

Annual Cumulated Index

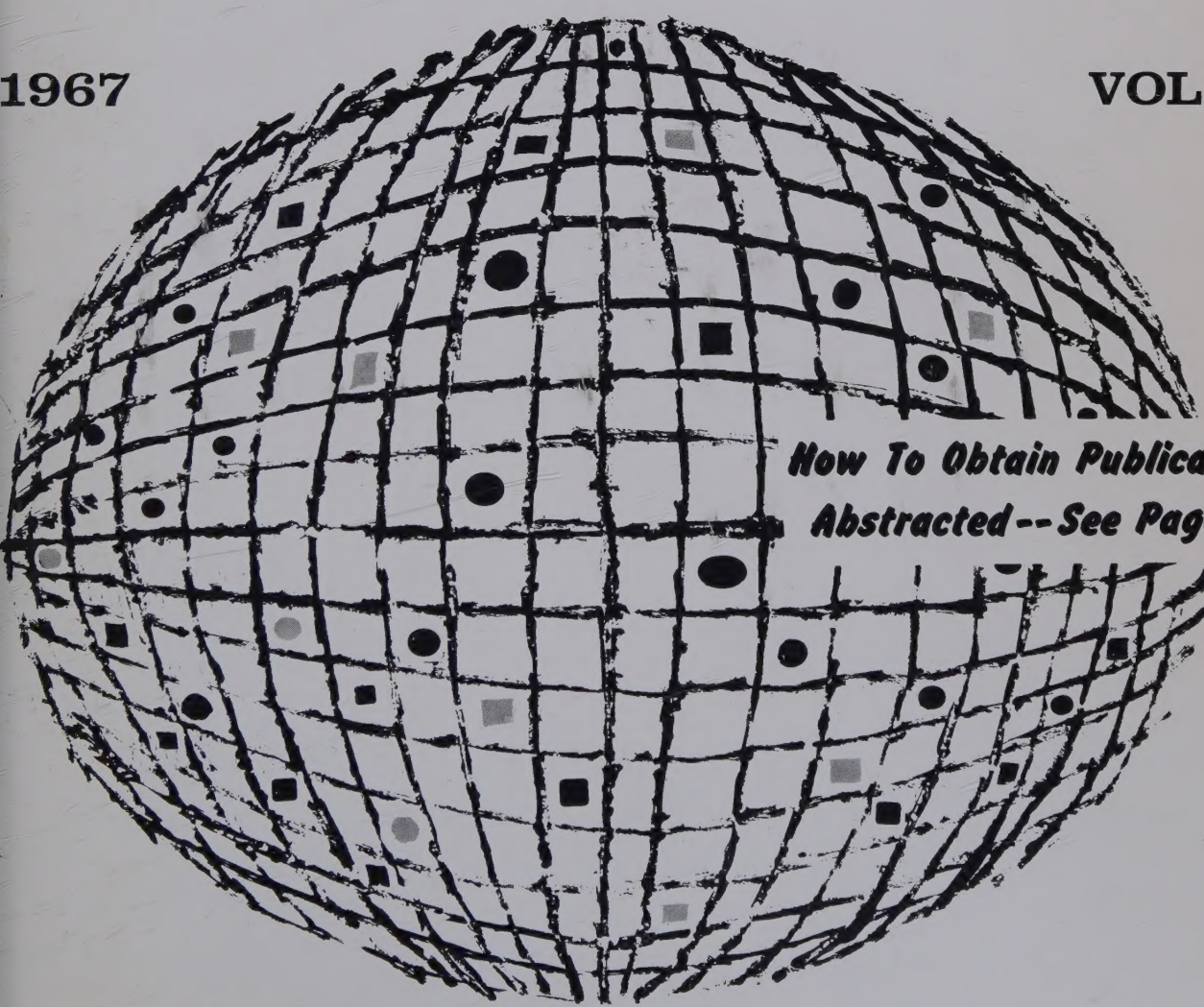
ACCESSION NOS. A67-10001 to A67-43116

INTERNATIONAL AEROSPACE ABSTRACTS

PART 2, SUBJECT INDEX, M - Z

1967

VOL. 7



*How To Obtain Publications
Abstracted -- See Page IV*

PUBLISHED BY THE TECHNICAL INFORMATION SERVICE
AMERICAN INSTITUTE OF AERONAUTICS AND ASTRONAUTICS

INTERNATIONAL AEROSPACE ABSTRACTS

Prepared and published by the TECHNICAL INFORMATION SERVICE,
AMERICAN INSTITUTE OF AERONAUTICS AND ASTRONAUTICS, INC., under
NATIONAL AERONAUTICS AND SPACE ADMINISTRATION
Contract No. NSR 33-003-009

T.L.
500
I57
vol. 7
index
pt. 2
NIC

ANNUAL CUMULATED INDEX

PART 2 SUBJECT INDEX, M - Z

VOLUME 7 JANUARY-DECEMBER 1967

ACCESSION NUMBERS A67-10001 to A67-43116

INTERNATIONAL AEROSPACE ABSTRACTS is published semimonthly by the Technical Information Service, American Institute of Aeronautics and Astronautics, Inc., at Phillipsburg, N. J.
Editorial and Subscription Offices: 750 Third Avenue, New York, N. Y. 10017
Telephone: 212 TN-7-8300 TWX: 212 867-7265

SUBSCRIPTION INFORMATION.

Semimonthly issues: United States and Possessions, 1 year, \$25 postpaid; Foreign Countries, 1 year, \$33 postpaid.

Cumulated Index Volumes: United States and Possessions, 1 year, \$25 postpaid; Foreign Countries, 1 year, \$33 postpaid.

Second-class postage paid at Phillipsburg, N. J.

Copyright © 1967 by the American Institute of Aeronautics and Astronautics, Inc.

CONTENTS

Pages

PART 1

INTRODUCTION	iii	
HOW TO OBTAIN PUBLICATIONS ABSTRACTED	iv	
CROSS REFERENCES	iv	
LIST OF PERIODICALS SCANNED	v	— xxi
SUBJECT INDEX, A - L	A1	— A894

PART 2

INTRODUCTION	iii	
HOW TO OBTAIN PUBLICATIONS ABSTRACTED	iv	
CROSS REFERENCES	iv	
SUBJECT INDEX, M - Z	A895	— A1871

PART 3

INTRODUCTION	iii	
HOW TO OBTAIN PUBLICATIONS ABSTRACTED	iv	
PERSONAL AUTHOR INDEX	B1	— B728
CONTRACT NUMBER INDEX	C1	— C69
MEETING PAPER AND REPORT NO. INDEX	D1	— D29
ACCESSION NUMBER INDEX	E1	— E148

STAFF, AIAA Administrator—Technical Information Programs, ROBERT R. DEXTER
STAFF, TECHNICAL INFORMATION SERVICE Director, JOHN J. GLENNON • Associate Director—
Administrative, THOMAS J. MESKEL • Associate Director—Technical, IRENE W. BOGOLUBSKY •
Manager—Information Systems, WILLIAM T. MORRIS, JR. • Index Editor, MILDRED C. OGDEN •
Supervisor—Abstracting Department, DAVID A. HOWELL • Chief Librarian, PATRICIA M. MARSHALL

Printed by Sheridan Printing Company, Inc.
 Phillipsburg, N. J.

INTRODUCTION

1127-19
INTERNATIONAL AEROSPACE ABSTRACTS (IAA) is an abstracting and indexing service covering the world's published literature in the field of aeronautics and space science and technology. IAA is issued semimonthly, on the 1st and 15th of each month.

Coverage of Published Literature

The following types of publications are covered in IAA:

- Periodicals (including government-sponsored journals) and books.
- Meeting papers and conference proceedings issued by professional societies and academic organizations.
- Translations of journals and journal articles.

Coverage of Reports ("Unpublished" Literature)

Abstracts and indexes of report literature are issued in SCIENTIFIC AND TECHNICAL AEROSPACE REPORTS (STAR), which is published by the Scientific and Technical Information Division, National Aeronautics and Space Administration.

By special arrangement between NASA and the American Institute of Aeronautics and Astronautics, IAA is issued in coordination with the twice-monthly schedule of STAR, which appears on the 8th and 23rd of each month.

IAA and STAR utilize both identical subject categories and indexes, which are described below.

Thus the two services provide comprehensive access to the national and international unclassified report and published literature of current significance to aerospace science and technology.

Arrangement of the Semimonthly Issues

IAA is arranged in two major sections:

- (1) Abstracts Section. This section contains complete bibliographic citations with informative abstracts, arranged by appropriate subject categories to facilitate scanning. The subject categories are numbered from 01 to 34, and the scope of each category is outlined in the Table of Contents and again at the beginning of each category in the Abstracts Section. Each abstract is prefixed by the IAA accession number.
- (2) Index Section. Four indexes are contained in this section: Subject, Personal Author, Meeting Paper and Report Number, and Accession Number. Each index is prefaced by explanatory notes to guide the user to the desired abstract.

Cumulated Indexes

Cumulated indexes are prepared and issued promptly at the end of each quarter year, with the 4th quarterly being the Annual Index.

Each cumulated index contains the following sections: A—Subject Index, B—Personal Author Index, C—Contract Number Index, D—Meeting Paper and Report Number Index, and E—Accession Number Index.

Guide to the Subject Indexes

A GUIDE TO THE SUBJECT INDEXES FOR STAR has been issued by the Scientific and Technical Information Division of NASA. This publication contains an alphabetic listing of the subject headings and cross-references used in both STAR and IAA indexes, which use the same subject terminology.

Subscribers to the IAA Cumulated Indexes may obtain copies of the guide by writing to the AIAA Technical Information Service, 750 Third Avenue, New York, N.Y. 10017.

Information regarding SCIENTIFIC AND TECHNICAL AEROSPACE REPORTS and the availability of INTERNATIONAL AEROSPACE ABSTRACTS to organizations having contractual arrangements with NASA may be obtained from the following address:

National Aeronautics and Space Administration
Scientific and Technical Information Division
Attention: Code USS-A
Washington, D. C. 20546

how to obtain publications abstracted

All publications abstracted are available from the AIAA Technical Information Service.

Document services are provided as follows:

- Paper copies of accessions announced in *IAA* and of other published articles in the TIS library are available at \$3.00 per document, regardless of the number of pages.
- Paper copies of accessions announced in *Scientific and Technical Aerospace Reports (STAR)* and of similar unpublished reports in the TIS library are available at the rate of \$0.25 per page, minimum order \$3.00.
- Microfiche of documents announced in *IAA* are available at the rate of \$0.50 per microfiche on demand. Documents available in this manner are identified by the symbol # following the accession number in the Abstracts Section and in the Meeting Paper and Report Number and the Accession Number Indexes.
- Minimum air-mail postage to foreign countries is \$1.00.

Address all inquiries and requests to:

TECHNICAL INFORMATION SERVICE
AMERICAN INSTITUTE OF AERONAUTICS
AND ASTRONAUTICS, INC.
750 Third Avenue, New York, N. Y. 10017

A number of publications, because of their special characteristics, are available only for reference in the library.

PLEASE REFER TO THE ACCESSION NUMBER WHEN REQUESTING PUBLICATIONS.

Telephone: 212 TN-7-8300
TWX: 212 867-7265

NOTE: The AIAA does not sell the publications abstracted except those issued by AIAA.

CROSS REFERENCES

The subject index includes two types of cross references to aid the user of the index in locating the material being sought:

1. "SEE" references (S) direct the user to alternate headings under which material on the subject will be found, for example:

COLUMBIUM
S NIOBIUM

2. "SEE ALSO" references (SA) refer the user to additional headings in the same subject area, for example:

LUMINESCENCE
SA ELECTROLUMINESCENCE

LIST OF SUBJECT HEADINGS OF
PUBLICATIONS

A Notation of Content, rather than the title of the publication, appears under each subject heading; it is listed under several subject headings which provide multiple access to the subject content of each accession. The IAA accession number is located under and to the right of the Notation of Content. It is preceded by numbers identifying the issue and page of International Aerospace Abstracts where the abstract is located.

To illustrate:

Issue Number	Page Number	Accession Number
	01	p0007 A67-11162

M**M-1 ROCKET ENGINE**

M-1 Engine Thrust Chamber Assembly test facilities and analog computer simulation during checkout
[AIAA PAPER 67-455] 18 p3019 A67-33929

M-1 engine system technology items noting thrust chamber assembly, gas generator, fuel turbopump, etc
[AIAA PAPER 67-520] 18 p3115 A67-33983

M-2 LIFTING BODY

Joint NASA-USAF lifting body flight test program and M2/F2, HL-10 and SV-5P research vehicles
06 p0947 A67-18197

M-REGION

Sporadic E layer stratification and morphology of M and N reflections produced by transparent and semitransparent E layer
05 p0799 A67-17029

High altitude atmospheric turbulence research on Reynolds number and vertical drift velocity gradients of M zone
05 p0799 A67-17030

Search for solar M-regions complicated by velocity decrease near active sun, considering corpuscular streams as enhanced solar wind
16 p2749 A67-31414

MA-1 FLIGHT DIRECTOR SYSTEM

Digital computers for built-in self-test in airborne weapon system, with examples of mechanized tests from F-106/MA-1 system
20 p3392 A67-36989

MACH INERTIA PRINCIPLE

London moment of rotating superconductors and relation to Lense-Thirring fields of general relativity
01 p0134 A67-10812

Mach principle as consequence of de Sitter universe filled with Dirac dust
05 p0847 A67-16803

Mach principle manifestation in Jordan extended gravitation theory, calculating rotation of local inertial frame induced by rotating shell of mass
23 p4027 A67-41147

MACH NUMBER**SA CRITICAL MACH NUMBER**

Supersonic MHD generator crisis possibility assuming quasi-one-dimensional nonheat-conducting approximation at small Reynolds numbers and plasma scalar conductivity
01 p0011 A67-10177

Fuel requirements for high altitude high-Mach number aircraft noting thermal stability, autooxidation, self-ignition, specific heat, etc
[DVL-599] 03 p0502 A67-13015

Base pressure measurements on sharp and blunt 9 degree cones at Mach 3.50 to 9.20
04 p0547 A67-14851

Mach number and temperature ratio effects on convective heat-transfer coefficient to flat plate through turbulent boundary layer in air and Stanton number calculation in terms of drag coefficient
04 p0731 A67-15820

Mach number effect on flutter characteristics of thin cantilever wings analyzed in transonic blowdown wind tunnel, presenting results as flutter speed ratios
05 p0747 A67-16440

Mach number effect on mixing lengths

and kinematic eddy viscosities in turbulent flat plate boundary layer

Tests at Mach 8 on cone, analyzing effect of roughness elements and variable entropy on transition and heat transfer distribution
[AIAA PAPER 67-199] 06 p0987 A67-18324

Hydrogen or nitrogen gas injection at various Mach numbers from nozzle in flat plate into Mach 2.72 free air stream
[AIAA PAPER 67-225] 06 p0940 A67-18444

Aerodynamic characteristics of Mars probe/lander configurations consisting of blunted cone, shell and spherical segment analyzed at various Mach numbers on ballistic range
[AIAA PAPER 67-167] 06 p0941 A67-18482

Specific impulse and thrust coefficient performance as function of flight Mach number and altitude for air augmented solid propellant propulsion vehicle using supersonic combustion
[AIAA PAPER 67-226] 06 p1097 A67-18517

Partial diaphragm when applying supersonic Mach box method for steady state condition and uniform downwash on wing compared with complete diaphragm
06 p0944 A67-18875

Laminar boundary layer separation length data in hypersonic flow show strong Mach number dependence
06 p0992 A67-18878

Effect of Mach number and specific heat ratio on distance of shock wave from end face of circular cylinder in axisymmetric flow
07 p1126 A67-19347

Pressure amplitude at resonance decreasing with increasing Mach number observed as effect of mean flow on wall damping of finite amplitude gas pulsations
07 p1168 A67-19576

Mach and cavitation number effects in fluid dynamic elements and circuits such as operating pressure limit, power consumption and output
08 p1320 A67-20455

Reynolds number and ratio with Mach number as similarity parameters in fluidic devices with significant compressibility and viscosity
08 p1283 A67-20471

Boundary layer transition measurements of contoured nozzle flow at hypersonic Mach numbers
08 p1320 A67-20584

BGK intermolecular collision model of sphere drag at high Knudsen numbers and low Mach numbers
08 p1322 A67-21140

Mach number effect on hypersonic flow past delta wing with blunt edges at zero angle of attack
10 p1590 A67-23036

Free flight response of two panels subjected to turbulent pressure fluctuations at supersonic Mach numbers
10 p1719 A67-23558

Asymptotic analysis of radiative Rayleigh problem in flow of compressible viscous heat-conducting radiating gray gas extended to high plate Mach numbers
11 p1774 A67-23855

Thirteen moment equation solved for problem of plane Couette flow by iteration scheme, showing functional dependence on Mach and Knudsen numbers
11 p1774 A67-23863

Rogallo wing aerodynamic characteristics compared for various wing configurations and Mach numbers for possible application to spacecraft recovery
11 p1869 A67-24093

Laminar heat transfer rate to two-dimensional blunt base in supersonic flow evaluated for varying Reynolds, flow and shock Mach numbers
11 p1882 A67-24222

Hypersonic transport design, considering payload vs range and weight and power plant, aerodynamic, structural and flight profile problems
11 p1744 A67-24579

Drag coefficients of hypersonic optimum bodies at nonoptimum Mach numbers
12 p1892 A67-25744

Model tests on free jet scramjet facility configurations at high Mach numbers, obtaining data on bypass flow pressure recovery and diffusion
13 p2089 A67-26830

Numerical solution of initial and boundary value Rayleigh problems for nonlinear Krook equation at large wall

velocities 13 p2102 A67-26968
Hemispheric pressure distributions, measuring effect of Mach number, hole size and angular position of hole on Pitot pressure 13 p2220 A67-27193

Vortices in plane flow behind circular cylinder at different Mach numbers, noting staggered pattern formation 14 p2296 A67-27988

Automatic fluoric gain changer circuit for flight control systems counteracting Mach number and altitude pressure effects 14 p2251 A67-28352

Performance of low energy-density electric shock tube in helium driver 14 p2293 A67-28752

Gas-ionizing shock wave with zero electrical conductivity of gas in front of shock wave and infinite conductivity behind 15 p2470 A67-29310

Shock wave shapes around spherical and cylindrical-nosed bodies, assuming hyperbolic profile asymptotic to freestream Mach angle or attached shock angle 15 p2417 A67-29448

Single-fluid model accounting for behavior of MHD shock producing devices with unseparated shock and driving current sheet 15 p2528 A67-29565

Laminar boundary layer transition in hypersonic shock tunnel of cone, noting effect of high Mach numbers and tip surface roughness, using surface heat transfer gauges 15 p2418 A67-30191

Optimum Mach number for nonequilibrium helium-cesium plasma flow in MHD generator, explaining effect of deceleration temperature and internal efficiency level on optimum pressure 16 p2604 A67-30570

Magnetoacoustic shock waves front in rarefied plasma disintegration at high Mach numbers as cause of increase in front wave duration and width 16 p2714 A67-31039

Mach number effect on location of head shock wave and flow stability at slightly supersonic velocities for various body shapes 16 p2593 A67-31129

Shock-wave separation dependence on bluntness degree, Mach number and gas type during supersonic motion of ellipsoids of revolution 16 p2675 A67-31130

Shape dependence of detached shock wave in supersonic gas flow of blunt-nosed models on Mach number, heat capacity and bluntness ratio 16 p2593 A67-31131

Position determination of sonic points on head shock wave and blunt body surface in ballistics showing Mach number and gas type effects 16 p2593 A67-31132

Rotor-hovering performance-prediction with test data showing discrepancy increase with wake contraction, blade loading, tip Mach number and blades number [AHS PAPER 100] 16 p2594 A67-31817

Helicopter rotor at high Mach numbers, noting thin blade tips and compressibility effects and tests in wind tunnel [AHS PAPER 102] 16 p2595 A67-31819

Nozzle and membrane effects on shock wave intensity in tube, showing graphically Mach number dependence upon initial pressure 17 p2837 A67-32345

Mach and Reynolds numbers effect on rarefied supersonic gas flow pattern near forward stagnation point of blunt body, noting decrease in density 18 p3028 A67-34209

Aerodynamic characteristics of Mars probe/lander configurations consisting of blunted cone, shell and spherical segment analyzed at various Mach numbers on ballistic range [AIAA PAPER 67-167] 19 p3169 A67-34816

Compressibility effects on airfoils during high subsonic and low speed stalls, considering Reynolds and Mach number effect 19 p3170 A67-35521

Dynamic stability analysis of bodies of revolution, in supersonic flow, using characteristics method [AIAA PAPER 67-807] 19 p3172 A67-35998

Axisymmetric flow equations for performance prediction of axial-flow turbomachines and stage

design 20 p3355 A67-36186
 Mean heat transfer coefficient at flat plate with turbulent boundary layer at zero incidence Mach numbers mean heat-transfer coefficient at flat plate with turbulent boundary layer at zero incidence 20 p3543 A67-36275
 Mach High altitude variable Mach number test cell for testing intake system of Concorde aircraft Olympus 593 20 p3414 A67-36497
 Laminar and turbulent free shear layers analysis unifying treatment of mixing layers, assessing Mach number, Prandtl number and temperature ratio effects on constant pressure mixing [ASME PAPER 67-HT-81] 20 p3551 A67-36759
 Diffracting shock wave profile for various corner angles and wall shock Mach numbers, comparing experimental and theoretical results 20 p3422 A67-36847
 Transpiration cooled vehicles correlation with compressible turbulent boundary layer with mass transfer, emphasizing high Mach number 20 p3423 A67-37256
 Stagnation-point flow of rarified gas, using linearized BGK model of Boltzmann equation with small Mach number 20 p3425 A67-37673
 Mach number effect on electron temperature structure of partially ionized monatomic and diatomic gas shocks 21 p3610 A67-37760
 Incident and reflected shocks from laminar and turbulent boundary layers measured over various Mach numbers 21 p3610 A67-37771
 Hydrogen or nitrogen gas injection at various Mach numbers from nozzle in flat plate into Mach 2.72 free air stream 21 p3610 A67-37800
 Stretched sail behavior in sonic, supersonic and hypersonic flows, discussing profile dependence on angle of attack and free-stream Mach number 21 p3563 A67-37889
 Transitional and turbulent boundary layers on cold flat plate in hypersonic flow noting bluntness, Reynolds and Mach numbers effects 21 p3615 A67-39080
 Supersonic aircraft evolution emphasizing Dassault series, Northrop T-38 and F-5 and Swedish Draken and Viggen 22 p3746 A67-39883
 Base pressure behind circular projection in Laval nozzles, measuring dependence on specific heat ratio at different Mach numbers by varying gas 22 p3741 A67-40021
 Multiple reflection of molecules effect on nonconvex wing aerodynamic characteristics for finite Mach number lateral free molecular flow 22 p3741 A67-40022
 Reattachment of two-dimensional compressible air jets to planes, discussing pressure maximum and inlet Mach numbers 22 p3786 A67-40068
 Advanced high Mach number aircraft secondary power system requirements, discussing high pressure hydraulic systems and complex pneumatic positioning control systems 22 p3749 A67-40341
 Nozzle form optimization from Mach distribution in supersonic region, defining perturbation functions 23 p3929 A67-41248
 Aircraft wing drag noting relation between Mach number, thickness chord ratio, aspect ratio, airfoil shape and wing configuration 23 p3930 A67-41306
 Transonic and supersonic grid wind tunnel loaned to Germany by NASA for testing blades 23 p3987 A67-41328
 Design characteristics of various SST, discussing Mach numbers and wing configuration 23 p3935 A67-41398
 Ar atomic beam produced by plasma burner measured for kinetic energy and Mach number 24 p4198 A67-42576
MACH-ZEHNDER INTERFEROMETER
 Mach-Zehnder interferometer study of fluctuations in turbulent wakes of slender cones and spheres in ballistic flight [AIAA PAPER 65-809] 01 p0007 A67-11166
 One-dimensional refractive index distribution using power series expansions for refractive index and ray traces obtained from relation of inhomogeneities and interference pattern of Mach-Zehnder interferometer 03 p0423 A67-13908
 Mach-Zehnder interferometer used with axisymmetric free flight models at hypersonic speeds, noting isopycnals and light gas gun 05 p0789 A67-17355
 Laser interferometry and photon scattering in high temperature plasma diagnostics 09 p1536 A67-21602
 Two-beam Mach-Zehnder and Michelson

interferometers using coherence properties of lasers, construction and applications 10 p1652 A67-22709
 New MZI technique for detecting fringe shift across discontinuity as in shock tube or in shock tunnel flow 12 p1926 A67-25938
 Behavior of electromagnetically accelerated shock waves investigated by Mach-Zehnder interferometer 15 p2488 A67-29663
 Time varying high density laser induced plasmas formed in high pressure gases studied using Mach-Zehnder interferometer 15 p2488 A67-29903
 Shock waves generated electromagnetically in T-tube studied with Mach-Zehnder interferometer 19 p3208 A67-35396
 Mach-Zehnder-Rozhdestvenski interferometer design for training studies of supersonic and subsonic gas flows and anomalous dispersion 20 p3452 A67-37556
 Heat transfer analysis using Mach-Zehnder interferometer with laser light source for applications to spacecraft electronics 21 p3731 A67-37959
 Strong blast waves and laser generated plasma dynamics in high pressure gas investigated using Mach-Zehnder interferometer and pressure probe measurements [AIAA PAPER 67-696] 21 p3672 A67-38725
MACHINE
 S DRAFTING MACHINE
 S FINITE-STATE MACHINE
 S GRINDING MACHINE
 S GROUND EFFECT MACHINE
 S MILLING MACHINE
 S READING MACHINE
 S ROTATING MACHINE
 S SEQUENTIAL MACHINE
 S TURBOMACHINE
 S WELDING MACHINE
 S ZETA MACHINE
MACHINE LANGUAGE
 SA ERROR DETECTING CODE
 SA FORTRAN
 Nonprocedural programming formal system for differentiation of mathematical formulas by digital computer 03 p0375 A67-13561
 Unsolvability of recognition of linear context-free language, searching for algorithm and generalizing to metalinear languages 03 p0375 A67-13562
 On-line computation and man-computer interactive languages, discussing JOSS, MADCAP and Klerer-May systems 11 p1756 A67-24249
 Properties of favorable coding schemes, applying results to text transmission through auditory and tactile senses 12 p1907 A67-26081
 Effects of placing restrictions on derivations of unrestricted rewriting systems 12 p1962 A67-26120
 Digital computer languages in relation to engineering design problems 13 p2073 A67-27189
 Problem oriented language for mechanical problems programming applied to steady state vibrations, static problems and stress-strain relation 14 p2276 A67-29000
 Computational error caused by finite word length of aerospace computers 15 p2439 A67-29596
 Interlocking plan for entire countdown checkout process by combining subsystems simulated as partially controlled stochastic process 15 p2441 A67-30166
 K-multiple automata for language recognition or generation, discussing generalization from simple to multiple automata 19 p3202 A67-35607
 Associative memory system of persistent current bit-cells using cryotrons in selection and control network 21 p3587 A67-37955
 Spatial filters for code translation and image sharpening produced by holograph in reasonably good approximation 24 p4159 A67-43097
MACHINE LEARNING
 Anthropotechnique as scientific discipline, discussing environmental layout, adaptation of machine to man and limits of intelligent machine handling 04 p0562 A67-14539
 Learning machines used for classifying measurement data of objects representable as points in n-dimensional space after training by forced learning 10 p1654 A67-22757
 Modified perceptron procedure for nonseparable cases, minimizing error probability and introducing reinforcement factors 12 p1961 A67-26064

Flight simulator experiments test plots ability to disregard senses and trust only flight control instruments 14 p2255 A67-28220
 Learning control systems, discussing adaptive time, searching, strategy, teaching, association, principle and behavior 22 p3776 A67-39412
 Learning threshold element circuit employing electrochemical controllable resistors as weight factors 22 p3809 A67-40480
MACHINE LIFE
 Soviet papers on friction and wear in machinery covering elastorheology and equilibrium stability of rigid rotor 22 p3811 A67-39315
 Soviet papers on dynamics and strength of machines, Issue 4 23 p4075 A67-40678
MACHINE RECOGNITION
 Unsolvability of recognition of linear context-free language, searching for algorithm and generalizing to metalinear languages 03 p0375 A67-13562
MACHINE STORAGE
 MECCA /mechanized catalog/ system designed to produce printed library catalogs and to generate data bank for later machine retrieval 02 p0207 A67-11812
MACHINE TOOL
 SA BELLOWS
 SA DIE
 SA DRILL
 SA PULLEY
 Pulsed lasers as machine tools for material removal, noting tests on titanium, aluminum oxide, steel, etc 04 p0628 A67-15308
 Fluidic digital rectilinear displacement indicator emphasizing transducer, logic circuitry and readout 08 p1281 A67-20456
 Spring controlled pneumatic switching units for switching machine operations and interlocking of machine controls 08 p1282 A67-20468
 Influence of explosive forming characteristics on springback based upon tests in forming of gore sections for Saturn V rocket 10 p1660 A67-23170
 Computer programming or software techniques in relation to hardware elements of computer graphics system [ASTME PAPER WES-7-02] 11 p1756 A67-24253
 Book on machining Alcoa aluminum covering Al alloys properties, requirements for machine tools, cutting conditions and compounds, finishing operations, etc 18 p3053 A67-33771
 Machines and machining technology for materials used in Mach-3 aircraft structures, discussing cutting fluids, cutter and best metal removal rate 21 p3631 A67-38014
 Plastic deformation during metal cutting, deriving metal deformation, cutting tool stressed state and temperature as function of particle trajectories 21 p3637 A67-38923
 Beryllium component machine tool installations and operation, discussing contamination protective systems for toxic dust 23 p4009 A67-40687
 Machining advantages and economy of annealed steels over maraged steels 23 p4010 A67-41352
 Graphics system for space vehicle design and flight plan via light pen, trajectory computation and performance curve display on scope [AIAA PAPER 67-897] 24 p4126 A67-43006
MACHINE TRANSLATION
 SA LANGUAGE PROGRAMMING
 Automatic mathematical translation /AMTRAN/ system, remote terminal conversational-mode computer system that eliminates need for specialist programmer for large class of routine problems 02 p0206 A67-11811
MACHINING
 SA ELECTROCHEMICAL MACHINING
 SA ELECTROLYTIC MACHINING
 SA FINISH
 SA SPARK EROSION MACHINING
 SA TOOLING
 SA ULTRASONIC MACHINING
 Book on thermal effects and cutting machinability of aircraft materials 03 p0427 A67-13190
 Single pulsed electron beam used in machining and imaging modes for creating machine scan device 04 p0623 A67-15316
 Copy machining of thin walled propulsion duct pivot support tube used in Bell V-STOL aircraft 06 p1008 A67-18724
 Machining techniques for paper-base and glass-base laminates of various grades for

printed circuit boards 08 p1334 A67-20742
Laser welding and machining - Seminar, Pennsylvania State University, June-July 1965 09 p1504 A67-22137
Synchro-turn system for precision machining of beryllium mirrors 10 p1659 A67-22988
Bending fatigue tests of unmachined, mechanically machined and chemically machined panels of aluminum and titanium alloys 10 p1669 A67-23437
Cut-off turning test on 40 mm Al bar, effect of mineral oil and kerosene on cutting depth and speed and of feed on tangential force and chip size 11 p1809 A67-24945
Machining damage in beryllium from single point turning and drilling 13 p2123 A67-27133
Semiconductor integrated circuit slices interconnection processes, using gas laser for thermal micromachining 14 p2281 A67-28023
Machining advantages and economy of annealed steels over maraged steels 23 p4010 A67-41352
Beryllium part fabrication by metal removal, discussing machining and surface treatment methods [SAE PAPER 670803] 24 p4159 A67-41990
MACLAURIN SERIES
Solution of second order differential equation containing continuous function expandable in Maclaurin series, using Volterra integral equation 02 p0260 A67-12668
Control system synthesis based on approximation principle using transfer function expansion in Maclaurin series 06 p0978 A67-18559
Deformed figures of Maclaurin spheroids from solving post-Newtonian hydrodynamic equations for uniformly rotating axisymmetric bodies 08 p1354 A67-21245
Gamma function concept for varying difference interval and complex argument 11 p1812 A67-23966
Asymptotic integration technique for small axisymmetrical oscillations of thin walled elastic shell of revolution for case of double reversal point 12 p2029 A67-25675
Maclaurin series expansion representation of generalized heat equation 13 p2147 A67-27454
MACROMOLECULE
Relation between acid-basic state and conductivity for polyaniline macromolecular semiconductors such as emeraldines 01 p0130 A67-10196
Water and internal acidity effect upon oligomeric polyanilines semiconductivity 01 p0130 A67-10197
Biological macromolecule detection using thiacarbocyanine dye and observation of absorption spectra changes 15 p2426 A67-29115
Nonlinear macroscopic rheological behavior of dilute suspensions of deformable spheres 17 p2887 A67-32280
MACROSCOPIC EQUATION
Validity of Onsager-Casimir reciprocal relations with the theoretical framework of macroscopic nonequilibrium thermodynamics 07 p1268 A67-19574
Hamilton-Jacobi solutions for Vlasov equation leading to nonsecular perturbation theory for macroscopic quantities 10 p1686 A67-23469
Plasma oscillations, discussing kinetics, macroscopic and Vlasov equations, Landau damping and beam instabilities [AFOSR-66-2823] 19 p3299 A67-35871
Fluctuating light scattering cross section and Lorentz-Lorenz refractive index formula derived from microscopic equations 20 p3483 A67-36174
Turbulence theory from local equilibrium breakdown macroscopic approach by imposing suitable conditions on correlation functions, discussing stochastic Navier-Stokes equations 22 p3782 A67-39500
MAGMA
SA LAVA
Magmatic origin of chondrule meteorites, considering structure, electron probe microanalysis, crystallization and equilibrium 13 p2200 A67-27234
MAGNESIUM
Magnesium wire as in-contact masking material, with surfaces precoated with thin silver layer 03 p0494 A67-13490
Fermi-Dirac statistics, transverse magnetoresistance and galvanomagnetic properties of hexagonal-close-packed Mg and Zn 03 p0495 A67-13511

Existence of cosmic-ray-produced Mg-28 radionuclide in rain 04 p0692 A67-14495
Mossbauer investigations of stoichiometric manganese-ferrite and two magnesium-manganese ferrites made at room and liquid nitrogen temperatures 04 p0676 A67-14925
Differential cross sections corresponding to excitation of seven states of residual nucleus in Al-Mg reaction at 20.9 Mev 05 p0849 A67-17381
Thermal conduction paths for magnesium joints in cordwood mounting of electronic parts in heat conducting plate 05 p0929 A67-17451
X-ray line broadening in deformed magnesium by Fourier analysis of line shapes and analysis of line widths, noting lattice distortion 07 p1210 A67-20108
Electrical resistance and weight increase measurements in aluminum and Al-Mg alloys, noting relation between oxidation rate and Mg content during annealing 08 p1341 A67-20796
Equilibrium temperatures of Fe and Mg ions in chondritic meteorites 08 p1400 A67-21266
Temperature dependence of magnetization and resistivity in SHF magnesium-aluminum ferrite 10 p1688 A67-22830
Gas-shielded stud welding of magnesium 12 p1950 A67-25739
UV spectra of Mg III and Mg IV investigated by sliding spark in vacuum, noting various ionization charges in vacuum 14 p2351 A67-28944
Vacuum effect on tensile, creep and fatigue properties of magnesium polycrystals and on tensile properties of oriented magnesium single crystals 15 p2503 A67-29561
Resonance line profiles for Ca II and Mg II in lower solar chromosphere, noting interlocking effect 19 p3325 A67-35504
Differential cross sections for inelastic large angle alpha particle scattering from unnatural parity states in Mg showing diffraction pattern 20 p3488 A67-36931
Twin lamellae in magnesium examined by electron microscopy reconfirms double twinning sequence 24 p4173 A67-42345
MAGNESIUM ALLOY
Tensile deformation behavior of commercial aluminum-5 percent magnesium alloy, correlating uneven yielding regions with occurrence of markings on specimen surface 01 p0093 A67-10060
High strength magnesium casting alloys for aerospace applications, based on heat treatment involving internal precipitation of hydride [SAE PAPER 660656] 01 p0094 A67-10615
Mg-Nd alloy structure development during plastic deformation at high temperature, noting lattice distortions and recrystallization process 02 p0255 A67-11868
Ti-Mg alloy production under high pressure, noting existence of solid solution of one weight-percent Mg 03 p0441 A67-13255
Magnesium alloys in aircraft and space vehicle construction, discussing production, processing and properties 04 p0638 A67-14983
High internal damping properties of magnesium alloy with zirconium addition 04 p0638 A67-15175
Longitudinal and shear wave velocities in polycrystalline sample of magnesium thorium alloy measured by pulse transmission technique as function of temperature [ASME PAPER 66-WA/MET-11] 04 p0639 A67-15375
High temperature steady state creep rate analysis of pure Ag and internally ionized Ag-Mg alloys 06 p1014 A67-17805
Aerospace castings from light ternary Mg-Li-Si alloy, discussing fabrication development 07 p1193 A67-20254
Static and fatigue properties of repair welded aluminum and magnesium premium quality castings 08 p1333 A67-20360
Kinetics of two-phase decomposition of solid solution of magnesium-aluminum alloy using X-ray analysis, noting grain orientation and size 08 p1342 A67-20810
Bond strength of magnesium alloys as affected by surface preparations, specific alloy and adhesive type 09 p1507 A67-22521
Roll fatigue tests of forged ZK60A-T5 magnesium and 2014-T6 aluminum wheels 10 p1661 A67-23439
Optical absorption of Al and some Al-Mg alloys in region from 0.7 to 2.0 ev investigated by conventional polarimetric reflection technique 10 p1696 A67-23773
Cerium addition effects on magnesium workability evaluated by sample elongation

in tension test and plate working limit in cold rolling 15 p2505 A67-30398
Magnesium and magnesium alloy corrosion, discussing treatments for prevention of various kinds of corrosion 20 p3466 A67-36637
Dilute magnesium addition effect on growth and shrinkage of dislocation loops in aluminum studied by isothermal annealing of thin foils 21 p3644 A67-38088
Aluminum magnesium alloys prepared by powder metallurgy and hot extrusion evaluated for tension, compression, impact, fatigue and creep 22 p3821 A67-40053
Spontaneous inflammability temperatures of Al, Mg and Al-Mg alloy powders measured noting moisture effect 22 p3919 A67-40325
Aluminum-magnesium alloy dislocation networks structure and formation investigated by thin foil technique after rapid solidification 23 p4017 A67-40658
High vacuum environment and vacuum outgassing time effects on magnesium alloys fatigue properties under constant load and reversed bending 24 p4172 A67-42037
MAGNESIUM COMPOUND
Lattice heat capacities, Debye temperatures, heat capacity, free formation energy and thermodynamic functions of groups II-IV semiconductors 23 p4047 A67-41533
MAGNESIUM FLUORIDE
Association energy of vacancy-impurity dipole obtained from electrical conductivity of magnesium fluoride-doped lithium fluoride at ambient temperature 12 p1978 A67-25149
Magnesium fluoride double Rochon prism used as polarizer or analyzer in vacuum UV wavelengths 15 p2491 A67-30425
Optical properties of magnesium fluoride in EUV from reflectivity measurements on crystal and thin films 18 p3099 A67-33692
MAGNESIUM OXIDE
Microprobe study of impurities in hot-pressed polycrystalline MgO compact and existence of significant grain boundary volume [JPL-TR-32-1015] 01 p0131 A67-10262
Compacting effect of additive oxides of Ti, Zr, Si, Fe, Zn and Al on hot pressing of MgO 01 p0102 A67-11243
Plasma arc tunnel tests show thermochemical heat of ablation of magnesite strongly dependent on stagnation enthalpy [AIAA PAPER 65-641] 03 p0449 A67-13061
Identification of molecular bands of spectrum of large sunspot, detecting presence of magnesium oxide 03 p0512 A67-13887
Forces holding hydroxyl ions to surfaces of MgO particles 04 p0642 A67-15087
UV optical properties and electronic band structure of magnesium oxide 13 p2181 A67-27167
Molecule dissociation in meteoric trains, discussing coordinate system to determine cross sections for dissociation of magnesium and silicon oxides 14 p2383 A67-27945
Plastic accommodation in Mg O idealized as linear array of continuously distributed edge dislocations to study crack nucleation 16 p2775 A67-31326
Magnesium oxide and lithium fluoride in far UV, noting refractive and absorption indices 16 p2734 A67-31881
Flow stress of fresh dislocations in titanium and vanadium doped MgO single crystals, measuring dependence on heat treatment and test temperature 18 p3097 A67-33492
Magnetic field induced hyperfine structure in mono- and divalent iron ions in magnesium and calcium oxide, showing evidence of paramagnetic resonance 20 p3506 A67-36211
Magnesium oxide single crystal electronic spectrum obtained from reflectance spectra, observing large plasma peak in energy loss function 20 p3509 A67-36508
Cathodoluminescence device for rapid identification of phase assemblages in solid state reaction system magnesium oxide-magnesium silicate /enstatite/ 21 p3630 A67-38848
Adsorbed ions and organic molecules effect on mobility of half-loops dislocation introduced by indenter into MgO surfaces 23 p4035 A67-40655
MAGNET
SA ELECTROMAGNET
SA FERRIMAGNET
SA SUPERCONDUCTING MAGNET
Behavior of magnet and ball in gravitational field in five-dimensional

continuum 01 p0060 A67-10366
Low power MPD arc thruster design and performance with radiation cooled electromagnets and permanent magnets [AIAA PAPER 67-50] 06 p1074 A67-18436
Periodic permanent magnet assemblies for traveling wave tube design, employing magnet stack design curves and demagnetization curves 09 p1476 A67-22210

MAGNETIC ABSORPTION

Oscillatory magnetoabsorption of direct transition in layer compound gallium selenide near absolute 06 p1060 A67-18918

MAGNETIC AMPLIFIER

Amplitudes and phase angles of harmonic components of output current of operating circuits of transistorized magnetic amplifiers 07 p1150 A67-19209
Effect of degree of coupling between resonator system and load on generation zones and regenerative amplification of pulsed magnetron, noting characteristics 08 p1305 A67-21271
Operation modes of electron beam generators with resonant oscillating systems and bipolar regenerative amplifiers developed from them 08 p1305 A67-21272
Choke-coupled magnetic amplifiers and amplifiers with rotational magnetization, considering multicycle and single-cycle amplification 21 p3593 A67-38290
Magnetron type microwave amplifier gain increase, discussing electron beam interaction region M-type device gain calculations 22 p3770 A67-39654

MAGNETIC ANNULAR ARC

Axial current distribution in exhaust of magnetic annular arc, examining effect of entrainment on thrust measurement 06 p1075 A67-18850

MAGNETIC ANNULAR SHOCK TUBE

/MAST/
Gas-ionizing shock wave with zero electrical conductivity of gas in front of shock wave and infinite conductivity behind 15 p2470 A67-29310
Magnetic annular arc /MAARC/ driven shock tube design, construction and performance, stressing radiation loss prevention 21 p3806 A67-37774

MAGNETIC ANOMALY

SA GEOMAGNETIC ANOMALY
Computer program for gravity and magnetic profiles across two-dimensional bodies of arbitrary shape 06 p0998 A67-18736
Space time distribution of magnetic activity during IGY, noting elliptical region about magnetic pole characterized by increased activity 17 p2848 A67-32950
Geomagnetic field structure determination by method used to divide geomagnetic field observed along limited magnetic profile derived from mathematical apparatus of correlation analysis 23 p3994 A67-40715
Electron content of topside ionosphere studied for equatorial anomaly during diurnal variations 24 p4148 A67-42063
Anomalous electron heating rate in plasma region traversed by magnetic shock wave obtained by electron velocity distribution observation 24 p4198 A67-42736

MAGNETIC CIRCUIT

High speed magnetic logic circuits for operation in nuclear radiation environment 02 p0219 A67-12161
Functional converters of magnetic type for mathematical operations with analog computers 09 p1498 A67-22032
Monograph on high power semiconductor-magnetic pulse generators, noting saturable inductors and silicon controlled rectifiers, circuit analysis, voltage regulator, etc 09 p1482 A67-22698
Moving coil and variable air gap electromagnetic actuators, discussing characteristics and applications 14 p2247 A67-28266
Displacement detector operating on Hall effect basis with differential magnetic circuit, including displacement transmitters with unified output 21 p3626 A67-38159
Pure magnetic integrated logic circuit for space research, noting improvement on speed factor 21 p3588 A67-38675

MAGNETIC COIL

Various magnetic coil systems and parameters for MHD generator use 01 p0011 A67-10050
Traveling field and coil symmetrization of induction machine with open magnetic loop 01 p0012 A67-10187
Plasma trap configuration parameters

inside solenoid wound about circular torus, noting magnetic surface distortion as function of screw axis period and curvature 01 p0121 A67-10342
Quantum paramagnetic traveling wave amplifier using rutile with admixture of chromium and combined with magnet with superconducting coil 05 p0825 A67-17161
Plasma trap configuration parameters inside solenoid wound about circular torus, noting magnetic surface distortion as function of screw axis period and curvature 11 p1843 A67-25015
Traveling field in gap of induction machines with open magnetic circuit created by linear winding load 16 p2723 A67-31583
Design schemes for magnetic systems of vortex MGD generators with external and internal winding 16 p2609 A67-31585
Various magnetic coil systems and parameters for MHD generator use 17 p2804 A67-33328
Coil and dipole systems for magnetic testing of large spacecraft 20 p3415 A67-36612

MAGNETIC COMPASS

Low weather minima flight control system consisting of autopilot, flight system and gyromagnetic compass 03 p0466 A67-14385

MAGNETIC CONTROL

SA ELECTROMAGNETIC CONTROL
Geomagnetic stabilization of satellite initially torque-stabilized, deriving motion equation 01 p0153 A67-10210
Transformation of transverse oscillations of electron flux by short magnetic lenses studied by eigenvector concept 02 p0214 A67-11900
Command laws for DC magnetic attitude control of spin-stabilized earth satellites by means of coils of axis parallel to spin, including effects of orbital eccentricity and magnetic dipole 07 p1257 A67-19361
Magnetic devices for microwave integrated circuits, discussing ferrite substrate use as medium for microstrip transmission lines 15 p2452 A67-29928
Magnetic device design optimization for satellite attitude control, noting equations and charts 15 p2572 A67-30385
Noise and dark current reduction in photomultiplier tubes by magnetic defocusing [SRCC-43] 19 p3193 A67-35314
Magnetically tunable multisection bandpass filter in ferrite-loaded evanescent waveguide 22 p3772 A67-39907

MAGNETIC CORE

Resistance losses of ferrite core in strong HF field determined using oscillogram analysis, noting possibilities in wide frequency range and complex magnetization 01 p0035 A67-10414
Natural oscillations in dissipative oscillatory circuits containing inductance coil with magnetized ferrite core in presence of strong HF field 01 p0037 A67-10544
Inductance coefficient dependence on geometric air gap of ferrite cup cores, showing use for design of stable resonance circuits 02 p0280 A67-11464
Elastic and inelastic flux switching, explaining different types of domain wall displacement in terms of variations of energy gradient vs wall position 05 p0774 A67-16832
Transistor circuit containing magnetic cores with rectangular hysteresis loop analyzed for switching processes using differential equations 20 p3399 A67-37114

MAGNETIC DIFFUSER

Momentum, heat and magnetic field diffusion in viscous, thermal and magnetic boundary layers of different thicknesses in MHD fluid 22 p3850 A67-39721

MAGNETIC DIPOLE

SA ELECTRIC DIPOLE
Effect of plasma outside cylindrical plasma column on dipole resonance, noting increased oscillation frequency and coupling of resonances 01 p0123 A67-10459
Laser characteristics of narrow band type I solar radio burst and magnetic dipole transitions in split Zeeman sublevels of hydrogen atoms of solar corona in ground level 02 p0322 A67-11652
Poloidal hydromagnetic plasmaspheric resonance under conditions representative of inner magnetosphere 02 p0276 A67-12563
Herman and Gibbons conclusions on radiation energy concentration in ionized gas shown to be erroneous 03 p0411 A67-12961
Electromagnetic excitation by vertical

magnetic dipole located above spiral anisotropic plane 04 p0586 A67-15672
Z component of geomagnetic field, determining parameters of sloping dipoles 05 p0802 A67-17149
Energy required to confine static shielded magnetic dipole field, immersed in highly conducting medium, by transient diamagnetic surface as function of dipole moment and disturbance 06 p1030 A67-17658
Quasi-MHD analysis of supersonic rarefied plasma flow near magnetic dipole 06 p1043 A67-18670
Relativistic theory for interaction of electric point charge and magnetic dipole 09 p1580 A67-22549
Limit energy of monopole in field of earth magnetic dipole 10 p1631 A67-22800
Diurnal variation of difference between dipole and measured field for quiet magnetosphere from Elektron satellite data 10 p1649 A67-23296
Two-dimensional model of magnetosphere to find equilibrium boundary between rarefied plasma and magnetic field of two-dimensional dipole 10 p1649 A67-23297
Stormer method solution of charged particle motion in field of magnetic dipole situated in external uniform magnetic field antiparallel to dipole magnetic moment vector 11 p1856 A67-24069
Synchrotron radiation of relativistic electrons in magnetic field of dipole 12 p1994 A67-25535
Charged particle motion in field of magnetic dipole situated in external magnetic field /magnetospheric G region/, using Stormer method 12 p1994 A67-25644
Monopole motion in magnetic dipole field, comparing electric and magnetic cases 14 p2378 A67-27920
Nondipole region of geomagnetic field at magnetosphere boundary and effect on boundary position on daylight side 14 p2308 A67-27931
Laser characteristics of narrow band type I solar radio burst and magnetic dipole transitions in split Zeeman sublevels of hydrogen atoms of solar corona in ground level 16 p2747 A67-31067
Geomagnetic eccentric dipole shown equivalent to multipoles superposition, giving geometric parameters and procedure for determining true magnetic poles 18 p3042 A67-34351
Chapman-Ferraro problem analyzed by impinging high speed hydrogen plasma stream against three-dimensional magnetic dipole, discussing boundary shape 19 p3288 A67-35366
Interaction of moving plasma with dipole magnetic field measured visually and with electric and magnetic probes 19 p3288 A67-35367
Interaction of plasma stream with three-dimensional magnetic dipole field, discussing current distribution in cavity 19 p3221 A67-35368
Coil and dipole systems for magnetic testing of large spacecraft 20 p3415 A67-36612
Stable height to distance to supporting magnetic field origin ratio for prominences, noting agreement with Kippenhahn-Schluter model 20 p3528 A67-37469
Z component of geomagnetic field, determining parameters of sloping dipoles 21 p3619 A67-38491
Magnetic dipole moments of moon, Mars and Venus using space probes, discussing solar wind near-earth planetary field interaction measurements [JPL-TR-32-1059] 21 p3709 A67-38992
Magnetized gyroscope magnetic moment effect on performance calculated, discussing drift from axis equilibrium state 22 p3796 A67-39231
Spherical and cylindrical dipole fields in different coordinate systems, discussing differential distances 23 p3975 A67-41211
Fourth order multipole parameters derived from spherical harmonic function coefficients for geomagnetic field potential 24 p4146 A67-41784
Limit energy of monopole in field of earth magnetic dipole 24 p4150 A67-42137
Horizontal telescope used for solar corona photography during total eclipse /1966/, determining radii passing through solar magnetic poles 24 p4227 A67-42153
Scattering from half-loop on conducting plane obtained through image theory,

considering electric and magnetic dipole contributions 24 p4121 A67-42265

MAGNETIC DISPERSION

Dispersion relation of electron impurities in gapless superconductors and effect on period and damping of Tomasch oscillations 01 p0130 A67-10154

Longitudinal electric field penetration into magnetoplasma layer in constant magnetic field 01 p0122 A67-10356

Radio wave guiding along electron density discontinuity in magnetotonic exosphere, noting low dispersion modes 01 p0027 A67-11259

Electromagnetic wave propagation along plasma column subjected to longitudinal magnetic field, calculating dispersion curves for two dipolar modes as function of wavelength and frequency 02 p0273 A67-12062

Effect of spin exchange scattering by magnetic impurities on electronic properties of superconductor 07 p1235 A67-20129

Longitudinal electric field penetration into magnetoplasma layer in constant magnetic field 11 p1844 A67-25029

Critical alternating-magnetization curves of permalloy films, clarifying theoretical experimental problems and effect of anisotropy field dispersion magnitude on curves 12 p1981 A67-25245

Thermal radiation characteristics of metallic surfaces, comparing metal dispersion relationships with experimental emissivity 13 p2130 A67-26439

Electromagnetic wave propagation, excitation and dispersion in metals in magnetic field 14 p2366 A67-28426

Time-growing instability existences in distributed parametric media using dispersion relation 19 p3195 A67-35620

Microwave delay-line techniques using YIG crystal, examining solid state dispersion characteristics 20 p3507 A67-36241

Data and theories on stationary spin waves in ferromagnetic thin layers, considering modes, dispersion law and spectra interpretation 20 p3507 A67-36318

Dispersion characteristics of geomagnetic micropulsation pearls, obtaining magnetospheric proton densities 21 p3617 A67-38127

MAGNETIC DOMAIN

SA SATURATION

Domain structure of strontium ferrite investigated by Bitter powder pattern method in basal planes, showing dependence on magnetic field intensity, temperature and thickness of crystals 04 p0673 A67-14482

Quasi-equilibrium states during pulse remagnetization of thin ferromagnetic films, discussing domain structure 08 p1367 A67-20604

Propagation of bounded domain with strong electric field in semiconductor with negative differential conductivity 09 p1557 A67-22558

Reverse magnetization spike domains analyzed for nucleation and growth 13 p2179 A67-27141

180 degree domain formation in ferroelectric crystals unaffected by presence of shorted electrodes due to surface layer properties differing from bulk 19 p3304 A67-35047

MAGNETIC EFFECT

SA BARKHAUSEN EFFECT

SA GEOMAGNETIC EFFECT

SA MEISSNER EFFECT

SA PHOTOELECTROMAGNETIC /PEM/ EFFECT

Spin-lattice relaxation time dependence on temperature and magnetic field in neutron-irradiated quartz with paramagnetic defects at helium temperature range 01 p0127 A67-10064

Anisotropy of Hall effect dependence on field and temperature in dysprosium crystal 01 p0133 A67-10743

Internal forced convection in viscoplastic fluids between two parallel plates with applied normal magnetic field 01 p0126 A67-11188

Luminescence front interaction with transverse magnetic field in electrodynamic shock tube 02 p0274 A67-12416

Mercury device for analyzing pressure distribution, velocity profiles and resistance coefficients of turbulent flow in channels of linear induction pumps under travelling magnetic field 04 p0670 A67-15521

Electromagnetic excitation by vertical magnetic dipole located above spiral anisotropic plane 04 p0586 A67-15672

Ferroacoustic resonance in yttrium ferrite galate crystals, noting effect of magnetic field on pulse amplitude 05 p0868 A67-17064

Gas laser behavior in magnetic field, analyzing data on magnetic effect, Zeeman effect and microwave pumping 06 p1011 A67-18168

Inductance, flow current and external magnetic field effects caused by diamagnetism of superconducting solenoid winding 06 p1051 A67-18207

Longitudinal magnetic field effect on convective heat transfer during turbulent MHD pipeflow of liquid Ga 06 p1044 A67-18682

Magnetic field effect on static shielding of point charge calculated, using Green function of inverse dielectric function of electron gas plasma 06 p1071 A67-18989

Acceleration of propellant in arcjet devices by thermal and self-magnetic forces, using various nozzle configurations 08 p1375 A67-20574

Interaction between layers of ferromagnetic films of different composition and coercivity separated by insulating quartz layer, obtaining films by vacuum deposition 08 p1369 A67-20811

Self-consistent description of warm stationary plasma in uniformly sheared magnetic field, noting shear rate current flow 08 p1364 A67-21402

Potential distribution in electron-collisionless plasma in weak magnetic field 08 p1365 A67-21412

Magnetic effect on injected plasma density and anomalous potential in semiconductor rods 09 p1552 A67-21761

Magnetic field inhomogeneity effect on electrically conducting fluid flow in Hall type generator duct 09 p1443 A67-21806

Paramagnetic Knight shift in metals and semiconductors as affected by temperature and magnetic and electric field intensity 09 p1554 A67-21972

Convective type drift instability in collisional and collisionless regimes due to magnetic shear effects driven by density gradient 10 p1685 A67-23462

Changes produced in urinary sodium, potassium, and calcium excretion in mice exposed to homogeneous magnetic field 10 p1600 A67-23819

Plasma flows from normal and coaxial electrode contact points of arc and effect of external forces by schlieren photography 10 p1687 A67-23849

Torque on sun calculated from solar wind motion, taking rotation and magnetic field effects into consideration 11 p1857 A67-23931

Flute instability in mirror confined plasmas assuming particle drift under external forces 11 p1830 A67-24004

Magnetic field effect on electromagnetic wave propagation through free carrier plasmas in semiconductors, considering Faraday configuration 11 p1840 A67-24663

Magnetic effect and collision in damping of electron Langmuir oscillations 11 p1842 A67-24965

Hydromagnetic wave propagation and energy transfer in stratified isothermal plasma embedded in parallel uniform gravity and magnetic fields 11 p1868 A67-25083

Nonhomogeneous turbulent motion of conducting fluid stabilized by longitudinal magnetic field 12 p1976 A67-28069

Polarization phenomena in gas laser in presence of magnetic field 12 p1954 A67-28236

Anisotropy of Hall effect dependence on field and temperature in dysprosium crystal 13 p2176 A67-26772

Aeromagneto flutter of plane duct of finite length 13 p2218 A67-26805

Fabrication and operation of divalent dysprosium doped calcium fluoride laser, discussing magnetic field effects, Q-switching, cooling, etc 13 p2127 A67-27086

Geomagnetic field influence on cosmic rays simulated by electron beam and terrella situated in vacuum tank 13 p2192 A67-27243

External magnetic field accelerating effect on constant-mass plasma clusters between parallel conductors 14 p2354 A67-27763

Nondipole region of geomagnetic field at magnetosphere boundary and effect on boundary position on daylight side 14 p2308 A67-27931

Magnetic activity at low latitudes during IGY 14 p2309 A67-27940

Arbitrary ionization ratio plasma conductivity in presence of constant and

uniform magnetic field 14 p2355 A67-27955

Observed micropulsation activity during meteor shower compared with predicted magnetic agitation value determined from equation by Chapman and Ashour 14 p2383 A67-28045

Radio whistlers occurrence relationship to solar and magnetic activities at various latitudes 14 p2265 A67-28413

Effects of strong coupling and spin-flip scattering by magnetic impurities on superconductors, calculating conductivity and surface impedance at finite temperatures 14 p2371 A67-28725

Thorium-gadolinium alloy magnetization curves confirming full Meissner effect, showing bulk properties of superconductors obey Abrikosov-Gorkov theory 14 p2373 A67-28859

Quantum oscillations of Nernst-Ettingshausen effect in indium arsenide 14 p2376 A67-29087

Magnetic moment of electron in HF plasma accelerator for case of negligible axial acceleration in resonance region 15 p2527 A67-29514

Nonlinear effects during titanium plasma source operation, investigating plasma nature and magnetic field effects on injector operation and plasma parameters 15 p2529 A67-29719

Ferroacoustic resonance in yttrium ferrite galate crystals, noting effect of magnetic field on pulse amplitude 15 p2538 A67-29795

Transverse magnetic field effect on induced emission of GaAs diodes 15 p2543 A67-30251

Satellite scintillation in auroral zone depends on time of observation and on magnetic activity 15 p2483 A67-30294

Field-aligned irregularities as effect of increased electron temperature in F-2 layer, analyzing heat production and loss mechanism [AGARDOGRAPH 95] 15 p2484 A67-30305

Transverse magnetic field effect on barrier wake oscillation in electrically conducting liquid 16 p2723 A67-31714

Superconductors and ferromagnetic domains proximity effects at critical temperature in resistive and tunneling effect measurements 17 p2912 A67-32271

Transverse magnetic field effect on turbulent MHD jet flow in bounded space, noting channel wall conductivity 17 p2901 A67-32565

Inductance, flow current and external magnetic field effects caused by diamagnetism of superconducting solenoid winding 17 p2922 A67-33221

Paramagnetic Knight shift in metals and semiconductors as affected by temperature and magnetic and electric field intensity 17 p2923 A67-33309

Tunneling into thin superconducting films in magnetic field, measuring field effect on density of states for finite mean free path 17 p2924 A67-33371

Magnetoelasticity/magnetoelastothermoelasticity theories concerned with externally applied magnetic field interacting effects on elastic/thermoelastic deformations of solid body 19 p3262 A67-35799

Gravitational and magnetic torque effects on rotational motion of asymmetric Pegasus satellite in circular orbit [AIAA PAPER 67-567] 19 p3335 A67-35963

Magnetic cut-off system for plasma jet, with plasma flux reduction 20 p3497 A67-36679

Ionogram data used to identify high absorption periods, analyzing diurnal variations of critical frequency F-2 layer showing no echo occurrences 20 p3432 A67-37275

Magnetic field effect on resistance coefficient of mercury flow in circular pipe 20 p3501 A67-37304

Gas laser behavior in magnetic field, analyzing data on magnetic effect, Zeeman effect and microwave pumping 20 p3462 A67-37591

Magnetic curvature effect on drift cyclotron instabilities, considering density gradients, Maxwell plasmas and resonance 21 p3661 A67-37749

Germanium conductivity dependence on surface and space charges in transverse magnetic field 21 p3676 A67-37862

Dynamic model for magnetic field effect on vibrations of clock balance wheel having magnetized cross bar 21 p3625 A67-37988

Electromagnetic forces and pressure and

hydraulic losses of turbulent mercury flow in annular channel under traveling magnetic field effect 21 p3666 A67-38249

Changes in electric resistance of ellipsoidal plasma probe in homogeneous magnetic field, deriving equations of potential and resistance 21 p3666 A67-38250
Superconducting critical temperature below Kondo temperature for metal solutions with magnetic impurities calculated, using Green function 21 p3680 A67-38350

Microscopic theory of zero-bias magnetic tunneling anomalies covering weak and strong coupling limits in p-n semiconductors and tunnel junctions 21 p3682 A67-38385

Magnetic separations performed on Jodzie howardite, showing uniform primordial gas enrichment indicating covariant solar planetary components 21 p3704 A67-38503

Magnetic field effect on flow field and drag of blunt body in partially ionized argon plasma, obtaining electron density and temperature [AIAA PAPER 67-729] 21 p3673 A67-38753

Flow velocity and magnetic field effects on characteristics of single controlled glow discharge in cesium seeded argon 21 p3674 A67-38888

Magnetic effect on polarization of resonance radiation in solar chromosphere 21 p3709 A67-38989

Ni plasma acceleration in axisymmetric electric discharge by self-induced magnetic field, determining reaction force 22 p3844 A67-39356

Electron density relation to output power in He-Ne laser and magnetic field effect, using microwave resonator technique 22 p3814 A67-39428

Magnetic shear effects on density gradient drift instabilities in plasma with plasma pressure to magnetic pressure ratio larger than electron-ion mass ratio 22 p3845 A67-39483

Direct Josephson current dependence on magnetic field in tunnel junctions noting temperature dependence of oscillation periods 22 p3857 A67-39504

Magnetic element impurity effects on semiconductor resistivity, calculating spin dependent scattering of free carriers 22 p3859 A67-39625

Explosion of ovoid copper wire conductors observed with pulsed X-rays noting effect of magnetic pressure 23 p4028 A67-41461

Static tufted magnetic field perturbing effect on solar atmosphere small scale structure, noting pressure, density and temperature changes [SR-15] 24 p4222 A67-41767

Electrical design of large lightweight solar array for electric propulsion type Mars-bound spacecraft, discussing magnetic effects and power losses 24 p4104 A67-42512

Transverse magnetic field effect on two-dimensional jet of incompressible fluid 24 p4198 A67-42565

MAGNETIC EQUATOR

SA GEOMAGNETIC EQUATOR

Lunar tide effects on ionospheric characteristics near magnetic equator, noting fluctuations in electron concentration 02 p0237 A67-11673

Fading characteristics of radio waves reflected from sporadic E layer of ionosphere over magnetic equator 03 p0406 A67-12824

Horizontal drift measurements in E and F regions of ionosphere over magnetic equator in India 03 p0407 A67-12829

Spread-F occurrence dependency on F layer height variations with time, season and longitude and plasma wave generation near geomagnetic equator 03 p0415 A67-14115

Diurnal and seasonal variation of total columnar ionospheric electron content at magnetic equator analyzed, using Faraday rotation technique 10 p1651 A67-23341

Diurnal variation of telluric currents near magnetic equator during IGY and IQSY suggests equatorial electrojet as main source for current 10 p1651 A67-23343

Ionospheric electric current measurement, determining vertical current density distribution and electron number density for geomagnetic field study 13 p2107 A67-26308

Ionization transport from equator along magnetic lines of force may contribute to formation of diurnal ionization anomaly of F region in intermediate zone 13 p2117 A67-27708

Geomagnetic ring current observations

using Elektron II satellite, noting location, orientation and structural features 14 p2308 A67-27928

Magnetic variation measurements at Addis Ababa indicate intermittent existence of inverse direction equatorial electrojet 15 p2478 A67-30070

Oblique sounding of transequatorial path [AGARDOGRAPH 95] 15 p2438 A67-30298

Spread-F occurrence studied using hourly soundings near magnetic equator [AGARDOGRAPH 95] 15 p2484 A67-30307

Magnetic storm effects on F-2 layer near equatorial zone boundary causing variations in critical frequency of layer 16 p2663 A67-30970

Lunar tide effects on ionospheric characteristics near magnetic equator, noting fluctuations in electron concentration 16 p2665 A67-31088

Reflection coefficients of sharply bounded ionosphere for plane waves incident from arbitrary direction at magnetic equator 16 p2632 A67-31863

Equatorial anomaly in F-2 layer of ionosphere, examining solar activity, seasonal variation relation to magnetic activity, lunar phase and heights 23 p3996 A67-41082

Cosmic ray equator position at zero meridian measured, noting substantial difference in location from magnetic equator position 23 p4059 A67-41135

MAGNETIC FIELD

SA ELECTROMAGNETIC FIELD

SA ELECTROMAGNETISM

SA FIELD EMISSION

SA GALACTIC MAGNETIC FIELD

SA GEOMAGNETIC FIELD

SA INTERPLANETARY MAGNETIC FIELD

SA INTERSTELLAR MAGNETIC FIELD

SA KERR EFFECT

SA LUNAR MAGNETIC FIELD

SA NONUNIFORM MAGNETIC FIELD

SA PLANETARY MAGNETIC FIELD

SA SELF-CONSISTENT FIELD /SCF/

SA SOLAR MAGNETIC FIELD

SA STELLAR MAGNETIC FIELD

SA TRAPPED MAGNETIC FIELD

High current discharge effect on magnetically confined argon laser 01 p0086 A67-10012

State density for highly doped semiconductor in magnetic field, obtaining results at near Fermi level energies and at bottom of conduction band 01 p0128 A67-10096

Efficiency criterion for semiconductors, using equations for flux density of electric current and energy for isotropic semiconductor in absence of magnetic field 01 p0129 A67-10103

Superconducting transition temperature and critical field curve for pure Ga single crystals 01 p0130 A67-10153

Braking of conducting gas by transverse magnetic field in rectangular channel, deriving one-dimensional channel flows 01 p0119 A67-10173

Hall effect in low temperature plasma consisting of combustion products with admixture of KOH under variable sign magnetic field, demonstrating potential gradient existence 01 p0120 A67-10175

Stationary free-surface mercury flow in channels under magnetic field, analyzing hydraulic jump and influence of field on location 01 p0120 A67-10179

Helical flow of conducting fluid between porous cylinders and disk electrodes in radial magnetic field, calculating electric power and efficiency 01 p0120 A67-10183

Motion equation solution to viscous conducting flow at inlet of diverging channel using difference method, noting magnetic field effect 01 p0120 A67-10184

Effect of electrode tips of MHD generator and induced magnetic field on fluid flow in generator analyzed, using approximation method 01 p0121 A67-10227

Magnetic surfaces of straight helical magnetic field in presence of axial current 01 p0122 A67-10344

Plasma density dependence of adiabatic motion of plasmoids in longitudinal magnetic field 01 p0122 A67-10351

Diffusion and lifetime of plasma charged particles in magnetic field covering instability, contraction, decay, recombination, etc 01 p0123 A67-10389

Maser oscillation intensity and frequency dependence on constant electric and

magnetic fields acting on molecular beam in front of resonator 01 p0089 A67-10390

Equilibrium of plasma excited by radio wave in low pressure gas in presence of magnetic field 01 p0124 A67-10811

London moment of rotating superconductors and relation to Lense-Thirring fields of general relativity 01 p0134 A67-10811

Intrinsic electric field of rarefied ion-electron plasma in external magnetic field and plasma stability, noting use of Galerkin method to determine plasma layer slippage 01 p0126 A67-11299

Superconductivity of second kind in thin film, considering geometry dependent upper critical fields 02 p0291 A67-11731

Critical field for second order transition of superconductor to normal state, noting effect of vortex structure 02 p0291 A67-11731

Q-spoiling of ruby laser by optical pumping in intense inhomogeneous magnetic field with reduced gain 02 p0253 A67-12500

Three-dimensional eigenmodes for collisionless electronic Vlasov plasma imbedded in magnetic field in electrostatic approximation, noting plasma stability 02 p0275 A67-12555

Electrolytic tank analog for magnetic field configurations in design of plasma containment device 02 p0279 A67-12693

Zero order Hamiltonian in perturbation theory for eigenvalue problems of atom in magnetic field 02 p0271 A67-12722

Angular and energy characteristics of proton beam in pulsed magnetic field determining probability of proton-neutron charge exchange for proton in forward flight 02 p0271 A67-12755

Differential method measurement of Hall effect in presence of large constant magnetic field 03 p0487 A67-12808

AC measurements on hard superconductors exposed to magnetic field obtaining critical surface current and density from voltage-time curves 03 p0487 A67-12809

Parametric resonance in plasma situated in magnetic field noting oscillation, frequency stability, kinetic equations, electric field effect, etc 03 p0475 A67-12931

Perturbation of electron density at large distances from body at high velocity in collisionless plasma under steady external magnetic field 03 p0475 A67-12939

Energy dissipation due to deformation of magnetic field in compressible conducting medium near zero field lines 03 p0470 A67-12940

Flute type instability of ideally conducting plasma in toroidal discharges with strong longitudinal magnetic field 03 p0476 A67-13343

Static theory of oscillations of relativistic plasma in uniform magnetic field 03 p0477 A67-13510

Effect of sudden change in magnetic field and/or pressure gradient on Hartmann flow, assuming stationary and nonconducting plates 03 p0482 A67-13745

Electron oscillations of uniform plasma slab in presence of strong magnetic field, noting orthogonality condition of normal modes density gradients and profile and dispersion relation 03 p0482 A67-13747

Wave propagation in rarefied two-component plasma situated in uniform constant magnetic field with finite Larmor radius 03 p0483 A67-13875

Solutions for nonlinear Ginzburg-Landau equations in cylindrical symmetry for type I superconductor 03 p0499 A67-13876

Channel flow of suddenly pressurized viscoelastic and electrically conducting fluid under influence of constant transverse magnetic field 03 p0483 A67-14035

Formula for second order correction factor derived for special case of static magnetic field with axial symmetry 03 p0484 A67-14040

Magnetic field geometric properties effect on magnetic moment and adiabatic invariants of charged particle motion 03 p0484 A67-14041

Plasma vortex filaments produced in pairs as shown by image converter photographs of interfaces between magnetic field and accelerated plasma 03 p0486 A67-14054

Transport and ionization properties of molecular gases in transverse magnetic field, using ionization chamber 03 p0474 A67-14358

Behavior of diamagnetic particles in moving magnetic field with respect to

- propulsion and MHD technology in space vehicles 04 p0687 A67-14546
- Dispersion and damping of oscillations in Maxwellian plasmas with zero order density gradients examined, using Vlasov and Maxwell equations 04 p0665 A67-15103
- Electromagnetic excitation of metallic cone, deriving systems of linear algebraic equations for coefficients of expansion of electric and magnetic fields 04 p0575 A67-15152
- Magnetic field finiteness effect on effectiveness of gyrotronic plasma waveguide excitation by coaxial line of force 04 p0665 A67-15165
- Plasma wave behavior in strong external magnetic field, discussing scattering at ions, wave transformations and nonlinear wave interactions 04 p0667 A67-15206
- Plasma flux interaction in magnetic multipole field, proving mutual polarization of interacting fluxes by photographic results 04 p0667 A67-15210
- Coaxial plasma source transition from high energy particle production to production of slow plasmoids, noting V-I characteristics and magnetic field distribution 04 p0667 A67-15212
- Charged particle distribution in hollow cylinder shaped positive plasma column during diffusion and helical instability in longitudinal magnetic field 04 p0668 A67-15281
- Operating possibility of axisymmetric electron beam so that plasma frequency will exceed electron cyclotron frequency of magnetic focusing field at some point or throughout beam 04 p0624 A67-15326
- Flux jumps in hard superconductor AC and DC magnetic fields 04 p0682 A67-15328
- Conical MHD flow of ideal conducting gas with Hall effect in magnetic field, deriving electrodynamic and energy characteristics 04 p0669 A67-15515
- Heat transfer in plane conducting fluid jet spreading over flat wall in transverse magnetic field, noting solution for temperature distribution for small MHD interaction parameters 04 p0670 A67-15520
- Cylindrical inductor with inhomogeneous field, analyzing case of strong field inhomogeneity when inductor radius is much greater than pole pitch 04 p0556 A67-15522
- Magnetic field structure in working space of linear multiphase inductive MHD generator 04 p0556 A67-15523
- Coefficient of hydraulic resistance derived for plane flow of electrically conducting fluid in traveling magnetic field 04 p0670 A67-15534
- Vector potential of magnetic field of any axisymmetric electric current distribution used to compute field of two model magnetospheric ring currents 04 p0617 A67-15535
- Magnetic field effect on velocity of electron drift produced by electrical field in dense plasma 04 p0671 A67-15580
- Kinetic theory of quantum electron gas coupled to radiation field under uniform external magnetic field 04 p0672 A67-15770
- Magnetic field effect on transport equation, presenting relationship between classical Boltzmann equation and corresponding quantum mechanical formalism 04 p0659 A67-15773
- Homogeneous anisotropic cosmological model with magnetic field for solution of Einstein gravitational and Maxwell equations in space filled with ideal matter 04 p0702 A67-15984
- Fields of two parallel wires immersed in plasma derived, obtaining formula for driving point impedance of probe 05 p0849 A67-16004
- Electric and magnetic field components produced by vertical and horizontal dipole antennas located at surface of conducting earth derived for quasi-static range 05 p0769 A67-16007
- Stationary and reflected shock wave produced in moving argon plasma interacting with stationary magnetic field 05 p0850 A67-16067
- Boltzmann equation for cosmic ray particle motion in random magnetic field 05 p0878 A67-16094
- High magnetic fields effect on cardiac activity in spontaneously excited isolated turtle heart by simultaneous and separate electrical and mechanical measurement 05 p0755 A67-16282
- Rotation and vibration of conducting circular cylinder in magnetic field, noting motion retardation due to induced electric current interaction with field 05 p0851 A67-16434
- Double resonance effects extended to case of stimulated emission in excited states of neon, using gas laser in transverse DC magnetic field 05 p0818 A67-16645
- Macroelectrodynamical equations for low temperature intermediate state of type I superconductors, noting magnetic field effect on structure 05 p0863 A67-16695
- Plasma stream translational energy transformation into random motion in connection with collisionless shock wave propagation along magnetic field 05 p0853 A67-16756
- Two-flow equations for stationary relativistic electron cloud in self-consistent crossed fields 05 p0774 A67-16907
- Pivoted slider bearing under external magnetic field analyzed, considering pad surface curvature 05 p0811 A67-16981
- Plane explosion in conducting gas with initial magnetic field having intensity vector directed at angle to plane 05 p0855 A67-17022
- Magnetoelastic vibrations due to step function of mechanical radial force acting on perfectly conducting isotropic elastic cylinder placed in magnetic field 05 p0847 A67-17278
- RF power oscillator for low pressure plasma production, noting work and grid coils and time and power controls 05 p0856 A67-17281
- Solution for parallel plates in steady state Hartmann flow extended to coaxial flow between concentric cylinders, noting role of magnetic field 05 p0856 A67-17356
- Ohm law in multicomponent nonisothermal plasmas derived as function of electric and magnetic fields and temperature and pressure gradients, using transport equation 05 p0857 A67-17422
- Transverse wave instabilities in collisionless hydrogen plasmas under magnetic field 05 p0858 A67-17429
- Plasma density, electron temperature and potential distribution measured across magnetic field, determining ion and electron-diffusion coefficients in plasma column 05 p0858 A67-17432
- Minimum B magnetic field geometry for LF oscillations in Cs plasma of Topsy Q device 05 p0859 A67-17444
- Limitation of Froehlich-Terreux quasi-superconducting state, discussing experimental and observational difficulties 06 p1047 A67-17654
- Aurora and ring current theory confirming role of hydromagnetic plasma flow and frozen-in field lines in geomagnetic storms 06 p0995 A67-17973
- Plasma instability in HF electric and constant magnetic field for sufficiently low pressure 06 p1039 A67-18081
- Coaxial plasma gun performance in longitudinal magnetic field, noting conditions of generation of single plasmoid 06 p1039 A67-18084
- Stability of flexible conductor in longitudinal magnetic field, using scalar potential to determine disturbed state 06 p1040 A67-18095
- Magnetic field effect on space charge neutralization in thin beam approximation [AIAA PAPER 67-83] 06 p1041 A67-18275
- Source model for predicting drag force on moving arc column in cross flow velocity and balancing magnetic field [AIAA PAPER 67-97] 06 p0986 A67-18280
- Polarization characteristics of ionized argon laser in magnetic field 06 p1011 A67-18542
- Stability of circular cylindrical shell in supersonic nonviscous conducting gas flow with unperturbed velocity, and under magnetic field 06 p1106 A67-18622
- Turbulent flow of mercury in flat channels plane perpendicular to magnetic field, noting reduction of flow resistance coefficient 06 p1044 A67-18678
- Magnetic field of cylindrical permanent magnet used as rotor of electromagnetic induction pump, determining induction components and permeances to fluxes 06 p0951 A67-18885
- Turbulent flow of electrically conducting fluid in pipe located in longitudinal magnetic field 06 p1044 A67-18889
- Size and shape of roughness projections effect on resistance coefficient during turbulent pipe flow in transverse magnetic field 06 p1044 A67-18690
- Forced motion of charged particle in magnetic field 06 p1045 A67-18743
- Charged particles motion in magnetic field with regular and random components, deriving kinetic equation for distribution function and then diffusion equation 06 p1037 A67-18800
- Perpendicular magnetic field induced change in electron temperature of current carrying semiconducting plates 06 p1054 A67-18805
- Transverse magnetic field effect on laminar radial flow of incompressible fluid between closely spaced parallel plates, presenting graphs of pressure distribution 06 p1046 A67-18829
- Generation of longitudinal plasma oscillation harmonics near electron cyclotron frequencies 06 p1046 A67-18831
- Electron double resonance for ionized impurity pairs in n-and p-type Si, noting splitting of resonance peaks and relaxation time of homopolar pair 06 p1068 A67-18970
- Electron motion in crossed fields with arbitrary ratio of electric and magnetic fields, considering simultaneously valence and conduction bands 06 p1069 A67-18978
- Superconductivity in germanium telluride, noting critical magnetic field data 06 p1069 A67-18981
- Transverse oscillation stability in quasi-one-dimensional flow of conducting gas in magnetic field 07 p1227 A67-19119
- Turbulent flow of conducting fluid with free surface in presence of crossed magnetic and electric fields 07 p1227 A67-19321
- Fluid mechanical model of electric arc balanced magnetically in gas flow, based on photographs showing arc must simulate solid body [AIAA PAPER 67-96] 07 p1240 A67-19437
- Anisotropic uniform model of universe with uniform intergalactic field 07 p1248 A67-19482
- Instability of inhomogeneous weakly ionized plasma in crossed electric and magnetic fields in quasi-approximation 07 p1228 A67-19508
- Wave coupling in varying density regions in hot anisotropic electron plasma, noting effect of angle width between propagation vector and static magnetic field 07 p1228 A67-19509
- Diamagnetic probe measurements of kinetic pressure of plasma in magnetic field 07 p1228 A67-19513
- Persistent current loops in hard superconducting wire formed when wire is magnetized by static transverse external field 07 p1232 A67-19554
- MHD phenomena in vortex ring in conducting fluid, noting intensification of initial field at high Reynolds numbers and self-excitation 07 p1229 A67-19684
- De Haas-Shubnikov effect observation method and application to measurements on bismuth 07 p1155 A67-19891
- Critical field for nucleation of superconductivity at tunneling barrier in magnetic field 07 p1235 A67-20131
- Effects of gases flowing in magnetic field analogous to galvanomagnetic Hall effect in conductors analyzed using oxygen 07 p1230 A67-20144
- Temperature dependence of critical field in superconducting vanadium 07 p1237 A67-20178
- MGD lubrication, obtaining motion equation of gas in electric or magnetic fields, velocity distributions, pressure differential equations, etc 07 p1192 A67-20210
- Current density distribution in MPD arc jet exhaust measured, using Hall effect sensors [AIAA PAPER 66-116] 08 p1375 A67-20573
- Source model for predicting aerodynamic drag on moving arc column in crossflow yields relationship between crossflow velocity and balancing magnetic field 08 p1356 A67-20579
- Energy loss of charged particles during passage through weakly turbulent plasma in magnetic field with HF oscillations 08 p1357 A67-20844
- Plasma instability in HF electric field perpendicular to given magnetic field under low pressures 08 p1357 A67-20847
- Equations for ionized positive plasma column of gas discharge between infinite dielectric planes under oblique magnetic field with component in direction of external electric field 08 p1358 A67-20849

Radial current density distribution in homopolar, noting deviation of magnetic field and nature of current distribution around anode 08 p1358 A67-20850

Bending effect of spectral lines in plasma created by rotating HF dipole in quasi-steady magnetic field 08 p1358 A67-20854

Shock wave propagation in plasma across magnetic field, solving problem via two-component hydrodynamic equation 08 p1358 A67-20858

Soviet lunar probe measurements of gamma spectrometry, magnetic and gravitational fields, corpuscular radiation intensity, etc 08 p1411 A67-20999

Landau type damping of plasma oscillations and Bernstein mode electrostatic propagation perpendicular to weak magnetic field 08 p1360 A67-21129

Particle loss through axisymmetric cusped magnetic field containment geometry, deriving adiabatic invariant for collisionless plasma 08 p1361 A67-21133

Rotating helical perturbations in Penning discharge plasma accompanying LF oscillations enhance particle transport across magnetic field 08 p1362 A67-21146

End losses from linear theta pinch estimated from self-consistent calculation of structure of plasma and confining magnetic field 08 p1362 A67-21149

Effective field for microwave breakdown for gas in external DC magnetic field and electric field valid for any stationary random signal 09 p1462 A67-21646

Parallel critical field calculation of tunneling barrier extended to all temperatures in dirty limit 09 p1552 A67-21745

Action of strong transverse magnetic field on supersonic current of ionized argon 09 p1540 A67-21787

Hall effect in low temperature plasma in nonhomogeneous magnetic field, describing measuring device 09 p1541 A67-21803

Zeeman effect in Ne-He gas laser operating in longitudinal magnetic field, noting dependence of frequency difference on field strength 09 p1512 A67-21920

Kinetics of nonuniform generation of longitudinal plasma waves by transverse wave beam with narrow spectrum, noting effect of magnetic field 09 p1545 A67-21995

Plasmoid density, electron temperature and radius variation during propagation through magnetic field, using electric and magnetic probes 09 p1545 A67-21996

Nonsymmetric oscillations in plasma in magnetic field arising from electron beam passage through plasma, deriving dispersion equation 09 p1545 A67-22003

Systems with toroidal magnetic field increasing toward periphery, considering method using skin effect of semiconductors 09 p1545 A67-22005

Electrostatic oscillations in dielectric, semiconductor and plasma in presence and absence of external magnetic field 09 p1555 A67-22011

Gardenhose instability for ultrarelativistic plasma in magnetic field, showing that instability criterion for particular non-Maxwellian distribution function is not met 09 p1546 A67-22229

Magnetic field shaping for convergent confined flow electron guns to create design data to reduce trial and error work 09 p1478 A67-22256

Solutions for field aligned flow past magnetic source using Green function, estimating energy dissipation rate 09 p1549 A67-22399

Faraday effect optical isolator for IR region using lead glass rod in magnetic field as nonreciprocal element 09 p1500 A67-22425

Continuous magnetic field satisfies conditions of stability, size, orientation, uniformity and controllability of maser type amplifier employing superconductor winding 09 p1516 A67-22482

Plasma column and plasma beam of same radius situated in coaxial waveguide under magnetic field, obtaining dispersion equation 09 p1465 A67-22551

Excitation and damping of drift waves in stable regime of ionized plasma radially confined by axial magnetic field 09 p1550 A67-22679

Auroral brightness variations related to magnetic field fluctuations, especially to pearl type fluctuations 10 p1632 A67-22811

Self-consistent field in HF plasma accelerator with static magnetic field

gradient 10 p1683 A67-22852

Electric fields due to electron-plasma and ion-acoustic waves associated with sunspot magnetic field variation as main cause of electron acceleration in solar flares 10 p1700 A67-23056

Low temperature alkali plasmas in strong magnetic fields interpreted in terms of collisional drift modes 10 p1684 A67-23073

Book on superconductivity of metals and alloys including fundamental properties, condensed state, analysis of Landau-Ginsburg equations, magnetic field effects, etc 10 p1690 A67-23160

Ambipolar diffusion of plasma cloud imbedded in ionized gas with homogeneous magnetic field, assuming electric current is not vanishing 10 p1648 A67-23293

Diurnal variation of difference between dipole and measured field for quiet magnetosphere from Elektron satellite data 10 p1649 A67-23296

Current instability in inhomogeneous plasma formed by drift and ion-acoustic waves with oscillation frequencies 10 p1685 A67-23461

First integrals of motion to determine stationary distribution function of charged particles and self-consistent magnetic field of plasma 10 p1685 A67-23464

Stability of plasma toroidal configurations under effect of component of magnetic field curvature which lies within magnetic surface 10 p1686 A67-23487

Perturbation theory developed to estimate magnetic surface stability against field irregularities, noting role of field resonances 10 p1686 A67-23488

Effect of varying magnetic field, vacuum and ion density at 27 MHz on properties of cylindrical argon plasma column, using capacitive and inductive coupling 10 p1686 A67-23504

Critical fields of thin superconducting films determined by specular reflection of electrons from surfaces 10 p1694 A67-23596

Deformation of velocity profile in inhomogeneous magnetic field, noting anisotropic conductivity of flow 10 p1686 A67-23670

Nonlinearity in V-I characteristic of type II superconductor situated in external magnetic field 10 p1696 A67-23775

Toroidal screw pinch equilibrium and stability in rapidly rising helical magnetic field, discussing experimental setup and results 11 p1827 A67-23888

Flute instability in low beta plasma in presence of nonuniform electric field perpendicular to magnetic field 11 p1828 A67-23891

Plasma ring acceleration produced by pulsed azimuthal electric field, noting magnetic field role in stabilization 11 p1828 A67-23893

Relativistic electron motion in mirror magnetic field interacting with axial electromagnetic wave calculated, comparing results with Seidl 11 p1828 A67-23895

Electromagnetic wave propagation in partially ionized paramagnetic gas in static magnetic field 11 p1751 A67-23970

Plasma stability research program facilities for study of helical instabilities in cesium arc plasmas in axial, Ioffe and other magnetic field configurations 11 p1829 A67-23998

Azimuthal modes of Kadomtsev plasma instability, describing subthreshold response spectra 11 p1829 A67-24001

Anomalous losses in plasma confined in magnetic field, correlating loss process with tube dimensions, electron temperature, gas pressure and magnetic field 11 p1829 A67-24002

Plasma diffusion across static magnetic fields in electrodeless E type RF discharges 11 p1830 A67-24008

Heat transfer of electrolyte solutions, noting effect of magnetic field on turbulent flow and empirical relation to calculate Nusselt number 11 p1831 A67-24024

Stormer method solution of charged particle motion in field of magnetic dipole situated in external uniform magnetic field antiparallel to dipole magnetic moment vector 11 p1856 A67-24069

Stability of pulsating plasma cylinder contained by time dependent magnetic field described by MHD equations 11 p1832 A67-24154

Impedance of strip antenna embedded in

dielectric layer overlain by cold plasma, considering reflection coefficient and static magnetic field effect 11 p1763 A67-24305

Radiation characteristics for slotted cylinder covered with magnetized inhomogeneous plasma sheath assuming parabolic electron density distribution 11 p1753 A67-24306

Ion-ion collision and shear stabilizing effect on resistive drift mode, applying dispersion relation with BGK collision operator 11 p1834 A67-24374

Minimum B magnetic field geometry effect on spontaneous oscillations and anomalous cross field plasma transport in TOPSY Q device with uniform axial magnetic field 11 p1835 A67-24388

Cooperative effect among electrons in presence of radial density gradient in cyclotron echo phenomena 11 p1836 A67-24391

Electrostatic turbulence in low beta plasma and influence on diffusion across magnetic field, noting heating system for plates of Q device 11 p1789 A67-24413

Polar bright surges at limb, showing frequency and parameters of occurrence 11 p1862 A67-24496

Dissipation of magnetic fields at neutral lines in two-dimensional field with two intersecting shocks 11 p1862 A67-24498

Two-dimensional steady MHD flow with resolution of neutral sheets into intermediate and slow waves 11 p1862 A67-24499

Magnetic field superposition technique for fast compression and long containment time of plasma in theta pinches 11 p1840 A67-24652

Frequency stabilization of gas laser by discriminant, using discharge tube with gain profile split by AC magnetic field 11 p1801 A67-24664

Q parameter of hydrogen maser measurement by method of no clock structure modification and by inhomogeneous magnetic field method 11 p1802 A67-24754

Current distribution of magnetic field in plasma coaxial injector indicating dominant role of Hall effect in plasma acceleration 11 p1841 A67-24854

Upper critical field limits for bulk type II superconductors 11 p1850 A67-24933

Current distribution in incompressible fluid flow in magnetic field at low Reynolds number, estimating Lorentz force effect 11 p1842 A67-24952

Asymptotic Krylov-Bogoliubov computation of moving charges interacting with space modulated magnetic fields 11 p1842 A67-24967

Magnetic surfaces of straight helical magnetic field in presence of axial current 11 p1843 A67-25017

Plasma density dependence of adiabatic motion of plasmoids in longitudinal magnetic field 11 p1844 A67-25024

Parametric resonance excitation of Alfvén waves by small LF modulation of DC magnetic field imposed on ideal MHD plasma 11 p1844 A67-25062

Gross behavior and properties of laboratory plasma generation with combined transverse and longitudinal ionizing currents parallel to magnetic field 11 p1845 A67-25098

Sunspot appearance and stars with pulsating magnetic field from Jensen theory of magnetic tubes 12 p2000 A67-25135

Annealing effect on damping rods for magnetic field stabilized satellites 12 p2011 A67-25212

Resistance of magnetic structure of Ni-Fe thin films deposited on metal substrate with anisotropic surface roughness to effect of orthogonal pulsed fields 12 p1980 A67-25238

UHF susceptibility of uniaxial magnetic films in weak fields far from ferromagnetic resonance 12 p1981 A67-25246

Generation rate of secondary HF wave from resonant interaction of two longitudinal waves in cold beam-plasma under external magnetic field 12 p1970 A67-25250

Negative-mass instability of cylindrical layer of relativistic electrons in geometrical configuration approximating Astron machine 12 p1970 A67-25254

Spectrum of longitudinal plasma oscillations noting instability under resonance condition 12 p1970 A67-25255

Microexplosion by optical breakdown of air in focus of laser beam, analyzing volume

- of concentrated plasma by measuring external magnetic field perturbation 12 p1952 A67-25336
- Dynamics of baroclinic geostrophic circumpolar vortex beta-plane flow in zonal magnetic field, noting applications to solar rotation, hydromagnetic dynamo theory, etc 12 p1963 A67-25338
- Arc rotation heat transfer effects in self-induced magnetic field plasma arc heaters used for aerodynamic tests 12 p2034 A67-25346
- MHD induction generator with variable fluid and magnetic field velocity noting high power of cascading generator 12 p1897 A67-25377
- Plasma propagation theory of arc retrograde motion in transverse magnetic field 12 p1974 A67-25400
- Steady state properties of collisionless cylindrical injected plasma of zero temperature in presence of longitudinal magnetic field steady state properties of collisionless cylindrical injected plasma of zero temperature in 12 p1974 A67-25455
- Stabilization of thermally ionized potassium plasma by applying shear to confining magnetic field 12 p1975 A67-25476
- Drift effect on diffusion spreading of plasma inhomogeneities in magnetic field, deriving expression for Fourier component potential and magnetic field perturbations 12 p1933 A67-25546
- Oscillations and stability of cylindrical shell in conducting gas flow in presence of magnetic field 12 p2021 A67-25581
- Response of superconducting sheath state of lead-indium in AC and DC magnetic fields studied, noting transition changes response of superconducting sheath state of lead-indium in AC and DC magnetic fields studied, 12 p1985 A67-25847
- Local magnetic field, ion density flow and electric field in plasma measured downstream of theta-pinch accelerator in presence of uniform guide field [AIAA PAPER 66-155] 12 p1975 A67-25895
- Containment of transparent plasma produced by field of traveling wave in circular waveguide, noting plasma ion-current distribution 12 p1976 A67-26066
- Nonhomogeneous turbulent motion of conducting fluid stabilized by longitudinal magnetic field 12 p1976 A67-26069
- Ionized multiwatt argon lasers, discussing relation between output power and discharge current, gas pressure, magnetic field and tube bore size 12 p1953 A67-26159
- Radial flow of two-dimensional viscous conducting fluid in wedge shaped channel under magnetic field, reducing flow equation to differential equation 12 p1977 A67-26180
- Primordial element formation, primordial magnetic fields and universe isotropy, showing correctness of big-bang relativistic theory, early anisotropy of universe, etc 12 p2010 A67-26240
- Electron-cyclotron wave instability in plasma noting dispersion relation, growth rate frequency, destabilizing effect of electrons, etc 13 p2163 A67-26286
- Magnetic field intensification in plasmas determined from solution of MHD equations, noting formation of time independent fields 13 p2163 A67-26292
- Earth bow plasma shock wave model with ion wave instabilities as principal shock structure [SR-2] 13 p2107 A67-26301
- Galactic cosmic ray intensity depression by convective region and by surrounding static barrier of expanding corona 13 p2191 A67-26323
- Solar activity effect on brightness and polarization of zodiacal light 13 p2109 A67-26332
- MHD generator two-dimensional incompressible flow, obtaining expressions for power output, velocity, electrical efficiency, etc 13 p2055 A67-26417
- Flow in MHD nozzles studied for hypothetical magnetic interaction parameter of unity order 13 p2165 A67-26592
- Shock wave propagation in cylindrical tube, comparing theoretical and experimental results concerning light front, pressure and magnetic field 13 p2094 A67-26641
- Finite ion Larmor radius effect on superposed fluid stability investigated for general perturbation direction, noting magnetically stabilized configurations become overstable 13 p2187 A67-26993
- Defects in irradiated silicon, analyzing electron paramagnetic resonance and electron-nuclear double resonance of aluminum vacancy pair 13 p2180 A67-27161
- Laminar motion equation for conducting gas jet expansion along plane wall in presence of transverse magnetic field solved in series form 13 p2168 A67-27304
- Electrostatic polarization of cylindrical plasma layer in external static magnetic field, discussing transverse charged particle drift in crossed fields 13 p2168 A67-27305
- Plane one-dimensional MHD flow in transverse magnetic field with magnetic Reynolds number equal to or greater than unity 13 p2169 A67-27311
- Laminar flow of incompressible conducting fluid in diffuser in presence of transverse magnetic field 13 p2169 A67-27313
- Alfven wave propagation in viscous incompressible infinitely conductive fluid under effect of gradually varying magnetic field 13 p2170 A67-27363
- Critical particle velocity and particles frozen in given point of magnetic field line, discussing effects of plasma compression and reflection levels 13 p2204 A67-27432
- Sunspot groups and chromospheric features associated with magnetic fields of active region in light of supergranular structure of solar atmosphere 13 p2204 A67-27434
- Experiment to represent sunspot model having mechanism of natural turbulent convection of liquid mercury inhibited in presence of magnetic field 13 p2171 A67-27437
- Electrodynamics equations for pure and doped two-band superconductors, studying upper critical magnetic field 13 p2184 A67-27630
- Flute type instability of ideally conducting plasma in toroidal discharges with strong longitudinal magnetic field 13 p2172 A67-27715
- Plasma acceleration under combined axial magnetic and electric fields, noting experimental setup and results 14 p2353 A67-27750
- External magnetic field accelerating effect on constant-mass plasma clusters between parallel conductors 14 p2354 A67-27763
- Two-dimensional steady flow analysis in channels with variable cross sections under strong magnetic field action, calculating velocity distribution by series expansion 14 p2355 A67-27902
- Pressure driven flow at high Hartmann number along annular channel between nonconducting circular cylinders 14 p2355 A67-27907
- Monopole motion in magnetic dipole field, comparing electric and magnetic cases 14 p2378 A67-27920
- Equilibrium of magnetic field confined by impact pressure of beam of ions for general direction of incidence of beam 14 p2310 A67-28046
- Cyclotron echo formation in rare gas and nitrogen afterglow plasma in presence of inhomogeneous magnetic field, stressing velocity-dependent collision frequency case 14 p2356 A67-28150
- Dispersion relation for two-component model of collisionless nonrelativistic plasma with external magnetic field acting on system 14 p2356 A67-28201
- Collisionless plasma flow around conducting sphere in uniform magnetic field 14 p2357 A67-28206
- Drift of theta pinch plasma due to asymmetry of magnetic field analyzed, using high speed photography 14 p2357 A67-28233
- Time varying magnetic field in shock tube, analyzing electric current diffusion layer 14 p2358 A67-28234
- Magnetic field, pressure and discharge current effects on saturation electron current of electrostatic probe used to measure magnetoplasma electron density 14 p2358 A67-28237
- Zeeman effect in Ne-He gas laser operating in longitudinal magnetic field, noting dependence of frequency difference on field strength 14 p2330 A67-28249
- Diffusion by microwave breakdown of weakly ionized helium plasma in metal chamber immersed in magnetic field 14 p2358 A67-28293
- Integral expression derived for current distribution on infinite antenna aligned with magnetic field immersed in plasma, using generalized eigenfunctions 14 p2284 A67-28378
- Flux density of variable radio sources with peculiar radio spectra 14 p2386 A67-28446
- Plane explosion in conducting gas with initial magnetic field having intensity vector directed at angle to plane 14 p2359 A67-28484
- Homogeneous anisotropic cosmological model with magnetic field for solution of Einstein gravitational equations and Maxwell equations in space filled with ideal matter 14 p2386 A67-28485
- Motion and dispersion of inhomogeneity in unbounded plasma in magnetic and electric fields 14 p2359 A67-28504
- Ion oscillations excitation by beam-plasma interaction near ion-plasma frequency, studying instability as function of magnetic field, plasma density and other parameters 14 p2360 A67-28553
- Superheating in cylindrical pure niobium by suppressing end effects 14 p2369 A67-28597
- Gas laser mode interaction in Zeeman laser, investigating transition in axial magnetic field 14 p2331 A67-28715
- Critical surface transport currents in type II superconductors interpreted by surface flux pinning model 14 p2370 A67-28718
- Two cases of critical surface current magnitude change in type II superconductors after transport current direction reversal 14 p2370 A67-28719
- Theory of pure type II superconductors in high magnetic fields, calculating ultrasonic attenuation coefficient 14 p2370 A67-28721
- Superconducting indium-bismuth alloy films immersed in strong magnetic fields parallel and perpendicular to surface, studying film thickness effect by tunneling technique 14 p2371 A67-28723
- Magnetic field effect on microwave surface impedance of superconducting tantalum measured in various temperature ranges via dielectric-resonator techniques 14 p2371 A67-28726
- Perturbation factors in angular correlation function for multidomain ferromagnetic materials determined taking into account magnetic field fluctuations 14 p2371 A67-28728
- Plasma wave drift in stellarator helical magnetic field, deriving equations for wave developing conditions 14 p2361 A67-28762
- AC and DC magnetic bearings efficient load support and development potentials [ASLE PREPRINT 67AM 6D-4] 14 p2325 A67-28788
- Mean flux density and polarization degree of radio emission from Jupiter in centimeter spectral range 14 p2389 A67-28837
- Perpendicular critical magnetic fields of superconducting aluminum, tin and gallium small grained films examined for superconducting transition temperature enhancement 14 p2373 A67-28860
- Blunt nosed reentry vehicle model with skewed magnetic field investigated in magnetoaerodynamic flow for possible bow shock distortion 14 p2244 A67-29049
- Diffusion due to ion-ion collisions between different ion species, stressing impurities diffusion in rotating plasmas 14 p2363 A67-29066
- Transverse diffusion coefficient of collisionless plasma in magnetic field measured, using variations in radial plasma column density 14 p2363 A67-29067
- Motion of ideally conducting gas near zero line of magnetic field in terms of MHD equations, obtaining exact solutions for two-dimensional nonstationary problem 14 p2363 A67-29076
- Density of states of pure type II superconductors in high magnetic fields, deriving approximate expression for Green function 15 p2533 A67-29089
- Screw instability in linear Hall accelerator 15 p2522 A67-29207
- Energetic plasma confined in magnetic mirrors shown to have little interaction with main plasma body 15 p2523 A67-29213
- Electrically conducting compressible viscous free jet in presence of transverse magnetic and electric fields solved analytically by perturbation technique 15 p2523 A67-29215
- Weak random initial magnetic field evolution in highly conducting isotropically turbulent fluid, noting exact initial growth expression of magnetic energy spectrum 15 p2469 A67-29223

Generation of quiescent variable-parameter arc plasma in strong magnetic field 15 p2523 A67-29228

Vorticity generation by interaction of waves with plasma in magnetic field 15 p2524 A67-29231

Soviet book on plasmoids covering coaxial plasma sources, magnetic field interaction and observation methods 15 p2524 A67-29243

Small nonpolarized plasmoids interacting with axisymmetric magnetic field, discussing penetration mechanism, equations of motion and magnetic moment 15 p2524 A67-29245

Longitudinal deformation of plasmoid interacting with axisymmetric magnetic field, noting expansion in homogeneous region 15 p2525 A67-29246

Radial deformation of premagnetized plasmoid interacting with increasing magnetic field 15 p2525 A67-29247

Plasmoid collisions in axisymmetric magnetic field studied spectrographically for energy density, radiative power, charged particle density, etc 15 p2525 A67-29248

Current layer motion in coaxial plasma gun, measuring discharge current, electric and magnetic fields and ejected ions at gun outlet 15 p2525 A67-29250

Coaxial plasma gun operating in longitudinal magnetic field, noting effect on plasmoid uniformity 15 p2525 A67-29253

Structure and magnetic field of plasmoids produced by conical induction source studied with probe-diagnostic method 15 p2526 A67-29255

Magnetic field influence on AC surface field effect in germanium resulting from change in sample conductance and not from change in surface barrier height 15 p2533 A67-29263

Temperature dependence of current carrier mobility in nickel and iron oxide, noting scattering due to magnetic field 15 p2533 A67-29315

Low temperature transport effects in n-type gallium antimonide at high magnetic fields, observing oscillatory behavior of Hall coefficient and transverse magnetoresistance 15 p2534 A67-29327

Electromagnetic excitation of metallic cone, deriving systems of linear algebraic equations for coefficients of expansion of electric and magnetic fields 15 p2435 A67-29339

Magnetic field finiteness effect on effectiveness of gyrotronic plasma waveguide excitation by coaxial line of force 15 p2526 A67-29352

Nonlinear oscillation theory for parametric resonance effect in gas lasers placed in stationary and variable magnetic field 15 p2498 A67-29468

Steady two-dimensional magnetic bottle in which moving, compressible and electrically conducting plasma is confined by horizontally aligned magnetic field 15 p2528 A67-29568

MHD boundary layer flow past seminfinit plate, applying fluctuating magnetic field to plate 15 p2510 A67-29631

Mathematical models for loss measurements in thin Permalloy films with ramp drives 15 p2536 A67-29649

Initially isotropic turbulence, characterized by three dimensionless numbers, suppressed by applying uniform magnetic field 15 p2471 A67-29656

Gravitational instabilities arising in plasma disk subjected to differential rotation in presence of magnetic field parallel to rotation axis 15 p2528 A67-29662

Plasma drift instability in discharge with oscillating electrons, measuring plasma vibration spectrum 15 p2528 A67-29711

Interaction between SHF field and created plasma in electron-cyclotron resonance state 15 p2529 A67-29715

Stationary concentration of charged particles in plasma created by uniform and nonuniform SHF magnetic field in electron-cyclotron resonance state 15 p2529 A67-29716

Density measurement of plasma discharge captured by magnetic field, considering linear and toroidal sections of collector 15 p2529 A67-29717

Plasma flow layer, acceleration and other parameters investigated under several operation conditions in coaxial plasma gun 15 p2529 A67-29718

Nonlinear effects during titanium plasma source operation, investigating plasma nature

and magnetic field effects on injector operation and plasma parameters 15 p2529 A67-29719

Experimental determination of hydrogen atom beam density after focusing by hexapolar magnet 15 p2520 A67-29720

Escalator effect by interaction of conduction and induction currents in niobium alloy wires 15 p2539 A67-29826

Macroelectrodynamical equations for low temperature intermediate state of type I superconductors, noting magnetic field effect on structure 15 p2539 A67-29866

Relaxation oscillations in n-type indium antimonide crystal under magnetic field effect and responsivity measurements in far IR 15 p2540 A67-29931

Inertial acceleration indicators which operate on magnetic-restraint principle, employing one or more permanent magnets to create magnetic field 15 p2489 A67-30087

Eddy currents in nonmagnetic conductors calculated by finite difference successive overrelaxation technique on digital computer 15 p2541 A67-30142

Difference leveling between electron and hole concentrations near junction by compensating charges of donors and acceptors with semiconductor space charges 15 p2542 A67-30242

Low temperature conductivity of semiconductors in electric and magnetic fields analyzed, noting electron-photon interactions and photon heating effect 15 p2542 A67-30248

Hall coefficient and reluctance dependence on magnetic field inductance in p-type cadmium tin arsenide samples from 250 to 411.7 degrees K 15 p2543 A67-30253

Plasma wave behavior in strong external magnetic field, discussing scattering at ions, wave transformations and nonlinear wave interactions 15 p2532 A67-30254

Plasma flux interaction in magnetic multipole field, proving mutual polarization of interacting fluxes by photographic results 15 p2532 A67-30258

Coaxial plasma source transition from high energy particle production to production of slow plasmoids, noting V-I characteristics and magnetic field distribution 15 p2532 A67-30260

Collision integral for Landau plasma in strong magnetic field to obtain time evolution of one-particle distribution function 15 p2532 A67-30382

Frequency shifting technique using auxiliary coil to produce magnetic field for masers in high power radar applications 15 p2439 A67-30392

Motion of particles trapped in magnetic field, discussing conditions leading to spiral family of trajectory curves 15 p2551 A67-30397

Motion of single-component electrically charged gas in elliptical cylindrical cavity analyzed for relative deformation when applying magnetic field 16 p2656 A67-30456

Boundary form of freely expanding plasma cloud in magnetic field determined, assuming plasma pressure equal to external magnetic field pressure 16 p2706 A67-30457

Pulsed discharge in transverse magnetic field noting relation between ionization instability and turbulent conductivity of nonequilibrium plasma 16 p2711 A67-30538

Effective conductivity tensor of nonhomogeneous plasma in homogeneous external magnetic field 16 p2711 A67-30539

He-Cs blow-down MPD facility, discussing generator duct feasibility, nonequilibrium ionization effects, performance and test results 16 p2853 A67-30549

MHD conversion of thermal energy contained in cesium-seeded noble gas examined for conditions governing disk-type ducts use 16 p2603 A67-30566

Steady-state mercury flow along open trough in transverse magnetic field, measuring electric and hydraulic characteristics and providing plasma motion model 16 p2713 A67-30578

AC MHD power generator and turbine described noting working fluid flow 16 p2805 A67-30581

Coulomb collisions effect on transverse wave along external magnetic field in dense plasma, noting damping of whistler mode and use of Fokker-Planck equation 16 p2713 A67-30608

Phenomenological theory for

thermomagnetic effects in type II superconductor flux flow state 16 p2724 A67-30609

Magnetic design of OGO and Pioneer solar probe including data on instrumentation, mechanical equipment, permanent magnets, test methods, etc 16 p2757 A67-30637

Magnetic field dependence of current oscillations in piezoelectric semiconductors 16 p2725 A67-30804

Nernst effect in type I superconductor, noting transverse voltages caused by longitudinal temperature gradients 16 p2727 A67-30819

Hall effect measurement in single crystal of arsenic at liquid helium temperatures in magnetic fields noting quantum oscillations 16 p2727 A67-30820

Steady laminar flow of viscous, incompressible, electrically conducting fluid in insulated rectangular channel, with imposed oblique transverse magnetic field 16 p2713 A67-30860

Electrostatic stability of finite-length plasmas immersed in magnetic field studied on mathematical model, discussing experiments with plasma-generating machines 16 p2714 A67-30871

Kelvin instability following velocity discontinuity in current-carrying cold collisionless plasmas under magnetic field, deriving dispersion relation and instability criteria from fluid equations 16 p2714 A67-30872

Two-flow equations for stationary relativistic electron cloud in self-consistent crossed fields 16 p2636 A67-30884

Collision plasma instability analysis based on MHD equations and ion motion along magnetic field 16 p2715 A67-31041

Helium plasma electron temperature and density dependence, with/without magnetic field, on pinch discharge 16 p2718 A67-31187

Field distribution in plasma waveguide at LF and large densities, noting dispersion properties of E and H waves 16 p2718 A67-31189

Turbulent channel flow of mercury in presence of uniform transverse magnetic field deducing skin friction coefficient 16 p2661 A67-31224

Turbulent channel flow of electrically conducting fluid in presence of magnetic field obtaining skin friction coefficient and velocity profiles 16 p2661 A67-31225

Drift instabilities in nonuniform collision-free plasma stabilized by magnetic shear noting longitudinal currents, electron and ion temperature gradients, etc 16 p2718 A67-31226

Bounce model pinch stability, noting plasma and field separation by thin surface, with anisotropies in velocity distribution and angular momentum considered 16 p2718 A67-31227

Numerical analysis of structure of one-dimensional unsteady magnetic compression waves propagating into collisionless plasma, using motion equations 16 p2719 A67-31232

Electrostatic wave effect on anisotropic relativistic proton plasma in magnetic field, noting instability 16 p2739 A67-31234

Plasma anomalous resistive instability shown independent from microinstability and caused by poor conductivity parallel to magnetic lines 16 p2720 A67-31240

Design guides for efficiency, bandwidth and resonant frequency derived from slot antenna analysis, using variational methods 16 p2638 A67-31334

Conducting Bingham plastic fluids considered as lubricants in rheostatic bearing in presence of constant magnetic field [ASME PAPER 67-LUBS-4] 16 p2682 A67-31382

Probe measurements of friction drag coefficient and velocity profile of turbulent flow of mercury in circular tube in presence of longitudinal magnetic field 16 p2721 A67-31394

Propagation of shear acoustic waves traveling parallel to magnetic field along symmetry direction in metal crystal 16 p2731 A67-31446

Forbush effect causing solar flares not originating from same active solar region, discussing long connection to sun and interlocking 16 p2739 A67-31458

Radio wave trapping and guiding along magnetic field lines by irregularities in

electron density 16 p2667 A67-31513
Faraday rotation satellite observations at closely spaced frequencies, allowing electron content figure determination 16 p2629 A67-31514
Slow oscillations of fluid in rotating cavity under magnetic field to evaluate Hide theory for nondipole drift of geomagnetic field 16 p2667 A67-31554
Nonlinear laser theory to calculate amplitudes, frequencies and beat frequencies of circularly polarized modes in laser with axial magnetic field 16 p2686 A67-31562
Solution of MHD boundary layers with magnetic field as exponential function of x coordinate, extended to transverse magnetic fields 16 p2722 A67-31570
Laminar jet flow of electrically conducting fluid over plane solid surface in transverse magnetic field solved using motion and continuity equations 16 p2722 A67-31571
Traveling field in gap of induction machines with open magnetic circuit created by linear winding load 16 p2723 A67-31583
Surface impedance of cylindrically stratified anisotropic ionosphere in presence of static magnetic field, calculating propagation parameters 16 p2631 A67-31853
Magnetic bottles leakage in fusion reactors, describing differences between microinstabilities and MHD theories 16 p2724 A67-31865
Magnetic field in moon proximity constructed from Lunik x satellite plasma and magnetic measurements 16 p2755 A67-31889
Lagrangian for interaction of electric charge with field induced by scalar magnetic charge to determine electrical dipole moment 17 p2883 A67-32100
Magnetic and electric charge interaction, noting neutrino electric dipole moment 17 p2887 A67-32101
Optimum energy conversion for MHD flows related to magnetic field value 17 p2898 A67-32180
Voltage induced by magnetic field using shock tube with high velocity ionized argon flow 17 p2898 A67-32184
Steady state plasma accelerators different from gas dynamic accelerators with Laval nozzles due to variety of waves, electric/magnetic fields, etc 17 p2898 A67-32185
Transverse magnetic field effects on heat transfer in turbulent flow of mercury in circular iron tube 17 p2899 A67-32186
Hall field intensity and asymptotic electron temperature of ionized argon-cesium mixture flow in transverse magnetic field with subsonic velocity 17 p2900 A67-32338
Superimposed electromotive force appearing in direction of magnetic field in presence of opposed spiral motion in turbulent field 17 p2842 A67-32341
Mercury flow in rotating torus with induction pump and magnetic field effect on flow studied for flow resistance 17 p2900 A67-32342
Microwave emission intensity from InSb, examining dependence on angle between DC electric and magnetic fields 17 p2914 A67-32815
Motion of shocks through chromosphere under guidance of magnetic fields 17 p2944 A67-32642
Josephson junction as ideal zero impedance voltage source with discrete voltage for simultaneous application of microwave and magnetic fields 17 p2915 A67-32657
Zero temperature cylindrical collisionless plasma in magnetic field studied for electrostatic instability, noting effect of radial velocities of electrons and ions 17 p2902 A67-32658
Duoplasmatron ion source study with Langmuir probe, finding that pressure dependent discharge characteristics relate to magnetic field radial components 17 p2902 A67-32659
Linear theory of collision-induced instability of partially ionized gases for waves propagating along external magnetic field 17 p2902 A67-32669
Hydromagnetic wave propagation in collisionless plasma based on Vlasov equation, finding Alfvén, magnetoacoustic and nonoscillating waves 17 p2902 A67-32673
Temperature dependence of upper critical

fields for clean superconductors of second kind, noting role of electron-reflection properties of surface 17 p2915 A67-32693
Static equilibrium for two-dimensional toroidal plasma configurations with inner fields and purely meridional electric currents 17 p2903 A67-32709
Relationship between microhardness of niobium and other variables characterizing superconductivity 17 p2915 A67-32720
Particle motion and plasma equilibrium in helical magnetic field, discussing magnetic surface phenomena 17 p2904 A67-32914
Plasma acceleration by SHF waves, worldwide research and results 17 p2904 A67-32915
Plasmoid motion in longitudinal, transverse and two-dimensional multipole magnetic fields, investigating electric fields and plasmoid parameters 17 p2904 A67-32916
Slipping instability of plasma flows, noting instability criteria for long and short wavelength oscillatory 17 p2905 A67-32925
Anomalous magnetic field charts for heights in ionosphere useful for studying auroras spatial distribution and sporadic E layer distribution 17 p2847 A67-32948
Cross sectional shape of magnetically balanced arc determined, noting elongation perpendicular to flow 17 p2906 A67-33033
Vlasov equation for anisotropic electron plasma in external magnetic field solved by Laplace transform of density perturbation in initial value problem 17 p2907 A67-33104
Charged particle beam guiding and focusing by helical magnetic multipole field for relativistic and nonrelativistic cases 17 p2908 A67-33112
Trapped plasma build-up in magnetic field by ionization of injected atomic beam, noting ionization cross section parameters 17 p2908 A67-33115
Steady state magnetic field in transition region between magnetosphere and bow shock by MHD equations, noting solution by approximation method 17 p2951 A67-33186
Fluctuating electric and magnetic fields due to plasma instabilities and stabilizing effect of mode coupling in collisionless plasma 17 p2909 A67-33229
Magnetic field annihilation rate prediction in current pinches attributed to magnetic energy dissipation by ways other than ohmic losses 17 p2909 A67-33248
Energy dissipation by relativistic charged particle and magnetic field containing it shown to exceed initial energy 17 p2952 A67-33320
Flow of viscous incompressible conducting fluid in channel with porous walls 17 p2910 A67-33352
Polarization properties of single mode operating gas laser in small axial magnetic field with initial cavity anisotropy 17 p2870 A67-33368
Mean free path effects on critical field and density of states of small superconducting spheres 17 p2924 A67-33370
Self-consistency equation for nucleation of superconductivity in presence of magnetic field 17 p2924 A67-33372
Magnetic field induced changes in Bardeen-Cooper-Schrieffer spectrum of electronic excitations in pure type I superconductor and effect on electromagnetic radiation absorption 17 p2925 A67-33374
Electronic contribution to thermal conductivity of pure type II superconductor in high magnetic field, noting rapid conductivity drop and strong anisotropy 17 p2925 A67-33376
Transition temperature of phonon-coupling superconductor merged with that of type II superconductor critical field to obtain strong coupling corrections to critical field 17 p2925 A67-33378
Magnetization in superconducting Mo measured in He 3 cryostat, noting transition temperatures and critical field 17 p2925 A67-33379
Skin effect in type II superconductor, observing flux penetration into single crystal cylinder immersed in LF alternating magnetic field 17 p2926 A67-33381
Magnetic diffusion effects in sunspot region assuming Schroeter value for electric conductivity 17 p2952 A67-33395
Eruption of solar flare of importance 2, describing evolution, associated optical and

radio phenomena, structure of longitudinal magnetic field, etc 17 p2939 A67-33397
Relation between current, voltage and magnetic field of weakly connected double-contact junctions in superconductors 17 p2926 A67-33406
Strong and weak magnetic field effects on qualitative characteristics of compressible media analyzed using Chaplygin-Sedov hodograph method 18 p3084 A67-33421
Magnetic field effect on Hall coefficient of p-type Ge-Si single crystal alloys 18 p3098 A67-33574
Spectral data and energy level diagrams from magnetic and electric field passage through barium cloud 18 p3036 A67-33606
Argon plasma injection effect into low pressure coaxial magnetic field noting pressure, flow speed, electron temperature, etc 18 p3084 A67-33647
Heat transfer due to flow of electrically conducting incompressible viscous fluid from rotating insulated disk under influence of axially oriented magnetic field 18 p3084 A67-33667
Relation between current and voltage in type II superconductors situated in transverse magnetic field in flux-flow regime 18 p3101 A67-33987
Magnetic field parallel component influence on depinning threshold of vortices in superconducting films 18 p3101 A67-33990
Determination of magnetic field of spreading currents in continuous conducting media separated by spheroidal surface 18 p3079 A67-34035
Stable deflection of homogeneous plasma stream by linearly increasing transverse magnetic field, neglecting particle collisions 18 p3087 A67-34036
Longitudinal magnetic field effect on radiation intensity of He-Ne laser operating in pulsed regime 18 p3061 A67-34043
Three-dimensional equation for wave propagation through inhomogeneous warm compressible plasma in inhomogeneous static magnetic field 18 p3088 A67-34071
Relationship between axial magnetic field necessary to extinguish oscillation from Brewster-angled laser and spontaneous intensity 18 p3061 A67-34200
Longitudinal magnetic field effect on conducting fluid turbulent flow found limited to dissipation mechanism occurrence 18 p3028 A67-34215
Ionosphere collision frequencies and densities studied by rocket measurements of magnetic field of VLF wave radiated from ground 18 p3041 A67-34233
Cyclotron instabilities of two-component electron plasma 18 p3089 A67-34295
Collision induced instability in semiconductor plasmas, noting system consisting of electrons and holes with transverse relative drift to static magnetic field 18 p3102 A67-34348
Charged particles motion in magnetic field with regular and random components, deriving kinetic equation for distribution function and then diffusion equation 18 p3083 A67-34419
Perpendicular magnetic field inducer change in electron temperature of current carrying semiconducting plates 18 p3102 A67-34424
Conduction band structure in n-type strontium titanate investigated by measuring oscillatory magnetoresistance in high magnetic fields 18 p3104 A67-34592
Detection properties of n-type InSb in microwave and IR ranges, studying impurity and magnetic field effects 19 p3300 A67-34762
Vortical structure of current and magnetic field distribution along superconducting film with magnetic field parallel to surface, discussing possible observation by optical diffraction 19 p3301 A67-34899
HF magnetic fields for plasma sheath with perpendicularly superimposed static magnetic field and resonance excitation of electron cyclotron waves 19 p3276 A67-35117
Impedance measurements of RF discharge in single turn coil with superimposed static magnetic field, noting dependences and two resonances 19 p3276 A67-35119
Transverse forces acting on arbitrarily curved current carrying plasma cylinder in transverse magnetic field 19 p3281 A67-35151
Column effects in arc interaction with transverse magnetic

fields 19 p3281 A67-35152
 Retrograde motion of electric arc discharge at low pressure with transverse magnetic field, including cathode vaporization 19 p3281 A67-35153
 Electric arcs in cross flow with variable magnetic field across electrode space 19 p3281 A67-35154
 Kinetic equation for inhomogeneous plasma in uniform external magnetic field, for application in studies of transport and high frequency wave phenomena 19 p3285 A67-35342
 Plane ionization wave propagation in uniform magnetic field compared with flame front expansion during slow burning 19 p3286 A67-35347
 Deuterium plasmoid structure, impurity distribution, passage through pulsed magnetic barrier and capture by longitudinal magnetic field with mirror geometry 19 p3288 A67-35364
 Experiments with thermally ionized cesium plasma in magnetic field with variable curvature 19 p3288 A67-35365
 Interaction of moving plasma with dipole magnetic field measured visually and with electric and magnetic probes 19 p3288 A67-35367
 Boundary layer structure between rarefied plasma and magnetic field solved in relativistic-invariant form 19 p3288 A67-35369
 Structure of shock waves in collision-free plasma at angle to external magnetic field studied by hydrodynamic equations 19 p3288 A67-35372
 Cylindrical plasma column subjected to axial magnetic field measured for electric field oscillations by movable probe within ionized gas 19 p3288 A67-35374
 UHF wave interaction between plasma and electron stream in magnetic field noting convective instability 19 p3291 A67-35382
 Beam-plasma interaction in magnetic field, studying microwave field distribution and emission 19 p3291 A67-35383
 Drift instabilities and related phenomena in inhomogeneous plasma confined by strong magnetic fields 19 p3292 A67-35388
 Theory demonstrating stability of current sheets of different shapes in coaxial accelerators 19 p3294 A67-35406
 Electric and magnetic field measurements in collisionless shock wave propagating through highly ionized magnetized plasma 19 p3294 A67-35408
 Ion cyclotron frequency wave generation in plasma confined in magnetic well for maximal density 19 p3295 A67-35419
 Velocity fields in solar atmosphere observed with magnetograph, studying magnetic field effect on oscillations amplitude and frequency 19 p3324 A67-35434
 Homogeneous MHD turbulence on large scale structure, finding asymptotic forms of velocity and magnetic field correlations 19 p3295 A67-35540
 Ion source using Penning discharge used to inject hydrogen ions into magnetic field 19 p3195 A67-35599
 Entropy and free energy functionals for collisionless plasma at equilibrium in adiabatic magnetic field 19 p3298 A67-35731
 Effect of angular direct current magnetic field on radiation of slot antenna located on metal cylinder covered by plasma sheath 19 p3184 A67-35811
 Dispersion equations and solution for transverse magnetic waves in parallel-plate waveguide partially filled with plasma slab, discussing existing modes 20 p3492 A67-36127
 Steady flow of perfectly conducting inviscid liquid past thin symmetrical airfoil of finite conductivity in aligned magnetic field 20 p3494 A67-36146
 Type II superconductor suspended on elastic fiber in magnetic field investigated for oscillation dampings 20 p3505 A67-36203
 Ultrasonic attenuation measurements at high magnetic fields in mixed state for clean and dirty limits 20 p3483 A67-36205
 Youngs modulus variation as function of external magnetic field in mixed state in niobium 20 p3464 A67-36221
 Electromagnetic properties of metal considered for strong quantization of electron states in magnetic field 20 p3464 A67-36224
 Propagation characteristics of ELF electromagnetic waves investigated below anisotropic ionosphere, considering magnetic

field 20 p3379 A67-36282
 Highly eccentric orbit satellite /HEOS/ for solar wind, cosmic ray and magnetic field data collection, noting design and mission program 20 p3531 A67-36412
 Bounded plasma flux in magnetic field, considering plasma polarization on magnetic field boundary, noting flux deceleration 20 p3497 A67-36682
 Inhomogeneous plasma instability from low pressure arc discharge in magnetic field 20 p3498 A67-36683
 Uniformly accelerated axisymmetric plasmoid isolation from pulsed accelerated walls in presence of external magnetic field, noting stable configuration 20 p3498 A67-36685
 Plasmoid instability from inhomogeneous flow along magnetic field 20 p3498 A67-36693
 Electromagnetic wave propagation in waveguides calculated together with electric and magnetic fields by perturbation method 20 p3382 A67-36862
 Stratosphere and mesosphere, discussing energetics, energy transfer, ionospheric currents, magnetic fields, atmospheric trace components, solar UV radiation measurements, etc 20 p3430 A67-36897
 Plasma stability in combined magnetic fields investigated for oscillation frequencies 20 p3500 A67-37048
 Motion of plasmoids injected axially in two-dimensional multipolar magnetic field, studying losses 20 p3500 A67-37061
 LF and HF wave excitation in homogeneous plasma with external magnetic field, obtaining differential and integral wave intensities 20 p3501 A67-37142
 Three-dimensional incompressible flow with colinear magnetic field, studying stability by numerical method 20 p3423 A67-37242
 Laminar MHD boundary layer over finite dielectric disk in presence of magnetic field, determining velocity profiles 20 p3501 A67-37305
 Sudden commencement and initial phase of magnetic storm explained in terms of currents induced in ionosphere 20 p3434 A67-37422
 Superconductors with overlapping bands, discussing copper pairing, heat capacity, critical field and ultrasonic attenuation 20 p3512 A67-37435
 Continuous DC EMF in semiconductor with symmetrical nonlinear conductivity analyzed in variable AC waveguide magnetic field 20 p3513 A67-37449
 Book on thermoelectric and thermomagnetic effects in metals, semimetals and semiconductors subjected to electric, magnetic and temperature fields, discussing transport theory 20 p3514 A67-37464
 Solar radio emission mechanism for spin transitions of neutron beta decay electrons in external magnetic field 20 p3520 A67-37522
 Current distribution of magnetic field in plasma coaxial injector indicating dominant role of Hall effect in plasma acceleration 20 p3502 A67-37537
 Electromagnetic shielding effectiveness of enclosure determined by measurement of perpendicular magnetic field along conducting wall surface, emphasizing continuity of seams 20 p3404 A67-37640
 Frequency characteristics of planar and spherical plasma resonance probes and RF impedance probe in magnetic field, considering equivalent electric circuit 20 p3503 A67-37670
 Plasma conductivity tensor in steady magnetic field in terms of electric field correlation using Kubo transport theory 20 p3503 A67-37692
 Magnetic field line trajectories in toroidal stellarators, discussing rotational transforms on last closed surface and perturbation effects 21 p3662 A67-37753
 Steady state theory of low pressure plasma discharge column in axial magnetic field derived, using moments of Boltzmann equation 21 p3662 A67-37756
 Electron-cyclotron harmonic resonances interactions in RFF excited electrodeless helium discharges, discussing magnetic field position measurement and plasma simulation 21 p3662 A67-37757
 Maser output pulsations by varying active particles entering resonator through electric or magnetic field 21 p3638 A67-37941

Two-port magnetoelastic delay performance obtained in YIG rod by injecting longitudinal elastic waves along axis 21 p3677 A67-38007
 Carrier spatial redistribution under magnetic field effect of current in semiconducting crystal with intrinsic conductivity noting I-V curve shape 21 p3678 A67-38098
 Transverse oscillation stability in quasi-one-dimensional flow of conducting gas in magnetic field 21 p3664 A67-38164
 Velocity profiles of boundary layer of conducting fluid rotating over stationary dielectric disk of infinite radius in magnetic field 21 p3665 A67-38246
 Steady motion of electrically conducting viscous fluid due to slow rotation of thin dielectric disk inside housing immersed in magnetic field 21 p3665 A67-38247
 Deformation of velocity profile in inhomogeneous magnetic field, noting anisotropic conductivity of flow 21 p3666 A67-38271
 Z-pinch in electron hole plasma observed by microwave probe method, noting no minimum current exists for semiconductors 21 p3666 A67-38356
 Parallel conducting flow along insulating pipe under applied magnetic field, elucidating singularities of Hartmann boundary layers 21 p3668 A67-38495
 Nonlinear oscillation theory for parametric resonance effect in gas lasers placed in stationary and variable magnetic field 21 p3641 A67-38549
 Rigid cylinder two-dimensional motion in rotating incompressible fluid compared to motion in isotropic incompressible conducting medium under magnetic field 21 p3668 A67-38552
 Velocity and pressure distributions and free shape of conducting liquid in rotating circular cylinder under magnetic and electric fields 21 p3668 A67-38561
 Instability of plasma with anisotropic ion velocity distribution, deriving equations for temperature variations and magnetic field energy changes 21 p3669 A67-38680
 Dispersion equation for frequency dependence on wave amplitude propagated in plasma placed in constant magnetic field causing longitudinal oscillations 21 p3669 A67-38681
 Probe for measuring three directional components of argon plasma magnetic field inside theta pinch conical coil, noting vortex structures [AIAA PAPER 67-659] 21 p3671 A67-38695
 Plasma acceleration by electromagnetic microwave discharge in static magnetic field gradient, discussing microwave-plasma energy transfer at electron cyclotron resonance [AIAA PAPER 67-660] 21 p3671 A67-38696
 Electrodynamical equations for pure and doped two-band superconductors, studying upper critical magnetic field 21 p3685 A67-38826
 Evidence for relationship between solar flares and magnetic fields explained by neutral point type model, considering smaller flares 21 p3699 A67-38988
 Convective motion of low pressure plasma confined by strong magnetic field taking into account heat and mass transfer 21 p3875 A67-39014
 Alfven two-dimensional problem extended to charged-particle motion in dipole magnetic field with electric field determining forbidden band size, shape and specular reflection points position 21 p3621 A67-39015
 Asymptotic formulas for propagating discontinuity diffusion in magnetoplasma, considering discontinuity shape, diffusion and lifetime 21 p3621 A67-39020
 Planet Jupiter research, noting unresolved questions of cosmology, interior structure and Great Red Spot 21 p3711 A67-39092
 Chapman-Enskog expansion applied to Fokker-Planck equation for plasma allows transport coefficients calculation without further approximation in presence/absence of magnetic field 22 p3843 A67-39266
 Finite discontinuity jump conditions for plasma in strong magnetic field determined by approximation and Maxwell equation, noting possible application to satellite data 22 p3843 A67-39269
 Empirical model of sunspot activity within

solar cycle limits indicating separate consideration of magnetic field generation and spot formation 22 p3879 A67-39300

Dielectric susceptibility and ion density measurement for polarized hydrogen plasma moving through transverse magnetic field 22 p3845 A67-39424

Mixed state existence in type I superconducting thin film, discussing microwave power absorption variation with perpendicular magnetic field 22 p3856 A67-39437

Limited instability and flux jumping variation with magnetic field for flux pinning and Lorentz forces equilibrium in mixed state of type II 22 p3856 A67-39438

LF permeabilities of superconductor due to surface currents calculated for magnetic field conditions 22 p3856 A67-39439

Dispersion relation for wave propagation in electro-magneto-ionic medium under electric and magnetic fields obtained using Maxwell-Boltzmann-Vlasov equations, discussing cut-off frequency 22 p3788 A67-39469

Thetatron gun plasma burst expanding freely in drift tube, discussing wall shorting effect inhibition method and measurements 22 p3846 A67-39485

Coordinate system with straight current and magnetic field lines used for hydromagnetic resistive interchange instabilities studies in toroidal configurations provides negative criterion generalization 22 p3846 A67-39486

Flux penetration and dissipation measured on superconducting niobium slab samples with tangential applied field studied for effect of thickness 22 p3857 A67-39491

Circular polarized magnetic field penetration into plasma cylinder noting penetration depth frequency dependence and MHD stability effect 22 p3846 A67-39508

Ion source using electron bombardment without magnetic source field, studying focusing and optimal operating conditions of electron accelerating system 22 p3847 A67-39641

Lande factors of neon atoms subjected to magnetic field and multimode laser irradiation measured by observing resonant saturations in fluorescent light emitted 22 p3815 A67-39651

Gravitational instability in anisotropic plasma including rotation effect 22 p3848 A67-39694

Incompressible finite conductivity tearing instability in hard-core pinch with constant applied axial magnetic field 22 p3848 A67-39695

Hot electron plasma confinement in magnetic mirror fields with compensating curvature, discussing experimental observations and hybrid configuration formation 22 p3849 A67-39698

Kinetic equations for electrons and photons in homogeneous plasma in strong magnetic field derived from Maxwell and classical motion equations 22 p3851 A67-39736

Magnetoacoustic attenuation in metals with Fermi surface, open orbits and magnetic breakdown calculated by solving Boltzmann equation via path-integral method generalization 22 p3861 A67-39995

Equations numerical integration for MHD fluid flows near critical point in presence of azimuthal magnetic field for several Alfvén and diffusion numbers 22 p3853 A67-40011

Resonant cavity electric field excitation placed in magnetic field near electron cyclotron frequency studied for expressions of self-excitation current 22 p3816 A67-40126

Atmosphere of Mars studied using three models generated to show high, mean and low density compositions to account for gravitational and magnetic fields 22 p3887 A67-40140

AC and DC magnetic bearings efficient load support and development potentials [ASLE PREPRINT 67AM 6D-4] 22 p3813 A67-40219

Radial electron density profile and critical longitudinal magnetic field for helical current convective instability in hollow plasma column via Langmuir probe measurements 22 p3853 A67-40234

Angular and energy characteristics of proton beam in pulsed magnetic field, determining probability of proton-neutron

charge exchange for proton in forward flight 22 p3842 A67-40255

N-type InSb microwave noise emission at low temperatures in low electric field regime, measuring magnetic field threshold and background continuum 22 p3864 A67-40345

Equilibrium configuration for non-spherical cold gas cloud permeated by magnetic field in gravitationally collapsed state 22 p3895 A67-40518

Rotation and magnetic field effects on single and multiple stars formation 22 p3895 A67-40519

RF size effects in plane parallel metal plate, discussing skin effect in magnetic fields, electron trajectories and spherical Fermi surface 22 p3868 A67-40551

Electrical conductivity or magnetic Reynolds number of shock produced plasma flow, discussing interaction between magnetic field and plasma flow 23 p4031 A67-40881

Turbulent plasma state and diffusion across magnetic field due to ion acoustic instability noting diffusion coefficient increment with instability excitation 23 p4032 A67-40905

Two-dimensional two-fluid nonlinear computer model applicable to low beta plasma interchange modes 23 p4033 A67-40995

Space time distribution of cosmic rays as function of plasma efflux from sun, magnetic field intensity, topology and scale irregularities 23 p4059 A67-41133

Unsteady continuity and motion equations describing F layer dynamic characteristics under time dependent electric and magnetic fields 23 p3996 A67-41178

Magnetic and electric dipole antennas located above earth surface, deriving quasi-static electric and magnetic field components 23 p3981 A67-41210

Flare positions relative to neutral line in longitudinal components of photospheric magnetic fields, stressing drift rate 23 p4060 A67-41231

Velocity fields in solar photosphere and chromosphere, discussing granulation, supergranulation, magnetic fields and oscillatory motions 23 p4068 A67-41276

G factor of holes in Ge and Si semiconductors computed in quasi-classical region noting dependence on hole moves relative to magnetic field 23 p4042 A67-41297

Two-stream instability in plasma analyzed using magnetic field association with charged particle motion and boundary effects 23 p4034 A67-41450

Magnetic field critical current density characteristics of Nb-Zr-Ti superconducting alloys, discussing peak effect and barrier height random distribution 23 p4044 A67-41451

Magnetic field of flux jumping in synthetic high field superconductors measured as function of temperature and field sweep rate 23 p4044 A67-41452

Rise rate dependence of transition current of superconducting solenoids on presence of electrical short circuit 23 p4045 A67-41457

Destruction of superconductivity in niobium by current and external magnetic field intensity 23 p4047 A67-41691

Two-phase mixture passing through magnetic field in MHD generator studied for effective electric conductivity 23 p3942 A67-41758

Electrical conductivity of high void fraction two-phase flow with and without magnetic field in MHD generator 23 p3942 A67-41759

Nonlinear growth of interstellar gas clouds and forces in three dimensions 24 p4223 A67-41812

Interstellar gas and magnetic field periodic system stability noting free-fall time 24 p4224 A67-41814

Upper critical nucleation field at free surface of superconductor backed by normal metal 24 p4200 A67-41862

Constant voltage steps of AC Josephson effect observed in drop-form junctions exposed to radiation 24 p4200 A67-41864

Oscillating magnetic field influence on Hall effect and resistance of superconducting niobium 24 p4201 A67-41870

Interaction between broadening plasmoid and external magnetic field assuming time dependent conductivity and magnetic field as function of time 24 p4195 A67-41929

Energy transfer in sunspot model with vertical magnetic field, noting magnetic pressure distribution and magnetohydrostatic equations 24 p4226 A67-41966

Nonlinear ferrite diaphragms in waveguides, discussing magnetic field effect on cavity tuning 24 p4119 A67-41972

Faraday rotation and ellipticity measurements in germanium and gallium arsenide at room temperature in weak magnetic fields 24 p4202 A67-41984

Auroral brightness variations related to magnetic field fluctuations, especially to pearl type fluctuations 24 p4150 A67-42148

Phonon assisted magnetoabsorption in direct band semiconductors 24 p4203 A67-42267

Electric and magnetic field measurement by energy density antenna applicable to reducing signal fading encountered on mobile radio transmission path 24 p4131 A67-42340

Omega phase precipitation and superconducting critical transport currents in Ti-Nb wire samples 24 p4173 A67-42347

Geomagnetic dynamo laboratory model self-excitation conditions determined from solutions of electrodynamic equations, diagramming magnetic field and current distribution 24 p4231 A67-42353

Hall potential difference for thin film in magnetic leakage field of domain interface between ferro-and ferrimagnetic 24 p4204 A67-42457

Transverse magnetic field effect on two-dimensional jet of incompressible fluid 24 p4198 A67-42565

Plasma dynamics with HF theta pinch discharges confined in magnetic field 24 p4198 A67-42575

Hydromagnetic flow stability in infinitely long cylindrical pipe with arbitrarily smooth cross section and applied radial magnetic field 24 p4198 A67-42693

Microwave absorption by magnetic field induced surface states in superconductors, showing anomalies consistent with quasi-particle decay 24 p4205 A67-42739

Boltzmann equation for cosmic ray particle motion in random magnetic field 24 p4213 A67-42770

Steady electric power from Cs seeded Ar plasma in nonequilibrium ionization flowing at high speed through magnetic field 24 p4109 A67-42895

MGD reentry flow regimes analyzed, noting increased bow shock standoff distance and drag, comparing in-flight and laboratory simulation 24 p4199 A67-42920

Compressible fluid with finite electrical conductivity in constant magnetic field hitting thin cylindrical obstacle, solving flow motion equations 24 p4199 A67-43080

Resonance rectification effects for wire probe in magnetoplasma observed in terms of warm plasma perpendicular permittivity component 24 p4199 A67-43101

MAGNETIC FIELD COIL

Abnormal internal phenomena in superconducting coil during magnetic excitation and S-N transition 05 p0871 A67-17482

Induction method for measuring plasma conductivity 07 p1230 A67-20105

Magnetic field curvature effects on low temperature alkali metal plasma column stability 11 p1830 A67-24007

Structural mass and shielded volume problems of unconfined magnetic space shields design 14 p2253 A67-29040

Gradient compensated large volume degausser noting inner and outer coils, magnetic field generators and construction and performance specifications 15 p2517 A67-29491

High-intensity and high-voltage current switching devices, noting strong pulsed magnetic field production 17 p2803 A67-32350

Toroidal stellarator magnetic trap with time-varying double coil magnetic field and external plasma injection 17 p2904 A67-32911

Direct solar to electric energy conversion using superconducting flux barrier, discussing superconductive phase change and magnetic properties 22 p3748 A67-40151

Liquid helium application in electromagnetic DC, LF and HF AC devices 22 p3838 A67-40397

Space magnetic environment simulation coil facility for spacecraft testing by mapping magnetic fields 24 p4138 A67-42030

MAGNETIC FIELD DISTURBANCE

Geomagnetic field disturbance due to earth passage through tail of Halley comet, 1910 II 02 p0236 A67-11654

Neutron component diurnal variation in cosmic radiation during period of coil type magnetic disturbances in tail of geomagnetic storm 02 p0306 A67-11656

Radio wave scattering and resonance scattering in wake of body moving in lower ionosphere plasma due to disturbance of electron concentration 02 p0192 A67-11657

Electrical current passage across neutral or ionized argon flow in presence of accelerating or decelerating magnetic field 03 p0478 A67-13605

VHF backscatter observations of radio auroral radar echo occurrence at sunspot maximum associated with spirals in geomagnetic latitude and time, magnetic disturbance levels and season 03 p0513 A67-14113

Magnetometer predictions of geomagnetic disturbances and intense sporadic E layer occurrences at various sunspot cycle times in auroral zone and effects on VHF absorption 03 p0415 A67-14118

Relation between magnetic activity and ionospheric disturbances in F-2 layer studied on basis of 30-year data 07 p1173 A67-19702

Magnetic disturbances at midlatitudes, noting origin from locally generated currents 07 p1174 A67-19709

Auroral occurrence rate at zenith as function of latitude for magnetically quiet and magnetically disturbed periods 07 p1178 A67-19817

Charge separation mechanism of auroral electrojets, noting enhanced ionospheric conductivity by electron bombardment 07 p1245 A67-19931

Dayside geomagnetic field disturbances in auroral oval monitored by satellite in polar orbit at 1100 km 08 p1329 A67-21487

Boundary variations of auroral oval zones, noting dependence on magnetic perturbation intensity 10 p1630 A67-22785

Semiannual variations of magnetic activity 10 p1630 A67-22796

Transverse magnetic field interaction with laminar boundary layer on rotating cone during reentry, assessing effect on spin and controlling torques 12 p1892 A67-25385

Earth magnetosphere at distances 7 to 11.7 earth radii obtained by Elektron satellites, noting differences between measured and calculated field vector 12 p1936 A67-25803

Interaction of shock-induced flow in ideal gas and transverse magnetic field analyzed for steady state and transient one-dimensional effects 13 p2162 A67-26280

Ion temperature gradients causing plasma instabilities when magnetic shear is present, deriving governing integral equation 13 p2162 A67-26284

Synoptic charting of high latitude geomagnetic field distribution during magnetic storm, discussing ring current behavior 14 p2309 A67-27942

Ionospheric micropulsations induced by enhanced conductivity of current due to meteors, noting end effect from finite ion trail length 14 p2383 A67-28044

Auroral zone electron precipitation occurring in strong transient magnetic disturbances observed by bremsstrahlung 14 p2310 A67-28056

Global response of topside ionosphere to magnetic disturbances at solar minimum studied from electron concentration measurements at 640 km 15 p2475 A67-29610

Flux-gate magnetometer device for determining attitude of satellite or rocket probe, considering magnet perturbation due to solar wind and solar storms 16 p2700 A67-30658

Geomagnetic field disturbance due to earth passage through tail of Halley comet, 1910, II 16 p2865 A67-31069

Neutron component diurnal variation in cosmic radiation during period of coil type magnetic disturbances in tail of geomagnetic storm 16 p2738 A67-31071

Radio wave scattering and resonance scattering in wake of body moving in lower ionosphere plasma due to disturbance of electron concentration 16 p2824 A67-31072

Flux observations in type II superconductors when changing magnetic field suddenly, with results used to deduce flux flow resistivity 18 p2730 A67-31169

Luminosity variations of comet 1963 III related to solar and geomagnetic disturbances caused by corpuscular solar particles 17 p2946 A67-32730

ULF radio emission associated with magnetic field disturbances, geomagnetic pulsations, auroras and exospheric particle acceleration 17 p2846 A67-32939

Polar magnetic disturbances accompanied by short period pulsations investigated with magnetogram for negative magnetic bay characteristics 17 p2847 A67-32943

Distribution of auroras during magnetically quiet and disturbed periods related to magnetosphere shape 17 p2849 A67-32965

Interpretation of multiple structure of auroral arc 18 p3035 A67-33598

Electrical current passage across neutral or ionized argon flow in presence of accelerating or decelerating magnetic field 18 p3091 A67-34470

Interplanetary magnetic field variation properties and effects on solar cosmic rays determined through Mariner II recordings employed to develop model 19 p3314 A67-35452

Soviet book on ionospheric geomagnetic disturbance prediction and short term radio propagation forecasting service 21 p3616 A67-37933

Evening sector polar magnetic substorm disturbance field morphology in transition region 21 p3616 A67-37998

Geomagnetic field polarity inversion, discussing reverse magnetization of volcanic rocks 21 p3621 A67-38982

Latitude variation of critical frequency of F-2 layer in equatorial region during geomagnetic disturbance, discussing ionization density 21 p3622 A67-39036

Nighttime E region electron concentration profile valley structure variations for quiet and disturbed geomagnetic activity 22 p3791 A67-39814

High energy cosmic ray shower detection combining perturbed magnetic field pulse and coincident optical radiation observations 23 p4051 A67-40812

Spread ionization in topside of ionosphere from satellite observations 24 p4148 A67-42060

Boundary variations of auroral oval zones, noting dependence on magnetic perturbation intensity 24 p4149 A67-42121

Semiannual variations of magnetic activity 24 p4149 A67-42132

MAGNETIC FIELD INTENSITY

Electromagnetic oscillation excitation in plasma beam, analyzing cases of weak and strong external magnetic fields 01 p0122 A67-10349

Dynamic dissipation of magnetic field, examining mechanism by which magnetic energy is converted directly into fast particle energy 01 p0146 A67-11277

Properties of solar and geophysical phenomena analyzed, concluding that magnetic field of corpuscular fluxes has forceless structure 02 p0311 A67-12590

Diffusion decay of discharge plasma with oscillating electrons in magnetic field 02 p0278 A67-12620

Motion of plasma through nonuniform transverse magnetic field, noting dependency of plasma motion solely on field intensity 02 p0278 A67-12623

Theoretical semiconductor electroconductivity dependence on intensities of strong electric and magnetic fields 03 p0490 A67-13158

Spin-lattice relaxation time of dirty type II superconductor alloys in mixed state in almost upper critical field 03 p0493 A67-13472

Temperature and magnetic field gradient effects on magnetothermomechanical interaction of viscous incompressible ferrofluid with cold wall 04 p0600 A67-14446

Domain structure of strontium ferrite investigated by Bitter powder pattern method in basal planes, showing dependence on magnetic field intensity, temperature and thickness of crystals 04 p0673 A67-14482

Plasma loss in single-ended Q device measured as function of magnetic field strength, obtaining diffusion coefficient directly 05 p0659 A67-17445

Motion of magnetic lines of force including analysis of fluids with finite high conductivity 06 p1030 A67-17561

Singularities of Faraday effect in n-type InSb in millimeter band at 77.8 degrees K as

function of sample thickness and magnetic field intensity 06 p1047 A67-17755

Average latitudinal drift of sunspots and migration of magnetic fields on sun 06 p1089 A67-18708

Changes in ultrasonic attenuation of superconducting niobium at low magnetic fields, considering effects of low critical field impurity phases 06 p1053 A67-18757

Magnetic field strength effects on excited acceptor states of semiconducting diamond determined, using Zeeman splittings of main excited lines 06 p1062 A67-18927

Axial magnetic field effect on Ne-He laser power output operating in regime of simultaneous generation of 3.39 and 0.6328 micron lines 07 p1196 A67-19601

Continuous transition from moving striation to helical oscillation in helium discharge plasma due to increase of applied magnetic field 09 p1538 A67-21570

Cosmos XLIX measurements of magnetic field intensity compared with calculation from spherical harmonic coefficients 10 p1632 A67-22812

Theoretical semiconductor electroconductivity dependence on intensities of strong electric and magnetic fields 10 p1690 A67-23106

Nonlinear dependence of current in electric field in thin semiconductor film in quantizing magnetic field 10 p1694 A67-23591

Dependence of ion current from RF ion source on plasma density at boundary and longitudinal magnetic field intensity 10 p1687 A67-23794

Low temperature alkali plasmas in magnetic fields in terms of collisional drift modes, determining steady state frequencies, amplitudes, etc 11 p1834 A67-24381

Instabilities in DC electron beam/plasma experiment noting dependence on beam current, magnetic field strength, beam velocity and plasma density 11 p1837 A67-24400

Electromagnetic oscillation excitation in plasma beam, analyzing cases of weak and strong external magnetic fields 11 p1844 A67-25022

Hall coefficient dependence on magnetic field intensity for n-type InSb single crystals at 77 degrees K 12 p1984 A67-25518

Sputnik III data application to plotting of total magnetic field intensity chart above U.S.S.R., using spherical harmonic analysis 12 p1933 A67-25652

Current carrier concentration gradient in InSb, investigating effect on transverse reluctance coefficient and Hall effect dependence on magnetic field intensity 13 p2173 A67-26360

Diffusion decay of discharge plasma with oscillating electrons in magnetic field 13 p2170 A67-27376

Motion of plasma through nonuniform transverse magnetic field, noting dependency of plasma motion solely on field intensity 13 p2170 A67-27379

Magnetic field amplification within sunspot groups, considering convective zone and viscosity 13 p2202 A67-27419

Model with hydrostatic gas pressure distribution to interpret equivalent widths of atomic and ionic lines in spectra of umbrae 13 p2203 A67-27426

One-dimensional plane shock wave propagation through hot dense plasmas under various energy and pressure conditions, noting magnetic field effect 14 p2356 A67-27957

Photographs of sunspots analyzed to obtain magnetic field strength data 14 p2384 A67-28076

Equatorial electrojet width and intensity analyzed with ground level magnetic field measurements from Peru and Nigeria 14 p2312 A67-28572

Superconducting solenoid producing oscillatory magnetic fields having peak to peak amplitudes, noting niobium-zirconium wire performance 14 p2288 A67-28747

Magnetic field strength effects on pulse and CW operation of large diameter ionized gas lasers 15 p2496 A67-29173

Coaxial helium-plasma source with superimposed azimuthal magnetic field, noting plasmoid density increase with magnetic field, plasmoid velocity and experimental setup 15 p2528 A67-29254

Magnetic trap electron capture lifetime dependence on magnetic field determined by

scattering by residual gas, noting adiabaticity parameter critical value 15 p2526 A67-29361

Line contours for Fe-I-6302.5 angstrom across sunspot in west solar limb measured simultaneously with magnetic field strengths and direction and Evershed velocity 15 p2554 A67-29460

HeNe laser output measured as function of axial magnetic field strength 15 p2498 A67-29512

Performance characteristics of Faraday and Hall MHD generators using strong magnetic fields and considering ion slip and finite electrode segmentation effects 16 p2599 A67-30527

Large combustion-driven, self-excited Faraday-type MHD generator having multi-or single-circuit net power output, discussing design 16 p2608 A67-30596

Solar cosmic ray observations, discussing emission spectrum, interplanetary particle distribution, diffusion coefficient, magnetic field strength, space-time distribution, etc 17 p2934 A67-32096

Electric field effect on magnetoresistance of p-type indium arsenide surface in high magnetic fields at low temperatures 17 p2911 A67-32206

MHD generators theory and operation including superheat conductivity, strong magnetic field generation and MGD flow structure in ducts 17 p2803 A67-32335

Spectrophotometric observations used to construct empirical curve relating radiation intensity and magnetic field strength in sunspots 17 p2946 A67-32728

Rotating field pinch dynamics in terms of temperature, pressure, plasma radius and magnetic field strength, noting energy transfer efficiency 17 p2908 A67-33108

Sigma components of line split in young sunspots magnetic fields measured with spectrocomparator, showing broadening of iron line in intergranular space 17 p2952 A67-33394

Hard superconductors electrical resistivity when subjected to increasing magnetic field, considering flux pinning and viscous motion of flux lines 18 p3098 A67-33518

Hall angle of various superconducting niobium-tantalum alloys in mixed state, noting dependence on current and temperature 18 p3098 A67-33519

Degradation, training and instability in superconducting coils, protection of windings and related problems of superconducting magnets for use in MHD generators 18 p3099 A67-33711

Temperature and magnetic field intensity dependence of microwave emission from n-type indium antimonide 18 p3101 A67-34016

Laser heating of plasma situated in strong longitudinal magnetic field 18 p3060 A67-34041

Shock wave argon ionization in constant magnetic field, showing attenuation decrease of microwave signal in plasma and modulus change curves 18 p3087 A67-34045

Weakly ionized inhomogeneous plasma in crossed fields, discussing magnetic field strength effect on stability against perturbations 18 p3089 A67-34296

Hall coefficient dependence on magnetic field intensity for n-type InSb single crystals at 77 degrees K 18 p3103 A67-34449

Structure of ion and electron currents axial emission from cathode measured as function of magnetic field intensity 19 p3277 A67-35121

Solar-flare short and long term forecasting, discussing magnetic-field configurations and gradients 19 p3314 A67-35269

Flux penetration and vortices formation in macroscopic type II superconductor shown to be favorable below thermodynamical critical field 20 p3508 A67-36426

Book on generation of high magnetic fields, discussing solenoids, cooling systems, superconducting and pulsed coils, etc 20 p3483 A67-36452

Discharge length influence on reflex discharge characteristics, considering conditions for charged particles extraction from discharge 20 p3498 A67-36686

Current distribution in MHD channel with strong magnetic field solved by reduction to Riemann type boundary value problem 20 p3500 A67-37047

Axial magnetic field effect on Ne-He laser

power output operating in regime of simultaneous generation of 3.39 and 0.6328 micron lines 20 p3462 A67-37340

Current carrier concentration gradient in InSb, investigating effect on transverse reluctance coefficient and Hall effect dependence on magnetic field intensity 21 p3680 A67-38317

Hard X-ray emission by hot electron plasma trapped in discharge tube due to magnetic field rise 21 p3667 A67-38413

Zero magnetic field in superconducting lead shell using Meissner effect 22 p3865 A67-40438

Helium RF discharge radiation temperature as magnetic field function measured, discussing enhanced diffusion role in radiation temperature determination 23 p4032 A67-40897

Solar magnetographs for defining strength and direction of magnetic field in solar atmosphere 24 p4223 A67-41769

Magnetic field intensity effect of sunspot group on source radio noise flux 24 p4209 A67-42136

Cosmos XLIX measurements of magnetic field intensity compared with calculations from spherical harmonic coefficients 24 p4150 A67-42149

Ar produced in capillary arc discharge, studying charged particle density and electron temperature dependence on magnetic field intensity 24 p4196 A67-42244

Intense continuous or long pulse magnetic fields in MHD generator, obtaining magnetic energy required for air gap, discussing superconducting magnets 24 p4098 A67-42414

MAGNETIC FILM

SA FERROMAGNETIC FILM

Structural and magnetic properties of /111/ films of permalloy produced epitaxially on epitaxial /111/ Ag on mica 04 p0676 A67-14931

Wall creeping in thin magnetic Ni-Fe films analyzed as function of thickness, field pulse amplitude, etc, comparing results with existing theories 11 p1845 A67-23953

UHF susceptibility of uniaxial magnetic films in weak fields far from ferromagnetic resonance 12 p1981 A67-25240

Soviet papers on structure and properties of metal films 17 p2920 A67-32887

Magnetics - Conference, Washington, D.C., April 1967 22 p3859 A67-39895

Chemical vapor deposition method to grow epitaxial YIG on YAG using high temperature hydrolysis oxidation at seed surface 22 p3860 A67-39896

Worm motion of domain walls in Permalloy films using Kerr magneto-optic apparatus under pulse drive with nanosecond rise time 22 p3860 A67-39901

Large angle flux reversal of Permalloy magnetic films investigated from experimental results of switching characteristics 22 p3860 A67-39903

High speed read-only memory with waffle iron structure noting ease of information change and high bit density 22 p3765 A67-39904

Magnetic film memory written and read by focused light studied using thermal cycle time and read bandwidth calculations 22 p3765 A67-39910

Demagnetizing fields in thin magnetic films, considering saturation, film thickness and anisotropy 24 p4204 A67-42338

MAGNETIC FORMING

Instrumentation and control for magnetic pulse metal forming including pulse generation, energy transfer, electrical operations, etc [SAE PAPER 660066] 01 p0078 A67-10569

Forming of refractory materials for rockets by explosive, magnetic and Dynapak forming and beam welding methods 01 p0079 A67-10638

MAGNETIC INDUCTION

Alfvén standing wave generation by current injection and/or electromagnetic induction in conducting liquid 02 p0272 A67-11520

Mathematical analysis of problems posed by electrostatic gyroscope with regard to suspension, starting, braking and effect of magnetic induction field on rotor 02 p0242 A67-12039

Origin of geomagnetic field, attributing paleomagnetic inversions to electromagnetism induction effects produced by solar corpuscular eruptions 02 p0326 A67-12063

X and Z components of ponderomotive forces acting on conductive strip of finite width in EM field produced by unidirectional inductor 04 p0556 A67-15525

Magnetic field of cylindrical permanent magnet used as rotor of electromagnetism induction pump, determining induction components and permeances to fluxes 06 p0951 A67-18685

Mean value of current in flat channel of MHD generator with short circuited electrodes taking into account induced fields 06 p0952 A67-18687

Electromagnetic induction in conducting sphere rotating in transverse field, extending results for steady state to unsteady rotation, determining magnetic moment 07 p1174 A67-19715

Induction method for measuring plasma conductivity 07 p1230 A67-20105

Effective electron and ion diffusion coefficients measured for positive magnetic field gradients show reduced plasma diffusion 08 p1364 A67-21400

Ion current from duoplasmatron ion source with expansion cuvette increased by superimposing weak magnetic induction in expansion zone and insulating cuvette walls 09 p1550 A67-22598

Frequency analysis of continuous and irregular geomagnetic pulsations measured by induction magnetometer 11 p1786 A67-24332

Performance characteristics of single wavelength liquid-metal MHD induction generator with end-loss compensation 12 p1897 A67-25375

Test program for induction coupled MHD generator using liquid sodium as working fluid, noting equivalent single phase circuit for electrical characteristics 12 p1897 A67-25376

Blowdown wind tunnel for He-K MHD generator, considering magnetically induced ionization, conductivity, gas temperature, etc 12 p1898 A67-25389

Explosively driven MHD generator, obtaining conversion efficiency dependence on magnetic Reynolds number, load-to-channel inductance ratio and magnetic/kinetic energies ratio 12 p1901 A67-25896

RF plasma torch coupling efficiency shown insensitive to input power and gas flow rate 12 p1976 A67-25925

Electromagnetic wave propagation characteristics in solid plasmas without magnetic induction, showing dynamic Hall effect 14 p2366 A67-28473

Production of crossed field and beam microwave tubes, noting demagnetization and coercive and inductance forces of various magnetic materials 15 p2447 A67-29753

Magnetically induced ionization in nonseeded helium and argon gas mixtures used to determine nonseeding operation of MHD generator in nonequilibrium ionization mode 16 p2711 A67-30542

Nonequilibrium plasma properties and generator performance due to magnetically induced ionization in closed loop facility using cesium seeded helium 16 p2602 A67-30557

Traveling field in gap of induction machines with open magnetic circuit created by linear winding load 16 p2723 A67-31583

Performance characteristics of helical electromagnetic induction pumps calculated taking into account effect of duct wall and liquid metal layer 16 p2609 A67-31584

Radio signals reflection by free radicals in ionosphere, observing predicted intensity and particle detection 17 p2817 A67-33233

Existence and stability conditions of several-quanta flux lines in type II superconductors 20 p3505 A67-36206

Vertical magnetic induction effect on nucleate boiling of mercury on horizontal heating surface [AICHE PAPER 20] 20 p3552 A67-36830

Operating characteristics of induction pump with asymmetrical current supply, calculating magnetic induction, currents and forces in liquid metal layer 20 p3365 A67-37307

Geomagnetic aperiodic variation effect on earth electric conductivity in electromagnetic induction theory for flat earth model 21 p3622 A67-39027

YIG magnetically induced elastic wave

dispersion, acoustic Faraday rotation and group velocity dispersion measured using Bragg diffraction 22 p3855 A67-39358

Magnetically induced circular dichroism and birefringence in ICI electronic spectrum, noting frequency dependence and molecular rotation effect 22 p3758 A67-39638

MAGNETIC INDUCTION PROBE

Hall coefficient tensor in single crystals of titanium measured at room temperature as function of crystallographic orientation in magnetic field 01 p0132 A67-10375

Pressure attenuation of transverse fringe effect in flat linear induction pumps 16 p2723 A67-31582

MAGNETIC INSTRUMENT

SA ELECTROMAGNETIC INSTRUMENT

Two magnetically geared microscope stages for nuclear track plates 02 p0247 A67-12696

Magnetic screening tests and use of parts sampling to control magnetic cleanliness for quality assurance 03 p0396 A67-13721

Explosive driven magnetic generator applied to investigate electric, optical and elastic properties of various substances, plasma physics and charged particle accelerator 05 p0786 A67-16365

Eddy current test systems using magnetic reaction analyzer with Hall element for detector, noting applications to welding, thickness measurement, stress monitoring, etc 09 p1502 A67-21869

Construction method for pulse generator in digital magnetic devices and current generators in magnetic deflecting system 10 p1613 A67-23449

Two-cycle shift register calculated, using magnetic element with rectangular hysteresis loop without shunting diode 11 p1769 A67-25042

Inertial acceleration indicators which operate on magnetic-restraint principle, employing one or more permanent magnets to create magnetic field 15 p2489 A67-30087

Design and performance of explosive driven magnetic generators, giving line drawings and current oscillograms 18 p2987 A67-33628

MAGNETIC MATERIAL

Principle magnetic properties of series of anisotropic alloys of Alnico type with 38 percent cobalt and coercive forces in excess of 2000 oe 01 p0093 A67-10518

High temperature electrical material evaluation for Rankine cycle [SAE PAPER 660682] 01 p0094 A67-10571

Regenerative thermomagnetic power devices, considering state equations for ferromagnetic material, power cycle and entropy change due to magnetization [ASME PAPER 66-WA/ENER-1] 04 p0555 A67-15414

High temperature cobalt iron alloy for square loop and power transformer applications 05 p0864 A67-16833

Magnetic delay line vibration isolation system as heart of airborne special purpose computer in USN E-2A early warning aircraft 05 p0779 A67-17458

Concentrations of black magnetic spherules plotted down red clay core from North Pacific, noting size distributions suggesting extraterrestrial origin 06 p1079 A67-17657

Saturation magnetization of mixed cadmium ferrites of spinel structure 06 p1050 A67-18182

Soviet book on magnetic switching elements in radio electronics covering magnetic materials properties with rectangular hysteresis, shift registers, logic circuits, etc 11 p1765 A67-24515

Soft magnetic materials metallurgy for several types of electrical equipment 13 p2178 A67-27140

Reverse magnetization spike domains analyzed for nucleation and growth 13 p2179 A67-27141

Magnetization ripple in multilayer films, noting dependence on copper layer 13 p2179 A67-27143

Optical exciton-magnon absorption in manganese fluoride, experimental results and theory of interactions 17 p2926 A67-33382

Regenerative thermomagnetic power devices, considering state equations for ferromagnetic material, power cycle and entropy change due to magnetization [ASME PAPER 66-WA/ENER-1] 18 p2989 A67-34128

Satellite stabilization in geomagnetic field by applying magnet to satellite axis and using damping elements of soft magnetic materials 21 p3713 A67-38375

Heating and quenching of aluminum and gallium substituted YIG changes magnetization of material due to cations redistribution process 22 p3860 A67-39913

Temperature stable ferrite materials for laminated memory arrays compatible with integrated semiconductor drive circuit 22 p3861 A67-39914

Magnetic materials and applications - Conference, London, September 1967 23 p4040 A67-41181

Deterioration in permanent magnets at high temperatures and procedures to minimize detrimental performance 23 p4041 A67-41182

Magnetically tunable microwave filters using MHD modes in ferrites 23 p3980 A67-41186

Chemical history of Fe traced in nebular material assuming preplanetary particles were similar to those presently discarded by sun 23 p4068 A67-41360

Magnetic impurities in tunnel junction barriers investigated for effect on junction resistance 24 p4200 A67-41865

Light propagation in electrically and magnetically anisotropic medium and diffraction by birefringent cylinder using coupled integrodifferential equations 24 p4119 A67-41889

Black magnetic spherules in Pleistocene and recent beach sands, investigating origin by electron microscopy 24 p4235 A67-42835

MAGNETIC MEASUREMENT

SA ELECTROMAGNETIC MEASUREMENT

SA FLUXMETER

Ionized gas electric conductivity measurement based on magnetic flux changes and deflection of lines of forces during gas-magnetic field interaction 03 p0478 A67-13604

Magnetic fields at various depths of solar atmosphere measured by Crimean Astrophysical Observatory double magnetograph 04 p0701 A67-15551

Elektron I and II satellite measurements on outer radiation belt, noting geomagnetic field distortion and boundary dependence on magnetic perturbations 05 p0880 A67-16110

Hysteresis losses in nonideal superconductors calculated, using phenomenological equations of flux motion 06 p1048 A67-17819

Magnetic field variation indicator based on Barkhausen effect 06 p1002 A67-17941

Dislocation density and magnetic hysteresis in superconducting state of 110-oriented Nb single crystals as function of angle of torsion 07 p1209 A67-19646

Induction method for measuring plasma conductivity 07 p1230 A67-20105

Device for visible recording of H component of geomagnetic field 12 p1941 A67-25556

Preliminary results of magnetic field measurements in vicinity of magnetosphere and interplanetary space from Mariner IV 12 p2007 A67-25822

Magnetization measurements in applied magnetic fields at cryogenic temperatures of dirty type II superconducting transition metal alloys 17 p2925 A67-33375

Magnetic field variation indicator based on Barkhausen effect 18 p3046 A67-33777

Ionized gas electric conductivity measurement based on magnetic flux changes and deflection of lines of forces during gas-magnetic field interaction 18 p3090 A67-34469

Thermoelectric and galvanomagnetic measurements on p-type bismuth compound, explaining anomalous rise in Hall coefficient with temperature and effective mass ratios change 18 p3105 A67-34632

Superconducting transition temperatures and low field magnetization of ceramic mixed Ba, Sr and Ca-Sr titanates, showing particle nature of specimens 19 p3302 A67-35037

Magnetometer with Gauss sensor describing n-type InSb pickup bridge instrument sensitivity 20 p3447 A67-36760

Weak magnetic field measurement using magnetic resonance, discussing electron nuclear resonance optical detectors, cesium vapor magnetometers and superconducting quantum interference device

/SQUID/ 22 p3799 A67-39771

Analogy between electric, thermal and magnetic phenomena considered in terms of molecular transfer theory, noting pure mathematical meaning with no physical content 22 p3837 A67-40213

Magnetization measurements for pure superconducting tin cylinders, discussing superheating effects 23 p4044 A67-41441

Elektron I and II satellite measurements on outer radiation belt, noting geomagnetic field distortion and boundary dependence on magnetic perturbations 24 p4214 A67-42786

MAGNETIC MEMORY

Measurement capabilities of linear digital displacement transducer with magnetically stored calibration 01 p0074 A67-11124

Design balances, tradeoffs and approaches to system design of various types of transistor-magnetic logic for aerospace timing 02 p0216 A67-12014

Piggyback twister /PBT/ magnetic memory for recording high impact data 02 p0242 A67-12019

Modeling of magnetic drum memory system using Markov chain based on historical data 03 p0400 A67-14220

System design decisions through static and rotating magnetic memories reliability as applied to command and control systems 08 p1299 A67-20665

Cryoelectric memory loop cell and hybrid organization system noting economy, high speed, mass storage, etc 12 p1915 A67-25887

Automatic multichannel system for data recording and processing obtained in studies of ionospheric structural inhomogeneities containing magnetic-tape memory and device for digital computer 13 p2119 A67-26561

Jackquard loom modification for assembling read-only braid transformer memories, describing self-contained model 13 p2123 A67-26803

Computer memory systems for handling Air Force information, discussing types of memory, storage techniques and device technologies 17 p2819 A67-32473

Nonvolatile block-oriented random access memory /BORAM/ combining thin magnetic films and scanning strain waves 18 p3012 A67-34347

High speed computer memory design using plated wire elements 19 p3189 A67-36065

Integrated circuit memory with 64 eight-bit words and compatible with high speed current-mode gates for high speed computers 19 p3189 A67-36066

Sonic film memory for digital information storage, discussing block-oriented random access memory /BORAM/ 19 p3189 A67-36067

Scientific data handling system using passive magnetostrictive multichannel delay line memory 20 p3390 A67-36251

Scintillation and dynamic range problems mitigated for Fourier spectrometry by rapid scanning 20 p3438 A67-36342

Nondestructively optically read ferroelectric bismuth titanate single crystal memory device 22 p3767 A67-39261

Mathematical model for linear memory arrays cross coupling problems, discussing signal distortion due to common mode capacitance effect 22 p3765 A67-39912

Temperature stable ferrite materials for laminated memory arrays compatible with integrated semiconductor drive circuit 22 p3861 A67-39914

MAGNETIC METAL

Magnetism and Magnetic Materials Conference, Washington, D.C., November 1966 13 p2178 A67-27137

Spin waves in two-band ferromagnetic metal assuming electron interaction via Coulomb potential 13 p2178 A67-27138

Possible superconductive pairing of two electrons separated by barrier leading to higher transition temperature for superconductors and superconductivity in magnetic metals 18 p3101 A67-33988

Alnico alloys containing Ti studied for columnar crystal growth, noting Ti content influence on crystal structure formation 21 p3645 A67-38376

Magnetic breakdown in metals covering one-electron theory, electronic motion, Bragg diffraction, de Hass-van Alven effect, coupled orbits and HF oscillations 22 p3866 A67-40552

MAGNETIC MIRROR

Injection of helical electron beams into

magnetic mirror trap, examining plasma lifetime, density and electron and ion energies produced 02 p0274 A67-12457

Effective capture of electrons in magnetic mirror trap with stationary field by pulse-type injection of helical electron beam 02 p0274 A67-12458

Thermally ionized cesium plasma confinement investigated in magnetic mirror geometry, in terms of collisional diffusion and end plate ion recombination 02 p0276 A67-12560

Plasma components transmission from occluded-hydrogen titanium-washer source into mirror machine along curved field lines of magnetic cusp 03 p0485 A67-14048

Instability in hot electron plasma in mirror field occurring suddenly in quietly decaying plasma generated by high power microwave 04 p0683 A67-14621

Hot electron plasma instability in magnetic mirror, discussing stabilization by cold plasma component and magnetic field line typing in conducting end plates 05 p0858 A67-17431

Minimum B magnetic field geometry for LF oscillations in Cs plasma of Topsy. Q device 05 p0859 A67-17444

Quasi-linear theory of loss cone instability of plasma confined in mirror type trap 08 p1359 A67-20899

Data correlation on nonadiabatic behavior of individual charged particles in magnetic fields 08 p1362 A67-21150

Hamiltonian function of particle in static magnetic field determined with cyclicity in two degrees of freedom 10 p1684 A67-22900

Action-angle coordinates for particle motion in magnetic mirror systems 10 p1684 A67-22901

Relativistic electron motion in mirror magnetic field interacting with axial electromagnetic wave calculated, comparing results with Seidl experiment 11 p1828 A67-23895

Energetic molecular hydrogen ions injected into resonant nonadiabatic magnetic mirror trap, studying particle mean lifetime, noting cold plasma stabilizing effect 12 p1969 A67-25248

Hydrogen plasma produced by coaxial gun located in magnetic mirror 13 p2163 A67-26291

Plasma EM instability in magnetic mirror configuration, solving linearized Vlasov equation for dispersion relation of transverse EM waves 13 p2164 A67-26293

Modulated electron beam interaction with plasma formed by beam causes ion heating to energies of hundreds of volts in magnetic mirror field 13 p2164 A67-26299

Energetic plasma confined in magnetic mirrors shown to have little interaction with main plasma body 15 p2523 A67-29213

Stabilization of ion cyclotron plasma in mirror machines by energy spreading and application of high frequency electric field 16 p2714 A67-30873

Flute instability for inhomogeneous plasma equilibria in inhomogeneous magnetic fields of mirror machines, solving Vlasov and Poisson equations 16 p2714 A67-30875

Flute instability in mirror machines at very low plasma densities, using variational principle for stability criterion derivation 16 p2714 A67-30876

Intense microwave radiation from high density plasma confined by magnetic mirror 17 p2894 A67-32145

Ion cyclotron instability potential and adiabatic compression of plasma in mirror machine, measuring plasma decay rate and potential 22 p3846 A67-39487

Hot electron plasma confinement in magnetic mirror fields with compensating curvature, discussing experimental observations and hybrid configuration formation 22 p3849 A67-39698

Cyclotron instability examined for plasma in magnetic mirror machines with anisotropic nonmonotonic ion distribution in velocity space 22 p3852 A67-39988

MAGNETIC MOMENT

Formula for second order correction factor derived for special case of static magnetic field with axial symmetry 03 p0484 A67-14040

Magnetic field geometric properties effect on magnetic moment and adiabatic invariants of charged particle motion 03 p0484 A67-14041

Electromagnetic induction in conducting sphere rotating in transverse field, extending results for steady state to unsteady rotation, determining magnetic moment 07 p1174 A67-19715

First order correction to magnetic moment invariant in Van Allen radiation belt 07 p1246 A67-19955

Magnetic moment variations of charge in combination static magnetic and HF field 10 p1683 A67-22843

Flight control magnetic source interaction with ionized gas induced by bow shock ahead of blunt body in hypersonic flow 10 p1592 A67-23143

Polarization of ytterbium isotopes in atomic state using optical pumping with resonance line, calculating magnetic moments 10 p1665 A67-23479

Induced magnetic moment and surface fields of ideal superconducting torus in uniform magnetic field calculated using Legendre functions 11 p1850 A67-24918

Optimization of injection location in HF plasma accelerators 13 p2165 A67-26586

Local magnetic moment derivation methods using magnetoresistivity data, estimating concentration and temperature dependence 13 p2177 A67-26990

Current damping, thermal expansion, radial oscillation, kinetic pressure and other dissipative processes effects on magnetic properties of plasmoids 15 p2524 A67-29244

Small nonpolarized plasmoids interacting with axisymmetric magnetic field, discussing penetration mechanism, equations of motion and magnetic moment 15 p2524 A67-29245

Magnetic moment of electron in HF plasma accelerator for case of negligible axial acceleration in resonance region 15 p2527 A67-29514

Escalation effect by interaction of conduction and induction currents in niobium alloy wires 15 p2539 A67-29828

Magnetic susceptibilities and anisotropies of manganous acetate tetrahydrate crystal measured at various temperatures 15 p2540 A67-30091

Magnetic moment under short wave electrostatic perturbations 18 p3093 A67-34755

Superconducting niobium wire magnetic moment and heat development during external magnetic field variation, discussing irreversible behavior 20 p3511 A67-37240

Satellite stabilization with respect to geomagnetic field obtained by applying moments of magnetic forces 21 p3713 A67-38589

Magnetized gyroscope magnetic moment effect on performance calculated, discussing drift from axis equilibrium state 22 p3796 A67-39231

Conduction electron ground state and anomalous magnetic moment in antiferromagnetic semiconductor, considering magnetic polaron 22 p3857 A67-39462

Magnetic moments of sublattices and of yttrium garnet calculated including biquadratic temperature dependent exchange 23 p4043 A67-41302

Mossbauer spectra of FeMo alloys for closed space compositions show overlap of disturbed surroundings of impurity iron atoms and magnetic moment 24 p4203 A67-42108

MAGNETIC PISTON

Neutron emissions by noncylindrical discharges of revolution, noting high pressure and impurities favoring airtight magnetic piston 10 p1683 A67-22844

MAGNETIC PROBE

Current distribution in eddy configuration of atmospheric gas discharge, noting flow surface deformation rate and measurement techniques 02 p0180 A67-12441

Anomalous skin depths and magnetic probe measurement of oscillating magnetic field penetrating into plasma cylinder 03 p0477 A67-13534

Infinite magnetic quadrupole channel, discussing operations in complete transverse plane phase space via 4×4 matrix transformations 08 p1332 A67-21172

Geomagnetic anomaly studied from equatorial ionosphere vertical probe observations in East Asian zone of Pacific ocean 14 p2308 A67-27937

Semiconductor galvanothermoelectric characteristics analyzed using all-metal device 19 p3228 A67-34989

MAGNETIC PROPERTY

SA HALL EFFECT

SA HYSTERESIS

SA INDUCTION

Electron resonance and magnetic properties of solid solution in bismuth ferrite and barium titanate system, obtaining phase diagram 01 p0127 A67-10063

Temperature dependence of complex initial magnetic permeability of cobalt-zinc ferrites over 0.1-2000 mc frequency range 01 p0128 A67-10079

Magnetic properties of YGa and YGaGd ferrites noting effect of increasing Gd content 01 p0136 A67-11052

Geomagnetic field intensity measurement, based on observation that ferromagnetic minerals cooled in weak magnetic field from above Curie temperature acquire thermoremanent magnetization 02 p0236 A67-11477

Activity of oxygen in liquid Fe-Pt alloy system, determining temperature and composition effect on equilibrium constant 02 p0256 A67-12708

Magnetic properties of pure and impure double-band superconductors in vicinity of upper critical field treated by almost-free-electron approximation 03 p0500 A67-14196

Temperature and thickness dependence of critical field of superconducting Sn films measured and compared with nonlocal theoretical models 05 p0864 A67-18899

Low temperature magnetic properties of superconducting Mo-Re alloys in fine wire form 07 p1236 A67-20135

Temperature dependence of magnetization and resistivity in SHF magnesium-aluminum ferrite 10 p1688 A67-22830

Magnetic resistance and Hall effect dependence on external electric field in semiconductors, noting difference for parabolic and nonparabolic law of carrier dispersion 10 p1695 A67-23661

Soviet book on magnetic switching elements in radio electronics covering magnetic materials properties with rectangular hysteresis, shift registers, logic circuits, etc 11 p1765 A67-24515

Synthetic pink-ruby crystal demagnetization characteristics when employed as coolant in cryostat, noting temperature dependence 11 p1851 A67-25033

Magnetic characteristics of ferromagnetic thin films obtained by ferromagnetic and spin wave resonance techniques 12 p1981 A67-25241

Rubidium nickel trifluoride transparent single crystal magnetic and optical properties analyzed, concluding compound is antiferromagnetic 12 p1984 A67-25747

Low noise SiFe sheet development and application, considering effects on magnetic properties 13 p2178 A67-27139

Approximate quantum numbers for d-band states in transition metals 13 p2179 A67-27155

Magnetic properties of meteorites, residual thermomagnetic capacity and determination of space magnetic fields 14 p2383 A67-27926

Magnetic properties of pure and impure double-band superconductors in vicinity of upper critical field treated by almost-free-electron approximation 14 p2369 A67-28541

Copper phthalocyanine single crystal measurements for electric, thermoelectric and galvanomagnetic properties 14 p2376 A67-29086

Current damping, thermal expansion, radial oscillation, kinetic pressure and other dissipative processes effects on magnetic properties of plasmoids 15 p2524 A67-29244

Magnetic properties of superconducting vanadium calculated from cellular model 16 p2726 A67-30816

High pressure electrodeless discharge in pure Ne and Xe and mixture of Kr and Xe, detailing effect of steady state magnetic field on Xe plasmoid 16 p2717 A67-31185

Magnetic, electric and SHF properties of oxides and solid solutions of bivalent europium from 1.6 to 300 degrees K 16 p2733 A67-31732

Book on intermetallic compounds discussing bonding, crystal structure, microstructure, formation, stability, kinetics, transformations and properties 16 p2692 A67-31867

Magnetic resistance and Hall effect dependence on external electric field in semiconductors, noting difference for parabolic and nonparabolic law of carrier

dispersion 17 p2924 A67-33342
 Hysteretic superconductor, showing trapped flux or remnant magnetic moment linear relationship with average internal field in low but not in high k superconductors 19 p3302 A67-35036
 Type II superconductors properties, studying Ginzburg-Landau equations, vortex lines, reversible magnetic behavior and irreversible phenomena in mixed state 19 p3307 A67-35868
 Ni-Fe-Mn alloy, Youngs modulus and magnetic saturation temperature dependence, noting order-disorder effects on Curie point 20 p3468 A67-37178
 Magnetic properties of relativistic equilibrium plasma in magnetic field studied in Boltzmann and quantum cases, using thermodynamic functions 20 p3502 A67-37557
 Spin-density waves effect on electronic properties and Fermi surface of antiferromagnetic metals 21 p3676 A67-37817
 Planetary magnetic fields calculated from meteorite magnetic properties and assumptions about cores and crusts 21 p3711 A67-39042
 Generalized Ginzburg-Landau parameters and magnetic properties of type II superconductors near upper critical field 22 p3857 A67-39440
 Fe rods in Fe-Sb matrix eutectic system, measuring rod diameter and Fe volume fraction effects on magnetic properties 23 p4039 A67-40884
 Flexible anisotropic ferrite magnets preparation, noting influence of blinder in orientation of crystals 23 p4041 A67-41183
 Domain structures in YIG slices after polishing strains elimination, noting spike domains 23 p4041 A67-41185
 High temperature strength and magnetic properties of cobalt-tungsten alloy for space power generator rotors 24 p4174 A67-42726

MAGNETIC PUMPING

SA ELECTROMAGNETIC PUMP

Transverse forces acting on arbitrarily curved current carrying plasma cylinder in transverse magnetic field 19 p3281 A67-35151
 Collisionless plasma heating by random magnetic fields using simple betatron model 21 p3662 A67-37762
 Monolithic magnetic double-balanced modulator, comparing patterns from working sample with theoretical conversion gain 22 p3773 A67-39916

MAGNETIC RELAXATION

Quantum mechanical theory of microwave nonresonant absorption and dielectric and magnetic relaxation in gases 01 p0116 A67-10145
 Magnetic field gradient relaxation mechanism by random excitation of transitions in F equals 1 level of ground state of hydrogen atoms in maser 05 p0817 A67-16635
 Relaxation phenomena role in MHD generator using nonequilibrium ionization, noting collisional and radiative recombination mechanisms 09 p1542 A67-21815
 High velocity shock waves obtained by magnetic pressure and relaxation processes, using electromagnetic shock tubes 11 p1832 A67-24034
 Relaxation effects in initially non-Maxwellian high temperature theta pinch using Fokker-planck equation for particle velocity distribution function relaxation effects in initially non-Maxwellian 13 p2163 A67-26288
 Nonlinear generalization of Schroedinger equation describing hidden variables effect solved for spin-1/2 magnetic moment relaxing in constant magnetic field 21 p3658 A67-38845
 Quasi-linear relaxation dynamics of unstable distribution function for potential drift waves, deriving law governing average wave number time variation 23 p4032 A67-40911
MAGNETIC RESONANCE
 SA FERROMAGNETIC RESONANCE
 SA NUCLEAR MAGNETIC RESONANCE
 SA PARAMAGNETIC RESONANCE
 SA PROTON MAGNETIC RESONANCE
 Optical pumping and double resonance used to study magnetic resonance and Zeeman effect 14 p2333 A67-28969
 Metastable atomic oxygen state observed in microwave discharge of molecular oxygen, noting g factor of 2 in strong

resonance 18 p3082 A67-34029
 Temperature dependence and anisotropy of high temperature ferrimagnetic microwave resonance linewidth of Si-doped YIG, showing valence exchange effect on losses 20 p3508 A67-38390
 Light beam propagation in atomic vapor, with atoms undergoing magnetic resonance, describing electromagnet wave polarization 20 p3458 A67-36435
 Magnetoresonant gyroscopes simulation by converting motion equations to rotating coordinates system 20 p3451 A67-37154
 Superconducting diode behavior in resonant electromagnet radiation field, studying current-voltage-magnetic field relationship 20 p3511 A67-37241
 Weak magnetic field measurement using magnetic resonance, discussing electron nuclear resonance optical detectors, cesium vapor magnetometers and superconducting quantum interference device /SQUID/ 22 p3799 A67-39771
 Geomagnetic perturbation data from high altitude nuclear weapon detonations, deriving theoretical model based upon MHD resonance, noting Alfvén wave behavior 22 p3792 A67-39932

MAGNETIC RIGIDITY

Cosmic ray intensity changes for various values of cut-off rigidity determined using barometric coefficient 02 p0307 A67-11667
 Atmospheric cosmic ray fluxes measured on series of USAF jet aircraft flights [AFCL-67-0099] 04 p0693 A67-14961
 Chemical composition of primary cosmic rays in moderate energy rigidity range with aid of satellite Proton I 05 p0877 A67-16087
 Change in cosmic ray cut-off rigidity caused by currents from trapped particle motion, according to Chapman-Akasofu radiation belt model 05 p0880 A67-16111
 Relation between cosmic ray cut-off rigidity and L parameter, solving approximately 7th degree algebraic equation 05 p0880 A67-16113
 Intensity of various secondary cosmic ray components in cut-off rigidity range from 0.3 to 10 Bev 05 p0881 A67-16124
 Geomagnetic cut-off rigidity effect on cosmic ray intensity and coupled coefficients 05 p0882 A67-16127
 Barometric effect of cosmic rays with allowance for changes in D/R / primary spectrum and cut-off 05 p0884 A67-17136
 Cosmic ray nucleonic component in Antarctic zone measured by neutron monitor, standardized and related to solar activity 10 p1699 A67-22862
 Primary cosmic ray proton and deuteron flux near geomagnetic equator determined by nuclear emulsion method 10 p1703 A67-23543
 Vertical cut-off rigidities for specific locations of geophysical interest computed from trajectory tracing process 13 p2191 A67-26325
 Cosmic ray particle trajectories for various cut-off rigidity values in different points on earth surface, noting integration of motion equations of charged particle 13 p2192 A67-27244
 Measurement of atmospheric cosmic ray fluxes over large portions of globe as comparison evaluation for different cut-off rigidity models 13 p2192 A67-27245
 Multi-aircraft measurements of cosmic ray spectrum and geomagnetic cut-off rigidity 13 p2193 A67-27246
 Cosmic ray intensity changes for various values of cut-off rigidity determined using barometric coefficient 16 p2738 A67-31082
 Latitude variation of effective geomagnetic cut-off rigidity of cosmic rays in presence of penumbra and constant geomagnetic field 17 p2934 A67-32094
 McIlwain coordinates correlated with vertical cut-off rigidities, estimating cosmic ray rigidities 17 p2936 A67-32537
 Spectral data on primary cosmic ray protons and helium nuclei analyzed, assuming solar cycle modulation due to diffusion-convection process 17 p2952 A67-33247
 Barometric effect of cosmic rays with allowance for changes in D/R / primary spectrum and cut-off 21 p3698 A67-38479
 Penumbra influence on cosmic ray effective cut-off rigidity calculated, noting

case of primary variations and constant magnetic field 21 p3699 A67-39017
 Cosmic ray trajectories in geomagnetic field, discussing asymptotic directions, rigidities, crossed telescope measurements and focusing effect 23 p4050 A67-40693
 Chemical composition of primary cosmic rays in moderate energy rigidity range with aid of satellite Proton I 24 p4212 A67-42763
 Change in cosmic ray cut-off rigidity caused by currents from trapped particle motion, according to Chapman-Akasofu radiation belt model 24 p4214 A67-42787
 Relation between cosmic ray cut-off rigidity and L parameter, solving approximately 7th degree algebraic equation 24 p4214 A67-42789
 Intensity of various secondary cosmic ray components in cut-off rigidity range from 0.3 to 10 Bev 24 p4215 A67-42800
 Geomagnetic cut-off rigidity effect on cosmic ray intensity and coupled coefficients 24 p4215 A67-42803

MAGNETIC SHIELDING

SA ELECTROMAGNETIC SHIELDING

Space satellite power converter-regulator design for minimum magnetic disturbance 05 p0754 A67-17462
 Energy required to confine static shielded magnetic dipole field, immersed in highly conducting medium, by transient diamagnetic surface as function of dipole moment and disturbance field 06 p1030 A67-17658
 Magnetic field effect on static shielding of point charge calculated, using Green function of inverse dielectric function of electron gas plasma 06 p1071 A67-18989
 Sensitive magnetic susceptibility measurements using superconducting circuits and magnetic shields 10 p1657 A67-23780
 Rare earth metal superconductive shielded magnetic lens for focusing high energy electrons 11 p1802 A67-24765
 Superconducting solenoid producing oscillatory magnetic fields having peak to peak amplitudes, noting niobium-zirconium wire performance 14 p2288 A67-28747
 Magnetic shielding properties of earth mantle obtained from power spectrum, deducing transfer function of mantle 14 p2314 A67-28887
 Structural mass and shielded volume problems of unconfined magnetic space shields design 14 p2253 A67-29040
 Transient plane wave magnetic field attenuation through semiinfinite plate using simplified Laplace transfer function, noting infinite product form for LPTF 16 p2626 A67-31349
 Thermal magnetic noise fluctuations reduction in superconductors below 4.2 degrees K 17 p2913 A67-32272

MAGNETIC SIGNAL

Specific storage volume and surface signal density in rotating magnetic data-storage devices investigated for capacity increase 19 p3186 A67-35584

MAGNETIC SPECTROSCOPY

Muon momenta, signs and densities in cosmic air showers determined, using magnet spectograph with visual display 06 p1076 A67-17651
 Slit size effect on magnetograph observations of solar magnetic field in near polar regions 06 p1082 A67-18015
 Inner zone trapped electron flux measurements by satellite indicating natural environment emergence from Starfish remnants 19 p3216 A67-35186
 Fast scanning 180 degree magnetic mass spectrometer for monitoring fast changes in residual gas compositions 20 p3448 A67-36875
 Solar magnetographs for defining strength and direction of magnetic field in solar atmosphere 24 p4223 A67-41769

MAGNETIC STORM

SA GEOMAGNETIC STORM

Planet rotation and orbiting of satellite Io modulations effect on maximum RF of storms 05 p0904 A67-17408
 Evening micropulsation events with rising midfrequency characteristics, discussing possible source mechanisms 07 p1182 A67-19947
 Low altitude electron trapping boundary collapse during magnetic storm due to field line extension into geomagnetic tail 11 p1785 A67-23943
 High energy particle precipitation into upper atmosphere at medium latitude after

magnetic storms, dependence on season and latitude and correlation with geomagnetic pulsation enhancement 12 p1991 A67-25113

Frequency spectrum of P1 2 micropulsation activity and relation to planetary magnetic activity 13 p2109 A67-26327

Effect of decrease in intensity of cosmic ray nuclear component during magnetic storms with sudden commencement studied by superposition of epochs 13 p2194 A67-27332

Blast wave driven by solar flare ejecting plasma cloud proposed as origin of energy density increase causing sudden commencement of magnetic storm 15 p2476 A67-29625

Magnetic storm effects on F-2 layer near equatorial zone boundary causing variations in critical frequency of layer 16 p2663 A67-30970

Sporadic E layer shows small negative relation to magnetic disturbances from 1958 to 1963 16 p2669 A67-31905

Polar cap anomalous absorption effects from ionosphere and geomagnetic field studies, noting correlation with magnetic storms 17 p2846 A67-32936

Balloon measurements of auroral X-rays, discussing flux and energy spectrum variations and bursts relation to magnetic storms 18 p3038 A67-33613

Auroral and polar magnetic substorms related to magnetic field lines reconnection in magnetosphere tail 18 p3117 A67-33615

Long-duration monochromatic emission with worldwide character in frequency spectrum of magnetic storm 18 p3041 A67-34193

Sudden commencement of November 13, 1960 caused by cosmic ray flare of November 12 20 p3517 A67-36284

Sudden commencement and initial phase of magnetic storm explained in terms of currents induced in ionosphere 20 p3434 A67-37422

Evening sector polar magnetic substorm disturbance field morphology in transition region 21 p3618 A67-37998

Absorption of VHF waves in whistler mode at low latitudes calculated for various ionospheric conditions during sunspot activity 21 p3617 A67-38065

Solar emissions and magnetic storms and auroras, discussing ring current, solar flux and Van Allen belt energetic particle density 21 p3620 A67-38978

Cause of cosmic radiation intensity increase before magnetic storms associated with Forbush effects 21 p3699 A67-39029

Cosmic ray diurnal variation during magnetic storms from neutron monitors and meson telescope data 23 p4058 A67-41124

Solar eclipse effects on topside ionosphere electron concentration, noting decrease for magnetic quiet conditions 24 p4148 A67-42059

MAGNETIC SURVEY

Structure of main geomagnetic field over Eurasia, noting difference in spectra over oceans and continents 07 p1173 A67-19697

MAGNETIC SUSCEPTIBILITY

Magnetic susceptibility studies show semiconductor to metal transition in titanium pentoxide and titanium trioxide, clarifying electronic nature of phase transition 01 p0132 A67-10376

Vibrational-rotational motion effect on electric and magnetic properties of diatomic molecules, calculating magnetic susceptibility and rotational magnetic moment 01 p0117 A67-10784

Photomagnetic susceptibility measured by means of induced short duration light flash, using germanium 06 p1001 A67-17938

Electron spin resonance of P doped Si at liquid He temperatures, obtaining paramagnetic susceptibility in metallic conduction region 06 p1068 A67-18972

SHF susceptibility of ferromagnetic thin films for constant magnetic fields far from electromagnetic resonance 08 p1367 A67-20605

Specific heat and magnetic susceptibility of yttrium solid solutions with magnetic impurities of Gd 08 p1369 A67-20870

Sensitive magnetic susceptibility measurements using superconducting circuits and magnetic shields 10 p1657 A67-23780

UHF susceptibility of uniaxial magnetic films in weak fields far from ferromagnetic resonance 12 p1981 A67-25240

Hole effective masses in p-type CdSb determined by measuring magnetoresistance effect and magnetic susceptibility 12 p1987 A67-26225

Magnetic susceptibilities and anisotropies of manganous acetate tetrahydrate crystal measured at various temperatures 15 p2540 A67-30091

Superconducting niobium and tantalum compounds investigated for maximum transition temperatures 16 p2728 A67-30818

Niobium stannide, V-Ga and V-Si paramagnetic susceptibility, elastic constants and electric resistivity temperature dependence 23 p4038 A67-40794

MAGNETIC SUSPENSION

Three-component wind tunnel balance capable of magnetically suspending test model 05 p0788 A67-16461

Roll control techniques for model suspended in electromagnet system 10 p1623 A67-23471

MAGNETIC SWITCHING

Design balances, tradeoffs and approaches to system design of various types of transistor-magnetic logic for aerospace timing 02 p0216 A67-12014

Three-port 35-GHz ferrite circulator latching switch, discussing geometric configurations, effects on performance characteristics, ferromagnetic materials selection, etc 08 p1304 A67-21225

DC motor with switching by magnetoresistant elements 21 p3571 A67-38225

MAGNETIC TAPE

Reconstructing serial pulse train from parallel data recorded on magnetic tape, examining flutter performance 02 p0242 A67-12021

Wave front reconstruction from magnetization distribution on magnetic tape, discussing possibilities based on magneto-optical Kerr effect, hypersonic wave generation and powder patterns 12 p1939 A67-25237

Packaging integrated circuit airborne tape control unit 12 p1911 A67-25273

Computerized microfilm or magnetic tape production for manned space station maintenance documentation 23 p4071 A67-40593

MAGNETIC TAPE RECORDER

Magnetic tape recorder for collection of flight loads data, examining development, test and specification 01 p0075 A67-11131

Magnetic recording of various types of monopulse, PPI and MTI radar signals, with application to airborne data acquisition recorder and ground reproducer 02 p0196 A67-12004

Tape recorder design for spaceborne data storage using isoelectric drive principle of peripherally driving tape packs to obtain high reliability 02 p0242 A67-12018

Analog magnetic recording in ground telemetry stations 03 p0418 A67-12896

Forced oscillation method measurement of aerodynamic coefficient of hypersonic blowdown wind tunnel 05 p0788 A67-16784

Comparative analysis of magnetization modes for magnetic storage of LF signals, using flux-sensitive and inductive reproducing heads in magnetic recorders 07 p1147 A67-19632

Magnetic recording process in dynamic magnetic storage method with bias magnetization, using Preisach magnetic particle model for case of static transparency in information carrier 07 p1147 A67-19633

Accident recording system for Concorde and protection from moisture, shock, fire and rough seas 12 p1939 A67-25231

Scan converter for Apollo TV performing time base conversion with destructive readout storage element and flicker correction with magnetic disk [SMPT PAPER 101-53] 12 p1904 A67-25468

Portable self-powered magnetic tape recorder for gathering data on vibration, temperature and shock on ground and in-flight aircraft 12 p1942 A67-25688

Magnetic tape simultaneous recording of radio atmospherics from broadband receivers and from waveform photographs, computing Fourier phase and pulse amplitude spectra 16 p2629 A67-31508

Data reduction system noting magnetic tape data collection, data transfer, random data analyzer, system analysis with transfer

function analysis, etc 20 p3442 A67-36460

MAGNETIC TRANSDUCER

High sensitivity inductive transducer using ferrite rings for measuring nutational oscillations of gyroscopic instruments 21 p3630 A67-38917

MAGNETIC TRAP

Symmetric inductor with multipole magnetic field for stable plasma confinement, calculating input parameters 01 p0012 A67-10188

Plasma trap configuration parameters inside solenoid wound about circular torus, noting magnetic surface distortion as function of screw axis period and curvature 01 p0121 A67-10342

Charged particle injection into magnetic traps through mirror, using annular electron gun 01 p0122 A67-10350

Plasma equilibrium in toroidal magnetic traps, discussing readjustment of small denominators in nondisturbance equation 01 p0123 A67-10508

Nuclear fusion, discussing magnetic confinement methods of hot plasma shell holding light nuclei 01 p0124 A67-10778

Decaying plasma density determined from high mode oscillations produced in magnetic trap with metallic chamber at 2000 to 6000 oe 02 p0274 A67-12464

Distortion of magnetic well in minimum-B system by plasma calculated, using hydromagnetic equilibria equations 02 p0276 A67-12561

Existence of exact solution to motion equations for charged particles in acute angled magnetic trap 03 p0486 A67-14064

Luna X lunar-orbiter satellite observations of charged particles in lunar ionosphere, using magnetic trap 03 p0513 A67-14066

Plasma behavior in magnetic trap with opposite fields, noting Coulomb ion-ion collisions and proton charge reversal 04 p0667 A67-15211

Plasma injected into magnetic trap with aid of conical theta pinch investigated to determine ion and electron energy, lifetime and charged particle concentration variation 04 p0668 A67-15279

Properties of dense plasma with preheated electrons in ion cyclotron resonance region, using magnetic mirror trap 05 p0853 A67-16755

Axisymmetric minimum average B configuration of triply connected system 05 p0809 A67-17446

Nonlinear theory on effect of drifting cone plasma instability on particle drift from adiabatic trap 05 p0860 A67-17545

Higher fast ion density achieved by fast neutral particle injection into closed-line magnetic trap 10 p1686 A67-23466

Effect of ion collisions and other terms on resistive-g instability in plasmas 11 p1826 A67-23873

Plasma parameter range for convective and absolute Harris instabilities, noting correlation with density 11 p1827 A67-23883

Stabilization of current driven helical waves in weakly ionized plasmas by magnetic wells of finite but small depth 11 p1827 A67-23885

Helical instability of positive plasma column in longitudinal magnetic field, using magnetic pickup coil 11 p1829 A67-23999

Outlook for controlled nuclear fusion process for industrial power generation, stressing plasma equilibrium preservation through magnetic trapping 11 p1831 A67-24015

Magnetic well stable to pure interchange instability and ballooning mode instability 11 p1839 A67-24544

Plasma trap configuration parameters inside solenoid wound about circular torus, noting magnetic surface distortion as function of screw axis period and curvature 11 p1843 A67-25015

Charged particle injection into magnetic traps through mirror, using annular electron gun 11 p1844 A67-25023

Plasma equilibrium in toroidal magnetic traps, discussing readjustment of small denominators in nondisturbance equation 11 p1844 A67-25071

Antisymmetric toroidal containment systems with line closure 12 p1970 A67-25251

Electron and ion temperature difference necessary to develop instability connected with loss cone of plasma with hot electrons placed in magnetic mirror

trap 12 p1971 A67-25334

Kinetic approximation of penetration of electric field into plasma layer situated in stationary magnetic field, determining plasma field 13 p2164 A67-26396

Existence of exact solution to motion equations for charged particles in acute angled magnetic trap 13 p2172 A67-27717

Magnetic trap electron capture lifetime dependence on magnetic field determined by scattering by residual gas, noting adiabaticity parameter critical value 15 p2526 A67-29361

Plasma behavior in magnetic trap with opposite fields, noting Coulomb ion-ion collisions and proton charge reversal 15 p2532 A67-30259

Motion of particles trapped in magnetic field, discussing conditions leading to spiral family of trajectory curves 15 p2551 A67-30397

Accelerated electrons effect on plasma in closed magnetic trap, measuring current flow, plasma density, X-ray/microwave radiation and light 16 p2717 A67-31186

Soviet book on plasma physics covering magnetic traps, acceleration, radiation, etc 17 p2903 A67-32909

Plasma injection into closed magnetic trap, studying effects of helical magnetic field on containment time, density, and cross section distribution 17 p2903 A67-32910

Toroidal stellarator magnetic trap with time-varying double coil magnetic field and external plasma injection 17 p2904 A67-32911

Ionization of media, sterile plasma production, dense plasma heating and plasma trap falling, by laser emission 17 p2904 A67-32917

Ambipolar potential-enhanced loss in magnetic trap reduced by potential difference in magnetic mirror throats dividing field 17 p2909 A67-33116

Stabilization conditions of isothermal plasma drift in magnetic trap for comparable electron and ion temperatures 21 p3663 A67-37936

Linear magnetically trapped plasma stability theory described from MHD or quasi-fluid point of view 22 p3853 A67-40075

Microwave production of plasma in trap at electron cyclotron resonance, investigating absorption and density 23 p4035 A67-41684

MAGNETIC VARIATION

Temporal variations in velocity of westward drift of nondipole geomagnetic field and negative correlation with solar activity 02 p0237 A67-11679

Monthly and seasonal variation of magnetic horizontal component in Eastern Africa on international quiet and disturbed days from February 1964 to January 1965 03 p0408 A67-12838

Origin of fluctuations in equatorial electrojet, discussing new type of geomagnetic variation, of polar origin 03 p0408 A67-12840

Lunar tidal variations in ionosphere in power spectrum analysis from geomagnetic data obtained during IGY 03 p0508 A67-12849

Recurrent variations of cosmic radiation during solar cycle 04 p0691 A67-14417

Variable polarization of magnetic star HD 71866 studied by observational program between January and April 1966 04 p0697 A67-14759

Height profile of Sq current in ionosphere, showing dependence on electric field direction 05 p0799 A67-16872

Changeability laws in quiet solar diurnal magnetic variations in 1964 and relation to state of ionosphere resulting from dynamo effect 05 p0802 A67-17147

Equatorial electrojet relationship with worldwide Sq currents 07 p1171 A67-19417

Ionization structure of polar auroras from spatial distribution of radar-reflecting zones, taking into account magnetic field variations 07 p1174 A67-19710

Latitude distribution curves of two quasi-circular zones of maximum magnetic activity along 12 consecutive meridians of local geomagnetic time 07 p1178 A67-19825

Mariner IV magnetometer data in earth magnetosheath analyzed to determine character of fluctuations in magnetic field 07 p1179 A67-19911

Normality of SD variation at dip-equatorial stations suggests origin beyond F layer 08 p1327 A67-21373

X-ray structural and spectral analysis of changes in lattice constant, linear expansion coefficient and K-absorption edge of iron and manganese in ferrite with spinel structure 08 p1372 A67-21492

Magnetic field variation at high latitude from quiet days in summer of IGY based on calculations for winter 10 p1632 A67-22810

Rapid magnetic variations near magnetic equator, determining principal characteristics 12 p1931 A67-25117

Lunar periodic variation of geomagnetic field on Khels Island in Franz Joseph Land 14 p2309 A67-27938

Current diagram plotting by graphical integration method for diurnal solar magnetic variations in especially quiet days 14 p2309 A67-27939

Magnetic variation measurements at Addis Ababa indicate intermittent existence of inverse direction equatorial electrojet 15 p2478 A67-30070

Daily geomagnetic variations superpositional nature studied by factorizing frequency functions describing day-to-day variability 16 p2664 A67-30971

Temporal variations in velocity of westward drift of nondipole geomagnetic field and negative correlation with solar activity 16 p2665 A67-31094

Rapid earth electromagnetic field variations used for plasma concentration and magnetosphere radius determination 17 p2846 A67-32937

Polar cap auroras frequency patterns relationship to worldwide storms 18 p3037 A67-33611

Magnetic variations relationship to magnetospheric perturbations, emphasizing particle participation near auroral zones 20 p3428 A67-36376

Daily magnetic variations over England, noting difference between values obtained for summer IQD and other days of year 20 p3429 A67-36870

Geomagnetic variations discussing attempts to explain 27-day recurrence tendency and to relate solar wind and magnetic indices 20 p3430 A67-36902

Superconducting niobium wire magnetic moment and heat development during external magnetic field variation, discussing irreversible behavior 20 p3511 A67-37240

Changeability laws in quiet solar diurnal magnetic variations in 1964 and relation to state of ionosphere resulting from dynamo effect 21 p3619 A67-38489

Geomagnetic field polarity inversion, discussing reverse magnetization of volcanic rocks 21 p3621 A67-38982

Incompressible hydromagnetic fluid oscillation in rotating spherical shell pervaded by strong toroidal and weak poloidal magnetic field for geomagnetic secular variation hypothesis 21 p3621 A67-38983

Deep subterranean electric conductivity using 30-year cyclic geomagnetic field variation data 21 p3622 A67-39025

Mariner IV flight magnetometer data, determining interplanetary field and geomagnetic variability 22 p3790 A67-39800

Rapid magnetic field variations observed in magnetosheath evaluated in terms of transverse modes of plasma wave propagation 23 p3995 A67-40804

Magnetic field variation at high latitude from quiet days in summer of IGY based on calculations for winter 24 p4150 A67-42147

MAGNETICALLY TRAPPED PARTICLE

SA GEOMAGNETICALLY TRAPPED PARTICLE

Distribution of charged particles of different energies escaping from magnetic trap in which spiral moving electron fluxes are created 02 p0274 A67-12459

Toroidal machine velocity space instabilities, rapidly saturating, with long time scale remaining relaxation 11 p1828 A67-23876

Polar auroral substorms, discussing mechanisms for dumping trapped particles 19 p3215 A67-35173

Inner zone trapped electron flux measurements by satellite indicating natural environment emergence from Starfish remnants 19 p3216 A67-35186

Hard X-ray emission by hot electron plasma trapped in discharge tube due to magnetic field rise 21 p3667 A67-38413

Temporary trapping device combining resonant perturbation and saddle point injection in Stormer potential configuration methods 22 p3849 A67-39697

MAGNETISM

SA DIAMAGNETISM

SA ELECTROMAGNETISM

SA FERRIMAGNETISM

SA FERROMAGNETISM

SA GALVANOMAGNETISM

SA GEOMAGNETISM

SA GYROMAGNETISM

SA HYDROMAGNETISM

SA PARAMAGNETISM

SA THERMOMAGNETISM

Piezomagnetic coefficients in magnetostrictive equations, permeability extrema and elastic moduli of Ni-Co-Mn ferrites 05 p0863 A67-16703

MAGNETITE

Magnetite crystals of asymmetrical shape observed in Alais, Ivuna and Orgueil carbonaceous meteorites noting particle corrosion 22 p3881 A67-39496

MAGNETIZATION

SA BARKHAUSEN EFFECT

SA KERR EFFECT

Magnetic properties of second kind superconductivity of indium-lead alloys as function of temperature down to 0.38 degrees K 05 p0864 A67-16893

Reverse magnetization and energy of anisotropy of single crystal ferromagnetic films 08 p1368 A67-20607

Type II superconductor voltage proportionality to time varying magnetic field under constant transport current and linear field sweep conditions 11 p1846 A67-24583

Porosity and particle size effects on magnetization curve of superconducting Nb sintered compacts with and without C added 12 p1978 A67-25139

Critical alternating-magnetization curves of permalloy films, clarifying theoretical experimental problems and effect of anisotropy field dispersion magnitude on curves 12 p1981 A67-25245

Structure effect on magnetization and critical current density in transverse magnetic field of superconducting V and Nb foils with different grain boundary orientations 12 p1986 A67-26067

Magnetization ripple in multilayer films, noting dependence on copper layer 13 p2179 A67-27143

Superconducting mixed state of concentrated Mo-Nb alloy, evaluating free area of Fermi surface in k space 16 p2726 A67-30812

Magnetization measurements in applied magnetic fields at cryogenic temperatures of dirty type II superconducting transition metal alloys 17 p2925 A67-33375

Thin superconducting films behavior in perpendicular magnetic fields, studying sample geometry effect on reversible magnetization curve 19 p3303 A67-35041

Book on electrodynamics of moving media, deriving force distribution using Hamiltonian and virtual power principles in relativistic formulations 20 p3500 A67-37087

Mathematical model describing magnetic damping in attitude control system of ESRO I satellite 21 p3678 A67-38216

Choke-coupled magnetic amplifiers and amplifiers with rotational magnetization, considering multicycle and single-cycle amplification 21 p3593 A67-38290

Nonideal type II superconductors, discussing flux motion and density, pinning force, magnetization, hysteresis, relaxation and energy loss 21 p3683 A67-38402

Dynamic energy losses in thin Ni-Fe films during magnetization reversal studied by observation of M-H loop 22 p3860 A67-39902

MAGNETO-OPTIC

Optical and magneto-optical phenomena in CdSnAs sub 2, discussing reflection and absorption spectrum, optical activity, double refraction, dielectric constant, etc 01 p0128 A67-10094

Optical reflection, transparency and Faraday effect for indium antimonide, calculating effective electron mass, relation between energy and wave number, etc 01 p0128 A67-10095

Photoconductivity resonances and recombination radiation in PbTe and InSb due to multiple photon interband transitions between Landau levels in high intensity

- magnetic fields 02 p0254 A67-12522
High magnetic field effect on interband semiconductor laser, particularly electromagnetic modes and coupling and threshold current 05 p0822 A67-16673
Linear and nonlinear magneto-optical phenomena in semiconductors, examining line and level broadening, cyclotron resonance with lasers, etc 06 p1060 A67-18916
Exciton and oscillatory magnetoabsorption spectra in layer type semiconductors in high magnetic fields 06 p1060 A67-18917
Oscillatory magnetoabsorption of direct transition in layer compound gallium selenide near absolute 06 p1060 A67-18918
Optical absorption and oscillatory magnetoabsorption in tellurium, noting interband transition and lack of inversion symmetry 06 p1060 A67-18919
Free carrier electro-magneto-optical phenomenon in semiconductors, noting conductivity tensor, Faraday effect, Derr effect and Voigt effect 09 p1558 A67-22602
Nonlinear excitation of electron plasmas in solids explained by mechanism of nonparabolic energy bands 10 p1689 A67-23075
Absorption coefficient of light in semiconductors in crossed electric and magnetic fields, examining conditions for Franz-Keldysh effect occurring in magnetic field 10 p1693 A67-23590
Interband magneto-optical phenomena involving linear single photon absorption and dispersion in semiconductors and semimetals 11 p1847 A67-24662
Rare earth metal superconductive shielded magnetic lens for focusing high energy electrons 11 p1802 A67-24765
Wave front reconstruction from magnetization distribution on magnetic tape, discussing possibilities based on magneto-optical Kerr effect, hypersonic wave generation and powder patterns 12 p1939 A67-25237
Magnetic deviation ion mass spectrometer for ionospheric rocket probes, noting onboard application 21 p3628 A67-38657
Magnetically induced circular dichroism and birefringence in ICI electronic spectrum, noting frequency dependence and molecular rotation effect 22 p3758 A67-39638
- MAGNETOACOUSTIC WAVE**
Cerenkov and cyclotron absorption of Alfvén and fast magnetoacoustic waves in plasma with gas-kinetic pressure in quasi-linear approximation 01 p0124 A67-10747
HF heating of dense plasma by resonance excitation of cyclotron-type ion waves and fast magnetoacoustic waves 02 p0274 A67-12460
MHD stability of dense plasma jets flowing into transverse magnetic field, discussing effect of conductivity and Hall factor 03 p0477 A67-13462
Harmonic response due to compressibility in traveling wave plasma devices, discussing magnetoacoustic resonances for case of cylindrical symmetry 03 p0485 A67-14051
Chapman-Joulet theorem for MHD detonation in shock tube blocked by stationary perfectly conducting surface, noting relation to magnetoacoustic wave 12 p1976 A67-26071
Transformation of magnetoacoustic waves in terms of ideal MHD by phase integrals method 12 p1976 A67-26072
Cerenkov and cyclotron absorption of Alfvén and fast magnetoacoustic waves in plasma with gas-kinetic pressure in quasi-linear approximation 13 p2168 A67-26776
Radiants associated with sonic, magnetosonic and Alfvén waves and definition in terms of distribution of delta operator of infinitesimal discontinuity 14 p2359 A67-28511
Heating of chromosphere above sunspot due to magnetoacoustic waves which develop into weak shock waves 15 p2551 A67-29142
Magnetoacoustic shock waves front in rarefied plasma disintegration at high Mach numbers as cause of increase in front wave duration and width 16 p2714 A67-31039
Hydromagnetic wave propagation in collisionless plasma based on Vlasov equation, finding Alfvén, magnetoacoustic and nonoscillating waves 17 p2902 A67-32673
LF acoustic/magnetoacoustic wave propagation in partially ionized plasmas studied within framework of macroscopic plasma dynamics, using dynamic adiabatic state equation 19 p3290 A67-35375
Energy dissipation of strong magnetosonic waves in rarefied plasma, discussing electrons ionizing collisions at wave front 19 p3293 A67-35402
Magnetoacoustic wave excitation and detection in rotating plasma accelerator, noting resonance and wave transition 19 p3298 A67-35746
Efficiency of plasma heating by HF field with excited magnetosonic wave due to energy absorption 21 p3669 A67-38678
Fast and slow magnetosonic wave propagation in plasma analyzed by Huygens principle 21 p3670 A67-38687
Alfvén, fast and slow magnetoacoustic and entropy hydromagnetic wave propagation in anisotropic collisionless magnetoplasma 22 p3843 A67-39268
Heating of chromosphere above sunspot due to magnetoacoustic waves which develop into weak shock waves 24 p4239 A67-43065
- MAGNETOELASTIC VIBRATION**
Spin-magnetophononic and magnetophononic oscillations of magnetic resistance in n-InAs 01 p0133 A67-10547
Spin-magnetophononic and magnetophononic oscillations of magnetic resistance in n-InAs 01 p0137 A67-11055
Magnetoelastic vibrations due to step function of mechanical radial force acting on perfectly conducting isotropic elastic cylinder placed in magnetic field 05 p0847 A67-17278
Natural magnetoelastic oscillations of circular cylindrical conducting shell 12 p2023 A67-25596
- MAGNETOELASTIC WAVE**
Approximate numerical solution used to calculate delay of z-directed magnetoelastic wave in yttrium iron garnet 01 p0138 A67-11321
Frequency selective parametric limiting by parallel pumping of subharmonic magnetoelastic waves in YIG 13 p2077 A67-26523
Excitation of magnetoelastic waves at 200 to 3000 mc at room temperature in yttrium garnet single crystals obtained by gradual crystallization from yttrium and ferric oxides 16 p2733 A67-31733
Two-port magnetoelastic delay performance obtained in YIG rod by injecting longitudinal elastic waves along axis 21 p3677 A67-38007
YIG magnetically induced elastic wave dispersion, acoustic Faraday rotation and group velocity dispersion measured using Bragg diffraction 22 p3855 A67-39358
Plane circularly polarized magnetoelastic and elastic wave scattering at plane discontinuity surface between ferromagnetic insulating medium and elastic medium 22 p3856 A67-39364
- MAGNETOELASTICITY**
Magnetoelasticity/magnetothermoelasticity theories concerned with externally applied magnetic field interacting effects on elastic/thermoelastic deformations of solid body 19 p3262 A67-35799
- MAGNETOELECTRIC MEDIUM**
Substantial size reduction of conical logarithmic antenna by loading with magnetodielectric material 02 p0212 A67-11612
Oscillatory magnetoconductance in inverted surfaces of p-type silicon 06 p1063 A67-18940
Relativistic electrodynamics of moving medium, discussing Maxwell-Minkowski equations, Born equations, field vector transformations, etc 09 p1533 A67-22449
Magnetolectric device development to measure and register weak signals in digital form in converters of automatic control systems 22 p3809 A67-40475
Measurements on YIG crystals showing magnetic crystal symmetry lowering by strong electric field 23 p4035 A67-40654
- MAGNETOGASDYNAMICS**
Generalized MGD equation for thrust in ramjet engine, with application to rocket engine and pulsed jet 03 p0503 A67-13086
Gas film MGD lubrication in transverse and tangential electromagnetic fields 05 p0810 A67-16273
Compressibility effect on dual solutions recurrence in MGD boundary layer over flat plate 06 p1041 A67-18134
- Quasi-one-dimensional MGD channel flow calculation methods, considering Hall effect, heat transfer, friction and potential drop near sectioned electrode 06 p1043 A67-18675
Hypercritical flows in MGD solved explicitly for exact solutions 07 p1230 A67-20120
MGD lubrication, obtaining motion equation of gas in electric or magnetic fields, velocity distributions, pressure differential equations, etc 07 p1192 A67-20210
Relations between rates of propagation of constant pressure, density, etc, for one-dimensional MGD flows 08 p1357 A67-20585
Protoplanetary cloud and evolution, noting Hoyle 'rotatory nebula and other hypotheses 09 p1563 A67-21633
Quasi-one-dimensional analysis of MGD, considering equations of continuity, state, current density, etc [AFOSR-87-1000] 09 p1540 A67-21792
Magnetofluid dynamics - AIAA Selected Reprint Series, Volume II 11 p1841 A67-24946
Transverse magnetic field interaction with laminar boundary layer on rotating cone during reentry, assessing effect on spin and controlling torques 12 p1892 A67-25385
Radiation MGD, considering flow problems with thermal radiation and electromagnetic field effect 12 p1975 A67-25889
Cylindrical screened electrode for measuring temperature plasma conductivity in MGD generator 13 p2055 A67-26434
Propagation of small disturbances in general three-dimensional unsteady nonequilibrium MGD, noting influence of various parameters 14 p2361 A67-28904
Ionizing detonation wave model with electrical conductivity jumping from zero to infinity characterized by exothermal energy release and magnetoacoustic speed propagation 15 p2528 A67-29567
Stratified layer flow of working fluid in duct of synchronous induction MGD generator studying stability by approximation 16 p2607 A67-30594
MHD generators theory and operation including superheat conductivity, strong magnetic field generation and MGD flow structure in ducts 17 p2803 A67-32335
Synchronous and asynchronous idealized induction alternating current MGD generators 17 p2803 A67-32340
Steady flow of ideal gas with conductivity past thin wedge in magnetic field studied for asymptotic properties of flow field 17 p2902 A67-32671
Interaction of planetary magnetic field with solar plasma studied using hypersonic analog, estimating energy transfer rate 17 p2951 A67-33208
Strong and weak magnetic field effects on qualitative characteristics of compressible media analyzed using Chaplygin-Sedov hodograph method 18 p3084 A67-33421
Stagnation pressure lower than atmospheric pressure in supersonic subatmospheric flow in magnetoaerodynamic generation nozzle, discussing Hall effects for energy conversion process 18 p3020 A67-34122
Supersonic free plasma jet with axial current, solving MGD equations for structure modifications due to self-magnetic forces 19 p3288 A67-35363
MGD shock wave with conductivity jump, correlating wave boundary to gas parameter 21 p3864 A67-38238
Current sheet propagation transition to steady pattern in pulsed plasma accelerator, noting breakdown and current characteristics [AIAA PAPER 67-656] 21 p3689 A67-38692
Propellants and propellant mixtures effects on MPD arc jet performance in test for ions and neutrals mixture acceleration to high velocity [AIAA PAPER 67-684] 21 p3688 A67-38715
Electro- and permanent magnet configurations using different materials analyzed, determining lowest mass magnet system for MPD arcs [AIAA PAPER 67-686] 21 p3692 A67-38717
Rotating current spoke in MPD engine, existence and connection with exhaust fluctuations [AIAA PAPER 67-689] 21 p3693 A67-38720
Insulator boundary layers in supersonic MGD channel noting heat transfer rate, current density, stagnation, pressure

distribution and skin friction
 [AIAA PAPER 67-717] 21 p3673 A67-38743
 Tensor conductivity effect on continuum and collisionless MPD flows past slender bodies
 [AIAA PAPER 67-731] 21 p3674 A67-38755
 Neutral carrier gas and slightly ionized plasma binary mixture model for nonhomogeneous seeding effects on rotating arc performance 21 p3674 A67-38885
 Flow velocity and magnetic field effects on characteristics of single controlled glow discharge in cesium seeded argon 21 p3674 A67-38888
 Imbedded magnetic field stabilization effect on infinitely conducting inviscid compressible relativistic MGD half-jet 22 p3850 A67-39706
 Boundary layer electric current temperature, velocity and density profile calculation on nonconducting MGD channel wall assuming smaller magnetic Reynolds number than unity 24 p4196 A67-42212
 One-dimensional steady MGD flow of polytropic gas with finite constant electric conductivity, noting flow patterns and oblique shock wave structure 24 p4198 A67-42707
 Steady electric power from Cs seeded Ar plasma in nonequilibrium ionization flowing at high speed through magnetic field 24 p4109 A67-42895
 MGD reentry flow regimes analyzed, noting increased bow shock standoff distance and drag, comparing in-flight and laboratory simulation 24 p4199 A67-42920

MAGNETOHYDRODYNAMIC ACCELERATION

MHD channel flow for given accelerator analyzed, based on magnetic and other interaction parameters for full range of possible exit states 01 p0014 A67-11195
 Acceleration mechanism in plasma current layer forming when strong magnetic field moves at high speed into initially stationary field-free plasma 02 p0274 A67-12341
 Plasma acceleration and retardation by magnetic standing waves 04 p0688 A67-14564
 Staustrahlrohr experiments in thermodynamic acceleration process for liquid metal of MHD converter for space vehicle propulsion 04 p0580 A67-15966
 Asymptotic solution for one-dimensional MHD generator scaling numerical values to obtain correct results for zero initial current and velocity 05 p0856 A67-17365
 Electrode geometry effect on current and potential distributions in MPD arcs 06 p1074 A67-18335
 Propellant injection through electrodes effect on potential distribution in MPD arc [AIAA PAPER 67-49] 06 p1074 A67-18435
 Pressure difference in cathode region of MPD accelerator as affected by plasma compression and magnetic field [AIAA PAPER 67-47] 06 p0951 A67-18466
 MHD flow past sonic velocity in channel of constant cross section, discussing conditions for smooth acceleration 13 p2169 A67-27309
 MHD resonance acceleration of plasma clusters and shock waves, showing advantage for parallel or coaxial conductor systems 14 p2354 A67-27762
 MHD accelerators for hypervelocity test facilities, showing Faraday accelerator is best suited to operation at high flow densities required 14 p2294 A67-29042
 Single-fluid model accounting for behavior of MHD shock producing devices with unseparated shock and driving current sheet 15 p2528 A67-29565
 Pressure difference in cathode region of MPD accelerator as affected by plasma compression and magnetic field [AIAA PAPER 66-47] 15 p2531 A67-30205
 Electrode feed system for segmented-electrode MHD accelerator to avoid power supplies/switch gear 19 p3177 A67-35774
 Pressure gauge for plasmas subjected to large dynamic electric and magnetic fields in accelerator channel of MHD wind tunnel 20 p3444 A67-36529
 Electrodeless slip-type MHD steady state acceleration of subsonic and supersonic high density gas flows for simulating reentry speeds and altitudes 21 p3607 A67-37778
 MPD Hall accelerator construction and operation using argon or helium propellants, measuring azimuthal velocities in plume

[AIAA PAPER 67-672] 21 p3691 A67-38705
 Distributions of current, potential, electron density and pressure and ion velocity vector orientation in MPD arc, verifying electromagnetic effects presence [AIAA PAPER 67-676] 21 p3671 A67-38709
 Lithium and ammonia MPD arc thrusters tests in low environmental pressure [AIAA PAPER 67-685] 21 p3692 A67-38716
 MPD plasma accelerator for spacecraft propulsion system, performance data and proposed acceleration mechanisms [AIAA PAPER 67-688] 21 p3693 A67-38719
 Fringing effects on electric efficiency variation with slip for cylindrical induction MHD device operable as accelerator, generator or Joule heater [AIAA PAPER 67-714] 21 p3673 A67-38740
 Hot shot nitrogen gas source for pulsed MHD accelerator to provide lunar reentry 21 p3608 A67-38863

MAGNETOHYDRODYNAMIC FLOW

Quasi-one-dimensional approximation for MGD equations 01 p0118 A67-10047
 Steady state two-coordinate problem of MGD solved for subsonic attached flow past simply connected profile 01 p0119 A67-10171
 MGD flows in channels analyzed, using transformation of hodograph for vortical velocity distribution 01 p0119 A67-10172
 MHD rotation of conducting viscoplastic fluid between two coaxial cylinders in crossed fields 01 p0120 A67-10180
 Surface roughness effect on laminar MHD flow through rectangular duct, deriving relation between transition friction factor and Reynolds and Hartmann numbers 01 p0120 A67-10186
 MHD boundary layer development on accelerated body treated by reducing partial to ordinary differential equation, using stream function 01 p0121 A67-10190
 Effect of electrode tips of MHD generator and induced magnetic field on fluid flow in generator analyzed, using approximation method 01 p0121 A67-10227
 Linear formulation of electromagnetic field effect on supersonic gas flow 01 p0125 A67-10980
 Saturation effect dependence on electrode surface temperature and bulk gas temperature in MHD generator duct 01 p0126 A67-11186
 Induction velometry measurement of average velocity of free jet of ionized gas influenced by transverse uniform magnetic field 02 p0272 A67-11881
 Shock wave formation due to nonlinear vibrations in tube containing fluid subjected to transverse magnetic field with plane heater at midsection and externally supplied energy 02 p0273 A67-12058
 Uniform velocity MHD channel flow of nonequilibrium plasma with tensor electroconductivity 02 p0275 A67-12552
 Analogy between turbulent MHD channel flow at high Reynolds numbers and moderate Hartmann numbers and turbulent boundary layer flow with suction 02 p0277 A67-12569
 Channel flow interaction of plasma from coaxial plasma gun with transverse magnetic field 02 p0277 A67-12618
 Motion of medium of variable electric conductivity in rectangular channel situated in magnetic field 03 p0478 A67-13621
 Current density distribution in two-electrode MHD channel operating in amplification and generation mode 03 p0479 A67-13686
 Free convective boundary layer flows of electrically conducting fluid in transverse magnetic field 03 p0481 A67-13734
 MHD flow past bodies in electroconductive viscous incompressible flow 03 p0482 A67-13743
 Channel flow of suddenly pressurized viscoelastic and electrically conducting fluid under influence of constant transverse magnetic field 03 p0483 A67-14035
 MHD lubrication flow in externally pressurized thrust bearing analyzed, including fluid inertia 04 p0627 A67-14461
 Magnetic autogeneration for decelerating and cooling effects on aircraft entering dense atmospheric layer 04 p0664 A67-14791
 Nonstationary flow of gas in transverse magnetic field, noting electric conductivity dependence on compressibility and temperature 04 p0665 A67-15178

Viscous friction and heat flux for partially ionized medium flowing in plane channel with anisotropic transport coefficients 04 p0666 A67-15189
 Electric potential and current density distribution in MHD channel allowing for anisotropy in conductivity 04 p0666 A67-15190
 Motion induced by electric and magnetic fields on initially static fluid between two concentric tubes [ASME PAPER 66-WA/FE-35] 04 p0668 A67-15366
 Combined free and forced convection over electrically insulating vertical plate of constant temperature with transverse magnetic field with plate moving up or down [ASME PAPER 66-WA/HT-38] 04 p0724 A67-15429
 Turbulent MHD flows in prismatic and cylindrical pipes, particularly pipes with slot shaped cross section 04 p0669 A67-15513
 Supersonic conducting gas flow in coaxial channel in magnetic field formed by currents flowing over plasma 04 p0669 A67-15514
 Conical MHD flow of ideal conducting gas with Hall effect in magnetic field, deriving electrodynamic and energy characteristics 04 p0669 A67-15515
 Linearly expanding MHD channel with solid electrodes, noting end effects relation to electrode dimensions 04 p0669 A67-15516
 Velocity field in MHD jet flow discharging into immersed bounded space 04 p0669 A67-15518
 Unsteady viscous fluid flow in MHD channel under action of pressure gradient solved for arbitrary load coefficient 04 p0669 A67-15519
 Heat transfer in plane conducting fluid jet spreading over flat wall in transverse magnetic field, noting solution for temperature distribution for small MHD interaction parameters 04 p0670 A67-15520
 Strain gauge measurements of resistance of sphere to MHD turbulent flow of mercury in rectangular tube 04 p0670 A67-15530
 Contactless flow meter, based on spatial MHD drifting, for flow velocity measurements on electroconductive fluid 04 p0624 A67-15531
 Zone of quasi-solid motion in MHD flows of viscoplastic fluids 04 p0670 A67-15532
 Reducible helical MHD flows, considering intrinsic formulations of equation for cases where vector products of fluid velocity and magnetic field equal zero 04 p0609 A67-15804
 MHD heat transfer in finite duct for fully developed flow conditions with arbitrary oriented applied magnetic field and variable heat flux boundary conditions 04 p0673 A67-15872
 Exact solution /by Hankel and Laplace transforms/ of unsteady motion of viscous MHD fluid in cylindrical vessel in axisymmetric constant strength magnetic field 05 p0850 A67-18134
 MHD steady laminar flow of viscous incompressible electrically conducting liquid in rectangular pipe between conducting plates 05 p0853 A67-18723
 Plasma flow velocity measurement in MHD channel using time-of-flight technique, noting experimental error 05 p0854 A67-18983
 Lie series formalism applied to solution of Bessel equation describing behavior of laminary oscillating MHD fluid 05 p0854 A67-16989
 Single parameter MHD flow of ideal incompressible infinitely electroconductive gas 05 p0855 A67-17114
 Solution for parallel plates in steady state Hartmann flow extended to coaxial flow between concentric cylinders, noting role of magnetic field 05 p0856 A67-17356
 Hydromagnetic compressible boundary layer flow past flat plate analyzed via von Karman integral method 05 p0794 A67-17361
 Laminar heat transfer in thermal viscous MHD flow past semiminfinite flat plate 05 p0857 A67-17416
 Heat transfer in short circuit generalized MHD Couette flow for velocity field and temperature distribution, when walls are at equal and unequal temperatures in transverse magnetic field 06 p1039 A67-18070
 Steady two-dimensional MHD flow of ideal inviscid perfectly conducting compressible fluid with one nonzero component 06 p1040 A67-18115

Dimensional analysis of turbulent MHD flow in interspace between two coaxial cylinders in rotating circular magnetic field and similarity criteria for EM power losses 06 p1042 A67-18548

Low magnetic Reynolds number two-dimensional and axisymmetric MHD flow of conducting ideal gas through supersonic nozzle 06 p1043 A67-18669

Quasi-MHD analysis of supersonic rarefied plasma flow near magnetic dipole 06 p1043 A67-18670

Hysteresis effects in steady laminar two-dimensional MHD flow of gas between moving planes and coaxial cylinders in TM field 06 p1043 A67-18671

Turbulent MHD boundary layer flow of constant-electroconductivity incompressible fluid past dielectric plate in TM field, for small magnetic Reynolds numbers 06 p1043 A67-18672

Leak current, friction and heat-transfer coefficients of compressible laminar boundary layer on insulator wall of MHD channel with anisotropic conductivity 06 p1043 A67-18673

Incompressible fluid flow in symmetric flat channel, for case of constant electric conductivity and low Reynolds number 06 p1043 A67-18676

Electrically conducting boundary layer flow past flat plate in TM field 06 p1043 A67-18677

Turbulent flow of mercury in flat channels plane perpendicular to magnetic field, noting reduction of flow resistance coefficient 06 p1044 A67-18678

Plastic flow effects on MHD Couette flow in annular gap between two coaxial cylinders in radial magnetic field 06 p1044 A67-18680

Longitudinal magnetic field effect on convective heat transfer during turbulent MHD pipeflow of liquid Ga 06 p1044 A67-18682

Wall profile construction of working zone of flat MHD channel with ideal conductors for both sides 06 p1044 A67-18691

Plasma flow in plane MHD channel in absence of longitudinal thermal flux, considering temperature dependence of heat transfer and viscous energy dissipation coefficients 06 p1045 A67-18811

Suction-preserved steady state vortex sheet on surface of infinite porous circular cylinder in viscous MHD liquid suddenly rotated about axis 06 p1046 A67-18891

MHD phenomena in vortex ring in conducting fluid, noting intensification of initial field at high Reynolds numbers and self-excitation 07 p1229 A67-19684

Steady flow of anisotropic conducting medium in half-space under influence of magnetic field 07 p1230 A67-20033

Wall conductance effect on MHD flow through finite cross section rectangular and circular channels 08 p1356 A67-20572

Plasma transport properties, discussing application of ionization level as indicator for electric conductivity and viscosity 08 p1357 A67-20591

Gas dynamics of nonisentropic two-dimensional MHD flow of ideal inviscid perfectly conducting compressible fluid 08 p1357 A67-20593

Gas ionizing shocks for plane flows with magnetic field lying in flow plane 08 p1358 A67-20895

Shock wave formation due to heat addition to one-dimensional flow of ideal inviscid conducting monatomic compressible fluid under transverse magnetic field 08 p1359 A67-20980

Iterative method for two-dimensional problem of incompressible viscous MHD free jet flow from thin slot in plane wall 08 p1361 A67-21143

Approximate solution of some nonstationary boundary layer problems with allowance for magnetic field, discussing nonsteady flow of viscous incompressible electrically conducting fluid past flat plate 08 p1362 A67-21202

Ionization and temperature measurement in MHD experiment, noting microwave interferometer response as electron density function and line reversal measurement 09 p1538 A67-21777

MHD of flows with hot electrons in MHD ducts at low magnetic Reynolds numbers, emphasizing boundary layer and shock wave

theory 09 p1541 A67-21797

Hydraulic approximation for calculating MHD flows in ducts 09 p1541 A67-21804

MHD flow of viscous conducting fluid jets and MHD flows with nonlinear temperature dependent conductivity 09 p1541 A67-21807

Nonequilibrium excitation influence on electron density in one-dimensional MFD channel flow 09 p1542 A67-21814

Direct current electrical discharge investigated in gas flow in magnetic field perpendicular to flow 09 p1542 A67-21816

Electric arc behavior in argon gas flowing through magnetic field, measuring flow velocity, electron temperature, spatial distribution, etc 09 p1543 A67-21824

Hysteresis effects in one-dimensional conducting gas flow through rectangular MHD converter channel with constant magnetic gap and variable electron spacing 09 p1444 A67-21859

Approximation of electrical conductivity change in ideally conducting gas in turbulent MGD flow 09 p1544 A67-21860

LF temperature pulsations in turbulent MHD flow of electrolyte 09 p1549 A67-22385

Solutions for field aligned flow past magnetic source using Green function, estimating energy dissipation rate 09 p1549 A67-22399

First approximation for MHD nozzle flows with end effects 09 p1550 A67-22589

MHD channel flow under transverse electromagnetic field, analyzing effect of various geometries and boundary conditions 10 p1684 A67-22875

Magnetoaerodynamic flow relations for axisymmetric blunt bodies with shock layers in shifting equilibrium 10 p1591 A67-23114

Inviscid two-dimensional flow using extension of Hele-Shaw analogy, noting axisymmetric, compressible and MHD cases 10 p1627 A67-23554

Dissipative wave propagation in linearized compressible MHD flow, constructing solution for arbitrary values of dimensionless parameters and field orientation 11 p1825 A67-23867

Heat transfer of electrolyte solutions, noting effect of magnetic field on turbulent flow and empirical relation to calculate Nusselt number 11 p1831 A67-24024

Solid body translational movement in viscous incompressible conductive flow in magnetic field solved for case of zero magnetic Reynolds number 11 p1832 A67-24055

Stability of pulsating plasma cylinder contained by time dependent magnetic field described by MHD equations 11 p1832 A67-24154

Two-dimensional steady MHD flow with resolution of neutral sheets into intermediate and slow waves 11 p1862 A67-24499

Green integrals extended to movement of incompressible viscous conductive fluid in which magnetic field is generated 11 p1840 A67-24620

Boundary layer behavior in fully ionized two-temperature plasma 11 p1840 A67-24670

Electric field in MHD channels in presence of near-electrode potential drop 11 p1840 A67-24871

Nonequilibrium MHD plasmas investigated for electrothermal instabilities noting effect of plane wave fluctuations 12 p1972 A67-25391

Behavior of high current arcs driven by strong external magnetic fields with respect to hypersonic flow generation by MHD forces 12 p1974 A67-25399

Electrode feed system for segmented electrode MHD wind tunnel 12 p1920 A67-25406

MHD of thin body in oblique fields 12 p1976 A67-25939

Transformation for uncoupling system of duct flow of conducting fluids under arbitrary oriented applied magnetic field 12 p1976 A67-25941

Extension of Loitsianskii hypothesis concerning localism of turbulent transfer processes in viscous flows to MHD flows, noting results for friction coefficient 12 p1976 A67-26070

Magnetic field intensification in plasmas determined from solution of MHD equations, noting formation of time independent fields 13 p2163 A67-26292

Rate of resistive diffusion of hydromagnetic equilibrium computed using expansion near magnetic axis 13 p2164 A67-26296

Flow in MHD nozzles studied for hypothetical magnetic interaction parameter of unity order 13 p2165 A67-26592

Hydraulic properties of duct of constant rectangular cross section functioning in closed circuit used to measure MHD flow velocity 13 p2165 A67-26593

Velocity measurement in electrically conducting fluid flow in presence of uniform magnetic induction normal to flow direction 13 p2167 A67-27206

Ionized gas flow past oscillating interface in presence of magnetic field, based on MHD boundary layer model with constant velocity profile 13 p2168 A67-27302

Steady three-dimensional flow of electrically conducting gas in working section of linear MHD channel 13 p2169 A67-27310

Plane one-dimensional MHD flow in transverse magnetic field with magnetic Reynolds number equal to or greater than unity 13 p2169 A67-27311

Resistance and heat transfer of plate situated in turbulent MHD boundary layer in compressible fluid 13 p2169 A67-27312

Hodograph transformation in two-dimensional problems of MHD of viscous flow 13 p2170 A67-27318

Channel flow interaction of plasma from coaxial plasma gun with transverse magnetic field 13 p2170 A67-27374

Boundary layer equations reduced to ordinary differential equations without using self-similarity assumptions, noting friction-drag and heat-transfer coefficient along MHD channel 14 p2356 A67-27978

Effect of finite magnetic Prandtl number on hydromagnetic flow past thin airfoil 14 p2240 A67-28142

Laminar boundary flow over dielectric disk with homogeneous magnetic field perpendicular to plane of disk, obtaining liquid velocity and electric field density 14 p2358 A67-28282

One-dimensional laminar MHD flow at hydrodynamic stabilization, discussing heat transfer, Hartmann flow, magnetic field, Prandtl number and Joule heating 14 p2358 A67-28283

Expansion of plane jet of conducting liquid in magnetic field 14 p2302 A67-28304

MHD flows in tubes in presence of longitudinal electric current 14 p2361 A67-28743

Flow of conducting incompressible viscous fluid near accelerated plate under parallel plate and magnetic field, noting velocity profiles and stress role 14 p2361 A67-28814

Magnetoaerodynamic drag and flight control available to vehicle entering earth atmosphere calculated, including induced magnetic fields effects and nonscalar conductivity 14 p2394 A67-29041

Blunt nosed reentry vehicle model with skewed magnetic field investigated in magnetoaerodynamic flow for possible bow shock distortion 14 p2244 A67-29049

MHD boundary layer flow past seminfinit plate, applying fluctuating magnetic field to plate 15 p2510 A67-29631

Current density distribution in MHD duct with segmented electrodes of finite size analytically described, noting experimental agreement 16 p2600 A67-30537

Oscillation spectrum of weakly ionized plasma current flowing normal to applied magnetic field discussed and analyzed in linear approximation using MHD model 16 p2712 A67-30546

Laminar and turbulent MHD flows of liquid sodium in rectangular duct with conducting walls, determining wall and magnetohydraulic losses 16 p2712 A67-30573

MHD flow of liquid mercury through circular pipes at high Hartmann and Reynolds numbers, plotting friction factors 16 p2712 A67-30576

Steady-state mercury flow along open trough in transverse magnetic field, measuring electric and hydraulic characteristics and providing plasma motion model 16 p2713 A67-30578

End losses in magnetohydrodynamic channels of linearly variable cross section determined using equivalent channel geometry 16 p2606 A67-30585

Striated layer flow of working fluid in duct of synchronous induction MGD generator studying stability by approximation 16 p2607 A67-30594

Steady laminar flow of viscous, incompressible, electrically conducting fluid in insulated rectangular channel, with imposed oblique transverse magnetic field 16 p2713 A67-30860

Kelvin instability following velocity discontinuity in current-carrying cold collisionless plasmas under magnetic field, deriving dispersion relation and instability criteria from fluid 16 p2714 A67-30872

Collision plasma instability analysis based on MHD equations and ion motion along magnetic field 16 p2715 A67-31041

MHD effect in shock tube, studying EMF induced in motion of transverse magnetoplasma 16 p2715 A67-31112

Monograph on upper atmosphere kinetics noting Boltzmann equations, MHD processes, thermal diffusion, etc 16 p2666 A67-31166

Simultaneous measurement of many aerodynamic, electrical and electromagnetic parameters in test time interval of several hundred microseconds of MHD augmented shock tunnel 16 p2656 A67-31262

Effect of temperature dependence of plasma conductivity on magnetohydrodynamic channel flows 16 p2721 A67-31392

Energy conservation law concerning electromagnetohydrodynamics of viscous electrically conducting fluid showing that total energy in fixed volume changes 16 p2721 A67-31549

Reduction of steady viscous magnetohydrodynamic flows having orthogonal magnetic and velocity field distributions to associated flows having zero magnetic field 16 p2721 A67-31552

Solution of MHD boundary layers with magnetic field as exponential function of x coordinate, extended to transverse magnetic fields 16 p2722 A67-31570

Laminar jet flow of electrically conducting fluid over plane solid surface in transverse magnetic field solved using motion and continuity equations 16 p2722 A67-31571

Transverse magnetic field effect upon convective heat transfer in turbulent flow in electrically conducting fluid in channel bounded by two parallel plates 16 p2722 A67-31572

Laminar flow of electrically-conducting fluid suddenly expanding in magnetic field calculated by approximate method 16 p2722 A67-31573

Hypersonic magnetohydrodynamic flow over blunt bodies for small magnetic Reynolds number hypersonic magnetohydrodynamic flow over blunt bodies for small magnetic Reynolds number hypersonic magnetohydrodynamic flow over blunt 16 p2594 A67-31579

Magnetic bottles leakage in fusion reactors, describing differences between microinstabilities and MHD theories 16 p2724 A67-31865

Optimum energy conversion for MHD flows related to magnetic field value 17 p2898 A67-32180

Transverse magnetic field effect on turbulent MHD jet flow in bounded space, noting channel wall conductivity 17 p2901 A67-32565

MHD flow, deriving equation system and boundary conditions for gas dynamic process 17 p2903 A67-32682

MHD of terrestrial liquid core noting geomagnetic field variation, earth mantle movements, etc 17 p2845 A67-32773

Nonuniform electrical conduction in MHD channels analyzed by differential equations 17 p2906 A67-33011

Kantorovich indirect variational method applied to MHD flow inside rectangular duct 17 p2906 A67-33038

MHD behavior of inviscid fluid in limit of infinite electrical conductivity and mobility exhibiting Hall effect 17 p2908 A67-33109

Steady state magnetic field in transition region between magnetosphere and bow shock by MHD equations, noting solution by approximation method 17 p2951 A67-33186

Quasi-one-dimensional approximation for MGD equations 17 p2910 A67-33325

Geometry of streamlines and field lines of MHD flow, using partial differential

equations 17 p2910 A67-33351

Speed deficits of oxyacetylene detonation waves passing through MHD channel in electromagnetic field explained by Hall effects altering boundary layer 18 p3086 A67-33825

Conditions of time-symmetry for four classes of flows, discussing instabilities 18 p3079 A67-34004

Leakage current on insulating walls in MHD channel calculations, evaluating variable electrical conductivity in plasma boundary layer plasma boundary layer leakage current on insulating walls in MHD 18 p3088 A67-34061

Perfect frictionless supersonic MHD gas flow model for shock wave control, noting nozzle geometry 18 p3088 A67-34123

Heat transfer in steady axisymmetric MHD flow near stagnation point, with series solutions for velocity, magnetic field and temperature 18 p3161 A67-34381

MHD jet converter research, reviewing basic equations, AC/DC generators and thermodynamic/ electric problems 19 p3268 A67-35062

Homogeneous MHD turbulence on large scale structure, finding asymptotic forms of velocity and magnetic field correlations 19 p3295 A67-35540

Electric arc blowing in plasma of nonuniform conductivity and inclusion of effect in MHD flow 19 p3298 A67-35760

Helicallly symmetric MHD flow of compressible fluid in circular plasma cylinder, considering waves and stability 20 p3492 A67-36132

Magneto-fluid and plasma dynamics - Conference, New York, April 1965 20 p3493 A67-36142

Plasma shock wave structure model, analyzing steady flow of electrically neutral fluid 20 p3493 A67-36144

Steady flow of perfectly conducting inviscid liquid past thin symmetrical airfoil of finite conductivity in aligned magnetic field 20 p3494 A67-36146

Compressible inviscid fluid MHD motion, stressing quasi-aligned field flows 20 p3496 A67-36272

Book on electromagnetodynamics of fluids covering MHD, astrophysics, plasma physics, etc 20 p3499 A67-36808

Rear stagnation point solution for viscous incompressible electrically conducting MHD flow 20 p3499 A67-36850

Laminar MHD boundary layer over finite dielectric disk in presence of magnetic field, determining velocity profiles 20 p3501 A67-37305

Boundary value problems solution in steady two-dimensional compressible MHD flow past thin body 21 p3660 A67-37742

Unsteady conducting fluid flow in MHD ducts with small magnetic Reynolds number and constant pressure 21 p3663 A67-37935

Energy indicators calculated for MHD channel flow with finite sectional electrodes and wide Hall parameter variations 21 p3665 A67-38242

Turbulent MHD boundary layer in liquid with linear pressure gradient, discussing numerical integration, flow velocity and magnetic field distribution 21 p3665 A67-38244

MGD boundary layer flow for thermally conducting flat plate, deriving equations for any heat transfer 21 p3675 A67-39090

Book on parallel laminar flow stability covering channel and pipe flows, jets, wakes, free shear and boundary layers 22 p3783 A67-39632

Perturbation theory for solving initial and boundary value problem in unsteady MHD flow past thin symmetrical bodies with inwardly diffusing magnetic field 22 p3850 A67-39707

Momentum, heat and magnetic field diffusion in viscous, thermal and magnetic boundary layers of different thicknesses in MHD fluid 22 p3850 A67-39721

Equations numerical integration for MHD fluid flows near critical point in presence of azimuthal magnetic field for several Alfven and diffusion numbers 22 p3853 A67-40011

Precise and approximate formulations for unsteady flows of conducting fluid in MHD channels with external electric circuit 22 p3853 A67-40023

Discontinuity conditions derived for nondissipative hydromagnetic shock surface flows, with jump relations from divergence form of MHD equations 22 p3854 A67-40317

Electromagnetic forces effects on steady rotating motions of conducting viscous incompressible fluids via adjustable local boundary layer first order approximation 23 p4031 A67-40604

Linear MHD flow characteristics variation with electric conductivity and gas flow rate changes, noting transverse magnetic flow variation with magnetic Reynolds number 23 p4033 A67-41284

Equation system for conducting perfect gas motion group analyzed leading to possible invariant solutions of system applicable to MHD equations 24 p4197 A67-42354

Continuous shock wave profile found in MHD fluid where Whitham condition for wave profile discontinuity is satisfied 24 p4143 A67-42356

Thermodynamic and electrical properties of MHD conversion fluid /K-seeded combustion products/ obtained by hydrocarbon fuel combustion, discussing electrical conductivity calculations 24 p4099 A67-42415

MHD lubrication flow in self-acting step type thrust bearing configuration, showing torque reduction 24 p4162 A67-42566

Hydromagnetic flow stability in infinitely long cylindrical pipe with arbitrarily smooth cross section and applied radial magnetic field 24 p4198 A67-42693

MAGNETOHYDRODYNAMIC GENERATOR

SA PLASMA GENERATOR

Optimization of working characteristics of MHD generator as power device 01 p0011 A67-10049

Various magnetic coil systems and parameters for MHD generator use 01 p0011 A67-10050

Azimuthal current effect on electrical efficiency of MHD vortex generator 01 p0120 A67-10174

Potential distribution between graphite and metallic electrodes of MHD generator in nonstationary heat conditions under induced or applied electric field 01 p0011 A67-10176

Supersonic MHD generator crisis possibility assuming quasi-one-dimensional nonheat-conducting approximation at small Reynolds numbers and plasma scalar conductivity 01 p0011 A67-10177

Electrical efficiency of MHD generator cycles, determining external load resistance 01 p0012 A67-10178

Fringe effects in plane induction MHD machine compared for different methods of determination 01 p0012 A67-10191

Effect of electrode tips of MHD generator and induced magnetic field on fluid flow in generator analyzed, using approximation method 01 p0121 A67-10227

MHD power generation, presenting electrical conduction in gases, seeding and ionization, equations, conversion efficiency, electrical losses, compressible flow theory and application to various cycles 01 p0013 A67-10556

Electrode tips and inhomogeneity of applied magnetic field effect on fluid flow of MHD generator 01 p0124 A67-10753

Electrode losses in MHD generators with nonequilibrium and equilibrium ionization compared, attributing differences to coupling between conductivity and local dissipation 01 p0014 A67-11159

Distribution of electromagnetic fields, density of forces and Joule losses with higher spatial harmonics in asymmetric type of MHD induction generator allowing for conducting walls 03 p0475 A67-13178

Mass flow from gas-vapor mixture to wall of recuperative heat-exchanger condenser 03 p0536 A67-13688

Electrical parameters of DC MHD generator with arbitrary connected electrodes 04 p0553 A67-14475

Design features of high velocity test stand with arc heater and MHD accelerator 04 p0595 A67-14543

Nonequilibrium plasma diagnostics of steady HF discharge in toroidal MHD plasma generator 04 p0553 A67-14580

Cylindrical inductor with inhomogeneous field, analyzing case of strong field inhomogeneity when inductor radius is much greater than pole pitch 04 p0556 A67-15522

Magnetic field structure in working space of linear multiphase inductive MHD generator 04 p0556 A67-15523

One-dimensional linear approximation of effects of magnetic and electric shunting of linear inductor edges on constant velocity MHD channel flow 04 p0556 A67-15524

Temperature and heat flux distribution in linear liquid-metal MHD device with direct cooling of winding 04 p0556 A67-15528

Magnetic Reynolds number determinations for inductive MHD generator and DC conductive MHD generator 04 p0670 A67-15533

Liquid metal MHD converter with multistage thermodynamic drive for use as power source in space vehicles as alternative to thermionic converter 04 p0559 A67-15965

Cryogenic techniques for space power generators based on superconductivity, discussing MHD converters 04 p0560 A67-15967

AC power generation by linear channel liquid metal MHD inductive generator 05 p0754 A67-17348

High electric power production for short periods, anticipating magnetoaerodynamic power stage combined with conventional alternators 06 p0949 A67-17567

Optimum MHD generators using anisotropic plasma, discussing conducting-gas MHD flow, Hall effect, ion slip effect, etc 06 p0950 A67-18089

Closed cycle MHD energy converter applications 06 p0951 A67-18668

Optimal power design of conduction type MGD generator 06 p0951 A67-18674

AC MHD generator with liquid metal working fluid operating under self-excitation conditions 06 p0951 A67-18683

Transient self-excitation in autonomous electromechanical system consisting of pump and MHD generator 06 p0952 A67-18686

Mean value of current in flat channel of MHD generator with short circuited electrodes taking into account induced fields 06 p0952 A67-18687

DC amplifier with capacitive feedback as correcting device in recording currents while studying magnetoplasma generator 06 p0952 A67-18693

MHD application for power conversion and generation, discussing methods and efficiency 06 p1076 A67-19023

Syringe injection system for seeding plasma with Na-K alloy in study of MHD power generation and propulsion 08 p1279 A67-20377

Electrical characteristics of linear segmented electrode Hall and Faraday MHD generators, noting power output reduction due to electrode voltage losses 08 p1283 A67-20578

Self-charging of temperature independent radioactive ultrafine particles for MHD power generation 08 p1283 A67-20647

Equivalent circuits of MHD generators with segmented electrodes electrically connected in various ways 08 p1286 A67-20738

MHD electrical power generation - Conference, Salzburg, July 1966, Volume I 09 p1536 A67-21773

Measuring apparatus for scalar and tensor plasma conductivity in AC MHD generators and accelerators 09 p1538 A67-21775

Argon-cesium plasma spectroscopy, describing equipment, ionization, conductivity, recombination, concentration, etc 09 p1538 A67-21779

Flow velocity, seeding ratio and electrical conductivity in seeded argon plasma, noting relation between plasma and MHD generator characteristics 09 p1539 A67-21780

Electrode conduction processes and segmented electrode-insulator ratio effects in MHD power generation experiments 09 p1539 A67-21785

Current-voltage characteristics of moving argon plasma, noting variation of plasma conductance with flush and filament electrodes 09 p1540 A67-21786

Measurements of conductivity, electron density and ionization rate of cesium in argon on alkali shock tube, describing MHD generator wind tunnel experiment 09 p1540 A67-21789

Relaxation process and magnitude of nonthermal ionization in MHD generator, describing experimental equipment and

results in xenon and in argon 09 p1540 A67-21790

Core and boundary layer flows in large scale MHD generator, noting viscous friction and heat transfer at walls 09 p1442 A67-21793

High voltage MHD generator consisting of n pairs of segmented electrodes series connected, noting no-load voltage as function of electrode pairs 09 p1442 A67-21795

Electrical parameters of DC MHD generator determined from equivalent circuits 09 p1471 A67-21796

Quasi-one-dimensional plasma motion in linear and radial Hall type MHD generator ducts 09 p1541 A67-21798

Optimum conditions for MHD power generation with Joulean dissipation derived from first and second law of thermodynamics 09 p1442 A67-21799

Minimum volume conditions for MHD conversion duct with known upstream and downstream stagnation 09 p1443 A67-21800

Minimization of MHD generator duct with fixed boundary values as criterion in determining expansion shape 09 p1443 A67-21801

Channel flow and power generation of MHD generator, stressing influence of nonequilibrium ionization 09 p1541 A67-21802

Plasma flow in series type MHD generator duct, noting optimum flow conditions and quasi-one-dimensional model 09 p1443 A67-21805

Magnetic field inhomogeneity effect on electrically conducting fluid flow in Hall type generator duct 09 p1443 A67-21806

Boundary layer at electrode and center of flow of plane MHD generator calculated numerically by one-dimensional theory for subsonic and supersonic velocities 09 p1443 A67-21808

Electric conductivity and kinetic energy in seeded and unseeded airflow MHD experiments in hypersonic shock tunnels for aerospace applications 09 p1542 A67-21809

Increased electric conductivity of gas in MHD generator obtained, using small auxiliary electrodes 09 p1443 A67-21810

Numerical solutions for range of operating conditions in segmented linear MPD generators, using He-Cs working fluids 09 p1443 A67-21811

MHD generator using nonseeded inert gas as working fluid 09 p1444 A67-21812

Relaxation phenomena role in MHD generator using nonequilibrium ionization, noting collisional and radiative recombination mechanisms 09 p1542 A67-21815

Conductivity of high density plasma of MHD generator, noting quantum phenomena associated with overlapping electron wave functions 09 p1543 A67-21818

Conductivity of working fluid in MHD generator using thermionic emission from suspended lanthanum conductivity of working fluid in MHD generator using thermionic emission from suspended lanthanum hexaboride 09 p1543 A67-21820

Auxiliary arc electrodes for solution to cold boundary layer and cathode emissivity problems in MHD generators 09 p1444 A67-21822

Nonsteady state processes in nonequilibrium plasma with local collisions, using Boltzmann kinetic equation for application in MHD generators 09 p1543 A67-21823

Temperature characteristics, electric conductivity, electrode drop and heat loss of acetylene combustion gas mixed with seed material and nitrogen used as MHD fluid 09 p1580 A67-22151

Electrode ends effect on flow of fluid in MHD generator, using iterative solution 09 p1549 A67-22563

Electrical conductivity tensor effect on flow in MHD generator, considering transport of ionized gas and solution of symmetric problem 09 p1550 A67-22575

Variational problem for flow of plasma with variable electrical conductivity in channel of MHD generator solved, using Lagrange method of multipliers 10 p1684 A67-23023

Space charge and eddy currents in ionized gas flow in MHD channel determined, showing effect of cold electrode boundary layer on electrical performance 11 p1746 A67-24874

Two-phase liquid metal cycle MHD conversion, discussing thermodynamic aspect, hot gas system and possibility for use in spacecraft and ground power plants 12 p1896 A67-25121

Partial differential equation of MHD converters, noting effects of converter width, side conductor materials and velocity distribution 12 p1896 A67-25374

Performance characteristics of single wavelength liquid-metal MHD induction generator with end-loss compensation 12 p1897 A67-25375

Test program for induction coupled MHD generator using liquid sodium as working fluid, noting equivalent single phase circuit for electrical characteristics 12 p1897 A67-25376

MHD induction generator with variable fluid and magnetic field velocity noting high power of cascading generator 12 p1897 A67-25377

Self-excited liquid metal MHD induction generator 12 p1897 A67-25378

Liquid metal MHD cycles with condensation by multistage injection of liquid 12 p1897 A67-25379

Linear induction MHD generator with cryogenically cooled coil windings for alleviating large gap and short stator problems 12 p1898 A67-25380

Three diagonal conducting wall MHD generators, discussing time averaged behavior, instabilities and working fluid conductivity 12 p1898 A67-25381

Solid fueled rocket powered MHD generators with high power densities 12 p1898 A67-25382

Large disk MHD generator studied for plasma properties and fluid mechanics, noting seed ionization effect on performance 12 p1972 A67-25386

Hall voltage reduction in linear MHD generators noting Lorentz force effect 12 p1898 A67-25387

Nonequilibrium MHD generator for closed and open cycles, noting K seed ionization by energy transfer from excited N molecules 12 p1898 A67-25388

Blowdown wind tunnel for He-K MHD generator, considering magnetically induced ionization, conductivity, gas temperature, etc 12 p1898 A67-25389

Transient acoustical response of uniform flow to turbulence and noise in MHD generators 12 p1899 A67-25390

MHD generator working fluid temperature reduction 12 p1973 A67-25395

Steady MHD electric power generation, flow velocity effect on single controlled glow discharge in cesium-seeded argon 12 p1974 A67-25402

Hot electrodes for open cycle MHD generators, noting refractory oxides 12 p1899 A67-25405

Explosively driven MHD generator, obtaining conversion efficiency dependence on magnetic Reynolds number, load-to-channel inductance ratio and magnetic/kinetic energies 12 p1901 A67-25896

MHD power generation using bifluid liquid metal system /such as Li and Cs/ with two-phase generation 12 p1901 A67-25897

Fringe effects in MHD generator channels, determining potential and current distribution and estimating losses 12 p1901 A67-26078

MHD generator two-dimensional incompressible flow, obtaining expressions for power output, velocity, electrical efficiency, etc 13 p2055 A67-26417

Finite length inductive MHD generator, solving inlet and outlet effects on boundary value problem 13 p2165 A67-26613

Influence of Hall effect and viscosity on flow relations and power output of MHD generator 13 p2165 A67-26642

Onsager formalism of irreversible thermodynamics applied to steady state laminar hydromagnetic energy conversion, analyzing nature of coupling 13 p2055 A67-27001

Graph analytical calculation of MHD generator channel 13 p2169 A67-27308

Direct current MHD generator having channel of constant cross section and using NaK as working fluid 13 p2056 A67-27315

Electromagnet design for experimental DC MHD generator 14 p2247 A67-27950

Electrodeless MGD power generation

during entry, using torque on magnet taken as rotating member of generator 15 p2422 A67-29443

Mathematical model of MHD induction generator, deriving electrical diagram 15 p2527 A67-29472

MHD generator with uniform rectangular duct, considering ion slip and Hall effect in case of two-dimensional flow 15 p2422 A67-29906

Change in pressure losses in MHD generators channel, obtained from pressure gradient relation to flow rate of conducting fluid 16 p2705 A67-30449

Unsteady flow of inviscid, electrically conducting but thermally nonconducting gas at small magnetic Reynolds numbers in MHD generator channel unsteady flow of inviscid electrically conducting but thermally nonconducting gas at small magnetic 16 p2706 A67-30451

Electricity from MHD - Conference, Salzburg, July 1966, Volume 2 16 p2706 A67-30512

Nonequilibrium tensor conductivity in argon-potassium plasma under MHD generator conditions 16 p2709 A67-30514

Wall conductance of insulating gaps between electrode segments shown as cause of inferior performance of MHD generators 16 p2599 A67-30526

Performance characteristics of Faraday and Hall MHD generators using strong magnetic fields and considering ion slip and finite electrode segmentation effects 16 p2599 A67-30527

Internal resistance, potential fall and current distribution for staggered electrode geometry in MHD generator of Faraday type 16 p2599 A67-30528

Current distribution in Faraday MHD generator measured with potassium resonance lines 16 p2599 A67-30529

Current and potential distribution for thermally-stable plasma of Faraday-type segmented electrode MHD generator, taking into account nonequilibrium ionization 16 p2599 A67-30530

Performance of linear series of MHD generators noting electrical properties, effect of electrode scattering, etc 16 p2600 A67-30531

MHD generator terminal values and other electric parameters deviations for various finite length electrodes connected in series 16 p2600 A67-30532

Hall effect in semiconducting electrode MHD generators, noting Joule heating losses, nonlinear electrical conductivity, etc 16 p2600 A67-30533

Arbitrary electrode MHD generator electrical characteristics, considering end effects and determining internal conduction matrix 16 p2600 A67-30534

Schwarz transformation methods for electrical studies of MHD generators with tensor conductivity 16 p2600 A67-30535

Steady flow of anisotropically conducting fluid in plane or annular channel of MHD generator with nonequilibrium plasma at small Reynolds numbers 16 p2600 A67-30541

Hot electron nonequilibrium plasma use in MHD generators, considering energy transfer, plasma stability, magnetogasdynamics, etc 16 p2601 A67-30545

Uniform flow ionization in MHD generators produced by electric arc investigated for preionized gas stream 16 p2712 A67-30547

Experiments and design of low temperature seeded inert gas MHD power generator operating in nonthermal ionization mode 16 p2601 A67-30548

He-Cs blow-down MPD facility, discussing generator duct feasibility, nonequilibrium ionization effects, performance and test results 16 p2653 A67-30549

Electrode-to-plasma conduction process effect on MHD generator performance, noting current saturation conditions and results 16 p2601 A67-30550

High temperature loop technology of closed cycle MPD generator, noting transport and reaction mechanisms within high temperature regions 16 p2601 A67-30551

Nonequilibrium plasma production via plasma electron heating with electric field induced in MHD generator 16 p2601 A67-30552

ARGAS closed MHD loop noting technical, constructional details, intended research

program and operational results 16 p2653 A67-30553

MHD power generation experiments with potassium seeded argon plasmas to study performance at Faraday and Hall parameters 16 p2601 A67-30554

Nonequilibrium ionization existence in sufficient magnitude to investigate closed loop MPD power generation feasibility at low temperatures, discussing explanation of saturation effect 16 p2602 A67-30555

Large nonequilibrium MHD generator design and preliminary performance, emphasizing electrode-wall shorting phenomenon in channel 16 p2602 A67-30556

Nonequilibrium plasma properties and generator performance due to magnetically induced ionization in closed loop facility using cesium seeded helium 16 p2602 A67-30557

Nonequilibrium linear MHD generator electrical characteristics, discussing power output and Hall potential reduction causes 16 p2602 A67-30558

Experiments with 100-kw MHD generator free from secondary effects by choosing MHD interaction parameter values greater than unity 16 p2602 A67-30559

Argon-potassium plasma electrical conductivity investigation showing that optimum increase in conductivity corresponds to optimum electrode length 16 p2602 A67-30560

Closed-loop MHD cycle efficiency through thermal efficiency as function of net MHD output density 16 p2603 A67-30561

Optimization of Brayton cycle consisting of heat source, MPD generator, recuperator, etc, in terms of thermal efficiency and specific power 16 p2603 A67-30562

Efficiency and thermodynamic parameters of possible closed-cycle flow schemes for base-load MHD generators 16 p2603 A67-30563

Preheated gas pulsed with shock waves studied for direct AC power production by MHD generator 16 p2603 A67-30564

Conductivity in Faraday generator with cesium-seeded argon calculated from energy balance of electrons 16 p2603 A67-30565

MHD conversion of thermal energy contained in cesium-seeded noble gas examined for conditions governing disk-type ducts use 16 p2603 A67-30566

MHD Brayton cycle power generation techniques, considering noble gases seeded with alkali metal vapors as working fluid 16 p2603 A67-30567

Jet compressors for closed Brayton cycle MPD to study momentum transfer of two high velocity gas or vapor streams of very different molecular weight 16 p2604 A67-30568

Criteria for use of Rankine MHD systems in space 16 p2604 A67-30569

Optimum Mach number for nonequilibrium helium-cesium plasma flow in MHD generator, explaining effect of deceleration temperature and internal efficiency level on optimum pressure 16 p2604 A67-30570

Generator parameters and thermal efficiencies optimization for gas-cooled MGD reactor system, studying temperature and partial-pressure relation to power density 16 p2604 A67-30571

Energy conversion with liquid metal working fluids in MHD converter, proposing stepwise injection and expansion to reduce impact losses 16 p2604 A67-30572

Electrical conductivity measurement of liquid-vapor potassium mixture flowing in circular steel tube simulating MHD oscillator conditions 16 p2712 A67-30575

Magnetohydrodynamic generators operating with two-phase liquid metal flows, describing design and performance 16 p2604 A67-30577

Effect of magnetic field gradients at inlet and outlet on linear two-dimensional induction MHD generator calculated by bilateral Laplace transform 16 p2605 A67-30579

Cryogenically cooled primary winding system for AC MHD generator, considering real machine data 16 p2605 A67-30580

AC MHD power generator and turbine described noting working fluid flow 16 p2605 A67-30581

Material limitations in MHD induction generator, discussing effect of conducting channel walls and thermal insulation on performance 16 p2605 A67-30582

Liquid metal magnetohydrodynamic power generation for space vehicle 16 p2605 A67-30583

use Fluid metal magnetohydrodynamic power conversion program results 16 p2606 A67-30584

Liquid metal energy converters using magnetohydrodynamic induction noting electrodynamic aspects 16 p2606 A67-30586

Liquid metal injection techniques used in magnetohydrodynamic converters 16 p2606 A67-30587

Magnetohydrodynamic generator functioning by emulsion consisting of gas or vapor in liquid metal 16 p2606 A67-30588

Liquid metal magnetohydrodynamic power generation systems using condensing ejector or two-phase jet pump 16 p2606 A67-30589

Magnetohydrodynamic liquid metal power conversion systems investigated using thermodynamic properties 16 p2606 A67-30590

Thermodynamics of injector of magnetohydrodynamic power unit using two-phase vapor-liquid metallic working fluid 16 p2607 A67-30591

Nonsteady combustion MHD open cycle generator improving power density by modulation of conductivity and particle velocity 16 p2607 A67-30595

Large combustion-driven, self-excited Faraday-type MHD generator having multi-or single-circuit net power output, discussing design 16 p2608 A67-30596

Maximum power density, maximum efficiency of diagonal wall generator, Faraday generators and Hall current generators compared 16 p2608 A67-30597

Carrusel magnetoaerodynamic generator, defining equations governing development of electric and thermodynamic properties of plasma 16 p2608 A67-30599

Linear and turbulent MHD generators of conduction type considering operating conditions, efficiency and energy conversion 16 p2608 A67-30600

Magnetohydrodynamic energy converters based on nonequilibrium plasmas for laser construction 16 p2686 A67-31576

Design schemes for magnetic systems of vortex MGD generators with external and internal winding 16 p2609 A67-31585

Thermodynamics of MHD converter cycles with previously mixed liquid metal used as working body, discussing thermal, electrical and energetic efficiency 16 p2610 A67-31780

Liquid-metal and plasma MHD systems for power generation in space environments, noting Rankine and Brayton cycles [JPL-TR-32-1129] 17 p2802 A67-32049

Coupling between free electron and molecular vibrational temperatures in plasma environments, noting energy distribution, application to MHD generation, etc 17 p2894 A67-32150

Low temperature plasma conductivity of combustion products, particularly of exhaust gases in duct of MHD oscillator 17 p2895 A67-32155

Low temperature plasma production in combustion chamber for use in MHD generators, giving equations for plasma composition 17 p2833 A67-32167

Diamagnetic properties of plasma described by extended field equations suggest existence of steady state inductive power transfer between plasma and magnetic fields 17 p2898 A67-32178

Open-cycle gas generator as power supply source for MHD generators, noting reduction of wall effects 17 p2802 A67-32179

Experiments of internal impedance of MHD generator show wide range of working conditions as slowly varying function of applied current 17 p2802 A67-32182

Partially ionized gases application to industry, stressing power units incorporating plasma converters, plasma electrolytic fuel elements and MHD generators 17 p2899 A67-32187

MHD generators theory and operation including superheat conductivity, strong magnetic field generation and MGD flow structure in ducts 17 p2803 A67-32335

Thermodynamic analysis of thermal cycles with MGD generator and steam or gas turbine, noting thermal efficiency 17 p2803 A67-32336

Synchronous and asynchronous idealized induction alternating current MGD generators 17 p2803 A67-32340

Optimization of working characteristics of

MHD generator as power device 17 p2804 A67-33327
 Various magnetic coll systems and parameters for MHD generator use 17 p2804 A67-33328
 Energy conversion methods, MHD power generation - Conference, London, November 1965 18 p3085 A67-33701
 Temperature and/or velocity modulation of plasmas for generating MHD power 18 p3085 A67-33702
 Current distribution in segmented electrode MHD duct and sufficient condition for preventing current leakage between adjacent segments of generator 18 p2987 A67-33703
 Current flow patterns in cross connected MHD generator with four electrodes 18 p2987 A67-33704
 Flow stability in MHD generators after extracting significant electrical power from gas 18 p2987 A67-33705
 Gas-borne suspensions of thermionically emitting particles as MHD working fluids 18 p3086 A67-33707
 Electrode and insulator behavior in experimental MHD generator electrically producing temperature modulation of gas stream 18 p2988 A67-33708
 Combination of monoclinic zirconia, second ceramic and metal in electrodes of MHD generators 18 p3099 A67-33709
 Physical chemistry of potassium sulphate at high temperatures and use for MHD seeding 18 p3086 A67-33710
 Degradation, training and instability in superconducting coils, protection of windings and related problems of superconducting magnets for use in MHD generators 18 p3099 A67-33711
 Buildup time for nonequilibrium argon ionization at inlet of MHD generator channel 18 p2989 A67-34048
 Two-phase liquid metal MHD generators, appraising friction losses and conductivity limitations 19 p3175 A67-34802
 MHD generators using liquid metals examined for advantages/limitations, discussing loop design 19 p3268 A67-35063
 Ceramic material requirements for MHD generator electrodes and duct walls, discussing tests in alkali-seeded plasma 20 p3472 A67-36114
 Open-cycle MHD generator thermal characteristics, direct thermal energy conversion into electricity and optimum front surface temperature 20 p3362 A67-36366
 Current distribution in MHD channel with strong magnetic field solved by reduction to Riemann type boundary value problem 20 p3500 A67-37047
 MHD transformation of heat energy into electricity, discussing plasmatron applications and plasma velocity and temperature measurements in MHD generators 21 p3664 A67-38236
 Fringing effects on electric efficiency variation with slip for cylindrical induction MHD device operable as accelerator, generator or Joule heater [AIAA PAPER 67-714] 21 p3673 A67-38740
 Linear nonequilibrium MHD generator channel, studying discharge structure and stability and convective and Lorentz forces effects on electric characteristics [AIAA PAPER 67-718] 21 p3673 A67-38744
 Cycle and separator efficiencies and specific radiator area compared for liquid alkali metal-lithium MHD power generators 21 p3572 A67-38864
 Linear MPD channel theory with heavy component in uniform state evaluated for investigation of electrical conductivity phenomena 22 p3747 A67-39277
 Large model superconducting magnet for MHD central-station power generation, discussing performance and specifications 22 p3749 A67-40399
 Comparison of flat channel linear MHD induction generator analysis stressing gross power output in constant current and voltage modes 23 p3942 A67-41737
 Two-phase mixture passing through magnetic field in MHD generator studied for effective electric conductivity 23 p3942 A67-41758
 Electrical conductivity of high void

fraction two-phase flow with and without magnetic field in MHD generator 23 p3942 A67-41759
 Liquid metal MHD converters with multistage injection condensation, calculating cyclic process efficiency through thermodynamics 24 p4098 A67-42085
 Plasma nonequilibrium electric conductivity in induced electric field investigated by MHD generator with Ar-K working fluid 24 p4196 A67-42209
 One-dimensional plasma flow variables relations analyzed in crossed electric and magnetic fields with small magnetic Reynolds numbers 24 p4196 A67-42216
 MHD generation of electric power, describing motion equations for conducting fluid in electromagnetic field and duct configurations 24 p4098 A67-42413
 Intense continuous or long pulse magnetic fields in MHD generator, obtaining magnetic energy required for air gap, discussing superconducting magnets 24 p4098 A67-42414
 Electric power generation with closed cycle MHD conversion fluid having gases with high equilibrium conductivity, discussing ionization and electrothermal instability 24 p4099 A67-42416
 Electric power generation using two-phase liquid-metal cycles in MHD converter, discussing liquid metal dynamics 24 p4099 A67-42417
 Energy conversion MHD channel of Faraday type using hot spacers and electrodes for control 24 p4106 A67-42526
 MPD energy conversion duct using heated inert gas working fluid, discussing Hall parameter operation and efficiency factors 24 p4109 A67-42898
MAGNETOHYDRODYNAMIC SHEAR HEATING
 Stability of plasma toroidal configurations under effect of component of magnetic field curvature which lies within magnetic surface 10 p1686 A67-23467
MAGNETOHYDRODYNAMIC STABILITY
 Oscillation of fluid metal droplet, free or immersed in fluid dielectric, in steady and uniform magnetic field 01 p0120 A67-10181
 Small oscillations of viscous liquid-metal droplet under capillary force and in presence of magnetic field 01 p0120 A67-10182
 MHD instability as mechanism responsible for destruction of conductor during electrical explosion 01 p0126 A67-11296
 Phenomenological approach to dispersion relation for hose instability of charged particle beam passing through plasma 02 p0272 A67-11525
 Distortion of magnetic well in minimum-B system by plasma calculated, using hydromagnetic equilibria 02 p0276 A67-12561
 Polarization of type Pcl hydromagnetic oscillations observed at two conjugate geomagnetic stations analyzed by magnetic tape recorder 03 p0406 A67-12818
 MHD stability of dense plasma jets flowing into transverse magnetic field, discussing effect of conductivity and Hall factor 03 p0477 A67-13462
 Hydromagnetic approximation in stability of axisymmetric mode in case of mercury cylinder enclosing copper rod with electric current 03 p0480 A67-13728
 Surface charge distribution effect on stability of conducting fluid in presence of magnetic field 03 p0481 A67-13731
 Stability of inviscid flows of perfectly conducting fluid between two concentric circular cylinders with axial volume current distribution 03 p0403 A67-13732
 Gravitational and magnetogravitational stability of rotating fluid layers of uniform thickness under Coriolis force and magnetic field 03 p0482 A67-13744
 Effect of sudden change in magnetic field and/or pressure gradient on Hartmann flow, assuming stationary and nonconducting plates 03 p0482 A67-13745
 Boundary layer type theory for compressible half-jet with aligned magnetic field 03 p0483 A67-14033
 Inviscid stability of incompressible half-jet under aligned magnetic field, determining neutrally stable eigenvalues 03 p0483 A67-14034
 Fluid interface instability suppression via feedback, noting stability criteria and parameters 03 p0482 A67-14036

Dense high temperature plasma produced by 30-kjoule theta pinch examined by IR maser-excited coupled resonator system [AIAA PAPER 66-151] 04 p0664 A67-14822
 MHD stability of plasma cylinder in time dependent magnetic field 04 p0671 A67-15643
 Drift waves in finite pressure plasma, noting oscillation caused instabilities induced by Alfvén type and slow magnetoacoustic wave interaction 05 p0852 A67-16693
 Negative critical Taylor number for stability of swirling fluid with variable density in circular magnetic field 05 p0859 A67-17442
 Hydromagnetic stability of dissipative flow between rotating permeable cylinders 06 p1040 A67-18129
 MHD phenomena in open electric arc, determining role in formation of plasma configurations of arc 06 p1044 A67-18688
 Finite-beta resistive instabilities of magnetospheric tails analyzed by applying hydromagnetic equations 07 p1244 A67-19923
 Combined Rayleigh-Taylor and Kelvin-Helmholtz instability for incompressible plasmas carrying uniform magnetic field including Hall current 08 p1359 A67-20902
 Plasma filament instability suppression by applying external magnetic field 09 p1545 A67-22069
 Numerical calculations of nonlinear behavior of MHD shock waves in dissipative medium 11 p1825 A67-23854
 Magnetic field curvature effects on low temperature alkali metal plasma column stability 11 p1830 A67-24007
 Stability of pulsating plasma cylinder contained by time dependent magnetic field described by MHD equations 11 p1832 A67-24154
 Solar corpuscular stream magnetic field theoretical model including hydromagnetic stability conditions and undisturbed solar wind 12 p1998 A67-25821
 Theoretical interpretation of fine structure observations of sunspots by stratoscope, discussing stability modes and sunspot umbras 13 p2203 A67-27423
 Stability of interstellar gas to perturbations in gas pressure, magnetic field and cosmic ray pressure from hydromagnetic viewpoint taking rotation into account 14 p2388 A67-28832
 Motion of ideally conducting gas near zero line of magnetic field in terms of MHD equations, obtaining exact solutions for two-dimensional nonstationary problem 14 p2363 A67-29076
 Drift waves in finite pressure plasma, noting oscillation caused instabilities induced by Alfvén type and slow magnetoacoustic wave interaction 15 p2530 A67-29864
 Energy conservation in magnetohydrodynamics of plasmas, noting energy equation in plasma 16 p2721 A67-31548
 Energy dissipation and transport coefficients temperature dependence effect on short wave perturbation development in magnetohydrodynamics 16 p2723 A67-31578
 Model of nonradiative energy transport in sunspots, in which Alfvén waves generated in convectively unstable layer propagate upward into overlying stable layer 19 p3330 A67-36079
 Hydromagnetic shock waves in dissipative plasma, considering nonevolutionary normal shock break-up and switch-on shock stability 20 p3493 A67-36143
 Slightly resistive plasma stability analyzed by asymptotic methods, studying small perturbation growth rate 20 p3493 A67-36145
 MHD instability of sub-Alfvén equations for zonal flow outside diurnally oscillating boundary layer of precessing spheroid 20 p3494 A67-36147
 Highly asymmetric equation for MHD resonance of guided poloidal mode solved using dipole coordinates 20 p3502 A67-37427
 Toroidal plasma instabilities analyzed, justifying use of two-dimensional slab models with varying gravitational field simulating magnetic lines curvature effect 21 p3661 A67-37747
 Flows superimposition on toroidal hydromagnetic equilibrium, stressing stationary motion of plasma layers between neighboring magnetic surfaces 21 p3661 A67-37751
 Linear nonequilibrium MHD generator channel, studying discharge structure and

- stability and convective and Lorentz forces effects on electric characteristics [AIAA PAPER 67-718] 21 p3673 A67-38744
- Circular polarized magnetic field penetration into plasma cylinder noting penetration depth frequency dependence and MHD stability effect 22 p3846 A67-39508
- MHD stability in two-fluid model examined for condition where resistivity and electron inertia are neglected 22 p3851 A67-39984
- Linear magnetically trapped plasma stability theory described from MHD or quasi-fluid point of view 22 p3853 A67-40075
- Relative equilibrium of liquid cylinder investigated for uniform rotation in uniform axial electric field 22 p3787 A67-40135
- Magnetogravitational instability of uniformly rotating compressible medium due to variable amplitude perturbations, stressing Jeans theory 23 p4033 A67-41019
- ### MAGNETOHYDRODYNAMIC TURBULENCE
- Attenuation of uniform turbulent motion in incompressible fluid located in magnetic field 03 p0479 A67-13629
- Second order spectral tensor equations governing turbulence occurring in presence of uniform magnetic field at low magnetic Reynolds numbers 03 p0483 A67-13883
- Certain dissipative mechanisms of homogeneous turbulence in presence of uniform magnetic field with small magnetic Reynolds number 04 p0662 A67-14414
- Growth of turbulent mercury jet issuing into low speed secondary flow and located in coaxial magnetic field 06 p1040 A67-18130
- MHD approximation of solar plasma fluxes observed by Mariner II as free rotating jets 07 p1243 A67-19802
- MHD equations for spectral energy tensors of weak homogeneous magnetoturbulent field and derivation of asymptotic decay law by method of steepest descent 08 p1359 A67-21122
- Velocity space diffusion from weak collisionless plasma turbulence in magnetic field 08 p1360 A67-21123
- Hydromagnetic wake around nonconducting sphere moving in current carrying fluid 08 p1324 A67-21410
- Magnetic and plasma observations of Explorer X and Mariner II confirmed that interplanetary shock waves give rise to sudden storm commencements magnetic and plasma observations of Explorer X 12 p2008 A67-25823
- Turbulent electrostatic shock in plasmas, discussing determination of structure by ion wave instabilities [SR-1] 13 p2162 A67-26281
- Transverse magnetic field effects on heat transfer in turbulent flow of mercury in circular iron tube 17 p2899 A67-32186
- Polarization of periodic pearl-type oscillations of geomagnetic field at magnetically conjugate points 17 p2850 A67-32974
- ### MAGNETOHYDRODYNAMIC WAVE
- Nonlinear MHD waves, examining hyperbolic systems of quasi-linear PDEs, simple wave and flow theory 01 p0126 A67-11252
- Magnetospheric plasma motion in terms of hydromagnetic wave theory, noting effect of variations of geomagnetic field and ionospheric plasma density [AFRL-66-803] 01 p0145 A67-11263
- MHD wave generation in sunspots, examining depth of solar magnetic layer that affects magnetic convection 01 p0151 A67-11283
- Poloidal hydromagnetic plasmaspheric resonance under conditions representative of inner magnetosphere 02 p0276 A67-12563
- Small amplitude wave propagation in incompressible conducting fluid 03 p0480 A67-13725
- Small amplitude wave propagation in ionized high temperature gas embedded in uniform magnetic field with Hall current 03 p0482 A67-13742
- Structure of MHD shock wave taking into account ionization process 04 p0669 A67-15517
- Fluxgate magnetometer onboard applications technology satellite for measuring MHD wave propagation within magnetosphere 04 p0626 A67-15723
- MHD wave propagation emphasizing viscosity, heat and electrical conductivity, Hall current, nonequilibrium phenomena and effect of medium 05 p0851 A67-18364
- MHD and ionizing shock waves and conservation laws 05 p0851 A67-18416
- solutions 05 p0851 A67-18416
- ELF and sub-ELF hydromagnetic waves in upper atmosphere observed using five rocketborne cesium magnetometers 05 p0798 A67-16869
- Oblique shock wave evolution in MHD 05 p0859 A67-17489
- Standing transverse hydromagnetic waves effect on longitudinal invariant of particle motion trapped along geomagnetic field 06 p0997 A67-18700
- Collisionless damping of magnetospheric MHD waves 07 p1172 A67-19541
- Propagation of magnetodynamic disturbance through loss ionosphere and entry into earth surface 07 p1174 A67-19718
- MHD wave theory for slow processes in ionosphere and magnetosphere 07 p1181 A67-19933
- Ionosphere-exosphere system response to bomb-like hydromagnetic source and resultant ground level magnetic fluctuations 07 p1181 A67-19940
- Cyclotron resonance instability of ion cyclotron and magnetosonic waves propagating at angle to magnetic field in infinite uniform plasma 08 p1359 A67-20898
- Latitude dependent plasmasphere oscillations, providing toroidal and standing wave solutions for MHD equations 08 p1365 A67-21407
- Field aligned currents in magnetosphere as explanation of geomagnetic fluctuation localization to region smaller than applicable hydromagnetic wavelength 08 p1402 A67-21476
- Polar auroras, considering types resulting from MHD wave heating of upper atmosphere, low energy particle penetration of atmosphere, etc 09 p1491 A67-21892
- Resonance in plasma magnetized by radial magnetic field solved, obtaining MHD wave equation, noting relation to micropulsations 09 p1545 A67-22196
- Hydromagnetic shock wave intensity decrease in nonuniform magnetosphere treated by Chisnell-Whitham method 10 p1634 A67-23053
- Hydromagnetic gradient waves theory extended to weakly ionized medium-density magnetized plasma of type expected in ionospheric E layer 11 p1783 A67-23923
- Hydromagnetic wave propagation and energy transfer in stratified isothermal plasma embedded in parallel uniform gravity and magnetic fields 11 p1868 A67-25083
- MHD wave propagation in magnetoplasma-filled waveguide, discussing pressure, current inertia, resistivity, etc 12 p1969 A67-25247
- Energetic particle interaction with hydromagnetic shock wave, noting case of particle in radiation belt 12 p1994 A67-25530
- Spacecraft rotation effect on measurement of hydromagnetic radiation in solar wind 12 p1934 A67-25782
- Long period hydromagnetic waves in magnetosphere and coupling to solar wind studied by Explorer XIV 12 p1937 A67-25812
- Chapman-Jouget theorem for MHD detonation in shock tube blocked by stationary perfectly conducting surface, noting relation to magnetoacoustic wave 12 p1976 A67-26071
- Ionospheric structure and micropulsations of geomagnetic field correlated, studying magnetodynamic wave damping and solar activity effects 13 p2114 A67-26856
- Infrasonic and hydromagnetic wave propagation in atmosphere and ionosphere measured by array of underwater and acoustic sensors 13 p2122 A67-27701
- Relativistic MHD shock wave stability in infinitely conducting plasma with magnetic field parallel to shock wave 15 p2523 A67-29216
- Polarization of complex wave form geomagnetic micropulsations of natural and artificial origin, using physical optics 15 p2476 A67-29620
- Fundamental relations for normal shock wave behavior in compressible fluid for classical and hydromagnetic cases 15 p2473 A67-30226
- Properties of irregularities responsible for spread-F, discussing hydromagnetic waves [AGARDOGRAPH 95] 15 p2484 A67-30303
- Magnetohydrodynamic wave dispersion theory at open end of semilinear plasma waveguide closed by conducting diaphragm 16 p2722 A67-31574
- Coaxial and magnetohydrodynamic waveguide matching obtaining reflection coefficient of former and wave amplitude of latter 16 p2722 A67-31575
- Diurnal characteristics of geomagnetic micropulsations noting period, amplitude, continuity, time of occurrence, etc, proving existence of hydromagnetic waves generated at magnetosphere 17 p2841 A67-32212
- Normal modes of hydromagnetic oscillations in rotating fluid sphere including ohmic dissipation, deriving dispersion relations 17 p2941 A67-32285
- Attenuation of natural hydromagnetic waves /PcI/ in ionosphere, noting amplitude reduction and particle distribution in magnetosphere 17 p2843 A67-32536
- Hydromagnetic wave propagation in collisionless plasma based on Vlasov equation, finding Alfvén, magnetoacoustic and nonoscillating waves 17 p2902 A67-32673
- Hydromagnetic mechanism explaining pulsating radio auroral echoes accompanying sudden commencements, considering Wentzel resonant interaction 17 p2845 A67-32766
- Pc 1 micropulsation signals classified as hydromagnetic whistlers and periodic hydromagnetic emissions, suggesting cyclotron instability process as generation mechanism of latter 17 p2853 A67-33253
- Inhomogeneous hydrodynamic motion and thermal particle velocities effect on MHD wave propagation 18 p3086 A67-34034
- Classification of small amplitude waves, surfaces of weak discontinuity and shock waves in ideal MHD medium obeying adiabatic state equation 19 p3294 A67-35409
- Coronal heating extent placed at 1.6 solar radii by 38 MHz radar investigation studies, noting agreement with coronal density calculation 20 p3528 A67-37477
- Proton mechanism of escape from earth magnetic field, analyzing charged particle in Alfvén wave field 20 p3520 A67-37667
- Diurnal variation of earth-ionosphere cavity resonances and properties and propagation of ELF, ULF and MHD waves 20 p3390 A67-37727
- Low amplitude MHD shock wave attenuation, assuming high magnetic Reynolds numbers and small excitation zone width 21 p3665 A67-38239
- Fast and slow magnetosonic wave propagation in plasma analyzed by Huygens principle 21 p3670 A67-38687
- Alfvén, fast and slow magnetoacoustic and entropy hydromagnetic wave propagation in anisotropic collisionless magnetoplasma 22 p3843 A67-39268
- Long period hydromagnetic propagation in theta model geomagnetic tail, deriving TM and TE modes equations 22 p3791 A67-39815
- Geomagnetic perturbation data from high altitude nuclear weapon detonations, deriving theoretical model based upon MHD resonance, noting Alfvén wave behavior 22 p3792 A67-39932
- Laminar nonrelativistic finite amplitude hydromagnetic wave propagation in low temperature ionized plasma, using two-fluid model 22 p3852 A67-39990
- Synchrotron X-ray radiation by high energy electrons in magnetic field with enhancement due to outward propagating hydromagnetic waves proposed as Crab Nebula emission mechanism 23 p4051 A67-40914
- Magnetically tunable microwave filters using MHD modes in ferrites 23 p3980 A67-41186
- Structure of quasi-steady-state MHD shock wave in plasma supersonic flow, analyzing width dependence magnetic field 24 p4195 A67-41937
- ### MAGNETOHYDRODYNAMICS
- SA ALFVEN WAVE
- SA FLUID MECHANICS
- SA HYDROMAGNETISM
- SA PINCH EFFECT
- SA PLASMA DYNAMICS
- Resonance conditions for maximum attainable induction acceleration of cylindrical plasma in space between two concentric glass tubes determined by solving MHD equations 01 p0119 A67-10168
- MHD effects during motion of dielectric shell in electrolyte in presence of external magnetic field 01 p0120 A67-10185

ULF recording of geohydromagnetic micropulsations 01 p0060 A67-10892
 /whistlers/
 Solutions of nonstationary equations of plane laminar MHD boundary layer, using transformation to specialized form of curvilinear coordinates 03 p0477 A67-13527
 MHD - Seminar, Indian Institute of Science, Bangalore, May 1963 03 p0479 A67-13722
 MHD and plasma physics and application to cosmic and geophysical phenomena 03 p0479 A67-13723
 MHD equations, discussing dimensional and nondimensional parameters, modifications of Maxwell equations, vorticity and rate of circulation change in viscous flow, etc 03 p0480 A67-13724
 Some MHD experiments dealing with various working media and with space propulsion 03 p0480 A67-13729
 MHD analysis of composite slider bearing using electroconductive lubricant such as liquid metal, in magnetic field perpendicular to bearing surface, for large and small Hartmann numbers [ASME PAPER 66-LUB-B] 05 p0811 A67-16275
 MHD effects in liquid crystals 05 p0846 A67-16736
 Role of negative ions in flames and of negative droplets in mercury vapor, noting use of isotopic tracer techniques and flame behavior as gaseous semiconductors 05 p0853 A67-16886
 Parametric method of calculating laminar boundary layer in MHD 06 p1044 A67-18879
 Differential equation of motion of meniscus of MHD fluid in capillary in TM field due to surface tension 06 p1044 A67-18881
 Solar physics and MHD model of sun 07 p1247 A67-19331
 Book on MGD and plasma motion including ionized gas, plasma flows, Alfvén wave propagation, shock waves, plasma boundary layer, etc 07 p1230 A67-19727
 Angular acceleration sensor for control system stabilization using MHD principles, obtaining transfer function 08 p1331 A67-20697
 Solid electrolytes used as MHD hot electrode materials between electron conductors 08 p1284 A67-20704
 Magnetothermoelastic mechanism of exploding wire effect under high intensity current surge in pulsed generator for hydrodynamic and magnetoelastic pumping 08 p1354 A67-21046
 Monograph on MHD containing bibliography of Italian and foreign works 08 p1366 A67-21499
 Theory of electrostatic probes in high pressure plasma, discussing ionization and recombination phenomena, diffusion boundary layer, spherical probe, etc 09 p1539 A67-21784
 Hall effect in low temperature plasma in nonhomogeneous magnetic field, describing measuring device 09 p1541 A67-21803
 Progress in aeronautical sciences, Volume 8 10 p1589 A67-22870
 Hamiltonian function of particle in static magnetic field determined with cyclicity in two degrees of freedom 10 p1684 A67-22900
 Action-angle coordinates for particle motion in magnetic mirror systems 10 p1684 A67-22901
 Lorentz invariance, momentum energy tensors and formulation of MHD problem 10 p1685 A67-23083
 Model ionosphere with homogeneous isotropic turbulence investigated for values of kinematic viscosity and dissipation rate of turbulent energy determined from rocket measurements 10 p1646 A67-23273
 Magnetofluid dynamics - AIAA Selected Reprint Series, Volume II 11 p1841 A67-24946
 Current distribution in incompressible fluid flow in magnetic field at low Reynolds number, estimating Lorentz force effect 11 p1842 A67-24952
 Variational principle extended to relativistic scalar hydrodynamics, deriving Hamilton equations 11 p1844 A67-25034
 Energy conversion by MHD 12 p1896 A67-25184
 Cesium seeded argon plasma at atmospheric pressure, noting electron heating effect on conductivity curve and applicability to MHD

conversion 12 p1970 A67-25253
 MHD engineering - Conference, Stanford University, March 1967 12 p1971 A67-25373
 Transformation of magnetoacoustic waves in terms of ideal MHD by phase integrals method 12 p1976 A67-26072
 Ponderomotive forces and geomagnetic westward drift in regard to MHD theory and earth core flows 13 p2114 A67-26855
 Invariant transformation of MGD equations where plane flow is situated in transverse magnetic field 13 p2166 A67-26895
 Sunspot structure, discussing photospheric model, magnetic field influence, MHD structure and energy balance, and photospheric and chromospheric parts 13 p2205 A67-27438
 Self-sustaining high temperature and electrically conducting gas layer formation observed in nonsteady interaction of compressible electrically conducting medium with magnetic field 14 p2355 A67-27839
 Book on mathematics of MHD which assumes that working fluid is Newtonian and obeys Ohm law in form appropriate to moving conductors 15 p2527 A67-29384
 Pulsed discharge in transverse magnetic field noting relation between ionization instability and turbulent conductivity of nonequilibrium plasma 16 p2711 A67-30538
 Electricity from MHD - Conference, Salzburg, Austria, July 1966, Volume 3 16 p2607 A67-30592
 Mhd boundary layer at various Reynolds numbers and magnetic Reynolds number conditions MHD boundary layer at various Reynolds numbers and magnetic Reynolds number conditions MHD boundary layer at various Reynolds numbers 16 p2722 A67-31569
 Magneto-Fanno flow shock tube experiments to determine one-dimensional MGD interactions between partially ionized gas flow and external magnetic field 17 p2898 A67-32183
 Applied MHD - Conference, Jena, East Germany, April 1966 17 p2899 A67-32334
 MHD boundary layer theory principles, demonstrating similarity solutions existing in incompressible fluid 17 p2901 A67-32348
 Heat transfer bibliography covering boundary layer, phase change, two-phase flow, channel flow, conduction, liquid metal, MHD, etc 17 p2969 A67-32450
 MHD open circuit solution, operating by means of ionized gases, may lead to very high temperature internal combustion heat machines, discussing heat cycles 18 p3115 A67-34120
 MHD conversion of heat into electricity noting nozzle behavior during long-lasting experiments, corrosion resistant conducting materials and electrical insulators 18 p2989 A67-34121
 MHD equation simplifications and MHD converter model for problem solving, discussing electrical and thermodynamic characteristics 18 p2989 A67-34125
 Existence and uniqueness of classical solutions of nonstationary boundary and initial value problem in MHD 20 p3497 A67-36430
 Wave propagation and flow past obstacle in fluid magnetodynamics 20 p3503 A67-37676
 Plasma hydromagnetic jump conditions derived from two-fluid plasma model, discussing relevance to collisionless plasma shock 21 p3682 A67-37784
 Relativistic magnetic hydrodynamics profile streamlining and hodograph transformation 21 p3664 A67-38237
 Boundary value problem describing conducting fluid motion in longitudinal magnetic field, considering magnetic Reynolds numbers, electric current density distribution and heat exchange 21 p3665 A67-38243
 Dimensional analysis method for determining similarity criteria for MHD processes in liquid metals and alloys 21 p3665 A67-38248
 Plasma rotation in MPD arc measured for electric and magnetic field distribution and current and electron density distribution [AIAA PAPER 67-655] 21 p3689 A67-38691
 Anode heat transfer in MPD arc, discussing configurations and thrusters [AIAA PAPER 67-673] 21 p3691 A67-38706
 Graduate text in general fluid mechanics covering magnetofluid dynamics and vector analysis 22 p3788 A67-40324
 Galilean invariance principle used to

analyze system of multicomponent MHD equations to select reference system describing motions and transfer processes across magnetic field 24 p4197 A67-42351
MAGNETOHYDROSTATICS
 SA FLUID MECHANICS
 SA HYDROMAGNETISM
 SA PLASMA PHYSICS
 Static magnetic field effect on normal distribution of pressure, temperature and density in solar atmosphere, considering sunspots and velocity field effects [AFCLR-66-879] 13 p2204 A67-27435
 Sunspot magnetic field affecting convective energy transport so that resulting pressure gradient together with gravity force balances magnetic field 13 p2204 A67-27436
 Variational technique involving Lagrange function representation of Grad magnetohydrostatic equation extended to symmetrical solenoid field 15 p2530 A67-29727
 Static equilibrium for two-dimensional toroidal plasma configurations with inner fields and purely meridional electric currents 17 p2903 A67-32709
 Energy transfer in sunspot model with vertical magnetic field, noting magnetic pressure distribution and magnetohydrostatic equations 24 p4226 A67-41966
MAGNETOIONIC PLASMA
 Radiation characteristics of current sources perpendicular to magnetostatic field for cylindrical column of free space surrounded by loss-free magnetoionic medium 08 p1357 A67-20715
 Cerenkov radiation due to point charge moving at uniform velocity parallel to magnetostatic field in unbounded magnetoionic medium 17 p2812 A67-32314
 Stream instabilities in magnetoionic plasmas in presence of DC magnetic field, noting possibilities of growing waves 19 p3292 A67-35389
 Electric and magnetic field measurements in collisionless shock wave propagating through highly ionized magnetized plasma 19 p3294 A67-35408
 Guided waves on infinite cylindrical cavity in magnetoionic medium noting wave solutions, phase velocity, plasma frequencies, etc 20 p3383 A67-37107
 Guided wave characteristics in infinite free space cylindrical cavity in magnetoionic medium noting resonance, transition, cut-off frequencies, phase velocity, etc 20 p3383 A67-37108
MAGNETOIONICS
 Radio wave guiding along electron density discontinuity in magnetoionic exosphere, noting low dispersion modes 01 p0027 A67-11259
 Radio communications disruptions during magnetoionic disturbances in ionosphere at high latitudes during decreasing solar activity 02 p0193 A67-11660
 Small amplitude electromagnet wave propagation in cold homogeneous ionospheric plasma including negative ions and immersed in static magnetic field 04 p0614 A67-14957
 Antenna orientation effect on polarization components of radio waves reflected from ionosphere, noting occurrence and properties of magnetoionic component of polarization 07 p1173 A67-19690
 Short term and averaged characteristics of nonreciprocal HF ionospheric single and multipath propagation paths 11 p1762 A67-24286
 Radio communications disruptions during magnetoionic disturbances in ionosphere at high latitudes during decreasing solar activity 16 p2624 A67-31075
 Altitude of lower boundary of ionosphere determined by electron density profile, considering absorption coefficient and magnetoionic signal components 16 p2669 A67-31906
 Exoionospheric communications system with ideal matched filter and signal processing at transmitter for increased range and secure coding possibilities 21 p3586 A67-38952
MAGNETOMETER
 Magnetic field intensity near moon measured by Luna X magnetometer, noting correlation with earth surface intensity 01 p0150 A67-10909
 Magnetometer predictions of geomagnetic disturbances and intense sporadic E layer

occurrences at various sunspot cycle times in auroral zone and effects on VHF absorption 03 p0415 A67-14118

Statistical properties of interplanetary magnetic field variations, charged particles propagation in solar system and photospheric processes analyzed, using Mariner II magnetometer 04 p0698 A67-14951

Fluxgate magnetometer onboard applications technology satellite for measuring MHD wave propagation within magnetosphere 04 p0626 A67-15723

Fluxgate magnetometer for OGO-E spacecraft in observing MHD waves and magnetic field structures in space 04 p0626 A67-15724

Proton precession magnetometer completely transistorized except for signal amplifier 05 p0807 A67-18712

Limitations in tilted fluxgate magnetometer data from Explorer XVIII satellite due to ambient dynamic field effects 07 p1182 A67-19943

Skylark rocket attitude in free space determined from solar and magnetic sensor data used in least squares method 08 p1406 A67-20508

Longitudinal and lateral axes orientation of uniformly rotating or rapidly rotating vehicle utilizing outputs from solar sensors and lateral magnetometer 08 p1409 A67-20538

Metrological characteristics of three-component magnetometers with ferromagnetic probes installed in Elektron II space station 11 p1789 A67-24079

Frequency analysis of continuous and irregular geomagnetic pulsations measured by induction magnetometer 11 p1786 A67-24332

Recording and analysis of geomagnetic pulsations of auroral zone and comparison with bremsstrahlung measurement, using two-magnetometer arrangement 15 p2474 A67-29524

Flux-gate magnetometer device for determining attitude of satellite or rocket probe, considering magnet perturbation due to solar wind and solar storms 16 p2700 A67-30658

Rubidium vapor magnetometer used for near earth orbiting spacecraft, instrumentation and in-flight performance 20 p3443 A67-36513

Magnetometer with Gauss sensor describing n-type InSb pickup bridge instrument sensitivity 20 p3447 A67-36760

Small alternating magnetic field modulation effects on sampled output of rubidium magnetometer with frequency counter 20 p3448 A67-36876

Weak magnetic field measurement using magnetic resonance, discussing electron nuclear resonance optical detectors, cesium vapor magnetometers and superconducting quantum interference device /SQUID/ 22 p3799 A67-39771

Analytic model for output voltage of fluxgate magnetometer, demonstrating excitation function and core squareness effects 22 p3800 A67-39911

Nuclear magnetometers for magnetospheric measurements from rockets 23 p3998 A67-40697

Rapid magnetic field variations observed in magnetosheath evaluated in terms of transverse modes of plasma wave propagation 23 p3995 A67-40804

MAGNETOMETRY

Approximate method of computing attitude of sounding rockets from magnetometer data 03 p0519 A67-13782

Kappa rocket sounding of ionospheric Sq-currents, using rubidium vapor magnetometer 05 p0799 A67-16871

IMP II satellite measurements of magnetic fields in interplanetary space by onboard monoaxial fluxgate magnetometers 14 p2310 A67-28052

Solution of incorrect magnetometric and gravimetric problems represented by integral equations of convolution type with unstable solutions 16 p2663 A67-30866

MAGNETOPLASMA

Energy required to confine static shielded magnetic dipole field, immersed in highly conducting medium, by transient diamagnetic surface as function of dipole moment and disturbance field 06 p1030 A67-17658

Vela II measurements of earth magnetopause and bow shock positions,

showing relationship to magnetic disturbance index and thus also to solar wind velocity 07 p1180 A67-19920

Magnetopause structure and attitude from Explorer XII observations 07 p1180 A67-19925

Magnetosheath field, geomagnetic activity index, magnetopause stability and interplanetary magnetic field influence on magnetospheric phenomena 07 p1182 A67-19953

Earth bow shock observations with Explorer XII satellite magnetometer 14 p2383 A67-28047

Transverse field growth studied for generation of magnetic field in boundary layer by currents along magnetopause produced by tangential solar wind 22 p3871 A67-39801

MAGNETOPLASMA

Weak longitudinal and transverse magnetic fields increase emf and optimum output voltage characteristics of thermionic diode introduced into autonomous mercury discharge plasma 01 p0034 A67-10135

Longitudinal electric field penetration into magnetoplasma layer in constant magnetic field 01 p0122 A67-10356

Reflection of vertically polarized exponentially varying electromagnetic waves by horizontally stratified magnetoplasma half-space 01 p0023 A67-10471

Performance capabilities of Hall current accelerators determined from parameters influencing anode power loss [AIAA PAPER 66-184] 01 p0125 A67-11160

Self-focusing of transverse electromagnetic plane waves in magnetoplasma 02 p0191 A67-11571

Modes of beam waveguide or beam waveguide resonator filled with axially magnetized plasma 02 p0213 A67-11619

Magnetically compressed plasma as high intensity source of near UV and visible radiation experimentally studied in dynamic pinch 02 p0272 A67-11880

Cold beam plasma interaction theory for finite transverse dimensions and finite magnetic fields determined by computer solution of dispersion relations 02 p0272 A67-11884

Ion motion effect on spectral region and energy density of Cerenkov excitation produced by charge moving in cold magnetoactive plasma 02 p0274 A67-12456

Kinetic theory for passage of electromagnetic wave through plasma layer in waveguide with metallic walls, assuming negligible transverse particle motion due to strong magnetic field 02 p0205 A67-12474

Sweep spectrometer study of effect of strong magnetic field on characteristics of plasma beam produced by titanium plasma source 02 p0278 A67-12622

Quasi-linear approximation of Cerenkov and cyclotron damping of electromagnetic waves in magnetoactive plasma, considering collisions of wave-absorbing resonance particles 03 p0475 A67-12934

Quasi-linear equations for inhomogeneous plasma in magnetic field applied to pumping of energy of Langmuir oscillations 03 p0475 A67-12936

Ion wave excitation due to Hall current compared with current parallel to static magnetic field in weakly ionized plasma on basis of two-fluid model 03 p0476 A67-13354

Experimental results of microwave absorption by magnetoplasma indicate peaks result from excited electromagnetic wave propagation 03 p0476 A67-13357

Attenuation of uniform turbulent motion in incompressible fluid located in magnetic field 03 p0479 A67-13629

Propagation of coupled electromagnetic, electron-acoustic and ion-acoustic waves in horizontally stratified and magnetized electron-ion plasma 03 p0372 A67-13991

Electron recombination in rapid cooling of magnetized plasma jet expanding into vacuum 03 p0486 A67-14195

Dispersion equation for electromagnetic waves propagating in uniform plasma layer along boundary parallel to external magnetic field 04 p0687 A67-15207

Convective effects role in exciting axisymmetric oscillations in plasma cylinder in magnetic field with aid of radius restricted electron beam 04 p0668 A67-15271

Kinetic theory of electromagnetic propagation in confined magnetoactive

plasma 04 p0668 A67-15272

Conical induction plasma gun construction in strongly preionized regime and results of electrostatic probe measurements made with discharge camera 04 p0668 A67-15280

Electrical noises of plasma of steady state HF discharge in magnetic field discussed from standpoint of universal plasma instability 04 p0671 A67-15640

Kinetic theory of electromagnetic wave propagation in layered plasma waveguide in strong magnetic field 05 p0761 A67-16341

Radiation resistance and modes of oriented electric dipole in loss-free magnetoplasma 05 p0853 A67-16848

LF oscillation 30 times greater than HF oscillation in plasma in magnetic field 05 p0854 A67-16897

Longitudinal propagation of SLF electromagnetic waves through plane-laminar magnetoactive ionospheric plasma 05 p0765 A67-16955

Perturbation theory of ion concentration at great distances from body rapidly moving in collisionless plasma in constant magnetic field 05 p0855 A67-17139

Nonlinear interaction of two electromagnetic waves in infinite cold magnetoactive plasma 05 p0766 A67-17230

Plasma loss in single-ended Q device measured as function of magnetic field strength, obtaining diffusion coefficient directly 05 p0859 A67-17445

Uncoupled form for plasma resonance probe in magnetic field obtained, using special coordinate transformation 06 p1041 A67-18145

Low power MPD arc thruster design and performance with radiation cooled electromagnets and permanent magnets [AIAA PAPER 67-50] 06 p1074 A67-18436

Kinetic equation for homogeneous nongyrotropic magnetoplasma, discussing collective effects and errors in Sundaresan analysis 06 p1042 A67-18574

Plasma stability with randomly fluctuating parameters for magnetic field with curved lines of force 06 p1045 A67-18790

Nonlinear second harmonic generation of current density in inhomogeneous magnetoplasma and reflected electromagnetic wave from free space interface 06 p1046 A67-18825

Time dependent behavior of diffusion of plasma inhomogeneities with or without particle drift 07 p1250 A67-19810

Current density distribution in MPD arc jet exhaust measured, using Hall effect sensors [AIAA PAPER 66-116] 08 p1375 A67-20573

Complex Doppler effect in dense cold magnetized plasma 08 p1357 A67-20818

Electromagnetic-wave radiation peculiarities in homogeneous anisotropic dispersive magnetic plasma 08 p1294 A67-20821

Self-focusing of longitudinal electromagnetic waves in nonlinear plasma in strong magnetic field 08 p1357 A67-20822

Electrodynamics properties of homogeneous magnetoactive plasmas including wave propagation, excitation, scattering, etc 08 p1358 A67-20863

Nonlinear constant profile plane waves in cold Vlasov hydrogen plasma under influence of external magnetic field 08 p1359 A67-20896

Quasi-shock structure in collision free plasma in magnetic field and comparison with bow shock on solar wind near earth 08 p1359 A67-20901

LF wave frequency-and amplitude-dependent transverse anomalous diffusion coefficient in fully ionized magnetoplasma in Q-machine 08 p1360 A67-21125

Kinetic equation for unstable homogeneous plasma in uniform magnetic field when subjected to sudden uniform electric field 08 p1360 A67-21127

Resonant frequencies of standing wave Bernstein modes propagating in magnetized homogeneous plasma columns and effects of anisotropy of unperturbed electron velocity and ambipolar-diffusional electric field 08 p1361 A67-21131

Anomalous diffusion and radial density profile in positive column with longitudinal magnetic field 08 p1362 A67-21148

Noise energy spectra created by wave-wave scattering of quasi-longitudinal waves in magnetoactive plasmas with different

- electron and ion temperatures 08 p1365 A67-21413
- Angular and frequency spectra of Cerenkov and cyclotron radiation from charged particle spiraling in cold magnetoplasma determined by Fourier transform method 09 p1562 A67-22228
- Spectral densities of electromagnetic fields of thermal radiation in magnetoplasma as related to radiation resistance of immersed antenna 09 p1464 A67-22448
- Quasi-static theory of cylindrical impedance probe for magnetoplasma extended to include vacuum sheath effects 09 p1549 A67-22451
- Electron plasma behavior and stability in presence of time dependent electric field 09 p1549 A67-22553
- Magnetized plasma oscillations for arbitrary initial distributions of electrons and ions, obtaining dispersion equation in fifth degree 09 p1550 A67-22617
- Electron-hole plasma pinch instability in InSb on application of longitudinal magnetic fields shows change to helical rotating plasma 10 p1683 A67-22760
- Drift cyclotron oscillations of inhomogeneous collision plasma propagating across magnetic field, taking into account particle collisions with aid of Landau collision integral 10 p1686 A67-23595
- Magnetic field curvature effects on low temperature alkali metal plasma column stability 11 p1830 A67-24007
- Physical stabilization mechanism of helical instability of positive column in longitudinal magnetic field due to quasi-linear effects 11 p1831 A67-24012
- Relativistic solution to normal incidence on semilinear longitudinal drifting homogeneous temperate magnetoplasma, obtaining reflected and transmitted waves 11 p1832 A67-24304
- Diffusion measurements in potassium magnetoplasmas based on volume plasma loss properties of variable length single-ended Q device 11 p1835 A67-24386
- LF drift waves effect upon anomalous transverse diffusion in fully ionized magnetoplasma, noting wave amplitude 11 p1835 A67-24387
- Longitudinal electric field penetration into magnetoplasma layer in constant magnetic field 11 p1844 A67-25029
- MHD wave propagation in magnetoplasma-filled waveguide, discussing pressure, current inertia, resistivity, etc 12 p1969 A67-25247
- Thermal ionization for low temperature plasma confined in magnetic field, examining magnetic field effect on ionization 12 p1975 A67-25757
- Performance capabilities of Hall current accelerators determined from parameters influencing anode power loss [AIAA PAPER 66-201] 12 p1975 A67-25892
- Nonuniform absorption of gyro-resonant microwave energy by electron gas used to produce helical configuration in magnetoplasmas 13 p2163 A67-26289
- Nondissipative plasma flow past magnetized cylinder in absence of electromagnetic field, noting current force relation to distance between conductor and cylinder surface 13 p2168 A67-27303
- Hollow electrically conducting fluid jet stabilization in presence of uniform magnetic field 13 p2169 A67-27314
- Sweep spectrometer study of effect of strong magnetic field on characteristics of plasma beam produced by titanium plasma source 13 p2170 A67-27378
- Critical particle velocity and particles frozen in given point of magnetic field line, discussing effects of plasma compression and reflection levels 13 p2204 A67-27432
- Ion density concentration in magnetic-field-aligned rotating plasma columns/plasma eddies/ 13 p2171 A67-27433
- Nonlinear harmonic generation in magnetoplasma using Boltzmann equation, noting sharp resonance peaks 14 p2358 A67-28236
- Magnetic field, pressure and discharge current effects on saturation electron current of electrostatic probe used to measure magnetoplasma electron density 14 p2358 A67-28237
- Integral expression derived for current distribution on infinite antenna aligned with magnetic field immersed in plasma, using generalized eigenfunctions 14 p2284 A67-28378
- Electron recombination in rapid cooling of magnetized plasma jet expanding into vacuum 14 p2360 A67-28540
- Magnetoplasma radiation by microwave pulse excitation at gyrofrequency harmonics, considering single particle approach 14 p2360 A67-28557
- Magnetactive plasma quasi-linear oscillations equations, determining damping decrements of plasma electric field components 14 p2361 A67-28753
- Propagation of coupled electromagnetic and electroacoustic waves in magnetized compressible stratified electron plasma 15 p2521 A67-29177
- Current strip in cold magnetoplasma, noting radiation resistance of Hertzian dipole for large frequency ranges 15 p2521 A67-29185
- Dispersion equation for electromagnetic waves propagating in uniform plasma layer along boundary parallel to external magnetic field 15 p2532 A67-30255
- Invariant solutions to nonlinear electromagnetic phenomena in dense plasma with nonequilibrium electric conductivity in variable magnetic field 16 p2712 A67-30543
- Oscillation spectrum of weakly ionized plasma current flowing normal to applied magnetic field discussed and analyzed in linear approximation using MHD model 16 p2712 A67-30546
- He-Cs blow-down MPD facility, discussing generator duct feasibility, nonequilibrium ionization effects, performance and test results 16 p2653 A67-30549
- Optimization of Brayton cycle consisting of heat source, MPD generator, recuperator, etc, in terms of thermal efficiency and specific power 16 p2603 A67-30562
- Carrousel magnetoaerodynamic generator, defining equations governing development of electric and thermodynamic properties of plasma 16 p2608 A67-30599
- MHD effect in shock tube, studying EMF induced in motion of transverse magnetoplasma 16 p2715 A67-31112
- Energy losses of modulated azimuthal current in magnetoplasma, discussing specifically electron cyclotron resonance 16 p2716 A67-31177
- Quasi-linear theory of plasma cyclotron instability, analyzing transverse oscillations propagating along external magnetic field 16 p2717 A67-31179
- Anomalous decay of discharge plasma with oscillating electrons in strong magnetic field, using diagrams 16 p2717 A67-31181
- Drift waves in fully ionized potassium magnetoplasma in single-ended Q machine, measuring effect on transverse diffusion coefficient 16 p2720 A67-31242
- Magnetoplasma diffusion equation of F-2 layer allowing electric currents and temperature variations, noting transverse drift of field 16 p2666 A67-31402
- Nonlinear interaction between weakly ionized helium magnetoplasma produced by HF discharge and microwave field 17 p2903 A67-32676
- Instability and related anomalous diffusion of magnetized weakly ionized hydrogen plasma of RF discharge in cylindrical geometry 17 p2908 A67-33113
- Dispersion effect on shock wave structure in magnetoplasma, analyzing role of wave front inclination angle to magnetic field 18 p3084 A67-33525
- Plasma stability with randomly fluctuating parameters for magnetic field with curved lines of force 18 p3086 A67-33732
- Beat frequency generation and multiplication and subsequent harmonic amplification in plasma-beam system, particular case of plane waves 18 p3087 A67-34037
- Laser heating of plasma situated in strong longitudinal magnetic field 18 p3060 A67-34041
- Frequency regions for Cerenkov radiation and power spectrum in collisionless magnetoplasma calculated using refractive index 18 p3090 A67-34428
- Stimulated coherent emission at upper hybrid resonance frequency from magnetoplasma excited by microwave pulse 18 p3090 A67-34466
- Collisionless electrostatic shock in magnetized plasma in absence of initial magnetic field 18 p3092 A67-34749
- Electron cyclotron resonance absorption of microwaves in oxygen magnetoplasma used to alter electron attachment and detachment rate coefficients 19 p3271 A67-35077
- Periodic spatial variations of parameters of positive column plasma in magnetic field along obstacle shadow due to electron wakes 19 p3273 A67-35093
- Wave propagation and electron beam-plasma interaction in plasma column inside magnetic field, measuring plasma characteristics and spatial distribution 19 p3275 A67-35107
- Plasma column in magnetic field created by diffusion from low pressure pulsed discharge in hydrogen, with plasma density dependent on gas pumping speed 19 p3275 A67-35108
- Spark perturbation of magnetic and electromagnetic fields, studying plasma-magnetic interaction and spark plasma characteristics 19 p3239 A67-35165
- Production and behavior of magnetically stabilized high density high temperature plasma, describing experiment 19 p3282 A67-35167
- Transport coefficients of fully ionized hydrogen plasma in magnetic field calculated from Fokker-Planck equation 19 p3286 A67-35350
- Alkali-metal magnetoplasma properties related to enhanced diffusion, showing relationship to beam-plasma interaction 19 p3287 A67-35360
- Interaction of moving plasma with dipole magnetic field measured visually and with electric and magnetic probes 19 p3288 A67-35367
- Interaction of plasma stream with three-dimensional magnetic dipole field, discussing current distribution in cavity 19 p3221 A67-35368
- Cyclotron harmonic wave propagation in warm magnetoplasmas predicted theoretically for perpendicular and oblique damping 19 p3288 A67-35371
- Inhomogeneous plasma stability, considering wave drift oscillations expanding across external magnetic field and flute instability in noncompensating plasma 19 p3292 A67-35393
- Electromagnetic wave reflection by stratified magnetoplasma, obtaining formulas providing perturbation effect on reflection coefficients 19 p3183 A67-35457
- Variational formula for antenna impedance in warm magnetoplasma, considering force and fluid-flux distribution 19 p3194 A67-35513
- Influence of Langmuir probe losses on ion-density measurements in thermal cesium plasma with homogeneous magnetic field 19 p3296 A67-35589
- Dispersion equation for electrodynamic boundary value problem of natural oscillations of cylindrical resonator with magnetoactive plasma 19 p3299 A67-36019
- Exchange invariance in dissipationless fluid systems, deriving conservation law and stability conditions and application to gyro-stabilized magnetoplasma 20 p3419 A67-36151
- Electromagnetic and pressure fields produced by current distributions in compressible magnetoplasmas determined using perturbation theory 20 p3496 A67-36312
- Plasma stability in combined magnetic fields investigated for oscillation frequencies 20 p3500 A67-37048
- Coupling coefficients for nonlinear interaction between two transverse waves and electron plasma wave in magnetic field 20 p3501 A67-37181
- Parametric resonance in magnetosonic waves through analysis of perturbed particle trajectories in modulated plasma field, determining velocity time dependence 20 p3501 A67-37296
- Partial solutions of equations describing axisymmetric unstable motions of gravitating rarefied magnetoplasma 20 p3502 A67-37663
- Resonance phenomena in bounded magnetoplasma shown on basis of dispersion relation as due to formation of standing waves of electromagnetic waves 20 p3503 A67-37671
- Plasma conductivity tensor in steady magnetic field in terms of electric field correlation using Kubo transport theory 20 p3503 A67-37692
- Electron-plasma oscillation damping in hot collisional plasma with external uniform

magnetic field investigated using Fokker-Planck equation 20 p3503 A67-37693

Radiation of monofrequency antenna in compressible magnetoplasma expressing far field as sum of modal plane waves 20 p3388 A67-37701

Ionization and recombination effects on MHD wave propagation through three-component magnetoplasma, deriving nonlinear motion equations 21 p3660 A67-37743

Kinetic theory of electromagnetic wave propagation in laminar plasma medium situated in steady HF or LF magnetic field normal to plasma layer interfaces 21 p3663 A67-37860

Dispersion equation of radioactive compressible nonviscous plasma with finite electric conductivity under gravitational and axial magnetic fields 21 p3663 A67-37918

Oscillation of liquid sodium drop in dielectric medium in presence of constant magnetic field 21 p3665 A67-38245

Perturbation theory of ion concentration at great distances from body rapidly moving in collisionless plasma in constant magnetic field 21 p3668 A67-38481

Electromagnetic wave propagation in plasma layer bounded by external constant magnetic field, using kinetic theory with Maxwell equations and distribution function 21 p3670 A67-38685

Spacecraft-space plasma electric equilibrium, discussing active spacecraft configurations for control [AIAA PAPER 67-702] 21 p3714 A67-38729

Electrostatic ion propulsion and KEMAN MPD thruster research in Germany [AIAA PAPER 67-724] 21 p3694 A67-38749

Asymptotic formulas for propagating discontinuity diffusion in magnetoplasma, considering discontinuity shape, diffusion and lifetime 21 p3621 A67-39020

Electromagnetic wave propagation in nonuniformly magnetized plasma with wave frequency near second electron cyclotron harmonic 22 p3843 A67-39263

Dispersion equation for extraordinary and plasma waves propagating through magnetoplasma perpendicular to external magnetic field studied near lower hybrid frequency 22 p3844 A67-39419

Helical electromagnetic wave scattering and transformation during propagation in magnetoplasma, considering fluctuations 22 p3846 A67-39501

Dispersion characteristics of surface waves excited in infinitely long axially magnetized cold plasma by electric dipole 22 p3847 A67-39621

Resonant particle diffusion of nonuniform plasma across magnetic field, calculating transport coefficients 22 p3848 A67-39687

Synchrotron radiation intensity of relativistic electron moving in anisotropic medium 22 p3851 A67-39735

Kinetic theory of electromagnetic propagation through magnetoactive plasma, determining reflection, transmission and absorption coefficients and plasma field configuration 22 p3761 A67-39758

Electromagnetic propagation in plasma layer in magnetic field, determining absorption coefficient 22 p3762 A67-40123

Antenna immersed in plasma problem solved using electromagnetic radiation in ionized medium principles 23 p3978 A67-40707

Charged particle gas interaction with EM field noting electron gas collective oscillations, EM wave propagation in anisotropic plasma and applications 23 p4037 A67-40759

Two and three-pulse echo trains stimulated in magnetoplasma by repeated electron cyclotron frequency pulsing studied with single particle collision theory 23 p4031 A67-40889

Secondary temperature resonances in magnetized plasma slab with nonsymmetric inhomogeneous density profile, noting spectrum degeneracy in symmetric nonuniform profile 23 p4034 A67-41359

Variations in parameters of magnetized plasmoids interacting in nonuniform fields determined by magnetic and electric probes 23 p4035 A67-41685

Wave propagation in plasma with anisotropic pressure studied using modified Burgers equations, examining effect of collisions 24 p4197 A67-42260

Galilean invariance principle used to

analyze system of multicomponent MHD equations to select reference system describing motions and transfer processes across magnetic field 24 p4197 A67-42351

Total head tube in combination with electrostatic probe used in supersonic plasma diagnostics, measuring plasma and shock wave front parameters 24 p4197 A67-42355

Design of gasdynamic shock tube described with measuring apparatus developed for studying ionized gas flows in magnetic field 24 p4139 A67-42357

Electromagnetic wave diffraction in magnetoactive plasma by conducting wedge using Laplace integral in rotating reference frame 24 p4123 A67-42706

Resonance rectification effects for wire probe in magnetoplasma observed in terms of warm plasma perpendicular permittivity component 24 p4199 A67-43101

Laser-irradiated plasma theoretical study indicating absorption enhancement in external magnetic field 24 p4199 A67-43104

MAGNETORESISTANCE

Solid state inductive element with magnetoresistance used for increase of Q 01 p0032 A67-10006

Geometrical /current distribution/ influence on magnetoresistance effect in indium antimonide and indium arsenide at 34 gc/s 01 p0132 A67-10467

Conductivity, Hall coefficient and magnetoresistance of monophase InSb films as function of film thickness 02 p0295 A67-11765

Anisotropy of electric resistivity, Seebeck and Hall coefficients and magnetoresistance of n-type single crystal ferric oxide /hematite/ containing tetravalent tin ion as impurity 02 p0299 A67-12085

Anisotropy of magnetoresistance and Hall effect in n-GaAs, discussing conduction band structure in vicinity of edge 03 p0487 A67-12806

Negative magnetoresistance of n-type InAs in longitudinal magnetic fields 03 p0490 A67-13156

Fermi-Dirac statistics, transverse magnetoresistance and galvanomagnetic properties of hexagonal-close-packed Mg and Zn 03 p0495 A67-13511

Transverse magnetoresistance and Hall effect measurements on n-type GaSb at various magnetic fields and temperatures, obtaining electron concentration and mobility 03 p0501 A67-14347

Longitudinal magnetoresistance anisotropy and Hall coefficient anisotropy in p-type indium antimonide, noting similarities with galvanomagnetic anisotropy of p-type germanium 04 p0674 A67-14609

Quantum oscillation of transverse and longitudinal magnetothermal emf in n-type indium antimonide compared with oscillations of transverse and longitudinal magnetoresistance and Hall coefficient 04 p0680 A67-15288

Transverse magnetoresistance of n-type InAs, noting temperature effect and correlation with quantum theory 04 p0681 A67-15293

Hall effect and magnetoresistance effect measured on p- and n-CdSb single crystals above 77 degrees K and magnetic fields up to 7500 gauss 06 p1054 A67-18824

Corbino magnetoresistance experiments for n-type surface layers on p-type indium arsenide crystals as function of surface electric field 06 p1064 A67-18941

Conduction band structure and anisotropy of electron scattering in n-GaAs, analyzing magnetoresistance and Hall effect 06 p1064 A67-18943

Hall coefficient and transverse magnetoresistance behavior in n-GaSb at 4.2 degrees K, using DC high magnetic fields 06 p1064 A67-18946

Quantum oscillations in magnetoresistance of n-type pure HgTe used to estimate electron effective mass and g value close to band edge 06 p1065 A67-18948

Energy surfaces of tellurium investigated with oscillatory magnetoresistance /Shubnikov-de Haas effect/ 06 p1065 A67-18949

Negative magnetoresistance in semiconductors caused by magnetic system in random lattice of impurity atoms 06 p1067 A67-18965

Magnetoresistance of heavily doped n-type

silicon at liquid He temperature noting dependence on field strength and temperature 06 p1067 A67-18967

Resistivity, magnetoresistance, Hall effect and thermal conductivity in n-type In-Sb at liquid He temperatures 06 p1068 A67-18968

Oscillatory magnetoresistance and Hall effect in single crystals of Sn-doped Bi to decrease Fermi energy 06 p1070 A67-18984

Resistivity, Hall coefficient and magnetoresistance of bismuth thin films at various temperatures, showing size dependence of effective mobilities of electrons and holes 06 p1070 A67-18985

De Haas-Shubnikov effect observation method and application to measurements on bismuth 07 p1155 A67-19891

Nonohmic conductivity in n-type GaAs accompanied by negative photoconductivity and giant magnetoresistance, noting electron injection at cathode 07 p1234 A67-20099

Negative magnetoresistance of n-type InAs in longitudinal magnetic fields 10 p1690 A67-23104

Exchange model of zero bias tunneling anomalies, discussing Hamiltonian, interference magnetic scattering and metal junctions 10 p1691 A67-23400

Hole effective masses in p-type CdSb determined by measuring magnetoresistance effect and magnetic susceptibility 12 p1987 A67-26225

Electromagnetic effect in n-type InSb samples, measuring magnetic resistance, Hall effect and magnetic EMF 13 p2174 A67-26368

Local magnetic moment derivation methods using magnetoresistivity data, estimating concentration and temperature dependence 13 p2177 A67-26990

Resistivity and magnetoresistance for metallic impurity conduction in phosphorus doped silicon at low temperature with various donor concentrations 14 p2365 A67-28232

Quantum oscillation of magnetoresistivity in n-type mercury telluride crystals, obtaining electron mass 14 p2369 A67-28598

Temperature dependence of electrical conductivity, Hall effect and resistance in transverse magnetic field for tin-doped InSb 15 p2534 A67-29385

Electric field effect on magnetoresistance of p-type indium arsenide surface in high magnetic fields at low temperatures 17 p2911 A67-32206

Book on effects of hot electrons associated with carrier concentration in semiconductors at very low temperatures 17 p2914 A67-32378

Shubnikov-de Haas and Gurevich-Firson oscillations of photomagnetic effect in n-InSb magnetic field 17 p2914 A67-32451

Electrical resistance of niobium single crystal at very low temperature from beginning of superconductivity transition 17 p2916 A67-32805

Operator for spin-phonon interaction between conduction electrons and polarization-induced longitudinal oscillations of semiconductor lattice 18 p3099 A67-33697

Conduction band structure in n-type strontium titanate investigated by measuring oscillatory magnetoresistance in high magnetic fields 18 p3104 A67-34592

Lorentz number, Hall coefficient, magnetoresistance and Hall mobility variations in n-type degenerate semiconductors 18 p3106 A67-34729

Magnetometer with Gauss sensor describing n-type InSb pickup bridge instrument sensitivity 20 p3447 A67-36780

Impurity conduction causing negative magnetoresistance in Cu doped n-type GaAs crystals at low temperature 20 p3513 A67-37440

Electromagnetic effect in n-type InSb samples, measuring magnetic resistance, Hall effect and magnetic EMF 21 p3680 A67-38324

Current carrier mobility, Hall effect and magnetoresistance in semiconductors with nonuniform ion distribution 22 p3858 A67-39507

Strong electric field effects on parabolic energy band semiconductor magnetoresistance and Hall coefficients, discussing scattering mechanisms 24 p4202 A67-41982

Maximum Corbino magnetoresistivity in indium antimonide single crystals, investigating impurity concentration and layer distribution 24 p4203 A67-42208

MAGNETOSONIC RESONANCE

Ferroacoustic resonance in yttrium ferrite galate crystals, noting effect of magnetic field on pulse amplitude 05 p0868 A67-17064
Cyclotron resonance instability of ion cyclotron and magnetosonic waves propagating at angle to magnetic field in infinite uniform plasma 08 p1359 A67-20898
Ferroacoustic resonance in yttrium ferrite galate crystals, noting effect of magnetic field on pulse amplitude 15 p2538 A67-29795
Magnetosonic resonances location in exosphere, showing diagram of Alfvén velocity profile 18 p3042 A67-34389
Parametric resonance in magnetosonic waves through analysis of perturbed particle trajectories in modulated plasma field, determining velocity time dependence 20 p3501 A67-37296

MAGNETOSPHERE

Dynamo theory interpretation of magnetospheric-ionospheric electric current system associated with N-S asymmetry of magnetic daily variation at time of equinox 01 p0057 A67-10113
Magnetospheric plasma motion in terms of hydromagnetic wave theory, noting effect of variations of geomagnetic field and ionospheric plasma density [AFCL-66-803] 01 p0145 A67-11263
Interaction of solar wind and frozen-in magnetic field with geomagnetic field inside and outside magnetosphere, comparing theory with satellite measurements 02 p0320 A67-11461
Integral intensity of charged particles diffusing through drift shells in earth magnetosphere with specific example for protons 02 p0306 A67-11550
Solar dynamics, with emphasis on solar wind interaction with magnetosphere of earth [AFCL-66-867] 02 p0326 A67-12246
Poloidal hydromagnetic plasmaspheric resonance under conditions representative of inner magnetosphere 02 p0276 A67-12563
Shape of magnetosphere of rectilinear flow in divergent plasma stream as function of plasma pressure 03 p0474 A67-12921
Charged particle motions calculated in model of earth magnetosphere including magnetic and electric field 03 p0410 A67-12953
Interchange of field lines between closed region of magnetosphere and open tail, explaining features of auroral breakup and geomagnetic bays 03 p0410 A67-12955
Solar wind-magnetosphere system simulation, testing hypothesis that observed convective pattern is established by earth rotation 03 p0506 A67-12959
Spatial distribution of energetic electrons in geomagnetic tail by analyzing counting rates from solid state detector on IMP I satellite 04 p0692 A67-14953
Vector potential of magnetic field of any axisymmetric electric current distribution used to compute field of two model magnetospheric ring currents 04 p0617 A67-15535
Geomagnetic and auroral storms provide information on interaction of solar plasma flows and magnetosphere 04 p0618 A67-15688
Nighttime magnetospheric auroral VLF hiss generation by suprathermal particle associated with coherent electron plasma radio emission 04 p0618 A67-15686
Fluxgate magnetometer for OGO-E spacecraft in observing MHD waves and magnetic field structures in space 04 p0626 A67-15724
Primary cosmic radiation in interplanetary space, lunar surface albedo and soft particle fluxes in magnetosphere measured by Luna X orbiter 05 p0875 A67-16053
Plasma observations in tail of terrestrial magnetosphere and circumlunar space by Luna X orbiter, using charged particle traps 05 p0875 A67-16054
Alfvén velocity distribution in magnetosphere to understand nature of geomagnetic micropulsation 05 p0795 A67-16062
Magnetic field observations by rockets and satellites 05 p0798 A67-16870
Solar corpuscular streams effect on magnetospheric loop and on earth rotational velocity 05 p0801 A67-17135
Micropulsation dynamic spectra showing nosed tones instead of usual tones explained by helium ion content increase in outer

magnetosphere 05 p0803 A67-17406
Radial temperature profile of magnetospheric plasma near equatorial plane observed by IMP 06 p0996 A67-18432
satellites
Planet Mercury magnetospheric scattering of solar-flare protons to earth, obtaining deflection angle [AIAA PAPER 87-150] 06 p1088 A67-18505
Collisionless damping of magnetospheric MHD waves 07 p1172 A67-19541
Small two-dimensional oscillations in XY plane for isothermal magnetosphere in uniform gravitational field, postulating Boltzmann equilibrium density 07 p1173 A67-19699
Corpuscular intrusions into earth magnetosphere involving entire auroral zone and occurring only on night side 07 p1174 A67-19713
Solar wind magnetic field as medium for plasma-magnetosphere interaction 07 p1243 A67-19803
Solar wind parameter variation, magnetosphere flux interaction and dependence of geomagnetic storm on magnetospheric conditions and geomagnetic field increase 07 p1243 A67-19804
Radio wave emission due to shock wave propagation in magnetospheric boundary and electromagnetic scattering in plasma wave field 07 p1243 A67-19808
Solar corpuscular stream magnetic field effect on change in orientation of geomagnetic field related to change in stream geoeffectiveness 07 p1243 A67-19827
Plasma sheet with enhanced energy density stretching across magnetotail as evidenced by Vela-IIB satellite observations 07 p1244 A67-19921
Magnetospheric distortion during geomagnetic storm on September 30, 1961, examining Explorer XII satellite evidence on ring currents 07 p1180 A67-19924
Electron energy spectra analyzed in earth magnetosphere using OGO 3, noting relation to radial distance 07 p1244 A67-19926
MHD wave theory for slow processes in ionosphere and magnetosphere 07 p1181 A67-19933
Magnetosheath field, geomagnetic activity index, magnetopause stability and interplanetary magnetic field influence on magnetospheric phenomena 07 p1182 A67-19953
Kinetic theory-plasma dynamics theory calculations of magnetospheric solar wind proton velocity distribution as function of particle speed 08 p1377 A67-21315
Quasi-trapped whistler mode propagation and generation by trapped electrons in magnetosphere, noting refraction index and wave reflection 08 p1327 A67-21462
Explorer XXXIII satellite magnetometric measurements of geomagnetic tail at distances beyond lunar orbit 08 p1402 A67-21468
Adiabatic invariant analysis of charged particle motion in model magnetosphere 08 p1378 A67-21474
Field aligned currents in magnetosphere as explanation of geomagnetic fluctuation localization to region smaller than applicable hydromagnetic wavelength 08 p1402 A67-21476
Tabulated altitudes, periods and velocities for Martian satellites in circular parking orbits 09 p1564 A67-21716
Polar auroras, considering types resulting from MHD wave heating of upper atmosphere, low energy particle penetration of atmosphere, etc 09 p1491 A67-21892
Field buildup during sudden commencement of magnetic storms in magnetosphere determined from MHD wave and solar wind pressure measurements 10 p1630 A67-22777
Cosmic ray neutron component intensity during magnetic perturbations, considering effect of magnetospheric deformation 10 p1699 A67-22781
Geomagnetic micropulsation excitation by solar wind flow around magnetosphere, noting surface wave propagation 10 p1699 A67-22797
Energy production sources in inner magnetospheric plasma near equatorial plane 10 p1634 A67-23058
Variations in position of mirror points of high energy electrons determined from Cosmos V satellite data 10 p1647 A67-23281

Diurnal variation of difference between dipole and measured field for quiet magnetosphere from Elektron satellite data 10 p1649 A67-23296
Two-dimensional model of magnetosphere to find equilibrium boundary between rarefied plasma and magnetic field of two-dimensional dipole 10 p1649 A67-23297
FR-I satellite data on VLF propagation in lower magnetosphere 10 p1649 A67-23301
First and second adiabatic invariants of charged particle motion in calculating trajectory in combined electric-magnetic field 10 p1651 A67-23395
Cosmic ray and space research through direct measurement of particles, radiation, magnetosphere, etc 11 p1856 A67-24105
Mechanical and electrical modes of energy transfer occurring in free and forced oscillations in earth magnetosphere 12 p2000 A67-25107
Charged particle motion in magnetosphere under sudden magnetic pulse, compiling Fokker-Planck equation for particle distribution function 12 p1992 A67-25118
Magnetosphere phenomena investigated via atmosphere model to explain planetary nebulas and eruptive solar prominences 12 p1992 A67-25119
Fast variations of electromagnetic field measured by satellites electron I and II used as indication of state of radiation belts and magnetosphere of earth fast variations of electromagnetic field measured 12 p1994 A67-25537
Charged particle motion and penetration of magnetosphere in proximity of neutral point as result of solar wind-geomagnetic field interaction 12 p1975 A67-25643
Charged particle motion in field of magnetic dipole situated in external magnetic field /magnetospheric G region/, using Stoermer method 12 p1994 A67-25644
IMP-I earth satellite magnetic field measurement experimental results including solar wind flow effects 12 p1936 A67-25802
Earth magnetosphere at distances 7 to 11.7 earth radii obtained by Elektron satellites, noting differences between measured and calculated field vector 12 p1936 A67-25803
Inflation of magnetosphere near 8 earth radii in Southern Hemisphere using Explorer XIV satellite 12 p1936 A67-25805
Low energy particles detected close to equatorial plane of magnetosphere by satellites Elektron and Cosmos 12 p1997 A67-25811
Magnetic field variations in magnetosphere at distances of 3 to 6 earth radii attributed to distribution of trapped radiation 12 p1997 A67-25814
Interplanetary medium including solar wind, geomagnetosphere and observation instruments 12 p2009 A67-26173
Magnetospheres of self-gravitating bodies with reference to radio sources and cosmic ray acceleration 12 p1999 A67-26251
Earth bow plasma shock wave model with ion wave instabilities as principal shock structure [SR-2] 13 p2107 A67-26301
OGO 3 observation of low energy protons and electrons in earth magnetosphere, noting narrow peak of relatively high low-energy particle intensities 13 p2190 A67-26312
Solar wind bulk velocity studied via Vela 3A bow shock crossings, noting velocity decrease when entering magnetosheath 13 p2190 A67-26320
Transient variations in magnetospheric boundary position 13 p2109 A67-26328
Magnetospheric regions of amplification of VLF emissions and micropulsations 13 p2115 A67-26858
Magnetosphere rotation problem in presence of solar wind analyzed for auroral particle acceleration, noting perturbing field of induced electric current 14 p2307 A67-27917
Nondipole region of geomagnetic field at magnetosphere boundary and effect on boundary position on daylight side 14 p2308 A67-27931
Earth bow shock observations with Explorer XII satellite magnetometer 14 p2383 A67-28047
IMP II satellite measurements of magnetic fields in interplanetary space by onboard monoaxial fluxgate magnetometers 14 p2310 A67-28052
VLF noise emissions originating in

ionosphere and magnetosphere with reference to ground-based, rocket and satellite observations 14 p2265 A67-28414

Magnetosphere, turbulent transition region and shock wave characteristics and dimensions examined with regard to possible active or passive interaction with moon 14 p2388 A67-28619

Simulation of magnetospheric effects for possible application to ionospheric probes 14 p2294 A67-29035

Plasma wind tunnel facility for producing steady flow high conductivity collisionless plasma simulating solar wind interaction with magnetosphere 14 p2294 A67-29036

Electrodynamic forces and torques on charged bodies moving through rarefied and partially ionized earth magnetosphere and upper atmosphere 14 p2362 A67-29039

Geomagnetic pulsations and auroral activity, using magnetosphere simplified model 15 p2474 A67-29505

Dayside distortion of geomagnetic field by solar wind beyond 3.5 earth radii measured and compared with three magnetosphere models 15 p2475 A67-29612

Blast wave driven by solar flare ejecting plasma cloud proposed as origin of energy density increase causing sudden commencement of magnetic storm 15 p2476 A67-29625

Upper atmosphere photoelectric processes contributing to low energy electron content of magnetosphere 16 p2664 A67-30973

Asymmetric proton injection into magnetosphere using Vlasov equation, with solution in terms of electric potential 16 p2668 A67-31403

Magnetospheric tail bursts of energetic electrons identified with auroral zone radiowave absorption 16 p2666 A67-31410

Relative, world-wide magnetospheric electron precipitation into lower, denser atmosphere determined, using conjugate point magnetospheric-ionospheric circuit model 16 p2667 A67-31510

Integral intensity of charged particles diffusing through drift shells in earth magnetosphere with specific example for protons 16 p2740 A67-31616

Low energy protons emitted by solar flare satellite observed inside and outside of magnetosphere, noting immediate access to polar caps 16 p2740 A67-31626

Magnetic field measurement with Lunik x near lunar orbit noting magnitude, time behavior and existence of terrestrial magnetic tail 16 p2755 A67-31888

Plasma concentration diagnostics by hydromagnetic probing method, determining concentration profile from latitude dependence of torsional vibrations 18 p2668 A67-31890

Diurnal characteristics of geomagnetic micropulsations noting period, amplitude, continuity, time of occurrence, etc, proving existence of hydromagnetic waves generated at magnetosphere 17 p2841 A67-32212

Electrical field distribution during injection of charged particles into two-dimensional model of magnetosphere 17 p2841 A67-32244

Charged particles with Alfvén velocities distribution in magnetosphere analyzed based on cold plasma density, emphasizing data of OGO A 17 p2899 A67-32256

F region and magnetosphere data obtained by incoherent-backscatter radar technique, studying ion and electron temperatures relationship to height, electron density profiles, etc 17 p2843 A67-32389

Attenuation of natural hydromagnetic waves /Pc1/ in ionosphere, noting amplitude reduction and particle distribution in magnetosphere 17 p2843 A67-32536

Magnetosphere and auroral phenomena including Van Allen radiation zones, satellite telemetry, solar wind fluctuations and cyclotron resonance phenomenon 17 p2844 A67-32664

Shock wave generation of electromagnetic radiation at magnetospheric boundary, discussing plasma oscillation excitation, plasma wave scattering, etc 17 p2846 A67-32935

Rapid earth electromagnetic field variations used for plasma concentration and magnetosphere radius determination 17 p2846 A67-32937

High altitude plasma-concentration diagnostics from magnetospheric oscillation

spectra 17 p2846 A67-32940

Distribution of auroras during magnetically quiet and disturbed periods related to magnetosphere shape 17 p2849 A67-32965

Model for distribution of thermal plasma in magnetosphere of Jupiter under assumption of corotation with planet 17 p2951 A67-33196

Whistler method detection of magnetospheric electric field associated with polar substorm 17 p2851 A67-33197

Fluid flow around magnetosphere boundary analyzed, noting geomagnetic field effect on hot plasma 17 p2853 A67-33252

Auroral oval between outer boundary of trapping region and ionosphere and dynamical and atomic interactions between magnetospheric plasma and neutral atmosphere 18 p3035 A67-33597

Static electric fields produced in magnetosphere and effects such as motion of visual and radio aurora and currents in ionosphere 18 p3035 A67-33600

Auroral and polar magnetic substorms related to magnetic field lines reconnection in magnetosphere tail 18 p3117 A67-33815

Ionospheric and magnetospheric neutral and charged particles temperature vertical distribution, noting effects producing variations 18 p3040 A67-34033

OGO-A satellite observations of hydromagnetic whistlers /pearls/ nature, showing linkage to magnetosphere 18 p3042 A67-34390

Alfvén and magnetosonic wave generation and propagation in magnetosphere, detailing azimuth number approaching infinity 18 p3042 A67-34391

Flux, energy distribution and density of ions and electrons in magnetosphere plasma during solar activity period determined by OGO-C electrostatic probes 19 p3217 A67-35200

Explorer 33 plasma measurements, discussing plasma flow parameter calculation methods, including plasma models and magnetospheric shape and size 19 p3319 A67-35245

Space research in West Germany noting ionospheric physics, magnetosphere and solar and cosmic radiation 19 p3321 A67-35293

Polish space research noting satellite position observations, geodetic computations, meteorology, cosmic physics, magnetosphere, medicine and biology 19 p3321 A67-35296

Magnetospheric boundary and standing shock wave for earth scaled down to apply to Mars 19 p3324 A67-35442

Geomagnetic field boundary observations by Explorer XII 19 p3222 A67-35453

Synoptical and monitoring projects for solar activity, interplanetary space, magnetosphere, ionosphere, aeronomy, etc 19 p3223 A67-35475

Earth radiation belts nature and plasma activity in magnetosphere 19 p3315 A67-35485

Geomagnetic micropulsation properties variation over last solar cycle and causes 19 p3325 A67-35486

Elliptic geocentric satellite orbit for measurements of magnetosphere-nearby space region, analyzing orbital lifetimes and perturbations 19 p3226 A67-36005

[AIAA PAPER 67-616] 19 p3226 A67-36005

Abnormally early eastward auroral motion appearance in evening and associated magnetospheric plasma shell motion 20 p3426 A67-36294

Instantaneous distribution patterns for aurora on polar region, discussing geoelectric field role in internal structure of magnetosphere 20 p3430 A67-36906

Diurnal variation investigated by rocket, discussing ionospheric electric currents and magnetosphere-ionosphere electric field 20 p3431 A67-36908

Irregular pulsations of diminishing periods /IPDP/, discussing cause and low energy electron flux variations 20 p3431 A67-37097

Geomagnetic tail at 1000 earth radii, noting possibility of magnetic force lines connected to earth and tail geometry 20 p3433 A67-37402

Low energy proton flux increases in outer radiation belt during quiet magnetic activity and correlation with magnetic bay appearances 20 p3519 A67-37408

Magnetosheath observations by Vela 3 at 18 earth radii, discussing substructure, shock crossings and pulsations 20 p3433 A67-37410

Pi micropulsation subtypes, one related to

charged particles impulsive bursts from magnetospheric tail and another related to auroral electrojet 20 p3433 A67-37414

Primary cosmic radiation in interplanetary space, lunar surface albedo and soft particle fluxes in magnetosphere measured by Luna X orbiter 21 p3697 A67-37840

Plasma observations in tail of terrestrial magnetosphere and circumlunar space by Luna X orbiter, using charged particle traps 21 p3697 A67-37841

Alfvén velocity distributions in magnetosphere used to understand nature of geomagnetic micropulsation 21 p3616 A67-37849

Solar corpuscular streams effect on magnetospheric loop and on earth rotational velocity 21 p3619 A67-38478

Micropulsation spectra /sonagrams/ indicating magnetosphere plasma resonances with recognizable modal pattern 21 p3619 A67-38513

ULF radiation in polar auroral zone explained via plasma beam instability, assessing perturbation of particle fluxes in magnetosphere 21 p3621 A67-39016

Smith gyrofrequency model for determination of vertical electron concentration distribution in magnetosphere, using whistling atmospherics data 21 p3621 A67-39022

Alfvén standing wave formation due to interaction of magnetosphere with geomagnetic pulsation 21 p3621 A67-39023

Irregular pulsations of decreasing period /IPDP/ events detected in magnetosphere, discussing strong correlation with magnetic index 22 p3789 A67-39497

Solar-terrestrial physics and magnetosphere Conference, Belgrade, August-September 1966 22 p3882 A67-39667

Fluid model for magnetosphere shape, calculating flow velocity, density and temperature between shock and boundary 22 p3883 A67-39671

Magnetospheric energetic charged particles interrelations, discussing electron and proton energy spectra, particle population domains, trapped radiation and solar wind kinetic energy 22 p3870 A67-39673

Ionospheric plasma electron density profile and plasma resonance effects at base of magnetosphere measured by rocketborne gyro-plasma probe 22 p3793 A67-40043

Magnetospheric free boundary representation synthesis problem, discussing relaxation solution, dipole moment and stream direction 22 p3854 A67-40347

Magnetospheric discrete VLF emissions, discussing gyroresonance extension, resonant electron and emission frequency 23 p3995 A67-40802

Field buildup during sudden commencement of magnetic storms in magnetosphere determined from MHD wave and solar wind pressure measurements 24 p4149 A67-42113

Cosmic ray neutron component intensity during magnetic perturbations, considering effect of magnetospheric deformation 24 p4209 A67-42117

Geomagnetic micropulsation excitation by solar wind flow around magnetosphere, noting surface wave propagation 24 p4209 A67-42133

MAGNETOSPHERIC ELECTRON DENSITY

SA IONOSPHERIC ELECTRON DENSITY

Lunar X-rays excited by electrons of magnetospheric tail provide information on chemical composition of moon 01 p0144 A67-10563

Luna X shielded gas-discharge counter data on soft corpuscular radiation, noting solar contribution to magnetospheric tail 01 p0145 A67-10907

Thermal plasma measurements in magnetosphere for electron and ion density and thermal profiles, noting Maxwell energy distribution and charge neutrality 10 p1649 A67-23295

Laminar composition structure and periodicity of variations with time in outer radiation belt investigated by solar radiation satellites 10 p1701 A67-23298

FR-1 satellite data on VLF propagation in lower magnetosphere 10 p1649 A67-23301

Magnetospheric model of Jupiter from numerical calculation of maximum number density of plasma 12 p2000 A67-25206

Magnetospheric electron density distribution determined from analytical

- calculations, using whistler travel-time integral 13 p2111 A67-26576
- Low latitude nose whistlers, estimating path latitude and electron density distribution in intermediate region of magnetosphere 14 p2306 A67-27882
- F region and magnetosphere observation by incoherent backscatter radar technique 14 p2265 A67-28410
- Magnetosphere-ionosphere coupling mechanisms at middle and low latitudes 14 p2312 A67-28411
- F-region electron-density perturbations transmitted to magnetically conjugate region, noting electrostatic coupling mechanism 16 p2667 A67-31509
- Electron density measurement in ionosphere-magnetosphere transition region using rocketborne gyroplasma swept frequency probe, discussing electron density profile and plasma medium 19 p3229 A67-35201
- Photoelectric contribution to magnetospheric electron density on basis of pitch redistribution of collision component 20 p3425 A67-36283
- Magnetospheric features, describing magnetic field distribution, electron and proton density, plasma instabilities, bow shock and solar wind 20 p3430 A67-36903
- MAGNETOSPHERIC INSTABILITY**
- Formation of magnetospheric plasma knee by combined action of magnetospheric convection and plasma escape from tail 04 p0693 A67-14964
- Fluxgate magnetometer onboard applications technology satellite for measuring MHD wave propagation within magnetosphere 04 p0628 A67-15723
- Conjugate ducting observation via fixed frequency topside-sounder satellite, estimating electron concentration difference 06 p0997 A67-18699
- Finite-beta resistive instabilities of magnetospheric tails analyzed by applying hydromagnetic equations 07 p1244 A67-19923
- Hydromagnetic shock wave intensity decrease in nonuniform magnetosphere treated by Chisnell-Whitham method 10 p1634 A67-23053
- Collective effects and centrifugal instability from charged solar wind particle injected into earth magnetosphere near neutral point 12 p1991 A67-25109
- Long period hydromagnetic waves in magnetosphere and coupling to solar wind studied by Explorer XIV 12 p1937 A67-25812
- Statistics relating plasmopause position to three magnetic indices to clarify relationship between equatorial geocentric distance to plasmopause and worldwide magnetic activity level 15 p2477 A67-29627
- Frequency shifts on whistler mode signals from stabilized VLF transmitter from ionosphere and magnetosphere effects, noting electron density 16 p2631 A67-31856
- Magnetic variations relationship to magnetospheric perturbations, emphasizing particle participation near auroral zones 20 p3428 A67-36376
- Auroral breakup relation to ring current interchange instability, studying dispersion relation effects 20 p3431 A67-37096
- Micropulsation pattern changes during magnetospheric transition from quiet to excited state, discussing influence of earth and long period and pearl-type pulsations 22 p3883 A67-39674
- Magnetospheric open split tail topology noting stability of geometry in all solar wind and interplanetary medium 22 p3792 A67-39820
- MAGNETOSPHERIC ION DENSITY**
- SA IONOSPHERIC ION DENSITY**
- Charged particle traps installed in Luna X providing evidence for moon passing through tail of earth magnetosphere, noting effect of solar wind 01 p0145 A67-10908
- Whistler recordings on thermal plasma motions and ionization density near magnetospheric knee, noting whistler attenuation VLF noise, ion effects, electron temperature, etc 05 p0795 A67-16011
- Thermal plasma measurements in magnetosphere for electron and ion density and thermal profiles, noting Maxwell energy distribution and charge neutrality 10 p1649 A67-23295
- Solar wind properties studied using Vela electrostatic analyzers, noting velocity ranges, proton temperature and ion density 13 p2190 A67-26319
- Helium ion effects in micropulsation spectrograms of outer magnetosphere 13 p2108 A67-26326
- Radio whistlers occurrence relationship to solar and magnetic activities at various latitudes 14 p2265 A67-28413
- Magnetospheric ion density measurement possibility from association of pulsating radio auroral echoes with sudden geomagnetic field fluctuations 14 p2313 A67-28574
- MAGNETOSPHERIC PROTON DENSITY**
- Rocket measurements of 1/2 to 4 mev trapped protons in near-equatorial magnetosphere [AFCL-66-865] 03 p0505 A67-12835
- Laminar composition structure and periodicity of variations with time in outer radiation belt investigated by solar radiation satellites 10 p1701 A67-23298
- Relation between electron and proton distributions and existence of electric fields in magnetosphere 12 p1936 A67-25808
- Low energy proton and electron outer radiation belt satellite Cosmos 41 indicate capture and acceleration mechanism 12 p1997 A67-25810
- Helium ion effects in micropulsation spectrograms of outer magnetosphere 13 p2108 A67-26326
- Solar proton flux measurement by balloon on July 7, 1966 in northern Scandinavia, with differential proton flux calculated for several energies 19 p3312 A67-35175
- Proton velocity distribution in solar wind flow around magnetosphere 20 p3518 A67-36653
- Energetic proton flux measurements in magnetosphere using sounding rocket, discussing radial diffusion 20 p3518 A67-36998
- Dispersion characteristics of geomagnetic micropulsation pearls, obtaining magnetospheric proton densities 21 p3617 A67-38127
- Temporal and spatial low energy solar proton intensity variations indicating interplanetary medium changes effects on magnetospheric configuration 22 p3873 A67-39813
- MAGNETOSTATIC AMPLIFIER**
- Ferromagnetic magnetostatic amplifier using various types of oscillations for pumping and signal amplification 04 p0583 A67-15168
- Ferromagnetic magnetostatic amplifier using various types of oscillations for pumping and signal amplification 15 p2443 A67-29354
- Transient growth of magnetostatic modes in yttrium garnet subject to pulsed longitudinal pumping 16 p2732 A67-31704
- MAGNETOSTATIC FIELD**
- Microwave echoes in axially magnetized yttrium iron garnet cylinders following application of two pulses, with second twice frequency of first 02 p0297 A67-11874
- Paramagnetic current formation due to volume resonator microwave field interaction with dense plasma subject to RF pressure and EPR in static magnetic field 07 p1228 A67-19512
- Nonlinear PDE for magnetostatic field with variable permeability in discontinuous medium solved with digital computer 07 p1132 A67-19795
- Radiation characteristics of current sources perpendicular to magnetostatic field for cylindrical column of free space surrounded by loss-free magnetotonic medium 08 p1357 A67-20715
- Nonlinear thermomagnetic wave theory and amplification in case of plasma instability 09 p1545 A67-22072
- Ion acceleration by drift resonance caused by crossed magnetostatic and space charge electrostatic fields 11 p1841 A67-24768
- Moment method treatment of collisionless plasma equilibria in confining magnetostatic fields, using Vlasov equation to determine distribution function of particles 14 p2360 A67-28554
- Asymptotic solution of oblique waves in inhomogeneous vertically magnetized plasma 14 p2361 A67-28922
- Electric field due to double grid excitation in circular waveguide partially filled with warm homogeneous plasma in infinite magnetostatic fields 19 p3290 A67-35379
- Stationary state of collisionless plasma in magnetostatic and potential fields, deriving distribution functions and concentration formulas 22 p3842 A67-39243
- Electrostatic and magnetostatic potentials for slender bodies of revolution in axially symmetric external fields 23 p4028 A67-40753
- MAGNETOSTRICTION**
- SA ELECTROSTRICTION**
- Oscillatory magnetostriction in GaSb, noting stress effect on energy bands 02 p0296 A67-11819
- Ferrite materials for resonators of magnetostrictive transducers and filters used in transmission and reception of ultrasonic waves 03 p0420 A67-13548
- Piezomagnetic coefficients in magnetostrictive equations, permeability extrema and elastic moduli of Ni-Co-Mn ferrites 05 p0863 A67-16703
- Structural and technological problems connected with miniature electromechanical filters 10 p1609 A67-22876
- Low noise SiFe sheet development and application, considering effects on magnetic properties 13 p2178 A67-27139
- Magnetostriction of trivalent Yb and Ce ions in YIG, measuring temperature dependence, noting exchange and interaction of crystal field splitting for Yb 22 p3855 A67-39363
- MAGNETRON**
- Text on high power electronics including cathodic losses in magnetrons, electrodynamic theory of grids, high frequency measurement, secondary electron emission and electromagnetic oscillations 03 p0379 A67-13301
- Space charge fields of planar magnetron calculated taking account of effect of conducting planes of cathode and anode 03 p0385 A67-13954
- Two-flow equations for stationary relativistic electron cloud in self-consistent crossed fields 05 p0774 A67-16907
- Radar phase locking technique applied to magnetron radar, measuring transmitted pulse phase with respect to stalo running at magnetron frequency 05 p0780 A67-17521
- Effect of degree of coupling between resonator system and load on generation zones and regenerative amplification of pulsed magnetron, noting characteristics 08 p1305 A67-21271
- Apparatus producing voltage pulses in X-band magnetrons operating on pulse lengths of tens of nanoseconds 09 p1479 A67-22262
- Two-flow equations for stationary relativistic electron cloud in self-consistent crossed fields 16 p2636 A67-30884
- Gas ionization and plasma heating by high power microwaves using X-band and S-band frequency magnetrons 19 p3276 A67-35115
- Current-voltage characteristics of low pressure discharge in magnetron, giving integral equations and current stability 19 p3277 A67-35120
- Structure of ion and electron currents axial emission from cathode measured as function of magnetic field intensity 19 p3277 A67-35121
- Sinusoidal frequency oscillations in DC magnetron plasmas discharge, determining magnetic field, anode current and voltage and gas pressure dependence 19 p3277 A67-35124
- Magnetron cut-off characteristics modification via altering electron cloud resonant properties by injecting positive ions in interaction space 20 p3489 A67-37105
- Injection locked pulsed magnetron in coherent echo detection system studied by observing echo pulses from acoustic delay medium 20 p3401 A67-37221
- MAGNUS EFFECT**
- Motion of flux lines in type II superconductors at zero temperature, discussing friction, Magnus and other forces 01 p0133 A67-10750
- Nonlinear motion theory for axisymmetric sounding missiles or rockets with Magnus moments, showing application to near pitch-roll resonance 08 p1407 A67-20515
- Yaw force /Magnus/ of spinning projectile at angle of attack measured, using balance device in wind tunnel [AIAA PAPER 66-753] 14 p2292 A67-28132
- Aerodynamic lift, studying production of cosmic energy level supporting mechanism, explaining electromagnetic Magnus effect for gravity-free device 20 p3484 A67-36821
- Dynamic flight stability characteristics of

5 inch projectile with nonlinear magnus moment, noting Mach number, wind tunnel data, etc 21 p3563 A67-37805

MAIN SEQUENCE STAR

Computing velocities and convective energy transport in stars of different spectral types and luminosities 05 p0899 A67-17071

Evolution of low mass Population I stars from main sequence to red giant branch in Hertzsprung-Russell diagram, through energy generation phases of p-p chain reactions /dominating over C-N cycle reactions/ and hydrogen burning 09 p1566 A67-22225

Neutrinos in stellar evolution and cosmological processes, discussing production processes 14 p2383 A67-27969

Effective temperature for late type stars with or without water vapor opacity calculated for several masses, determining convective energy transport efficiency 24 p4224 A67-41818

MAINTAINABILITY

Rules for maximizing component accessibility when designing electronic equipment 01 p0078 A67-10166

System effectiveness critical activities covering reliability, maintainability, quality, design guides, etc, for aerospace industry 01 p0170 A67-11333

Maintainability diagnosis techniques and fields of application to electronic equipment, examining entropic methods, decreasing probability methods and linear analysis techniques 01 p0041 A67-11342

Reliability and maintainability demonstration at Rome Air Development Center, discussing test methods 01 p0084 A67-11360

Maintainability, reliability and operational flexibility of manned orbital space station [AIAA PAPER 66-933] 02 p0331 A67-12252

Integration of reliability, maintainability and other engineering disciplines, discussing objectives of program management [AIAA PAPER 66-859] 02 p0343 A67-12260

Analytic method for measurement of value of increased reliability or maintainability, using maintenance float as criterion [AIAA PAPER 65-734] 03 p0426 A67-12917

IEEE Automatic Support Systems Symposium for Advanced Maintainability, Clayton, Missouri, November 1966 03 p0397 A67-14201

Maintainability efforts in support of Acceptance Checkout Equipment/Apollo-Spacecraft /ACE-S/C/ program 03 p0398 A67-14205

Mathematical models properties analyzed for system reliability and maintainability, namely mission availability, discussing relationship to failure and action rate and time constraint 05 p0813 A67-17252

Systematic approach using weight factor for apportioning mean corrective times of equipment based upon maintainability, usage and reliability data 08 p1315 A67-20670

Lockheed C-5 quantitative maintainability program and application to air vehicle utilization and cost effectiveness 11 p1745 A67-24939

Interconnecting techniques for modules contained by printed circuit boards, noting usage of pin sockets and effect on maintainability and reliability 12 p1910 A67-25266

Engine design to reduce overall cost and improve power plant component for flight schedule reliability [SAE PAPER 670330] 12 p1990 A67-25872

Probability and prediction techniques related to maintainability discussed with application to early design, time constraints and maintenance goals 16 p2681 A67-30439

Revision of military terminology for weapon systems considering human factors, safety and maintainability and reliability relations 16 p2780 A67-30440

Maintainability program task requirements covered by Military Standard 470 16 p2781 A67-30441

Maintainability prediction procedures applicable to systems and equipment as described in DOD handbook 16 p2781 A67-30442

Design disclosure format /DDF/ linking program managers, review teams and contractors 16 p2781 A67-30443

Immediate, delayed and cyclic maintenance policies for phased array radar systems 16 p2634 A67-30446

Maintainability system operating parallel with cruise-mode spacecraft attitude-control system, noting application to Ranger III spacecraft 16 p2763 A67-31646

Reliability and maintainability Conference, Cocoa Beach, Florida, July 1967, Volume 6 18 p3055 A67-34648

Nature and magnitude of differences between intrinsic and operational reliability and maintainability characteristics, suggesting reconciliation approach 18 p3057 A67-34661

Maintainability technology and controls developed during F-111 design 18 p2986 A67-34663

Maintainability demonstration results and experience, describing field and plant testing procedures and controls 18 p3007 A67-34669

Development and application of Monte Carlo logistic simulation model for measuring system availability dependence on reliability, maintainability and logistic support 18 p3021 A67-34674

Maintainability risk analysis using analytical model with gamma distribution 18 p3021 A67-34685

Manned mission reliability and maintainability requirements in future systems 18 p2995 A67-34686

Maintainability and reliability cost effectiveness program /MARCEP/ applied to logic and computer limitation problems 18 p2995 A67-34689

Characteristics of immediate, delayed and cyclic maintenance of phased planar array radar systems, considering outage availability effects 18 p3005 A67-34693

Ground system design approach integrating reliability and maintainability with performance requirements, using Saturn V simulation as example 18 p3139 A67-34694

Reliability and maintainability case histories 18 p3005 A67-34696

Maintainability demonstration methods and statistical techniques for test data reduction 18 p3163 A67-34700

Operational computerized system for automatic surveillance of reliability and maintainability of spacecraft hardware 18 p3021 A67-34701

Maintenance time reduction for multimode airborne weapons through built-in test equipment and integrated program 21 p3601 A67-38947

Maintainability problems analyzed noting Apollo/ Saturn program 23 p4070 A67-40581

Life cycle cost covering accessibility, automated fault isolation, corrosion control, maintenance, etc 23 p4085 A67-40586

MAINTENANCE

SA AIRCRAFT MAINTENANCE

SA SPACE MAINTENANCE

In-service reliability analysis in reducing maintenance costs and spares requirements 01 p0083 A67-11352

Queueing theory applied to phased array radar maintenance problems, specifically replacement and repair of transmitter and/or receiver modules 08 p1292 A67-20668

Maintenance replication rate and spares provisioning measurement using Laplace transform 16 p2634 A67-30444

Impact of microelectronics on utilization and training of maintenance personnel 18 p2994 A67-34342

Development and maintenance of equipment containing integrated circuits, discussing processing, fault isolation and human error 18 p3016 A67-34670

Maintenance and support factors effects on systems availability described by mathematical models, giving applications in tradeoff studies 18 p3163 A67-34695

Nuclear methods and techniques applied to maintenance and checkout of complex electronic and electromechanical systems, discussing radiation-matter interaction, etc 20 p3449 A67-36981

Operational readiness of redundant system, deriving system readiness factor formula for operating and idle redundancy 20 p3451 A67-37158

Complex technical systems servicing, considering operation cost as optimization criterion 22 p3812 A67-39746

MAJORITY CARRIER

Gamma radiation and fast neutron effects on dark resistance, photoconductivity, majority carrier mobility, recombination

kinetics, etc, in CdS single crystal 01 p0128 A67-10086

Majority carrier current flow in metal-semiconductor barriers according to theory incorporating Schottky diffusion theory and Bethe thermionic emission theory 03 p0494 A67-13476

Current carrier behavior during field and diffusion injection of electron hole plasma into semiconductor 06 p1049 A67-17865

Carrier-carrier scattering influence on Hall effect and on minority-majority carrier mobility in graphite 06 p1063 A67-18938

Nonequilibrium charge carrier lifetime in indium antimonide single crystals with Ge and Au impurities 08 p1367 A67-20414

Temperature dependence of small signal AC field effect kinetics in silicon within 170-300 K, considering majority carriers and one energy level theory 13 p2176 A67-26708

Current-voltage characteristics of clamped metal/p-silicon diodes 18 p3009 A67-33475

Current-voltage characteristic of metal semiconductor point contact, taking into account rectifying effect of junction gap and majority and minority current carrier 18 p3097 A67-33476

Polarity reversal with DC bias in hot-carrier microwave diode 19 p3198 A67-36038

Majority and minority carrier lifetimes in n-type GaAs single crystals, measuring injection level dependence 20 p3512 A67-37436

MAMMAL

SA CAT

SA DOG

SA GUINEA PIG

SA MAN

SA MONKEY

SA RABBIT

SA RAT

Interspecies communication involving human and mammalian brain as computer with programs and metaprograms [AAS PAPER 66-77] 07 p1135 A67-20000

Mammalian porcine thyrocalcitonin extract effect on concentrations of serum calcium and phosphate in catfish 20 p3372 A67-37277

MAN

Biological clocks and cycles in man, lower animals and plants, discussing circadian rhythms 13 p2058 A67-26607

MAN-MACHINE SYSTEM

SA HUMAN ENGINEERING

SA HUMAN FACTOR

Reactive display system for optimum man/computer communication with time-sharing capabilities 01 p0029 A67-10670

Digitally-driven display system for graphic man-computer communication in aerospace industry 01 p0029 A67-10671

Interactions and relationships between man and machine in flight guidance 02 p0185 A67-11551

Monograph on system philosophy of automatic learning systems in application to autopilots, discussing man-aircraft system cybernetics, human behavior, environmental effects, etc 02 p0186 A67-12084

Operation and control of satellite equipment, discussing automatic, semiautomatic, human and telefactor /man-extension system/ methods [AIAA PAPER 66-918] 02 p0204 A67-12250

Water-immersion weightlessness simulation to determine astronaut EVA capabilities and man-machine interfaces [AIAA PAPER 66-903] 02 p0187 A67-12270

Performance requirements of dynamic flight simulators and visual display systems in man-machine flight control problems 03 p0395 A67-13385

Shared memory computer display system provides test bed for man-machine interaction, noting hardware and software design concepts 03 p0375 A67-13633

IEEE Automatic Support Systems Symposium for Advanced Maintainability, Clayton, Missouri, November 1966 03 p0397 A67-14201

Man-machine interface and automatic test operations in Saturn S-IVB system 03 p0398 A67-14204

Anthropotechnique as scientific discipline, discussing environmental layout, adaptation of machine to man and limits of intelligent machine handling 04 p0562 A67-14539

Programmable display synthesizing system for man-machine communications research based on electronic animation technique 05 p0786 A67-16314

Large space environmental simulation chamber design problems arising due to man-rated feature 05 p0788 A67-16618

Medical, design and operational aspects of quality requirements for reliability of man-rated space environment simulation chambers 05 p0788 A67-16621

Mockup of manned hardware systems in industrial design, describing application to LRV and LEM development, crew compartment design for undersea craft /DSRV/, etc 05 p0757 A67-17378

Man-computer graphics for computer aided design 05 p0768 A67-17514

Applications of computer generated displays, technologies and systems design in man-machine interaction 05 p0769 A67-17520

Man-machine interaction in visual displays of computer output 07 p1148 A67-19658

Pilot-aircraft compatibility in landing approach 07 p1136 A67-19888

Manual control dynamics for single loop systems facilitating man-machine system design 07 p1162 A67-19907

Small helicopter flight test report, discussing testing procedures on 14 models of one-man rotorcraft [AIAA PAPER 67-264] 07 p1129 A67-20041

Man-machine simulations for Apollo navigation, guidance and control system [AIAA PAPER 67-242] 07 p1136 A67-20063

Critical tracking task for man-machine research related to operator effective delay time 07 p1136 A67-20171

Inclusive classified bibliography pertaining to modeling human operator as element in automatic control system 07 p1137 A67-20173

Integrated cockpit research in man-machine relationship in aircraft 08 p1350 A67-20666

Psychology and space flight 09 p1454 A67-22056

Measurement and control methods in aircraft-instrument-pilot loop, noting human limitations in possibilities of automation computer applications 09 p1457 A67-22459

Man-computer system for aerospace problems, discussing terminology, methods of organization, problem solution, numerical analysis, etc 11 p1755 A67-24246

On-line computation and man-computer interactive languages, discussing JOSS, MADCAP and Klerer-May systems 11 p1756 A67-24249

Man-Computer Graphics /MCG/ allows operator control through oscilloscope via light sensitive pen 11 p1756 A67-24251

Selection of space cabin atmospheres including pressure, fire and blast hazard, humidity and temperature control, etc 11 p1748 A67-24262

Man-rated space simulation facility, emphasizing checkout and qualification of systems 12 p1921 A67-25689

Mechanization effect on man-machine relationships in flight test engineering analysis 13 p2052 A67-26423

Telefactor system in control of space operations, describing master-slave manipulator servomechanism with TV network and electronic communication link 13 p2063 A67-27213

Man-machine compatibility in very low altitude flight determined by two-phase controlled field experiments on obstruction avoidance task 14 p2256 A67-27742

Space exploration by automatic, manned and remote-controlled space flight systems, noting applications, limitations, transmission power and distance effects 14 p2256 A67-28036

Neutral buoyancy /water immersion/ technique for simulated space crewman performance, noting psychophysiological, man-machine and anthropomorphic parameters affecting space station design 15 p2431 A67-29282

Water-immersion weightlessness simulation to determine astronaut EVA capabilities and man-machine interfaces [AIAA PAPER 66-903] 15 p2431 A67-29439

Surveyor guidance program for midcourse and terminal information, noting redundancy in design, decision making telecommunications, etc 15 p2514 A67-29599

Visual analysis console for automatic information handling systems providing rapid data display and operator communications with high speed digital computers 15 p2488 A67-29737

Human factors information utilization by

designers, noting test results on conceptual drawing of equipment configuration according to design specifications 15 p2431 A67-29897

Optimization of man-machine environmental interface problems in framework of large-scale and long-term space operations [AAS PAPER 67-80] 15 p2432 A67-29947

Human response model identification in manual control system applied to study of stability and performance of man-machine system 15 p2432 A67-30315

Graphic information acquisition, processing and analysis noting requirements, application of computer, etc 16 p2781 A67-30636

Manrating of space environment simulators, emphasizing integration of physical facility requirements and operation procedure to provide safety 17 p2807 A67-31960

Lunar pogo stick, discussing velocities, horizontal and vertical displacements and weight estimates of man-carrying vehicle 17 p2832 A67-32065

Computer graphics for surface generation, stressing Coons surfaces and parametric representation 17 p2820 A67-32783

Controllability methods on VTOL transporters, developing model of pilot dynamic reaction to aircraft 18 p2993 A67-33457

Systems engineering in computer-driven CRT displays for man-machine communication, emphasizing hardware-software tradeoffs and communication-transmission factors systems engineering in computer-driven CRT 18 p3005 A67-33499

Human factors and anthropotechnology in development of weapon systems 18 p2993 A67-33643

Control display linkages tested with human subjects for response time 18 p2993 A67-34338

Interactionist models of human performance in complex system or formal work organization, discussing multidimensional models 18 p2994 A67-34654

Human engineering research to aid system designers to optimize mans role as control element in space systems 18 p2995 A67-34687

Systems approach combining human experience and logic with computer technology to implement navigation management function 19 p3254 A67-35313

Program providing man-machine communication for electronic circuit analyses using time sharing computer 19 p3186 A67-35619

Programming system design for incremental data assimilation in open ended man-computer information systems 19 p3187 A67-35680

Man-machine graphical communication device for real time monitoring with automated checkout 20 p3446 A67-36589

Devices for information exchange between man and machine, emphasizing video display equipment 21 p3577 A67-38158

Man-machine design for Apollo spacecraft navigation, guidance and control systems 22 p3830 A67-39180

Anthropotechnical reliability establishing methods considering ability of man to assimilate amount of information in unit of time 22 p3754 A67-39280

All-weather landing systems for automatic and manual control, considering Category II and III operations 22 p3831 A67-39611

Pilot and automatic control function coordination in piloting and landing aircraft, discussing precision problems, safety and development of new processes 22 p3831 A67-39750

Evaluation and analysis of critical human performance for rating man-machine interface 22 p3755 A67-40154

Spacecraft flight control and computerized systems, discussing redundant systems, integrated circuits and simulation for man-machine interaction and lack of response 22 p3908 A67-40336

Feedback changes effects on reaction time in stopping chronometer 22 p3756 A67-40536

Computer applications in electronic circuits design, discussing optimal man/computer interface and data handling processes 24 p4126 A67-42477

Integrated thermoelectric SNAP-8 Rankine power system for manned lunar base missions, studying man-system interactions

effect on design criteria 24 p4185 A67-42544

Automatic flight management of future high performance aircraft [AIAA PAPER 67-847] 24 p4183 A67-42963

Human Error Research and Analysis Program /HERAP/ for man-machine system, investigating pilot error and performance and aircraft accident prevention [AIAA PAPER 67-848] 24 p4117 A67-42984

Aircraft fuselages, wings, fillets, ducts and other free form surfaces defined using man-machine graphical interaction with computer [AIAA PAPER 67-895] 24 p4126 A67-43004

Man-computer system for aircraft design and manufacture emphasizing graphic and analytical routines [AIAA PAPER 67-898] 24 p4127 A67-43007

Time factor in onboard checkout and in-flight maintenance of manned spacecraft, discussing mission events and man-machine interaction [AIAA PAPER 67-950] 24 p4245 A67-43034

MANAGEMENT

S PERSONNEL

S PROGRAM MANAGEMENT

S WEAPON SYSTEM MANAGEMENT

MANAGEMENT PLANNING

SA PRODUCT DEVELOPMENT

Optimum design safety for VTOL aircraft, noting noise and vibration elimination [AIAA PAPER 66-813] 01 p0008 A67-10031

Carrier Onboard Delivery aircraft, discussing cost effectiveness by reduced delivery time of critical spare parts [AIAA PAPER 66-790] 01 p0009 A67-10533

Aerospace ground equipment management problems solved by program ensuring proper recognition by contractor and customer management [SAE PAPER 660686] 01 p0169 A67-10590

Total systems management technique applied to ground equipment management in development and production of weapons system [SAE PAPER 660687] 01 p0169 A67-10591

Space support, discussing functions during planning phases, constraints, systems engineering approach and integration of subplans into unified scheme [SAE PAPER 660688] 01 p0049 A67-10592

Space and weapon system support facilities acquisition and management systemization by government and industry [SAE PAPER 660692] 01 p0050 A67-10621

Administrative considerations in systems effectiveness programs [SAE PAPER 660731] 01 p0170 A67-10631

Optimized distribution of personnel reduction in naval overhaul and repair activities with minimum reduction in readiness 01 p0016 A67-10932

Rolls-Royce use of computers in engineering, manufacturing and marketing operations 01 p0031 A67-11199

Reliability Symposium, San Francisco, January 1966 01 p0081 A67-11332

Findings, conclusions and recommendations of Weapon System Effectiveness Industry Advisory Committee /WSEIAC/, noting concept of cost effectiveness 01 p0170 A67-11334

Inaccurate estimate effect on national budgets when evaluating systems efficiency 01 p0170 A67-11349

British procurement procedures for military aircraft noting cost estimate, feasibility study, development contract and production stages 02 p0343 A67-12242

History of selected reliability and maintainability committees and interested government agencies [AIAA PAPER 66-856] 02 p0343 A67-12259

Capabilities of passenger aircraft for short-range operations, noting design and economic suitability [AIAA PAPER 66-945] 03 p0361 A67-14022

Software configuration management by engineering methods, considering application to automatic support equipment /ASE/ for Saturn S-IVB stage 03 p0538 A67-14221

British-French cooperation in aeronautics, discussing Concorde SST, variable geometry aircraft, Olympus 593 turbojet, etc 03 p0362 A67-14379

Configuration management, method for current and precise documentation which attempts to assure customer and builder that final hardware is what they agreed on 04 p0739 A67-14424

Advanced feedback system simulation technique for strategic planning in business,

noting manpower allocation 04 p0739 A67-14498

Group dynamics approach to resistance or counterpart of planning, conversion and management of automatic data processing systems design [ASME PAPER 66-WA/MBT-10] 04 p0740 A67-15334

Management control systems, incompatibility between risk and controls, relations between government and contractors and implementation procedures [ASME PAPER 66-WA/MGT-16] 04 p0740 A67-15335

Ancillary benefits of automated R and D resources allocation system used as aid to management of USAF laboratory include data retrieval and effective management planning [ASME PAPER 66-WA/MGT-18] 04 p0740 A67-15336

Management of development, design, contracting, construction, checkout and acquisition in ballistic missile program 05 p0929 A67-16620

ESRO II satellite project, describing systems and program management 05 p0905 A67-16728

Quality evaluation review technique /QERT/ for management facilitation of program planning and scheduling, noting time and cost estimation 05 p0930 A67-17246

Support of NASA quality requirements by Defense Contract Administration Services Regions 05 p0930 A67-17262

Launch vehicle parameter design for optimal support of communications satellites 06 p1093 A67-17678

Economical hanging of commercial aircraft as implemented by Spanish airfleet 06 p0947 A67-18028

Educational problems including costs, teacher training, management, government support, etc 06 p1120 A67-19042

Organization of U.S. geodetic satellite program, discussing responsibilities for various phases of operation 07 p1269 A67-19758

European satellite triangulation network, discussing scientific, technical and organizational aspects 07 p1176 A67-19761

Static firing ground testing of Saturn launch vehicle [AIAA PAPER 67-234] 07 p1165 A67-20057

VTOL technique and advanced aircraft design 07 p1130 A67-20220

Management systems planning for control and information systems for Voyager project, with attention to work breakdown and scheduling [AAS PAPER 66-141] 08 p1429 A67-20966

Planning-Programming-Budgeting System /PPBS/ implementation by Federal agencies and relation to space activities [AAS PAPER 66-150] 08 p1430 A67-20970

Titan III program, considering DOD and USAF development of improved system acquisition policies and regulations [AAS PAPER 66-154] 08 p1430 A67-20972

NASA management and program trend line analysis [AAS PAPER 66-156] 08 p1430 A67-20973

Planned interdependency incentive method /PIIM/ for Gemini program at lowest cost and best performance [AAS PAPER 66-157] 08 p1430 A67-20974

Management aspects of design and development of Gemini spacecraft noting program organization, management techniques and personnel motivation [AAS PAPER 66-158] 08 p1430 A67-20975

Interface management of aerospace systems noting associated disciplines, documentation, contractor interrelationships and procuring agencies [AAS PAPER 66-159] 08 p1430 A67-20976

Management of engineering changes in manufacturing processes to prevent design or systems deficiencies resulting from poor control of changes 08 p1430 A67-21049

Management of aircraft hydraulic vacuum, delcing system and pneumatic components 09 p1581 A67-22127

Reliability management techniques for Projects Mercury, Gemini and F-4 Phantom II aircraft 09 p1582 A67-22288

Procedures for aircraft and spacecraft contractual arrangements to procure reliable systems, considering costs, qualification tests, etc 10 p1660 A67-23430

Economic impact of defense and space

programs 10 p1735 A67-23629

Management methods in military equipment development to be used with aircraft 11 p1885 A67-24655

Improvements in management control of complex projects, considering network analysis 11 p1885 A67-24656

Aerospace company management characteristics and problems 12 p2041 A67-25742

Planning and decision-making system in technological evolution and revolution 13 p2231 A67-27506

Systems approach as systematic investigation of research, engineering and management activities for technological or sociological gain 13 p2231 A67-27513

Planning-Programming-Budgeting System /PPBS/ implementation by Federal agencies and relation to space activities [AAS PAPER 66-150] 13 p2232 A67-27551

Titan III program, considering DOD and USAF development of improved system acquisition policies and regulations [AAS PAPER 66-154] 13 p2232 A67-27552

Management scheme for Apollo program 13 p2233 A67-27553

NASA management and program trend line analysis [AAS PAPER 66-156] 13 p2233 A67-27555

Interface management of aerospace systems noting associated disciplines, documentation, contractor interrelationships and procuring agencies [AAS PAPER 66-159] 13 p2233 A67-27556

Planned interdependency incentive method /PIIM/ for Gemini program at lowest cost and best performance [AAS PAPER 66-157] 13 p2233 A67-27558

Management aspects of design and development of Gemini spacecraft noting program organization, management techniques and personnel motivation [AAS PAPER 66-158] 13 p2233 A67-27559

Project NERO /near earth rescue and operations/ design study of MIT students as part of advanced space systems engineering course 13 p2214 A67-27700

Commercial forms of aluminum alloys, production, applications and marketing 14 p2336 A67-27812

Management aspects of technological capability within large hardware systems business 14 p2409 A67-28697

Management role in making technical and administrative decisions regarding type of telemetry system 14 p2272 A67-28698

Optimum design safety for VTOL aircraft, noting noise and vibration elimination [AIAA PAPER 66-813] 15 p2419 A67-29411

Spacecraft system performance vs component reliability, discussing practical aspects of software tools for management purposes 15 p2493 A67-29607

Project initiation emphasizing market, product /design, cost and timing/ and resources to market 15 p2583 A67-29667

Defense procurement procedures and task of project manager 15 p2583 A67-29668

Analysis of management methods applicable to aerospace industry, considering introduction of integrated information systems 15 p2583 A67-29669

Advanced space vehicle planning analyzed from economic approach to decision making, noting cost decrease with time 15 p2586 A67-29833

Fixed wing reusable horizontal landing boosters, comparing weight, cost, technical difficulty and availability 15 p2567 A67-29836

Flight data of X-15 research aircraft noting development, operation and economic aspects of performance 15 p2420 A67-29848

Reusable booster concept, economic justification, cost characteristics and management planning 15 p2569 A67-29850

Spaceport facilities, technology and economics 15 p2467 A67-29943

Space tourism potential, cost estimate of equipment, management, etc [AAS PAPER 67-127] 15 p2558 A67-29965

Management control system for technical, production, financial and contractual management of large scale or technical industry programs [AAS PAPER 67-153] 15 p2583 A67-29969

Launch operations requirements for future space programs

[AAS PAPER 67-37] 15 p2467 A67-30109

Management and cost factors involved in operation of modern integrated missile range 15 p2468 A67-30121

[AAS PAPER 67-59] 15 p2583 A67-30221

Network planning - Conference, London, June 1967

Applications of Program Evaluation and Review Technique /PERT/ in NASA 15 p2583 A67-30222

Critical Path Analysis /CPA/ system based on network techniques, coordinating separate development programs of ELDO member states 15 p2583 A67-30223

Planning integration of Boeing 747 jet aircraft into commercial airline [AIAA PAPER 67-394] 15 p2421 A67-30361

Reliability management under fixed-price contracts 15 p2584 A67-30403

Supplier control and reliability, discussing adequate input supply and output monitoring 15 p2584 A67-30407

Quality cost accounting and management decisions in performance of various functions 15 p2584 A67-30420

Sampling plan for destructive testing relating quality protection to cost 15 p2584 A67-30421

Design disclosure format /DDF/ linking program managers, review teams and contractors 16 p2781 A67-30443

Lunar orbiter quality assurance program emphasizing management, design, procurement, fabrication, quality control, etc 16 p2783 A67-31625

Aircraft accident prevention dynamics and data recording role noting repetitive causal factors, limitations and information loss 17 p2796 A67-32218

Carrier Onboard Delivery aircraft, discussing cost effectiveness by reduced deliver time of critical spare parts 17 p2797 A67-32572

Capabilities of passenger aircraft for short range operations, noting design and economic suitability [AIAA PAPER 66-945] 17 p2797 A67-32583

AFSCM 375-5 as methodology for system engineering, discussing management, documentation, applications, development, operation, design, etc 18 p3161 A67-33494

PERT /Program Evaluation and Review Technique/ planning method gives project management means for controlling project to accomplish task in shortest possible time 18 p3161 A67-33634

Hybrid simulators used for aerospace and military programs consisting of analog computers, digital computers and interface units for handling data flow 18 p3019 A67-33635

Control engineering in systems management applied to missile control and guidance 18 p3162 A67-33636

Systems thinking and systems management in rocket motor manufacture 18 p3111 A67-33638

Role in management of specification trees portraying interrelationship of requirement documents, specifications and standards applicable to particular program 18 p3162 A67-34671

System safety management/engineering procedures and techniques for safety requirements application 18 p3163 A67-34691

Short haul air transportation potentials and problems, considering legislative, administrative and financial aspects of implementation and planning 19 p3347 A67-34977

Airspace and ground environment systems approach to air transportation planning 19 p3348 A67-34978

Potential capital and profits growth in air transportation, discussing government, management and industry 19 p3348 A67-34979

Systems approach combining human experience and logic with computer technology to implement navigation management function 19 p3254 A67-35313

Retrofit accountability system requirements, environment, purpose and future applications 20 p3556 A67-36541

Quality program planning criteria for NASA contracts involving NPC 20 p3558 A67-36603

Planned introduction of Boeing 747 into airline service noting advances in technology for passenger comfort, cargo handling and rate reduction 20 p3361 A67-37441

Commercial aircraft planning and design

considering technology, market environment and manufacturers desires and capabilities 20 p3556 A67-37446

Principal investigator task evaluation, discussing responsibility for instruments, prelaunch operation, operational program establishment, processing, analyzing and publishing of results [AIAA PAPER 67-630] 20 p3534 A67-37614

National space program planning viewpoint of Executive Branch of Federal Government [AIAA PAPER 67-628] 20 p3556 A67-37619

Lessons from spacecraft industry experiences in 1960s and trends for 1970s, discussing subsystem performance experience, data acquisition, contracting, reliability, etc [AIAA PAPER 67-639] 20 p3557 A67-37622

Trends in contracting that will influence spacecraft design and development in 1970s [AIAA PAPER 67-641] 20 p3557 A67-37623

Space electronic program management and requirement integration, discussing functional or matrix type organization and project organization 21 p3734 A67-38215

Life cycle cost concept adaptation by DOD affecting logistics engineer, discussing reliability relation, maintainability, etc 23 p4084 A67-40580

Cost estimating techniques for military and NASA programs, comparing spacecraft resource forecasting with expenditure estimates [AIAA PAPER 67-809] 24 p4259 A67-42966

Advanced systems planning with limited funds in terms of payoff from advancing technology through R and D [AIAA PAPER 67-811] 24 p4259 A67-42967

Commuter airline planning using systems analysis to examine technical, managerial, legal and economic aspects [AIAA PAPER 67-843] 24 p4259 A67-42981

Lunar exploration planning methodology for after post-Apollo landing based on equipment evolution [AIAA PAPER 67-865] 24 p4238 A67-42988

Vehicle flight readiness review, technique for assuring maximum probability of mission success [AIAA PAPER 67-888] 24 p4140 A67-43001

U.S. launch operations techniques emphasizing launch site testing prior to launch [AIAA PAPER 67-889] 24 p4140 A67-43002

AGM-69A program-management system using CRT display for PERT/Time and Cost Control data translation [AIAA PAPER 67-920] 24 p4260 A67-43019

Deep-Space Network /DSN/ planning, discussing support for lunar and planetary flight support and applied research applications [AIAA PAPER 67-975] 24 p4260 A67-43051

MANEUVER

SA FLIGHT CONTROL

SA SATELLITE MANEUVER

SA SELF-MANEUVERING UNIT

SA SPACE RENDEZVOUS MANEUVER

SA SPACECRAFT MANEUVER

Transient buffet loads on wings due to gust or maneuver 13 p2215 A67-26533

Captured Air Bubble /CAB/ vehicle stability tests [AIAA PAPER 67-349] 14 p2246 A67-28731

MANEUVERABLE SATELLITE

Interception satellite thrust and steering optimization for pursuing maneuverable satellite, analyzing both evader and pursuer sides with differential game concept 24 p4182 A67-42908

Large plane changes by synergetic maneuver with drag cancelled by thrust, noting reduced efficiency due to high altitude L/D decay 24 p4242 A67-42911

MANEUVERABLE SPACECRAFT

Maneuvering propulsion problems for spacecraft attitude control 01 p0142 A67-11401

Maneuvering-range constraints effects on lifting-vehicle design parameters as velocity increments, propellant consumption, heating rates and acceleration tolerance [AIAA PAPER 66-961] 02 p0332 A67-12288

Maneuvering-range constraints effects on lifting-vehicle design parameters as velocity increments, propellant consumption, heating rates and acceleration 13 p2212 A67-26829

Remote maneuvering unit control during satellite inspection in simulated conditions 14 p2258 A67-28669

Liquid-bipropellant pressure-fed propulsion systems in lower thrust range and use for spacecraft maneuvering 16 p2736 A67-30707

Design for throttling and pulsing operation of rocket engine, discussing test data [AIAA PAPER 67-506] 18 p3113 A67-33970

Variable geometry entry spacecraft making secondary use of extendable wings in space as antenna and as radiators 20 p3532 A67-36560

Thrust augmented maneuvering /TAM/ for lifting reentry vehicle compared with other glide vehicles using lift/drag ratio 20 p3533 A67-36584

MANGANESE

Mossbauer investigations of stoichiometric manganese-ferrite and two magnesium-manganese ferrites made at room and liquid nitrogen temperatures 04 p0676 A67-14925

Ultramafic rock content of Na, Mn, Cr, Sc and Co determined by neutron activation technique 07 p1183 A67-20142

MANGANESE ALLOY

Manganese aluminide precipitation effect on primary recrystallization in metal systems, indicating softening processes in metals 06 p1015 A67-17810

Carbide forming elements effect on kinetics of isothermal transformation of austenite and mechanical properties of manganese-molybdenum steel 07 p1199 A67-19239

Rare earth metal/manganese alloys analyzed by amalgam process 07 p1210 A67-20111

Electrical resistance of manganin coil to 7 kbar and 200 degrees C, use as pressure indicator at elevated temperatures provided correction due to shift of resistance at different temperatures is made 08 p1353 A67-20373

Niobium effect on structure and properties of chromium-manganese steels as active nitride and carbide forming agent increases deformation resistance 08 p1343 A67-21206

Structural studies of FeNi-FeNiMn type thin films with ferro-antiferromagnetic coupling by Lorentz electron microscopy 24 p4206 A67-43109

MANGANESE COMPOUND

Crystallization phase in Pbnm orthorhombic space group of yttrium manganite under pressure and high temperature 09 p1557 A67-22572

Magnetic ordering effect on electrical properties of antiferromagnetic semiconductor MnTe indicate temperature anomaly above 440 degrees K 12 p1982 A67-25326

Magnetic susceptibilities and anisotropies of manganous acetate tetrahydrate crystal measured at various temperatures 15 p2540 A67-30091

Optical exciton-magnon absorption in manganese fluoride, experimental results and theory of interactions 17 p2926 A67-33382

Luminescence decay kinetics of trivalent Nd ions in antiferromagnetic Rb manganese fluoride, showing mechanism of transfer process of excitation energy of Mn ions 20 p3506 A67-36218

MANGANESE ION

Magnetic susceptibilities and anisotropies of manganous acetate tetrahydrate crystal measured at various temperatures 15 p2540 A67-30091

MANGANESE OXIDE

Neel temperature in NiO and MnO with divalent Fe measured using Mossbauer effect 12 p1985 A67-25844

N-type Hall effect in high temperature Li doped ceramic sample of MnO, measuring electric transport properties 22 p3858 A67-39521

MANGLER TRANSFORMATION

Approximate method of treating three-dimensional laminar incompressible boundary layer equations when cross flow is small [ASME PAPER 66-WA/FE-34] 04 p0607 A67-15365

MANIFOLD

Asymptotic behavior of curvature tensor in certain asymptotically Euclidean Riemannian space-time manifold 11 p1819 A67-24763

Proof of Kupka and Smale approximation theorem concerning differential equations defined on compact manifold 13 p2146 A67-27095

Liapunov subcenter manifold, showing that

real C-1 Hamiltonian system of ODEs has m distinct two-dimensional invariant manifolds 17 p2877 A67-32558

Bogolubov existence theorem for one-dimensional integral manifold and two-dimensional local integral manifold extended to Hilbert space 17 p2879 A67-32879

Dyadic formalism to prove Herglotz-Noether theorem for flat manifolds [JPL-TR-32-1125] 17 p2879 A67-32929

Exhaust manifold design for two-cycle diesel engine with turbosupercharger using physical simulation, discussing simulation criteria for gasdynamic processes 21 p3696 A67-38908

MANNED AIRCRAFT

Manned hypersonic vehicle /MHV/ design, considering performance, shape, size, propulsion, etc 03 p0360 A67-13792

MANNED ORBITAL LABORATORY /MOL/

Communications requirements for manned deep space missions, using optical links, with PPM, PCM/PL and coherent reception for each link [AIAA PAPER 66-317] 06 p0961 A67-17706

Manned orbital laboratory for biological research, discussing experimental possibilities and requirements on spacecraft 08 p1287 A67-21070

Manned orbiting laboratories for surveying natural resources using advanced remote sensing techniques 08 p1325 A67-21072

Simulator studies of MOL tracking experiments 08 p1317 A67-21105

Telemetry, tracking and command /TTC/ communications, emphasizing 1970 requirements for manned and unmanned earth-orbital, lunar and planetary missions 13 p2074 A67-27449

Onboard data management systems for manned space laboratory performing experiments, development tests and quasi-operational data gathering 16 p2633 A67-30669

Manned orbiting laboratories for exploring planets by remote sensing and planetary encounter missions compared to landing and flyby 19 p3332 A67-35336

Ultrareliable six redundant sensor attitude reference system for Manned Orbital Laboratory /MOL/ with limited sparing capability 21 p3624 A67-37786

MANNED ORBITAL RESEARCH LABORATORY /MORL/

Manned Orbital Research Laboratory /MORL/ design studies stressing stabilization and control and electric power subsystems, water supply, etc [AIAA PAPER 66-932] 02 p0332 A67-12277

Digital simulation program for systems design of long-duration space station of MORL type [AIAA PAPER 67-206] 06 p0981 A67-18512

Advanced low thrust propulsion systems and propellants evaluation for stationkeeping and stability control of NASA Manned Orbital Research Laboratory [AIAA PAPER 66-226] 07 p1240 A67-19365

MORL system reliability analysis, discussing Monte Carlo simulation, major parameters, constraints, program contingencies, etc 08 p1411 A67-21073

Manned Orbital Research Laboratory /MORL/ design and utilization 08 p1414 A67-21545

Manned Orbital Research Laboratory design and flight control characteristics 09 p1572 A67-22872

Manned orbital research laboratory /MORL/ examining experimental program, design, mission definition, logistics, cost 16 p2756 A67-30623

Manned space mission requirements and application of space power technology to multipurpose space stations, noting operation of Pu-238 isotope/Brayton cycle unit 17 p2953 A67-31979

Resistojet control system for MORL analyzed for requirements and applications [AIAA PAPER 67-721] 21 p3714 A67-38747

SNAP-8 type reactors and shield subsystems for MORL and manned lunar base plants, discussing Rankine and thermoelectric power conversion systems 24 p4186 A67-42546

Orbital research hospital design for utilizing zero and low gravity therapeutic value in treating physiological conditions [AIAA PAPER 67-833] 24 p4243 A67-42976

Manned orbiting space station operation in association with unmanned observatory, comparing gimbal mounted, free floating,

tethered and firmly fixed modes
[AIAA PAPER 67-926] 24 p4245 A67-43022

MANNED ORBITAL SPACE STATION /MOSS/

Maintainability, reliability and operational flexibility of manned orbital space station
[AIAA PAPER 66-933] 02 p0331 A67-12252

Rotating artificial gravity system for manned orbital vehicles and stations requiring no expenditure of propulsive mass to attain full vehicle rotation
05 p0906 A67-17203

Future manned earth orbital flights
[AAS PAPER 67-26] 15 p2562 A67-30101

Design integration of reactor, shielding and power conversion systems for manned earth orbital station
24 p4186 A67-42547

Design requirements of reactor power systems for manned earth orbital space station
24 p4186 A67-42548

Commercial earth orbital manned space station power system requirements, estimating operational and logistical costs for isotope and reactor designs
[AIAA PAPER 67-879] 24 p4187 A67-42998

MANNED ORBITAL TELESCOPE /MOT/

Manned planetary exploration, Mercury and Gemini flight programs and projected goals of Apollo Applications Program
12 p2002 A67-25233

Pointing control system /PCS/ for Apollo Telescope Mount /ATM/ for solar observations
[AIAA PAPER 67-534] 19 p3334 A67-35936

Radiance of debris cloud ejected from manned spacecraft, effect on optical environment and astronomical observations
20 p3525 A67-37099

MANNED REENTRY

Manned lifting body flight test program, noting NASA M2-F2 and HL-10 and USAF SV-5P
[AIAA PAPER 66-838] 03 p0519 A67-14127

Structures, materials and thermal protection systems for future manned reentry vehicles, emphasizing crew compartment compatible materials
[AIAA PAPER 66-987] 03 p0520 A67-14143

Manned spacecraft design, discussing range hardware and software development and future entry vehicle programs
[AAS PAPER 67-36] 15 p2571 A67-30108

Manned flight simulators suitable to space research, discussing types, phases of development, operational and performance features, etc
16 p2654 A67-30761

Feasibility of short radius centrifuge incorporation in space station, testing radius effects on operator performance of tasks
23 p3965 A67-41567

MANNED SPACE FLIGHT

SA SPACE FLIGHT STRESS

Weather and cloud photography during Gemini space flights and effect on interpretation of satellite weather pictures
01 p0109 A67-11393

Biomedical data from U.S. manned space flight experience including cardiovascular and central nervous systems, blood composition changes, etc
01 p0016 A67-11394

Requirements and alternate systems approaches for extravehicular operations in space
[AFAPL-CONF-67-6] 01 p0018 A67-11400

Propulsion systems including chemical, nuclear, etc, for manned interplanetary mission
01 p0142 A67-11402

Human capability to perform support functions in space
01 p0018 A67-11405

Voice communications and control facilities at mission control center in Houston for support of manned space program conducted by NASA
02 p0229 A67-12120

Scheduling and simulation of manned orbital operations using modular system of computer programs
[AIAA PAPER 66-907] 02 p0230 A67-12249

Space station role in manned space flight noting mission goals, earth, moon and planet-oriented applications, etc
[AIAA PAPER 66-906] 02 p0332 A67-12272

Effects of space station logistic requirements on design of spacecraft configurations with various hypersonic lift/drag ratios, comparing payload, cost, etc
[AIAA PAPER 66-958] 02 p0332 A67-12286

Bioengineering parameters influencing life support systems for manned exploration of moon including mission duration and closed regenerable systems
02 p0230 A67-12310

Physiological telemetry application in long space flights for medical examination and control during space flight
02 p0187 A67-12323

Gemini manned space flight program
02 p0327 A67-12363

Space radiation monitoring system aboard manned spacecraft to provide solutions to medical problems and safety of flight guidelines for mission
02 p0188 A67-12387

Launch operation requirements for manned space flight in 1970s
[AIAA PAPER 66-865] 03 p0397 A67-14130

Mission design, operations planning and flight preparation for manned orbital space missions
[AIAA PAPER 66-904] 03 p0519 A67-14131

Human space navigation in vicinity of earth and in and out of solar system
04 p0695 A67-14517

Beryllium properties and treatment for use in manned space flight noting thermal stress resistance, toxicity, honeycomb structures, etc
04 p0635 A67-14563

Scheduling manned space flight missions
04 p0704 A67-14902

Integration of life support system and propulsion system for manned interplanetary space missions
04 p0563 A67-15245

Piloted space flight simulation at Langley Research Center
[ASME PAPER 66-WA/AV-2] 04 p0599 A67-15395

Postulates on microbial hazards of astronauts in prolonged isolation based on studies with animals with locked flora
05 p0755 A67-18281

Optimum trajectory control for minimum heating paths during manned vehicle reentry at hyperbolic speeds
[AIAA PAPER 67-59] 06 p1095 A67-18268

Mars stopover mission with Venus swingby technique, discussing velocity requirements, trip times and initial mass in earth orbit
[AIAA PAPER 67-27] 06 p1085 A67-18332

Megawatt ion-propulsion power conditioning system design for manned interplanetary missions, noting payload-mass ratio problems, advantages, etc
[AIAA PAPER 67-52] 06 p1075 A67-18449

Nuclear or electric propulsion for planetary exploration, noting configuration and capabilities
06 p1098 A67-19019

Dental aspects of manned spaceflight, discussing preventive measures
06 p0954 A67-19030

Manned interplanetary flights before Mars landing, using Saturn-Apollo technology
06 p1092 A67-19031

Scientific value of manned lunar exploration
06 p1093 A67-19036

Projected ten-year manned exploration of lunar surface
06 p1093 A67-19037

Apollo manned lunar landings, system hardware, operational problems and development of lunar surface experiments package /ALSEP/
[AIAA PAPER 67-116] 07 p1163 A67-19438

Planned encounters with asteroids in manned missions to Mars for observational purposes, using computer program
[AAS PAPER 66-124] 07 p1254 A67-19983

Venus swingby trajectory for manned Mars mission as possibility in 1978-1986
[AAS PAPER 66-125] 07 p1254 A67-19984

Lunar surface accessibility study for manned lunar orbit rendezvous missions, discussing nonfree return and translunar trajectories
[AAS PAPER 66-131] 07 p1255 A67-19990

Testing of three individual propulsion systems of lunar module space vehicle in preparation for man-rated flight service
[AIAA PAPER 67-258] 07 p1166 A67-20073

Post Apollo space exploration - AAS Meeting, Chicago, May 1965
08 p1391 A67-21064

Post Apollo space flight technology, discussing recoverable and reusable booster rockets, spacecraft, life support systems, etc
08 p1391 A67-21065

Apollo extension systems, discussing current space technology and accomplishments
08 p1391 A67-21066

Manned vs unmanned space exploration, discussing increased mechanization of operation
08 p1392 A67-21067

Human performance on earth and in space noting depth perception, visual acuity, walking ability, reaction time,

etc 08 p1289 A67-21068

Experimental program for orbiting biomedical/ behavioral laboratory, discussing functions
08 p1287 A67-21069

Space astronomy program development, discussing manned orbital observatory concept and instrumentation
08 p1392 A67-21071

System concepts, combinations and missions for lunar exploration using LEM
08 p1316 A67-21082

LEM Truck concept based on Apollo hardware, delivering payloads for increase of lunar staytime and radius of operations
08 p1316 A67-21084

Manned planetary mission possibilities, stressing Mars exploration, noting trajectory planning, propulsion, crew requirements, etc
08 p1394 A67-21099

Gemini ground support system extension to cover Apollo program, stressing launch complex, deep space tracking, S-band linkage, communications satellite, etc
08 p1317 A67-21281

All-digital real time display system for ground monitoring of manned space flight including computers, software, output devices, etc
09 p1483 A67-21677

Extended manned lunar surface operations in study of lunar origin and history with respect to solar system
09 p1568 A67-22408

Four alternative plans for future U.S. space programs
10 p1710 A67-23636

Electric propulsion for manned interplanetary mission evaluated in light of new optimum planetary transfer trajectories of power-limited flight
11 p1859 A67-24342

Prolonged weightlessness exposure and expected effects on man
12 p1902 A67-25725

Weightlessness and manned space flight medical data to date
12 p1902 A67-25727

Manned spaceflight RF radiation communications systems including voice, telemetry, tracking and ranging, up data and TV
12 p1907 A67-25993

Radiation hazards and safety requirements for lunar and Mars manned space flights, discussing radiosensitivity, restoration and permissible doses
13 p2059 A67-26781

Medical testing, research and control during manned space flights, discussing diagnostic algorithms for onboard computer and frequency of data collection
13 p2062 A67-26782

Prophylaxis for negative effect of hypokinesia on human cardiovascular system
13 p2059 A67-26784

Planned encounters with asteroids in manned missions to Mars for observational purposes, using computer program
[AAS PAPER 66-124] 13 p2209 A67-27537

Venus swingby trajectory for manned Mars mission as possibility in 1978-1986
[AAS PAPER 66-125] 13 p2209 A67-27538

Lunar surface accessibility study for manned lunar orbit rendezvous missions, discussing nonfree return and translunar trajectories
[AAS PAPER 66-131] 13 p2209 A67-27542

Manned interplanetary program planning, suggesting basic parameters for manned trip to Mars and Venus
13 p2210 A67-27546

Space exploration by automatic, manned and remote-controlled space flight systems, noting applications, limitations, transmission power and distance effects
14 p2256 A67-28036

Radiation levels on Gemini IV flight including Van Allen belt and South Atlantic Anomaly
15 p2425 A67-29105

Free-running circadian oscillations noting nature of driving oscillation, physiology of circadian organization and relation to manned space flight
15 p2425 A67-29107

Radiation hazard to man from solar proton events
15 p2429 A67-29450

Nonhardware aspects of space navigation - Conference, Los Angeles, March 1967
15 p2513 A67-29504

Navigational technique for manned interplanetary missions, noting resemblance to traditional nautical technique
15 p2514 A67-29508

Optimization of man-machine environmental interface problems in framework of large-scale and long-term space operations
[AAS PAPER 67-80] 15 p2432 A67-29947

Future manned earth orbital flights
[AAS PAPER 67-28] 15 p2562 A67-30101

Future manned planetary missions

including flybys and landings, describing vehicle configurations and technological requirements
 [AAS PAPER 67-28] 15 p2562 A67-30103
 Support requirements for future manned space programs
 [AAS PAPER 67-58] 15 p2562 A67-30120
 Spacecraft design for manned planetary landings noting mission characteristics, navigation requirements, crew housing, etc
 16 p2756 A67-30625
 Physiological diagnostic information collection in prolonged space flight and data handling transmission systems
 16 p2617 A67-30763
 Methodology for numerically defining international magnitude of space rescue requirements
 16 p2781 A67-30771
 Cosmic radiation protection during manned space flight, considering use of radiation warning devices and protective drugs
 16 p2612 A67-30901
 Automation problems in space-flight operative medical control, giving equations of changes in physiological indices
 16 p2618 A67-30902
 Human psychological reactions to space flight problems, investigating effects of weightlessness, immobility and confinement on cosmonaut health and ability
 16 p2612 A67-30903
 Prolonged space flight effects on crew members health concerning crew selection test methods
 16 p2613 A67-30911
 Medicophysiological aspects of NASA program stressing cardiovascular, muscular and osseous problems
 16 p2614 A67-31538
 Manned space mission requirements and application of space power technology to multipurpose space stations, noting operation of Pu-238 isotope/Brayton cycle unit
 17 p2953 A67-31979
 Mars stopover mission with Venus swingby technique, discussing velocity requirements, trip times and initial mass in earth orbit
 [AIAA PAPER 67-27] 17 p2940 A67-32059
 Biopotential detection, recording and design noting electrocardiogram and electroencephalogram use to monitor weightlessness in manned space programs
 17 p2807 A67-32666
 Biotelemetry improvements in manned space flights, emphasizing bit rate reduction required for electrocardiogram data transmission to earth
 17 p2807 A67-32900
 Radiation and weightlessness effect on human organism in space flights, discussing galactic cosmic, solar and Van Allen belt radiation
 18 p3116 A67-33700
 Nuclear propulsion for manned Mars expedition, discussing engine and launch optimization, computer simulation, performance, trip times, velocity, weight, etc
 [AIAA PAPER 67-510] 18 p3077 A67-33974
 Man-rating F-1 engine, noting capabilities and future plans
 [AIAA PAPER 67-519] 18 p3115 A67-33982
 Manned mission reliability and maintainability requirements in future systems
 18 p2995 A67-34686
 MARCEP mathematical and mission simulation models to evaluate parameters affecting maintainability of long duration manned space flights
 18 p3138 A67-34688
 Optimum trajectory control for minimum heating paths during manned vehicle reentry at hyperbolic speeds
 [AIAA PAPER 67-59] 19 p3331 A67-34815
 Psychological/psychotechnical selection of French cosmonauts with reference to ballistic, orbital and space flight
 19 p3179 A67-35066
 Australian space research, discussing support to Apollo and U.S. manned space flight programs, ionospheric observations, satellite information, etc
 19 p3320 A67-35286
 Economic benefits from space systems used to survey food producing areas and weather
 19 p3350 A67-35650
 Mission simulator for manned space flight support used for real time training
 20 p3414 A67-36538
 Space suit support loop for use within manned space cabin simulator
 20 p3374 A67-36548
 Spacecraft computers role on advanced manned missions
 20 p3391 A67-36549
 Orpheus program for space flight safety using lifeboat rescue of astronauts on Apollo and other manned missions
 20 p3532 A67-36572

Radar designation by computer and real time reentry tracking for future Apollo manned space flight
 20 p3381 A67-36592
 Plasma volume, red blood cell mass and erythrocyte survival determination before and after space flight
 20 p3372 A67-37429
 Operational and cost-influencing characteristics of low orbit space operations compared from manned orbital base and earth base
 [AIAA PAPER 67-654] 20 p3530 A67-37631
 Apollo lunar landing mission strategy development concerning guidance, control and landing and propulsion systems
 22 p3897 A67-39166
 Alternate mission modes for manned Mars exploration
 22 p3886 A67-40136
 Rankine cycle power plant for electric propulsion manned Mars mission analysis of system characteristics and mission duration effect
 22 p3869 A67-40173
 Manned space flight predicted exposure effects vs actual medical findings
 23 p3945 A67-41067
 Oxygen regeneration life support system for multiple mission manned space flights evaluated with subsystem model
 [SAE PAPER 670849] 24 p4115 A67-42000
 Multi-kilowatt photovoltaic power system design for manned earth orbital mission
 24 p4104 A67-42511
 Nuclear electric space power plant with Rankine cycle for plausible Mars manned mission, discussing mission requirements and reactor elements
 24 p4186 A67-42549
 Manned space flight safety through mission trajectory design, considering hardware, software and operational constraints
 [AIAA PAPER 67-822] 24 p4243 A67-42970
 Manned space flight safety, discussing system design, operations planning, staffing, training and simulation
 [AIAA PAPER 67-824] 24 p4243 A67-42971
 Space flight emergency contingency planning for survival, evaluating physiological effects and remedial system effectiveness
 [AIAA PAPER 67-825] 24 p4116 A67-42972
 Apollo historical perspectives, background to U.S. man on moon decision in mid-1961, rocket booster development and space mobility
 [AIAA PAPER 67-839] 24 p4259 A67-42978
 Manned spacecraft recovery safety noting operational testing of postlanding systems, recovery support and retrieval procedures for Apollo
 [AIAA PAPER 67-852] 24 p4243 A67-42985
 Apollo manned Lunar Module /LM/ earth orbital development missions, reviewing key subsystems and technical problems
 [AIAA PAPER 67-863] 24 p4244 A67-42987
 Lunar exploration planning methodology for after-post-Apollo landing based on equipment evolution
 [AIAA PAPER 67-865] 24 p4238 A67-42988
 Commercial earth orbital manned space station power system requirements, estimating operational and logistical costs for isotope and reactor designs
 [AIAA PAPER 67-879] 24 p4187 A67-42998
 Man in space programs, examining costs and benefits
 [AIAA PAPER 67-927] 24 p4117 A67-43023
 Mathematical model for identification and control of systems safety in manned space programs using Monte Carlo techniques
 [AIAA PAPER 67-936] 24 p4245 A67-43026
 Manned planetary mission global network for continuous tracking, communication telemetry and TV transmission
 [AIAA PAPER 67-976] 24 p4125 A67-43052
 Long term manned space mission system effectiveness and reliability through interchangeability and redundancy noting optimization, tradeoffs, maintenance and spares
 [AIAA PAPER 67-984] 24 p4166 A67-43056
MANNED SPACECRAFT
 SA APOLLO SPACECRAFT
 SA GEMINI SPACECRAFT
 SA LUNAR EXCURSION MODULE /LEM/
 SA MERCURY CAPSULE
 SA UNMANNED SPACECRAFT
 SA VOSKHOD MANNED SPACECRAFT
 Reliability estimation techniques adaptable to computer implementation for complex manned systems
 01 p0031 A67-11338
 Crew performance evaluation via

behavioral and psychophysiological tests in Lunex II simulated lunar mobile laboratory
 01 p0017 A67-11392
 Manned geophysical observations from satellites as training ground for planetary research, especially Venus atmosphere
 01 p0155 A67-11395
 Manned lifting entry vehicle capability, minimum weight, variable geometry, retractable landing engines, etc
 [AIAA PAPER 66-959] 02 p0332 A67-12287
 Manned spacecraft atmosphere selection, experimenting with 100 percent oxygen at 258 mm Hg, noting toxicity, toleration, substitution of helium for nitrogen, etc
 02 p0187 A67-12319
 Expandable and modular structures for support on manned space missions, reviewing inflatable, chemically rigidizable, unfurlable and elastic recovery structures
 02 p0333 A67-12342
 Meteorological experiments possible in manned earth orbital spacecraft with aid of remote sensing of electromagnetic radiation
 02 p0239 A67-12379
 Manned meteorology experiments aboard earth satellite including ozone concentration, noctilucent clouds, spectral airglow and albedo, precipitation map, etc
 [AIAA PAPER 66-885] 03 p0513 A67-14020
 Onboard checkout equipment design requirements, considering hardware and software for manned spacecraft flight
 03 p0399 A67-14212
 Rankine cycle power plant characteristics for electric propulsion manned Mars mission
 [AIAA PAPER 66-894] 03 p0504 A67-14274
 Satellite role in worldwide meteorology, discussing global observation, observation platforms, manned satellites, and remote sensing and data collection of satellite instrumentation
 05 p0837 A67-16383
 Sensitivity of manned planetary spacecraft design to shield weight, onboard radiation and uncertainties in space environment radiation
 07 p1258 A67-19376
 Soft landing of manned spacecraft on lunar surface
 07 p1258 A67-19429
 Meteorological studies from manned spacecraft, discussing interpretation of cloud pictures and optical inhomogeneity of troposphere and stratosphere
 07 p1221 A67-20008
 Selection of space cabin atmospheres including pressure, fire and blast hazard, humidity and temperature control, etc
 11 p1748 A67-24262
 Lubricant selection for lunar missions and manned spacecraft based on compatibility with oxygen-rich environment, propellant, anodic coatings and sliding friction behavior in vacuum
 [ASLE PAPER 66AM-7A2] 13 p2123 A67-27100
 Materials evaluation and selection for compatibility with manned spacecraft environment
 15 p2507 A67-29551
 Apollo manned space flight program including mission profile, spacecraft and constituent systems
 16 p2756 A67-30626
 Research potential of manned earth orbiting spacecraft in meteorology
 16 p2759 A67-30687
 Manned meteorology experiments aboard earth satellite including ozone concentration, noctilucent clouds, spectral airglow and albedo, precipitation map, etc
 19 p3213 A67-34824
 Navigation and guidance analysis of Mars probe launched from manned flyby spacecraft for 1975-1976
 [AIAA PAPER 67-546] 19 p3257 A67-35945
 Design of time-shared multifunction display medium to improve guidance and control displays in manned spacecraft
 [AIAA PAPER 67-552] 19 p3257 A67-35949
 Electromagnetic interference and tape recorder jitter control problems in data management system for manned spacecraft
 20 p3442 A67-36468
 Aerocruise maneuver for optimizing orbital plane change with respect to cruise speed
 20 p3532 A67-36552
 Radiance of debris cloud ejected from manned spacecraft, effect on optical environment and astronomical observations
 20 p3525 A67-37099
 Human engineering performance data for equipment design for manned space systems, discussing zero gravity maintenance and repair

[AIAA PAPER 67-653] 20 p3375 A67-37630
Design and construction of power supply without hookup cables for manned lunar vehicle 21 p3571 A67-38337
Manned lifting reentry vehicle optimization using Optimum Compromise between Conflicting Operational Factors /OCCOF/ computer 22 p3902 A67-39947
Viscous degradation of hypersonic lift-drag ratio in manned spacecraft, noting free stream Mach and Reynolds numbers 22 p3742 A67-40113
Manned spacecraft space radiation monitoring system requirements and criteria to indicate biological response 23 p3966 A67-41589
Manned spacecraft water supply microbial contamination detection using firefly bioluminescent reaction 23 p3968 A67-41627
Vehicle volume and design criteria for manned lunar roving vehicles investigated by evaluating subjects performance under prolonged simulated lunar environment 23 p3970 A67-41658
Legal problems associated with telecommunications and meteorological satellites and with launching and retrieval of manned spacecraft 24 p4257 A67-42387
Large area solar array design for photovoltaic system for manned space systems based on orbital perturbations and mechanical and thermal environment considerations 24 p4105 A67-42516
Manned orbiting space station operation in association with unmanned observatory, comparing gimbal mounted, free floating, tethered and firmly fixed modes [AIAA PAPER 67-926] 24 p4245 A67-43022
Astronaut role in balanced in-flight testing for manned spacecraft [AIAA PAPER 67-949] 24 p4245 A67-43033
Time factor in onboard checkout and in-flight maintenance of manned spacecraft, discussing mission events and man-machine interaction [AIAA PAPER 67-950] 24 p4245 A67-43034

MANOMETER

VIM-1 vacuum gauge using inverse-magnetron type manometric transducer for measuring rarefied gas pressure 03 p0425 A67-14268
Manometer for measuring gas pressure from current required to heat platinum wire to certain temperature 06 p1003 A67-18192
Absolute manometer of Knudsen for any temperature ratios and arbitrary accommodation coefficient on boundaries 08 p1331 A67-20867
Micrometer U-tube manometers for medium vacuum measurements 08 p1332 A67-21493
VIM-1 vacuum gauge using inverse-magnetron type manometric transducer for measuring rarefied gas pressure 14 p2321 A67-28778
Electric manometer using electrolytic fluid for low velocity measurements with Pitot tube 16 p2875 A67-31210

MANPOWER

S PERSONNEL

MANUAL

S HANDBOOK

S INSTALLATION MANUAL

MANUAL CONTROL

Computer design test program to automate checkout process of Saturn I and V space boosters gradually while retaining manual checkout 01 p0051 A67-11427
Information model for manual control of astronaut motion and space orientation in free space 02 p0188 A67-12330
Extension of manual control to liquid rocket engine necessary to enable pilot to save primary mission or to change to planned secondary mission 04 p0703 A67-14426
Manual control dynamics for single loop systems facilitating man-machine system design 07 p1182 A67-19907
Manual thrust vector control development for Apollo Command and Service Module Stabilization and Control System [AIAA PAPER 67-243] 07 p1260 A67-20043
Simulation of pursuit-evasion differential game using variational method, comparing performance of human pilot to optimal pursuer 07 p1138 A67-20170
Critical tracking task for man-machine research related to operator effective delay time 07 p1136 A67-20171

Manual guidance for interplanetary flight by graphical methods, nomographs and relevant general equations 08 p1352 A67-21104
Simulator studies of MOL tracking experiments 08 p1317 A67-21105
Manual calculation and navigation of spacecraft orbiting near planets 08 p1352 A67-21112
Near planet orbital navigation by astronauts, celestial surfaces of position combine to define unique three-dimensional position of observer 09 p1526 A67-22388
Optical ranging technique for orbital rendezvous with manual checking of automatic equipment 09 p1527 A67-22395
Kinematic analysis of deviation from aircraft-missile line for designing electronic missile firing simulator, with manual telecontrol comprising controlled precession gyroscope for last integration 09 p1486 A67-22419
Verbal-analytical model of human operator performance in compensatory tracking 10 p1618 A67-22733
Analytic measure for difficulty of human control as constrained by capability, training and stress 13 p2061 A67-26709
Space exploration by automatic, manned and remote-controlled space flight systems, noting applications, limitations, transmission power and distance 14 p2256 A67-28036
Linearized manual space navigation incorporating redundant measurements to compensate for instrumentation inaccuracies 14 p2347 A67-28128
Sine wave tracking, studying operator manual control performance 17 p2808 A67-33179
Computer simulated flights of manual control for VTOL IFR operations indicate display and control subsystem deficiencies 17 p2808 A67-33183
Human controller as adaptive low pass filter to track signal contaminated with noise 18 p2994 A67-34340
Human engineering research to aid system designers to optimize man's role as control element in space systems 18 p2995 A67-34687
Reliability contribution of pilot using manual backup control for first stage of Saturn V tested using simulation [AIAA PAPER 67-554] 19 p3335 A67-35951
Manual altitude and attitude control effects on short-period handling quality requirements 19 p3175 A67-35974
Manual optimal guidance scheme using predictive display applied to launch vehicles during boost for continuous generation of predicted fuel-optimal trajectory 19 p3259 A67-35989
Manual control stationkeeping simulation, studying tether visual rendezvous techniques and fuel economy [AIAA PAPER 67-617] 19 p3337 A67-36006
Digital computer test program for automatic checkout of Saturn launch vehicles allowing manual intervention 20 p3391 A67-36574
Predictor display instrument for optimal manual control, noting use in manned spacecraft missions and time factor 20 p3447 A67-36840
Manual steering problem and function of lunar module /LM/ manual hybrid guidance system, with automatic guidance system produced trajectory 22 p3898 A67-39176
All-weather landing systems for automatic and manual control, considering Category II and III operations 22 p3831 A67-39611
Inverted pendulum and VTOL control experiments with and without motion cues, discussing various motion effects 22 p3755 A67-40087
Cylindrical solid state oxygen generators, discussing manual and remote electrical activation 23 p3968 A67-41621
Hand-held sextant capability in in-flight spacecraft navigation measurements [AIAA PAPER 67-775] 24 p4183 A67-42943

MANUFACTURING

Packaging, manufacturing and design techniques used in total-system-in-box concept for integrated circuits 01 p0039 A67-11116
Unified treatment of costs yields and reliability in semiconductor manufacture 01 p0171 A67-11380
Printed circuits handbook covering fabrication, design, assembly, soldering,

testing, etc 08 p1334 A67-20739
Research and development for better manufacturing emphasizing hydrothermal growth of ruby crystal 09 p1505 A67-22143
Cutting tool and cutting fluid evaluation, economic considerations for aerospace manufacturing [ASTME PAPER WES-7-27] 11 p1798 A67-24256

Productibility of aerospace products with regard to machinability of aluminum alloy [ASTME PAPER WES-7-29] 11 p1798 A67-24257

Soviet book on production of gas turbine engines covering manufacturing methods, automation of operations, tooling, etc 11 p1798 A67-24516

Microelectronic failure mechanism, examining manufacture and processing methods and production of uniform and versatile material 19 p3193 A67-35029

Microelectronics fabrication in terms of specific systems, discussing input and waste piping systems design, electrical distribution, exhaust, contamination control, etc 19 p3193 A67-35030

Zero gravity orbital manufacturing noting free fall casting and blowing and zero gravity surface tension casting and foaming, discussing Serpentiator System engineering [AIAA PAPER 67-842] 24 p4165 A67-42980

Economic exploitation of lunar mineral resources for near earth orbit manufacturing [AIAA PAPER 67-872] 24 p4238 A67-42993

MANY-BODY PROBLEM

Phase-space collision domains corresponding to hard-sphere N-body problem in gas transport theory 01 p0112 A67-10144

Equations governing divergent many-body behavior within BBGKY hierarchy in Boltzmann approximation for cut-off potentials, noting nondivergent nature of solutions 01 p0118 A67-10915

Computational methods in stellar dynamics noting n-body problem approach, continuum technique and statistical method 06 p1081 A67-17780

Qualitative methods in n-body problem concerned with masses motion in inertial space under gravity, solving motion equation 06 p1081 A67-17781

Numerical analysis and third integral applications to n-body problem in stellar dynamics and relation to celestial mechanics 08 p1380 A67-20381

Dynamical irreversible evolution of gas with short range repulsive forces, using n-particle distribution function with many-body interactions 11 p1824 A67-25077

Runge-Kutta-Fehlberg method for systems of ordinary first and second order differential equations applied to numerical solution of many-body problem 15 p2561 A67-30052

Real trajectories of n-body problem calculated by convergent integral iterations on basis of differential equations for motion of centers of gravity 16 p2750 A67-31441

Intrinsic optical excitation spectrum of crystalline solids for hole or electron localization, considering many-body relaxation effects influencing photoemission 16 p2732 A67-31698

Periodic trajectories in n stationary attracting centers field, using arbitrary gravitational law 18 p3127 A67-34271

Regularization of restricted three-body problem extended to case where three primaries of any mass revolve in circular orbits around common center of mass and fourth body of infinitesimal mass moves in their field 18 p3136 A67-34589

Quantum-mechanical treatment of free-bound approximation for eigenstates and canonical partition function for plasma system in thermodynamic equilibrium 19 p3285 A67-35345

Motion equation for four-body system attracting one another according to Newtonian law, obtaining series of functions converging toward solution 19 p3328 A67-35899

Many-body system interaction with quasi-particle with assigned orbit, discussing applications to transport coefficient, plasma stability, etc 20 p3495 A67-36155

Quantum mechanical accounting for materials optical properties, considering electronic structure 20 p3515 A67-37717

Two-body relaxation term in N-body self-

- p>gravitating gases of one and three dimensions and validity of Vlasov equation 22 p3894 A67-40508
-
- p>Small stellar systems evolution, double star formation and bound subgroups occurrence after condensation from collapsed cloud calculated numerically 22 p3896 A67-40521
-
- MANY-PARTICLE THEORY**
-
- p>Solution to Bogolubov differential equation for distribution functions of particle system by functional integration technique 12 p1962 A67-26174
-
- p>Eigenstates of particle mixing matrices and relation to physical antiparticles 16 p2705 A67-31565
-
- p>Free energy of N-particle system with far-reaching intramolecular interaction, using collective variables 18 p3085 A67-33670
-
- p>Classical scalar plasma with relativistic Hartree equilibrium approximation for energy, entropy and state equation noting effect of linear perturbation 22 p3842 A67-39209
-
- p>Multiparticle mechanism of cosmic ray-atomic nuclei interactions assuming particle formation 24 p4218 A67-42842
-
- MAP**
-
- p>SA ASTRONOMICAL MAP
-
- p>SA CHART
-
- p>SA LUNAR MAP
-
- p>SA RADAR CLUTTER MAP
-
- p>SA RADAR MAP
-
- p>SA RELIEF MAP
-
- p>SA WEATHER MAP
-
- p>Updating application of aerial photographs to scale of map based on radio altimeter data 03 p0419 A67-13262
-
- p>Synthetic target scenes generation technique by general purpose digital computer for early analytical evaluation of sensor concepts 11 p1791 A67-24456
-
- p>Sea-level pressure specification from 700-mb height by applying screening regression techniques to 17 years of synoptic data 13 p2114 A67-26740
-
- p>Double exposure holographic formation of contour map over diffusely reflecting surface, using immersion method with liquids of different refractive indexes 16 p2670 A67-30612
-
- p>Ground track location on contour map for flying terrain elevation profile, using digital computer 19 p3232 A67-35926
-
- p>Moving map display as cockpit navigation device useful when flying erratic routes at low altitude 23 p4003 A67-41283
-
- MAPPING**
-
- p>SA CARTOGRAPHY
-
- p>SA CONFORMAL MAPPING
-
- p>SA FIXED POINT
-
- p>SA FLUX MAPPING
-
- p>SA PHOTOGRAMMETRY
-
- p>SA TOPOGRAPHY
-
- p>Geometrical evaluation of line-scan images for mapping, noting imagery systems 01 p0059 A67-10316
-
- p>Geodetic satellites determination of positions of earth surface points, earth shape, gravitational field parameters, direct mapping and navigation 01 p0154 A67-10852
-
- p>Tropospheric pressure-altitude data by satellite radiometric topography mapping, using oxygen absorption band centered at 5 mm 02 p0262 A67-12367
-
- p>Continuous single-value mapping of straight line segment in partially ordered system of attracting sets 03 p0461 A67-14061
-
- p>Effects of unmodeled errors on minimum variance estimators, with application to tracking complex self-calibration estimation scheme [AAS PAPER 66-107] 07 p1216 A67-19967
-
- p>Power series technique applied to single edge notches in semilinear region in plane elasticity problems, using mapping function and Muskhelishvili theory 08 p1414 A67-20347
-
- p>Onboard device locating present and future orbital satellite position through microfilm map dependent on satellite motion equation 08 p1352 A67-21525
-
- p>Multiple wavelength and source holography with constant depth contours superimposed used in cross section tracing or contour mapping 10 p1652 A67-22710
-
- p>Lapunov theorem extension to onto mappings in compact sets 10 p1673 A67-22850
-
- p>Planetary mapping mission system requirements for photography, IR and radar imagery, radar reflectivity and spectroscopy with data analysis
-
- p>techniques 11 p1859 A67-24438
-
- p>Effect of unmodeled errors on minimum variance estimators, with application to tracking complex self-calibration estimation scheme [AAS PAPER 66-107] 13 p2154 A67-27525
-
- p>Geodetic satellites determination of positions of earth surface points, earth shape, gravitational field parameters, direct mapping and navigation 14 p2394 A67-28241
-
- p>Potentialities of space cartographic systems evaluated for geometric map accuracy and economic aspects [AAS PAPER 67-106] 15 p2478 A67-29960
-
- p>Aerial electronic photomapping and geodetic surveying system describing track-keeping navigation and vertically measuring 16 p2879 A67-31801
-
- p>World maps indicating geomagnetically conjugate locations and L parameters 17 p2844 A67-32547
-
- p>Cosmic radiation anisotropy variation with time and direction described on intensity contour map, noting application for neutron monitors data reduction 17 p2938 A67-33209
-
- p>Contour maps of percentage occurrence of earth echoes observed on Alouette I ionograms, noting noise level 17 p2852 A67-33236
-
- p>Continuous wave signals from Lunar Orbiter I after reflection from lunar surface, noting mapping use 17 p2817 A67-33364
-
- p>Mapping of Fabry-Perot interferometer plates defects by measuring apparatus function peak displacement, describing measurement setup 20 p3440 A67-36358
-
- p>Point-to-point mapping technique in combination with variational calculus for solving optimum control problems for piecewise linear dynamic systems 22 p3776 A67-39776
-
- p>Algorithm for piecewise smooth point-to-point mapping of straight line onto straight line to determine various motions 22 p3777 A67-39778
-
- p>Mapping of fluctuation field of space and earth environment by electromagnetic techniques 22 p3884 A67-39949
-
- p>Notch stress theory, discussing mapping function and elliptic integral solutions 22 p3913 A67-40004
-
- p>Gravity gradiometer digital computer program for simulated rotating gravitational mass sensor and gradient contour mapping 23 p4000 A67-41218
-
- MARAGING STEEL**
-
- p>Mossbauer spectroscopy used to study precipitation reactions in 17-7 PH stainless steel and in 18Ni-8Co-5Mo maraging steel 02 p0256 A67-12705
-
- p>Aging of Ni containing maraging steel and related alloys analyzed by electrical resistivity, X-ray diffraction and hardness measurements, noting nature of Co-Mo interaction 03 p0440 A67-13250
-
- p>Fracture toughness and critical defect sizes with welds of 18 percent nickel maraging steels 03 p0446 A67-13554
-
- p>Maraging steel properties, discussing composition, strengthening mechanism, tensile and impact toughness, mechanical and fatigue properties, etc 04 p0640 A67-15458
-
- p>Internal friction in 18 percent Ni maraging steel noting rapid dislocation recovery, independence of temperature and age hardening characteristics 05 p0828 A67-16468
-
- p>Local buckling strength of high strength axially compressed maraging steel cylinders circumferentially prestressed with high strength epoxy-protected fiberglass filament windings 05 p0923 A67-17211
-
- p>Maraging, 15CDV6 and 40CDV20 steel for missile and aircraft construction 05 p0830 A67-17269
-
- p>Rotating beam S-N fatigue curves for 18 percent Ni maraging steel bars subjected to heat treatments 06 p1014 A67-17800
-
- p>Heating rate influence on transformations in 18 percent nickel maraging steel 06 p1018 A67-18378
-
- p>Fusion welding of nickel maraging steel to lower strength steels to produce leaf spring subjected to tensile impact loading 07 p1198 A67-19213
-
- p>Composite material application to solid fuel rocket motor cases, discussing performance characteristics, manufacturing techniques, etc 09 p1578 A67-22513
-
- p>Pressure vessel design with ultrahigh strength steels, material strength variations, fracture toughness, minimum defect size and materials melting and fabrication practice [ASME PAPER 67-MET-18] 12 p2031 A67-25954
-
- p>Theoretical strength with iron-nickel maraging steels 12 p1957 A67-26125
-
- p>Effect of small cold deformation preceding aging in nickel maraging steel 13 p2132 A67-26575
-
- p>Maraging steels retaining toughness at cryogenic temperatures by suitable heat treatment 13 p2142 A67-27677
-
- p>Microstructural features of Ni maraging steel weldments related to fracture toughness properties 16 p2692 A67-31868
-
- p>Thermal nitridation of maraging steels, noting effects on mechanical properties 17 p2875 A67-33046
-
- p>Maraging stainless steel for high temperature applications, discussing properties, heat treatment and solution temperature effect 17 p2875 A67-33049
-
- p>Effectiveness of butt-welded joints and optimum heat treatment conditions for thin sheets of maraging steel containing 18 percent nickel 18 p3054 A67-34259
-
- p>Maraging steels development, discussing mechanical properties, metal working, etc 22 p3819 A67-39388
-
- p>Microsegregation and grain boundary liquation in heat affected zone of 18-Ni maraging steel welds 22 p3812 A67-39448
-
- p>Hot rolling finishing temperature and cooling rate effects on aged 250 grade 18 Ni maraging steel fracture toughness 22 p3822 A67-40057
-
- p>Primary and secondary strengthening precipitates in 18Ni/250/Al, V and Ti maraging steels 22 p3822 A67-40059
-
- p>Materials selection for external structures of transport aircraft flying at Mach 3 speeds, noting characteristics of maraging steels 23 p4019 A67-41045
-
- p>Machining advantages and economy of annealed steels over maraged steels 23 p4010 A67-41352
-
- p>Shear spun 300-grade maraging steel evaluated for pressure vessel applications, discussing fracture toughness [ASM PAPER C6-2.4] 23 p4020 A67-41412
-
- p>Corrosion and hydrogen embrittlement resistant nickel stainless maraging steel with bcc martensite crystal structure for pressure vessel applications 24 p4161 A67-42328
-
- MARE**
-
- S LUNAR MARE**
-
- MARINE NAVIGATION**
-
- p>Navigational satellite in aiding ships and aircraft in positioning, meteorology, communications, search and rescue, etc 01 p0111 A67-11390
-
- p>Competition and integration between maritime and air transport 08 p1429 A67-20770
-
- p>Navy navigation satellite system developed by APL, using Doppler frequency measurements for navigation fix 10 p1677 A67-23183
-
- p>Admiralty principles extended to occurrences involving aircraft flight over navigable water 12 p2040 A67-25486
-
- p>Automatic satellite navigation and communication system for aircraft and ships using cooperating ground stations 16 p2700 A67-30695
-
- p>Automatic position determination for ships using active navigation satellite systems, discussing communications potential and safety 19 p3254 A67-35310
-
- p>Satellite navigation systems requirements including Loran, inertial navigation and Navy systems 23 p4025 A67-41363
-
- MARINER II SPACE PROBE**
-
- p>Planetary proximity influence on motion of planetoid, with application to solar influence on Venus as studied by Mariner II 02 p0321 A67-11495
-
- p>Wide range vibrating-reed Mariner II electrometer, describing components, performance characteristics and results 02 p0241 A67-11681
-
- p>Composition and energy spectra of primary cosmic radiation in low energy regions from observations of Mariner II and Explorer VII 02 p0310 A67-12582
-
- p>Statistical properties of interplanetary magnetic field variations, charged particles propagation in solar system and photospheric processes analyzed, using Mariner II magnetometer 04 p0698 A67-14951
-
- p>Corpuscular stream parameters based on

data from Mariner II concerning cosmic ray variations on earth surface during geomagnetic storms 05 p0881 A67-16121

Masses of moon and Venus and astronomical unit determined from Mariner II Doppler data, noting sources of error 05 p0895 A67-16575

MHD approximation of solar plasma fluxes observed by Mariner II as free rotating jets 07 p1243 A67-19802

Solar wind plasma properties, noting relation between positive ion component and interplanetary magnetic field as measured by Mariner II [JPL-TR-32-1107] 13 p2190 A67-26304

Venus brightness temperature and atmosphere and Mars atmosphere sounded by Mariner II space probe, noting data on Mars magnetic field 14 p2322 A67-28964

Interplanetary magnetic field data by Mariner II compared to ground-based standard magnetograms and micropulsation recordings for October 7, 1962 geomagnetic storm 17 p2844 A67-32540

Corpuscular stream parameters based on data from Mariner II concerning cosmic ray variations on earth surface during geomagnetic storms 24 p4214 A67-42797

MARINER IV SPACE PROBE

Environment, mission requirements and subsystem interfaces effect on space vehicle structure [SAE PAPER 660673] 01 p0153 A67-10580

Canals on bright areas of Mars surface, from comparisons of observer sketches and Mariner IV photographs and Doppler spectroscopic results for dark areas 01 p0149 A67-10887

Mariner IV midcourse 50-lb thrust pressure-controlled monopropellant hydrazine propellant system, predicting impulse and velocity error as function of burn time [AIAA PAPER 66-948] 02 p0304 A67-12282

Absorptivity standard instrument to investigate solar absorptance of four surfaces used for spacecraft temperature control for Mariner IV on Mars mission [AIAA PAPER 65-650] 03 p0448 A67-13055

Half-scale thermal model of Mariner IV spacecraft tested in simulated solar environment [AIAA PAPER 66-23] 03 p0517 A67-13066

Martian craters, crater analysis techniques, impact velocities, etc., compared to lunar cratering and possibility of biological existence from Mariner IV photographs 04 p0696 A67-14736

Mariner IV Space Data Automation System /SDAS/ computer reliability design, pellet component concept, testing, interconnection and welding techniques 05 p0777 A67-17254

Martian surface in Mariner IV photographs 06 p1083 A67-18159

Martian lithosphere and rift valleys from Mariner IV data 06 p1092 A67-19005

Mariner IV magnetometer data in earth magnetosheath analyzed to determine character of fluctuations in magnetic field 07 p1179 A67-19911

Mariner IV trajectory analysis and importance of flight-path selection in construction of basic mission profile [AIAA PAPER 65-516] 08 p1413 A67-21507

Mariner IV spacecraft modification for Venus mission, discussing extent of changes 09 p1571 A67-21682

Polarity patterns of interplanetary magnetic field observed by Mariner IV during solar rotations 11 p1857 A67-23942

Pseudocolor technique, noting applicability to TV data presentation from space vehicles 11 p1789 A67-24250

Preliminary results of magnetic field measurements in vicinity of magnetosphere and interplanetary space from Mariner IV 12 p2007 A67-25822

Martian daytime atmosphere from zero to 50 km presenting spherical particle terminal velocities and possible sizes for obscurations, using Mariner IV occultation 13 p2195 A67-26316

Martian surface in Mariner IV photographs 16 p2741 A67-30503

Scientific instrument integration into Mariner IV spacecraft and prelaunch testing for flexible performance 16 p2757 A67-30640

Canopus star sensor used for roll control of Mariner IV spacecraft 16 p2699 A67-30654

Mariner IV spacecraft and mission 18 p3123 A67-34148

Visible brightness features in Mariner IV photographs of Mars interpreted as clouds 18 p3123 A67-34149

Mariner IV photographs of Mars, discussing mission objectives, functioning of camera system and interpretation of pictures 18 p3123 A67-34150

Radio occultation measurement of Martian atmosphere over two regions by Mariner IV space probe 18 p3123 A67-34151

Ground instrumentation system for Mariner IV occultation experiment, using Doppler frequency perturbation method for Mars atmospheric parameters determination 18 p3049 A67-34498

Control and measurement of temperatures of Mariner IV 18 p3052 A67-34514

Polymeric materials used for selected subsystems of Mariner IV space probe [JPL-TR-32-1031] 19 p3334 A67-35889

Mariner IV midcourse 50-lb thrust pressure-controlled monopropellant hydrazine propellant system, predicting impulse and velocity error as function of burn time 21 p3712 A67-37797

Mariner IV flight magnetometer data, determining interplanetary field and geomagnetic variability 22 p3790 A67-39800

Flight performance and power system design of Mariner IV Mars probe 23 p3939 A67-41509

MARINER PROGRAM

Ranger and Mariner spacecraft temperature control design, test and flight results 03 p0517 A67-13071

Mariner space vehicles design evolution noting contribution to future space flights through measurement of atmospheric density of Mars 24 p4241 A67-42399

Spacecraft structural criteria for lightweight photovoltaic solar arrays development, discussing Mariner type panel designs and power-to-weight ratios 24 p4108 A67-42557

MARINER SPACE PROBE

Structural design and temperature control influence on configuration of Mariner space probes 01 p0156 A67-11440

Mariner Venus 1967 space probe, obtaining atmospheric pressure density and refractive index from radio signal frequency, intensity and phase changes [AIAA PAPER 67-118] 06 p1085 A67-18310

Measurements performed from Mariner type probe during intercept with comet complement measurements performed from ground-based astronomical observatories by direct sampling 08 p1393 A67-21098

Mariner Venus 1967 space probe, obtaining atmospheric pressure density and refractive index from radio signal frequency, intensity and phase changes [AIAA PAPER 67-118] 22 p3886 A67-40094

Mariner space vehicles design evolution noting contribution to future space flights through measurement of atmospheric density of Mars 24 p4241 A67-42399

MARKOV CHAIN

Markovian division process application for solving multicomponent preventive maintenance, work sampling and search theory problems 01 p0108 A67-10930

Markov chains used in construction of reliability mathematical models for systems with dependence between components, noting differential equations 01 p0085 A67-11383

Stochastic process estimate of frequency and duration of weather events, using Monte Carlo simulation of probability distributions 02 p0261 A67-12079

Modeling of magnetic drum memory system using Markov chain based on historical data 03 p0400 A67-14220

Electronic generation of stochastic step processes defined by stationary Markov chains 07 p1162 A67-20195

Correlation functions and power spectra of stochastic processes with statistical structure defined by stationary Markov chains 07 p1217 A67-20196

Addenda to processes defined on finite Markov chain 09 p1524 A67-21680

Generalized maximum likelihood estimators with proof of asymptotic efficiency, considering Markov chain and stochastic difference 11 p1812 A67-24098

Information theoretic derivation of limit theorem for Markov chain with countable

number of states and constant transition probabilities 11 p1770 A67-24421

Algorithm for minimal realization of linear finite-dimensional dynamical system displayed by Markov parameters 14 p2291 A67-28066

Total number and number of distinct particles in equilibrium system of recurrent Markov processes 14 p2345 A67-28907

Final probabilities of ergodic Markov chain calculated by methods based on topological properties of stochastic graph 22 p3777 A67-39830

Communication constraint in ATC system modeled with Markov chain, noting data collection and reduction and data link utilization [AIAA PAPER 67-868] 24 p4124 A67-42991

MARKOV PROCESS

Direct and inverse Markov problem in complex region 01 p0104 A67-10286

Fluctuation noise effects on phase-locked automatic frequency control system obtained using Markov processes, determining phase difference probability density and statistical characteristics 01 p0037 A67-10713

Limiting theorem for weak convergence of solutions of differential equations with random right hand part to Markov process 01 p0106 A67-10922

Comparison of nonlinear and linear filtration in sense of minimum of mean square error of Markov process hidden in noise 01 p0106 A67-10923

Probabilistic structure of and establishment time for group synchronization in time-division-multiplex /binary code/ transmission systems 01 p0027 A67-11238

Real time data transmission systems with error detection, block retransmission capabilities and buffer storage unit treated as Markov process 02 p0194 A67-11810

Stability of stochastic difference systems in case of continuous perturbations subject to Markov random effect 03 p0467 A67-13111

Optimum processes in systems with distributed parameters described by partial differential equations 04 p0647 A67-15874

Simulation of controlled diffusion-type Markov processes applied to two stochastic equations related to problem of misadjustment on analog computer 05 p0768 A67-16263

Duality and a priori estimates in Markovian nonlinear stochastic optimal control problems 05 p0784 A67-16778

Linear fractional programming application to Markov renewal programming, determining stationary optimal policy for cost/time minimization 07 p1218 A67-20269

Stochastic Markov model for transient amplitude variation in systems with damped free vibration compared with deterministic solution 10 p1724 A67-23709

Nonequilibrium process in one dimension in presence of constant and oscillating electric field, using distribution function 11 p1824 A67-25078

Compact encoding of stationary Markov sources 12 p1919 A67-26085

Asymptotic study of Markov stationary discrete time and finite number of states decision process 14 p2291 A67-28510

Stochastic Liapunov function existence demonstrated for continuous strong Markov process with certain stochastic stability properties 15 p2458 A67-29898

Derivation of moments of continuous stochastic system 15 p2459 A67-30131

Finite dimensional approximations of optimal nonlinear filters for class of large-noise, nonlinear, continuous-time problems 16 p2651 A67-31680

All Markov transition functions in denumerable state space satisfying prescribed initial condition with given matrix 17 p2878 A67-32734

Homogeneous continuous Markov process without discontinuities of second kind and form of infinitesimal operator 17 p2878 A67-32735

Martin boundary for invariant Markov processes investigated on group of affine transformations of straight line 17 p2878 A67-32736

General variational theorem for rigid perfectly plastic materials developed using Hill and Markov maximum plastic work principles, noting possible unified derivation of principles 18 p3143 A67-34006

Markov processes applied to

synchronization failure in phase-lock AFC loop subjected to external fluctuations 18 p3000 A67-34086

Ergodic properties of additive functionals of recurrent Markov processes 18 p3071 A67-34182

Design of optimal waveforms for optimal estimation or prediction of state of linear dynamical system in presence of Markov and white noise 19 p3201 A67-34965

Hybrid computer Monte Carlo techniques for solving partial differential equations of continuous Markov processes 19 p3188 A67-36057

Optimum detection of Markov signals against noise background in case of discrete time 20 p3408 A67-37039

Optimal nonlinear filtering, deriving differential equations for probability density or state vector for noise corrupted system 21 p3603 A67-38442

Invariant measure existence condition derived for Markov processes, with several ergodic theorems for homogeneous Markov processes proved, noting transfer functions 22 p3827 A67-39877

Integral equation with transfer function density restrictions defining characteristic function of Markov process functional, deriving several limit theorems 22 p3827 A67-39878

MARS /PLANET/

SA EARTH-MARS RENDEZVOUS TRAJECTORY

Radio observations of Mercury, Venus and Mars, discussing concepts concerning planets physical condition 03 p0509 A67-13317

Martian craters, crater analysis techniques, impact velocities, etc, compared to lunar cratering and possibility of biological existence from Mariner IV photographs 04 p0696 A67-14736

Mars constitution examined on assumption of similarity to earth, noting Emden equation and Lyttleton results 05 p0902 A67-17290

Quantitative estimation of liquid water content on Mars from thickness of snow blanket on planet polar cap 06 p1084 A67-18167

Continental-oceanic boundaries of earth and relevance to tectonic speculations about moon and planets, noting role of radiogenic heat 06 p1091 A67-19003

Photographic observation of lunar topography and Mars 07 p1247 A67-19332

Trajectory characteristics of high thrust Mars missions and effect on other aspects of mission planning 07 p1248 A67-19358

Residuals in right ascension and declination of Mars observations made with astrolabe in France 07 p1250 A67-19723

Venus swingby trajectory for manned Mars mission as possibility in 1978-1986 [AAS PAPER 66-125] 07 p1254 A67-19984

Flight trajectories to moon, Venus and Mars 08 p1394 A67-21115

Martian radius determined by measuring gravity field at known surface points [JPL-TR-32-1091] 09 p1569 A67-22682

Compiled data for Mars apparition in 1967 giving general visibility conditions, phases, seasons and positions of Mars and earth 10 p1710 A67-23562

Martian entry condition analyzed as nonequilibrium flow field phenomenon, noting chemical kinetics and radiation behind shock wave in gas mixtures [AIAA PAPER 67-322] 12 p1930 A67-26037

Space flight to Mars, discussing medical problems originating from changing gravitational fields, meteorite dangers, radiation and psychological considerations 13 p2061 A67-26338

Evolutionary manned interplanetary exploration program with modular elements used for flyby, orbital capture and Mars landing, noting influence of Apollo program 13 p2199 A67-26827

Venus swingby trajectory for manned Mars mission as possibility in 1978-1986 [AAS PAPER 66-125] 13 p2209 A67-27538

Inconsistency in Martian surface pressure as calculated by Gray explained, using Leighton and Murray observations 14 p2389 A67-28842

Launching of space probes and data obtained on radiation particles and magnetic fields in space 14 p2392 A67-28960

Venus brightness temperature and atmosphere and Mars atmosphere sounded

by Mariner II space probe, noting data on Mars magnetic field 14 p2322 A67-28964

Pasteur Probe, assay of asymmetry of D, L amino acids in detection of Martian life 15 p2433 A67-29116

Radio observations of Mercury, Venus and Mars, discussing concepts concerning planets physical condition 16 p2741 A67-30493

Quantitative estimation of liquid water content on Mars from thickness of snow blanket on planet polar cap 16 p2742 A67-30511

Entry/Lander vehicle for Mars mission discussed in terms of gross payload, basic vehicle and preentry system 16 p2756 A67-30629

Automated biological laboratory /ABL/, comprehensive integrated system for detection of life on Mars 16 p2762 A67-31488

Mars polar cap size changes, color and visibility from observations in 1963 17 p2942 A67-32330

Nuclear propulsion for manned Mars expedition, discussing engine and launch optimization, computer simulation, performance, trip times, velocity, weight, etc [AIAA PAPER 67-510] 18 p3077 A67-33974

Radio and radar observations of Mercury, Venus and Mars 18 p3123 A67-34144

Mariner IV spacecraft and mission 18 p3123 A67-34148

Mars emission spectrum computed for two atmospheric models, presenting weighting functions for different wave numbers 18 p3125 A67-34159

Mars landing guidance requirements for unmanned lander after separation from interplanetary flyby space vehicle 21 p3655 A67-37783

21.2 cm spectra of Jupiter, Venus, Mars and Saturn noting mean effective brightness temperatures 21 p3709 A67-38993

Nuclear electric space power plant with Rankine cycle for plausible Mars manned mission, discussing mission requirements and reactor elements 24 p4186 A67-42549

Satellite rise and set time of distant primary and occultation interaction determined for case of Martian satellite 24 p4238 A67-42925

MARS ATMOSPHERE

Mars atmosphere entry probe configuration, aerodynamic characteristics, flow field, stability augmentation, instrumentation, thermal shielding, data handling and communications 01 p0156 A67-11424

Aerodynamic, thermodynamic and structural design aspects of flight capsule entering low density Mars atmosphere from orbit 01 p0156 A67-11432

Model of nonequilibrium properties of high temperature carbon dioxide and other gas mixtures in connection with studies for vehicles entering Martian atmosphere 01 p0008 A67-11436

Composition and surface pressure of Martian atmosphere determined from photographic spectrum of Mars obtained at March 1965 opposition 02 p0323 A67-11695

Carbon dioxide abundance at 200 degrees K determined from high dispersion IR spectrograms of Mars 03 p0514 A67-14309

Mechanism regulating total amount of earth and Mars atmosphere transparent to visible and IR radiation 06 p0995 A67-18052

Guided propulsive solution to Mars atmosphere-decelerated soft landing vehicle trajectory [AIAA PAPER 67-170] 06 p1029 A67-18508

Mars atmospheric composition and laminar convective heating and ablation studied to predict performance of heat protection systems during entry 06 p1119 A67-18849

Inviscid equilibrium gas stability characteristics for pointed and spherically blunt bodies in unsteady supersonic flight in Mars atmosphere 07 p1258 A67-19380

Carbon dioxide abundance and surface pressure of Martian atmosphere, noting self-broadening correction 08 p1400 A67-21250

Response of fungi to diurnal temperature extremes, describing soil, simulated Martian temperature regime and fungi growth 09 p1454 A67-21991

High dispersion spectrograms of Mars examined for water vapor presence, results indicate amount depends on size of polar cap [JPL-TR-32-1048] 09 p1568 A67-22235

Elevation differences between Martian

dark areas /maria/ and bright areas /deserts/, discussing surface pressure and temperature 10 p1706 A67-22957

Martian transient phenomena correlations among mass motion of water in atmosphere, polar cap growth and white cloud appearance frequency 11 p1862 A67-24501

Voyager project goals, orbital operations, capsule descent, navigational systems, etc 12 p2002 A67-25232

Martian atmosphere models with different composition, pressure and temperature 12 p2003 A67-25685

Mars atmospheric composition determination by shock layer radiometry technique during probe experiment [AIAA PAPER 67-293] 12 p2009 A67-26009

Martian daytime atmosphere from zero to 50 km presenting spherical particle terminal velocities and possible sizes for obscurations, using Mariner IV occultation 13 p2195 A67-26316

Mars atmosphere and ionosphere analyzed by measuring effect on radio occultation of planet, determining shape, atmosphere density profile, diurnal variations, etc [JPL-TR-32-1157] 13 p2199 A67-26819

Planetary quarantine constraints, noting prevention of Martian atmosphere contamination 15 p2424 A67-29098

System design of automated laboratory and associated entry vehicle for unmanned Martian exploration 16 p2653 A67-30628

Voyager project goals, orbital operations, capsule descent, navigational systems, etc 16 p2751 A67-31487

Carbon dioxide ions with electrons dissociative recombination measurements with microwave-afterglow differentially pumped quadrupole mass-spectrometer apparatus, noting Martian atmosphere model [SRCC-55] 17 p2888 A67-32828

Radiative relaxation times for temperature perturbations in CO₂ with small water vapor admixture under conditions similar to Martian atmosphere, discussing dynamical phenomena 17 p2951 A67-33187

Radio occultation measurement of Martian atmosphere over two regions by Mariner IV space probe 18 p3123 A67-34151

Mars atmosphere surface pressure, radiative equilibrium temperatures, sunlight resonance scattering distribution, etc 18 p3123 A67-34152

Martian atmosphere circulation model from Mariner IV occultation experiment, studying lateral eddy viscosity, winds, surface temperature and stress 18 p3124 A67-34153

Martian atmosphere transparency and visibility of surface details in blue and UV light, showing dark and semitone areas intensity, etc 18 p3124 A67-34154

Martian clouds analysis and topographical relationships, discussing white and yellow classification and frequency of occurrences 18 p3124 A67-34156

Atomic and molecular processes in Cytherean, Martian and Jovian upper atmospheres 18 p3124 A67-34158

Ground instrumentation system for Mariner IV occultation experiment, using Doppler frequency perturbation method for Mars atmospheric parameters determination 18 p3049 A67-34498

Effective braking height /EBH/ for small interplanetary particles of cosmic velocity entering Martian upper atmosphere 18 p3135 A67-34541

Venus and Mars atmosphere and surface studied by radio astronomy 19 p3317 A67-34796

Magnetospheric boundary and standing shock wave for earth scaled down to apply to Mars 19 p3324 A67-35442

Soviet book on planetary physics covering Martian, Venusian and Mercurian atmospheres, Venusian surface temperature and Jovian radio emission 21 p3707 A67-38933

Atmosphere of Mars studied using three models generated to show high, mean and low density compositions to account for gravitational and magnetic fields 22 p3887 A67-40140

Spherical entry vehicle used to define planetary atmosphere structure and composition from dynamic response during entry, discussing aerodynamic characteristics 22 p3907 A67-40177

Martian atmosphere component due to proton penetration into atmosphere from

solar wind, suggesting radio occultation by Mars orbiter 23 p4063 A67-40799

MARS ENVIRONMENT

Subsonic and supersonic parachutes for soft landing on Mars, discussing aerodynamic coefficients, descent rate, dynamic stability, inflation, porosity and wind effects, etc 04 p0551 A67-14574

McDonnell Martian Environmental Simulation Facility, analyzing sand and dust storm behavior at low pressures 07 p1248 A67-19386

Tabulated altitudes, periods and velocities for Martian satellites in circular parking orbits 09 p1564 A67-21716

Reassessment of COSPAR recommendations concerning planetary quarantine and spacecraft sterilization, particularly for Martian environment 10 p1601 A67-23579

Microhill hypothesis for Martian wave of darkening noting developments 11 p1859 A67-24223

Low barometric pressure, high carbon dioxide concentration and water availability on simulated Mars environment related to survival and growth of bacillus cereus 15 p2426 A67-29111

Soil, moisture and other requirements for microorganism survival in simulated Martian environment 19 p3177 A67-35220

Planetary quarantine problem for Martian survival of microorganisms investigated, using systems analysis 19 p3180 A67-35274

Internal and surface Martian geology synthesis, investigating parameters favoring organic growth and sites for exploration 19 p3323 A67-35334

Growth of terrestrial microorganisms on Mars noting possibility of planetary contamination 19 p3178 A67-35896

Subsonic and supersonic parachutes for soft landing on Mars, discussing aerodynamic coefficients, descent rate, dynamic stability, inflation, porosity and wind effects, etc 20 p3356 A67-36408

Survival and growth of Bacillus cereus and B. subtilis in simulated Martian environment of diurnal temperature cycling and low moisture and oxygen level 20 p3372 A67-37160

Martian sand and dust storms simulation and abrasive effects on spacecraft surface coatings, noting similarity with Earth deserts 24 p4227 A67-42038

MARS EXCURSION MODULE/MEM/

Mars/Venus flyby missions with manned Mars landers, showing trajectory profile for mission 05 p0902 A67-17221

MARS PROBE

SA MARINER SPACE PROBE

Mars atmosphere entry probe configuration, aerodynamic characteristics, flow field, stability augmentation, instrumentation, thermal shielding, data handling and communications 01 p0156 A67-11424

Mars/Venus flyby missions with manned Mars landers, showing trajectory profile for mission 05 p0902 A67-17221

Mars stopover mission with Venus swingby technique, discussing velocity requirements, trip times and initial mass in earth orbit [AIAA PAPER 67-27] 06 p1085 A67-18332

Aerodynamic characteristics of Mars probe/lander configurations consisting of blunted cone, shell and spherical segment analyzed at various Mach numbers on ballistic range [AIAA PAPER 67-167] 06 p0941 A67-18482

Trajectory possibilities for Venus swingby mission and role in manned exploration of Mars [AIAA PAPER 66-37] 07 p1248 A67-19363

Communication parameters associated with Martian flyby probes and with lander and manned vehicles 07 p1145 A67-19870

Data transmission capabilities of Mars probes and landing capsules [AAS PAPER 66-62] 07 p1146 A67-19998

Orbital reconnaissance of Mars in 1971 using modified Lunar Orbiter spacecraft, noting photographic system, trajectory, launch system, etc 09 p1570 A67-21681

System design of Voyager-class Mars Probe/ Lander, considering selections of entry aeroshell, landed capsule and descent and postimpact instrumentation 10 p1714 A67-23756

Geometric restraints on orbit about Mars noting trajectories of unmanned Mars

exploration satellite, payload, orbit inclination, etc 16 p2745 A67-30748

Mars stopover mission with Venus swingby technique, discussing velocity requirements, trip times and initial mass in earth orbit [AIAA PAPER 67-27] 17 p2940 A67-32059

Aerodynamic characteristics of Mars probe/lander configurations consisting of blunted cone, shell and spherical segment analyzed at various Mach numbers on ballistic range [AIAA PAPER 67-167] 19 p3169 A67-34816

Navigation and guidance analysis of Mars probe launched from manned flyby spacecraft for 1975-1976 [AIAA PAPER 67-546] 19 p3257 A67-35945

Guidance system requirements for unmanned Martian propulsive landing capsule [AIAA PAPER 67-619] 19 p3260 A67-36008

Alternate mission modes for manned Mars exploration 22 p3886 A67-40136

MARS SPACECRAFT

SA MARINER SPACE PROBE

Two superlight ablative compositions /SLA-741 and SLA-561/ developed for Mars Lander thermal protection, examining superiority to conventional low density charring ablators [SAE PAPER 660654] 01 p0103 A67-10614

Rankine cycle power plant characteristics for electric propulsion manned Mars mission [AIAA PAPER 66-894] 03 p0504 A67-14274

Hardware design and production problems in launch and at separation for minimizing earth bacteria biocontamination Martian lander 04 p0562 A67-14425

Soft landing problems for unmanned Mars entry noting parachute system, descent time, sensing system constraints, extreme wind environment, etc 04 p0706 A67-15236

Solar electric spacecraft performance in specific Mars orbiter-lander mission evaluated, using characteristic length concept 06 p1074 A67-18276

Sensing techniques for initiating parachute deployment on Mars lander vehicle [AIAA PAPER 67-202] 06 p0948 A67-18302

Planned encounters with asteroids in manned missions to Mars for observational purposes, using computer program [AAS PAPER 66-124] 07 p1254 A67-19983

Progressive mission capability of Mars capsule, examining feasibility of increased scientific payload weights by increase of mission profile [AAS PAPER 66-58] 07 p1255 A67-19995

Manned planetary mission possibilities stressing Mars exploration, noting trajectory planning, propulsion, crew requirements, etc 08 p1394 A67-21099

Superlight ablative systems for Mars Lander thermal protection 10 p1672 A67-23724

Interplanetary transit and atmospheric entry of unmanned vehicle landing on Mars surface, with reference to heat shield technology [JPL-TR-32-1145] 12 p2034 A67-25715

Planned encounters with asteroids in manned missions to Mars for observational purposes, using computer program [AAS PAPER 66-124] 13 p2209 A67-27537

Superlight ablative systems for Mars Lander thermal protection 22 p3826 A67-40088

Rankine cycle power plant for electric propulsion manned Mars mission analysis of system characteristics and mission duration effect 22 p3869 A67-40173

Performance and feasibility of staged propulsion during terminal phase of Mars soft landing [AIAA PAPER 67-987] 24 p4246 A67-43059

MARS SURFACE

Canals on bright areas of Mars surface, from comparisons of observer sketches and Mariner IV photographs and Doppler spectroscopic results for dark areas 01 p0149 A67-10887

Spectral scans of Mars and region of moon in IR range obtained with 82-inch telescope reduced, using scans of moon and sun, to spectral reflectivity curve 02 p0319 A67-11454

IR colorimetry of Martian bright and dark areas indicates correlations with limonite terrestrial rocks and volcanic ash 02 p0319 A67-11456

Physical simulation design of Martian surface environment in form of physically enclosed environmental

chamber 02 p0230 A67-12350

Carbon dioxide condensation on Martian polar caps 04 p0694 A67-14494

IR spectra of Mars bright areas compared with terrestrial rock, drawing conclusions regarding Mars mineralogy and detrital cover 05 p0896 A67-18717

Martian surface in Mariner IV photographs 06 p1083 A67-18159

Iron hydroxide formation in producing surface color of Mars 06 p1083 A67-18160

Photographic mapping of Martian surface with electrically propelled solar-powered photographic spacecraft placed into near polar orbit [AIAA PAPER 67-88] 06 p1096 A67-18438

Martian topography influence on formation of temperature bright patches 06 p1088 A67-18644

Frost phenomena on Mars examined on basis of Martian wave of darkening, noting necessity of deliquescent salts to attract and retain water on surface 06 p1089 A67-18645

Martian and lunar craters and volcanic activity 06 p1089 A67-18648

Martian lithosphere and rift valleys from Mariner IV data 06 p1092 A67-19005

Voyager type landers on Mars surface noting instrumentation, operation, reliability, etc [AAS PAPER 66-61] 07 p1259 A67-19997

Incremental and cumulative methods for analysis of diameter-frequency relation for craters, with special application to moon 08 p1385 A67-20932

Crustal features of moon and Mars analyzed for mantle convections, noting correspondence to spherical harmonics of various orders 08 p1397 A67-21208

Radar observation of Mars, noting mean reflection coefficient for signals returned by near center disk sections 09 p1563 A67-21632

Surveyor system and camera design for photographic mission on Mars surface 09 p1570 A67-21680

Ground observations of Martian relief during 1967 optimum period 09 p1565 A67-22014

Martian transient phenomena correlations among mass motion of water in atmosphere, polar cap growth and white cloud appearance frequency 11 p1862 A67-24501

Observations with birefringent interferometer and photoelectric spectrophotometer of Martian surface materials composition, noting strong band at 3.1 micron suggesting hydrated minerals 11 p1865 A67-24603

Radar measurements of Doppler spectra and power reflectivity of Mars interpreted as surface elevation differences between dark and bright areas 11 p1867 A67-24776

Spectrometric investigation of Mars in five spectral regions applied to color analysis of Martian continents and oceans for probable coloring of Martian vegetation 11 p1867 A67-24845

Martian surface in Mariner IV photographs 16 p2741 A67-30503

Iron hydroxide formation in producing surface color of Mars 16 p2741 A67-30504

Martian secular changes and dark area regeneration attributed to movement of sand, dust and wind caused by elevation and slope differences 16 p2747 A67-30989

Statistical correlation of latitude with time of maximum darkening of Mars dark areas, noting consistency of 2 models 16 p2749 A67-31401

Mars polar cap size changes, color and visibility from observations in 1963 17 p2942 A67-32330

Matter density and other physical properties of Martian surface estimated from radio and IR observations 18 p3119 A67-33860

Visible brightness features in Mariner IV photographs of Mars interpreted as clouds 18 p3123 A67-34149

Mariner IV photographs of Mars, discussing mission objectives, functioning of camera system and interpretation of pictures 18 p3123 A67-34150

Martian atmosphere transparency and visibility of surface details in blue and UV light, showing dark and semitone areas intensity, etc 18 p3124 A67-34154

Martian surface atmospheric pressure via photometric observations of Phobos eclipses 18 p3124 A67-34155

Relation between surface pressure and

atmospheric brightness in optically thin Rayleigh scattering atmosphere, considering application to Mars 18 p3134 A67-34536

Venus and Mars atmosphere and surface studied by radio 19 p3317 A67-34796

astronomy 19 p3317 A67-34796

Internal and surface Martian geology synthesis, investigating parameters favoring organic growth and sites for exploration 19 p3323 A67-35334

Direct and relay links capabilities for returning data to earth from Mars lander compared on effective radiated power basis [AIAA PAPER 67-647] 20 p3387 A67-37627

Radar cross section of Mars, discussing spectral analysis, echo delay and radar echoes from Jupiter 21 p3706 A67-38617

Impact crater size vs incidence analyzed statistically in study of validity of time dependence on saturation for moon and Mars 23 p4066 A67-41007

Photometric data on Mars opposition effect /nonlinear brightness surge at zero alpha phase angle/ noting phase curve steepness 24 p4226 A67-41838

MARTENSITIC STEEL

Weldability of quenched and tempered martensitic alloy steels of low to medium carbon content, particularly carbon-nickel-cobalt alloys 01 p0081 A67-11041

Electron microscopic structure and lattice defects of martensite in commercially pure titanium 06 p1017 A67-17966

Transformation twins in titanium, discussing relationship between twins and martensite crystal, using electron microscopy 06 p1017 A67-17967

Thermal mechanical treatments influence on strength, toughness and environmental failure resistance of low alloy high strength martensitic steel 11 p1806 A67-24363

Martensitically hardened high strength stainless steel, physical properties, heat treatment effects, etc 11 p1810 A67-25103

Cumulative strain behavior of nickel-chromium alloy and chromium martensitic type steel under action of cyclic loading 12 p2015 A67-25420

Electron microscopy used to investigate various defects forming in phase resulting from martensitic transformation 17 p2874 A67-32896

Crack nucleation in high strength low alloy steel, comparing fatigue processes in quenched and tempered martensite with those in pure metals 18 p3064 A67-34082

Endurance fatigue characteristics of weldable martensitic stainless steel, giving data for butt and spot welds 22 p3811 A67-39447

Aging of iron-nickel-titanium alloys during heating in reverse martensitic alpha to gamma transformation process, investigating phase parameter changes 22 p3820 A67-39824

Corrosion and hydrogen embrittlement resistant nickel stainless maraging steel with bcc martensite crystal structure for pressure vessel applications 24 p4161 A67-42328

MASER

SA GAS MASER

SA INFRARED MASER

SA LASER

SA TRAVELING WAVE MASER

Masers and lasers from Einstein discovery of stimulated emission to present 01 p0089 A67-10503

Negative absorption in cosmic radio sources of synchrotron radiation 04 p0700 A67-15200

Generalized Callen-Welton theorem applied to calculation of maser oscillations in amplification and generation regimes, determining noise spectral energy and spectral line width 05 p0762 A67-18350

X-band ruby maser design with liquid hydrogen cooling for high gain at low pumping power 07 p1194 A67-19131

Temperature dependence of paramagnetic resonance spectral shifts in chromium-doped titanium oxide crystal of cross relaxation rutile maser 07 p1196 A67-19676

Microwave receivers with low noise - Colloquium, Paris, May 1966 09 p1481 A67-22477

Continuous magnetic field satisfies conditions of stability, size, orientation, uniformity and controllability of maser type amplifier employing superconductor 09 p1516 A67-22482

Dependence of intrinsic noise temperature of ruby reflection maser on helium bath

temperature and chromium trioxide doping, using circulator 10 p1665 A67-23505

Anomalous polarization of four cosmic OH lines predicted from states of polarization in OH maser amplifier 13 p2161 A67-27289

Miniature cryogenic refrigeration systems design for masers and parametric amplifiers, investigating efficiency and contamination 14 p2277 A67-27775

Maser effect hypothesized as cause of 21 cm radiation in clouds of interstellar hydrogen in galactic corona 15 p2551 A67-29139

Soviet book on radio physics quantum amplifiers covering lasers, maser, paramagnetic resonance, etc 19 p3238 A67-34799

Bandwidths of reflex multicavity solid state masers containing active material in cavities 20 p3462 A67-37328

Design and operation of three-cavity solid state ruby maser 20 p3462 A67-37329

Quantum theory of maser oscillator model consisting of radiation field mode interacting with 3-level atoms 22 p3814 A67-39436

Maser effect hypothesized as cause of 21 cm radiation in clouds of interstellar hydrogen in galactic corona 24 p4239 A67-43062

MASER OUTPUT

Oscillation frequency of maser oscillator calculated using perturbation theory, noting traveling wave effect 01 p0089 A67-10395

Traveling wave maser consisting of paramagnetic crystal /chromium doped rutile/, slow wave circuit and ferrite isolator, discussing performance, stagger tuning, etc 02 p0251 A67-11787

Fluctuation measurements in amplitude of oscillation of ammonia beam maser 09 p1513 A67-22043

H-band coupled cavity transmission maser noting bandwidth gain and low noise temperature operation 10 p1665 A67-23441

Ruby maser operating with microrefrigerator at low temperature, noting broadband and bandwidth 11 p1800 A67-24467

Frequency shifting technique using auxiliary coil to produce magnetic field for masers in high power radar applications 15 p2439 A67-30392

Population inversion and spin-lattice relaxation effect on maser operation 19 p3304 A67-35547

Maser output pulsations by varying active particles entering resonator through electric or magnetic field 21 p3638 A67-37941

Laser and maser noise quantum theory emphasizing equations of motion and fluctuation problem, deriving density matrix equation 23 p4011 A67-40762

Czochralski ruby shows high inversion ratio when used as microwave maser material 24 p4205 A67-42813

MASER RESONATOR

Chromium-doped rutile suitability as active material in solid state maser resonator 01 p0088 A67-10246

Maser oscillation intensity and frequency dependence on constant electric and magnetic fields acting on molecular beam in front of resonator 01 p0089 A67-10396

Amplitude and frequency characteristics of hydrogen-atom beam maser 02 p0251 A67-11574

Two-frequency volume resonator with independent tuning within wide frequency band 02 p0214 A67-11911

Oscillation amplitude modulation in ammonia beam maser oscillator with single cavity followed by two cavities in cascade 05 p0817 A67-18636

Oscillation of maser with sinusoidal distribution of resonator field along axis of molecular motion 05 p0826 A67-17234

Intrinsic noise temperature measurement in reflection type cavity maser 06 p1010 A67-17892

L-band rutile traveling wave maser, discussing slowing factor and inverted susceptibility 09 p1514 A67-22270

Atomic and molecular frequency standards, reviewing ammonia and hydrogen masers and Cs, Tl and Rb gas frequency standards 14 p2333 A67-28975

Amplification characteristics of multicavity masers, determining Q-factor using chain matrix A formalism 19 p3241 A67-38027

Maser output pulsations by varying active particles entering resonator through electric or magnetic field 21 p3638 A67-37941

Resonant cavity electric field excitation placed in magnetic field near electron cyclotron frequency studied for expressions of self-excitation current 22 p3816 A67-40128

MASK

Photolithographic and metal aperture masks for integrated and thin film circuit manufacturing 13 p2124 A67-27390

MASKING

Magnesium wire as in-contact masking material, with surfaces precoated with thin silver layer 03 p0494 A67-13490

Design and fabrication of germanium Esaki diodes emphasizing development of planar process, using conventional oxide masking techniques 13 p2083 A67-27572

MASS

S AIR MASS

S CRITICAL MASS

S ELECTRON MASS

S PARTICLE MASS

S PLANETARY MASS

S SCHMIDT NUMBER

S STELLAR MASS

S VARIABLE MASS SYSTEM

MASS BALANCE

Fiber reinforced rotor blades, discussing composite material selection for research, mass balance, dynamic response tuning and material design properties 03 p0453 A67-13416

Resonance oscillations and rotations in mechanical systems having n-dimensional quasi-static vector analyzed and applied to triaxial ellipsoid with unbalanced mass 10 p1680 A67-23409

Book on principles of continua with applications 12 p1966 A67-25557

Lumped parameter model for monopropellant hydrazine reaction chamber developed, using mass and energy balance and reaction and diffusion rate coefficients 17 p2927 A67-31974

Roll-rate reversal dispersion effects of ballistic reentry body due to mass and aerodynamic asymmetries 22 p3742 A67-40117

Small perturbation analysis on mass conservation stability in solid propellant combustor, discussing parametric model 23 p4084 A67-41721

Soviet book on molecular flow in vessels covering mass balance, energy exchange, rarefied gas, etc 24 p4191 A67-42359

MASS DISTRIBUTION

Discrepancies between various mass models of galactic systems, commenting on rotation curves 02 p0324 A67-11768

Mass distribution of meteoric bodies and relation to autocorrelation function of disintegrated planetary surface 02 p0329 A67-12495

Semiconductor character of mercury selenide determined by analyzing variation of band-edge effective mass as function of composition of HgSe-CdTe alloys 03 p0499 A67-13886

Velocity, energy and concentration fields in laminar boundary layers with arbitrarily distributed mass transfer at surface 04 p0603 A67-14643

Meteoritic body distribution by energies noting consistency with mass distribution 04 p0701 A67-15228

Variability of conveyor belt velocity during loading and operation, unloading and stopping under load analyzed, using distribution theory 05 p0908 A67-18043

Distribution of instantaneous value of amplitude of signal after scattering on meteor trails 07 p1250 A67-19721

Imparting motion to system of two masses coupled by linear elastic shaft in infinite set of piecewise continuous loads, by variational method of influence functions 08 p1354 A67-21047

Free molecular flow rate and mass distributions through various length cylindrical nozzles 09 p1488 A67-22106

Relation between human mechanical impedance and coupling of human center of mass to environment, noting transfer function 09 p1456 A67-22370

Effect of mass distribution and loading sequence on elastic rod, solving eigenvalue problem by Galerkin method 10 p1715 A67-22912

Mass distribution of meteoric bodies and relation to autocorrelation function of disintegrated planetary surface 10 p1709 A67-23363

Flexibility and mass distribution effect on

vibration response of general continuous structures
[ASME PAPER 67-VIBR-44]

11 p1873 A67-24196

Natural and forced lateral vibration analysis of free-free beam by integration and finite difference methods, considering influence coefficients
[ASME PAPER 67-VIBR-54]

11 p1873 A67-24202

Post-Galilean transformation to which Einstein-Infeld-Hoffmann motion equation is invariant, considering transformation to center of mass system

12 p1965 A67-25125

Free oscillations of closed freely supported cylindrical shell of concentrated mass, determining frequency and bending moments

12 p2025 A67-25604

Vibrational mode behavior of rotating gravitational mass sensors and sensor design to minimize nonideal effect of manufacturing and external disturbances

12 p1945 A67-25919

Surface mass addition into turbulent boundary layer for attaining equilibrium velocity profiles, determining development from start of injection

12 p1930 A67-25929

Nonrelativistic theory of rotating configurations in terms of gravitational potential, center mass density and variable angular velocity

14 p2382 A67-27833

Structural mass and shielded volume problems of unconfined magnetic space shields design

14 p2253 A67-29040

Stability of prismatic shaft rotating with constant angular velocity as function of mass and setting point of rotating mass

16 p2766 A67-31151

Line element not precluding peculiar motions or assuming isotropy and homogeneity of mass distribution of universe, considering kinematical consequences

18 p3117 A67-33427

Superdense cosmical object model, discussing negative mass defect necessary for expansion to diffuse state

18 p3133 A67-34433

Dynamic modeling of complex rotor system to determine critical velocities, noting influence of number of mass concentrations on accuracy

21 p3689 A67-37951

Shape of line of deflection in systems subjected to flexural vibrations of rotating weightless shaft supporting eccentrically distributed mass points or disks

21 p3636 A67-38831

Gravity gradiometer digital computer program for simulated rotating gravitational mass sensor and gradient contour mapping

23 p4000 A67-41218

Meteor mass distribution, estimating exponent constant in cumulative influx formula

24 p4225 A67-41828

Mechanical system motion with point moving on surface, imposing limitations on system mass distribution, obtaining fixed coordinate system

24 p4188 A67-42302

MASS FLOW

Cryogenic fluid mass flow measurement methods, noting flow meter calibration

03 p0421 A67-13768

Temperature distribution in argon plasma jet with variable mass flow measured, using grating spectrometer

[ASME PAPER 66-WA/HT-50]

04 p0669 A67-15434

Unsteady heat transfer in tubes resulting from changes in heat flow, gas mass flow rate and acoustic balance

04 p0733 A67-15844

Empirical expression for resistance of small bore tubes to turbulent flow of compressible fluid in terms of mass flow and total head

08 p1320 A67-20461

Mass limiting two-phase flow compared in straight tube and in nozzle

13 p2093 A67-26541

Monte Carlo approach to transition and free molecular flow problems having mass as well as thermal motion of molecules

13 p2101 A67-26967

Cryogenic fluid mass flow measurement methods, noting flow meter calibration

13 p2121 A67-27633

Simple impact position model for predicting subsonic mass flow for opposing axisymmetric jet

14 p2303 A67-28331

Large combustion-driven, self-excited Faraday-type MHD generator having multi-or single-circuit net power output, discussing design

16 p2608 A67-30596

Separation streamline for massive blowing in free stream for model injected into arc tunnel flow

[AIAA PAPER 66-457] 17 p2839 A67-33007

Local mass flux and local impact pressure measurement in arc jet exhaust flow fields

17 p2861 A67-33029

Radial instreaming mass flow effect on cylindrically-symmetric arc with transpiration cooling, noting heat flux reduction

19 p3280 A67-35148

Compressible boundary layer-inviscid flow interactions in entrance region of internal flows, including shock tube boundary layer and effects of mass injection or suction

[ASME PAPER 67-HT-2] 20 p3421 A67-36701

Hydraulic resistance coefficient of rotating tubes, taking into account centrifugal mass forces effect on flow inside tube

20 p3421 A67-36793

Electromagnetically driven confined viscous vortex flow with high positive radial Reynolds numbers, solving energy equation for temperature distribution

[AIAA PAPER 67-730] 21 p3674 A67-38754

Oscillating mass flow characteristics in modified Moore variometer configuration for step, triangular and infrasonic functions

23 p4000 A67-41221

Stellar and planetary magnetic field formation theory based on concept of existing ionized turbulent mass flow on these celestial bodies

24 p4230 A67-42352

MASS FLOW FACTOR

SA NOZZLE GEOMETRY

Mass effect on blast wave equations of shock generation by secondary injection of fluid into hypersonic flow

01 p0141 A67-11179

Cathode phenomena in plasma thrusters with self-magnetic acceleration low mass-flow rates

19 p3297 A67-35600

Boundary layer effect on mass flow parameter and ram efficiency of submerged intakes

20 p3360 A67-37490

MASS FLOW RATE

Graphs for momentum flux and mass flow calculations for use in subsonic compressible flow

01 p0007 A67-11268

Helium 2 film free convection heat transfer, discussing mathematical analysis for vertical flat plate and horizontal circular cylinder

[ASME PAPER 65-WA/HT-10] 03 p0536 A67-14007

Thrust and mass flow rate of supersonic nozzle with and without internal separation

04 p0602 A67-14568

Electromagnetic measurement of motion of explosion products behind detonation wavefront, calculating isentrope from mass velocity distribution

04 p0606 A67-15184

Thermal choking in various devices having mixing processes between two flows with different stagnation enthalpies as possible limitation of mass flow rate

[ONERA-TP-411] 05 p0792 A67-16934

Hydrogen arcjet plume spectroscopy, examining exhaust at various H mass flow rates

05 p0874 A67-17357

Low rate gas flow meter noting sealing and controlling of piston, differential pressure meter and DC servoamplifier

06 p1000 A67-17753

Propellant injection through electrodes effect on potential distribution in MPD arc

[AIAA PAPER 67-49] 06 p1074 A67-18435

Critical mass flow rate existence for maximum thrust from MPD arc jet

06 p1075 A67-18866

Free molecular flow through circular orifice at high pressure ratios, discussing mass flux measurement methods

14 p2300 A67-28179

Compressible fluid flow in capillary tubes, discussing reduction in variation of pressure difference/mass flow ratio

14 p2303 A67-28350

Aircraft flow meters for simultaneous rate and volume measurements, examining equations of motion

16 p2671 A67-31006

Fluidic fuel control system for subsonic combustion ramjet engine, describing components, breadboard model and performance characteristics

[AIAA PAPER 67-497] 18 p3113 A67-33961

Lithium and ammonia MPD arc thrusters tests in low environmental pressure

[AIAA PAPER 67-685] 21 p3692 A67-38716

Mass flow rate, viscosity and conductivity changes effects on single needle colloid

thruster

[AIAA PAPER 67-530] 21 p3696 A67-38957

Swirling mass flow in supersonic nozzle indicates discharge coefficient falls nonlinearly with swirl

22 p3739 A67-39527

Mass efflux of Poiseuille flow over naturally permeable wall, discussing boundary layer effect

24 p4144 A67-42571

MASS RATIO

SA PAYLOAD MASS RATIO

SA PROPELLANT MASS RATIO

Cyclotron absorption in n type lead telluride with wide range of carrier concentrations, showing increase in transverse effective mass and decrease in anisotropic mass ratio

03 p0493 A67-13352

Extension of mass range of monopole mass spectrometer and effects on resolving power, sensitivity and mass discrimination, for partial pressure analysis

06 p1000 A67-17747

Equilateral position stability of equilibrium in planar restricted problem of three bodies for mass ratio values

13 p2205 A67-27477

Launch vehicle performance and engineering trade-off, considering mass fraction, weight reduction, specific impulse, losses and stage selection

16 p2762 A67-31489

Vehicle mass requirements for optimal high and low thrust propulsion systems for manned and unmanned planetary missions

20 p3533 A67-37125

Low pressure solid rocket motor design and application, noting advantages in high mass ratio performance and operational disadvantages

20 p3516 A67-37131

Magnetic shear effects on density gradient drift instabilities in plasma with plasma pressure to magnetic pressure ratio larger than electron-ion mass ratio

22 p3845 A67-39483

Mass species abundance ratio of hydrogen ion beam from Oak Ridge type duoplasmatron ion source, discussing pressure dependent characteristics

23 p4034 A67-41436

MASS SPECTROMETER

Miniaturized magnetic-type mass spectrometer for multigas analysis in high performance aircraft

01 p0068 A67-10957

Tandem mass spectrometers for study of ion-molecule reactions, noting ion gun, deceleration lens and collision chamber

02 p0247 A67-12690

Intensity and energy distribution of solar plasma determined by mass spectrometers which can separate hydrogen and helium components of plasma stream

02 p0247 A67-12692

Mass spectrometer resolution improved by variable focus at any arbitrary ion current through three-element unipotential lens

02 p0248 A67-12700

Extension of mass range of monopole mass spectrometer and effects on resolving power, sensitivity and mass discrimination, for partial pressure analysis

06 p1000 A67-17747

Ionic composition measurements of topside ionosphere from mass spectrometer flown on Explorer XXXI satellite

06 p0996 A67-18646

Rocketborne RF mass spectrometers use in study of atmospheric composition at high altitudes, discussing sampling

09 p1491 A67-21895

RF mass spectrometer with small dimensions and power requirements and high sensitivity designed for analysis of upper atmosphere ion and neutral composition

12 p1941 A67-25651

Satellite sealed subsystems individual leak rates in thermal-vacuum environment measured with mass spectrometer

12 p1921 A67-25690

Mass spectrometers operational performance characteristics, effects on sensitivity decay rate related to time. pressure and ionizing current

12 p1942 A67-25694

Three-channel particle spectrometer with semiconductor detectors and tunnel diode discriminators noting noise immunity, high signal level output, etc

12 p1944 A67-25853

Nighttime topside ionosphere composition, measuring concentrations of H, He and O by mass spectrometry

13 p2108 A67-28310

Lower E-region positive ion concentrations measured at time of declining solar activity by rocket installed mass spectrometer

14 p2310 A67-28049

Extraterrestrial life detection based on catalysis of oxygen exchange between labeled oxyanions and water, noting equipment 15 p2426 A67-29113

Variable field Thomson mass spectrograph application to analysis of mass composition of plasmoids 15 p2526 A67-29258

Carbon dioxide ions with electrons dissociative recombination measurements with microwave-afterglow differentially pumped quadrupole mass-spectrometer apparatus, noting Martian atmosphere model [SRCC-55] 17 p2888 A67-32826

Ion-molecule reactions in propane studied using mass and energy resolved ion beams in tandem mass spectrometer 17 p2810 A67-33264

Lower thermosphere composition and mean molecular weight analyzed for diurnal and latitude effects, using mass spectrometric measurements 19 p3220 A67-35265

Fast scanning 180 degree magnetic mass spectrometer for monitoring fast changes in residual gas compositions 20 p3448 A67-36875

Magnetic deviation ion mass spectrometer for ionospheric rocket probes, noting onboard application 21 p3628 A67-38657

D-region mobility and constituents abundance spectrometer device based on continuum concepts 22 p3799 A67-39816

Ionospheric ion-neutral reactions studied by photoionization mass spectrometer, noting temperature independent reactions 22 p3793 A67-40077

Rare gas isotopic analysis using ruby pulsed laser and mass spectrometer 22 p3816 A67-40241

Cold cathode ion source /CCIS/ quadrupole mass spectrometer for ultrahigh residual gas analysis 23 p4000 A67-41217

MASS SPECTROMETRY

Gas chromatographic and mass spectrometric analysis of chlamydospores of *Ustilago maydis*, *U. nuda* and *Sphacelotheca reiliana* for hydrocarbon content 03 p0363 A67-13594

Vapor composition, evaporation rate and vapor pressure above chromium carbides determined by effusion method combined with mass spectrometry 03 p0456 A67-14193

Mass spectrometric study of energy distribution of ions of accelerated plasma produced by coaxial source 04 p0668 A67-15216

Book on mass spectrometry principles and application to ion and neutral atom composition of upper atmosphere 04 p0624 A67-15587

Mass spectrometric determination of amino acid sequence from oligopeptides 04 p0566 A67-15613

Mass spectrometer in physiological research or in medical monitoring 05 p0758 A67-16279

Mass spectrometry of plasma ionic constituents, identifying monatomic and polyatomic ionic species in gaseous plasma by isotopic techniques 05 p0851 A67-16381

Mass spectrometric observation of ions formed during shock wave heating of gaseous krypton and xenon at 3600 to 7800 degrees K 05 p0795 A67-17440

Molecular beam technique for mass spectrometric sampling of high temperature systems at high atmospheric pressure [AIAA PAPER 67-37] 06 p0956 A67-18305

Upper atmospheric rocket sounding experiment during solar eclipse over Brazil, noting instrumentation and participating agencies 06 p0981 A67-18382

Mass spectrometric investigation of composition of negative ion sputtering products of solid metal surfaces under cesium ion bombardment 06 p1036 A67-18425

Vertical distribution of neutral composition of atmosphere between 100 and 200 km, comparing mass spectrometer with optical measurement 07 p1169 A67-19097

Rare earth compound and Ba abundances in Bununu howardite 07 p1249 A67-19537

Photoionization mass spectrometer for ion-molecule reaction studies, determining ion residence times, drift velocities, diffusion coefficients and ion temperatures 07 p1137 A67-20187

Photoionization mass spectrometer for charge transfer reaction analysis 07 p1137 A67-20188

Mass spectrometric detection of cosmic-ray-produced krypton isotope in meteorites

and possibility of Kr-Kr dating 07 p1256 A67-20228

Soviet lunar probe measurements of gamma spectrometry, magnetic and gravitational fields, corpuscular radiation intensity, etc 08 p1411 A67-20999

Gas desorption following Q-switched laser beam bombardment of tungsten target in vacuum 08 p1338 A67-21310

Pumping power of liquid nitrogen cooled cryosurface, showing reduced efficiency in presence of nitrogen via mass spectrometry 09 p1503 A67-22117

System, incorporating Teflon membrane, to selectively remove carrier gas from column effluent prior to entry into mass spectrometer 10 p1602 A67-22946

High resolution gas chromatography combined with mass spectrometry applied to analysis of pyrolysis products of isoprene from 300 to 1000 degrees C 10 p1602 A67-22947

Mass spectrometric measurements of upper atmosphere temperature 10 p1639 A67-23214

Mass spectrometric investigations of interaction of atmospheric ions with molecules of rocket gas release 10 p1640 A67-23215

Analytical methods using mass spectrometry and gas chromatography for contaminants affecting component reliability in gases enclosed within electronic components 10 p1611 A67-23310

Cryogenic stability, kinetics and energetics of lower boron hydrides explored with negative results, using mass spectrometry 10 p1603 A67-23385

Aliphatic hydrocarbons in meteorites, examining distribution of isoprenoid and other compounds via gas chromatography and mass spectrometry 10 p1709 A67-23489

Radioactive krypton content in stone meteorites determined via mass spectrometry, deriving spall ratios and radiation ages 11 p1866 A67-24692

Mass spectrometer and helium gas application in NDT for deleterious leaks in double-wall vessels for storing and shipping liquid oxygen and nitrogen 12 p1948 A67-25288

Upper atmospheric composition data compared, showing erroneous nature of Hinteregger and Pokhunkov measurements on oxygen-nitrogen ratio 12 p1934 A67-25789

Reactions between alkane and cycloalkane molecular ions analyzed, using conventional and tandem mass spectrometry 12 p1903 A67-25969

Dissociation energy of nitrous oxide reconciled with electron physics data 12 p1904 A67-26230

Bennett type RF spectrometer analysis of low pressure plasma discharge, noting effusion current determination 14 p2314 A67-27753

Complex organic compounds analysis by fast-electrical-scanning high resolution mass spectrometry and gas chromatography 14 p2259 A67-28425

Mass spectrometric analysis of sedimentary rocks for Sr-Rb and Sr isotopic composition from Bosumtwi crater, Ghana 14 p2314 A67-28952

Multiple ionization of rare gases analyzed in mass spectrometer with trapped ion source, noting energies of metastable levels 15 p2519 A67-29189

Fast hydrogen ion generation in coaxial plasma source to determine point in gun chamber where fast particles arise 15 p2525 A67-29251

Mass spectrometric study of energy distribution of ions of accelerated plasma produced by coaxial source 15 p2532 A67-30264

Secondary ion generation in flames by electron impact noting application of mass-spectrometry and hydrocarbon fuels analysis 16 p2780 A67-31520

Preignition phase of solid propellant burning, determining concentration of volatilized species as function of surface temperature 17 p2927 A67-33028

Trapping of hydrogen ions in molybdenum, titanium, tantalum and zirconium measured by mass spectrometric technique 17 p2810 A67-33384

Single gallium arsenide crystals sputtered by normally incident low energy argon ions in mass spectrometer

source 18 p3106 A67-34639

Knudsen cell used in mass spectrometry of thermodynamics of refractory substances vaporization 19 p3242 A67-34864

Primordial rare gases abundances in unequilibrated ordinary chondrites determined by mass spectrometry 19 p3317 A67-34912

Micrometeoroid collection experiments flown on Gemini IX and Gemini XII analyzed, using optical and electron microscopy and mass spectrometry 19 p3339 A67-35196

Refractory metals and compounds vaporization study, using Knudsen effusion method and mass spectrometry for vapor tension and vaporization energy 20 p3463 A67-36116

Mass spectrometry of titanium subfluorides at high temperatures, determining sublimation pressures and heat and dissociation energy 20 p3377 A67-37135

Existence of ozone difluoride established by low temperature experiments and correlation with mass spectrometric EPR, IR and NMR 20 p3377 A67-37136

Molecular flow mass spectrometer analysis of porous metal membranes for gases of different molecular weights 20 p3378 A67-37499

Ion mobility and reactions in argon measured using Townsend and Tyndall techniques with mass analysis 20 p3492 A67-37690

Impurity sources in hermetic electronic packaging investigated using mass spectrography and gas chromatography, comparing packaging techniques 21 p3636 A67-38632

Ionization potentials of clustered sodium atoms measured, describing experiment involving mass spectrometry 21 p3660 A67-39109

Mass spectrometric method for measuring double charge exchange cross sections of low energy positive ions, investigating current distribution 22 p3797 A67-39427

Photolysis of gaseous and liquid benzene, analyzing gaseous products by gas chromatography and mass spectrometry 22 p3757 A67-39443

Mass spectrometry used for simultaneous measurements of adsorption and crystal nucleation processes 23 p4043 A67-41355

Microwave plasma observed using spectroscopic and mass spectrometric techniques, discussing standing wave operation mode, emission and resonance lines 23 p4034 A67-41435

Mass spectrometric analysis of electrolyte degradation during electrolysis in sulfuric acid silica gel cell for oxygen recovery 23 p3970 A67-41705

Mass spectrometric study of oxygen adsorption, determining condensation coefficient and tungsten surface work function for various concentrations 24 p4172 A67-42073

Aliphatic hydrocarbons isolated from Trinidad Lake asphalt by gas chromatography and mass spectrometry appear to be unlike hydrocarbons 24 p4149 A67-42100

MASS SPECTROSCOPY

High resolution mass spectra obtained from fast magnetic scans of gas chromatographic effluents 03 p0367 A67-13336

Hydrogen arcjet plume spectroscopy, examining exhaust at various H mass flow rates 05 p0874 A67-17357

Structures and stereochemistry of clivonine and clivimine analyzed through mass spectroscopy and nuclear magnetic resonance 09 p1458 A67-22059

Measurements of positive ion composition of mesosphere and ionospheric D layer from rocket experiments 10 p1645 A67-23264

Mass of shaped charge accelerator generated fragments determined via high speed flash X-ray photography of projectiles in flight 11 p1790 A67-24448

Modified Thomson mass spectroscopy for visual observation of energy spectra of ion component of plasmoid 15 p2486 A67-29260

Nitrogen, oxygen and hydrogen determined by spark-source mass spectrography, noting reduction of instrument blank levels 15 p2433 A67-29403

Ionization processes in hot products of combustion processes /flame gases/ as weak plasma media noting flame properties, mass

spectroscopy, electron concentration, etc 17 p2967 A67-32140

MASS SPECTRUM

SA MOLECULAR SPECTRUM

Competing alternative pathways for formation of particular ion in mass spectra of substituted benzophenones 01 p0018 A67-10105

Mass spectra of amino ketones and amino alcohols and related substances 09 p1458 A67-22057

Production of charged double pion in pi plus-proton scattering, noting isobar model failure to explain enhancement at 400 Mev 19 p3266 A67-36100

Particle mass spectrum development in rocket nozzle, assuming droplet growth by collision and agglomeration as dominant mechanism 20 p3516 A67-37130

Pulsed ion flow energy and mass spectra analyzer suitable for 1 to 3 msec duration and time variation over 10 msec 24 p4158 A67-42741

MASS TRANSFER

SA ENERGY TRANSFER

Mass transfer and first order boundary layer effects on sharp cone drag [AIAA PAPER 66-33] 01 p0007 A67-11161

Hypersonic flow over blunt flat plate with surface mass transfer 01 p0007 A67-11180

Mass flow from gas-vapor mixture to wall of recuperative heat-exchanger condenser 03 p0536 A67-13688

Heat and mass transfer from vertical plates boundary layer in convection at low Reynolds number by interferometry [ASME PAPER 65-WA/HT-39] 03 p0404 A67-14011

Heat and mass transfer processes in rotationally symmetrical tank partially filled with liquid and subjected to external heating and acceleration in direction of longitudinal axis 04 p0720 A67-14577

Velocity, energy and concentration fields in laminar boundary layers with arbitrarily distributed mass transfer at surface 04 p0603 A67-14643

Soviet papers on laminar boundary layer flow and heat and mass transfer 04 p0721 A67-14708

Hydrogen and helium injection effect on local heat transfer to porous surface from dissociated turbulent boundary layer [ASME PAPER 66-WA/HT-24] 04 p0725 A67-15444

Mass transfer measurements of paradichloro benzene cylinders at various turbulent intensities and angles of attack, showing free flow turbulence effect on local mass transfer coefficient 04 p0548 A67-15493

Phenomenological theory of mass transfer in binary systems near critical point applied to particular boundary value problems 04 p0727 A67-15683

Mass transfer and hydrodynamics of gas jet injection into liquid surface, deriving empirical equations for hollow truncated point formed around injection point 04 p0727 A67-15754

Mass and heat transfer data from sweptback circular cylinders in Mach 2 wind tunnel with Reynolds number 100,000 04 p0549 A67-15824

Heat transfer - AICE International Conference, Chicago, August 1966, Volume 3, Single phase, mass transfer and vibrations 04 p0732 A67-15837

Surface property effects on effectiveness of mass transfer cooling in laminar boundary layers with hydrogen injected into free stream of nitrogen or carbon dioxide 04 p0733 A67-15840

Gas flow, convective heat transfer, enthalpy rise and surface mass transfer for bodies in cross flow, with application to circular cylinder 04 p0733 A67-15841

Equilibrium temperatures of mass transfer cooled walls in high speed flow of absorbing-emitting gas 04 p0737 A67-15864

Heat and mass transfer research - AICE Symposium, Detroit, December 1966, Part 2 05 p0925 A67-16269

Mass transfer perturbations about reversed flow profiles of Stewartson, noting computation of solutions to Falkner-Skan equation 05 p0794 A67-17369

Transient linear transfer problem solution via integral equations for corresponding boundary value problems 06 p1117 A67-18390

Reynolds number scaling theory for hypersonic ablation, deriving heat and mass

transfer relationship [AIAA PAPER 67-155] 06 p1117 A67-18478

Diffusion mass exchange model for thermal and hydrodynamic processes 07 p1267 A67-19328

Mass transfer rates of Nb-based alloys in high temperature Li determined in thermal convection loops under dynamic flow conditions 07 p1223 A67-19463

Carbon and nitrogen mass transfer rates by liquid potassium in 16 thermal convection loops of type 316 stainless steel with niobium/one-percent-zirconium and stainless steel tabs at 1200 to 1600 degrees F 07 p1223 A67-19465

Book on physical processes of heat and mass transfer including thermal conductivity and potential and various integral procedures 07 p1268 A67-20039

Simultaneous effects of heat and mass transfer on properties of stagnation point flows analyzed over full range of velocity gradients 08 p1276 A67-20568

Integral method to study surface chemistry interaction due to combustion and attendant mass transfer on isothermal graphite cone in nonsimilar boundary layer flow 08 p1320 A67-20570

Skin friction drag of constant property turbulent boundary layer with uniform injection, corrections of experimental law-of-wall and velocity-defect law concepts 10 p1625 A67-23111

Heat and mass transfer during stationary adiabatic vaporization of water ethanol and carbon tetrachloride 11 p1882 A67-24319

Mass transfer rates for axisymmetrically rotating bodies, using diffusion controlled electrode reaction system 12 p2033 A67-25277

Cathode spot phenomena in pulsed vacuum arc utilized for electric microthrusters, testing cathode materials by mass and momentum transfer measurements 12 p1989 A67-25403

Low density shock layer structure on cylinders at Mach 4 noting magnitude, location of disturbances, existence of shock wave-like flows, recession of leading edge, etc 14 p2299 A67-28173

Criterion expressions for Nusselt numbers of mass transfer in two-phase film system at high Prandtl numbers which describe physical properties of both phases 14 p2405 A67-28303

Differential equations for heat and mass transfer in laminar boundary layer of binary gas mixture flow past porous wet flat plate 14 p2242 A67-28307

Two-dimensional mixed boundary value problem of heat and mass transfer with characteristic equation containing multiple roots 14 p2406 A67-28312

Inertial criterion relation for determining effect of mass transfer, phase transformation, and Kossovich number on heat and mass transfer 14 p2406 A67-28313

References on heat and mass transfer 15 p2580 A67-29780

Prediction of large rocket nozzle material performance using semiempirical technique, noting mathematical models for internal and external heat and mass transfer 15 p2547 A67-29993

Kinetics of gas-solid reactions at high temperatures, noting mass transfer coefficients attainable, temperature discontinuities, stagnation lines, etc 15 p2582 A67-30022

Flat plate, simultaneous heat and mass transfer for Newtonian fluids in free convection analyzed, using group theory 15 p2582 A67-30217

Heat transfer in stagnation-point laminar boundary layer with mass injection and absorption of incident radiation 16 p2658 A67-30941

Boundary layer theory applied to solution of problems of combined heat and mass transfer, using approximate single-parameter integral method 16 p2594 A67-31202

Book on similarity theory applications to heat and mass transfer in moving medium 17 p2970 A67-32464

Soviet book on heat and mass transfer, Volume 6 17 p2971 A67-33067

Classical heterogeneous combustion and aerospace research, discussing multiple factor approach and mass transfer operations 18 p3150 A67-33801

S-shaped boiling curves analyzed in terms of nucleation characteristics of heat transfer

surface, correlating temperature driving force and density of centers 18 p3160 A67-34164

Mass-transfer coefficients through plane surface in liquid-liquid systems, examining interphase turbulence effect 19 p3345 A67-35566

Simultaneous heat and mass transfer in laminar free convection boundary layer at vertical surface with moving interface 19 p3346 A67-35613

Mass transfer cooling of carbon dioxide-nitrogen binary system in laminar boundary layer, stressing dissociation effect [ASME PAPER 67-HT-70] 20 p3550 A67-36750

Heat and mass transfer conditions in ablation of shear thinning and thickening fluids investigated at stagnation point [ASME PAPER 67-HT-78] 20 p3551 A67-36756

Approximation integral method for solution of coupled equations of heat and mass transfer in porous medium, discussing nonlinear and linear problems 20 p3553 A67-36938

Fuel cell performance under operating conditions of local nonuniformity in temperature, concentration, potential or current simulated with computer program 20 p3363 A67-37014

Unsteady transverse diffusion of passive impurity and mass and heat transfer in granular layer described by cell type models 20 p3554 A67-37054

Acoustic vibration effect on heterogeneous mass transfer at sphere surface in high Prandtl number liquids 20 p3554 A67-37068

Transpiration cooled vehicles correlation with compressible turbulent boundary layer with mass transfer, emphasizing high Mach number 20 p3423 A67-37256

Soviet book on boundary layer of non-Newtonian fluids covering hydrodynamics, heat transfer and mass transfer 20 p3424 A67-37546

Book on fluid dynamics of multiphase systems covering momentum, heat and mass transfers and chemical reactions 20 p3425 A67-37728

Mass injection effect on compressible three-dimensional laminar boundary layers analyzed for nonreacting gas, using conservation equations for flow velocity profiles 21 p3613 A67-38852

Convective motion of low pressure plasma confined by strong magnetic field taking into account heat and mass transfer 21 p3675 A67-39014

Surface mass transfer effects on viscous hypersonic shock layer of blunt body including suction and injection of air into air 22 p3743 A67-40417

Differential equation system for reacting laminar boundary layer heat and mass transfer solved analytically, noting compressible gas and porous foil filter 23 p4081 A67-40744

Three-dimensional heat conduction, heat and mass transfer and thermoelasticity problems solved by approximate method using functional parameters 23 p4083 A67-41290

Dynamic mass transfer equation for design parameters of regenerable absorption beds for carbon dioxide removal in spacecraft life support system [SAE PAPER 670842] 24 p4115 A67-41996

Heat and mass transfer processes in reacting laminar boundary layer flow with steady high speed gas flow 24 p4143 A67-42284

Heat and mass transfer in chemically reacting gas mixture compressible boundary layer, determining temperature in reaction zone and on porous plate surface 24 p4256 A67-42734

Colloidal electrodynamic energy converters analyzed on basis of power plant specific mass 24 p4109 A67-42888

Limit diffusion flux on rotating ring electrode surface in turbulent regime, determining mass transfer constant 24 p4146 A67-43112

MAST

S MAGNETIC ANNULAR SHOCK TUBE

/MAST/

MATERIAL

S ABLATING MATERIAL

S AIRFRAME MATERIAL

S ANISOTROPIC MATERIAL

S BITUMINOUS MATERIAL

S BUILDING MATERIAL

S COMPOSITE MATERIAL
 S DIELECTRIC MATERIAL
 S FOAMED MATERIAL
 S HIGH TEMPERATURE MATERIAL
 S IMPREGNATED MATERIAL
 S INTERSTELLAR MATERIAL
 S LAMINATED MATERIAL
 S MAGNETIC MATERIAL
 S MOLDING MATERIAL
 S NONABLATING MATERIAL
 S ORGANIC MATERIAL
 S ORTHOTROPIC MATERIAL
 S PARAELECTRIC MATERIAL
 S PHOTOELASTIC MATERIAL
 S PHOTOELECTRIC MATERIAL
 S PLASTIC MATERIAL
 S POROUS MATERIAL
 S PYROLYTIC MATERIAL
 S RADIOACTIVE MATERIAL
 S RADOME MATERIAL
 S REACTOR MATERIAL
 S REFRACTORY MATERIAL
 S REINFORCED MATERIAL
 S SELF-LUBRICATING MATERIAL
 S STRUCTURAL MATERIAL
 S THERMOELECTRIC MATERIAL
 S TRANSLUCENT MATERIAL
 S TRANSPARENT MATERIAL
 S VITREOUS MATERIAL

MATERIAL REMOVAL
 SA MACHINING
 Book on nontraditional machining processes covering process parameters, shape and materials applications, tooling, chemical removal, etc 14 p2328 A67-28893
 Hydraulic component material properties relationship to particulate material removed due to cavitation, showing particle size distribution definition 20 p3469 A67-37366
 Machines and machining technology for materials used in Mach-3 aircraft structures, discussing cutting fluids, cutter and best metal removal rate 21 p3631 A67-38014
 Electrochemical shaping precision analysis, discussing efficiency, current losses, energy consumption, surface geometry and electrolyte properties 22 p3812 A67-39543
 Potential energy release of stressed elastic body due to material removal and crack extension 22 p3911 A67-39679
 Machining advantages and economy of annealed steels over maraged steels 23 p4010 A67-41352

MATERIAL TESTING
 SA ENVIRONMENTAL TESTING
 SA FAILURE
 SA FATIGUE
 SA NONDESTRUCTIVE TESTING
 Materials for use as rolling-contact bearing lubricants in liquid hydrogen environment 01 p0077 A67-10119
 Physical and environmental effects on energy dissipation characteristics of balsa wood [SAE PAPER 660657] 01 p0103 A67-10616
 Two-phase flow and material attrition problems for Rankine cycle liquid metal power plants [ASME PAPER 66-GT/CLC-4] 01 p0014 A67-10872
 Temperature control of orbital Titan III-C transtage space booster, noting thermal design, configuration and materials test program support 02 p0335 A67-12395
 Ultrahigh vacuum envelopes design, fabrication and use, emphasizing choice of materials and outgassing load 02 p0250 A67-12452
 Material strength parameter /coupling modulus/ dependence on crack propagation velocity when accounting for rupture kinetics 03 p0529 A67-14166
 Material failure modes in engine components and improved structural design problems 03 p0505 A67-14387
 Nondestructive material testing - International Colloquium, Aachen, West Germany, December 1965 04 p0641 A67-14586
 Nondestructive testing by oscillatory methods of viscoelastic properties of high molecular weight polymers as functions of frequency and temperature 04 p0641 A67-14587
 Mean strain cumulative damage and effect in low cycle fatigue of 2024-T351 aluminum alloy, covering strain cycling, fatigue life, residual ductility, etc [ASME PAPER 65-WA/MET-5] 05 p0827 A67-16214
 Heating and cooling rates, hold time at maximum temperature, phase temperature

between temperature and strain cycling effects on thermal fatigue of stainless steel 05 p0921 A67-17085
 Ultrahigh vacuum effects on flow and fracture behavior of molybdenum 06 p1016 A67-17897
 Reciprocity principle of Equivalent Sun Hours /ESH/ as means of spacecraft material testing 06 p0980 A67-18365
 Hot gas tunnel for determination of material behavior under convective heat transfer conditions similar to that existing in rocket combustion chambers [AIAA PAPER 67-106] 06 p0981 A67-18473
 Test program to evaluate characteristics of existing Atlas engine boots in flight environment and provide parameters for design change [AIAA PAPER 67-277] 07 p1241 A67-20054
 Aircraft exfoliation corrosion, discussing methods for prevention in fastener holes 07 p1210 A67-20087
 Boron filament epoxy resin composites test program relative to mechanical design of reentry vehicle structure 08 p1345 A67-20424
 Laser beam effect on hydrodynamic bearings, discussing microcracks and critical energy, explaining breakdowns 08 p1337 A67-20840
 Static and transient strain measurement in aerospace structural materials using extensometer and compressive test jig, determining Young modulus, creep rate, etc 08 p1420 A67-20907
 Surface blistering of metals due to low energy hydrogen ion bombardment, determining solar absorptance change in gold-plated specimens 08 p1343 A67-21520
 Thermoelectric generator modules with Si-Ge alloys, discussing material preparation and generator fabrication 09 p1445 A67-22180
 Material combination and hardness effect in rolling contact fatigue life of high speed tool steel, stainless steel and wear resistant materials 09 p1505 A67-22191
 Nondestructive testing in calculating inherent reliability and improving reliability of manufactured product 09 p1506 A67-22304
 Aircraft reliability as function of fatigue life of welded joints noting static strength variation, S-N curve and multiple safety factor 09 p1506 A67-22471
 Epoxy adhesive properties dependence on application variables according to test methods of MIL-A-8623 adhesive specification 09 p1523 A67-22525
 Fatigue mechanism of materials, deriving parametric differential equations from group of postulates 09 p1578 A67-22546
 Behavior of metals, graphites and reinforced plastics for reentry nose cones tested, using rocket engine exhaust flame as heat source 10 p1698 A67-23480
 Thin plate targets response to hypervelocity impact to determine effectiveness of meteoroid bumpers composed of two layers of distinct materials 10 p1725 A67-23716
 Refractory materials for hypersonic vehicle leading edges 10 p1670 A67-23723
 Glass-fabric reinforced plastic shells fabrication and full scale structural evaluation 10 p1727 A67-23732
 Long time mechanical and thermal stability of polymeric materials predicted from accelerated testing at increased temperature-time relations 10 p1672 A67-23743
 Argon laser design for long life noting ion sputtering and gas clean-up 11 p1800 A67-24242
 Tensile strength retaining characteristics of aluminum alloys determined after varied soaking periods at various elevated temperatures 11 p1805 A67-24271
 Electronic computer usage to control temperature during creep and long term strength tests of heat resistant steels 11 p1877 A67-24818
 Multiposition grips for automatic mounting of metal or plastic specimens for low temperature mechanical tests 11 p1877 A67-24819
 Nondestructive testing methods noting applicability to flaw detection and quality control 12 p1948 A67-25138
 Cathode spot phenomena in pulsed vacuum arc utilized for electric microthrusters, testing cathode materials by mass and momentum transfer

measurements 12 p1989 A67-25403
 Crack propagation kinetics by thermal fluctuation induction, considering endurance and breakdown of metallic and semimetallic materials 12 p2029 A67-25666
 Light sources used for solar simulation testing in terms of operational characteristics and effect of different spectral irradiance characteristics on thermal control coatings 12 p1925 A67-25723
 Dynamic testing of crushable materials for planetary impact attenuation systems, noting Voyager and Ranger Lunar Capsule 12 p1956 A67-25731
 Double cantilever beam specimen for determining plain strain fracture toughness of metals 12 p1956 A67-25946
 Low to moderately high temperature emissometer, based on calorimetric method, to measure total hemispherical emittance of metals and coatings in vacuum [AIAA PAPER 67-299] 12 p1946 A67-26014
 Thermal modeling applicability to steady state and transient conditions, considering material property changes with temperature [AIAA PAPER 67-305] 12 p2036 A67-26020
 Spacecraft thermal control coating experiments, discussing unreliability of degradation results due to failure to measure radiation properties, UV wavelength dependence and micrometeoroid damage [AIAA PAPER 67-329] 12 p2038 A67-26043
 Material deformation, showing functional dependence of thermodynamic potential on state parameters in theory of plasticity, creep and relaxation 12 p1938 A67-26197
 Dynamic and physical testing of metals, discussing yield point, plastic deformation and oscillation damping characteristics 13 p2215 A67-26452
 Apparatus for programming thermal cycles in fatigue tests of materials 13 p2218 A67-26797
 Atlas booster materials compatibility with fluorine oxidizers 13 p2186 A67-27687
 Filament wound sleeve seal impregnated with solid lubricants dissipates heat in rubbing contact zone and provides wear characteristics for use in air compressor [ASLE PREPRINT 67AM 7A-3] 14 p2326 A67-28791
 Elastomeric materials thermostability in simulated spacecraft environment tested to obtain ignition point values 15 p2466 A67-29545
 Solid rocket components exposure to elevated temperatures, hard vacuum and UV radiation during space flight and reentry 15 p2507 A67-29548
 Thermal control materials for spacecraft, considering UV spectral distribution, radiation energy and flux, oxygen bleaching, etc 15 p2579 A67-29552
 Nonmetallic materials for unmanned spacecraft 15 p2507 A67-29553
 Gemini window contamination due to outgassing of silicones 15 p2507 A67-29555
 Organic dielectric materials for spacecraft, selection and evaluation 15 p2508 A67-29556
 Electron beam probing of semiconductor materials and devices 15 p2450 A67-29813
 Reinforcing fiber orientation effect on elastic moduli of materials, noting results on long and finite fibers 15 p2576 A67-30178
 Bulk elastic deformation of continuous medium with coaxial stress-strain deviators, analyzing deformations in body with specified boundary conditions 15 p2576 A67-30181
 Cerium addition effects on magnesium workability evaluated by sample elongation in tension test and plate working limit in cold rolling 15 p2505 A67-30398
 Solar simulation, comparing techniques for reproducing space thermal radiation environment with sun characteristics 16 p2654 A67-30674
 Effect of drilled holes on notch toughness of iron alloys, noting impact and slow bending testing, notch toughness improvement, etc 16 p2688 A67-31304
 Materials rolling contact fatigue strength measured by tester intended to serve as screening device [ASME PAPER 67-LUBS-3] 16 p2676 A67-31381
 Sinusoidal vibration generator consisting of two rigid vibrodynes connected by synchronized shaft for testing structural material 16 p2776 A67-31556
 Compaction pressure and sintering

temperature effect on initiation and propagation of cracks during bend testing of Ni and Mo specimens 16 p2691 A67-31586

Experimental assembly for measuring true heat capacity of heat resistant insulating materials during natural cooling at temperatures from 1200 to 2400 degrees K 16 p2678 A67-31784

Effects of repeated loading of materials and structures - Conference, Mexico City, September 1966, Volume 3 17 p2957 A67-32027

Effects of repeated loading of materials and structures - Conference, Mexico City, September 1966, Volume 6 17 p2958 A67-32029

Thermal conductivities below one degree K of various very pure metals, noting normal and superconducting states 17 p2912 A67-32265

Engine materials investigated for optimum low cycle fatigue resistance by pull-pull and rotating-beam fatigue testing techniques [SAE PAPER 670336] 17 p2874 A67-32986

Alloys for failure-safe structures tested, determining fracture toughness, fatigue strength and stress-corrosion cracking resistance 17 p2875 A67-33048

Radioscopy for testing cast-steel parts, welding seams, etc, noting radiation protection, radioscope video control and information storage 18 p3045 A67-33737

Microwave measurement methods for nondestructive material testing, discussing efficiency, advantages and applications 18 p3045 A67-33740

Ultrasonic probes calibration for evaluation of propagating ultrasonic wave during nondestructive testing of materials 18 p3046 A67-33744

Design and construction of equipment for oxygen, nitrogen and hydrogen determination in aerospace materials [ONERA-TP-466] 18 p2998 A67-34461

Sapphire whisker reinforced aluminum composites fabrication and evaluation [ASTM PAPER 2] 18 p3070 A67-34568

Atmospheric corrosion resistance of titanium alloys [ASTM PAPER 31] 18 p3068 A67-34579

Problem of manufacturing space vehicles with rigidly controlled cleanliness and biological contamination for missions to other planets 18 p2995 A67-34677

Collection of papers of high purity metals and alloys, discussing properties fabrication and testing 19 p3243 A67-34923

Fabrication, structure, possible failure and testing of coated refractory metals in applications for space technology 19 p3245 A67-34959

Microelectronic failure mechanism, examining manufacture and processing methods and production of uniform and versatile material 19 p3193 A67-35029

Deformation characteristics of light concrete statistically compared to second concrete, determined through parameter similarity 19 p3341 A67-35630

Polymeric materials used for selected subsystems of Mariner IV space probe [JPL-TR-32-1031] 19 p3334 A67-35889

Mechanical characteristics of materials determined using circular bending 20 p3537 A67-36476

Testing apparatus for rapid determination of tensile strength of fine filaments 20 p3537 A67-36522

AMICON 8000 kw plasma facility for simulating reentry environments for material and thermodynamic tests 20 p3415 A67-36551

Brittle-ductile materials thermal shock characteristics explained by strains and elastic energy, noting ductile materials withstand more strains before failure 20 p3538 A67-36673

Relation of testing and service performance - ASTM Conference, Atlantic City, June 1966 20 p3416 A67-36697

Product reliability dependence on scatter extent determination in fatigue life, recommending testing in S-N diagram short life region 20 p3538 A67-36699

High insulating effectiveness required of cryogenic insulations, evaluating insulation capacities of powders, fibers, foams, honeycomb, etc 20 p3553 A67-36885

Lifetime of structural sections subjected to creep deformation at high temperatures, showing relation to energy dissipation forces 20 p3540 A67-37058

Boron filament behavior in rotating-beam fatigue test 20 p3470 A67-37390

Stress corrosion characteristics of Ti alloy evaluated using cantilever beam testing procedure 20 p3470 A67-37465

Laboratory equipment for R and D on fibrous refractory materials 21 p3649 A67-37883

Black and white surface coating materials exposed to simulated solar radiation in vacuum, noting deterioration of white coatings 21 p3650 A67-37960

Contaminant control in space cabins by systematic screening of materials and supplies used, noting significance of test temperature 21 p3577 A67-38077

Comparative investigation of strain gauge testing methods 21 p3628 A67-38100

Adhesives for bonding overlay materials to substrates for high speed hydrofoils, describing water tunnel and rotating arm tests 21 p3632 A67-38131

Cross-wire resistance welded metal joints for aerospace electronic packing assemblies, investigating embedment, mechanical strength and materials evaluation 21 p3635 A67-38629

Failure mechanisms in semiconductor components under thermomechanical and electrical stresses for D2 satellite application 21 p3601 A67-39061

Microwave use in measuring burning rate of solid propellant rocket motors and in detection of porosity in nonconducting materials 22 p3795 A67-39198

Microcracking susceptibility studies of Inconel 718 weld heat affected zones, noting hot ductibility, weld circle patch and fillerless fusion welding tests 22 p3818 A67-39222

Creep properties of sheet materials in SST environment for selection of optimal airframe materials 22 p3818 A67-39225

Thermally stable polymers, discussing synthesis and testing on pilot plant and laboratory undeveloped stages 22 p3825 A67-39856

Aluminum magnesium alloys prepared by powder metallurgy and hot extrusion evaluated for tension, compression, impact, fatigue and creep 22 p3821 A67-40053

Spray and brush repair of zinc oxide-potassium silicate spacecraft thermal control paint, describing tests, surface preparation and coating application 22 p3828 A67-40111

Thermal diffusivities of thermal energy storage materials from solid surface temperature measurements, discussing advantages of transient method [ASME PAPER 66-WA/ENER-5] 22 p3919 A67-40349

Superorbital reentry environments, discussing materials, test environments and heat factors 22 p3919 A67-40383

Materials selection for external structures of transport aircraft flying at Mach 3 speeds, noting characteristics of maraging steels 23 p4019 A67-41045

Testing machine operated by hydraulic pressure for mechanical properties of materials at medium rates of strain 23 p4079 A67-41332

Fracture toughness and stress corrosion cracking of titanium alloy weldments indicating resistance differences between base metal and weldment 24 p4161 A67-42329

Lubricants, metal high temperature and atmospheric environments effects on gear load-carrying capacity [ASME PAPER 67-LUB-27] 24 p4164 A67-42685

Structural problems in high power solar photovoltaic arrays technology, discussing configuration, materials selection, thermal control coatings and tests 24 p4251 A67-42897

Signal processing and control computer system for materials research noting use in viscoelastic studies of crystalline polymers 24 p4126 A67-42930

MATERIALS EROSION

Two-phase flow and material attrition problems for Rankine cycle liquid metal power plants [ASME PAPER 66-GT/CLC-4] 01 p0014 A67-10872

Cavitation erosion in Hawker Siddeley Trident hydraulic system and steps to find solution 05 p0753 A67-16748

Leakages in hydraulic system of Hawker Siddeley Trident jet transport due to

cavitation erosion 07 p1132 A67-20149

Material corrosion control techniques, considering initial structure design, coatings application and protective coatings specifications 11 p1773 A67-24940

Gas turbine blade erosion from dust, discussing momentum separators and erosion-resistant coating 12 p1990 A67-25947

Lunar environment effects on Surveyor I components, particularly white paint degradation as function of time 15 p2579 A67-29451

Mechanism of electrode erosion by supersonic flame jets during pulsed discharge 16 p2724 A67-31775

Small particle bombardment of stone and iron meteorites, obtaining comparative erosion rates 21 p3704 A67-38504

Erodibility of solid propellants subjected to rapid flow of gas past burning surface 22 p3887 A67-39538

Erosion processes and outflow phenomena in ZnS rocket fuel, noting aluminum addition and gas leaks effects 24 p4206 A67-42579

MATERIALS SCIENCE

SA CERAMICS

SA METALLURGY

SA PLASTIC MATERIAL

Materials for structural usage in high altitude/ high temperature supersonic transports, comparing aluminum, titanium, etc, alloys for mechanical and physical properties [SAE PAPER 660665] 01 p0094 A67-10573

Effects of subsonic, supersonic, hypersonic and orbital environments on structures [SAE PAPER 660671] 01 p0160 A67-10578

Nondestructive testing /NDT/ of materials, components and systems for Saturn-Apollo program 02 p0250 A67-12631

Total normal emittance of various oxidation-resistant materials to very high temperatures in air determined, using special apparatus [AIAA PAPER 65-655] 03 p0447 A67-13035

Book on thermal effects and cutting machinability of aircraft materials 03 p0427 A67-13190

Magnesium wire as in-contact masking material, with surfaces precoated with thin silver layer 03 p0494 A67-13490

Synthesis conditions for materials of B-Al-N system determined by sintering mixtures of BN plus Al and AlN plus B powder in nitrogen atmosphere 03 p0456 A67-13544

Materials for energy transducers used in detection, generation or measurement of ultrasonic waves and materials for electrical filters 03 p0495 A67-13547

Ferrite materials for resonators of magnetostrictive transducers and filters used in transmission and reception of ultrasonic waves 03 p0420 A67-13548

Material selection and structural design problems for hypersonic vehicles 03 p0525 A67-13793

S-, Se- or Te-based nonoxide chalcogenide glassy systems for airborne IR optical equipment materials 03 p0456 A67-14390

Cryogenic temperature resistant plastics in space program, discussing insulation, adhesives, seals, gaskets and expulsion of cryogenic propellant in zero gravity environment [SAE PAPER 660638] 04 p0642 A67-15788

Internal stress calculation in multilayer materials 05 p0919 A67-16590

Materials evolution with high resistance to creep, mechanical and thermal fatigue, corrosion and impact, for gas turbine blades 05 p0829 A67-16744

Clothing hygiene with particular reference to aerospace problems 06 p0954 A67-17998

Fine structure and microstructural effects on control of magnetic, electrical, optical, thermal and mechanical properties of eutectic alloys 06 p1018 A67-18409

Metallic fibers development, noting research for continuous filaments, whiskers, staple fibers, materials, strength, etc 06 p1019 A67-18558

Soviet papers on structure and properties of aviation steels and alloys 07 p1198 A67-19238

Soviet book on high temperature strength of materials noting test stands, stresses, loads, applications to jet and rocket technologies, etc 07 p1208 A67-19299

Materials for large space power systems - Symposium, American Nuclear Society,

Washington, D.C., November 1965 07 p1222 A67-19459
Materials technology presently available for advanced Rankine systems including nuclear fuels, refractory metal alloys, electrical materials and stainless steel 07 p1223 A67-19460
Materials and fin tube geometry effects on ultimate size and mass of space radiator 07 p1223 A67-19461
Book on strength of materials covering energy density, plastic flow deformations, friction heating and fracture 08 p1414 A67-20307
Machining techniques for paper-base and glass-base laminates of various grades for printed circuit boards 08 p1334 A67-20742
Mechanical behavior of fiber reinforced materials, discussing elastic properties, failure theories, stress analysis, fracture toughness, structural design, etc 08 p1342 A67-20904
Materials failure laws based on combined analysis of cracks and fractures 09 p1575 A67-22166
Load, vibration, temperature, surface oxides, etc, effect on wear resistance of materials for aircraft gas turbine engines 09 p1506 A67-22194
Metal working problems involving sheet metal, powder metallurgy, extrusion, nondestructive testing and concerning high strength, refractory and superalloys [SAE PAPER 670098] 09 p1509 A67-22540
Gallium arsenide - International Symposium, Reading, Berks., England, September 1966 10 p1613 A67-23509
Solid motor case technology, evaluating materials, fabrication, segmented case joint design and cost comparisons for large rocket motors 10 p1661 A67-23703
Cutting tool and cutting fluid evaluation, economic considerations for aerospace manufacturing [ASTME PAPER WES-7-27] 11 p1798 A67-24256
Structural and mechanical properties of lunar maria surface material derived from satellite and earth-based data 11 p1864 A67-24557
Preparation and properties of electronic materials for radiative processes control - AIME Conference, Boston, August 1966 11 p1847 A67-24734
Pressure vessel design with ultrahigh strength steels, material strength variations, fracture toughness, minimum defect size and materials melting and fabrication practice [ASME PAPER 67-MET-18] 12 p2031 A67-25954
Book on engineering properties of ceramic materials covering high melting materials, physical, thermal and mechanical properties, thermal stress, oxidation, corrosion resistance, etc 12 p1960 A67-26201
Advances in materials - Symposium, Manchester, England April 1964 13 p2132 A67-26691
Gas discharge effects on materials employed in thermonuclear research 13 p2132 A67-26692
Materials requirements for aircraft turbojet and ramjet engines 13 p2187 A67-26694
Dislocation behavior in crystalline materials, examining agreement between theory and experiment 13 p2132 A67-26695
Nature of glassy state, reviewing nucleation, crystallization, chemical, physical, and electrical properties and transformation of glasses 13 p2143 A67-26696
Temperature and environmental effects on mechanical behavior of metals 13 p2132 A67-26697
Handbook of materials and techniques for vacuum devices covering high temperature properties, materials selection, joining processes, etc 14 p2339 A67-28829
Effects of space environment on materials - Conference, St. Louis, April 1967 15 p2505 A67-29534
Nonmetallic materials for unmanned spacecraft 15 p2507 A67-29553
Threaded fastener design and manufacture 15 p2493 A67-29650
Material processing in microelectronics with laser beam noting solid state lasers, power density, pulse frequency, etc 15 p2493 A67-29682
Epoxy casting resins as structural material in electronic industry, with tables of various

hardener characteristics, viscosities, epoxy equivalents, etc 15 p2508 A67-29683
Cost reduction of space vehicle structures and materials [AAS PAPER 67-81] 15 p2575 A67-29948
Beryllium wire manufacture and uses, noting properties, drawing techniques, annealing effects, reinforcing filament use, etc 16 p2687 A67-30488
Material limitations in MHD induction generator, discussing effect of conducting channel walls and thermal insulation on performance 16 p2605 A67-30582
Photoelastic stress analysis on bonded interface of strip with different end configurations noting stress concentration, bonding problems, etc 16 p2764 A67-30933
Book on ultrasonic machining of intractable materials covering basic principles, vibrator design, machine tools, technology, processes involved and applications 17 p2865 A67-32200
Strength increase of parts or system to prevent fatigue failure, noting bulk and material considerations and elimination of fretting, scoring, corrosion, sharp corners, etc 17 p2962 A67-32824
Materials engineering for electronic hardware, discussing design, development and construction, including tables on metallic finishes, coatings for printed wiring, etc 17 p2865 A67-33047
NERVA program, reactor and nonnuclear component development, full-scale testing, engine program, facilities and materials research [AIAA PAPER 67-487] 18 p3076 A67-33953
Highly purified silicone junction coating resins and silicone molding compound for microelectronic packaging 18 p3069 A67-34564
Strain-energy function of hyperelastic material in terms of extension ratios, with natural rubber as example 18 p3145 A67-34642
Research areas in future NASA program covering materials, energy conversion, guidance, instrumentation, etc 19 p3349 A67-35645
Materials technology expansion in electronics industry, discussing complete equipment components processed on semiconductor slices and large scale integrated electronics 19 p3198 A67-36054
Materials of high vacuum technology, Volume 1, Metals and metalloids 20 p3463 A67-36134
Development of Indian sources of aerospace metals evaluated, noting availability, potential, priority of materials and research facilities 20 p3464 A67-36187
Synthetics in aircraft and rocket construction, recommending duroplastics 20 p3473 A67-36453
Properties of pressed and sintered products of powder metallurgy, noting strength and ductility increase with increase in density 20 p3465 A67-36496
Equations of state of matter at high pressures and temperatures, discussing temperature density regions, theoretical calculations, etc 20 p3485 A67-36929
Aircraft structural form optimized through changes in geometry 20 p3542 A67-37531
Low temperature and irradiation environment effects on mechanical properties of engineering materials 20 p3418 A67-37532
Materials in airlift technology noting adaptation of titanium and beryllium 20 p3471 A67-37533
Man-made organic polymer properties and characteristics, considering crystallization, cross-linking and polymeric chain stiffening for structural applications 20 p3474 A67-37713
Laboratory equipment for R and D on fibrous refractory materials 21 p3649 A67-37883
Thick film design considerations covering material and micropart selection, circuit cost, reliability, substrate size and delivery schedule 21 p3596 A67-38346
High structural efficiency of aircraft materials emphasizing fatigue characteristics, fracture toughness and corrosion resistance 22 p3823 A67-40332
Thermal stress fracture of brittle ceramics studied for effect of relaxation by creep at high temperature under conditions of quasi-static heat flow 22 p3915 A67-40386
Soviet book on present state of semiconductor technology covering theory,

material properties and semiconductor devices 23 p3978 A67-40797
Property changes of semiconductor materials during processing, discussing photoelectric methods, resistivity derivative, recombination parameters and mechanical stresses 23 p4043 A67-41364
Structural defects in Ge and Si alloyed semiconductor junction devices caused by improper technological processing, noting microscopic photographs 23 p4043 A67-41365
Advanced fasteners - SAE Conference, Los Angeles, October 1967 24 p4160 A67-42076
Basic guidelines for fastener system selection for use in exotic environment with unusual stress condition 24 p4160 A67-42077
Fastener applications for gas turbine engines noting materials selection and design 24 p4160 A67-42079
Threaded fasteners for application to aerospace structures noting preload, torque and lubrication 24 p4160 A67-42080
Materials development and testing in orbiting laboratory noting zero gravity benefits [AIAA PAPER 67-815] 24 p4139 A67-42969
MATERIALS TESTING REACTOR
Low dose reactor irradiation effect on temperature dependence of dynamic modulus and internal friction of as-deposited pyrolytic graphite 23 p4021 A67-41075
MATHEMATICAL MODEL
SA FLOW GRAPH
SA POISSON PROCESS
Model of retinal receptor incorporating various feedback control processes consistent with physiological and psychological evidence 01 p0044 A67-10465
Nonlinear dispersive wave propagation analyzed by linearization, obtaining solution as Fourier integral through differential equation 01 p0024 A67-10737
Statistical-dynamical model for total chemical reaction cross sections using activated complex concept and integral equation 01 p0019 A67-10884
Absorption spectra models analyzed for use in IR radiation propagation in atmosphere 01 p0109 A67-11043
Solution of boundary value problems describing two-dimensional flow in plastic regions 01 p0185 A67-11304
Cerenkov radiation of beam-plasma system into dielectric, using mathematical model and mode coupling theory 01 p0040 A67-11314
Mathematical model for determining optimal maximum operating times for aircraft engines, using discrete failure rate to determine cost effectiveness 01 p0141 A67-11340
Markov chains used in construction of reliability mathematical models for systems with dependence between components, noting differential equations 01 p0085 A67-11383
Nonuniform damage in silicon solar cells produced by proton irradiation 02 p0182 A67-11682
Equations for one-dimensional model of macroscopically homogeneous linearly elastic medium of complex structure with spatial dispersion 02 p0337 A67-11952
PCM/TDM and influence of channel on signal determined, using mathematical model 02 p0202 A67-12130
Human pilot dynamic characteristics effects on manual satellite attitude control system stability, using root locus analysis of mathematical models 02 p0186 A67-12226
Numerical integration of solar orbit in model of galactic system 02 p0330 A67-12714
Statistical model of cost of elements of system undergoing gradual breakdown, giving optimal distribution of mean relative deviations of input and output parameters 03 p0389 A67-13090
Mathematical model selected for unstable heat exchange process with single-phase incompressible heat conductor 03 p0535 A67-13119
Periodic oscillations in model of thermal convection, noting flow direction and speed 04 p0719 A67-14646
Two-dimensional dynamic model of diurnal variation of thermosphere 04 p0611 A67-14651
Mathematical model for adaptive signal preprocessor, noting eye adaptation to changes in signal intensity and bandwidth 04 p0563 A67-14799
Human body response to acceleration according to various models

[ASME PAPER 66-WA/BHF-13] 04 p0564 A67-15402
Dynamic systems identification by digital computer modeling in state space formulation of ordinary differential equation [ASME PAPER 66-WA/AUT-10] 04 p0593 A67-15418
Mathematical flow-intermittance model for turbulent patterns, noting viscosity effects 04 p0609 A67-15755
Small oscillations of viscous incompressible fluid in container with free surface under action of potential force field 05 p0791 A67-16373
Mathematical theory of dimensional analysis and similitude, application to spacecraft thermal design and experimental results 05 p0926 A67-16514
Mathematical model of aircraft nucleonic fuel gauging facility system allowing performance evaluation and optimization by computer techniques 05 p0842 A67-16542
Q-switched ruby laser configuration with feedback control, noting frequency and instability correlation with theoretical results obtained from mathematical model 05 p0822 A67-16676
Mathematical models properties analyzed for system reliability and maintainability, namely mission availability, discussing relationship to failure and action rate and time constraint 05 p0813 A67-17252
Collisionless theory of plasma sheath near infinite planar electrodes, developing new sheath model incorporating microscopic boundary conditions 05 p0857 A67-17424
Stability theorem for damped dynamic systems based on commutativity of class of mathematical models 06 p1099 A67-17844
Differential equations and mathematical models for gas flows with chemical activity and radiative effects, particularly effects of reentry and propulsion 06 p0983 A67-17785
Inverse problems of potential theory analyzed for uniqueness of solution 06 p1023 A67-17861
Mathematical model for potential heating from gamma radiation source, determining transient temperature distribution for materials used in nuclear rockets 06 p1116 A67-18363
Computer program and mathematical model for design of electrostatic colloid thruster [AIAA PAPER 67-84] 06 p1075 A67-18499
Data requirements for medium period weather prediction, discussing mathematical models and meteorological satellites 06 p1028 A67-18998
Mathematical reliability of model for vibrating field lines used to explain micropulsation observations 07 p1182 A67-19950
Mathematical model for condensation point of first order phase transitions, examining free energy singularity and metastable phase 07 p1268 A67-20089
Black Brant III sounding rocket analyzed via mathematical model to predict temperature distribution in ablation material 08 p1425 A67-20531
Mathematical models for use in hybrid computer simulation for design of Integrated Helicopter Avionics System /IHAS/, analyzing operational modes of automatic flight control system /AFCS/ 08 p1350 A67-20658
Error model digital computer program applied to lunar surface hybrid navigation concepts, noting accuracy requirements from 1972 to 1985 08 p1351 A67-20675
Cosmological principle and field equations used in analysis of Einstein, de Sitter, Friedmann and Hoyle-Narlikar models 09 p1563 A67-21652
Mathematical model of microscopically heterogeneous medium undergoing elastoplastic deformation, deriving equations for stress-strain distribution under uniaxial loading 09 p1575 A67-21931
Dynamic simulation of linear differential equations 09 p1469 A67-22820
Matrix methods applied to graphs, giving proof for matrix tree theorem 10 p1673 A67-22832
Geometric interpretation of product form of inverse applied to sparse matrices in linear programming, using graph theory 10 p1673 A67-22833
Plane problem of rigid die penetration into elastic medium solved, using divergent

series form 10 p1721 A67-23671
Charge separation effects in Ferraro-Rosenbluth cold plasma sheath model, using relativistic treatment 11 p1825 A67-23869
Electromagnetic wave propagation across land-sea boundary on flat earth near coastline 11 p1751 A67-23967
Approximate normal mode technique, providing solution to sinusoidal and white noise randomly excited damped linear multi-degree of freedom system, for application to mathematical model [ASME PAPER 67-VIBR-2] 11 p1871 A67-24164
Unidirectional vibration isolation systems, discussing viscous damping, Coulomb damping transmissibility and resonance characteristics [ASME PAPER 67-VIBR-21] 11 p1796 A67-24180
Equations for turbomachinery blades vibration control noting energy exchange, stress amplitude, mechanical damping, etc [ASME PAPER 67-VIBR-49] 11 p1797 A67-24199
Mathematical analysis of electrochemical machining phenomena, discussing behavior predicting equations [ASTME PAPER WES-7-09] 11 p1798 A67-24254
Axisymmetric deformation of elastic slab with external crack interpreted as steady state problem of heat conduction 11 p1813 A67-24313
Finite difference network model method with error tolerance for spacecraft heat transfer calculation 11 p1883 A67-24356
Mathematical model of flooded random surface and applications to lunar terrain 11 p1863 A67-24556
Air traffic control systems analyzed by simulation techniques 12 p1964 A67-25229
Characterization and equivalent model construction technique for class of nonlinear systems mathematically described, constructing zero memory systems and systems with memory 12 p1919 A67-25285
Verification of thermal mathematical model for artificial satellite using thermal vacuum chamber, noting error analysis [AIAA PAPER 67-304] 12 p2036 A67-26019
Rough metal surface bidirectional reflectance, using Davies and Beckmann models [AIAA PAPER 67-319] 12 p2037 A67-26034
Mathematical model for predicting temperature and life of silver-zinc battery system in spacecraft [AIAA PAPER 67-334] 12 p1901 A67-26048
Diffusion flame stability criteria for one-dimensional model at unity Lewis number 13 p2221 A67-26260
Dynamic filtering fundamentals, considering mathematical modeling 13 p2086 A67-26414
Model equation for circadian periodicity 13 p2058 A67-26629
Analytical expressions for multiply scattered light mean intensity and light source function in homogeneous planetary atmosphere derived using mathematical model 13 p2113 A67-26683
Geometrical model for calculation of solar heat fluxes reflected from planet onto plate 13 p2201 A67-27342
Three-dimensional flow of ideal fluid past body enveloped by air cavern, deriving normal velocity components 14 p2239 A67-27985
Model of inviscid, incompressible and variable density airflow in long channel over mountain treated 14 p2346 A67-28004
Model for solid rocket motor instability caused by chamber and propellant combustion characteristics, relating instabilities 14 p2404 A67-28113
Mathematical model describing nonlinear behavior of vortex valve in fluid circuits, noting effect of swirl on vortex valve flow characteristics 14 p2251 A67-28341
Synthesis of optimal controls for nonlinear plant described by second order differential equation 14 p2291 A67-28383
Intake aerodynamics of upper wing surface studied with two-dimensional potential flow models and suction models, considering inlet problems 14 p2243 A67-28702
Equations describing forces of

electromagnetic wave interaction with spherical plasmoid in free space 14 p2361 A67-28806
Moon thermal history investigated using thermal model, comparing results with astrophysical and geological evidence including melting and fluid convection effects 14 p2390 A67-28888
Skin effect in plasma theory for case of nonlocality of relation between current and electric field 15 p2522 A67-29211
Solution for shock wave of bimodal distribution using Bhatnagar-Gross-Krook models, noting symmetry property destruction and recovery by using modified BGK model 15 p2470 A67-29226
Computational worst error algorithm for linear systems and quadratic error criteria, showing flowgraph and computer execution results 15 p2457 A67-29367
Recursive algorithm for identification of time varying parameters of system, noting use for matrix inversion 15 p2509 A67-29371
Mathematical model used to determine influence of nonlinear induced roll moment and yawing moment on dynamic stability of cruciform tailed bomb 15 p2416 A67-29428
Mathematical model of MHD induction generator, deriving electrical diagram 15 p2527 A67-29472
Statistical model for size effect in electrical conduction 15 p2517 A67-29485
Surveyor spacecraft reliability from test data, examining assessment outputs, basic definitions and mathematical models 15 p2493 A67-29608
Characteristics and mathematical model of junction field effect devices with small length-to-width ratios 15 p2446 A67-29636
Mathematical models for loss measurements in thin Permalloy films with ramp drives 15 p2536 A67-29649
Flattening of ellipsoid of revolution considered as mathematical surface for solution of geodetic problems 15 p2477 A67-29744
Advanced space vehicle planning analyzed from economic approach to decision making, noting cost decrease with time 15 p2566 A67-29833
Modular distance measurement using geometric model for electronic continuous wave distance measuring equipment 15 p2511 A67-29893
Steady state and transient analysis of digital phase-locked loops 15 p2458 A67-29939
Stress states, structure deformation, failure criteria and constitutive relations in structural design noting tensile, strip and lap shear test and continuum model 15 p2575 A67-29977
Prediction of large rocket nozzle material performance using semiempirical technique, noting mathematical models for internal and external heat and mass transfer 15 p2547 A67-29993
Model for velocity coupled axial mode combustion instability in solid propellant rocket motors, noting computer studies 15 p2547 A67-29997
Velocity limitations of accelerated plasma by momentum loss due to electrode impact of accelerated ions, proposing modified snowplow model 15 p2531 A67-30030
Book on creation and use of computer simulation models and routines for study of systems 15 p2440 A67-30133
Thermal conductivity variation of double-base solid propellants under acoustic irradiation compared with polymethyl methacrylate 15 p2545 A67-30199
Stochastic model to structural fatigue, obtaining probability distribution for number of load repetitions necessary for fatigue failure 15 p2578 A67-30270
Accuracy of mathematical models in control system identification estimated on basis of deterministic test signals for simulation in time and frequency domains 15 p2461 A67-30318
Technique based on Fokker-Planck equation for estimating statistics of randomly varying parameters in dynamic systems with known differential equation 15 p2461 A67-30323
Systems with asymmetric nonlinearities analyzed and synthesized by setting up mathematical model applicable to control and adaptive systems 15 p2463 A67-30333
Evolutionary concept for mass

transportation system [AIAA PAPER 67-381] 15 p2420 A67-30351
 Permutation modulation systems comparison based on proved-best criterion of alphabet size and minimum distance between signal vectors 15 p2439 A67-30384
 Energy and momentum exchange model for interaction of gas particle with solid body surface 16 p2619 A67-30458
 Current density distribution in MHD duct with segmented electrodes of finite size analytically described, noting experimental agreement 16 p2600 A67-30537
 Electrostatic stability of finite-length plasmas immersed in magnetic field studied on mathematical model, discussing experiments with plasma-generating machines 16 p2714 A67-30871
 Yield variation of excited hydrogen atoms formed by charge exchange with gas target thickness described by analytical model 16 p2714 A67-30874
 Motion stability of earth-orbiting nonsymmetrical satellite with elastically-connected moving parts studied by Liapunov analysis on mathematical model 16 p2762 A67-30962
 Book on analytical methods in vibrations covering general mathematical formulations of common features of various vibrating systems 16 p2765 A67-30999
 Electric field distribution inside local superconductor carrying steady case analyzed using Ginzburg-Landau equation, noting strong compressibility effect 16 p2731 A67-31171
 Electronic states and transitions of zirconium oxide, noting Franck-Condon factors and r centroids, calculated from Morse model 16 p2704 A67-31173
 Bounce model pinch stability, noting plasma and field separation by thin surface, with anisotropies in velocity distribution and angular momentum considered 16 p2718 A67-31227
 Analytical plasma flow model for acceleration process in Hall current device, noting final velocity derivation, temperature, critical velocity, etc 16 p2719 A67-31237
 Crack extension and propagation experiments defining plane-stress regime and providing rationale for Dugdale-Muskellshvili model, noting stress-strain relations 16 p2769 A67-31286
 Crags propagating crack model extended to general elastic anisotropy deriving general theory for tensile or shear stress fracture propagation 16 p2770 A67-31291
 Mechanical strength of medium formulated as microscopic behavior in continuum obtaining time-dependent macroscopic fracture strength 16 p2771 A67-31295
 Minimum realization of linear time-varying nonanticipative system characterized by its impulse response matrix 16 p2697 A67-31426
 Relative, world-wide magnetospheric electron precipitation into lower, denser atmosphere determined, using conjugate point magnetospheric-ionospheric circuit model 16 p2667 A67-31510
 Radio ray divergence in ionosphere using computer techniques, noting ionospheric models and limitations 16 p2629 A67-31512
 Optimal feedback control system design to account for differences between physical system and mathematical model in terms of parameters 16 p2647 A67-31641
 Behavior of high-order linear control systems analyzed using Liapunov second method, by finding low-order model with closely approximate response behavior of high order linear control systems analyzed, using Liapunov second method, 16 p2647 A67-31648
 Control of output variables in discrete multivariable system at steady state noting design, application and performance 16 p2649 A67-31668
 Lumped parameter model for monopropellant hydrazine reaction chamber developed, using mass and energy balance and reaction and diffusion rate coefficients 17 p2927 A67-31974
 Exact stability criteria for kinetics equations of coupled-core nuclear reactors, using Pontryagin theorem and models for time-distribution of coupling neutrons [ASME PAPER 66-WA/AUT-16] 17 p2882 A67-32015
 Integral multiplicity calculation procedure for meson component of cosmic rays based

on three-dimensional elementary event model, noting meteorological effects 17 p2934 A67-32104
 Model for hemispherical cratering of structural metals by hypervelocity impact, determining elastic-plastic threshold stress by true tensile strength measurement 17 p2958 A67-32217
 Mathematical model for global atmospheric circulation prediction and mean properties in terms of tensor algebra 17 p2843 A67-32466
 Long term gyro drift rate evaluation involving time series detrending and autoregression, periodogram, autocorrelation, spectral density and mathematical model analysis 17 p2858 A67-32486
 Nonlinear filter for homing missile tracking noise problem, noting computational requirements and feasibility by filter implementation model for different assumptions 17 p2882 A67-32526
 Millimeter radiation from 3C 273 17 p2944 A67-32635
 Automatic control systems, discussing open and closed loop control systems, mathematical model analysis and developments 17 p2830 A67-32788
 Ionizing radiation effect on field effect MOST transistors, noting irradiation degradations 17 p2919 A67-32856
 One-dimensional three-body problem, noting shell model for two particles and coordinate transformation 17 p2888 A67-32926
 Plane wave propagation in kinetic theory, discussing Boltzmann equation use and asymptotic results beyond critical frequency 17 p2905 A67-32927
 Critical speed control by squeeze-film oil damper between two nonrotating parts in parallel with flexible bearing support, using mathematical model [SAE PAPER 670347] 17 p2865 A67-32989
 Law for velocity distribution through wall boundary layers derived from eddy viscosity model, considering turbulent shear variation and Reynolds number effect 17 p2839 A67-33008
 Static /time-discrete/ electrical model for mathematical analogy of heat transfer processes and application to solution of nonlinear heat conduction equations 17 p2821 A67-33079
 Equations for one-dimensional model of macroscopically homogeneous linearly elastic medium of complex structure with spatial dispersion 17 p2965 A67-33269
 Three-space optical resonator model, deriving properties responsible for undesired natural frequencies suppression, noting selection characteristics 18 p3058 A67-33528
 Control engineering in systems management applied to missile control and guidance 18 p3162 A67-33636
 Mathematical model for thermal and chem-ionization processes in turbulent nonequilibrium afterburning rocket exhausts plume, studying neutral and charged species distribution 18 p3152 A67-33820
 Ejector ramjet and ducted rocket evaluation by analytical models for various flight trajectories, noting specific impulse improvement [AIAA PAPER 67-437] 18 p3112 A67-33915
 Boundary layer combustion in hybrid rockets from simplified model comprising convective transport and chemical kinetic factors, analyzing fuel regression rate [AIAA PAPER 67-471] 18 p3157 A67-33941
 Hydrogen-air reaction kinetics analyzed using standing wave normal shock, noting wall effects, ignition delay and recombination [AIAA PAPER 67-479] 18 p3157 A67-33948
 Physical and chemical conditions in rocket combustion chamber during starting transients and steady operation described by mathematical model intended for parametric studies [AIAA PAPER 67-517] 18 p3158 A67-33980
 Mathematical model for computer diagnosis of system failure, developing optimal policy for searching malfunctions with observable symptoms 18 p3006 A67-34065
 Perfect frictionless supersonic MHD gas flow model for shock wave control, noting nozzle geometry 18 p3088 A67-34123
 MHD equation simplifications and MHD converter model for problem solving,

discussing electrical and thermodynamic characteristics 18 p2989 A67-34125
 Slow response of cadmium selenide thin film transistors related to trapping levels in insulator 18 p3015 A67-34557
 Development and application of Monte Carlo logistic simulation model for measuring system availability dependence on reliability, maintainability and logistic support 18 p3021 A67-34674
 Saturn V reliability analysis model used by management for predicting performance probabilities 18 p3138 A67-34684
 Maintainability risk analysis using analytical model with gamma distribution 18 p3021 A67-34685
 MARCEP mathematical and mission simulation models to evaluate parameters affecting maintainability of long duration manned space flights 18 p3138 A67-34688
 Maintainability and reliability cost effectiveness program /MARCEP/ applied to logic and computer limitation problems 18 p2995 A67-34689
 Maintenance and support factors effects on systems availability described by mathematical models, giving applications in tradeoff studies 18 p3163 A67-34695
 Reliability analysis and mathematical models to evaluate crew safety applicable to system safety analysis, discussing component failure data, failure mode effect, etc 18 p3139 A67-34704
 Mathematical model of rigid, long space-body spinning at constant rate about symmetry axis for optimal attitude control calculations 19 p3331 A67-34777
 Gyroscope circuit model and oscillation behavior analyzed through nonlinear differential equation derived from Euler equation 19 p3227 A67-34843
 Flowgraph models of thermal and electrical parameters interaction in solid state devices, examining performance characteristics, system stability, etc 19 p3191 A67-34845
 Linear networks having reciprocal and nonreciprocal elements obtained using numerical-code circuit model 19 p3201 A67-34906
 One-dimensional models for constricted anomalous glow discharge investigated for various applications 19 p3274 A67-35100
 Inner zone electron intensity distribution model for solar activity minimum 19 p3219 A67-35238
 Flexural center location and torsional rigidity of bar calculated using elasticity theory and variational calculus 19 p3340 A67-35512
 Inhomogeneous cylindrical plasma column oscillations with perturbations, finding density-independent mode 19 p3295 A67-35564
 Stratified shear flow instability examined through two classical models 19 p3210 A67-35611
 Statistical band model applied to NO fundamental vibration band, discussing transmittance measurements and validity of linear region criterion 19 p3266 A67-35681
 Mathematical model for optimization problem obtaining equations generalizing Bellman equation 19 p3205 A67-35908
 Gradient method of parametric identification of processes through mathematical model 19 p3206 A67-35915
 Lunar landing module Doppler radar system in guidance navigation and control system, studying mathematical model performance 19 p3260 A67-36011
 Potential delta well model for barrier in solid state tunneling 19 p3308 A67-36039
 Mathematical models of multichannel radio equipment in presence of noise, including guidance and coordinate measurement systems 19 p3185 A67-36095
 Plasma shock wave structure model, analyzing steady flow of electrically neutral fluid 20 p3493 A67-36144
 Quasi-linear plasma waves model, considering Vlasov approximation, deriving distribution functions and electric field equations solution 20 p3494 A67-36149
 Transistor admittance parameters for mathematical model formulation representing small signal operations, for wideband transistor amplifier design 20 p3394 A67-36236
 Linear operation of diffused planar transistor in common emitter connection

studied by mathematical models 20 p3396 A67-36377

Equivalent circuits derived by mathematical model from experimental data on diffused planar transistor 20 p3396 A67-36378

Screened electron-phonon interaction effect on mobility of conduction electrons in semiconductors at low temperatures 20 p3509 A67-36433

Intermodulation interference effect on PCM/FM error rates studied using power series as mathematical model 20 p3380 A67-36563

Nilsson model used to derive expressions for nuclear matrix elements, considering forbidden beta decay of spheroidal-shaped nuclei 20 p3488 A67-36662

Effect of deviation of inlet fluid temperature change from step change on maximum slopes of transient response curves [ASME PAPER 67-HT-79] 20 p3551 A67-36757

Maximum strengths of aluminum alloy and metal columns under parameter variation, using mathematical model 20 p3538 A67-36780

Signal model with white noise fitted to time series, discussing signal proportion estimation methods 20 p3476 A67-36788

Stochastic models for forecasting seasonal and nonseasonal time series using iterative method 20 p3477 A67-36790

Weak electromagnetic decays of hyperons in broken SU(3) model 20 p3489 A67-37093

Mean error and optimal structures for multidimensional extremal systems with random noise obtained from steady process 20 p3409 A67-37112

Burning in unmixed reactants for high enthalpy inviscid flow of opposed streams studied for one-step reaction model and Lewis-Semenov number unity 20 p3554 A67-37132

Baroclinic quasi-geostrophic prediction of geopotential field using two-parameter model 20 p3481 A67-37236

Mathematical models of flow and filtration performance of wire cloth filter media in series and parallel configuration 20 p3365 A67-37364

Mathematical model simulation of horseshoe crab eye lateral inhibition for nervous system pattern transformation, discussing human visual pattern recognition process 20 p3375 A67-37543

Secondary dose equivalent model for calculating secondary proton and neutron doses determined, using random sampling techniques 20 p3482 A67-37551

Stagnation-point flow of rarified gas, using linearized BGK model of Boltzmann equation with small Mach number 20 p3425 A67-37673

Mathematical model for potential heating from gamma radiation source, determining transient temperature distribution for materials used in nuclear rockets 21 p3730 A67-37793

P-n-p-n diode noise measured by standard techniques and explained using theoretical model, considering internal feedback and additional amplification 21 p3589 A67-37820

Ionospheric pulse absorption study of measurements taken in Bulgaria during solar eclipse of May 1966 21 p3616 A67-37995

Mathematical model describing magnetic damping in attitude control system of ESRO I satellite 21 p3678 A67-38216

Plane problem of rigid die penetration into elastic medium solved, using divergent series form 21 p3719 A67-38272

Printed circuit thermal design, discussing edge-to-center temperature gradient and circuit board models 21 p3594 A67-38330

Analytical expressions for multiply scattered light, mean intensity and light source function in homogeneous planetary atmosphere derived using mathematical model 21 p3618 A67-38427

Thermal stress analysis of epoxy encapsulants using mathematical model for predicting performance in thermal shock 21 p3723 A67-38630

Thin plate idealization to Hrennikoff lattice model framework for linear stiffness method analysis 21 p3728 A67-38877

Geomagnetic field configuration and time change using dipole vector, noting variation role 21 p3620 A67-38979

Geomagnetic field intensity influence on atmospheric C-14 production, using two-reservoir model 21 p3620 A67-38981

Mathematical models for retrieval systems for future extravehicular operations, discussing rotational and translational motion and constraint equations 22 p3753 A67-39157

Vacancy concentration in dislocation enhanced diffusion model as explanation of phosphorus and boron anomalous diffusion in silicon 22 p3855 A67-39346

Carrier concentration dependence of thermoelectric power and Hall mobility of undoped and doped lead telluride explained by two-valence model 22 p3857 A67-39490

Flux penetration and dissipation measured on superconducting niobium slab samples with tangential applied field studied for effect of thickness 22 p3857 A67-39491

Combustion in solid propellant rocket engines using mathematical model 22 p3867 A67-39539

Kramers problem for rarefied gas flow, calculating slip coefficient for various collision frequency models, noting only slight model dependence 22 p3841 A67-39718

Mathematical model for solution of anisotropic diffusion equations of solar cosmic ray propagation 22 p3872 A67-39809

Magnetic film memory written and read by focused light studied using thermal cycle time and read bandwidth calculations 22 p3765 A67-39910

Analytic model for output voltage of fluxgate magnetometer, demonstrating excitation function and core squareness effects 22 p3800 A67-39911

Mathematical model for linear memory arrays cross coupling problems, discussing signal distortion due to common mode capacitance effect 22 p3765 A67-39912

Thomson motion equation derivation for variable mass system extended for flight simulation equations for variable mass inertially guided system 22 p3832 A67-40099

Computer program and mathematical model for design of electrostatic colloid thruster [AIAA PAPER 67-84] 22 p3868 A67-40101

Speedy generation of space flight guidance command signals and comparative analysis of operational schemes for generating guidance signals 22 p3832 A67-40145

Optimization of staged ejector systems noting mathematical model development to represent performance characteristics 22 p3787 A67-40150

Propellant sloshing effect on vehicle dynamics under zero gravity conditions studied by programming motion equation into digital simulation of spacecraft, control and propellant 22 p3907 A67-40180

Mathematical model for studying liquid slosh effects on rendezvous dynamics by incorporating sloshing dynamics into vehicle motion equation 22 p3888 A67-40189

Wake turbulence regimes for flows behind typical hypersonic bodies 22 p3743 A67-40222

Mathematical model for vibrating characteristics of structures in statistical mechanics framework, noting closeness to Green function rather than to mode concept [ONERA-TP-467] 22 p3915 A67-40385

Air damping effect on structural fatigue failure evaluated mathematically as power function relating stress to number of cycles 22 p3915 A67-40405

Logistics resource development and approaches to life cycle economics in 1970s 23 p4085 A67-40587

Yielding behavior of materials and structures examined via one-dimensional models noting stress-strain relations 23 p4072 A67-40605

Natural frequency vibration mode of turbine blades calculated by approximate theory of integral evaluation yield discrete models 23 p4076 A67-40684

Two-dimensional two-fluid nonlinear computer model applicable to low beta plasma interchange modes 23 p4033 A67-40995

Cylindrical antenna admittance taking into account antenna to coaxial line junction geometry, using magnetic current mathematical model 23 p3980 A67-41205

Electrically thick cylindrical antenna driven by delta function generator, discussing numerical solutions to two different mathematical models 23 p3980 A67-41206

CdS solar cell model, discussing p-n junction, CdS and copper sulfide properties and microscopic junction formation and behavior 23 p4046 A67-41486

Distributed model for photovoltaic cell via nonlinear least square techniques, discussing p-n silicon cells 23 p4046 A67-41487

Photovoltaics - IEEE conference, Cocoa Beach, Florida, March 1967, Volume 2: Spacecraft power systems, solar cell mathematical model 23 p3938 A67-41509

Mathematical technique to determine probabilities associated with critical system performance capability measured under varying human and environmental conditions 23 p3964 A67-41541

Small perturbation analysis on mass conservation stability in solid propellant combustor, discussing parametric model 23 p4084 A67-41721

Mathematical model of linear guidance law to dynamical system, noting reduction of two-point boundary value class error 23 p4026 A67-41732

Gravitational torque mechanism for radial outward angular momentum transport in solar nebula 24 p4223 A67-41790

Space distribution function of Knudsen gas in closed volume investigated using gas model noting dependence of time 24 p4190 A67-41902

Laser radiation model of superimposed coherent and incoherent radiation determining statistics of photons 24 p4166 A67-41903

Thermal testing techniques for solar probe spacecraft using analytical and experimental models 24 p4139 A67-42043

Mathematical methods for incorporating thermodynamic data into least squares fit 24 p4177 A67-42083

Distributive circuit element model for computation of optimum gridding of solar cells 24 p4098 A67-42086

High energy proton data from Telstar 1 satellite used to develop mathematical models of proton spatial distribution 24 p4210 A67-42334

Statistical model for multiple particle production process based on unitary symmetry concept of strong interactions, comparing results with quark model results 24 p4193 A67-42861

Mathematical model to aid in determination of need for technological advances in transportation [AIAA PAPER 67-799] 24 p4258 A67-42960

System-safety mathematical model for commercial jet airplanes using fault-tree modeling technique [AIAA PAPER 67-910] 24 p4096 A67-43017

Mathematical model for identification and control of systems safety in manned space programs using Monte Carlo techniques [AIAA PAPER 67-936] 24 p4245 A67-43026

MATHEMATICAL STATISTICS

Exact solutions derived for problems of mathematical expectation and density distribution of maxima for two types of nonstationary random processes 03 p0461 A67-13948

Computing methods and techniques in aircraft testing, discussing measurements, application of mathematical statistics, etc 09 p1469 A67-22455

Book on design and analysis of scientific experiments covering statistical estimation theory in design and testing of hypotheses, emphasizing computational techniques 12 p1961 A67-25560

Multiparameter data sorting technique for one-parameter information represented by simple distribution described by appropriate transformation coefficients 12 p1909 A67-25863

Handbook of engineering sciences, Volume 1, Basic sciences 13 p2155 A67-26266

Book on shift register sequence theory, discussing applications in communications, computers and switching theory 19 p3187 A67-35832

Mathematical statistics methods for nonreabsorbed spectral line widths and shifts and optical density in plasma 20 p3471 A67-37801

Testing procedures for null hypothesis sensitive to ordered alternatives where at least one inequality is strict 21 p3650 A67-37780

Aircraft empty weight equations as function of takeoff weight, using mathematical statistics 21 p3567 A67-38041

Optimal choice of prototype set by mathematical-statistics estimation theory, using active part of set for identifying

control image 21 p3605 A67-39113
 Statistical significance of mathematical and logical foundations of information processing method applied to meteor stream 23 p4070 A67-41690

MATHEMATICAL TABLE
 Designing antisymmetrically loaded conical shells and elastic systems consisting of rings, plates and shells for machine elements 08 p1424 A67-21427
 German-English index of mathematical tables for science and technology 08 p1431 A67-21541
 Physical electronics formulas tabulated, with solid state physics variables dimensionally coded and resultant nondimensional products cataloged, using computer routine 20 p3506 A67-36235

MATHEMATICS
SA ALGEBRA
SA CALCULUS
SA GEOMETRY
 Book on electronics reliability, calculation and design 03 p0377 A67-13232
 Failure occurrence paradox capable of resolution by small change of attitude 04 p0584 A67-15480
 Mathematical studies of mechanics of solids in Rumania, noting use of matrices, Fourier expansions, stresses, shock waves, etc 05 p0920 A67-16797
 Extreme points of copositive quadratic forms constituting closed convex cone in Euclidean space 05 p0836 A67-17045
 Space mathematics - Seminar, Cornell University, July-August 1963, Part 2 06 p1079 A67-17761
 Space mathematics - Seminar, Cornell University, July-August 1963, Part 1 06 p1080 A67-17771
 Space mathematics - Seminar, Cornell University, July-August 1963, Part 3 06 p0983 A67-17782
 Applied mathematics of space program fluid mechanics and aerodynamics 06 p0983 A67-17783
 Mathematical calculation and role in flight mechanics 06 p0947 A67-18018
 Monograph on integral equations covering Fredholm and Volterra equations, applications to theory of differential equations, properties of Cauchy type integrals, etc 08 p1348 A67-20761
 Mathematical methods for digital computers, Volume 2, covering programming languages, numerical linear algebra, etc 09 p1467 A67-22044
 Book on geometric programming detailing theory of mathematical method for optimizing engineering design 09 p1469 A67-22435
 Mathematical methods for two classes of variational problems analogous to optical reflection and optical refraction in connection with rocket flight 10 p1678 A67-23425
 Thermoelastic piecewise homogeneous bodies 12 p2013 A67-25259
 Shells of revolution under axisymmetric loading analyzed within ideally plastic shell theory, examining mathematical difficulties of shell carrying capacity 12 p2029 A67-25637
 Applied mathematics and mechanics - Symposium, Darmstadt Technical University, April 1966 13 p2156 A67-26605
 Numerical values of coefficients for four different implicit Runge-Kutta formulas 13 p2146 A67-26743
 Fourier series solutions of boundary-value and mixed problems in mathematical physics by integrating partial differential equations 14 p2348 A67-28287
 Possible permutations producing cyclic permutations in theorems for component interactions in mechanical systems 14 p2349 A67-28745
 Mathematical methods of celestial mechanics and astronautics - Conference, West Germany, March 1964 15 p2558 A67-30034
 Electrodynamically coupled system consisting of RCL circuit, transformer and mechanical system analyzed by mathematical analogy and analog computer 15 p2440 A67-30081
 Computerized mathematical procedures application in advanced large-scale automated systems 16 p2634 A67-31568
 Incorrect problems of mathematical physics examined and illustrated by classical Cauchy problem for Laplace

equation 16 p2698 A67-31736
 Book on engineering mathematics covering differential equation solutions by numerical method, partial differential equations, Fourier series, integrals, vector analysis, etc 17 p2876 A67-31930
 Mathematical programming on analog computers solved by saddle point and extremum methods, using differential equations 17 p2817 A67-32225
 Soviet papers on mathematical physics covering solution of boundary value problems, structural analyses, etc 17 p2884 A67-32887
 Numerical calculation and applied mathematics - Conference, Lille, France, 1964 18 p3071 A67-33751
 Long time behavior of weakly interacting nonlinear waves, emphasizing mathematical features common to physical situations 18 p3079 A67-34002
 Linear algebra describing equilibrium chemical systems and complex chemical mixtures, discussing hydrogen-fluorine coupling reaction at elevated temperatures 18 p2997 A67-34124
 Anharmonic method of photogrammetry rectification point by point, deriving positions from minimum control data 24 p4158 A67-42604
 Vector space convexity and nonmonotonicity proof, discussing 34-dimensional linear space and 1-simplicial convexity 24 p4179 A67-42729

MATHIEU FUNCTION
SA RAYLEIGH EQUATION
 Single mode analysis of dynamic buckling of imperfection-sensitive elastic structure prone to catastrophic failure under time dependent load 14 p2396 A67-28083
 Numerical recursion method for calculation of characteristic exponent of Mathieu differential equation 22 p3827 A67-39744

MATRIX
SA GRID
SA S-MATRIX
SA SCATTERING MATRIX
 Fiber strengthening theory, taking into account stress transfer between matrix and fiber in both elastic and plastic regions 03 p0449 A67-13257
 Synthesis method for immittance matrix with grounded unity gain amplifier /GUGA/ as only active element 03 p0393 A67-13979
 Carbon dioxide solid matrix study of carbon trioxide production, IR spectrum and molecular structure 05 p0759 A67-16838
 Solid propellant polymeric binder chemistry and high speed computer calculations of performance characteristics 08 p1373 A67-20875
 Linear transformation of normalized static capacitance matrix used to describe TEM propagation on array of parallel conductors 08 p1304 A67-21224
 Continuous filament reinforcement data, analyzing boron and silicon carbide for metal matrix applications 10 p1668 A67-23010
 [ASTME PAPER WES-7-75] 13 p2159 A67-27730
 Comparison of steady state operator of Prigogine with T-matrix 13 p2159 A67-27730
 Atomic collisions with negative ions, deriving transition matrices for resonance reactions and scatterings to analyze rearrangement process of associative electron detachment 14 p2350 A67-28149
 Metal matrices reinforcement by whiskers demonstrating high strength at high temperatures [ASME PAPER 67-DE-35] 14 p2328 A67-28876
 Memory device for matrix time meter, discussing use of logic thyatron to improve stability of memory matrix 16 p2674 A67-31119

MATRIX ALGEBRA
 Undetermined coefficients method for obtaining particular solution of linear ordinary system with constant coefficients, solving final matrix equation 01 p0105 A67-10729
 Nonsingular linear transformation of time-invariant linear dynamic system into canonical /phase-variable/ form 01 p0048 A67-11223
 Solution method for determinantal equation of matrix polynomial 02 p0258 A67-11799
 Quadratic performance criteria for discrete control systems, using Liapunov

matrix equation and digital computer program 02 p0225 A67-12074
 Gust reduction equations governing numerical procedure for transforming to inertial frame continuous records of air turbulence velocity via matrix methods [AIAA PAPER 66-987] 02 p0246 A67-12290
 Sinkhorn theorem on diagonal equivalence of nonnegative matrix to stochastic matrix, using Mennon homogeneous positive nonlinear operator T and uniqueness of eigenvectors of T 04 p0645 A67-15082
 Mathematical theory of dimensional analysis and similitude, application to spacecraft thermal design and experimental results 05 p0928 A67-16514
 System of n first order differential equations relating coordinates and time, using matrix methods for solution 06 p1022 A67-17773
 Stress-strain and Hooke law in orthotropic elasticity presented through matrix algebra and tensor coordinates 06 p1108 A67-18656
 Solution of ill-conditioned linear equations when matrix of coefficients is not sparse or otherwise specialized, noting error analyses of elimination methods 09 p1468 A67-22045
 Algorithm for analyzing general electric circuits with lumped parameters in transient state by automatic digital computer 09 p1469 A67-22440
 Matrix methods applied to graphs, giving proof for matrix tree theorem 10 p1673 A67-22832
 Geometric interpretation of product form of inverse applied to sparse matrices in linear programming, using graph theory 10 p1673 A67-22833
 Explicit invariant forms of factor equations for factorization of secular equations by group 10 p1674 A67-23377
 Book on matrices for structural analysis, including elementary algebra and detailed arithmetic of matrix methods applied to structure theory 10 p1719 A67-23476
 Anisotropic vector functions of vector argument connected with crystal symmetry 11 p1812 A67-24148
 Optimal smoothing filter and smoothing error covariance matrix equations for discrete linear systems, using orthogonal projection 11 p1770 A67-24422
 Liapunov functions generated by transformation of Companion matrix to Routh or Schwarz canonical forms, for asymptotically stable linear time-invariant multivariable systems 11 p1814 A67-24942
 Numerical methods for elliptic problems, discussing application of finite difference and solution of large algebraic systems 14 p2342 A67-28156
 Number of completely nonsingular $n \times n$ matrices with elements 0, 1 14 p2345 A67-28934
 Necessary and sufficient conditions to ensure existence of unique solutions of equations for 'active networks' 15 p2456 A67-29238
 Modular distance measurement using geometric model for electronic continuous wave distance measuring equipment 15 p2511 A67-29893
 Book on structural matrix analysis for engineers, giving examples of matrix algebra practical application and methods of linear equation investigation 16 p2784 A67-30966
 Book on analytical methods in vibrations covering general mathematical formulations of common features of various vibrating systems 16 p2765 A67-30999
 Necessary and sufficient conditions for decoupling time-invariant linear multivariable system by state variable feedback, discussing transfer matrix consequences 16 p2652 A67-31692
 Inversion of symmetrical matrices by computer, noting storage space advantages 17 p2820 A67-32802
 Book on computer solution of linear matrix algebraic systems and errors involved, discussing Gaussian elimination, FORTRAN, ALGOL and PL/I programs, etc 17 p2821 A67-32825
 Statistical techniques for missile injection error analysis, discussing direct and adjoint methods 19 p3254 A67-34780
 Determining sign of second variation in optimal control theory 19 p3202 A67-35756
 Analog computer solution of linear algebraic equations system modified to

- eliminate negative coefficients, guaranteeing computational system stability 19 p3187 A67-36032
- Linear equation system with coefficient matrix of multiple diagonal bands solved by direct method, reducing numerical solution error 20 p3476 A67-36675
- Differential and Clifford matrix algebra relationship in relativity theory, generalizing Dirac and quaternion algebras to Riemann spaces 21 p3656 A67-37923
- ### MATRIX ANALYSIS
- #### SA JACOBI MATRIX METHOD
- Hartree-Fock-Slater calculation of internal conversion coefficients for magnetic multipoles for yttrium-87 with 0.05 or 0.15 mc-square gamma energy values 01 p0116 A67-10203
- Matrix analysis of resonant vibration stability conditions 01 p0113 A67-10675
- Determination of maximum number of nonzero elements in nonnegative matrix and first power for which maximum density is assumed 01 p0105 A67-10731
- Control system analysis and design using parameter space method 01 p0047 A67-11216
- Algorithm for reducing linear time-invariant differential systems to state form applied to systems described by transfer functions 01 p0047 A67-11219
- State variable equation transformation to phase variable canonical form 01 p0047 A67-11222
- Matrix formulation of output controllability conditions for dynamic systems 01 p0048 A67-11293
- Identity of uniqueness and convergence constants of interpolation problems, discussing Abel-Goncharov function 02 p0258 A67-11624
- Optimal value of reactance of microwave parametric element 02 p0214 A67-11912
- Matrices of scattering transmission wave and normed cascade parameters of linear passive 2/m plus m/ terminal networks 02 p0221 A67-12528
- Electron collision cross section resonance mechanism analyzed via matrix methods, noting threshold effect application to electron scattering 03 p0470 A67-13219
- Conditions of solvability of Chaplygin problem 03 p0458 A67-13339
- Liapunov function of ninth order system represented by differential equation which, in phase variable form, can be represented by matrix equation 03 p0392 A67-13682
- Exact difference replacement for hyperbolic equation system where $n \times n$ symmetric matrices become coefficients of vectors in two-dimensional space 03 p0460 A67-13880
- Commuting inverses of singular square matrix A existing only if dimension of A null space equals multiplicity of zero root in characteristic equation 03 p0460 A67-13938
- Necessary and sufficient condition that generalized inverse of matrix A /denoted A plus/ commutes with A is that A plus can be expressed as polynomial in A with scalar coefficients 03 p0461 A67-13939
- Main properties of quasi-Cesaro method of summability 03 p0461 A67-13940
- Mathematical formulation relating modal distribution of truncation errors to matrix conditioning and loading type on structure 03 p0526 A67-13969
- Triangular iteration method of vector-matrix equation, noting role of continuous function 03 p0462 A67-14328
- Taper in thickness of wing for special case of linear type analyzed, using triangular elements for matrix displacement method 04 p0707 A67-14441
- Book of physics and mathematics as foundation for application of satellites to geodesy including spherical harmonics, matrices, orbital geometry, statistical implications and data analysis 04 p0611 A67-14466
- Minimization of number of arithmetical operations in matrix transformation process 04 p0644 A67-14729
- Stiffness matrix evaluation on basis of strain energy 04 p0709 A67-14813
- Modification of Potter method of Gaussian elimination for solving eigenvalue problems of buckling and free vibrations of shells of revolution 04 p0656 A67-14839
- Brownell approach for computing selected eigenvalues of matrix which can be applied in case of self-adjoint matrices 04 p0644 A67-14866
- Book on lamda-matrices for treating linear vibrating systems 04 p0644 A67-14869
- Implicit difference methods for initial boundary value problems based on Wiener-Hopf factorization 04 p0645 A67-15085
- Continuation of norms given at subring of matrix ring 04 p0646 A67-15257
- New matrix formula for obtaining inverse Laplace transformation [ASME PAPER 66-WA/AUT-3] 04 p0646 A67-15420
- Distributed parameter transmission matrix analysis of bending vibrations of nonuniform elastic beam [SAE PAPER 660719] 04 p0716 A67-15782
- Three-dimensional elastic problem of bodies of revolution, deriving Lamé and generalized Hooke equations in matrix form 05 p0916 A67-16226
- Vibrations of disk-drum rotor analyzed using matrix equation of discrete model 05 p0810 A67-16230
- Matrix method formulation of vibration and stability problems yielding upper bounds for natural frequencies 05 p0917 A67-16301
- Matrix analysis of small signal microwave frequency conversion based on linear operation of semiconductor diode 05 p0772 A67-16449
- Error estimation in linear matrix equation systems by rounding-off inaccuracies 05 p0834 A67-16721
- Operational calculus for functions of one continuous and one discrete variable 05 p0834 A67-16725
- Jordan form matrix algorithm of Wasow for reducing systems of first order ordinary differential equations with turning point 05 p0835 A67-16779
- Liapunov matrix equation solved by introducing skew symmetric matrix 05 p0835 A67-16950
- Matrix displacement approach to discrete element structural analysis for thin shell instability, emphasizing determination of membrane force distribution 05 p0925 A67-17352
- Reduction of systems of linear differential equations to generalized L-diagonal form 05 p0836 A67-17487
- Stability theorem for damped dynamic systems based on commutativity of class of mathematical models 06 p1099 A67-17644
- Matrix and vector computational procedures for solution of partial and ordinary differential equations 06 p1022 A67-17788
- Cruise error analysis for strapdown inertial navigation system with pulse torqued instruments in presence of small amplitude oscillations 06 p0947 A67-18007
- Invariants of triangular shell element stiffness matrices associated with polyhedral deflection distribution, discussing effect of geometry [AIAA PAPER 67-114] 06 p1103 A67-18356
- Nonsimilar solution to complex boundary layer problems, using matrix concept to integral relations via Taylor series expansion of parameters [AIAA PAPER 67-218] 06 p0988 A67-18364
- Matrix method determination of time response of time invariant linear systems to range of deterministic functions 06 p0978 A67-18402
- Matrix error analysis compared to algorithm optimization problems of numerical analysis [AIAA PAPER 67-142] 06 p1024 A67-18475
- Nonequilibrium boundary layer problem solution by direct treatment of two-point boundary value problem [AIAA PAPER 67-219] 06 p0990 A67-18515
- Book on computer matrix analysis of structures 06 p1105 A67-18520
- Time-weighted minimal energy control of nth order plant 06 p0977 A67-18531
- Matrix equations approximating integral equations of radiative energy transfer 06 p1118 A67-18551
- Sufficient conditions of absolute stability of nonlinear discrete systems based on matrix majorant concept 06 p0978 A67-18793
- Two generalized matrix forms of linear estimates for spaceship motion derived, based on maximum probability criterion 07 p1247 A67-19096
- Matrix techniques for finding geomagnetic field strength in solar ecliptic coordinate system 07 p1170 A67-19111
- Algebraic theory of finite systems of linear inequalities based on Minkowski theorem and boundary solution principle 07 p1216 A67-19582
- State transition partial derivatives for computing normal matrices in tracking analysis [AAS PAPER 66-108] 07 p1253 A67-19968
- Unitary and orthogonal invariants of square matrices 07 p1217 A67-20024
- Infinite magnetic quadrupole channel discussing operations in complete transverse plane phase space via 4×4 matrix transformations 08 p1332 A67-21172
- Givens-Householder method for computing eigenvalues and eigenvectors of real symmetric matrix 09 p1468 A67-22046
- Law of propagation of covariance in matrix form obtained from least squares adjustment 10 p1674 A67-23004
- Phonemic analysis of consonants in helium speech 10 p1597 A67-23312
- Finite element approach for determining rms deflections and stresses in randomly acoustically excited complex aerospace elastic structures 10 p1724 A67-23710
- Discrete element method for plastic analysis of complex built-up structures subjected to cyclic loading causing membrane stress and stress reversal 10 p1725 A67-23713
- Straightforward method consistent with virtual work principle for accelerating convergence to exact solution in shell analysis by matrix displacement method 10 p1725 A67-23714
- Dissipative gyroscopic force effects on mechanical system, noting necessary and sufficient conditions for stability and controllability 11 p1818 A67-24146
- Discrete mass technique for vibration analysis of thin shells [ASME PAPER 67-VIBR-23] 11 p1872 A67-24182
- Systematic design of matrix network, consisting of hybrids with phase delays in interconnecting lines, used for antenna beam steering 11 p1763 A67-24300
- Trajectory measurement errors for powered spacecraft using matrix analysis [AIAA PAPER 64-650] 11 p1817 A67-24335
- Ordinary waves in viscoelastic mediums analyzed, using Green tensor relation to Kirchhoff tensor 11 p1877 A67-24750
- Nonradial oscillations of homogeneous sphere examined on basis of general fourth order problem 11 p1819 A67-24783
- Green matrix estimates for homogeneous parabolic boundary value problems, showing proof of integral operator 11 p1813 A67-24850
- Matrix algorithm for calculating mean square error for synthesis of optimum control systems 13 p2087 A67-26612
- Time optimum control in n-dimensional linear dynamic system with constant coefficients determined by matrix method 13 p2087 A67-26619
- Dynamic properties of elastic one-and two-dimensional continua using matrix method on digital computer and Hermitian polynomials 13 p2218 A67-26621
- Interval arithmetic methods used for error bounding in matrix calculations of linear equations 13 p2147 A67-27170
- Analytical representations of admittance matrix of transistors, describing methods of obtaining quality coefficients, equivalent circuit synthesis, etc 13 p2081 A67-27199
- Radiation diffusion in medium of finite optical thickness, computation of source function and tabulation of matrices 14 p2382 A67-27832
- Electric network analogy for square matrix inversion 14 p2292 A67-28902
- Strong approximation of continuously differentiated function by means of differentiated expressions of finite line matrix 14 p2345 A67-28940
- Direct matrix method for analysis of critical loads and associated buckling modes for struts having various end constraints 14 p2403 A67-29017
- Matrix inversion formula applied to moving media electrodynamics and scaling operator in Lorentz transformation 15 p2509 A67-29175
- Recursive algorithm for identification of time varying parameters of system, noting use for matrix inversion 15 p2509 A67-29371
- Sufficient condition providing nonlinear

sampled system with set of initial conditions 15 p2458 A67-29473

Perturbation method for solution of linear matrix differential equations subject to initial and two-point boundary conditions applied to transmission lines 15 p2511 A67-30018

Quasi-isomorphic response of perturbed systems for slow coefficient variation of matrix system differential equation 15 p2512 A67-30050

Technique based on dimensional analysis for deriving set of dimensionless parameters in problems involving large number of variables, using matrix calculations 15 p2518 A67-30078

Matrix calculation of structures by parallel methods of forces and displacements [ONERA-TP-412] 15 p2576 A67-30125

Recursive formula for updating determinant of covariance matrix of state estimation error after incorporation of measurement 15 p2512 A67-30213

Limitations of observability and controllability of dynamic system determined, using approximation of performance matrix and iterative procedure 15 p2461 A67-30316

Arbitrary electrode MHD generator electrical characteristics, considering end effects and determining internal conduction matrix 16 p2600 A67-30534

Book on structural matrix analysis for engineers, giving examples of matrix algebra practical application and methods of linear equation investigation 16 p2764 A67-30966

Matrix method calculation for frequency, deformation, forces and moments of variable cross section in rotating turbine blade during natural bending oscillation 16 p2766 A67-31150

Book on matrix methods of structural analysis emphasizing force and displacement methods, noting civil and aircraft construction applications 16 p2767 A67-31253

Minimum realization of linear time-varying nonanticipative system characterized by its impulse response matrix 16 p2697 A67-31426

Electron-phonon interaction calculation for solid state transition metals justifying matrix element presented and using augmented plane wave 16 p2731 A67-31447

Linear algebraic equations arising from least squares estimation problem, noting Gaussian elimination process on matrices 16 p2647 A67-31651

Optimal trajectories for linear discrete system with respect to minimax criteria using standard programming code 16 p2650 A67-31670

Distributed parameter concepts of propagation, reflection and characteristic termination applied to dynamic analysis and control of bending vibration 16 p2776 A67-31686

Irreducible tensorial components of two-electron operator and second-order density matrix for spin-projected single-determinantal wave function 16 p2705 A67-31759

Computer method using coefficient linearity along diagonal of matrices to calculate N/h profiles of ionosphere 16 p2669 A67-31897

Riemann matrix in linear symmetric-hyperbolic systems of partial differential equations with constant coefficients in two-space and one-time variables 17 p2876 A67-32031

Minimizing nonlinear function of several variables without constraints, solution obtained by combination of interpolation techniques and Levenberg method 17 p2818 A67-32426

Matrix generalization of polar coordinate transformation to second order matrix differential system 17 p2877 A67-32563

Boundary value problem of linear partial differential equation reduced to linear equation system with block-tridiagonal matrix by difference approximation 17 p2820 A67-32801

Differential transport equation system in n-dimensional anisotropic space solved using matrices, discussing heat conduction equations 17 p2972 A67-33070

Stability and instability of tridiagonal linear system, noting application to stability analysis of differential equation system 18 p3070 A67-33644

Transition probabilities for molecular

collision excitation by differential equation matrix, approximations, perturbation theory, etc 18 p3081 A67-33785

Book on linear multiport synthesis covering time-invariant networks, matrix analysis, realizability considerations, network theory, etc 18 p3018 A67-34367

Sufficient conditions of absolute stability of nonlinear discrete systems based on matrix majorant concept 18 p3018 A67-34458

Deformation behavior of matrix and fibers in aluminum-boron and copper-tungsten composites studied by X-ray lattice strain techniques 18 p3067 A67-34570

Factors degrading reliability in use phase, developing analysis method for determining optimum corrective measures 18 p3057 A67-34667

Algorithm for computing matrix Riccati equation solution in optimization problems 19 p3249 A67-34781

First order perturbation solution for transition matrix relating errors at one point of two-body orbit to errors at later point 19 p3317 A67-34832

Alternating direction implicit /ADI/ method variant for elliptic and parabolic partial differential equations 19 p3250 A67-34868

Immittance and transmission matrices concepts applied to mechanical systems vibration, presenting formulations properties and interrelationships 19 p3261 A67-34960

Implications and ramifications of theory of cutouts in displacement method 19 p3343 A67-35771

Linear optimal control technique for flexible-booster control system design, showing drift minimum model with matrix transformations for closed-loop dynamics 19 p3336 A67-35988

Amplification characteristics of multicavity masers, determining Q-factor using chain matrix A formalism 19 p3241 A67-36027

Quasi-spectrum concept applied to square matrix for study of class of stochastic matrices 19 p3251 A67-36049

Electron tunneling through thin dielectric films and damping relation to electron energy calculated, using band model and matrix methods 20 p3508 A67-36424

Triangular finite element under plane stress analyzed using stiffness matrix, including in-plane concentrated moments and nodal rotation 20 p3538 A67-36676

Cross-spectral method application problems in feedback system analysis, identification and linear time invariant system 20 p3407 A67-36785

COSMOS, Courtaulds system for matrix operations and statistics 20 p3391 A67-36932

Skin stringer panel rows natural frequencies and normal modes predicted by transfer matrix method 20 p3539 A67-37008

Reliability criteria of systems with recovery, noting mean time to failure of system and mean time of system operation between failures 20 p3454 A67-37037

Orthonormalized vector reference in coupling between symmetrical tensors in continuum mechanics, deriving expansion coefficients 21 p3717 A67-37971

Master matrix containing initial values of geomagnetic inclination and gyrofrequencies for storage in computer memory to calculate ionospheric vertical profiles 21 p3623 A67-39046

Matrix method proposed for systems of linear differential equations governing satellite attitude control in elliptical orbits, considering integral criteria calculation 22 p3897 A67-39160

General theory advanced for analysis of statically loaded elastic structures using concept of finite members interconnected in finite loaded joints 22 p3911 A67-39559

Stiffness matrix for shallow rectangular shell element and application of finite element displacement method 23 p4073 A67-40628

Serial/matrix technique extended to give multivariable linear system responses defined in state space terms 23 p3983 A67-40646

Stability criterion derivation involving Markov determinants using second method of Liapunov 23 p4022 A67-40648

Fixed point probability row vector of regular or ergodic transition matrices simplified using generalized matrix inversion theory 23 p4023 A67-41032

Cosmic ray variations over celestial sphere investigated by matrices applied to distribution model 23 p4059 A67-41134

Maxwell-Euler equations reformulated into equivalent matrix integral equation, obtaining dispersion relation from integral equation kernel for compressible electron plasma 23 p3974 A67-41204

Matrix method for analyzing systems of gimbaled mirrors, prisms and ray projectors 23 p4003 A67-41323

Matrix displacement method for coupled bending-bending vibrations of pretwisted blading 23 p4078 A67-41329

Nonequilibrium boundary layer problem solution by direct treatment of two-point boundary value problem [AIAA PAPER 67-219] 23 p3991 A67-41715

Matrix version of Kalman-Yacubovich lemma for deriving stability conditions for continuous time dynamical systems with m-feedback nonlinearities 23 p3985 A67-41726

Graphical construction and electrical simulation for predetermining index and thickness of multilayer surfaces and filters 24 p4187 A67-41873

Controllability and observability of parallel and tandem connections of two linear time invariant differential systems of Jordan canonical form representation 24 p4135 A67-42181

MATRIX STRESS CALCULATION

Whisker strength measurement methods, noting role in reinforcement of ductile metal matrices 01 p0163 A67-11152

Stiffness techniques based on numerical integration for explicit calculation of displacement functions and derivatives in subroutine 01 p0163 A67-11173

Shells of revolution analyzed under symmetric and antisymmetric loading by matrix displacement method 01 p0164 A67-11191

Matrix-Holzer method for predicting free vibration modes of clustered launch vehicles in bending applied to first eight modes of Saturn I model 02 p0337 A67-11931

Beam-column analysis by finite element method, establishing end load-deformation relationship via stiffness matrices 03 p0523 A67-13457

Inertia constants of rigid bodies determined, using ground vibration tests [ONERA-TP-386] 05 p0786 A67-16476

TRIAX 6 element for axisymmetric analysis by matrix displacement method 05 p0922 A67-17105

Finite element method for problems in structural mechanics extended to beam vibration including shear and rotary inertia effects 05 p0924 A67-17284

Elastic-plastic plane stress configuration analysis by matrix displacement method, using quadrilateral finite elements 06 p1111 A67-18883

Shell structures solved numerically, using network of partial panels 08 p4147 A67-20556

Stiffness and consistent mass matrices for finite cylindrical shell element with admissible displacement state 10 p1717 A67-23128

Fiber aspect ratio, residual stress state and geometry of multifiber arrays studied in terms of influence on local stress concentration and matrix reinforcement 10 p1671 A67-23705

Energy techniques and matrix method for computer programming of dynamic response due to random and harmonic loading on structural systems [ASME PAPER 67-VIBR-56] 11 p1873 A67-24203

Matrix integral equations to calculate critical stresses and natural frequencies of oscillation of thin walled isotropic shells of revolution 12 p2022 A67-25585

Bent and twisted bars analysis using finite element method 14 p2399 A67-28133

Matrix calculation of structures by parallel methods of forces and displacements [ONERA-TP-412] 15 p2576 A67-30125

Shells of revolution with curved elements noting rigid body displacements in analysis by matrix displacement method 17 p2963 A67-33042

Metal matrix composites compression-microstrain behavior at room temperature, discussing stress-strain curve, Youngs modulus, yielding, etc [ASTM PAPER 6] 18 p3067 A67-34571

Strain distribution in aluminum filament

reinforced metal, investigating matrix plastic behavior and residual stresses, etc [ASTM PAPER 8] 18 p3067 A67-34573

Stiffness matrix of thin flat triangular elements of nonzero Gaussian curvature derived by reducing geometrical idealization errors 19 p3342 A67-35750

Matrix method for calculating behavior of rod of constant cross section stressed by bending and stretching or compression loading 19 p3343 A67-35815

Triangular elements under linearly varying strain used in matrix displacement method analysis of stability of membranes of arbitrary anisotropy 20 p3535 A67-36196

Unidirectional fiber-reinforced composite under axial load, discussing power series along with point matching techniques for solving interface, matrix and filament stresses 20 p3474 A67-37268

Stiffness matrix of unsymmetric nodal ring element for matrix displacement analysis of rib stiffened conical shells 22 p3914 A67-40191

MATTER

S ANTIMATTER

S EXTRATERRESTRIAL MATTER

S ROTATING MATTER

MAXIMUM PRINCIPLE

SA COMPLEX VARIABLE

SA PONTRYAGIN PRINCIPLE

Propellant-and time-optimum trajectories with thrust vector rotational velocity at flight beginning and termination taken as additional boundary condition analyzed, using maximum principle 01 p0146 A67-10209

Parameter optimization in systems subject to worst bounded disturbance that maximizes chosen performance index 01 p0046 A67-11204

Optimization of control systems with nonlinear plants, using Pontryagin maximum principle 02 p0224 A67-11511

Optimal feedback control for finite state systems with suitable performance criterion, using maximum principle applied to time-sharing computer systems 02 p0227 A67-12172

Navigation measurement optimization using Pontryagin maximum principle as necessary and sufficient condition to obtain smallest possible uncertainty 02 p0265 A67-12384

Optimal transfer of finite thrusting vehicle between circular coplanar orbits 02 p0330 A67-12719

Upper and lower bounds for solutions to transport equation obtained, using collocation method and maximum principle [DVL-479] 04 p0602 A67-14509

Maximum problem solution with quadratic nonconcave objective functions and linear inequalities as constraints 04 p0644 A67-14772

Optimality conditions for nonlinear discrete systems, showing that at limit these conditions become Pontryagin maximum principle for continuous systems 05 p0782 A67-16320

Pontryagin maximum principle for optimal control problem with constraints on control function 06 p0978 A67-18584

Two generalized matrix forms of linear estimates for spaceship motion derived, based on maximum probability criterion 07 p1247 A67-19096

Optimality conditions of systems containing components with distributed parameters 07 p1159 A67-19138

Pontryagin maximum principle, discussing singular and nonsingular extremals classification by numerical integration techniques 07 p1162 A67-20273

Automatic control with prediction, discussing optimal least time systems for trajectories satisfying maximum principle 10 p1608 A67-23322

Extension of Pontryagin maximum principle to variable control region, using Hamilton equation 11 p1812 A67-24208

Elastic-plastic body and elastic work hardening materials under static loading, using maximum principle for computing procedures 11 p1876 A67-24622

Penalty function method used for bounded phase coordinate optimal control problem for linear discrete systems with quadratic cost functionals 11 p1771 A67-24891

Gradient acceleration technique for solving optimal systems with unbounded control 11 p1771 A67-24896

Optimum three-dimensional ascent trajectories in model gravitational field

using maximum principle 12 p2000 A67-25211

Pontryagin maximum principle application to solution of one-dimensional minimum time rendezvous problem for thrust limited rocket with initial and final mass specified 12 p2012 A67-25922

Nonequilibrium processes, analyzing required number of additional conditions and region of applicability of most probable distribution function, noting relation to Boltzmann equation 13 p2100 A67-26954

Optimization of system described by differential and finite differential equations when including constraints 15 p2455 A67-29119

Space vehicle optimal control, studying maximum principle application, developing numerical algorithms of dynamic programming type and describing variational problems 16 p2742 A67-30664

Dynamic programming used for proof of distributed parameter maximum principle, exemplifying with boundary condition 16 p2852 A67-31687

Generalized linear programming applied to control theory noting use of differential equations 17 p2829 A67-32430

Iterative solution of boundary value problem for optimal trajectory, applying smoothing procedure 17 p2830 A67-32869

Quantum formulas for optimal filtration of useful electromagnetic signal in noise background based on maximum misinformation principle 18 p2999 A67-33533

Optimum thrust direction for horizontal jet flight of maximum duration determined, using variational calculus 18 p3138 A67-33557

Interpolation methods for solving nonlinear algebraic/transcendental equations applied to maximum principle boundary value problems 18 p3071 A67-33879

Optimality conditions for nonlinear discrete systems, showing that at limit these conditions become Pontryagin maximum principle for continuous systems 18 p3017 A67-33871

General variational theorem for rigid perfectly plastic materials developed using Hill and Markov maximum plastic work principles, noting possible unified derivation of principles 18 p3143 A67-34006

Optimal control methods of Bellman and Pontryagin, discussing maximum rule and dynamic programming for optimization in presence of constraints 18 p3018 A67-34284

Phase relationships between self-locked modes in lasers and agreement with predictions based on maximum emission principle 18 p3062 A67-34640

Local properties of limiting surfaces, giving hypothesis for surface separating two unconnected regions 19 p3204 A67-35903

Phase-locking effects between longitudinal modes in lasers, treating several-mode oscillations 20 p3456 A67-36171

Payload and trajectories determination for consumption optimization for missiles moving in constant gravitational field, using Pontryagin maximum principle 20 p3531 A67-36409

Second order nonlinear parabolic type partial differential equations with divergence structure, noting role of maximum principle 20 p3475 A67-36502

Laminar film boiling on thin wire, determining heat-transfer coefficient and vapor dome spacing and diameter [ASME PAPER 67-HT-62] 20 p3549 A67-36744

Valentine method for maximum principle problem solution, reducing to nonlinear differential equation system with special boundary conditions 20 p3477 A67-37029

Search for extremum of real function in presence of noise, using maximum principle 20 p3477 A67-37111

Maximum information principle applied to search for minimum of function 20 p3477 A67-37195

Maximum principle application to optimal control procedure, minimizing transient response and decreasing effect of random changes in system parameters 20 p3410 A67-37232

Maximum principle for hereditary processes optimal control with constant time lag and parameters 20 p3412 A67-37583

Book on calculus of variations and optimal control theory covering function maximum and minimum theory, fixed end-point problem, etc 21 p3853 A67-38799

Fuel optimal control conditions in attitude

correction of satellite in circular orbit determined using maximum principle, solving resulting boundary value problem 21 p3715 A67-39153

Steady flow extremum principles for incompressible viscous fluid generalized to liquid flow containing suspended solid bodies and drops of another liquid 24 p4144 A67-42567

MAXIMUM USABLE FREQUENCY

Maximum usable frequency for single discontinuity radio line calculated taking horizontal ionization gradients into account 10 p1604 A67-22794

F scatter, flutter fading and maximum usable frequency phenomenology from HF radio propagation studies near equator 15 p2438 A67-30297

Frequency limitations of field effect transistor as amplifier in connection with impurity profile, discussing figure of merit 22 p3767 A67-39275

Maximum usable frequency for single discontinuity radio line calculated taking horizontal ionization gradients into account 24 p4120 A67-42130

MAXWELL DISTRIBUTION

Microwave frequency measurements of radiation temperature of nitrogen afterglow plasma with Maxwellian electron velocity distributions 01 p0119 A67-10147

Numerical integration of averaged cross section for electron induced resonance charge exchange and ionization of accelerated beam of hydrogen atoms 02 p0278 A67-12629

Maxwellian and delta distribution models of reflected atoms in terms of mass, momentum and energy exchange 05 p0749 A67-17109

Necessary conditions for equilibrium of Maxwell-Boltzmann distribution using analyticity of S-matrix 05 p0849 A67-17115

Landau damping and growth applied to electron plasma waves for Maxwellian velocity distribution in slab and cylindrical geometries 08 p1365 A67-21403

Gardenhose instability for ultrarelativistic plasma in magnetic field, showing that instability criterion for particular non-Maxwellian distribution function is not met 09 p1546 A67-22229

Plasma potential and particle energies in cesium plasma measured by simultaneous observation of ion and electron energy spectra 09 p1548 A67-22338

Thermal plasma measurements in magnetosphere for electron and ion density and thermal profiles, noting Maxwell energy distribution and charge neutrality 10 p1649 A67-23295

Oriented velocity and temperature relaxation in Coulomb type plasma with particle velocities distributed according to Maxwellian law, evaluating Coulomb collisions effect on plasma components 10 p1685 A67-23410

Formation of Maxwell and non-Maxwell distribution in gases, noting reduction of time reversible to time irreversible equations 12 p1968 A67-26114

Third order Vlasov equation solved for nonlinear plasma oscillations in classical nonrelativistic collisionless Maxwell distribution electron gas 13 p2162 A67-26283

Maxwell dispersion of particles of molecular gas flow at wall of circular channel described by integral equation, determining particles experiencing mirror intercollisions 13 p2158 A67-26671

Steady state forced sound propagation in semiminfinite gas induced by oscillating plane piston reflecting particles with Maxwellian distribution 13 p2100 A67-26957

Numerical integration of averaged cross section for electron induced resonance charge exchange and ionization of accelerated beam of hydrogen atoms 13 p2171 A67-27387

Boltzmann equation and deduced moment equations containing moments up to fourth order in arbitrary orthogonal curvilinear coordinates 14 p2297 A67-27998

Electron mobility and temperature due to electric field in polar semiconductor investigated assuming displaced Maxwellian velocity distribution 14 p2375 A67-29065

Electric field effect in terms of drifted Maxwellian distribution, considering nonparabolic electron scattering where dominant energy-loss mechanism is optical

polar mode scattering 14 p2376 A67-29088
 Exact solutions for spatial distribution of potential within space-charge region of non-degenerate semiconductor in contact with metal 16 p2727 A67-30850
 Hot carrier galvanomagnetic characteristics of n-type germanium of intermediate carrier concentration, noting Maxwellian 16 p2731 A67-31172
 Chemical processes in low temperature plasmas, stressing nonequilibrium characteristics, temperature and collision factors, ionization and particle excitation 17 p2809 A67-32188
 Shock thickness for monatomic Maxwell molecule gas calculated using conservation and moment equations 18 p3030 A67-34753
 Theta pinch plasma sheath and fields time development for relaxing radial electric field 21 p3662 A67-37754
 Circular planar satellite electrostatic probe theory based on reversible particle trajectories, showing relation between boundary curve in velocity space and current-voltage characteristics 21 p3625 A67-37899
 Relaxation toward Maxwell distribution function of classical gas with initial nonequilibrium distribution function as velocity modulus function 22 p3782 A67-39406
 Ionized plasma electric conductivity calculation using Druyvesteyn and Maxwellian distribution for electrons and ions respectively 22 p3851 A67-39725
 Globular star cluster, initial gravitational collapse and dynamical mixing, discussing numerical analyses for homogeneous spherical cluster with Maxwell velocity distribution 22 p3894 A67-40509
 Energy distribution deviation of electrons emitted from plasma or solid via Maxwell distribution, deriving kinetic reflection coefficient in thermionic emission current expression 23 p4047 A67-41688

MAXWELL EQUATION
 Maxwell-Green tensor relating forces to displacements in structural elastic beam, showing role of Maxwell influence coefficient 02 p0336 A67-11482
 Locally Maxwellian solution of Boltzmann kinetic equation 03 p0459 A67-13632
 Maxwell equations for time-dependent fields integrated directly by using scalar-vector analog of Green theorem and Dirac delta function 03 p0469 A67-13716
 Electromagnetic field of accelerating charge using Coulomb law, relativity transformation relations, charge conservation, Newton third law, etc 03 p0469 A67-13719
 MHD equations, discussing dimensional and nondimensional parameters, modifications of Maxwell equations, vorticity and rate of circulation change in viscous flow, etc 03 p0480 A67-13724
 Dispersion and damping of oscillations in Maxwellian plasmas with zero order density gradients examined, using Vlasov and Maxwell equations 04 p0665 A67-15103
 Electromagnetic field in induction type plasma generator in steady state, from Maxwell equations and heat conservation equations 04 p0671 A67-15612
 Wave excitation in compressible partially ionized plasma by electromagnetic and acoustic /or mechanical/ sources, describing set of linearized hydrodynamic and Maxwell equations 05 p0859 A67-17436
 Soviet book on electromagnetic shock waves associated with not-very-high powers, using Maxwell-Lorentz equations 06 p1031 A67-17949
 Galerkin-Ritz method application to Maxwell waveguide equations for calculation of propagation constant of rectangular guide with transverse ferrimagnetic core 07 p1152 A67-19590
 Relation of magnetization of any homogeneous isotropic ellipsoid to local field and external applied magnetic field deduced from Maxwell equations and potential theory 07 p1234 A67-20127
 Exact solutions of Einstein-Maxwell equation of Petrov class N when propagation vector of gravitational field is hypersurface orthogonal 07 p1218 A67-20281
 Scattered particle intensity inside and outside finite medium determined from Maxwell and Schroedinger equations 09 p1531 A67-21631
 Monochromatic wave interaction with

isotropic electron-plasma, determining field and surface wave generated on basis of Maxwell equations 09 p1464 A67-22012
 Relativistic electrodynamics of moving medium, discussing Maxwell-Minkowski equations, Born equations, field vector transformations, etc 09 p1533 A67-22449
 EH solutions of Maxwell equations describing guided electromagnetic waves in homogeneous isotropic medium at velocity of light 09 p1465 A67-22550
 Vlasov equation for stationary distribution function of charged particles in plasma and self-consistent solution of Maxwell equations 10 p1685 A67-23463
 Oblique incidence of electromagnetic wave on plasma half-space 13 p2065 A67-26290
 Collective effects in collisionless plasmas in laboratory in case of Vlasov-Maxwell equations with Landau damping 14 p2362 A67-29037
 Nonrelativistic approximation for electromagnetic radiation in conducting medium moving with uniform velocity with respect to source 15 p2521 A67-29194
 Shock tube measurement of plasma electric conductivity, using Maxwell equation for quasi-steady state electromagnetic field 16 p2673 A67-31111
 Book on electromagnetic radiation discontinuities presenting solution of Helmholtz and harmonic Maxwell equations and derivation of discontinuities formulas by generalized functions 16 p2629 A67-31628
 Transverse and longitudinal waves in infinite nonrelativistic collisionless plasma, using Maxwell equation 18 p3093 A67-34750
 Approximation method for Einstein-Maxwell field equations successive solution applied to Weyl canonical problems and field equations for point particle 19 p3282 A67-35576
 Plasma wave influences on metal surface reflectivity investigated using Maxwell equation, calculating dielectric constant and conductivity 19 p3262 A67-35581
 Progressing wave method for linear partial differential equation systems, including Maxwell equations, applied to electromagnetic waves from moving sources 19 p3184 A67-35665
 Linear electromagnetic oscillations in homogeneous plasma described by motion and Maxwell equations 20 p3492 A67-38129
 Galerkin-Ritz method application to Maxwell waveguide equations for calculation of propagation constant of rectangular guide with transverse ferrimagnetic core 20 p3401 A67-37327
 Diffraction by cylinder in locally uniaxial medium with azimuthal optic axis, using Maxwell equation solution for plasma frequency 20 p3389 A67-37705
 Electromagnetic wave propagation in plasma layer bounded by external constant magnetic field, using kinetic theory with Maxwell equations and distribution function 21 p3670 A67-38685
 Finite discontinuity jump conditions for plasma in strong magnetic field determined by approximation and Maxwell equation, noting possible application to satellite data 22 p3843 A67-39269
 Electromagnetic wave propagation in moving media filled waveguides noting nondispersive dielectric and cold plasma cases 22 p3759 A67-39361
 Nonlinear theory of longitudinal plasma waves, formulating distribution function and Maxwell equation for electric field 22 p3845 A67-39421
 Kinetic equations for electrons and photons in homogeneous plasma in strong magnetic field derived from Maxwell and classical motion equations 22 p3851 A67-39736
 Steady laser oscillation by Maxwell equations, with allowance for diffusion effects, shows no qualitative changes in field distribution pattern 22 p3815 A67-39759
 Wave propagation in wave optics transition to geometrical optics in general relativity theory using series expansion 23 p4027 A67-41146
 Einstein-Maxwell fields exact solutions constructed from Einstein vacuum fields, discussing vacuum metric and transformations 23 p4028 A67-41150
 Maxwell-Euler equations reformulated into equivalent matrix integral equation, obtaining dispersion relation from integral equation kernel for compressible electron

plasma 23 p3974 A67-41204
 Maxwell equations solved for Gaussian beam form in anisotropic medium, discussing laser applications 24 p4167 A67-42092

MAXWELL FLUID
 Exact solutions to kinetic moment equations of monatomic gas in absence of external forces to case of mixture of monatomic Maxwellian gases with external forces 03 p0401 A67-12869
 Relaxation theory and eigenvalue theory for linearized collision integrals for mixtures of Maxwell fluid 08 p1355 A67-21116
 Molecules 08 p1355 A67-21116
 Electron streaming instability of plasmas with zero order density gradients from variational analysis of Vlasov-and Maxwellian-plasma perturbation wave propagation 08 p1360 A67-21128
 Asymptotic properties of solutions to kinetic coefficient equation system, noting mass velocity dependence on time 10 p1625 A67-23042
 Instability of Maxwellian fluid flow in pipe analyzed using Galerkin method 11 p1778 A67-24216
 Branch cut contribution to longitudinal electric field in relativistic Maxwell plasma using non-Laplace transformation procedure 22 p3854 A67-40319

MAXWELL-MOHR METHOD
 General theory advanced for analysis of statically loaded elastic structures using concept of finite members interconnected in finite loaded joints 22 p3911 A67-39559

MCDONNELL MILITARY AIRCRAFT S F-4 AIRCRAFT
MCLEOD GAUGE
 Pressure measurement with McLeod type gauge in presence of saturated vapors condensed during 21 p3627 A67-38384

MEAN FREE PATH
 Abnormal skin effect in thin films of noble metals near IR, taking into account wave penetration and magnitude of conducting electrons mean free path 02 p0288 A67-11723
 V-I tunneling characteristics and energy gap anisotropy of Pb-Bi superconducting alloy, discussing mean free path 03 p0501 A67-14341
 Electron motion in gases in pressure range where electron mean free path is comparable to or less than chamber length, showing effect on ion currents 04 p0662 A67-15769
 Simple method for determining mean free path of primary electrons in plasma 07 p1229 A67-19515
 Probe measurements of intermediate and high pressure plasmas in cases where mean free path of particles is greater than probe dimension 09 p1539 A67-21783
 Thin electrostatic sheath adjacent to body immersed in flowing weakly ionized continuum plasma analyzed for arbitrary Debye length mean free path ratios 11 p1825 A67-23868
 Diffusion phenomena of increasing mean free path with altitude in rarefied gas analyzed, incorporating gravitational field effect in Boltzmann equations 13 p2099 A67-26952
 Thermal accommodation coefficients determination in temperature jump region 15 p2580 A67-29883
 Titanium plasma source design features, performance, ion mean free path, energy spectrum and energy distribution 17 p2904 A67-32912
 Spectral data on primary cosmic ray protons and helium nuclei analyzed, assuming solar cycle modulation due to diffusion-convection process 17 p2952 A67-33247
 Mean free path effects on critical field and density of states of small superconducting spheres 17 p2924 A67-33370
 Tunneling into thin superconducting films in magnetic field, measuring field effect on density of states for finite mean free path 17 p2924 A67-33371
 Kinetic thermodynamics applied to real gas transport properties analysis by generalization of mean-free-path theory 20 p3543 A67-36185
 Shock wave thickness in hydrogen gas as function of shock speed and postshock plasma mean free path 22 p3783 A67-39723
 Surface superconductivity in dilute Ta-Nb

alloy ascribed to decrease in mean free path due to lattice defects 23 p4036 A67-40657
 Charged particles zenithal angular distributions determined by photorecordings for mean energies of 60 Gev 24 p4217 A67-42831
 Cross section of inelastic interactions and free path between nuclear active cosmic particles and lead nuclei at high energies 24 p4219 A67-42844
 Cosmic particle recording facility at Tskhra-Tskaro, giving data on free path of nuclear active particles in carbon with high energies 24 p4219 A67-42845

MEASURE THEORY

Statistical theory using calibration data to evaluate multielement system for measuring properties of cryogenic propellants and high temperature thrusting devices 01 p0069 A67-11026
 Ergodic theory of measurable partitions in Lebesgue space, extending Rokhlin-Sinai theory of increasing to flows generated by automorphism 04 p0644 A67-14756
 Connection between flow spectrum and velocity, obtaining continuous spectrum upon velocity change to equivalent invariant measure 06 p0983 A67-17860
 Lebesgue space in measure theory on Borel sets and Banach algebra over compact semigroups 07 p1214 A67-19211
 Proof of continuity of Haar measurable almost periodic functions 17 p2876 A67-32385
 All Markov transition functions in denumerable state space satisfying prescribed initial condition with given matrix 17 p2878 A67-32734
 Plasma measuring methods relation to plasma properties noting photography, optics, particle analysis, etc 18 p3090 A67-34378

MEASUREMENT

S ACTINOMETRY
 S ASTROMETRY
 S BODY MEASUREMENT
 S BODY MEASUREMENT /BIOL/
 S CALORIMETRY
 S DENSITY MEASUREMENT
 S DEPTH MEASUREMENT
 S DOWNRANGE MEASUREMENT
 S DRAG MEASUREMENT
 S ELECTRIC MEASUREMENT
 S ELECTROMAGNETIC MEASUREMENT
 S FLOW MEASUREMENT
 S FREQUENCY MEASUREMENT
 S FRICTION MEASUREMENT
 S GONIOMETRY
 S GRAVIMETRY
 S HOT-WIRE MEASUREMENT
 S HUMIDITY MEASUREMENT
 S IMPEDANCE MEASUREMENT
 S MAGNETIC MEASUREMENT
 S METROLOGY
 S NOISE MEASUREMENT
 S OPTICAL MEASUREMENT
 S PHOTOGRAPHIC MEASUREMENT
 S PHOTOMETRY
 S PLASMA FLUX MEASUREMENT
 S POLARIMETRY
 S PRECIPITATION PARTICLE MEASUREMENT
 S PRESSURE MEASUREMENT
 S PSYCHOMETRICS
 S RADAR MEASUREMENT
 S RADIATION MEASUREMENT
 S RADIOMETRY
 S RANGE MEASUREMENT
 S ROCKET MEASUREMENT
 S SATELLITE MEASUREMENT
 S SIGNAL MEASUREMENT
 S SOUND MEASUREMENT
 S SPECTROMETRY
 S SPECTROPHOTOMETRY
 S STOICHIOMETRY
 S STRESS MEASUREMENT
 S SYNOPTICAL MEASUREMENT
 S TEMPERATURE MEASUREMENT
 S THRUST MEASUREMENT
 S TIME MEASUREMENT
 S TRAJECTORY MEASURING SYSTEM
 S VELOCITY MEASUREMENT
 S VIBRATION MEASUREMENT
 S WIND MEASUREMENT
 S WIND VELOCITY MEASUREMENT

MEASURING APPARATUS

SA DISTANCE MEASURING EQUIPMENT
 SA FLOW METER
 SA FLUXMETER
 SA HELIOMETER
 SA HYGROMETER
 SA INTERFEROMETER

SA ION GAUGE
 SA IONIZATION GAUGE
 SA MACH-ZEHNDER INTERFEROMETER
 SA MAGNETOMETER
 SA MANOMETER
 SA MASS SPECTROMETER
 SA MCLEOD GAUGE
 SA MICROMETER
 SA PENETROMETER
 SA PHOTOMETER
 SA PIEZOELECTRIC PRESSURE GAUGE
 SA PIRANI GAUGE
 SA PLASTOMETER
 SA POLARIMETER
 SA POTENTIOMETER
 SA PRESSURE GAUGE
 SA RADAR ALTIMETER
 SA RADIO ALTIMETER
 SA REFLECTOMETER
 SA REFRACTOMETER
 SA RESISTANCE THERMOMETER
 SA SHOCK MEASURING APPARATUS
 SA SONIC ANEMOMETER
 SA TORQUE MEASURING APPARATUS
 SA TURBULENCE MEASURING APPARATUS
 SA VIBRATION MEASURING APPARATUS

Recording assembly for measurement of flexural and torsional moduli and internal friction at various frequencies and temperatures of small samples, using constant amplitude undamped oscillations 01 p0062 A67-10163

Doppler-Fezeau frequency effect in ionospheric satellites measuring device based on wave refraction 01 p0057 A67-10233

Photoelectric components and electronic measurement techniques in reception and demodulation of HF modulated laser beams 01 p0088 A67-10300

AC differential correlator for measuring small delays between two identical binary output waveforms 01 p0037 A67-10482

One-trap probe measurement of ionospheric electron density, electron temperature, plasma space potential relative to vehicle potential of sounding rocket, mean ion mass, composition and temperature 01 p0064 A67-10565

Amplitude-dependent internal friction and defect structures measured in aluminum excited longitudinally by mechanical resonator 01 p0067 A67-10842

Statistical theory using calibration data to evaluate multielement system for measuring properties of cryogenic propellants and high temperature thrusting devices 01 p0069 A67-11026

Liquid metal level measurements using thermocouple type probes as tank sensors, noting usage of electrical resistance of probe sheath 01 p0070 A67-11027

Electron current and positive ion current in flames measured by improved single-probe technique using grid and ring electrode 01 p0070 A67-11068

Analog device for measuring coefficient of space-time signal correlations and applications to statistical mechanics of turbulent fluids and random noise 01 p0054 A67-11090

Electric-resistance strain gauge measuring techniques at high temperatures 01 p0071 A67-11096

Response of temperature sensor bonded to metal strip pulse-heated by capacitor discharge technique 01 p0071 A67-11100

Capacitive pressure transducer featuring exceptional sensitivity, hysteresis, resolution and repeatability, detailing sensing element and measuring circuit design 01 p0071 A67-11102

Measurement capabilities of linear digital displacement transducer with magnetically stored calibration 01 p0074 A67-11124

Variable-reluctance pressure transducer with pressure sensor assembly weight reduction for lightweight aerospace requirements 01 p0075 A67-11136

Apparatus for measuring temperature dependence of thermoconductivity coefficient, thermal emf and specific electroresistance of cermet cylindrical shells 01 p0076 A67-11248

Automatic and semiautomatic devices for measuring scintillation of stellar images from traces of stars 02 p0242 A67-11994

Instrument designed for rapid measurement of surface deformations of 210-ft radio telescope at Parkes,

Australia 02 p0229 A67-12069
 Requirements for radiation detection and measuring systems in aerospace environment, considering safety, design, circuit techniques, etc 02 p0220 A67-12208
 Transistor noise coefficient measuring device for 30 kHz to 1.5 MHz frequency range 02 p0223 A67-12798
 Minimum noise coefficient of various types of common-base transistors at 1 kHz to 1.5 MHz frequencies 02 p0224 A67-12799
 Optical properties of semiconductors by measuring spectral emittance of transparent and opaque solids and measurements on materials used in IR optics [AIAA PAPER 65-654] 03 p0418 A67-13034
 Total normal emittance of various oxidation-resistant materials to very high temperatures in air determined, using special apparatus [AIAA PAPER 65-655] 03 p0447 A67-13035
 Chronotron type device for measuring zenith and azimuth angles of slope of axes of extensive air showers 03 p0425 A67-14263
 Algorithms in ZAM-2 computer program to calculate recording error parameters of linear scale measuring device 04 p0621 A67-14918
 Turning-arm apparatus operating in rarefied gas chamber and low pressure wind tunnel for drag measurements 04 p0596 A67-14993
 Dynamic elastic modulus of thin rod at elevated temperatures measured in terms of rapid-heating induced longitudinal oscillation [ASME PAPER 66-WA/MET-12] 04 p0712 A67-15376

Construction method for rms-optimal digital smoothing devices, noting case of astatic systems 05 p0782 A67-16268

MacLeod and type U vacuumeters using liquid for pressure measurement 05 p0804 A67-16303

Nucleonic cryogenic quality meter design and development and fluid monitoring through hydrogen vent line on Saturn S-IVB stage under orbital conditions 05 p0842 A67-16540

Two base-resistance measuring methods based on reverse-voltage-transfer-ratio measurement 05 p0807 A67-16949

Liquid hydrogen pressure, temperature, flow and liquid level measuring techniques 05 p0807 A67-17019

Automatic three-dimensional model measuring machine using data programming for aircraft contour measurement 05 p0811 A67-17047

Metrology requirements for Apollo project, noting control and measuring equipment and calibration procedures 05 p0814 A67-17263

Atmospheric charge density measurement by Faraday cage and Obolensky filter 05 p0803 A67-17384

Thin film dielectric constant and loss tangent measured by HF capacitance meter 05 p0871 A67-17483

Vacuum effect on sintering temperature, describing measuring apparatus and results 06 p1006 A67-17559

Magnetic field variation indicator based on Barkhausen effect 06 p1002 A67-17941

Small signal MIS capacitance vs bias characteristics measured over wide range of biases and sweep speeds 06 p1002 A67-17979

Measurement techniques used in wind tunnel and free atmosphere parachute tests 06 p0979 A67-18017

Pressure sensor consisting of aluminum membrane for measuring pressure distribution in parachute canopy 06 p1002 A67-18021

Varactor diode measurement by transmission methods under natural resonance conditions 06 p0969 A67-18122

Sensing techniques for initiating parachute deployment on Mars lander vehicle [AIAA PAPER 67-202] 06 p0948 A67-18302

Supersonic combustion measurements by thrust system method, optical probe and gas-sample probe technique [AIAA PAPER 67-223] 06 p1004 A67-18462

Hydraulics of electromagnetic liquid-metal metering device with constant inlet pressure, noting dose value dependence on parameters and operating conditions 06 p0951 A67-18684

Three-channel IR-UV rocket radiometer for onboard measurement of exhaust plumes under severe high altitude environmental

conditions 06 p1005 A67-18714
 Measuring equipment for critical current density of superconductors in strong magnetic field 06 p1005 A67-18722
 Radiosonde radiometer to measure long wave emission from earth and intervening atmosphere during night 06 p1005 A67-18742
 Laser extensometer measuring small dimensional changes of specimen in tensile testing furnace at high temperatures 06 p1012 A67-18778
 Confocal resonator wave meter used to obtain frequency resolution of 10 MHz at 100 GHz 06 p0972 A67-18835
 Motor driven cup anemometer and freely rotating cup anemometer in free and artificial flows 06 p1006 A67-18836
 Semiconductor loaded E plane T waveguide junction spectrometer for microwave measurement of transport parameters in semiconductors 08 p1329 A67-20375
 Pneumatic grating for complete measuring system, considering fluidic techniques 08 p1330 A67-20439
 Scatterometer measuring radar backscattering for prediction of terrain characteristics 08 p1293 A67-20682
 Rocket engine thrust measuring system for accuracy analysis 08 p1375 A67-20779
 Measuring technology and automation - Conference, Dusseldorf, October 1965 08 p1313 A67-21004
 Coordinates determining relative altitudes on lunar surface obtained through coordinate measuring instrument 08 p1398 A67-21216
 Instrument design for analyzing biaxial strain field in thin plate under creep, noting use of moire effect 08 p1332 A67-21461
 Measuring techniques and limitations as related to small reflections in precision coaxial transmission line 09 p1495 A67-21624
 Millimeter confocal wavemeter calibration and stability 09 p1470 A67-21625
 Thermophysical parameters of semiconductors measured with same instrument set through pulse method, for quality control application 09 p1495 A67-21655
 Device measuring uniaxial pressure effect on transmission factor of semiconductors in low absorption region 09 p1551 A67-21657
 X-ray diffraction techniques and apparatus for measuring residual stresses in metals [SAE PAPER 670151] 09 p1502 A67-21771
 Measuring apparatus for scalar and tensor plasma conductivity in AC MHD generators and accelerators 09 p1538 A67-21775
 Dual observation method for determining photoelastic parameters in scattered light 09 p1574 A67-21840
 Device for measuring potential fluctuations in turbulent flow of distilled water 09 p1501 A67-22562
 Theodolite Astro-2 observation of azimuth and position of moving satellite 10 p1655 A67-22985
 Measuring Hall effect in high specific resistance materials by using alternating magnetic field and DC current 10 p1691 A67-23502
 Distribution curves of ion density and condensation particle concentration in layers of atmosphere near sea level, noting criteria for instruments 10 p1657 A67-23695
 Sensitive magnetic susceptibility measurements using superconducting circuits and magnetic shields 10 p1657 A67-23780
 Plane layer type apparatus for measuring thermal conductivities and accommodation coefficients of gases over wide pressure 10 p1658 A67-23783
 Complex measuring instrumentation effect upon tilt table response 10 p1602 A67-23823
 Ionized shock-nitrogen conductivity measured by four-electrode device 11 p1832 A67-24057
 General atmospheric circulation, observation methods and apparatus 11 p1815 A67-24328
 Light velocity measurement using hollow cathode discharge in Ne-H laser 11 p1818 A67-24479
 Dielectric constant of very low loss materials at mm wavelengths measured by oversized rectangular waveguide technique 11 p1792 A67-24764
 Larenz, two-line and calorimetric methods for plasma jet temperature measurements 11 p1793 A67-24825

Direct microthrust measurement on swinging gate test stand with equalization network 11 p1774 A67-25014
 Langmuir probe and microwave transmission methods compared for plasma density measurement 12 p1939 A67-25256
 Null-yaw and fixed direction multihole probes for aerodynamic measurements, describing calibration charts and error sources 12 p1940 A67-25352
 Satellite measurement of low energy electrons and protons in auroral regions, discussing use of instruments with variable energy electrostatic thresholds and postacceleration techniques 12 p1944 A67-25851
 Nanosecond fluorimeter for measuring emission kinetics of chromophores 12 p1946 A67-25981
 Vacuum integrating sphere for in situ spectral reflectance measurements of carbon dioxide cryodeposits from 0.5 to 10 microns [AIAA PAPER 67-298] 12 p1926 A67-26013
 Low to moderately high temperature emissometer, based on calorimetric method, to measure total hemispherical emittance of metals and coatings in vacuum [AIAA PAPER 67-299] 12 p1946 A67-26014
 Zeeman effect in measuring magnetic fields of sun and stars, noting apparatus 12 p2010 A67-26235
 Holographic imaging methods for improving luminosity, detection and resolution of spectroscopic and astronomical instruments 12 p1948 A67-26238
 Foundation of theory of physical dimensions 13 p2157 A67-26806
 Motion equations and middle position equations for damping of stochastic oscillation in measuring apparatus pointer 13 p2119 A67-26822
 Spectral characteristics of small scale refractive index fluctuations in troposphere using radar echoes 13 p2068 A67-26790
 Restoration of distorted signals for linear and nonlinear process converters 13 p2088 A67-27021
 Image and other techniques to measure and reduce stray and scattered light in sunspot photometry, emphasizing possibility of using partial solar eclipse 13 p2203 A67-27424
 Nozzle thermocouple for low flow rate measurement of high temperature gases, discussing calibration curves and taking into account Reynolds number effect 13 p2121 A67-27464
 Phase and amplitude measurements of laser wavefront using laser phase-locked loop 13 p2129 A67-27494
 Apparatus for determining impurity distribution in semiconductor structure 14 p2317 A67-28281
 Tropospheric refractive index variation measurement technique 14 p2264 A67-28394
 Photoelectric two-cell polarimeter with rotating achromatic half-wave plane noting wavelength restriction 14 p2319 A67-28563
 Scale grating with moire fringe effect, noting attachment to Zeiss 3030 coordinate measuring instrument 14 p2319 A67-28590
 Chronotron type device for measuring zenith and azimuth angles of slope of axes of extensive air showers 14 p2321 A67-28775
 Electronic polarimeter applied to Stokes parameter measurement of lunar surface, determining reflected light ellipticity 15 p2552 A67-29147
 Soviet book on plasmoids covering coaxial plasma sources, magnetic field interaction and observation methods 15 p2524 A67-29243
 Telemetry systems for gun launched upper atmosphere probes 15 p2436 A67-29412
 Pulse measuring system for observing structure of pulsed signals in rectangular phase-time coordinates 15 p2444 A67-29414
 Gravitational acceleration determination noting reversible pendulum, free fall and symmetrical free motion methods 15 p2517 A67-29507
 Absolute spectral reflectance measurement in solar region in vacuo for applications to thermal control coatings 15 p2487 A67-29542
 Apparatus for direct weight loss recording of space materials 15 p2466 A67-29543
 DC and aC parameters of germanium tunnel diodes in 3 to 5 millamp range measured by ammeter dC and AC parameters of germanium tunnel diodes in 3 to 5 millamp range measured by ammeter 15 p2449 A67-29807

Electron density and temperature in plasma measured, using self-focused laser beams 15 p2488 A67-29902
 Automatic measurement of diurnal resonance frequency variations of earth/ionosphere cavity 15 p2489 A67-30071
 Handbook of electronic instruments and measurement techniques covering tools and instruments, components and equipment testing 15 p2490 A67-30232
 Probe for measuring energy transfer between satellite surface and upper atmosphere 16 p2670 A67-30646
 Analog-to-digital conversion method for measuring weak currents, giving diagram of measuring circuit 16 p2635 A67-30672
 Shock wave velocity measurement using photoelectric, piezoelectric ionization and continuous scanning methods 16 p2673 A67-31106
 Theodolitic device for measuring coordinates of center of gravity of photographed missile in flight 16 p2674 A67-31120
 Dynamics of electromechanical metering servosystems calculated by harmonic linearization method 16 p2644 A67-31380
 Mid-IR spectral emittance measuring apparatus, discussing range of performance, systems response, etc 16 p2677 A67-31429
 Experimental assembly for measuring true heat capacity of heat resistant insulating materials during natural cooling at temperatures from 1200 to 2400 degrees K 16 p2678 A67-31784
 Ellipsometer measurements to obtain estimates of refractive index and thickness of weakly absorbing isotropic, homogeneous slab 16 p2703 A67-31877
 Pressure measuring instrumentation response requirements for computing decay rate in solid propellant termination systems 17 p2926 A67-32069
 Circuitry and operation of instrument measuring entire DC response of tunnel diodes, describing measurement method 17 p2823 A67-32298
 Pressure measuring apparatus for direct gas pressure measurements in millitorr ranges 17 p2855 A67-32351
 Gas laser applications in construction, mechanics, communications, biology and medicine for control, measurement and experimental work 17 p2867 A67-32366
 RF attenuation measurement methods and standards 17 p2815 A67-32607
 Laser energy and power measurement, discussing radiation attenuation devices, measurement standards, etc 17 p2867 A67-32612
 Temperature autostabilizing nonlinear dielectric element /TANDEL/ for electric measurement circuits and measurement transducers 17 p2828 A67-32829
 Micrometeoritic cloud existence near earth refuted by satellite incidence-frequency measurements, describing satellite measuring devices 17 p2850 A67-32975
 Probe for total enthalpy measurements in arc jet exhausts 17 p2971 A67-33030
 Main characteristics of Saphir measurement system, definition of parameters to be measured and design problems 17 p2861 A67-33131
 Apparatus for measuring temperature dependence of thermoconductivity coefficient, thermal EMF and specific electroresistance of cermet cylindrical shells 17 p2861 A67-33171
 Modified hot-wire thermal conductivity cell for measuring effects of finite length, pressure and temperature on heat transfer from wire in rare gases 17 p2863 A67-33357
 Devices for flight speed measurement 18 p3019 A67-33461
 Electrodynamic transducer for liquid-borne ultrasonic pulse intensity measurements, considering limits, inductance and measuring system dimensions 18 p3043 A67-33463
 Ultrasonic probes calibration for evaluation of propagating ultrasonic wave during nondestructive testing of materials 18 p3046 A67-33744
 Laser energy output measured using formed calibrated hollow sphere of thin insulated copper wire as calorimeter 18 p3046 A67-33747
 Magnetic field variation indicator based on Barkhausen effect 18 p3046 A67-33777
 Grid electrostatic probe for ionospheric measurement of electron density and

temperature, examining measurement errors due to environmental disturbances 18 p3048 A67-34225

Phase measuring equipment and instrumental performance of radio tracking station at Winkfield 18 p3048 A67-34240

Plasma measuring methods relation to plasma properties noting photography, optics, particle analysis, etc 18 p3090 A67-34378

Solar radiation-balance measuring device using polyethylene film to give protection from wind effects 19 p3227 A67-34855

Apparatus for measuring metal/alloy hot hardness using indenter static impression and unilateral flattening 19 p3227 A67-34930

Semiconductor galvanothermometric characteristics analyzed using all-metal device 19 p3228 A67-34989

Instrumentation and microelectronic measuring methods based on nondestructive IR and UV techniques used in operation of superconductive cryogenic memory 19 p3193 A67-35028

Point-by-point measurements of magnitude and phase of repetitive pulsed time functions using commercial equipment 19 p3182 A67-35031

Instrument for measuring group delay time of microwave four-poles, using backward-wave tube as wave generator 19 p3193 A67-35032

Arglow measurement apparatus and procedure at Tehran University 19 p3224 A67-35488

Mass-transfer coefficients through plane surface in liquid-liquid systems, examining interphase turbulence effect 19 p3345 A67-35566

Laminar-turbulent boundary layer transition over aircraft components measured by method using negative-temperature-coefficient resistors compared to hot wire measurements 19 p3230 A67-35573

Installation for measuring wear rate, friction force, etc. of plane surfaces in alternating motion 20 p3453 A67-36198

Design, construction and operation of multichannel photoelectric spectrometer, using Fabry-Perot etalon and axicon 20 p3439 A67-36353

Mapping of Fabry-Perot interferometer plates defects by measuring apparatus function peak displacement, describing measurement setup 20 p3440 A67-36358

Multi-input photomultiplier pulse height photographic recording system using dual beam oscilloscope for cosmic ray experiments 20 p3444 A67-36525

Pressure gauge for plasmas subjected to large dynamic electric and magnetic fields in accelerator channel of MHD wind tunnel 20 p3444 A67-36529

Acoustic problems from SST and multimillion pound thrust launch vehicles studied at Eastern Test Range, using Launch Acoustics Measuring System /LAMS/ 20 p3415 A67-36593

Magnetometer with Gauss sensor describing n-type InSb pickup bridge instrument sensitivity 20 p3447 A67-36760

Small alternating magnetic field modulation effects on sampled output of rubidium magnetometer with frequency counter 20 p3448 A67-36876

Gravimetry, discussing absolute determinations, navigation, NBS measurements, etc 20 p3448 A67-36894

Measuring methods for high energy molecules accommodation coefficients, determining dependence on energy, incidence angle, surface nature and outgassing 20 p3489 A67-36939

Airflow velocity measurement device in cylindrical or rectangular tubes at low gas pressures 20 p3451 A67-37300

Holographic measurement of surface strains noting fringe pattern for displacements 21 p3625 A67-37944

Soviet monograph on high speed measuring methods in gasdynamics and plasma physics, discussing high temperature plasma and shock wave production 21 p3625 A67-37964

Fatigue indicating meter attachment to integrate fatigue damage over any load/time spectra 21 p3719 A67-38130

Industrial electronics measurement and control - Conference, Budapest, August 1967 21 p3591 A67-38157

Narrow and wide passband measurements of LRBA liquid propellant motors using test bench automatic measurement equipment 21 p3607 A67-38202

Measuring assembly containing logarithmic-response electrometric amplifiers for sounding rockets 21 p3592 A67-38222

Piezoresistance effect measurement in PbTe single crystals, obtaining coefficients for principal valence band through hydrostatic and uniaxial stresses in several crystallographic directions 21 p3683 A67-38389

Calibration for pyrometer with different surface heat transfer coefficients of black and gold strip 21 p3627 A67-38446

Electrometer and varactor devices for onboard low current measurements in space probes 21 p3599 A67-38634

Receiving system for telemetering with orientable antenna error-measuring signal receiver and servo loops 21 p3599 A67-38645

Instrumentation systems for measuring thrust and electric power input of electromagnetism induction plasma thruster [AIAA PAPER 67-739] 21 p3695 A67-38761

Pressure gauge using acoustic techniques designed for gas pressure measurements, discussing limitations, sensitivity and experimental results 21 p3630 A67-38787

Noise measurement and instrumentation used 21 p3630 A67-38900

Measuring device for frequency and resistance change measurements in quartz crystals due to temperature variations 21 p3601 A67-38975

Hydrogen integrator in pulsed mode of operation used to determine current pulse integrals 22 p3795 A67-39228

Permeability and permittivity values of homogeneous samples obtained by making transmission or reflection measurements in waveguides or coaxial cables 22 p3796 A67-39276

Electromechanical servosystem in conjunction with inductive pickup circuit for thrust measurements in jet engine bed tests 22 p3797 A67-39536

Weak magnetic field measurement using magnetic resonance, discussing electron nuclear resonance optical detectors, cesium vapor magnetometers and superconducting quantum interference device /SQUID/ 22 p3799 A67-39771

Optical transfer function relation between image aberration and diffraction, describing measuring methods 22 p3837 A67-40072

Thermal conductivity measurements of insulating materials at cryogenic temperatures - ASTM Conference, Philadelphia, February 1967, Committee C-16 22 p3802 A67-40289

Guarded hot plate technique for measuring thermal conductivity of low conductivity materials at cryogenic temperatures 22 p3802 A67-40290

Guarded hot plate apparatus for measuring thermal conductance of multilayer cryogenic insulation under vacuum conditions 22 p3802 A67-40291

Thermal conductivities of cryogenic insulation systems determined by two methods using calorimetry measurement of boil-off rate of liquid cryogen 22 p3802 A67-40292

Heat flow meter apparatus for rapidly measuring thermal conductivity of flat insulation specimens under cryogenic temperatures 22 p3802 A67-40293

Double-guarded cold plate apparatus for measuring thermal conductivity of multilayer insulations, powders, fibers and foams 22 p3803 A67-40294

Cryogenic insulation thermoconductivity measuring apparatus operable at high vacuum and nonsteady state conditions 22 p3803 A67-40295

Guarded cold flat plate calorimeter for measuring insulation thermoconductivity 22 p3803 A67-40296

Cryogenic thermoconductivity heat flow meter apparatus for felt, powder and block materials at atmospheric pressure 22 p3803 A67-40298

High temperature microhardness of semiconductors determined by method measuring indentation diagonals of cooled single crystal specimens 22 p3804 A67-40302

Thermal diffusivities of thermal energy storage materials from solid surface temperature measurements, discussing advantages of transient method

[ASME PAPER 66-WA/ENER-5]

Gravity meter based on levitated superconducting ball over persistent current magnet 22 p3919 A67-40349

Magnetoelectric device development to measure and register weak signals in digital form in converters of automatic control systems 22 p3809 A67-40432

Reversible counter using decimal register compared to conventional flip-flop counters 22 p3809 A67-40475

Design and operation of loudness level meter /8051A/ which uses analog switching circuits 22 p3809 A67-40479

Measuring device for aerodynamic coefficients during wind tunnel tests by forced oscillation method 22 p3809 A67-40570

Large diameter helicopter rotors and V/STOL propellers /axis tilting in vertical plane/ testing system of wind tunnel and aerodynamic torque measuring apparatus 23 p3986 A67-40575

Airport glide slope visual range determination with single-ended transmissometer by measuring transmission between photosensitive detector and laser light source 23 p3999 A67-41027

Helium-neon laser device for mirror spacing changes by optical heterodyning, discussing application to piezoelectricity 23 p4014 A67-41031

Multiplace metabolimeter closed circuit system with servo-driven volume meter for animal oxygen consumption in gaseous artificial environments 23 p3999 A67-41088

East-west asymmetry effect in cosmic rays obtained together with ionizing and hard components, using crossed telescope 23 p4060 A67-41137

Compensation method for longitudinal slot effects on propagation constant and characteristic impedance of rectangular waveguide used in standing wave meter 23 p4000 A67-41220

Drop-across-reactance method found satisfactory for accurate current measurements in high voltage RF plasma discharges 23 p4001 A67-41224

Computer-operated following ellipsometer for monitoring buildup and removal of thin anodic oxide film 23 p4001 A67-41260

ISA Conference, Chicago, September 1967, Volume 22, Part I, Measurement standards instrumentation 23 p4003 A67-41334

Comparison calibration techniques for vibration transducers using quartz accelerometer 23 p4003 A67-41337

ISA Conference, Chicago, September 1967, Volume 22, Part II, Physical and mechanical measurement instrumentation 23 p4004 A67-41367

Thermal radiation properties measurement for materials in spacecraft design, discussing apparatus, instruments, techniques, devices and methods 23 p4003 A67-41368

Radiative and convective heat flux measuring instruments calibration for aerospace industry 23 p4006 A67-41375

ISA Conference, Chicago, September 1967, Volume 22, Part IV, Applications in industry and science 23 p4008 A67-41423

Human systolic and diastolic blood pressure measuring apparatus and method 23 p4008 A67-41424

Electronic ellipsometer for measurement of very small changes in elliptically polarized light, discussing refractive index, Kerr effect and calibration 24 p4152 A67-41901

Thermal diffusivity measuring device for conducting or insulating flat samples by short signal method 24 p4153 A67-41906

Calibration of optical pyrometers using gold point black body and sectorized disks 24 p4155 A67-42292

Charge time determined as circuit constants function in designing linear detectors 24 p4158 A67-42716

Electronic polarimeter applied to Stokes parameter measurement of lunar surface, determining reflected light ellipticity 24 p4239 A67-43070

Measuring instrument for assessing digital data transmission channels performance using bit error counting combined with peak telegraph distortion 24 p4159 A67-43116

MECHANICAL DRAWING

Three-dimensional variation diagrams for control of calculations in optimum design [ASME PAPER 66-WA/MD-9]

Man-computer graphics for computer aided design 04 p0629 A67-15345
Computer programming or software techniques in relation to hardware elements of computer graphics system [ASTME PAPER WES-7-02] 05 p0768 A67-17514
Costs and savings of computer graphics systems used for preparing and maintaining aerospace engineering drawings [AIAA PAPER 87-899] 11 p1756 A67-24253
MECHANICAL ENGINEERING 24 p4127 A67-43008
Mechanical design of parabolic steerable antenna structure of 150-ft diam having superior accuracy and resonant frequency resulting from high stiffness-to-weight ratio 03 p0396 A67-13752
Quality control and internal combustion aircraft engine reliability from mechanical engineering viewpoint 05 p0812 A67-17243
Applied mechanics - IME Conference, Cambridge, England, April 1966 12 p2013 A67-25407
Short duration shock machine 12 p1923 A67-25707
Book on elasticity covering engineering, Cartesian tensor and vector-dyadic notation, etc 14 p2395 A67-27891
Environmental conditions effect on engineering systems, considering vibration, climatics, pressure, radiation, corrosion, dust penetration, etc 15 p2492 A67-29502
Engineering approach to nonelectric reliability in design, stressing mechanical aspects 15 p2495 A67-30415
MECHANICAL IMPEDANCE
Mechanical impedance of device moving in liquid at resonance, determining viscoelastic magnitudes of Newtonian and non-Newtonian liquids under different dynamic conditions 02 p0240 A67-11521
Mechanical impedance testing and analysis for spacecraft with single firing 08 p1422 A67-21285
Relation between human mechanical impedance and coupling of human center of mass to environment, noting transfer function 09 p1456 A67-22370
Distributed parameter concepts of propagation, reflection and characteristic termination applied to dynamic analysis and control of bending vibration 16 p2776 A67-31886
Immittance and transmission matrices concepts applied to mechanical systems vibration, presenting formulations properties and interrelationships 19 p3261 A67-34960
Aircraft cabin noise due to fuselage vibration reduced, using mechanical impedance [SAE PAPER 670873] 24 p4248 A67-42010
MECHANICAL OSCILLATOR
Radiophysical measurement of small amplitude mechanical oscillations of self-oscillator by means of mechanical-electric converters and effects of natural line width on minimum amplitudes 05 p0805 A67-16357
Global method application to vibration problems, discussing present trends in experimental methods [ONERA-TP-405] 05 p0919 A67-16478
Electric analog and mechanical model used to investigate single particle impact dampers 07 p1262 A67-19410
Theorems concerning eigenvalue problems and oscillatory conditions for multiple degree of freedom mechanical systems 07 p1224 A67-20103
Oscillation of oscillator with elastically hereditary and weakly nonlinear characteristics, applying operational method to analysis in terms of hereditary creep theory 11 p1876 A67-24682
Electrodynamic exciter of mechanical vibration noting design, operation and characteristics 22 p3780 A67-39553
MECHANICAL PROPERTY
SA BRITTLENESS
SA CREEP
SA DEFORMATION
SA DUCTILITY
SA ELASTICITY
SA FAILURE
SA FATIGUE
SA FRACTURE
SA HARDNESS
SA PERMEABILITY
SA PHOTOELASTICITY
SA PLASTICITY
SA SHEAR STRAIN

SA THERMAL STRESS
Mechanical properties and corrosion resistance of titanium alloy forgings used as compressor parts 01 p0093 A67-10546
Materials for structural usage in high altitude/ high temperature supersonic transports, comparing aluminum, titanium, etc, alloys for mechanical and physical properties [SAE PAPER 660665] 01 p0094 A67-10573
Deformation processing of beryllium with respect to mechanical properties, economics and manufacturing considerations, examining production techniques [SAE PAPER 660634] 01 p0078 A67-10608
Mechanical property data on Lockalloy /82 Be, 38 Al/ and comparison with other lightweight structural metals [SAE PAPER 660652] 01 p0094 A67-10613
High strength magnesium casting alloys for aerospace applications, based on heat treatment involving internal precipitation of hydride [SAE PAPER 660656] 01 p0094 A67-10615
Mechanical property and structural changes in titanium alloys subjected to high temperature thermomechanical treatment 01 p0095 A67-10641
X-ray diffraction-Fourier series analysis and electron microscopy analysis of annealing effects on structural properties of cold worked dispersion-strengthened alloys 01 p0097 A67-10698
Transverse oscillated electron beam welding procedures of D6AC steel and mechanical properties evaluation show comparable results to corresponding gas tungsten arc welds 01 p0080 A67-10946
Tensile testing machine measuring mechanical properties under conditions of rapidly applied stresses 01 p0102 A67-11086
Sonic analysis for determining performance and mechanical integrity of turbine engines by using phase-locked filter and frequency ratio 01 p0076 A67-11141
Whisker strength measurement methods, noting role in reinforcement of ductile metal matrices 01 p0163 A67-11152
Mechanical properties of high polymer solid in terms of microbehavior as result of deformation and orientation, expressing anisotropic relaxation function as time dependent function 02 p0297 A67-11873
Strain-hardening and temperature dependence of mechanical properties of ternary ordered alloys on nickel-iron base 02 p0255 A67-12875
Multidirectional reinforced epoxy plastics in testing mechanical response to stress 03 p0451 A67-13401
Graphite fiber reinforced epoxy resin matrix composites, determining mechanical properties 03 p0452 A67-13402
Beryllium wire reinforced epoxy-plastic composites in mechanical testing under various loadings 03 p0442 A67-13404
Mechanical properties of continuous filament-graphite matrix composite in 0.50 inch diameter rod form, discussing limitation of binder phase and interface 03 p0453 A67-13412
General and mechanical property requirements for metal matrix composite materials used for aircraft gas turbine compressor blades 03 p0443 A67-13418
Anisotropy effect of continuous filament composites on material strength, noting dependency on test specimen configuration in evaluation of mechanical properties 03 p0523 A67-13446
Behavior and fatigue strength of graphite during testing, plotting curves in semilogarithmic coordinates 04 p0641 A67-14599
Stress concentration effect on fatigue strength of mechanically heterogeneous welds 04 p0636 A67-14600
Nickel effect on tensile strength, impact toughness and cold shortness threshold of low carbon steel 04 p0636 A67-14750
Oxygen content effect on mechanical properties and phase transformations of VT 16 titanium alloy during thermal treatment 04 p0637 A67-14942
Superplastic effect in cr-30 at pct Co alloy, noting low temperature bend ductility in quenched metastable single phased and near equilibrium conditions 05 p0829 A67-16474
Refractory metal alloys mechanical

properties, metallurgical behavior and applications 05 p0829 A67-16741
Materials evolution with high resistance to creep, mechanical and thermal fatigue, corrosion and impact, for gas turbine blades 05 p0829 A67-16744
Structure and mechanical properties of molybdenum-niobium system monocrystalline melts prepared by electron beam zonal melting 05 p0830 A67-17024
Recrystallization and polygonization of pure and impure metals, noting role of vacancy supersaturation 05 p0830 A67-17311
Temperature, admixtures, structural state and deformation rate on mechanical properties of refractory metals in niobium-tantalum and molybdenum-tungsten groups 05 p0831 A67-17502
Cold plastic deformation, rolling direction and annealing temperature effect on mechanical properties of sheet niobium at room and high temperature 05 p0831 A67-17504
Structure and mechanical properties of niobium alloys containing vanadium and titanium, showing relation between behavior in thermal etching and content of alloying element 05 p0831 A67-17505
Mechanical properties and chemical composition of industrial niobium VN2 and VN2A at low temperatures 05 p0832 A67-17506
Microstructure and mechanical properties as functions of degree of deformation of pressed rods of Tsm2A alloy at 1300 degrees C 05 p0832 A67-17509
Hardness, microhardness, electric resistance and toughness results tabulated for polycrystalline nonalloyed molybdenum 05 p0832 A67-17510
Plasticity of cast molybdenum improved by vacuum-annealing at temperatures from 900 to 1200 degrees C 05 p0832 A67-17511
Fusion weld evaluation in 2014-T6 material by eddy current, electric conductivity and hardness plots, noting aging effects, mechanical property degradation, etc 06 p1007 A67-17640
Niobium addition effect on mechanical properties of steel, noting improvement of tensile strength and cold brittleness threshold decrease 06 p1018 A67-18235
Mechanical and structural properties of three-dimensionally reinforced plastic, noting composite cylinder [AIAA PAPER 87-171] 06 p1020 A67-18296
Effects of 450 and 600 degrees F exposures on mechanical properties of glass-fiber polyimide resin sandwich panels to be used on large skin areas of SST aircraft [AIAA PAPER 87-174] 06 p1021 A67-18484
Mechanical properties of continuous carbon filament/graphite binder composite including tensile, compressure, flexure, fatigue and shear properties [AIAA PAPER 87-173] 06 p1021 A67-18509
Orientation effects in mechanical behavior of anisotropic structural materials - Astm Symposium, Seattle, October-November 1985 06 p1107 A67-18653
Thermally activated deformation relating flow stress to square root of dislocation density 06 p1053 A67-18755
Boron fibers and reinforced plastic composites, noting mechanical and physical properties, application, etc 06 p1021 A67-18855
Carbide forming elements effect on kinetics of isothermal transformation of austenite and mechanical properties of manganese-molybdenum steel 07 p1199 A67-19239
Ce and Pr effect on structure, hardness and mechanical properties of cast steel at 800 degrees C 07 p1199 A67-19242
Hydrogen effect on high temperature plasticity failure and mechanical properties of titanium shown to be similar to that caused by strain 07 p1200 A67-19248
Quenching from alpha region and subsequent tempering effect on mechanical properties of titanium alloy VT5-1 07 p1200 A67-19249
Mechanical properties of alloys of systems Al-Zn-Li and Al-Zn-Li-Mg 07 p1201 A67-19253
Small additions of refractory elements effect on structure and properties of sheets of Al-Zn-Mg alloy in various states 07 p1201 A67-19254
Small additions of refractory elements

effect on structure and properties of aluminum alloy castings containing Zn and Mg 07 p1201 A67-19255

Phase diagram of titanium-rich alloys of system Ti-Al, measuring resistivity and hardness through X-ray diffraction, thermal analysis, etc 07 p1204 A67-19267

Structural changes in titanium alloys during heat treatment 07 p1205 A67-19271

Fine structure of two-phase alloys of titanium VT14 and structures effect on mechanical properties 07 p1205 A67-19274

Oxygen effect on mechanical property and heat resistance of alloys AT3 and AT8 07 p1205 A67-19276

Alloying effect on elastic modulus, strength and plasticity of titanium in temperature range from - 196 to 800 degrees 07 p1206 A67-19280

Heat treatment effect on mechanical properties and structure of Ti alloys, noting phase state variation as function of quenching temperature 07 p1206 A67-19282

Hydrogen brittleness in Ti alloys, noting conditions of development 07 p1206 A67-19283

Titanium alloy mechanical and physical characteristics, noting dependence on chemical and phase composition 07 p1206 A67-19285

Heat treatment effect on yield point, impact toughness and plasticity characteristics of Ti alloys 07 p1207 A67-19286

AT13 Ti alloy preparation noting physical and mechanical properties and heat treatment induced phase transformation 07 p1207 A67-19287

Mechanical properties and heat resistance of titanium alloyed with low and high proportions of Al and Sn 07 p1207 A67-19289

Surface defects effect on mechanical properties of sheet metal under tension and bending, tracking brittle fracture to stress concentrators 07 p1263 A67-19751

Tensile and bending strengths as suitability criteria of pressworking of materials 07 p1192 A67-19755

Mechanical and electrical performance requirements of satellite communications antenna using Cassegrain configuration, noting relation to design 07 p1157 A67-20092

Mechanical properties of alloys in descriptive approach, noting data on precipitation hardening, plastic strain and creep 07 p1211 A67-20176

Heat treatment optimization for precipitation hardening superalloys, devising mathematical model for test sequence 07 p1192 A67-20249

Fabrication, properties, deformation and fracture of silica fiber reinforced aluminum, noting effect of heat treatment and stress rupture 07 p1211 A67-20260

Unalloyed titanium properties dependence on deformation and temperature 07 p1211 A67-20290

Microstructural changes effect on mechanical properties of nickel base superalloys, with particular attention to wrought alloys 08 p1340 A67-20362

Reinforced plastics - SPI Conference, Washington, D.C., January-February 1967 08 p1344 A67-20420

Mechanical property correlation between high performance composites and cast epoxy resin data 08 p1344 A67-20423

Inorganic continuous ceramic fibers production, properties and application 08 p1345 A67-20426

Constitutive equation describing stress-strain behavior of metallic and nonmetallic materials for strain rate 08 p1417 A67-20560

Compression strength and strain of solid propellants, noting internal loads developed during burning process 08 p1373 A67-20720

Mechanics and chemistry of solid propellants - Symposium on Naval Structural Mechanics, Purdue University, April 1965 08 p1418 A67-20872

Reinforcement of solid propellants and use of high strength wires and cylinders 08 p1374 A67-20889

Mechanical properties of unfilled and filled elastomers 08 p1420 A67-20890

Tape production process from noncontinuous boron fibers, noting mechanical properties and process parameters 08 p1335 A67-20911

Elastic moduli of filled systems, discussing effects of filler size, shape, concentration,

agglomeration, etc 08 p1421 A67-20916

Lunar surface mechanical properties at Surveyor landing site according to telemetry data and photographs 08 p1386 A67-20942

Structure and mechanical properties of extruded Ni-Al-oxide cermet materials, noting high compression strength 09 p1517 A67-21876

Carbon fibers of high strength and high breaking strain noting heat treatment, structure and mechanical properties 09 p1520 A67-21988

Postquenching deformation effect on mechanical properties and creep resistance of aluminum alloys 09 p1519 A67-22156

[ONERA-TP-423] Structural adhesives bonding - Symposium, Stevens Institute of Technology, Hoboken, September 1965 09 p1521 A67-22499

Mechanical properties of polybenzimidazole resin show suitability for metal-to-metal and sandwich composite adhesives and high and cryogenic temperatures 09 p1523 A67-22518

Microstructural dislocation tangling and related changes in tensile properties of Hastelloy X-280 following thermomechanical treatments 10 p1688 A67-23174

Gas saturated layer effects on VT5 titanium alloy mechanical properties variation with temperature 10 p1670 A67-23642

Threaded fastener reliability factors noting mechanical testing 11 p1795 A67-24040

Bell X-22A VTOL research vehicle, assessing mechanical and aerodynamic characteristics, variable stability and control system, etc 11 p1743 A67-24097

Titanium-chromium-vanadium system isohardness and isothermal diagrams and characteristic micrographs 11 p1806 A67-24362

Soviet book on ideal plasticity theory covering basic assumptions, general theorems, Tresca yield condition, etc 11 p1875 A67-24511

Structural and mechanical properties of lunar maria surface material derived from satellite and earth-based data 11 p1864 A67-24557

Solothane 113 urethane rubber composition analyzed via constant strain rate tests, noting birefringent sensitivity and optical transmission properties 11 p1811 A67-24615

Composite structure of glass with crystalline aluminum oxide and zirconium oxide inclusions tested for strength and elastic properties 11 p1811 A67-24642

Tantalum alloy slip line observations, stress-strain curves, yield stresses and anisotropic elastic constants in compression deformation 11 p1810 A67-25091

Mechanical properties of zone melt molybdenum single crystals as affected by orientation and gas 11 p1810 A67-25092

Impurities Martensitically hardened high strength stainless steel, physical properties, heat treatment effects, etc 11 p1810 A67-25103

Testing instrument for determination of lead wire mechanical properties and bond strengths within semiconductor devices 12 p1911 A67-25270

Low temperature mechanical properties of E1827 alloy investigated under static uniaxial elongation, noting ultimate strength increases with decreasing temperature 12 p1955 A67-25370

Molybdenum and niobium effect on structure and physical properties of austenitic Cr-Mn steels with or without nickel 12 p1955 A67-25439

Alloy 718 composition, microstructure and heat treatment behavior correlated with mechanical properties, noting strengthening and oxidation resistance [ASME PAPER 67-MET-5] 12 p1956 A67-25949

Effect of V, Zr, and Y additions on mechanical properties of 1 mm sheet molybdenum 13 p2130 A67-26392

Soviet papers on mechanism of metal breakdown 13 p2130 A67-26446

Dynamic and physical testing of metals, discussing yield point, plastic deformation and oscillation damping 13 p2215 A67-26452

Temperature and environmental effects on mechanical behavior of metals 13 p2132 A67-26697

Beryllium and other hexagonal metals mechanical properties compared under neutron irradiation, elucidating causes of

beryllium embrittlement 13 p2135 A67-27102

Hydrogen and nitrogen effect on ductility of beryllium purified by zone refining 13 p2136 A67-27103

Plastic flow in beryllium under fluid pressure at room temperature 13 p2139 A67-27123

High purity beryllium mechanical properties obtained by double electrolysis 13 p2139 A67-27126

Influence of grain-size purity relation beryllium fabrication and resulting mechanical properties 13 p2139 A67-27127

Mechanical properties of beryllium-aluminum alloy sheet with improved fabricability 13 p2140 A67-27128

Microalloying beryllium for improved sintering characteristics and mechanical properties 13 p2140 A67-27130

Mechanical properties of beryllium with emphasis on influence of anisotropy in forming and grain size in powder metallurgy 13 p2140 A67-27134

Statistical analysis of beryllium cross-rolled sheet, hot pressed block and ring rolled forgings 13 p2140 A67-27135

Thermodynamics of elastic materials using corollary of Clausius-Duhem inequality 13 p2224 A67-27145

Testing techniques for electroformed thin shells noting tensile properties determination 13 p2219 A67-27184

Aluminum oxide whiskers structure and properties 13 p2141 A67-27186

Alloying elements effect on austenite hardening of high-nickel-content chromium-nickel steels during cold plastic deformation 13 p2142 A67-27285

UV radiation effect on mechanical characteristics of polyethylene terephthalate film in vacuum and atmospheric pressure 13 p2184 A67-27624

Klegcell G-300 mechanical and thermal properties tested for thermal insulation for cryogenic stage for liquid hydrogen on space vehicle 13 p2228 A67-27659

Mechanical properties of several nickel-base alloys at room and cryogenic temperatures 13 p2142 A67-27676

Maraging steels retaining toughness at cryogenic temperatures by suitable heat treatment 13 p2142 A67-27677

Thermal processing of precipitation-hardenable aluminum alloys, noting changes in structural and mechanical properties 14 p2335 A67-27804

Commercial aluminum casting alloys physical and mechanical properties 14 p2335 A67-27807

Design factors for aluminum castings 14 p2323 A67-27813

Aluminum impact extrusion process design 14 p2323 A67-27814

Aluminum alloy forgings design 14 p2323 A67-27815

Elastic moduli of composite materials with anisotropic filaments 14 p2398 A67-28101

Nondestructive determination of mechanical properties of refractory materials by ultrasonic and radiometric measurements 14 p2340 A67-28258

High temperature strength of thermomechanical nickel dependent upon previous thermal and mechanical history, measuring elastic strain energy in matrix 14 p2337 A67-28418

Creep behavior at different stresses approximated through density of dislocation velocity, deriving strain time relation 14 p2400 A67-28420

Large parabolic radio astronomy antennas, discussing design and performance of current and next generation dishes 14 p2284 A67-28430

Structure and mechanical properties of molybdenum-niobium system monocrystalline melts prepared by electron beam zonal melting 14 p2338 A67-28491

Molybdenum ductility improvement by electrowinning with yttrium 14 p2338 A67-28616

Titanium alloys research and development for aeronautics industry 14 p2338 A67-28627

Behavior study of titanium alloys of interest to aeronautics industry, stressing creep resistance 14 p2338 A67-28628

Evaluating mechanical and corrosion suitability of materials [ASME PAPER 67-DE-7] 14 p2339 A67-28666

Polyphenyl ether physical, chemical and mechanical properties, noting experimental

results and fluid performance in closed pump loops 14 p2341 A67-28953

Vacuum effect on tensile, creep and fatigue properties of magnesium polycrystals and on tensile properties of oriented magnesium single crystals 15 p2503 A67-29561

Hydrogen treatment effects on molybdenum ductility, noting grain-size and heat treatment contribution to strain-to-fracture difference at various deformation pressures 15 p2503 A67-29562

Hardness, toughness, stress relaxation, corrosion resistance, etc., of niobium-aluminum alloy with stable elastic modulus 15 p2504 A67-29973

Temperature homogenization effect on structure of industrial aluminum, determining mechanical properties dependency on Fe/Si ratio 15 p2504 A67-29975

Mechanical response of highly filled elastomer in complex triaxial tensile stress field, demonstrating dewetting effect, need for more testing, etc. 15 p2575 A67-29978

Book on mechanical properties of ordered alloys including formation of superlattices 15 p2504 A67-30028

Fatigue failure prevention noting load redistributing, stress concentration reduction, critical section size increases, mean stress reduction, etc. 15 p2494 A67-30098

Third 260-inch diameter solid propellant rocket engine test firing 15 p2548 A67-30150

Positive effect of carbon on microstructure and mechanical properties of niobium alloys 16 p2687 A67-30845

Microhardness and microstructure of annealed industrial nickel fillings studied, noting results obtained at 300 degrees C 16 p2687 A67-30846

Hardness, electrical resistance and phase composition on Ni-Mo alloy during annealing, discussing phase transformations 16 p2687 A67-30847

Inclusion problems involving tubular shells of isotropic incompressible materials yielding large deformations 16 p2766 A67-31099

Collection of articles on complex semiconductors investigating conductivity, thermal, electrical and other properties, and preparation methods 16 p2729 A67-31154

Alloy steels response to dynamic strain aging in quenched, tempered and ausformed conditions, plotting strength and toughness against straining and tempering temperatures 16 p2688 A67-31306

Titanium alloys crystal structures determined using single crystal X-ray and powder neutron diffraction method, noting mechanical properties temperature dependence and martensitic transition 16 p2688 A67-31307

Inclusion type, forging ratio and heat treatment effect on properties of longitudinal and transverse steel specimens 16 p2689 A67-31310

High pressure hydrogen environment effects on mechanical properties of steels at high temperatures 16 p2689 A67-31327

Microstructure stability of aluminum reinforced with Al-Ni whiskers, noting tensile strength and mechanical property dependence on temperature 16 p2690 A67-31372

Sapphire whiskers mechanical behavior obtained by static tension testing 16 p2694 A67-31523

Mechanical properties used to estimate low cycle fatigue behavior in creep range of components in high-temperature systems 16 p2777 A67-31813

Book on intermetallic compounds discussing bonding, crystal structure, microstructure, formation, stability, kinetics, transformations and properties 16 p2692 A67-31887

Evaluation of plasticity, durability and impact ductility of nonbrittle austenitic steel during high and low temperatures 17 p2873 A67-32767

Mechanical properties of titanium alloys at room and cryogenic temperatures 17 p2873 A67-32768

Mechanical properties of welded junctions of rolled sheets of aluminum alloys at room and cryogenic temperatures 17 p2873 A67-32769

Powder-metallurgical methods using mechanical filing, isostatic pressing and high

vacuum-high temperature sintering for fabrication of airfoil turbine-blade blocks 17 p2865 A67-32821

Structure and substructure effect on thin film properties, discussing vacuum deposition mechanism of metals, alloys, dielectrics and semiconductors 17 p2920 A67-32888

Neutron bombardment effect on niobium mechanical properties shown to depend on metal purity 17 p2874 A67-32898

High strength Ti alloys in development of compressor blades, considering yield strength, impact energy absorption, ductility, fracture toughness and fatigue resistance [SAE PAPER 670335] 17 p2874 A67-32985

Heat treatment of nickel superalloys for high temperature applications, showing solution-temperature effect on mechanical properties 17 p2865 A67-33045

Thermal nitridation of maraging steels, noting effects on mechanical properties 17 p2875 A67-33046

Multipass welded Hastelloy joint age embrittlement from exposure in inert atmosphere at high temperature, stressing ductility, tensile and hardness tests 17 p2866 A67-33199

Densification and wear resistance of hot pressed pure and binary systems of diboride established with TaC and other refractory additives 17 p2875 A67-33407

Tensometric properties of silicon whiskers and acicular single crystals studied under static and dynamic loads, estimating suitability as strain gauge sensors 18 p3097 A67-33473

Temperature and composition effect on ductility transitions, yield stress and dislocation pinning strength in iron base alloys due to change in slip 18 p3063 A67-33485

Molecular theories for polymer elastic and viscoelastic properties near glass transition region [AIChE PAPER 67-488] 18 p3143 A67-33954

Iron-chromium-bauxite cermets preparation and properties 18 p3065 A67-34260

Mo, V, Re, Zr and Ti additions effect on mechanical properties, forming stability and recrystallization temperature of Ta alloy with Nb 18 p3065 A67-34293

Mechanical property and structural changes in titanium alloys subjected to high temperature thermomechanical treatment 18 p3066 A67-34405

Nickel effect on tensile strength, impact toughness and cold shortness threshold of low carbon steel 18 p3066 A67-34408

Mechanical behavior of boron-aluminum composites subject to stress, strain and temperature, discussing melt infiltration, powder metallurgy and diffusion bonding production [ASTM PAPER 9] 18 p3067 A67-34574

Mechanical behavior of fiber-reinforced aluminum and effect on engineering application [ASTM PAPER 10] 18 p3070 A67-34575

Composite material with titanium strength-weight ratio and aluminum safety for aerospace vehicle construction [ASTM PAPER 15] 18 p3067 A67-34576

Structural reinforced plastic composite materials for cryogenic temperature application evaluated noting tensile, compression, shear, flexural and bearing properties [ASTM PAPER 16] 18 p3070 A67-34577

Alloying volatile metals with refractory metals in Nb-Zn system, noting thermal analysis and microhardness determination 19 p3243 A67-34926

Book on coatings of high temperature materials covering properties and characteristics and coated refractory metals 19 p3244 A67-34956

Refractory metals physical, mechanical and chemical properties when coated with oxidation resistant coatings 19 p3244 A67-34958

High modulus carbon fiber fracture path, orientation and crystallite size effects on physical properties 19 p3248 A67-35425

Plane elastic strip with stress-free edges concept studied, noting mechanical coherence for elasticity and bending, expressing results by meromorphic function 19 p3340 A67-35450

Thermal and thermomechanical treatments effect on structure and mechanical

properties of Fe-Ni-base alloy with Al and Ti additions 19 p3247 A67-35834

Viscoelastic behavior of pure gum rubbers and relationship between filler characteristics and mechanical properties of inert filled composite materials 19 p3249 A67-35888

Physicochemical and mechanical properties of refractory materials at high temperature - Conference, Paris, June-July 1965 20 p3471 A67-36109

Refractory properties and mechanical characteristics of graphites and carbons, discussing maximum compatibility temperature of graphite 20 p3472 A67-36110

Temperature effect on mechanical properties of solids with high melting point, with quasi-static hardness as strength measure at high temperatures 20 p3463 A67-36111

Mechanical characteristics of materials determined using circular bending 20 p3537 A67-36476

Carbide inclusions and distribution effect on fatigue behavior of open hearth and electric-arc furnace steels 20 p3464 A67-36478

Properties of pressed and sintered products of powder metallurgy, noting strength and ductility increase with increase in density 20 p3465 A67-36496

Ceramic materials fracture and deformation mechanisms, discussing stress role 20 p3473 A67-36645

Durability and electrical conductivity of metallic fiber materials noting influence of oxidation on properties 20 p3466 A67-36912

Heat treating effects on molybdenum properties and structural characteristics 20 p3466 A67-36967

Tungsten sheets examined for recrystallization, grain growth and ductile-brittle transition temperature /DBTT/ as function of thermal treatment and grain size 20 p3467 A67-37119

Group IV and V metal carbides ball-milled to determine mechanical strain effects 20 p3467 A67-37122

Titanium plasticity and durability under large temperature range as affected by Re, Ta, Pd and La alloying elements 20 p3468 A67-37175

Beta-Ti alloy mechanical properties variation with hydrogen content for various temperatures and hydrogen embrittlement mechanism 20 p3468 A67-37176

Unidirectionally solidified eutectic alloys noting materials preparations for thermoelectric, magnetic, optical and electronic applications 20 p3469 A67-37359

Unidirectional solidification of cast nickel-base superalloys, effect on creep behavior, stress-rupture properties and thermal shock resistance 20 p3469 A67-37383

Nickel-base single crystal superalloy tensile and creep properties, comparing single and multiple slip orientations 20 p3470 A67-37387

Low temperature and irradiation environment effects on mechanical properties of engineering materials 20 p3418 A67-37532

Electron beam welded D6AC steel plates evaluated after heat treated condition /stress relief/ for mechanical properties 20 p3456 A67-37695

Brazing alloys and high remelt and conventional techniques developed and evaluated for use in tantalum honeycomb structures 20 p3456 A67-37696

Man-made organic polymer properties and characteristics, considering crystallization, cross-linking and polymeric chain stiffening for structural applications 20 p3474 A67-37713

Metals, ceramics, glasses and polymers combined as composite materials, reviewing mechanical properties and considering applications to engineering design 20 p3475 A67-37714

Poly/phenylene/hydrazide fibers mechanical properties, thermal stability and potential application 21 p3648 A67-37876

High strength high modulus glass fibers, discussing mechanical properties and design 21 p3648 A67-37879

Fiber reinforced plastic composite strength and elastic modulus dependence on fiber properties, volume content, directional orientation and matrix load transfer properties 21 p3649 A67-37882

Prestressing effects on stress-strain diagram of monodirectional transversely

isotropic glass fiber reinforced plastic 21 p3650 A67-37911

Temperature, admixtures, structural state and deformation rate on mechanical properties of refractory metals in niobium-tantalum and molybdenum-tungsten groups 21 p3644 A67-38029

Cold plastic deformation, rolling direction and annealing temperature effect on mechanical properties of sheet niobium at room and high temperature 21 p3644 A67-38032

Structure and mechanical properties of niobium alloys containing vanadium and titanium, showing relation between behavior in thermal etching and content of alloying element 21 p3644 A67-38033

Mechanical properties and chemical composition of industrial niobium and alloys VN2 and VN2A at low temperatures 21 p3644 A67-38034

Microstructure and mechanical properties as functions of degree of deformation of pressed rods of TsM2A alloy at 1300 degrees C 21 p3644 A67-38037

Hardness, microhardness, electric resistance and toughness results tabulated for polycrystalline nonalloyed molybdenum 21 p3644 A67-38038

Plasticity of cast molybdenum improved by vacuum-annealing at temperatures from 900 to 1200 degrees C 21 p3644 A67-38039

Low temperature effect on physical and mechanical properties of engineering materials and cryogenic fluids, discussing heat generation and removal at rubbing surfaces 21 p3633 A67-38141

External ear replica for acoustical testing noting sensing element, ear canal and eardrum impedance 21 p3577 A67-38148

Cold forming properties and handling of stainless steels and superalloys noting contained extrusion and warm heading techniques 21 p3634 A67-38177

Ceramics operating without protective atmospheres at ultrahigh temperatures, discussing tolerance formation, mechanical properties and working processes 21 p3650 A67-38194

Metal mechanical properties determination during deformation by uniform ultrasonic loading 21 p3722 A67-38450

Visual characteristics of welded wire joints, discussing correlation with metallurgical and mechanical properties 21 p3636 A67-38631

Microchemical and microhardness properties of parallel gap welds for microstructure interpretation of metal joint 21 p3636 A67-38633

Carbon content effect on properties and structures of nickel and nickel-iron base superalloys 22 p3818 A67-39223

Oxidation process and mechanical properties of austenitic steels and alloys under prolonged loading at high temperatures, giving stress-durability diagrams 22 p3819 A67-39322

Heat treatment effects on mechanical properties of steel-forged gas turbine rotor shafts, including microcracks formation and growth and structural strength 22 p3819 A67-39323

Maraging steels development, discussing mechanical properties, metal working, etc 22 p3819 A67-39388

Low pressure diffusion welding and brazing process producing joints with mechanical properties close to titanium 6Al-4V 22 p3811 A67-39446

Composite material mechanical characteristics, discussing organic polymeric materials application in wide temperature range 22 p3825 A67-39855

High performance engineering thermoplastic /Polymer 360/ mechanical and electrical properties and environmental factors effects 22 p3825 A67-39858

Phase transformations in commercial titanium alloys compared for mechanical properties, emphasizing decomposition of metastable beta phases on quenching, aging or deformation 22 p3822 A67-40055

Twinning and low temperature mechanical properties of high purity polycrystalline niobium and molybdenum, discussing grain size effects 22 p3823 A67-40208

Lithium in electrolyte and active metallic nickel formation effects on capacity and plate mechanical strength in alkaline storage batteries 22 p3748 A67-40229

Softening and incipient recrystallization temperature of deformed niobium during annealing measured by X-ray analysis and mechanical properties 22 p3823 A67-40328

Book on linear mechanics of elastic structures covering work and energy, Saint Venant theory of torsion, stress analysis, etc 23 p4071 A67-40566

Surveyor I landing site soil data covering mechanical, optical, thermal and electrical properties 23 p4064 A67-40950

Testing machine operated by hydraulic pressure for mechanical properties of materials at medium rates of strain 23 p4079 A67-41332

Property changes of semiconductor materials during processing, discussing photoelectric methods, resistivity derivative, recombination parameters and mechanical stresses 23 p4043 A67-41364

Surface waves in medium with coupled stresses, using Cosserat type medium for analysis of properties 23 p4079 A67-41417

Electromechanical and photomechanical effects on microhardness in semiconductors 23 p4045 A67-41472

Rare earth metals effect on mechanical properties of austenitic chromium steel at high temperatures 24 p4169 A67-41920

Diagrams of specific strength of materials made of fibrous compositions 24 p4246 A67-41921

Positive effect of Zr on nickel plasticity, showing elimination of hot brittleness within wide range of temperatures 24 p4169 A67-41922

Deformable aluminum alloys low temperature mechanical properties 24 p4170 A67-41923

Aluminum alloy sheet welds with high silicon and magnesium content analyzed for tensile properties and fracture toughness 24 p4161 A67-42330

Cryogenic mechanical properties of poly(ethylene terephthalate) film studied for effects of stretch and heat set temperature and time 24 p4176 A67-42469

High temperature strength and magnetic properties of cobalt-tungsten alloy for space power generator rotors 24 p4174 A67-42726

Atom arrangement in crystalline materials considering lattice, planes and structure, discussing effect on mechanical properties, particularly friction 24 p4164 A67-42733

MECHANICAL RESONANCE

Amplitude-dependent internal friction and defect structures measured in aluminum excited longitudinally by mechanical resonator 01 p0067 A67-10842

Method of averages in solving resonance problems in wave mechanics 10 p1679 A67-22842

Forced nonlinear vibration of Duffing type experimentally simulated with models of isolating systems, obtaining response curves [ASME PAPER 67-VIBR-35] 11 p1873 A67-24192

Dynamic stability of structures, discussing parametric resonance, impulsive loading, circulatory loads, aeroelastic and buckling problems 14 p2396 A67-28079

Maximum gravitational radiation detection range for binary stellar system analyzed by mechanically resonant antennas 15 p2563 A67-30162

GaAs single crystals excited to stable longitudinal vibrations by supersonic absorption, determining resonance curve 17 p2914 A67-32401

Solar system resonances emphasizing nongravitational forces in resonance formation and asteroid collision formation of Kirkwood gaps 23 p4062 A67-40623

Resonance in unbounded traveling and standing /harmonic oscillations/ waves, demonstrating equivalence of resonance states using wave equations 23 p4079 A67-41416

MECHANICAL SYSTEM

Stability analysis of steady state dynamic holonomic mechanical systems using Rouse, Kelvin, Poincare and Chetaev theorems 02 p0267 A67-11959

Integral variational principles in mechanics when initial position and velocity are known 02 p0267 A67-11965

Unreliability of mean-time-between-failures concept as standard quality measure for mechanical systems 02 p0249 A67-12426

Mechanical system with two degrees of

freedom conditioned for oscillatory motion, using differential equations 05 p0908 A67-16042

Variability of conveyor belt velocity during loading and operation, unloading and stopping under load analyzed, using distribution theory 05 p0908 A67-16043

Vibrations of disk-drum rotor analyzed using matrix equation of discrete model 05 p0810 A67-16230

Iteration method of general linear programming on digital computer using penalty functions compared to equilibrium problem of mechanical system 05 p0781 A67-16259

Galilean relativity principle in analytic mechanics of holonomous systems with infinite degrees of freedom 05 p0846 A67-16735

Steady state rotations in perturbed autonomous systems 05 p0847 A67-17475

Stability of steady motions of holonomic mechanical systems in cyclic coordinates, using method based on theorems of Routh, Poincare, Kelvin and Chetaev 06 p1031 A67-17838

Theorems on interaction of parts of mechanical system with smooth holonomic constraints 07 p1224 A67-20038

Equations describing orbital plane rotation of satellites, noting analogy between equations for oscillations of mechanical system with one degree of freedom 09 p1564 A67-21887

Resonance oscillations and rotations in mechanical systems having n-dimensional quasi-static vector analyzed and applied to triaxial ellipsoid with unbalanced mass 10 p1680 A67-23409

Mechanical systems with automatic retardation /self-braking/ for application to brake mechanism and frictional transmission, analyzing Painleve paradoxes 10 p1680 A67-23607

Dissipative gyroscopic force effects on mechanical system, noting necessary and sufficient conditions for stability and controllability 11 p1818 A67-24146

Parametric coupling analyzed in electrical RLC circuit coupled with mechanical system through nonlinear inductance [ASME PAPER 67-VIBR-30] 11 p1797 A67-24188

Manipulators for astronauts using anthropomorphic mechanical hands and arms controlled by bilateral servo system in exoskeletal master 11 p1749 A67-25011

Equations for small oscillations of mechanical system with solid components divided into groups by system of generalized coordinates 12 p1967 A67-25661

Short duration shock machine 12 p1923 A67-25707

Mechanical cascade toroidal servo flight control system tested using simulator [SAE PAPER 670269] 12 p1895 A67-25867

Universal endurance criterion for machine structural elements sustaining complex stresses, based on machine part lifetime assessment 12 p2032 A67-25964

Theoretical design of equivalent mechanical system naturally matched to self-oscillating system 13 p2216 A67-26626

Motion of variable-mass mechanical system with friction described by 3N equations 13 p2159 A67-27709

Stability and nonlinear vibrations of mechanical systems under harmonic excitation 14 p2397 A67-28087

Possible permutations producing cyclic permutations in theorems for component interactions in mechanical systems 14 p2349 A67-28745

Motion of holonomic mechanical system of points with variable mass under action of active forces 15 p2517 A67-29464

Two coupled resonant mechanical circuits with parameter in coupling element allowed to vary periodically 15 p2494 A67-29772

Electrodynamically coupled system consisting of RCL circuit, transformer and mechanical system analyzed by mathematical analogy and analog computer 15 p2440 A67-30081

Liquid spring design characteristics noting fluid characteristics, precharge fluid pressure, friction, efficiency, gland configuration and application requirements 15 p2494 A67-30097

Unsteady motion stability over given time interval of mechanical systems described by

nonlinear differential equations 16 p2702 A67-31052

Sinusoidal vibration generator consisting of two rigid vibrodynes connected by synchronized shaft for testing structural material 16 p2776 A67-31556

Adaptive controller synthesis for unstable mechanical system driven by bang-bang actuator adaptive controller synthesis for unstable mechanical system driven by bang-bang actuator 16 p2648 A67-31656

Ventilatory mechanical system response to stepwise-increasing pressure stress studied with Laplace-Carson transform, giving characteristics of linear differential equation governing system 17 p2807 A67-32238

Stability of equilibrium of nonconservative continuous systems with slight damping 17 p2959 A67-32414

Incipient cavitation calculation in hydrodynamics as example for applying quadratic programming to mechanical system subject to one-sided constraints 17 p2838 A67-32429

Synthesis of mechanical system with variator having drive unit in steady or steadily increasing motion, deriving and solving dynamic equations 17 p2885 A67-32967

Stability of steady motions of holonomic mechanical systems in cyclic coordinates, using method based on theorems of Routh, Poincare, Kelvin and Chetaev 17 p2886 A67-33216

Stability analysis of steady state dynamic holonomic mechanical systems using Rouse, Kelvin, Poincare and Chetaev theorems 17 p2886 A67-33276

Integral variational principles in mechanics when initial position and velocity are known 17 p2887 A67-33282

Rotating device for transmitting motion through walls of ultrahigh vacuum chambers, using circular motion of bellows envelope and internal gearing 17 p2863 A67-33358

Stability of rotation about symmetry axis of unsteady mechanical system consisting of gyrost at with fixed point and flywheel, deriving motion equations 18 p3078 A67-33556

Number of feasible information networks with single channel redundancy for remote control of telemechanical system 18 p3016 A67-33572

Soviet book on unsteady oscillations of mechanical systems with any number of degrees of freedom 18 p3078 A67-33678

Combination paramagnetic resonance in mechanical system containing rotating body, giving procedure for approximate determination of oscillation amplitude and resonant zone boundaries 21 p3625 A67-37990

Equilibrium stability conditions for mechanical system of solid bodies derived using Liapunov function 21 p3626 A67-37991

Book on simulation of mechanical systems giving analytical, graphic and analog computer methods 21 p3588 A67-38252

Independent variable changes in dynamical systems and applications to systems regularization, giving canonical and Lagrangian motion equations with tensor notation 23 p4027 A67-41006

Light gas gun model launching technique with advantages of aerodynamic and mechanical methods of sabot stripping 23 p3988 A67-41751

Stability of ideal mechanical system with damping forces, obtaining motion equations 23 p4028 A67-41757

Two-axis gimbal system for solar simulation spacecraft testing, demonstrating intermediate axis internal drive system and outer axis drive input 24 p4153 A67-42044

Mechanical system motion with point moving on surface, imposing limitations on system mass distribution, obtaining fixed coordinate system 24 p4188 A67-42302

Book on stability of nonlinear mechanical systems covering qualitative methods, one degree of freedom systems, etc 24 p4188 A67-42375

Spacecraft long life and reliability, examining mechanical and electronic equipment margin testing problem [AIAA PAPER 67-880] 24 p4244 A67-43000

MECHANICAL TWINNING

Plastic deformation of single crystals of vanadium by bending and compressing at 298 and 77 degrees K showed etching but no evidence of mechanical twinning 18 p3101 A67-34077

Twinning and low temperature mechanical

properties of high purity polycrystalline niobium and molybdenum, discussing grain size effects 22 p3823 A67-40208

MECHANICS

SA BIOMECHANICS

SA CELESTIAL MECHANICS

SA CLASSICAL MECHANICS

SA CONTINUUM MECHANICS

SA ELECTROMECHANICS

SA FAULT MECHANICS

SA FLIGHT MECHANICS

SA FLUID MECHANICS

SA FRACTURE MECHANICS

SA HYDRODYNAMICS

SA KINETICS

SA ORBITAL MECHANICS

SA PHOTOMECHANICS

SA QUANTUM MECHANICS

SA SPACE MECHANICS

SA STATISTICAL MECHANICS

SA THERMOMECHANICS

Mechanics Conference, Ukrainian Academy of Sciences, Institute of Mechanics, Kiev, April 1966 01 p0157 A67-10214

Applied mechanics - Japan National Congress, Kyoto University, September 1964 05 p0844 A67-16415

Mathematical studies of mechanics of solids in Rumania, noting use of matrices, Fourier expansions, stresses, shock waves, etc 05 p0920 A67-16797

Theoretical derivation of self-extension velocities of storable tubular extendible member /STEM/ 06 p1008 A67-18594

Advances in applied mechanics, Volume 9, covering hydrodynamic stability, free oscillations, nonlinear vibrations and viscoplasticity 08 p1352 A67-20308

Theoretical and applied mechanics - Conference, Haifa, May 1966 11 p1871 A67-24117

Variational methods solutions for thin shell deformation 12 p2027 A67-25621

Applied mathematics and mechanics - Symposium, Darmstadt Technical University, April 1966 13 p2156 A67-26605

Collection of papers on advances in applied mechanics, volume 10 19 p3262 A67-35797

Book on linear mechanics of elastic structures covering work and energy, Saint Venant theory of torsion, stress analysis, etc 23 p4071 A67-40566

MECHANISM

Book on functional mechanisms for engineering design, presenting kinematic characteristics of output motion, planar linkage and spatial cycloidal crank and flexural mechanisms 20 p3454 A67-36766

MECHANIZATION

Mechanization effect on man-machine relationships in flight test engineering analysis 13 p2052 A67-26423

MEDICAL ELECTRONICS

Time division multiplexing system for LF bioelectric signals, noting operation parameters and modes 02 p0216 A67-12075

Physiological monitoring applied to man in space environment, emphasizing overall philosophy including need and results of monitoring [AIAA PAPER 66-928] 04 p0563 A67-14625

Cutaneous sensitivity communications, discussing information situations, applications and subsystems 09 p1456 A67-22375

Physiological diagnostic information collection in prolonged space flight and data handling transmission 16 p2617 A67-30763

Biopotential detection, recording and design noting electrocardiogram and electroencephalogram use to monitor weightlessness in manned space programs 17 p2807 A67-32666

MEDICAL EQUIPMENT

Long-term biomedical instrumentation in Air Force space program 01 p0017 A67-11029

Telemetering and programming equipment used by CERMA in nose cones of rockets containing cats and rats in state of weightlessness 03 p0366 A67-13928

Aerospace technology information transfer to biology and medicine [AIAA PAPER 66-952] 03 p0366 A67-14023

Miniature multichannel pulse-duration-modulated multiplex telemetry unit for medical monitoring of human subjects pulse, temperature, airflow, etc, under stress 14 p2259 A67-28688

Long term biomedical monitoring of human heart rate through lithium chloride impregnated balsa electrodes, noting space flight application 15 p2431 A67-29918

Digital cardiachometer design noting binary counter, clock, operation cycle, etc 15 p2432 A67-29921

Electrophysiological tests performed onboard Voskhod I noting apparatus recording electroencephalograph, electrooculogram, dynamogram and motion coordination in writing of astronauts 16 p2616 A67-30760

Emergency dental kit for prolonged space flight, discussing filler materials 23 p3965 A67-41564

Vibrocadiogram used as cardiovascular monitor, applying signal averaging methods for parameter evaluation during severe subject stress 23 p3959 A67-41660

Vibrophonocardiograph developed for use in shirt-sleeve flight environment, previous design miniaturized without sacrificing performance characteristics 23 p3970 A67-41661

Equipment integration for Apollo Application Program /AAP/ physiological experiments, discussing design and dimensions [AIAA PAPER 67-846] 24 p4117 A67-42982

MEDICAL PERSONNEL

SA FLIGHT SURGEON

Aeromedical examiner relationship to accident prevention, discussing standardization of psychological approach 23 p3963 A67-41539

Aerospace nursing, present applications and future implications 23 p3968 A67-41622

MEDICAL PROGRESS

Millimeter wave radiometry to study atmospheric properties, topographic relief, planets, medical and industrial research 14 p2265 A67-28402

Retinal photocoagulation using solid state laser 14 p2333 A67-28973

Book on aviation and space medicine problems 22 p3752 A67-40532

MEDICINE

SA AEROSPACE MEDICINE

SA BIOLOGY

SA CASE HISTORY

SA CLINICAL MEDICINE

SA DENTISTRY

SA FIRST AID

SA HISTOLOGY

SA NEUROSCIENCE

SA PSYCHIATRY

SA RADIATION MEDICINE

SA RADIOLOGY

Space technology utilization in detection and prevention of cardiovascular disease, discussing instrumentation for monitoring microcirculatory system [AIAA PAPER 66-951] 02 p0187 A67-12285

Laser applications to telemetry, radar, navigation, telecommunications, medicine, boring and welding 14 p2333 A67-28974

MEDIUM

S CONDUCTING MEDIUM

S ELASTIC MEDIUM

S GYROTROPIC MEDIUM

S INTERGLACTIC MEDIUM

S ISOTROPIC MEDIUM

S MAGNETOELECTRIC MEDIUM

MEISSNER EFFECT

Thorium-gadolinium alloy magnetization curves confirming full Meissner effect, showing bulk properties of superconductors obey Abrikosov-Gorkov theory 14 p2373 A67-28859

Zero magnetic field in superconducting lead shell using Meissner effect 22 p3865 A67-40438

MELIN TRANSFORM

S LAPLACE TRANSFORM

MELTING

SA ARC MELTING

SA LIQUEFACTION

SA VACUUM MELTING

SA ZONE MELTING

Powder metallurgy techniques for thermoelectric materials particularly lead telluride, germanium bismuth telluride and zinc antimonide 01 p0099 A67-10709

Controlled solidification in casting, ingot-making and other processes including composites and highly undercooled melts 03 p0442 A67-13305

Laser radiation effect on solids, noting laser properties, temperature rise, melting, vaporization and particle emission of

materials 09 p1513 A67-22144
 Premelting of predetermined sites in sodium-potassium alloys studied by transmission UV microscopy 14 p2339 A67-29032
 Thermal conductivity model for planetary igneous differentiation, discussing melting behavior as function of pressure and temperature 17 p2942 A67-32387
 Linear melting curve of fayalite up to 40 kb determined, using piston cylinder and thermocouples 21 p3617 A67-38190

MELTING POINT

One-dimensional freezing of semiinfinite isotropic homogeneous liquid-solid system with temperature-varying thermal properties 01 p0166 A67-10758
 Modulus of elasticity of metals and titanium alloys as function of electron structure and binding 07 p1206 A67-19279
 Melting temperatures of ZrC-HfC, TaC-ZrC and TaC-HfC compacts obtained via Pirani method 09 p1518 A67-21879
 Electron beam welding in vacuum and in atmosphere, describing rapid positioning, workpiece guidance, beam control and observation 09 p1503 A67-22119
 Temperature resistant elements and compounds for use above 3000 degrees F, considering melting points, atomic radii and densities 14 p2340 A67-28380
 Relative enthalpy and thermodynamic properties of beryllium aluminate from room temperature to melting point 15 p2508 A67-29764
 Melting point and microhardness of carbon-saturated TIC-VC solid solutions, noting temperature of eutectic of TIC-VC with graphite 16 p2691 A67-31588
 Changes in experimental relationship between preexponential factor in diffusion equation and activation energy for solid solutions 19 p3243 A67-34928
 Spectral emittance of melting or decomposing polystyrene determined, describing apparatus and experimental technique 20 p3446 A67-36663
 Molybdenum-boron system structural diagram, noting carbon effect on phase equilibria and temperature 20 p3468 A67-37177
 TiNi-TiFe system equilibrium diagram, studying melting points and heat treatment effects on microstructure 20 p3468 A67-37179
 Binary molybdenum-carbon system investigated using X-ray, metallographic, thermoanalytical and melting-point techniques 20 p3470 A67-37389
 Change patterns in melting point and forbidden bandwidth for anion and cation substituted compounds of AIIIBV group 21 p3676 A67-37932

MEM
S MARS EXCURSION MODULE /MEM/ MEMBRANE
SA DIAPHRAGM
SA EARDRUM
 Nonlinear membrane equations for extremely thin shell of revolution of very deformable material, assuming large displacements, rotations and strains 10 p1730 A67-23836
 Semipermeable Ag membrane as electron collector in oxygen diffusion process for cesium thermionic energy converters 11 p1746 A67-24923
 Flexural wave velocity-amplitude relation indicates possibility of stationary waves for fixed ratio of wave amplitude and spinning membrane angular velocity 14 p2403 A67-29016
 Finite inflation of isotropic elastic toroidal membrane possessing strain-energy function by uniform internal pressure 17 p2956 A67-31932
 Axisymmetric response of semiinfinite truncated cone striking smooth rigid obstacle, determining early stages of motion 17 p2960 A67-32422
 Stress-strain distribution in clamped membrane during stamping, deriving formulas for plastic deformation of metals 21 p3632 A67-38061
 Calculation method for mono-, two- and three-spar wings including membranes and plate, discussing stress formulas 21 p3722 A67-38525
 Zinc penetration through regenerated cellulose membrane separators shown to be growth mechanism in silver-zinc

cell 22 p3758 A67-40227
MEMBRANE ANALOGY
 Flexible membrane hydrostatic air bearing, determining membrane shape, pressure distribution and air gap by Navier-Stokes and membrane analogy equations [ASME PAPER 67-LUB-1] 24 p4162 A67-42668

MEMBRANE FORCE

Large deformations of circular membrane attached to ring subjected to action of uniform load 04 p0708 A67-14795
 Elastic cylindrical shell under arbitrary impulsive pressure distribution, discussing membrane and flexural stresses 05 p0909 A67-16139
 Matrix displacement approach to discrete element structural analysis for thin shell instability, emphasizing determination of membrane force 05 p0925 A67-17352
 Discrete element method for plastic analysis of complex built-up structures subjected to cyclic loading causing membrane stress and stress reversal 10 p1725 A67-23713
 Existence of solution for equilibrium problem of circular symmetrically loaded membrane with stress free contour proven by Chaplygin method 11 p1876 A67-24680
 Nozzle and membrane effects on shock wave intensity in tube, showing graphically Mach number dependence upon initial pressure 17 p2837 A67-32345
 Membrane stress state of spiral coiled tube surface, reducing stress components to second order differential equation 22 p3913 A67-40009

MEMBRANE STRUCTURE

Plastic deformation including instability of circular membrane subject to hydrostatic pressure, obtaining stress-strain curve 01 p0161 A67-10776
 Iterative solution for large deflection analysis of rotationally symmetric nonlinear membranes 04 p0715 A67-15658
 Optimum thin wall pressure vessels of anisotropic materials of monolithic and filamentary construction [ASME PAPER 66-APM-BB] 04 p0717 A67-15915
 Governing equation for bending of multilayered sandwich elastic plates composed of n membranes developed by variational method 06 p1110 A67-18857
 Shock wave profile in shock tube at different distances from plasma source determined, using perforated sliding membrane 09 p1489 A67-22329
 Plastic analysis of cylindrical shell deflections noting support against sliding, shell with clamped edges and with longitudinal force and membrane solution 10 p1715 A67-22922
 Triangular elements under linearly varying strain used in matrix displacement method analysis of stability of membranes of arbitrary anisotropy 20 p3535 A67-36196
 Molecular flow mass spectrometer analysis of porous metal membranes for gases of different molecular weights 20 p3378 A67-37499
 Nonlinear ferrite diaphragms in waveguides, discussing magnetic field effect on cavity tuning 24 p4119 A67-41972

MEMBRANE THEORY

Asymptotic theory of elastic plate dynamics, deriving displacement equations and boundary conditions 01 p0162 A67-10822
 Toroidal shell of circular cross section free of bending under uniform normal hydrostatic pressure 02 p0336 A67-11589
 Boundary layer phenomenon in nonlinear membrane theory, investigating problem of closing hole in membrane having John strain energy density 03 p0525 A67-13823
 Moire method in determining dynamic response of thin membranes 03 p0531 A67-14362
 Asymptotic distribution of natural frequencies of plane membrane with separable variables 04 p0708 A67-14671
 Variable thickness tension shell in nonlinear membrane analysis 04 p0709 A67-14843
 Axisymmetric deformation of shallow shells of revolution, noting membrane solutions 05 p0917 A67-16245
 Axisymmetric vibration modes of cylindrical-hemispherical membrane tank partly filled with liquid

[AIAA PAPER 67-75] 06 p0986 A67-18273
 Analytical solution for axially symmetric membranes made of neo-Hookean materials solved by simultaneous differential equations 06 p1107 A67-18652
 Membrane solution of spirally corrugated shell under axial and torsional loading determined from thin shell bending equations 06 p1110 A67-18856
 Stability of membrane solution in nonlinear plate and shell theory 07 p1263 A67-20032
 Scalar wave equation of annular membrane for origin symmetric motion and arbitrary initial and boundary conditions 08 p1415 A67-20476
 Second order equations of motion for free axisymmetric deformation of thin spherical shells, discussing membrane and composite mode of solution 08 p1416 A67-20490
 Asymptotic and particular solutions of conical shells subjected to lateral normal loads, discussing membrane forces, bending effects and boundary conditions for moments and shearing force 09 p1573 A67-21754
 Matched asymptotic expansions for solution of singular perturbation problem of stresses and deformations in pressurized toroidal membrane 11 p1871 A67-24086
 Cartesian formulation of membrane theory, discussing equations of equilibrium, strain energy, variation formulation and boundary conditions 11 p1875 A67-24431
 Perturbation solutions for finite inflation, under internal pressure, of elastic toroidal membrane of circular cross section 11 p1879 A67-25002
 Flexible filament under transverse impact from sphere, considering friction forces 19 p3341 A67-35704
 Vibrating annular membrane problem, including load per unit area and asymmetry of load and vibration, using finite transform derivation 20 p3539 A67-37006

MEMORY

SA KINESTHESIS
SA LEARNING
SA MAGNETIC MEMORY
SA TRAINING
 Automatic checkout system based on digital instrumentation with input of two bits and variable data rate resulting from use of memory storage 03 p0398 A67-14203
 Pupillary diametric size as indicator of load on human memory 05 p0756 A67-16587
 Airborne environment, compatibility and memory for airborne software 08 p1297 A67-20631
 Micrometazoa as model systems for studying physiology of memory at cellular level, examining habituation and maze behavior 20 p3369 A67-36657
 Closed loop stepping motor as mechanical memory and time optimal control and digital servomechanism applications 21 p3570 A67-37787
 Diffusion model of perceptual memory process when observer compares two consecutive stimuli, noting visual and auditory discrimination 21 p3576 A67-39097
 Perceptual motor-skills forgetting in simple printing task, attributing decrements to retroactive interferences 21 p3576 A67-39099
 Reinforcement intervals /RI/ effect in paired-associate learning using within-subjects, noting error dependence on RI 21 p3576 A67-39100
 Short term memory of paired associates studied using continuous technique, noting recall as function of number of interpolated pairs 22 p3750 A67-39318
 Recall of two messages of equal word number presented with words of one message sequentially alternating with other 22 p3754 A67-39587
 Biochemical model for long term sequential memory in nervous system, introducing network serving as clock to maintain temporal order of stored events 24 p4116 A67-42698

MEMORY STORAGE UNIT

Multistable memory consisting of series of cascaded bistable tunnel diodes with low resolution time 01 p0037 A67-10660
 Fast-acting memory storage advances for data processing application, noting classification of types 01 p0029 A67-10663
 Monolithic ferrite space memory system of minimum weight, power consumption and

- high reliability 02 p0208 A67-12162
Shared memory computer display system provides test bed for man-machine interaction, noting hardware and software design concepts 03 p0375 A67-13633
Logic and memory circuits and operational dynamics of system of pulsed elements operating on tunnel diodes 05 p0772 A67-16451
Exponential smoothing for prediction of reliability growth having advantages of tracking data precisely while retaining in memory only few historical statistics 05 p0811 A67-16828
Performance characteristics of cryotron memory cell for receiving pulses arriving at input from current magnitude 06 p0966 A67-18242
Superconducting switching and storage elements, examining physical properties, cryotron and continuous film memory cell 06 p0972 A67-18433
Read-only memory composed of MOS-FETs on single silicon chip 07 p1155 A67-19845
Image storage tubes /cathode ray tubes with memory device to store visual information/ 07 p1189 A67-20157
Random access storage of program for airborne digital computer system 08 p1297 A67-20628
Determination of length of deductive circuits of recycling memories and oscillators 08 p1302 A67-20835
Serial comparison technique for coding systems where weight of ascending bit is equal or greater than previous bit 11 p1756 A67-24266
Current stretch sensing for removing limitations to usable density of cryotron storage cells of random access memories 11 p1765 A67-24625
Integrated memory arrays, discussing packaging methods and comparing monolithic and hybrid large scale integration 14 p2280 A67-28014
PSIN /P region, Seminsulating region, N region/ diode array fabrication, performance, characteristics and applications 14 p2282 A67-28029
Prefix coding of histograms for minimal storage 14 p2272 A67-28703
Digital command and experimental data storage system for OAO 16 p2633 A67-30670
Satellite onboard multichannel systems for information processing, discussing construction, quick response memory and block diagrams 16 p2633 A67-30673
Memory device for matrix time meter, discussing use of logic thyatron to improve stability of memory matrix 16 p2674 A67-31119
Computer memory systems for handling Air Force information, discussing types of memory, storage techniques and device technologies 17 p2819 A67-32473
High density cryotron array production in associative memory application, using lock-out design feature 18 p3014 A67-34556
Fast thin film main memory system design noting 200 nsec cycle time and 180 nsec access time 19 p3189 A67-36063
Rotationally switched rod memory system with 100 nsec cycle time, discussing cost and performance factors 19 p3189 A67-36064
High speed computer memory design using plated wire elements 19 p3189 A67-36065
Static and dynamic electronic memories used in data processing 20 p3390 A67-36250
Scientific data handling system using passive magnetostrictive multichannel delay line memory 20 p3390 A67-36251
Semipermanent optical memory design using laser light source, acoustic light deflector and hologram array as information storage elements for address selection 20 p3390 A67-36511
Memory-cell circuit employing Esaki diodes negative resistance characteristic, developing small memory pulse amplitude useful in minimizing cycle time 20 p3397 A67-36769
Associative memory system of persistent current bit-cells using cryotrons in selection and control network 21 p3587 A67-37955
Packaging of IC core memory for aerospace use, discussing design and production of boards 21 p3595 A67-38338
Packaging of satellite plated wire memory components including memory plane stack, electronic circuit modules and interconnections 21 p3595 A67-38339
Nondestructively optically read ferroelectric bismuth titanate single crystal memory device 22 p3767 A67-39261
Magnetics - Conference, Washington, D.C., April 1967 22 p3859 A67-39895
Large capacity cryoelectric random access memories, examining three-wire cells and hybrid system for batch fabrication, redundancy, electric parameters, tolerances and noise 22 p3764 A67-39898
Nondestructive readout technique for superconductive memory cells, application and comparison with previous methods 22 p3765 A67-39899
High speed read-only memory with waffle iron structure noting ease of information change and high bit density 22 p3765 A67-39904
Magnetic film memory written and read by focused light studied using thermal cycle time and read bandwidth calculations 22 p3765 A67-39910
MOSFET integrated circuits for use in analog computers noting simplicity and switching qualities for control of hybrid devices 22 p3775 A67-40465
High level transistor/transistor logic 16-bit memory element function, characteristics and applications 23 p3975 A67-40698
MENTAL PERFORMANCE
SA PSYCHOMOTOR PERFORMANCE
Adrenal cortical activity changes correlated with pathological emotional states 06 p0952 A67-17848
Noise and vibration effect on human mental work capacity with increasing time limitation indicating efficiency reduction 16 p2614 A67-30917
Central factor influence in pure tone induced auditory fatigue while performing threshold tracking or other mental activity 21 p3576 A67-39060
Cockpit environment thermal stress effect on psychological test performance and biomedical parameters 22 p3753 A67-40539
MENTAL STRESS
SA ANXIETY
SA DEPERSONALIZATION
Stress-related and other physiological variables on jet aircraft pilots participating in storm penetration and perimeter flights 17 p2805 A67-31955
MERCURY /MA-1/ FLIGHT
S MA-1 FLIGHT DIRECTOR SYSTEM
MERCURY /METAL/
Stationary free-surface mercury flow in channels under magnetic field, analyzing hydraulic jump and influence of field on location 01 p0120 A67-10179
Mercury ion rocket propulsion system compared to cesium ion system 02 p0305 A67-12338
Hydromagnetic approximation in stability of axisymmetric mode in case of mercury cylinder enclosing copper rod with electric current 03 p0480 A67-13728
Mercury photosensitized oxidation of tetrafluoroethylene, noting reaction process and parameters 04 p0567 A67-15950
Capture cross section of photons by zinc and mercury atoms in germanium determined from integral voltaic photosensitivity, using black body as radiation source 05 p0868 A67-17066
Growth of turbulent mercury jet issuing into low speed secondary flow and located in coaxial magnetic field 06 p1040 A67-18130
Temperature variation in wall of square channel due to heat transfer to turbulent flow of water and Hg 07 p1265 A67-19126
Ion thruster, including mercury feed system and shielded neutralizer, designed and tested for spacecraft station keeping and attitude control [AIAA PAPER 66-247] 10 p1698 A67-23120
Mercury abundance in various meteorite and rock types determined by neutron activation analysis, relating data to evolution of meteorites and earth 11 p1858 A67-24064
Experiment to represent sunspot model having mechanism of natural turbulent convection of liquid mercury inhibited in presence of magnetic field 13 p2171 A67-27437
Mercury abundance in chondrite meteorites determined by neutron activation and separation by volatilization over temperature range 13 p2210 A67-27603
Liquidus curves of various metals with mercury at high temperatures, obtaining corrosion rates and data on grain boundaries penetration 15 p2502 A67-29261
Capture cross section of photons by zinc and mercury atoms in germanium determined from integral voltaic photosensitivity, using black body as radiation source 15 p2538 A67-29797
MHD flow of liquid mercury through circular pipes at high Hartmann and Reynolds numbers, plotting friction factors 16 p2712 A67-30576
Steady-state mercury flow along open trough in transverse magnetic field, measuring electric and hydraulic characteristics and providing plasma motion model 16 p2713 A67-30578
Turbulent channel flow of mercury in presence of uniform transverse magnetic field deducing skin friction coefficient 16 p2861 A67-31224
Probe measurements of friction drag coefficient and velocity profile of turbulent flow of mercury in circular tube in presence of longitudinal magnetic field 16 p2721 A67-31394
Spatial correlation coefficients and transverse temperature perturbation scales during turbulent nonisothermal flow of mercury in circular pipe 16 p2724 A67-31776
Transverse magnetic field effects on heat transfer in turbulent flow of mercury in circular iron tube 17 p2899 A67-32186
Resonance effect in low energy or low velocity Li-Hg total scattering cross section 18 p3082 A67-34031
Partial molal entropies of doubly ionized aqueous Zn, Cd and mercurous and mercuric ions calculated, using literature data 20 p3376 A67-36792
Magnetic field effect on resistance coefficient of mercury flow in circular pipe 20 p3501 A67-37304
Longitudinal ultrasound attenuation in polycrystalline superconducting mercury at 9.3 GHz, studying temperature dependence 20 p3514 A67-37568
Temperature variation in wall of square channel due to heat transfer to turbulent flow of water and Hg 21 p3731 A67-38170
Electromagnetic forces and pressure and hydraulic losses of turbulent mercury flow in annular channel under traveling magnetic field effect 21 p3666 A67-38249
Liquid mercury equation of state and electrical resistivity at high temperatures and pressures 21 p3686 A67-39104
Liquid mercury conductor flow in annular gap electromagnetically accelerated by Lorentz force, showing restricted nonexistence proof for inviscid problem 23 p3992 A67-41742
MERCURY /PLANET/
Frequencies of radar echoes from Mercury and Venus measured, for testing Doppler formula 01 p0026 A67-10920
Radio observations of Mercury, Venus and Mars, discussing concepts, concerning planets physical condition 03 p0509 A67-13317
Trajectory modes for manned and unmanned missions to Mercury, 1980-2000 [AIAA PAPER 67-28] 06 p1086 A67-18333
Planet Mercury magnetospheric scattering of solar-flare protons to earth, obtaining deflection angle [AIAA PAPER 67-150] 06 p1088 A67-18505
Solar oblateness indication of solar quadrupole moment effect on Mercury perihelion precession solar oblateness indication of solar quadrupole moment effect on Mercury perihelion precession 08 p1354 A67-21429
Solar oblateness effect on quadrupole moment and on perihelion of Mercury 10 p1709 A67-23487
Polarization properties of Mercury explained by surface only, so there is no polarimetric evidence for atmosphere on Mercury 12 p2010 A67-26244
Cross section and angular scattering law for Venus and Mercury from delay and Doppler frequency shift radar echo measurements 15 p2556 A67-29870
Venus and Mercury intrinsic rotation rates and surface radar reflectivity of former from radar echo measurements 15 p2556 A67-29872
Radio observations of Mercury, Venus and Mars, discussing concepts concerning planets physical condition 16 p2741 A67-30493
Solar spin-down problem, noting oblateness effect on perihelion precession of

Mercury 17 p2940 A67-32208
 Rotation and heating of planet Mercury, examining insolation and surface temperatures from coupling of orbital and rotational periods 17 p2940 A67-32210
 Planetary influences on sunspot formation and disappearance showing periodicity in Zurich relative daily sunspot number 17 p2943 A67-32439
 Radio and radar observations of Mercury, Venus and Mars 18 p3123 A67-34144
 Criticism of classical theory of Mercury rotation period equal to revolution around sun 18 p3125 A67-34191
 Trajectory modes for manned and unmanned missions to Mercury, 1980-2000 21 p3700 A67-37782
 Solar oblateness and Mercury perihelion advance, showing turbulent viscosity forces acting on photospheric meridional currents as possible distortion cause 21 p3701 A67-37963
 Soviet book on planetary physics covering Martian, Venusian and Mercurian atmospheres, Venusian surface temperature and Jovian radio emission 21 p3707 A67-38933
 Mercury radio emission observation yielding average brightness temperature and planetocentric phase angle relation 22 p3889 A67-40240
 Upper limit of carbon dioxide abundance in Mercury atmosphere 24 p4225 A67-41836
 Incompatibility of microwave phase effects measurements in Mercury thermal emission with simple model for thermal behavior of planet surface 24 p4226 A67-41837
 Thermophysical research requirements for Venus Lander, Jupiter Entry Probe and Mercury Orbiter planetary exploration missions 24 p4227 A67-42041

MERCURY ARC

CW He-Ne laser compared with mercury arc source, obtaining Raman spectra of carbon tetrachloride by three methods of excitation 03 p0438 A67-13912
 Low density electron bombardment ion engine, particularly mercury engine and Cs gas discharge ion engine, for electrostatic propulsion 04 p0689 A67-15020
 Hologram of cold mercury arc spectrum obtained by triangle path interferometer 09 p1497 A67-21766
 Water cooled mercury arc discharge lamp for room temperature optimum optical pumping of CW lasers 12 p1952 A67-25331
 Iso-irradiance contours close to high pressure mercury arc lamp [AIAA PAPER 67-315] 12 p2037 A67-26030
 Mercury fed plasma bridge neutralizers for in-flight operation of SERT II electron bombardment ion thruster [AIAA PAPER 67-670] 21 p3691 A67-38704

MERCURY CAPSULE

Maximum temperature profile in phenolic resin-siliceous fiber heat shields on ICBM and Mercury spacecraft [AIAA PAPER 65-638] 03 p0533 A67-13058

MERCURY COMPOUND

Semiconductor character of mercury selenide determined by analyzing variation of band-edge effective mass as function of composition of HgSe-CdTe alloys 03 p0499 A67-13886
 Three-component semiconducting compound corresponding to stoichiometry of mercury thallium sulphide, noting properties 07 p1233 A67-19650
 Resistivity, Hall effect and thermoelectric power of mercury selenide from 77 to 500 degrees K 09 p1557 A67-22556
 EPR applied to investigation of various semiconductors containing iron, and Mn at liquid nitrogen temperature 14 p2373 A67-28968

MERCURY LIGHT

Multiple pass effects in laser pumping cavities, noting mercury lamp performance 10 p1662 A67-22743

MERCURY PROJECT

Structural safety of Mercury and Gemini vehicles, noting fail-safe and fracture tolerant design [SAE PAPER 660681] 01 p0154 A67-10585
 Manned planetary exploration, Mercury and Gemini flight programs and projected goals of Apollo Applications Program 12 p2002 A67-25233
 NASA earth orbital photographic experiments planned for 1967-1969 as supplement to Mercury and Gemini efforts 12 p1940 A67-25433

Gemini program engineering aspects compared to Gemini/Mercury, discussing basic design rules adopted and Apollo Applications Project objectives 22 p3904 A67-40064

MERCURY TELLURIDE

Vacuum evaporation of HgTe thin film, examining thermal treatment, electric properties as function of thickness, etc 02 p0280 A67-11463
 Semiconductor lasers and fast IR detectors, discussing InAs, InSb and three types of mercury cadmium telluride detectors 05 p0821 A67-16668
 Band structure of n-type HgTe by use of model of band structure based on observation of Shubnikov-de Haas effect 05 p0864 A67-16900
 Absorption measurements of 139-Gc microwaves for very high purity mercury telluride, deducing electron effective mass 06 p1047 A67-17653
 Mercury telluride thin film properties and fabrication methods 06 p1050 A67-18185
 Quantum oscillations in magnetoresistance of n-type pure HgTe used to estimate electron effective mass and g value close to band edge 06 p1065 A67-18948
 Conduction band structure and scattering processes of cadmium mercury telluride mixed crystal determined from thermoelectric power, effective mass and electron mobility 12 p1979 A67-25178
 Quantum oscillation of magnetoresistivity in n-type mercury telluride crystals, obtaining electron mass 14 p2369 A67-28598

MERCURY VAPOR

Resonances in low pressure mercury vapor discharge due to natural resonance modes of cylindrical plasmas 02 p0273 A67-12097
 Role of negative ions in flames and of negative droplets in mercury vapor, noting use of isotopic tracer techniques and flame behavior as gaseous semiconductors 05 p0853 A67-16886
 Large scale expansion nozzle control by heterogeneous nucleation and mercury vapor and drop growth processes in nitrogen flow [AIAA PAPER 66-85] 10 p1733 A67-23125
 First azimuthally varying mode in mercury vapor plasma discharge, predicting growth of hose-like instability of electron beam 11 p1841 A67-24928
 Lightweight flight prototype mercury ion engine system development and testing [AIAA PAPER 66-216] 13 p2188 A67-26823
 Dispersion relations of moving striations in rare gases, noting wave nature and dependence on discharge current 15 p2472 A67-29733
 Secondary ionization processes in mercury vapor, calculating relative populations of excited and metastable atoms per ion pair 19 p3265 A67-35090
 Current growth rate instabilities in high current mercury vapor discharges, giving image converter photographs 19 p3265 A67-35091
 Comparison of experimental and theoretical results on electron beam produced mercury-vapor discharge 19 p3290 A67-35380
 Vertical magnetic induction effect on nucleate boiling of mercury on horizontal heating surface [AIChE PAPER 20] 20 p3552 A67-36830
 Gaseous mercury discharges through orifice as ion beam neutralizer for electrostatic thrusters [AIAA PAPER 67-669] 21 p3691 A67-38703
 Measurement of cesium and mercury ion-atom resonance charge exchange cross section [AIAA PAPER 67-682] 21 p3660 A67-38713
 Neutralizer for large mercury thruster systems using hollow cathode forming plasma bridge neutralizer for large mercury thruster systems using hollow cathode forming plasma bridge [AIAA PAPER 67-871] 21 p3697 A67-38958
 Ion wave dispersion relation in mercury vapor plasma, explaining cut-off frequency dependence on electron drift velocity 22 p3842 A67-39207
 Hollow cathode mercury laser providing improved performance, stability and reproducibility 23 p4016 A67-41226

MERIDIONAL FLOW

Cyclogenetic processes from baroclinic instability occurring in zonal and meridional flow 06 p1027 A67-18602

Northern Hemispheric mean meridional circulation determined, using angular momentum and continuity equations 09 p1490 A67-21549

Variations in position of mirror points of high energy electrons determined from Cosmos V satellite data 10 p1647 A67-23281

Mean meridional motions in biennial wind oscillation in wind structure of low latitude stratosphere 13 p2151 A67-26738

Effect of ozone on mean meridional circulation in upper atmosphere and mesosphere 16 p2666 A67-31098

Cyclogenesis due to baroclinic instability in zonal and meridional basic current showing relationship by superimposing perturbation 19 p3252 A67-35528

Stratospheric mean adiabatic vertical motion and temporal correlations with temperature, isobaric height, zonal/meridional wind and horizontal kinetic energy computed based on seasonal averages 19 p3224 A67-35529

Zonal winds studied by meridional sections from observations made during same months over several years 20 p3480 A67-36965

Large scale eddy terms for balancing mean meridional circulation in winter, discussing terms magnitudes in different latitudes 22 p3828 A67-39326

Photoelectric micrometer for automatic determination of meridian passage times, describing tracking servomechanism and collimation measurements device 22 p3881 A67-39515

Ekman pumping in solar core noting slow meridional-current distribution in spinning core determined by energy balance 24 p4225 A67-41834

MESON

SA BARYON
 SA KAON
 SA MUON
 SA PION

Temperature effect on diurnal variation of meson intensity at high latitudes, finding wave maximum amplitude in spring 05 p0796 A67-16117

Diurnal variation of hard component near minimum solar activity, emphasizing temperature effects 17 p2932 A67-32080

Integral multiplicity calculation procedure for meson component of cosmic rays based on three-dimensional elementary event model, noting meteorological effects 17 p2934 A67-32104

Relationship between geomagnetic storms with sudden commencements and perturbations of southern and northern components of meson distribution in Northern Hemisphere 17 p2938 A67-32796

Cosmic-ultrahigh-energy heavy nuclei and fragmentation products producing multiple mesons 20 p3518 A67-37092

Temperature effect on diurnal variation of meson intensity at high latitudes, finding wave maximum amplitude in spring 24 p4152 A67-42793

MESON-BARYON RESONANCE

Hypothesis of meson resonances produced in cosmic ray interactions, explaining multiple birth characteristics of secondary particles 02 p0314 A67-12745

Algebra of factorized Regge pole residues applied to obtain relations between meson-baryon and baryon-baryon exchange processes 16 p2705 A67-31627

Production of charged double pion in pi plus-proton scattering, noting isobar model failure to explain enhancement at 400 Mev 19 p3266 A67-36100

Hypothesis of meson resonances produced in cosmic ray interactions, explaining multiple birth characteristics of secondary particles 22 p3876 A67-40247

Positive rho meson and doubly positive nucleon-pion resonance generation in 2.34 GeV/c 24 p4193 A67-42856

MESON-NUCLEON INTERACTION

Calculation of neutron generation by mu-mesons for various depths in earth 02 p0312 A67-12607

Nucleon-nucleon interaction - Conference, University of Florida, March 1967 20 p3490 A67-37612

Positive rho meson and doubly positive nucleon-pion resonance generation in 2.34 GeV/c 24 p4193 A67-42856

Negative pion-and proton-nucleon reactions at 17 and 24 GeV/c, using Lobachevskii-Einstein velocity space images method to

obtain kinematics 24 p4193 A67-42858
MESOSPHERE
 Meteorological Rocket Network /MRN/
 probing of stratosphere and lower
 mesosphere and analysis of acquired
 data 02 p0239 A67-12535
 Atmospheric temperature and wind
 velocity in mesosphere measured by rocket
 grenade method 05 p0798 A67-16857
 Book on structure of stratosphere and
 mesosphere noting rocket exploration
 results, synoptic observations, solar control
 over temperature variations,
 etc 07 p1172 A67-19603
 Mean noon profile of mesospheric electron
 number density at 35 degrees S latitude
 preceding solar eclipse 08 p1378 A67-21483
 Rocket measurement of diurnal variation
 of ozone profiles above maximum
 concentration level 10 p1638 A67-23202
 Mesosphere ice point temperature, atomic
 oxygen concentration and total density
 measurement with heat
 recorder 10 p1656 A67-23207
 Measurements of positive ion composition
 of mesosphere and ionospheric D layer from
 rocket experiments 10 p1645 A67-23264
 Possible major effect of minor neutral
 constituents of mesosphere on free electron
 density in D layer 10 p1645 A67-23265
 Ionosphere-stratosphere coupling and
 effect of atmospheric seasonal variations on
 plasma behavior 10 p1645 A67-23266
 Heat radiative flux divergences and
 equilibrium temperature distribution with
 altitude calculated for heat regime modeling
 radiative transfer conditions in stratosphere
 and mesosphere 10 p1647 A67-23275
 Rocket probe measurements indicate
 existence of maximum ion concentration in
 stratosphere and lower ion concentration at
 equator than at
 midlatitudes 10 p1648 A67-23284
 Effect of variation of vertical air density
 profile on relative optical air mass for
 ARDC standard model atmosphere 1959
 compared with
 measurements 10 p1652 A67-23622
 Multiple air scattering in mesosphere as
 function of zenith distance of sun and
 brightness of twilight sky 11 p1785 A67-23957
 Rocket probe measurements indicate
 existence of maximum ion concentration in
 stratosphere and lower ion concentration at
 equator than at
 midlatitudes 12 p1933 A67-25650
 Seasonal variations and attenuation of
 ionospheric absorption, using A3
 method 14 p2312 A67-28570
 Water vapor and atomic oxygen
 concentration in mesosphere measured by
 meteorological rocket 16 p2665 A67-31097
 Effect of ozone on mean meridional
 circulation in upper atmosphere and
 mesosphere 16 p2666 A67-31098
 Mesospheric wind components via rocket
 measurements of Northern and Southern
 Hemispheres, noting semiannual wind
 fluctuation near equator 18 p3030 A67-33552
 Biennial oscillations effect on spring wind
 reversal in stratosphere and mesosphere,
 showing transition date dependence on
 geographical location and
 height 18 p3074 A67-34352
 Mesosphere winds and turbulence
 observed by forming aluminum oxide smoke
 trails 18 p3043 A67-34496
 Mesospheric temperature possible
 relationship to occurrence of noctilucent
 clouds studied using rocket
 soundings 19 p3251 A67-34951
 Density, temperature, water vapor and
 atomic oxygen concentration in mesosphere
 measured by heat method 19 p3216 A67-35183
 Rocket sampling of noctilucent cloud
 particles in mesopause 19 p3216 A67-35194
 Daytime ozone density distribution of
 mesospheric layer measured by using UV
 photometers in rockets 19 p3217 A67-35203
 Quasi-biennial zonal wind and temperature
 oscillation in stratosphere and mesosphere,
 discussing periodicity and oscillation
 model 19 p3220 A67-35272
 Temperature and wind profiles in
 stratosphere and mesosphere during winter
 and summer determined by grenade
 soundings, noting diurnal
 variations 19 p3226 A67-35924
 Stratosphere and mesosphere, discussing
 energetics, energy transfer, ionospheric
 currents, magnetic fields, atmospheric trace

components, solar UV radiation
 measurements, etc 20 p3430 A67-36897
 Rocket measurements above England,
 noting relation of temperature maximum at
 stratopause to mesospheric wind
 maximum 20 p3480 A67-36966
 High velocity tropospheric winds at 40 to
 60 km altitude, discussing supergradient and
 subgradient winds and energy transport to
 mesosphere possibilities 22 p3793 A67-40032
METABOLIC WASTE
SA WASTE DISPOSAL
 Urinary loss of calcium, phosphorus,
 nitrogen, sodium and chloride in men under
 prolonged bed rest at ground level or at
 simulated altitudes 07 p1134 A67-19857
 [SAM-TR-66-296]
 Metabolism of dihydroxyphenylalanine in
 human subjects 09 p1454 A67-21982
METABOLISM
SA ADRENAL METABOLISM
SA CALCIUM METABOLISM
SA CARBOHYDRATE METABOLISM
SA ENERGY REQUIREMENT
SA ENZYME ACTIVITY
SA LIPID METABOLISM
SA OXYGEN CONSUMPTION
SA OXYGEN METABOLISM
SA PHOSPHORYLATION
SA PHOTOSYNTHESIS
SA PROTEIN METABOLISM
 Space flight acceleration, vibration and
 ionizing radiation effects on body functions,
 oxidizing metabolism of central nervous
 system and fission processes of hemopoietic
 tissues 01 p0015 A67-10336
 Bed recumbency effect on ventilatory,
 metabolic and cardiac response to bicycle
 ergometer test, noting possible preventive
 effect of muscular exercises and venous
 occlusion 01 p0016 A67-10949
 Metabolic work requirement of man
 wearing pressure suit and associated
 biomechanical characteristics while
 locomoting on lunar gravity
 simulator 02 p0189 A67-12393
 Metabolic reaction of deer mice to
 temperature and altitude, analyzing various
 enzyme systems 04 p0561 A67-14593
 Subgravity traction simulation experiments
 to determine effects on metabolic rates
 during walking on
 treadmill 05 p0755 A67-16280
 Closed ecological systems and endogenous
 formation of CO in plant and animal
 tissues 07 p1136 A67-19107
 Adapted Mueller-Franz portable breath-
 powered respirometer utilizing scuba-gear
 for measuring underwater
 metabolism 09 p1455 A67-21722
 Bronchial tube diameter makes possible
 alveolar ventilation with minimum
 metabolism or entropy production in
 musculature 09 p1454 A67-21986
 Genetic transcription as affected by
 ionizing radiation and hydrogen
 peroxide 11 p1747 A67-24786
 Cardiac changes under hypoxia,
 experimental morphological
 study 13 p2058 A67-26756
 Metabolic rates during lunar gravity
 simulation 13 p2062 A67-26922
 Plants in low gravity environment
 simulated by 2 rpm clinostat with horizontal
 axis, studying growth direction and
 respiratory metabolism 15 p2426 A67-29114
 Rats exposed to simulated altitude studied
 for acute changes in iodine metabolism,
 noting dichotomy between thyroidal iodine
 uptake and secretion
 rates 15 p2428 A67-29279
 Physiological reaction of human body to
 applied stimuli, developing method
 evaluating metabolism 16 p2612 A67-30907
 Water-salt metabolism changes during
 prolonged confinement in bed following
 exposure to acceleration indicating
 dehydration and
 decalcification 16 p2613 A67-30916
 Biostasis /suspended animation/ by frozen
 storage investigated for application to
 interstellar voyages, noting possible damage
 prevention during space
 trips 19 p3181 A67-35325
 Hypokinesia effects on nitrogen
 metabolism of rats 20 p3368 A67-36261
 Synthesis of single cycle of natural
 metabolic processes to be used as basis of
 space-vehicle self-sufficient life support
 systems 20 p3368 A67-36262
 Autotrophic and heterotrophic carbon

dioxide fixation regulation in
 Hydrogenomonas, discussing two Calvin cycle
 enzymes 20 p3370 A67-36797
 Factors involved in use of thymine by
 uninfected cells in metabolism of
 Escherichia coli 20 p3370 A67-36799
 Oxidative phosphorylation effects on
 energy metabolism of Thibacillus thioparus
 in cell-free system 20 p3371 A67-36927
 Chronic hypercapnia effects on pH level,
 Ca and P metabolism and electrolyte
 metabolism in normal sedentary
 man 23 p3955 A67-41605
 Physical capabilities and work potential of
 man in terms of physiological elements and
 methodology 23 p3959 A67-41662
 Origin of life on earth, formation of
 nucleic acid molecules and metabolic
 mechanism 24 p4112 A67-42052
METAL
SA ALKALI METAL
SA ALKALINE EARTH METAL
SA ALLOY
SA ANTIMONY
SA BARIUM
SA BERYLLIUM
SA BISMUTH
SA BORON
SA CADMIUM
SA CALCIUM
SA CERIUM
SA CESIUM
SA CHROMIUM
SA COBALT
SA COPPER
SA DYSPROSIUM
SA EUROPIUM
SA FUSED METAL
SA GADOLINIUM
SA GALLIUM
SA GERMANIUM
SA GOLD
SA HAFNIUM
SA HOLMIUM
SA INDIUM
SA IRIIDIUM
SA IRON
SA LANTHANIDE
SA LANTHANUM
SA LEAD
SA LIGHT METAL
SA LIQUID METAL
SA LITHIUM
SA MAGNESIUM
SA MAGNETIC METAL
SA MANGANESE
SA MERCURY /METAL/
SA MOLYBDENUM
SA NEODYMIUM
SA NICKEL
SA NIOBIUM
SA NOBLE METAL
SA NONMETAL
SA NOTCHED METAL
SA OSMIUM
SA PALLADIUM
SA PLATINUM
SA PLUTONIUM
SA POLISHED METAL
SA POTASSIUM
SA POWDERED METAL
SA RARE EARTH
SA REFRACTORY METAL
SA RHENIUM
SA RUBIDIUM
SA RUTHENIUM
SA SAMARIUM
SA SCANDIUM
SA SHEET METAL
SA SILVER
SA SODIUM
SA STRONTIUM
SA TANTALUM
SA THORIUM
SA TITANIUM
SA TRANSITION ELEMENT
SA TUNGSTEN
SA ULTRAPURE METAL
SA URANIUM
SA VANADIUM
SA YTTERBIUM
SA YTTRIUM
SA ZINC
SA ZIRCONIUM
 Physical properties of metals influence on
 friction, adhesion, wear and welding
 tendency in vacuum 03 p0428 A67-13271
 Single crystal whisker composite
 methodology in plastics, metals and
 ceramics, emphasizing alignment and
 handling problems 03 p0453 A67-13410

Plastic deformation of isotropic tubular samples of steel, brass, copper and duralumin under complex loading at constant stress rate 03 p0530 A67-14169

Book on dynamic strength, brittleness, plasticity and ductility of metals 05 p0907 A67-16031

Unfamiliar metals properties and potentialities from viewpoint of metallurgist 05 p0830 A67-17088

Reliability and temperature stability of metals used for contacts and interconnections on semiconductor devices 06 p0971 A67-18246

Phase and structural transformations in metals and alloys studied with aid of exoelectronic emission 07 p1201 A67-19257

Energy balance criteria during slow crack growth and at inception of catastrophic rupture in high strength ductile metals, noting necking phenomena in tensile test 08 p1421 A67-20953

Metal deficiencies, UV excesses and other color anomalies in solar type disk population stars 08 p1400 A67-21249

Simulation of stress-strain state of metal under elastoplastic deformation, based on models used in polarization-optical techniques, analyzing stresses in high polymers 08 p1423 A67-21330

Elastoplastic properties of copper, aluminum alloys and brass under explosive load, noting increased temperature effect on elastoplastic wave parameters 10 p1668 A67-23092

Book on electron radiation damage in semiconductors and metals covering lattice defects, alloys, atom displacement, EPR testing, etc 12 p1986 A67-25890

Effect of metals and alloys on thermal stability of Avtur 50 aviation kerosene from ASTM-CRC and high temperature coker tests 13 p2185 A67-26703

Beryllium and other hexagonal metals mechanical properties compared under neutron irradiation, elucidating causes of beryllium embrittlement 13 p2135 A67-27102

General model for semiconductor-to-metal transition 13 p2180 A67-27163

Metal-to-semiconductor transition measurements of hydrostatic pressure shift and uniaxial stress of temperature 13 p2180 A67-27164

Physical properties of metals influence on friction, adhesion, wear and welding tendency in vacuum 14 p2324 A67-28000

Electromagnetic wave propagation, excitation and dispersion in metals in magnetic field 14 p2366 A67-28426

Transitional impurity effects on superconducting critical temperature of normal metals, stressing localized states with no magnetic moments 14 p2371 A67-28727

Thermoelectric power increase in low temperature metals not explained by residual resistivity in simple model calculation 15 p2540 A67-30096

Phonon drag part of thermoelectric power in metals formula, by assuming electron scattering description by relaxation time 16 p2731 A67-31445

Thermal conductivities below one degree K of various very pure metals, noting normal and superconducting states 17 p2912 A67-32265

Current-voltage characteristic of metal semiconductor point contact, taking into account rectifying effect of junction gap and majority and minority current carrier 18 p3097 A67-33476

Book on electrodeposition of metals in ultrasonic field, discussing effects on electrode potentials, concentration polarization, deposition rate, etc 19 p3235 A67-34914

Diffusion saturation methods of alloy surfaces by metals and metalloids classified by physicochemical characteristics of active phase of diffusing element 19 p3242 A67-34916

Collection of papers of high purity metals and alloys, discussing properties fabrication and testing 19 p3243 A67-34923

Dimensional changes of metals under simultaneous effects of thermal cycling and external load due to surplus point defects directional displacement 19 p3244 A67-34929

Reports on progress in physics, Volume 29, Part I, covering creep in metals and plasma spectroscopy 19 p3263 A67-35853

Logarithmic, diffusion and high

temperature creep in 19 p3248 A67-35854

metals 19 p3248 A67-35854

Development of Indian sources of aerospace metals evaluated, noting availability, potential, priority of materials and research facilities 20 p3464 A67-36187

Electromagnetic properties of metal considered for strong quantization of electron states in magnetic field 20 p3464 A67-36224

Metal mechanical properties determination during deformation by uniform ultrasonic loading 21 p3722 A67-38450

Metal creep behavior under step function stress application including elastic and plastic deformation 23 p4018 A67-40717

METAL ALLOY

S ALLOY

METAL BONDING

Titanium carbide coating depositions on steel and subsequent annealing redistribution of elements in interface 01 p0093 A67-10301

Ultrahigh vacuum installation using ion-getter pumps for analysis of adhesion between plastics and metals in space environment 02 p0228 A67-11552

Bonding mechanism between metals and ceramics, noting glass penetration theory 02 p0255 A67-12060

General and mechanical property requirements for metal matrix composite materials used for aircraft gas turbine compressor blades 03 p0443 A67-13418

Metal addition effect on grain growth of matrix oxides, noting inhibitive results in most cases 04 p0642 A67-15086

Antonov An-24V Soviet high wing monoplane and use of electrical spot welding and metal bonding in construction 06 p0944 A67-17597

Adhesive types and characteristics suitable for aluminum bonding 06 p1020 A67-18062

Cold hardened metal adhesive /Agomet E/, discussing polymerization, pot time, setting and temperature 07 p1193 A67-20291

Design of three types of bonded metal-to-metal joints, discussing advantages of theoretical over empirical methods 09 p1576 A67-22501

Single stage bonding of tapered aluminum honeycomb panels employing wrap-around skins and nonperforated core 09 p1507 A67-22507

Adhesive bonding of solid propellants in rocket motors, emphasizing propellant liner interface and bonding at interface 09 p1578 A67-22514

Polybenzimidazole /PBI/ structural adhesives for bonding stainless steel, beryllium and titanium 09 p1523 A67-22517

Mechanical properties of polybenzimidazole resin show suitability for metal-to-metal and sandwich composite adhesives and high and cryogenic temperatures 09 p1523 A67-22518

Surface preparation for aluminum and bond strength dependence on cure temperature, humidity and impurities 09 p1507 A67-22519

Metal surface preparation by mechanical and chemical processing for adhesive bonding 09 p1507 A67-22520

Bond strength of magnesium alloys as affected by surface preparations, specific alloy and adhesive type 09 p1507 A67-22521

Structural adhesives for fabricating large one-piece hemispherical bulkheads, noting effect of radiation and high vacuum 09 p1578 A67-22523

Adhesive systems for substructure bonding to solid ablators and to honeycomb operating in extreme environments 09 p1578 A67-22524

Ultrasonic spot welding of dissimilar metals, discussing bond mechanisms and threshold curves relating clamping force, power level and weld strength 12 p1950 A67-25737

Fracture toughness of 7075-T6 and -T651 sheet, plate and multilayered adhesive bonded panels, showing independence of thickness and number of layers [ASME PAPER 67-MET-4] 12 p1956 A67-25948

Dynamic and physical testing of metals, discussing yield point, plastic deformation and oscillation damping characteristics 13 p2215 A67-26452

Book on adhesive bonding Alcoa aluminum covering techniques, applications including

aircraft and military uses, classifications, etc 13 p2143 A67-27177

Heat removal from high density packaged electronics by bonded metallic heat sink [ASME PAPER 67-DE-47] 14 p2408 A67-28880

Metallic couples ultrahigh vacuum adhesion experiments show contaminant dispersal as major barrier 15 p2492 A67-29493

Metallic adhesion between Mo-Mo and Ti-Ti couples, showing contact resistance useful in determining contamination at conducting interface 17 p2871 A67-32465

Steady thermal strains measurement in aero and industrial turbine and engine components, discussing fine wire behavior, bonding agent, performance, requirements, etc 18 p3143 A67-33900

Semimonocoque aluminum alloy glider design features, recommending integral construction with metal bonding or combination metal bonding and riveting 18 p3054 A67-34374

Flip-chip bonding and dimensional transformation, low cost microcircuit production technique 18 p3014 A67-34549

Properties of adhesive bonding compared with spot welding and riveting in aircraft industry 19 p3236 A67-35821

Surface treatment of metal to ensure strength of bonded joints, discussing causes of aluminum-alloy corrosion during pickling 19 p3237 A67-35822

Drawing technique for bundles of sheathed superalloy wires noting sheathing, stress relief, interfilament welding and oxide bonding 21 p3643 A67-37878

Mechanical thermal pulse techniques for precision bonding, emphasizing band and join type connection and bonding to unstripped plastic insulated wires and cables 21 p3635 A67-38625

Visual characteristics of welded wire joints, discussing correlation with metallurgical and mechanical properties 21 p3636 A67-38631

Polyt IV glider wing noting bonded aluminum sheet/honeycomb sandwich shell 22 p3811 A67-39302

Electroplating for fabricating fibrous composite materials noting advantages of low temperatures and absence of mechanical working 22 p3819 A67-39560

Adhesives to bond metal linings to filament-wound cryogenic pressure vessels evaluated by test series simulating fabrication and service conditions 23 p4010 A67-41347

Fabrication under tensile stress of large double contour composite structures, obtaining improved bonding [ASM PAPER C6-21.2] 23 p4010 A67-41410

Adhesive system for structural bonding of fiberglass reinforced polyester to itself and to metal 24 p4175 A67-42421

METAL CARBIDE

RF spark source mass spectrometer to detect and identify trace amounts of vapor molecular carbide species for refractory metal carbides 03 p0367 A67-13228

Superconducting critical temperatures of nonstoichiometric transition metal carbides and nitrides, correlating data with valence electron concentration 03 p0491 A67-13256

Superconductivity and transition temperature of technetium and technetium carbide 05 p0860 A67-16389

Reduced thermodynamic potentials of large classes of refractory metal carbides and nitrides 11 p1804 A67-23901

Electric, thermal and physical properties of pyrolytic carbides and nitrides of group IV metals 11 p1804 A67-23903

Hall effect and electrical resistance of ZrC-NbC and TaC-HfC alloys at room temperature 11 p1804 A67-23904

Superconductivity transition temperatures of metal carbides, showing stoichiometry as main feature for maximum temperature 19 p3303 A67-35040

Cesium vapor treatment effect on work function of high melting Ta and Zr carbides, evaporation products and graphite 19 p3176 A67-35080

Group IV and V metal carbides ball-milled to determine mechanical strain effects 20 p3467 A67-37122

METAL COATING

Coatings of nickel, chromium and Cu on SiC and aluminum oxide whiskers by electroforming and metalizing, using electron microscope

techniques 03 p0444 A67-13434
Schottky barrier photodiodes with
antireflection coating on metal film for fast
and efficient optical
detectors 04 p0582 A67-15078
Coated filaments effect in controlling
composite microstructures for several metal-
graphite and metal-boron systems
[AIAA PAPER 67-175] 06 p1019 A67-18441
Thermal properties and environmental
stability of barrier layer anodized aluminum
surfaces in space, noting emittance and
absorption values 10 p1671 A67-23744
Fiber reinforced metal coating by passing
silica through molten aluminum, discussing
freezing by radial conduction of heat into
fiber 12 p1954 A67-25292
Electrophoretic coating of metals
compared with cathodic and anodic
synthetic depositions 18 p3054 A67-34098
Plasma arc deposition and gas pressure
bonding technique for producing defect-free
uniform iridium protective coatings for
graphite reentry
structures 20 p3465 A67-36607
Destructive and nondestructive testing of
thickness of oxide coatings on Al and Al
alloys 22 p3798 A67-39552

METAL COMBUSTION

SA SOLID PROPELLANT IGNITION
Metal fiber addition to basic propellant
increases burning rate 05 p0872 A67-17215
Techniques for study of metal combustion
in rocketry including particle burning, bulk
metal and metal vapor combustion and low
temperature oxidation
[AIAA PAPER 67-66] 06 p1072 A67-18437
Aluminum particle combustion in solid
rocket grains, noting drop formation
mechanism and droplet combustion analysis
[ONERA-TP-486] 17 p2926 A67-32697
Heterogeneous reaction in metal
combustion for vapor-phase burning noting
collision efficiency 18 p3149 A67-33797
High temperature kinetics of bulk
beryllium metal combustion in hydrogen-
oxygen-water vapor system, studying flame
environments, thermal balance,
etc 18 p3151 A67-33809
Spectral brightness of metal chelate liquid
fuel-air flames
[CI PAPER 67-2] 19 p3309 A67-34997
Aluminum particle combustion noting
changes from preignition to burnout, flame
structure, particle geometry, etc
[WSCI PAPER 66-3] 22 p3919 A67-40224
Technical feasibility of rocket propellant
combinations involving metal combustion and
chemical heating of excess
H 24 p4206 A67-42403

METAL COMPOUND

SA ORGANOMETALLIC COMPOUND
Internal friction in 18 percent Ni maraging
steel noting rapid dislocation recovery,
independence of temperature and age
hardening characteristics 05 p0828 A67-16468
Chemical behavior of metallic elements
predicted by periodic table, noting formation
of liquid and solid metallic solutions, binary
and complex metallides and nature of
chemical bond 06 p1018 A67-18233
Semiconductor-to-metal transitions in
transition metal
compounds 13 p2181 A67-27165
Alloying volatile metals with refractory
metals in Nb-Zn system, noting thermal
analysis and microhardness
determination 19 p3243 A67-34926
Composite technology emphasizing fiber-
reinforced metal matrix composites,
discussing filaments, plastics, ceramics,
fabrication methods, etc 21 p3643 A67-37953
New semiconductor compounds derived by
cross substitution of group IV
semiconductors, giving thermal properties
and phase diagrams 23 p4036 A67-40720

METAL CORROSION

Corrosion detection of metal surface
under protective coating, using beta
radiation probe 02 p0245 A67-12218
Simplified neutron activation technique
for analyzing metallic wear from aircraft
hydraulic systems, computing activities of
desired radioisotopes by cookbook
procedure 02 p0249 A67-12221
Impurity effect /primarily O/ in reactions
between liquid alloys and solid metals
undergoing deformation 06 p1017 A67-17951
Corrosion tests of W-, Mo-, Rh-based
materials for compatibility in lithium at
2500, 2800 and 3000 degrees

F 07 p1208 A67-19466
Corrosive media effects on fatigue
strength and endurance limits of three Al
alloys used in aircraft
components 08 p1341 A67-20598
Oxygen solubility in fused carbonates and
corrosion behavior of Ag and Cu oxide, air
and carbon dioxide cathodes in molten
carbonate fuel cells 09 p1458 A67-22182
Metallurgical and fluid dynamic results of
2000-hr endurance test at high temperatures
on two-stage 200 hp turbine in wet
potassium vapor
[ASME PAPER 67-GT-9] 11 p1745 A67-24797
Simple and stress corrosion problems in
aircraft design emphasizing protection of
joints 12 p1954 A67-25127
Qualitative and quantitative prediction of
corrosive environments effects on
transducer performance
[ASME PAPER 67-MET-14] 12 p1945 A67-25952

Beryllium corrosion in carbon dioxide
under pressure at high
temperatures 13 p2136 A67-27108
Book on stress corrosion of metals
covering mechanisms, resistance techniques
and tests 13 p2141 A67-27174
Corrosion of metals by flowing liquid
fluorine compounds 13 p2143 A67-27688
Stress corrosion resistance and control for
aluminum alloys, noting types, causes and
methods 14 p2335 A67-27806
High temperature corrosion and
evaporation of Haynes 25 and Hastelloy X-
280 in atmospheres of oxygen, carbon
monoxide, carbon dioxide, water vapor and
methane 14 p2336 A67-28148
Liquidus curves of various metals with
mercury at high temperatures, obtaining
corrosion rates and data on grain boundaries
penetration 15 p2502 A67-29261
Cladding effect on corrosion resistance
and fatigue behavior of duralumin, noting
role of alternating stresses in cladding
layer 15 p2504 A67-29827
Ultrahigh vacuum and air fatigue testing
of aluminum alloy observing corrosion
process influence on mechanism by
latter 16 p2689 A67-31369
Hydrogen coverage at metal surface
during dissolution in corrosion
process 18 p3066 A67-34368
Atmospheric corrosion resistance of
titanium alloys 18 p3068 A67-34579
[ASTM PAPER 31] 20 p3465 A67-36634
Book on light metals
corrosion 20 p3465 A67-36634
Aluminum corrosion behavior stressing
surface oxide film
condition 20 p3465 A67-36635
Beryllium corrosion occurrence, causes,
effects, prevention and advantages over
steel and aluminum 20 p3465 A67-36636
Magnesium and magnesium alloy corrosion,
discussing treatments for prevention of
various kinds of corrosion 20 p3468 A67-36637
Titanium susceptibility to corrosion,
achieving protection by passive self-healing
films forming on metal
surface 20 p3466 A67-36638
Automatic apparatus for flooding or
spraying test specimens with liquid
corrosive media according to predetermined
program 21 p3715 A67-37827
Performance of wide variety of
exceptional metals studied for corrosion and
temperature resistance characteristics in
atomic power application 23 p4018 A67-40899

METAL CRYSTAL

Carbon diffusion in refractory metals with
bcc lattice at temperatures of 1100 to 1600
degrees C, considering activation energy and
frequency factor 01 p0101 A67-10937
Degree of strain effect on kinetics of
recrystallization of nickel and niobium
monocrystals investigated by electron beam
fusion in vacuum 01 p0101 A67-10940
Crystal orientation of grains during fatigue
and plastic deformation analyzed on copper
using X-ray diffraction, noting crystal
behavior 02 p0254 A67-11467
Soviet monograph on vacuum arc melting
of titanium alloy ingots noting crystallization
process, structural changes and properties of
end-products 03 p0447 A67-13925
Test on nickel and aluminum of Bailey-
Orowan equation in relation to work
hardening and recovery in
creep 04 p0640 A67-15623
Flow characteristics of Fe single crystals

and behavior of
imperfections 04 p0640 A67-15793
Soviet papers on growth and imperfections
of metallic crystals 05 p0826 A67-16074
Electron beam zonal fusion growth of Mo,
W and Ta single crystals without using
crucible 05 p0827 A67-16079
Dislocation mechanisms for prismatic and
basal slip in Ti at low temperatures,
measuring critical shearing stress and
temperature dependence of activation
volume 05 p0828 A67-16467
Growth condition effect on perfection of
single crystals of niobium examined, using
X-ray diffraction
techniques 05 p0828 A67-16470
Ternary alloys compounded with Ti, Zr,
Hf, Fe, Ni, Co, Cu, Al, Ga, noting crystalline
structures 05 p0830 A67-16919
Structures of divalent and trivalent metals
in terms of pseudopotentials and second
order perturbation theory 05 p0869 A67-17189
Metal resistivity change due to multiple
point imperfections and lattice distortions,
noting aggregate effect estimation from
scattering power of isolated
defects 05 p0830 A67-17190
Recrystallization and polygonization of
pure and impure metals, noting role of
vacancy supersaturation 05 p0830 A67-17311
Sputtering yields of aluminum, copper and
titanium measured as function of cesium ion
energies for use as electrodes on cesium ion
engines
[AIAA PAPER 66-203] 05 p0871 A67-17349
Tantalum interaction with nitrogen and air
show retardation of grain
growth 05 p0832 A67-17507
Hardness, microhardness, electric
resistance and toughness results tabulated
for polycrystalline nonalloyed
molybdenum 05 p0832 A67-17510
Metal single crystal use in structural
design of stress resisting
devices 06 p1013 A67-17795
Metallographic, X-ray and electron
microscope studies of dislocation
substructure and fatigue life extension in
bending-fatigued Al and Ag
crystals 06 p1013 A67-17798
Manganese aluminide precipitation effect
on primary recrystallization in metal
systems, indicating softening processes in
metals 06 p1015 A67-17810
Electron microscopic structure and lattice
defects of martensite in commercially pure
titanium 06 p1017 A67-17966
Transformation twins in titanium,
discussing relationship between twins and
martensite crystal, using electron
microscopy 06 p1017 A67-17967
High temperature condensed phase
equilibria in Ti-W-O system examined, using
sealed capsule technique 06 p1018 A67-18371
Metallic fibers development, noting
research for continuous filaments, whiskers,
staple fibers, materials, strength,
etc 06 p1019 A67-18558
Thermally activated deformation relating
flow stress to square root of dislocation
density 06 p1053 A67-18755
Small additions of refractory elements
effect on structure and properties of sheets
of Al-Zn-Mg alloy in various
states 07 p1201 A67-19254
Small additions of refractory elements
effect on structure and properties of
aluminum alloy castings containing Zn and
Mg 07 p1201 A67-19255
Specific stacking fault energy of deformed
fcc metals determined from electron
microscope diffraction contrast of stacking
fault dipoles 07 p1208 A67-19637
Dislocation theory of slip geometry and
temperature dependence of flow stress in
bcc metals 07 p1209 A67-19641
DC resistivity due to electron scattering
from vacancy, octahedral and tetrahedral
interstitials in beryllium computed by
diffraction model concept of
pseudopotentials in metal
theory 07 p1209 A67-19643
Structure of rolling texture of bcc metals
and alloys under various external
deformation conditions 07 p1210 A67-20107
X-ray line broadening in deformed
magnesium by Fourier analysis of line
shapes and analysis of line widths, noting
lattice distortion 07 p1210 A67-20108
Strain rate dependence of critical shear
stress in cadmium single crystals used in

activation energy
determination 07 p1234 A67-20109

Chondrite metallic minerals, thermal history and parent planets noting nickel, taenite and kamacite crystal components 08 p1397 A67-21207

X-ray structural and spectral analysis of changes in lattice constant, linear expansion coefficient and K-absorption edge of iron and manganese in ferrite with spinel structure 08 p1372 A67-21492

Single crystal film structure of fcc metals evaporated in ultrahigh vacuum onto alkali halide surfaces cleaved in air and in situ 09 p1552 A67-21671

Eutectic alloys of heavy metal phases with InP compound analyzed, noting phase orientation parallel to solidification direction 09 p1552 A67-21880

Anisotropy of electronic metal work functions for zero and high electric fields perpendicular to surface measured by field emission and thermionic techniques 09 p1450 A67-22356

Tensile strength and cross sectional area measurement of aluminum oxide whiskers 10 p1669 A67-23326

Eutectics use in composite material by growing single crystal whiskers aligned inside matrix 10 p1669 A67-23637

Stress corrosion cracking of titanium alloys, noting tensile test data, crack propagation in salt solution and in pure solvents and metallurgical and electrochemical factors 10 p1670 A67-23701

Hydrostatic pressure effect on surface microstructure, dislocation substructure and stress-strain behavior of beryllium 11 p1805 A67-24110

Entropy function relationship to properties of pure metals, noting correlation with lattice parameters at 298 degrees K 11 p1805 A67-24360

Temperature dependence of elastic constants of molybdenum single crystals measured, using thin rod resonance techniques 11 p1809 A67-24908

Stress and temperature dependence of motion of edge dislocations in nickel single crystals 11 p1809 A67-24920

Direct observation on precipitation and aging behavior in Cu-Ti alloys by transmission electron microscopy 11 p1809 A67-24948

Deformation of crystalline solids - Conference, Ottawa, August 1966, Part 2 11 p1810 A67-25089

Failure mode at tip of crack predicted using cleavage strength and shear strength of perfect crystals, noting tungsten and iron 11 p1880 A67-25090

Mechanical properties of zone melt molybdenum single crystals as affected by orientation and gas impurities 11 p1810 A67-25092

Beryllium single crystal dislocation and twinning induced by compression deformation 11 p1810 A67-25093

Alloy 718 composition, microstructure and heat treatment behavior correlated with mechanical properties, noting strengthening and oxidation resistance [ASME PAPER 67-MET-5] 12 p1956 A67-25949

Temperature dependence of bcc metals elastic limit at low temperature, assuming sessile-dissociated screw dislocations formation during microdeformation, stressing stacking fault energy effect 13 p2130 A67-26438

Soviet papers on mechanism of metal breakdown 13 p2130 A67-26446

Stress dependence of dislocation configuration in deformed niobium 13 p2133 A67-27010

Dislocation velocity measurements and thermally activated motion in molybdenum 13 p2133 A67-27011

Electron microscope observations on matrix precipitation in beryllium 13 p2136 A67-27106

Dynamics of beryllium lattice noting dispersion curves of wave frequencies 13 p2137 A67-27109

Plastic behavior of zone refined and prestrained beryllium single crystals 13 p2137 A67-27111

Microstrain c-axis compression test on two Be-4.37 wt percent Cu crystals, detecting nonbasal pyramidal slip system and compression twinning 13 p2137 A67-27114

Transmission electron microscopy of dislocation structure produced in beryllium by specific deformation 13 p2138 A67-27116

Electron microscope study of cold working and tempering of beryllium single crystals 13 p2138 A67-27117

Ternary alloys compounded with Ti, Zr, Hf, Fe, Ni, Co, Cu, Al, Ga, noting crystalline structures 14 p2337 A67-28259

Molybdenum ductility improvement by electrowinning with yttrium 14 p2338 A67-28616

Amplitude dependence of energy dissipation due to internal friction in metals and alloys of various lattice types under near-resonance loading 15 p2504 A67-29970

Propagation of shear acoustic waves traveling parallel to magnetic field along symmetry direction in metal crystal 16 p2731 A67-31446

Soviet book on study of defects of crystalline structure of metals and alloys including X-ray analysis of aluminum single crystals, radiation effects on niobium, etc 17 p2874 A67-32894

X-ray spectral analysis of bent aluminum single crystals with crystallographic plane parallel to reflecting surface of crystal 17 p2874 A67-32895

Barium adsorption on individual crystal planes of tungsten field emitter studied for thermally equilibrated and unequilibrated adsorbate layers 17 p2922 A67-33259

Pressurization produced free dislocations effect on yielding and fracture in bcc metals 18 p3063 A67-33484

Magnetic field effect on Hall coefficient of p-type Ge-Si single crystal alloys 18 p3098 A67-33574

Field ion microscopy of Ni-Mo alloys 18 p3065 A67-34364

Growth rate of oxide and other dielectric contact films on metal crystals computed for ionic diffusion and electron tunneling 18 p3103 A67-34590

Particle growth during coalescence of fine phases of metallic alloys 19 p3245 A67-35469

Fractional order peaks in low energy electron diffraction /LEED/ patterns from single crystal metal surfaces 19 p3246 A67-35783

Nickel aluminide structure, examining arrangement of Ti, Cr and W in lattice via X-ray spectroscopy 20 p3467 A67-37116

Niobium and niobium alloy structural changes during heating after pressing and rolling deformation 21 p3644 A67-38031

Tantalum interaction with nitrogen and air show retardation of grain growth 21 p3644 A67-38035

Hardness, microhardness, electric resistance and toughness results tabulated for polycrystalline nonalloyed molybdenum 21 p3644 A67-38038

Spontaneous decomposition of helical dislocations in metal crystal into row of pinched-off loops plus straight dislocation line 21 p3677 A67-38092

Surface states effect on frequency dependence of elements of equivalent circuit of n-type semiconductor/metal contact 22 p3859 A67-39578

Elastic constants and interatomic interaction parameters of niobium alloyed with tantalum, titanium and vanadium 22 p3820 A67-39789

Carbon diffusion in refractory metals with bcc lattice at temperatures of 1100 to 1600 degrees C, considering activation energy and frequency factor 22 p3820 A67-39791

Degree of strain effect on kinetics of recrystallization of nickel and niobium monocrystals investigated by electron beam fusion in vacuum 22 p3820 A67-39793

Twinning and low temperature mechanical properties of high purity polycrystalline niobium and molybdenum, discussing grain size effects 22 p3823 A67-40208

Aluminum-magnesium alloy dislocation networks structure and formation investigated by thin foil technique after rapid solidification 23 p4017 A67-40658

Ti additive effect on aluminum oxide particle growth in Ni matrix from 1000 to 1350 degrees C 24 p4171 A67-41959

Thermal vacancies in Ni-Al investigated by comparing separately determined dilatometric and lattice parameter of /100/ single crystal 24 p4173 A67-42165

METAL CUTTING

Cutting and milling processes in aeronautical industry, effect on costs and production rates 03 p0427 A67-13024

Thermal field of cutting area of aircraft structural material analyzed, using differential equations of thermoconductivity 03 p0427 A67-13191

Thermodynamics of metal cutting process, assuming plastic deformation accompanied by successive melting and solidification of metal area under deformation 03 p0427 A67-13192

Classification of experimental methods used in analysis of thermal phenomena during metal cutting 03 p0427 A67-13194

Determining dependences of criteria for metal cutting processes from studies of thermal effects 03 p0428 A67-13195

Wheel trimming quality effect on thread grinding temperature for aircraft materials 03 p0428 A67-13196

Cutting temperature and heat distribution in cutting tool and blank in superhigh speed cutting process for deformable aluminum alloys 03 p0428 A67-13197

Cut-off turning test on 40 mm Al bar, effect of mineral oil and kerosene on cutting depth and speed and of feed on tangential force and chip size 11 p1809 A67-24945

Heat flux requirements for cutting low-plasticity metal sheets on lathe, noting thermal effect 14 p2325 A67-28654

Machinability of high strength steels, titanium alloys and refractory alloys, examining cutting and RF current induction for heat treatment 15 p2505 A67-30128

Book on machining Alcoa aluminum covering Al alloys properties, requirements for machine tools, cutting conditions and compounds, finishing operations, etc 18 p3053 A67-33771

Plasma arc for high quality cutting and piercing of thick metals 20 p3456 A67-37694

Machines and machining technology for materials used in Mach-3 aircraft structures, discussing cutting fluids, cutter and best metal removal rate 21 p3631 A67-38014

Photoelectric device measuring cutting-tool temperature for automatic control of state of cutting edges 21 p3626 A67-38059

Computer controlled metal cutting, discussing prospects, difficulties and need for systematic mathematical study 21 p3637 A67-38920

Photoelectric method for measuring temperatures in metal cutting 21 p3631 A67-38921

Plastic deformation during metal cutting, deriving metal deformation, cutting tool stressed state and temperature as function of particle trajectories 21 p3637 A67-38923

METAL FATIGUE

Rolling-element bearings design and material processing for special conditions, noting stress and fatigue 01 p0079 A67-10726

Fatigue strength of riveted joints as affected by material properties, rivet placement and fabrication method 03 p0521 A67-13023

Titanium alloy forging tests covering notched tension, compression, shear, bearing, fracture toughness and smooth and axial fatigue 03 p0446 A67-13552

Fatigue mechanisms for fcc metals and alloys, reviewing research on crack initiation and propagation 03 p0447 A67-13800

Fatigue cracks and fatigue cycles effect on brittle fracture behavior of annealed 4140 steel [ASME PAPER 66-WA/MET-17] 04 p0639 A67-15332

Protecting turbomachinery from unstable and oscillatory flow, noting resonance effect [ASME PAPER 66-WA/GT-13] 04 p0690 A67-15370

Shearing stress failure theory for high cycle fatigue employing rotating principal stress axes and nonsynchronous stresses [ASME PAPER 66-WA/MET-9] 04 p0712 A67-15374

Fatigue strength of smooth and notched steel samples subject to bending in single plane, discussing effect of form of stress cycle on failure rate 05 p0923 A67-17181

Fatigue crack propagation in sheet metal, noting usefulness of McClintock formula 05 p0924 A67-17332

Fatigue crack growth in metal due to plastic deformation, predicting crack growth

coefficient 05 p0924 A67-17333
Fiber diameter, length and discontinuity effects on fatigue properties of fiber-reinforced metal 06 p1099 A67-17712
Endurance and creep of chromium steels with extended thermal treatment 06 p1018 A67-18228
Crack growth rate and measurements of temperature effect on low pressure fatigue of Al 06 p1019 A67-18561
Mechanical properties of alloys in descriptive approach, noting data on precipitation hardening, plastic strain and creep 07 p1211 A67-20176
Monograph on creep and creep rupture as applied to aeronautics field noting problems in boundary and initial value, stability, stressed state, etc 07 p1264 A67-20301
Test method for metal resistance to thermal fatigue under active creep conditions 09 p1519 A67-22168
Correlation among room temperature creep stresses, fatigue and proportional limit in titanium alloys 10 p1669 A67-23325
Random-loading fatigue crack growth behavior of airframe aluminum and titanium alloys under sinusoidal, narrow band and broad band random loading 10 p1669 A67-23434
Flight load maneuver data for fatigue evaluation of F-4 series aircraft 10 p1594 A67-23435
Scatter factor for fatigue life of aluminum aircraft structures subjected to identical loading histories 10 p1594 A67-23436
Bending fatigue tests of unmachined, mechanically machined and chemically machined panels of aluminum and titanium alloys 10 p1669 A67-23437
Roll fatigue tests of forged ZK60A-T5 magnesium and 2014-T6 aluminum wheels 10 p1661 A67-23439
Satellite material problems in corrosion, fatigue failure, vacuum degradation, etc 10 p1670 A67-23740
Constant-amplitude reverse bend stress fatigue testing device for extreme high vacuum, testing aluminum 10 p1658 A67-23781
Nickel-base alloy static and dynamic creep test, examining fatigue zone fracture surface 11 p1806 A67-24364
Metallurgical investigations by electron microscopy of rolling contact fatigue, elucidating mechanisms of failure due to shearing stress 12 p1954 A67-25329
Double cantilever beam specimen for determining plain strain fracture toughness of metals 12 p1956 A67-25946
ASTM 1964 references on fatigue 12 p2032 A67-26093
Soviet papers on mechanism of metal breakdown 13 p2130 A67-26446
Temperature and environmental effects on mechanical behavior of metals 13 p2132 A67-26697
Metal matrix composite fatigue behavior in tension-tension loading as function of volume fraction 14 p2337 A67-28422
Dynamic components thermal characteristics determination by IR optic techniques, studying metal fatigue, wear and friction phenomena 14 p2328 A67-28873
Intermediate principal stress effect on fatigue of thick wall steel tubes under triaxial stresses 15 p2573 A67-29402
Creep behavior of materials in nuclear reactors, gas turbines and electric power plants, noting aluminum alloy and high temperature material fatigue 15 p2502 A67-29506
Concorde structural development noting effects of temperature on fatigue and creep strength of aluminum alloys [AIAA PAPER 67-402] 15 p2578 A67-30369
Electron fractography and analytical fracture mechanics application to fatigue crack propagation, noting stress-intensity-factor role 16 p2771 A67-31296
Cycles required to start crack, and cycles for crack propagation to failure estimated for notched specimen 16 p2771 A67-31297
Fatigue crack growth rates in metals under random loading correlated to cyclic load tests 16 p2774 A67-31320
Low cycle fatigue behavior of metals at creep range temperature related to equivalent ductility and strain rate 16 p2774 A67-31321
Metal fatigue studied with X-ray

diffraction technique 16 p2774 A67-31322
Mechanical properties used to estimate low cycle fatigue behavior in creep range of components in high-temperature systems 16 p2777 A67-31813
Temperature effect on low-cycle fatigue behavior of Udimet 700 superalloy, noting internal and surface cracking 16 p2693 A67-31870
Cumulative fatigue at root of circular notch of coupon type aluminum alloy specimens subjected to low cycle compression-tension strains 17 p2957 A67-32028
Fatigue strength calculated using fracture criterion for multiaxial alternating stress and combined alternating bending and torsional stresses 17 p2960 A67-32632
Crack nucleation in high strength low alloy steel, comparing fatigue processes in quenched and tempered martensite with those in pure metals 18 p3064 A67-34082
Electron fractography applied to fatigue studies of fracture appearance, morphology of striations and fracture surface microdetails [ASTM PAPER 42] 18 p3068 A67-34580
Electron fractographic techniques for failure analysis, examining fracture direction, differentiation between hydrogen embrittlement and stress corrosion in steels and cyclic stress 18 p3145 A67-34581
Short time tensile and long time creep-rupture properties of HF and HH iron-chromium-nickel alloys at high temperatures [ASTM PAPER 52] 18 p3068 A67-34582
Cumulative damage observed for biaxial fatigue stress tests on tubular steel specimens 19 p3341 A67-35552
Elongation and failure of chromium-molybdenum-vanadium steel analyzed from creep test results 20 p3464 A67-36477
Carbide inclusions and distribution effect on fatigue behavior of open hearth and electric-arc furnace steels 20 p3464 A67-36478
Structural changes due to fatigue in cladding layer of alloy D16AT studied by X-ray diffraction 21 p3642 A67-37826
Initial tension and compression effects on fatigue strength of aluminum alloy structures during plastic cold working 22 p3911 A67-39549
Metal stress relaxation effects under cyclic thermal loads, with endurance vs stress relaxation diagrams 22 p3912 A67-39686
Gaseous environment influence on fatigue fracture mode in quenched and tempered ultrahigh strength steel investigated by fractographic analysis 22 p3821 A67-40051
Parallel contours of fracture surface at optical magnifications obtained by method based on microhardness indentations 22 p3823 A67-40300
Tensile mean stress effect on dormancy of fatigue edge crack in mild steel 23 p4079 A67-41344
Fatigue crack propagation - ASTM Conference, Atlantic City, June-July 1966 24 p4247 A67-41941
Crack propagation rate and residual static strength of fatigue cracked Ti and steel cylinders for SST design 24 p4247 A67-41943
Metal fatigue in controlled gaseous environment stressing test variables effects on crack propagation mechanism 24 p4248 A67-41945
High strength aluminum alloy panel resistance to fatigue crack propagation, discussing axial load fatigue machine 24 p4170 A67-41949
Tensile to shear transition behavior of fatigue crack fronts during cycling of sheet materials, noting correlation of shear with crack stress intensities 24 p4170 A67-41950
Fatigue microcrack and macrocrack propagation in aluminum alloys, discussing continuum mechanics approach 24 p4248 A67-41952
Fatigue crack propagation in ultrahigh strength steels, noting rate sensitivity to moisture and plane strain fracture toughness 24 p4171 A67-41953
High vacuum environment and vacuum outgassing time effects on magnesium alloys fatigue properties under constant load and reversed bending 24 p4172 A67-42037
Protecting turbomachinery from unstable and oscillatory flow, noting resonance effect [ASME PAPER 66-WA/GT-13]

Steel dislocation structure under adsorption fatigue investigated by electron microscope, discussing surface active medium effect 24 p4207 A67-42462
Metal-fatigue failure indicator-predictor gauge by correlating resistance changes with fatigue damage [AIAA PAPER 67-794] 24 p4251 A67-42955
METAL FILM
SA THIN FILM
Change in resistance of titanium films deposited in high vacuum from argon ion bombardment, noting dependence on energy value 01 p0129 A67-10099
Variation of effective conductivity of thin metallic film with surface charge calculated by Boltzmann transport equation used with Fuchs-Sondheimer boundary conditions 01 p0130 A67-10204
Surface effects in quasi-classical energy quantization of conduction electron subject to arbitrary law of dispersion in metallic film 01 p0133 A67-10748
Ellipsometer study of anomalous absorption in very thin dielectric films on evaporated metals 01 p0138 A67-11075
Surface color explained using backscattering angle and diffraction properties of germanium films vacuum deposited onto heated substrate 01 p0138 A67-11076
Quantum dimensional effects in bismuth films by tunnel spectroscopy, showing energy dependence of state density having form of step function 02 p0281 A67-11632
Vacuum deposited metal film structure analyzed over wide temperature range, using electron diffraction and electron microscopy techniques 02 p0285 A67-11705
Peculiarities of substructure of thin metal films produced by condensation in vacuum studied by multibeam interferometric technique 02 p0285 A67-11706
Kinetics of formation of thin continuous films from isolated three-dimensional nuclei 02 p0286 A67-11709
Surface structure effect of evaporation deposited film and substrate crystal on epitaxy of film studied by electron diffraction and electron microscope 02 p0286 A67-11710
Epitaxial deposition of Van Arkel zirconium on sodium chloride and calcium fluoride cleavages at various temperatures 02 p0286 A67-11711
Electron microscopy study using replica technique of cross section of films of Al and Si vacuum deposited on glass substrates reveal columnar growth of polycrystalline film 02 p0287 A67-11712
Quantitative in situ X-ray diffractometer investigations of evaporated metal films and after annealing treatments ranging up to 370 degrees C 02 p0287 A67-11713
Ti, Zr and La boride thin films by chemical conversion of thin films of these metals with gaseous boron hydrides 02 p0287 A67-11715
Substrate temperature effect on structure of evaporated alloy thin films 02 p0287 A67-11716
Internal stresses of thin metallic and dielectric films, discussing methods for stress measurement, stress models and formulas 02 p0287 A67-11717
Optical properties of thin metallic films relative to electronic structure in microcrystals 02 p0288 A67-11722
Abnormal skin effect in thin films of noble metals near IR, taking into account wave penetration and magnitude of conducting electrons mean free path 02 p0288 A67-11723
Karmers-Kronig dispersion relationship for simultaneous determination of index and thickness of thin metallic film 02 p0289 A67-11726
Photoelectric efficiency of thin gold films illuminated from free surface side and support side 02 p0289 A67-11730
Photoelectric emission of metal films with electronic structure evolving with film thickness 02 p0290 A67-11731
Capacitance and optical thickness of fatty acid monolayers sandwiched between Al-films 02 p0290 A67-11732
Angular distribution of secondary electrons emitted at reverse side of aluminum films 02 p0290 A67-11734
Contact effect between superconductor

and normal conductor and between two different superconductors, noting transition temperature 02 p0291 A67-11740

Shifts in normal state conductivity and superconducting transition temperature due to charge carrier changes in In, Tl and Sn films 02 p0291 A67-11741

Low seated interfaces effect on electron transport in thin continuous metal films in presence of magnetic or electric fields 02 p0292 A67-11743

Electric resistance of titanium evaporated films in thickness range of path length effects 02 p0292 A67-11744

Effects of order-disorder state and film thickness on structure and electric conductivity of evaporated nickel, titanium and silver films 02 p0292 A67-11745

Electron conduction in discontinuous metal films by transport of activated charge carrier creation and by tunneling for island sizes 02 p0292 A67-11746

Electric resistance of discontinuous thin gold films as function of time and temperature 02 p0292 A67-11747

Electric conductivity in microcrystalline metal films in theory based on Kubo type formula and Bardeen-Harrison-Stratton treatment of tunneling 02 p0292 A67-11748

Thermoelectric power of series of gold films, noting thickness effect on electron diffusion and phonon drag 02 p0293 A67-11749

Semiconductor-metal-semiconductor structure with metal vapor deposited, analyzing voltage-current characteristics for amplifier technology 02 p0293 A67-11754

Semiconducting properties of lead telluride thin films, analyzing electron transport phenomena 02 p0294 A67-11756

Resistivity, temperature coefficient of resistivity and Hall coefficient as function of bismuth film thickness, showing that size quantization of films leads to semiconductor metals 02 p0300 A67-12509

Low voltage photomeasurements in metal-insulator-metal films with opposing photocurrent separation 02 p0301 A67-12519

Single crystal transistor with metallic base, noting frequency, V-I and power characteristics, radiation resistance, etc 02 p0221 A67-12530

Solar absorbance and thermal emittance of aluminum coated with vacuum deposited films of aluminum oxide of various thicknesses [AIAA PAPER 65-656] 03 p0448 A67-13036

Ohm law deviation in island-structure thin metallic films and current dependence on field strength 03 p0490 A67-13159

Figure contact resistance between Al and Cr sputtered conductive and resistive films 03 p0491 A67-13248

Photoelectron emission from aluminum-aluminum oxide-gold film system with electric field in dielectric 03 p0492 A67-13295

Metal-semiconductor surface barrier and prediction using concepts of covalent and ionic crystals 03 p0494 A67-13475

Majority carrier current flow in metal-semiconductor barriers according to theory incorporating Schottky diffusion theory and Bethe thermionic emission theory 03 p0494 A67-13476

Parametric amplification and sideband oscillations in structured superconducting Sn thin films 03 p0496 A67-13568

Ion beam generation for drilling thin metallic coatings deposited on glass-ceramic substrates 03 p0432 A67-14269

Photoelectron emission from aluminum-aluminum oxide-gold film system with electric field in dielectric 04 p0674 A67-14720

Temperature dependence of migration of double positioning boundaries during growth of gold films inside electron microscope 04 p0675 A67-14924

Structural and magnetic properties of /111/ films of permalloy produced epitaxially on epitaxial /111/ Ag on mica 04 p0676 A67-14931

Environmental effects on mechanical behavior of metals in vacuum and gases normally found in atmosphere, considering surface oxide layer 04 p0638 A67-14996

Vaporization of thin metallic films with focused laser beam, comparing theoretical and experimental results prepared by using pulsed high pressure helium-neon laser 04 p0630 A67-15478

Grain oriented growth in beryllium

condensates, discussing acicular structure of transverse sections of films 04 p0641 A67-15979

Iron and chromium films prepared at 4 degrees K analyzed by radial distribution, showing electron diffraction patterns of amorphous state 05 p0866 A67-16976

Oxidation of vacuum-deposited bismuth films, determining ionic and electronic transport numbers 06 p1013 A67-17659

Ohmic contacts prepared by chemical deposition of metal films on gallium arsenide 06 p1050 A67-17939

Mercury telluride thin film properties and fabrication methods 06 p1050 A67-18185

Tungsten films with fcc structure obtained by ion beam sputtering in vacuum onto substrates of glass, rock salt and mica at various temperatures 07 p1232 A67-19557

Film resistance effect on low impedance tunneling measurements 07 p1234 A67-20101

Electrical and thermal conductivity of tin films investigated in search for surface superconductivity induced by electric field 10 p1688 A67-22765

Substrate metal hardness effect on performance of molybdenum disulphide films, noting wear rates 10 p1659 A67-22867

Vapor deposition of thin films by decomposition of metallic alcoholates in luminescent discharge plasma 10 p1696 A67-23692

Wall creeping in thin magnetic Ni-Fe films analyzed as function of thickness, field pulse amplitude, etc, comparing results with existing theories 11 p1845 A67-23953

Optical transmission and electrical properties of complementary metallic meshes fabricated by formation of complement of agglomerated thin films 11 p1845 A67-24142

Depression of superconducting transition temperature in narrow tin films, noting condition for maximum microwave enhancement of critical current 11 p1846 A67-24563

Measurement of radiation reflectivity scattered from optical surfaces in far UV, noting role of overcoating with metallic films 11 p1819 A67-24666

Pore formation, lifetime and microstructure of thin electrolytic metal films under load and high temperature at grain boundaries 12 p1955 A67-25448

Low temperature deposition of amorphous films of transition metals and alloys, noting atomic arrangement, comparing with case of metals condensed in crystalline state 12 p1982 A67-25451

Thermal radiation properties of oxide films of variable thickness on metal substrates, using radio-recording spectrophotometer at various wavelengths [AIAA PAPER 67-286] 12 p1958 A67-26003

Temperature-dependent thermoconductivity of metal film on insulation laminations in relation to bulk parent material in insulation systems of cryogenic propellants [AIAA PAPER 67-295] 12 p2035 A67-26010

High stability metal thin film resistors applied to thin film circuits, noting substrate properties and pattern design 12 p1918 A67-26209

Surface effects in quasi-classical energy quantization of conduction electron subject to arbitrary law of dispersion in metallic film 13 p2176 A67-26777

Nonequilibrium states in metal-to-semiconductor junction resulting from emission of high energy holes and hot free electrons in same direction 13 p2176 A67-26861

Vacuum deposition techniques for production of optical film materials for neutral density filters and sunglasses, discussing dielectric, metallic, reflecting and semitransparent films 13 p2158 A67-27076

Structure and properties of thin films in terms of deposition conditions, noting conditions for continuity, surface roughness, grain size, lattice defect density, crystalline orientation, purity, etc [AIAA PAPER 66-727] 13 p2054 A67-27591

Single crystal transistor with metallic base, noting frequency, V-I and power characteristics, radiation resistance, etc 14 p2279 A67-28007

Nature of photoelectromotive force of cadmium selenide with Cu, Ag, Au, Pt vacuum-deposited on

surface 14 p2367 A67-28527

Evaluation method for deposited thin film interfacial interconnections 14 p2369 A67-28613

Li film structure on compact tungsten faces by diffraction method, using free electron beams 14 p2372 A67-28760

Ion beam generation for drilling thin metallic coatings deposited on glass-ceramic substrates 14 p2325 A67-28779

Optical properties of thin aluminum and silver layers subjected to proton beam bombardment 14 p2373 A67-28855

Measurement of resistance of thin metal films and kinetics of charge drain from surface 15 p2485 A67-29126

Temperature distribution from local regions of microscopically thin film junctions of metal structures, noting effect on average temperature 15 p2444 A67-29415

Structure of thin tungsten films as function of nature and temperature of substrate, noting partial crystallization of fcc structure 15 p2535 A67-29477

Gold, silver, copper and tin condensed films, investigating dependence of structure and conductivity on substrate material 15 p2540 A67-30122

Density, crystallinity and electric properties of thin metal films deposited on rotating cylindrical substrate 16 p2727 A67-30899

Sapphire whisker strength coated with thin metal film determined at room and elevated temperatures 16 p2694 A67-31522

Strength and durability in friction tests of soft, vacuum deposited, thin-metal gold film lubricants, noting dependence on film-substrate interface 16 p2684 A67-31816

Electron-mirror microscopy for intermediate-state pattern of superconducting samples noting bulk, thin sheet and lead films 17 p2912 A67-32266

Soviet papers on structure and properties of metal films 17 p2920 A67-32887

Molybdenum/tungsten films obtained by thermal decomposition in vacuum analyzed, noting surface morphological changes with temperature changes 17 p2921 A67-32892

Ohmic contacts prepared by chemical deposition of metal films on gallium arsenide 18 p3100 A67-33775

Degree of blackness of normal black body radiation for various metals, studying temperature and kinetic relations and blackness of opaque oxide films 18 p3064 A67-34052

Adsorption, surface reaction and mutual displacement of carbon monoxide, carbon dioxide and oxygen on titanium film, using mass spectrometer 19 p3244 A67-34941

Measurement of work function changes of nickel films for oxygen and hydrogen chemisorption 19 p3246 A67-35787

Structural defects of reciprocally oriented polycrystalline bismuth-antimony films analyzed by moire method 20 p3510 A67-36813

Solid lubricants including powders, solid dispersions, resin bonded dry film and soft metal films, discussing metal oxide lubricant effect on graphite 20 p3455 A67-37263

Physical properties of thin layers of cadmium telluride-metal systems analyzed for metal concentration and temperature of base at time of deposition 20 p3513 A67-37448

Pore formation, lifetime and microstructure of thin electrolytic metal films under load and high temperature at grain boundaries 21 p3646 A67-38827

Hall coefficient and mobility measured for annealed polycrystalline and epitaxially grown gold, silver and copper films, discussing size effect 22 p3855 A67-39355

Dynamic energy losses in thin Ni-Fe films during magnetization reversal studied by observation of M-H loop 22 p3860 A67-39902

Electrically tunable low pass filter using Permalloy films near resonance 22 p3772 A67-39906

Superconductivity enhancement in fine grained tungsten films, discussing structural changes and theoretical models 23 p4036 A67-40702

Resistance properties of thin continuous Au, Ag, Cu and Al films influenced by superimposed thin films, discussing resistance change and surface scattering 23 p4039 A67-40879

Nature of photoelectromotive force of

cadmium selenide with Cu, Ag, Au, Pt vacuum-deposited on surface 23 p4039 A67-40934

Evaporated thin Au and Ni films electric conductivity measurements, obtaining electron mean free path and bulk resistivity 23 p4040 A67-41016

Temperature effect on structure of W films prepared by triode pulverization at low pressure and low power 23 p4041 A67-41194

Deposited Al layer thickness on Si determined using X-ray spectrometric technique 24 p4200 A67-41803

Change of conductivity with temperature measurements for stabilized amorphous bismuth films 24 p4200 A67-41866

Electron beam retarding potential method to measure work function changes resulting from Cs, oxygen and hydrogen adsorption on TiO_2 single crystal 24 p4201 A67-41892

Ti thin films use as getter in electron microscopy of Mo particles at high temperature with minimum oxidation 24 p4172 A67-41978

METAL FOIL

Metal photocathodes as secondary standards for absolute intensity measurements in vacuum UV 03 p0499 A67-13910

Strains, slip lines and onset of cracks in thin chromium foils investigated by electron microscopy 04 p0640 A67-15977

Titanium alloy thin foil preparation using window method and electropolishing conditions, noting phase transformation 10 p1668 A67-23175

Solar wind trapping in solids using ion bombardment of aluminum foils at various energies and temperatures 11 p1825 A67-25079

Spacecraft thermal joint conduction study covering surface conditions, external pressure, use of various fillers and parent materials and vacuum environment [AIAA PAPER 67-316] 12 p2037 A67-26031

Structure effect on magnetization and critical current density in transverse magnetic field of superconducting V and Nb foils with different grain boundary orientations 12 p1986 A67-26067

Commercial forms of aluminum alloys, production, applications and marking 14 p2336 A67-27812

Electric vortex-field integrator using aluminum foil sheet and external field to simulate circular flow about wing profile at various angles of attack 17 p2834 A67-32905

Thin self-supporting beryllium foils preparation for use as atomic and molecular ion beam targets 17 p2866 A67-33360

Fatigue-damage evaluation system for transport aircraft, noting use of cumulative strain gauge that stores strain history 18 p3142 A67-33897

Penetration rates of thin aluminum foil sensors of Ariel II satellites compared with flux measured by microphone detectors in vicinity of earth 21 p3722 A67-38494

Multiple reflective metal foil structure with separating matrix transient thermal response, determining number of radiation shields for given thermal protection 22 p3919 A67-40115

Aluminum-magnesium alloy dislocation networks structure and formation investigated by thin foil technique after rapid solidification 23 p4017 A67-40658

METAL FORMING

SA EXPLOSIVE FORMING

Instrumentation and control for magnetic pulse metal forming including pulse generation, energy transfer, electrical operations, etc [SAE PAPER 660066] 01 p0078 A67-10569

Deformation in niobium and tantalum by wire drawing at room temperature, producing changes in shape and position of X-ray diffraction peak 01 p0095 A67-10686

Wing-fuselage section panels of hypersonic aircraft built by brazing refractory honeycomb 10 p1660 A67-23171

Integrally formed compression panel efficiencies compared with other aerospace panel concepts 10 p1729 A67-23769

Heat resistance of Ni alloys with oxides noting experimental procedure, and effect of various additives 16 p2690 A67-31433

Flow stress of aluminum related to strain, strain rate and temperature, discussing compression testing machine and results 18 p3064 A67-34078

Material point displacement velocity field of bending elements of sheet during profile shaping by roll forming, determining stress-strain condition 21 p3631 A67-38052

Work of deformation during expansion of tubular blanks with varying hardening characteristics under uniform loading 21 p3631 A67-38054

Honsel Plastic Mold /HPM/ process for high surface quality, discussing cost, materials and solidification time 21 p3637 A67-38976

METAL FUEL

Metallic material compatibility with medium energy hypergolic propellant components hydrazine/UDMH and nitrogen tetroxide, used in ELDO rocket 01 p0139 A67-10211

Hybrid fuel regression rate, discussing oxydizer flow rate and burner pressure interdependence [AIAA PAPER 66-113] 05 p0873 A67-17347

Erosion processes and outflow phenomena in ZnS rocket fuel, noting aluminum addition and gas leaks 24 p4206 A67-42579

METAL-GAS SYSTEM

Stable size and reaction of molten metal droplets with rarefied atmosphere as consequence of surface oxide film, treating beryllium 10 p1733 A67-23124

Trapping of hydrogen ions in molybdenum, titanium, tantalum and zirconium measured by mass spectrometric technique 17 p2810 A67-33384

High temperature kinetics of bulk beryllium metal combustion in hydrogen-oxygen-water vapor system, studying flame environments, thermal balance, etc 18 p3151 A67-33809

METAL HALIDE

Tungsten powder compacts impregnation technique by metallic halides solutions, obtaining even distribution of metal 14 p2338 A67-28614

METAL ION

Potentials of zero charge of gold, silver and mercury electrodes as affected by cations and respective metal ion interaction 11 p1749 A67-23920

Mono- and polycrystalline samples of Al and Cu bombardment by argon ions in presence of oxygen and by oxygen and nitrogen ions under vacuum 14 p2351 A67-28513

Relation between changes in ferrite lattice parameter at magnetic conversion temperature and changes in ferrite metal ion charges due to electron exchange 18 p3095 A67-33444

Charge transfer role in formation and maintenance of molecular and metal-ion layer in E region of ionosphere 19 p3217 A67-35204

Partial molal entropies of doubly ionized aqueous Zn, Cd and mercurous and mercuric ions calculated, using literature data 20 p3376 A67-36792

Excitation effect on single electron charge transfer collisions of Fe ions in various gases determined with different excited states of ions 23 p4030 A67-40976

METAL JOINT

SA SOLDERED JOINT

SA WELDED JOINT

Plasma arc welding produces butt type joints in thick titanium aerospace structures [SAE PAPER 660646] 01 p0078 A67-10609

Effect of locking dovetail joint geometry on static strength 03 p0528 A67-14077

Soft metal enclosed in higher-melting-point metal forming seal bakeable at temperatures above 500 degrees C 04 p0630 A67-15633

Heat transfer through metal to metal joints, determining influence of number of real contact points and compressive load 04 p0735 A67-15854

Threaded fastener developments for critical joint design requirements, considering strength, temperature, weight and cost 05 p0810 A67-16166

Thermal conduction paths for magnesium joints in cordwood mounting of electronic parts in heat conducting plate 05 p0929 A67-17451

Diffusion welding of aluminum alloys and austenitic stainless steel tubular joints 07 p1190 A67-19214

Aircraft hollow control rods with threaded joints noting compression and

testing 07 p1192 A67-19753

Blank heating processes in production by pressworking of seamless adapters for detachable tube joints 07 p1192 A67-19754

Stress distribution in dovetail compressor blade joint analyzed using frozen stresses method 08 p1424 A67-21335

Pulsed laser welding process, discussing wire-to-wire welds, sheet-to-sheet welds and circuit board weldings 09 p1504 A67-22139

Design of three types of bonded metal-to-metal joints, discussing advantages of theoretical over empirical methods 09 p1576 A67-22501

Simple and stress corrosion problems in aircraft design emphasizing protection of joints 12 p1954 A67-25127

Spacecraft thermal joint conduction study covering surface conditions, external pressure, use of various fillers and parent materials and vacuum environment [AIAA PAPER 67-316] 12 p2037 A67-26031

Book on adhesive bonding Alcoa aluminum covering techniques, applications including aircraft and military uses, classifications, etc 13 p2143 A67-27177

Dissimilar metal transition joints employing roll-bonded and friction welded components 13 p2124 A67-27685

Permanent joints for Agena pressure systems, discussing retention of pressurized gases in connector tubing system 17 p2801 A67-31984

Metal-to-metal seal for separable joints /Bobbin seal/ utilizing elastic and plastic responses of seal structure and interface 17 p2864 A67-31993

Hydraulic tubing permanent joints, made by induction-brazing method, for installation on A-7A Corsair II 17 p2801 A67-32007

High vacuum enclosure problems solved by use of magnetic seal for joints of large valves and degassing by direct heating of wall surfaces 17 p2802 A67-32300

Glued metal joints properties analyzed from test results by method using theory of probability and statistical sample 21 p3716 A67-37950

Cross-wire resistance welded metal joints for aerospace electronic packing assemblies, investigating embedment, mechanical strength and materials evaluation 21 p3635 A67-38629

Microchemical and microhardness properties of parallel gap welds for microstructure interpretation of metal joint 21 p3636 A67-38633

Electron beam welding of high temperature metals in vacuum 22 p3812 A67-39541

Beryllium braze joining for light stiff components noting structural examples and fabrication techniques, with reference to Apollo SNAP-27 radiator housing [SAE PAPER 670805] 24 p4159 A67-41991

METAL-METAL BONDING

Chemical behavior of metallic elements predicted by periodic table, noting formation of liquid and solid metallic solutions, binary and complex metallides and nature of chemical bond 06 p1018 A67-18233

Creep measurement associated with adhesive bonding of aircraft structures, particularly creep of metal-metal lap joints and bonded sandwich structures creep measurement associated with adhesive bonding 09 p1522 A67-22505

Design, production and experience of bonded structures in Europe for aerospace applications 09 p1577 A67-22511

Friction welding of dissimilar metals by inertial process, considering effects of flywheel rotation and weld-interface velocity and pressure [ASTME PAPER WES-7-51] 10 p1660 A67-23006

Alloy 718 composition, microstructure and heat treatment behavior correlated with mechanical properties, noting strengthening and oxidation resistance [ASME PAPER 67-MET-5] 12 p1956 A67-25949

Effective gap thickness and gap number relation determined from correlation of parameters of thermal contact conductance [AIAA PAPER 67-317] 12 p2037 A67-26032

Dissimilar metal transition joints employing roll-bonded and friction welded components 13 p2124 A67-27685

Interband states in vicinity of

metallurgical junction, deriving formula for depletion layer capacitance of abrupt junctions with interface states 14 p2373 A67-28929

Chemical reactions in Ni-Ti-Nb system, examining via X-ray diffraction formation of ternary intermetallic compounds 16 p2691 A67-31593

X-ray structural and diffraction analysis of Mo-Ni-Bo system at high temperatures noting isothermal sections of phase diagram 16 p2691 A67-31595

METAL OXIDE

Sintering of crystalline oxides through volume diffusion, noting sintering rates 01 p0096 A67-10693

Electrical and optical properties of solid solutions formed by beta manganese and chromium dioxide within wide composition range, showing magnetic semiconductor behavior 01 p0134 A67-10755

Equilibrium carbon monoxide pressures measured by torsion effusion studies of reaction of graphite with hafnium and uranium dioxides at high temperatures 01 p0018 A67-10763

Compacting effect of additive oxides of Ti, Zr, Si, Fe, Zn and Al on hot pressing of MgO 01 p0102 A67-11243

Tunnel-current measurements of sandwich configurations, determining metal/metal-oxide work function 02 p0295 A67-11764

Fibering of oxides by hot deformation in metal matrices of unalloyed columbium or tantalum, preparing composites by powder metallurgy 03 p0441 A67-13273

Metal addition effect on grain growth of matrix oxides, noting inhibitive results in most cases 04 p0642 A67-15086

Optical self-absorption and dielectric constant of cadmium oxide thin film in case of high electron degeneration 04 p0683 A67-15655

Oxide dispersion hardening of intermetallic NiAl and FeAl compounds for improved high temperature strength 06 p1014 A67-17803

Stable size and reaction of molten metal droplets with rarefied atmosphere as consequence of surface oxide film, treating beryllium 10 p1733 A67-23124

Ultrahigh vacuum cold welding in dynamic load elevated temperature environment, noting surface oxide in vacuum 10 p1670 A67-23742

Energy distribution of electron tunneling through metal-insulator-metal diode noting dependence on temperature, film thickness and voltage 12 p1982 A67-25449

Thin film capacitor dielectrics of silicon oxides and various metal oxides, noting influence on vacuum deposited compounds 12 p1918 A67-26210

Book on high temperature oxidation of metals and alloys, fundamental aspects and reaction mechanisms 13 p2141 A67-27176

Temperature resistant elements and compounds for use above 3000 degrees F, considering melting points, atomic radii and densities 14 p2340 A67-28380

Lead, copper and cobalt oxides effects upon ignition kinetics of paraffinic and aromatic fuels 14 p2407 A67-28550

Surface reactions and structure determinations of oxides of niobium, tantalum and vanadium with /110/ surfaces from CO and oxygen absorption 15 p2504 A67-29881

Durability and electrical conductivity of metallic fiber materials noting influence of oxidation on properties 20 p3466 A67-36912

Solid lubricants including powders, solid dispersions, resin bonded dry film and soft metal films, discussing metal oxide lubricant effect on graphite 20 p3455 A67-37263

Magnetic impurities in tunnel junction barriers investigated for effect on junction resistance 24 p4200 A67-41865

Titanium-magnesium and titanium-beryllium oxides physical properties under electron bombardment in vacuum indicate usability for SHF oscillation energy absorbers 24 p4202 A67-42069

METAL OXIDE SEMICONDUCTOR /MOS/

Linearity of MOS transistor as variable resistor improved by keeping substrate floating and connecting substrate to drain 01 p0036 A67-10439

Model describing effect of ionizing radiation on metal-oxide-silicon surfaces, showing relation to study of defect

structure of silica 01 p0036 A67-10475

Effects of aluminum electrode and hydrogen atom on MOS structure during annealing 01 p0137 A67-11069

Silicon-tantalum oxide system prepared by reactive sputtering, noting characteristics of MOS diode of system 01 p0137 A67-11071

Integratable gyrator using metal oxide semiconductor and bipolar transistors whose circuit enables high Q factor inductances to be derived from low loss capacitors 01 p0041 A67-11329

Ion transport on and through thin oxide layers of MOS structure investigated by charge comparison method 02 p0293 A67-11750

Surface origin of LF noise power spectrum demonstrated via silicon MOS field effect structures 02 p0296 A67-11820

Junction type field effect transistors and metal oxide semiconductor devices for switching functions in digital circuitry 02 p0215 A67-11971

Small signal RF amplification of VHF MOS transistors, considering TA2840 triode and TA7010 dual-insulated-gate transistors used as VHF amplifiers 02 p0218 A67-12101

DC and RF I-V characteristics, device fabrication and structure of epitaxial depletion mode n-type MOS-FET 02 p0218 A67-12103

Microelectronic applications of silicon-on-sapphire /SOS/ and MOS-FET large scale arrays /LSA/ 02 p0219 A67-12108

MOS capacitance measurements combined with neutron activation analysis, showing positive charge increase at oxidized silicon surfaces by sodium presence 02 p0300 A67-12518

Hertzian relaxation spectra of MOS structures showing existence of two absorption regions 03 p0493 A67-13453

Surface state density effect on electron mobility in Si inversion layer of MOS-FET 03 p0496 A67-13577

MOS-FET amplifier RC network design 03 p0382 A67-13670

MOS-FET broadband frequency doubler circuit 03 p0382 A67-13671

Properties of silicon dioxide-silicon system, examining oxidation process and electrical properties of metal oxide silicon /MOS/ structure 03 p0500 A67-14181

Designing with MOS field effect transistors 03 p0388 A67-14182

Signal distortion arising from nonlinear /parabolic/ transconductance voltage characteristics of MOS /metal oxide silicon/ transistor determined experimentally by distortion measurement techniques 03 p0388 A67-14183

Transistor and integrated circuits applications including high input impedance amplifier using MOSFET transistor, pulse forming circuit, stable sawtooth generator, etc 04 p0579 A67-14402

Energy distribution of surface states at steam-grown silicon-silicon dioxide interfaces determined by LF differential capacitance measurements of MOS structures 04 p0683 A67-15622

Ionizing radiation effects on silicon planar bipolar transistors determine degradation mechanisms 04 p0588 A67-15707

Insulated gate field effect transistors with silicon dioxide and silicon nitride insulation under electron irradiation, noting gate turn-on voltage reduction and source-drain leakage elimination 04 p0588 A67-15713

I-V characteristics shift and radiation hardening of Mos transistors for low ionizing dose level 04 p0589 A67-15714

Space radiation effect on MOSFET and metal-silicon nitride-silicon devices, noting protective methods 04 p0589 A67-15715

Instability effect in n-channel silicon MOS transistors bombarded with ionizing radiation 04 p0589 A67-15716

Transient response of MOS transistors and integrated circuits to ionizing radiation 04 p0589 A67-15719

Impurity concentration profiles in silicon epitaxial wafer determined, using MOS capacitors 05 p0866 A67-16985

Orientation dependence of surface charge on anodized indium antimonide from MOS capacitance measurements 05 p0869 A67-17093

Pulse response of MOSFET and depletion layer FET 05 p0778 A67-17324

Illumination effect on capacitance of metal-SiO-Si system with various

biases 07 p1152 A67-19591

Read-only memory composed of MOS-FETs on single silicon chip 07 p1155 A67-19845

Self-healing electric breakdown in MOS structures noting magnitude duration, temperature and propagation characteristics 07 p1157 A67-19904

Second breakdown in N-channel MOS transistor 07 p1157 A67-19906

IR photovoltaic response, quantum efficiency and V-I characteristics of InSb MOS structures 09 p1551 A67-21577

Positive charge drift induced by hydrogen heating in silicon dioxide film on MOS transistor 09 p1552 A67-21763

Effects of dry and wet preoxidation on characteristics of MOS transistor using silicon 09 p1552 A67-21768

Insulated gate to obtain depletion in channel of MOS-FET transistor, noting inversion layer and frequency response 09 p1475 A67-22202

Thin film silicon-on-sapphire deep depletion MOS transistors 09 p1475 A67-22203

Temperature dependence of threshold voltage, effective mobility in inversion layer and channel conductance of MOS transistor below saturation 09 p1475 A67-22204

Semiconductor dielectric interface characterization from study of complex capacity of metal/oxide/semiconductor structures 09 p1557 A67-22557

MOS structure studied by measuring variations in capacitance and charge injection into oxide 09 p1558 A67-22586

Exchange model of zero bias tunneling anomalies, discussing Hamiltonian, interference magnetic scattering and metal junctions 10 p1691 A67-23400

Metal-beryllium oxide bond for semiconductors noting mechanical and electrical strength, thermal conductivity and refractivity 10 p1696 A67-23691

Conductance-and capacitance-voltage curves of MOS capacitors analyzed for temperature dependence of inversion layer frequency response in n-type silicon 11 p1846 A67-24234

Substrate doping, source bias and bulk contact effect upon DC characteristics of silicon MOS transistors 12 p1916 A67-26068

Semiconductor integrated circuits, discussing hybrid, multichip and beam-lead methods in digital and linear circuit applications 12 p1917 A67-26203

Semiconductor devices for microcircuits, discussing MOS FET, metal base transistor, etc 12 p1918 A67-26208

MOS transistor digital switch integrating methods, presenting operating conditions and design factors for IC inverter 12 p1918 A67-26218

Static and dynamic behavior of large pulsed signal behavior of n-type MOSFET below and in constriction /pinch/ region 13 p2076 A67-26487

Anomalous shift in gate threshold voltage of high transconductance p-channel MOSFETs during exposure to space-like radiation 13 p2076 A67-26516

Ultrasensitive miniature temperature sensor using pyroelectric material on gate of MOS transistor 13 p2119 A67-26517

Charge motion on outer silicon oxide surface of MOS structure, estimating surface resistance and dependency on humidity and other factors 13 p2176 A67-26707

Charge equation of enhancement-type MOS transistors, determining waveforms and switching times of resistor-coupled switching circuit 13 p2078 A67-26786

Book on MOSFET covering device theory, characteristics and usage in discrete and integrated circuit form and application to practical circuit design 13 p2079 A67-26997

Metal oxide silicon transistors as high performance analog switching elements, noting design and performance 14 p2281 A67-28018

Threshold voltage control for complementary pair MOS transistors, discussing techniques used 14 p2281 A67-28019

Gate capacitance storage property of p-channel enhancement MOSTs used in achieving low power consumption values 14 p2281 A67-28020

MOSTSIM 2 computer program for design of integrated circuits 14 p2281 A67-28021

Light sensitive arrays based on photodiodes combined with MOS devices

analyzed for use of image, pattern detection and other applications 14 p2282 A67-28026

Advances in microelectronics, emphasizing role of MOS transistors 14 p2285 A67-28458

Two opposing tunnel currents

determination through transition zone of metal-oxide-metal structure 14 p2367 A67-28515

MOS transistor channel conductance measured as function of gate voltage, noting variation with temperature 14 p2289 A67-28924

DC operation of FET at liquid helium temperature noting transfer and drain characteristics similar to those at room temperature 14 p2290 A67-28926

Military radar intercept calculator, discussing small size, low power supply, high performance and MOS memory 15 p2439 A67-29161

Transconductance and voltage gain of MOS/FET using hafnium dioxide 15 p2442 A67-29171

Substrate resistivity effect on threshold of surface inversion in MOS system, deriving expression for threshold voltage vs impurity concentration 15 p2446 A67-29638

MOS transistor HF behavior noting phase shift, frequency dependence, etc 15 p2449 A67-29805

MOS oxide-film thickness estimation by extrapolating MOS capacitance-voltage curve into accumulation region at high negative bias 15 p2539 A67-29815

Space-charge limited ionic currents in MOS structure oxide film, noting relationship between interface ion trapping rate and SCL currents 15 p2539 A67-29825

Metal oxide semiconductor field effect transistor /MOSFET/ Inverter transient response determination, noting mobility dependency on gate voltage 15 p2452 A67-29940

GaAs epitaxial layer in transistors with silicon nitride insulator surpasses silicon MOS device in power gain, frequency response and temperature range 15 p2455 A67-30391

Surface charge density of MOS as affected by bias and temperature treatment 16 p2724 A67-30602

MOS and bipolar integrated circuits compared, noting MOS IC advantages 16 p2637 A67-31194

MOS instabilities from ion drift, temperature dependent deep trapping and fast interface states from temperature stress, noting instabilities elimination techniques 17 p2823 A67-32195

Effects of electric fields and configurations on thermal annealing and radiation hardening of MOSFETs 17 p2916 A67-32835

Electron bombardment effect on insulated-gate and junction-gate FETs and MOS IC indicates FET resistance to ionizing radiation 17 p2918 A67-32850

MOST behavior under irradiation studied for defect creation and ionization, charge displacements and preexistent trap ionization 17 p2918 A67-32852

Ionizing radiation effect on field effect MOST transistors, noting irradiation degradations 17 p2919 A67-32856

Slowly decaying broad maximum of parallel conductance explained by tunneling for surface states near Si-silicon oxide interface 18 p3101 A67-34018

Radiation effects in metal-insulator-semiconductor /MIS/ devices, noting shift and shape change in characteristic curve 18 p3012 A67-34345

Design of large scale integrated MOS-FET devices for general logic circuit applications 18 p3014 A67-34554

MOSFET approach to small scale integration of large scale circuits 18 p3014 A67-34555

Universal array of complementary-symmetry MOS transistors applied to missile and surface radar beam steering phase array storage unit 18 p3015 A67-34563

MOS and silicon transistors for design of logarithmic amplifiers for space instrumentation 19 p3194 A67-35463

Space environment effects on integrated circuits, discussing FET-MOS type 19 p3196 A67-35675

LF noise in MOS-FET, discussing relationship to drain current and power dissipation 19 p3198 A67-36044

Tunneling characteristics of metal-oxide-silicon semiconductors, observing band structure and interface-state densities influences 19 p3308 A67-36045

MOS devices electrical characteristics controlled by physical parameters studied for approximate relations between loads, potentials and surface fields 20 p3507 A67-36319

MOS transistor advantages in integrated circuits 20 p3395 A67-36320

Radiation effects on MOS devices, analyzing electrical characteristics degradation mode and conduction threshold voltage variation 20 p3396 A67-36321

MOS transistors handling, mounting and utilization compared to FETs 20 p3396 A67-36322

MOS element utilization as impedance transformer at output of ceramic ferroelectric subminiaturized pressure pickup 20 p3435 A67-36323

Reliability evaluation of MOS large scale integration devices, using simplified circuit to test individual small elements 20 p3398 A67-36800

Semiconductivity of molybdenum-oxygen systems, analyzing solid phase effect on solution mechanism 20 p3510 A67-36816

Tracer experiments using tritiated ethanol on surface of MOS capacitor to indicate field-induced proton transport 20 p3510 A67-36857

Cobalt 60 gamma radiation effect on MOS diodes fabricated on silicon substrates, noting surface state and oxide charge densities 20 p3510 A67-36961

Inverse layer effect on p-type silicon MOS structure surface, examining deviation from equilibrium space charge theory 20 p3511 A67-37141

Illumination effect on capacitance of metal-SiO₂-Si system with various biases 20 p3401 A67-37330

Field effect devices noting insulated gate transistor, thin single crystal silicon film deposition on sapphire single crystal, etc 21 p3590 A67-38064

MOS transistors surface properties and leakage current affected by gold, showing positive charge production 21 p3678 A67-38150

Integrated MOS-FET analog gate for pointing and logic of space telemetry switch 21 p3592 A67-38227

Radiation effect on MOS transistors in D-2 satellite telemetry coder 21 p3593 A67-38230

MOSFET gate breakdown nondestructively determined by measurement of leakage component 21 p3598 A67-38574

MOS-FET signal distortion avoided by taking into account turn-on voltage dependence on source bias 21 p3600 A67-38847

Switching behavior equations derived for FET with solutions applied to MOS and junction gate FET circuits 21 p3602 A67-39069

Solid state photosensitive devices combining p-n diodes and MOS circuitry noting application in electrical readout, image and pattern detection 22 p3796 A67-39332

Noise factor variations with source resistance for MOST in common-gate and common-source connections, showing advantage of low noise operation 22 p3773 A67-40309

Clean MOS structure bias and temperature /BT/ treatment at high electric fields causing electrochemical reaction affecting surface charge density 22 p3774 A67-40461

MOSFET integrated circuits for use in analog computers noting simplicity and switching qualities for control of hybrid devices 22 p3775 A67-40465

Book on MOS-FET device operation and characteristics, discussing circuit parameters and digital applications 23 p3983 A67-41766

Monolithic integrated circuit design, considering thin film circuits, hybrid techniques and MOS devices 24 p4132 A67-42687

METAL PARTICLE

Models of reflection nebulae light for single scattering, pure or modified by internal nebular extinction, on spherical grains imitating dielectric or metallic particles 11 p1861 A67-24487

Sputtering yields and energy-transfer efficiency measurements by ion beam

sputtering of liquid metals indicate no justification for incorporation into low thruster

[AIAA PAPER 67-683] 21 p3692 A67-38714

Plastic deformation during metal cutting, deriving metal deformation, cutting tool stressed state and temperature as function of particle trajectories 21 p3637 A67-38923

Equilibrium angular distribution function computer calculations for cascade particle numbers in iron and lead reveal dependence on primary particle energy 24 p4221 A67-42873

METAL PLATE

SA FLANGE

Griffith energy criterion and stress-strain environmental criterion for fractures in brittle cracked metallic plate 03 p0523 A67-13467

Elevated-temperature tensile testing of thin Rene 41, Hastelloy X and TD Nickel sheet 03 p0446 A67-13553

Combined elastic solutions-finite difference method for bending of compressible or incompressible rectangular metal plate beyond elastic limit 05 p0907 A67-16017

Heat treatment effect on structure, hardness, microhardness and corrosion resistance of VT1 titanium and OT4 titanium manganese-aluminum alloy sheets 06 p1018 A67-18236

Micrographs of thin Ti layers through electron microscope showing dislocation distribution 11 p1806 A67-24428

Commercial forms of aluminum alloys, production, applications and marketing 14 p2336 A67-27812

Optical and stereoscan microscope scanning combined with X-ray microanalysis used to investigate results on collection surfaces of space probes 19 p3339 A67-35197

Laser thermal and radiation effect on metals, discussing mechanical damage 21 p3646 A67-39011

High speed read-only memory with waffle iron structure noting ease of information change and high bit density 22 p3765 A67-39904

RF size effects in plane parallel metal plate, discussing skin effect in magnetic fields, electron trajectories and spherical Fermi surface 22 p3866 A67-40551

Crack propagation through mild steel plates investigated by method using stress values at several places near crack and at crack tip 23 p4074 A67-40665

Transient displacement and strain distributions in fracturing notched magnesium plate, using moire-fringe technique and Q-spooled laser 23 p4076 A67-40736

METAL POWDER

S POWDERED METAL

METAL PROPELLANT

Techniques for study of metal combustion in rocketry including particle burning, bulk metal and metal vapor combustion and low temperature oxidation [AIAA PAPER 67-66] 06 p1072 A67-18437

Liquid and solid rocket propellants, examining use of metals as fuels 14 p2376 A67-27877

Combustion rate and subsurface activity of metallized burning polymers, stressing heat conduction role and applications to propellant combustion [CI PAPER 67-3] 19 p3344 A67-34998

METAL REINFORCEMENT

Filament-matrix interactions in metal matrix composites considered as liquid phase layer formation by interdiffusion 03 p0442 A67-13309

Fiber-metal composites with properties related by law-of-mixture relationship 03 p0442 A67-13310

Tensile strength affecting factors in metals reinforced with strong fibers 03 p0442 A67-13311

Ceramic material strength improvement by refractory metal fiber reinforcement, noting strontium zirconate-molybdenum systems 03 p0450 A67-13312

Technique for producing continuous metallic filaments with diameter of less than 7.5 microns and composites 03 p0443 A67-13408

Thermodynamic compatibility of B, SiC, BN, boron carbide and tin nitride with various metal matrices in fiber-reinforced composites 03 p0443 A67-13429

Silicon carbide filament properties, fabrication and use as reinforcement of metal matrix composites, noting strength retention at high temperatures 03 p0445 A67-13439

Fiber reinforced metals 03 p0456 A67-13893

Fiber diameter, length and discontinuity effects on fatigue properties of fiber-reinforced metal 06 p1099 A67-17712

Fabrication, properties, deformation and fracture of silica fiber reinforced aluminum, noting effect of heat treatment and stress rupture 07 p1211 A67-20260

Nickel composite with tungsten filament and aluminum oxide whiskers, noting parameters of tensile strength after annealing 08 p1342 A67-20909

Book on composite materials covering theory of metal strengthening, dispersion, fiber strengthened materials, material potentials, etc 11 p1807 A67-24634

Fiber reinforcement theory, considering strengthened metal behavior at elevated temperatures and under work hardening conditions 11 p1807 A67-24635

Fiber strengthening processes, advantages and limitations of fiber for composite systems and incorporation in metal matrices 11 p1811 A67-24637

Ultrasonic energy applied to several metallurgical processes, exploring possible application to metal reinforcement 14 p2337 A67-28321

Filament-metal matrix composites for high temperature range, discussing kinetic phenomena [ASTM PAPER 1] 18 p3066 A67-34567

Mechanical behavior of fiber-reinforced aluminum and effect on engineering application [ASTM PAPER 10] 18 p3070 A67-34575

Tensile properties of fiber-reinforced metals, discussing failure at notch root 20 p3464 A67-36417

Metal composite materials for higher temperature resistance utilizing filaments, fibers and whiskers, discussing machinability and testing 21 p3643 A67-37954

METAL SHELL

Local buckling strength of high strength axially compressed maraging steel cylinders circumferentially prestressed with high strength epoxy-protected fiberglass filament windings 05 p0923 A67-17211

Forming closed contour shells by straining with expandable punch 07 p1191 A67-19750

Zero magnetic field in superconducting lead shell using Meissner effect 22 p3865 A67-40438

METAL SPRAYING

S PLASMA ARC METAL SPRAYING

METAL SURFACE

Time dependent perturbation theory applied to calculating probability field ionization as function of atom-metal separation 01 p0116 A67-10206

Periodic surface distortion of molten layer in axisymmetric flat stagnation regions of cylindrical iron and copper rods 01 p0102 A67-11190

Boundary conditions at interface between superconductor-superconductor and superconductor metal 03 p0489 A67-12937

Spectral emittance of metallic and nonmetallic materials, discussing surface roughness effects [AIAA PAPER 65-675] 03 p0467 A67-13042

Heat transfer between metallic surfaces in contact [AIAA PAPER 65-661] 03 p0534 A67-13067

Book on molecular physics of boundary friction on metal surfaces 03 p0429 A67-13333

Evaporation process and pore development in alloy samples under tensile stresses 03 p0424 A67-14058

Total specular reflectance of rough metal surfaces calculated, using Maxwell equations and approximation via Kirchhoff diffraction theory [AIAA PAPER 65-424] 04 p0723 A67-15232

Incipience, growth and detachment of boiling bubbles in saturated distilled water from artificial nucleation sites of given geometry and size in heated metal surface 04 p0734 A67-15847

Arc formation at metal surface in hydrogen plasma analyzed at various gas pressures, using Penning discharge, noting heat treatment effect on hydrogen 05 p0850 A67-16066

Titanium surface alloying in aluminum

melts at temperatures from 700 to 1000 degrees C 05 p0828 A67-16328

Surface plasma wave dispersion in metals, noting method for solving Kulik equation 05 p0864 A67-16761

Surface current excitation by electromagnetic and electrokinetic waves on metal cylinder immersed in uniform collisionless isotropic plasma 06 p0962 A67-18075

Mass spectrometric investigation of composition of negative ion sputtering products of solid metal surfaces under cesium ion bombardment 06 p1036 A67-18425

Apparatus used to study exoelectronic emission from metallic surfaces, detailing Geiger counter, high voltage rectifier, scaling device and counting rate meter 07 p1201 A67-19256

Surface defects effect on mechanical properties of sheet metal under tension and bending, tracking brittle fracture to stress concentrators 07 p1263 A67-19751

Soviet book on electron properties of metals and alloys 08 p1371 A67-21490

Cryogenic low pressure seal to seal aluminum or stainless steel flanges 08 p1336 A67-21498

Surface preparation for aluminum and bond strength dependence on cure temperature, humidity and impurities 09 p1507 A67-22519

Currents caused by light pressure on metal surface and in flare plasma when laser beam hits surface 10 p1664 A67-23333

Microstructural variations of Ti-Mo-Al alloys due to stress corrosion cracking, noting increased resistance through heat treatment [ASME PAPER 67-GT-5] 11 p1808 A67-24793

Computer analysis of curve for total emission from group of separate localized emission points on surface of high vacuum metallic cathode 11 p1820 A67-24922

Preparation and characterization of metal surfaces for study of emittance properties as function of surface roughness and oxidation [AIAA PAPER 67-318] 12 p1957 A67-26033

Rough metal surface bidirectional reflectance, using Davies and Beckmann models [AIAA PAPER 67-319] 12 p2037 A67-26034

Closed form solution for determining total emissivity of metals and radiation conductivity of radiation shield for nongray metallic surfaces at low temperature [AIAA PAPER 67-335] 12 p2038 A67-26049

Thermal radiation characteristics of metallic surfaces, comparing metal dispersion relationships with experimental emissivity 13 p2130 A67-26439

Depolarization of linearly polarized EM waves backscattered from rough metals and inhomogeneous dielectrics with known statistical properties 13 p2158 A67-26878

Thermal accommodation of rare gases on clean metal surfaces, computing energy interaction with linear nearest-neighbor lattice 13 p2098 A67-26941

Thermal accommodation coefficient measurements with rare gases and metals and alkali metal sets 13 p2223 A67-26942

Thermal accommodation coefficient of rare gases on clean tungsten surfaces with gas temperature above room temperature 13 p2223 A67-26943

Noble gas molecular beam quasi-specular scattering from metal surfaces noting effects of beam incidence angle, molecular weight and gas temperature 13 p2099 A67-26949

Lobular scattering of 1 eV energy chopped argon beams from silver, mica and brass surfaces, noting distributions and contamination effects 13 p2099 A67-26950

Thermal phenomena arising upon projectile impact on metal surface 13 p2220 A67-27383

Machinery wear, galling and scuffing reduction by using graphite and molybdenum disulfide as dry film lubricants 14 p2324 A67-27999

Metallic couples ultrahigh vacuum adhesion experiments show contaminant dispersal as major barrier 15 p2492 A67-29493

Surface reactions and structure determinations of oxides of niobium, tantalum and vanadium with /110/ surfaces from CO and oxygen absorption 15 p2504 A67-29881

Reduced blackness coefficients measured

for coaxial system of tungsten-molybdenum surfaces by calorimetric method 16 p2780 A67-31778

Mechanisms of atomic recombination at surfaces analyzed, considering behavior of insulators and semiconductor oxides 18 p2997 A67-33794

Metal surface property improvement by thermal-spray coating noting flame plating 18 p3055 A67-34483

Absorption of oxygen upon clean nickel surface and beginning of oxidation 19 p3244 A67-34937

Interaction of oxygen with tungsten surface at room temperature 19 p3244 A67-34940

Plasma wave influences on metal surface reflectivity investigated using Maxwell equation, calculating dielectric constant and conductivity 19 p3262 A67-35581

Electromagnetic radiation reflectivity on metal surface investigated using microscopic model to derive fields and boundary conditions 19 p3262 A67-35582

Absorbance and emittance of metal surfaces determined via cyclic incident radiation, noting error computation and method accuracy 19 p3346 A67-35742

Structure of surfaces - Conference, Durham, N.C., November 1966 19 p3246 A67-35782

Fractional order peaks in low energy electron diffraction /LEED/ patterns from single crystal metal surfaces 19 p3246 A67-35783

Surface bombardment damage on molybdenum and tungsten crystals by inert gas ions 19 p3246 A67-35784

Low energy electron diffraction /LEED/ observations of interaction of tungsten surface with adsorbates 19 p3246 A67-35785

Cold welding tendencies and frictional studies of clean metal combinations under ultra high vacuum 19 p3237 A67-35839

Axial residual stress determination in metal surface layers based on measuring strains 19 p3343 A67-35844

Electron emission utilized in evaluating metal surface properties, particularly sintered material porosity 19 p3247 A67-35849

Factors influencing secondary electron emission produced by high energy molecular beam impact on metal surface 20 p3488 A67-36438

Aluminum corrosion behavior stressing surface oxide film condition 20 p3465 A67-36635

Vertical magnetic induction effect on nucleate boiling of mercury on horizontal heating surface [AICHE PAPER 20] 20 p3552 A67-36830

Surface plasma oscillations at optical frequencies detected by radiation from optical grating metal surface, measuring dispersion relation 20 p3514 A67-37569

Surface geometrical variations in electrochemical shaping process for hydrodynamic removal of dissolved processed metal, deriving partial differential equations 21 p3636 A67-38897

Photoelectric method for measuring temperatures in metal cutting 21 p3631 A67-38921

Epitaxial growth of gold on cadmium iodide surface studied with transmission electron microscopy, discussing diffraction patterns and substrates preparation 21 p3687 A67-39140

Surface states effect on current-voltage characteristics of metal-semiconductor contact from kinetic coefficients of electron exchange 22 p3858 A67-39570

Hemispherical reflectance of metal surfaces investigated for relation of wavelength and surface roughness 22 p3920 A67-40420

Chemical milling of aluminum alloy parts by dimensional etching, discussing protective coatings 23 p4009 A67-40641

Temperature of metal surface irradiated by giant pulse laser beam by measuring energy of emitted thermal ions 23 p4015 A67-41035

Frictional processes of metal surfaces under boundary lubrication conditions emphasizing initiation of seizure 23 p4010 A67-41063

Oxygen diffusion through lubricant to metal surface examined for influence in corrosive wear

- [ASLE PAPER 67-LC-4] 24 p4164 A67-42743
Limit diffusion flux on rotating ring
electrode surface in turbulent regime,
determining mass transfer
constant 24 p4146 A67-43112
- METAL VAPOR**
High temperature reaction between
refractory whiskers of silicon nitride and Al
and Ni, observing results by electron
microscopy 03 p0445 A67-13528
Laser radiation effect on metals, noting
disintegration mechanism, indentation
formation and vapor
formation 08 p1337 A67-20856
Transverse separation of rare gas-metal
vapor mixture components in positive
nonisothermal plasma column in plain-
symmetric glow discharge 09 p1545 A67-21998
Electron sources from arc discharge
plasma in metal vapor, using copper and tin
cathodes 09 p1548 A67-22327
Alkali metal vapor and inert gas mixtures
with alkali seeding radiation properties,
noting nonequilibrium argon-krypton plasma
parameter determination in electrical
discharge 16 p2710 A67-30522
Physical properties of binary pulsed
discharge plasma in helium and argon
seeded with Cs and K
vapor 16 p2711 A67-30525
Hydrodynamics of liquid-gaseous metal
mixture flowing through nozzles, discussing
heat exchange rate and condensation
effects 16 p2656 A67-30574
Electrical conductivity measurement of
liquid-vapor potassium mixture flowing in
circular steel tube simulating MHD oscillator
conditions 16 p2712 A67-30575
Fluid metal magnetohydrodynamic power
conversion program
results 16 p2606 A67-30584
Thermodynamic characteristics and plasma
parameters of lithium vapor in wide
pressure and high temperature
range 16 p2721 A67-31389
Lithium plasma source current-voltage
characteristics in vacuum, obtaining
parameters valid for arcs burning under
atmospheric pressure and nonzero magnetic
fields 17 p2906 A67-33089
Multiquantum photoionization applied to
laser-induced breakdown thresholds in
cesium and rubidium
vapors 19 p3241 A67-35810
Valveless metal vapor feed system for use
in pulsed plasma accelerators employing
mercury as propellant
[AIAA PAPER 67-738] 21 p3695 A67-38760
Evaporated metallic contacts to conducting
strontium titanate single crystals measured
for electric properties evaporated metallic
contacts to conducting strontium titanate
single crystals measured
for 23 p4038 A67-40874
Excitation effect on single electron charge
transfer collisions of Fe ions in various
gases determined with different excited
states of ions 23 p4030 A67-40976
Device for metering variety of metals for
high vacuum evaporation designed for thin
film metal-insulator-metal diodes
fabrication 23 p4001 A67-41223
Phenomena between evaporated metal and
semiconductor surface affecting potential
barrier by metal electrons extraction
potential and semiconductor fast state
concentration 24 p4204 A67-42410
Real gases examined for application as
working fluid in Brayton cycle power plant,
considering radiator area reduction to
Rankine cycle 24 p4102 A67-42488
- METAL WORKING**
SA BRAZING
SA CUTTING
SA FINISH
SA FORGING
SA GRINDING
SA HARDENING
SA MELTING
SA SMELTING
Deformation processing of beryllium with
respect to mechanical properties, economics
and manufacturing considerations, examining
production techniques
[SAE PAPER 660634] 01 p0078 A67-10608
Titanium crossbeam design and fabrication
[SAE PAPER 660647] 01 p0079 A67-10610
Titanium fabrication techniques for XB-70
and space booster
[SAE PAPER 660650] 01 p0079 A67-10611
Metal and alloy heat treatment
Intensification with ultrasonic techniques
improve steel recrystallization,
etc 01 p0095 A67-10640
Mechanical property and structural
changes in titanium alloys subjected to high
temperature thermomechanical
treatment 01 p0095 A67-10641
Metastable phase formation in Ti alloys,
noting nature and properties of different
phases 01 p0095 A67-10642
Powder metallurgy - International
Conference, New York, June 1965, Volume 2,
Applications 01 p0097 A67-10696
Book on thermal effects and cutting
machinability of aircraft
materials 03 p0427 A67-13190
Hardening during plastic deformation of
steel samples under compression, deriving
stress-strain state in cutting
process 03 p0427 A67-13193
Plasma needle arc process for welding,
brazing and cutting very thin metals for
extremely low current
work 03 p0430 A67-13690
Electrochemical machining, discussing
relationship between total current, applied
potential, electrolyte flow rate, electrolyte
conductivity and electrode gap
[ASME PAPER 66-PROD-5] 03 p0432 A67-13833
Soviet monograph on vacuum arc melting
of titanium alloy ingots noting crystallization
process, structural changes and properties of
end-products 03 p0447 A67-13925
Capacitor pressure sensor produced by
furnace brazing molybdenum to itself and to
zircon with pure copper and Cu-Au-Ni filler
metals 04 p0630 A67-15460
Superconductivity in aged Zr-Nb alloys,
noting transition temperature increase of
quenched alloy upon
aging 05 p0828 A67-18469
Microscopic hole drilling into metals by
laser beams, noting energy and power
correlation with hole
magnitude 07 p1190 A67-19090
Heat treatment effect on mechanical
properties and structure of Ti alloys, noting
phase state variation as function of
quenching temperature 07 p1206 A67-19282
Heat resistance of Ti alloy after
thermomechanical treatment, noting
properties as long lifetime structural
material 07 p1206 A67-19284
AT13 Ti alloy preparation noting physical
and mechanical properties and heat
treatment induced phase
transformation 07 p1207 A67-19287
VT15 titanium alloy weld properties as
affected by machining and postwelding heat
treatment 07 p1208 A67-19294
Deformation speed effect on structural
changes in Ti, noting test results at 600
degrees C 07 p1209 A67-19735
Soviet book on new elements in
technology of
pressworking 07 p1191 A67-19746
Maximum permissible angle in beveling,
springiness of beveled part and heating
effect on beveling process analyzed,
considering loading 07 p1191 A67-19747
Compression process for hollow cylindrical
blanks using integration method, viewing
deformation as sum of sequential stages of
small dislocations 07 p1191 A67-19748
Forming closed contour shells by straining
with expandable punch 07 p1191 A67-19750
Blank heating processes in production by
pressworking of seamless adapters for
detachable tube joints 07 p1192 A67-19754
Tensile and bending strengths as
suitability criteria of pressworking of
materials 07 p1192 A67-19755
Electron microscope analysis of stress
corrosion crack failure 07 p1211 A67-20250
Satellite structure from Be-10c alloy,
properties compared with Al and joining
methods 07 p1192 A67-20251
Aerospace castings from light ternary Mg-
Li-Si alloy, discussing fabrication
development 07 p1193 A67-20254
Fracture behavior of Ti alloys in aqueous
environment, noting process to increase
fracture toughness 08 p1340 A67-20364
Structural changes and changes in elastic
properties of cold rolled Ti and Zr during
recrystallization heating 08 p1342 A67-21003
Electrical characteristics of thin film
nickel-chromium resistors dependency on
variation in processing parameters including
source and film composition, deposition rate,
etc 09 p1555 A67-22103
Electron beam welding in vacuum and in
atmosphere, describing rapid positioning,
workpiece guidance, beam control and
observation 09 p1503 A67-22119
Metal working problems involving sheet
metal, powder metallurgy, extrusion,
nondestructive testing and concerning high
strength, refractory and superalloys
[SAE PAPER 670098] 09 p1509 A67-22540
Roll fatigue tests of forged ZK60A-T5
magnesium and 2014-T6 aluminum
wheels 10 p1661 A67-23439
Cutting tool and cutting fluid evaluation,
economic considerations for aerospace
manufacturing
[ASTME PAPER WES-7-27] 11 p1798 A67-24256
Productibility of aerospace products with
regard to machinability of aluminum alloy
[ASTME PAPER WES-7-29] 11 p1798 A67-24257
Nb embrittlement by H at ambient
temperatures under work hardening effect,
noting correlation between elastic limit and
deformability in H 11 p1808 A67-24427
Future Air Force requirements for base
metal forms and metal-working techniques
including hot strength alloy forgings, fine
wire, etc 12 p1948 A67-25286
Molybdenum and niobium effect on
structure and physical properties of
austenitic Cr-Mn steels with or without
nickel 12 p1955 A67-25439
Effect of small cold deformation preceding
aging in nickel maraging
steel 13 p2132 A67-26575
Metal working methods, discussing high
hydrostatic pressure, pressurized liquid,
extrusion and high rate 13 p2123 A67-26699
Electron microscope study of cold working
and tempering of beryllium single
crystals 13 p2138 A67-27117
Machining damage in beryllium from
single point turning and
drilling 13 p2123 A67-27133
Specifying temper for stainless steel
tubing, noting properties of various
techniques 13 p2124 A67-27175
Aluminum, Volume 2, Design and
application 14 p2322 A67-27811
Methods for transformation of titanium
alloys by forging or die stamping to meet
particular requirements 14 p2324 A67-28630
Book on nontraditional machining
processes covering process parameters,
shape and materials applications, tooling,
chemical removal, etc 14 p2328 A67-28893
Internal friction of annealed and cold-
worked niobium and tantalum wires
containing oxygen and nitrogen measured,
noting cold-work peaks in addition to Snoek
peaks 15 p2503 A67-29748
Machinability of high strength steels,
titanium alloys and refractory alloys,
examining cutting and RF current induction
for heat treatment 15 p2505 A67-30126
Extremal principle of possible
simultaneous variations of stressed and
strained states which follows from origin of
virtual velocities 15 p2576 A67-30182
Cerium addition effects on magnesium
workability evaluated by sample elongation
in tension test and plate working limit in
cold rolling 15 p2505 A67-30398
Weldability test method, developing rig
which permits arc welding in argon
atmosphere with TIG
electrode 16 p2681 A67-30833
Inclusion type, forging ratio and heat
treatment effect on properties of
longitudinal and transverse steel
specimens 16 p2689 A67-31310
Book on machining Alcoa aluminum
covering Al alloys properties, requirements
for machine tools, cutting conditions and
compounds, finishing operations,
etc 18 p3053 A67-33771
Electrostream process for drilling very
small diameter holes in superalloys for gas
turbine and nozzle vane fabrication
[ASTME PAPER MR67-141] 18 p3054 A67-34175
Shear-spinning technique for
manufacturing molybdenum alloy missile
nose tips 18 p3054 A67-34365
Metal and alloy heat treatment
intensification with ultrasonic techniques
improve steel properties, recrystallization,
etc 18 p3066 A67-34404
Mechanical property and structural

changes in titanium alloys subjected to high temperature thermomechanical treatment 18 p3066 A67-34405

Metastable phase formation in Ti alloys, noting nature and properties of different phases 18 p3066 A67-34406

Broadening of Debye-Scherrer line profiles and structure recovery studied in cold-worked Ti, Zr and Hf specimens by X-ray analysis 19 p3247 A67-35835

High velocity metalworking /HVM/ techniques, applying transient pressure to specific workpiece area 20 p3454 A67-36886

Group IV and V metal carbides ball-milled to determine mechanical strain effects 20 p3467 A67-37122

Plasma arc for high quality cutting and piercing of thick metals 20 p3456 A67-37694

Machines and machining technology for materials used in Mach-3 aircraft structures, discussing cutting fluids, cutter and best metal removal rate 21 p3631 A67-38014

Niobium and niobium alloy structural changes during heating after pressing and rolling deformation 21 p3644 A67-38031

Characteristic method for determining stress field and plastic deformation mechanism during cutting, notching and punching processes 21 p3632 A67-38060

Stress-strain distribution in clamped membrane during stamping, deriving formulas for plastic deformation of metals 21 p3632 A67-38061

Giant forging press for aircraft and aerospace components 21 p3634 A67-38198

Volume strains in metals during pressworking and rolling 21 p3637 A67-38922

Electron beams applied during pressworking of sheet materials to provide temperatures favorable to microstructure defect healing 21 p3637 A67-38927

Heat treatment effects on mechanical properties of steel-forged gas turbine rotor shafts, including microcracks formation and growth and structural strength 22 p3819 A67-39323

Maraging steels development, discussing mechanical properties, metal working, etc 22 p3819 A67-39388

Hot rolling finishing temperature and cooling rate effects on aged 250 grade 18 Ni maraging steel fracture toughness 22 p3822 A67-40057

Heavy section forgings of Ti and high tensile strength Ti alloys with thicknesses up to 10 inches 22 p3822 A67-40197

Closed die forging of nickel base superalloys for large turbine wheel components [ASM PAPER C6-18.4] 23 p4010 A67-41401

Beryllium part fabrication by metal removal, discussing machining and surface treatment methods [SAE PAPER 670803] 24 p4159 A67-41990

METALLIC PLASMA

Nonisothermal alkali plasma collisional drift instability in radial electric field 11 p1834 A67-24380

Calculation of thermal excitation function and optimum temperature and pressure of atom and ion spectral line shift in two-component plasma 11 p1840 A67-24580

Alkaline-metal-plasma machine design, studying operating modes with electric probes 18 p3091 A67-34631

Discharge plasmas in hollow cathodes investigated using photography, showing mercury vapor and inert gas plasmas form homogeneous or laminar positive plasma columns 19 p3274 A67-35102

Alkali-metal magnetoplasma properties related to enhanced diffusion, showing relationship to beam-plasma interaction 19 p3287 A67-35360

Comparison of experimental and theoretical results on electron beam produced mercury-vapor discharge 19 p3290 A67-35380

Ceramic material requirements for MHD generator electrodes and duct walls, discussing tests in alkali-seeded plasma 20 p3472 A67-36114

Laser-created alumina plasma ion-energy spectrum, measuring plasma characteristics with pentagrid energy analyzer 24 p4199 A67-43102

METALLOGRAPHY

Deformation speed effect on structural changes in Ti, noting test results at 600 degrees C 07 p1209 A67-19735

Microstructure interpretation of 5Al-2.5Sn titanium alloy, examining high optical magnification and polarized light illumination 08 p1340 A67-20365

X-ray diffraction and metallographic investigation show iron meteorites shock at pressures of at least 130 kbar 10 p1705 A67-22954

Corrosion test on turbine blades with nickel and cobalt base conducted in burner rigs, using metallographic examinations [ASME PAPER 67-GT-2] 11 p1808 A67-24790

Soviet papers on mechanism of metal breakdown 13 p2130 A67-26446

State diagram structure of Ti-Cu system examined using metallographic, thermographic, X-ray and microhardness analyses 13 p2131 A67-26473

Niobium-cobalt alloys constitution, determining equilibrium diagram by thermal analysis, microscopic metallography and X-ray diffraction techniques 14 p2338 A67-28615

Book on mechanical properties of ordered alloys including formation of superlattices 15 p2504 A67-30028

Aluminum welded joints investigated by radiographic and metallographic methods for bubbles and cracks 18 p3053 A67-33743

Structure and decomposition of Goose Lake meteorite and fragments 19 p3323 A67-35424

Binary molybdenum-carbon system investigated using X-ray, metallographic, thermoanalytical and melting-point techniques 20 p3470 A67-37389

Electron beam welded D6AC steel plates evaluated after heat treated condition /stress relief/ for mechanical properties 20 p3456 A67-37695

Electrolytic polishing technique for bright field etch of Be specimens 24 p4173 A67-42349

METALLURGY

SA FRACTOGRAPHY

SA HYDROMETALLURGY

SA POWDER METALLURGY

SA SMELTING

Three-component diffusion theory applied to calculation of three-component metallic solid solutions, examining interstitial and substitutional systems with different boundary conditions 02 p0256 A67-12707

Refining, forming and utilization of metals, discussing high pressure forming, vacuum degassing and superplasticity 03 p0440 A67-13198

Refractory metal alloys rating on basis of weldability emphasizing metallurgical considerations, taking into account process control and welding as thermal process 05 p0830 A67-16829

New metals replacing steels noting titanium, beryllium and niobium in French industry 06 p1017 A67-17994

Soviet papers on metallochemistry of titanium alloys [JPL-TR-32-807] 07 p1202 A67-19259

International Vacuum Congress, Stuttgart, June-July 1965, Volume 2, Part III 09 p1484 A67-22116

Gas saturated layer effects on VT5 titanium alloy mechanical properties variation with temperature 10 p1870 A67-23642

Stress corrosion cracking of titanium alloys, noting tensile test data, crack propagation in salt solution and in pure solvents and metallurgical and electrochemical factors 10 p1870 A67-23701

Future Air Force requirements for base metal forms and metal-working techniques including hot strength alloy forgings, fine wire, etc 12 p1948 A67-25286

Metallurgy of beryllium - Conference Grenoble, France, May 1965 metallurgy of beryllium - Conference, Grenoble, France, May 1965 13 p2134 A67-27101

Soft magnetic materials metallurgy for several types of electrical equipment 13 p2178 A67-27140

Quality control in electron beam welding, discussing design, metallurgical aspects, etc 13 p2124 A67-27168

Aluminum, Volume 1, Properties, physical metallurgy and phase diagrams 14 p2334 A67-27801

Ultrasonic energy applied to several metallurgical processes, exploring possible application to metal reinforcement 14 p2337 A67-28321

Titanium alloys research and development for aeronautics industry 14 p2338 A67-28627

Technological, physical, mechanical and heat resistance properties of new titanium alloy developed on titanium aluminide 16 p2691 A67-31590

Plasma technology in industry, discussing Polish-made plasma torch design and operation and plasmatron and spraying applications 17 p2865 A67-32189

Metallurgical aspects of nitrided component application in unmanned satellite drive systems to remedy sliding wear and increase reliability 18 p3058 A67-34676

Soviet book on high temperature nonmetallic thermocouples and sheaths covering thermal control automation of metallurgical processes, thermoelectric and refractory properties, electrodes, electromotive force, etc 19 p3227 A67-34922

Soviet metallurgical, chemical and electrochemical studies and industrial applications of titanium 24 p4169 A67-41918

METAMORPHISM

Chondrites metamorphosis and equilibrium, studying iron oxide and rare gas content, petrological factors and material formation 18 p3134 A67-34494

Ferrous ion order-disorder in meteoritic pyroxenes, using Moosbauer iron 57 absorption, noting metamorphic history of chondrites 21 p3702 A67-38128

METASTABLE ATOM

Metastable phase formation in Ti alloys, noting nature and properties of different phases 01 p0095 A67-10642

Electron density enhancement in thermal plasma by metastable atoms, computing ionization by method of Lagrange multipliers 02 p0272 A67-11519

Metastable exciton states of cadmium and lead iodide obtained from fundamental reflectivity spectra 06 p1060 A67-18915

Microwave and optical measurements of decay of neutral metastable and charged species in flowing He afterglow 08 p1356 A67-21300

Atomic beam source for metastable Ca atoms in measuring population numbers from absorption lines 09 p1534 A67-21564

Helium-neon CW laser oscillation at 1.1523 microns observed in high velocity gas flow system, using rapid mixing of metastable helium atoms with initially unexcited neon 09 p1510 A67-21568

Bohn ionization equation applied to helium plasma to include effect of He 2 energy levels 09 p1544 A67-21883

Molecular metastables produced in positive column of helium discharge by electron excitation 09 p1548 A67-22368

Ionization coefficients in helium over pressure range near to atmospheric show destruction of metastable states in gas accounts for dependence on electric field 10 p1681 A67-22962

Energetic metastable diatomic oxygen molecule excited by electron impact studied with high sensitivity molecular beam apparatus 10 p1682 A67-23386

Gamma decay of Se 73 and Se 81 isomeric pairs with half-lives, energies and decay schemes 11 p1822 A67-23980

Electronic absorption spectrum observed during cyanogen azide flash photolysis 13 p2177 A67-26988

Superconducting transitions of three metastable states of Ga 17 p2915 A67-32707

Noise analysis in He-Ne laser during RF and DC excitation, noting relation between critical frequency and lifetime of metastable atom 18 p3058 A67-33648

Active medium radial variation in density of neon atoms metastable level as explanation of anomalous laser oscillation 18 p3060 A67-34013

Metastable atomic oxygen state observed in microwave discharge of molecular oxygen, noting g factor of 2 in strong resonance 18 p3082 A67-34029

Metastable phase formation in Ti alloys, noting nature and properties of different phases 18 p3066 A67-34406

Secondary ionization processes in mercury vapor, calculating relative populations of excited and metastable atoms per ion pair 19 p3265 A67-35090

Electronic energy transfer between metastable argon and nitrogen molecule, noting rotational enhancement 20 p3487 A67-36228

Metastable helium atom altitude distribution and 10830 angstrom radiation

emission rate, discussing possible explanation of helium loss from atmosphere 20 p3427 A67-36310

Direct excitation in argon gas from metastable state to upper laser state compared with two-step excitation 20 p3460 A67-36860

Energy level behavior of metastable alkali atoms against autoionization and radiative decay 20 p3492 A67-37691

Lifetime decrease of metastable state of chromium ion in ruby and emerald due to temperature raise, showing radiative transition 21 p3676 A67-37816

Energy difference between metastable levels of hydrogen-like atom determined by measuring lifetime in electrostatic field, yielding average Lamb shift in Li ion 22 p3839 A67-39202

Spontaneous annealing models of lithium-diffused Si solar cells, discussing defect compensation and metastable defect formation 23 p3941 A67-41523

Phonon annihilation during decay of two metastable fluorescent states of ionized Ba compound 24 p4205 A67-42737

METAZOAN

Micrometazoa as model systems for studying physiology of memory at cellular level, examining habituation and maze behavior 20 p3369 A67-36657

METEOR

SA ASTEROID

SA CEPHEID

SA LEONID METEOR

SA PERSEID METEOR

SA QUADRANTID METEOR

SA RADIO METEOR

SA SPORADIC METEOR

Meteor luminescence during atmospheric motion, obtaining radiation coefficient as function of cross sections of particle excitation and pulse transfer processes 01 p0151 A67-11287

Meteor sighting probability and problem of actual number of meteors 03 p0511 A67-13815

Antimatter in meteors from interpretation of mean gamma radiation intensity measurements 04 p0698 A67-14940

Soviet papers on physics of comets and meteors 05 p0888 A67-16199

Rotating shutter telescopic observation for optical measurement of faint meteor velocity 05 p0897 A67-16805

Difference of dynamic and photometric mass of meteors cannot be explained in terms of differences in constants of drag and light curve equations alone 05 p0897 A67-16806

Diffusion influence on radio determination of meteor velocity by diffraction method 05 p0897 A67-16807

Heat emission from compression shock layer about meteors in thermodynamic equilibrium 05 p0903 A67-17313

Pumping medium power lasers using artificial meteors to produce intense gas glow in compression wave 06 p1009 A67-17757

Bright meteoric orbits according to photographic observations at Dushanbe and Odessa 06 p1084 A67-18165

Theory and experiment relating to interplanetary bodies larger than molecules but smaller than asteroids 07 p1246 A67-19054

Sporadic E ionization and anomalous increase in rate of radar meteor counts during 1963 in mid-latitude European stations 07 p1172 A67-19424

Upper atmosphere temperature, pressure and density determined by photographic observations of meteors, based on calculating height of homogeneous atmosphere 07 p1174 A67-19708

Microwave reflection from region with nonuniform hydrometeor for case where dimensions vary greatly and relation to wavelength is arbitrary 11 p1754 A67-24981

Photographic meteor observations 1957-1961 at Kiev 13 p2196 A67-26495

Meteor orbital elements according to photographic observations 13 p2196 A67-26496

Meteor hyperbolic motion and geocentric trajectory determination 13 p2196 A67-26497

Drag effects on meteoric bodies studied by photographic observations 13 p2196 A67-26499

Number of fragments in meteor fragmentation 13 p2197 A67-26500

Developments in techniques of meteor

spectral observations 13 p2197 A67-26503

Effective diffusion cross section for meteor atoms in atmosphere, using Thomas-Fermi-Dirac and dumbbell molecule models 13 p2111 A67-26553

Photographic determination of meteor masses, examining dependence of radiation coefficient 13 p2198 A67-26555

Goniometric measurements of two angles defining direction of incoming 30 MHz wave reflected by meteor streams, using radio link 14 p2390 A67-28900

Bright meteoric orbits according to photographic observations at Dushanbe and Odessa 16 p2741 A67-30509

Near-earth meteor flux estimate through luminous efficiency and ionizing probability application to data on radio and photographic meteor fluxes 19 p3319 A67-35217

Meteor mass distribution, estimating exponent constant in cumulative influx formula 24 p4225 A67-41828

Absolute radar echo duration dependence on meteoroid mass calculated for various velocities 24 p4228 A67-42268

METEOR I ROCKET

Wind velocity and direction measurements by radar tracking of chaff /dipoles/ clouds 19 p3219 A67-35247

METEOR BURST

Meteor burst radio propagation channel clock synchronization experiment to determine frequency offset between two remotely located frequency standards 09 p1494 A67-21618

METEOR DUST CLOUD

Linear electron density measurement in meteor trains using radio echo observations of Geminids 1963 stream 05 p0889 A67-16206

Meteor stream relation to natural ice nuclei and precipitation 13 p2205 A67-27461

Tektite field origin hypotheses including terrestrial and lunar 15 p2551 A67-29093

METEOR HAZARD

Space vehicle hazard due to focusing of meteor streams by earth in antiradiant direction 12 p2002 A67-25656

Mission profiles involving new materials for missile and space structures reviewed for progress in computer applications 22 p3915 A67-40330

Leakage rate due to meteoroid penetration of single and multiple hulled spacecraft, discussing effect on internal pressure 24 p4251 A67-42928

METEOR SHOWER

Mass distribution of meteoric bodies and relation to autocorrelation function of disintegrated planetary surface 02 p0329 A67-12495

Micrometeoroid sampling with Luster sounding rocket during Leonid meteor shower, detailing contamination control program 04 p0699 A67-14966

Observed meteor luminosity and deceleration compared with theoretical values 05 p0889 A67-16209

Atmospheric tides deduced from drifts of ionized meteor trains observed by Doppler shift of echoes 05 p0803 A67-17405

Aerobee rocket measurement in sampling of micrometeoroid debris during peak of Leonid meteor shower 10 p1707 A67-23237

Number and total mass of meteor particles captured by earth atmosphere from cosmic space to closed geocentric orbits 10 p1708 A67-23242

Mass distribution of meteoric bodies and relation to autocorrelation function of disintegrated planetary surface 10 p1709 A67-23363

Periodicity of precipitation singularities and relation to period of comets and meteor streams 11 p1815 A67-24329

Relationship between Pons-Winnecke comet and certain types of meteor showers 13 p2196 A67-26498

Sporadic E layer formation and possible creation of more favorable conditions by high meteor activity 13 p2201 A67-27391

Meteor stream relation to natural ice nuclei and precipitation 13 p2205 A67-27461

Observed micropulsation activity during meteor shower compared with predicted magnetic agitation value determined from equation by Chapman and Ashour 14 p2383 A67-28045

Ferromagnetic dust concentration variations in upper atmosphere during meteor shower 16 p2668 A67-31707

Meteoritic satellites of earth, estimating capture region 17 p2941 A67-32324

Vertical distribution of meteor showers obtained by measuring distribution in decay times of underdense radio echoes 20 p3321 A67-36303

Micrometeorite flux rate for Leonid shower measured with Luster sounding rocket collecting surface 20 p3528 A67-37424

Contamination control program developed for investigation and elimination of contaminant particles from 1965 Leonid Meteor Shower micrometeoroids collected by rocket payload 23 p3986 A67-40850

Experimental facilities to test antimatter hypothesis of comets and meteoric swarms 23 p4069 A67-41689

METEOR SLAG

Meteoritic matter obtained by piezoelectric pickups applied to Luna X, noting impact frequency for interplanetary space 01 p0150 A67-10910

METEOR TRAIL

Statistical properties of echoes from meteoric trails during forward scattering, determining diurnal variations for number, duration and fill factor of reflected signals 01 p0025 A67-10791

Linear electron density in meteoric trails determined not by vaporization rate but by number of meteoric atoms moving together with body at given moment 02 p0322 A67-11677

Ionization efficiency and cross section of meteor trails during collision between particles of meteoric vapor and air molecules 02 p0329 A67-12494

Mass distribution of meteoroid flux determined by relating frequency distribution of durations of radar echoes from meteor trails 03 p0516 A67-14348

Plasma resonance measurement from radio wave scattering in cylindrical tubes which simulate meteor trail models 04 p0700 A67-15226

Meteor train drift observation, describing apparatus and data processing used by Kharkov Polytechnic Institute 05 p0889 A67-16208

Upper atmospheric turbulence measurements based on radiolocational observation of meteor trains 05 p0796 A67-16211

Upper atmospheric turbulence and wind measurement by radio reflection from meteor tail 05 p0802 A67-17382

Distribution of instantaneous value of amplitude of signal after scattering on meteor trails 07 p1250 A67-19721

Solar cycle variations in atmospheric density deduced from meteor observations and rocket measurements in mesopause and thermosphere 10 p1638 A67-23204

Ionization efficiency and cross section of meteor trails during collision between particles of meteoric vapor and air molecules 10 p1709 A67-23362

Anomalous high diffusion coefficients determined from dispersion of chemical contaminant releases and long lasting meteor trails at various altitudes 12 p1935 A67-25792

Meteor trains detection and study of motions in upper atmosphere using Garchy meteor radar with continuous wave 13 p2195 A67-26467

Ferrite-diode system with automatic gating of signal reflection used in radar wind velocity observations to reduce pulse interferences produced by meteor trails 13 p2197 A67-26505

Diurnal, annual and seasonal variations of high altitude turbulent motions in upper atmosphere through observation of meteor trails by coherent pulse method 13 p2110 A67-26506

Meteor distribution estimation attempted through radar observation, measuring kinetic energy level, velocity and electron distribution in meteor trails 13 p2197 A67-26507

Initial radius of ionized meteor track, taking into account dependence of effective diffusion cross section of meteor atoms in atmosphere on relative velocity 13 p2198 A67-26554

Diurnal and seasonal variations in radio echo observations from meteoric trains during forward ultrashortwave scattering 14 p2383 A67-27924

Molecule dissociation in meteoric trains,

discussing coordinate system to determine cross sections for dissociation of magnesium and silicon oxides 14 p2383 A67-27945

Ionospheric micropulsations induced by enhanced conductivity of current due to meteors, noting end effect from finite ion trail length 14 p2383 A67-28044

Satellite-launched artificial meteors discussing use, system concept, orbit considerations, cost, acceleration and separation 16 p2758 A67-30645

Linear electron density in meteoric trails determined not by vaporization rate but by number of meteoric atoms moving together with body at given 16 p2747 A67-31092

Radar observation of meteor echoes in upper atmosphere, particularly deionization of processes in meteor 16 p2749 A67-31251

Probability of perceiving meteor determined on basis of observation by independent counting method by group of observers 16 p2751 A67-31460

Atmospheric trajectories of faint telescopic meteors observed by separate stations simultaneously and probability of plotting 16 p2751 A67-31461

Color indices of visible meteors observed by naked eye and through color filters noting brightness dependence and meteor train distribution 16 p2751 A67-31462

Soviet book on meteors in earth atmosphere studied by radar discussing meteor trails, upper atmosphere winds, etc 16 p2754 A67-31866

Distribution of meteoritic matter in solar system determined, using radar observations and astronomical photography 17 p2941 A67-32321

Helio-centric dust cloud noting correlation of meteor and comet model with observations 17 p2842 A67-32325

Processing results of meteor photographs using panchromatic films and program-controlled exposure time 17 p2942 A67-32328

Observational results consisting of meteor trail photographs for determining processes responsible for relative intensity of brightness and trail 20 p3530 A67-37665

Statistical significance of mathematical and logical foundations of information processing method applied to meteor stream 23 p4070 A67-41690

METEORITE

SA ACHONDRITE

SA ASTEROID

SA BRUDERHEIM METEORITE

SA CARBONACEOUS METEORITE

SA CHONDRITE

SA ELEMENT ABUNDANCE

SA IRON METEORITE

SA IVUNA METEORITE

SA MICROMETEORITE

SA MICROMETEOROID

SA ORGUEIL METEORITE

SA STONY METEORITE

SA TUNGUSK METEORITE

Classical meteoric ablation theory generalized to include thermal radiation, conduction and meteoroid heat capacity in causing fragmentation 01 p0147 A67-10357

Absolute age of earth, heavy elements and meteorites determined by radioactive decay measurements, comparing present and initial ratios of uranium 235 and 238 02 p0329 A67-12496

Cosmic radiation investigated by using meteorites 02 p0310 A67-12580

Meteorites from asteroids in hypothesis based on chemical composition, structure and gas absorption age 04 p0702 A67-15562

Change in intensity and forms of energy spectrum effects on accuracy of measuring values of meteorite preentry dimensions, weight and degree of ablation 05 p0887 A67-16099

Primary cosmic radiation intensity determined with help of nuclear particle tracks in moldavites and meteorites 05 p0887 A67-16100

Fireballs associated with meteorite fall at Barwell 05 p0898 A67-16928

Neutron produced phosphorus 32 measurement in Barwell and St. Severin meteorites 06 p1078 A67-17604

Meteoritic origin from planetary disintegration 06 p1089 A67-18659

Tracks of primary cosmic rays with atomic number greater than or equal to 20 in

meteorites, discussing relationship between track length and particle mass 07 p1245 A67-19942

Spectrum of meteorite luminescence emission after irradiation with protons and UV radiation, using spectrophotometer 08 p1390 A67-21021

Origin of chondrites implied by short period and long period nuclides created by neutron fluxes 10 p1704 A67-22849

Absolute age of earth, heavy elements and meteorites determined by radioactive decay measurements, comparing present and initial ratios of uranium 235 and 238 10 p1709 A67-23364

Hypersthene chondrite origin and history studied using noble gas content and shock and reheating by X-ray diffraction 11 p1865 A67-24602

Disintegration of meteoric bodies in terrestrial atmosphere, disputing conclusion of Kramer 12 p2002 A67-25552

Techniques for determining cosmic ray age and stable and radioactive nuclide production rates in meteorites 14 p2380 A67-27968

Cosmic origin of tektites indicated by factors other than chronology 14 p2385 A67-28145

Chondritic meteorites two-dimensional classification grid based on chemical and petrologic subdivisions 14 p2391 A67-28949

Planetary magnetic fields calculated from meteorite magnetic properties and assumptions about cores and crusts 21 p3711 A67-39042

Change in intensity and forms of energy spectrum effects on accuracy of measuring values of meteorite preentry dimensions, weight and degree of ablation 24 p4238 A67-42775

Primary cosmic radiation intensity determined with help of nuclear particle tracks in moldavites and meteorites 24 p4238 A67-42776

Cosmogenic radioactivity in freshly fallen meteorites measured and compared to calculate terrestrial and exposure ages and spatial and time dependence 24 p4238 A67-42884

METEORITE COLLISION

Ion engine arcing frequency from micrometeoroid impact [AIAA PAPER 66-205] 02 p0302 A67-11936

Origin of Mouna Nong type tektites detached by meteoritic impact, considering lunar origin based on diffusion rates in silicates 06 p1078 A67-17562

Meteoritic influx and crater formation on moon, noting Apollo type asteroids and cometary nuclei 08 p1389 A67-21017

Meteoritic bombardment damage to lunar surface with reference to terrestrial craters and hypervelocity impact 08 p1389 A67-21018

Ries Kessel meteoritic crater /Germany/ analyzed by Fourier data smoothing technique, noting impact center, entry direction, etc 11 p1884 A67-24559

Space flight to Mars, discussing medical problems originating from changing gravitational fields, meteorite dangers, radiation and psychological considerations 13 p2061 A67-26338

Generalization of Oepik theory of planetary bodies collision to include case where orbits of both colliding bodies are ellipses 14 p2384 A67-28055

Micrometeoritic cloud existence near earth refuted by satellite incidence-frequency measurements, describing satellite measuring devices 17 p2850 A67-32975

Lunar surface particles geocentric trajectories, giving perigee distance and velocity curves 18 p3120 A67-33866

Tektite formation and flight from large meteorite impact, discussing blast expansion flow 20 p3530 A67-37527

Possibility of antimatter meteor reaching earth surface on basis of collision theory between matter and antimatter 22 p3882 A67-39589

Penetration depth of hypervelocity impact craters photographed by Luna and Ranger vehicles indicate granular lunar surface 23 p4065 A67-41003

METEORITE DENSITY

Time variance of earth-moon distance, discussing meteoroidal accretion mechanism effect on capture phenomena 02 p0319 A67-11453

Meteoritic body distribution by energies

noting consistency with mass distribution 04 p0701 A67-15228

Statistical characteristics of meteor radio echoes in Geminides stream noting duration, amplitudes, intervals and ranges 05 p0889 A67-16205

Orbit calculation of 12,500 meteors in earth vicinity based on radar observations of radiants and velocities 09 p1563 A67-21635

Meteor particle density study based on photographic observations 13 p2197 A67-26501

Ballistic aspects, structure and destructive power of Tungusk meteorite do not support thermal explosion 15 p2558 A67-30010

hypothesis 20 p3530 A67-37534

Frothing-sloughing ablation concept explains density variations of cometary meteors obtained from photographic and radar observations 17 p2943 A67-32541

Ballistic aspects, structure and destructive power of Tungusk meteorite do not support thermal explosion 20 p3530 A67-37534

METEORITIC COMPOSITION

Cometary origin of Tungusk meteorite of 1908 supported by analysis of space trajectory and observed nightglow at time of fall 01 p0151 A67-11274

Polycyclic aromatic hydrocarbon distribution in Cold Bokkeveld and Orgueil meteorites 02 p0320 A67-11476

Cosmic ray variations studied by effects on Zaisan chondrite 02 p0310 A67-12581

Crystal morphological features of Tucson meteorite 03 p0510 A67-13350

Lanthanide abundance variation and coordination number, comparing abundances in terrestrial and meteoritic materials with average chondrite 03 p0413 A67-13507

Australites, Henbury impact glass and subgreywacke, comparison of abundances of 51 elements 03 p0512 A67-13900

Tunguska meteorite composition, evaluating validity of theory attributing nucleon-antinucleon annihilation to antimatter composition 04 p0701 A67-15546

Meteorite size prior to entering atmosphere, noting radius and use of isotope activity nomogram 04 p0702 A67-15751

Total carbon abundances in enstatite chondrites 05 p0886 A67-16024

Primordial argon and metamorphism of chondrites 05 p0886 A67-16025

Chemical analysis of stony meteorites, noting analytical procedures and results 05 p0895 A67-16581

Multiplicity of bolides of Barwell meteorites, examining validity of conclusion reached by Miles and Meadows 05 p0898 A67-16889

Niningerite composition and optical, physical and crystallographic properties 07 p1247 A67-19064

Comets hypothesized to consist of antimatter originating from parts of galaxy consisting entirely of antimatter 07 p1247 A67-19098

Diffusive fractionation and two-component models for trapped meteoritic neon and isotopic composition of neon in carbonaceous chondrites 07 p1249 A67-19536

Petrology and mineralogy of British Museum noncarbonaceous chondrites and relative abundance of primitive and recrystallized variants by isochemical recrystallization near 900 degrees C 07 p1249 A67-19538

Chemical and mineralogical composition of roedderite found in Indarch meteorite, presenting electron probe analysis and X-ray diffraction pattern optical data 07 p1255 A67-20012

Iron-rich silicates significance in Mezo-Madaras chondrite [AFCL-87-0012] 07 p1256 A67-20013

Mass spectrometric detection of cosmic-ray-produced krypton isotope in meteorites and possibility of Kr-Kr dating 07 p1256 A67-20228

Concentration of Ni, Ga and Ge in series of Odessa and Canyon Diablo meteorite specimens 08 p1385 A67-20936

Origin of fissionogenic Xe isotopes in Pasamonte achondrite 08 p1386 A67-20938

Chondrite metallic minerals, thermal history and parent planets noting nickel, taenite and kamacite crystal components 08 p1397 A67-21207

Hexagonal diamond content of Canyon Diablo and Goalpara meteorites 08 p1400 A67-21264

- Equilibrium temperatures of Fe and Mg ions in chondritic meteorites 08 p1400 A67-21266
- Bununu meteorite /pyroxene-plagioclase achondrite/ composition and structure 09 p1564 A67-21736
- Occurrence, decomposition kinetics and phase equilibria of cohenite, noting almost exclusive presence in meteorites containing 8 percent Ni 09 p1564 A67-21737
- Ge and Ga concentration in selected Fe meteorites used to determine quantization in terms of multiple parent body hypothesis and planetary fractionation processes 09 p1564 A67-21738
- Trace element concentration in iron meteorites determined using lithium drifted Ge semiconductor detector 09 p1569 A67-22686
- Composition of Marthas Vineyard and selected Georgia tektites mutually related to silica-rich bediasites 09 p1569 A67-22687
- Cosmogenic tritium content in Sikhote Alin iron meteorite irradiated with reactor neutrons 09 p1569 A67-22688
- Xenon 129 and tellurium 128 formation intervals in chondritic meteorites as measure of neutron induced isotope production by solar nucleosynthesis 09 p1570 A67-22694
- Origin of chondrites implied by short period and long period nuclides created by neutron fluxes 10 p1704 A67-22849
- Meteoritic matter investigation with Venus II and Zond III probes, discussing impact rate and distribution along flight path 10 p1708 A67-23241
- Meteoritic, solar and terrestrial rare earth distribution abundance in chondritic or ordinary stony meteorites 10 p1651 A67-23428
- Aliphatic hydrocarbons in meteorites, examining distribution of isoprenoid and other compounds via gas chromatography and mass spectrometry 10 p1709 A67-23489
- Maskelynite-bearing stony meteorites, noting absence of crystalline structure 10 p1709 A67-23494
- Parameters and shock wave characteristics of Tunguska explosion, postulating reaction mechanism 10 p1710 A67-23611
- Orgueil carbonaceous meteorite composition and mineral texture including petrogenesis and origin of organic content and mineralized microstructures 10 p1710 A67-23628
- Chemical and mineralogical composition of meteorites found in Australia, Africa, Ireland and Java 10 p1712 A67-23807
- Chemical and mineralogical composition and structure of Belly River, Bluff, Bremer Voerde and Modoc meteorites 10 p1712 A67-23808
- Neutron activation analysis for terrestrial and meteoritic rock major element abundance, noting possible application to extraterrestrial surface analysis 11 p1749 A67-23976
- Mercury abundance in various meteorite and rock types determined by neutron activation analysis, relating data to evolution of meteorites and earth 11 p1858 A67-24064
- Cosmochemical considerations, from thermodynamical viewpoint, of formation processes of earth, planets and meteorites 11 p1864 A67-24600
- Electron microprobe analysis for examining oxidation reduction mechanism in iron meteorites 11 p1865 A67-24606
- Radioactive krypton content in stone meteorites determined via mass spectrometry, deriving spall ratios and radiation ages 11 p1866 A67-24692
- Amphibole richterite found in graphite nodules of iron meteorite, using electron microprobe and X-ray powder diffraction 11 p1868 A67-24873
- German book on space chemistry covering age and origin of earth, meteorites, tektites and impactites 12 p1903 A67-25427
- Meteorite age and related problems of cosmic chemistry 12 p1903 A67-25429
- Tektites and impactites composition and origin 12 p1903 A67-25430
- Tektite origin, composition, identification, strewn fields and configurations 12 p2009 A67-26232
- Developments in techniques of meteor spectral observations 13 p2197 A67-26503
- Meteor radiation and methods of meteor spectrography, discussing chemical composition, spectral characteristics, green oxygen line and photoelectrical color sensors 13 p2197 A67-26504
- Analysis of eucrite-type meteorite which fell on June 10, 1939 near Chervonyi Kut in Ukraine 13 p2197 A67-26508
- Enstatite characteristics in enstatite achondrite meteorites, discussing mineralogy and composition 13 p2200 A67-27236
- Low pressure diffusion of carbon to nucleation sites and graphite growth in cubic morphology suggested as origin of cliftonite in meteorites 14 p2384 A67-28144
- Rutile in meteorites, noting presence of titanium oxide as result of electron microprobe studies 14 p2386 A67-28476
- Nogoya type II carbonaceous chondrite noting cosmogenic, radiogenic and primordial noble gas components 14 p2390 A67-28890
- Neutron activation analysis to determine trace elements in iron meteorites 14 p2391 A67-28947
- Lamellar troilite occurrence and origin in iron meteorites 14 p2391 A67-28948
- Farmington chondrite meteorite observations show two small granular cristobalite xenoliths surrounded by thin diopside clinopyroxene reaction rim 15 p2556 A67-29647
- Isotope fractionation processes and reproducibility of age of iron meteorites studied from cosmic ray exposure ages 15 p2556 A67-29664
- Meteorological conditions, acoustic phenomena and fireballs associated with meteorite fall at Barwell, England 15 p2562 A67-30083
- Preferred shape orientation of olivine crystals in porphyritic chondrules suggesting drawing from larger magma bodies 16 p2619 A67-30986
- Light and heavy rare gases content in St Severin meteorite and iron-enriched fractions 16 p2750 A67-31435
- El Taco meteorite samples analyzed for rare gas concentrations, comparing with rare gas data from Campo del Cielo and North Chile meteorites 16 p2750 A67-31439
- Petrographic and microprobe analysis of unequilibrated ordinary chondrites, studying textural, mineralogical and chemical characteristics 16 p2750 A67-31451
- Olivine composition in chondrites relative abundances and classification 16 p2751 A67-31455
- Chemical analyses of stony meteorite and iron meteorite with silicate inclusions 16 p2751 A67-31456
- Infrared reflectance and optical constants of tektites for origin mode, noting constituent dependence on geographic location 16 p2753 A67-31697
- Spallation and fissiogenic xenon and krypton content in Pasamonte achondrite as evidence for extinct radioactivity in meteorites 16 p2754 A67-31747
- Slow motion gamma spectrometry for measurement of sodium 24 abundance in Saint Severin meteorite, evaluating modes of formation 16 p2754 A67-31790
- Chondrites metamorphosis and equilibrium, studying iron oxide and rare gas content, petrological factors and material formation 18 p3134 A67-34494
- Structure and decomposition of Goose Lake meteorite and fragments 19 p3323 A67-35424
- Abundance of volatile elements in meteorites, comparing chondrite decrease for evidence of fractionations in solar nebula 20 p3526 A67-37173
- Quantitative analysis of new mineral /gentnerite/ found in Odessa meteorite 20 p3529 A67-37526
- Parameters and shock wave characteristics of Tunguska explosion, postulating reaction mechanism 20 p3530 A67-37535
- Meteorite minerals characteristic constituents, describing crystalline form, frequency of occurrence, percentage, nature and terrestrial effects 21 p3700 A67-37766
- Chemical analysis and normative mineral composition of Winona meteorite, showing relation to chondrites 21 p3702 A67-38067
- Chondrites solidification age measured via rubidium-strontium pairs in component minerals, using phase separation method 21 p3702 A67-38125
- Rare earth elements distribution and component minerals in Bruderheim meteorite, using phase separation method 21 p3702 A67-38126
- Paraffinic hydrocarbons composition in Orgueil, Murray, Mokola and other meteorites identified by gas chromatography 21 p3703 A67-38501
- Meteoritic organic chemical analyses since 1900, considering volatile materials distribution and carbonaceous chondrites 21 p3704 A67-38502
- Magnetic separations performed on Jodzie howardite, showing uniform primordial gas enrichment indicating covariant solar planetary components 21 p3704 A67-38503
- Small particle bombardment of stone and iron meteorites, obtaining comparative erosion rates 21 p3704 A67-38504
- Krypton isotope composition in three unequilibrated and two gas rich chondrites, with correction for cosmic ray spallation 22 p3881 A67-39494
- Strontium and rubidium 87 measurements on iron meteorite silicate inclusions, with age determination at 4.4 to 4.8 billion years 22 p3881 A67-39495
- Possibility of antimatter meteor reaching earth surface on basis of collision theory between matter and antimatter 22 p3882 A67-39589
- Fremont Butte, Colorado, meteorite noting external form, structure and composition 23 p4069 A67-41448
- Anoka, Minnesota, iron meteorite noting composition, chemistry, structure and cooling rate 23 p4069 A67-41449
- Indium concentrations determined by neutron activation in petrological suite of L-group chondrites 23 p4069 A67-41474
- Iodine isotope mass-yield distributions from spontaneous plutonium 242 fission, discussing heavy xenon isotopes from extinct plutonium 244 in meteorites 24 p4191 A67-42450
- Chlorine abundance and distribution in iron meteorites from neutron activation analysis and metallographic examination, discussing terrestrial contamination effects 24 p4232 A67-42610
- Iron meteorite with partially preserved fusion crust from atmospheric flight noting martensitic structures due to rapid cooling 24 p4232 A67-42611
- Chromite composition in chondrites using electron microprobe technique, discussing petrographic origin and vanadium abundance 24 p4232 A67-42612
- Hypersthene chondrite postformational history, discussing native copper and ilmenite content of Newmann lamellae and flowage 24 p4232 A67-42613
- Crystalline variation and chemical composition of meteorite found at Marburg, West Germany 24 p4232 A67-42614
- Iodine, uranium and tellurium abundances in various achondrites, chondrites and mesosiderites from neutron activation analysis 24 p4233 A67-42616
- Precious metal concentrations in carbonaceous and enstatite chondrites using neutron activation analysis 24 p4233 A67-42617
- Type I carbonaceous chondrite flakes from British Columbia meteorite fall 24 p4233 A67-42618
- Achondrites and mesosiderites containing brecciated structures indicate magnetic differentiation, recrystallization, refragmentation and ejection from parent body 24 p4233 A67-42619
- Coexisting sphalerite, troilite and daubreelite in Odessa meteorite and sphalerite inclusions in kamacite in Odessa and Canon Diablo analyzed for chemical composition 24 p4233 A67-42620
- Galactic cosmic ray solar cycle and secular variations in bombardment of meteorites at average meteoroid solar distance and 1 AU from radioactive isotope ratios 24 p4210 A67-42622
- Preatmospheric hypervelocity impact black glass in Cachari eucrite studied by optical microscopy, electron microprobe and X-ray diffraction 24 p4233 A67-42623
- Shaw meteorite noting chondrite composition, lack of chondrite structure and Ca content suggesting high crystallization temperature 24 p4234 A67-42624
- Brianite and panethite in Dayton very fine octahedrite phosphate-silicate nodules 24 p4234 A67-42625
- Xenon data from Murray and Renazzo carbonaceous chondrites reinterpreted, discussing large presence of fissiogenic

xenon 24 p4234 A67-42626
Cl, Br and I abundances in carbonaceous chondrites analyzed by neutron activation in estimating primordial halogen abundance ratios 24 p4234 A67-42628
Khor Temiki aubrite meteorite composition and structure 24 p4234 A67-42629
Al 26 content of stony meteorites by coincidence spectrometry noting cosmic ray exposure ages for eight meteorites 24 p4234 A67-42630
Li isotopic composition and abundance in chondrites and iron meteorites measured, noting implications for earth and meteoritic parent body formation 24 p4235 A67-42632
Coexisting minerals and interstitial groundmass of chondrules of Mezo-Madaras chondrite 24 p4235 A67-42633
Solar and galactic low energy cosmic ray nuclear ionizing and interaction effects on meteorite surface isotopic composition, estimating particle fluxes 24 p4210 A67-42634
Black magnetic spherules in Pleistocene and recent beach sands, investigating origin by electron microscopy 24 p4235 A67-42635
Canon Diablo octahedrite quantitative chemical and modal mineralogical composition variations in rim and plain components 24 p4235 A67-42636
Stony meteorite Fe, Ni, Co, Ca, Cr and Mn concentration determined by X-ray fluorescence 24 p4235 A67-42638
Aromatic compounds in benzene eluate fractions from carbonaceous chondrites by high resolution capillary gas-liquid chromatography 24 p4236 A67-42640
Total carbon content and primordial rare gases in chondrites 24 p4236 A67-42641
Chromite and chromite chondrules in chondrites noting formation at very high temperatures and rapid cooling 24 p4236 A67-42642
Concentration and distribution of phosphorus in kamacite and taenite in Mount Edith medium octahedrite determined by electron probe microanalysis 24 p4236 A67-42643
Silicon abundances in chondrules from different chondrites by neutron activation analysis 24 p4236 A67-42644
Alkali, alkaline earth and rare earth elements distribution in chondrite component minerals 24 p4236 A67-42646
Antimony abundance in meteorites, tektites and terrestrial rock by neutron activation analysis 24 p4236 A67-42647
Mezo-Madaras chondrite polymict structure differs from structure in light-dark meteorites 24 p4237 A67-42648
Tektite composition considered from results of high temperature vapor fractionation of silicates 24 p4237 A67-42649
Iron meteorite chemical classification, measuring Ni, Ga, Ge and Ir concentrations for Fe groups and pallasites 24 p4237 A67-42650
Olivine and pyroxene composition distribution in type II carbonaceous chondrites, discussing metamorphic effects and gas-dust fractionation 24 p4237 A67-42651
Isotope ratios of fission and spallation xenon in meteorites from abundance data analysis by least squares method 24 p4238 A67-42886
METEORITIC COMPRESSION
Microscopic and X-ray diffraction study of octahedrite shock history 24 p4234 A67-42631
METEORITIC CRATER
Volcanism triggered by meteoritic impact suggested from comparison of volcanic and impact data, noting terrestrial, lunar and Martian craters 02 p0319 A67-11455
Meteorite crater in northern Chile with dimensions of 455 m average diameter and 31 m average depth 02 p0325 A67-11859
Lunar cratering statistics interpretation in terms of meteoroid impact hypothesis, noting equilibrium distribution function [AAS PAPER 66-183] 08 p1387 A67-20958
Astrobleme in Australia analyzed for origin of eruptive gas 10 p1706 A67-22956
Ries Kessel meteoritic crater /Germany/ analyzed by Fourier data smoothing technique, noting impact center, entry direction, etc 11 p1864 A67-24559
Terrestrial origin hypothesis for tektites, moldavites and impact glass supported by krypton-argon and fission track measurements 11 p1866 A67-24693
Peculiarities of dispersion of matter resulting from meteorite impact on lunar

surface as explanation of concentric nature of structure of crater 12 p2002 A67-25646
Mass spectrometric analysis of sedimentary rocks for Sr-Rb and Sr isotopic composition from Bosumtwi crater, Ghana 14 p2314 A67-28952
Deformation in Sudbury structure, Ontario, suggests petrographic evidence for origin by meteorite impact 15 p2473 A67-29158
Chemical analysis of meteorite impact glass from separated areas across Henbury strewnfield 16 p2667 A67-31452
Lunar surface evolution model implying partial melting due to impacts as only cause of primitive plutonic activity 20 p3525 A67-36948
Theoretical lunar crater formation data compared to experimental measurements, discussing lunar crater structures and crater fields 22 p3879 A67-39297
METEORITIC DAMAGE
Ranger photographs of lunar surface noting erosion and fragmentation by meteorite bombardment 08 p1390 A67-21026
Meteoritic penetration through obstacle theoretically considered 11 p1869 A67-24076
Meteoritic penetration through relatively thin shield 11 p1869 A67-24077
Possible degradation effects produced in uncovered and covered N/P silicon solar cells by simulated micrometeoroid exposure 15 p2423 A67-30219
Man-rated space-vehicle structural design considering space environment loads and material requirements, noting applicability of existing methods 16 p2756 A67-30630
Penetration rates of thin aluminum foil sensors of Ariel II satellites compared with flux measured by microphone detectors in vicinity of earth 21 p3722 A67-38494
Simulated micrometeoroid bombardment effect on n/p Si and CdS solar cells performance 23 p3941 A67-41521
Leakage rate due to meteoroid penetration of single and multiple hulled spacecraft, discussing effect on internal pressure 24 p4251 A67-42928
METEORITIC DUST
Soviet rocket and satellite observation of meteoric dust from 1957 through 1966 05 p0887 A67-16057
Solid interplanetary matter in vicinity of moon observed by Luna X piezoelectric pickups attached to orbiter 05 p0887 A67-16058
Meteoritic dust accumulations at low latitudes in upper atmosphere evidenced by observation of noctilucent clouds, estimating scattering function 05 p0802 A67-17329
Concentrations of black magnetic spherules plotted down red clay core from North Pacific, noting size distributions suggesting extraterrestrial origin 06 p1079 A67-17657
Meteoritic dust particle effect on steady state distribution of electrons and ions in lower ionosphere, deriving expression for recombination coefficient from auroral radio absorption data 06 p0995 A67-18074
Intense diurnal activity in sporadic E layer interpreted as effect of Omicron-Cetid meteoric stream 10 p1633 A67-22896
Micrometeoritic particle condensation in vicinity of earth measured by Elektron II satellite 12 p2008 A67-25825
Daily and seasonal changes in numbers, dimensions and shapes of micrometeoritic particles over period of two years, discussing origin 19 p3327 A67-35878
Braking and heating effects of atmosphere on meteors in zodiacal dust to 1-meter size, discussing interaction at air cap, entry, etc 20 p3525 A67-36949
Soviet rocket and satellite observation of meteoric dust /1957 through 1966/ 21 p3701 A67-37844
Solid interplanetary matter in vicinity of moon observed by Luna X piezoelectric pickups attached to orbiter 21 p3701 A67-37845
METEORITIC IONIZATION
Meteoritic ion pair production probability by total ablation of micron-size Fe particles in air and Ar as function of particle velocity 08 p1399 A67-21241
Intense diurnal activity in sporadic E layer interpreted as effect of Omicron-Cetid meteoric stream 10 p1633 A67-22896
Correlation between diurnal meteor activity and twilight emission of ionized calcium H and K lines confirmed by

Quadrantides swarm observations 11 p1857 A67-24756
Ionization and diffusion cross sections of Ca, Fe, Si and Mg atoms of disintegrated meteors 12 p2002 A67-25551
Sporadic E layer generated by meteoritic ionization noting critical frequency 13 p2111 A67-26601
Near-earth meteor flux estimate through luminous efficiency and ionizing probability application to data on radio and photographic meteor fluxes 19 p3319 A67-35217
Meteor activity radar observations and simultaneous ionosphere probe to establish relation between sporadic E layer ionization and sporadic meteors 21 p3623 A67-39040
Sporadic E blanketing frequencies during November 1965 as indicator of wind structure in lower ionosphere and meteor influx 23 p3995 A67-40806
METEORITIC MICROSTRUCTURE
Galactic and solar nucleosynthesis, determining formation of meteorites on basis of decay of nucleides Pu 244 and I 129 02 p0320 A67-11472
Friable structure of meteorites, examining disintegration under aerodynamic pressure in atmosphere 03 p0509 A67-13205
Optical activity in meteorite organic matter, recording observation of low amplitude 03 p0510 A67-13592
Neutron exposure ages of meteorites, estimating amount of shielding which surrounds samples in space from Co-60 and Ar-39 activity data 06 p1082 A67-17871
Correlation of meteoroid environments in solar system, analyzing meteor mass measurement results, hypervelocity impact and solar electromagnetic radiation effects [AIAA PAPER 67-151] 06 p1085 A67-18319
Rare earth compound and Ba abundances in Bununu howardite 07 p1249 A67-19537
Origin of fossil charged particle tracks in meteorites such as cosmic radiation, fission of U 238, meson jets, spallation recoils, etc 07 p1245 A67-19941
Lunar resources for space and planetary exploration, discussing application of solar radiation, extraction of mineral resources from meteorites, etc 09 p1568 A67-22406
Isotopic composition of krypton in high and low calcium achondrites, noting measurement results 09 p1569 A67-22685
Track densities and production rates with increase of heavy cosmic nuclei inside meteorite 09 p1570 A67-22690
Chemical and mineralogical composition and structure of Belly River, Bluff, Bremer Voorde and Modoc meteorites 10 p1712 A67-23808
Chemical composition of indochinites, determining nonuniform distribution of elements via electron microprobe counts 11 p1866 A67-24695
Cosmic ray spallation and special anomaly in achondrites 11 p1866 A67-24696
Magmatic origin of chondrule meteorites, considering structure, electron probe microanalysis, crystallization and equilibrium 13 p2200 A67-27234
Deformation in Sudbury structure, Ontario, suggests petrographic evidence for origin by meteorite impact 15 p2473 A67-29158
Radiation level on lunar surface noting degree of danger to astronaut, solar activity effect, creation of secondary emission, etc 16 p2737 A67-30782
Fusion crust of meteorites noting similar properties and relations in zonal arrangement of mineral associations in their formation 16 p2750 A67-31437
Iron and iron-stony meteorites cooling rates in relation to Ni content and Widmanstätten structure suggest development in different thermal environments 16 p2750 A67-31453
Condensation path of cooling gas of solar composition calculated considering barriers to homogeneous nucleation of condensed phase 16 p2751 A67-31454
External features of South Vietnamese tektites noting structure, surface characteristics and possible formation mechanism 17 p2947 A67-32774
Fremont Butte, Colorado, meteorite noting external form, structure and composition 23 p4069 A67-41448
Anoka, Minnesota, iron meteorite noting composition, chemistry, structure and cooling rate 23 p4069 A67-41449

- Correlation of meteoroid environments in solar system, analyzing meteor mass measurement results, hypervelocity impact and solar electromagnetic radiation effects [AIAA PAPER 67-151] 23 p4070 A67-41719
- Preatmospheric hypervelocity impact black glass in Cachalir eucrite studied by optical microscopy, electron microprobe and X-ray diffraction 24 p4233 A67-42623
- Microscopic and X-ray diffraction study of octahedrite shock history 24 p4234 A67-42631
- Mezo-Madaras chondrite polymict structure differs from structure in light-dark meteorites 24 p4237 A67-42648
- ## METEOROID
- Thermal testing of critical systems module of meteoroid detection satellite without attaching sensor arrays 02 p0334 A67-12378
- Near-earth meteoroid flux measurements for spacecraft design [AIAA PAPER 67-152] 06 p1085 A67-18291
- ## METEOROID CRATER
- Effectiveness of meteoroid shielding from hypervelocity impact penetration and cratering 01 p0155 A67-11406
- Laboratory calibration of piezoelectric transducer used as micrometeoroid impact gauge 15 p2486 A67-29410
- ## METEOROID HAZARD
- Impact physics and meteoroid population, with particular reference to space flight problems and research in high velocity impact 04 p0705 A67-15000
- Designing methods for meteoroid impact emphasizing minimum weight shield arrangement [ASME PAPER 67-DE-45] 14 p2402 A67-28878
- Astronomical and satellite measurements of meteoroid environment of spacecraft in solar system 15 p2555 A67-29535
- ## METEOROID PROTECTION
- High speed photographic equipment, analyzing gun launching of vehicles in upper atmosphere and design of protection system against space vehicle failure due to meteorites 01 p0068 A67-10968
- Effectiveness of meteoroid shielding from hypervelocity impact penetration and cratering 01 p0155 A67-11406
- Meteoroid protection system designs for optimum orbital space laboratories and manned interplanetary spacecraft 10 p1713 A67-23700
- Thin plate targets response to hypervelocity impact to determine effectiveness of meteoroid bumpers composed of two layers of distinct materials 10 p1725 A67-23716
- Chemical, mechanical and chemical-mechanical self-sealant systems incorporated in spacecraft walls for micrometeoroid protection 10 p1673 A67-23748
- Laboratory calibration of piezoelectric transducer used as micrometeoroid impact gauge 15 p2486 A67-29410
- Space electronic equipment design, considering incorporation of vibration, vacuum, micrometeoroid and radiation protection 21 p3591 A67-38209
- ## METEOROLOGICAL BALLOON
- Global weather forecasting system of meteorological balloons 03 p0464 A67-14278
- Horizontal tropospheric probe using constant altitude balloons 09 p1525 A67-22560
- Satellite tracking of ghost balloons used for data collection on atmospheric circulation in troposphere and stratosphere [AAS PAPER 67-103] 15 p2420 A67-29958
- Trajectory analysis of EOLE meteorological balloons flights in troposphere over Southern Hemisphere 19 p3332 A67-35276
- Equations for spherical superpressure balloon vertical rise in calm air 24 p4095 A67-42927
- ## METEOROLOGICAL FLIGHT
- Inertial navigation equipment applied to meteorological research, using aircraft for vertical gust measurement 06 p1002 A67-18025
- Satellite Infrared Spectrometer /SIRS/ flown by balloon for cloud top and surface temperatures 22 p3829 A67-40370
- Ice nucleating properties of meteoritic material 24 p4231 A67-42371
- ## METEOROLOGICAL INSTRUMENT
- ### SA ANEMOMETER
- ### SA HYGROMETER
- Microwave radiometric meteorological observations using twin-horn antenna technique, noting antenna resolution 01 p0108 A67-10314
- Problems encountered in preparation of final meteorological radiation tapes, using Tiros IR radiation data 01 p0108 A67-10320
- Fill factor of radar beams reflected from meteorological targets of various forms derived, taking antenna radiation pattern into account 01 p0025 A67-10790
- Integrating hemispherical system for creating indoor artificial diffusing sky used in calibrating meteorological pyranometers 03 p0419 A67-13078
- Ozone determination by electrochemical and colorimetric methods compared for effects of sensor cell aging 03 p0413 A67-13931
- Meteorological instrumentation for measuring physical characteristics of atmosphere 04 p0649 A67-14686
- M-60 radsonde measurement reliability, comparing coupled pair subjected to same shocks and direct solar radiation 04 p0625 A67-15606
- Fog penetrating imaging device using germanium panel, horn and waveguide 05 p0809 A67-17512
- Papers from Scientific Research Institute of Hydrometeorological Instrument Design covering radiosonde, sensing elements, etc 07 p1187 A67-19736
- Continuous automatic and portable instrument for ice nuclei detection and counting 10 p1654 A67-22818
- Constant temperature difference hot thermocouple anemometer, discussing operation principle and performance 10 p1654 A67-22822
- Airport traffic control tower instrument panel displaying continuously telemetered data on current weather conditions of runway complex 10 p1656 A67-23087
- Nimbus I spacecraft overall characteristics, performance and major subsystems, particularly performance of meteorological sensors 16 p2759 A67-30685
- Mechanically and electrically simple cup-type anemometer developed with starting speed of 6 cm/sec and linear response 21 p3628 A67-38581
- ## METEOROLOGICAL PROBE
- High altitude balloon soundings, noting balloon construction 01 p0010 A67-10934
- Clear air turbulence characteristics in terms of measuring systems and reduction methods [AIAA PAPER 66-966] 02 p0262 A67-12289
- Magnetic activity effect on sporadic E region drifts, comparing plot of K index vs drift velocities 03 p0413 A67-13684
- Vertical ozone distribution in atmosphere and transport processes, noting results of tracer experiments 03 p0414 A67-14090
- Radar and airborne instrumentation sampling of atmosphere, noting linked mode or one-one comparison between returned radar signal and meteorological probe 04 p0570 A67-14685
- Radar measurement of vertical density profiles of clouds and precipitation 04 p0650 A67-14689
- Multivariate statistical analysis of wind sounding data, applying high degree of correlation between two wind parameters and empirical density function [AIAA PAPER 66-353] 05 p0838 A67-17214
- Laser application to meteorology, discussing Rayleigh, aerosol and Raman scattering, system configuration and measurement problems 07 p1194 A67-19091
- Meteorological telemetry system for gun launched probes for high altitude research 08 p1292 A67-20664
- Fluctuations in measurements of hurricane clouds, determining frequency domains for dominant mode of activity via variance spectrum analysis 10 p1676 A67-22817
- High resolution measurement of air temperatures and temperature differences applied in conjunction with data processing equipment 10 p1654 A67-22821
- Meteorological probes using GHOST balloons for wind measurements 10 p1594 A67-23197
- Vertical atmospheric flow mean velocity determination within fixed area from wind probe observations at fixed points 11 p1816 A67-24523
- Neutral upper atmosphere winds near equator, discussing sodium vapor rocket observation results 12 p1934 A67-25790
- Numerical methods for calculating pseudoadiabatic characteristics of saturated air parcels 17 p2879 A67-32549
- Clear air turbulence characteristics in terms of measuring systems and reduction methods [AIAA PAPER 66-966] 17 p2880 A67-32581
- Empirical orthogonal functions, determining vertical atmospheric temperature profiles from radiometric satellite measurements 22 p3828 A67-39325
- ## METEOROLOGICAL ROCKET
- ### SA RAVEN ROCKET
- ### SA SOUNDING ROCKET
- Meteorological Rocket Network /MRN/ probing of stratosphere and lower mesosphere and analysis of acquired data 02 p0239 A67-12535
- Rocket vehicles for synoptic meteorology, evaluating vehicle concepts, performance characteristics and costs 08 p1404 A67-20497
- Packaged liquid power plants for meteorological rockets, design and performance 08 p1408 A67-20523
- Experimental Inter-American Meteorological Rocket Network /EXAMETNET/ for Southern Hemisphere research 08 p1350 A67-20549
- Meteorological rocket network observations of complex circulation system in middle and upper atmosphere 10 p1643 A67-23247
- Meteorological rocket measurement of wind patterns noting velocities, turbulences, stratospheric diffusion coefficients, etc 13 p2117 A67-27611
- Water vapor and atomic oxygen concentration in mesosphere measured by meteorological rocket 16 p2665 A67-31097
- Soviet meteorological rocket observation and research, basic techniques and program results 23 p4025 A67-41447
- ## METEOROLOGICAL SATELLITE
- ### SA ESSA SATELLITE
- ### SA NIMBUS SATELLITE
- ### SA SYNCHRONOUS METEOROLOGICAL SATELLITE /SMS/
- ### SA TIROS SATELLITE
- Tiros satellite photography used to forecast British Isles weather 12 to 24 hr in advance 01 p0108 A67-10225
- Anisotropy of reflected solar radiation from various surfaces as measured with aircraft-mounted radiometer 01 p0146 A67-10318
- Weather satellites, discussing photographic and radiation measuring equipment and automatic picture transmission 01 p0109 A67-10768
- Weather and cloud photography during Gemini space flights and effect on interpretation of satellite weather pictures 01 p0109 A67-11393
- Cloud cover space photography by Voskhod I and Voskhod II to determine spatial structure of clouds of various types and fields of brightness 01 p0110 A67-11429
- Tropospheric pressure-altitude data by satellite radiometric topography mapping, using oxygen absorption band centered at 5 mm 02 p0262 A67-12367
- Meteorological experiments possible in manned earth orbital spacecraft with aid of remote sensing of electromagnetic radiation 02 p0239 A67-12379
- Worldwide meteorological data acquisition capability proposal for improving upper air observations, noting satellite system role 02 p0231 A67-12383
- Line scan TV for earth observation satellites noting camera design, coverage, systems effectiveness and performance results 02 p0335 A67-12398
- Weather satellite system determining worldwide occurrence and distributions of thunderstorms and associated atmospheric effects 02 p0262 A67-12399
- Maritime precipitation analyzed using radar data and satellite photographs of cloud cover 02 p0262 A67-12404
- Meteorological satellites ESSA II and Nimbus II and British ground facilities for receiving cloud cover pictures 03 p0424 A67-13913
- Manned meteorology experiments aboard earth satellite including ozone concentration, noctilucent clouds, spectral airglow and albedo, precipitation map, etc [AIAA PAPER 66-885] 03 p0513 A67-14020
- Meteorological satellites noting necessity of radiation

measurements 04 p0648 A67-14409
 Supersatellite technology and advantages of larger automaton craft including superweather, superremote sensor, superutility, supersurveillance and superscientific satellite systems 04 p0703 A67-14601
 Nimbus II AVCS, APT, HRIR and MRIR sensory data analysis 04 p0613 A67-14801
 Weather satellite for automatic photo transmission, noting Tiros and Nimbus 04 p0651 A67-15454
 Soviet papers on planetary atmospheric circulation and artificial earth satellites 04 p0651 A67-15467
 Vortex structures of cloud systems from meteorological satellite data 04 p0651 A67-15468
 Atmospheric sounding of twilight phenomena in upper layers, solar ray illumination techniques and solar ray color spectral variation 04 p0617 A67-15475
 Satellite determination of cloud distribution over sky by azimuthal measurements from single point 04 p0652 A67-15476
 Satellite role in worldwide meteorology, discussing global observation, observation platforms, manned satellites, and remote sensing and data collection of satellite instrumentation 05 p0837 A67-16383
 Tiros satellite development and Tiros operational satellite /TOS/ system noting design, camera orientation, spin-rate control, etc 06 p1096 A67-18412
 Oxygen A band near 7600 angstroms used by Gemini V astronauts to measure cloud top altitude, showing method of computing correction factor 06 p1026 A67-18563
 Data requirements for medium period weather prediction, discussing mathematical models and meteorological satellites 06 p1028 A67-18998
 Graphical method by which small local users of meteorological satellite pictures can identify geographical position of features in image [AIAA PAPER 66-439] 07 p1184 A67-19373
 Meteorological data classification system using computer based level logical-tree method 10 p1676 A67-22820
 Digital /chirp/ radiosonde for meteorological and earth satellite measurements employing pulse bursts from voltage controlled oscillator 10 p1655 A67-22823
 Soviet book on practical utilization of observational data from meteorological satellites covering radiation and cloud cover, emphasizing weather forming systems analysis, aerological and synoptical data comparisons, etc 10 p1676 A67-23017
 Space technology developments for World Weather Watch, discussing satellites role in weather forecasting, meteorological sensor and instrumentation 10 p1677 A67-23369
 ESSA meteorological satellite system noting mission requirements, design and performance [SMPT PAPER 101-56] 12 p2011 A67-25472
 Legal problems of space research connected with telecommunication and meteorological activity 12 p2042 A67-26142
 Space activities effect on International Civil Aviation Organization including navigational problems, aircraft communication, meteorological data and technological advances 12 p2043 A67-26151
 Legal and political aspects of International meteorological data collection and distribution system, including use of satellites 12 p2044 A67-26153
 Tiros satellites characteristics including ESSA I 15 p2565 A67-29762
 Spaceport meteorology by satellite observation of earth atmosphere and cloud systems [AAS PAPER 67-47] 15 p2513 A67-30115
 Meteorological and Communication Satellites, Congress, Athens, September 1965, Volume 4 meteorological and communication satellites - IAF Conference, Athens, September 1965, Volume 4 16 p2759 A67-30684
 Worldwide meteorological satellite system, operation, structure and functions 16 p2759 A67-30686
 Research potential of manned earth orbiting spacecraft in meteorology 16 p2759 A67-30687
 Tropospheric water vapor analysis via

Tiros IV satellite, determining spatial and temporal temperature, humidity and mass variations 17 p2880 A67-32550
 Error factors in cloud and underlying surface temperature determination from weather satellites in various spectral intervals 18 p3073 A67-33558
 Satellite tracking of cloud formation on earth shadow side, calculating outgoing radiation intensity under cloudless and cloudy sky 18 p3074 A67-33564
 Manned meteorology experiments aboard earth satellite including ozone concentration, noctilucent clouds, spectral airglow and albedo, precipitation map, etc 19 p3213 A67-34824
 Application satellite program, discussing meteorological and communications satellites, noting ESSA I, Syncom, etc 19 p3333 A67-35635
 Meteorological satellite program results, discussing Tiros satellites cloud pictures, storm warning, etc 19 p3253 A67-35637
 Economic benefits from space systems used to survey food producing areas and weather 19 p3350 A67-35650
 Satellites role in World Weather Watch /WWW/ program for weather analyses and forecasts 19 p3253 A67-35656
 Image dissector camera providing high resolving power, photometric fidelity and long life for use in meteorological satellite 20 p3445 A67-35541
 Atmospheric energetics, discussing stratospheric-tropospheric energetics differences, atmospheric radiation balance distribution, meteorological satellite data, computer studies of atmospheric circulation, etc 20 p3429 A67-36895
 Meteorological satellites data interpretation and application 20 p3430 A67-36900
 Radiation balance chart of earth atmosphere system for evaluation of radiation receivers on Nimbus II satellite 20 p3431 A67-36964
 Triaxial attitude control stabilization for second-generation /TIROS/ meteorological satellite 22 p3897 A67-39156
 TIROS satellite program accomplishments since 1960, describing operational system, TOS ground-station network and ESSA satellites 22 p3899 A67-39608
 Legal problems associated with telecommunications and meteorological satellites and with launching and retrieval of manned spacecraft 24 p4257 A67-42387
 Advanced meteorological satellite objectives, discussing storm warnings, weather forecasting and atmospheric pollution 24 p4240 A67-42392
METEOROLOGICAL SERVICE
 Weather forecasting - Symposium, Vienna, September 1965 06 p1026 A67-18598
 Soviet book on aeronautical meteorology noting atmospheric conditions, clouds, ice formation, flight data utilization, Soviet Civil Aviation services, etc 07 p1220 A67-19579
METEOROLOGICAL STATION
 Polarization measurements and noctilucent cloud observation over North America 02 p0239 A67-12534
 Meteorological observatory on moon for observations of earth atmosphere and cloud cover and solar activity 04 p0597 A67-15066
 Meteorological observations of earth from lunar surface 12 p1920 A67-25648
 Equatorial electrojet currents studied from IGY data from South American stations 24 p4148 A67-42065
 Sq currents in American equatorial zone during IGY 24 p4148 A67-42066
METEOROLOGY
 SA AEROLOGY
 SA AERONOMY
 SA ATMOSPHERIC CONDITION EFFECT
 SA ATMOSPHERIC ENERGETICS
 SA CLIMATOLOGY
 SA CLOUD PHYSICS
 SA HYDROMETEOROLOGY
 SA MICROMETEOROLOGY
 SA NUCLEAR METEOROLOGY
 SA POLAR METEOROLOGY
 SA RADIO METEOROLOGY
 SA SYNOPTIC METEOROLOGY
 SA TROPICAL METEOROLOGY
 Worldwide meteorological data acquisition capability proposal for improving upper air observations, noting satellite system role 02 p0231 A67-12383

Meteorological problems connected with design and future operations of supersonic transport, noting particular hazards of mountain-like cumulonimbus clouds 04 p0652 A67-15542
 Derivation of accurate solution of equation for geopotential field prognosis using only simple invariant-group solutions and meteorological terminology 05 p0837 A67-16489
 Spherical harmonics integration of low order spectral form of primitive meteorological equations 06 p1025 A67-18051
 Vertical interpolation of data from constant pressure to constant density surfaces for meteorological purposes 06 p0999 A67-18741
 Meteorological studies from manned spacecraft, discussing interpretation of cloud pictures and optical inhomogeneity of troposphere and stratosphere 07 p1221 A67-20008
 Real time meteorological system providing prelaunch impact prediction for unguided high altitude rocket firings, noting computer program 08 p1314 A67-20543
 Meteorology - Conference, Liblice, Czechoslovakia, October 11 p1815 A67-24325
 Dispersion equations obtained for numerical forecasting of meteorological fields from basic hydrothermodynamic equations, using Reynolds stresses 13 p2149 A67-26272
 Millimeter waves in atmospheric research, discussing radar meteorology, radiometry, etc 13 p2072 A67-27493
 Real time meteorological system for ballistic high altitude multistage rocket trajectory, computation and prediction 13 p2091 A67-27610
 Synthesized summary of reports on radio propagation in nonionized media, noting meteorological radar and precipitation effect 14 p2264 A67-28393
 Meteorological conditions, acoustic phenomena and fireballs associated with meteorite fall at Barwell, England 15 p2562 A67-30083
 Soviet book on cosmic rays including solar-diurnal, 11-year and 27-day variations, temperature effect, geomagnetic field effect, etc 17 p2930 A67-32077
 Integral multiplicity calculation procedure for meson component of cosmic rays based on three-dimensional elementary event model, noting meteorological effects 17 p2934 A67-32104
 Soviet book on aeronautical meteorology covering wind and cloud effects on takeoff, landing and supersonic flying in storms and jet stream layers 18 p3074 A67-33676
 Lightning theories from Mount San Salvatore /Switzerland/ observations, noting corona currents 18 p3074 A67-33995
 Soviet collection of articles on atmospheric physics 19 p3213 A67-34850
 Long term global integrations of primitive meteorological equations for free surface model, using spherical polar coordinates 19 p3252 A67-35058
 Space research in Brazil, discussing rocket launching facility, meteorological experiments, X-ray astronomy, satellite observations, etc 19 p3320 A67-35285
 Polish space research noting satellite position observations, geodetic computations, meteorology, cosmic physics, magnetosphere, medicine and biology 19 p3321 A67-35296
 Rumanian space research in meteorology, fluid mechanics, space medicine, etc 19 p3321 A67-35305
 IQSY South African participation, reviewing meteorology, geomagnetism, aurora, airglow, ionosphere, cosmic rays, etc 19 p3315 A67-35477
 IQSY program in U.S.S.R. /1964-1966/ including meteorology, aurora studies, solar activity, etc 19 p3223 A67-35482
 National IQSY research programs /1964-1965/ 19 p3325 A67-35497
 Position, shape and motion of large scale cirrus bands relationship to meteorological properties of upper troposphere 19 p3252 A67-35527
 Bad weather landing of VTOL aircraft noting landing profiles, meteorological parameters and control system 20 p3361 A67-36455
 Vertical energy transfer from stationary disturbances induced by topography and

diabatic heat sources and sinks, using primitive motion 20 p3480 A67-36504

ATS-1 spin scan camera experiment for photographic recording of weather motions 20 p3446 A67-36610

Cross-spectrum analysis in meteorology, considering property fluxes and time series, discussing turbulent energy flux, solar activity, etc 20 p3480 A67-36786

Meteorology, goals and methods, prospects for effective utilization of satellites and new techniques 20 p3480 A67-36823

Real time meteorological system providing prelaunch impact prediction for unguided high altitude rocket firings, noting computer program 21 p3607 A67-37812

Frequency of noctilucent clouds studied as function of meteorological conditions of mesopause 21 p3618 A67-38447

Tethered sonde for micrometeorological soundings of lower atmosphere noting pressure transducer, servoswitching system, thermistor, hygistor, data acquisition, etc 21 p3628 A67-38582

High velocity tropospheric winds at 40 to 60 km altitude, discussing supergradient and subgradient winds and energy transport to mesosphere possibilities 22 p3793 A67-40032

Atmospheric density, temperature and composition altitude variation measured by satellite observation of laser backscatter Raman component 22 p3806 A67-40366

ATS-1 spin scan camera experiment for photographic recording of weather motions 24 p4156 A67-42405

METER

S ACCELEROMETER

S ALTIMETER

S ANEMOMETER

S BAROMETER

S BOLOMETER

S CALORIMETER

S CONDUCTIVITY METER

S DIFFRACTOMETER

S DILATOMETER

S DOSIMETER

S DYNAMOMETER

S ELECTROMETER

S FIELD INTENSITY METER

S FLOW METER

S FLUXMETER

S GAS METER

S GAUGE

S GRAVIMETER

S HELIOMETER

S HYGROMETER

S INDICATOR

S MAGNETOMETER

S MEASURING APPARATUS

S MICROMETER

S PLASTOMETER

S POLARIMETER

S POTENTIOMETER

S PYRANOMETER

S RATE METER

S REFLECTOMETER

S REFRACTOMETER

S SEISMOMETER

S SPECTROMETER

S TACHOMETER

S VOLTMETER

S WATTMETER

METHACRYLATE

S METHYL METHACRYLATE

S POLYMETHYL METHACRYLATE

METHANE

SA NITROMETHANE

Nonlinear equations for equilibrium composition of combustion products from methane burned with ionizing admixtures over various temperature and pressure ranges 01 p0139 A67-10046

Dissociation pressures of mixed gas hydrates predicted from data for hydrates of methane, propane and nitrogen with water 02 p0190 A67-12234

Size distribution of electron avalanches in methane gas under electric field no longer satisfy Furry distribution due to first Townsend ionization 03 p0473 A67-13463

Mean values of methane wavelengths in Uranus spectrum measured for determination of atmospheric temperature 03 p0515 A67-14327

Spectral study of Jupiter, Saturn and rings of Saturn, determining methane concentration in cloud layers 04 p0701 A67-15557

Experimental equipment for chemical

reaction analysis in fluid systems based on study of partial oxidation of methane at high pressures 05 p0759 A67-17540

Exothermal reaction zone in one-dimensional shock wave in argon diluted oxygen-hydrogen and methane-oxygen mixtures 07 p1267 A67-19309

Normal flame propagation rates for methane-air mixtures at high pressures 07 p1239 A67-19313

Uranus and Neptune spectral absorptions compared with laboratory spectra obtained with very long optical paths indicate methane role in planetary absorption 08 p1397 A67-21213

Derivation and computer method solution of equations describing thermodynamic equilibrium of gaseous products from oxidative combustion of methane 11 p1881 A67-24023

CH concentration measurement in flash photolysis of methane by means of kinetic spectroscopy 12 p1904 A67-26228

Liquidified natural gas application to SST, noting improvement in engine performance with use of methane 13 p2185 A67-27439

Methylene role in atmospheric tritiated methane, specifically nitric oxide interference 13 p2117 A67-27604

Pool boiling of methane over pressure range from 1 atm to critical pressure in both nucleate and stable film boiling regimes 13 p2229 A67-27667

Reaction of atomic oxygen with methane studied by photolysis of ozone-methane mixtures dissolved in liquid argon [JPL-TR-32-1109] 14 p2259 A67-28297

Burning velocities, temperatures and burnt gas composition of flammable methane-rich perchloric acid mixtures 14 p2406 A67-28544

Sensitized ignitions of methane and oxygen mixtures, with nitrogen oxides and inert gases added, and suggested reaction mechanisms 14 p2407 A67-28549

Nonlinear equations for equilibrium composition of combustion products from methane burned with ionizing admixtures over various temperature and pressure ranges 17 p2927 A67-33324

Prebiotic synthesis of monocarboxylic acids suggested from mixture of methane and water exposed to semicorona discharge 19 p3181 A67-35882

Atmospheric absorption of gas laser radiation at two wavelengths noting dependence on gas pressure and amount of methane 20 p3463 A67-37668

Jupiter atmosphere, interior and surface properties, speculating on possibility of life in spite of presence of noxious gases 21 p3703 A67-38191

Hydrocarbons transformation mechanism and kinetics at low pressures in glow discharge noting three-way decomposition 22 p3757 A67-39585

METHOD

S APPROXIMATION METHOD

S ASYMPTOTIC METHOD

S BOUNDARY CONTRACTION METHOD

S BRIDGMAN METHOD

S CHAPMAN-ENSKOG METHOD

S CHARACTERISTIC METHOD

S COMPUTER METHOD

S CROCCO METHOD

S ELECTROMAGNETIC METHOD

S ENCKE METHOD

S FINITE DIFFERENCE METHOD

S FOUR-BODY METHOD

S GALERKIN METHOD

S HODOGRAPH METHOD

S JACOBI MATRIX METHOD

S LEAST SQUARES METHOD

S LIGHTHILL METHOD

S MAXWELL-MOHR METHOD

S MOIRE METHOD

S MOMENT METHOD

S MONTE CARLO METHOD

S NEWTON-RAPHSON METHOD

S OPTICAL METHOD

S POINT MATCHING METHOD

S RAYLEIGH-RITZ METHOD

S RELAXATION METHOD

S RITZ AVERAGING METHOD

S SCHMIDT METHOD

S SONOGRAM METHOD

S STROMGREN METHOD

S TEST METHOD

S VARIATION METHOD

S VON ZEIPPEL METHOD

S WING FLOW METHOD TEST

METHYL

Crossed molecular beam kinetics of reactive asymmetry of oriented methyl iodide polar molecules reacting with rubidium 06 p0955 A67-17831

Ethylene oxide and methyl bromide mixture for spacecraft sterilization, discussing penetrating power, effect on components and packing and toxicity 15 p2430 A67-29101

METHYL ALCOHOL

Engine-oil-operated water/methanol system provides boosted takeoff power and maintains takeoff power at elevated temperatures 05 p0873 A67-16233

In situ reforming methanol air cell design, construction and expected performance 09 p1445 A67-22186

Direct and indirect methods of using methanol in fuel cells 14 p2253 A67-29022

Radial distribution functions for liquid methanol and ethanol at room temperature, observing intermolecular hydrogen bonding 20 p3378 A67-37560

METHYL HALIDE

Crossed molecular beam kinetics of reactive asymmetry of oriented methyl iodide polar molecules reacting with rubidium 06 p0955 A67-17831

METHYL HYDRAZINE

Gas chromatography and IR spectrophotometry used to examine monomethyl hydrazine air oxidation, showing evidence of surface catalyzed reaction 21 p3578 A67-38841

Monomethylhydrazine effects on metabolism and heat balance using various calorimetric methods 23 p3954 A67-41601

Toxic metabolic effects of MMH, discussing methemoglobinemia as indicator of exposure dosage in animal study 23 p3955 A67-41602

METHYL METHACRYLATE

SA POLYMETHYL METHACRYLATE

Ionizing radiation effect on polymers used in electronics, producing temporary effects also found in mineral insulators like anodic tantalum oxide 17 p2917 A67-32841

METHYL NITRATE

Criticality criteria and temperature profiles in thermal explosions, studying exothermic decomposition of gaseous methyl nitrate 18 p3156 A67-33851

METROLOGY

Sonoholograms, techniques and information content 04 p0625 A67-15678

Metrology requirements for Apollo project, noting control and measuring equipment and calibration procedures 05 p0814 A67-17263

Accuracy ratio and traceability of flow metrology noting uncertainty values, cryogenic standards, gas leakage detection, etc 05 p0809 A67-17377

Fundamental problems of metrology - Symposium, Warsaw, April 1967 10 p1654 A67-22755

Measurement interpreted as information process in terms of exactly defined basic concepts of information theory 10 p1654 A67-22756

Learning machines used for classifying measurement data of objects representable as points in n-dimensional space after training by forced learning 10 p1654 A67-22757

Laser interferometers for metrology applications, considering sources of error 15 p2501 A67-30411

Laser research and development in France and applications to holography, metrology and gyros 17 p2868 A67-32745

Laser application as research tool and for ranging and metrology noting laser availability and performance 23 p4015 A67-41050

Correlation calculus applied in metrology, estimating correlation coefficient 23 p4008 A67-41397

MEXICO

Mexican space research activities noting studies in meteorology, aeronomy, solar radiation, communications, tracking, astronomy and geomagnetism 19 p3321 A67-35298

MI-10 HELICOPTER

S MIL MI-10 HELICOPTER

MIAZINE

S PYRIMIDINE

MICA

Antifrictional properties of mica and

boron nitride for use instead of graphite as solid lubricant in cermet packing materials 01 p0081 A67-11246

Chemical stability of silver graphite, molybdenum disulfide, zinc oxide, boron nitride, muscovite and phlogopite mica solid lubricants 10 p1659 A67-22829

Reflectance, transmittance and absorptance of muscovite type mica as function of thickness measured, using prism and grating spectrophotometers [AIAA PAPER 67-288] 12 p1958 A67-26005

Antifrictional properties of mica and boron nitride for use instead of graphite as solid lubricant in cermet packing materials 17 p2866 A67-33169

MICHELSON INTERFEROMETER

Michelson type interferometer for Nimbus meteorological satellite to obtain vertical temperature, humidity and ozone profile 02 p0246 A67-12365

Optical paths and variable-contrast interference at Michelson interferometer which adds two groups of two laser coherent waves 06 p1009 A67-17636

Spectral transmission of far IR Michelson interferometer with dielectric film beam-dividers 06 p1005 A67-18716

Balloon-borne high resolution Fourier interference spectrometers analyzed in terms of IR Michelson interferometer and near IR cats-eye interferometer [JPL-TR-32-1071] 07 p1184 A67-19391

IR spectroscopy using Michelson interferometer coupled with computer and wave analyzer 07 p1190 A67-20272

Fringe counting in laser interferometers and phase quadrature signals for bidirectional counting at good efficiency without mechanical or optical complications 09 p1493 A67-21613

Two-beam Mach-Zehnder and Michelson interferometers using coherence properties of lasers, construction and applications 10 p1652 A67-22709

Venus atmosphere spectra obtained by Michelson interferometer, finding HCl lines consistent with 2-mm Amagat of gas [JPL-TR-32-1106] 11 p1863 A67-24510

Optical interferometry in plasma diagnostics, discussing degree of ionization, time dependent electron density distribution, etc 12 p1976 A67-26073

Michelson interferometer with laser source analyzed for beam frequency and wavelength, refraction coefficient, etc 15 p2486 A67-29467

Michelson interferometer and ring laser compared for measurement of relativistic rotational effects of earth 17 p2883 A67-32361

Two-beam interferometric spectroscopy, discussing digital computers role and duality of spectral and angular measurements 19 p3232 A67-35872

Asymmetric interferogram for spectral transmittance measurements in magnitude and phase obtained by far IR Michelson interferometer 20 p3437 A67-36335

Fourier spectroscopy in far IR for routine investigation through Michelson and lamellar grating interferometers 20 p3437 A67-36340

Doppler widths from plasma UV lines using fast scan Michelson interferometer 20 p3438 A67-36343

Balloon-borne Michelson interferometer for far IR solar spectrometry 20 p3438 A67-36344

Upper limit of arc for hydroxyl /OH/ emission region associated with radio source W3, using Michelson interferometer consisting of two spaced radio telescope stations 20 p3523 A67-36648

Michelson interferometer with laser source analyzed for beam frequency and wavelength, refraction coefficient, etc 21 p3628 A67-38548

Two-tilt compensating interferometers, using vector form of reflection law 22 p3796 A67-39236

Temperature dependence and electro-optic coefficients in lithium niobate single crystal measured, noting relationship in paraelectric perovskites 22 p3863 A67-40235

Airborne multiple scan interferometry for low temperature IR emission spectral distribution of minerals 22 p3807 A67-40368

Laser interferometric velocity measurements of moving objects, discussing accuracy improvements by recorder resolution power increase and atmospheric and seismic disturbance

elimination 23 p3997 A67-40571

Michelson interferometer used as tunable mirror in laser resonators, obtaining internal modulation of initial intensity 23 p4013 A67-40902

ADP electro-optic crystal in laser emission control tested in beam deflection device and Michelson interferometer modulator, noting refractive index changes 24 p4167 A67-42239

Atmospheric spectral analysis of planets and stars by using computer, telescope and interferometer system 24 p4232 A67-42572

MICROANALYSIS

Rapid micro dry combustion determination of carbon, hydrogen and nitrogen in high explosives 05 p0759 A67-17154

Monograph on electron microprobe X-ray analyzer and application in mineralogy 10 p1603 A67-23632

MICROBALANCE

Vacuum microbalance techniques - Conference on Vacuum Microbalance Techniques, Princeton, September 1965, Volume 5 04 p0619 A67-14730

Thermomolecular flow effect caused by transverse and longitudinal forces, calculating force on hangdown fiber in microbalance 04 p0620 A67-14732

Longitudinal thermomolecular flow theories at intermediate pressures, comparing similarities and discrepancies in forces acting on hangdowns or samples in microbalance measurements 04 p0603 A67-14733

Impulse measurements of small electric engines by vacuum microbalance technique, also suitable for average thrust measurements in millipound and micropound ranges 04 p0620 A67-14734

MICROBE

S MICROORGANISM

MICROBIOLOGY

SA CULTURE TECHNIQUE

Gulliver radioisotopic biochemical probe to detect extraterrestrial life 05 p0806 A67-16548

Microbial cell population - statistics and dynamics 05 p0757 A67-17156

Problem of manufacturing space vehicles with rigidly controlled cleanliness and biological contamination for missions to other planets 18 p2995 A67-34677

Pedoscope use in soil microbiological studies including ecology, infection susceptibility, etc 19 p3179 A67-35205

Biological life support system for regenerating closed atmosphere by photosynthesis, using gas exchange between man and microalgae 19 p3180 A67-35236

Desiccated microbial populations of lyophilized Staphylococcus epidermidis cells and Bacillus subtilis spores studied for synergism in ethylene oxide-methyl bromide sterilization 19 p3180 A67-35279

Reduction of microbial shedding from humans, comparing and evaluating clothing and surgical mask use 20 p3374 A67-36802

Microorganism shedding by human beings studied by isolation of specific sources and washing or sanitizing of arms 20 p3374 A67-36803

Comparative microbial contamination levels in clean rooms used for assembly and test of lunar spacecraft 23 p3961 A67-40851

Numerical estimation of microbial contamination on surfaces of spacecraft using swab samples, environmental settling strips and air samples 23 p3962 A67-40853

Indigenous biological flora of human male subjects in closed environment and effects of diet on fecal flora 23 p3957 A67-41842

Origin of round body structures in Orgueil meteorite 24 p4113 A67-42455

MICROCIRCUIT

SA PRINTED CIRCUIT

Welmer triode with contact rectifier for use as component of microminiature radio circuits, noting effect of contact rectification on current-voltage characteristics and amplifying power of such triodes 01 p0035 A67-10397

Ceramic-based microcircuit manufacturing techniques 02 p0249 A67-12182

Transient radiation effects on microcircuits 04 p0588 A67-15701

Adaptable large scale integrated military and space systems, discussing microelectronic circuit, logistics and dynamic redundancy 08 p1311 A67-20665

Thin film circuit technology, discussing application to distributed parameter devices,

cost, reliability, miniaturization, design flexibility, performance characteristics and manufacturing materials 08 p1301 A67-20789

Thick film hybrid microcircuit technology, fabrication and performance characteristics 08 p1301 A67-20790

Planar packaging concepts for avionics equipment systems and circuit boards developed from extensive use of microcircuits and thin film circuits [SAE PAPER 670251] 11 p1758 A67-23984

Microelectronics technique, particularly integrated circuits, basic theory and research 12 p1917 A67-26202

Large scale monolithic integration of subassemblies combined with upside-down assembly technique for more complex low cost high performance microcircuits 13 p2077 A67-26658

High Noise Immunity Logic Family /HNIL/ digital switching microcircuits for long distance signal transmission operating at high voltage 14 p2282 A67-28028

Evaluation method for deposited thin film interfacial interconnections 14 p2369 A67-28613

Microelectronic amplifiers, emphasizing reliability improvement and decreased sensitivity to parameter changes 15 p2443 A67-29239

Electron beam probing of semiconductor materials and devices 15 p2450 A67-29813

Secondary electron detector for electronic microcircuits bombarded by electron beam used to observe potential distribution in junction breakdown 15 p2453 A67-30065

Semiconductor field development, discussing component reliability and miniaturization 17 p2823 A67-32299

Aircraft electric power systems and future use of solid state high power devices, integrated microcircuits and solid rotor generator 17 p2804 A67-32512

Linear microcircuits evaluation and application covering offset voltage and current, noise properties, input impedance, etc 18 p3013 A67-34548

Flip-chip bonding and dimensional transformation, low cost microcircuit production technique 18 p3014 A67-34549

Monolithic or thin film microcircuits design and performance limitations resolved by combining characteristics of thick and thin films 18 p3014 A67-34552

MOSFET approach to small scale integration of large scale circuits 18 p3014 A67-34555

Operating and performance characteristics of helium-neon pulsed gas laser, discussing application to integrated microcircuits fabrication 22 p3813 A67-39333

Ti thin film microcircuit fabrication and electrical properties 23 p3977 A67-40661

Polished glass substrates for thin film microcircuits, analyzing surface resistivity and optical transmittance changes due to heat treatment 23 p4043 A67-41366

MICROCRACK

Minimum alternating stress causing given length microcrack to grow and macrocrack growth rate 16 p2774 A67-31317

MICRODENSITOMETER

Microdensitometry in retrieval of data recorded on photographic film 06 p1001 A67-17791

Photographically recorded information retrieval by isodensitometry [SMPTE PAPER 101-89] 12 p1941 A67-25473

Lunar charting for selenocentric coordinates from densitometric analysis and altitude measurements, using photometric methods and Isodensitracer 18 p3049 A67-34333

Moon elevation profiles and lunar slopes determined by photometry and isodensitometric measurements of Ranger IX photographs 18 p3133 A67-34335

Cauchy domes in Mare Tranquillitatis, deriving relief pictures with photometry 23 p4066 A67-41013

MICROELECTRONICS

SA THICK FILM

Ninety-eight-channel microelectronic PCM multiplexer-encoder design and development qualified to Apollo spacecraft environments 01 p0026 A67-10864

All-weather carrier landing system using precision tracking radar and microelectronic data link aboard carrier 01 p0026 A67-10969

NASA program for microelectronic circuit and space vehicle

reliability 01 p0042 A67-11364
Integrated ceramic printed and thin film
circuitry in microelectronic
technology 01 p0043 A67-11385
Make-before-break contacts effect on
degree of complexity of film and hybrid
microelectronic nodes 02 p0215 A67-11913
Hybrid thin film microelectronics
circuitry, using tantalum films as basis for
passive components 02 p0218 A67-12107
Microelectronic applications of silicon-on-
sapphire /SOS/ and MOS-FET large scale
arrays /LSA/ 02 p0219 A67-12108
Microstructural analysis multiple electron-
photon cascade resonance amplifier response
to sine-square radio 03 p0376 A67-13091
Transient radiation response mechanisms
in monolithic microcircuits using p-n
junction isolation from 04 p0589 A67-15721
Book on applied microelectronics for
system and subsystem designer 05 p0775 A67-17035
Circuit element types and technology for
design engineers 05 p0776 A67-17036
Microelectronics in digital subsystems of
logic, memory, input/output and power
supply 05 p0784 A67-17037
LF analog-linear circuitry and reduction of
electromechanical control system
requirements to realizable microelectronic
circuits 05 p0776 A67-17038
HF analog microcircuits in sensors for
information transmission systems, noting
problems of precision and high power
05 p0776 A67-17039
Trends in microelectronics and related
technology 05 p0776 A67-17040
Design technique for inertial navigation
instruments makes it possible to package
within instrument electronics necessary to
control and operate each of its
facilities 05 p0779 A67-17464
Modular system for packaging
microelectronic flat packs and miniature
discrete electronic components 05 p0779 A67-17465
Book on introduction to microelectronics
including integrated circuits, thin film
devices, etc 07 p1158 A67-20280
Microelectronic radar intercept calculator
/RIC/ for ground-controlled intercept
capability when used with air search radar
feeding information to PPI display 08 p1293 A67-20690
IR techniques for reliability enhancement
of microelectronics 10 p1610 A67-22977
Monte Carlo and direct calculation
methods analyzed in connection with
microelectronic circuit designs 10 p1610 A67-22978
Automatic flight control development for
general aviation, discussing fluidics,
electropneumatic servoactuator and
microelectronics 12 p1895 A67-25505
[SAE PAPER 670255] Heat sterilization in microelectronic
assemblies 12 p1914 A67-25683
Implant telemetry techniques and
associated problems and potential of
microelectronics 12 p1903 A67-26171
Microelectronics technique, particularly
integrated circuits, basic theory and
research 12 p1917 A67-26202
Thin film integrated circuit technology,
discussing reliability, production, packaging,
components, etc 12 p1917 A67-26204
High density circuit assembly system
emphasizing micromodule method 12 p1917 A67-26205
Micropower electronics noting effects of
input capacitance and container and wiring
capacitances on HF characteristics 12 p1917 A67-26206
Microminiature circuits in space
electronics 12 p1918 A67-26216
Microwave design techniques for
calculating even and odd mode characteristic
impedances of miniature microstrip
transmission lines 13 p2071 A67-27445
Advances in microelectronics, emphasizing
role of MOS transistors 14 p2285 A67-28458
Simulated space effects on microelectronic
device materials 15 p2466 A67-29549
Material processing in microelectronics
with laser beam noting solid state lasers,
power density, pulse frequency, etc 15 p2493 A67-29682
Microelectronics practice and possible use
of space for fabrication

[AAS PAPER 67-79] 15 p2452 A67-29946
Cathode sputtering, evaporation and
anodic oxidation for thin film deposition in
integrated circuit technology 15 p2453 A67-30066
Book on microelectronics in U.S. covering
semiconductor and thin film integrated
circuits, hybrid circuits, fabrication,
applications, etc 16 p2637 A67-31255
Twenty-eight volt monolithic integrated
logic circuit suitable for aircraft
applications 16 p2642 A67-31725
Soviet book on semiconductor technology
and microelectronics covering photoelectric
functional converters, junction
characteristics, etc 18 p3008 A67-33467
Photoelectric functional converters
application to semiconductor
microelectronics and optoelectronic
circuits 18 p3008 A67-33468
Digital and analog computers evolution,
discussing microelectronics, speed, accuracy,
bulk and human brain 18 p3010 A67-33551
Impact of microelectronics on utilization
and training of maintenance
personnel 18 p2994 A67-34342
Microelectronics for expanding economy -
IEEE Conference, St. Louis, June
1967 18 p3013 A67-34547
Large scale integration of circuits studied
for high yield, using concept of redundancy
adjustment of probability 18 p3014 A67-34553
Automatic IC mask artwork generating
system for large scale integration
environment, describing hardware, software
and performance 18 p3055 A67-34558
Thin film hybrid subaudio active filter
design and fabrication, discussing power
consumption, circuit breadboard
performance, etc 18 p3015 A67-34559
Microelectronic systems design problems
and solutions, discussing system adaptability
concept and influence on design methods
and technology 18 p3015 A67-34561
Microelectronics technology extended to
microwave frequencies, considering
development of solid state devices and
ICs 18 p3015 A67-34562
Highly purified silicone junction coating
resins and silicone molding compound for
microelectronic packaging 18 p3069 A67-34564
Vacuum systems for microelectronic
device fabrication, detailing pumping
methods and related equipment 19 p3236 A67-35020
Photomask application to microelectronics
chip and die fabrication, discussing systems
for step-and-repeat operation elimination in
image array making 19 p3236 A67-35021
Processes and instrumentation for forming
contacts on microelectronics
devices 19 p3236 A67-35022
Instrumentation and microelectronic
measuring methods based on nondestructive
IR and UV techniques used in operation of
superconductive cryogenic memory 19 p3193 A67-35028
Microelectronic failure mechanism,
examining manufacture and processing
methods and production of uniform and
versatile material 19 p3193 A67-35029
Microelectronics fabrication in terms of
specific systems, discussing input and waste
piping systems design, electrical distribution,
exhaust, contamination control, etc 19 p3193 A67-35030
Deep space navigation and guidance
technology, emphasizing simplification of
onboard navigation procedures 19 p3255 A67-35856
Microelectronic circuit packages,
discussing interconnection wiring and
optimization 21 p3594 A67-38333
Microelectronic performance degradation
resistance under thermal sterilization cycling
conditions 21 p3596 A67-38344
Electronic packaging - SAE Conference,
New York, February 1967 21 p3634 A67-38618
IR monitoring technique to improve
accuracy of welding inspection using voltage
feedback to regulate output 21 p3634 A67-38620
Soviet papers on semiconductor technology
and microelectronics 22 p3768 A67-39587
Guidance and navigation sensors and
systems, discussing spacecraft facilitated by
microelectronics, computer technology,
optimal filtering and gyroscopic sensor
design 22 p3834 A67-40335
Microelectronic integrated checkout
equipment interfacing subsystems under test

with test subsystem [AIAA PAPER 67-952] 24 p4133 A67-43036
MICROGRAPHY
SA PHOTOMICROGRAPHY
Neutron bombardment effect on titanium
and chromium carbides before and after
heat treatment, giving results of X-ray and
micrographical analyses, electric resistance,
brittleness and microhardness measurements 03 p0447 A67-13639
Rhesus monkeys liver damage after
irradiation by penetrating protons 14 p2254 A67-28064
Titanium alloys research and development
for aeronautics industry 14 p2338 A67-28627
High strength high modulus carbon fiber
microstructure, studying crystallite size,
orientation effect, electron micrographs and
X-ray diffraction 19 p3248 A67-35426
Dislocation in field-ion micrograph
analyzed by computer-simulated Ranganathan
hypothesis using Moore shell model 19 p3266 A67-35603
Field-ion micrograph indexing noting
equivalence of pseudostereographic
projection to Brandon proposals for pole
identification 24 p4154 A67-42173
MICROINSTRUMENTATION
Planar packaging concepts for avionics
equipment systems and circuit boards
developed from extensive use of
microcircuits and thin film circuits
[SAE PAPER 670251] 11 p1758 A67-23984
Miniature transducers for shock tunnel
instrumentation, noting compensating system
to reduce spurious signals from pressure
and skin friction acceleration 22 p3809 A67-40463
MICROMEROGRAPH
S PARTICLE SIZE
MICROMETEORITE
Centimeter-and millimeter scale roughness
of lunar surface produced by micrometeorite
impact 01 p0150 A67-10893
Micrometeorite flux through thin
aluminum foil determined using Ariel II
satellite 12 p2008 A67-25824
Micrometeoritic particle condensation in
vicinity of earth measured by Elektron II
satellite 12 p2008 A67-25825
Zodiacal dust explained by radioactive Al
26 deposited in marine sediments and
brought by micrometeorites exposed to solar
protons 15 p2553 A67-29157
Ionization in E region due to influx of
micrometeorites 17 p2943 A67-32542
Effective collection time for collecting
cosmic dust in altitude ranges of cosmic and
terminal velocities of particles, using
rockets 19 p3318 A67-35195
Electromagnetic radiation, elementary
particles and micrometeorites effects on
earth satellites 19 p3327 A67-35672
Daily and seasonal changes in numbers,
dimensions and shapes of micrometeoritic
particles over period of two years,
discussing origin 19 p3327 A67-35878
Micrometeorite flux rate for Leonid
shower measured with Luster sounding
rocket collecting surface 20 p3528 A67-37424
Penetration rates of thin aluminum foil
sensors of Ariel II satellites compared with
flux measured by microphone detectors in
vicinity of earth 21 p3722 A67-38494
MICROMETEOROID
Ion engine arcing frequency from
micrometeoroid impact [AIAA PAPER 66-205] 02 p0302 A67-11936
Aerobee rocket measurement in sampling
of micrometeoroid debris during peak of
Leonid meteor shower 10 p1707 A67-23237
Micrometeoroid damage of n-p silicon and
CdS solar cells 13 p2056 A67-27440
Laboratory calibration of piezoelectric
transducer used as micrometeoroid impact
gauge 15 p2486 A67-29410
Possible degradation effects produced in
uncovered and covered N/P silicon solar
cells by simulated micrometeoroid
exposure 15 p2423 A67-30219
Micrometeoroid collection experiments
flown on Gemini IX and Gemini XII
analyzed, using optical and electron
microscopy and mass spectrometry 19 p3339 A67-35196
Space electronic equipment design,
considering incorporation of vibration,
vacuum, micrometeoroid and radiation
protection 21 p3591 A67-38209
Body porosity effect on hypervelocity
impact, computing pressure, velocity, density

and specific internal energy profiles 22 p3912 A67-39748

Puncture sealing of meteoroid penetration in spacecraft, giving mechanical and chemical methods and self-sealing tile inner shell process 22 p3913 A67-39885

Contamination control program developed for investigation and elimination of contaminant particles from 1965 Leonid Meteor Shower micrometeoroids collected by rocket payload 23 p3986 A67-40850

MICROMETEOROID EXPLORER

S EXPLORER XXIII SATELLITE

MICROMETEOROLOGY

Analysis of additional terms in Reynolds flux equation when under unsteady conditions, using wind and temperature measurements, noting role in micrometeorology 02 p0238 A67-12077

MICROMETER

Micrometer U-tube manometers for medium vacuum measurements 08 p1332 A67-21493

Photoelectric micrometer for automatic determination of meridian passage times, describing tracking servomechanism and collimation measurements device 22 p3881 A67-39515

MICROMINIATURIZATION

Feasibility of employing BIT and fault-isolation circuits made possible by microminiaturization techniques applied to advanced avionics systems [AIAA PAPER 67-268] 07 p1167 A67-20077

Planar and sandwich resistor structures in Si thin film integrated circuits 08 p1302 A67-20793

Microelectronic frequency discrimination techniques based on analyzing whole functional block and searching for circuit configurations 14 p2282 A67-28024

Feasibility of employing BIT and fault-isolation circuits made possible by microminiaturization techniques applied to advanced avionics systems [AIAA PAPER 67-268] 17 p2834 A67-32590

Microminiaturization problems associated with design and preparation of solid state Si microdiode matrices 22 p3769 A67-39580

Microminiaturized matrix preparation using welded and diffused Si diodes assembled in two groups of perpendicular metal strips 22 p3769 A67-39581

Solid state multilayer circuits preparation for use in microminiaturization, stressing advantages over printed circuits 22 p3774 A67-40327

MICROMINIATURIZED ELECTRONIC EQUIPMENT

Aviation avionics microelectronic devices stressing reliability, maintenance, circuitry, etc [SAE PAPER 670253] 11 p1758 A67-23985

Silk screen techniques used for film circuitry implementation on integral sensor telemetry transmitter with standard components 12 p1911 A67-25272

Microminiaturizable transistorized circuit for generating wide frequency range high Q inductances from semiconductor devices for integrated selective circuits 13 p2081 A67-27201

Thin films as passive and active electrical components in microminiaturization, noting characteristics obtained by vacuum evaporation, cathode sputtering, diffusion and epitaxial growth 15 p2447 A67-29684

Microelectronics practice and possible use of space for fabrication [AAS PAPER 67-79] 15 p2452 A67-29946

Microminiaturized systems for fault analysis and indication design and application to built-in test equipment 20 p3449 A67-36983

500 to 1000 MHz ultrahigh RF hybrid amplifier fabricated with microelectronic multilayer thin film technique, noting performance of components 21 p3596 A67-38342

Soviet book on microminiaturized aerospace digital computers noting production problems, reliability, electronics, storage units and foreign computers 21 p3588 A67-38765

MICROORGANISM

SA ALGAE

SA BACTERIA

SA CULTURE /BIOL/

SA FUNGUS

SA PLANKTON

SA VIRUS

Postulates on microbial hazards of astronauts in prolonged isolation based on studies with animals with locked flora 05 p0755 A67-16281

Comparative evaluation of methods for determining microbial contamination on various types of surfaces 10 p1601 A67-23348

Rocket and balloon-borne exposure study of terrestrial microorganism survival in space 15 p2424 A67-29097

Spacecraft sterilization for microflora and microorganisms using dry heat for instruments, liquid straining and gas for surfaces 15 p2430 A67-29100

Ecological patterns of microorganisms in desert soils 15 p2426 A67-29112

Exobiology and effect of physical factors on microorganisms 15 p2427 A67-29117

Preservation of viable microbes in anabiosis in potassium salts determined improbable by failure to grow bacteria 15 p2427 A67-29118

Ultrasonic energy, used for removing microorganisms from various surfaces for enumeration, noting texture, pretreatment and heat effects on recovery efficiency 19 p3179 A67-34911

Continuous synchronous culture of photosynthetic microorganism *Chlorella* cultivated in illuminated and dark stirred tanks 19 p3177 A67-34913

Lethal effect of solar UV radiations on dried *Coliphage* T-1 exposed to space at sounding rocket altitudes 19 p3177 A67-35184

Soil, moisture and other requirements for microorganism survival in simulated Martian environment 19 p3177 A67-35220

Terrestrial microorganisms survival in space, noting inactivation effect by solar radiation 19 p3178 A67-35221

Terrestrial microorganism survival in space aboard Gemini satellite, discussing lethal effects of solar radiation 19 p3178 A67-35223

Analytical model for microbial population survival times during heat sterilization studied for spacecraft applications, considering environment and exposure time 19 p3180 A67-35264

Ionospheric and stratospheric UV radiation effects on survival of microorganisms 19 p3178 A67-35271

Planetary quarantine problem for Martian survival of microorganisms investigated, using systems analysis 19 p3180 A67-35274

Desiccated microbial populations of lyophilized *Staphylococcus epidermidis* cells and *Bacillus subtilis* spores studied for synergism in ethylene oxide-methyl bromide sterilization 19 p3180 A67-35279

Growth of terrestrial microorganisms on Mars noting possibility of planetary contamination 19 p3178 A67-35896

Microbiological organisms in jet aircraft wing fuel tanks as major corrosion sources, with fuel additives tested to inhibit microbial growth 20 p3515 A67-36485

Microorganism shedding by human beings studied by isolation of specific sources and washing or sanitizing of arms 20 p3374 A67-36803

Survival and growth of *Bacillus cereus* and *B. subtilis* in simulated Martian environment of diurnal temperature cycling and low moisture and oxygen level 20 p3372 A67-37160

Pyrolysis gas chromatography method for life detection and chemical identification of microorganisms 20 p3378 A67-37500

Microbial interaction in closed system by simulating space flight conditions, noting degree of crowding effect on buildup 21 p3577 A67-38899

Assessment of microbial contamination on surfaces of space hardware by ultrasonics 23 p3962 A67-40852

Potential contamination of equipment by primate passenger during 30-day earth orbit, studying skin, body particulate matter and indigenous microflora 23 p3944 A67-40856

Human microbial shedding using sterile stainless steel shedding chamber, discussing clean room clothing reducing shed rate 23 p3962 A67-40857

Microbial interaction factors determined between men and environment in closed systems 23 p3962 A67-40858

Germ sampling at high altitudes using hydroaeroscopes attached to conventional aircraft 23 p3963 A67-41072

Long term space mission sanitation,

personal hygiene and body cleansing to control microbe populations on body surface and teeth 23 p3967 A67-41611

Manned spacecraft water supply microbial contamination detection using firefly bioluminescent reaction 23 p3968 A67-41627

Indigenous microflora as determined in men undergoing simulated space conditions, considering microbic shock postulated on long term missions 23 p3958 A67-41656

Microbial contamination of jet aircraft fuel systems [SAE PAPER 670869] 24 p4206 A67-42007

MICROPHONE

Pressure calibration methods for testing response of microphones in difficult conditions of temperature, pressure and frequency 09 p1484 A67-21938

Noise cancelling devices for converting noise into equivalent electric energy, noting pressure, differential and throat microphones 15 p2489 A67-30088

Noise discrimination microphones in aircraft, discussing performance characteristics, design, construction, applications, clarity, size, etc 18 p2994 A67-34399

MICROPULSATION

SA GEOMAGNETIC MICROPULSATION

Helium ion effects in micropulsation spectrograms of outer magnetosphere 13 p2108 A67-26328

Ionospheric micropulsations induced by enhanced conductivity of current due to meteors, noting end effect from finite ion trail length 14 p2383 A67-28044

Observed micropulsation activity during meteor shower compared with predicted magnetic agitation value determined from equation by Chapman and Ashour 14 p2383 A67-28045

ELF and micropulsations phenomena divided into earth-ionosphere cavity resonances and regular and irregular pulsations 14 p2266 A67-28415

MICROROCKET

Microrocket technology, deriving propellant consumption equations and explaining numerical coefficient variation 15 p2545 A67-29452

Control rockets covering very low thrust operation, gas generation problems, gas expansion, etc 20 p3516 A67-36881

MICROSCOPE

SA ELECTRON MICROSCOPE

SA ION MICROSCOPE

Holographic interference pattern magnification and observation by looking through objective end of microscope 02 p0242 A67-12027

Two magnetically geared microscope stages for nuclear track plates 02 p0247 A67-12696

Reflected light microscope for viewing unstained brain and ganglion cells 18 p2991 A67-34530

Prototype model of petrographic microscope for lunar and planetary missions, discussing design and fabrication 19 p3229 A67-35320

MICROSCOPY

SA ELECTRON MICROSCOPY

SA MICROGRAPHY

SA PHOTOMICROGRAPHY

SA ULTRAVIOLET MICROSCOPY

Holography using bright field microscopy and examination a posteriori in reconstruction by dark field, phase contrast or interference microscopy 04 p0618 A67-14496

Holography characteristics and possible future uses noting properties, resolution limits and depth of field of high resolution holographic microscopy 18 p3043 A67-33546

MICROSTRUCTURE

SA METEORITIC MICROSTRUCTURE

SA SYNTHETIC MICROSTRUCTURE

Powder metallurgical techniques for controlling porosity microstructures including powder selection, pore forming additives, compaction and sintering 01 p0100 A67-10723

Structural sensitivity of plastic properties of molybdenum alloys produced by electron beam fusion, investigating microstructure, failure in bending tests and grain fragmentation 01 p0101 A67-10936

Arc radiation and selective solute vaporization from arc spot region of weld pool used to explain formation of overlap segregation in aluminum alloy

- weldments 01 p0080 A67-10947
Microstructure and microhardness of evaporated thin films as function of temperature of substrate during condensation 02 p0286 A67-11707
Microstructure effect on creep deformation mechanisms in polycrystalline ceramic oxides including grain size, subgrain structure, porosity, diffusional creep and dislocation movement 03 p0449 A67-13304
Anisotropy of thermal expansion and microstructural changes due to thermal stresses 03 p0446 A67-13564
Elastic modulus, Youngs modulus and Poisson ratio for solids containing foreign inclusions imbedded in matrix 03 p0524 A67-13785
Microstructure and mechanical properties as functions of degree of deformation of pressed rods of Tsm2A alloy at 1300 degrees C 05 p0832 A67-17509
Transmission electron microscopy analysis of microstructural phase properties of Ti-8Al-1V-1Mo alloy after duplex and mill annealing treatments 06 p1013 A67-17797
Cyclic load and temperature effects on creep behavior of Ni-base alloy Mar-M 200 between 1800 and 1900 degrees F 06 p1014 A67-17802
Tensile tests performed on alpha titanium between -321 and 75 degrees F, discussing ductile-to-brittle transition, microcrack formation and brittle fracture mechanics 06 p1014 A67-17807
Heat treatment and microstructural observations in wrought Ni-base superalloy Udmet 700 in static creep, determining fracture and deformation properties 06 p1015 A67-17809
Macroscopic brittle fracture theory for structural microheterogeneities effect on maximum macrostresses in plates with hyperbolic notches under tensile loads 06 p1100 A67-17950
Fine structure and microstructural effects on control of magnetic, electrical, optical, thermal and mechanical properties of eutectic alloys 06 p1018 A67-18409
Microstructural and X-ray analysis of intermediate phases of Ti-Ir and Ti-Rh intermetallic compounds, including microhardness and fusion point variations 07 p1204 A67-19263
Microstructure of alloys of Ti-Fe and Ti-Cr-Fe systems, determining phase composition and incipient melting temperature 07 p1204 A67-19269
Ternary system Ti-Al-V alloys analyzed using thermal, microstructural, etc. methods, plotting solidus surface in crystallization region of beta-solid solution 07 p1205 A67-19273
Microstructural changes effect on mechanical properties of nickel base superalloys, with particular attention to wrought alloys 08 p1340 A67-20362
Microstructure interpretation of 5Al-2.5Sn titanium alloy, examining high optical magnification and polarized light illumination 08 p1340 A67-20365
Micromechanical failure mechanism of fiber reinforced plastics under tension, compression and shear 08 p1344 A67-20422
Microstructural dislocation tangling and related changes in tensile properties of Hastelloy X-280 following thermomechanical treatments 10 p1688 A67-23174
Microstructural study of adhesive behavior of powdered bakelite in intergrain pores of carbon-graphite compacts in terms of capillary attraction forces 11 p1810 A67-23900
Microstructure of aluminum alloys analyzed for composition, fabrication and thermal treatment, using electron microscopy 14 p2334 A67-27803
Titanium-vanadium alloy microstructure investigated under quenching and aging through electron microscopy 14 p2338 A67-28423
Soviet atmospheric turbulence studies considering microstructure, wave propagation in turbulent atmosphere, turbulent exchange in atmospheric ground layers, etc 14 p2346 A67-28763
Gold, silver, copper and tin condensed films, investigating dependence of structure and conductivity on substrate material 15 p2540 A67-30122
Ti-Zr-C and Ti-Hf-C alloy X-ray and microstructural studies noting homogenizing, annealing, quenching and phase equilibria 15 p2505 A67-30388
Positive effect of carbon on microstructure and mechanical properties of niobium alloys 16 p2687 A67-30845
Microhardness and microstructure of annealed industrial nickel filings studied, noting results obtained at 300 degrees C 16 p2687 A67-30846
Microstructure stability of aluminum reinforced with Al-Ni whiskers, noting tensile strength and mechanical property dependence on temperature 16 p2690 A67-31372
Microstructural features of Ni maraging steel weldments related to fracture toughness properties 18 p2692 A67-31868
Maximum shear stress dependence on composite materials microstructure, noting filler and binder role 18 p3069 A67-34170
High strength high modulus carbon fiber microstructure, studying crystallite size, orientation effect, electron micrographs and X-ray diffraction 19 p3248 A67-35426
TiNi-TiFe system equilibrium diagram, studying melting points and heat treatment effects on microstructure 20 p3468 A67-37179
Microstructure and mechanical properties as functions of degree of deformation of pressed rods of Tsm2A alloy at 1300 degrees C 21 p3644 A67-38037
Microchemical and microhardness properties of parallel gap welds for microstructure interpretation of metal joint 21 p3636 A67-38633
Heat treatment effect on microstructure and notch-bar rupture life of INCONEL alloys 21 p3646 A67-38776
Hot-cracking and microstructure characteristics in weld heat resistant Ni alloys evaluated by synthetic specimen technique 22 p3819 A67-39449
Structural sensitivity of plastic properties of molybdenum alloys produced by electron beam fusion, investigating microstructure, failure in bending tests and grain fragmentation 22 p3820 A67-39790
Cleavage, plastic, creep, fatigue and other types of fracture noting initiation, propagation, mode, behavior, microstructure and appearance 23 p4019 A67-41033
Dislocation of aluminum during creep investigated for change in block structure 23 p4020 A67-41301
Transmission electron microscopy for microstructure observations at growing fatigue crack tips in aluminum alloys, discussing plastic dislocation morphology and density 24 p4170 A67-41947
Microstructure of SGBF graphite under tensile and compressive stresses noting crack generation in layer planes [ACS PAPER 6-N-66F] 24 p4175 A67-42372
MICROTHRUST
Microthrust ion engine system with thrust vector control, using ion beam deflection [AIAA PAPER 66-204] 04 p0706 A67-15241
Electric propulsion for satellite applications, noting cesium contact microthrustor ion engine system [AIAA PAPER 67-80] 07 p1240 A67-19435
Permanent magnet low thrust engines performance and tests, starting from cesium electron bombardment ion microthrustor [AIAA PAPER 67-81] 07 p1240 A67-19436
Solid propellant highly restartable electric trigger microthrustor, noting triggering electrode and feed system 11 p1746 A67-25013
Direct microthrust measurement on swinging gate test stand with equalization network 11 p1774 A67-25014
Design and performance characteristics of electrothermal microthrust systems for spacecraft functions [AIAA PAPER 67-423] 18 p2988 A67-33907
Primary electric propulsion application to satellite and other space missions, considering auxiliary systems and experimental thruster systems [AIAA PAPER 67-426] 18 p3112 A67-33910
Permanent magnet low thrust engines performance and tests, starting from cesium electron bombardment ion microthrustor 21 p3689 A67-37790
Radioisotope heating to provide ionizer temperatures in contact ion thrusters [AIAA PAPER 67-734] 21 p3695 A67-38757
Pulsed vacuum arc microthrustor noting various performance data and advantages [AIAA PAPER 67-737] 21 p3695 A67-38759
Colloid microthrustor technology, discussing stationkeeping application, energy loss, diagnostic techniques, etc [AIAA PAPER 67-531] 22 p3867 A67-39200
Primary electric propulsion application to satellite and other space missions, considering auxiliary systems and experimental thruster systems [AIAA PAPER 67-426] 24 p4208 A67-42901
MICROWAVE
Millimeter and centimeter radio wave propagation in near sea level tropospheric waveguides 02 p0191 A67-11569
Book on microwave engineering including transmission lines, resonators, waveguides, antennas, tubes, etc 04 p0583 A67-15269
Microwave and optical measurements of decay of neutral metastable and charged species in flowing He afterglow 08 p1356 A67-21300
Reconstructions of visible images from reduced scale replicas of polarized microwave holograms 09 p1496 A67-21709
Microwave amplification by electron beam interaction with cesium plasma 13 p2166 A67-26726
Microwave amplification when electron beam passes through cesium plasma, noting noise figure dependence on tube pressure 21 p3668 A67-38605
MICROWAVE ANTENNA
SA LUNEBERG LENS
SA RADAR ANTENNA
Polarization pattern dependence on phase-amplitude distribution of field at microwave antenna aperture 02 p0214 A67-11905
Computer and curve tracer method to generate photo masters for printed circuit microwave antennas, transmission lines and filters 03 p0383 A67-13790
Transition zone anechoic chambers for field checkout, production and radiation testing of microwave antennas 03 p0397 A67-14102
Microwave data link system development for deep space communication 04 p0568 A67-14499
Microwave scanning antennas, Volume 3, Array systems 07 p1151 A67-19544
Microwave scanning antennas, Volume 2, Array theory and practice 07 p1154 A67-19780
Mutual coupling and edge effects in finite scanning arrays 07 p1154 A67-19784
Miniaturized C-band digital latching phase shifter for combined advantages of waveguide and stripline design 08 p1305 A67-21227
Maximum signal transfer theorem for radio wave transmission, scattering and subsequent detection 09 p1462 A67-21611
Basic design differences illustrating paraboloidal reflector variations, noting factors contributing to or detracting from antenna efficiency 10 p1613 A67-23413
Criterion of accuracy for given approximate current distribution based on difference between variationally computed stationary and nonstationary antenna impedances 11 p1759 A67-24131
Waveguide discontinuity problems solved through matrix iterative analysis 11 p1760 A67-24237
Current distribution and input admittance of infinitely long cylindrical antenna driven by slice generator and immersed in anisotropic plasma 11 p1761 A67-24284
Systematic design of matrix network, consisting of hybrids with phase delays in interconnecting lines, used for antenna beam steering 11 p1763 A67-24300
Nylon trailing line antenna application, operation and performance 11 p1743 A67-24359
Contribution of propagation factors in terrestrial atmosphere to noise received by antenna at hyperfrequencies 12 p1904 A67-25308
Receiver-antenna system in radio astronomy, discussing low noise, thermal signal reception and acquisition of information limited by internal or external noise 12 p1914 A67-25309
Phased-array microwave antenna system for scanning simultaneous targets whose distance and direction are changing rapidly 13 p2083 A67-27566
Phase lock techniques applied to microwave antenna arrays noting problems, advantages, properties, etc 15 p2451 A67-29922
Large aperture, low noise, steerable antennas for ground station commercial

satellite communication networks 16 p2641 A67-31532

Narrow beam microwave integrated circuit phased array system design for tactical communications satellite requirements 17 p2956 A67-32497

Satellite influence on microwave antenna design, discussing mount designs, multifunctional antenna feed systems, structural analysis and geometries for microwave antennas 21 p3593 A67-38233

Omnidirectional double slot array of thin X-band rectangular waveguides, noting design for slot conductance and power handling capacity 23 p3977 A67-40699

MICROWAVE APPARATUS

Phase locking, mode selection and noise problems in synchronous operation of microwave silicon avalanche diode oscillators to obtain large coherent output power 01 p0033 A67-10016

Epitaxial gallium arsenide Gunn effect oscillators in generating continuous wave oscillation 01 p0033 A67-10026

Charged particle motion in field of traveling electromagnetic waves used in studies for microwave amplifiers, particle accelerators, etc 01 p0022 A67-10352

Microwave spaced-cavity refractometer for measuring small-scale variations of refractive index, wind speed, temperature, etc, in lower atmosphere 01 p0025 A67-10816

Microwave power generation by avalanche-transit time diodes, noting noise and excess heat problems 01 p0040 A67-11255

Three representative microwave systems of different transmitting capacity currently in serial production 02 p0220 A67-12203

Gallium arsenide microwave diodes prepared by vapor phase growth method with highest combination of reverse breakdown voltages and cut-off frequencies 03 p0379 A67-13477

Trimode four channel monopulse bridge with reduced microwave components 03 p0383 A67-13828

Meteorological instrumentation for measuring physical characteristics of atmosphere 04 p0649 A67-14686

Ground station for space communications and radar and radio physics, noting use of Cassegrain antenna computer guided pointing control, plug-in equipment box, etc 04 p0596 A67-15047

Fast switching microwave phase shifters for high power array radars, describing drive control techniques 04 p0581 A67-15053

Thin film piezoelectric transducers properties used in microwave acoustic delay lines and phonon generators for analysis of phonon-phonon interactions in dielectric materials 04 p0621 A67-15116

Radio electronics, discussing quantum electronics, lasers, microwave devices and technology, plasma physics, etc 06 p0968 A67-18072

Avalanche drift diode and application in microwave technology, analyzing dynamic negative resistance formation, volt-ampere characteristics and output power 06 p0970 A67-18169

Properties determining phase linearity of microwave devices, noting effects of cascaded devices on system performance 06 p0972 A67-18578

Microwave feedback radiometers using electromechanical and all-electronic systems 07 p1155 A67-19875

Semiconductor loaded E plane T waveguide junction spectrometer for microwave measurement of transport parameters in semiconductors 08 p1329 A67-20375

Phase linearity of microwave component and interaction of cascaded devices, giving analysis of two-port device 08 p1303 A67-21029

Solid state microwave square law detectors, comparing threshold response for unit video bandwidth using Noise Equivalent Power /NEP/ concept 08 p1304 A67-21220

Electronics methods used in laser technology and vice versa, emphasizing microwave photoelectronic devices, self-consistent gas discharges at optical frequencies, etc 08 p1338 A67-21269

Low temperature components for data processing, low noise amplifiers and microwave technology, noting superconductor elements like cryotron 09 p1463 A67-21760

Microwave receivers with low noise - Colloquium, Paris, May 1966 09 p1481 A67-22477

Local oscillators with standardized frequencies in conjunction with central mixer used as wideband noise receiver for increased sensitivity 09 p1481 A67-22480

Pulsed oscillations of microwave Gunn effect oscillator in n-type single crystal GaAs 10 p1609 A67-22838

Integrated circuit technology for microwave equipment including guidelines and system design 10 p1610 A67-22973

Nonreciprocal ferrite devices at microwave frequencies, detailing circulator and isolator components 11 p1758 A67-24060

Charged particle motion in field of traveling electromagnetic waves used in studies for microwave amplifiers, particle accelerators, etc 11 p1755 A67-25025

High resistance region effect in neighborhood of linear junction on series resistance analyzed for microwave varactor design 12 p1912 A67-25280

Low noise level microwave receivers - Conference, Paris, May 1966, Part 2 12 p1912 A67-25294

Planetary atmospheric composition study under ambient conditions using instrument involving very high Q Fabry-Perot microwave cavities 12 p1946 A67-25986

Low temperature refrigeration for microwave systems - Conference, Frankfurt am Main, April 1966 14 p2277 A67-27774

Stirling type closed cycle cooling system for masers and other microwave electronic devices 14 p2278 A67-27784

Progress in linear circuit theory, discussing scattering matrices, broadband matching and distributed and mixed lumped networks 14 p2291 A67-28460

Microwaves and laser links for spacecraft-earth communications noting limitations by external noise effects, atmospheric turbulence, fabrication tolerances, etc 14 p2273 A67-28799

RCA papers on defense electronic products including search radar, superconductor devices, data and spacecraft communications, speech recognition 14 p2274 A67-28910

Performance of electron tube and solid state devices in microwave region, comparing low noise amplifier devices 14 p2289 A67-28913

Design procedures for practical elliptic function filter with high selectivity in very compact configuration, noting bandpass and band-stop applications 15 p2444 A67-29453

Electron tube requirements for space applications noting size, weight, environmental parameters, etc 15 p2447 A67-29752

Ion beam generation and applications, discussing duoplasmatron, RF source, contact ionization source and Penning discharge 15 p2488 A67-29756

Multipactor suppression properties of Ti, Cr, V and Ta determined using special electromagnetic cavities 15 p2448 A67-29757

Special plastics for low loss microwave transmission devices, describing electrical properties 15 p2508 A67-29930

Output noise power spectrum properties of X-band ruby maser oscillator, noting frequency dependence on electromagnetic energy and cavity losses 16 p2685 A67-31055

Solid state microwave delay lines noting advantages, operation principles, fixed variable construction, etc 16 p2637 A67-31106

Microwave ferrite devices describing applications at metric and decimetric wavelengths, at very low temperatures and at high power levels 17 p2828 A67-32744

Carbon dioxide ions with electrons dissociative recombination measurements with microwave afterglow differentially pumped quadrupole mass-spectrometer apparatus, noting Martian atmosphere model [SRCC-55] 17 p2888 A67-32826

Design considerations for reliable microwave power packs noting redundancy, independent module system and intrinsic reliability 18 p3010 A67-33665

Microwave measurement methods for nondestructive material testing, discussing efficiency, advantages and applications 18 p3045 A67-33740

Microwave experimental technique for continuous velocity measurement of shock and contact discontinuities bounding air

plasma generated in cylindrical hypersonic shock tube 18 p3020 A67-34105

Gunn effect semiconductor oscillator for generating microwave power using GaAs 18 p3013 A67-34525

Solid state pulsed carrier IF-AGC system design for microwave receivers noting input network, video circuit, AGC loop gain, etc 18 p3016 A67-34597

Strip transmission lines used for microwave circuits noting applications, design data, discontinuity information, etc 19 p3191 A67-34945

Microwave direction-finding receiver with digital output for blind aircraft landing and navigational uses 19 p3254 A67-35551

Epitaxial gallium arsenide FET electrical characteristics, noting structural details and feasibility for use at microwave frequencies 19 p3196 A67-35629

Oscillation conditions of microwave tunnel diode theoretically and experimentally evaluated for mounting at feed point of semicircular loop antenna 19 p3198 A67-35660

Instrument-landing system including microwave apparatus 19 p3255 A67-35807

Electromagnetic wave generation and amplification extended from LF microwaves up to optical band 20 p3380 A67-36488

Avalanche drift diode and application in microwave technology, analyzing dynamic negative resistance formation, volt-ampere characteristics and output power 20 p3404 A67-37592

Plasma acceleration by electromagnetic microwave discharge in static magnetic field gradient, discussing microwave-plasma energy transfer at electron cyclotron resonance [AIAA PAPER 67-660] 21 p3671 A67-38696

Microwave use in measuring burning rate of solid propellant rocket motors and in detection of porosity in nonconducting materials 22 p3795 A67-39186

Systems with low noise factor and high selectivity tuned by varying pumping frequency 22 p3767 A67-39370

Standing wave ratio and impedance measurement method for rectangular waveguides at microwave frequencies 22 p3767 A67-39371

Magnetron type microwave amplifier gain increase, discussing electron beam interaction region M-type device gain calculations 22 p3770 A67-39654

Design formulas for predicting dependence of resistance and reactance of diffused microwave p-n diodes on reverse bias voltage 22 p3770 A67-39730

Microwave mixing with weakly coupled Josephson superconducting diodes, discussing - Fourier components 22 p3865 A67-40439

Unilateral parametric amplifier using two varactor diode low pass filter with pumping phase difference, noting bandwidth and gain 24 p4128 A67-41969

Optical communications systems capable of microwave bandwidths evaluated experimentally and theoretically 24 p4123 A67-42805

Czochralski ruby shows high inversion ratio when used as microwave maser material 24 p4205 A67-42813

MICROWAVE ATTENUATION

Quantum mechanical theory of microwave nonresonant absorption and dielectric and magnetic relaxation in gases 01 p0116 A67-10145

Microwave modulation of helium-neon laser intensity studied as function of temperature and electron density 01 p0088 A67-10260

Attenuation characteristics of unsupported resistive thin film applied to one face of dielectric vane in microwave attenuator 01 p0039 A67-10899

Temperature dependence of phase shift in magnesium-copper ferrite-chromite phase shifter as affected by microwave permeability 02 p0301 A67-12672

Electron paramagnetic resonance of photosensitive donors in zinc oxide with oxygen vacancies 06 p1054 A67-18832

Waveguide resonant-iris bandpass filter with very wide passband and stopbands that provide transmission and attenuation characteristics for use with microwave generators 07 p1151 A67-19426

Measurement of attenuation of 8.6 mm wavelength radiation in rain, relation to rate

of rainfall, using corner reflectors 07 p1146 A67-20201

Dielectric relaxation of gases and sharp rise in microwave absorption coefficient in Cytherean atmosphere 08 p1401 A67-21372

Antenna height protection against microwave diffraction fading determined, using digital computer to evaluate residue series for grazing conditions 09 p1464 A67-22444

Microwave oscillation-amplifying L-band platinotron tube to amplify peak power of radar transmitter 10 p1605 A67-23061

Atmospheric attenuation at millimeter wavelength measured noting correlation with weather conditions and solar flux effect 11 p1751 A67-23971

Microwave surface absorption in static magnetic field affects surface resistance of superconducting alloys 11 p1846 A67-24584

Microwave attenuation standard derived using waveguide below critical frequency as voltage divider to determine losses in components 13 p2067 A67-26488

X-band attenuation by rocket exhaust plume measured with AM/PM noise for various propellant systems 15 p2436 A67-29429

Light attenuation measurement in chilled silicon noting attenuation increase with incident intensity 16 p2685 A67-30870

Correlation of rainfall rate with attenuation at various frequencies of microwaves 16 p2625 A67-31341

Microwave attenuation change and harmonic generation by n-type GaAs in strong microwave electric fields, determining current density relation to field strength 17 p2913 A67-32310

Temperature compensated electronically controlled ferrite attenuator design and performance 17 p2825 A67-32524

RF attenuation measurement methods and standards 17 p2815 A67-32607

Attenuation of lunar microwave emission measured by artificial moon method, determining phase dependence of lunar temperature 18 p3119 A67-33861

Shock wave argon ionization in constant magnetic field, showing attenuation decrease of microwave signal in plasma and modulus change curves 18 p3087 A67-34045

MICROWAVE CIRCUIT

Cut-off frequency of varactor diode defined for variable series resistance factor 01 p0036 A67-10466

Solid state microwave telemetry transmitters, discussing power generation, stability, modulation /AM, PM and FM/, environmental effects and circuitry 02 p0216 A67-12008

Gunn effect semiconductors and contact preparation techniques, noting excitation of oscillations and amplification characteristics in GHz range 02 p0220 A67-12198

Measurement of sticking coefficient for thermal electrons in oxygen and air, using microwave circuits 02 p0274 A67-12466

Transient analysis of TEM mode four-port microwave networks by flow graph techniques, with application to branch line coupler, phase shifter and ring hybrid 04 p0591 A67-14861

Microwave varactor tuned transistor oscillator design, considering collector base multiplication, oscillation and load matching conditions and theoretical tuning curve 04 p0581 A67-14864

Power reflection technique for high quality varactor diode characterization 08 p1304 A67-21221

Isolation bandwidth characteristics of Y circulator junction modified by external tuning elements 09 p1474 A67-22087

Noise generation in Gunn diodes suggests dependence on avalanching of charges in bulk material, making bulk oscillations irregular 09 p1556 A67-22263

Microwave frequency oscillations obtained from p-n junction diodes reversed-biased into avalanche region, noting dependence on temperature and impedance of microwave circuit 09 p1479 A67-22265

Processing techniques for integrated microwave circuits using silicon-on-sapphire /SOS/ transistors for high frequency power outputs 10 p1610 A67-22972

Exact calculation of electrical performance of rectangular waveguide T-junction having arbitrary cross section used to find equivalent circuit 11 p1767 A67-24732

Nonuniform distributed network problems solved by Lie algebras 12 p1919 A67-25979

Single crystal YIG phase shifter performance noting improved output with proper microwave circuit design 13 p2076 A67-26479

Composite resonant system behavior with and without stub tuner, tabulating internal, external, loaded Qs and coupling coefficient 13 p2076 A67-26480

Microelectronic frequency discrimination techniques based on analyzing whole functional block and searching for circuit configurations 14 p2282 A67-28024

Microwave modules using integrated circuits 15 p2451 A67-29926

Balanced broadband microwave transistor amplifiers using tantalum integrated circuitry 15 p2452 A67-29927

Hybrid microwave integrated circuits, discussing use of planar and passivated chip devices 15 p2452 A67-29929

Parametric negative resistance range and impedance matrix element values of microwave Read avalanche diode 15 p2453 A67-30016

Electronic components - IEEE and EIA Conference, Washington, May 1967 16 p2641 A67-31721

Narrow beam microwave integrated circuit phased array system design for tactical communications satellite requirements 17 p2956 A67-32497

Solid state microwave device technology concerning generators, low noise and control devices, discussing computerized technique for circuit analysis and design 18 p3015 A67-34595

Strip transmission lines used for microwave circuits noting applications, design data, discontinuity information, etc 19 p3191 A67-34945

Design and stability of wideband tunnel diode amplifiers for microwave radiolink receivers 20 p3395 A67-36248

Monograph on waveguide junctions theory and microwave network analysis, stressing model characteristic definition and impedance 20 p3399 A67-36950

Microwave characteristics of coaxial mounted tunnel diodes investigated by equivalent circuit parameters 21 p3602 A67-39070

Transistor parameters effect on microwave-circuit performance, tradeoffs and relation between tradeoffs, circuit performance and design 22 p3775 A67-40467

MICROWAVE COUPLING

Microwave mixing in paramagnetic crystal using traveling wave maser with ruby as mixer element, noting frequency conversion 01 p0086 A67-10003

Equivalent circuit synthesis for microwave band pass filter design consisting of interdigital or comb structure EM line-coupled resonators 07 p1149 A67-19132

Properties of real radiators and effects of mutual coupling between pairs noting impedance, pattern and polarization characteristics 07 p1154 A67-19782

Behavior of infinite arrays including radiation pattern approach yielding expressions for gain and periodic structure approach yielding input impedance variation with scan angle 07 p1154 A67-19783

Sensitivity of dielectric rod terminal impedance to surface wave coupling when no resonance regions exist within energy-carrying cross section 07 p1158 A67-20299

Advances in microwaves, Volume 1, covering stanford accelerator design, directional couplers, waveguide singular integral equations, Lie algebras, microwave network application, etc advances in microwaves, Volume 1, covering 12 p1906 A67-25975

Directional coupler classification 12 p1915 A67-25977

Microwave power coupling from waveguide to helicon mode in doped indium antimonide by placing aluminum oxide cones on semiconductor surface 12 p1986 A67-26160

Mode correspondence between circular and square multimode tapered waveguide, noting similar behavior of coupling mechanism of waveguides 15 p2444 A67-29454

MICROWAVE FILTER

SA WAVEGUIDE

Ring trapped mode resonator for use in microwave filters, developing expressions for unloaded Q and resonant frequency in

transverse electric mode 02 p0217 A67-12091

Optimum microwave filters with even number of sections, using first order Chebyshev polynomial to obtain equivalent circuit 10 p1613 A67-23444

Waveguide discontinuity problems solved through matrix iterative analysis 11 p1760 A67-24237

Characteristics of waveguide resonant-iris filters for microwave generators 13 p2083 A67-27444

Superconducting microwave filters, discussing minimum insertion loss, loss dependence on various factors and effect of peak fields on maximum power 14 p2289 A67-28915

Impedance wall validity range for microwave structure, discussing tunable filter 17 p2816 A67-32787

Microwave direct-coupled cavity filter design using single insertion loss formula for case of Chebyshev equal-ripple characteristic 17 p2828 A67-33084

Coaxial and strip-line passive microwave components stressing design of hybrid junctions, microwave mixers, filters, etc 19 p3195 A67-35549

Magnetics - Conference, Washington, D.C., April 1967 22 p3859 A67-39895

Microwave pulse compression filter using dispersive characteristics of propagating magnetostatic spin waves in single crystal YIG rods 22 p3773 A67-39908

Magnetically tunable microwave filters using MHD modes in ferrites 23 p3980 A67-41186

Low loss mechanically or magnetically tunable 1 to 12 GHz hybrid ferrimagnetic dielectric microwave bandpass filter with improved power handling 24 p4132 A67-42808

MICROWAVE FREQUENCY

Coherent microwave power at K-band frequencies from indium antimonide structures, presenting theory of two-stream interaction in transverse magnetic field 01 p0131 A67-10371

Microwave mixer point contact diode with X-band intermediate frequency for good value of conversion loss 01 p0036 A67-10438

Dielectric behavior and point imperfections of high temperature KCl in microwave frequency range 02 p0299 A67-11896

Mode switching in tunnel diode, noting change from relaxation to microwave oscillation mode 02 p0217 A67-12090

Experimental results of microwave absorption by magnetoplasma indicate peaks result from excited electromagnetic wave propagation 03 p0476 A67-13357

Book on microwave breakdown in gases covering electron collisions, Boltzmann equation for ionized gas, breakdown in atmosphere, etc 03 p0369 A67-13559

Nanosecond pulse microwave breakdown in air 04 p0657 A67-15120

Microwave integrated circuits combining tantalum thin film technology and beam lead devices, noting fabrication, advantages and performance 05 p0770 A67-16241

Matrix analysis of small signal microwave frequency conversion based on linear operation of semiconductor diode 05 p0772 A67-16449

Amplifier using electro-optic junction modulator combined with photodetector, showing gain at microwave frequencies 05 p0774 A67-16822

Microwave surface resistance of type II superconductors, from simultaneous measurements of real part of surface impedance and magnetization 05 p0871 A67-17375

Spectra of unlocked driven semiconductor oscillators observed with millimeter wave reflex klystrons, noting gradual controllable frequency pulling 05 p0780 A67-17522

Absorption measurements of 139-Gc microwaves for very high purity mercury telluride, deducing electron effective mass 06 p1047 A67-17653

Electroconductivity variations in CdS and CdSe single crystals with SHF electric field strength, intensity of bias lighting and temperature in minus 70 to plus 70 degrees C interval 08 p1370 A67-20996

Absolute value of photoconductivity in polycrystalline high resistivity CdS and CdSe SHF field and experimental determination of barrier amplification factor and intercrystalline barrier

height 08 p1370 A67-20997
 Optimization of design of input-output matching networks for transistor microwave frequency amplifiers, using computer program 08 p1305 A67-21228
 Precision power measurements of spacecraft CW signal level with microwave noise standards, noting Mariner IV application [JPL-TR-32-1070] 09 p1495 A67-21622
 Upper frequency limit prediction method for Gunn oscillations 09 p1556 A67-22264
 Temperature effect on microwave-gain characteristics of bulk GaAs amplifier, interpreting results in terms of changing carrier concentration 10 p1612 A67-23371
 Nonreciprocal ferrite devices at microwave frequencies, detailing circulator and isolator components 11 p1758 A67-24060
 Magnetic field effect on electromagnetic wave propagation through free carrier plasmas in semiconductors, considering Faraday configuration 11 p1840 A67-24663
 Packaging method for integrated microwave transistor amplifier constructed on ceramic substrates 12 p1910 A67-25265
 RF communication converter miniaturization and packaging techniques 12 p1911 A67-25271
 Breakdown voltage characteristics of Ge bonded diode in relation to microwave oscillation, noting avalanche breakdown 12 p1914 A67-25458
 Spin wave interaction in YIG with acoustic, magnetoplastic and relaxation oscillations excited by laser and microwave 12 p1953 A67-25749
 Thin film superconducting bridge behavior in microwave field noting dependence of deviation from classical rectification on frequency, power, temperature and bridge width 12 p1985 A67-25848
 Broadband microwave frequency translator using latching ferrite phase shifter 13 p2075 A67-26477
 Solid state semiconductor microwave power generator design, analyzing spurious oscillations rejection problem 13 p2081 A67-27204
 Frequency multiplication of microwaves by field electron emission in superconducting cavity 14 p2278 A67-27787
 Solar flux density absolute microwave spectra 14 p2385 A67-28441
 Magnetoplasma radiation by microwave pulse excitation at gyrofrequency harmonics, considering single particle approach 14 p2360 A67-28557
 Solar radio emission spectroheliograms at different millimeter wave frequencies 14 p2388 A67-28834
 Microwave frequency superconductor materials, applying bulk and thin film properties to filter, amplifier, oscillator, junction and Josephson effect devices 14 p2289 A67-28917
 Microwave power generating semiconductor oscillators noting negative resistance effect, construction of Gunn oscillator diode, etc 15 p2445 A67-29583
 Magnetic devices for microwave integrated circuits, discussing ferrite substrate use as medium for microstrip transmission lines 15 p2452 A67-29928
 Communication with and by space vehicles at ghz frequencies, using atmospheric windows [AAS PAPER 67-94] 15 p2478 A67-29954
 Tunable microwave-frequency light modulator consisting of rectangular cross section coaxial cavity with two electro-optical crystals 15 p2501 A67-30141
 Dielectric constant measurement of solids at microwave frequencies, noting performance of solid dielectrics as temperature function 16 p2678 A67-31720
 Large dynamic range, high-burnout microwave varistor diode construction and planar technique for Schottky barrier diode array fabrication described 16 p2642 A67-31723
 IMPATT diode operation based on combination of avalanche-current multiplication and transit-time delay to produce negative resistance 17 p2824 A67-32832
 Differential phase-shift measurements at UHF and microwave frequencies, discussing standards, techniques and uncertainties in characteristics 17 p2815 A67-32608
 Nonlinear interaction between weakly

ionized helium magnetoplasma produced by HF discharge and microwave field 17 p2903 A67-32676
 Gallium arsenide single crystal lattice dielectric constant measured noting broad resonance 18 p3101 A67-34010
 Microelectronics technology extended to microwave frequencies, considering development of solid state devices and ICs 18 p3015 A67-34562
 Interaction between electrostatic and guided electromagnetic wave, considering plasma wave amplification by pumping at microwave frequency 18 p3091 A67-34643
 Instrument for measuring group delay time of microwave four-poles, using backward-wave tube as wave generator 19 p3193 A67-35032
 Gas ionization and plasma heating by high power microwaves using X-band and S-band frequency magnetrons 19 p3276 A67-35115
 Pulsed operation of large-area silicon p-n junction avalanche diode oscillators for microwave frequencies 19 p3196 A67-35627
 Microwave sound generation by transient heating of material surface with laser pulses 20 p3457 A67-36386
 Resonance frequency shift analysis of autostabilized light modulator at microwave frequencies noting heat transfer, transition temperature, etc 20 p3459 A67-36503
 Radiometric technique for absolute temperature measurement of microwave noise sources under field conditions 20 p3444 A67-36521
 RF power meter design having coaxial thin film thermocouple in-line detector to sample incident power 21 p3589 A67-37916
 Microwave and acoustic frequency holography and possible application to target shape recognition and inverse scattering in radar 21 p3626 A67-38063
 Microwave characteristics of coaxial mounted tunnel diodes investigated by equivalent circuit parameters 21 p3602 A67-39070
 Balanced SHF transducer for microwave receiver input with separate signal and heterodyne lines coupled by directional bond openings, noting decoupled inputs 22 p3772 A67-39875
 Superconductors for high-Q microwave cavities construction, noting unloaded Q and resonant frequency measurements and surface properties 22 p3865 A67-40431
 Series and parallel pulse forming feed networks for generating microwave signals, comparing output parameters and limitations 22 p3774 A67-40444
 Noise in polarized Si semiconductor avalanche junctions at RF and microwave frequencies noting determination of impact ionization parameters 23 p3980 A67-41189
 Microwave absorption by magnetic field induced surface states in superconductors, showing anomalies consistent with quasi-particle decay 24 p4205 A67-42739

MICROWAVE INTERFEROMETER

Multibeam microwave interferometer measurement of radial distribution of electron density in plasma 01 p0119 A67-10169
 Electron scattering cross section of argon and atomic oxygen measured, using microwave interferometer for analysis of plasma produced in shock tube 03 p0472 A67-13320
 Microwave interferometer reliability for plasma diagnostics in magnetic field 05 p0851 A67-16521
 Time dependence of electron density in afterglow of electrodeless discharge in hydrogen plasma measured, using microwave interferometer 07 p1229 A67-19682
 Ionization and temperature measurement in MHD experiment, noting microwave interferometer response as electron density function and line reversal measurement 09 p1538 A67-21777
 Plasma diagnostics by microwave interferometry in MHD channel using open waveguide, calculating field distribution and propagation characteristics 09 p1539 A67-21781
 Microwave interferometer for measurement of effective recombination coefficient of decaying argon-cesium plasma with hot electrons at various argon pressures 09 p1542 A67-21817
 Lecher system with finlines providing transition to waveguides for incorporation in

microwave interferometers with high spatial resolution 10 p1658 A67-23785
 Microwave interferometer with dielectric rods as waveguides for measuring electron density in small volume inside plasma 13 p2120 A67-26859
 Microwave transmission measurements of electrical properties of shock ionized air noting dielectric constant, electron density, conductivity, attenuation, etc 15 p2470 A67-29490
 Electron density behind shock front of discharge plasma measured using interferometer 19 p3230 A67-35395
 Light deflection by solar gravity measuring method using radar interferometer 20 p3485 A67-36995
 Axial electron density profile in weakly ionized seeded argon plasma expanding through supersonic nozzle determined experimentally using microwave [AIAA PAPER 67-704] 21 p3872 A67-38731

MICROWAVE PLASMA PROBE
 Plasma diagnostics, comparing microwave toroidal resonator, cylindrical resonator and probe methods 03 p0477 A67-13466
 Effective diffusive scattering cross section of electrons in He and Ar plasma with K vapor additions and in pure K, based on DC plasma conductivity and microwave generator Q-factor 04 p0673 A67-15972
 Plasma electron density range measurable by microwave extended by phase angle being expanded by impedance transformation 05 p0854 A67-16982
 Microwave receiver with no separate local oscillator for plasma scattering experiments 06 p1000 A67-17617
 Controlled nonreciprocal microwave device using Faraday rotation in solid state plasma 09 p1474 A67-22090
 Lecher system with finlines providing transition to waveguides for incorporation in microwave interferometers with high spatial resolution 10 p1658 A67-23785
 Plasma stability, discussing flute and Kadomtsev instabilities and possibility of anomalous diffusion for confined steady state 11 p1831 A67-24011
 Electron number densities measured behind shock wave in pressure-driven shock tube by microwave resonant cavity technique and by electrostatic quasi-Langmuir probe 11 p1790 A67-24451
 Transient ionization levels of hypersonic velocity projectile wakes measured by open microwave resonators phase shift 11 p1790 A67-24452
 Microwave reflection analysis of plasma surface phenomena, noting dependence on electron density and collision frequency 11 p1844 A67-25097
 Ionization rate in helium, argon and xenon plasmas determined by microwave technique 12 p1970 A67-25291
 Electron density and collision rate of shock produced plasma measured with X-band microwave reflection probe 19 p3293 A67-35398
 Langmuir probe collection of ions in low density plasma flows, with electron density agreeing with microwave data 19 p3297 A67-35591
 Faraday effect in microwave region used for electron density determination in argon and helium low pressure plasmas and comparison with cyclotron radiation data 19 p3297 A67-35592
 Complex reflection coefficient for finite-width boundary used for plasma diagnostics in high electron-density range, discussing modeling errors 20 p3499 A67-36959
 Z-pinch in electron hole plasma observed by microwave probe method, noting no minimum current exists for semiconductors 21 p3866 A67-38356
 Microwave methods of plasma diagnostics based on attenuation, reflection or refraction measurements compared to double probe density measuring technique 21 p3670 A67-38688
 Plasma spatial electron density distribution from refraction of microwave beams with several frequency components 21 p3670 A67-38689
 Turbulence effect on accuracy of microwave cut-off measurements of plasma density suggests electromagnetic wave scattering 22 p3845 A67-39430
 Microwave plasma observed using

spectroscopic and mass spectrometric techniques, discussing standing wave operation mode, emission and resonance lines 23 p4034 A67-41435

Microwave production of plasma in trap at electron cyclotron resonance, investigating absorption and density 23 p4035 A67-41684

Kinetic behavior of electrons in air plasmas containing electrophilic gasses studied with microwaves behind reflected shock waves 24 p4196 A67-42196

MICROWAVE PROBE

Interdependent microwave radar-and radiometer-sensor measurements of backscatter and albedo characteristics of earth surface 01 p0021 A67-10333

Frequency doubling by varactor diode, expressing principal parameters as function of normalized amplitude of input voltage 01 p0039 A67-10856

Diagnostic measurement techniques for statistical properties of ionized particles of equilibrium turbulent plasma, using electrostatic probe and high resolution microwave probe 02 p0275 A67-12550

Excitation of probe near semiconductor 07 p1154 A67-19790

Microwave loss in reflex plasma discharge determined from microwave energy decay measurements 08 p1363 A67-21311

Free electron density and effective collision frequency of ionized argon in wake of shock wave measured, using microwave probe methods 11 p1775 A67-24017

Density measurements in Q-device by resonance fluorescence scattering, Langmuir probe and microwave methods compared, examining causes of discrepancy 11 p1838 A67-24405

Microwave thermography used to measure microwave optical field patterns, using Czerny IR thermosensitive transducer process 12 p1939 A67-25196

Ultrasonic devices for coherent optical systems, discussing CdS transducers, laser scanners and microwave signal processing 15 p2500 A67-29912

Microwave methods applied to plasma diagnostics restricted to steady state plasma 17 p2901 A67-32349

Antenna field strength measurement above 1 GHz, discussing formulas for high accuracy gain determination, multipath interference and antenna separation 17 p2815 A67-32609

Josephson junction as ideal zero impedance voltage source with discrete voltage for simultaneous application of microwave and magnetic fields 17 p2915 A67-32657

Plasma produced by shock wave in low pressure gas measured for phase angle by microwave reflection probes 18 p3088 A67-34076

Plasma bunches-microwave interaction showing electron energy and plasma ions velocity increase 19 p3291 A67-35384

MICROWAVE RADIATION

Junction perfection in coherent microwave oscillation in avalanche p-n silicon diodes 01 p0036 A67-10449

Time varying energy distribution of high energy electrons producing solar microwave impulsive bursts and X-ray bursts by emission of gyrosynchrotron radiation 01 p0145 A67-11145

Two-layer model of lunar surface analyzed, using criteria of transparency to microwave radiation 02 p0324 A67-11700

Balloon observation of thermal radio emission of molecular oxygen in terrestrial atmosphere 02 p0237 A67-11852

Microwave echoes in axially magnetized yttrium iron garnet cylinders following application of two pulses, with second twice frequency of first 02 p0297 A67-11874

Synthesis and sidelobe reduction of unequally spaced antenna arrays with uniform or stepped amplitude distribution, achieving desirable radiation characteristics 02 p0217 A67-12095

Microwave radiation measurements from internal plasma resonance of positive column near electron cyclotron harmonic frequencies 03 p0476 A67-13355

Instabilities in drifting semiconductor plasma, noting dispersion curve and collision ionization for longitudinal oscillations 03 p0496 A67-13674

Quantitative expression of technique for observing 5-mm self-emission from oxygen of earth atmosphere to obtain vertical sense

[RASSA PAPER 1-10-144] 03 p0418 A67-14251

Anomalous pulsed microwave emission at cyclotron frequency in partially ionized plasmas analysis extended to show that emission is not stationary with time 04 p0663 A67-14615

Instability in hot electron plasma in mirror field occurring suddenly in quietly decaying plasma generated by high power microwave 04 p0663 A67-14621

Interpretations of microwave emission from Venus through experiments in which anomalous signals have been observed in X-band from glow discharges 04 p0699 A67-14952

Gas discharge in argon maintained within waveguide by microwave signal at cyclotron resonance, observing second harmonic radiation 05 p0850 A67-16046

Microradiowave absorption in air by water vapor dimers 06 p0963 A67-18206

Microwave third harmonic generation in homogeneous semiconductors at low temperatures, noting ionized impurity scattering effect 08 p1368 A67-20701

Linearized perturbation equations integrated for cosmological model, giving energy density fluctuations, rotational perturbations, gravity waves and estimated anisotropy of microwave radiation 08 p1398 A67-21233

Second order coherence theory noting microwave experiments with radiation sources simulated by noise tubes, coherence function factorization and spectral modulation of superposed beams 09 p1510 A67-21584

Nondestructive testing of dielectric materials by microwave techniques 10 p1660 A67-23014

Dog experiments, determining microwave radiation effects on physiological response 10 p1600 A67-23824

Polarization of cosmic OH 18-cm radiation 11 p1864 A67-24565

Slotted inhomogeneous waveguide propagation behavior investigated, using transverse equivalent network 11 p1766 A67-24691

Brightness distribution of radio emission over solar disk during solar activity minima determined from radioheliograms 12 p2001 A67-25226

Element production in early stages of homogeneous expanding universe and within stars, noting nature of background microwave radiation 12 p2010 A67-26239

Sudden cosmic noise absorption correlated with solar microwave flux to establish daily mean value 13 p2190 A67-26311

Large microwave field and small parallel DC field applied across GaAs sample altering conductivity related to carrier velocity-field characteristic 14 p2369 A67-28601

Spectrographic observations of late stages of limb flare by achromatic coronagraph 14 p2381 A67-28835

Microwave harmonic generation from Josephson junction noting radiation waveguide coupling, bias point, input power level and Josephson equations 15 p2535 A67-29492

Interaction between SHF field and created plasma in electron-cyclotron resonance state 15 p2529 A67-29715

Stationary concentration of charged particles in plasma created by uniform and nonuniform SHF magnetic field in electron-cyclotron resonance state 15 p2529 A67-29716

Nonlinear effects during titanium plasma source operation, investigating plasma nature and magnetic field effects on injector operation and plasma parameters 15 p2529 A67-29719

Microwave emission from magnetic-field-free electron hole plasma in p-type InSb at 77 degrees K 15 p2539 A67-29820

Excess cosmic microwave background temperature of 2 degrees K at 1.5 cm wavelength 15 p2551 A67-30161

Brightness temperature reduction of Venus at decimeter wavelengths determined from 49.1 cm measurements 16 p2749 A67-31409

Intense microwave radiation from high density plasma confined by magnetic mirror 17 p2894 A67-32145

Microwave emission phenomena from n and p type indium antimonide, noting no essential difference 17 p2914 A67-32375

Microwave emission intensity from InSb,

examining dependence on angle between DC electric and magnetic fields 17 p2914 A67-32615

Upper limit data about reported very low temperature distributed-source microwave background radiation and small-scale angular distribution 17 p2945 A67-32653

Photo-induced microwave response of SbSI crystals to variations in reflection coefficient indicates photodiodelectric effect 17 p2915 A67-32675

Radiation from array of parallel plate waveguide with thick walls excited by TEM modes 17 p2828 A67-33085

Microradiowave absorption in air by water vapor dimers 17 p2817 A67-33219

Temperature and magnetic field intensity dependence of microwave emission from n-type indium antimonide 18 p3101 A67-34016

Collision induced instability in semiconductor plasmas, noting system consisting of electrons and holes with transverse relative drift to static magnetic field 18 p3102 A67-34348

Microwave radio observations of total sun eclipse made in Canada in 1963, discussing solar radio emission [AD-642463] 18 p3133 A67-34487

Venus surface temperature and microwave emission, discussing ionospheric model, greenhouse effect, microdischarge model, radio aurora, etc 18 p3135 A67-34543

Detection properties of n-type InSb in microwave and IR ranges, studying impurity and magnetic field effects 19 p3300 A67-34762

Ground based solar electromagnetic radiation environment studies in visible and radio windows 19 p3323 A67-35332

Beam-plasma interaction in magnetic field, studying microwave field distribution and emission 19 p3291 A67-35383

High power microwave radiation from nonequilibrium plasma discharge near electron cyclotron frequency 19 p3291 A67-35386

Microwave noise radiation and scattering from cylindrical plasma column, studying dissipative processes on emission spectrum 19 p3291 A67-35387

Hyperfine structure of ground state of helium 3 microwave transition radiation from galactic H II regions 19 p3330 A67-36074

Ionization-enhanced microwave resonant radiation from model rocket exhausts studied using Dicke type radiometer 20 p3543 A67-36233

Plasma absorption of microwaves, noting 20 resonant maxima near harmonics of electron cyclotron frequency 20 p3498 A67-36692

Solar flare microwave radio bursts, suggesting synchrotron radiation from relativistic positrons, calculating positron yield and synchrotron spectrum 20 p3519 A67-37101

Electron drift velocity and mobility in InSb calculated from conductivity and Hall effect measurements, noting microwave emission occurrence 20 p3514 A67-37544

Electron temperature of shock-heated argon plasma determined by measuring microwave noise radiation and absorption 21 p3660 A67-37741

Resonance and noise microwave emission thresholds for InSb electron hole plasma subject to crossed electric and magnetic fields, noting Hall effect 21 p3683 A67-38403

Microwave radiation from plasma beam interaction, measuring radiation intensity as function of discharge current 21 p3668 A67-38416

Steady state plasma in strong microwave electric field acting on electron component 22 p3845 A67-39431

35 GHz second harmonic generation power and conversion efficiency in low pressure gas discharge, noting pressure and gas species variations 22 p3854 A67-40316

N-type InSb microwave noise emission at low temperatures in low electric field regime, measuring magnetic field threshold and background continuum 22 p3864 A67-40345

Atmospheric temperature profile to 75 km by remote sounding, using satellite measurement of molecular oxygen resonance line at 5 mm 22 p3806 A67-40360

Airborne measurement of microwave emission from earth surface and atmosphere for potential application of radiometry to

weather satellite reconnaissance 22 p3806 A67-40361

Microwave background radiation angular distribution anisotropy lower limit estimated from perturbations of cosmological model 22 p3892 A67-40498

Solar type IV burst centimeter and decimeter polarization and spectral variabilities examined in helical electron stream cyclotron radiation hypothesis for solar corona model 23 p4050 A67-40776

Equivalent temperature of cosmic microwave background radiation at 3.2 cm wavelength, discussing Dicke type radiometer and error sources 23 p4063 A67-40922

Microwave background in steady state universe explained by starlight absorption and microwave reemission by interstellar dust, discussing young spiral galaxies 24 p4226 A67-41875

MICROWAVE RADIOMETER

Microwave radiometric meteorological observations using twin-horn antenna technique, noting antenna resolution 01 p0108 A67-10314

Interdependent microwave radar and radiometer-sensor measurements of backscatter and albedo characteristics of earth surface 01 p0021 A67-10333

Microwave radiometry application to navigation, thermonuclear diagnostics, astronomical temperature measurements, etc 03 p0367 A67-12805

Traveling wave maser in radiometry receiver 12 p1951 A67-25295

UHF intensity-modulated light emanating from plasma observed with aid of photomultiplier radiometer 13 p2167 A67-27082

Sky brightness temperature measurements at various millimeter wavelengths for possible isotropic electromagnetic emission in universe 17 p2935 A67-32230

Quasar sources studies set limits on possible density inhomogeneity magnitudes in universe by measuring cosmic microwave background isotropy and homogeneity 20 p3525 A67-36868

Satellite-borne superheterodyne radiometer for measuring stratospheric temperature utilizing millimeter wave spectrum of molecular oxygen 21 p3584 A67-38669

Microwave and mm radiometric sensor for passive satellite reconnaissance of earth atmosphere and terrain thermal noise 22 p3805 A67-40353

Langmuir probes investigated by comparing measurements in ionized He afterglow by cylindrical double probes and by gated microwave radiometer and resonant cavity 24 p4197 A67-42261

MICROWAVE REFLECTOMETRY

Microwave swept frequency measurements on RF transmission line systems and development of VSWR and insertion loss test set 01 p0039 A67-11038

Millimeter microwave transmission and reflection through 50 angstrom superconducting tin and indium films near critical temperature 10 p1688 A67-22764

Electrostatic probe and VHF microwave reflectometry study of nitrogen flow around models in hotshot wind tunnels, determining plasma sheath physical characteristics 11 p1839 A67-24445

Microwave reflection from region with nonuniform hydrometeor for case where dimensions vary greatly and relation to wavelength is arbitrary 11 p1754 A67-24981

Surface density gradient and collision frequency effects on polarization of microwaves reflected from plasma surface 13 p2164 A67-26300

Parallel plate transmission system for reflection, diffraction and transmission measurements at microwaves, noting design criteria 18 p3002 A67-34224

Microwave refraction technique for determining electron density profiles in transient plasma column 19 p3295 A67-35517

MICROWAVE RESONANCE

Optical resonator theory and applications in lasers and microwaves 06 p1000 A67-17572

Paramagnetic current formation due to volume resonator microwave field interaction with dense plasma subject to RF pressure and EPR in static magnetic field 07 p1228 A67-19512

Optimal conditions of thermostability of

anisotropic spherical ferrite microwave resonator with various orientations 07 p1153 A67-19597

Microwave quasi-optical ring resonator formed by mirrors 09 p1513 A67-22088

Relationship between domain transit frequency and cavity controlled frequency of thin Gunn devices 11 p1759 A67-24130

Extension of stripline circulator operation calculation by Davies and Cohen to include wider range of stripline geometries 13 p2076 A67-26482

Electron density variation, collision frequency and phase shift in standing striations in positive column 14 p2353 A67-27758

Diffusion by microwave breakdown of weakly ionized helium plasma in metal chamber immersed in magnetic field 14 p2358 A67-28293

Magnetic field effect on microwave surface impedance of superconducting tantalum measured in various temperature ranges via dielectric-resonator techniques 14 p2371 A67-28726

Electron wave resonances in bounded plasmas, examining application to average plasma density measurement 17 p2896 A67-32163

Coupling factor between microwave resonator and transmission line determined by oscillographic recording of microwave field 18 p3010 A67-33508

Resonance method for measuring microwave resonators Q-factor and its small variations 19 p3191 A67-34982

Electron cyclotron resonance absorption of microwaves in oxygen magnetoplasma used to alter electron attachment and detachment rate coefficients 19 p3271 A67-35077

Temperature dependence and anisotropy of high temperature ferrimagnetic microwave resonance linewidth of Si-doped YIG, showing valence exchange effect on losses 20 p3508 A67-36390

Optimal conditions of thermostability of anisotropic spherical ferrite microwave resonator with various orientations 20 p3401 A67-37336

Electron density relation to output power in He-Ne laser and magnetic field effect, using microwave resonator technique 22 p3814 A67-39428

MICROWAVE SCATTERING

Born approximation theory of nonlinear scattering of microwaves from oscillating plasma column, noting diffraction patterns and frequency shifts 01 p0027 A67-11324

Absolute intensity and angular distribution of microwaves scattered from oscillating plasma column, noting diffraction patterns and frequency shifts 01 p0027 A67-11325

UHF dispersion in barium titanate ferroelectric crystals explained as microwave scattering 03 p0497 A67-13701

Bistatic radar cross section of underdense turbulent plasma measured at X-band and results compared with theoretical scattering model 05 p0760 A67-15999

Long distance propagation of ultrashort radio waves by ionospheric scattering in subpolar region, noting graphs of signal level changes 07 p1144 A67-19707

Sporadic E layer in middle latitude by method of forward ultrashort wave scattering 10 p1630 A67-22792

Nondestructive testing of dielectric materials by microwave techniques 10 p1660 A67-23014

Directional coupler classification 12 p1915 A67-25977

Scattering method for observing plasma instability near electron gyrofrequency harmonics 16 p2715 A67-31062

Resonance methods for microwave measurement of scattering matrix of two-port reciprocal junction 18 p3002 A67-34223

X-band propagation over rough earth when illuminated by radiation, studying scattering problems 20 p3388 A67-37647

Microwave scattering cross section for turbulent weakly ionized plasma column, noting square root of mean square plasma density fluctuation limit for Born approximation 22 p3850 A67-39722

Sporadic E layer in middle latitude by method of forward ultrashort wave scattering 24 p4149 A67-42128

MICROWAVE SPECTRUM

Nuclear magnetic resonance and microwave spectra of some deuterio

derivatives of 2, 4-dicarbaclavoheptaborane-7/7 01 p0019 A67-11146

[JPL-TR-32-1038]

Gas laser pumped microwave emission for producing controlled excited state population for RF spectroscopy of neon 05 p0817 A67-16638

Emission microwave spectroscopy of OCS, observing coherent ringing, coherent radiation modulation and pulse echoes 06 p1032 A67-18208

Excitation and propagation of Bernstein modes in nonuniform plasmas near electron cyclotron harmonics 08 p1361 A67-21130

Correction of calculations of Einstein A coefficient for transition of OH 09 p1532 A67-21989

Plasma stabilization by HF electromagnetic fields, noting mode spectrum spacing along sample axis and dependence on field strength 10 p1686 A67-23585

Phase locking experimental data on injection locked X-band Gunn effect microwave oscillators 11 p1759 A67-24128

Microwave spectral brightness measurements of Venus compared with several model atmospheres 11 p1865 A67-24601

Microwave radiometric measurements of planetary disk temperature of Venus, Mars, Jupiter and Saturn 11 p1869 A67-25094

Thermal properties of moon by comparing IR and microwave measurements of spectrum with theoretical calculation of upper layer temperature distribution [AIAA PAPER 67-289] 12 p2009 A67-26006

Microwave spectroscopy of organic semiconductors, examining EPR of chemical bonds in energy transfer 14 p2366 A67-28505

Astronomical radio telescope control, noting altazimuth and equatorial modes of operation, overall accuracy, etc 15 p2492 A67-29532

Electron-photon cascade process in intergalactic space, noting role of microwave radiation in gamma ray astronomy 15 p2550 A67-29750

Microwave spectrum and observation at 6 cm wavelength of Venus to determine total intensity and polarization of radiation 16 p2747 A67-30987

Microwave radiations of Jupiter, deriving equivalent black body temperature, magnetic field data, radiation belts data and electron energy 21 p3710 A67-38995

Earth atmosphere humidity profiles and cloud densities interpreted from 1 cm microwave absorption measurement, water vapor resonance and radiosonde measurement 22 p3806 A67-40359

Incompatibility of microwave phase effects measurements in Mercury thermal emission with simple model for thermal behavior of planet surface 24 p4226 A67-41837

MICROWAVE SWITCHING

Microwave direction-finding systems based on amplitude comparison for use with pulse or continuous wave signals, noting switching system 02 p0198 A67-12067

X sub L band waveguide switches using p-i-n diodes for switching elements in SPST, SP2T, SP4T and SP8T microwave switches 04 p0580 A67-14863

Monolithic IC design of diodes and X-band microswitch transmission line fabricated on Si substrate 06 p0968 A67-18053

Second and third harmonics produced by p-i-n diode in microwave switching application 13 p2075 A67-26478

Flip-flop type current mode switching circuits, discussing features incorporated and performance 14 p2280 A67-28012

Design concept for microwave integrated circuits, noting realization and performance evaluation 14 p2280 A67-28013

Metal oxide silicon transistors as high performance analog switching elements, noting design and performance 14 p2281 A67-28018

Gate capacitance storage property of p-channel enhancement MOSTs used in achieving low power consumption values 14 p2281 A67-28020

Variation of series resistance and junction capacity in tunnel diodes used in microwave switching 15 p2449 A67-29808

MICROWAVE TRANSMISSION

Microwave negative conductance due to traveling space charge waves in n-type GaAs 01 p0133 A67-10487

Electric motor energized by microwaves in

waveguides at S-band, investigating speed, torque and frequency characteristics 02 p0183 A67-12116

Transmittance increase of silicon film when illuminated by silicon dioxide layer in long wave IR spectrum 03 p0488 A67-12891

Radio propagation in microwave terrestrial model waveguide of variable surface impedance, using reciprocity theorem 04 p0570 A67-14865

Communications requirements for manned deep space missions, using optical links, with PPM, PCM/PL and coherent reception for each link [AIAA PAPER 66-317] 06 p0961 A67-17706

TALAR ground-to-aircraft microwave transmission landing approach system for use in conjunction with instrument landing system /ILS/ crosspointer indicator 06 p1028 A67-17721

Transmittance increase of silicon film when illuminated by silicon dioxide layer in long wave IR spectrum 06 p1054 A67-18769

Waveguide resonant-iris bandpass filter with very wide passband and stopbands that provide transmission and attenuation characteristics for use with microwave generators 07 p1151 A67-19426

Echo pulses in YIG crystal noting influence of lateral elastic HF signals 08 p1366 A67-20313

Twofold phase modulation in meters of microwave reflection and transmission coefficients 08 p1295 A67-21276

Spatial coherence measurement in 3.2 mm horizontal transmission, considering amplitude and phase fluctuations received in two spaced antennas 09 p1461 A67-21599

Radar information transmission using wideband microwave links and conventional display techniques 09 p1465 A67-22637

Millimeter microwave transmission and reflection through 50 angstrom superconducting tin and indium films near critical temperature 10 p1688 A67-22764

Design equations and computer calculated curves to achieve varactor-tuned octave bandwidth transistor oscillators by using transmission line 10 p1613 A67-23412

H-band coupled cavity transmission maser noting bandwidth gain and low noise temperature operation 10 p1665 A67-23441

Langmuir probe and microwave transmission methods compared for plasma density measurement 12 p1939 A67-25256

Material properties and capabilities of different types of optical waveguides including iterative electromagnetic wave beams, reflecting pipes, fiber guides, etc 12 p1906 A67-25976

Microwave methods for electric resistivity measurements of semiconductor materials, noting application to GaAs 12 p1916 A67-25999

Geographical location and optical path length effects upon fade margin required for desired propagation reliability of microwave signals 13 p2066 A67-26406

Field solution of TE sub k zero mode wave incidence on inductive irris in rectangular waveguide 13 p2066 A67-26475

Microwave design techniques for calculating even and odd mode characteristic impedances of miniature microstrip transmission lines 13 p2071 A67-27445

Flexwell waveguide as low loss flexible microwave transmission line 13 p2084 A67-27581

Millimeter wave attenuation measurement in rain using low height antennas 14 p2274 A67-28923

Microwave transmission measurements of electrical properties of shock ionized air noting dielectric constant, electron density, conductivity, attenuation, etc 15 p2470 A67-29490

Gunn effect as only solid state effect capable of producing high output power in microwave range in pulsed and continuous operation, noting physical nature 15 p2536 A67-29530

Microwave rocket propulsion through direct electromagnetic heating of gas and powered by wireless ground-transmitted microwaves 16 p2736 A67-30712

Microwave flux-flow resistivity transitions observed for strongly paramagnetically limited titanium-vanadium alloys 16 p2727 A67-30821

Solid state microwave delay lines noting advantages, operation principles, fixed

variable construction, etc 16 p2637 A67-31196

Resistive antenna receiving properties determined via transmitting antenna driving-point impedance and short circuit current 16 p2638 A67-31338

System for information transmission over optical path using microwave subcarrier, noting satisfactory SNR 17 p2812 A67-32237

Plasma resonances, deriving relations between coefficients for transmission, reflection and emission of microwaves and explaining collision-free discharge 17 p2907 A67-33105

Parallel plate transmission system for reflection, diffraction and transmission measurements at microwaves, noting design criteria 18 p3002 A67-34224

Microwave transmission through quiescent cesium plasma studied, noting apparatus for thermal ionization studies 19 p3288 A67-35370

Polarity reversal with DC bias in hot-carrier microwave diode 19 p3198 A67-36038

Microwave delay-line techniques using YIG crystal, examining solid state dispersion characteristics 20 p3507 A67-36241

Instrument errors in HF radio rangefinder 20 p3446 A67-36632

Permeability and permittivity values of homogeneous samples obtained by making transmission or reflection measurements in waveguides or coaxial cables 22 p3796 A67-39276

Microwave multichannel communication system using PCM, noting low power output requirement and suitability for digital data transmission 22 p3763 A67-40460

Operating principles of Y-shaped ferrite circulator, discussing temperature and power variations effects on sensitivity 23 p4041 A67-41213

Radio signals from clouds to yield information on cloud physics, using superheterodyne microwave receivers 24 p4124 A67-42883

MICROWAVE TUBE

Input admittance and susceptance of microwave tetrode 01 p0038 A67-10829

Self-activating microwave cold cathode crossed field amplifiers for modulation circuits in complex radar systems 03 p0387 A67-14121

High grade oxide ceramics for making dielectrically transparent insulating structures in microwave power tube 04 p0641 A67-14856

Pulsed radar transmitter research in U.K., noting beam type microwave tubes, solid state switches, hydrogen thyatrons, etc 04 p0581 A67-15052

Cylindrical electronic microwave tubes, deriving expressions for zero and first approximations of physical parameters 05 p0774 A67-16906

Microwave and optical generation and amplification - International Conference, Cambridge, England, September 1966 09 p1476 A67-22251

Microwave oscillation-amplifying L-band platinotron tube to amplify peak power of radar transmitter 10 p1605 A67-23061

Ignitor-contributed noise deleterious effect on low noise radar receivers, noting influence of TR device inserted in front of receiver 10 p1611 A67-23329

Traveling wave tube amplifiers for communications systems noting amplitude transfer function, two-tone and FM intermodulation, etc 10 p1613 A67-23440

Electron beam experimental methods for current density distributions, electron velocities and determining parameters for microwave tube design 11 p1758 A67-24094

Energy conservation analysis of step in negative resistance region of voltage-current characteristic curve of oscillating tunnel diode 11 p1759 A67-24132

Cathode noise voltage in low current arc at atmospheric pressure as function of arc cathode surface state 14 p2354 A67-27764

Production of crossed field and beam microwave tubes, noting demagnetization and coercive and inductance forces of various magnetic materials 15 p2447 A67-29753

Book on microwave valves covering technique and behavior of common devices 16 p2638 A67-30864

Cylindrical electronic microwave tubes, deriving expressions for zero and first approximations of physical parameters 16 p2638 A67-30883

Phase and amplitude characteristics of microwave amplifiers obtained from response to short input pulse 17 p2827 A67-32791

Instrument for measuring group delay time of microwave four-poles, using backward-wave tube as wave generator 19 p3193 A67-35032

Crossed field cascade tubes as frequency oscillators and microwave generators, discussing improved performance and interaction efficiency of devices 22 p3775 A67-40559

MICTURITION

S URINATION

MID-LATITUDE ATMOSPHERE

Position of tropopause in middle latitude jet flow 02 p0240 A67-12642

Geomagnetic activity effect on electron concentration at heights of 100 and 110 km 05 p0801 A67-17143

Winter radio absorption anomaly at middle latitudes theory in terms of temperature and nitric oxide distributions in D region 07 p1171 A67-19415

Sporadic E ionization and anomalous increase in rate of radar meteor counts during 1963 in mid-latitude European stations 07 p1172 A67-19424

Statistical distribution of monthly median noon critical frequency of F-2 layer from ionospheric stations at mid-latitudes, auroral regions and at polar cap 07 p1174 A67-19703

Magnetic disturbances at midlatitudes, noting origin from locally generated currents 07 p1174 A67-19709

Sporadic E layer in middle latitude by method of forward ultrashort wave scattering 10 p1630 A67-22792

Rocket probe measurements indicate existence of maximum ion concentration in stratosphere and lower ion concentration at equator than at midlatitudes 10 p1648 A67-23284

Atomic ions of meteoric origin indicated as source of midlatitude E region in IQSY rocket measurement 10 p1648 A67-23289

Rocket probe measurements indicate existence of maximum ion concentration in stratosphere and lower ion concentration at equator than at midlatitudes 12 p1933 A67-25650

Geomagnetic activity effect on electron concentration at heights of 100 and 110 km 21 p3619 A67-38485

Diurnal, latitudinal and seasonal variations of midlatitude topside ionosphere electron density profiles and plasma scale heights calculated from Alouette I ionograms 23 p3994 A67-40775

OH Meinel band, nitrogen dioxide continuum and O IS to 1D transitions maxima altitudes in midlatitude night airglow emissions from rocket radiometer measurements 23 p3995 A67-40813

Sporadic E layer in middle latitude by method of forward ultrashort wave scattering 24 p4149 A67-42128

MIDCOURSE GUIDANCE

SA GUIDANCE SYSTEM

Recursive space navigation applied to navigating in near orbit of planet by measuring directions to known landmarks 01 p0110 A67-11157

Mathematical technique of midcourse guidance for spin stabilized interplanetary spacecraft, specifically computer simulation for flight to Jupiter 02 p0264 A67-12369

Reconnaissance missions to outer solar system using energy derived from midcourse planetary encounter 05 p0893 A67-16520

Propellant requirements for unmanned lunar and interplanetary soft landing vehicles presented with equations that couple injection, midcourse and terminal phases [AAS PAPER 66-129] 07 p1241 A67-19988

Propellant requirements for unmanned lunar and interplanetary soft landing vehicles presented with equations that couple injection, midcourse and terminal phases [AAS PAPER 66-129] 13 p2214 A67-27540

Feedback from observations introduced into midcourse guidance correction program, showing optimal random feedback solution obtained for deterministic optimal feedback control problems 16 p2701 A67-31657

Linear continuous time stochastic optimal control process, obtaining optimum performance achievable as function of total

effort at initiation of optimization period 17 p2830 A67-33012

MIE SCATTERING FUNCTION

Mie scattering and plane wave diffraction theory for small angle light dispersion from sphere 01 p0112 A67-10131

Volume scattering of Mie spherical particle polydispersion and irregular particles 10 p1679 A67-22747

Radiation absorption and scattering by small spherical solid carbon particles in wavelength range 0.2 to 40 μ calculated by classical Mie theory [AIAA PAPER 66-134] 10 p1682 A67-23146

Models of reflection nebulae light for single scattering, pure or modified by internal nebular extinction, on spherical grains imitating dielectric or metallic particles 11 p1861 A67-24487

Collective scattering cross section and collective spectral extinction of Mie scattering with logarithmic Gaussian distributions 13 p2150 A67-26432

Visible continuous spectrum of comets rules out hypothesis of iron particles major role in scattering solar light 15 p2554 A67-29515

Volume backscattering functions and optical extinction coefficients for visible and IR radiation and selected cloud models 17 p2817 A67-33293

Computational scheme for calculation of Mie cross sections of absorbing particles 19 p3184 A67-35688

MIGRATION

S ELECTROMIGRATION

MIL MI-10 HELICOPTER

Mi-10 Soviet flying crane, very high four-wheeled landing gear enables it to drive over load and clamp it by hydraulically operated grips 02 p0181 A67-12201

MILITARY AIRCRAFT

Optimization of aircraft design for counter-insurgency /COIN/ operations using digital computers and wind tunnel tests, considering cost effectiveness [AIAA PAPER 66-779] 01 p0009 A67-10526

Cost effectiveness of optimum military aircraft system, evaluating design alternatives in hardware and support concepts via Monte Carlo simulation and high speed digital computers [AIAA PAPER 66-786] 01 p0009 A67-10530

Oxygen system for military aircraft pilot using electrochemical cell to extract oxygen from atmospheric air [AIAA PAPER 66-787] 01 p0012 A67-10531

Digital computer program SYNAC for parametric synthesis and performance analysis of military aircraft [AIAA PAPER 66-795] 01 p0009 A67-10535

Reliability improvement effect on cost in tactical aircraft, examining obsolescence, risk factor determination, etc 01 p0170 A67-11350

Distribution of maintenance manhour intervals for tasks on military aircraft compared with logarithmic normal distribution, presenting histograms and cumulative distributions 01 p0171 A67-11382

British procurement procedures for military aircraft noting cost estimate, feasibility study, development contract and production stages 02 p0343 A67-12242

Lockheed C-141A military transport and engineering evaluation for civil certification and military acceptance, noting commercial C-5A 03 p0361 A67-14018

Lockheed 500, derivative of USAF C-5A transport, discussing logistic capabilities, economics and representative approaches [AIAA PAPER 66-1019] 03 p0362 A67-14152

Human engineering aspects of design of future military high performance aircraft, noting automatic control and display system requirements 04 p0562 A67-14535

V/STOL military transports purchase decisions based on analyses of operational employment, engineering design and economic utility 04 p0551 A67-14803

Military pilot escape, survival, search and rescue 05 p0752 A67-17102

Preflight and operational status test set /PTS/ for radiation testing of electronic equipment on military aircraft 08 p1303 A67-21059

Aircraft gas turbine and fuel control design to meet engine requirement in broad environmental challenges [SAE PAPER 670140] 09 p1560 A67-22541

Flight load maneuver data for fatigue

evaluation of F-4 series aircraft 10 p1594 A67-23435

Military aircraft characteristics and performance evaluation procedure 11 p1885 A67-25102

Avionics system development for V/STOL tactical aircraft, emphasizing onboard electrical system 13 p2053 A67-27222

Strike aircraft design noting weapons compatibility, use of analytical and scale testing techniques, etc 15 p2418 A67-29396

Avionics, ordnance and military aircraft as totally integrated system, noting need of accurate navigation, target accuracy and improved communications 15 p2444 A67-29398

Four combat aircraft designs /tailless delta, swept wing, variable geometry and VTO aircraft/ using same bypass engines /Pratt Whitney-SNECMA TF-306s/ 15 p2419 A67-29670

Jaguar, Franco-British military aircraft designed for combat training and tactical support during 1970s 15 p2420 A67-30127

Digital onboard checkout system for SST and other commercial/military aircrafts to discover in-flight malfunctions digital onboard checkout system for SST and other commercial/military aircraft to discover in-flight 16 p2596 A67-31493

Mirage III-G, variable-geometry military aircraft evaluation considering multiple-mission capability 16 p2597 A67-31539

Landing gear for operating off rough terrain and unprepared airstrips in OV-10A Bronco aircraft for counter insurgency 17 p2794 A67-31989

Requirements and disadvantages of proposed escape systems for fixed and rotary wing Army aircraft 17 p2794 A67-31998

Tactical aircraft survivability in North and South Vietnam, discussing missile and interceptor ineffectiveness and limited-war considerations for aircraft 17 p2796 A67-32434

Structural design for gust loads on USAF aircraft based on continuous turbulence and failure probabilities 18 p2986 A67-34653

A-7A aircraft maintenance guarantee and role of training 18 p2987 A67-34681

IR technology influence on military aircraft design 19 p3173 A67-35932

Performance requirements and design aspects of variable sweep aircraft, examining swing pivot systems 20 p3361 A67-36498

Aircraft design by statistical methods, presenting samples for interceptor fighter, shorthaul jet and light twin-engine cargo aircraft 20 p3361 A67-37170

TSIS fire control equipment family, considering maximum cost effectiveness, discussing use in Dassault Mirage M-5 and RCAF CF-5 aircraft 20 p3364 A67-37244

Digital computer program SYNAC for parametric synthesis and performance analysis of military aircraft 21 p3568 A67-38534

Soviet papers on aircraft construction and techniques used by Air Force covering theory, engines, design, manufacture and operation 21 p3568 A67-38901

Cost effectiveness of digital and voice accident recorders in small fighter and military aircraft for low level missions, reconnaissance, flight testing and training 21 p3631 A67-39129

Environmental control for high performance military aircraft covering air conditioning, temperature and pressure control and oxygen supply systems 21 p3572 A67-39130

Utility aircraft costs lower than specialized aircraft in meeting mixed mission requirements in counterinsurgency environment, considering changes, uncertainty and logistics 22 p3745 A67-39618

Supersonic aircraft evolution emphasizing Dassault series, Northrop T-38 and F-5 and Swedish Draken and Viggen 22 p3746 A67-39883

Parametric investigation of propulsion system effect on takeoff weight of VTOL subsonic ground combat aircraft 23 p3934 A67-41315

Human blood circulation times during weightlessness produced by parabolic flight 23 p3959 A67-41698

MILITARY AVIATION

Production program and MAC operational experience of C-141A jet cargo transport [AIAA PAPER 66-791] 01 p0009 A67-10534

Reliability matrix analysis of AFSCM 375 management system 01 p0171 A67-11375

West German wartime military air transport requirements regarding fleet size and composition 04 p0551 A67-14566

Tracking in air traffic control environment, noting differences with military environment and cooperative tracking methods 04 p0654 A67-15060

F-111 type hydraulic power supply system design for supersonic aircraft using ground support equipment and military materials 05 p0752 A67-16159

Future French Air Force combat aircraft limited to Mirage F-III or Franco-British Jaguar project variable geometry types 10 p1585 A67-23621

Aviation insurance characteristics, types of policy in force and regulations applying under internal law 14 p2409 A67-28933

Astronautics education for RAF and USAF officers 16 p2782 A67-30786

Computer memory systems for handling Air Force information, discussing types of memory, storage techniques and device technologies 17 p2819 A67-32473

AFSCM 375-5 as methodology for system engineering, discussing management, documentation, applications, development, operation, design, etc 18 p3161 A67-33494

AH-56A weapons system design approach, detailing avionics 19 p3196 A67-35666

Transall C 160 aircraft wings, fuselage, tail surfaces, landing gear and power units 20 p3361 A67-36633

Minimizing time for deployment of infantry force by airlift analyzed by computer procedures based on loading, effectiveness and productivity 20 p3361 A67-37529

Computerized system for calculating spares quantities and providing overall adequacy within monetary, weight or volume constraint 23 p4085 A67-40583

Short haul military requirements /1970-1980/, considering assault and logistic airlifts supporting ground forces and V/STOL aircraft [SAE PAPER 670827] 24 p4093 A67-41992

Military flight clothing tested in actual survival conditions for ability of subject to withstand moderate sea water environment [AIAA PAPER 67-968] 24 p4118 A67-43046

MILITARY HELICOPTER

SA 330 turbine-powered assault helicopter, noting flight tests, speed, altitude, transport capabilities, etc 04 p0550 A67-14468

Helicopter design noting speed, maneuverability, handling, carrying capacity and disk loading 11 p1743 A67-23993

Requirements for operating characteristics of single and twin gas turbine engines for military helicopters noting system response, deceleration, fuel control, etc 16 p2736 A67-30929

Ch-54 A Flying Crane helicopter, discussing use in Vietnam in terms of field supply, transportation to Vietnam, etc [AHS PAPER 126] 16 p2598 A67-31841

Requirements and disadvantages of proposed escape systems for fixed and rotary wing Army aircraft 17 p2794 A67-31998

In-flight escape of helicopter personnel using Navy fuselage capsule, describing devices for recovery, protection and survival 17 p2794 A67-31999

AH-56A /AAFSS/ safety engineering, failure effects method, Army role, etc 18 p2987 A67-34690

Combat helicopters with reference to Huey/Cobra noting stub wings, armor protection, rotor and weapon systems 23 p3932 A67-40619

Light Observation Helicopter Avionics Package /LOHAP/, designed for OH-6A Cayuse helicopter, providing communications and navigational capabilities 23 p3980 A67-40927

MILITARY PSYCHIATRY

Treatment of psychiatric diseases in ground staff and aircrew, discussing psychopharmacology in aeronautical medicine 23 p3967 A67-41603

MILITARY SPACECRAFT

Initial defense communication satellite and military requirements 03 p0369 A67-13826

Characteristics and performance of synchronous satellite military communication system 06 p0979 A67-17668

Economics of military space launching systems 15 p2566 A67-29830

Navy Navigation Satellite System,

discussing naval and civilian application and improved gravitational field model 19 p3255 A67-35638

MILITARY TECHNOLOGY

SA DEFENSE

Mission reliability and effectiveness analysis of Army Missile Command weapon systems 01 p0154 A67-10627

Findings, conclusions and recommendations of Weapon System Effectiveness Industry Advisory Committee /WSEIAC/, noting concept of cost effectiveness 01 p0170 A67-11334

Radar data handling and display systems used with pulsed radars, detailing military type for use of weapons control officer 04 p0578 A67-15057

Military prime contract awards distribution with respect to states 07 p1269 A67-19470

NORAD installation in Cheyenne Mountain, Colorado, describing data processing equipment and performance 07 p1148 A67-19840

Nortronics NDC-1051 computer design and performance for military airborne applications 08 p1296 A67-20625

Requirements for military communications for flexible response, noting limitations /survivability, error rate, delay time, cost, etc/ and Digital Distributed Communications Network /DDC/ 09 p1463 A67-21676

Criterion characterizing adhesive joints in structural bonding of military materiel 09 p1522 A67-22500

Laser applications in military technology including precision measurement, secure communication, target location, etc 10 p1664 A67-23070

Management methods in military equipment development to be used with aircraft 11 p1885 A67-24655

Electronic package design for rugged military field service 12 p1911 A67-25268

Military electronics equipment packaging, discussing integrated circuits, module board design, interconnectors, nuclear radiation effect, heat dissipation, power supply design and cooling 13 p2083 A67-27447

U.S. international telecommunications requirements through 1975 14 p2272 A67-28704

Military surveillance satellite for high resolution photography noting design, application and projected performance 15 p2564 A67-29400

Revision of military terminology for weapon systems considering human factors, safety and maintainability and reliability relations 16 p2780 A67-30440

Maintainability program task requirements covered by Military Standard 470 16 p2781 A67-30441

Maintainability prediction procedures applicable to systems and equipment as described in DOD handbook 16 p2781 A67-30442

Air Force rescue radio equipment evolution, describing models 17 p2814 A67-32516

Reliability studies for optimization of aerospace systems and military engineering design and manufacture 18 p3053 A67-33637

Passive electronics countermeasure device /chaff/ consisting of metal strips to produce radar echoes 18 p3001 A67-34118

AMICON 8000 kw plasma facility for simulating reentry environments for material and thermodynamic tests 20 p3415 A67-36551

Ground vertical loop radio antenna for army use noting shape, performance, mobility, etc 20 p3399 A67-36884

TSIS fire control equipment family, considering maximum cost effectiveness, discussing use in Dassault Mirage M-5 and RCAF CF-5 aircraft 20 p3364 A67-37244

Book on reusable protective packaging of military, electronic and aerospace instruments and systems 22 p3771 A67-39832

Life cycle cost concept adaptation by DOD affecting logistics engineer, discussing reliability relation, maintainability, etc 23 p4084 A67-40580

U.S. space flight affairs and decisions /1957-1967/ 23 p4086 A67-40918

MILITARY WEAPON TRANSPORT VEHICLE

Continuous mechanical ladder for troop/cargo lowering and retrieval from CH-47 helicopter 17 p2804 A67-32518

MILKY WAY

Milky Way galaxy mechanism and

evolution, examining correlation between period of pulsation of intrinsic variable and galactic velocity 03 p0516 A67-14334

UV radiation observed beyond atmosphere in winter Milky Way, noting nebula detection and photographic apparatus 18 p3125 A67-34190

Search for IR stars at various temperature ranges reveals dense interstellar clouds, cool Mira Stars and circumstellar clouds 20 p3523 A67-36647

MILLIMETER WAVE

SA MICROWAVE

Impedance measurement of silver bonded Ge diode at X band and in mm wave region, improving performance by usage in breakdown region 01 p0033 A67-10028

Locked oscillation of silicon p-n junction avalanche diodes in 50 to 140 GHz range 01 p0035 A67-10436

Millimeter and centimeter radio wave propagation in near sea level tropospheric waveguides 02 p0191 A67-11569

Millimeter wavelength transmission line deficiencies reduced by using channeling systems in form of elastic dielectric tape on which are mounted thin metallic strips 04 p0575 A67-15167

Raindrop and melting hailstone absorption, scattering and backscatter cross sections of millimeter waves in satellite communications and weather radars 04 p0577 A67-15685

Spectra of unlocked driven semiconductor oscillators observed with millimeter wave reflex klystrons, noting gradual controllable frequency pulling 05 p0780 A67-17522

Step recovery diode utility extension, obtaining high efficiency from harmonic generators in millimeter wavelengths 05 p0780 A67-17529

Singularities of Faraday effect in n-type InSb in millimeter band at 77.8 degrees K as function of sample thickness and magnetic field intensity 06 p1047 A67-17755

Confocal resonator wave meter used to obtain frequency resolution of 10 MHz at 100 GHz 06 p0972 A67-18835

Measurement of attenuation of 8.6 mm wavelength radiation in rain, relation to rate of rainfall, using corner reflectors 07 p1146 A67-20201

Millimeter wave satellite communications, considering propagation, orbital and system design parameters, antenna pointing and satellite and ground equipment 08 p1292 A67-20671

Absorption coefficient of water vapor in relative windows of transparency for millimeter and submillimeter radio waves 08 p1294 A67-20817

Direct-coupled confocal resonators used as band pass filters at mm wavelengths 08 p1305 A67-21229

Radiometric maps of brightness temperature contours on lunar disk from measurements of 3.3 mm wavelength thermal emission [JPL-TR-32-1058] 08 p1399 A67-21242

Millimeter confocal wavemeter calibration and stability 09 p1470 A67-21625

Point contact electrically formed semiconductor junction diodes, discussing harmonic generation by various material combinations 09 p1474 A67-22086

Down-converter in reflection cavity configuration using bulk semiconductors as detection medium, considering optimum conditions 09 p1515 A67-22277

Ultrarapid AM of hyperfrequency mm wave in waveguide 09 p1465 A67-22568

Detection and measurement of mm wave difference frequency between two near laser lines, using optical heterodyne 11 p1803 A67-24832

Submillimeter-wave measurements for water-vapor detection from jet aircraft flying in stratosphere 13 p2114 A67-26795

Millimeter waves in atmospheric research, discussing radar meteorology, radiometry, etc 13 p2072 A67-27493

Medium power millimeter wave klystron /Laddertron/ construction and characteristics 14 p2278 A67-27800

Millimeter wave radiometry to study atmospheric properties, topographic relief, planets, medical and industrial research 14 p2265 A67-28402

Solar radio emission spectroheliograms at different millimeter wave frequencies 14 p2388 A67-28834

Millimeter wave attenuation measurement

in rain using low height antennas 14 p2274 A67-28923

Nonuniformity of mm wave detected by wideband frequency sweep control backward wave oscillator 16 p2643 A67-30896

Millimeter wave resonant interferometer capable of measuring spatial distribution of electrons in low density transient plasma column subject to perturbation 16 p2675 A67-31263

Path diversity in millimeter waves propagation through rain for various frequency 16 p2625 A67-31343

Millimeter wave passive radiometry noting design, capability, detectability and aerial reconnaissance 17 p2814 A67-32521

Absorption by atmospheric oxygen and rain of mm waves, using device permitting continuous frequency variation 18 p3002 A67-34230

Oblique incidence millimeter wave technique using ray theory for measuring collisionless plasma electron density profile 20 p3496 A67-36311

Millimeter wave reflectance for semiconductor panel, air space and metal reflector arranged planarly, discussing reflectance variation with conductivity and complete absorption 20 p3510 A67-37025

Satellite-borne, superheterodyne radiometer for measuring stratospheric temperature utilizing millimeter wave spectrum of molecular oxygen 21 p3584 A67-38669

Solar RF radiation in mm wavelength evaluated for information on solar flare activity 22 p3882 A67-39591

35 GHz second harmonic generation power and conversion efficiency in low pressure gas discharge, noting pressure and gas species variations 22 p3854 A67-40316

Microwave and mm radiometric sensor for passive satellite reconnaissance of earth atmosphere and terrain thermal noise 22 p3805 A67-40353

Coherent high power millimeter and submillimeter wave generation by various free electron beam devices, noting periodic beam has greatest development potential 22 p3774 A67-40443

Compensation method for longitudinal slot effects on propagation constant and characteristic impedance of rectangular waveguide used in standing wave meter 23 p4000 A67-41220

MILLING

SA CHEMICAL MILLING

Titanium mill products intended to meet requirements of C5A and SST aircraft, describing specially designed mill processing equipment 01 p0079 A67-10612

Cutting and milling processes in aeronautical industry, effect on costs and production rates 03 p0427 A67-13024

Beryllium part fabrication by metal removal, discussing machining and surface treatment methods [SAE PAPER 670803] 24 p4159 A67-41990

MILLING MACHINE

Numerically controlled milling for producing three-dimensional curved surfaces for turbomachinery [SAE PAPER 670096] 09 p1509 A67-22539

MILNE EQUATION

Duhamel principle for internal radiation field in inhomogeneous finite atmosphere based on existence and uniqueness theorem for Milne integral equation 24 p4189 A67-42598

MILNE-THOMSON METHOD

S RUNGE-KUTTA INTEGRATION

MINERAL

SA BAUXITE

SA CALCITE

SA COHENITE

SA GARNET

SA GRAPHITE

SA HEMATITE

SA INDOCHINITE

SA LAVA

SA ROCK

SA SOIL

SA WURTZITE

Geomagnetic field intensity measurement, based on observation that ferromagnetic minerals cooled in weak magnetic field from above Curie temperature acquire thermoremanent magnetization 02 p0236 A67-11477

Photon beam transmission measurement

- technique for determining bone mineral content in vivo 23 p3945 A67-41087
- MINERAL OIL**
- Thermal stability and degradation of n-hexadecane, mineral oils, and oligomers measured as function of time and temperature 16 p2695 A67-31754
- Life tests of tapered roller bearings in mineral oils and synthetic fluids, demonstrating lubrication effect on contact fatigue crack propagation [ASME PAPER 67-LUB-20] 24 p4163 A67-42678
- MINERALOGY**
- SA PETROLOGY**
- IR spectra of Mars bright areas compared with terrestrial rock, drawing conclusions regarding Mars mineralogy and detrital cover 05 p0896 A67-16717
- Chemical and mineralogical composition of roedderite found in Indarch meteorite, presenting electron probe analysis and X-ray diffraction pattern optical data 07 p1255 A67-20012
- Bununu meteorite /pyroxene-plagioclase achondrite/ composition and structure 09 p1564 A67-21736
- Monograph on electron microprobe X-ray analyzer and application in mineralogy 10 p1603 A67-23632
- Chemical and mineralogical composition of meteorites found in Australia, Africa, Ireland and Java 10 p1712 A67-23807
- Enstatite characteristics in enstatite achondrite meteorites, discussing mineralogy and composition 13 p2200 A67-27236
- Detection of mineral resources by orbiting satellite photography, using remote sensor techniques 19 p3225 A67-35655
- Quantitative analysis of new mineral /gentnerite/ found in Odessa meteorite 20 p3529 A67-37526
- Meteorite minerals characteristic constituents, describing crystalline form, frequency of occurrence, percentage, nature and terrestrial effects 21 p3700 A67-37766
- Mineral deposits on moon noting probable magmatic segregation, fumarole products, carbonaceous deposits, etc 21 p3711 A67-39119
- Airborne multiple scan interferometry for low temperature IR emission spectral distribution of minerals 22 p3807 A67-40368
- Canon Diablo octahedrite quantitative chemical and modal mineralogical composition variations in rim and plain components 24 p4235 A67-42636
- Economic exploitation of lunar mineral resources for near earth orbit manufacturing [AIAA PAPER 67-872] 24 p4238 A67-42993
- MINIATURE ELECTRONIC EQUIPMENT**
- SA MICROMINIATURIZED ELECTRONIC EQUIPMENT**
- Structural and technological problems connected with miniature electromechanical filters 10 p1609 A67-22876
- RF communication converter miniaturization and packaging techniques 12 p1911 A67-25271
- Design for active filters via eight-pin miniature component 14 p2283 A67-28288
- Hybrid microwave integrated circuits, discussing use of planar and passivated chip devices 15 p2452 A67-29929
- Aerospace electrical and electronic equipment reliability requirements with reference to technology of miniature electrical connection devices 15 p2454 A67-30230
- Miniature electrostatic accelerometer featuring suspension and force rebalance systems, discussing performance, applications and accuracy acceleration measurement 17 p2858 A67-32484
- Nonreciprocity in YIG filters employing stripline or miniature coaxial line construction 22 p3772 A67-39905
- MINIATURIZATION**
- SA MICROMINIATURIZATION**
- Measurement capabilities of linear digital displacement transducer with magnetically stored calibration 01 p0074 A67-11124
- Miniaturized high shock package utilizing FM-modulated 19.8 megacycle transmitter and piezoresistive accelerometer for measuring deceleration profiles 02 p0242 A67-12011
- Nonrechargeable batteries for miniaturized components, discussing dry, electrochemical, alkaline and mercury cells 07 p1131 A67-19531

- Microwave design techniques for calculating even and odd mode characteristic impedances of miniature microstrip transmission lines 13 p2071 A67-27445
- Semiconductor field development, discussing component reliability and miniaturization 17 p2823 A67-32299
- Laser welding and welding processes noting evolution as specialized tool to supplement present welding equipment 21 p3635 A67-38622
- MINIMUM DRAG**
- Nonaxisymmetric nose section of bodies of revolution having minimum drag at high supersonic speed 06 p0936 A67-17737
- Minimum drag body with specified center of pressure 10 p1592 A67-23155
- Parameterization of minimum-drag slender pointed cone situated in viscous hypersonic gas flow 13 p2050 A67-26882
- Optimum shape variations of minimum-drag body with given lifting force and volume solved through Euler equations 14 p2239 A67-27983
- Interval size effect on minimum drag coefficients and optimum shapes of bodies of revolution determined from Newtonian impact theory 15 p2416 A67-29407
- Minimum drag for slender body in hypersonic flow, assuming pressure coefficient is modified Newtonian and surface-averaged skin friction coefficient is constant 15 p2416 A67-29408
- MINITRACK OPTICAL TRACKING SYSTEM /MOTS/**
- Geos A space vehicle, discussing orbital motion, instrumentation and operation 07 p1259 A67-19759
- Optical and radio orbit tracking facilities, analyzing data accuracy levels, minitrack functions, etc 09 p1464 A67-22055
- Orbit determination from Minitrack observations, discussing effects of ionospheric refraction, atmospheric drag and earth tesseral harmonics 18 p3126 A67-34244
- Low perigee satellite orbit determination by visual observation, comparing directional accuracy and orbital elements with Minitrack and Baker-Nunn 18 p3126 A67-34247
- MINKOWSKI THEORY**
- Exact solutions of Einstein-Maxwell equation of Petrov class N when propagation vector of gravitational field is hypersurface orthogonal 07 p1218 A67-20281
- Relativistic electrodynamics of moving medium, discussing Maxwell-Minkowski equations, Born equations, field vector transformations, etc 09 p1533 A67-22449
- Moments of distribution function of perfect fluid calculated and used in studies of orthogonal polynomials on Minkowski hyperboloid 12 p1966 A67-25144
- Energy variation of two-body system due to gravitational radiation studied within framework of Minkowski theory 12 p1966 A67-25145
- Book on electrodynamics of moving media, deriving force distribution using Hamiltonian and virtual power principles in relativistic formulations 20 p3500 A67-37087
- MINOR CIRCLE TURN**
- Optimizing constant and variable parameter of minor circle solution for lateral maneuvering on spherical planet 02 p0333 A67-12335
- MINORITY CARRIER**
- SA MAJORITY CARRIER**
- Electron mobility in p-type indium antimonide, noting entrainment of minority carriers by majority 01 p0129 A67-10098
- Maximum alloying temperature and cooling rate of p-n junctions effect on volt-ampere characteristics of silicon diode and minority carrier lifetime 01 p0039 A67-11053
- Switching from transmission direction to barrier direction in junction diode at high injection levels 02 p0223 A67-12877
- Linear theory of self-excitation of oscillations in semiconductors in presence of large current density inhomogeneity 03 p0489 A67-13147
- Bulk minority carrier lifetime measured directly in solar cell by measuring short circuit current decay constant which is dependent on cell thickness and carrier type 04 p0554 A67-15128
- Temperature and impurity ion concentration effect on minority carrier mobility in degenerate gallium arsenide 04 p0679 A67-15143

- Dynamic resistance of Si p-n junction and diffusion length for minority carriers measured, using pulsed electron beam irradiation 04 p0584 A67-15317
- Nonohmic contacts, metal semiconductor point contact and soldered contact instead of p-n junctions used to measure diffusion length for minority carriers 04 p0584 A67-15481
- Emitter barrier capacitance effect on frequency characteristic of current amplification factor in drift transistors with accelerating field for minority carriers 04 p0585 A67-15502
- Minority carrier lifetime dependence on injection level, obtaining recombination center parameters for neutron irradiated germanium, using photoconductivity 04 p0684 A67-15692
- Lithium interaction with radium induced damage in silicon solar cells to produce center preserving minority carrier lifetime 04 p0556 A67-15703
- Anomalous permanent changes in transistor gain after low exposure dosage of electron and/or gamma radiation related to recombination current-component buildup 04 p0588 A67-15705
- Surface photoelectromotive force in GaAs type semiconductors with short duration minority carriers 04 p0686 A67-15969
- Diffusion and melting techniques used to determine effect of Ni, W, Ti and Ta impurities on lifetime of minority carriers in n-base of silicon p-n junctions 05 p0865 A67-16967
- Nanosecond lifetime measurement for minority carriers in long diodes 05 p0775 A67-17004
- Effect of local states in forbidden band on electron processes in n-GaP crystals, diagramming absorption and photoluminescence excitation spectra 05 p0868 A67-17063
- Storage time of drift transistors calculated as function of minority carriers effective lifetime 05 p0776 A67-17094
- Carrier-carrier scattering influence on Hall effect and on minority-majority carrier mobility in graphite 06 p1063 A67-18938
- Transport coefficients for minority carrier scattering in InSb 07 p1209 A67-19652
- Nonequilibrium charge carrier lifetime in indium antimonide single crystals with Ge and Au impurities 08 p1367 A67-20414
- Linear theory of self-excitation of oscillations in semiconductors in presence of large current density inhomogeneity 10 p1689 A67-23096
- Electron capture coefficient of A-centers in silicon at helium temperatures 10 p1694 A67-23649
- Undamped plasma oscillations in nonpolar semiconductors doped with impurities in external electric field, determining phase velocity 11 p1846 A67-24472
- Gallium arsenide electron photon transistor electrical properties at cryogenic and room temperature, determining total internal quantum yield of photons 11 p1765 A67-24475
- Drift field, field gradient and diffused impurity effects on minority carriers and quantum efficiency in silicon photocells 11 p1746 A67-24914
- Temperature and impurity ion concentration effect on minority carrier mobility in degenerate gallium arsenide 12 p1979 A67-25166
- Optical quenching of photoconductivity in silicon resulting from minority carrier capture by centers created by irradiation 13 p2173 A67-26358
- Stress effect on minority carrier mobility and concentration in germanium and silicon p-n junctions under uniaxial compression 14 p2364 A67-27825
- Measurement of variable Hall electromotive force component created by illumination of thin low resistance germanium samples by modulated 14 p2368 A67-28529
- Doping distribution optimum for minimizing minority carrier transit time through base to improve overall HF performance of diodes and transistors 14 p2287 A67-28676
- Dislocation-free Ge structural and electrical characteristics after cooling, considering quenching defects effect 14 p2372 A67-28761

Steady state one-dimensional carrier distribution in depth for electron beam excitation of semiconductors computed, including diffusion and surface recombination 15 p2442 A67-29180
Effect of local states in forbidden band on electron processes in n-GaP crystals, diagramming absorption and photoluminescence excitation spectra 15 p2538 A67-29794
Minority carrier lifetime in p-silicon, analyzed varying temperature and injection level and studying recombination 16 p2725 A67-30807
Specific resistance, EMF, Hall effect, and minority-carrier lifetime measurement of germanium whiskers bombarded by high energy electrons from linear accelerator 16 p2732 A67-31479
Impurity effect on annealing behavior of irradiated silicon studied via isothermal annealing of minority carrier lifetime 17 p2921 A67-33051
Electron capture coefficient of A-centers in silicon at helium temperatures 17 p2923 A67-33330
Current-voltage characteristic of metal semiconductor point contact, taking into account rectifying effect of junction gap and majority and minority current carrier 18 p3097 A67-33476
Thermal stabilization of inverse current of p-n junction by additional gate for minority carriers extraction 18 p3009 A67-33478
Irradiation effect on minority carrier lifetime for p-n junction devices in epitaxial film and single crystal forms 19 p3306 A67-35670
Semiconductor metal diodes operation principles, emphasizing lack of minority carrier storage 20 p3509 A67-36491
Majority and minority carrier lifetimes in n-type GaAs single crystals, measuring injection level dependence 20 p3512 A67-37436
Optical quenching of photoconductivity in silicon resulting from minority carrier capture by centers by irradiation 21 p3679 A67-38315
Base region thickness, minority carrier lifetime and impurity concentration effects on conduction characteristics of silicon diodes and thyristors 21 p3597 A67-38523
Electrical conductivity, Hall coefficient and thermo-EMF measurements in Zn and Te doped gallium antimonide crystals for minority carrier role in impurity conduction 21 p3687 A67-39141
Measuring method for minority carriers recombination rate at base surfaces of n-m/ contact without passing DC through contact 22 p3858 A67-39575
Measurement of variable Hall electromotive force component created by illumination of thin low resistance germanium samples by modulated light 23 p4039 A67-40936
MINUTEMAN ICBM
Physical and management aspects of reliability of integrated circuits for Minuteman II 01 p0042 A67-11367
Minuteman missile site selection and investigation program, considering field reconnaissance, data compilation and formulation 05 p0787 A67-16607
Operational phase of Minuteman program [AAS PAPER 66-162] 08 p1430 A67-20977
Cost improvement for Minuteman II integrated circuits from failure rate reduction, using failure mode model and measurement system 09 p1480 A67-22305
Operational phase of Minuteman program [AAS PAPER 66-162] 13 p2233 A67-27557
Statistical service life prediction based on propellant grain structural integrity for Minuteman third stage motor, noting grain stress analysis 15 p2547 A67-29996
Built-in test features in Minuteman II intercontinental ballistic missile weapons system electronics, discussing ground equipment including self-test features and status display techniques 20 p3417 A67-36973
MINUTEMAN TRANSPORTER-ERECTOR
Missile handling, from primitive techniques to Titan III ICBM mobile service towers 05 p0787 A67-16613
MIDOSIS
S VISION
MIRROR
SA BEAM SPLITTER
SA MAGNETIC MIRROR

SA PARABOLOIDAL MIRROR
SA ROTATING MIRROR
Adjustment procedure for laser with polygonal resonator, noting spatial mirror adjustment in addition to angular adjustment 01 p0087 A67-10162
Optical methods and equipment used in checking surface finish and volume and surface inhomogeneities of active media and interferometric mirrors of lasers 03 p0436 A67-13143
Performance characteristics for pulse type Ar laser with external interferential system of quasi-confocal spherical mirrors 03 p0438 A67-14188
Beryllium as substrate for mirrors of catadioptric lenses, noting strain-induced aberration 03 p0470 A67-14391
Extremely high reflective dielectric mirror coatings with zinc selenide for laser resonator cavities and interference filters 04 p0634 A67-15654
Laser mirror design in lens form for decoupling diffraction limited parallel beam, based on theorems concerning Gaussian beam imaging and behavior 05 p0826 A67-17327
Spherical coupler for fastening mirrors and plane-parallel plates at Brewster angle in gas laser 06 p1011 A67-18394
Resonator Q-modulation technique observation of central dip tuning in modulated power output of gas laser with moving mirror 06 p1011 A67-18758
Internal mirror reflections elimination in laser beam output intensity distribution by filtering device 09 p1512 A67-22042
Synchro-turn system for precision machining of beryllium mirrors 10 p1659 A67-22988
Proton radiation effects on mirror reflectance in high vacuum at various temperatures, degradation by blistering found to be highly temperature-dependent [AIAA PAPER 67-341] 12 p1957 A67-26055
Point holograms, reconstituting wavefronts from high quality lenses and mirrors and use as optical elements for replacing lenses in optical systems 18 p3048 A67-34194
Fabry-Perot interferometer for emission spectra time variations observed by employing electromechanical system to vary mirror motion speed 22 p3809 A67-40416
Lloyd mirror experiment applied to testing flatness of large surfaces, using moire technique for visualizing and measuring fringe deviation 23 p4002 A67-41263
MIRROR POINT
Amplification factor of circular polarization antennas calculated by mirror image method 02 p0209 A67-11505
Variations in position of mirror points of high energy electrons determined from Cosmos V satellite data 10 p1647 A67-23281
Coulomb interaction influence upon electron distribution in radiation belts at low altitudes in magnetic anomaly region 10 p1702 A67-23299
Amplification factor of circular polarization antennas calculated by mirror image method 14 p2283 A67-28069
Fokker-Planck equation describing distribution of geomagnetically trapped electrons as function of longitude, time, energy and mirror-point field intensity 22 p3791 A67-39808
MISS-DISTANCE
In-flight instrumentation for prompt miss distance measurement using gamma ray techniques 05 p0841 A67-16533
MISSILE
SA AIR TO AIR MISSILE
SA AIR TO SURFACE MISSILE
SA ANTAREAS MISSILE
SA ANTI-AIRCRAFT MISSILE
SA BALLISTIC MISSILE
SA BLACK BRANT III MISSILE
SA BLACK BRANT V MISSILE
SA BLACK BRANT MISSILE
SA BLUE STREAK MISSILE
SA GUIDED MISSILE
SA POLARIS MISSILE
SA SERGEANT MISSILE
SA SUPERSONIC COMBUSTION RAMJET MISSILE /SCRAM/
SA SURFACE TO SURFACE MISSILE
SA TALOS MISSILE
SA TARTAR MISSILE
SA TERRIER MISSILE
SA TITAN I ICBM

SA TITAN II ICBM
Experimental aerodynamics, Volume 2, covering simulation, transonic, supersonic and hypersonic domains 09 p1437 A67-22215
Missile dynamic behavior analysis using linear aeroballistic theory in conjunction with numerical computations of motion equation 14 p2395 A67-29058
Missiles and aerospace vehicles sciences - AAS Conference, Huntsville, Alabama, December 1966, Volume 1 22 p3900 A67-39926
MISSILE ANTENNA
High altitude research rocket HF telemetering remote control signal receivers, antennas and earth station, discussing design and circuitry of transmitter antenna 19 p3193 A67-35061
Analog simulation of electromagnetic radiation from antenna of revolution in vacuum and plasma via networks, discussing rocket nose cone shapes 23 p3977 A67-40578
MISSILE CASE
X-ray image transformation, transmission and amplification directly into video signals for inspection of missile case walls and weldments 10 p1622 A67-22929
MISSILE CONSTRUCTION
Forming of refractory materials for rockets by explosive, magnetic and Dynapak forming and beam welding methods 01 p0079 A67-10638
Maraging, 15CDV6 and 40CDV20 steel for missile and aircraft construction 05 p0830 A67-17269
Pressure measurement at stagnation point of cylindrical missile with spherical nose cone during free flight in ballistic testing 16 p2593 A67-31123
Shear-spinning technique for manufacturing molybdenum alloy missile nose tips 18 p3054 A67-34365
Missiles and aerospace vehicles sciences - Conference, Huntsville, Alabama, December 1966, Volume 2 22 p3904 A67-40134
Honeycomb sandwich structures for aircraft and missile construction, discussing panel configurations 23 p4077 A67-41047
Book on analysis and design of missile structure covering load and stress analysis 23 p4071 A67-41501
MISSILE CONTROL
SA HOMING
Servo control system selection for air-launched missile with Homing guidance system, reviewing four major designs of torque-proportional hardware 02 p0182 A67-11842
Optimum terminal missile maneuver and evasion strategy with Gaussian process 03 p0465 A67-13267
Optical system consisting of polarized laser beams for monitoring missile attitude during early launch phase 04 p0619 A67-14505
Spin scale factor of Frick for scaling body fixed motion equations analyzed, deriving near optimum factor and near maximum time interval of integration for spinning missiles 05 p0906 A67-17362
Feasibility of pure-fluid missile control system demonstrated by systems analyses, preflight tests and flight tests 07 p1257 A67-19360
Final value homing missile guidance 07 p1221 A67-19383
Missile and aircraft control systems design, discussing root locus and stability curve methods for solving characteristic equation 09 p1483 A67-22489
Missile guidance accuracy, examining motion in central gravitational field along trajectory 15 p2572 A67-30177
Elimination of electrical transients in high performance sleeve induction motors for missile guidance control systems 16 p2609 A67-31664
Nonlinear filter for homing missile tracking noise problem, noting computational requirements and feasibility by filter implementation model for different assumptions 17 p2882 A67-32526
Stochastic differential game with missile and radar, using linear theory in finding optimal strategies 18 p3075 A67-33495
Control engineering in systems management applied to missile control and guidance 18 p3162 A67-33636
Statistical techniques for missile injection error analysis, discussing direct and adjoint methods 19 p3254 A67-34780
Built-in tests /BIT/ for AN/AWG-10 Missile Control System 20 p3417 A67-36990

Z-transform and W-transform theory applied to dynamic compensation of linear sampled data control systems for attitude control of large booster 21 p3713 A67-38027
Blue Streak launch vehicle control system, discussing destabilizing resonance effects, hydraulic system, propellant movement in tanks and testing 21 p3570 A67-38102
Missile and space support systems reliability, flight equipment and redundancy 22 p3781 A67-40342

MISSILE DEFENSE

Data utilization in Air Defense Command /ADC/ weapon systems management 13 p2233 A67-27560

MISSILE DEFENSE SYSTEM

Parameter management applied to roll rate control in ballistic missile target system /BMTS/ with fin incidence 08 p1407 A67-20516
Parameter management applied to roll rate control in ballistic missile target system /BMTS/ with fin incidence 21 p3712 A67-37801

MISSILE DESIGN

SA MAGNUS EFFECT

Design of gust alleviation controls for boost phase flight of missiles incorporating random winds, time-varying missile dynamics, control problem, etc [AIAA PAPER 66-969] 02 p0332 A67-12292

Ordnance systems and devices noting composition, function, operation and testing procedures 04 p0557 A67-15734

Shortcomings in complex reentry system design caused by human factors 09 p1456 A67-22290

Soviet book on pilotless aircraft and missiles covering jet engine design, automatic control, radio engineering and aircraft aerodynamics 15 p2564 A67-29242

Laser-energized explosive device /LEED/ for pyrotechnic device actuation noting power source, ruby laser, metallic fiber-optic conductor, missile design, etc 17 p2803 A67-32437

Nonlinear filter for homing missile tracking noise problem, noting computational requirements and feasibility by filter implementation model for different assumptions 17 p2882 A67-32526

Main characteristics of Saphir measurement system, definition of parameters to be measured and design problems 17 p2861 A67-33131

Solid propellant engines treated for constant missile volume and mass 18 p3137 A67-34360

Solid propellant rocket motor-body shape as additional variable used to achieve given thrust-time program 18 p3115 A67-34361

Fault tree analysis concept development for predicting possible undetected safety hazards within complex missile systems 19 p3331 A67-34827

Solid propellant space propulsion technology covering developments in missiles, launch vehicles, fabrication and range of application 22 p3869 A67-40334

Book on analysis and design of missile structure covering load and stress analysis 23 p4071 A67-41501

MISSILE LAUNCHER

SA LAUNCH VEHICLE

SA MOBILE MISSILE LAUNCHER

Launching missiles safely from advanced marine systems 10 p1621 A67-22769

MISSILE RANGE

White Sands Missile Range instrumentation modernization program, discussing advanced range testing, reporting and control /ARTRAC/ system, telemetry and electronic and optical sensors 02 p0229 A67-12003

Management and cost factors involved in operation of modern integrated missile range [AAS PAPER 67-59] 15 p2468 A67-30121

MISSILE ROLL CONTROL

Interceptor missile adaptive roll autopilot with new dither principle in simulated testing of stability 01 p0111 A67-11203

Design procedure for slender multistage fast-burning rockets, noting modified flexural behavior and aerodynamic load 08 p1416 A67-20529

Vector equation for determining missile maximum roll rate for effective navigation ratio and time constant for guidance systems 11 p1816 A67-24215

Two-channel control system for

programmed roll of rapidly rotating carrier rocket, analyzing efficiency 22 p3898 A67-39175

MISSILE SIGNATURE

Cool burning smokeless propellants for gas generator applications and low signature missiles evaluated against criteria 15 p2544 A67-29981

MISSILE SIMULATOR

Three and six degrees of freedom missile subsystem design analysis using flight simulation by hybrid computer 05 p0789 A67-17515

Kinematic analysis of deviation from aircraft-missile line for designing electronic missile firing simulator, with manual telecontrol comprising controlled precession gyroscope for last integration 09 p1486 A67-22419

MISSILE STABILIZATION

Linear and nonlinear three-dimensional longitudinal stability coefficients from free flight measurements aboard missiles 04 p0703 A67-14553

MISSILE SYSTEM

Mission reliability and effectiveness analysis of Army Missile Command weapon systems [SAE PAPER 660725] 01 p0154 A67-10627

Thermal model for transient heat transfer analysis of missile guidance systems for prediction of operating temperature 02 p0263 A67-12104

Missile handling, from primitive techniques to Titan III ICBM mobile service towers 05 p0787 A67-18613

Nuclear radiation damage to circuit elements of missile FM/FM telemetry system, analyzing changes in electric characteristics 14 p2271 A67-28685

Low cost accurate mechanical timers [ASME PAPER 67-DE-39] 14 p2321 A67-28877

Control engineering in systems management applied to missile control and guidance 18 p3162 A67-33638

Universal array of complementary-symmetry MOS transistors applied to missile and surface radar beam steering phase array storage unit 18 p3015 A67-34563

Fault tree analysis concept development for predicting possible undetected safety hazards within complex missile systems 19 p3331 A67-34827

Aerospace system power conditioning design optimization, treating efficiency, regulation, EMI, BITE, primary power, size, weight, radiation hardening and cost [AIAA PAPER 67-985] 24 p4110 A67-43057

MISSILE TEST

Reliability tests on aerospace and missile systems research and development component assemblies 01 p0085 A67-11376

Optical instrumentation for missile and space vehicle testing 10 p1655 A67-22993

Systems thinking and systems management in rocket motor manufacture 18 p3111 A67-33638

Reliability demonstration during category II and III testing of missile and airborne radar fire control system, emphasizing coordination between factory and field 18 p3138 A67-34652

Tactical checkout missile test installations for Terrier, Tartar and Talos missiles 20 p3416 A67-36971

MISSILE TEST RANGE

Computer applications to test scheduling problem against probabilistic demand in heuristic environment [AAS PAPER 67-46] 15 p2467 A67-30114

Firing range for investigating Reynolds number effect on flow around bodies having complex design at transonic and supersonic velocities 16 p2655 A67-31116

Photographic recording by shadow method for alignment of optical equipment in firing range used to determine aerodynamic characteristics of various missiles 16 p2674 A67-31117

MISSILE TRACKING

Deep space and missile tracking antennas - ASME Conference, New York, November-December 1966 03 p0383 A67-13748

Sound-ranging technique for locating supersonic missiles 05 p0766 A67-17282

Mobile Cinetheodolite Mount design and operation for missile tracking 06 p1001 A67-17794

Frequency effects in radar return from turbulent weakly ionized missile wakes, obtaining relationship between radar cross

section and electron density distribution [AIAA PAPER 67-23] 06 p0963 A67-18258

Instrumental accuracy of missile range instrumentation systems, discussing error sources, detection and correction 10 p1605 A67-23002

General problem of least squares solved using method of Lagrange multipliers 10 p1674 A67-23003

Aircraft detection and in-flight tracking by real time computers, assessing role in missile and satellite tracking 13 p2153 A67-26666

Stability analysis of minimum variance estimations used to self-calibrate missile tracking instrumentation complex 13 p2120 A67-26815

Evaluation and calibration of missile and space tracking systems including test-by-test analysis, lofted rockets, self-calibrating systems, etc 16 p2621 A67-30682

Handbook of telemetry and remote control considering position measuring, missile guidance, flight control, data processing, feedback information, communications, etc 16 p2633 A67-31916

IR imaging system with multiple target capability for measuring IR radiation emitted by missiles during launch, boost and reentry 18 p3052 A67-34532

Data analysis and reduction studies for calibration of missile tracking systems using near earth satellite 20 p3381 A67-36604

MISSILE TRAJECTORY

Mayer technique in calculus of variation for constrained error coefficient criterion function for missile trajectory optimization in aerospace guidance and control 02 p0265 A67-12389

Altitude control system with optimized guidance device which reduces flight altitude of guided low trajectory missiles over sea surface 04 p0652 A67-14562

High accuracy tracking system for measurement of missile and rocket trajectories during lift-off phase 05 p0762 A67-16530

Wind variability effect on impact point of launch vehicle with reference to range safety at Western Test Range [AIAA PAPER 67-187] 06 p0980 A67-18323

Capabilities, goals and scientific and engineering problems associated with missile trajectory analysis, detailing tracking equipment [AAS PAPER 67-43] 15 p2438 A67-30112

Wind variability effect on impact point of launch vehicle with reference to range safety at Western Test Range 19 p3207 A67-34834

Payload and trajectories determination for consumption optimization for missiles moving in constant gravitational field, using Pontryagin maximum principle 20 p3531 A67-36409

MISSILE VIBRATION

Reduction and analysis of nonstationary missile flight vibration data, obtaining power spectral density 23 p4007 A67-41385

MISSILE WING

Minuteman missile site selection and investigation program, considering field reconnaissance, data compilation and formulation 05 p0787 A67-16607

MISSION

S FLYBY MISSION

S SPACE MISSION

MISSION PLANNING

Environment, mission requirements and subsystem interfaces effect on space vehicle structure [SAE PAPER 660673] 01 p0153 A67-10580

Mission reliability and effectiveness analysis of Army Missile Command weapon systems [SAE PAPER 660725] 01 p0154 A67-10627

DOD/NASA management practice program ensuring identification, communication and achievement of mission success requirement [SAE PAPER 660729] 01 p0170 A67-10629

Human capability to perform support functions in space 01 p0018 A67-11405

Integrated logistics system capable of supporting earth orbital operations and sufficiently flexible for demanding applications of space and lunar operations [AIAA PAPER 66-864] 02 p0331 A67-12262

Bioengineering parameters influencing life support systems for manned exploration of moon including mission duration and closed regenerable systems 02 p0230 A67-12310

- First orbit rendezvous mission planning with no ground support after spacecraft liftoff, considering propellant costs, procedural timing, terminal approach, etc 02 p0333 A67-12343
- Velocity requirements for orbital transfer and selection criteria for comet missions from 1967 to 1986 03 p0510 A67-13491
- Titan III launch vehicle for multiple payload delivery into precise space trajectory [AIAA PAPER 66-836] 03 p0519 A67-14125
- Mission design, operations planning and flight preparation for manned orbital space missions [AIAA PAPER 66-904] 03 p0519 A67-14131
- Rankine cycle power plant characteristics for electric propulsion manned Mars mission [AIAA PAPER 66-894] 03 p0504 A67-14274
- Scheduling manned space flight missions 04 p0704 A67-14902
- Space vehicle vs ground systems reliability [SAE PAPER 660691] 04 p0740 A67-15790
- Mathematical models properties analyzed for system reliability and maintainability, namely mission availability, discussing relationship to failure and action rate and time constraint 05 p0813 A67-17252
- Design, operational characteristics and testing of ion engine for spacecraft propulsion, considering mission analysis, orbit parameters and spacecraft orientation [AIAA PAPER 67-87] 06 p1074 A67-18342
- Planetology and space mission planning - Conference, New York, November 1965 06 p1090 A67-18993
- Terrestrial and planetary biospheres, tabulating probability values for matching 06 p0953 A67-19007
- Planetary transportation model application to space program 06 p1093 A67-19032
- Specification and evaluation of space projects and programs, noting model construction and planning 06 p1093 A67-19033
- Planning of manned scientific planetary missions, distinguishing critical experiments, taxonomic knowledge and precursor knowledge 06 p1093 A67-19034
- Space mission planning in planetary environments, discussing methods and planetological parameters 06 p1093 A67-19035
- Trajectory characteristics of high thrust Mars missions and effect on other aspects of mission planning 07 p1248 A67-19358
- Venus swingby trajectory for manned Mars mission as possibility in 1978-1986 [AAS PAPER 66-125] 07 p1254 A67-19984
- Approximate method for predicting lunar satellite lifetimes and application to lunar orbit mission analysis [AAS PAPER 66-130] 07 p1255 A67-19989
- Lunar surface accessibility study for manned lunar orbit rendezvous missions, discussing nonfree return and translunar trajectories [AAS PAPER 66-131] 07 p1255 A67-19990
- Progressive mission capability of Mars capsule, examining feasibility of increased scientific payload weights by increase of mission profile [AAS PAPER 66-58] 07 p1255 A67-19995
- LM guidance and control systems performance verification [AIAA PAPER 67-244] 07 p1165 A67-20064
- Solid and hybrid propulsion relationship to sounding rocket vehicle design and mission analysis, particularly application to synoptic meteorology 08 p1374 A67-20492
- Apollo spacecraft, discussing performance of Command and Service Module with typical payloads 08 p1412 A67-21077
- Apollo Extension System for lunar surface missions, discussing extension of mission time by unmanned LEM laboratory 08 p1316 A67-21083
- Mission requirements for unmanned exploration of solar system including energy and flight time, noting thrust vs ballistic vehicles 08 p1393 A67-21096
- Manned planetary mission possibilities stressing Mars exploration, noting trajectory planning, propulsion, crew requirements, etc 08 p1394 A67-21099
- Nuclear rocket engine design for near-optimum vehicle performance for mission capability 08 p1412 A67-21107
- Gemini experiments program, examining crew integration, mission planning and prelaunch operations 10 p1713 A67-23243
- Computer application to aerospace missions, discussing operation and equipment parameters, reliability, man-machine interaction, etc 11 p1756 A67-24248
- Venus swingby trajectory for manned Mars mission as possibility in 1978-1986 [AAS PAPER 66-125] 13 p2209 A67-27538
- Approximate method for predicting lunar satellite lifetimes and application to lunar orbit mission analysis [AAS PAPER 66-130] 13 p2209 A67-27541
- Lunar surface accessibility study for manned lunar orbit rendezvous missions, discussing nonfree return and translunar trajectories [AAS PAPER 66-131] 13 p2209 A67-27542
- Manned interplanetary program planning, suggesting basic parameters for manned trip to Mars and Venus 13 p2210 A67-27546
- Space rescue mission planning and targeting by computer 15 p2555 A67-29609
- Space transportation systems, considering recovery facilities, reusable boosters, cost, etc 15 p2568 A67-29846
- Apollo/Saturn V vehicle launching site, assembly building and lunar flight 15 p2569 A67-29849
- Support requirements for future manned space programs [AAS PAPER 67-56] 15 p2562 A67-30120
- Spacecraft design for manned planetary landings noting mission characteristics, navigation requirements, crew housing, etc 16 p2756 A67-30625
- Comet mission study using space probes boosted by Atlas Agena and Atlas Centaur launch vehicles for interception from 1967 to 1975 16 p2745 A67-30750
- Evaluation of relative scientific effectiveness of various lunar exploration programs through analysis of results from hypothetical missions to selected earth-analog sites 16 p2747 A67-30991
- Primary electric propulsion systems for deep space missions with reference to SERT II program and compatibility with other spacecraft programs [AIAA PAPER 67-424] 18 p3111 A67-33908
- Problem areas within cryogenic chemical and nuclear propulsion systems for space missions, noting available technology and limitations [AIAA PAPER 67-454] 18 p3110 A67-33928
- Nuclear propulsion for manned Mars expedition, discussing engine and launch optimization, computer simulation, performance, trip times, velocity, weight, etc [AIAA PAPER 67-510] 18 p3077 A67-33974
- Apollo Applications Program objectives, discussing revisitation and reuse of hardware left in orbit, in-flight maintenance for long duration space missions, etc 18 p2994 A67-34657
- Mission risk appraisal technique for identification and quantification of high risk areas for unmanned interplanetary missions 18 p3163 A67-34682
- Strategy of holding higher performance rocket engines for critical missions analyzed statistically for increased payload 19 p3311 A67-34829
- Planetary quarantine and biological search strategy, discussing Voyager-Mars mission configuration, sterilization, back-contamination and decisions 19 p3180 A67-35233
- Method for assigning numerical value to space scientific payload effectiveness toward satisfying mission goals 19 p3322 A67-35319
- Interplanetary transfer trajectory simulation, discussing planet ephemeris, coordinate systems, low and high powered and coasting segments 19 p3322 A67-35321
- Software aspects of space navigation including computer programming, mission planning, error analysis and reliability realization 19 p3187 A67-35858
- Effective guidance and control redundancy for spacecraft configurations and mission outcomes, discussing computer systems [AIAA PAPER 67-555] 19 p3257 A67-35952
- Multiplanet mission for Jupiter, Saturn, Uranus and Neptune, using swingby technique for probe launched in late 1970s [AIAA PAPER 67-613] 19 p3329 A67-36002
- Iterative guidance mode /IGM/ applied to effective gravity vector prediction, acceleration measurement of noise sensitivity and energy limitations [AIAA PAPER 67-620] 19 p3260 A67-36009
- Mission simulator for manned space flight support used for real time training 20 p3414 A67-36538
- Spacecraft computers role on advanced manned missions 20 p3391 A67-36549
- Launch operations optimization for mission planning through analysis of performance data from past programs 20 p3532 A67-36557
- Flight phase constraints effect on design of Voyager orbiter-capsule mission 20 p3532 A67-36564
- Apollo Range Instrumentation Aircraft /ARIA/ deployment model to determine flight plans for support of translunar injection phase of Apollo mission 20 p3361 A67-36600
- Quality program planning criteria for NASA contracts involving NPC 200-3 20 p3556 A67-36602
- Vehicle mass requirements for optimal high and low thrust propulsion systems for manned and unmanned planetary missions 20 p3533 A67-37125
- Minimizing time for deployment of infantry force by airlift analyzed by computer procedures based on loading, effectiveness and productivity 20 p3361 A67-37529
- Scientist role in automated laboratory for remote biological exploration of planets [AIAA PAPER 67-632] 20 p3375 A67-37615
- General purpose unmanned spacecraft and multimission applications satellite possibilities [AIAA PAPER 67-635] 20 p3534 A67-37620
- Spacecraft computer managed laboratory /CML/ for flexible decision making in space missions of 1970s [AIAA PAPER 67-643] 20 p3393 A67-37624
- Operational and cost-influencing characteristics of low orbit space operations compared from manned orbital base and earth base [AIAA PAPER 67-654] 20 p3530 A67-37631
- Data on crew workload in C-141 aircraft used for extended mission living and working schedules, showing major disruptions in regular patterns 21 p3576 A67-38073
- Low thrust Jupiter flyby mission analysis for interplanetary vehicles with solar electric propulsion [AIAA PAPER 67-708] 21 p3706 A67-38735
- Approximate method for electric propulsion missions analysis, determining system components effects on performance [AIAA PAPER 67-709] 21 p3693 A67-38736
- Test and control planning concepts for space travel projects, considering third stage of booster rocket Europa I 22 p3921 A67-39281
- Space research experiments reliability requirements, considering structural components, project planning and measuring methods adaptation to ambient conditions 22 p3899 A67-39283
- Mission flight profile, considering thrust failure prior to attaining orbital speed, analyzing instantaneous impact point /IIP/ 22 p3831 A67-39610
- Secondary payload for Saturn launch vehicle evaluation according to experiment/mission effectiveness and compatibility by computer program methodology 22 p3903 A67-39950
- Multiple payload mission planning for multiple and single earth orbits and apogee motor delivery, evaluating cost and performance 22 p3903 A67-39952
- Solar probe mission planning, evaluating high temperature electronics capability and high flux GaAs solar cell efficiency 22 p3903 A67-39956
- Alternate mission modes for manned Mars exploration 22 p3886 A67-40136
- Lunar missions evaluated for scientific effectiveness via use of earth analogs assuming hypothetical terrestrial objectives parallel to lunar program 22 p3887 A67-40142
- Mission planning for post-Apollo period including selection of lunar landing sites and definition of preferred scientific activity 22 p3888 A67-40144
- Unmanned 0.1 AU /Icarus/ solar probe preliminary design, discussing thermal control and power supply problems unmanned 0.1 AU /ICARUS/ solar probe preliminary design, discussing thermal control and power 22 p3906 A67-40152
- Earth orbital mission utilizing propellant transfer techniques based on fluid management under low gravity

environment 22 p3906 A67-40163
Mission profiles involving new materials for missile and space structures reviewed for progress in computer applications 22 p3915 A67-40330
Power systems for long duration missions including photovoltaic solar energy, thermoelectric, Brayton cycle and thermionic conversion systems, discussing solid state components 22 p3749 A67-40339
Planning and design of Voyager for future interplanetary flight, discussing RTG and spacecraft system redundancy 23 p4071 A67-40867
NASA space program planning and proposed progress in 1970s 23 p4086 A67-40921
Biosatellite II, mission objectives and planned experiments 24 p4240 A67-41897
Integrated design requirements of SNAP-8 Rankine power system for manned lunar base mission, discussing mission requirements and reactor shield system 24 p4185 A67-42545
Impact of future aeronautical vehicles on development test facility planning [AIAA PAPER 67-780] 24 p4139 A67-42947
Manned space flight safety through mission trajectory design, considering hardware, software and operational constraints [AIAA PAPER 67-822] 24 p4243 A67-42970
Manned space flight safety, discussing system design, operations planning, staffing, training and simulation [AIAA PAPER 67-824] 24 p4243 A67-42971
Apollo manned Lunar Module /LM/ earth orbital development missions, reviewing key subsystems and technical problems [AIAA PAPER 67-863] 24 p4244 A67-42987
Lunar exploration planning methodology for after post-Apollo landing based on equipment evolution [AIAA PAPER 67-865] 24 p4238 A67-42988
Lunar transportation systems for exploration logistics support after first Apollo flight, feasibility, candidates, selection and evolution [AIAA PAPER 67-873] 24 p4244 A67-42994
Vehicle flight readiness review, technique for assuring maximum probability of mission success [AIAA PAPER 67-888] 24 p4140 A67-43001
U.S. launch operations techniques emphasizing launch site testing prior to launch [AIAA PAPER 67-889] 24 p4140 A67-43002
Spaceborne computer-managed laboratory for experiments and instruments control in future space missions [AIAA PAPER 67-957] 24 p4140 A67-43040
R and D deep space communication system planning methodology for comparing laser, IR and mm wave possibilities, analyzing tradeoff and optimizations [AIAA PAPER 67-973] 24 p4260 A67-43050
Manned planetary mission global network for continuous tracking, communication telemetry and TV transmission [AIAA PAPER 67-976] 24 p4125 A67-43052

MITOCHONDRIA
Nonphosphorylating respiration of mitochondria from brown adipose tissue of rats, providing example of electron transport 02 p0185 A67-12527

MITOSIS
SA CELL DIVISION
Chromosome configuration and mitosis impairment in micropores Tradescantia paludosa due to space flight effects of Voshkod I 07 p1133 A67-19109
Gravity effect on liver regeneration in rats measured by mitotic count 20 p3372 A67-36963

MITSUBISHI MU-2 AIRCRAFT
Quality control around twin turboprop utility plane MU-2 at experimental stage 05 p0812 A67-17245

MIXED FLOW
Turbulence in free shear layer in mixing region of circular jet, comparing statistical characteristics of mathematical and physical models [AIAA PAPER 65-805] 01 p0054 A67-11164
Instability of gravitating slipstreams or mixed streams and cloud fragmentation of interstellar gas 03 p0511 A67-13877
Intersecting turbulent jet mixing studied for velocity fields, pressure and temperature 04 p0609 A67-15592
Thermal choking in various devices having

mixing processes between two flows with different stagnation enthalpies as possible limitation of mass flow rate [ONERA-TP-411] 05 p0792 A67-16934
Gas dynamics and geometry in mixing zone of Freon 12, air and helium jets in wake air flow, determining effect of jet velocity, gas density, etc 06 p0982 A67-17743
Thermodynamic flow analysis of feasibility of coolant gas addition to nozzle flow for improved particle formation efficiency in mixed flow colloid thruster [AIAA PAPER 67-85] 06 p0941 A67-18500
Three-way valve design for flow deflection, separation and mixing 08 p1286 A67-21535
Rotating blades cascade performance in mixed flow turbomachines, noting flow characteristics and slip factors 12 p1892 A67-25350
Upstream velocity profile effect on free mixing of jets with ambient fluid 14 p2240 A67-28107
Mixing patterns and flow configurations in model for determining combustion performance in well-stirred reactor 18 p3154 A67-33833
Type II superconductors properties, studying Ginzburg-Landau equations, vortex lines, reversible magnetic behavior and irreversible phenomena in mixed state 19 p3307 A67-35868
Cascade flow in mixed flow pumps and turbines, solving boundary value problems for stream function by relaxation method 20 p3356 A67-36421
Laminar and turbulent free shear layers analysis unifying treatment of mixing layers, assessing Mach number, Prandtl number and temperature ratio effects on constant pressure mixing [ASME PAPER 67-HT-81] 20 p3551 A67-36759
Two-dimensional turbulent mixing of supersonic reacting and nonreacting gases studied with square shock tube 21 p3606 A67-37772
One-dimensional compound-compressible nozzle gas flow theory, discussing choking phenomenon and three-dimensional computer calculations 23 p3927 A67-40603
Gas-air mixing in coaxial flow engine based on one-dimensional ejector theory at subsonic flow velocities, discussing chamber design gas-air mixing in coaxial flow engine based on one-dimensional ejector theory at subsonic flow 23 p4048 A67-40638
Solution for flow through circular array of blades contained between two surfaces of revolution separated by small variable distance obtained by Ackeret method 23 p3927 A67-40726
Mixing effect in dual flow turbojet engines analyzed to obtain better conversion of combustion into kinetic energy 23 p3931 A67-41317
Momentum equation integration to determine two mixing parallel subsonic streams interface 23 p3991 A67-41667
Mixed flow of five plane turbulent air jets discharged into atmosphere through slotted nozzles 24 p4143 A67-42285

MIXER
Three equivalent circuits of transistor mixer 05 p0784 A67-16943
Local oscillators with standardized frequencies in conjunction with central mixer used as wideband noise receiver for increased sensitivity 09 p1481 A67-22480
Parametric double pumping mixer of down converter type for multiple-beam low noise receiving antenna 12 p1913 A67-25302
Coaxial and strip-line passive microwave components stressing design of hybrid junctions, microwave mixers, filters, etc 19 p3195 A67-35549
Receiver mixer design characteristics effect on prediction of spurious response levels 20 p3405 A67-37648

MIXING
S JET MIXING
S LAMINAR MIXING
S PREMIXED FLAME
S SIGNAL MIXING
S TURBULENT MIXING
MIXING LENGTH FLOW THEORY
Generalized mixing length argument in turbulent diffusion, obtaining integral equation for continuous case 04 p0603 A67-14648
Mixing length flow theory of turbulent incompressible flow integral diffusion model

extended for boundary layer, channel and Couette flows 04 p0609 A67-15811
Computing velocities and convective energy transport in stars of different spectral types and luminosities 05 p0899 A67-17071
Mach number effect on mixing lengths and kinematic eddy viscosities in turbulent flat plate boundary layer [AIAA PAPER 67-199] 06 p0987 A67-18324
Suction requirements for elimination of turbulent boundary layer separation in adverse pressure gradient, based on mixing rate hypothesis and von Karman momentum integral [AIAA PAPER 67-197] 06 p0988 A67-18442
Peripheral jet behavior in hovercraft described via modified mixing theory 06 p0991 A67-18752
Experiment to represent sunspot model having mechanism of natural turbulent convection of liquid mercury inhibited in presence of magnetic field 13 p2171 A67-27437
Karman similarity hypothesis extended to cylindrical geometry to establish conditions for universal velocity similarity in fully turbulent rotating flows [ASME PAPER 67-APM-23] 17 p2838 A67-32416
Lower thermal boundary layer of solar convection zone within framework of mixing length theory 18 p3133 A67-34376
Mixing-length velocity profile in boundary layers with transpiration, discussing Tennekes theory and turbulent kinetic energy change rate 19 p3211 A67-35752
Base pressure calculation of stepped axisymmetric body in supersonic flow based on turbulent mixing 22 p3740 A67-39944
Solar hydrogen convection zone mean stratification derived from mixing length theory, discussing zone structure dependence on temperature and density dependence of opacity 23 p4068 A67-41278
Penetrative motion of individual elements in earth atmosphere and prediction of velocity field from convective overshoot 23 p4024 A67-41279
Partial differential equation in lubricant pressure based on mixing-length theory, presenting full journal bearings in turbulent and laminar regimes 23 p4010 A67-41342
Integral turbulent transfer model using velocity distribution function to develop mixing length flow theory 24 p4141 A67-41933

MIXTURE
S BINARY MIXTURE
S GAS MIXTURE
S LIQUID-GAS MIXTURE
MOBILE MISSILE LAUNCHER
Mobile launch concept of Launch Complex 39 in which mobile launcher and crawler transporter are used to transport vehicle from vehicle assembly building to launch site 02 p0228 A67-11837
Saturn V Mobile Launcher configuration, design and testing 02 p0228 A67-11840
Mobile launcher and crawler transporter facilities for Apollo/Saturn V launch exploration vehicle 05 p0787 A67-16611
Mobile launch concept for Apollo/Saturn V lunar landing mission, discussing structural composition, functions and performance of launcher [AIAA PAPER 67-247] 07 p1165 A67-20065
CNES rocket probe mobile launching unit for auroras, eclipses and Van Allen belt layer experiments 21 p3609 A67-39051

MOBILITY
SA ELECTRON MOBILITY
SA HOLE MOBILITY
SA ION MOBILITY
Preparation temperature and condensation rate effect on current carrier mobility in lead selenide and telluride films 01 p0128 A67-10089
Photo-Hall effect and photoconductivity on compensated p-InSb at low temperatures, examining temperature dependence of carrier mobility 01 p0128 A67-10093
Current-carrier scattering in germanium telluride 01 p0129 A67-10097
Intrinsic damping and eddy current-limited domain wall mobility in Ni-Fe alloy ferromagnetic thin films 02 p0298 A67-11890
Carrier mobility and concentration in epitaxial silicon layers obtained by vacuum sublimation 03 p0498 A67-13869
Temperature variation of electric

conductivity and carrier mobility in diffused germanium resistors doped with antimony for thermometry 05 p0773 A67-16464

Vibration absorbers effectiveness determined using stiffness and mobility method, noting detuning [ASME PAPER 67-VIBR-65] 11 p1873 A67-24206

Rigid articulated pressure suits, discussing design, construction and operation for low external pressure, mobility requirements, etc 16 p2618 A67-30779

Resistance and Hall effect measurements on PbTe thin films prepared by vacuum evaporation on amorphous or oriented substrates 19 p3307 A67-35795

Energy dependent mobility in small signal analysis of waves in semiconductors 22 p3864 A67-40310

MODAL RESPONSE

Statistical dependence effect of normal mode response of complex structures to random excitation 01 p0163 A67-11172

Dynamic programming recursive estimation of modal trajectory for nonlinear non-Gaussian noise and comparison with Bayesian estimation and case of Gaussian white noise 01 p0047 A67-11214

Shear deformation and rotary inertia effects on modal data of nonuniform beam, with complex behavior defined by ordinary differential equations 08 p1416 A67-20533

Individual section dampers relation to modal damping of series mass spring in lumped parameter systems 10 p1729 A67-23770

Panels response to oscillating and to moving shock waves, discussing mode excitation, magnification factor, Bessel function, etc 20 p3539 A67-37001

Angular divergence of solid state laser radiation for case of variable resonator and pump parameters 21 p3640 A67-38367

Launch vehicle response in lateral vibration modes to nonstationary random transonic buffeting excitation 22 p3907 A67-40167

Mode acceleration method for axisymmetric dynamic response due to time dependent loading in spherical and cylindrical shells 22 p3914 A67-40190

MODE

S COUPLED MODE

S FAILURE MODE

S LASER MODE

S PROPAGATION MODE

S SCHUMANN MODE

MODE OF VIBRATION

S VIBRATION MODE

MODE SEQUENCE

Plasma stabilization by HF electromagnetic fields, noting mode spectrum spacing along sample axis and dependence on field strength 10 p1686 A67-23585

P-n junction diode frequency doubler operating in charge-storage/step-recovery mode efficiency and power output 20 p3395 A67-36315

Multimode monopulse feed system optimum aperture distribution determination, obtaining maximum rate of signal change on axis 22 p3763 A67-40313

MODE SHAPE

Dynamic rubber wheel model to supplement digital computer analysis for prediction of frequencies, mode shapes and stress distributions of vibrating rotor stages [ASME PAPER 66-WA/GT-8] 04 p0712 A67-15364

Natural frequencies and mode shapes for axisymmetric vibration of thin elastic and ellipsoidal shells 04 p0714 A67-15424

Resonant frequencies compared with associated mode shapes of truncated conical shells with both edges free 10 p1718 A67-23455

Vibratory motions of turbine blades, considering frequency determination, tangential mode, stress, damping and excitation source [ASME PAPER 67-VIBR-66] 11 p1798 A67-24207

Natural frequency and mode shape for nonuniform simply supported beam, using Fourier series to approximate deflection, mass and inertia moment 11 p1874 A67-24429

Vibration characteristics of cantilever type pretwisted turbine blading, considering effects of taper, calculating frequencies and mode shapes 12 p2014 A67-25414

Sawtooth voltage oscillation of triangular

shape for pulse width modulation pulse shapers 13 p2089 A67-27704

Natural frequencies and mode shapes of pressurized circular cylinders with flexible stringers and attached point-mass [AIAA PAPER 66-449] 14 p2399 A67-28120

Mode correspondence between circular and square multimode tapered waveguide, noting similar behavior of coupling mechanism of waveguides 15 p2444 A67-29454

Flat-top pulse waveform with high transmission efficiency, confined spectra and good electromagnetic compatibility 20 p3388 A67-37654

Mode-matching technique for bifurcated anisotropic waveguide, discussing Bresler biorthogonality relationships to derive anisotropic guide mode equations 20 p3407 A67-37712

Natural frequencies and mode shapes determined for circular cylindrical shell closed by elastic plate 23 p4080 A67-41750

Asymptotic functional dependences and eigenvalues of guided wave modes in uniform and nonuniform structures deduced by ray-optical techniques 24 p4124 A67-42807

MODE TRANSFORMER

Mode transformation due to slightly tilted waveguide tube treated as boundary value problem 01 p0040 A67-11233

MODEL

S AIRCRAFT MODEL

S ASTRONOMICAL MODEL

S ATMOSPHERE MODEL

S BIOLOGICAL MODEL

S DUMMY

S DYNAMIC MODEL

S ENVIRONMENT MODEL

S GUTENBERG MODEL

S LIGHTHILL MODEL

S MATHEMATICAL MODEL

S SCALE MODEL

S SPACECRAFT MODEL

S THREE-FLUID MODEL

S TWO-FLUID MODEL

S WIND TUNNEL MODEL

MODULATED CONTINUOUS WAVE

High power visible CW gas laser beam generation, modulation and deflection for application to visual display technology [SMPTE PREPRINT 100-6] 03 p0438 A67-13801

MODULATION

S AMPLITUDE MODULATION

S CARRIER MODULATION

S DELTA MODULATION

S DEMODULATION

S FREQUENCY MODULATION

S INTERMODULATION

S IONOSPHERIC CROSS MODULATION

S OPTICAL MODULATION

S PHASE MODULATION

S PULSE AMPLITUDE MODULATION /PAM/

S PULSE CODE MODULATION /PCM/

S PULSE DURATION MODULATION /PDM/

S PULSE FREQUENCY MODULATION /PFM/

S PULSE MODULATION

S PULSE POSITION MODULATION /PPM/

S PULSE TIME MODULATION /PTM/

S PULSE WIDTH MODULATION /PWM/

S SINGLE-SIDEBAND MODULATION

S TRAVELING WAVE MODULATION

S VELOCITY MODULATION

MODULATION TECHNIQUE

Radiant flux modulation using two lattices, for case of rectangular aperture with uniform flux distribution 01 p0022 A67-10423

Book on modulation, resolution and signal processing in radar, sonar and related systems 03 p0372 A67-14233

Transmitter modulation choice for nonconventional radar system, taking into account scanning antenna modulation effects 04 p0572 A67-15029

Book on phase coherent communication principles based on statistical communication theory, discussing coherent receivers and analog and digital modulation systems 04 p0576 A67-15616

Multiple access modulation techniques /frequency-division, time-division, spread-spectrum and pulse-address/ for use in communications satellites 06 p0960 A67-17694

Time division multiple access /TDMA/ modulation technique for satisfying anticipated demand by many small users for communication satellite

facilities 06 p0961 A67-17695

Reflection coefficients of plasma waveguide measured by determining wave modulation coefficients 06 p1039 A67-18083

Resonator Q-modulation technique observation of central dip tuning in modulated power output of gas laser with moving mirror 06 p1011 A67-18758

Transmission methods, analyzing noise threshold, signal bunching, etc 07 p1141 A67-19339

Noise modulation effect on signal distortion by analyzing signal components in terms of noise parameters and of undistorted signal 07 p1147 A67-20240

LF modulation technique used aboard Canadian ionospheric research satellite ISIS-A for tape recording of signals with VLF components 08 p1298 A67-20662

Transmission methods in satellite communications and power level decrease by noise reduction 09 p1463 A67-21758

Modulation pyrometer measuring plasma temperature from spectral line intensity 09 p1499 A67-22328

Omega navigation system composed of eight transmitters will give worldwide coverage on frequencies 10.2 kc and 13.6 kc 09 p1527 A67-22627

Cross correlation and statistical dependence between envelope and frequency deviation of sine wave plus random noise, noting possible application to frequency demodulation 11 p1753 A67-24646

Satellite Telecommunications with Automatic Routing /STAR/ system modulation techniques, channel capacity and Start-Stop /SS/ operation 13 p2067 A67-26718

Satellite Telecommunications with Automatic Routing /STAR/ system transmission system operation and modulation techniques 13 p2068 A67-26719

Satellite telecommunication with automatic routing noting switching concept and modulating methods 13 p2087 A67-26721

Laser communication system for black and white tv signal transmission noting focusing, noise level and light modulation laser communication system for black and white TV signal transmission noting focusing, noise 13 p2068 A67-26724

Low pass high pass time-varying filter combination with stopband attenuation obtained by outphasing in quadrature-modulation arrangement 13 p2078 A67-26787

Modulation and demodulation methods for multiplex telemetry, discussing PCM, PSK and SSB 14 p2271 A67-28682

Solar wind modulation of low energy galactic cosmic radiation, estimating primary source spectra, proton and helium fluxes 15 p2550 A67-29614

Permutation modulation systems comparison based on proved-best criterion of alphabet size and minimum distance between signal vectors 15 p2439 A67-30384

Troposcatter techniques reviewed proposing analog voice waveform conversion into digital form by delta modulation or PCM for upgrading present operational systems 16 p2628 A67-31492

Cosmic ray intensity 11-year variation energy characteristics, discussing spectrum bending due to integral modulation in interplanetary space 17 p2932 A67-32083

Cosmic ray intensity, discussing modulation due to earth heliolatitude variation 17 p2932 A67-32086

Hollow anode glow discharge noting motion of ions and electrons in beam configuration 19 p3195 A67-35598

Selective modulation spectrometry, discussing problem of spectrometry without slit 20 p3438 A67-36348

Utility charts for evaluation of data modulation methods 20 p3380 A67-36543

Modulation systems in satellite communications evaluated by criteria of baseband signal noise ratio, signal power, frequency band requirements, etc 20 p3383 A67-36956

Frequency bands and modulation methods for space communication system 21 p3581 A67-38235

Modulation transfer theory for frequency response of optical system in temporal or spatial domains, discussing Fourier series and transform [SMPTE PAPER 102-47] 22 p3808 A67-40380

Nuclear cosmic ray component intensity variation related to 27-day solar activity

variation in Elektron II and IV analysis of modulating effect 23 p4055 A67-41104
 Secular modulation of cosmic ray intensity in interplanetary space using Parker diffusion model 23 p4057 A67-41117

MODULATOR

SA DEMODULATOR
 SA ELECTRON TUBE
 SA LIGHT MODULATOR
 SA OPTICAL MASER MODULATOR
 Pulse shape formed during discharge of chain-type artificial line 01 p0038 A67-10719
 Input admittance of parametric diode of reactance modulator with nonlinear losses 02 p0221 A67-12425
 Modulation linearity improvement using separate analyzer assembly with each electro-optic crystal 09 p1511 A67-21643
 Traveling wave electro-optic modulator tested at 6328 angstroms with CW drive power 09 p1471 A67-21644
 Power jet and single control bubble region portion of fluid jet modulator modeled for studying static and dynamic properties 14 p2248 A67-28271
 IR modulator utilizing field-induced free carrier absorption, with expressions for modulation index in terms of geometrical and physical properties of materials 15 p2491 A67-30428
 Monolithic magnetic double-balanced modulator, comparing patterns from working sample with theoretical conversion gain 22 p3773 A67-39916
 Nonreciprocal waveguide device consisting of ferrite loaded coaxial branch and crystal diode useful as isolator, modulator and filter 22 p3774 A67-40459
 Modulator-demodulator device using phase shifts between signals in successive time intervals to speed handling of data in HF band 22 p3764 A67-40557

MODULE

SA COMMAND MODULE
 SA ELECTRONIC MODULE
 SA LANDING MODULE
 SA LUNAR EXCURSION MODULE /LEM/
 SA MARS EXCURSION MODULE /MEM/
 SA SERVICE MODULE
 SA SPACECRAFT MODULE
 Modular xenon solar simulator for large area solar simulation, discussing source, transfer optical system and Cassegrain module, including fill-in optics 12 p1925 A67-25735

Universal internal communications system /UICS/ for interconnecting avionic system components, using single coaxial cable and modules 17 p2813 A67-32472
 Test facility for 5000 mw nuclear rocket propulsion modules, discussing effect on design and flight conditions duplication [AIAA PAPER 67-465] 18 p3020 A67-33936

MODULUS

SA BULK MODULUS
 SA DYNAMIC MODULUS
 SA ELASTIC MODULUS
 SA YOUNGS MODULUS
 Shear modulus effect on stress distribution of planar array of screw dislocations near bimetallic welded half-planes interface 11 p1804 A67-24107
 Increasing modulus maximum of integral function relation to moduli of coefficients of power series 11 p1813 A67-24520

MOHR CIRCLE

Mohr circle geometric representation of transformation of two-dimensional symmetric stress tensors in using complex variable vectors /phasors/ 04 p0657 A67-14850

MOIRE METHOD

Moire method in determining dynamic response of thin membranes 03 p0531 A67-14362
 Moire patterns in determining partial derivatives of displacement components 05 p0909 A67-16142
 Moire pattern method of determining fringes representing constant curvature of bent plates 05 p0921 A67-16827
 Moire method of surface strain measurement 07 p1262 A67-19387
 Instrument design for analyzing biaxial strain field in thin plate under creep, noting use of moire effect 08 p1332 A67-21461
 Moire fringes as parametric curves 09 p1574 A67-21837
 Moire patterns of modified intensity distribution analyzed, ascertaining fringe sharpening and

multiplication 11 p1875 A67-24612
 Theoretical calculations for minimum anticlastic cross section deformations of thin elastic strips with optimally tapered edges verified by moire method 11 p1875 A67-24613
 Flexural vibrations of plates studied by moire method for nodes, antinodes, local amplitude and phase distributions 12 p1966 A67-25293
 Scale grating with moire fringe effect, noting attachment to Zeiss 3030 coordinate measuring instrument 14 p2319 A67-28590
 Transient analysis of displacement, strain and stress fields around running crack tip in epoxy plate with central notch using Moire method 16 p2775 A67-31325
 Moire topography techniques for partial slope and macroscopic curvature measurements of cylindrical and conical shells due to loading 17 p2960 A67-32455
 Moire stress analysis technique for transferring grid without master contact 17 p2855 A67-32456
 Holographic moire patterns as white light viewing technique for aerodynamic flow visualization 19 p3232 A67-35699
 Optical system using moire patterns to measure refractive index gradients in boundary layer, showing relation to temperature and density gradient [ASME PAPER 67-HT-3] 20 p3447 A67-36702
 Structural defects of reciprocally oriented polycrystalline bismuth-antimony films analyzed by moire method 20 p3510 A67-36813
 Hologram-moire interferometry for transparent objects of moderate optical quality 21 p3624 A67-37853
 Transient displacement and strain distributions in fracturing notched magnesium plate, using moire-fringe technique and Q-spooled laser 23 p4076 A67-40736
 Book on two-dimensional and surface strain measurement for industrial application including strain gauges, photoelasticity and moire methods 23 p4077 A67-40791
 Aperture system using moire fringe method to execute spectral scan for Fabry-Perot spectrometer 23 p4001 A67-41258
 Lloyd mirror experiment applied to testing flatness of large surfaces, using moire technique for visualizing and measuring fringe deviation 23 p4002 A67-41263
 Moire patterns generated on computer printout when superimposing sampling grid over two-dimensional function to be plotted 24 p4158 A67-42809

MOISTURE

Moisture effect on slow crack propagation in thin sheets of SAE 4340 steel under static and cyclic loading [ASME PAPER 66-WA/MET-6] 04 p0639 A67-15340
 Soil, moisture and other requirements for microorganism survival in simulated Martian environment 19 p3177 A67-35220

MOISTURE METER

S HYGROMETER

MOL

S MANNED ORBITAL LABORATORY

/MOL/

MOLAB

S LUNAR MOBILE LABORATORY

/MOLAB/

MOLDAVITE

Primary cosmic radiation intensity determined with help of nuclear particle tracks in moldavites and meteorites 05 p0887 A67-16100
 Terrestrial origin hypothesis for tektites, moldavites and impact glass supported by krypton-argon and fission track measurements 11 p1866 A67-24693
 Tektite origin, composition, identification, strewn fields and configurations 12 p2009 A67-26232
 Cosmic origin of tektites indicated by factors other than chronology 14 p2385 A67-28145
 Primary cosmic radiation intensity determined with help of nuclear particle tracks in moldavites and meteorites 24 p4238 A67-42776

MOLDING MATERIAL

Highly purified silicone junction coating resins and silicone molding compound for microelectronic packaging 18 p3069 A67-34564
 Slip casting of niobium carbide powders noting effects of dispersed phase contents,

pH variation and temperature on molding properties 20 p3466 A67-36909
 Influence of palladium additives and sintering temperature on tungsten molding noting shrinkage, density, microhardness, durability and microstructure 20 p3466 A67-36910
 Honsel Plastic Mold /HPM/ process for high surface quality, discussing cost, materials and solidification time 21 p3637 A67-38976

MOLECULAR ABSORPTION

Atomic and molecular absorption and emission in middle UV region of electromagnetic spectrum, noting energy levels, electronic transitions and oscillator strengths 04 p0660 A67-14692
 Continuous absorber effect on spectral line reversal gas phase temperature measurement [AIAA PAPER 67-108] 06 p1004 A67-18503
 Solar radiation passage through earth atmosphere in triplet lines O I, considering molecular hydrogen absorption and brightness distribution of radiation 14 p2378 A67-27862
 Zinc penetration through regenerated cellulose membrane separators shown to be growth mechanism in silver-zinc cell 22 p3758 A67-40227

MOLECULAR BEAM

SA ATOMIC CLOCK

Maser oscillation intensity and frequency dependence on constant electric and magnetic fields acting on molecular beam in front of resonator 01 p0089 A67-10396
 Nozzle type molecular beam measuring distribution of speeds after scattering incident beam from solid surface 05 p0849 A67-17276
 Change in temperature conditions during growth of epitaxial germanium films from molecular beam in vacuum 06 p1046 A67-17551
 Crossed molecular beam kinetics of reactive asymmetry of oriented methyl iodide polar molecules reacting with rubidium 06 p0955 A67-17831
 Molecular beam technique for mass spectrometric sampling of high temperature systems at high atmospheric pressure [AIAA PAPER 67-37] 06 p0956 A67-18305
 Density and direction of gas molecular flow through tube and aperture measured by ionization detector 09 p1489 A67-22107
 Modulated molecular beam apparatus with chopper used in conjunction with field emission microscope for studies of atomic interactions with surfaces 09 p1499 A67-22114
 Energetic metastable diatomic oxygen molecule excited by electron impact studied with high sensitivity molecular beam apparatus 10 p1682 A67-23386
 Molecular beam electric resonance /MBER/ spectrometer for hyperfine structure of rubidium fluoride 11 p1821 A67-23961
 Molecular beam chamber for cryopumping studies and capture coefficient data 11 p1773 A67-24344
 Differential reaction cross section and internal excitation function from K and Br molecule crossed beam velocity analysis 11 p1750 A67-24991
 Momentum accommodation coefficients of variable angle of incidence of monochromatic argon molecular beams 13 p2098 A67-26946
 Normal and tangential momentum accommodation coefficients in low density facility 13 p2098 A67-26947
 Noble gas molecular beam quasi-specular scattering from metal surfaces noting effects of beam incidence angle, molecular weight and gas temperature 13 p2099 A67-26949
 Lobular scattering of 1 ev energy chopped argon beams from silver, mica and brass surfaces, noting distributions and contamination effects 13 p2099 A67-26950
 Surface interaction of free molecular flows or molecular beams, considering state variables in highly rarefied gas in Maxwellian equilibrium, stagnation temperature, etc 13 p2159 A67-27299
 Axial and radial velocity distributions in axisymmetric free jets of pure gases and binary gas mixtures, noting molecular beam production 14 p2301 A67-28183
 Nonequilibrium aspects of fluid mechanics of freely expanding jet analyzed, using aerodynamic molecular beam

system 14 p2301 A67-28184
Time of flight distribution measurement of weak molecular beam, noting limitations due to signal to noise ratio 14 p2316 A67-28185
Intensity and velocity distribution in molecular beams from nozzle sources, discussing physical processes responsible for formation 14 p2301 A67-28186
Kantrowitz-Grey molecular beam generator performance, noting high source pressure due to high pumping speed, background gas scattering, etc 14 p2316 A67-28189
Charge exchange method for production of molecular beams, noting production of plasma by RF discharge and ion beam generation 14 p2316 A67-28190
Molecular beam apparatus for measuring collision cross section and velocity distribution of sputtered particles 14 p2316 A67-28191
Molecular beam apparatus for determining momentum accommodation coefficients for neutral particle - surface interactions 14 p2316 A67-28192
Velocity distributions in surface scattered molecular beams, proposing broadband lock-in beam detection for signal to noise enhancement 14 p2317 A67-28195
Mechanisms operating in lasers employing optical transitions of molecules in fluids 14 p2331 A67-28471
Critical temperatures and phase composition of films obtained by vacuum deposition of sublimed cadmium telluride 15 p2537 A67-29706
Short duration shock tube molecular beam in helium and oxygen, giving test arrangement and data comparisons 17 p2835 A67-33361
Factors influencing secondary electron emission produced by high energy molecular beam impact on metal surface 20 p3488 A67-36438
Rapid adiabatic cooling of gas systems for population inversion states 21 p3638 A67-37942
Frequency stability of molecular beam laser in space environment during prolonged continuous and repeatedly interrupted operation 21 p3582 A67-38594
Critical temperatures and phase composition of films obtained by vacuum deposition of sublimed cadmium telluride 24 p4199 A67-41776

MOLECULAR BONDING

Reformation processes effect on stress-time-to-fracture behavior of solids, considering governing differential equation 08 p1423 A67-21302
Radial distribution functions for liquid methanol and ethanol at room temperature, observing intermolecular hydrogen bonding 20 p3378 A67-37560
Hydrogen peroxide and disulphane molecules force constant and vibrational spectra investigation indicates little change in elastic properties 22 p3757 A67-39583
Bond formation effect on electron scattering cross sections for molecular H, N and O 23 p4029 A67-40966

MOLECULAR CHAIN

SA CRYSTAL LATTICE
Admissible configurations and diffusive motions of molecular chains on quadratic lattice narrow channels 08 p1356 A67-21299
Kinetic mechanisms in combustion peninsula of three-limit explosion reactions with trace inhibitors, studying quadratic chain-breaking processes by static method 18 p3156 A67-33848
Density, morphology and melting data on extended chain linear polyethylene and high molecular weight polymethylene crystallized from melt under high pressure 20 p3474 A67-37398
Free energy of polymer solid consisting of entangled long chain molecules when deformed by elastic strain 22 p3828 A67-40201

MOLECULAR COLLISION

SA ATOMIC COLLISION
Vibrational excitation and dissociative attachment in bombardment of hydrogen molecules by electrons of energies up to about 12 eV 01 p0117 A67-10782
Improved Monte Carlo method for calculating steady state monatomic rarefied-gas flows, using computer for calculating possibility of collision in given geometrical cell 01 p0055 A67-11292

Excitation of vibrational degrees of freedom in molecular collision from vibrational relaxation data and molecular beam elastic scattering experiments 01 p0118 A67-11302
Close-coupling calculation of resonant structure of scattering amplitude of excited-state atoms and molecules in continuum 03 p0471 A67-13221
Potassium atom reactive scattering from oriented methyl iodine molecules, determining variation of chemical reactivity over molecular surface 03 p0367 A67-13524
Molecular gas laser Q-switching techniques, determining rotational collision sections for carbon dioxide and cross sections for vibrational relaxation 05 p0816 A67-16632
Rotational relaxation times for homonuclear diatomic molecules 06 p1037 A67-19043
Molecular quadrupole moments and shape parameters derived from viscosities and second virial coefficients 06 p1038 A67-19047
Relaxation theory and eigenvalue theory for linearized collision integrals for mixtures of Maxwell fluid molecules 08 p1355 A67-21116
Models for collision processes and changes of degree of freedom in kinetic equation for polyatomic gases 08 p1323 A67-21386
Calculation of effective excitation cross sections of hydrogen atoms for collisions with nitrogen molecules and hydrogen atoms 09 p1534 A67-21850
Transmission probability describing free molecular flow through vacuum systems obtained via Monte Carlo program 09 p1488 A67-22104
Collision induced far IR absorption in rare gas mixtures with emission spectrum calculation 09 p1535 A67-22382
Ion motion under influence of electric field and density gradient with charge transfer collision between ions and neutral gas background 13 p2162 A67-26269
Interactions of homonuclear diatomic gas molecules with fcc solid surfaces calculated by digital computer 13 p2098 A67-26938
Discrete ordinate technique for nonlinear Boltzmann equation for hard sphere molecules, considering pseudoshock relaxation 13 p2102 A67-26973
Monte Carlo evaluation of Boltzmann collision integral for translational relaxation and plane steady shock problems 13 p2103 A67-26974
Transport coefficient expressions for collisions between rigid diatomic molecules, using perturbation method 14 p2259 A67-28298
Inelastic collisions of proton beam with carbon monoxide target molecules, determining ionization cross section and charge transfer 14 p2390 A67-28943
Gas condensation near comet nucleus as source of formation of entire dust component of comet coma 15 p2552 A67-29153
Lyman-alpha radiation emission from ion-target-gas collision measured for various projectile energies 17 p2889 A67-33224
Kinetics of coupled atomic recombination and vibrational de-excitation in continuously expanding gas flow 18 p3081 A67-33781
Rate of vibration-vibration energy exchange in gas mixtures 18 p3081 A67-33783
Transition probabilities for molecular collision excitation by differential equation matrix, approximations, perturbation theory, etc 18 p3081 A67-33785
Compound state resonances in molecular collisions, stressing scattering cross sections behavior for deuterium-xenon 19 p3286 A67-35881
Ion-molecule collision cross section determined from pressure broadening of ion cyclotron resonance lines at high electric field/pressure ratio 22 p3840 A67-39365
Reaction rates and yield for multichannel molecular collisions, introducing observable yield operator in theory, using motion equations 22 p3757 A67-39635
Monte Carlo method for molecular vacuum pump calculation, noting applicability to molecule-boundary and molecule-molecule collision conditions 22 p3785 A67-40012
Compound state resonances in atom/molecule collisions below first excitation threshold 23 p4029 A67-40959

Cross section data for molecular oxygen and electron collision processes, discussing elastic scattering, attachment, rotational transitions and Born cross section 23 p4030 A67-41481
Gas condensation near comet nucleus as source of formation of entire dust component of comet coma 24 p4239 A67-43076

MOLECULAR DIFFUSION

Diffusion and dissociation of CO molecules in solar atmosphere 01 p0151 A67-11284
Specific radioactivity of Sb-124 and effect on diffusion of antimony in Sb-doped n-type Ge single crystals and Ga-doped p-type Ge single crystals 03 p0500 A67-14067
Laminar electrohydrodynamic flow in plane diffusor, taking into account molecular diffusion of space charge 04 p0668 A67-15277
Admissible configurations and diffusive motions of molecular chains on quadratic lattice narrow channels 08 p1356 A67-21299
Sorption process for determining sticking probability of molecules on surface of sorbents, diffusion coefficient of molecules through sorbents and adsorption isotherms 09 p1533 A67-22115
Anomalous high diffusion coefficients determined from dispersion of chemical contaminant releases and long lasting meteor trails at various altitudes 12 p1935 A67-25792
High temperature diffusion of potassium in single crystal and polycrystalline molybdenum 15 p2504 A67-29972
Simultaneous ejection of two vapor trails of different atomic mass, examining turbopulse phenomena of atmospheric turbulence 17 p2853 A67-33254

MOLECULAR DISSOCIATION

SA ATOMIC RECOMBINATION
Competing alternative pathways for formation of particular ion in mass spectra of substituted benzophenones 01 p0018 A67-10105
Shock tube measurement of dissociation energy of NH radical in reflected shocks through nitrogen-hydrogen-krypton and ammonia-krypton mixtures 01 p0117 A67-10787
Diatomic gas flow past blunt bodies, noting effect of oscillation and dissociation relaxation on mean energy 02 p0180 A67-12465
Nitric oxide molecular laser obtained by dissociation of NO-Cl in pulsed electrical discharge 02 p0253 A67-12510
Rate equation for dissociation and recombination of diatomic molecules 03 p0473 A67-13521
Diffusion theory of vibration-dissociation coupling used to analyze transient effects in dissociation reactions behind shock waves 03 p0474 A67-14025
Equilibrium constants and internal energies of hydrogen molecular ion calculated as function of temperature and pressure, using partition function 04 p0697 A67-14807
Role of solar photon and corpuscular radiation in dissociation and ionization of water molecules in cometary atmospheres 05 p0888 A67-16203
Tetrafluoroethylene dissociation in nitrogen behind shock waves and thermoequilibrium constants studied, using shock tube and optical absorption spectroscopy 05 p0759 A67-16840
Absolute cross section for dissociation of hydrogen ion by electron impact measured, using cross beam technique 09 p1535 A67-22377
Hydrogen-molecule ion dissociation by electron collision, noting various transition states 09 p1535 A67-22378
Photometric measurements of eclipses of artificial solar satellite 1960 Eta 2 at sunrise and sunset in Lyman alpha and violet spectral range 10 p1706 A67-23221
Dissociation energy of nitrous oxide reconciled with electron physics data 12 p1904 A67-26230
Exciton molecule formation in semiconductors in case of large radius exciton, determining dissociation energy and temperature 13 p2173 A67-26363
Upper atmosphere hydrodynamic equation additional terms account for hydrodynamic effects of dissociative recombination and ion molecule reactions 13 p2112 A67-26670
Molecule dissociation in meteoric trains, discussing coordinate system to determine

cross sections for dissociation of magnesium and silicon oxides 14 p2383 A67-27945

Critical temperatures and phase composition of films obtained by vacuum deposition of sublimed cadmium telluride 15 p2537 A67-29706

Dissociation cross section of hydrogen molecule exchange excited by electron impact from ground to triplet state, using one-center wave functions 15 p2521 A67-30379

Multicomponent reacting laminar boundary layer in chemical equilibrium solved using Stefan-Maxwell relations 16 p2658 A67-30937

Elementary processes in low temperature plasma 17 p2893 A67-32135

Electric quadrupole-quadrupole and dipole-octupole forces contribution to dispersion energy for axially symmetric molecules, noting resonance 17 p2887 A67-32353

Carbon dioxide ions with electrons dissociative recombination measurements with microwave-afterglow differentially pumped quadrupole mass-spectrometer apparatus, noting Martian atmosphere model [SRCC-55] 17 p2888 A67-32826

Production mechanism of atomic nitrogen ions in upper atmosphere, showing predominance of nitrogen molecule dissociative

photolionization 17 p2851 A67-33204

Isotope effect in hydrogen molecule dissociative attachment at low energy, noting short negative-ion formation lifetime and long separation time 17 p2889 A67-33223

Energy distributions of hydrogen and deuterium ions from dissociative ionization of hydrogen and deuterium 17 p2889 A67-33226

Nitrogen oxide and carbon dioxide high pressure unimolecular decomposition noting high pressure rate constants, transition probabilities, potential surface shape, etc 18 p3082 A67-33793

Vibrational and/or chemical relaxation effects behind various shock waves in hypersonic air streams determined for equilibrium and nonequilibrium conditions 19 p3169 A67-34813

Surface ionization of atoms and molecules on nonmetals, determining work functions and activation energies for dissociation 19 p3264 A67-35083

Inviscid hypersonic axisymmetric flow over cylinder and sphere near stagnation point, including dissociation and detached shock wave 19 p3171 A67-35722

Photodissociation of hydrogen molecules in H I regions of interstellar medium, evaluating lifetime and density 19 p3331 A67-36085

Angular distribution of products in electron impact dissociation of hydrogen molecule calculated following Born approximation for scattering amplitude 20 p3487 A67-36231

Coolant passage axial curvature effect on heat transfer to endothermically dissociating supercritical nitrogen tetroxide [ASME PAPER 67-HT-59] 20 p3549 A67-36741

Exciton molecule formation in semiconductors in case of large radius exciton, determining dissociation energy and temperature 21 p3680 A67-38320

Dissociation and recombination of diatomic molecules by invert third bodies described by stochastic theory 22 p3756 A67-39386

Critical temperatures and phase composition of films obtained by vacuum deposition of sublimed cadmium telluride 24 p4199 A67-41776

MOLECULAR ELECTRONICS

Uniform electric field quadrupole polarizabilities and shielding factors for S-state atoms and ions, demonstrating independence of factors from existence of field gradient 03 p0472 A67-13321

MOLECULAR ENERGY

SA NUCLEAR ENERGY

Radiative lifetimes of UV molecular transitions, analyzing emission spectrum in vacuum monochromator 06 p1035 A67-17828

Extended average energy approximation of first order perturbation wave function, proposing procedure for multidimensional problems 07 p1137 A67-20186

Activities and relative partial molar free energies of CuPt alloys, noting formation mechanism, ordering temperatures, etc 17 p2872 A67-32739

Measuring methods for high energy

molecules accommodation coefficients, determining dependence on energy, incidence angle, surface nature and outgassing 20 p3489 A67-36939

Total energy of beryllium hydride molecule analyzed, using difference between SCF energies and single determinant wave function 20 p3377 A67-37139

Chemical bond calculations with high temperature chemistry, discussing hydride molecular energy, dissociation energies and diatomic molecules 21 p3578 A67-38394

Integrated and Integral Hellmann-Feynman formulas for isoelectronic molecular process energy difference 22 p3757 A67-39637

Total energy of beryllium hydride molecule as sum of SCF, correlation and relativistic energy and SCF error by LCAO-MO method 24 p4118 A67-41926

MOLECULAR FLOW

SA FREE MOLECULAR FLOW

Formulation of problem of large-scale fluid mechanics, based on definition of characteristic flow parameters, applied to molecular flows 03 p0404 A67-13882

Transverse and longitudinal Knudsen forces account for experimentally observed thermomolecular flow forces by extension of theory in intermediate pressure range 04 p0603 A67-14731

Thermomolecular flow effect caused by transverse and longitudinal forces, calculating force on hangdown fiber in microbalance 04 p0620 A67-14732

Longitudinal thermomolecular flow theories at intermediate pressures, comparing similarities and discrepancies in forces acting on hangdowns or samples in microbalance measurements 04 p0603 A67-14733

Boltzmann equation applicability to flows satisfying condition of molecular chaos, noting role of Knudsen layer 06 p1022 A67-17724

Nonisothermal changes in properties and composition during chemical and physical reactions, noting application to Knudsen cell vaporization [ATAA PAPER 67-156] 06 p0956 A67-18321

Boltzmann equation for rarefied gas flows between two parallel infinite plates for Maxwellian, hard sphere and BGK models 08 p1355 A67-21117

Cesium vapor flow from orifices and tubes into vacuum analyzed, noting dependence of angular distribution and center line intensity on Knudsen numbers 08 p1324 A67-21495

Nonuniform molecular density, pumping power and gas temperature distribution in evacuated space simulator 09 p1503 A67-22118

Velocity distribution function of re-emitted molecules effect on slip flow boundary conditions 13 p2102 A67-26970

Molecular speed ratio in low density flows determined via stagnation point heat transfer and flat plate heat transfer measurements 14 p2301 A67-28182

Pure molecular flow coupled with surface diffusion applied to cesium transport 15 p2520 A67-29494

Free molecular flow region, calculating drag on plate, sphere and general body, considering drag effect on satellite orbit 15 p2561 A67-30045

Molecular flow mass spectrometer analysis of porous metal membranes for gases of different molecular weights 20 p3378 A67-37499

Molecular gas flow through cylindrical tube, using wall pressure distribution to measure pump speed 21 p3610 A67-37823

Soviet book on molecular flow in vessels covering mass balance, energy exchange, rarefied gas, etc 24 p4191 A67-42359

MOLECULAR FORMING

Interstellar molecule formation as result of chemical exchange reactions between atoms of interstellar gas and atoms chemically bound to interstellar grains 02 p0323 A67-11689

Triatomic molecules formation and abundance in solar photosphere estimated for thermodynamic equilibrium 18 p3119 A67-33858

MOLECULAR GAS

Inelastic collisions of electrons with diatomic molecules, noting effect on speed of energy exchange in nonhomogeneous plasma 01 p0118 A67-10044

Quantum mechanical theory of microwave nonresonant absorption and dielectric and

magnetic relaxation in gases 01 p0116 A67-10145

Identical particles gas with velocities distributed regularly in plane, analyzing compression and relaxation waves present in six- and eight-velocity models 01 p0051 A67-10228

Atmospheric radio wave absorption coefficient and altitude determined and linked to effects of colliding paramagnetic oxygen molecules 01 p0022 A67-10391

Total atmospheric attenuation measurement at 3.2 Ghz due primarily to nonresonance absorption of molecular oxygen 02 p0237 A67-11855

Exact vibrational matrix elements for molecular hydrogen and intensity of quadrupole rotation-vibration spectrum 03 p0515 A67-14324

Perturbation treatment of diatomic hydrogen ion, improving polarized hydrogen-atom treatment by using zero-order wave function 03 p0474 A67-14333

Transport and ionization properties of molecular gases in transverse magnetic field, using ionization chamber 03 p0474 A67-14358

Molecular hydrogen features in spectra of Saturn and Uranus 04 p0696 A67-14738

Hydrogen and helium injection effect on local heat transfer to porous surface from dissociated turbulent boundary layer [ASME PAPER 66-WA/HT-24] 04 p0725 A67-15444

Hydrogen molecule excitation by electron impact extended to D excited state, noting values for oscillator strength 04 p0662 A67-15767

Oxygen atoms reaction with tetrafluoroethylene in presence of molecular oxygen 04 p0567 A67-15949

Atmospheric radio wave absorption at wavelengths ranging from 1.36 to 3.0 mm, determining absorption coefficients of molecular oxygen and water vapor 05 p0761 A67-16343

Excitation and relaxation mechanisms for closed molecular gas laser 05 p0816 A67-16631

Molecular fluxes in lunar atmosphere relationship to gas source distribution, surface temperature and gas emission laws 05 p0904 A67-17404

Dipole-dipole molecular interaction contribution to thermodynamics and state equation of excited molecular gas, noting dissociation possibility 06 p0991 A67-18802

Emission spectra of nitrogen excited by electron beam of 0.1 to 20 kev and oxygen and air bombarded by 13-kev electrons 07 p1225 A67-19099

Spatial growth of ionization in molecular hydrogen, using thin film cathode 07 p1226 A67-19853

Emission occurring when mixing molecular nitrogen with helium ion following charge transfer analyzed spectroscopically 08 p1326 A67-21358

Monte Carlo computer program for calculating molecular gas flow with axisymmetric vacuum structures, showing applications on pumping speed test domes and measuring apparatus for sticking coefficients 09 p1488 A67-22105

Excitation and photon emission rates of auroral nitrogen first and second positive group 10 p1650 A67-23338

Shock tube study of oscillator strength of diatomic molecular carbon Swan bands 11 p1750 A67-25066

Energetic molecular hydrogen ions injected into resonant nonadiabatic magnetic mirror trap, studying particle mean lifetime, noting cold plasma stabilizing effect 12 p1969 A67-25248

Maxwell dispersion of particles of molecular gas flow at wall of circular channel described by integral equation, determining particles experiencing mirror intercollisions 13 p2158 A67-26671

Molecular laser action on vibrational-rotational transitions between low lying vibrational levels on hydrogen and deuterium halides 13 p2127 A67-27018

Gas condensation near comet nucleus as source of formation of entire dust component of comet coma 15 p2552 A67-29153

Thermal conductances in collisionless gas between coaxial cylinders and concentric spheres obtained for arbitrary thermal accommodation coefficients 15 p2579 A67-29566

Energy exchange between electron gas and molecular gas shown to depend on composition of latter, for application of nonequilibrium plasma 16 p2710 A67-30521

Molecular nitrogen rotational relaxation time by probing of supersonic free jet 16 p2705 A67-31757

Upper limit on concentration of molecular hydrogen in interstellar space by comparison of Lyman bands in absorption spectra of early type stars and laboratory source 17 p2945 A67-32651

Gaseous chemical reaction dynamics analyzed with monochromatic laser light-induced photocatalysis 17 p2868 A67-32772

Lifetime and diffusion coefficient of lowest excited state of molecular nitrogen from intensity decay measurements of Vegard-Kaplan band 17 p2889 A67-33243

Inelastic collisions of electrons with diatomic molecules, noting effect on speed of energy exchange in nonhomogeneous plasma 17 p2890 A67-33322

Rate constant for gas phase recombination of atomic and molecular oxygen into ozone, discussing M effect 18 p3082 A67-34030

Dipole-dipole molecular interaction contribution to thermodynamics and state equation of excited molecular gas, noting dissociation possibility 18 p3029 A67-34421

Molecular oxygen absorption line equivalent widths measurement at 5 mm wavelength obtained from model atmosphere to determine earth atmospheric temperature 20 p3427 A67-36370

Electron impact excitation and ionization cross sections data of molecular nitrogen synthesized using modified Born approximation 20 p3489 A67-37418

Optical absorption, refractivity and electron scattering used to construct model dipole spectrum of molecular nitrogen and calculate dipole properties 24 p4190 A67-42096

Gas condensation near comet nucleus as source of formation of entire dust component of comet 24 p4239 A67-43076

Submillimeter wave laser resonator mode calculation using laser-resonator interferometry 24 p4169 A67-43105

MOLECULAR INTERACTION

Intermolecular double resonance and Overhauser effect in organic liquids 01 p0019 A67-10825

Chemiluminescent gas phase reactions involving electronically excited oxygen molecules trimethylaluminum and diborane near 3 millitorr 01 p0019 A67-11007

Four-linked rare earth chelate with sodium ion obtained with benzoylaceton and europium, analyzing molecular and ionic transitions by absorption and emission spectra 02 p0251 A67-11518

Hydrogen bonding of derivatives of guanosine and cytidine soluble in chloroform studied in IR, confirming geometrical specificity in two-stranded nucleic acids 02 p0190 A67-11585

Quasi-stationary techniques for calculating energies and widths of resonances occurring in electron-atom and electron-molecule scattering 02 p0269 A67-12449

Tandem mass spectrometers for study of ion-molecule reactions, noting ion gun, deceleration lens and collision chamber 02 p0247 A67-12690

Transport properties of model fluid whose molecules interact according to square-well potential used to calculate transport coefficients of krypton, xenon and argon 04 p0720 A67-14507

Electric conductivity of hexamethylbenzene explained by molecular interaction conductivity change at transition point 05 p0871 A67-17379

Diffusion-viscosity coupling in stationary flow of nitrous oxide-carbon dioxide mixture in case of Maxwellian intermolecular forces 05 p0794 A67-17380

Dipole-dipole molecular interaction contribution to thermodynamics and state equation of excited molecular gas, noting dissociation possibility 06 p0991 A67-18802

Jovian atmosphere simulation with energy from corona discharge, producing simple organic molecules 07 p1246 A67-19057

Intermolecular forces in methyl chloride and benzene calculated using spherical shell central potential theory 07 p1138 A67-20191

Molecular association in Na, K and Cs

vapors, noting existence of dimer and tetramer molecules 08 p1355 A67-21033

Excess tunnel current due to inelastic electron molecule interactions near metal insulator interface 10 p1689 A67-23074

Hydrolysis of phthalimide ring with carboxylate group linked through alkyl group as anionic intramolecular catalyst 10 p1602 A67-23159

Momentum and energy imparted by collisions of gas molecules with atoms of cold rigid wall for arbitrary interaction potential 13 p2050 A67-26883

Surface interaction of free molecular flows or molecular beams, considering state variables in highly rarefied gas in Maxwellian equilibrium, stagnation temperature, etc 13 p2159 A67-27299

Treatise on adhesion and adhesives, Volume 1, Theory 14 p2340 A67-27793

Coupling between free electron and molecular vibrational temperatures in plasma environments, noting energy distribution, application to MHD generation, etc 17 p2894 A67-32150

Energy level shifts due to atom confinement by conducting walls 17 p2888 A67-32390

Short range intermolecular interaction of two ground state hydrogen molecules, using rigorous valence bond approach and population analysis 17 p2890 A67-33262

Contribution to friction coefficient from time correlations between hard and soft molecular interactions evaluated, using linear trajectory approximation 17 p2890 A67-33263

Free energy of N-particle system with far-reaching intramolecular interaction, using collective variables 18 p3085 A67-33670

Atomic and molecular processes in Cytherean, Martian and Jovian upper atmospheres 18 p3124 A67-34158

Dipole-dipole molecular interaction contribution to thermodynamics and state equation of excited molecular gas, noting dissociation possibility 18 p3029 A67-34421

Low-energy electron collisions and interactions with atoms and molecules, discussing vibrational excitation, ion formation, ionization cross section, etc 19 p3264 A67-35068

Intermolecular hydrogen bonds energies estimated for organic semiconductors in ground and first excited states 20 p3512 A67-37301

Temperature dependence of far IR collision-induced absorption as probe of rare gas mixtures interatomic potentials 20 p3490 A67-37587

Binary gas mixtures transport coefficients calculation, comparing experimental and theoretical values of viscosity and thermoconductivity dependent upon interaction between unlike molecules 21 p3733 A67-39064

Long range retarded interaction energies, obtaining energy term coefficient from minimal principle using Karplus and Kolker method 22 p3757 A67-39636

Multiple reflection of molecules effect on nonconvex wing aerodynamic characteristics for finite Mach number lateral free molecular flow 22 p3741 A67-40022

Ionospheric ion-neutral reactions studied by photoionization mass spectrometer, noting temperature independent reactions 22 p3793 A67-40077

Analogy between electric, thermal and magnetic phenomena considered in terms of molecular transfer theory, noting pure mathematical meaning with no physical content 22 p3837 A67-40213

Two-photon absorption theory extension to include vibronic mixing between different electronic states using two-photon laser excitation of polycyclic atomic molecules 23 p4013 A67-40964

Intermediate range intermolecular forces with overlapping wave functions and exchange effects calculated for ionized H molecule using perturbation theory 23 p4029 A67-40971

Protective effect of substrates against ionizing radiation on enolase and lactic dehydrogenase [SAM-TR-66-264] 24 p4111 A67-41841

Atomic Cs vapor experimental values for heat-transfer coefficient used to determine Cs atoms and molecules interaction potentials 24 p4253 A67-42211

Hydrodynamic solution for shock wave parameters of monatomic gases assuming exponential molecular interaction potentials and absence of mass forces 24 p4142 A67-42271

Intermolecular forces theory, considering hydrogen atom interaction through Born-Oppenheimer approximation and variational calculations [WIS-TCI-249] 24 p4191 A67-42666

MOLECULAR ION

Approximate molecular orbitals, Part I 03 p0474 A67-14351

Approximate molecular orbitals, Part II 03 p0474 A67-14352

Molecular nitrogen ion emission in twilight, discussing intensities, rotational distribution, charge transfer zenith measurement and ion-atom interchange reaction 05 p0803 A67-17409

Doppler profiles of nocturnal green line /5577 angstroms/ nonthermal emission resulting from molecular oxygen ion dissociative recombination [AFCRL-67-0443] 05 p0803 A67-17411

Substituent effects on unimolecular ion decomposition reactions, noting role of Hammett equation and electron energies 06 p0954 A67-17568

Vertical and horizontal variations of intensities of auroral OI and molecular nitrogen ion emissions 08 p328 A67-21480

Dominant ionic species in cesium plasma diode determined as atomic cesium ion rather than molecular cesium ion 09 p1448 A67-22337

Diatomic molecular ion composition and variation of effective recombination coefficient in ionosphere in terms of altitude, time of day, solar activity, temperature, etc 10 p1630 A67-22788

Reactions between alkane and cycloalkane molecular ions analyzed, using conventional and tandem mass spectrometry 12 p1903 A67-25969

Molecular nitrogen and oxygen ions colliding with atomic sodium examined in crossed-beam experiment for resonance charge transfers 16 p2705 A67-31758

Ion-molecular reactions of hydrogen with inert gases caused by low energy electrons in low temperature plasmas, considering energy level populations, reaction cross sections, etc 17 p2808 A67-32141

Photoelectron energy measurement and Franck-Condon factors for vibrational transitions of molecular ions when ejected by He resonance line 17 p2888 A67-32356

He-He ground state and first excited state potentials obtained from differential scattering cross sections 17 p2889 A67-33257

Density contour determination for magnetically confined plasma by energetic molecular ion beam probe of plasma and atomic ion measurement from collisional dissociation 17 p2910 A67-33356

Thin self-supporting beryllium foils preparation for use as atomic and molecular ion beam targets 17 p2866 A67-33360

Fractional excitation and ionization for argon beam extracted from arc-heated supersonic free jet, noting molecular ions and neutralization 18 p3082 A67-34028

Charge transfer role in formation and maintenance of molecular and metal-ion layer in E region of ionosphere 19 p3217 A67-35204

Negatively ionized ozone and diatomic oxygen concentration ratio determined from physicochemical processes for 10-60 km range 19 p3219 A67-35249

Molecular and atomic ion concentration in earth upper atmosphere observed from low altitude satellite, discussing diurnal variation and solar effect 19 p3220 A67-35262

Absolute electron impact excitation cross section of 3914 angstrom band of positively ionized nitrogen molecule 20 p3450 A67-37104

IR absorption in alkali-halide crystals containing molecular ion impurities caused by intralonic vibrations 20 p3511 A67-37140

Mass species abundance ratio of hydrogen ion beam from Oak Ridge type duoplasmatron ion source, discussing pressure dependent characteristics 23 p4034 A67-41436

Diatomic molecular ion composition and variation of effective recombination coefficient in ionosphere in terms of altitude, time of day, solar activity, temperature, etc 24 p4149 A67-42124

MOLECULAR ORBIT

- Perturbation treatment for molecular configuration using product of atomic or molecular orbitals as zero-order wave function 06 p1034 A67-17826
- Relation between Slater screening constants and interchangeability of atomic orbitals 10 p1682 A67-23378
- Molecular orbital electron charge density pictures, noting representation close to Hartree-Fock calculation method 10 p1682 A67-23379
- Chemical effects in X-ray spectra and inner shell photoelectron spectra of sulfur and chlorine-oxygen anions and molecular orbital method 18 p2998 A67-34520

MOLECULAR OSCILLATION

- Oscillatory relaxation of heavy two-atom molecules during single-quantum energy transitions in light-gas medium 02 p0269 A67-12422
- Wave interaction dynamics of far IR electromagnetic radiation generation by coherent molecular vibrations or phonons excited by stimulated Raman scattering and resonant phase matching condition 04 p0657 A67-15113
- Relaxation problem of two-level molecule in dense resonance medium 05 p0762 A67-16351
- Oscillation amplitude modulation in ammonia beam maser oscillator with single cavity followed by two cavities in cascade 05 p0817 A67-16636
- Oscillator strength of atomic and ionic lines, normalization of NBS gf values and solar abundances of alkali metals 07 p1256 A67-20167
- Collisional excitation of Si ion from ground state to autoionization levels at coronal temperatures 07 p1256 A67-20168
- Rotational temperatures of CO molecule oscillative-rotational bands in solar atmosphere refute assumed temperature nonuniformities 09 p1563 A67-21626
- Molecular vibrational rotational parameters measured with IR heterodyning technique 09 p1535 A67-22136
- Activation energy of molecular relaxation processes in terms of areas under loss factor and reciprocal temperature curves 14 p2259 A67-28299

MOLECULAR OSCILLATOR

- Coherent resonant absorption and emission in IR and visible spectrum, discussing Lorentz oscillator and Dicke spin model of radiating molecule 15 p2519 A67-29190
- Trajectory systems, discussing atomic clock and laser based equipment design, operation and performance [ONERA-TP-446] 15 p2554 A67-29376

MOLECULAR PHYSICS

- Perturbation theory in molecular quantum physics using variational principles 02 p0270 A67-12722
- Book on molecular physics of boundary friction on metal surfaces 03 p0429 A67-13333
- Atomic and molecular chemophysical processes in shock waves derived from high temperature thermal energy transfer including instrumentation, relaxation, ionization and spectroscopy 22 p3786 A67-40074

MOLECULAR PUMP

- Molecular sink for simulated testing of spacecraft components noting vessel construction, vacuum pump system, molecular trap array, etc 18 p3019 A67-33547

MOLECULAR ROTATION

- Trifluoramine oxide IR spectrum measured, determining structure, symmetry and rotational, vibrational and thermodynamic properties 15 p2433 A67-29880
- Laser emission from HF molecules rotational transition initiated by pulsed electrical discharge, listing wavelengths 19 p3241 A67-36103
- Electronic energy transfer between metastable argon and nitrogen molecule, noting rotational enhancement 20 p3487 A67-36228
- Hyperfine structure in rotational spectrum of HDO and deuterium oxide analyzed by beam maser spectroscopy, evaluating coupling constants 20 p3461 A67-37287
- Low energy electron scattering from hydrogen molecules in ground electronic and vibrational states, calculating rotational excitation cross section 20 p3491 A67-37687
- Molecular band spectra of CN emission assuming Gaussian rotational line

- profile 23 p4030 A67-41695
- IR lasers using vibrational rotational transitions of carbon dioxide 24 p4166 A67-41799

MOLECULAR SIEVE

- Molecular sieves using regenerable carbon dioxide solid adsorbents for spacecraft life support systems 20 p3374 A67-36611
- Molecular sieves as casings filler for semiconductor devices, discussing stabilization of electrical parameters and absorptive capacity of synthetic zeolites 23 p4042 A67-41274

MOLECULAR SPECTROSCOPY

- Molecular spectroscopy of illumination effects on cobalt activated ZnS exposed to ruby laser pulses 01 p0090 A67-10683
- Quantitative intensity of weak carbon dioxide triad in 1 micron spectral region obtained, using pressure broadening techniques 06 p1031 A67-17870
- Book on IR spectroscopy covering molecular spectroscopy, lattice vibrations, semiconductor electronic effects, IR detectors, far IR, etc book on IR spectroscopy covering molecular spectroscopy, lattice vibrations, semiconductor 08 p1353 A67-20762
- Central tuning dip in power output of continuous wave submillimeter molecular laser to measure radiative lifetime and collision line broadening 11 p1803 A67-24932
- Fluor molecule emission spectrum between 4500 and 8500 angstroms, discussing results of rotational vibration analysis [DVL-624] 11 p1750 A67-25003
- Molecular spectroscopy of illumination effects on cobalt activated ZnS exposed to ruby laser pulses 11 p1804 A67-25072
- Reactions between alkane and cycloalkane molecular ions analyzed, using conventional and tandem mass spectrometry 12 p1903 A67-25969
- Spectroscopic techniques for plasma parameter measurements in high temperature range, discussing methods employed and experimental setups 15 p2533 A67-30424
- Temperature dependence of thermodynamic functions of polyatomic gases at high temperatures 16 p2704 A67-31391
- Hyperfine structure in rotational spectrum of HDO and deuterium oxide analyzed by beam maser spectroscopy, evaluating coupling constants 20 p3461 A67-37287
- Scaling law derived from small angle scattering theory, interpreting data in spectroscopic manner to deduce potentials and interactions between electronic states 22 p3839 A67-39205

MOLECULAR SPECTRUM

- Paramagnetic resonance of praseodymium and uranium ions in calcium fluoride analyzed via fitting to spin Hamiltonian 01 p0129 A67-10146
- Nuclear magnetic resonance and microwave spectra of some deuterio derivatives of 2, 4-dicarbaheptaheptaborane/7/[JPL-TR-32-1038] 01 p0019 A67-11146
- Electron angular distribution in copper and gold thin films attributed to individual close interaction scattering phenomena 02 p0297 A67-11834
- Laser induced breakdown of complex organic molecules in vapor state, noting emission accompanied by formation of partially dissociated hot gas 02 p0252 A67-12451
- Identification of molecular bands of spectrum of large sunspot, detecting presence of magnesium oxide 03 p0512 A67-13887
- Molecular nitrogen and oxygen properties, calculating Hartree-Fock value for energy in ground state 04 p0680 A67-14693
- Collision induced dissociation of deuterium by argon and nitrogen examined with angular ion scattering apparatus, determining kinetic energy and angular distribution 05 p0848 A67-16834
- Intensity distribution in rotational structure of molecular spectra bands upon excitation by ion impacts 06 p1035 A67-17877
- Thermodynamic functions of diatomic gases with molecules in 3-sigma electron state 07 p1225 A67-19121
- Self-broadening coefficients of spectral lines of absorbing atmospheric gases measured in comparison with line

- broadening effects of nitrogen 10 p1678 A67-22715
- Flash spectroscopy apparatus with Q-switched ruby laser, discussing molecular electronic excitation 10 p1663 A67-22854
- Spectrum of second order Raman lines in coupling of radiation and matter, using Green function 10 p1663 A67-22855
- Condon local geometry of molecular spectrum determined by plotting intensities on Deslandres diagram 10 p1681 A67-22959
- Level populations and energy loss rate of electrons during nonelastic collisions with impurity molecules in weakly ionized two-temperature plasma 11 p1831 A67-24019
- 1/s line intensity distribution function for molecular spectra representation using growth curves calculated for Lorentz lines 11 p1822 A67-24416
- Expression for electron contribution to Stark broadening, using impact approximation with Lewis or Debye cut-offs 11 p1823 A67-24491
- CH molecule solar spectral observations interpreted using several upper photosphere models and assuming local thermodynamic equilibrium approximation 11 p1861 A67-24495
- Spatial correlation and molecular properties in extended Hartree-Fock calculations, deriving first and second order density matrices for ground state of H, Li and F 11 p1824 A67-24993
- Molecular spectra of sunspots and solar disk 13 p2203 A67-27428
- Conversion process and ESR in gamma-irradiated dihydrothymine noting reaction rate 14 p2259 A67-28300
- Stimulated inverse Raman effect, noting experimental laser setup and theory based on optical phonon emission 14 p2333 A67-28985
- Electronic, vibrational and rotational temperatures in laser-produced flames measured spectroscopically 15 p2433 A67-29879
- Exciting molecular emission spectra in cold plasma free of electrode-induced impurities by superhigh frequency source 16 p2704 A67-31478
- Permafrost layer existence beneath lunar surface, noting possible detection techniques 17 p2952 A67-33250
- Laser excited vibrational fluorescence measurements in carbon dioxide noting energy transfer rates, system kinetics, radiative coupling, etc 18 p3060 A67-34027
- Selective enhancement of molecular spectra of HD and diatomic deuterium in argon and krypton discharges 18 p3083 A67-34518
- Thermodynamic functions of diatomic gases with molecules in 3-sigma electron state 21 p3659 A67-38186
- Boron oxide identified as radiating species causing molecular fluorescence spectrum in upper atmosphere at twilight 21 p3623 A67-39123
- Molecular band spectra of CN emission assuming Gaussian rotational line profile 23 p4030 A67-41695

MOLECULAR STRUCTURE

SA RAMAN SCATTERING

- Molecular pair distribution function in perfect crystalline solids, using method based on cell cluster theory 05 p0758 A67-16129
- Carbon dioxide solid matrix study of carbon trioxide production, IR spectrum and molecular structure 05 p0759 A67-16838
- Zr-Mo, Ca-Mo and Ni-Cr cermets, noting preparation and structural defects 05 p0830 A67-17034
- Crossed molecular beam kinetics of reactive asymmetry of oriented methyl iodide polar molecules reacting with rubidium 06 p0955 A67-17831
- X-ray crystal structural analysis of tetraethyl titanate and monomethyltriethyl titanate, determining reason for difference in color 06 p0955 A67-17849
- Changes in giant molecule structure of polypropylene films under action of laser pulses analyzed by optical microscopy 07 p1211 A67-19169
- Atmospheric mixing time and lifetime of atomic and molecular oxygen at high altitude, noting agreement with barometric distribution law, concentration pattern, etc 07 p1178 A67-19813
- Structures and stereochemistry of

clivonine and clivimine analyzed through mass spectroscopy and nuclear magnetic resonance 09 p1458 A67-22059

Anodic oxidation and molecular structure influence on performance of normal saturated hydrocarbons in fuel cells 10 p1595 A67-22927

Effective diffusion cross section for meteor atoms in atmosphere, using Thomas-Fermi-Dirac and dumbbell molecule models 13 p2111 A67-26553

Shock structure in diatomic gas described using Mott-Smith bimodal distribution function, including relaxation effects 15 p2469 A67-29217

Trifluoramine oxide IR spectrum measured, determining structure, symmetry and rotational, vibrational and thermodynamic properties 15 p2433 A67-29880

Kinetics of difluoromethylene-nitric oxide reaction, describing experimental apparatus, reaction mechanism, molecule structure and calculating heat of molecule formation 16 p2620 A67-31760

Relation between molecular structure of In and Sb semiconductor compounds and fine structure of X-ray absorption spectra 18 p3095 A67-33441

Liquid crystal - Conference, Kent State University, August 1965, Part III 18 p2991 A67-33633

Zr-Mo, Ca-Mo and Ni-Cr cermet, noting preparation and structural defects 18 p3066 A67-34455

Existence of ozone difluoride established by low temperature experiments and correlation with mass spectrometric EPR, IR and NMR 20 p3377 A67-37136

MOLYBDENUM THEORY

Atomic and molecular time-dependent quantum-mechanical perturbation theory with differential equation formulation within Hartree-Fock approximation 02 p0268 A67-12725

Thermodynamic properties of real air, deriving expressions for expansion in isothermal-isentropic mode from subcritical temperatures to 1500 degrees K 04 p0738 A67-15914

NBS polyisobutylene relaxation modulus and Rouse functions for torsional molecular vibrations and internal rotation in viscoelastic theory of amorphous polymers 08 p1346 A67-20878

Molecular theories for polymer elastic and viscoelastic properties near glass transition region [AIAA PAPER 67-488] 18 p3143 A67-33954

MOLYBDENUM WEIGHT

Molecular weight sensitivity of thermoconductivity of polydimethylsiloxane and polyethyleneglycol 01 p0103 A67-10295

Gel permeation chromatography for analytical fractionation of propellant binder prepolymers and separating and purifying labile binder ingredients 04 p0686 A67-14472

Transport of free molar energy in system in interdiffusion 09 p1581 A67-22597

Intrinsic viscosity of linear homogeneous polystyrenes in decalin and toluene over large temperature ranges and molecular weights 10 p1602 A67-23384

Molecular sizes of diphenylpyridine nucleotide linked dehydrogenases of representative animal, plant and microbial species 11 p1750 A67-24784

Mechanism for bounding quarks to atomic systems of low molecular weight 13 p2109 A67-26330

Motion and continuity equations for atomic and molecular oxygen density solved numerically as time dependent problem 16 p2664 A67-30975

IR lattice spectra of rare earth iron garnets noting absorption in low frequency bands and molecular weights 16 p2733 A67-31880

Lower thermosphere composition and mean molecular weight analyzed for diurnal and latitude effects, using mass spectrometric measurements 19 p3220 A67-35265

Earth density/pressure relation and mantle and core mean atomic weight used to construct mass-mean density curve for planets 24 p4231 A67-42448

Ultrahigh molecular weight poly(ethylene terephthalate)/ synthesized, studying catalyst, particle size, reaction temperature and time and carrier gas flow rate 24 p4176 A67-42467

Molecular weight and amino acid

composition of chromatium ferredoxin 24 p4113 A67-42653

MOLYBDENUM

SA DIATOMIC MOLECULE

SA MACROMOLECULE

SA POLYATOMIC MOLECULE

SA TRIATOMIC MOLECULE

Methods for calculating interaction potentials of atoms, molecules and ions 03 p0473 A67-13613

Methods for calculating interaction potentials of atoms, molecules and ions 18 p3083 A67-34478

Linear/nonlinear molecule optical properties obtainable from light scattering in gas by strong optical field 20 p3488 A67-36437

MOLTEN-SALT ELECTROLYTE

Operational economy of dip brazing method of joining aluminum and reliability of ultrasonic printout procedures for inspection of assemblies 10 p1660 A67-23007

Operation, structure, performance and application of solid, molten and aqueous electrolyte fuel cells 14 p2253 A67-29023

MOLYBDENUM

Interdiffusion of niobium and molybdenum over 1400-2300 degrees C range using diffusion couples, determining activation energy values 01 p0100 A67-10767

Crystal layer dislocation structure of cold rolled molybdenum foil investigated by electron microscopy 01 p0101 A67-10939

Structural orientation, purity and perfection of molybdenum single crystals grown by zonal electron-beam melting process 02 p0255 A67-11867

Solubility of carbon in Mo, Re and W determined by isothermal carburization method 03 p0439 A67-12845

Thermostability of ceramic coatings applied to W and Mo during cooling, in terms of temperature-dependent elastic modulus and linear expansion coefficients 03 p0446 A67-13638

Electron diffraction scanner structural analysis of Ta and Mo very thin film growth 04 p0677 A67-15101

Molybdenum grain boundary relaxation and embrittling effect of interstitial impurity additions 05 p0829 A67-16505

Structure and mechanical properties of molybdenum-niobium system monocrystalline melts prepared by electron beam zonal melting 05 p0830 A67-17024

Hardness, microhardness, electric resistance and toughness results tabulated for polycrystalline nonalloyed molybdenum 05 p0832 A67-17510

Plasticity of cast molybdenum improved by vacuum-annealing at temperatures from 900 to 1200 degrees C 05 p0832 A67-17511

Ultrahigh vacuum effects on flow and fracture behavior of molybdenum 06 p1016 A67-17897

Austenitic chrome-manganese steel structure and properties as function of nitrogen, molybdenum and niobium 06 p1017 A67-18184

Molybdenum effect on properties of chromium-nickel alloy, noting hardness and strength 06 p1018 A67-18229

Molybdenum and molybdenum alloy stress-rupture characteristics at 2200 degrees C for arc-cast and wrought sintered material 06 p1019 A67-18854

Corrosion tests of W, Mo, Rh-based materials for compatibility in lithium at 2500, 2800 and 3000 degrees 07 p1208 A67-19466

Temperature dependence of relaxation-type ultrasound attenuation maxima in plastic deformation of molybdenum and niobium single crystals 08 p1367 A67-20419

Plastic flow peculiarities analysis based on X-ray diffraction effects obtained by deforming single crystal molybdenum of various orientations 08 p1342 A67-20809

Thermal diffusivity and specific heat of molybdenum at high temperatures measured, using variable heating in induction furnace 09 p1517 A67-21866

Performance of thermionic converters, discussing voltage output, interelectrode spacing, rhenium-rhenium and rhenium-molybdenum electrode systems 09 p1449 A67-22343

Temperature dependence of elastic constants of molybdenum single crystals measured, using thin rod resonance techniques 11 p1809 A67-24908

Mechanical properties of zone melt molybdenum single crystals as affected by orientation and gas impurities 11 p1810 A67-25092

Effect of V, Zr, and Y additions on mechanical properties of 1 mm sheet molybdenum 13 p2130 A67-26392

Brittle fracture at grain boundaries in samples of electron-beam molybdenum prepared by forging in air after extrusion 13 p2130 A67-26447

Dislocation velocity measurements and thermally activated motion in molybdenum 13 p2133 A67-27011

Molybdenum polycrystal plastic strain rate in pre-yield region studied by successive stress relaxation method for dislocation density and mobility characteristics 14 p2337 A67-28230

Structure and mechanical properties of molybdenum-niobium system monocrystalline melts prepared by electron beam zonal melting 14 p2338 A67-28491

Molybdenum ductility improvement by electrowinning with yttrium 14 p2338 A67-28616

Hydrogen treatment effects on molybdenum ductility, noting grain-size and heat treatment contribution to strain-to-fracture difference at various deformation pressures 15 p2503 A67-29562

High temperature diffusion of potassium in single crystal and polycrystalline molybdenum 15 p2504 A67-29972

Carbon monoxide chemisorption on polycrystalline molybdenum studied by radiotracer, noting desorption at various temperatures as time function 15 p2434 A67-30099

High purity single crystal molybdenum electrical resistivity dependence on deformation 16 p2689 A67-31370

Vanadium and molybdenum effect on properties and phase transformations of titanium chromide 16 p2691 A67-31591

Reduced blackness coefficients measured for coaxial system of tungsten-molybdenum surfaces by calorimetric method 16 p2780 A67-31778

Metallic adhesion between Mo-Mo and Ti-Ti couples, showing contact resistance useful in determining contamination at conducting interface 17 p2871 A67-32465

Thermostability of ceramic coatings applied to W and Mo during cooling, in terms of temperature-dependent elastic modulus and linear expansion coefficients 17 p2875 A67-33172

Fatigue characteristics of chromium-molybdenum steels subjected to various heat treatments, comparing tension-compression and torsion 18 p3065 A67-34258

Molybdenum interband transitions noting low energy optical property anomalies and origin of two absorption bands 20 p3466 A67-36865

Heat treating effects on molybdenum properties and structural characteristics 20 p3466 A67-36967

Oxygen determination in molybdenum using vacuum extraction 20 p3467 A67-37121

Hardness, microhardness, electric resistance and toughness results tabulated for polycrystalline nonalloyed molybdenum 21 p3644 A67-38038

Plasticity of cast molybdenum improved by vacuum-annealing at temperatures from 900 to 1200 degrees C 21 p3644 A67-38039

Molybdenum heat resistance improvement after structural polygonization by deformation and annealing, describing durability dependence on treatment conditions 22 p3819 A67-39324

Crystal layer dislocation structure of cold rolled molybdenum foil investigated by electron microscopy 22 p3820 A67-39792

Twinning and low temperature mechanical properties of high purity polycrystalline niobium and molybdenum, discussing grain size effects 22 p3823 A67-40208

Oxygen interstitial solid solubility in niobium, noting decrease with addition of tungsten and molybdenum 22 p3823 A67-40211

Ti thin films use as getter in electron microscopy of Mo particles at high temperature with minimum oxidation 24 p4172 A67-41978

MOLYBDENUM ALLOY

Work function of solid solutions of tungsten with molybdenum and tantalum

explained by surface adsorption effects 01 p0093 A67-10092

Structural sensitivity of plastic properties of molybdenum alloys produced by electron beam fusion, investigating microstructure, failure in bending tests and grain fragmentation 01 p0101 A67-10936

X-ray microstructural and chemical analysis of sintering of zirconium diboride-molybdenum disilicide alloys 01 p0102 A67-11242

Eliminating solidification cracks in arc-melted ingots of high strength crack-prone Mo-TiC type alloy by capping with unalloyed molybdenum 02 p0248 A67-12704

Electron beam zonal vacuum fusion growth of Mo-Nb alloy single crystals 05 p0827 A67-16080

Titanium, zirconium and hafnium effect on recrystallization temperature and strength of alloys of molybdenum with carbon 05 p0832 A67-17508

Small additions of Y, La, Hf, V, Ti and Zr on structure of cleaved surfaces and viscosity of Mo cermet materials 07 p1198 A67-19184

Carbide forming elements effect on kinetics of isothermal transformation of austenite and mechanical properties of manganese-molybdenum steel 07 p1199 A67-19239

Isothermal transformation diagrams for titanium-molybdenum alloys 07 p1199 A67-19243

Low temperature magnetic properties of superconducting Mo-Re alloys in fine wire form 07 p1236 A67-20135

Substructural strengthening of carbide precipitation hardened molybdenum alloy by swaging and wire drawing 11 p1805 A67-24108

Superconducting mixed state of concentrated Mo-Nb alloy, evaluating free area of Fermi surface in k space 16 p2726 A67-30812

Hardness, electrical resistance and phase composition on Ni-Mo alloy during annealing, discussing phase transformations 16 p2687 A67-30847

Cleaved surfaces of Mo cermet binary alloys structures annealed and fractured under static bending loads studied for surface properties 17 p2871 A67-32133

Structures in Mo-Re and W-Re systems examined by X-ray powder techniques, discussing occurrence of chromium oxide type structure 17 p2873 A67-32813

X-ray, microstructural and chemical analysis of sintering of zirconium diboride-molybdenum disilicide alloys 17 p2875 A67-33167

Shear-spinning technique for manufacturing molybdenum alloy missile nose tips 18 p3054 A67-34365

Thermal exposure effect on recrystallization and ductility of TZM molybdenum alloy sheet and foil 19 p3234 A67-34793

Alloying effect on temperature and strain rate sensitivity of niobium-molybdenum bcc metal 19 p3246 A67-35730

Tungsten-molybdenum alloy heat-resistant properties noting vacuum testing and subjection to plastic deformation, with results related to molybdenum content and temperature 20 p3467 A67-36968

Molybdenum-boron system structural diagram, noting carbon effect on phase equilibria and temperature effects 20 p3468 A67-37177

Titanium, zirconium and hafnium effect on recrystallization temperature and strength of alloys of molybdenum with carbon 21 p3644 A67-38036

Structural sensitivity of plastic properties of molybdenum alloys produced by electron beam fusion, investigating microstructure, failure in bending tests and grain fragmentation 22 p3820 A67-39790

HF fatigue tests in high vacuum environment on recrystallized molybdenum base alloy TiC for elevated temperature fatigue 22 p3822 A67-40058

Mossbauer spectra of FeMo alloys for closed space compositions show overlap of disturbed surroundings of impurity iron atoms and magnetic moment 24 p4203 A67-42108

MOLYBDENUM CARBIDE

Room temperature microhardness anisotropy, slip and twinning in molybdenum carbide single crystals noting orientation

dependence, elastic modulus, electric resistivity and measurement techniques 03 p0441 A67-13254

Titanium carbide-molybdenum carbide interaction and structure of resulting Ti-Mo-C 07 p1203 A67-19261

Solid solution properties of niobium carbide-molybdenum carbide alloy, noting changes in electron structure 14 p2337 A67-28284

High superconducting transition temperatures in molybdenum carbide compounds stressing crystal structures 19 p3245 A67-35729

Binary molybdenum-carbon system investigated using X-ray, metallographic, thermoanalytical and melting-point techniques 20 p3470 A67-37389

Carbon thermodynamic activity in molybdenum carbide alloyed with small additions of Fe, Ni and Ti 24 p4171 A67-41962

MOLYBDENUM COMPOUND

Isotope effects on superconducting transition temperature of molybdenum boride and tungsten 06 p1047 A67-17642

Substrate metal hardness effect on performance of molybdenum disulfide films, noting wear rates 10 p1659 A67-22887

MOLYBDENUM OXIDE

Ion temperature, cell temperature, cell voltage and current in electrolytic technique for reproducible growth of molybdenum IV/oxide crystals 15 p2533 A67-29295

Semiconductivity of molybdenum-oxygen systems, analyzing solid phase effect on solution mechanism 20 p3510 A67-36816

Fast production of semiconductor and refractory metals by reducing silicon tetrachloride and molybdenum trioxide with hydrogen in electric discharge 21 p3681 A67-38358

MOLYBDENUM SULFIDE

Lubrication and bearing problems in space environment, noting molybdenum disulfide and silicones 05 p0811 A67-16932

Ball bearing life operating in vacuum with molybdenum disulfide and oils as lubricant [ASLE PAPER 66AM 7A3] 08 p1335 A67-21036

Chemical stability of silver graphite, molybdenum disulfide, zinc oxide, boron nitride, muscovite and phlogopite mica solid lubricants 10 p1659 A67-22829

Molybdenum disulfide compacts pressurized by explosive forming, determining specific gravity, hardness, compressive and tensile properties, etc 16 p2695 A67-31753

Molybdenum sulfide solid lubricant oxidation characteristics analyzed by thermogravimetry [ASLE PAPER 67-LC-14] 24 p4165 A67-42748

Synthetic molybdenum sulfide film examined for lubricating performance under extreme pressure conditions in air and immersed in fluids [ASLE PAPER 67-LC-15] 24 p4165 A67-42749

MOMENT

S BENDING MOMENT

S DIPOLE MOMENT

S HINGE MOMENT

S INERTIA MOMENT

S LOADING MOMENT

S MAGNETIC MOMENT

S NUCLEAR-ELECTRIC MOMENT

S PITCHING MOMENT

S ROLLING MOMENT

MOMENT DISTRIBUTION

Moments of distribution function of perfect fluid calculated and used in studies of orthogonal polynomials on Minkowski hyperboloid 12 p1966 A67-25144

Displacements, stresses and moments in orthotropic and bimetallic cylindrical shells under radial concentrated forces determined via computer method 12 p0205 A67-25608

Finite rotation of body due to revolutions of internal flywheels determined assuming total kinetic moment of system is zero 12 p1966 A67-25658

Local magnetic moment derivation methods using magnetoresistivity data, estimating concentration and temperature dependence 13 p2177 A67-26990

Particle momentum distributions derived from relativistic quantum statistical mechanics 13 p2161 A67-27398

Differential equations determining time-dependent torsional moment and stresses in

thin walled rods in creep presence 17 p2821 A67-32830

Air suction effect on moment characteristics of cranked slender profile, determining boundary layer control 21 p3564 A67-38043

Calculated stressed state of short thin walled shells under transverse loads and torsional moments 21 p3726 A67-38797

MOMENT EQUATION

Rotating gyroscope with conical cup on ball support, deriving expressions for moments of forces imposed by support 01 p0064 A67-10419

Aerodynamic heating from turbulent boundary layer to swept surface symmetrical to surface line dividing flow obtained from momentum and energy integral equations 04 p0549 A67-15825

Statistical linearization of nonlinear aerodynamic coefficient of angle-of-attack moment of aircraft 04 p0549 A67-15884

Moments of output coordinates of nonlinear system determined by algorithm based on approximation method, applied to automatic control system 09 p1525 A67-22079

Thirteen moment equation solved for problem of plane Couette flow by iteration scheme, showing functional dependence on Mach and Knudsen numbers 11 p1774 A67-23863

Plasma models and methods used to study wave propagation phenomena, considering particle orbit, single species moment equations, velocity distribution function, etc 12 p1975 A67-25527

Book on principles of continua with applications 12 p1966 A67-25557

Equilibrium equations of Vlasov engineering moment theory of shells of variable curvature 12 p0201 A67-25577

Asymptotic methods of obtaining refined solutions for zero moment equations of concentrated loads applied to shells with Gaussian curvature 12 p0208 A67-25630

Distribution function and temperatures in monatomic gas under steady expansion into vacuum determined by integrating Bhatnagar-Gross-Krook /BGK/ model equation and moment equations respectively 13 p2104 A67-26982

Nonequilibrium effects in spherical free jet expansions of polyatomic gases and gas mixtures, obtaining moment equations for flow field development 13 p2104 A67-26983

Geomagnetic field analytical representation, giving equations for moments and distribution of equivalent set of dipoles 14 p2309 A67-27948

Boltzmann equation and deduced moment equations containing moments up to fourth order in arbitrary orthogonal curvilinear coordinates 14 p2297 A67-27998

Moment stress effect on natural oscillation frequency, deriving motion equations of circular cylindrical shell 14 p2401 A67-28735

Derivation of moments of continuous stochastic system 15 p2459 A67-30131

Three-dimensional turbulent boundary layer flow over infinite swept wing calculated using entrainment and momentum integral equations 16 p2657 A67-30617

Velocity distribution functions in statistical theory of turbulence, deriving moment equations and comparing properties with kinetic theory 16 p2660 A67-31220

Shock thickness for monatomic Maxwell molecule gas calculated using conservation and moment equations 18 p3030 A67-34753

Compressible laminar spanwise boundary layer, on yawed infinite cylinder with disturbed suction calculated using momentum equation 19 p3342 A67-35724

Solution to moment equations for near-equilibrium spherically-symmetric expanding flows by using Bernstein-Greene-Kruskal theory for Boltzmann equation 19 p3212 A67-35764

Helly problem of moment theory and optimum approximation of finite defect by subspace elements of continuous functions, examining uniqueness and existence 21 p3653 A67-38400

Moment-kinematic and moment-energetic characteristics of servomotors applied to point and functional problems of servomechanisms in space 24 p4098 A67-42094

MOMENT METHOD

Solution to boundary value problem of generalized moment theory of elasticity, determining mean displacement of

microinhomogeneous elastic body 02 p0337 A67-11953
Plane problems of moment theory of elasticity for plane weakened by finite number of circular apertures, obtaining uniqueness of solutions 02 p0338 A67-11954
Energy spectra of avalanche electrons in copper, iron, aluminum and graphite determined by method of moments, considering polarization of medium and multiple scattering 02 p0316 A67-12768
Kinetic moment in celestial mechanics, noting application to satellite orbit determination in terrestrial gravitational field 03 p0510 A67-13456
Unsteady temperature fields in structures calculated by moments 07 p1266 A67-19145
Mott-Smith type moment method and restricted variational principle determinations of shock structure 08 p1355 A67-21141
Statistical basis for modified moment theory of elasticity that takes into account contribution of all deformation-tensor-component gradients to deformation energy 09 p1574 A67-21914
Thin electrostatic sheath adjacent to body immersed in flowing weakly ionized continuum plasma analyzed for arbitrary Debye length mean free path ratios 11 p1825 A67-23868
Kinetic theory description of flow over right circular cylinder at low speed based on Lees moment method 13 p2102 A67-26969
Boundary value problems involving shallow cylindrical shells of given arbitrary configuration solved, using Vlasov moment theory 14 p2395 A67-27837
Moment method treatment of collisionless plasma equilibria in confining magnetostatic fields, using Vlasov equation to determine distribution function of particles 14 p2360 A67-28554
Theorems derived from approximate methods of analysis applied to collocation, moment and Galerkin methods for solving linear integral and differential equations 14 p2344 A67-28671
Solution to boundary value problem of generalized moment theory of elasticity, determining mean displacement of microinhomogeneous elastic body 17 p2965 A67-33270
Plane problems of moment theory of elasticity for plane weakened by finite number of circular apertures, obtaining uniqueness of solutions 17 p2966 A67-33271
Lagrange interpolation pattern synthesis technique using moment criterion for optimum pattern approximation by nonuniform antenna array 18 p3012 A67-34430
Momentum integral method applied to two-dimensional flow problem between flat plates 20 p3420 A67-36420
Steady state theory of low pressure plasma discharge column in axial magnetic field derived, using moments of Boltzmann equation 21 p3662 A67-37756
Vlasov equation solved by taking continuous spectrum of infinite matrix belonging to moment equations into account, obtaining Landau damping results 22 p3852 A67-39992
Energy spectra of avalanche electrons in copper, iron, aluminum and graphite determined by method of moments, considering polarization of medium and multiple scattering 22 p3877 A67-40270

MOMENTUM
SA ANGULAR MOMENTUM
Transverse-momentum distribution of secondaries from high energy nuclear interactions in accelerator energy region interpreted by statistical model 13 p2195 A67-27580
Momentum and energy of gravitational waves in terms of relativity theory 15 p2518 A67-30005
Momentum and energy of gravitational waves in terms of relativity theory momentum and energy of gravitational waves in terms of relativity theory 18 p3079 A67-33763
Momentum equation examined by curvature of streamlines downstream from shock wave 22 p3783 A67-39727

MOMENTUM ENERGY
Turbulent energy dissipation rates, eddy fluxes of sensible heat, momentum and kinetic energy measured above

nonhomogeneous surface 02 p0238 A67-12076
Uniform property turbulent boundary layer heat transfer calculation, using solution of integral momentum and kinetic energy equations 04 p0731 A67-15821
Radiation pressure of electromagnetic and acoustic waves calculated from momentum of incident and scattered wave trains 05 p0846 A67-16583
Muon momenta, signs and densities in cosmic air showers determined, using magnet spectrophotograph with visual display 06 p1076 A67-17651
Lorentz invariance, momentum energy tensors and formulation of MHD problem 10 p1685 A67-23083
Accidental degeneracy of hydrogen atom levels using Schroedinger equation, deriving eigenfunctions 18 p3083 A67-34072
Energy-momentum density and superpotentials in privileged frame of reference, giving results due to Einstein and Freud pseudotensors 19 p3261 A67-35048
Polytrope structure from integrodifferential equation assuming metric, energy momentum tensor for static spherical symmetry and polytropic equation of state 21 p3658 A67-38615

MOMENTUM PRECESSION
Coupling mechanism of earth liquid core and mantle during luni-solar precession 24 p4151 A67-42315

MOMENTUM THEORY
Optimal control of one-dimensional distributed oscillatory system and wave processes using momentum theory and propagating method 01 p0044 A67-10493
Motion laws for variable mass system, discussing versions of law and problem of angular momentum 01 p0113 A67-10507
Momentum loss rate by conduction electrons of polar semiconductors for known energy and momentum distribution 02 p0280 A67-11486
Radial momentum equation of flow outward from axisymmetric turbulent wall air jet impinging on solid surface 05 p0792 A67-16819
Plasma expansion in magnetic field, showing dominating effect of initial outward momentum 05 p0858 A67-17428
Artificial heat conduction mechanism, introducing viscosity term into momentum and energy equations to account for shock discontinuities in flow problems 06 p0992 A67-18830
Optical transitions in semiconductors satisfying principle of momentum conservation through mutual interaction between free current carriers 06 p1059 A67-18912
Behavior of momentum effect jet interaction proportional amplifier using flow visualization on water table and large scale pneumatic model 08 p1282 A67-20460
Moment stresses in thermoelasticity for medium described in terms of displacement and rotational vectors 10 p1720 A67-23599
Optimal control of one-dimensional distributed oscillatory system and wave processes using momentum theory and propagating method 10 p1621 A67-23615
Static operating characteristics of vented single-stage momentum exchange proportional amplifiers, noting applicability for compressible and incompressible flow regimes 14 p2250 A67-28329
Book on aerodynamics of V/STOL aircraft emphasizing use of momentum and finite wing theories, considering deflection of trailing vortex system 14 p2243 A67-28678
Ground effect of static circular peripheral jet, comparing derived relations between jet flow, base pressure and hover height with experimental model results 15 p2415 A67-29262
Regions forbidden to motion in three-body problem determined in barycentric coordinate system for nonzero modulus of momentum vector 18 p3117 A67-33627
Relativity theory accounting for energy conservation properties in elementary particle interactions and small size and high energy emission of quasars 22 p3892 A67-40499
Momentum equation integration to determine two mixing parallel subsonic streams interface 23 p3991 A67-41667
Mechanical system motion with point moving on surface, imposing limitations on system mass distribution, obtaining fixed

coordinate system 24 p4188 A67-42302

MOMENTUM TRANSFER
Ionized impurity scattering mechanisms causing energy and momentum losses in n-type InSb below 77 degrees K 01 p0134 A67-10806
Observed differences between lateral transport rates of heat and chemical species and of momentum in turbulent free shear flows accounted for by model [AIAA PAPER 65-810] 01 p0054 A67-11167
Low energy total and momentum-transfer scattering cross sections for electrons on He and Ar compared, using modified effective range formulas 03 p0471 A67-13319
Electron scattering cross section of argon and atomic oxygen measured, using microwave interferometer for analysis of plasma produced in shock tube 03 p0472 A67-13320
Momentum transfer during impact, penetration depth, crater form and mass loss at various velocities, using spherical aluminum projectiles and aluminum targets 04 p0710 A67-15005
Electron cyclotron echo production from plasmas by repeated pulsing, developing theory based on electron neutral momentum transfer collisions 04 p0665 A67-15105
Momentum transfer mechanism in separated flow region of rectangular cavity facing oncoming turbulent boundary layer [AFCR-66-851] 04 p0610 A67-15924
Momentum transfer accompanying ionizing impact of electrons against atoms of inert gases 06 p1037 A67-18426
Four-momentum transfer, inelasticity and mass of target isobars in cosmic ray jets 07 p1246 A67-20278
Momentum interaction principle used in experiments to produce proportional fluid amplifier, discussing geometry and characteristics 08 p1282 A67-20464
Electron transport phenomena in thermionic converter plasmas, emphasizing electron-ion collisions to electron momentum transfer collision frequency 09 p1450 A67-22351
Turbulent transfer in diabatic conditions, deriving formulas for wind and temperature profiles 10 p1677 A67-23574
Matched pulses for two-layer laminates, discussing complete energy transfer to base and uniform momentum transfer 10 p1724 A67-23707
Symmetrical jets and wakes in streaming flow with pressure gradient, noting time-mean profiles of particular pressure fields 11 p1741 A67-24047
Momentum and energy transfer effects on gas kinetic equations of nonequilibrium flows, analyzing diffusion problem 11 p1780 A67-24536
Double shutter drift tube for measuring electron drift velocities and momentum transfer cross sections in methane, ethane, ethylene, etc 11 p1824 A67-24994
Momentum transfer of positively ionized nitrogen molecule incident on copper target, measuring accommodation coefficient with torsion balance 13 p2098 A67-26945
Momentum accommodation coefficients of variable angle of incidence of monochromatic argon molecular beams 13 p2098 A67-26946
Normal and tangential momentum accommodation coefficients in low density facility 13 p2098 A67-26947
Three-layer atmospheric model for use in two-dimensional diffusion equation for steady state conditions incorporating eddy diffusion of momentum 13 p2153 A67-27607
Molecular beam apparatus for determining momentum accommodation coefficients for neutral particle surface interactions 14 p2316 A67-28192
Asymptotic curve for single arbitrary reflection of atom from plane with weak surface roughness, calculating total momentum and energy fluxes 14 p2351 A67-28636
Geostrophic wind angular momentum transport at 500 mb in Northern Hemisphere, using zonal harmonic analysis, noting quasi-biennial cycle 15 p2512 A67-29201
Control moment gyro as attitude control actuator for spacecraft, noting advantages over other momentum transfer systems 15 p2486 A67-29307
Rapid acquisition of sun in solar energy

conversion systems based on momentum exchange from rotating flywheels to platform 15 p2423 A67-30130

Energy and momentum exchange model for interaction of gas particle with solid body surface 16 p2619 A67-30458

Jet compressors for closed Brayton cycle MPD to study momentum transfer of two high velocity gas or vapor streams of very different molecular weight 16 p2604 A67-30568

Momentum transfer collision frequency for electrons in cesium plasmas from electrical conductivity and plasma properties measurement in cesium arc column 16 p2719 A67-31236

Flow analysis of compressible fluid in wake behind body positioned symmetrically with respect to flow direction, using momentum and energy conservation equations 19 p3170 A67-35610

Control moment gyro /CMG/ and use in space-vehicle attitude-control system, emphasizing control laws [AIAA PAPER 67-589] 19 p3336 A67-35985

Momentum amplifier based on primary, secondary and control jet momentum flux interaction 20 p3362 A67-36120

Electron beam deflection by standing light wave of laser shows momentum transfer resulting in Bragg relationship for reflection angle 20 p3461 A67-37185

Book on fluid dynamics of multiphase systems covering momentum, heat and mass transfers and chemical reactions 20 p3425 A67-37728

Plasma model kinetic equation, discussing collision operator approximating momentum and energy transfer rates 22 p3843 A67-39265

Numerical solution of Poiseuille flow with variable fluid properties, solving coupled momentum and energy equations [ASME PAPER 66-WA-FE-22] 23 p3989 A67-40930

Gravitational torque mechanism for radial outward angular momentum transport in solar nebula 24 p4223 A67-41790

Momentum and heat transfer in axisymmetric turbulent free jets exhausting into quiescent air, using finite difference technique 24 p4092 A67-42608

MONATOMIC GAS

Structure of shock wave in monatomic gas analysis using orthogonal polynomial solution of Boltzmann equation, noting Mott-Smith distribution function 02 p0234 A67-12541

Exact solutions to kinetic moment equations of monatomic gas in absence of external forces to case of mixture of monatomic Maxwellian gases with external forces 03 p0401 A67-12869

Shock wave structure in steady state monatomic relativistic gas 05 p0793 A67-17112

Sound propagation in dilute monatomic gas confined in box and in unconfined rarefied monatomic gas assuming unidirectional perturbation of velocity distribution 13 p2100 A67-26955

Generalized spatially uniform distribution functions for monatomic rarefied gas describing one-dimensional heat transfer in nonuniform flow 13 p2100 A67-26958

Orthogonal polynomial method to determine distribution function for equilibrium of single species two-temperature gas mixture 13 p2102 A67-26972

Distribution function structure in gas kinetic flows as given by BGK model in plane weak shock in monatomic gas 13 p2104 A67-26981

Distribution function and temperatures in monatomic gas under steady expansion into vacuum determined by integrating Bhatnagar-Gross-Krook /BGK/ model equation and moment equations respectively 13 p2104 A67-26982

Similarity solution to laminar boundary layer heat transfer from monatomic gas to cooled wall with no applied electric or magnetic fields [JPL-TR-32-1143] 15 p2523 A67-29219

Boundary conditions for Navier-Stokes equations in rarefied monatomic gas with distribution function given a priori 15 p2470 A67-29234

Thermal accommodation coefficients determination in temperature jump region 15 p2580 A67-29883

Numerical calculations of interactions of monatomic gas particles with ideal and contaminated crystal surfaces at epithelial

energies 15 p2434 A67-30197

Continuous spectrum emission from free-bound and free-free electron transitions into field of monatomic gas ion using shock tube 16 p2673 A67-31109

Physical parameter determination for monatomic gas flow based on energy balance, taking into account heating and ionization in thermal nonequilibrium 17 p2837 A67-32337

Shock thickness for monatomic Maxwell molecule gas calculated using conservation and moment equations 18 p3030 A67-34753

Transient heat transfer through monatomic collisionless ideal gas enclosed between parallel walls analyzed for step change in one wall temperature [ASME PAPER 67-HT-53] 20 p3548 A67-36735

Mach number effect on electron temperature structure of partially ionized monatomic and diatomic gas shocks 21 p3610 A67-37760

Multiphoton absorption in monatomic gases causing ionization of atom applied to plasma production by intense radiation from lasers 24 p4190 A67-42098

Hydrodynamic solution for shock wave parameters of monatomic gases assuming exponential molecular interaction potentials and absence of mass forces 24 p4142 A67-42271

MONITOR

SA IN-FLIGHT MONITORING

SA RADIO FREQUENCY MONITORING

Monitoring events occurring during testing of space vehicle by data compression techniques and time shared computer-controlled checkout system [SAE PAPER 680696] 01 p0049 A67-10593

Air monitoring instruments used in detection and control of air pollution 01 p0050 A67-11037

Wideband multichannel transient monitoring system for detection and analysis of electrical transient 05 p0809 A67-17537

Instrument landing system transmitter monitors for automatic blind landing, noting near field monitors and internal monitors 07 p1222 A67-19654

Aircraft noise monitoring system for Zurich airport 13 p2052 A67-26535

Radio propagation influence on performance of azimuth channel of ILS defining characteristics of ILS signals relevant to monitor design 13 p2154 A67-26986

Continuous monitoring and control of primary mirror figure of orbiting, diffraction limited astronomical telescope for optimum performance 16 p2680 A67-31802

Vacuum system pressure measuring and monitoring by remote control methods as used in Gemini spacecraft test program 17 p2859 A67-32593

Soviet book on photoelectric sensors in monitoring, control and regulation systems noting design principles, operational requirements, etc 18 p3011 A67-33716

Intensity and uniformity monitor for solar simulators using thermopile as detector 19 p3207 A67-34835

Soviet papers on thermoelectric measurements and monitoring 22 p3801 A67-40212

Vibrocadiogram used as cardiovascular monitor, applying signal averaging methods for parameter evaluation during severe subject stress 23 p3959 A67-41660

Passive sensing techniques for remote monitoring of nonelectronic systems [AIAA PAPER 67-774] 24 p4158 A67-42942

MONKEY

Cellular biochemical thermoregulation and organic mass changes in cold and heat-acclimatized monkeys 04 p0560 A67-14582

Responses of lateral geniculate nucleus of monkey to light increment and decrement and encoding of brightness 04 p0561 A67-14592

MONOCHROMATIC RADIATION

Intensity dependent frequency shift in spectral output of monochromatic giant pulse lasers measured, using Fabry-Perot interferometer 01 p0088 A67-10251

Surface photopotential of cadmium sulphide single crystals under monochromatic illumination in alternating electric field, using voltage modulation method 01 p0134 A67-10807

Laser characteristics of narrow band type I solar radio burst and magnetic dipole

transitions in split Zeeman sublevels of hydrogen atoms of solar corona in ground level 02 p0322 A67-11652

Horizon studies for monochromatic radiation following Lambert-Beer law of transmission, noting Chapman theory on exponential distribution of atmospheric constituent of absorption 04 p0613 A67-14697

Harmonic generation by traveling waves in nonlinear dispersive medium for quasi-monochromatic signals, obtaining correlation function and spectrum of second harmonic for Gaussian processes 04 p0657 A67-15146

Width of spectral absorption line of water vapor at lambda equals 0.92 mm measured with aid of monochromatic radiation source and radiometer with thermal indicator 05 p0761 A67-16342

Antenna synthesis for wide band radiation reception using Fredholm integral equation 05 p0774 A67-16912

Diathermy, derivation of equation relating monochromatic/integral radiation energy ratio of solid material of fluid heat emitter to temperature 07 p1211 A67-19130

Absorption laws for spectral-line broadening due to propagation of intense monochromatic radiation through dielectric medium 08 p1294 A67-20816

Integral hemispherical and monochromatic radiative capacity of carbon compounds at high temperatures 09 p1497 A67-21877

Quantum mechanical theory of interference between independent nonmonochromatic light beams using nonmonochromatic modes of radiation field 10 p1663 A67-22866

Monochromatic longitudinal wave amplification by charged particle beam in nonlinear plasma, noting amplitude dependence on coordinate 10 p1686 A67-23587

High power laser emitting monochromatic radiation at single frequency applicable in spectroscopy, telemetry and telecommunication 14 p2330 A67-28469

Absorption law for weak lines in semiinfinite homogeneous scattering atmosphere for isotropic scattering 14 p2314 A67-28848

Spectral energy distribution of source 3C 446 between August 17 and December 12, 1966 14 p2369 A67-28850

Homogeneity of solar prominences studied photographically in monochromatic light 14 p2382 A67-28941

Harmonic generation by traveling waves in nonlinear dispersive medium for quasi-monochromatic signals, obtaining correlation function and spectrum of second harmonic for Gaussian processes 15 p2517 A67-29333

Laser characteristics of narrow band type I solar radio burst and magnetic dipole transitions in split Zeeman sublevels of hydrogen atoms of solar corona in ground level 16 p2747 A67-31067

Abnormally high photostresses in semiconductor films under monochromatic light studied, using angular dependence observation technique 17 p2921 A67-32970

Design criteria for narrow optical passband filters used in reception of nonparallel modulated monochromatic radiation 17 p2862 A67-33291

Long-duration monochromatic emission with worldwide character in frequency spectrum of magnetic storm 18 p3041 A67-34193

Optical instrumentation for auroral and afterglow studies with applications of grating spectroscopic systems, monochromators, interferometers and photometers 23 p3996 A67-41256

MONOCHROMATOR

High resolution echelle monochromator and use in measuring ion temperature of He plasma 04 p0663 A67-14787

Photoionization and absorption coefficients of nitric oxide gas measured, using vacuum UV monochromator 06 p1037 A67-18573

Spectrum of quiet sun between 30 and 128 angstroms analyzed in November 1965, using rocketborne grating monochromator with Geiger detector 09 p1566 A67-22232

Chromospheric solar radiation measured during solar eclipse with UV monochromator, using electromagnetic radiation photomultipliers 15 p2565 A67-29573

Monochromator for measuring spectral distribution of laser light scattered by high temperature plasmas 19 p3230 A67-35593

Remote control of monochromator prism

- rotation using balanced-bridge system to regulate flow 20 p3451 A67-37308
- Spectral irradiances determined by conventional prism monochromator and by system employing narrow bandpass interference filters 21 p3656 A67-37850
- MONOCOQUE CYLINDER**
- Blaxial buckling behavior of 45 degrees eccentric-stiffened waffle cylinders using prediction theory 19 p3341 A67-35525
- MONOCULAR VISION**
- Correlation between heart rate, landing error and field of view for binocular and monocular sphere of vision of jet pilots 09 p1455 A67-21717
- MONOMOLECULAR LAYER**
- Reactive properties of p-n semiconductor structures at high injection levels for monomolecular electron-hole recombination 06 p1049 A67-17866
- MONOPLANE**
- Antonov An-24V Soviet high wing monoplane and use of electrical spot welding and metal bonding in construction 06 p0944 A67-17597
- German SIAT 223 Flamingo sports, trainer and cross-country aircraft, noting design, components and tabulated technical data 18 p2985 A67-33641
- MONOPOLE ANTENNA SYSTEM**
- Limit energy of monopole in field of earth magnetic dipole 10 p1631 A67-22800
- Radiation field of monopole antenna hinged on spherical conducting support calculated with Green function technique 13 p2081 A67-27200
- Data representing monopole antenna voltage breakdown in simulated Mars and Venus atmospheres 19 p3197 A67-35829
- Electrically thick monopole transmitting antenna integral equation for current distributions and admittance 23 p3981 A67-41207
- Limit energy of monopole in field of earth magnetic dipole 24 p4150 A67-42137
- MONOPROPELLANT**
- Self-deflagration process of hydrazine diphosphate studied for three suggested pressure regimes 14 p2376 A67-28551
- Combustion of pure liquid monopropellant droplet burning in own combustion products at low Reynolds numbers 14 p2376 A67-28552
- High density moisture-proof noncrystalline family of gas generator propellants, surveying burning rates, physical properties and application 15 p2544 A67-29980
- Lumped parameter model for monopropellant hydrazine reaction chamber developed, using mass and energy balance and reaction and diffusion rate coefficients 17 p2927 A67-31974
- Nitrate ester monopropellants studied for heat-up, ignition and combustion in high temperature nitrogen gas under moderate/high pressures, noting burning rates [AIAA PAPER 67-480] 18 p3158 A67-33949
- High density moisture-proof noncrystalline family of gas generator propellants, surveying burning rates, physical properties and application 24 p4207 A67-42921
- MONOPULSE ANTENNA**
- X-band Cassegrainian tracking antenna for space rendezvous position and rate information for navigation and guidance computations 04 p0569 A67-14502
- High efficiency S-band monopulse focal point tracking feed, discussing aperture geometry design theory 08 p1300 A67-20654
- Broadband monopulse three-element tracking feeds for spherical Luneberg lens scanning antenna, discussing radiator design, radiation pattern and cross coupling between error channels 15 p2451 A67-29924
- Cassegrain monopulse feed system using end-fire pyrold radiators 15 p2451 A67-29925
- Systematic boresight and off-boresight tracking errors in planar monopulse phased rectangular arrays produced by analog phase shifters with nonlinear transfer characteristics 17 p2825 A67-32617
- Equivalent circuit of two-port antennae with application to magic-T systems 18 p3013 A67-34527
- Squinted, sum and difference radiation patterns interrelationships for amplitude monopulse antennas with impedance mismatch and mutual coupling between feeds 19 p3197 A67-35824
- Multimode monopulse feed system optimum aperture distribution determination, obtaining maximum rate of signal change on axis 22 p3763 A67-40313
- MONOPULSE RADAR**
- Error equation for accuracy of monopulse radar in search mode applied to monopulse radar systems, using logarithmic normalization 01 p0022 A67-10446
- Signal and clutter model of monopulse radar tracking errors 02 p0201 A67-12114
- Complex indicated angle extension of monopulse normalized error signal used to locate unresolved targets 02 p0201 A67-12115
- Trimode four channel monopulse bridge with reduced microwave components 03 p0383 A67-13828
- Radiation monopulse passage through amplifying and absorbing media having form of rods 03 p0374 A67-14329
- C-band traveling wave maser for monopulse radar, analyzing saturation, recovery, duplexing and gain phase stability 08 p1293 A67-20691
- MONOXIDE**
- S CARBON MONOXIDE**
- MONTE CARLO METHOD**
- Monte Carlo techniques use of random numbers, noting Buffon needle problem, Laplace equation, number generation and radar target detection simulation 01 p0104 A67-10158
- Cost effectiveness of optimum military aircraft system, evaluating design alternatives in hardware and support concepts via Monte Carlo simulation and high speed digital computers [AIAA PAPER 66-786] 01 p0009 A67-10530
- Infinitely divisible distributions of first passage times and hitting points in ordinary random walk solved by Bessel functions 01 p0106 A67-10735
- Differentially coherent phase-shift keying system analyzed under wide range of signal and noise conditions 01 p0025 A67-10861
- Improved Monte Carlo method for calculating steady state monatomic rarefied-gas flows, using computer for calculating possibility of collision in given geometrical cell 01 p0055 A67-11292
- Stochastic process estimate of frequency and duration of weather events, using Monte Carlo simulation of probability distributions 02 p0261 A67-12079
- Intranuclear cascades of nucleon-nucleus interaction calculated on basis of Fermi gas model, using Monte Carlo method and three-dimensional relativistic kinematics 02 p0314 A67-12748
- Monte Carlo method for calculating longitudinal and transverse development of extensive air showers, considering fluctuations 02 p0318 A67-12784
- Monte Carlo computer program for simulation of thermal radiation among opaque surfaces in vacuum [ASME PAPER 65-WA/HT-40] 03 p0537 A67-14009
- Monte Carlo simulation provides realistic analysis of set of stochastic processes involved in flow within maintenance and logistics system 03 p0400 A67-14223
- Book on Monte Carlo method, method of statistical trials 03 p0462 A67-14256
- Exodus method /modified Monte Carlo method/ which does not use random numbers and can be applied to any problem admitting nodal network [ASME PAPER 66-WA/HT-61] 04 p0646 A67-15436
- Monte Carlo method analysis of rarefied gas heat transfer between parallel plates in terms of temperature, density and Knudsen number 04 p0728 A67-15807
- Angular distribution of radiation at boundary of homogeneous diffusion sphere, with isotropic central point source calculated by Monte Carlo method 05 p0838 A67-16491
- Computer simulated calculation of simple fluid properties using Monte Carlo method 05 p0927 A67-16890
- Monte Carlo technique in predicting antenna performance 05 p0775 A67-16969
- Asymmetrical angular elastic scattering distribution of electrons on helium atoms, using Monte Carlo method 06 p1034 A67-17648
- Histogram construction via algebraic Monte Carlo method, determining simultaneous effect of several input statistical variables on output variable [AIAA PAPER 67-210] 06 p1024 A67-18326
- Comparison between Monte Carlo and PERT models, noting PERT errors and Monte Carlo simulation for Voyager spacecraft development [AIAA PAPER 67-209] 06 p1097 A67-18513
- Book on electromagnetic wave propagation and turbulent media covering invariant imbedding method, turbulence generation, statistical methods of analysis, etc 08 p1295 A67-20984
- Monte Carlo simulation studies for fatigue data analysis of rolling-contact bearings, using Weibull equation [ASLE PAPER 66AM 1B2] 08 p1336 A67-21038
- MORL system reliability analysis, discussing Monte Carlo simulation, major parameters, constraints, program contingencies, etc 08 p1411 A67-21073
- Repetitive analog computer for Monte Carlo method solution of linear stochastic programming problems 08 p1299 A67-21198
- Ionization calorimeter performance simulation using Monte Carlo simulation 09 p1497 A67-21900
- Numerical quadrature methods of Romberg, Chebyshev and Monte Carlo, noting analytic function and program for machine evaluation 09 p1468 A67-22047
- Transmission probability describing free molecular flow through vacuum systems obtained via Monte Carlo program 09 p1488 A67-22104
- Monte Carlo computer program for calculating molecular gas flow with axisymmetric vacuum structures, showing applications on pumping speed test domes and measuring apparatus for sticking coefficients 09 p1488 A67-22105
- Monte Carlo calculations of impurity band states in degenerate semiconductor 09 p1558 A67-22618
- Monte Carlo and direct calculation methods analyzed in connection with microelectronic circuit designs 10 p1610 A67-22978
- High density one-component plasma radial distribution determination by Born-Green-Yvon integral 13 p2162 A67-26282
- Angular distribution of radiation at boundary of homogeneous diffusion sphere, with isotropic central point source calculated by Monte Carlo method 13 p2155 A67-26346
- General algorithm for solving atmospheric optics problem applicable to short wave radiation transfers of atmospheres with various light scattering, using Monte Carlo method 13 p2151 A67-26684
- Couette flow and heat transfer of rarefied gas between parallel plates analyzed by Monte Carlo method 13 p2223 A67-26961
- Monte Carlo approach to transition and free molecular flow problems having mass as well as thermal motion of molecules 13 p2101 A67-26967
- Monte Carlo calculation of kinetics of chemically reacting multicomponent gas for finite number of particles followed through random collision processes 13 p2102 A67-26971
- Monte Carlo evaluation of Boltzmann collision integral for translational relaxation and plane steady shock problems 13 p2103 A67-26974
- High energy muon flux in air showers at sea level determined, using semi-Monte Carlo method 13 p2195 A67-27579
- Atmospheric optics problems solved by Monte Carlo method, presenting results in tabular and graphical form 14 p2313 A67-28767
- Monte Carlo method applied to heat conduction problems, discussing steady state and transient situations with linear and nonlinear boundary conditions [ASME PAPER 65-WA/HT-1] 15 p2578 A67-29318
- Statistical probability distribution for determining systematic errors of potentiometer multiplier by Monte Carlo method /static testing/ 16 p2633 A67-30464
- Reverse Monte Carlo method for circuit analysis, noting computer analysis of sense amplifier 16 p2633 A67-30475
- Random signal treatment by Monte Carlo method for cutting tool applications 16 p2643 A67-30922
- Monte Carlo evaluation of linear-and eigenvector-method for estimation of pulse transfer function of linear, time-invariant

dynamic feedback system 16 p2653 A67-31695
 Linear/Monte Carlo method performance evaluation of intercept/rendezvous guidance and navigation for advanced space missions 17 p2882 A67-32493
 Impurity atoms and defects distributions in Si and Ge bombarded by different ions of medial energies calculated by Monte Carlo method 17 p2916 A67-32839
 Phonon spectrum of Si calculated by Monte Carlo method, determining Si thermodynamic functions 18 p3098 A67-33629
 Synthesis of radar ambiguity functions via burst-pulse time-frequency waveform coding, employing Bayesian statistical analysis 18 p3000 A67-34109
 Modified Monte Carlo procedure using partitioning method and stratified sampling 18 p3072 A67-34396
 Electron flow in low density argon gas diode analyzed by Monte Carlo method 18 p3091 A67-34641
 Development and application of Monte Carlo logistic simulation model for measuring system availability dependence on reliability, maintainability and logistic support 18 p3021 A67-34674
 Risk assessment techniques for design, fabrication and testing of complex spacecraft noting component reliability, Bayesian statistics, Monte Carlo technique, etc 18 p3138 A67-34683
 Hybrid computer Monte Carlo techniques for solving partial differential equations of continuous Markov processes 19 p3188 A67-36057
 Nonlinear circuits analyzed by Monte Carlo method for computer synthesis 20 p3407 A67-36331
 Two-point boundary value problem approximate solution using Monte Carlo path integral calculation 20 p3475 A67-36481
 System reliability prediction and confidence limits for several component failure probability distributions, using Monte Carlo simulation on digital computer 20 p3455 A67-37314
 Monte Carlo method to determine derivatives of radiation doses in optimization of shape and composition of protective shields 21 p3577 A67-38425
 General algorithm for solving atmospheric optics problem applicable to short wave radiation transfers of atmospheres with various light scattering, using Monte Carlo method 21 p3618 A67-38428
 Minimum variance simulation for satellite attitude determination reliability using magnetic and solar measurements 21 p3715 A67-39150
 Repetitive analog computer for Monte Carlo method solution of linear stochastic programming problems 22 p3764 A67-39865
 Free and near-free molecular flow via cylindrical ducts using Monte Carlo method and high speed digital computer 22 p3784 A67-39946
 Lunar rendezvous spacecraft guidance system performance for various initial conditions and instrument errors simulated by Monte Carlo computer program 22 p3832 A67-39965
 Monte Carlo method for molecular vacuum pump calculation, noting applicability to molecule-boundary and molecule-molecule collision conditions 22 p3785 A67-40012
 Rocket engine cluster thrust and moment vectors analyzed statistically for thrust misalignment 22 p3869 A67-40170
 Intranuclear cascades of nucleon-nucleus interaction calculated on basis of Fermi gas model, using Monte Carlo method and three-dimensional relativistic kinematics 22 p3876 A67-40250
 Monte Carlo method for calculating longitudinal and transverse development of extensive air showers, considering fluctuations 22 p3878 A67-40286
 Light gas escape flux from atmosphere velocity and angular distributions near critical level using Monte Carlo analysis 24 p4224 A67-41823
 Electron photon cascades in lead scintillator devices investigated using Nagel Monte Carlo calculations for energies between 100 and 440 Mev 24 p4191 A67-42439
 Mathematical model for identification and control of systems safety in manned space programs using Monte Carlo techniques [AIAA PAPER 67-936] 24 p4245 A67-43026

MOON

SA EARTH-MOON SYSTEM
 SA HILL LUNAR THEORY
 SA LUNAR ATMOSPHERE
 SA LUNAR BASE
 SA LUNAR COMMUNICATION
 SA LUNAR COMPOSITION
 SA LUNAR CRATER
 SA LUNAR CRUST
 SA LUNAR DISK
 SA LUNAR DUST
 SA LUNAR ECHO
 SA LUNAR ECLIPSE
 SA LUNAR EFFECT
 SA LUNAR ENVIRONMENT
 SA LUNAR EVOLUTION
 SA LUNAR EXCURSION MODULE
 /LEM/
 SA LUNAR EXPLORATION
 SA LUNAR FAR SIDE
 SA LUNAR FLIGHT
 SA LUNAR GEOLOGY
 SA LUNAR GRAVITATION
 SA LUNAR GRAVITATIONAL EFFECT
 SA LUNAR IONOSPHERE
 SA LUNAR LANDING
 SA LUNAR LANDING MODULE
 SA LUNAR LANDING SITE
 SA LUNAR LAUNCH
 SA LUNAR LIMB
 SA LUNAR LOGISTICS
 SA LUNAR LUMINESCENCE
 SA LUNAR MAGNETIC FIELD
 SA LUNAR MAP
 SA LUNAR MARE
 SA LUNAR MOBILE LABORATORY
 /MOLAB/
 SA LUNAR OBSERVATORY
 SA LUNAR OCCULTATION
 SA LUNAR ORBIT
 SA LUNAR ORBITAL RENDEZVOUS
 /LOR/
 SA LUNAR PERTURBATION
 SA LUNAR PHASE
 SA LUNAR PHOTOGRAPH
 SA LUNAR PHOTOGRAPHY
 SA LUNAR PROBE
 SA LUNAR PROGRAM
 SA LUNAR ROVING VEHICLE /LRV/
 SA LUNAR SATELLITE
 SA LUNAR SCATTERING
 SA LUNAR SEISMOGRAPH
 SA LUNAR SHADOW
 SA LUNAR SOIL
 SA LUNAR SPACECRAFT
 SA LUNAR SURFACE
 SA LUNAR SURFACE VEHICLE
 SA LUNAR TEMPERATURE
 SA LUNAR TIDE
 SA LUNAR TOPOGRAPHY
 SA LUNAR TRACKING
 SA LUNAR TRAJECTORY
 Masses of moon and Venus and astronomical unit determined from Mariner II Doppler data, noting sources of error 05 p0895 A67-16575
 Photographic observation of lunar topography and Mars 07 p1247 A67-19332
 Lunar external gravitational field, topographic surface and moments of inertia [AAS PAPER 66-189] 08 p1387 A67-20962
 Physics of moon and environment - Conference, London, June 1965 08 p1388 A67-21008
 Book on moon in space age covering lunar motion around gravity center, nature of lunar soil, lunar satellite perturbations, etc 08 p1395 A67-21156
 Lunar rotation about center of gravity, optical libration and physical libration in selenocentric coordinates 08 p1395 A67-21157
 Dependence of thermal conductivity of lunite on temperature, noting properties of moon surface 09 p1565 A67-21987
 Political ramifications of lunar landings, noting UN resolution concerning national possession of moon 13 p2230 A67-26339
 Moon and planets - Conference, Vienna, May 1966 18 p3120 A67-34134
 Moon mechanical ellipticity determined by modification of Habibullin method adapted to Schrutka-Rechtenstamm artifact 18 p3128 A67-34304
 Moon physical libration in longitude 18 p3129 A67-34306
 Lunar forced physical librations calculation improved by using digital computer programmed to generate iterative solutions 18 p3129 A67-34307
 Moon Blink project for detecting red or blue temporary color

phenomena 18 p3134 A67-34535
 Penetrating particles in cosmic radiation deep underground in Kolar gold field experiment, discussing muon-neutrino interaction 24 p4210 A67-42582
MOON-EARTH TRAJECTORY
 SA EARTH-MOON TRAJECTORY
 Geocentric initial conditions for motion of bodies leaving moon surface after initial instantaneous thrust 01 p0148 A67-10387
 Three-impulse orbital transfer from lunar orbits and earth reentry trajectory applications [AAS PAPER 66-134] 07 p1255 A67-19993
 Three-impulse orbital transfer from lunar orbits and earth reentry trajectory applications [AAS PAPER 66-134] 13 p2210 A67-27544
 Earth-moon and moon-earth trajectory parameters related to lunar orbit conditions for synthesizing lunar orbit trajectory 13 p2210 A67-27616
 Moon-earth trajectories, with formulas for given angular ranges of flight, obtaining optimum velocity to depart from lunar gravitational field 21 p3704 A67-38584
MOON ILLUSION
 Lunar parallax determination by four methods 08 p1395 A67-21158
MORL
 S MANNED ORBITAL RESEARCH LABORATORY /MORL/
MORPHOLOGICAL INDEX
 Lunar crater classification by morphological types discussing ring structures 16 p2747 A67-30984
MORPHOLOGY
 SA LUNG MORPHOLOGY
 Fracture mechanism for formation of dimpled fracture surface morphology 06 p1105 A67-18562
 Energy, time and physical morphology of atmosphere, hydrosphere and lithosphere surfaces 06 p1091 A67-18994
 Morphology of lunar craters from Ranger photographs, noting distribution and possible competing processes of crater formation and destruction 11 p1865 A67-24608
 Cardiac changes under hypoxia, experimental morphological study 13 p2058 A67-26756
 Schroeter rule and modification of lunar crater impact morphology 13 p2210 A67-27602
 Morphological behavior of damped type geomagnetic pulsations associated with storm sudden commencements and sudden impulses 17 p2851 A67-33211
 Worldwide morphology of atomic oxygen nightglows 18 p3032 A67-33580
 Worldwide auroral morphology, discussing latitude and local time distribution and temporal variations 18 p3032 A67-33581
 Human-hair-root activity during short term deprivation of protein 19 p3177 A67-34954
 Auroral substorms, examining energy spectrum and flux of precipitating particles and morphology 20 p3431 A67-37100
 Evening sector polar magnetic substorm disturbance field morphology in transition region 21 p3616 A67-37998
 Morphology of Jupiter decametric radio sources 21 p3710 A67-38997
 Additive elements studied for influence on morphology, nature and hot plasticity of sulfides in austenitic stainless steels 21 p3646 A67-39077
 Compact and dispersed cosmic matter using morphological approach to discovery, invention and research in astronomy 22 p3890 A67-40429
MORPHOTROPISM
 SA CRYSTAL STRUCTURE
 Enthalpy changes in ammonium perchlorate during linear heating, noting crystal structure transformation and subsequent decomposition 14 p2376 A67-28903
MORSE POTENTIAL
 Pitzer acentric factor relationship to Morse intermolecular potential function appears to hold only for normal fluids 07 p1138 A67-20193
MOSS
 S METAL OXIDE SEMICONDUCTOR /MOS/
MOSAIC
 Mosaic construction and image analysis for Surveyor TV pictures 08 p1333 A67-21504
MOSS
 S MANNED ORBITAL SPACE STATION /MOSS/

MOSSBAUER EFFECT

Motion sensing using Mossbauer nuclear resonance effect with radiation source located on body in motion and detector in controlled motion 01 p0062 A67-10156

Mossbauer spectroscopy used to study precipitation reactions in 17-7 PH stainless steel and in 18Ni-8Co-5Mo maraging steel 02 p0256 A67-12705

Scattering amplitude for multipole mixtures in Mossbauer effect determined, from which can be derived absorption cross section and complex refractive index 04 p0660 A67-14758

Mossbauer investigations of stoichiometric manganese-ferrite and two magnesium-manganese ferrites made at room and liquid nitrogen temperatures 04 p0676 A67-14925

Mossbauer nuclear resonance fluorescence effect spectrometer using Doppler principle, with applications to aerospace 05 p0843 A67-16544

Time analysis of Mossbauer spectrum variation and isometric shift of source Te-125m in PbTe absorber following neutron irradiation in reactor 09 p1559 A67-22661

Neel temperature in NiO and MnO with divalent Fe measured using Mossbauer effect 12 p1985 A67-25844

Ferrous ion order-disorder in meteoritic pyroxenes, using Mossbauer iron 57 absorption, noting metamorphic history of chondrites 21 p3702 A67-38128

Mossbauer spectra of FeMo alloys for closed space compositions show overlap of disturbed surroundings of impurity iron atoms and magnetic moment 24 p4203 A67-42108

MOT

S MANNED ORBITAL TELESCOPE /MOT/

MOTION

S ANGULAR MOTION

S BROWNIAN MOTION

S DOMAIN WALL MOTION

S EARTH MOTION

S HARMONIC MOTION

S HEAD MOVEMENT

S HEAVING MOTION

S ION MOTION

S LIBRATIONAL MOTION

S ORBITAL MOTION

S PARTICLE MOTION

S PLANETARY MOTION

S SPACECRAFT MOTION

S VERTICAL MOTION

S WAVE MOTION

MOTION EQUATION

SA BALANCE EQUATION

Motion equation solution to viscous conducting flow at inlet of diverging channel using difference method, noting magnetic field effect 01 p0120 A67-10184

Geomagnetic stabilization of satellite initially torque-stabilized, deriving motion equation 01 p0153 A67-10210

Plasma density dependence of adiabatic motion of plasmoids in longitudinal magnetic field 01 p0122 A67-10351

Charged particle motion in field of traveling electromagnetic waves used in studies for microwave amplifiers, particle accelerators, etc 01 p0022 A67-10352

Levi-Civita regularized equations of elliptic motion of particle influenced by massive primary and perturbed by smaller primary, Part I, Trigonometric series solution 01 p0147 A67-10379

Levi-Civita regularized equation of elliptic motion of particle influenced by massive primary and perturbed by smaller primary, Part II, Applications to circular and collision orbits 01 p0147 A67-10380

Existence of class of quasi-periodic solutions of three-body problem for near-circular inclined planetary and lunar orbits, Part I 01 p0148 A67-10382

Encke special perturbation method of integrating motion equations of near-earth satellites modified to eliminate first-order effects of earth oblateness 01 p0148 A67-10383

Difference equations of absolute motion applied to universal rendezvous guidance scheme 01 p0110 A67-10427

Small-perturbation hover dynamics motion equations, characteristic modes, stability derivatives and dimensional analysis [SAE PAPER 660578] 01 p0010 A67-10570

Energy functionals and universal integrals of motion for force field symmetric about

axis of rotation 01 p0113 A67-10680

Lateral motion of simply supported axially loaded viscoelastic column governed by system of linear ordinary differential equations with periodic coefficients 01 p0106 A67-10732

Motion equations of gyrost at around fixed point reduced to two-equation system 01 p0067 A67-10821

Asymptotic theory of elastic plate dynamics, deriving displacement equations and boundary conditions 01 p0162 A67-10822

Certain solutions to problem of motion of solid body with clamped point in homogeneous gravitational force field 01 p0114 A67-10990

Singularity in motion equations of closed loop optimal guidance systems 01 p0111 A67-11224

Interaction between atoms of solid surface and gas phase, obtaining closed-form solution of motion equations 01 p0118 A67-11295

Disturbance theory linearized initial value problems for free trajectories passively moving above smooth earth surface 02 p0320 A67-11465

Analytic solution in terms of modified Bessel functions of synergetic turn in exponential atmosphere, using spacecraft engines only for drag cancellation and orbit trimming 02 p0331 A67-11938

[AIAA PAPER 66-487] Stability analysis of steady state dynamic holonomic mechanical systems using Rouse, Kelvin, Poincare and Chetaev theorems 02 p0267 A67-11959

Body of revolution bounded by sphere rolling on stationary sphere with force function of applied forces dependent on only one coordinate 02 p0267 A67-11960

Solid body motion equation about stationary point fixed at earth surface 02 p0267 A67-11961

Variational problem of optimal motion in gravitational field, for limited-power propulsion system in combination with energy accumulator and engine with limited jet velocity 02 p0327 A67-12332

Weight factor effects on optimal motion parameters of variable mass system with limited velocity jet propulsion in gravitational field 02 p0327 A67-12333

Collision paths of free particle in Newtonian gravitational field examined, using analogy of circular restricted three-body problem 02 p0328 A67-12403

Symmetry groups of motion equation determined, using generators of Lie spatial groups 02 p0268 A67-12424

Qualitative dynamic stability analysis of motion equations with two zeros and trajectories near singular line 03 p0467 A67-12887

Linearized motion equation of self-adaptive systems with stabilized frequency characteristics, considering effect of control and noise signals in basic control loop 03 p0390 A67-13101

Axially symmetric motion of elastic spherical sandwich shell, determining natural frequencies and effects of shear deformation, normal stress and rotatory inertia 03 p0522 A67-13212

Motions of asymmetrical rigid body subjected to no-power forces 03 p0468 A67-13349

Exact field equations for motion of hyperelastic rod derived from general three-dimensional theory 03 p0522 A67-13391

Stability regions for compressible fluid squeeze-film journal bearing of infinite length, considering motion along axis [ASME PAPER 66-LUB-15] 03 p0431 A67-13758

Existence of exact solution to motion equations for charged particles in acute angled magnetic trap 03 p0486 A67-14064

Discrete gyroscopic servocontrol in presence of multidimensional random noise, ensuring optimal reproduction of input signal 03 p0465 A67-14157

Natural and forced oscillations of sphere-array moving with collisions, analyzing quasi-elastic properties of system 03 p0432 A67-14182

Auxiliary system considered simultaneously with given dissipative system in variational formulations, noting motion equations 03 p0530 A67-14175

Refraction of plane shock wave by

interface between different gases, reducing motion equation to polynomial of degree 12 04 p0601 A67-14465

Behavior of diamagnetic particles in moving magnetic field with respect to propulsion and MHD technology in space vehicles 04 p0687 A67-14546

Motion equation and measurement of angles of aircraft closely approaching vertical plane, using new coordinate system 04 p0704 A67-14776

Third integral of motion in series form derived by Contopoulos combined with known energy and field integrals describes orbits of axisymmetric star systems 04 p0699 A67-14981

Aperiodic motion of two bodies of variable mass across canonical cross section, constructing osculating orbit and deriving equations for variation rate 04 p0700 A67-15202

Relative motion of body about satellite in orbit, determining impulses which cause body to remain in satellite vicinity 04 p0706 A67-15249

Principles of suboptimal perturbation guidance and methods for polynomial approximation of guidance matrices 04 p0655 A67-15629

First transcendent integrals of motion equations of heavy solid about fixed point 04 p0659 A67-15756

Impulsively thrusting rocket and bounded thrust rocket in relation to Newton law of motion, obtaining rigorous equation of motion 04 p0707 A67-15881

Program selection for motion equations, parameters and control functions maximizing composite flight vehicle probability of delivering payload to given region 04 p0552 A67-15882

Motion theory of discrete defects in linear elastic continuum 05 p0908 A67-16038

Variational problem of rocket dynamics in homogeneous gravitational field in empty space reduced to differential equation system 05 p0904 A67-16049

Eddy current damping effect on motion equation of magnetization vector in thin ferromagnetic film switching by coherent rotation 05 p0860 A67-16070

Book on aerogasdynamics in relation to rocket and aviation technology including shock waves, rarefaction flow, heat transfer, skin friction, etc 05 p0747 A67-16173

Stresses in solids moving during loading, using velocity vector and strain rate tensor as variables for instantaneous state of body motion 05 p0914 A67-16194

Piston motion effect on flow uniformity in hypersonic gun tunnel, using perforated plate technique to prevent piston fluctuation 05 p0791 A67-16430

Instability modes of cantilevered bars induced by fluid flow through attached pipes, examining cases of torsional and transverse flutter and torsional buckling 05 p0921 A67-16882

Integral motion equations of rigid body with cavity partly filled with viscous incompressible fluid with free surface 05 p0921 A67-17005

Motion analysis of elastic deformable body visualized as rigid frame and elastic particles 05 p0923 A67-17183

Spin scale factor of Frick for scaling body fixed motion equations analyzed, deriving near optimum factor and near maximum time interval of integration for spinning missiles 05 p0906 A67-17362

Approximation for low thrust trajectory without singularity at escape and having correct behavior up to and beyond escape, using motion equation 05 p0903 A67-17363

Steady oblique nonlinear waves in warm collision-free plasma 05 p0857 A67-17425

Three and six degrees of freedom missile subsystem design analysis using flight simulation by hybrid computer 05 p0789 A67-17515

Mechanics of celestial bodies including problems on Newton gravitation law, motion equations, two-body problem, Kepler law, etc 06 p1030 A67-17772

Restricted problem of three bodies, two of which are assumed to be point masses, determining motion of third body 06 p1081 A67-17779

Qualitative methods in n-body problem concerned with masses motion in inertial space under gravity, solving motion

- equation 06 p1081 A67-17781
- Orbital decay, considering drag force expression, motion equation, atmospheric structure, King-Hele theory, etc 06 p1081 A67-17786
- Successive approximations determining radiation pressure effect on and disturbing function of motion equations of artificial satellite 06 p1081 A67-17787
- Improving estimates of solutions of linear perturbed-motion equations of mechanical systems with variable coefficients 06 p1023 A67-18038
- Stabilization of gyrostabilizer using motion equations as given by Volterra 06 p1002 A67-18043
- Comet model construction assuming rectangular coordinates system, noting particle motion initial velocity and repelling acceleration 06 p1084 A67-18205
- Inverse method of structural analysis of automatic control systems described by nonlinear differential motion equations 06 p0976 A67-18238
- Self-preserving turbulent jet ejector, solving equations of motion to determine system geometry corresponding to flow conditions [AIAA PAPER 67-127] 06 p0988 A67-18456
- Regularization of motion equations in computation of vehicle trajectory going near singularity [AIAA PAPER 67-26] 06 p1087 A67-18464
- Differential equation of motion of meniscus of MHD fluid in capillary in TM field due to surface tension 06 p1044 A67-18681
- Motion about fixed point of solid body with cavity filled with viscous incompressible fluid 06 p0991 A67-18810
- Small oscillations and stability of hyperelastic incompressible rectangular strip under uniformly distributed biaxial load 06 p1111 A67-18892
- Near wake uniqueness and criticality condition in Crocco-Lees mixing theory, obtaining critical point from boundary layer equations of motion [AIAA PAPER 67-65] 07 p1168 A67-19433
- Lagrangian dynamical system determined under parametric form of motions applied to two- and three-body problems 07 p1216 A67-19722
- Integrodifferential motion equations for Jupiter satellites 07 p1250 A67-19724
- Modification of Encke perturbation method for computing satellite orbits, obtaining integration of motion equations [AAS PAPER 66-93] 07 p1252 A67-19957
- Motion of near lunar satellite in initially circular orbit analyzed by integrating equations for time rates of change of orbit elements [AAS PAPER 66-95] 07 p1252 A67-19959
- Constructing formal integrals, in form of power series, of time independent Hamiltonian system near equilibrium point [AAS PAPER 66-102] 07 p1216 A67-19964
- Theorems on interaction of parts of mechanical system with smooth holonomic constraints 07 p1224 A67-20038
- Nearly commensurable periods in restricted problem of three bodies, calculating long period variations in interior 2/1 case, noting solutions to Poincare problem 08 p1381 A67-20391
- Selection of constants defining reference orbit of planet and use in differential equations of motion 08 p1382 A67-20394
- Second order equations of motion for free axisymmetric deformation of thin spherical shells, discussing membrane and composite mode of solution 08 p1416 A67-20490
- Error in application of WKB method to linearized postburnout equation of motion of sounding rocket 08 p1406 A67-20510
- Nonlinear motion theory for axisymmetric sounding missiles or rockets with Magnus moments, showing application to near pitch-roll resonance 08 p1407 A67-20515
- Nonlinear equations of motion of bifilar pendulum without using suspension geometry or inertia properties of suspended body 08 p1354 A67-20922
- Dynamical effects of heat absorption or rejection on flow of electrically charged fluid considered within special relativity framework 08 p1426 A67-20923
- Numerical integration of restricted problem of three bodies for finding lunar trajectories, using motion equations and Taylor series 08 p1396 A67-21181
- Restricted problem of three bodies analyzed using Birkhoff variables and power series representing motion equations, obtaining coefficients for collision orbit 08 p1396 A67-21182
- Motion equations for ionized irregularity of finite length applied to barium ion cloud, deriving expression for ionospheric electric field 08 p1326 A67-21357
- Onboard device locating present and future orbital satellite position through microfilm map dependent on satellite motion equation 08 p1352 A67-21525
- Airborne guidance computations using prescribed-H-method, representing two-body motion in inertial space, presenting equations for target hitting, circular orbit, etc 08 p1352 A67-21532
- Relativistic rotation of perigee of satellite determined from first integral of motion equation 09 p1563 A67-21858
- Graphical analysis of rotor flutter in hover using modified Theodorsen function 09 p1573 A67-21743
- Gradient method solution for class of optimal control problems, minimizing mean square value of finite state components of object in motion 09 p1482 A67-21871
- Elliptic type orbit determination in generalized problem of two stationary centers by integration in quadratures of motion equations of satellite 09 p1565 A67-21902
- Motion equations and boundary conditions for viscous liquid, noting operator characteristics of viscosity coefficients near critical point 09 p1487 A67-21909
- Unstable motion of incompressible viscous fluid in interspace between concentric spheres 09 p1487 A67-21928
- Coulomb friction in gyroscopic system analyzed, solving motion equation 09 p1498 A67-22033
- Nonlinear system response to pulse excitation, solving problem via Poincare perturbation method 09 p1533 A67-22153
- Motion induced by sources and sinks distributed along vertical boundary of rotating fluid, noting role of Ekman layers 09 p1489 A67-22416
- Turbulent fluctuations in rotationally symmetrical jet, obtaining velocity profiles from integration of motion equations 09 p1490 A67-22548
- Hydrodynamic coefficients of equations of perturbed motion for body with cavity in form of circular cylinder with flat bottom 10 p1624 A67-23032
- Dynamic analysis of sandwich plate with clamped edges executing plane strain motions, using variational motion equation and Galerkin method 10 p1717 A67-23138
- Trajectory of rebounding detonation wave in approximate analytic solution of nonlinear equation of motion 10 p1626 A67-23152
- Semianalytical solution of motion of satellite in lunar orbit, considering perturbations due to lunar and earth gravity and solar attraction 10 p1706 A67-23185
- Wind shear theory of formation of temperate zone blanketing sporadic E layers, noting motion equation for ions in ionospheric E region 10 p1644 A67-23258
- First integrals of motion to determine stationary distribution function of charged particles and self-consistent magnetic field of plasma 10 p1685 A67-23464
- Temperature of moving body in relativistic frame of reference 10 p1680 A67-23497
- Motion equations used in determining lateral stability and control derivatives for STOL aircraft 10 p1595 A67-23551
- Longitudinal perturbed motion of aircraft with free-floating canard, obtaining differential equation corresponding to characteristic equation 10 p1595 A67-23606
- Dynamic behavior of multidimensional system described by ODE 10 p1675 A67-23608
- Differential equations of motion for permanent rotation heavy gyro with fixed point 10 p1657 A67-23668
- Motion stability of dynamic system whose equation has two small positive roots 10 p1681 A67-23680
- Motion equations for planar simulation of flexible Saturn IB launch vehicles under in-flight winds using Appell equation, noting sloshing mode 10 p1713 A67-23750
- Wall law for thick turbulent boundary layer with sublayer thickness compared to radius of transverse curvature, analyzing motion equations 10 p1629 A67-23847
- Numerical finite difference solution of three-dimensional equations of motion for laminar natural convection, noting Navier-Stokes equation 11 p1774 A67-23861
- Relativistic electron motion in mirror magnetic field interacting with axial electromagnetic wave calculated, comparing results with Seldi experiment 11 p1828 A67-23895
- Torque on sun calculated from solar wind motion, taking rotation and magnetic field effects into consideration 11 p1857 A67-23931
- Diurnally oscillating component of thermospheric east-west pressure acceleration at equator, noting balancing effect of viscous diffusion, ion distribution, etc 11 p1785 A67-23939
- Classical equation of motion of extended monopole charged particle without preacceleration or runaway solutions 11 p1821 A67-23977
- Singular characteristics of dynamic systems with steady state motion, noting effect of constantly acting small perturbations 11 p1818 A67-24147
- Laplace stability of motion of heavy rigid body with fixed point moving along spherical surface 11 p1818 A67-24163
- Gyroscopic moment effect on critical speeds of shaft-disk system mounted in short end bearings, obtaining frequency equations [ASME PAPER 67-VIBR-9] 11 p1795 A67-24169
- Frequency response, equation of motion, elastic restraint and structural flexibility of gyroscopic vibration absorber, noting antiresonant frequency functions [ASME PAPER 67-VIBR-13] 11 p1795 A67-24173
- Influence of internal friction on high speed rotor stability using motion equation, noting bearing support flexibility and damping role [ASME PAPER 67-VIBR-14] 11 p1795 A67-24174
- Rotor supported in fluid film journal bearings, eliminating self-excited vibrations through motion equation [ASME PAPER 67-VIBR-28] 11 p1797 A67-24186
- Incompressible Newtonian fluid applied to dynamic reversibility of flows, analyzing motion equation and possible integration of Navier-Stokes equation 11 p1778 A67-24273
- Stability of bilaterally symmetrical object towed in air along straight line, obtaining characteristic equation as test for lateral or longitudinal stability 11 p1743 A67-24309
- Error accumulation in numerical integration of motion equation analyzed for circular satellite orbits 11 p1859 A67-24317
- Reentry guidance by threshold network storage of precomputed optimum commands, using analogy of surface approximation problem in N plus one-dimensional space [AIAA PAPER 66-52] 11 p1869 A67-24338
- Motion of hollow body filled with viscous fluid at large Reynolds numbers, determining Zhukovskii potentials and examining small oscillations 11 p1782 A67-24673
- Dynamic effects on satellite motion of mechanical deformations in stabilizing system, deriving equations for rotational motion about center of inertia 11 p1870 A67-24674
- Random motion transport relation to heat propagation noting tensor characteristics, entropy effects and path dependence 11 p1819 A67-24757
- Instability zone of electrometer, noting relation to parametric resonance of needle and Hill equation form of needle motion 11 p1877 A67-24758
- Variational principle as basis for dynamics of elastic shell theory, discussing motion described by Timoshenko type equation 11 p1877 A67-24853
- Plasma density dependence of adiabatic motion of plasmoids in longitudinal magnetic field 11 p1844 A67-25024
- Charged particle motion in field of traveling electromagnetic waves used in studies for microwave amplifiers, particle accelerators, etc 11 p1755 A67-25025
- Reading errors of oscillating plant mounted gyrocompass assuming gyromoment

- compensation and no friction, determining motion through differential equation 11 p1794 A67-25045
- Energy functionals and universal integrals of motion for force field symmetric about axis of rotation 11 p1821 A67-25069
- Charged particle motion in magnetosphere under sudden magnetic pulse, compiling Fokker-Planck equation for particle distribution function 12 p1992 A67-25118
- Post-Galilean transformation to which Einstein-Infeld-Hoffmann motion equation is invariant, considering transformation to center of mass system 12 p1965 A67-25125
- General solution for motion equation of rotating shaft with changing angular velocity, noting transition through critical speed 12 p1949 A67-25408
- Variational principles and reciprocity theorems for dynamic problems of elastic shell theory, particularly motion described by linear equations of Timoshenko type theory 12 p2019 A67-25563
- Optimum propulsion control law selection for limited motion capacity in mass accumulation regime determined, considering two-dimensional problem of vehicle motion 12 p1989 A67-25659
- Equations for small oscillations of mechanical system with solid components divided into groups by system of generalized coordinates 12 p1967 A67-25661
- Green function theory of nonlinear transport coefficients 12 p1967 A67-25846
- Second order solutions to motion equations governing satellite rendezvous in elliptical orbit 12 p2012 A67-25931
- Nonlinear oscillation effect on motion equation of elastic object under free flight conditions 12 p2032 A67-25966
- Integration of abbreviated motion equations for gyroscopes, obtaining expressions for gimbal errors 12 p1945 A67-25967
- One-dimensional heat flow to confined ideal gas solved on digital computer, discussing energy equations, thermal gradient induced fluid motion, etc [AIAA PAPER 67-337] 12 p2039 A67-26051
- Conditional stability of class of controlled systems, noting aircraft controlled by autopilot 12 p1919 A67-26104
- Magnetic field intensification in plasmas determined from solution of MHD equations, noting formation of time independent fields 13 p2163 A67-26292
- Motion equations and middle position equations for damping of stochastic oscillation in measuring apparatus pointer 13 p2119 A67-26622
- Separated compression shock circulation in front of wedge profiles at high Mach numbers 13 p2049 A67-26640
- Three-dimensional supersonic flow for ideal fluids using Euler motion equation 13 p2050 A67-26648
- Dynamic equations for interacting connected rigid bodies 13 p2212 A67-26838
- Flow and heat transfer in viscous fluid layer expanding over rotating disk, calculating energy and motion equations 13 p2224 A67-27050
- Laminar motion equation for conducting gas jet expansion along plane wall in presence of transverse magnetic field solved in series form 13 p2168 A67-27304
- Coupled nonlinear equations integration in boundary layer theory with specific reference to heat transfer near stagnation point in three-dimensional flow 13 p2224 A67-27463
- Equilateral position stability of equilibrium in planar restricted problem of three bodies for mass ratio 13 p2205 A67-27477
- Integrals of motion in three-dimensional restricted three-body problem as generalizations of angular momentum 13 p2205 A67-27480
- Modification of Encke perturbation method for computing satellite orbits, obtaining integration of motion equations [AAS PAPER 66-93] 13 p2207 A67-27517
- Motion of near lunar satellite in initially circular orbit analyzed by integrating equations for time rates of change of orbit elements [AAS PAPER 66-95] 13 p2207 A67-27519
- Motion of variable-mass mechanical system with friction described by 3N equations 13 p2159 A67-27709
- Existence of exact solution to motion equations for charged particles in acute angled magnetic trap 13 p2172 A67-27717
- Integrals of motion-equations for charged particles in axisymmetric magnetic field derived using perturbation theory 14 p2353 A67-27752
- Steady slow motion of time-independent non-Newtonian liquid through tapered tube, deriving motion equations 14 p2294 A67-27822
- Mathematical investigation of satellite motion in vicinity of critical inclination, analyzing singularity 14 p2384 A67-28077
- Stability problems in control system of Saturn launch vehicles 14 p2393 A67-28085
- Modulation of L/D and bank angle to achieved heading, range and trajectory stabilization, using closed form equations 14 p2347 A67-28114
- Elastic rod, string or torsional member under effect of accelerating axial load, solving differential equation of motion in fixed end condition 14 p2399 A67-28140
- Method of averaging applied to solution of canonical equation system describing particle motion at high altitude in gravitational field of nonspherical planet 14 p2388 A67-28637
- Numerical solutions of Poisson and motion equations for electron gun design, examining truncation error via perturbation theory 14 p2287 A67-28677
- Gas laser quantum theory, deriving motion equation for radiation-density matrix 14 p2332 A67-28716
- Moment stress effect on natural oscillation frequency, deriving motion equations of circular cylindrical shell 14 p2401 A67-28735
- Computer programs for calculating curvature tensors and motion equations [JPL-TR-32-1122] 14 p2276 A67-28847
- Helicopter rotor and pylon stability investigated through motion equation 14 p2246 A67-29048
- Missile dynamic behavior analysis using linear aeroballistic theory in conjunction with numerical computations of motion equation 14 p2395 A67-29058
- Motion of ideally conducting gas near zero line of magnetic field in terms of MHD equations, obtaining exact solutions for two-dimensional nonstationary problem 14 p2363 A67-29076
- Cometary orbit evolution of Jupiter family, considering influence of Jupiter 15 p2553 A67-29155
- Small nonpolarized plasmoids interacting with axisymmetric magnetic field, discussing penetration mechanism, equations of motion and magnetic moment 15 p2524 A67-29245
- Earth-pointing satellite attitude control system using gravity gradient stabilization, deriving motion equations 15 p2564 A67-29329
- Analytic solution obtained for minimum impulse transfer between two neighboring low eccentricity orbits 15 p2554 A67-29405
- Motion equation for nonideal relativistic electron gas, reviewing hydrodynamics obtained from Landau 15 p2527 A67-29517
- Motion of solid body with rotating flywheels rotating at constant velocities relative to inertial space and body 15 p2493 A67-29686
- Selection of two regularizing functions reduced to one by evaluating relations between them in restricted three-body problem 15 p2557 A67-29875
- Mass point motion in central mass gravitational field determined from mass point position and velocity coordinates, obtaining Kepler orbits 15 p2559 A67-30035
- Motion analysis near triangular libration point within framework of elliptic restricted three-body problem 15 p2559 A67-30036
- Perturbation theory applied to periodic motions in three-body restricted problem 15 p2560 A67-30040
- High altitude satellites orbital curves, considering moon effect 15 p2560 A67-30044
- Lapunov functions generating methods applicable to nonlinear and linear autonomous systems 15 p2511 A67-30048
- Set of linearized motion equation for ferry vehicle to obtain optimal-thrust during rendezvous attempt with orbital satellite 15 p2571 A67-30049
- Motion equations of heavy symmetrical gyroscope in gimbal suspension, noting integrals of second approximation 15 p2490 A67-30174
- Missile guidance accuracy, examining motion in central gravitational field along trajectory 15 p2572 A67-30177
- Motion equations of astatic gyroscope with vertical rotor axis, with allowance for aircraft motion over pitch, roll and yaw angles 16 p2670 A67-30465
- Precession theory of compensating gyroazimuth, discussing random disturbances reduction by introducing electric mismatch of both sensitive elements 16 p2670 A67-30467
- Motion and continuity equations for atomic and molecular oxygen density solved numerically as time dependent problem 16 p2664 A67-30975
- Aircraft flow meters for simultaneous rate and volume measurements, examining equations of motion 16 p2671 A67-31006
- Theorems defining class of motions of system of mass points of given mass in Lobachevskii space 16 p2702 A67-31011
- Approximate calculation of coefficients in equation for perturbed motion of rigid body containing liquid 16 p2765 A67-31051
- Invariant curves dissolution and nonapplicability of third integrals explained examining perturbation values and initial conditions and resonance phenomena 16 p2748 A67-31140
- Numerical analysis of structure of one-dimensional unsteady magnetic compression waves propagating into collisionless plasma, using motion equations 16 p2719 A67-31232
- Fluid motion in shallow trapezoidal container, noting dimensionless quantity relating frequencies to volume and rim dimensions, sloshing modes, eigenvalues, etc 16 p2661 A67-31421
- Free vibrations of freely supported toroidal shell, noting elastic motion equations in terms of toroidal coordinates and boundary conditions applicable to polar motion 16 p2775 A67-31423
- Real trajectories of n-body problem calculated by convergent integral iterations on basis of differential equations for motion of centers of gravity 16 p2750 A67-31441
- Laminar jet flow of electrically conducting fluid over plane solid surface in transverse magnetic field solved using motion and continuity equations 16 p2722 A67-31571
- Second order incompressible fluid equation of motion, compatibility equation and dissipation function 16 p2663 A67-31703
- Lagrange equations of perfect fluid flow linked to datum point and geometric surface arbitrarily moved within flow 16 p2663 A67-31709
- Equation derived for accurate approximation of viscous friction coefficient in spool and nozzle-flapper preamplifier stages of electrohydraulic servovalve 16 p2610 A67-31915
- Optimal control for aircraft gust alleviation using frequency domain theory and short period mode approximation 17 p2795 A67-32036
- Lateral-directional stability equations for aircraft with nonzero product of inertial flying along steep flight path gradient 17 p2796 A67-32219
- Motion of dynamically symmetric satellite under action of gravitational moments, discussing stability and nonlinear oscillations 17 p2955 A67-32243
- Restricted three-body problem in post-Newtonian approximation, obtaining equations of motion 17 p2943 A67-32441
- Thin airfoils in radiation gas dynamics, formulating linearized theory for plane steady motion via Fourier transform and obtaining solution for absorption coefficient 17 p2791 A67-32556
- Periodic solution of boundary value problem involving motion equation of viscous fluid 17 p2838 A67-32681
- Nonstationary plane and axisymmetric flows, discussing acoustic and Oswatitsch theories, velocity potentials, differential equations of motion, etc 17 p2839 A67-32713
- Three-body problem of Jupiter satellites orbits under solar influence, computing initial elements, determining orbital stability and solving satellite motion equations 17 p2946 A67-32753
- Stability analysis of deformable space vehicle in torque free state noting gravitational effect, stability of spin motion, characteristic motion equations, etc 17 p2956 A67-32779
- Synthesis of mechanical system with

variator having drive unit in steady or steadily increasing motion, deriving and solving dynamic equations 17 p2885 A67-32967

Regularization of motion equations in computation of vehicle trajectory near singularity [AIAA PAPER 67-26] 17 p2948 A67-33039

Motion of lunar images in focal plane of horizontal telescope without coelostat arrangement 17 p2950 A67-33130

Cross sectional strain and stress distributions in cylindrical elastic bars subjected to pressure-step and velocity-impact loading [ASME PAPER 67-APM-33] 17 p2965 A67-33158

Comet model construction assuming rectangular coordinates system, noting particle motion initial velocity and repelling acceleration 17 p2951 A67-33215

Stability analysis of steady state dynamic holonomic mechanical systems using Rouse, Kelvin, Poincare and Chetaev theorems 17 p2886 A67-33276

Body of revolution bounded by sphere rolling on stationary sphere with force function of applied forces dependent on only one coordinate 17 p2886 A67-33277

Solid body motion about stationary point fixed at earth surface 17 p2886 A67-33278

Frequency spectrum of annihilation operator for system of harmonic oscillators using motion equation obtained through Hamiltonian 17 p2870 A67-33316

Elastic-plastic rods theory using thermodynamical restrictions, examining straight rod motions 17 p2966 A67-33348

Variable mass body rectilinear unsteady motion equations for movement at various levels in viscous fluid 18 p3023 A67-33426

Electron bunching in sweep klystron, deriving electric field equation, motion equations and continuity criteria for arbitrary charge density distribution 18 p3010 A67-33501

Motion equation of non-Newtonian fluids in initial section of cylindrical tube 18 p3024 A67-33539

Motion equation of system of two banked wings near solid surface with optimum circulation distribution 18 p3024 A67-33542

Stability of rotation about symmetry axis of unsteady mechanical system consisting of gyrostat with fixed point and flywheel, deriving motion equations 18 p3078 A67-33556

Incompressible fluid flow past semilinear flat plate during ejection of another fluid from plane surface into main flow solved using motion equations 18 p3025 A67-33571

Soviet book on nonlinear problems of motion of compressible fluid with small disturbances, investigating pressure fronts, neighborhoods of wave fronts, etc 18 p3025 A67-33715

Gyromotor electromechanical moment effect on drift of triaxial gyrostat stabilizer exposed to platform vibrations, formulating rotor motion equations 18 p3047 A67-33992

Book on variational principles of mechanics covering basic concepts, calculus of variation, equations of motion, etc 18 p3079 A67-34100

Integral motion equations of rigid body with cavity partly filled with viscous incompressible fluid with free surface 18 p3028 A67-34267

Inertial motion of solid body in space of constant curvature, obtaining solution to differential equation 18 p3079 A67-34372

Effective braking height /EBH/ for small interplanetary particles of cosmic velocity entering Martian upper atmosphere 18 p3135 A67-34541

Book on methods for applying principles of dynamics to engineering problems covering three-dimensional approach, free-body system and derivation of motion equations 18 p3080 A67-34566

Integrals of motion in plane elliptic restricted three-body problems for orbits with small eccentricity near primaries 18 p3136 A67-34588

Solid body of variable mass with cavities filled with ideal incompressible fluid, analyzing differential equations of motion 18 p3080 A67-34604

Circular planform peripheral jet ground effect machine heaving motion analyzed using motion equations 19 p3172 A67-34867

Apparent forces of analytical mechanics for several cases of

motion 19 p3261 A67-35049

Behavior of finite-amplitude disturbances periodic in motion direction for plane parallel laminar flows studied, using partial differential equations 19 p3208 A67-35051

Nonrelativistic charged particle transport in geomagnetic dipole field under effect of electromagnetic pulses obtained, using Fokker-Planck equation 19 p3313 A67-35212

Ohm law extended to electrical conduction of partially ionized plasmas and nonneutral ionized gases 19 p3287 A67-35356

Turbulent velocity fluctuations dynamics in and outside viscous sublayer examined by linearizing motion equation around known mean velocity profile 19 p3209 A67-35414

Combustion rocket engines thermodynamic cycle and specific impulse values, considering motion equations and plasma engines 19 p3311 A67-35571

Restricted three-body problem with two masses under Newtonian gravitation and third obeying semi-Newtonian laws 19 p3327 A67-35664

Motion equations of classical point particles determined by known Euclidean symmetry of space 19 p3262 A67-35709

Motion equation for four-body system attracting one another according to Newtonian law, obtaining series of functions converging toward solution 19 p3328 A67-35899

Motion equations of spin-stabilized rocket under thrust with jet damping, variable mass and momentum effects and all angular disturbances 19 p3334 A67-35938

Multiple scaling for analyzing flight vehicle performance and dynamic behavior [AIAA PAPER 67-560] 19 p3335 A67-35957

Ascent and descent gravity turn trajectories of rocket in constant gravitational field, considering drag forces in motion equation [AIAA PAPER 67-596] 19 p3336 A67-35992

Linear electromagnetic oscillations in homogeneous plasma described by motion and Maxwell equations 20 p3492 A67-36129

MHD instability of sub-Alfven equations for zonal flow outside diurnally oscillating boundary layer of precessing spheroid 20 p3494 A67-36147

Guiding center plasma theory /GCP/ stability, potential, Vlasov and motion equations, etc 20 p3494 A67-36152

Turbulent flow in circular duct, obtaining velocity distribution 20 p3419 A67-36276

Steady flow equations with symmetry of revolution, obtaining first integrals for perfect fluid 20 p3420 A67-36395

Inertial effects of rotor on synchronous motion of simply supported and cantilever arrangements of rotor shaft systems 20 p3453 A67-36500

Vertical energy transfer from stationary disturbances induced by topography and diabatic heat sources and sinks, using primitive motion equations 20 p3480 A67-36504

Spherical coordinates from integration of 20 asteroids differential motion equations including Jupiter, Saturn perturbation and orbital element determinations 20 p3523 A67-36629

Motion theory of comet Wolf I during 1918-1925 revolution which included close approach to Jupiter in 1922 20 p3524 A67-36659

Vibrating elastic bar motion equation reduced to integral equations system for solutions to boundary value problems 20 p3476 A67-36667

Book on functional mechanisms for engineering design, presenting kinematic characteristics of output motion, planar linkage and spatial cycloidal crank and flexural mechanisms 20 p3454 A67-36766

Solution drops motion in diffusing binary gas mixture, analyzing velocity 20 p3421 A67-36812

Doppler effect wave radiation experiment correction equations developed for source, observer and medium motion 20 p3486 A67-37005

Equations of motion of continuous single loop adaptive control system with scan modulated parameters, noting stability analysis method 20 p3408 A67-37044

Magnetoresonant gyroscopes simulation by converting motion equations to rotating coordinates system 20 p3451 A67-37154

Gyrotachometer errors in measuring

object angular velocity and acceleration relative to one axis, deriving differential equations of motion 20 p3451 A67-37155

Fokker-Planck equation for distribution function over laser observable values derived from quantum-mechanical laser master equation by expanding statistical operator 20 p3461 A67-37182

Semiconductor laser light field amplitude equation of van der Pol oscillator derived and shown valid for optical band-to-band transitions 20 p3461 A67-37184

Motion equations of incompressible nonisothermal fluid jet studied by closed similarity solutions, obtaining temperature distributions 20 p3423 A67-37209

Relativistic elasticity, discussing solution of field equations in transient unidirectional motion 20 p3486 A67-37279

Finite amplitude elastic wave motions with only constitutive nonlinearities 20 p3540 A67-37282

Motion equations for elastically deforming body containing cavity partly filled with ideal fluid 20 p3481 A67-37380

Parameters for motion of flight vehicle as solid body and for elastic deformations 20 p3482 A67-37381

Fresnel integrals for quadratures of motion for undamped vibrator, deriving equation for envelope of maximum amplitude 20 p3541 A67-37485

Variational principle as basis for dynamics of elastic shell theory, discussing motion described by Timoshenko type equation 20 p3542 A67-37541

Two-body problem in classical mechanics, proving existence and quantization of circular orbits 20 p3487 A67-37581

Corrective force selection for bringing nonlinear discrete system to predetermined phase space point in fixed instant of time 20 p3487 A67-37659

Ionization and recombination effects on MHD wave propagation through three-component magnetoplasma, deriving nonlinear motion equations 21 p3660 A67-37743

Variational problem of rocket dynamics in homogeneous gravitational field in empty space reduced to differential equation system 21 p3701 A67-37836

Energy accumulator and constant power propulsion system for near-circular orbit space maneuvering, considering two-vehicle encounter 21 p3689 A67-37985

Motion equations of astatic gyroscope mounted on rocking base and with friction in Cardan suspension axes 21 p3626 A67-38042

Hydraulic servodrive with supply source, control valve, actuator and feedback components analyzed for stability, deriving motion equations 21 p3570 A67-38048

Differential equations of motion for permanent rotation heavy gyro with fixed point 21 p3627 A67-38269

Motion stability of dynamic system whose equation has two small positive roots 21 p3657 A67-38281

Different motion equations equivalence for nonholonomic systems from Chaplygin method 21 p3657 A67-38303

Transient gas motions for various waves, analyzing motion equations and classifying integral curve fields 21 p3565 A67-38556

Optimal control for nonlinear dynamic systems with/without invariant properties investigated for departures from optimal motion 21 p3656 A67-38586

Mathematical models for retrieval systems for future extravehicular operations, discussing rotational and translational motion and constraint equations 22 p3753 A67-39157

Statistical method for determining satellite orientation and rotation based on differential motion equation 22 p3878 A67-39166

Satellite-gyroscope asymptotic equilibrium positions obtained by general motion equation, calculating gravitational and aerodynamic moment effects 22 p3898 A67-39187

Fast and slow oscillatory spinning of aircraft, examining equations of motion by approximate methods based on Brodetsky analysis 22 p3744 A67-39197

Motion equation derivation permitting analysis of gyrosystems mounted on fixed or moving plants, determining instrumental errors 22 p3795 A67-39230

Charged particle motion equation derivation in guiding center approximation in lowest order through Northrop averaging process 22 p3843 A67-39264

Linear equations of motion of concentrated defect in elastic medium using variational principle 22 p3909 A67-39292

Approximate shell theory for unrestricted elastic deformation, discussing treatment of motion equations 22 p3909 A67-39293

Optimal control of quasi-linear system perturbed motion, developing approximation method 22 p3778 A67-39305

Large scale eddy terms for balancing mean meridional circulation in winter, discussing terms magnitudes in different latitudes 22 p3828 A67-39326

Synchronous motions in dynamic bearing system of nonlinear plants with one degree of freedom interacting through weak coupling 22 p3836 A67-39395

Computer formulation of motion equations using tensor calculus to extend area of application of digital computers 22 p3827 A67-39418

Closed form solution for two-dimensional reentry trajectories by transforming motion equations into Bernoulli with two arbitrary functions of inclination, considering constant gravitational field 22 p3881 A67-39526

Doppler effect method application to satellites and space vehicles motion, giving formulas for satellite velocity, orbital shape and position 22 p3831 A67-39588

Reaction rates and yield for multichannel molecular collisions, introducing observable yield operator in theory, using motion equations 22 p3757 A67-39635

Plasma stability investigated using constants of motion for solution of Vlasov equation 22 p3849 A67-39700

Kinetic equations for electrons and photons in homogeneous plasma in strong magnetic field derived from Maxwell and classical motion equations 22 p3851 A67-39736

Self-similar solutions to motion equations are possible for internal heat generation in confined supersonic flow, assuming constant transport properties 22 p3784 A67-39781

Numerical program integrating motion equation of charged particles from realistic geomagnetic field model, with trajectory calculations for solar cosmic rays 22 p3872 A67-39810

Plane motion of container formed by two concentric cylinders and radial partitions partly filled with small vibrating ideal fluid 22 p3786 A67-40029

Velocity distribution determination method for supersonic flow around zero incidence cones in equilibrium air, discussing motion equation and flow field parameters 22 p3742 A67-40098

Thomson motion equation derivation for variable mass system extended for flight simulation equations for variable mass inertially guided system 22 p3832 A67-40099

Propellant sloshing effect on vehicle dynamics under zero gravity conditions studied by programming motion equation into digital simulation of spacecraft, control and propellant 22 p3907 A67-40180

Mathematical model for studying liquid slosh effects on rendezvous dynamics by incorporating sloshing dynamics into vehicle motion equation 22 p3888 A67-40189

Three-dimensional periodic motion about collinear Lagrangian equilibrium points, determining motion, variational and orbit equations and numerical integration 22 p3889 A67-40427

Motion of small spherical particles entering upper atmosphere of earth with cosmic velocities studied for terminal velocities 22 p3890 A67-40472

Dynamical interaction of interplanetary particles with upper atmosphere studied by simplification of motion equation 22 p3890 A67-40473

Hydraulic angular acceleration sensor motion equation obtained by kinetostatic method 22 p3809 A67-40477

Error of three degrees of freedom astatic gyro motion owing to viscous friction moments in suspension in case of irregular rocking of base 22 p3810 A67-40484

Energy dissipation and motion equations of superfluid helium flow through pores, describing technique to detect critical velocity in wide channels 22 p3839 A67-40550

Electromagnetic forces effects on steady

rotating motions of conducting viscous incompressible fluids via adjustable local boundary layer first order approximation 23 p4031 A67-40604

Dynamics of electrohydraulic servomechanism /transducer-amplifier/ for transforming signals into forces for displacing spacecraft control mechanism, examining motion equations 23 p3935 A67-40637

Nonlinear problems of parametric excitation of rings solved by equations, considering normally and centrally directed pressures 23 p4074 A67-40651

Principles developed for founding of unified field theory of gravitation and electromagnetism, with space-time geodesics as charged particle motion equation 23 p4028 A67-40659

Axisymmetric vibrations of homogeneous and sandwich spherical shells obtained from generalized variational motion equations including thickness-shear deformation effect 23 p4075 A67-40687

Real gas jet equations of motion, energy and continuity derived, transformed and solved for mixing region, discussing approximate state equation construction 23 p3989 A67-40729

Laser and maser noise quantum theory emphasizing equations of motion and fluctuation problem, deriving density matrix equation 23 p4011 A67-40782

Discretization error analyzed for accumulation during numerical solution of equations of orbital motion 23 p4023 A67-40864

Independent variable changes in dynamical systems and applications to systems regularization, giving canonical and Lagrangian motion equations with tensor notation 23 p4027 A67-41006

Rigorously geodetic inertial motion of extended object in Einstein gravitational field, using relativistic hydrodynamics 23 p4027 A67-41148

Unsteady continuity and motion equations describing F layer dynamic characteristics under time dependent electric and magnetic fields 23 p3996 A67-41178

Turbulent boundary layer energy and motion equations, heat transfer through layers, energy exchange and phenomenological relations 23 p3991 A67-41249

Normal modes of stellar internal motions, considering turbulent convection equations and weak-coupling approximation 23 p4068 A67-41277

Penetrative motion of individual elements in earth atmosphere and prediction of velocity field from convective overshoot 23 p4024 A67-41279

Spin characteristics of VJ 101 C VTOL airplane via numerical integration of motion equations including mass coupling effects and nonlinear aerodynamics 23 p3934 A67-41313

Latitude variation and motion of instantaneous pole from astronomical stations during IGY, using differential method for coordinate system 23 p3997 A67-41350

Dynamic longitudinal stability of rigid glider towed by rigid aircraft with elastic cable subjected to aerodynamic loads, deriving motion differential equations 23 p3935 A67-41418

Imploding shocks and detonations propagation investigated by similarity solution extended to early imploding processes, using Oshima quasi-similar approximation 23 p3992 A67-41722

Model for compressible free jet with moving environment in core and developed region of exhaust plume 23 p3992 A67-41731

Dynamic impossibility of free stream velocity distributions admitting similarity solutions, calculating laminar boundary layers 23 p3992 A67-41741

Stability of ideal mechanical system with damping forces, obtaining motion equations 23 p4028 A67-41757

Population noise in semiconductor laser junctions calculated by quantum mechanical Langevin method 24 p4166 A67-41887

Atoms interaction with solid body surface, noting pair interaction law effect on characteristic energy accommodation coefficient and motion equation solution 24 p4190 A67-41938

Orbital elements and motion equations of periodic comet Harrington for five perihelion times before 24 p4226 A67-41964

Discovery 24 p4226 A67-41964

Motion equations for mean orbital and osculating elements of particle rotating in gravitational field of aspherical planet 24 p4228 A67-42274

Minimizing maximum control deviation problem reduced to motion equation numerical integration 24 p4188 A67-42301

MHD generation of electric power, describing motion equations for conducting fluid in electromagnetic field and duct configurations 24 p4098 A67-42413

Cometary orbit evolution of Jupiter family, considering influence of Jupiter 24 p4240 A67-43078

Compressible fluid with finite electrical conductivity in constant magnetic field hitting thin cylindrical obstacle, solving flow motion equations 24 p4199 A67-43080

Integration of motion equations of second order incompressible fluid 24 p4146 A67-43106

MOTION PERCEPTION

Effect of image smear and dimension on target recognition measured on differently oriented, moved and remote Landolt C 09 p1455 A67-21723

Stimulus thresholds for perception of angular acceleration in man 15 p2427 A67-29267

Mathematical model for otolithic organs used to analyze human spatial orientation 16 p2610 A67-30753

Vestibular, tactual and proprioceptive information in judging Coriolis rotation and attitudes during rotation and pitching on piloted flight simulator 22 p3751 A67-39605

Inverted pendulum and VTOL control experiments with and without motion cues, discussing various motion effects 22 p3755 A67-40087

MOTION PICTURE

SA CINEMATOGRAPHY

Picture generation by computer for concept demonstration, subsequently photographed with automated microfilm camera 08 p1299 A67-21050

Time varying electromagnetic field pattern of prolate spheroid antenna with rotationally symmetric current distribution motion pictures generated by computer 11 p1758 A67-24115

Rapid deformation in tubular blank during expansion by pulsed loading studied by high speed motion picture photography 21 p3631 A67-38055

Moving point trajectory recorded by hologram 21 p3627 A67-38347

Gemini booster launch photographic recording with 50 cameras collecting engineering data and motion pictures of prelaunch, launch and postlaunch 22 p3807 A67-40372

MOTION SICKNESS

Correlation of airsickness in early flight training with subjective anxiety 21 p3575 A67-38086

Airsickness early in flight training indicates high levels of anxiety and attrition potentials and poor prognosis 23 p3963 A67-41544

Habituation transference in Coriolis stimulation for change from passive lateral chair tilts to various active head tilts during rotation 23 p3953 A67-41585

Nervous and humoral mechanisms of extralabyrinthine effects on vegetative disturbances during space flight factors 24 p4111 A67-41843

MOTION SICKNESS DRUG

Antimotion sickness drugs and placebos effect on altering motion sickness susceptibility in Skyraider aircraft aerobatics and Slow Rotation Room dial test 21 p3574 A67-38083

MOTION STABILITY

Steady motion stability of heavy homogeneous body of revolution on absolutely rough horizontal plane 01 p0115 A67-10992

Stability of steady state motions of solid body with one attached point located in potential force field 02 p0267 A67-11963

Stability in the sense of Liapunov, Poincare, Lagrange and others for dynamical systems 02 p0268 A67-12502

Stabilization of steady state motion of controlled system described by nonlinear

differential equations with time delays 03 p0392 A67-13588
 Stability problem of steady motions, using differential equations with time delay 03 p0468 A67-13616
 Stability of motion of gyro suspension, noting gyrohorizon compass operation for constant suspension point and angular velocities 03 p0424 A67-14158
 Liapunov stability of gyroscope motion, with Cardan suspension center moving over earth surface 03 p0424 A67-14179
 Poincare method applied to moon motion in vicinity of equilibrium configuration, using equations of linear variation 06 p1031 A67-17775
 Stability of steady motions of holonomic mechanical systems in cyclic coordinates, using method based on theorems of Routh, Poincare, Kelvin and Chetaev 06 p1031 A67-17838
 Perturbed motion stability in critical cases, examining canonical systems 06 p1032 A67-18034
 Stabilization of steady motions of nonlinear control system in critical case of pair of pure imaginary roots 06 p0975 A67-18035
 Sufficient conditions for stabilization of motion of nonstationary controlled system 06 p0975 A67-18036
 Motion stability concepts of synthesis of control devices, with example for harmonic oscillator 06 p1032 A67-18243
 Optimum control of motion stability of solid body with fixed point, using gyrostabilizer rotors 06 p1034 A67-18617
 Liapunov function for motion stability of solid body on earth surface having fixed point and internal gyro 06 p1004 A67-18619
 Motion instability of liquid in interspace between two rotating spheres when ratio of radii approaches 2 06 p0992 A67-18820
 Sufficient conditions for stability of solutions of nonlinear nonautonomous equation, examining pendulum of variable length 09 p1533 A67-22154
 Stability of radial motion of spherical gas bubble in incompressible inviscid fluid under external pressure 10 p1624 A67-23028
 Stability of rotational motion of body with cavity containing ideal fluid, considering fluid motion as potential flow, determining velocity potential and inertia moments 10 p1679 A67-23031
 Longitudinal perturbed motion of aircraft with free-floating canard, obtaining differential equation corresponding to characteristic equation 10 p1595 A67-23606
 Stability of integrals of differential equations for periodic motions 10 p1680 A67-23666
 Stability of linear integro-differential equations for processes with distributed parameters 10 p1681 A67-23667
 Kinematic nonlinearities effect on existence, properties and stability of vibrations in unison of particle with two degrees of freedom 11 p1818 A67-24085
 Quasi-static analysis of nonsynchronous response effect of gas bearing pivoted pad design variables and application to operating machinery [ASME PAPER 67-VIBR-15] 11 p1796 A67-24175
 Analytical expression for steady state rate of electric domain movement in semiconductors in terms of electric field distribution at domain center 11 p1846 A67-24482
 Motion stability during final time interval for case of two zero roots determined by analysis of nonlinear functions structure 11 p1813 A67-24518
 Stability of motion of plane boundary interface between two different density coupled fluid jets analyzed to determine role of viscosity in drop formation 11 p1782 A67-24959
 Stability of motions of satellite with rotor and cavity with liquid, reducing problem to solution of minimum change in potential energy of system 13 p2213 A67-27319
 Linear effects of oscillations of liquids in right circular cylinder, determining stability of forced oscillations 14 p2296 A67-27984
 Stability of motion of continuous dynamical systems analyzed via computing machines 14 p2348 A67-28080
 Mark 19 Sperry gyrocompass with SGN 4 inertial platform 14 p2322 A67-28989

Conservative systems motion stability, generalizing precession and nutation of gyroscope with respect to noncyclic coordinate 15 p2518 A67-29685
 Motion stability described by differential equations of perturbed motion 15 p2518 A67-29695
 Liapunov direct method applied to Hermite theorem on number of positive real part zeros of complex polynomial and stability theory of linear motions 15 p2458 A67-29699
 Motion stability of earth-orbiting nonsymmetrical satellite with elastically-connected moving parts studied by Liapunov analysis on mathematical model 16 p2762 A67-30962
 Unsteady motion stability over given time interval of mechanical systems described by nonlinear differential equations 16 p2702 A67-31052
 Statistical probability for motion stability of nonlinear stochastic systems during time interval, discussing oscillation stability of pendulum with randomly oscillating bearing 16 p2703 A67-31145
 Three-body problem of Jupiter satellites orbits under solar influence, computing initial elements, determining orbital stability and solving satellite motion equations 17 p2946 A67-32753
 Stability of steady motions of holonomic mechanical systems in cyclic coordinates, using method based on theorems of Routh, Poincare, Kelvin and Chetaev 17 p2886 A67-33216
 Stability of steady state motions of solid body with one attached point located in potential force field 17 p2886 A67-33280
 Airfoil unsteady motion problem near screen in incompressible fluid with given horizontal/vertical velocity 18 p2981 A67-33410
 Steady motion of craft with aerial lifting surfaces over rough water, defining conditions for safe operation 18 p3022 A67-33415
 Stability of motion of symmetrical rotor gyrostat about fixed point on rotating earth surface 18 p3078 A67-33555
 Wave number and Rayleigh numbers effect on stability of two-dimensional convection in layer heated from below 18 p3159 A67-34003
 Book on theory of orbits covering restricted problem of three bodies, two bodies in rotating coordinate system and periodic orbits 18 p3120 A67-34032
 Existence and stability of rectilinear translation motions of blunt body submerged in potential flow of incompressible fluid at rest at infinity 18 p3027 A67-34183
 Critical stability cases of almost periodic motions, showing reduction to solution of differential equations of steady motion 18 p3080 A67-34602
 Nonlinear analysis of earth-moon system motion stability in three dimensions near L4 libration point when perturbed by sun 19 p3328 A67-35962
 Impact characterization and length, determining contact energy with Hertz equation and integrating nonlinear differential equation for system motion 20 p3483 A67-36195
 Sufficient conditions for statistical stability of motion in nonlinear systems 20 p3409 A67-37225
 Free vibrations and motion stability during extremum drift for one-and multidimensional pulsed optimal systems 20 p3411 A67-37374
 Book on mechanics of controlled body including control system realization, motion programming, dynamic error assessment and three-dimensional problems 20 p3482 A67-37459
 Laplace transformation of solution of linear differential equations with variable coefficients and time lags, analyzing motion stability 20 p3478 A67-37579
 Stability of integrals of differential equations for periodic motions 21 p3657 A67-38267
 Stability of linear integro-differential equations for processes with distributed parameters 21 p3657 A67-38268
 Automatic check system for investigation of dynamic characteristics of stabilization system for carrier and space vehicle, noting system reliability 22 p3830 A67-39172

Algorithm for piecewise smooth point-to-point mapping of straight line onto straight line to determine various motions 22 p3777 A67-39778
 Validity of Liapunov first approximation theorems for motion stability when not satisfying power series terms 22 p3837 A67-39881
 Stable motion of rarefied plasma ions and electrons in crossed electric and magnetic fields 22 p3853 A67-40024
 Nonlinear steady motions produced by stable stratification in rapidly rotating fluid, discussing Ekman layers 23 p3990 A67-41170
 Indirectly corrected gyro vertical used to determine vertical on power plant, considering random plant motion and gyroscopic drift 24 p4155 A67-42298
 Gravity oriented satellite coupled librational motion in circular orbit analyzed for motion stability by numerical methods 24 p4231 A67-42384
 Dynamic response of large flexible space systems subjected to motion inputs and arbitrary force, analyzing joined Timoshenko beams 24 p4240 A67-42395
 Stationary motion stability of gyrostat satellite in Newtonian force field, defining body position in coordinate system 24 p4241 A67-42400
 Vector Liapunov function existence during conditionally or asymptotically stable motion 24 p4189 A67-42690

MOTOR
 S ELECTRIC MOTOR
 S PULSE MOTOR
 S ROCKET STEERING MOTOR
 S SERVOMOTOR
 S SYNCHRONOUS MOTOR
 S TORQUE MOTOR

MOTOR CASE
 SA ROCKET MOTOR CASE
 Filamentary materials for wound structures, particularly rocket motor cases, noting fabrication equipment, physical properties, etc 11 p1811 A67-25008

MOTOR SYSTEM
 Moment of aerodynamic resistance calculated for gyromotors operating in H and He, examining laminar flow near rotor 01 p0064 A67-10418
 High speed fluidic logic circuitry for pneumatic stepping motor 14 p2251 A67-28351
 Sailplanes with self-contained launching apparatus noting minimum performance, motor propulsion and auxiliary equipment 22 p3744 A67-39303

MOTOR SYSTEM /BIOL/
 Prolonged confinement in small chambers effect on biodynamic processes of walking and other movements in special positions 16 p2613 A67-30914
 Inertia and muscle tone level effects on intermittence sampling frequency in hand movement control system 17 p2808 A67-33180
 Animal study for motor reflexes under simulated weightlessness and during gravitational pulses 20 p3367 A67-36258
 Hypokinesia effects on nitrogen metabolism of rats 20 p3368 A67-36261
 Human sensor-motor coordination testing in simulated weightlessness 20 p3368 A67-36263
 Perceptual motor-skills forgetting in simple printing task, attributing decrements to retroactive interferences 21 p3576 A67-39099
 Transverse accelerations remote aftereffect on conditioned alimentary reflexes of rats, discussing prolonged depression of higher nervous activity 23 p3943 A67-40771
 Algorithm for processing primary motor characteristics of human motions on digital computer 24 p4114 A67-41857
 Motion coordination under conditions of intermittent acceleration and weightlessness during parabolic aircraft flight 24 p4112 A67-41858

MOTS
 S MINITRACK OPTICAL TRACKING SYSTEM /MOTS/

MOUNT
 S CHASSIS
 S FUSELAGE MOUNTING
 S PYLON MOUNTING
 S RIGID MOUNTING

MOUNTAIN
 Physical model of turbulence used in developing forecasting scheme of clear air turbulence /CAT/ over mountains

- [AIAA PAPER 67-184] 06 p1026 A67-18298
Physical model of turbulence used in developing forecasting scheme of clear air turbulence /CAT/ over 17 p2880 A67-32552
Mountains
Mountain wave and air turbulence program using high altitude research aircraft measurements and stressing 24 p4181 A67-42275
- MOUNTAIN INHABITANT**
S ALTITUDE ACCLIMATIZATION
MOVING TARGET INDICATOR /MTI/
RADAR
Magnetic recording of various types of monopulse, PPI and MTI radar signals, with application to airborne data acquisition recorder and ground reproducer 02 p0196 A67-12004
Quantum size in analog-to-digital conversion and effect on quantization noise in output of moving target indicator /MTI/ radar processors 04 p0570 A67-14873
Moving target indication /MTI/ in theory and technique including description of delay lines, stalos, transistors, phase detectors and modulator 04 p0573 A67-15037
SDS radar, surveillance radar designed to detect moving targets on ground extended to detection of low flying aircraft 04 p0573 A67-15038
Optical range gated filter for detecting moving targets in clutter background, using laser beam for application to MTI radar 08 p1293 A67-20687
Video mapping technique making possible radar moving target indication for permanent echoes only 12 p1909 A67-25128
Radar resolution performance in moving target determined by cross section of desired target compared with combined cross section of all interfering targets 12 p1907 A67-26083
Doppler effect method for measuring effective scatter area in laboratory 15 p2443 A67-29286
Dual-antenna AMTI radar ground clutter cancellation and signal enhancement 18 p3001 A67-34117
Radar moving target indicating filters performance, describing method for including target Doppler frequency statistics in gain probability 20 p3386 A67-37498
Digital simulation of clutter rejection MTI radars 20 p3388 A67-37651
Approximate method for evaluation of processing loss in delay line MTI receiver 22 p3758 A67-39211
Degradation of moving clutter attenuation efficiency due to Doppler-frequency shift in MTI radar systems 23 p3972 A67-40642
- MTI**
S MOVING TARGET INDICATOR /MTI/
RADAR
MU-2 AIRCRAFT
S MITSUBISHI MU-2 AIRCRAFT
MULTICHANNEL RECEIVER
Multichannel Data Logging System for recording short-term simultaneous analog data from 25 to 100 parallel input channels 01 p0076 A67-11142
PPM-frequency time hopping for multichannel communication system to transmit digital data over tropospheric scatter path 02 p0202 A67-12131
Multichannel sequential detection in case of reception through independent multiple channels with noise 05 p0765 A67-16953
Limitations in conventional radar compared to new multichannel radar with discontinuous pulse compression 13 p2070 A67-27203
Satellite onboard multichannel systems for information processing, discussing construction, quick response memory and block diagrams 16 p2633 A67-30673
Information capacity dependence on number of frequency-divided channels of optical communication system, investigating information loss in channel-separating receiver 16 p2623 A67-30882
Circuit of automatic multichannel secondary particle recorder of SKL type for cosmic ray station, using azimuthal muon telescope and neutron supermonitor 17 p2854 A67-32098
Mathematical models of multichannel radio equipment in presence of noise, including guidance and coordinate measurement systems 19 p3185 A67-36095
Contour-volumetric displays for processing and handling data in nuclear experiment 20 p3450 A67-36986
Optimum multichannel system utilization for receiving regular signal against background noise 20 p3384 A67-37197
Spurious response identifying equations for more realistic P and Q values on multiple conversion 20 p3404 A67-37636
Equations for mode analysis in multichannel extremal control systems with harmonic probe signals, discussing synthesis of optimizers and phase shift automatic compensation 22 p3777 A67-39864
Multichannel image data handling and processing system using multispectral analysis for remote agricultural sensing and surveying from aerospace platforms 24 p4157 A67-42435
- MULTICHANNEL TRANSMITTER**
Optimum telemetry system characteristics for shock, vibration and acoustic measurements and data bandwidth sufficiency 02 p0196 A67-12009
Time combined with frequency division multiplex multichannel communication system for transmission of digital information over tropospheric scatter communication channel 02 p0203 A67-12132
Radio system passband increase and multichannel intercorrelation signal processing for increasing noise rejection for limited analysis time 11 p1772 A67-24984
Multichannel radar formula for discriminating power in distance corresponding to time resolution 18 p3002 A67-34228
Probability of signal detection and accuracy of measurement in fluctuating multichannel system 24 p4120 A67-42223
- MULTILAUNCH TECHNIQUE**
Multiple payload and multipurpose spacecraft evaluated for cost reduction in USAF space operations [AIAA PAPER 67-636] 20 p3535 A67-37621
- MULTILAYER STRUCTURE**
SA HONEYCOMB
SA LAMINATE
SA SANDWICH CONSTRUCTION
Low voltage photomeasurements in metal-insulator-metal films with opposing photocurrent separation 02 p0301 A67-12519
Stability problems of sandwich plates, considering buckling and wrinkling 02 p0341 A67-12713
Value and sign of phase jump taking place during light reflection from multilayer dielectric film 03 p0467 A67-12892
Multilayer insulation system materials and design data for use on spacecraft in temperature range from 300 to 800 degrees K [AIAA PAPER 65-663] 03 p0534 A67-13069
Yield surfaces for nonhomogeneous shells of revolution 03 p0523 A67-13501
Elastic axisymmetric deformation of circular two-layer plate with closely spaced rod couplings compliant to radial shear 03 p0527 A67-14070
Tension and bending of two-layer rods under nonuniform heating and loading 03 p0527 A67-14071
Helicon wave propagation along multilayered structure, calculating Bloch waves, fields and dispersion 04 p0665 A67-15119
Interconnection patterns for slice-level subsystems of integrated circuits 04 p0585 A67-15490
Approximate solution of thermoelectricity equation for multilayer cylinder in constant-temperature medium 04 p0738 A67-15891
Axisymmetric motions of Timoshenko type cylindrical shells composed of two elastic isotropic layers of different materials and thicknesses connected by perfect bond 04 p0717 A67-15909
Lifting capacity of two-layer cylindrical shell made of different elastically hardening materials, considering temperature effect 05 p0912 A67-16180
Internal stress calculation in multilayer materials 05 p0919 A67-16590
Temperature distribution in two-layer plate during welding by laser light flux 05 p0814 A67-17548
Validity of equations for bending, natural oscillations and stability of three-layer solid circular plate with rigid filling and asymmetric structure 06 p1106 A67-18628
Value and sign of phase jump taking place during light reflection from multilayer dielectric film 06 p1034 A67-18770
Governing equation for bending of multilayered sandwich elastic plates composed of n membranes developed by variational method 06 p1110 A67-18857
Equations for nonstationary temperature field of n-layer plate, noting convective heat transfer on free surface of plate 07 p1267 A67-19327
Interaction between layers of ferromagnetic films of different composition and coercivity separated by insulating quartz layer, obtaining films by vacuum deposition 08 p1369 A67-20811
Visual observation of internal circuitry and interconnections of multilayer boards through failure analysis technique 08 p1307 A67-21419
Large deflection of asymmetrically layered plate, using parametric expansion techniques to extract system of differential equations governing scaling of stresses and displacement component for boundary conditions 09 p1574 A67-21756
Nondestructive testing techniques for multilayer printed wiring boards stressing axial transverse laminography and mutual coupling 09 p1502 A67-21867
Bending oscillations of hinged and clamped three-layer beams 09 p1575 A67-22219
Vibration characteristics of two-layered plates of arbitrary thickness and differing materials, noting coupling effect between flexure and extension 10 p1718 A67-23140
Stress distribution prediction in multilayered circular cylinder subjected to combined bending and axial loading exhibiting multilinear stress-strain relationships 10 p1724 A67-23706
Matched pulses for two-layer laminates, discussing complete energy transfer to base and uniform momentum transfer 10 p1724 A67-23707
Vacuum multilayer insulation for cryogenic space propulsion vehicles noting self-evacuation system and calorimetric test 10 p1734 A67-23728
Deformation of laminated shell structures under axisymmetric loading, deriving differential equation by considering boundary conditions at both ends 10 p1731 A67-23846
Composite loss factor and natural frequencies of vibrating beams composed of alternate layers of elastic and viscoelastic material [ASME PAPER 67-VIBR-6] 11 p1871 A67-24166
Constrained layer damping mechanism for optimum performance of plates, beams and tubular structures, using viscoelastic material [ASME PAPER 67-VIBR-26] 11 p1872 A67-24184
V-I characteristics of In and Ge structures with negative resistance, noting effect of four-layer substructures 11 p1765 A67-24474
C-band traveling wave maser using printed circuit technology results in reduced structure size, perfect contact between structure and ruby, etc 11 p1801 A67-24727
Bending theory for sandwich plates solved by Galerkin method assuming load distribution over upper and lower faces of plate 11 p1880 A67-25095
Electronic packaging technique in thin film technology using flip-chip bonding and MTFI techniques 12 p1910 A67-25264
Bending of three-layer plate freely supported along four edges in presence of variable surface heating 12 p2022 A67-25588
Three-layer shell with lightweight filler under creep studied for initial forms of equilibrium 12 p2024 A67-25598
Variational derivation of nonlinear equilibrium equations for three-layer conical shell with rigid incompressible filler under external pressure 12 p2025 A67-25609
Critical stresses of compressed three-layer cylindrical shell of asymmetrical structure in presence of variable temperature 12 p2026 A67-25614
Rectangular three-layer plate thermoelectric oscillations due to random pulses analyzed using series expansion 12 p2027 A67-25625
Natural oscillation frequency of multilayer shells of revolution with nonsymmetrical structure containing rigid filler and

subjected to transverse load 12 p2027 A67-25626

Resolvent equations of shallow multilayer shells of regular structure to solve problems involving calculations of strength, stability and oscillations 12 p2029 A67-25668

Fracture toughness of 7075-T6 and -T651 sheet, plate and multilayered adhesive bonded panels, showing independence of thickness and number of layers [ASME PAPER 67-MET-4] 12 p1956 A67-25948

Magnetization ripple in multilayer films, noting dependence on copper layer 13 p2179 A67-27143

Minimum weight combinations of shields and spacers for lowest heat flux, noting mounting technique and leakage effect 13 p2228 A67-27653

Propellant leakage degradation of multilayer insulation system of cryogenic storage tank 13 p2186 A67-27654

Effective thermal conductivity parameter for multilayered insulation 13 p2228 A67-27656

Thickness, material type, environmental and surface emittance of radiation shield effects on thermal performance of multilayer insulation system 13 p2228 A67-27660

Evaluation method for deposited thin film interfacial interconnections 14 p2369 A67-28613

Lamellar troilite occurrence and origin in iron meteorites 14 p2391 A67-28948

Stability equation of multilayer sandwich plates with isotropic homogeneous facing layers and orthotropic homogeneous core layers 15 p2577 A67-30267

Langmuir-Blodgett multimonoayers of stearic acid investigated as thin film dielectric 16 p2728 A67-31020

Thermal stresses in three-layer cylindrical sandwich shell of finite length with rigid filler having temperature as function of radius only 16 p2765 A67-31049

Reliability of multilayer printed wiring boards as interconnection device 16 p2642 A67-31726

Solderless-wrap lightweight interconnection board for Lunar Module landing radar, noting manufacturing details 16 p2642 A67-31919

Ionospheric observations of thick layer structure accompanying auroral activity, emphasizing ionization profiles, electric fields, aurora generation and global distribution 18 p3039 A67-33620

Bending oscillations of hinged and clamped three-layer beams 18 p3141 A67-33770

Stress anomaly effect on structural integrity of Teflon laminates determined by photoelastic techniques 18 p3142 A67-33894

Forced bending oscillations for three-layer cylindrical shell under pulsed internal pressure 19 p3338 A67-34878

Multilayer cantilever beam subjected to varying load, studying cases where slip region propagates from edge to interior 19 p3341 A67-35579

Stress-strain relationships for single layer used to obtain stress distribution in orthotropic laminates subjected to axial and shear stresses [ASME PAPER 66-WA/RP-5] 20 p3542 A67-37611

Multilayer board compared to two-sided board circuits, discussing circuit reliability, flexibility, cost, packaging density, etc 21 p3594 A67-38332

500 to 1000 MHz ultrahigh RF hybrid amplifier fabricated with microelectronic multilayer thin film technique, noting performance of components 21 p3596 A67-38342

Multilayer circuit board fabrication, giving data on operational and standby failures 21 p3596 A67-38345

Soviet papers on strength and stability of elements of thin walled structures 21 p3723 A67-38778

Elastic stability of three-layer cylindrical shell filled with corrugated metallic sheets under combined loads, deriving linear equations 21 p3724 A67-38786

Compression strength analysis of plane and cylindrical multilayer skin panels reinforced by corrugated fillers, determining critical load and local stability loss 21 p3725 A67-38787

Two-layer circular cylindrical shell stability under axial compression with transverse displacements, analyzing axisymmetric deformation of longitudinal strip 21 p3725 A67-38793

Triple layer cylindrical shells stability beyond elastic limit studied based on plastic deformations, loading principle and shallow shell theory 21 p3727 A67-38838

Three layer cylindrical shell stability in elastic and inelastic domains under separate and joint loads, considering filler layer deformation 21 p3727 A67-38840

Three layer cylinders and cylindrical and plane panel optimum parameters using critical stress expressions from nonlinear elasticity theory 21 p3729 A67-38915

Dielectric thin film negative resistors for oscillator circuits compared to multilayer p-n-p-n structures for output frequency voltage temperature dependence 22 p3769 A67-39576

Multiple reflective metal foil structure with separating matrix transient thermal response, determining number of radiation shields for given thermal protection 22 p3919 A67-40115

Calorimeter for evacuated multilayer insulation materials to evaluate performance and measure heat transfer rate and thermoconductivity 22 p3803 A67-40297

Solid state multilayer circuits preparation for use in microminiaturization, stressing advantages over printed circuits 22 p3774 A67-40327

Singular solutions for bending stresses in loaded infinite three-layer plate 23 p4079 A67-41415

Graphical construction and electrical simulation for predetermining index and thickness of multilayer surfaces and filters 24 p4187 A67-41873

Electromagnetic wave propagation through two-layer shielded dielectric waveguide using dispersion equation 24 p4129 A67-42192

Cryogenic flexibility of single and multiple ply thin polymeric film tested for porosity, cycle life and film thickness relation 24 p4176 A67-42468

Long term cryogenic propellant storage in space, considering rigid open cell polyurethane foam as spacer in multilayer insulation system 24 p4254 A67-42480

Repetitive circuit arrays combined with multilayer interconnections using discretionary wiring to improve array yield 24 p4132 A67-42688

MULTIMODE RESONATOR

Function of symmetrical gas-laser resonator analyzed to determine angle of divergence of laser beams generated by various transverse electromagnetic wave modes 14 p2332 A67-28854

Optimum energy coupling of multimode gas laser determined experimentally 14 p2333 A67-28971

Three-space optical resonator model, deriving properties responsible for undesired natural frequencies suppression, noting selection characteristics 18 p3058 A67-33528

Cylindrical Fabry-Perot resonator, determining resonant modes by applying boundary conditions, noting eigenvalue and eigenfunction roles 18 p3060 A67-34024

Function of symmetrical gas-laser resonator analyzed to determine angle of divergence of laser beams generated by various transverse electromagnetic wave modes 19 p3242 A67-36106

Longitudinal mode generation in ruby laser emission operating in single pulse regime with resonant mirror reflector 24 p4169 A67-42894

MULTIPACTOR

Multipactor in T-R switch for improved recovery time 03 p0383 A67-13827

Multipactor suppression properties of Ti, Cr, V and Ta determined using special electromagnetic cavities 15 p2448 A67-29757

MULTIPATH PROPAGATION

Test program on air-to-air propagation between two jet aircraft at high altitude and path lengths up to maximum radio line-of-sight, considering antenna gain and multipath fading 02 p0202 A67-12122

Fading and multipath propagation mechanism for communication links involving satellites and aircraft with antenna beams, assuming fading models and estimating margins required for FSK

teletype transmission 06 p0960 A67-17673

Field strength measurements in multipath field using linear and circular probing 07 p1142 A67-19448

Error rate expression for canonic binary receivers, evaluating performance of incoherent detection 14 p2272 A67-28706

Digital error performance of transportable troposcatter facility evaluated as function of path length 17 p2811 A67-32118

Perturbing factors in avionics communications noting drawbacks and advantages of satellite utilization, possible commercial applications, etc 17 p2813 A67-32498

Modes of boresight shift in conical-scan and sequential-lobing types of amplitude sensitive angle-tracking antennas 17 p2814 A67-32523

Antenna field strength measurement above 1 GHz, discussing formulas for high accuracy gain determination, multipath interference and antenna separation 17 p2815 A67-32609

Multipath effect measurement in propagation path at UHF frequencies from synchronous satellite to aircraft 17 p2816 A67-32626

Higher order mode excitation by multipath propagation in deep fading of receiving horn-reflector antenna 20 p3385 A67-37355

Multipath cell with White mirror system using carbon dioxide and molecular nitrogen gas mixture for gas laser amplifier and oscillator operation 21 p3625 A67-37854

Exolospheric communications system with ideal matched filter and signal processing at transmitter for increased range and secure coding possibilities 21 p3586 A67-38952

Error probability for binary signaling through multipath channel with receiver waveform comprising white Gaussian noise and time delayed frequency-shifted signal 24 p4121 A67-42341

MULTIPHASE FLOW

Stability of one-dimensional polyphase flow in porous medium studied using theory of servomechanisms 16 p2609 A67-31713

Book on fluid dynamics of multiphase systems covering momentum, heat and mass transfers and chemical reactions 20 p3425 A67-37728

MULTIPLE-DEGREE-OF-FREEDOM SYSTEM

Solving quasi-linear automatic system with n degrees of freedom in cases of incommensurable frequencies by approximation method 10 p1673 A67-22935

Effective degrees of freedom of vibrating structure 10 p1718 A67-23153

Frequency spectrum of annihilation operator for system of harmonic oscillators using motion equation obtained through Hamiltonian 17 p2870 A67-33316

Random vibration testing by multiple electrodynamic exciter technique, analyzing electromechanics and structural feedback 19 p3339 A67-34961

Subharmonic and summed and differential harmonic oscillations in multiple-degree-of-freedom system with asymmetric nonlinear spring characteristics, studying stability 22 p3910 A67-39408

Error of three degrees of freedom astatic gyro motion owing to viscous friction moments in suspension in case of irregular rocking of base 22 p3810 A67-40484

Longitudinal oscillations with multiple degree of freedom obtained over sections of adopted stress-strain diagram, characterizing elastoplastic properties 23 p4076 A67-40683

MULTIPLEX TRANSMISSION

Ninety-eight-channel microelectronic PCM multiplexer-encoder design and development qualified to Apollo spacecraft environments 01 p0026 A67-10864

Multiplex electrohydraulic actuators development, noting fault detection and feedback signals to prevent output drift 05 p0754 A67-16752

Communications satellite system efficiency enhanced by using automatic adaptive voice multiplexer in ground terminal equipment 06 p0960 A67-17676

Multiple access modulation techniques /frequency-division, time-division, spread-spectrum and pulse-address/ for use in communications satellites 06 p0960 A67-17694

Asynchronous delta modulation system for cases with no time division multiplexing such as asynchronous multiplex communication 10 p1606 A67-23063

Multiple internal communications system concept using single coaxial cable handling information transfer by integrated circuits 13 p2083 A67-27448

Airborne radio telemetry equipment transmitting in-flight data to ground station for monitoring and analysis, using frequency- and time-division multiplexing 14 p2261 A67-28038

Modulation and demodulation methods for multiplex telemetry, discussing PCM, PSK and SSB 14 p2271 A67-28682

Miniature multichannel pulse-duration-modulated multiplex telemetry unit for medical monitoring of human subjects pulse, temperature, airflow, etc., under stress 14 p2259 A67-28688

Universal internal communications system /UICS/ for interconnecting avionic system components, using single coaxial cable and modules 17 p2813 A67-32472

Probability density function of ratio of two nonzero mean Gaussian random variables derived and applied to calibrated signal using noisy calibration 17 p2816 A67-32624

Computer application to planning and operating simultaneous access European ground station network 18 p3003 A67-34355

Solid state devices operational characteristics from applications in transmission technology 20 p3394 A67-36242

Multiple internal communications system dealing with diversified information forms, discussing flexibility, reliability and other advantages for weapon systems 20 p3381 A67-36567

Microwave multichannel communication system using PCM, noting low power output requirement and suitability for digital data transmission 22 p3763 A67-40460

MULTIPLEXER

SA FREQUENCY-DIVISION MULTIPLEXING

SA ORTHOGONAL WAVEFORM MULTIPLEXING

SA TIME DIVISION MULTIPLEX

Communication system engineering handbook covering system design, programming, modeling, switching, multiplexing, etc 14 p2269 A67-28508

Near IR grating spectrometer converted to multiplex instrument by adding encoding disk in spectrum plane 20 p3437 A67-36339

High data rate storage system for Nimbus B tested by simulation 20 p3445 A67-36547

MULTIPLIER

SA ELECTRON MULTIPLIER

SA FREQUENCY MULTIPLIER

SA LAGRANGE MULTIPLIER

SA PHOTOMULTIPLIER

Distribution function for probability density of random process at output of multiplier acted upon by envelopes consisting of Gaussian noise and pulse signal 05 p0767 A67-17397

Analog multiplier using p-n junction dynamic capacitance, noting decays in RC circuit current 14 p2290 A67-28928

Linear signal multiplier using thermally stable InSb, InAs or GaAs sensors with Hall effect voltage linearly dependent on control current 15 p2444 A67-29386

Large scale integration of arithmetic functions utilizing pcosocnd circuits, noting ease of fabrication, flexibility and module multipliers 15 p2452 A67-29936

Stability of feedback systems containing single odd monotonic nonlinearity 24 p4136 A67-42187

Logarithmic nature of I-V characteristics of silicon junction diodes for design of analog multiplier with differential operational amplifier 24 p4131 A67-42478

MULTIPLIER PHOTOTUBE

S PHOTOMULTIPLIER

MULTIPOLAR FIELD

Hartree-Fock-Slater calculation of internal conversion coefficients for magnetic multipoles for yttrium-87 with 0.05 or 0.15 mc-square gamma energy values 01 p0116 A67-10203

Plasma confinement by HF multipole electromagnetic field, noting role of potential accompanying rotating magnetic field 11 p1839 A67-24425

Internal conversion electron spectrum for samarium 155 to europium 155 transmutation, noting multipolarities and new lines 16 p2733 A67-31706

Plasmoid motion in longitudinal,

transverse and two-dimensional multipole magnetic fields, investigating electric fields and plasmoid parameters 17 p2904 A67-32916

MULTIPROGRAMMING

Multiprogramming system for computer controlled telemetry data reduction system 02 p0206 A67-11807

Low cost time delay and multiple programmer for space research 12 p1909 A67-25230

MULTIPROPELLANT

Double-and multiple-based nitrate propellants and gunpowders with tabulated characteristics analyzed, particularly nitrocellulose-nitroglycerin, diglycol-dinitrate, nitroguanidine and ammonium nitrate compounds 13 p2185 A67-26337

MULTISTAGE COMPRESSOR

Multistage gas-bearing helium compressor development 13 p2057 A67-27681

Attenuation of circumferential inlet distortion in multistage axial compressors, predicting flow field and pressure distortion via zero axial clearance approximation [AIAA PAPER 67-415] 18 p2982 A67-33902

Stage operation compensation in multistage axial compressor during operating regimes variations along flow length 20 p3516 A67-37084

Boundary between stable operation of multistage axial flow compressor and rotational flow separation region, using variational condition 21 p3689 A67-38046

Handley Page Jetstream power plant, propeller design, turboprop engine operation and control 22 p3868 A67-40131

MULTISTAGE ROCKET

Multistage rocket motion optimization in uniform gravitational field formulated as coupled variational problem 13 p2213 A67-27321

Peak altitude of multistage sounding rocket vertical trajectory in vacuum determined by dimensionless graphs 16 p2762 A67-31247

Initial weight prediction of single and multistage launching vehicles by coordinating practical and theoretical aspects 16 p2762 A67-31490

Multistage rocket advantages compared to single stage rocket with respect to attainment of characteristic velocity 20 p3534 A67-37297

MULTISTAGE ROCKET VEHICLE

Guidance equations for multistage boosters offer target change on launch pad and in flight 02 p0265 A67-12718

Three-stage Black Arrow satellite launcher, detailing guidance system used in first and second stages and system used to rotate third stage 03 p0519 A67-13929

Task distribution, overall network, flow diagram and data processing of PERT method controlling development of ELDO-A rocket third stage 16 p2783 A67-31632

Development, reliability and acceptance tests for third stage of ELDO satellite launcher, discussing components, time schedules, personnel training, etc 18 p3136 A67-33639

MULTISTAGE VEHICLE

Optimal stage sizes and trajectory for multistage launch vehicle determined by various techniques [AAS PAPER 66-113] 07 p1259 A67-19972

Optimal stage sizes and trajectory for multistage launch vehicle determined by various techniques [AAS PAPER 66-113] 13 p2214 A67-27529

Unsteady aerodynamic forces due to gusts on supersonic bodies of revolution 19 p3172 A67-36001

MULTIVIBRATOR

Static characteristics of series connected tunnel diodes used in determining pulse duration and recovery time of driven multivibrator 03 p0377 A67-13236

Multiple correlation applications in design analysis of high reliability critical circuits 05 p0777 A67-17249

Cancellation of unwanted spectral components in FM multivibrator system by generating cancelling component in square law device 07 p1145 A67-19871

Crystal frequency stabilization in relaxation-oscillator circuit, showing similar use in astable multivibrator instead of LC circuit 20 p3384 A67-37215

CR self-oscillation circuits, discriminating CR oscillators from astable, monostable and bistable multivibrators 21 p3604 A67-38601

MUON

Charge ratio of cosmic ray muons determined by particle collection in small and wide angular ranges about vertical 01 p0144 A67-10783

High energy cosmic ray muons studied, using ionization calorimeter and hodoscope counters 02 p0317 A67-12770

Interactions of superhigh energy muons in cosmic ray nonelectromagnetic cascade showers 02 p0317 A67-12771

Superhigh energy particle accelerators and energy spectra of cosmic ray muons in electron photon cascades 02 p0317 A67-12772

Integral energy spectra and angular distribution of muons, comparing computational and experimental data 02 p0317 A67-12773

Spatial and angular particle distributions in muon-generated electron photon cascade, using spark chamber muon detectors 02 p0317 A67-12774

Absorption curve and energy spectrum of high energy muons 02 p0317 A67-12775

EAS with zenith angle between 30 and 45 degrees and fixed number of muons and electrons 02 p0318 A67-12777

Muon groups at depth of 40 mwe not responsible for substantial energy leakage from extensive air showers 02 p0318 A67-12779

Muon flux measurement with aid of spark chamber at depth of 20 mwe used for spatial distribution near axis of extensive air showers 02 p0318 A67-12780

Positive-to-negative charge ratio of high energy cosmic ray muons 03 p0506 A67-13518

Primary cosmic ray spectrum at high energies and spectra of gamma rays and muons in atmosphere 04 p0692 A67-14857

Muon momenta, signs and densities in cosmic air showers determined, using magnet spectrograph with visual display 06 p1076 A67-17651

Large atmospheric jets with low muon content explained by presence of hypothetical primary cosmic photons with very high energies 09 p1562 A67-22559

Energy loss of high energy muons caused by nuclear interaction and fluctuation due to passage through great thickness of material corrected for standard 10 p1703 A67-23690

High energy muon flux in air showers at sea level determined, using semi-Monte Carlo method 13 p2195 A67-27579

Solar-diurnal variations of neutron and muon components of cosmic rays based on IGY data, analyzing temperature effect 17 p2931 A67-32079

Solar diurnal wave from underground muon detectors and relationship to solar activity over 11-year cycle, noting phase changes 18 p3116 A67-33514

Cosmic radiation dose, estimating contributions due to mu meson and electron-photon cascade shower components 18 p2990 A67-33516

High energy cosmic ray muons investigated, using ionization calorimeter and hodoscope counters 22 p3877 A67-40272

Interactions of superhigh energy muons in cosmic ray nonelectromagnetic cascade showers 22 p3877 A67-40273

Superhigh energy particle accelerators and energy spectra of cosmic ray muons in electron photon cascades 22 p3877 A67-40274

Integral energy spectra and angular distribution of muons, comparing computational and experimental data 22 p3877 A67-40275

Spatial and angular particle distributions in muon-generated electron photon cascade, using spark chamber muon detectors 22 p3877 A67-40276

Absorption curve and energy spectrum of high energy muons 22 p3877 A67-40277

EAS with zenith angle between 30 and 45 degrees and fixed number of muons and electrons 22 p3877 A67-40279

Muon groups at depth of 40 mwe not responsible for substantial energy leakage from extensive air showers 22 p3877 A67-40281

Muon flux measurement with aid of spark chamber at depth of 20 mwe used for spatial distribution near axis of extensive air showers 22 p3877 A67-40282

Plonic and muonic K-series X-rays studied by liquid He scintillation counter, obtaining separation peaks 24 p4192 A67-42735

Air shower muon generation altitude determination from relative positive-negative muon distribution shift 24 p4220 A67-42863

Shower producing capability of various particle groups at 40 mwe below ground, evaluating muon energy spectra 24 p4220 A67-42865

High energy cosmic ray muon integral angular and integral spectrum below earth surface 24 p4222 A67-42877

Muon properties investigated for mean energy by spark calorimeter at various depths 24 p4222 A67-42879

Bremsstrahlung due to collision of muon with electron at rest, discussing energy photons role 24 p4194 A67-42880

Photonuclear interaction effect on large angle scattering of high energy muons 24 p4222 A67-42881

MUSCLE

SA ELECTROCARDIOGRAPHY

Muscle system participation in bending and straightening of elbow joint muscle system participation in bending and straightening of elbow joint 07 p1133 A67-19346

Minimal value of artificial gravity for normal electroactivity of skeletal muscles determined for otherwise weightless condition 13 p2057 A67-26457

MUSCULAR FATIGUE

Maximum aerobic work correlation with anthropometric and spirometric parameters, studying ventilatory capacity coefficient 16 p2614 A67-31472

MUSCULAR FUNCTION

SA HEART FUNCTION

SA KINESIS

Heat balance and ventilation of human body in pressure suit 09 p1455 A67-21731

Factors in recovery from performance decrement, activation, inhibition and warm-up [NAVTRADEVEN-IH-72] 24 p4114 A67-41809

Exclusion effect of afferent signalization on tonic function of iliotibial muscle in frogs exposed to acetylcholine 24 p4112 A67-41852

MUSCULAR STRENGTH

Weightlessness simulation by bed rest and water immersion, evaluating validity of protective measures, recovery time and tilt response 15 p2424 A67-29102

Maximal muscular static force vs physical stress measurement for optimal work conditions 23 p3954 A67-41598

MUSCULAR SYSTEM

S MOTOR SYSTEM /BIOL/

MUSCULAR TONUS

Inertia and muscle tone level effects on intermittent sampling frequency in hand movement control system 17 p2808 A67-33180

Exclusion effect of afferent signalization on tonic function of iliotibial muscle in frogs exposed to acetylcholine 24 p4112 A67-41852

MUSKELSHVILI PRINCIPLE

Power series technique applied to single edge notches in semilinear region in plane elasticity problems, using mapping function and Muskelshvili theory 08 p1414 A67-20347

MUTATION

SA GENETICS

Killing and mutagenic efficiencies of heavy ionizing particles in Arabidopsis thaliana 06 p0953 A67-18379

Sporulation mutations induced by heat in Bacillus subtilis 08 p1287 A67-20983

Genetic transcription as affected by ionizing radiation and hydrogen peroxide 11 p1747 A67-24786

Cell survival rates and mutation development in Chlorella vulgaris plants carried by Cosmos 20 p3367 A67-36256

Space genetics, discussing space environment exposure of experimental animals as cause of mutations, hereditary damage, etc 24 p4113 A67-42053

MYSTERE XX AIRCRAFT

S DASSAULT MYSTERE XX AIRCRAFT

N

N-156 AIRCRAFT

S F-5 AIRCRAFT

N-P JUNCTION

SA P-N JUNCTION

Current carrier distribution in GaAs-Ge

heterojunctions measured for energy band diagram 15 p2542 A67-30241

I-V curve related to state densities on both sides of n-p junction of tunneling system 16 p2725 A67-30808

Attenuating electron waves in crystals corresponding to energy values in forbidden band used in calculating current across n-p junction 21 p3879 A67-38311

High energy proton irradiation and annealing of n and p type Si, comparing proton and electron damage 23 p4047 A67-41519

Li containing p-on-n and n-on-p Si cell degradation by bombardment noting carrier removal damage, annealing and radiation damage resistance 23 p3941 A67-41524

N-P-N JUNCTION

Epitaxial diffused integrated circuit structure containing p-n-p and n-p-n transistors 01 p0033 A67-10021

Planar transistor stability under X-ray irradiation, showing drifts of variable importance according to type of transistor /p-n-p or n-p-n/ 03 p0387 A67-13996

Double diffused n-p-n gallium arsenide transistor, discussing ways oxygen modifies p-n junctions to increase voltage breakdown 10 p1617 A67-23537

Lateral bipolar n-p-n transistors fabricated using heteroepitaxial films of silicon on sapphire 13 p2078 A67-26779

Silicon negative-resistance junction diodes, studying n-p-n structure and diode characteristics dependence on light, temperature, voltage and frequency 16 p2636 A67-30898

N-STAGE PROCESS

Discrete time control /multistage/ version of Berkovitz nonlinear programming problem 07 p1183 A67-20276

Runge-Kutta integrations for all seasons by proceeding in blocks of N steps compared to predictor-corrector methods 21 p3652 A67-38173

N-TYPE SEMICONDUCTOR

Variable effect of external electrical field on IR photoconductivity of thin n-and p-type silicon samples with low bulk impurity contents 01 p0128 A67-10076

Microwave negative conductance due to traveling space charge waves in n-type GaAs 01 p0133 A67-10487

Spin-magnetophononic and magnetophononic oscillations of magnetic resistance in n-InAs 01 p0133 A67-10547

Ionized impurity scattering mechanisms causing energy and momentum losses in n-type InSb below 77 degrees K 01 p0134 A67-10806

X-ray irradiation effect on electrophysical properties of n-and p-type germanium, determining absorption coefficient 01 p0136 A67-11044

Spin-magnetophononic and magnetophononic oscillations of magnetic resistance in n-InAs 01 p0137 A67-11055

Voltage induced by electron beam in n-and p-type germanium bars having inhomogeneous resistivity distribution, obtaining equations from one-dimensional model 01 p0137 A67-11059

Thermally grown silicon dioxide and resulting silicon-silicon dioxide interface, noting potential difference effect on n-type inversion layer 02 p0293 A67-11753

External electron emission measurement from polished n-germanium and n-silicon surfaces 02 p0296 A67-11830

Impulse measurements of temperature conduction in n-type semiconductors 02 p0297 A67-11848

Electron beam scanning technique measurement of diffusion lengths in Si and GaP p-n junctions and recombination rate of dislocations in n-type Si 02 p0298 A67-11887

Deep-level localized current oscillations in n-type silicon crystal 02 p0298 A67-11892

Anisotropy of electric resistivity, Seebeck and Hall coefficients and magnetoresistance of n-type single crystal ferric oxide /hematite/ containing tetravalent tin as impurity 02 p0299 A67-12085

DC and RF I-V characteristics, device fabrication and structure of epitaxial depletion mode n-type MOS-FET 02 p0218 A67-12103

Dependence of conductivity on microhardness of p-doped n-type silicon, examining effect of gamma radiation 02 p0300 A67-12477

Potential distribution, I-V characteristics and pulse shape of n-type Ge with sealed-in Sn, In-Sb, Sn-Sb and Pb-Sb contacts in strong electrical field 02 p0300 A67-12480

Anisotropy of magnetoresistance and Hall effect in n-GaAs, discussing conduction band structure in vicinity of edge 03 p0487 A67-12806

Dependence of peak inverse voltage of n-Si and p-Ge on specific resistance and concentration and mobility of current carriers 03 p0488 A67-12817

Microhardness of n-type InSb single crystals and crack formation near indentation area 03 p0489 A67-13093

Steady state photoconductivity and photomagnetic effect in single crystals of n-type GaAs with various carrier concentrations 03 p0490 A67-13151

Negative magnetoresistance of n-type InAs in longitudinal magnetic fields 03 p0490 A67-13156

Optical or inertial electron mass dependence on N-concentration in IR spectrum of n-type GaAs monocrystal with S, Se and Te impurities 03 p0490 A67-13161

Local diffusion of Ga into Sb-doped Ge samples from Ga-doped silicon dioxide films prepared in specially designed vacuum ampoule 03 p0491 A67-13175

Hall mobility, Seebeck and Nernst coefficients measured in temperature range from about 100 to 350 degrees K for scattering mechanisms of conduction electrons in n type CdS 03 p0493 A67-13351

Cyclotron absorption in n type lead telluride with wide range of carrier concentrations, showing increase in transverse effective mass and decrease in anisotropic mass ratio 03 p0493 A67-13352

Electric current oscillation mode beyond Gunn effect threshold in n-type GaAs 03 p0496 A67-13669

Instability of Sb and Au-doped n-type germanium during carrier injection, examining current-voltage and frequency characteristics and illumination effects 03 p0499 A67-13955

Secondary breakdown relaxation oscillations and I-V characteristics of point contact n-type Ge diode 03 p0386 A67-13964

Transverse magnetoresistance and Hall effect measurements on n-type GaSb at various magnetic fields and temperatures, obtaining electron concentration and mobility 03 p0501 A67-14347

Seebeck and Hall coefficients, electrical and thermal conductivity and figure of merit measured as function of dopant concentration of n-type CuBr doped bismuth antimonide telluride 03 p0501 A67-14350

Space charge wave velocity in semiconductors, noting recombination type instability 04 p0678 A67-14928

Wave propagation in n-type semiconductor with negative differential resistance 04 p0678 A67-15129

Open circuit voltage and short circuit current capability of solar energy converter photoelement made of single crystal n-type indium phosphide 04 p0679 A67-15141

Nonsinusoidal periodic oscillations observed in high resistivity n-type silicon compensated by zinc and phosphorus 04 p0679 A67-15142

Quantum oscillation of transverse and longitudinal magnetothermal emf in n-type indium antimonide compared with oscillations of transverse and longitudinal magnetoresistance and Hall coefficient 04 p0680 A67-15288

Temperature and doping level effect on conduction band edge of n-type semiconductors, noting doublet shifts resulting in narrower forbidden energy gaps 04 p0681 A67-15292

Transverse magnetoresistance of n-type InAs, noting temperature effect and correlation with quantum theory 04 p0681 A67-15293

Transverse magnetic field effect on thermoelectric properties of n-type polycrystals of bismuth-antimony alloys containing 0, 5, 12 and 19 percent antimony in bismuth [ASME PAPER 66-WA/ENER-4] 04 p0682 A67-15368

Displacement effects in n-and p-type silicon when exposed to energetic radiation, using electron spin resonance and galvanomagnetic

- techniques 04 p0684 A67-15689
- Defect impurity relation in electron damaged p-type silicon and electron irradiation effect on float zone n-type silicon 04 p0684 A67-15690
- Impurity microsegregation substructure in n-and p-type bismuth telluride crystals grown according to Bridgman method, measuring electrical properties, thermal emf, Hall constant, etc 05 p0861 A67-16498
- Band structure of n-type HgTe by use of model of band structure based on observation of Shubnikov-de Haas effect 05 p0864 A67-16900
- LF photocurrent oscillation in high resistivity n-type GaAs, noting relation between amplitude temperature and light intensity 05 p0866 A67-16987
- Photoemission of electrons from conduction and valence bands of n-type degenerate Si into thermally grown silicon dioxide layers 05 p0870 A67-17195
- Frequency modes of Gunn effect oscillator 05 p0872 A67-17531
- Inelastic scattering of carbon dioxide laser radiation by mobile Landau-level electrons in n-InSb 06 p1009 A67-17723
- Singularities of Faraday effect in n-type InSb in millimeter band at 77.8 degrees K as function of sample thickness and magnetic field intensity 06 p1047 A67-17755
- Annealing of fast neutron damage in impurity conducting n-type Ge, noting small activation energy in resistivity below 10 degrees K 06 p1050 A67-18146
- Hall effect and resistivity in n-GaAs with Si as shallow donor, obtaining ionization energy and impurity band conduction values 06 p1052 A67-18570
- Far IR lattice bands in n-type indium antimonide single crystal 06 p1059 A67-18908
- Conduction band structure and anisotropy of electron scattering in n-GaAs, analyzing magnetoresistance and Hall effect 06 p1064 A67-18943
- Hall coefficient and transverse magnetoresistance behavior in n-GaSb at 4.2 degrees K, using DC high magnetic fields 06 p1064 A67-18946
- Quantum oscillations in magnetoresistance of n-type pure HgTe used to estimate electron effective mass and g value close to band edge 06 p1065 A67-18948
- Nonlinear galvanomagnetic effects due to hot electrons in n-type InSb in quantum limit 06 p1065 A67-18953
- Time dependence of V-I curves in n-type In-Sb at low temperatures, determining electron-hole pair generation rate 06 p1066 A67-18955
- Gunn effect in GaAs caused by field induced transfer of electrons from high to low conduction band valleys 06 p1067 A67-18961
- Magnetoresistance of heavily doped n-type silicon at liquid He temperature noting dependence on field strength and temperature 06 p1067 A67-18967
- Far IR resonant absorption in n-type silicon analyzed, considering donor-pair conduction dominant mechanism 06 p1068 A67-18974
- Fluorescence of n-and p-type gallium arsenic phosphide under optical excitation 07 p1232 A67-19635
- Nonohmic conductivity in n-type GaAs accompanied by negative photoconductivity and giant magnetoresistance, noting electron injection at cathode 07 p1234 A67-20099
- Optical spectrum of normal excitons in deformed and nondeformed n-type Ge single crystal layers for four orientations 08 p1367 A67-20409
- Photoionization cross section of negatively charged In atoms in n-type silicon from comparison of intrinsic photoconductivity with impurity photoconductivity 08 p1367 A67-20410
- Electron mobility measurements in n-type SiC polytypes noting temperature dependence 08 p1370 A67-21294
- Resistivity variation in n-type germanium pellet measured with focused electron beam, showing position dependence of diffusion length as cause of error 09 p1473 A67-22018
- Large area 200-v planar voltage-variable capacitance diodes 09 p1475 A67-22207
- Conduction electrons interaction with deformation potential and piezoelectric phonons to explain hot electron results in n-type InSb, taking into account screening of scattering potential 09 p1558 A67-22619
- Electron-hole plasma pinch instability in InSb on application of longitudinal magnetic fields shows change to helical rotating plasma 10 p1683 A67-22760
- Pulsed oscillations of microwave Gunn effect oscillator in n-type single crystal GaAs 10 p1609 A67-22838
- Surface treatment effect in field effect anomaly of cleaved and etched n-type indium antimonide at high magnetic fields 10 p1688 A67-22903
- Steady state photoconductivity and photomagnetic effect in single crystals of n-type GaAs with various carrier concentrations 10 p1690 A67-23100
- Negative magnetoresistance of n-type InAs in longitudinal magnetic fields 10 p1690 A67-23104
- Optical or inertial electron mass dependence on N-concentration in IR spectrum of n-type GaAs monocrystal with S, Se and Te impurities 10 p1690 A67-23108
- Gunn effect oscillators constructed from epitaxially grown n-type GaAs on n-plus substrate to obtain CW oscillations with frequencies from 3 to 35 gc 10 p1615 A67-23530
- Semiconductor conductivity in strong SHF electric fields, measuring dielectric constant and Fourier component 10 p1657 A67-23587
- Strong electrical field effect on Faraday effect in n-type InSb 10 p1695 A67-23683
- Negative immittance converter circuits deducible from one basic NIC, noting similarity to Stelmel vacuum tube circuits 11 p1769 A67-24129
- Bulk reverse current in diffused Si power rectifiers, interpreting reverse characteristics in terms of thermal pair production 11 p1760 A67-24144
- Conductance-and capacitance-voltage curves of MOS capacitors analyzed for temperature dependence of inversion layer frequency response in n-type silicon 11 p1846 A67-24234
- LF current oscillations excitation in n-type semiconductors analyzed using dispersion equation, noting role of external electric field 11 p1849 A67-24870
- Edge dislocations effect on electrical noise in n-type silicon analyzed and results compared with Shockley-Read model 11 p1849 A67-24906
- Barrier height between tungsten silicide films and n-type silicon base determined, using photoelectric response measurements 11 p1850 A67-24924
- Wave propagation in n-type semiconductor with negative differential resistance 12 p1978 A67-25153
- Open circuit voltage and short circuit current capability of solar energy converter photoelement made of single crystal n-type indium phosphide 12 p1979 A67-25164
- Nonsinusoidal periodic oscillations observed in high resistivity n-type silicon compensated by zinc and phosphorus 12 p1979 A67-25165
- Hall effect and thermoelectric power in doped, conductive titanium oxide ceramics, noting dependence on doping concentration 12 p1982 A67-25452
- Scattering mechanisms and role of interelectron collisions in n-Pb-Te and certain other semimetals analyzed by concentration dependence of mobility and thermal EMF 12 p1983 A67-25514
- Hall coefficient dependence on magnetic field intensity for n-type InSb single crystals at 77 degrees K 12 p1984 A67-25518
- Lifetime for nonequilibrium current carriers in n-type indium antimonide crystals from generation-recombination noise measurements at various temperatures 12 p1984 A67-25523
- P-and n-type silicon spectral emissivity measured at several temperatures and wavelengths for carrier concentrations and direct current resistivities [AIAA PAPER 67-302] 12 p1958 A67-26017
- Current voltage characteristics of alloyed p-n junctions in n-type InAs, discussing contribution of tunnel current 12 p1986 A67-26099
- IR surface photoconductivity of silicon as function of surface potential and current carrier parameters 13 p2174 A67-26397
- HF photoconductive phase responses in single crystal n-type indium arsenide, deriving carrier lifetimes 14 p2364 A67-28104
- Resistivity and Hall effect oscillations in antimony doped n-type germanium crystals in metallic impurity conduction state 14 p2365 A67-28231
- Resistivity and magnetoresistance for metallic impurity conduction in phosphorus doped silicon at low temperature with various donor concentrations 14 p2365 A67-28232
- Schubnikow-De Haas oscillation analysis in n-type bismuth telluride indicates multivalley conduction band structure 14 p2369 A67-28596
- Quantum oscillation of magnetoresistivity in n-type mercury telluride crystals, obtaining electron mass 14 p2369 A67-28598
- Unique determination for parameters of surface recombination centers in n-type germanium 15 p2534 A67-29326
- Semiconductors 15 p2534 A67-29326
- Low temperature transport effects in n-type gallium antimonide at high magnetic fields, observing oscillatory behavior of Hall coefficient and transverse magnetoresistance 15 p2534 A67-29327
- Relaxation oscillations in n-type indium antimonide crystal under magnetic field effect and responsivity measurements in far IR 15 p2540 A67-29931
- One-dimensional propagation of stable negative-resistance domains for carriers interacting with single type of impurity level 16 p2727 A67-30852
- Pulsed resistivity and Hall effect measurements of n-type GaAs in high electric fields at room temperature below microwave oscillation threshold 16 p2731 A67-31449
- Radiative recombination mechanisms in photoluminescence of n-type InP, discussing emission bands 16 p2732 A67-31450
- Microwave emission phenomena from n and p type indium antimonide, noting no essential difference 17 p2914 A67-32375
- Shubnikov-de Haas and Gurevich-Firson oscillations of photomagnetic effect in n-InSb magnetic field 17 p2914 A67-32451
- Disordered regions produced by fast neutron irradiation effect on semiconductor properties of silicon 17 p2919 A67-32859
- N-type germanium photoconductivity spectrum studied after bombardment with electrons at very low temperatures 17 p2919 A67-32860
- Annealing kinetics of n-type germanium exposed to electron bombardment at cryogenic temperature 17 p2919 A67-32861
- Strong electrical field effect on Faraday effect in n-type InSb 17 p2924 A67-33344
- Temperature and magnetic field intensity dependence of microwave emission from n-type indium antimonide 18 p3101 A67-34016
- Scattering mechanisms and role of interelectron collisions in n-Pb-Te and certain other semimetals analyzed by concentration dependence of mobility and thermal EMF 18 p3103 A67-34445
- Hall coefficient dependence on magnetic field intensity for n-type InSb single crystals at 77 degrees K 18 p3103 A67-34449
- Lifetime for nonequilibrium current carriers in n-type indium antimonide crystals from generation-recombination noise measurements at various temperatures 18 p3103 A67-34454
- Conduction band structure in n-type strontium titanate investigated by measuring oscillatory magnetoresistance in high magnetic fields 18 p3104 A67-34592
- Electrical characteristics of degenerate n-type germanium diode with gold or indium as metallic element 18 p3105 A67-34635
- Lorentz number, Hall coefficient, magnetoresistance and Hall mobility variations in n-type degenerate semiconductors 18 p3106 A67-34729
- Au and P doped n-type Si, noting formation of p-type surface layer of increasing thickness when heat treated 19 p3299 A67-34761
- Detection properties of n-type InSb in microwave and IR ranges, studying impurity and magnetic field effects 19 p3300 A67-34762
- Temperature dependence of electric conductivity and Hall effect in epitaxial layers of undoped and Fe-doped n-type Ga-As samples 19 p3300 A67-34770
- Fast neutron irradiation effect on electrical conductivity and Hall effect in Zn doped n-type indium arsenide single

crystals 19 p3301 A67-34771
 Neutron irradiation effect on n-type and p-type semiconductors thermophysical parameters 19 p3307 A67-35874
 Simultaneous diffusion of gallium and arsenic in silicon from gallium arsenide source, obtaining profiles at various temperatures 19 p3308 A67-38035
 IR emission in n-type gallium arsenide samples exhibiting current oscillations due to electron-phonon coupling 20 p3508 A67-38423
 Magnetometer with Gauss sensor describing n-type InSb pickup bridge instrument sensitivity 20 p3447 A67-38760
 Potential field distribution in n-GaAs devices before and after switching indicate carrier generation in narrow region near anode 20 p3510 A67-38853
 Majority and minority carrier lifetimes in n-type GaAs single crystals, measuring injection level dependence 20 p3512 A67-37436
 I-V characteristics of many-valley semiconductors in strong electric field deviating from Ohm law with scattering by phonons 20 p3513 A67-37439
 Impurity conduction causing negative magnetoresistance in Cu doped n-type GaAs crystals at low temperature 20 p3513 A67-37440
 Current runaway effects in n-cadmium telluride suggest current-density controlled resistivity caused by hole-electron pairs avalanche 21 p3877 A67-38006
 Electron beam method for measuring resistivity variation in germanium semiconductors, calculating diffusion lengths 21 p3879 A67-38254
 Volt-ampere characteristics of n-type GaAs at high fields above Gunn threshold, showing saturation, space charge effect and current controlled negative resistance 21 p3879 A67-38260
 Quantum transport theories for calculating multiple scattering in doped semiconductors 21 p3882 A67-38386
 Moving high field domain and current saturation in optically excited n-InSb 21 p3883 A67-38404
 N-type Hall effect in high temperature Li doped ceramic sample of MnO, measuring electric transport properties 22 p3858 A67-39521
 Surface states effect on frequency dependence of elements of equivalent circuit of n-type semiconductor/metal contact 22 p3859 A67-39578
 Energy state of recombination level of thermally hardened silicon diode base, considering spatial lifetime of minority carriers 22 p3773 A67-39920
 Interband and free carrier Faraday rotation in n-type InAs at room and low temperature, determining conduction band parameters 22 p3883 A67-40204
 N-type InSb microwave noise emission at low temperatures in low electric field regime, measuring magnetic field threshold and background 22 p3864 A67-40345
 Size effects in platelets of multivalley bipolar semiconductors with long scattering and electron-hole recombination times, studying electric pinch effect 23 p4042 A67-41292
 Impact ionization avalanche plasma production and instabilities in InSb at low temperatures, measuring current variation with electric field strength 24 p4204 A67-42344
 Lifetimes of n-type Cd-Hg-Te alloy, showing Hall-Shockley-Read type recombination at low temperatures 24 p4205 A67-42864

NA-300 AIRCRAFT
S OV-10 AIRCRAFT
NACELLE
 Isolated nacelle design for high by-pass ratio turbofan engines, particularly pylon mounted engine [SAE PAPER 680732] 01 p0140 A67-10632
 Nacelle design for high inlet pressure recovery and low external cowl drag, for high by-pass fan engine subsonic aircraft [SAE PAPER 680733] 01 p0140 A67-10633
 Aerodynamics of nacelle used in selection and integration of exhaust systems producing highest thrust-minus drag cruise performance [SAE PAPER 680734] 01 p0140 A67-10634

Aerodynamic design of Boeing 737 covering data of analytical studies, wind tunnel and flight tests, aerodynamic parameters and drag, flap system size, efficiency, wing geometry and handling qualities [AIAA PAPER 65-739] 03 p0354 A67-12906
 Aerodynamic design of Boeing 737 covering data of analytical studies, wind tunnel and flight tests, aerodynamic parameters and drag, flap system size, efficiency, wing geometry and handling qualities [AIAA PAPER 65-739] 08 p1279 A67-21043
 Engine nacelle location, size and shape effects on drag due to wing thickness and drag due to lift [AIAA PAPER 66-665] 17 p2791 A67-32567

NANOSECOND
 Rotationally switched rod memory system with 100 nsec cycle time, discussing cost and performance factors 19 p3189 A67-36064
 Multistage receiver protector recovery period measurement, discussing nanosecond reaction time 21 p3589 A67-37819

NAPHTHALENE
 Electric conductivity of naphthalene and beta-methylnaphthalene in liquid and solid state as affected by electric field 06 p1049 A67-17857
 Crystal growth, nucleation, supercooling, solidification, glass forming and kinetics of 1, 3, 5-tri-alpha-naphthylbenzene 17 p2809 A67-33255
 Absorption of optical photons in molecular crystals, noting results of laser output on naphthalene 20 p3457 A67-36326

NARCOSIS
 Metabolic depression in animals exposed to air after living in helium-oxygen environment, suggesting denitrogenation period effect 23 p3944 A67-40823

NASA PROGRAM
SA APOLLO APPLICATIONS PROGRAM
 /AAP/
SA SPACE PROGRAM
 NASA-sponsored satellite geodesy program using Baker-Nunn camera, noting station positions and gravitational potential determination 01 p0056 A67-10040
 NASA program involving orbiting satellite studies of natural and cultural resources 01 p0168 A67-10326
 System reliability improvements based on design and reliability experience producing increased success percentage of NASA systems from 62 to 87 percent 01 p0083 A67-11345
 NASA program for microelectronic circuit and space vehicle reliability 01 p0042 A67-11364
 Role of large solid propellant rocket motor in U.S. space program noting design, technology, testing, cost, thrust-vector control systems, etc 01 p0142 A67-11447
 Voice communications and control facilities at mission control center in Houston for support of manned space program conducted by NASA 02 p0229 A67-12120
 NASA research on visual problems of extended spaceflight 02 p0189 A67-12408
 Integration, testing and launching of flight hardware for Apollo/Saturn V space vehicle at Kennedy Space Center [AIAA PAPER 66-837] 03 p0397 A67-14126
 NASA FM telemetry system for data acquisition and processing from Ariel satellites including methods for storage, transmission, handling, etc 04 p0568 A67-14437
 NASA quality assurance program and NASA industry quality relationships, particularly for large space systems procurement 05 p0930 A67-17242
 Product identification and traceability standards for space system quality assurance program for NASA space systems 05 p0930 A67-17251
 Support of NASA quality requirements by Defense Contract Administration Services Regions 05 p0930 A67-17262
 NASA geodetic satellite program noting Beacon Explorer, Geos I and Pageos 07 p1176 A67-19757
 New aerospace-related technology in nonaerospace applications, noting NASA and petroleum industry 07 p1269 A67-20263
 Unmanned spacecraft program costs estimation through empirical studies of past and current NASA programs

[AAS PAPER 66-149] 08 p1429 A67-20969
 Implementation of NASA NPC 250-1 /Reliability Program Provisions for Space Systems Contractors/ as applied to Saturn V Mechanical Ground Support Equipment Program 09 p1582 A67-22292
 Electron microscope and microprobe measurements of luster flight samples, discussing particle size distribution and nondispersible chemical analysis 10 p1707 A67-23238
 Gemini experiments program, examining crew integration, mission planning and prelaunch operations 10 p1713 A67-23243
 Space technology developments for World Weather Watch, discussing satellites role in weather forecasting, meteorological sensor and instrumentation 10 p1877 A67-23369
 NASA earth orbital photographic experiments planned for 1967-1969 as supplement to Mercury and Gemini efforts 12 p1940 A67-25433
 Scientific research using NASA CV-990 aircraft 13 p2090 A67-27258
 Unmanned spacecraft program costs estimation through empirical studies of past and current NASA programs [AAS PAPER 66-149] 13 p2232 A67-27550
 Communication satellite program research 14 p2269 A67-28455
 U.S. international telecommunications requirements through 1975 14 p2272 A67-28704
 NASA applications technology stressing stabilization and pointing systems, data retrieval, etc [AAS PAPER 67-77] 15 p2557 A67-29944
 NASA space applications and future possibilities noting ATS-I satellite for cloud photography, omnidirectional aircraft antennas and Apollo Applications Program [AAS PAPER 67-89] 15 p2583 A67-29951
 Applications of Program Evaluation and Review Technique /PERT/ in NASA 15 p2583 A67-30222
 French satellite FR-1 to be launched in late 1965 by NASA for ionospheric studies, noting instrumentation, data transmission, etc 16 p2757 A67-30641
 San Marco project, joint effort of NASA and Italian Space Commission to launch satellite for atmospheric and ionospheric measurements 16 p2757 A67-30642
 Unmanned exploration of moon, summarizing results on surface structure, back side and material composition 16 p2748 A67-31199
 Medicophysiological aspects of NASA program stressing cardiovascular, muscular and osseous problems 16 p2814 A67-31538
 German Azur research satellite program design, instrumentation, payload, etc, and NASA role 18 p3162 A67-33640
 Control integration for lunar mapping 18 p3131 A67-34321
 Optical and stereoscopic microscope scanning combined with X-ray microanalysis used to investigate results on collection surfaces of space probes 19 p3339 A67-35197
 NASA observations for orbit determination from Goddard Range and Range Rate system compared to OGO-B observations 19 p3319 A67-35218
 U.S. space research program /1966/, national organization, international participation, space vehicle research and experiments related to future programs 19 p3322 A67-35307
 Research areas in future NASA program covering materials, energy conversion, guidance, instrumentation, etc 19 p3349 A67-35645
 Early autumn stratospheric circulation of Southern Hemisphere investigated by meteorological rocket observations 19 p3253 A67-35920
 Upgraded Saturn V vehicles and intermediate payload Saturn vehicles, studying costs, flexibility, performance and boost-assist components 20 p3531 A67-36539
 Changing role of technical writers and editors during next decade 20 p3556 A67-36587
 Quality program planning criteria for NASA contracts involving NPC 200-3 20 p3556 A67-36602
 Liquid rocket propellants use in U.S. space program, particularly Apollo project, discussing future trends 20 p3515 A67-36880
 Automation techniques for stage checkout in Saturn program noting equipment, time

factor, etc 20 p3417 A67-36975
Onboard Checkout System /OCS/ design, considering system selection techniques, design development, equipment, etc, with orientation on OCS design by NASA/MSC 20 p3417 A67-36988
Hypersonic flight programs, considering Air Force, Navy and NASA research programs on scramjets 20 p3517 A67-37447
High resolution interferometer data from radio source 3C 273 recorded at NASA deep space stations in Australia 21 p3712 A67-39122
Mississippi Test Facility /MTF/ of NASA noting rocket testing facilities, scientific laboratories and industrial complex 23 p3986 A67-40588
Progress in various space programs noting NASA role 23 p4086 A67-40668
Evolution of U.S. space program since inception and future manned and unmanned exploration 23 p4086 A67-40917
U.S. space flight affairs and decisions /1957-1967/ 23 p4086 A67-40918
U.S. exploration of solar system with unmanned spacecraft 23 p4086 A67-40920
NASA space program planning and proposed progress in 1970s 23 p4086 A67-40921
AZUR project /first German satellite/ cooperation with NASA, testing, signal recording, etc 23 p4071 A67-41326
Transonic and supersonic grid wind tunnel loaned to Germany by NASA for testing blades 23 p3987 A67-41328
Environmental control and life support system design for NASA Biosatellite program, discussing experimental results [SAE PAPER 870839] 24 p4114 A67-41995
White Sands Test Facility /WSTF/ constructed by NASA for hot firing tests of lunar module at simulated altitude 24 p4138 A67-42031
ESRO II satellite project objectives, design, testing program and mission requirements 24 p4241 A67-42402
NASA test program to evaluate performance and design point characteristics of 3-kw closed recuperated Brayton cycle power conversion system 24 p4102 A67-42486
NACA transition to NASA noting factors shaping development of government space research policy [AIAA PAPER 87-838] 24 p4259 A67-42977
Apollo historical perspectives, background to U.S. man on moon decision in mid-1961, rocket booster development and space mobility [AIAA PAPER 87-839] 24 p4259 A67-42978
Economic exploitation of lunar mineral resources for near earth orbit manufacturing [AIAA PAPER 87-872] 24 p4238 A67-42993
NASA National Space Science Data Center operation [AIAA PAPER 87-946] 24 p4260 A67-43032
NATIONAL AERONAUTICS AND SPACE ACT
Statute of National Aeronautics and Space Act of 1958 which forbids issuance of patent 05 p0929 A67-18771
NATIONAL LAUNCH VEHICLE PROGRAM
Economics of military space launching systems 15 p2566 A67-29830
NATURAL FREQUENCY
Expansion of E type symmetrical oscillations in axisymmetrical delay systems used in calculation of cylindrical resonators 01 p0035 A67-10394
Discrete element technique applied to natural vibrations of deep spherical shells satisfying geometric and force boundary conditions 01 p0164 A67-11184
Resonances in low pressure mercury vapor discharge due to natural resonance modes of cylindrical plasmas 02 p0273 A67-12097
Dynamic stability and critical flutter of axial-flow-turbine blades in cascade, for natural frequencies slightly mismatched 03 p0520 A67-12880
Von Zepel transformation solution small divisor problem arising from natural frequencies of orbital resonance motion of 24-hr artificial satellite 03 p0457 A67-13162
Axially symmetric motion of elastic spherical sandwich shell, determining natural frequencies and effects of shear deformation, normal stress and rotatory inertia 03 p0522 A67-13212
Formulation of dynamic three-dimensional problem of homogeneous isotropic and linearly elastic bodies in terms of

stresses 03 p0523 A67-13459
Plane oscillations of elastic pendulum with shaft undergoing bending deformation, determining principal zone of instability for action by longitudinal harmonic force 03 p0469 A67-14161
Natural and forced oscillations of sphere-array moving with collisions, analyzing quasi-elastic properties of system 03 p0432 A67-14162
Asymptotic distribution of natural frequencies of plane membrane with separable variables 04 p0708 A67-14871
Convective excitation of ionic oscillations in plasma by inhomogeneous electron beam as result of spatial gradient of distribution function 04 p0668 A67-15270
Transient thermal stress and associated natural frequency variations in circular disk elements [ASME PAPER 66-WA/MD-2] 04 p0629 A67-15347
Natural frequencies and mode shapes for axisymmetric vibration of thin elastic and ellipsoidal shells 04 p0714 A67-15424
Aircraft skin panel fatigue failure under hypersonic conditions, noting effect of natural vibration frequency and axisymmetric oscillations 05 p0916 A67-16229
Forced parametric oscillations in linear system, obtaining solutions for case where excitation frequency is twice natural frequency 05 p0916 A67-16243
Maximum slope method for obtaining natural frequency and damping ratio of highly damped second order systems from time history data 06 p1100 A67-18012
Coupled system of thin elastic shells, giving response to static or harmonically oscillating loads or to unloaded natural frequencies and mode shapes, using Green matrix [AIAA PAPER 87-45] 06 p1103 A67-18351
Sommerfeld effect in linear oscillating system with randomly variable natural frequency 07 p1261 A67-19140
Shear deformation and rotary inertia effects on modal data of nonuniform beam, with complex behavior defined by ordinary differential equations 08 p1416 A67-20533
Numerical procedure for proportioning members of complex structure with specified natural vibrational frequency based on finite element idealization 08 p1417 A67-20554
Frequency broadening of natural oscillations of optical resonator upon interaction with two-level atom in electromagnetic field 08 p1337 A67-20868
Solid rocket engine propellant grain structural dynamics including elastic and viscoelastic deformations, stress and shear vibration modes, natural frequency calculations, etc, using Fourier inversions and transforms 08 p1376 A67-20883
Internally modulated gas laser at 100 and 4000 MHz, describing electromagnetic field in Fabry-Perot resonator in terms of natural oscillation modes and coupling 09 p1514 A67-22269
Composite loss factor and natural frequencies of vibrating beams composed of alternate layers of elastic and viscoelastic material [ASME PAPER 87-VIBR-6] 11 p1871 A67-24166
Vibrational experiments with honeycomb type core sandwich beams on lowest natural frequency, node locations and damping, noting core shear flexibility [ASME PAPER 87-VIBR-11] 11 p1872 A67-24171
Determination of proper frequencies of vibration of thick-bladed turbine disk with interaction between disk, blades and shrouding [ASME PAPER 87-VIBR-52] 11 p1797 A67-24201
Vibration in cylindrical shafts, noting high stresses due to low mechanical damping, existence of two natural frequencies, etc 12 p1949 A67-25411
Natural frequencies of bladed disks calculated from 12 p2014 A67-25417
Matrix integral equations to calculate critical stresses and natural frequencies of oscillation of thin walled isotropic shells of revolution 12 p2022 A67-25585
Eigenvalue density in problems involving oscillations of elastic plates and shells,

establishing existence of natural frequency bunching point 12 p2022 A67-25586
Oscillations of cylindrical shell containing compressible gas perturbed by heat induced shock wave 12 p2023 A67-25595
Natural magnetoelastic oscillations of circular cylindrical conducting shell 12 p2023 A67-25596
Natural oscillations of elastic truncated conical shells of revolution under composite static load 12 p2026 A67-25613
Natural frequencies of free longitudinal oscillations of circular rod with random parameters determined by modified Krylov-Bogolubov asymptotic method 12 p2031 A67-25957
Polar coordinate analysis of free oscillations of circular plates with loosely clamped edges under large deflections, obtaining Duffing equation 12 p2031 A67-25963
Electrical simulation of finite difference calculations of problems of bending and natural oscillations of circular, annular and sector plates 12 p2032 A67-25968
Multidegree of freedom linear system analysis by dividing method for relations between system constants and solutions 13 p2156 A67-26527
Self-excited systems sensitivity function maximum value attained via time dependency on natural frequency and damping factor only 13 p2216 A67-26627
Natural frequencies of elastic toroids experimentally determined compared with theoretical results 13 p2219 A67-27091
Pilot techniques for determining aircraft longitudinal short period dynamics /natural frequency and damping ratio/ for standard analysis 14 p2244 A67-27741
Natural frequencies and mode shapes of pressurized circular cylinders with flexible stringers and attached point-mass [AIAA PAPER 86-449] 14 p2399 A67-28120
Moment stress effect on natural oscillation frequency, deriving motion equations of circular cylindrical shell 14 p2401 A67-28735
Bounds for natural frequency eigenvalues of simply supported uniform beam with constant end load and uniformly distributed axial load 14 p2403 A67-29005
Timoshenko beam equations modification necessary to account for normal pressure and Poisson ratio effects for application to thin walled circular tubes 14 p2403 A67-29013
Stability of systems with controlled plant and correcting system, based on analysis of stabilizability conditions in certain natural frequency regions 15 p2518 A67-30176
Sommerfeld effect in linear oscillating system with randomly variable natural frequency 17 p2965 A67-33217
Three-space optical resonator model, deriving properties responsible for undesired natural frequencies suppression, noting selection characteristics 18 p3058 A67-33528
Soviet book on numerical methods for calculating natural oscillation frequencies of liquids in bounded volumes 18 p3026 A67-33772
Natural frequencies of vibration of supported sandwich plate [SESA PAPER 1175] 18 p3143 A67-33901
Upper bounds for cantilever beam natural oscillation frequency error determined when approximately calculated frequency values approach exact values of problem 18 p3143 A67-34168
Estimation method for lower bounds of natural frequencies of circular closed cylindrical shell 19 p3338 A67-34876
Free axisymmetric oscillations of reinforced, closed, cylindrical circular shells, discussing natural frequencies and bending oscillations 19 p3338 A67-34877
Dispersion equation for electrodynamic boundary value problem of natural oscillations of cylindrical resonator with magnetoactive plasma 19 p3299 A67-36019
Skin stringer panel rows natural frequencies and normal modes predicted by transfer matrix method 20 p3539 A67-37008
Frequency and mode configurations of natural symmetric oscillations of elastically clamped cylindrical shells solved by characteristic equation 21 p3717 A67-37974
Ideal incompressible fluid axisymmetrical oscillations in elastic cylindrical shell, determining normal modes and natural frequencies of shell and

fluid 21 p3613 A67-38789

Natural frequencies and shape of axisymmetric oscillations of thin spherical shell under initial stress calculated via boundary value problem, using computer method 21 p3725 A67-38791

Self-oscillations of axial compressor blades, taking into account variation in natural frequency of flexural vibrations between blades 21 p3727 A67-38835

Minimum mass bar design for axial vibration of beam with load distribution at specified natural frequency 21 p3728 A67-38890

Natural vibration frequencies of cylindrically orthotropic circular plate with linearly variable thickness, solving differential equation of motion 21 p3728 A67-38898

Hollow torus axisymmetric circumferential natural vibration eigenfrequencies and eigenmodes dependence on thickness and torus radius ratio 22 p3908 A67-39289

Steady random natural frequency variation and subharmonic resonance, discussing periodic right hand side Duffing type equation describing system 22 p3836 A67-39405

Output SNR dependence on difference between input signal and natural frequencies for quasi-optimal linear filters, noting improvement for mismatched input 22 p3761 A67-39867

Homogeneous and sandwich spherical caps axisymmetric vibration natural frequencies solved approximately, noting application to shallow and spherical shell problems 23 p4073 A67-40617

Natural frequency vibration mode of turbine blades calculated by approximate theory of integral evaluation yield discrete models 23 p4076 A67-40684

Hysteresis loop measurement using Sonntag fatigue machine which produces sinusoidal force at 30 Hz fixed frequency 23 p4078 A67-41227

Natural frequencies and mode shapes determined for circular cylindrical shell closed by elastic plate 23 p4080 A67-41750

NATURAL SATELLITE

Observations of 24 comets, 11 minor planets and Jupiter VIII, using computer 01 p0148 A67-10386

Planet rotation and orbiting of satellite Io modulations effect on maximum RF of storms 05 p0904 A67-17408

Integrodifferential motion equations for Jupiter satellites 07 p1250 A67-19724

Solution within planetary theory with no secular terms in metric elements applied to problem of first order theory of Vesta disturbed by Jupiter 07 p1250 A67-19725

Unidentified satellite as explanation of abnormal perturbations in Saturn ring 11 p1866 A67-24770

Meridian observation of Jupiter for planet position determination, analyzing discrepancies between ephemerides and observations, noting random error 11 p1868 A67-25087

Stimulation of Jupiter radio emission by Io 12 p2000 A67-25204

Satellites Europa, Ganymede, Callisto and Amalthea show no effect on probability or spectral character of decametric radio emission of Jupiter 12 p2010 A67-26243

Cosmogonic hypotheses evaluation based on relation between oblateness, mass and number of satellites of planets of solar system 13 p2198 A67-28765

Meteoritic satellites of earth, estimating capture region dimensions 17 p2941 A67-32324

Phobos and Deimos origin in equatorial circular orbits or asteroid capture and tidal modification 18 p3125 A67-34160

Nonthermal radio emission from Jupiter atmosphere, studying Io modulation effect 19 p3317 A67-34933

Janus / Saturn tenth satellite/ discovery on December 15, 1966, noting orbit in ring plane and period 20 p3527 A67-37399

VLF radio reception anomalies explained by ephemeral natural satellite still in orbit, assuming reflections taking place near satellite perigee 21 p3582 A67-38514

Lunar gravitational fields based on Cassini and Euler rotation laws compared with solar, Saturnian and Jovian effects on Saturn and Jupiter satellites 24 p4229 A67-42311

Satellite rise and set time of distant

primary and occultation interaction determined for case of Martian satellite 24 p4238 A67-42925

NAVDAC

Program checkout facility designed to perform operational checkout of navigation systems by analyzing system under simulated conditions 09 p1484 A67-21833

NAVIER-STOKES EQUATION

SA REYNOLDS EQUATION

Heat transfer and equilibrium temperature of heat conducting sharp cones in supersonic rarefied gas flow at zero angle of attack 01 p0007 A67-10977

Unsteady laminar flow of incompressible fluid in gap between parallel disks with gap width varying with time, obtaining solutions for Navier-Stokes and thermal energy equations 02 p0231 A67-11469

Slow periodic motions of viscous incompressible fluid past sphere in infinitely long circular cylinder, using Navier-Stokes motion equations 04 p0602 A67-14618

Kinetic theory of gases through certain correlation functions known as product densities used to explain transitions from gaseous to liquid state 04 p0608 A67-15466

Difference scheme for calculating one-dimensional steady and unsteady Navier-Stokes equations for compressible gas flows 06 p0982 A67-17727

Navier-Stokes equations for two-dimensional sonic flow of viscous heat-conducting gas assuming particle velocity close to sound speed, studying asymptotic pattern 06 p0937 A67-18031

Vortex periodicity in wakes as function of Reynolds and Rossby numbers, solving nonlinear viscous Navier-Stokes equations [AIAA PAPER 67-34] 06 p0987 A67-18349

Free boundary flows of viscous liquid, analyzing Stokes flow at zero Reynolds number 06 p0990 A67-18641

Approximations to Navier-Stokes equations corresponding to steady two-dimensional incompressible viscous flow about circular cylinders 07 p1167 A67-19156

Numerical solution to time dependent Navier-Stokes equation for transient supersonic flow around right circular cylinder, using explicit-implicit finite difference method 07 p1169 A67-19625

Perturbation of two-dimensional viscous flows in finite region, noting exact solution of Navier-Stokes equation 08 p1319 A67-20352

Navier-Stokes equation for viscous incompressible fluid flow between stationary and uniformly moving parallel plates with uniform suction along stationary plate 08 p1322 A67-21179

Initial and boundary value problems in compressible fluid flow with moving boundaries governed by Navier-Stokes equation 08 p1322 A67-21384

Cauchy problem for nonstationary linearized Navier-Stokes equations for fixed container partially filled with liquid 09 p1532 A67-21873

Phonon lifetime variation effect on stimulated Brillouin and Raman scattering in gases by temperature, pressure and laser power variation and comparison with Stokes gain theories 10 p1662 A67-22758

Interaction of transverse distributed surface vibration with adjacent laminar flow, superimposing oscillatory pressure and velocity field developed in boundary layer fluid over idealized steady fluid flow 10 p1623 A67-22861

One-dimensional compressible flow, considering buoyancy forces as closed-form solution of Navier-Stokes equations for unknown temperature-dependent coefficient of viscosity 10 p1625 A67-23135

Navier-Stokes equation solution in region with smooth boundary, using linear elliptic equations 10 p1675 A67-23676

Stability of almost stationary periodic solution of Navier-Stokes equation, examining spectrum of relevant stationary problem 10 p1675 A67-23677

Numerical finite difference solution of three-dimensional equations of motion for laminar natural convection, noting Navier-Stokes equation transformation 11 p1774 A67-23861

Shock wave structure theory using Navier-Stokes character of shock wings and measured thickness, noting dependence on number density 11 p1775 A67-23879

Incompressible Newtonian fluid applied to dynamic reversibility of flows, analyzing motion equation and possible integration of Navier-Stokes equation 11 p1778 A67-24723

Motion of hollow body filled with viscous fluid at large Reynolds numbers, determining Zhukovskii potentials and examining small oscillations 11 p1782 A67-24673

Viscous flow around spheres, considering mass efflux effect, using Navier-Stokes equations and finite difference methods 12 p1927 A67-25282

Navier-Stokes equations solved by finite difference methods at low Reynolds numbers for viscous flow around sphere, noting no flow separation 12 p1927 A67-25283

Thermal convection in rotating fluid annulus analyzed using Navier-Stokes equations as initial value problem 12 p1963 A67-25339

Navier-Stokes asymptotic solutions for large Reynolds number flows, emphasizing incompressible axial flow past semilinear circular cylinders 12 p1930 A67-26179

Regularity properties in time variable of solutions of n-dimensional Navier-Stokes system 13 p2145 A67-26509

Regularity properties in temporal variable of solutions of n-dimensional Navier-Stokes system, using various interpolation methods 13 p2145 A67-26604

Dynamic characteristics of pneumatic transmission lines in regulation loops noting parameters effects, calculation methods, etc 13 p2055 A67-26799

Rarefied multicomponent gas flow boundary conditions over subliming wall determined through Navier-Stokes approximation, noting distribution function of each component 13 p2105 A67-27054

Stability of solutions of Navier-Stokes equations for boundary value problem and convergence to steady state 13 p2106 A67-27455

Navier-Stokes equations governing flow linearized by using weak solution technique 14 p2295 A67-27894

Heat conductivity effect on various one-dimensional flows solved by numerical integration of Navier-Stokes equations 14 p2296 A67-27980

Two-dimensional unsteady Navier-Stokes equations for compressible viscous gas in closed region, examining convective flow and heat transfer 14 p2296 A67-27987

Supersonic viscous flow near blunt body stagnation line, using Navier-Stokes equations 14 p2240 A67-27993

Viscous hypersonic flow past leading edge of sharp flat plate analyzed, using Navier-Stokes equation and velocity slip and temperature jump wall boundary conditions 14 p2299 A67-28162

One-dimensional small signal linear model of fluid transmission line using finite lumped parameter elements and Navier-Stokes equations 14 p2247 A67-28265

Linear symmetric modes of propagation for viscous compressible liquid in rigid and elastic conduits analyzed using Navier-Stokes equations [ASME PAPER 67-FE-12] 14 p2304 A67-28361

Boundary conditions for Navier-Stokes equations in rarefied monatomic gas with distribution function given a priori 15 p2470 A67-29234

Reproductive property of Navier-Stokes equations, generalizing notion of periodicity 15 p2510 A67-29462

Time independent two-dimensional Navier-Stokes equations solutions from singular perturbation theory, determining properties 16 p2657 A67-30828

Circular vortex ring motion and decay in incompressible flow field considered for Navier-Stokes equations solution by boundary layer technique 16 p2660 A67-31212

Cone and disk laminar flows of power-law fluids similarity solution by Navier-Stokes equation 17 p2793 A67-33040

Separation and stall of impulsively started elliptic cylinder including interactions between boundary layer and outer flow [ASME PAPER 67-APM-31] 17 p2840 A67-33157

Motion equation of non-Newtonian fluids in initial section of cylindrical tube 18 p3024 A67-33539

Flow past circular cylinder started impulsively from rest, reexamining Navier-

Stokes equations 18 p3026 A67-34008
Parameters of viscous supersonic compressible gas flow past corner, giving smooth coupling conditions for Navier-Stokes and boundary layer solutions 18 p3027 A67-34205
Numerical solutions of hypersonic sharp leading edge flows, with full time-dependent Navier-Stokes equations solved 18 p2984 A67-34739
Infinitesimal driven plane wave characteristics in uniform plasma with finite electron drift velocity found, using Navier-Stokes and Poisson equations, energy conservation continuity and perfect gas law 19 p3290 A67-35376
Regularity of generalized solutions of general nonlinear and nonstationary Navier-Stokes equations, improving differential properties by data smoothness 19 p3209 A67-35445
Hypersonic rarefied flow past sharp leading edge of flat plate noting incomplete compression phenomenon 19 p3171 A67-35735
Supersonic viscous gas flow around body of revolution involving perturbation damping, analyzing Navier-Stokes and heat transfer equations for flow chart 20 p3357 A67-36810
Hypersonic weak-interaction similarity solutions for viscous heat-conducting compressible flow past flat plate, using Navier-Stokes equations 20 p3357 A67-36849
Finite difference scheme based on Douglas-Rachford implicit alternating direction method for nonstationary Navier-Stokes equation initial value problems 20 p3423 A67-37213
Properties of kinetic energy and squared vorticity in two-dimensional inviscid turbulent flow, using Navier-Stokes equation and conservation laws 21 p3609 A67-37735
Exact solutions of incompressible Navier-Stokes equation for irrotational Beltrami nonconvective two-dimensional swirl and axially symmetric cross flows 21 p3609 A67-37737
Navier-Stokes equation solution in region with smooth boundary, using linear elliptic equations 21 p3652 A67-38277
Stability of almost stationary periodic solution of Navier-Stokes equation, examining spectrum of relevant stationary problem 21 p3653 A67-38278
Turbulence theory from local equilibrium breakdown macroscopic approach by imposing suitable conditions on correlation functions, discussing stochastic Navier-Stokes equations 22 p3782 A67-39500
Navier-Stokes differential equations for unsteady incompressible viscous fluid motion solution method, considering quadratic inertial terms 22 p3783 A67-39682
Navier-Stokes equations asymptotic solutions used for gas flow laminar boundary layer calculation near corner of body where supersonic gas flow passes through low pressure region 22 p3785 A67-40018
Local existence, uniqueness and regularity theorems for Cauchy problem solution for Navier-Stokes system in space 24 p4177 A67-42155
Papers on fluid mechanics and singular perturbations including Navier-Stokes equations, boundary layer theory, etc 24 p4141 A67-42167
Flexible membrane hydrostatic air bearing, determining membrane shape, pressure distribution and air gap by Navier-Stokes and membrane analogy equations [ASME PAPER 67-LUB-1] 24 p4162 A67-42668

NAVIGATION

S AIR NAVIGATION
S CELESTIAL NAVIGATION
S COLLISION AVOIDANCE NAVIGATION
S INERTIAL NAVIGATION
S INTERPLANETARY NAVIGATION
S LONG RANGE NAVIGATION
S LORAN
S MARINE NAVIGATION
S ONBOARD NAVIGATION
S PLOTTING
S POLAR NAVIGATION
S RADAR NAVIGATION
S RADIO NAVIGATION
S SPACE NAVIGATION
S STAR TRACKER
S TRIANGULATION

NAVIGATION AID

Navigation aids for ATC, discussing ground reference aids in terms of accuracy 09 p1530 A67-22649
Long range navigation aids for use as possible alternative to existing aids in interface between en route and terminal area 09 p1531 A67-22655
TACAN off-track airborne navigation computer and suitable indicator provide nonradial straight course as aid to ATC 09 p1531 A67-22658
Inertial navigation system and onboard navigation course computer evaluated, noting performance data and circular error 15 p2515 A67-29742
Experimental transmissions for navigation system monitored over 8500 km path to determine phase variations of VLF signals, for use in design of radio navigation aid 15 p2515 A67-30134
Long distance air navigation aids, stressing supersonic flight safety requirements 16 p2701 A67-31248
VLF transmitter design criteria and characteristics for global time and navigation signal network 17 p2824 A67-32494
Laser gyroscopes as aid to navigation and guidance, discussing principle, advantages, etc 17 p2868 A67-32726
Microwave direction-finding receiver with digital output for blind aircraft landing and navigational uses 19 p3254 A67-35551
Navy Navigation Satellite System, discussing naval and civilian application and improved gravitational field model 19 p3255 A67-35638
Ground-based radio aids to navigation as represented by existing major systems 19 p3255 A67-35857
NAVIGATION AND GUIDANCE
SA HOMING
Strap-down inertial navigation system compared with gimbaled system, noting methods of attitude reference and angular readout 01 p0110 A67-10489
ISA National Aerospace Instrumentation Symposium, Philadelphia, May 1966 01 p0072 A67-11108
Apollo Guidance and Navigation System positioning by electrically torquing gyros, discussing error sources 01 p0073 A67-11115
Digital computers for navigation and guidance solving design problem by combining general purpose /GP/ and digital differential analyzer /DDA/ approaches to produce hybrid computer 01 p0111 A67-11258
Minimum tracking data in guidance technique functioning comparable to proportional navigation homing system, noting tests in computer simulations and in laboratory model 02 p0263 A67-12158
Voyager spacecraft guidance and control system analysis, examining systems design requirements, problems of redundancy implementation for critical functions and gyro system 02 p0265 A67-12381
Navigation measurement optimization using Pontryagin maximum principle as necessary and sufficient condition to obtain smallest possible uncertainty 02 p0265 A67-12384
Short wave and very short wave direction finding from aircraft 03 p0465 A67-13394
Apollo guidance and navigation by computer holding fixed program with diverse and flexible applications 05 p0809 A67-17550
State space method for navigation problems of nominal trajectories 06 p1028 A67-17927
Solar perturbation effect on motion near collinear earth-moon libration points [AIAA PAPER 67-24] 06 p1064 A67-18259
Electronic clocks, with frequency and phase variation negligible, as means of making air and space navigation exact 07 p1222 A67-19681
Apollo external visual simulation display systems, discussing optical methods applied during navigation, guidance and control tests [AIAA PAPER 67-253] 07 p1189 A67-20085
Manual guidance for interplanetary flight by graphical methods, nomographs and relevant general equations 08 p1352 A67-21104
Omega navigation system composed of eight transmitters will give worldwide coverage on frequencies 10.2 kc and 13.6 kc 09 p1527 A67-22627
Direct view storage tubes for radar

displays 09 p1528 A67-22628
Flight testing of radio navigation aids for civil aviation noting techniques, telescope and typical test 09 p1528 A67-22629
Direct method for determining space directions and adjustment of satellite triangulation net 10 p1637 A67-23181
Vector equation for determining missile maximum roll rate for effective navigation ratio and time constant for guidance systems 11 p1816 A67-24215
Horizon sensor data processing with compensation for statistical properties of errors, noting application of optimal filtering theory 11 p1817 A67-24336
Navigation of SST with respect to optimum trajectory, flight system and traffic control 13 p2153 A67-26710
Past and future development in communication, components and guidance for space application 13 p2072 A67-27504
Kalman filter divergence control, noting analytical and empirical modification methods 14 p2347 A67-28116
Navigation and guidance functions performed in typical space-exploration mission 14 p2347 A67-28363
Computer partitioning for long term reliability in space, noting requirements for various phases of operation 15 p2439 A67-29306
Avionics, ordnance and military aircraft as totally integrated system, noting need of accurate navigation, target accuracy and improved communications 15 p2444 A67-29398
Nonhardware aspects of space navigation - Conference, Los Angeles, March 1967 15 p2513 A67-29594
Lunar module onboard guidance equipment design, noting operational strategies, control systems, etc 15 p2514 A67-29601
Steering laws synthesis for explicit guidance, noting generalization and solution of closed loop equations 15 p2514 A67-29603
Software tools for certifying operational flight programs 15 p2440 A67-29604
Commercial automatic inertial navigator for subsonic and supersonic aircraft provides global navigation and guidance within ATC limits without dependence on external aids 15 p2514 A67-29739
Proposed worldwide navigation, communication and traffic control system for all weather to guide aircraft and vessels, locate distressed vehicles and direct rescue operations at sea [AAS PAPER 67-102] 15 p2515 A67-29957
Spacecraft design for manned planetary landings noting mission characteristics, navigation requirements, crew housing, etc 16 p2756 A67-30625
Advanced range and orbit determination /AROD/ using airborne equipment to originate control and tracking signals by checking ground stations 16 p2701 A67-31491
Computational limitations of onboard orbiting computers such as fixed point arithmetic, limited word length and solution techniques 17 p2881 A67-32056
Linear/Monte Carlo method performance evaluation of intercept/rendezvous guidance and navigation for advanced space missions 17 p2882 A67-32493
Self-optimizing dual input Wiener digital filter by live input data processing derived for zero mean input case, noting applications to hybrid navigation systems 17 p2882 A67-32527
Automatic position determination for ships using active navigation satellite systems, discussing communications potential and safety 19 p3254 A67-35310
Deep space navigation and guidance technology, emphasizing simplification of onboard navigation procedures 19 p3255 A67-35856
Navigation requirements of V/STOL aircraft in high density urban areas 19 p3256 A67-35863
Navigation and guidance analysis of Mars probe launched from manned flyby spacecraft for 1975-1978 [AIAA PAPER 67-546] 19 p3257 A67-35945
Book on star trackers and systems design including technology, use for navigation and guidance, reference frames, error sources, atmospheric effects, etc 20 p3481 A67-36136
Navigation and guidance requirements of advanced single-stage-to-orbit reusable launch vehicle investigated to determine

- necessary modifications 20 p3481 A67-36576
 Man-machine design for Apollo spacecraft navigation, guidance and control systems 22 p3830 A67-39180
 Missiles and aerospace vehicles sciences - Conference, Huntsville, Alabama, December 1966, Volume 2 22 p3904 A67-40134
 Geopolitical factors connected with navigation satellite operation and control [AIAA PAPER 67-960] 24 p4260 A67-43041
- NAVIGATION INSTRUMENT**
SA INERTIAL PLATFORM
 Mark XII and XIV microcircuit computers for real-time navigational computation on military and civil aircraft 01 p0029 A67-10668
 Microwave radiometry application to navigation, thermonuclear diagnostics, astronomical temperature measurements, etc 03 p0367 A67-12805
 Apollo guidance and navigation by computer holding fixed program with diverse and flexible applications 05 p0809 A67-17550
 Maximum data recovery from interplanetary reconnaissance probe by returning vehicle to earth vicinity, using space velocity meter as navigation instrument 08 p1332 A67-21102
 Omnigraph airborne navigation equipment with small digital computer and closed loop display 09 p1526 A67-22389
 Omega receiver navigation set for high performance aircraft lane-position resolution 09 p1526 A67-22391
 VHF ILS equipment achieves necessary instrumental accuracy for automatic landing operation 09 p1529 A67-22643
 STAN 37-38-39, designed to meet operational requirements of category III all-weather landings and providing ground beacon requirements of ILS systems 09 p1529 A67-22645
 Divergence from and oscillation about nominal path in proportional navigation homing system 11 p1817 A67-24226
 Gemini VII star sightings analyzed, using handheld space sextant in Gemini VI, discussing effect of bias, timing angle measurement and trajectory errors 13 p2154 A67-26817
 Mark 19 Sperry gyrocompass with SGN 4 inertial platform 14 p2322 A67-28989
 Air navigation, classical methods, instrumentation and air traffic control 15 p2513 A67-29092
 Guidance and navigation sensors and systems, discussing spacecraft facilitated by microelectronics, computer technology, optimal filtering and gyroscopic sensor design 22 p3834 A67-40335
 Light Observation Helicopter Avionics Package /LOHAP/, designed for OH-6A Cayuse helicopter, providing communications and navigational capabilities 23 p3980 A67-40927
 Moving map display as cockpit navigation device useful when flying erratic routes at low altitude 23 p4003 A67-41283
- NAVIGATION SATELLITE**
SA TRANSIT SATELLITE
 AN/SRN-9 Integral Doppler equipment for use with navigation satellites to determine ship position at sea 05 p0839 A67-17388
 Thermal design of navigational satellites, obtaining reduction in discrepancy between operational orbital temperatures and preflight calculations through thermal vacuum testing 09 p1572 A67-22062
 Navy navigation satellite system developed by APL, using Doppler frequency measurements for navigation fix 10 p1877 A67-23183
 Navigation satellites of next decade, discussing services for air and sea intercontinental transportation vehicles [AAS PAPER 67-101] 15 p2570 A67-29956
 Proposed worldwide navigation, communication and traffic control system for all weather to guide aircraft and vessels, locate distressed vehicles and direct rescue operations at sea 15 p2515 A67-29957
 Automatic position determination for ships using active navigation satellite systems, discussing communications potential and safety 19 p3254 A67-35310
 Worldwide navigation satellite system in next decade, studying economical, organizational, technological, operational and safety aspects 19 p3255 A67-35658
 Influence of navigational requirements and technology on design of navigation-satellite system 19 p3256 A67-35862
 Navigation satellites for information during movements of manned/unmanned terrestrial vehicles containing position determination, communications and weather relay service and scientific sensors 22 p3831 A67-39524
 Solar cell power systems design and control technique for use in satellite programs, specifically transit 3B and 4A, ionosphere Beacon satellite, etc 23 p3938 A67-41507
 Geopolitical factors connected with navigation satellite operation and control [AIAA PAPER 67-960] 24 p4260 A67-43041
- NAVIGATION SYSTEM**
SA DIGITAL NAVIGATION SYSTEM
 KC-70 low cost inertial navigation system noting use of inertial sensors and digital computers 01 p0076 A67-11256
 Self-contained orbital navigation system using earth-horizon measurements in 14-16 mu carbon dioxide absorption band, using Kalman linear filter theory 02 p0263 A67-11925
 Autonomous satellite navigation based on repeatedly measuring angular position of ejected test probe relative to stars 02 p0264 A67-12311
 Position finding techniques based on precise observations of satellite orbits for ATC purposes 03 p0465 A67-13025
 X-ray and gamma ray navigation systems for helicopter formation flying, examining accuracy and scanning requirements 04 p0653 A67-14605
 System Utilizing Signal-processing for Automatic Navigation, for moving vehicles, using time delays and frequency multiplication 04 p0653 A67-14870
 Airborne Doppler navigation techniques and configurations 04 p0653 A67-15041
 Proportional navigation, emphasizing time-varying behavior of basic parameters, applied to exoatmospheric interception of satellite 04 p0654 A67-15550
 Navigation functional display requirements associated with early manned lunar exploration vehicles 04 p0655 A67-15662
 Supersonic transport navigation system accuracy, reliability, directional measurement, inertial speed, etc 07 p1221 A67-19068
 Navigation system test by phase shifter, noting signal generator which simulates omnirange systems 07 p1155 A67-19839
 Error model digital computer program applied to lunar surface hybrid navigation concepts, noting accuracy requirements from 1972 to 1985 08 p1351 A67-20675
 Precise pole-to-pole navigation system without use of special grids or transverse computational modes 09 p1526 A67-21830
 UHF distance measuring equipment /DME/ using new type of ground beacon and only thermionic devices in transmitter power stage 09 p1530 A67-22650
 Seastations in conjunction with submarine cables for aviation communication, navigation and air traffic control 09 p1530 A67-22652
 Performance errors analysis of navigation using inertial guidance and radar tracking 11 p1817 A67-24334
 Doppler radar and Doppler navigation system capabilities, applications, cost and reliability for supersonic and subsonic aircraft [SAE PAPER 670328] 12 p1964 A67-25870
 Inertial navigation system including aircraft interfaces, system modes of operation and performance [SAE PAPER 670329] 12 p1964 A67-25871
 Sensor stability conditions for two rotor gyrocompass on sea-going ship turning in circle 13 p2118 A67-26373
 Earth-based navigation for two-spacecraft missions using analytical techniques for POLYDOP tracking data 13 p2155 A67-27526
 Rate measuring strapdown inertial navigation systems, describing gas bearing gyros and three-axis ring laser 14 p2348 A67-29080
 Navigational technique for manned interplanetary missions, noting resemblance to traditional nautical technique 15 p2514 A67-29598
 Surveyor guidance program for midcourse and terminal information, noting redundancy in design, decision making
- telecommunications, etc 15 p2514 A67-29599
 Experimental transmissions for navigation system monitored over 8500 km path to determine phase variations of VLF signals, for use in design of radio navigation aid 15 p2515 A67-30134
 Operational accuracy of inertial navigation system as function of accelerometer and integrator error 16 p2699 A67-30468
 Principle of recursive navigation 16 p2700 A67-30656
 New navigation system/ADVANCE/ consisting of two-degrees-of-freedom gyro and accelerometer noting UTM grid-zone distribution system 16 p2701 A67-30928
 Advanced range and orbit determination /AROD/ using airborne equipment to originate control and tracking signals by checking ground stations 16 p2701 A67-31491
 Airborne optical satellite tracking, discussing accuracy limitations and comparing to ground stations 16 p2630 A67-31799
 Aerial electronic photomapping and geodetic surveying system describing track-keeping navigation and verticality measuring 16 p2679 A67-31801
 Optimum mixer-filter for aircraft navigation systems consisting of inertial platform aided by Doppler and/or Loran designed, using Kalman filtering 17 p2825 A67-32525
 Unidentified landmark navigation from orbiting vehicle by computer simulation, noting instrumentation accuracies 17 p2882 A67-33018
 Navigation system for long range transport aircraft providing accurate and reliable fixing, discussing takeoff and landing 19 p3254 A67-35312
 Systems approach combining human experience and logic with computer technology to implement navigation management function 19 p3254 A67-35313
 Navigation system for concorde aircraft, considering inertial navigation 19 p3255 A67-35805
 Ground-based radio aids to navigation as represented by existing major systems 19 p3255 A67-35857
 Air traffic control, navigation techniques, requirements and equipment for general aviation to end of century 19 p3256 A67-35861
 Strapdown inertial reference and navigation system initial alignment utilizing coordinate-transformation matrix computer [AIAA PAPER 67-556] 19 p3257 A67-35953
 Lunar landing module Doppler radar system in guidance navigation and control system, studying mathematical model performance 19 p3260 A67-36011
 Initial-convergence examination of Kalman filter for various autonomous navigation modes [AIAA PAPER 67-623] 19 p3260 A67-36012
 Correlation position device for autonomous orbital navigation system 20 p3481 A67-36553
 Navigational system accuracy and breakdown detection, discussing efficiency criterion for logic device operation 20 p3399 A67-37069
 Air traffic control /ATC/ in 1970s, discussing airports, electronic facilities and collision avoidance 20 p3482 A67-37441
 Automatic navigation trends, discussing cost effectiveness, transportation objectives and application rate 22 p3831 A67-39465
 Inertial navigation system operation errors on moving power plant due to inaccurate initial data feeding into computer 24 p4182 A67-42300
- NEAR INFRARED**
 Abnormal skin effect in thin films of noble metals near IR, taking into account wave penetration and magnitude of conducting electrons mean free path 02 p0288 A67-11723
 Absolutely calibrated radiometer for CW laser radiation in visible and near IR bands which relies on heat flow through standard thermal impedance 09 p1502 A67-22615
 Multiple scattering and finite detector bandwidth effects on shape of absorption features in atmospheric scattering 11 p1862 A67-24502
 Black body radiation deduced by analyzing spectrum of lightning in near IR at very high temperatures 11 p1816 A67-24755
 Small optical rotations in near IR measured by ring laser, discussing dynamic

- behavior of polarization state 13 p2128 A67-27345
- Multiphonon orbit-lattice relaxation of lower lying excited states of Dy doped lanthanum chloride investigated, using IR fluorescence and quantum counter techniques 19 p3302 A67-35035
- Near IR laser transitions in pure helium studied with scanning Fabry-Perot interferometer, determining fine structure components in upper laser levels 22 p3817 A67-40488
- NEBULA**
- SA CRAB NEBULA
- SA PLANETARY NEBULA
- SA SOLAR NEBULA
- UV radiation observed beyond atmosphere in winter Milky Way, noting nebula detection and photographic apparatus 18 p3125 A67-34190
- Physical parameters of IR nebula discovered in Orion 19 p3330 A67-36080
- NEGATIVE CONDUCTANCE**
- Gunn effect noting negative bulk conductivity, creation of external negative conductance and zones with different field intensities in semiconductor crystals 01 p0130 A67-10253
- Oscillations associated with S type current controlled negative resistance in semiconductors gallium arsenide samples, examining LF instability 01 p0133 A67-10473
- Microwave negative conductance due to traveling space charge waves in n-type GaAs 01 p0133 A67-10487
- Negative photoconductivity in germanium, noting breakdown and negative conductivity in In region, volt-ampere characteristics, etc 02 p0297 A67-11835
- Gallium arsenide negative conductance amplifiers used in calculation of negative mobility 02 p0221 A67-12512
- Negative magnetoresistance of n-type InAs in longitudinal magnetic fields 03 p0490 A67-13156
- Behavior of resonator quantum devices, using oscillating circuit with quasi-linear negative conductance 03 p0379 A67-13293
- Small signal theory of space charge limited unipolar diodes, calculating impedance and negative conductance 04 p0582 A67-15097
- Stability of state of semiconductors with absolute negative conductivity 05 p0868 A67-17059
- Effect of load mismatch on laser output, determining nonlinear dependence of equivalent negative conductance as function of oscillation amplitude in laser resonator cavity 08 p1338 A67-21270
- Negative magnetoresistance of n-type InAs in longitudinal magnetic fields 10 p1690 A67-23104
- Microwave amplification and negative conductance for GaAs, InP and CdTe 11 p1850 A67-24916
- Stability of state of semiconductors with absolute negative conductivity 15 p2538 A67-29790
- Transistor current-voltage characteristics when controlled by space-charge and transit-time effects, obtaining large negative conductances at HF 17 p2824 A67-32302
- Nonuniform stationary states of current in semiconductors having S-shaped current-voltage characteristics 19 p3301 A67-34900
- Negative differential conductivity in semiconductor in acoustic instability mode and connection with sound amplification and number of electron traps 21 p3678 A67-38097
- Negative differential conductivity in viscous semiconductor with stationary sound wave propagating under sound amplification conditions 21 p3681 A67-38352
- Gunn effect, describing electron transfer, domain propagation and space charge instabilities in GaAs 22 p3841 A67-40073
- NEGATIVE FEEDBACK**
- S DEGENERATION**
- NEGATIVE RESISTANCE DEVICE**
- Negative resistance of waveguide-mounted tunnel diode decrease with frequency suggested as source of oscillations at frequencies above cut-off 01 p0032 A67-10001
- Stabilization scheme for certain active networks, examining compensated one-port Y in simple amplifier connection 01 p0033 A67-10015
- Oscillation frequency and breakdown voltage in GaAs p-n junction reverse-biased into avalanche region due to negative resistance arising from transit time effect 01 p0137 A67-11070
- Modes of electric circuit with two reactive elements and nonlinear negative resistance investigated by piecewise linear approximation 02 p0224 A67-11580
- Negative resistance and current density in double-injection filaments in seminsulating Si 02 p0298 A67-11886
- Cadmium selenide single crystals subjected to gas discharge saturation of current-voltage characteristic, noting section with negative differential resistance 03 p0489 A67-13146
- Feedback effect on current voltage characteristic of device with negative feedback and reactivity of device in negative resistance region 03 p0380 A67-13583
- Tunnel-diode amplifier sensitivity gain due to negative resistance variation 03 p0382 A67-13668
- Book on network theory of negative-resistance tunnel diode linear and nonlinear sinusoidal circuits and application to amplifiers 03 p0383 A67-13817
- Stripe pattern characteristic of voltage-controlled negative resistance and LF electric oscillation observed in SbSI due to diffraction effect 04 p0674 A67-14619
- Wave propagation in n-type semiconductor with negative differential resistance 04 p0678 A67-15129
- Negative differential resistances and inductive effects in alpha-modified SiC p-n junction diodes 04 p0679 A67-15136
- Book on semiconductor devices with negative resistance having decreasing section in volt-ampere characteristics 05 p0770 A67-16171
- GaAs p-s-l-n diode exhibiting negative resistance, allowing assembly into X-Y matrix and electrical pulsing into emitting or nonemitting state 05 p0771 A67-16312
- Amplitude effect reduced on performance of nonlinear circuits by using shunt circuit, pseudolinear laws, and negative resistances, reviewing self-adaptive systems 05 p0785 A67-17271
- Current-controlled NDR, electron-hole generation and switching to higher current lower voltage state in GaAs 05 p0870 A67-17275
- Small signal negative resistance and avalanche region of impact ionization avalanche transit time /IMPATT/ diodes, particularly Read diodes 05 p0777 A67-17319
- Negative resistance regions in Si Zener diodes explained in terms of impact ionization and junction breakdown combination 06 p0968 A67-17814
- Avalanche drift diode and application in microwave technology, analyzing dynamic negative resistance formation, volt-ampere characteristics and output 06 p0970 A67-18169
- Magnetoresistance of heavily doped n-type silicon at liquid He temperature noting dependence on field strength and temperature 06 p1067 A67-18967
- Algorithm determining negative resistance intervals in parametric amplifier 08 p1299 A67-20334
- Semiconductor-insulator-semiconductor structure as negative resistance, noting V-I characteristics under various conditions 08 p1370 A67-21292
- Cadmium selenide single crystals subjected to gas discharge saturation of current-voltage characteristic, noting section with negative differential resistance 10 p1689 A67-23095
- Negative immittance converter circuits deducible from one basic NIC, noting similarity to Steimel vacuum tube circuits 11 p1789 A67-24129
- Current flow through plasma sheath into magnetized plasma, noting negative resistance characteristics of sheath upon ion cyclotron frequency 11 p1837 A67-24397
- V-I characteristics of In and Ge structures with negative resistance, noting effect of four-layer substructures 11 p1785 A67-24474
- Breakdown and switching in CdS single crystals, noting formation of negative resistance and thickness effect on performance 11 p1847 A67-24729
- Volt-ampere characteristics of diffused silicon n-n junctions with negative resistance analyzed, noting preparation technique 11 p1768 A67-24859
- P-type Au compensated Si diode with negative resistance, determining reversed conductivity recovery time 11 p1768 A67-24861
- Low bias non-Esaki current in tunneling p-n junction diodes with large excess currents 11 p1768 A67-24926
- Wave propagation in n-type semiconductor with negative differential resistance 12 p1978 A67-25153
- Hall EMF measurement in base of negative resistance silicon diode 12 p1917 A67-26097
- Transient characteristics of doped silicon diodes with negative resistance, determining electron lifetime vs current, noting space charge role 13 p2076 A67-26489
- Distributed tunnel diode amplifier design noting magnitude of attenuation by shunt for LF and HF [AFOSR-67-1406] 13 p2079 A67-26876
- Operation and electrical characteristics of bulk negative resistance semiconductor devices 13 p2183 A67-27562
- Negative-resistance Gunn effect in gallium arsenide and indium phosphide due to field excited electron transfer 14 p2366 A67-28474
- HF negative resistance in dielectric diodes with high density of shallow traps taking into account transit time 14 p2367 A67-28521
- Space-charge-wave growth and differential negative resistance conditions in two-valley semiconductors obtained from impedance 15 p2442 A67-29179
- Microwave power generating semiconductor oscillators noting negative resistance effect, construction of Gunn oscillator diode, etc 15 p2445 A67-29583
- Parametric negative resistance range and impedance matrix element values of microwave Read avalanche diode 15 p2453 A67-30016
- One-dimensional propagation of stable negative-resistance domains for carriers interacting with single type of impurity level 16 p2727 A67-30852
- Silicon negative-resistance junction diodes, studying n-p-n structure and diode characteristics dependence on light, temperature, voltage and frequency 16 p2636 A67-30898
- Analog-to-code converter using negative resistance of unijunction transistor, noting construction and results 16 p2636 A67-30900
- Negative-resistance in evaporated silicon films at room and liquid-nitrogen temperatures believed due to double injection 16 p2728 A67-31035
- IMPATT diode operation based on combination of avalanche-current multiplication and transit-time delay to produce negative resistance 17 p2824 A67-32332
- Niobium alloy semiconductor structures with nonlinear negative resistance, giving volt-ampere characteristics 18 p3009 A67-33472
- Au, Zn or Ni doped silicon diodes studied for current distribution over base cross section with negative resistance 18 p3010 A67-33577
- Laminar-turbulent boundary layer transition over aircraft components measured by method using negative-temperature-coefficient resistors compared to hot wire measurements 19 p3230 A67-35573
- Stability criterion for bandpass tunnel diode amplifier, determining limitations on diode series inductance as function of negative resistance 19 p3196 A67-35662
- Semiconductor negative resistance devices to achieve analog to digital conversion 20 p3390 A67-36252
- Controlled differential negative resistance silicon junction diodes with cadmium alloyed base 20 p3397 A67-36696
- Memory-cell circuit employing Esaki diodes negative resistance characteristic, developing small memory pulse amplitude useful in minimizing cycle time 20 p3397 A67-36769
- Impurity conduction causing negative magnetoresistance in Cu doped n-type GaAs crystals at low temperature 20 p3513 A67-37440
- Avalanche drift diode and application in microwave technology, analyzing dynamic negative resistance formation, volt-ampere characteristics and output

power 20 p3404 A67-37592
Dielectric thin film negative resistors for oscillator circuits compared to multilayer p-n-p structures for output frequency voltage temperature dependence 22 p3769 A67-39576
Nonreciprocal parametric amplifier obtained by using parametric elements in frequency inverting case without unguide or circulator 22 p3771 A67-39838

NEODYMIUM
Radiation of giant pulses of superluminescence by highly excited active medium of Nd glass with rapid cut-in of amplification 01 p0091 A67-10837
Temperature dependence of threshold for stimulated emission of Nd trivalent ion in several host lattices estimated from intensity variation of laser active fluorescence component 01 p0091 A67-10855
Mg-Nd alloy structure development during plastic deformation at high temperature, noting lattice distortions and recrystallization process 02 p0255 A67-11868
Fluorescent emission of neodymium laser triggered by Pockels effect as function of population inversion 03 p0436 A67-13201
Output spectra of Nd doped YAG and ruby lasers, determining mechanisms responsible for observed overall linewidths 05 p0820 A67-16660
Terminal level lifetime and fluorescence line of neodymium doped glass influence on dynamics and efficiency of Q-spoiled laser 05 p0822 A67-16675
Neodymium doped optical glasses for laser technology 05 p0824 A67-16855
Calcium fluoride-cerium fluoride with neodymium additions as active medium for lasers, discussing absorption and luminescence spectra and induced radiation 05 p0825 A67-16922
Neodymium glass laser time characteristics and spectral changes during conversion to traveling wave laser 06 p1012 A67-18782
Neodymium glass laser with spherical mirror resonator in stationary regime 06 p1012 A67-18783
Stimulated emission, absorption spectra and luminescence of neodymium-activated YAG crystals in pulsed laser 09 p1513 A67-22068
Design characteristics and operation of continuous neodymium laser 09 p1516 A67-22665
Calcium fluoride-cerium fluoride with neodymium additions as active medium for lasers, discussing absorption and luminescence spectra and induced radiation 14 p2330 A67-28262
Laser transition absorption cross section at room temperature for neodymium ion in yttrium-aluminum garnet determined by two methods 14 p2331 A67-28713
Neodymium activated alpha-gagarinite crystal laser, noting ternary fluoride systems characterized by optical centers 15 p2496 A67-29360
Measurement of position of polarization plane of radiation emitted by neodymium-glass laser 15 p2499 A67-29758
Absorption, fluorescence and laser emission spectra of triply ionized neodymium yttrium in compound below room temperature 16 p2726 A67-30810
Neodymium glass laser time characteristics and spectral changes during conversion to traveling wave laser 18 p3059 A67-33724
Neodymium glass laser with spherical mirror resonator in stationary regime 18 p3059 A67-33725
Laser frequency variation and emission kinetics during generation process, investigating spectra at scanning rate and pumping energy ranges 18 p3061 A67-34619
Neodymium doped calcium tungstate single crystals synthesized, obtaining continuous laser action 20 p3458 A67-36494
Laser induced gas electrical breakdown theories, predicting high threshold field strengths invalidated by single mode, phase-locked and laser measurements 20 p3459 A67-36851
Phonon spectrum of neodymium trichloride crystal lattice determined from polarized vibronic transition spectra and Zeeman effect of trivalent Pr and Nd impurity ions 22 p3840 A67-39434

NEODYMIUM COMPOUND
Sublimation and gaseous equilibria involving neodymium fluorides and barium

fluorides 03 p0367 A67-13519
Neodymium-glass laser using spontaneous amplified emission in nonresonant system to obtain high brightness output pulse 04 p0633 A67-15100
Heat capacity and Debye temperature of NdS, LaSe and LaTe 05 p0867 A67-17056
Giant pulse formation theory, measuring shape and duration of neodymium glass laser pulses for various values of inverse population 06 p1010 A67-17876
Dielectric properties including permittivity, losses, polarization, impurity conduction and forbidden bandwidths of thin films of praseodymium, cerium and neodymium fluorides 08 p1370 A67-20995
Heat capacity and Debye temperature of NdS, LaSe and LaTe 15 p2538 A67-29787

NEON
Microwave modulation of helium-neon laser intensity studied as function of temperature and electron density 01 p0088 A67-10260
Coupling of pulse powers in TEM of up to 80 mw from He-Ne laser at 6328 angstroms 03 p0437 A67-13678
Construction methods of DC operated He/Ne laser tubes using optical contact bonds 04 p0631 A67-14763
Double resonance effects extended to case of stimulated emission in excited states of neon, using gas laser in transverse DC magnetic field 05 p0818 A67-16845
WKB approximation of quantum radial distribution function for neon intermolecular pair potential taking into account particle exchange effect 06 p1038 A67-19044
Diffusive fractionation and two-component models for trapped meteoritic neon and isotopic composition of neon in carbonaceous chondrites 07 p1249 A67-19536
Radial particle density profile in neon negative glow plasma in cylindrical discharge tube measured by double probe method 08 p1362 A67-21288
Population inversion of neon levels in He-Ne microwave discharge as affected by pressure and power scattered by unit discharge volume 09 p1512 A67-21924
Stimulated emission in negative luminescence region of He-Ne glow discharge, noting effect of pressure and volt current 09 p1512 A67-21925
Recombination processes determined from data of time dependence of spectral line intensities and number density in decay plasmas produced in neon and helium-neon mixtures 09 p1548 A67-22360
Oscillator strengths for extreme UV resonance lines of ions in neon isoelectronic sequence calculated, based on single configurations in intermediate coupling 12 p1968 A67-26247
Line-narrowing effect induced by laser radiation applied to measurements of isotope shifts for two optical transitions in neon 13 p2127 A67-27080
Population inversion of neon levels in He-Ne microwave discharge as affected by pressure and power scattered by unit discharge volume 14 p2330 A67-28253
Electron thermal diffusivity in room temperature neon afterglow plasma measured using Tonks-Dattner resonance, noting independence of electron density 15 p2532 A67-30381
Cesium-neon mixture effect on thermionic-emission converter operation measured in experimental tube with plane electrodes, discussing volt-ampere characteristics 16 p2810 A67-31783
Helium and neon content and isotopic composition in iron meteorites, noting He 3 deficiency in hexahedrites due to tritium loss 17 p2942 A67-32359
Two peaks in emission from low pressure helium or neon discharge simulating plasma slab with second peak corresponding to plasma cut-off frequency 17 p2901 A67-32369
Active medium radial variation in density of neon atoms metastable level as explanation of anomalous laser oscillation 18 p3060 A67-34013
Mobility and diffusion of neon positive ions in neon, deriving ion energy and collisional cross section 19 p3271 A67-35074
Photon transmission delaying processes and secondary ionization growth time dependence on overvoltage in neon 19 p3264 A67-35086
Relative photon scattering cross sections

for He and Ne at Lyman alpha, describing measurement technique 20 p3489 A67-37431
Landé factors of neon atoms subjected to magnetic field and multimode laser irradiation measured by observing resonant saturations in fluorescent light emitted 22 p3815 A67-39651
Excited levels mean life in multiply ionized oxygen and neon measured by beam-foil technique 23 p4029 A67-40955

NEPTUNE
Neptunian planet-satellite system, discussing orbital motion of Triton 01 p0148 A67-10385
Resonance relation between orbits of Neptune and Pluto established by numerical integration 08 p1381 A67-20392
Uranus and Neptune spectral absorptions compared with laboratory spectra obtained with very long optical paths indicate methane role in planetary absorption 08 p1397 A67-21213

NERNST HEAT THEOREM
Hall mobility and Nernst-Ettingshausen effect in Zn and Cd-doped p-type GaAs at temperatures from 90 to 800 degrees K 03 p0491 A67-13174
Pressure rise in ionized He plasma cylinder due to Nernst effect 10 p1686 A67-23777
Tin and indium superconducting films transverse voltages due to longitudinal temperature gradients calculated for entropy per flux quantum 24 p4205 A67-43098

NERVA
S NUCLEAR ENGINE FOR ROCKET VEHICLE /NERVA/

NERVOUS SYSTEM
SA AUTONOMIC NERVOUS SYSTEM
SA BRAIN
SA CENTRAL NERVOUS SYSTEM
SA CEREBRAL CORTEX
SA CEREBROSPINAL FLUID
SA END PLATE
SA NEUROLOGY
SA NEURON
SA NEUROSCIENCE
SA PERIPHERAL NERVOUS SYSTEM
SA SPINAL CORD
Effects of 1, 1, 3-tricyano-2-aminopropene /TCAP/ on incorporation of protein and nucleic acid precursors into frog nervous system in vitro 04 p0560 A67-14408
Responses of lateral geniculate nucleus of monkey to light increment and decrement and encoding of brightness 04 p0561 A67-14592
Metabolic cerebellum changes under nonlethal hypoxia, noting system compensation during symptomatic stages and destruction of Purkinje cells at critical stages 04 p0561 A67-14629
Mammalian neuron networks for visual pattern recognition, noting equivalence of processing by memory neurons with matrix multiplication 04 p0563 A67-14798
Spontaneous discharges from single units in cochlear nucleus after destruction of cochlea, noting results of animal study 06 p0952 A67-17847
Terminal connections of spinothalamic and distribution in human thalamus, noting pain relay question 06 p0953 A67-18775
Electric stimulation of crossed olivocochlear cats and effect on auditory nerve responses 08 p1287 A67-20483
Acoustic waveform procession to auditory centers of brain, discussing transformations used by animals 09 p1454 A67-21686
Immediate and subsequent effects of brain damage in rats, using closed field intelligence tests 09 p1454 A67-22058
Analysis of brain wave records from Gemini flight GT-VII by computations to be used in 30-day primate flight 15 p2425 A67-29104
Prolonged confinement in small chambers effect on biodynamic processes of walking and other movements in special positions 16 p2613 A67-30914
Evoked potential display procedures yielding photographic superposition of large number of average responses 19 p3179 A67-34955
Mathematical model simulation of horseshoe crab eye lateral inhibition for nervous system pattern transformation, discussing human visual pattern recognition process 20 p3375 A67-37543
Sensory deprivation in space medicine, discussing irritation spectrum leading to

- pathological changes in psychic processes of test subjects 24 p4111 A67-41842
- Biochemical model for long term sequential memory in nervous system, introducing network serving as clock to maintain temporal order of stored events 24 p4116 A67-42698
- ## NETHERLANDS
- Fluid dynamics, structures and operations research and development at Netherlands National Aerospace Laboratory 02 p0231 A67-12640
- Space research organizational structure in Netherlands noting programs and experiments 19 p3321 A67-35299
- ## NETWORK
- SA CIRCUIT
- SA COUPLING NETWORK
- SA DEEP SPACE NETWORK /DSN/
- SA ELECTRIC NETWORK
- SA GRID
- SA ITERATIVE NETWORK
- SA LOGIC NETWORK
- SA QUADRUPOLE NETWORK
- SA RC NETWORK
- SA RLC NETWORK
- SA SATELLITE NETWORK
- SA SATELLITE TRACKING AND DATA ACQUISITION NETWORK
- Three-resistor thin film network possessing minimum sensitivity to random variations in individual components compared with single thin film resistor with same terminal impedance 04 p0593 A67-15487
- Gaseous laser output expressed in single or two-line oscillations as function of pumping rates and transition probabilities, considering concept of equivalent network 05 p0825 A67-16979
- Computer analysis, design and optimization of linear electronic networks 13 p2088 A67-26747
- ## NETWORK ANALYSIS
- Stabilization scheme for certain active networks, examining compensated one-port Y in simple amplifier connection 01 p0033 A67-10015
- Maximum power gain and admittance matrix for neutralized amplifier stages with three-terminal amplifier devices /electron tubes and transistors/ 01 p0035 A67-10432
- Network analysis by digital computer covering methods and programs for ladder networks, nodal, electronic circuit and state variable analysis, etc 01 p0028 A67-10462
- Flowgraph teaching techniques, discussing problem formulation, construction procedures and symbolic and numerical evaluation in network analysis 01 p0030 A67-11042
- Electronic Circuit Analysis Program /ECAP/, integrated system of digital computer programs producing DC, AC or transient network analyses from circuit topology, excitation, etc 01 p0031 A67-11338
- Combining IBM ECAP and propagation-of-variance moment method computer program for improved reliability circuit analysis 01 p0043 A67-11377
- Potential difference variation in circuits consisting of diode, capacitance and active resistor 02 p0209 A67-11509
- Modes of electric circuit with two reactive elements and nonlinear negative resistance investigated by piecewise linear approximation 02 p0224 A67-11580
- Ferrite-based microelements as quasi-resonant RC circuits 02 p0214 A67-11907
- Electromagnetic, circuit theory, quantum and statistical mechanics laws for conduction electrons in low and high injection p-n junctions 02 p0299 A67-12105
- Matrices of scattering transmission wave and normed cascade parameters of linear passive 2/m plus m/ terminal networks 02 p0221 A67-12528
- Network analysis shortcut by topological representation of impedance in node and loop equations 03 p0389 A67-12963
- Temperature determination for collector p-n junction of transistors in class B power amplifier by thermal equivalent circuit analysis 03 p0378 A67-13249
- AEDNET system of digital computer programs for on-line simulation of nonlinear networks and oscilloscope display 03 p0375 A67-13665
- Book on network theory of negative-resistance tunnel diode linear and nonlinear sinusoidal circuits and application to amplifiers 03 p0383 A67-13817
- Slot couplings of rectangular single-mode waveguides analyzed by equivalent circuit and concentrated parameter methods 03 p0385 A67-13952
- Automatic malfunction analysis /AMA/ technique providing space-vehicle test engineer with listing of all component failures that could cause abnormal indication at any observable monitoring point 03 p0399 A67-14213
- Switching circuit malfunctions analysis, discussing modeling for failure, simulation of failure and timing problems and sequential networks 03 p0394 A67-14219
- Book on circuitry for RF, AM and FM electronic communication systems 03 p0388 A67-14272
- Balancing network of reactance modulated amplifier with semiconductor diode capacitance, noting parametric oscillation at pumping generator frequency 04 p0579 A67-14450
- Transient analysis of TEM mode four-port microwave networks by flow graph techniques, with application to branch line coupler, phase shifter and ring hybrid 04 p0591 A67-14861
- Digital computer-aided circuit sensitivity analysis using symbols, with example of band pass filter analysis 04 p0578 A67-15088
- Analogous tube and transistor tuned feedback amplifier analysis and use of nonunidirectional active network as amplifying element 04 p0586 A67-15670
- Accuracy analysis method for radioelectronic circuits, noting statistical test method 04 p0586 A67-15671
- Network analysis with state variables describing system stored energy 05 p0781 A67-16022
- Three equivalent circuits of transistor mixer 05 p0784 A67-16943
- Effects of parameters of series circuit on current pulse in active load, using computer to calculate series circuit 05 p0785 A67-17470
- Varactor diode measurement by transmission methods under natural resonance conditions 06 p0969 A67-18122
- Performance characteristics of cryotron memory cell for measuring pulses arriving at input from current magnitude 06 p0966 A67-18242
- Peaking circle graphical method for solving 3-DB points in second order systems 06 p0971 A67-18244
- Solar array output protection against individual cell failures, considering effects of paralleling 06 p0951 A67-18420
- Parallel equivalent circuit parameters and Q-factor of cylindrical cavity resonator in TM sub 010 mode 07 p1153 A67-19813
- Circuit and system theory - Allerton Conference, University of Illinois, October 1966 08 p1307 A67-20317
- Reciprocal time domain analysis of RC networks, thin film networks and minority carrier devices 08 p1310 A67-20340
- Equivalent circuits of MHD generators with segmented electrodes electrically connected in various ways 08 p1286 A67-20738
- Integrated circuit in optimal design of aerospace systems, discussing potential low cost and use in computer analyses of circuits 08 p1303 A67-21060
- Electrical parameters of DC MHD generator determined from equivalent circuits 09 p1471 A67-21796
- Algorithm for analyzing general electric circuits with lumped parameters in transient state by automatic digital computer 09 p1469 A67-22440
- Normal form and stability of coupled nonlinear RLC networks with possible interconnected elements of like type 10 p1618 A67-22703
- Network analysis and synthesis using centrally located tree to generate connected linear graph trees 10 p1618 A67-22704
- Matrix methods applied to graphs, giving proof for matrix tree theorem 10 p1673 A67-22832
- Boundary between applicability ranges of network and steepest descent methods in equation integration of Timoshenko theory in analysis of plate deformation 11 p1871 A67-24159
- Improvements in management control of complex projects, considering network analysis 11 p1885 A67-24656
- Qualitative analysis of nonlinear systems described by ordinary or partial differential equations or by functional equations 14 p2291 A67-28452
- Functional-analytic techniques providing understanding of some nonlinear circuits action on input to output signal production 14 p2291 A67-28453
- On-line nonlinear circuit design, discussing computer program for evaluating performance resulting from modifications 15 p2442 A67-29169
- Necessary and sufficient conditions to ensure existence of unique solutions of equations for active networks 15 p2456 A67-29238
- Balancing network of reactance modulated amplifier with semiconductor diode capacitance, noting parametric oscillation at pumping generator frequency 15 p2443 A67-29287
- Electronic device modeling criteria expressing physical structure, representing significant properties and leading to useful equivalent circuits for circuit analysis 15 p2452 A67-30013
- Network planning - Conference, London, June 1967 15 p2583 A67-30221
- Applications of Program Evaluation and Review Technique /PERT/ in NASA 15 p2583 A67-30222
- Critical Path Analysis /CPA/ system based on network techniques, coordinating separate development programs of ELDO member states 15 p2583 A67-30223
- Reverse Monte Carlo method for circuit analysis, noting computer analysis of sense amplifier 16 p2633 A67-30475
- General equation for suppressor controlled transconductance of pentode useful for circuit analysis 16 p2635 A67-30794
- Network-diagram methods theory, discussing CPM, PERT, MPM, noting applications to technology and sociology 16 p2783 A67-31631
- Book on integrated and active network analysis and synthesis including integrated device operation, basic characteristics and network techniques 17 p2830 A67-32732
- Semiconductor device and transient ionizing radiation effects on monolithic integrated circuits 17 p2828 A67-32836
- Solid state microwave device technology concerning generators, low noise and control devices, discussing computerized technique for circuit analysis and design 18 p3015 A67-34595
- Sensitivity coefficients through flowgraphic representation of network function, discussing algorithmic computer program 19 p3200 A67-34846
- Stability range of feedback networks determined with respect to independent circuit parameter using root hodographs 19 p3201 A67-34910
- Pulse compression in unmatched dispersive networks noting phase characteristic matched to signal received 20 p3379 A67-36380
- Monograph on waveguide junctions theory and microwave network analysis, stressing model characteristic definition and impedance 20 p3399 A67-36950
- Series/parallel connection of redundant elements in thermopile shown to increase reliability of array over simple series of thermoelectric elements 20 p3363 A67-36958
- CR self-oscillation circuits, discriminating CR oscillators from astable, monostable and bistable multivibrators 21 p3604 A67-38601
- Soviet monograph on multiphase relaxation oscillators including circuit analysis for use in automation, telemechanics and radio engineering 22 p3768 A67-39464
- Functional analysis of transistor amplifier with multiloop feedback, deriving equation for transfer constant 22 p3769 A67-39577
- Final probabilities of ergodic Markov chain calculated by methods based on topological properties of stochastic graph 22 p3777 A67-39830
- Transistorized LF LC filter with positive and negative feedback, analyzing circuit to increase Q-factor and narrow passband 22 p3772 A67-39869
- Electronic network analysis using topological techniques of signal flow graphs, flow graphs and k-trees 22 p3778 A67-40556
- ## NETWORK SYNTHESIS
- Gyrator-RC filter synthesis procedure, noting open circuit voltage of network

configuration 01 p0032 A67-10008
Pulse frequency multistable devices whose states differ, along with output voltage, by generated pulse rate 01 p0043 A67-10239
Book on fluid power circuits and controls engineering 01 p0012 A67-10305
Semiconductor device measuring pulsed nanosecond currents produced in detectors by alpha particles 01 p0065 A67-10651
Time measurement with semiconductor device, noting parameter variation effect and experimental results 01 p0066 A67-10652
Circuit design measuring travel time required by low energy particle of varying mass 01 p0066 A67-10654
Neutron spectrometric measurements, discussing starting time determination and conversion of travel time into amplitude spectrum 01 p0066 A67-10656
Time expansion device for photomultiplier circuit for high pulse frequency using recording system, readout, thin film memory and simulation unit 01 p0029 A67-10662
Binary compound transistors, calculating parameters using T-shaped equivalent circuits 01 p0038 A67-10828
Capacitive pressure transducer featuring exceptional sensitivity, hysteresis, resolution and repeatability, detailing sensing element and measuring circuit design 01 p0071 A67-11102
All-pass RC filter network design for constant signal delay in LF systems, noting cascade phase characteristics 01 p0045 A67-11197
Stability theory based on functional methods, examining feedback system with linear time invariant and nonlinear elements 01 p0046 A67-11208
Stability theory application to control, circuit theory and aerospace systems 01 p0047 A67-11221
Reliable electronic design by suppression of adverse interactions among system levels 01 p0083 A67-11348
Inductance coefficient dependence on geometric air gap of ferrite cup cores, showing use for design of stable resonance circuits 02 p0280 A67-11464
Standard frequency transfer to local oscillator, removing modulation and producing continuous stable carrier 02 p0210 A67-11530
Graphical method of analyzing nonlinear problems of fluidic circuits 02 p0182 A67-11775
Shielded coupled strip transmission line with three center conductors, noting electrical behavior, cross section dimension evaluation from characteristic immittances, etc 02 p0193 A67-11777
Synthesis of TEM directional couplers and fixed phase shifters consisting of multiple parallel coupled quarter wave sections 02 p0214 A67-11778
Wideband elliptic-function band-stop transmission line filter design, computing characteristic impedances of filter element 02 p0214 A67-11779
Design technique predicting hot spot temperature and location in thin film circuit, determining power rating 02 p0215 A67-11972
Electronic equipment for measuring peak and valley currents of tunnel diodes 02 p0216 A67-12037
Q-active filter for narrow-band noise measurement in LF range 02 p0216 A67-12038
National Electronics Conference, Chicago, October 1968 02 p0199 A67-12086
Subnanosecond time interval measurements with recirculating transmission line memory 02 p0243 A67-12092
Signal suppression in ferrite frequency selective limiters evaluated using parametric subharmonic generator model 02 p0217 A67-12093
Six-port circulator with common pair of ferrite disks serving multiple junctions, used in frequency separation networks and tunnel diode amplifiers 02 p0217 A67-12094
Swept frequency modulation program, emphasizing lack of design information for optimizing performance and networks design with large time bandwidth products 02 p0202 A67-12124
Cryogenic associative memory system for information retrieval 02 p0208 A67-12163
Iterative realization of pattern recognition networks consisting of multilayer of linear threshold elements 02 p0208 A67-12174

Conformal mapping for obtaining loci of complex variables without tedious calculations demonstrated, using simple T filter 02 p0227 A67-12176
Fluidic oscillators, negative-and positive-gain operational amplifiers and cascade circuits 03 p0363 A67-13233
Equivalent circuit for four-layer dinistor with frequency independent elements, noting dependence of network elements on dinistor parameters 03 p0377 A67-13238
Dinistor trigger circuits with counting input, discussing flip-flop 03 p0377 A67-13239
Aluminum-titanium dioxide-silicon varactor equivalent circuit, noting measurement of parameters 03 p0377 A67-13240
Computer role in electronic systems design for higher reliability at lower cost 03 p0375 A67-13712
Synthesis of networks incorporating semiuniform loss by transformation into networks with near ideal reactances 03 p0393 A67-13974
Synthesis technique for RC network using two distributed RC elements, one negative impedance converter and one lumped capacitor 03 p0393 A67-13975
Synthesis method for immittance matrix with grounded unity gain amplifier /GUGA/ as only active element 03 p0393 A67-13979
Stability criterion for PWM feedback systems containing one integrating element 03 p0393 A67-13984
Differential far-end-operated half-echo suppressor design for telephone circuits with long propagation time 03 p0371 A67-13990
Telemetry design factors, discussing interference problems, antenna design, oscillator stability, preamplifiers, etc 03 p0372 A67-14120
Short triple electric and light pulse generation noting equipment design and performance 03 p0388 A67-14270
Autopilot programmer design for automatic guidance in approach and stabilization along course of aerial photography aircraft 03 p0465 A67-14284
Radar, range instrumentation and measurement systems 04 p0568 A67-14497
Universal circuit concept for fulfilling any electronic function 04 p0591 A67-14504
Synthesis procedure for distributed filters based on elliptic function or Cauer parameter lumped element prototype 04 p0580 A67-14859
Microwave varactor tuned transistor oscillator design, considering collector base multiplication, oscillation and load matching conditions and theoretical tuning curve 04 p0581 A67-14864
Lumped electric circuit device producing dispersion for pulse compression system noting design 04 p0574 A67-15054
Dispersive network of apparatus producing dispersion in pulse compression system, noting role of relatively low center frequency 04 p0574 A67-15055
Traveling wave field effect transistors, discussing method of increasing transconductance and cut-off frequency 04 p0582 A67-15096
Electrical properties of slotted waveguide bridge section based on symmetric terminal network theory and classical thermodynamical methods 04 p0582 A67-15147
Three-wire-line interdigital filters of Chebyshev and elliptic function characteristic for broad bandwidth 05 p0775 A67-16946
Equivalent circuit of piezoelectric quartz pressure transducer used with measuring circuit with small input resistance for solving gasdynamic problems 05 p0808 A67-17111
Fluidic circuit design, testing and performance noting transfer functions and differentiating and integrating circuits 05 p0754 A67-17200
Multiple correlation applications in design analysis of high reliability critical circuits 05 p0777 A67-17249
PCM telemetry system for satellite test vehicle of ELDO program using transistorized printed circuit technology 06 p0957 A67-17613
Synthesis of potentially bistable oscillator configurations serving as prototypes for integrated nearly sinusoidal applications 06 p0967 A67-17812

Synthesis of capacitive converters of angular displacements into digital code 06 p1003 A67-18175
Smoothing filter with output controlled parallel transistors, discussing empirical and experimental formulas and approximate circuit calculation 06 p0971 A67-18215
Equivalent circuit synthesis for microwave band pass filter design consisting of interdigital or comb structure EM line-coupled resonators 07 p1149 A67-19132
Monograph on internal state assignment problems in sequential machine circuit synthesis 07 p1147 A67-19208
Asynchronous control of information transmission in networks consisting of independent sequential circuits 07 p1161 A67-19884
Poles and zeros of amplifier transfer functions using digital computer, noting role in network analysis 07 p1157 A67-20091
Relation among sampling theorem, Z transformation and time series method for applications to network analysis 07 p1146 A67-20194
Topological properties of networks containing resistors, capacitors, self-inductors and controlled current generators 07 p1162 A67-20200
Pole-zero sensitivity minimization with respect to active and passive elements in active RC circuit design 08 p1308 A67-20322
Algorithms for dichotomous representation of macrocircuits, considering computer programs and establishment of flow graphs 08 p1299 A67-20326
Nonlinear DC circuits analyzed by digital computer for application to path integrals and stability problems 08 p1346 A67-20333
Fabrication concepts for large scale integration /LSI/ circuits 08 p1300 A67-20634
Design and layout of printed circuits 08 p1301 A67-20740
Device for parallel combination of radio transmitters 08 p1294 A67-20777
Convex programming procedure yielding algorithm for tuning out system from possible resonance zone 08 p1353 A67-20837
Chopper circuit theory and design methods with DC amplifier comparison 08 p1302 A67-20991
Linear transformation of normalized static capacitance matrix used to describe TEM propagation on array of parallel conductors 08 p1304 A67-21224
Optimization of design of input-output matching networks for transistor microwave frequency amplifiers, using computer program 08 p1305 A67-21228
Zener diode function generator eliminates need for external reference voltage source 08 p1307 A67-21538
Computer logic device development, discussing interdependence of various components and packaging methods 09 p1466 A67-21683
Input resistance and noise performance of multiple idler parametric amplifiers 09 p1474 A67-22084
Isolation bandwidth characteristics of Y circulator junction modified by external tuning elements 09 p1474 A67-22087
Circuit load effects on microwave properties of Gunn diodes, discussing equivalent circuit and graphical analysis of quenched and inhibited modes of operation 09 p1479 A67-22268
Monograph on high power semiconductor-magnetic pulse generators, noting saturable inductors and silicon controlled rectifiers, circuit analysis, voltage regulator, etc 09 p1482 A67-22698
Current-voltage characteristics of Esaki diode composite circuit 10 p1609 A67-22837
Functional properties of semiconductor devices and integrated circuits, considering network design 10 p1610 A67-22976
Optimum microwave filters with even number of sections, using first order Chebyshev polynomial to obtain equivalent circuit 10 p1613 A67-23444
Binary compound transistors, calculating parameters using T-shaped equivalent circuits 10 p1613 A67-23459
Synthesis of time functions with finite number of discontinuities by constructing functional scheme of system from Laplace transform of output 11 p1769 A67-24122
Definition, realizability and design of active gyrator, using two controlled current sources to obtain deal impedance inverting

characteristics 11 p1789 A67-24127
 Negative immittance converter circuits
 deducible from one basic NIC, noting
 similarity to Steimel vacuum tube
 circuits 11 p1769 A67-24129
 Cut-off frequency of drift transistor,
 discussing function of drift field
 parameter 11 p1759 A67-24143
 Theoretical realizability, design and
 stability of ideal gyrator with two
 operational amplifiers and resistance
 network 11 p1760 A67-24232
 Systematic design of matrix network,
 consisting of hybrids with phase delays in
 interconnecting lines, used for antenna beam
 steering 11 p1763 A67-24300
 Optical lossless double pass network
 synthesis techniques using birefringent
 crystals extended to complex and real
 transmittance amplitudes 11 p1818 A67-24418
 Network analysis of frequency stability of
 quartz generators, showing possible
 reduction through additional HF cascades
 introduction into feedback
 loop 11 p1768 A67-24982
 Relay testing under operational voltages
 and currents, discussing timing circuits and
 sequencing and computer inputs
 outputs 12 p1922 A67-25698
 Active filter design combining flat
 amplitude response with flat time
 delay 12 p1915 A67-25973
 P-i-n diode switches, discussing driving
 techniques for series and parallel biased
 switches, pulse leakage and RF turn-off
 delay minimization 12 p1917 A67-26194
 Thin film integrated circuit, discussing
 development of large value resistors and
 capacitors 12 p1918 A67-26219
 Compensation technique for improving
 stability of certain nonlinear autonomous
 systems by addition of zero
 networks 13 p2086 A67-26413
 Single crystal YIG phase shifter
 performance noting improved output with
 proper microwave circuit
 design 13 p2076 A67-26479
 Composite resonant system behavior with
 and without stub tuner, tabulating internal,
 external, loaded Qs and coupling
 coefficient 13 p2076 A67-26480
 Distributed tunnel diode amplifier design
 noting magnitude of attenuation by shunt
 for LF and HF
 [AFOSR-87-1406] 13 p2079 A67-26876
 Five classes of automated general purpose
 computer program for circuit design
 analysis 13 p2074 A67-27492
 Oscillation discharge by reactive circuit
 elements in two-terminal line controlled by
 movable poles of circuit in complex
 plane 13 p2085 A67-27723
 Bennett type RF spectrometer analysis of
 low pressure plasma discharge, noting
 effusion current
 determination 14 p2314 A67-27753
 Flip-flop type current mode switching
 circuits, discussing features incorporated and
 performance 14 p2280 A67-28012
 Design concept for microwave integrated
 circuits, noting realization and performance
 evaluation 14 p2280 A67-28013
 Integrated memory arrays, discussing
 packaging methods and comparing monolithic
 and hybrid large scale
 integration 14 p2280 A67-28014
 Thin film technique interconnecting
 integrated circuits by ultrasonic welding and
 multilayer thin film conductor
 networks 14 p2280 A67-28016
 Microelectronic technique application to
 active filter design, noting monolithic
 realization of operational
 amplifier 14 p2280 A67-28017
 Threshold voltage control for
 complementary pair MOS transistors,
 discussing techniques
 used 14 p2281 A67-28019
 MOSTSIM 2 computer program for design
 of integrated circuits 14 p2281 A67-28021
 Microelectronic frequency discrimination
 techniques based on analyzing whole
 functional block and searching for circuit
 configurations 14 p2282 A67-28024
 Fluidic pulse switching network hazards at
 high operating speeds, suggesting digital
 computer simulation to anticipate and
 rectify hazards before hardware
 fabrication 14 p2251 A67-28348
 Linear lumped component three-terminal
 transformerless RC circuits analyzed using

digital computers 14 p2291 A67-28459
 Progress in linear circuit theory,
 discussing scattering matrices, broadband
 matching and distributed and mixed lumped
 networks 14 p2291 A67-28460
 All-pass networks design method using
 algorithm and computer program for
 communications system
 application 14 p2274 A67-28914
 Design chart for parameter derivation of
 basic digital synthesizer, noting advantage in
 handling of tradeoffs 14 p2276 A67-28919
 Frequency domain instability criteria
 generated from stability criteria for time
 varying and nonlinear feedback
 problems 15 p2455 A67-29167
 Gyrator type circuit which requires only
 three amplifiers and which, when terminated
 with capacitor, can replace ungrounded
 inductor 15 p2456 A67-29240
 Electrical properties of slotted waveguide
 bridge section based on symmetric terminal
 network theory and classical
 thermodynamical methods 15 p2443 A67-29334
 Microwave power generating
 semiconductor oscillators noting negative
 resistance effect, construction of Gunn
 oscillator diode, etc 15 p2445 A67-29583
 Fast warmup crystal oscillator, noting
 advantages and applications in equipment
 requiring low power consumption and
 frequency stability 15 p2445 A67-29584
 Thermal, mechanical and electrical design
 of stable quartz crystal oscillator used for
 Geos satellite to generate RF carriers and
 Doppler system timing
 signals 15 p2445 A67-29585
 Phase lock loop of synchronized time code
 translator, noting design and
 application 15 p2445 A67-29587
 Pull-in range in feedback synchronization,
 discussing multistage filter and results
 obtained with graphical, computer and
 theoretical methods 15 p2446 A67-29588
 Acquisition behavior of phase locked
 loops, determining time and pull in range of
 loop for input step in
 frequency 15 p2446 A67-29590
 Oscillator with lumped parameter
 superconducting L-C tank circuit, noting
 frequency variations as function of
 temperature 15 p2451 A67-29916
 Two-port network design applied to FET
 in common source and common gate
 amplifier configuration 15 p2451 A67-29917
 Special preprocessing circuit for cardiac
 beat recognition discriminates against noise
 artifacts in
 electrocardiogram 15 p2432 A67-29920
 Cauer polynomials forming procedure
 suitable for synthesis of LC ladder filters
 without mutual coupling, giving design
 procedure of Cauer filter
 network 15 p2452 A67-29935
 Computer aided network sensitivity
 analysis 15 p2440 A67-29937
 Worst distribution analysis for statistical
 circuit design 15 p2455 A67-30406
 Multilayer printed circuit board system for
 interconnecting microelectronic components
 noting application of X-ray, ultrasonic, beta-
 ray, etc to process
 control 16 p2681 A67-30476
 Smoothing filter with output controlled
 parallel transistors, discussing empirical and
 experimental formulas and approximate
 circuit calculation 16 p2635 A67-30481
 Book on analysis and synthesis of tunnel
 diode circuits including equivalent circuits,
 amplifiers, etc 16 p2636 A67-30997
 Applied synthesis technique using
 feedback and command controller elements
 for strongly interacting multivariable control
 systems, illustrated by flight control system
 design 16 p2649 A67-31661
 Synthesis technique applying Liapunov
 theory for state vector tracking of nonlinear
 multivariable control systems illustrated by
 reactor control design 16 p2649 A67-31662
 Necessary and sufficient conditions for
 decoupling time-invariant linear
 multivariable system by state variable
 feedback, discussing transfer matrix
 consequences 16 p2652 A67-31692
 Waveguide mounted tunnel-diode oscillator
 noting equivalent circuit, power output,
 frequency, etc 17 p2822 A67-32037
 Temperature compensated electronically
 controlled ferrite attenuator design and
 performance 17 p2825 A67-32524
 Parallel electro-optical technique for

implementing linear threshold adaptive
 networks 17 p2860 A67-32616
 Book on integrated and active network
 analysis and synthesis including integrated
 device operation, basic characteristics and
 network techniques 17 p2830 A67-32732
 Radiation-hardened semiconductor
 electronic circuit design, noting radiation
 environment existing in spacecraft nuclear
 generator vicinity 17 p2919 A67-32857
 Monolithic operational amplifiers with
 simplified frequency-compensated network
 using minimum stages and integrated circuit
 components 17 p2828 A67-32899
 Combined electrical modeling technique
 for solution of two-and three-dimensional
 problems of unsteady heat
 conduction 17 p2973 A67-33081
 Design of receiver circuitry for IR
 surveillance system having high signal
 detectability 17 p2862 A67-33289
 Identification, coding and enumeration of
 distinguishable subnetwork configurations
 employing combinatorial
 analysis 18 p3016 A67-33496
 Algorithms for dichotomous representation
 of macrocircuits, considering computer
 programs and establishment of flow
 graphs 18 p3005 A67-33498
 Automatic AM control noting
 proportionate variation of carrier level to
 signal volume 18 p2998 A67-33502
 Number of feasible information networks
 with single channel redundancy for remote
 control of telemechanical
 system 18 p3016 A67-33572
 Initial loss in TWT with lossless slow
 wave circuit connection to drift tube,
 expressing field components by sums of
 normal modes 18 p3010 A67-33645
 Synthesis of time optimal control for
 discrete plants described by difference
 equations, deriving algorithm defining
 surface in phase space of
 variables 18 p3017 A67-33872
 Book on linear multiport synthesis
 covering time-invariant networks, matrix
 analysis, realizability considerations, network
 theory, etc 18 p3018 A67-34367
 Enhancement of signal to noise ratio of
 turbulence measurements by cross
 correlation and heat transfer
 transducer 18 p3050 A67-34499
 Monolithic or thin film microcircuits
 design and performance limitations resolved
 by combining characteristics of thick and
 thin films 18 p3014 A67-34552
 Large scale integration of circuits studied
 for high yield, using concept of redundancy
 adjustment of probability 18 p3014 A67-34553
 MOSFET approach to small scale
 integration of large scale
 circuits 18 p3014 A67-34555
 High density cryotron array production in
 associative memory application, using lock-
 out design feature 18 p3014 A67-34556
 Geocentric trajectories for particles of
 single class 18 p3018 A67-34666
 Synthesis of potentially bistable oscillator
 configurations serving as prototypes for
 integrated nearly sinusoidal applications
 [AIAA PAPER 65-363] 19 p3227 A67-34821
 Optimal design of RC lines distributed
 parameter systems using gradient technique
 and variational calculus 19 p3200 A67-34841
 Internal states minimization of sequential
 machines by developing
 algorithm 19 p3200 A67-34844
 Electronic circuit theoretical analysis
 noting nonlinear and qualitative
 processes 19 p3200 A67-34904
 Linear networks having reciprocal and
 nonreciprocal elements obtained using
 numerical-code circuit
 model 19 p3201 A67-34906
 Equivalent transformation of electronic
 circuits having nonreciprocal elements
 studied by methods of component
 connection 19 p3201 A67-34908
 Strip transmission lines used for
 microwave circuits noting applications,
 design data, discontinuity information,
 etc 19 p3191 A67-34945
 RC oscillators based on silicon n-p-n
 transistors for radio frequencies, analyzing
 active all-pass phase-shift
 circuit 19 p3191 A67-34946
 Single-mesh circuits design for driving
 xenon flashlamps, solving normalized
 nonlinear differential
 equation 19 p3192 A67-35015

Program providing man-machine communication for electronic circuit analyses using time sharing 19 p3186 A67-35619

Circuit design and performance to convert DC input voltage to pulse train with width proportional to input 19 p3197 A67-35702

Flowgraph models describing relationships between thermal and electrical parameters of devices and associated circuits 19 p3206 A67-36034

System/semiconductor interface with complex integrated circuits, examining different designs 19 p3199 A67-36055

High speed computer memory design using plated wire elements 19 p3189 A67-36065

Book on linear active network theory, emphasizing related circuit theory 20 p3407 A67-36119

Design and characteristics of solid state UHF transmitters and receivers applicable in color TV systems 20 p3395 A67-36249

Nonlinear circuits analyzed by Monte Carlo method for computer synthesis 20 p3407 A67-36331

State space equations formulated for general class of nonlinear networks, deriving block diagram of relationships 20 p3407 A67-36332

Thyratron circuit for generating high repetition rate high energy pulses, discussing design considerations and modifications 20 p3397 A67-36527

Multiple-winding choke design replacing separate inductors in filtering circuit and reducing power supply size and weight 20 p3399 A67-36882

Harmonic linearization, estimating quality of oscillatory transients in nonsearching self-adjusting systems described by high order differential equations 20 p3408 A67-37045

Capacitance reduction in active RC synthesis noting RLC, transfer functions, canonic sections, etc 20 p3409 A67-37109

Modulo control algorithms application in circuit for finding residues 20 p3392 A67-37153

Waveguide-below-cutoff bandpass filter theoretical design using equivalent circuit of filter to derive attenuation and bandpass properties 20 p3400 A67-37217

Frequency locked loop FM demodulator with high noise threshold 20 p3385 A67-37352

Timing considerations in sequential fluid power circuits design in terms of stray delay concept and safety of asynchronous circuit 20 p3365 A67-37362

Amplification factor stabilization or variance of transistorized radio astronomy receivers, discussing circuit diagram, performance and reliability 20 p3403 A67-37517

Sequential circuits design possessing distinguishing sequences and with very short fault detection experiments 21 p3588 A67-38183

Noise generator for calibration of radio receiver working in 1-2.6 MHz range during rocket flight 21 p3592 A67-38221

Flexible circuitry method of electronic packaging stressing use of flat cables 21 p3595 A67-38336

CR self-oscillation circuits, discriminating CR oscillators from astable, monostable and bistable multivibrators 21 p3604 A67-38601

Transistor oscillator design stressing output, efficiency and frequency stability at maximum load conductance 21 p3598 A67-38602

Operational analysis and DC design of Esaki diode pair bistable circuit used in high speed counting network performed by analog computer 21 p3604 A67-38603

Electronic circuit packaging in Apollo lunar module signal conditioning equipment 21 p3635 A67-38628

Aircraft construction techniques for terminating cables by pressure type connections, examining design factors 21 p3572 A67-39074

Essential additional operator, essential transformed system and cross correlation function methods for self-adjusting circuit design, considering sign of gradient component 21 p3604 A67-39110

Microminiaturized matrix preparation using welded and diffused Si diodes assembled in two groups of perpendicular metal strips 22 p3769 A67-39581

Solid state multilayer circuit preparation

for use in microminiaturization, stressing advantages over printed circuits 22 p3774 A67-40327

Surveyor TV power conditioning circuit and product design, discussing weight saving features, reliability and magnetic housing 22 p3807 A67-40374

Transistor parameters effect on microwave-circuit performance, tradeoffs and relation between tradeoffs, circuit performance and design 22 p3775 A67-40467

Varactor inductance effects on design varactor tuned circuits above 50 MHz 23 p3982 A67-41504

Unipolar-bipolar transistor hybrids for stable temperature independent current generators, detailing circuit design 24 p4128 A67-41895

Radiation resistance and reactance of thin film inductor in microwave integrated circuit determined using Fourier transform 24 p4128 A67-41924

Limiter circuits for NERVA reactor control, discussing design requirements and operation 24 p4183 A67-42472

Computer applications in electronic circuits design, discussing optimal man/computer interface and data handling processes 24 p4126 A67-42477

Electrical design of large lightweight solar array for electric propulsion type Mars-bound spacecraft, discussing magnetic effects and power losses 24 p4104 A67-42512

Monolithic integrated circuit design, considering thin film circuits, hybrid techniques and MOS devices 24 p4132 A67-42687

Repetitive circuit arrays combined with multilayer interconnections using discretionary wiring to improve array yield 24 p4132 A67-42688

Gigahertz tunnel diode logic, static and dynamic behavior of circuits under DC worst case tolerance analysis, timing analysis, etc 24 p4133 A67-42825

Linear optimal control in systems with uncertain parameters, noting application to design of compensating network for flexible booster for uncertain value of first bending mode 24 p4137 A67-42903

Asynchronous finite state sequential nonlinear controller synthesis with few flip-flops for dynamic space vehicle systems [AIAA PAPER 67-988] 24 p4127 A67-43060

NEUMANN PROBLEM

Neumann problems of Laplace equation with nonhomogeneous boundary conditions in theory of probe measurements of parameters of semiconductor films 01 p0136 A67-10997

Thermoelastic wave expansion in infinite medium discussed on basis of Duhamel-Neumann equation 04 p0715 A67-15577

Numerical solution of Fredholm integral equation of second kind with real analytic and periodic functions, noting eigenvalues 07 p1216 A67-19883

Elastic potential used to study Green and Neumann tensors through series expansion for Dirichlet problem 19 p3341 A67-35541

NEURAL NET

S ARTIFICIAL INTELLIGENCE

NEUROLOGY

SA DYSBARISM

Identification and localization of center median nucleus of Luys, noting CM projects primarily upon putamen 08 p1288 A67-21356

Pathogenesis of focal neurological dysbarism in pilots during altitude decompression sickness 10 p1600 A67-23827

NEURON

Absolute threshold of cat optic nerves determined by inspection of poststimulus time histograms, computed from responses of identical flashes of white light 10 p1598 A67-23581

NEURON TRANSMISSION

Mammalian neuron networks for visual pattern recognition, noting equivalence of processing by memory neurons with matrix multiplication 04 p0563 A67-14798

Waveforms of spike potentials form neurons in anteroventral cochlear nucleus indicate spikes are composed of three components 08 p1286 A67-20367

Vestibular stimulation effect on activity of neurons of optical cortex of curarized cats under vertical acceleration 13 p2058 A67-26758

NEUROPHYSIOLOGY

SA PSYCHOPHYSIOLOGY

Life sciences in fiscal year 2001, advanced concepts with emphasis on neurophysiological and behavioral problems 13 p2061 A67-27505

Neurophysiology of anesthesia 15 p2429 A67-29294

Soviet papers on certain problems of space neurophysiology 23 p3942 A67-40763

NEUROSCIENCE

Comparative neurosciences research program suggestions 07 p1135 A67-19864

NEUTRAL BEAM

Charge density modulation from plasma-beam interaction 20 p3504 A67-36157

Cross section measurement for charge transfer reactions, using crossed ion and neutral beam configuration and product ion mass analysis in nitrogen dioxide production 20 p3377 A67-37404

Mercury fed plasma bridge neutralizers for in-flight operation of SERT II electron bombardment ion thruster [AIAA PAPER 67-670] 21 p3691 A67-38704

Quasi-neutral ion beam focusing by axisymmetric electromagnetic field with closed electron drift, noting ion velocity distribution effects for longitudinal and azimuthal components 23 p4035 A67-41682

NEUTRAL ELEMENT

Intergalactic atomic neutral hydrogen detection in emission in clusters of galaxy and in noncluster field 03 p0514 A67-14318

Rate equations for nonequilibrium excitation of neutral helium in plasmas of moderate density solved and compared with population densities 11 p1844 A67-25075

Resonance transition probabilities in intermediate coupling for some neutral nonmetals, noting radiative lifetime measurements by phase shift 12 p1968 A67-26246

Rotational velocity of neutral hydrogen subsystem in outer regions of Galaxy outside galactic plane 17 p2950 A67-33163

NEUTRAL PARTICLE

Charged and neutral particles collision effect on LF oscillations in weakly ionized plasma in crossed electric and magnetic fields 06 p1046 A67-18827

Plasma-neutral coupling in ionospheric motions having short durations compared with time between neutral particle collisions with ions 08 p1325 A67-21151

Neutral particle densities of nitrogen, molecular and atomic oxygen and argon in upper atmosphere, noting density profile irregularities, diffusive separation altitude, etc 10 p1639 A67-23213

Ionosphere as binary two-temperature gas and transfer coefficients for elastic collisions based on Boltzmann equation 10 p1640 A67-23220

Possible major effect of minor neutral constituents of mesosphere on free electron density in D layer 10 p1645 A67-23265

Auroral intensity ratio of green line of atomic oxygen and first negative band of nitrogen, showing rise in electron temperature above neutral particle temperature 16 p2686 A67-31413

Formation of high energy plasma in toroidal system by neutral atom injection, discussing differential equations 17 p2908 A67-33110

Solar wind perturbation of uncharged interplanetary dust particle orbits, calculating particle lifetime 17 p2951 A67-33234

Ionospheric and magnetospheric neutral and charged particles temperature vertical distribution, noting effects producing variations 18 p3040 A67-34033

Arctic upper atmosphere neutral gas composition and altitude distribution studied, using meteorological rockets 19 p3219 A67-35251

Propellants and propellant mixtures effects on MPD arc jet performance in test for ions and neutrals mixture acceleration to high velocity [AIAA PAPER 67-684] 21 p3688 A67-38715

Ionospheric and magnetospheric temperature measurements using rockets and satellites including neutral particle, ion and electrons 22 p3871 A67-39677

Neutral atmospheric temperatures calculated from data provided by incoherent scatter soundings of ionosphere 22 p3794 A67-40474

Neutral and charged particle trapping using waves, discussing wave attenuation

from particle interaction, plasma waveguide and laser beam trapping 23 p4017 A67-41681

Electron neutral heat transfer in plasmas, obtaining data on electron thermal diffusivity from pulsed heat flow experiments in helium 24 p4194 A67-41872

Optimization of high energy neutral particles source /Eollon/ measurements, noting application to atomic collisions problem 24 p4153 A67-41912

Search for neutral particles other than muons with high penetration capability from heavy mass or passivity at 40 mwe depth 24 p4220 A67-42866

NEUTRALIZATION

Magnetic field effect on space charge neutralization in thin beam approximation [AIAA PAPER 67-83] 06 p1041 A67-18275

Electron space-charge neutralization in design of thermionic /heat-to-electricity/ converters 08 p1286 A67-21177

Neutralizer for large mercury thruster systems using hollow cathode forming plasma bridge neutralizer for large mercury thruster systems using hollow cathode forming plasma bridge [AIAA PAPER 67-671] 21 p3697 A67-38958

NEUTRINO

SA ANTINEUTRINO

Neutrino flux recording for temperature determination of sun interior, discussing thermonuclear reactions 01 p0152 A67-11301

Solar neutrino-electron interaction and use of boron-cycle solar neutrino fluxes to determine existence of neutrino and antineutrino scattering effects 02 p0317 A67-12776

Davis radiochemical experiment for detection of solar neutrinos and sampling techniques for detecting high energy atmospheric neutrinos 03 p0516 A67-14338

Plasma neutrino process as accelerating mechanism for evolution in UV dwarfs 08 p1396 A67-21180

Star collapse observation by detection of high energy neutrino fluxes produced by catastrophic star contraction 09 p1561 A67-21630

Neutrino theory and application to astronomy 09 p1563 A67-21651

Limit energy of monopole in field of earth magnetic dipole 10 p1631 A67-22800

Anisotropic cosmological solution with energy density determined only by neutrinos moving along one axis, noting expansion 10 p1708 A67-23334

Lifetime of atomic state against decay induced by lepton coupling, estimating neutrino power radiation and astrophysical implications 11 p1821 A67-23959

High energy photons, cosmic X-rays and hard radiation production mechanisms in interstellar gas, galactic halo and intergalactic medium 14 p2380 A67-27964

Neutrinos in stellar evolution and cosmological processes, discussing production processes 14 p2383 A67-27969

Gravitational fields for observation of soft cosmic neutrino and neutretto background predicted by different cosmological theories 15 p2555 A67-29641

Supernova explosion and collapse theory using relativistic hydrodynamics 16 p2752 A67-31541

Cross section of Helium 3 reaction calculated for possible solar neutrino source 16 p2741 A67-31921

Magnetic and electric charge interaction, noting neutrino electric dipole moment 17 p2887 A67-32101

Neutrino occurrence in universe noting postcreation and relic neutrinos, energy density, relic neutrino concentration, cosmic ray-neutrino interaction, etc 17 p2940 A67-32102

Solar neutrino-electron interaction and use of boron-cycle solar neutrino fluxes to determine existence of neutrino and antineutrino scattering effects 22 p3877 A67-40278

Solar neutrino astrophysics, universal neutrino sea, high energy neutrinos, neutrino detectors, stellar energy production, solar thermometry and gravitational constant time variation 23 p4056 A67-41111

Limit energy of monopole in field of earth magnetic dipole 24 p4150 A67-42137

Neutrino behavior in beta decay, proton-neutrino and proton-proton reactions,

discussing astronomical implications of neutrino radiation 24 p4227 A67-42197

High energy neutrino flux from atmosphere studied in South African gold mine using liquid scintillation detector 24 p4210 A67-42581

Penetrating particles in cosmic radiation deep underground in Kolar gold field experiment, discussing muon-neutrino interaction 24 p4210 A67-42582

Solar neutrino observation, considering inverse nuclear beta decay and elastic scattering by orbital electrons 24 p4210 A67-42583

NEUTRON

SA FAST NEUTRON

SA SLOW NEUTRON

SA THERMAL NEUTRON

Temperature effect in neutron component of cosmic rays and seasonal changes in intensity affected by interplanetary magnetic field 02 p0307 A67-11666

Calculation of neutron generation by mu-mesons for various depths in earth 02 p0312 A67-12607

Neutron collision cross section and calculation of energy loss of displaced Si atoms to ionization 03 p0494 A67-13481

Neutron production in cosmic radiation, neutron measurements and geophysical effects 06 p1077 A67-17875

Cosmic ray nucleonic component in Antarctic zone measured by neutron monitor, standardized and related to solar activity 10 p1699 A67-22862

Primary cosmic radiation composition effect on secondary emission, examining flux, spectra, nucleon interactions, proton component and neutrons 14 p2380 A67-27966

Temperature effect in neutron component of cosmic rays and seasonal changes in intensity affected by interplanetary magnetic field 16 p2738 A67-31081

Statistical correlation between phase and amplitude in first harmonic solar-diurnal variation of neutron component, noting longitude effect 17 p2931 A67-32078

Solar-diurnal variations of neutron and muon components of cosmic rays based on IGY data, analyzing temperature effect 17 p2931 A67-32079

Statistical analysis of solar-diurnal and semidiurnal variations of cosmic ray neutron component with respect to geomagnetic field perturbations 17 p2932 A67-32081

Relation between frequency distribution of sudden changes in cosmic ray intensity and solar-diurnal variation 17 p2932 A67-32082

27-day cycle variation in various noncosmic ray electromagnetic complex phenomena 17 p2932 A67-32084

Cosmic ray secondary nucleon production of multiple neutrons observed and energy spectra measured, using multiplicity monitor 20 p3452 A67-37407

Nuclear interactions mechanisms analyzed by method allowing comparison with Feynmann diagram, determining necessary information for analysis 24 p4193 A67-42859

NEUTRON ABSORBER

Time analysis of Mossbauer spectrum variation and isometric shift of source Te-125m in PbTe absorber following neutron irradiation in reactor 09 p1559 A67-22661

Complementary variational principles in neutron diffusion theory 11 p1824 A67-24632

Invariant imbedding method applied to energy dependent neutron radiation penetration problems in thick and heterogeneous shields 11 p1817 A67-25063

NEUTRON ACTIVATION

Neutron activation analysis applied to determination of Ar 40 and K 41 content of iron meteorites 02 p0326 A67-12045

Simplified neutron activation technique for analyzing metallic wear from aircraft hydraulic systems, computing activities of desired radioisotopes by cookbook procedure 02 p0249 A67-12221

Lithium fluoride thermoluminescent responses to neutrons, studying first and second order kinetics of decay and phosphor experiment 04 p0685 A67-15710

Neutron activation analysis of Si, Fe, Al, Mg and O content of lunar and planetary surfaces 05 p0843 A67-16546

Trace element concentration in iron meteorites determined using lithium drifted Ge semiconductor detector 09 p1569 A67-22686

Neutron activation analysis for terrestrial

and meteoritic rock major element abundance, noting possible application to extraterrestrial surface analysis 11 p1749 A67-23976

Fast neutron activation cross sections of Se and Fe measured, noting subshell closure effect and isomer ratio 11 p1822 A67-23979

Mercury abundance in various meteorite and rock types determined by neutron activation analysis, relating data to evolution of meteorites and earth 11 p1858 A67-24064

Mercury abundance in chondrite meteorites determined by neutron activation and separation by volatilization over temperature range 13 p2210 A67-27603

Neutron activation analysis to determine trace elements in iron meteorites 14 p2391 A67-28947

Element abundance in various chondrite groups determined by neutron activation technique 14 p2391 A67-28950

Chromium distribution in laser rubies with neutron activation autoradiography 20 p3458 A67-36427

Tracer experiments using tritiated ethanol on surface of MOS capacitor to indicate field-induced proton transport 20 p3510 A67-36857

Uranium content of chondrites measured by thermal neutron activation and delayed neutron counting 21 p3704 A67-38505

Indium concentrations determined by neutron activation in petrological suite of L-group chondrites 23 p4069 A67-41474

Chlorine abundance and distribution in iron meteorites from neutron activation analysis and metallographic examination, discussing terrestrial contamination effects 24 p4232 A67-42610

Iodine, uranium and tellurium abundances in various achondrites, chondrites and mesosiderites from neutron activation analysis 24 p4233 A67-42616

Precious metal concentrations in carbonaceous and enstatite chondrites using neutron activation analysis 24 p4233 A67-42617

Silicon abundances in chondrules from different chondrites by neutron activation analysis 24 p4236 A67-42644

Antimony abundance in meteorites, tektites and terrestrial rock by neutron activation analysis 24 p4236 A67-42647

NEUTRON BOMBARDMENT

Spin-lattice relaxation time dependence on temperature and magnetic field in neutron-irradiated quartz with paramagnetic defects at helium temperature range 01 p0127 A67-10064

Neutron irradiation effect on twinning behavior and transition temperature of niobium-vanadium alloy 02 p0256 A67-12709

Neutron bombardment effect on titanium and chromium carbides before and after heat treatment, giving results of X-ray and micrographical analyses, electric resistance, brittleness and microhardness measurements 03 p0447 A67-13639

Neutron energy deposition in silicon in ionization and elastic interactions calculated, noting effects of atomic recoils 04 p0684 A67-15688

Neutron induced degradation of carrier lifetime in n- and p-type silicon containing oxygen and dopant impurities 04 p0684 A67-15691

Minority carrier lifetime dependence on injection level, obtaining recombination center parameters for neutron irradiated germanium, using photoconductivity 04 p0684 A67-15692

Transient annealing following pulsed neutron exposure in silicon transistors and solar cells as function of temperature and injection level 04 p0684 A67-15693

Annealing behavior and uniaxial stress response of radiation induced defects in Si causing 1.8, 3.3 and 3.9 micron IR absorption bands examined via EPR studies 05 p0870 A67-17194

Annealing of fast neutron damage in impurity conducting n-type Ge, noting small activation energy in resistivity below 10 degrees K 06 p1050 A67-18146

Impurity states in CdTe analyzed by examining changes in electrical and optical properties after thermal-neutron bombardment 06 p1062 A67-18928

Absorption spectra and photoluminescence in n- and p-type GaAs before and after neutron and electron

irradiation 06 p1062 A67-18933
 Annealing of neutron irradiation induced changes in impurity conduction in Sb-doped Ge 06 p1068 A67-18969
 Creep ductility, stress rupture and high temperature irradiation embrittlement of neutron-irradiated Hastelloy N 08 p1343 A67-21195
 Electrical conductivity measurement of He 3 plasma induced by neutron irradiation 09 p1542 A67-21813
 Fast neutron irradiated p-type silicon single crystals electric and photoelectric properties 10 p1691 A67-23404
 Invariant imbedding method applied to energy dependent neutron radiation penetration problems in thick and heterogeneous shields 11 p1817 A67-25063
 Beryllium and other hexagonal metals mechanical properties compared under neutron irradiation, elucidating causes of beryllium embrittlement 13 p2135 A67-27102
 Crystal dislocation in InSb by fast neutron bombardment assuming displacement wedges with electron type conductivity 15 p2541 A67-30234
 Fast neutron bombardment and temperature effects on conductivity, photoconductivity and resistivity of Si single crystals, determining energy levels of defects 15 p2541 A67-30236
 Neutron irradiation effects in pure Mo, noting formation of prismatic dislocation loops 17 p2872 A67-32740
 Clustering in AL-GP zone alloys after low temperature neutron irradiation 17 p2872 A67-32742
 Temperature, resistivity and injection level dependence of recombination processes in neutron irradiated silicon explained by two-level recombination model 17 p2916 A67-32837
 Radiation effects on silicon transistor parameter behavior characteristics 17 p2917 A67-32843
 Neutron and Co gamma rays radiation effect on lithium drifted p-n silicon detectors 17 p2917 A67-32846
 Low temperature thermal conductivity measurement of fast-neutron-irradiated silicon and germanium, showing difference between bombardment induced scattering in two materials 17 p2919 A67-32855
 Disordered regions produced by fast neutron irradiation effect on semiconductor properties of silicon 17 p2919 A67-32859
 Neutron bombardment effect on niobium mechanical properties shown to depend on metal purity 17 p2874 A67-32898
 Damage regions in Si, GaAs and InSb irradiated with monoenergetic neutrons determined, using electron microscopy 17 p2922 A67-33060
 Effect of irradiation of silicon by fast neutrons on switching time of alloy diode synthesized on silicon base 20 p3508 A67-36402
 Secondary neutron spectral data measured by proton recoil spectrometer from targets bombarded by 160 Mev protons 23 p4028 A67-40739
 Li interactions with complex damage clusters produced by neutrons in Si solar cells, discussing annealing, radiation hardening and energy dependence 23 p3940 A67-41520
 Fast neutron radiation damage in narrow base p-n-p-n devices compared to one-dimensional theory, showing superiority to bipolar transistors 24 p4130 A67-42248
 Neutron irradiation effect on thermal conductivity of silicon at low temperature noting annealing stage 24 p4206 A67-43110

NEUTRON COUNTER
SA GEIGER COUNTER
 Barometric pressure coefficient, correcting terrestrial neutron monitor intensities, dependency on magnitude variations related to changes of atmospheric water vapor content 03 p0505 A67-12958
 Cosmic radiation anisotropy variation with time and direction described on intensity contour map, noting application for neutron monitors data reduction 17 p2938 A67-33209
 Uranium content of chondrites measured by thermal neutron activation and delayed neutron counting 21 p3704 A67-38505
 Solar diurnal variation and sudden changes in cosmic ray intensity from yearly neutron component data 23 p4058 A67-41123
 Cosmic ray intensity measurement data

from Soviet 1966 expedition in Arctic Ocean 23 p4060 A67-41138
 Solar neutron observations with boron fluoride counter on OSO-1, discussing absence of diurnal variation 23 p4061 A67-41236

NEUTRON CROSS SECTION
 Intensity of ionizing and neutron component of cosmic rays, noting correlation for sporadic cyclic variations and solar activity cycles 05 p0879 A67-16103
 Neutron exposure ages of meteorites, estimating amount of shielding which surrounds samples in space from Co-60 and Ar-39 activity data 06 p1082 A67-17871
 Fast neutron activation cross sections of Se and Fe measured, noting subshell closure effect and isomer ratio 11 p1822 A67-23979
 S-process theory of heavy element formation in solar system confirmed by measuring neutron capture cross sections 24 p4224 A67-41817
 Intensity of ionizing and neutron component of cosmic rays, noting correlation for sporadic cyclic variations and solar activity cycles 24 p4213 A67-42779

NEUTRON DECAY
 Modes in spatial distribution of neutron density within cosmic ray neutron monitor, each mode having distinct lifetime, using diffusion theory 04 p0661 A67-15615
 Satellite-borne detection of decay protons as test of solar neutron observation 17 p2937 A67-32544
 Solar radio emission mechanism for spin transitions of neutron beta decay electrons in external magnetic field 20 p3520 A67-37522

NEUTRON DETECTOR
 Charged particle solid state detectors, considering neutron intensity and energy and spectral and/or dose measurements 02 p0244 A67-12210
 Solar particles zones of incidence during maximum and minimum solar activity 02 p0310 A67-12574
 Fast and slow neutrons detected by proportional and scintillation counters 02 p0312 A67-12606
 Hysteresis effect on cosmic ray intensity of solar cycle variations 07 p1242 A67-19620
 Barometric coefficient for neutron monitor noting long term and altitude dependence 07 p1188 A67-19954
 Recoil proton detectors used for rocket measurements of fast neutron intensity above Fort Churchill, Canada, during 1964 and 1965 12 p1998 A67-25828
 Directional neutron detector using liquid scintillator for low mev energy range for rocket and satellite experiments 12 p1945 A67-25860
 Reception vectors for first and second spherical harmonics of cosmic ray distribution calculated for neutron monitor stations 21 p3699 A67-39018
 Deuterium-tritium plasma temperature measurement using neutron detector, assuming Kerr cell ruby laser produced thermonuclear reaction heating in gas 23 p4031 A67-40892
 Radiation resistant silicon diode fast neutron monitors, discussing fission spectra and leakage currents in damaged diodes 24 p4183 A67-42473

NEUTRON DIFFRACTION
 Neutron diffraction in ordered nickel-manganese alloys with near equilibrium distribution of atoms over lattice points 05 p0863 A67-16758

NEUTRON DISTRIBUTION
 Book on natural neutron background of atmosphere and earth crust including effect of primary and secondary cosmic radiation, solar neutrons, presence in rocks, etc 01 p0143 A67-10042
 Variation of seasonal diurnal distribution of sudden changes in cosmic ray neutron component intensity related to solar activity changes 05 p0881 A67-16118
 Solar diurnal variation of cosmic ray neutron component in Antarctic during minimum activity period, using harmonic analysis 05 p0881 A67-16119
 Seasonal changes in solar diurnal and semidiurnal variations of cosmic ray neutron component due to earth rotation axis and anisotropy sources 05 p0885 A67-17138
 Rotation of vector of solar diurnal variation in intensity of cosmic radiation neutron component during solar activity minimum 05 p0885 A67-17497

Geophysical and heliophysical characteristics for enhanced cosmic radiation intensity during magnetic storm in February 1959 05 p0885 A67-17498

Latitudinal effect on neutron-monitor data taken by Soviet ship in North Pacific, obtaining relation between coupling constant and cut-off rigidity 17 p2933 A67-32092
 Seasonal changes in solar diurnal and semidiurnal variations of cosmic ray neutron component due to earth rotation axis and anisotropy sources 21 p3700 A67-39048
 Low latitude cosmic ray neutron monitor multiplicity distribution, discussing monitor geometry and latitude 22 p3874 A67-40047
 Variation of seasonal diurnal distribution of sudden changes in cosmic ray neutron component intensity related to solar activity changes 24 p4214 A67-42794
 Solar diurnal variation of cosmic ray neutron component in Antarctic during minimum activity period, using harmonic analysis 24 p4214 A67-42795

NEUTRON EMISSION
 Nuclear radiation intensity effect on switching time of fast diodes, examining produced stability changes 01 p0066 A67-10655
 Neutron spectrometric measurements, discussing starting time determination and conversion of travel time into amplitude spectrum 01 p0066 A67-10656
 Nuclear physics of neutron emission in stellar interiors, reaction rates of neutron-producing processes evaluated with optical model of nucleus and uncertainties assessed 03 p0508 A67-14315
 Magnitude of lunar neutron emission due to cosmic rays estimated from atmospheric measurements 05 p0879 A67-16105
 Energetic neutrons relationship to sub solar flare 06 p1076 A67-17602
 Cosmic ray neutron component intensity during magnetic perturbations, considering effect of magnetospheric deformation 10 p1699 A67-22781
 Neutron emissions by noncylindrical discharges of revolution, noting high pressure and impurities favoring airtight magnetic piston 10 p1683 A67-22844
 Neutron irradiation effect on n-type and p-type semiconductors thermophysical parameters 19 p3307 A67-35874
 Thermonuclear origin of neutron emission in theta pinch plasma, determining ion temperature from scattering of ruby laser beam 22 p3843 A67-39244
 Intensity of ionizing and neutron components measured in stratosphere as function of geomagnetic rigidity, obtaining coupling coefficients for cosmic ray variations 23 p4059 A67-41136
 Cosmic ray neutron component intensity during magnetic perturbations, considering effect of magnetospheric deformation 24 p4209 A67-42117
 Magnitude of lunar neutron emission due to cosmic rays estimated from atmospheric measurements 24 p4213 A67-42781

NEUTRON FLUX
SA ATMOSPHERIC NEUTRON FLUX
 Neutron component diurnal variation in cosmic radiation during period of coil type magnetic disturbances in tail of geomagnetic storm 02 p0308 A67-11658
 Neutron-group fluxes and variations with solar activity during IYQS observed by Elektron II 02 p0310 A67-12583
 Elektron satellite observations on primary cosmic radiation, noting correlation between intensity variation and neutron component intensity 05 p0880 A67-16109
 Neutron produced phosphorus 32 measurement in Barwell and St. Severin meteorites 06 p1078 A67-17604
 Neutron induced dimensional changes in turbostratic carbons used as coatings on nuclear fuel particles, presenting densification curves 08 p1346 A67-21542
 Origin of chondrites implied by short period and long period nuclides created by neutron fluxes 10 p1704 A67-22849
 Neutron component diurnal variation in cosmic radiation during period of coil type magnetic disturbances in tail of geomagnetic storm 16 p2738 A67-31071
 Temperature effect measurement of neutron cosmic ray component, noting results of Chicago and Hobart geophysical stations 17 p2933 A67-32088
 New lower upper limit on solar neutron

- flux at energies greater than 60 mev for emission during quiet times 17 p2936 A67-32532
- Neutron transport and radiative transfer analysis via generating function technique, confining analysis to one energy model 17 p2876 A67-32557
- Low latitude neutron fluxes for PCN and quiet solar period, noting solar proton production of neutrons 20 p3519 A67-37406
- Solar cycle primary cosmic radiation variation above magnetosphere and radiation belts at stratosphere and surface, using neutron monitors and space vehicle measurements 23 p4055 A67-41101
- Elektron satellite observations on primary cosmic radiation, noting correlation between intensity variation and neutron component intensity 24 p4214 A67-42785
- NEUTRON PHYSICS**
- Solar cosmic ray multiple neutron production increase on January 28, 1967 from Antarctica cosmic ray neutron monitor measurements 22 p3874 A67-40048
- NEUTRON SCATTERING**
- Lunar and planetary surface elemental analysis technique by analysis of gamma rays resulting from inelastic scattering of neutrons 05 p0843 A67-16545
- NEUTRON SOURCE**
- Fixed voltage, fixed energy and variable voltage variable energy pulsed neutron devices and applications in nuclear propulsion, radiation dosimetry, velocity measurements, etc 02 p0266 A67-12216
- Plasma-particle distribution function in infinite system of alternating positive and negative electrodes, evaluating high-velocity neutron source effectiveness 16 p2718 A67-31193
- NEUTRON SPECTROMETRY**
- Directional neutron spectrometer for events in which neutron is scattered by first scintillator into second 12 p1945 A67-25859
- NEUTRON SPECTRUM**
- Solar cosmic ray generation during chromospheric flares, noting increased neutron intensity 05 p0880 A67-16112
- Coupling coefficients of cosmic ray neutron component according to data from schooner Zaria 05 p0882 A67-16125
- Primary cosmic ray spectrum changes from differential response functions and specific yield functions of neutron monitors 17 p2936 A67-32533
- Secondary neutron spectral data measured by proton recoil spectrometer from targets bombarded by 160 Mev protons 23 p4028 A67-40739
- Neutron and proton spectra anomalies from proton-nucleon interactions in 100 Mev region 24 p4192 A67-42731
- Solar cosmic ray generation during chromospheric flares noting increased neutron intensity 24 p4214 A67-42788
- Coupling coefficients of cosmic ray neutron component according to data from schooner Zaria 24 p4215 A67-42801
- NEUTRON STAR**
- Calculation of gravitational radiation from pulsating and rotating objects according to weak field limit formula of general relativity and applied to neutron star 09 p1562 A67-22227
- Brans-Dicke theory of gravitational scalar field effect on structure of neutron cold spherical stellar model analyzed and compared with relativity 11 p1864 A67-24596
- Neutron star structure and evolution from presupernovae stars including gravitational collapse and neutrino emission processes 12 p2007 A67-25768
- Scalar gravitational fields in pulsating stars, calculating scalar wave radiation rate and star relaxation time 17 p2952 A67-33319
- Critical comments on Shklovsky model for newly identified X-ray source Sco XR-1 20 p3527 A67-37394
- Vibrating neutron stars, discussing damping, heating, energy storage and X-ray emission possibilities at 1000 years range 22 p3882 A67-39619
- NEW ZEALAND**
- Bird hazard to aircraft at Auckland International Airport, examining geographical features, history, species, daily movement patterns and seasonal abundances 15 p2419 A67-29672
- NEWCOMB DERIVATIVE**
- Newcomb entropy method extended to stability analysis of plasma in zero magnetic field 08 p1362 A67-21144
- NEWTON-RAPHSON METHOD**
- Quasi-Newton methods in nonlinear equation solving and unconstrained optimization 02 p0259 A67-11801
- Newton-Raphson quasi-linearization applied to orbit determination from angular data, range and range rate, noting linear differential equations controlling orbit 05 p0894 A67-16563
- Newton-Raphson method generalized for solution of two-point boundary value problems of nonlinear optimal control theory for digital solution 06 p0974 A67-17923
- Algorithm encountered while solving trajectory optimization problems, discussing variational concepts, indirect, gradient, second variation and generalized Newton-Raphson methods 06 p1082 A67-17932
- Iterative numerical method for solving equations of single variable by using several approximations applied to parallel processing environment 13 p2148 A67-27487
- Newton-Raphson computational procedure for finding extremal control policies for nonlinear processes 15 p2456 A67-29363
- Stationary Newton method for nonlinear functional equations in Banach spaces, formulating convergence conditions 16 p2697 A67-31332
- Modified adjoint method and Friedrichs operator equation solution for two-point boundary value problems 21 p3652 A67-38025
- Trajectory optimization initial value problem, considering various conditions, methods of solution and reentry heating minimization 21 p3703 A67-38440
- NEWTON SECOND LAW**
- Impulsively thrusting rocket and bounded thrust rocket in relation to Newton law of motion, obtaining rigorous equation of motion 04 p0707 A67-15881
- NEWTON THEORY**
- Numerical study of Newtonian potential perturbation effects on satellite motion about planet 02 p0321 A67-11496
- Separation points occurring in Newtonian theory of hypersonic flow locally treated by modifying shock layer equations, thus verifying free layer theory 04 p0545 A67-14463
- Hodographic theory of Newtonian mechanics for trajectory hodograph analysis, noting powered trajectories and multiple body problems 08 p1384 A67-20618
- Calculation method for concentrated forces arising at intersection line of two surfaces due to interaction of shock layers, based on Newton law 10 p1590 A67-23035
- Newtonian analogues of trigonometric and exponential functions studied by series 13 p2148 A67-26851
- Shear-free flows of gravitating gas investigated on basis of Newtonian mechanics 14 p2348 A67-28580
- Interval size effect on minimum drag coefficients and optimum shapes of bodies of revolution determined from Newtonian impact theory 15 p2416 A67-29407
- Real trajectories of n-body problem calculated by convergent integral iterations on basis of differential equations for motion of centers of gravity 16 p2750 A67-31441
- Book on methods for applying principles of dynamics to engineering problems covering three-dimensional approach, free-body system and derivation of motion equations 18 p3080 A67-34566
- Restricted three-body problem with two masses under Newtonian gravitation and third obeying semi-Newtonian laws 19 p3327 A67-35664
- Upper limit for condensation of fluctuations in primordial fireball determined by considering effects of radiative diffusion 21 p3711 A67-39120
- General convergence theorems for Newton method applied to convex operators for partially ordered topological linear spaces 23 p4023 A67-40863
- NEWTONIAN FLUID**
- Mechanical impedance of device moving in liquid at resonance, determining viscoelastic magnitudes of Newtonian and non-Newtonian liquids under different dynamic conditions 02 p0240 A67-11521
- Optimum hypersonic shapes for outer flow region, using Newtonian approximative model 10 p1589 A67-22734
- Incompressible Newtonian fluid applied to dynamic reversibility of flows, analyzing motion equation and possible integration of Navier-Stokes equation 11 p1778 A67-24273
- Heat transfer from laminar Newtonian flow through cooled elliptic tubes with variable cross sections 12 p2033 A67-25215
- Energy equation for laminar flow of compressible Newtonian fluid, calculating temperature profiles of fluid 13 p2224 A67-27049
- Steady slow motion of time-independent non-Newtonian liquid through tapered tube, deriving motion equations 14 p2294 A67-27822
- Book on mathematics of MHD which assumes that working fluid is Newtonian and obeys Ohm law in form appropriate to moving conductors 15 p2527 A67-29384
- Flat plate, simultaneous heat and mass transfer for Newtonian fluids in free convection analyzed, using group theory 15 p2582 A67-30217
- Turbulent heat-transfer coefficients and eddy diffusivity profiles for momentum and heat in Newtonian and non-Newtonian fluids, giving equation for data correlation 19 p3344 A67-34869
- Critical Reynolds number of laminar-turbulent transition for Newtonian flow in rectangular ducts to verify minimum in curve as function of duct aspect ratio 19 p3210 A67-35616
- Lift-drag ratio attainable by slender flat-top body at supersonic speeds, considering Newtonian pressure distribution and constant skin friction 20 p3359 A67-37124
- Soviet book on boundary layer of non-Newtonian fluids covering hydrodynamics, heat transfer and mass transfer 20 p3424 A67-37546
- NIACIN**
- S NICOTINIC ACID**
- NICHROME**
- Density, crystallinity and electric properties of thin metal films deposited on rotating cylindrical substrate 16 p2727 A67-30899
- NICKEL**
- Degree of strain effect on kinetics of recrystallization of nickel and niobium monocrystals investigated by electron beam fusion in vacuum 01 p0101 A67-10940
- Effects of order-disorder state and film thickness on structure and electric conductivity of evaporated nickel, titanium and silver films 02 p0292 A67-11745
- Constant load creep test determination of creep ductility and dimensional instability of nickel at 500 and 525 degrees 02 p0256 A67-12702
- Nickel effect on tensile strength, impact toughness and cold shortness threshold of low carbon steel 04 p0636 A67-14750
- Longitudinal Kerr and Faraday effects in Ni and permalloy films using photoelectric polarization spectrometer, choosing various refractive indices and gyroelectric constants 05 p0865 A67-16972
- X-ray Debye temperature thermal variation measurements of pure nickel and chromium 06 p1015 A67-17850
- K-absorption spectrum of Ni as function of concentration of alloying elements and arrangement of atoms of alloying elements into Ni crystal lattice 06 p1017 A67-17952
- Nickel composite with tungsten filament and aluminum oxide whiskers, noting parameters of tensile strength after annealing 08 p1342 A67-20909
- Concentration of Ni, Ga and Ge in series of Odessa and Canyon Diablo meteorite specimens 08 p1385 A67-20936
- Self-lubricating properties of composites of porous nickel and nickel-chromium alloy impregnated with barium fluoride-calcium fluoride eutectic [ASLE PAPER 66AM 1C2] 08 p1335 A67-21035
- Chondrite metallic minerals, thermal history and parent planets noting nickel, taenite and kamacite crystal components 08 p1397 A67-21207
- Cryogenic hydrogen-oxygen ignition with hydrogen-gas entrained Raney nickel as catalyst 09 p1579 A67-21706
- Welding of niobium and nickel alloys by high energy pulsed laser, noting weld joint 09 p1505 A67-22147
- Fuel cell hydrogen electrodes prepared from preactivated Raney-Nickel catalyst powders 09 p1445 A67-22185
- Niobium and nickel as thermionic

converter collector materials, comparing characteristics 09 p1447 A67-22331

Stress and temperature dependence of motion of edge dislocations in nickel single crystals 11 p1809 A67-24920

Width of ferromagnetic resonance curve in nickel and permalloy thin films as function of preparation and thermal treatment techniques 12 p1981 A67-25244

Testing techniques for electroformed thin shells noting tensile properties determination 13 p2219 A67-27184

Ni XIX, Cu XX and Zn XXI spectra observation using vacuum spark chamber 14 p2389 A67-28840

Microhardness and microstructure of annealed industrial nickel filings studied, noting results obtained at 300 degrees C 16 p2687 A67-30846

Inelastic differential scattering cross sections and angular distribution of Ni first-excited-state protons determined by distorted wave calculation 17 p2888 A67-32733

Nickel effect on tensile strength, impact toughness and cold shortness threshold of low carbon steel 18 p3066 A67-34408

Adsorption of oxygen upon clean nickel surface and beginning of oxidation 19 p3244 A67-34937

Adsorption effect of various metals on electrical conductivity and Hall effect of thin nickel films 20 p3504 A67-36166

Temperature effect on Ni thermal diffusivity measured using ruby laser pulse 21 p3640 A67-38262

Degree of strain effect on kinetics of recrystallization of nickel and niobium monocrystals investigated by electron beam fusion in vacuum 22 p3820 A67-39793

In-plane and out-of-plane ferromagnetic resonance line widths in Ni single crystal platelets noting cubic crystalline anisotropy at 25.92 GHz 22 p3884 A67-40245

Nickel on chromium carbide base cermet polishing by synthetic diamond wheels shown to have little effect on strength 24 p4159 A67-41963

NICKEL ALLOY
SA INCONEL
SA PERMALLOY

Modulated structure of aged Ni-Al alloys, including electron micrograph and phase diagram studies of particle growth kinetics 01 p0092 A67-10056

Nickel-base superalloys hardened in part by precipitation of gamma phase examined by X-ray diffraction techniques 01 p0095 A67-10687

Nickel-thoria powder produced by pressure hydrometallurgy techniques and dispersion-strengthened by compaction and rolling, noting tensile stress-rupture properties revealed by optical and electron microscopy 01 p0097 A67-10697

Sintered Ni-base heat resistant alloys, discussing composition-creep strength relation, grain size, prealloyed-powder production and thermal and structural shock properties 01 p0098 A67-10700

Weldability of quenched and tempered martensitic alloy steels of low to medium carbon content, particularly carbon-nickel-cobalt alloys 01 p0081 A67-11041

Strain-hardening and temperature dependence of mechanical properties of ternary ordered alloys on nickel-iron base 02 p0255 A67-12675

Light and electron microscopy used with X-ray diffraction and X-ray fluorescence analysis to study effects of temperatures and stress on As-cast nickel-base superalloy 02 p0256 A67-12706

Fracture toughness and critical defect sizes with welds of 18 percent nickel maraging steels 03 p0446 A67-13554

Decay of K-state in Ni-Cr, Ni-Cr-Mo and Fe-Ni-Cr-Mo alloys studied in terms of electric conductivity during plastic deformation 04 p0635 A67-14429

Phase work hardening of austenitic Fe-Ni alloys in phase transformation process 04 p0635 A67-14430

Stability of austenite in some Fe-Cr-Ni alloys under low temperature strain 04 p0636 A67-14753

Forging and solution treating nickel-chromium alloy 718 to investigate notch ductility and uniform grain size 04 p0640 A67-15459

Neutron diffraction in ordered nickel-manganese alloys with near equilibrium

distribution of atoms over lattice points 05 p0863 A67-16758

Cyclic load and temperature effects on creep behavior of Ni-base alloy Mar-M 200 between 1800 and 1900 degrees F 06 p1014 A67-17802

Heat treatment and microstructural observations in wrought Ni-base superalloy Udimet 700 in static creep, determining fracture and deformation properties 06 p1015 A67-17809

Hydrostatic pressure effect on dispersion of gamma prime phase in precipitation heat treatment of nickel-base superalloy 06 p1016 A67-17902

Molybdenum effect on properties of chromium-nickel alloy, noting hardness and strength 06 p1018 A67-18229

Nickel-chromium alloys with niobium in study of precipitation hardening and hardness 06 p1018 A67-18230

Heat resistant nickel-based alloys for gas turbine blades and disks 06 p1018 A67-18232

Heating rate influence on transformations in 18 percent nickel maraging steel 06 p1018 A67-18378

Hot cracking and strain-age cracking in heat affected zone of Rene 41 alloy weldments 07 p1198 A67-19215

Microstructural changes effect on mechanical properties of nickel base superalloys, with particular attention to wrought alloys 08 p1340 A67-20362

Ni-graphite antifriction composites capable of high temperature operation with good lubrication properties and oxidation resistance under dry friction conditions 08 p1341 A67-20599

Sessile drop technique to study effect of atmosphere and alloy additions of Ti and Cr on surface tension and contact angle of N on sapphire substrated at 1500 degrees C 08 p1343 A67-21543

Fracture behavior of creep resistant alloy steel and nickel-chromium alloy subjected to cyclic loading at elevated temperatures 09 p1517 A67-21556

Structure and mechanical properties of extruded Ni-Al-oxide cermet materials, noting high compression strength 09 p1517 A67-21876

Deoxidative capacity and activity of titanium in nickel-chromium alloys 09 p1518 A67-21964

Phase transformations in heat treated nickel-rich Ni-Co-Cr-Al-Ti-C cast alloys noting sigma formation 10 p1668 A67-23173

Titanium carbide dispersion-strengthened nickel by internal carburization, with fair ductility and stress rupture properties at high temperatures 11 p1806 A67-24361

Nickel-base alloy static and dynamic creep test, examining fatigue zone fracture surface 11 p1806 A67-24364

High strength nickel base alloy with improved oxidation resistance up to 2200 degrees F for applicability to gas turbine engine components [ASME PAPER 67-GT-1] 11 p1808 A67-24789

Gas turbine bucket alloy improvement via heat treatment, noting performance evaluation results from creep rupture tests [ASME PAPER 67-GT-55] 11 p1808 A67-24811

Hardening and softening of nickel-alumina alloys 12 p1955 A67-25365

Cumulative strain behavior of nickel-chromium alloy and chromium martensitic type steel under action of cyclic loading 12 p2015 A67-25420

Welding technique for thick nickel-base alloy using gas tungsten arc, noting inspection techniques, tensile test results, etc 12 p1950 A67-25736

Theoretical strength with iron-nickel maraging steels 12 p1957 A67-26125

Structure, composition and morphology of carbide phases of nickel superalloy 13 p2131 A67-26573

Effect of small cold deformation preceding aging in nickel maraging steel 13 p2132 A67-26575

Interaction between phases of nickel aluminum-nickel titanium pseudobinary system, determining concentration dependence of properties of system 13 p2142 A67-27286

Mechanical properties of several nickel-base alloys at room and cryogenic temperatures 13 p2142 A67-27676

Heat resistance in air of dispersion hardened nickel alloys containing certain

oxides prepared by powder metallurgy methods 14 p2336 A67-27867

High temperature strength of thermomechanical nickel dependent upon previous thermal and mechanical history, measuring elastic strain energy in matrix 14 p2337 A67-28418

Polyhedral boundary precipitations of complex heat resistant nickel alloy in carbide phase caused by boron and cerium 14 p2338 A67-28674

Internal friction in nickel chromium alloys heated to annealing temperature, noting 530 and 800 degree peaks and origin of latter 14 p2338 A67-28675

Alloyed Ni-Be alloys properties, discussing influence of Mo, W, B, V and Co on heat resistance without impairing physical properties 15 p2504 A67-29974

Hardness, electrical resistance and phase composition on Ni-Mo alloy during annealing, discussing phase transformations 16 p2687 A67-30847

Heat resistance of Ni alloys with oxides noting experimental procedure, and effect of various additives 16 p2690 A67-31433

Microstructural features of Ni maraging steel weldments related to fracture toughness properties 16 p2692 A67-31868

Formation and degradation mechanisms of aluminide coatings on Ni-base superalloys, discussing experimental procedures 16 p2693 A67-31871

Elastic constants of directionally solidified Ni base superalloy considering consequences of anisotropy to design analysis 16 p2693 A67-31874

Dispersed aluminum oxides effect on size of nickel grains in sintered or extruded nickel-aluminum oxide cermets, studying compressive strength dependence 17 p2871 A67-31924

Powder-metallurgical methods using mechanical filing, isostatic pressing and high vacuum-high temperature sintering for fabrication of airfoil turbine-blade blocks 17 p2865 A67-32821

Values of rigidity coefficient and space occupied by vacancy compared for deformed nickel samples 17 p2874 A67-32897

Heat treatment of nickel superalloys for high temperature applications, showing solution-temperature effect on mechanical properties 17 p2865 A67-33045

Strength characteristics of single crystals of nickel aluminide /gamma phase/, discussing temperature and orientation dependence of work hardening 18 p3064 A67-34079

Coherent precipitation hardening theory treats yielding in nickel base alloy containing coherent stress-free ordered particles as dynamic process 18 p3064 A67-34080

Stability of austenite in some Fe-Cr-Ni alloys under low temperature strain 18 p3066 A67-34411

Nickel-base alloys refractory-melt reactions in vacuum induction melting investigated by measuring contact angles from photographs, noting carbon contact angles from photographs noting carbon effect 19 p3242 A67-34786

Structural transformations in alnico alloy with titanium studied by X-ray 19 p3245 A67-35467

Diffusion of nickel in solid solution and two-phase alloys of nickel-titanium system 19 p3245 A67-35468

Abnormal X-ray interference pattern change during aging of nickel-beryllium alloys 19 p3245 A67-35471

Thermal and thermomechanical treatments effect on structure and mechanical properties of Fe-Ni-base alloy with Al and Ti additions 19 p3247 A67-35834

Nickel aluminide structure, examining arrangement of Ti, Cr and W in lattice via X-ray spectroscopy 20 p3467 A67-37116

Hardening during deformation in stoichiometric nickel manganite alloy noting temperature effect, surface characteristics and electric resistance 20 p3467 A67-37118

Ni-Fe-Mn alloy, Youngs modulus and magnetic saturation temperature dependence, noting order-disorder effects on Curie point 20 p3468 A67-37178

Unidirectional solidification of cast nickel-base superalloys, effect on creep behavior, stress-rupture properties and thermal shock resistance 20 p3469 A67-37383

Nickel-base single crystal superalloy tensile and creep properties, comparing single and multiple slip orientations 20 p3470 A67-37387
 Temperature /K-state/ effect on dislocation blocking stresses in nickel alloy studied by mechanical hysteresis method 20 p3471 A67-37558
 Strain age cracking characteristics in welded Rene 41 nickel base alloy, discussing test procedure used with circular patch test to evaluate contributing factors 20 p3471 A67-37698
 Oxidation mechanisms for nickel-aluminum alloys studied for effects of temperature and alloy composition 21 p3645 A67-38773
 Plastic deformation of single-crystal Ni-Al investigated for temperature, orientation and strain-rate dependence of tensile flow 21 p3645 A67-38774
 Chemical diffusion coefficients and heats of activation in nickel-aluminum intermetallic phases and solid solution calculated from layer growth experiments 21 p3645 A67-38775
 Powder X-ray structural analysis of compounds of Nb-Ni and Ta-Ni systems, establishing homogeneity region for NbNi 21 p3646 A67-38973
 Carbon content effect on properties and structures of nickel and nickel-iron base superalloys 22 p3818 A67-39223
 Astroloy /Ni base superalloy/ disks for jet engine application, discussing chemical composition, basic ingot structure, forging and heat treatment 22 p3818 A67-39226
 Temperature dependence of ferromagnetic parallel resonance line width in Ni-Fe alloy films, stressing surface oxidation role 22 p3855 A67-39350
 Hot-cracking and microstructure characteristics in weld heat resistant Ni alloys evaluated by synthetic specimen technique 22 p3819 A67-39449
 Primary and secondary strengthening precipitates in 18Ni/250/Al, V and Ti maraging steels 22 p3822 A67-40059
 Fatigue behavior of Cr steel and Ni-Cr alloy examined for influence of direction of first loading stroke of push-pull testing 23 p4019 A67-41155
 Closed die forging of nickel base superalloys for large turbine wheel components [ASM PAPER C6-18.4] 23 p4010 A67-41401
 Ni-Cr superalloy oxidation and sulfidation, relating sulfidation resistance of uncoated Ni superalloys to matrix Cr content [ASM PAPER C6-18.5] 23 p4020 A67-41406
 Soviet studies of Ni- and Fe-based heat resistant aging alloys and aircraft gas turbine technology 24 p4169 A67-41919
 Positive effect of Zr on nickel plasticity, showing elimination of hot brittleness within wide range of temperatures 24 p4169 A67-41922
 Thermal vacancies in Ni-Al investigated by comparing separately determined dilatometric and lattice parameter of /100/ single crystal 24 p4173 A67-42165
 Stress-rupture properties of composites containing refractory metal fibers and nickel alloys evaluated at high temperatures 24 p4174 A67-42475
 Khor Temiki aubrite meteorite composition and structure 24 p4234 A67-42629

NICKEL-CADMIUM BATTERY
 VR 3, 5 DS cadmium-nickel sealed battery for space applications 07 p1131 A67-19528
 Sealed Ni-Cd battery developments including oxygen recombination, temperature effect, separator reliability, electrochemical failure modes, etc 09 p1445 A67-22177
 Isotope analysis of iron migration in Ni-Cd cells with pocket electrodes 09 p1458 A67-22178
 Sealed Ni-Cd batteries with pocket plates and sintered plates, considering operational aspects 09 p1446 A67-22189
 Battery charger system for aircraft application noting nickel-cadmium battery, logic circuitry, wide environmental operation conditions, etc 17 p2804 A67-32515
 Bipolar Ni-Cd cells for ruby lasers and power sources to yield high energy pulses for firing pyrotechnic devices 19 p3175 A67-34803
 High power thyristor used with battery to operate pulse repeating sonar transducer 22 p3747 A67-39255
 Lithium in electrolyte and active metallic

nickel formation effects on capacity and plate mechanical strength in alkaline storage batteries 22 p3748 A67-40229

NICKEL COMPOUND
 Deformation properties of polycrystalline and single crystal specimens of intermetallic compound NiAl studied as function of testing temperature and composition 01 p0092 A67-10059
 Nickel hydroxide structure, discussing effect of current, charge and electrolyte concentration on production rate 09 p1458 A67-22183
 Chemical reactions in Ni-Ti-Nb system, examining via X-ray diffraction formation of ternary intermetallic compounds 16 p2691 A67-31593
 Frozen vacancies effect on microhardness and electrical resistance of nickel ferrite and yttrium garnet 18 p3097 A67-33480
 Ceramic-to-metal sealing method based on use of ductile nickel-titanium intermetallic compound as braze 20 p3454 A67-36518

NICKEL OXIDE
 Thermal emittance of nickel as function of oxide thickness measured, using filament in vacuum technique and microphotography [AIAA PAPER 65-673] 03 p0440 A67-13041
 Neel temperature in NiO and MnO with divalent Fe measured using Mossbauer effect 12 p1985 A67-25844
 Temperature dependence of current carrier mobility in nickel and iron oxide, noting scattering due to magnetic field 15 p2533 A67-29315

NICKEL PLATING
 Nickel protective coating on large parts through chemical reduction of nickel salt by sodium hypophosphite, discussing technological and economic aspects 14 p2324 A67-28609

NICOTINE
 Purification and properties of nicotine oxidase suggest metalloflavoprotein having riboflavin 5-phosphate 20 p3376 A67-37032

NICOTINIC ACID
 Hydrazine effect, alone and with nicotinic acid, on oxygen consumption, respiratory quotient, carbohydrate pool and heat losses in rats studied using gradient calorimeter 18 p2992 A67-34714

NIGHT IONOSPHERE
SA AIRGLOW
 Nighttime F layer irregularities at equator responsible for scintillation of signals from radio sources and satellites 03 p0407 A67-12828
 Seasonal variation in temperature in nighttime F region through analysis of emission intensity of oxygen red line and upper atmosphere structure 06 p0996 A67-18431
 Ten years ionospheric drift measurements in LF range 07 p1171 A67-19420
 Corpuscular intrusions into earth magnetosphere involving entire auroral zone and occurring only on night side 07 p1174 A67-19713
 Seasonal observations of nocturnal ionospheric absorption, noting connection with structural state of sporadic E layer 09 p1491 A67-21930
 Boundary variations of auroral oval zones, noting dependence on magnetic perturbation intensity 10 p1630 A67-22785
 Vertically moving perturbations in nighttime ionosphere studied from vertical ionospheric sounding data, discussing type A4 which develops in F layer near maximum ionization 10 p1631 A67-22805
 Hydrogen and He UV glow in night sky as ion and electron source, estimating intensities and ionization rate 10 p1633 A67-22949
 Subsonic parachute-borne blunt probes for charged particle measurement in ionosphere 10 p1645 A67-23260
 Atomic ions of meteoric origin indicated as source of midlatitude E region in IQSY rocket measurement 10 p1648 A67-23289
 Nocturnal decline of ionospheric airglow 6300 angstrom line intensity due to diatomic oxygen ion-electron recombination 10 p1649 A67-23294
 Behavior of nighttime equatorial F-2 layer under ambipolar diffusion and electrodynamic drift 11 p1784 A67-23935
 Connection between sub-ELF ionospheric emissions at night and high negative ion concentration, noting ion-acoustic wave excitation 11 p1787 A67-24399

Nighttime ionosphere maintained by downward flux of electrons from protonosphere as shown by columnar electron contents measurements, noting decay rate 13 p2107 A67-26305
 Nighttime topside ionosphere composition, measuring concentrations of H, He and O by mass spectrometry 13 p2108 A67-26310
 Cosmic noise intensity at 25 MHz noting nighttime variation dependence on solar activity 13 p2201 A67-27392
 Characteristic enhancement of forbidden doublet in nitrogen excitation observed in night airglow during traveling ionospheric F region perturbation 15 p2474 A67-29479
 Nighttime profiles calculated with allowance for ionization beyond lower bound of frequency range of ionospheric station 16 p2669 A67-31896
 Upper atmospheric nightglow emission intensity measured finding continuous excitation of oxygen atoms as energy reservoir 16 p2670 A67-31918
 IQSY electrophotometric and spectrometric measurements of annual and nighttime variations in rotational temperatures and integral intensity of hydroxyl emission bands 17 p2849 A67-32957
 Hydrogen distribution in upper atmosphere and geocorona, relating H-alpha emission increase to solar activity decrease 17 p2849 A67-32961
 H-alpha diurnal and seasonal intensity variations in geocorona indicating hydrogen content build-up during night 17 p2851 A67-33202
 Aurora Borealis and airglow history, discussing sunspot cycle influence, theories concerning origin, etc 18 p3032 A67-33579
 Worldwide morphology of atomic oxygen nightglows 18 p3032 A67-33580
 Bates theory of atomic oxygen excitation in upper atmosphere as cause of F layer nightglow emissions 18 p3038 A67-33616
 Nocturnal recombination processes in ionospheric F region for nitrogen and oxygen based on 5200 and 6300 angstrom lines 18 p3040 A67-33693
 Day-and nighttime electron and ion density profiles in lower ionosphere deduced from blunt probe theory and measurements 19 p3218 A67-35213
 Day-and nighttime electron density profiles in ionospheric D layer 19 p3218 A67-35227
 Attachment coefficient and transport velocity in nighttime F region from backscatter N-h profiles, determining loss term integration 20 p3426 A67-36287
 Night airglow research during IQSY noting correlation of low activity with sunspot minimum 20 p3430 A67-36905
 Latitude, altitude and local time variation of forces controlling 100 to 700 km atmospheric winds, noting effects on ionospheric phenomena 21 p3654 A67-37994
 Ion formation rate in F-2 layer under nocturnal ionospheric conditions, determining electron densities 21 p3623 A67-39037
 Nighttime E region electron concentration profile valley structure variations for quiet and disturbed geomagnetic activity 22 p3791 A67-39814
 Nighttime variation of ionospheric winds over Barbados via luminous trails measurements, obtaining steady state components for seasonal variations 23 p3995 A67-40807
 Ionospheric electron content and OI nightglow in Hawaii, discussing ionization density increases throughout bottomside F layer 24 p4147 A67-41878
 Diurnal variations of electron concentration in topside ionosphere studied at low and middle latitudes using satellite data, noting secondary nighttime maximum 24 p4148 A67-42064
 Boundary variations of auroral oval zones, noting dependence on magnetic perturbation intensity 24 p4149 A67-42121
 Vertically moving perturbations in nighttime ionosphere studied from vertical ionospheric sounding data, discussing type A4 which develops in F layer near maximum ionization 24 p4150 A67-42142
 Geomagnetic field aligned irregularities, explaining ionospheric E-region scattered wave propagation 24 p4120 A67-42150

NIGHT SKY
 Night sky phenomena and atmospheric

attenuation of light from Beta Canis Majoris
photographed from Gemini
IX 01 p0151 A67-10965

Auroral spectrograph data,
1959 02 p0238 A67-12036

Zodiacal light brightness variation during
solar activity cycle 03 p0413 A67-13454

Doppler profiles of nocturnal green line
/5577 angstroms/ nonthermal emission
resulting from molecular oxygen ion
dissociative recombination
[AFCL-67-0443] 05 p0803 A67-17411

Azimuth stabilization of balloons, using
frictionless bearing to decouple
gondola 07 p1191 A67-19403

Electron and ion emissions from hydrogen
and helium UV glows in nighttime
ionosphere 10 p1633 A67-23049

Space correlation of main emission lines
for night sky emission spectra and altitude
distribution of sodium
luminescence 10 p1647 A67-23279

Rocketborne photometer data analysis of
night sky airglow and spectrum in 6300
angstrom region 11 p1786 A67-24072

Photoelectric scanning observations of
night airglow for two spectral lines of
OI 14 p2306 A67-27788

Nightglow continuum
emission 14 p2313 A67-28576

Nightglow measurements noting intensity
relation to spread-F and sporadic E
[AGARDOGRAPH 95] 15 p2485 A67-30308

IQSY and IGY comparison of night airglow
OI latitude observations 16 p2667 A67-31517

Upper limit on mean mass density of
luminous matter in universe from brightness
of night sky 17 p2944 A67-32638

Soviet book on polar auroras and night
airglow 17 p2848 A67-32951

Drift azimuths, sizes and displacements of
spatial inhomogeneities in oxygen atom
emission at 5577 angstroms during night
airglow 17 p2848 A67-32952

Night airglow brightness spatial
distribution observed by photoelectric
photometry in 5893 angstrom band, including
isophotes charts and emission-inhomogeneity
drift histogram 17 p2848 A67-32953

Nightglow emission structure and variation
at airglow equator, discussing predawn and
storm effects, intensity variations with solar
cycle, OH bands, etc 18 p3036 A67-33607

Kinetic temperature measurements of 5577
angstrom line night airglow with Fabry-
Perot interferometer, discussing nightly
mean temperatures 18 p3037 A67-33609

High latitude night sky emissions observed
by photographic spectrography, examining
oxygen, nitrogen and hydrogen
lines 18 p3037 A67-33610

Height profile of atomic oxygen 6300
angstrom emission in night airglow
determined by rocket
photography 19 p3215 A67-35177

Hydrogen and hydroxyl emissions in
nightglow 19 p3223 A67-35483

Evening auroral activity characterized by
westward traveling surges occurring not
within auroral zone 20 p3426 A67-36291

Low energy, positive ion flux from inner
radiation zone, noting losses due to charge
exchange, night sky emissions and
lifetimes 21 p3697 A67-37996

Profile of night sky hydrogen Lyman alpha
emission line determined using data from
rocketborne hydrogen-filled filter
tube 22 p3790 A67-39805

OH Meinel band, nitrogen dioxide
continuum and O I_s to I_D transitions
maxima altitudes in midlatitude night
airglow emissions from rocket radiometer
measurements 23 p3995 A67-40813

Radiometer using black plate with
radiation toward night sky balanced by IR
radiation transfer in vacuum
system 24 p4152 A67-41787

NIGHT VISION

Effects of anthocyanin glucosides on night
vision of airport approach
controllers 04 p0561 A67-14633

Effects of irritation of vestibular
apparatus on adaptability of human eye to
darkness, studying rate of recovery of
sharpness of vision 16 p2614 A67-30918

Low light level TV as aid to nighttime air
rescue, describing ionoscope and image
orthicon of camera
system 17 p2859 A67-32506

Night and day carrier landing pilot

performance, noting altitude position
estimation inaccuracy as contribution to
higher accident rate 23 p3968 A67-41618

Brightness thresholds and reading ability
tests evaluated for male subjects under
varied simulated conditions of altitude and
oxygen breathing 23 p3959 A67-41694

NIKE-APACHE ROCKET

Artificial shock wave from TNT explosion
in aurora, in attempt to determine effects
on auroral emission and
temperature 03 p0413 A67-13374

Electron density profiles of Nike-Apache
rocket observations of nitric oxide ionization
by Lyman alpha radiation in E region at
sunrise 03 p0415 A67-14114

Instrument testing for 625 A1 research
satellite with Nike-Apache BRD-A1 high
altitude research rocket 13 p2119 A67-28581

Input impedance of short dipole antennas
on Nike-Apache rocket 15 p2444 A67-29504

NIKE-CAJUN ROCKET

Rotating vane electric field meter system
flown on Nike-Cajun sounding rocket to
determine electrostatic potential on vehicle
throughout flight 01 p0074 A67-11126

Nike-Cajun rocket investigation of
equatorial D and E region parameters and
effect on electrojet 10 p1648 A67-23288

NIKE ROCKET

Nike rocket boosted 20-ft-diam ribbon
parachute for deployment at dynamic
pressures above 400 psf 13 p2054 A67-27598

NIKE-TOMAHAWK ROCKET

Payload-apogee altitude performance,
static stability and dynamic motions of
Tomahawk vehicle analyzed for ability to
meet 100 km sounding rocket
requirement 08 p1404 A67-20494

Nose selection and vehicle motion
dynamics for second stage of two-stage
sounding rocket system, discussing nose
shapes effect on altitude performance,
overall vehicle stability, bending moments,
etc 08 p1406 A67-20513

Nike-Tomahawk rocket aeroelastic
behavior, noting occurrence of large extra-
atmospheric coning angles 08 p1416 A67-20534

Nike-Tomahawk rocket aeroelastic
behavior, noting occurrence of large extra-
atmospheric coning angles 24 p4242 A67-42912

NIMBUS SATELLITE

Stereo interpretation of Nimbus II
automatic picture transmission photography
for cloud patterns 02 p0241 A67-11970

Michelson type interferometer for Nimbus
meteorological satellite to obtain vertical
temperature, humidity and ozone
profile 02 p0246 A67-12365

Thermal control of Nimbus spacecraft by
utilizing semipassive and passive thermal
control elements to maintain temperature of
overall spacecraft, subsystems and
components 02 p0335 A67-12391

Nimbus II AVCS, APT, HRIR and MRIR
sensory data analysis 04 p0613 A67-14801

Program for radiol isotopic power on
Nimbus B spacecraft provided by SNAP-19
generators 05 p0843 A67-16553

PCM telemetry unit for Nimbus B
spacecraft noting applications and
performance 05 p0767 A67-17463

Nimbus power supply subsystems 1960-
1969, discussing regulation techniques,
battery and maximum power point
tracking 08 p1283 A67-20649

Material considerations in establishing
failure mechanism of Nimbus solar array
drive 10 p1713 A67-23741

Shutter type thermal control system
design for Nimbus spacecraft
[AIAA PAPER 67-309] 12 p2012 A67-26024

High data rate storage for Nimbus B
satellite noting signal processing, checkout
and retrieval operations 14 p2276 A67-28918

Nimbus I spacecraft overall characteristics,
performance and major subsystems,
particularly performance of meteorological
sensors 16 p2759 A67-30685

Variability in human estimation of total
cloud cover data by satellite-photograph
interpretation, noting use of Nimbus I
photographs 17 p2880 A67-32555

High data rate storage system for Nimbus
B tested by simulation 20 p3445 A67-36547

Thermal design of electronic packaging of
Nimbus satellite control
system 21 p3594 A67-38328

NIMONIC ALLOY

Thermal fatigue cycling of nimonic 80A

solid cylinder specimen restrained by
clamps 16 p2775 A67-31323

Two-stage heat treatment effect on
strength of high temperature Nimonic 80
alloy noting high brittleness, grain size and
boundaries and fracture
propagation 23 p4019 A67-41076

Long term strength limit and fracture
propagation of AKN22 /Nimonic 80/ alloy
welds and AKN22-16/13 CrNi steel
composites welds 23 p4019 A67-41079

NIMPHE

S HYDRAZINE ENGINE /NIMPHE/

NIObIUM

Deformation in niobium and tantalum by
wire drawing at room temperature,
producing changes in shape and position of
X-ray diffraction peak 01 p0095 A67-10686

Interdiffusion of niobium and molybdenum
over 1400-2300 degrees C range using
diffusion couples, determining activation
energy values 01 p0100 A67-10767

Degree of strain effect on kinetics of
recrystallization of nickel and niobium
monocrystals investigated by electron beam
fusion in vacuum 01 p0101 A67-10940

Variations in tensile and creep-rupture
properties of niobium caused by nitrogen
additions that produce single-phase and two-
phase structures studied at room and high
temperatures 02 p0256 A67-12703

Low energy electron diffraction
techniques for niobium /110/ surface, noting
argon ion bombardment 02 p0257 A67-12729

Columbium additions to stainless steel for
steam turbine blading 03 p0446 A67-13543

Niobium and tantalum oxides from
decomposition of zircon-pyrochlor
concentrate by silicon
fluorides 04 p0637 A67-14941

Degree of deformation effect on
superconducting properties of niobium and
vanadium 04 p0686 A67-15986

Growth condition effect on perfection of
single crystals of niobium examined, using
X-ray diffraction
techniques 05 p0828 A67-16470

Cold plastic deformation, rolling direction
and annealing temperature effect on
mechanical properties of sheet niobium at
room and high
temperature 05 p0831 A67-17504

LF high-Q resonances in mixed state of
pure outgassed Ne 06 p1048 A67-17818

New metals replacing steels noting
titanium, beryllium and niobium in French
industry 06 p1017 A67-17994

Austenitic chrome-manganese steel
structure and properties as function of
nitrogen, molybdenum and
niobium 06 p1017 A67-18184

Nickel-chromium alloys with niobium in
study of precipitation hardening and
hardness 06 p1018 A67-18230

Changes in ultrasonic attenuation of
superconducting niobium at low magnetic
fields, considering effects of low critical
field impurity phases 06 p1053 A67-18757

Solution hardening in niobium by Ta, V,
Zr and W, showing linearity with
composition and relationship to sum of
atomic size and elastic modulus
differences 07 p1209 A67-19642

Steady states in annealing of niobium and
tantalum in oxygen atmosphere, noting
relation of pressure to
temperature 07 p1210 A67-20110

Niobium and tantalum purification from
interstitial impurities by high vacuum
annealing, noting effect on electric
resistivity 07 p1210 A67-20112

Temperature dependence of relaxation-
type ultrasound attenuation maxima in
plastic deformation of molybdenum and
niobium single crystals 08 p1367 A67-20419

Niobium effect on structure and
properties of chromium-manganese steels as
active nitride and carbide forming agent
increases deformation
resistance 08 p1343 A67-21206

Josephson and ordinary tunneling currents
for two-band model superconductor, treating
niobium-tin junction 09 p1551 A67-21687

Thermal conductivity coefficient and
integral hemispherical degree of blackness
of niobium at temperatures above 1000
degrees C 09 p1517 A67-21856

Welding of niobium and nickel alloys by
high energy pulsed laser, noting weld
joint 09 p1505 A67-22147

Niobium and nickel as thermionic

converter collector materials, comparing characteristics 09 p1447 A67-22331
 Temperature dependence of thermal diffusivity of tantalum and niobium 11 p1804 A67-24035
 Nb embrittlement by H at ambient temperatures under work hardening effect, noting correlation between elastic limit and deformability in H 11 p1806 A67-24427
 Porosity and particle size effects on magnetization curve of superconducting Nb sintered compacts with and without C added 12 p1978 A67-25139
 Stress dependence of dislocation configuration in deformed niobium 13 p2133 A67-27010
 Nb-N system diagram for five stable nitride phases, giving two reactions governing high temperature phase fields 14 p2337 A67-28419
 Degree of deformation effect on superconducting properties of niobium and vanadium 14 p2366 A67-28489
 Superheating in cylindrical pure niobium by suppressing end effects 14 p2369 A67-28597
 Stress vs strain curves and slip systems in compression and tension of niobium single crystals 14 p2339 A67-29030
 Electron microscope study of dislocation structures in deformed niobium single crystals 14 p2339 A67-29031
 Internal friction of annealed and cold-worked niobium and tantalum wires containing oxygen and nitrogen measured, noting cold-work peaks in addition to Snoek peaks 15 p2503 A67-29748
 Relationship between microhardness of niobium and other variables characterizing superconductivity 17 p2915 A67-32720
 Electrical resistance of niobium single crystal at very low temperature from beginning of superconductivity transition 17 p2916 A67-32805
 Oxygen concentration and strain rate effect on yield point phenomenon in electron beam refined niobium, showing relation to dislocation multiplication 18 p3063 A67-33486
 Impurities in high-purity niobium determined chemically and spectroscopically 19 p3243 A67-34927
 Peltier and Ettingshausen effects in flux-flow state of superconducting niobium, considering contribution to entropy flow 19 p3304 A67-35535
 Youngs modulus variation as function of external magnetic field in mixed state in niobium 20 p3464 A67-36221
 Superconducting niobium wire magnetic moment and heat development during external magnetic field variation, discussing irreversible behavior 20 p3511 A67-37240
 Dynamic microstrain of niobium, considering purity and temperature effects, obtaining activation energy band spectrum 20 p3469 A67-37385
 Characteristics of niobium annealed at 2000 C, describing texture development and crystal perfection variation with annealing time 20 p3470 A67-37391
 Cold plastic deformation, rolling direction and annealing temperature effect on mechanical properties of sheet niobium at room and high temperature 21 p3644 A67-38032
 Nuclear relaxation time measurement in superconducting niobium near upper critical field 21 p3684 A67-38563
 Surface superconductivity of cylindrical niobium samples, discussing microscopic surface roughness and approximate character of theory 21 p3685 A67-38802
 Flux penetration and dissipation measured on superconducting niobium slab samples with tangential applied field studied for effect of thickness 22 p3857 A67-39491
 Degree of strain effect on kinetics of recrystallization of nickel and niobium monocrystals investigated by electron beam fusion in vacuum 22 p3820 A67-39793
 Twinning and low temperature mechanical properties of high purity polycrystalline niobium and molybdenum, discussing grain size effects 22 p3823 A67-40208
 Oxygen interstitial solid solubility in niobium, noting decrease with addition of tungsten and molybdenum 22 p3823 A67-40211
 Softening and incipient recrystallization temperature of deformed niobium during

annealing measured by X-ray analysis and mechanical properties 22 p3823 A67-40326
 Anisotropic energy gap measurements in niobium single crystals by tunneling 22 p3865 A67-40440
 Superconducting niobium energy gap determination by tunneling experiments 23 p4036 A67-40703
 Thermal conductivity of clean and dirty type II superconductors, discussing finite temperature gradient effect on niobium 23 p4036 A67-40704
 Destruction of superconductivity in niobium by current and external magnetic field intensity 23 p4047 A67-41691
 Oscillating magnetic field influence on Hall effect and resistance of superconducting niobium 24 p4201 A67-41870
NIOBIUM ALLOY
 Oxidation test and mechanical property data to determine suitability of columbium and tantalum alloys as thermal protective materials for use in multicycle earth reentry vehicles [SAE PAPER 860660] 01 p0094 A67-10618
 Fabrication of columbium alloy liquid metal loop to study boiling and condensing characteristics of Na and K up to 1000 degrees F with gas tungsten arc welding in helium atmosphere 01 p0080 A67-10945
 Neutron irradiation effect on twinning behavior and transition temperature of niobium-vanadium alloy 02 p0256 A67-12709
 Continuous gas deposition of trinobium-tin alloy on moving refractory wire without reaction chamber contamination by by-products 03 p0500 A67-14065
 Niobium-aluminum alloys elasticity, shear cubic compressibility moduli, Poisson ratio, characteristic temperature and crystal lattice structure 04 p0635 A67-14431
 Electron beam zonal vacuum fusion growth of Mo-Nb alloy single crystals 05 p0827 A67-16080
 X-ray structural analysis of superconducting Nb based alloys, noting two-phase region in annealed samples 05 p0863 A67-16690
 Refractory metal alloys mechanical properties, metallurgical behavior and applications 05 p0829 A67-16741
 Structure and certain properties of niobium-tantalum alloys containing tungsten and molybdenum show these alloying elements form continuous series of hard solutions 05 p0831 A67-17503
 Structure and mechanical properties of niobium alloys containing vanadium and titanium, showing relation between behavior in thermal etching and content of alloying element 05 p0831 A67-17505
 Mechanical properties and chemical composition of industrial niobium VN2 and VN2A at low temperatures 05 p0832 A67-17506
 Mass transfer rates of Nb-based alloys in high temperature Li determined in thermal convection loops under dynamic flow conditions 07 p1223 A67-19463
 Li, Na, K, Rb and Cs vacuum tests as coolants and working fluids in high temperature compact space power plant 07 p1223 A67-19464
 Carbon and nitrogen mass transfer rates by liquid potassium in 16 thermal convection loops of type 316 stainless steel with niobium/one-percent-zirconium and stainless steel tabs at 1200 to 1600 degrees F 07 p1223 A67-19465
 Carburization of niobium and tantalum-base alloys through exposure to gaseous mixture of benzene-hydrogen, noting results of creep rupture tests 08 p1341 A67-20785
 Phase diagram of Nb-Ti-Zr system and superconducting properties of alloys 09 p1518 A67-22029
 Niobium alloy for elevated temperature strength, considering weldability, liquid metal corrosion resistance and fabricability to form mill products by using zirconium and carbon 09 p1519 A67-22397
 Effect of vanadium, zirconium, tantalum and tungsten concentration on Youngs modulus of niobium, noting temperature dependence and changes in elastic properties 09 p1519 A67-22398
 Niobium self-diffusion in alloys with tungsten, showing dependence on specimen composition 13 p2141 A67-27283
 Continuous gas deposition of trinobium-

tin alloy on moving refractory wire without reaction chamber contamination by by-products 13 p2185 A67-27721
 Niobium-cobalt alloys constitution, determining equilibrium diagram by thermal analysis, microscopic metallography and X-ray diffraction techniques 14 p2338 A67-28615
 Magnet consisting of superconductive solenoid of niobium-zirconium wire with ferromagnetic insertions 15 p2422 A67-29127
 Escalation effect by interaction of conduction and induction currents in niobium alloy wires 15 p2539 A67-29826
 X-ray structural analysis of superconducting Nb based alloys, noting two-phase region in annealed samples 15 p2539 A67-29860
 Hardness, toughness, stress relaxation, corrosion resistance, etc., of niobium-aluminum alloy with stable elastic modulus 15 p2504 A67-29973
 Superconducting mixed state of concentrated Mo-Nb alloy, evaluating free area of Fermi surface in k space 16 p2726 A67-30812
 Niobium alloys under annealing and aging analyzed, noting formation of oxide, nitride and carbide phases followed by coagulation and brittleness 16 p2687 A67-30844
 Positive effect of carbon on microstructure and mechanical properties of niobium alloys 16 p2687 A67-30845
 Niobium-iron binary alloys structural study, noting phase instabilities for various added impurities 17 p2871 A67-32042
 Relaxation processes for oxygen in solid solution in niobium demonstrating clustering of atoms into groups [AD-642957] 17 p2871 A67-32628
 Neutron bombardment effect on niobium mechanical properties shown to depend on metal purity 17 p2874 A67-32898
 Critical parameters for vanadium-niobium alloys superconduction, giving curves for transition temperature and measuring critical electric fields 17 p2874 A67-32973
 Far IR measurements used to determine superconducting energy gap widths in niobium alloys 17 p2925 A67-33373
 Niobium alloy semiconductor structures with nonlinear negative resistance, giving volt-ampere characteristics 18 p3009 A67-33472
 Mo, V, Re, Zr and Ti additions effect on mechanical properties, forming stability and recrystallization temperature of Ta alloy with Nb 18 p3065 A67-34293
 Alloying volatile metals with refractory metals in Nb-Zn system, noting thermal analysis and microhardness determination 19 p3243 A67-34926
 Alloying effect on temperature and strain rate sensitivity of niobium-molybdenum bcc metal 19 p3246 A67-35730
 Zirconium addition effect on dynamic strengthening temperature range of niobium alloys, discussing process mechanism 20 p3468 A67-37123
 Critical surface between superconducting and normal state determined for commercial niobium stannide ribbon and Nb-Zr wire 20 p3512 A67-37346
 Structure and certain properties of niobium-tantalum alloys containing tungsten and molybdenum show these alloying elements form continuous series of hard solutions 21 p3644 A67-38030
 Niobium and niobium alloy structural changes during heating after pressing and rolling deformation 21 p3644 A67-38031
 Structure and mechanical properties of niobium alloys containing vanadium and titanium, showing relation between behavior in thermal etching and content of alloying element 21 p3644 A67-38033
 Mechanical properties and chemical composition of industrial niobium and alloys VN2 and VN2A at low temperatures 21 p3644 A67-38034
 Generalized Ginzburg-Landau parameters and magnetic properties of type II superconductors near upper critical field 22 p3857 A67-39440
 Elastic constants and interatomic interaction parameters of niobium alloyed with tantalum, titanium and vanadium 22 p3820 A67-39789
 Factors affecting tensile ductility minimum behavior of silicide coated niobium alloys investigated in air for intermediate temperature range 22 p3821 A67-40052

Interstitial oxygen solubility in niobium using X-ray diffraction, micrographic and thermal techniques, discussing lattice structure 22 p3823 A67-40209

Lattice parameter of bcc Nb-Hf alloy with interstitial solid solution of oxygen 22 p3823 A67-40210

High oxygen Nb-Ti alloy solid solution critical superconducting current density and workability dependence on Th, Gd and Y solute content 23 p4036 A67-40705

Coated columbium alloy potential as turbine vanes in gas turbine power plants, discussing stress rupture strength, oxidation erosion and thermal fatigue lives [ASM PAPER C6-1.4] 23 p4020 A67-41402

Interstitial solid solubility of N in Nb and Nb binary alloys containing Hf, Mo and W as function of pressure and temperature 24 p4172 A67-41976

Hf, Mo and W influence on maximum interstitial solid solubility of N in Nb rich ternary systems 24 p4172 A67-41977

NIOBIUM CARBIDE

Temperature dependence of grain size in nonstoichiometric NbC between 1600 and 3300 degrees K in vacuum and Ar 01 p0102 A67-11245

Single conduction band approximation of nature of increase with temperature of thermal conductivity of ZrC and NbC in terms of scattering and Fermi energy 11 p1804 A67-23902

Solid solution properties of niobium carbide-molybdenum carbide alloy, noting changes in electron structure 14 p2337 A67-28284

Orthorhombic, low temperature alpha modification of niobium and vanadium carbide 16 p2691 A67-31598

Temperature dependence of grain size in nonstoichiometric NbC between 1600 and 3300 degrees K in vacuum and Ar 17 p2875 A67-33168

Slip casting of niobium carbide powders noting effects of dispersed phase contents, pH variation and temperature on molding properties 20 p3466 A67-36909

WC-NbC-Co alloys oxidation resistance in air studied by sintering powdered WC and NbC with Co, finding oxidation rate linear function of time 22 p3820 A67-39565

Niobium carbide enthalpy, heat content and heat capacity variation in homogeneity domain from 1300 to 2500 degrees K 24 p4171 A67-41958

Solubility of niobium carbide in gamma iron determined from experiments using Fe-Nb alloy in equilibrium with hydrogen-methane mixtures 24 p4173 A67-42348

NIOBIUM COMPOUND

Polarized radiation measurements of far IR absorption coefficient and refractive indices in lithium niobium oxide 03 p0496 A67-13571

X-ray analysis of Nb-Ni-Al solid solutions, noting solubility of Nb and construction of phase diagram 04 p0638 A67-15204

Equilibrium diagram of niobium-nickel system determined by thermal analysis, microscopical metallography and X-ray techniques 05 p0828 A67-16387

Dislocation density and magnetic hysteresis in superconducting state of 110-oriented Nb single crystals as function of angle of torsion 07 p1209 A67-19646

Tunable lithium niobate optical oscillator with external mirrors 09 p1510 A67-21576

Minimum N and O content in degassing determined from equilibrium pressures in Nb-O and Ta-O systems 09 p1518 A67-22125

Space vehicle potentiometer, noting niobium diselenide lubricant and minimum frictional torque 14 p2325 A67-28770

High field type II superconductors, analyzing flux jumps 14 p2373 A67-28916

Stabilization of current intensity in superconducting coils noting two characteristic intensities, measurements of niobium compounds, effects of added copper, etc 16 p2607 A67-30593

Superconducting niobium and tantalum compounds investigated for maximum transition temperatures 16 p2726 A67-30818

Niobium and tantalum nitrides physical properties including microhardness, electric and thermal conductivities, Hall coefficient and thermal EMF 22 p3861 A67-39917

Ferroelectric, electro-optic and dielectric properties of tetragonal potassium-niobate-strontium-niobate crystal 24 p4204 A67-42366

NIOBIUM OXIDE

Spectral response of short circuit photocurrent of niobium pentoxide metal diodes 04 p0582 A67-15125

Anodic oxides of titanium, tantalum and niobium from thin dielectric film preparations compared, determining nature and characteristics 13 p2175 A67-26654

NIOBIUM STANNIDE

Increase in superconducting critical current density in diffusion layers of proton-irradiated niobium stannide and decrease at higher dosage 06 p1048 A67-17817

Circuit Q of self-resonant coil of niobium stannide at RF low temperatures 11 p1767 A67-24726

Niobium stannide for refrigerated RF preselectors for interference reduction in radio communications, stressing high Q factors 22 p3865 A67-40435

NITRATE

SA AMMONIUM NITRATE

SA HYDRAZINE NITRATE

SA METHYL NITRATE

SA PENTAERYTHRITOL TETRANITRATE /PETN/

SA SODIUM NITRATE

Clathrates exhibiting metallic conductivity and superconductivity at specific temperatures, noting transition temperature of nitrate salt 01 p0135 A67-10917

NITRATE ESTER

Flame propagation effects and combustion chemistry of nitrate ester or double base solid propellants 08 p1374 A67-20877

Nitrate ester monopropellants studied for heat-up, ignition and combustion in high temperature nitrogen gas under moderate/high pressures, noting burning rates [AIAA PAPER 67-480] 18 p3158 A67-33949

NITRIC ACID

Propagation velocity and other characteristics of detonations in liquid mixtures of nitropropane 2 and nitric acid, noting relation to initial temperature and water content 04 p0726 A67-15495

Nitric acid decomposition process by irradiation determined by photolysis of nitrogen dioxide [JPL-TR-32-1128] 14 p2260 A67-28782

NITRIC OXIDE

Ionospheric D-region concentration of neutral NO estimated, based on dissimilarity of sunspot cycle variation 01 p0056 A67-10111

Nitric oxide molecular laser obtained by dissociation of NO-Cl in pulsed electrical discharge 02 p0253 A67-12510

Dispersion of refractive index of NO in fundamental vibration-rotation band 03 p0468 A67-13473

Electron density profiles of Nike-Apache rocket observations of nitric oxide ionization by Lyman alpha radiation in E region at sunrise 03 p0415 A67-14114

Upper atmospheric oxygen atom concentration profiles obtained via wind tunnel simulation of NO releases [AFCLR-67-0053] 04 p0615 A67-14971

Photoionization and absorption coefficients of nitric oxide gas measured, using vacuum UV monochromator 06 p1037 A67-18573

Winter radio absorption anomaly at middle latitudes theory in terms of temperature and nitric oxide distributions in D region 07 p1171 A67-19415

Photoionization yield and absorption coefficient of nitric oxide at various wavelengths in 580-1350 angstrom region, using H sub 2 emission sources 10 p1681 A67-22738

Reaction rate kinetics of combination of H atoms with NO plus third body /M/ compared with H and O atoms plus M relative to argon 11 p1749 A67-24238

Methylene role in atmospheric tritiated methane, specifically nitric oxide interference 13 p2117 A67-27604

Atomic oxygen density profiles obtained from radiation intensity resulting from nitric oxide reaction 14 p2293 A67-28199

Chemiluminescent rate constant increase in reaction of nitric oxide and oxygen in upper atmosphere explained by clustering of former 15 p2434 A67-29884

Combustion of hydrogen and hydrazine with nitrous and nitric oxide noting flame speeds and flammability limits of ternary mixtures at sub atmospheric pressures 16 p2779 A67-31519

Electron temperature/ion temperature

ratio and oxygen atom ratio to sum of oxygen molecule and nitric oxide in F-1 layer obtained by radar 17 p2843 A67-32529

Nitric oxide production reaction rate measured in shock-heated air at high temperatures, with nitric oxide concentration determined by IR emission 18 p2997 A67-33791

Ionization in ethylene flames at atmospheric pressure, using nitric oxide as oxidizer and electrostatic probe 18 p3107 A67-33804

Gas phase reactions of hydrazine with nitrogen dioxide, nitric oxide and oxygen, determining reaction rates, activation energy and order 18 p3109 A67-33837

NO role in sunrise E region compared to Barth NO distribution, determining density profiles, relative ion ratios, etc 19 p3216 A67-35191

Statistical band model applied to NO fundamental vibration band, discussing transmittance measurements and validity of linear region criterion 19 p3266 A67-35681

Nitric oxide reaction with triphenylmethylperoxy radical investigated in connection with study on reversible reaction 20 p3377 A67-37138

NITRIDATION

Thermal nitridation of maraging steels, noting effects on mechanical properties 17 p2875 A67-33046

Metallurgical aspects of nitrided component application in unmanned satellite drive systems to remedy sliding wear and increase reliability 18 p3058 A67-34676

Surface hardening of titanium alloys by carbon and nitrogen, using high-frequency induction heating 19 p3242 A67-34919

NITRIDE

SA ALUMINUM NITRIDE

SA BORON NITRIDE

SA SILICON NITRIDE

SA TANTALUM NITRIDE

Refractory metal chlorides reacted with methane and nitrogen in hydrogen jet to form carbides and nitrides 03 p0440 A67-12925

Reduced thermodynamic potentials of large classes of refractory metal carbides and nitrides 11 p1804 A67-23901

Electric, thermal and physical properties of pyrolytic carbides and nitrides of group IV metals 11 p1804 A67-23903

Methods of producing coatings based on metal-like high temperature materials 19 p3244 A67-34957

NITRILE

SA ACETONITRILE

Alpha aminonitriles formation by electric discharge through anhydrous methane and ammonia mixture, showing hydrolysis to amino acid as possible bearing on chemical evolution 20 p3369 A67-36764

NITRO COMPOUND

Double and multiple-based nitrate propellants and gunpowders with tabulated characteristics analyzed, particularly nitrocellulose-nitroglycerin, diglycol-dinitrate, nitroguanidine and ammonium nitrate compounds 12 p2185 A67-26337

Catalytic effect of thermal polyanhydride-alpha-amino acids on hydrolysis of p-nitrophenylacetate, noting role of histidine residues 13 p2065 A67-26732

NITROAMINE

S CYCLOTRIMETHYLENE

TRINITRAMINE /RDX/

NITROCELLULOSE

Decomposition and stability of diphenylamine compounds in nitrocellulose powder, determining activation energies 15 p2543 A67-29889

Calorimetric investigation of role of ballistic modifier in nitrocellulose propellants combustion [CI PAPER 67-1] 19 p3309 A67-34996

NITROGEN

SA LIQUID NITROGEN

SA VEGARD-KAPLAN BAND

Electron collisions in nitrogen studied by mass spectrometer, measuring dissociative ionization cross section of nitrogen 01 p0117 A67-10779

Three-body and wall recombination coefficients of atomic nitrogen, using electron spin resonance spectrometer for concentration measurements 01 p0117 A67-10883

Ion extraction and plasma sheath formation in nitrogen discharge studied by

quadrupole mass-spectrometric sampling probe, noting ion current ratio dependence on probe potential 02 p0272 A67-11889

Dissociation pressures of mixed gas hydrates predicted from data for hydrates of methane, propane and nitrogen with water 02 p0190 A67-12234

Role of amplification due to impacts of second kind in emission of nitrogen and CO molecular bands in mixture of nitrogen-argon and CO-Ar in glow discharge 02 p0270 A67-12674

Nitrogen adsorption at room temperature on atomically clean polycrystalline rhenium, noting dependence of sticking coefficient upon surface coverage and temperature 02 p0257 A67-12728

Absorption spectrum of activated nitrogen produced by microwave discharge in 600-1100 angstrom region [AFRL-67-0109] 03 p0473 A67-13520

Kinetics of degassing of tantalum-nitrogen solid solutions by annealing in high vacuum at various high temperatures 04 p0637 A67-14909

Low density gas flow through short tubes at densities varying from continuum to free-molecule regime, noting nitrogen flow [ASME PAPER 66-WA-PID-8] 04 p0606 A67-15331

Electric breakdown in gas discharges in nitrogen and hydrogen at high pressure 04 p0681 A67-15652

Surface property effects on effectiveness of mass transfer cooling in laminar boundary layers with hydrogen injected into free stream of nitrogen or carbon dioxide 04 p0733 A67-15840

Hugoniot-Rankine conditions, dissociation and ionization of hydrogen and nitrogen gas behind high speed shock wave and radiation effects 05 p0790 A67-16036

Self-absorption of radiation in high temperature plasma jet of hydrogen, argon and nitrogen 05 p0851 A67-16522

Nitrogen wavelengths obtained from precision measurements of various nitrogen lines, using vacuum UV spectrograph 05 p0846 A67-16781

Stimulated emission in triplet system of nitrogen molecule produced by pulsed laser discharge, identifying lines and interpreting intensity distribution in rotational band spectrum 05 p0824 A67-16785

Rapid micro dry combustion determination of carbon, hydrogen and nitrogen in high explosives 05 p0759 A67-17154

Tantalum interaction with nitrogen and air show retardation of grain growth 05 p0832 A67-17507

Nitrogen behavior in Cr-Y alloy of varying interstitial concentration and thermal history 06 p1016 A67-17898

Austenitic chrome-manganese steel structure and properties as function of nitrogen, molybdenum and niobium 06 p1017 A67-18184

Trace fluorocarbon effect on vibrational relaxation in nitrogen shock waves studied by UV spectrophotometric technique 06 p0955 A67-18251

Atmospheric nitrogen contamination effect on tensile creep of chromium-tantalum alloys 06 p1018 A67-18369

Nitrogen and oxygen excitation by proton shocks, measuring emission cross sections of radiation and analyzing vibrational structure 06 p1037 A67-18706

Verbal communication intelligibility in man-rated altitude simulator with nitrogen or helium added to oxygen atmosphere 08 p1287 A67-20484

Color phenomena on moon 08 p1396 A67-21165

Emission occurring when mixing molecular nitrogen with helium ion following charge transfer analyzed spectroscopically 08 p1326 A67-21358

Electric conductivity of high temperature nitrogen jet as affected by impurity particles of potassium, metals and metal oxides 09 p1547 A67-22321

Effects of additions of carbon, nitrogen or oxygen on properties of vapor deposited tungsten 09 p1519 A67-22348

Large scale expansion nozzle control by heterogeneous nucleation and mercury vapor and drop growth processes in nitrogen flow [AIAA PAPER 66-85] 10 p1733 A67-23125

Correlation of nitrogen vibrational-translational relaxation times for various

measuring methods, noting temperature distribution of rate 10 p1733 A67-23151

Excitation and photon emission rates of auroral nitrogen first and second positive group 10 p1650 A67-23338

Superfine structure of EPR spectrum of nitrogen in silicon carbide as function of nitrogen concentration and sample temperature 10 p1694 A67-23650

Electrostatic probe and VHF microwave reflectometry study of nitrogen flow around models in hotshot wind tunnels, determining plasma sheath physical characteristics 11 p1839 A67-24445

Eckert reference temperature yields approximations for heat transfer, skin friction and recovery temperature in high speed laminar diatomic nitrogen and carbon dioxide boundary layers 11 p1883 A67-24576

Human lung gas mixing efficiency estimated, using residual lung nitrogen content curve 11 p1747 A67-24628

Dissociation energy of nitrous oxide reconciled with electron physics data 12 p1904 A67-26230

Temperature and density measurements in supersonic free jets of nitrogen and shock waves 13 p2093 A67-26279

Pulsed UV laser using nitrogen noting synchronization characteristics, stability, peak power, etc 13 p2126 A67-26700

Potato radiation resistivity improvement in conditions of anoxia 13 p2058 A67-26755

Comparison of effect of various diluent gases in evoking flyer bends in simulated orbital flights 13 p2062 A67-26916

Thermal accommodation coefficient of nitrogen and helium on nitrogen covered tungsten above room temperature 13 p2223 A67-26944

Hydrogen and nitrogen effect on ductility of beryllium purified by zone refining 13 p2136 A67-27103

Critical two-phase flow of nitrogen and oxygen through orifices characterized by mass-limited conditions 13 p2106 A67-27669

Propagation rate of LF acoustic waves in low pressure glow discharge in nitrogen 14 p2354 A67-27759

Cyclotron echo formation in rare gas and nitrogen afterglow plasma in presence of inhomogeneous magnetic field, stressing velocity-dependent collision frequency case 14 p2356 A67-28150

Nitrogen, oxygen and hydrogen determined by spark-source mass spectrography, noting reduction of instrument blank levels 15 p2433 A67-29403

Characteristic enhancement of forbidden doublet in nitrogen excitation observed in night airglow during traveling ionospheric F region perturbation 15 p2474 A67-29479

Nitrogen presence in solar material, using measurements of high resolution spectrophotometric record of Fraunhofer spectrum [AFRL-67-0479] 15 p2554 A67-29516

Laser output reduced by rare gas impurities in molecular neutral CO and nitrogen gas lasers 15 p2500 A67-29910

Molecular nitrogen rotational relaxation time by probing of supersonic free jet 16 p2705 A67-31757

Forbidden nitrogen I lines in IR solar spectrum, computing oscillation frequencies, nitrogen abundance and equivalent widths, comparing predictions to observational results 17 p2948 A67-32819

Trace fluorocarbon effect on vibrational relaxation in nitrogen shock waves studied by UV spectrophotometric technique [AIAA PAPER 67-11] 17 p2809 A67-33035

Rate constant of atomic oxygen ions reaction with vibrationally excited nitrogen molecules 17 p2889 A67-33201

Cross sections for electron capture by protons measured for various energies in nitrogen, argon and helium 17 p2889 A67-33227

Lifetime and diffusion coefficient of lowest excited state of molecular nitrogen from intensity decay measurements of Vegard-Kaplan band 17 p2889 A67-33243

Superfine structure of EPR spectrum of nitrogen in silicon carbide as function of nitrogen concentration and sample temperature 17 p2923 A67-33331

Nitrate ester monopropellants studied for heat-up, ignition and combustion in high temperature nitrogen gas under moderate/high pressures, noting burning

rates [AIAA PAPER 67-480] 18 p3158 A67-33949

Volt-ampere characteristics of long free-burning convection-free DC and AC arcs in nitrogen, argon and carbon dioxide 19 p3280 A67-35149

Electric conductance exponential decay in column of wall stabilized nitrogen arc after current interruption 19 p3282 A67-35157

Electronic energy transfer between metastable argon and nitrogen molecule, noting rotational enhancement 20 p3487 A67-36228

Hypokinesia effects on nitrogen metabolism of rats 20 p3368 A67-36261

Approximate electron radial functions for uniformly charged nucleus /UCN/ used in analyzing boron 12 and nitrogen 12 beta decay spectra 20 p3488 A67-36915

Simultaneous oscillation in UV and IR and interaction of 1st and 2nd plus ve system of bands in molecular nitrogen laser 20 p3461 A67-37292

Langley Hypersonic Nitrogen Facility flow evaluation covering pitot pressure survey of nozzle wall boundary layer, centerline and Mach number 21 p3607 A67-37777

Nitrogen role in oxidation of titanium in air at elevated temperatures studied by spectrographic analysis 21 p3643 A67-37828

Tantalum interaction with nitrogen and air show retardation of grain growth 21 p3644 A67-38035

Fine structure of nitrogen 14 resonance in hydrazine analyzed for Zeeman effect 21 p3688 A67-38418

Hot shot nitrogen gas source for pulsed MHD accelerator to provide lunar reentry 21 p3608 A67-38863

Critical fluid flow rate analysis of two-phase nitrogen at stagnation pressure of 25 psia 22 p3784 A67-39967

Interstitial solid solubility of N in Nb and Nb binary alloys containing Hf, Mo and W as function of pressure and temperature 24 p4172 A67-41976

Two-photon absorption in alkali halide crystal via gas laser noting F center formation 24 p4187 A67-42361

Density variation in shock tube across nonstationary shock wave separating from nitrogen gas fluorescence excited by fast electron beam 24 p4145 A67-42663

Excitation time of electronic states on nitrogen molecule at high temperatures 24 p4194 A67-42890

NITROGEN ATOM

Nitrogen atoms recombination in fast flow system using photometry, determining atom concentration, noting nitrogen afterglow intensity 06 p0956 A67-18760

Oxygen atoms association and combination with nitrogen atoms, determining rate constants of reactions 06 p0956 A67-18761

Chemiluminescence of upper atmospheric NI and rocket probe measurement of NI atom concentration at night 07 p1182 A67-19951

Rydberg series in extreme UV observed in absorption spectrum of helium-nitrogen discharges and active nitrogen [AFRL-66-835] 17 p2888 A67-32629

NITROGEN COMPOUND

SA PSEUDOURREA

Energetic and angular studies of argon deuteride and nitrogen deuteride positive ion formation using angular ion scattering apparatus 05 p0848 A67-16835

Chemical problems concerning specifications and use of nitrogen peroxide and unsymmetrical dimethyl hydrazine as propellants 06 p1071 A67-17612

Ti stress corrosion in nitrogen tetroxide, detailing investigative techniques [ASM PAPER C6-2.2] 23 p4020 A67-41409

NITROGEN FLUORIDE

Vibrational force constants of nitrogen fluoride, using lone pair of electrons model 01 p0117 A67-10764

Nitrogen fluorides synthesis in nitrogen plasma jet intermixed with gaseous fluorides 02 p0190 A67-12235

Enthalpy of formation and dissociation of explosion of mixtures of hydrogen and excess nitrogen trifluoride 06 p0955 A67-17985

Enthalpy of reaction of sulfur and nitrogen trifluoride 06 p0955 A67-17986

NITROGEN ION

Molecular nitrogen ion emission in twilight, discussing intensities, rotational

distribution, charge transfer zenith measurement and ion-atom interchange reaction 05 p0803 A67-17409

Vertical and horizontal variations of intensities of auroral OI and molecular nitrogen ion emissions 08 p1328 A67-21480

Ionized shock-nitrogen conductivity measured by four-electrode device 11 p1832 A67-24057

Momentum transfer of positively ionized nitrogen molecule incident on copper target, measuring accommodation coefficient with torsion balance 13 p2098 A67-26945

Volume emission profile vs height of positively ionized nitrogen molecule first negative band at 4278 angstroms 16 p2666 A67-31408

Production mechanism of atomic nitrogen ions in upper atmosphere, showing predominance of nitrogen molecule photoionization 17 p2851 A67-33204

Nocturnal recombination processes in ionospheric F region for nitrogen and oxygen based on 5200 and 6300 angstrom lines 18 p3040 A67-33693

Nitrogen ion drift velocities in plasma jet flowing into vacuum chamber noting ion mobilities in parent and foreign gas 19 p3271 A67-35075

Absolute electron impact excitation cross section of 3914 angstrom band of positively ionized nitrogen molecule 20 p3450 A67-37104

Electron-ion three-body recombination rate in nonequilibrium dense nitrogen plasma measured spectroscopically [AIAA PAPER 67-703] 21 p3672 A67-38730

NITROGEN OXIDE

Two sound-absorption maxima in liquid nitrogen tetroxide resulting from relaxation of dissociation equilibrium 01 p0019 A67-10841

Overlapping of bands of nitrogen oxide, CO and carbon dioxide in 4.5 micron region determined for inversion experiments 02 p0246 A67-12368

Spontaneous-emission probability and absolute intensity for IR absorption band of nitrous oxide 03 p0467 A67-12854

Oxidation by nitrous oxide, nitric oxide, nitrogen dioxide and ozone, considering various reactions 04 p0566 A67-15095

Fluorescence decay time of NO, determining transition moment 05 p0848 A67-18837

Chemiluminescence from oxygen atom-hydrazine flames suggesting excited NO formed by energy transfer 06 p1072 A67-17987

Atomization, mixing and reaction characteristics of hydrazine and nitrogen tetroxide injected from quadlet element [AIAA PAPER 67-107] 06 p1072 A67-18308

Fractional volume abundance of atmospheric nitrous oxide, considering photodissociation, microbiological reactions and mixing 08 p1327 A67-21369

Chemiluminescent radiation from interaction of nitric oxide with atmospheric ozone for PCA conditions [AFOSR-67-1379] 10 p1702 A67-23345

Aerobee rocket sounding of ionospheric sporadic E layer, noting abundance of metallic ions in layer and NO above and below 11 p1784 A67-23926

Nitric acid decomposition process by irradiation determined by photolysis of nitrogen dioxide [JPL-TR-32-1128] 14 p2260 A67-28782

Nitrogen oxide and carbon dioxide high pressure unimolecular decomposition noting high pressure rate constants, transition probabilities, potential surface shape, etc 18 p3082 A67-33793

Gas phase reactions of hydrazine with nitrogen dioxide, nitric oxide and oxygen, determining reaction rates, activation energy and order 18 p3109 A67-33837

Effect of additives on hydrazine nitrogen trioxide droplet flame structure and burning rate [AIAA PAPER 67-482] 18 p3158 A67-33951

Additives effect on ignition delay and pressure of hypergolic hydrazine-nitrogen tetroxide propellant systems 19 p3310 A67-35012

Atomization, mixing and reaction characteristics of hydrazine and nitrogen tetroxide injected from quadlet element [AIAA PAPER 67-107] 19 p3310 A67-35766

Coolant passage axial curvature effect on

heat transfer to endothermically dissociating supercritical nitrogen tetroxide [ASME PAPER 67-HT-59] 20 p3549 A67-38741

Cross section measurement for charge transfer reactions, using crossed ion and neutral beam configuration and product ion mass analysis in nitrogen dioxide production 20 p3377 A67-37404

Combustion characteristics of hydrazine type propellants and resultant reactions in low thrust engines prior to ignition 21 p3687 A67-37798

Kinetics of flames propagating in hydrogen-nitrous oxide mixtures diluted with inert gases 23 p4082 A67-41142

NITROGEN PLASMA

Thermal conductivity of nitrogen plasma in cascade arc, solving Elenbaas-Heller equation 19 p3287 A67-35358

Density and temperature measurements of high temperature nitrogen plasma jet using schlieren photographic method 19 p3231 A67-35595

Streaming thermal plasma /STP/ devices, discussing plasma jet synthesis of HCN from cold methane and thermal nitrogen plasma 21 p3578 A67-38393

Electrical conductivity of nitrogen plasma seeded with potassium, noting nonuniform temperature profile in flow [AIAA PAPER 67-716] 21 p3673 A67-38742

NI plasma acceleration in axisymmetric electric discharge by self-induced magnetic field, determining reaction force 22 p3844 A67-39356

NITROGLYCERIN

Powder admixtures influence on critical diameter of detonation of solid, continuous and macroscopically homogeneous explosive, noting inorganic admixtures role 04 p0723 A67-15197

Time dependent temperature profile for stationary nitroglycerin powder combustion process 07 p1267 A67-19312

NITROMETHANE

Gas phase pyrolysis kinetics of tetranitromethane, noting pressure effect and rate equation of thermal decomposition 01 p0019 A67-10765

Mass velocity profile measured using electromagnetic device to record emf changes in metal probe embedded in nitromethane flow 06 p1112 A67-17953

Initiation of explosive reaction in liquid mixture of tetranitromethane and benzene by methane-oxygen detonation 06 p1112 A67-17954

Unconfined nitromethane transient initiation, determining differential conservation, state and reaction rate equations, using two-dimensional computations 18 p3153 A67-33824

Photolysis and pyrolysis of nitromethane and methyl nitride using flash photolysis and kinetic spectroscopy 18 p2998 A67-34276

NITROPROPANE

Propagation velocity and other characteristics of detonations in liquid mixtures of nitropropane 2 and nitric acid, noting relation to initial temperature and water content 04 p0728 A67-15495

NITROSO COMPOUND

Dissociative recombination rate of auroral ionization 02 p0236 A67-11861

Thermoconductivity of nitrosyl bromide at 290-900 degrees K and 200-600 torr measured by hot filament techniques 11 p1881 A67-24022

Dissociative recombination rate of auroral ionization 16 p2665 A67-31076

Photosynthesis of nitrosoformaldehyde and identification of spectrum consisting of diffuse band 18 p2998 A67-34277

NITROSOL

Dissociative recombination coefficient of nitrosyl ion with electrons 04 p0567 A67-15765

NOBLE GAS

S RARE GAS

NOBLE METAL

Abnormal skin effect in thin films of noble metals near IR, taking into account wave penetration and magnitude of conducting electrons mean free path 02 p0288 A67-11723

Inverse Hall effect of noble metals alloyed with B-group metals as affected by residual resistivity and phonon scattering 04 p0682 A67-15465

Temperature dependence of residual resistivity of diffusing ions for

electromigration of silver in copper and gold and self-diffusion of copper in aluminum 07 p1209 A67-19647

Partial sum rules for transition and noble metals having resonant D state 07 p1238 A67-20216

Potentials of zero charge of gold, silver and mercury electrodes as affected by cations and respective metal ion interaction 11 p1749 A67-23920

Defect interaction and diffusion zone of short gold-silver couples 18 p3064 A67-34081

Alloying effect on diffusion thermopower in relation to Fermi surface variations in dilute silver-gold alloys [JPL-TR-32-1095] 24 p4200 A67-41840

NOCTILUCENT CLOUD

Polarization measurements and noctiluculent cloud observation over North America 02 p0239 A67-12534

Meteoritic dust accumulations at low latitudes in upper atmosphere evidenced by observation of noctiluculent clouds, estimating scattering function 05 p0802 A67-17329

Criticism of photometric results of Ney and Peplin findings regarding link layer in terrestrial atmosphere 05 p0802 A67-17330

IGY study of noctiluculent clouds indicates occurrence over North America as frequently as in Europe and U.S.S.R. 07 p1218 A67-19052

Fogle theory concerning possible latitudinal shift of noctiluculent clouds, using cloud occurrence frequency 10 p1677 A67-23501

Noctiluculent cloud formation by agglomeration of oxygen/ozone molecules in mesosphere layers 17 p2879 A67-32323

Mesospheric temperature possible relationship to occurrence of noctiluculent clouds studied using rocket soundings 19 p3251 A67-34951

Rocket sampling of noctiluculent cloud particles in mesopause 19 p3216 A67-35194

Brightness and contrast study of noctiluculent clouds in twilight layer indicating preferability of satellite observation 20 p3434 A67-37426

Frequency of noctiluculent clouds studied as function of meteorological conditions of mesopause 21 p3618 A67-38447

Motion of small spherical particles entering upper atmosphere of earth with cosmic velocities studied for terminal velocities 22 p3890 A67-40472

Noctiluculent cloud fine structure wave form due to visibility through ice condensed on dust particles in wave-like pattern 24 p4146 A67-41791

NODE

Network analysis shortcut by topological representation of impedance in node and loop equations 03 p0389 A67-12963

Sensor beam, scan mode and perinadir nadir angle determination for Tiros IR data using simplified graph method 13 p2117 A67-27612

NOISE

SA AERODYNAMIC NOISE

SA AIRCRAFT NOISE

SA BACKGROUND NOISE

SA BOUNDARY LAYER NOISE

SA CONTINUOUS NOISE

SA COSMIC NOISE

SA GAUSSIAN NOISE

SA IMPULSE NOISE

SA IONOSPHERIC NOISE

SA JET NOISE

SA RADIO NOISE

SA RANDOM NOISE

SA ROCKET ENGINE NOISE

SA SHOT NOISE

SA SIGNAL NOISE

SA SIGNAL TO NOISE RATIO

SA SOLAR NOISE

SA SPECTRAL NOISE

SA SYNCHROTRON NOISE

SA THERMAL NOISE

SA WHITE NOISE

Book on statistical communications theory, digital communications, AM and FM CW communications, binary communications and noise 01 p0021 A67-10306

Mean time analysis of PCM synchronization, noting pattern synchronization in presence of noise 02 p0197 A67-12020

Photomultiplier noise amplitude distribution and causal external factors 03 p0388 A67-14260

Noise figure of low noise to TWT

- obtained by calculating equivalent noise impedance stage by stage 05 p0773 A67-16510
- Excess noise and oscillations in gold-doped germanium photodiodes attributed to generation-recombination fluctuations of large bulk resistance 06 p0971 A67-18220
- Noise sources and characteristics, discussing incidental radio 06 p0965 A67-18834
- Sufficient conditions for asymptotic invariance of Bayes estimate of regression coefficient for nonstationary noise 10 p1619 A67-22952
- Photomultiplier noise amplitude distribution and causal external factors 14 p2288 A67-28772
- Second derivative of two-probe current measurement method for determining electron energy distribution in gas discharge, noting low sensitivity to noise 20 p3498 A67-36687
- Wave transformation effect on inhomogeneous plasma radiation noise, applying results to stable plasma thermal radiation 20 p3498 A67-36691
- Semiconductor device noise theory emphasizing junction diodes, bipolar transistors and field effect transistors 22 p3770 A67-39773
- NOISE ATTENUATION**
- Cassegrain feed for 85-ft-diam antenna of planetary radar system noting operative conditions, polarization capabilities and performance data 04 p0596 A67-15048
- Low 1/f noise mixer diodes, comparing Schottky barrier diode with backward diode type 05 p0780 A67-17528
- Noise modulation effect on signal distortion by analyzing signal components in terms of noise parameters and of undistorted signal 07 p1147 A67-20240
- Noise injection and coherent detection to extend RF attenuation measurement range of series IF substitution 09 p1495 A67-21623
- Research approaches to alleviation of airport community noise 13 p2053 A67-26539
- Control system identification for noise corrupted input/output data, using algorithmic approach and iteration procedure 15 p2461 A67-30320
- Normalization of noise produced by life support systems in spaceship cabins during prolonged flights 16 p2617 A67-30762
- Vibrophonocardiographic techniques for monitoring cardiac dynamics in flight environment 17 p2806 A67-31954
- Noise control of aircraft auxiliary power units, noting installation of special acoustic materials 17 p2800 A67-31977
- Roller traction drive unit for extremely quiet power transmission compared with planetary-gear drive [AIAA PAPER 67-429] 18 p3053 A67-33913
- Superheterodyne receiver operating in K-band having solid state low noise characteristics 18 p3011 A67-34068
- Commercial aircraft noise system solution, considering engines, nacelles, operational procedures and airport options [AIAA PAPER 67-761] 23 p3933 A67-40992
- NOISE ELIMINATION**
- Electrical system design and integration in UK-3 scientific satellite, noting noise control for receiver 01 p0156 A67-11423
- Noise-rejection characteristics of signal detector based on zero counting of random process 02 p0194 A67-11902
- Noise rejection properties of time discrimination method of pulsed signals improved by using exponential rather than selecting function 02 p0194 A67-11909
- Radio astronomical observation technique, eliminating tropospheric radiation noise fluctuation effects on telescope 02 p0198 A67-12033
- Noise-rejecting spatial filters in signal pattern recognition 03 p0368 A67-13276
- Noise rejection of various types of modulation in data transmission with multiple noise 04 p0568 A67-14454
- Government agencies activity in dealing with alleviation of aircraft noise 05 p0929 A67-16386
- Excess photon noise in detected photocurrent of multimode laser for uncoupled and phase locked modes 05 p0815 A67-18623
- Aircraft noise control at international airports with special reference to Heathrow 05 p0752 A67-17101
- Recognition of fading signals transmitted by channels with unknown parameters, considering optimum reception technique based on arbitrary law 05 p0767 A67-17399
- Filtering problem in numerical weather forecasting, discussing use of truncated diagnostic and complete primitive field equations 06 p1027 A67-18601
- Analog circuit for presenting fixed pulse output corresponding to each cardiac cycle of given electrocardiogram and highly unresponsive to noise 09 p1455 A67-21715
- Spaced antenna reception by quadratic addition of signals providing efficient operation at various statistical characteristics of radio channel 10 p1607 A67-23447
- Radio system passband increase and multichannel intercorrelation signal processing for increasing noise rejection for limited analysis time 11 p1772 A67-24984
- Noise rejection of remote control command information transmission in system with comparison circuit, using error detecting and correcting codes 11 p1772 A67-25041
- Aircraft noise acceptability criteria noting political-legal aspects 13 p2053 A67-26537
- Nonlinear correction method for determining orbital parameters of space vehicle, using residuals and least squares technique 14 p2384 A67-28127
- Noise rejection of various types of modulation in data transmission with multiple noise 15 p2435 A67-29291
- Noise cancelling devices for converting noise into equivalent electric energy, noting pressure, differential and throat microphones 15 p2489 A67-30088
- Noise suppression in p-n junction biased in direction of current, noting effect of space charge on current fluctuation 15 p2543 A67-30252
- Nonlinear filter for homing missile tracking noise problem, noting computational requirements and feasibility by filter implementation model for different assumptions 17 p2882 A67-32526
- Combined control system of extremal plant with alpha system corrector and open loop part, describing noise, disturbance and efficiency factors 17 p2830 A67-33099
- Noise removal and deconvolution techniques applied to resolution of beam collision experiments 17 p2886 A67-33261
- Separation of magnetic noise caused by ferromagnetic bodies in geomagnetic field 22 p3795 A67-39227
- Large capacity cryoelectric random access memories, examining three-wire cells and hybrid system for batch fabrication, redundancy, electric parameters, tolerances and noise 22 p3764 A67-39898
- NOISE HAZARD**
- Global examination of growth of aircraft noise nuisance in vicinity of airports, determining index of community 05 p0751 A67-16385
- Global examination of growth of aircraft noise nuisance in vicinity of airports, determining index of community 09 p1439 A67-21702
- Vibration response of Apollo shell structures to acoustic and aerodynamic noise 12 p2012 A67-25728
- Fluidic pulse switching network hazards at high operating speeds, suggesting digital computer simulation to anticipate and rectify hazards before hardware fabrication 14 p2251 A67-28348
- Apollo mission launch noise and physiological effects on crew 18 p2996 A67-34718
- V/stol concepts for short haul commercial aircraft compared for gross weight, operating cost, gust sensitivity and noise levels [AIAA PAPER 67-938] 24 p4096 A67-43028
- NOISE INTENSITY**
- Flame noise in spherical volume of combustible gas confined within soap bubble and spark ignited, noting relation between radiated sound and flame movement and combustion 01 p0168 A67-11290
- Radiation absorption by ionized hydrogen in plane of galaxy to explain brightness profiles for declination minus 37 degrees 02 p0307 A67-11688
- Phase and amplitude fluctuation of gas and solid state lasers, accounting for noise caused by pumping, incoherent decay, lattice vibrations and atomic collisions 04 p0632 A67-14949
- Noise effect on ideal relay element with lagging feedback analyzed using Kolmogoroff equations, comparing performance with ideal forcing element connected to linear amplifier 05 p0782 A67-16321
- Noise factor dependence on frequency in tunnel-diode frequency mixers 05 p0777 A67-17172
- Large ground antenna performance with solar noise jamming 05 p0780 A67-17524
- Component, due to recombination-generation process, of overall noise from semiconductors under electric current, measuring probability densities by statistics 06 p0966 A67-17588
- Intrinsic noise temperature measurement in reflection type cavity maser 06 p1010 A67-17892
- Solar radio noise storm model, determining intensities for various frequency separations 07 p1256 A67-20169
- Equalization and cancellation model of binaural unmasking applied to data on interaural just-noticeable differences 08 p1290 A67-20482
- Steady state beam induced plasma parameters and behavior when affected by HF noise oscillations and effect on electron concentration in plasma 09 p1545 A67-21997
- Wave propagation and noise in gas discharge at low pressure, noting luminescence fluctuations 09 p1545 A67-22220
- Edge dislocations effect on electrical noise in n-type silicon analyzed and results compared with Shockley-Read model 11 p1849 A67-24906
- Time discretization method applied to determination of peak duration distribution of normal noise envelope 11 p1754 A67-24987
- Low noise level microwave receivers - Conference, Paris, May 1966, Part 2 12 p1912 A67-25294
- Signal duration effect on detection in presence of masking noise by human auditory system, using electric analogy for testing purposes 12 p1903 A67-26126
- Intermediate and HF noise of probes immersed in gas discharges explained by space charge sheath and bulk plasma noises 12 p1948 A67-26226
- Diurnal cyclic intensity variations of atmospheric radio noise at stations widely spaced over globe 13 p2111 A67-26571
- Atmospheric noise properties possible influence on communication, measuring intensities and short term amplitude functions 14 p2266 A67-28416
- Signal field energy distribution optimization ensuring minimum error dispersion during digital information transmission through channels with noise fluctuations 16 p2823 A67-31014
- One-dimensional probability distribution density of sum of pulsed and fluctuation noises 16 p2823 A67-31016
- Output noise power spectrum properties of X-band ruby maser oscillator, noting frequency dependence on electromagnetic energy and cavity losses 16 p2885 A67-31055
- Contour maps of percentage occurrence of earth echoes observed on Alouette I ionograms, noting noise level 17 p2852 A67-33236
- Wave propagation and noise in gas discharge at low pressure, noting luminescence fluctuations 18 p3086 A67-33764
- Noise effect on ideal relay element with lagging feedback analyzed using Kolmogoroff equations, comparing performance with ideal forcing element connected to linear amplifier 18 p3017 A67-33873
- Design and characteristics/gain, noise factor and bandwidth of parametric amplifier 19 p3194 A67-35548
- Visual noise induction methods investigated at seven noise levels, discussing pattern comparisons by 46 subjects 20 p3372 A67-37000
- Semiconductor laser light field amplitude equation of van der Pol oscillator derived and shown valid for optical band-to-band transitions 20 p3461 A67-37184
- IR laser rangefinder using neodymium doped rods, noting noise peak value and advantages over ruby laser 22 p3799 A67-39780
- Perceived noise level measurement procedure applied to aircraft noise exposure using Kryter techniques 23 p4027 A67-41143

Cockpit noise levels of various airline aircraft noting propeller effect 23 p3964 A67-41556

Structure of image of diffused surface in coherent illumination investigated for mean intensity and noise-like obscuring component 24 p4155 A67-42336

Radio noise data compared for transmission lines, automotive traffic and RF stabilized arc welders 24 p4123 A67-42718

NOISE MEASUREMENT

Cooling effect of emission current on square wave modulated noise diode cathode 01 p0033 A67-10024

Noise factor of linear receiving systems in quantum and classical regions, noting role of dual push-pull amplifier and frequency converter 01 p0022 A67-10393

Stochastic approximation theory to obtain algorithms for recovery of functions, using noisy measurements taken at randomly selected points 01 p0028 A67-10450

Thermal, excess and shot noise in transducers, examining CW signal generator method for measuring average noise factor 01 p0039 A67-11196

Perceived noise level calculator for immediate and continuous measurement in PNDB to overcome time delay 02 p0266 A67-11471

Measurement and control of corona-generated noise in aircraft, noting charge rate during takeoff via potential gradient method 02 p0190 A67-11501

Q-active filter for narrow-band noise measurement in LF range 02 p0216 A67-12038

Noise level and noise voltage measurements and noise frequency spectra of passive semiconductor resistors, thermistors, Ge rectifying diode and logarithmic diode 02 p0223 A67-12797

Transistor noise coefficient measuring device for 30 kHz to 1.5 MHz frequency range 02 p0223 A67-12798

Minimum noise coefficient of various types of common-base transistors at 1 kHz to 1.5 MHz frequencies 02 p0224 A67-12799

FAA study of jet takeoff and landing noise effect on population around airport, establishing numerical value of noisiness 03 p0358 A67-12979

Noises in quantum amplifier due to heat fluctuations and spontaneous emission of active microparticles, discussing negative temperature state 03 p0368 A67-13139

Transistor life expectancy and failure predictions from LF noise measurements 03 p0389 A67-14277

Approximation method for calculating autocorrelation function of quantized noise 04 p0567 A67-14405

Aircraft noise measurement evaluation and control, discussing monitoring and mapping 04 p0551 A67-14591

Conditional probability density of phase derivative of narrow-band normal noise determined for case when noise envelope is greater than electric field 04 p0575 A67-15162

Noise spectra of double base diode for case of uniform field in base and comparison with experimental noise measurements 04 p0585 A67-15619

Electronic testing of transmitters and receivers noting AM and FM systems sensitivity, noise figures and image rejection 04 p0590 A67-15727

Radiation noise effect on laser optical properties, noting density vs resonator characteristics, energy spectrum, etc 08 p1337 A67-20839

Sidereal time recorder used with riometer for detection of radio noise absorption in ionosphere 08 p1329 A67-21489

Noise comparators and associated thermal standards to provide noise source calibration facilities at S-and X-bands 09 p1495 A67-21621

Noise and pressure measurement in difficult conditions of vibrations and temperature for use in pressure-transducer design of jet and rocket systems 09 p1497 A67-21939

Human response to comparative sounds from aircraft and objective measurement of reference sound, determining acceptable noise levels 09 p1456 A67-21940

Automatic aircraft-noise monitoring equipment at Frankfurt airport to measure noise levels during takeoff and maintain them within regulations 09 p1484 A67-21941

Flicker noise characterization in silicon

planar transistor 09 p1474 A67-22041

Simple diode parametric amplifier, discussing bandwidth and noise measurements and compensating circuits for gain-frequency response improvement 09 p1474 A67-22085

Signal and noise response of Ge avalanche photodiodes noting design, fabrication, LF photomultiplication and static V-I characteristics 09 p1475 A67-22200

Noise measurements on pulsed four-cavity electrostatically focused S-band klystrons 09 p1477 A67-22253

Microwave receivers with low noise Colloquium, Paris, May 1986 09 p1481 A67-22477

Local oscillators with standardized frequencies in conjunction with central mixer used as wideband noise receiver for increased sensitivity 09 p1481 A67-22480

Maser for traveling waves over large cm wave band used as low noise amplifier 09 p1482 A67-22481

Comparison of electron tubes, transistors and FET noise figures as function of source impedance of generator 10 p1610 A67-22924

Ignitor-contributed noise deleterious effect on low noise radar receivers, noting influence of TR device inserted in front of receiver 10 p1611 A67-23329

Dependence of intrinsic noise temperature of ruby reflection maser on helium bath temperature and chromium trioxide doping, using circulator 10 p1665 A67-23505

Transistor noise coefficient dependence on acoustic frequency, temperature, emitter current and collector voltage 11 p1769 A67-25037

Twelve-channel parallel action noise spectrum analyzer for LF noise measurement, using transistorized negative feedback amplifier 11 p1769 A67-25038

Hyperfrequency receiver noise temperature measurement, calculating gain stability influence 12 p1952 A67-25296

Noise calculation in parametric amplifier using approximation method 12 p1913 A67-25300

Lifetime for nonequilibrium current carriers in n-type indium antimonide crystals from generation-recombination noise measurements at various temperatures 12 p1984 A67-25523

Aircraft noise and siting of major airport 13 p2089 A67-26536

Noise measurement in p-n junction diodes 13 p2079 A67-26875

Accuracy of SNR measurement as function of noise power and signal parameter 13 p2070 A67-27045

Intermodulation noise calculated for case of distortion variable in any way with frequency 13 p2070 A67-27195

VLF noise emissions originating in ionosphere and magnetosphere with reference to ground-based, rocket and satellite observations 14 p2265 A67-28414

Device design for measurement of noise factor of RF transistor 14 p2286 A67-28587

Minimum value of noise constant of tunnel diode, noting occurrence beyond point of inflection on I-V characteristic curve 14 p2290 A67-28930

Conditional probability density of phase derivative of narrow-band normal noise determined for case when noise envelope is greater than electric field 15 p2435 A67-29349

Recursive formula for updating determinant of covariance matrix of state estimation error after incorporation of measurement 15 p2512 A67-30213

Discrete interval binary-noise perturbation signal application for identification and compensation of three-variable self-adaptive flight control system 15 p2572 A67-30319

Noise measurement covering principles, switching radiometer, sources, factors and temperature 17 p2814 A67-32604

Noise analysis in He-Ne laser during RF and DC excitation, noting relation between critical frequency and lifetime of metastable atom 18 p3058 A67-33648

Lifetime for nonequilibrium current carriers in n-type indium antimonide crystals from generation-recombination noise measurements at various temperatures 18 p3103 A67-34454

Microwave noise radiation and scattering from cylindrical plasma column, studying dissipative processes on emission spectrum 19 p3291 A67-35387

Electron fluctuations variance and correlation coefficients computed for sensitized GaAs, comparing noisiness of deep recombination levels 19 p3306 A67-35732

Multistage linear dynamic systems with sequentially correlated noise, evaluating filtering, prediction and smoothing procedures 19 p3206 A67-35941

LF noise in MOS-FET, discussing relationship to drain current and power dissipation 19 p3198 A67-36044

Radiometric technique for absolute temperature measurement of microwave noise sources under field conditions 20 p3444 A67-36521

P-n-p-n diode noise measured by standard techniques and explained using theoretical model, considering internal feedback and additional amplification 21 p3589 A67-37820

Noise measurement and instrumentation used 21 p3630 A67-38900

Metal bolometer impedance and noise generation, discussing Johnson and temperature fluctuation noises 22 p3797 A67-39343

Noise factor variations with source resistance for MOST in common-gate and common-source connections, showing advantage of low noise operation 22 p3773 A67-40309

Perceived noise level measurement procedure applied to aircraft noise exposure using Kryter techniques 23 p4027 A67-41143

Aircraft flyover noise recording system, considering calibration, weather tape recording and synchronization system equipment 23 p3999 A67-41145

Noise in polarized Si semiconductor avalanche junctions at RF and microwave frequencies noting determination of impact ionization parameters 23 p3980 A67-41189

Background noise measurement results using statistical model for vortex velocities, obtaining noise spectrum for type II superconductors 24 p4200 A67-41869

NOISE METER

S VELA PROJECT

NOISE PROPAGATION

Noise stability for wideband analog methods of information transmission based on analysis of probability distribution density, using normal rms error and anomalous error probability 03 p0369 A67-13581

Noise and signal fluctuation effects on angle tracking radar with amplitude comparison system 07 p1147 A67-20239

NOISE REDUCTION

Pump noise contribution to total noise of LF parametric converter, analyzing effect of magnitude of bridge out-of-balance voltage 01 p0032 A67-10002

Method of coherent addition of signals to calculate noise resistance of diversity reception 01 p0024 A67-10718

Jet aircraft noise alleviation problems near national airports noting noise limits fixations, engine noise reduction, steeper takeoff and landings, etc [AIAA PAPER 66-909] 02 p0181 A67-12274

VTOL jet transport noise effect on surrounding habitats and guidelines for airport design 03 p0357 A67-12973

Transmission of random sound and vibration through double wall analyzed by general method applicable to acoustics and thermodynamics 03 p0468 A67-13214

Noise reduction in FM receivers with negative frequency feedback by reducing IF bandwidth 03 p0381 A67-13662

Paraelectrics as prospective materials for UHF amplifiers with very low noise level 03 p0382 A67-13711

Noise coefficient minimization for traveling wave tube, with account of current interception at delay system input 03 p0386 A67-13961

Turbulence as producer of noise in proportional fluid amplifiers, considering signal and noise at receiver entrance in terms of stagnation pressure 04 p0557 A67-15919

Nonstationary problem of linear filtering in presence of additive noise solved by computer simulation 05 p0782 A67-16262

Strakhov method determination of optimum numerical filter for extraction of potential field signal from random noise background 05 p0787 A67-17390

Hovercraft noise problem compared with surface transport, noting siting of terminals

- and noise reduction techniques 06 p0946 A67-17915
- Amplitude bounded noise and random measurement error smoothing, noting increased efficiency and possibility of narrow band application 06 p0975 A67-18217
- Noise suppression on adaptive identification control systems, using series model 06 p0978 A67-18560
- Jet engine noise sources, discussing noise radiation patterns, penalties for improved specific fuel consumption, etc 09 p1559 A67-21701
- Acoustic noise and control - Conference, London, January 1967 09 p1532 A67-21937
- Methods to minimize sonic boom ground exposure, considering aircraft design and maneuverability as function of altitude 09 p1439 A67-21942
- Blocking effect due to interference in parametric amplifier, discussing relation between gain and blocking frequency 10 p1609 A67-22834
- Jet flame stabilization and audible noise reduction using ultrasonic acoustic energy 11 p1883 A67-24842
- Vibrational mode behavior of rotating gravitational mass sensors and sensor design to minimize nonideal effect of manufacturing and external disturbances 12 p1945 A67-25919
- Atmospheric long range spectral transmissivity measured by single beam photometer with recording potentiometer added to reduce beam noise 13 p2119 A67-26689
- Ultralow noise receiver configurations for cryogenically cooled microwave traveling wave masers and parametric amplifiers 14 p2260 A67-27776
- Proportional momentum beam deflection fluid amplifier design 14 p2249 A67-28327
- Aspect ratio effect on noise in proportional fluid 14 p2250 A67-28330
- Stability in electronic equipment 14 p2285 A67-28438
- Transmission noise control to achieve helicopter cabin noise levels comparable to fixed wing jet aircraft, discussing system phasing of planetary gears [ASME PAPER 67-DE-58] 14 p2328 A67-28883
- Noise cancelling devices for converting noise into equivalent electric energy, noting pressure, differential and throat microphones 15 p2489 A67-30088
- Program for perceived noise levels reduction on ground of turbofan-powered commercial transport by acoustically absorbent lining of ducts [AIAA PAPER 66-389] 15 p2548 A67-30357
- Concorde jet engine silencer concept and characteristics [AIAA PAPER 67-391] 15 p2549 A67-30359
- Cabin noise reduction in DC-9 by tuned vibration absorbers attached to engine support structure [AIAA PAPER 67-401] 15 p2421 A67-30368
- Amplitude bounded noise and random measurement error smoothing, noting increased efficiency and possibility of narrow band application 16 p2642 A67-30483
- Laboratory equipment protection from vibration environment, noting instrumentation and results 17 p2833 A67-32066
- Subjective/objective measurement types required for systematic aircraft noise regulation around airports, based on maximum permissible noise exposure criterion 17 p2795 A67-32121
- Added narrow band noises and tones influence on subjective response to shaped white noise 17 p2795 A67-32125
- Thermal magnetic noise fluctuations reduction in superconductors below 4.2 degrees K 17 p2913 A67-32272
- Low noise parametric down-converter by using two incommensurable pumping generators, noting gain bandwidth product and minimum noise temperature 17 p2824 A67-32315
- Coding system using pulse interval modulation and providing reduced quantizing noise in received message developed from decaying-step approximation of signal waveforms 17 p2813 A67-32320
- JT9D engine design from viewpoint of incorporated noise reduction features [SAE PAPER 670331] 17 p2929 A67-32984
- V/STOL all-weather operation developments noting navigation and communications, operations under icing and noise problems [SAE PAPER 670348] 17 p2798 A67-32990
- Reduced noise rejection regions in receiver of PSK telemetry signals in narrow band concentrated noise, using phase and polarity comparison methods 18 p3000 A67-34085
- High resolution holograms using Fresnel biprism to reduce noise 18 p3053 A67-34620
- Noise and dark current reduction in photomultiplier tubes by magnetic defocusing [SRCC-43] 19 p3193 A67-35314
- Noise wave amplitude reduction method by suitable initial wind field adaptation to pressure field studied for applications to divergent barotropic model 19 p3253 A67-35530
- Spectrometer SNR improvement without affecting resolution by using larger inlet and outlet slit openings 20 p3441 A67-36365
- Provision of additional metropolitan airport facilities to accommodate supersonic transportation noting noise abatement, traffic growth and off-airport processing 20 p3556 A67-37444
- Signal to noise ratio for optical solar spectra, describing low noise level spectrometer 21 p3624 A67-37730
- Atmospheric long range spectral transmissivity measured by single beam photometer with recording potentiometer added to reduce beam noise 21 p3627 A67-38431
- Noise reduction in residential areas near landing strips using Tu-124 aircraft studied with suggested takeoff and landing piloting techniques 21 p3569 A67-38928
- Output noise variance minimization, calculating smoothing coefficients for discrete time invariant filters used in sampled data systems 21 p3801 A67-38949
- Airport terminal facilities - Conference, Houston, April 1967 22 p3778 A67-39373
- Development of major air terminal buildings at Canadian airports by maximum operational capacity, land availability, noise contours and capital investment 22 p3779 A67-39377
- Airport requirements for V/STOL and short haul air transportation, stressing need for solution of noise problem 22 p3779 A67-39381
- Future improvements in aeronautical field covering noise control, centralization, TV communication, ultimate speed, sonic boom and nuclear cargo aircraft 22 p3746 A67-39846
- Boeing SST competition, cost, operation, design, airport noise and sonic boom 22 p3746 A67-39882
- Prospects for lower noise levels of current and future aircraft, considering noise reduction at source /engine/ and greater separation distance from affected community 23 p3933 A67-40725
- Aircraft auxiliary power unit noise control, considering acoustical materials and installation techniques 23 p3935 A67-41144
- Aircraft cabin noise due to fuselage vibration reduced, using mechanical impedance [SAE PAPER 670873] 24 p4248 A67-42010
- Conceptual aircraft suitability for short haul transportation systems, discussing operation, design, noise factors, flight profiles and V/STOL certification rules [AIAA PAPER 67-771] 24 p4095 A67-42939
- Short haul VTOL air transportation airport-community noise problem, examining propulsion systems and site planning [AIAA PAPER 67-867] 24 p4096 A67-42990
- V/STOL and STOL concepts as applied to short haul transportation [AIAA PAPER 67-941] 24 p4097 A67-43031
- NOISE SPECTRUM**
- Noise spectra measurements performed on two Read diode and two Gunn oscillators by reflection cavity microwave discriminator technique 01 p0033 A67-10017
- Spectrum of galactic radio emission measured using diode noise sources whose output spectra is calibrated for various frequencies 01 p0147 A67-10360
- Frequency doubling by varactor diode, expressing principal parameters as function of normalized amplitude of input voltage 01 p0039 A67-10856
- Surface origin of LF noise power spectrum demonstrated via silicon MOS field effect structures 02 p0296 A67-11820
- Passive detection of sonar target in presence of Gaussian noise background with unknown spectral quantities 02 p0217 A67-12087
- Coherent homodyne detection at 10.6 micrometers with aluminum-doped silicon photoconductor, presenting noise spectra and voltage 03 p0438 A67-13989
- Fluctuation spectra of amplitude and frequency of reflex klystron oscillations excited by fluctuation noise /Schottky effect/ 04 p0583 A67-15169
- Noise spectra of double base diode for case of uniform field in base and comparison with experimental noise measurements 04 p0585 A67-15619
- Generalized Callen-Welton theorem applied to calculation of maser oscillations in amplification and generation regimes, determining noise spectral energy and spectral line width 05 p0762 A67-16350
- Multilayer technique for evaporation of ohmic contacts onto CdS, noting V-I characteristics and noise spectrum of recrystallized layer 06 p1050 A67-18142
- Device for measurement of photocurrent noise spectra in semiconductors at 1 cps to 5 kc 06 p0970 A67-18194
- Plasma stability with randomly fluctuating parameters for magnetic field with curved lines of force 06 p1045 A67-18790
- Nonlinear instability of nonisothermal plasma in external electric field, determining ion-acoustic noise spectrum and time dependent variations in kinetic energy of plasma electrons and ions 06 p1045 A67-18801
- Passage of pulsed coherent useful and noise signals through two-channel time discriminator 07 p1140 A67-19237
- Noise energy spectra created by wave-wave scattering of quasi-longitudinal waves in magnetoactive plasmas with different electron and ion temperatures 08 p1365 A67-21413
- FM noise source in cavity controlled Gunn effect oscillator 09 p1474 A67-22040
- Input resistance and noise performance of multiple idler parametric amplifiers 09 p1474 A67-22084
- Noise generation in Gunn diodes suggests dependence on avalanching of charges in bulk material, making bulk oscillations irregular 09 p1556 A67-22263
- Narrowband optical heterodyne detection, describing InAs photodiode arrangement 10 p1654 A67-22752
- Background noise curve of geomagnetic variations, attributing minimum spectral energy on ground to existence of permanent static solar wind component 10 p1632 A67-22856
- Generation-recombination and modulation noise power spectrum of high purity p-type InSb at 77 degrees K 10 p1893 A67-23566
- Noise in space charge limited current in CdS single crystal at low injection level 10 p1696 A67-23772
- Quantum noise theory for lasers, obtaining rate equations and noise sources with moments appropriate to shot noise and amplitude spectrum 11 p1799 A67-24239
- Dynamic correspondence between electromagnetic field density matrix and associated classical random problem, obtaining means of quantum operators through Fokker-Planck equation 11 p1799 A67-24240
- Diffusion of particles across magnetic lines in dense and quiescent plasma compared with Bohm and collisional values 11 p1835 A67-24383
- Transition to turbulence in thermal plasma examined, using model based on coupled Van der Pol oscillators, noting noise spectrum rise 11 p1836 A67-24390
- Noise spectral distribution and instability in germanium and silicon photodiodes 11 p1765 A67-24473
- Twelve-channel parallel action noise spectrum analyzer for LF noise measurement, using transistorized negative feedback amplifier 11 p1768 A67-25038
- Photoconductivity kinetics and regeneration recombination noise spectrum of p-InSb crystals, showing association with hole capture, lifetime and alloying impurity 12 p1883 A67-25512
- Computer calculation of noise temperature of high gain antennas, noting application to

design and analysis of paraboloidal and Cassegrain systems 12 p1917 A67-26195

Noise figure expression using normal mode amplitudes for crossed field amplifiers 13 p2079 A67-26874

Cavitation correlation with sound pressure and vibration acceleration in closed circuit hydrodynamic tunnel, showing cavitation noise spectrum 14 p2295 A67-27870

Radio noise spectrum on VLF bands in ionosphere observed by sounding rocket K-9M-19 14 p2307 A67-27886

Statistics of fluctuation processes occurring at outputs of filter/discriminator/integrator system acted upon by wideband noise 14 p2283 A67-28279

Electrostatic waves in LF noise bands as cause of diffuse traces observed by Louette satellite ionospheric probe electrostatic waves in LF noise bands as cause of diffuse traces observed by Alouette satellite 14 p2312 A67-28518

Postsampling exponential first order digital filter and application to data reduction for trend analysis and noisy phenomena 14 p2288 A67-28687

Influence of higher order contributions to correlation function of intensity fluctuation in laser near threshold determined using Fokker-Planck equation 15 p2496 A67-29091

Fluctuation spectra of amplitude and frequency of reflex klystron oscillations excited by fluctuation noise /Schottky effect/ 15 p2443 A67-29355

X-band attenuation by rocket exhaust plume measured with AM/PM noise for various propellant systems 15 p2436 A67-29429

Nonlinear effects during titanium plasma source operation, investigating plasma nature and magnetic field effects on injector operation and plasma parameters 15 p2529 A67-29719

Temperature dependent noise spectra of InSb single crystals, noting deep energy level and impurity energy 15 p2541 A67-30235

Heating of ions in current carrying nonisothermal plasma deriving noise spectral density and electron and ion distribution functions 16 p2715 A67-31047

Atmospheric noise data for various frequencies and various latitudes and longitudes 16 p2632 A67-31861

Pearl period shift explained by model showing proton effect and limited spectrum MHD noise 17 p2847 A67-32946

Performance of matched filtering system related to degree of displacement for uniform and nonuniform spectral densities 17 p2862 A67-33295

Frequency spectra of excess noise in semiconductor devices due to characteristics fluctuations after applying signal 17 p2828 A67-33383

Plasma stability with randomly fluctuating parameters for magnetic field with curved lines of force 18 p3086 A67-33732

Noise in injection-synchronized oscillators, deriving inequality 18 p3011 A67-34221

Nonlinear instability of nonisothermal plasma in external electric field, determining ion-acoustic noise spectrum and time dependent variations in kinetic energy of plasma electrons and ions 18 p3090 A67-34420

Photoconductivity kinetics and regeneration recombination noise spectrum of p-InSb crystals, showing association with hole capture, lifetime and alloying impurity 18 p3103 A67-34443

Mean flow refraction and temperature differences between mixing layer and outside fluid effect on HF component of jet noise 19 p3173 A67-34962

FM signals demodulation and negative feedback modulation, deriving signal to noise ratio and noise spectrum formulas 19 p3183 A67-35562

Noise spectral density measured at low temperature in sensitized GaAs, studying relaxation time, temperature effect, etc 19 p3307 A67-35733

Noise generator for calibration of radio receiver working in 1-2.6 MHz range during rocket flight 21 p3592 A67-38221

HF noise spectrum of drain and gate currents of junction FET computed from current series expansion 21 p3597 A67-38569

LF noise spectrum of p-n junction using arbitrary pulse duration distribution

functions 22 p3858 A67-39573

Laser and maser noise quantum theory emphasizing equations of motion and fluctuation problem, deriving density matrix equation 23 p4011 A67-40782

Ionizing radiation effects on dark current and noise pulse spectrum of photomultiplier tubes used in balloon and satellite X-ray observations 23 p4000 A67-41216

Background noise measurement results using statistical model for vortex velocities, obtaining noise spectrum for type II superconductors 24 p4200 A67-41869

Population noise in semiconductor laser junctions calculated by quantum mechanical Langevin method 24 p4166 A67-41887

Distant atmospheric waveform at night analyzed using digital computer for VLF phase spectra 24 p4149 A67-42068

NOISE STORM

Origin of solar type I noise storm radiation seen in cyclotron radiation from electron streams gyrating in spot field configurations in corona 07 p1244 A67-19852

Solar radio noise storm model, determining intensities for various frequency separations 07 p1256 A67-20169

Active region corona and type I bursts supposedly generated by plasma oscillations excited by electron beam 08 p1377 A67-21445

Type III solar radio bursts, noting association with noise storms and radio condensations 10 p1704 A67-22889

38 MHz solar burst duration, bandwidth, amplitude, number and polarization characteristics noting possible generating mechanisms 20 p3520 A67-37476

NOISE SUPPRESSOR

HF conducted and radiated RF interference suppression by dielectric and magnetic absorption, pseudoresonant or interfacial loss and artificial skin effect 01 p0024 A67-10500

Optimum reception criteria for double beam channels with fluctuating noise, signal phase and amplitude 02 p0205 A67-12532

Noise rejection properties of threshold devices with storage circuit calculated on basis of intersection probability of fixed level by storage circuit output voltage 02 p0205 A67-12533

Suppressor applications of nozzles in reduction of sound power level generated in exhaust jet wake and ground surface deterioration from VTOL lift jets 03 p0350 A67-12916

Quantum size in analog-to-digital conversion and effect on quantization noise in output of moving target indicator /MTI/ radar processors 04 p0570 A67-14873

Clutter suppression by complex weighting of coherent pulse train 04 p0570 A67-14878

Acoustic liners to suppress screech in hydrogen-oxygen engines 04 p0691 A67-15988

Extended plug nozzles in suppression of jet noise in small turbojet engines [SAE PAPER 870157] 09 p1561 A67-22544

Optimum linear receiver for noisy PAM system using criterion of mean square interference 11 p1752 A67-24134

Circuit for discriminating neutrons, gammas and charged particles from each other in phoswich scintillator 12 p1945 A67-25857

Optimum reception criteria for double beam channels with fluctuating noise, signal phase and amplitude characteristics 14 p2261 A67-28009

Noise rejection properties of threshold devices with storage circuit calculated on basis of intersection probability of fixed level by storage circuit output voltage 14 p2261 A67-28010

Noise suppression in p-n junction biased in direction of current, noting effect of space charge on current fluctuation 15 p2543 A67-30252

Radar waveforms for suppression of extended clutter, discussing confinement of matched filter response in delay and Doppler or ambiguity function 16 p2625 A67-31270

Noise discrimination microphones in aircraft, discussing performance characteristics, design, construction, applications, clarity, size, etc 18 p2994 A67-34399

Noise rejecting algorithms for ODE solutions with computer, using redundancy, placement of control and feedback

techniques 20 p3392 A67-37224

NOISE THRESHOLD

Multichannel sequential detection in case of reception through independent multiple channels with noise 05 p0765 A67-18553

Threshold value lowering in synchronous demodulation, determining output SNR as function of input SNR 06 p1294 A67-20771

Transmission methods in satellite communications and power level decrease by noise reduction 09 p1463 A67-21758

Defining noise margins on noise immunity in binary electrological systems, discussing static /steady state/, with graphs for exemplary integrated logical units 09 p1469 A67-22097

Threshold signals and optimal modulation parameters of analog methods of transmitting information under conditions of ideal reception 10 p1604 A67-22964

Threshold region of FM signals having carrier modulated by Gaussian baseband signal 11 p1752 A67-24124

Discriminator threshold and SNR above threshold response when demodulating FM signal undergoing selective fading 14 p2273 A67-28711

Voice modulation effect on phase-lock demodulator for single channel voice communication extending definition of threshold for optimum link design 16 p2629 A67-31529

Threshold value of SNR of radar system in target detection against reflecting background, deriving block diagram consisting of linear group, detector and integrator 17 p2816 A67-32684

Effect of unconditional stability of loop in phase lock demodulator on threshold performance of loop, noting transfer functions role 17 p2816 A67-32782

Frequency locked loop FM demodulator with high noise threshold 20 p3385 A67-37352

Asymptotic relative efficiency of mixed statistical threshold tests with Gaussian samples 20 p3412 A67-37495

FM/PM and FM/FM radio telemetry in proportional and constant band covering regulation, SNR, noise threshold, etc 21 p3587 A67-39050

Threshold discrimination for two unknown a priori probability signals against noise background, using stochastic approximation in algorithm 24 p4134 A67-41795

Generation-recombination noise voltage in IR detector materials, discussing impurity and intrinsic photoconductors 24 p4201 A67-41909

NOISE TOLERANCE

FAA study of jet takeoff and landing noise effect on population around airport, establishing numerical value of noisiness 03 p0358 A67-12979

Subjective/objective measurement types required for systematic aircraft noise regulation around airports, based on maximum permissible noise exposure criterion 17 p2795 A67-32121

Subjective evaluation of relative annoyance of sonic booms, explosions and jet aircraft noise 18 p2986 A67-34393

Continuous /24 hr/ wide band noise effect on human body, discussing subjective/objective fatigue 20 p3369 A67-36670

Binary and tetravalent signals quantitative comparison for noise sensitivity by computing transmission matrix during transmission via linear channel 22 p3761 A67-39787

NOMENCLATURE

Lawful concept of heavenly bodies 12 p2042 A67-26138

Nomenclature applicable to juridical norms regulating outer atmosphere and space activities 12 p2043 A67-26150

Revision of military terminology for weapon systems considering human factors, safety and maintainability and reliability relations 16 p2780 A67-30440

NOMOGRAPH

Calculation of scale functions of alignment nomogram as applied to sets of functions 01 p0104 A67-10279

Engineering method of calculating Fresnel coefficients based on use of nomograms 02 p0286 A67-11910

Ramjet external-combustion engine noting design of trailing edge, nomograms of pressure, temperature, thrust component, etc 04 p0688 A67-14578

- Pneumatic transmission line model for use in fluidic control systems, noting nomographs determining gain-vs-frequency curves 05 p0753 A67-16237
- Clear air turbulence relation to various ranges of Richardson number, noting set of nomograms for number estimation 05 p0838 A67-16709
- Nomograms and tables for calculation of Richardson number in relation to forecasting of clear air turbulence 05 p0838 A67-16710
- Manual guidance for interplanetary flight by graphical methods, nomographs and relevant general equations 08 p1352 A67-21104
- Nomograms for analysis and synthesis of astatic automatic control systems 10 p1621 A67-23851
- Approximate determination of satellite lifetime by nomogram constructed on basis of known upper atmosphere density data 13 p2213 A67-27324
- Nomogram to predict SNR for certain laser setups 14 p2330 A67-28289
- Nomograph construction for earth pointing cameras, evaluating imaging system effectiveness as ground resolution and scale factor, plotting system performance characteristics 22 p3800 A67-40106
- NON-NEWTONIAN FLOW**
- Infinite length journal bearing performance of non-Newtonian fluids with shear dependent viscosity in analytical investigation at constant temperature 05 p0810 A67-16274
- Book on quantitative relationships for non-Newtonian systems, considering classification and fluid behavior of materials with anomalous flow properties 08 p1322 A67-21268
- Plane Poiseuille flow calculations extended to Couette flow between coaxial circular cylinders, plotting flow velocity curves 09 p1490 A67-22595
- Approximate iterative calculation of non-Newtonian supersonic gas flow past highly blunt bodies 11 p1741 A67-24156
- Viscoelastic fluid isotropic turbulence decay approximating non-Newtonian effects by perturbation method 22 p3787 A67-40221
- Non-Newtonian elastoviscous channel flow between rigid boundaries solved by asymptotic expansion in lubrication approximation 24 p4145 A67-43086
- NON-NEWTONIAN FLUID**
- Hydrodynamic thermal explosion of stationary axisymmetric non-Newtonian fluid in infinitely long cylindrical tube 01 p0052 A67-10681
- Internal forced convection in viscoplastic fluids between two parallel plates with applied normal magnetic field 01 p0126 A67-11188
- Numerical solutions of equations of motion and energy for heating of non-Newtonian fluids in rectilinear axisymmetric laminar flow in circular tubes extended to case of cooling at constant tube-wall temperature 04 p0720 A67-14510
- Numerical solution of motion and energy equations for non-Newtonian fluid flow in tubes of circular cross section with heat transfer to or from fluid 05 p0925 A67-16271
- Hydrodynamic thermal explosion of stationary axisymmetric non-Newtonian fluid in infinitely long cylindrical tube 11 p1783 A67-25068
- Friction factors and velocity profiles in turbulent flow of viscoelastic non-Newtonian fluid, noting correlation between frictional characteristics and Reynolds number 12 p1929 A67-25904
- Laminar natural convection heat transfer between vertical plate and power-law fluid with high Prandtl number 16 p2780 A67-31553
- Stationary laminar boundary layer equations of Ostwald-de Waele power law fluids, flow and temperature boundary layer differential equation 17 p2836 A67-32262
- Solutions
- Existence of affine solutions in natural convection along vertical flat heating plate, deriving expressions for thermal and dynamic boundary layers 18 p3025 A67-33685
- Heat transfer in steady flow of non-Newtonian fluid between two walls with periodic deformation considered, using perturbation method 18 p3161 A67-34616
- Arbitrary internal heat generation terms in energy equation effect upon limiting Nusselt number for heat transfer to pipeline flow of non-Newtonian fluids [AICHE PAPER 12] 20 p3552 A67-36826
- Viscous non-Newtonian fluid radial flow between circular disks solved, using model equation reduced to power law equation 21 p3612 A67-38381
- NONABLATING MATERIAL**
- Reflectance of pyrolytic graphite and phenolic nylon chars for radiant heat rejection from nonablating heat shield 15 p2579 A67-29434
- NONADIABATIC THEORY**
- Data correlation on nonadiabatic behavior of individual charged particles in magnetic fields 08 p1362 A67-21150
- Excitation cross sections for protons incident on atomic hydrogen calculated by nonadiabatic method 20 p3491 A67-37686
- Self-similar solutions to motion equations are possible for internal heat generation in confined supersonic flow, assuming constant transport properties 22 p3784 A67-39781
- NONCONDENSIBLE GAS**
- Condensation heat transfer in presence of noncondensables, interfacial resistance, superheating, variable properties and diffusion 04 p0720 A67-14644
- Pressure measurement with McLeod type gauge in presence of saturated vapors condensed during compression 21 p3627 A67-38384
- NONDESTRUCTIVE TESTING**
- SA DESTRUCTIVE TESTING**
- SA FLAW DETECTION**
- Integrated circuit reliability and nondestructive testing, noting component failure analysis, self-maintenance, network parameter determination, etc 02 p0224 A67-11526
- Gamma and X-radiographic radioactive sources for nondestructive testing of hydrogenous materials such as rubber, adhesives and explosives in steel or other metal assemblies 02 p0249 A67-12220
- Cholesteric liquid crystals and use in visualizing small thermal gradients for thermal nondestructive testing 02 p0250 A67-12538
- Sonic resonator for nondestructive testing of composite structure operating only from one accessible surface 02 p0250 A67-12630
- Nondestructive testing /NDT/ of materials, components and systems for Saturn-Apollo program 02 p0250 A67-12631
- Nondestructive test methods for monitoring service hardware during boron composite material development and correlation with results of destructive tests 03 p0455 A67-13447
- Nondestructive ultrasonic detection of surface or internal flaws 03 p0430 A67-13549
- Nondestructive material testing - International Colloquium, Aachen, West Germany, December 1965 04 p0641 A67-14586
- Nondestructive testing by oscillatory methods of viscoelastic properties of high molecular weight polymers as functions of frequency and temperature 04 p0641 A67-14587
- Nondestructive testing /NDT/ developments noting radiography for quality control, ultrasonic, continuous wave, resonance and pulse echo methods and applications to Polaris program 04 p0706 A67-15263
- Equilibrium photocurrents in silicon switching diodes from nondestructively measured electrical parameters 04 p0588 A67-15698
- Nondestructive test development to meet inspection requirements of advanced aircraft design, discussing titanium fusion and resistance spot welds and adhesive bonding honeycomb components 05 p0808 A67-17087
- Nondestructive quality control testing, discussing thermoelectric, magnetic particle and fluorescent penetrant, ultrasonic and linear measurement 05 p0813 A67-17259
- Eddy current conductivity technique for monitor of heat effects in nondestructive testing of 2014 Al alloy weldments 05 p0813 A67-17260
- Fusion weld evaluation in 2014-T6 material by eddy current, electric conductivity and hardness plots, noting aging effects, mechanical property degradation, etc 05 p1007 A67-17640
- Ultrasonic techniques for nondestructive testing for Saturn honeycomb heat shields 07 p1192 A67-20166
- Reinforced plastics - SPI Conference, Washington, D.C., January-February 1967 08 p1344 A67-20420
- Nuclear magnetic resonance and nuclear quadrupole resonance techniques for nondestructive testing of reinforced plastics for curing and internal stresses 08 p1345 A67-20425
- Nondestructive testing techniques for multilayer printed wiring boards stressing axial transverse laminography and mutual coupling 09 p1502 A67-21867
- Nondestructive testing techniques in radiation vulnerability analysis of electronic systems, noting ionization effects and permanent damage in semiconductors 09 p1471 A67-21868
- Silicon oxide film thickness determined from intensity of reflected light 09 p1553 A67-21954
- Nondestructive tests designed to increase reliability of coated specimens by elucidating failure mechanisms 09 p1519 A67-22303
- Nondestructive testing in calculating inherent reliability and improving reliability of manufactured product 09 p1506 A67-22304
- Direct measurement of aeroelastic parameters of aircraft wings, using dynamically similar models fitted on auxiliary rocket devices 09 p1576 A67-22462
- Ultrasonic nondestructive inspection of adhesively bonded components, discussing pulse echo reflection, pulsed through transmission and sweep frequency coupling methods and scanning equipment 09 p1507 A67-22526
- Quality control system for adhesive bonding using Fokker bond tester ultrasonic resonance instrument 09 p1508 A67-22527
- Metal working problems involving sheet metal, powder metallurgy, extrusion, nondestructive testing and concerning high strength, refractory and superalloys [SAE PAPER 670098] 09 p1509 A67-22540
- Ultrasonic inspecting technique for reinforced plastic components and adhesive bonds of solid propellant booster nozzles 10 p1659 A67-22930
- IR techniques for reliability enhancement of microelectronics 10 p1610 A67-22977
- Nondestructive testing of dielectric materials by microwave techniques 10 p1660 A67-23014
- X-radiographic nondestructive testing and inspection for quality control of electronic and electromechanical devices including printed circuits, encapsulated modules, thin films, etc 10 p1611 A67-23311
- Large part inspection via ultrasonic and eddy current techniques, discussing surface and discontinuity dimension analysis 10 p1660 A67-23324
- Monograph on electron microprobe X-ray analyzer and application in mineralogy 10 p1603 A67-23632
- Nondestructive testing in aircraft industry evaluated, considering role in aircraft structural design, crack detection, etc 11 p1799 A67-24654
- Nondestructive testing methods noting applicability to flaw detection and quality control 12 p1948 A67-25138
- Mass spectrometer and helium gas application in NDT for deleterious leaks in double-wall vessels for storing and shipping liquid oxygen and nitrogen 12 p1948 A67-25288
- Welding technique for thick nickel-base alloy using gas tungsten arc, noting inspection techniques, tensile test results, etc 12 p1950 A67-25736
- Nondestructive testing techniques for turbojet engines noting advantage of planned inspection [SAE PAPER 670339] 12 p1950 A67-25876
- X-ray sensitive TV system with image enlargement for nondestructive testing [SAE PAPER 670362] 12 p1950 A67-25882
- Radiographic screening of relays for detection of solder balls, broken leads, cracks, etc 13 p2084 A67-27695
- Relay testing for Saturn program including vibration scan, radiographic inspection, etc 13 p2084 A67-27696
- Ultrasonic flaw detection of hidden cracks in turbine blades 14 p2395 A67-27872
- Nondestructive determination of mechanical properties of refractory materials by ultrasonic and radiometric measurements 14 p2340 A67-28258

Diffused base transistor impurity concentration measured nondestructively to determine structure 15 p2448 A67-29801

Nondestructive determination of stress distribution in three-layer tempered glass aircraft windshield by scattered-light photoelastic method 15 p2575 A67-30033

Multilayer printed circuit board system for interconnecting microelectronic components noting application of X-ray, ultrasonic, beta-ray, etc to process control 16 p2681 A67-30476

Electroinductive defectoscope circuitry and operation described noting use for fatigue cracks observation in threaded components 16 p2681 A67-31917

X-ray spectrometer with cold cathode, discussing equipment design, principles, operation and performance 17 p2853 A67-32046

Nondestructive testing - Conference, Warsaw, October 1966, Volume 1 18 p3044 A67-33733

Nondestructive testing - Conference, Warsaw, October 1966, Volume 2 18 p3045 A67-33738

Microwave measurement methods for nondestructive material testing, discussing efficiency, advantages and applications 18 p3045 A67-33740

Ultrasonic probes calibration for evaluation of propagating ultrasonic wave during nondestructive testing of materials 18 p3046 A67-33744

Design and development of IR signature analysis technique for nondestructive testing of electronic and electromechanical assemblies 18 p3052 A67-34512

Graphite material strength prediction by nondestructive test techniques consisting of bulk density and eddy current measurements [ASTM PAPER 54] 18 p3070 A67-34584

Microcircuit nondestructive IR inspection and equipment used for mask alignments 19 p3192 A67-35025

Instrumentation and microelectronic measuring methods based on nondestructive IR and UV techniques used in operation of superconductive cryogenic memory 19 p3193 A67-35028

Ultrasonics as nondestructive means of measuring residual stresses 20 p3537 A67-36475

Integrated nondestructive testing for determining weld integrity of space vehicles 20 p3454 A67-36586

IR scanning nondestructive testing program for microwelds to evaluate quality 20 p3454 A67-36666

Nondestructive testing of electronic circuits with fiber optic scintillators, vidicon data sampling and pattern recognition displays, discussing TV data handling 20 p3449 A67-36982

MOSFET gate breakdown nondestructively determined by measurement of leakage component 21 p3598 A67-38574

Quality control methods to ensure thin film circuitry integrity and reliability, showing need for better nondestructive testing techniques 21 p3635 A67-38623

Destructive and nondestructive testing of thickness of oxide coatings on Al and Al alloys 22 p3798 A67-39552

Nondestructive inspection of composite structures in helicopter rotor blades, discussing structure, loading and quality control capability 22 p3812 A67-39857

Performance reliability of reinforced plastics for structural load-bearing components using nondestructive testing, defining material-energy interactions 22 p3826 A67-39860

Electronic or electromechanical failure-prone component pinpointing using various nondestructive testing methods 23 p4009 A67-40912

Electronic assembly loose parts detection system using nondestructive vibration testing 23 p4005 A67-41369

Fail-safe design, nondestructive testing and inspection facilities at design stage for aircraft structures 24 p4250 A67-42442

Ultrasonic monitoring technique for fatigue damage and crack formation and propagation in aircraft structures [AIAA PAPER 67-793] 24 p4251 A67-42954

NONELECTRONIC APPARATUS

Passive sensing techniques for remote monitoring of nonelectronic systems

[AIAA PAPER 67-774] 24 p4158 A67-42942

NONEQUILIBRIUM

SA EQUILIBRIUM

Nonequilibrium effects in spherical free jet expansions of polyatomic gases and gas mixtures, obtaining moment equations for flow field development 13 p2104 A67-26983

Existence in alkali-metal-seeded rare gases of mode of nonequilibrium electric discharge with constricted positive column 17 p2910 A67-33385

NONEQUILIBRIUM FLOW

Model of nonequilibrium properties of high temperature carbon dioxide and other gas mixtures in connection with studies for vehicles entering Martian atmosphere 01 p0008 A67-11436

Nonequilibrium expansion of high temperature diatomic gas through hypersonic convergent-divergent nozzle 02 p0180 A67-12547

Hypersonic flow of air past circular cylinder with nonequilibrium oxygen dissociation, including dissociation of free stream 03 p0351 A67-13000

Finite difference solution to nonsimilar laminar mixing of streams undergoing nonequilibrium chemical reactions 04 p0609 A67-15816

Matched asymptotic expansions method for perturbation problem of nearly equilibrium dissociating boundary layer flow 05 p0792 A67-16818

Continuum viscous nonequilibrium flow partial differential equations in thin shock layer 05 p0750 A67-17335

Reacting gas flow in nozzle in one-dimensional formulation taking into account nonequilibrium course of chemical reactions 06 p0935 A67-17728

Hypersonic flow past sphere by relaxing gas with internal degrees of freedom in nonequilibrium 06 p0935 A67-17731

Discontinuous solutions in supersonic reacting gas flows under nonequilibrium conditions 06 p0984 A67-18112

Near-field solution for nonequilibrium transonic flow around corner near transonic-frozen flow field 06 p0942 A67-18587

Dissociational rate constants and vibrational relaxation times modifications, considering coupling of vibrational and dissociational nonequilibrium of expanding gas in nozzle [AIAA PAPER 66-520] 06 p0992 A67-18851

Nonequilibrium effects on shock wave reflection coefficient 06 p0992 A67-18885

Supersonic flow velocity and density probe for direct measures of mass and momentum influx, noting solution of H-T diagram of argon and probe criteria 09 p1497 A67-21776

Effect of underheating on development of boiling crisis in two-phase nonequilibrium flows 10 p1732 A67-23018

Momentum and energy transfer effects on gas kinetic equations of nonequilibrium flows, analyzing diffusion problem 11 p1780 A67-24536

Ionized fluid flow analyzed by multilayer theory to evaluate energy transfer mechanisms, noting temperature and compositional nonequilibrium effects 11 p1780 A67-24537

Propagation of small disturbances in general three-dimensional unsteady nonequilibrium MGD, noting influence of various parameters 14 p2361 A67-28904

Weakly perturbed supersonic flows in presence of arbitrary number of nonequilibrium physicochemical processes 15 p2472 A67-29688

Nonequilibrium-transition patterns of quasi-one-dimensional dissociating-gas flow through diverging supersonic nozzle 19 p3211 A67-35759

Coles equation representing nonequilibrium turbulent boundary layer without transpiration 19 p3212 A67-35776

Nonequilibrium quasi-one-dimensional nozzle flows in limit when relaxation time is large compared with characteristic flow time 19 p3172 A67-35800

Thin optimum wing contour constructing procedure having minimum wave drag in supersonic flow solved by linear approximation, obtaining numerical values for parameters 22 p3741 A67-40017

Variational formulation and Rayleigh-Ritz method for nonequilibrium viscous incompressible flows, obtaining velocity and temperature distributions 22 p3788 A67-40422

Shock curvature and flow variable gradients at tip of pointed axisymmetric body in nonequilibrium flow, solving linear differential equations and singularity 23 p3928 A67-41176

Variational methods for nonequilibrium thermodynamic processes based on fluctuation theory, noting application to viscous heat conducting flows 24 p4255 A67-42554

NONEQUILIBRIUM IONIZATION

Spatial distributions of free electrons in near wakes of spheres in hypersonic flight [AIAA PAPER 66-55] 04 p0547 A67-14820

Spatial growth of ionization in molecular hydrogen, using thin film cathode 07 p1226 A67-19853

Nonequilibrium ionization of gas-solid suspension expanding supersonically in nozzle as function of charge distribution 07 p1227 A67-20258

Channel flow and power generation of MHD generator, stressing influence of nonequilibrium ionization 09 p1541 A67-21802

Relaxation phenomena role in MHD generator using nonequilibrium ionization, noting collisional and radiative recombination mechanisms 09 p1542 A67-21815

Excited atoms effect on nonequilibrium ionization of partially ionized plasma in direct energy conversion systems, using Klein effect 09 p1543 A67-21821

Nonequilibrium ionization and radiation effect on shock wave attenuation calculated using linearized theory 11 p1774 A67-23856

Current and potential distribution for thermally-stable plasma of Faraday-type segmented electrode MHD generator, taking into account nonequilibrium ionization 16 p2599 A67-30530

Magnetically induced ionization in nonseeded helium and argon gas mixtures used to determine nonseeding operation of MHD generator in nonequilibrium ionization mode 16 p2711 A67-30542

Nonequilibrium ionization existence in sufficient magnitude to investigate closed loop MPD power generation feasibility at low temperatures, discussing explanation of saturation effect 16 p2602 A67-30555

Large nonequilibrium MHD generator design and preliminary performance, emphasizing electrode-wall shorting phenomenon in channel 16 p2602 A67-30556

Nonequilibrium plasma properties and generator performance due to magnetically induced ionization in closed loop facility using cesium seeded helium 16 p2602 A67-30557

Physical parameter determination for monatomic gas flow based on energy balance, taking into account heating and ionization in thermal nonequilibrium 17 p2837 A67-32337

Atomic nitrogen-oxygen mixtures ion concentration enhancement in hydrocarbons presence, discussing atom recombination rate, etc 18 p3107 A67-33805

Buildup time for nonequilibrium argon ionization at inlet of MHD generator channel 18 p2989 A67-34048

Steady electric power from Cs seeded Ar plasma in nonequilibrium ionization flowing at high speed through magnetic field 24 p4109 A67-42895

NONEQUILIBRIUM PLASMA

Uniform velocity MHD channel flow of nonequilibrium plasma with tensor electroconductivity 02 p0275 A67-12552

Stationary waves and nonstationary multibeam flows in plasma with arbitrary electron velocity distribution 03 p0486 A67-14198

Nonequilibrium plasma diagnostics of steady HF discharge in toroidal MHD plasma generator 04 p0553 A67-14580

Fluctuation-dissipative ratio between correlation functions of fluctuating parameters and dissipative properties in thermodynamic-nonequilibrium systems with spatial dispersion 04 p0673 A67-15968

Nonequilibrium excitation influence on electron density in one-dimensional MFD channel flow 09 p1542 A67-21814

Modified Chapman-Enskog method for obtaining transport properties of nonequilibrium partially ionized gas, giving hydrodynamic equations 11 p1775 A67-23866

Rate equations for nonequilibrium excitation of neutral helium in plasmas of

moderate density solved and compared with population densities 11 p1844 A67-25075

Hall voltage reduction in linear MHD generators noting Lorentz force effect 12 p1898 A67-25387

Nonequilibrium MHD generator for closed and open cycles, noting K seed ionization by energy transfer from excited N molecules 12 p1898 A67-25388

Nonequilibrium MHD plasmas investigated for electrothermal instabilities noting effect of plane wave fluctuations 12 p1972 A67-25391

Kinetic equation for completely ionized plasma generalized for several particle species case 13 p2165 A67-26585

Plasma-radiation interaction represented by Compton effect, utilizing Boltzmann term developed according to powers of perturbation caused by electron motion 13 p2165 A67-26598

Nonequilibrium line radiation for generalized Lorentz profiles in spherical plasma of large optical thickness 13 p2166 A67-26728

Simple model atom selection for electron density calculation in low temperature nonequilibrium Cs plasmas 13 p2171 A67-27441

Stationary waves and nonstationary multibeam flows in plasma with arbitrary electron velocity distribution 14 p2360 A67-28543

Nonequilibrium tensor conductivity in argon-potassium plasma under MHD generator conditions 16 p2709 A67-30514

Electrical conductivity and electron energy balance in nonequilibrium plasma calculated over wide range of conditions on basis of ionization theory 16 p2709 A67-30516

Electron concentration and temperature, gas temperature, electrical field intensity and conductivity of Hg-Cs nonequilibrium plasma 16 p2709 A67-30517

Electron number density and number density of electronic states calculated from rate equations for noble gas seeded with alkali metal 16 p2710 A67-30518

Solution of Boltzmann and rate equations for electron distribution function and state populations in nonequilibrium MHD plasmas 16 p2710 A67-30519

Energy exchange between electron gas and molecular gas shown to depend on composition of latter, for application of nonequilibrium plasma 16 p2710 A67-30521

Alkali metal vapor and inert gas mixtures with alkali seeding radiation properties, noting nonequilibrium argon-krypton plasma parameter determination in electrical discharge 16 p2710 A67-30522

Electrical characteristics of low current arc discharge in magnetic field determining effect of nonequilibrium plasma on conductivity 16 p2710 A67-30524

Pulsed discharge in transverse magnetic field noting relation between ionization instability and turbulent conductivity of nonequilibrium plasma 16 p2711 A67-30538

Steady flow of anisotropically conducting fluid in plane or annular channel of MHD generator with nonequilibrium plasma at small Reynolds numbers 16 p2600 A67-30541

Invariant solutions to nonlinear electromagnetic phenomena in dense plasma with nonequilibrium electric conductivity in variable magnetic field 16 p2712 A67-30543

Hot electron nonequilibrium plasma use in MHD generators, considering energy transfer, plasma stability, magnetogasdynamics, etc 16 p2601 A67-30545

Optimum Mach number for nonequilibrium helium-cesium plasma flow in MHD generator, explaining effect of deceleration temperature and internal efficiency level on optimum pressure 16 p2604 A67-30570

Particle energy distribution in low temperature nonequilibrium plasma in diffusion approximation description 16 p2720 A67-31386

Magnetohydrodynamic energy converters based on nonequilibrium plasmas for laser construction 16 p2686 A67-31576

Amplifying electromagnetic radiation in nonequilibrium decaying plasma of various degrees of ionization, taking into account kinetics 16 p2723 A67-31577

Electron velocity distribution function in nonequilibrium plasma having spatial distribution governed by electron-electron and inelastic collisions 16 p2723 A67-31768

Correlation of measurement data on electrical conductivity of nonequilibrium plasma with impurities 17 p2895 A67-32153

Chemical processes in low temperature plasmas, stressing nonequilibrium characteristics, temperature and collision factors, ionization and particle excitation 17 p2809 A67-32188

Local electronic energy balance formulation, including radiative transport effect in nonuniform seeded plasma, described by two-temperature model 17 p2906 A67-33010

Experiments on equilibrium and nonequilibrium electrical conductivity of seeded combustion products and theory of nonequilibrium ionization and recombination 18 p3085 A67-33706

Energy and intensity density of radiation emitted by semiinfinite nonequilibrium electron plasma with non-Maxwellian particle distribution calculated, based on general fluctuation theory 19 p3267 A67-34902

Kinetic equation for inhomogeneous plasma in uniform external magnetic field, for application in studies of transport and high frequency wave phenomena 19 p3285 A67-35342

Plane ionization wave propagation in uniform magnetic field compared with flame front expansion during slow burning 19 p3286 A67-35347

High power microwave radiation from nonequilibrium plasma discharge near electron cyclotron frequency 19 p3291 A67-35386

Characteristics of nonequilibrium cesium plasma subjected to continuous electric field 19 p3294 A67-35417

Electric arc blowing in plasma of nonuniform conductivity and inclusion of effect in MHD flow 19 p3298 A67-35760

Plasma kinetic theory, discussing BBGKY hierarchy, nonequilibrium processes and unstable plasma kinetic equations 20 p3495 A67-36154

Book on statistical theory of nonequilibrium processes in plasma, using microscopic equations to obtain two first moments of random functions 20 p3499 A67-36951

Energy transfer and electron conduction in nonequilibrium argon arc column at one atmosphere [AIAA PAPER 67-693] 21 p3672 A67-38722

Electron-ion three-body recombination rate in nonequilibrium dense nitrogen plasma measured spectroscopically [AIAA PAPER 67-703] 21 p3672 A67-38730

Linear nonequilibrium MHD generator channel, studying discharge structure and stability and convective and Lorentz forces effects on electric characteristics [AIAA PAPER 67-718] 21 p3673 A67-38744

Quasi-one-dimensional nonequilibrium argon plasma flow equation, discussing kinetic model with atom-atom and electron-atom impact ionization 22 p3850 A67-39708

Emissivity expressions and absorption coefficients developed for plasma particles interacting with electromagnetic field and at equilibrium 22 p3854 A67-40527

Shock wave produced optically-thin nonequilibrium plasmas studied using Rankine-Hugoniot calculations for properties, varying electron/ion temperature ratio [DVL-635] 24 p4194 A67-41860

Statistical entropy of nonequilibrium plasma assuming binary correlation functions, obtaining distribution function equation 24 p4196 A67-42158

Kinetic behavior of electrons in air plasmas containing electrophilic gasses studied with microwaves behind reflected shock waves 24 p4196 A67-42196

NON-EQUILIBRIUM RADIATION

Radiation intensity and causes of radiation peak of nonequilibrium gas following strong shock waves 18 p3083 A67-34059

NON-EUCLIDEAN GEOMETRY

Invariant properties of partially polarized electromagnetic waves analyzed in Poincare and Cayley-Klein models of hyperbolic space, using geometric constructions 09 p1460 A67-21588

NONGRAY ATMOSPHERE

SA GRAY GAS

Radiant heat transfer from nongray surfaces with external radiation [AIAA PAPER 66-21] 03 p0533 A67-13043

Nongray model atmospheres of Jovian

planets constructed for different relative concentrations of helium and diatomic hydrogen and various likely effective temperatures as chief sources of thermal opacity 09 p1567 A67-22237

Closed form solution for determining total emissivity of metals and radiation conductivity of radiation shield for nongray metallic surfaces at low temperature [AIAA PAPER 67-335] 12 p2038 A67-26049

Radiative energy transfer through nongray medium bounded by two flat surfaces, obtaining temperature distribution and heat flux values 15 p2578 A67-29130

Structure of strong shock wave studied for simple models of nongray radiative transfer 16 p2658 A67-30938

Radiative heat transfer in nonisothermal nongray gas model, measuring absorption and emission in carbon dioxide and water gases [ASME PAPER 66-WA/HT-25] 20 p3555 A67-37607

Integrated intensities for thermal radiation heat transfer in nongray nonscattering gas approximated, deriving effective absorption coefficient 22 p3920 A67-40442

NONHOLONOMIC EQUATION

Singular characteristics of dynamic systems with steady state motion, noting effect of constantly acting small perturbations 11 p1818 A67-24147

Different motion equations equivalence for nonholonomic systems from Chaplygin method 21 p3657 A67-38303

Mechanical system motion with point moving on surface, imposing limitations on system mass distribution, obtaining fixed coordinate system 24 p4188 A67-42302

NONLINEAR EQUATION

SA BERNOULLI EQUATION

SA LINEAR EQUATION

Nonlinear equations for equilibrium composition of combustion products from methane burned with ionizing admixtures over various temperature and pressure ranges 01 p0139 A67-10046

Extension of Waltman theorems regarding oscillation and asymptotic behavior of solutions of nonlinear differential equation, proving solution existence for initial value problem 01 p0105 A67-10730

Nonlinear dispersive wave propagation analyzed by linearization, obtaining solution as Fourier integral through differential equation 01 p0024 A67-10737

Parabolic equation derivative solution applying results to boundary value problems, Cauchy problem and nonlinear equation 01 p0106 A67-10901

Nonlinear equations of shell equilibrium, considering slew, elongation and shear 01 p0162 A67-10903

Numerical solution of nonlinear differential equations governing finite axisymmetric deformation of thin shells of revolution 01 p0164 A67-11176

Continued fraction rational approximations to solution of second-order nonlinear equation, including Riccati equations treated by Merkes, Scott and Fair 02 p0258 A67-11558

Nonlinear Sturm-Liouville BVP with random forcing function 02 p0258 A67-11587

Quasi-Newton methods in nonlinear equation solving and unconstrained optimization 02 p0259 A67-11801

Existence theorems for nonlinear boundary value problems 02 p0260 A67-12738

Exact and approximate solutions to Cauchy problem for nonlinear wave equation in affine connection field theory 03 p0457 A67-13171

Stabilization of steady state motion of controlled system described by nonlinear differential equations with time delays 03 p0392 A67-13588

Self-sustained periodic solution in nonlinear difference differential equation proved under appropriate assumptions for various parameters 03 p0459 A67-13655

Exact monotonic and approximate oscillatory solutions of nonlinear differential equations of high order 03 p0460 A67-13656

Solutions for nonlinear Ginzburg-Landau equations in cylindrical symmetry for type I superconductor 03 p0499 A67-13876

Patching method applied to nonlinear differential equation of forced oscillation of second order relay system with damping 03 p0393 A67-13901

Stability of forced oscillations described by second order nonlinear differential equation determined by Pinnl asymptotic method 03 p0530 A67-14177

Rational approximation of generalized Duffing equation, damped mass spring oscillator equation and generalized second order Riccati equation 04 p0647 A67-15660

Nonlinear equations for supercritical axisymmetric elastic deformation of circular cylindrical shell under longitudinal impact from rigid body 05 p0907 A67-16015

Nonlinear boundary value problem with small parameter multiplying highest derivative 05 p0835 A67-16737

Nonlinear equations of traveling wave tube solved approximately, taking account of relativistic effects 05 p0776 A67-17164

Nekrasov method application to construction of algorithm for small solutions to nonlinear integral equations, using recursion techniques 05 p0836 A67-17488

Two variable expansion procedure for approximate asymptotic solution to nonlinear differential equation 06 p1022 A67-17789

Newton-Raphson method generalized for solution of two-point boundary value problems of nonlinear optimal control theory for digital solution 06 p0974 A67-17923

Inverse method of structural analysis of automatic control systems described by nonlinear differential motion 06 p0976 A67-18238

General nonlinear law of hereditary creep 06 p1107 A67-18636

Periodic vibrations of systems governed by nonlinear PDEs, examining perturbation method, transverse vibrations of bar, string, beam and membrane and sound waves in enclosure 06 p1034 A67-18640

Nonlinear problems of thin plate bending, using successive approximations 06 p1108 A67-18661

Numerical solutions of nonlinear differential equations - Conference, U.S. Army Mathematics Research Center, Madison, May 1966 07 p1212 A67-19152

Variability and nonvariability of solutions to second order nonlinear differential equations 07 p1213 A67-19172

Convergence of solution of nonlinear functional equations, noting iteration processes applications 07 p1215 A67-19329

Nonlinear PDE for magnetostatic field with variable permeability in discontinuous medium solved with digital computer 07 p1132 A67-19795

Computer program for axisymmetric nonlinear behavior of stiffened elastic shells of revolution with variable thickness, calculating collapse pressures [AIAA PAPER 66-529] 08 p1417 A67-20558

Nonlinear equations of motion of bifilar pendulum without using suspension geometry or inertia properties of suspended body 08 p1354 A67-20922

Monograph on existence theorems for nonlinear equations, using functional analysis in Banach space 08 p1348 A67-21175

Existence theorems of algebraic integral equations /AIR/ with nonlinear functionals 09 p1524 A67-21649

Sufficient conditions for stability of solutions of nonlinear nonautonomous equation, examining pendulum of variable length 09 p1533 A67-22154

Explicit bounds for solutions of certain second order nonlinear differential equations 10 p1674 A67-22967

Class of nonlinear operators and necessary and sufficient condition of solvability of quasi-linear elliptic equations 10 p1674 A67-23076

Existence, uniqueness and stability investigation of periodical solutions for nonlinear hyperbolic partial differential equations 10 p1674 A67-23387

Numerical solution of class of nonlinear high order differential equations with two-point asymptotic boundary conditions for thermal boundary layers in laminar and turbulent flow 10 p1627 A67-23560

Nonlinear membrane equations for extremely thin shell of revolution of very deformable material, assuming large displacements, rotations and strains 10 p1730 A67-23836

Nonlinear system of partial differential equations describing one-dimensional combustion process of gas mixture 11 p1882 A67-24158

Series method of solving boundary value problems for nonlinear ordinary differential equations 11 p1814 A67-25050

Nonlinear equations of shell equilibrium, considering slew, elongation and shear 11 p1880 A67-25073

Nonlinear equations of thin shell theory, especially equilibrium equations, taking into account displacements, elongations and shear, noting linearization in stability problems 12 p2025 A67-25605

Variational derivation of nonlinear equilibrium equations for three-layer conical shell with rigid incompressible filler under external pressure 12 p2025 A67-25609

Equilibrium equations modified in nonlinear theory of thin walled elastic shells 12 p2028 A67-25634

Resolvent equations of shallow multilayer shells of regular structure to solve problems involving calculations of strength, stability and oscillations 12 p2029 A67-25668

Upper and lower bounds on distance between zeros of components of solutions of second order ordinary nonlinear differential equations 12 p1961 A67-26062

Nonlinear equations in gas dynamics for turbulent nonpotential flows, emphasizing geometry of characteristic surfaces and numerical calculation 12 p1931 A67-26199

Stability of discontinuous solutions of gas dynamic equations noting doubtful case with imaginary eigenvalues 13 p2093 A67-26379

Electron generator with oscillatory anode circuit nonlinear differential equation analyzed by linearizing, applying algorithm to obtain computer solution 13 p2144 A67-26393

Solvable convergent difference schemes for nonlinear elliptic equations using variational method applied to differential equation 13 p2145 A67-26445

Iteration solution for system of equations for nonlinear deflection and stability of anisotropic plates 13 p2217 A67-26632

Discrete ordinate technique for nonlinear Boltzmann equation for hard sphere molecules, considering pseudoshock relaxation 13 p2102 A67-26973

Iterative methods for solving nonlinear least squares problems by choosing linear nonsingular transformations of finite-dimensional Euclidean space 13 p2147 A67-27171

Mysovskikh theorem concerning convergence of Newton method for finding zeros of nonlinear operators between Banach spaces 13 p2147 A67-27172

Asymptotic behavior of parameter-dependent nonlinear functional equations arising in signal reconstruction study 13 p2147 A67-27451

Convergence of methods of tangential parabolas and hyperbolas used in nonlinear equation solution with nondifferentiable operators convergence of methods of tangential parabolas and hyperbolas used in nonlinear equation solution 13 p2149 A67-27619

Nonlinear differential equation for shock wave of several circular arc airfoils integrated to give shock wave location 14 p2239 A67-27797

Nonlinear equation systems solved using parameters and varying them to original form while simultaneously tracing roots 14 p2342 A67-27975

Nonlinear inviscid transonic flow in throat of two-dimensional curved nozzle, using approximate method [ASME PAPER 67-FE-11] 14 p2242 A67-28360

Synthesis of optimal controls for nonlinear plant described by second order differential equation 14 p2291 A67-28383

Constructing example of isolated stationary point 14 p2343 A67-28387

Integral equations in automatic control theory, deriving theorem which leads to Popov frequency domain stability criterion 14 p2292 A67-28635

Space-time region division method for reducing nonlinear heat conduction to subordinate linear multilayer system problems, assuming stationary time characteristics and coordinates 14 p2408 A67-28804

Numerical solution of Cauchy problem class of nonlinear integrodifferential equations 14 p2344 A67-28896

Nonlinear partial differential equations of stellar evolution theory solved under

assumption of spherical symmetry of star 14 p2392 A67-28995

Reproductive property of Navier-Stokes equations, generalizing notion of periodicity 15 p2510 A67-29462

Bifurcation of nonlinear operator equations to determine steady state axisymmetric homogeneous fluid flows between rotating cylinders 15 p2494 A67-29693

Extension of Vainberg method for studying nonlinear integral equations with aid of Hart theorem to cover Urysohn type equations 15 p2511 A67-29888

Integrodifferential equation solvability by investigation of adjoint Cauchy problem 15 p2511 A67-29890

Nonlinear differential equations of systems describable by state model solved by incremental linearization technique 15 p2458 A67-29908

Invariant solutions to nonlinear electromagnetic phenomena in dense plasma with nonequilibrium electric conductivity in variable magnetic field 16 p2712 A67-30543

Uniqueness and existence of Cauchy problem solution considering Dirichlet limits, studying convergence requirements 16 p2695 A67-30829

Nontrivial real or complex solutions of nonlinear integral equations of Hammerstein type bifurcating from identically vanishing solution 16 p2695 A67-30858

Existence theorems for systems of nonlinear integral equations of Hammerstein type with positive definite kernels 16 p2687 A67-30859

Algorithm for statistical estimation of nonlinear function of signal containing noise 16 p2643 A67-30921

Unsteady motion stability over given time interval of mechanical systems described by nonlinear differential equations 16 p2702 A67-31052

Numerical solution of nonlinear integral equations with variable upper limit, applicable to Cauchy and boundary value problems 16 p2696 A67-31142

Stress-strain state determination of nonlinear plate with circular holes, deriving boundary conditions and basic equations 16 p2766 A67-31147

Monotone iterations for nonlinear elliptic differential equations in boundary-value problems applied to Gauss-Seidel methods 16 p2697 A67-31331

Stationary Newton method for nonlinear functional equations in Banach spaces, formulating convergence conditions 16 p2697 A67-31332

Stabilization method for solution of boundary value problems for second order nonlinear ordinary differential equation 16 p2698 A67-31482

Nonlinear equations governing complex chemical and phase equilibria derived from thermodynamic principles and supplemented by solving algorithms and practical applications 16 p2820 A67-31815

Minimizing nonlinear function of several variables without constraints, solution obtained by combination of interpolation techniques and Levenberg method 17 p2818 A67-32426

Properties of solutions of second order nonlinear nonautonomous ordinary differential equations from study of truncated version of equation 17 p2879 A67-32884

Static /time-discrete/ electrical model for mathematical analogy of heat transfer processes and application to solution of nonlinear heat conduction equations 17 p2821 A67-33079

Nonlinear equations for equilibrium composition of combustion products from methane burned with ionizing admixtures over various temperature and pressure ranges 17 p2927 A67-33324

Interpolation methods for solving nonlinear algebraic/transcendental equations applied to maximum principle boundary value problems 18 p3071 A67-33679

Nonlinear hyperbolic equation solution formulation based on Riemann invariants 18 p3072 A67-34288

Cauchy problem solution for certain functional equations in complete linear normalized space extended to include nonlinear space 18 p3073 A67-34603

Single-mesh circuits design for driving

- xenon flashlamps, solving normalized nonlinear differential equation 19 p3192 A67-35015
- Plasma-metal interface electric field intensity, deriving dimensionless formula from nonlinear second order differential equation 19 p3277 A67-35125
- Regularity of generalized solutions of general nonlinear and nonstationary Navier-Stokes equations, improving differential properties by data smoothness 19 p3209 A67-35445
- Prestressed-shell buckling, using Budianskii-Koiter tensor nonlinear equilibrium equations by numerical analysis 19 p3343 A67-35778
- Nonlinear features of geostrophic adjustment in one-dimensional barotropic atmosphere number 19 p3253 A67-35917
- Impact characterization and length, determining contact energy with Hertz equation and integrating nonlinear differential equation for system motion 20 p3483 A67-36195
- Nonlinear approximation of thin elastic plane plates noting influence of elastic medium and strain tensor deformations 20 p3535 A67-36279
- Thin rectangular vortex wing in uniform flow, solving nonlinear equations by successive approximations 20 p3356 A67-36439
- Two-point boundary value problem, approximate solution using Monte Carlo path integral calculation 20 p3475 A67-36481
- Second order nonlinear parabolic type partial differential equations with divergence structure, noting role of maximum principle 20 p3475 A67-36502
- Analytic design of optimal digital controller, resolving problem of choice of weighting coefficients of functional representing generalized rms estimate of transient 20 p3408 A67-37046
- Variational equations solved by numerical integration along with nonlinear differential equations with less computing and storage and higher accuracy 20 p3478 A67-37212
- Approximate solutions for nonlinear differential equations to study periodic motions for analysis of pressure relief system 20 p3366 A67-37369
- Velocity field in axisymmetric boundary layer described by nonlinear partial differential equations 20 p3425 A67-37677
- Asymptotic behavior of solutions for nonlinear differential equations 20 p3479 A67-37720
- Integration of Cauchy problem for class of nonlinear higher order partial differential equations 21 p3651 A67-37901
- Solution behavior of second order nonlinear differential equation with restriction on one constant 21 p3651 A67-37922
- Convective heat flow nonlinear equations for fluid sphere having heat sources expressed in Boussinesq approximation as perturbation of steady state conduction solution 21 p3731 A67-37926
- Convergence of perturbed Galerkin method to construct general theory of approximate methods for nonlinear equations 21 p3653 A67-38419
- Nonlinear generalization of Schroedinger equation describing hidden variables effect solved for spin-1/2 magnetic moment relaxing in constant magnetic field 21 p3658 A67-38845
- Discontinuous systems proved for stability and instability, using almost-reducible linear approximations 21 p3654 A67-38850
- Switching behavior equations derived for FET with solutions applied to MOS and junction gate FET 21 p3602 A67-39069
- Ferromagnetic magnetization curve approximated for analytical solutions of boundary value problems in nonlinear electrodynamics, obtaining Riemann functions 22 p3836 A67-39420
- Tanh γ form laminar mixing layer and nonlinear inviscid equation two-dimensional solutions with linearized stability theory perturbations 22 p3782 A67-39528
- Propagation anomalies of atmospheric acoustic signals of nuclear explosions due to nonlinearities and refraction 22 p3790 A67-39645
- Extension of nonlinear TWT equations to floating drift relativistic klystron, noting formulas for first harmonic of current in two-and three-cavity klystron 22 p3770 A67-39655
- Saint Venant principle in linear and nonlinear plane elasticity in two-dimensional isotropic body 22 p3912 A67-39743
- Nonlinear hyperbolic equations of compressible duct flow solved using centered difference method, compared with method of characteristics 22 p3784 A67-39945
- Nonlinear differential equations describing extensional motion of dumbbell satellite solved on digital computer 22 p3886 A67-40086
- Corrections for three results in asymptotic solution of nonideal Bose-Einstein particle system nonlinear integral equations 23 p4026 A67-40718
- Nonlinear differential equations solutions extended analytically by parameter substitution method applied to Rayleigh equation 23 p4023 A67-40926
- Second order accurate approximation to advection terms in hydrodynamics equations noting aliasing effects, amplitude and phase errors and stability 23 p4024 A67-40994
- Turbulence onset from small eddies in shear flow analyzed by nonlinear approach 23 p3990 A67-41173
- Numerical solution for two-point nonlinear boundary value problem of n-order ordinary differential equation 24 p4177 A67-41914
- Free carrier effect on higher harmonic generation in semiconductors from nonlinear Boltzmann equation 24 p4202 A67-41985
- Sampling interval criteria with nonlinear integrands in discrete-continuous feedback control systems, obtaining performance surfaces in object function-parameter space 24 p4134 A67-42024
- Canonical decomposition of nonlinear error covariance difference equation derived for discrete estimation problems 24 p4177 A67-42188
- Stabilization method for solution of boundary value problems for second order nonlinear ordinary differential equation 24 p4177 A67-42198
- Temperature field within multidimensional body in nonlinear heat conduction process in terms of known temperature distribution along coordinates 24 p4254 A67-42254
- Nonlinear analysis of cellular convection induced by surface tension in finite amplitude heated liquid layer, discussing prediction of hexagonal flow pattern 24 p4255 A67-42569
- Nonlinear equation solution existence in real Hilbert space with linear and nonlinear operator 24 p4178 A67-42721
- Second order nonlinear differential equation derived for pressure-time curve required for ideal solid propellant rocket motor 24 p4208 A67-42923
- Nonlinear partial differential equations - Conference, University of Delaware, December 1985 24 p4179 A67-43081
- Viscous flow stability between concentric rotating cylinders with Taylor vortices, deriving velocity and pressure perturbation nonlinear partial differential equations 24 p4145 A67-43083
- Ad hoc exact solution techniques for nonlinear partial differential equations noting physical applications 24 p4180 A67-43085
- Non-Newtonian elastoviscous channel flow between rigid boundaries solved by asymptotic expansion in lubrication approximation 24 p4145 A67-43086
- Integral equations for nonlinear problems in partial differential equations, including Volterra, boundary value and initial value problems 24 p4180 A67-43088
- Nonlinear electrical problems requiring partial differential equations including magnetic saturation, parametric amplifier, electron tube, traveling wave amplifier and semiconductor diodes 24 p4133 A67-43089
- NONLINEAR FEEDBACK**
- Saturated transistor logic circuit using rectifier diodes to provide nonlinear current feedback from collector to base of transistor 01 p0038 A67-10817
- Stability theory based on functional methods, examining feedback system with linear time invariant and nonlinear elements 01 p0046 A67-11208
- Functional integration analysis of exponential behavior of nonlinear feedback control systems 01 p0047 A67-11211
- Onset of periodic oscillations in nonlinear feedback systems 05 p0785 A67-17267
- Pulse interference inhibition in AM signals reception by nonlinear negative feedback loop in HF cascades of receiving device 05 p0785 A67-17471
- Parametric coupling analyzed in electrical RLC circuit coupled with mechanical system through nonlinear inductance [ASME PAPER 67-VIBR-30] 11 p1797 A67-24188
- Functional-analytic techniques providing understanding of some nonlinear circuits action on input to output signal production 14 p2291 A67-28453
- Continuous nonlinear feedback law for controlling thrust direction to produce minimum time spacecraft rendezvous with nonmaneuvering target 16 p2758 A67-30651
- Coupled systems stability constraints and oscillatory behavior, discussing feedback path nonlinearities using differential equations 19 p3200 A67-34849
- Prediction-comparison system for data compression, noting nonlinear error feedback and advantage of closed-loop predictor 20 p3412 A67-37497
- Popov method extension for absolute stability of nonlinear feedback systems containing distributed elements 23 p3984 A67-40870
- Simultaneous self-starting oscillations at unrelated frequencies in feedback loop containing one nonlinearity, calculating equivalent linear gain 23 p3984 A67-41157
- NONLINEAR FILTER**
- Comparison of nonlinear and linear filtration in sense of minimum of mean square error of Markov process hidden in noise 01 p0106 A67-10923
- Spontaneous emission spectra and ratio of number of photons in various oscillation modes of laser with nonlinear filter type lock 02 p0251 A67-11573
- Optimum signal reception against non-Gaussian noise background in presence of white Gaussian noise 03 p0368 A67-13274
- Sharp cut-off nonlinear filter design with jump effect for rapid gain increase with small frequency increment 03 p0368 A67-13981
- Optimal multichannel nonlinear filtering problem of minimum variance estimation of state of n-dimensional nonlinear system subject to stochastic disturbance 04 p0592 A67-15084
- Hybrid nonlinear optical filter exhibiting different transmission properties in opposite paths applied to CRT display 05 p0804 A67-16306
- Synthesis of optimal nonlinear filters of Volterra type approximating kernels of filters by orthonormal functions 05 p0782 A67-16318
- Filtering for nonlinear dynamical systems with white Gaussian noise processes 06 p1029 A67-18532
- Optimal extremal control systems synthesized by nonlinear filtering compared to those synthesized by correlation method of control 08 p1313 A67-21328
- Filter theory method applied in solving analytical construction problems for optimal controllers, noting existence of Fourier transform and Pally-Wiener condition 09 p1482 A67-22078
- Dynamical equations for optimal nonlinear filtering and representation of conditional expectation as solution to stochastic differential equation 13 p2146 A67-27094
- Optimal nonlinear filter construction for steady-state random process correction using iterative method 16 p2636 A67-30925
- Finite dimensional approximations of optimal nonlinear filters for class of large-noise, nonlinear, continuous-time problems 16 p2651 A67-31680
- Nonlinear filter for homing missile tracking noise problem, noting computational requirements and feasibility by filter implementation model for different assumptions 17 p2882 A67-32526
- Synthesis of optimal nonlinear filters of Volterra type approximating kernels of filters by orthonormal functions 18 p3017 A67-33869
- Estimation and filtering in discrete linear systems with reference to Gaussian statistical hypothesis 19 p3250 A67-35910
- Nonlinear sequential estimation problem from noisy measurement data using

nonstatistical least squares formulation, obtaining approximate solution to two-point boundary value problem 20 p3410 A67-37319
Optimal nonlinear filtering, deriving differential equations for probability density or state vector for noise corrupted system 21 p3603 A67-38442

NONLINEAR PROGRAMMING SA DUAL CONTROL PROBLEM

Algorithm based on penalty functions to determine hyperplane used as iterative solution for separating convex sets 01 p0028 A67-10495
Nonlinear solution method incorporated in computer program for analysis of abnormally operating circuits considering catastrophic part failure modes 01 p0031 A67-11337
Structural design optimization by nonlinear programming noting Sequential Unconstrained Minimization Technique, use of variable metric, Powell direct search method, etc 02 p0209 A67-12711
Constrained minimization problems in finite-dimensional spaces in unified approach 03 p0458 A67-13269
Maximum problem solution with quadratic nonconcave objective functions and linear inequalities as constraints 04 p0644 A67-14772
Discrete time control /multistage/ version of Berkovitz nonlinear programming problem 07 p1163 A67-20276
Algorithm based on penalty functions to determine hyperplane used as iterative solution for separating convex sets 10 p1608 A67-23617
Nonlinear programming model for launch vehicle design and costing 12 p2013 A67-26193
Nonlinear programming in Banach space, considering saddle value problem 13 p2147 A67-27453
Dual formulation of variational problems with differential inequality constraints, noting relation between mathematical programming and variational calculus 14 p2345 A67-28908
Interior penalty method for inequality constrained optimal control problems concerning convergence rapidly 16 p2651 A67-31677
Book on nonlinear programming covering various methods and use in control 17 p2818 A67-32424
Mathematical methods of nonlinear programming, discussing convexity, quasi-convexity, gradient, Taylor series and quadratic approximations 17 p2818 A67-32425
Solving general integer programs, investigating cutting methods, rounding algorithm, branch and bound method and partition method 17 p2819 A67-32427
Hypothesis of convexity of economic function for generalizing problem of inequalities in nonlinear stochastic programming 17 p2819 A67-32428
Symmetry and self-duality in nonlinear programming investigated for class of nondifferentiable convex problems 20 p3475 A67-36482
Constrained minimization problem extended to necessary conditions for characterizing noninferior points to determine vector-valued criteria in finite dimensional spaces 20 p3478 A67-37576
Optimal control problem solving by Legendre polynomial expansions and relating function sequence correspondence approximated by finite nonlinear programming 23 p3983 A67-40647

NONLINEAR SYSTEM SA LINEAR SYSTEM

Nonlinearities such as limitation of linear characteristics, dead band, hysteresis, etc, in aircraft gas turbine control system 01 p0011 A67-10167
Difference equations of nonlinear sampled data systems and resultant recurrence formula for system response calculation 01 p0043 A67-10201
Periodic solutions for difference-differential autonomous nonlinear oscillatory system with one degree of freedom 01 p0113 A67-10290
Comparison of variances evaluated by Kolmogorov and Volterra techniques for phase locked loop subjected to white Gaussian input 01 p0044 A67-10480
Periodic regimes in two-channel automatic systems with nonlinear element in single channel part of loop, showing cross connections effect on

auto-oscillations 01 p0023 A67-10494
Real time digital simulation of linear and nonlinear control systems with large sampling intervals, determining optimization criterion by nonlinear multipoint boundary value problem 01 p0045 A67-10674
Optimal nonlinear feedback control derived from quartic and higher order performance criteria 01 p0046 A67-11206
Asymptotic stability of nonlinear systems, noting application to systems with control and Liapunov function 01 p0048 A67-11318
Optimization of control systems with nonlinear plants, using Pontryagin maximum principle 02 p0224 A67-11511
Nonlinear servo devices examined, using simplified form of harmonic-equivalent method obtained from multilinear characteristics 02 p0224 A67-11529
Sufficient condition for absolute bounded-input-bounded-output stability for certain class of nonlinear sampled data feedback systems 02 p0224 A67-11586
Nonlinear transformations of probability measures in functional spaces, noting application of random-process theory 02 p0259 A67-11922
Stability analysis of nonlinear stochastic systems in presence of random and Gaussian perturbations, determining validity of law of large numbers and amplified law of large numbers 02 p0267 A67-11958
Equilibrium equations, boundary conditions and constitutive relations for nonlinear theory of elastic directed curves, examining double stress without moment 02 p0267 A67-12057
Shock wave formation due to nonlinear vibrations in tube containing fluid subjected to transverse magnetic field with plane heater at midsection and externally supplied energy 02 p0273 A67-12058
Tabular adaptive predictive model for trajectory following control of nonlinear plant with switched two-level input 02 p0225 A67-12136
On-line estimation of states and parameters for noisy discrete nonlinear dynamic system 02 p0226 A67-12153
Sequential suboptimal adaptive control of nonlinear systems, considering generation of optimum closed-loop control for startup dynamics of nuclear reactor 02 p0226 A67-12156
Describing function determination for case of piecewise linear-nonlinear characteristics with discontinuities of first kind 02 p0227 A67-12682
Analog computer solution to autonomous systems with one degree of freedom capable of self-excited oscillation or excited by external periodic force 02 p0209 A67-12712
Soviet book on theory of automatic control systems of regular linear, special linear and nonlinear types 03 p0390 A67-13108
Structural design of optimal control for n-order nonlinear plant, using variational calculus 03 p0391 A67-13185
Invariant control device synthesis in multidimensional nonlinear automatic control systems 03 p0391 A67-13187
Necessary and sufficient conditions of invariance and autonomy of multidimensional nonlinear automatic control systems with right-hand discontinuities in describing differential equations 03 p0391 A67-13188
Existence theorems for periodic solutions of coupled nonlinear systems of two or more degrees of freedom, including normal mode vibrations 03 p0524 A67-13654
AEDNET system of digital computer programs for on-line simulation of nonlinear networks and oscilloscope display 03 p0375 A67-13665
Asymptotic rate of convergence of Gauss-Seidel type iterative processes for nonlinear difference equations 03 p0460 A67-13881
Popov stability of distributed parameter dynamical systems with multiple nonlinearities 04 p0591 A67-14419
Statistical linearization for minimization of mean square error between time derivatives for actual and model outputs for zero and special memory nonlinearities 04 p0591 A67-14420
Signal stabilization by linearization of time independent nonlinearities using extra signal and nonlinearity, noting role of pulse width modulation

[ASME PAPER 66-WA/AUT-21]

04 p0592 A67-15392
Equivalent gain and error response of hysteretic system to Gaussian inputs 04 p0593 A67-15637
Pulse type nonlinear automatic systems and systems with single nonlinear element 04 p0593 A67-15753
Normal modal vibrations for some damped n degree of freedom nonlinear systems 04 p0659 A67-15935
Simple waves for nonlinear system of partial differential equations applied to multidimensional compressible inviscid flows 05 p0790 A67-16045
Stability of control systems with distributed parameters and hysteresis-curve-type nonlinearity for various critical cases of system characteristic equation 05 p0781 A67-16250
Optimal filtration of nonlinear functional of Gaussian signal, obtaining expressions for kernels of optimal filter 05 p0782 A67-16317
Optimality conditions for nonlinear discrete systems, showing that at limit these conditions become Pontryagin maximum principle for continuous systems 05 p0782 A67-16320
Higher harmonics computation of nonlinear steady oscillation in arbitrary system 05 p0846 A67-16438
Gain adjustment of nonlinear time variant control systems with random inputs 05 p0783 A67-16444
Periodic and almost periodic limiting operational conditions for control systems with nonlinear units 05 p0784 A67-17020
Frequency criteria of absolute stability of nonlinear control systems with periodically varying parameters 05 p0784 A67-17238
Transient analysis of control system with nonlinear damping and frequency 05 p0785 A67-17301
Resonance in nonlinear dissipative systems subjected to periodic stimulating force 05 p0847 A67-17486
Approximation techniques generating algorithm for iteratively solving sequential optimization of nonlinear control systems 06 p0974 A67-17930
Stabilization of steady motions of nonlinear control system in critical case of pair of pure imaginary roots 06 p0975 A67-18035
Control law determination procedure for structural synthesis of combined automatic control systems for nonlinear plants 06 p0976 A67-18237
Dynamic characteristics of nonlinear automatically controlled plants 06 p0976 A67-18241
Boundary curves for jump resonance criteria of nonlinear control systems and conditions-in second order servo system with idealized saturation 06 p0977 A67-18526
Design procedure for meeting step-input specifications in piecewise single-valued nonlinear multivariate control system design 06 p0978 A67-18720
Sufficient conditions of absolute stability of nonlinear discrete systems based on matrix majorant concept 06 p0978 A67-18793
Differential descent in solution of multidimensional variation problem as applied to nonlinear system 07 p1212 A67-19136
Galerkin procedure for multipoint boundary value problems of general nonlinear systems 07 p1213 A67-19160
Nonlinear self-adjusting system with linear prediction analyzed by digital computer 07 p1160 A67-19200
Forced oscillations in nonlinear resonant circuit employing p-n junction capacitance 07 p1150 A67-19235
Growth of solutions of forced oscillations of nonlinear oscillator driven by white noise 07 p1218 A67-20268
Geometric analysis of vibration of nonlinear systems with one degree of freedom 08 p1353 A67-20311
Stochastic input passage through class of nonlinear systems, developing functional relations between statistical properties 08 p1308 A67-20324
Transient response of autonomous nonlinear systems examined using Liapunov function, obtaining time constant 08 p1310 A67-20341
Stability and transient response of nonlinear control systems treated by

- parameter plane techniques and describing function theory 08 p1310 A67-20342
- Parameter plane analysis of forced oscillations and jump resonance phenomena in nonlinear systems with periodic forced signals 08 p1311 A67-20343
- Generalized Zubov formulation from Liapunov function of limit cycle behavior in third order nonlinear systems 08 p1311 A67-20345
- Perturbation technique used to study random response of airplanes to effect of runway roughness 08 p1279 A67-20480
- Harmonic response and jump phenomena in closed loop systems with dynamic range type nonlinearity under sudden sinusoidal excitation 08 p1312 A67-20721
- Nonlinear continuum mechanics of viscoelastic materials with application to solid propellants 08 p1419 A67-20879
- Nonlinear viscoelastic fluids, discussing Couette flow, steady flow, periodic motion, wave propagation, thermomechanical coupling, etc 08 p1419 A67-20881
- Insensitivity zone used for stabilizing nonlinear automatic control systems 08 p1313 A67-21323
- Stability region for automatic nonlinear control systems unstable as whole 09 p1532 A67-21913
- Moments of output coordinates of nonlinear system determined by algorithm based on approximation method, applied to automatic control system 09 p1525 A67-22079
- Nonlinear automatic system with logical device analyzed in presence of external action, obtaining harmonic linearization coefficients 09 p1482 A67-22080
- Synthesis of control device for one class of nonlinear sampled data systems, obtaining processes with minimum control time 09 p1483 A67-22082
- Lorentz transform applied to solution of problem in interaction of waves within nonlinear medium 09 p1465 A67-22478
- Normal form and stability of coupled nonlinear RLC networks with possible interconnected elements of like type 10 p1618 A67-22703
- Self-excited oscillations of nonlinear servosystems examined, applying expression for generalized transmittance of nth order system 10 p1618 A67-22851
- Stability of automatic control systems with nonlinearity and nonunique equilibrium state 10 p1619 A67-23318
- Periodic regimes in two-channel automatic systems with nonlinear element in single channel part of loop, showing cross connections effect on auto-oscillations 10 p1608 A67-23618
- Dynamic theory of vibration damping by controlled impact in forced oscillations in two-mass nonlinear system 10 p1721 A67-23683
- Nonlinear behavior of elastic structural systems, approximating displacement patterns, stress-strain ratios, post buckling behavior, etc 10 p1726 A67-23717
- Power flow formulas for white noise driven vibratory systems, estimating average oscillation amplitude and plastic strain accumulation rate 10 p1731 A67-23841
- Nonlinear hydrodynamic stability theory of one-dimensional detonations based on perturbation techniques, detailing cases of ideal gas unimolecular reactions 11 p1774 A67-23857
- Nonlinear sampled system with parameters in functional dependence on sign of error at discrete instants of sampling 11 p1769 A67-24056
- Kinematic nonlinearities effect on existence, properties and stability of vibrations in unison of particle with two degrees of freedom 11 p1818 A67-24085
- Absolute extrema of certain integrals from method for finding corresponding functions with prescribed endpoints 11 p1812 A67-24087
- Averaging method in nonlinear mechanics, discussing results of Bogolubov studies 11 p1818 A67-24089
- Forced nonlinear vibration of Duffing type experimentally simulated with models of isolating systems, obtaining response curves [ASME PAPER 67-VIBR-35] 11 p1873 A67-24192
- Nonlinear automatic control with random parameters, noting change of system operator as function of disturbances on system 11 p1770 A67-24211
- Material hysteresis model for transient dynamic analysis 11 p1874 A67-24358
- Optimal solutions to mixed initial boundary value problems for control processes described by semilinear hyperbolic partial differential equations in two independent variables 11 p1770 A67-24423
- Nonlinear mechanics of plasma-like distributed system studied with Q machine, noting mode locking 11 p1839 A67-24550
- Local and overall stability of nonlinear discrete system with variable modes consisting of linear filter preceded by impulse modulator 11 p1770 A67-24751
- Characterization and equivalent model construction technique for class of nonlinear systems mathematically described, constructing zero memory systems and systems with memory 12 p1919 A67-25285
- Nonlinear oscillation effect on motion equation of elastic object under free flight conditions 12 p2032 A67-25966
- Stability and asymptotic behavior of perturbed nonlinear systems of ordinary differential equations 12 p1961 A67-26060
- Higher order resonance rotations of arbitrary order of nonlinear system 12 p1967 A67-26102
- Third order Vlasov equation solved for nonlinear plasma oscillations in classical nonrelativistic collisionless Maxwell distribution electron gas 13 p2162 A67-26283
- Almost periodicity of bounded solutions to nonlinear systems in n-dimensional Euclidean space 13 p2144 A67-26381
- Compensation technique for improving stability of certain nonlinear autonomous systems by addition of zero networks 13 p2086 A67-26413
- Stability and asymptotic stability conditions for coefficients of system of linear first order differential equations 13 p2144 A67-26443
- Alserman problem concerning absolute stability of zero solution to nonlinear third order system of differential equations 13 p2087 A67-26616
- Two component equivalent of two-stream distribution function solution to plane Couette flow, studying nonlinear effects 13 p2101 A67-26965
- Analog computer application in linear, nonlinear and time-varying systems 13 p2072 A67-26995
- Restoration of distorted signals for linear and nonlinear process converters 13 p2088 A67-27021
- Stability and nonlinear vibrations of mechanical systems under harmonic excitation 14 p2397 A67-28087
- Dynamic buckling under step loading studied on basis of general nonlinear theory of elastic stability 14 p2397 A67-28089
- Nonlinear dynamic response of thin walled shells of revolution 14 p2397 A67-28090
- Qualitative analysis of nonlinear systems described by ordinary or partial differential equations or by functional equations 14 p2291 A67-28452
- Nonlinear imaging phenomena discussed in connection with holography, describing holoscopes permitting three-dimensional magnification in real time 14 p2319 A67-28495
- Associated force field applied to phase trajectories of nonlinear systems, analyzing conditions of conservatism and normalization 14 p2349 A67-28744
- Necessary and sufficient conditions for boundary of absolute stability domain of nonlinear automatic control systems 15 p2455 A67-29120
- Frequency domain instability criteria generated from stability criteria for time varying and nonlinear feedback problems 15 p2455 A67-29167
- On-line nonlinear circuit design, discussing computer program for evaluating performance resulting from modifications 15 p2442 A67-29169
- Newton-Raphson computational procedure for finding extremal control policies for nonlinear processes 15 p2456 A67-29363
- Fokker-Planck-Kolmogorov method analysis of nonlinear systems described by stochastic partial differential equations 15 p2517 A67-29658
- Solution stability of parametric nonlinear differential equation system, noting validity of Popov criterion 15 p2518 A67-29660
- Two coupled resonant mechanical circuits with parameter in coupling element allowed to vary periodically 15 p2494 A67-29772
- Difficulties arising in applying Liapunov first method to solution of canonical systems and ways to overcome them 15 p2511 A67-29885
- Nonlinear system analysis by subdividing total motion of system into fast and slow components, noting application to control systems 15 p2458 A67-29886
- Existence conditions of periodic solution of equations describing nonlinear oscillations of thin plates with allowance for damping and application of Galerkin method 15 p2575 A67-29887
- Liapunov functions generating methods applicable to nonlinear and linear autonomous systems 15 p2511 A67-30048
- Three-step nonlinear analysis procedure for nonlinear stability for position-control servomechanical system applications 15 p2459 A67-30143
- Nonlinear nonconservative systems stability analysis by approximate method based on principle of energy conservation 15 p2519 A67-30194
- Statistical dispersion methods for identification of nonlinear controlled plants 15 p2462 A67-30324
- Systems with asymmetric nonlinearities analyzed and synthesized by setting up mathematical model applicable to control and adaptive systems compensation 15 p2463 A67-30333
- Random instability of nonlinear oscillations of dynamic system with time behavior described by equation 16 p2702 A67-30447
- Second order conductivity tensor of isotropic electron gas theory, using thermodynamic Green functions 16 p2713 A67-30803
- Types of closed characteristics in bounded region of two-dimensional autonomous differential equation systems 16 p2695 A67-30856
- Nonlinear automatic control systems with random processes studied using orthogonal polynomials with Hermitian series expansion 16 p2643 A67-30924
- Transient processes in nonlinear automatic control systems 16 p2643 A67-30926
- Free undamped oscillations of nonlinear conservative systems with several degrees of freedom with small nonlinearities 16 p2765 A67-31048
- Natural oscillations of inertial vertical with nonlinear correction, determining oscillation frequencies and damping rates 16 p2675 A67-31146
- Nonlinear laser theory to calculate amplitudes, frequencies and beat frequencies of circularly polarized modes in laser with axial magnetic field 16 p2686 A67-31562
- Optimal control problem for nonlinear systems with constrained sample times 16 p2646 A67-31635
- Synthesis technique applying Liapunov theory for state vector tracking of nonlinear multivariable control systems illustrated by reactor control design 16 p2649 A67-31662
- Nonlinear discrete system equivalence of integral pulse frequency modulation /ipfm/ feedback systems, discussing Lagrange stability criterion 16 p2652 A67-31685
- Describing functions for nonlinearity consisting of bang-bang with dead zone characteristic followed by linear integrator with constrained integration range 16 p2652 A67-31690
- Identification of continuous, nonlinear, time-dependent, single-input single-output systems represented by Volterra functional series model and stochastic approximation 16 p2653 A67-31694
- Hardware characteristics of control moment gyro /CMG/, determining nonlinearity effects on performance by simulation 17 p2853 A67-31995
- Boundary value problems containing positive linear differential operators and monotone functions of dependent variable analyzed via nonlinear heat generation 17 p2967 A67-32040
- Tolerance of nonlinearities in input transducer of time-varying optimal control systems, using Liapunov function 17 p2829 A67-32307
- Oscillating circuit with nonlinear capacitance in free oscillating regime, obtaining formula for envelope of free oscillation differing from exponent 17 p2829 A67-32311

Variational principles and methods of approximation for nonself-adjoint and nonlinear systems 17 p2969 A67-32449

Critical heat flux value nonlinearly dependent on liquid bulk underheating to saturation temperature, deriving empirical formula 17 p2970 A67-32460

Liapunov subcenter manifold, showing that real C-1 Hamiltonian system of ODEs has m distinct two-dimensional invariant manifolds 17 p2877 A67-32558

Frequency response of nonlinear system, analyzing saturation characteristic of amplifier by digital computer 17 p2821 A67-32933

Stability analysis of nonlinear stochastic systems in presence of random and Gaussian perturbations, determining validity of law of large numbers and amplified law of large numbers 17 p2886 A67-33275

State variable difference equation method for HF solution of ordinary differential equations in digital simulation with nonlinearity 18 p3005 A67-33662

Optimal filtration of nonlinear functional of Gaussian signal, obtaining expressions for kernels of optimal filter 18 p3016 A67-33868

Optimality conditions for nonlinear discrete systems, showing that at limit these conditions become Pontryagin maximum principle for continuous systems 18 p3017 A67-33871

Long time behavior of weakly interacting nonlinear waves, emphasizing mathematical features common to physical situations 18 p3079 A67-34002

Uniqueness of response of nonlinear continuous servosystem subjected to any signal 18 p3017 A67-34185

Sufficient conditions of absolute stability of nonlinear discrete systems based on matrix majorant concept 18 p3018 A67-34458

Bang-bang control using adaptive-predictive model applied to least-square error trajectory control of settling-time nonlinear systems 19 p3199 A67-34784

Parabola test for absolute stability, replacing Popov test for nonlinear sectors having nonzero lower bound 19 p3199 A67-34785

Algebraic method applied for control optimization of nonlinear systems, acquiring asymptotic stability by using Liapunov function 19 p3199 A67-34825

Gyroscope circuit model and oscillation behavior analyzed through nonlinear differential equation derived from Euler equation 19 p3227 A67-34843

Nonlinear bending theory of sandwich plates with orthotropic layers 19 p3342 A67-35716

Dynamic identification of loop system consisting of square-law operator, with behavior function of input signal and initial conditions 19 p3206 A67-35916

Nonlinear analysis of earth-moon system motion stability in three dimensions near L4 libration point when perturbed by sun 19 p3328 A67-35962

Nonlinear resonant coupling between damped and undamped vibrations for damping roll in TRAAC and elastic dumbbell satellites [AIAA PAPER 67-568] 19 p3329 A67-35964

Parameter optimization by modified sequential random perturbation technique using hybrid computer, considering initial conditions and analog computer errors effect, for dynamic systems 19 p3188 A67-36058

Nonlinear circuits analyzed by Monte Carlo method for computer synthesis 20 p3407 A67-36331

State space equations formulated for general class of nonlinear networks, deriving block diagram of relationships 20 p3407 A67-36332

Optimum output-input characteristic of memoryless nonlinear system determined from solution of integral equation 20 p3407 A67-36382

Valentine method for maximum principle problem solution, reducing to nonlinear differential equation system with special boundary conditions 20 p3477 A67-37029

Input signal level for stability loss or self-oscillations automatic control in system, using analysis for nonlinear systems with forced vibrations 20 p3408 A67-37041

Maximum probability criterion on output coordinates of system for selection of

parameters of optimal nonlinear control system 20 p3408 A67-37042

Stability of periodic solution of nonlinear systems with coefficients dependent on amplitude and frequency 20 p3408 A67-37043

Statistical linearization of nonsingle valued nonlinearities considered as multidimensional inertialess functions of dependent variables 20 p3408 A67-37073

Bridge circuits with nonlinear resistances, calculating statistical characteristics by graphical method for functional transformer 20 p3451 A67-37151

Oscillation index in qualitative assessment of equilibrium converging processes in nonlinear systems 20 p3409 A67-37200

Sufficient conditions for statistical stability of motion in nonlinear systems 20 p3409 A67-37225

Necessary condition for optimal control in nonlinear automatic control system determined, using method of successive approximations 20 p3410 A67-37229

Suboptimal controller generating linear combination of state coordinates shown to give optimal performance when using linear controller preceding relay 20 p3410 A67-37251

Second order nonlinear optimal control system for various performance criteria using Pontryagin principle 20 p3410 A67-37252

He-Ne laser light intensity distribution cumulants for nonlinear oscillation threshold operation 20 p3461 A67-37289

Nonlinear fluid mechanical systems design using numerical least squares method in fitting second order differential equation to straight line approximation of state variable 20 p3366 A67-37368

Numerical methods for linear optimal control problems, noting applicability of algorithms to certain nonlinear problems 20 p3411 A67-37375

Nonlinear automatic control systems characteristics analyzed for various possible error accumulations 20 p3412 A67-37382

Thermodynamics of nonlinear materials with internal state variables, analyzing evolution equation, dynamic stability, dissipation, etc 20 p3555 A67-37563

Corrective force selection for bringing nonlinear discrete system to predetermined phase space point in fixed instant of time 20 p3487 A67-37659

Nonlinear elastic anisotropic wedge deformation for short time loading moment applied to apex, approximating stress function 20 p3542 A67-37680

Asymptotic series in theory of nonlinear systems of ordinary differential equations 20 p3479 A67-37718

Estimates for solutions to nonlinear boundary value problems for second order differential equation 20 p3479 A67-37719

Almost periodicity of bounded solutions to nonlinear systems in n-dimensional Euclidean space 20 p3479 A67-37726

Dynamic flight stability characteristics of 5 inch projectile with nonlinear Magnus moment, noting Mach number, wind tunnel data, etc 21 p3563 A67-37805

Deflection and stresses in corrugated diaphragm rigidly clamped on contour with distributed pressure and concentrated central force, using finite difference approximation 21 p3717 A67-37977

Nonresonant third order dielectric susceptibility coefficients of gases measured in four-wave mixing experiment to calculate harmonic radiation in laser beam 21 p3639 A67-38008

Dynamic theory of vibration damping by controlled impact in forced oscillations in two-mass nonlinear system 21 p3720 A67-38284

Nonlinear equilibrium equation system derived for shells of revolution, considering shell stability 21 p3721 A67-38304

Nonlinear mechanical model with mathematical pendulums for solid bodies containing nonlinearly oscillating liquid in motion 21 p3612 A67-38307

Advances in control systems, Theory and applications Volume 5, covering optimal control and optimization advances in control systems, Theory and applications, Volume 5, covering optimal control 21 p3603 A67-38438

Steady state plant performance optimization for unknown dynamic characteristics, determining periodic input signal 21 p3603 A67-38439

Polygonal approximation method for systems with nonlinear characteristics analyzed using continuous functions 21 p3657 A67-38551

Optimal control for nonlinear dynamic systems with/without invariant properties investigated for departures from optimal motion 21 p3656 A67-38586

Electromagnetic wave focusing in nonlinear medium with small nonlinear polarizability 21 p3670 A67-38684

Computer program based on tracking function method setup for investigating nonlinear second order autonomous system stability and boundedness 21 p3604 A67-39076

Invariance principle proposed for controller analytical design for nonlinear invariant systems by reducing problem to quasi-linear problem 21 p3604 A67-39111

Wave correlation evolution in uniformly turbulent weakly nonlinear systems 22 p3843 A67-39267

Quasi-periodic solutions of nonlinear systems of differential equations containing small parameter 22 p3827 A67-39304

Magnus version of first harmonic approximation method for nonlinear systems engineering, using analog computer simulation for accuracy examination 22 p3776 A67-39327

Subharmonic and summed and differential harmonic oscillations in multiple-degree-of-freedom system with asymmetric nonlinear spring characteristics, studying stability 22 p3910 A67-39408

Nonlinear theory of longitudinal plasma waves, formulating distribution function and Maxwell equation for electric field 22 p3845 A67-39421

Stability and response time of quantified pulse-position modulation feedback control circuit consisting of nonlinear sampler and first order continuous part 22 p3776 A67-39647

Maximum stresses with changes in Poisson ratio for thin parallelogramic panels with nonlinear behavior 22 p3911 A67-39666

Problem solving method based on averaging over periodic functions for steady waves in nonlinear one-dimensional distributed systems, deriving approximate equations 22 p3815 A67-39761

Standing waves in hot plasma traversed by quasi-neutral charged particle flux including numerical analysis of elongated wave occurrences 22 p3853 A67-40124

Forced resonant nonlinear oscillation of liquid in cylindrical tank 22 p3787 A67-40192

Optical properties of new and stable nonlinear optical ferroelectric potassium lithium niobate single crystal 22 p3863 A67-40236

Modulated signal nonlinear distortions from AC-system resulting from system components nonlinearities 22 p3763 A67-40478

Elliptically polarized electromagnetic wave propagation in homogeneous infinite plasma, solving Vlasov equations of nonlinear theory by successive approximation 23 p4030 A67-40597

Nonlinear system suboptimal feedback control technique based on method for determining approximate solutions for Hamilton-Jacobi-Bellman equation 23 p3983 A67-40645

Nonlinear problems of parametric excitation of rings solved by equations, considering normally and centrally directed pressures 23 p4074 A67-40651

Differential equations maximum parameter values for single mass nonlinear system passage through resonance point determined with approximate methods based on small parameter method 23 p4026 A67-40686

Laser light production and properties based on quantum mechanical equations, describing nonlinear interaction radiation and matter 23 p4011 A67-40761

Methods of increasing rate of convergence in convergence processes for improper integral of first kind 23 p4022 A67-40861

Popov method extension for absolute stability of nonlinear feedback systems containing distributed elements 23 p3984 A67-40870

Stability analysis of two-dimensional nonlinear multivariable systems with nonlinearities, finding limit cycle of symmetric and antisymmetric cases from characteristic equations 23 p3984 A67-41160

Nonlinear steady motions produced by

stable stratification in rapidly rotating fluid, discussing Ekman layers 23 p3990 A67-41170

Explicit nonlinear numerical integration method for solution of large systems of ordinary differential equations 23 p4024 A67-41394

Inverse problem of synthesizing optimum control for nonlinear systems 23 p3985 A67-41672

Nonlinear sampled data system instability, discussing arbitrary single-valued nonlinearities and arbitrary modulation law /PAM, PWM or PFM/ 23 p3985 A67-41674

Matrix version of Kalman-Yacubovich lemma for deriving stability conditions for continuous time dynamical systems with m-feedback nonlinearities 23 p3985 A67-41726

Light beam self-focusing, discussing electromagnetic interaction in nonlinear medium, refractive index dependence on wave intensity and geometrical optics 24 p4187 A67-41770

Book on nonlinear theory of thin shells covering deformation and stress state, surface kinetics, momentum conservation, etc 24 p4246 A67-41800

Nonlinear ferrite diaphragms in waveguides, discussing magnetic field effect on cavity tuning 24 p4119 A67-41972

Integral pulse FM effect on feedback control, obtaining stability of equivalent nonlinear discrete system 24 p4135 A67-42182

Bounded-input bounded-output stability on nonlinear time varying discrete control system using Liapunov function 24 p4135 A67-42183

Transient behavior of autonomous nonlinear control system phase space domains, finding relative stability domains for special time dependent Liapunov function 24 p4135 A67-42186

Stability of feedback systems containing single odd monotonic nonlinearity 24 p4136 A67-42187

Laser emission nonlinear effects for materials with internal induced absorption noting pulse elongation and spatial smoothing 24 p4168 A67-42370

Book on stability of nonlinear mechanical systems covering qualitative methods, one degree of freedom systems, etc 24 p4188 A67-42375

Asynchronous finite state sequential nonlinear controller synthesis with few flip-flops for dynamic space vehicle systems [AIAA PAPER 87-988] 24 p4127 A67-43060

Synergetic approach to problems of nonlinear dispersive wave propagation interaction 24 p4125 A67-43093

NONLINEARITY

SA LINEARITY

SA VOLTERRA EQUATION

Analytic performance calculation for varactor frequency doubler with various degrees of nonlinearity 01 p0040 A67-11234

Artificial nonlinearization method of solving linear second order equations with variable coefficients, with application to two-dimensional electromagnetic propagation along inhomogeneous dielectric layers 02 p0191 A67-11572

Dynamic behavior of electric angle drive unit in linear automatic control system, noting nonlinearities 02 p0227 A67-12197

Optical nonlinearities due to conduction band electrons in InAs, InSb, GaAs and PbTe studied, using Q-switched carbon dioxide laser radiation 02 p0254 A67-12524

Impedance matching conditions, gain nonlinearity and bistable mode instability in solid state parametric frequency converters 03 p0381 A67-13637

Quantum study of optical nonlinearities in absorbing materials, energy transfer between optical waves, laws of nonlinear reflection and coherence effects 04 p0657 A67-14881

Probability density of oscillating system with piecewise-linear characteristic under action of exponentially correlated random force 05 p0844 A67-18014

Stability and asymptotic stability of control systems with multiple nonlinearities and inputs, using frequency criterion in connection with transfer function 06 p0973 A67-17601

Resonance transition of hinged ponderable rod with nonlinear supports 06 p1109 A67-18666

Electric field induced optical refractivity changes /Franz-Keldysh effect/ and nonlinear light scattering, light beam

deflection and modulation in neutron-irradiated Si at 95 degrees K 07 p1231 A67-19487

Self-focusing of longitudinal electromagnetic waves in nonlinear plasma in strong magnetic field 08 p1357 A67-20822

Nonlinearity caused by relativistic mass effect leading to radiation maxima of plasma excited by two pulses at electron gyrofrequency 11 p1827 A67-23889

System with two nonlinearities separated by high pass filter, obtaining joint describing function 11 p1760 A67-24275

Nonlinear correction method for determining orbital parameters of space vehicle, using residuals and least squares technique 14 p2384 A67-28127

Linearization of oscillation differential equations containing even nonlinearities, using asymptotic polynomials 14 p2344 A67-28810

Boundary conditions influence on flutter critical boundary character considering nonlinearities of physical nature 18 p2776 A67-31471

Asymptotic stability criterion for autonomous feedback system with single odd monotonic nonlinearity, using functional analysis 18 p2646 A67-31639

Finite amplitude elastic wave motions with only constitutive nonlinearities 20 p3540 A67-37282

Nonlinearity of unsteady gasdynamic processes in internal combustion engine exhaust systems, using unsteady sources and sinks 21 p3689 A67-38044

Multivariable Popov criterion application to stable and to state feedback law linear finite-dimensional systems, noting toleration of nonlinearities 23 p3984 A67-41158

Stability analysis of two-dimensional nonlinear multivariable systems with nonlinearities, finding limit cycle of symmetric and antisymmetric cases from characteristic equations 23 p3984 A67-41160

Photographic film nonlinearities effect in holographic recording of coherent wavefront using two-beam interferometry, describing phenomenological model 23 p4002 A67-41269

NONMETAL

SA CERAMICS

SA METAL

SA PLASTIC MATERIAL

Spectral emittance of metallic and nonmetallic materials, discussing surface roughness effects [AIAA PAPER 85-875] 03 p0467 A67-13042

Powdered and fired ceramic materials 03 p0449 A67-13199

UVFD-1 ultrasonic velocimetric flow detector for inspection of nonmetallic laminated structures and products 09 p1502 A67-22096

Combining two or more nonmetallic substances noting applications of fiber reinforced, particulate filled and laminated composites 10 p1871 A67-23013

Resonance transition probabilities in intermediate coupling for some neutral nonmetals, noting radiative lifetime measurements by phase shift 12 p1968 A67-26246

Gemini window contamination due to outgassing of silicones 15 p2507 A67-29555

Surface ionization of atoms and molecules on nonmetals, determining work functions and activation energies for dissociation 19 p3284 A67-35083

NONOHMIC EFFECT

Current-voltage characteristics peculiarities of fine cadmium sulfide single crystals with nonohmic contacts 02 p0296 A67-11831

Optical phonons role in determining form of free carrier distribution function in semiconductors and nonohmic behavior of strongly piezoelectric crystals 06 p1065 A67-18952

Nonohmic electrical conduction of semiconducting thin films in strong electric fields analyzed using electron temperature approximation 20 p3506 A67-36219

N-type InSb hot electron and nonohmic effects, noting low temperature and magnetic and electric field dependence of Hall coefficient and resistivity 21 p3683 A67-38405

NONUNIFORM MAGNETIC FIELD

Motion of plasma through nonuniform transverse magnetic field, noting dependency of plasma motion solely on field

intensity 02 p0278 A67-12623

Motion of plasma through nonuniform transverse magnetic field, noting dependency of plasma motion solely on field intensity 13 p2170 A67-27379

Plasma finite orbits instability due to plasma particle shift, discussing collision frequency role 19 p3287 A67-34896

Transverse magnetic field retardation of flowing plasma in electromagnetic shock tube noting conductivity 20 p3496 A67-36214

Effect of energy redistribution between ion and electron components of plasma flow in nonuniform magnetic field, deriving relativistic and polarization corrections to classical theory 20 p3500 A67-37050

Plasma stability in nonuniformly oriented magnetic field at guiding center limit 22 p3848 A67-39688

Variations in parameters of magnetized plasmoids interacting in nonuniform fields determined by magnetic and electric probes 23 p4035 A67-41885

Demagnetizing fields in thin magnetic films, considering saturation, film thickness and anisotropy 24 p4204 A67-42338

NONUNIFORM PLASMA

Temperature-dependent wave propagation in slightly inhomogeneous hot nonuniform plasma, examining positive column of mercury vapor discharge 02 p0193 A67-11782

Longitudinal and transverse waves transformation in nonuniform plasma 04 p0668 A67-15276

Oscillations of nonuniform plasma column 04 p0668 A67-15278

Conductivity of plasma capacitors in inhomogeneous plasma found to increase with frequency due to density gradient and resonance 12 p1969 A67-25194

Laser beam acceleration of inhomogeneous plasma by imparting high energies to oncoming ions 12 p1969 A67-25198

Flute oscillations in bounded nonuniform plasmas and effect of incoherently precessing ions, noting variational methods and perturbation analysis 14 p2360 A67-28555

Effective conductivity tensor of nonhomogeneous plasma in homogeneous external magnetic field 16 p2711 A67-30539

Drift instabilities in nonuniform collision-free plasma stabilized by magnetic shear noting longitudinal currents, electron and ion temperature gradients, etc 16 p2718 A67-31226

Electromagnetic wave propagation in nonuniformly magnetized plasma with wave frequency near second electron cyclotron harmonic 22 p3843 A67-39263

Resonant particle diffusion of nonuniform plasma across magnetic field, calculating transport coefficients 22 p3848 A67-39687

Electromagnetic wave absorption and transformation in resonant layer of nonuniform plasma at oblique incidence 24 p4119 A67-42071

NONVISCOUS FLOW

Hydrodynamic stability Cauchy problem for continuous spectrum of two-dimensional parallel flow of nonviscous incompressible fluid 03 p0402 A67-13172

Rayleigh problem in hydrodynamic stability for two-dimensional parallel flow of nonviscous incompressible fluid 13 p2106 A67-27456

Longitudinal wall curvature effect on boundary layer flow stability and generalization of Rayleigh theorems for nonviscous instability 23 p3992 A67-41733

NORMAL DISTRIBUTION

Counting errors and amplitude spectra distortion in detectors for statistical characteristics of information contained in signals 01 p0066 A67-10653

Curves of probability of detection vs signal to noise ratio for log-normal signals in Gaussian noise, considering correlated and uncorrelated signals 07 p1144 A67-19868

Structural reliability determined when stress and strength distributions are described by normal statistical distribution 09 p1575 A67-22298

Amplitude distributions of solar photospheric fluctuations 10 p1711 A67-23795

Static magnetic field effect on normal distribution of pressure, temperature and density in solar atmosphere, considering sunspots and velocity field effects [AFCLR-86-679] 13 p2204 A67-27435

Computer method analysis of electron temperature and density behavior on basis

of glow discharge for plasma electron balance equation solution 14 p2353 A67-27755

Sensitivity tests required to verify nonnormality in sample population, studied by computer simulation techniques 16 p2634 A67-31525

Random variables generation in computer, explaining procedure for beta and chi-square variates and normal distribution 19 p3188 A67-36056

ELF waveforms spectral estimation at discrete frequencies of each polarity used for statistical comparison of mean spectra show normal distribution 22 p3789 A67-39474

Asymmetry and peakedness variation from normal distribution of random process at output of linear filter matched with broadband PM and PPM signal 22 p3761 A67-39868

NORMAL FORCE DISTRIBUTION

Discrete method strength calculation for round cylindrical shells applicable to computer solution of normal external loading problems 02 p0339 A67-12442

Normal force and pitching moment values for interference on body, wing and overall body-wing obtained, using pressure distribution integration 04 p0545 A67-14439

Asymptotic and particular solutions of conical shells subjected to lateral normal loads, discussing membrane forces, bending effects and boundary conditions for moments and shearing 09 p1573 A67-21754

Displacement and stress distribution in shallow spherical shell under concentrated loads including normal force, tangential force and bending 21 p3730 A67-39087

NORMAL SHOCK WAVE

Solid particle drag, convective heat transfer and ablation effects on structure of normal shock wave in nonreacting mixture of gas and ablating dust, using Runge-Kutta integration 08 p1427 A67-21120

Normal shock relations in adiabatic constant area ducts used to connect properties on two sides of shock in steady one-dimensional flow 15 p2470 A67-29441

Fundamental relations for normal shock wave behavior in compressible fluid for classical and hydromagnetic cases 15 p2473 A67-30226

Oblique, normal and transverse ionizing shock waves 18 p3092 A67-34733

NORTH AFRICA

SA EGYPT

Geodetic linking of France and North Africa by synchronous photographs of Echo I satellite 07 p1176 A67-19767

NORTH AMERICA

Polarization measurements and noctilucent cloud observation over North America 02 p0239 A67-12534

NORTH AMERICAN MILITARY AIRCRAFT

S X-15 AIRCRAFT

S XB-70 AIRCRAFT

NORTHERN HEMISPHERE

Northern Hemisphere synoptic auroral charts on polar projection 02 p0238 A67-12035

Interdiurnal temperature variability distribution in northern hemispheric stratosphere in January and July, based on synoptic weather maps 04 p0816 A67-15473

Critical ionization frequencies in F-2 layer in near-polar region observed at Northern Hemisphere high latitude 07 p1179 A67-19832

Northern Hemispheric mean meridional circulation determined, using angular momentum and continuity equations 09 p1490 A67-21549

Normal distributions of various quantities related to radiation budgets of tropospheric column, earth surface and troposphere-earth system over Northern Hemisphere 13 p2116 A67-27458

Vertical distribution of heating rate by radiative processes over Northern Hemisphere presented in zonal cross sections 13 p2116 A67-27459

Solar activity cycle effect on northern hemisphere pressure field solar activity cycle effect on Northern Hemisphere pressure field 13 p2117 A67-27632

Seasonal and latitudinal magnetic activity variations in Northern Hemisphere, investigating time-space characteristics of K index 14 p2309 A67-27943

Geostrophic wind angular momentum transport at 500 mb in Northern

Hemisphere, using zonal harmonic analysis, noting quasi-biennial cycle 15 p2512 A67-29201

Zonal and meridional distributions of 5-day averaged outgoing long wave radiation and relation to Northern Hemisphere circulation 17 p2879 A67-32548

Quasi-biennial oscillation in ozone in northern Hemisphere harmonically analyzed 19 p3225 A67-35921

NORTHROP MILITARY AIRCRAFT

S F-5 AIRCRAFT

NOSE CONE

SA ABLATING NOSE CONE

SA ROCKET NOSE CONE

Nonaxisymmetric nose section of bodies of revolution having minimum drag at high supersonic speed 06 p0936 A67-17737

Diamant third stage and nose cone 07 p1258 A67-19522

Behavior of metals, graphites and reinforced plastics for reentry nose cones tested, using rocket engine exhaust flame as heat source 10 p1698 A67-23480

These nose cones in supersonic flight, calculating aerodynamic coefficients from trajectory and flight phases 13 p2051 A67-27291

Short conical spiral antennas for trajectory plotting of small nose cones 14 p2279 A67-27900

Pressure measurement at stagnation point of cylindrical missile with spherical nose cone during free flight in ballistic testing 16 p2593 A67-31123

Bluntness influence on nose cone heating in laminar flow in supersonic flight investigated to determine optimum design of rocket or space vehicle nose 20 p3359 A67-37185

Static pressure probe nose derived from supersonic slender body theory and shaped for subsonic speeds 21 p3564 A67-38535

Nose bluntness and cone angle effects on base pressure and heating in laminar hypersonic flow regime, using free flight telemetry technique 21 p3565 A67-38882

Dynamic destabilization for hypersonic flow around slender cone with severely blunt nose analyzed by blast wave analogy 22 p3742 A67-40109

NOTCH

SA PARABOLIC NOTCH

Notch steepness of open circuit transfer function of loaded exponentially tapered RC notch filter 01 p0041 A67-11317

Plastic yielding effect on stress and deformation of edge notch subject to longitudinal shearing stress 03 p0523 A67-13469

Thickness effect on fatigue crack propagation in notched clad sheet under cyclic tensile loading and transition from tensile fracture mode to shear mode 03 p0532 A67-14386

Elastic-plastic torsion of shafts with hyperbolic notches solved for Ramberg-Osgood and bilinear stress-strain curve 04 p0627 A67-14977

Antennas featuring steerable notch in omnidirectional pattern as alternative to narrow beam antenna for certain applications 16 p2638 A67-31335

NOTCH SENSITIVITY

Plastic flow of axially symmetric notched bars pulled in tension, obtaining load factors 01 p0159 A67-10401

Titanium alloy forging tests covering notched tension, compression, shear, bearing, fracture toughness and smooth and axial fatigue 03 p0446 A67-13552

Forging and solution treating nickel-chromium alloy 718 to investigate notch ductility and uniform grain size 04 p0640 A67-15459

Aluminum content effect on stress-rupture properties of chromium-molybdenum-vanadium steel, noting notch sensitivity and ductility 16 p2693 A67-31869

Mechanical properties of titanium alloys at room and cryogenic temperatures 17 p2873 A67-32768

Mechanical properties of welded junctions of rolled sheets of aluminum alloys at room and cryogenic temperatures 17 p2873 A67-32769

Tensile properties of fiber-reinforced metals, discussing failure at notch root 20 p3464 A67-36417

NOTCH STRENGTH

Stress concentration in annular rotor with

notch /or crack/ on inner surface, using integral equation 01 p0159 A67-10276

Design strength of plane notched elements under single mode vibration, obtaining equation for fatigue stress concentration factor 05 p0919 A67-16592

Macroscopic brittle fracture theory for structural microheterogeneities effect on maximum macrostresses in plates with hyperbolic notches under tensile loads 06 p1100 A67-17950

Stresses in elastic half-plane with rectilinear notch 06 p1101 A67-18181

Power series technique applied to single edge notches in semiinfinite region in plane elasticity problems, using mapping function and Muskhelishvili theory 08 p1414 A67-20347

Stress concentration factors for two circular notches of variable radius and position superposed at edges of strip 09 p1574 A67-21839

Plane notch stresses in viscoelastic materials with equations obtained from three-dimensional elasticity theory 10 p1720 A67-23578

Stress concentration factor role in evaluating notch toughness of aluminum alloy 13 p2220 A67-27185

Notch toughness of some aluminum alloy castings at cryogenic temperatures 13 p2221 A67-27672

Effect of drilled holes on notch toughness of iron alloys, noting impact and slow bending testing, notch toughness improvement, etc 16 p2688 A67-31304

Stress analysis of semiinfinite plate containing reinforced notch on one side under uniform tension 17 p2961 A67-32777

Loading frequency influence on endurance characteristics of V95 aluminum alloy notched for stress concentration 21 p3644 A67-38051

Notch stress theory, discussing mapping function and elliptic integral solutions 22 p3913 A67-40004

Stress distribution in shear-strained Cosserat prism containing deep notch 22 p3913 A67-40005

Elastic strain energy change rate as related to notch depth considered for edge notches with finite radius 23 p4074 A67-40664

Tensile properties and notch toughness of aluminum alloy sheet and welded joints evaluated at room and subzero temperatures 23 p4020 A67-41348

NOTCHED METAL

Continuity gauge measurement of crack growth on flat and curved surfaces at cryogenic temperatures 01 p0102 A67-11028

Stress-strain state in elastoplastic range of notched Duralumin strip studied by photoelastic coatings 12 p2032 A67-26105

Cycles required to start crack, and cycles for crack propagation to failure estimated for notched specimen 16 p2771 A67-31297

Fatigue crack growth rates in metals under random loading correlated to cyclic load tests 16 p2774 A67-31320

Cumulative fatigue at root of circular notch of coupon type aluminum alloy specimens subjected to low cycle compression-tension strains 17 p2957 A67-32028

Elastic strain energy change rate as related to notch depth considered for edge notches with finite radius 23 p4074 A67-40664

Transient displacement and strain distributions in fracturing notched magnesium plate, using moire-fringe technique and Q-spoiled laser 23 p4076 A67-40736

NOTCHED STEEL

Fatigue strength of smooth and notched steel samples subject to bending in single plane, discussing effect of form of stress cycle on failure rate 05 p0923 A67-17181

NOVA

SA SUPERNOVA

Optical identification of position of X-ray astronomical source Sco X-1, noting similarity of certain properties with old novae 02 p0324 A67-11772

NOVA OUTBURST

X-ray emission from old novae noting possibility that hot coronas may arise from vibration 02 p0308 A67-12032

Thermonuclear reactions occurring in supernova shock wave propagating through stellar envelope 18 p3136 A67-34726

Novae and supernovae outbursts, suggesting mechanism which can account for

both phenomena and for other problems
concerned with quasi-stellar sources
/quasars/ 24 p4231 A67-42451

NOZZLE

SA ANNUAL NOZZLE
SA CONICAL NOZZLE
SA CONVERGENT-DIVERGENT NOZZLE
SA CONVERGENT NOZZLE
SA DE LAVAL NOZZLE
SA DIVERGENT NOZZLE
SA EXHAUST NOZZLE
SA HYPERSONIC NOZZLE
SA JET NOZZLE
SA ROCKET NOZZLE
SA SONIC NOZZLE
SA SPIKE NOZZLE
SA SUPERSONIC NOZZLE
SA TURBINE NOZZLE
SA WIND TUNNEL NOZZLE

Irregularly spaced nozzle vanes effect
upon blade vibration in radial flow gas
turbine
[ASME PAPER 67-VIBR-42] 11 p1797 A67-24195

NOZZLE EFFICIENCY

Method for matching jet engine intake and
ejector pumping characteristics to evaluate
static and in-flight performance of air-
augmented nozzles, considering external
aerodynamics influence
[AIAA PAPER 65-596] 03 p0350 A67-12903
Space simulator application to
development of space rocket propulsion
systems, examining test problems of low
pressure space engines
[AIAA PAPER 67-257] 07 p1164 A67-20052
Thrust chamber nozzle performance
degradation with energy release and
expansion ratio 13 p2188 A67-26847
Simulation of dynamic performance of
pneumatic rebound-nozzle signal converters
by analog computer 13 p2056 A67-27240
Prediction of large rocket nozzle material
performance using semiempirical technique,
noting mathematical models for internal and
external heat and mass transfer
15 p2547 A67-29993
Multiple exhaust nozzles for advanced
nuclear rocket engines noting design and
performance prediction procedures
22 p3834 A67-40160

NOZZLE EXPANSION

Optimum nozzle contours for expansion of
Lighthill idealized dissociating gas in one-
dimensional flow determined by methods of
variational calculus 02 p0305 A67-12353
Source flow expansion of partially ionized
gas into vacuum for predicting flow
properties of low density free jet plasma
expansions
[AIAA PAPER 67-99] 06 p1041 A67-18281
Minimization of MHD generator duct with
fixed boundary values as criterion in
determining expansion shape
09 p1443 A67-21801
Large scale expansion nozzle control by
heterogeneous nucleation and mercury vapor
and drop growth processes in nitrogen flow
[AIAA PAPER 66-85] 10 p1733 A67-23125
Thrust chamber nozzle performance
degradation with energy release and
expansion ratio 13 p2188 A67-26847
Hydraulic analog for qualitative analysis of
flow field of expansion-deflection
nozzle 14 p2297 A67-28136
Air gauge circuit analysis extended to
fluidic restrictor circuits and complex
resistor circuits, using Bernoulli and
continuity equations 14 p2252 A67-28353
Jet reattachment for inclined walls at low
Reynolds numbers and moderate nozzle
aspect ratios
[ASME PAPER 67-FE-25] 14 p2305 A67-28369
Two-dimensional expansion-deflection
nozzle studied for internal pressure
distribution and resultant thrust
determination 14 p2244 A67-29050
Air condensation in hypersonic wind
tunnel strongly related to flow expansion
rate 16 p2657 A67-30708
Ionization of low temperature supersonic
plasma jets, noting kinetics of elementary
processes, gas dynamic parameters and
effects of combustion and alkali metal
admixture 17 p2896 A67-32170
Kinetics of coupled atomic recombination
and vibrational de-excitation in continuously
expanding gas flow 18 p3081 A67-33781
Axial electron density profile in weakly
ionized seeded argon plasma expanding
through supersonic nozzle determined

experimentally using microwave
interferometer
[AIAA PAPER 67-704] 21 p3672 A67-38731
Limiting driven conditions corresponding
to optimum expansion and low density shock
tube flow for overexpanded
nozzle 21 p3609 A67-38886

NOZZLE FLOW

Flow field about subsonic jet exhausting
into quiescent and low velocity air stream
[AIAA PAPER 65-704] 01 p0055 A67-11254
Centrifugal pump with vapor core
principle combined with spill nozzle for
application to aero engine fuel and reheat
systems 01 p0014 A67-11267
Plasma effects in nozzle flow of
hypersonic shock tunnel using air, obtaining
electron density profile 01 p0126 A67-11442
Supersonic jet from finite length nozzle in
supersonic stream at angle of attack,
analyzing flow characteristics by using
linearized theory 02 p0177 A67-11523
Reynolds number effects and initial
conditions effects on development of free
shear in mixing layer from constant area
nozzle 02 p0231 A67-11559
Transonic plane gas flow equations with
algebraic self-similar solutions used for
analysis of flow in various
nozzles 02 p0178 A67-11951
Gas flow of two-phase medium in Laval
nozzle in presence of small particle lags in
velocity and temperature in one-dimensional
formulation 03 p0349 A67-12865
Two-dimensional nonvortical shock-wave
gas flow through Laval
nozzle 03 p0350 A67-12886
Hypersonic low density wind tunnel for
high Mach numbers and stagnation
temperatures, analyzing measurements made,
noting heater, nozzle, diffuser,
etc 04 p0595 A67-14561
Nozzle exhaust plumes of rockets or
supersonic ramjets with diffusion flames as
source of UV radiation 04 p0721 A67-14702
Experimental data compared to theory for
expansion of high temperature air in
equilibrium and nonequilibrium flow through
Mach number 10 contoured nozzle
[AIAA PAPER 66-2] 05 p0750 A67-17340
Reacting gas flow in nozzle in one-
dimensional formulation taking into account
nonequilibrium course of chemical
reactions 06 p0935 A67-17726
Thermodynamic flow analysis of feasibility
of coolant gas addition to nozzle flow for
improved particle formation efficiency in
mixed flow colloid thruster
[AIAA PAPER 67-85] 06 p0941 A67-18500
Three-dimensional internal flows in
intakes and exhaust nozzles computed by
combined characteristics and finite
difference method
[AIAA PAPER 67-224] 06 p0942 A67-18516
Laval nozzle configuration for sharply
bounded carbon dioxide jet in
vacuum 06 p0943 A67-18781
Dissociational rate constants and
vibrational relaxation times modifications,
considering coupling of vibrational and
dissociational nonequilibrium of expanding
gas in nozzle
[AIAA PAPER 66-520] 06 p0992 A67-18851
Approximate analysis of subsonic
compressible flow in annular nozzle of short
duct fan engines and inner wall curvature
effect on pressure distributions
06 p0944 A67-18871
Nonconventional rocket propulsion systems
performance and base environment
characteristics evaluated, using separate cold
flow and combustion models
[AIAA PAPER 67-256] 07 p1241 A67-20072
Nonequilibrium ionization of gas-solid
suspension expanding supersonically in
nozzle as function of charge
distribution 07 p1227 A67-20258
Boundary layer transition measurements of
contoured nozzle flow at hypersonic Mach
numbers 08 p1320 A67-20584
Oscillatory isentropic flow through nozzles
solved numerically, using Tsien proof of
nonsingularity of solution 08 p1375 A67-20775
Heat transfer effect in converging-
diverging nozzle flow, considering polytropic
process 08 p1278 A67-21526
Free molecular flow rate and mass
distributions through various length
cylindrical nozzles 09 p1488 A67-22106
First approximation for
MHD nozzle flows
with end effects 09 p1550 A67-22589

Model for gas particle exhaust flow from
under expanded nozzles 10 p1592 A67-23154
One-dimensional flow through nozzle and
stability of weakly ionized plasma with
induced Hall current 11 p1832 A67-24155
Wind tunnel test program for simulation
of gas-particle rocket exhaust plume,
separated flow around nozzle and base
recirculation
[AIAA PAPER 66-767] 11 p1773 A67-24351
Conducting gas flow in jet in front of
electromagnetic accelerator nozzle exit
region analyzed, giving jet shape and
parameter distribution 11 p1842 A67-24951
Nonstationary gas jet stream formation
following shock wave outflowing from
nozzle, obtaining calculation
method 12 p1929 A67-25674
Expression derived for vibrational
relaxation in recombining expanding nozzle
exhaust gas, assessing effect of chemical
reactions on this mechanism 12 p1929 A67-25755
Mass limiting two-phase flow compared in
straight tube and in
nozzle 13 p2093 A67-26541
Flow in MHD nozzles studied for
hypothetical magnetic interaction parameter
of unity order 13 p2185 A67-26592
Similar solution of compressible laminar
boundary layer equations for Laval nozzle
flow contour 13 p2049 A67-26639
Nozzle thermocouple for low flow rate
measurement of high temperature gases,
discussing calibration curves and taking into
account Reynolds number effect 13 p2121 A67-27464
Hydraulic analog for qualitative analysis of
flow field of expansion-deflection
nozzle 14 p2297 A67-28136
Discharge characteristics of sharp and
round edged orifices in transition regime
noting variation of pressure ratio, magnitude
of Knudsen and Reynolds numbers,
etc 14 p2300 A67-28180
Nonequilibrium aspects of fluid mechanics
of freely expanding jet analyzed, using
aerodynamic molecular beam
system 14 p2301 A67-28184
Intensity and velocity distribution in
molecular beams from nozzle sources,
discussing physical processes responsible for
formation 14 p2301 A67-28186
Electron beam analysis of skimmer
influence on nozzle beam
formation 14 p2301 A67-28187
Apparent mass of supersonic jet stream
under off-design flow conditions 14 p2242 A67-28302
Incompressible fluid flow in convergent
nozzle with finite aspect ratio, predicting
offset on nozzle flow and jet
reattachment 14 p2303 A67-28334
Nonlinear inviscid transonic flow in throat
of two-dimensional curved nozzle, using
approximate method
[ASME PAPER 67-FE-11] 14 p2242 A67-28380
Two-dimensional expansion-deflection
nozzle studied for internal pressure
distribution and resultant thrust
determination 14 p2244 A67-29050
Nozzle type similarity solution to
axisymmetric viscous transonic equation,
describing shock wave development at
nozzle throat 15 p2417 A67-29654
Gas-liquid droplet behavior in geometric
nozzle for constant difference between
phase velocities, determining appropriate
nozzle profile 15 p2472 A67-29777
Supersonic jet expelled from plane nozzle
solved by characteristic method to
determine family of rarefaction waves and
nozzles 16 p2656 A67-30455
Hydrodynamics of liquid-gaseous metal
mixture flowing through nozzles, discussing
heat exchange rate and condensation
effects 16 p2656 A67-30574
Physical parameter determination for
monatomic gas flow based on energy
balance, taking into account heating and
ionization in thermal nonequilibrium 17 p2837 A67-32337
Nozzle and membrane effects on shock
wave intensity in tube, showing graphically
Mach number dependence upon initial
pressure 17 p2837 A67-32345
Boundary layer effect on primary wave
propagation and gas states behind reflected
wave in shock tube with
nozzle 17 p2837 A67-32346
Vectoring and nonvectoring nozzles of

different geometries for lift and lift/cruise engines 17 p2982 A67-32569

Transonic plane gas flow equations with algebraic self-similar solutions used for analysis of flow in various nozzles 17 p2841 A67-33268

Short duration shock tube molecular beam in helium and oxygen, giving test arrangement and data comparisons 17 p2835 A67-33361

Laval nozzle configuration for sharply bounded carbon dioxide jet in vacuum 18 p2982 A67-33723

Book on analysis and design of pneumatic systems covering nozzle flow, transfer functions, root locus, plenum chambers, servoactuator, etc 18 p2988 A67-33754

Stagnation pressure lower than atmospheric pressure in supersonic subatmospheric flow in magnetoaerodynamic generation nozzle, discussing Hall effects for energy conversion process 18 p3020 A67-34122

Liquid hydrogen pumping for Phoebus reactor, discussing feed systems, nozzles, configurations, design, testing, etc [AIAA PAPER 67-478] 18 p3077 A67-34402

Swirl effect on nozzle flow applied to solid propellant nozzles assuming irrotational flow so that tangential velocity field has free vortex characteristics 19 p3311 A67-34826

Oscillations of electric arcs with superimposed gas flow in cylindrical nozzle and rectangular channel, determining critical Reynolds number [DVL-629] 19 p3280 A67-35147

Diffusion of free isothermal turbulent jet of incompressible fluid flowing from nozzle into coaxial surrounding uniform stream 19 p3209 A67-35443

Turbulent boundary layer and heat-transfer coefficients for air in conical nozzles, noting uncooled inlet length and convergence angle effects [ASME PAPER 67-HT-28] 20 p3357 A67-36721

Langley Hypersonic Nitrogen Facility flow evaluation covering pitot pressure survey of nozzle wall boundary layer, centerline and Mach number 21 p3607 A67-37777

Base pressure behind circular projection in Laval nozzles, measuring dependence on specific heat ratio at different Mach numbers by varying gas 22 p3741 A67-40021

Polytropic exponent along axis shown to approach adiabatic exponent at throat of convergent-divergent nozzle 22 p3742 A67-40112

Quasi-cylindrical approximation theory on swirling nozzle flow in relation to spin effect on rocket nozzle performance 22 p3742 A67-40118

Liquid surface tension effect on maximum particle size in two-phase nozzle flow, discussing drag exerted by accelerating gas stream 22 p3787 A67-40225

Optimum blowing angle of gas into supersonic nozzle determined by supersonic wind tunnel investigation of flow interaction 22 p3743 A67-40452

One-dimensional compound-compressible nozzle gas flow theory, discussing choking phenomenon and three-dimensional computer calculations 23 p3927 A67-40603

Shadow photography study of underexpanded nozzle ejected supersonic turbulent jet off-design behavior, discussing static pressure distribution, boundary layer and Mach number effect 23 p3928 A67-40732

Flow coefficient of various nozzles discharging into unbounded atmosphere for wall pressure distribution of potential rotational flow, using rheoelectric tank 23 p3989 A67-41140

Numerical method together with stable difference scheme used to calculate sub-, trans- and supersonic flows in Laval nozzle inverse problem 24 p4091 A67-42180

Approximate single parameter solution for compressible turbulent boundary layer in supersonic diffuser 24 p4144 A67-42586

NOZZLE GEOMETRY

Nozzle wall shape design based on Mach waves generation appearing when supersonic gas expands about corner 03 p0352 A67-13816

Supersonic nozzle producing lift force without downward deflection analyzed by characteristics method 04 p0545 A67-14440

Nozzle submergence loss in solid propellant rocket engine, correlating loss percentage of specific impulse with

dimensionless groups 05 p0875 A67-17366

SST nozzle geometry for high efficiency operation over large exhaust pressure variation 06 p0942 A67-18745

Flow restricting devices, describing basic and special throttles and nozzles 09 p1442 A67-21647

Control of multishaft jet engines, discussing compressor geometry, afterburner and engine fuel flow, nozzle area effects, etc [SAE PAPER 670139] 09 p1559 A67-21770

Extended plug nozzles in suppression of jet noise in small turbojet engines [SAE PAPER 670157] 09 p1561 A67-22544

Starting phenomenon on reversed nozzle and multishock types of supersonic intakes 10 p1590 A67-22918

Nozzle thrust increase through gas flow rotation noting dependence on nozzle length 10 p1590 A67-23027

Optimum thrust nozzle contours for chemically reacting gas flows, obtaining set of partial differential equations for gas dynamic properties [AIAA PAPER 66-638] 10 p1592 A67-23118

Plasmatron jet with vortical air stabilization of arc, correlating jet structure with nozzle geometry and electrode polarity 11 p1832 A67-24027

Optimum geometry for rectilinear diffuser with rectangular, conical or annular cross section noting flow regime, performance characteristics and boundary layer effect 11 p1741 A67-24050

Isentropic compression due to motion of heavy piston in gun tunnel noting nozzle throat effect on motion and stagnation pressure 11 p1773 A67-24577

Rocket nozzle design to reduce gas misalignment noting turning moment, nozzle geometry, cold gas tests, static and flight trials of motors, etc 15 p2547 A67-29995

Third 260-inch diameter solid propellant rocket engine test firing 15 p2548 A67-30150

Stresses due to external forces and moments acting on elastic nonradial circular cylindrical nozzle attached to spherical shell 17 p2959 A67-32409

Vectoring and nonvectoring nozzles of different geometries for lift and lift/cruise engines 17 p2928 A67-32569

Supersonic aircraft nozzle system aerodynamic performance at subsonic speeds [AIAA PAPER 67-452] 18 p2983 A67-33926

Scramjet engine nozzle contours noting expansion-deflection, bell, plug and arbitrary annular nozzles, with optimum nozzle design and computer program for performance prediction [AIAA PAPER 67-453] 18 p2983 A67-33927

Cathode phenomena in plasma thrusters with self-magnetic acceleration low mass-flow rates [DVL-631] 19 p3297 A67-35600

Laval nozzles performance under off-design conditions, noting shock wave formation in region of supersonic velocity 21 p3564 A67-38420

Design, fabrication and performance of 10-millipound resistojets operating on hydrogen or ammonia, describing heat exchanger and nozzle geometry [AIAA PAPER 67-664] 21 p3690 A67-38699

Optimization analysis for axisymmetric rocket motor nozzle design based on assumptions for gas particle flow [AIAA PAPER 66-538] 21 p3565 A67-38875

Nozzle form optimization from Mach distribution in supersonic region, defining perturbation functions 23 p3929 A67-41248

Fluidic digital component design utilizing wave phenomena produced by two interacting low entropy pneumatic jets, discussing nozzle geometry and fluidic oscillators 23 p3936 A67-41421

Efficiency of conical thrust nozzles with various lengths and cone angles, determining optimization coefficient 24 p4093 A67-42922

NOZZLE THRUST COEFFICIENT

Nuclear rockets employing multiple exhaust nozzles, noting performance gain occurring because of high temperature capability of refractory nozzles [AIAA PAPER 66-925] 03 p0466 A67-14135

Nozzle requirements for hypersonic vehicle at transonic conditions, noting results of tests in high velocity wind tunnel 04 p0545 A67-14536

Nozzle thrust increase through gas flow rotation noting dependence on nozzle length 10 p1590 A67-23027

Two-dimensional expansion-deflection nozzle studied for internal pressure distribution and resultant thrust determination 14 p2244 A67-29050

Boundary layer effect on thrust of small rocket engines with high expansion ratio nozzles 16 p2736 A67-30706

Vectoring and nonvectoring nozzles of different geometries for lift and lift/cruise engines 17 p2928 A67-32569

Aerodynamic suckdown results obtained in investigation of VTOL ground-proximity effects 17 p2791 A67-32588

Efficiency of conical thrust nozzles with various lengths and cone angles, determining optimization coefficient 24 p4093 A67-42922

NOZZLE WALL

Nozzle ablations studied based on chemical mechanism, discussing pure on reinforced phenolic resin [ONERA-TP-475] 14 p2404 A67-27896

Shock tunnel experiments with hypersonic turbulent boundary layer flow over flat plates with blunt and sharp leading edges and wall of expansion nozzle 16 p2659 A67-30954

NRX-A REACTOR

S NUCLEAR ENGINE FOR ROCKET VEHICLE /NERVA/

NUCLEAR AIRCRAFT

Future improvements in aeronautical field covering noise control, centralization, TV communication, ultimate speed, sonic boom and nuclear cargo aircraft 22 p3746 A67-39846

NUCLEAR AUXILIARY POWER

SA SNAP PROGRAM

SNAP-8 powered Brayton cycle system for large space stations noting components and overall design 24 p4102 A67-42490

SNAP-8, nuclear electric power-conversion system /PCS/ designed for operation in space, using liquid metals as working fluids 24 p4184 A67-42497

NUCLEAR EFFECT

Solar and galactic low energy cosmic ray nuclear ionizing and interaction effects on meteorite surface isotopic composition, estimating particle fluxes 24 p4210 A67-42634

NUCLEAR-ELECTRIC MOMENT

Polarization of ytterbium isotopes in atomic state using optical pumping with resonance line, calculating magnetic moments 10 p1865 A67-23479

NUCLEAR-ELECTRIC POWER SUPPLY

Apollo-Saturn program automatic checkout systems, discussing ground support equipment facility automation, computer software and checkout technique applications to nuclear electronic systems 20 p3533 A67-36977

Nuclear electric space power plant with Rankine cycle for plausible Mars manned mission, discussing mission requirements and reactor elements 24 p4186 A67-42549

NUCLEAR-ELECTRIC PROPULSION

Space trajectory analysis of nuclear-electric propelled vehicle 13 p2199 A67-27169

Thermionic reactor with uranium diodes core array, describing in-pile reactor uses, arcjet, heat pipe and conceptual design components [AIAA PAPER 67-498] 18 p3076 A67-33962

NUCLEAR EMULSION

Nuclear emulsion measurements of primary cosmic ray alpha particle flux over Hyderabad during high solar activity in 11-year cycle 03 p0506 A67-13720

Energy spectrum of cosmic ray heavy nuclei, using stack of nuclear emulsions exposed during Quiet Sun on balloon flight 04 p0892 A67-14960

Low energy heavy nuclei analyzed by slicing emulsion in connection with solar activity studies 06 p1076 A67-17634

Cosmic ray nuclei observed from satellites and balloons by nuclear emulsions in stacks of plastic sheets 06 p1076 A67-17641

Proton energy spectrum obtained from nuclear emulsion measurements on Gemini IV and V missions 07 p1244 A67-19855

Trapped proton flux data from nuclear photographic emulsions 08 p1378 A67-21472

Primary cosmic ray proton and deuteron flux near geomagnetic equator determined by nuclear emulsion method 10 p1703 A67-23543

He 3 nuclei in low energy primary cosmic radiation determined, using stack of nuclear emulsions 12 p1993 A67-25479

Charge spectrum of heavy cosmic ions of iron group in ionographic emulsions exposed

- in satellite 12 p1999 A67-25829
Radiation doses measured by onboard dosimeters and those fastened to space suits of crews of Voskhod I and Voskhod II compared, noting radiation composition analysis - by means of nuclear emulsions 14 p2256 A67-27863
Fragmentation parameters of multicharge component of heavy cosmic ray nuclei on emulsion hydrogen 17 p2936 A67-32251
Cosmic ray nuclei fragmentation without particle production, noting nuclear emulsions and high energy 17 p2936 A67-32363
Unexpected excess of primary cosmic ray helium nuclei flux value in nuclear photographic emulsions 17 p2939 A67-33237
Ionizing radiation received by biological tissue during space flights measured by nuclear-emulsion 20 p3368 A67-36260
Antiproton abundance upper limit in low energy galactic cosmic radiation determined by exposing nuclear stack to residual atmosphere 20 p3518 A67-36872
Photoemulsion data analysis of high energy nuclear interactions in nuclear emulsions exposed to air showers during flights 24 p4192 A67-42827
Stack of alternating lead layers, nuclear emulsions, X-ray films with graphite cosmic-ray receiving shield on top used for determining distribution in time of events 24 p4217 A67-42832
- NUCLEAR ENERGY**
Data on fragmentation of energy in nuclear reactions in atmospheric showers compared with calculations results for predicted energy 02 p0316 A67-12764
Energy dependence of isotopic composition of primary helium nuclei, considering ionization loss, fragmentation and solar modulation 03 p0505 A67-12956
Average energy of bond between like atoms 06 p0956 A67-18609
Physics and efficiency of direct conversion of heat, light, nuclear, thermonuclear and chemical energy to electrical energy, avoiding mechanical energy 10 p1597 A67-23507
Symmetry principles at high energy - Conference, University of Miami, January 1967 22 p3840 A67-39582
Data on fragmentation of energy in nuclear reactions in atmospheric showers compared with calculations results for predicted energy 22 p3876 A67-40266
Thermoelectric nuclear energy conversion device operating inside reactor fuel element, discussing conversion efficiency 24 p4186 A67-42551
Relativistic particles producing ionization bursts studied for energy spectrum recorded during operation of stack of ionization chambers alternating with lead and graphite layers 24 p4218 A67-42834
Energy flux fluctuation of nuclear active component in extensive air shower stem for given fixed muon and electron numbers 24 p4220 A67-42867
- NUCLEAR ENGINE FOR ROCKET VEHICLE /NERVA/**
Instrumentation and control /I and C/ system for ground test of Nerva propulsion system 03 p0395 A67-13384
Controls and control experimental program for nuclear rocket engine employing hot bleed cycle [AIAA PAPER 66-1005] 03 p0466 A67-14150
Nuclear power and propulsion systems for space applications, discussing present and future technologies [AAS PAPER 67-132] 15 p2516 A67-29967
Twin spool zero-NPSP /net positive suction pressure/ turbopump selected for NERVA rocket after assessing turbopump, engine, vehicle and mission related systems [AIAA PAPER 67-476] 18 p3075 A67-33946
NERVA radiation effects tests at cryogenic temperatures [AIAA PAPER 67-477] 18 p3076 A67-33947
NERVA program, reactor and nonnuclear component development, full-scale testing, engine program, facilities and materials research [AIAA PAPER 67-487] 18 p3076 A67-33953
Ground technology program for nuclear rocket development, discussing NERVA and KIWI programs 18 p3077 A67-34706
NERVA engine development, discussing NRX tests and Phoebus reactor tests for high temperature and power operation 20 p3482 A67-36571
Configuration selection of turbopump for hot-bleed cycle nuclear engine, discussing performance optimization factors 22 p3834 A67-40162
NERVA components including nozzle and associated hot gas bleed port, turbopump, control valve, pressure vessel and thermocouples 22 p3834 A67-40172
Nuclear subsystem controls and instrumentation for NERVA noting automatic startup, override, power and temperature controller 24 p4183 A67-42471
Limiter circuits for NERVA reactor control, discussing design requirements and operation 24 p4183 A67-42472
Nuclear rocket propulsion development, hot test results, one broadband engine configuration and flight stage planning [AIAA PAPER 67-981] 24 p4187 A67-43054
- NUCLEAR EXPLOSION**
SA HIGH ALTITUDE NUCLEAR DETECTION STUDIES /HANDS/ SA STAR FISH PROJECT SA UNDERGROUND NUCLEAR EXPLOSION SA VELA PROJECT
Characteristics of different plasmas produced by nuclear explosions at high altitude on radar systems 04 p0569 A67-14506
Physical pattern of high altitude fission cloud and motion of gamma and beta fission fragments captured by geomagnetic field and observed by Cosmos satellite 07 p1242 A67-19102
Ionospheric disturbances from high altitude nuclear detonations observed as changes in F-2 layer critical frequency 07 p1181 A67-19939
Ionosphere-exosphere system response to bomb-like hydromagnetic source and resultant ground level magnetic fluctuations 07 p1181 A67-19940
Nuclear blast interaction with bow shock of reentry vehicle and effect on structural materials 12 p1929 A67-25730
F layer critical frequency perturbations due to low altitude nuclear explosion 13 p2107 A67-26309
Nuclear explosion effects on radio propagation, noting new ionization in ionosphere and radio signals generation 14 p2266 A67-28417
Radioactivity, using Cs137 isotope as radioactive agent, in civilian Norwegian pilots 15 p2429 A67-29283
Polarization of complex wave form geomagnetic micropulsations of natural and artificial origin, using physical optics 15 p2476 A67-29620
Nuclear explosion effects on atmospheric pressure, electron density, and F-2 layer height, noting dependence on time, season, etc 15 p2478 A67-30087
Strong ionospheric effects observed on ionograms after high altitude detonation including changes in F layer critical frequency, height and spread [AGARDOGRAPH 95] 15 p2484 A67-30306
Artificial red aurora created in southern conjugate region by atmospheric nuclear burst 16 p2664 A67-30977
Emission time history for red 6300 angstrom atmospheric emission from atomic oxygen produced by nuclear explosion 16 p2664 A67-30978
Structure and decay of artificial radiation belt produced by high altitude nuclear explosion 17 p2936 A67-32534
Auroral position, motion and brightness measurements from high altitude nuclear tests in 1962 18 p3036 A67-33603
Afterglows from atmospheric nuclear detonations related to natural airglow and aurora 18 p3036 A67-33604
Optical IR characteristics of long-time afterglow from high altitude nuclear detonations 18 p3036 A67-33605
Propagation anomalies of atmospheric acoustic signals of nuclear explosions due to nonlinearities and refraction effects 22 p3790 A67-39645
Star Fish high altitude nuclear explosion effect on electron loss rate in F-2 region 22 p3793 A67-40082
Nongravitational and splitting effects in comet motion and rotating comet nucleus model, using push-effect hypothesis for post-explosion analysis nongravitational and splitting effects in comet motion and
- rotating comet nucleus model, using 23 p4062 A67-40673
- NUCLEAR FUEL**
SA FUEL ELEMENT SA REACTOR FUEL
Materials technology presently available for advanced Rankine systems including nuclear fuels, refractory metal alloys, electrical materials and stainless steel 07 p1223 A67-19460
Multigroup diffusion theory analysis of gas-core /cavity/ nuclear rocket engine 08 p1352 A67-21196
- NUCLEAR FUSION**
Nuclear fusion, discussing magnetic confinement methods of hot plasma shell holding light nuclei 01 p0124 A67-10778
Pinch effect in containing fusion reaction 03 p0481 A67-13733
Fusion propulsion for interstellar missions, examining requirements for detection of extra solar life 06 p1076 A67-19027
Outlook for controlled nuclear fusion process for industrial power generation, stressing plasma equilibrium preservation through magnetic trapping 11 p1831 A67-24015
Plasma instability as obstacle to controlled nuclear fusion noting causes, effects, forbiddenness phenomenon, etc 11 p1831 A67-24016
Plasma microinstability theory, predicting dangerous instability above critical density, discussing applications to very high temperature plasma experiments 20 p3495 A67-36153
Nuclear fusion control and relativistic high density matter acceleration, discussing amplification effect application to plasma theory, plasma RF confinement and acceleration 22 p3851 A67-39772
Cyclotron instability examined for plasma in magnetic mirror machines with anisotropic nonmonotonic ion distribution in velocity space 22 p3852 A67-39988
- NUCLEAR GYROSCOPE**
Efficient inertial navigation system with He 2 superfluid persistent current gyro element having small drift rate 22 p3808 A67-40395
- NUCLEAR HEAT**
Nuclear heated thermionic converter construction, V-I characteristics and comparison with electrical heating 09 p1451 A67-22359
- NUCLEAR INTERACTION**
Effect of fluctuations on systematic error in determination of energy characteristics of nuclear interactions in photoemulsion in presence of energy threshold 02 p0312 A67-12605
Nuclear cascade process in iron absorber of ionization calorimeter, comparing empirical and experimental values 02 p0248 A67-12747
Intranuclear cascades of nucleon-nucleus interaction calculated on basis of Fermi gas model, using Monte Carlo method and three-dimensional relativistic kinematics 02 p0314 A67-12748
Peripheral nonelastic interactions described, using amplitude characteristics of elastic cosmic ray particle interaction and complex orbital moment technique 02 p0315 A67-12749
Nuclear interaction similarity with Dirac monopole interaction with electromagnetic field, noting equality in number of conservation laws acting in either interaction 02 p0271 A67-12751
Characteristics of transverse pulse produced by secondary particles created in active nuclear particle collision 02 p0271 A67-12752
Angular and energy characteristics of proton beam in pulsed magnetic field, determining probability of proton-neutron charge exchange for proton in forward flight 02 p0271 A67-12753
Ionization calorimeter measurements of energy transmission by photons in cosmic nuclear-active pion and nucleon interactions with various nuclei 02 p0316 A67-12763
Nucleon interaction generating high energy gamma rays, discussing photon and energy spectra of electron photon cascade, pion generation and gamma quantum detection in atmospheric nuclear interactions 02 p0316 A67-12763
Isobaric pions role in interaction between nucleons and pions on one hand and nuclei

- of air atoms on other 02 p0319 A67-12786
 Massive star behavior during final
 catastrophic evolution stages, stressing
 effect of electron type neutrino interactions,
 using numerical hydrodynamics coupled with
 energy transfer methods 03 p0516 A67-14340
 Giant airshower recorder using liquid
 scintillators to record collision of cosmic
 rays with atmospheric
 nuclei 03 p0508 A67-14388
 Lithium interaction with radium induced
 damage in silicon solar cells to produce
 center preserving minority carrier
 lifetime 04 p0556 A67-15703
 Relativistic interaction energies between
 atoms in degenerate states determined,
 using Breit-Pauli
 approximation 05 p0848 A67-16839
 Nucleon radius from pion-nucleon phase
 shift, assuming nucleon is p-wave bound
 state of pion and nucleon, using Gelfand-
 Levitan formalism
 [AIAA PAPER 67-213] 06 p1036 A67-18368
 Exponent in expression relating nuclear
 interaction cross section to atomic weight of
 absorber determined from absorption path
 of nuclear active particles of cosmic
 radiation 06 p1078 A67-18795
 Cosmic ray nucleon interaction with high
 energies, estimating transition probability
 and interaction cross section of baryon in
 passive state 10 p1703 A67-23586
 Energy loss of high energy muons caused
 by nuclear interaction and fluctuation due
 to passage through great thickness of material
 corrected for standard
 rock 10 p1703 A67-23690
 Measurement of quark flux with 2/3
 charge of electron reaching sea level with
 relativistic velocities 11 p1823 A67-24598
 Diffusion of protons and nuclei having
 elastic interactions at 27 GeV/c, using
 probability distribution for events outside
 Gaussian limit of multiple
 scattering 13 p2160 A67-26436
 Transverse-momentum distribution of
 secondaries from high energy nuclear
 interactions in accelerator energy region
 interpreted by statistical
 model 13 p2195 A67-27580
 Nucleon-nucleon collisions, analyzing pair
 production, electromagnetic cascade,
 secondary interactions,
 etc 16 p2703 A67-30965
 Fragmentation parameters of multicharge
 component of heavy cosmic ray nuclei on
 emulsion hydrogen 17 p2936 A67-32251
 Cosmic ray nuclei fragmentation without
 particle production, noting nuclear emulsions
 and high energy 17 p2936 A67-32363
 Exponent in expression relating nuclear
 interaction cross section to atomic weight of
 absorber determined from absorption path
 of nuclear active particles of cosmic
 radiation 18 p3116 A67-34414
 Cosmic ultrahigh-energy heavy nuclei and
 fragmentation products producing multiple
 mesons 20 p3518 A67-37092
 Cosmic ray physics - Conference, Moscow,
 November 1965 22 p3874 A67-40246
 Nuclear cascade process in iron absorber
 of ionization calorimeter, comparing
 empirical and experimental
 values 22 p3801 A67-40249
 Intranuclear cascades of nucleon-nucleus
 interaction calculated on basis of Fermi gas
 model, using Monte Carlo method and three-
 dimensional relativistic
 kinematics 22 p3876 A67-40250
 Peripheral nonelastic interactions
 described, using amplitude characteristics of
 elastic cosmic ray particle interaction and
 complex orbital moment
 technique 22 p3876 A67-40251
 Nuclear interaction similarity with Dirac
 monopole interaction with electromagnetic
 field, noting equality in number of
 conservation laws acting in either
 interaction 22 p3841 A67-40253
 Characteristics of transverse pulse
 produced by secondary particles created in
 active nuclear particle
 collision 22 p3841 A67-40254
 Angular and energy characteristics of
 proton beam in pulsed magnetic field,
 determining probability of proton-neutron
 charge exchange for proton in forward
 flight 22 p3842 A67-40255
 Ionization calorimeter measurements of
 energy transmission by photons in cosmic
 nuclear-active pion and nucleon interactions
 with various nuclei 22 p3876 A67-40263
 Nucleon interaction generating high
 energy gamma rays, discussing photon and
 energy spectra of electron photon cascade,
 pion generation and gamma quantum
 detection in atmospheric nuclear
 interactions 22 p3876 A67-40265
 Isobaric pions role in interaction between
 nucleons and pions on one hand and nuclei
 of air atoms on other 22 p3878 A67-40288
 Reentrant cosmic ray albedo intensity,
 considering nuclear interaction and
 trajectory spiraling
 effects 23 p4050 A67-40808
 Penetrating particles in cosmic radiation
 deep underground in Kolar gold field
 experiment, discussing muon-neutrino
 interaction 24 p4210 A67-42582
 Neutron and proton spectra anomalies
 from proton-nuclei interactions in 100 Mev
 region 24 p4192 A67-42731
 Photoemulsion data analysis of high
 energy nuclear interactions in nuclear
 emulsions exposed to air showers during
 flights 24 p4192 A67-42827
 Shower particles angular distribution
 investigated using Wilson cloud chamber,
 obtaining agreement with results by
 kinematic methods 24 p4217 A67-42828
 Secondary particles angular distribution in
 showers studied with cloud chamber,
 ionization calorimeter and counters to
 identify particles causing shower asymmetry
 and symmetry 24 p4217 A67-42829
 Multiple charged particle production
 process mean characteristics determined for
 several energy levels 24 p4217 A67-42830
 Stack of alternating lead layers, nuclear
 emulsions, X-ray films with graphite cosmic-
 ray receiving shield on top used for
 determining distribution in time of
 events 24 p4217 A67-42832
 Energy fraction transfer to neutral pions
 during interactions with heavy nuclei
 measured for several energy levels, using
 ionization calorimeter 24 p4218 A67-42833
 High energy gamma quanta from high
 energy cosmic particle interaction with
 carbon and air nuclei, noting three
 superhigh energy electron/photon cascades
 recorded 24 p4218 A67-42835
 High energy nucleon interactions with X-
 ray films and nuclear emulsions aboard
 aircraft, with diagram of gamma quanta
 energy spectra 24 p4218 A67-42836
 Characteristic of high energy nucleon-
 nucleus interaction, analyzing changes due to
 structural buildup 24 p4192 A67-42839
 Multiparticle mechanism of cosmic ray-
 atomic nuclei interactions assuming particle
 formation 24 p4218 A67-42842
 Effective cross section of inelastic
 interaction between high energy protons and
 carbon nuclei monitored by Proton I and
 II 24 p4219 A67-42843
 Cross section of inelastic interactions and
 free path between nuclear active cosmic
 particles and lead nuclei at high
 energies 24 p4219 A67-42844
 Cosmic particle recording facility at
 Tskhra-Tskaro, giving data on free path of
 nuclear active particles in carbon with high
 energies 24 p4219 A67-42845
 Nuclear cosmic particle interactions cross
 section in iron, using Bartlett S-function for
 particle free path
 determination 24 p4219 A67-42846
 High energy cosmic ray nuclear interaction
 cross section dependence on interacting
 material atomic weight determined by
 ionization calorimeter and Geiger
 counters 24 p4219 A67-42847
 Cross section of inelastic interaction
 between cosmic ray neutrons and carbon
 nuclei at energies of 100
 GeV 24 p4219 A67-42848
 Nuclear active cosmic ray particles and Fe
 atom nuclei inelastic interaction cross
 section 24 p4219 A67-42849
 Nuclear cascade avalanche absorption in
 Fe analyzed by ionization
 calorimeter 24 p4219 A67-42850
 Effective lambda and sigma hyperons and
 K-meson production cross section
 dependence on target element atomic weight
 during cosmic rays interaction with various
 nuclei 24 p4220 A67-42851
 Secondary particle pulse spectra and mean
 inelasticity coefficient dependence on
 particle multiplicity and primary proton
 energy in 20 GeV/c proton-proton
 interactions 24 p4193 A67-42854
 Negative pion and proton-nucleon reactions
 at 17 and 24 GeV/c, using Lobachevskii-
 Einstein velocity space images method to
 obtain kinematics 24 p4193 A67-42858
 Nuclear interactions mechanisms analyzed
 by method allowing comparison with
 Feynmann diagram, determining necessary
 information for analysis 24 p4193 A67-42859
 Statistical model for multiple particle
 production process based on unitary
 symmetry concept of strong interactions,
 comparing results with quark model
 results 24 p4193 A67-42861
 Extensive air showers accompanying high
 energy nuclear active particles, discussing
 nuclear interaction processes and energy
 transformation 24 p4220 A67-42864
 Photonuclear interaction effect on large
 angle scattering of high energy
 muons 24 p4222 A67-42881
- ### NUCLEAR MAGNETIC RESONANCE
- Nuclear magnetic resonance and
 microwave spectra of some deuterio
 derivatives of 2, 4-
 dicarbalcloheptaborane-7/7
 [JPL-TR-32-1038] 01 p0019 A67-11146
 Gradient-elastic tensor of ions in sodium
 chloride and sodium bromide crystals
 determined from effects of static elastic
 strain on nuclear magnetic
 resonance 02 p0280 A67-11485
 Nuclear magnetic resonance /NMR/ used
 to measure gelation times, rates of
 polymerization and nature of volatiles
 included in raw material
 resins 03 p0429 A67-13448
 Nuclear magnetic resonance and nuclear
 quadrupole resonance techniques for
 nondestructive testing of reinforced plastics
 for curing and internal
 stresses 08 p1345 A67-20425
 Two energy gaps in superconducting
 compounds studied by NMR
 techniques 08 p1371 A67-21443
 Structures and stereochemistry of
 clivonine and clivimine analyzed through
 mass spectroscopy and nuclear magnetic
 resonance 09 p1458 A67-22059
 Optical transient nutation effect in carbon
 dioxide laser 11 p1802 A67-24829
 Associated nonuniform electron-nucleus
 oscillations in ferromagnetic substances
 studied to determine feasibility of maser,
 using magnetic-reversal nuclear magnetic
 resonance 16 p2686 A67-31731
 Book on thermodynamics of irreversible
 phenomenon in liquid metals including
 Onsager symmetry relations,
 phenomenological theory, nuclear magnetic
 resonance, galvano- and thermomagnetic
 phenomenon, etc 17 p2968 A67-32233
 Linear autodyne circuit allowing
 sensitivity control irrespective of oscillation
 level useful in NMR lines 19 p3202 A67-35791
 Transition temperature, Knight shift and
 NMR line width variation in V-Au
 compounds as function of atomic
 ordering 22 p3858 A67-39520
 Ti isotopes nuclear magnetic resonance in
 hexagonal Ti metal showing d-like
 conduction-electron states at Fermi level by
 spin-lattice relaxation
 time 24 p4203 A67-42109
- ### NUCLEAR METEOROLOGY
- Cosmic ray variations classification and
 origin, taking into account possible
 interference between
 meteorological
 effects 05 p0877 A67-16082
 Lower atmosphere nucleonic component
 measurement, noting attenuation coefficient
 dependence on atmospheric
 depth 17 p2842 A67-32364
 Cosmic ray variations classification and
 origin taking into account possible
 interference between meteorological
 effects 24 p4212 A67-42758
- ### NUCLEAR PARTICLE
- SA BARYON
 SA MESON
 SA MUON
 SA NEUTRON
 SA POSITRON
 SA PROTON
 Energy moments of inverse problem in
 theory of nuclear cascade determined, using
 first order Volterra integral
 equation 02 p0317 A67-12769
 Temporal variations of nuclear flux of
 primary cosmic radiation of Elektron II and
 IV satellites, discussing Forbush effect in

nuclear and neutron components 05 p0877 A67-16085
 High energy primary gamma quanta flux outside atmosphere estimated with aid of Proton I satellite 05 p0877 A67-16088
 Primary cosmic radiation intensity determined with help of nuclear particle tracks in moldavites and meteorites 05 p0887 A67-16100
 Exponent in expression relating nuclear interaction cross section to atomic weight of absorber determined from absorption path of nuclear active particles of cosmic radiation 06 p1078 A67-18795
 CdTe properties evaluated through pulse height response of surface barrier devices to monoenergetic alpha particles normally incident to surface 08 p1356 A67-21308
 Device for studying high energy nuclear active particles of cosmic rays interaction and determination of energy spectrum 12 p1947 A67-26095
 Diffusion of protons and nuclei having elastic interactions at 27 GeV/c, using probability distribution for events outside Gaussian limit of multiple scattering 13 p2160 A67-26436
 Exponent in expression relating nuclear interaction cross section to atomic weight of absorber determined from absorption path of nuclear active particles of cosmic radiation 18 p3116 A67-34414
 Adjustment and test of 300 Mev proton extraction system for NASA 600 Mev synchrocyclotron 20 p3413 A67-36182
 Nuclear active particles energy spectrum obtained on mountain tops, investigating absolute flux by using ionization calorimeter 21 p3698 A67-38293
 Energy moments of inverse problem in theory of nuclear cascade determined, using first order Volterra integral equation 22 p3842 A67-40271
 Temporal variations of nuclear flux of primary cosmic radiation of Elektron II and IV satellites, discussing Forbush effect in nuclear and neutron components 24 p4212 A67-42761
 High energy primary gamma quanta flux outside atmosphere estimated with aid of Proton I satellite 24 p4212 A67-42764
 Primary cosmic radiation intensity determined with help of nuclear particle tracks in moldavites and meteorites 24 p4238 A67-42776
 Extensive air showers accompanying high energy nuclear active particles, discussing nuclear interaction processes and energy transformation 24 p4220 A67-42864

NUCLEAR PHYSICS

SA FEYNMAN DIAGRAM
 SA PLASMA PHYSICS
 SA REACTOR PHYSICS

Zero order Hamiltonian in perturbation theory for eigenvalue problems of atom in magnetic field 02 p0271 A67-12723
 Variational perturbation equations and time-independent Schroedinger equation for two-, three- and four-electron atoms 02 p0271 A67-12724
 Atomic and molecular time-dependent quantum-mechanical perturbation theory with differential equation formulation within Hartree-Fock approximation 02 p0268 A67-12725
 Nuclear physics of neutron emission in stellar interiors, reaction rates of neutron-producing processes evaluated with optical model of nucleus and uncertainties assessed 03 p0508 A67-14315
 Multichannel photoionization of atomic systems obtained with dipole approximation assuming LS coupling, using wave functions 07 p1226 A67-19498
 Intermediate vector bosons as unobservable particles described by renormalizable Lagrangian in indefinite metric space 13 p2161 A67-27578
 Close-coupling calculations of positions and widths of lowest-lying autoionizing D states in helium 16 p2704 A67-31167
 Ground state hyperfine splitting of singly charged helium calculations by Zwanziger and Sternheim evaluated by examining error corrections by Fortson et al 20 p3488 A67-36694
 Excited nuclei electromagnetic de-excitation rate by inelastic scattering in stellar particles calculated as function of temperature, density, transition energy and multipole functions 21 p3660 A67-38846

Atomic and molecular chemicophysical processes in shock waves derived from high temperature thermal energy transfer including instrumentation, relaxation, ionization and spectroscopy 22 p3786 A67-40074

NUCLEAR POWER

Nuclear power supplies for electrical propulsion including liquid metal reactor-potassium Rankine, Brayton, MHD power conversion and thermionic reactor [AIAA PAPER 66-1021] 03 p0363 A67-14153
 Space-power subsystems, evaluation of power sources 04 p0558 A67-15954
 Radioisotope sources and nuclear reactors as energy sources for space vehicles 04 p0558 A67-15959
 Fast and thermal reactors with thermionic converters in reactor core and nuclear system with converters outside core analyzed for power supply for space vehicles 04 p0559 A67-15964
 Nuclear power systems for future communications satellites noting reactor, radioisotope, power system and thermoelectric power conversion equipment 06 p1029 A67-17687
 Nuclear power and propulsion systems for space applications, discussing present and future technologies [AAS PAPER 67-132] 15 p2516 A67-29967
 Optimization of Brayton cycle consisting of heat source, MPD generator, recuperator, etc, in terms of thermal efficiency and specific power 16 p2603 A67-30562
 German lighter than air technical and economic travel problems of medium speed dirigibles using helium and nuclear power drives 22 p3745 A67-39751

NUCLEAR POWER CONVERSION

Rankine and Brayton cycles for spacecraft power generation, discussing operation principles, advantages and performance characteristics 01 p0112 A67-11428
 Outlook for controlled nuclear fusion process for industrial power generation, stressing plasma equilibrium preservation through magnetic trapping 11 p1831 A67-24015
 High temperature high power gas diodes and thyatrons for large nuclear electrical space power systems, noting parameters of design and performance 15 p2448 A67-29755
 Book on electromechanical, direct and nuclear energy conversion covering transducer design, nuclear structure, photoelectric conversion, reactor theory, thermionic conversion, etc 22 p3749 A67-40329
 Design integration of reactor, shielding and power conversion systems for manned earth orbital station 24 p4186 A67-42547
 Design requirements of reactor power systems for manned earth orbital space station 24 p4186 A67-42548
 Advanced radioisotope thermoelectric generator/RTG/ system designs employing SiGe direct radiating power conversion subsystems 24 p4110 A67-42899

NUCLEAR POWER PLANT

Space energy supply plant with nuclear energy sources, noting transformer design 04 p0558 A67-15958
 Thermodynamic limits on specific work and specific impulse of adiabatic chemical engines and nuclear engines [AIAA PAPER 67-227] 06 p1029 A67-18445
 Integrated design requirements of SNAP-8 Rankine power system for manned lunar base mission, discussing mission requirements and reactor shield system 24 p4185 A67-42545
 Nuclear electric space power plant with Rankine cycle for plausible Mars manned mission, discussing mission requirements and reactor elements 24 p4186 A67-42549
 Parametric analysis and system optimization of nuclear reactor heated Brayton cycle space power plants, discussing turbomachinery performance and shielding weight factors 24 p4186 A67-42550
 Reentry vehicle design characteristics and requirements for safe reentry of radioactive power sources, discussing heat protection systems [AIAA PAPER 67-966] 24 p4246 A67-43044

NUCLEAR PROPULSION

SA THERMONUCLEAR PROPULSION

Fixed voltage, fixed energy and variable voltage variable energy pulsed neutron devices and applications in nuclear

propulsion, radiation dosimetry, velocity measurements, etc 02 p0266 A67-12216
 Solar and nuclear-electric propulsion thrusters including ion engines, plasma engines, arc jets, resistojets, etc [AIAA PAPER 66-830] 02 p0303 A67-12253
 Nuclear propulsion systems development for U.S. space program 02 p0266 A67-12336
 Direct ballistic gravity-assisted ballistic and nuclear electric low thrust flight modes for interplanetary exploration 02 p0327 A67-12366
 Radioisotope application to spacecraft propulsion and integrated power noting potential sources, thruster design concepts and mission types 04 p0655 A67-14554
 Atomic power-supply system for space vehicles built in West Germany using sintered U-Y and U-Zr fuel elements 04 p0655 A67-14558
 Program for radioisotopic power on Nimbus B spacecraft provided by SNAP-19 generators 05 p0843 A67-16553
 Nuclear thermionic propulsion system with low specific weight as interplanetary propulsion system [AIAA PAPER 67-229] 06 p1029 A67-18519
 Nuclear or electric propulsion for planetary exploration, noting configuration and capabilities 06 p1098 A67-19019
 MHD application for power conversion and generation, discussing methods and efficiency 06 p1076 A67-19023
 Solid, liquid and gaseous core and radioisotope nuclear rocket engines, discussing thrust levels and other characteristics 06 p1030 A67-19024
 Nuclear pulse propulsion, discussing principles of operation of contained and uncontained systems 06 p1030 A67-19025
 Nuclear pulse propulsion activities of last decade and current research 06 p1030 A67-19026
 SNAP-10A and SNAP-8, discussing reactor thermoelectric space power program 08 p1352 A67-21052
 Nuclear rocket engine design for near-optimum vehicle performance for mission capability 08 p1412 A67-21107
 Radioisotope application to spacecraft propulsion and integrated power noting potential sources, thruster design concepts and mission types 13 p2155 A67-26578
 Space propulsion technology and mission capabilities in fiscal year 2001 13 p2189 A67-27502
 Future space transportation techniques and mission applications in solar system 13 p2213 A67-27508
 Absorption of thermal radiation from gaseous fuel by transparent wall of nuclear light bulb rocket engine [AIAA PAPER 66-619] 15 p2516 A67-29426
 Nuclear power and propulsion systems for space applications, discussing present and future technologies [AAS PAPER 67-132] 15 p2516 A67-29967
 Lighter-than-air, nuclear-powered dirigible described giving details on capacity, safety and mode of propulsion 16 p2597 A67-31787
 Nuclear reactors for space propulsion and onboard power supply, including conversion systems 18 p3075 A67-33654
 Problem areas within cryogenic chemical and nuclear propulsion systems for space missions, noting available technology and limitations [AIAA PAPER 67-454] 18 p3110 A67-33928
 Test facility for 5000 mw nuclear rocket propulsion modules, discussing effect on design and flight conditions duplication [AIAA PAPER 67-465] 18 p3020 A67-33936
 Nuclear propulsion for aircraft, discussing reactor compactness and shielding techniques [AIAA PAPER 67-508] 18 p3076 A67-33972
 Nuclear propulsion for manned Mars expedition, discussing engine and launch optimization, computer simulation, performance, trip times, velocity, weight, etc [AIAA PAPER 67-510] 18 p3077 A67-33974
 Combined electric constant low thrust and chemical or nuclear high thrust space propulsion systems for interplanetary missions [AIAA PAPER 67-511] 18 p3114 A67-33975
 Potassium Rankine cycle turboelectric space power system, emphasizing vapor fin type of condensing radiator 20 p3364 A67-37018

- NERVA components including nozzle and associated hot gas bleed port, turbopump, control valve, pressure vessel and thermocouples 22 p3834 A67-40172
- Lithium-boiling potassium test facility to investigate transient and steady state characteristics of Rankine cycle system for application to spacecraft nuclear-electric propulsion 24 p4183 A67-42492
- Gaseous nuclear rocket engine propulsion, reviewing fluid mechanics, radiant heat transfer, transparent walls, nuclear criticality, coaxial flow reactor, etc [AIAA PAPER 67-783] 24 p4187 A67-42948
- Nuclear rocket propulsion development, hot test results, one breadboard engine configuration and flight stage planning [AIAA PAPER 67-981] 24 p4187 A67-43054
- ### NUCLEAR RADIATION
- #### SA GAMMA RADIATION
- #### SA POST-BLAST NUCLEAR RADIATION
- High speed nuclear electronics - Colloquium, Polytechnic Institute and Nuclear Study Center, Grenoble, France, February 1966 01 p0065 A67-10649
- Nuclear radiation intensity effect on switching time of fast diodes, examining produced stability changes 01 p0066 A67-10655
- Semiconductor surface barrier Si n-type detector yielding fast resolution curve in alpha-gamma radiation coincidence experiment 01 p0066 A67-10657
- Soviet and other papers on nuclear emission detectors, using electron-optical light amplifiers 01 p0069 A67-11006
- Neutron collision cross section and calculation of energy loss of displaced Si atoms to ionization 03 p0494 A67-13481
- Book on nuclear radiation effects on electronic systems including radiation shielding, nuclear instrumentation systems and electronic design techniques 04 p0583 A67-15267
- Nuclear and space radiation effects - IEEE Conference, Stanford University, July 1966 04 p0586 A67-15687
- Nuclear radiation characteristics pertinent to propagation of signals for measurement of range and bearing 05 p0839 A67-16532
- Fission or radioisotopic nuclear radiation applied to laser pumping, discussing forms, sources, power, solid state and molecular gas lasers, energy transfer, optical fluorescence and cut-off phenomenon 05 p0814 A67-16547
- Width of l band of p-i-n nuclear emission detector during Li ion drift through doped Si semiconductor detector 05 p0872 A67-17500
- Creep rupture, fatigue strength and brittle-ductile transition of aluminum as affected by nuclear radiation 13 p2133 A67-27090
- Measurement of thermal conductivity of irradiated foam-type insulation materials 13 p2228 A67-27662
- Disturbance of capacitive liquid level gauges by nuclear radiation 13 p2122 A67-27684
- Nuclear radiation damage to circuit elements of missile FM/FM telemetry system, analyzing changes in electric characteristics 14 p2271 A67-28685
- Adhesives for nuclear powered spacecraft tested for pressure, temperature and radiation effects 15 p2508 A67-29560
- Book on radioisotope measurement applications in engineering covering nuclear radiation, gas detectors, scintillation, etc 15 p2516 A67-29900
- Soviet and other papers on nuclear emission detector, using electron-optical light amplifiers 16 p2670 A67-30494
- Response of capacitors irradiated by pulses of transient nuclear radiation 17 p2828 A67-32863
- Lunar exploration by nuclear experiment, discussing instrument specifications for neutron gamma measurements 19 p3229 A67-35318
- Radioisotope heating to provide ionizer temperatures in contact ion thrusters [AIAA PAPER 67-734] 21 p3695 A67-38757
- Hazards of rocket launching noting propellant toxicity, airborne fragmentation, inadvertent ignition and nuclear radiation 22 p3900 A67-39884
- Environmental simulation for aerospace vehicle, discussing vibration, shock and high temperature testing and space and nuclear radiation simulation 22 p3781 A67-40343
- Nuclear cosmic ray component intensity variation related to 27-day solar activity variation in Elektron II and IV analysis of modulating effect 23 p4055 A67-41104
- Nuclear radiation damage to circuits noting Compton effect, ionization current effects, resistance drops, electron-hole pair formation, etc 24 p4132 A67-42702
- ### NUCLEAR REACTION
- #### SA FISSION
- #### SA FUSION
- #### SA INELASTIC SCATTERING
- #### SA RESONANCE SCATTERING
- Apparatus for investigating nucleon reactions with approximate energy greater than 100,000 bev, including Cerenkov and scintillation counters and spark chambers 02 p0316 A67-12765
- Elimination of certain contradictions in data concerning high energy cosmic rays explained by means of hypothesis of existence of passive S-state of baryon 02 p0316 A67-12766
- Recoil ranges of products from reactions of Cu-65 with 11-35-mev He-3 ions 03 p0473 A67-13926
- Radioactive isotopes in iron meteorite used to determine cosmic ray origin and to study nuclear processes in early history of solar system 05 p0877 A67-16084
- Evolution of 2.25 M star from main sequence to helium burning phase noting lifetimes, nuclear burning of core, stellar mass fraction and stellar model algorithm 09 p1566 A67-22226
- Change in critical mass of large reflector moderated gaseous-fueled cavity reactor due to presence of hot hydrogen gas in cavity 12 p1965 A67-25908
- Absolute cross sections and isomeric yield ratios for d,p reactions up to 15 mev in various metals 14 p2350 A67-27790
- Information on early history of solar system material obtained for neutron buildup processes of heavy element synthesis in stars 15 p2519 A67-29156
- Internal conversion electron spectrum for samarium 155 to europium 155 transmutation, noting multipolarities and new lines 16 p2733 A67-31706
- Spallation and fissionlike xenon and krypton content in Pasamonte achondrite as evidence for extinct radioactivity in meteorites 16 p2754 A67-31747
- Cross section of Helium 3 reaction calculated for possible solar neutrino source 16 p2741 A67-31921
- Gamma ray schemes of resonances in silicon 29-phosphorus 30 reaction for resonant and bound levels of phosphorus 30 properties 16 p2705 A67-31922
- Laser pulse duration effect on photonuclear processes, as affected by matter-radiation interactions, observing ionization in gases and surface photoeffects 19 p3238 A67-34897
- Proton, neutron and alpha particle emission rates for heavy nuclei in elevated temperatures calculated and tabulated 20 p3490 A67-37553
- Apparatus for investigating nucleon reactions with approximate energy greater than 100,000 Bev, including Cerenkov and scintillation counters and spark chambers 22 p3876 A67-40267
- Elimination of certain contradictions in data concerning high energy cosmic rays explained by means of hypothesis of existence of passive S-state of baryon 22 p3877 A67-40268
- Energetic nuclear bombardment effects on stellar surface element abundance calculated with statistical theory in A magnetic variable star abundance anomaly 24 p4228 A67-42263
- Abundance anomalies in stellar surface layers by proton and alpha particle bombardment caused nucleus breakdown and buildup to lower and higher mass numbers respectively 24 p4228 A67-42264
- Three-body problem application to nuclear reactions involving neutron, proton and heavy nucleus, parametrizing two-body interactions in terms of s-wave separable potentials 24 p4191 A67-42593
- Radioactive isotopes in iron meteorite used to determine cosmic ray origin and to study nuclear processes in early history of solar system 24 p4212 A67-42760
- Isotope ratios of fission and spallation xenon in meteorites from abundance data analysis by least squares method 24 p4238 A67-42886
- ### NUCLEAR REACTOR
- ### S REACTOR
- ### NUCLEAR REACTOR MATERIAL
- Nuclear and engineering ceramics - Conference, Harwell, Berks., England, October 1965 12 p1964 A67-25210
- Power supply and transformation equipment in satellites, discussing batteries, fuel cells, nuclear reactors and solar energy 14 p2252 A67-28566
- Creep behavior of materials in nuclear reactors, gas turbines and electric power plants, noting aluminum alloy and high temperature material fatigue 15 p2502 A67-29506
- Hydrogen solubility in eutectic sodium-potassium mixture, noting usefulness as nuclear reactor coolants, and dependence on pressure and temperature variations 16 p2619 A67-30620
- Computer analysis of critical fuel solution reactors with arrays of large diameter voids 16 p2702 A67-31814
- Thermionic space power systems, examining solar, radioisotope and nuclear reactors as heat sources, discussing power density and electrode affinity 17 p2802 A67-32050
- Instability of gas-cooled nuclear reactor passages in steady laminar flow studied by time-dependent analysis 19 p3260 A67-35743
- Hybrid simulation for analysis and design of nuclear reactors feedback control systems 19 p3189 A67-36068
- Pu 239 fueled fast spectrum nuclear reactor spacecraft power supply design for 1 kwe noting cost, control, heat transfer and optimization 24 p4185 A67-42538
- ### NUCLEAR RESEARCH
- Instrumentation in space and laboratory - Conference, Boston, October 1966 12 p1943 A67-25850
- Nuclear methods and techniques applied to maintenance and checkout of complex electronic and electromechanical systems, discussing radiation-matter interaction, etc 20 p3449 A67-36981
- Contour-volumetric displays for processing and handling data in nuclear experiment 20 p3450 A67-36986
- ### NUCLEAR ROCKET
- ### SA POODLE ROCKET ENGINE
- Fluid mechanics of mixtures whose components are at large deviation from equilibrium with one another, considering propulsion system application 01 p0055 A67-11439
- Optimum nozzle contours for expansion of Lighthill idealized dissociating gas in one-dimensional flow determined by methods of variational calculus 02 p0305 A67-12353
- Nuclear Rocket propulsion development, noting nuclear rocket engine test program [AIAA PAPER 66-829] 03 p0466 A67-14124
- Nuclear rockets employing multiple exhaust nozzles, noting performance gain occurring because of high temperature capability of refractory nozzles [AIAA PAPER 66-925] 03 p0466 A67-14135
- Rover testing facilities of Nuclear Rocket Development Station in Nevada [AIAA PAPER 66-1003] 03 p0397 A67-14148
- Testing of NRX/EST and NRX-A5 with emphasis on startup capability, engine control and high temperature operation [AIAA PAPER 66-1004] 03 p0466 A67-14149
- Controls and control experimental program for nuclear rocket engine employing hot bleed cycle [AIAA PAPER 66-1005] 03 p0466 A67-14150
- Transient heat transfer and thermal stresses for nuclear rocket due to sudden hydrogen coolant flow increase [ASME PAPER 66-WA/NE-4] 04 p0656 A67-15373
- Optimum control of flow rate through nuclear rocket with constraint on thermal stress in fuel elements [ASME PAPER 66-WA/AUT-6] 04 p0656 A67-15419
- Liquid hydrogen use in nuclear rocket testing, noting Kiwi reactor, Dewar system, transfer line, etc 05 p0789 A67-17013
- Delayed energy produced by fission product decay when restart of nuclear rocket engine is considered, noting effects of cooldown requirements [AIAA PAPER 66-551] 05 p0844 A67-17222
- Mathematical model for potential heating from gamma radiation source, determining

transient temperature distribution for materials used in nuclear rockets 06 p1116 A67-18363

Replacement of chemical launching rockets by advanced propulsion system, with particular reference to nuclear rocket 07 p1242 A67-20264

Multigroup diffusion theory analysis of gas-core /cavity/ nuclear rocket engine 08 p1352 A67-21196

NERVA program, reactor and nonnuclear component development, full-scale testing, engine program, facilities and materials research [AIAA PAPER 67-487] 18 p3076 A67-33953

Gas core reactor, discussing application of fissionable gas to heat hydrogen propellant in nuclear rocket reactor [AIAA PAPER 67-499] 18 p3076 A67-33963

Economical feasibility of open and closed cycle vortex-stabilized gaseous nuclear rocket engines, investigating vortex flow characteristics [AIAA PAPER 67-500] 18 p3076 A67-33964

Recirculation zone in fluid mechanics experiments on cylindrical cavity simulating gas-core nuclear rocket as heavy gas reservoir, discussing flow patterns [AIAA PAPER 67-502] 18 p3076 A67-33966

Safety program for nuclear rocket engine testing, discussing role of cryogenics 20 p3482 A67-36565

Mathematical model for potential heating from gamma radiation source, determining transient temperature distribution for materials used in nuclear rockets 21 p3730 A67-37793

Multiple exhaust nozzles for advanced nuclear rocket engines noting design and performance prediction procedures 22 p3834 A67-40160

Cryogenic valve testing facility for nuclear rockets using liquid hydrogen at high pressures and flow rates 23 p3936 A67-41425

Gaseous nuclear rocket engine propulsion, reviewing fluid mechanics, radiant heat transfer, transparent walls, nuclear criticality, coaxial flow reactor, etc [AIAA PAPER 67-783] 24 p4187 A67-42948

Nuclear rocket propulsion development, hot test results, one breadboard engine configuration and flight stage planning [AIAA PAPER 67-981] 24 p4187 A67-43054

NUCLEAR SCATTERING

SA RESONANCE SCATTERING

Change in critical mass of large reflector moderated gaseous-fueled cavity reactor due to presence of hot hydrogen gas in cavity 12 p1965 A67-25908

Generalized potentials for medium energy inelastic nuclear scattering derived with projection operator method 14 p2350 A67-27789

Peak energy dependence on atomic number in inelastic alpha particle scattering at 24.8 Mev by Ni 58, Cu, Ag, Ta and Au 21 p3659 A67-38401

NUCLEAR SHIELDING

Nuclear propulsion for aircraft, discussing reactor compactness and shielding techniques [AIAA PAPER 67-508] 18 p3076 A67-33972

Hardening technique for circuits using electrical shielding to withstand radiation effects of nuclear war 20 p3399 A67-36883

Parametric analysis and system optimization of nuclear reactor heated Brayton cycle space power plants, discussing turbomachinery performance and shielding weight factors 24 p4186 A67-42550

NUCLEAR SPECTROSCOPY

SA ISOTOPE SHIFT

Surface barrier diffused-junction lithium-compensated silicon and lithium-compensated germanium particle detectors for aerospace application 02 p0245 A67-12212

Mossbauer nuclear resonance fluorescence effect spectrometer using Doppler principle, with applications to aerospace 05 p0843 A67-16544

Line-narrowing effect induced by laser radiation applied to measurements of isotope shifts for two optical transitions in neon 13 p2127 A67-27080

Nuclear spectroscopy and solar neutrino astrophysics 16 p2753 A67-31734

NUCLEAR SPIN

Paramagnetic resonance of praseodymium and uranium ions in calcium fluoride analyzed via fitting to spin Hamiltonian 01 p0129 A67-10146

Temperature and purity dependence of nuclear-spin relaxation time in type II superconductor gapless region and volume average of density states on Fermi surface 03 p0499 A67-13937

Nonexponential electron spin cross relaxation measurement in dilute ruby 17 p2924 A67-33369

Resonance absorption and zero-field nuclear spin relaxation in normal and superconducting aluminum, studying phase change 19 p3303 A67-35044

Optically pumped vapor rotatory power as optical pumping experiment monitoring technique, discussing specific rotatory power and refractive index dependence on light frequency 22 p3816 A67-40320

Nongravitational effects in Halley comet motion and arbitrarily rotating comet nucleus model, noting push-effect hypothesis 23 p4062 A67-40672

Nongravitational and splitting effects in comet motion and rotating comet nucleus model, using push-effect hypothesis for post-explosion analysis nongravitational and splitting effects in comet motion and rotating comet nucleus model, using 23 p4062 A67-40673

Very long nuclear spin relaxation times in gaseous He by suppressing He surface interactions measured in highly spin polarized samples 24 p4191 A67-42247

NUCLEAR STRUCTURE

Hartree-Fock-Slater calculation of internal conversion coefficients for magnetic multipoles for yttrium-87 with 0.05 or 0.15 mc-square gamma energy values 01 p0116 A67-10203

Fast neutron activation cross sections of Se and Fe measured, noting subshell closure effect and isomer ratio 11 p1822 A67-23979

Absolute cross sections and isomeric yield ratios for /d,p/ reactions up to 15 mev in various metals 14 p2350 A67-27790

Atom arrangement in crystalline materials considering lattice, planes and structure, discussing effect on mechanical properties, particularly friction 24 p4184 A67-42733

NUCLEAR WARFARE

Hardening technique for circuits using electrical shielding to withstand radiation effects of nuclear war 20 p3399 A67-36883

NUCLEATE BOILING

SA HEAT TRANSFER

Nucleate boiling mechanism in superheated binary mixtures obtained from extension of theories of van Wijk, Vos and van Stralen by Scriven and Brulijn 04 p0720 A67-14637

Comparison of temperature differences for similar liquids boiling on various surfaces, with graph correlating heat flux/temperature difference data 04 p0721 A67-14645

Rapid depressurization transients effect on saturated pool boiling system from stainless steel surface 04 p0734 A67-15848

Zero gravity effects on boiling from flat horizontal surface for various subcoolings, fluid properties and heat transfer rates 12 p2034 A67-25720

Pool boiling of methane over pressure range from 1 atm to critical pressure in both nucleate and stable film boiling regimes 13 p2229 A67-27687

Dimensional analysis of heat transfer correlations for nucleate boiling in free convection, including critical heat flux conditions 14 p2408 A67-28932

Heat transfer in cryogenic range, noting heat flux measurements, use of semiconductors, etc 16 p2780 A67-31533

Thermal problems peculiar to cryogenics stored in reduced gravity environment 17 p2968 A67-32010

Nucleate boiling heat transfer correlations graphically estimated for design purposes to compute heat flux and wall superheat 17 p2968 A67-32033

Vapor volumetric fraction during forced convection, calculating true local vapor weight, volumetric fraction, location of bubble departure, etc 18 p3160 A67-34163

S-shaped boiling curves analyzed in terms of nucleation characteristics of heat transfer surface, correlating temperature driving force and density of centers 18 p3160 A67-34164

Heat transfer characteristics of several aliphatic hydrocarbons in nucleate and film boiling during forced flow in heated tubes [ASME PAPER 67-HT-7] 20 p3544 A67-36705

Ultrasonic field effects on nucleating fluid in flash boiling system and heat transfer dependence on bubble density parameters [ASME PAPER 67-HT-11] 20 p3545 A67-36709

Rohsenow nucleate pool-boiling data correlation, stressing coefficients dependence on surface preparation and liquid-surface combination [ASME PAPER 67-HT-33] 20 p3547 A67-36723

Sinusoidal surface vibration effect on nucleate pool boiling reveals lowered surface temperature for low heat flux, LF and high acceleration [ASME PAPER 67-HT-49] 20 p3548 A67-36731

Surface vibration effect on nucleate pool boiling, measuring heat-transfer coefficient and proposing mechanism [ASME PAPER 67-HT-58] 20 p3549 A67-36740

Gravitational effect upon nucleate boiling analyzed by experimentation on all levels up to maximum attainable by apparatus available [AIChE PAPER 4] 20 p3552 A67-36826

Vertical magnetic induction effect on nucleate boiling of mercury on horizontal heating surface [AIChE PAPER 20] 20 p3552 A67-36830

Bubble frequency, departure diameter and rise velocity relationship in nucleate boiling 20 p3553 A67-36934

Model for straight fin nucleate boiling onset criterion, discussing boiling section length expression, heat flux and temperature profile 22 p3919 A67-40387

NUCLEATION

Normal region distribution in superconducting solenoid measured after quenching by varying quenching current 01 p0137 A67-11065

Nucleation theories, emphasizing relation with oriented growth of thin films condensing on solid foreign substrate 02 p0285 A67-11702

Nucleation of epitaxial SiC on Si surfaces 02 p0299 A67-11894

Incidence, growth and detachment of boiling bubbles in saturated distilled water from artificial nucleation sites of given geometry and size in heated metal surface 04 p0734 A67-15847

Critical field for nucleation of superconductivity at tunneling barrier in magnetic field 07 p1235 A67-20131

Nucleation during pulse remagnetization of thin films, showing domain structure of formation, growth of nuclei, etc 08 p1367 A67-20603

Heat-transfer coefficients during dropwise condensation on randomly distributed nucleation sites analyzed through computer simulated model 08 p1426 A67-20925

Large scale expansion nozzle control by heterogeneous nucleation and mercury vapor and drop growth processes in nitrogen flow [AIAA PAPER 66-85] 10 p1733 A67-23125

Growth mechanisms and crystalline quality of diamond type compounds and crystals in III-V and II-VI groups 13 p2177 A67-27009

Critical fields in strong coupling superconductors, using Ginsburg-Landau equations 19 p3303 A67-35042

Equilibrium state of two-dimensional lattice liquid-gas system using cluster variation method for nucleation and thin film growth studies 23 p4040 A67-40967

Velocity distribution of evaporated Au and incident velocity on nucleation of Au on rocksalt studied by velocity selector 23 p4009 A67-41015

NUCLEATION PROCESS

Polarized light crystallization microanalysis for supercooled water droplets with additives applied to spherical single crystals of ice during droplet freezing 01 p0109 A67-11010

Crystal and biological nucleation processes and mechanisms and roles of energy, charged particles, shocks, grain size and impurities 04 p0565 A67-15080

Nuclear-bubble hypothesis for inception of hydraulic cavitation examined, using free-jet test 04 p0606 A67-15123

Impurity effects on nucleation of Se vapor onto Pyrex glass noting degree of critical supersaturation, production of phase with nonequilibrium structure, etc 11 p1821 A67-24992

Nucleation of titanium and titanium oxide thin films correlation to thickness obtained from fluorescent intensity

measurement 12 p1981 A67-25276
 Condensation spectrum evolution of cloud droplets 13 p2151 A67-26690
 Reverse magnetization spike domains analyzed for nucleation and growth 13 p2179 A67-27141
 Fracture stresses of cracked plates and flow stresses of polycrystalline aggregates as related to stresses and strains at ends of plano-discontinuities 16 p2769 A67-31285
 Condensation path of cooling gas of solar composition calculated considering barriers to homogeneous nucleation of condensed phase 16 p2751 A67-31454
 Self-consistency equation for nucleation of superconductivity in presence of magnetic field 17 p2924 A67-33372
 Critical supersaturations for homogeneous nucleation of ethanol, hexane, etc., investigated using thermal diffusion cloud chamber 20 p3555 A67-37562
 Condensation spectrum evolution of cloud droplets 21 p3654 A67-38432
 Path-probability method applied to thin film nucleation and growth on substrate by vapor deposition, deriving kinetic equations 23 p4040 A67-40968
 Mass spectrometry used for simultaneous measurements of adsorption and crystal nucleation processes 23 p4043 A67-41355
 Bi and Ag nucleation on evaporated substrates studied as function of substrate temperature and impinging flux using electron microscopy 23 p4044 A67-41455
 Upper critical nucleation field at free surface of superconductor backed by normal metal 24 p4200 A67-41862

NUCLEIC ACID

SA CHROMOSOME

SA DEOXYRIBONUCLEIC ACID /DNA/

Hydrogen bonding of derivatives of guanosine and cytidine soluble in chloroform studied in IR, confirming geometrical specificity in two-stranded nucleic acids 02 p0190 A67-11585

Nucleic acid molecule reproduction discussing probability of life development under favorable environmental circumstances 16 p2611 A67-30767

Factors involved in use of thymine by uninfected cells in metabolism of *Escherichia coli* 20 p3370 A67-36799

Nucleic acid metabolism in Chinese hamster fibroblasts grown in vitro noting effects of concentrations of sodium azide 21 p3575 A67-38798

Origin of life on earth, formation of nucleic acid molecules and metabolic mechanism 24 p4112 A67-42052

NUCLEON

High energy interaction of nucleons with complex nuclei described by model of cascade-type nucleon and pion multiplication within nucleus 02 p0312 A67-12604

Ionizing accompaniment of near 170 bev nucleons at 2000 m altitude recorded by spark chamber /Geiger counter/ ionization chamber apparatus 02 p0312 A67-12609

Pion energy transmission during inelastic interaction of cosmic particles with Pb nuclei 02 p0315 A67-12756

Ionization calorimeter measurements of energy transmission by photons in cosmic nuclear-active pion and nucleon interactions with various nuclei 02 p0316 A67-12761

Nucleon interaction generating high energy gamma rays, discussing photon and energy spectra of electron photon cascade, pion generation and gamma quantum detection in atmospheric nuclear interactions 02 p0316 A67-12763

Apparatus for investigating nucleon reactions with approximate energy greater than 100,000 bev, including Cerenkov and scintillation counters and spark chambers 02 p0316 A67-12765

Self-consistent three-body calculation of pion-nucleon scattering using off-energy shell theory 04 p0660 A67-14858

Flight test of nucleonic fuel gauge, discussing photon-matter interaction principles, ground test calibration data, aircraft environment and gauge performance 05 p0841 A67-16537

Continuous nucleonic oil quantity gauging system requiring no tank penetrations 05 p0842 A67-16538

Nucleonic quality gauging system for two-phase hydrogen pipeline 05 p0842 A67-16539

Nucleonic cryogenic quality meter design and development and fluid monitoring

through hydrogen vent line on Saturn S-IVB stage under orbital conditions 05 p0842 A67-16540

Mathematical model of aircraft nucleonic fuel gauging facility system allowing performance evaluation and optimization by computer techniques 05 p0842 A67-16542

Nucleon radius from pion-nucleon phase shift, assuming nucleon is p-wave bound state of pion and nucleon, using Gelfand-Levitan formalism 06 p1036 A67-18368

[AIAA PAPER 67-213] Proton II satellite measurements of intensity of nuclear component of primary cosmic radiation 09 p1561 A67-21897

Existence of nucleon bound state in PIN channel investigated through nonperturbative S-matrix in absence of forces arising from inelastic states 11 p1822 A67-23978

Primary cosmic radiation composition effect on secondary emission, examining flux, spectra, nucleon interactions, proton component and neutrons 14 p2380 A67-27966

Lower atmosphere nucleonic component measurement, noting attenuation coefficient dependence on atmospheric depth 17 p2842 A67-32364

Cosmic ray secondary nucleon production of multiple neutrons observed and energy spectra measured, using multiplicity monitor 20 p3452 A67-37407

Pion energy transmission during inelastic interaction of cosmic particles with Pb nuclei 22 p3876 A67-40258

Ionization calorimeter measurements of energy transmission by photons in cosmic nuclear-active pion and nucleon interactions with various nuclei 22 p3876 A67-40263

Nucleon interaction generating high energy gamma rays, discussing photon and energy spectra of electron photon cascade, pion generation and gamma quantum detection in atmospheric nuclear interactions 22 p3876 A67-40265

Apparatus for investigating nucleon reactions with approximate energy greater than 100,000 Bev, including Cerenkov and scintillation counters and spark chambers 22 p3876 A67-40267

Characteristic of high energy nucleon-nucleus interaction, analyzing changes due to structural buildup 24 p4192 A67-42839

Pion nucleon inelastic collisions at 17 GeV/c momentum, discussing proton pulse spectra and ionization losses 24 p4192 A67-42853

NUCLEON-NUCLEON SCATTERING Spectra of outgoing protons for various targets using scintillation counter, interpreting data by means of impulse-approximation calculation 02 p0269 A67-11862

Intranuclear cascades of nucleon-nucleus interaction calculated on basis of Fermi gas model, using Monte Carlo method and three-dimensional relativistic kinematics 02 p0314 A67-12748

Cosmic ray nucleon interaction with high energies, estimating transition probability and interaction cross section of baryon in passive state 10 p1703 A67-23586

Phase shift analysis of nucleon-pion coupling, noting discrepancy between empirical and theoretical results 11 p1823 A67-24599

Nucleon-nucleon collisions, analyzing pair production, electromagnetic cascade, secondary interactions, etc 16 p2703 A67-30965

Nucleon-nucleon interaction - Conference, University of Florida, March 1967 20 p3490 A67-37612

Intranuclear cascades of nucleon-nucleus interaction calculated on basis of Fermi gas model, using Monte Carlo method and three-dimensional relativistic kinematics 22 p3876 A67-40250

Proton-proton and pion and kaon elastic scattering from protons at high energy, deriving approximate formula for differential cross section, noting nucleon structure 24 p4193 A67-42855

Negative pion and proton-nucleon reactions at 17 and 24 GeV/c, using Lobachevskii-Einstein velocity space images method to obtain kinematics 24 p4193 A67-42858

NUCLEOSIDE SA RIBONUCLEIC ACID /RNA/ Phosphorylation of nucleosides with polyphosphoric acid 13 p2065 A67-26807

NUCLEOSYNTHESIS

Galactic and solar nucleosynthesis, determining formation of meteorites on basis of decay of nucleides Pu 244 and I 129 02 p0320 A67-11472

He abundance in sun suggests He stellar nucleosynthesis was responsible for increase in He abundance in interstellar gas between formation of sun and present time 17 p2947 A67-32763

Origin of elements, discussing element formation and abundances, nucleosynthesis and cosmological theories 19 p3263 A67-35869

Core of two solar masses of gravitationally collapsing star, analyzing hydrodynamics, heating, helium 4 formation, neutron decay, nucleosynthesis, light output and mass ejection 22 p3882 A67-39622

NUCLEOTIDE

S PYRIDINE NUCLEOTIDE

S RIBONUCLEIC ACID /RNA/

NUCLEUS

SA HEAVY NUCLEUS

SA ICE NUCLEUS

Hellum isotope formation in cosmic rays during light nuclei fragmentation due to high energy proton interaction 05 p0878 A67-16093

Cosmic ray nuclei observed from satellites and balloons by nuclear emulsions in stacks of plastic sheets 06 p1076 A67-17641

Identification and localization of center median nucleus of Luys, noting CM projects primarily upon putamen 08 p1288 A67-21356

Factors affecting current methods of sizing Altken nuclei 13 p2152 A67-26865

Liquid nuclei formation at condensation centers in atmosphere analyzed for various degrees of saturation 14 p2346 A67-27908

Statistical properties of optical variability of 3C 273 suggesting quasar nucleus as single body 20 p3521 A67-36297

Hellum isotope formation in cosmic rays during light nuclei fragmentation due to high energy proton interaction 24 p4213 A67-42769

Characteristic of high energy nucleon-nucleus interaction, analyzing changes due to structural buildup 24 p4192 A67-42839

Fast He nuclei from photoemulsion nuclear splitting induced by proton and antiproton bombardment 24 p4193 A67-42860

NUCLIDE

S RADIOACTIVE NUCLIDE

NULL HYPOTHESIS

Testing procedures for null hypothesis sensitive to ordered alternatives where at least one inequality is strict 21 p3650 A67-37780

NULL ZONE

Interaction between different layers of homosphere, discussing separating and null layers and vertical interaction 13 p2115 A67-26864

Electromagnetic scattering from free-space impedance homogeneous spheres, discussing null production in backscattering cross section 23 p3973 A67-40882

NUMBER

S FROUDE NUMBER

S GRASHOF NUMBER

S KNUDSEN NUMBER

S LAVAL NUMBER

S LEWIS NUMBER

S MACH NUMBER

S NUSSELT NUMBER

S PECLET NUMBER

S QUANTUM NUMBER

S RANDOM NUMBER

S RAYLEIGH NUMBER

S REYNOLDS NUMBER

S RICHARDSON NUMBER

S SCHMIDT NUMBER

S SIMILARITY NUMBER

S STANTON NUMBER

NUMBER THEORY

Two proofs for Cauchy inequality between arithmetical and geometrical means of set of nonnegative numbers 04 p0643 A67-14728

Fundamental theorems on ordinals in inner models of set theory 04 p0646 A67-15608

Bombieri theorem on primes in arithmetic progression applied to proof of Hardy-Littlewood statement on representation of integers 06 p1025 A67-18733

Cyclotomic numbers of order 18 with applications to difference sets 13 p2146 A67-26735

NUMERICAL ANALYSIS

Numerical analysis showing dependence of

vacuum plasma accelerator geometrical and electrical parameters on plasma acceleration kinematics 01 p0122 A67-10347

Accelerated gradient method for numerical solution of parameter optimization problems with nonlinear constraints 01 p0104 A67-10428

Functional analysis of plane problem of elastostatic theory for multiply-connected regions with given surface traction 01 p0160 A67-10516

Numerical method to obtain emission coefficients from emitted spectral intensities for asymmetrical plasma sources such as atomic spectral argon line 01 p0115 A67-11073

Quasi-Newton methods in nonlinear equation solving and unconstrained optimization 02 p0259 A67-11801

Language and system design of numerical analysis problem solving system /NAPSS/ 02 p0206 A67-11803

Kantorovich theorem, Goodman-Lance method and two-point boundary value problems, noting numerical results obtained on IBM 7094 computer 02 p0259 A67-11836

FAA study of jet takeoff and landing noise effect on population around airport, establishing numerical value of noisiness 03 p0358 A67-12979

Numerical method for estimating capacity of arbitrary surface noting relation to Dirichlet problem 03 p0462 A67-14342

Numerical analysis of unsteady viscous fluid flow past circular cylinder, noting effect of Reynolds number 04 p0602 A67-14617

Elasticity and shell theory solutions for long circular cylindrical shells compared by numerical analysis 04 p0709 A67-14811

Modification of Potter method of Gaussian elimination for solving eigenvalue problems of buckling and free vibrations of shells of revolution 04 p0656 A67-14839

Numerical solution of Wiener-Hopf equation in statistical identification of linear dynamic plant 04 p0644 A67-14903

Difference approximation with second order accuracy of numerical solution for parabolic type equations 05 p0834 A67-16372

Numerical analysis of constraint effects on trial function selection in variational calculus problem of pure torsional vibration of cantilever beam of thin walled open cross section 05 p0917 A67-16418

Numerical solution of two-dimensional quasi-linear hyperbolic systems using characteristic method, obtaining approximate equations 05 p0834 A67-16436

Numerical procedure for optimizing stability of linear dynamic system by applying steepest descent method 05 p0845 A67-16437

Numerical handling of data in statistical study of servomechanism, noting circuitry and random function generator 06 p0966 A67-17586

Autocorrelation program for moving from study arrangement to data band readable in Fortran 06 p0965 A67-17587

Time-independent radiative transfer through circular cylindrical medium, using numerical methods 06 p1111 A67-17874

Book on numerical inversion of Laplace transform for computers 06 p1023 A67-17942

Flow field of finite bladed propeller in forward flight regime, analyzing harmonic content, noting fluctuating part of velocity component 06 p0937 A67-18004

Error estimation in numerical prediction of ionospheric index 06 p0995 A67-18049

Numerical method solution of nonlinear two-point boundary value problem associated with optimum transfer of spacecraft [AIAA PAPER 67-58] 06 p1023 A67-18267

Matrix error analysis compared to algorithm optimization problems of numerical analysis [AIAA PAPER 67-142] 06 p1024 A67-18475

Numerical calculation of critical hot spot thermal explosion conditions for plane slab, cylindrical and spherical symmetry 07 p1264 A67-19071

Numerical solutions of nonlinear differential equations - Conference, U.S. Army Mathematics Research Center, Madison, May 1966 07 p1212 A67-19152

Error bounds in numerical solution of ordinary differential equations, considering monotonic majorants 07 p1213 A67-19154

Second order method for nonlinear optimal control problems resulting in Riccati differential equations 07 p1213 A67-19155

Numerical solution of hydrodynamic equations adaptable to finite difference methods 07 p1167 A67-19157

Oscillating variables of flow past cylinder, calculating magnitude and frequency of lift 07 p1168 A67-19258

Numerical solution of Fredholm Integral equation of second kind with real analytic and periodic functions, noting eigenvalues 07 p1216 A67-19883

Combination numerical-analytical approach to ascent trajectory optimization 07 p1253 A67-19971

Accelerated gradient method for numerical solution of parameter optimization with nonlinear constraints [AAS PAPER 66-118] 07 p1217 A67-19977

Numerical analysis and third integral applications to n-body problem in stellar dynamics and relation to celestial mechanics 08 p1380 A67-20381

Numerical wing analysis in steady or unsteady supersonic flow, calculating pressure coefficient, local loads and generalized forces from deformation law or wing slope 08 p1278 A67-20800

Van der Monde systems and numerical differentiation based on Neville formula 08 p1349 A67-21194

Self-consistent field approximation to ion-beam-plasma boundary interaction noting effect on ion beam structure, boundary conditions and resulting current density 08 p1363 A67-21307

Soviet book on numerical solution of nonlinear boundary value problems for differential equation systems, determining eigenvalues and eigenfunctions 08 p1349 A67-21337

General purpose quadrature method for numerical evaluation of specific definite integrals 09 p1524 A67-21834

Numerical analysis and programming techniques for orbit determination 09 p1467 A67-21835

Root squaring and subresultant /RSSR/ routine as root finder for polynomial equations with real coefficients 09 p1468 A67-22050

Book on linear vibration theory including generalized properties and numerical methods 09 p1576 A67-22423

Elastic-plastic analysis showing relationship between tangent modulus and initial strain methods 10 p1728 A67-23718

Summation of convergent series for cyclotron harmonic wave dispersion for numerical and analytic work 11 p1827 A67-23886

Man-computer system for aerospace problems, discussing terminology, methods of organization, problem solution, numerical analysis, etc 11 p1755 A67-24246

Atmospheric distortion effect on signal reception by large dimensional antennas, obtaining numerical estimates for various parameters 11 p1753 A67-24439

Numerical and photoelastic solutions compared for uniform edge loading, obtaining pressure calibration by means of shear stress measurement 11 p1876 A67-24616

Numerical analysis showing dependence of vacuum plasma accelerator geometrical and electrical parameters on plasma acceleration kinematics 11 p1844 A67-25020

General formula for numerical solution of ODE of any order and linear and nonlinear systems 12 p1960 A67-25434

Book on design and analysis of scientific experiments covering statistical estimation theory in design and testing of hypotheses, emphasizing computational techniques 12 p1961 A67-25560

Discrete analysis in plate and shell theory based on method of constructing difference equation, using strain energy of system 12 p2023 A67-25591

Singularities causing numerical instabilities used in steady gas dynamic Cauchy problem solution, exemplifying with supersonic blunt body 12 p1893 A67-25932

Iso-irradiance contours close to high pressure mercury arc lamp [AIAA PAPER 67-315] 12 p2037 A67-26030

High density one-component plasma radial distribution determination by Born-Green-Yvon Integral 13 p2162 A67-26282

Surface temperature of one-dimensional homogeneous thermally isotropic body impervious to radiation 13 p2222 A67-26610

Existence of three-dimensional solution of

boundary layer equations of viscous incompressible flow in neighborhood of stagnation point 13 p2050 A67-26912

Drag coefficient for cylinder rotating in rarefied gas, comparing numerical method and approximate analytical solution 13 p2101 A67-26963

Mysovskikh theorem concerning convergence of Newton method for finding zeros of nonlinear operators between Banach spaces 13 p2147 A67-27172

Frequency shift in emission spectrum of complex atom in uniform electric field, noting numerical results for Al I 13 p2168 A67-27208

Iterative numerical method for solving equations of single variable by using several approximations applied to parallel processing environment 13 p2148 A67-27487

Numerical solution of boundary value problem for quasi-linear equation 13 p2148 A67-27498

Combination numerical-analytical approach to ascent trajectory optimization [AAS PAPER 66-112] 13 p2208 A67-27528

Iteration process by difference scheme for numerical solution to Dirichlet problem of two-dimensional Poisson equation 13 p2148 A67-27613

Optimum trajectories between material points moving along same orbit in gravitational field of spherically symmetric central body, obtaining numerical solutions for circular initial orbit 14 p2382 A67-27852

Numerical solution of linear differential equation and Volterra linear integral equation of second kind based on Lobatto four-point quadrature formula 14 p2342 A67-27977

Transverse normal loading of doubly periodic unidirectional elastic fiber reinforced infinite elastic matrix 14 p2398 A67-28098

Numerical analysis of boundary layer separation effect on evolution of wake, noting sensitivity to initial velocity profile 14 p2297 A67-28129

Numerical methods for elliptic problems, discussing application of finite difference and solution of large algebraic systems 14 p2342 A67-28156

Chapman-Enskog method modified for formulation of multicomponent laminar boundary layer problem for numerical solution 15 p2469 A67-29220

First order finite difference numerical analysis of thin elastic orthotropic and inhomogeneous cylindrical shells with small deformations from external forces 15 p2574 A67-29471

Numerical analysis of PDEs with singular coefficients, noting equivalence of stability and convergence 15 p2510 A67-29519

High accuracy alternating direction implicit difference schemes for biharmonic, heat conduction and Laplace equations 15 p2510 A67-29520

Generating time series for amount of solar radiation falling on horizontal surface of unit area at top of atmosphere per unit time 15 p2477 A67-29628

Reflection coefficient for electromagnetic wave in circular cylindrical shock tube incident on moving plasma calculated numerically 15 p2531 A67-29905

Noncircular cylindrical shell of orthotropic material under distributed load numerically analyzed by shell theory 15 p2578 A67-30272

Numerical techniques for process identification in automatic control systems, discussing methods such as autocorrelation, spectral density, differential approximation, etc 15 p2460 A67-30310

MHD generator terminal values and other electric parameters deviations for various finite length electrodes connected in series 16 p2600 A67-30532

Numerical approximation of evolution equation solution for linear and nonlinear operators by finite difference method 16 p2696 A67-31198

Numerical calculations for two-dimensional Benard convection between rigid boundaries compared with other results 16 p2660 A67-31215

Thermal plasma column instability concept applied to determine Kauffmann Criterion, calculating production coefficient, V-I characteristics, etc 16 p2719 A67-31229

Elasto-plastic stresses and strains in cracked plates analyzed by numerical

method, noting stress singularities and stress-strain fields 16 p2769 A67-31287

Numerical methods for elliptic partial differential equations with coefficients singular on boundary portion, constructing barrier functions and establishing existence and convergence theorems 16 p2697 A67-31330

Abel integral inverter discussing design, construction and performance of analog computer for solution of Abel integral equation 16 p2634 A67-31428

Algebra of factorized Regge pole residues applied to obtain relations between meson-baryon and baryon-baryon exchange processes 16 p2705 A67-31627

Numerical calculations of parameters of steady state HF high pressure vortical discharge of argon in air 16 p2723 A67-31769

Numerical analysis of ionospheric radio wave propagation, examining, attenuation polarization and power flow as function of electron density profiles 16 p2631 A67-31857

Numerical Fourier transform calculations for pulse testing procedures for controlled time function input systems 17 p2883 A67-32018

Sokolov method of averaging functional corrections for treatment of radiant interchange between surfaces 17 p2967 A67-32068

Cross sectional shape and thickness ratio variation effect on maximum high lift/drag ratio examined, using flat-topped conical bodies 17 p2789 A67-32071

Three-dimensional laminar boundary layer flow, calculating skin friction and velocity profiles 17 p2790 A67-32284

Book on nonlinear programming covering various methods and use in control 17 p2818 A67-32424

Waveguide discontinuity problems solution by digital computer 17 p2827 A67-32792

Numerical analytical method for periodic systems described by ordinary differential equations 17 p2879 A67-32877

Numerical methods for solving thermal explosion and combustion problems on electronic computers, examining Cauchy problems solutions 17 p2973 A67-33075

Book on control systems and linear vibrational mechanical systems emphasizing use of analog and digital computers, frequency response, complex plane and root locus plots, FORTRAN method, etc 17 p2822 A67-33133

Axisymmetric two-dimensional elastic wave propagation equations for finite elastic bar, considering continuous and discontinuous loadings at impact end [ASME PAPER 67-APM-22] 17 p2964 A67-33151

Numerical calculation and applied mathematics - Conference, Lille, France, 1964 18 p3071 A67-33751

First order generalized planetary theory from Poisson form, deriving trigonometric expansion of disturbing functions, periodic inequalities, etc 18 p3120 A67-33865

Thermal perturbations on fused silica primary mirror in orbiting space telescope, with numerical analysis of radiation transfer in telescope tube 18 p3046 A67-33880

Supersonic flow past smooth body with internal duct incident at angle of attack 18 p2984 A67-34212

Combination variational-difference numerical method applied to nonlinear boundary value problems, noting numerical functional minimization 18 p3071 A67-34264

Numerical solutions of hypersonic sharp leading edge flows, with full time-dependent Navier-Stokes equations solved 18 p2984 A67-34739

Alternating direction implicit /ADI/ method variant for elliptic and parabolic partial differential equations 19 p3250 A67-34868

Electronic circuits containing vacuum tubes and transistors analyzed by computer method using Bellert's algebra of structural numbers 19 p3201 A67-34907

Numerical differentiation and smoothing of equally and nonequally spaced experimental data in independent variable 19 p3250 A67-35615

Grid functions from nodal values on rectangular surface used to solve potential equation by finite difference method 19 p3342 A67-35717

Prestressed-shell buckling, using

Budlanskil-Kolter tensor nonlinear equilibrium equations by numerical analysis 19 p3343 A67-35778

Revised London theory of superconductivity destruction by current, using numerical methods for optimum phase-boundary configuration 20 p3505 A67-36208

Correlations between elastic limit, tensile strength and elongation in foundry aluminum alloys used in control reliability 20 p3465 A67-36479

Linear equation system with coefficient matrix of multiple diagonal bands solved by direct method, reducing numerical solution error 20 p3476 A67-36675

Analytical method yielding solutions for transient steady heat conduction in bodies with arbitrary boundary and initial conditions [ASME PAPER 67-HT-44] 20 p3547 A67-36726

Fabry-Perot resonator with nonuniform reflectors, analyzing resonant modes amplitude/phase distribution and diffraction/reflection losses 20 p3447 A67-36767

Numerical spectrum analysis procedures, discussing fast Fourier transform techniques, classical spectrum windows and complex demodulation process for time series studies 20 p3476 A67-36784

Temperature dependent viscosity effects on heat transfer and drag on wedge-shaped body, calculating boundary layers on surface 20 p3421 A67-36824

Optimum control problems solved by numerical methods based on variation in state space 20 p3477 A67-37035

Effect of energy redistribution between ion and electron components of plasma flow in nonuniform magnetic field, deriving relativistic and polarization corrections to classical theory 20 p3500 A67-37050

Fourth order parabolic partial differential equation solution by explicit and implicit finite difference methods 20 p3478 A67-37211

Numerical methods for linear optimal control problems, noting applicability of algorithms to certain nonlinear problems 20 p3411 A67-37375

Flow due to rotating disk with center sink solved numerically by considering flow unsteady [ASME PAPER 67-FE-8] 20 p3425 A67-37599

One-dimensional nonstationary compressible gas flow studied with variational calculus, obtaining approximate analytical periodical solutions 20 p3360 A67-37678

Full wave solutions for coupled modes corresponding to ionospheric propagation in vacuum, stressing numerical swamping problem 20 p3389 A67-37710

Modified adjoint method and Friedrichs operator equation solution for two-point boundary value problems 21 p3652 A67-38025

Finite conductivity effect on two-dimensional plasma flow in coaxial channel solved numerically, obtaining steady state flow regime by build-up method 21 p3665 A67-38240

Satellite with symmetry axis perpendicular to orbit analyzed for rotational motion, determining instability for eccentric orbit, noting gravitational effect 21 p3713 A67-38588

Numerical solution of compressible boundary layer stability equations including perpendicular flow velocity component terms 21 p3614 A67-38854

Scattering from hard surface solved numerically assuming constant potentials, relating potential present values to retarded values and to incident field 21 p3658 A67-39058

Surface temperatures of two rubbing bodies and heat partition between them determined numerically, using Fredholm integral equation solution 21 p3638 A67-39091

Basic equation derived for I-V characteristics of p-n-p-n device with graphical solution for related p-n junctions 22 p3768 A67-39251

Large scale eddy terms for balancing mean meridional circulation in winter, discussing terms magnitudes in different latitudes 22 p3828 A67-39326

Stabilizing effect of ion-ion collisions on collisional types of interchange instability, giving numerical solution of relevant normal mode equations 22 p3845 A67-39484

Numerical computations for resistive plasma drift instabilities in conducting cylinder, noting finite boundary conditions

effect 22 p3848 A67-39693

Laminar heat transfer computing method for spherically blunted cone at angle of attack requiring small numerical calculations 22 p3740 A67-39937

Nonlinear hyperbolic equations of compressible duct flow solved using centered difference method, compared with method of characteristics 22 p3784 A67-39945

Electrostatic gyro characteristics, design implications, numerical analysis of parameters and corresponding drift rates 22 p3800 A67-40185

Weighting function calculation for remote temperature sensing of terrestrial atmosphere using selective chopper radiometer 22 p3805 A67-40356

Global star cluster, initial gravitational collapse and dynamical mixing, discussing numerical analyses for homogeneous spherical cluster with Maxwell velocity distribution 22 p3894 A67-40509

Interstellar gas cloud gravitational collapse for models initially in gravitational equilibrium without mass motions, analyzing cooling and density distribution effects numerically 22 p3895 A67-40514

One-dimensional unstable cloud hydrodynamics analyzed numerically, noting collapse primarily in center and little density growth in outer region 22 p3895 A67-40515

General Pythagorean three-body problem solved completely using numerical method 23 p4062 A67-40624

Cauchy problem for heat equation noting error analysis for numerical procedure and Stefan problem solution 23 p4081 A67-40860

Discretization error analyzed for accumulation during numerical solution of equations of orbital motion 23 p4023 A67-40864

Electrically thick cylindrical antenna driven by delta function generator, discussing numerical solutions to two different mathematical models 23 p3980 A67-41206

Numerically computed power outputs and efficiency of continuous room temperature ruby lasers in good agreement with theoretical model 23 p4017 A67-41465

Numerical solution for two-point nonlinear boundary value problem of n-order ordinary differential equation 24 p4177 A67-41914

Gravity oriented satellite coupled librational motion in circular orbit analyzed for motion stability by numerical methods 24 p4231 A67-42384

Multifrequency radar system performance, obtaining expression for detection probability as frequency number, false alarm probability and integrated pulse number function 24 p4122 A67-42408

Irrational gas jet impinging on and depressing infinite liquid surface, discussing streamlines and rippling 24 p4144 A67-42585

Semimplicit numerical methods for time transient gas-lubrication Reynolds equation stressing numerical stability [ASME PAPER 67-LUB-18] 24 p4163 A67-42677

Numerical procedure for structural systems analysis, discussing computer application to hydrodynamic, electric, magnetic, thermodynamic, elastostatic and elastodynamic problems [AIAA PAPER 67-955] 24 p4127 A67-43038

Numerical solution methods for partial differential equations, discussing dynamic programming, Laplace transform and quadrature technique methods 24 p4180 A67-43084

NUMERICAL CONTROL

Numerically controlled milling for producing three-dimensional curved surfaces for turbomachinery [SAE PAPER 670096] 09 p1509 A67-22539

Automatic positioning control and problems in normalizing programming codes used in numerical control 14 p2276 A67-28956

Liapunov second method and extensions used in control problems of differential systems 15 p2574 A67-29633

Direct numerical control by computer of 150 heating circuits for safe kinetic heating test simulation of flying conditions for large supersonic aircraft 17 p2820 A67-32748

Canonical form of filtering problems with solution identical to control problem 19 p3205 A67-35911

NUMERICAL INTEGRATION

SA RUNGE-KUTTA INTEGRATION

Continuous automatic interval computation for numerical integration of initial value problem 01 p0105 A67-10515

Stiffness techniques based on numerical integration for explicit calculation of displacement functions and derivatives in subroutine 01 p0163 A67-11173

Numerical study of Newtonian potential perturbation effects on satellite motion about planet 02 p0321 A67-11496

Fourier integral calculation using Hurwitz and Zweifel numerical integration method and Euler transformation 02 p0258 A67-11557

Current density resulting from integration over energy of transport equation applicable to dielectric film 02 p0295 A67-11763

Numerical solution of ordinary differential equations at remote terminal, commenting on integration in on-line mode 02 p0259 A67-11802

Numerical integration of averaged cross section for electron induced resonance charge exchange and ionization of accelerated beam of hydrogen atoms 02 p0278 A67-12629

Numerical integration of solar orbit in model of galactic system 02 p0330 A67-12714

Algorithm for numerical calculation of three-dimensional boundary layer of incompressible fluid 03 p0401 A67-12876

Supersonic underexpanded jet interacting with obstacle in numerical solution using integral relations and characteristics 03 p0350 A67-12879

Numerical determination of axisymmetric equilibrium shapes of interface between two nonmixing liquids uniformly rotating in vessel under weak centrifugal and capillary forces and zero gravity conditions 03 p0402 A67-12882

Characteristics method in numerical solution of one-dimensional problems of propagation 03 p0458 A67-13348

Approximation method for computation of radiation patterns from circular apertures and reflectors by single integration at wide angles and large Fresnel numbers 03 p0384 A67-13844

Static electrointegrator for numerical solution of boundary layer theory problems for incompressible fluid and compressible gas 04 p0603 A67-14642

Variational approximation of normal velocity on oscillating wings including linear approximation, numerical integration and comparison to least squares method 04 p0547 A67-14842

Stability and error analysis of Runge-Kutta-Fehlberg numerical integration method 04 p0645 A67-14986

Book on numerical realization of variational methods, discussing Hilbert space elements, Ritz and Bubnov-Galerkin stability processes, spectral and nonlinear problems, etc 04 p0645 A67-15009

Numerical analysis of crack propagation in cyclic loaded structures, taking into account load ratio and instability at onset of fast fracture [ASME PAPER 66-WA/MET-4] 04 p0711 A67-15342

Boundary layer equations for pseudoplastic fluids solved for exact numerical solutions, specifically near stagnation point 04 p0609 A67-15599

Exterior Dirichlet problem for reduced wave equation treated by numerical method 05 p0835 A67-16738

Numerical integration of quasi-geostrophic atmospheric model with asymmetric zonal current 06 p0999 A67-18739

Partial diaphragm when applying supersonic Mach box method for steady state condition and uniform downwash on wing compared with complete diaphragm 06 p0944 A67-18875

Heat transfer in compressed gas evacuated from container, using numerical integration of state equation 07 p1267 A67-19324

Gravitational field of any primary determined using observations of satellites in orbit about primary, noting numerical integration technique and special perturbation methods [AAS PAPER 66-109] 07 p1253 A67-19969

Invariant imbedding and numerical integration of boundary value problem for unstable linear systems of ordinary differential equations 07 p1218 A67-20214

Pontryagin maximum principle, discussing singular and nonsingular extremals classification by numerical integration techniques 07 p1182 A67-20273

Solutions of fifth order Runge-Kutta equations 08 p1347 A67-20369

Two methods of numerical construction of derivatives involved in inversion of Laplace transform 08 p1347 A67-20370

Numerical analysis of plane restricted three-body problem with two bodies of equal mass moving on circular orbit 08 p1380 A67-20386

Resonance relation between orbits of Neptune and Pluto established by numerical integration 08 p1381 A67-20392

Harmonic series of coordinates of moon in three-body problem of sun-earth-moon treated by numerical method 08 p1382 A67-20395

Aerodynamic stability coefficients determined from sounding rocket flight data, using computer program for numerically integrating six degrees of freedom motion equations 08 p1407 A67-20517

Spectral stability criteria for numerical integration procedure using Z transforms, specifically finite difference operators 08 p1296 A67-20600

Numerical solution methods for variational problems of flight dynamics 08 p1348 A67-21114

Numerical integration of restricted problem of three bodies for finding lunar trajectories, using motion equations and Taylor series 08 p1396 A67-21181

Numerical solution of sequential decision problems involving parabolic equations with moving boundaries 08 p1349 A67-21256

Numerical solution of integrodifferential equations 08 p1349 A67-21261

Stability of stepwise solution methods of initial value problems for second order differential equations 09 p1524 A67-21935

Stability of Fehlberg method when applied to solution of initial value problems for second order differential equations 09 p1524 A67-21936

Numerical quadrature methods of Romberg, Chebyshev and Monte Carlo, noting analytic function and program for machine evaluation 09 p1488 A67-22047

Numerical integration of dispersion relation for electron beam in plasma 09 p1546 A67-22313

Symmetrical equilibrium flow past blunt body at superorbital reentry conditions calculated by integrating motion equations across shock layer 10 p1591 A67-23109

Numerical calculations of blast waves by standard and Hartree techniques compared with analytical results and application of Richardson extrapolation method 10 p1625 A67-23110

Radial flow of compressible fluids between disks solved through simpler form instead of numerical integration of differential equations 10 p1593 A67-23475

Numerical solution of class of nonlinear high order differential equations with two-point asymptotic boundary conditions for thermal boundary layers in laminar and turbulent flow 10 p1627 A67-23560

Numerical solution methods of invariant imbedding equation for reflection function of spherical shell with absorption and isotropic multiple scattering 10 p1680 A67-23634

Error accumulation in numerical integration of motion equation analyzed for circular satellite orbits 11 p1859 A67-24317

Calculating method for parachute opening forces, system velocity, cloth pressure loading and filling time for horizontal and vertical deployment 11 p1743 A67-24348

Flight time estimation methods for iterative solutions of optimum trajectories by numerical integration 11 p1859 A67-24436

Hydrodynamic stability problems solved through approximate and numerical methods involving eigenvalue spectrum and Orr-Sommerfeld equation for parallel flow 11 p1781 A67-24552

Gradient acceleration technique for solving optimal systems with unbounded control 11 p1771 A67-24896

Modified quasi-linearization method for numerically solving trajectory optimization problems with undetermined terminal time 12 p2008 A67-25913

Relaxation time for spatially homogeneous electron gas calculated by direct numerical integration of linearized Fokker-Planck equation 13 p2164 A67-26297

Zeta transformation applied to numerical integration operator to determine stability of solution to system of linear differential equations on digital differential analyzer 13 p2072 A67-26348

Unified method of numerical quadrature for integrands of certain complex analytic functions, obtaining asymptotic expansion of error functional 13 p2145 A67-26734

One-dimensional transport equations of p-n junction in steady state solved numerically 13 p2078 A67-26781

Numerical integrations of equation for turbulent diffusion in atmosphere 13 p2152 A67-26863

Numerical integration of averaged cross section for electron induced resonance charge exchange and ionization of accelerated beam of hydrogen atoms 13 p2171 A67-27387

Plane problems of elasticity theory solved numerically using conformal mapping 13 p2220 A67-27621

Heat conductivity effect on various one-dimensional flows solved by numerical integration of Navier-Stokes equations 14 p2296 A67-27980

Synthesis of field distribution over aperture of antenna radiating maximum portion of power into given solid space angle 14 p2283 A67-28274

General formulation and solution methods of electromagnetic wave diffraction and scattering problems 14 p2268 A67-28448

Numerical solution of Cauchy problem class of nonlinear integrodifferential equations 14 p2344 A67-28896

Cometary orbit evolution of Jupiter family, considering influence of Jupiter 15 p2553 A67-29155

Order and asymptotic form of error of numerical methods for solving initial value problem for differential equations 15 p2471 A67-29632

Orbit of Halleys comet integrated ahead to next apparition /1988/ and predicts time perihelion passage 15 p2557 A67-29874

Perturbation theory methods as applied to first order differential equation 15 p2560 A67-30041

Error assessment in numerical integration for ordinary differential equations applied to many-body problem 15 p2512 A67-30053

Numerical solutions to differential equations governing earth electric field near surface obtained by Runge-Kutta method 16 p2664 A67-30974

Invariant curves dissolution and nonapplicability of third integrals explained examining perturbation values and initial conditions and resonance phenomena 16 p2748 A67-31140

Celestial mechanics and adaptation of perturbation methods and numerical integration techniques to stellar dynamics 16 p2748 A67-31141

Numerical solution of nonlinear integral equations with variable upper limit, applicable to Cauchy and boundary value problems 16 p2696 A67-31142

Two-dimensional viscous fluid flow with formulation and solution of weak shock reflection problems by numerical method 16 p2662 A67-31534

Optimization of numerical solution to linear ordinary differential equation with homogeneous boundary value conditions 16 p2698 A67-31546

Optimal control and convex programming, discussing problem of admissible investment program control for production constraints 17 p2829 A67-32431

Predictor-corrector for solving ordinary differential equations, discussing influence of rounding-off errors on accuracy of solution 18 p3071 A67-34286

Parallel numerical integration formulas for differential equations 18 p3072 A67-34395

Fokker-Planck damping introduced into Fourier-Hermite representation of Vlasov equation produces Landau and Van Kampen treatments 18 p3030 A67-34754

Single-step numerical integration stability analysis applied to linear differential equations with known root locations 19 p3249 A67-34839

Long term global integrations of primitive

meteorological equations for free surface model, using spherical polar coordinates 19 p3252 A67-35058

Atmospheric spectra and related quantities calculated, obtaining radiation spectral distribution by radiative transfer equation, comparing results with other studies 19 p3220 A67-35260

Numerical integration solution for finite elastoplastic deflections of circularly symmetrical plates 19 p3340 A67-35511

Conditions for optimal planar intermediate-thrust /singular/ trajectory in inverse-square-law field analyzed graphically 19 p3333 A67-35749

Numerical digital computer solution of parabolic partial differential equations with two-point boundary conditions, using method of lines 20 p3391 A67-36820

Probability characteristics of oscillating satellite motion, considering random parameter scatter and atmospheric density variations, with expectation obtained by numerical integration 20 p3485 A67-36922

Variational equations solved by numerical integration along with nonlinear differential equations with less computing and storage and higher accuracy 20 p3478 A67-37212

Multiple integration method for determining coefficients and differential equation order for linear dynamic systems 20 p3412 A67-37378

Turbulent MHD boundary layer in liquid with linear pressure gradient, discussing numerical integration, flow velocity and magnetic field distribution 21 p3665 A67-38244

Eigenstate variables for representation of optimum orbital transfer problems, discussing numerical integrations 22 p3878 A67-39154

Charge model for unsaturated and saturated p-n-p dynamic behavior using numerical integration techniques 22 p3766 A67-39249

Glider towing cable configuration taking into account aerodynamic drag forces, using digital computer for numerical calculations and integrations 22 p3745 A67-39551

Numerical recursion method for calculation of characteristic exponent of Mathieu differential equation 22 p3827 A67-39744

Lagrange multipliers in two-point boundary condition problems for trajectory optimization estimated by direct method 22 p3885 A67-39963

Equations numerical integration for MHD fluid flows near critical point in presence of azimuthal magnetic field for several Alfvén and diffusion numbers 22 p3853 A67-40011

Numerical integration of Eros orbital motion normals, obtaining earth-moon mass and various astronomical constants 23 p4061 A67-40621

Spin characteristics of VJ 101 C VTOL airplane via numerical integration of motion equations including mass coupling effects and nonlinear aerodynamics 23 p3934 A67-41313

Explicit nonlinear numerical integration method for solution of large systems of ordinary differential equations 23 p4024 A67-41394

Minimizing maximum control deviation problem reduced to motion equation numerical integration 24 p4188 A67-42301

Finite difference integration method for predicting flow velocity and temperature distribution of gaseous diffusion flame in axisymmetrical combustion chamber 24 p4091 A67-42383

Frequency Response and direct numerical integration of governing differential equations, considering gas-lubricated tilting-pad journal bearing stability [ASME PAPER 67-LUB-8] 24 p4162 A67-42672

Terrestrial gravity anomalies influence on satellite orbits treated by analytical numerical integration 24 p4237 A67-42686

Cometary orbit evolution of Jupiter family, considering influence of Jupiter 24 p4240 A67-43078

Integration of motion equations of second order incompressible fluid 24 p4146 A67-43106

NUSSELT NUMBER

Analytic approximation method for thermal convection at large Rayleigh numbers 04 p0721 A67-14649

Turbulent boundary layer-flat surface interfacial Stefan-Nusselt flow effects on apparent kinetics of heterogeneous chemical reactions in forced convective systems 04 p0567 A67-15681

Mass transfer and hydrodynamics of gas jet injection into liquid surface, deriving empirical equations for hollow truncated point formed around injection point 04 p0727 A67-15754

Finite difference solution of parabolic equation for laminar heat transfer in inlet of rectangular duct as function of wall temperature and Nusselt number for different aspect ratios 04 p0728 A67-15805

Convective heat transfer from bluff bodies analyzed, particularly small electrically heated cylinders at low Reynolds numbers, noting correlation with Nusselt and Prandtl numbers 04 p0732 A67-15831

Energy methods of subcritical convective instability theory and critical Rayleigh number dependence on Nusselt number 05 p0926 A67-16816

Asymptotic properties of fluid temperature field and Nu numbers in nonstationary heat transfer during passage of laminar flow of viscous incompressible fluid through rectilinear channel 07 p1265 A67-19125

Criterion expressions for Nusselt numbers of mass transfer in two-phase film system at high Prandtl numbers which describe physical properties of both phases 14 p2405 A67-28303

Nusselt results concerning heat transfer extended to include surface tension effect on heat transfer coefficient 17 p2970 A67-32461

Local heat-transfer coefficients of turbine blades, evaluating local Nusselt number distribution, Reynolds numbers, and turbulent flow effects 20 p3515 A67-36451

Convection initiation Rayleigh number in closed cell and Nusselt number-Rayleigh number relation after convection initiation [ASME PAPER 67-HT-4] 20 p3544 A67-36703

Arbitrary internal heat generation terms in energy equation effect upon limiting Nusselt number for heat transfer to pipeline flow of non-Newtonian fluids [AIChE PAPER 12] 20 p3552 A67-36828

Heat transfer in fully developed laminar flow through rectangular and isosceles triangular ducts, determining Nusselt numbers 20 p3553 A67-36940

Asymptotic properties of fluid temperature field and Nu numbers in nonstationary heat transfer during passage of laminar flow of viscous incompressible fluid through rectilinear channel 21 p3731 A67-38169

Cooling of cylinder moving through fluid assuming fluid properties permit boundary layer approximations 22 p3918 A67-39782

NUTATIONAL OSCILLATION

Acceleration perturbations, gravity gradient torques and nutational motions effects on pendulums and gyrocompasses used as vertical indicating devices 01 p0064 A67-10644

Couple due to distant mass acting on nonspherical object determined, considering luni-solar precession and nutation variability 08 p1031 A67-17778

Nutation divergence during atmosphere exit of spin stabilized probe shown to be analogous to pendulous gyro with time dependent spring 08 p1406 A67-20511

Optical transient nutation effect in carbon dioxide laser 11 p1802 A67-24829

Viscous friction in axes of gyroscope suspension further damping of nutational oscillations and increases precession oscillations of inertial vertical 11 p1794 A67-25051

Freely precessible gyroscope viscous fluid nutation damping response to translational and vibration accelerations near critical frequencies 12 p1942 A67-25679

Conservative systems motion stability, generalizing precession and nutation of gyroscope with respect to noncyclic coordinate 15 p2518 A67-29685

High sensitivity inductive transducer using ferrite rings for measuring nutational oscillations of gyroscopic instruments 21 p3630 A67-38917

NUTRITION

SA DIET

SA FOOD

SA SPACE FLIGHT FEEDING

Functional or reactive hypoglycemia as potential cause of flight accidents, showing alimentary behavior of pilot brings about apparition of hypoglycemic phases 14 p2254 A67-28216

Human hair-root activity during short term deprivation of protein 19 p3177 A67-34954

Simultaneous copolymerization of Leuchs anhydrides of 18 amino acids common to protein, discussing nutritional significance 20 p3377 A67-37397

NUTRITIONAL REQUIREMENT

Effects of various diets and simulated space conditions on human waste and water consumption applied to life support system development 02 p0188 A67-12339

Food quality design for Gemini and Apollo space programs 05 p0757 A67-17261

Gastroenterology in space medicine and physiological basis of cosmonaut nutrition 13 p2058 A67-26752

Biological value of plant proteins for closed life-support system, studying diet effects on rats 16 p2612 A67-30908

Oxygen toxicity relation to nutrition, hormonal secretion and age factors, discussing experiments on rats 23 p3956 A67-41632

NUTS AND BOLTS

Threaded fastener reliability factors noting mechanical testing 11 p1795 A67-24040

Threaded fastener design and manufacture 15 p2493 A67-29650

NYLON

SA POLYAMIDE

Relation between effective porosity and differential pressure of rigid steel and elastic nylon ribbon grids of various forms and porosities 06 p0844 A67-17630

Ablative properties of nylon-phenolic materials used in fabrication of composite heat shield with low residual stresses 09 p1523 A67-22506

Ablative behavior of low and high density phenolic nylon in diffusion controlled surface combustion regime [AIAA PAPER 67-328] 12 p2038 A67-26042

Space environmental effects on filled elastomers, nylon parachute material and adhesion of metals 15 p2506 A67-29540

NYSTAGMUS

SA EYE MOVEMENT

Caloric nystagmus in man clarified by test in weightless phase of parabolic flight 15 p2428 A67-29277

Visual arousal interaction and specificity of nystagmic habituation 17 p2805 A67-31958

Habituation transference in Coriolis stimulation for change from passive lateral chair tilts to various active head tilts during rotation 23 p3953 A67-41585

O-RING SEAL

Gland design variation effects in gaseous helium seal performance from O-ring permeation measurements at pressures up to 1000 psi 17 p2801 A67-31992

O STAR

Kinematic, spectroscopic and photometric data for pygmy stars /blue ultradwarfs/ 17 p2945 A67-32645

O and B stars surveyed with 154 cm Catalina reflector show discrepancies from mean interstellar polarization-wavelength dependence near Orion 23 p4062 A67-40626

OAO

Orbiting radio telescope for cosmic radio wave frequency and amplitude detection 02 p0334 A67-12360

OAO satellites for astronomical experiments, discussing planning and specific features 06 p1098 A67-19048

Space astronomy program development, discussing manned orbital observatory concept and instrumentation 08 p1392 A67-21071

Large orbital observatories design for permanent residence, noting atmospheric control and vehicle stabilization 09 p1572 A67-22673

OAO structure for measuring absolute stellar energy in UV region 10 p1712 A67-22991

Explorer type compared to Orbiting Observatory type satellites regarding weight,

volume, reliability, data transmission, power, etc 12 p2012 A67-25785

Digital command and experimental data storage system for OAO 16 p2633 A67-30670

Attitude control for orbiting astronomical observatories, noting system design and performance characteristics 16 p2763 A67-31689

Continuous monitoring and control of primary mirror figure of orbiting, diffraction limited astronomical telescope for optimum performance 16 p2680 A67-31802

Manned orbiting laboratories for exploring planets by remote sensing and planetary encounter missions compared to landing and flyby 19 p3332 A67-35336

Small and large orbiting observatory satellites compared for operational needs, interference problems, scheduling and multisampling of space phenomena [AIAA PAPER 67-634] 20 p3534 A67-37616

SNR performance of SEC vidicon image storage tube at optimum and reduced readout rates 22 p3773 A67-39961

Manned orbiting space station operation in association with unmanned observatory, comparing gimbal mounted, free floating, tethered and firmly fixed modes [AIAA PAPER 67-926] 24 p4245 A67-43022

OBLATENESS

Encke special perturbation method of integrating motion equations of near-earth satellites modified to eliminate first-order effects of earth oblateness 01 p0148 A67-10383

Earth oblateness effect on torque experienced in nonuniform geogravitational field by satellite with unequal principal moments of inertia 01 p0154 A67-11194

Cosmogonic hypotheses evaluation based on relation between oblateness, mass and number of satellites of planets of solar system 13 p2198 A67-26765

Solar oblateness and Mercury perihelion advance, showing turbulent viscosity forces acting on photospheric meridional currents as possible distortion cause 21 p3701 A67-37963

Lunar orbit precession due to quadrupole moment of sun arising from solar oblateness 23 p4066 A67-41014

OBLIQUE COORDINATE

TM and TE mode uncoupling in oblique wave scattering from radially inhomogeneous cylinders 22 p3763 A67-40308

OBLIQUE SHOCK WAVE

Oblique shock detection in conical nozzle with circular arc throat, noting measurement techniques 04 p0547 A67-14833

Deflection angle of supersonic gas flow with oblique shock wave and heat input in wake, choosing minimum entropy variation as measure of system optimality 04 p0550 A67-15898

Steady oblique nonlinear waves in warm collision-free plasma 05 p0857 A67-17425

Oblique shock wave evolution in MHD 05 p0859 A67-17489

Asymmetric interaction of supersonic vehicle intercepted with oblique shock wave [AIAA PAPER 67-180] 06 p0989 A67-18486

Magnetic and plasma observations of Explorer X and Mariner II confirmed that interplanetary shock waves give rise to sudden storm commencements magnetic and plasma observations of Explorer X 12 p2008 A67-25823

High altitude jet structure for two-dimensional and axisymmetric cases with very large exit/ambient pressure ratio 15 p2418 A67-30208

Propagation of strong ionizing front at arbitrary oblique angle relative to magnetic field, determining limits to value of electric field ahead of shock 17 p2908 A67-33114

Oblique, normal and transverse ionizing shock waves 18 p3092 A67-34733

Vibrational excitation effects on shock wave behavior calculated analytically by linearizing problem 19 p3212 A67-35773

Oblique interaction between supersonic vehicle in free flight and plane shock wave simulated, noting large unbalanced force 21 p3807 A67-37776

One-dimensional steady MGD flow of polytropic gas with finite constant electric conductivity, noting flow patterns and oblique shock wave structure 24 p4198 A67-42707

OBSERVATION

S CELESTIAL OBSERVATION

S RADAR OBSERVATION

S RADIO ECHO OBSERVATION

S RADIO OBSERVATION

S SATELLITE OBSERVATION

S SOLAR RADIATION OBSERVATION

S VISUAL OBSERVATION

OBSERVATORY

S ASTRONOMICAL OBSERVATORY

S GEOPHYSICAL OBSERVATORY

S LUNAR OBSERVATORY

S SOLAR OBSERVATORY

OCCULTATION

SA LUNAR OCCULTATION

SA STELLAR OCCULTATION

Mars atmosphere and ionosphere analyzed by measuring effect on radio occultation of planet, determining shape, atmosphere density profile, diurnal variations, etc [JPL-TR-32-1157] 13 p2199 A67-26819

Sun illumination time of artificial earth satellite moving in elliptical orbit 13 p2200 A67-27338

Computing transits of outer planets /Jupiter to Pluto/ over solar disk, as seen from another outer planet 17 p2948 A67-33095

Solar radio noise source position determined during occultation caused by partial solar eclipse of May 20, 1966 17 p2953 A67-33403

Ground instrumentation system for Mariner IV occultation experiment, using Doppler frequency perturbation method for Mars atmospheric parameters determination 18 p3049 A67-34498

Satellite rise and set time of distant primary and occultation interaction determined for case of Martian satellite 24 p4238 A67-42925

OCEAN

SA ATLANTIC OCEAN

SA PACIFIC OCEAN

Geomagnetic anomalies over Pacific-Antarctic ridge and distribution of causal bodies with reference to field reversal 04 p0611 A67-14493

Cloud vorticity effects on ocean roughness, from Tiros autumnal observations 04 p0651 A67-15469

OCEANOGRAPHY

Remote sensing of environment - USAF and USN Symposium, University of Michigan, Ann Arbor, April 1966 01 p0057 A67-10307

Radiation and scattering of transient gravity waves by thin vertical plates in deep ocean 06 p0985 A67-18188

Oceanographic measurements with instrumented satellites, examining surface temperature surface waves, tides, albedo, heat flux and coordination of airborne and seaborne sensing systems 06 p0999 A67-19000

High resolution radar correlometer measurement of spatial correlation radius of RF radiation scattered by disturbed ocean surface 08 p1294 A67-20819

Aircraft instrumentation for oceanographic measurement platform including radiation thermometer, wave meter and expendable bathythermograph 09 p1441 A67-22498

[AIAA PAPER 66-695] Global ocean data acquisition by remote sensor operating from spacecraft for oceanographic studies 15 p2477 A67-29698

Space utilization by joint venture approach, discussing communications, ocean studies, etc 19 p3350 A67-35651

Structure and properties of glass-ceramics noting applications to space and oceanographic exploration 20 p3473 A67-36596

OCULAR CIRCULATION

Existence of fovea in human retina explained by blood supply interference with steady and acute vision 02 p0184 A67-11473

Bilateral conjunctival hyperemia attributed to cardio-hemo-respiratory decompensation 04 p0561 A67-14628

Tonometric and tonographic investigations of intraocular tension in hypoxia 06 p0953 A67-17995

OGIVE

SA ELLIPSOID

Controlling radar cross section of long thin bodies by employing corrugated structures operating in nonpropagating mode 03 p0370 A67-13862

OGO

Energy spectra and abundances of elements He through Si of galactic cosmic ray above 20 mev per nucleon in nuclear charge range between 2 and

26 02 p0307 A67-11687

OGO experiments including earth atmosphere, magnetosphere, earth-sun system, etc 02 p0334 A67-12359

Geomagnetic field values obtained from OGO-2 satellite-mounted rubidium vapor magnetometer 10 p1641 A67-23244

IMP-II and OGO-I measurements on plasma characteristics in transition region between solar wind and geomagnetic field 12 p1997 A67-25806

Nuclear abundances of galactic and solar cosmic rays, discussing detector electronics system for measurement of particle energy spectrum 12 p1944 A67-25852

OGO communication system design and flight test 12 p1907 A67-25994

Magnetic design of OGO and Pioneer solar probe including data on instrumentation, mechanical equipment, permanent magnets, test methods, etc 16 p2757 A67-30637

Electronic checkout, environmental qualification and integration of OGO by spacecraft simulator and performance analysis system 16 p2654 A67-30639

Large sun-oriented deployable solar array for OGO design, fabrication and flight performance 24 p4104 A67-42508

OGO-A

Charged particles with Alfvén velocities distribution in magnetosphere analyzed based on cold plasma density, emphasizing data of OGO A 17 p2899 A67-32256

OGO-A satellite observations of hydromagnetic whistlers /pearls/ nature, showing linkage to magnetosphere 18 p3042 A67-34390

Alpha particle proton ratio of geomagnetic field from data from charged-particle telescope on OGO 1 20 p3519 A67-37412

Energetic protons from March 24, 1966 solar flare observed with OGO 1 satellite scintillation counter 23 p4060 A67-41233

OGO-B

Airglow lines measured through photometers on OGO-II satellite, noting nadir and zenith airglow 10 p1660 A67-23278

NASA observations for orbit determination from Goddard Range and Range Rate system compared to OGO-B observations 19 p3319 A67-35216

OGO-C

Electron energy spectra analyzed in earth magnetosphere using OGO 3, noting relation to radial distance 07 p1244 A67-19926

OGO 3 observation of low energy protons and electrons in earth magnetosphere, noting narrow peak of relatively high low-energy particle intensities 13 p2190 A67-26312

Flux, energy distribution and density of ions and electrons in magnetosphere plasma during solar activity period determined by OGO-C electrostatic probes 19 p3217 A67-35200

Charged particles of extraterrestrial ring current during geomagnetic storms, with Ogo 3 measurements of proton and electron differential energy spectrums 20 p3432 A67-37401

OH-6 HELICOPTER

Avionics equipment development for Cayuse helicopter, discussing design with respect to weight, size, maintainability and other logistical considerations [AHS PAPER 105] 18 p2680 A67-31822

Light Observation Helicopter Avionics Package /LOHAP/, designed for OH-6A Cayuse helicopter, providing communications and navigational capabilities 23 p3980 A67-40927

OHM LAW

Ohm law deviation in island-structure thin metallic films and current dependence on field strength 03 p0490 A67-13159

Ohm law in multicomponent nonisothermal plasmas derived as function of electric and magnetic fields and temperature and pressure gradients, using transport equation 05 p0857 A67-17422

Two-fluid theory for plasma stability, obtaining equation on velocity field perturbation by considering Ohm law, stress tensor with Larmor radius and viscosity from collisions 10 p1685 A67-23465

Book on mathematics of MHD which assumes that working fluid is Newtonian and obeys Ohm law in form appropriate to moving conductors 15 p2527 A67-29384

Ionization wave velocity in nonisothermal, low temperature plasma discussed, using

generalized Ohm law, law of conservation of electron energy and SAHA equation 16 p2711 A67-30540
 Ohm law extended to electrical conduction of partially ionized plasmas and nonneutral ionized gases 19 p3287 A67-35356
 Gold-doped silicon diode space charge and oscillation effect, discussing deviation from Ohm law at lowest voltages 19 p3198 A67-36043
 Transport process instability theory, discussing collisionless plasma transport phenomena and relation to Ohm law 20 p3495 A67-36156
 Dense hydrogen plasma ohmic heating in quasi-stationary discharge without external magnetic field, obtaining stable impurity-free plasma column 24 p4195 A67-41939

OHMIC LOSS

Antenna characteristics of Dwingeloo radio telescope, determining directivity, response pattern, ohmic loss, etc 18 p3008 A67-33433

OIL

SA LUBRICATING OIL

SA MINERAL OIL

SA PETROLEUM

Technical characteristics of Peschanyi Island oil and feasibility study of technological process for aviation oil production 04 p0627 A67-14742
 Continuous nucleonic oil quantity gauging system requiring no tank penetrations 05 p0842 A67-16538
 Oils and shales from 3 million to 2.7 billion years old analyzed for hydrocarbon content, using gas chromatography and mass spectrometry 05 p0797 A67-16580

OLEFIN

Orientation of free radicals in addition reactions with unsymmetrical monoolefins 09 p1459 A67-22366

OLIVINE

Preferred shape orientation of olivine crystals in porphyritic chondrules suggesting drawing from larger magma bodies 16 p2619 A67-30986
 Olivine composition in chondrites relative abundances and classification 16 p2751 A67-31455
 Linear melting curve of fayalite up to 40 kb determined, using piston cylinder and thermocouples 21 p3617 A67-38190

OMNIDIRECTIONAL ANTENNA

Directive gain and impedance calculated for ring array of antennas that concentrate radiated power in plane of ring and are omnidirectional 02 p0211 A67-11595
 Omnidirectional slot antenna with two slots resonant at frequencies nearly octave apart and fed by single common waveguide 04 p0590 A67-15904
 Optimum illumination for maximum power transfer between two opposed rotationally symmetric antennas 11 p1762 A67-24291
 NASA space applications and future possibilities noting ATS-I satellite for cloud photography, omnidirectional aircraft antennas and Apollo Applications Program [AAS PAPER 67-89] 15 p2583 A67-29951
 Omnidirectional radiation pattern for S-band telemetry on rockets more than 1/2 ft in diameter by small electrical separation of antennas [AAS PAPER 67-51] 15 p2454 A67-30116
 Antennas featuring steerable notch in omnidirectional pattern as alternative to narrow beam antenna for certain applications 16 p2638 A67-31335
 Despun antenna system for satellite stabilized by rotation around axis perpendicular to orbital plane 21 p3591 A67-38204
 Telemetry antenna of instrument container of D-1 satellites 21 p3592 A67-38218
 Omnidirectional double slot array of thin X-band rectangular waveguides, noting design for slot conductance and power handling capacity 23 p3977 A67-40699

ON-LINE PROGRAMMING

Numerical solution of ordinary differential equations at remote terminal, commenting on integration in on-line mode 02 p0259 A67-11802
 Digital communications system evaluator /DICOSE/ using stored program processor coupled with communication channel arrays to provide real time on-line system 02 p0230 A67-12127
 AEDNET system of digital computer programs for on-line simulation of nonlinear networks and oscilloscope

display 03 p0375 A67-13665
 On-line digital computer used in optimizing control by prediction, including quadratic and steady state value 05 p0784 A67-18524
 Phaseplot, on-line graphical output parametric display technique, noting hardware realizations and software requirements 13 p2073 A67-27063
 Digital computer used for on-line control of jet engine 13 p2074 A67-27190
 On-line nonlinear circuit design, discussing computer program for evaluating performance resulting from modifications 15 p2442 A67-29169
 Synthesis and design of on-line self-organizing control of multiple goal, multiple actuator systems 16 p2848 A67-31854
 Adaptation technique for on-line steady-state optimizing control using updated control algorithm 16 p2848 A67-31855
 DIALOG /computer implemented retrieval system/ capabilities, design, philosophy and performance 17 p2819 A67-32468
 Iterative on-line reliability calculation of automatically repaired space computer, noting reliability and performance 17 p2820 A67-32501
 Radar system using real-time on-line computer applied to adaptive control of beam direction and transmitter modulation 17 p2816 A67-32790
 Computerized method for on-line data analysis, elucidating SLIP language, request, processing, interpretation, time sharing, background activity, etc 17 p2821 A67-32865

ONBOARD NAVIGATION

Onboard digital computer navigation, guidance and control of reentry and aerospace vehicles 06 p1028 A67-17922
 Onboard device locating present and future orbital satellite position through microfilm map dependent on satellite motion equation 08 p1352 A67-21525
 Book on range instrumentation covering optical, radar, support systems, etc 10 p1604 A67-22992
 Computational limitations of onboard orbiting computers such as fixed point arithmetic, limited word length and solution techniques 17 p2881 A67-32056
 Systems recommended to meet area navigation requirements, considering pictorial display/ course line computer /PD/CLD/ application 17 p2881 A67-32391
 Deep space navigation and guidance technology, emphasizing simplification of onboard navigation procedures 19 p3255 A67-35856
 Satellite attitude by onboard radio antennas method 21 p3583 A67-38637
 Compact air-to-ground laser rangefinder onboard helicopter nose section 23 p3999 A67-41028
 Time factor in onboard checkout and in-flight maintenance of manned spacecraft, discussing mission events and man-machine interaction [AIAA PAPER 67-950] 24 p4245 A67-43034
 Spaceborne computer-managed laboratory for experiments and instruments control in future space missions [AIAA PAPER 67-957] 24 p4140 A67-43040

ONE-DIMENSIONAL FLOW

One-dimensional compressible gas-channel flow under thermal and mechanical effects analyzed within generalized energy coordinates 01 p0119 A67-10170
 Parametric representation derived for one-dimensional nonsteady flows, considering two distinct solutions of Martin Monge-Ampere equation 01 p0052 A67-10520
 Stability of solutions to general equations of steady state one-dimensional relaxed flow of perfect gas mixtures 02 p0305 A67-12353
 Gas flow of two-phase medium in Laval nozzle in presence of small particle lags in velocity and temperature in one-dimensional formulation 03 p0349 A67-12865
 Transformation of unknown functions and independent variables entering into differential equations for motion of nonviscous nonheat-conducting gas 03 p0403 A67-13628
 Transverse wave behavior in reactive flow, analyzing refraction or reflection of acoustic

waves at shock front, obtaining comparison of behavior in corresponding real flows 03 p0405 A67-14026
 One-dimensional steady state gas compression flow undergoing thermodynamic relaxation processes 03 p0405 A67-14258
 Differential equations for local interfacial and wall shear stresses for one-dimensional annular two-phase flow 04 p0735 A67-15857
 Group classification by Cartan method of equations of one-dimensional plane wave gas flow 04 p0611 A67-15982
 Approximate solutions for uniform gas cloud expansion into vacuum with attention to inaccuracies 06 p0993 A67-18890
 Relations between rates of propagation of constant pressure, density, etc, for one-dimensional MGD flows 08 p1357 A67-20585
 Shock wave formation due to heat addition to one-dimensional flow of ideal inviscid conducting monatomic compressible fluid under transverse magnetic field 08 p1359 A67-20980
 Quasi-one-dimensional analysis of MGD, considering equations of continuity, state, current density, etc [AFOSR-67-1000] 09 p1540 A67-21792
 Quasi-one-dimensional plasma motion in linear and radial Hall type MHD generator ducts 09 p1541 A67-21798
 Nonequilibrium excitation influence on electron density in one-dimensional MFD channel flow 09 p1542 A67-21814
 Structural equations with variable coefficients for nonstationary one-dimensional gas flows, using Cartan method 09 p1487 A67-21912
 Flow of ideal gas behind shock wave of finite amplitude analyzed, based on equation for one-dimensional adiabatic motion 10 p1624 A67-23033
 One-dimensional compressible flow, considering buoyancy forces as closed-form solution of Navier-Stokes equations for unknown temperature-dependent coefficient of viscosity 10 p1625 A67-23135
 Invariant transformation for pulse and continuity equations of one-dimensional unstabilized motions of ideal compressible fluid 10 p1628 A67-23678
 Nonlinear hydrodynamic stability theory of one-dimensional detonations based on perturbation techniques, detailing cases of ideal gas unimolecular reactions 11 p1774 A67-23857
 One-dimensional flow through nozzle and stability of weakly ionized plasma with induced Hall current 11 p1832 A67-24155
 Calculation of weight flow and velocity for real gas, obtaining correction factor 11 p1779 A67-24355
 Strong plane shock attenuation from impact studied with numerical method of characteristics for one-dimensional unsteady flow, showing late-stage equivalence 11 p1820 A67-24905
 Parameters of gas behind incident and reflected shock waves calculated, using gas dynamic and chemical equilibrium equations for one-dimensional problem 12 p1930 A67-28134
 Plane one-dimensional MHD flow in transverse magnetic field with magnetic Reynolds number equal to or greater than unity 13 p2169 A67-27311
 Stability of arbitrary one-dimensional hydrodynamical flow in quasi-isothermal case 13 p2105 A67-27413
 Heat conductivity effect on various one-dimensional flows solved by numerical integration of Navier-Stokes equations 14 p2286 A67-27980
 Group classification by Cartan method of equations of one-dimensional plane wave gas flow 14 p2305 A67-28483
 Solution for shock wave of bimodal distribution using Bhatnagar-Gross-Krook models, noting symmetry property destruction and recovery by using modified BGK model 15 p2470 A67-29228
 Normal shock relations in adiabatic constant area ducts used to connect properties on two sides of shock in steady one-dimensional flow 15 p2470 A67-29441
 Compression shocks in one-dimensional steady flow of Lighthill ideal dissociating gas studied, using semiempirical relation for relaxation equation 15 p2471 A67-29578
 Heat addition in channels of variable cross section area discussed for one-dimensional, inviscid flow of ideal gases with constant

specific heat ratio 16 p2591 A67-30944
Limits of applicability of methods based on one-dimensional model employing Reynolds analogy for gas flow in pipes 16 p2660 A67-31203
Stability of one-dimensional polyphase flow in porous medium studied using theory of servomechanisms 16 p2609 A67-31713
Magneto-Fanno flow shock tube experiments to determine one-dimensional MGD interactions between partially ionized gas flow and external magnetic field 17 p2898 A67-32183
Initial phase of expansion of two-component plasma into vacuum analyzed, using extension of Sedov homogeneous relative deformation method 18 p3084 A67-33423
Constructing solution of Cauchy initial value problem when Riemann function is unknown for one-dimensional linear viscoelasticity 18 p3139 A67-33428
Hydrodynamic structure of exothermic reaction zone behind one-dimensional shock fronts in gaseous detonation studied by optical method 18 p3153 A67-33827
Equations of one-dimensional aerothermodynamic flow of dissociating gas 20 p3420 A67-36599
One-dimensional nonstationary compressible gas flow studied with variational calculus, obtaining approximate analytical periodical solutions 20 p3360 A67-37678
Invariant transformation for pulse and continuity equations of one-dimensional unstabilized motions of ideal compressible fluid 21 p3612 A67-38279
One-dimensional compound-compressible nozzle gas flow theory, discussing choking phenomenon and three-dimensional computer calculations 23 p3927 A67-40603
Gas-air mixing in coaxial flow engine based on one-dimensional ejector theory at subsonic flow velocities, discussing chamber design gas-air mixing in coaxial flow engine based on one-dimensional ejector theory at subsonic flow 23 p4048 A67-40638
One-dimensional plasma flow variables relations analyzed in crossed electric and magnetic fields with small magnetic Reynolds numbers 24 p4196 A67-42216
Correction to parametric representations of nonsteady one-dimensional flows 24 p4145 A67-42691
One-dimensional steady MGD flow of polytropic gas with finite constant electric conductivity, noting flow patterns and oblique shock wave structure 24 p4198 A67-42707
ONE-WAY SPACE FLIGHT
Propulsion sources for one-way unmanned subrelativistic interstellar probes, discussing interaction with deep space environment for vehicle control 19 p3322 A67-35316
OPACITY
Atmosphere model for pure helium star including only helium I and II transitions and electron scattering in calculating opacity 14 p2387 A67-28578
Mean absorption coefficient for optically thin plasma derived taking into account radiative losses, noting electron and ion temperature ratios 16 p2706 A67-30459
Protonosphere heating by photoelectrons escaping from F region, estimating protonosphere opacity and daytime escape flux 19 p3221 A67-35280
Absorption coefficient of radiative transfer equation and high temperature air opacity 20 p3485 A67-36930
Atmospheric opacity and extraterrestrial radio source intensity related by improved Taylor series technique using least squares method [JPL-TR-32-1115] 23 p4062 A67-40733
OPERATION
S EXTRAVEHICULAR OPERATION
S PREFLIGHT OPERATION
OPERATIONAL CALCULUS
Book on differential and difference equations including first order equations, linear equations, Laplace transforms, numerical and series solutions, etc 02 p0260 A67-12473
Exact solution /by Hankel and Laplace transforms/ of unsteady motion of viscous MHD fluid in cylindrical vessel in axisymmetric constant strength magnetic field 05 p0850 A67-16134
Operational calculus for functions of one

continuous and one discrete variable 05 p0834 A67-16725
Mikusinski operator solution of partial integrodifferential equations 07 p2125 A67-19471
Weinstein results for pointwise monotone growth and convexity extended in norm to certain Cauchy problems of second order differential equations 12 p1961 A67-26063
Two-dimensional operator calculus for solving all second order linear partial differential equations of two dimensions 13 p2146 A67-26745
OPERATIONAL HAZARD
Detonation characteristics evaluation of solid-composite propellant, noting hazards study program /Project SOPHY/ and critical geometry theory 15 p2544 A67-29999
Helicopter cargo restraint system program meeting prescribed operational and safety requirements [AHS PAPER 124] 16 p2598 A67-31839
OPERATIONAL PROBLEM
Maintainability, reliability and operational flexibility of manned orbital space station [AIAA PAPER 66-933] 02 p0331 A67-12252
Apollo manned lunar landings, system hardware, operational problems and development of lunar surface experiments package /ALSEP/ [AIAA PAPER 67-116] 07 p1163 A67-19438
Oscillation of oscillator with elastically hereditary and weakly nonlinear characteristics, applying operational method to analysis in terms of hereditary creep theory 11 p1876 A67-24682
Linear amplitude characteristics in synthesis of instrumental servosystems with saturated components such as amplifiers 11 p1794 A67-25040
Turboramjet engine transition phase noting problems in passing from turbojet to ramjet operation 12 p1988 A67-25185
Airline operation, reliability, personnel and training techniques [SAE PAPER 670343] 12 p2041 A67-25879
NASA STADAN and Apollo network antenna systems, analyzing tracking antenna systems, command systems and operational problems 14 p2287 A67-28681
Starter cartridges for jet engines, discussing operational problems and mechanical design, igniter and propellant development, etc 15 p2423 A67-29982
Air traffic control operations forecasting, stressing proposed STOL and VTOL port [AIAA PAPER 67-398] 15 p2515 A67-30365
Characteristics, operation, technology and reliability of telemetering systems for ESRO I, HEOS A, TD 1 and TD 2 including control factors and coding systems 17 p2816 A67-32747
V/STOL all-weather operation developments noting navigation and communications, operations under icing and noise problems [SAE PAPER 670348] 17 p2798 A67-32990
Generation and loading of triple point hydrogen for high performance aircraft, boosters and spacecraft [AIAA PAPER 67-468] 18 p3110 A67-33938
Relationship between acceptance test and operational reliability studied by multiple regression analysis 18 p3138 A67-34668
Operational readiness of redundant system, deriving system readiness factor formula for operating and idle redundancy 20 p3451 A67-37158
Small and large orbiting observatory satellites compared for operational needs, interference problems, scheduling and multisampling of space phenomena [AIAA PAPER 67-634] 20 p3534 A67-37616
Preliminary spacecraft concept for real time operational space environment monitoring system 22 p3901 A67-39928
SST fleet size, flight time, station stop time, seat mile costs, fuel consumption, noise and sonic boom problems affecting airline economics [AIAA PAPER 67-749] 23 p3933 A67-40983
OPERATIONS RESEARCH
SA WAR GAME
Space systems performance, components and modes of operation, showing merits in terms of entire space program 08 p1431 A67-21108
Accelerometer use for operational load measurements in aircraft, emphasizing automatic counting technique 11 p1880 A67-25059

Prediction techniques developed under storage technology program, including nonoperating and operating time periods to determine operational readiness 15 p2495 A67-30416
Operational system for handling and processing aerospace-system human-factors task data in government/contractor environment 18 p2994 A67-34343
Nature and magnitude of differences between intrinsic and operational reliability and maintainability characteristics, suggesting reconciliation approach 18 p3057 A67-34661
Development of quantitative logistics performance parameters related to time, resources and cost in Concept Formulation Phase and Contractual Definition Phase 18 p3162 A67-34678
Static and dynamic inventory control models for logistics planning and operational readiness with cost constraints 18 p3162 A67-34680
Operational and cost-influencing characteristics of low orbit space operations compared from manned orbital base and earth base [AIAA PAPER 67-654] 20 p3530 A67-37631
Hot shot tunnel F operation as combustion test facility using air, discussing oxygen depletion, particle contamination and reservoir decay 21 p3606 A67-37775
Book on optimization covering inequality constraints, decomposition strategy, direct methods, etc 22 p3775 A67-39270
Cost estimating techniques for military and NASA programs, comparing spacecraft resource forecasting with expenditure estimates [AIAA PAPER 67-809] 24 p4259 A67-42986
Manned space flight safety, discussing system design, operations planning, staffing, training and simulation [AIAA PAPER 67-824] 24 p4243 A67-42971
OPERATIVE TEMPERATURE
Entropy applied to theory of fuel cells, noting effect of operating temperature 14 p2252 A67-29018
Gain control of common emitter cascade by varying transistor regime, taking into account effect of operating frequency and temperature 16 p2637 A67-31027
Low noise parametric down-converter by using two incommensurable pumping generators, noting gain bandwidth product and minimum noise temperature 17 p2824 A67-32315
Maximum heating temperature of smallest particles of polydisperse material in two-phase flow by approximation method 17 p2970 A67-32462
High modulus high strength inorganic filament windings tested for tension and buckling-critical structures, considering weight decrease and operating temperature increase 19 p3245 A67-35553
Heat transfer dependence in cavity of closed evaporative thermosyphon on device inclination angle and coolant filled fraction of cavity 21 p3625 A67-37913
OPERATOR
SA DIFFERENTIAL OPERATOR
SA HAMILTONIAN
SA INTEGRAL OPERATOR
SA RAYLEIGH-RITZ METHOD
Sinkhorn theorem on diagonal equivalence of nonnegative matrix to stochastic matrix, using Mennon homogeneous positive nonlinear operator T and uniqueness of eigenvectors of T 04 p0645 A67-15082
Harmonic analysis of accuracy of reproduction in digital form of operators selecting period of time quantization, duration of analog-to-digital conversion, etc 05 p0781 A67-16258
Solution concept definition for integral equation with discontinuous operator 05 p0835 A67-16938
Inequalities for difference and pseudodifferential operators, providing sharp form of Garding inequality 06 p1025 A67-18642
Mikusinski operator solution of partial integrodifferential equations 07 p1215 A67-19471
Critical tracking task for man-machine research related to operator effective delay time 07 p1136 A67-20171
Spectral stability criteria for numerical integration procedure using Z transforms, specifically finite difference

operators 08 p1296 A67-20600
 Generalization of multistep methods for ordinary differential equations, noting associated operators and local discretization error 08 p1348 A67-21191
 Operator calculus, based on momentum operator choice, designed to take account of finite domain of wave functions in quantum mechanics 10 p1682 A67-23349
 Quantumstatistical thermodynamics with several temperatures for indivisible observation level 10 p1733 A67-23477
 Dynamic correspondence between electromagnetism field density matrix and associated classical random problem, obtaining means of quantum operators through Fokker-Planck equation 11 p1799 A67-24240
 Schroeder fixed point theorem for convergence rate of iteration series extended to concave operators which need not remain constant 14 p2345 A67-28937
 Computer aided network sensitivity analysis 15 p2440 A67-29937
 Operators spectrum properties and corresponding singular eigenfunctions encountered in plasma problems, showing application to initial and boundary value problems 20 p3494 A67-36148
 Reaction rates and yield for multichannel molecular collisions, introducing observable yield operator in theory, using motion equations 22 p3757 A67-39635
 General convergence theorems for Newton method applied to convex operators for partially ordered topological linear spaces 23 p4023 A67-40863

OPERATOR PERFORMANCE
SA ASTRONAUT PERFORMANCE
SA PILOT PERFORMANCE
 Human pilot dynamic characteristics effects on manual satellite attitude control system stability, using root locus analysis of mathematical models 02 p0186 A67-12226
 Adaptive functions of man in vehicle control systems 07 p1221 A67-19194
 Inclusive classified bibliography pertaining to modeling human operator as element in automatic control system 07 p1137 A67-20173
 Optimal type of strategy of remote control and force sensitive and stable feedback presentation in master-slave manipulators with transmission delay 09 p1456 A67-22374
 Panel layout for rectilinear instruments 14 p2257 A67-28661
 Remote maneuvering unit control during satellite inspection in simulated conditions 14 p2258 A67-28669
 Comparison of operator performance when using rotary selector, thumbwheel and digital pushbutton switches 15 p2430 A67-29135
 Human factors information utilization by designers, noting test results on conceptual drawing of equipment configuration according to design specifications 15 p2431 A67-29897
 Compensatory tracking experiments between single and two-axis tracking systems, determining training effects on model parameters of human operator 17 p2808 A67-33178
 Sine wave tracking, studying operator manual control performance 17 p2808 A67-33179
 Radar target designation tracking performance in simulated high speed low altitude aircraft, using closed loop analyses 17 p2830 A67-33181
 Continuous exposure to random vertical vibrations studied for effects on compensatory tracking performance, noting decrement by peak vibration acceleration power location 18 p2993 A67-34336
 Human operator performance in continuous pursuit tracking with advanced and delayed visual display 18 p2994 A67-34339
 Quantification for effective human performance implementation into system designs during conceptual, design and acquisition phases 18 p2994 A67-34655
 Electronic system for measuring operator information retrieval in bimensory configuration, using video-record radar set and playback 20 p3419 A67-37639
 Adaptive processes of human operator during control tasks involving sudden change of controlled plant dynamics 21 p3576 A67-37948
 Performance characteristics in zero potential energy manual task, discussing

work output 21 p3577 A67-38074
 Feasibility of short radius centrifuge incorporation in space station, testing radius effects on operator performance of tasks 23 p3965 A67-41567
 Factors in recovery from performance decrement, activation, inhibition and warm-up [NAVTRADEVCEIN-IH-72] 24 p4114 A67-41809

OPHTHALMODYNAMOMETRY
 Blackout experimentation results, discussing centrifugation and ophthalmodynamometry blackout production and visual system effects 22 p3752 A67-39607

OPHTHALMOLOGY
 Medical complications of contact lenses and aeromedical implications 18 p2993 A67-34723

OPTICAL ABSORPTION
 Oscillations of optical absorption in cadmium sulfide in strong electric fields, noting electron transfer between Wannier discrete level 01 p0127 A67-10070
 Ellipsometer study of anomalous absorption in very thin dielectric films on evaporated metals 01 p0138 A67-11075
 Exciton and impurity states in optical absorption spectra of nonmetallic crystals in pseudopotential theory 02 p0281 A67-11489
 Optical absorption edge in cadmium telluride, noting impurity bands and dependence on energy and temperature 02 p0281 A67-11492
 Cadmium telluride optical absorption edge due to exciton creation with simultaneous absorption of longitudinal optical phonons calculated by perturbation theory 02 p0281 A67-11493
 Normal and abnormal optical absorption in thin zinc sulfide films with excited states in forbidden band surfaces 02 p0288 A67-11724
 Optical absorption spectra of hexagonal red HgS single crystals at self-absorption edge at temperatures from 20.4 to 310 degrees K 02 p0300 A67-12476
 Attenuation length of photoexcited electrons in evaporated layers of CuBr estimated by measuring photoemission yield as function of thickness 03 p0500 A67-14332
 Near UV optical constants of lanthanum fluoride 03 p0470 A67-14400
 Quantum study of optical nonlinearities in absorbing materials, energy transfer between optical waves, laws of nonlinear reflection and coherence effects 04 p0657 A67-14881
 Vanadium charge compensator in laser calcium tungstate, determining vanadium positions via electron spin resonance 04 p0633 A67-15306
 Optical self-absorption and dielectric constant of cadmium oxide thin film in case of high electron degeneration 04 p0683 A67-15655
 Saturable optical absorption of light flux from high intensity Q-switched ruby laser 05 p0822 A67-16677
 Damage in glass induced by linear absorption of laser radiation non-Q-spoiled 05 p0824 A67-16794
 L-and K-band absorption due to optical transitions starting from ground state of F center in alkali halide 05 p0864 A67-16801
 Tetrafluoroethylene dissociation in nitrogen behind shock waves and thermoequilibrium constants studied, using shock tube and optical absorption spectroscopy 05 p0759 A67-16840
 Optical absorption due to direct intervalence band transitions in Ge, noting effect of lattice temperature 05 p0869 A67-17192
 Optical absorption and oscillatory magnetoabsorption in tellurium, noting interband transition and lack of inversion symmetry 06 p1060 A67-18919
 Hall effect, electrical resistivity and optical transmission data and Co impurities in GaP studied via crystal field theory 06 p1061 A67-18926
 Light scattering influence on effective value of extinction coefficient considered as function of optical parameters of medium and of angular characteristics of source and receiver 07 p1221 A67-20007
 Optical absorption, photoconductivity and p-n junction in cadmium telluride 08 p1368 A67-20734
 Oscillations of optical absorption in cadmium sulfide in strong electric fields, noting electron transfer between Wannier

discrete level 08 p1371 A67-21453
 IR absorption in high purity boron films, showing absence of absorption peaks at 2-15 microns 09 p1533 A67-22132
 Characteristic optical density and equilibrium of alkyl-sodium and aromatic hydrocarbons as function of temperature and wavelengths, correlating electron affinity with enthalpy values 09 p1458 A67-22214
 Optical absorption of Al and some Al-Mg alloys in region from 0.7 to 2.0 eV investigated by conventional polarimetric reflection technique 10 p1696 A67-23773
 Radiation pressure on vanes of rotary actuator of spacecraft radiation orientation system 12 p2011 A67-25655
 Optical and paramagnetic resonance of ytterbium ions in calcium fluoride, obtaining correlation between site geometry and optical absorption 12 p1984 A67-25843
 Temperature dependence of electrical conductivity and Hall effect of barium-titanate crystals reduced by hydrogen, observing electron spin resonance and optical absorptions 14 p2363 A67-27824
 Optical absorption coefficient due to conduction electrons in nondegenerate semiconductors derived using Plakida method, noting light scattering 14 p2372 A67-28808
 Book on problems of optics covering emission, absorption, diffraction, dispersion, etc 14 p2349 A67-29006
 Mean absorption coefficient for optically thin plasma derived taking into account radiative losses, noting electron and ion temperature ratios 16 p2706 A67-30459
 Saturated neon absorption inside helium laser, noting output power peak caused by Lamb dip effect 16 p2685 A67-31033
 Ellipsometer measurements to obtain estimates of refractive index and thickness of weakly absorbing isotropic, homogeneous slab 16 p2703 A67-31877
 Kronig-Penney model for electron potential in crystal adapted to semiconductor, discussing cubic lattice 17 p2914 A67-32386
 Radiation kinetics of laser with resonator having lens system and low absorption nonlinear medium, showing time shift of kinetic curve 17 p2868 A67-32663
 Optical exciton-magnon absorption in manganese fluoride, experimental results and theory of interactions 17 p2926 A67-33382
 Martian surface atmospheric pressure via photometric observations of Phobos eclipses 18 p3124 A67-34155
 Shock tube experiments conducted on mixtures of fine solid particles and gases 20 p3414 A67-36516
 Optical third-harmonic generation in rare gases, comparing coefficients with Kerr effect coefficients 21 p3639 A67-37962
 LiF crystals doped with Ti studied for electrical and optical properties, finding atomically dispersed Ti fractions in form of doubly positively charged centers 21 p3687 A67-39137
 Electron-electron interaction effect on Li soft X-ray emission spectrum, liquid metal optical absorption and alkali metal dielectric response 23 p4037 A67-40760
 Intervening galaxy effect on radiation from distant objects, studying Faraday rotation, 21-cm absorption, optical scattering and absorption lines 24 p4223 A67-41810
 Optical absorption, refractivity and electron scattering used to construct model dipole spectrum of molecular nitrogen and calculate dipole properties 24 p4190 A67-42096
 Phonon assisted magnetoabsorption in direct band semiconductors 24 p4203 A67-42267

OPTICAL AMPLIFIER
 Short pulse Q-switched laser with variable pulse length 05 p0817 A67-16641
 Laser mode combination tones detected by coupled high resolution optical amplifier corresponding to simultaneously oscillating frequencies 09 p1511 A67-21747
 Optical detectors for images and selected radiation signals using Bendix Channeltron multiplier, describing types, properties and applications 17 p2858 A67-32480
 Neodymium-glass laser amplifier gain saturation investigation using laser driving signal, discussing Schulz-DuBois steady state theory and inversion density 22 p3813 A67-39349

OPTICAL BEAM SCANNING

- IR and visible images of eclipsed moon made from scan data and magnetically recorded analog signals from observation of total lunar eclipse on December 19, 1964 04 p0697 A67-14741
- Conductivity changes in thin layer of silicon oxide induced by electron beam of scanning electron microscope 04 p0682 A67-15318
- Data record and readout systems dependence on precise spot and line scan methods, using diffraction limited spots of laser generated light 04 p0623 A67-15321
- Diffraction limited performance achieved for flying spot recording and readout, using concentric optical system, applied to laser scanner 04 p0658 A67-15322
- Thermal high resolution recording using moving laser spot on metallic and organic thin films 05 p0815 A67-16586
- Parametric fluctuations of spatially restricted light beam in turbulent atmosphere 05 p0766 A67-17229
- Electron beam spatial scanning of coherent emission of GaAs junction laser at low temperatures, making current distribution nonuniform 06 p1011 A67-18150
- Geos A space vehicle, discussing orbital motion, instrumentation and operation 07 p1259 A67-19759
- Optical beam deflection method based on polarization change of acoustically deflected light as compared to incident beam 09 p1510 A67-21574
- Resistivity variation in n-type germanium pellet measured with focused electron beam, showing position dependence of diffusion length as cause of error 09 p1473 A67-22018
- Laser light deflecting methods, detailing scanlaser, laser resonator combining features of laser and cathode ray tube 13 p2128 A67-27237
- High precision CRT display system using raster beam positioning and computer-generated digital video 20 p3447 A67-36807
- Debye-Sears effect in one-dimensional Fresnel zone plate moving at acoustic velocity causes scanning of focal spots 22 p3835 A67-39242
- Laser radiation in calibration of spectrometer scanning function by duplicating spatial coherence characteristics of radiation 23 p4014 A67-41023
- OPTICAL CORRECTION PROCEDURE**
- SA LENS DESIGN**
- Adjustment procedure for laser with polygonal resonator, noting spatial mirror adjustment in addition to angular adjustment 01 p0087 A67-10162
- Laser brightness gain and single transverse mode operation by compensation for thermal distortion with external mirror 05 p0819 A67-16656
- Diffraction based criteria use for image quality in automatic optical design, reviewing aberration tolerance theory 06 p1030 A67-17573
- Remote sensing cross-beam cross correlation methods of determining spatially resolved average thermodynamic properties [AIAA PAPER 67-149] 06 p1004 A67-18477
- Pencil-beam radio telescope adjustment via methods of control of surface of optical telescopes 07 p1189 A67-20244
- Prisms for dispersion compensation and single plane diffraction grating as correcting element for achromatizing white light reconstruction of two-beam surface hologram 09 p1492 A67-21567
- OPTICAL COUPLING**
- Coupling mechanism in passive Q-switching operation between filaments at different regions of ruby laser rod 01 p0090 A67-10813
- Optical coupling using gallium arsenide laser for variation of frequency of diode emission through small change in current density 05 p0814 A67-16390
- Photoconductivity, edge emission spectrum, longitudinal optical phonon coupling and eigenfrequencies for linear chain of Cd-Se-Cd-S-Cd... atoms 05 p0870 A67-17196
- Transversal mode excitation in electrostrictively operated scanning interferometer and optical matching to laser cavity 09 p1492 A67-21563
- Radiation from two optically coupled cavities of compound laser identical in time and spectral composition without tuning one cavity to other 17 p2868 A67-32661

- Laser mirror transmissivity optimization in high power optical cavities noting reflection coefficient selection 19 p3241 A67-35701
- Cross correlated photons of laser used to determine correlation functions by applying thermodynamic Green function 24 p4168 A67-42594
- Optical coupling of photomultiplier tube to acrylic plastic using clear silicone potting compound 24 p4158 A67-42700
- Functional half-adder using optical coupling in injection laser noting design criteria and mode propagation delay 24 p4169 A67-42822
- OPTICAL DENSITY**
- Multiparametric diagnostic technique for optically dense plasma 03 p0486 A67-14187
- Composite heat transfer and viscous friction of moving gray medium with large optical density, using laminar boundary layer equation, noting hydrodynamic state role 04 p0722 A67-14713
- Density effect on Sommerfeld diffraction problem 04 p0715 A67-15583
- Effect of variation of vertical air density profile on relative optical air mass for ARDC standard model atmosphere 1959 compared with measurements 10 p1652 A67-23622
- Inversion of spectroscopic integral equation which relates emission coefficient to integrated intensity distribution for optically thin and asymmetrical light source 12 p1968 A67-26175
- Solar X-ray measurement with satellite noting radio noise flux, absorption in atmosphere and optical density changes 17 p2939 A67-33242
- Mathematical statistics methods for nonreabsorbed spectral line widths and shifts and optical density in plasma 20 p3471 A67-37601
- Semiconducting alloys of gallium investigated by photometric method using gallium and xylene orange 22 p3804 A67-40299
- OPTICAL EMISSION**
- Luminescence and conductivity of CdS single crystals, noting temperature effect and release mechanism of trapped electrons and holes 01 p0134 A67-10820
- GaAs p-s-i-n diode exhibiting negative resistance, allowing assembly into X-Y matrix and electrical pulsing into emitting or nonemitting state 05 p0771 A67-16312
- Optical phonon production, showing existence of electric field strength range at low temperature scattering in which phonon emission results in electron stoppage 06 p1010 A67-17884
- Stimulated two quantum radiation in optical range for transitions occurring between discrete levels of impurity crystals or free atoms 06 p1010 A67-17885
- Microwave optical field distribution patterns visualized using IR thermosensitive transducer method 11 p1792 A67-24714
- GaAs laser diode noting peak optical power, spectra and role of individual diodes in stack operation 11 p1802 A67-24745
- Detectability of ion recombination free-free emission from H II regions 12 p2011 A67-26252
- Sco XR-1 source model corresponding to neutron star in state of accretion as possible explanation of X-ray emission power from source 13 p2189 A67-26262
- Book on problems of optics covering emission, absorption, diffraction, dispersion, etc 14 p2349 A67-29006
- Coherency relation between quasi-periodic X-ray and optical pulsations in auroras 17 p2844 A67-32543
- Relationship between radio galaxies and quasars, observing two sources of moderate distance, noting intense optical emission of limited intensity or duration 20 p3521 A67-36296
- Flare X-ray emission period determined, noting maximum radio emission and optical intensity 21 p3699 A67-38965
- Image radiance distribution of confined plasma in circular tubes noting absence of distortion 22 p3842 A67-39234
- Laser beam cross section variation during free space propagation and through optical systems, discussing He-Ne laser radiation 23 p4011 A67-40724
- Satellite and ground based measurements of incident proton neutral hydrogen flux and Balmer alpha optical emission in auroral hydrogen arc 23 p3995 A67-40803

- High energy cosmic ray shower detection combining perturbed magnetic field pulse and coincident optical radiation observations 23 p4051 A67-40812
- Atmospheric scintillation effects on optical data channel for application to laser radar noting SNR role 23 p3975 A67-41266
- Longitudinal mode generation in ruby laser emission operating in single pulse regime with resonant mirror reflector 24 p4169 A67-42894
- OPTICAL EMISSION SPECTROSCOPY**
- Spectral characteristics of two-photon optical excitation and light emission from CdSe semiconductor laser with modulated Q-factor 04 p0633 A67-15299
- Differential Stark effect in second excited state of alkali metal atoms described, using electric field level crossing spectroscopy 06 p1035 A67-17830
- Electronic, vibrational and rotational temperatures in laser-produced flames measured spectroscopically 15 p2433 A67-29879
- All-electronic, ultra-fast scanning spectrometer utilizing image dissector for power spectral density function measurements of rapidly time varying optical emission 16 p2680 A67-31803
- Design problems in IR optical systems including materials limitation, reflection losses, environmental requirements, etc 18 p3078 A67-33566
- Signal to noise ratio for optical solar spectra, describing low noise level spectrometer 21 p3624 A67-37730
- Spectroscopic investigations of emission under free generation and Q-switching conditions of mixed-fluoride crystal lasers 21 p3682 A67-38370
- Solar corona spectra during total eclipse /1966/ using polaroid camera 24 p4154 A67-42157
- OPTICAL EQUIPMENT**
- Photoelectric optical imaging system survival in earth radiation belt, noting noise level and total energy absorption 02 p0243 A67-12055
- Power signal to noise ratios for coherent and noncoherent optical detection, for optimization of optical systems 02 p0243 A67-12056
- Optical methods and equipment used in checking surface finish and volume and surface inhomogeneities of active media and interferometric mirrors of lasers 03 p0436 A67-13143
- Fabrication of improved focos and field flatteners and evaluation of optical performance in terms of modulation transfer function (MTF), vignetting and T-number measurements [SMPT PREPRINT 100-3] 03 p0469 A67-13802
- Optical system consisting of polarized laser beams for monitoring missile attitude during early launch phase 04 p0619 A67-14505
- Laser displays application, performance and status of existing devices 06 p1001 A67-17887
- Radio electronics, discussing quantum electronics, lasers, microwave devices and technology, plasma physics, etc 06 p0968 A67-18072
- Light source devices for electronic functions, discussing p-n junction 07 p1231 A67-19081
- TV camera to be used by Apollo astronauts noting integrated circuits, optical system, light intensifier, etc 09 p1499 A67-22175
- Faraday effect optical isolator for IR region using lead glass rod in magnetic field as nonreciprocal element 09 p1500 A67-22425
- Photographing satellites, using optical system and image converter for determining coordinates 10 p1606 A67-23184
- All-mirror Schmidt telescope system for space research providing easier switchover from photography to slitless spectroscopy 10 p1657 A67-23561
- Procedure and auxiliary equipment used to focus optical elements of gas laser 12 p1952 A67-25364
- Articulated optical pickup system for scale model simulation providing pitch, roll and yaw motions and fixed perspective point 12 p1941 A67-25470
- Determining theoretical minimum signal that can be detected by optical detection system noting dependence on integration

time, noise, etc [SMPTE PAPER 101-91] 12 p1905 A67-25475
JPL solar simulator design, fabrication and performance 12 p1925 A67-25733
Parameters of multiple-scattered optical radiation applied to laser communication system design 12 p1906 A67-25988
Interplanetary space environment effects on spacecraft optical equipment noting thermal design [JPL-TR-32-1098] 13 p2144 A67-27358
Solid state lasers and pulsed ruby lasers for continuous and quasi-continuous operation, noting applications in micromachining 14 p2331 A67-28559
Optical system consisting of circular sweep camera for recording useful streak images on Polaroid film 14 p2320 A67-28748
Photographic recording by shadow method for alignment of optical equipment in firing range used to determine aerodynamic characteristics of various missiles 16 p2674 A67-31117
Rotating mirror streak cameras, noting development history and future needs 16 p2675 A67-31249
High resolution UV spectrograph with echelle, noting optical line-up for photographing H-Lyman alpha line at 1216 angstroms 16 p2680 A67-31875
Spherical and chromatic aberrations, astigmatism and field error of catadioptric telescope, determining resolving power with various methods 17 p2855 A67-32327
Exhaust gases effect on satellites optical equipment calculated by determining propane attitude-control jet gas flow parameters 18 p3137 A67-34359
Optical system for computer counting and analyzing aerosol particles on photofilm 19 p3227 A67-34861
Miniature optically immersed thermistor bolometer arrays employed for earth atmospheric horizon scanning from orbiting vehicles 19 p3231 A67-35684
Examination of ability of man to determine drift angle of spacecraft with optical sight [AIAA PAPER 67-624] 19 p3337 A67-36013
Semipermanent optical memory design using laser light source, acoustic light deflector and hologram array as information storage elements for address selection 20 p3390 A67-36511
Optical glass selection for design of double-lens objective for IR region of spectrum, considering aberrations 20 p3451 A67-37157
Three-dimensional hologram reconstruction and image speckle, considering three-dimensional boundary value problem 20 p3451 A67-37309
Imaging systems of ground-viewing satellite, discussing TV, lasers, radar, etc 20 p3452 A67-37310
Articulated optical pickup system for scale model simulation providing pitch, roll and yaw motions and fixed perspective point 23 p3988 A67-41502
Installation problems of head-up displays in commercial aircraft 24 p4152 A67-41896
Digital computer and coherent optical image processing techniques compared, reviewing data transfer schemes and available hardware 24 p4125 A67-42438
Character recognition via holography using Gabor principle of two coherent waves falling simultaneously on photographic plate 24 p4157 A67-42456

OPTICAL FILTER
SA INFRARED FILTER
Properties of uranyl-doped glass for application as saturable optical filter for use with lasers 01 p0032 A67-10009
Autonomous space navigation system using optical spatial filter techniques for recognition and tracking of planetary surfaces and star fields 02 p0264 A67-12316
Gallium arsenide crystal properties for use in optical filter 03 p0488 A67-12858
UV technology, discussing radiation sources, photodetectors, filters, polarizers, reflective coatings, etc 04 p0619 A67-14704
Hybrid nonlinear optical filter exhibiting different transmission properties in opposite paths applied to CRT display 05 p0804 A67-16306
Automatic dielectric film filter method in spectrophotometry 05 p0805 A67-16370
Multilayer interference filter having various transmission characteristics,

emphasizing filters with narrow stop bands used to eliminate laser beam hazard 07 p1224 A67-19400
Ruby laser mode locking and mode competition using RG-8 filter as passive modulator 07 p1197 A67-20147
Optical range gated filter for detecting moving targets in clutter background, using laser beam for application to MTI radar 08 p1293 A67-20687
Matched filter detection of target shape in photographs using both coherent and incoherent illuminations 09 p1496 A67-21712
Spectral differentiation and hologram filtering in reducing optical signal comparison to signal correlation 09 p1497 A67-21826
Internal mirror reflections elimination in laser beam output intensity distribution by filtering device 09 p1512 A67-22042
Selective surface obtained experimentally by deposition of stack of thin layers 09 p1558 A67-22599
Design criteria for narrow optical passband filters used in reception of nonparallel modulated monochromatic radiation 17 p2862 A67-33291
Performance of matched filtering system related to degree of displacement for uniform and nonuniform spectral densities 17 p2862 A67-33295
Optical system devised to alter relative harmonic coefficients and eliminating ringing effects for photographs represented in two-dimensional Fourier series applied to lunar photography 18 p3047 A67-33998
Filter with hyperfine doublet splitting using Paschen-Back effect for optical pumping 22 p3816 A67-40321
Fabry-Perot etalon resonator studied for incidence angles for use as filter, test instrument and control device for laser output 22 p3809 A67-40469
Self-synchronization of axial modes of LF oscillations of laser giant pulse intensity with saturable filters 23 p4013 A67-40908
Highly reflective coatings and interference filters for silicon solar cells on spinning spacecraft on near-sun mission 23 p3937 A67-41490
Improved dipole shutter, optical transparency for protection against high intensity flashes 23 p3965 A67-41565
Graphical construction and electrical simulation for predetermining index and thickness of multilayer surfaces and filters 24 p4187 A67-41873

OPTICAL GENERATOR
Elements of laser communication system including transmission media, terminals, generators, modulators, etc 09 p1462 A67-21675
Amplification and detection of high power TW laser pulses, noting superradiance limit 09 p1514 A67-22273
Sum generation of tunable two-frequency pulse output of gain-switched ruby laser 20 p3458 A67-36389

OPTICAL HETERODYNE
Continuously variable optical delay line using acoustic waves to diffract and frequency shift portion of argon ion laser beam 02 p0253 A67-12517
Optical mixing due to conduction band electrons in semiconductor 02 p0254 A67-12525
Optimum processing of photocell output to produce Poisson photoelectron flux 03 p0368 A67-13282
Optical heterodyne technique detecting stimulated Brillouin scattering, noting frequency shift demodulation arising from ruby laser light incidence on quartz crystal 05 p0823 A67-16688
Spatially resolved He-Ne laser heterodyne measurements of electron number densities in weakly ionized Ar pulsed discharges 05 p0856 A67-17272
High power carbon dioxide laser heterodyne detection of beats and linewidth measurements 06 p1010 A67-17891
Heterodyne and photon counting receivers compared for optical communications 07 p1185 A67-19398
Signal to noise ratio of optical-heterodyne detection system as affected by atmospheric distortion of optical wave front 07 p1144 A67-19786
Molecular vibrational rotational parameters measured with IR heterodyning technique 09 p1535 A67-22136

Narrowband optical heterodyne detection describing InAs photodiode arrangement 10 p1654 A67-22775
Detectability of coherent optical signal against incoherent Gaussian background noise radiation in heterodyne receiver with laser local oscillator 11 p1800 A67-24411
Laser for remote vibration measurement and detection without mechanical contact with structure under test 11 p1798 A67-24433
Detection and measurement of mm wave difference frequency between two near laser lines, using optical heterodyne 11 p1803 A67-24833
Heterodyne detector of submillimeter radiation using CN maser as continuous wave source of coherent radiation 12 p1951 A67-25220
Heterodyne signal amplitude dependence on optical path length difference for oscillating axial modes in multimode gas laser 13 p2128 A67-27344
Atmospheric modulation noise in optical heterodyne receiver, deriving signal power variance and mean-square frequency spread from propagation statistics for wave structure function 16 p2630 A67-31800
Harmonic mixing and heterodyne detection of laser radiation 19 p3240 A67-35622
Lasers for wideband planetary communication, describing heterodyne receiver and transmitter designs 20 p3381 A67-36566
Minimum detectable signal and frequency response of mercury-doped germanium detector, measuring response time and SNR through optical heterodyne techniques 21 p3590 A67-38000
Directional characteristics in optical heterodyne detection processes including finite sources, bandwidth, random phase sources and rough surfaces 23 p4012 A67-40877
Hellum-neon laser device for mirror spacing changes by optical heterodyning discussing application to piezoelectricity 23 p4014 A67-41033
Optical communications systems capable of microwave bandwidths evaluated experimentally and theoretically 24 p4123 A67-42200

OPTICAL IMAGE
SA IMAGE CONTRAST
SA RETINAL IMAGE
Pilot experiment, recording simultaneous optical image position, atmospheric temperature fluctuations and wind direction 01 p0108 A67-10255
Operational notation characterizing basic optical elements as block diagrams gives results identical to those of Fresne Kirchhoff diffraction formula 01 p0028 A67-10433
Resolution limit imposed by atmospheric turbulence on image of ground object obtained by long exposure photography from high altitudes 01 p0109 A67-11088
Lower atmospheric layer and meteorological conditions effect on oscillations of image of artificial source of light 02 p0238 A67-11988
Oscillations in turbulence angle observations of quality of star images considering role of synoptic front 02 p0261 A67-11999
Photoelectric recording of scintillation of stellar images by function of nature of scintillation while carrying out observations 02 p0326 A67-11999
Fluctuation of stellar images and analysis of systematic errors in guidance of telescope as result of atmospheric refraction and flexure of telescope barrel 02 p0241 A67-11999
Automatic and semiautomatic devices for measuring scintillation of stellar images from traces of stars 02 p0242 A67-11999
Coherence theory and linear system analysis applied to optical image processing in incoherent and coherent illumination 02 p0267 A67-12244
Hologram copying by laser technique using original hologram as object for second hologram 03 p0426 A67-14333
Dirichlet theorem and coherent imaging, discussing form of Fourier functions for Fraunhofer diffraction at infinity 07 p1185 A67-19400
Quality of optical images and physical receivers including both curve of modulation transfer and noise 07 p1146 A67-20136

Imaging properties of gas lens, discussing ray trajectory, ray matrix lens formula, optical transfer function, etc 09 p1498 A67-22083

Mosaic of photosensors for solid state imaging, discussing electro-optical conversion, structure and characteristics 09 p1476 A67-22209

Apparent rotation of spectral lines as viewed through holograms, obtaining equations for angular change of image position 10 p1653 A67-22717

Optical effects of thermal structure in lower atmosphere 10 p1679 A67-22745

Hologram copies by recording interference pattern between undiffracted and diffracted waves 10 p1654 A67-22754

Holography/recording light in three dimensions/, noting virtual and real images and color production 10 p1657 A67-23623

Restoration of digitized turbulence-degraded images by corrective processing of harmonic representation according to measured optical transfer function 11 p1789 A67-24414

Optical image recording, storage and reproduction using Gudden-Pohl effect 15 p2487 A67-29470

Optical image producing method of complex ultrasonic field using light diffraction of laser beam 15 p2487 A67-29498

Optical image reconstruction from sampled hologram using wavefront reconstruction technique 15 p2488 A67-29819

Motion of lunar images in focal plane of horizontal telescope without coelostat arrangement 17 p2950 A67-33130

Linear least squares filtering of distorted images, stressing turbulent atmosphere effect 18 p3047 A67-33882

Reflected light microscope for viewing unstained brain and ganglion cells 18 p2991 A67-34530

Computer program for handling of transform between spatial coordinate representation and spatial frequency representation of image 18 p3007 A67-34599

Cathode study using electron images of recording storage tube cathodes 19 p3197 A67-35813

Corrective image deconvolution of smearing caused by extended instrument functions in optical imaging possible by holographic Fourier transform division 20 p3435 A67-36204

Statistical properties of optical variability of 3C 273 suggesting quasar nucleus as single body 20 p3521 A67-36297

Electromagnetic point source in presence of planar interface between two anisotropic media, obtaining far fields through Fourier integral and ray optical calculation 20 p3388 A67-37703

Stellar detectors components, describing optical receiving, image tracking and photometric devices 21 p3628 A67-38651

Maximum likelihood method used as criterion in processing optical images propagated through turbulent atmosphere 21 p3586 A67-38954

Optical transfer function relation between image aberration and diffraction, describing measuring methods 22 p3837 A67-40072

Nomograph construction for earth pointing cameras, evaluating imaging system effectiveness as ground resolution and scale factor, plotting system performance characteristics 22 p3800 A67-40106

Nonpseudoscopic real image production from arbitrary hologram using different geometries for reference and reconstructed waves 23 p3998 A67-40701

Diffraction and image formation in coherent and noncoherent light with relation to Fourier transform 23 p3972 A67-40708

Matrix method for analyzing systems of gimbaled mirrors, prisms and ray projectors 23 p4003 A67-41323

Structure of image of diffused surface in coherent illumination investigated for mean intensity and noise-like obscuring component 24 p4155 A67-42336

Two-dimensional optical image analysis program for image prediction and enhancement, discussing transfer function 24 p4157 A67-42433

OPTICAL INSTRUMENT

SA ENDSCOPE
SA INFRARED DETECTOR
SA INTERFEROMETER
SA MICROSCOPE

SA PHOTOELECTRIC APPARATUS

SA REFLECTOMETER
SA RING LASER
SA STROBOSCOPE
SA TELESCOPE

High resolution optical shaft angle encoder with gallium arsenide diodes as light sources and compatible with integrated circuit techniques 01 p0073 A67-11113

Dynalens optical element characterized by variable-geometry fluid prism that deflects beam of light or electromagnetic energy 01 p0075 A67-11132

Lasers applied to photo-optical instrumentation problems, detailing schlieren systems, interferometry, high speed streak photography and transmissometer 02 p0245 A67-12243

Book on modern optical engineering covering image formation, aberrations, prisms and mirrors, stops and apertures, etc 03 p0468 A67-13365

Neodymium-glass laser using spontaneous amplified emission in nonresonant system to obtain high brightness output pulse 04 p0633 A67-15100

Laser microprobe used to study small inclusions in metals 04 p0634 A67-15461

Viewing system for laser operating in production shop 06 p1009 A67-17792

Mobile Clnetheodolite Mount design and operation for missile tracking 06 p1001 A67-17794

Bibliography on lasers covering modes, scattering mechanisms, quantum electrodynamics, matter-radiation interaction, plasma, holography and optics 06 p1010 A67-17890

Book on reticles in electro-optical devices 08 p1353 A67-20757

Design of simplified noneclipse coronagraph, describing optical system and basic performance characteristics of instrument 09 p1495 A67-21636

Microwave and optical generation and amplification - International Conference, Cambridge, England, September 1966 09 p1476 A67-22251

Interferoscope used in testing large glass panels for aircraft camera windows 10 p1652 A67-22701

Optical instrumentation for missile and space vehicle testing 10 p1655 A67-22993

Film camera and video transmission system onboard Lunar Orbiter II 10 p1657 A67-23624

Oscillating plateholder for determining instantaneous focal length of large telescopes 11 p1791 A67-24459

Solar continuous spectrum observations indicating limb darkening around 2500 angstroms, using optical system mounted on Veronique rocket 12 p2007 A67-25820

Oscillation characteristics and special features of doubly segmented laser, noting maximum suppression of unwanted modes 12 p1953 A67-26221

Book on gas laser origin, development, properties and construction 14 p2329 A67-27799

Clinographic polariscope for surface measurement of stress-strain in building materials, noting operation and results 14 p2395 A67-27973

Performance of single lens objective for coronagraph noting resolution, scattered-light background brightness, etc 15 p2485 A67-29151

Large screen displays for group interaction simulation noting cost factors, techniques and performance characteristics 15 p2486 A67-29302

Ultrasonic devices for coherent optical systems, discussing CdS transducers, laser scanners and microwave signal processing 15 p2500 A67-29912

Color TV laser display using Ne-He and argon-ion laser in modulation and scanning system 15 p2489 A67-29914

Airborne photo-optical instrumentation - Conference, Cocoa Beach, Florida, February 1967 16 p2678 A67-31791

Airborne long focal length photographic system environmental effects studied with Cassegrainian type Maksutov telescope 16 p2678 A67-31793

Optical system for earth observation satellite with line-scan television for weather forecasting discussing photometry and fiber optics 16 p2679 A67-31797

Photo-optical instrumentation for

biosatellite 30-day orbiting primate mission discussing adverse environmental effects and other constraints regarding requirements 16 p2680 A67-31806

Moire stress analysis technique for transferring grid without master contact 17 p2855 A67-32456

Optical means for enhancing quantum efficiency of tri-alkali photocathode, discussing standing wave pattern in spaced-reflective and reflective photocathodes 17 p2861 A67-33287

Point holograms, reconstituting wavefronts from high quality lenses and mirrors and use as optical elements for replacing lenses in optical systems 18 p3048 A67-34194

Development of kinetheodolites for satellite tracking 18 p3048 A67-34238

Holographic interferometry in fractional-fringe density plasmas, discussing sensitivity and advantages of combined method 19 p3232 A67-35691

Design, fabrication and testing to enable optical systems to resist space environmental degradation 20 p3445 A67-36568

Reflectometer based on goniometer design employing beam reversal and beam splitter for measuring exit beam intensity 20 p3448 A67-36955

High magnification microscopes for semiconductor research noting advantages of illumination system and light sources 21 p3630 A67-38895

Book on optical interferometry from coherence theory viewpoint, considering wave front and amplitude division, interference spectroscopy, multiple and laser interference, etc 21 p3658 A67-39066

Two-tilt compensating interferometers, using vector form of reflection law 22 p3796 A67-39236

Devices to help pilot detection of aircraft evaluated for systematic relationship between detection functions under fixated conditions and in visual search 22 p3755 A67-39848

Modulation transfer theory for frequency response of optical system in temporal or spatial domains, discussing Fourier series and transform 22 p3808 A67-40380

Optical system models based on gallium-arsenide laser techniques for SNR measurements 23 p4014 A67-41026

Optical instrumentation for auroral and afterglow studies with applications of grating spectroscopic systems, monochromators, interferometers and photometers 23 p3996 A67-41256

Optics for Queen Elizabeth II telescope noting design, tolerance, quartz mirror and test procedures 23 p4001 A67-41257

Dual beam bidirectional reflectance attachment permitting sample plane tilting in spectroscopic measurements 23 p4002 A67-41261

Reactive optical information processing maximum efficiency from phase object in laser cavity, discussing modulation depth and power gain 23 p4002 A67-41270

Ion optical system for extraction of dense ion beams from plasma discharges, studying beam forming characteristics via automatic trajectory tracer model 23 p4034 A67-41463

Electronic ellipsometer for measurement of very small changes in elliptically polarized light, discussing refractive index, Kerr effect and calibration 24 p4152 A67-41901

Internal light applied to opaque-faced edge-lighted plastic display panels [SAE PAPER 670196] 24 p4097 A67-41986

Optical detector using length of single mode optical waveguide with photodetector at output for null detection 24 p4133 A67-42817

Performance of single lens objective for coronagraph noting resolution, scattered-light background brightness, etc 24 p4158 A67-43074

OPTICAL MASER MODULATOR
SA LIGHT MODULATOR

Ruby laser mode locking and mode competition using RG-8 filter as passive modulator 07 p1197 A67-20147

OPTICAL MEASUREMENT
SA ELECTRONIC PHOTOGRAPHY

Optical surface roughness measurement using coherent radiation produced by helium-neon laser sigma-polarized at 6328

angstroms 01 p0020 A67-10020
Background noise effect on low level light intensity measurement of microsecond transient discharge 02 p0243 A67-12185
Optical observation of brightest X-ray source in Scorpius, giving tabulated data as function of radius 05 p0892 A67-16414
Line width of CW Ga-As lasers measured using homodyne detection and autocorrelation 05 p0821 A67-16670
Spectral radiance of low current graphite arc anode determined, using high accuracy spectroradiometer 05 p0846 A67-16787
Rotating shutter telescopic observation for optical measurement of faint meteor velocity 05 p0897 A67-16805
Photomagnetic susceptibility measured by means of induced short duration light flash, using germanium 06 p1001 A67-17938
Error due to multiple propagation in distance measurement by comparison of modulation phases on transmitted and reflected laser beam 07 p1186 A67-19606
Optical incremental shaft resolver using plastic radial gratings 08 p1331 A67-20864
Microwave and optical measurements of decay of neutral metastable and charged species in flowing He afterglow 08 p1356 A67-21300
Laser effect on electron gas and excited state populations in xenon discharges 08 p1338 A67-21306
Calorimetric measurement of pulsed ruby laser output energy 09 p1510 A67-21615
Optical signal modulation to measure noise figure at UHF of photoparametric amplifier, using silicon mesa diode as both photodetector and varactor diode 09 p1476 A67-22208
Holography for particle size analysis noting wave formation and reconstruction, hologram camera, etc 10 p1653 A67-22748
Beam wavelength and laser intensity effect on attenuation in carbon disulfide induced by ruby laser indicate two-photon absorption 10 p1667 A67-23776
Measuring method for beam divergence of Q-switched ruby laser rods 10 p1667 A67-23782
Laser for remote vibration measurement and detection without mechanical contact with structure under test 11 p1798 A67-24433
Quasi-stellar objects red shift and optical magnitude measurements, noting discrepancies with zero and nonzero cosmological constant 11 p1863 A67-24508
Laser holography combined with schlieren techniques to measure ray deviations in optically inhomogeneous field of transient phenomenon 11 p1794 A67-24927
Upper atmospheric composition data compared, showing erroneous nature of Hinteregger and Pokhunkov measurements on oxygen-nitrogen ratio 12 p1934 A67-25789
Reflectance, transmittance and absorbance of muscovite type mica as function of thickness measured, using prism and grating spectrophotometers [AIAA PAPER 67-288] 12 p1958 A67-26005
Phase and amplitude measurements of laser wavefront using laser phase-locked loop 13 p2129 A67-27494
Laser measurements and standards of energy, power, attenuation and frequency stability, using pulsed ruby and gas lasers as radiation source 14 p2319 A67-28392
IR spectrum evaluation procedures and optical measurement as applied to atmosphere physics 14 p2311 A67-28401
OH emission in H II region W3, using improved equipment 14 p2389 A67-28845
Pasteur Probe, assay of asymmetry of D, L amino acids in detection of Martian life 15 p2433 A67-29116
Development of plasmoid density due to laser ionization measured using Fabry-Perot interferometer 15 p2527 A67-29474
Fluid flow measurement through optical radiation detection, determining local velocities and image-space motion 15 p2488 A67-29768
Spectrometers, utilizing interference filter wedges, for field use, especially in hostile environments 15 p2491 A67-30430
Probability distribution of number of photons and integrated intensity relation to normal and antinormal ordering of field operators in quantum optics 16 p2685 A67-30826
Light attenuation measurement in chilled

silicon noting attenuation increase with incident intensity 16 p2685 A67-30870
Concentration profile of normal and excited mercury atoms in shock wave front and wake, noting gas density and electron concentration profiles 16 p2673 A67-31108
Calibration system for PRESS optical aircraft program utilizing portable collimators 16 p2679 A67-31796
Interference from laser light beam superposition at single photon level, noting existence of fringes 17 p2866 A67-32277
Energy loss function of thin film deposited metals, using optical measurement method 17 p2913 A67-32294
GaAs laser reflectance measurements of tactical landing terrain samples 17 p2858 A67-32483
Very high optical resolution via lunar occultation noting experimental technique 17 p2945 A67-32646
Laser applications utilizing power density for studying reflectance, Raman spectra, photography, holography, etc 17 p2868 A67-32691
Perspective and path length effects on determination of spatial distribution of auroral luminosity from optical observations 17 p2851 A67-33206
Optical instrument for measurement and control of tube flares in connections in liquid propulsion systems 18 p3054 A67-34366
Arlow measurement apparatus and procedure at Tehran University 19 p3224 A67-35488
Searchlight brightness measurements for vertical turbidity layer of troposphere using computing scattering functions 19 p3225 A67-35532
Optical system using moiré patterns to measure refractive index gradients in boundary layer, showing relation to temperature and density gradient [ASME PAPER 67-HT-3] 20 p3447 A67-36702
Radiance of debris cloud ejected from manned spacecraft, effect on optical environment and astronomical observations 20 p3525 A67-37099
Optical metagalactic radiation measured by spacecraft photographic and photometric methods, reviewing Olbers paradox and night sky brightness measurements 20 p3526 A67-37127
Bezold-Brucke hue shift measurements in color naming situation using optical system 22 p3835 A67-39238
Wind and cloudiness effects on terrestrial scintillation based on visual estimates and measurements 22 p3828 A67-39240
Diamond electronic structure studied by absolute reflectance measurements, obtaining dielectric response function over broad energy range 22 p3862 A67-39999
CdTe photoemission absolute energies determined by correlating electron energy distribution structure with structure in optical data 22 p3862 A67-40001
Optical transfer function relation between image aberration and diffraction, describing measuring methods 22 p3837 A67-40072
EM radiation reflection, absorption and transmission through dielectric medium measured, studying other aspects by electric dipole oscillator model 23 p4037 A67-40757
Venus surface temperature measured using difference between optical and radar radii, cloud temperatures and adiabatic lapse rate 24 p4225 A67-41827
Ariel III satellite attitude determination using optical glint technique 24 p4240 A67-41877
Optical measurement of atmospheric refractive index gradient showing approximate accuracy and simplicity for reasonably large gradients 24 p4188 A67-42093

OPTICAL METHOD

Coherent optical systems for processing data collected by sidelooking synthetic-aperture radars 01 p0022 A67-10430
Interferential method of testing high resolution photographic emulsions, using laser as light source 01 p0091 A67-10832
Holograms with incoherent illumination, noting patterns produced and resolution parameters 01 p0070 A67-11081
Optical frequency translation of pulses from mode locked laser, noting Doppler shifts of large magnitude 02 p0253 A67-12506
Absorption of electromagnetic energy in gases in centimeter range waves measured, using optical-acoustic method of signal

changes 03 p0418 A67-12895
Optical methods and equipment used in checking surface finish and volume and surface inhomogeneities of active media and interferometric mirrors of lasers 03 p0436 A67-13143
Holograms of objects immersed in water and illuminated by 7-mc sound waves and reconstruction of optical images from sound holograms using laser light 03 p0420 A67-13570
Focused image holography with extended sources for real image in proximity of hologram plate 03 p0420 A67-13574
Method for recording Fresnel transformations of two- and three-dimensional scenes illuminated by spatially incoherent light 03 p0423 A67-13907
Holography, discussing color reproduction, character recognition and vision by sound or ultrasound 04 p0623 A67-15301
Holographic laboratory experiments, discussing Lippman method and imagery through diffusing media contour line implantation 04 p0623 A67-15302
Laser application to radar signal processing and communications equipment 04 p0576 A67-15303
Clear air turbulence detection with laser radar, noting airborne equipment and results 04 p0650 A67-15304
Time constants of thermocouples as function of parameters on which they depend, using schlieren phenomena 04 p0624 A67-15417
Temperature stresses in plane elements by unsteady heat fields examined via polarization optical method 05 p0914 A67-16195
Amplitude spectrum of turbulent flow rate fluctuations at flame temperatures measured via photoelectric method 05 p0927 A67-16942
Communications requirements for manned deep space missions, using optical links, with PPM, PCM/PL and coherent reception for each link [AIAA PAPER 66-317] 06 p0961 A67-17706
Optical method observations of phase transition of ferroelectric monocrystal SbSI 06 p1047 A67-17758
Smear camera used to measure detonation front velocity of explosive or propellant 06 p1001 A67-17793
Absorption of electromagnetic energy in gases in centimeter range waves measured, using optical-acoustic method of signal changes 06 p1006 A67-18772
Laser digital devices, discussing use as switching circuit in digital computer 07 p1194 A67-19088
Microscopic hole drilling into metals by laser beams, noting energy and power correlation with hole magnitude 07 p1190 A67-19090
Moiré method of surface strain measurement 07 p1262 A67-19387
Image distances and relative intensities for zone plates determined from holographic theory 07 p1185 A67-19401
Smithsonian observatory tracking network and geodetic results 07 p1177 A67-19777
Steady state laser design, comparing balance method with method based on quasi-classical theory 07 p1197 A67-20245
UV imaging system for lunar missions to detect luminescing minerals on lunar surface 08 p1331 A67-21079
Multispectral photography for AES missions, describing lunar color studies [AFCLR-66-796] 08 p1331 A67-21081
Polarization-optical method for investigation of stresses - All-Union Conference, Leningrad, June 1964 08 p1423 A67-21329
Nonstationary thermoelastic stresses analyzed using photoelastic technique based on polarized light 08 p1423 A67-21334
Error signal generation method to control laser frequency of laser oscillator 08 p1339 A67-21378
Aerosol particle velocity measurement using optical compensation and photoelectric particle counter 08 p1428 A67-21422
Low spatial frequency white light hologram production on Diazo materials 09 p1493 A67-21572
Cylindrical optics in converting laser emission into second harmonic in ADP and KDP crystals, obtaining high conversion efficiency 09 p1511 A67-21916
Hologram fixation by Gabor single beam

method, using gas laser as light source 09 p1511 A67-21919

Stress measurement in metal components with photoelastic coatings and thin walled structures, using reflected light 09 p1575 A67-22169

Photooptical system for determining velocity of projectile after target penetration 09 p1502 A67-22623

Barium Q plasma device for optical diagnosis of oscillatory microinstabilities compared with Langmuir probe 11 p1838 A67-24406

Quantitative schlieren interferometry, measuring thermal distributions near heated vertical plate and horizontal cylinder 11 p1791 A67-24668

Hall voltage reduction in linear MHD generators noting Lorentz force effect 12 p1898 A67-25387

Dual camera for Lunar Orbiter, design, performance and hardware modifications [SMPT PAPER 101-47] 12 p1940 A67-25465

Advances in communication systems, Volume 2 12 p1906 A67-25987

Optical computing principles, techniques and configurations for communication problems noting Fourier transform, coding, etc 12 p1907 A67-25990

Optical interferometry in plasma diagnostics, discussing degree of ionization, time dependent electron density distribution, etc 12 p1976 A67-26073

Cloud height measurement by optical method compared with vertical radar procedure 13 p2152 A67-26866

Image transmission through optical fiber, discussing reconstruction of refracted image via holography 13 p2120 A67-27209

Optical interference method of two-dimensional Fourier transform with spatially incoherent illumination to derive relations for transforms of images 13 p2121 A67-27290

Error analysis shows laser-radar method improves accuracy of astronomical parameters of earth-moon system, taking into account physical libration 13 p2200 A67-27327

Flow visualization, discussing schlieren process in light of Toepler, fine focusing, microscopic, phase contrast and field absorption processes 14 p2315 A67-27974

Cylindrical optics in converting laser emission into second harmonic in ADP and KDP crystals, obtaining high conversion efficiency 14 p2329 A67-28245

Hologram fixation by Gabor single beam method, using gas laser as light source 14 p2329 A67-28248

Coherent radiation frequency conversion and nonlinear optics methods, including stimulated Raman scattering and Mandelstam-Brillouin scattering 14 p2330 A67-28467

Amplitude spectrum of turbulent flow rate fluctuations at flame temperatures measured via photoelectric method 14 p2406 A67-28490

Scale grating with moire fringe effect, noting attachment to Zeiss 3030 coordinate measuring instrument 14 p2319 A67-28590

Slit width effect on accuracy of equivalent width measurements, noting results with 10 angstrom/mm plates 14 p2319 A67-28591

Dynamic components thermal characteristics determination by IR optic techniques, studying metal fatigue, wear and friction phenomena [ASME PAPER 67-DE-24] 14 p2328 A67-28873

Semiconductor laser output power varied by decreasing inverse population through heating electron-hole gas by intense optical radiation 15 p2496 A67-29236

Transposition into holography of optical visualization methods by linking ultrahigh speed camera and solid state laser 15 p2487 A67-29481

Local turbulent properties of supersonic jet exhaust measured optically by crossed beam correlation technique 16 p2591 A67-30943

Collection of papers on aerophysical studies of supersonic flows covering shock tube experiments, gas density, interferometer and photographic measurements, etc 16 p2672 A67-31101

Shadow method analysis of shock wave interaction with fixed bodies in shock tube at small and medium supersonic Mach numbers 16 p2673 A67-31105

High speed spark photography with electronic equipment, describing generating

and control units and optical techniques for shock wave observation 16 p2674 A67-31127

Atmospheric ozone vertical distribution, discussing optical measurement method 16 p2676 A67-31375

Ultrashort light pulses, discussing laser modes, Q-switching pulse duration measurements, etc 16 p2686 A67-31741

Silicon oxide and nitride film thickness determined with interference technique, using spectrophotometer in UV and visible wavelength range 17 p2854 A67-32191

Frequency and wavelength stabilization of gas lasers, noting wavelength shifts due to gas pressure and gain variations 17 p2815 A67-32611

Spectral purity of Ebert type far IR grating spectrometer determined, noting experimental technique 17 p2863 A67-33300

Holographic testing of large optical surfaces, using laser sources and interferometer guidance 17 p2863 A67-33301

Optical methods used for study of ruby crystals uniformity, discussing Twyman interferometer design 18 p3098 A67-33576

Hydrodynamic structure of exothermic reaction zone behind one-dimensional shock fronts in gaseous detonation studied by optical method 18 p3153 A67-33827

Radiative heating of H and He containing suspension of solid particle absorbers, noting proportionality between gas particle dispersion decrease and energy absorption [AIAA PAPER 67-501] 18 p3158 A67-33965

Soviet and foreign studies of atmospheric oxygen by optical and spectral methods 19 p3214 A67-34857

On-the-ground optical determination method of stratospheric aerosol particle numbers and sizes from ruby laser radiation measurement scattering 19 p3225 A67-35531

Differential geometry and vector analysis used to design axisymmetric lens of arbitrary shape for observing phenomena in arbitrary flow field of revolution 21 p3610 A67-37810

Holographic measurement of surface strains noting fringe pattern for displacements 21 p3625 A67-37944

Optical system performance and atmosphere attenuation, analyzing absorption and scattering phenomena in terms of weather conditions 22 p3828 A67-39612

Spherical electromagnetic wave refraction on heterogeneous parabolic plasma layer using beam optics 22 p3760 A67-39737

Optical technique with laser source for range measurements noting use of dispersion between two different light wavelengths 22 p3800 A67-40139

Parallel contours of fracture surface at optical magnifications obtained by method based on microhardness indentations 22 p3823 A67-40300

Wind tunnel hypersonic flow visualizations under low flow density conditions, comparing schlieren and phase-contrast methods 23 p3985 A67-40568

Determination of coordinates from satellite observations noting triangulation method and optical technique 23 p3994 A67-40700

Optical elastohydrodynamic system for evaluation of lubricants using interference pattern obtained from metal ball rolling against plate glass [ASLE PAPER 67-LC-12] 24 p4164 A67-42747

Asymptotic functional dependences and eigenvalues of guided wave modes in uniform and nonuniform structures deduced by ray-optical techniques 24 p4124 A67-42807

OPTICAL MODULATION

Optical modulator using electro-optic effect in lithium tantalate for PCM transmission systems operating at 224 megacycle bit rate 01 p0033 A67-10013

Microwave modulation of helium-neon laser intensity studied as function of temperature and electron density 01 p0088 A67-10260

Light modulation at hyperfine frequencies in optically pumped potassium vapor, noting detection techniques, optical absorption and dispersion 02 p0251 A67-11818

Giant coherent light pulse generation by Q-factor modulated laser 03 p0433 A67-12941

Self-modulation characteristics of carbon dioxide laser and use in measuring detector response and atmospheric propagation characteristics 03 p0439 A67-14399

Single mode output power modulation analysis of saturation and gain of gas lasers and effects of excitation density modulation and resonator Q modulation 04 p0633 A67-15111

Magneto-optical modulation of IR emission of He-Ne gas laser 04 p0633 A67-15139

Frequency conversion at optical wavelengths of doubly modulated light, using LF photodetectors as receivers 04 p0575 A67-15170

Intracavity time-varying perturbation of losses in gas laser using diamagnetic Faraday effect in glasses analyzed in connection with output intensity 05 p0818 A67-16646

Equation for dynamical behavior of laser, solving case of deep modulation of output, noting pulsation problems 05 p0820 A67-16682

Single mode output power modulation study of saturation and gain of gas laser 05 p0823 A67-16686

Internal modulation of IR gas laser using cadmium sulfide or selenide single crystals 05 p0824 A67-16914

Periodic automodulation of radiation and possibility of generating giant pulses in three-level laser with inhomogeneously excited active medium 05 p0826 A67-17233

Semiconductor mirror for Q-factor modulation of laser resonator 06 p1012 A67-18789

Electric field induced optical refractivity changes /Franz-Keldysh effect/ and nonlinear light scattering, light beam deflection and modulation in neutron-irradiated Si at 95 degrees K 07 p1231 A67-19487

Rate equations for gas discharge modulation of He-Ne laser 07 p1195 A67-19492

Error due to multiple propagation in distance measurement by comparison of modulation phases on transmitted and reflected laser beam 07 p1186 A67-19606

Photon counting distributions and intensity fluctuations of modulated laser beams 07 p1197 A67-20125

Modulation linearity improvement using separate analyzer assembly with each electro-optic crystal 09 p1511 A67-21643

Traveling wave electro-optic modulator tested at 6328 angstroms with CW drive power 09 p1471 A67-21644

Laser mode-locking during resonator Q-factor modulation 09 p1513 A67-22065

Control of laser action, noting feedback theory conception and geometrical optics of laser modulation 09 p1513 A67-22146

Internally modulated gas laser at 100 and 4000 MHz, describing electromagnetic field in Fabry-Perot resonator in terms of natural oscillation modes and coupling 09 p1514 A67-22269

Laser beam modulation by atmospheric turbulence as function of receiving aperture size, range and atmospheric conditions 11 p1799 A67-24236

Transmission of large number of instrumentation channels over parallel pulse-modulated light beams, using electro-optical mosaic sources and detectors 11 p1764 A67-24444

Rapid vapor phase growth of high resistivity GaP for electro-optic modulators, noting high electron mobility 11 p1848 A67-24747

Magneto-optical modulation of IR emission of He-Ne gas laser 12 p1951 A67-25162

SNR and transmission error probability in pulse modulated optical communication 13 p2067 A67-26663

UHF intensity-modulated light emanating from plasma observed with aid of photomultiplier radiometer 13 p2167 A67-27082

Frequency conversion at optical wavelengths of doubly modulated light, using LF photodetectors as receivers 15 p2443 A67-29356

Internal modulation of IR gas laser using cadmium sulfide or selenide single crystals 16 p2685 A67-30891

Potassium dihydrogen phosphate inside laser cavity to achieve HF modulation 17 p2869 A67-33297

Semiconductor mirror for Q-factor modulation of laser resonator 18 p3059 A67-33731

Optical subcarrier communications, noting use space-oriented missions and RF

techniques optical subcarrier communications, noting use in space-oriented missions and RF 20 p3378 A67-36183

Wave field behind transmission grating illuminated by plane wave examined by Fourier spectrometry based on grating resonances 20 p3437 A67-36338

Optical communication systems modulation, discussing TV link, modulator, optical waveguides and materials availability 22 p3759 A67-39330

Modulation transfer theory for frequency response of optical system in temporal or spatial domains, discussing Fourier series and transform [SMPT PAPER 102-47] 22 p3808 A67-40380

Michelson interferometer used as tunable mirror in laser resonators, obtaining internal modulation of initial intensity 23 p4013 A67-40902

Modulation transfer functions of various solar recording films using interference device, giving detectability threshold of two-dimensional emulsion patterns 23 p4001 A67-41237

Plasma discharge instability effect on gas laser operation, discussing moving layers self-excitation and laser beam modulation 24 p4188 A67-42561

OPTICAL PATH

Radiant heating by inhomogeneous hot gases, determining spectral transmittances of inhomogeneous optical paths using Curtis-Godson approximation 02 p0342 A67-12050

Silicon solar cell to measure solar radiation intensity, discussing effect of optical path length ratio and atmospheric constituents 03 p0419 A67-13079

Density dependence of refractive index of air and phase and group refractive index as function of pressure, temperature and composition 05 p0838 A67-16783

Interferometer for small optical path difference measurements, noting high sensitivity and environmental stability 05 p0807 A67-16789

Optical paths and variable-contrast interference at Michelson interferometer which adds two groups of two laser coherent waves 06 p1009 A67-17636

Ruby laser cavity losses measurement by Fabry-Perot resonance 10 p1662 A67-22740

Near IR atmospheric absorption over 25-km horizontal path at sea level 10 p1629 A67-22744

Energy propagation and partial self-focusing in laser beam 10 p1663 A67-22847

Multiple scattering and finite detector bandwidth effects on shape of absorption features in atmospheric scattering 11 p1862 A67-24502

Geographical location and optical path length effects upon fade margin required for desired propagation reliability of microwave signals 13 p2066 A67-26406

Prediction of total emissivity of nitrogen-broadened and self-broadened hot water vapor 13 p2155 A67-26493

Heterodyne signal amplitude dependence on optical path length difference for oscillating axial modes in multimode gas laser 13 p2128 A67-27346

Pulse modulated data channel operation over parallel optical paths, noting advantages inherent in simple processing and control circuitry 14 p2272 A67-28699

Atmosphere effect on laser beam scintillation measurements after propagating over 8 km path near ground for various collector sizes and environmental conditions 16 p2686 A67-31879

Mean-square value and autocorrelation function for fluctuations of geometrical optical paths 18 p3000 A67-34025

Frame-camera interferogram data for Nd-doped glass rod during laser pumping analyzed through optical path length changes 18 p3062 A67-34623

Pump radiation induced optical distortion in Nd-doped glass laser rods measured and compared to theory 18 p3062 A67-34625

Holographic interferometry by superimposed holograms before or after photographic development 19 p3232 A67-35890

Pulse width of ultrashort light pulses measured by Michelson type arrangement of nonlinear optics 20 p3456 A67-36172

Holography by amplitude division, eliminating destructive interference by using optical prism 20 p3435 A67-36200

Absorption of optical photons in molecular crystals, noting results of laser output on naphthalene 20 p3457 A67-36326

Two-dimensional displays conversion to three-dimensional, using uniaxial crystals to vary optical path length and digital control with electro-optic polarization switches 20 p3447 A67-36806

Displacement effects analyzed for one beam of laser streak interferometer relative to another on image intensity distribution 22 p3795 A67-39199

Optical mixing process for study of polarized light in wedge shaped cells of Raman active medium 23 p4017 A67-41433

OPTICAL POLARIZATION

Binary detection probability for optical polarization modulation communication system using Gaussian approximation, noting signal to noise ratio 01 p0026 A67-10866

Barium titanate single crystals at infrared frequencies investigated for polarization, effective permittivity and coercive field 03 p0497 A67-13697

Lamb self-consistent theory and rate equation approximation study of magnetic depolarization of vapor and polarization of monomode gas laser in magnetic field 05 p0818 A67-16644

Electron mobility in AlSb, GaP and GaSb calculated by combining effects of optical polar and deformation potential scattering 06 p1067 A67-18964

Polarization and brightness temperature distributions across lunar disk observed with Parkes radio telescope at various wavelengths 07 p1251 A67-19854

Optical rotation of lipids extracted from soils, sediments and Orgueil carbonaceous meteorite 08 p1289 A67-21173

Longitudinal mode oscillations of gas laser when resonator length changes with time, noting polarization and amplitude change related to growth of new oscillation 08 p1338 A67-21314

Two-plate polarizer rendering worst cross polarization with arbitrary vane angles and differential phase shifts 09 p1474 A67-22089

Prismatic wideband directional couplers of Brewster angle type, discussing basic theories, frequency characteristics, insertion loss and directivity 10 p1606 A67-23065

Polarization of ytterbium isotopes in atomic state using optical pumping with resonance line, calculating magnetic moments 10 p1665 A67-23479

Optical lossless double pass network synthesis techniques using birefringent crystals extended to complex and real transmittance amplitudes 11 p1818 A67-24418

Wavelength dependence of polarization of IR star in Cygnus measured by far IR lead sulfide photopolarimeter 11 p1863 A67-24509

Linear polarization of Crab Nebula, Cygnus A and other radio sources observed at wavelength of 21.3 cm, using radio telescope 13 p2198 A67-26714

X-ray laser resonator proposal involving three-dimensional puckered ring arrangement of crystals at Bragg angle, discussing polarization losses 13 p2126 A67-27012

Combination tones generation by interaction of orthogonal gas laser oscillations, showing dependence on polarization states and primary oscillations 13 p2126 A67-27015

Thermal stresses and displacement in flat wedges using optical polarization method 13 p2219 A67-27058

Small optical rotations in near IR measured by ring laser, discussing dynamic behavior of polarization state 13 p2128 A67-27345

Linear polarization of discrete radio sources at 6 cm wavelength 13 p2206 A67-27483

Photoelectric two-cell polarimeter with rotating achromatic half-wave plane noting wavelength restriction 14 p2319 A67-28563

Electric field effect in terms of drifted Maxwellian distribution, considering nonparabolic electron scattering where dominant energy-loss mechanism is optical polar mode scattering 14 p2376 A67-29086

Measurement of position of polarization plane of radiation emitted by neodymium-glass laser 15 p2499 A67-29758

Small scale trapping of laser beam and frequency shift in Raman radiations observed under various polarization

conditions 16 p2684 A67-30607

Polarization and angle of arrival fluctuations for plane wave propagated through turbulent medium 16 p2625 A67-31344

Intrinsic optical polarization of Taurus IR source 19 p3330 A67-36081

Optical polarimetric observations of quasi-stellar objects 19 p3331 A67-36083

Beta Lyrae intrinsic polarization amount and phase dependence in visual, blue and UV light observed, analyzing polarization curves 20 p3528 A67-37471

Polarized and depolarized scattering from perfectly conducting rough surface, theory based on Fourier transform and small perturbations polarized and depolarized scattering from perfectly conducting rough surface, using theory 22 p3782 A67-40076

Zodiacal light and interplanetary dust, discussing brightness, polarization, color, spectrum and dust cloud about earth 22 p3794 A67-40426

Emission wavelength selection in multicolor-emission noble gas laser using linear polarization control device 23 p4014 A67-41025

Optically active alpha amino acids synthesized from alpha keto acids by hydrogenolytic asymmetric transamination 24 p4119 A67-42703

OPTICAL POWER LIMITER

Single frequency light from argon FM laser with external lithium niobate modulator, discussing overall conversion efficiency and distortion reduction 10 p1664 A67-22906

OPTICAL PROPERTY

Optical and magneto-optical phenomena in CdSnAs sub 2, discussing reflection and absorption spectrum, optical activity, double refraction, dielectric constant, etc 01 p0128 A67-10094

Optical harmonic generation and first order sum and difference frequencies in plane parallel crystal plate within framework of phenomenological theory 01 p0089 A67-10361

Electrical and optical properties of solid solutions formed by beta manganese and chromium dioxide within wide composition range, showing magnetic semiconductor behavior 01 p0134 A67-10755

Nonlinear optical materials properties discussed on basis of Soviet and foreign studies involving lasers 01 p0115 A67-11011

Optical characteristics, including refractive indices, of thin layer amorphous titanium oxide films 01 p0115 A67-11048

Optical transmittance of fused silica at elevated temperatures, showing shift in UV to IR absorption with increasing temperature 01 p0138 A67-11074

Interferometric technique for measuring thickness and optical constant of thin antimony trisulfide films 02 p0288 A67-11721

Optical properties of thin metallic films relative to electronic structure in microcrystals 02 p0288 A67-11722

Optical constants of silver solid solutions with gold addition, noting dependence of refractive index, absorption coefficient and conduction electrons on impurity concentration 02 p0255 A67-11870

Soviet papers on optical instability of earth atmosphere 02 p0261 A67-11982

Paint film thickness of spacecraft coatings, effect on spectral directional reflectance and binormal transmittance in far IR [AIAA PAPER 65-653] 03 p0447 A67-13033

Optical properties of semiconductors by measuring spectral emittance of transparent and opaque solids and measurements on materials used in IR optics [AIAA PAPER 65-654] 03 p0418 A67-13034

Spectral emittance of metallic and nonmetallic materials, discussing surface roughness effects [AIAA PAPER 65-675] 03 p0467 A67-13042

Optical and electrical properties of barrier layers in Cu doped GaP, discussing intensity region of superlinearity dependence on temperature and IR light 03 p0491 A67-13202

Low energy electron-helium atom scattering, using formal optical potential in variational expression for scattering phase shifts 03 p0471 A67-13318

Optical activity in meteorite organic matter, recording observation of low amplitude 03 p0510 A67-13592

Optical properties of evaporated barium

films investigated at various wavelengths, using ultrahigh vacuum
reflectometer 03 p0499 A67-13909
IR spectral emittance measurements of optical materials by comparison with black body radiation at same temperature 03 p0470 A67-14392
Ground tests of 2.3-m-diam models of foldable foam-reinforced plastic paraboloidal mirrors for satellite energy supply system and optimization of optical characteristics 04 p0558 A67-15957
Light sensitivity of diffused Si phototransistor and of system of two cascade coupled phototransistors 05 p0770 A67-16169
Optical properties of thin indium films of varying thicknesses 05 p0862 A67-16599
Nonlinear instability of optical frequencies in partially ionized plasma, noting nonlinear frequency buildup for strong plasma waves 05 p0852 A67-16691
Optical constants of Ge in XUV verified using Kronig-Kramers dispersion relation, optical oscillator strength sum rule, correlation methods and electron energy loss distribution 05 p0864 A67-16784
Optical harmonic generation and first order sum and difference frequencies in plane parallel crystal plate within framework of phenomenological theory 06 p1009 A67-17619
Relation between optical and radio properties of quasars 06 p1086 A67-18374
Optical properties of interstellar grains, noting complex index of refraction as function of wavelength 06 p1087 A67-18410
Optical properties of zinc oxide analyzed by exposing samples to mechanical and thermal treatments and UV radiation [AIAA PAPER 67-214] 06 p1052 A67-18514
IR spectra of undoped and Li doped ZnSe and CdS 06 p1059 A67-18911
Impurity states in CdTe analyzed by examining changes in electrical and optical properties after thermal-neutron bombardment 06 p1062 A67-18928
Niningerite composition and optical, physical and crystallographic properties 07 p1247 A67-19064
Crystal symmetry, optical properties and ferroelectric polarization of barium titanate single crystals 07 p1234 A67-20096
Infinite plate consisting of monopolar semiconductor of given thickness under effect of electric field results in change in galvanomagnetic, piezoresistance and optical properties 08 p1367 A67-20416
Space environment effect on refractive optical systems, particularly solar radiation effect on optical properties of glass 08 p1330 A67-20644
Radiation noise effect on laser optical properties, noting density vs resonator characteristics, energy spectrum, etc 08 p1337 A67-20839
Quantum theory of optical coherence in twisted convolution formalism 08 p1354 A67-20871
Lunar surface optical properties and IR emission [AAS PAPER 66-185] 08 p1387 A67-20960
Optical quenching effect and spectral distribution of photoconductivity and optical transmission of KRS-5 single crystals 09 p1552 A67-21673
Nonparaxial imaging, magnification and aberration properties in holography, examining point source object 09 p1496 A67-21707
Transmission of artificial quartz at room temperature, obtaining optical constants in far IR region 09 p1553 A67-21917
Uniaxial stress and static electric field effects on energy band structure of strontium titanate and derivation of optical selection rules in region of perturbed crystals 10 p1891 A67-23403
Refractive index of microwave lenses made of ferrite material changed by varying DC magnetic field 11 p1752 A67-24125
Lunar optical properties simulated with commercial Portland cement and maroon and black coloring powders, noting blue-green color index discrepancy 11 p1885 A67-24609
Optical and laser properties of trivalent Nd and Eu ion doped yttrium orthovanadate 11 p1847 A67-24739
Microwave thermography used to measure microwave optical field patterns, using Czerny IR thermosensitive transducer

process 12 p1939 A67-25196
Nonlinear optical materials properties discussed on basis of Soviet and foreign studies involving lasers 12 p1966 A67-25361
Rubidium nickel trifluoride transparent single crystal magnetic and optical properties analyzed, concluding compound is antiferromagnetic 12 p1984 A67-25747
Emittance properties of sintered oxides treated by method of empirical generalization and by method involving comparison of emittance in air and in vacuum [AIAA PAPER 67-301] 12 p1958 A67-26016
Optical materials properties analyzed for UV induced degradation under vacuum conditions [AIAA PAPER 67-344] 12 p1959 A67-26058
Far UV transmitting windows, particularly lithium fluoride, and response measurements below 2000 angstroms, noting fabrication on solar blind materials 12 p1947 A67-26161
Formulas for using wave plates in ellipsometry 13 p2158 A67-26879
Piezotransmission measurements of phonon-assisted transitions in semiconductors 13 p2179 A67-27157
UV optical properties and electronic band structure of magnesium oxide 13 p2181 A67-27167
Absorption and fluorescence characteristics of Nd-doped phosphate glasses used as laser material 13 p2128 A67-27229
Control efficiency and perfect cut-off of beam current of controlled electron guns, noting focusing properties and variation in focusing with voltage 14 p2276 A67-27767
Reflection coefficient and separation of real and imaginary parts of optical index in nonmetal band-to-band transition model semiconductor 14 p2384 A67-27956
Transmission of artificial quartz at room temperature, obtaining optical constants in far IR region 14 p2365 A67-28246
Optical properties of thin aluminum and silver layers subjected to proton beam bombardment 14 p2373 A67-28855
Optical constants of ionic crystals at low temperatures determined from reflection spectra, noting correlation between absorption coefficient, magnitude and phonon difference processes 14 p2374 A67-28986
Optical characteristics of cosmic and terrestrial surfaces, noting color distribution on moon, asteroids, stony meteorites, etc 15 p2516 A67-29152
Reflectance of pyrolytic graphite and phenolic nylon chars for radiant heat rejection from nonablating heat shield 15 p2579 A67-29434
Refractory material as component of silicate binder having stable optical and physical properties under simulated space conditions 15 p2506 A67-29547
Asbestos reinforced plastics evaluated for physical and optical properties, thermal-vacuum and UV resistance 15 p2507 A67-29550
Nonlinear instability of optical frequencies in partially ionized plasma, noting nonlinear frequency buildup for strong plasma waves 15 p2530 A67-29862
Optical properties of moon quantitatively compared with powder samples, bombarded with ions from hydrogen discharge plasma 16 p2753 A67-31744
Reflectance and optical constants of evaporated iridium films measured in vacuum ultraviolet 16 p2733 A67-31878
Magnesium oxide and lithium fluoride in far UV, noting refractive and absorption indices 16 p2734 A67-31881
Source size effect on resolution in Fourier transform holography comparing theoretical and experimental results 16 p2681 A67-31883
Optical properties of Mg layers evaporated in ultrahigh vacuum, noting results of reflectivity measurements 17 p2913 A67-32292
Optical behavior of graphite as interstellar matter, discussing appearance as metal or dielectric particle, extinction and optical conductivity 18 p3117 A67-33513
Optical properties of magnesium fluoride in EUV from reflectivity measurements on crystal and thin films 18 p3099 A67-33692
Satellite technique for sounding atmospheric optical properties and height distribution of ozone and aerosols 18 p3040 A67-33853

Four types of holographic imaging systems, discussing optical properties and divergence and convergence 18 p3046 A67-33879
Graphical integration method for calculating optical characteristics of materials used in solar radiation spectral measurements 18 p2990 A67-34492
Two-channel single-pulse neodymium glass laser with 180 joule pulse, performance and optical features 19 p3239 A67-34986
Impurity effect on optical properties of interstellar graphite particles, examining wavelength dependence of absorption coefficient and refractive index of coals 19 p3323 A67-35423
Secular behavior of optical properties of X-ray emitting object near Cygnus X-2 19 p3331 A67-36084
Tellurium nonlinear optical properties including absorption and refraction indices, discussing second harmonic radiation generation 20 p3507 A67-36324
Upper atmosphere optical properties determined by simultaneous twilight balloon and ground measurements, establishing twilight sky luminance ratios to solar luminance 20 p3427 A67-36369
Linear/nonlinear molecule optical properties obtainable from light scattering in gas by strong optical field 20 p3488 A67-36437
Magnesium oxide single crystal electronic spectrum obtained from reflectance spectra, observing large plasma peak in energy loss function 20 p3509 A67-36508
Optimization for selection of optical coating patterns of external surfaces of spacecraft for temperature control [ASME PAPER 67-HT-55] 20 p3548 A67-36737
Molybdenum interband transitions noting low energy optical property anomalies and origin of two absorption bands 20 p3466 A67-36865
Sterically controlled synthesis of optically active alpha-amino acids from alpha-keto acids by reductive amination 20 p3376 A67-36874
Si optical and electrical properties and energy levels with Mg as donor impurity 20 p3510 A67-36916
Quantum mechanical accounting for materials optical properties, considering electronic structure 20 p3515 A67-37717
Hologram-moire interferometry for transparent objects of moderate optical quality 21 p3624 A67-37853
Single crystals of lithium-meta-niobate evaluated for nonlinear optical quality, using gas laser and interferometer 21 p3677 A67-38010
AlN single crystal thermal stable semiconductor optical/electrical properties, measuring space-charge-limited current and photocurrent 21 p3684 A67-38522
Nondestructively optically read ferroelectric bismuth titanate single crystal memory device 22 p3767 A67-39261
Optical properties of new and stable nonlinear optical ferroelectric potassium lithium niobate single crystal 22 p3863 A67-40236
Optical characteristics of wideband pulse compression system using Brillouin scattering for compressing time duration of frequency swept pulses of acoustic wave 23 p4012 A67-40869
Surveyor I landing site soil data covering mechanical, optical, thermal and electrical properties 23 p4064 A67-40950
Polished glass substrates for thin film microcircuits, analyzing surface resistivity and optical transmittance changes due to heat treatment 23 p4043 A67-41366
Radiation field asymmetry and anomalous beam angle divergence of ruby lasers linked to dislocations in ruby crystals prepared by Verneuil method 24 p4186 A67-42070
Ferroelectric, electro-optic and dielectric properties of tetragonal potassium-niobate-strontium-niobate crystal 24 p4204 A67-42366
Optical characteristics of cosmic and terrestrial surfaces, noting color distribution on moon, asteroids, stony meteorites, etc 24 p4190 A67-43075
OPTICAL PUMPING
CW laser using 3-inch ruby crystals with 15 percent mirror transmission, pumping power of double threshold value and 1.6 watt power output 01 p0088 A67-10244
Approximate absolute values of pumping

power, threshold power and critical excess population for ruby laser determined from relative flash tube intensity
 measurements 01 p0088 A67-10245

Laser action in optically pumped CN, discussing vibrational-rotational transitions 01 p0089 A67-10370

Flashlight /incoherent/ pumping of visible and IR, InSb and CdS-CdSe lasers 01 p0089 A67-10447

Decay cross section of pumped metastable He atoms in HeNe laser 01 p0090 A67-10511

Radiation from high energy level transitions excited in He-Ne laser during optical pumping with He lamp 01 p0090 A67-10513

Optical pumping with diode laser into Fabry-Perot resonator face of thin highly-absorbing semiconductor, noting variable mode spacing including single mode output 01 p0091 A67-10879

Laser characteristics of narrow band type I solar radio burst and magnetic dipole transitions in split Zeeman sublevels of hydrogen atoms of solar corona in ground level 02 p0322 A67-11652

Light modulation at hyperfine frequencies in optically pumped potassium vapor, noting detection techniques, optical absorption and dispersion 02 p0251 A67-11818

Q-spilling of ruby laser by optical pumping in intense inhomogeneous magnetic field with reduced gain 02 p0253 A67-12505

Temperature tuning of lithium niobate optical parametric oscillator in visible spectrum, noting generated frequency dependence on pump frequency and longitudinal mode distribution 02 p0253 A67-12511

Pumping of organic dyes in organic solvents, using pulsed ruby laser 02 p0253 A67-12515

Measurement method for spin relaxation and longitudinal decay of optically pumped vapors in weak magnetic fields 02 p0248 A67-12699

Luminescence of alcoholic solution of europium chelate at low temperatures, noting changes in intensity of optical excitation at various energy levels 03 p0433 A67-12894

Volume density of heat sources in ruby laser rod by numerical integration of pumping and absorption spectra 03 p0434 A67-13117

Kinetic equation derivation from density matrix for case of quantum generation of secondary optical harmonic in laser cavity under various optical pumping conditions 03 p0435 A67-13127

Influence of polarized atoms diffusion on spatial distribution of optically oriented atoms 03 p0437 A67-13388

Parametric amplification of far IR in Te crystal pumped by carbon dioxide laser 03 p0437 A67-13572

Crystal absorption and lamp emission spectra for CW pumping of Nd-doped YAG by water-cooled Kr arcs 03 p0437 A67-13576

Spontaneous emission in inversely populated medium examined for uniform ruby rod laser with uniform pumping distribution 03 p0438 A67-14186

Spin relaxation times of ground state of atomic cesium in aromatic gases measured using optical pumping, noting dependency on temperature 04 p0660 A67-14611

SFH oscillator construction using multiphonon processes that occur in gases during dipole interactions 04 p0580 A67-14749

Spin echo and free decay signals in Rubidium optical pumping analyzed, using pulse method and light modulation technique 04 p0632 A67-14770

Emission from tellurium single crystal pumped by two waves from carbon dioxide laser 04 p0632 A67-14914

Trivalent neodymium doped glass laser with internal imperfections due to optical pumping examined via optical metallography, transmission electron microscopy and electron diffraction techniques 04 p0632 A67-14927

Ferromagnetic magnetostatic amplifier using various types of oscillations for pumping and signal amplification 04 p0583 A67-15168

Fraction of luminous energy captured by optical pumping lasers in given geometrical configuration, obtaining functioning threshold depending only on

crystal 04 p0634 A67-15498

Abrupt transmission change during ruby laser emission resulting from pumping with xenon flash lamp 04 p0634 A67-15649

Fission or radioisotopic nuclear radiation applied to laser pumping, discussing forms, sources, power, solid state and molecular gas lasers, energy transfer, optical fluorescence and cut-off phenomenon 05 p0814 A67-16547

Loss measurement for ruby laser resonant cavity, comparing thresholds for R sub 1 and R sub 2 line operation 05 p0819 A67-16655

Optically pumped ruby noting absorption and emission spectrum, transition stages and phonon terminated amplification 05 p0820 A67-16658

Tunable Raman laser obtained by electron mobility subjected to magnetic field, noting threshold pump power 05 p0823 A67-16684

Hydrogen atom excitation by Lyman alpha radiation absorption in electric field 05 p0848 A67-16795

Threshold of parametric oscillator system with idler modes in same frequency spacing as laser pump source 05 p0824 A67-16823

Gaseous laser output expressed in single or two-line oscillations as function of pumping rates and transition probabilities, considering concept of equivalent network 05 p0825 A67-168979

Pumping medium power lasers using artificial meteors to produce intense gas glow in compression wave 06 p1009 A67-17757

Extension of paper on saturable absorber giant pulse lasers to include effects of finite absorber lifetime on pulse parameters, noting pump role 06 p1011 A67-18148

Gas laser behavior in magnetic field, analyzing data on magnetic effect, Zeeman effect and microwave pumping 06 p1011 A67-18168

Semiconductor lasers using single and double photon optical excitation 06 p1013 A67-18930

YAG solid state laser system, discussing output, theoretical limits, performance characteristics, etc 07 p1194 A67-19084

Book on lasers, light amplifiers and oscillators noting optical resonators, optical pumping, pulsed lasers, etc 07 p1195 A67-19469

Optimal design of elliptical pumping chambers from numerical calculations containing all geometric sizes of pumping lamps and laser rods and reflectivity of walls 07 p1195 A67-19490

Ruby laser irradiation by similar laser situated at right angle to first results in radiation intensity reduction of irradiated laser 08 p1338 A67-21204

Energy coupling measurement through electrodeless discharges in coaxial tubes, discussing parameters, dynamic processes, etc 08 p1338 A67-21291

Time dependent behavior of laser pumped ruby maser at low temperature 08 p1511 A67-21765

Gallium arsenide laser pumped by Stokes component of induced Raman scattering in liquid nitrogen of Q-modulated ruby laser light 09 p1512 A67-21973

Small size CW He-Ne laser pumped by resonant cavity, examining current-voltage characteristics and current dependence of output power 09 p1513 A67-22170

Design characteristics and operation of continuous neodymium laser 09 p1516 A67-22665

Multiple pass effects in laser pumping cavities, noting mercury lamp performance 10 p1662 A67-22743

Photon absorption coefficients measured in active and passive regions of electron-beam-pumped semiconductor laser 10 p1664 A67-22909

Polarization of ytterbium isotopes in atomic state using optical pumping with resonance line, calculating magnetic moments 10 p1665 A67-23479

Ruby laser output energy losses when passing from normal to passive Q-switched operation 11 p1800 A67-24241

Ruby laser generation spectrum width analyzed interferometrically as function of mirror spacing and pumping power 12 p1952 A67-25325

Water cooled mercury arc discharge lamp for room temperature optimum optical pumping of CW lasers 12 p1952 A67-25331

Automatic photographic recording of laser output energy vs excitation energy obtained

from fluorescence of ruby used to integrate laser light 12 p1952 A67-25333

Premature generation breakdown in ruby laser, noting effect of additional media on pumping level/generation time ratio 12 p1953 A67-25445

Spatial modulation in populations of optically pumped ruby investigated for possible application to analysis of space and time distribution of laser beam 13 p2126 A67-26860

Optical fluorescence, thermally tunable over significant portion of visible and near IR spectrum, from phase-matched parametric system 13 p2127 A67-27081

Deformed laser resonator mode, studying diffraction losses, amplitude and phase distribution during pumping pulse 13 p2127 A67-27087

Effectiveness of coupling between light source and active medium in optically pumped laser 13 p2128 A67-27230

Pumping efficiency of optically pumped laser, considering electric energy conversion, absorption, etc 13 p2129 A67-27349

Diffraction losses in resonator cavity decreased by thermal deformation of neodymium-glass crystal due to pumping with periodic pulses 13 p2130 A67-27629

Mechanisms operating in lasers employing optical transitions of molecules in fluids 14 p2331 A67-28471

Optical pumping and double resonance used to study magnetic resonance and Zeeman effect 14 p2333 A67-28969

Atomic and molecular frequency standards, reviewing ammonia and hydrogen masers and Cs, Tl and Rb gas frequency standards 14 p2333 A67-28975

Magnetic field strength effects on pulse and CW operation of large diameter ionized gas lasers 15 p2496 A67-29173

Ferromagnetic magnetostatic amplifier using various types of oscillations for pumping and signal amplification 15 p2443 A67-29354

Electron spin resonance measurement of ground state population in ruby rod during optical pumping 15 p2497 A67-29389

Giant pulse time evolution influenced by pump-induced material inhomogeneities studied by analyzing laser rate equations 15 p2498 A67-29484

Temperature measurement of ruby laser rods during pulsed pumping from birefringence dependence on temperature and resulting thermoelastic stresses 15 p2499 A67-29721

ZnS two-photon absorption spectrum to establish two-photon pumping capabilities of semiconducting crystals 15 p2500 A67-29816

General relations for amplification and oscillation development in optically pumped alkali vapor maser derived and applied to rubidium 85 15 p2501 A67-30095

Master equation for statistical operator of laser mode leads to photon number distribution for arbitrary pumping 15 p2501 A67-30124

Direct lasing of conventional ruby rods requiring 200-joule xenon pump deriving energy from chemical reaction 15 p2502 A67-30437

Laser action of ruby and neodymium glass rods in case of axicon pumping 16 p2684 A67-30460

Three-level maser detector for far IR using double-quantum pumping 16 p2684 A67-30606

Laser characteristics of narrow band type I solar radio burst and magnetic dipole transitions in split Zeeman sublevels of hydrogen atoms of solar corona in ground level 16 p2747 A67-31067

Output power of gas laser with numerous axial-oscillation modes calculated as function of resonator length and pumping power 17 p2866 A67-31926

Continuous IR chemical maser action in carbon dioxide, using chemi-optical resonant pumping 17 p2866 A67-32275

Atomic frequency standards, noting cesium and thallium atomic beam devices, H maser, rubidium gas cells, optical pumping, etc 17 p2860 A67-32601

Frequency variation of ruby laser optically pumped by flash lamp, noting effect of phthalocyanine solution 17 p2868 A67-32705

Optically pumped alkali metal vapors orientation checking by light pulse method, noting relaxation curve 17 p2869 A67-32811

Single laser pulse generation noting high peak power, subnanosecond time duration, optical cavity length, etc 17 p2869 A67-33063

Gallium arsenide laser pumped by Stokes component of induced Raman scattering in liquid nitrogen of Q-modulated ruby laser light 17 p2870 A67-33310

Optical parametric oscillator with ruby laser pumping, noting values of electro-optic and rotational tuning 18 p3059 A67-34011

Vacuum UV and X-ray lasers from electron ejection from inner shells of atoms through photoionization 18 p3060 A67-34015

Laser frequency variation and emission kinetics during generation process, investigating spectra at scanning rate and pumping energy ranges 18 p3061 A67-34619

Pump induced optical distortion in isotropic laser materials analyzed using Fermat principle, predicting ray refraction, beam divergence, etc 18 p3062 A67-34624

Pump radiation induced optical distortion in Nd-doped glass laser rods measured and compared to theory 18 p3062 A67-34625

Transverse-mode distribution of emission intensity of solid state laser with plane mirrors 20 p3459 A67-36688

Device for automatic recording of laser emission and of energy of pumping pulse 20 p3460 A67-37149

High efficiency optical pumping system for crystal laser rods with application to CW output 20 p3461 A67-37290

Gas laser behavior in magnetic field, analyzing data on magnetic effect, Zeeman effect and microwave 20 p3462 A67-37591

Vibrational energy levels leading to laser oscillation in UV, noting process using Lyman discharge 21 p3638 A67-37855

Immersion effect on concentrating and increasing pump flux of laser incident on absorbing core, considering rod and sphere 21 p3638 A67-37857

Induced three-photon combination scattering kinetics applied to laser pumping 21 p3638 A67-37867

Optical pumping of sodium vapor with deuterium light, discussing optical transparency in excited state mixing cross sections 21 p3639 A67-38018

Solid state CW optically pumped microwave masers using divalent Tm in calcium fluoride and strontium fluoride hosts 21 p3640 A67-38454

Premature generation breakdown in ruby laser, noting effect of additional media on pumping level/generation time ratio 21 p3642 A67-38819

Diffraction losses in resonator cavity decreased by thermal deformation of neodymium-glass crystal due to pumping with periodic pulses 21 p3642 A67-38825

Optically pumped vapor rotatory power as optical pumping experiment monitoring technique, discussing specific rotatory power and refractive index dependance on light frequency 22 p3816 A67-40320

Filter with hyperfine doublet splitting using Paschen-Back effect for optical pumping 22 p3816 A67-40321

Optically pumped Rb in collisions with Kr inducing relaxation, noting two different correlation times due to kinetic collisions and metastable states 23 p4012 A67-40792

Energy detection of multipulse returns from optically rough target using Q-switched laser 23 p4016 A67-41265

Cesium vapor pumping by intensive polarized light used for studying Cs buffer gas collision influence on pumping cycle and Zeeman transitions effect on polarization 23 p4016 A67-41291

Two-photon absorption in semiconductor laser in relation to upper limit of transmission power 24 p4200 A67-41863

Density 24 p4200 A67-41863

Efficiency of optical system of solid state laser with cathode luminescence pumping 24 p4169 A67-42892

OPTICAL PYROMETER

Radiation techniques for surface temperature measurement, considering optical and radiation pyrometers, projection thermography and photographic techniques 01 p0062 A67-10274

Black body radiation equation approximating Planck equation in intermediate region with optical pyrometry application 05 p0807 A67-16788

Modulation pyrometer measuring plasma temperature from spectral line intensity 09 p1499 A67-22328

Temperature measurement in hypersonic gun tunnel, using modified line reversal two-beam optical pyrometer with measurements in shock layer at front of cylinder 09 p1486 A67-22413

Refractory oxides solidification points measurement using optical-pyrometer method 20 p3472 A67-36118

Calibration of optical pyrometers using gold point black body and sectorized disks 24 p4155 A67-42292

OPTICAL RADAR

SA LIDAR

Output characteristics of half-wave mode Kerr cell ruby oscillator used as optical radar for clear air turbulence /CAT/ detection 02 p0198 A67-12053

Dual beam wind measurement by incoherent radar 04 p0648 A67-14675

Cassegrain feed for 85-ft-diam antenna of planetary radar system noting operative conditions, polarization capabilities and performance data 04 p0596 A67-15048

GaAs room temperature laser diode application to communication and radar systems 07 p1194 A67-19086

Radar evidence for atmospheric dust layers around 80 km altitude 13 p2109 A67-26333

Backscattered light intensity from laser beam for measuring atmospheric density variations, discussing optimization of sensitivity 13 p2072 A67-27609

Lunar studies by laser techniques, considering optics, principles for distinguishing between useful and noise signals, precision of measurements, etc 14 p2386 A67-28468

Laser ranging using reflectors proposed for investigating lunar motion and various lunar parameters 18 p3130 A67-34317

Stratospheric aerosol concentrations observed by optical radar echoes compared with expected return from molecular atmosphere to obtain vertical profile 18 p3042 A67-34493

Optical determination accuracy of satellite orbits, investigating orbit elements by Gaussian averaging calculation assuming elliptical orbit 22 p3830 A67-39161

80 km atmospheric backscattering enhancement detected by optical radar 22 p3759 A67-39558

Airport glide slope visual range determination with single-ended transmissometer by measuring transmission between photosensitive detector and laser light source 23 p3999 A67-41027

Atmospheric scintillation effects on optical data channel for application to laser radar noting SNR role 23 p3975 A67-41266

Earth science and resource studies with orbiting imaging radars onboard space vehicles [AIAA PAPER 67-767] 24 p4258 A67-42936

OPTICAL RANGEFINDER

Optical ranging technique for orbital rendezvous with manual checking of automatic equipment 09 p1527 A67-22395

Pulsed ruby laser rangefinder with high maximum repetition frequency and digital range readout for data acquisition for determining airborne target trajectories 09 p1465 A67-22622

Laser rangefinder limit for rocket, balloon or satellite trajectory, noting effects of various parameters related to source, receiver, etc 10 p1663 A67-22881

Optical ranging system with high power chemical laser noting performance characteristics 15 p2500 A67-29913

IR laser rangefinder using neodymium doped rods, noting noise peak value and advantages over ruby laser 22 p3799 A67-39780

Lasers as light source in optical telemetry, discussing laser radiation, solid state and gas lasers and critical parameters 22 p3800 A67-39981

Compact air-to-ground laser rangefinder onboard helicopter nose section 23 p3999 A67-41028

IR Q-switched neodymium glass laser rangefinder performance and advantages 23 p3999 A67-41029

Performance limits of laser rangefinder for design of all-weather terrestrial

rangefinder, discussing echo signal, backscatter noise and TPG 23 p3999 A67-41040

Laser application as research tool and for ranging and metrology noting laser availability and performance 23 p4015 A67-41050

OPTICAL REFLECTIVITY

Value and sign of phase jump taking place during light reflection from multilayer dielectric film 03 p0467 A67-12892

Directional reflective coating consisting of cylindrical dielectric fibers oriented perpendicular to absorbing substrate [AIAA PAPER 65-671] 03 p0467 A67-13039

Bidirectional reflectance measurements to determine optical degradation induced by UV radiation [AIAA PAPER 65-672] 03 p0419 A67-13040

Temperature and doping level effect on conduction band edge of n-type semiconductors, noting doublet shifts resulting in narrower forbidden energy gaps 04 p0681 A67-15292

Change of polarization state of ray due to multiple internal reflections within many-sided reflectors 04 p0657 A67-15307

Q-switched laser operation observed using liquid selenium mirror as reflector in ruby laser measuring reflectivity changes 05 p0822 A67-16679

Nonlinear optical reflection laws governing direction, polarization and intensity of second harmonic light generated in reflection 06 p1030 A67-17571

Value and sign of phase jump taking place during light reflection from multilayer dielectric film 06 p1034 A67-18770

Metastable exciton states of cadmium and lead iodide obtained from fundamental reflectivity spectra 06 p1060 A67-18915

Internal mirror reflections elimination in laser beam output intensity distribution by filtering device 09 p1512 A67-22042

Laser mode selection by internal reflection prisms 10 p1662 A67-22742

Room temperature electroluminescence spectra of several materials with Ge, zinc blende and wurtzite structures by electrolyte technique 10 p1691 A67-23401

Mathematical methods for two classes of variational problems analogous to optical reflection and optical refraction in connection with rocket flight 10 p1678 A67-23425

Models of reflection nebulae light for single scattering, pure or modified by internal nebular extinction, on spherical grains imitating dielectric or metallic particles 11 p1861 A67-24487

Measurement of radiation reflectively scattered from optical surfaces in far UV, noting role of overcoating with metal films 11 p1819 A67-24666

Multiply reflective laser detector diode design, showing internal reflection effect for trapping light in silicon due to large refractive index 11 p1802 A67-24737

Photoemission study of electronic structure of CdTe, considering two strong reflectivity peaks in optical reflectivity spectrum [AFCLR-67-0405] 12 p1983 A67-25478

Lunar figure and orbit parameters measured by optical location method 12 p2002 A67-25647

Material properties and capabilities of different types of optical waveguides including iterative electromagnetic wave beams, reflecting pipes, fiber guides, etc 12 p1906 A67-25976

Bidirectional spectroradiometer for reflectance of solid and powder samples [AIAA PAPER 67-313] 12 p1946 A67-26028

Rough metal surface bidirectional reflectance, using Davies and Beckmann models [AIAA PAPER 67-319] 12 p2037 A67-26034

Proton radiation effects on mirror reflectance in high vacuum at various temperatures, degradation by blistering found to be highly temperature-dependent [AIAA PAPER 67-341] 12 p1957 A67-26055

Vacuum deposition techniques for production of optical film materials for neutral density filters and sunglasses, discussing dielectric, metallic, reflecting and semitransparent films 13 p2158 A67-27076

Transmittance and reflectance measurements on wirecloth and metallic meshes using vacuum grating spectrometer

for design of transmission band pass filter in far IR 13 p2121 A67-27354

Absolute reflectance of RbI and KI between 300 and 77 degrees K, noting spin orbit interaction effects and values of dielectric parameters 15 p2520 A67-29768

Tables of Fresnel intensity reflectances from classical electrodynamics noting characteristics for amplitude minima, polarization maxima and 90 degrees phase difference [RE-TR-67-7] 15 p2518 A67-29769

Output energy for ruby laser with parallel mirrors for varying excitation energies, pulse lengths, mirror reflectivities and losses due to absorption, scattering and reflection 15 p2502 A67-30427

Infrared lattice vibration spectra of II-VI compounds analyzed by Drude dispersion, obtaining transverse-optical-mode frequency 16 p2724 A67-30603

Optical reflection spectra of GaS, GaSe, and GaTe single crystal semiconductors in electron volt band energy range 16 p2730 A67-31159

Evaporation of thin films of high melting point materials by focused laser beam and reflectance and relative transmittance in vacuum UV 18 p3059 A67-33885

Diffuse reflected and transmitted spectral line profile calculations for uniform noncoherently scattering media 19 p3183 A67-35555

Reflectivity spectra of YIG and YGG crystals, observing YTG structure attributed to charge transfer enhanced crystal field transitions reflectivity spectra of YIG and YGG crystals, observing YIG structure attributed to charge 22 p3863 A67-40238

EM radiation reflection, absorption and transmission through dielectric medium measured, studying other aspects by electric dipole oscillator model 23 p4037 A67-40757

Lunar surface luminance transient enhancement noting photoabsorbing color center formation, increased reflectivity and photoluminescence, photoionization and photoemission 23 p4065 A67-41004

Radiative heat transfer for light reflection and transmission by optically thick scatterers with three-term phase function, obtaining asymptotic formulas 24 p4147 A67-41820

OPTICAL RESONANCE

Photoconductivity resonances and recombination radiation in PbTe and InSb due to multiple photon interband transitions between Landau levels in high intensity magnetic fields 02 p0254 A67-12522

Wave interaction dynamics of far IR electromagnetic radiation generation by coherent molecular vibrations or phonons excited by stimulated Raman scattering and resonant phase matching condition 04 p0657 A67-15113

Ruby laser with nonresonant feedback due to radiation scattering, showing use as optical frequency standard 05 p0818 A67-16642

Optical and paramagnetic resonance of ytterbium ions in calcium fluoride, obtaining correlation between site geometry and optical absorption 12 p1984 A67-25843

Validity range for weak turbulence theory in case of wave resonant interaction mechanism, treating Fokker-Planck and nonlinear optics approximations 19 p3298 A67-35792

Far IR maser oscillators with water and deuterium oxide, presenting construction and operating characteristics 21 p3639 A67-38253

He-Ne laser pulse delay when excited in optical resonator noting dependence on gas pressures 24 p4187 A67-42207

OPTICAL RESONATOR

Laser producing two or three light pulses in sequence with interval between pulses mechanically controlled by optical wedge inserted into resonator 01 p0087 A67-10181

Frequency stability of double beam ammonia laser with thermostatic quartz resonators on 3-2 line 01 p0088 A67-10247

Single mode approximation of parametric excitation and self-excitation of oscillations in Fabry-Perot resonator filled with nonlinear dispersive medium 02 p0251 A67-11575

Optical resonator theory stressing electromagnetic boundary value problem 02 p0267 A67-12026

Ruby laser pumping threshold energy, divergence angle and output power as affected by resonator length 03 p0433 A67-12855

Ruby laser generation from two R lines by prismatic light dispersion in resonator 03 p0433 A67-13095

Regenerative radiation from neon line in He-Ne laser, using spherical reflectors in resonator 03 p0434 A67-13096

Possible oscillation modes in cylindrical solid state laser and dependence of pumping threshold, output power and divergence angle on resonator length 03 p0435 A67-13129

Linear phase distortions of plane resonator with tilted mirrors and effects on generation of stimulated emission in ruby crystal laser 03 p0435 A67-13130

Tunable dispersion resonator and broadening of laser emission spectral range to obtain operating frequency other than fundamental 03 p0435 A67-13131

Steady state laser radiation during relaxation, discussing time-dependent spectral composition, oscillation modes and polarization characteristics 03 p0435 A67-13134

Pulsed laser Q-factor modulation using nonlinear resonator functions in absorbing medium 03 p0438 A67-13135

Oscillation types for gas-laser semiconcentric resonator 03 p0437 A67-13286

Radiative power amplification of He-Ne laser with nearly confocal resonators 03 p0438 A67-14190

Light absorption in transparent materials measured using thermal lens method 03 p0439 A67-14395

Performance of GaAs semiconductor laser with resonator, noting dependence of forbidden zone width and absorption coefficient on free carrier concentration and incident photon energy 04 p0634 A67-15759

General theory for parametric oscillation in optical region 05 p0817 A67-16639

Laser brightness gain and single transverse mode operation by compensation for thermal distortion with external mirror 05 p0819 A67-16656

Electron densities in helium plasma measured by laser amplifier with maximum gain and minimum bandwidth at point nearest threshold 05 p0820 A67-16663

Suppression of undesirable axial modes in gas laser oscillating at several frequencies obtained by filling with active gas mixture each of two coupled Fabry-Perot type resonators 05 p0826 A67-17326

Passband narrowing due to coupling between passive oscillating system and active substance contained in resonator cavity represented by RLC circuit 05 p0780 A67-17474

Operation of synchronized neodymium laser time variable reflection (TVR)/oscillator, using single pockels cell to obtain Q-switching and cavity dumping 05 p0826 A67-17525

Optical resonator theory and applications in lasers and microwaves 06 p1000 A67-17572

Resonator Q-modulation technique observation of central dip tuning in modulated power output of gas laser with moving mirror 06 p1011 A67-18758

Semiconductor mirror for Q-factor modulation of laser resonator 06 p1012 A67-18789

Book on lasers, light amplifiers and oscillators noting optical resonators, optical pumping, pulsed lasers, etc 07 p1195 A67-19469

Tuning of gas laser resonator 07 p1195 A67-19505

Synthesis of traveling wave regime in complex optical resonator with additional external mirrors 07 p1198 A67-19600

Frequency broadening of natural oscillations of optical resonator upon interaction with two-level atom in electromagnetic field 08 p1337 A67-20868

Stokes light generated in off-axis resonator for quantitative measurements of stimulated Raman effect in self-focusing materials 08 p1339 A67-21375

Gain saturation effect on oscillating modes of optical masers 08 p1339 A67-21377

Frequency stability of He-Ne lasers analyzed by heterodyning two laser resonators 09 p1509 A67-21558

Tunable lithium niobate optical oscillator with external mirrors 09 p1510 A67-21576

Polarization of waves generated by annular laser resonators of triangular shape, obtaining directions of electric field vectors 09 p1512 A67-21923

Adjustment of compound gas laser resonator provides increase of stimulated emission output without lengthening resonator 09 p1512 A67-21985

Wave synchronization in gas laser with ring resonator cavity 09 p1513 A67-22063

Laser mode-locking during resonator Q-factor modulation 09 p1513 A67-22065

Gas laser frequency and emitted power dependence on resonator tuning 09 p1513 A67-22070

Microwave quasi-optical ring resonator formed by mirrors 09 p1513 A67-22088

Frequency stabilization of Zeeman laser, using intensity crossover region with cavity tuning between oscillations on two orthogonally circularly polarized axial modes 09 p1513 A67-22134

Gain curves in multifrequency optical oscillators, measuring vanishing frequencies as function of losses in resonator, noting attenuation in laser discharge tube 09 p1514 A67-22271

Coupled laser quenching and transient buildup in rate equation analysis, noting spike suppression 09 p1514 A67-22274

Ruby laser cavity losses measurement by Fabry-Perot resonance 10 p1662 A67-22740

Longitudinal modes of carbon dioxide laser cavity by varying optical length of cavity 10 p1663 A67-22846

Giant pulse generation range in transverse direction after Q-switching in ruby laser, examining resonator properties 10 p1666 A67-23584

Optimum illumination for maximum power transfer between two opposed rotationally symmetric antennas 11 p1762 A67-24291

Toroidal laser resonator, analyzing modal properties of inner field and optical stability of beam 12 p1951 A67-25197

Periodic variations of oscillation modes in He-Ne laser as result of resonator length increase 12 p1952 A67-25437

Gaseous laser oscillations in Fabry-Perot resonator with corner-cube prism noting alignment characteristics 12 p1953 A67-25454

Raman laser physics covering gain formula, stimulated and spontaneous scattering and cavities 12 p1953 A67-26124

X-ray laser resonator proposal involving three-dimensional puckered ring arrangement of crystals at Bragg angle, discussing polarization losses 13 p2126 A67-27012

Deformed laser resonator mode, studying diffraction losses, amplitude and phase distribution during pumping pulse 13 p2127 A67-27087

Interferometry of resonator modes in submillimeter wave laser 13 p2129 A67-27347

Amplitude, phase distribution and output beam characteristics in transverse modes of unstable optical cavities analyzed using pulsed gas laser 13 p2129 A67-27350

Electromagnetic radiation equilibrium in gas lasers, studying effect of cavity length variations on linewidth 14 p2329 A67-27952

Polarization of waves generated by annular laser resonators of triangular shape, obtaining directions of electric field vectors 14 p2330 A67-28252

High power laser emitting monochromatic radiation at single frequency applicable in spectroscopy, telemetry and telecommunication 14 p2330 A67-28469

Interaction between oppositely moving traveling waves in helium-neon laser with annular resonator 14 p2332 A67-28856

800 mm and 1265 mm optical resonator He-Ne lasers, obtaining maximum output power and application as Raman spectroscopy light source 14 p2333 A67-28972

Modes in unstable optical resonators and lens waveguides, noting spherical wave characteristics of geometrical eigenmodes 15 p2497 A67-29391

Semiconductor laser generating oscillations in external cavity, finding Brewster window effective in suppressing modes within crystal 15 p2498 A67-29511

Radiation polarization in ruby laser with resonator shaped like rectangular parallelepiped 15 p2499 A67-29701

Angular distribution of laser radiation and variation in beam direction of stimulated radiation as function of misadjustment angle

of resonator mirrors 15 p2500 A67-29759
 Quantum paramagnetic amplifiers in USSR, discussing physical characteristics and operation of resonators in decimeter band, antenna systems for noise reduction, etc 16 p2623 A67-31024
 Nonaxial oscillation modes in He-Ne laser interaction with spherical mirror resonator confocal cavity 16 p2685 A67-31038
 Light field distribution in optical resonator of Fabry-Perot type
 Interferometer with nonparallel mirrors, using Airy function for localizing field concentration planes 17 p2853 A67-31925
 Output power of gas laser with numerous axial-oscillation modes calculated as function of resonator length and pumping power 17 p2866 A67-31926
 Radiation kinetics of laser with resonator having lens system and low absorption nonlinear medium, showing time shift of kinetic curve 17 p2868 A67-32663
 Fabry-Perot resonator excitation using integral equations corresponding to boundary value functions 17 p2868 A67-32667
 Fabry-Perot resonator free oscillations defined by complex frequency, obtaining diffraction loss and resonant frequency 17 p2868 A67-32668
 Three-space optical resonator model, deriving properties responsible for undesired natural frequencies suppression, noting selection characteristics 18 p3058 A67-33528
 Temperature gradient in steady state thermally operated solid state lasers, calculating end face curvatures and light paths for resonator mode correction 18 p3059 A67-33714
 Semiconductor mirror for Q-factor modulation of laser resonator 18 p3059 A67-33731
 Cylindrical Fabry-Perot resonator, determining resonant modes by applying boundary conditions, noting eigenvalue and eigenfunction roles 18 p3060 A67-34024
 Spectrum of continuous action laser with confocal resonator, showing mode degeneration association with phase distortions of wave front caused by mirror defects 18 p3060 A67-34039
 Interaction between oppositely moving traveling waves in helium-neon laser with annular resonator 19 p3242 A67-36107
 Isotope shifts measurement in IR with variable length laser cavity 20 p3439 A67-36355
 Measurement of variation of formation time of Q-switched ruby laser as function of loop gain 20 p3458 A67-36432
 Fabry-Perot resonator with nonuniform reflectors, analyzing resonant modes amplitude/phase distribution and diffraction/reflection losses 20 p3447 A67-36767
 Modes and eigenvalues of symmetric cylindrical Fabry-Perot laser resonator with circular output-coupling apertures 20 p3460 A67-37024
 Synthesis of traveling wave regime in complex optical resonator with additional external mirrors 20 p3462 A67-37339
 Diffraction coefficient of open laser resonators coupled in series, discussing boundary conditions 21 p3638 A67-37864
 Fabry-Perot etalon resonator studied for incidence angles for use as filter, test instrument and control device for laser output 22 p3809 A67-40469
 Intrinsic modes of spherical mirror resonators, noting parameters identifying beams generated by such resonators 23 p3998 A67-40709
 Laser emission mode splitting of CN laser, discussing wavelength to resonance length and Fabry-Perot interferometer permitting line splitting observation 23 p4012 A67-40893
 Michelson interferometer used as tunable mirror in laser resonators, obtaining internal modulation of initial intensity 23 p4013 A67-40902
 Analysis of laser with selective resonator indicating stimulated emission basic characteristics determined by active medium band shape and Q-factor curve 23 p4013 A67-40907
 Optically concentrated laser radiation beam properties using plane and spherical faced ruby resonators 23 p4016 A67-41322
 Radiation polarization in ruby laser with resonator shaped like rectangular parallelepiped 24 p4186 A67-41771

Maxwell equations solved for Gaussian beam form in anisotropic medium, discussing laser applications 24 p4187 A67-42092
 Frequency and intensity of laser light analyzed for reaction of coupled optical resonator 24 p4188 A67-42574
 Divergence angles of helium-neon laser radiation, discussing resonator with spherical mirrors with unequal curvature radii 24 p4169 A67-42891
 Submillimeter wave laser resonator mode calculation using laser-resonator interferometry 24 p4169 A67-43105
OPTICAL SATELLITE TRACKING PROGRAM
 French optical satellite observation network 14 p2270 A67-28569
OPTICAL SENSOR
 Unusual optical detection characteristics in multiplier phototube when monitoring circuit bandwidth is extended 05 p0807 A67-16791
 Sensors of electromagnetic radiation in UV, visible and IR ranges, noting improvement through automatic data processing 06 p1006 A67-19013
 Articulated optical pickup system for scale model simulation providing pitch, roll and yaw motions and fixed perspective point 12 p1941 A67-25470
 Star tracker using camera tube sensors and electronic scanning noting system errors reduction 13 p2154 A67-27491
 Radar, IR and laser sensors production trends for airborne reconnaissance 15 p2485 A67-29163
 Electronic equipment for generating delay times corresponding to missile velocity during optical recording by numerous sensors distributed along ballistic firing range 16 p2674 A67-31118
 Continuous monitoring and control of primary mirror figure of orbiting, diffraction limited astronomical telescope for optimum performance 16 p2680 A67-31802
 Optical detectors for images and selected radiation signals using Bendix Channeltron multiplier, describing types, properties and applications 17 p2858 A67-32480
 Bicrystals use in optical receivers based on bicrystal interface anomalies 20 p3457 A67-36238
 Attitude control methods compared for use in rockets collecting data in UV region from various stars 20 p3531 A67-36411
 Integrated circuit for TV camera including photosensitive array and self-scanned solid state image sensor 23 p3998 A67-40868
 Articulated optical pickup system for scale model simulation providing pitch, roll and yaw motions and fixed perspective point 23 p3988 A67-41502
OPTICAL SIGNAL
SA VISUAL SIGNAL
 Coherent radio emission of extensive air showers determined from known threshold energy of optical signal 02 p0318 A67-12783
 Low loss phase modulator for optical signals, using piezoelectric effect 04 p0576 A67-15506
 Optimal reception of narrow band signals emerging from photomultiplier 05 p0764 A67-16913
 Contrast transfer characteristics of n tuple models of retinal receptive fields as function of optical signal size or spatial frequency 05 p0757 A67-17303
 Optical information transformation using incoherent and coherent light 06 p0999 A67-17570
 Supersensitive laser light detector for wideband receivers to approach theoretical SNR limit set by noise in signal 07 p1194 A67-19085
 Background limit to sensitivity of point to point optical communication obtained through signal to noise ratio of optical point detectors under BLIP condition 09 p1462 A67-21641
 Spectral differentiation and hologram filtering in reducing optical signal comparison to signal correlation 09 p1497 A67-21826
 Heterodyne signal amplitude dependence on optical path length difference for oscillating axial modes in multimode gas laser 13 p2128 A67-27346
 Optimal reception of narrow band signals emerging from photomultiplier 16 p2623 A67-30890
 Visual noise induction methods

investigated at seven noise levels, discussing pattern comparisons by 46 subjects 20 p3372 A67-37000
 Ultrashort optical pulse propagation in two-level medium, describing pulse shapes by solving partial differential equation 20 p3461 A67-37286
 Coherent radio emission of extensive air showers determined from known threshold energy of optical signal 22 p3878 A67-40285
 Optical mixing of two low level signals in atomic states of He-Ne laser noting amplitude modulation of visible laser output 23 p4012 A67-40891
 Optical signal detector performance, deriving outlet electron distribution function 24 p4166 A67-41797
 Aperture usage for random optical communication channel through turbulent atmosphere 24 p4124 A67-42814
OPTICAL SPECTRUM
 Spectra and intensity vs excitation level and spatial distribution vs current density determined for optical radiation by electron excited cadmium sulfide 02 p0251 A67-11828
 Space bandwidth signal spectral analysis using multichannel optical system and two-dimensional optical system with increased frequency resolution 02 p0243 A67-12049
 Lasers used to extend RF plasma diagnostic procedures to optical frequencies by interferometric and Thomson diffusion methods 03 p0477 A67-13474
 Two-phonon IR absorption and Raman scattering spectra to provide information about phonon spectra of crystals and phonon-electron interaction in filled valence bands 06 p1059 A67-18907
 Electromagnetic radiation at satellite-borne sensor, discussing spectral, spatial and temporal distributions of radiation energy intensity 06 p1006 A67-19010
 Laser spectroscopy, discussing advantages, precision attainable, line shape and position measurements 07 p1194 A67-19087
 Optical spectrum of normal excitons in deformed and nondeformed n-type Ge single crystal layers for four orientations 08 p1367 A67-20409
 Gas laser frequency and emitted power dependence on resonator tuning 09 p1513 A67-22070
 Accelerated method for spectral calculation of optical parameters of solar radiation 13 p2211 A67-27625
 Intrinsic optical excitation spectrum of crystalline solids for hole or electron localization, considering many-body relaxation effects influencing photoemission 16 p2732 A67-31698
 Spectrum and excitation mechanisms in aurora, discussing variations, excitation, ionization, hydrogen lines and temperature measurement 18 p3032 A67-33582
 Quasi-stellar radio source optical spectrum observed, identifying spectral lines and determining red shift 18 p3118 A67-33854
 Spectrum of continuous action laser with confocal resonator, showing mode degeneration association with phase distortions of wave front caused by mirror defects 18 p3060 A67-34039
 Absorption, reflection and emission spectra of gold chloride at low temperatures 18 p3101 A67-34187
 Photon generation threshold energy temperature dependence for gallium-arsenic epitaxial injection lasers 19 p3238 A67-34773
 Spectral characteristics of solid state laser with large angular divergence of light, showing contribution from degenerate modes 19 p3239 A67-34903
 Raman scattering for overdamped soft optic vibrational mode in barium titanate, giving temperature dependence of Raman spectrum 23 p4038 A67-40796
OPTICAL THICKNESS
 Limb intensity profiles at center of hydrogen alpha calculated for several simple models of absorption coefficient at line center, showing abrupt changes in gradient 02 p0323 A67-11693
 Convective heat transfer in radiating gas, examining boundary layer equations and boundary conditions involving luminescence 03 p0532 A67-12866
 Electron density, optical thickness and temperature of ruby laser-induced carbon plasma 05 p0852 A67-18654
 Nonlinear three-dimensional radiative transfer solved by method of self-consistent

optical depths 07 p1248 A67-19485
 Selective surface obtained experimentally by deposition of stack of thin layers 09 p1558 A67-22599
 Spectroscopic methods for measuring plasma temperatures from 1000 to 10,000 degrees K, distinguishing optically thick and thin media 12 p1968 A67-25188
 Inversion of spectroscopic integral equation which relates emission coefficient to integrated intensity distribution for optically thin and asymmetrical light source 12 p1968 A67-26175
 Nonequilibrium line radiation for generalized Lorentz profiles in spherical plasma of large optical thickness 13 p2166 A67-26728
 Maximeter in monitoring thin films differing in optical thickness 13 p2181 A67-27232
 Radiation diffusion in medium of finite optical thickness, computation of source function and tabulation of matrixes 14 p2382 A67-27832
 Behavior at infinity of specific intensity in plane-parallel atmosphere 14 p2391 A67-28946
 Quasi-equilibrium number density of excited atoms and electronic transition rate in decaying optically-thick helium and hydrogen plasmas, considering Penning ionization 16 p2715 A67-31168
 Ellipsometer measurements to obtain estimates of refractive index and thickness of weakly absorbing isotropic, homogeneous slab 16 p2703 A67-31877
 Line width vs optical thickness in pulsed argon-ion laser used to determine level population in plasma 17 p2867 A67-32452
 Electron temperature of H II region related to high temperature main sequence stars determined as function of electron density and radiation dilution factor 19 p3325 A67-35503
 Role of Rosseland approximation in convection-radiation interaction, considering flow of gray gas in laminar boundary layer [ASME PAPER 67-HT-9] 20 p3545 A67-36707
 Volumetric absorption coefficient effect on Rosseland equilibrium radiative heat transfer and temperature profiles in optically thick fluid flowing past flat plate 20 p3553 A67-36936
 Bouguer law applicability for describing narrow collimated light beams attenuation in scattering media in terms of optical thickness 20 p3462 A67-37666
 Attenuation of continuous and pulsed laser emission studied for various thicknesses of artificial water fog 22 p3816 A67-39921
 Light reflection and transmission by thick optical atmosphere according to phase function 24 p4147 A67-41819
 Radiative heat transfer for light reflection and transmission by optically thick scatterers with three-term phase function, obtaining asymptotic formulas 24 p4147 A67-41820
 Graphical construction and electrical simulation for predetermining index and thickness of multilayer surfaces and filters 24 p4187 A67-41873

OPTICAL TRACKING
SA MINITRACK OPTICAL TRACKING
 SYSTEM /MOTS/
 Optical and UHF Doppler /UDOP/ tracking for lift-off phase of Saturn SA-5 launch vehicle 03 p0368 A67-13383
 U.S. Coast and Geodetic Survey satellite triangulation program based on optical tracking of passive satellites simultaneously from two or more mobile camera stations 07 p1176 A67-19764
 Trajectory determination from optical and radar data of spacecraft [JPL-TR-32-950] 08 p1384 A67-20621
 Book for amateurs on observing earth satellites including methods and discoveries about upper atmosphere and shape of earth 10 p1608 A67-23620
 Soviet book on IR and optical devices for vehicle guidance and homing covering light propagation, radiation from targets, airborne missile homing systems, etc 11 p1791 A67-24514
 Satellite tracking, noting radar, radar and laser methods, and visual and photographic observations 16 p2630 A67-31765
 Airborne optical satellite tracking, discussing accuracy limitations and comparing to ground stations 16 p2630 A67-31799

Radio, radar and optical methods for close earth satellites tracking, advantages and limitations 18 p3003 A67-34235
 Schmidt satellite cameras to record trail from bearing and elevation fixed in relation to earth, detailing optical system of Royal Radar Establishment /RRE/ camera 18 p3048 A67-34237
 Indonesian space center, describing radar and optical tracking systems, launch complex telemetry system, etc 19 p3207 A67-35234
 Graphical method predicting latitudes where satellites in circular orbit are visible, in both Northern and Southern Hemispheres 19 p3182 A67-35268
 Greek space research noting satellite optical tracking, solar photosphere and chromosphere, atmospheric electricity and solar eclipse measurements 19 p3320 A67-35292
 Optical data acquisition by NASA for National Geodetic Satellite Program flash photography 20 p3382 A67-36888
 Optical and IR wideband communication between earth and interplanetary spacecraft, discussing tracking, detectors, pointing and beam formation 22 p3782 A67-39960

OPTICAL TRANSITION
 Optical transmission and transition in semiconductor single crystals of various unit cells, considering bismuth tellurium sulfide 02 p0289 A67-11725
 Transition to detonation in gaseous medium experimentally studied, based on self-sustained detonation front and adaptation of amplitude modulated giant pulse laser system 03 p0535 A67-13500
 Optical transitions and k conservation in crystalline solids explained in terms of localization of hole produced by excitation 04 p0674 A67-14526
 Allowed and forbidden direct interband optical transitions in anisotropic semiconductors, using effective mass theory for exciton, solving Schroedinger equation 04 p0674 A67-14610
 Spin echo and free decay signals in Rubidium optical pumping analyzed, using pulse method and light modulation technique 04 p0632 A67-14770
 Light emission spectrum changes due to forced transitions during passage through finite volume with negative absorption factor 04 p0709 A67-14812
 High resolution spectroscopy using Zeeman-tuned IR maser oscillating at transitions between 3 and 9 microns 05 p0816 A67-16633
 Optical transitions in semiconductors satisfying principle of momentum conservation through mutual interaction between free current carriers 06 p1059 A67-18912
 Optical transitions at isoelectronic traps in GaP and ZnTe, presenting fluorescent spectra 06 p1062 A67-18929
 Diffuse polychromatic light reflection from infinitely deep one-dimensional medium of atoms with three energy levels, with all interlevel transitions allowed 07 p1248 A67-19484
 Relative intensities and cascade transition ratio in CW Ar II laser near 4103.9 angstroms 07 p1195 A67-19560
 Center frequency shifts of 6328 angstrom neon transition in Zeeman discharge cell measured in terms of discharge current and gas pressure 07 p1197 A67-20100
 Laser transition in B 2, Br 2 and Sn in pulsed discharges of boron chloride, hydrogen bromide and stannic chloride respectively 08 p1339 A67-21379
 Multiple-photon radiative transitions in strongly doped semiconductor, noting state density 10 p1694 A67-23652
 Temperature dependence of total intensity in difference band systems, difference transitions between nondegenerate vibrations compared with carbon dioxide band 11 p1821 A67-23960
 Optical transient nutation effect in carbon dioxide laser 11 p1802 A67-24829
 Absolute frequency measurement and spectroscopy of gas laser transitions in far IR, analyzing Zeeman effect 11 p1802 A67-24830
 Superradiant transition in high gain pulsed laser 11 p1803 A67-24841
 Radio astronomical investigations of 18 cm ground state lambda doublet transition of OH suggest maser amplification of radiation

takes place in interstellar medium 13 p2198 A67-26715
 Optical double-quantum transition in which atom passes from one Zeeman sublevel to another by absorption and successive reemission of optical photons 13 p2127 A67-27079
 Line-narrowing effect induced by laser radiation applied to measurements of isotope shifts for two optical transitions in neon 13 p2127 A67-27080
 Frequency measurement of gas laser transitions in heavy water and acetylene discharges 16 p2685 A67-30824
 Multiple-photon radiative transitions in strongly doped semiconductor, noting state density 17 p2923 A67-33333
 Energy band structure of crystals of groups IV, III-V and II-VI and magnesium silicide type crystals 18 p3095 A67-33448
 Spectra of noble gases in 4-micron region, using IR spectrometer equipped with cooled lead sulphide detector 18 p3082 A67-33876
 Tabulation of accidental coincidences between fundamental frequency of one laser and harmonic or subharmonic frequencies of another, as necessary condition for frequency translation between lasers 19 p3240 A67-35700
 Spectral analysis of K alpha type X-ray transitions in solar atmosphere and laboratory plasma 19 p3331 A67-36086
 Laser emission from HF molecules rotational transition initiated by pulsed electrical discharge, listing wavelengths 19 p3241 A67-36103
 Circular polarization in j equals l to j equals zero transition in gas laser shown due to different atomic relaxation processes rates 21 p3640 A67-38353
 Near IR laser transitions in pure helium studied with scanning Fabry-Perot interferometer, determining fine structure components in upper laser levels 22 p3817 A67-40488
 Laser lines observation in Freon-He mixtures in CW gas discharge 22 p3817 A67-40489
 Carbon disulfide P-branch transitions with J equals 28 to 46 for 001-100 vibrational transition identified as laser lines in N-carbon disulfide gas system 23 p4011 A67-40789
 Spectrum line observation of decay transition of structure of gas laser 23 p4016 A67-41324
 Phonon assisted magnetoabsorption in direct band semiconductors 24 p4203 A67-42267
 Separate studies of power and collision broadening of gas laser transition showing proportional DC laser power to square of gain 24 p4169 A67-43103

OPTICS
SA ABERRATION
SA ATMOSPHERIC REFRACTION
SA CASSEGRAIN OPTICS
SA CRYSTAL OPTICS
SA DIFFRACTION PATH
SA DIFFRACTION PATTERN
SA ELECTRO-OPTICS
SA ELECTRON OPTICS
SA FIBER OPTICS
SA FOCUS
SA GEOMETRICAL OPTICS
SA INTERFEROMETRY
SA PHYSICAL OPTICS
 Book on modern optical engineering covering image formation, aberrations, prisms and mirrors, stops and apertures, etc 03 p0468 A67-13365
 Glass in refractive space optics, discussing UV solarization and athermalization [SMPT PREPRINT 100-34] 03 p0469 A67-13808
 Optical problems when making IR astrophysical observations with balloon-borne telescope noting data documentation, focusing, image slicer, spectrometer, aberration correction, etc 07 p1184 A67-19388
 Space environment effect on refractive optical systems, particularly solar radiation effect on optical properties of glass 08 p1330 A67-20644
 Equivalent classical source for weakly coupled quantum-mechanical source, estimating approximation extent 13 p2159 A67-27732
 Atmospheric optics problems solved by Monte Carlo method, presenting results in tabular and graphical

- p form 14 p2313 A67-28767
-
- Book on problems of optics covering emission, absorption, diffraction, dispersion, etc 14 p2349 A67-29006
-
- Solving Schroedinger equation with initial coherent radiation state 20 p3485 A67-36866
-
- Atmospheric optics and radiation transfer covering sky brightness, solar insulation, earth radiance and albedo, etc 20 p3430 A67-36899
-
- DODGE satellite TV cameras for black and white, plus color picture transmission with photometric analysis and camera optics 20 p3452 A67-37573
-
- Developments in optics and applications in industry - Conference, Sussex, April 1967 22 p3836 A67-39328
-
- Optical communication system components, discussing cost and potential information capacity factors in picture phone and newspaper transmission facilities 22 p3759 A67-39329
-
- Coherent optics technology, presenting effective black body temperature of six radiation sources and output and pulse duration of four laser sources 22 p3817 A67-40351
-
- Dynamical processes in solid state optics - Conference, Oiso, Japan, August-September 1966, Part 1 23 p4037 A67-40756
-
- Boeing 20-ft solar simulator alignment, calibration, cleanliness, optical system, xenon light sources and vacuum system 24 p4139 A67-42045
-
- OPTIMAL CONTROL**
-
- Successive approximations to determine vector in theory of optimal control 01 p0043 A67-10236
-
- Optimum tests for check of working order of system with minimal material losses of safe or fault system 01 p0043 A67-10240
-
- Accelerated gradient method for numerical solution of parameter optimization problems with nonlinear constraints 01 p0104 A67-10428
-
- Conjugate gradients method extended to function space for optimal control 01 p0044 A67-10483
-
- Direct and inverse problems of optimization of quadratic functional in linear autonomous and controlled systems 01 p0044 A67-10490
-
- Optimal control system for linear plant with modulus limited control actions 01 p0044 A67-10491
-
- Invariant and optimal linear systems with periodic parameters analyzed by transfer function calculation 01 p0044 A67-10492
-
- Optimal control of one-dimensional distributed oscillatory system and wave processes using momentum theory and propagating method 01 p0044 A67-10493
-
- Real time digital simulation of linear and nonlinear control systems with large sampling intervals, determining optimization criterion by nonlinear multipoint boundary value problem 01 p0045 A67-10674
-
- Existence, uniqueness and reversion theorems, necessary optimality criteria and nonfixed time case for optimal control problem of n-dimensional linear parabolic equations 01 p0105 A67-10679
-
- Markovian division process application for solving multicomponent preventive maintenance, work sampling and search theory problems 01 p0106 A67-10930
-
- Three-dimensional problem of optimizing motion of two-stage rocket in homogeneous parallel force field with limited thrusts in engine of both stages 01 p0154 A67-10993
-
- Linear optimal control techniques used as synthesis tool in designing control system for Short Range Station Keeping /SRSK/ task of assault helicopter, noting closed loop dynamics 01 p0111 A67-11201
-
- Parameter optimization in systems subject to worst bounded disturbance that maximizes chosen performance 01 p0046 A67-11204
-
- Optimal nonlinear feedback control derived from quartic and higher order performance criteria 01 p0046 A67-11206
-
- Quasi-optimum control law for minimum-time bounded acceleration rendezvous in plane 01 p0111 A67-11212
-
- Existence and uniqueness theorem of Riccati equation arising in solution of optimal linear regulator problems in Hilbert space 01 p0047 A67-11213
-
- Deterministic optimal control, discussing Bellman dynamic programming method, Pontryagin maximum principle, orbital transfer, interplanetary guidance, etc 01 p0047 A67-11220
-
- Singularity in motion equations of closed loop optimal guidance 01 p0111 A67-11224
-
- Closed loop realization of optimum control law superior to open loop implementation for linear system not asymptotically stable or subject to random disturbances 01 p0048 A67-11225
-
- Learning control system seeking optimum point of bimodal static characteristics by polynomial conjecture 01 p0048 A67-11236
-
- Optimal transfer between hyperbolic orbits in Newtonian field of attraction of heavy sphere of nonzero radius 01 p0152 A67-11411
-
- Optimization of control systems with nonlinear plants, using Pontryagin maximum principle 02 p0224 A67-11511
-
- Bryson gradient method of constructing optimal control laws applied to algorithm for numerical solution of variational problems in optimal control theory 02 p0224 A67-11535
-
- Linearly-approximated characteristics of maneuvers correcting near-planet positions of spacecraft with pulsed flight velocity characteristics 02 p0321 A67-11536
-
- Synthesis of optimum discrete control for eventual state of linear stochastic system, reducing problem to solution of Bellman functional equation 02 p0225 A67-11957
-
- Tabular adaptive predictive model for trajectory following control of nonlinear plant with switched two-level input 02 p0225 A67-12136
-
- Optimum control of antenna pointing direction and space vehicle height subject to random disturbance 02 p0219 A67-12147
-
- Iterative procedure for computing fixed-time fuel-optimal controls for problem of hitting hypersphere centered at origin at state space 02 p0303 A67-12149
-
- Suboptimal solutions for class of linear regulator problems with soft saturation constraints, noting Hamilton-Jacobi equation 02 p0226 A67-12150
-
- Iterative procedure for changing constraint minimization problem to mathematical programming formulation in solving discrete terminal control problem 02 p0226 A67-12152
-
- Projection principle for minimization of variance of squared error 02 p0259 A67-12154
-
- Systemic computational technique for designing specific optimal controller, considering performance index 02 p0226 A67-12155
-
- Optimal feedback control for finite state systems with suitable performance criterion, using maximum principle applied to time-sharing computer systems 02 p0227 A67-12172
-
- Weight factor effects on optimal motion parameters of variable mass system with limited velocity jet propulsion in gravitational field 02 p0327 A67-12333
-
- Mayer technique in calculus of variation for constrained error coefficient criterion function for missile trajectory optimization in aerospace guidance and control 02 p0265 A67-12389
-
- Optimal rocket trajectories, discussing role and significance of intermediate thrust arcs of rocket extremals in vacuum 02 p0335 A67-12397
-
- Describing function determination for case of piecewise linear-nonlinear characteristics with discontinuities of first kind 02 p0227 A67-12682
-
- Structural design optimization by nonlinear programming noting Sequential Unconstrained Minimization Technique, use of variable metric, Powell direct search method, etc 02 p0209 A67-12711
-
- Optimal transfer of finite thrusting vehicle between circular coplanar orbits 02 p0330 A67-12719
-
- Synthesis of linear automatic control system with constant parameters for integral Q-factor, noting effect of small parameters on properties of optimum system 03 p0390 A67-13097
-
- Soviet papers on complex control systems 03 p0390 A67-13180
-
- Spatially distributed system for optimal filtration of useful signal in random noise fields 03 p0391 A67-13181
-
- Characteristic function method for solving optimal control problems and sufficient conditions for existence of absolute minimum 03 p0457 A67-13183
-
- Structural design of optimal control for n-order nonlinear plant, using variational calculus 03 p0391 A67-13185
-
- Asymptotic control problem of n-dimensional systems solved by functional analytic techniques 03 p0391 A67-13265
-
- Equivalence relations for optimal control problems classification and algorithm construction 03 p0391 A67-13266
-
- General variational problem and necessary conditions formulated in setting of locally convex linear topological space 03 p0458 A67-13268
-
- Constrained minimization problems in finite-dimensional spaces in unified approach 03 p0458 A67-13269
-
- Linear optimal systems with time delays 03 p0392 A67-13270
-
- Optimality principle in mean for optimum averaging of controls of stochastic systems 03 p0392 A67-13595
-
- Optimal control problems, considering arbitrary piecewise-continuous function with finite number of discontinuities of first kind 03 p0392 A67-13626
-
- Soviet monograph on mathematical methods of optimum control 03 p0392 A67-13714
-
- Monograph on self-adaptive servocontrol systems, discussing transfer function optimization, frequency filter structure, noise problems, etc 03 p0393 A67-13715
-
- Quadratic programming applied to design of digitally compensated sampled data control system 03 p0393 A67-13902
-
- Linear optimal control via root square locus to design simple effective structural bending control for four XB-70 coupled longitudinal bending modes [AIAA PAPER 66-970] 03 p0361 A67-14142
-
- Suboptimal policies for fuel optimal control and energy optimal control problems for linear time invariant system obtained, using Liapunov functions 04 p0590 A67-14418
-
- Target homing of tracking systems receiving signal packages only in absence of fading 04 p0591 A67-14659
-
- Optimum control problems for systems described by differential equation with deviating argument 04 p0591 A67-14667
-
- Optimal temperature control design using IBM 7094 digital computer program for thermal environment simulation of stabilized multisurfaced earth-orbiting spacecraft structure [ASME PAPER 66-WA/HT-44] 04 p0724 A67-15430
-
- Optimal control of systems described by elliptic differential operators 04 p0593 A67-15491
-
- Principles of suboptimal perturbation guidance and methods for polynomial approximation of guidance matrices 04 p0655 A67-15629
-
- Optimum processes in systems with distributed parameters described by partial differential equations 04 p0647 A67-15874
-
- Optimality of totally singular vector controls governing dynamical systems and extension of Green theory approach to higher dimensions to evaluate optimality of such controls 04 p0594 A67-15875
-
- Exhaustive equivalence classes of optimal systems with separable controls 04 p0594 A67-15876
-
- Minimum norm control for linear time-varying system by fixed point method 04 p0594 A67-15878
-
- Necessary conditions from second variation, via transformed accessory minimum problem, for class of singular Bolza problems, including singular optimal control problems 04 p0594 A67-15879
-
- Successive approximations applied to optimal control equation for self-similar viscous Couette flow between one stationary and one moving wall 04 p0610 A67-15885
-
- Book on optimal control theory of deterministic dynamical systems governed by ordinary differential equations in presence of control and state constraints 04 p0594 A67-15943
-
- General theory of variational problems of optimum control incorporating calculus of variations and Pontryagin maximum principle 04 p0647 A67-15981
-
- Optimization of linear control systems when placing step limitations on control, using functional analysis 05 p0781 A67-16251
-
- Synthesis problem of optimum dynamic

characteristics of multivariate linear control systems with random input signals 05 p0781 A67-16252

Optimum control of two-dimensional oscillating system when placing limitations on control, using Butkovskii L-problem of moments 05 p0781 A67-16253

Optimal control problem of variable structure system, deriving necessary and sufficient conditions for existence of trajectories 05 p0781 A67-16256

Comparison of nonoptimum and optimum strategies in dual control of inertialess plants in presence of noise in feedback loop 05 p0781 A67-16257

Synthesis of stochastic optimal control for case of discrete input of feedback vector, noting dependency on coordinates characterizing probability density of plant vector 05 p0782 A67-16316

Optimal filtration of nonlinear functional of Gaussian signal, obtaining expressions for kernels of optimal filter 05 p0782 A67-16317

Synthesis of optimal nonlinear filters of Volterra type approximating kernels of filters by orthonormal functions 05 p0782 A67-16318

Optimality conditions for nonlinear discrete systems, showing that at limit these conditions become Pontryagin maximum principle for continuous systems 05 p0782 A67-16320

Controllability region and correctness of formulation of optimal problem 05 p0783 A67-16358

Synthesis and control strategy of optimal final value linear system under random environment statistically considered, using Bellman dynamic programming 05 p0783 A67-16442

Optimum switching function of relay servosystem subjected to stationary Gaussian random input found by perturbation method 05 p0783 A67-16445

Optimal steering and cut-off reelight in orbital transfers, using orbital parameters as state variables for greater accuracy in calculations 05 p0905 A67-16519

Multiparameter self-adaptive control by pole-zero cancellation with simple structure and fast response 05 p0783 A67-16523

On-line digital computer used in optimizing control by prediction, including quadratic and steady state value 05 p0784 A67-16524

Duality and a priori estimates in Markovian nonlinear stochastic optimal control problems 05 p0784 A67-16778

Burning, staging and thrust direction programs for range maximization of particle in planar motion under downward gravitational acceleration and linear drag 05 p0905 A67-16780

Bang-bang control for feedback systems, applying computer to optimization of switching time from state to state of linear systems 05 p0784 A67-16854

Optimal stabilization of small oscillations of body around center of mass in central field 05 p0901 A67-17117

Optimal Wiener values of filter parameters in phase-lock loop, noting possibility of improved performance despite deviations 06 p0973 A67-17615

Adaptive utilization of communication satellite systems optimizing dynamic traffic handling of combined ground and satellite communications complex, noting network configurations 06 p0959 A67-17670

Parametric analysis, penalty-effectiveness tradeoff and system selection for communications satellites, using block digital computer synthesis with subroutines for operational requirements [AIAA PAPER 66-330] 06 p0960 A67-17693

Linear frequency-domain analysis technique for examining stability and performance characteristics in optimal-control design of control systems 06 p0973 A67-17718

Brachistochrone problem analyzed using variational calculus and optimal control theory 06 p0973 A67-17770

Advances in control systems, Volume 3, covering reentry and aerospace vehicle guidance and control, BVP techniques, optimal control, Kalman filtering techniques and state space methods for navigation problems 06 p0973 A67-17921

Newton-Raphson method generalized for solution of two-point boundary value

problems of nonlinear optimal control theory for digital solution 06 p0974 A67-17923

Existence theorems in optimal control theory of linear and nonlinear systems 06 p0974 A67-17924

Minimum normed operator application to optimal terminal control system problems 06 p0974 A67-17925

Book on advances in control systems including algorithms for sequential optimization, trajectory optimization, optimal control, etc 06 p0974 A67-17929

Approximation techniques generating algorithm for iteratively solving sequential optimization of nonlinear control systems 06 p0974 A67-17930

Optimum control of multidimensional and multilevel systems, discussing linear systems, load distribution, cyclic optimization and aggregated systems 06 p0974 A67-17933

Optimal control of linear stochastic systems with complexity constraints applied to sampled data system 06 p0975 A67-17934

Convergence rate of method of gradients relationship to singularity of second variation operator in optimal programming problems 06 p0975 A67-17935

Closedness of set of trajectories or of solutions of contingent equation used in existence problems of optimal control and variational calculus 06 p0975 A67-18100

Optimal regime conditions in engineering calculation of generating device with self-parametric frequency multiplication, using nonlinear inductance in ultrasonic frequency range 06 p0970 A67-18171

Optimal threshold level resulting in minimum residual probability of distortion in transmission of pulse coded signals in systems with information feedback 06 p0975 A67-18218

Optimal one-dimensional truncated signal distribution ensuring optimal capacity or differential entropy 06 p0976 A67-18219

Numerical method solution of nonlinear two-point boundary value problem associated with optimum transfer of spacecraft [AIAA PAPER 67-58] 06 p1023 A67-18267

Optimum trajectory control for minimum heating paths during manned vehicle reentry at hyperbolic speeds 06 p1095 A67-18268

Dual control of plant with random amplification factor as Bayesian problem 06 p0976 A67-18408

Fixed time fuel-optimal controls computed by iterative procedure developed by Pontryagin principle 06 p1097 A67-18522

Optimization of stochastic dynamic system with noisy output 06 p0977 A67-18525

Weight factor of optimizing functional determined by distribution of roots for analytical design of optimal controls 06 p0977 A67-18547

Pontryagin maximum principle for optimal control problem with constraints on control function 06 p0978 A67-18584

Optimal parameter problem of controlled dynamic systems, considering antagonism between designer and nature, applying results to space flight mechanics 06 p1088 A67-18616

Optimum control of motion stability of solid body with fixed point, using gyrostabilizer rotors 06 p1034 A67-18617

Optimal power design of conduction type MGD generator 06 p0951 A67-18674

Optimality conditions of systems containing components with distributed parameters 07 p1159 A67-19138

Second order method for nonlinear optimal control problems resulting in Riccati differential equations 07 p1213 A67-19155

Self-adaptive control systems theory - IFAC Symposium, Teddington, Middx., England, September 1965 07 p1159 A67-19192

Cost function gradient estimation for optimum control of nonlinear stochastic systems 07 p1159 A67-19193

Optimal control system having nonunique solution of Pontryagin equation and having separatrix between two strategies 07 p1160 A67-19203

Search limit cycle frequency and magnitude in single dimensional optimizing systems with nonlinear function modeling of performance measurement process 07 p1161 A67-19206

Optimal conditions of thermostability of anisotropic spherical ferrite microwave

resonator with various orientations 07 p1153 A67-19597

Closed form general complete solution to linear time invariant second-order optimal filter 07 p1161 A67-19791

Minimum energy problems in Hilbert function space for continuous and discrete linear systems, noting operator transformation into linear differential equations 07 p1216 A67-19908

Sufficient conditions of optimality for discrete controlled systems 07 p1162 A67-20023

Reliability in optimal control problems in terms of probability of faultless operation 07 p1162 A67-20027

Optimum stability of body with fixed point, using stabilizing gyros 07 p1224 A67-20028

Simulation of pursuit-evasion differential game using variational method, comparing performance of human pilot to optimal pursuer 07 p1136 A67-20170

Pontryagin maximum principle, discussing singular and nonsingular extremals classification by numerical integration techniques 07 p1162 A67-20273

Caratheodory unified approach to Hamilton-Jacobi theory in variational calculus problems of optimal control 07 p1162 A67-20275

Discrete time control /multistage/ version of Berkovitz nonlinear programming problem 07 p1163 A67-20276

Optimal control for linear system with respect to performance functional which includes trajectory sensitivity 08 p1309 A67-20327

Sensitivity of index of performances to variations in plant parameter for open and closed loop optimal control with one or two degrees of freedom 08 p1309 A67-20328

Extremal control problem of undamped oscillatory plant analyzed using bounded phase-coordinate control theory 08 p1309 A67-20330

Optimal control systems without complex controllers using variational calculus, for application to submarine diving control 08 p1309 A67-20331

Conjugate gradient minimization method in function space 08 p1310 A67-20337

Optimal design of pneumatic control jet of fluid amplifier to obtain maximum logic gain 08 p1282 A67-20459

Third order control system saturation, considering approximate solution to third order bang-bang system 08 p1312 A67-20722

Dynamic programming for control system synthesis, noting invariant embedding and optimality principle use in optimum design problems 08 p1312 A67-20752

Self-optimizing and adaptive control systems achieved by feedback action or performance index optimization 08 p1312 A67-20753

Multivariable control systems with random inputs for nonlinear and linear cases 08 p1312 A67-20754

Optimal control analysis of system behavior described by linear stochastic differential equations 08 p1313 A67-21325

Optimal extremal control systems synthesized by nonlinear filtering compared to those synthesized by correlation method of control 08 p1313 A67-21326

Optimal transfer of thrust limited vehicle between coplanar circular orbits 09 p1571 A67-21694

Optimization problem associated with fuel consumption for control of satellite orientation by means of active system 09 p1571 A67-21696

Gradient method solution for class of optimal control problems, minimizing mean square value of finite state components of object in motion 09 p1482 A67-21871

Existence and uniqueness theorem for functional equation of optimal control problems, noting stability of solution 09 p1524 A67-21874

Plasma in flat-electrode accelerator, examining optimum accelerator length associated with equilibrium between acceleration processes in plasma and diffusive scattering of plasmoid 09 p1545 A67-22001

Optimal control of elastic flight vehicles, describing axis oscillations by equations of beam with variable cross section 09 p1439 A67-22075

Variation of functional determined on trajectories of differential equation systems with discontinuities, discussing application to optimal control problems 09 p1525 A67-22076

Synthesis of optimal Liapunov-Bellman function, noting sequential solution method for independent variables and method using first order partial differential equation 09 p1525 A67-22077

Filter theory method applied in solving analytical construction problems for optimal controllers, noting existence of Fourier transform and Pally-Wiener condition 09 p1482 A67-22078

Optimal control of variable structure system in presence of perturbation, discussing quality control and preservation of sliding plane 09 p1483 A67-22081

Optimizing reliability level in conceptual phase system to ultimately yield operational systems of desired capability, illustrating with C-130/C-141 transport aircraft study 09 p1582 A67-22293

Survey and bibliography of works on optimum control system design and statistical signal descriptions 09 p1483 A67-22386

Optimum transient response for bang-bang control system with finite time control activation 09 p1483 A67-22609

Optimum control and prediction in designing self-adjusting controllers for linear systems with correlated disturbances 10 p1618 A67-22732

Optimal discrete binary system of electrical control of beam position of phased linear antenna array 10 p1611 A67-22982

Quasi-linearization determination of optimum finite thrust and impulsive orbital transfers 10 p1706 A67-23130

Nonlinear programming and control problems in terms of variations, maximum principle and dynamic programming 10 p1619 A67-23418

Computation difficulty in optimal control law for dynamical system, noting three optimal conditions 10 p1619 A67-23419

Differential games, particularly pursuit of one controlled object by another terminating in shortest time 10 p1620 A67-23421

Stability of optimal control problem in nonlinear process and linear regulator 10 p1620 A67-23423

Optimal control for investment program, obtaining solution through convex programming 10 p1620 A67-23426

Direct and inverse problems of optimization of quadratic functional in linear autonomous and controlled systems 10 p1621 A67-23612

Optimal control system for linear plant with modulus limited control actions 10 p1621 A67-23613

Invariant and optimal linear systems with periodic parameters analyzed by transfer function calculation 10 p1621 A67-23614

Optimal control of one-dimensional distributed oscillatory system and wave processes using momentum theory and propagating method 10 p1621 A67-23615

Optimal control of maneuver induced vibration in flexible aerospace vehicles 10 p1714 A67-23754

Synthesis of near optimum high order control systems from simple convenient control functions equivalent with respect to sign 10 p1621 A67-23850

Optimum linear receiver for noisy PAM system using criterion of mean square interference 11 p1752 A67-24134

Automatic optimization problem for linear Diophantine plant via analysis of discrete extremal problems 11 p1770 A67-24209

Dynamic programming and Liapunov function for optimization of systems employing digital controllers 11 p1770 A67-24210

Stochastic optimal control with noisy observations, obtaining Hamilton-Jacobi stochastic equation in function space [ASME PAPER 66-WA/FE-6] 11 p1770 A67-24276

Satellite attitude control in elliptic orbit 11 p1869 A67-24337

Reentry guidance by threshold network storage of precomputed optimum commands, using analogy of surface approximation problem in N plus one-dimensional space [AIAA PAPER 66-52] 11 p1869 A67-24338

Optimal smoothing filter and smoothing error covariance matrix equations for

discrete linear systems, using orthogonal projection 11 p1770 A67-24422

Optimal solutions to mixed initial boundary value problems for control processes described by semilinear hyperbolic partial differential equations in two independent variables 11 p1770 A67-24423

Solution of optimal control problems using hybrid computers 11 p1770 A67-24426

Optimum distributed parameter system described by N-dimensional wave equation with unconstrained boundary control function 11 p1770 A67-24889

Optimum control integral criterion function for class of distributed parameter systems subject to control signal saturation 11 p1770 A67-24890

Penalty function method used for bounded phase coordinate optimal control problem for linear discrete systems with quadratic cost functionals 11 p1771 A67-24891

Analogue computer applied to solve two-point boundary value problem for fourth order optimal control problem with applied Pontryagin maximum principle 11 p1771 A67-24893

Gradient acceleration technique for solving optimal systems with unbounded control 11 p1771 A67-24896

Existence, uniqueness and reversion theorems, necessary optimality criteria and nonfixed time case for optimal control problem of n-dimensional linear parabolic equations 11 p1814 A67-25067

Statistical analysis of optimum control system design by parameter adjustment, finding systems transfer function through Wiener-Hopf integral 11 p1772 A67-25082

Optimum propulsion control law selection for limited motion capacity in mass accumulation regime determined, considering two-dimensional problem of vehicle motion 12 p1989 A67-25659

Pontryagin maximum principle application to solution of one-dimensional minimum time rendezvous problem for thrust limited rocket with initial and final mass specified 12 p2012 A67-25922

Root trajectory theory use in automation schemes for analysis and synthesis of optimum control systems, outlining applications 13 p2085 A67-26394

Matrix algorithm for calculating mean square error for synthesis of optimum control systems 13 p2087 A67-26612

Optimal control theory in design of aerodynamic shapes, flight paths, guidance and control logic, data processing logic, etc 13 p2072 A67-26814

Direct numerical method for finding optimal values of functionals and associated velocity fields in plastic limit analysis 13 p2219 A67-27153

Design and optimal performance considerations on application of derived rate increment feedback to satellite attitude control systems in limit cycle and acquisition systems 13 p2212 A67-27297

Optimal suspension systems synthesis, discussing dynamic programming theory 13 p2159 A67-27300

Space vehicle flight control with minimum total characteristic velocity, determining optimum points for applying correcting acceleration 13 p2213 A67-27320

Multistage rocket motion optimization in uniform gravitational field formulated as coupled variational problem 13 p2213 A67-27321

High performance aerodynamic vehicle design noting configuration variables, optimum performance parameters, vehicle force characteristics, optimization of hypersonic aircraft performance, etc [AIAA PAPER 66-486] 13 p2054 A67-27584

Regularization method for maximum height ascent of rocket uniformly approximating control function by gradient projection method 13 p2149 A67-27618

Optimal transients for third order system with stepwise external controls, determining switching surfaces 13 p2089 A67-27705

Optimality principle in mean for optimum averaging of controls of stochastic systems 14 p2290 A67-27841

Optimum trajectories between material points moving along same orbit in gravitational field of spherically symmetric central body, obtaining numerical solutions for circular initial orbit 14 p2382 A67-27852

Optimum stabilization of axisymmetric

satellite by system of n reactive jets 14 p2393 A67-27854

Minimum of maximum overload in braking of vehicle in atmosphere, examining aerodynamic lift on basis of Pontryagin maximum principle 14 p2393 A67-27855

Optimum control of earth satellites and space vehicles and stable solutions of orbits in orbital mechanics 14 p2393 A67-27879

Synthesis of optimal controls for nonlinear plant described by second order differential equation 14 p2291 A67-28383

Dual formulation of variational problems with differential inequality constraints, noting relation between mathematical programming and variational calculus 14 p2345 A67-28908

Optimal control of random dynamical systems analyzed, using first order vector differential or difference equations 14 p2292 A67-29062

Frequency domain instability criteria generated from stability criteria for time varying and nonlinear feedback problems 15 p2455 A67-29167

Optimal control applications of Fletcher-Reeves conjugate gradient minimization method and comparison with second variational technique 15 p2456 A67-29362

Newton-Raphson computational procedure for finding extremal control policies for nonlinear processes 15 p2456 A67-29363

Parametric input/output relation of approximate controller with optimized performance index, obtaining specific optimal control designed in regard to worst initial state 15 p2456 A67-29365

Sensitivity of cost functional in optimal control system with random variable parameters, noting system performance detection techniques 15 p2457 A67-29368

Extent of system parameter change insuring system performance within specified limit 15 p2457 A67-29369

Optimal averaging theories of controls of dynamic systems 15 p2458 A67-29687

Linear single input optimal cooperative rendezvous problem with quadratic performance index solved using variational calculus 15 p2458 A67-29909

Optimal final value control theory, applying variational calculus and functional analysis to control function selection for dynamic systems 15 p2459 A67-30020

Set of linearized motion equation for ferry vehicle to obtain optimal-thrust during rendezvous attempt with orbital satellite 15 p2571 A67-30049

Backward and forward algorithms of dynamic programming for time dependent systems, noting advantages of forward algorithm for optimization of system 15 p2440 A67-30157

Optimal statistical adaptive model used in defining characteristics of control plants 15 p2461 A67-30321

Method of dynamic characteristics, determining controlled plant performance during operation 15 p2462 A67-30328

Process identification by cyclic parameter adjustment with automatic iteration, using analog and hybrid computers 15 p2465 A67-30342

Optimal control theory applied to extremum control in dynamic programming equation derivation for simplified extremum control problem 15 p2465 A67-30343

Optimal threshold level resulting in minimum residual probability of distortion in transmission of pulse coded signals in systems with information feedback 16 p2642 A67-30484

Optimal one-dimensional truncated signal distribution ensuring optimal capacity or differential entropy 16 p2643 A67-30485

Fuel optimum guidance law to achieve required velocity 16 p2700 A67-30655

Synthesis of optimal linear control system coupled with vehicle configuration design technique for guidance parameters and temperature accumulation along optimum entry trajectories 16 p2758 A67-30660

Space vehicle optimal control, studying maximum principle application, developing numerical algorithms of dynamic programming type and describing variational problems 16 p2742 A67-30664

Determining control functions and choosing parameters governing transfer of dynamic system from initial to final state 16 p2744 A67-30732

Extrapolation of time series with discrete Laguerre polynomials, deriving general recursion relation for expansion coefficients 16 p2697 A67-31418

Bryson gradient method of constructing optimal control laws applied to algorithm for numerical solution of variational problems in optimal control theory 16 p2644 A67-31601

Linearly-approximated characteristics of maneuvers correcting near-planet positions of spacecraft with pulsed flight velocity characteristics 16 p2752 A67-31602

Quantization error effect for digital control system design 16 p2646 A67-31637

Optimal feedback control system design to account for differences between physical system and mathematical model in terms of parameters 16 p2647 A67-31641

Suboptimal control of large scale dynamic system consisting of two weakly coupled subsystems using aggregation 16 p2647 A67-31645

Off-line training technique achieving practical closed loop, suboptimal control laws and controllers 16 p2648 A67-31653

Adaptation technique for on-line steady-state optimizing control using updated control algorithm 16 p2648 A67-31655

Feedback from observations introduced into midcourse guidance correction program, showing optimal random feedback solution obtained for deterministic optimal feedback control problems 16 p2701 A67-31657

Suboptimal control function sequence generation by combining approximation in control policy space with stability criteria from direct method of Liapunov 16 p2648 A67-31658

Suboptimal, adaptive solutions to sampled data problem for quadratic performance index minimization by obtaining control law and sampling scheme 16 p2649 A67-31660

Control of output variables in discrete multivariable system at steady state noting design, application and performance 16 p2649 A67-31668

Algebraic characterization of optimal singular control for autonomous linear plants, using explicit closed form representation of singular strip 16 p2649 A67-31669

Optimal trajectories for linear discrete system with respect to minimax criteria using standard programming code 16 p2650 A67-31670

Linear pulse frequency modulated control systems, noting upper and lower bounds of optimal performance 16 p2650 A67-31671

Sensitivity analysis application to nonlinear system modeling and compensation noting minimization procedure parameter determination and performance index 16 p2650 A67-31674

Optimal control of measurement subsystems within feedback control systems 16 p2650 A67-31676

Interior penalty method for inequality constrained optimal control problems concerning convergence rapidity 16 p2651 A67-31677

Conjugate gradients providing convergent means to solve optimal-control problems for linear systems with quadratic performance index 16 p2651 A67-31678

Optimal feedback control calculation for launch vehicle synthesizing optimal controller with sensitivity constraints to reduce trajectory dispersion 16 p2763 A67-31679

Optimum filtering and control of randomly-sampled linear and nonlinear systems with Gaussian or non-Gaussian statistics, synthesizing generalized Kalman filter 16 p2651 A67-31683

Optimal control of dynamic systems with minimax type performance index, discussing application of proposed method of solution 17 p2829 A67-32014

Optimal control for aircraft gust alleviation using frequency domain theory and short period mode approximation 17 p2795 A67-32036

First variation theory in extremal problems, noting generalization of classical variational problems and optimal control problems for functions with single independent variable 17 p2876 A67-32043

Computational limitations of onboard orbiting computers such as fixed point arithmetic, limited word length and solution

techniques 17 p2881 A67-32056

Optimum control of space vehicle motion along binormal to circular reference orbit for minimum fuel consumption criterion 17 p2955 A67-32255

Tolerance of nonlinearities in input transducer of time-varying optimal control systems, using Liapunov function 17 p2829 A67-32307

Book on nonlinear programming covering various methods and use in control 17 p2818 A67-32424

Optimal control and convex programming, discussing problem of admissible investment program control for production constraints 17 p2829 A67-32431

Synthesis of optimum discrete control for eventual state of linear stochastic system, reducing problem to solution of Bellman functional equation 17 p2831 A67-33274

Stochastic differential game with missile and radar, using linear theory in finding optimal strategies 18 p3075 A67-33495

Quantum formulas for optimal filtration of useful electromagnetic signal in noise background based on maximum misinformation principle 18 p2999 A67-33533

Synthesis of stochastic optimal control for case of discrete input of feedback vector, noting dependency on coordinates characterizing probability density of plant vector 18 p3016 A67-33867

Optimal filtration of nonlinear functional of Gaussian signal, obtaining expressions for kernels of optimal filter 18 p3016 A67-33868

Synthesis of optimal nonlinear filters of Volterra type approximating kernels of filters by orthonormal functions 18 p3017 A67-33869

Optimality conditions for nonlinear discrete systems, showing that at limit these conditions become Pontryagin maximum principle for continuous systems 18 p3017 A67-33871

Mathematical model for computer diagnosis of system failure, developing optimal policy for searching malfunctions with observable symptoms 18 p3006 A67-34065

Synthesis of optimal and quasi-optimal sampled data control systems applied to various order plants 18 p3017 A67-34281

Requirements of optimal controller for system with constraints imposed on control magnitude 18 p3018 A67-34283

Optimal control methods of Bellman and Pontryagin, discussing maximum rule and dynamic programming for optimization in presence of constraints 18 p3018 A67-34284

Optimum short term screen tests developed for integrated circuits 18 p3018 A67-34649

Relationship of management to reliability aspects during Athena program 18 p3138 A67-34651

Book on optimal control covering theory and application of linear algebra, vector analysis, Euclidean space, Pontryagin principle, etc 18 p3018 A67-34758

Mathematical model of rigid, long space-body spinning at constant rate about symmetry axis for optimal attitude control calculations 19 p3331 A67-34777

Algorithm for computing matrix Riccati equation solution in optimization problems 19 p3249 A67-34781

Optimum trajectory control for minimum heating paths during manned vehicle reentry at hyperbolic speeds [AIAA PAPER 67-59] 19 p3331 A67-34815

Algebraic method applied for control optimization of nonlinear systems, acquiring asymptotic stability by using Liapunov function 19 p3199 A67-34825

Indices optimal diagnostic value using mathematical evaluation of information theory 19 p3186 A67-34889

Design of optimal waveforms for optimal estimation or prediction of state of linear dynamical system in presence of Markov and white noise 19 p3201 A67-34965

Empirical formulas for optimal operation of extremal controllers, design data generation and cost index determination 19 p3201 A67-34992

Determining sign of second variation in optimal control theory 19 p3202 A67-35756

Computer solution of optimal control problems by finite difference method 19 p3202 A67-35886

Identification, optimization and stability

of automatic systems - Conference, Slacay, France, May 1965 19 p3203 A67-35901

Dynamic system with state at any instant represented by point in Euclidean space of n dimensions 19 p3203 A67-35902

Local properties of limiting surfaces, giving hypothesis for surface separating two unconnected regions 19 p3204 A67-35903

Pontryagin principle extension by mathematical formulation modification 19 p3204 A67-35904

Invariant integral from use of Noether theorem of calculus of variations applied to optimal control problem 19 p3204 A67-35906

Mathematical model for optimization problem obtaining equations generalizing Bellman equation 19 p3205 A67-35908

Identification problem solution by gradient and Newtonian methods, using algorithm simplified by sensitivity function 19 p3205 A67-35914

Singular optimal control and attitude problem in rocket guidance [AIAA PAPER 67-582] 19 p3258 A67-35977

Linear optimal control technique for flexible-booster control system design, showing drift minimum model with matrix transformations for closed-loop dynamics 19 p3336 A67-35988

Manual optimal guidance scheme using predictive display applied to launch vehicles during boost for continuous generation of predicted fuel-optimal trajectory 19 p3259 A67-35989

Simulation evaluation of closed form lifting reentry guidance [AIAA PAPER 67-597] 19 p3259 A67-35993

Correlations between elastic limit, tensile strength and elongation in foundry aluminum alloys used in control reliability 20 p3465 A67-36479

Launch operations optimization for mission planning through analysis of performance data from past programs 20 p3532 A67-36557

Predictor display instrument for optimal manual control, noting use in manned spacecraft missions and time factor 20 p3447 A67-36840

Functional analysis applied to optimum control by reduction of variational problem to finite dimensional analysis and calculation of algorithms for use with digital computer 20 p3477 A67-37034

Optimum control problems solved by numerical methods based on variation in state space 20 p3477 A67-37035

Maximum probability criterion on output coordinates of system for selection of parameters of optimal nonlinear control system 20 p3408 A67-37042

Analytic design of optimal digital controller, resolving problem of choice of weighting coefficients of functional representing generalized rms estimate of transient 20 p3408 A67-37046

Noise effect on synthesis of discrete systems with and without feedback channel for transmitting continuous messages, using binary signal and criterion of minimum rms error 20 p3383 A67-37071

Dynamic programming for optimal algorithm for extremal control in presence of noise at system input and output 20 p3408 A67-37072

Closure and convexity of attainable control sets in finite and infinite dimensions, noting Liapunov theorem 20 p3408 A67-37075

Existence theorems for linear optimal control problems with nonlinear cost functionals 20 p3408 A67-37076

Linear optimal stationary control system with state dependent white noise disturbances described by differential equation 20 p3408 A67-37077

Extremal systems having auto-oscillating optimizers and controlled plants, investigating performance improvement by complex modification of input signal 20 p3409 A67-37110

Computer programming method for analysis of complex systems 20 p3392 A67-37194

Optimal system determined from maximum probability criteria of target hitting 20 p3410 A67-37226

Minimum control system optimization, noting adaptation with respect to minimum mean square error, statistical criterion calculation, etc 20 p3410 A67-37227

Switching surface construction using one

to one correspondence between points in controllability region and points on surface of nth order system 20 p3410 A67-37230

Accuracy problems in control systems, discussing error assessment and accuracy estimates of optimal control 20 p3410 A67-37231

Maximum principle application to optimal control procedure, minimizing transient response and decreasing effect of random changes in system 20 p3410 A67-37232

Suboptimal controller generating linear combination of state coordinates shown to give optimal performance when using linear controller preceding relay 20 p3410 A67-37251

Second order nonlinear optimal control system for various performance criteria using Pontryagin principle 20 p3410 A67-37252

Optimal control theory for distributed parameter systems using dynamic programming, showing use in two-point boundary control problems involving partial differential equations 20 p3410 A67-37320

Optimal control theory for linear distributed parameter systems, presenting solution algorithms and computational results for several problems 20 p3411 A67-37321

Optimal conditions of thermostability of anisotropic spherical ferrite microwave resonator with various orientations 20 p3401 A67-37336

Complex multiaircraft control systems with hierarchical control structure with imposed universal optimality criterion 20 p3411 A67-37373

Free vibrations and motion stability during extremum drift for one-and multidimensional pulsed optimal systems 20 p3411 A67-37374

Numerical methods for linear optimal control problems, noting applicability of algorithms to certain nonlinear problems 20 p3411 A67-37375

Distributed receiving system for optimal filtration of random field of space-distributed source 20 p3385 A67-37376

Aircraft flight dynamics optimized in angle of attack by variational calculus, analyzing control system 20 p3361 A67-37377

Constrained minimization problem extended to necessary conditions for characterizing noninferior points to determine vector-valued criteria in finite dimensional spaces 20 p3478 A67-37576

Optimality and invariance conditions for linear free-time problem 20 p3412 A67-37582

Maximum principle for hereditary processes optimal control with constant time lag and parameters 20 p3412 A67-37583

Book on optimal control theory covering Fourier and Laplace transforms, automatic control, mathematical theories, etc 21 p3602 A67-37829

Generalized Legendre-Clebsch condition applied to singular arc trajectory solutions of state and adjoint equations for optimal control 21 p3602 A67-38023

Plant parameter uncertainties sensitivity constraint for optimal linear control synthesis, discussing Wiener-Hopf equation condition 21 p3602 A67-38026

Book on optimal adaptive control systems, detailing material on game theory for use in control system design 21 p3603 A67-38266

Advances in control systems, Theory and applications Volume 5, covering optimal control and optimization advances in control systems, Theory and applications, Volume 5, covering optimal control 21 p3603 A67-38438

Steady state plant performance optimization for unknown dynamic characteristics, determining periodic input signal 21 p3603 A67-38439

Set of states reachable in given time in control problem determined by heuristic and rigorous methods 21 p3603 A67-38441

Optimal nonlinear filtering, deriving differential equations for probability density or state vector for noise corrupted system 21 p3603 A67-38442

Computational considerations for trajectory optimization in bounded state space, discussing necessary and sufficient condition 21 p3604 A67-38443

Optimal control for nonlinear dynamic systems with/without invariant properties investigated for departures from optimal motion 21 p3656 A67-38586

Book on calculus of variations and optimal control theory covering function maximum and minimum theory, fixed end-point problem, etc 21 p3653 A67-38799

Mathematical programming problem for automating design of optimum thin walled systems, noting stress-strain state factors 21 p3728 A67-38903

Time optimal flight trajectories in planar and spatial pursuit problems with constraints on pursuer, using Pontryagin maximum principle 21 p3712 A67-39151

Eigenstate variables for representation of optimum orbital transfer problems, discussing numerical integrations 22 p3878 A67-39154

Single-axis time and fuel supoptimal /superior optimal/ control for spacecraft attitude control obtained via bang-bang manipulation of damping and jet commands 22 p3897 A67-39155

Stochastic optimal control algorithm for pursuit process in problem of encounter of two cosmic objects 22 p3878 A67-39183

Optimal flexible strategies for pulsed correction of close-to-nominal space vehicle trajectory, using fuel reserve limitation criterion 22 p3878 A67-39186

Active control of space vehicles orientation, discussing optimal and rational control and rotational motion braking problems 22 p3899 A67-39189

Optimal algorithm for single parameter linear and nonlinear correction of interplanetary flight, noting application to space vehicle approach to designated planet 22 p3830 A67-39193

Book on optimization covering inequality constraints, decomposition strategy, direct methods, etc 22 p3775 A67-39270

Optimal control of quasi-linear system perturbed motion, developing approximation method 22 p3776 A67-39305

Optimal transfer function of static systems calculated, using measured data and substitution for higher order transitions through jointly operating PI controller 22 p3776 A67-39335

Open loop adaptive optimal control, calculating plant dynamic sensitivity coefficients for unknown disturbances, using digital computer on feedback path 22 p3776 A67-39411

Learning control systems, discussing adaptive time, searching, strategy, teaching, association, principle and behavior 22 p3776 A67-39412

Lift reduction and increase of helicopter maximum speed by controlling optimum angle of attack of rotor blades over surface of revolution 22 p3744 A67-39548

Weight factor of optimizing functional determined by distribution of roots for analytical design of optimal controls 22 p3776 A67-39747

Point-to-point mapping technique in combination with variational calculus for solving optimum control problems for piecewise linear dynamic systems 22 p3776 A67-39776

Dynamics of single channel extremal systems having plants in linear and nonlinear elements and control units in form of self-oscillating type optimizer 22 p3777 A67-39777

Approximation method for solution of Bellman equation in optimal control problems 22 p3777 A67-39828

Equations for mode analysis in multichannel extremal control systems with harmonic probe signals, discussing synthesis of optimizers and phase shift automatic compensation 22 p3777 A67-39864

Book on continuous and scanning control systems optimization and random processes theory including numerical techniques, harmonic analysis and Gaussian transformation 22 p3777 A67-40070

Variational calculus for optimal attitude acquisition/stabilization controller synthesis for spinning and nonspinning space vehicles 22 p3904 A67-40105

Suboptimal feedback solution to guidance and control in minimum time and fuel for low thrust orbital transfer 22 p3832 A67-40146

Rapidly converging iterative solutions to Min-H strategy applicable to trajectory optimization and payload maximization 22 p3888 A67-40148

Booster autopilot in bounded phase

coordinates subject to disturbances, determining extremal control as function of time 22 p3833 A67-40149

Lateral stability augmentation of supersonic aircraft using linear multichannel state-vector optimal feedback control 22 p3746 A67-40155

Suboptimal linear control laws involving parameter optimization 22 p3777 A67-40156

Terminal guidance problem involving optimal control for deviations in systems with transport lag 22 p3833 A67-40158

Optimum sensitivities of control function with respect to vehicle parameter changes and state variables without using finite differences 22 p3833 A67-40159

Optimum process theory methods applied to calculus of variations, examining sufficient conditions for optimality principle 22 p3778 A67-40446

Linear servosystem parametric optimization and application to satellite attitude control, discussing selective and gradient methods 23 p4070 A67-40577

Nonlinear system suboptimal feedback control technique based on method for determining approximate solutions for Hamilton-Jacobi-Bellman equation 23 p3983 A67-40645

Optimal control problem solving by Legendre polynomial expansions and relating function sequence correspondence approximated by finite nonlinear programming 23 p3983 A67-40647

Parameter invariance problem for linear systems solved by obtaining necessary and sufficient conditions for invariance in optimal control systems 23 p3984 A67-41159

Parameter variation of optimal linear control systems with quadratic performance index /Lapapunov 23 p3985 A67-41161

Optimal control systems synthesis using dynamic programming and closed loop system 23 p3985 A67-41671

Inverse problem of synthesizing optimum control for nonlinear systems 23 p3985 A67-41672

Optimal control of maneuver induced vibration in flexible aerospace vehicles 23 p4071 A67-41725

Book on adaptive control and optimization techniques covering basic mathematics, computer methods, differential equations, time domain, etc 24 p4133 A67-41793

Optimum stabilization system for manned space station with asymptotic damping of initial angular momentum 24 p4240 A67-42088

Design of approximately optimal feedback controllers for systems with bounded states 24 p4134 A67-42178

Penalty function approach for inequality constrained optimal control problems 24 p4135 A67-42180

Dynamic programming, deriving successive sweep method for optimal control problems, discussing discrete algorithm for numerical problems 24 p4136 A67-42694

Synthesis of automatic systems optimum in mean noting difficulties arising from no restrictions on control law 24 p4137 A67-42722

Linear optimal control in systems with uncertain parameters, noting application to design of compensating network for flexible booster for uncertain value of first bending mode 24 p4137 A67-42903

OPTIMIZATION

SA BOLZA PROBLEM

SA FLIGHT OPTIMIZATION

SA TRAJECTORY CONTROL

SA TRAJECTORY OPTIMIZATION

Gain optimization for antenna arrays for determination of maximum expected gain and required excitations when finding random errors in amplitudes and phases of excitations 01 p0032 A67-10005

Optimum design safety for VTOL aircraft, noting noise and vibration elimination [AIAA PAPER 66-813] 01 p0008 A67-10031

Optimization of working characteristics of MHD generator as power device 01 p0011 A67-10049

Optimization of directive gain and SNR of arbitrary antenna array with or without constraint on array Q-factor 01 p0035 A67-10431

Overall system performance optimization for specified cost 01 p0170 A67-10630

Optimal subsonic flow diffusers based on

Walz laminar and turbulent boundary layer theory 01 p0006 A67-10648

Direction finder accuracy optimization, considering automatic tracking of target angular coordinates 01 p0024 A67-10721

Optimum frame frequency and virtual exposure coefficient determination for high- and superhigh-speed cameras 01 p0067 A67-10831

Reliability optimization relation to program time and costs and schedule for cost reduction keeping time constant 01 p0085 A67-11384

Optimization of size of film negative for aerial cameras on grounds of economic efficiency 02 p0240 A67-11532

Approximation theory of optimum performance of nonuniformly spaced arrays 02 p0212 A67-11613

Quasi-Newton methods in nonlinear equation solving and unconstrained optimization 02 p0259 A67-11801

Power signal to noise ratios for coherent and noncoherent optical detection, for optimization of optical systems 02 p0243 A67-12058

Continuous linear programming problems with time delays in constraints, noting construction of solutions to dual problem from solution to primal problem 02 p0207 A67-12059

Fuselage optimization for short haul transport aircraft 02 p0181 A67-12199

Least squares gradient method for boundary value and optimization problems found in flight mechanics and astrodynamics 02 p0260 A67-12372

Optimization of display configurations for group viewing 03 p0365 A67-13299

Lagrange multiplier matrix in minimum weight and fully stressed optimum structural design techniques 03 p0525 A67-13966

Optimization of power plant of short range aircraft accounting for high by-pass ratios 04 p0687 A67-14530

Optimal flexure solution for Saint Venant problem in circular cylinder, using Papkovitch-Neuber stress functions [ASME PAPER 66-WA/APM-19] 04 p0714 A67-15410

Information theory assessment of optimizing criteria and approximation for steady state gain of optimum filter, based on Wiener type 04 p0586 A67-15639

Deflection angle of supersonic gas flow with oblique shock wave and heat input in wake, choosing minimum entropy variation as measure of system optimality 04 p0550 A67-15898

Optimal plastic design of minimum cost structural beams with failure under given loads [ASME PAPER 66-WA/APM-22] 04 p0718 A67-15927

Integrated circuit adoption for optimal mixture with remaining discrete devices, particularly gimbal loops 05 p0770 A67-16236

Optimum design of bar profile, considering bending and torsion effect and variation of wall thickness 05 p0916 A67-16242

Numerical procedure for optimizing stability of linear dynamic system by applying steepest descent method 05 p0845 A67-16437

Optimal processes in sampled data control system 06 p0976 A67-18404

Matrix error analysis compared to algorithm optimization problems of numerical analysis [AIAA PAPER 67-142] 06 p1024 A67-18475

Optimal guidance equations for ascent trajectories into circular orbits, developing feedback guidance loop for real onboard control system [AIAA PAPER 67-56] 06 p1029 A67-18495

Gyrostad transfer motion from initial stage to predicted orientation maneuver with minimum consumption, using Pontryagin method 07 p1184 A67-19149

Optimal design of elliptical pumping chambers from numerical calculations containing all geometric sizes of pumping lamps and laser rods and reflectivity of walls 07 p1195 A67-19490

Waveform and filter design for acceptable performance in clutter environment 07 p1145 A67-19880

Effects of unmodeled errors on minimum variance estimators, with application to tracking complex self-calibration estimation scheme

[AAS PAPER 66-107] 07 p1216 A67-19967

Optimization of Saturn vehicle, considering interaction of guidance, control and propellant utilization systems

[AAS PAPER 66-117] 07 p1222 A67-19975

Multiparameter sensitivity index for control systems noting synthesis method for minimization of sensitivity 08 p1309 A67-20329

Optimization of design of input-output matching networks for transistor microwave frequency amplifiers, using computer program 08 p1305 A67-21228

Optimum transformation of linear system with minimal rms error from given point to fixed delta-environment of another given point 08 p1313 A67-21322

Input-output information transfer through correlation function of electromagnetic fields, obtaining optimization of system 09 p1461 A67-21603

Optimization of thermionic diode, with electrical conduction and heat transport represented by differential equations 09 p1448 A67-22336

Book on geometric programming detailing theory of mathematical method for optimizing engineering design 09 p1469 A67-22435

Optimum filtration of signals in presence of arbitrary interference, using orthogonal function series 10 p1607 A67-23443

Optimum microwave filters with even number of sections, using first order Chebyshev polynomial to obtain equivalent circuit 10 p1613 A67-23444

Optimization techniques for linear matched filters to obtain maximum signal to noise ratio for certain signal waveforms 10 p1621 A67-23573

Optimization problem described by differential equations and related to Bellman equation 10 p1675 A67-23681

Computation of optimal estimators synthesis reduced through partitioning of system state vector 11 p1764 A67-24443

Convex polyhedron theorem in determining whole set of optimal solutions in linear programming 11 p1814 A67-24979

Primary illumination laws for parabolic reflector for maximum quality factor determined, considering multimode sources for cold antennas 12 p1913 A67-25307

Variability factors in fabrication of miniature printed glaze resistors and circuits evaluated to obtain optimal process control criteria 12 p1916 A67-25998

SR-N4 hovercraft, optimum size for coastal waters, structural features, performance, control, etc 12 p1895 A67-26168

Nonlinear programming model for launch vehicle design and costing 12 p2013 A67-26193

Optimization of injection location in HF plasma accelerators 13 p2165 A67-26586

Optimal value of target function in optimization theory 13 p2087 A67-26618

Computer analysis, design and optimization of linear electronic networks 13 p2088 A67-26747

Condenser parameter effect on maximum heat transport in heat pipes for nonradiative and radiative cases 13 p2222 A67-26844

Thermal behavior of vehicle entering earth atmosphere at velocities approaching 15 km/sec 13 p2224 A67-27325

Optimum utilization of aerodynamic forces in aircraft maneuvers 13 p2213 A67-27326

Self-adjustable orthogonal digital filters for system identification and optimization 13 p2088 A67-27409

Sufficiency proofs for problem of optimum transversal contour of slender conical body 13 p2051 A67-27457

Effect of unmodeled errors on minimum variance estimators, with application to tracking complex self-calibration estimation scheme [AAS PAPER 66-107] 13 p2154 A67-27525

Optimization of Saturn vehicle, considering interaction of guidance, control and propellant utilization systems [AAS PAPER 66-117] 13 p2155 A67-27532

Optimal methods of escape from helicopter, examining rotor avoidance during ejection 14 p2256 A67-27745

Intermediate-thrust arcs in central force field satisfying optimality conditions, noting that motions are degenerate solutions of Euler equations 14 p2382 A67-27850

Optimum trajectory of pulsed coplanar

orbital transfer in central Newtonian force field with restrictions placed on distance to attracting center 14 p2382 A67-27851

Stationary property of random process approximating anomalous magnetic field, noting optimum filtering 14 p2309 A67-27946

Optimum shape variations of minimum-drag body with given lifting force and volume solved through Euler equations 14 p2239 A67-27983

Optimal structural design with failure probability constraints 14 p2399 A67-28122

Optimum pressure drop in compressed air driven turbine as function of initial pressure in air cylinder and turbine parameters 14 p2252 A67-28652

Feedback control theory for constant temperature hot-wire anemometers using differential equation applied to frequency response optimization 14 p2320 A67-28750

Directivity factor of linear antenna array with Chebyshev radiation pattern 14 p2289 A67-28862

Optimization of system described by differential and finite differential equations when including constraints 15 p2455 A67-29119

Quantizer optimal design for closed-loop dynamic and open-loop static systems 15 p2456 A67-29364

Optimum design safety for VTOL aircraft, noting noise and vibration elimination [AIAA PAPER 66-813] 15 p2419 A67-29411

Optimum system for signal detection with single-band noise modulation during carrier suppression, noting receiving system 15 p2436 A67-29413

Formulation and analysis of class of optimization problems based on contraction mappings in theory underlying dynamic programming 15 p2511 A67-29891

Phase lock techniques applied to microwave antenna arrays noting problems, advantages, properties, etc 15 p2451 A67-29922

Optimization of man-machine environmental interface problems in framework of large-scale and long-term space operations [AAS PAPER 67-80] 15 p2432 A67-29947

Hertz and Mindlin problems for fourth order paraboloids in contact generalized, minimizing microslips and annulus of slip [ASME PAPER 67-APM-12] 15 p2505 A67-30149

Optimization of Brayton cycle consisting of heat source, MPD generator, recuperator, etc, in terms of thermal efficiency and specific power 16 p2603 A67-30562

Optimal maneuvers for space rendezvous between earth satellite and propelled vehicle on circular orbits, studying fuel consumption and rendezvous time 16 p2758 A67-30652

Polynomial substitution formulas for complicated equations of multipoint boundary value and optimization problems in flight mechanics and astrodynamics 16 p2695 A67-30733

Optimal system determination for recognition and separation of useful signal combined with noise nonlinearly 16 p2643 A67-30923

Dollar consequence functions for producer and consumer risks due to product faults noting optimization 16 p2782 A67-31257

Voice modulation effect on phase-lock demodulator for single channel voice communication extending definition of threshold for optimum link design 16 p2629 A67-31529

Optimization of numerical solution to linear ordinary differential equation with homogeneous boundary value conditions 16 p2696 A67-31546

Sampled data feedback control system using quadratic programming to determine optimum compensator 16 p2646 A67-31636

Optimization for linear vibration isolators considering vibration clearance tradeoff for random base motion 16 p2703 A67-31642

Self-optimizing, type-one system design discussing steady state optimization problem 16 p2649 A67-31666

Optimum estimation of linear dynamic systems with stochastic transition and output model matrices, independent from one sample point to next, with known mean and covariance 16 p2652 A67-31693

Computer program for optimizing performance of high resolution airborne

photo-optical recording system using modulation transfer function analysis 16 p2678 A67-31792

Optimum speed capability evaluation of aerial weapons system in relation to value and cost, noting aircraft performance characteristics 16 p2783 A67-31830

Linear programming algorithm for optimizing channel assignments in satellite communication systems 17 p2810 A67-32111

Plasma propulsion for interplanetary flight, discussing optimization of specific impulse, weight distribution and flight path 17 p2928 A67-32226

Linear programming algorithm for optimizing life support systems of space vehicles in terms of minimum weight/efficiency ratio 17 p2807 A67-32254

Multidigit delta modulation system using individual optimized stages developed by successive approximation of message waveform 17 p2812 A67-32319

Hertz and Mindlin problems for fourth order paraboloids in contact generalized, minimizing microslips and annulus of slip [ASME PAPER 67-APM-12] 17 p2871 A67-32411

Mathematical methods of nonlinear programming, discussing convexity, quasi-convexity, gradient, Taylor series and quadratic approximations 17 p2818 A67-32425

Optimum mixer-filter for aircraft navigation systems consisting of inertial platform aided by Doppler and/or Loran designed, using Kalman filtering 17 p2825 A67-32525

Program producing optimum structural design configurations when restrictions on variables and aims of design are given as input data [AIAA PAPER 66-531] 17 p2960 A67-32577

Design criteria for narrow optical passband filters used in reception of nonparallel modulated monochromatic radiation 17 p2862 A67-33291

Optimization of working characteristics of MHD generator as power device 17 p2804 A67-33327

Optimal thrust-weight ratio for lifting engines of VTOL aircraft 18 p3110 A67-33544

Reliability studies for optimization of aerospace systems and military engineering design and manufacture 18 p3053 A67-33637

Selection rigidity and code step optimum parameters for communications channel symmetry 18 p3000 A67-34088

Second, third and fourth order phase locked loops performance characteristics compared for optimum selection, calculating integrated square error and peak error 18 p3001 A67-34116

Maximum shear stress dependence on composite materials microstructure, noting filler and binder role 18 p3069 A67-34170

Symmetrical traveling-wave antenna design with given sidelobe level and amplification factor, determining coupling coefficient and maximum utilization factor 18 p3011 A67-34178

Optimal control methods of Bellman and Pontryagin, discussing maximum rule and dynamic programming for optimization in presence of constraints 18 p3018 A67-34284

Factors degrading reliability in use phase, developing analysis method for determining optimum corrective measures 18 p3057 A67-34667

Optimal discrete filter corresponding to given analog filter for minimum mean square error 19 p3199 A67-34782

Pulse-width modulated control system optimization, with necessary conditions derived by variational calculus, and numerical solution to resulting boundary value problem 19 p3199 A67-34783

Optimal design of RC lines distributed parameter systems using gradient technique and variational calculus 19 p3200 A67-34841

Laser mirror transmissivity optimization in high power optical cavities noting reflection coefficient selection 19 p3241 A67-35701

Minimax fuel requirement of aircraft angular stabilization for undetermined inertial moment probability distribution 19 p3202 A67-35887

Duality method in dynamic optimization problem 19 p3204 A67-35907

Spacecraft performance, operation and design optimization solved by variational analysis [AIAA PAPER 67-557] 19 p3174 A67-35954

Parameter optimization by modified sequential random perturbation technique using hybrid computer, considering initial conditions and analog computer errors effect, for dynamic systems 19 p3188 A67-36058

Variational procedure for sequential decoding scheme with mean error probability dependence on code limitation approximately same as for optimal decoding 19 p3185 A67-36096

Optimal multidimensional systems for discriminating and detecting signals dependent on finite number of random parameters and combined with noise 19 p3185 A67-36097

Integral equations for weight function of optimum filter and correlation function of random absolute error 20 p3408 A67-37040

Optimal geometry of certain isolated heat-conducting circular fins cooled by radiation 20 p3554 A67-37067

Optimum redundancy of multistage parallel systems using variational technique to maximize profit 20 p3556 A67-37316

Wind perturbation effects on performance of radio telescope servosystems, giving method for determining optimal system parameters 20 p3403 A67-37519

Aircraft structural form optimized through changes in geometry 20 p3542 A67-37531

Constrained minimization problem extended to necessary conditions for characterizing noninferior points to determine vector-valued criteria in finite dimensional spaces 20 p3478 A67-37578

Intermodulation due to nonlinearities in transistor amplifiers, discussing design guidelines for optimizing 20 p3404 A67-37634

Optimization problem described by differential equations and related to Bellman equation 21 p3653 A67-38282

Advances in control systems, Theory and applications Volume 5, covering optimal control and optimization advances in control systems, Theory and applications, Volume 5, covering optimal control 21 p3603 A67-38438

Optimum discharge chamber configuration of permanent magnet mercury-bombardment thruster for SERT II mission [AIAA PAPER 67-668] 21 p3691 A67-38702

Optimization analysis for axisymmetric rocket motor nozzle design based on assumptions for gas particle flow [AIAA PAPER 66-538] 21 p3565 A67-38875

Minimum mass bar design for axial vibration of beam with load distribution at specified natural frequency 21 p3728 A67-38890

Graphic optimization technique for mass reduction in solar powered ion propulsion system with acceptable reliability constraint [AIAA PAPER 67-701] 21 p3697 A67-38960

Optimal parameters of transfer function of low thrust power limited engines by approximate solution of differential equation 22 p3898 A67-39181

Book on optimization covering inequality constraints, decomposition strategy, direct methods, etc 22 p3775 A67-39270

Optimal shock absorbers synthesis, showing reduction to variational problem and equations for one degree of freedom mass 22 p3776 A67-39394

Fredholm equation solution and minimax theory for p-dimensional vector signal detection against p-dimensional Gaussian noise background 22 p3762 A67-39876

Manned lifting reentry vehicle optimization using Optimum Compromise between Conflicting Operational Factors /OCCOF/ computer program 22 p3902 A67-39947

Optimization of staged ejector systems noting mathematical model development to represent performance characteristics 22 p3787 A67-40150

Optimum blowing angle of gas into supersonic nozzle determined by supersonic wind tunnel investigation of flow interaction 22 p3743 A67-40452

Optimum relative angular velocity selected for cooled high temperature gas turbine stages, discussing blade mean cooling depth and cooling heat 22 p3870 A67-40456

Blade airfoil sections two-dimensional aerodynamic characteristics studied in wind tunnel for aerodynamic optimization calculation of helicopter rotors 23 p3927 A67-40576

Nonlinear sampled data automatic control

system optimization by statistical method 23 p3985 A67-41673

Optimal output effect for spatial temporal processing of signals in presence of multiplicative and additive signal fluctuations 24 p4120 A67-42232

Systems optimization methodology to analyze radioisotope thermoelectric generators /RTG/ for spacecraft applications, discussing computer program 24 p4184 A67-42504

Analysis of satellite power systems for maximum utilization of power 24 p4108 A67-42540

Optimization of capillary pumping of microgrooved heat pipes, discussing transport equation 24 p4255 A67-42552

Automatic systems optimization, adaptation and learning 24 p4138 A67-42697

Interception satellite thrust and steering optimization for pursuing maneuverable satellite, analyzing both evader and pursuer sides with differential game concept 24 p4182 A67-42908

Efficiency of conical thrust nozzles with various lengths and cone angles, determining optimization coefficient 24 p4093 A67-42922

OPTIMUM THRUST PROGRAMMING

Optimal one-and two-impulse orbital transfer maneuvers, considering shallowly intersecting coplanar orbits 01 p0148 A67-10426

Optimal transfer of finite thrusting vehicle between circular coplanar orbits 02 p0330 A67-12719

Optimal steering and cut-off reflight in orbital transfers, using orbital parameters as state variables for greater accuracy in calculations 05 p0905 A67-16519

Optimum thrust programming for sounding rocket extended by reducing state to single variable to obtain sufficient conditions for specific extremal solution 05 p0906 A67-17225

Minimum fuel transfer between circular or elliptic orbits in central gravitational field 08 p1384 A67-20620

Numerical solution methods for variational problems of flight dynamics 08 p1348 A67-21114

Optimum thrust nozzle contours for chemically reacting gas flows, obtaining set of partial differential equations for gas dynamic properties [AIAA PAPER 66-638] 10 p1592 A67-23118

Book on mechanics of low thrust space flight covering physical principles and generalized characteristics of engine systems, problems in optimization of space vehicles, etc 13 p2211 A67-26460

Determining control functions and choosing parameters governing transfer of dynamic system from initial to final state 16 p2744 A67-30732

Variational problem for optimum acceleration of low thrust vehicle that attains hyperbolic velocity after departure from near circular orbit 16 p2744 A67-30737

Optimal transfers between coplanar and coaxial orbits /any duration/ 16 p2745 A67-30739

Second partial derivatives of position and velocity vectors components developed with respect to same vectors components at arbitrary epoch 16 p2696 A67-30960

Optimum control of space vehicle motion along binormal to circular reference orbit for minimum fuel consumption criterion 17 p2955 A67-32255

Optimum thrust direction for horizontal jet flight of maximum duration determined, using variational calculus 18 p3136 A67-33557

Thrust and drag response to heat input directly behind and before body moving supersonically or subsonically 21 p3563 A67-37887

Optimum consumption of inert mass working fluid in limited discharge velocity engine in terms of final speed gain 21 p3689 A67-37986

Saturn V S-IVB stage propellant slosh amplification minimization at boost thrust termination analysis, simulating slosh wave motion by time varying nonlinear spring-mass model 22 p3903 A67-39970

Thrust history to produce maximum altitude for two-stage launch vehicle determined using simplifying assumptions and atmospheric drag 22 p3904 A67-40089

Thrust staging for optimum thrust program without coasting phase for ascent from low orbit 23 p4071 A67-41314

ORBIT

S ORBITING RADIO BEACON
IONOSPHERIC SATELLITE

ORBIT

S CIRCULAR ORBIT
S EARTH ORBIT
S ELECTRON ORBIT
S ELLIPTICAL ORBIT
S EQUATORIAL ORBIT
S HELIOCENTRIC ORBIT
S HYPERBOLIC ORBIT
S LARMOR ORBIT
S LUNAR ORBIT
S MOLECULAR ORBIT
S PARKING ORBIT
S PERIODIC ORBIT
S PLANETARY ORBIT
S POLAR ORBIT
S SATELLITE ORBIT
S SPACECRAFT ORBIT
S SPIN-ORBIT INTERACTION
S STATIONARY ORBIT
S TRANSFER ORBIT
S TROJAN ORBIT
S TWENTY-FOUR HOUR ORBIT
S TWO-BODY ORBIT

ORBIT CALCULATION

SA AIRBORNE RANGE AND ORBIT
DETERMINATION /AROD/

Orbits, altitudes, viewing geometry,
coverage and resolution pertinent to
satellite observations of earth and
atmosphere 01 p0147 A67-10325

Neptunian planet-satellite system,
discussing orbital motion of
Triton 01 p0148 A67-10385

Orbital 2-1 periodic resonance in
neighborhood of equilateral equilibrium
points of restricted
problem 02 p0321 A67-11497

Satellite orbit calculation using cylindrical
coordinates 02 p0321 A67-11547

Analytic solution in terms of modified
Bessel functions of synergetic turn in
exponential atmosphere, using spacecraft
engines only for drag cancellation and orbit
trimming [AIAA PAPER 66-487] 02 p0331 A67-11938

Minimum initial velocity and
corresponding orbital inclination of satellite
in Keplerian motion 02 p0327 A67-12334
Numerical integration of solar orbit in
model of galactic system 02 p0330 A67-12714

Book of physics and mathematics as
foundation for application of satellites to
geodesy including spherical harmonics,
matrices, orbital geometry, statistical
implications and data analysis 04 p0611 A67-14466

Five-comet probe mission, discussing
velocity requirements for launch from earth
orbit, cometary brightness, weight
requirements and possible carrier
rockets 04 p0695 A67-14532

Onboard guidance scheme as backup to
earth-based orbit determination techniques
and for approach navigation and orbit
correction in planetary capture
maneuver 04 p0654 A67-15234

Satellite orbit inclination, longitude of
ascending node and nodal period obtained
from synchronous
observations 05 p0894 A67-16555

Preliminary analysis of INTEROBS
program observations in Hungary, noting
determination of changes in period of
satellite 05 p0763 A67-16556

Simultaneous visual tracking data reduction
for satellite period 05 p0763 A67-16558

Satellite orbital parameters determined
from visual observations 05 p0894 A67-16559

Satellite orbit major axis determination by
using coincidence of time when satellite
crosses plane of tracking station parallel
with time of crossing topocentric celestial
equator 05 p0894 A67-16560

Satellite trajectory determination through
high accuracy observations, using short
arcs 05 p0894 A67-16561

Orbital elements determination from
reduced Baker-Nunn observations of
satellites, noting disturbance by resonance
effects of earth gravitational potential
sectorial and tesseral
harmonics 05 p0763 A67-16562

Newton-Raphson quasi-linearization applied
to orbit determination from angular data,
range and range rate, noting linear
differential equations controlling
orbit 05 p0894 A67-16563

Perturbed motion of satellite with small

orbital eccentricities 05 p0905 A67-16570

Tracking geometry and dynamics of lunar
satellite, estimating orbital elements and
lunar gravitational field parameters through
earth based range and range rate
observations [AIAA PAPER 66-39] 05 p0902 A67-17207

Eckert-Brouwer orbit correction formula
in general perturbations theory, expressed
in rectangular coordinates and variation of
astronomical elements, applied to planetary
theory 05 p0904 A67-17391

Three-body problem of orbital motion,
examining periodic librations of planetoid
around triangular equilibrium
point 06 p1079 A67-17762

Particle motion in vicinity of triangular
libration point in earth-moon system solved
in form of analytical expressions with time-
dependent coordinates 06 p1079 A67-17763

Long period of nonperiodic librational
motion about equilateral points of restricted
three-body problem 06 p1080 A67-17765

Nonperiodic librational motions in
restricted three-body problem for relatively
elliptic motion of two finite
masses 06 p1080 A67-17766

Kalman filter, modern version of Gaussian
least squares method linear estimation of
orbital elements of celestial
body 06 p0974 A67-17926

Pacific equilibrium longitude for
stationary satellite, discussing processing of
Syncom III data, drift rate calculations, etc
[AIAA PAPER 67-91] 06 p1086 A67-18338

Preliminary circular orbit determination
from single state of range-only data
[AIAA PAPER 67-92] 06 p1088 A67-18501

Modification of Encke perturbation
method for computing satellite orbits,
obtaining integration of motion equations
[AAS PAPER 66-93] 07 p1252 A67-19957

Complete error budget of ballistic flight
orbit prediction including force model error
effects [AAS PAPER 66-106] 07 p1253 A67-19966

State transition partial derivatives for
computing normal matrices in tracking
analysis [AAS PAPER 66-108] 07 p1253 A67-19968

Gravitational field of any primary
determined using observations of satellites
in orbit about primary, noting numerical
integration technique and special
perturbation methods [AAS PAPER 66-109] 07 p1253 A67-19969

Data smoothing, signal processing and
exact minimum mean square error
procedures 07 p1218 A67-20287

Selection of constants defining reference
orbit of planet and use in differential
equations of motion 08 p1382 A67-20394

Reference orbit for integration through
boundaries of activity spheres, replacing six
osculating Keplerian reference
orbits 08 p1383 A67-20590

Rocket maneuvers for rendezvous with
propulsionless target satellite in elliptic
orbit 08 p1410 A67-20640

Manual guidance for interplanetary flight
by graphical methods, nomographs and
relevant general
equations 08 p1352 A67-21104

Restricted problem of three bodies
analyzed using Birkhoff variables and power
series representing motion equations,
obtaining coefficients for collision
orbit 08 p1398 A67-21182

Satellite orbit effect on establishment of
global communications
network 08 p1296 A67-21505

Orbit calculation of 12,500 meteors in
earth vicinity based on radar observations of
radiants and velocities 09 p1563 A67-21635

Elliptic type orbit determination in
generalized problem of two stationary
centers by integration in quadratures of
motion equations of
satellite 09 p1565 A67-21902

Polynomial approximation method for
determining satellite orbits from large-time-
interval trajectory
measurements 11 p1858 A67-24066

Horizon sensor data processing with
compensation for statistical properties of
errors, noting application of optimal filtering
theory 11 p1817 A67-24336

Asymptotic calculation of effect of small
tangential thrust on satellite motion problem
solved for satellite orbit in first and second
approximation 11 p1870 A67-24684

High order tesseral harmonic effects on
satellite orbit calculation 12 p2008 A67-25831
Orbit, luminescence and spectrum of July
5, 1962 bolide orbit, luminescence and
spectrum of July 5, 1962 bolide orbit,
luminescence and spectrum of July 5,
1962 13 p2197 A67-26502

Modification of Encke perturbation
method for computing satellite orbits,
obtaining integration of motion equations
[AAS PAPER 66-93] 13 p2207 A67-27517

Orbit determination of stationary satellites
through data analysis, noting perturbation
effect and estimation of Early Bird satellite
orbit 13 p2208 A67-27522

Complete error budget of ballistic flight
orbit prediction including force model error
effects [AAS PAPER 66-106] 13 p2208 A67-27524

Laser applications to satellite tracking,
orbit calculation and atmospheric
studies 14 p2331 A67-28608

Orbit of Halleys comet integrated ahead to
next apparition /1986/ and predicts time
perihelion passage 15 p2557 A67-29874

Mass point motion in central mass
gravitational field determined from mass
point position and velocity coordinates,
obtaining Kepler orbits 15 p2559 A67-30035

Molniva type communication satellite,
discussing optimum orbital requirements for
maximum coverage, phasing,
etc 16 p2742 A67-30698

Geometric restraints on orbit about Mars
noting trajectories of unmanned Mars
exploration satellite, payload, orbit
inclination, etc 16 p2745 A67-30748

Orbit determination between two radii
vectors with specified periaapsis radius
distance 16 p2746 A67-30959

Birkhoff normalization of Hamiltonian
function in neighborhood of stable
equilibrium position in connection with
Trojan orbits in three-body
problem 16 p2747 A67-30985

Invariant curves dissolution and
nonapplicability of third integrals explained
examining perturbation values and initial
conditions and resonance
phenomena 16 p2748 A67-31140

Advanced range and orbit determination
/AROD/ using airborne equipment to
originate control and tracking signals by
checking ground stations 16 p2701 A67-31491

Satellite orbit calculation using cylindrical
coordinates 16 p2752 A67-31613

Airborne Astrographic Camera System
using meteor orbit theory to observe
reentry trajectory discussing data reduction
theory and photo-optical
instrumentation 16 p2679 A67-31795

Orbital analysis - Conference, London,
October 1966 18 p3125 A67-34234

Luna IX and Luna X near moon, studying
injection phase, orbit and landing phase
from transmitted frequency
observations 18 p3003 A67-34242

Satellite orbit determination, observation,
dynamical theory, perturbations, drag,
computation, etc 18 p3126 A67-34243

Orbit determination from Minitrack
observations, discussing effects of
ionospheric refraction, atmospheric drag and
earth tesseral harmonics 18 p3126 A67-34244

Balloon satellite orbital elements predicted
in advance by computation of solar
radiation, gravitational perturbations,
etc 18 p3126 A67-34246

Low perigee satellite orbit determination
by visual observation, comparing directional
accuracy and orbital elements with Minitrack
and Baker-Nunn 18 p3126 A67-34247

Echo I orbit determined from field-
reduced Baker-Nunn
observations 18 p3127 A67-34248

Economical transfers between Keplerian
orbits in time-free case, considering
hyperbolas, exterior ellipses and launching
orbits [ONERA-TP-482] 18 p3133 A67-34465

Error effect in continuous Kalman filters
used in orbit determination problems,
deriving error bounds
formula 19 p3199 A67-34779

Upper atmosphere rotational speed
determined by analyzing changes in
satellites orbital
inclinations 19 p3216 A67-35182

NASA observations for orbit determination
from Goddard Range and Range Rate system
compared to OGO-B

observations 19 p3319 A67-35216
 Conventional guidance-problem parameters and basic parameters applicable to Surveyor in relation to accuracy of lunar landing 19 p3257 A67-35943
 Orbit determination for Lunar Orbiter, describing computer program and studying Doppler residuals [AIAA PAPER 67-545] 19 p3328 A67-35944
 Orbital evolution of comet Daniel over 400 years, examining approaches to earth and discovery role 20 p3522 A67-36619
 Intersection points for satellite orbit and earth shadow /shadow equation/ solved for small eccentricities by iteration method 20 p3523 A67-36624
 Differential coefficients of asteroids Gerda, Flora and Juno in heliocentric coordinate system including Jupiter and Saturn perturbations 20 p3523 A67-36627
 Spherical coordinates from integration of 20 asteroids differential motion equations including Jupiter, Saturn perturbation and orbital element determinations 20 p3523 A67-36629
 Comet Wolf I orbit evolution over 400 years /1660-2060/, accounting for planetary perturbations and considering secular deceleration 20 p3524 A67-36660
 Possibility of common origin for comets Wolf I and Barnard 20 p3524 A67-36661
 Satellite orbit determination by measuring arrival angle of two transmitted waves with different frequencies 20 p3382 A67-36774
 Electronic satellite position and motion measurement for satellite geodesy, with rapid data reduction, day-night capability and optical accuracy 20 p3383 A67-36889
 Satellite orbit adjustment, stationkeeping and attitude control of typical earth-and sun-synchronous satellites by electric propulsion systems [AIAA PAPER 67-719] 21 p3694 A67-38745
 Definitive orbit of comet Pereyra derived from positional observations 21 p3707 A67-38963
 Spacecraft ephemeris, orbit compatibility and scheduling in AAP mission experiments 22 p3885 A67-39959
 Pacific equilibrium longitude for stationary satellite, discussing processing of Syncom III data, drift rate calculations, etc [AIAA PAPER 67-91] 22 p3886 A67-40085
 Soviet book on motion of artificial satellites in earth gravitational field covering perturbation theory, force field, algorithms for calculations, etc 23 p4063 A67-40734
 Satellite rise and set time of distant primary and occultation interaction determined for case of Martian satellite 24 p4238 A67-42925

ORBIT DECAY
 Satellites in near-circular decaying polar orbits experience drag forces at equatorial latitudes greater than those at polar latitudes 04 p0706 A67-15233
 Orbital decay, considering drag force expression, motion equation, atmospheric structure, King-Hele theory, etc 06 p1081 A67-17786
 Equations of motion for earth satellite indicate greater significance for atmospheric resistance than gravitational effect 06 p1083 A67-18040
 Semiannual effect on satellite orbit decay, correlating with difference in latitude between perigee and subsolar point 07 p1251 A67-19850
 Upper atmosphere density determined from satellite braking 08 p1325 A67-21002
 Earth aerospace thermodynamic properties from 100 to 100,000 km alt predicted, considering diurnal and extreme solar activity variations for engineering applications 13 p2114 A67-26821
 Satellite orbit analysis and computer program for earth zonal harmonics determination, considering orbit elements and gravitational constants [AAS PAPER 66-91] 13 p2116 A67-27516
 Upper-atmosphere density determination methods, with comparison of orbital decay and instrument 18 p3041 A67-34254
 Multiphonon orbit-lattice relaxation of lower lying excited states of Dy doped lanthanum chloride investigated, using IR fluorescence and quantum counter techniques 19 p3302 A67-35035
 Satellite earth crashing time and place calculated, providing observation

possibilities 19 p3184 A67-35831
 Elliptic geocentric satellite orbit for measurements of magnetosphere-nearby space region, analyzing orbital lifetimes and perturbations [AIAA PAPER 67-616] 19 p3226 A67-36005
 Alouette I and Explorer XX /S-48/ spin behavior explained by solar heating of antennas and solar radiation pressure 21 p3712 A67-37784

ORBIT EQUATION
 Case of integrability of equations of perturbed motion of satellite under action of Newtonian force 01 p0151 A67-10994
 Exact solutions in theory of orbits using Hamilton-Jacobi and Laplace equations 05 p0903 A67-17294
 Satellite motion for all inclinations around oblate planet with potential including second and fourth zonal harmonics 08 p1382 A67-20396
 Solution of motion equations for lunar satellites in near equatorial plane using transformation of variables 08 p1383 A67-20582
 Equations describing orbital plane rotation of satellites, noting analogy between equations for oscillations of mechanical system with one degree of freedom 09 p1584 A67-21887
 Optimum trajectory of pulsed coplanar orbital transfer in central Newtonian force field with restrictions placed on distance to attracting center 14 p2382 A67-27851
 Optimal interorbital transfers between near-circular noncoplanar closely spaced orbits described in terms of linearized theory 15 p2563 A67-30389
 Three-dimensional periodic motion about collinear Lagrangian equilibrium points, determining motion, variational and orbit equations and numerical integration 22 p3889 A67-40427

ORBIT PERTURBATION
SA SATELLITE PERTURBATION
 Levi-Civita regularized equations of elliptic motion of particle influenced by massive primary and perturbed by smaller primary, Part I, Trigonometric series solution 01 p0147 A67-10379
 Levi-Civita regularized equation of elliptic motion of particle influenced by massive primary and perturbed by smaller primary, Part II, Applications to circular and collision orbits 01 p0147 A67-10380
 Existence of class of quasi-periodic solutions of three-body problem for near-circular inclined planetary and lunar orbits, Part I 01 p0148 A67-10382
 Orbital resonance caused by tesseral harmonics, examining perturbations of synchronous satellite in eccentric orbits 02 p0328 A67-12400
 Perturbed trajectories computation in earth-moon system by replacing gravitational forces with single inverse square force 02 p0330 A67-12717
 Aperiodic motion of two bodies of variable mass across canonical cross section, constructing osculating orbit and deriving equations for variation 04 p0700 A67-15202
 Eckert-Brouwer orbit correction formula in general perturbations theory, expressed in rectangular coordinates and variation of astronomical elements, applied to planetary theory 05 p0904 A67-17391
 Orbit position control based on solar pressure on plane sail structure and hollow thin-skinned lenticular shape of passive communications satellites [AIAA PAPER 66-313] 06 p1094 A67-17703
 Orbit perturbation induced by omitting certain harmonics in expansion of earth gravity potential, evaluating covariance integrals [AIAA PAPER 67-93] 06 p1084 A67-18278
 Satellite under perturbing acceleration having constant modulus and directed along normal to osculating plane of orbit, calculating rotation of orbital plane 06 p1088 A67-18620
 Lunar gravitational field and effect on motion of lunar satellite 08 p1395 A67-21163
 Perturbation of lunar satellite due to lengthening of one of lunar axes 08 p1396 A67-21164
 Motion of lunar satellite, noting principal perturbations due to nonspherical lunar gravity and earth attraction, considering moon libration and solar small

forces 08 p1397 A67-21184
 Orbital behavior and stationkeeping propulsion requirements for synchronous satellites, considering solar radiation and earth oblateness effects 09 p1571 A67-21697
 Orbital disturbances of satellite produced by zonal harmonics of gravitational field 09 p1584 A67-21884
 Orbit perturbations due to tesseral harmonics contained in series expansion of gravitational potential determined using computer program 09 p1467 A67-21885
 Orbit determination of stationary satellites through data analysis, noting perturbation effect and estimation of Early Bird satellite orbit 13 p2208 A67-27522
 Approximate analytical solution for satellite circular orbits subjected to small tangential thrust or drag 14 p2384 A67-28117
 Evolution of short-period comet orbits /1660-2060/ taking into account perturbing effects of outer planets 15 p2552 A67-29154
 Cometary orbit evolution of Jupiter family, considering influence of Jupiter 15 p2553 A67-29155
 Lunar communications using satellites in astrodynamical aspects of lunar orbital stability and effective communications zone 16 p2622 A67-30730
 Secular and periodic perturbations of orbits of artificial satellites of earth and moon by attraction of external bodies 16 p2746 A67-30981
 Heliocentric orbits of former Jupiter satellites, relating direct or retrograde satellite to heliocentric semimajor axis as asteroid 17 p2946 A67-32754
 Solar wind perturbation of uncharged interplanetary dust particle orbits, calculating particle lifetime 17 p2951 A67-33234
 Orbit determination from Minitrack observations, discussing effects of ionospheric refraction, atmospheric drag and earth tesseral harmonics 18 p3126 A67-34244
 Satellite orbit perturbations in theories determining earth gravitational field, observing relation to departures from Keplerian ellipse 18 p3041 A67-34249
 Satellite orbit perturbation analysis for lunar gravitational field determination using von Zeipel transformation 18 p3131 A67-34325
 First order perturbation solution for transition matrix relating errors at one point of two-body orbit to errors at later point 19 p3317 A67-34832
 Elliptic geocentric satellite orbit for measurements of magnetosphere-nearby space region, analyzing orbital lifetimes and perturbations [AIAA PAPER 67-616] 19 p3226 A67-36005
 Atmospheric drag influence on orbital elements of satellites having highly eccentric orbits 20 p3522 A67-36616
 Differential coefficients of asteroids Gerda, Flora and Juno in heliocentric coordinate system including Jupiter and Saturn perturbations 20 p3523 A67-36627
 Spherical coordinates from integration of 20 asteroids differential motion equations including Jupiter, Saturn perturbation and orbital element determinations 20 p3523 A67-36629
 Cometary astronomy problems from contemporary celestial mechanics viewpoint, considering short-period comets and orbital perturbations caused by Jupiter 20 p3524 A67-36658
 Comet Wolf I orbit evolution over 400 years /1660-2060/, accounting for planetary perturbations and considering secular deceleration 20 p3524 A67-36660
 Possibility of common origin for comets Wolf I and Barnard 20 p3524 A67-36661
 Janus /Saturn tenth satellite/ discovery on December 15, 1966, noting orbit in ring plane and period 20 p3527 A67-37399
 Orbit perturbation induced by omitting certain harmonics in expansion of earth gravity potential, evaluating covariance integrals 21 p3700 A67-37785
 Upper atmosphere angular velocity determined from changes in satellite orbital inclinations, noting increase with height 21 p3619 A67-38512
 Circular orbit stability in planetary axisymmetric gravitational and dipole magnetic fields 22 p3880 A67-39404
 Shape of earth studied for irregularities other than flattening at poles as revealed by perturbation of artificial satellite

- orbits 22 p3792 A67-39894
 Solar radiation pressure perturbations on large planar reflector satellite orbit 22 p3903 A67-39953
 Scaled Unsöld approximation for Hartree-Fock function in perturbation expansion 23 p4030 A67-40977
 Relation between earth-moon orbital inclinations indicates incompatibility of dynamical figures with assumptions of hydrostatic equilibrium and homogeneous density distribution 24 p4229 A67-42320
 Terrestrial gravity anomalies influence on satellite orbits treated by analytical numerical integration 24 p4237 A67-42686
 Evolution of short period comet orbits /1660-2060/ taking into account perturbing effects of outer planets 24 p4239 A67-43077
 Cometary orbit evolution of Jupiter family, considering influence of Jupiter 24 p4240 A67-43078
- ORBITAL ASSEMBLY**
 Systems application in orbital launch operations [AIAA PAPER 66-908] 03 p0519 A67-14132
- ORBITAL CALCULATION**
 Satellite orbit computation program with element representation based on drag-free perturbation theory coupled with differential correction procedure 08 p1383 A67-20403
 Titan III system capability for space support and logistics, discussing parameters of assessment 08 p1412 A67-21076
 Elliptic restricted three-body problem solved for eigenvalues and orbital series solutions of Lagrangian triangular point 08 p1397 A67-21214
 Periodic comet observation methods and orbital results 10 p1705 A67-29226
 Independent cometary orbit correction permitting checkout of initial coordinate and velocity components 11 p1868 A67-25084
 Rate of satellite turn in elliptical orbit calculated by introducing nondimensional angle, deriving master curves, noting applicability to attitude control systems 12 p2000 A67-25124
 Earth gravitational field eccentricity effect on deviation of satellites from Kepler ellipse orbits 13 p2200 A67-27322
 Orbiting navigation with compensation for periodic errors, using modified Kalman filtering technique 15 p2513 A67-29595
 High altitude satellites orbital curves, considering moon effect 15 p2560 A67-30044
 Satellite visibility calculation for individual ground stations of telemetry and tracking network as function of orbital injection parameters 15 p2561 A67-30047
 Heliocentric dust cloud noting correlation of meteor and comet model with observations 17 p2842 A67-32325
 Smithsonian Astrophysical Observatory Differential Orbit Improvement program for lunar orbits, with selenocentric reference system 18 p3132 A67-34327
 Lambert theorem used to find required trajectory to effect rendezvous in space 19 p3332 A67-34828
 Digital computer simulation of orbital launch window problem for departure-trajectory analyses [AIAA PAPER 67-615] 19 p3329 A67-36004
 Autonomous solution to orbital navigation problem yielding direct measure of orbital parameters 22 p3830 A67-39179
 Optimal filtering theory for horizon sensor data processing for orbital navigation, examining statistical characteristics 22 p3834 A67-40196
- ORBITAL ELEMENT**
 Orbital elements of satellite determined from three position coordinates and three velocity components 01 p0149 A67-10788
 Variant of analytical determination /in terms of osculating-orbit elements/ of moments of entry into and emergence from earth shadow of artificial satellite 02 p0321 A67-11548
 Dynamical effect of explosive phenomena in comet Halley and nuclear rotation based on 1909-1911 observations 04 p0694 A67-14469
 Improvement of orbital elements of comet Grigg-Skjellerup, using all observations made during previous appearances 04 p0701 A67-15451
 Tungusk comet trajectory and orbit with radiant in constellation Cetus 05 p0889 A67-16210
 Perturbations of satellite orbital elements caused by pressure of solar radiation reflected from earth 05 p0894 A67-16566
 Zonal harmonics determination through satellite observations processed using computer program, noting necessity for increased number of satellites [AAS PAPER 66-91] 07 p1183 A67-19956
 Motion of near lunar satellite in initially circular orbit analyzed by integrating equations for time rates of change of orbit elements [AAS PAPER 66-95] 07 p1252 A67-19959
 Isotropic mass loss effect on binary star system orbital elements and period eccentricity relationship 08 p1380 A67-20385
 Asymmetric distribution of asteroids in heliocentric latitude and longitude 10 p1705 A67-22894
 Proposal for computation of unknown parts of gravitation field of earth from successive satellite passages 10 p1636 A67-23180
 Independent cometary orbit correction permitting checkout of initial coordinate and velocity components 11 p1868 A67-25084
 Meteor orbital elements according to photographic observations 13 p2196 A67-26496
 Geocentric orbital elements determined from quasi-simultaneous direction observations to satellites 13 p2199 A67-26852
 Motion of near lunar satellite in initially circular orbit analyzed by integrating equations for time rates of change of orbit elements [AAS PAPER 66-95] 13 p2207 A67-27519
 Planetary masses, radii and orbital element and astronomic unit determinations from radar time delay and Doppler shift measurements 15 p2556 A67-29871
 Orbit of Halleys comet integrated ahead to next apparition /1986/ and predicts time perihelion passage 15 p2557 A67-29874
 Computational method for high altitude atmosphere density, orbital elements, drag coefficients and potentials from satellite displacement and velocity measurements 15 p2562 A67-30069
 Variant of analytical determination /in terms of osculating-orbit elements/ of moments of entry into and emergence from earth shadow of artificial satellite 16 p2752 A67-31614
 Injun III rocket orbital parameters determined by optical and radar observations to provide inclination values for studying upper atmosphere rotational speed 17 p2952 A67-33251
 Balloon satellite orbital elements predicted in advance by computation of solar radiation, gravitational perturbations, etc 18 p3126 A67-34246
 Determination of Love number of earth from variations of orbital inclinations of satellites 18 p3041 A67-34250
 Air drag effect on six Cosmos satellites orbits having low perigee, discussing diurnal air density variation at 280 km height 18 p3042 A67-34256
 Atmospheric drag influence on orbital elements of satellites having highly eccentric orbits 20 p3522 A67-36616
 Corrected orbital data for 60 minor planets, giving osculating elements for asteroids 20 p3522 A67-36618
 Orbital evolution of comet Daniel over 400 years, examining approaches to earth and discovery role 20 p3522 A67-36619
 Artificial earth satellite orbital element accuracy, describing least squares method of choosing time intervals for reducing errors 20 p3523 A67-36625
 Spherical coordinates from integration of 20 asteroids differential motion equations including Jupiter, Saturn perturbation and orbital element determinations 20 p3523 A67-36629
 Distribution asteroids in space studied by computer analysis from selected plots of orbital elements 20 p3524 A67-36654
 Optical determination accuracy of satellite orbits, investigating orbit elements by Gaussian averaging calculation assuming elliptical orbit 22 p3830 A67-39161
 Orbital element periodic variations for satellite motion about oblate planet with low and moderate eccentricity 22 p3880 A67-39313
 Soviet ephemeris of minor planets for 1968 covering orbital elements, opposition dates, time, etc 22 p3884 A67-39925
 Orbital elements and motion equations of periodic comet Harrington for five perihelion times before 24 p4226 A67-41964
- discovery 24 p4226 A67-41964
 Motion equations for mean orbital and osculating elements of particle rotating in gravitational field of aspherical planet 24 p4228 A67-42274
- ORBITAL LAUNCH**
 Systems application in orbital launch operations [AIAA PAPER 66-908] 03 p0519 A67-14132
 Unmanned Jupiter space flights, discussing requirements for flyby, Orbiter and low thrust missions 07 p1249 A67-19570
 Optimization of extra-atmospheric phase of orbital ascent by assumption of certain hypotheses concerning atmosphere transit cost and nonnegligible-aerodynamic atmosphere thickness 17 p2946 A67-32695
 Diamant satellite series, describing design and construction of Diapason and Diadem orbital satellites 17 p2956 A67-32746
 Spacecraft in lunar exploration by type and properties, emphasizing soft landing and orbiting mooncraft 20 p3526 A67-37249
- ORBITAL MECHANICS**
 Graphical methods for solutions to orbital mechanics problems involving equations derived from Newton and Kepler laws 05 p0901 A67-17206
 Topology of three-dimensional integral surface projection of section of energy integral by third integral 08 p1380 A67-20382
 Lunar orbit evolution caused by tidal friction in earth and moon interiors 09 p1563 A67-21634
 Optimum control of earth satellites and space vehicles and stable solutions of orbits in orbital mechanics 14 p2393 A67-27879
 Optimal interorbital transfers between near-circular noncoplanar closely spaced orbits described in terms of linearized theory 15 p2563 A67-30389
 Echo I orbit determined from field-reduced Baker-Nunn observations 18 p3127 A67-34248
 Von Zepel method and Hamiltonian perturbation mechanics used for orbits at resonance with tesseral harmonics of geopotential 19 p3328 A67-35959
 Artificial satellite motion determination of external earth gravity field compared with surface measurements, orbit theory, etc 20 p3432 A67-37205
 Book on astronautics covering rocket theory, celestial mechanics and space problems 21 p3703 A67-38434
 Matrix method to calculate energy eigenvalues and orbital wave functions for various singlet states of helium isoelectronic sequence 22 p3841 A67-40202
- ORBITAL MOTION**
 Comet orbits classification noting distributions of eccentricities, inclinations and perihelion ecliptic coordinates 01 p0146 A67-10232
 Effect of meridional wind on satellite orbit inclination 01 p0146 A67-10255
 Cometary motion in outer solar system region, taking galactic nucleus as perturbing body 01 p0151 A67-11286
 Stability in the sense of Liapunov, Poincare, Lagrange and others for dynamical systems 02 p0268 A67-12502
 Resonance phenomena associated with small divisor in third integral of orbital motion 03 p0457 A67-13164
 Kinetic moment in celestial mechanics, noting application to satellite orbit determination in terrestrial gravitational field 03 p0510 A67-13456
 Motion of satellite inside resisting atmosphere 04 p0696 A67-14737
 Ascent or descent from initially Keplerian orbit by constant low thrust analyzed by two-variable expansion procedure 04 p0704 A67-14828
 Early Bird hydrogen peroxide control system maneuvers to place satellite into final stationary position 06 p1093 A67-17663
 Long period features of motion of Trojan planets in vicinity of equilateral triangle configurations 06 p1079 A67-17764
 Restricted problem of three bodies, two of which are assumed to be point masses, determining motion of third body 06 p1081 A67-17779
 Qualitative methods in n-body problem concerned with masses motion in inertial space under gravity, solving motion equation 06 p1081 A67-17781
 Geos A space vehicle, discussing orbital motion, instrumentation and

- operation 07 p1259 A67-19759
U.S. Passive Geodetic Satellite, describing fabrication, structural integrity, flight preparation, launch, etc 07 p1259 A67-19760
Dynamic behavior of large flexible bodies in orbital motion around gravitating center, emphasizing response and stability of elastic degrees of freedom 08 p1383 A67-20562
Earth rotational and orbital motions interrelated by Loitsianskii theorem for turbulent fluid motion 12 p1932 A67-25190
Second order solutions to motion equations governing satellite rendezvous in elliptical orbit 12 p2012 A67-25931
Nonlinear correction method for determining orbital parameters of space vehicle, using residuals and least squares technique 14 p2384 A67-28127
Spinor representation of energetic identities of Kepler motion, showing identity of Lambert theorem for position triangle and Stumpf theorem for velocity triangle 15 p2561 A67-30054
Rotational analysis theorem concerning earth satellite motion about angular-momentum vector with respect to inertial reference frame 15 p2519 A67-30209
Deviation of path of orbiting body calculated from nominal or reference trajectory 16 p2744 A67-30729
Material elasticity effects on planar librational motion of rigid satellite under action of gravity 16 p2761 A67-30743
Finite collision time for artificial celestial body moving under influence of Newtonian force from attractive center 16 p2745 A67-30744
Orbits and trajectories for plane motion of material point in conservative field of force 16 p2748 A67-31138
Aerocruise maneuver for optimizing orbital plane change with respect to cruise speed 20 p3532 A67-36552
Motion theory of comet Wolf I during 1918-1925 revolution which included close approach to Jupiter in 1922 20 p3524 A67-36659
Comet Wolf I orbit evolution over 400 years /1660-2060/, accounting for planetary perturbations and considering secular deceleration 20 p3524 A67-36660
Probability characteristics of osculating satellite motion, considering random parameter scatter and atmospheric density variations, with expectation obtained by numerical integration 20 p3485 A67-36922
Energy accumulator and constant power propulsion system for near-circular orbit space maneuvering, considering two-vehicle encounter 21 p3689 A67-37985
Differential correction vectors for non-Keplerian reference orbits, reexamining rotating ellipses in Hansen type intermediaries 21 p3705 A67-38612
Optimal flexible strategies for pulsed correction of close-to-nominal space vehicle trajectory, using fuel reserve limitation criterion 22 p3878 A67-39186
Triaxial orbital orientation control algorithm for space vehicle with incomplete angular position information 22 p3899 A67-39191
Protogalactic survival during metagalactic formation due to favorable orientation of equatorial planes to orbital planes 22 p3894 A67-40511
Corrected derivation of earth-moon mass and various astronomical constants from Eros orbital motion 23 p4061 A67-40620
Numerical integration of Eros orbital motion normals, obtaining earth-moon mass and various astronomical constants 23 p4061 A67-40621
Nongravitational effects in Halley comet motion and arbitrarily rotating comet nucleus model, noting push-effect hypothesis 23 p4062 A67-40672
Nongravitational and splitting effects in comet motion and rotating comet nucleus model, using push-effect hypothesis for post-explosion analysis nongravitational and splitting effects in comet motion and rotating comet nucleus model, using 23 p4062 A67-40673
Discretization error analyzed for accumulation during numerical solution of equations of orbital motion 23 p4023 A67-40864
Jacobi high energy ellipsoid orbits in barred spirals valid at galactic time scales 23 p4063 A67-40898
Time reversible difference procedures including Lorentz and continuity equations, relativistic orbits and gyrocenter motion 23 p4027 A67-40996
Spurious nucleus behind solid 1910 Halley Comet nucleus hypothesized as explanation for anomalous positional residuals 23 p4065 A67-41001
Orbital elements and motion equations of periodic comet Harrington for five perihelion times before discovery 24 p4226 A67-41964
ORBITAL RENDEZVOUS
SA EARTH ORBITAL RENDEZVOUS /EOR/
SA LUNAR ORBITAL RENDEZVOUS /LOR/
SA SPACECRAFT ORBITAL RENDEZVOUS
Rendezvous maneuver between vehicle and target in free orbital flight in central gravitational field, deriving low acceleration program for elliptical target orbit 01 p0152 A67-10208
Evasive guidance and maneuvering during terminal phase of co-orbital rendezvous 02 p0330 A67-11926
First orbit rendezvous mission planning with no ground support after spacecraft liftoff, considering propellant costs, procedural timing, terminal approach, etc 02 p0333 A67-12343
Optimal tradeoff function where expense is increased for saving time in orbital transfer to rendezvous, considering impulse modes 02 p0328 A67-12407
Requirements of economical and effective orbital logistics support system [AIAA PAPER 66-863] 03 p0519 A67-14129
Gemini program evaluation, discussing information gained from experiments performed during flights [AIAA PAPER 66-1027] 04 p0704 A67-14979
Finite thrust explicit guidance law for nearly circular orbital rendezvous 05 p0906 A67-17208
Gemini rendezvous experience, describing flight test cycles, type of maneuvers needed, ground and onboard support systems, etc [AIAA PAPER 67-272] 07 p1260 A67-20081
Optical ranging technique for orbital rendezvous with manual checking of automatic equipment 09 p1527 A67-22395
Rendezvous between spacecraft and target flying in elliptic orbit of arbitrary eccentricity solved, using new approach [AIAA PAPER 66-537] 14 p2394 A67-28115
Set of linearized motion equation for ferry vehicle to obtain optimal-thrust during rendezvous attempt with orbital satellite 15 p2571 A67-30049
Accuracy of satellite orbit prediction for rendezvous mission related to ground-based tracking network sensors by digital computer simulation 15 p2441 A67-30165
Optimal maneuvers for space rendezvous between earth satellite and propelled vehicle on circular orbits, studying fuel consumption and rendezvous time 16 p2758 A67-30652
Requirements of economical and effective orbital logistics support system [AIAA PAPER 66-863] 19 p3331 A67-34809
Manual control stationkeeping simulation, studying tether visual rendezvous techniques and fuel economy [AIAA PAPER 67-617] 19 p3337 A67-36006
Mass optimal trajectory problems with variable endpoints solved using initial and terminal coasting arcs 22 p3884 A67-39955
Adaptive terminal guidance scheme for circular orbit rendezvous to provide near optimal trajectory 22 p3832 A67-39964
Two-finite burns minimum fuel rendezvous problem using dual phase plane description, determining control law 22 p3888 A67-40147
ORBITAL SIMULATOR
SA HIGH VACUUM ORBITAL SIMULATOR /HIVOS/
Scheduling and simulation of manned orbital operations using modular system of computer programs [AIAA PAPER 66-907] 02 p0230 A67-12249
Optimal temperature control design using IBM 7094 digital computer program for thermal environment simulation of stabilized multisurfaced earth-orbiting spacecraft structure [ASME PAPER 66-WA/HT-44] 04 p0724 A67-15430
Computer programming to predict performance of complex orbit navigation systems using simulation of landmark visibility from orbit as model 09 p1467 A67-21832
Numerical analysis and programming techniques for orbit determination 09 p1467 A67-21835
Apparatus for simulating spatial turn in artificial satellite and feasibility of developing turns in near-earth space by applying force perpendicular to orbital plane 09 p1484 A67-22095
Thermal gradients on surface of orbiting cylindrical stabilization boom determined, using computer simulation of earth orbital environment 16 p2764 A67-30957
Biaxial satellite motion simulator for large space-simulation chamber, discussing temperature and pressure simulation 18 p3021 A67-34611
ORBITAL SPACE STATION
SA MANNED ORBITAL SPACE STATION /MOSS/
Space station operations in navigation and tracking, communication coverage, abort recovery, etc 12 p2012 A67-25743
Integrated launch/reentry vehicle reusability via tip tank concept 15 p2567 A67-29837
Design requirements for commercial orbital space stations intended for weather forecasting, agricultural prediction and industrial research [AAS PAPER 67-113] 15 p2557 A67-29961
Design and operation of orbital space station, determining orbit altitude, payload weight, tracking and communication system support requirements, recovery operations, etc 16 p2761 A67-30961
Orbiting Energy Depot, discussing fuel regeneration and resupply to enable use of fuel cells combined with nuclear power as main onboard power 22 p3902 A67-39948
Multi-kilowatt photovoltaic power system design for manned earth orbital mission 24 p4104 A67-42511
Materials development and testing in orbiting laboratory noting zero gravity benefits [AIAA PAPER 67-815] 24 p4139 A67-42969
Manned orbiting space station operation in association with unmanned observatory, comparing gimbal mounted, free floating, tethered and firmly fixed modes [AIAA PAPER 67-926] 24 p4245 A67-43022
ORBITAL TRANSFER
SA HOHMANN ORBITAL TRANSFER
SA IMPULSE ORBITAL TRANSFER
Deterministic optimal control, discussing Bellman dynamic programming method, Pontryagin maximum principle, orbital transfer, interplanetary guidance, etc 01 p0047 A67-11220
Optimal transfer between hyperbolic orbits in Newtonian field of attraction of heavy sphere of nonzero radius 01 p0152 A67-11411
Maneuvering-range constraints effects on lifting-vehicle design parameters as velocity increments, propellant consumption, heating rates and acceleration tolerance [AIAA PAPER 66-961] 02 p0332 A67-12288
Flight path control in software system for Lunar Orbiter, discussing optimization program for midcourse aim point and lunar injection point 02 p0265 A67-12382
Necessary conditions for optimal fixed-time powered transfers with multiple coasts and thrusts between circular orbits 02 p0328 A67-12402
Optimal tradeoff function where expense is increased for saving time in orbital transfer to rendezvous, considering impulse modes 02 p0328 A67-12407
Optimal transfer of finite thrusting vehicle between circular coplanar orbits 02 p0330 A67-12719
Lifting reentry vehicles for achieving orbital plane changes by synergistic maneuvers [AIAA PAPER 66-960] 03 p0520 A67-14141
Orbital transfer by hyperbolic encounter maneuver in perturbed gravity fields 04 p0895 A67-14541
Comparison of performance of atom-ion and colloidal thruster systems for orbital transfers, noting influence of various parameters on mission capabilities 04 p0688 A67-14560
Optimal interorbital transfer between

elliptical orbits in central Newtonian force field analyzed in terms of minimum characteristic velocity 05 p0886 A67-16047

Plane problem of optimum interorbital transfer in central Newtonian force field, classifying initial orbits and transfer trajectories 05 p0886 A67-16048

Optimal steering and cut-off reight in orbital transfers, using orbital parameters as state variables for greater accuracy in calculations 05 p0905 A67-16519

ELDO-PAS configuration consisting of fourth-stage addition to three-stage Europa I launcher, with apogee motor integrated in satellite, for telecommunications 06 p1093 A67-17557

Rendezvous problem of ascent and injection into transfer orbit and terminal phase 06 p1082 A67-17790

Numerical method solution of nonlinear two-point boundary value problem associated with optimum transfer of spacecraft [AIAA PAPER 67-58] 06 p1023 A67-18267

Optimal coplanar orbit transfer treated by Contensou-Busemann approach with metric tensor completed by smallest possible convex hull 06 p1090 A67-18886

Optimum energy transfer from hyperbolic orbit in Newtonian central force field in absence of transfer time limitations 07 p1247 A67-19094

Plane optimum transfer of point of variable mass between two elliptical orbits in centrally directed Newtonian force field 07 p1247 A67-19095

Orbital change problems using Busemann configuration space combined with geometrical properties inherent to Keplerian orbits

[AAS PAPER 66-122] 07 p1254 A67-19981

Transfer from elliptical orbit to coplanar hyperbolic asymptote treated in terms of limited classes of one-and two-impulse maneuvers

[AAS PAPER 66-127] 07 p1255 A67-19986

Interplanetary trajectories for vehicles using high and low thrust propulsion systems, considering three two-body transfers and role of hyperbolic excess speeds

[AAS PAPER 66-128] 07 p1241 A67-19987

Abort velocity requirements for three-burn transfer maneuver out of lunar polar orbit

[AAS PAPER 66-133] 07 p1255 A67-19992

Minimum fuel transfer between circular or elliptic orbits in central gravitational field 08 p1384 A67-20620

Expressions showing possibilities to change independently all orbital elements of spacecraft by means of small continuous thrusts achieved through electric propulsion 08 p1413 A67-21365

Optimal transfer of thrust limited vehicle between coplanar circular orbits 09 p1571 A67-21694

Rendezvous between coplanar circular orbits, comparing Hohmann transfer with simple bielliptic method 09 p1564 A67-21695

Optimization in terms of energy expenditure of problem of interorbital one- and two-pulse satellite transfer in central gravitational field 09 p1564 A67-21888

Tunguska meteorite transfer from heliocentric to geocentric orbit proved impossible by computer calculation 11 p1868 A67-24847

Computer iteration scheme for calculating arbitrary hyperbolic transfer orbit in field of attracting center, based on Gaussian equations 12 p2002 A67-25640

Maneuvering-range constraints effects on lifting-vehicle design parameters as velocity increments, propellant consumption, heating rates and acceleration 13 p2212 A67-26829

Lifting reentry vehicles for achieving orbital plane changes by synergetic maneuvers

[AIAA PAPER 66-960] 13 p2212 A67-26846

Interplanetary trajectories for vehicles using high and low thrust propulsion systems, considering three two-body transfers and role of hyperbolic excess speeds

[AAS PAPER 66-128] 13 p2214 A67-27539

Euler-Lambert equation for orbital transfer in Newtonian field solved by approximate method 14 p2383 A67-27865

Nongeometric derivation of solution equations for cotangential orbital

transfer 14 p2384 A67-28134

Space vehicle optimal control, studying maximum principle application, developing numerical algorithms of dynamic programming type and describing variational problems 16 p2742 A67-30664

Minimum-fuel transfers of moving body between infinitely close elliptical Keplerian orbits in central Newtonian field, considering propulsion system models 16 p2744 A67-30738

Optimal transfers between coplanar and coaxial orbits /any 16 p2745 A67-30739

Meteoritic satellites of earth, estimating capture region dimensions 17 p2941 A67-32324

Economical transfers between Keplerian orbits in time-free case, considering hyperbolas, exterior ellipses and launching orbits

[ONERA-TP-482] 18 p3133 A67-34465

Comparison of performance of atom-ion and colloidal thruster systems for orbital transfers, noting influence of various parameters on mission capabilities 20 p3515 A67-36407

Variable thickness insulation system for transport of hydrogen propellant into earth orbit for docking transfer to lunar and interplanetary mission vehicles

[ASME PAPER 67-HT-50] 20 p3548 A67-36732

Optimal interorbital transfer between elliptical orbits in central Newtonian force field analyzed in terms of minimum characteristic velocity 21 p3701 A67-37834

Plane problem of optimum interorbital transfer in central Newtonian force field, classifying initial orbits and transfer trajectories 21 p3701 A67-37835

Eigenstate variables for representation of optimum orbital transfer problems, discussing numerical integrations 22 p3878 A67-39154

Satellite maneuverability in orbit using hypothetical elliptical orbit to demonstrate formulas used 22 p3882 A67-39563

Mass optimal trajectory problems with variable endpoints solved using initial and terminal coasting arcs 22 p3884 A67-39955

Suboptimal feedback solution to guidance and control in minimum time and fuel for low thrust orbital transfer 22 p3832 A67-40146

Thrust staging for optimum thrust program without coasting phase for ascent from low orbit 23 p4071 A67-41314

Synchronous orbit communication satellite electric thruster, considering space charge neutralized ion accelerator 23 p4049 A67-41428

Large plane changes by synergetic maneuver with drag cancelled by thrust, noting reduced efficiency due to high altitude L/D decay 24 p4242 A67-42911

ORBITAL VELOCITY

Minimum initial velocity and corresponding orbital inclination of satellite in Keplerian motion 02 p0327 A67-12334

Velocity requirements for orbital transfer and selection criteria for comet missions from 1967 to 1986 03 p0510 A67-13491

Gravity loss in motion of body propelled from vicinity of planet into space trajectory 04 p0695 A67-14515

Relative motion of body about satellite in orbit, determining impulses which cause body to remain in satellite vicinity 04 p0706 A67-15249

Propellant cost optimization using minimum characteristic velocity solutions for extra-atmospheric part of rocket ascent trajectory, emphasizing final elliptical orbit of arbitrary orientation 10 p1704 A67-22877

Independent cometary orbit correction permitting checkout of initial coordinate and velocity components 11 p1868 A67-25084

Optimum trajectories between material points moving along same orbit in gravitational field of spherically symmetric central body, obtaining numerical solutions for circular initial orbit 14 p2382 A67-27852

Topocentric velocity of artificial satellite determined by introducing two pairs of unitary vectors in orbital plane 15 p2556 A67-29745

Minimum velocity increment for bielliptic transfer between noncoplanar circular orbits 20 p3528 A67-37128

Doppler effect method application to satellites and space vehicles motion, giving

formulas for satellite velocity, orbital shape and position 22 p3831 A67-39588

Mission flight profile, considering thrust failure prior to attaining orbital speed, analyzing instantaneous impact point /IIP/ 22 p3831 A67-39610

ORBITING ASTRONOMICAL OBSERVATORY /OAO/

S OAO

S OSO

ORBITING DIPOLE

Radar measurements confirm West Ford dipoles reentered lower atmosphere in accord with predictions 04 p0618 A67-15941

ORBITING GEOPHYSICAL OBSERVATORY /OGO/

S OGO

ORBITING RADIO BEACON IONOSPHERIC SATELLITE

Transhorizon propagation modes from signals transmitted by orbiting radio beacon ionospheric satellite /ORBIS/, showing paths sustained by ionospheric ducts or usual hop modes

[RASSA PAPER 1-10-146] 03 p0373 A67-14253

ORBIS satellite experimental results, noting long range propagation at night and during sunrise

[RASSA PAPER 1-10-147] 03 p0373 A67-14254

ORBITING SATELLITE

Oscillatory motions of orbiting body around center of mass, noting stability of these librations if amplitude is always limited in time 01 p0153 A67-10411

Vapor replacement in propellant feed duct with subcooled liquid to meet engine starting requirement of space vehicle parked in orbit

[AIAA PAPER 66-975] 02 p0305 A67-12297

Meteorological experiments possible in manned earth orbital spacecraft with aid of remote sensing of electromagnetic radiation 02 p0239 A67-12379

Solar radiation increase using orbiting reflector satellite, discussing illumination capability

[AAS PAPER 67-118] 15 p2570 A67-29964

Deviation of path of orbiting body calculated from nominal or reference trajectory 16 p2744 A67-30729

Motion stability of earth-orbiting nonsymmetrical satellite with elastically-connected moving parts studied by Liapunov analysis on mathematical model 16 p2762 A67-30962

Photo-optical instrumentation for biosatellite 30-day orbiting primate mission discussing adverse environmental effects and other constraints regarding requirements 16 p2680 A67-31806

Large orbiting astronomical telescope design, discussing minimum waver, high resolution image recording, compactness and thermal warpage 18 p3043 A67-33493

Detection of mineral resources by orbiting satellite photography, using remote sensor techniques 19 p3225 A67-35655

Computer program for calculating optimal launch windows for orbiting satellites 19 p3190 A67-36071

Rubidium vapor magnetometer used for near earth orbiting spacecraft, instrumentation and in-flight performance 20 p3443 A67-36513

Upper atmosphere density measurement systematic errors in orbiting pressure gauges by neglecting adsorption and desorption 20 p3450 A67-37103

ORBITING SOLAR OBSERVATORY /OSO/

S OSO

ORDNANCE

SA WEAPON

Ordnance systems and devices noting composition, function, operation and testing procedures 04 p0557 A67-15734

ORE

S MINERAL

ORGAN

S ESOPHAGUS

ORGAN WEIGHT

Effects of long term repeated short treatments of mice with hyperbaric oxygen on organ and body weights and hematologic and histologic development 13 p2060 A67-26926

ORGANIC ALUMINUM COMPOUND

Upper atmospheric wind measurement by artificial cloud method which releases sodium at twilight and trimethyl aluminum at night 05 p0798 A67-16858

ORGANIC CHEMISTRY

Monograph on organic chemistry of hydrazine 05 p0758 A67-16073
Book on organic semiconductors emphasizing physical methods, organic chemicals and solid state theory 08 p1372 A67-21506

ORGANIC COMPOUND

SA AROMATIC COMPOUND

Laser induced breakdown of complex organic molecules in vapor state, noting emission accompanied by formation of partially dissociated hot gas 02 p0252 A67-12451

Pumping of organic dyes in organic solvents, using pulsed ruby laser 02 p0253 A67-12515

Luminescence spectra of terbium complex compounds with pyrazolone derivatives 03 p0433 A67-12888

LCAO MO calculation of charge carrier mobility in hydrogen phthalocyanine 03 p0495 A67-13525

Organic composites reinforced with single crystal fibers manufactured, using fiberization of whiskers 05 p0832 A67-16167

Halley comet head diameter change determined by converting propane and ethylene molecules in photon and corpuscular radiation field of sun 05 p0888 A67-16202

Two-photon absorption in organic dyes for various wavelengths, extinction coefficients and concentrations 05 p0815 A67-16626

Laser beam effect on benzene and other organic compounds, noting formation of dark readily coagulating deposit 05 p0759 A67-17028

Electric conductivity of hexamethylbenzene explained by molecular interaction conductivity change at transition point 05 p0871 A67-17379

Luminescence spectra of terbium complex compounds with pyrazolone derivatives 06 p1012 A67-18768

Jovian atmosphere simulation with energy from corona discharge, producing simple organic molecules 07 p1246 A67-19057

Beta hydroxyvaline synthesis, resolution and configuration 07 p1137 A67-20014

Probability of effervescence of superheated liquids as function of temperature and pressure, analyzing N-pentane and hexane under isobaric heating and reduced pressure 09 p1580 A67-21907

Sedimentary rock analysis for aliphatic hydrocarbons, discussing methods and results 10 p1709 A67-23488

Fluorescein family organic dyes exhibiting laser action when excited by ruby and neodymium second harmonics 12 p1953 A67-25748

Complex organic compounds analysis by fast-electrical-scanning high resolution mass spectrometry and gas chromatography 14 p2259 A67-28425

Polyphenyl ether physical, chemical and mechanical properties, noting experimental results and fluid performance in closed pump loops 14 p2341 A67-28953

Special grade RDX for exploding bridge wire initiators noting chemical/physical properties and performance 14 p2377 A67-28955

Temperature dependence of electrical conductivity in organic semiconductors, examining compounds during transition from solid to liquid state 20 p3508 A67-36404

Alpha aminonitriles formation by electric discharge through anhydrous methane and ammonia mixture, showing hydrolysis to amino acid as possible bearing on chemical evolution 20 p3369 A67-36764

Organic dyes as broadband pulsed light amplifiers, noting input frequency relation to laser oscillation 20 p3460 A67-36855

Lactic dehydrogenases of H4 and M4 type, preparation and catalytic and enzymological properties 20 p3377 A67-37159

Classification of 2-oxazolidones, examining preparation, physical chemistry, properties and polymerized derivatives 23 p3971 A67-41041

Na-acenaphthene reaction temperature dependence, studying optical density, precipitation, ion pair formation, coupling constants and hyperfine structure [JPL-TR-32-1144] 24 p4118 A67-42326

1, 3-diones and beta-ketoesters with cobalt for room temperature curing of unsaturated polyester resins by organic peroxide 24 p4175 A67-42420

polyester resins by organic peroxide 24 p4175 A67-42420

ORGANIC FLUORINE COMPOUND

Temperature dependence and reaction energetics of free radical addition of trifluoroacetonitrile to ethylene 09 p1459 A67-22364

Free radical addition of perfluoroacetonitrile to vinyl fluoride, noting formation of one isomeric compound 09 p1459 A67-22365

Linear fluorinated hydrocarbon polymer oils and grease mixtures with low molecular weight polytetrafluoroethylene thickener as lubricant for liquid fueled rocket motors [ASLE PREPRINT 87AM 8A-4] 14 p2327 A67-28796

Triplet-to-singlet conversion of difluoromethylene radical by self-annihilation, noting reactions with oxygen atoms 20 p3378 A67-37561

ORGANIC LASER

Spectral narrowing and tunability over wide spectral range demonstrated in solid/liquid dye lasers using diffraction gratings as cavity reflectors 15 p2500 A67-29817

Rose bengal saturable filter for production of high peak power neodymium laser pulses by regeneration switching 20 p3457 A67-36175

ORGANIC LIQUID

Intermolecular double resonance and Overhauser effect in organic liquids 01 p0019 A67-10825

Dynamic-seal technology in applications employing liquid metals, gas and standard organic fluids for ground, aerospace and space turbomachinery [ASME PAPER 87-DE-50] 14 p2328 A67-28881

Longitudinal turbulence intensities, autocorrelations, energy spectra and peak energy dissipation frequencies for organic solvents flowing in smooth round tubes 24 p4141 A67-41927

Organic Rankine cycle power system using monoisopropylbiphenyl (MIPB) as working fluid noting advantages 24 p4103 A67-42494

Rankine cycle power plants using organic working fluids considered for near-term application 24 p4103 A67-42495

ORGANIC MATERIAL

Hydrogen peroxide oxidation and ozonolysis of polymer type material in coal, kerogen and Orgueil meteorite 08 p1289 A67-21174

Biological macromolecule detection using thiacarbocyanine dye and observation of absorption spectra changes 15 p2426 A67-29115

Organic dielectric materials for spacecraft, selection and evaluation 15 p2508 A67-29556

Man-made organic polymer properties and characteristics, considering crystallization, cross-linking and polymeric chain stiffening for structural applications 20 p3474 A67-37713

Meteoritic organic chemical analyses since 1900, considering volatile materials distribution and carbonaceous chondrites 21 p3704 A67-38502

Electronic transitions optical saturations in polyatomic organic molecules with high intensity laser radiation, discussing relation to bleaching of dyes 22 p3817 A67-40487

Photocurrents and photopotentials in organic solids, discussing atomic bonding effect 23 p4045 A67-41484

ORGANIC PHOSPHORUS COMPOUND

Stereospecific addition of organophosphides to terminal alkynes 04 p0565 A67-14522

Organic phosphate shown as inhibitory factor from B. stearothermophilus for attachment of amino acids to transfer RNA 20 p3370 A67-36798

ORGANIC SEMICONDUCTOR

Book on organic semiconductors emphasizing physical methods, organic chemicals and solid state theory 08 p1372 A67-21506

Dark and photo-conductivity of organic semiconductors, noting measurement techniques and effect of purity, materials, pressure, etc 19 p3302 A67-34995

Intermolecular hydrogen bonds energies estimated for organic semiconductors in ground and first excited states 20 p3512 A67-37301

Conductivity and IR absorption spectra of organic semiconductors in polycrystalline, melt and liquid states 22 p3861 A67-39922

ORGANISM

SA ANIMAL STUDY

SA MICROORGANISM

Electromechanical system for study of plant or organism growth and development in compensated gravitational fields 11 p1793 A67-24822

ORGANOMETALLIC COMPOUND

SA CHELATE COMPOUND

Laser generation through rare earth chelate solutions, requirements for working solutions and apparatus 10 p1664 A67-23068

Carbonyl compounds reaction with N-salicylideneglycinatoaquocopper (II)/syntheses of beta-hydroxy alpha-amino acid from glycine 20 p3376 A67-36877

ORGANOMETALLIC POLYMER

Hole mobility produced by single pulses of electrons in films of polyvinyl acetate semiconductors with sputtered gold electrodes, determining relation between film conductivity and mobility 15 p2537 A67-29703

Composite material mechanical characteristics, discussing organic polymeric materials application in wide temperature range 22 p3825 A67-39855

Hole mobility produced by single pulses of electrons in films of polyvinyl acetate semiconductors with sputtered gold electrodes, determining relation between film conductivity and mobility 24 p4199 A67-41773

ORGUEIL METEORITE

Optical rotation of lipids extracted from soils, sediments and Orgueil carbonaceous meteorite 08 p1289 A67-21173

Hydrogen peroxide oxidation and ozonolysis of polymer type material in coal, kerogen and Orgueil meteorite 08 p1289 A67-21174

Orgueil carbonaceous meteorite composition and mineral texture including petrogenesis and origin of organic content and mineralized microstructures 10 p1710 A67-23628

Electron microscopy of biological-like structures in Orgueil carbonaceous meteorite 13 p2210 A67-27583

Magnetite crystals of asymmetrical shape observed in Alais, Ivuna and Orgueil carbonaceous meteorites noting particle corrosion 22 p3881 A67-39496

Origin of round body structures in Orgueil meteorite 24 p4113 A67-42455

ORIENTATION

S INSTRUMENT ORIENTATION

S SATELLITE ORIENTATION

S SPACE ORIENTATION

S SPATIAL ORIENTATION

ORIFICE

SA DUCT

Elastic orifice compensator in externally pressurized gas bearings for flow control, noting increased bearing stiffness 01 p0077 A67-10123

Airflow instability with square edge circular orifice, discussing hysteresis effect on discharge coefficient 04 p0601 A67-14487

Critical two-phase flow of nitrogen and oxygen through orifices characterized by mass-limited conditions 13 p2106 A67-27669

Frictional pressure drop for isothermal incompressible flow in isosceles triangular duct, with correlations for laminar and turbulent flow 14 p2243 A67-28365

Incompressible two-phase mixed flow through sharp edge orifice including shear force between phases 14 p2305 A67-29012

Cavitation in spool control valve orifices, showing effect on flow discharge coefficient over range of conditions 20 p3366 A67-37371

Force defect coefficient method applied to calculation of compressible jet flow discharge for asymmetric two-dimensional orifice 23 p3936 A67-41330

ORIGIN

SA PLANETARY ORIGIN

Tektites and impactites composition and origin 12 p1903 A67-25430

ORION AIRCRAFT

S P-3 AIRCRAFT

ORION CONSTELLATION

IR star in Orion nebula noting photometric result, comparing IR flux with energy distribution of black body as function of wavelength 09 p1567 A67-22239

Physical parameters of IR nebula discovered in Orion 19 p3330 A67-36080

Far UV spectra of brighter stars in

vicinity of epsilon Orionis photographed with objective spectrograph carried by rocket 22 p3882 A67-39555

O and B stars surveyed with 154 cm Catalina reflector show discrepancies from mean interstellar polarization-wavelength dependence near Orion 23 p4062 A67-40626

IR nebula in Orion as protocluster with massive stars imbedded in opaque dust cloud, discussing collapse and lifetime 24 p4225 A67-41829

ORION PROJECT

Nuclear pulse propulsion, discussing principles of operation of contained and uncontained systems 06 p1030 A67-19025

ORLICZ SPACE

Jackson theorem on optimal approximations of periodic functions with r -th derivative belonging to metric generalized to case of Orlicz space 02 p0259 A67-11872

OROGRAPHY

SA MOUNTAIN

SA TOPOLOGY

Numerical method for calculation of finite amplitude orographic disturbances by using finite difference algorithm 05 p0837 A67-16484

Numerical method for calculation of finite amplitude orographic disturbances by using finite difference algorithm 13 p2150 A67-26340

Orographic factors effect on stratospheric pressure field, obtaining ascending vertical fluxes and heat input equations, discussing refractive index for atmospheric perturbations 13 p2112 A67-26672

ORTHICON

SA IMAGE ORTHICON TUBE

Image orthicon TV system and application to auroral observations, noting data acquisition mechanism 06 p0993 A67-17563

Image degradation comparison between photographic and image orthicon systems, discussing image orthicon receptor advantages when used for space applications 20 p3446 A67-36606

ORTHO-PARA CONVERSION

Liquid hydrogen production techniques in purification, ortho-para conversion and refrigeration 05 p0789 A67-17017

ORTHOGONAL FUNCTION

Orthogonal expansions in physical boundary value problems characterized by homogeneous differential equation with inhomogeneous boundary data 01 p0106 A67-10734

Structure of shock wave in monatomic gas analysis using orthogonal polynomial solution of Boltzmann equation, noting Mott-Smith distribution function 02 p0234 A67-12541

Limiting conditions for polynomials orthonormal on unit circle for nonnegative summable 2π -periodic weight function 03 p0456 A67-12885

Method of approximating functions with aid of orthonormal systems and single channel optimization, using analog computer 05 p0788 A67-16264

Polynomials orthogonal with respect to contours, examining analytic function representation via Fourier series expansion of such polynomials 06 p1025 A67-18695

Proof that Tandoni theorem gives best estimate for convergence rates of orthogonal series 09 p1524 A67-21911

Decomposition, in orthogonal universal vectors, of electromagnetic universal force created by point charge animated by universal velocity and acceleration 09 p1534 A67-22590

Optimum filtration of signals in presence of arbitrary interference, using orthogonal function series 10 p1807 A67-23443

Moments of distribution function of perfect fluid calculated and used in studies of orthogonal polynomials on Minkowski hyperboloid 12 p1966 A67-25144

Orthogonal polynomial method to determine distribution function for equilibrium of single species two-temperature gas mixture 13 p2102 A67-26972

Self-adjustable orthogonal digital filters for system identification and optimization 13 p2088 A67-27409

General method based on reciprocity theorem developed for problem solutions in elasticity theory 14 p2402 A67-28740

Pressure distribution in subsonic flow for vertical stabilizer calculated, using orthogonal function theory 18 p2982 A67-33655

Biorthogonality relation derived between eigenfunctions of operator representing linearized anisotropic multifluid warm plasma and eigenfunctions of adjoint operator 20 p3503 A67-37711

Mode-matching technique for bifurcated anisotropic waveguide, discussing Bresler biorthogonality relationships to derive anisotropic guide mode equations 20 p3407 A67-37712

Orthogonal signaling in sequential decision feedback on communication over additive white Gaussian noise channel, obtaining expression for error probability 22 p3775 A67-39295

Empirical orthogonal functions, determining vertical atmospheric temperature profiles from radiometric satellite measurements 22 p3828 A67-39325

Integral equations with integral operators and excitation frequencies for forced oscillation, solving friction via orthogonal iteration approximation 22 p3916 A67-40454

Existence and form of orthogonality condition on natural vibrational modes of linear elastic shell under boundary conditions 23 p4073 A67-40616

Orthogonal transformation of neighboring quantum states into classical two-component plasmas, using WKB approximation 24 p4195 A67-42107

ORTHOGONAL WAVEFORM MULTIPLEXING

OPW calculation of six symmetry points in wurzite Brillouin zone of CdS, using pseudopotential techniques 06 p1058 A67-18903

ORTHOSTATIC TOLERANCE

9-alpha-fluorohydrocortisone and venous occlusive cuffs effects on plasma volume and orthostatic tolerance following 28 to 78 days of bed rest 01 p0016 A67-10960

Absolute bed rest and recumbent exercise during bed rest effects on pulse rate response to submaximal work, cardiovascular functional capacity /maximal oxygen intake/, physical work capacity and orthostatic tolerance 05 p0755 A67-16283

Cardiovascular changes due to orthostasis, evaluating influence of intravascular instrumentation on orthostatic tolerance of normal men 06 p0953 A67-18776

Cardiovascular response of 37 patients with heart disease to prolonged passive upright tilt compared with normal subjects 07 p1135 A67-19866

Diurnal rhythm of cardiovascular responses to active orthostasis and Schneider test performance in function diagnostics of peripheral cycle regulation [DVL-620] 11 p1747 A67-25035

Weightlessness simulation by bed rest and water immersion, evaluating validity of protective measures, recovery time and tilt response 15 p2424 A67-29102

Plasma volume and tilt table response of humans to water immersion deconditioning experiments, using extremity cuffs to study protective effect 15 p2428 A67-29271

Hemodynamic modifications produced by orthostatism noting changes in cardiac frequency, arterial pressure and central blood volume produced 16 p2616 A67-30754

Human brain hemodynamics during prolonged hypokinesia including orthostatic and bed-rest tests, using rheoencephalographic technique 20 p3368 A67-36266

Human experiments to study somnolent and precollaptoic /collaptoic/ states when falling asleep and during prolonged standing tests 20 p3368 A67-36268

Human response to low intensity long duration transverse acceleration, discussing increase in splanchnic blood flow during centrifugation and orthostatic intolerance 23 p3958 A67-41652

ORTHOTROPIC CYLINDER

Elastic general instability of orthotropically stiffened cylinders under axial compression [AIAA PAPER 66-139] 01 p0183 A67-11154

Critical axial compression buckling loads of orthotropic cylinders having stiffening patterns analyzed, considering three instability failure modes 10 p1728 A67-23760

Torsional buckling stress of orthotropic cylindrical shells with high order terms due to internal pressure rise 11 p1876 A67-24701

Torsional wave propagation in anisotropic

nonuniform cylindrical rod for constant and variable Youngs moduli 13 p2218 A67-26902

Nonaxisymmetric temperature fields for orthotropic hollow cylinder and sphere solved using Bessel functions, noting heat transfer between external and internal surfaces 15 p2579 A67-29697

Orthotropic circular cylindrical shell of elastic material instability under combined torsion and hydrostatic pressure investigated for simply supported and clamped ends 17 p2963 A67-33016

Orthotropically stiffened cylinders elastic instability under torsional load 23 p4080 A67-41741

ORTHOTROPIC MATERIAL

Material orthotropy effect on directions of principal stresses and strains in fiberglass and boron composites 06 p1108 A67-18654

Anisotropic sandwich constructions characteristics for orthotropic materials used for facings and cores, considering stiffness and buckling 06 p1108 A67-18655

Stress-strain and Hooke law in orthotropic elasticity presented through matrix algebra and tensor coordinates 06 p1108 A67-18656

Elastic interaction between dislocation loops and straight dislocations in orthotropic anisotropic materials analyzed for various graphite configurations 08 p1346 A67-20797

Plane thermal stress at insulated hole under uniform heat flow in orthotropic medium 10 p1730 A67-23838

Brittle strength of orthotropic materials investigated for proposed phenomenological fracture condition 14 p2399 A67-28103

Yield conditions for plastically incompressible isotropic and orthotropic materials with different yield stress in tension and compression, without using hydrostatic terms 19 p3339 A67-35053

Buckling analysis of sandwich beams with elastic orthotropic cores under axial compression 20 p3537 A67-36841

Orthotropic laminated layer with heat emission investigated for thermoconductivity and temperature stress distribution 21 p3731 A67-38299

ORTHOTROPIC PLATE

Stability of rectangular elastic orthotropic plates under distributed and concentrated loads, noting glass fiber reinforced plates 02 p0339 A67-12240

Variational analysis of BVP of natural oscillations of orthotropic plates 02 p0341 A67-12663

Bending of orthotropic plates and beams supported by elastic layer under uniform transverse load, noting effect of length-width ratio change 03 p0520 A67-13017

Bending of orthotropic sandwich plates in differential equation derived based on variational method 04 p0709 A67-14844

Minimum potential energy principle and Rayleigh-Ritz method derivation of flutter equations for flat rectangular orthotropic panels 05 p0924 A67-17350

Yielding and brittle cracking of orthotropic strip, using Wiener-Hopf technique and asymptotic method for isotropic case 06 p1102 A67-18317

Axisymmetric buckling of orthotropic circular plates with variable thickness in terms of lateral plate deflection and stress distribution 11 p1876 A67-24660

Geometrically nonlinear theory of elastic stability of anisotropic shells and linear stability of orthotropic plates, using differential equations 12 p2028 A67-25628

Laminar natural convection heat transfer between vertical plate and power-law fluid with high Prandtl number 16 p2780 A67-31553

Nonlinear bending theory of sandwich plates with orthotropic layers 19 p3342 A67-35716

Differential equations for stressed thin orthotropic plates of variable thickness derived and solved in cylindrical coordinates 20 p3539 A67-36919

Thermal stresses in orthotropic sandwich plate solved by boundary value and stress distribution 20 p3541 A67-37298

Stress-strain relationships for single layer used to obtain stress distribution in orthotropic laminates subjected to axial and shear stresses [ASME PAPER 66-WA/RP-5] 20 p3542 A67-37611

Natural vibration frequencies of cylindrically orthotropic circular plate with linearly variable thickness, solving

- differential equation of motion 21 p3728 A67-38898
- Bending of orthotropic strip to anticlastic surface by uniform moment, determining strain along neutral axis, bending moment and couple action 22 p3913 A67-40008
- Viscoelastic behavior of laminated orthotropic plates, discussing single layer or homogeneous orthotropic viscoelastic plate problem 22 p3914 A67-40108
- ORTHOTROPIC SHELL**
- Finite element method structural analysis of laminated orthotropic shell of revolution 03 p0524 A67-13787
- Simulation of isotropic and structurally orthotropic shells by laminated models and constructing limiting relations between generalized stresses 03 p0530 A67-14170
- Dynamic response of cylindrical sandwich shell under axially symmetric moving ring load, considering steady state behavior 04 p0713 A67-15404
- Initial equilibrium state stability of multilayer orthotropic circular cylindrical shell based on anisotropic shell theory 05 p0919 A67-16585
- Generalized Stodola iteration method for computer analysis of axisymmetric buckling of ring-stiffened orthotropic shells of revolution [AIAA PAPER 67-109] 06 p1103 A67-18339
- Axisymmetric plane-strain vibrations of thick layered orthotropic shell under internal and external pressures analyzed, using Fourier series for eigenmodes determination 08 p1415 A67-20487
- Unsymmetric free vibrations of orthotropic sandwich shells of revolution treated by Rayleigh-Ritz technique 08 p1417 A67-20555
- Locally loaded orthotropic shells of revolution under radial concentrated forces 12 p2021 A67-25575
- Stressed and strained state of orthotropic cylindrical shell weakened by circular hole 12 p2021 A67-25578
- Tensometry method to study stress concentration around circular hole in orthotropic glass-fiber reinforced cylindrical shell 12 p2021 A67-25579
- Displacements, stresses and moments in orthotropic and bimetallic cylindrical shells under radial concentrated forces determined via computer method 12 p2025 A67-25608
- Large deformations of zero moment orthotropic shells of revolution under action of inertial loads caused by centrifugal acceleration of shells 12 p2028 A67-25629
- First order finite difference numerical analysis of thin elastic orthotropic and inhomogeneous cylindrical shells with small deformations from external forces 15 p2574 A67-29471
- Noncircular cylindrical shell of orthotropic material under distributed load numerically analyzed by shell theory 15 p2578 A67-30272
- Stability of reinforced thin structurally-orthotropic cylindrical shell problem, discussing rib eccentricity, axial compression load, torsional load, etc 19 p3338 A67-34874
- Anisotropic composites viscoelastic analysis applied to orthotropic cylinder pressurization, glass fiber cooling and relaxation shear moduli problems 20 p3474 A67-37287
- Buckling loads in orthotropic circular cylindrical shells under simultaneous longitudinal and external peripheral pressure stresses 22 p3912 A67-39752
- OSCILLATING CYLINDER**
- Oscillations of circle solved, using method of elastic oscillations of plane with circular cut 04 p0708 A67-14788
- Kollmann theory on critical rpm of hollow shells of revolution containing liquid, explaining unstable oscillations appearance in supercritical region 06 p1100 A67-17992
- Free and forced oscillation of disks and right circular cylinders rotating in free stream, noting turbulent wake flow 06 p1101 A67-18136
- Pressure measurements on surface and in wake of circular cylinder at rest and in vortex excited oscillation at subcritical Reynolds numbers [ASME PAPER 67-VIBR-31] 11 p1777 A67-24189
- Cylinders of rectangular section as aeroelastic nonlinear oscillators, theory of galloping oscillation and force measurements on stationary cylinder
- [ASME PAPER 67-VIBR-50]
- Vibrational frequency and amplitude effects on heat transfer intensity from vibrating cylinder into circular channel at low Reynolds numbers 20 p3554 A67-37303
- Oscillation stability of rotating cylindrical shell filled with ideal incompressible weightless fluid, determining instability region distribution 21 p3721 A67-38302
- OSCILLATING FLOW**
- Small oscillations of viscous liquid-metal droplet under capillary force and in presence of magnetic field 01 p0120 A67-10182
- Flow induced by infinite flat oscillating plate in incompressible dusty gas 02 p0234 A67-12548
- Axisymmetric sloshing oscillations of liquid in U-tube type connected cylindrical tanks, obtaining velocity, pressure and wave height 03 p0522 A67-13213
- Density wave type flow oscillations in boiling Freon 11 examined, noting effects of partial evaporation superheat and liquid inlet temperature on stability [ASME PAPER 66-WA/HT-49] 04 p0725 A67-15433
- Mass and oscillation damping of rigid sphere in cylindrical tube containing viscous liquid [ASME PAPER 66-WA/UNT-5] 04 p0608 A67-15442
- Oscillation effect on instantaneous local heat transfer in forced convection from cylinder measured by optical method and theoretically calculated by power series expansion method 04 p0733 A67-15843
- Lagrange variational equation application to dynamic stability problems of plates in gas flow 05 p0923 A67-17188
- Damping of liquid oscillations in cylindrical tanks, determining rigid and flexible baffle loss coefficients, baffle efficiency and maximum bending stress [AIAA PAPER 66-97] 05 p0793 A67-17210
- Oscillating variables of flow past cylinder, calculating magnitude and frequency of lift 07 p1168 A67-19258
- Oscillatory isentropic flow through nozzles solved numerically, using Tsien proof of nonsingularity of solution 08 p1375 A67-20775
- Shock wave formation due to heat addition to one-dimensional flow of ideal inviscid conducting monatomic compressible fluid under transverse magnetic field 08 p1359 A67-20980
- Transverse oscillations of vortex free fluid in circular cylinder with horizontal generatrix, determining first natural frequency by Rayleigh method 09 p1574 A67-21891
- Interaction of transverse distributed surface vibration with adjacent laminar flow, superimposing oscillatory pressure and velocity field developed in boundary layer fluid over idealized steady fluid flow 10 p1623 A67-22861
- Hydrodynamic drawing together problem for aerosol particles oscillating in sonic field at small Reynolds numbers, showing optimal field frequency-approach velocity correspondence 10 p1627 A67-23643
- Pressure measurements on surface and in wake of circular cylinder at rest and in vortex excited oscillation at subcritical Reynolds numbers [ASME PAPER 67-VIBR-31] 11 p1777 A67-24189
- Flow induced vibrations of rigid plate in narrow channels, noting flow rate dependence on channel width [ASME PAPER 67-VIBR-32] 11 p1777 A67-24190
- Thermal and ablative lag induced by periodic heat input to oscillating flat plate in high velocity flow, showing crossover from dynamically stabilizing to destabilizing condition as oscillation frequency increases [AIAA PAPER 67-336] 12 p2039 A67-26050
- Ionized gas flow past oscillating interface in presence of magnetic field, based on MHD boundary layer model with constant velocity profile 13 p2168 A67-27302
- Unsteady heat transfer in tube in presence of variable gas flow rate 17 p2967 A67-32129
- Free convection oscillatory flow from horizontal plate having periodic temperature variations analyzed for LF and HF ranges 17 p2969 A67-32445
- Unsteady plane parallel flow stability of viscous electrically conducting incompressible fluid in oscillating magnetic field 17 p2910 A67-33350
- Hydrodynamic drawing together problem for aerosol particles oscillating in sonic field at small Reynolds numbers, showing optimal field frequency-approach velocity correspondence 18 p3029 A67-34412
- Transition in oscillating boundary layer flows studied for various parameters effect 19 p3209 A67-35413
- Oscillation and stability of two irregular thin elastic cylindrical shells in potential flow of compressible fluid 21 p3720 A67-38296
- Boiler inlet impedance frequency response in single tube heat exchanger when pumped with oscillating flow 22 p3916 A67-39390
- Oscillating mass flow characteristics in modified Moore variometer configuration for step, triangular and infrasonic functions 23 p4000 A67-41221
- Energy equation solution procedure for heat transfer across two-dimensional oscillating laminar boundary layer 23 p4082 A67-41243
- OSCILLATING WING**
- Aerodynamic forces of oscillating lifting surfaces of large aspect ratio in subsonic range investigated by approximation method 03 p0351 A67-12996
- Aerodynamics of slender wings executing simple harmonic oscillations and having leading edge separation 03 p0352 A67-13894
- Free stream conditions approaching oscillating body in low speed wind tunnel, employing unsteady Bernoulli equation 03 p0352 A67-13899
- Variational approximation of normal velocity on oscillating wings including linear approximation, numerical integration and comparison to least squares method 04 p0547 A67-14842
- Unsteady aerodynamic forces on thin wing oscillating in transonic flow, discussing acoustic ray paths and signal transmission times [AIAA PAPER 67-16] 06 p0943 A67-18841
- Bending torsional flutter of uniform swept wing with velocity component aerodynamic strip theory [AIAA PAPER 66-475] 06 p1110 A67-18860
- Unsteady supersonic flow about conical wing fuselage system with LF harmonic oscillatory motion 07 p1127 A67-20224
- Sub-or supersonic wing leading edge in unsteady supersonic flow, presenting discontinuities in vibration modes and calculating wing stress forces 10 p1590 A67-22879
- Matched asymptotic expansion for singular pressure loading behavior for oscillating wings or control surface edges 10 p1593 A67-23712
- Solution of voltterra type equation for oscillations of thin profiles of grid in incompressible inviscid flow 13 p2218 A67-26899
- Dither and sinusoidal incidence variations effect on control wing hinge moments of transonic-supersonic rolling maneuvering guided missile [AIAA PAPER 66-755] 17 p2789 A67-32062
- Analog computer method application for determining critical frequency and critical flutter speed of wing having torsional bending vibrations in airflow 21 p3718 A67-37992
- Oscillating infinitely thin wing profile in inviscid subsonic compressible flow, deriving perturbation pressure 23 p3929 A67-41250
- OSCILLATION**
- SA ELECTRON OSCILLATION
- SA FORCED OSCILLATION
- SA FREE OSCILLATION
- SA HARMONIC OSCILLATION
- SA HYDROFOIL OSCILLATION
- SA ION OSCILLATION
- SA LATERAL OSCILLATION
- SA MOLECULAR OSCILLATION
- SA NUTATIONAL OSCILLATION
- SA PERIODIC OSCILLATION
- SA PLASMA OSCILLATION
- SA PRESSURE OSCILLATION
- SA SELF-OSCILLATION
- SA STABLE OSCILLATION
- SA TIDAL OSCILLATION
- SA TRANSIENT OSCILLATION
- SA TRANSVERSE OSCILLATION
- SA VIBRATION

Oscillation of fluid metal droplet, free or immersed in fluid dielectric, in steady and uniform magnetic field 01 p0120 A67-10181

Steady state elastic oscillations in case of plane deformation for infinite plane weakened by round arbitrarily arranged holes 01 p0159 A67-10224

Gunn effect semiconductors and contact preparation techniques, noting excitation of oscillations and amplification characteristics in GHz range 02 p0220 A67-12198

Instability of nonlinear stationary oscillations of potential in electron-ion flows useful in distribution functions of ions and electrons 03 p0470 A67-12935

Franck-Condon factors and transition probabilities of electron oscillatory transfers in diatomic molecules 03 p0471 A67-13314

Quasi-rotational oscillatory solution to equation system with arbitrary degree of freedom with respect to parameter in given region 03 p0468 A67-13338

Formulation of dynamic three-dimensional problem of homogeneous isotropic and linearly elastic bodies in terms of stresses 03 p0523 A67-13459

Damped oscillations and velocity of sound waves in semiconductors and metals in presence of strong magnetic field 03 p0501 A67-14370

Entanglement effect of plasma and magnetic branches of oscillations in antiferromagnetic semiconductors on LF expanding plasma waves in strong electric fields 04 p0678 A67-15133

Oscillations of derivatives of almost periodic functions obtained with aid of Kronecker-Weyl theorem 04 p0646 A67-15259

Bubnov-Galerkin and energy method solutions of stability and oscillatory motion equations for conical shell under inertial loading 04 p0717 A67-15890

Mechanical system with two degrees of freedom conditioned for oscillatory motion, using differential equations 05 p0908 A67-16042

Optimum control of two-dimensional oscillating system when placing limitations on control, using Butkovskii L-problem of moments 05 p0781 A67-16253

Generalized Callen-Welton theorem applied to calculation of maser oscillations in amplification and generation regimes, determining noise spectral energy and spectral line width 05 p0762 A67-16350

Quantum oscillations of Hall effect and longitudinal and transverse reluctance in n-indium antimonide, noting spin splitting and temperature and electron concentration effect on oscillation maximum 05 p0861 A67-16394

Phugoid trajectories of ballistic reentry of hypothetical glider into variable density atmosphere 05 p0847 A67-17009

Oscillatory motion of pendulum-gyroscope system near given position of relative stability 06 p1002 A67-18042

Estimating interval of nonoscillation of finite difference equation 06 p1024 A67-18556

Electronic analog detection and separation of oscillations slightly differing in amplitude 06 p1109 A67-18667

Graphical and analytical solutions to wave propagation in inhomogeneous media in conditions of wave number variations oscillating along coordinate 06 p1034 A67-18814

Theorems concerning eigenvalue problems and oscillatory conditions for multiple degree of freedom mechanical systems 07 p1224 A67-20103

Resonance oscillations and rotations in mechanical systems having n-dimensional quasi-static vector analyzed and applied to triaxial ellipsoid with unbalanced mass 10 p1680 A67-23409

Averaging method in nonlinear mechanics, discussing results of Bogolubov studies 11 p1818 A67-24089

Energy conservation analysis of step in negative resistance region of voltage-current characteristic curve of oscillating tunnel diode 11 p1759 A67-24132

Astatic gyroscope accuracy dependence on random fluctuations of dry friction moment when under oscillatory motion of bearings, giving correlation function of error dispersion 11 p1794 A67-25044

Reading errors of oscillating plant mounted gyrocompass assuming gyromoment compensation and no friction, determining

motion through differential equation 11 p1794 A67-25045

Entanglement effect of plasma and magnetic branches of oscillations in antiferromagnetic semiconductors on LF expanding plasma waves in strong electric fields 12 p1978 A67-25157

Rectangular three-layer plate thermoelastic oscillations due to random pulses analyzed using series expansion 12 p2027 A67-25625

Damping of plane sinusoidal wave in cold collisionless plasma, studying supercritical amplitude oscillatory process 13 p2171 A67-27615

Resistivity and Hall effect oscillations in antimony doped n-type germanium crystals in metallic impurity conduction state 14 p2365 A67-28231

Oscillation pendulum equation solution properties, noting existence of certain bifurcation value of parameter 14 p2348 A67-28382

Oscillation of rod in gas stream investigated for nonlinear factor effect on oscillations 14 p2243 A67-28639

Franck-Condon factors and transition probabilities of electron oscillatory transfers in diatomic molecules 16 p2703 A67-30490

Magnetic field dependence of current oscillations in piezoelectric semiconductors 16 p2725 A67-30804

Two-body system connected on circular orbit by spherical hinge examined for plane oscillations, finding all equilibrium positions with respect to orbital coordinate 17 p2954 A67-32242

Dynamic phenomena in two identical cylindrical shells placed side by side in inviscid supersonic flow of compressible fluid 18 p3024 A67-33540

Phugoid trajectories of ballistic reentry of hypothetical glider into variable density atmosphere 18 p3079 A67-34272

Conduction band structure in n-type strontium titanate investigated by measuring oscillatory magnetoresistance in high magnetic fields 18 p3104 A67-34592

Oscillation conditions of microwave tunnel diode theoretically and experimentally evaluated for mounting at feed point of semicircular loop antenna 19 p3196 A67-35660

Quasi-biennial oscillation in ozone in northern Hemisphere harmonically analyzed 19 p3225 A67-35921

Oscillation index in qualitative assessment of equilibrium converging processes in nonlinear systems 20 p3409 A67-37200

Number of degrees of freedom for observation of motion of steady signal from uncontrolled plant 22 p3836 A67-39775

Estimating interval of nonoscillation of finite difference equation 23 p4022 A67-40822

OSCILLATION FREQUENCY

SA PLASMA FREQUENCY

Negative resistance of waveguide-mounted tunnel diode decrease with frequency suggested as source of oscillations at frequencies above cut-off 01 p0032 A67-10001

Recording assembly for measurement of flexural and torsional moduli and internal friction at various frequencies and temperatures of small samples, using constant amplitude undamped oscillations 01 p0062 A67-10163

Generation of current oscillations by electroacoustic effects in semiconducting cadmium sulfide 01 p0130 A67-10199

Oscillation frequency of maser oscillator calculated using perturbation theory, noting traveling wave effect 01 p0089 A67-10395

Maser oscillation intensity and frequency dependence on constant electric and magnetic fields acting on molecular beam in front of resonator 01 p0089 A67-10396

Effect of plasma outside cylindrical plasma column on dipole resonance, noting increased oscillation frequency and coupling of resonances 01 p0123 A67-10459

Oscillation modes in film with free boundaries, determining phonon density 01 p0136 A67-11049

Oscillation frequency and breakdown voltage in GaAs p-n junction reverse-biased into avalanche region due to negative resistance arising from transit time effect 01 p0137 A67-11070

Pressure coupled combustion dynamics of solid propellants analyzed as function of propellant variables, oscillation frequency and combustion pressure 01 p0143 A67-11448

Deep-level localized current oscillations in

n-type silicon crystal 02 p0298 A67-11892

Vibration of entire multifrequency system reduced to single frequency resonance when frequency passes through zero, illustrated with solar system 02 p0267 A67-11917

Diatomic gas flow past blunt bodies, noting effect of oscillation and dissociation relaxation on mean 02 p0180 A67-12465

Plasma electron density and formation determined, using Fabry-Perot resonator 02 p0275 A67-12469

Temperature tuning of lithium niobate optical parametric oscillator in visible spectrum, noting generated frequency dependence on pump frequency and longitudinal mode distribution 02 p0253 A67-12511

Parametric resonance in plasma situated in magnetic field noting oscillation, frequency stability, kinetic equations, electric field effect, etc 03 p0475 A67-12931

Frequency spectrum of micropulsations analysis from records taken at station near geomagnetic equator 03 p0410 A67-12954

Anomalous skin depths and magnetic probe measurement of oscillating magnetic field penetrating into plasma cylinder 03 p0477 A67-13534

Gas squeeze film stiffness and damping torques on circular disk oscillating about diameter [ASME PAPER 66-LUB-4] 03 p0432 A67-13762

Spectral analysis of HF oscillations with phase modulated fluctuation as functions of phase dispersion and spectral form of modulating fluctuations 03 p0393 A67-13950

Eigenfrequencies of elastic plate containing cavities filled with incompressible moving fluid, obtaining eigenfrequencies dependence on velocity of fluid motion 03 p0530 A67-14173

Steady state regime and stability of two-photon laser, noting field dependence of intensity and duration of frequency pulse and resonance excitation curves 04 p0631 A67-14745

Field and charge density distributions in semiconductor with hot electrons, showing domain movement type oscillations due to stationary wave propagation 04 p0680 A67-15286

General theory for parametric oscillation in optical region 05 p0817 A67-16639

Pulsating gravitational collapse from point of view of external observer, noting oscillation period and distortion of contraction expansion symmetry 05 p0896 A67-16692

Onset of oscillation in He-Ne laser analyzed using Lamb theory, obtaining time constant value for population of lower laser level 05 p0824 A67-16821

Electron beam excitation as possible explanation of relation between enhanced diffusion and HF oscillation in plasma 05 p0854 A67-16896

LF oscillation 30 times greater than HF oscillation in plasma in magnetic field 05 p0854 A67-16897

Transient behavior of He-Ne lasers under pulsed HF excitation, discussing rate equations representing atomic population density and photon 05 p0825 A67-16980

Phase locked oscillations of silicon avalanche diodes noting hysteresis 05 p0775 A67-16984

LF photocurrent oscillation in high resistivity n-type GaAs, noting relation between amplitude temperature and light intensity 05 p0866 A67-16987

Stationarity conditions for FM oscillations with noise modulated frequency 05 p0766 A67-17167

Oscillation of maser with sinusoidal distribution of resonator field along axis of molecular motion 05 p0826 A67-17234

Suppression of undesirable axial modes in gas laser oscillating at several frequencies obtained by filling with active gas mixture each of two coupled Fabry-Perot type resonators 05 p0826 A67-17326

Frequency modes of Gunn effect oscillator 05 p0872 A67-17531

Excess noise and oscillations in gold-doped germanium photodiodes attributed to generation-recombination fluctuations of large bulk resistance 06 p0971 A67-18220

Fundamental frequency of natural

oscillations of plate, using integrodifferential equations derived from elasticity theory in form of power series 06 p1108 A67-18662

Periodic oscillation mode of time invariant feedback system containing relay determined, using state space approach 06 p0978 A67-18719

Charged and neutral particles collision effect on LF oscillations in weakly ionized plasma in crossed electric and magnetic fields 06 p1046 A67-18827

Quantum oscillations in magnetoresistance of n-type pure HgTe used to estimate electron effective mass and g value close to band edge 06 p1065 A67-18948

Oscillations in conductivity of electron-hole plasma in semiconductors due to nonlinearity of volt-ampere characteristics 06 p1070 A67-18988

Sommerfeld effect in linear oscillating system with randomly variable natural frequency 07 p1261 A67-19140

Equations of pulsations of spherically symmetrical configurations in general relativity theory, considering oscillation frequency and instability of singular sphere 07 p1248 A67-19483

LF resonance oscillations in cylindrical plasma column, considering ionization mechanism of Philips Ionization Gauge /PIG/ discharge 07 p1229 A67-19674

Mathematical reliability of model for vibrating field lines used to explain micropulsation observations 07 p1182 A67-19950

Energy loss of charged particles during passage through weakly turbulent plasma in magnetic field with HF oscillations 08 p1357 A67-20844

Rotating helical perturbations in Penning discharge plasma accompanying LF oscillations enhance particle transport across magnetic field 08 p1362 A67-21146

Frequency and phase locking of laser oscillators by externally injected signal 08 p1338 A67-21309

Longitudinal mode oscillations of gas laser when resonator length changes with time, noting polarization and amplitude change related to growth of new oscillation 08 p1338 A67-21314

Laser mode combination tones detected by coupled high resolution optical amplifier corresponding to simultaneously oscillating frequencies 09 p1511 A67-21747

Transverse oscillations of vortex free fluid in circular cylinder with horizontal generatrix, determining first natural frequency by Rayleigh method 09 p1574 A67-21891

Gunn diode efficiency for mixed resonant transit time and suppressed modes, using dynamic drift velocity field strength characteristic 09 p1474 A67-22039

Microwave frequency oscillations obtained from p-n junction diodes reversed-biased into avalanche region, noting dependence on temperature and impedance of microwave circuit 09 p1479 A67-22265

Gunn diode self-pumped parametric oscillator, showing power derived from variation of domain capacity at second harmonic of oscillation frequency 09 p1479 A67-22267

Pulsed oscillations of microwave Gunn effect oscillator in n-type single crystal GaAs 10 p1609 A67-22838

Method of averages in solving resonance problems in wave mechanics 10 p1679 A67-22842

Computer simulation of GaAs Gunn diode in resonant circuit noting frequency, efficiency and load characteristics 10 p1612 A67-23370

Current instability in inhomogeneous plasma formed by drift and ion-acoustic waves with oscillation frequencies 10 p1685 A67-23461

Gunn effect oscillators constructed from epitaxially grown n-type GaAs on n-plus substrate to obtain CW oscillations with frequencies from 3 to 35 10 p1615 A67-23530

Nonlinearity caused by relativistic mass effect leading to radiation maxima of plasma excited by two pulses at electron gyrofrequency 11 p1827 A67-23889

Electron plasma frequency instability, correlating coherent deceleration of electron beam with compression of interference pattern 11 p1827 A67-23890

LF instabilities and anomalous plasma processes in cesium discharge and thermal plasmas 11 p1829 A67-24000

Unidirectional vibration isolation systems, discussing viscous damping, Coulomb damping transmissibility and resonance characteristics [ASME PAPER 67-VIBR-21] 11 p1796 A67-24180

Amplitude control of wind induced oscillation in antenna system through cross section shape [ASME PAPER 67-VIBR-39] 11 p1777 A67-24194

Dispersion relation for LF oscillations in plasma with negative ions derived in three-fluid approximation 11 p1834 A67-24375

Cesium plasma measurements to determine steady state parameters and LF oscillation characteristics 11 p1834 A67-24379

Low temperature alkali plasmas in magnetic fields in terms of collisional drift modes, determining steady state frequencies, amplitudes, etc 11 p1834 A67-24381

One-dimensional weak plasma turbulence, noting structure of spectra for various oscillation frequencies 11 p1837 A67-24393

Elastic properties of tektites measured using resonant sphere technique 11 p1864 A67-24558

Local and overall stability of nonlinear discrete system with variable modes consisting of linear filter preceded by impulse modulator 11 p1770 A67-24751

Oscillating libration orbits with period rigorously commensurable in rational fraction to basic long period 11 p1866 A67-24775

Nonradial oscillations of homogeneous sphere examined on basis of general fourth order problem 11 p1819 A67-24783

Optical transient nutation effect in carbon dioxide laser 11 p1802 A67-24829

Subharmonic oscillations in tunnel diode circuits analyzed, including solutions to forced pumping oscillations and frequency characteristic equations 11 p1768 A67-24858

LF current oscillations excitation in n-type semiconductors analyzed using dispersion equation, noting role of external electric field 11 p1849 A67-24870

Single mode He-Ne laser, noting discontinuities in power output and inhomogeneous nature of gain curve 12 p1951 A67-25147

Electronegative plasma kc oscillations during glow discharge, measuring variations of frequency and longitudinal and radial intensity 12 p1970 A67-25261

UHF oscillations in GaAs thin epitaxial layers deposited on isolating substrates of same material 12 p1981 A67-25279

Stabilization of thermally ionized potassium plasma by applying shear to confining magnetic field 12 p1975 A67-25476

Resonance properties of semiconductor with moving electrical domains, showing periodic variation with illumination intensity 12 p1983 A67-25517

Lower modes and frequencies of natural elastic oscillations of vessel formed by liquid-filled shell of revolution taking into account fluid surface wave and shell inertia 12 p2020 A67-25566

Approximate method for determining free oscillation frequencies of hinged rectangular plate with variable thickness 12 p2021 A67-25574

Matrix integral equations to calculate critical stresses and natural frequencies of oscillation of thin walled isotropic shells of revolution 12 p2022 A67-25585

Natural magnetoelastic oscillations of circular cylindrical conducting shell 12 p2023 A67-25596

Nonlinear oscillations of elastic plates under simultaneous effect of harmonic and random load 12 p2024 A67-25597

Free oscillations of closed freely supported cylindrical shell of concentrated mass, determining frequency and bending moments 12 p2025 A67-25604

Initial imperfection effects on free oscillation frequencies of cylindrical shell under static axial load 12 p2026 A67-25619

Equation for relation between critical stresses of cylindrical shell loading and minimum natural-oscillation frequency of unloaded shell 12 p2027 A67-25623

Asymptotic method of integrating differential equations applied to analysis of

axisymmetrical oscillations of thin elastic LF shells of revolution 12 p2027 A67-25624

Natural oscillation frequency of multilayer shells of revolution with nonsymmetrical structure containing rigid filler and subjected to transverse load 12 p2027 A67-25628

Oscillation frequency and frequency density distribution equations derived for thin elastic shells of revolution clamped along two parallels, using differential equations 12 p2027 A67-25627

Equations for small oscillations of mechanical system with solid components divided into groups by system of generalized coordinates 12 p1967 A67-25661

Natural frequencies of free longitudinal oscillations of circular rod with random parameters determined by modified Krylov-Bogolubov asymptotic method 12 p2031 A67-25957

Polar coordinate analysis of free oscillations of circular plates with loosely clamped edges under large deflections, obtaining Duffing equation 12 p2031 A67-25963

Thermal and ablative lag induced by periodic heat input to oscillating flat plate in high velocity flow, showing crossover from dynamically stabilizing to destabilizing condition as oscillation frequency increases [AIAA PAPER 67-336] 12 p2039 A67-26050

Shock tube analysis of oscillation relaxation in iodine between 1000 and 3800 degrees K 12 p1930 A67-26115

Transient variations in magnetospheric boundary position 13 p2109 A67-26328

Oscillation effect on power and time characteristics of ruby laser output with variable threshold ratios of axial and inner radiation modes 13 p2125 A67-26398

Frequencies of turbine blade vibrations calculated by iteration method, considering coupling between bending and torsion 13 p2217 A67-26744

Lateral bipolar n-p-n transistors fabricated using heteroepitaxial films of silicon on sapphire 13 p2078 A67-26779

Combination tones generation by interaction of orthogonal gas laser oscillations, showing dependence on polarization states and primary oscillations 13 p2126 A67-27015

Oscillation discharge by reactive circuit elements in two-terminal line controlled by movable poles of circuit in complex plane 13 p2085 A67-27723

Resonant oscillation in Penning discharge when electron motion around plasma column perturbs plasma 14 p2355 A67-27828

Moment stress effect on natural oscillation frequency, deriving motion equations of circular cylindrical shell 14 p2401 A67-28735

Elastic vibrations in superconductors noting vortex effects, weaknesses of elastic moduli changes and decrease in ultrasonic attenuation 14 p2375 A67-28988

Pulsed power output for microwave GaAs oscillator biased into avalanche, with diodes grown by liquid phase epitaxy 15 p2442 A67-29172

Current dependent modes in pulsed avalanche diodes 15 p2442 A67-29174

General resistive instabilities of self-pinched cylindrically symmetric beam of charged particles passing through ohmic plasma channel 15 p2522 A67-29198

Subjective responses to oscillation in yaw 15 p2427 A67-29269

Microrocket technology, deriving propellant consumption equations and explaining numerical coefficient variation 15 p2545 A67-29452

Nonlinear oscillation theory for parametric resonance effect in gas lasers placed in stationary and variable magnetic field 15 p2498 A67-29468

Vortex wakes of vibrating cylinders at low Reynolds numbers noting change in geometry along span 15 p2471 A67-29653

Electromagnetic surface wave propagation in plasma, studying oscillation spectra dependence on surface wave field amplitude 15 p2529 A67-29712

Pulsating gravitational collapse from point of view of external observer, noting oscillation period and distortion of contraction expansion symmetry 15 p2556 A67-29863

Relaxation oscillations in n-type indium antimonide crystal under magnetic field

effect and responsivity measurements in far IR 15 p2540 A67-29931

Plasma spectrum, discussing electromagnetic oscillation damping on boundary of two media with different electrical properties 15 p2531 A67-30073

Random instability of nonlinear oscillations of dynamic system with time behavior described by equation 16 p2702 A67-30447

Hall effect measurement in single crystal of arsenic at liquid helium temperatures in magnetic fields noting quantum oscillations 16 p2727 A67-30820

Strong reflection from underlying surface effect on range-only radar measurements, deriving phase angle between side-and carrier-frequency oscillation 16 p2624 A67-31030

Natural oscillations of inertial vertical with nonlinear correction, determining oscillation frequencies and damping rates 16 p2675 A67-31146

Matrix method calculation for frequency, deformation, forces and moments of variable cross section in rotating turbine blade during natural bending oscillation 16 p2766 A67-31150

Waveguide mounted tunnel-diode oscillator noting equivalent circuit, power output, frequency, etc 17 p2822 A67-32037

Gradient stabilization of cryogenic liquids in pendulum and sloshing motions, noting response to kinetic energy input, oscillation frequency period and stability criteria 17 p2836 A67-32053

Thermomagnetic oscillation effect in arsenic, bismuth and antimony using cryostat, noting field strength variation 17 p2912 A67-32267

Confocal ruby laser mode structure analyzed for relation between mode number and spiking regularity, noting frequency hopping 17 p2867 A67-32402

Free convection oscillatory flow from horizontal plate having periodic temperature variations analyzed for LF and HF ranges 17 p2969 A67-32445

Shubnikov-de Haas and Gurevich-Firson oscillations of photomagnetic effect in n-InSb magnetic field 17 p2914 A67-32451

Radiation from two optically coupled cavities of compound laser identical in time and spectral composition without tuning one cavity to other 17 p2868 A67-32661

Electronically swept coherent frequency synthesizer for various bands 17 p2827 A67-32799

Forbidden nitrogen I lines in IR solar spectrum, computing oscillation frequencies, nitrogen abundance and equivalent widths, comparing predictions to observational results 17 p2948 A67-32819

Dynamic system single- and multifrequency random oscillations described by differential-difference equations and solved through probability distribution 17 p2885 A67-32876

Single frequency vibrations of beams and girders solved by applying asymptotic methods 17 p2962 A67-32881

Vibrational temperature determined from relative populations of upper oscillation levels of auroras indicates latitude independence 17 p2849 A67-32963

Arc oscillation in argon in cross flow facility noting parameter ranges, electrode spacing effects, etc 17 p2906 A67-33037

Radial hydromagnetic oscillation frequency of plasma cylinder, calculating g-factor and plasma mass 17 p2909 A67-33117

Power spectrum of pulsating aurora measured at HF, noting relation to modulation mechanism in flux of primary particles 17 p2850 A67-33193

Sommerfeld effect in linear oscillating system with randomly variable natural frequency 17 p2965 A67-33217

Spin-exchange frequency pulling of ground state hyperfine transition in atomic hydrogen analyzed for self-excited oscillation in hydrogen maser 17 p2889 A67-33225

Coherent electromagnetic oscillation from voltage biasing of superconducting weak link producing coupled quantum oscillators 17 p2926 A67-33380

Soviet book on numerical methods for calculating natural oscillation frequencies of liquids in bounded volumes 18 p3026 A67-33772

Spurious phase modulation reduction in multistage frequency multiplier using lumped-selection filters, determining cut-off

angle in multiplying cascades 18 p3000 A67-34087

Upper bounds for cantilever beam natural oscillation frequency error determined when approximately calculated frequency values approach exact values of problem 18 p3143 A67-34168

Noise in injection-synchronized oscillators, deriving inequality 18 p3011 A67-34221

Resonance properties of semiconductor with moving electrical domains, showing periodic variation with illumination intensity 18 p3103 A67-34448

LF oscillations built up in bipropellant rocket engine equipped with pressurized feeding system 19 p3311 A67-35052

Intense HF oscillations from plasma-beam interaction in cold cathodes PIG reflex discharge 19 p3275 A67-35109

Sinusoidal frequency oscillations in DC magnetron plasmas discharge, determining magnetic field, anode current and voltage and gas pressure 19 p3277 A67-35124

Velocity fields in solar atmosphere observed with magnetograph, studying magnetic field effect on oscillations amplitude and frequency 19 p3324 A67-35434

Nonlinear interaction between two waves of multiple frequencies in communication line, nonlinear line capacitance being periodic function of line length 19 p3185 A67-36021

Quasi-CW oscillation at 4880 angstrom of wide-bore AR II ion laser by plasma inductive excitation 20 p3458 A67-36387

Mutual pulling system between two klystrons, deriving equations for pulling bandwidth and for various system responses 20 p3398 A67-36772

Organic dyes as broadband pulsed light amplifiers, noting input frequency relation to laser oscillation quenching 20 p3460 A67-36855

Panel response to oscillating and to moving shock waves, discussing mode excitation, magnification factor, Bessel function, etc 20 p3539 A67-37001

Plasma stability in combined magnetic fields investigated for oscillation frequencies 20 p3500 A67-37048

Triode system of reflex klystron, stressing creation of modulated SHF oscillations device 20 p3451 A67-37148

Potential linear theory applied to oscillatory profiles moving at uniform velocity inside ideal fluid 20 p3424 A67-37593

Frequency and mode configurations of natural symmetric oscillations of elastically clamped cylindrical shells solved by characteristic equation 21 p3717 A67-37974

Gunn effect applied to GaAs crystals for use as diodes, discussing current-voltage characteristics 21 p3684 A67-38444

Frequency stabilization of laser oscillator against reference laser amplifier, noting residual AM effects 21 p3641 A67-38461

Nonlinear oscillation theory for parametric resonance effect in gas lasers placed in stationary and variable magnetic field 21 p3641 A67-38549

Transistor oscillator design stressing output, efficiency and frequency stability at maximum load conductance 21 p3598 A67-38602

Soviet papers on HF properties of plasma including heating, stability, theory, electromagnetic wave scattering, etc 21 p3668 A67-38677

Two-mode laser beam electromagnetic field statistical properties tend to Bose-Einstein form 21 p3642 A67-39117

Monograph on frequency stabilization of LF oscillator by servo method, showing improved SNR of passband 21 p3587 A67-39126

Plasma continuity equations, deriving oscillation frequency equations for LF oscillations in partially ionized gases 22 p3844 A67-39383

Ultrasonic wave absorption in high purity gallium single crystals in magnetic field, observing large magnitude geometric oscillations at cryogenic temperature 22 p3859 A67-39653

Integral equations with integral operators and excitation frequencies for forced oscillation, solving friction via orthogonal iteration approximation 22 p3916 A67-40454

Slide wire strain gauge to measure static

strains and stresses at high temperatures 22 p3809 A67-40476

Oscillations of polytropic and compressible cylinders investigated by small perturbation method noting separate mode of gravitational instability 22 p3896 A67-40526

Current oscillations in Co-doped Si p-n diode devices noting SCL I-V characteristics 23 p3978 A67-40788

Self-synchronization of axial modes of LF oscillations of laser giant pulse intensity with saturable filters 23 p4013 A67-40908

Simultaneous self-starting oscillations at unrelated frequencies in feedback loop containing one nonlinearity, calculating equivalent linear gain 23 p3984 A67-41157

Thermal development method used for observing and recording laser oscillations from output of nitrogen-carbon dioxide systems 24 p4166 A67-41908

Titanium-magnesium and titanium-beryllium oxides physical properties under electron bombardment in vacuum indicate usability for SHF oscillation energy absorbers 24 p4202 A67-42069

Fundamental statistical oscillation characteristics expressions for quasi-harmonic self-excited oscillators with low noise and many degrees of freedom 24 p4129 A67-42225

Read type and avalanche type oscillations in silicon varactor diodes, noting parasitic series resistance and electric field peak effects 24 p4133 A67-42820

Separate studies of power and collision broadening of gas laser transition showing proportional DC laser power to square of gain 24 p4169 A67-43103

OSCILLATOR

SA BACKWARD WAVE OSCILLATOR

SA ELECTRON TUBE

SA HARMONIC OSCILLATOR

SA MECHANICAL OSCILLATOR

SA MOLECULAR OSCILLATOR

SA PARAMETRIC OSCILLATOR

SA SUBHARMONIC OSCILLATOR

SA SYNCHRONIZED OSCILLATOR

SA VACUUM TUBE OSCILLATOR

Noise spectra measurements performed on two Read diode and two Gunn oscillators by reflection cavity microwave discriminator technique 01 p0033 A67-10017

Epitaxial gallium arsenide Gunn effect oscillators in generating continuous wave oscillation 01 p0033 A67-10026

Amplitudes of two-mass single-spring system, using Rayleigh approach to determination of eigenfrequencies 01 p0159 A67-10282

Oscillation frequency of maser oscillator calculated using perturbation theory, noting traveling wave effect 01 p0089 A67-10395

Locked oscillation of silicon p-n junction avalanche diodes in 50 to 140 GHz range 01 p0035 A67-10436

Optimal control of one-dimensional distributed oscillatory system and wave processes using momentum theory and propagating method 01 p0044 A67-10493

Harmonic linearization technique to examine characteristics of oscillatory circuits with nonlinear capacitors 01 p0038 A67-10715

Constant phase local oscillator distributing signals for radio telescope, measuring phase length of transmission line 02 p0212 A67-11608

Emission of point oscillator located in medium having permittivity varying according to traveling wave law 02 p0192 A67-11643

Improved frequency stability and specific transistor characteristics of transistor oscillators with AGC 02 p0216 A67-11981

Bulk GaAs Gunn effect oscillators and amplifiers and electron transfer between high mobility and low mobility conduction bands 02 p0218 A67-12099

Logarithmic conversion of input-signal amplitudes into pulse numbers, using oscillatory circuit 02 p0221 A67-12419

H-2 Stokes Raman oscillator operating at 9755 angstroms, finding performance as expected of laser oscillators with beam instability not developed 02 p0253 A67-12516

Fluidic oscillators, negative-and positive-gain operational amplifiers and cascade circuits 03 p0363 A67-13233

Quartz self-excited oscillator employing Hartley oscillator circuit 03 p0378 A67-13289

Frequency oscillations in oscillator with double-loop delayed

feedback 03 p0378 A67-13291
 Relationships involving power and efficiency of self-excited tunnel diode oscillator, calculating effect of parasitic TD parameters and circuit 03 p0381 A67-13584
 Internal modulation and heterodyning in construction of highly linear large-deviation VHF solid state FM oscillator /FMO/ 03 p0381 A67-13636
 Avalanche transit time diode used as sideband translator and combination local oscillator-mixer at X-band 03 p0381 A67-13666
 Phase locking of pulsed Gunn oscillators with 0.3 to 1 microsecond pulse widths in S-band 03 p0382 A67-13672
 Transistor hybrid equivalent circuit of large amplitude sinusoidal voltage used in design of LC oscillators, power amplifiers, etc 03 p0387 A67-13998
 Steady state oscillation regime of one-dimensional oscillator determined by replacing arbitrarily shaped hysteresis loop with ellipse of equivalent area, noting higher harmonics effect 03 p0530 A67-14176
 SHF oscillator construction using multiphonon processes that occur in gases during dipole interactions 04 p0580 A67-14749
 Microwave varactor tuned transistor oscillator design, considering collector base multiplication, oscillation and load matching conditions and theoretical tuning curve 04 p0581 A67-14864
 Vertical hydrogen beam oscillator serving as atomic clock, noting design principle and operation 04 p0632 A67-14898
 Pneumatic oscillator producing triangular waveforms of pressure vs time, using freely floating disk [ASME PAPER 66-WA/AUT-4] 04 p0555 A67-15388
 Isocline method used to analyze quasi-linear equation for single-loop self-excited oscillator with periodically varying bias voltage and resonant frequency radio signal 04 p0586 A67-15676
 Pulsed high energy ionizing radiation effects on behavior and output frequency of electronic quartz oscillator crystals 04 p0685 A67-15700
 Hydrogen molecule excitation by electron impact extended to D excited state, noting values for oscillator 04 p0662 A67-15767
 Simultaneous free and parametric oscillations of elastic cylindrical shell of infinite length and subsonic flow of ideal gas in shell 04 p0717 A67-15888
 Main properties of phase automatic frequency control, using standard signal as additional action on self-excited oscillator 05 p0764 A67-16904
 X-band Gunn oscillator with dielectric tuning system 05 p0775 A67-16951
 Doppler effect on emission spectrum and energy of moving oscillator and intensity of surface wave excited by it 05 p0765 A67-17160
 RF power oscillator for low pressure plasma production, noting work and grid coils and time and power controls 05 p0856 A67-17281
 FM in quartz oscillators, deriving nonlinear distortion and frequency deviation factors and analyzing effect of destabilizing factors 05 p0767 A67-17400
 Input device for quadrupole amplifiers in form of sequential oscillators with inductive coupling used to widen frequency band of output 05 p0785 A67-17472
 Spectra of unlocked driven semiconductor oscillators observed with millimeter wave reflex klystrons, noting gradual controllable frequency pulling 05 p0780 A67-17522
 Operation of synchronized neodymium laser time variable reflection /TVR/ oscillator, using single pockels cell to obtain Q-switching and cavity dumping 05 p0826 A67-17525
 Synthesis of potentially bistable oscillator configurations serving as prototypes for integrated nearly sinusoidal applications 06 p0967 A67-17812
 Performance of transferred electron oscillators produced by alloying Sn contacts on to epitaxial GaAs 06 p0971 A67-18225
 Impact excitation of oscillation with oscillating circuit in anode and cathode 07 p1150 A67-19236
 Book on lasers, light amplifiers and oscillators noting optical resonators, optical

pumping, pulsed lasers, etc 07 p1195 A67-19469
 Short pulse start/stop control of tunnel diode oscillator 07 p1153 A67-19608
 Vapor phase epitaxial deposition of n-type GaAs contact layers for Gunn effect X-band oscillators 07 p1153 A67-19609
 Growth of solutions of forced oscillations of nonlinear oscillator driven by white noise 07 p1218 A67-20268
 Analysis of uncontrolled synchronized self-excited oscillator 08 p1302 A67-20829
 Determination of length of deductive circuits of recycling memories and oscillators 08 p1302 A67-20835
 Continuous waves from synchronized pulsed bulk GaAs oscillators operating in microwave region 09 p1471 A67-21645
 FM noise source in cavity controlled Gunn effect oscillator 09 p1474 A67-22040
 Upper frequency limit prediction method for Gunn oscillations 09 p1556 A67-22264
 Troubleshooting problems in oscillator circuit solved via Bayesian computer program simulating critical behavior 09 p1456 A67-22369
 Local oscillators with standardized frequencies in conjunction with central mixer used as wideband noise receiver for increased sensitivity 09 p1481 A67-22480
 High stability clocks for trajectory measurement with oscillator, using atomic or molecular transitions [ONERA-TP-459] 10 p1655 A67-22880
 Design equations and computer calculated curves to achieve varactor-tuned octave bandwidth transistor oscillators by using transmission line 10 p1613 A67-23412
 Epitaxial advantages over melt grown GaAs in construction of continuous wave and pulsed Gunn effect oscillators 10 p1616 A67-23531
 Gunn effect devices high efficiency achievement, considering circuit and material from theoretical and experimental viewpoint 10 p1616 A67-23535
 Optimal control of one-dimensional distributed oscillatory system and wave processes using momentum theory and propagating method 10 p1621 A67-23615
 Amplifier and self-excited oscillator employing reflex klystron with phase locking 11 p1757 A67-23907
 Phase locking experimental data on injection locked X-band Gunn effect microwave oscillators 11 p1759 A67-24128
 Relationship between domain transit frequency and cavity controlled frequency of thin Gunn devices 11 p1759 A67-24130
 Telemetry transmitters using solid state wideband microwave voltage-controlled oscillators 11 p1753 A67-24442
 Phase locking in phase plane on modulation of driver and self-excited oscillator, using differential equation 11 p1754 A67-24725
 Shock tube study of oscillator strength of diatomic molecular carbon Swan bands 11 p1750 A67-25066
 Explanation of anomalies of experimental static current-voltage characteristics of GaAs tunnel diode oscillators 12 p1917 A67-26098
 Oscillator strengths for extreme UV resonance lines of ions in neon isoelectronic sequence calculated, based on single configurations in intermediate coupling 12 p1968 A67-26247
 Amplitude and frequency fluctuations in flicker noise region of transistorized quartz oscillator 13 p2075 A67-26395
 Two 8-cascade tunnel diode oscillators with HF oscillations and low resonant resistance 13 p2078 A67-26750
 Wideband tank circuit using ferromagnetic core with negative frequency characteristic in induction coil 13 p2071 A67-27277
 Laser gas-discharge tube /without resonator/ amplification relations, considering stimulating radiation, noting application as oscillator 14 p2328 A67-27771
 Circuit for multifrequency ionospheric probing, with basic frequency scanning unit containing sawtooth pulse oscillator 14 p2315 A67-27949
 Radio interferometer design with superlong base compensating for phase fluctuations 14 p2261 A67-28068
 Jet driven fluoric oscillator 14 p2251 A67-28344
 Book on theory and practice of transistor circuits covering oscillator theory, transistor

noise, frequency modulation, band filter linkage, etc 14 p2290 A67-29007
 Volt-ampere characteristics of gallium arsenide tunnel diode oscillators 15 p2443 A67-29285
 Racalator as alternative to frequency synthesis noting design principles, operation and results 15 p2445 A67-29586
 Plasma characteristics and instability when plasma waves lead to current oscillations in bulk semiconductor 15 p2450 A67-29814
 Main properties of phase automatic frequency control, using standard signal as additional action on self-excited oscillator 16 p2623 A67-30880
 Nonuniformity of mm wave detected by wideband frequency sweep control backward wave oscillator 16 p2643 A67-30896
 Tunnel diode oscillator design from averaged and normalized current-voltage characteristics 16 p2637 A67-31028
 Waveguide mounted tunnel-diode oscillator noting equivalent circuit, power output, frequency, etc 17 p2822 A67-32037
 Averaging principle applied to stochastic differential equations describing oscillatory system subject to white noise effects 17 p2885 A67-32878
 Interferometer operated with independent oscillators and without wide bandwidth communication link between elements, making operation possible at very long base lines 17 p2864 A67-33363
 Coherent electromagnetic oscillation from voltage biasing of superconducting weak link producing coupled quantum oscillators 17 p2926 A67-33380
 Oscillator analysis for particular class of adiabatic invariants 18 p3117 A67-33686
 Operating spectrum of tunnel diode oscillator developed according to waveguide techniques, determining optimal requirements 18 p3011 A67-34232
 Gunn effect semiconductor oscillator for generating microwave power using GaAs 18 p3013 A67-34525
 Synthesis of potentially bistable oscillator configurations serving as prototypes for integrated nearly sinusoidal applications [AIAA PAPER 65-363] 19 p3227 A67-34821
 RC oscillators based on silicon n-p-n transistors for radio frequencies, analyzing active all-pass phase-shift circuit 19 p3191 A67-34946
 Pulsed operation of large-area silicon p-n junction avalanche diode oscillators for microwave frequencies 19 p3196 A67-35627
 Cooling and illumination effect on Gunn oscillators resulting in abrupt shift from transit-time frequency mode to higher frequency 19 p3305 A67-35628
 Boundary value problem of oscillatory system with time lag quasi-linear partial differential equation 19 p3251 A67-36050
 Semiconductor laser light field amplitude equation of van der Pol oscillator derived and shown valid for optical band-to-band transitions 20 p3461 A67-37184
 High stability quartz master oscillator for D-1 satellite transmitter control 21 p3591 A67-38206
 Far IR maser oscillators with water and deuterium oxide, presenting construction and operating characteristics 21 p3639 A67-38253
 Linear oscillator forced motion subjected to harmonic AM perturbations studied for servomechanisms 21 p3658 A67-38554
 Transistor oscillator design stressing output, efficiency and frequency stability at maximum load 21 p3598 A67-38602
 Amplifier and self-excited oscillator employing reflex klystron with phase locking 21 p3600 A67-38935
 Monograph on frequency stabilization of LF oscillator by servo method, showing improved SNR of passband 21 p3587 A67-39126
 Quantum theory of maser oscillator model consisting of radiation field mode interacting with 3-level atoms 22 p3814 A67-39436
 Soviet monograph on multiphase relaxation oscillators including circuit analysis for use in automation, telemechanics and radio engineering 22 p3788 A67-39464
 Ruby rods in concentric spherical cavities observing spiking, mode structure and output energy 22 p3817 A67-40485
 Fluidic digital component design utilizing

wave phenomena produced by two interacting low entropy pneumatic jets, discussing nozzle geometry and fluidic oscillators 23 p3936 A67-41421
Silicon avalanche oscillators under continuous operation at millimeter wavelengths, discussing efficiency and power densities 24 p4133 A67-42815

OSCILLATORY COMBUSTION S COMBUSTION INSTABILITY

OSCILOGRAPH

SA BARKHAUSEN EFFECT
Oscillogram interpretation during ultrasonic inspection of turbine and compressor blades 06 p1007 A67-18098
Impact bending and tension processes using drop hammer technique evaluated with improved method using oscillography for high quality load-time measurements 13 p2215 A67-26391
Nanosecond baseband pulse rise time measurement, discussing real time and sampling oscillography, pulse comparison, basic instrumentation, etc 17 p2814 A67-32603
Successive release evaluation by periodometer and memory oscillograph of viscous damping of one degree of freedom system 17 p2884 A67-32698
Coupling factor between microwave resonator and transmission line determined by oscillographic recording of microwave field 18 p3010 A67-33508
Phase delayed triggering of oscillographs using ring type potentiometer to produce phase displacements by mechanical rotation 22 p3799 A67-39754
Q-switched laser single pulse visual recording by oscillograph with storage tube/photodiode combination 22 p3817 A67-40415

OSCILLOSCOPE

Oscilloscope plotting of Langmuir probe and double probe characteristics corresponding to time varying plasma properties 12 p1947 A67-26122
Oscilloscope recording of mechanical rotation rate using semiconductor photoelectric effect 22 p3796 A67-39341

OSEEN APPROXIMATION

Injection from half-plane located in steady viscous flow in Oseen approximation, noting skin friction 01 p0052 A67-10793
Oseen flow past semilinear plate and vertical force formulated by integral equations solved for drag and lifting singularities distribution, using Wiener-Hopf technique 08 p1319 A67-20350
Oseen equations inadequacy in ensuring uniqueness for flow past infinite body 08 p1319 A67-20351
Laminar diffusion flame in Oseen flow, identifying limiting case with stoichiometric Burke-Schumann flame and frozen flow 09 p1579 A67-21548
Counterpart of Stokes hydrodynamical paradox for linearized viscous fluid flow obtained from application of singular perturbation to Oseen equations 16 p2657 A67-30827

OSMIUM

Re and Os abundances in various chondrites determined by neutron activation analysis, noting fractionation 24 p4235 A67-42637

OSO

Calibration procedures for earth albedo experimental package of Orbiting Solar Observatory 02 p0246 A67-12401
Ames emissivity experiment on OSO-II to measure thermal radiation properties of temperature control coatings exposed to space environment [AIAA PAPER 65-651] 03 p0448 A67-13056

OSO-I

Upper limits on cosmic gamma ray flux obtained using OSO-I and sodium iodide scintillation counters 12 p1995 A67-25763
Solar gamma-ray flux in high energy region analyzed using OSO-I satellite 14 p2381 A67-28057
Solar neutron observations with boron fluoride counter on OSO-I, discussing absence of diurnal variation 23 p4061 A67-41236

OSO-II

Albedo and earth-radiation measurements from OSO-II compared with other results, noting limb-brightening effect [AIAA PAPER 67-330] 12 p1938 A67-26044

OTOLITH

Extraterrestrial vestibular research in

orientation of humans in space, noting possible disorders due to radiation and lack of protection 15 p2425 A67-29106
Mathematical model for otolithic organs used to analyze human spatial orientation 16 p2610 A67-30753
Vestibular organ acceleration while walking at lunar and earth gravity 23 p3953 A67-41584

OTOLOGY

Aeromedical problems associated with surgical procedures for relief of otosclerosis 13 p2060 A67-26928

OUTER RADIATION BELT

SA INNER RADIATION BELT

SA VAN ALLEN BELT

Temporal variations of intensities of electrons of various energy ranges trapped in outer radiation zone measured by research satellite Injun III 04 p0693 A67-14962

Correlation of time variations of proton and electron intensity of outer radiation belt and dependence on geomagnetic environment 07 p1243 A67-19828

Laminar composition structure and periodicity of variations with time in outer radiation belt investigated by solar radiation satellites 10 p1701 A67-23298

Low energy proton and electron outer radiation belt satellite Cosmos 41 indicate capture and acceleration mechanism 12 p1997 A67-25810

Magnetic field variations in magnetosphere at distances of 3 to 6 earth radii attributed to distribution of trapped radiation 12 p1997 A67-25814

Equatorial measurement of intensity of protons with energies greater than 400 kev and electrons with energies greater than 2 mev in outer radiation belt center in 1964 13 p2191 A67-26544

Relativistic-electron diffusion wave in outer radiation belt recorded by device mounted on Cosmos XII satellite in high geomagnetic latitudes 13 p2191 A67-26545

Time variations of electron intensity in outer radiation belt observed by satellites, studying electron radial diffusion and drift velocity 19 p3313 A67-35257

Low energy proton flux increases in outer radiation belt during quiet magnetic activity and correlation with magnetic bay appearances 20 p3519 A67-37408

Outer Van Allen radiation zone intensity maximum position dependence on electron energy and magnetic activity, noting relation to diffusion theory 22 p3870 A67-39620

Energetic outer radiation belt electron spectra spatial and time variations 22 p3873 A67-39822

OUTPUT

SA FREQUENCY STABILITY

SA LASER OUTPUT

SA MASER OUTPUT

Maximal error estimation arising from delay in output functions of servomechanisms provided bandwidth, maximum oscillation and slope are known 08 p1286 A67-20780

Input-to-output amplitude and phase modulation characteristics derived for multicavity klystron amplifiers 19 p3197 A67-35809

Optimum output-input characteristic of memoryless nonlinear system determined from solution of integral equation 20 p3407 A67-36382

Duration of dynamic system output for given input time calculated by computer programming 22 p3784 A67-39336

Optimal output effect for spatial temporal processing of signals in presence of multiplicative and additive signal fluctuations 24 p4120 A67-42232

OV-10 AIRCRAFT

Flight test program of North American OV-10A COIN /counter-insurgency/ aircraft 06 p0947 A67-18199

OV-10A aircraft testing in landing and takeoff from fields, jungle clearings and primitive roadways 10 p1594 A67-23391

Landing gear for operating off rough terrain and unprepared airstrips in OV-10A Bronco aircraft for counter insurgency 17 p2794 A67-31989

OVER-WATER FLIGHT

Tilt and vertical float program of Naval Air Systems Command comprising four studies covering factors involved in any open ocean aircraft 03 p0354 A67-12901

Bertin type air cushion vehicles, examining power supply and refinements required for over-water application 03 p0358 A67-12977

Problems involved in ditching business aircraft on ocean and subsequent recovery 14 p2245 A67-28319

OVERVOLTAGE

Photon transmission delaying processes and secondary ionization growth time dependence on overvoltage in neon 19 p3284 A67-35086

OV2 /ORBITING VEHICLE-2/

General utility spacecraft family, orbital bus and multiple orbit/payload launch missions for reducing unmanned space research and development costs [AIAA PAPER 67-637] 20 p3534 A67-37617

OXIDASE

Purification and properties of nicotine oxidase suggest metalloflavoprotein having riboflavin 5-phosphate 20 p3376 A67-37032

OXIDATION

SA COMBUSTION

SA ELECTROCHEMICAL OXIDATION

Oxidation and ablation characteristics of tantalum in hyperthermal arc tunnel filled with oxygen-nitrogen mixtures 01 p0102 A67-11153

Free radicals in gas phase oxidation and spontaneous ignition reactions 02 p0341 A67-11502

Properties of Si-Si interface subjected to thermal oxidation in dry and wet oxidizing gases, thermal decomposition of ethyltriethoxysilane and vacuum evaporation of SiO and quartz 02 p0293 A67-11751

Properties of silicon dioxide-silicon system, examining oxidation process and electrical properties of metal oxide silicon /MOS/ structure 03 p0500 A67-14181

Oxidation of Al-2 percent aluminum oxide SAP type alloy foil heated in situ and observed by hot stage transmission microscopy, electron diffraction and motion picture micrography 04 p0635 A67-14513

Monograph on low temperature oxidation including kinetic mechanism, oxidation of various compounds, knock phenomenon, etc 04 p0565 A67-15089

Oxidation processes by treatment of composite and elementary reactions, noting chain reactions and chain branching 04 p0565 A67-15090

Hydrogen oxidation noting explosive property as function of temperature, pressure, composition, etc 04 p0565 A67-15091

Carbon monoxide reaction with oxygen noting effects of various hydrogen-containing compounds, discrepancies in explosion limits, etc 04 p0565 A67-15092

Carbon disulphide oxidation noting self-ignition temperature, explosion limits, reaction products, cool flame propagation, etc 04 p0566 A67-15093

Hydrogen sulfide oxidation, role of temperature and pressure, determining explosion levels 04 p0566 A67-15094

Oxidation by nitrous oxide, nitric oxide, nitrogen dioxide and ozone, considering various reactions 04 p0566 A67-15095

Mercury photosensitized oxidation of tetrafluoroethylene, noting reaction process and parameters 04 p0567 A67-15950

Structural changes during oxidation of chromium-yttrium alloys determined by measuring gain in weight per unit surface of samples heated in SiH₄ or molybdenum oven in open aluminum tubes 05 p0827 A67-16327

Steady state kinetics and microstructures of simultaneous internal oxidation and external scale formation of Cu-Zr and Cu-Zr-Re alloys in pure oxygen at 1000 degrees C 05 p0828 A67-16471

Two oxidation mechanisms for Ti-Al alloys based on increased diffusion rate and decreased oxidation rate 05 p0829 A67-16492

Titanium oxidation characteristics, determining activation energy of scale formation, oxygen absorption of base metal and total oxygen 05 p0829 A67-16759

Oxidation of vacuum-deposited bismuth films, determining ionic and electronic transport numbers 06 p1013 A67-17659

Gas phase oxidation of diborane in furnace-heated vessels and flash photolysis 06 p0955 A67-18058

Ni, Si and Nb effect on oxidation of binary alloys of titanium in air at high temperature, discussing heat

resistance 07 p1205 A67-19275
Sulfur compound in carbonaceous
chondrites explained by oxidation of troilite
by oxygen and HOOH 07 p1249 A67-19539
Oxidation of tantalum coated with
aluminum and aluminum-chromium alloys at
high temperatures and various oxygen
pressures, using X-ray diffraction, electron
microscopy, etc 08 p1341 A67-20764
Electrical resistance and weight increase
measurements in aluminum and Al-Mg alloys,
noting relation between oxidation rate and
Mg content during 08 p1341 A67-20796
annealing 08 p1341 A67-20796
Deoxidative capacity and activity of
titanium in nickel-chromium
alloys 09 p1518 A67-21964
Oxygen chemisorption and oxidation on
tungsten ribbon studied by flash desorption,
using mass spectrometer 09 p1457 A67-22023
Reaction rate of oxygen jet impinging on
tungsten samples at high temperature and
various pressures, noting activation energy
and diffusion effect 09 p1457 A67-22026
Anodic oxidation and molecular structure
influence on performance of normal
saturated hydrocarbons in fuel
cells 10 p1595 A67-22927
Derivation and computer method solution
of equations describing thermodynamic
equilibrium of gaseous products from
oxidative combustion of
methane 11 p1881 A67-24023
Rate of formation of tungsten oxide in
porous sample, noting increase in rate of
oxidation due to porosity
effect 11 p1809 A67-24915
Book on high temperature oxidation of
metals and alloys, fundamental aspects and
reaction mechanisms 13 p2141 A67-27178
Ultrahigh vacuum and air fatigue testing
of aluminum alloy observing corrosion
process influence on mechanism by
latter 16 p2689 A67-31369
Slow oxidation of n-octane vapor /oxygen/
nitrogen mixtures at reduced pressures and
temperatures 16 p2779 A67-31518
High temperature oxidation of titanium at
reduced oxygen pressures governed by
dissolution of oxygen in
metal 17 p2873 A67-32812
Two oxidation mechanisms for Ti-Al alloys
based on increased diffusion rate and
decreased oxidation rate 17 p2875 A67-33175
Oxide films on silicon, discussing silica
glass properties, junction formation, surface
protection/passivation, device structures and
oxidation techniques 18 p3096 A67-33454
Measurements of induction period,
ammonia consumption rate after induction
and radiation from electronically excited OH
radicals in ammonia-oxygen
reaction 18 p3155 A67-33836
Interaction of oxygen with tungsten
surface at room 19 p3244 A67-34940
criticism of McCarroll statement on oxide
formation on tungsten surface at room
temperature 19 p3244 A67-34942
Ignition and extinction characteristics of
liquid fuel droplets burning in oxidizing
atmosphere calculated, using finite rate
kinetics 19 p3214 A67-35000
Ethylene-oxygen reaction in shock waves,
studying induction period and time
dependency of mixture composition,
ionization and
chemiluminescence 20 p3376 A67-36232
Durability and electrical conductivity of
metallic fiber materials noting influence of
oxidation on properties 20 p3466 A67-36912
Oxidative phosphorylation effects on
energy metabolism of *Thiobacillus thioautotrophicus*
in cell-free system 20 p3371 A67-36927
Nitrogen role in oxidation of titanium in
air at elevated temperatures studied by
spectrographic analysis 21 p3643 A67-37828
Gas chromatography and IR
spectrophotometry used to examine
monomethyl hydrazine air oxidation, showing
evidence of surface catalyzed
reaction 21 p3578 A67-38841
Oxidation of ultrahigh purity Co at various
oxygen pressures and at high
temperatures 23 p4018 A67-40872
Ti thin films use as getter in electron
microscopy of Mo particles at high
temperature with minimum
oxidation 24 p4172 A67-41978
OXIDATION RESISTANCE
Oxidation resistant thermal protection

materials for 4000 degrees F high velocity
air environment 01 p0094 A67-10617
[SAE PAPER 660659]
Titanium shavings application preventing
iron oxidation during 01 p0095 A67-10643
heating 01 p0095 A67-10643
Total normal emittance of various
oxidation-resistant materials to very high
temperatures in air determined, using
special apparatus 03 p0447 A67-13035
[AIAA PAPER 65-655]
Thermo-oxidative stability of
polyphenylene resins in asbestos reinforced
laminates 03 p0451 A67-13400
Phenothiazine carboxylic acid esters as
improved antioxidants in stable and sludge-
free synthetic oils 09 p1520 A67-21705
Electron microprobe analysis for
examining oxidation reduction mechanism in
iron meteorites 11 p1865 A67-24606
Cobalt alloys precipitation hardening
behavior, oxidation, thermal shock resistance
and stress rupture 11 p1808 A67-24704
High strength nickel base alloy with
improved oxidation resistance up to 2200
degrees F for applicability to gas turbine
engine components 11 p1808 A67-24789
[ASME PAPER 67-GT-1]
Alloy 718 composition, microstructure and
heat treatment behavior correlated with
mechanical properties, noting strengthening
and oxidation resistance 12 p1956 A67-25949
[ASME PAPER 67-MET-5]
Beryllium oxidation in high temperature
range 13 p2136 A67-27107
Stability of titanium-aluminum alloys
during oxidation in air 13 p2142 A67-27287
Oxidation resistant-coated refractory alloy
systems for use on reentry
vehicles 15 p2466 A67-29537
Solid self-lubricating materials
mechanically strong and resisting oxidation
for high temperature air applications,
examining friction-wear
characteristics 16 p2683 A67-31752
Experiments on oxidation kinetics of
refractory metals in undissociated and partly
dissociated oxygen-chlorine
mixtures 17 p2971 A67-33021
Titanium shavings application preventing
iron oxidation during 18 p3066 A67-34407
heating 18 p3066 A67-34407
Refractory metals physical, mechanical and
chemical properties when coated with
oxidation resistant 19 p3244 A67-34958
coatings 19 p3244 A67-34958
Fabrication, structure, possible failure and
testing of coated refractory metals in
applications for space
technology 19 p3245 A67-34959
Refractory metals and oxidation protection
noting coating materials, application
methods, etc 20 p3463 A67-36133
Ceramic-to-metal sealing method based on
use of ductile nickel-titanium intermetallic
compound as braze 20 p3454 A67-36518
Scaling resistance of nickel and cobalt
binary alloys investigated to determine heat
resistance as function of
composition 20 p3467 A67-37115
Compositional changes at alloy/oxide
interface during protective oxidation
calculated using finite difference
method 20 p3468 A67-37247
Amine-tin antioxidant systems for aliphatic
hydrocarbons and related alkyl substituted
fluids 20 p3474 A67-37594
Vapor deposition-prepared continuous
silicon carbide filaments for use as
reinforcement in high strength oxidation-
resistant structural plastic
composite 21 p3648 A67-37881
Oxidation mechanisms for nickel-aluminum
alloys studied for effects of temperature
and alloy composition 21 p3645 A67-38773
Oxidation process and mechanical
properties of austenitic steels and alloys
under prolonged loading at high
temperatures, giving stress-durability
diagrams 22 p3819 A67-39322
WC-NbC-Co alloys oxidation resistance in
air studied by sintering powdered WC and
NbC with Co, finding oxidation rate linear
function of time 22 p3820 A67-39565
Chromate conversion process applicable to
IC interconnecting aluminization reveals
defective areas under normal quality control
procedures 22 p3771 A67-39835
Hafnium-tantalum coated refractory metals

investigated for use in high temperature
rocket motors 22 p3821 A67-39891
Barrier system for oxidation resistant
protective coating for high temperature
protection of refractory
coatings 23 p4018 A67-40900
Ni-Cr superalloy oxidation and sulfidation,
relating superalloy resistance of uncoated Ni
superalloys to matrix Cr content
[ASM PAPER C6-18.5] 23 p4020 A67-41406
Slurry coating applied to aerospace
refractory metal component for oxidation
protection 23 p4020 A67-41407
[ASM PAPER C6-1.5]
Strength and oxidation tests evaluated for
coated fasteners in extreme temperature
use 24 p4160 A67-42078
Chemical interactions in formation of
oxidation resistant solid lubricant composites
of tungsten diselenide-gallium alloys for use
in ball bearing systems 24 p4164 A67-42745
[ASLE PAPER 67-LC-6]
Molybdenum sulfide solid lubricant
oxidation characteristics analyzed by
thermogravimetry 24 p4165 A67-42748
[ASLE PAPER 67-LC-14]
OXIDE
SA ALUMINUM OXIDE
SA BERYLLIUM OXIDE
SA BORIC OXIDE
SA BORON OXIDE
SA CALCIUM OXIDE
SA CHROMIUM OXIDE
SA COPPER OXIDE
SA DEUTERIUM OXIDE
SA ETHYLENE OXIDE
SA GERMANIUM OXIDE
SA HAFNIUM OXIDE
SA IRON OXIDE
SA LEAD OXIDE
SA LITHIUM OXIDE
SA MAGNESIUM OXIDE
SA MANGANESE OXIDE
SA METAL OXIDE
SA MOLYBDENUM OXIDE
SA NICKEL OXIDE
SA NIOBIUM OXIDE
SA NITROGEN OXIDE
SA PEROXIDE
SA PROPYLENE OXIDE
SA SILICON OXIDE
SA TANTALUM OXIDE
SA TITANIUM OXIDE
SA TRIFLUOROAMINE OXIDE
SA TRIOXIDE
SA TUNGSTEN OXIDE
SA URANIUM OXIDE
SA VANADIUM OXIDE
SA YTTRIUM OXIDE
SA ZINC OXIDE
SA ZIRCONIUM OXIDE
Polarized radiation measurements of far
IR absorption coefficient and refractive
indices in lithium niobium
oxide 03 p0496 A67-13571
Electrochemical properties of solid
refractory oxides for high temperature fuel
cells 08 p1284 A67-20703
Hot electrodes for open cycle MHD
generators, noting refractory
oxides 12 p1899 A67-25405
Emittance properties of sintered oxides
treated by method of empirical
generalization and by method involving
comparison of emittance in air and in
vacuum 12 p1958 A67-28016
[AIAA PAPER 67-301]
Dissociation energy of nitrous oxide
reconciled with electron physics
data 12 p1904 A67-28230
Design and fabrication of germanium Esaki
diodes emphasizing development of planar
process, using conventional oxide masking
techniques 13 p2083 A67-27572
Estimation of statistical sums of states of
groups of oxides and fluorides at high
temperatures 16 p2704 A67-31390
Temperature dependence of oxide
hardness relative to other materials,
comparing oxide hardness data to carbide
data 20 p3472 A67-36113
OXIDE FILM
Optical characteristics, including refractive
indices, of thin layer amorphous titanium
oxide films 01 p0115 A67-11048
Stresses and stress relaxation in thin
oxide films deposited by various methods on
glass substrates from elastic or plastic
deformation at elevated
temperatures 02 p0288 A67-11719
Ion transport on and through thin oxide

layers of MOS structure investigated by charge comparison method 02 p0293 A67-11750

Thermal emittance of nickel as function of oxide thickness measured, using filament in vacuum technique and microphotography [AIAA PAPER 65-673] 03 p0440 A67-13041

Schottky emission as rate limiting factor in thermal oxidation of metals 04 p0677 A67-14947

Environmental effects on mechanical behavior of metals in vacuum and gases normally found in atmosphere, considering surface oxide layer 04 p0638 A67-14996

Impurity distribution in epitaxial films at film/substrate interface after oxidation under different oxidation conditions for silicon planar devices 05 p0869 A67-17095

Conductivity changes in flash evaporated p-GaAs films caused by field effect and optical and thermal excitation at temperatures about 100 degrees K 07 p1232 A67-19564

Oxide film surface effect on electrophysical characteristics of Ge surface, noting potential changes and recombination rate 08 p1367 A67-20412

Surface oxide films and lifetime of vacancies in thin crystals analyzed for pure aluminum and dilute aluminum alloys 08 p1369 A67-20794

Insulated gate to obtain depletion in channel of MOS-FET transistor, noting inversion layer and frequency response 09 p1475 A67-22202

Thin film silicon-on-sapphire deep depletion MOS transistors 09 p1475 A67-22203

Tin oxide films in microscopic quantities on glass and quartz substrates studied for transparency, reflectivity and roughness 12 p1982 A67-25324

Thermal radiation properties of oxide films of variable thickness on metal substrates, using radio-recording spectrophotometer at various wavelengths [AIAA PAPER 67-286] 12 p1958 A67-26003

Photoengraving and use as precision processing technique 12 p1951 A67-26213

Anodic oxides of titanium, tantalum and niobium from thin dielectric film preparations compared, determining nature and characteristics 13 p2175 A67-26654

Anisotropy in thin dielectric films of tantalum and titanium anodic oxide from various measurements explained by transistor-like model 13 p2175 A67-26655

MOS oxide-film thickness estimation by extrapolating MOS capacitance-voltage curve into accumulation region at high negative bias 15 p2539 A67-29815

Oxide films on silicon, discussing silica glass properties, junction formation, surface protection/passivation, device structures and oxidation techniques 18 p3096 A67-33454

Degree of blackness of normal black body radiation for various metals, studying temperature and kinetic relations and blackness of opaque oxide films 18 p3064 A67-34052

Growth rate of oxide and other dielectric contact films on metal crystals computed for ionic diffusion and electron tunneling 18 p3103 A67-34590

Image-force effects in normal state tunneling through lead-oxide-lead junctions exhibiting Josephson effect [JPL-TR-32-1154] 18 p3106 A67-34647

Water adsorption on oxide covered surface of germanium, studying chemisorption dependence on p-type doping 19 p3301 A67-34935

Interaction between environment, oxide layer and surface slip formation in aluminum during cyclic bending 19 p3247 A67-35788

Lossless small-area Josephson junction analyzed from viewpoint of quantum dynamics, considering system of two superconducting plates 20 p3505 A67-36207

Aluminum corrosion behavior stressing surface oxide film condition 20 p3465 A67-36635

Space environmental effect on lubricants and rolling element bearings, comparing evaporative losses of solid and liquid lubricants 21 p3633 A67-38143

Diode volt-ampere characteristics, considering space charge in base barrier layer and rear contact oxide film, noting vertical section appearing on direct branch 21 p3593 A67-38291

Structural properties of Si anodic oxide

layers studied by X-ray analysis, using Laue photograph method 21 p3681 A67-38360

Oxidation mechanisms for nickel-aluminum alloys studied for effects of temperature and alloy composition 21 p3645 A67-38773

Structures of glow discharge and evaporated silicon oxide films determined by measuring intensity of electron wave scattering at large angles, describing measurement method 21 p3687 A67-39139

Destructive and nondestructive testing of thickness of oxide coatings on Al and Al alloys 22 p3798 A67-39552

Computer-operated following ellipsometer for monitoring buildup and removal of thin anodic oxide film 23 p4001 A67-41260

Cathode outer oxide surface heating for pulsed emission current measured in intervals between retarding current pulses and different repetition frequencies 24 p4129 A67-42231

High temperature thermal insulation consisting of thin refractory metal foils separated by thin refractory oxide layers 24 p4103 A67-42501

OXIDIZER

SA LIQUID OXIDIZER

SA PROPELLANT OXIDIZER

Working equations for dimensions and orientation of impinging propellant sheets in liquid rocket engine 02 p0182 A67-11946

Quenching diameter of premixed fuel-oxidizer flames by volatile inhibitors, noting nature of oxidizers, particularly oxygen 02 p0342 A67-12031

Gaseous ammonia composite solid propellant ignition upon contact with oxidizing vapors such as perchloric acid vapor 06 p1073 A67-18869

OXYGEN

SA AIRCRAFT BREATHING APPARATUS

SA HIGH PRESSURE OXYGEN

SA LIQUID OXYGEN /LOX/

SA OZONE

Atmospheric radio wave absorption coefficient and altitude determined and linked to effects of colliding paramagnetic oxygen molecules 01 p0022 A67-10391

Cylindrical resonator for high precision measurements of sound absorption in oxygen 01 p0067 A67-10838

Mach interactions and propagation mode of spinning detonation wave front in stoichiometric oxyhydrogen 02 p0232 A67-11564

Oxygen impurity effect on recrystallization temperature of annealed and rolled tantalum 02 p0255 A67-11866

Tropospheric pressure-altitude data by satellite radiometric topography mapping, using oxygen absorption band centered at 5 mm 02 p0282 A67-12367

Heats of adsorption of hydrogen and oxygen on semiconductors of zinc blende type calculated, using Clausius-Clapeyron and Bering-Serpinskii equations 03 p0496 A67-13646

Oxygen adsorption on tungsten crystal face studied by back-reflection low energy electron diffraction 03 p0447 A67-13647

Virtual transitions to low-lying continuum states in oxygen 04 p0659 A67-14478

Oxygen content effect on mechanical properties and phase transformations of VT 16 titanium alloy during thermal treatment 04 p0637 A67-14942

Neutron induced degradation of carrier lifetime in n- and p-type silicon containing oxygen and dopant impurities 04 p0684 A67-15691

Heat transfer to end wall of shock tube behind reflected shock wave in oxygen dissociated to varying degrees and at high temperatures 04 p0729 A67-15813

Doppler profiles of nocturnal green line /5577 angstroms/ nonthermal emission resulting from molecular oxygen ion dissociative recombination [AFCLR-67-0443] 05 p0803 A67-17411

Hartree, Hartree and Swirles calculations for oxygen repeated with superposition of configurations in determining wave functions and energy 06 p1034 A67-17647

Impurity effect /primarily O/ in reactions between liquid alloys and solid metals undergoing deformation 06 p1017 A67-17951

O-to-Fe ratio determined in active solar corona from intensity ratio of O-8 to Fe-17 lines and in quiet corona from O-7 to Fe-14

ratio 06 p1083 A67-18068

Oxygen A band near 7600 angstroms used by Gemini V astronauts to measure cloud top altitude, showing method of computing correction factor 06 p1026 A67-18563

Nitrogen and oxygen excitation by proton shocks, measuring emission cross sections of radiation and analyzing vibrational structure 06 p1037 A67-18706

Oxygen effect on mechanical property and heat resistance of alloys AT3 and AT8 07 p1205 A67-19276

Exothermal reaction zone in one-dimensional shock wave in argon diluted oxygen-hydrogen and methane-oxygen mixtures 07 p1267 A67-19309

Oxygen photochemical equilibrium above 150 km, assuming dominant role of radiative recombination above 120 km 07 p1178 A67-19814

Steady states in annealing of niobium and tantalum in oxygen atmosphere, noting relation of pressure to temperature 07 p1210 A67-20110

Oxygen precipitation consisting of point defects as explanation of structural changes of silicon single crystals during thermal treatment 08 p1370 A67-21205

Vertical and horizontal variations of intensities of auroral OI and molecular nitrogen ion emissions 08 p1328 A67-21480

Extraterrestrial life detection method based on catalysis of isotopic oxygen exchange between water and oxygen-containing anions 09 p1454 A67-22015

Ozone formation in photolysis of oxygen and oxygen-helium mixture as function of pressure and temperature 09 p1457 A67-22025

Reaction rate of oxygen jet impinging on tungsten samples at high temperature and various pressures, noting activation energy and diffusion effect 09 p1457 A67-22026

Kinetics and mechanism of cathodic oxygen reduction reaction on metal electrodes 09 p1458 A67-22188

Effects of additions of carbon, nitrogen or oxygen on properties of vapor deposited tungsten 09 p1519 A67-22348

Oxygen as steady state electronegative additive in cesium thermionic converter shown to improve performance without surface corrosion 09 p1450 A67-22355

Large amplitude variations of intensity of oxygen emission in night airglow and structure of lower thermosphere 10 p1634 A67-23051

Energetic metastable diatomic oxygen molecule excited by electron impact studied with high sensitivity molecular beam apparatus 10 p1682 A67-23386

Reaction rate kinetics of combination of H atoms with NO plus third body /M/ compared with H and O atoms plus M relative to argon 11 p1749 A67-24238

Semipermeable Ag membrane as electron collector in oxygen diffusion process for cesium thermionic energy converters 11 p1746 A67-24923

Molecular oxygen densities in range 70-90 km determined by rocket measurements of atmospheric absorption of solar UV radiation in Southern Hemisphere 12 p1934 A67-25786

Radical concentrations and decays in lean hydrogen-nitrogen-oxygen flames 13 p2221 A67-26261

Injection coefficients of hydrogen and oxygen during buildup of discharge in homogeneous electric field 13 p2160 A67-26813

Critical two-phase flow of nitrogen and oxygen through orifices characterized by mass-limited conditions 13 p2106 A67-27669

Photoelectric scanning observations of night airglow for two spectral lines of OI 14 p2306 A67-27788

Kinetic energy distribution of ions produced by dissociative attachment dependence on ion thermal energy and electron affinity of oxygen 14 p2350 A67-28151

Mono- and polycrystalline samples of Al and Cu bombardment by argon ions in presence of oxygen and by oxygen and nitrogen ions under vacuum 14 p2351 A67-28513

Sensitized ignitions of methane and oxygen mixtures, with nitrogen oxides and inert gases added, and suggested reaction mechanisms 14 p2407 A67-28549

Nitrogen, oxygen and hydrogen determined by spark-source mass

spectrography, noting reduction of instrument blank levels 15 p2433 A67-29403
Chemiluminescent rate constant increase in reaction of nitric oxide and oxygen in upper atmosphere explained by clustering of former 15 p2434 A67-29884
Adsorptive interaction of oxygen with tungsten surface 15 p2434 A67-30100
High temperature vapor fractionation of silicate glass related to variations of oxygen isotopes in tektites 15 p2564 A67-30394
Oxygen concentration and strain rate effect on yield point phenomenon in electron beam refined niobium, showing relation to dislocation multiplication 18 p3063 A67-33486
Gas phase reactions of hydrazine with nitrogen dioxide, nitric oxide and oxygen, determining reaction rates, activation energy and order 18 p3109 A67-33837
Reaction zones of ammonia-oxygen and hydrazine decomposition flames, measuring temperature and concentration profiles 18 p3155 A67-33838
Spectrophotometric study of multiple reaction zones of premixed trimethylaluminum-oxygen flames, emphasizing microstructure 18 p3109 A67-33840
Oxygenic concentrations in primitive earth atmosphere, discussing Martian atmosphere composition 18 p3041 A67-34095
Decomposition of polytetrafluoroethylene in glow discharge studied using helium, helium plus oxygen or oxygen as carrier gas 18 p2998 A67-34369
Currents in copper phthalocyanine thin films measured as function of temperature and ambient noting effect on conductivity, trap density, etc 18 p3104 A67-34627
Soviet and foreign studies of atmospheric oxygen by optical and spectral methods 19 p3214 A67-34857
Adsorption, surface reaction and mutual displacement of carbon monoxide, carbon dioxide and oxygen on titanium film, using mass spectrometer 19 p3244 A67-34941
Negatively ionized ozone and diatomic oxygen concentration ratio determined from physicochemical processes for 10-60 km range 19 p3219 A67-35249
Adsorption of oxygen on tungsten surface, discussing electron diffraction 19 p3246 A67-35786
Oxygen determination in molybdenum using vacuum extraction 20 p3467 A67-37121
Inelastic electron impact cross sections for ionization and vibrational excitation of atmospheric molecular oxygen 20 p3489 A67-37419
Triplet-to-singlet conversion of difluoromethylene radical by self-annihilation, noting reactions with oxygen atoms 20 p3378 A67-37561
Oxidized silicon surface properties affected by diffused oxygen and gold, finding parasitic n-type layer formations and positive surface charge production 21 p3678 A67-38149
Oxygen concentration in silicon semiconductors, discussing oxygen properties and effects on carrier lifetime, surface etching and dislocations 21 p3682 A67-38363
Lattice parameter of bcc Nb-Hf alloy with interstitial solid solution of oxygen 22 p3823 A67-40210
Atmospheric temperature profile to 75 km by remote sounding, using satellite measurement of molecular oxygen resonance line at 5 mm 22 p3806 A67-40360
Excited levels mean life in multiply ionized oxygen and neon measured by beam-foil technique 23 p4029 A67-40955
Gallium oxide desorption rate and activation energy after O adsorption on GaAs (111) surface 23 p4045 A67-41464
Solid chemical state O for spacecraft noting advantages over liquid and high pressure gas, discussing storage, handling, losses, shelf life, availability and containers 23 p3967 A67-41608
Mass spectrometric study of oxygen adsorption, determining condensation coefficient and tungsten surface work function for various concentrations 24 p4172 A67-42073
Apollo spacecraft H-O chemical to electric energy converting fuel cell performance degradation resulting from O electrode contamination due to inert diluent impurities in O supply 24 p4106 A67-42525

OXYGEN AFTERGLOW

IQSY and IGY comparison of night airglow OI latitude observations 16 p2667 A67-31517
Electron cyclotron resonance absorption of microwaves in oxygen magnetoplasma used to alter electron attachment and detachment rate coefficients 19 p3271 A67-35077

OXYGEN APPARATUS

Oxygen concentration system for aviator breathing 18 p2995 A67-34717

OXYGEN ATOM

Perfluorocyclopropane production in reaction of oxygen atoms with tetrafluoroethylene 01 p0018 A67-10762
Chemiluminescent gas phase reactions involving electronically excited oxygen molecules trimethylaluminum and diborane near 3 millitorr 01 p0019 A67-11007
Electron excitation cross section of transitions between spin multiplets of ground state of neutral oxygen atom calculated, using continuous state Hartree-Fock formulation 03 p0472 A67-13322
Upper atmospheric oxygen atom concentration profiles obtained via wind tunnel simulation of NO releases [AFCLR-67-0053] 04 p0615 A67-14971
Excited states in negative atomic oxygen ion, giving estimates of electron-atom interaction 04 p0661 A67-15764
Oxygen atoms reaction with tetrafluoroethylene in presence of molecular oxygen 04 p0567 A67-15949
Spectrum of glow during gas phase reaction of germanium tetrahydride with atomic oxygen, observing new bands of D-X system 06 p0955 A67-17655
Reaction rate of oxygen atom with C3F6 and hydrocarbons 06 p0955 A67-17983
Oxygen atoms association and combination with nitrogen atoms, determining rate constants of reactions 06 p0956 A67-18761
Cross sections for photodetachment of electron from negative atomic oxygen ion 07 p1225 A67-19497
Mesosphere ice point temperature, atomic oxygen concentration and total density measurement with heat recorder 10 p1656 A67-23207
Spatial inhomogeneities in green line of atomic oxygen, using electrophotometry during airglow 13 p2111 A67-26567
Reaction of atomic oxygen with methane studied by photolysis of ozone-methane mixtures dissolved in liquid argon [JPL-TR-32-1109] 14 p2259 A67-28297
Chemiluminescent reactions of atomic oxygen with carbonyl sulfide and hydrogen sulfide in flow system as function of reaction time and reactant concentrations 14 p2260 A67-28781
Adsorptive interaction of oxygen with tungsten surface 15 p2434 A67-30100
Motion and continuity equations for atomic and molecular oxygen density solved numerically as time dependent problem 16 p2664 A67-30975
Emission time history for red 6300 angstrom atmospheric emission from atomic oxygen produced by nuclear explosion 16 p2664 A67-30978
Water vapor and atomic oxygen concentration in mesosphere measured by meteorological rocket 18 p2665 A67-31097
Oxygen caused bright spots in field ion microscope patterns of tungsten, noting oxygen variation effects 16 p2693 A67-31873
Upper atmospheric nightglow emission intensity measured finding continuous excitation of oxygen atoms as energy reservoir 16 p2870 A67-31918
Electron temperature/ion temperature ratio and oxygen atom ratio to sum of oxygen molecule and nitric oxide in F-1 layer obtained by radar 17 p2843 A67-32529
Coherency relation between quasi-periodic X-ray and optical pulsations in auroras 17 p2844 A67-32543
Relaxation processes for oxygen in solid solution in niobium demonstrating clustering of atoms into groups [AD-642957] 17 p2871 A67-32628
Negative oxygen ion reaction rate constants for ion loss processes in ionospheric D region obtained by laboratory measurement 17 p2851 A67-33195
Rate constant of atomic oxygen ions reaction with vibrationally excited nitrogen molecules 17 p2889 A67-33201
Production modes, physical deactivation with related electronic energy transfer and

chemical reactions of D oxygen atoms, noting significance for upper atmosphere 17 p2809 A67-33203
Worldwide morphology of atomic oxygen nightglows 18 p3032 A67-33580
Bates theory of atomic oxygen excitation in upper atmosphere as cause of F layer nightglow emissions 18 p3038 A67-33616
Atomic oxygen effect on vibrational relaxation of oxygen in shock waves at high temperatures, using laser schlieren technique 18 p3081 A67-33784
Metastable atomic oxygen state observed in microwave discharge of molecular oxygen, noting g factor of 2 in strong resonance 18 p3082 A67-34029
Adsorption of oxygen upon clean nickel surface and beginning of oxidation 19 p3244 A67-34937
Density, temperature, water vapor and atomic oxygen concentration in mesosphere measured by heat method 19 p3216 A67-35183
Auroral excitation of atomic oxygen forbidden lines, giving photon emission rate vs zenith angle 20 p3426 A67-36301
Auroras /ordinary and type with forbidden emission of atomic oxygen/, examining wind-aurora relation 22 p3790 A67-39675

OXYGEN BIFLUORIDE

Reaction mechanism between oxygen difluoride and diborane based on visual observation, gas composition and pressure-temperature relationships [CI PAPER 67-10] 19 p3309 A67-35005

OXYGEN BREATHING

Manned spacecraft atmosphere selection, experimenting with 100 percent oxygen at 258 mm Hg, noting toxicity, toleration, substitution of helium for nitrogen, etc 02 p0187 A67-12319
Experiments showing occurrence of aero-ateletasis in pilots exposed to high G forces, breathing oxygen and using anti-G suit 09 p1453 A67-21733
Human lung gas mixing efficiency estimated, using residual lung nitrogen content curve 11 p1747 A67-24626
Contaminant control in oxygen for breathing in aviation solved by gas chromatography 12 p1902 A67-25173
Lung, liver, kidney and heart pathology of dogs, monkeys, rats and mice exposed for 2 to 13 weeks to pure oxygen atmosphere at reduced pressure 13 p2059 A67-26918
True air life support system, describing concept for deriving fixed percentage binary gas from two steady state cryogenic liquids 13 p2064 A67-27638
Effects of breathing pure oxygen under pressure on autonomous regulatory systems /nervous, respiratory, circulatory/ of man 14 p2257 A67-28225
Pulmonary mechanics associated with oxygen toxicity and suggested physiological test for susceptibility to effects of oxygen 15 p2429 A67-29280
Spacecraft cabin atmosphere, comparing pure oxygen with two-gas atmosphere 16 p2617 A67-30776
Contaminant concentration in liquid breathing oxygen of aircraft converter determined by gas chromatography 16 p2619 A67-31475
Oxygen concentration system for aviator breathing 18 p2995 A67-34717
Alkaline concentrator appears superior to acid and solid units for possible onboard generation of oxygen 23 p3963 A67-41543
Reactions of animals exposed to pure oxygen space cabin atmosphere for 235 days, noting no systematic toxicity 23 p3952 A67-41574
Lung changes relation to fatal outcome of 100 percent oxygen exposure 23 p3958 A67-41649
Brightness thresholds and reading ability tests evaluated for male subjects under varied simulated conditions of altitude and oxygen breathing 23 p3959 A67-41694

OXYGEN COMPOUND

SA DIOXANE

SA OXIDE

Refractory oxides solidification points measurement using optical-pyrometer method 20 p3472 A67-36118

OXYGEN CONSUMPTION

Physical fitness of man with respect to manual labor, oxygen deficiency and acceleration 03 p0364 A67-13924
Compatibility of artificial gas mixtures dependent on carbon dioxide and oxygen

partial pressures 04 p0562 A67-14573
Heat metabolism in working men while isolated from environment by water-cooled suit and environmental chamber [ASME PAPER 66-WA/HT-45] 04 p0564 A67-15431
Absolute bed rest and recumbent exercise during bed rest effects on pulse rate response to submaximal work, cardiovascular functional capacity /maximal oxygen intake/, physical work capacity and orthostatic tolerance 05 p0755 A67-16283
Long term effects of oxygen environment on rat colony at 210 mm Hg absolute showed no significant physiological changes and no difficulty in readaptation 05 p0755 A67-16285
Titanium oxidation characteristics, determining activation energy of scale formation, oxygen absorption of base metal and total oxygen 05 p0829 A67-16759
Adapted Mueller-Franz portable breath-powered respirometer utilizing scuba-gear for measuring underwater metabolism 09 p1455 A67-21722
Physical exercise effect on oxygen consumption at decreased pressure 17 p2806 A67-31963
Polarographic and mass gas flowmeter sensors incorporated into bench model for on-line continuous determination of oxygen consumption in human subjects 18 p2995 A67-34711
Hydrazine effect, alone and with nicotinic acid, on oxygen consumption, respiratory quotient, carbohydrate pool and heat losses in rats studied using gradient calorimeter 18 p2992 A67-34714
Hydrazine effect on carbohydrate metabolism in vivo and in vitro, studying hyperlactatemia, hypoglycemia, oxygen consumption inhibition, etc 18 p2992 A67-34720
Oxygen consumption and phosphorylation processes relation studied in rats for high altitude stability 20 p3367 A67-36259
Brain tissue respiratory processes of rabbits subjected to hypergravity and acute hypoxia noting no significant difference between experimental and control animals 23 p3943 A67-40770
Metabolic depression in animals exposed to air after living in helium-oxygen environment, suggesting denitrogenation period effect 23 p3944 A67-40823
Multiplace metabolimeter closed circuit system with servo-driven volume meter for animal oxygen consumption in gaseous artificial environments 23 p3999 A67-41088
Oxygen consumption rate during ambulatory lunar surface exploration, describing lunar simulator 23 p3966 A67-41597
Physiological measurements in obtaining energy expenditure and workloads during simulated lunar surface mission 23 p3959 A67-41657
Inert gas effect on oxygen consumption in living tissue studied by polarographic and Warburg techniques 23 p3960 A67-41706
Oxygen diffusion through lubricant to metal surface examined for influence in corrosive wear [ASLE PAPER 67-LC-4] 24 p4164 A67-42743

OXYGEN DEFICIENCY
SA ANOXIA
SA HYPOXIA
Aminasine injection and electrolysis effects on formatio reticularis of animals after exposure to hypoxia 20 p3367 A67-36255
Central nervous system, adenohypophysis and adrenal glands relation in oxygen deficiency 20 p3369 A67-36669
Treatment of hypoxia by determining primary site of oxygen tension attenuation in transfer from respiratory environment to cellular level 23 p3953 A67-41591
Hypoxia warning systems, discussing spurious warning avoidance and mask mounted sensor 23 p3968 A67-41629
Arterial and venous blood of brain and mixed venous blood of heart measured in dogs exposed to simulated altitude, noting body deoxygenation 24 p4111 A67-41851

OXYGEN FLUORIDE
Oxygen difluoride propellant system design and operational experience at Arnold Center [AIAA PAPER 67-279] 07 p1164 A67-20049

OXYGEN METABOLISM
Upper torso exercises effect compared

with torque maneuvers effect on oxygen metabolism under reduced gravity conditions 01 p0017 A67-10959
Oxygen balance of organism during prolonged accelerations, noting disturbed gas exchange between alveoles and capillaries 02 p0188 A67-12329
Individual phospholipids in hemispheres of rat brains and rate of turnover of phosphate groups during oxygen deprivation 04 p0562 A67-15548
Oxygen metabolism changes in muscular and brain tissues of animals exposed to prolonged transverse accelerations, examining oxygen consumption and body temperature 16 p2612 A67-30905
Effect upon cardiovascular system of weightlessness simulated by immersion in brine 17 p2805 A67-31952
Physical exercise effect on oxygen consumption at decreased pressure 17 p2806 A67-31963
Functional relation between oxidation, metabolism, blood flow volume rate and brain temperature in rats exposed to vibration, noting temperature decrease and blood supply and oxygen consumption stimulation 23 p3943 A67-40769
Metabolic depression in animals exposed to air after living in helium-oxygen environment, suggesting denitrogenation period effect 23 p3944 A67-40823
Cerebral blood flow and metabolism during combined hypoxia and hypercapnia, noting cerebral vasodilatation effect 23 p3945 A67-41080
Multiplace metabolimeter closed circuit system with servo-driven volume meter for animal oxygen consumption in gaseous artificial environments 23 p3999 A67-41088

OXYGEN PRODUCTION
Oxygen, carbohydrates, proteins, etc, produced by unicellular algae through photosynthesis, finding optimum efficiency of process 02 p0186 A67-11861
Chemical aspects of evolution of terrestrial atmosphere, noting role of photolysis in oxygen production 03 p0414 A67-14089
Aerojet Carbothermal Process for oxygen manufacture from lunar resources, discussing experimental results from research operations 08 p1316 A67-21092
Contaminant control in oxygen for breathing in aviation solved by gas chromatography 12 p1902 A67-25173
Production modes, physical deactivation with related electronic energy transfer and chemical reactions of D oxygen atoms, noting significance for upper atmosphere 17 p2809 A67-33203
Biological problems in prolonged space voyages including oxygen replacement, water supply and food 19 p3179 A67-35209
Cylindrical solid state oxygen generators, discussing manual and remote electrical activation 23 p3968 A67-41621
Mass spectrometric analysis of electrolyte degradation during electrolysis in sulfuric acid silica gel cell for oxygen recovery 23 p3970 A67-41705

OXYGEN RECOMBINATION
Atmospheric mixing time and lifetime of atomic and molecular oxygen at high altitude, noting agreement with barometric distribution law, concentration pattern, etc 07 p1178 A67-19813
Nocturnal recombination processes in ionospheric F region for nitrogen and oxygen based on 5200 and 6300 angstrom lines 18 p3040 A67-33693
Carbon monoxide and atomic oxygen recombination in expansion wave of single-pulse shock tube at high temperatures 18 p2997 A67-33790
Rate constant for gas phase recombination of atomic and molecular oxygen into ozone, discussing M effect 18 p3082 A67-34030
Recombination and bremsstrahlung continuum radiation measurements of atomic and ionic oxygen in plasma 19 p3299 A67-36093

OXYGEN SENSOR
Quantitative expression of technique for observing 5-mm self-emission from oxygen of earth atmosphere to obtain vertical sense [RASSA PAPER 1-10-144] 03 p0418 A67-14251
Polarographic and mass gas flowmeter sensors incorporated into bench model for on-line continuous determination of oxygen

consumption in human subjects 18 p2995 A67-34711

OXYGEN SPECTRUM
Absorption spectrum of condensed oxygen in 1.26 to 0.3 micron region 01 p0116 A67-10509
Oxygen spectra in daylight, twilight and during eclipse 07 p1173 A67-19662
Brightness variations of oxygen in day and twilight airglow observed by balloon-borne instruments 07 p1173 A67-19663
Oxygen IV transition multiplet relative intensities for measuring decay rates, using triply ionized emitters 10 p1678 A67-22718
Rydberg series energy levels of oxygen molecule, comparing theoretical calculations with experimental results 10 p1681 A67-22887
Diurnal and latitudinal variations in 5577 angstrom zenith nightglow intensity compared with 6300 angstrom calibrations 10 p1650 A67-23337
Auroral green lambda 5577 of oxygen atom analyzed from glow discharge emission, proposing excitation mechanism on basis of intensity variations 11 p1824 A67-24934
Correlation of monthly and nightly green line 5577 Angstroms /OI/ airglow intensity with sunspot number and 10.7 cm flux 16 p2749 A67-31404
Solar spectrum observations in oxygen regions, describing prism-grating spectrometer, photoelectric recording and scan-averaging by digital computer [AFCL-67-0478] 16 p2749 A67-31417
Drift azimuths, sizes and displacements of spatial inhomogeneities in oxygen atom emission at 5577 angstroms during night airglow 17 p2848 A67-32952
Optical observations of daytime aurora by means of atomic-oxygen-emission interferometry 17 p2852 A67-33212
Ionospheric electron temperature incoherent backscatter measurements confirming predawn enhancement of 6300 angstroms airglow 18 p3039 A67-33624
Height profile of atomic oxygen 6300 angstrom emission in night airglow determined by rocket photography 19 p3215 A67-35177
Nitrogen and oxygen dayglow emissions observed during total solar eclipse of May 1965, studying emission/continuum intensity ratio 20 p3427 A67-36368
Cloud measurements from Gemini 5 from reflected solar radiation spectra of oxygen A band region 22 p3807 A67-40369
Ionospheric electron content and OI nightglow in Hawaii, discussing ionization density increases throughout bottomside F layer 24 p4147 A67-41878

OXYGEN SYSTEM
Oxygen system for military aircraft pilot using electrochemical cell to extract oxygen from atmospheric air [AIAA PAPER 66-787] 01 p0012 A67-10531
Oxygen pressure vessels for prototype BAC/Sud-Concorde manufactured from stainless steel 06 p0952 A67-18734
Environmental control for high performance military aircraft covering air conditioning, temperature and pressure control and oxygen supply systems 21 p3572 A67-39130
Fire in Apollo 204 spacecraft noting alterations in oxygen and electrical systems, escape hatch, materials and communications 22 p3900 A67-39888
Spacecraft atmosphere selection covering physiological, engineering and fire criteria, evaluating oxygen diluent and recovery 22 p3755 A67-39889
Composite propulsion systems for aerospace missions, considering Mach range, specific impulse, oxygen source, design characteristics, capabilities and limitations 22 p3868 A67-39890
Hydrogen peroxide oxygen-water supply system as backup for long space flights noting storage tanks, catalytic reactor and heat exchanger 22 p3747 A67-39893
Flame mechanism experiments for solid material surface, measuring flame velocity, stressing space capsule fire hazard minimization 22 p3904 A67-40110
Alkaline concentrator appears superior to acid and solid units for possible onboard generation of oxygen 23 p3963 A67-41543
Emergency oxygen supply systems for aircraft, discussing simplicity, standardization, safety, reliability and maintenance

[AIAA PAPER 87-965] 24 p4110 A67-43043

OXYGEN TENSION

- Cannulation of renal capsular lymphatics in anesthetized dogs, testing if lymph fluid can serve to assess tissue oxidation 06 p0952 A67-17853
- Book on positive pressure breathing as means for acceptable arterial oxygen tension at altitudes above 40,000 ft and effects of raised intrapulmonary pressure 08 p1288 A67-21500
- Relationship between oxygen tension and radiosensitivity in complex biological system 17 p2806 A67-31962
- Hematologic effects of increased oxygen tension, discussing mechanisms of erythrocyte-oxygen interactions 18 p2991 A67-34710
- Rat adrenal gland responses to increased oxygen tension at ambient temperature, noting oxygen critical threshold partial pressure affecting survival 23 p3950 A67-41538
- Treatment of hypoxia by determining primary site of oxygen tension attenuation in transfer from respiratory environment to cellular level 23 p3953 A67-41591
- Arterial oxygen tension during acceleration recorded on anesthetized greyhounds using microelectrode and physiological gas analyzer 23 p3958 A67-41653
- Increased oxygen tension causing increased free radical flux in rat kidney tissue akin to ionizing radiation exposure 23 p3958 A67-41654

OXYGEN TOXICITY

- Mice inoculated with tetanus exposed to high pressure oxygen /OHP/ under immediate and delayed administration 09 p1453 A67-21727
- Absorptional atelectasis breathing oxygen at simulated altitude, discussing prevention by using inert gas 09 p1453 A67-21732
- Hepatic effects of breathing pure oxygen for eight months upon rats, dogs and monkeys 10 p1600 A67-23818
- Acetylative capacity and lipid metabolic changes and readjustment to normality in rats in oxygen-rich environment 14 p2256 A67-28588
- Blood pressure changes and pulmonary edema in rat associated with hyperbaric oxygen 15 p2428 A67-29275
- Proliferative pulmonary lesions in monkeys exposed to high concentrations of oxygen at 600 to 760 mm Hg pressure 15 p2428 A67-29276
- Pulmonary mechanics associated with oxygen toxicity and suggested physiological test for susceptibility to effects of oxygen 15 p2429 A67-29280
- Pure oxygen effect on activity of lysosomal aryl sulfatase in brain, liver and liver tissue homogenates from rats 18 p2992 A67-34719
- Comparative pathology of animals continuously exposed to varied concentrations of carbon tetrachloride vapor in altitude chamber 21 p3573 A67-38070
- Lung changes resulting from prolonged exposure to 100 percent oxygen at 550 mm Hg suggest media erosion and evidence of hypertrophy and hyperplasia 22 p3751 A67-39601
- Vitamins A and E deficiency effects on rats exposed to pure oxygen noting less weight gain and growth 23 p3952 A67-41568
- Reactions of animals exposed to pure oxygen space cabin atmosphere for 235 days, noting no systematic toxicity 23 p3952 A67-41574
- Oxygen toxicity relation to nutrition, hormonal secretion and age factors, discussing experiments on rats 23 p3956 A67-41632
- Rats exposed to different hyperoxic atmospheres for 20 days studied for toxic lipids formation 24 p4112 A67-41854

OXYGEN TREATMENT

- Cardiovascular changes and vasodepressor effect in reoxygenation of cats 03 p0364 A67-14290
- Crystal structure defects and electroconductivity variations in CdS single crystals in oxygen ambient and effects of various surface treatments 05 p0862 A67-16605
- Acute hyperbaric oxygenation histological effects on pulmonary circulation of rabbits 16 p2614 A67-31473
- Zirconium-niobium alloys investigated for

- oxygen impurity effects on critical current density and superconducting properties 19 p3243 A67-34925
- Differential cross sections for elastic scattering of alpha particles by oxygen, giving angular distributions and resonances 21 p3659 A67-38517
- Differential cross sections of elastic scattering of alpha particles by oxygen, measuring angular distributions 21 p3659 A67-38518
- OXYGEN 18
 - Extraterrestrial life detection based on catalysis of oxygen exchange between labeled oxyanions and water, noting equipment 15 p2426 A67-29113

OZONE

- Vertical distribution of ozone measured by rocket, using UV absorption 02 p0238 A67-12065
- Michelson type interferometer for Nimbus meteorological satellite to obtain vertical temperature, humidity and ozone profile 02 p0246 A67-12365
- Seasonal and yearly variations of atmospheric ozone sounded by electrochemical ionosonde 03 p0405 A67-12804
- Latitude distribution of ozone at high altitudes, deduced from radiance of earth daylight atmosphere, measured with satellite-borne radiometer 03 p0410 A67-12948
- Ozone determination by electrochemical and colorimetric methods compared for effects of sensor cell aging 03 p0413 A67-13931
- Time-dependent photochemical model for space-time variations of oxygen allotropes in 20 to 100 km layer 03 p0414 A67-14087
- Vertical ozone distribution in atmosphere and transport processes, noting results of tracer experiments 03 p0414 A67-14090
- Laser radar returns from lower troposphere compared with vertical ozone distributions indicate inverse relationship 04 p0612 A67-14676
- Atmospheric ozone in middle UV spectral region, noting vertical distribution, destruction by solar radiation, lifetime below layer in photochemical equilibrium, etc 04 p0612 A67-14694
- Oxidation by nitrous oxide, nitric oxide, nitrogen dioxide and ozone, considering various reactions 04 p0566 A67-15095
- Chemical reaction effect on heat transfer in thermally decomposing ozone system 05 p0925 A67-16270
- Statistical method of calculation of atmospheric thermal, conservative and dynamic characteristics using measured ozone distribution 05 p0796 A67-16488
- Atmospheric ozone distribution, air flows and temperature at high altitudes in equatorial latitudes of Atlantic Ocean 05 p0799 A67-17026
- Ozone concentration in commercial jet aircraft measured for possible seasonal and meteorological correlation 06 p0947 A67-18008
- North American ozonesonde network investigation of isentropic and vertical distribution of ozone mixing ratio in lower stratosphere in May 1963 06 p0996 A67-18446
- Statistical characteristics of atmospheric ozone distribution, determining autocorrelation and cross correlation functions, concentration and temperature profiles 07 p1170 A67-19357
- Soviet papers on optical radiation and ozonometric studies of atmosphere 07 p1219 A67-19451
- Techniques for calculating vertical distribution of atmospheric ozone from intensity of solar UV radiation at various altitudes 07 p1172 A67-19456
- Analytical method for solving nonstationary one-dimensional equation of ozone transport 07 p1172 A67-19457
- Local peculiarities of vertical distribution of ozone in equatorial and polar regions for different turbulent dynamic models of stratosphere 07 p1173 A67-19696
- Solar UV reflection and scattering from earth atmosphere, use in determining total concentration and vertical distribution of ozone 07 p1178 A67-19815
- Hydrogen peroxide oxidation and ozonolysis of polymer type material in coal, kerogen and Orgueil meteorite 08 p1289 A67-21174
- Ozone formation in photolysis of oxygen and oxygen-helium mixture as function of pressure and temperature 09 p1457 A67-22025

- Atmospheric scattering of solar flux in UV noting radiation transfer for airborne detector, air component absorption coefficient and spectra from rocket flight 10 p1629 A67-22736
- Rocket measurement of diurnal variation of ozone profiles above maximum concentration level 10 p1638 A67-23202
- Average distribution and time variation of ozone in stratosphere and mesosphere in study of contribution of photochemical reactions involving hydrogen 10 p1645 A67-23263
- Atmospheric ozone data on basis of meteorological observations and synoptic maps on ship in Atlantic 11 p1785 A67-23958
- Vertical distribution of ozone over Tallahassee, noting maximum and minimum density altitudes, seasonal variations, etc 11 p1787 A67-24555
- Rayleigh scattering and Lambert ground reflection effect on solar energy absorbed by ozone in earth molecular atmosphere evaluated on basis of transfer equation 12 p1932 A67-25341
- Statistical method of calculation of atmospheric thermal, conservative and dynamic characteristics using measured ozone distribution 13 p2109 A67-26344
- Vertical distribution of tropospheric and stratospheric ozone based on observations of U.S. ozonometric stations at various latitudes 14 p2308 A67-27927
- Radio probe to derive relations between ozone content of lower stratosphere and origin of air in layers 15 p2474 A67-29525
- Effect of ozone on mean meridional circulation in upper atmosphere and mesosphere 16 p2666 A67-31098
- Ozone generator and calibrator, noting design principles, operation performance and results 16 p2676 A67-31374
- Atmospheric ozone concentration measurement using potassium iodide method 16 p2676 A67-31376
- Atmospheric ozone vertical distribution, measurement, discussing equipment design and underlying principles of method 16 p2676 A67-31377
- Satellite technique for sounding atmospheric optical properties and height distribution of ozone and aerosols 18 p3040 A67-33853
- Rate constant for gas phase recombination of atomic and molecular oxygen into ozone, discussing M effect 18 p3082 A67-34030
- Atmospheric ozone content compared for discrepancies between theoretical and experimental results for vertical, latitudinal and seasonal variations 19 p3214 A67-34856
- Negatively ionized ozone and diatomic oxygen concentration ratio determined from physicochemical processes for 10-60 km range 19 p3219 A67-35249
- Quasi-biennial oscillation in ozone in northern Hemisphere harmonically analyzed 19 p3225 A67-35921
- Total atmospheric ozone from satellite measurements of solar UV reflected radiation determined, using atmospheric model with Rayleigh scattering 19 p3226 A67-35923
- Surface air radioactivity and ozone measurements in Antarctica reveal fission product yearly oscillation 20 p3429 A67-36871
- Ozone parameters determination from measurements of radiation backscattered by earth atmosphere 22 p3794 A67-40365
- Vertical distribution of thermal stability in lower stratosphere compared with atmospheric ozone from ozone and temperature soundings 22 p3829 A67-40471
- UV light photolyzing ozone dispersed in solid carbon dioxide matrix causes formation of new substance showing IR absorption 23 p3971 A67-40970
- Solar radiant energy attenuation by atmospheric ozone, deriving transmission function relation to ozone content 24 p4181 A67-41915
- Radiation measurement from satellite, discussing observation of ozone absorption band 24 p4181 A67-42397

OZONE FLUORIDE

- Existence of ozone difluoride established by low temperature experiments and correlation with mass spectrometric EPR, IR and NMR 20 p3377 A67-37136

OZONOSPHERE

- Daytime ozone density distribution of mesospheric layer measured by using UV

photometers in rockets 19 p3217 A67-35203
 Medium wave and global UV radiation,
 relative sunspot number and ozone density
 measurements and 22 p3873 A67-40030

P

P-3 AIRCRAFT

Corrosion control requirements of P-3
 Orion aircraft, including six steps to
 corrosion control and remedial
 measures 01 p0011 A67-11012
 Orion P-3 electrical power system changes
 effect on weapons system, noting power
 distribution and generation 09 p1452 A67-22677
 Air conditioning system of P-3 aircraft,
 noting redesign to include auxiliary power
 unit for functioning during ground
 operation 20 p3363 A67-36512

P-I-N DIODE

Impurity concentration and electric field
 distribution determined in drift region of
 silicon p-i-n detectors from capacity as
 function of reverse voltage 02 p0296 A67-11823
 X sub L band waveguide switches using p-
 i-n diodes for switching elements in SPST,
 SP2T, SP4T and SP8T microwave
 switches 04 p0580 A67-14863
 Electroluminescence, photoconductivity
 and I-V characteristics of niobium-niobium
 oxide-gold diode and possible existence of p-
 i-n junction in oxide 04 p0582 A67-15104
 GaAs p-s-i-n diode exhibiting negative
 resistance, allowing assembly into X-Y
 matrix and electrical pulsing into emitting
 or nonemitting state 05 p0771 A67-16312
 Width of I band of p-i-n nuclear emission
 detector during Li ion drift through doped
 Si semiconductor detector 05 p0872 A67-17500
 Monolithic IC design of diodes and X-band
 microswitch transmission line fabricated on
 Si substrate 06 p0968 A67-18053
 P-I-n diode structure and behavior under
 direct and reverse-bias conditions 06 p0969 A67-18121
 P-I-n diode switches, discussing driving
 techniques for series and parallel biased
 switches, pulse leakage and RF turn-off
 delay minimization 12 p1917 A67-26194
 Second and third harmonics produced by
 p-i-n diode in microwave switching
 application 13 p2075 A67-26478
 Noise measurement in p-i-n junction
 diodes 13 p2079 A67-26875
 PSIN /P region, Seminsulating region, N
 region/ diode array fabrication, performance,
 characteristics and applications 14 p2282 A67-28029
 Total resistance of p-i-n diode calculated
 assuming high injection levels in base and
 moderate frequencies 14 p2286 A67-28530
 Direct and indirect converters emphasizing
 preconcentration of solar radiation, noting
 thermophotovoltaic generators of p-i-n
 type 16 p2608 A67-30713
 IMPATT diode operation based on
 combination of avalanche-current
 multiplication and transit-time delay to
 produce negative resistance 17 p2824 A67-32332
 Gold-doped silicon diode space charge and
 oscillation effect, discussing deviation from
 Ohm law at lowest voltages 19 p3198 A67-36043
 Design formulas for predicting dependence
 of resistance and reactance of diffused
 microwave p-i-n diodes on reverse bias
 voltage 22 p3770 A67-39730
 Current oscillations in Co-doped Si p-i-n
 diode devices noting SCL I-V
 characteristics 23 p3978 A67-40788
 Total resistance of p-i-n diode calculated
 assuming high injection levels in base and
 moderate frequencies 23 p3980 A67-40937

P-N JUNCTION
 Surface effect on temperature, I-V and
 watt-ampere characteristics of p-n junction
 semiconductor injection laser diode as
 coherent light source 01 p0087 A67-10077
 Volt-ampere characteristics and other
 properties of GaAs lasers with tellurium and
 Zn-doped epitaxial p-n junction 01 p0087 A67-10080
 Diffusion parameters and solubility of Cd
 in InAs measured with aid of radioactive
 isotopes compared with diffusion coefficient
 measurement by p-n junction method 01 p0128 A67-10082
 Minimum spectral line width, threshold
 current density, radiation-peak displacement
 and possible recombination mechanism for
 GaSb laser diode p-n junctions in coherent
 radiation 01 p0087 A67-10085
 Coherent emission of indium arsenide
 phosphide p-n junction 01 p0087 A67-10101
 Efficient electroluminescence at 300
 degrees K from GaAs diode amphoteric
 dopant Si as dominant impurity on both
 sides of p-n junction 01 p0131 A67-10368
 Temperature dependence of optical
 phonon mean free paths and mean energy
 loss per collision predict avalanche
 multiplication and voltage breakdown of Si
 and Ge p-n junctions 01 p0132 A67-10374
 Locked oscillation of silicon p-n junction
 avalanche diodes in 50 to 140 GHz
 range 01 p0035 A67-10436
 Junction perfection in coherent microwave
 oscillation in avalanching p-n silicon
 diodes 01 p0036 A67-10449
 Continuous coherent radiation of GaAs
 semiconductor laser with epitaxial p-n
 junction at ambient temperature of 77
 degrees K 01 p0090 A67-10548
 Charge collection velocity in
 semiconductor particle energy detector
 expressed in terms of electron and hole
 motion and induced charges 01 p0065 A67-10650
 Maximum alloying temperature and cooling
 rate of p-n junctions effect on volt-ampere
 characteristics of silicon diode and minority
 carrier lifetime 01 p0039 A67-11053
 Continuous coherent radiation of GaAs
 semiconductor laser with epitaxial p-n
 junction at ambient temperature of 77
 degrees K 01 p0091 A67-11056
 Oscillation frequency and breakdown
 voltage in GaAs p-n junction reverse-biased
 into avalanche region due to negative
 resistance arising from transit time
 effect 01 p0137 A67-11070
 Checking ohmic back contact on
 semiconductor wafers before fabrication of
 diode, using four-point probe 01 p0077 A67-11315
 Maximum power transformed by nonlinear
 capacitance of semiconductor diode on
 closed p-n junction 02 p0210 A67-11510
 Strong injection in nondegenerated p-n
 junction producing electron-hole plasma in n
 region near junction 02 p0296 A67-11827
 Different crystallization conditions and
 effect on Se surface structures on
 properties of p-n heterojunctions in Se-CdSe
 and Se-CdS rectifying cells and
 photocells 02 p0297 A67-11849
 Solution grown epitaxial red light emitting
 p-n junctions in GaP preparation, electrical
 and optical properties, examining I-V
 characteristics 02 p0297 A67-11876
 Electron beam scanning technique
 measurement of diffusion lengths in Si and
 GaP p-n junctions and recombination rate of
 dislocations in n-type Si 02 p0298 A67-11887
 Implantation of Cs and Na ions into p-type
 silicon, effect on hot electron emission from
 p-n junction 02 p0299 A67-11897
 Electromagnetic, circuit theory, quantum
 and statistical mechanics laws for conduction
 electrons in low and high injection p-n
 junctions 02 p0299 A67-12105
 Electron microscopy analysis of
 microinhomogeneities in commercial Si used
 in preparation of p-n junction devices 02 p0257 A67-12434
 Photovoltaic effect in p-n junctions of
 lead tin telluride diodes indicate potential
 for IR detection throughout 8-14 microns
 atmospheric window 02 p0221 A67-12514
 Transition time dependence between
 avalanche and second breakdown on input
 power to p-n silicon junction, noting thermal
 effects in semiconductors 02 p0222 A67-12650
 DC parametric device in which capacitance
 variation of silicon p-n junctions due to
 input signal causes FM 03 p0377 A67-13106
 Injection peculiarity in heterojunctions
 arising from band discontinuities which
 favor hole injection over electron
 injection 03 p0490 A67-13154
 Intensity of light emitted by individual
 microplasmas of silicon p-n junctions
 increases with voltage to maximum and then
 decreases 03 p0491 A67-13176
 Parametric excitation of spectrotron with
 controllable p-n junction capacitance and

intrinsic voltage feedback 03 p0378 A67-13241
 Radial distribution of excess current
 carriers in base of p-n junction transistor
 with high injection levels 03 p0378 A67-13244
 Excitation of parametron with p-n junction
 capacitance produced by inverted impurity
 concentration gradient in base of
 junction 03 p0378 A67-13246
 Temperature determination for collector
 p-n junction of transistors in class B power
 amplifier by thermal equivalent circuit
 analysis 03 p0378 A67-13249
 Epitaxially grown junction as nonlinear
 transmission line 03 p0379 A67-13294
 Temperature effect on electron emission
 and stability of p-n junction using silicon
 and silicon carbide 03 p0494 A67-13487
 Shunting of input current into collector
 region of planar triode 03 p0386 A67-13963
 GaP electroluminescent junctions,
 considering feasibility of
 electroluminescence applications where
 human eye is detector 04 p0581 A67-15077
 Emission spectra and I-V characteristics of
 diffusion p-n junctions in InP and
 spontaneous radiative recombination in
 presence of small current 04 p0679 A67-15138
 V-I characteristics of p-n junctions on In-
 Sb base, noting effects of surface etching,
 temperature and impurity
 concentration 04 p0680 A67-15157
 Fabrication technique and characteristics
 of photovoltaic energy converters produced
 by bombarding p-type Si with phosphorus
 ions 04 p0680 A67-15284
 Recombination radiation from Ga-Sb p-n
 junctions, noting spectral composition as
 function of current density and impurity
 concentration 04 p0681 A67-15297
 Radiative recombination in space charge
 layer of p-n junction in silicon carbide
 determined from I-V characteristics and
 capacitance 04 p0681 A67-15298
 Dynamic resistance of Si p-n junction and
 diffusion length for minority carriers
 measured, using pulsed electron beam
 irradiation 04 p0584 A67-15317
 Nonohmic contacts, metal semiconductor
 point contact and soldered contact instead
 of p-n junctions used to measure diffusion
 length for minority carriers 04 p0584 A67-15481
 Scanning electron microscope used as
 conductive probe to measure depletion layer
 widening in silicon diode as function of
 applied voltage 04 p0584 A67-15483
 Surface aspects of thermal degradation of
 GaAs p-n junction lasers and tunnel
 diodes 04 p0585 A67-15620
 Forward current, electroluminescent
 intensity and short circuit current during
 bombardment as function of 2-mev electron
 irradiation 04 p0685 A67-15704
 Transient radiation response mechanisms
 in monolithic microcircuits using p-n
 junction isolation from substrate 04 p0589 A67-15721
 Radiation intensity dependence for various
 spectral bands of diffused gallium arsenide
 p-n junctions on current density 05 p0861 A67-16391
 Radiative interband recombination in
 strong electric field of p-n junction,
 calculating radiation intensity as function of
 quantum energy and applied
 voltage 05 p0863 A67-16689
 Current and hole distribution calculated
 for p-n junction acted upon by sinusoidal
 voltage of arbitrary amplitude-small injection
 level 05 p0865 A67-16910
 Temperature effect on impact ionization
 coefficient in SiC semiconductor p-n
 junctions with reversed current in strong
 electric field 05 p0865 A67-16916
 Emission from p-n junctions in crystals of
 InP-GaAs solid solution 05 p0865 A67-16941
 Tunnel diode capacitance relation to
 displacement interpreted in terms of
 impurity drift in nonuniform field of p-n
 junction in highly doped germanium
 diodes 05 p0865 A67-16959
 Diffusion and melting techniques used to
 determine effect of Ni, W, Ti and Ta
 impurities on lifetime of minority carriers in
 n-base of silicon p-n junctions 05 p0865 A67-16967
 Tunneling through junctions with
 nonuniform electric field, calculating
 probabilities and currents by WKB
 method 05 p0866 A67-16973
 Microplasma effects arising in avalanche

type breakdown in deep-seated large-area p-n junction in silicon 05 p0867 A67-17052

Volt-ampere characteristics of epitaxial GaP-GaAs heterojunctions 05 p0867 A67-17054

Antimony diffusion into germanium using vacuum furnace, giving graphs with variation of antimony concentration and depth of diffused p-n junction 05 p0869 A67-17089

Silicon p-n junction avalanche breakdown voltages obtained from formula for ionization coefficient 05 p0869 A67-17090

Bias voltage dependence of capacitance in n-type silicon p-n junctions with voltage breakdown 05 p0869 A67-17171

Combination of approximations method for natural oscillations in circuit containing p-n junction capacitance and nonlinear inductance 05 p0777 A67-17237

Similarity theory applied to electron processes in p-n junctions 06 p1048 A67-17854

X-ray effect on conductivity, carrier concentration and mobility in Si crystals and Si p-n junction 06 p1048 A67-17855

X and electron irradiation effect on current-voltage characteristics of p-n junctions in gallium 06 p1049 A67-17859

Parametric action in back biased p-n junctions carrying injected currents, discussing photoparametric frequency converters, transistor amplifiers and frequency doublers 06 p0969 A67-18106

Surface generation-recombination and channel effects on p-n junctions and transistors exposed to ionizing radiation 06 p1054 A67-18822

Recombination radiation of p-n junctions in GaAs with and without Fabry-Perot cavity, discussing nonequilibrium current carrier kinetics and I-V characteristics 06 p1063 A67-18934

Landau quantization and removal of spin degeneracy effect on capacitance of p-n junction 06 p1065 A67-18951

Avalanche multiplication in Ge and GaAs p-n junctions, comparing experimental and theoretical ionization rates, predicting voltage breakdown 06 p1065 A67-18954

Light source devices for electronic functions, discussing p-n junction 07 p1231 A67-19081

Forced oscillations in nonlinear resonant circuit employing p-n junction capacitance 07 p1150 A67-19235

Electric field induced IR absorption in GaAs p-n junction diodes 07 p1231 A67-19553

Current constriction in p-n junction under thermal breakdown, deriving expressions for terminal voltage and radius of constriction 07 p1157 A67-19901

Area of Safe Operation for transistors in switching mode defined, using thermal feedback model 07 p1157 A67-19902

Magnetic effect on photoresponse of illuminated InAs p-n junctions 07 p1237 A67-20181

Recombination radiation from GaAs p-n junctions with and without Fabry-Perot resonator, noting parameter dependence on current density 08 p1337 A67-20413

Photovoltaic emf of silicon solar cell illuminated by ruby laser 08 p1285 A67-20732

Optical absorption, photoconductivity and p-n junction in cadmium telluride 08 p1368 A67-20734

Pulsed sinusoidal bridge for simultaneous measurement of volt-capacitance and volt-ampere characteristics of relaxing p-n junction barriers 08 p1303 A67-20998

Surface effect on temperature, I-V and watt-ampere characteristics of p-n junction semiconductor injection laser diode as coherent light source 08 p1339 A67-21455

Volt-ampere characteristics and other properties of GaAs lasers with tellurium and Zn-doped epitaxial p-n junction 08 p1340 A67-21457

Diffusion parameters and solubility of Cd in InAs measured with aid of radioactive isotopes compared with diffusion coefficient measurement by p-n junction method 08 p1371 A67-21459

Ionization coefficient in selenium p-n step junction of rectifier cell 09 p1551 A67-21656

Hole electron product of p-n junctions, plotting numerical results for electrostatic potential, quasi-Fermi levels and carrier concentration of n-p junction 09 p1553 A67-21946

Stress-dependence of Si p-n junctions with dense generation-recombination centers,

showing that shifts in bias I-V characteristics are due to bandgap changes 09 p1553 A67-21947

High Injection theories of p-n junction, commenting on corrections made in connection with junction voltage 09 p1472 A67-21953

Hydrostatic pressure and temperature effect on current-voltage characteristics of tunnel p-n junctions in gallium arsenide 09 p1554 A67-21977

Spatial variation of quasi-Fermi potentials in symmetrical step and linearly graded p-n junctions 09 p1556 A67-22201

Output and emission spectra of p-n junction diodes analyzed in connection with laser effect in GaSb 09 p1516 A67-22600

CdS solar cell model noting spectral response, V-I characteristic and temperature variation 10 p1596 A67-23164

Capacitance of abrupt p-n heterojunctions and effects of interface states, noting capacitance-voltage characteristics 10 p1612 A67-23372

Transient component in breakdown voltage of silicon p-n junction rectifiers in region of intermittent microplasma conduction 10 p1612 A67-23375

Tunneling assisted photon absorption process /Franz-Keldysh effect/ in semiconductor junctions studied, using differential photocurrent response 10 p1691 A67-23402

Double diffused n-p-n gallium arsenide transistor, discussing ways oxygen modifies p-n junctions to increase voltage breakdown 10 p1617 A67-23537

Avalanche multiplication of current carriers at low temperatures in p-n junctions of InAs, determining carrier ionization coefficient and dependence on electrical field 10 p1695 A67-23660

Conductivity of almost intrinsic infinite p-n junction semiconductor, noting volume charge effect on behavior of junction 10 p1695 A67-23662

Stimulated emission in GaSb injection lasers with steep flat p-n junction, noting dependence of luminescence intensity on current density 10 p1667 A67-23665

P-n junction capacitance in transition region currents obtained by integral of holes or electron concentration 11 p1759 A67-24136

Traveling wave IR and sub-mm light modulator design using free carrier absorption in reverse biased p-n junction diodes 11 p1759 A67-24137

Dimensions effect on efficiency of radiant energy cells 11 p1745 A67-24437

LF noise fluctuation anomalies in narrow doped germanium p-n junctions at low temperatures 11 p1765 A67-24476

High efficiency pulsed gallium arsenide avalanche diode 11 p1767 A67-24722

P-n junction fabrication in vapor phase grown GaAs-P alloys resulting in room temperature injection laser, thereby extending operation into visible spectrum 11 p1802 A67-24741

Low bias non-Esaki current in tunneling p-n junction diodes with large excess currents 11 p1768 A67-24926

Emission spectra and I-V characteristics of diffusion p-n junctions in InP and spontaneous radiative recombination in presence of small current 12 p1979 A67-25161

Semiconductor diode light sources, discussing phenomenon of p-n junction luminescence and potential application in optical displays and data transmission 12 p1979 A67-25169

High resistance region effect in neighborhood of linear junction on series resistance analyzed for microwave varactor design 12 p1912 A67-25280

Voltage breakdown in selectively diffused p-n junction, analyzing dependence on radius of junction curvature 12 p1982 A67-25453

Influence of deep level impurities on uniaxial stress effect of Ge p-n junction 12 p1983 A67-25456

Volt-ampere characteristics of diffused p-n junctions in epitaxial GaAsP film obtained by gas transport 12 p1984 A67-25519

Current voltage characteristics of alloyed p-n junctions in n-type InAs, discussing contribution of tunnel current 12 p1986 A67-26099

Attenuating electron waves in crystals corresponding to energy values in forbidden

band used in calculating current across n-p junction 13 p2172 A67-26354

Electric and photoelectric properties of p-n junction obtained by thermal diffusion of copper into n-ZnS-Cl single crystals 13 p2172 A67-26355

One-dimensional transport equations of p-n junction in steady state solved numerically 13 p2078 A67-26781

Electric field distribution in p region, space charge layer and n region of p-n abrupt junction germanium diode at room temperature 13 p2078 A67-26788

Surface fields effect on breakdown voltage of planar silicon p-n junctions 13 p2079 A67-26873

Scanning microscope for studying Si p-n junctions by electron or ion bombardment 13 p2120 A67-27069

Stroboscopic electron mirror microscope observations of Si p-n junctions in pulsed regime 13 p2120 A67-27070

Scanning electron microscope observations of p-n junctions using small periodic bias voltages 13 p2177 A67-27072

Evaporated silicon thin-film transistors operating by field effect conductivity modulation of n-type inversion layer at p-type film surface 13 p2083 A67-27573

Electrical and energy performance of high efficiency GaAs solar cells compared to silicon photocells, discussing temperature effect and p-n junction depth 13 p2056 A67-27623

Stress effect on minority carrier mobility and concentration in germanium and silicon p-n junctions under uniaxial compression 14 p2364 A67-27825

Origin of excessive reverse current in silicon p-n junction, discussing surface layer channel formation 14 p2283 A67-28040

Maximum power transformed by nonlinear capacitance of semiconductor diode on closed p-n junction 14 p2283 A67-28073

Apparatus for determining impurity distribution in semiconductor structure 14 p2317 A67-28281

Emission from p-n junctions in crystals of InP-GaAs solid solution 14 p2366 A67-28486

Performance characteristics of nonstoichiometrically doped p-n junctions in Cd-Hg-Te alloy operated as IR photovoltaic detector 14 p2366 A67-28496

Characteristics of electroluminescent p-n junctions prepared on base of beryllium-doped silicon carbide 14 p2367 A67-28524

Nature of photoelectromotive force of cadmium selenide with Cu, Ag, Au, Pt vacuum-deposited on surface 14 p2367 A67-28527

Injection electroluminescence of p-n junctions in GaP doped with tellurium, zinc, ZnO, etc 14 p2368 A67-28531

Double injection and oscillations of current-voltage dependence of alloyed diodes prepared on basis of p-type gallium phosphide 14 p2286 A67-28594

Analog multiplier using p-n junction dynamic capacitance, noting decays in RC circuit current 14 p2290 A67-28928

Computer solution for current density, continuity and Poisson equation to obtain electron density and electrostatic potential in p-n junction 14 p2290 A67-28931

Pulsed power output for microwave GaAs oscillator biased into avalanche, with diodes grown by liquid phase epitaxy 15 p2442 A67-29172

V-I characteristics of p-n junctions on InSb base, noting effects of surface etching, temperature and impurity concentration 15 p2534 A67-29344

P-n semiconductor junction widening due to impurity diffusion and drift, noting first order differential equations describing space-charge width variation with time 15 p2535 A67-29488

Current saturation phenomena in junction-gate field effect transistor 15 p2446 A67-29637

Microplasma effects arising in avalanche type breakdown in deep-seated large-area p-n junction in silicon 15 p2538 A67-29783

Volt-ampere characteristics of epitaxial GaP-GaAs heterojunctions 15 p2538 A67-29785

Space charge varactor compared to p-n junction varactor, noting applications 15 p2449 A67-29804

Radiative interband recombination in strong electric field of p-n junction, calculating radiation intensity as function of

- quantum energy and applied voltage 15 p2539 A67-29859
- Difference leveling between electron and hole concentrations near junction by compensating charges of donors and acceptors with semiconductor space charges 15 p2542 A67-30242
- Noise suppression in p-n junction biased in direction of current, noting effect of space charge on current fluctuation 15 p2543 A67-30252
- Effect of capture levels on current-voltage characteristic of semiconductor p-n diode with ohmic back contact 16 p2635 A67-30471
- Reactive characteristics of diffused p-n junctions in p-and n-silicon at high injection levels and in strong electric fields 16 p2726 A67-30817
- Current and hole distribution calculated for p-n junction acted upon by sinusoidal voltage of arbitrary amplitude-small injection level 16 p2727 A67-30887
- Temperature effect on impact ionization coefficient in SiC semiconductor p-n junctions with reversed current in strong electric field 16 p2727 A67-30893
- Surface etching effects on positively sloped current-voltage characteristics of p-n junctions in fused indium antimonide 16 p2730 A67-31161
- Surface leakage current and reverse current flow in silicon p-n junction diode affected by positive ion bombardment and oxygen adsorption 17 p2911 A67-32202
- Stress effect on electric properties of p-n junction of semiconductor diodes and means of control 17 p2912 A67-32252
- Impurity diffusion and segregation effects in p-n junctions in compensated solution grown GaP 17 p2921 A67-33053
- Hydrostatic pressure and temperature effect on current-voltage characteristics of tunnel p-n junctions in gallium arsenide 17 p2923 A67-33314
- Avalanche multiplication of current carriers at low temperatures in p-n junctions of InAs, determining carrier ionization coefficient and dependence on electrical field 17 p2924 A67-33341
- Conductivity of almost intrinsic infinite p-n junction semiconductor, noting volume charge effect on behavior of junction 17 p2924 A67-33343
- Stimulated emission in GaSb injection lasers with steep flat p-n junction, noting dependence of luminescence intensity on current density 17 p2870 A67-33346
- Thermal stabilization of inverse current of p-n junction by additional gate for minority carriers extraction 18 p3009 A67-33478
- Amplitude modulation using varicaps and p-n junction in transistorized transmitter, analyzing HF oscillator 18 p2999 A67-33507
- Probability of tunneling across impurity level of p-n junction 18 p3099 A67-33695
- Structural dislocations effect on formation of microplasmas during avalanche breakdown of silicon p-n junction 18 p3099 A67-33698
- Spectral and recombination radiation intensity changes from indium phosphide diode under different uniaxial compressions 18 p3100 A67-33718
- Volt-ampere characteristics of diffused p-n junctions in epitaxial GaAsP film obtained by gas transport technique 18 p3103 A67-34450
- Thin film resistor used to improve performance of picosecond silicon integrated digital circuit with p-n junction isolation 18 p3014 A67-34551
- Effect of dislocations in GaAs single crystals on diffused p-n junctions structure and recombination radiation parameters 19 p3300 A67-34768
- Electrical characteristics of GaAs p-n diffusion junctions used as solar cells 19 p3300 A67-34769
- Threshold current density dependency on photon energy in diffused and epitaxial p-n junction GaAs injection lasers 19 p3238 A67-34774
- Copper-doping technique for obtaining p-n junctions in sintered cadmium sulfide polycrystals, suitable for use in photoelectric converters 19 p3304 A67-35427
- Pulsed operation of large-area silicon p-n junction avalanche diode oscillators for microwave frequencies 19 p3196 A67-35627
- Irradiation effect on minority carrier lifetime for p-n junction devices in epitaxial film and single crystal forms 19 p3306 A67-35670
- Flowgraph models describing relationships between thermal and electrical parameters of devices and associated circuits 19 p3206 A67-36034
- Depletion layer capacitance of p-n step junction with inclusion of effect of spillover charge as function of voltage 20 p3504 A67-36167
- Dimensions effect on efficiency of radiant energy cells 20 p3362 A67-36239
- Photovoltaic cell characteristics, emphasizing energy conversion processes and quantum efficiency determination 20 p3362 A67-36240
- P-n junction diode frequency doubler operating in charge-storage/step-recovery mode efficiency and power output 20 p3395 A67-36315
- Current creep in selenium rectifier and effect on local conductivity channels in p-n junction of rectifier 20 p3508 A67-36403
- Electrical conductivity variation of low and high resistance germanium due to X-ray radiation absorption 20 p3508 A67-36405
- Operation of Hall generator with variable thickness active layer 20 p3401 A67-37220
- Electric and photoelectric properties of p-n junction obtained by thermal diffusion of copper into n-ZnS-Cl single crystals 21 p3679 A67-38312
- Solution grown GaAs laser diodes with Fabry-Perot cavity, measuring threshold current density variation with reciprocal laser diode length 21 p3641 A67-38457
- P-n junction devices static behavior assuming Van Roosbroeck differential equations in bulk and transition regions 21 p3598 A67-38571
- Microwave characteristics of coaxial mounted tunnel diodes investigated by equivalent circuit parameters 21 p3602 A67-39070
- Limitations imposed on performance of large area p-n junctions by quality of silicon material, discussing defect-free processing techniques 22 p3766 A67-39247
- Concentric ring junction to prevent surface breakdown in planar p-n junctions 22 p3766 A67-39252
- Avalanche breakdown voltage in Si planar p-n junctions studied for relation to impurity gradient 22 p3766 A67-39256
- Planar diffused p-n junction profile geometry using scanning electron microscope and electron probe with computer calculations 22 p3855 A67-39360
- LF noise spectrum of p-n junction using arbitrary pulse duration distribution functions 22 p3858 A67-39573
- Recombination centers in silicon transistor emitter-base junctions causing anomalous base current component studied via temperature dependence of forward characteristics 22 p3770 A67-39732
- Characteristics of electroluminescent p-n junctions prepared on base of beryllium-doped silicon carbide 23 p4039 A67-40931
- Nature of photoelectromotive force of cadmium selenide with Cu, Ag, Au, Pt vacuum-deposited on surface 23 p4039 A67-40934
- Injection electroluminescence of p-n junctions in GaP doped with tellurium, zinc, ZnO, etc 23 p4039 A67-40938
- Light emission spots one to one correspondence with microplasmas in GaP p-n junctions 23 p4043 A67-41437
- P-n junction performance with depletion layer subjected to sudden extreme carrier density generation noting significant local distortion 23 p4044 A67-41453
- Electromagnetic mode propagation in anisotropic dielectric p-n junction waveguide models noting Pockel effect of electric field on light 23 p3982 A67-41466
- Lifetime measurements of GaAs diodes determined from p-n junction impedance 23 p3982 A67-41468
- CdS solar cell model, discussing p-n junction, CdS and copper sulfide properties and microscopic junction formation and behavior 23 p4046 A67-41486
- Distributed model for photovoltaic cell via nonlinear least square techniques, discussing p-n silicon cells 23 p4046 A67-41487
- Li containing p-on-n and n-on-p Si cell degradation by bombardment noting carrier removal damage, annealing and radiation damage resistance 23 p3941 A67-41524
- Spectral response of p-n semiconductor heterojunction, considering absorption effects and photocurrent loss 24 p4202 A67-41981
- Planar dielectric waveguide excitation at p-n junctions by externally incident electromagnetic field 24 p4121 A67-42337
- ### P-N-P JUNCTION
- Epitaxial diffused integrated circuit structure containing p-n-p and n-p-n transistors 01 p0033 A67-10021
- Abnormal diffusion of base dopant impurities in shallow double-diffused structures in silicon, noting cooperative diffusion in enhanced or retarded penetration of base region 02 p0298 A67-11877
- Planar transistor stability under X-ray irradiation, showing drifts of variable importance according to type of transistor /p-n-p or n-p-n/ 03 p0387 A67-13996
- Failure mechanisms in silicon transistors deduced from step stress tests 04 p0584 A67-15482
- Electron induced ionization and displacement damage in n-p-n and p-n-p transistors at medium and low powers 04 p0588 A67-15706
- Switching process for silicon p-n-p structures, deriving relations for delay and response times and transient period as function of parameters 05 p0865 A67-16911
- Diffused base transistor impurity concentration measured nondestructively to determine structure 15 p2448 A67-29801
- Switching process for silicon p-n-p structures, deriving relations for delay and response times and transient period as function of parameters 16 p2727 A67-30888
- Germanium pulse switching triode with fused p-n-p junction 18 p3009 A67-33477
- P-n-p diode volt-ampere characteristic qualitative calculation, analyzing device negative resistance with avalanche multiplication 21 p3593 A67-38289
- P-n-p transistor overcomes bandwidth and switching time deficiencies to enhance minority carrier transport 21 p3598 A67-38570
- ### P-N-P-N JUNCTION
- #### SA N-P-N JUNCTION
- Semiconductor negative resistance devices to achieve analog to digital conversion 20 p3390 A67-36252
- P-n-p-n diode noise measured by standard techniques and explained using theoretical model, considering internal feedback and additional amplification 21 p3589 A67-37820
- P-n-p-n triode turn-off characteristics showing forward biased center junction, establishing general turn-off criterion 21 p3591 A67-38154
- Reverse transient in p-n-p-n triode when reverse pulse is applied to gate 21 p3598 A67-38573
- Charge model for unsaturated and saturated p-n-p-n dynamic behavior using numerical integration techniques 22 p3766 A67-39249
- Basic equation derived for I-V characteristics of p-n-p-n device with graphical solution for related p-n junctions 22 p3766 A67-39251
- General three-terminal p-n-p-n triode turn-on criterion equation derived and simplified for practical external-circuit arrangements 22 p3770 A67-39731
- Fast neutron radiation damage in narrow base p-n-p-n devices compared to one-dimensional theory, showing superiority to bipolar transistors 24 p4130 A67-42248
- ### P-TYPE SEMICONDUCTOR
- Variable effect of external electrical field on IR photoconductivity of thin n-and p-type silicon samples with low bulk impurity contents 01 p0128 A67-10076
- Photo-Hall effect and photoconductivity on compensated p-InSb at low temperatures, examining temperature dependence of carrier mobility 01 p0128 A67-10093
- Electron mobility in p-type indium antimonide, noting entrainment of minority carriers by majority 01 p0129 A67-10098
- X-ray irradiation effect on electrophysical properties of n-and p-type germanium, determining absorption coefficient 01 p0136 A67-11044
- Voltage induced by electron beam in n-and p-type germanium bars having inhomogeneous resistivity distribution, obtaining equations from one-dimensional model 01 p0137 A67-11059

Proton irradiation effect on Hall coefficient, resistivity and magnetoresistance of p-type bismuth telluride single crystals 02 p0298 A67-11882

Implantation of Cs and Na ions into p-type silicon, effect on hot electron emission from p-n junction 02 p0299 A67-11897

Temperature and stress dependence of electron lifetime in p-type Si-B and Ge-Zn between 1.5 and 4.2 degrees K 02 p0301 A67-12523

Dependence of peak inverse voltage of n-Si and p-Ge on specific resistance and concentration and mobility of current carriers 03 p0488 A67-12817

Hall effect in semiconductors containing two species of current carriers, p-type PbTe and GeTe, taking into account temperature dependence of energy gap 03 p0489 A67-13148

Hall mobility and Nernst-Ettingshausen effect in Zn and Cd-doped p-type GaAs at temperatures from 90 to 800 degrees K 03 p0491 A67-13174

Longitudinal magnetoresistance anisotropy and Hall coefficient anisotropy in p-type indium antimonide, noting similarities with galvanomagnetic anisotropy of p-type germanium 04 p0674 A67-14609

Electrical conductivity of p-GaSe single crystals in strong electric fields 04 p0676 A67-14929

Uniaxial compression effect on two jump conductivity processes occurring in p-type silicon 04 p0679 A67-15145

Fabrication technique and characteristics of photovoltaic energy converters produced by bombarding p-type Si with phosphorus ions 04 p0680 A67-15284

Displacement effects in n-and p-type silicon when exposed to energetic radiation, using electron spin resonance and galvanomagnetic techniques 04 p0684 A67-15689

Defect impurity relation in electron damaged p-type silicon and electron irradiation effect on float zone n-type silicon 04 p0684 A67-15690

Impurity microsegregation substructure in n-and p-type bismuth telluride crystals grown according to Bridgman method, measuring electrical properties, thermal emf, Hall constant, etc 05 p0861 A67-16498

Large signal AC field effect measurements on A and B real surfaces of InSb exposed to different ambients 05 p0862 A67-16604

Shallow donor introduction in p-type Ga-As laser results in increased efficiency of radiative recombination 05 p0826 A67-17280

Anomalous temperature dependence of IR absorption in p-type germanium attributed to phonon induced effects 06 p1060 A67-18913

Impurity states in CdTe analyzed by examining changes in electrical and optical properties after thermal-neutron bombardment 06 p1062 A67-18928

Oscillatory magnetoconductance in inverted surfaces of p-type silicon 06 p1063 A67-18940

Corbino magnetoresistance experiments for n-type surface layers on p-type indium arsenide crystals as function of surface electric field 06 p1064 A67-18941

Galvanomagnetic effects and band structure of p-type cadmium antimonide 06 p1064 A67-18942

Negative magnetoresistance in semiconductors caused by magnetic system in random lattice of impurity atoms 06 p1067 A67-18965

Fluorescence of n-and p-type gallium arsenic phosphide under optical excitation 07 p1232 A67-19635

Piezoresistance measurement in p-type Ge as function of pressure and impurity concentration at 77 and 300 degrees K 07 p1233 A67-19644

Second breakdown and degradation in Ge alloy junctions, noting failure mechanism and preventive surface treatment 07 p1157 A67-19905

Coherent radiation generation in electron-hole indium antimonide plasma, discussing emission spectrum 08 p1367 A67-20418

Hall effect on hot carriers in p-type Ge semiconductor in microwave field as function of field strength 08 p1369 A67-20993

Thin film silicon-on-sapphire deep depletion MOS transistors 09 p1475 A67-22203

Temperature dependence of threshold

voltage, effective mobility in inversion layer and channel conductance of MOS transistor below saturation 09 p1475 A67-22204

Hall effect in semiconductors containing two species of current carriers, p-type PbTe and GeTe, taking into account temperature dependence of energy gap 10 p1689 A67-23097

Fast neutron irradiated p-type silicon single crystals electric and photoelectric properties 10 p1691 A67-23404

Generation-recombination and modulation noise power spectrum of high purity p-type InSb at 77 degrees K 10 p1693 A67-23566

Impurity photoconductivity spectra of p-type germanium at low temperatures, noting parameters of relative depth of equidistant minima oscillations 10 p1693 A67-23583

Space-charge-limited currents in p-type silicon noting I-V characteristics, theoretical values agreement, Hall coefficient measurements correlation, etc 11 p1845 A67-24135

Uniaxial compression effect on two jump conductivity processes occurring in p-type silicon 12 p1979 A67-25168

Photoconductivity kinetics and regeneration recombination noise spectrum of p-InSb crystals, showing association with hole capture, lifetime and alloying impurity 12 p1983 A67-25512

P-and n-type silicon spectral emissivity measured at several temperatures and wavelengths for carrier concentrations and direct current resistivities [AIAA PAPER 67-302] 12 p1958 A67-26017

Hole effective masses in p-type CdSb determined by measuring magnetoresistance effect and magnetic susceptibility 12 p1987 A67-26225

Carrier distribution function in degenerate p-type germanium in presence of hole scattering on acoustic phonons, considering heating in arbitrary electric and magnetic fields 13 p2181 A67-27281

P-type GaAs laser excited by Q-switched ruby laser at liquid nitrogen temperature, noting spectral shift due to Burstein effect 14 p2329 A67-27831

Hall coefficient, electrical resistivity and Seebeck coefficient of p-type lead telluride measured, using two-valence band model 14 p2367 A67-28520

P-type silicon IR photoconductivity burst in nonequilibrium field 14 p2368 A67-28536

Microwave emission from magnetic-field-free electron hole plasma in p-type InSb at 77 degrees K 15 p2539 A67-29820

Hall coefficient and reluctance dependence on magnetic field inductance in p-type cadmium tin arsenide samples from 250 to 411.7 degrees K 15 p2543 A67-30253

Cobalt 60 gamma radiation effect on set of B-doped p-type silicon samples, giving radiation-induced defects. 16 p2724 A67-30472

Minority carrier lifetime in p-silicon, analyzed varying temperature and injection level and studying recombination 16 p2725 A67-30807

Electric field effect on magnetoresistance of p-type indium arsenide surface in high magnetic fields at low temperatures 17 p2911 A67-32206

Microwave emission phenomena from n and p type indium antimonide, noting no essential difference 17 p2914 A67-32375

Disordered regions produced by fast neutron irradiation effect on semiconductor properties of silicon 17 p2919 A67-32859

Current-voltage characteristics of clamped metal/p-silicon diodes 18 p3009 A67-33475

Photoconductivity kinetics and regeneration recombination noise spectrum of p-InSb crystals, showing association with hole capture, lifetime and alloying impurity 18 p3103 A67-34443

Surface recombination velocities relationship in depletion, inversion and accumulation surface layers of p-type silicon, using ambipolar carrier transport formulation 18 p3104 A67-34593

Thermoelectric and galvanomagnetic measurements on p-type bismuth compound, explaining anomalous rise in Hall coefficient with temperature and effective mass ratios change 18 p3105 A67-34632

Thin films of cuprous sulfide, selenide and telluride prepared by flash evaporation, discussing resistivity and absorption coefficient 18 p3106 A67-34637

Localized vibrational modes of lithium in lithium diffused p-type Ga-As doped with Mn, Cd or Zn 18 p3106 A67-34644

Water adsorption on oxide covered surface of germanium, studying chemisorption dependence on p-type doping 19 p3301 A67-34935

Neutron irradiation effect on n-type and p-type semiconductors thermophysical parameters 19 p3307 A67-35874

Active impurities concentration in p-type semiconductors by measuring temperature at zero thermoelectric potential 19 p3308 A67-35875

Nonequilibrium current carrier lifetime in p-type InSb samples alloyed with Cu and Ge, noting hole concentration and temperature effects 20 p3510 A67-36761

Intrinsic and impurity photoconductivity kinetics over wide temperature and illumination range of p-type indium sulfide single crystals obtained by zone melting 21 p3676 A67-37859

Impurities compensated p-type cadmium antimonide single crystals, determining Hall effect temperature dependence and specific resistance 21 p3676 A67-37868

Hall effect measurements on heat treated and quenched p-type silicon crystals, noting donor centers appearance due to vacancy cluster 21 p3687 A67-39138

Silicon AC strain gauges performance investigated by employing oriented p-Si crystals operating in static and dynamic modes 22 p3798 A67-39569

P-type silicon IR photoconductivity burst in nonequilibrium field effect 23 p4040 A67-40943

P-I-n structures obtained from p-type Si by Li drift studied for carriers collection efficiency and potential path distributions 23 p4044 A67-41456

Impact ionization avalanche plasma production and instabilities in InSb at low temperatures, measuring current variation with electric field strength 24 p4204 A67-42344

PACIFIC OCEAN

Atmospheric circulation in weak easterly region in troposphere over northwest Pacific in summer 10 p1677 A67-23499

PACKAGING

SA CONTAINER

SA ELECTRONIC PACKAGING

Apollo computer design mechanical packaging, implementing heat and vibration model to conduct thermal vibration and sealing tests 05 p0814 A67-17460

Thermal, mechanical stress and moisture resistance reliability tests of plastic encapsulated transistors 15 p2444 A67-29457

Fluoride and electronic integrated circuits compared, presenting state of art in packaging 16 p2610 A67-31722

Slough characteristics measuring methods for clean packaging materials, considering Taber-Abraser, tumble-box and reciprocating-stylus method 23 p3986 A67-40847

PACKING

Antifrictional properties of mica and boron nitride for use instead of graphite as solid lubricant in cermet packing materials 01 p0081 A67-11246

Antifrictional properties of mica and boron nitride for use instead of graphite as solid lubricant in cermet packing materials 17 p2866 A67-33169

PACKING DENSITY

High speed automatic testing of semiconductor devices, discussing wafers and integrated circuits 15 p2449 A67-29812

High density packaging technique for aerospace electronic equipment of reliable and long-life qualities 20 p3397 A67-36603

Electronic circuit packaging in Apollo lunar module signal conditioning equipment 21 p3635 A67-38628

PADE APPROXIMATION

Rational approximations to incomplete elliptic integral of first and second kinds derived by main diagonal Pade approximations 18 p3072 A67-34397

PAIN

Terminal connections of spinothalamic and distribution in human thalamus, noting pain relay question 06 p0953 A67-18775

PAINT

SA FILLER

SA FINISH

Lunar environment effects on Surveyor I

components, particularly white paint degradation as function of time 15 p2579 A67-29451

PAIR PRODUCTION

Pair production in irradiated semiconductors within framework of plasmon decay, considering variation of radiation ionization energies with band gap energy 06 p1063 A67-18935

Experimental verification of predictions of conventional quantum electrodynamic vacuum effects by Compton and other scattering techniques 09 p1534 A67-22021

Energy loss of high energy muons caused by nuclear interaction and fluctuation due to passage through great thickness of material corrected for standard rock 10 p1703 A67-23690

Lifetime of atomic state against decay induced by lepton coupling, estimating neutrino power radiation and astrophysical implications 11 p1821 A67-23959

Relativistic velocity shock wave propagation in stellar high temperature high density plasmas with pair production, thermonuclear reactions and neutrino emissions 14 p2355 A67-27953

Electron cascade showers, examining elementary processes, general behavior, three-dimensional theories and large angle single scattering 14 p2379 A67-27961

Hypothesis attributing most energetic cosmic ray proton source to powerful radio galaxies noting pair production effect on cosmic ray sources 16 p2738 A67-30822

Nucleon-nucleon collisions, analyzing pair production, electromagnetic cascade, secondary interactions, etc 16 p2703 A67-30965

Possible superconductive pairing of two electrons separated by barrier leading to higher transition temperature for superconductors and superconductivity in magnetic metals 18 p3101 A67-33988

Light absorption of single-band semiconductor calculated from wave function of electron-hole pairs located near charged impurities, obtaining pair lifetime 19 p3300 A67-34767

Antiproton production by primary cosmic ray collisions with atmospheric nuclei compared with interstellar gas 21 p3620 A67-38843

PAKISTAN

Pakistan space research noting facilities, sounding rocket experiments and satellite- and ground-based observations 19 p3321 A67-35297

PALEONTOLOGY

Paleontological evidence of earth rotation rate 24 p4151 A67-42318

PALLADIUM

Stability of palladium oxide resistive glaze films, describing process variables affecting resistivity and TCR 09 p1473 A67-22019

Influence of palladium additives and sintering temperature on tungsten molding noting shrinkage, density, microhardness, durability and microstructure 20 p3466 A67-36910

PALLADIUM ALLOY

Plastic deformation effect on resistivity and Hall effect of copper-palladium and gold-palladium alloys 13 p2133 A67-27005

Recovery of deformed copper-palladium and gold-palladium alloys by isothermal and isochronal annealing, noting vacancy and interstitial migration 13 p2133 A67-27007

PAM

S PULSE AMPLITUDE MODULATION /PAM/

PANEL

SA CONTROL PANEL

SA CURVED PANEL

SA PLATE

SA RECTANGULAR PANEL

SA WING PANEL

Shell structures solved numerically, using network of partial panels 08 p1417 A67-20556

Integrally formed compression panel efficiencies compared with other aerospace panel concepts 10 p1729 A67-23769

Stress-strain state of short cylindrical shell and square panel under axial compression hinged along edges 14 p2402 A67-28897

Maximum stresses with changes in Poisson ratio for thin parallelogramic panels with nonlinear behavior 22 p3911 A67-39666

PANEL FLUTTER

Aircraft skin panel fatigue failure under

hypersonic conditions, noting effect of natural vibration frequency and axisymmetric oscillations 05 p0916 A67-16229

Minimum potential energy principle and Rayleigh-Ritz method derivation of flutter equations for flat rectangular orthotropic panels 05 p0924 A67-17350

Unsteady aerodynamic field with application to panel flutter in low supersonic flow 08 p1418 A67-20608

Free flight response of two panels subjected to turbulent pressure fluctuations at supersonic Mach numbers 10 p1719 A67-23558

Flutter of panels mounted on wedges in hypersonic flow of perfect gas, neglecting acoustic waves 10 p1593 A67-23735

Identical flutter boundaries of multibay and one-bay panels with clamped edges in high and low supersonic regions 12 p2030 A67-25930

Flutter amplitude of stressed panels analyzed in terms of amplification ratios 14 p2399 A67-28139

Stability boundaries and critical frequencies for sem infinite elastically restrained plate determined at different boundary stiffnesses 15 p2575 A67-29858

Lapunov functional for aeroelastic divergence noting application to partial differential equations 15 p2575 A67-30021

Boundary conditions influence on flutter critical boundary character considering nonlinearities of physical nature 16 p2776 A67-31471

Aeroelastic stability of two-dimensional flat panels in subsonic and transonic flow, noting flutter and divergence 16 p2776 A67-31545

Flutter of flat panels at low supersonic speeds, describing mounting which makes it possible to change tension of panel during testing at constant Mach number [ONERA-TP-487] 17 p2961 A67-32699

Ionization effect on external pressure determination for high velocity gas flows past plates and shells with flutter 18 p2981 A67-33424

Flutter of simply supported thin isotropic parallelogramic flat panels in supersonic flow 19 p3342 A67-35751

Panels response to oscillating and to moving shock waves, discussing mode excitation, magnification factor, Bessel function, etc 20 p3539 A67-37001

Skin stringer panel rows natural frequencies and normal modes predicted by transfer matrix method 20 p3539 A67-37008

Panel flutter analysis of hinged closed circular cylindrical shell in supersonic gas flow, considering axial compression and structural damping 21 p3725 A67-38788

Flutter of two cylindrical panels bonded by elastic filler in supersonic gas flow, showing flutter velocity increase with increasing filler elasticity 22 p3910 A67-39455

Mathematical model, representing two-dimensional panel fluttering in supersonic flow, to study stability criterion via Lapunov second method 23 p4081 A67-41752

PANORAMIC SCANNING

Geometrical evaluation of line-scan images for mapping, noting imagery systems 01 p0059 A67-10316

Soviet papers on photogrammetric processing and interpretation of aerial photographs 14 p2318 A67-28370

Scanning and transformation of panoramic lunar surface photographs 14 p2319 A67-28373

Analytical reduction of panoramic and strip photography to equivalent frame photography 15 p2486 A67-29299

Global ocean data acquisition by remote sensor operating from spacecraft for oceanographic studies 15 p2477 A67-29698

Analysis of lunar surface panoramas transmitted by automatic station Lunik IX after soft landing 18 p3122 A67-34138

Carrier frequency measurement accuracy using panoramic radio receiver, discussing statistical estimate of errors using two different reading methods 22 p3772 A67-39871

PAPER CHROMATOGRAPHY

Metabolism of dihydroxyphenylalanine in human subjects 09 p1454 A67-21982

Amino acid formation by formamide thermal decomposition, noting support for hydrogen cyanide oligomerization hypothesis 20 p3376 A67-36700

PARA HYDROGEN

Physical properties of liquid

hydrogen 05 p0928 A67-17012

Liquid and gas viscosity correlation at 1 atm with reduced density for parahydrogen 05 p0873 A67-17224

Density-temperature formulae for coexisting liquid and vapor and for freezing liquid para hydrogen 06 p1118 A67-18521

PARABOLA

Simultaneous effect of transverse curvature and fluid injection on boundary layer flow over parabola of revolution, obtaining iterative solution to differential equation 01 p0055 A67-11175

Harmonic components of current of HF transistor under sinusoidal excitation, using piecewise parabolic approximation 05 p0772 A67-16456

Hertz and Mindlin problems for fourth order paraboloids in contact generalized, minimizing microslips and annulus of slip [ASME PAPER 67-APM-12] 15 p2505 A67-30149

Hertz and Mindlin problems for fourth order paraboloids in contact generalized, minimizing microslips and annulus of slip [ASME PAPER 67-APM-12] 17 p2871 A67-32411

PARABOLIC EQUATION

Solvability of degenerated parabolic boundary value problem in Euclidean space cylinder and relation to homogeneous Dirichlet problem 01 p0105 A67-10677

Existence, uniqueness and reversion theorems, necessary optimality criteria and nonfixed time case for optimal control problem of n-dimensional linear parabolic equations 01 p0105 A67-10679

Parabolic equation derivative solution applying results to boundary value problems, Cauchy problem and nonlinear equation 01 p0106 A67-10901

Convergence theorem for second-order linear three-level difference scheme for class of quasi-linear parabolic differential equation 02 p0258 A67-11556

Free boundary problem for parabolic equation proving existence and uniqueness theorems for certain initial conditions 02 p0258 A67-11626

Parabolic convolution type equations in bounded cylindrical and noncylindrical regions, discussing smooth operators in half-space 02 p0259 A67-11871

Generalized solutions to second order linear or quasi-linear uniform parabolic equation 02 p0259 A67-11916

Necessary conditions for stability of trivial solutions of parabolic systems of partial differential equations 03 p0456 A67-12861

Contour integral method applied to solution of three-dimensional mixed problem for second order parabolic equation under mixed type boundary conditions containing time differentiation 03 p0457 A67-13115

Pointwise bounds for solutions of first initial boundary value problem for second order semilinear parabolic equation 03 p0460 A67-13821

Existence theorem for periodic solutions to parabolic boundary value problem involving reduction to solvable operator equation 03 p0460 A67-13835

Parabolic conditions for general second order PDE, discussing bicharacteristic condition, initial boundary value problem, Monge-Ampere equations and quasi-linear equation systems 03 p0461 A67-14105

Pointwise bounds for solutions of semilinear parabolic equation, presenting existence theorems 04 p0647 A67-15739

Difference approximation with second order accuracy of numerical solution for parabolic type equations 05 p0834 A67-16372

Pointwise bounds for linear and nonlinear second initial boundary value problem of parabolic type 05 p0836 A67-17046

Error estimate for approximate solution of linear parabolic equation using Kantorovich theorem on functional analysis in normalized space 05 p0836 A67-17108

Parabolic equations with continuous coefficients 07 p1212 A67-19139

Solution approximation for nonlinear parabolic PDEs, using linear combination of finite set of selected functions 07 p1213 A67-19159

Existence of solutions to differential and integrodifferential equations possessing asymptotic parabolas 07 p1214 A67-19174

Trace formulas of difference between two ordinary differential operators of higher

order 07 p1214 A67-19175

Structure of solutions to elliptic and parabolic equations with one separable variable concerning combined action of convective and conductive transport 07 p1214 A67-19177

Modification of functional scheme of Chaplygin method applied to solution of first boundary value problem for class of quasi-linear second order parabolic equation 07 p1215 A67-19220

Solvability of Cauchy problem for second order linear parabolic equations in classes of exponentially increasing functions 07 p1216 A67-19584

Schauder type boundary estimates for solution of directional-derivative problem of parabolic equation in noncylindrical region 08 p1348 A67-21153

Numerical solution of sequential decision problems involving parabolic equations with moving boundaries 08 p1349 A67-21256

Plane viscous problem of gas motion through weak straight line discontinuity of acceleration, noting formation of boundary layer 11 p1742 A67-24687

Existence, uniqueness and reversion theorems, necessary optimality criteria and nonfixed time case for optimal control problem of n-dimensional linear parabolic equations 11 p1814 A67-25067

Representation and uniqueness theorems for second order linear parabolic partial differential equations 12 p1961 A67-26061

Convergence considerations on second order method of parabolic equations approximate solution 13 p2148 A67-27473

Single parameter family of two-layer difference schemes with decomposing operators for general linear second order parabolic equations with mixed derivatives and variable coefficients 13 p2149 A67-27614

Difference methods for parabolic equations and alternating direction implicit methods for elliptic equations 14 p2342 A67-28155

Two-dimensional mixed boundary value problem of heat and mass transfer with characteristic equation containing multiple roots 14 p2406 A67-28312

Uniqueness of solutions for Cauchy problem and some boundary value problems of general parabolic systems in class of increasing Holder 14 p2344 A67-28894

Uniqueness theorems for Adler fourth and fifth boundary value problems for heat conduction differential equation 14 p2409 A67-28936

Finite difference solution of third boundary value problem for heat conduction equation, obtaining conditions for coefficients from stability requirements 15 p2510 A67-29521

Finite difference method solution of periodic parabolic problem solution subject to nonlinear boundary condition 15 p2510 A67-29522

Finite difference method of solving degenerate elliptic and parabolic equations 15 p2511 A67-30008

Uniqueness and existence of Cauchy problem solution considering Dirichlet limits, studying convergence requirements 16 p2695 A67-30829

Numerical calculation of self-focusing of axisymmetric electromagnetic-wave packets in nonabsorbing cubic isotropic media based on parabolic equation 16 p2628 A67-31504

Time optimal control for parabolic equations, proving bang-bang principle, smoothness, existence of minimum, etc 17 p2877 A67-32559

Parabola test for absolute stability, replacing Popov test for nonlinear sectors having nonzero lower bound 19 p3199 A67-34785

Alternating direction implicit /ADI/ method variant for elliptic and parabolic partial differential equations 19 p3250 A67-34868

Second order nonlinear parabolic type partial differential equations with divergence structure, noting role of maximum principle 20 p3475 A67-36502

Numerical digital computer solution of parabolic partial differential equations with two-point boundary conditions, using method of lines 20 p3391 A67-36820

Fourth order parabolic partial differential equation solution by explicit and implicit

finite difference methods 20 p3478 A67-37211

Inversion formulas for parabolic functions solution to vibration equation in diffraction at paraboloid of revolution 21 p3652 A67-38110

Wave propagation in inhomogeneous half-space with refractive index depending on two coordinates analyzed, using parabolic equation method 21 p3580 A67-38114

Pointwise bounds for perturbed parabolic and elliptic equations using known bounds for corresponding strictly differential problems, noting Rayleigh-Ritz procedure 21 p3652 A67-38174

Inequality for pointwise bounds of second initial boundary value problem for second order semilinear parabolic equation, noting Rayleigh-Ritz method 21 p3652 A67-38176

Cauchy problem for second order parabolic partial differential equation 22 p3827 A67-39432

Analysis of system described by heat equation where disturbance propagates with infinite speed as function of time 23 p4024 A67-41086

Solution for coupled system of parabolic partial differential equations describing reactants diffusion and heat conduction in gas phase 23 p4048 A67-41764

Finite difference method for degenerate elliptic and parabolic equations involving various boundary value problems 24 p4178 A67-42269

Extrapolated Crank-Nicolson difference scheme for quasi-linear parabolic equations 24 p4180 A67-43091

PARABOLIC FLIGHT

Caloric nystagmus in man clarified by test in weightless phase of parabolic flight 15 p2428 A67-29277

Human blood circulation times during weightlessness produced by parabolic flight 23 p3959 A67-41698

Motion coordination under conditions of intermittent acceleration and weightlessness during parabolic aircraft flight 24 p4112 A67-41858

PARABOLIC NOTCH

Diffraction of plane harmonic horizontally polarized shear waves by parabolic cylinder, obtaining dynamic shear-stress concentration for parabolic notch and rigid parabolic insert [ASME PAPER 66-WA/APM-13] 04 p0713 A67-15405

PARABOLIC REFLECTOR

Asymmetrically truncated parabolic antenna in three-dimensional problem, noting effect of shifting radiator 02 p0209 A67-11506

Multielement scanning feed system for parabolic cylindrical antenna by controlling phase and amplitude of signal radiating from each element 02 p0211 A67-11800

Polarization angle of linear feed antenna on polar mounted paraboloid relative to az-el coordinate system 02 p0212 A67-11611

Radiation pattern and standing wave ratio for antenna system consisting of paraboloidal cylindrical reflector and frequency-independent feed 02 p0213 A67-11644

Lambda 1 distribution in circular aperture energizer for low noise parabolic antennas 02 p0214 A67-11796

Angular section errors effect on directive gain coefficient of parabolic antenna with automatic phasing 02 p0215 A67-11875

Long wave spacecraft antenna design, deployment and stabilization, noting environmental effects such as thermal expansion, solar pressure, etc [AIAA PAPER 66-848] 02 p0221 A67-12258

Statistical analysis of sidelobe region of offset-feed parabolic reflector antenna 03 p0382 A67-13673

Structural and mechanical concept, design and testing of fully steerable radome-enclosed parabolic Haystack antenna 03 p0396 A67-13750

Design, fabrication and erection of 210-ft parabolic fully steerable tracking antenna for deep space instrumentation facility /DSIF/ 03 p0383 A67-13751

Mechanical design of parabolic steerable antenna structure of 150-ft diam having superior accuracy and resonant frequency resulting from high stiffness-to-weight ratio 03 p0396 A67-13752

Computer derivation of best-fit hyperbolic and parabolic surfaces using total parameter variation method 03 p0388 A67-14122

Radio source MSH 21-23 observation during lunar occultation, using parabolic antenna and switched-type gain modulated receiver 03 p0515 A67-14326

Erectable antenna design for S-band communications between lunar surface and earth during lunar stay portion of Apollo mission 04 p0569 A67-14501

Lunar occultation of celestial radio sources noting brightness distribution and spectral resolution 05 p0891 A67-16402

Ground-based steerable paraboloid spherical reflector and multiplane type antennas, noting cost per unit area for unit wind speed of 30 mph and frequency of 1400 mc, performance, restrictions, etc [AIAA PAPER 66-324] 06 p0967 A67-17685

Cosmic X-ray source scanning for 21 cm wavelength radiation, using radiometer and parabolic reflector 07 p1247 A67-19063

Cross-polarization radiation of axisymmetric mirror 08 p1305 A67-21277

Radio telescope of cross shaped wideband antennas of parabolic cylinder type 08 p1318 A67-21339

Wideband feed for cross shaped antennas of parabolic cylinder type 08 p1306 A67-21340

Large radio telescope using short wave parabolic reflectors 08 p1318 A67-21342

Parabolic reflector with shields protecting feed from extraneous radio waves 08 p1318 A67-21343

Large size parabolic reflector with small deformation constructed with multibearing suspension 08 p1318 A67-21344

Sidelobes and amplification factors of narrow beam parabolic antennas in near zone 08 p1306 A67-21348

Elastic deformation due to structural weight sustained by 22-meter parabolic reflector of RT-22 radio telescope of U.S.S.R. Physics Institute 08 p1424 A67-21354

Elastic strains created in parabolic reflector /radio telescope antenna/ mounted on four supports by weight of structure in vertical position 08 p1424 A67-21355

Basic design differences illustrating paraboloidal reflector variations, noting factors contributing to or detracting from antenna efficiency 10 p1613 A67-23413

Feed system design for spherical reflector illumination specifying required field distribution and primary gain 11 p1761 A67-24281

Reflection coefficient of parabolic reflector antenna illuminated by horn radiator with sector shaped radiation pattern 11 p1767 A67-24718

Parabolic Cassegrain antenna with low noise temperature for space telecommunication station 12 p1913 A67-25304

Circular and rectangular radiation sources of large extent described by means of radiometric antennas 12 p1913 A67-25306

Primary illumination laws for parabolic reflector for maximum quality factor determined, considering multimode sources for cold antennas 12 p1913 A67-25307

Computer calculation of noise temperature of high gain antennas, noting application to design and analysis of paraboloidal and Cassegrain systems 12 p1917 A67-26195

Parabolic reflectors providing auxiliary solar energy for space stations and spacecraft, manufacturing and testing procedures 13 p2211 A67-26335

Direct TV reception from satellites, discussing cost of Yagi and parabolic antennas, noting output tube 13 p2066 A67-26336

Solar concentrator technology, discussing design requirements of space power conversion devices and manufacturing methods 13 p2055 A67-26826

Asymmetrically truncated parabolic antenna in three-dimensional problem, noting effect of shifting radiator 14 p2283 A67-28070

Large parabolic radio astronomy antennas, discussing design and performance of current and next generation dishes 14 p2284 A67-28430

Noncircular and asymmetrical aperture radio telescopes, considering cylindrical paraboloid, Pulkova and Kraus type Nancy telescopes 14 p2284 A67-28431

Deflections and stresses of paraboloidal shells of revolutions under gravity loads for applications to paraboloidal reflector antenna construction 16 p2763 A67-30678

Design and electrical properties of 25-meter Cassegrainian antenna installed at Ralston ground station for radio communications via satellites 16 p2622 A67-30699

Correcting feed for Arecibo ionospheric Observatory reflector noting antenna gain 16 p2639 A67-31359

Soviet book on radio telescopes covering design and construction principles, structural considerations, astronomical data, antennas, parabolic reflectors, etc 17 p2831 A67-31934

Radio telescope of cross shaped wideband antennas of parabolic cylinder type 17 p2831 A67-31935

Wideband feed for cross shaped antennas of parabolic cylinder type 17 p2822 A67-31936

Large radio telescope using short wave parabolic reflectors 17 p2831 A67-31938

Parabolic reflector with shields protecting feed from extraneous radio waves 17 p2822 A67-31939

Large size parabolic reflector with small deformation constructed with multibearing suspension 17 p2831 A67-31940

Sidelobes and amplification factors of narrow beam parabolic antennas in near zone 17 p2822 A67-31944

Elastic deformation due to structural weight sustained by 22-meter parabolic reflector of RT-22 radio telescope of U.S.S.R. Physics Institute 17 p2956 A67-31950

Elastic strains created in parabolic reflector /radio telescope antenna/ mounted on four supports by weight of structure in vertical position 17 p2956 A67-31951

Cassegrain antenna gain and noise temperature with dual reflector system derived from feed pattern and system geometry 17 p2824 A67-32395

Structural rigidity of rotating parabolic reflector obtained by solving elastic strain problem 20 p3542 A67-37511

Rigidity estimation of parabolic reflector by comparison with beam resting on two bearings 20 p3542 A67-37512

Parabolic cylindrical reflector beam waveguide, discussing conduction and diffraction losses of TE and TM modes 21 p3583 A67-38608

Phase distribution in antenna aperture for small displacement of antenna feed from focal point calculated on basis of theorem proved 22 p3762 A67-39870

Pencil-beam antenna with field distribution fluctuation determined for resolving power by mean square measuring of radiation pattern, detailing parabolic reflectors with rough surfaces 22 p3763 A67-40125

Very large array /VLA/ of radio telescopes designed based on Ryle aperture synthesis principle, consisting of parabolic antennas and used for radio maps 23 p3978 A67-40798

Lunar crater utilization as LF radio astronomy parabolic reflector, noting electromagnetic characteristics [AIAA PAPER 67-904] 24 p4125 A67-43012

PARABOLOIDAL MIRROR

Ground tests of 2.3-m-diam models of foldable foam-reinforced plastic paraboloidal mirrors for satellite energy supply system and optimization of optical characteristics 04 p0558 A67-15957

Procedure and auxiliary equipment used to focus optical elements of gas laser 12 p1952 A67-25384

Afocal field corrector for astronomical telescopes with paraboloidal mirrors 17 p2862 A67-33296

PARACHUTE

SA RECOVERY PARACHUTE

SA RIBBON PARACHUTE

Mechanical construction of two types of Gerdien condenser rocket probes, noting instrumentation racks and inflatable parachutes for descent 03 p0518 A67-13368

Inflatable parachute system developed for deceleration of ionospheric probe instrumentation descending after expulsion from rocket 03 p0359 A67-13369

Subsonic and supersonic parachutes for soft landing on Mars, discussing aerodynamic coefficients, descent rate, dynamic stability, inflation, porosity and wind effects, etc 04 p0551 A67-14574

Soft landing problems for unmanned Mars entry noting parachute system, descent time, sensing system constraints, extreme wind environment, etc 04 p0706 A67-15236

Time-dependent pressure distribution in parachute canopy during inflation measured by special transducers 06 p0945 A67-17631

Measurement techniques used in wind tunnel and free atmosphere parachute tests 06 p0979 A67-18017

Pressure sensor consisting of aluminum membrane for measuring pressure distribution in parachute canopy 06 p1002 A67-18021

Aerodynamic and structural data on supersonic decelerators, determining problem areas and voids [AIAA PAPER 67-201] 06 p0948 A67-18301

Sensing techniques for initiating parachute deployment on Mars lander vehicle [AIAA PAPER 67-202] 06 p0948 A67-18302

Multistage parachute recovery systems used for aerial delivery systems, escape from aircraft and recovery of spacecraft [AIAA PAPER 66-25] 08 p1413 A67-21513

Aerodynamic problem of steady potential flow and added mass in unsteady motion of idealized hemispherical parachute 09 p1438 A67-22485

High altitude parachute systems test techniques for analysis of inflation, stability variations porosity, effects at low dynamic pressure, etc 15 p2419 A67-29433

Aerial delivery concepts including drag cones, lift platforms, gliding parachutes, ballute parachute, ultrafast-opening parachute, etc 17 p2796 A67-32519

Load prediction method necessitated by minimum weight and volume requirements for spacecraft recovery system, considering nonuniform opening of parachutes in cluster 17 p2797 A67-32578

Locating general drop zone and desired impact point, identifying receiving unit and dropping supplies for aerial delivery systems 17 p2797 A67-32587

Subsonic and supersonic parachutes for soft landing on Mars, discussing aerodynamic coefficients, descent rate, dynamic stability, inflation, porosity and wind effects, etc 20 p3356 A67-36408

Correction technique validity determined by comparing parachute determined winds with chaff-determined wind profiles 21 p3854 A67-38186

Parachute stress analysis during inflation, evaluating magnitude and distribution of snap stress to prevent canopy failure 21 p3568 A67-38538

PARACHUTE FABRIC

Metering and pumping equipment for test channel for high altitude permeability tests of parachute cloth, noting permeability of MIL-C-7350 B, type I 02 p0182 A67-12789

Calculating method for parachute opening forces, system velocity, cloth pressure loading and filling time for horizontal and vertical deployment 11 p1743 A67-24348

Space environmental effects on filled elastomers, nylon parachute material and adhesion of metals 15 p2506 A67-29540

PARACHUTING

LW-3B escape system for low and medium performance V/STOL aircraft 17 p2794 A67-32000

Evolution and future objectives of ejection-seat escape systems design, noting characteristics and deficiencies in conventional ejection seats 17 p2795 A67-32002

Continuous EKG recording during free fall parachuting, discussing tachycardia as normal response 23 p3964 A67-41560

Parachute descent training for USAF pilots using Para-Sail ascending parachute 23 p3967 A67-41609

PARAELECTRIC MATERIAL

Electro-optical properties of paraelectric perovskites indicating origin in polarization 02 p0296 A67-11821

Paraelectrics as prospective materials for UHF amplifiers with very low noise level 03 p0382 A67-13711

Far IR reflectivity of potassium tantalate analyzed as function of temperature, noting soft mode as temperature lowers towards Curie temperature far IR reflectivity of potassium tantalate 10 p1688 A67-22766

Dielectric and electro-optic properties of lead magnesium niobate, noting second order ferroelectric transition 11 p1803 A67-24834

PARAGLIDER

Guided high altitude sounding rocket with

paraglider recovery system that attains normal flight attitude upon atmospheric entry without control 04 p0703 A67-14547

Recoverable high altitude rocket space probe with paraglider 07 p1259 A67-19573

PARALLAX

Model atmospheres and astronomical and parallax refraction 07 p1174 A67-19716

Lunar parallax determination by four methods 08 p1395 A67-21158

PARALLEL

Initial value problem for hydrodynamic instability of parallel flow of inviscid fluid 08 p1319 A67-20309

Parallelism between edges of aerial photographs and line of flight achieved by automatic rotation 16 p2671 A67-31031

PARALLEL PLATE

Mutual coupling between TEM and TE 01 parallel-plate waveguides calculated, using wedge diffraction techniques 02 p0211 A67-11596

Interference between plane surfaces in supersonic gas flow between two rectangular parallelepipeds 03 p0403 A67-13630

Diffuse reflection of radiation from nonstationary plane-parallel layer solved on basis of Ambartsumian invariance principle 04 p0695 A67-14657

Idempotent method solution of transport equations for radiative heat transfer in nonisothermal anisotropic scattering medium between two parallel plates [ASME PAPER 66-WA/HT-28] 04 p0725 A67-15441

Interferometer measurements of laminar forced convection in entrance region between parallel flat plates [ASME PAPER 66-WA/HT-16] 04 p0608 A67-15449

Monte Carlo method analysis of rarefied gas heat transfer between parallel plates in terms of temperature, density and Knudsen number 04 p0728 A67-15807

Parallel Couette and Poiseuille flows of multicomponent viscous plasma in presence of pressure gradient and electric field 05 p0854 A67-16894

Solution for parallel plates in steady state Hartmann flow extended to coaxial flow between concentric cylinders, noting role of magnetic field 05 p0856 A67-17356

Spherical coupler for fastening mirrors and plane-parallel plates at Brewster angle in gas laser 06 p1011 A67-18394

Transverse magnetic field effect on laminar radial flow of incompressible fluid between closely spaced parallel plates, presenting graphs of pressure distribution 06 p1046 A67-18829

Laminar flow between parallel plates for arbitrary initial velocity distribution and time varying pressure gradient 10 p1629 A67-23842

Heat transfer of fully developed laminar flow of Bingham material between parallel plates and linearly varying wall temperature noting equations of state, velocity and temperature distribution 11 p1883 A67-24944

Heat transfer for gas with internal degrees of freedom between parallel plates, noting temperature profiles and jumps 13 p2100 A67-26959

Nonlinear heat transfer between parallel plates, using ellipsoidal statistical model of Boltzmann equation 13 p2223 A67-26960

Couette flow and heat transfer of rarefied gas between parallel plates analyzed by Monte Carlo method 13 p2223 A67-26961

Temperature distribution for asymmetric heat transfer in turbulent flow between parallel plates 15 p2469 A67-29133

Transverse magnetic field effect upon convective heat transfer in turbulent flow in electrically conducting fluid in channel bounded by two parallel plates 16 p2722 A67-31572

Turbulent thermal convection properties measured in air between constant temperature horizontal plates, discussing structure 17 p2968 A67-32281

Radiation from array of parallel plate waveguide with thick walls excited by TEM modes 17 p2828 A67-33085

Parallel plate transmission system for reflection, diffraction and transmission measurements at microwaves, noting design criteria 18 p3002 A67-34224

Energy equation for laminar convective

heat transfer in combined hydrodynamic and thermal entrance region bound by parallel flat plates
[ASME PAPER 67-HT-48] 20 p3548 A67-36730

Atmospheric turbulence and diffusion, detailing turbulent energy and thermal variance budgets measurements, parallel plate convection, air pollution, etc 20 p3480 A67-36898

Heat transfer of gas between parallel plates including radiation and rarefaction effects treated, using kinetic theory 20 p3553 A67-36935

Parallel plate antenna for LF transmission and reception in conducting medium 22 p3773 A67-40307

Velocity and pressure distributions and flow field for laminar incompressible source flow between two coaxial parallel disks rotating at different speeds 23 p3988 A67-40602

Radiation from infinite aperiodic array of parallel plate waveguides, using Wiener-Hopf technique for edge effect evaluation 23 p3978 A67-40825

Cylindrical antenna admittance taking into account antenna to coaxial line junction geometry, using magnetic current mathematical model 23 p3980 A67-41205

Unstable radiant heat interaction between two plane parallel infinite plates of finite thickness analyzed to determine thermal stabilization processes 24 p4254 A67-42257

PARAMAGNETIC AMPLIFIER

Microwave mixing in paramagnetic crystal using traveling wave maser with ruby as mixer element, noting frequency conversion 01 p0086 A67-10003

21-cm-wave radiospectrometer with quantum paramagnetic amplifier for investigating radio lines of hydrogen 02 p0241 A67-11638

Active time of two-level quantum paramagnetic amplifier increased by using only portion of spin packets, noting effect of EPR line 04 p0633 A67-15159

Quantum paramagnetic traveling wave amplifier using rutile with admixture of chromium and combined with magnet with superconducting coil 05 p0825 A67-17161

Active time of two-level quantum paramagnetic amplifier increased by using only portion of spin packets, noting effect of EPR line 15 p2496 A67-29346

Quantum paramagnetic amplifiers in USSR, discussing physical characteristics and operation of resonators in decimeter band, antenna systems for noise reduction, etc 16 p2623 A67-31024

Ruby as active material for traveling wave maser /TWM/ noting advantages 24 p4167 A67-42238

PARAMAGNETIC RESONANCE

SA ELECTRON PARAMAGNETIC RESONANCE

Paramagnetic resonance of praseodymium and uranium ions in calcium fluoride analyzed via fitting to spin Hamiltonian 01 p0129 A67-10146

Electron spin resonance absorption spectrum of Pt in YAG at low temperatures, noting ionic orientation 03 p0492 A67-13326

Electron spin resonance of P doped Si at liquid He temperatures, obtaining paramagnetic susceptibility in metallic conduction region 06 p1068 A67-18972

Temperature dependence of paramagnetic resonance spectral shifts in chromium-doped titanium oxide crystal of cross relaxation rutile maser 07 p1196 A67-19676

Paramagnetic resonance absorption spectrum of cerium in yttrium-gallium-garnet host crystal 08 p1371 A67-21312

Flexible plate elastic stability under effect of suddenly applied and short term forces 12 p2024 A67-25599

Two-phonon absorption in ultrasonic paramagnetic resonance of uranium-doped calcium fluoride, relating wave attenuation to ultrasonic intensity and magnetic field angular variation 14 p2365 A67-28295

Soviet book on radio physics quantum amplifiers covering lasers, maser, paramagnetic resonance, etc 19 p3238 A67-34799

Magnetic field induced hyperfine structure in mono- and divalent iron ions in magnesium and calcium oxide, showing evidence of paramagnetic resonance 20 p3506 A67-36211

Combination paramagnetic resonance in mechanical system containing rotating body,

giving procedure for approximate determination of oscillation amplitude and resonant zone boundaries 21 p3625 A67-37990

PARAMAGNETISM

SA NUCLEAR MAGNETIC RESONANCE

Zeeman field spatial orientation of paramagnetic spin-lattice relaxation for 2T2 states in rhombic symmetry, emphasizing application to Fe-doped potassium cobalticyanide and potassium ferricyanide 01 p0129 A67-10150

Gas laser spectroscopic analysis of hyperfine structure, paramagnetic properties, radiative lifetimes and Doppler-broadened transition saturation behavior of excited states of Xe 129 04 p0661 A67-15462

Paramagnetic current formation due to volume resonator microwave field interaction with dense plasma subject to RF pressure and EPR in static magnetic field 07 p1228 A67-19512

Pauli-paramagnetic superconductivity in Ti-16 at. percent Mo from specific heat measurements 07 p1235 A67-20130

States density in vicinity of Fermi surface obtained from values of paramagnetic susceptibility for gold-palladium alloys 13 p2133 A67-27006

Surface current change between critical paramagnetic and critical diamagnetic induced by temperature variation in type II superconductor immersed in static magnetic field 14 p2365 A67-28296

Microwave flux-flow resistivity transitions observed for strongly paramagnetically limited titanium-vanadium alloys 16 p2727 A67-30821

Paramagnetic and electrical properties of organic polyvinyl-acetate-based semiconductor films irradiated with electrons before and after heating 18 p3099 A67-33694

Specific heat of superconductors containing paramagnetic impurities calculated, noting effect of ordering impurity spins 19 p3303 A67-35045

PARAMETER

S COLLISION PARAMETER

S STOKES PARAMETER

PARAMETRIC AMPLIFIER

Impedance measurement of silver bonded Ge diode at X band and in mm wave region, improving performance by usage in breakdown region 01 p0033 A67-10028

Two-stage parametric amplifier using GaAs cooled in closed cycle cryogenic refrigeration system applied to satellite communications 01 p0033 A67-10029

Reflection-type amplifier in downrange guidance system, examining noise figure optimization, pump power requirements, bandwidth and input resistance 01 p0035 A67-10410

Ground station receiver for satellite communication which utilizes liquid-helium-cooled parametric amplifier at top producing extremely low noise temperature 01 p0023 A67-10469

Gunn effect domain traveling wave parametric amplifier pumped by periodic impedance variations in boundary conductor of microstrip transmission line 01 p0040 A67-11309

Degenerate parametric amplifiers in interferometry, discussing noise temperature and pump locking 02 p0240 A67-11622

Low noise parametric self-resonance amplifiers with bandwidths, discussing use of high diode Q-factor 02 p0220 A67-12204

Microstructural analysis multiple electron-photon cascade resonance amplifier response to sine-square radio signal 03 p0376 A67-13091

Traveling wave parametric amplifier circuit with series connected varactor diode 03 p0380 A67-13504

Parametric amplification and sideband oscillations in structured superconducting Sn thin films 03 p0496 A67-13568

Parametric amplification of far IR in Te crystal pumped by carbon dioxide laser 03 p0437 A67-13572

Balancing network of reactance modulated amplifier with semiconductor diode capacitance, noting parametric oscillation at pumping generator 04 p0579 A67-14450

Parametric amplifiers and lasers 05 p0814 A67-16361

Input device for quadrupole amplifiers in form of sequential oscillators with inductive

coupling used to widen frequency band of output 05 p0785 A67-17472

Upper sideband effect in parametric amplifier on positive conductance and negative resistance of circuits, deriving noise figure expression 06 p0966 A67-17575

S-band parametric amplifier pumped at J-band using balanced idler circuit with two varactor diodes incorporated in one encapsulation 06 p0966 A67-17580

Parametric action in back biased p-n junctions carrying injected currents, discussing photoparametric frequency converters, transistor amplifiers and frequency doublers 06 p0969 A67-18106

Varactor diode impedance behavior in parametric amplifiers under low temperature conditions 07 p1152 A67-19551

Algorithm determining negative resistance intervals in parametric amplifier 08 p1299 A67-20334

Input resistance and noise performance of multiple idler parametric amplifiers 09 p1474 A67-22084

Simple diode parametric amplifier, discussing bandwidth and noise measurements and compensating circuits for gain-frequency response improvement 09 p1474 A67-22085

Optical signal modulation to measure noise figure at UHF of photoparametric amplifier, using silicon mesa diode as both photodetector and varactor diode 09 p1476 A67-22208

Two positive kinetic power waves coupled in interaction for DC pumped quadrupole amplifier having low noise and high efficiency 09 p1478 A67-22260

Blocking effect due to interference in parametric amplifier, discussing relation between gain and blocking frequency 10 p1609 A67-22834

Amplification processes in parametrically regenerated circuit with simultaneous complex variation of capacitance and attenuation 10 p1607 A67-23446

Parametric amplifiers of high gain stability for radio astronomy noting very low SNR and optimum noise temperature 12 p1912 A67-25298

Parametric amplifier varactor characteristics, construction methods and qualities for hyperfrequency low noise parametric amplification 12 p1913 A67-25299

Noise calculation in parametric amplifier using approximation method 12 p1913 A67-25300

Low noise amplifiers at Fucino for reception from Early Bird satellite 12 p1913 A67-25301

Microwaves parametric amplification experiments in superconducting Josephson tunnel junctions, showing signal amplification as function of temperature, absorption dip of rutile resonator, etc 12 p1915 A67-25745

Parametric coupling between two waves noting losses 13 p2086 A67-26511

Parametric amplifiers incorporating two varactor diodes, noting in-phase pumping for unilateral operation and large potential bandwidth 13 p2078 A67-26785

Miniature cryogenic refrigeration systems design for masers and parametric amplifiers, investigating efficiency and contamination 14 p2277 A67-27775

Ultralow noise receiver configurations for cryogenically cooled microwave traveling wave masers and parametric amplifiers 14 p2260 A67-27776

Two-stage parametric amplifier system cooled to 20 degrees K, as low noise amplifier in receiving equipment for satellite communication 14 p2278 A67-27780

Two-stage fixed-tuned parametric amplifier for satellite communications earth stations, considering circulator development and varactor 14 p2278 A67-27781

Low temperature parametric amplifiers, discussing varactors, circulators and demands on cooling 14 p2278 A67-27783

Parametric amplifiers as reliable low noise broadband microwave amplifiers 14 p2286 A67-28465

Low noise amplifiers in radio astronomy 14 p2286 A67-28466

Microwave frequency superconductor materials, applying bulk and thin film properties to filter, amplifier, oscillator, junction and Josephson effect

devices 14 p2289 A67-28917

Balancing network of reactance modulated amplifier with semiconductor diode capacitance, noting parametric oscillation at pumping generator frequency 15 p2443 A67-29287

Two coupled resonant mechanical circuits with parameter in coupling element allowed to vary periodically 15 p2494 A67-29772

Space charge varactor compared to p-n junction varactor, noting applications 15 p2449 A67-29804

Gain-bandwidth product of parametric reflection amplifiers with line-type resonators 15 p2454 A67-30145

Low noise parametric down-converter by using two incommensurable pumping generators, noting gain bandwidth product and minimum noise temperature 17 p2824 A67-32315

Design and characteristics/gain, noise factor and bandwidth of parametric amplifier 19 p3194 A67-35548

Lower frequency pumped parametric amplifier with three idler frequencies 19 p3195 A67-35626

Microwave amplifier using varactor diode with coaxial signal, lumped element idler and waveguide pump circuit for broadband radio link at 20 db 20 p3401 A67-37357

Reduction of RF interference in reflection-type parametric amplifiers covering spurious responses, amplifier saturation, intermodulation and cross modulation 20 p3406 A67-37655

Systems with low noise factor and high selectivity tuned by varying pumping frequency 22 p3767 A67-39370

Nonreciprocal parametric amplifier obtained by using parametric elements in frequency inverting case without uniglide or circulator 22 p3771 A67-39838

Superconducting parametric amplifier for measurements of small DC voltages in low impedance circuits 22 p3866 A67-40441

Two varactor diode bandpass filter for parametric amplifier, analyzing bandwidth vs gain 24 p4128 A67-41968

Unilateral parametric amplifier using two varactor diode low pass filter with pumping phase difference, noting bandwidth and gain 24 p4128 A67-41969

Parametric amplification of traveling wave tube through coupled wave method noting role of phase velocities of space charge waves 24 p4130 A67-42241

Nonlinear electrical problems requiring partial differential equations including magnetic saturation, parametric amplifier, electron tube, traveling wave amplifier and semiconductor diodes 24 p4133 A67-43089

PARAMETRIC DIODE

SA VARACTOR DIODE

Varactor diode series resistance loss responsible for bandwidth loss in parametric delay lines used for signal processing 01 p0027 A67-11323

Signal suppression in ferrite frequency selective limiters evaluated using parametric subharmonic generator model 02 p0217 A67-12093

Input admittance of parametric diode of reactance modulator with nonlinear losses 02 p0221 A67-12425

Cylindrical electronic microwave tubes, deriving expressions for zero and first approximations of physical parameters 05 p0774 A67-16906

Field equations for spreading resistance of variable capacitance diode and point contact variable resistance diode derived in terms of frequency, material characteristics and physical parameters 11 p1767 A67-24731

Parametric negative resistance range and impedance matrix element values of microwave Read avalanche diode 15 p2453 A67-30016

Cylindrical electronic microwave tubes, deriving expressions for zero and first approximations of physical parameters 16 p2636 A67-30883

Diode function generator for empirical functions representation 22 p3775 A67-40562

PARAMETRIC FREQUENCY CONVERTER

Pump noise contribution to total noise of LF parametric converter, analyzing effect of magnitude of bridge out-of-balance voltage 01 p0032 A67-10002

Input impedances calculated for parametric up-converters, examining overall signal behavior 02 p0220 A67-12205

DC parametric device in which capacitance variation of silicon p-n junctions due to input signal causes FM 03 p0377 A67-13106

Impedance matching conditions, gain nonlinearity and bistable mode instability in solid state parametric frequency converters 03 p0381 A67-13637

PARAMETRIC OSCILLATOR

Nonlinear servo devices examined, using simplified form of harmonic-equivalent method obtained from multilinear characteristics 02 p0224 A67-11529

Single mode approximation of parametric excitation and self-excitation of oscillations in Fabry-Perot resonator filled with nonlinear dispersive medium 02 p0251 A67-11575

Temperature tuning of lithium niobate optical parametric oscillator in visible spectrum, noting generated frequency dependence on pump frequency and longitudinal mode distribution 02 p0253 A67-12511

Parametric amplification and sideband oscillations in structured superconducting Sn thin films 03 p0496 A67-13568

Amplitude and phase of weak signals at low signal to noise ratio, using parametric oscillators for signal phase quantization 04 p0620 A67-14748

Phase determination of signal components generated by parametric oscillator by synchronizing oscillator with respect to difference between frequencies of components 04 p0583 A67-15171

General theory for parametric oscillation in optical region 05 p0817 A67-16639

Threshold of parametric oscillator system with idler modes in same frequency spacing as laser pump source 05 p0824 A67-16823

Stability analysis of parametric phase-locked subharmonic tunnel diode oscillator circuits capable of bistable phase operation 07 p1153 A67-19610

Tunable lithium niobate optical oscillator with external mirrors 09 p1510 A67-21576

Gunn diode self-pumped parametric oscillator, showing power derived from variation of domain capacity at second harmonic of oscillation 09 p1479 A67-22267

Instability zone of electrometer, noting relation to parametric resonance of needle and Hill equation form of needle motion 11 p1877 A67-24758

Parametric resonance excitation of Alfvén waves by small LF modulation of DC magnetic field imposed on ideal MHD plasma 11 p1844 A67-25062

Optical fluorescence, thermally tunable over significant portion of visible and near IR spectrum, from phase-matched parametric system 13 p1217 A67-27081

Plasma acceleration under combined axial magnetic and electric fields, noting experimental setup and results 14 p2353 A67-27750

Oscillation pendulum equation solution properties, noting existence of certain bifurcation value of parameter 14 p2348 A67-28382

Phase determination of signal components generated by parametric oscillator by synchronizing oscillator with respect to difference between frequencies of components 15 p2443 A67-29357

Optical parametric oscillator with ruby laser pumping, noting values of electro-optic and rotational tuning 18 p3059 A67-34011

Parametric excitation in plasma located in oscillating electric field due to density gradient, showing predominance on electron-ion coupling 20 p3503 A67-37672

Stimulated Raman scattering in IR active nontotally symmetric vibration of alpha quartz crystal, noting parametric oscillation 21 p3641 A67-38459

PARAMETRON

Excitation of parametron with p-n junction capacitance produced by inverted impurity concentration gradient in base of junction 03 p0378 A67-13246

Single circuit parametron with pulsed balance-modulated pumping voltage, showing existence of two independent subharmonic components 18 p3005 A67-33503

PARITY

Radiative recombination processes involving neutral donors and acceptors in silicon and germanium, describing extrinsic luminescence bands 22 p3862 A67-39998

PARKING ORBIT

Transfer from elliptical orbit to coplanar hyperbolic asymptote treated in terms of limited classes of one-and two-impulse maneuvers 07 p1255 A67-19986

Tabulated altitudes, periods and velocities for Martian satellites in circular parking orbits 09 p1564 A67-21716

PARTIAL DIFFERENTIAL EQUATION

SA BIHARMONIC EQUATION

SA HEAT EQUATION

SA HYPERBOLIC EQUATION

SA KINETIC EQUATION

SA LAGRANGE MULTIPLIER

SA PARABOLIC EQUATION

SA POISSON EQUATION

SA STURM-LIOUVILLE PROBLEM

Sanders equation for circular cylindrical elastic shell reduced to fourth order PDE 01 p0159 A67-10400

Second-order effects in propagation of elastic waves through homogeneous isotropic media 01 p0113 A67-10405

Parametric representation derived for one-dimensional nonsteady flows, considering two distinct solutions of Martin Monge-Ampere equation 01 p0052 A67-10520

Fundamental solutions to certain singular partial differential equations with constant coefficients, using Bessel iteration operator and Fourier-Bessel transforms 01 p0105 A67-10676

Nonlinear MHD waves, examining hyperbolic systems of quasi-linear PDEs, simple wave and flow theory 01 p0126 A67-11252

Block successive overrelaxation method /BSOR/ compared with direct method for solving fourth order partial differential equation 02 p0258 A67-11800

Cauchy problem for Euler-Poisson-Darboux equation solved for all values of time and specified values of parameter 02 p0260 A67-12431

Necessary conditions for stability of trivial solutions of parabolic systems of partial differential equations 03 p0456 A67-12861

Existence and uniqueness theorem and upper and lower Chaplygin function approximations for solutions of Cauchy problem for quasi-linear first order PDE 03 p0456 A67-12884

Necessary and sufficient conditions of invariance and autonomy of multidimensional nonlinear automatic control systems with right-hand discontinuities in describing differential equations 03 p0391 A67-13188

Exact field equations for motion of hyperelastic rod derived from general three-dimensional theory 03 p0522 A67-13391

Mathematical physics PDE problems solved by combined method using Fourier integral transform and theory of Riemann boundary value problem 03 p0459 A67-13589

Cauchy problem of odd-order equations that are correct according to Petrovskii 03 p0459 A67-13644

Asymptotic rate of convergence of Gauss-Seidel type iterative processes for nonlinear difference equations 03 p0460 A67-13881

Parabolic conditions for general second order PDE, discussing bicharacteristic condition, initial boundary value problem, Monge-Ampere equations and quasi-linear equation systems 03 p0461 A67-14105

Goursat problem of first order nonlinear hyperbolic equations, introducing characteristic parameters with reduction to standard form 03 p0462 A67-14109

Boundary value and contact problem solution using elasticity theory for transversely isotropic layer 03 p0529 A67-14165

Book on propagation, reflection and superposition of shock waves in ideal gases based on theory of hyperbolic nonlinear PDEs 04 p0601 A67-14467

Elasticity problem treated by method of reduction to second order partial differential equations 04 p0710 A67-14911

Book on main linear boundary value problems for second order linear partial differential equations and systems of such equations satisfying ellipticity 04 p0645 A67-15006

Optimum processes in systems with distributed parameters described by partial differential equations 04 p0647 A67-15874

Simple waves for nonlinear system of partial differential equations applied to

multidimensional compressible inviscid flows 05 p0790 A67-16045
 Moire patterns in determining partial derivatives of displacement components 05 p0909 A67-16142
 Degeneration of solutions of well-posed systems of first order partial differential equations when particular parameter approaches zero 05 p0836 A67-17315
 Brachistochrone problem analyzed using variational calculus and optimal control theory 06 p0973 A67-17770
 Matrix and vector computational procedures for solution of partial and ordinary differential equations 06 p1022 A67-17788
 Wave propagation in random medium, examining stochastic PDEs, solutions and method of regularization 06 p1032 A67-18101
 Inviscid linearized perturbations of supersonic entropy layers analyzed, using approximating partial differential equations by simultaneous ordinary differential equations [AIAA PAPER 67-6] 06 p0938 A67-18249
 Characteristics method applied to one-dimensional propagation problem, considering Massau grid and using partial differential equation 06 p0990 A67-18585
 Periodic vibrations of systems governed by nonlinear PDEs, examining perturbation method, transverse vibrations of bar, string, beam and membrane and sound waves in enclosure 06 p1034 A67-18640
 Nonlinear PDEs of two-valley model of Gunn effect materials, noting microscopic transport configurations 06 p1067 A67-18962
 Well posed problems for PDEs, discussing continuous dependence and error bounds 07 p1213 A67-19158
 Solution approximation for nonlinear parabolic PDEs, using linear combination of finite set of selected functions 07 p1213 A67-19159
 Mikusinski operator solution of partial integrodifferential equations 07 p1215 A67-19471
 Existence and uniqueness of 2k-fold continuously differentiable solutions to Dirichlet problem for nonlinear integrodifferential equations 07 p1215 A67-19476
 Eigenfunction expansion of self-adjoint operator generated by elliptic differential boundary value problem with eigenvalue in boundary condition 07 p1215 A67-19581
 Numerical solution to time dependent Navier-Stokes equation for transient supersonic flow around right circular cylinder, using explicit-implicit finite difference method [AIAA PAPER 67-221] 07 p1169 A67-19625
 Nonlinear PDE for magnetostatic field with variable permeability in discontinuous medium solved with digital computer 07 p1132 A67-19795
 Higher order perturbations of elements in three-body problem determined using methods of Krylov-Bogolubov and Poincare [AAS PAPER 66-99] 07 p1252 A67-19862
 State transition partial derivatives for computing normal matrices in tracking analysis [AAS PAPER 66-108] 07 p1253 A67-19868
 Singular perturbation problems for partial differential equations 07 p1217 A67-20019
 Partial differential equations for plate motion, considering transverse shear and rotary inertia, solved for plates bounded by elliptical and hyperbolic cylinders 08 p1416 A67-20489
 Fiber reinforced composite material behavior examined from shear loading tests, using finite difference analysis for representative PDEs 08 p1420 A67-20908
 Truncated elliptic systems of partial differential equations for reducing two-point boundary value problems in vector space to initial value problems by projection 08 p1348 A67-21192
 Numerical solution of sequential decision problems involving parabolic equations with moving boundaries 08 p1349 A67-21256
 Partial differential equations for displacement and stress functions of shallow shells expressed as Bessel functions 09 p1573 A67-21664
 Synthesis of optimal Liapunov-Bellman function, noting sequential solution method for independent variables and method using first order partial differential

equation 09 p1525 A67-22077
 General Fuchs type theorem for partial differential equations applicable to hypergeometric functions with two variables 09 p1525 A67-22574
 Goursat problem for partial differential equation shown not to possess classical solution even under suitable hypothesis 09 p1525 A67-22624
 Modified first boundary value problem for linear elliptic nonself-adjoint partial differential equation in two-dimensional plane 10 p1674 A67-23077
 Optimum thrust nozzle contours for chemically reacting gas flows, obtaining set of partial differential equations for gas dynamic properties [AIAA PAPER 66-638] 10 p1592 A67-23118
 Reduction of PDE system of heat transfer, using Hermitian approximating polynomials to obtain solution to initial system 10 p1608 A67-23323
 Navier-Stokes equation solution in region with smooth boundary, using linear elliptic equations 10 p1675 A67-23676
 Boundary value problem solution governed by system of partial differential equations applied to analysis of curved thin walled shells of revolution 10 p1729 A67-23765
 Nonlinear system of partial differential equations describing one-dimensional combustion process of gas mixture 11 p1882 A67-24158
 Legendre polynomial form of slender body motion in spherical coordinate systems generalized for axially symmetric harmonic functions in three dimensions with validity for Helmholtz equation 11 p1812 A67-24310
 Green matrix estimates for homogeneous parabolic boundary value problems, showing proof of integral operator 11 p1813 A67-24850
 Partial differential equation of MHD converters, noting effects of converter width, side conductor materials and velocity distribution 12 p1896 A67-25374
 Vlasov variational method application to stressed state of flexible plates and shells, linearizing partial differential equations by successive loadings 12 p2020 A67-25570
 Partial differential equations applied to calculation of extended cylindrical shells under arbitrary curvilinear and rectilinear edge loading 12 p2022 A67-25582
 Representation and uniqueness theorems for second order linear parabolic partial differential equations 12 p1961 A67-26061
 Elasticity problems for bounded connected region consisting of finite number of rectangles solved by relaxation techniques 13 p2215 A67-26372
 Fundamental solution of thermoelectricity equations for thin walled shallow shells and infinite plates with various instantaneous interval heat sources 13 p2221 A67-26374
 Mixed problem for linear hyperbolic partial differential equation asymptotically represented and reduced to boundary value problem and Cauchy problem 13 p2144 A67-26377
 First boundary value problem for second order elliptic partial differential equations, analyzing smoothness and continuity of generalized solution 13 p2144 A67-26378
 Finite length inductive MHD generator, solving inlet and outlet effects on boundary value problem 13 p2165 A67-26613
 Stewartson-Crocco equations solved by differential method for compressible laminar boundary layers 13 p2094 A67-26649
 Two-dimensional operator calculus for solving all second order linear partial differential equations of two dimensions 13 p2146 A67-26745
 Thermal boundary layer equation reduced to ordinary differential equation for flat plate with given heat conductivity 13 p2224 A67-27048
 Elliptic regularization for symmetric positive system of linear first order partial differential equations with irregular boundaries 13 p2147 A67-27178
 Characteristic initial value problem for linear second order hyperbolic partial differential equation 13 p2147 A67-27180
 Steady three-dimensional flow of electrically conducting gas in working section of linear MHD channel 13 p2169 A67-27310
 Single parameter family of two-layer difference schemes with decomposing

operators for general linear second order parabolic equations with mixed derivatives and variable coefficients 13 p2149 A67-27614
 Hilbert space methods in elliptic partial differential equations 14 p2341 A67-27849
 Time dependent viscous flow between two rotating spheres analyzed by extension of numerical methods 14 p2296 A67-27905
 Nonlinear equation systems solved using parameters and varying them to original form while simultaneously tracing roots 14 p2342 A67-27975
 Stability and asymptotic behavior of dynamical systems defined by autonomous functional or partial differential equation and conditions for applying Liapunov theorem 14 p2342 A67-28081
 Partial differential equations for three-dimensional inviscid flow solved for flow field over blunt body shapes at various angles of attack, for application to Apollo spacecraft [AIAA PAPER 66-413] 14 p2240 A67-28110
 Hyperbolic difference equations, reviewing Courant-Friedrichs-Lewy paper in light of recent developments 14 p2342 A67-28154
 Numerical methods for elliptic problems, discussing application of finite difference and solution of large algebraic systems 14 p2342 A67-28156
 Difference method for solution of plane problems in dynamic elasticity, noting equations of dynamic/elastic deformations under plain strain conditions 14 p2400 A67-28256
 Fourier series solutions of boundary-value and mixed problems in mathematical physics by integrating partial differential equations 14 p2348 A67-28287
 Continuous solutions of Cauchy problem for linear first order PDEs with discontinuous coefficients, noting conditions imposed 14 p2344 A67-28905
 Uniqueness theorems for Adler fourth and fifth boundary value problems for heat conduction differential equation 14 p2409 A67-28936
 Nonlinear partial differential equations of stellar evolution theory solved under assumption of spherical symmetry of star 14 p2392 A67-28995
 Parameter and domain dependence of eigenvalues of elliptic partial differential equations 15 p2509 A67-29461
 Saltykov method applied to second type partial differential dynamics equations of first class 15 p2510 A67-29518
 Numerical analysis of PDEs with singular coefficients, noting equivalence of stability and convergence 15 p2510 A67-29519
 Finite difference method solution of periodic parabolic problem solution subject to nonlinear boundary condition 15 p2510 A67-29522
 Fokker-Planck-Kolmogorov method analysis of nonlinear systems described by stochastic partial differential equations 15 p2517 A67-29658
 Liapunov functional for aeroelastic divergence noting application to partial differential equations 15 p2575 A67-30021
 Eddy currents in nonmagnetic conductors calculated by finite difference successive overrelaxation technique on digital computer 15 p2541 A67-30142
 Stability equation of multilayer sandwich plates with isotropic homogeneous facing layers and orthotropic homogeneous core layers 15 p2577 A67-30267
 Large deflection bending of simply supported rectangular sandwich plates with isotropic core under uniform normal pressure, solving governing differential equations by digital computer 15 p2577 A67-30269
 Uniqueness and existence of Cauchy problem solution considering Dirichlet limits, studying convergence requirements 16 p2695 A67-30829
 Successive overrelaxation iterative method for solving elliptic partial differential equations 16 p2695 A67-30830
 Numerical methods for elliptic partial differential equations with coefficients singular on boundary portion, constructing barrier functions and establishing existence and convergence theorems 16 p2697 A67-31330
 Monotone iterations for nonlinear elliptic differential equations in boundary-value problems applied to Gauss-Seidel

methods 16 p2697 A67-31331
 Stationary Newton method for nonlinear functional equations in Banach spaces, formulating convergence conditions 16 p2697 A67-31332
 Pointwise bounds for solution of Cauchy problem for nonlinear and linear elliptic system, noting application to biharmonic equation 16 p2697 A67-31422
 Riemann matrix in linear symmetric-hyperbolic systems of partial differential equations with constant coefficients in two-space and one-time variables 17 p2876 A67-32031
 Control theory of hyperbolic PDEs examined, noting application to distributed parameter systems 17 p2877 A67-32561
 Cauchy problem for homogeneous linear difference scheme with constant complex coefficients, giving stability lemmas 17 p2877 A67-32677
 MHD flow, deriving equation system and boundary conditions for gas dynamic process 17 p2903 A67-32682
 Boundary value problem of linear partial differential equation reduced to linear equation system with block-tridiagonal matrix by difference approximation 17 p2820 A67-32801
 Rotational motions of second order autonomous systems, proposing determining algorithm 17 p2885 A67-32883
 Scattering problem for partial difference equations with finite perturbation and inverse problem determining perturbation 17 p2817 A67-32885
 Linear continuous time stochastic optimal control process, obtaining optimum performance achievable as function of total effort at initiation of optimization period 17 p2830 A67-33012
 Static /time-discrete/ electrical integrators for solution of boundary layer equations 17 p2821 A67-33080
 Asymptotic stability of homogeneous system of partial differential equations in stratification wave theory, introducing source function for local plasma disturbance effect 17 p2907 A67-33101
 Geometry of streamlines and field lines of MHD flow, using partial differential equations 17 p2910 A67-33351
 Constructing solution of Cauchy initial value problem when Riemann function is unknown for one-dimensional linear viscoelasticity 18 p3139 A67-33428
 Transonic jet flow study with electric analogy methods, solving Frankl and Tricomi problems for mixed type PDE 18 p2982 A67-33684
 Iterative methods for integration of linear partial differential equations, determining relaxation factor 18 p3071 A67-33753
 Book on variational principles of mechanics covering basic concepts, calculus of variation, equations of motion, etc 18 p3079 A67-34100
 Alternating direction implicit /ADI/ method variant for elliptic and parabolic partial differential equations 19 p3250 A67-34868
 Complex partial differential equations solutions by channel analog memory used with analog computer 19 p3186 A67-34966
 Behavior of finite-amplitude disturbances periodic in motion direction for plane parallel laminar flows studied, using partial differential equations 19 p3208 A67-35051
 Longitudinal surface curvature effects on steady, two-dimensional incompressible laminar boundary layers, noting partial differential equations, computer solution, velocity profile, etc 19 p3209 A67-35415
 Progressing wave method for linear partial differential equation systems, including Maxwell equations, applied to electromagnetic waves from moving sources 19 p3184 A67-35665
 Automatic control systems general theory with distributed parameters and delay, proving existence and uniqueness of solutions of partial differential equations solutions 19 p3251 A67-36048
 Boundary value problem of oscillatory system with time lag quasi-linear partial differential equation 19 p3251 A67-36050
 Hybrid computer Monte Carlo techniques for solving partial differential equations of continuous Markov processes 19 p3188 A67-36057
 Ram effect similarity criteria

determination from partial differential equation system noting composite similarity, simulation possibilities, continuity equation, etc 20 p3419 A67-36190
 Second order nonlinear parabolic type partial differential equations with divergence structure, noting role of maximum principle 20 p3475 A67-36502
 Linear equation system with coefficient matrix of multiple diagonal bands solved by direct method, reducing numerical solution error 20 p3476 A67-36675
 Heat exchanger transfer functions obtained from linearization of partial differential equations [ASME PAPER 67-HT-5] 20 p3544 A67-36704
 Numerical digital computer solution of parabolic partial differential equations with two-point boundary conditions, using method of lines 20 p3391 A67-36820
 First boundary value problem for linear elliptic differential equations involving two small parameters 20 p3477 A67-36942
 Fourth order parabolic partial differential equation solution by explicit and implicit finite difference methods 20 p3478 A67-37211
 Ultrashort optical pulse propagation in two-level medium, describing pulse shapes by solving partial differential equation 20 p3461 A67-37286
 Optimal control theory for distributed parameter systems using dynamic programming, showing use in two-point boundary control problems involving partial differential equations 20 p3410 A67-37320
 Formulating Cauchy problem and mixed problem for second order self-adjoint equation, establishing initial data and boundary value dependence 20 p3479 A67-37657
 Velocity field in axisymmetric boundary layer described by nonlinear partial differential equations 20 p3425 A67-37677
 Integration of Cauchy problem for class of nonlinear higher order partial differential equations 21 p3651 A67-37901
 Green function for SH-line source in wedge-shaped medium with apex removed by circular cylinder, determining reflected and refracted fields 21 p3579 A67-37925
 Navier-Stokes equation solution in region with smooth boundary, using linear elliptic equations 21 p3652 A67-38277
 Linear boundary value problem for system of first order partial differential equations having real and imaginary characteristics 21 p3653 A67-38398
 Trajectory optimization initial value problem, considering various conditions, methods of solution and reentry heating minimization 21 p3703 A67-38440
 Surface geometrical variations in electrochemical shaping process for hydrodynamic removal of dissolved processed metal, deriving partial differential equations 21 p3636 A67-38897
 Partial differential equations with more equations than unknowns investigated for solution by reducing integrable systems to ordinary differential equations 21 p3654 A67-39095
 Closed form equation with variable segregation coefficient for single pass zone melting in binary alloy systems 22 p3856 A67-39368
 Cauchy problem for second order parabolic partial differential equation 22 p3827 A67-39432
 Partial differential equations solution in heat transfer between incompressible fluid and porous medium 22 p3917 A67-39640
 Representation of characteristic surfaces of unsteady axisymmetric flow and steady three-dimensional supersonic flow by hyperbolic system of quasilinear differential equations 22 p3785 A67-40010
 Thin circular elastic plate under uniform compressive thrust, with nonlinear boundary value problems involving partial differential equations for buckled states 22 p3916 A67-40525
 Elastic wave problems involving one space variable solved by hyperbolic partial differential equations 23 p4072 A67-40610
 Partial differential equation in lubricant pressure based on mixing-length theory, presenting full journal bearings in turbulent and laminar regimes 23 p4010 A67-41342
 Cauchy problem solution for linear partial differential equation with coefficients which are functions of three-dimensional variable,

deriving maximal class of uniqueness of solution 23 p4024 A67-41692
 Solution for coupled system of parabolic partial differential equations describing reactants diffusion and heat conduction in gas phase 23 p4048 A67-41764
 Complex Fourier transform technique in variable coefficient partial differential equations applied to Cauchy-Kowalewski and Petrowski-Leray theorems 24 p4178 A67-42202
 Caratheodory method in variational calculus and partial differential equations, discussing coordinate-free invariance usage and extremal theory 24 p4178 A67-42203
 Equation system for conducting perfect gas motion group analyzed leading to possible invariant solutions of system applicable to MHD equations 24 p4197 A67-42354
 Extended dynamical systems in Banach space and use of invariance principle for stability theory of partial differential equations 24 p4178 A67-42652
 Hyperbolic noninvariance in partial differential equations, discussing existence theorems for nonhyperbolic initial value problem systems 24 p4178 A67-42727
 Existence theorems for partial and ordinary differential equation solutions, discussing boundary value problems for nonlinear differential equation class 24 p4178 A67-42728
 Nonlinear partial differential equations - Conference, University of Delaware, December 1965 24 p4179 A67-43081
 Similarity analysis of partial differential equations, discussing free parameter analysis, variables separation method, group theory approach and dimensional analysis 24 p4180 A67-43082
 Viscous flow stability between concentric rotating cylinders with Taylor vortices, deriving velocity and pressure perturbation nonlinear partial differential equations 24 p4145 A67-43083
 Numerical solution methods for partial differential equations, discussing dynamic programming, Laplace transform and quadrature technique 24 p4180 A67-43084
 Ad hoc exact solution techniques for nonlinear partial differential equations noting physical applications 24 p4180 A67-43085
 Non-Newtonian elastoviscous channel flow between rigid boundaries solved by asymptotic expansion in lubrication approximation 24 p4145 A67-43086
 Two-and three-dimensional laminar viscous boundary layer flow nonlinear partial differential equations solved analytically, studying difference equation substitution 24 p4145 A67-43087
 Integral equations for nonlinear problems in partial differential equations, including Volterra, boundary value and initial value problems 24 p4180 A67-43088
 Nonlinear electrical problems requiring partial differential equations including magnetic saturation, parametric amplifier, electron tube, traveling wave amplifier and semiconductor diodes 24 p4133 A67-43089
 Difference methods for soft solutions to partial differential equations, discussing initial value problem 24 p4180 A67-43090
 Synergetic approach to problems of nonlinear dispersive wave propagation interaction 24 p4125 A67-43093
PARTIAL PRESSURE
 Compatibility of artificial gas mixtures dependent on carbon dioxide and oxygen partial pressures 04 p0562 A67-14573
 Extension of mass range of monopole mass spectrometer and effects on resolving power, sensitivity and mass discrimination, for partial pressure analysis application 06 p1000 A67-17747
 Trigger discharge gauge compared with ionization gauge and partial pressure analyzer 06 p0950 A67-17749
 Physiologically inert gas continuous labelling of pulmonary circulation in one lung compartment and measurement of partial pressure of gas in arterial blood by gas chromatography 07 p1133 A67-19477
 Minimum N and O content in degassing determined from equilibrium pressures in Nb-O and Ta-O systems 09 p1518 A67-22125
 Generator parameters and thermal efficiencies optimization for gas-cooled MGD reactor system, studying temperature and

partial-pressure relation to power density 16 p2604 A67-30571
Thin films of cuprous sulfide, selenide and telluride prepared by flash evaporation, discussing resistivity and absorption coefficient 18 p3106 A67-34637
Reaction mechanism between oxygen difluoride and diborane based on visual observation, gas composition and pressure-temperature relationships [CI PAPER 67-10] 19 p3309 A67-35005
Collection efficiency of plane acting as pump in vacuum system, discussing parameter measurements, partial pressure analyzer and kinetic theory values 23 p4004 A67-41354
Altitude chamber studies of passively pressurizing partial pressure suit for possible use by SST crew 23 p3969 A67-41647

PARTICLE
SA ANTIPARTICLE
SA CHARGED PARTICLE
SA ELEMENTARY PARTICLE
SA METAL PARTICLE
SA NEUTRAL PARTICLE
SA NUCLEAR PARTICLE
SA PENETRATING PARTICLE
SA PLASMA-PARTICLE INTERACTION
SA PRECIPITATION PARTICLE MEASUREMENT
SA QUARK
SA RADIOACTIVE PARTICLE
SA RELATIVISTIC PARTICLE
SA TRAPPED PARTICLE
Quark radio wave line detection from quasars in galaxies with history of high intensity cosmic rays 08 p1400 A67-21246
Radial particle density profile in neon negative glow plasma in cylindrical discharge tube measured by double probe method 08 p1362 A67-21288

PARTICLE ACCELERATION
Identical particles gas with velocities distributed regularly in plane, analyzing compression and relaxation waves present in six-and eight-velocity models 01 p0051 A67-10228
Dynamic dissipation of magnetic field, examining mechanism by which magnetic energy is converted directly into fast particle energy 01 p0146 A67-11277
Cesium ion beam generation by accelerating cesium in space charge sheath located between ionizer and plasma filled region [AIAA PAPER 66-927] 02 p0303 A67-12251
Cosmic ray electromagnetic acceleration mechanism, calculating motion of charged relativistic particles in applied fields 02 p0311 A67-12586
Production of low energy cosmic ray electrons, investigating energy inputs to injected secondary electrons by possible low magnitude solar electric field and possible galactic Fermi acceleration 02 p0312 A67-12635
Trapped particle acceleration by magnetic fluctuation produced by ionospheric currents derived from observations of sharp energy groups of high energy electrons 03 p0409 A67-12942
Electromagnetic field of accelerating charge using Coulomb law, relativity transformation relations, charge conservation, Newton third law, etc 03 p0469 A67-13719
Propulsion through drag interaction between magnetically-accelerated iron particle suspension and air [AIAA PAPER 66-926] 03 p0504 A67-14136
Tritium production in atmosphere by galactic cosmic rays, by solar flare accelerated particles and accretion from sun 04 p0613 A67-14855
Electron and ion acceleration by cosmic plasma waves, examining contribution of these processes to radiation belt formation 04 p0701 A67-15555
Solar charged particles acceleration and propagation through interplanetary space, galactic cosmic ray origin, radiation belt structure, etc, analyzed from space data 05 p0883 A67-16877
Charged particle excitation by random electromagnetic field, obtaining velocity distribution function via all-order perturbation method 06 p1040 A67-18102
Statistical particle acceleration in turbulent plasma 08 p1358 A67-20861
Galactic radio sources noting disk model brightness distribution, relativistic particle

energies, continuous particle acceleration and ratio between proton and electrical component of cosmic radiation 09 p1563 A67-21629
Electric fields due to electron-plasma and ion-acoustic waves associated with sunspot magnetic field variation as main cause of electron acceleration in solar flares 10 p1700 A67-23056
Solar flares as acceleration mechanisms for relativistic and subrelativistic particles 10 p1700 A67-23056
Oriented velocity and temperature relaxation in Coulomb type plasma with particle velocities distributed according to Maxwellian law, evaluating Coulomb collisions effect on plasma components 10 p1885 A67-23410
Classical equation of motion of extended monopole charged particle without preacceleration or runaway solutions 11 p1821 A67-23977
Ion acceleration region demonstrated by coupling two HF magnetic field gradient accelerators 11 p1841 A67-24767
Ion acceleration by drift resonance caused by crossed magnetostatic and space charge electrostatic fields 11 p1841 A67-24768
Obstacles at variable angles attached to pendulum with two degrees of freedom used to study high speed impact of solid particles 12 p1926 A67-25956
Preferential acceleration of heavy nuclei on sun compared with ionizing power of primary particles 13 p2195 A67-27341
Electrode shape design for cylindrical charged-particle beam formation 14 p2320 A67-28650
Solitary waves, discussing electron and ion acceleration and transfer mechanism of solar wind ion kinetic energy to electrons 15 p2475 A67-29613
Accelerated electrons effect on plasma in closed magnetic trap, measuring current flow, plasma density, X-ray/microwave radiation and light emission 16 p2717 A67-31186
Ionization loss effect on energy spectra of cosmic ray nuclei undergoing Fermi acceleration 17 p2930 A67-32041
Solar cosmic ray generation, discussing chromospheric eruptions, spectra, chemical and nuclear composition, particle acceleration, etc 17 p2934 A67-32095
Statistical particle acceleration mechanism in plasmas noting Cerenkov acceleration, particle state changes, wave generation, etc 17 p2905 A67-32921
Acceleration mechanisms of isolated plasma particles under effect of weak or strong field with frequency of order of Langmuir frequency of electron 17 p2905 A67-32922
Nonadiabatic theory for plasma behavior in strong electric field, discussing plasma instability conditions 17 p2905 A67-32924
ULF radio emission associated with magnetic field disturbances, geomagnetic pulsations, auroras and exospheric particle acceleration 17 p2846 A67-32939
Microwave and type IV solar bursts, examining gyrosynchrotron emission and various electron acceleration mechanisms 17 p2939 A67-33391
Energy transport, cosmic ray particle storage and triggering mechanism in solar flares, considering relation with stellar flares 17 p2939 A67-33398
Earth radiation belts nature and plasma activity in magnetosphere 19 p3315 A67-35485
Particle acceleration in solar flares and relative abundance of various nuclei among energetic solar particles 19 p3315 A67-35492
Reversible betatron acceleration mechanism during geomagnetic storm 20 p3434 A67-37425
Propellants and propellant mixtures effects on MPD arc jet performance in test for ions and neutrals mixture acceleration to high velocity [AIAA PAPER 67-684] 21 p3688 A67-38715
Kaufman thruster with curved stainless steel accelerating-grid system, studying operation, efficiency, plasma instability, etc [AIAA PAPER 67-725] 21 p3694 A67-38750
Cosmic rays interaction with solar and terrestrial magnetic fields, noting interplanetary plasma flows and solar activity 21 p3699 A67-39006
Fast electrons formation mechanism during flares ascribed to fast proton

deceleration in flare region rather than high energy particle ionization 21 p3699 A67-39013
Dynamic processes in tail of Morehouse comet, discussing velocity measurements, structures and acceleration variations 22 p3888 A67-40205
Heavy nuclei intensity during solar cosmic ray intensity increase accompanying chromospheric flares, proposing magnetic field dynamic dissipation acceleration mechanism for charged particles 23 p4056 A67-41113
Cosmic ray acceleration mechanisms for fast particle generation under outer space conditions 23 p4057 A67-41114
Cesium ion beam generation by accelerating cesium in space charge sheath located between ionizer and plasma filled region [AIAA PAPER 66-927] 23 p4049 A67-41736
Abundance anomalies in stellar surface layers by proton and alpha particle bombardment caused nucleus breakdown and buildup to lower and higher mass numbers respectively 24 p4228 A67-42264
Gravitational effect on free falling electrons in vacuum, showing gravitational induction of electric field outside metal surface 24 p4189 A67-42740

PARTICLE ACCELERATOR
SA BETATRON
SA ELECTRON ACCELERATOR
SA ELECTRON GUN
SA LINEAR ACCELERATOR
Superhigh energy particle accelerators and energy spectra of cosmic ray muons in electron photon cascades 02 p0317 A67-12772
Explosive driven magnetic generator applied to investigate electric, optical and elastic properties of various substances, plasma physics and charged particle accelerator 05 p0786 A67-16365
Particle accelerator - Conference, Washington, D.C., March 1967 20 p3413 A67-36180
Sulfur hexafluoride gas handling system for potential drop particle accelerator, considering design, fabrication and performance 20 p3413 A67-36181
Adjustment and test of 300 Mev proton extraction system for NASA 600 Mev synchrocyclotron 20 p3413 A67-36182
Mass flow rate, viscosity and conductivity changes effects on single needle colloid thruster [AIAA PAPER 67-530] 21 p3696 A67-38957
Superhigh energy particle accelerators and energy spectra of cosmic ray muons in electron photon cascades 22 p3877 A67-40274

PARTICLE BEAM
SA MOLECULAR BEAM
SA NEUTRAL BEAM
SA PROTON BEAM
Magnetic surfaces of straight helical magnetic field in presence of axial current 01 p0122 A67-10344
Phenomenological approach to dispersion relation for hose instability of charged particle beam passing through plasma 02 p0272 A67-11525
Hazards to man on moon from flare-produced solar particle beams and galactic radiation, noting estimate for life shortening 02 p0189 A67-12394
Magnetic field effect on space charge neutralization in thin beam approximation [AIAA PAPER 67-83] 06 p1041 A67-18275
Electron-ion beam interaction with confined plasma in strong magnetic field, noting ion-sound excitation 08 p1358 A67-20857
Energetic particle scattering by laboratory plasmas, deriving expressions for scattering coefficients in terms of electric field autocorrelation function 08 p1361 A67-21136
Spectrum of ionic waves in plasma located in electrical field and interacting with charged particle beam, obtaining dispersion equation 09 p1544 A67-21846
Density attenuation within crossed particulate beams analyzed under steady state interaction, giving more exact solution than Beer law approximation 11 p1818 A67-24318
Ionic waves in plasma in electric field interacting with beam of charged particles at relaxation time, using dispersion equation 11 p1841 A67-24869
Magnetic surfaces of straight helical magnetic field in presence of axial current 11 p1843 A67-25017

Electrode shape design for cylindrical charged-particle beam formation 14 p2320 A67-28650
 General resistive instabilities of self-pinch cylindrically symmetric beam of charged particles passing through ohmic plasma channel 15 p2522 A67-29198
 Active corpuscular plasma diagnostics method applied to hydrogen plasma study 15 p2526 A67-29257
 Charged particle beam passage through plasma, detailing excitation of one-dimensional oscillation expanding perpendicularly to boundary of semilinear plasma 16 p2716 A67-31176
 Dispersion equations for long wavelength beam instability propagating through homogeneous plasma 17 p2895 A67-32160
 Charged particle beam guiding and focusing by helical magnetic multipole field for relativistic and nonrelativistic cases 17 p2908 A67-33112
 Noise removal and deconvolution techniques applied to resolution of beam collision experiments 17 p2886 A67-33261
 Hot plasma corpuscular diagnostics methods, noting particle beam determination of hot plasma density, electron temperature and plasma electric fields 19 p3296 A67-35586
 Electrode configurations producing various intense charged particle beams, deriving algorithm applicable to three-dimensional problems 24 p4153 A67-41928
 Particle streams with greater than 1 TeV energy analyzed by Lobachevskii-Einstein velocity space images method 24 p4193 A67-42857

PARTICLE CHARGING

SA CHARGED PARTICLE

Self-charging of temperature independent radioactive ultrafine particles for MHD power generation 08 p1283 A67-20647
 Meteoritic ion pair production probability by total ablation of micron-size Fe particles in air and Ar as function of particle velocity 08 p1399 A67-21241
 Preformed micron and submicron-sized solid particles for colloidal propulsion, investigating particle feeding and charging [AIAA PAPER 67-727] 21 p3688 A67-38751

PARTICLE CLOUD

Low energy proton distribution in geomagnetic coordinates obtained from Elektron satellite measurements 05 p0880 A67-16108
 Volume scattering of Mie spherical particle polydispersion and irregular particles 10 p1879 A67-22747
 Book on fluid dynamics of multiphase systems covering momentum, heat and mass transfers and chemical reactions 20 p3425 A67-37728
 Rotation and pressure gradient effects on gravitational instability of collapsing gas clouds, discussing subsequent fragmentation 22 p3893 A67-40501
 Interstellar gas cloud collision, heating, possible gravitational instability and subsequent cooling 22 p3894 A67-40513
 Interstellar gas cloud gravitational collapse for models initially in gravitational equilibrium without mass motions, analyzing cooling and density distribution effects numerically 22 p3895 A67-40514
 Collapsing gas cloud noting instability for density fluctuations, rise of turbulence and fragmentation phenomena 22 p3895 A67-40516
 Fragmentation and excess angular momentum problems in star formation theories, examining relevance to simplifying assumptions and physical situation 22 p3895 A67-40517
 Equilibrium configuration for nonspherical cold gas cloud permeated by magnetic field in gravitationally collapsed state 22 p3895 A67-40518
 Zonal method of determining radiative heat transfer between gray particle cloud and surrounding gray walls of enclosing system 24 p4253 A67-42252
 Low energy proton distribution in geomagnetic coordinates obtained from Elektron satellite measurements 24 p4214 A67-42784

PARTICLE COLLISION

SA MOLECULAR COLLISION

Cross sections for double electron capture by two 50-kev protons in single collisions with hydrogen and inert gas target 01 p0115 A67-10140
 Levi-Civita regularized equation of elliptic

motion of particle influenced by massive primary and perturbed by smaller primary, Part II, Applications to circular and collision orbits 01 p0147 A67-10380
 Atmospheric radio wave absorption coefficient and altitude determined and linked to effects of colliding paramagnetic oxygen molecules 01 p0022 A67-10391
 Meteor luminescence during atmospheric motion, obtaining radiation coefficient as function of cross sections of particle excitation and pulse transfer processes 01 p0151 A67-11287
 Photon interaction in plasma, determining energy density and collision frequency 02 p0272 A67-11583
 Collision paths of free particle in Newtonian gravitational field examined, using analogy of circular restricted three-body problem 02 p0328 A67-12403
 Ionization efficiency and cross section of meteor trails during collision between particles of meteoric vapor and air molecules 02 p0329 A67-12494
 Interference induced elongation of light scattering indicatrix of particle conglomeration 02 p0263 A67-12671
 Peripheral nonelastic interactions described, using amplitude characteristics of elastic cosmic ray particle interaction and complex orbital moment technique 02 p0315 A67-12749
 Characteristics of transverse pulse produced by secondary particles created in active nuclear particle collision 02 p0271 A67-12752
 Methods for calculating interaction potentials of atoms, molecules and ions 03 p0473 A67-13613
 Kinetic equations derived for plasma with particle interactions 03 p0481 A67-13735
 Small amplitude wave propagation in equilibrium plasma studied using collision model proposed by Bhatnagar, Gross and Krook 03 p0481 A67-13738
 Electron thermal conductivity of fully ionized Lorentz gas, determining energy transfer from Landau damping of plasma waves and collision parameters 03 p0484 A67-14039
 Self-consistent three-body calculation of pion-nucleon scattering using off-energy shell theory 04 p0680 A67-14858
 Partially ionized two-temperature plasma, deriving distribution function of first approximation associated with viscosity 04 p0668 A67-15186
 Energy transfer rate between electrons and ions in plasma, noting velocity dependence of Coulomb logarithm 04 p0672 A67-15775
 Thrust generation from neutral particle sputtering from solid target, noting advantages such as storage, operating life, etc 05 p0873 A67-16515
 Collision induced dissociation of deuterium by argon and nitrogen examined with angular ion scattering apparatus, determining kinetic energy and angular distribution 05 p0848 A67-16834
 Charged particle collisions effect on drift instability of low pressure plasma studied, using Landau collision integral as model collision integral 05 p0860 A67-17546
 Charged and neutral particles collision effect on LF oscillations in weakly ionized plasma in crossed electric and magnetic fields 06 p1046 A67-18827
 Ambipolar diffusion theory for describing diffusion of nonuniformities in ionosphere including F region 07 p1230 A67-19717
 Correction of Fatkullin expressions for LF conductivities of homogeneous plasma in presence of electron-ion collisions in ionosphere 07 p1179 A67-19834
 Plasma-neutral coupling in ionospheric motions having short durations compared with time between neutral particle collisions with ions 08 p1325 A67-21151
 Microwave loss in reflex plasma discharge determined from microwave energy decay measurements 08 p1363 A67-21311
 Electrostatic probe theory in moderately ionized gas taking into account effect of electron-ion collisions 08 p1324 A67-21393
 Transition of extensive air showers in atmosphere with determination of lateral structure, mean free path and inelasticity 08 p1377 A67-21437
 Nonsteady state processes in nonequilibrium plasma with local collisions,

using Boltzmann kinetic equation for application in MHD generators 09 p1543 A67-21823
 Calculation of effective excitation cross sections of hydrogen atoms for collisions with nitrogen molecules and hydrogen atoms 09 p1534 A67-21850
 Average diffusion cross section for elastic collisions of electrons with heavy particles, comparing calculated and measured values 09 p1534 A67-21864
 Ionization calorimeter performance simulation using Monte Carlo 09 p1497 A67-21900
 Diffused base punchthrough avalanche transistor /PAT/ at high recurrence frequency having capacitance dependence of pulse width 10 p1609 A67-22839
 Low temperature alkali plasmas in strong magnetic fields interpreted in terms of collisional drift modes 10 p1884 A67-23073
 Atmospheric reaction with energetic particles and resultant production of atomic oxygen, atomic nitrogen and nitric oxide 10 p1637 A67-23191
 Occurrence of collisions between ionized and neutral particles based on analysis of spectrum diffused by E region 10 p1646 A67-23268
 Ionization efficiency and cross section of meteor trails during collision between particles of meteoric vapor and air molecules 10 p1709 A67-23362
 Drift cyclotron oscillations of inhomogeneous collision plasma propagating across magnetic field, taking into account particle collisions with aid of Landau collision integral 10 p1686 A67-23595
 Density attenuation within crossed particulate beams analyzed under steady state interaction, giving more exact solution than Beer law approximation 11 p1818 A67-24318
 Microwave reflection analysis of plasma surface phenomena, noting dependence on electron density and collision frequency 11 p1844 A67-25097
 Braking of bodies moving in rarefied plasma 12 p1892 A67-25536
 Obstacles at variable angles attached to pendulum with two degrees of freedom used to study high speed impact of solid particles 12 p1926 A67-25956
 Device for studying high energy nuclear active particles of cosmic rays interaction and determination of energy spectrum 12 p1947 A67-26095
 Maxwell dispersion of particles of molecular gas flow at wall of circular channel described by integral equation, determining particles experiencing mirror intercollisions 13 p2158 A67-26671
 Lobular scattering of 1 ev energy chopped argon beams from silver, mica and brass surfaces, noting distributions and contamination effects 13 p2099 A67-26950
 Monte Carlo calculation of kinetics of chemically reacting multicomponent gas for finite number of particles followed through random collision processes 13 p2102 A67-26971
 Coordinated experiments on auroras to understand particle-atmosphere interaction, emphasizing aircraft phase of measurement 13 p2115 A67-27256
 Molecular beam apparatus for measuring collision cross section and velocity distribution of sputtered particles 14 p2316 A67-28191
 Linearized Fokker-Planck kinetic equation, describing approach to equilibrium of test electrons injected into electron plasma in thermal equilibrium 14 p2356 A67-28203
 Coefficient for electron ion recombination during triple particle collision, using Boltzmann kinetic equations 14 p2363 A67-29077
 Plasmoid collisions in axisymmetric magnetic field studied spectrographically for energy density, radiative power, charged particle density, etc 15 p2525 A67-29248
 Transforms for regularizing two-body collisions in plane two-and three-body systems with aid of conformal mapping and function theory 15 p2559 A67-30037
 Condensed phase particle growth in rocket nozzle by particle collision and coalescence [AIAA PAPER 66-639] 15 p2548 A67-30200
 Nucleon-nucleon collisions, analyzing pair production, electromagnetic cascade, secondary interactions,

etc 16 p2703 A67-30965
 Temperature gradient effect on stability of inhomogeneous magnetically-confined plasma with frequent ion collisions 16 p2720 A67-31239
 Recharge cross section in collisions of slow atoms or ions involving interparticle transfer of one electron 16 p2705 A67-31781
 Long-lived impact excitation states of particles measured from cross section of nonelastic collision with second particle 17 p2809 A67-32142
 Chemical processes in low temperature plasmas, stressing nonequilibrium characteristics, temperature and collision factors, ionization and particle excitation 17 p2809 A67-32188
 Excited state and steady state populations in high pressure plasma with heavy particle collisional ionization and electron-ion recombination 17 p2909 A67-33228
 Noise removal and deconvolution techniques applied to resolution of beam collision experiments 17 p2886 A67-33261
 Stable deflection of homogeneous plasma stream by linearly increasing transverse magnetic field, neglecting particle collisions 18 p3087 A67-34036
 Methods for calculating interaction potentials of atoms, molecules and ions 18 p3083 A67-34478
 Ionizing and charge transfer processes following heavy particle collisions in ionized gas analyzed using spectroscopic technique 19 p3264 A67-35069
 Convergence of solutions for AC and DC electric conductivity of plasma with collisions 19 p3286 A67-35352
 Absorption lines in quasi-stellar source analysis to obtain estimates of either particle density in absorbing region or distance between continuum source and absorber 19 p3330 A67-36082
 Relaxation of carbon dioxide pulsed laser levels by collisions with hydrogen, showing gain dependence on hydrogen pressure 20 p3457 A67-36384
 Particle mass spectrum development in rocket nozzle, assuming droplet growth by collision and agglomeration as dominant mechanism 20 p3516 A67-37130
 Antiproton production by primary cosmic ray collisions with atmospheric nuclei compared with interstellar gas 21 p3620 A67-38843
 Plasma model kinetic equation, discussing collision operator approximating momentum and energy transfer rates 22 p3843 A67-39265
 Chapman-Enskog transport collision integrals calculated for repulsive and attractive screened Coulomb potentials in ionized gases 22 p3850 A67-39717
 Kinetic equations for electrons and photons in homogeneous plasma in strong magnetic field derived from Maxwell and classical motion equations 22 p3851 A67-39736
 Peripheral nonelastic interactions described, using amplitude characteristics of elastic cosmic ray particle interaction and complex orbital moment 22 p3876 A67-40251
 Characteristics of transverse pulse produced by secondary particles created in active nuclear particle collision 22 p3841 A67-40254
 Interstellar gas cloud collision, heating, possible gravitational instability and subsequent cooling 22 p3894 A67-40513
 HF conductivity of partially ionized plasma in long wavelength limit, treating particle interactions by BBGKY and Boltzmann collision integral methods 23 p4031 A67-40888
 Two and three-pulse echo trains stimulated in magnetoplasma by repeated electron cyclotron frequency pulsing studied with single particle collision theory 23 p4031 A67-40889
 Capture, ionization and ionization capture in collisions of protons with argon atoms 23 p4030 A67-41687
 Electron neutral heat transfer in plasmas, obtaining data on electron thermal diffusivity from pulsed heat flow experiments in helium 24 p4194 A67-41872
 Relaxation of anisotropic plasmas based on Fokker-planck equation assuming elliptic distribution during process 24 p4198 A67-42440
 Electrical conductivity of ionized plasma taking into account particle impenetrability,

using Boltzmann and collision at distance integrals 24 p4198 A67-42662
 Air shower nuclear active component spectra noting need for mechanism of energy transfer from nucleons into electron-photon avalanches 24 p4220 A67-42862
 Shower producing capability of various particle groups at 40 mwe below ground, evaluating muon energy 24 p4220 A67-42865
 Bremsstrahlung due to collision of muon with electron at rest, discussing energy photons role 24 p4194 A67-42880

PARTICLE COUNTER

High temperature operation of diamond counters for nuclear particles 01 p0068 A67-10927
 Operational alpha counting characteristics for point plane counter in air working in corona streamer mode 02 p0241 A67-11680
 Physical characteristics affecting detection efficiency of Geiger counters, proportional counters and ion chambers used in space measurements of particles 02 p0244 A67-12209
 Silicon integrated circuit data encoder for Isis A satellite particle counting experiment, noting design and construction 05 p0770 A67-16292
 Proton precession magnetometer completely transistorized except for signal amplifier 05 p0807 A67-16712
 Cosmic ray intensity variations using gas discharge counters onboard Soviet satellites, noting Forbush effects 05 p0884 A67-17025
 Spark counter for recording fission fragments in presence of high intensity alpha radiation 06 p1001 A67-17936
 Transistorized electron counter using tunnel diodes, noting 06 p1004 A67-18391
 Aerosol particle velocity measurement using optical compensation and photoelectric particle counter 08 p1428 A67-21422
 Dead time instability effect on neutron monitor performance 10 p1699 A67-22799
 Measurement of cosmic ray intensity by Zond III automatic space probe 10 p1701 A67-23230
 Distribution curves of ion density and condensation particle concentration in layers of atmosphere near sea level, noting criteria for instruments 10 p1657 A67-23695
 Rise time in solid state detectors, considering equivalent circuit, plasma, time, etc 11 p1789 A67-24103
 Need for increased sampling rates of particle counters to improve monitoring system performance for clean room sampling and leak testing of HEPA filters 23 p3961 A67-40843
 In-Line-Filter-Holder and Counter /ILFHC/ designed for high and low pressure systems to verify particulate cleanliness levels in modern fluid systems 23 p3935 A67-40846
 Primary proton energy spectrum determination by particle energy measurements with ionization calorimeters and particle counters onboard space stations 23 p4054 A67-41092
 Cosmic ray measurements during low geomagnetic activity using scintillation, gas discharge and semiconductor proton counters mounted on Cosmos satellite 23 p4055 A67-41099
 Auroral zone phenomena analyzed using rocketborne counters 23 p3997 A67-41333
 Dead time instability effect on neutron monitor performance 24 p4209 A67-42135

PARTICLE DECAY

Directional correlation of first forbidden beta group and gamma ray in decay of antimony at four beta energies 02 p0269 A67-11863
 Plastic deformation and aging effect on kinetics of beta phase decay, dispersion and alpha phase distribution of TC6 by optical and electron microscopy and measurements of hardness and mechanical properties in tension 04 p0640 A67-15976
 Solar wind effect on cathode scattering of cosmic dust particles in earth proton belt and shortening of lifetime of captured particles 06 p1078 A67-18162
 Pair production in irradiated semiconductors within framework of plasmon decay, considering variation of radiation ionization energies with band gap energy 06 p1063 A67-18935
 Particle loss through axisymmetric cusped magnetic field containment geometry,

deriving adiabatic invariant for collisionless plasma 08 p1361 A67-21133
 Radical concentrations and decays in lean hydrogen-nitrogen-oxygen flames 13 p2221 A67-26261
 Solar wind effect on cathode scattering of cosmic dust particles in earth proton belt and shortening of lifetime of captured particles 16 p2737 A67-30506
 Nonleptonic sigma decay modes described by four complex amplitudes with phases given by time-reversal invariance 19 p3263 A67-34892
 Average dwell times and velocities of Ba, Sr, Li, Tl, Sn, Bi, Be, Zn, and Hg in arc plasma 19 p3281 A67-35155
 Luminescence decay kinetics of trivalent Nd ions in antiferromagnetic Rb manganes fluoride, showing mechanism of transfer process of excitation energy of Mn ions 20 p3506 A67-36218
 Nilsson model used to derive expressions for nuclear matrix elements, considering forbidden beta decay of spheroidal-shaped nuclei 20 p3488 A67-36662
 Approximate electron radial functions for uniformly charged nucleus /UCN/ used in analyzing boron 12 and nitrogen 12 beta decay spectra 20 p3488 A67-36915
 Weak electromagnetic decays of hyperons in broken SU(3) model 20 p3489 A67-37093
 Solar proton event /February 1965/, time history of low energy protons was more complex than that of higher energy particles 22 p3872 A67-39812
 Solar neutrino observation, considering inverse nuclear beta decay and elastic scattering by orbital electrons 24 p4210 A67-42583
 Phonon annihilation during decay of two metastable fluorescent states of ionized Ba compound 24 p4205 A67-42737
 Microwave absorption by magnetic field induced surface states in superconductors, showing anomalies consistent with quasi-particle decay 24 p4205 A67-42739
 Isobar decay mechanism for high energy pion generation in cosmic rays propagating through atmosphere 24 p4218 A67-42841

PARTICLE DETECTOR

SA ELECTRON DETECTOR

SA NEUTRON DETECTOR

L-3 rocket observation of proton and electron fluxes at high altitudes, using solid state detectors 01 p0144 A67-10564
 Charge collection velocity in semiconductor particle energy detector expressed in terms of electron and hole motion and induced charges 01 p0065 A67-10650
 Rocket measurement of proton energy spectra and pitch angle distribution associated with auroral radio absorption, using solid state surface barrier detector 01 p0061 A67-11261
 Charge composition of cosmic radiation, noting results for charges 1/3 e and 2/3 e, experimental setup, etc 02 p0306 A67-11500
 Charged particle solid state detectors, considering neutron intensity and energy and spectral and/or dose measurements 02 p0244 A67-12210
 Surface barrier diffused-junction lithium-compensated silicon and lithium-compensated germanium particle detectors for aerospace application 02 p0245 A67-12212
 Detection of slow neutrons escaping from atmosphere by counters filled with boron fluoride onboard high altitude balloons 02 p0312 A67-12599
 400-kev electrons precipitation in auroral zone measured with solid state detector mounted on polar satellite 03 p0410 A67-12952
 Fluctuations and broadening of energy-loss spectrum of charged particles passing through semiconductor detectors 03 p0491 A67-13224
 Determining total number of charged particles in extensive atmospheric shower and position of axis of shower 03 p0507 A67-14059
 Multiplate spark chamber as linear high energy electron and photon detector 03 p0425 A67-14264
 Davis radiochemical experiment for detection of solar neutrinos and sampling techniques for detecting high energy atmospheric neutrinos 03 p0516 A67-14338
 High-counting-rate particle detector for balloon sounding of atmospheric

top 04 p0621 A67-14899

Spatial distribution of energetic electrons in geomagnetic tail by analyzing counting rates from solid state detector on IMP I satellite 04 p0692 A67-14953

Plasma observations in tail of terrestrial magnetosphere and circumlunar space by Luna X orbiter, using charged particle traps 05 p0875 A67-16054

Cosmic ray nuclei observed from satellites and balloons by nuclear emulsions in stacks of plastic sheets 06 p1076 A67-17641

Sun generated high and low energy protons analyzed, using semiconductor detectors during flights of interplanetary probes 06 p1077 A67-17841

Satellite measurement of low energy electrons and protons in auroral regions, discussing use of instruments with variable energy electrostatic thresholds and postacceleration techniques 12 p1944 A67-25851

Three-channel particle spectrometer with semiconductor detectors and tunnel diode discriminators noting noise immunity, high signal level output, etc 12 p1944 A67-25853

Channel multiplier instrument measuring low energy electron and proton auroral fluxes from polar orbiting satellites 12 p1944 A67-25855

Nanosecond fluorimeter for measuring emission kinetics of chromophores 12 p1946 A67-25981

Far UV transmitting windows, particularly lithium fluoride, and response measurements below 2000 angstroms, noting fabrication on solar blind materials 12 p1947 A67-26161

Transmission energy characteristics of spherical plate electrostatic analyzers from external sources of electrons and protons 14 p2320 A67-28746

Multiplate spark chamber as linear high energy electron and photon detector 14 p2321 A67-28776

Cosmic ray mu-meson intensities at different altitudes at equator measured as function of zenith and azimuth, using scintillation counter telescope 15 p2549 A67-29184

Laser light photon counting statistics using probability density for laser light intensity 15 p2498 A67-29513

Meteoritic satellites of earth, estimating capture region dimensions 17 p2941 A67-32324

Primary cosmic ray spectrum changes from differential response functions and specific yield functions of neutron monitors 17 p2936 A67-32533

Radio signals reflection by free radicals in ionosphere, observing predicted intensity and particle detection 17 p2817 A67-33233

Low energy H and He isotope detection in cosmic radiation at solar minima via balloon mounted scintillation counter 17 p2939 A67-33246

On-the-ground optical determination method of stratospheric aerosol particle numbers and sizes from ruby laser radiation measurement scattering 19 p3225 A67-35531

Switched Proton Electron Channeltron Spectrometer /SPECS/ developed for measurement of charged particles in space 20 p3443 A67-36517

Alpha particle proton ratio of geomagnetic field from data from charged-particle telescope on OGO 1 20 p3519 A67-37412

Plasma observations in tail of terrestrial magnetosphere and circumlunar space by Luna X orbiter, using charged particle traps 21 p3697 A67-37841

Semiconductor detector for information on charged particles of cosmic radiation, studying characteristics of instrument 21 p3629 A67-38664

Reception vectors for first and second spherical harmonics of cosmic ray distribution calculated for neutron monitor stations 21 p3699 A67-39018

Back collection of charge due to ionizing alpha or beta particles by silicon p-n junction detector with space charge width less than range 22 p3797 A67-39345

Solar proton event /February 1965/, time history of low energy protons was more complex than that of higher energy particles 22 p3872 A67-39812

Charge spectrum of very heavy cosmic ray primaries studied from balloon observations in photographic emulsion detector for Texas

atmosphere 23 p4050 A67-40676

High energy cosmic ray shower detection combining perturbed magnetic field pulse and coincident optical radiation observations 23 p4051 A67-40812

Mobile laser transceiver for atmospheric targets detection, discussing real time technique for determining atmospheric function 23 p4014 A67-41022

PARTICLE DIFFUSION

Crossed electric and magnetic fields effect on quasi-liquefaction process of nonconducting particles by electrolyte 01 p0121 A67-10189

Integral intensity of charged particles diffusing through drift shells in earth magnetosphere with specific example for protons 02 p0306 A67-11550

Cosmic rays from solar flare and interplanetary space properties, covering particle scattering and magnetic field induced one-dimensional particle diffusion 02 p0310 A67-12575

Relative dispersion of particle pairs in homogeneous turbulence using Lagrangian-history direct interaction closure approximation for convected scalar field, obtaining Richardson diffusion equation 03 p0405 A67-14031

Relative diffusion of liquid particles in turbulent flow with shear, deriving formulas 05 p0837 A67-16490

Angular distribution of radiation at boundary of homogeneous diffusion sphere, with isotropic central point source calculated by Monte Carlo method 05 p0838 A67-16491

Electron-concentration distribution in ionospheric F-2 layer with vertical distribution of electron-ion gas 07 p1178 A67-19821

Domain formation process during passage of current through multivalley semiconductor when electron intervalley scattering drift length exceeds diffusion length 09 p1555 A67-22074

Neutral particle densities of nitrogen, molecular and atomic oxygen and argon in upper atmosphere, noting density profile irregularities, diffusive separation altitude, etc 10 p1639 A67-23213

Three stages of solar cosmic rays entry into polar cap atmosphere due to differential arrival of solar electrons, protons and alpha particles 11 p1855 A67-23925

Diffusion of particles across magnetic lines in dense and quiescent plasma compared with Bohm and collisional values 11 p1835 A67-24383

Complementary variational principles in neutron diffusion theory 11 p1824 A67-24632

Transverse diffusion of particle perpendicular to magnetic field by assembly of random Alfvén waves explains increase in electric field energy 11 p1840 A67-24753

Relative diffusion of liquid particles in turbulent flow with shear, deriving formulas 13 p2093 A67-26345

Angular distribution of radiation at boundary of homogeneous diffusion sphere, with isotropic central point source calculated by Monte Carlo method 13 p2155 A67-26346

Diffusion of protons and nuclei having elastic interactions at 27 GeV/c, using probability distribution for events outside Gaussian limit of multiple scattering 13 p2160 A67-26436

Steady state forced sound propagation in semilinear gas induced by oscillating plane piston reflecting particles with Maxwellian distribution 13 p2100 A67-26957

Interplanetary particle diffusion model analysis in terms of energy, position in space, direction and time 13 p2193 A67-27250

Sonagrams for micropulsations, computer simulated, using equations for cyclotron instability and quasi-linear diffusion of protons in bounded plasma 15 p2476 A67-29618

Integral intensity of charged particles diffusing through drift shells in earth magnetosphere with specific example for protons 16 p2740 A67-31616

Solar proton diffusion data for model of quiescent interplanetary medium 17 p2937 A67-32539

Earth radiation belts nature and plasma activity in magnetosphere 19 p3315 A67-35485

Cosmic ray diffusion in interplanetary

magnetic field, examining statistical homogeneity and isotropy 20 p3520 A67-37473

Proton mechanism of escape from earth magnetic field, analyzing charged particle in Alfvén wave field 20 p3520 A67-37667

Secular modulation of cosmic ray intensity in interplanetary space using Parker diffusion model 23 p4057 A67-41117

Cosmic ray anisotropy in solar system, considering diurnal variation in terms of anisotropic diffusion 23 p4058 A67-41121

PARTICLE EMISSION

SA QUANTUM GENERATOR

Particle emission from surface interacting with laser beam 02 p0252 A67-12180

Total energy of slow particle radio emission and real delta electron emission determined in extensive air showers 02 p0318 A67-12782

Noises in quantum amplifier due to heat fluctuations and spontaneous emission of active microparticles, discussing negative temperature state 03 p0368 A67-13139

Extensive near-vertical air shower analysis at sea level for nucleon-air-nucleus and pion-air-nucleus interaction 03 p0506 A67-13517

Emission of electrically charged and film producing particles from sputter ion pumps, describing experimental facility and two methods for examination 07 p1190 A67-20283

Relativistic mechanism of electromagnetic wave scattering at velocity fluctuations and emission from plasma in external field 08 p1295 A67-20831

Polar auroras, considering types resulting from MHD wave heating of upper atmosphere, low energy particle penetration of atmosphere, etc 09 p1491 A67-21892

Laser radiation effect on solids, noting laser properties, temperature rise, melting, vaporization and particle emission of materials 09 p1513 A67-22144

Emission of particles, causing geomagnetic storms, without accompanying radio effects 11 p1787 A67-24594

Nanosecond fluorimeter for measuring emission kinetics of chromophores 12 p1946 A67-25981

Nilsson model used to derive expressions for nuclear matrix elements, considering forbidden beta decay of spheroidal-shaped nuclei 20 p3488 A67-36662

Proton, neutron and alpha particle emission rates for heavy nuclei in elevated temperatures calculated and tabulated 20 p3490 A67-37553

Laser application to high temperature research, discussing high temperature production using lasers, high temperature plasma and laser-irradiated surface particle emission 21 p3640 A67-38392

Solar wind geomagnetic field interactions during disturbed conditions, discussing solar particle emissions, solar plasma activity, ring and ionospheric currents 22 p3870 A67-39672

Total energy of slow particle radio emission and real delta electron emission determined in extensive air showers 22 p3878 A67-40284

Solar flare energetic X-ray events detected by onboard satellite ionization chambers, studying relationship to radio burst and space particle emission 23 p4060 A67-41232

PARTICLE FLUX

Rms particle numbers calculated for electrons and photons in three-dimensional theory of electromagnetic showers 01 p0143 A67-10543

Radial transport of cesium plasma governed by resistive diffusion as shown by stellarator experiments in which surface recombination losses within plasma volume were negligibly small 01 p0125 A67-10914

Azimuthal asymmetry in distribution of shower particles around shower axis, using Geiger-Müller counter telescopes 01 p0145 A67-11230

Radial extension of corpuscular flux from chromospheric flares and duration of earth immersion in flux 02 p0306 A67-11653

Energy spectrum of variations in cosmic ray intensity and changes in spectrum with decreasing solar activity calculated for additional particle flux 02 p0311 A67-12597

High energy cosmic ray interactions analyzed at 3340 m above sea level, using Wilson cloud chambers, gas discharge counters, ionization calorimeter, etc 02 p0248 A67-12746

Spatial and angular particle distributions

in muon-generated electron photon cascade, using spark chamber muon detectors 02 p0317 A67-12774

Muon flux measurement with aid of spark chamber at depth of 20 mwe used for spatial distribution near axis of extensive air showers 02 p0318 A67-12780

Nuclear emulsion measurements of primary cosmic ray alpha particle flux over Hyderabad during high solar activity in 11-year cycle 03 p0506 A67-13720

Continuous flux of solar protons entering earth atmosphere important in energy balance of ionosphere and sun [RASSA PAPER 1-10-140] 03 p0417 A67-14248

Primary cosmic radiation in interplanetary space, lunar surface albedo and soft particle fluxes in magnetosphere measured by Luna X orbiter 05 p0875 A67-16053

Temporal variations of nuclear flux of primary cosmic radiation of Elektron II and IV satellites, discussing Forbush effect in nuclear and neutron components 05 p0877 A67-16085

High energy primary gamma quanta flux outside atmosphere estimated with aid of Proton I satellite 05 p0877 A67-16088

Cosmos 53 satellite radiation data using on board gas discharge counter 05 p0879 A67-16107

Electromagnetic waves produced by charge traveling at constant velocity in medium with convective instability 05 p0762 A67-16353

Solar proton flux measurement with balloon-borne detectors in northern Scandinavia 05 p0882 A67-16740

Altitude variation of cosmic ray intensity in atmosphere, checking accuracy of flux data from rockets and satellites 05 p0883 A67-16879

Rocket sounding of intensity distribution of proton and electron fluxes at high altitudes, noting secondary particle emission from radiation belt 05 p0883 A67-16880

LF photocurrent oscillation in high resistivity n-type GaAs, noting relation between amplitude temperature and light intensity 05 p0866 A67-16987

Concentration and density distributions of particle flux near body moving in rarefied plasma 05 p0855 A67-17122

Molecular fluxes in lunar atmosphere relationship to gas source distribution, surface temperature and gas emission laws 05 p0904 A67-17404

Energy spectrum of levels appearing in silicon single crystals irradiated by integral fluxes of fast electrons, neutrons and gamma quanta 05 p0872 A67-17547

Energy and angular distributions of neutral atoms and charge-exchange ions from mercury electron bombardment thruster, determining particle effluxes [AIAA PAPER 67-82] 06 p1075 A67-18498

Proton energy spectrum obtained from nuclear emulsion measurements on Gemini IV and V missions 07 p1244 A67-19855

Satellite measurement of low energy proton precipitation in auroral zone during magnetically quiet period 07 p1245 A67-19930

Lunar water sources, considering hydrous minerals, cold trapped volatile products of volcanic origin and dispersed hydrates 08 p1317 A67-21093

Differential energy spectra and fluxes of charged splash and reentrant albedo proton measurement of cosmic radiation in various energy ranges 08 p1377 A67-21467

Trapped proton flux data from nuclear photographic emulsions 08 p1378 A67-21472

Anisotropic proton velocity distribution obtained from solar wind measurements on Pioneer VI spacecraft 08 p1378 A67-21475

Star collapse observation by detection of high energy neutrino fluxes produced by catastrophic star contraction 09 p1561 A67-21630

Ionospheric absorption as indicator of particle flux below point of long radio wave reflection, noting relation to solar cosmic rays 09 p1561 A67-21844

Polar cap absorption with solar cosmic ray properties from balloons and relation to processes in terrestrial atmosphere 10 p1637 A67-23189

Polar glow aurora, discussing optical emissions generated by solar cosmic ray protons and alpha particles, energy spectrum, atmospheric and ionospheric absorption effect, etc 10 p1637 A67-23190

High altitude balloon top collections of cosmic dust shows evidence of absence of crystal structure in particles 10 p1708 A67-23239

Plasma flows from normal and coaxial electrode contact points of arc and effect of external forces by schlieren photography 10 p1687 A67-23849

Lateral distribution of radio emission flux of extensive air showers /EAS/ of cosmic rays 12 p1940 A67-25337

Low energy particles detected close to equatorial plane of magnetosphere by satellites Elektron and Cosmos 12 p1997 A67-25811

Primary cosmic radiation composition effect on secondary emission, examining flux, spectra, nucleon interactions, proton component and neutrons 14 p2380 A67-27966

Pressure gradient in duoplasmatron ion source as function of parameters of discharge 14 p2359 A67-28512

Sonagrams for micropulsations, computer simulated, using equations for cyclotron instability and quasi-linear diffusion of protons in bounded plasma 15 p2476 A67-29618

Expulsion of ions from comets toward sun examined for source, dissociation and ionization of parent particles, velocity, etc 16 p2746 A67-30979

Radial extension of corpuscular flux from chromospheric flares and duration of earth immersion in flux 16 p2738 A67-31068

One-dimensional charged particle flow in bounded system, particularly overlapping steady state zero-temperature flow approximation solutions, noting instabilities 16 p2704 A67-31233

Drift waves in fully ionized potassium magnetoplasma in single-ended Q machine, measuring effect on transverse diffusion coefficient 16 p2720 A67-31242

Relationship between geomagnetic storms with sudden commencements and perturbations of southern and northern components of meson distribution in Northern Hemisphere 17 p2938 A67-32796

Power spectrum of pulsating aurora measured at HF, noting relation to modulation mechanism in flux of primary particles 17 p2850 A67-33193

Unexpected excess of primary cosmic ray helium nuclei flux value in nuclear photographic emulsions 17 p2939 A67-33237

Auroral particle fluxes and effects from coordinated satellite-, aircraft- and ground-based measurements 18 p3034 A67-33590

Atmospheric emissions and electron and proton precipitation latitude and diurnal variations measurements from satellite-borne photometric studies 18 p3039 A67-33623

Hysteretic superconductor, showing trapped flux or remnant magnetic moment linear relationship with average internal field in low but not in high k superconductors 19 p3302 A67-35036

Thermomdiffusion term in particle flux equation, showing large electron temperature variation across low voltage arc plasma 19 p3279 A67-35140

Solar proton flux measurement by balloon on July 7, 1966 in northern Scandinavia, with differential proton flux calculated for several energies 19 p3312 A67-35175

Zodiacal dust particle flux measurements from OGO 3 and Mariner IV spacecraft in cisunar and interplanetary space 19 p3318 A67-35185

Primary diffuse X-ray flux and spectrum found isotropic by balloon measurements made in three particular directions 19 p3313 A67-35244

Irregular pulsations of dimming periods /IPDP/, discussing cause and low energy electron flux variations 20 p3431 A67-37097

Auroral substorms, examining energy spectrum and flux of precipitating particles and morphology 20 p3431 A67-37100

Low energy proton flux increases in outer radiation belt during quiet magnetic activity and correlation with magnetic bay appearances 20 p3519 A67-37408

Micrometeorite flux rate for Leonid shower measured with Luster sounding rocket collecting surface 20 p3528 A67-37424

Primary cosmic radiation in interplanetary space, lunar surface albedo and soft particle fluxes in magnetosphere measured by Luna X orbiter 21 p3697 A67-37840

Low energy, positive ion flux from inner

radiation zone, noting losses due to charge exchange, night sky emissions and lifetimes 21 p3697 A67-37996

Nuclear active particles energy spectrum obtained on mountain tops, investigating absolute flux by using ionization calorimeter 21 p3698 A67-38293

Concentration and density distributions of particle flux near body moving in rarefied plasma 21 p3668 A67-38465

ULF radiation in polar auroral zone explained via plasma beam instability, assessing perturbation of particle fluxes in magnetosphere 21 p3621 A67-39016

Interplanetary magnetic field normal to ecliptic plane influence on interplanetary cosmic ray flux, discussing solar origin of field 21 p3699 A67-39019

Temporal periodicity of 10 cps observed in flux of auroral electrons by rocketborne radiation detectors 22 p3790 A67-39795

Intense fluxes of charged particles associated with disturbances in interplanetary medium during 1966 22 p3871 A67-39797

Cosmic ray propagation processes studied from measurement of anisotropic character of cosmic radiation 22 p3871 A67-39798

Standing waves in hot plasma traversed by quasi-neutral charged particle flux including numerical analysis of elongated wave occurrences 22 p3853 A67-40124

High energy cosmic ray interactions analyzed at 3340 m above sea level, using Wilson cloud chambers, gas discharge counters, ionization calorimeter, etc 22 p3801 A67-40248

Spatial and angular particle distributions in muon-generated electron photon cascade, using spark chamber muon detectors 22 p3877 A67-40276

Muon flux measurement with aid of spark chamber at depth of 20 mwe used for spatial distribution near axis of extensive air showers 22 p3877 A67-40282

Proton energy spectrum azimuthal asymmetry measured with telescopes using scintillation and Cerenkov counters 23 p4054 A67-41096

Satellite and probe data analysis on ionizing component, primary cosmic rays and albedo particle flux intensity near atmospheric outer boundary 23 p4055 A67-41098

Resolution and geometrical factor determination for isotropic proton fluxes by using pencil beam and measurements over many angles and positions 23 p4001 A67-41225

High energy neutrino flux from atmosphere studied in South African gold mine using liquid scintillation detector 24 p4210 A67-42581

Temporal variations of nuclear flux of primary cosmic radiation of Elektron II and IV satellites, discussing Forbush effect in nuclear and neutron components 24 p4212 A67-42761

High energy primary gamma quanta flux outside atmosphere estimated with aid of Proton I satellite 24 p4212 A67-42764

Cosmos 53 satellite radiation data using onboard gas discharge counter 24 p4213 A67-42783

Cascade particles interaction functions with substance determined by inverse problem method 24 p4221 A67-42875

PARTICLE INTENSITY

Increase with latitude of Forbush effects and secular variations in cosmic ray intensity explained by worldwide data obtained with meson detectors 02 p0311 A67-12596

Vector electric field and particle intensity measurements from sounding rocket launched into visible aurora 08 p1329 A67-21486

Scattered particle intensity inside and outside finite medium determined from Maxwell and Schroedinger equations 09 p1531 A67-21631

Cosmic ray protons and helium nuclei intensity measured as function of energy or magnetic rigidity, determining particle intensity gradient under equilibrium conditions for diffusion 09 p1562 A67-22241

Cosmic ray neutron component intensity during magnetic perturbations, considering effect of magnetospheric deformation 10 p1699 A67-22781

Polarized pyrometric probe applied to hot

and dense plasmas, ascertaining particle energies and densities 11 p1789 A67-24410
Stochastic differential equations for obtaining probability distribution of cosmic ray particles counted in given time interval sounding rocket detector 12 p1996 A67-25783
OGO 3 observation of low energy protons and electrons in earth magnetosphere, noting narrow peak of relatively high low-energy particle intensities 13 p2190 A67-26312
Rocket sampling of noctilucent cloud particles in mesopause 19 p3216 A67-35194
Cosmic ray neutron component intensity during magnetic perturbations, considering effect of magnetospheric deformation 24 p4209 A67-42117
Rocket measurements in auroral zone, considering proton and electron intensities, energy spectra and angular distribution 24 p4209 A67-42262
Penetrating component of high energy cosmic rays below ground measured for intensity 24 p4221 A67-42876

PARTICLE MASS

Relativistic mass-velocity relationship in empirical verification involving data on electron-proton parameters 09 p1531 A67-21650
He 3 nuclei in low energy primary cosmic radiation determined, using stack of nuclear emulsions 12 p1993 A67-25479
Densities of individual meteoritic, glacial and volcanic spherules, suggesting nonvolcanic origin of polar spherules 14 p2390 A67-28886
Supersonic gas-particle flow with chemical reactions 15 p2469 A67-29225
Particle mass not related to velocity with respect to other particles velocity explained in terms of relativistic uniformly accelerated motion 22 p3837 A67-39879
Absolute radar echo duration dependence on meteoroid mass calculated for various velocities 24 p4228 A67-42268
Search for neutral particles other than muons with high penetration capability from heavy mass or passivity at 40 mwe depth 24 p4220 A67-42866

PARTICLE MOTION

SA ELECTRON MOBILITY

Charged particle motion in field of traveling electromagnetic waves used in studies for microwave amplifiers, particle accelerators, etc 01 p0022 A67-10352
Particle deflection techniques for determining electrostatic field strengths, detailing application to surface field strengths for isolated spacecraft 01 p0074 A67-11129
Magnetic particle motion, analyzing effect of earth electric dipole field 02 p0311 A67-12585
Cosmic ray electromagnetic acceleration mechanism, calculating motion of charged relativistic particles in applied fields 02 p0311 A67-12586
Charged particle motions calculated in model of earth magnetosphere including magnetic and electric field 03 p0410 A67-12953
Criterion equations describing motion of fluid particle in conducting medium in presence of electromagnetic field and crossed electrical and magnetic fields 03 p0475 A67-13177
Motion of charged particles in constant electromagnetic fields, noting effect of drift motion 03 p0481 A67-13737
Idealized steady motion of aerosol particles and inertial deposition theory 03 p0404 A67-13836
Magnetic field geometric properties effect on magnetic moment and adiabatic invariants of charged particle motion 03 p0484 A67-14041
Charged particle motion in random magnetic field, describing time evolution of particle distribution in pitch angle and position in terms of Fokker-Planck coefficients 03 p0508 A67-14317
Statistical properties of interplanetary magnetic field variations, charged particles propagation in solar system and photospheric processes analyzed, using Mariner II magnetometer 04 p0698 A67-14951
Shock wave propagation in gas-dust medium, examining motion and velocities of gas and dust at distance approaching infinity 04 p0701 A67-15556
Boltzmann equation for cosmic ray particle motion in random magnetic

field 05 p0878 A67-16094
Earnshaw conjecture refuted for particle in three-dimensional lamellar motion 05 p0792 A67-16726
Plasma stream translational energy transformation into random motion in connection with collisionless shock wave propagation along magnetic field 05 p0853 A67-16756
Oscillation in finite plasma with two types of boundaries, showing dynamics of particles 05 p0859 A67-17448
Motion of magnetic lines of force including analysis of fluids with finite high conductivity 06 p1030 A67-17561
Plasmoid structure produced by coaxial plasma gun with interchangeable polarity electrodes, noting experimental setup, particle velocity, density, energy, etc 06 p1040 A67-18085
Linear nonrelativistic motion of charged particle in field of traveling electromagnetic wave 06 p0975 A67-18087
Perturbed motion of comet in medium of constant low density in solar Schwarzschild field, using quasi-Newton approximation, considering electromagnetic and gravitational fields 06 p1084 A67-18164
Standing transverse hydromagnetic waves effect on longitudinal invariant of particle motion trapped along geomagnetic field 06 p0997 A67-18700
Forced motion of charged particle in magnetic field 06 p1045 A67-18743
Charged particle motion in magnetic field under action of laser emission 06 p1012 A67-18787
Charged particles motion in magnetic field with regular and random components, deriving kinetic equation for distribution function and then diffusion equation 06 p1037 A67-18800
Physical pattern of high altitude fission cloud and motion of gamma and beta fission fragments captured by geomagnetic field and observed by Cosmos satellite 07 p1242 A67-19102
First order correction to magnetic moment invariant in Van Allen radiation belt 07 p1246 A67-19955
Invariance principle applied to motions of material particle that do not depend on particle mass 07 p1224 A67-20026
Energy loss of charged particles during passage through weakly turbulent plasma in magnetic field with HF oscillations 08 p1357 A67-20844
Rotating helical perturbations in Penning discharge plasma accompanying LF oscillations enhance particle transport across magnetic field 08 p1362 A67-21146
Adiabatic invariant analysis of charged particle motion in model magnetosphere 08 p1378 A67-21474
Cosmic ray effects on solar system and on galactic scale, discussing energy spectrum, particle diffusion and motion, solar wind, etc 09 p1562 A67-22530
Hamiltonian function of particle in static magnetic field determined with cyclicity in two degrees of freedom 10 p1684 A67-22900
Action-angle coordinates for particle motion in magnetic mirror systems 10 p1684 A67-22901
Anisotropic cosmological solution with energy density determined only by neutrinos moving along one axis, noting expansion 10 p1708 A67-23334
East-West motion of auroras analyzed in Idaho using radar echoes, noting velocity, direction reversal, etc 10 p1651 A67-23344
Hamilton-Jacobi solutions for Vlasov equation leading to nonsecular perturbation theory for macroscopic quantities 10 p1686 A67-23469
Polar magnetic substorms noting flux tube flow, proposing structure for substorm current system [JPL-TR-32-1094] 11 p1784 A67-23928
Charged particle motion in static magnetic fields without axial symmetry derived, employing Lagrange equation in transformed coordinate system and Alfvén motion 11 p1855 A67-23929
Stormer method solution of charged particle motion in field of magnetic dipole situated in external uniform magnetic field antiparallel to dipole magnetic moment vector 11 p1856 A67-24069
Kinematic nonlinearities effect on existence, properties and stability of

vibrations in unison of particle with two degrees of freedom 11 p1818 A67-24085
Thermal dissipation of energy in ionized cesium plasma, obtaining plasma oscillation excitation which destroys electron drift motion 11 p1837 A67-24394
Charged particle motion in field of traveling electromagnetic waves used in studies for microwave amplifiers, particle accelerators, etc 11 p1755 A67-25025
Hamiltonian for free particle of arbitrary spin and mass formulated in terms of spin matrix polynomials, noting independence of expansion coefficients 11 p1824 A67-25074
Collective effects and centrifugal instability from charged solar wind particle injected into earth magnetosphere near neutral point 12 p1991 A67-25109
Charged particle motion in magnetosphere under sudden magnetic pulse, compiling Fokker-Planck equation for particle distribution function 12 p1992 A67-25118
High velocity particles and slower corpuscles penetration into lower ionosphere occurring after solar flare explained by Sweet mechanism 12 p1993 A67-25134
Charged particle motion and penetration of magnetosphere in proximity of neutral point as result of solar wind-geomagnetic field interaction 12 p1975 A67-25643
Charged particle motion in field of magnetic dipole situated in external magnetic field /magnetospheric G region/, using Stoermer method 12 p1994 A67-25644
Vertical cut-off rigidities in South Atlantic analyzed via sixth degree simulation of geomagnetic field, obtaining results from trajectory analysis of cosmic rays [AFCR-67-0082] 12 p1996 A67-25774
Time dependent large scale electric potential field effect on motion of geomagnetically trapped particles 12 p1997 A67-25809
Martian daytime atmosphere from zero to 50 km presenting spherical particle terminal velocities and possible sizes for obscuration, using Mariner IV occultation 13 p2195 A67-26316
Proton mobility in ice when limited by lattice scattering calculated, using Boltzmann transport equation 13 p2160 A67-26991
Cosmic ray particle trajectories for various cut-off rigidity values in different points on earth surface, noting integration of motion equations of charged particle 13 p2192 A67-27244
Inverse problem of relativistic motion of point of variable mass 13 p2159 A67-27362
Critical particle velocity and particles frozen in given point of magnetic field line, discussing effects of plasma compression and reflection levels 13 p2204 A67-27432
Idealized steady motion of aerosol particles and inertial deposition theory 13 p2107 A67-27712
Monopole motion in magnetic dipole field, comparing electric and magnetic cases 14 p2378 A67-27920
Plasma-vehicle interaction, discussing charged particle motion about small vehicle in ionospheric orbit 14 p2357 A67-28209
Method of averaging applied to solution of canonical equation system describing particle motion at high altitude in gravitational field of nonspherical planet 14 p2388 A67-28637
Electrodynamic forces and torques on charged bodies moving through rarefied and partially ionized earth magnetosphere and upper atmosphere 14 p2362 A67-29039
Particle velocity distribution calculation in current-carrying electron-proton plasma by Lenard-Balescu-Guernsey form of Fokker-Planck equation 15 p2522 A67-29204
Fourier-Hermite solutions of Vlasov equations for electron motion against positive neutralizing background examined in linearized limit, noting Landau damping recovery 15 p2509 A67-29205
Radiation by charged particle moving in spiral line between two adjacent dielectric surfaces, deriving equations for spectral density of radiation components 15 p2520 A67-29714
Motion of particles trapped in magnetic field, discussing conditions leading to spiral family of trajectory curves 15 p2551 A67-30397
Perturbed motion of comet in medium of constant low density in solar Schwarzschild field, using quasi-Newton approximation, considering electromagnetic and gravitational

fields 16 p2741 A67-30508
 Dispersion equation for stability of steady turbulent state obtained from perturbation theory and applied to drift cyclotron instability of plasma 16 p2719 A67-31230
 Microscopic interpretation of generalized Helmholtz equation, considering particle in charged gas in adiabatic flow as rotating cylinder model 16 p2720 A67-31245
 Two-dimensional motion of charged particles in electromagnetic field, noting magnitude of forbidden band as function of particle energy 16 p2740 A67-31885
 Quartz sand particles descending motion and heat transfer in gas vertical tube, determining temperature profile 17 p2967 A67-32132
 Representation of rotating gaseous emission rings in eclipsing binary systems by periodic orbits around more massive component in restricted three-body problem 17 p2944 A67-32640
 Zero temperature cylindrical collisionless plasma in magnetic field studied for electrostatic instability, noting effect of radial velocities of electrons and ions 17 p2902 A67-32658
 Particle motion and plasma equilibrium in helical magnetic field, discussing magnetic surface phenomena 17 p2904 A67-32914
 Motion of small solid particles suspended in steady isotropic and locally uniform turbulent gas flow 18 p3025 A67-33626
 Charged particle motion in magnetic field under action of laser emission 18 p3059 A67-33729
 Highly ionized two-fluid plasma confined magnetically analyzed for stability 18 p3086 A67-33986
 Inhomogeneous hydrodynamic motion and thermal particle velocities effect on MHD wave propagation 18 p3086 A67-34034
 Charged particles motion in magnetic field with regular and random components, deriving kinetic equation for distribution function and then diffusion 18 p3083 A67-34419
 Effective braking height /EBH/ for small interplanetary particles of cosmic velocity entering Martian upper atmosphere 18 p3135 A67-34541
 Closed-cycle generator using gasdynamic forces to transport charged particles against opposing electric field, noting enthalpy role 19 p3175 A67-34801
 Effective collection time for collecting cosmic dust in altitude ranges of cosmic and terminal velocities of particles, using rockets 19 p3318 A67-35195
 Sensors used in cosmic dust experiments studied for response to microparticle hypervelocity impacts, noting relationship to velocity 19 p3229 A67-35210
 Nonrelativistic charged particle transport in geomagnetic dipole field under effect of electromagnetic pulses obtained, using Fokker-Planck equation 19 p3313 A67-35212
 Approximation method for Einstein-Maxwell field equations successive solution applied to Weyl canonical problems and field equations for point particle 19 p3262 A67-35576
 Dispersion relation for microinstabilities in finite plasma noting relation to particle motion 20 p3496 A67-36215
 Motion of plasmoids injected axially in two-dimensional multipolar magnetic field, studying losses 20 p3500 A67-37061
 Faster-than-light particles with spacelike four-momentum within special relativity theory, discussing quantum field theory rejection of objections 20 p3486 A67-37091
 Particle paths in central force field derived through second order differential equation for inverse separation, noting perturbation potential determination 20 p3526 A67-37254
 Proton mechanism of escape from earth magnetic field, analyzing charged particle in Alfvén wave field 20 p3520 A67-37667
 Vector equation describing particle motion under Newtonian force used for velocity and equation of particle path through application of law of areas 21 p3658 A67-38553
 Alfvén two-dimensional problem extended to charged-particle motion in dipole magnetic field with electric field determining forbidden band size, shape and specular reflection points 21 p3621 A67-39015
 Interplanetary magnetic field magnitude

determination by considering particle motion along magnetic lines of force and trajectories divergence in earth vicinity during cosmic ray bursts 21 p3700 A67-39030
 Unsteady spherically symmetric gas flows with gas particle radial velocity proportional to distance from symmetry center 22 p3739 A67-39216
 Thermal particles parallel velocity and transverse spatial diffusion coefficients found by studying test particle motion in weakly turbulent Vlasov magnetoplasma 22 p3849 A67-39702
 Particle mass not related to velocity with respect to other particles velocity explained in terms of relativistic uniformly accelerated motion 22 p3837 A67-39879
 Cosmic ray fluctuations without imposing limitations on particle scattering, deriving expressions using three-dimensional cascade shower theory 22 p3873 A67-39880
 Motion of small spherical particles entering upper atmosphere of earth with cosmic velocities studied for terminal velocities 22 p3890 A67-40472
 Dynamical interaction of interplanetary particles with upper atmosphere studied by simplification of motion equation 22 p3890 A67-40473
 Drift equation supplemented by collision terms for describing interplanetary regular magnetic field and solar wind velocity fluctuation effects on cosmic ray propagation 23 p4056 A67-41105
 Electron multiplier detection efficiency for positive ions determined as function of incoming ion energy, velocity and degree of ionization 23 p4000 A67-41219
 Two-stream instability in plasma analyzed using magnetic field association with charged particle motion and boundary effects 23 p4034 A67-41450
 Autopropulsion of gas bubble by rocket effect noting equivalent particle concept and applications to boiling, flow and cavitation erosion 24 p4141 A67-41904
 Motion equations for mean orbital and oscillating elements of particle rotating in gravitational field of aspherical planet 24 p4228 A67-42274
 Boltzmann equation for cosmic ray particle motion in random magnetic field 24 p4213 A67-42770

PARTICLE PRODUCTION

Book on natural neutron background of atmosphere and earth crust including effect of primary and secondary cosmic radiation, solar neutrons, presence in rocks, etc 01 p0143 A67-10042
 Calculation of neutron generation by mu-mesons for various depths in earth 02 p0312 A67-12607
 Secondary particle generation in satellite walls due to 0.1 to 20 bev pi-mesons and protons 02 p0312 A67-12610
 Hypothesis of meson resonances produced in cosmic ray interactions, explaining multiple birth characteristics of secondary particles 02 p0314 A67-12745
 Electron-photon shower measurement using ionization calorimeter type device 02 p0271 A67-12755
 Ionization calorimeter photoemulsion measurements at mountain altitudes, determining formation mechanism of high energy pions in primary cosmic radiation 02 p0315 A67-12760
 Positive-to-negative charge ratio of high energy cosmic ray muons 03 p0506 A67-13516
 Charged gas expansion with particle production, noting parameters and applicability to cosmological model of Hoyle 04 p0606 A67-15185
 Coaxial plasma source transition from high energy particle production to production of slow plasmoids, noting V-I characteristics and magnetic field distribution 04 p0667 A67-15212
 Deuterium nuclei generation in galactic cosmic radiation 05 p0878 A67-16096
 Cross section of proton production for molecular ion beams of hydrogen passing through lithium plasma 05 p0852 A67-16600
 Neutron production in cosmic radiation, neutron measurements and geophysical effects 06 p1077 A67-17875
 Thermodynamic flow analysis of feasibility of coolant gas addition to nozzle flow for improved particle formation efficiency in mixed flow colloid thruster [AIAA PAPER 67-85] 06 p0941 A67-18500

Energy spectrum of primary electron flux and brightness of auroral light measured by rockets in active auroras used to derive electron production rate 10 p1650 A67-23306
 Energetic macroscopic particle production noting possible application in controlled thermonuclear power 12 p1966 A67-25252
 Apparatus for particulate smokes generation, control and sampling, noting combination with angular scanning spectropolarimeter 12 p1946 A67-25982
 Particle momentum distributions derived from relativistic quantum statistical mechanics 13 p2161 A67-27398
 Thermodynamical, dynamical, and possible third mechanisms responsible for features in high energy cosmic ray interactions and multiple production of shower secondaries 14 p2379 A67-27962
 High energy photons, cosmic X-rays and hard radiation production mechanisms in interstellar gas, galactic halo and intergalactic medium 14 p2380 A67-27964
 Neutrinos in stellar evolution and cosmological processes, discussing production processes 14 p2383 A67-27969
 Coaxial plasma source transition from high energy particle production to production of slow plasmoids, noting V-I characteristics and magnetic field distribution 15 p2532 A67-30260
 Eigenstates of particle mixing matrices and relation to physical antiparticles 16 p2705 A67-31565
 Cosmic ray nuclei fragmentation without particle production, noting nuclear emulsions and high energy 17 p2936 A67-32363
 Solar flare effect on electron production and electron density in lower ionosphere 17 p2936 A67-32382
 Energy spectrum and production rates for secondary antiprotons from inelastic collisions of high energy galactic cosmic radiation with interstellar gas nuclei 19 p3316 A67-36098
 Production of charged double pion in pi plus-proton scattering, noting isobar model failure to explain enhancement at 400 Mev 19 p3266 A67-36100
 Cosmic ultrahigh-energy heavy nuclei and fragmentation products producing multiple mesons 20 p3518 A67-37092
 Low latitude neutron fluxes for PCN and quiet solar period, noting solar proton production of neutrons 20 p3519 A67-37408
 Cosmic ray secondary nucleon production of multiple neutrons observed and energy spectra measured, using multiplicity monitor 20 p3452 A67-37407
 Solar cosmic ray multiple neutron production increase on January 28, 1967 from Antarctica cosmic ray neutron monitor measurements 22 p3874 A67-40048
 Hypothesis of meson resonances produced in cosmic ray interactions, explaining multiple birth characteristics of secondary particles 22 p3876 A67-40247
 Electron-photon shower measurement using ionization calorimeter type device 22 p3842 A67-40257
 Ionization calorimeter photoemulsion measurements at mountain altitudes, determining formation mechanism of high energy pions in primary cosmic radiation 22 p3876 A67-40262
 Low pressure argon ion laser cold emission cathode, considering electron production by cathode sputtering owing to self-sustained arc discharge 22 p3817 A67-40413
 Intensities of cosmic ray produced deuterium and tritium in atmosphere measured from high altitude balloons 23 p3995 A67-40811
 Makeup low energy spectra and electron component of cosmic rays and solar particle production with curves for element abundance 23 p4053 A67-41090
 Cosmic ray acceleration mechanisms for fast particle generation under outer space conditions 23 p4057 A67-41114
 Neutron component intensity variation and particle generation on sun during chromospheric flares and electromagnetic radiation during solar activity cycle 23 p4057 A67-41116
 Neutrino behavior in beta decay, proton-neutrino and proton-proton reactions, discussing astronomical implications of neutrino radiation 24 p4227 A67-42197
 Deuterium nuclei generation in galactic

cosmic radiation 24 p4213 A67-42772
Multiple charged particle production process mean characteristics determined for several energy levels 24 p4217 A67-42830
Relativistic particles producing ionization bursts studied for energy spectrum recorded during operation of stack of ionization chambers alternating with lead and graphite layers 24 p4218 A67-42834
Isobar decay mechanism for high energy pion generation in cosmic rays propagating through atmosphere 24 p4218 A67-42841
Multiparticle mechanism of cosmic ray-atomic nuclei interactions assuming particle formation 24 p4218 A67-42842
Effective lambda and sigma hyperons and K-meson production cross section dependence on target element atomic weight during cosmic rays interaction with various nuclei 24 p4220 A67-42851
Positive rho meson and doubly positive nucleon-pion resonance generation in 2.34 GeV/c 24 p4193 A67-42856
Fast He nuclei from photoemulsion nuclear splitting induced by proton and antiproton bombardment 24 p4193 A67-42860
Statistical model for multiple particle production process based on unitary symmetry concept of strong interactions, comparing results with quark model results 24 p4193 A67-42861
Air shower muon generation altitude determination from relative positive-negative muon distribution shift 24 p4220 A67-42863

PARTICLE PROPERTY

Mechanism leading to superconductivity even for particles with purely repulsive forces between them, examining general theory for weak short-ranged pair forces between particles 01 p0129 A67-10151
Track method analysis of phase transitions in particle growth and evaporation rate during combustion process 08 p1428 A67-21421
Rarefied gas flow dynamic behavior during reaction with gas measuring device mounted on moving plant 09 p1487 A67-21896
Atmospheric dust content estimation, using solar radiation depletion by particulate matter and separating attenuation by gases and water vapor 10 p1700 A67-23086
Solar and galactic particle spectra and composition measured with cosmic ray telescope mounted on satellite 13 p2193 A67-27249
Particle density and material functions of gases of random composition, calculating values without regard to reaction dissociation 15 p2543 A67-29090
Diffusion coefficient dependence on solar particle energy and distance from sun noting time variation 16 p2740 A67-31892
Gamma ray schemes of resonances in silicon 29-phosphorus 30 reaction for resonant and bound levels of phosphorus 30 properties 16 p2705 A67-31922
Neutrino behavior in beta decay, proton-neutrino and proton-proton reactions, discussing astronomical implications of neutrino radiation 24 p4227 A67-42197

PARTICLE SIZE

Experimental verification of Shifrin-Perelman method of determining spectrum of dispersed atmospheric aerosol particles from spectral transmittance 01 p0108 A67-10130
Rapid method of calculating effective spectral parameters of aerosol dimensions 01 p0108 A67-10132
Optical scattering cross sections for polydispersions of dielectric spheres, showing dependence on ratio of third to second moment of shape and size distribution function 01 p0115 A67-10177
Particle size measurements based on use of optical mean scattering cross sections 01 p0070 A67-10178
Temperature dependence of grain size in nonstoichiometric NbC between 1600 and 3300 degrees K in vacuum and Ar 01 p0102 A67-11245
Diffuse spectral reflectance of optically thick cloud and powder layers composed of particles with strong IR resonance, noting effect of particle size 03 p0467 A67-13047
[AIAA PAPER 65-667]
High temperature single solid particle plasma generation by focused giant pulse Q-spooled ruby laser beam irradiation of LiH suspended in vacuum electric fields 03 p0485 A67-14047

Effect of gravitational changes on aerosol deposition in lungs of man, noting particle size and alveolar region 09 p1452 A67-21724
Holography for particle size analysis noting wave formation and reconstruction, hologram camera, etc 10 p1653 A67-22748
Electron microscope and microprobe measurements of luster flight samples, discussing particle size distribution and nondispersive chemical analysis 10 p1707 A67-23238
Magnetically coupled superconducting films, showing fluxon size as function of film thickness 10 p1896 A67-23774
Impact and abrasion wear of axial and centrifugal helicopter compressor stages due to dust intake, showing direct proportionality to impact velocity and particle size 11 p1853 A67-24531
Porosity and particle size effects on magnetization curve of superconducting Nb sintered compacts with and without C added 12 p1978 A67-25139
Lunar soil density problem investigated by sieving clean powders of different materials with different grain sizes and drop heights under ultrahigh vacuum 12 p2000 A67-25207
Coherent ordered precipitates formation in Ni-Cr-Al alloy, discussing spacing, shape and size of gamma prime particles as function of time 12 p1954 A67-25344
Electrical conductivity measurements of NaCl as function of particle size and temperature used to study subsurface diffusion 12 p1987 A67-26191
Martian daytime atmosphere from zero to 50 km presenting spherical particle terminal velocities and possible sizes for observations, using Mariner IV occultation 13 p2195 A67-26316
Theory of nephelometric method for measuring transparency and structure of atmospheric aerosols 13 p2151 A67-26685
Factors affecting current methods of sizing Aitken nuclei 13 p2152 A67-26665
Aluminum powders and aluminum powder metallurgy products properties, discussing powder and particle applications in metallurgy 14 p2335 A67-27809
Burning rate vs pressure and other factors as function of composite solid propellant composition and oxidizer particle size distribution 15 p2580 A67-29985
Polarimetric properties of simulated lunar surface, showing polarization effect on particle size 16 p2754 A67-31749
Variation of friction and wear of solid lubricant film with thickness theory based on junction and wear particle size 16 p2683 A67-31751
Dispersed aluminum oxides effect on size of nickel grains in sintered or extruded nickel-aluminum oxide cermets, studying compressive strength 17 p2871 A67-31924
Aluminum particle combustion in solid rocket grains, noting drop formation mechanism and droplet combustion analysis [ONERA-TP-486] 17 p2926 A67-32697
Temperature dependence of grain size in nonstoichiometric NbC between 1600 and 3300 degrees K in vacuum and Ar 17 p2875 A67-33168
Rocket chamber pressure influence on particle size measurements of heterogeneous combustion products of solid propellants containing aluminum 18 p3109 A67-33839
General quantum relativity theory in real universe with large radius and elementary particle structure 18 p3080 A67-34728
Size-frequency distribution of particles and craters and optical, thermal, radio and other properties of lunar surface obtained from Surveyor I landing 19 p3318 A67-35179
Integrodifferential equations for product surface area changes and grinding process development obtained by assuming proportionality between fracturing probability and particle size 19 p3236 A67-35725
Daily and seasonal changes in numbers, dimensions and shapes of micrometeoritic particles over period of two years, discussing origin 19 p3327 A67-35878
Hydraulic component material properties relationship to particulate material removed due to cavitation, showing particle size distribution definition 20 p3469 A67-37366
Lunar surface materials choice narrowing method via albedo, color and polarization property examinations to find possible

candidates for lunar surface model 21 p3701 A67-37897
Liquid surface tension effect on maximum particle size in two-phase nozzle flow, discussing drag exerted by accelerating gas stream 22 p3787 A67-40225
RF size effects in plane parallel metal plate, discussing skin effect in magnetic fields, electron trajectories and spherical Fermi surface 22 p3866 A67-40551
Centrifugal disk photosedimentometer used for size analysis of latex emulsions 23 p3972 A67-41066
Laser macrophotography for size distribution of particulate debris dispersed from ablating zirconium alloy specimen in hyperthermal wind tunnel ablation testing 23 p4006 A67-41380
Contamination control for Titan IIIB program, discussing MAPS, membrane filter technique, environment cleanliness control and particulate spectra 23 p3938 A67-41499
Spray coating particle flow rate dependence on plasma jet flow velocity, specific weight and particle size measured by high speed filming 24 p4159 A67-41961
Ice nucleating properties of meteoritic material 24 p4231 A67-42371

PARTICLE THEORY

SA MANY-PARTICLE THEORY

Second and third virial coefficient of quantum gas expressed in terms of two-particle scattering amplitude, starting from cluster expansion of partition function 05 p0849 A67-17316
Solution to chain of kinetic gas equations, showing effect of fast reversible and slow irreversible processes on particle distribution function 05 p0847 A67-17541
Evaporation process of particles in high temperature gas stream under nonadiabatic conditions 08 p1428 A67-21424
Thirteen-moment equations solved obtaining theory of thermal force acting on spherical particle for entire range of Knudsen numbers 16 p2861 A67-31221
Particle theory analysis of electromagnetic and electrostatic instabilities due to anisotropic velocity distributions 16 p2722 A67-31560
Interaction of three-dimensional model of gas with solid surface, discussing atomic velocity distribution from surface reflection, energy and momentum accommodation coefficients, etc 19 p3264 A67-34936
Asymmetry in angular distribution of secondary particles in cosmic ray showers 24 p4218 A67-42838

PARTICLE TRACK

Two magnetically geared microscope stages for nuclear track plates 02 p0247 A67-12696
Primary cosmic radiation intensity determined with help of nuclear particle tracks in moldavites and meteorites 05 p0887 A67-16100
Origin of fossil charged particle tracks in meteorites such as cosmic radiation, fission of U 238, meson jets, spallation recoils, etc 07 p1245 A67-19941
Tracks of primary cosmic rays with atomic number greater than or equal to 20 in meteorites, discussing relationship between track length and particle mass 07 p1245 A67-19942
Track densities and production rates with increase of heavy cosmic nuclei inside meteorite 09 p1570 A67-22690
Solar wind particle propagation and scattering path in interplanetary space according to data of 11-yr cosmic ray variations 12 p1991 A67-25115
Processing and obtaining phase holograms of elementary particle tracks in gelatin bubble and emulsion chambers 18 p3049 A67-34387
Vector equation describing particle motion under Newtonian force used for velocity and equation of particle path through application of law of areas 21 p3658 A67-38553
Primary cosmic radiation intensity determined with help of nuclear particle tracks in moldavites and meteorites 24 p4238 A67-42776

PARTICLE TRAJECTORY

Levi-Civita regularized equations of elliptic motion of particle influenced by massive primary and perturbed by smaller primary, Part I, Trigonometric series solution 01 p0147 A67-10379
Geocentric initial conditions for motion of

bodies leaving moon surface after initial instantaneous thrust 01 p0148 A67-10387

Fluid flow through parallel cylinders when flow incidence is lateral and Reynolds numbers are small, determining particles trajectories 06 p0991 A67-18819

Effect of higher harmonics of geomagnetic field on cosmic ray trajectories, noting reception cones of Soviet stations 07 p1243 A67-19685

Focusing of charged particles with pair of concentric spherical grids 10 p1658 A67-23784

Toroidal machine velocity space instabilities, rapidly saturating, with long time scale remaining 11 p1826 A67-23876

Solar wind region magnitude, scattering transport path of particles and spectral variation of magnetic inhomogeneities analyzed on basis of 11-year cosmic ray cycle 11 p1855 A67-23930

Asymptotic Krylov-Bogolubov computation of moving charges interacting with space modulated magnetic fields 11 p1842 A67-24967

Characteristic effects of deformed geomagnetic field on trajectories and asymptotic directions of arrival of medium energy cosmic rays 12 p1998 A67-25819

Particle trajectory analysis with perturbation series, noting position and velocity error estimation for restricted three-body problems 16 p2749 A67-31425

Spherical analysis of geomagnetic maps to determine asymptotic directions of cosmic rays for Soviet station network 17 p2933 A67-32091

Trajectories of auroral charged particles accelerated in geomagnetic tail computed, using fields of magnetosphere reconnection model 18 p3038 A67-33614

Lunar surface particles geocentric trajectories, giving perigee distance and velocity curves 18 p3120 A67-33866

Particle trajectories analysis for drift instability mechanism, considering resonant and nonresonant particles 19 p3267 A67-34890

Parametric resonance in magnetosonic waves through analysis of perturbed particle trajectories in modulated plasma field, determining velocity time dependence 20 p3501 A67-37296

Particle trajectories for two model configurations of electric and magnetic fields in geomagnetic tail, noting application to auroral acceleration 20 p3433 A67-37415

Partial solutions of equations describing axisymmetric unstable motions of gravitating rarefied magnetoplasma 20 p3502 A67-37663

Circular planar satellite electrostatic probe theory based on reversible particle trajectories, showing relation between boundary curve in velocity space and current-voltage characteristics 21 p3625 A67-37899

Plastic deformation during metal cutting, deriving metal deformation, cutting tool stressed state and temperature as function of particle trajectories 21 p3637 A67-38923

Interplanetary magnetic field magnitude determination by considering particle motion along magnetic lines of force and trajectories divergence in earth vicinity during cosmic ray bursts 21 p3700 A67-39030

Numerical program integrating motion equation of charged particles from realistic geomagnetic field model, with trajectory calculations for solar cosmic rays 22 p3872 A67-39810

Cosmic ray trajectories in geomagnetic field, discussing asymptotic directions, rigidities, crossed telescope measurements and focusing effect 23 p4050 A67-40693

Cosmic ray equator position at zero meridian measured, noting substantial difference in location from magnetic equator position 23 p4059 A67-41135

Nuclear cosmic particle interactions cross section in iron, using Bartlett S-function for particle free path determination 24 p4219 A67-42846

PARTICULATE FILTER

Hydraulic component material properties relationship to particulate material removed due to cavitation, showing particle size distribution definition 20 p3469 A67-37366

In-Line-Filter-Holder and Counter /ILFHC/ designed for high and low pressure systems to verify particulate cleanliness levels in modern fluid systems 23 p3935 A67-40846

Sampling bottle with valves and high

pressure filter holder for fuel and oxidizer, by weighing bottle before and after sampling amount of fuel passing through filter can be calculated 23 p3998 A67-40849

Supercleaning processes for Lunar Orbiter calling for personnel training, clean room garments, chemical cleaners, special packaging and inspection for particulate contamination 23 p3962 A67-40854

Contamination control for Titan IIIB program, discussing MAPS, membrane filter technique, environment cleanliness control and particulate spectra 23 p3938 A67-41499

PARTITION FUNCTION

Quantum mechanical perturbation theory calculation of upper and lower bounds of energy eigenvalues using partitioning methods 02 p0269 A67-12727

Ergodic theory of measurable partitions in Lebesgue space, extending Rokhlin-Sinai theory of increasing to flows generated by automorphism 04 p0644 A67-14756

Equilibrium constants and internal energies of hydrogen molecular ion calculated as function of temperature and pressure, using partition function 04 p0697 A67-14807

Lower bound procedure in quantum mechanical energy equation eigenvalue problem by partitioning and bracketing Hilbert space 05 p0848 A67-16836

Second and third virial coefficient of quantum gas expressed in terms of two-particle scattering amplitude, starting from cluster expansion of partition function 05 p0849 A67-17316

LSI application to computer design using functional partition of control and data path structures 08 p1298 A67-20638

Computation of optimal estimators synthesis reduced through partitioning of system state vector 11 p1764 A67-24443

Partition functions applicability at high temperatures 14 p2405 A67-28131

Numerical realization of partitioning method in case of rectangular plate bending with end loading, using bar scheme 15 p2576 A67-30180

Quantum statistics of high temperature plasma in thermodynamical balance, introducing effective potentials for partition function evaluation and calculating free energy 18 p3089 A67-34300

Modified Monte Carlo procedure using partitioning method and stratified sampling 18 p3072 A67-34396

Quantum-mechanical treatment of free-bound approximation for eigenstates and canonical partition function for plasma system in thermodynamic equilibrium 19 p3285 A67-35345

Partition function of partially ionized hydrogen two-component plasma 19 p3285 A67-35346

Lanthanide partition coefficient for crystallization under calcium effect, noting inflectional pattern for inverse ionic radius variation 21 p3617 A67-38123

PASSENGER

Optimum passenger handling in long haul air transportation for various airport facilities [AIAA PAPER 66-843] 02 p0181 A67-12257

Passenger volume handled and area accommodated by commercial airports in West Germany 03 p0538 A67-12978

Pilots and passengers protection and escape from aircraft after accident 03 p0361 A67-14096

Airline terminal building concept to provide practical approach to terminal complex design [SAE PAPER 67-0320] 17 p2835 A67-32981

Airlines and governmental regulatory agencies controlling competition, new entry and rate policies relationship, examining all-cargo carrier and passenger trunk line 19 p3349 A67-34980

Legal and financial problems in obtaining airline tickets for third persons 20 p3555 A67-36300

Philadelphia International Airport facility planning based on forecasts, population and business growth, economic factors and historic trends 21 p3734 A67-38805

Master plan for Philadelphia International Airport to accommodate increased air travel, cargo and jet aircraft 21 p3808 A67-38806

Airport wheel hub terminal circumscribed by two satellite buildings noting passenger vehicular access, pedestrian movement,

aircraft servicing, etc 21 p3608 A67-38807

Aircraft terminal apron design, considering passenger convenience, variations in aircraft configuration and changes in aircraft mix and loading facilities 22 p3779 A67-39379

Problems of handling people on future giant aircraft noting reservations, ticketing, boarding procedures and baggage-handling functions 22 p3780 A67-39382

Airport planning in 1970s noting environment compatibility, crosswind tolerance, passenger volume, automobile parking and metropolitan access [AIAA PAPER 67-760] 23 p3987 A67-40991

PASSIVE SATELLITE

SA ECHO SATELLITE

Combined effect of aerodynamic and gravity torques on stability of motion of passive satellites investigated by Liapunov direct method 04 p0704 A67-14827

Post-Echo II passive communication satellites and systems and results of Comsat systems [AIAA PAPER 66-312] 06 p0961 A67-17702

Orbit position control based on solar pressure on plane sail structure and hollow thin-skinned lenticular shape of passive communications satellites [AIAA PAPER 66-313] 06 p1094 A67-17703

U.S. Passive Geodetic Satellite, describing fabrication, structural integrity, flight preparation, launch, etc 07 p1259 A67-19760

U.S. Coast and Geodetic Survey satellite triangulation program based on optical tracking of passive satellites simultaneously from two or more mobile camera stations 07 p1176 A67-19764

Optimum control of earth satellites and space vehicles and stable solutions of orbits in orbital mechanics 14 p2393 A67-27879

Acquisition phase of satellite with passive magnetic attitude stabilization, discussing programming difficulties and modified Rayleigh model for German 625A-1 satellite 22 p3898 A67-39173

PATCH TEST

Strain age cracking characteristics in welded Rene 41 nickel base alloy, discussing test procedure used with circular patch test to evaluate contributing factors 20 p3471 A67-37696

PATENT

Criteria used by Government patent departments in screening and evaluating inventions for patent applications 07 p1269 A67-19467

Government patent policy 12 p2040 A67-25487

PATH

S DIFFRACTION PATH

S ELECTRON PATH

S FLIGHT PATH

S GLIDE PATH

S MULTIPATH PROPAGATION

S OPTICAL PATH

S TRAJECTORY

PATHOLOGICAL EFFECT

Correlation of changes in serum enzyme behavior in rats with pathological injuries due to short transverse decelerations 06 p0953 A67-17996

Hazards of laser radiation, mechanisms, control and management 10 p1601 A67-23328

Pathogenesis of focal neurological dysbarism in pilots during altitude decompression sickness 10 p1600 A67-23827

Monograph on theory of decompression sickness and application to diving tables, including calculation of critical size of localized bubbles formed from dissolved nonrespiration-involved gases in tissues [DVL-623] 11 p1748 A67-25036

Prolonged weightlessness exposure and expected effects on man 12 p1902 A67-25725

Comparison of effect of various diluent gases in evoking flyer bends in simulated orbital flights 13 p2062 A67-26916

Lung, liver, kidney and heart pathology of dogs, monkeys, rats and mice exposed for 2 to 13 weeks to pure oxygen atmosphere at reduced pressure 13 p2059 A67-26918

Physiological effects in baboon of prolonged decompressions simulating loss of cabin pressure 13 p2060 A67-26924

Acceleration problems in astronautics noting axis determination and effect on human body 20 p3371 A67-36822

Space cabin environmental changes studied for susceptibility of mice to viral infection 21 p3574 A67-38080

Traumatic sickness in dogs due to high

gravity impact noting enzymatic activity changes and immunizing reaction 21 p3575 A67-38509

Microbic shock in human organism during prolonged space flight due to intestinal tract flora variation from food consumption lacking variety 22 p3750 A67-39334

Trauma in lateral impact at high entrance velocity compared with rearward and forward facing body orientations of baboons when restrained by lap belt only 22 p3750 A67-39594

Aircraft/bird collision noting dispersion, flock detection and windshield protection 23 p3934 A67-41070

Energy transfer effects on pathophysiological responses of guinea pigs and bradycardia response in monkeys under minus G impact acceleration 23 p3955 A67-41610

Pathological effects, including carcinogenesis following proton whole body irradiation in rats 23 p3958 A67-41645

Sensory deprivation in space medicine, discussing irritation spectrum leading to pathological changes in psychic processes of test subjects 24 p4111 A67-41842

Clinicopsychopathological method applied to analysis of hallucination, depersonalization and similar effects resulting from exposure to extremal factors from standpoint of space psychology 24 p4112 A67-41856

PATHOLOGY

SA DISEASE

SA HUMAN PATHOLOGY

Comparative pathology of animals continuously exposed to varied concentrations of carbon tetrachloride vapor in altitude chamber 21 p3573 A67-38070

PATIENT

S DISEASE

PATTERN

S DIFFRACTION PATTERN

S FLOW PATTERN

S WIDMANSTATTEN PATTERN

PATTERN DISTRIBUTION

Radiation patterns and impedance plots of sleeve antenna over band with frequency ratio of 4 to 1 02 p0212 A67-11607

Interconnection patterns for slice-level subsystems of integrated circuits 04 p0585 A67-15490

Correction for gain computations based on pattern integration during translational motion of antenna 11 p1763 A67-24297

Method of radiation pattern synthesis for equally and unequally spaced arrays 14 p2285 A67-28451

Anechoic chamber characteristics, noting indoor antenna pattern measurements and transmission attenuation variations 16 p2640 A67-31364

Electron-mirror microscopy for intermediate-state pattern of superconducting samples noting bulk, thin sheet and lead films 17 p2912 A67-32266

Auroral particle precipitation, establishing latitude vs time pattern from gross statistical data on optical-and radio-auroral phenomena 17 p2850 A67-33191

Antenna characteristics of Dwingeloo radio telescope, determining directivity, response pattern, ohmic loss, etc 18 p3008 A67-33433

Lagrange interpolation pattern synthesis technique using moment criterion for optimum pattern approximation by nonuniform antenna array 18 p3012 A67-34430

Structural defects of reciprocally oriented polycrystalline bismuth-antimony films analyzed by moire 20 p3510 A67-36813

Electron-interference experiment using laser light, discussing electron wave function phase change and electron interference pattern displacement 20 p3460 A67-36999

Fourier transform application to automatic pattern recognition, using photographic plate to record plane intensity distribution 22 p3764 A67-39331

Phase distribution in antenna aperture for small displacement of antenna feed from focal point calculated on basis of theorem proved 22 p3762 A67-39870

Antenna linear array design with limited amplitude tapering, showing desirable pattern characteristics in partially uniform array 23 p3978 A67-40827

PATTERN RECOGNITION

SA AUTOMATIC PATTERN

RECOGNITION

Algorithm based on affine transformation

of plane figures used to compare images of written letters of 01 p0028 A67-10541

Step procedure for synthesizing circular aperture patterns 02 p0212 A67-11609

Mean time analysis of PCM synchronization, noting pattern synchronization in presence of noise 02 p0197 A67-12020

Pattern recognition preprocessing by similarity functionals, examining relationship between measurement, selection and feature definition 02 p0207 A67-12137

Pattern recognition systems with fixed linear structure changing to nonlinear as result of repetitive generation and selection of relations among input measurements 02 p0208 A67-12141

Compound statistical decision theory for pattern recognition based on Bayes conditional probability 02 p0208 A67-12164

Abstraction problem in pattern classification, using algorithms with convergence properties 02 p0208 A67-12173

Iterative realization of pattern recognition networks consisting of multilayer of linear threshold elements 02 p0208 A67-12174

Dispersion method of spontaneous subdivision of image space into compact sets /images/ 03 p0374 A67-13081

Image recognition systems compared with constant indeterminate and random prototypes 03 p0374 A67-13082

Noise-rejecting spatial filters in signal pattern recognition 03 p0388 A67-13276

Pattern recognition, property filtering and lunar feature data experiments coupled with Tiros cloud photographs demonstrate preprocessing for systems design 03 p0376 A67-13805

Error correcting method for star pattern and constellation identification 04 p0619 A67-14552

Stripe pattern characteristic of voltage-controlled negative resistance and LF electric oscillation observed in SbSI due to diffraction effect 04 p0674 A67-14619

Self-organizing approach to structure adaptation in pattern recognition applied to handwritten numerals, spoken vowels and EEGs 04 p0578 A67-14797

Mammalian neuron networks for visual pattern recognition, noting equivalence of processing by memory neurons with matrix multiplication 04 p0563 A67-14798

Nonlinear recognition procedures, discussing probability distribution approximation by orthogonal expansion and by-product of low order conditional probabilities 04 p0578 A67-14800

Contrast transfer characteristics of n tuple models of retinal receptive fields as function of optical signal size or spatial frequency 05 p0757 A67-17303

Iterative computation of a posteriori probability for M-ary nonsupervised adaptation 06 p0965 A67-17947

Consistency technique for associating parts of patterns and results of computer simulation 06 p0965 A67-18057

Integrated film reading and display system, discussing characteristics of waveform display/ analyzer subsystems and scanning/recording requirements 07 p1148 A67-19742

Error correcting method for star pattern and constellation identification process 13 p2153 A67-26579

EEG baselines covering wide range of states of wakefulness and sleep in astronaut candidates estimated by computation and pattern recognition techniques 13 p2062 A67-26921

Input/output model of system with finite settling time, using error correcting technique employed in pattern recognition 15 p2460 A67-30314

Parallel electro-optical technique for implementing linear threshold adaptive networks 17 p2860 A67-32616

Learning in unknown stationary environment using stochastic approximation, discussing Bayesian interference, pattern recognition, automatic control and statistical communications 18 p3070 A67-33497

Nonlinear decision surfaces determined by pattern-recognizing adaptive threshold device via generation of polynomial discriminant functions and computer

programs 18 p3006 A67-34064

Pattern recognition machine construction and design, using reading machine as example 18 p3006 A67-34383

High resolution flying-spot scanner as input device for computer simulation of optical character-recognition systems 18 p3006 A67-34403

Redundancy reduction techniques and error correction coding of digital communication systems including waveform, pattern recognition, vocoding, etc 18 p3004 A67-34613

Formula manipulation by computer, noting simplification, pattern matching, complex number handling, etc 19 p3187 A67-35678

Automatic unique acquisition of Canopus for roll control of interplanetary spacecraft, discussing identification, discrimination and calibration 19 p3258 A67-35980

[AIAA PAPER 67-585] Coherent light applications in holography and spatial filtering including Fourier transform holography and pattern recognition 20 p3457 A67-36333

Nondestructive testing of electronic circuits with fiber optic scintillators, vidicon data sampling and pattern recognition displays, discussing TV data handling 20 p3449 A67-36982

Automatic test system employing optical and electrical input signals based on pattern recognition with CRT display 20 p3392 A67-36991

Visual noise induction methods investigated at seven noise levels, discussing pattern comparisons by 46 subjects 20 p3372 A67-37000

Mathematical model simulation of horseshoe crab eye lateral inhibition for nervous system pattern transformation, discussing human visual pattern recognition process 20 p3375 A67-37543

Digital switching functions and pattern recognition realization through computer-programable algorithm for designing feed-forward threshold logic nets 21 p3588 A67-38182

Pattern recognition model as self-learning algorithm noting Nagy and Shelton scheme 24 p4137 A67-42821

PAVEMENT Concrete pavement performance at ten civil airports, examining durability of surfaces, jointing subbase thickness and maintenance 02 p0229 A67-11841

PAYLOAD SA INSTRUMENT PACKAGE SA PIGGYBACK SYSTEM Scientific lunar payload communications system 02 p0196 A67-11999

Rocket payload with weight of 9 lb for release of sodium and lithium in aurora for study of D-region ion concentration and emission 03 p0413 A67-13375

Titan III launch vehicle for multiple payload delivery into precise space trajectory [AIAA PAPER 66-836] 03 p0519 A67-14125

Design and instrumentation of Rubis research rocket payload for analysis of geomagnetic and electric fields 04 p0703 A67-14565

Laboratory payload concept of automated laboratories for planetary exploration, noting systems engineering advantages 04 p0706 A67-15237

Analytical solution to determine rocket design for maximum payload energy 04 p0706 A67-15240

ELDO guidance station in Australia for control of third stage and orbit placement of payload, noting Interferometric complex 04 p0654 A67-15625

Program selection for motion equations, parameters and control functions maximizing composite flight vehicle probability of delivering payload to given region 04 p0552 A67-15882

Items affecting information transmitted from payload landed on remote planet to earth via communications satellite including orbit, transmission policy and orbit injection error effect on communication capability [AIAA PAPER 66-314] 06 p1094 A67-17704

Design and instrumentation of Rubis research rocket payload for analysis of geomagnetic and electric fields 07 p1258 A67-19572

Instrument integration for landing capsule payloads of planetary missions, considering

functional operation, environmental constraints and interface definition [AIAA PAPER 66-59] 07 p1188 A67-19996

Payload-apogee altitude performance, static stability and dynamic motions of Tomahawk vehicle analyzed for ability to meet 100 km sounding rocket requirement 08 p1404 A67-20494

Controlled recovery of payloads from high altitudes and at large glide distances, using Para-Fall 08 p1409 A67-20545

Operational aspects and techniques of rocket payload recovery from sea and air noting recovery forces, aids, problem areas, location of recovery control, etc 08 p1409 A67-20546

Optimum weight ratio for space vehicle with solar energy operated engine, noting dependence on distance from sun, trajectory optimization, etc 09 p1571 A67-21886

Radioisotope heated hydrogen thrusters for propelling high energy upper stage, discussing performance, payload advantages and high energy kick stage [AIAA PAPER 67-509] 18 p3113 A67-33973

Initial defense communications satellite program giving payload characteristics and orbit analysis of 15 military launchings 18 p3137 A67-34612

Strategy of holding higher performance rocket engines for critical missions analyzed statistically for increased payload 19 p3311 A67-34829

Method for assigning numerical value to space scientific payload effectiveness toward satisfying mission goals 19 p3322 A67-35319

Unmanned rough-landing survival capsules design considerations for potential planetary payloads 19 p3332 A67-35335

Optimal payload lifting and nonlifting trajectories of winged boost-launch vehicle [AIAA PAPER 67-558] 19 p3335 A67-35955

Up-rated Saturn V vehicles and intermediate payload Saturn vehicles, studying costs, flexibility, performance and boost-assist components 20 p3531 A67-36539

Post-Saturn launch vehicle, discussing multipurpose, variable payload boosters, usability, noise levels, etc 20 p3533 A67-36613

Secondary payload for Saturn launch vehicle evaluation according to experiment/mission effectiveness and compatibility by computer program methodology 22 p3903 A67-39950

Multiple payload mission planning for multiple and single earth orbits and apogee motor delivery, evaluating cost and performance 22 p3903 A67-39952

Payload integration process for space experimentation 22 p3922 A67-39962

Rapidly converging iterative solutions to Min-H strategy applicable to trajectory optimization and payload maximization 22 p3888 A67-40148

Solid propellant motors relative performance as related to intermediate payload missions, considering reusable liquid strap-on stages for post-Saturn payloads [DOUGLAS PAPER-4452] 24 p4240 A67-42388

Launching and ballistic flight of Rubis IV rocket, discussing scientific preparation and payload testing 24 p4241 A67-42573

Saturn V payload capabilities uprating by building block approach using solid propellant rocket motor, noting cost factor and mission flexibility [AIAA PAPER 67-907] 24 p4244 A67-43014

Lunar applications of spent Saturn V-S-IVB/IU stage concept, discussing payload capabilities [AIAA PAPER 67-986] 24 p4246 A67-43058

PAYLOAD MASS RATIO

Saturn V launch vehicle, discussing payload-mass ratio, capabilities and modification possibilities 06 p1098 A67-19020

Optimal stage sizes and trajectory for multistage launch vehicle determined by various techniques [AAS PAPER 66-113] 07 p1259 A67-19972

VTOL/STOL aircraft evaluation via performance characteristics 07 p1130 A67-20219

Advanced structures and materials in future launch vehicles evaluated by design synthesis technique for component weight reduction, equivalent payload gained and cost ratio 10 p1723 A67-23699

Optimal stage sizes and trajectory for multistage launch vehicle determined by various techniques [AAS PAPER 66-113] 13 p2214 A67-27529

Effect of payload weight, density and type on performance and design of reusable launch systems 15 p2568 A67-29841

Concorde aircraft fuel, discussing fuel transfer, problem of boiling, in-flight environment simulation, payload/mass ratio, etc 16 p2734 A67-31809

Discontinuous integrands in calculus of variations formulations of trajectory optimization and maximum payload problems with discontinuous state variables 22 p3827 A67-39954

PCM

S PULSE CODE MODULATION /PCM/

PD-808 AIRCRAFT

S PIAGGIO-DOUGLAS PD-808 AIRCRAFT

PUM

S PULSE DURATION MODULATION /PDM/

PECLET NUMBER

Heat transfer in fuel cell battery held in isothermal bath, giving charts for maximum temperatures at different Peclet numbers 20 p3364 A67-37016

Porous cermet tubular element fire barriers of stainless steel powder for increased safety in gas flame processes, determining critical Peclet values 24 p4159 A67-41957

PEGASUS SATELLITE

Pegasus thermal control louver system characteristics determined by environmental chamber testing, noting testing configuration [AIAA PAPER 67-308] 12 p2036 A67-26023

Thermal control coating degradation data from aluminum case containing four sensors aboard Pegasus spacecraft [AIAA PAPER 67-331] 12 p2038 A67-26045

Gravitational and magnetic torque effects on rotational motion of asymmetric Pegasus satellite in circular orbit [AIAA PAPER 67-567] 19 p3335 A67-35963

PELTIER EFFECT

SA THOMSON EFFECT

Peltier and Ettingshausen effects in flux-flow state of superconducting niobium, considering contribution to entropy flow 19 p3304 A67-35535

PEM EFFECT

S PHOTOELECTROMAGNETIC /PEM/ EFFECT

PENDULUM

SA GYROSCOPIC PENDULUM

Periodic motions of pendulum with vibrating point of suspension 01 p0113 A67-10288

Acceleration perturbations, gravity gradient torques and nutational motions effects on pendulums and gyrocompasses used as vertical indicating devices 01 p0064 A67-10644

Nonlinear equations of motion of bifilar pendulum without using suspension geometry or inertia properties of suspended body 08 p1354 A67-20922

Sufficient conditions for stability of solutions of nonlinear nonautonomous equation, examining pendulum of variable length 09 p1533 A67-22154

Oscillation pendulum equation solution properties, noting existence of certain bifurcation value of parameter 14 p2348 A67-28382

Poincare continuation method using simple pendulum problem, deriving elliptic functions as power series [AIAA PAPER 67-564] 19 p3250 A67-35960

PENDULUM APPARATUS

Plane oscillations of elastic pendulum with shaft undergoing bending deformation, determining principal zone of instability for action by longitudinal harmonic force 03 p0469 A67-14161

Obstacles at variable angles attached to pendulum with two degrees of freedom used to study high speed impact of solid particles 12 p1926 A67-25956

Gravitational acceleration determination noting reversible pendulum, free fall and symmetrical free motion methods 15 p2517 A67-29507

Statistical probability for motion stability of nonlinear stochastic systems during time interval, discussing oscillation stability of pendulum with randomly oscillating bearing 16 p2703 A67-31145

Nature of axis coupling for Kater pendulum assuming weightless rod and mass point loads 17 p2883 A67-31929

Motion rate of pendulum with two antennas moving in electromagnetic field

with standing wave measured by correlation meter 21 p3631 A67-39115

PENETRATING PARTICLE

Penetrating radiation measurement on moon surface obtained by Luna IX spacecraft 08 p1385 A67-20841

Three stages of solar cosmic rays entry into polar cap atmosphere due to differential arrival of solar electrons, protons and alpha particles 11 p1855 A67-23925

Invariant imbedding method applied to energy dependent neutron radiation penetration problems in thick and heterogeneous shields 11 p1817 A67-25063

Airglow and enhanced penetrating electromagnetic radiation in southern radiation anomaly observed with scintillation crystal during aircraft flight 12 p1996 A67-25775

Space-time distribution of heavy penetrating particles in extensive air showers, applying scale transformation properties of distribution to integration over primary particle spectrum 15 p2550 A67-29749

Fission-particle damage formation in semiconducting layer structures, using model based on thermal spike 17 p2918 A67-32849

Color contrast penetration method for crack detection in aircraft engines and motor car parts 18 p3045 A67-33739

Penetrating particles in cosmic radiation deep underground in Kolar gold field experiment, discussing muon-neutrino interaction 24 p4210 A67-42582

Search for neutral particles other than muons with high penetration capability from heavy mass or passivity at 40 mwe depth 24 p4220 A67-42866

Penetrating component of high energy cosmic rays below ground measured for intensity 24 p4221 A67-42876

Hard component penetration of cosmic rays investigated by ionization calorimeter and hodoscope counters 24 p4222 A67-42878

PENETRATION

SA CRATERING

SA FRAGMENTATION

SA IMPACT

SA PROJECTILE PENETRATION

SA TARGET PENETRATION

Penetration factor along grid of plane triode calculated from nomograms 05 p0774 A67-16937

Qualitative and quantitative descriptions of penetration of solids by high power density electron beams in welding, calculating penetration vs welding velocity and current curves 06 p1008 A67-18696

Vitreous silica and molten Al reaction, penetration rate of Al, reaction rate and effect of Bi and Sb on rates by lamellar compound formation 10 p1669 A67-23381

High velocity particles and slower corpuscles penetration into lower ionosphere occurring after solar flare explained by Sweet mechanism 12 p1993 A67-25134

Diffusion, solubility and electrical behavior of lithium in gallium antimonide 16 p2726 A67-30811

Penetration rates of thin aluminum foil sensors of Ariel II satellites compared with flux measured by microphone detectors in vicinity of earth 21 p3722 A67-38494

PENETRATION BALLISTICS

Meteoritic penetration through obstacle theoretically considered 11 p1869 A67-24076

Concepts of wind drift and lateral maneuver applied in flight mechanics 17 p2798 A67-32591

PENETROMETER

Omnidirectional penetrometer for lunar surface parametric impact testing and certification of safe soft-landing site for Apollo LEM 01 p0074 A67-11123

Polarization-diversity telemetry receivers for combining FM/FM penetrometer data, noting signal fading 02 p198 A67-12024

PENNING DISCHARGE

Anomalous diffusion arising from LF flute instability in Penning discharge, measurements of turbulent fields used to determine statistical transport rates 02 p0276 A67-12559

Arc formation at metal surface in hydrogen plasma analyzed at various gas pressures, using Penning discharge, noting heat treatment effect on hydrogen 05 p0850 A67-16066

Rotating helical perturbations in Penning discharge plasma accompanying LF

oscillations enhance particle transport across magnetic field 08 p1362 A67-21146
 Resonant oscillation in Penning discharge when electron motion around plasma column perturbs plasma 14 p2355 A67-27828
 Quasi-equilibrium number density of excited atoms and electronic transition rate in decaying optically-thick helium and hydrogen plasmas, considering Penning ionization 16 p2715 A67-31168
 Penning cell discharge ignition in high vacuum magnetic field in terms of Townsend avalanche theory, with discharge-ignition curves 19 p3272 A67-35089
 Intense HF oscillations from plasma-beam interaction in cold cathodes PIG reflex discharge 19 p3275 A67-35109
 Penning ionization gauge discharge nonlinear response to VHF signals, discussing resonance behavior 19 p3275 A67-35110
 Ion source using Penning discharge used to inject hydrogen ions into magnetic field 19 p3195 A67-35599

PENNING GAUGE

Calibration of low pressure Penning gas discharge gauge and stability of discharge modes 06 p0950 A67-17748
 Trigger discharge gauge compared with ionization gauge and partial pressure analyzer 06 p0950 A67-17749
 Response of trigger discharge gauge, noting ion current component 06 p0950 A67-17750

PENTAERYTHRITOL TETRANITRATE

/PETN/

Lead azide and pentaerythrite tetranitrate explosion triggered by laser radiation 07 p1195 A67-19315

PEPTIDE

Pituitary enzymes hydrolyzing aminoacyl arylamides and relation to peptidases 01 p0015 A67-10488
 Mass spectrometric determination of amino acid sequence from oligopeptides 04 p0566 A67-15613
 Synthesis of biologically pertinent peptides under possible primordial conditions 24 p4118 A67-42606

PERCEPTION

S AUDITORY PERCEPTION
 S COLOR PERCEPTION
 S CUTANEOUS PERCEPTION
 S DEPTH PERCEPTION
 S MOTION PERCEPTION
 S RECOGNITION
 S SENSORY PERCEPTION
 S SIZE PERCEPTION
 S SPATIAL PERCEPTION
 S VISUAL PERCEPTION

PERCEPTRON

Image recognition systems compared with constant indeterminate and random prototypes 03 p0374 A67-13082
 Computer simulation of perceptron predicting result of cyclic process 07 p1147 A67-19150
 Modified perceptron procedure for nonseparable cases, minimizing error probability and introducing reinforcement factors 12 p1961 A67-28064
 Perceptron system for correcting average line position of open loop portion of control system, discussing pole interaction and self-organization 17 p2830 A67-33098

PERCEPTUAL DEPRIVATION

S SENSORY DEPRIVATION

PERCEPTUAL SPEED

Skilled response organization, discussing stimulus coherence, tracking task, spatial and temporal coherence, secondary task, sequence length and task coding 14 p2254 A67-28034
 Intermittent visual stimulus influence on perceptual motor skills in aviation 14 p2258 A67-28668

PERCHLORATE

S AMMONIUM PERCHLORATE
 S HYDRAZINE PERCHLORATE
 S POTASSIUM PERCHLORATE

PERCHLORIC ACID

Gaseous ammonia composite solid propellant ignition upon contact with oxidizing vapors such as perchloric acid vapor 06 p1073 A67-18869
 Burning velocities, temperatures and burnt gas composition of flammable methane-rich perchloric acid mixtures 14 p2406 A67-28544
 Flame properties of flammable ethylene-rich perchloric acid mixtures 14 p2406 A67-28545

Flame properties of flammable ethane-rich perchloric acid mixtures 14 p2406 A67-28546
 Chemical structure of premixed flames of methane and perchloric acid vapor diluted with argon obtained in terms of composition, temperature and velocity profiles 18 p3109 A67-33841
 Catalyzed ignition of composite propellant fuels in presence of perchloric acid studied for acceleration of rate of acid decomposition 23 p4048 A67-41761

PERFECT GAS

SA IDEAL GAS

Perfect gases reacting mixture flows formulated for system of differential equations 06 p0955 A67-18114
 Rational approximation method for calculating supersonic axisymmetric flow of perfect gas around given blunt body 06 p0943 A67-18846
 Supersonic flow of ideal thermodynamically perfect gas from nozzle into medium at rest 10 p1591 A67-23037
 Calculation of weight flow and velocity for real gas, obtaining correction factor 11 p1779 A67-24355
 Moments of distribution function of perfect fluid calculated and used in studies of orthogonal polynomials on Minkowski hyperboloid 12 p1966 A67-25144
 Vibration of cylindrical shell containing flowing incompressible perfect fluid 13 p2215 A67-26528
 Plane shock wave propagation in inviscid perfect gas colliding with right angle obstacle, determining flow in perturbed region 14 p2296 A67-27979
 Integral relation method analysis of supersonic gas flow past blunt body of revolution 17 p2791 A67-32679
 Relaxation toward Maxwell distribution function of classical gas with initial nonequilibrium distribution function as velocity modulus function 22 p3782 A67-39406
 Integral solution for massive blowing on slender hypersonic wedges and cones in laminar flow, assuming homogeneous nonreacting perfect gas mixtures 23 p3932 A67-41743
 Equation system for conducting perfect gas motion group analyzed leading to possible invariant solutions of system applicable to MHD equations 24 p4197 A67-42354

PERFLUOROALKANE

Linear fluorinated hydrocarbon polymer oils and grease mixtures with low molecular weight polytetrafluoroethylene thickener as lubricant for liquid fueled rocket motors [ASLE PREPRINT 67AM 8A-4]

Perfluorocyclobutane-fluorine combustion studies and measurement of detonation velocities and limits [CI PAPER 67-23] 19 p3345 A67-35013

PERFORATED PLATE

Stress concentration in plate weakened by infinite sequence of uniform holes and subject to elastoplastic strain 02 p0337 A67-11844
 Plastic zone expansion near circular hole in plate under pure shearing stress 02 p0337 A67-11845
 Stress concentration near elastic ring-reinforced hole in elongated nonlinear plate 02 p0341 A67-12865
 Stress concentration in sheet with circular opening subjected to biaxial tension 04 p0711 A67-15198
 Stressed state of anisotropic half-plane weakened by finite number of elliptical holes with centers on straight line perpendicular to boundary of half-plane 05 p0907 A67-16018
 Tensile stress concentration near rhombic hole taking into account physical nonlinearity of aluminum brass plate 05 p0907 A67-16020
 Two-dimensional photoelasticity analysis of stress concentration in plate with large number of uniformly spaced circular holes under biaxial loading 05 p0918 A67-16423
 Piston motion effect on flow uniformity in hypersonic gun tunnel, using perforated plate technique to prevent piston fluctuation 05 p0791 A67-16430
 Stress distribution at rigid ring-reinforced curvilinear hole in spherical shell 05 p0922 A67-17178
 Streak and open shutter photography of planar detonation wave in channel

transmitting through orifice, obtaining induction distance for transition from deflagration to detonation 06 p1119 A67-18596
 Elastic equilibrium of circular plate with elliptical hole and tight washer, determining stress-strain state 06 p1106 A67-18631
 Stress concentration in infinite incompressible plate with circular hole under bilateral tension analyzed, using variational method 06 p1107 A67-18634
 Dynamic stress concentration for plate with square hole, using approximate method of boundary shape perturbation and conformal mapping 06 p1109 A67-18665
 Second order elastic effects in infinite isotropic compressible medium with elliptic hole subjected to uniform tangential force at boundary 07 p1263 A67-19729
 Small twist superposed on nonuniform large extensions in circular sheet with small hole 07 p1263 A67-19730
 Stress distribution in elastic plate with circular hole, noting particular cases of general solution for simple boundary tractions 08 p1422 A67-21167
 Thin plate reinforcement around holes in plane sheets subjected to stresses at infinity 10 p1719 A67-23472
 Geometrically nonlinear effects of stress concentrations at holes in thin plate with large deformations 11 p1878 A67-24878
 Concentration of force and moments near circular holes in shells of revolution with large elastic displacements 11 p1878 A67-24879
 Stress concentration near holes in perturbed shallow shells of revolution 11 p1878 A67-24880
 Shear modulus magnitude effect on stress concentration at circular hole in cylindrical shell for various ratios of Youngs moduli 11 p1878 A67-24881
 Plane stress state near circular hole in infinite anisotropic plate of rigid-plastic nonhardening material 11 p1879 A67-24882
 Plastic zone about circular hole in infinite plate under uniform hydrostatic tension 11 p1879 A67-24887
 Stressed and strained state of infinite plate lying on elastic base weakened by finite number of arbitrarily located circular holes 11 p1879 A67-25053
 Elastic-plastic deformation around circular hole in plate under cyclic loading, recording strain distributions, development of plastic zone, etc 12 p2016 A67-25423
 Stress field in infinite plate with three circular holes under action of concentrated forces determined by solving associated boundary value problem 12 p2016 A67-25435
 Equivalent reinforcement and contour of symmetrically shaped hole corresponding to plate subjected to bilateral tension 12 p2019 A67-25564
 Semifinite thin plate with circular inclusion under uniform tension 13 p2215 A67-26525
 Stress concentrations around shaped holes in plates under uniform tension, deriving formulas by perturbation method 15 p2577 A67-30268
 Stress distribution in thin plates containing curvilinear holes of various shapes 16 p2766 A67-31100
 Stress-strain state determination of nonlinear plate with circular holes, deriving boundary conditions and basic equations 16 p2766 A67-31147
 Soviet book on supersonic gas flows in perforated boundaries covering flow characteristics, dynamic property, supersonic nozzles, velocity regulation, etc 17 p2789 A67-32019
 Analytic solution for finite radial expansion and consecutive unloading of circular hole in infinite elastic-plastic plate of initially varying thickness 17 p2966 A67-33347
 Elastic stress distribution in infinite plate having circular hole, applying coupled stresses theory 18 p3140 A67-33666
 Stress concentration near curvilinear hole in infinite plate subjected to biaxial uniform stress field at infinity 18 p3144 A67-34172
 Threshold equilibrium of brittle plate with polygonal hole in biaxial tension-compression 19 p3343 A67-35845
 Critical loads required for crack propagation terminating at curvilinear hole edge in plate decreasing with decreasing radius of corners 19 p3343 A67-35846

Critical loading for crack propagation in structures weakened by holes 19 p3344 A67-35847

Slip band length in plate with circular hole determined in terms of linear theory of elasticity 19 p3344 A67-35848

Stress-strain state in braces across elliptical hole in elastic plate, obtaining solution for eccentric load 21 p3721 A67-38305

Laser thermal and radiation effect on metals, discussing mechanical damage 21 p3646 A67-39011

Stress distribution on boundaries of two unequal circular holes in infinite plate determined by mapping region conformally onto annulus 21 p3730 A67-39086

Anisotropic plate with two elliptical holes studied for stresses under edge load by solving linear algebraic equations infinite system 22 p3910 A67-39452

Stress intensity factors for infinite plate subjected to cylindrical bending with radial cracks from internal hole 23 p4073 A67-40615

Soviet book on elasticity and plasticity covering perforated plates and shells and elastohereditary media 23 p4077 A67-40748

Elastic bending of thin shells and plates perforated with holes in various arrays, calculating stress distribution and concentration 23 p4077 A67-40749

Optimal reinforcements of cuts in stressed plates, considering displacements and conditions in discrete points of contact contour 24 p4249 A67-42105

PERFORATION

Three-dimensional stress concentration around cylindrical hole in seminfinite elastic body 05 p0909 A67-16140

Perforated plenum technique for direct forced air cooling of electronic equipment inside rack enclosure 08 p1303 A67-21061

PERFORMANCE

S AIRCRAFT PERFORMANCE

S ASTRONAUT PERFORMANCE

S HELICOPTER PERFORMANCE

S HUMAN PERFORMANCE

S MENTAL PERFORMANCE

S OPERATOR PERFORMANCE

S PILOT PERFORMANCE

S PROPULSION SYSTEM PERFORMANCE

S PSYCHOMOTOR PERFORMANCE

S SPACECRAFT PERFORMANCE

PERFORMANCE CHARACTERISTICS

Heat flux measurement with narrow view angle radiometers, discussing equipment design, performance characteristics and results 01 p0069 A67-11021

Sonic analysis for determining performance and mechanical integrity of turbine engines by using phase-locked filter and frequency ratio generator 01 p0076 A67-11141

Parameter optimization in systems subject to worst bounded disturbance that maximizes chosen performance index 01 p0046 A67-11204

Analytic performance calculation for varactor frequency doubler with various degrees of nonlinearity 01 p0040 A67-11234

Learning control system seeking optimum point of bimodal static characteristics by polynomial conjecture 01 p0048 A67-11236

Performance and design characteristics of solid state microwave converters for converting VLF telemetry receivers to L-and S-bands 02 p0196 A67-12006

Quadratic performance criteria for discrete control systems, using Liapunov matrix equation and digital computer program 02 p0225 A67-12074

Computational method for optimization of infinite time control problem for linear systems and quadratic indexes of performance 02 p0226 A67-12148

Klystron amplifier performance, noting increased efficiency by using double interaction in output circuit 02 p0222 A67-12531

Shared memory computer display system provides test bed for man-machine interaction, noting hardware and software design concepts 03 p0375 A67-13633

Ferric-doped-rutile 8 mm traveling wave maser, noting operating range and performance characteristics 03 p0438 A67-13986

Performance characteristics for pulse type Ar laser with external interferential system

of quasi-confocal spherical mirrors 03 p0438 A67-14188

Working diagrams, performance characteristics and loss mechanisms of ejector and compressor for mixing two liquid or two gas streams 03 p0353 A67-14305

Mean square error vs parameter curves determines applicability of perturbation method 04 p0591 A67-14421

Performance characteristics and bearing load-deflection equations of shaft supported by n roller bearings [ASME PAPER 66-WA/LUB-4] 04 p0629 A67-15339

Computer method for predicting servo positioner performance 05 p0753 A67-16235

Planar integrated circuit technology and beam lead sealed junctions, noting fabrication techniques, performance and applications 05 p0770 A67-16240

Performance characteristics of tunnel diode autodyne frequency converters 05 p0774 A67-16917

Performance-weight relations and shape parameters for Maxwell structures design, considering filament wound isotensoid container and tension shell decelerator 06 p1111 A67-18884

YAG solid state laser system, discussing output, theoretical limits, performance characteristics, etc 07 p1194 A67-19084

CW interference and white noise effect on second order phase lock loop, using reciprocal of loop mean square phase error as index of performance 07 p1161 A67-19878

LM guidance and control systems performance verification [AIAA PAPER 67-244] 07 p1165 A67-20064

Optimal control for linear system with respect to performance functional which includes trajectory sensitivity 08 p1309 A67-20327

Sensitivity of index of performances to variations in plant parameter for open and closed loop optimal control with one or two degrees of freedom 08 p1309 A67-20328

Terrier two-stage sounding rocket design, fabrication, flight testing and performance characteristics 08 p1408 A67-20527

High energy booster and upper stage combinations for space research, discussing mission capabilities, cost factors, reliability, etc 08 p1412 A67-21075

Low temperature characteristics of Ga-As varactor diode junction properties, calculating spreading resistance 09 p1471 A67-21827

Inert gas effect on performance characteristics of cesium thermionic converter, noting saturation current increase 09 p1444 A67-22008

BAC 111 hydraulic system, discussing service experience, reliability, maintenance, performance characteristics, etc 09 p1444 A67-22128

Solar cell system for UK-3 satellite, discussing design, material selection, development and fabrication 09 p1445 A67-22179

Theoretical and experimental basis of high performance Mg-air cells, discussing development and performance 09 p1445 A67-22187

Interface between reliability cost and performance resulting from application of microelectronics to Sergeant Artillery Guided Missile Ground Electronics 09 p1572 A67-22309

Reliability methodology in design and development stage, discussing component stresses, performance variation, etc 09 p1572 A67-22310

Aircraft sensor systems, discussing recording and evaluation tasks and performance characteristics 09 p1501 A67-22454

Statistical dynamics applications to evaluate system dynamic characteristics from operational data 09 p1469 A67-22460

Constant temperature difference hot thermocouple anemometer, discussing operation principle and performance 10 p1654 A67-22822

Future French Air Force combat aircraft limited to Mirage F-III or Franco-British Jaguar project variable geometry types 10 p1595 A67-23621

JR 100 H lift jet engine height control studies by NAL 11 p1852 A67-24267

Sheath helix antenna with conducting

core, noting variation of operation characteristics with core size and pitch angle 11 p1760 A67-24277

Nylon trailing line antenna application, operation and performance 11 p1743 A67-24359

Radiometer system with photomultiplier tube for measuring absolute radiation from hypervelocity projectile flow fields 11 p1790 A67-24447

Thin film thermal radiation detector noting construction, calibration, performance, error sources and advantages of pyroelectric over thin film gauges 11 p1790 A67-24454

Performance characteristics of photosensors and limitation by statistical fluctuation in absorption rate of light quanta in primary photoprocess 11 p1766 A67-24627

Low speed wind tunnel design, structure, performance and cost 11 p1773 A67-24640

Push-pull electrostatic loudspeaker for aircraft cockpit, helmet and ear-insert communication 11 p1767 A67-24702

Antenna aperture and array effect on characteristics and performance of radio direction finder 11 p1794 A67-25005

Linear amplitude characteristics in synthesis of instrumental servosystems with saturated components such as amplifiers 11 p1794 A67-25040

Military aircraft characteristics and performance evaluation procedure 11 p1885 A67-25102

Tandem cascade of airfoils slow speed performance flow characteristics 12 p1891 A67-25349

Performance characteristics of single wavelength liquid-metal MHD induction generator with end-loss compensation 12 p1897 A67-25375

Lunar Orbiter photographic system design including film processing, image conversion, relay, reconstitution, performance, characteristics, etc [SMPT PAPER 101-46] 12 p1940 A67-25464

High quality film processing in Lunar Orbiter spacecraft photo system, noting separate environmental control system [SMPT PAPER 101-49] 12 p1941 A67-25467

Vidicon TV design modifications for spacecraft applications noting reduced power requirements, improvement of heaters, narrowing of bandwidth, etc [SMPT PAPER 101-51] 12 p1914 A67-25471

Thrust reversers for business jet aircraft noting limitations, performance gains, technical aspects of analysis and testing, etc [SAE PAPER 670235] 12 p1989 A67-25493

Growth and operational capabilities of turboprop and reciprocating engines [SAE PAPER 670236] 12 p1989 A67-25494

Cessna tandem twin aerodynamics noting propeller slipstream variation effects, comparing front and rear engine operation [SAE PAPER 670243] 12 p1894 A67-25498

Accelerometer mountings evaluated covering attachment, calibration, resonance frequencies, tension-compression, bending, shear interface and cantilever effect 12 p1942 A67-25680

Mass spectrometers operational performance characteristics, effects on sensitivity decay rate related to time, pressure and ionizing current 12 p1942 A67-25694

Relay, connector and switch operation simulation, discussing design and performance of chatter and transfer detectors 12 p1943 A67-25702

Reverberation chamber for high intensity acoustic testing of specimen subjected to directionally predetermined spectral distribution of acoustic energy field 12 p1924 A67-25712

JPL solar simulator design, fabrication and performance 12 p1925 A67-25733

R/D on water launched space probes, discussing operation, applications and results 12 p2012 A67-25839

Solid and liquid propellants, considering minimum specific propellant consumption in connection with fuel selection for auxiliary power systems [SAE PAPER 670205] 12 p1987 A67-25866

Dielectric isolation of integrated circuit via ceramic medium, discussing technique, testing and results 12 p1916 A67-25997

SR-N4 hovercraft, optimum size for coastal waters, structural features, performance, control, etc 12 p1895 A67-26168

Nonlinear programming model for launch vehicle design and costing 12 p2013 A67-26193

Preferential epitaxial growth method for electrical element isolations in IC, noting no lattice defect effect on electrical characteristics of element 12 p1918 A67-26217

Oscillation effect on power and time characteristics of ruby laser output with variable threshold ratios of axial and inner radiation modes 13 p2125 A67-26398

Book on mechanics of low thrust space flight covering physical principles and generalized characteristics of engine systems, problems in optimization of space vehicles, etc 13 p2211 A67-26460

Single crystal YIG phase shifter performance noting improved output with proper microwave circuit design 13 p2076 A67-26479

Semiconductor device fabrication and operation, analyzing silicon, germanium, silicon carbide, InSb and GaAs 13 p2176 A67-26693

Structural evaluation of sheet beryllium fabricated by three different methods 13 p2140 A67-27136

High performance aerodynamic vehicle design noting configuration variables, optimum performance parameters, vehicle force characteristics, optimization of hypersonic aircraft performance, etc [AIAA PAPER 66-486] 13 p2054 A67-27584

Thickness, material type, environmental and surface emittance of radiation shield effects on thermal performance of multilayer insulation system 13 p2228 A67-27660

Size and power requirements of liquid helium temperature refrigerators 13 p2057 A67-27679

Optimum efficiency of high power klystrons for operation in fourth and fifth TV band, noting space charge effect 14 p2277 A67-27773

Book on gas laser origin, development, properties and construction 14 p2329 A67-27799

Klystron amplifier performance, noting increased efficiency by using double interaction in output circuit 14 p2279 A67-28008

Design concept for microwave integrated circuits, noting realization and performance evaluation 14 p2280 A67-28013

Monolithic circuits for RF communications systems 14 p2282 A67-28027

PSIN /P region, Seminsulating region, N region/ diode array fabrication, performance, characteristics and applications 14 p2282 A67-28029

Aperture efficiency of Parkes radio telescope reflector for decimeter and centimeter wavelengths obtained through celestial radio source 14 p2282 A67-28035

Flow processes and static and dynamic performance characteristics of axisymmetric fluid jet modulator and single receiver-diffuser studied experimentally 14 p2248 A67-28269

Static and dynamic characteristics of interaction region for fluid jet and receiver-load system, examining stability conditions 14 p2248 A67-28270

Power jet and single control bubble region portion of fluid jet modulator modeled for studying static and dynamic properties 14 p2248 A67-28271

Static and dynamic performance of pancake vortex flow field and application to pressure amplification 14 p2248 A67-28272

Laminar NOR unit feasibility, operating characteristics and performance 14 p2250 A67-28335

Principle of operation and static performance data of fluoric AND gate, using wall attachment principle 14 p2251 A67-28337

Static operating characteristics of diaphragm pneumatic logic device 14 p2275 A67-28347

Two-dimensional curved diffuser design by comparison with flow regime and performance data, obtaining diffuser shape and pressure distribution criteria [ASME PAPER 67-FE-6] 14 p2242 A67-28358

Large parabolic radio astronomy antennas, discussing design and performance of current and next generation 14 p2284 A67-28430

Spherical reflector radio telescope design, performance and application, describing

parameters of Tokyo, Lockheed, Nancay and Arecibo 14 p2284 A67-28432

Y-shape, T-shape and hollow circle arrays, considering u-v plane coverage, number of antenna elements, etc 14 p2285 A67-28436

Performance characteristics of nonstoichiometrically doped p-n junctions in Cd-Hg-Te alloy operated as IR photovoltaic detector 14 p2366 A67-28496

Scale grating with moire fringe effect, noting attachment to Zeiss 3030 coordinate measuring instrument 14 p2319 A67-28590

Power advantage of optimum system achieved with suboptimum feedback function for sequential binary detection system 14 p2292 A67-28707

Smoke generator control and performance for flow visualization applications [JPL-TR-32-1117] 14 p2293 A67-28751

Wear lifetimes for three greases thickened with submicron boron nitride powder [ASLE PREPRINT 67AM 2C-2] 14 p2325 A67-28785

RF design of communication satellite earth stations, discussing receiving, sensitivity parameters, etc 14 p2273 A67-28798

Fluorine compounds as propellants in upper stage propulsion units, discussing properties, suitability and performance 14 p2377 A67-28979

Japanese weather radar facility featuring network relay equipment functioning in PPI/RHI mode, noting parabolic horn antenna 14 p2290 A67-28998

Operation, structure, performance and application of solid, molten and aqueous electrolyte fuel cells 14 p2253 A67-29023

Fuel cells such as KOH, high temperature and ion exchanger diaphragm noting applications and performance characteristics 14 p2253 A67-29025

Performance of single lens objective for coronagraph noting resolution, scattered-light background brightness, etc 15 p2485 A67-29151

Large screen displays for group interaction simulation noting cost factors, techniques and performance characteristics 15 p2486 A67-29302

Supersonic inlets for jet aircraft, discussing positioning of terminal shock at intake for most efficient engine performance 15 p2415 A67-29303

Parametric input/output relation of approximate controller with optimized performance index, obtaining specific optimal control designed in regard to worst initial state 15 p2456 A67-29365

Sensitivity of cost functional in optimal control system with random variable parameters, noting system performance detection techniques 15 p2457 A67-29368

Extent of system parameter change insuring system performance within specified limit 15 p2457 A67-29369

Gradient compensated large volume degausser noting inner and outer coils, magnetic field generators and construction and performance specifications 15 p2517 A67-29491

Racalator as alternative to frequency synthesis noting design principles, operation and results 15 p2445 A67-29586

Spacecraft system performance vs component reliability, discussing practical aspects of software tools for management purposes 15 p2493 A67-29607

Multichannel field effect transistor theory and experiment 15 p2446 A67-29635

High temperature high power gas diodes and thyatrons for large nuclear electrical space power systems, noting parameters of design and performance 15 p2448 A67-29755

Systems approach to reliability, integrating cost and performance and demonstrating tradeoff decisions 15 p2448 A67-29800

Fixed wing reusable horizontal landing boosters, comparing weight, cost, technical difficulty and availability 15 p2567 A67-29836

Effect of payload weight, density and type on performance and design of reusable launch systems 15 p2568 A67-29841

MHD generator with uniform rectangular duct, considering ion slip and Hall effect in case of two-dimensional flow 15 p2422 A67-29906

Optical ranging system with high power chemical laser noting performance characteristics 15 p2500 A67-29913

Detonation characteristics evaluation of solid-composite propellant, noting hazards study program /Project SOPHY/ and critical geometry theory 15 p2544 A67-29999

Emitter-base voltage vs collector-current characteristic used to study stability of parallel pairs of HF high power transistors 15 p2453 A67-30017

Management and cost factors involved in operation of modern integrated missile range [AAS PAPER 67-59] 15 p2468 A67-30121

Reliability, performance requirements and environment in which system must operate 15 p2583 A67-30128

Method of dynamic characteristics, determining controlled plant performance during operation 15 p2462 A67-30328

Multichannel photometer for space applications requiring low weight and power, no moving parts and high sensitivity divided in four electrically and optically distinct quadrants 15 p2491 A67-30433

Bell Model 266 composite VTOL aircraft, discussing tilting rotor principle for conversion from helicopter to aircraft 16 p2595 A67-30495

Wall conductance of insulating gaps between electrode segments shown as cause of inferior performance of MHD generators 16 p2599 A67-30526

Performance characteristics of Faraday and Hall MHD generators using strong magnetic fields and considering ion slip and finite electrode segmentation effects 16 p2599 A67-30527

Performance of linear series of MHD generators noting electrical properties, effect of electrode scattering, etc 16 p2600 A67-30531

High temperature loop technology of closed cycle MPD generator, noting transport and reaction mechanisms within high temperature regions 16 p2601 A67-30551

MHD power generation experiments with potassium seeded argon plasmas to study performance at Faraday and Hall parameters 16 p2601 A67-30554

Maximum power density, maximum efficiency of diagonal wall generator, Faraday generators and Hall current generators compared 16 p2608 A67-30597

Linear and turbulent MHD generators of conduction type considering operating conditions, efficiency and energy conversion 16 p2608 A67-30600

High pressure liquid propellant rocket engines, noting high thrust, smaller engine dimensions, and combustion chamber cooling 16 p2735 A67-30704

Manned flight simulators suitable to space research, discussing types, phases of development, operational and performance features, etc 16 p2654 A67-30761

General equation for suppressor controlled transconductance of pentode useful for circuit analysis 16 p2635 A67-30794

Performance characteristics of tunnel diode autodyne frequency converters 16 p2636 A67-30894

Requirements for operating characteristics of single and twin gas turbine engines for military helicopters noting system response, deceleration, fuel control, etc 16 p2736 A67-30929

Angle diversity performance of wire-grid lens antenna determined using statistical analysis 16 p2639 A67-31361

Launch vehicle performance and engineering trade-off, considering mass fraction, weight reduction, specific impulse, losses and stage selection 16 p2762 A67-31489

Performance characteristics of helical electromagnetic induction pumps calculated taking into account effect of duct wall and liquid metal layer 16 p2609 A67-31584

Suboptimal, adaptive solutions to sampled data problem for quadratic performance index minimization by obtaining control law and sampling scheme 16 p2649 A67-31660

Linear pulse frequency modulated control systems, noting upper and lower bounds of optimal performance indices 16 p2650 A67-31671

Sensitivity analysis application to nonlinear system modeling and compensation noting minimization procedure parameter determination and performance index 16 p2650 A67-31674

Analysis of discrete nonlinear time-varying systems, noting computational simplicity,

application to feedback system, etc 16 p2650 A67-31675

Attitude control for orbiting astronomical observatories, noting system design and performance characteristics 16 p2763 A67-31689

Hyperfrequency amplification using electric field effect for conduction modulation of single crystal germanium sheet 16 p2732 A67-31705

Airborne ground profiler using CW and pulsed lasers range finders discussing performance 16 p2679 A67-31798

Airborne photographic systems defining performance criteria for quantitative analysis and application of transfer functions for evaluation 16 p2680 A67-31804

Ultraviolet camera lenses for space flight use discussing techniques for testing and evaluating performance 16 p2680 A67-31805

Hueycobra helicopter design and configuration noting maneuverability range, endurance, crew protection, weapons system, etc [AHS PAPER 113] 16 p2598 A67-31829

X-ray spectrometer with cold cathode, discussing equipment design, principles, operation and performance 17 p2853 A67-32046

Forced-erasure decoding of fading and nonfading channels compared with correlation and digital decoding 17 p2811 A67-32114

Hall parameter instability and conductivity analysis applied to performance characteristics of subsonic flow generator 17 p2898 A67-32181

Ionization fluctuations due to interaction between shower particles and absorbing component of ionization calorimeter and effect on accuracy of energy measurement 17 p2855 A67-32250

Miniature electrostatic accelerometer featuring suspension and force rebalance systems, discussing performance, applications and accuracy acceleration measurement 17 p2858 A67-32484

Linear/Monte Carlo method performance evaluation of intercept/rendezvous guidance and navigation for advanced space missions 17 p2882 A67-32493

IBM CP-2 militarized digital computer noting design, maintainability and performance 17 p2820 A67-32500

Relative merits of atomic frequency standards, discussing limitations, future outlook and applications 17 p2860 A67-32602

Bowtie radar display effectiveness in target detection compared with conventional Plan Position Indicator /PPI/ [TR-750-7] 17 p2807 A67-32630

Aerospace industry quality control requirements and specification, noting small business role 17 p2974 A67-32818

System performance in electrooptical telemetry noting receiver, transmitter, silicon photodiode, shot, thermal and background noise, etc 17 p2817 A67-32931

Integrated electronic display for V/STOL flight evaluated, considering vehicle dynamics, handling qualities, etc, and presenting performance data 17 p2861 A67-33182

Performance of matched filtering system related to degree of displacement for uniform and nonuniform spectral densities 17 p2862 A67-33295

Supercavitating engines noting design principles, performances of existing models and connection between parameters 18 p3023 A67-33417

Supercavitating engines, defining optimum curvature and thickness distribution, performance optimization, etc 18 p3023 A67-33418

Hydrazine as single component fuel for gas generators and rocket engines, noting advantages and performance characteristics 18 p3106 A67-33459

Performance characteristics of photodiodes with photoelectric cells as light-source position sensors 18 p3009 A67-33470

Turbofan jet propulsion system reversed-thrust, discussing momentum net change, external drags, clamshell and annular targets and cascade reversers [AIAA PAPER 67-418] 18 p2982 A67-33905

Design and performance characteristics of electrothermal microthrust systems for spacecraft functions [AIAA PAPER 67-423] 18 p2988 A67-33907

AC motor design for operation in He in cryogenic to room temperature range, noting performance parameters and design considerations [AIAA PAPER 67-456] 18 p2988 A67-33930

Micro-orifice injector rocket motors covering efficiency, nominal thrust, size, performance, cooling, design factors, etc [AIAA PAPER 67-462] 18 p3113 A67-33933

Subcooled liquid and slush hydrogen fuels effects on space vehicle design and performance, discussing propulsion, insulation, pressurization, venting, management, etc [AIAA PAPER 67-467] 18 p3137 A67-33937

Value analysis technique to compare competing high performance insulation systems on basis of differences in performance and cost [AIAA PAPER 67-469] 18 p3162 A67-33939

Michelson type carbon dioxide laser for AC discharge analysis, noting apparatus design and performance results 18 p3060 A67-34014

Step recovery varactors in constant-component and microstrip CW duplexers 18 p3011 A67-34067

Second, third and fourth order phase locked loops performance characteristics compared for optimum selection, calculating integrated square error and peak error 18 p3001 A67-34116

Development of quantitative logistics performance parameters related to time, resources and cost in Concept Formulation Phase and Contractual Definition Phase 18 p3162 A67-34678

Ground system design approach integrating reliability and maintainability with performance requirements, using Saturn V simulation as example 18 p3139 A67-34694

Flowgraph models of thermal and electrical parameters interaction in solid state devices, examining performance characteristics, system stability, etc 19 p3191 A67-34845

Two-channel single-pulse neodymium glass laser with 180 joule pulse, performance and optical features 19 p3239 A67-34986

Magnetic electron multiplier performance as photomultiplier in EUV spectral region 19 p3231 A67-35683

Feedback control system using pneumatic computing components and vibration isolators for automatic platform tilt stabilization, performance characteristics, etc [AIAA PAPER 67-548] 19 p3208 A67-35946

Sulfur hexafluoride gas handling system for potential drop particle accelerator, considering design, fabrication and performance 20 p3413 A67-36181

Solid state devices operational characteristics from applications in transmission technology 20 p3394 A67-36242

Performance characteristics of XB-70 flight test data acquisition system 20 p3442 A67-36467

HF transistor design principles, considering current technology 20 p3396 A67-36493

TRKI-12 predetection receiver/recorder subsystem examined for performance characteristics 20 p3380 A67-36550

Relation of testing and service performance - ASTM Conference, Atlantic City, June 1966 20 p3418 A67-36697

Ground vertical loop radio antenna for army use noting shape, performance, mobility, etc 20 p3399 A67-36884

Inertial guidance system in ELDO-A satellite launch vehicle performance assessed using onboard computer 20 p3481 A67-37187

Mathematical models of flow and filtration performance of wire cloth filter media in series and parallel configuration 20 p3365 A67-37364

Performance factors affecting size, shape and operation of piston and bore including hydraulic lock, viscous drag, oil contamination, etc 20 p3366 A67-37387

Multielement correlation type arrays response to several point sources studied by extending spectral method 20 p3403 A67-37510

Performance of hydrogen driven shock tube investigated for usefulness, considering shock wave attenuation and helium driver performance 21 p3605 A67-37769

Magnetic annular arc /MAARC/ driven shock tube design, construction and

performance, stressing radiation loss prevention 21 p3606 A67-37774

High pressure hypersonic gun tunnel calibration with performance estimation method compared with tests, discussing high altitude Mach 10 flight simulation 21 p3607 A67-37779

Electrostatic getter-ion pump performance, giving pumping speeds, pressure and starting characteristics, residual gas composition and operating life 21 p3624 A67-37822

Fibers of ordered aromatic copolyamides, performance characteristics and resistance to degradation at high temperature 21 p3647 A67-37873

Performance characteristics in zero potential energy manual task, discussing work output 21 p3577 A67-38074

AH-56A Cheyenne compound aircraft weapon system and major subsystems, discussing fire control, navigation system and performance characteristics 21 p3568 A67-38133

System effectiveness analysis with particular attention to availability, concepts and sample results 21 p3734 A67-38184

Gemini spacecraft antennas performance during reentry into ionized medium, discussing electron concentration profiles, nonearth atmosphere extrapolation and antenna breakdown effect 21 p3591 A67-38210

Coupler type bend for double layer pillbox antennas, discussing measurements for performance characteristics 21 p3597 A67-38565

Steady flow ammonia MPD arc jet thruster propulsion performance, discussing test chamber pressure variation, thrust data and cooling systems [AIAA PAPER 67-690] 21 p3696 A67-38930

Data compression and error control coding in space telemetry analyzed, using performance measures similar to distortion function 21 p3586 A67-38950

Operating and performance characteristics of helium-neon pulsed gas laser, discussing application to integrated microcircuits fabrication 22 p3813 A67-39333

Hovercraft principle application noting development, sea-keeping problems, predicted capability and costs 22 p3745 A67-39663

Design formulas for predicting dependence of resistance and reactance of diffused microwave p-i-n diodes on reverse bias voltage 22 p3770 A67-39730

Performance reliability of reinforced plastics for structural load-bearing components using nondestructive testing, defining material-energy interactions 22 p3826 A67-39860

Nomograph construction for earth pointing cameras, evaluating imaging system effectiveness as ground resolution and scale factor, plotting system performance characteristics 22 p3800 A67-40106

Optimization of staged ejector systems noting mathematical model development to represent performance characteristics 22 p3787 A67-40150

Weather effects on exposed and enclosed earth based satellite communications antenna systems, discussing performance characteristics under various meteorological conditions 22 p3763 A67-40408

Performance of wide variety of exceptional metals studied for corrosion and temperature resistance characteristics in atomic power application 23 p4018 A67-40899

Performance limits of laser rangefinder for design of all-weather terrestrial rangefinder, discussing echo signal, backscatter noise and TPG 23 p3999 A67-41040

Parameter variation of optimal linear control systems with quadratic performance index /Liapunov function/ 23 p3985 A67-41161

Deterioration in permanent magnets at high temperatures and procedures to minimize detrimental performance 23 p4041 A67-41182

P-n junction performance with depletion layer subjected to sudden extreme carrier density generation noting significant local distortion 23 p4044 A67-41453

High enthalpy supersonic wind tunnel performance, analyzing Teflon model stagnation ablation 23 p3931 A67-41477

Decreasing thickness and temperature

variation effects on solar cell performance 23 p3937 A67-41489

Solar cell integral covers, discussing solar simulation, vacuum and thermal tests, performance characteristics, etc 23 p3937 A67-41491

Vibrophonocardiograph developed for use in shirt-sleeve flight environment, previous design miniaturized without sacrificing performance characteristics 23 p3970 A67-41661

Isolation effects in constant environment on cycles of physiological functions and performance levels of man 23 p3959 A67-41697

Handbook on HF directional antennas covering performance characteristics and applications 24 p4128 A67-41794

Proportional characteristics and signal limiting capabilities of fluoric operational amplifier, discussing analog gain block performance 24 p4098 A67-41988

Solid propellant motors relative performance as related to intermediate payload missions, considering reusable liquid strap-on stages for post-Saturn payloads [DOUGLAS PAPER-4452] 24 p4240 A67-42388

Design parameters and performance characteristics for overdriven varactor upper sideband upconverter /USBUC/ 24 p4131 A67-42446

NASA test program to evaluate performance and design point characteristics of 3-kw closed recuperated Brayton cycle power conversion system 24 p4102 A67-42486

SET VIII Thermionic generator, evaluating operational and long term performance characteristics for space applications 24 p4103 A67-42499

Thermionic converter arrays output characteristics determined as function of interconnection resistance, failure modes and patterns, etc 24 p4103 A67-42500

Cascaded and segmented thermoelectric module design, discussing SiGe and PbTe elements and performance 24 p4184 A67-42506

Large sun-oriented deployable solar array for OGO design, fabrication and flight performance 24 p4104 A67-42508

Solar array as primary electrical power source of Pioneer deep space probes, comparing performance data with test and design data 24 p4105 A67-42514

Solar cell array flight systems, discussing flight experience, design and fabrication history 24 p4105 A67-42518

Parametric analysis of heat pipes, design, operation principles and performance capabilities 24 p4255 A67-42553

Performance characteristics of active channel of insulated gate FET for application as high gain HF amplifier 24 p4133 A67-42824

Reliability assessment test program for determining capabilities and limitations of 2 kw hydrogen-oxygen fuel cell stacks 24 p4109 A67-42896

Heat pipe performance in zero gravity field, discussing isothermal operation of water heat pipe in earth orbit 24 p4256 A67-42926

Water immersion simulation, studying astronaut performance characteristics in Gemini and proposed Apollo missions [AIAA PAPER 67-773] 24 p4116 A67-42941

V/STOL and STOL concepts as applied to short haul transportation [AIAA PAPER 67-941] 24 p4097 A67-43031

Reentry vehicle design characteristics and requirements for safe reentry of radioactive power sources, discussing heat protection systems [AIAA PAPER 67-966] 24 p4246 A67-43044

Performance of single lens objective for coronagraph noting resolution, scattered-light background brightness, etc 24 p4158 A67-43074

PERFORMANCE DECUREMENT

Dose levels and hangover effect of secobarbital on simulated pilotage performance 03 p0366 A67-14291

Space charge and eddy currents in ionized gas flow in MHD channel determined, showing effect of cold electrode boundary layer on electrical performance 11 p1746 A67-24874

Phase shifts in human circadian system noting individual differences, performance deficit, physiological changes and dissociation from time zone

displacements 15 p2425 A67-29108

Diagnostic devices for sensing performance deterioration and mechanical malfunctions in supersonic aircraft engines [SAE PAPER 670363] 17 p2930 A67-33000

Nonuniform electrical conduction in MHD channels analyzed by differential equations 17 p2906 A67-33011

Simulated micrometeoroid bombardment effect on n/p Si and CdS solar cells performance 23 p3941 A67-41521

Apollo spacecraft H-O chemical to electric energy converting fuel cell performance degradation resulting from O electrode contamination due to inert diluent impurities in O supply 24 p4106 A67-42525

PERFORMANCE PREDICTION

Electronic system reliability prediction without relying exclusively on failure rate information 01 p0042 A67-11372

Game theory of economic incentive payment reliability demonstration and prediction 01 p0171 A67-11374

Diffuser use in low density hypersonic wind tunnel and method of evaluating global performance for diffusers with conical inlet followed by cylindrical mixing section 05 p0748 A67-16763

Digital computer simulation model implementation in prelaunch prediction of Saturn V launch vehicle system performance [AIAA PAPER 67-205] 06 p1096 A67-18344

Monte Carlo and direct calculation methods analyzed in connection with microelectronic circuit designs 10 p1610 A67-22978

Inequality to derive error estimation of performance of automatic pulse servosystem inside interval of discreteness 11 p1772 A67-25039

Military aircraft characteristics and performance evaluation procedure 11 p1885 A67-25102

Cesium thermionic diode parameters including added noble gas pressure effect for ignited mode performance prediction and optimization 12 p1896 A67-25262

Radial gas turbine losses, obtaining rotor loss coefficients, discussing flow pattern for performance prediction 12 p1891 A67-25347

High speed radial turbine rotor temperature distribution measured for pattern prediction of temperature 12 p1988 A67-25354

Iso-irradiance contours close to high pressure mercury arc lamp [AIAA PAPER 67-315] 12 p2037 A67-26030

Satellite launch vehicle performance analysis based on velocity requirements and gravity and drag losses for applications to booster configurations 14 p2394 A67-28701

Probability and prediction techniques related to maintainability discussed with application to early design, time constraints and maintenance goals 16 p2681 A67-30439

Maintainability prediction procedures applicable to systems and equipment as described in DOD handbook 16 p2781 A67-30442

Optimum performance of propulsion acceleration calculated by approximation method, noting earth-Mars transfer and Jupiter and Saturn missions 16 p2760 A67-30735

Reliability prediction relationship to system support costs, computing factors for undersupport and oversupport of tactical missile system 16 p2782 A67-31256

Rotor-hovering performance-prediction with test data showing discrepancy increase with wake contraction, blade loading, tip Mach number and blades number [AHS PAPER 100] 16 p2594 A67-31817

Rotor blade compressibility effects on helicopter performance, describing flight test techniques and data analyses and comparing prediction and test results [AHS PAPER 103] 16 p2595 A67-31820

Computer program for synthesizing and analyzing performance of preliminary designs of hypervelocity cruise vehicles 17 p2819 A67-32474

Scramjet engine nozzle contours noting expansion-deflection, bell, plug and arbitrary annular nozzles, with optimum nozzle design and computer program for performance prediction [AIAA PAPER 67-453] 18 p2983 A67-33927

Graphite material strength prediction by nondestructive test techniques consisting of bulk density and eddy current

measurements

[ASTM PAPER 54] 18 p3070 A67-34584

Reliability prediction prospects for electronic products, considering factory-to-target progress and reliability factors 18 p3057 A67-34672

Saturn V reliability analysis model used by management for predicting performance probabilities 18 p3138 A67-34684

Reliability prediction, modeling and analysis activities in Apollo program 18 p3139 A67-34697

Digital computer simulation model implementation in prelaunch prediction of Saturn V launch vehicle system performance [AIAA PAPER 67-205] 19 p3331 A67-34807

Axisymmetric flow equations for performance prediction of axial-flow turbomachines and stage design 20 p3355 A67-36186

Prelaunch checkout in 1970s, discussing vehicle subsystems, prelaunch requirements and operations and launch site technology 20 p3415 A67-36579

Lunar Orbiter power subsystem reliability tradeoff, methodology, performance prediction, etc 20 p3363 A67-36594

Performance prediction calculations for double junction n-p-n silicon solar cells, discussing simplified model limits and space radiation environment 21 p3571 A67-38232

Thermal stress analysis of epoxy encapsulants using mathematical model for predicting performance in thermal shock 21 p3723 A67-38630

Maintenance time reduction for multimode airborne weapons through built-in test equipment and integrated program 21 p3601 A67-38947

Perturbation scheme for linear system performance determination based on component performance information 21 p3654 A67-39063

Performance prediction of low solidity cascades from potential flow calculations 21 p3566 A67-39079

Steady tunnel operation effects on tracked hovercraft air cushion performance, discussing tunnel entrance problems 22 p3746 A67-40067

Multiple exhaust nozzles for advanced nuclear rocket engines noting design and performance prediction procedures 22 p3634 A67-40160

Configuration selection of turbopump for hot-bleed cycle nuclear engine, discussing performance optimization factors 22 p3834 A67-40162

Prediction of Saturn V launch vehicle effectiveness during prelaunch phase using computer simulation [SMPT PAPER 102-27] 22 p3908 A67-40371

Large model superconducting magnet for MHD central-station power generation, discussing performance and specifications 22 p3749 A67-40399

Flexible integrated deployable solar cell array design, environmental testing and performance prediction 23 p3939 A67-41511

Computer program for predicting silicon solar cell current-voltage characteristics as function of incident solar intensity and cell temperature over heliocentric distances 23 p3939 A67-41513

Multifaceted solar array performance determination 24 p4104 A67-42509

Electromagnetic compatibility prediction using statistical descriptions of case emission and susceptibility 24 p4132 A67-42712

AIDS data processing and analysis system for automated fault diagnosis and equipment trend prediction, describing methods applied to aircraft [AIAA PAPER 67-792] 24 p4126 A67-42953

PERFUSION

Theoretical lung with equal ventilation-perfusion ratio used to study determinants in inert gas elimination 21 p3575 A67-38515

PERIGEE

Relativistic rotation of perigee of satellite determined from first integral of motion equation 09 p1563 A67-21658

Maximum and minimum eclipse time of earth satellites with circular and elliptical orbits, considering dependence on argument of orbital perigee 13 p2201 A67-27339

PERIOD EQUATION

Almost periodicity of bounded solutions to nonlinear systems in n-dimensional Euclidean space 13 p2144 A67-26381

Almost periodicity of bounded solutions to nonlinear systems in n-dimensional Euclidean space 20 p3479 A67-37726

PERIODIC FUNCTION

Periodic solutions for difference-differential autonomous nonlinear oscillatory system with one degree of freedom 01 p0113 A67-10290

Asymptotic behavior of characteristic exponents and associated eigenfunctions for periodic differential difference equations 01 p0105 A67-10521

Lateral motion of simply supported axially loaded viscoelastic column governed by system of linear ordinary differential equations with periodic coefficients 01 p0106 A67-10732

Jackson theorem on optimal approximations of periodic functions with r-th derivative belonging to metric generalized to case of Orlicz space 02 p0259 A67-11872

Existence of periodic solutions for infinite system of integro-differential equation 02 p0260 A67-12537

Book on conductive heat transfer covering lumped, integral and differential formulations, two-and three-dimensional periodic functions, unsteady problems, Laplace transforms, etc 03 p0535 A67-13075

Cauchy problem of odd-order equations that are correct according to Petrovskii 03 p0459 A67-13644

Optimal approximations by trigonometric polynomials for classes of periodic functions belonging to Banach space invariant 03 p0459 A67-13645

Existence theorems for periodic solutions of coupled nonlinear systems of two or more degrees of freedom, including normal mode vibrations 03 p0524 A67-13654

Self-sustained periodic solution in nonlinear difference differential equation proved under appropriate assumptions for various parameters 03 p0459 A67-13655

Existence theorem for periodic solutions to parabolic boundary value problem involving reduction to solvable operator equation 03 p0460 A67-13835

Continuous periodic function approximation by Fourier series 03 p0462 A67-14108

Response curves of steady state forced vibrations, cosinelike functions and periodic functions possessing amplitude 04 p0656 A67-14444

Quasi-periodic solutions for sets of differential equations containing small parameter 04 p0643 A67-14660

Existence of periodic solution for set of quasi-linear differential equations 04 p0643 A67-14662

Existence and evaluation of solution for periodic boundary value problem of set of ordinary differential equations 04 p0643 A67-14668

Oscillations of derivatives of almost periodic functions obtained with aid of Kronecker-Weyl theorem 04 p0646 A67-15259

Fourier series approximation of functions with structural properties differing with segments of domain of definition 05 p0836 A67-17107

Uniform almost periodic functions with Fourier indices having one, and only one, limit point 06 p1023 A67-17836

Asymptotic stability of periodic solutions of nonautonomous quasi-linear systems with two degrees of freedom 06 p0975 A67-18037

Periodic solutions of elliptical and restricted four-body problems about libration points of restricted three-body problem [AAS PAPER 66-101] 07 p1252 A67-19963

Periodic solutions of hyperbolic equations containing small parameter by extending Cesari method for differential equations 07 p1218 A67-20213

Periodic solutions of three-dimensional restricted problem, noting existence of orbits for various combinations of eccentricity and inclination 08 p1396 A67-21183

Existence, uniqueness and stability investigation of periodical solutions for nonlinear hyperbolic partial differential equations 10 p1874 A67-23387

Stability of integrals of differential equations for periodic motions 10 p1880 A67-23866

Gamma function concept for varying difference interval and complex

argument 11 p1812 A67-23966

Galerkin method applied to approximation of periodic solution of system of singular differential equations 11 p1819 A67-24762

Multidimensional linear differential equations with almost periodic coefficients analyzed for error of exact solution 11 p1814 A67-24977

Problem of Vallee-Poussin type for linear hyperbolic equations with spatial variable coefficients 11 p1814 A67-25049

Closed contour for equation expressing periodic solutions of second order differential equations 12 p1982 A67-26184

Extension of Zygmund approximation series to two dimensions, noting periodic function role 14 p2345 A67-28938

Behavior of quasi-linear stochastic differential equations with one degree of freedom subjected to effect of random periodic excitation 16 p2696 A67-31009

Conditions for stability of solutions of second order linear differential equation with periodic coefficients 16 p2696 A67-31010

Fourier coefficients determination by calculating trapezoidal-rule approximations 16 p2697 A67-31333

Proof of continuity of Haar measurable almost periodic functions 17 p2876 A67-32385

Transformation of van der Pol equation into piecewise linear differential equation, determining periodic solution from asymptotic expansion 17 p2878 A67-32712

Distribution coefficients for impurities in gallium and indium arsenides as periodic function of atomic weight decreasing with increasing atomic number 18 p3102 A67-34289

Periodic solutions for quasi-harmonic time-lag system, proposing calculation for periodic regimes in form of integral series 18 p3079 A67-34371

Nonlinear interaction between two waves of multiple frequencies in communication line, nonlinear line capacitance being periodic function of line length 19 p3185 A67-36021

Stability of periodic solution of nonlinear systems with coefficients dependent on amplitude and frequency 20 p3408 A67-37043

Stress analysis in theory of circular cylindrical shell weakened by doubly periodic system of identical circular holes 20 p3542 A67-37664

Stability of integrals of differential equations for periodic motions 21 p3657 A67-38267

Attitude continuous instability regions in parameter space and resonance frequency of spinning unsymmetrical satellite noting periodic processes 22 p3899 A67-39311

Problem solving method based on averaging over periodic functions for steady waves in nonlinear one-dimensional distributed systems, deriving approximate equations 22 p3815 A67-39761

PERIODIC ORBIT

Analytic continuation method proof of existence of class of periodic orbits of three-dimensional three-body problem, Part II 01 p0148 A67-10381

Existence of class of quasi-periodic solutions of three-body problem for near-circular inclined planetary and lunar orbits, Part I 01 p0148 A67-10382

Orbital 2-1 periodic resonance in neighborhood of equilateral equilibrium points of restricted problem 02 p0321 A67-11497

Generalization of Whittaker formula for periodic orbits to fields with arbitrary attraction law 06 p1082 A67-18039

Isotropic mass loss effect on binary star system orbital elements and period eccentricity relationship 06 p1380 A67-20385

Elliptic restricted problem of periodic Trojan orbit and nonperiodic librational frequency and angular motion of Jupiter 08 p1381 A67-20388

Periodic solutions for restricted three-body problem 08 p1384 A67-20619

Natural families of periodic orbits, using generalized Hill equation 13 p2205 A67-27476

Stromgren family of periodic orbits in restricted problem 13 p2205 A67-27479

Orbits in Copenhagen problem asymptotic at L4 and genealogy 13 p2205 A67-27481

Family of periodic orbits around triangular libration points in restricted three-body problem 15 p2557 A67-29876

Canonical elements for variables of Levi-Civita regularizing binary collisions in

restricted three-body problem, noting existence of periodic orbits 15 p2557 A67-29878

Comet missions, discussing spacecraft exploration criteria for short period and long period first-apparition comets 16 p2745 A67-30749

Representation of rotating gaseous emission rings in eclipsing binary systems by periodic orbits around more massive component in restricted three-body problem 17 p2944 A67-32640

Book on theory of orbits covering restricted problem of three bodies, two bodies in rotating coordinate system and periodic orbits 18 p3120 A67-34032

Bounded isoenergetic displacement of periodic orbits in restricted circular three-body problem 18 p3135 A67-34542

Orpheus program for space flight safety using lifeboat rescue of astronauts on Apollo and other manned missions 20 p3532 A67-36572

Three-dimensional periodic motion about collinear Lagrangian equilibrium points, determining motion, variational and orbit equations and numerical integration 22 p3889 A67-40427

Book on celestial mechanics covering Laplace-Newcombe method, Hill planet and lunar methods and periodic orbits methods using differential equations 23 p4069 A67-41429

Orbital elements and motion equations of periodic comet Harrington for five perihelion times before discovery 24 p4226 A67-41964

PERIODIC OSCILLATION

Dispersion relation of electron impurities in gapless superconductors and effect on period and damping of Tomasch oscillations 01 p0130 A67-10154

Energy dissipation and heating due to oscillation of polymers whose rheological properties are described by elastic heredity theory, considering homogeneous and reinforced plastics 01 p0102 A67-10220

Periodic motions of pendulum with vibrating point of suspension 01 p0113 A67-10288

Periodic regimes in two-channel automatic systems with nonlinear element in single channel part of loop, showing cross connections effect on auto-oscillations 01 p0023 A67-10494

Oscillation theorems for second order differential equations 01 p0105 A67-10522

Forced periodic vibrations of homogeneous isotropic uniformly thick plate with free edges reduced to Fredholm integral equation 03 p0524 A67-13624

Periodic oscillations in model of thermal convection, noting flow direction and speed 04 p0719 A67-14464

Nonsinusoidal periodic oscillations observed in high resistivity n-type silicon compensated by zinc and phosphorus 04 p0679 A67-15142

Onset of periodic oscillations in nonlinear feedback systems 05 p0785 A67-17267

Plane elastic problem for bodies with almost periodic fast oscillating elastic parameters, obtaining asymptotic solution for boundary value problems 06 p1106 A67-18625

Periodic oscillation mode of time invariant feedback system containing relay determined, using state space approach 06 p0978 A67-18719

Difference assessment between secular and long period perturbations generated by similar initial conditions for celestial mechanics problems 09 p1563 A67-21637

Periodic regimes in two-channel automatic systems with nonlinear element in single channel part of loop, showing cross connections effect on auto-oscillations 10 p1608 A67-23616

Oscillating libration orbits with period rigorously commensurable in rational fraction to basic long period 11 p1866 A67-24775

Nonsinusoidal periodic oscillations observed in high resistivity n-type silicon compensated by zinc and phosphorus 12 p1979 A67-25165

Periodic variations of oscillation modes in He-Ne laser as result of resonator length increase 12 p1952 A67-25437

Sawtooth voltage oscillation of triangular shape for pulse width modulation pulse

shapers 13 p2089 A67-27704
 Linearization of oscillation differential equations containing even nonlinearities, using asymptotic polynomials 14 p2344 A67-28810
 Stellar pulsational instability phenomena calculated numerically for infinitesimal amplitude of central core 14 p2392 A67-28996
 Perturbation theory applied to periodic motions in three-body restricted problem 15 p2560 A67-30040
 Operational accuracy of inertial navigation system as function of accelerometer and integrator error 16 p2699 A67-30468
 Short-period oscillations of auroral cosmic noise absorption 16 p2689 A67-31910
 Space-time properties of hydroxyl emission observed by spectrophotoelectrometry, giving diagrams of periodic variations and measurement errors 17 p2848 A67-32954
 Polarization of periodic pearl-type oscillations of geomagnetic field at magnetically conjugate points 17 p2850 A67-32974
 Coefficients of odd zonal harmonics in terrestrial gravitation evaluated from orbital eccentricity analysis of artificial satellites 17 p2853 A67-33249
 Critical stability cases of almost periodic motions, showing reduction to solution of differential equations of steady motion 18 p3080 A67-34602
 Gyroscope circuit model and oscillation behavior analyzed through nonlinear differential equation derived from Euler equation 19 p3227 A67-34843
 Periodic spatial variations of parameters of positive column plasma in magnetic field along obstacle shadow due to electron wakes 19 p3273 A67-35093
 Quasi-biennial zonal wind and temperature oscillation in stratosphere and mesosphere, discussing periodicity and oscillation model 19 p3220 A67-35272
 Intrinsic frequencies and modes of periodic free vibrations of homogeneous beam with weakly nonlinear boundary conditions of Duffing type 19 p3340 A67-35509
 Approximate solutions for nonlinear differential equations to study periodic motions for analysis of pressure relief system 20 p3366 A67-37369
 Magnetosheath observations by Vela 3 at 18 earth radii, discussing substructure, shock crossings and pulsations 20 p3433 A67-37410
 Odd and even photomagnetic effect oscillations in InSb, measuring EMF at low temperatures and strong fields 21 p3677 A67-38095
 Orbital element periodic variations for satellite motion about oblate planet with low and moderate eccentricity 22 p3880 A67-39313
 Monograph on variable stars of RR Lyrae type covering spectrophotometric investigations of periodic brightness fluctuations and oscillations 22 p3880 A67-39463
 Algorithm for piecewise smooth point-to-point mapping of straight line onto straight line to determine various motions 22 p3777 A67-39778
 Moving striation modes observed in periodic sidelight intensity oscillations of He-Ne laser 22 p3816 A67-40312
 Advances in astronomy and astrophysics, Volume 5, covering zodiacal light, periodic oscillations, sunspot groups, etc 22 p3889 A67-40425
 Three-dimensional periodic motion about collinear Lagrangian equilibrium points, determining motion, variational and orbit equations and numerical integration 22 p3889 A67-40427
 Averaging method for studying system oscillations over infinite time interval subject to pulsed action 23 p4027 A67-40925
 Stability boundary of periodic oscillation described by third order differential equations near Liapunov critical case 24 p4137 A67-43108

PERIODIC PROCESS

Natural and forced oscillations of sphere-array moving with collisions, analyzing quasi-elastic properties of system 03 p0432 A67-14162
 Existence, convergence and divergence of periodic solutions for normal mode vibrations of system subject to small

perturbations 04 p0656 A67-14448
 Periodical components of fluctuations in chemical processes of Piccardi D-test 06 p0994 A67-17638
 Nonperiodic librational motions in restricted three-body problem for relatively elliptic motion of two finite masses 06 p1080 A67-17766
 Galerkin procedure for multipoint boundary value problems of general nonlinear systems 07 p1213 A67-19160
 Terrestrial behavior under action of time dependent periodic potential, treating earth as Maxwell body for shear processes 08 p1325 A67-21211
 Periodic limiting regime for sets of difference equation 11 p1813 A67-24517
 Pulsating model of closed universe, noting ordinary matter time-dependent scalar field interaction and equation for nonvanishing pressure 11 p1868 A67-24867
 Model equation for circadian periodicity 13 p2058 A67-26629
 Weighted mean latitudes of sunspots of new cycle during years of minimum solar activity, determining 15 p2552 A67-29145
 Linear integrodifferential equations describing oscillatory processes, with asymptotic solutions in terms of parameter μ through WKB method 15 p2509 A67-29232
 Reproductive property of Navier-Stokes equations, generalizing notion of periodicity 15 p2510 A67-29462
 Periodic solution of boundary value problem involving motion equation of viscous fluid 17 p2838 A67-32681
 Numerical analytical method for periodic systems described by ordinary differential equations 17 p2879 A67-32877
 Averaging method extended to physical systems described by differential equations simultaneously dependent on almost periodic fast time and periodic slow time 17 p2885 A67-33140
 Periodic fluctuations of cosmic ray diurnal variation statistically studied, using neutron and meson component data 20 p3518 A67-36993
 Irregular pulsations of decreasing period /IPDP/ events detected in magnetosphere, discussing strong correlation with magnetic index 22 p3789 A67-39497
 Weighted mean latitudes of sunspots of new cycle during years of minimum solar activity, determining 24 p4239 A67-43068

PERIODICITY

SA LONG PERIOD EFFECT

Reproductive property of Navier-Stokes equations, generalizing notion of periodicity 15 p2510 A67-29462
 Planetary influences on sunspot formation and disappearance showing periodicity in Zurich relative daily sunspot number 17 p2943 A67-32439
 Galactic anisotropies observation, giving procedure for detecting periodicities and data on sidereal daily variation amplitude 19 p3315 A67-35484
 Photometric observation data on Jupiter atmospheric activity /1964-1965/ noting three-month periodic change 22 p3879 A67-39299
 Temporal periodicity of 10 cps observed in flux of auroral electrons by rocketborne radiation detectors 22 p3790 A67-39795
 Periodicity of sunspot groups covering number and importance characteristics, formation frequency and long term spot period 22 p3890 A67-40428
 Cosmic ray diurnal anisotropy component annual means variation with two solar cycles 23 p4051 A67-40817

PERIPHERAL JET

Lift augmentation parameters in peripheral jets in proximity of ground, namely jet thickness, height from ground and jet curtain inclination [ASME PAPER 66-APM-R]

Peripheral jet behavior in hovercraft described via modified mixing theory 06 p0991 A67-18752
 Ground effect of static circular peripheral jet, comparing derived relations between jet flow, base pressure and hover height with experimental model results 15 p2415 A67-29262
 Amplification factor of air-cushion vehicles and its physical significance for bell-and

peripheral-jet concepts 16 p2596 A67-31444
 Circular planform peripheral jet ground effect machine heaving motion analyzed using motion equations 19 p3172 A67-34867
 Peripheral jet air cushion vehicle circular platform design, discussing dimensionless design parameter determination from operating height, translational speed and weight 22 p3745 A67-39726
 Peripheral jet GEM pitching characteristics analysis by longitudinal static stability and dynamic pitching motion 22 p3745 A67-39837
PERIPHERAL NERVOUS SYSTEM
 Diurnal rhythm of cardiovascular responses to active orthostasis and Schneider test performance in function diagnostics of peripheral cycle regulation [DVL-620] 11 p1747 A67-25035
 Peripheral auditory system model relating all-or-none activity of nerve fibers to acoustic stimulation 17 p2806 A67-32044
 Peripheral venous renin levels changes used to evaluate angiotensin system response to acceleration 23 p3960 A67-41700

PERMALLOY

Longitudinal Kerr and Faraday effects in Ni and permalloy films using photoelectric polarization spectrometer, choosing various refractive indices and gyroelectric constants 05 p0865 A67-16372
 Width of ferromagnetic resonance curve in nickel and permalloy thin films as function of preparation and thermal treatment techniques 12 p1981 A67-25244
 Critical alternating-magnetization curves of permalloy films, clarifying theoretical experimental problems and effect of anisotropy field dispersion magnitude on curves 12 p1981 A67-25245
 Mathematical models for loss measurements in thin Permalloy films with ramp drives 15 p2536 A67-29649
 Theoretical concepts about coercive forces in Permalloy films, considering variations as function of applied stress 17 p2920 A67-32889
 External stress effect on coercive force in Permalloy film 17 p2920 A67-32890
 Dependence of electric resistance of thin Permalloy films on substrate temperature during evaporation and vacuum heat treatment 20 p3514 A67-37555
 Worm motion of domain walls in Permalloy films using Kerr magneto-optic apparatus under pulse drive with nanosecond rise time 22 p3860 A67-39901
 Large angle flux reversal of Permalloy magnetic films investigated from experimental results of switching characteristics 22 p3860 A67-39903
 Electrically tunable low pass filter using Permalloy films near resonance 22 p3772 A67-39906
 Structural studies of FeNi-FeNiMn type thin films with ferro-antiferromagnetic coupling by Lorentz electron microscopy 24 p4206 A67-43109

PERMEABILITY

SA DIELECTRIC PERMEABILITY

Permittivity and permeability of smooth convex body, using ray tracing technique for vector fields 01 p0020 A67-10014
 Temperature dependence of complex initial magnetic permeability of cobalt-zinc ferrites over 0.1-2000 mc frequency range 01 p0128 A67-10079
 Metering and pumping equipment for test channel for high altitude permeability tests of parachute cloth, noting permeability of MIL-C-7350 B, type I fabric 02 p0182 A67-12789
 Piezomagnetic coefficients in magnetostrictive equations, permeability extrema and elastic moduli of Ni-Co-Mn ferrites 05 p0863 A67-16703
 Permeability of porous materials of refractory compounds, determining experimentally relation between gas permeability, porosity and particle size 09 p1517 A67-21875
 Gland design variation effects in gaseous helium seal performance from O-ring permeation measurements at pressures up to 1000 psi 17 p2801 A67-31992
 LF permeabilities of superconductor due to surface currents calculated for magnetic field conditions 22 p3856 A67-39439

PEROXIDE

SA HYDROGEN PEROXIDE

1, 3-diones and beta-ketoesters with cobalt for room temperature curing of unsaturated

polyester resins by organic
peroxide 24 p4175 A67-42420

PERSEID METEOR
Perselid meteor brightness studied from
data of photoelectric observations by use of
electronic multiplier 11 p1867 A67-24846

PERSONALITY
SA DEPERSONALIZATION
Second order personality factor analysis
applied to air traffic control
specialists 13 p2063 A67-26929
Nonphysical forces /human soul and
personality/ analyzed to explain validity
limits of laws of physics, discussing
Descartes dualism, quantum mechanics,
coincidences, determinism,
etc 18 p3077 A67-33500

PERSONALITY ASSESSMENT
Naval jet replacement pilot training
failures examined for significant
data 23 p3966 A67-41579

PERSONNEL
SA ASTRONAUT
SA FLYING PERSONNEL
SA MEDICAL PERSONNEL
SA PILOT
SA SPACECREW
Group dynamics approach to resistance or
counterpart of planning, conversion and
management of automatic data processing
systems design
[ASME PAPER 66-WA/MBT-10] 04 p0740 A67-15334
Impact of microelectronics on utilization
and training of maintenance
personnel 18 p2994 A67-34342

PERSONNEL SELECTION
SA PHYSICAL EXAMINATION
SA PILOT SELECTION
Optimized distribution of personnel
reduction in naval overhaul and repair
activities with minimum reduction in
readiness 01 p0016 A67-10932
Advanced feedback system stimulation
technique for strategic planning in business,
noting manpower
allocation 04 p0739 A67-14498
Blood pressure response to carotid sinus
pressure in normal and vasomotor instability
subjects evaluated for personnel selection
for flying training 05 p0756 A67-16290
Spacecraft habitability, discussing chemical
and bacteriological changes, air
contamination and biological compatibility
for crew selection 13 p2061 A67-26754
Research astronaut 13 p2062 A67-26763
Prolonged space flight effects on crew
members health concerning crew selection
test methods 16 p2613 A67-30911
Airline pilot recruitment, role, capability
and training 18 p2993 A67-34073
Manpower planning concept assuring
personnel availability for space
missions 18 p3162 A67-34679
Tape recorder for routine auditory
screening of civil aviation personnel and
criticism of whispered voice auditory
test 18 p2993 A67-34725
Psychological/psychotechnical selection of
French cosmonauts with reference to
ballistic, orbital and space
flight 19 p3179 A67-35066
European approaches to physiological and
psychotechnical selection and training of
cosmonauts 20 p3375 A67-36925
Clean room justification guidelines
including contracts, proposals, work loads,
environmental requirements, equipment and
personnel selection 23 p3987 A67-40855
Naval jet replacement pilot training
failures examined for significant
data 23 p3966 A67-41579
Medical support for SR-71 aircraft crew
members, describing crew selection, flight
preparation and medical
examinations 23 p3966 A67-41600
Motion coordination under conditions of
intermittent acceleration and weightlessness
during parabolic aircraft
flight 24 p4112 A67-41858

PERSPECTIVE
SA DEPTH PERCEPTION
Earth azimuthal perspective projections
/cosmographic projections/ in space
photograph interpretation 03 p0419 A67-13264
Holographic technique for restoration of
third-dimension information in recording of
conventionally focused
photographs 07 p1188 A67-19788

Perspective and path length effects on
determination of spatial distribution of
auroral luminosity from optical
observations 17 p2851 A67-33206

PERSPIRATION
S SWEATING
PERT PROJECT
Comparison between Monte Carlo and
PERT models, noting PERT errors and
Monte Carlo simulation for Voyager
spacecraft development
[AIAA PAPER 67-209] 06 p1097 A67-18513
F-111 fixed price contract management,
discussing weapon system management,
acquisition, controls and techniques to
circumvent inherent problems
[AAS PAPER 66-153] 08 p1430 A67-20971
F-111 fixed price contract management,
discussing weapon system management,
acquisition, controls and techniques to
circumvent inherent problems f-111 fixed
price contract management, discussing
weapon system management, acquisition,
controls
[AAS PAPER 66-153] 13 p2233 A67-27554
Applications of Program Evaluation and
Review Technique /PERT/ in
NASA 15 p2583 A67-30222
Network-diagram methods theory,
discussing CPM, PERT, MPM, noting
applications to technology and
sociology 16 p2783 A67-31631
Task distribution, overall network, flow
diagram and data processing of PERT
method controlling development of ELDO-A
rocket third stage 16 p2783 A67-31632
PERT /Program Evaluation and Review
Technique/ planning method gives project
management means for controlling project to
accomplish task in shortest possible
time 18 p3161 A67-33634

PERTURBATION
SA LUNAR PERTURBATION
SA ORBIT PERTURBATION
SA PLASMA PERTURBATION
SA SATELLITE PERTURBATION
SA SECULAR PERTURBATION
Perturbation estimation theorems and
stability of plane steady curvilinear flows of
ideal fluid 03 p0402 A67-12883
Automatic adjustment of amplification
factor of control systems in response to
perturbation 03 p0389 A67-13080
Existence, convergence and divergence of
periodic solutions for normal mode
vibrations of system subject to small
perturbations 04 p0656 A67-14448
Optimum switching function of relay
servosystem subjected to stationary Gaussian
random input found by perturbation
method 05 p0783 A67-18445
Stability and asymptotic behavior of
perturbed nonlinear systems of ordinary
differential equations 12 p1961 A67-26060
F layer critical frequency perturbations
due to low altitude nuclear
explosion 13 p2107 A67-26309

PERTURBATION THEORY
Time dependent perturbation theory
applied to calculating probability field
ionization as function of atom-metal
separation 01 p0116 A67-10206
Concentration of stresses around
curvilinear holes in thin shells solved with
nonlinear law of elasticity, reducing problem
by boundary shape perturbation
method 01 p0158 A67-10218
Oscillation frequency of maser oscillator
calculated using perturbation theory, noting
traveling wave effect 01 p0089 A67-10395
Effective mass Hamiltonian for conduction
band g factor anisotropy of indium
antimonide in magnetic
field 01 p0134 A67-10785
Differential equation solution by
separation of multiplicative derivative, by
perturbation method, by reduction to
Volterra equation and by integral
series 01 p0107 A67-11250
Unsteady interaction between blunt bodies
and shock wave, comparing reflected shock
wave velocity decrease for plane spherically
blunted cylinders 01 p0008 A67-11294
Cadmium telluride optical absorption edge
due to exciton creation with simultaneous
absorption of longitudinal optical phonons
calculated by perturbation
theory 02 p0281 A67-11493
Harmonic analysis of perturbed satellite
motion from exact solution for point motion
about two fixed centers

[ONERA-TP-420] 02 p0320 A67-11494
Numerical study of Newtonian potential
perturbation effects on satellite motion
about planet 02 p0321 A67-11496
Shock wave formation due to nonlinear
vibrations in tube containing fluid subjected
to transverse magnetic field with plane
heater at midsection and externally supplied
energy 02 p0273 A67-12058
Near circular orbit of satellite in
terrestrial gravitational field analyzed, using
approximate solution of perturbed Kepler
motion 02 p0327 A67-12373
Stability in the sense of Liapunov,
Poincare, Lagrange and others for dynamical
systems 02 p0268 A67-12502
Perturbation theory for solving Vlasov
equation for strong plasma turbulence, using
statistical set of exact particle
orbits 02 p0275 A67-12551
Singular perturbation theory of
differential equations applied in control
engineering, noting asymptotic expansion of
solution 02 p0227 A67-12681
Perturbation theory and quantum
mechanical applications - Seminar, University
of Wisconsin, Madison, October
1965 02 p0270 A67-12721
Perturbation theory in molecular quantum
physics using variational
principles 02 p0270 A67-12722
Zero order Hamiltonian in perturbation
theory for eigenvalue problems of atom in
magnetic field 02 p0271 A67-12723
Variational perturbation equations and
time-independent Schroedinger equation for
two-, three-and four-electron
atoms 02 p0271 A67-12724
Atomic and molecular time-dependent
quantum-mechanical perturbation theory
with differential equation formulation within
Hartree-Fock
approximation 02 p0268 A67-12725
Stationary methods in continuous spectra
perturbation theory of nonrelativistic
quantum-mechanical scattering in Hilbert
space 02 p0268 A67-12726
Quantum mechanical perturbation theory
calculation of upper and lower bounds of
energy eigenvalues using partitioning
methods 02 p0269 A67-12727
Harmonic approximation of infinite crystal
dynamics problem, noting collisional case
and action of external force on
atoms 03 p0520 A67-12930
Formulated conditions for proving
existence of invariant surfaces of system not
circumscribed by ordinary perturbation
theory 03 p0456 A67-13110
Stability of stochastic difference systems
in case of continuous perturbations subject
to Markov random effect 03 p0467 A67-13111
Perturbation theory analysis of spatial
dispersion effects on frequency addition in
crystals 03 p0434 A67-13125
Quasi-rotational oscillatory solution to
equation system with arbitrary degree of
freedom with respect to parameter in given
region 03 p0468 A67-13338
Periodic perturbations accumulation in
linear system with one degree of
freedom 03 p0469 A67-14178
Perturbation treatment of diatomic
hydrogen ion, improving polarized hydrogen-
atom treatment by using zero-order wave
function 03 p0474 A67-14333
Approximate molecular orbitals, Part
I 03 p0474 A67-14351
Mean square error vs parameter curves
determines applicability of perturbation
method 04 p0591 A67-14421
Velocity profiles for infinite cylindrical
journal bearing, using small eccentricity
perturbation calculation and modified
Reynolds number as parameter
[ASME PAPER 66-WA/APM-17] 04 p0630 A67-15408
Laminar free convection of radiation
absorbing-emitting fluid along flat plate
noting interaction effects, solving problem
by singular perturbation 04 p0727 A67-15682
Elektron I and II satellite measurements
on outer radiation belt, noting geomagnetic
field distortion and boundary dependence on
magnetic perturbations 05 p0880 A67-18110
Change in cosmic ray cut-off rigidity
caused by currents from trapped particle
motion, according to Chapman-Akasofu
radiation belt model 05 p0880 A67-18111
Relation between cosmic ray cut-off
rigidity and L parameter, solving

- approximately 7th degree algebraic equation 05 p0880 A67-16113
- Temperature perturbation in Thomas-Fermi functions for atom radius as related by Gilvray to simpler Feynman-Metropolis-Teller case 05 p0848 A67-16132
- Motion of cosmic radiation source effect on frequency spectrum of amplitude and phase fluctuations in turbulent atmosphere 05 p0761 A67-16344
- Energy spectrum of semiconductor compounds with chalcopyrite structure analyzed, using perturbation theory, noting changes resulting from crystalline and spin-orbital interactions 05 p0861 A67-16393
- Stability and dynamical response of small portions of differentially rotating stellar disks, noting decaying nonaxisymmetrical instabilities, epicyclic frequency, surface density, etc 05 p0892 A67-16410
- Intracavity time-varying perturbation of losses in gas laser using diamagnetic Faraday effect in glasses analyzed in connection with output intensity 05 p0818 A67-16646
- Evolution of nonlinear perturbations in plasmas, noting physical meaning of self-similar solution based on Korteweg-de Vries equation 05 p0853 A67-16698
- Matched asymptotic expansions method for perturbation problem of nearly equilibrium dissociating boundary layer flow 05 p0792 A67-16818
- Supersonic flow around elliptic cone with symmetrical fins, determining perturbation velocity via Germain method 05 p0749 A67-16844
- Matrix solution to free motion of point in randomly perturbed resisting medium in rotating aspherical geogravitational field 05 p0901 A67-17110
- Perturbation theory of ion concentration at great distances from body rapidly moving in collisionless plasma in constant magnetic field 05 p0855 A67-17139
- Structures of divalent and trivalent metals in terms of pseudopotentials and second order perturbation theory 05 p0869 A67-17189
- Time-invariant system of linear perturbation equations for error analyses of rocket boost inertial navigation systems 05 p0839 A67-17353
- Eckert-Brouwer orbit correction formula in general perturbations theory, expressed in rectangular coordinates and variation of astronomical elements, applied to planetary theory 05 p0904 A67-17391
- Closed form for perturbation terms of linear Boltzmann equation 05 p0847 A67-17438
- Perturbation treatment for molecular configuration using product of atomic or molecular orbits as zero-order wave function 06 p1034 A67-17826
- Perturbed motion of comet in medium of constant low density in solar Schwarzschild field, using quasi-Newton approximation, considering electromagnetic and gravitational fields 06 p1084 A67-18164
- Orbital guidance and rendezvous in inverse square central force field using perturbation method, considering elliptical and circular orbits [AIAA PAPER 67-55] 06 p1028 A67-18265
- Numerical method solution of nonlinear two-point boundary value problem associated with optimum transfer of spacecraft [AIAA PAPER 67-58] 06 p1023 A67-18267
- Astrodynamic perturbation theory in which perturbed space-vehicle motion is described in terms of osculating hodograph applied to lunar landing [AIAA PAPER 67-25] 06 p1085 A67-18304
- Periodic vibrations of systems governed by nonlinear PDEs, examining perturbation method, transverse vibrations of bar, string, beam and membrane and sound waves in enclosure 06 p1034 A67-18640
- Dynamics of spherical gyroscope considered as automatic control system operating in presence of random perturbation 06 p1006 A67-18791
- Three-photon ionization transition rates for alkali atoms, using quantum defect Coulomb functions to evaluate perturbation formula 07 p1195 A67-19496
- Integrodifferential motion equations for Jupiter satellites 07 p1250 A67-19724
- Solution within planetary theory with no secular terms in metric elements applied to problem of first order theory of Vesta disturbed by Jupiter 07 p1250 A67-19725
- Modification of Encke perturbation method for computing satellite orbits, obtaining integration of motion equations [AAS PAPER 66-93] 07 p1252 A67-19857
- Higher order perturbations of elements in three-body problem determined using methods of Krylov-Bogolubov and Poincare [AAS PAPER 66-99] 07 p1252 A67-19862
- Gravitational field of any primary determined using observations of satellites in orbit about primary, noting numerical integration technique and special perturbation methods [AAS PAPER 66-109] 07 p1253 A67-19969
- Singular perturbation problems for partial differential equations 07 p1217 A67-20019
- Extended average energy approximation of first order perturbation wave function, proposing procedure for multidimensional problems 07 p1137 A67-20186
- Instability and periodic solutions in nonlinear feedback systems obtained using perturbation theory of Hale and Cesari 08 p1310 A67-20339
- Three-body problem with all perturbations of first order represented by elliptic integrals 08 p1381 A67-20390
- Application limit of inviscid small perturbation theory to secondary flow in cascade, comparing experimental and calculated vortex strength 08 p1275 A67-20406
- Perturbation technique used to study random response of airplanes to effect of runway roughness 08 p1279 A67-20480
- Coefficient of major axis of symmetry of spherical harmonic in satellite oscillations 08 p1383 A67-20587
- Reference orbit for integration through boundaries of activity spheres, replacing six osculating Keplerian reference orbits 08 p1383 A67-20590
- Self-focusing of longitudinal electromagnetic waves in nonlinear plasma in strong magnetic field 08 p1357 A67-20822
- Induced radiation at high photon densities, noting applicability of perturbation theory to multiphoton resonance radiation of lasers 08 p1337 A67-20823
- Ellipticities of moon for radial shift and rotation of unperturbed orbit of close satellite in plane of instantaneous motion 08 p1396 A67-21178
- Linearized perturbation equations integrated for cosmological model, giving energy density fluctuations, rotational perturbations, gravity waves and estimated anisotropy of microwave radiation 08 p1398 A67-21233
- Nonlinear plasma wave equation in periodic solutions obtained by perturbation scheme 08 p1364 A67-21398
- Inclination variation with time of 24-hr low inclination orbits perturbed by solar-lunar gravitation 08 p1402 A67-21508
- Electromagnetic wavefront perturbations from plane wave propagation resolved into random tilt and residual phase perturbation 09 p1461 A67-21596
- Flow of ideal compressible electrically conducting fluid in traveling wave accelerator, using multiple coordinate method to approximate small perturbation solution 09 p1544 A67-21849
- Optimal control of variable structure system in presence of perturbation, discussing quality control and preservation of sliding plane 09 p1483 A67-22081
- Nonlinear system response to pulse excitation, solving problem via Poincare perturbation method 09 p1533 A67-22153
- Perturbation technique based on hydraulic analogy for estimating optimum efficiency and performance of axial flow compressor from description of geometry and aerodynamic environment 09 p1560 A67-22491
- Longitudinal stability of rigid glider in towed flight, calculating lift coefficients for various rope-plane configurations 09 p1441 A67-22607
- Existence, uniqueness and stability investigation of periodical solutions for nonlinear hyperbolic partial differential equations 10 p1674 A67-23387
- Scattering of circularly polarized electromagnetic wave in Coulomb field, noting coalescence of two-wave quanta into one quantum of double frequency 10 p1666 A67-23594
- Numerical solution methods of invariant imbedding equation for reflection function of spherical shell with absorption and isotropic multiple scattering 10 p1680 A67-23634
- Perturbation theory applied to study of electron states and interband optical transfers in strong electric fields of semiconductors 10 p1695 A67-23659
- Stability of almost stationary periodic solution of Navier-Stokes equation, examining spectrum of relevant stationary problem 10 p1675 A67-23677
- Nonlinear hydrodynamic stability theory of one-dimensional detonations based on perturbation techniques, detailing cases of ideal gas unimolecular reactions 11 p1774 A67-23857
- Wave propagation in hot plasma in cylindrical waveguide with arbitrary axial magnetic field, treating boundary value problem by perturbation expansion 11 p1826 A67-23874
- Matched asymptotic expansions for solution of singular perturbation problem of stresses and deformations in pressurized toroidal membrane 11 p1871 A67-24086
- Singular characteristics of dynamic systems with steady state motion, noting effect of constantly acting small perturbations 11 p1818 A67-24147
- Power series solutions of singular vibration problems converted to quotient of polynomials by transformation into continued fractions, using perturbation technique [ASME PAPER 67-VIBR-7] 11 p1872 A67-24167
- Parametric coupling analyzed in electrical RLC circuit coupled with mechanical system through nonlinear inductance [ASME PAPER 67-VIBR-30] 11 p1797 A67-24188
- Strong small perturbation solutions for steady supersonic flows of inert or reacting gas mixtures around plane corner 11 p1778 A67-24230
- Gravitational instability due to small irregularities and implications for early universe and galaxy formation 11 p1860 A67-24483
- Soviet book on theory of inertial navigation, autonomous systems 11 p1817 A67-24513
- Visual presentation of geomagnetic displays using normal ionospheric current system with line separation inversely proportional to field perturbation intensity 11 p1788 A67-24699
- Stability of points of equilibrium in restricted problem as influenced by perturbations of Coriolis force 11 p1866 A67-24773
- Undetermined coefficient method compared with confluent hypergeometric functions for solving first order perturbation equation for refractive index of He 11 p1813 A67-24787
- Possible initial perturbations development into galaxies with dissipative effects associated with transport processes treated via Boltzmann equation 11 p1867 A67-24838
- Perturbation solutions for finite inflation, under internal pressure, of elastic toroidal membrane of circular cross section 11 p1879 A67-25002
- Comet P/Wolf I motion perturbations of six planets, searching ephemeris for perihelion in August 1967 11 p1868 A67-25085
- Drift effect on diffusion spreading of plasma inhomogeneities in magnetic field, deriving expression for Fourier component potential and magnetic field perturbations 12 p1933 A67-25546
- Linearized Crocco equation for zero pressure gradient and constant viscosity density product applied to boundary layer problem 12 p1929 A67-25907
- Approximate technique using perturbation theory in analyzing microwave interaction with gyrotropic media 12 p1908 A67-26183
- Dispersion equations obtained for numerical forecasting of meteorological fields from basic hydrothermodynamic equations, using Reynolds stresses 13 p2149 A67-26272
- Plasma-radiation interaction represented by Compton effect, utilizing Boltzmann term developed according to powers of perturbation caused by electron motion 13 p2165 A67-26598
- Unsteady perturbation effect of external velocity on laminar boundary

layer 13 p2094 A67-26645
 Linear relations between ballistic
 perturbation coefficients for main problem
 of external ballistics 13 p2211 A67-26705
 Gas-solid energy exchange model, studying
 harmonic oscillator and free
 particle 13 p2098 A67-26939
 Unified theory of gas-solid energy transfer
 in perturbation approximation, examining
 physical principles 13 p2223 A67-26940
 Viscous fluid flow stability in boundary
 layer on plate, applying perturbation
 method, calculating critical values of
 modified Reynolds numbers 13 p2105 A67-27051
 Modification of Encke perturbation
 method for computing satellite orbits,
 obtaining integration of motion equations
 [AAS PAPER 66-93] 13 p2207 A67-27517
 Integrals of motion-equations for charged
 particles in axisymmetric magnetic field
 derived using perturbation theory 14 p2353 A67-27752
 Stability, probability and reliability
 relationship presented together with
 statistical problems in structural
 stability 14 p2396 A67-28082
 Dynamic buckling under step loading
 studied on basis of general nonlinear theory
 of elastic stability 14 p2397 A67-28089
 Transport coefficient expressions for
 collisions between rigid diatomic molecules,
 using perturbation method 14 p2259 A67-28298
 Flute oscillations in bounded nonuniform
 plasmas and effect of incoherently
 precessing ions, noting variational methods
 and perturbation analysis 14 p2360 A67-28555
 Constant and variable coefficient initial
 and boundary value problems for second
 order differential equations 14 p2343 A67-28626
 Numerical solutions of Poisson and motion
 equations for electron gun design, examining
 truncation error via perturbation
 theory 14 p2287 A67-28677
 Perturbation factors in angular correlation
 function for multidomain ferromagnetic
 materials determined taking into account
 magnetic field fluctuations 14 p2371 A67-28728
 Stability of interstellar gas to
 perturbations in gas pressure, magnetic field
 and cosmic ray pressure from hydromagnetic
 viewpoint taking rotation into
 account 14 p2388 A67-28832
 Compressible flow analysis in three-
 dimensional curved duct using small
 perturbation method 14 p2305 A67-28976
 Equation of state for Debye continuum
 governing nonlinear propagation of
 perturbations terminating in shock wave at
 distance 14 p2374 A67-28982
 Boundary perturbation theory in
 electromagnetism noting application to
 conducting sphere with surface
 perturbation 15 p2435 A67-29186
 Electrically conducting compressible
 viscous free jet in presence of transverse
 magnetic and electric fields solved
 analytically by perturbation
 technique 15 p2523 A67-29215
 Constitutive equations describing small
 perturbations on viscometric flows, noting
 relations with stress-relaxation moduli
 flow 15 p2469 A67-29222
 Perturbation stability in thermodynamic
 parameters of isotropic expanding universe
 which contains matter and radiation in
 equilibrium 15 p2554 A67-29459
 Evolution of nonlinear perturbations in
 plasmas, noting physical meaning of self-
 similar solution based on Korteweg-de Vries
 equation 15 p2530 A67-29869
 Difficulties arising in applying Liapunov
 first method to solution of canonical systems
 and ways to overcome them 15 p2511 A67-29885
 Nonlinear system analysis by subdividing
 total motion of system into fast and slow
 components, noting application to control
 systems 15 p2458 A67-29886
 Perturbation method for solution of linear
 matrix differential equations subject to
 initial and two-point boundary conditions
 applied to transmission lines 15 p2511 A67-30018
 Commensurability cases of asteroid and
 Jupiter within framework of secular
 perturbation theory 15 p2559 A67-30038
 Perturbation theory applied to periodic

motions in three-body restricted
 problem 15 p2560 A67-30040
 Perturbation theory methods as applied to
 first order differential equation 15 p2560 A67-30041
 Quasi-isomorphic response of perturbed
 systems for slow coefficient variation of
 matrix system differential equation 15 p2512 A67-30050
 Spinor representation of energetic
 identities of Kepler motion, showing identity
 of Lambert theorem for position triangle
 and Stumpf theorem for velocity triangle 15 p2561 A67-30054
 Spinor algebra application to Fourier
 series transformation of spherical harmonics
 expansion representing earth gravitational
 potential at space location 15 p2561 A67-30055
 Discrete interval binary-noise perturbation
 signal application for identification and
 compensation of three-variable self-adaptive
 flight control system 15 p2572 A67-30319
 Feedback control system for hologram
 interference fringe stabilization, noting
 phase disturbances due to different
 effects 15 p2491 A67-30432
 Perturbed motion of comet in medium of
 constant low density in solar Schwarzschild
 field, using quasi-Newton approximation,
 considering electromagnetic and gravitational
 fields 16 p2741 A67-30508
 Asymptotic calculation of satellite orbit
 evolution in noncentral gravitational field of
 earth 16 p2743 A67-30724
 Time of flight expressed in terms of
 perturbed true anomaly in case of large
 eccentricities 16 p2743 A67-30726
 Deviation of path of orbiting body
 calculated from nominal or reference
 trajectory 16 p2744 A67-30729
 Counterpart of Stokes hydrodynamical
 paradox for linearized viscous fluid flow
 obtained from application of singular
 perturbation to Oseen equations 16 p2657 A67-30827
 Time independent two-dimensional Navier-
 Stokes equations solutions from singular
 perturbation theory, determining
 properties 16 p2657 A67-30828
 Motion in ternary stellar system consisting
 of central body and close and distant
 companions 16 p2746 A67-30956
 Second partial derivatives of position and
 velocity vectors components developed with
 respect to same vectors components at
 arbitrary epoch 16 p2696 A67-30960
 Approximate calculation of coefficients in
 equation for perturbed motion of rigid body
 containing liquid 16 p2765 A67-31051
 Invariant curves dissolution and
 nonapplicability of third integrals explained
 examining perturbation values and initial
 conditions and resonance phenomena 16 p2748 A67-31140
 Celestial mechanics and adaptation of
 perturbation methods and numerical
 integration techniques to stellar
 dynamics 16 p2748 A67-31141
 Dispersion equation for stability of steady
 turbulent state obtained from perturbation
 theory and applied to drift cyclotron
 instability of plasma 16 p2719 A67-31230
 Axial nonuniform perturbations of
 electromagnetic propagating structures
 analyzed, using nonlinear phase progression
 from perturbation theory of quantum
 mechanics 16 p2626 A67-31345
 Iterative technique for calculating
 electromagnetic propagating structures with
 nonuniform gross perturbations obtaining
 convergence improvement 16 p2626 A67-31346
 Particle trajectory analysis with
 perturbation series, noting position and
 velocity error estimation for restricted
 three-body problems 16 p2749 A67-31425
 Plasma conductivity measurement,
 applying Fishbeck nonperturbing
 method 17 p2896 A67-32165
 Stability conditions for gas stabilized DC
 electric arc in plasma-arc torch determined,
 using small perturbation technique
 schematic feed circuit 17 p2897 A67-32173
 Analyses of small and large-deflection
 problems of clamped skewed plates under
 uniform pressure 17 p2958 A67-32407
 Hamiltonian formalism for collisionless
 electron plasma nonlinear kinetics using
 quantum statistical perturbational
 treatment 17 p2902 A67-32670
 Scattering problem for partial difference

equations with finite perturbation and
 inverse problem determining perturbation 17 p2817 A67-32885
 Approximate solution for hypersonic flow
 past unyawed cone by small disturbance
 stream function equation 17 p2793 A67-33024
 Perturbation theory applied to study of
 electron states and interband optical
 transfers in strong electric fields of
 semiconductors 17 p2924 A67-33340
 Action variables to take account of
 essential characteristics of Delaunay lunar
 theory 18 p3118 A67-33687
 Transition probabilities for molecular
 collision excitation by differential equation
 matrix, approximations, perturbation theory,
 etc 18 p3081 A67-33785
 Transient heat conduction in
 inhomogeneous solids with periodic
 temperature boundary conditions, using
 Keller perturbation method 18 p3159 A67-34007
 Satellite orbit determination, observation,
 dynamical theory, perturbations, drag,
 computation, etc 18 p3126 A67-34243
 Balloon satellite orbital elements predicted
 in advance by computation of solar
 radiation, gravitational perturbations,
 etc 18 p3126 A67-34246
 Weakly ionized inhomogeneous plasma in
 crossed fields, discussing magnetic field
 strength effect on stability against
 perturbations 18 p3089 A67-34296
 Dynamics of spherical gyroscope
 considered as automatic control system
 operating in presence of random
 perturbation 18 p3049 A67-34456
 Long range first order interaction between
 two excited hydrogen atoms yielding
 perturbation energy matrix, discussing
 diagonalization process 18 p3083 A67-34517
 Traveling ionospheric disturbances effect
 on and measurement of direction of
 movement of downcoming F-2 region
 perturbation 18 p3043 A67-34526
 Heat transfer in steady flow of non-
 Newtonian fluid between two walls with
 periodic deformation considered, using
 perturbation method 18 p3161 A67-34616
 Schwarzschild criterion validity, reducing
 initial value problem for hydrodynamic
 perturbation equation to time independent
 problem 18 p3029 A67-34737
 Integration of regularizing canonical and
 corresponding Hamilton-Jacobi equation
 applied to two-body problem for
 construction of perturbation
 theory 19 p3249 A67-34795
 Nonlinear effect of gravitational instability
 in expanding universe, calculating second-
 order density perturbations by iteration
 method 19 p3317 A67-34891
 Radiation field interaction with particles
 in assemblage of electrons and atoms or ions
 using perturbation theory and Liouville
 equation 19 p3284 A67-35339
 Langevin similarity theorem applied to
 ballistic perturbation theory, deriving
 formulation containing temperature gradient,
 descent acceleration and kinetic height
 parameters 19 p3326 A67-35578
 Gravitational waves, calculating velocity of
 propagation using perturbation
 method 19 p3262 A67-35708
 Nonlinear features of geostrophic
 adjustment in one-dimensional barotropic
 atmosphere number 19 p3253 A67-35917
 Von Zepel method and Hamiltonian
 perturbation mechanics used for orbits at
 resonance with tesseral harmonics of
 geopotential 19 p3328 A67-35959
 Hansen planetary theory representing
 position of disturbed planet as deviation in
 time and space from position of fictitious
 planet with Keplerian motion
 [AIAA PAPER 67-565] 19 p3328 A67-35961
 Nonlinear analysis of earth-moon system
 motion stability in three dimensions near L4
 libration point when perturbed by
 sun 19 p3328 A67-35962
 Electromagnetic and pressure fields
 produced by current distributions in
 compressible magnetoplasmas determined
 using perturbation theory 20 p3496 A67-36312
 Electromagnetic wave propagation in
 waveguides calculated together with electric
 and magnetic fields by perturbation
 method 20 p3382 A67-36882
 Perturbation scheme deriving geomagnetic
 Euler potentials applied to magnetospheric
 model with solar wind

effect 20 p3434 A67-37423
 Kato perturbation theorems applied to ordinary differential equations in Banach space 20 p3478 A67-37575
 Variational approximation for ground state of perturbed Schrodinger equation with single variable wave function 20 p3479 A67-37600
 Perturbation method using stream function for investigating anisotropic wave propagation describable by hyperbolic differential equations 21 p3811 A67-37891
 Method for determining physical interactions in system of bodies with arbitrary perturbations, using vector form equation 21 p3657 A67-37987
 Spin-spin coupling constants from perturbation-variation and first order perturbed trial function assumptions 21 p3658 A67-38003
 Indium antimonide hole surfaces approximated within second order perturbation theory, discussing energy contours, Baguley cyclotron resonance data and maximum energy value 21 p3679 A67-38255
 Stability of almost stationary periodic solution of Navier-Stokes equation, examining spectrum of relevant stationary problem 21 p3653 A67-38278
 Perturbation theory of ion concentration at great distances from body rapidly moving in collisionless plasma in constant magnetic field 21 p3668 A67-38481
 Stability and instability properties of differential system, discussing matrix and roots 21 p3653 A67-38558
 Perturbation scheme for linear system performance determination based on component performance information 21 p3654 A67-39063
 Statistical properties of perturbations in rocket path determined to minimize statistical quantities 22 p3878 A67-39182
 Shock structure in kinetic theory of gases, solving Krook model of Boltzmann equation with small perturbation technique 22 p3782 A67-39196
 Optimal control of quasi-linear system perturbed motion, developing approximation method 22 p3776 A67-39305
 Dissociation and recombination of diatomic molecules by invert third bodies described by stochastic theory 22 p3756 A67-39386
 Magnetic element impurity effects on semiconductor resistivity, calculating spin dependent scattering of free carriers 22 p3859 A67-39625
 Damping constant of electromagnetic wave in plane parallel waveguide with ferrite resonant isolator, using perturbation theory, considering dielectric and magnetic losses 22 p3770 A67-39659
 Perturbation theory for solving initial and boundary value problem in unsteady MHD flow past thin symmetrical bodies with inwardly diffusing magnetic field 22 p3850 A67-39707
 Quasi-linear perturbation expansion used to study evolution of localized disturbance in plasma 22 p3851 A67-39985
 Polarized and depolarized scattering from perfectly conducting rough surface, theory based on Fourier transform and small perturbations polarized and depolarized scattering from perfectly conducting rough surface, using theory 22 p3762 A67-40076
 Relative equilibrium of liquid cylinder investigated for uniform rotation in uniform axial electric field 22 p3787 A67-40135
 Viscoelastic fluid isotropic turbulence decay approximating non-Newtonian effects by perturbation method 22 p3787 A67-40221
 Nonlinear hydrodynamic equation term effects on rotational fluid motion in galactic plane, discussing velocity perturbations and discontinuities 22 p3893 A67-40502
 Josephson effect and quantum coherence measurements in superconductors and superfluids, discussing perturbation theory and tunnel junctions interference effects 22 p3866 A67-40549
 Soviet book on motion of artificial satellites in earth gravitational field covering perturbation theory, force field, algorithms for calculations, etc 23 p4063 A67-40734
 Perturbing gravitational potential of earth expanded with Taylor series along earth relief levels 23 p3996 A67-40859
 Intermediate range intermolecular forces

with overlapping wave functions and exchange effects calculated for ionized H molecule using perturbation theory 23 p4029 A67-40971
 Perturbed region behind diffracting shock wave on plane-walled convex corners at supersonic speed 23 p3990 A67-41172
 Nozzle form optimization from Mach distribution in supersonic region, defining perturbation functions 23 p3929 A67-41248
 Propagation of signals in transmission lines with distributed capacitance and conductance for nonlinear parameters 23 p3982 A67-41396
 Small perturbation analysis on mass conservation stability in solid propellant combustor, discussing parametric model 23 p4084 A67-41721
 Temperature variations of satellite with radiatively coupled isothermal inner shell having heat source analyzed via perturbation method for differential equations 24 p4253 A67-42051
 Papers on fluid mechanics and singular perturbations including Navier-Stokes equations, boundary layer theory, etc 24 p4141 A67-42167
 Perturbation theory definitions and overlap theorem proved and applied to small Reynolds number flows 24 p4142 A67-42168
 Singular perturbation methods for two-dimensional lifting low Reynolds number flow 24 p4091 A67-42169
 Prandtl limit behavior near zero skin friction, with perturbation methods generalizing Poiseuille and Couette flows 24 p4142 A67-42170
 Elektron I and II satellite measurements on outer radiation belt, noting geomagnetic field distortion and boundary dependence on magnetic perturbations 24 p4214 A67-42786
 Change in cosmic ray cut-off rigidity caused by currents from trapped particle motion, according to Chapman-Akasofu radiation belt model 24 p4214 A67-42787
 Relation between cosmic ray cut-off rigidity and L parameter, solving approximately 7th degree algebraic equation 24 p4214 A67-42789
 Uniformization of asymptotic expansions, constructing counterterms by nesting increasing number of extensions for both secular and singular perturbation terms 24 p4190 A67-43094
 Perturbation theory for exchange forces using Brillouin and Schrodinger equations 24 p4194 A67-43115

PETN

S PENTAERYTHRITOL TETRANITRATE

/PETN/

PETROGRAPHY

SA ROCK

Microscopic particles from various deposits analyzed for possible extraterrestrial origin 09 p1570 A67-22693
 Orgueil carbonaceous meteorite composition and mineral texture including petrogenesis and origin of organic content and mineralized microstructures 10 p1710 A67-23628
 Deformation in Sudbury structure, Ontario, suggests petrographic evidence for origin by meteorite impact 15 p2473 A67-29158
 Petrographic and microprobe analysis of unequilibrated ordinary chondrites, studying textural, mineralogical and chemical characteristics 16 p2750 A67-31451
 Prototype model of petrographic microscope for lunar and planetary missions, discussing design and fabrication 19 p3229 A67-35320
 Chromite composition in chondrites using electron microprobe technique, discussing petrographic origin and vanadium abundance 24 p4232 A67-42612

PETROLEUM

SA KEROSENE

New aerospace-related technology in nonaerospace applications, noting NASA and petroleum industry 07 p1269 A67-20263

PETROLOGY

SA METAMORPHISM

SA ROCK

Ultramafic rock content of Na, Mn, Cr, Sc and Co determined by neutron activation technique 07 p1183 A67-20142
 UV reflectance measurements of granitic, gabbroic and serpentine rocks used to identify lunar silicates 09 p1569 A67-22689
 Neutron activation analysis for terrestrial and meteoritic rock major element

abundance, noting possible application to extraterrestrial surface analysis 11 p1749 A67-23976
 Mercury abundance in various meteorite and rock types determined by neutron activation analysis, relating data to evolution of meteorites and earth 11 p1858 A67-24064
 IR spectral techniques for satellite geodetic surveying, discussing spectral matching techniques for discriminating between different types of rocks [AIAA PAPER 67-284] 12 p1938 A67-26001
 Chondritic meteorites two-dimensional classification grid based on chemical and petrologic subdivisions 14 p2391 A67-28949
 Lunar surface rocks viscosity, volcanic origin, etc, with reference to Flamsteed Ring putative magma 15 p2553 A67-29159
 Electron microprobe analysis of quartz and alumina darkening upon solar wind ion bombardment, noting existence of iron, tungsten and carbon in samples 16 p2753 A67-31745
 Lunar surface materials choice narrowing method via albedo, color and polarization property examinations to find possible candidates for lunar surface model 21 p3701 A67-37897
 Geomagnetic field polarity inversion, discussing reverse magnetization of volcanic rocks 21 p3821 A67-38882
 Indium concentrations determined by neutron activation in petrological suite of L-group chondrites 23 p4069 A67-41474
 Chemical analysis of glass bombs from Ries crater area investigated for textural differences due to shock melting and cooling rates 24 p4233 A67-42621

PFM

S PULSE FREQUENCY MODULATION

/PFM/

PH FACTOR

Enzymatic activity and inhibition, thermal stability and electrophoretic properties of induced and constitutive acid phosphatases of *Escherichia coli* 10 p1598 A67-23397
 Acid-base relation of blood and cerebrospinal fluid with respect to respiratory regulation studied in man at high altitude 17 p2806 A67-32333
 Slip casting of niobium carbide powders noting effects of dispersed phase contents, pH variation and temperature on molding properties 20 p3466 A67-36909
 Dog adaptation to increased carbon dioxide levels in normoxic environment, noting effects on arterial pH and bicarbonate level 23 p3950 A67-41537
 Chronic hypercapnia effects on pH level, Ca and P metabolism and electrolyte metabolism in normal sedentary man 23 p3955 A67-41605

PHANTOM AIRCRAFT

S F-4 AIRCRAFT

PHARMACOLOGY

SA DRUG

Pharmacology in prolonged space flight noting increasing resistance of organism to extremal flight factors, use of pharmaceuticals during flight, etc 02 p0185 A67-12320
 Effects of radiation protective pharmacological agents /cystamine, serotonin AET, strychnine, etc/ on animals subjected to centrifugation, for application to astronauts 12 p1902 A67-25654
 Pilot self-medication causes and dangers, classifying dangerous drugs and studying effects on pilot performance 16 p2614 A67-31474
 Drugs for protection and stimulation of biological functions of spacecrews, noting experimental results on transverse-acceleration resistance of animals 20 p3367 A67-36254
 Antimotion sickness drugs and placebos effect on altering motion sickness susceptibility in Skylab aircraft aerobatics and Slow Rotation Room dial test 21 p3574 A67-38083
 Treatment of psychiatric diseases in ground staff and aircrew, discussing psychopharmacology in aeronautical medicine 23 p3967 A67-41603
 Pharmacological alterations of vibration tolerance 23 p3955 A67-41613
 Reactivity of animals to caffeine and strychnine during transverse acceleration aftereffects 24 p4111 A67-41850

PHARYNX

Intrapulmonary pressures chosen during

immersion in thermally neutral water, comparing transpharyngeal and transthoracic pressure gradients for various breathing devices 22 p3751 A67-39604

PHASE

S GAS PHASE
S LIQUID PHASE
S LUNAR PHASE
S RETURN-TO-EARTH PHASE
S SINGLE-PHASE FLOW
S SOLID PHASE
S TWO-PHASE FLOW
S TWO-PHASE SYSTEM
S VAPOR PHASE

PHASE ANGLE

Plasma electron density range measurable by microwave extended by phase angle being expanded by impedance transformation 05 p0854 A67-16982
Hypothetical control system with 30 db/decade attenuation characteristic and constant phase margin of 45 degrees, presenting phase angle stabilization technique that improves actual systems 06 p0977 A67-18416
Five to fifty MHz direct reading phase meter with hundredth degree precision 09 p1494 A67-21620
Parallel operation of same frequency transmitters on common antenna examining several designs 16 p2637 A67-31003
Strong reflection from underlying surface effect on range-only radar measurements, deriving phase angle between side-and carrier-frequency oscillation 16 p2624 A67-31030
Plasma produced by shock wave in low pressure gas measured for phase angle by microwave reflection probes 18 p3088 A67-34076
Satellite orbit determination by measuring arrival angle of two transmitted waves with different frequencies 20 p3382 A67-36774
Hard limiter effect on test signal phase angle, considering single and two interfering signals 21 p3586 A67-38955
Mercury radio emission observation yielding average brightness temperature and planetocentric phase angle relation 22 p3889 A67-40240
Photometric data on Mars opposition effect /nonlinear brightness surge at zero alpha phase angle/ noting phase curve steepness 24 p4226 A67-41838

PHASE CHANGE

Dysprosium crystalline structure and phase transition from helioid antiferromagnetism to paramagnetism 01 p0133 A67-10744
Transistor behavior in phase inverter at LF as function of type /p-n-p or n-p-n/ and value of internal capacity 01 p0038 A67-10770
Phase reversal in lunar variations of critical frequencies of F-2 layer at Waltair, India 01 p0060 A67-11232
Surface temperature of deflagrating ammonium perchlorate crystals calculated from crystal phase transition thickness [AIAA PAPER 67-68] 06 p1073 A67-18469
Phase equilibrium and physicochemical properties of titanium aluminide-titanium stannide-zirconium quasi-ternary alloy 07 p1204 A67-19264
Phase state of thin layers of vapor deposited InTe with 50-60 percent Te 08 p1369 A67-20994
Analytic solutions of heat equation for case when both temperature and heat flow rate are prescribed at single fixed boundary applied to phase change problems 08 p1428 A67-21432
General method of averaging applied to slightly damped librations problem in perturbed one degree of freedom system 08 p1424 A67-21435
X-ray analysis of lattice structure of terbium crystals at 120 to 300 degrees K 09 p1555 A67-22066
Intermediate phases in alloys of Ti with Ir, Rh and Qs indicate possibility of polymorphism 13 p2131 A67-26472
Dysprosium crystalline structure and phase transition from helioid antiferromagnetism to paramagnetism 13 p2176 A67-26773
Average heat of atomization in correlating composition and temperature limits of stability of NaCl type structure among IV-VI compound semiconductors 13 p2184 A67-27570
Solution of one-dimensional diffusion equation of heat flow normal to surfaces, prescribing potential and flow rate along moving parametric curve 14 p2405 A67-28254

Fluoric solar attitude control device functioning as sensor and actuator, noting design principles and operation 17 p2954 A67-31982
Solar diurnal wave from underground muon detectors and relationship to solar activity over 11-year cycle, noting phase changes 18 p3116 A67-33514
Resonance absorption and zero-field nuclear spin relaxation in normal and superconducting aluminum, studying phase change 19 p3303 A67-35044
FM laser frequency stabilization employing stabilization discriminant derived from residual phase variation and laser beat note 19 p3240 A67-35622
Stress field on epitaxial dislocation line in weakly alloyed titanium, calculating energy of phase boundary and contribution of latter to plastic deformation 20 p3487 A67-37117
Phase relationship between solar activity changes and changes in solar wind parameters over 11-year cycle 20 p3519 A67-37395
HF oscillators phase bridge based on phase synchronization of identical and adjacent frequencies 21 p3590 A67-37947
Surface temperature of deflagrating ammonium perchlorate crystals calculated from crystal phase transition thickness [AIAA PAPER 67-68] 21 p3688 A67-38859
Qualitative and quantitative variation in alloy phase composition with temperature and age hardening length, studying structural diagram 22 p3818 A67-39321
Phase distribution in antenna aperture for small displacement of antenna feed from focal point calculated on basis of theorem proved 22 p3762 A67-39870
Iron titanium oxides and oxygen fugacity in volcanic rocks noting temperature effect 22 p3792 A67-39975
Anodic oxidation usable for efficient phase analysis technique for V-Ga alloys, identifying interference colors in absence of oxygen impurities 23 p4036 A67-40713
Critical temperature near superconducting phase transition investigated for alloys and pure superconductors 24 p4200 A67-41867
Distant atmospheric waveform at night analyzed using digital computer for VLF phase spectra 24 p4149 A67-42068
Array antenna directive pattern scanning utilizing difference in phase lead between heterodyne and converted signals at feeder 24 p4130 A67-42234
Pump frequency reduction in Adler tubes, examining spatial harmonics of quadrupole structure field and suggesting use of cophase connection 24 p4130 A67-42240

PHASE COHERENCE

Book on phase coherent communication principles based on statistical communication theory, discussing coherent receivers and analog and digital modulation systems 04 p0578 A67-15618
Signal design problem of optimal waveforms for transmission through phase incoherent channel 06 p0962 A67-17945
Sum radiation frequency generation by ruby and neodymium lasers in KDP crystals 07 p1196 A67-19734
Timing error and noisy phase reference joint effect on system performance of coded partially phase coherent reception 17 p2811 A67-32118
Injection locked pulsed magnetron in coherent echo detection system studied by observing echo pulses from acoustic delay medium 20 p3401 A67-37221

PHASE CONTRAST

Phase objects observation method using spatial filtering and Hilbert transform 20 p3458 A67-36388
Wind tunnel hypersonic flow visualizations under low flow density conditions, comparing schlieren and phase-contrast methods 23 p3985 A67-40568
Holography /phase-recording of diffracted wavelets/ for phase contrast and stroboscopy, interferometry in polarized light and 3-D photoelasticity 23 p3999 A67-41179

PHASE CONTROL

Standard frequency transfer to local oscillator, removing modulation and producing continuous stable carrier 02 p0210 A67-11530
Constant phase local oscillator distributing signals for radio telescope, measuring phase length of transmission line 02 p0212 A67-11608

Phase separation and synchronization during separation of AM signals with overlapping frequency spectra 05 p0764 A67-16903
Main properties of phase automatic frequency control, using standard signal as additional action on self-excited oscillator 05 p0764 A67-16904
Automatic phase control /APC/ loop for stabilization of phase shift in RF amplifier 05 p0778 A67-17395
Approximation method of determining statistical characteristics of phase coordinates of linear automatic control systems 06 p0978 A67-18792
Two-phase phase control valve with reactive compensating resistances, based on two-phase transformer with axisymmetric irreversible rotating magnetic field 07 p1150 A67-19319
Phase compensation technique for signals received at widely spaced antennas and processed at central location 07 p1155 A67-19876
Lock-on band determination for inertial system of phase automatic frequency control in presence of fluctuation noises 11 p1750 A67-23910
Two-mirror antenna with automatic phase error control, noting experimental model correlation 13 p2080 A67-27024
Phase distribution in laser aperture based on analysis of radiation in Fresnel zone 13 p2127 A67-27029
Continuous second harmonic generation of 2572 angstrom argon II laser, noting optimum phase matching, power dependence on crystal temperature, etc 15 p2497 A67-29392
Phase separation and synchronization during separation of AM signals with overlapping frequency spectra 16 p2622 A67-30879
Main properties of phase automatic frequency control, using standard signal as additional action on self-excited oscillator 16 p2623 A67-30880
Approximation method of determining statistical characteristics of phase coordinates of linear automatic control systems 18 p3018 A67-34457
Doppler frequency measurement error due to short fading relative to time constant of automatic phase control loop 21 p3584 A67-38674
Lock-on band determination for inertial system of phase automatic frequency control in presence of fluctuation noises 21 p3585 A67-38938
Steady random process phase overshoot length distribution determined over given level as well as relationships for mean value and distribution 24 p4136 A67-42194

PHASE DEMODULATOR

Wideband phase-leading quadrupoles with circuit breakers and effect on envelope of modulated signal 13 p2085 A67-27706
FM signals demodulation and negative feedback modulation, deriving signal to noise ratio and noise spectrum formulas 19 p3183 A67-35562
Radio interferometry at Diane satellite tracking station, noting synchronous demodulation technique 21 p3587 A67-39052

PHASE DETECTOR

Moving target indication /MTI/ in theory and technique including description of delay lines, stalos, transistors, phase detectors and modulator 04 p0573 A67-15037
Amplitude and phase detection for determined signal with nonstationary noise, using generalization of Levin method 05 p0767 A67-17402
Automatic phase sensor for waveguide combiner in S-band ground tracking and space communication network 07 p1149 A67-19051
Large base phase meter design 07 p1186 A67-19587
Fast phase fluctuations of signal reflected from F-2 layer 07 p1144 A67-19819
Doppler frequency-measuring tracking system in which tracking filter or retuned heterodyne is used for definition of signal with unknown frequency 10 p1607 A67-23452
Extended phase detector for phase-lock loop receivers 13 p2075 A67-26408
Soviet book on SHF radio receivers covering theoretical and engineering aspects of component design, control, signal

detection, etc 17 p2822 A67-32020
 Large base phase meter 20 p3452 A67-37324
 design
 Radar station with antenna system for three target coordinates simultaneous measurements 21 p3582 A67-38498
 Frequency doubler and divider using transistorized synchronized switching phase detectors with closed feedback circuit 22 p3762 A67-39872
 Oscillating circuits with nonlinear active elements amplitude and phase frequency characteristics graphically plotted, noting effects on frequency devices 24 p4136 A67-42191
 SHF phase meters used in plasma diagnostics classified to facilitate proper phase meter selection for specific application 24 p4154 A67-42218

PHASE DEVIATION

Synthesis of phase synchronization system providing maximum level filtering of external fluctuation noise, using generalized integral criterion 03 p0393 A67-13949
 Mean and mean square directivity factor of antenna array in presence of phase and amplitude distortions 04 p0583 A67-15164
 Phase determination of signal components generated by parametric oscillator by synchronizing oscillator with respect to difference between frequencies of components 04 p0583 A67-15171
 Radio interferometer design with superlong base compensating for phase fluctuations 14 p2261 A67-28068
 Subjective responses to oscillation in yaw 15 p2427 A67-29269
 Mean and mean square directivity factor of antenna array in presence of phase and amplitude distortions 15 p2443 A67-29351
 Phase determination of signal components generated by parametric oscillator by synchronizing oscillator with respect to difference between frequencies of components 15 p2443 A67-29357
 Standard scintillation index method for describing ionospheric effects, discussing power calibration, scaling, deviations, etc 19 p3220 A67-35256
 Coherent responder used in distance Doppler tracking system, obtaining radial distance by using phase compression 21 p3656 A67-38650
 Odd value correlation coefficient and wave amplitude fluctuation effects on mean radiation pattern and antenna amplification losses 23 p3977 A67-40599

PHASE DIAGRAM

Phase diagram of W-Zr-Ti ternary alloy 01 p0093 A67-10291
 Value and sign of phase jump taking place during light reflection from multilayer dielectric film 03 p0467 A67-12892
 X-ray and thermal analyses and phase diagram of titanium chromide-tantalum chromide-niobium chromide solid solution at high temperatures 03 p0447 A67-13640
 Liapunov function of ninth order system represented by differential equation which, in phase variable form, can be represented by matrix equation 03 p0392 A67-13682
 Pressure composition diagrams of thallium rich portion of thallium-indium system at high pressure-temperature 04 p0635 A67-14511
 Microscopic and X-ray analysis of cast and annealed W-Mo-Ti alloys, plotting polythermal cross sections 04 p0638 A67-15203
 X-ray analysis of Nb-Ni-Al solid solutions, noting solubility of Nb and construction of phase diagram 04 p0638 A67-15204
 X-ray study of phase composition of refractory alloys carbide solid solutions noting hardness, electric resistance and elastic deformation energy of crystal lattice 04 p0638 A67-15205
 Book on structure of metallic alloy including phase diagram of vanadium-gallium system 05 p0827 A67-16325
 Phase diagram of vanadium-gallium system by differential thermal analysis of thirty-five 10-g V-Ga alloy samples prepared in arc oven 05 p0827 A67-16326
 High temperature condensed phase equilibria in Ti-W-O system examined, using sealed capsule technique 06 p1018 A67-18371
 Value and sign of phase jump taking place during light reflection from multilayer dielectric film 06 p1034 A67-18770
 Isothermal transformation diagrams for

titanium-molybdenum alloys 07 p1199 A67-19243
 Phase composition and structure of alloys in aluminum corner of system Al-Cu-Cd-Mn with constant manganese concentration of 0.7 percent at 500 degrees 07 p1201 A67-19251
 Phase diagrams of various titanium-phosphorus compounds and mixtures with up to 45 atomic percent P and microstructural characteristics of Ti-P alloys 07 p1203 A67-19262
 Microstructural and X-ray analysis of intermediate phases of Ti-Ir and Ti-Rh intermetallic compounds, including microhardness and fusion point variations 07 p1204 A67-19263
 Mutual diffusion characteristics of titanium-tungsten mixtures at high temperatures, noting discontinuity on concentration curve due to two-phase region presence 07 p1204 A67-19266
 Phase diagram of titanium-rich alloys of system Ti-Al, measuring resistivity and hardness through X-ray diffraction, thermal analysis, etc 07 p1204 A67-19267
 Microstructure of alloys of Ti-Fe and Ti-Cr-Fe systems, determining phase composition and incipient melting temperature 07 p1204 A67-19269
 Phase diagram of Ti-V-C system based on phase equilibria, using X-ray diffraction, microhardness measurements, etc 07 p1204 A67-19270
 Ternary system Ti-Al-V alloys analyzed using thermal, microstructural, etc, methods, plotting solidus surface in crystallization region of beta-solid 07 p1205 A67-19273
 Occurrence, decomposition kinetics and phase equilibria of cohenite, noting almost exclusive presence in meteorites containing 8 percent Ni 09 p1564 A67-21737
 Phase diagram of Nb-Ti-Zr system and superconducting properties of alloys 09 p1518 A67-22029
 Ternary phase diagram of Mo-Ti-Zr system from eleven isothermal cross sections 11 p1808 A67-24856
 Quenching examination of phase equilibrium in system lead oxide-titanium oxide-zirconium oxide, determining isotherms lines, melting points, etc 12 p1986 A67-26188
 Systems producing germanide phases noting phase diagrams of germanides of s-elements, ds-elements, fds-elements and sp-elements 13 p2175 A67-26469
 Interaction between phases of nickel aluminum-nickel titanium pseudobinary system, determining concentration dependence of properties of system 13 p2142 A67-27286
 Aluminum, Volume 1, Properties, physical metallurgy and phase diagrams 14 p2334 A67-27801
 Aluminum alloy systems physical and structural characteristics and phase diagrams 14 p2334 A67-27802
 Phase equilibrium diagrams of Al alloy systems, designating solid phases by chemical symbols and allotropic or polymorphic forms by prefixing Greek letters 14 p2335 A67-27810
 Phase diagrams of elementary auroral disturbance and restoration on earth daylight side 14 p2309 A67-27941
 Nb-N system diagram for five stable nitride phases, giving two reactions governing high temperature phase fields 14 p2337 A67-28419
 Circadian rhythms detection, estimating parameters by cosinor procedure for temporal morphology aspects evaluation 14 p2255 A67-28480
 Zn-Sb intermetallic compounds preparation for single crystals in semiconductor phase 14 p2372 A67-28826
 Premelting of predetermined sites in sodium-potassium alloys studied by microscopy 14 p2339 A67-29032
 Pulse-time modulation of first kind and block diagram of pulse time modulator studied for control system applications 15 p2455 A67-29122
 Heat resistance of Ti alloys, emphasizing significance of chemical interactions, polymorphic transformations and phase diagrams for high temperature performance 15 p2504 A67-30007

Ti-Zr-C and Ti-Hf-C alloy X-ray and microstructural studies noting homogenizing, annealing, quenching and phase equilibria 15 p2505 A67-30388
 Phase composition of titanium containing slag formed during alloying of stainless steel with titanium, noting titanium oxidation 16 p2887 A67-30842
 Phase equilibrium in cross section of Ti-Al-Cr-Fe-Si-B system 16 p2887 A67-30849
 Nagelberg formula locating Fresnel region phase center of aperture antennas examined by calculating phase patterns of radiation field 16 p2839 A67-31357
 Metallography, roentgenography and differential thermal analysis of composition temperature ranges of chromium-germanium phases 16 p2691 A67-31592
 X-ray structural and diffraction analysis of Mo-Ni-Bo system at high temperatures noting isothermal sections of phase diagram 16 p2691 A67-31595
 Nonstoichiometry of zirconium oxide and relation to tetragonal-cubic inversion in zirconium oxide 16 p2694 A67-31597
 X-ray and thermal analyses and phase diagram of titanium chromide-tantalum chromide-niobium chromide solid solution at high temperatures 17 p2875 A67-33173
 Phase diagrams for axisymmetric and asymmetric antennas analyzed by Kirchhoff integral method 18 p3010 A67-33504
 Molybdenum-boron system structural diagram, noting carbon effect on phase equilibria and temperature effects 20 p3468 A67-37177
 Ti-Al alloys ordering transformation studied by electron microscopy and electron and X-ray diffraction, showing existence of three phase fields 20 p3470 A67-37386
 Chemical diffusion coefficients and heats of activation in nickel-aluminum intermetallic phases and solid solution calculated from layer growth experiments 21 p3645 A67-38775
 Phase and chemical compositions of structural components forming in iron-nickel-chromium alloys with aluminum and titanium content 22 p3820 A67-39788
 New semiconductor compounds derived by cross substitution of group IV semiconductors, giving thermal properties and phase diagrams 23 p4036 A67-40720
 Omega phase precipitation and superconducting critical transport currents in Ti-Nb wire samples 24 p4173 A67-42347
 Translucent material /Zyttrite/ obtained from cubic phase stabilization of Y and Zr alkoxides at low temperatures, noting high surface activity 24 p4175 A67-42373

PHASE ERROR

Variation of antenna amplification ratio with distance as function of phase error at antenna aperture with exciter off-focus as error source 01 p0035 A67-10392
 Model distribution for phase error in second-order phase locked loop used to complement analytical model in signal to noise region [JPL-TR-32-1017] 01 p0026 A67-10865
 Linear phase distortions of plane resonator with tilted mirrors and effects on generation of stimulated emission in ruby crystal laser 03 p0435 A67-13130
 Imperfect excitation effect on vibration test results such as admittance, phase curve, damping coefficient, etc 05 p0920 A67-16769
 Properties determining phase linearity of microwave devices, noting effects of cascaded devices on system performance 06 p0972 A67-18578
 Radio telescope antenna phase errors due to structural rigidity and fabrication accuracy 08 p1306 A67-21346
 Basic design differences illustrating paraboloidal reflector variations, noting factors contributing to or detracting from antenna efficiency 10 p1613 A67-23413
 Feedback control system for hologram interference fringe stabilization, noting phase disturbances due to different effects 15 p2491 A67-30432
 Radio telescope antenna phase errors due to structural rigidity and fabrication accuracy 17 p2822 A67-31942
 Linear minimum variance estimation for random signal with complex phase errors, considering signal processing and optical propagation 18 p3001 A67-34111
 Second, third and fourth order phase locked loops performance characteristics

compared for optimum selection, calculating integrated square error and peak error 18 p3001 A67-34116
Near-threshold behavior of phase-locked devices, noting phase error processes 20 p3385 A67-37350
Incompatibility of microwave phase effects measurements in Mercury thermal emission with simple model for thermal behavior of planet surface 24 p4226 A67-41837

PHASE FADING

Phase cancellation of sinusoidal signals in presence of Gaussian noise for comparison and threshold decision schemes 01 p0025 A67-10860
MF and HF portions of radio spectrum relationship to communication systems, presenting amplitude and phase variation in conjunction with effects of fading, time and frequency spread and atmospheric noise [IEEE PAPER 19-CP-65-482] 11 p1755 A67-25080

Experimental determination of compression and rarefaction shock waves structure causing high pressure phase formation and decay in potassium halides 23 p3989 A67-40906

PHASE LOCK

SA DELAY LOCK

Phase locking, mode selection and noise problems in synchronous operation of microwave silicon avalanche diode oscillators to obtain large coherent output power 01 p0033 A67-10016

Locked oscillation of silicon p-n junction avalanche diodes in 50 to 140 GHz range 01 p0035 A67-10436

Trigger circuits for generating sharply defined rectangular waves phase locked to repetitive signal 01 p0036 A67-10451

Comparison of variances evaluated by Kolmogorov and Volterra techniques for phase locked loop subjected to white Gaussian input 01 p0044 A67-10480

Aircraft-to-ground communications using Applications Technology Satellite B as repeater in VHF COM 01 p0024 A67-10665

Fluctuation noise effects on phase-locked automatic frequency control system obtained using Markov processes, determining phase difference probability density and statistical characteristics 01 p0037 A67-10713

Model distribution for phase error in second-order phase locked loop used to complement analytical model in signal to noise region [JPL-TR-32-1017] 01 p0026 A67-10865

Sonic analysis for determining performance and mechanical integrity of turbine engines by using phase-locked filter and frequency ratio generator 01 p0076 A67-11141

Limiting SNR determines, for given initial detuning, probability close to unity of phase jumps in phase locked AFC system 03 p0380 A67-13580

Phase locking of pulsed Gunn oscillators with 0.3 to 1 microsecond pulse widths in S-band 03 p0382 A67-13672

Reflex klystron operation modes such as phase locked amplifier, regenerative amplifier, detector and mixer 03 p0387 A67-14101

Phase locked laser loop for amplitude and phase measuring device for coherent optical wave fronts 04 p0632 A67-15076

Phase lock system used to receive and correctly utilize signals from distant transmitter 04 p0585 A67-15814

Excess photon noise in detected photocurrent of multimode laser for uncoupled and phase locked modes 05 p0815 A67-16623

Phase locked oscillations of silicon avalanche diodes noting hysteresis 05 p0775 A67-16984

Radar phase locking technique applied to magnetron radar, measuring transmitted pulse phase with respect to state running at magnetron frequency 05 p0780 A67-17521

Spectra of unlocked driven semiconductor oscillators observed with millimeter wave reflex klystrons, noting gradual controllable frequency pulling 05 p0780 A67-17522

Centering accuracy, off-course sensitivity, mean modulation depth and relative tone phase of ILS signal measurement improved by phase locked detection technique 06 p0957 A67-17577

Optimal Wiener values of filter

parameters in phase-lock loop, noting possibility of improved performance despite deviations 06 p0973 A67-17615

Stability analysis of parametric phase-locked subharmonic tunnel diode oscillator circuits capable of bistable phase operation 07 p1153 A67-19610

CW interference and white noise effect on second order phase lock loop, using reciprocal of loop mean square phase error as index of performance 07 p1161 A67-19878

Filtering properties of frequency-stability transport circuits of molecular beam generator, noting design considerations for high efficiency 08 p1305 A67-21274

Probability of signal acquisition by phase locked oscillator system operating in frequency search mode, determining maximum admissible search rate without noise 08 p1295 A67-21275

Frequency and phase locking of laser oscillators by externally injected signal 08 p1338 A67-21309

Phase locking of longitudinal modes of gas laser by cavity mirror translation at constant velocity 09 p1510 A67-21575

Self-locking of He-Ne lasers at various mirror separations by controlling oscillation frequency with intracavity modulator 09 p1516 A67-22432

Phase locking systems and problems of frequency shifts and Doppler effect 10 p1620 A67-23508

Amplifier and self-excited oscillator employing reflex klystron with phase locking 11 p1757 A67-23907

Phase locking experimental data on injection locked X-band Gunn effect microwave oscillators 11 p1759 A67-24128

Phase locking in phase plane on modulation of driver and self-excited oscillator, using differential equation 11 p1754 A67-24725

Extended phase detector for phase-lock loop receivers 13 p2075 A67-26408

Nonlinear theory of internally loss modulated laser including effect of arbitrary atomic line shape, saturation and mode pulling 13 p2127 A67-27084

Phase and amplitude measurements of laser wavefront using laser phase-locked loop 13 p2129 A67-27494

Spontaneous visible light emission due to laser action in carbon dioxide laser plasma, examining plasma current change with phase-lock technique 14 p2331 A67-28494

Highly adaptive phase lock coherent receiving system fulfilling requirements of data and Doppler tracking receivers 14 p2271 A67-28691

Block coded frequency multiplexed PM communication system design and performance, considering simplification, cost and weight 14 p2271 A67-28694

Phase lock loop of synchronized time code translator, noting design and application 15 p2445 A67-29587

Approximate solution to nonlinear problem of pull-in range of phase locked loops, noting filter configurations and methods of analysis 15 p2446 A67-29589

Acquisition behavior of phase locked loops, determining time and pull in range of loop for input step in frequency 15 p2446 A67-29590

Phase lock techniques applied to microwave antenna arrays noting problems, advantages, properties, etc 15 p2451 A67-29922

Steady state and transient analysis of digital phase-locked loops 15 p2458 A67-29939

Phase-locked radio interferometer for satellite tracking 16 p2621 A67-30679

First slip time of phase locked loop of arbitrary order shown as solution of first order linear differential equation 17 p2811 A67-32117

Markov processes applied to synchronization failure in phase-lock AFC loop subjected to external fluctuations 18 p3000 A67-34086

Apollo ranging code with phase locked loop for bit synchronization, plotting SNR vs error probability and acquisition time 18 p3000 A67-34102

Random characteristics of second order phase locked loop with Gaussian noise input, using digital simulation 18 p3017 A67-34104

Satellite tracking simultaneous-lobing monopulse receiving system utilizing

polarization diversity in coherent and noncoherent operational modes 18 p3020 A67-34110

Second, third and fourth order phase locked loops performance characteristics compared for optimum selection, calculating integrated square error and peak error 18 p3001 A67-34116

Unlock behavior of second order phase locked loop with and without interfering carriers 18 p3018 A67-34346

Phase relationships between self-locked modes in lasers and agreement with predictions based on maximum emission principle 18 p3062 A67-34640

Phase-locking effects between longitudinal modes in lasers, treating several-mode oscillations 20 p3456 A67-36171

Pulse width of ultrashort light pulses measured by Michelson type arrangement of nonlinear optics 20 p3456 A67-36172

Laser induced gas electrical breakdown theories, predicting high threshold field strengths invalidated by single mode, phase-locked and laser measurements 20 p3459 A67-36851

Injection locked pulsed magnetron in coherent echo detection system studied by observing echo pulses from acoustic delay medium 20 p3401 A67-37221

Near-threshold behavior of phase-locked devices, noting phase error processes 20 p3385 A67-37350

Amplifier and self-excited oscillator employing reflex klystron with phase locking 21 p3600 A67-38935

Phase locked automatic frequency control regulated phase distortion effects on radar signal mean peak power at matched receiver filter output 22 p3761 A67-39762

Formation of short ruby laser light pulse and repetition frequency control using mode locking with saturable absorbers 23 p4015 A67-41036

PHASE LOCK DEMODULATOR

Threshold performance of limiter discriminator phase locked demodulator and FM feedback demodulator 06 p0969 A67-18107

FM feedback system for lunar orbiter signal demodulation, discussing system composition and performance 06 p0975 A67-18108

Threshold reduction in phase locked loop by retarding phase of return signal from voltage controlled oscillator to phase detector 06 p0969 A67-18109

Intermodulation distortion of phase-locked loop demodulator as influenced by system parameters 14 p2273 A67-28708

Internal and coupling modulation and mode locking of continuous ruby laser 15 p2499 A67-29729

Voice modulation effect on phase-lock demodulator for single channel voice communication extending definition of threshold for optimum link design 16 p2629 A67-31529

Effect of unconditional stability of loop in phase lock demodulator on threshold performance of loop, noting transfer functions role 17 p2816 A67-32782

PHASE MODULATION

SA FREQUENCY MODULATION

Terminology of phase-difference modulated signal reception, noting coherent, correlation and autocorrelation methods 01 p0025 A67-10830

Spectral analysis of HF oscillations with phase modulated fluctuation as functions of phase dispersion and spectral form of modulating fluctuations 03 p0393 A67-13950

S-band direct phase modulator using varactor diodes with extremely linear phase characteristics 04 p0580 A67-14596

Two-dimensional characteristic function and probability-distribution density of random process which is phase modulated by normal noise 04 p0575 A67-15161

Low loss phase modulator for optical signals, using piezoelectric effect 04 p0576 A67-15506

Code-division-multiplex decentralized control system for communication satellites based on use of pseudorandom PM signals of wide bandwidth 06 p0959 A67-17672

Image restoration via phase holograms, noting applications to deteriorated photographic negatives and positives 08 p1331 A67-20842

System characteristics of tunnel diode amplifiers, discussing noise figure,

intermodulation, AM-PM conversion, etc 09 p1481 A67-22479

Omega navigation system composed of eight transmitters will give worldwide coverage on frequencies 10.2 kc and 13.6 kc 09 p1527 A67-22627

Parameters of simultaneous amplitude phase modulation of periodic cosmic ray variations obtained from satellite observations 10 p1698 A67-22779

Cosmic ray intensity variation detection with respect to sidereal time on basis of simultaneous amplitude phase modulation 10 p1698 A67-22780

AC background in phase of output oscillation of multistage frequency multipliers attributed to presence of HF harmonics in automatic bias circuit 10 p1613 A67-23448

Terminology of phase-difference modulated signal reception noting coherent, correlation and autocorrelation methods 10 p1607 A67-23460

Phase locking in phase plane on modulation of driver and self-excited oscillator, using differential equation 11 p1754 A67-24725

Intensity fluctuations of waves diffracted by deeply modulated random phase screen 13 p2071 A67-27403

Wideband phase-leading quadrupoles with circuit breakers and effect on envelope of modulated signal 13 p2085 A67-27706

Block coded frequency multiplexed PM communication system design and performance, considering simplification, cost and weight 14 p2271 A67-28694

Variable data rate modem for digital signal transmission on HF radio circuits 14 p2272 A67-28705

Modulation indexes for two-channel phase coherent communication system determining data rate yielding predetermined bit-error probability [JPL-TR-32-1118] 14 p2273 A67-28709

Two-dimensional characteristic function and probability-distribution density of random process which is phase modulated by normal noise 15 p2435 A67-29348

Pulse measuring system for observing structure of pulsed signals in rectangular phase-time coordinates 15 p2444 A67-29414

Possible directional pattern forms obtainable for single-ring circular arrays, using Fourier harmonic analysis technique 15 p2454 A67-30138

Electronic technique producing quadrature signal from laser feedback interferometer 15 p2502 A67-30436

Graphical technique for phase-modulated deep-space communications links resulting in optimum power division between carrier and sine and square-wave carriers 16 p2625 A67-31258

Sunrise variations of phase and amplitude of vlf signals over single long path interpreted as interference between waveguide modes 16 p2631 A67-31851

Cosmic ray variations methodology, considering solar system geometry, interstellar cosmic ray gradient, phase and amplitude modulation, etc 17 p2934 A67-32103

Simultaneous amplitude and phase modulation of periodic cosmic ray variations by using two frequencies 17 p2934 A67-32106

Spurious phase modulation reduction in multistage frequency multiplier using lumped-selection filters, determining cut-off angle in multiplying cascades 18 p3000 A67-34087

Coaxial and strip-line passive microwave components stressing design of hybrid junctions, microwave mixers, filters, etc 19 p3195 A67-35549

C-band solid state YIG serrodyne theory and operation, outlining phase velocity modulation of magnetostatic modes 19 p3196 A67-35661

Scheme for obtaining zero beats using broad range of phase frequency modulations for direct determination of laser frequencies 19 p3241 A67-36024

Design and performance of frequency multiplexed phase-modulated communication systems 20 p3385 A67-37353

Electro-optic phase modulation of visible and IR light by p-n, p-i-n and metal semiconductor junctions and heterojunctions, noting propagation modes 21 p3684 A67-38453

Synchronous detection for signal phase gap measurements and Diana type satellite

tracking, discussing hypothetical carrier 21 p3583 A67-38644

Frequency limitations of PCM communication, determining PCM/PM and PCM/FM power spectra for hybrid modulation spectra 21 p3584 A67-38652

FM/PM and FM/FM radio telemetry in proportional and constant band covering regulation, SNR, noise threshold, etc 21 p3587 A67-39050

Reactive optical information processing maximum efficiency from phase object in laser cavity, discussing modulation depth and power gain 23 p4002 A67-41270

Parameters of simultaneous amplitude phase modulation of periodic cosmic ray variations obtained from satellite observations 24 p4209 A67-42115

Cosmic ray intensity variation detection with respect to sidereal time on basis of simultaneous amplitude phase modulation 24 p4209 A67-42116

PHASE SHIFT

Magnetic susceptibility studies show semiconductor to metal transition in titanium pentoxide and titanium trioxide, clarifying electronic nature of phase transition 01 p0132 A67-10376

All-pass RC filter network design for constant signal delay in LF systems, noting cascade phase characteristics 01 p0045 A67-11197

Synthesis of TEM directional couplers and fixed phase shifters consisting of multiple parallel coupled quarter wave sections 02 p0214 A67-11778

Optimal value of reactance of microwave parametric element 02 p0214 A67-11912

Temperature dependence of phase shift in magnesium-copper ferrite-chromite phase shifter as affected by microwave permeability 02 p0301 A67-12672

Phase shift dependence on ferrite permeability tensor of reversible ferrite phase shifter 02 p0301 A67-12673

Stability analysis of spectrotron with external feedback based on time delay, inertia of nonlinear quadrupole and circuit phase shifts 03 p0377 A67-13092

Interferometric holography in diffused light, obtaining interferogram of phase shifting object 03 p0420 A67-13451

Minimum phase shift low pass filters with given departure from constant attenuation and given nonlinearity of phase response in passband 03 p0380 A67-13579

Stochastic analysis of energy spectrum of output signal of phase shift modulator in PCM systems 04 p0571 A67-14895

Fast switching microwave phase shifters for high power array radars, describing drive control techniques 04 p0581 A67-15053

Radiative lifetimes of UV multiplets in Si, P, S, O, Ne 2 and Ar 2 measured via phase shift method, correcting for transition cascading 05 p0892 A67-18411

Excess carrier lifetime in semiconductors by measuring photoconductive phase shift of spreading resistance under point contact 05 p0861 A67-16501

Multielement antenna scanning grid-phasing method having random function distribution at aperture 05 p0776 A67-17159

Automatic phase control /APC/ loop for stabilization of phase shift in RF amplifier 05 p0778 A67-17395

Optical method observations of phase transition of ferroelectric monocrytal SBI 06 p1047 A67-17758

Nucleon radius from pion-nucleon phase shift, assuming nucleon is p-wave bound state of pion and nucleon, using Gelfand-Levitan formalism [AIAA PAPER 67-213] 06 p1036 A67-18368

Small signal nonlinear amplitude distortion and phase shift measurement in TWT 07 p1151 A67-19427

Variational bound method applied to calculation of lower bounds on S-wave phase shifts for scattering of electrons by hydrogen atoms 07 p1226 A67-19499

Phase variation dependence at receiver output on polarization of wave incident on antenna of phase measuring system 07 p1144 A67-19694

Navigation system test by phase shifter, noting signal generator which simulates omnirange systems 07 p1155 A67-19839

Variational bounds on eigenphase shifts in scattering theory obtained by SB and R

approaches 08 p1355 A67-20865

Phase linearity of microwave component and interaction of cascaded devices, giving analysis of two-port device 08 p1303 A67-21029

X-band circularly polarized nonreciprocal ferrite phase shifter for phased array antennas 08 p1305 A67-21226

Miniaturized C-band digital latching phase shifter for combined advantages of waveguide and stripline design 08 p1305 A67-21227

Track method analysis of phase transitions in particle growth and evaporation rate during combustion 08 p1428 A67-21421

LF test generator producing ramp output for phase shift detection in electronic systems at different input voltages 08 p1307 A67-21537

FM of RC generator by connecting parametric voltage transducer output to phase shift network and applying generated voltage to transducer input through matching network 09 p1496 A67-21692

Triangular low filament laser diodes, considering alteration of internal reflection to achieve phase shift phenomena 10 p1662 A67-22716

Computer calculation of induced circulations and influence coefficients for turbine blades with arbitrary profiles and oscillation shift 10 p1591 A67-23044

Diode type lossless network description with excellent transient response and less settling time than conventional branch-line coupler phase shifter 10 p1613 A67-23414

Phase shift as quantitative measure of relationship between surface convection and charge relaxation 11 p1825 A67-23862

Existence of nucleon bound state in PIN channel investigated through nonperturbative S-matrix in absence of forces arising from inelastic states 11 p1822 A67-23978

Free electron density and effective collision frequency of ionized argon in wake of shock wave measured, using microwave probe methods 11 p1775 A67-24017

Independent control of angular location of independent zeros of directional pattern for linear array 11 p1762 A67-24290

Systematic design of matrix network, consisting of hybrids with phase delays in interconnecting lines, used for antenna beam steering 11 p1763 A67-24300

Transient ionization levels of hypersonic velocity projectile wakes measured by open microwave resonators phase shift 11 p1790 A67-24452

Saturation effect on phase shift of traveling wave masers and reflex type cavity masers 11 p1800 A67-24468

Phase shift analysis of nucleon-pion coupling, noting discrepancy between empirical and theoretical results 11 p1823 A67-24599

Photometric studies of eclipses of Echo I and II satellites, noting period of rotation from luminosity curves and 180 degree phase shift 12 p2008 A67-25832

Phase measurements of VLF transmission over long distance transequatorial path 12 p1906 A67-25942

Active filter design combining flat amplitude response with flat time delay 12 p1915 A67-25973

Broadband microwave frequency translator using latching ferrite phase shifter 13 p2075 A67-26477

Single crystal YIG phase shifter performance noting improved output with proper microwave circuit design 13 p2076 A67-26479

Parametric amplifiers incorporating two varactor diodes, noting in-phase pumping for unilateral operation and large potential bandwidth 13 p2078 A67-26785

Microwave interferometer with dielectric rods as waveguides for measuring electron density in small volume inside plasma 13 p2120 A67-26859

Phase shift between electron temperature, luminous intensity and electron density in stratified positive column of glow discharge 14 p2353 A67-27757

Electron density variation, collision frequency and phase shift in standing striations in positive column 14 p2353 A67-27758

Instrumentation using quantum effects in

weakly coupled superconductors 14 p2375 A67-29043
 Phase shifts in human circadian system noting individual differences, performance deficit, physiological changes and dissociation from time zone displacements 15 p2425 A67-29108
 Phase shift lifetime of excess carriers in semiconductors under sinusoidal injection, showing decrease as injection frequency increases 15 p2533 A67-29264
 Temperature dependence of lifetime and Hall coefficient in InSb, measuring lifetime by phase shift method, concluding that recombination centers are lattice defects 15 p2535 A67-29483
 MOS transistor HF behavior noting phase shift, frequency dependence, etc 15 p2449 A67-29805
 Thermoelectric power increase in low temperature metals not explained by residual resistivity in simple model calculation 15 p2540 A67-30096
 Segmented two-stage waveguide-slot scanning antennas with intersegment phase shifters connected in series in transmission line 16 p2637 A67-31026
 Axial nonuniform perturbations of electromagnetic propagating structures analyzed, using nonlinear phase progression from perturbation theory of quantum mechanics 16 p2626 A67-31345
 Necessity of incremental phase shift during IF time delay steering of antenna array main beam 16 p2639 A67-31354
 Systematic clockwise rotation of asymmetry axis of main phase decrease during geomagnetic storm 16 p2666 A67-31412
 Energy level shifts due to atom confinement by conducting walls 17 p2888 A67-32390
 Differential phase-shift measurements at UHF and microwave frequencies, discussing standards, techniques and uncertainties in characteristics 17 p2815 A67-32608
 Systematic boresight and off-boresight tracking errors in planar monopulse phased rectangular arrays produced by analog phase shifters with nonlinear transfer characteristics 17 p2825 A67-32617
 Microwave ferrite devices describing applications at metric and decimetric wavelengths, at very low temperatures and at high power levels 17 p2826 A67-32744
 Low noise transistorized amplifier at 408 MHz for synthesis 17 p2827 A67-32785
 Radiotelescope 17 p2827 A67-32785
 Time resolved measurements of phase fluctuations of coherent beam at emergence from turbulent layer 17 p2817 A67-33304
 Michelson type carbon dioxide laser for AC discharge analysis, noting apparatus design and performance 18 p3060 A67-34014
 Friedel sum rule applied to semiconductors, discussing Born approximation role 18 p3104 A67-34591
 Nonleptonic sigma decay modes described by four complex amplitudes with phases given by time-reversal invariance 19 p3263 A67-34892
 RC oscillators based on silicon n-p-n transistors for radio frequencies, analyzing active all-pass phase-shift circuit 19 p3191 A67-34946
 Microwave photon interaction with superconducting tunneling currents measured in aluminum-indium junctions, extended to tin-lead junctions, discussing phase shift 19 p3303 A67-35046
 Transient effects of changes in applied radio frequency power to which latching ferrite phase shifters could be subjected in array applications 19 p3196 A67-35663
 Phase shift method for obtaining radiative lifetimes by electron collisions current 20 p3488 A67-36665
 Bias in coherency estimation resulting from phase changes 20 p3476 A67-36787
 Electron-interference experiment using laser light, discussing electron wave function phase change and electron interference pattern displacement 20 p3460 A67-36999
 Excess carrier lifetime in semiconductors by measuring photoconductive phase shift of spreading resistance under point contact 20 p3512 A67-37317
 Spaced antenna array radiation pattern frequency control analyzed for relationship between arrival angle and heterodyne

frequency 20 p3402 A67-37506
 Despun antenna design, functioning and performance for communications satellites, discussing pattern, scanning and phase shifters 21 p3591 A67-38205
 Ferroelectric phase shifter temperature compensation, showing reduction in sensitivity by connecting in series two different ferroelectric materials 21 p3679 A67-38219
 Unstable light scattering in atmospheric models studied in relation to medium optical properties, using phase shift measurement 21 p3627 A67-38448
 Phase delayed triggering of oscillographs using ring type potentiometer to produce phase displacements by mechanical rotation 22 p3799 A67-39754
 Equations for mode analysis in multichannel extremal control systems with harmonic probe signals, discussing synthesis of optimizers and phase shift automatic compensation 22 p3777 A67-39864
 S-band rectangular digital phase shifter combining advantages of waveguide design with compactness of strip transmission line structure 22 p3773 A67-39909
 Modulator-demodulator device using phase shifts between signals in successive time intervals to speed handling of data in HF band 22 p3764 A67-40557
 Experimental determination of compression and rarefaction shock waves structure causing high pressure phase formation and decay in potassium halides 23 p3989 A67-40906
 Approximate methods for solving heat transfer problems with phase change, considering applicability to Stefan problem 23 p4084 A67-41749
PHASE-SHIFT KEYING
 Differentially coherent phase-shift keying system analyzed under wide range of signal and noise conditions 01 p0025 A67-10861
 Integrated circuit eliminating pilot tones in digital data by simultaneously phase modulating binary data and bit-timing signals on carrier 02 p0194 A67-11797
 Scheme reducing decoding failures due to atmospheric noise in coherent-phase-shift-keyed data transmissions by ground wave 05 p0767 A67-17523
 Optimal Wiener values of filter parameters in phase-lock loop, noting possibility of improved performance despite deviations 06 p0973 A67-17615
 Spectra and joint correlation function for PSK signal modulation 10 p1604 A67-22979
 Book on communication principles emphasizing digital radio communication system design, frequency and binary phase shift keying, filtering, fading, etc 16 p2624 A67-31254
 Reduced noise rejection regions in receiver of PSK telemetry signals in narrow band concentrated noise, using phase and polarity comparison 18 p3000 A67-34085
 Deep space communication system using sequential decoding, binary phase-shift keying and 8-level quantized decisions 20 p3384 A67-37349
PHASE-SPACE INTEGRAL
 Control region construction in phase space for linear differential equation system 02 p0224 A67-11627
 Abruptly varying random processes with determinate deflection, discussing phase space in form of Banach space 04 p0646 A67-15260
 Infinite magnetic quadrupole channel, discussing operations in complete transverse plane phase space via 4 x 4 matrix transformations 08 p1332 A67-21172
 Transformation of magnetoacoustic waves in terms of ideal MHD by phase integrals method 12 p1976 A67-26072
 Superposition approximation for dense gases and liquids equilibrium theory, using phase-space distribution functions from maximization of information entropy 18 p3078 A67-33669
 Correlation function method in superconductivity theory, formulating electric current density in terms of distribution function in phase space 18 p3100 A67-33712
 Synthesis of time optimal control for discrete plants described by difference equations, deriving algorithm defining surface in phase space of

variables 18 p3017 A67-33872
 Two-stream instability calculations from phase-space boundary motion, using Vlasov equation in distribution function 21 p3662 A67-37763
 Transient behavior of autonomous nonlinear control system phase space domains, finding relative stability domains for special time dependent Liapunov function 24 p4135 A67-42186
PHASE-SWITCHING INTERFEROMETER
 Radio star fadeouts and radio propagation 15 p2563 A67-30287
 Broadband radio star Cassiopeia A scintillations observed with swept frequency interferometer 15 p2563 A67-30288
 Radio star Cassiopeia A scintillations and spread-F in auroral zone [AGARDOGRAPH 95] 15 p2482 A67-30289
PHASE TRANSFORMATION
 Spontaneous electro-optical effect in triglycin sulfate crystals spectrally studied, noting changes in double refraction along three crystallographic axes during ferroelectric phase transition 01 p0129 A67-10138
 State variable equation transformation to phase variable canonical form 01 p0047 A67-11222
 Nonsingular linear transformation of time-invariant linear dynamic system into canonical /phase-variable/ form 01 p0048 A67-11223
 Liquid propulsion systems operating in space and resulting problems of phase transformation, noting plug formation and flow stoppage 01 p0055 A67-11386
 Kamacite and taenite superstructures and metastable tetragonal phase in iron meteorite 03 p0510 A67-13334
 Superconducting-to-mixed state phase transformation in type II superconductors in applied magnetic field and accompanying onset of vortex filaments at surfaces 03 p0501 A67-14372
 Phase work hardening of austenitic Fe-Ni alloys in phase transformation process 04 p0635 A67-14430
 Mohr circle geometric representation of transformation of two-dimensional symmetric stress tensors in using complex variable vectors /phasors/ 04 p0657 A67-14850
 Oxygen content effect on mechanical properties and phase transformations of VT 18 titanium alloy during thermal treatment 04 p0637 A67-14942
 Effect of structure of beta titanium alloy on crack propagation resistance 04 p0641 A67-15985
 Superplastic effect in cr-30 at. pct Co alloy, noting low temperature bend ductility in quenched metastable single phased and near equilibrium conditions 05 p0829 A67-16474
 Phase recrystallization effect on structure and mechanical properties of cast monophase titanium alloys 05 p0830 A67-16760
 Transmission electron microscopy study of phase transformations of Ti-8Al-1Mo-1V alloy 06 p1014 A67-17804
 Diffusion and nondiffusion transformations in titanium alloys, noting martensitic transformation 06 p1018 A67-18231
 Isothermal transformations in hypo-and hypereutectoid titanium-chromium alloys 07 p1200 A67-19244
 Hydrogen distribution between phases in /alpha and beta/ titanium alloys at various temperatures 07 p1200 A67-19246
 Hydrogen effect on processes occurring in alloy VT3-1 during aging shown to increase beta phase 07 p1200 A67-19247
 Phase and structural transformations in metals and alloys studied with aid of exoelectronic emission 07 p1201 A67-19257
 Mechanical properties and heat resistance of titanium alloyed with low and high proportions of Al and Sn 07 p1207 A67-19289
 Phase transformations and welding characteristics of alpha and /alpha plus beta/ titanium alloys 07 p1207 A67-19292
 Mathematical model for condensation point of first order phase transitions, examining free energy singularity and metastable phase 07 p1268 A67-20089
 X-ray structural study of phase transformations during heat treatment of VT3-1 titanium alloy 09 p1518 A67-22030
 Phase transformations in heat treated

nickel-rich Ni-Co-Cr-Al-Ti-C cast alloys
noting sigma formation 10 p1668 A67-23173
Titanium alloy thin foil preparation using
window method and electropolishing
conditions, noting phase
transformation 10 p1668 A67-23175
Transformation of magnetoacoustic waves
in terms of ideal MHD by phase integrals
method 12 p1976 A67-26072
Performance of two versions of
continuously operating electromechanical
SHF phase converter 13 p2081 A67-27047
Inertial criterion relation for determining
effect of mass transfer, phase
transformation, and Kossovich number on
heat and mass transfer 14 p2406 A67-28313
Effect of structure of beta titanium alloy
on crack propagation
resistance 14 p2338 A67-28488
Temperature dependence of complex
permittivity and spontaneous polarization of
SbSI single-crystal whiskers in phase
transformation region 15 p2537 A67-29707
Second order phase transitions in ionic
crystals caused by vibronic interaction
analogous to Jahn-Teller effect in ideal
crystals 16 p2726 A67-30813
Niobium alloys under annealing and aging
analyzed, noting formation of oxide, nitride
and carbide phases followed by coagulation
and brittleness 16 p2687 A67-30844
Hardness, electrical resistance and phase
composition on Ni-Mo alloy during annealing,
discussing phase
transformations 16 p2687 A67-30847
Vanadium and molybdenum effect on
properties and phase transformations of
titanium chloride 16 p2691 A67-31591
Nonstoichiometry of zirconium oxide and
relation to tetragonal-cubic inversion in
zirconium oxide 16 p2694 A67-31597
Niobium-iron binary alloys structural
study, noting phase instabilities for various
added impurities 17 p2871 A67-32042
Formulas for potential temperatures
derived from thermodynamic principles,
considering four stages of reversible
adiabatic transformation of humid
air 17 p2844 A67-32566
Hydrogen effect on stability of beta phase
in alloy VT15 18 p3065 A67-34291
Physical changes in exploding wires before
gas ionization observed by X-ray technique,
studying resistivity variation with
density 19 p3261 A67-35161
Dynamic equations for adiabatic changes
of state for mixtures of partially ionized
gases with chemical
reactions 19 p3286 A67-35348
Structural transformations in alnico alloy
with titanium studied by
X-ray 19 p3245 A67-35467
Temperature dependence of electrical
conductivity in organic semiconductors,
examining compounds during transition from
solid to liquid state 20 p3508 A67-36404
Parabolic cylindrical reflector beam
waveguide, discussing conduction and
diffraction losses of TE and TM
modes 21 p3583 A67-38608
Superconducting property of kappa phase
in Bi-Sn alloy at high pressure, with
determination of transition to
superconducting state and temperature
interval to keep stable
state 22 p3857 A67-39460
Lattice type gas heat capacity
discontinuity near critical
point 22 p3790 A67-39509
Aging of iron-nickel-titanium alloys during
heating in reverse martensitic alpha to
gamma transformation process, investigating
phase parameter changes 22 p3820 A67-39824
Bainite beta to alpha transformation in
titanium-oxygen system, using high
temperature metallography
techniques 22 p3821 A67-39825
Phase transformations in commercial
titanium alloys compared for mechanical
properties, emphasizing decomposition of
metastable beta phases on quenching, aging
or deformation 22 p3822 A67-40055
Omega phase morphology by transmission
electron microscopy of Ti-Nb indicating
ellipsoids with major axes parallel to /111/
directions in matrix 23 p4017 A67-40653
Temperature dependence of complex
permittivity and spontaneous polarization of
SbSI single-crystal whiskers in phase
transformation region 24 p4199 A67-41777
Triggering controller dynamic model with

magnetolectric drive, examining phase
volume by point transformation
technique 24 p4155 A67-42297
PHASE VELOCITY
Internal gravity-shear waves in
troposphere for two-and three-layer model
of air density and horizontal velocity, noting
phase velocities 02 p0238 A67-12190
ELF and VLF wave propagation in earth-
ionosphere waveguide at wide frequency
range, giving amplitude spectra and mean
phase velocity for day and
night 06 p0994 A67-17970
Tabulation and plotting of VLF radio wave
diurnal phase changes as function of
frequency and path 07 p1142 A67-19450
Symmetric wave propagation in cylindrical
waveguide filled with inhomogeneous
plasma, calculating phase
velocities 07 p1158 A67-20242
Envelope and phase velocities for laser
pulse propagating in nonlinear dielectric
with intensity dependent index of
refraction 09 p1511 A67-21748
Electron beam plasma amplification
measurements in interaction region by
nonperturbing technique, measuring RF
growth, phase velocity,
etc 11 p1841 A67-24907
Gas-liquid droplet behavior in geometric
nozzle for constant difference between
phase velocities, determining appropriate
nozzle profile 15 p2472 A67-29777
Nonlinear dependence of phase velocity on
wave amplitude during electromagnetic
propagation in plasma waveguide, describing
test apparatus 16 p2718 A67-31191
Magnetic tape simultaneous recording of
radio atmospherics from broadband receivers
and from waveform photographs, computing
Fourier phase and pulse amplitude
spectra 16 p2629 A67-31508
Coupling between slow waves and
convective instabilities in solids, showing
interaction inhibition for electron drift
velocities greater than phase
velocity 18 p3101 A67-34017
Phase velocity and attenuation of ionic
plasma waves in weakly ionized gases
measured in absence and presence of
external magnetic fields 19 p3290 A67-35378
Phase velocity and attenuation of
audiofrequency electromagnetic waves to
derive electron density
profiles 20 p3426 A67-36288
Wave propagation in ferrite-filled
rectangular waveguide with transverse
magnetization 20 p3382 A67-36864
Guided waves on infinite cylindrical cavity
in magnetoionic medium noting wave
solutions, phase velocity, plasma frequencies,
etc 20 p3383 A67-37107
Guided wave characteristics in infinite
free space cylindrical cavity in magnetoionic
medium noting resonance, transition, cut-off
frequencies, phase velocity,
etc 20 p3383 A67-37108
Ion cyclotron wave propagation in plasma,
considering Larmor radius effects, quasi-
static dispersion relation, phase velocity and
cyclotron resonance 21 p3661 A67-37750
Isolated longitudinal wave pulse amplitude
and phase velocity dependence on trapped
particle density in ion-electron and electron-
positron plasmas 21 p3669 A67-38683
Acoustic ion waves phase velocity and
attenuation constant measurements verify
predicted dependence on ion mass, with
attenuation due to ion-neutral
collisions 21 p3675 A67-39054
Electromagnetic wave propagation in
moving media filled waveguides noting
nondispersive dielectric and cold plasma
cases 22 p3759 A67-39361
Bifilar complementary loaded helical
antenna, determining radiation patterns,
near field amplitudes and phase
velocities 23 p3979 A67-40834
Coupled electromagnetic whispering
gallery modes in large dielectric cylinders,
discussing circumferential phase velocity,
boundary region and axial wave
number 23 p3974 A67-41203
Plasma waves generation by transverse
waves as function of phase relation of
interaction 23 p4034 A67-41678
Parametric amplification of traveling wave
tube through coupled wave method noting
role of phase velocities of space charge
waves 24 p4130 A67-42241

PHASED ARRAY
Impedance matching of infinite phased
array by dielectric sheets, noting radiation
pattern dependence on beam scan
angle 01 p0040 A67-11312
Phasing system using steered beam of
coherent light for RF
array 01 p0027 A67-11320
Directive gain and impedance calculated
for ring array of antennas that concentrate
radiated power in plane of ring and are
omnidirectional 02 p0211 A67-11595
Computer program for optimizing network
components and evaluation of improvement
of planar array match by compensation
through contiguous element
coupling 02 p0211 A67-11597
Angular section errors effect on directive
gain coefficient of parabolic antenna with
automatic phasing 02 p0215 A67-11975
Stationary phase technique synthesis of
continuous linear antenna and integral
equation for determining radiation
pattern 03 p0378 A67-13284
Automatic checkout and monitoring of
phased array radar
system 04 p0595 A67-14500
Beam scanning and beam forming
techniques for phased-array radar, noting
frequency and phase scan
methods 04 p0596 A67-15049
Electronic scanning of antenna beams,
reducing feed complexity of large phased
array by grouping of elements, tapering and
array thinning 04 p0581 A67-15050
Monte Carlo technique in predicting
antenna performance 05 p0775 A67-16969
Self-phased arrays and remote phase
synchronization 07 p1152 A67-19549
Queueing theory applied to phased array
radar maintenance problems, specifically
replacement and repair of transmitter
and/or receiver modules 08 p1292 A67-20668
Thinned aperture computed lens /TACOL/
of hard point demonstration array radar
/HAPDAR/ phased array radar
system 08 p1315 A67-20679
X-band circularly polarized nonreciprocal
ferrite phase shifter for phased array
antennas 08 p1305 A67-21226
Optimal discrete binary system of
electrical control of beam position of phased
linear antenna array 10 p1611 A67-22962
Phased array antenna impedance matched
for all scan angles assuming connecting
circuits are lossless 11 p1758 A67-23975
Simulator measurements of active
impedance of phased array antenna element
at two different scan angles by single
element in waveguide 11 p1763 A67-24299
Determinants of electronically steerable
antenna arrays 12 p1917 A67-26158
Phased-array microwave antenna system
for scanning simultaneous targets whose
distance and direction are changing
rapidly 13 p2083 A67-27566
Immediate, delayed and cyclic maintenance
policies for phased array radar
systems 16 p2634 A67-30446
Superlimiting phased-array receiving
system in two-source
environment 16 p2638 A67-31271
Narrow beam microwave integrated circuit
phased array system design for tactical
communications satellite
requirements 17 p2956 A67-32497
Systematic boresight and off-boresight
tracking errors in planar monopulse phased
rectangular arrays produced by analog phase
shifters with nonlinear transfer
characteristics 17 p2825 A67-32617
Radiation from array of parallel plate
waveguide with thick walls excited by TEM
modes 17 p2828 A67-33085
Universal array of complementary-
symmetry MOS transistors applied to missile
and surface radar beam steering phase array
storage unit 18 p3015 A67-34563
Characteristics of immediate, delayed and
cyclic maintenance of phased planar array
radar systems, considering outage availability
effects 18 p3005 A67-34693
Transient effects of changes in applied
radio frequency power to which latching
ferrite phase shifters could be subjected in
array applications 19 p3196 A67-35663
Irradiance due to square array of circular
apertures from scalar Fresnel-Kirchhoff
diffraction theory, giving plots of Fresnel
diffraction patterns 22 p3835 A67-39235

- Coherent amplification properties of antireflective coated GaAs diodes considered for application to phased array 22 p3813 A67-39254
- Linear and planar phased array antennas investigated for radiation impedance as function of scan variable 24 p4130 A67-42339
- High gain phased array for satellite transmission using feedback to correct phase and amplitude parameters variations 24 p4124 A67-42816
- PHENOL**
- SA EPOXY RESIN
- Ablative behavior of low and high density phenolic nylon in diffusion controlled surface combustion regime [AIAA PAPER 67-328] 12 p2038 A67-26042
- PHENOL RESIN**
- Nuclear magnetic resonance /NMR/ used to measure gelation times, rates of polymerization and nature of volatiles included in raw material 03 p0429 A67-13448
- Mineral additive effect on thermal stability of phenolic resins in inert and oxidative atmospheres at atmospheric pressure [ONERA-TP-324] 09 p1520 A67-22155
- Nozzle ablations studied based on chemical mechanism, discussing pure on reinforced phenolic resin [ONERA-TP-475] 14 p2404 A67-27896
- PHENOMENON**
- S CHORUS PHENOMENON
- S LEIDENFROST PHENOMENON
- S PHYSIOLOGICAL PHENOMENON
- S THERMONUCLEAR PHENOMENON
- PHENOTHIAZINE**
- Phenothiazine carboxylic acid esters as improved antioxidants in stable and sludge-free synthetic oils 09 p1520 A67-21705
- PHENYL**
- S POLYPHENYL
- PHOEBUS NUCLEAR REACTOR**
- Phoebus 1B test /high-power-density reactors for space propulsion/ noting reactor design for fuel-element testing [AIAA PAPER 67-486] 18 p3076 A67-33952
- Liquid hydrogen pumping for Phoebus reactor, discussing feed systems, nozzles, configurations, design, testing, etc [AIAA PAPER 67-478] 18 p3077 A67-34402
- NERVA engine development, discussing NRX tests and Phoebus reactor tests for high temperature and power operation 20 p3482 A67-36571
- Nuclear rocket propulsion development, hot test results, one breadboard engine configuration and flight stage planning [AIAA PAPER 67-981] 24 p4187 A67-43054
- PHONEME**
- Phonemic analysis of consonants in helium speech 10 p1597 A67-23312
- PHONON**
- Temperature dependence of heat-pulse propagation in sapphire at low temperature intervals, noting phonon mean free path 01 p0131 A67-10341
- Spin-magnetophononic and magnetophononic oscillations of magnetic resistance in n-InAs 01 p0133 A67-10547
- Oscillation modes in film with free boundaries, determining phonon density 01 p0136 A67-11049
- Spin-magnetophononic and magnetophononic oscillations of magnetic resistance in n-InAs 01 p0137 A67-11055
- Theory of second sound in semiconductors caused by long wave phonons interacting with current carriers in absence of external field 03 p0490 A67-13152
- Lattice vibration spectra and energies of two-phonon summation bands and reststrahlen bands in gallium arsenide phosphide single crystals 03 p0495 A67-13514
- Light absorption and photolization of shallow impurity levels in semiconductors during acoustic phonon scattering 04 p0678 A67-15135
- Magnon phonon scattering relaxation time as function of temperature and wave vector, calculating thermal conductivity of YIG 05 p0869 A67-17191
- Photoconductivity, edge emission spectrum, longitudinal optical phonon coupling and eigenfrequencies for linear chain of Cd-Se-Cd-S-Cd... atoms 05 p0870 A67-17196
- Temperature dependence of three-phonon processes in solids noting application to Si, Ge, GaAs and InSb 05 p0870 A67-17198
- Superconducting tunnel diode for quantum generation and detection of incoherent phonons, discussing I-V characteristics 06 p1011 A67-18211
- Two-phonon IR absorption and Raman scattering spectra to provide information about phonon spectra of crystals and phonon-electron interaction in filled valence bands 06 p1059 A67-18907
- Optical phonons role in determining form of free carrier distribution function in semiconductors and nonohmic behavior of strongly piezoelectric crystals 06 p1065 A67-18952
- Current saturation and phonon amplification induced instabilities in CdS crystals 06 p1066 A67-18958
- Phonon lifetime variation effect on stimulated Brillouin and Raman scattering in gases by temperature, pressure and laser power variation and comparison with Stokes gain theories 10 p1682 A67-22758
- Theory of second sound in semiconductors caused by long wave phonons interacting with current carriers in absence of external field 10 p1690 A67-23101
- Light absorption and photolization of shallow impurity levels in semiconductors during acoustic phonon scattering 12 p1978 A67-25159
- Carrier distribution function in degenerate p-type germanium in presence of hole scattering on acoustic phonons, considering heating in arbitrary electric and magnetic fields 13 p2181 A67-27281
- Two-phonon absorption in ultrasonic paramagnetic resonance of uranium-doped calcium fluoride, relating wave attenuation to ultrasonic intensity and magnetic field angular variation 14 p2365 A67-28295
- Phonons and hypersound - Conference, University of Grenoble, March-April 1966 14 p2373 A67-28980
- Phonon scattering at point defects theory found to disagree with experimental results on InSb-InTe 16 p2730 A67-31156
- Phonon drag part of thermoelectric power in metals formula, by assuming electron scattering description by relaxation time 16 p2731 A67-31445
- Book on effects of hot electrons associated with carrier concentration in semiconductors at very low temperatures 17 p2914 A67-32378
- Multiphonon orbit-lattice relaxation of lower lying excited states of Dy doped lanthanum chloride investigated, using IR fluorescence and quantum counter techniques 19 p3302 A67-35035
- Superconducting bismuth investigated using tunnel effect method to measure electron energy spectrum gap and phonon spectrum distribution 21 p3685 A67-38801
- X-ray diffusion from thermal agitation oscillations coupled with plasma waves in indium antimonide, discussing phonon-plasmon interactions and Hall effect measurements 22 p3859 A67-39652
- IR absorption and Raman scattering spectra of diagonal cubic crystal structures 23 p4037 A67-40758
- Light polarization and intensity for Raman scattering from plasmons and phonons in GaAs 23 p4038 A67-40795
- Phonon annihilation during decay of two metastable fluorescent states of ionized Ba compound 24 p4205 A67-42737
- Electron tunneling into superconductors to investigate pressure induced energy shifts in Pb phonon spectrum 24 p4206 A67-43100
- PHONON BEAM**
- Optical phonons role in thermal conductivity of GaSb doped with Zn and Te in temperature range 80 to 600 degrees K 03 p0488 A67-12811
- Optical phonon production, showing existence of electric field strength range at low temperature scattering in which phonon emission results in electron stoppage 06 p1010 A67-17884
- X-ray diffusion intensity by transverse polarization phonons in indium antimonide at various temperature ranges 19 p3307 A67-35793
- Symmetry of phonons and rules of corresponding selection for IR absorption and Raman diffusion for two phonons 23 p4026 A67-40689
- PHOSPHATE**
- SA ADENOSINE TRIPHOSPHATE /ATP/
- SA AMMONIUM PHOSPHATE
- SA POTASSIUM PHOSPHATE
- Individual phospholipids in hemispheres of rat brains and rate of turnover of phosphate groups during oxygen deprivation 04 p0562 A67-15548
- Absorption and fluorescence characteristics of Nd-doped phosphate glasses used as laser material 13 p2128 A67-27229
- Fluorimetric technique for phosphatase activity in soil based on beta-naphthol release from sodium-beta-naphthylphosphate 14 p2254 A67-28067
- Organic phosphate shown as inhibitory factor from B. stearothermophilus for attachment of amino acids to transfer RNA 20 p3370 A67-36798
- Brianite and panethite in Dayton very fine octahedrite phosphate-silicate nodules 24 p4234 A67-42625
- PHOSPHIDE**
- SA GALLIUM PHOSPHIDE
- SA INDIUM PHOSPHIDE
- Phase diagrams of various titanium-phosphorus compounds and mixtures with up to 45 atomic percent P and microstructural characteristics of Ti-P alloys 07 p1203 A67-19262
- Band-to-band radiative recombination in compounds of gallium and indium with phosphorus, arsenic and antimony 12 p1979 A67-25177
- PHOSPHINE**
- Reaction of lithium diphenyl phosphide with diphenylacetylene producing high yields of stereochemically pure vinyl phosphides in presence of primary or secondary amine 04 p0565 A67-14523
- PHOSPHOR**
- SA RADIOPHOSPHOR
- Visual display of output patterns of IR lasers using heat sensitive phosphors 09 p1500 A67-22433
- PHOSPHORESCENCE**
- SA AFTERGLOW
- Radioisotope and phosphor research and increased brightness of self-luminous devices 05 p0842 A67-16543
- Spectroscopic properties of mixed complexes with two different ligand groups surrounding lanthanide ion, discussing energy transfer and absorption 23 p3971 A67-40747
- PHOSPHORIC ACID**
- Phosphorylation of nucleosides with polyphosphoric acid 13 p2065 A67-26807
- Condensation of cytidylic acid in presence of polyphosphoric acid 13 p2065 A67-27183
- PHOSPHORUS**
- Isolation-diffusion of phosphorus in silicon with low surface concentration, with applicability to preparation of integrated solid state circuits 02 p0223 A67-12736
- Phosphorus-diffusion method in silicon with thin phosphorus containing layer used to produce working area of planar strain gauges 02 p0248 A67-12737
- Calculation of dislocation precipitated profile for ideal complimentary error-function diffusion profile of phosphorus in silicon 07 p1234 A67-19890
- P atoms distribution in doped surface layer of silicon photoconverter for various thermodiffusion conditions exhibiting typical concentration curves 12 p1982 A67-25322
- Slope 12 p1982 A67-25322
- Gamma ray schemes of resonances in silicon 29-phosphorus 30 reaction for resonant and bound levels of phosphorus 30 properties 16 p2705 A67-31922
- X-ray K spectra of phosphorus absorption and emission in indium, gallium and boron phosphide semiconductors and red phosphorus 18 p3095 A67-33440
- Phosphorus concentration influence on epitaxial silicon layers growth and electrical characteristics 21 p3681 A67-38362
- Anomalous phosphorus diffusion in Si at high surface concentrations explained by excess vacancy generation at edge jogs on gliding dislocations 22 p3855 A67-39347
- Defects in surface layer of silicon crystals during deep diffusion of phosphorus studied by X-ray diffraction 23 p4042 A67-41295
- Concentration and distribution of phosphorus in kamacite and taenite in Mount Edith medium octahedrite determined by electron probe microanalysis 24 p4236 A67-42643

PHOSPHORUS COMPOUND

SA ORGANIC PHOSPHORUS COMPOUND

Excitation of phosphor suspensions in solid dielectric by mechanical energy analyzed via impact 01 p0113 A67-10354

Excitation of phosphor suspensions in solid dielectric by mechanical energy analyzed via impact 11 p1851 A67-25027

IR vibrational and Raman spectra of thiophosphoryl trichloride, thiophosphoryl dichlorodifluoride, thiophosphoryl trifluoride and thiophosphoryl 23 p4041 A67-41242

PHOSPHORUS 32

Neutron produced phosphorus 32 measurement in Barwell and St. Severin meteorites 06 p1078 A67-17604

PHOSPHORYLATION

Nonphosphorylating respiration of mitochondria from brown adipose tissue of rats, providing example of electron transport 02 p0185 A67-12527

Phosphorylation of nucleosides with polyphosphoric acid 13 p2065 A67-26807

Oxygen consumption and phosphorylation processes relation studied in rats for high altitude stability 20 p3367 A67-36259

Oxidative phosphorylation effects on energy metabolism of *Thiobacillus thioautotrophicus* in cell-free system 20 p3371 A67-36927

PHOSWICH SCINTILLATION

Circuit for discriminating neutrons, gammas and charged particles from each other in phoswich scintillator 12 p1945 A67-25857

PHOTIC STIMULATION

Human reaction to intermittent photic stimulation in environmental chamber under IFR conditions 17 p2807 A67-31966

PHOTOCATALYSIS

Gaseous chemical reaction dynamics analyzed with monochromatic laser light-induced photocatalysis 17 p2868 A67-32772

PHOTOCATHODE

SA PHOTOTUBE

Metal photocathodes as secondary standards for absolute intensity measurements in vacuum 03 p0499 A67-13910

UV Multiple beam interference in opaque photocathodes, determining intensity function via multiplication of amplitude by complex conjugate 07 p1185 A67-19407

Translucent and opaque photocathodes analysis 07 p1185 A67-19408

Optical means for enhancing quantum efficiency of tri-alkali photocathode, discussing standing wave pattern in spaced-reflective and reflective photocathodes 17 p2861 A67-33287

PHOTOCHEMICAL REACTION

Time-dependent photochemical model for space-time variations of oxygen allotropes in 20 to 100 km layer 03 p0414 A67-14087

Chemical and photochemical reactions controlling ion composition of atmosphere between 150 and 300 km 07 p1170 A67-19100

Oxygen photochemical equilibrium above 150 km, assuming dominant role of radiative recombination above 120 km 07 p1178 A67-19814

Electron density variation from photochemical rates in equatorial F layer during October 1959 solar eclipse 10 p1651 A67-23342

Photochemical reaction and turbulent diffusion effect studied using mesospheric model, establishing relation between composition and dynamic state 13 p2113 A67-26681

Nitric acid decomposition process by irradiation determined by photolysis of nitrogen dioxide [JPL-TR-32-1128] 14 p2260 A67-28782

Free atomic sodium distribution in daytime upper atmosphere, noting thin layer formation and radiative transfer theory 15 p2475 A67-29616

Book on ionospheric chemistry, noting chemical and photochemical reactions above 60 km, and ionization processes 16 p2619 A67-31252

Photochemical reaction and turbulent diffusion effect studied using mesospheric model, establishing relation between composition and dynamic state 21 p3618 A67-38426

PHOTOCHEMISTRY

Photochemical cells and site involved in

visual adaptation, reporting

electroretinogram data 06 p0953 A67-18643

Vacuum UV resonance lamp design to eliminate difficulty of window seal caused by discharge 08 p1329 A67-20354

Semiconductor substrate photochemical processing and coating photoresistant techniques 12 p1916 A67-25996

Photochemical analysis of diurnal variations of electron concentration and temperature of upper

ionosphere 16 p2669 A67-31902

Photochemical study of propyne with 2062-A iodine line 24 p4118 A67-42327

PHOTOCONDUCTIVE CELL

Surface hole photoconductivity for pressed metal anode CdS ohmic cathode system, noting spectral distribution dependency on crystal heat treatment and air humidity 11 p1849 A67-24871

PHOTOCONDUCTIVITY

Variable effect of external electrical field on IR photoconductivity of thin n- and p-type silicon samples with low bulk impurity contents 01 p0128 A67-10076

Gamma radiation and fast neutron effects on dark resistance, photoconductivity, majority carrier mobility, recombination kinetics, etc., in CdS single crystal 01 p0128 A67-10086

Photo-Hall effect and photoconductivity on compensated p-InSb at low temperatures, examining temperature dependence of carrier mobility 01 p0128 A67-10093

Photon modulation of tunnel emission produced by IR irradiation of thin film semiconductor sandwich of aluminum-aluminum trioxide-tellurium-gold 01 p0131 A67-10369

Surface photopotential of cadmium sulphide single crystals under monochromatic illumination in alternating electric field, using voltage modulation method 01 p0134 A67-10807

Oscillatory low temperature photoconductive spectral response of p-type indium antimonide as function of electric field strength and temperature 02 p0280 A67-11487

Oscillatory semiconductor photoconductivity dependence on photon energy periodic in longitudinal-optical phonon energy treated by Boltzmann equation, noting elastic scattering 02 p0280 A67-11488

Thin layers of crystallized cadmium telluride of high electron mobility analyzed for electrical properties and photoconductivity 02 p0294 A67-11759

High resistivity silicon single crystals, discussing carrier lifetime, photoconductivity and recombination levels 02 p0297 A67-11832

Negative photoconductivity in germanium, noting breakdown and negative conductivity in In region, volt-ampere characteristics, etc. 02 p0297 A67-11835

Photoconductivity resonances and recombination radiation in PbTe and InSb due to multiple photon interband transitions between Landau levels in high intensity magnetic fields 02 p0254 A67-12522

Differential method measurement of Hall effect in presence of large constant magnetic field 03 p0487 A67-12808

Steady state photoconductivity and photomagnetic effect in single crystals of n-type GaAs with various carrier concentrations 03 p0490 A67-13151

Free current carrier formation in molecular crystal, examining dependence of photoconductivity on magnetic field intensity 03 p0501 A67-13469

Semiconductor photoconductivity dependence on external radiation frequency, examining electron-phonon interaction 03 p0502 A67-14374

Current voltage characteristics of Cd-GaSe-Bi diode structure, rectification coefficient, activation energy and photocurrent spectral distribution 04 p0676 A67-14930

Electroluminescence, photoconductivity and I-V characteristics of niobium-niobium oxide-gold diode and possible existence of p-I-n junction in oxide 04 p0582 A67-15104

Spectral response of short circuit photocurrent of niobium pentoxide metal diodes 04 p0582 A67-15125

Photoconductivity and negative resistance caused by carrier lifetime change in response to change in injection level in SiC p-n junctions 04 p0680 A67-15156

Excess carrier lifetime in semiconductors by measuring photoconductive phase shift of spreading resistance under point contact 05 p0861 A67-16501

Photoconductivity, edge emission spectrum, longitudinal optical phonon coupling and eigenfrequencies for linear chain of Cd-Se-Cd-S-Cd... atoms 05 p0870 A67-17196

Impurity IR photoconductivity of silicon surface doped with gold 05 p0871 A67-17491

Photoconductivity of silicon alloyed with gold and zinc at various temperatures 05 p0871 A67-17492

Device for measurement of photocurrent noise spectra in semiconductors at 1 cps to 5 kc 06 p0970 A67-18194

Cooling requirements for intrinsic photoconductive IR detector, comparing theory and experiment 06 p1005 A67-18713

Current saturation and phonon amplification induced instabilities in CdS crystals 06 p1066 A67-18958

Supersensitive laser light detector for wideband receivers to approach theoretical SNR limit set by noise in signal 07 p1194 A67-19085

Spectral distribution of photoconductance and conductance glow curves of CdS single crystals after vacuum heat treatment 07 p1237 A67-20179

Optical absorption, photoconductivity and p-n junction in cadmium telluride 08 p1368 A67-20734

Absolute value of photoconductivity in polycrystalline high resistivity CdS and CdSe SHF field and experimental determination of barrier amplification factor and intercrystalline barrier height 08 p1370 A67-20997

Effect of surface recombination and parasitic capacitance on linear buildup of photoconductivity in semiconductors, noting germanium photoresistor 09 p1551 A67-21668

Optical quenching effect and spectral distribution of photoconductivity and optical transmission of KRS-5 single crystals 09 p1552 A67-21673

Fluctuation levels and induced photoconductivity in vitreous semiconductor thallium selenide and arsenic telluride mixture 09 p1553 A67-21969

Steady state photoconductivity and photomagnetic effect in single crystals of n-type GaAs with various carrier concentrations 10 p1690 A67-23100

Fast neutron irradiated p-type silicon single crystals electric and photoelectric properties 10 p1691 A67-23404

Impurity photoconductivity spectra of p-type germanium at low temperatures, noting parameters of relative depth of equidistant minima oscillations 10 p1693 A67-23583

Temperature dependence of Hall constant and photoconductivity kinetics of gallium antimonide with different tellurium content 10 p1694 A67-23651

Surface hole photoconductivity for pressed metal anode CdS ohmic cathode system, noting spectral distribution dependency on crystal heat treatment and air humidity 11 p1849 A67-24871

Photoconductivity kinetics and regeneration recombination noise spectrum of p-InSb crystals, showing association with hole capture, lifetime and alloying impurity 12 p1983 A67-25512

Optical quenching of photoconductivity in silicon resulting from minority carrier capture by centers created by irradiation 13 p2173 A67-26358

IR surface photoconductivity of silicon as function of surface potential and current carrier parameters 13 p2174 A67-26397

HF photoconductive phase responses in single crystal n-type indium arsenide, deriving carrier lifetimes 14 p2364 A67-28104

Cadmium sulfide crystal photoconductivity peaks near band edge, noting heat treatment, temperature and defects 14 p2364 A67-28229

Depth of capture levels determined from temperature dependence of kinetics of gamma-conductivity or photoconductivity of cadmium sulfide 14 p2367 A67-28526

Measurement of variable Hall electromotive force component created by illumination of thin low resistance germanium samples by modulated 14 p2368 A67-28529

P-type silicon IR photoconductivity burst

in nonequilibrium field effect 14 p2368 A67-28536

Semiconductor photoconductivity kinetics as affected by surface recombination, considering bi-and monopolar photoconductivity 14 p2372 A67-28756

Photoconductivity and negative resistance caused by carrier lifetime change in response to change in injection level in SiC p-n junctions 15 p2534 A67-29343

Light interaction with solids, discussing photoconductivity and phototropy 17 p2913 A67-32373

N-type germanium photoconductivity spectrum studied after bombardment with electrons at very low temperatures 17 p2919 A67-32860

Silicon photoconductivity measurements after electron irradiation at cryogenic temperature 17 p2920 A67-32864

Minority carrier trapping analyzed from transient decay of photoconductivity in n-type polycrystalline films of InAs 17 p2922 A67-33064

Fluctuation levels and induced photoconductivity in vitreous semiconductor thallium selenide and arsenic telluride mixture 17 p2923 A67-33306

Temperature dependence of Hall constant and photoconductivity kinetics of gallium antimonide with different tellurium content 17 p2923 A67-33332

Photoconductivity kinetics and regeneration recombination noise spectrum of p-InSb crystals, showing association with hole capture, lifetime and alloying impurity 18 p3103 A67-34443

Space charge limited currents in copper phthalocyanine thin films measured as function of voltage, temperature, thickness and illumination 18 p3104 A67-34626

Red luminescent band and photoconductivity in cadmium sulfide single crystal, discussing IR quenching of photocurrent 19 p3300 A67-34764

Impurity photoconductivity in cadmium sulfide energy levels at red luminescence centers depth 19 p3300 A67-34765

Dark and photo-conductivity of organic semiconductors, noting measurement techniques and effect of purity, materials, pressure, etc 19 p3302 A67-34995

Photomagnetic effect and kinetic photoconductivity in cadmium sulfide single crystals, determining lifetime and mobility of nonequilibrium holes 20 p3504 A67-36158

Two-photon photoconductivity in pulsed ruby laser excited cadmium sulfide, determining carrier density and density dependence on light intensity 20 p3456 A67-36164

Excess carrier lifetime in semiconductors by measuring photoconductive phase shift of spreading resistance under point contact 20 p3512 A67-37317

Intrinsic and impurity photoconductivity kinetics over wide temperature and illumination range of p-type indium sulfide single crystals obtained by zone melting 21 p3676 A67-37859

Current carrier recombination processes in pure, preheated and Cu-doped GaAs, studying temperature and concentration dependence of intrinsic and impurity photoconductivity 21 p3676 A67-37863

Optical quenching of photoconductivity in silicon resulting from minority carrier capture by centers by irradiation 21 p3679 A67-38315

AIN single crystal thermostable semiconductor optical/electrical properties, measuring space-charge-limited current and photocurrent 21 p3684 A67-38522

Photoconductivity measurements for chromium doped seminsulating gallium arsenide, discussing response peak and possible mechanisms 22 p3855 A67-39348

Photoconductivity in cadmium sulfide crystals induced by light from ruby laser with Q-factor modulation, showing photocurrent dependence on laser power 22 p3814 A67-39511

Depth of capture levels determined from temperature dependence of kinetics of gamma-conductivity or cadmium sulfide 23 p4039 A67-40933

Measurement of variable Hall electromotive force component created by illumination of thin low resistance germanium samples by modulated

light 23 p4039 A67-40936

P-type silicon IR photoconductivity burst in nonequilibrium field effect 23 p4040 A67-40943

Semiconducting diamonds photoconductive response measured noting correlation with activation energy 23 p4044 A67-41454

Photocurrents and photopotentials in organic solids, discussing atomic bonding effect 23 p4045 A67-41484

Space charge layers on surfaces of lead sulfide photoconducting film noting Hall coefficients 24 p4204 A67-42363

PHOTOCONDUCTOR

Laser saturation of photoconductivity and determination of imperfection parameters in sensitive photoconductors such as single crystal of cadmium 02 p0251 A67-11879

Coherent homodyne detection at 10.6 micrometers with aluminum-doped silicon photoconductor, presenting noise spectra and voltage 03 p0438 A67-13989

Photoexcited electron lifetimes measured in extrinsic germanium photoconductors using Doppler shift and rotating mirror square light pulse method 06 p1005 A67-18715

IR detectors analyzed for dependences of detectivities on temperature, noting noise role 24 p4201 A67-41907

Generation-recombination noise voltage in IR detector materials, discussing impurity and intrinsic photoconductors 24 p4201 A67-41909

PHOTODETACHMENT

SA PLANE WAVE

Photodetachment probability for Cs and negative I due to simultaneous absorption of two ruby quanta 05 p0815 A67-16627

Single- and double-quantum photodetachment of negative ions, giving cross sections for electron elastic scattering 07 p1225 A67-19494

Cross sections for photodetachment of electron from negative atomic oxygen ion 07 p1225 A67-19497

Corpuscular streams and photodetachment of electrons reaction effect on formation of D layer of ionosphere 09 p1491 A67-21894

Electron affinity of helium measured by analyzing energy of electrons photodetached from negative helium ions beam passing through laser electromagnetic field 22 p3815 A67-39614

PHOTODETECTOR

Schottky barrier photodiodes with antireflection coating on metal film for fast and efficient optical detectors 04 p0582 A67-15078

Frequency conversion at optical wavelengths of doubly modulated light, using LF photodetectors as receivers 04 p0575 A67-15170

Optical signal modulation to measure noise figure at UHF of photoparametric amplifier, using silicon mesa diode as both photodetector and varactor diode 09 p1476 A67-22208

Photon modulated tunneling in Te-Al oxide-Al structures, noting increased spectral response and detection range 10 p1689 A67-22907

Detectability of coherent optical signals against incoherent Gaussian background noise radiation in heterodyne receiver with laser local oscillator 11 p1800 A67-24419

Frequency conversion at optical wavelengths of doubly modulated light, using LF photodetectors as receivers 15 p2443 A67-29356

Laser light photon counting statistics using probability density for laser light intensity 15 p2498 A67-29513

Avalanche photodiode model with guarding for active area 15 p2452 A67-30014

Criteria for optimized avalanche photodiode design and for best semiconductor material choice based on carrier multiplication process 15 p2453 A67-30015

Time constants of fast photodetectors measured, using mercury wetted relay and epitaxial indium arsenide diode laser 18 p3046 A67-33746

Solid state photosensitive devices combining p-n diodes and MOS circuitry noting application in electrical readout, image and pattern detection 22 p3796 A67-39332

Image tubes to obtain signal and noise solutions, determining Noise Equivalent

Power /NEP/, Detectivity Star and Detective Quantum Efficiency 22 p3805 A67-40352

Schottky photodiode narrow spectral response in Spicer absorption diffusion model shown to exist only in rapidly changing absorption coefficient region 23 p3981 A67-41272

Optical signal detector performance, deriving outlet electron distribution function 24 p4166 A67-41797

Optical detector using length of single mode optical waveguide with photodetector at output for null detection 24 p4133 A67-42817

PHOTODIODE

Design principles and reliability of extensometric sensor with photodiode for static and dynamic study of deformation processes 04 p0621 A67-14919

Schottky barrier photodiodes with antireflection coating on metal film for fast and efficient optical detectors 04 p0582 A67-15078

Solid state diode matrix display using gallium phosphide light sources to investigate use as data recording device 05 p0771 A67-16313

Excess noise and oscillations in gold-doped germanium photodiodes attributed to generation-recombination fluctuations of large bulk resistance 06 p0971 A67-18220

GaAs p-n-i-n diode as light activated switch, noting electrical and optical properties 08 p1306 A67-21295

Signal and noise response of Ge avalanche photodiodes noting design, fabrication, LF photomultiplication and static V-I characteristics 09 p1475 A67-22200

Optical signal modulation to measure noise figure at UHF of photoparametric amplifier, using silicon mesa diode as both photodetector and varactor diode 09 p1476 A67-22208

Solid state celestial trackers development with special reference to photodiode, noting silicon photovoltaic sensor 09 p1526 A67-22394

GaAs laser diodes in pulse operation at liquid nitrogen temperature, comparing reflection and diffraction losses with absorption losses 10 p1666 A67-23521

Noise spectral distribution and instability in germanium and silicon photodiodes 11 p1765 A67-24473

Multiplex reflective laser detector diode design, showing internal reflection effect for trapping light in silicon due to large refractive index 11 p1802 A67-24737

Light sensitive arrays based on photodiodes combined with MOS devices analyzed for use of image, pattern detection and other applications 14 p2282 A67-28026

Avalanche photodiode model with guarding for active area geometry 15 p2452 A67-30014

Criteria for optimized avalanche photodiode design and for best semiconductor material choice based on carrier multiplication process 15 p2453 A67-30015

System performance in electrooptical telemetry noting receiver, transmitter, silicon photodiode, shot, thermal and background noise, etc 17 p2817 A67-32931

Performance characteristics of photodiodes with photoelectric cells as light-source position sensors 18 p3009 A67-33470

Coordinate photodiode matrix with photocells positioned at current-conducting busbar intersections, describing preparation technique 18 p3009 A67-33471

Photodiode holder design for ITT FW-114A high speed planar photodiode for monitoring giant pulse laser output 20 p3397 A67-36528

Short circuit photocurrent of avalanche photodiode, determining frequency response and multiplication effect on bandwidth 22 p3787 A67-39362

Schottky photodiode narrow spectral response in Spicer absorption diffusion model shown to exist only in rapidly changing absorption coefficient region 23 p3981 A67-41272

PHOTODISSOCIATION

Diffusion and dissociation of CO molecules in solar atmosphere 01 p0151 A67-11284

Fractional volume abundance of atmospheric nitrous oxide, considering photodissociation, microbiological reactions and mixing 08 p1327 A67-21369

Photodissociation of hydrogen molecules in H I regions of interstellar medium, evaluating lifetime and density 19 p3331 A67-38085

PHOTOELASTIC MATERIAL

Plasticity and creep problems solution using conventional elastic optically active materials 08 p1423 A67-21331

Solothane 113 urethane rubber composition analyzed via constant strain rate tests, noting birefringent sensitivity and optical transmission properties 11 p1811 A67-24615

PHOTOELASTIC STRESS MEASUREMENT

Elastic behavior of load cell operating on variable capacitance principle designed to fit spaces restricted in one dimension 01 p0034 A67-10296

Elastoplastic deformation under plane stress conditions determined, using method of photoelastic coatings 02 p0336 A67-11628

Stress calculation comparison of computer data and photoelastic data for series of pressure vessels with hemispherical and torispherical heads [ASME PAPER 66-WA/PVP-5] 04 p0719 A67-15931

Dynamic stress concentration due to elastic wave analyzed by high speed photoelasticity to clarify difference between dynamic and static stress distribution 07 p1262 A67-19414

Photoelastic stress measurement techniques for birefringent high polymers extended to two- and three-dimensional linear viscoelasticity problems 08 p1420 A67-20887

Mechanical stresses in silicon single crystal containing p-n junction and ohmic contact measured by photoelastic method, determining birefringence 08 p1423 A67-21332

Dual observation method for determining photoelastic parameters in scattered light 09 p1574 A67-21840

Numerical and photoelastic solutions compared for uniform edge loading, obtaining pressure calibration by means of shear stress measurement 11 p1876 A67-24616

Photoelastic coating technique for measuring stress distribution in blades vibrating in resonant modes 12 p2014 A67-25415

Stress-strain state in elastoplastic range of notched Duralumin strip studied by photoelastic coatings 12 p2032 A67-26105

Three-dimensional photoelasticity and determination of axes of birefringents and change in phase by scattering polarized light 13 p2219 A67-27092

Nondestructive determination of stress distribution in three-layer tempered glass aircraft windshield by scattered-light photoelastic method 15 p2575 A67-30033

Photoelastic stress analysis on bonded interface of strip with different end configurations noting stress concentration, bonding problems, etc 16 p2764 A67-30933

Stress waves propagating in half-space due to point load on surface studied initially in three-dimensional dynamic photoelasticity 17 p2959 A67-32415

Thermal perturbations on fused silica primary mirror in orbiting space telescope, with numerical analysis of radiation transfer in telescope tube 18 p3046 A67-33880

Stress anomaly effect on structural integrity of Teflon laminates determined by photoelastic techniques 18 p3142 A67-33894

Stress calculation comparison of computer data and photoelastic data for series of pressure vessels with hemispherical and torispherical heads [ASME PAPER 66-WA/PVP-5] 18 p3143 A67-34127

Deformations and residual stresses in polycrystalline microstructures, using photoelastic coating method 20 p3540 A67-37059

Stress concentration of plane curved beams with uniform cross section determined from photoelastic experiments 20 p3540 A67-37210

Birefringent properties of Voigt type viscoelastic medium and Noll hydrostatic material during stress relaxation 21 p3657 A67-38409

Book on two-dimensional and surface strain measurement for industrial application including strain gauges, photoelasticity and moiré methods 23 p4077 A67-40791

Frozen stress photoelastic technique used to determine hoop and radial stresses at

hole boundaries for different flat disk configurations 23 p4077 A67-41154

Suitability of finite element method for stresses in composite materials, examining single broken fiber in matrix 23 p4077 A67-41156

Holography /phase-recording of diffracted wavelets/ for phase contrast and striae, interferometry in polarized light and 3-D photoelasticity 23 p3999 A67-41179

PHOTOELASTICITY

Two-dimensional photoelasticity analysis of stress concentration in plate with large number of uniformly spaced circular holes under biaxial loading 05 p0918 A67-16423

Moiré pattern method of determining fringes representing constant curvature of bent plates 05 p0921 A67-16827

Total relative retardation in three-dimensional photoelastic model viewed under polarized light 07 p1264 A67-20259

Plastic strain distributions in polycrystalline austenitic stainless steel and titanium, using photoelastic coating 08 p1343 A67-21333

Nonstationary thermoelastic stresses analyzed using photoelastic technique based on polarized light 08 p1423 A67-21334

Stress measurement in metal components with photoelastic coatings and thin walled structures, using reflected light technique 09 p1575 A67-22169

Immersion technique measurement of gravitational stresses using two- and three-dimensional photoelasticity [ASME PAPER 67-APM-11] 17 p2964 A67-33146

Threshold power dependence on temperature and photoelasticity for stimulated Brillouin scattering in crystalline and fused quartz 24 p4204 A67-42365

Total principal constraints on I curves in two-dimensional photoelastic medium 24 p4251 A67-42658

PHOTOELECTRIC APPARATUS

Photoelectric components and electronic measurement techniques in reception and demodulation of HF modulated laser beams 01 p0088 A67-10300

ASL 70-mm photoelectric system in studying approach and landing parameters for aircraft design and testing 01 p0075 A67-11133

Photoelectric optical imaging system survival in earth radiation belt, noting noise level and total energy absorption 02 p0243 A67-12055

Amplitude spectrum of turbulent flow rate fluctuations at flame temperatures measured via photoelectric method 05 p0927 A67-16942

Airborne photoelectric device for registration of cloud drops 07 p1189 A67-20009

Far UV transmitting windows, particularly lithium fluoride, and response measurements below 2000 angstroms, noting fabrication on solar blind materials 12 p1947 A67-26161

Meteor radiation and methods of meteor spectrography, discussing chemical composition, spectral characteristics, green oxygen line and photoelectrical color sensors 13 p2197 A67-26504

Amplitude spectrum of turbulent flow rate fluctuations at flame temperatures measured via photoelectric method 14 p2406 A67-28490

Photoelectric measurement of planetary disk diameter and center-to-limb darkening 16 p2753 A67-31716

Diurnal variations in He twilight emission intensity determined using photoelectric spectrometer 17 p2849 A67-32958

Soviet book on photoelectric sensors in monitoring, control and regulation systems noting design principles, operational requirements, etc 18 p3011 A67-33716

Photographic systems and photoelectric scanner for observation of solar annular eclipse 18 p3049 A67-34312

Digital recording double Fabry-Perot spectrometer, discussing pressure difference control system 20 p3440 A67-36363

Photoelectric device measuring cutting-tool temperature for automatic control of state of cutting edges 21 p3626 A67-38059

Photoelectric method for measuring temperatures in metal cutting 21 p3631 A67-38921

Photoelectric polarimeter for measuring rotational, electro-optical and electrogyrational effects and optical activity in ferroelectrics 21 p3631 A67-38969

Oscilloscope recording of mechanical rotation rate using semiconductor photoelectric effect 22 p3796 A67-39341

Photoelectric micrometer for automatic determination of meridian passage times, describing tracking servomechanism and collimation measurements device 22 p3881 A67-39515

Magnetoelectric device development to measure and register weak signals in digital form in converters of automatic control systems 22 p3809 A67-40475

Photoelectric records of DE and LZE in solar photosphere velocity fields, analyzing oscillations onset and lifetimes 23 p4066 A67-41229

Property changes of semiconductor materials during processing, discussing photoelectric methods, resistivity derivative, recombination parameters and mechanical stresses 23 p4043 A67-41364

Vertical distribution of cloud condensation nuclei in free atmosphere investigated by flow type onboard photoelectric apparatus to calculate washout coefficients 24 p4181 A67-42163

PHOTOELECTRIC CELL

SA PHOTOCONDUCTIVE CELL

Different crystallization conditions and effect on Se surface structures on properties of p-n heterojunctions in Se-CdSe and Se-CdS rectifying cells and photocells 02 p0297 A67-11849

Optimum processing of photocell output to produce Poisson photoelectron flux 03 p0368 A67-13282

Thin film photoconverters using silicon, cadmium sulfide and cadmium telluride 04 p0553 A67-14664

GaP electroluminescent junctions, considering feasibility of electroluminescence applications where human eye is detector 04 p0581 A67-15077

Spectral sensitivity and temperature characteristics of light generated pairs of photoelectric converters 07 p1131 A67-19105

Drift field, field gradient and diffused impurity effects on minority carriers and quantum efficiency in silicon photocells 11 p1746 A67-24914

Optimum multiscade photocell constructing procedure from half-cells of arbitrary number, size and shape 13 p2174 A67-26370

Stimulation of photosensitivity of cadmium sulfide single crystals by chemical etching 13 p2174 A67-26401

Photoelectric two-cell polarimeter with rotating achromatic half-wave plane noting wavelength restriction 14 p2319 A67-28563

High resolution spectroscopy, using incoherent light mixed with coherent laser light, for astronomical purposes 17 p2854 A67-32234

Soviet book on semiconductor technology and microelectronics covering photoelectric functional converters, junction characteristics, etc 18 p3008 A67-33467

Photoelectric functional converters application to semiconductor microelectronics and optoelectronic circuits 18 p3008 A67-33468

Transverse-conduction photopotentiometer operating as functional energy converter, calculating resistive layer required for device operation 18 p3009 A67-33469

Performance characteristics of photodiodes with photoelectric cells as light-source position sensors 18 p3009 A67-33470

Coordinate photodiode matrix with photocells positioned at current-conducting busbar intersections, describing preparation technique 18 p3009 A67-33471

Germanium photovoltaic cells as solar conversion devices [ONERA-TP-478] 18 p2990 A67-34464

Copper-doping technique for obtaining p-n junctions in sintered cadmium sulfide polycrystals, suitable for use in photoelectric converters 19 p3304 A67-35427

Thin film cadmium telluride solar cells, discussing efficiencies and photoelectric properties of junction 21 p3679 A67-38224

Photovoltaics - IEEE Conference, Cocoa Beach, Florida, March 1967, Volume 1, Thin film cells 23 p3936 A67-41482

PHOTOELECTRIC EMISSION

Photoelectron emission from aluminum-aluminum oxide-gold film system with electric field in dielectric 03 p0492 A67-13295

Visible and X-ray photoelectric emissions

- in layers of Se-As-Tl intrinsic semiconductor films in vacuum 03 p0498 A67-13838
- Attenuation length of photoexcited electrons in evaporated layers of CuBr estimated by measuring photoemission yield as function of thickness 03 p0500 A67-14332
- Photoelectron emission from aluminum-aluminum oxide-gold film system with electric field in dielectric 04 p0674 A67-14720
- Relativistic photoelectric cross section for two electrons of K-shell computed, using numerical program 04 p0661 A67-15763
- Surface photoelectromotive force in GaAs type semiconductors with short duration minority carriers 04 p0686 A67-15969
- Reduced X-ray photoelectric current in modified Bayard-Alpert ion gauge for vacuum pressure measurements below 10 to minus tenth torr 05 p0805 A67-16462
- Dember effect, bulk photovoltaic effect and current density in illuminated inhomogeneous semiconductor 05 p0863 A67-16702
- LF photocurrent oscillation in high resistivity n-type GaAs, noting relation between amplitude temperature and light intensity 05 p0866 A67-16987
- Photoemission of electrons from conduction and valence bands of n-type degenerate Si into thermally grown silicon dioxide layers 05 p0870 A67-17195
- High power laser beam polarization direction effects on electron emission from Ag surface 06 p1012 A67-18759
- Potential on hot body in plasma as function of surface temperature and plasma characteristics, considering case where photoemission is present 07 p1251 A67-19812
- UV solar radiation absorption in upper atmosphere determined from measurement of photoelectron currents emitted by planar metallic orthogonal photocathodes onboard Cosmos II satellite 10 p1647 A67-23282
- Field emission from sharply pointed CdS single crystals photon-enhanced by illumination from pulsed argon-ion laser 11 p1845 A67-24133
- Optically excited electrons of X minima in gallium arsenide 11 p1803 A67-24998
- Visible and X-ray photoelectric emissions in layers of Se-As-Tl intrinsic semiconductor films in vacuum 13 p2184 A67-27719
- Intrinsic optical excitation spectrum of crystalline solids for hole or electron localization, considering many-body relaxation effects influencing photoemission 16 p2732 A67-31698
- Photoelectric contribution to magnetospheric electron density on basis of pitch redistribution of collision component 20 p3425 A67-36283
- Auroral excitation of atomic oxygen forbidden lines, giving photon emission rate vs zenith angle 20 p3426 A67-36301
- Field induced photoelectron emission /FPE/ from Si surface barrier diodes, discussing FPE measurement using xenon arc lamp and grating monochromator 23 p3980 A67-40890
- PHOTOELECTRIC MATERIAL**
- High voltage photo-emf in epitaxial zinc telluride films grown on halide substrates 05 p0868 A67-17061
- Distribution of capacitive photo-emf over surface of semiconductor determined by measuring value created by scanning surface of sample with narrow modulated-light beam 08 p1367 A67-20415
- Optical materials properties analyzed for UV induced degradation under vacuum conditions [AIAA PAPER 67-344] 12 p1959 A67-26058
- High voltage photo-EMF in epitaxial zinc telluride films grown on halide substrates 15 p2538 A67-29792
- Generation-recombination noise voltage in IR detector materials, discussing impurity and intrinsic photoconductors 24 p4201 A67-41909
- PHOTOELECTRIC PHOTOMETRY**
- Water vapor lines in spectrum of Venus obtained by photoelectric scanning of spectrum 02 p0324 A67-11769
- Photoelectric recording of scintillation of stellar images by function of nature of scintillation while carrying out observations 02 p0326 A67-11991
- Red-green-IR three-beam high resolution photoelectric photometry during lunar eclipse for lunar colorimetric studies 04 p0696 A67-14735
- Large star fields outside earth atmosphere, using wide-angled photoelectric photometer for simultaneous UV and visible spectrum measurements of sky brightness 04 p0700 A67-15073
- Visual, photographic and photoelectric methods for comet polarimetry 05 p0890 A67-16334
- Photoelectric observation results of short period variable DQ Cepheid star 05 p0891 A67-16405
- Photometry of integrated light of Venus, inferring presence of ice in atmosphere from halo effect of brightness dispersion 05 p0892 A67-16407
- Calculation method for energetic photoelectric photometry system for tracing behind radiative source or for distance measurement 08 p1331 A67-21055
- Photospheric brightness fluctuations recorded photoelectrically across solar disk center simultaneously for two regions of continuum, deriving autocorrelation functions and spatial power spectra 10 p1711 A67-23796
- Perseld meteor brightness studied from data of photoelectric observations by use of electronic multiplier 11 p1867 A67-24846
- Barrier height between tungsten silicide films and n-type silicon base determined, using photoelectric response measurements 11 p1850 A67-24924
- Spatial inhomogeneities in green line of atomic oxygen, using electrophotometry during airglow 13 p2111 A67-26567
- Photoelectric observation of Fraunhofer line profiles by high dispersion solar spectrograph 13 p2198 A67-26706
- Photoelectric scanning observations of night airglow for two spectral lines of OI 14 p2306 A67-27788
- Photoelectric measurements of continuum intensity differences and concave grating spectra of faculae and undisturbed photosphere 14 p2378 A67-27846
- High luminosity spectrograph using inverse Wadsworth mounting constructed for recording auroral spectra in far UV 14 p2315 A67-28157
- Solar corona temperature from intensity gradients measured during total eclipse of May 30, 1965 14 p2387 A67-28564
- Photoelectric solar spectroscopy at Nice Observatory, discussing suitability of location and results obtained 14 p2387 A67-28592
- Two-color photoelectric photometry of earthshine, determining earth albedos 15 p2477 A67-29626
- Photoelectric method measuring separation of head shock wave from supersonically-moving body, detailing equipment design and operation 16 p2674 A67-31128
- Night airglow brightness spatial distribution observed by photoelectric photometry in 5893 angstrom band, including isophotes charts and emission-inhomogeneity drift histogram 17 p2848 A67-32953
- Difference between ephemerals and universal time based on observations of lunar occultations 17 p2950 A67-33129
- Hydrogen emission lines photoelectric measures in Ton 1542 indicates radiative recombination in upper levels and sharp intensity increase in red ascribed to nonthermal sources 18 p3120 A67-33997
- Temperature field and electron concentration in electric arc moving along parallel electrodes in magnetic field, giving propagation rate, arc intensity, etc 18 p3087 A67-34046
- Martian surface atmospheric pressure via photometric observations of Phobos eclipses 18 p3124 A67-34155
- Corona temperature and logarithmic intensity gradients determined by pointwise three-color photoelectric photometry during solar eclipse 19 p3318 A67-35017
- Airglow measurement apparatus and procedure at Tehran University 19 p3224 A67-35488
- Photoelectric recording of Raman spectra excited by ruby laser 19 p3240 A67-35546
- Design, construction and operation of multichannel photoelectric spectrometer, using Fabry-Perot etalon and axicon 20 p3439 A67-36353
- Low intensity photoelectric signal detection by Fabry-Perot spectrometer using SNR enhancing method 20 p3439 A67-36356
- Computer method for evaluating hyperfine structure recordings obtained by photoelectric Fabry-Perot interferometer 20 p3440 A67-36357
- Calculation method for energetic photoelectric photometry system for tracing behind radiative source or for distance measurement 22 p3797 A67-39417
- PHOTOELECTRICITY**
- X-ray radiation effect on p-n junctions of germanium diodes, noting changes in V-I characteristics 01 p0136 A67-11047
- Anomalous photocurrent generation in transistors, noting carrier generation and transport processes 04 p0685 A67-15696
- Equilibrium photocurrents in silicon switching diodes from nondestructively measured electrical parameters 04 p0588 A67-15698
- Elliptical polarization of Crab Nebula radiation possibly explained without synchrotron hypothesis by analyzing photoelectric observations of Stokes parameters 05 p0882 A67-16593
- Illumination effect on capacitance of metal-SiO-Si system with various biases 07 p1152 A67-19591
- Electric and photoelectric properties of p-n junction obtained by thermal diffusion of copper into n-ZnS-Cl single crystals 13 p2172 A67-26355
- Nature of photoelectromotive force of cadmium selenide with Cu, Ag, Au, Pt vacuum-deposited on surface 14 p2367 A67-28527
- Upper atmosphere photoelectric processes contributing to low energy electron content of magnetosphere 16 p2664 A67-30973
- Thermophotovoltaic conversion efficiency evaluation based on theory of photoelement operation 16 p2609 A67-31398
- Photo-induced microwave response of SbSI crystals to variations in reflection coefficient indicates photodiodelectric effect 17 p2915 A67-32675
- Illumination effect on capacitance of metal-SiO-Si system with various biases 20 p3401 A67-37330
- Electric and photoelectric properties of p-n junction obtained by thermal diffusion of copper into n-ZnS-Cl single crystals 21 p3679 A67-38312
- Nature of photoelectromotive force of cadmium selenide with Cu, Ag, Au, Pt vacuum-deposited on surface 23 p4039 A67-40934
- PHOTOELECTROMAGNETIC /PEM/ EFFECT**
- Hall coefficient and transverse magnetoresistance behavior in n-GaSb at 4.2 degrees K, using DC high magnetic fields 06 p1064 A67-18946
- Magnetic effect on photoresponse of illuminated InAs p-n junctions 07 p1237 A67-20181
- PHOTOELECTROMAGNETIC DETECTOR**
- Translucent and opaque photocathodes analysis 07 p1185 A67-19408
- Cathodoluminescence detector for electron microprobe, noting components and use 16 p2677 A67-31432
- Photoelectromagnetic detector spectral sensitivity, magnetoresistance and time constants with optically polished thin elements fabricated from Ge, InAs, GaSb and InSb single crystals 24 p4154 A67-42243
- PHOTOELECTRON**
- Continuous helium-neon laser used to obtain short intense light pulses and to study kinetics of autophotoelectronic emission of high resistivity silicon 03 p0436 A67-13142
- High altitude vertical photoelectron distribution from electron concentration measurements by Cosmos V and IMP I and II 05 p0795 A67-16061
- Dead time corrections to photocount distributions using time interval probability density of counts, noting application to laser light 06 p1009 A67-17652
- Photoelectron energy measurement and Franck-Condon factors for vibrational transitions of molecular ions when ejected by He resonance line 17 p2888 A67-32356
- Protonosphere heating by photoelectrons escaping from F region, estimating protonosphere opacity and daytime escape flux 19 p3221 A67-35280
- Dayglow photoelectron excitation rate from electron energy loss calculations, with energy transfer functions calculated from photoelectrons produced by UV solar radiation 20 p3434 A67-37421

High altitude vertical photoelectron distribution from electron concentration measurements by Cosmos V and IMP I and II 21 p3615 A67-37848

PHOTOENGRAVING

Photoengraving and use as precision processing technique 12 p1951 A67-26213

Chemical milling technique for space vehicle chassis and circuitry production, noting similarity and differences with photoengraving and printed circuit techniques 16 p2683 A67-31739

PHOTOGRAMMETRY

SA AERIAL PHOTOGRAPHY

SA MAPPING

Photogrammetric refraction in high altitude surveying for isothermal atmosphere and for atmospheric polytropic through altitude of 11 km 05 p0808 A67-17033

Photogrammetric network for large-area phototriangulation using star-tracking airborne cameras, discussing theoretical and technical aspects 06 p0994 A67-17716

U.S. Coast and Geodetic Survey satellite triangulation program based on optical tracking of passive satellites simultaneously from two or more mobile camera stations 07 p1176 A67-19764

BMK ballistic camera with equatorial and azimuthal mount for stellar geodetic satellite tracking and punch card controlled mono- and stereocomparators 07 p1188 A67-19773

Triangulation by photogrammetric use of geodetic satellites and data reduction methods 07 p1177 A67-19777

Stekometer with automatic recorder for use in analytic photogrammetry for mapping and engineering surveys 09 p1497 A67-21751

Errors, due to inaccurate tentative aerial observations, in determination of identification points for vertical aerial photography 13 p2118 A67-26464

Soviet papers on photogrammetric processing and interpretation of aerial photographs 14 p2318 A67-28370

Aerial and space photography for forestry 14 p2321 A67-28827

Three-photo orientation solution to analytic aerotriangulation problem, investigating mathematical concepts and computer programming methods 15 p2486 A67-29298

Analytical reduction of panoramic and strip photography to equivalent frame photography 15 p2486 A67-29299

Aerial electronic photomapping and geodetic surveying system describing track-keeping navigation and verticality measuring 16 p2679 A67-31801

Photogrammetric refraction in high altitude surveying for isothermal atmosphere and for atmospheric polytropic through altitude of 11 km 21 p3627 A67-38265

Anharmonic method of photogrammetry rectification point by point, deriving positions from minimum control data 24 p4158 A67-42604

PHOTOGRAPH

S CLOUD PHOTOGRAPH

S LUNAR PHOTOGRAPH

PHOTOGRAPH INTERPRETATION

Remote sensing techniques and data evaluation and processing in geography 01 p0058 A67-10308

Geometrical evaluation of line-scan images for mapping, noting imagery systems 01 p0059 A67-10316

Lunar crater photographs obtained by Ranger VIII and IX compared with those of laboratory craters overlain with granular material, for depth interpretation [JPL-TR-32-1021] 02 p0320 A67-11459

Interpretation of built-up areas in cities and industrial sites from aerial photographs 02 p0240 A67-11533

Interpretations of lunar crater erosion other than used by Jaffe from Ranger VII pictures 02 p0325 A67-11860

Stereo interpretation of Nimbus II automatic picture transmission photography for cloud patterns [AFCR-66-805] 02 p0241 A67-11970

Positions of Echo satellites during reentry stage observed at Aslago in 1964 03 p0509 A67-13105

Earth azimuthal perspective projections /cosmographic projections/ in space photograph interpretation 03 p0419 A67-13264

Plasma vortex filaments produced in pairs as shown by image converter photographs of interfaces between magnetic field and

accelerated plasma 03 p0486 A67-14054

Aerial photograph interpretation of landscape in terms of tone, texture and stereo effect 04 p0619 A67-14529

Aerial photograph physics in correct and faulty colors, discussing recognition of relation between landscape and photographic density 05 p0804 A67-16064

Communications of Lunar and Planetary Laboratory /University of Arizona/, Volume 4, covering Ranger VII records 05 p0896 A67-16713

Ranger VII photographic interpretation and lunar surface structures 05 p0896 A67-16714

Wall of large circular formation on moon shown on Orbiter photographs as convex body resembling flow of viscous lava 05 p0901 A67-17202

General purpose computer used in automatic photointerpretation process in relation to pattern recognition 05 p0768 A67-17513

Fluid mechanical model of electric arc balanced magnetically in gas flow, based on photographs showing arc must simulate solid body [AIAA PAPER 67-96] 07 p1240 A67-19437

Geodetic linking of France and North Africa by synchronous photographs of Echo I satellite 07 p1176 A67-19767

TV pictures of Surveyor I compartment radiators taken on June 11 and July 12, 1966, discussing cause of some changes in dust locations 08 p1386 A67-20944

Ranger photographs of lunar surface noting erosion and fragmentation by meteorite bombardment 08 p1390 A67-21026

Pictures of moon taken by Ranger, Surveyor and Orbiter spacecraft analyzed for origin, history, libration, temperature and properties 08 p1401 A67-21428

Matched filter detection of target shape in photographs using both coherent and incoherent illuminations 09 p1496 A67-21712

Boulder size distribution in Luna IX surface photographs 09 p1570 A67-22692

Selenological analysis of Ranger IX photographs, examining origin and age of craters and mountain chains 10 p1705 A67-22898

Cloud photographs obtained on board ATS-I satellite with camera equipped with reflecting telescope show feasibility of short-lived weather systems from synchronous altitude 10 p1657 A67-23367

Lunar photography by refractor and reflector telescopes at Pic du Midi Observatory 10 p1710 A67-23563

Saturn edgewise rings rapid fading and brightness variation on disk 10 p1710 A67-23564

Reductive determination of refraction-free photographic coordinates of lunar limb profile points and disk points 11 p1860 A67-24458

Systematic errors in earthward coordinates of selenodetic points, noting results of triangulation 11 p1860 A67-24461

Measures and reductions for 1868 points on Yerkes lunar photograph No. 1269, listing uncorrected and refraction-free photographic coordinates 11 p1860 A67-24463

Lunar soil composition determined to be porous fine-grain moderately cohesive rock powder, from Surveyor I and Luna IX pictures 11 p1865 A67-24607

Catalog for interpretation of objects in eastern sector of far side of moon 11 p1867 A67-24844

Ground based conversion of Lunar Orbiter II video signals into photographic images, describing reconstruction electronics, signal processor, etc 12 p1940 A67-25466

Photographically recorded information retrieval by isodensitometry [SMPT PAPER 101-89] 12 p1941 A67-25473

Rotational velocity of Venus spots based on sidereal rotation measurements 13 p2198 A67-26588

Theoretical interpretation of fine structure observations of sunspots by stratoscope, discussing stability modes and sunspot umbras 13 p2203 A67-27423

Soviet papers on photogrammetric processing and interpretation of aerial photographs 14 p2318 A67-28370

Panoramic photograph processing theory 14 p2318 A67-28372

Scanning and transformation of panoramic lunar surface photographs 14 p2319 A67-28373

Monochromatic photographs through filters for observation of shading variation in intensity of solar emission between center and edge of solar disk 14 p2387 A67-28517

Aerial and space photography for forestry 14 p2321 A67-28827

Number of rays and brightness of Comet Morehouse derived from photographs taken with Greenwich reflector 16 p2742 A67-30666

Lunar surface bearing strength estimate from Orbiter II photograph, noting Sabine D crater measurement as potential landing site for Surveyor and Apollo [JPL-TR-32-1156] 16 p2746 A67-30931

Theodolite device for measuring coordinates of center of gravity of photographed missile in flight 16 p2674 A67-31120

Variability in human estimation of total cloud cover data by satellite-photograph interpretation, noting use of Nimbus I photographs 17 p2880 A67-32555

Lunar surface photographs taken by Luna IX and Surveyor I showing linear and circular ground features, rock blocks and dust 17 p2948 A67-33094

Lunar surface and U.S. Ranger program significance and interpretation 18 p3121 A67-34137

Analysis of lunar surface panoramas transmitted by automatic station Lunik IX after soft landing 18 p3122 A67-34138

Visible brightness features in Mariner IV photographs of Mars interpreted as clouds 18 p3123 A67-34149

Mariner IV photographs of Mars, discussing mission objectives, functioning of camera system and interpretation of pictures 18 p3123 A67-34150

Nickel-base alloys refractory-melt reactions in vacuum induction melting investigated by measuring contact angles from photographs, noting carbon contact angles from photographs noting carbon effect 19 p3242 A67-34786

Detection of mineral resources by orbiting satellite photography, using remote sensor techniques 19 p3225 A67-35655

Moon probe photographs studied to ascertain moon surface material, structural condition and carrying capacity for future landings on moon 19 p3327 A67-35830

Everhart comet and various minor planets positions through photographic observations at Tartu 20 p3522 A67-36622

Various minor planets positions from photographic observations at Crimean Astrophysical Observatory 20 p3523 A67-36630

Cavitation erosion noting high speed motion picture photographic analysis of kinematic structure of cavitation zone 20 p3420 A67-36631

Surveyor I spacecraft location and identification on moon surface by photographs taken by Orbiter III 20 p3524 A67-36649

Automated system for growth and analysis of bacterial colonies using environmental chamber and computer controlled flying-spot scanner 20 p3453 A67-37598

Observational results consisting of meteor trail photographs for determining processes responsible for relative intensity of brightness and trail length 20 p3530 A67-37665

Penetration depth of hypervelocity impact craters photographed by Luna and Ranger vehicles indicate granular lunar surface 23 p4065 A67-41003

Forestry applications for remote sensing from earth orbiting vehicles for inventory and evaluation of resources [AIAA PAPER 67-765] 24 p4258 A67-42934

PHOTOGRAPHIC APPARATUS

Weather satellites, discussing photographic and radiation measuring equipment and automatic picture transmission 01 p0109 A67-10768

High speed photographic equipment, analyzing gun launching of vehicles in upper atmosphere and design of protection system against space vehicle failure due to meteorites 01 p0068 A67-10968

Zone plate free from chromatic aberration and application to three-color holography 03 p0420 A67-13681

Photographic technique for photometric comet observations, noting automatic polarograph and high transmission meniscus telescope 05 p0890 A67-16333

Aerial photographic techniques and

equipment, noting use in reconnaissance and mapping 06 p1000 A67-17583

Laser line-scanning photographic system, discussing possible extraterrestrial applications 06 p1006 A67-19011

Filmed data and computers - Seminar, Photo-Optical Instrumentation Engineers Society, Boston, June 1966 07 p1148 A67-19741

Surveyor system and camera design for photographic mission on Mars surface 09 p1570 A67-21680

Holography for particle size analysis noting wave formation and reconstruction, hologram camera, etc 10 p1653 A67-22748

Goniometric measurement accuracy of aerial camera photogrammetric distortion 11 p1793 A67-24864

Lunar Orbiter photographic system readout for image conversion to video signals [SMPT PAPER 101-45] 12 p1940 A67-25463

Lunar Orbiter photographic system design including film processing, image conversion, relay, reconstitution, performance, characteristics, etc [SMPT PAPER 101-46] 12 p1940 A67-25464

Dual camera for Lunar Orbiter, design, performance and hardware modifications [SMPT PAPER 101-47] 12 p1940 A67-25465

Automatic laser tracker system for close-up photographic coverage of rocket test [SMPT PAPER 101-90] 12 p1905 A67-25474

Two-phase gas-liquid flow photography equipment and techniques, with applications to droplet mass transfer, flow pattern determination, etc 16 p2671 A67-30840

High speed spark photography with electronic equipment, describing generating and control units and optical techniques for shock wave observation 16 p2674 A67-31127

Airborne photo-optical instrumentation - Conference, Cocoa Beach, Florida, February 1967 16 p2678 A67-31791

Airborne photographic instrumentation system for photometric observation of total solar eclipse, noting automatic tracking system 16 p2678 A67-31794

Interference and spectroscopic devices improving photographic detection of astronomical telescopes on ground and in space 18 p3048 A67-34189

UV radiation observed beyond atmosphere in winter Milky Way, noting nebula detection and photographic apparatus 18 p3125 A67-34190

Antares triaxial tracking camera noting mounting, electronic and optical systems and performance techniques 19 p3229 A67-35267

TV in lunar environment, discussing development and performance of instrument used during Surveyor I mission 21 p3629 A67-38658

Plasmoid propagation at high pressures, emphasizing Bostick buttons performance compared to electromagnetic shock tube, describing button gun and photographic equipment 21 p3674 A67-38771

Aerial color photography advantages over black and white, discussing exposure, processing and viewing 22 p3797 A67-39450

PHOTOGRAPHIC DEVELOPER

Wide latitude low gamma Ilford Phenidone /POTA/ developer for astronomical and scientific photography 06 p1002 A67-17976

High quality film processing in Lunar Orbiter spacecraft photo system, noting separate environmental control system [SMPT PAPER 101-49] 12 p1941 A67-25467

PHOTOGRAPHIC EMULSION

Interferential method of testing high resolution photographic emulsions, using laser as light source 01 p0091 A67-10832

Noise limitations in obtaining three-dimensional images by holographic techniques, considering graininess of photographic emulsion 01 p0067 A67-10834

Effect of fluctuations on systematic error in determination of energy characteristics of nuclear interactions in photoemulsion in presence of energy threshold 02 p0312 A67-12605

Film cooling technique for color photographs of astronomical objects to diminish effects of reciprocity failure and increase light sensitivity 06 p1002 A67-17975

Wavelength dependence of characteristic curve of photographic emulsion 06 p1002 A67-17977

Model predicting effects of finite hologram emulsion resolving power on field

range recorded in hologram and resolution in reconstructed image 06 p1004 A67-18543

Holographic evaluation of spatial frequency response of photographic emulsions 07 p1186 A67-19493

Image restoration via phase holograms, noting applications to deteriorated photographic negatives and positives 08 p1331 A67-20842

Trapped proton flux data from nuclear photographic emulsions 08 p1378 A67-21472

Distribution of photons from point image in photographic emulsion calculated using diffusion equation, deriving limits on point spread functions and corresponding modulation transfer functions 09 p1496 A67-21708

High intensity reciprocity failure in Kodak 649-F spectroscopic plates revealed by holograms obtained with Q-switched ruby laser 09 p1496 A67-21711

Energy spectrum of primary cosmic ray alpha particles measured by nuclear photographic emulsion, estimating geomagnetic cut-off 09 p1562 A67-22418

Photographic technique for obtaining solar image in rays of Lyman alpha line spectrum, using quartz crystal 11 p1793 A67-24862

Pulsed ruby laser to obtain Fourier holograms in light reflected from diffusely scattering objects, discussing relaxation of resolving power of photographic emulsions 12 p1939 A67-25335

Heavy cosmic ions recorded on ionographic emulsions exposed on polar satellite 12 p1999 A67-25830

Unexpected excess of primary cosmic ray helium nuclei flux value in nuclear photographic emulsions 17 p2939 A67-33237

Experimental techniques in making multicolor white light reconstructed holograms, discussing signal to noise ratio, coherent light and photographic emulsion 17 p2862 A67-33299

Emulsion shrinkage effect on hologram image space 17 p2863 A67-33303

Resolution improvement of earth-based lunar photography, discussing film speeds, emulsions, etc 18 p3049 A67-34332

Sensitivity of film with and without image intensifier compared, using emulsion densities as function of number of incident quanta 22 p3796 A67-39278

Charge spectrum of very heavy cosmic ray primaries studied from balloon observations in photographic emulsion detector for Texas atmosphere 23 p4050 A67-40676

Modulation transfer functions of various solar recording films using interference device, giving detectability threshold of two-dimensional emulsion patterns 23 p4001 A67-41237

Three-beam holographic interferometry using only one exposure of photographic emulsion 23 p4001 A67-41259

PHOTOGRAPHIC FILM

Space bandwidth theorem for Fresnel and Fraunhofer holograms, taking into account effects of photographic film 01 p0071 A67-11083

Optimization of size of film negative for aerial cameras on grounds of economic efficiency 02 p0240 A67-11532

Negative lens property responsible for reconstruction of original scene in full three-dimensional reality 03 p0420 A67-13676

Microdensitometry in retrieval of data recorded on photographic film 06 p1001 A67-17791

High resolution aerial photography, detailing photographic films, optical design, camera systems and methods of system analysis 08 p1330 A67-20645

Selective imaging of objects in range using pulsed laser illuminator synchronized with Kerr cell camera, obtaining elimination of film exposure due to backscatter in turbid atmosphere 08 p1337 A67-20683

Dynamic range of data processor /correlator/ associated with synthetic aperture mapping radar system, considering film grain noise 08 p1293 A67-20688

Print-etch and negative-pattern image transfer techniques for fabrication 08 p1334 A67-20743

Fresnel microzone plates for X-ray images of sun 10 p1707 A67-23232

Spatially modulated laser recording parameters, emphasizing beam intensity ratio to signal beam, offset angle film transfer

characteristic and recording wavelength 13 p2129 A67-27351

Film transport methods and other factors relating to high speed frame cinematography 14 p2315 A67-27871

Optical system consisting of circular sweep camera for recording useful streak images on Polaroid film 14 p2320 A67-28748

Hypersensitization procedure for spectroscopic plates, minimizing nonuniformities of plate fog by use of stop bath 18 p3047 A67-33883

Tracking of GEOS-A satellite by Riga station, explaining negatives reduction 19 p3182 A67-35235

Application of double-exposure holographic interferometry technique by using tri-X Pan film for hologram recording 19 p3232 A67-35693

Recording and display programs illustrating relative capabilities of thermoplastic and direct electron beam on photographic film recording 20 p3449 A67-36984

Film resolution limitation on hologram size, Rayleigh resolution and interference pattern recording 22 p3796 A67-39259

Photographic film nonlinearities effect in holographic recording of coherent wavefront using two-beam interferometry, describing phenomenological model 23 p4002 A67-41269

PHOTOGRAPHIC MEASUREMENT

SA PHOTOGAMMETRY

Diffusion coefficient of lithium in p-type silicon determined by method using electrophotographic developing agents 01 p0127 A67-10061

Radiation techniques for surface temperature measurement, considering optical and radiation pyrometers, projection thermography and photographic techniques 01 p0062 A67-10274

Airborne surface temperature measurement relating surface appearances to radiation parameters 01 p0063 A67-10327

Lunar disk color index derivation by applying method of photographic photometry in UV and IR spectral regions 02 p0329 A67-12493

Spectrographic observation of quasi-stellar and Haro-Luyten objects, noting hydrogen absorption spectra and emission wavelengths 03 p0511 A67-13652

CW He-Ne laser compared with mercury arc source, obtaining Raman spectra of carbon tetrachloride by three methods of excitation 03 p0438 A67-13912

Solar radio burst analysis from spectral diagrams noting sudden beginning, precursory activity and succession of isolated peaks and islands 04 p0692 A67-14588

Micrometric measurement of absolute and relative heights of 163 unobtrusive points on lunar surface, comparing values of Maedler, Schmidt and U.S. Army Map Service 04 p0700 A67-15177

Photographic measurement of plasma jet velocity using time shift in brightness fluctuation 04 p0666 A67-15188

Plasma flux interaction in magnetic multipole field, proving mutual polarization of interacting fluxes by photographic results 04 p0667 A67-15210

Photographic comet photometry as technique for studying comet brightness 05 p0890 A67-16332

Visual, photographic and photoelectric methods for comet polarimetry 05 p0890 A67-16334

Various photometric standard systems assessed, noting use of photographic plates and filters in agreement with UVB system 05 p0805 A67-16335

Wind tunnel study of boundary layer transition structure on ogive nose cylinders aligned parallel to flow [AIAA PAPER 67-129] 06 p0939 A67-18314

Turbulence effect on burning velocity and physical structure of flame surface in turbojet-afterburner-like combustion chamber 07 p1265 A67-19073

Image distances and relative intensities for zone plates determined from holographic theory 07 p1185 A67-19401

Dust cloud moons of earth, discussing results of photographic measurements 07 p1256 A67-20165

Compressed air gun for impulsively loading structures, measuring response by high speed photographic technique 08 p1414 A67-20374

Laser photography, discussing equipment used and shadowgraphs obtained in free flight range 08 p1330 A67-20595

Solar corona observations of Surveyor I, discussing extent of measurable radiance and occurrence of streamer 08 p1386 A67-20943

Diffusion coefficient of lithium in p-type silicon determined by method using electrophotographic developing agents 08 p1371 A67-21447

Photooptical system for determining velocity of projectile after target penetration 09 p1502 A67-22623

Maksutov-Cassegrain type telescope for rocket mounting, design and performance 10 p1654 A67-22751

Lunar disk color index derivation by applying method of photographic photometry in UV and IR spectral regions 10 p1708 A67-23361

Roughness data and statistical analysis of off-runway landing areas in Canada, using aerial photography for profile measurement 10 p1622 A67-23388

Steady state plasma belt in dipole magnetic field, measuring spatial variation of density and temperature, electron spin, gyration, etc 11 p1828 A67-23940

Mass of shaped charge accelerator generated fragments determined via high speed flash X-ray photography of projectiles in flight 11 p1790 A67-24448

Communications of lunar and planetary laboratory, Volume 5, University of Arizona 11 p1860 A67-24457

Goniometric measurement accuracy of aerial camera photogrammetric distortion 11 p1793 A67-24864

TV subsystem of Surveyor I, discussing operation-design constraints, camera configuration, video sequence, etc [SMPT PAPER 101-43] 12 p1904 A67-25461

Zero gravity effects on boiling from flat horizontal surface for various subcoolings, fluid properties and heat transfer rates 12 p2034 A67-25720

Photographic determination of meteor masses, examining dependence of radiation coefficient 13 p2198 A67-26555

Solar flare observation with monochromatic heliograph at Mitaka 14 p2384 A67-28095

Electron beam analysis of skimmer influence on nozzle beam formation 14 p2301 A67-28187

Shutter speed and illumination data for cinematographic documentation of total solar eclipse 15 p2555 A67-29576

Plasma flux interaction in magnetic multipole field, proving mutual polarization of interacting fluxes by photographic results 15 p2532 A67-30258

Lunar crater classification by morphological types discussing ring structures 16 p2747 A67-30984

Airborne photographic systems defining performance criteria for quantitative analysis and application of transfer functions for evaluation 16 p2680 A67-31804

Hydrodynamic field of falling sphere in viscous liquid within cylindrical container noting streamlines, velocity variations, etc 17 p2837 A67-32288

Time dependent self-compressed pinch-discharge radiation characteristics in various gases analyzed photographically for luminescence distribution, spectral composition, etc 17 p2904 A67-32918

Elliptical patterns on emission lines of argon plasma jets attributed to anthalation backing during hypersensitization of film 17 p2863 A67-33305

Heliometer replaced by long focus photographic refractor used for moon rotation constant determination 18 p3129 A67-34308

Discharge plasmas in hollow cathodes investigated using photography, showing mercury vapor and inert gas plasmas form homogeneous or laminar positive plasma columns 19 p3274 A67-35102

Photographic techniques for atmospheric attenuation in air to ground visibility 20 p3441 A67-36399

Optical metagalactic radiation measured by spacecraft photographic and photometric methods, reviewing Olbers paradox and night sky brightness measurements 20 p3526 A67-37127

Altitude variation of air scattering

coefficient determined from brightness profile measurements of haze at planet limb, using spacecraft photography 20 p3432 A67-37238

Complex structure elimination in shock wave region of T-tube, discussing discharge plasma, shock wave trajectories and photographic observation 21 p3612 A67-38257

Q-switched laser use as light source for photographing droplets in spray containing fluorescent dye excited by second harmonic of ruby light 22 p3797 A67-39492

Maximum current and total light output of triggered lightning strokes at close range upon ship deck, noting photographs of discharge 22 p3793 A67-39979

Observation of annular solar eclipse of 1966 from Madrid, noting photographs application for occulted region chord measurements 22 p3888 A67-40200

Horizontal telescope used for solar corona photography during total eclipse /1966/, determining radii passing through solar magnetic poles 24 p4227 A67-42153

PHOTOGRAPHIC RECORDING

Holographic techniques for recording and reconstructing three-dimensional objects 01 p0062 A67-10192

NASA program involving orbiting satellite studies of natural and cultural resources 01 p0168 A67-10326

Focused image holography with extended sources for real image in proximity of hologram plate 03 p0420 A67-13574

Lunar landing sites from photographic reconnaissance by Lunar Orbiter II 05 p0888 A67-16154

Bright meteoric orbits according to photographic observations at Dushanbe and Odessa 06 p1084 A67-18165

Streak and open shutter photography of planar detonation wave in channel transmitting through orifice, obtaining induction distance for transition from deflagration to detonation 06 p1119 A67-18596

Holographic technique for restoration of third-dimension information in recording of photographs 07 p1188 A67-19788

3-D imagery and holograms of objects illuminated in white light photographed through fly eye lens 07 p1189 A67-20098

Image restoration via phase holograms, noting applications to deteriorated photographic negatives and positives 08 p1331 A67-20842

Planetary mapping mission system requirements for photography, IR and radar imagery, radar reflectivity and spectroscopy with data analysis 11 p1859 A67-24438

Three-dimensional film plane hologram recording of object without external source reference beams 11 p1793 A67-24828

Ground based conversion of Lunar Orbiter II video signals into photographic images, describing reconstruction electronics, signal processor, etc 12 p1940 A67-25466

Photographically recorded information retrieval by isodensitometry [SMPT PAPER 101-89] 12 p1941 A67-25473

Holography applied to radio frequencies, noting recording technique with locally produced reference wave 13 p2119 A67-26518

Holography developments and applications, with emphasis on recording and transmitting pictorial information 13 p2121 A67-27565

High luminosity spectrograph using inverse Wadsworth mounting constructed for recording auroral spectra in far UV 14 p2315 A67-28157

Holograms of three-dimensional objects, discussing experimental setup and results 15 p2489 A67-30077

Bright meteoric orbits according to photographic observations at Dushanbe and Odessa 16 p2741 A67-30509

Velocity measurement and image recording of freely moving objects during ballistic tests by electronic and photographic methods 16 p2874 A67-31126

Photographic recording of fast moving plasma clouds during pulsed discharges in rarefied gas using Topler apparatus 16 p2721 A67-31396

Chromosphere and corona UV emission spectrum provided by sounding rocket using photographic recordings 16 p2752 A67-31625

Airborne camera system for high altitude photography of rocket and spacecraft vehicle

launchings describing development 16 p2679 A67-31800

Coronal condensation analysis observed photographically during total solar eclipse, finding good correspondence of loop system spatial trajectories to force line configurations 17 p2945 A67-32690

Space research effects on science and technology, noting fields of application 17 p2974 A67-32771

Soviet book on first panoramic views of lunar surface covering Lunik IX soft landing, data on morphological and geological characteristics of landing site, etc 17 p2948 A67-32966

Geomagnetic time and latitude distribution of magnetic disturbances at auroral and polar cap latitudes 18 p3032 A67-33583

Cinematographic observations of fast auroral variations 18 p3033 A67-33587

Geos satellite observational technique in France 19 p3182 A67-35237

Application of double-exposure holographic interferometry technique by using tri-X Pan film for hologram recording 19 p3232 A67-35693

Thermoplastic-resin film with UV sensitive dispersed compound for carbon-dioxide laser-radiation photography 19 p3240 A67-35694

Enhancement of faint photographic spectra using signal averaging digital computer 19 p3232 A67-35698

Flow pattern caused by low speed splash of liquid drop into pool computer examined, obtaining configuration plots various splash stages 19 p3212 A67-35895

SIMAC spectrography, discussing brightness, speed, etc, of electronic camera and photographic plate recording 20 p3439 A67-36350

Photographically recorded spectra for absolute intensity processed by computer program, providing digitally recorded densities on magnetic tape 21 p3624 A67-37851

Plasma component velocity distribution and multiple plasmoid production indicated in spectrograms from high speed photography of coaxial injector discharge 21 p3664 A67-37939

Rapid deformation in tubular blank during expansion by pulsed loading studied by high speed motion picture photography 21 p3631 A67-38055

Oxygen-hydrogen mixtures burning characteristics in shock wave tube, studying ignition processes with schlieren photographs 21 p3731 A67-38366

Simultaneous UV photographs and radar cross section measurements of Venus, discussing atmospheric motion and rotation 21 p3705 A67-38611

Spacecraft design, solar powering, electric propulsion and side-looking radar for planetary surface observation mission on Mars or Venus [AIAA PAPER 67-712] 21 p3714 A67-38739

Fourier transform application to automatic pattern recognition, using photographic plate to record plane intensity distribution 22 p3764 A67-39331

Photographic research of small scale meteorological disturbances /cloud formations/ observed by Tiros satellites 22 p3829 A67-39972

Gemini booster launch photographic recording with 50 cameras collecting engineering data and motion pictures of prelaunch, launch and postlaunch 22 p3807 A67-40372

Venus rotation, discussing radar and optical and UV photography observations 23 p4063 A67-40800

Charged particles zenithal angular distributions determined by photorecordings for mean energies of 80 Gev 24 p4217 A67-42831

PHOTOGRAPHIC RECORDING INSTRUMENT

UV technology, discussing radiation sources, photodetectors, filters, polarizers, reflective coatings, etc 04 p0619 A67-14704

Brightness angular velocity and geometry of moving object relationship to camera parameter to determine exposure and focal length and contrast for optimum recording 05 p0808 A67-17032

Construction and operational characteristics of device for photographic recording of gyroscopic pendulum

trajectory 06 p1003 A67-18177
 Stekometer with automatic recorder for use in analytic photogrammetry for mapping and engineering surveys 09 p1497 A67-21751
 Photographic technique for obtaining solar image in rays of Lyman alpha line spectrum, using quartz crystal 11 p1793 A67-24862
 Automatic photographic recording of laser output energy vs excitation energy obtained from fluorescence of ruby used to integrate laser light 12 p1952 A67-25333
 Design and operation of all-reflecting Schmidt camera 14 p2319 A67-28562
 Photographic recording by shadow method for alignment of optical equipment in firing range used to determine aerodynamic characteristics of various missiles 16 p2674 A67-31117
 Computer program for optimizing performance of high resolution airborne photo-optical recording system using modulation transfer function analysis 16 p2678 A67-31792
 Airborne Astrographic Camera System using meteor orbit theory to observe reentry trajectory discussing data reduction theory and photo-optical instrumentation 16 p2679 A67-31795
 Photo-optical instrumentation for biosatellite 30-day orbiting primate mission discussing adverse environmental effects and other constraints regarding requirements 16 p2680 A67-31806
 Electron beam and laser beam line scan recorders requirements, limits, applications and techniques 17 p2857 A67-32470
 Rastering nanosecond laser sensitizer for materials responsive to short duration signals, discussing recording, sensitometric and measuring subsystem 17 p2858 A67-32482
 Photographic systems and photoelectric scanner for observation of solar annular eclipse 18 p3049 A67-34312
 Multi-input photomultiplier pulse height photographic recording system using dual beam oscilloscope for cosmic ray experiments 20 p3444 A67-36525
 Hologram reconstruction of objects in fog-like medium 20 p3450 A67-37027
 Brightness angular velocity and geometry of moving object relationship to camera parameter to determine exposure and focal length and contrast for optimum recording 21 p3627 A67-38264
 Holography /phase-recording of diffracted wavelets/ for phase contrast and striae, interferometry in polarized light and 3-D photoelasticity 23 p3999 A67-41179
 Modulation transfer functions of various solar recording films using interference device, giving detectability threshold of two-dimensional emulsion patterns 23 p4001 A67-41237
 Photographic film nonlinearities effect in holographic recording of coherent wavefront using two-beam interferometry, describing phenomenological model 23 p4002 A67-41269
PHOTOGRAPHIC TRACKING
SA CINETHODOLITE
 Photogrammetric network for large-area phototriangulation using star-tracking airborne cameras, discussing theoretical and technical aspects 06 p0994 A67-17716
 Position determination for mobile luminous objects in sky by triangulation, using ballistic photographic chambers in positions pinpointed by star sightings 07 p1188 A67-19770
 Simulator studies of MOL tracking experiments 08 p1317 A67-21105
 Thermal and momentum eddy diffusivities computed from wind profile and turbulence of rocket released chemical clouds 08 p1328 A67-21478
 Photographing satellites, using optical system and image converter for determining coordinates 10 p1606 A67-23184
 Spectrum and scales of upper atmospheric turbulence determined by photographic tracking 13 p2108 A67-26314
 Radar, radio, photographic and visual satellite tracking methods 15 p2437 A67-30084
 Satellite tracking, noting radar, radar and laser methods, and visual and photographic observations 16 p2630 A67-31765
 Gravity data from lunar orbiter tracking, discussing Kepler element role 18 p3131 A67-34326
 Image motion compensation tracking study for earth reconnaissance from space, investigating computer and manual tracking

modes, control dynamics and gain and magnification 18 p2993 A67-34337
PHOTOGRAPHY
 SA AERIAL PHOTOGRAPHY
 SA ALL-SKY PHOTOGRAPHY
 SA ASTRONOMICAL PHOTOGRAPHY
 SA CLOUD PHOTOGRAPHY
 SA COLOR PHOTOGRAPHY
 SA ELECTRO-OPTICS
 SA ELECTRONIC PHOTOGRAPHY
 SA FRACTOGRAPHY
 SA FRAME PHOTOGRAPHY
 SA HELIOGRAPHY
 SA INFRARED PHOTOGRAPHY
 SA LUNAR PHOTOGRAPHY
 SA PHOTOMICROGRAPHY
 SA RADAR PHOTOGRAPHY
 SA RADIOGRAPHY
 SA ROCKET PHOTOGRAPHY
 SA SATELLITE PHOTOGRAPHY
 SA SCHLIEREN PHOTOGRAPHY
 SA SHADOW PHOTOGRAPHY
 SA SPACE PHOTOGRAPHY
 SA SPARK PHOTOGRAPHY
 SA STEREOSCOPIC PHOTOGRAPHY
 SA STREAK PHOTOGRAPHY
 SA X-RAY PHOTOGRAPHY
 Fabrication of improved Focons and field flatteners and evaluation of optical performance in terms of modulation transfer function /MTF/, vignetting and T-number measurements [SMPT PREPRINT 100-3]
 Weather satellite for automatic photo transmission, noting Tiros and Nimbus 04 p0651 A67-15454
 Correct method for affine transformation of model in processing of superwide angle photographs on autoradiograph 09 p1496 A67-21750
 Three-dimensional photography based on laser derived hologram, examining split-beam technique 10 p1655 A67-23072
 Laser applications utilizing power density for studying reflectance, Raman spectra, photography, holography, etc 17 p2868 A67-32691
PHOTOIONIZATION
 Proposed modification of Wetzel model of direct ionization by primary continuum in light of recent steady state precursor electron density measurements ahead of Ar shocks 01 p0118 A67-11193
 Light absorption and photoionization of shallow impurity levels in semiconductors during acoustic phonon scattering 04 p0678 A67-15135
 Photodetachment probability for Cs and negative I due to simultaneous absorption of two ruby quanta 05 p0815 A67-16627
 Photoionization and absorption coefficients of nitric oxide gas measured, using vacuum UV monochromator 06 p1037 A67-18573
 Three-photon ionization transition rates for alkali atoms, using quantum defect Coulomb functions to evaluate perturbation formula 07 p1195 A67-19496
 Multichannel photoionization of atomic systems obtained with dipole approximation assuming LS coupling, using wave functions 07 p1226 A67-19498
 Spectral dependence of impurity photocurrent in single crystal CdS specimens in constant illumination 07 p1234 A67-20025
 Photoionization mass spectrometer for ion-molecule reaction studies, determining ion residence times, drift velocities, diffusion coefficients and ion temperatures 07 p1137 A67-20187
 Photoionization mass spectrometer for charge transfer reaction analysis 07 p1137 A67-20188
 Photoionization cross section of negatively charged In atoms in n-type silicon from comparison of intrinsic photoconductivity with impurity photoconductivity 08 p1367 A67-20410
 Quantum mechanical theory for IR absorption by excitons due to photoionization and intraband lattice scattering 09 p1552 A67-21670
 Photoionization by spin-dependent electric dipole and spin-dependent magnetic quadrupole transitions with polarized electron spin 09 p1535 A67-22379
 Plasma source in which collimated photon beam generates plasma by single quantum photoionization of rarefied gas 09 p1549 A67-22426
 Photoionization yield and absorption

coefficient of nitric oxide at various wavelengths in 580-1350 angstrom region, using H sub 2 emission sources 10 p1681 A67-22738
 Direct ionization and secondary excitation in proton auroras, noting magnitude of contribution by various processes 11 p1784 A67-23927
 Sco X-1 physical characteristics noting ionization, possible stellar wind and pressure equilibrium effects 11 p1862 A67-24506
 Light absorption and photoionization of shallow impurity levels in semiconductors during acoustic phonon scattering 12 p1978 A67-25159
 Microexplosion by optical breakdown of air in focus of laser beam, analyzing volume of concentrated plasma by measuring external magnetic field perturbation 12 p1952 A67-25336
 Positive ion production during illumination of cesium vapor-filled thermionic cell with laser beam 12 p1973 A67-25396
 Neutral silicon photoionization cross sections for continuous UV absorption measured near ionization limits by shock tube technique 12 p1968 A67-26248
 Photoionization quantum yield in intrinsic-absorption region of cadmium selenide films 14 p2372 A67-28853
 Photoionization study of diatomic-ion formation in argon, krypton and xenon by collision process [AFRL-66-785] 17 p2888 A67-32631
 Photoadsorption of X-rays by interstellar gas using photoionization cross sections, showing neon K edge as distinctive feature of spectrum 17 p2937 A67-32752
 Production mechanism of atomic nitrogen ions in upper atmosphere, showing predominance of nitrogen molecule dissociative photoionization 17 p2851 A67-33204
 Spectral dependence of impurity photocurrent in single crystal CdS specimens in constant illumination 18 p3100 A67-33759
 Vacuum UV and X-ray lasers from electron ejection from inner shells of atoms through photoionization 18 p3060 A67-34015
 Laser pulse duration effect on photonuclear processes, as affected by matter-radiation interactions, observing ionization in gases and surface photoeffects 19 p2338 A67-34897
 Multiple-photon ionization of atoms and molecules in strong varying electromagnetic field, measuring ionization probability dependence on field intensity 19 p3265 A67-35164
 Multiquantum photoionization applied to laser-induced breakdown thresholds in cesium and rubidium vapors 19 p3241 A67-35810
 Ionospheric ion-neutral reactions studied by photoionization mass spectrometer, noting temperature independent reactions 22 p3793 A67-40077
 Lunar surface luminance transient enhancement noting photoabsorbing color center formation, increased reflectivity and photoluminescence, photoionization and photoemission 23 p4065 A67-41004
PHOTOLUMINESCENCE
 Spectral distribution of relative quantum yield of photoluminescence in polycrystalline cadmium sulfide films 01 p0133 A67-10510
 Luminescence spectrum of CuCl at low temperatures excited by double photon absorption from high intensity laser beam 06 p1010 A67-17822
 Absorption spectra and photoluminescence in n-and p-type GaAs before and after neutron and electron irradiation 06 p1062 A67-18933
 Surface recombination velocities and diffusion lengths in GaAs determined by variation of cathodoluminescence intensity with voltage of exciting electron beam 06 p1063 A67-18936
 Fluorescence of n-and p-type gallium arsenic phosphide under optical excitation 07 p1232 A67-19635
 Heat radiative flux divergences and equilibrium temperature distribution with altitude calculated for heat regime modeling radiative transfer conditions in stratosphere and mesosphere 10 p1647 A67-23275
 Chemical impurities and native defects observed in GaAs using photoluminescence at 20 degrees K, noting role of optical activation energy 11 p1848 A67-24742

- Nanosecond fluorimeter for measuring emission kinetics of chromophores 12 p1946 A67-25981
- Radiative recombination mechanisms in photoluminescence of n-type InP, discussing emission bands 16 p2732 A67-31450
- Lunar surface luminescence transient enhancement noting photoabsorbing color center formation, increased reflectivity and photoluminescence, photoionization and photoemission 23 p4065 A67-41004
- PHOTOLUMINESCENT BAND**
- Radiative recombination processes involving neutral donors and acceptors in silicon and germanium, describing extrinsic luminescence bands 22 p3862 A67-39998
- PHOTOLYSIS**
- Laser action in optically pumped CN, discussing vibrational-rotational transitions 01 p0089 A67-10370
- Combination flash photolysis-flash pyrolysis system with timing circuit, using Tektronix pulse generators and ignitron circuit for firing spectroscopic lamp 02 p0247 A67-12689
- Chemical aspects of evolution of terrestrial atmosphere, noting role of photolysis in oxygen production 03 p0414 A67-14089
- Possible stabilization of AgCl crystals against solar radiation effects by addition of Cu, Ni, Zn, Cs, S or Hg 04 p0685 A67-15752
- Vacuum UV photolysis of solid ethane films, measuring product distributions, presenting evidence for quenching of excited ethane and ethylene 05 p0758 A67-16128
- Vacuum UV flash photolysis kinetic spectroscopy apparatus 05 p0807 A67-16782
- Photolysis of hydrazine vapor in vacuum UV, examining emission as function of pressure and photolysis time 07 p1138 A67-20190
- Ozone formation in photolysis of oxygen and oxygen-helium mixture as function of pressure and temperature 09 p1457 A67-22025
- CH concentration measurement in flash photolysis of methane by means of kinetic spectroscopy 12 p1904 A67-26228
- Electronic absorption spectrum observed during cyanogen azide flash photolysis 13 p2177 A67-26988
- Nitric acid decomposition process by irradiation determined by photolysis of nitrogen dioxide [JPL-TR-32-1128] 14 p2260 A67-28782
- Photolysis and pyrolysis of nitromethane and methyl nitride using flash photolysis and kinetic spectroscopy 18 p2998 A67-34276
- Photolysis of gaseous and liquid benzene, analyzing gaseous products by gas chromatography and mass spectrometry 22 p3757 A67-39443
- UV light photolyzing ozone dispersed in solid carbon dioxide matrix causes formation of new substance showing IR absorption 23 p3971 A67-40970
- Nondisturbing turbulent flow measurements applied to viscous sublayer in smooth square pipe, showing linear velocity gradient in layer adjacent to wall 24 p4144 A67-42607
- PHOTOMAGNETIC EFFECT**
- Steady state photoconductivity and photomagnetic effect in single crystals of n-type GaAs with various carrier concentrations 03 p0490 A67-13151
- Photomagnetic susceptibility measured by means of induced short duration light flash, using germanium 06 p1001 A67-17938
- Steady state photoconductivity and photomagnetic effect in single crystals of n-type GaAs with various carrier concentrations 10 p1690 A67-23100
- Shubnikov-de Haas and Gurevich-Firson oscillations of photomagnetic effect in n-InSb magnetic field 17 p2914 A67-32451
- Photomagnetic effect and kinetic photoconductivity in cadmium sulfide single crystals, determining lifetime and mobility of nonequilibrium holes 20 p3504 A67-36158
- Odd and even photomagnetic effect oscillations in InSb, measuring EMF at low temperatures and strong fields 21 p3877 A67-38095
- PHOTOMECHANICS**
- Photomechanical effect in germanium, noting dependence of mechanical properties on quantity of impurity concentration 04 p0680 A67-15285
- Photomechanical effect in metals, discussing influence of impurities and heat treatment 13 p2174 A67-26400
- Electromechanical and photomechanical effects on microhardness in semiconductors 23 p4045 A67-41472
- PHOTOMETER**
- SA SPECTROPHOTOMETER**
- Sodium dayglow emission measurement by Zeeman photometer, presenting calculation of radiant energy absorption by sodium vapor in magnetic field 03 p0409 A67-12945
- Airglow lines measured through photometers on OGO-II satellite, noting nadir and zenith airglow 10 p1660 A67-23278
- Determining theoretical minimum signal that can be detected by optical detection system noting dependence on integration time, noise, etc [SMPT PAPER 101-91] 12 p1905 A67-25475
- Atmospheric long range spectral transmissivity measured by single beam photometer with recording potentiometer added to reduce beam noise 13 p2119 A67-26689
- Multichannel photometer for space applications requiring low weight and power, no moving parts and high sensitivity divided in four electrically and optically distinct quadrants 15 p2491 A67-30433
- Fuel consumption precision measurements for low thrust auxiliary rockets using impeller wheel and photometric devices [AIAA PAPER 67-507] 18 p2989 A67-33971
- Atmospheric long range spectral transmissivity measured by single beam photometer with recording potentiometer added to reduce beam noise 21 p3627 A67-38431
- PHOTOMETRY**
- SA ASTRONOMICAL PHOTOMETRY**
- SA PHOTOELECTRIC PHOTOMETRY**
- SA SPECTROPHOTOMETRY**
- SA TELEPHOTOMETRY**
- SA ULTRAVIOLET PHOTOMETRY**
- SA VISUAL PHOTOMETRY**
- Low voltage photomeasurements in metal-insulator-metal films with opposing photocurrent separation 02 p0301 A67-12519
- Photometric analysis of twilight halo photographs by Vostok VI spacecraft 03 p0415 A67-14227
- Zodiacal-light photometric measurements, analyzing effect of twilight radiation on observable brightness 04 p0617 A67-15558
- Sonoholograms, techniques and information content 04 p0625 A67-15678
- Soviet papers on problems of comet photometry 05 p0890 A67-16329
- Various photometric standard systems assessed, noting use of photographic plates and filters in agreement with UVB system 05 p0805 A67-16335
- Criticism of photometric results of Ney and Peplin findings regarding link layer in terrestrial atmosphere 05 p0802 A67-17330
- Photometric measurements on deviations from equilibrium state in burnt gases of laminar premixed shielded flames at atmospheric pressure [AIAA PAPER 67-9] 06 p1072 A67-18345
- Nitrogen atoms recombination in fast flow system using photometry, determining atom concentration, noting nitrogen afterglow intensity 06 p0956 A67-18760
- Photometric analysis of twilight halo photographs by Vostok VI spacecraft 12 p1932 A67-25483
- Photometric investigations of simulated lunar surfaces confirm high porosity and low albedo without postulating necessity for fine dust layer 12 p2003 A67-25740
- Photometric studies of eclipses of Echo I and II satellites, noting period of rotation from luminosity curves and 180 degree phase shift 12 p2008 A67-25832
- Atomic-absorption flame photometric instrumentation and techniques 13 p2120 A67-26811
- Image and other techniques to measure and reduce stray and scattered light in sunspot photometry, emphasizing possibility of using partial solar eclipse 13 p2203 A67-27424
- Photometric auroral observations and geomagnetic field fluctuation magnetograms compared, noting relation between geomagnetic and auroral pulsations 14 p2309 A67-27944
- Photometric theory of artificial satellite eclipse by earth with application to atmospheric study 16 p2745 A67-30746
- Airborne photographic instrumentation system for photometric observation of total solar eclipse, noting automatic tracking system 16 p2678 A67-31794
- Optical system for earth observation satellite with line-scan television for weather forecasting discussing photometry and fiber optics 16 p2679 A67-31797
- Supernovae photometric properties, considering mean absolute photographic magnitude at maximum light, brightness decline rate, etc 18 p3119 A67-33857
- Photometric determination of moon limb shape during annular solar eclipse, using rotating prisms 18 p3129 A67-34313
- Photometric methods for determination of lunar relief 18 p3132 A67-34328
- Lunar charting for selenocentric coordinates from densitometric analysis and altitude measurements, using photometric methods and Isodensitracer 18 p3049 A67-34333
- Moon shape determined from topocentric terminator deviation, using photometry 18 p3132 A67-34334
- Moon elevation profiles and lunar slopes determined by photometry and Isodensitometric measurements of Ranger IX photographs 18 p3133 A67-34335
- Shadow photometer conversion to various interferometer types for studying inhomogeneous three-dimensional fluid flows in transparent media 19 p3228 A67-34985
- Slope derivation from lunar orbiter photography using photometric model and computer program 19 p3230 A67-35322
- DODGE satellite TV cameras for black and white, plus color picture transmission with photometric analysis and camera optics 20 p3452 A67-37573
- Stellar detectors components, describing optical receiving, image tracking and photometric devices 21 p3628 A67-38651
- Photometric observation data on Jupiter atmospheric activity /1964-1965/ noting three-month periodic change 22 p3879 A67-39299
- Luminance of lunar surface site predicted by direct solar and earth reflected illumination together with local albedo variations 22 p3887 A67-40143
- Soviet book on atmospheric visibility noting photometry, range, threshold, runway visual range, atmospheric transmittance and atmospheric boundary layer problems 23 p4024 A67-40600
- Cauchy domes in Mare Tranquillitatis, deriving relief pictures with photometry 23 p4066 A67-41013
- PHOTOMICROGRAPHY**
- Microhardness of n-type InSb single crystals and crack formation near indentation-area 03 p0489 A67-13093
- Quasi-equilibrium states during pulse remagnetization of thin ferromagnetic films, discussing domain structure 08 p1367 A67-20604
- Qualitative and quantitative prediction of corrosive environments effects on transducer performance [ASME PAPER 67-MET-14] 12 p1945 A67-25952
- Brittle fracture at grain boundaries in samples of electron-beam molybdenum prepared by forging in air after extrusion 13 p2130 A67-26447
- Electro-optical spectrograph producing dynamic spectrograph continuous in both frequency and time 14 p2319 A67-28444
- Optical system for computer counting and analyzing aerosol particles on photofilm 19 p3227 A67-34861
- PHOTOMULTIPLIER**
- Time resolving capabilities of RCA C-70045, 56 AVP and XP 1020 photomultipliers 01 p0067 A67-10659
- Time expansion device for photomultiplier circuit for high pulse frequency using recording system, readout, thin film memory and simulation unit 01 p0029 A67-10662
- Self-locking modes in argon ion laser, observing subnanosecond pulsation of laser output with wideband photomultiplier 02 p0253 A67-12503
- Cerenkov radiation induced by cosmic ray in end-on photomultiplier and resultant fundamental noise limitation 02 p0247 A67-12686
- Twyman-Green arrangement of interferometer with narrow laser beam and twin photomultipliers, examining strong

shocks in argon in 15.2 cm shock tube 02 p0247 A67-12688
 Photomultiplier noise amplitude distribution and causal external factors 03 p0388 A67-14260
 Comet photometry for measuring weak fluxes of light produced by heavenly bodies, analyzing photoelectromultipliers 05 p0805 A67-16336
 Unusual optical detection characteristics in multiplier phototube when monitoring circuit bandwidth is extended 05 p0807 A67-16791
 Optimal reception of narrow band signals emerging from 05 p0764 A67-16913
 Photomultiplier tubes for satellite instrumentation, discussing application as circuit components and star trackers 07 p1185 A67-19397
 UV sensitivity increase in sodium salicylate photomultiplier combination 07 p1185 A67-19405
 Calculation method for energetic photoelectric photometry system for tracing behind radiative source or for distance measurement 08 p1331 A67-21055
 Signal and noise response of Ge avalanche photodiodes noting design, fabrication, LF photomultiplication and static V-I characteristics 09 p1475 A67-22200
 Light emission by gas under action of intense laser radiation studied by high speed high sensitivity photomultiplier 09 p1516 A67-22583
 Photomultipliers in DC output mode for extreme UV 10 p1653 A67-22737
 Background noise produced by high energy radiation incident on photomultiplier tube, stressing differences between tubes in number of small pulses produced 10 p1618 A67-23809
 Radiometer system with photomultiplier tube for measuring absolute radiation from hypervelocity projectile flow fields 11 p1790 A67-24447
 UHF intensity-modulated light emanating from plasma observed with aid of photomultiplier radiometer 13 p2167 A67-27082
 Travel-time effects on quasi-steady state operation characteristics occurring from electron optical characteristics of two-grid-controlled photomultiplier 14 p2277 A67-27769
 Photomultiplier noise amplitude distribution and causal external factors 14 p2288 A67-28772
 Chromospheric solar radiation measured during solar eclipse with UV monochromator, using electromagnetic radiation photomultipliers 15 p2565 A67-29573
 Optimal reception of narrow band signals emerging from 16 p2623 A67-30890
 Photomultiplier gate for stimulated spontaneous light scattering discrimination, showing high cut-off efficiency, linearity and absence of spurious effect 17 p2863 A67-33353
 Noise and dark current reduction in photomultiplier tubes by magnetic defocusing [SRCC-43] 19 p3193 A67-35314
 Magnetic electron multiplier performance as photomultiplier in EUV spectral region 19 p3231 A67-35683
 Multi-input photomultiplier pulse height photographic recording system using dual beam oscilloscope for cosmic ray experiments 20 p3444 A67-36525
 Calculation method for energetic photoelectric photometry system for tracing behind radiative source or for distance measurement 22 p3797 A67-39417
 Ionizing radiation effects on dark current and noise pulse spectrum of photomultiplier tubes used in balloon and satellite X-ray observations 23 p4000 A67-41216
 Optical coupling of photomultiplier tube to acrylic plastic using clear silicone potting compound 24 p4158 A67-42700

PHOTON

Large atmospheric jets with low muon content explained by presence of hypothetical primary cosmic photons with very high energies 09 p1562 A67-22559
 High energy photons, cosmic X-rays and hard radiation production mechanisms in interstellar gas, galactic halo and intergalactic medium 14 p2380 A67-27964
 Probability distribution of number of

photons and integrated intensity relation to normal and antinormal ordering of field operators in quantum optics 16 p2685 A67-30826
 Photon transmission delaying processes and secondary ionization growth time dependence on overvoltage in neon 19 p3264 A67-35086
 High photon energy densities generation and concept of exponential amplifier for use as laser probes 19 p3240 A67-35692
 Extensive air showers due to extragalactic primary photons demonstrated, considering production process 19 p3316 A67-35796
 Induced three-photon combination scattering kinetics applied to laser pumping 21 p3638 A67-37867
 Two-mode laser beam electromagnetic field statistical properties tend to Bose-Einstein form 21 p3642 A67-39117

PHOTON ABSORPTION

SA TOWNSEND DISCHARGE
 Optical absorption edge in cadmium telluride, noting impurity bands and dependence on energy and temperature 02 p0281 A67-11492
 Spontaneous emission spectra and ratio of number of photons in various oscillation modes of laser with nonlinear filter type lock 02 p0251 A67-11573
 Laser saturation of photoconductivity and determination of imperfection parameters in sensitive photoconductors such as single crystal of cadmium 02 p0251 A67-11879
 Photoconductivity resonances and recombination radiation in PbTe and InSb due to multiple photon interband transitions between Landau levels in high intensity magnetic fields 02 p0254 A67-12522
 Frequency dependent two-photon absorption radiation-matter interaction and secondary harmonic generation in n-and p-type impurity semiconductors 03 p0435 A67-13126
 Attenuation length of photoexcited electrons in evaporated layers of CuBr estimated by measuring photoemission yield as function of thickness 03 p0500 A67-14332
 Light absorption by free current carriers role in kinetic equations of semiconductor laser/radiation system 03 p0439 A67-14376
 Photon scattering in three-dimensional semimfinite medium for constant frequency and survival probability 04 p0695 A67-14655
 Two-photon absorption in organic dyes for various wavelengths, extinction coefficients and concentrations 05 p0815 A67-16626
 Oscillation in CdS crystal by ruby laser induced two-photon excitation, noting proportionality of absorption coefficient to light beam intensity 05 p0821 A67-16667
 Multiphoton absorption processes, coherence of radiation fields and statistical properties of laser light 05 p0823 A67-16681
 Capture cross section of photons by zinc and mercury atoms in germanium determined from integral voltaic photosensitivity, using black body as radiation source 05 p0868 A67-17066
 Two-photon absorption spectrum of single crystal CdS, using polarized light and precise geometry 06 p1011 A67-18209
 Coherent radiation interaction with two-level atoms system in single mode approximation, obtaining equation for time dependent number of photon emission and absorption 06 p1012 A67-18804
 Semiconductor lasers using single and double photon optical excitation 06 p1013 A67-18930
 Three-photon ionization transition rates for alkali atoms, using quantum defect Coulomb functions to evaluate perturbation formula 07 p1195 A67-19496
 Distribution of photons from point image in photographic emulsion calculated using diffusion equation, deriving limits on point spread functions and corresponding modulation transfer functions 09 p1496 A67-21708
 Mosaic of photosensors for solid state imaging, discussing electro-optical conversion, structure and characteristics 09 p1476 A67-22209
 Photon absorption coefficients measured in active and passive regions of electron-beam-pumped semiconductor laser 10 p1664 A67-22909
 Tunneling assisted photon absorption process /Franz-Keldysh effect/ in

semiconductor junctions studied, using differential photocurrent response 10 p1691 A67-23402
 Beam wavelength and laser intensity effect on attenuation in carbon disulfide induced by ruby laser indicate two-photon absorption 10 p1667 A67-23776
 Interband magneto-optical phenomena involving linear single photon absorption and dispersion in semiconductors and semimetals 11 p1847 A67-24662
 High resistivity regions in silicon exposed to photon bombardment 13 p2173 A67-26364
 Two photon stepwise absorption of low power He-Ne laser light in erbium doped yttrium oxide and lanthanum fluoride crystals 13 p2177 A67-27013
 Optical double-quantum transition in which atom passes from one Zeeman sublevel to another by absorption and successive reemission of optical photons 13 p2127 A67-27079
 Combined resonance transition in indium antimonide induced by single photon absorption 13 p2178 A67-27083
 Absorption probability for photons traversing photon gases with different spectra 13 p2161 A67-27733
 Opacity of universe to high energy photons, estimating spectra and absorption probability 13 p2161 A67-27734
 Capture cross section of photons by zinc and mercury atoms in germanium determined from integral voltaic photosensitivity, using black body as radiation source 15 p2538 A67-29797
 ZnS two-photon absorption spectrum to establish two-photon pumping capabilities of semiconducting crystals 15 p2500 A67-29816
 Radiation transport in spectral lines as photon absorptions and emissions, discussing contemporary theories, approximation methods and applications 17 p2893 A67-32143
 Interference from laser light beam superposition at single photon level, noting existence of fringes 17 p2866 A67-32277
 Probabilities for two-photon absorption processes induced by coherent and thermal light when acting on atomic system 17 p2870 A67-33317
 Coherent radiation interaction with two-level atoms system in single mode approximation, obtaining equation for time dependent number of photon emission and absorption 18 p3061 A67-34423
 Statistics of electron avalanche generating secondary effect at cathode through photon emission, obtaining excited molecule distribution 19 p3265 A67-35087
 Two-photon photoconductivity in pulsed ruby laser excited cadmium sulfide, determining carrier density and density dependence on light intensity 20 p3456 A67-36184
 Simultaneous absorption of two photons by transparent material at radiation frequency corresponding to only one photon 20 p3457 A67-36325
 Absorption of optical photons in molecular crystals, noting results of laser output on naphthalene 20 p3457 A67-36326
 High resistivity regions in silicon exposed to photon bombardment 21 p3680 A67-38321
 Precursor IR resonance radiation from hypervelocity ablating vehicles observed and related to photon absorption and water vapor presence in air 22 p3917 A67-39712
 Two-photon absorption theory extension to include vibronic mixing between different electronic states using two-photon laser excitation of polycyclic atomic molecules 23 p4013 A67-40964
 Ionization fronts stability, finding no instabilities for strong D type fronts 24 p4224 A67-41816
 Two-photon absorption in semiconductor laser in relation to upper limit of transmission power 24 p4200 A67-41863
 Multiphoton absorption in monatomic gases causing ionization of atom applied to plasma production by intense radiation from lasers 24 p4190 A67-42098
 Two-photon absorption in alkali halide crystal via gas laser noting F center formation 24 p4167 A67-42361
 Escape probability of photon from homogeneous plane parallel medium, discussing coherent scattering process and integral equation 24 p4191 A67-42596

PHOTON BEAM

Polya distribution describing photon correlations in ionizing laser beams enables differentiation between various multiphoton ionization processes 03 p0438 A67-13982

Multiphoton ionization of krypton atom by ruby laser radiation 06 p1037 A67-18796

Photon counting distributions and intensity fluctuations of modulated laser beams 07 p1197 A67-20125

Plasma source in which collimated photon beam generates plasma by single quantum photoionization of rarefied gas 09 p1549 A67-22426

Angular distribution of laser radiation and variation in beam direction of stimulated radiation as function of misadjustment angle of resonator mirrors 15 p2500 A67-29759

Electron beam and laser beam line scan recorders requirements, limits, applications and techniques 17 p2857 A67-32470

Multiphoton ionization of krypton atom by ruby laser radiation 18 p3083 A67-34415

Photon beam transmission measurement technique for determining bone mineral content in vivo 23 p3945 A67-41087

PHOTON DENSITY

Photon interaction in plasma, determining energy density and collision frequency 02 p0272 A67-11583

First and second order correlation functions for field obtained by superposition of two laser modes through Youngs experiment, used to determine coherence and statistical properties 02 p0254 A67-12634

Excess photon noise in detected photocurrent of multimode laser for uncoupled and phase locked modes 05 p0815 A67-16623

Particle number fluctuation in single cell of Kastler photon set, discussing statistical properties of laser emission in multimode excitation regime 07 p1196 A67-19599

Induced radiation at high photon densities, noting applicability of perturbation theory to multiphoton resonance radiation of lasers 08 p1337 A67-20823

Laser light photon counting statistics using probability density for laser light intensity 15 p2498 A67-29513

Primary cosmic radiation and interaction in atmosphere studied during minimum solar activity by balloon flights to determine effect of latitude on secondary photons 15 p2550 A67-29533

Master equation for statistical operator of laser mode leads to photon number distribution for arbitrary pumping 15 p2501 A67-30124

He-Ne laser light intensity distribution cumulants for nonlinear oscillation threshold operation 20 p3461 A67-37289

Particle number fluctuation in single cell of Kastler photon set, discussing statistical properties of laser emission in multimode excitation regime 20 p3462 A67-37338

Laser radiation photon number and amplitude fluctuations quantum mechanical calculation by deriving two coupled equations 22 p3815 A67-39784

Laser radiation model of superimposed coherent and incoherent radiation, determining statistics of photons 24 p4166 A67-41903

PHOTON-ELECTRON INTERACTION

Energy transfer into electron-photon avalanche by high energy nucleons compared to data of air shower and particle spectra 01 p0144 A67-10745

Homogeneous transfer equation in line formation, noting correlation between thermalization length and line source function of two-level atom 02 p0266 A67-11698

Excitation and transport of electrons in metals studied by thin film methods 02 p0289 A67-11728

Film thickness dependence of photoelectric effect of surface and volume in single electron excitation by photon absorption 02 p0289 A67-11729

Threshold current density dependency on photon energy in gallium arsenide laser diodes 03 p0379 A67-13480

Optical absorption due to direct intervalence band transitions in Ge, noting effect of lattice temperature 05 p0869 A67-17192

Induced radiation at high photon densities, noting applicability of perturbation theory to multiphoton resonance radiation of

lasers 08 p1337 A67-20823

Excitation and photon emission rates of auroral nitrogen first and second positive group 10 p1650 A67-23338

Compton effect produced by thermal photons on relativistic electrons in solar atmosphere 12 p2002 A67-25528

Energy transfer into electron-photon avalanche by high energy nucleons compared to data of air shower and particle spectra 13 p2192 A67-28774

Magnetoquantum-electric effect in solid state plasmas based on displacement of centers of carrier cyclotron orbits 13 p2184 A67-27691

Electron density and temperature in plasma measured, using self-focused laser beams 15 p2488 A67-29902

Optical properties of Mg layers evaporated in ultrahigh vacuum, noting results of reflectivity measurements 17 p2913 A67-32292

Threshold current density dependency on photon energy in diffused and epitaxial p-n junction GaAs injection lasers 19 p3238 A67-34774

Microwave photon interaction with superconducting tunneling currents measured in aluminum-indium junctions, extended to tin-lead junctions, discussing phase shift 19 p3303 A67-35046

Relative photon scattering cross sections for He and Ne at Lyman alpha, describing measurement technique 20 p3489 A67-37431

Bremsstrahlung due to collision of muon with electron at rest, discussing energy photons role 24 p4194 A67-42880

PHOTONIC PROPULSION

Electric and photon propulsion systems in German-American research 16 p2736 A67-30710

PHOTOPRODUCTION

Extensive air showers due to extragalactic primary photons demonstrated, considering production process 19 p3316 A67-35796

PHOTORECEPTOR

Inhibitory effect of light from cool white fluorescent lamps on growth of yeast, alga and protozoa 06 p0952 A67-17872

Image degradation comparison between photographic and image orthicon systems, discussing image orthicon receptor advantages when used for space applications 20 p3446 A67-36606

PHOTOREDUCTION

Tracking of GEOS-A satellite by Riga station, explaining negatives reduction 19 p3182 A67-35235

PHOTORESISTIVITY

Semiconductor substrate photochemical processing and coating photoresistant techniques 12 p1916 A67-25996

PHOTORESISTOR

S RESISTOR

PHOTOSPHERE

Spectral equivalent linewidths of four solar faculae and adjacent undisturbed photosphere sections 01 p0151 A67-11285

Hydrodynamics of lower solar photosphere, examining connection between small-scale oscillatory Doppler shifts and exponentially decaying continuum 03 p0511 A67-13650

Computation of electric conductivity in sunspots and photosphere from empirically determined linear logarithmic relation 03 p0511 A67-13814

Hydrogen line intensity decrease in solar photosphere and chromosphere, noting agreement with Schroedinger equation results 03 p0512 A67-14004

Photospheric bridges over sunspots studied by meniscus photoheliograph at Tashkent Astronomical Observatory 04 p0701 A67-15552

Solar hydrogen convection zone interaction with photosphere restricted to relation of convection theory to granulation and supergranulation 05 p0899 A67-17070

Coronal temperature and temperature distribution in transition region between chromosphere and corona, assuming photospheric wave propagation as essentially one-dimensional 05 p0900 A67-17077

LF gravitational-acoustic and internal gravity mode wave propagation in temperature-stratified photosphere-low chromosphere region and solar atmospheric resonant responses 08 p1399 A67-21236

Solar spectrum reexamination determining lower limit for C12/C13 isotopic abundance ratio in photosphere 09 p1566 A67-22231

[AFCRL-67-0480]

Generation of oscillations in solar atmosphere by separate granules modeled by bottom zone of isothermal gravitating photospheric layer overlaid by hot corona 10 p1704 A67-22721

Horizontal motions of solar granulation toward supergranulation from data of granule coordinates and velocities 10 p1704 A67-22723

Homogeneous solar photosphere and lower chromosphere model in hydrostatic and local thermodynamic equilibrium, reproducing continuous and line spectrum 11 p1858 A67-24112

CH molecule solar spectral observations interpreted using several upper photosphere models and assuming local thermodynamic equilibrium approximation 11 p1861 A67-24495

Sunspot groups configuration preceding and following formation of type IV radio burst flares 12 p1992 A67-25130

Type IV bursts and associated active regions 12 p1993 A67-25131

Monochromatic UV photographs of limb of sun analyzed for evidence of solar granulation in 2000 angstrom spectral range 12 p2001 A67-25220

Rapid rotation of solar interior 12 p1994 A67-25526

Evershed effect observations suggest existence of two or more streams in both photospheric and chromospheric Evershed flows 13 p2204 A67-27429

Sunspot structure, discussing photospheric model, magnetic field influence, MHD structure and energy balance, and photospheric and chromospheric parts 13 p2205 A67-27438

Photoelectric measurements of continuum intensity differences and concave grating spectra of faculae and undisturbed photosphere 14 p2378 A67-27846

Relation between number of photospheric granules and Wolf sunspot number 14 p2387 A67-28582

Distinction between macro-and microturbulence in solar photosphere studied from line profiles 17 p2944 A67-32641

Photospheric mean alpha hydrogen radiation intensity profile computed for various heights above solar surface taking into account limb-darkening effect 17 p2946 A67-32729

Surface helium abundance in blue horizontal branch and halo B stars, considering depletion mechanism 17 p2947 A67-32764

Interplanetary sector structure observed by IMP-I satellite compared with photospheric magnetic field and plage structure observations 17 p2953 A67-33400

Small scale magnetic fields observed in photosphere explained by sunspots made invisible by lateral heat influx 17 p2953 A67-33404

Triatomic molecules formation and abundance in solar photosphere estimated for thermodynamic equilibrium 18 p3119 A67-33858

Corona observation within one solar radius of photosphere, identifying emission lines and explaining continuous spectrum and Fraunhofer lines reduced depth 19 p3318 A67-35055

Solar oblateness and Mercury perihelion advance, showing turbulent viscosity forces acting on photospheric meridional currents as possible distortion cause 21 p3701 A67-37963

Photoelectric records of DE and LZE in solar photosphere velocity fields, analyzing oscillations onset and lifetimes 23 p4066 A67-41229

Flare positions relative to neutral line in longitudinal components of photospheric magnetic fields, stressing drift rate 23 p4060 A67-41231

Velocity fields in solar photosphere and chromosphere, discussing granulation, supergranulation, magnetic fields and oscillatory motions 23 p4068 A67-41276

Static tufted magnetic field perturbing effect on solar atmosphere small scale structure, noting pressure, density and temperature changes [SR-15] 24 p4222 A67-41787

Magnetic changes in solar atmosphere, discussing current-free field configurations using solar magnetograms and photospheric

field effect 24 p4222 A67-41768
 Mean intensity photospheric H-alpha radiation profile for prominences in solar corona, noting profile dependence on height, velocity and direction 24 p4209 A67-41965
 IR C atom multiplet in solar spectrum at 10,700 angstroms, noting C abundance dependence on convective velocities and deviations from black body function and local thermodynamic equilibrium 24 p4237 A67-42655
PHOTOSTRESS
 Abnormally high photostresses in semiconductor films under monochromatic light studied, using angular dependence observation technique 17 p2921 A67-32970
PHOTOSYNTHESIS
 SA CHLOROPHYLL
 SA METABOLISM
 Oxygen, carbohydrates, proteins, etc, produced by unicellular algae through photosynthesis, finding optimum efficiency of process 02 p0186 A67-11861
 Construction of lunar microcosm, considering recycling based on photosynthesis 02 p0185 A67-12313
 Fluorescence induction in isolated chloroplasts analysis yielding method to determine amount of light used in process 07 p1134 A67-19846
 Photosynthesis of nitrosoformaldehyde and identification of spectrum consisting of diffuse band 18 p2998 A67-34277
 Continuous synchronous culture of photosynthetic microorganism *Chlorella* cultivated in illuminated and dark stirred tanks 19 p3177 A67-34913
 Biological life support system for regenerating closed atmosphere by photosynthesis, using gas exchange between man and microalgae 19 p3180 A67-35236
 Indigenous biology in Venus clouds, proposing isopycnic float bladder macroorganism ingesting water and minerals blown up from surface by pinocytosis 22 p3750 A67-39556
PHOTOTRANSISTOR
 Diffusely transmitting integrating sphere with solid state photodiode used in laser output measurement 01 p0089 A67-10445
 Light sensitivity of diffused Si phototransistor and of system of two cascade coupled phototransistors 05 p0770 A67-16169
PHOTOTROPISM
 Light interaction with solids, discussing photoconductivity and phototropy 17 p2913 A67-32373
 Thermophototropic model providing active thermal control in spacecraft surface functions as variable absorbance coating to compensate for solar irradiation changes 21 p3730 A67-37792
PHOTOTUBE
 SA ELECTRON TUBE
 SA PHOTOMULTIPLIER
 S-band traveling wave phototube operating with He-Ne laser noting performance, design and methods of operation 09 p1479 A67-22279
 Directional neutron spectrometer for events in which neutron is scattered by first scintillator into second 12 p1945 A67-25859
 Equivalent resistance of traveling wave phototube for large modulation index 16 p2636 A67-30897
PHOTOVISCOELASTICITY
 Internally banded polariscope incorporated into transparent model for three-dimensional photoviscoelastic material studies 03 p0531 A67-14364
 Tensile analog data reduction technique for determination of principal stress differences history at points of two nonhomogeneous photoviscoelastic models 05 p0921 A67-16826
 Photoelastic stress measurement techniques for birefringent high polymers extended to two- and three-dimensional linear viscoelasticity problems 08 p1420 A67-20887
PHOTOVOLTAGE
 Photovoltage measurement across lifetime junction produced by electron irradiation and by changing surface recombination velocity 11 p1850 A67-24917
 Anomalous photovoltages in CdSe and CdS thin layers 13 p2175 A67-26429
 Heat treatment effect in various gaseous media on electrical properties of CdTe films with abnormally high photovoltage, noting structural stabilization 22 p3861 A67-39924

PHOTOVOLTAIC CELL
 Silicon solar cell to measure solar radiation intensity, discussing effect of optical path length ratio and atmospheric constituents 03 p0419 A67-13079
 CdS thin film solar cells history, design, fabrication and performance 04 p0553 A67-14474
 Optimum gridline spacing for photovoltaic cells operating at high solar fluxes, noting maximum power point efficiency dependence on cell and geometric parameters and solar flux level [ASME PAPER 66-WA/SOL-1] 04 p0555 A67-15381
 Electric thrusters and electric propulsion, examining overall efficiency as function of specific impulse 05 p0874 A67-16933
 Semiconducting compounds for thin film photovoltaic devices using GaAs crystals, considering absorption coefficient 08 p1284 A67-20725
 Semiconductor thin film properties for photovoltaic cell applications 08 p1368 A67-20727
 Electrical and photovoltaic properties of PbS-Si heterostructures 12 p1980 A67-25180
 Silicon photocells at high luminous flux concentrations, noting increase in multiplicity of power with series resistance 13 p2058 A67-27622
 Solar energy conversion into electric power by GaAs and Si cells analyzed, using photovoltaic cell theory 15 p2536 A67-29503
 Spatial distribution of radiation damage in solids determined by spectral analysis of photovoltaic current of photovoltaic cell 16 p2728 A67-30815
 Optimum grid line spacing for photovoltaic cells operating at high solar fluxes, noting maximum power point efficiency dependence on cell and geometric parameters and solar flux level [ASME PAPER 66-WA/SOL-1] 18 p2989 A67-34129
 Annealing under continuous irradiation in p-on-n silicon solar cells with lithium diffused in N region 19 p3306 A67-35671
 Photovoltaic cell characteristics, emphasizing energy conversion processes and quantum efficiency determination 20 p3362 A67-36240
 Solar photovoltaic cell design for lower temperature operation, noting application to near-sun missions 21 p3570 A67-37789
 Integrating pyranometer operating on silicon photovoltaic solar cell for use by climatological stations and mesoscale networks 21 p3628 A67-38580
 Photocurrents and photopotentials in organic solids, discussing atomic bonding effect 23 p4045 A67-41484
 Cadmium sulfide film cell photovoltaic effect and mechanism, discussing cell structure and spectral response 23 p4046 A67-41485
 Distributed model for photovoltaic cell via nonlinear least square techniques, discussing p-n silicon cells 23 p4046 A67-41487
 Photovoltaics - IEEE conference, Cocoa Beach, Florida, March 1967, Volume 2, Spacecraft power systems, solar cell mathematical model 23 p3938 A67-41505
 Photovoltaics - IEEE Conference, Cocoa beach, March 1967, Volume 3, Radiation and micrometeoroid effects on solar cells, lithium in silicon cells 23 p3940 A67-41516
PHOTOVOLTAIC CONVERSION
 Photovoltaic effect application to conversion of solar radiation to electrical energy, presenting pictorial explanation of solar cell 01 p0013 A67-10553
 Fabrication technique and characteristics of photovoltaic energy converters produced by bombarding p-type Si with phosphorus ions 04 p0680 A67-15284
 Dimensions effect on efficiency of radiant energy cells 11 p1745 A67-24437
 Characteristics of photovoltaic solar converters, discussing drift field, wrap around and epitaxial webbed silicon cells, minimum film thickness and radiation damage 17 p2801 A67-32048
 Dimensions effect on efficiency of radiant energy cells 20 p3362 A67-36239
 Photovoltaic cell characteristics, emphasizing energy conversion processes and quantum efficiency determination 20 p3362 A67-36240
 Power systems for long duration missions including photovoltaic solar energy,

thermoelectric, Brayton cycle and thermionic conversion systems, discussing solid state components 22 p3749 A67-40339
 Multifaceted solar array performance determination 24 p4104 A67-42509
 Multi-kilowatt photovoltaic power system design for manned earth orbital mission 24 p4104 A67-42511
 Large area solar array design for photovoltaic system for manned space systems based on orbital perturbations and mechanical and thermal environment considerations 24 p4105 A67-42516
PHOTOVOLTAIC EFFECT
 Photovoltaic effect application to conversion of solar radiation to electrical energy, presenting pictorial explanation of solar cell 01 p0013 A67-10553
 Film thickness dependence of photoelectric effect of surface and volume in single electron excitation by photon absorption 02 p0289 A67-11729
 Photoelectric efficiency of thin gold films illuminated from free surface side and support side 02 p0289 A67-11730
 Photoelectric emission of metal films with electronic structure evolving with film thickness 02 p0290 A67-11731
 Photovoltaic effect in thin telluride layers and in contacts between layers and various metal electrodes, noting dependence on angle of deposition 02 p0294 A67-11758
 Photovoltaic effect in p-n junctions of lead tin telluride diodes indicate potential for IR detection throughout 8-14 microns atmospheric window 02 p0221 A67-12514
 Optical and electrical properties of barrier layers in Cu doped GaP, discussing intensity region of superlinearity dependence on temperature and IR light 03 p0491 A67-13202
 Anomalous photovoltaic effect in semiconductor Ge, Si, CdTe and GaAs thin films due to photodiffusion and microtransitions 04 p0685 A67-15758
 Dember effect, bulk photovoltaic effect and current density in illuminated inhomogeneous semiconductor 05 p0863 A67-16702
 Semiconductor surface photovoltage under small signal conditions, when quasi-equilibrium approximation will be valid in space charge layer 06 p1047 A67-17600
 Photovoltaic and photoresistant effects in cadmium sulfide thin films with recombination centers 08 p1368 A67-20728
 Photovoltaic emf of silicon solar cell illuminated by ruby laser 08 p1285 A67-20732
 Photovoltaic effect in cell prepared by CdTe film deposition and copper telluride flash evaporation 08 p1285 A67-20733
 Oriented growth of thick films of CdTe deposited on quartz plates in vacuum, discussing photovoltaic effect 12 p1982 A67-25450
 Performance characteristics of nonstoichiometrically doped p-n junctions in Cd-Hg-Te alloy operated as IR photovoltaic detector 14 p2366 A67-28496
 Lifetime gradient and Dember photovoltages in n and p type germanium and silicon semiconductors 23 p4045 A67-41483
 Cadmium sulfide film cell photovoltaic effect and mechanism, discussing cell structure and spectral response 23 p4046 A67-41485
 CdTe thin film solar cell, examining spectral response, sputtered Pt photovoltaic barrier-forming method and integrated array fabrication 23 p4046 A67-41495
 Isochronal annealing effects on photovoltaic properties of n-on-p Si solar cells irradiated by energetic proton 23 p3940 A67-41518
 Poly-N-vinyl carbazole-iodine charge transfer photovoltaic effect spectral and intensity dependence, noting possible radiation detection and energy conversion applications [JPL-TR-32-1138] 24 p4201 A67-41899
 Photoelectromagnetic detector spectral sensitivity, magnetoresistance and time constants with optically polished thin elements fabricated from Ge, InAs, GaSb and InSb single crystals 24 p4154 A67-42243
PTHALATE
 S POLYETHYLENE TEREPHTHALATE
PHYSICAL CHEMISTRY
 Physicochemical properties of Ti-Al-O solid solutions 07 p1203 A67-19280
 Phase diagrams of various titanium-

phosphorus compounds and mixtures with up to 45 atomic percent P and microstructural characteristics of Ti-P alloys 07 p1203 A67-19262

Physicochemistry of substances under impact compression, considering thermodynamic parameters, phase transformation and compressibility curves 11 p1749 A67-24324

Monograph on equilibrium statistical thermodynamics using quantum mechanics 20 p3554 A67-37271

Atomic and molecular chemicophysical processes in shock waves derived from high temperature thermal energy transfer including instrumentation, relaxation, ionization and spectroscopy 22 p3786 A67-40074

Physicochemical combustion of turbulent air-fuel mixture in straight flow combustion chambers, noting effects of various factors and intensification methods 22 p3921 A67-40448

PHYSICAL ENDURANCE

SA WORK CAPACITY

Physical capabilities and work potential of man in terms of physiological elements and methodology 23 p3959 A67-41662

Restoration of cardiovascular integrity in post myocardially infarcted aviation personnel 23 p3971 A67-41709

PHYSICAL EXAMINATION

SA PERSONNEL SELECTION

Medical testing, research and control during manned space flights, discussing diagnostic algorithms for onboard computer and frequency of data collection 13 p2062 A67-26762

Ballistographic, glucose and Masterov methods applied to pilot examination for coronary defects 14 p2255 A67-28223

Pilot medical examination frequency and effect on safety 18 p2992 A67-34722

Glucose loading effects on electrocardiogram of pilot applicants evaluated for injection before and after diabetes test 21 p3573 A67-38068

PHYSICAL EXERCISE

SA MUSCULAR FATIGUE

SA WORK CAPACITY

Upper torso exercises effect compared with torque maneuvers effect on oxygen metabolism under reduced gravity conditions 01 p0017 A67-10959

Maximum aerobic work correlation with anthropometric and spirometric parameters, studying ventilatory capacity coefficient 16 p2614 A67-31472

Physical exercise effect on oxygen consumption at decreased pressure 17 p2806 A67-31963

Heat and exercise induced hypohydration effects upon physical performance of women, showing some deterioration in cardiovascular system 20 p3372 A67-37033

Conductive cooling method for pressure applications in body heat loss promotion at high exercise rate 23 p3964 A67-41558

Optimum cooling in ventilated impermeable clothing using ambient air over range of simulated physiological activity 23 p3967 A67-41604

PHYSICAL FACTOR

Origin of elements, discussing element formation and abundances, nucleosynthesis and cosmological theories 19 p3263 A67-35869

Physical parameters of IR nebula discovered in Orion 19 p3330 A67-36080

PHYSICAL FITNESS

SA FLIGHT FITNESS

SA MUSCULAR STRENGTH

Physical fitness of man with respect to manual labor, oxygen deficiency and acceleration 03 p0364 A67-13924

Flight simulator acceptance and role in pilot training and checking in UK 13 p2064 A67-27272

European approaches to physiological and psychotechnical selection and training of cosmonauts 20 p3375 A67-36925

Data on crew workload in C-141 aircraft used for extended mission living and working schedules, showing major disruptions in regular patterns 21 p3576 A67-38073

Middle aged pilot medical fitness for flying, noting age-accident statistics, changes in skill, performance, senses and responses 22 p3756 A67-40535

Age limitations of flying personnel taking into account physical condition and

professional capabilities 22 p3756 A67-40542
Rentgenographic kymography in evaluating cardiovascular apparatus in middle aged pilots 22 p3753 A67-40543

PHYSICAL OPTICS

Wave scattering by smooth and rough finite cylinder situated in layer with randomly varying dielectric constant analyzed by approximation of physical optics 05 p0762 A67-16349

Acoustic waves omnidirectional scattering by rough imperfectly reflecting surfaces analyzed using physical optics method 10 p1680 A67-23314

Electromagnetic wave scattering from plasmas calculated in context of physical optics, noting that radar cross section for plasmas with finite conductivity is polarization dependent 11 p1820 A67-24913

Soviet book on physical optics 12 p1967 A67-26131

Electromagnetic sensing of absolute rotation with self-oscillating laser version of Sagnac Interferometer 14 p2349 A67-28812

Polarization of complex wave form geomagnetic micropulsations of natural and artificial origin, using physical optics 15 p2476 A67-29620

Envelope representation of fluctuating classical wave amplitude of stationary optical fields [SR-4] 15 p2518 A67-29767

Radio telescope design, considering sensitivity and resolving power, discussing classical optics and multiplicative antenna based telescope 23 p3980 A67-41081

PHYSICAL PROPERTY

X-ray irradiation effect on electrophysical properties of n-and p-type germanium, determining absorption coefficient 01 p0136 A67-11044

Condensation mechanism and effect on physical properties of thin films 02 p0285 A67-11704

Physical characteristics affecting detection efficiency of Geiger counters, proportional counters and ion chambers used in space measurements of particles 02 p0244 A67-12209

Physical and functional characteristics of contoured amplifying semiconductor radiation detectors for use in missile and satellite instrumentation 02 p0244 A67-12211

Physical properties of metals influence on friction, adhesion, wear and welding tendency in vacuum 03 p0428 A67-13271

X-ray study of phase composition of refractory alloys carbide solid solutions noting hardness, electric resistance and elastic deformation energy of crystal lattice 04 p0638 A67-15205

Physical parameters, absolute values and discovery dates of comets observed from 1954 through 1960 05 p0886 A67-16030

Physical properties of liquid hydrogen 05 p0928 A67-17012

Physical and chemical behavior of elements and chemical compounds, considering electron configurations, using condensed-state atom model 06 p1035 A67-17843

Physical properties of transition elements, alloys and compounds in terms of stable electron configurations, using Samsonov theory 06 p1035 A67-17844

Transpiration, torsion and gravimetric effusion experiments to obtain thermal functions and approximate composition of vapors over solid beryllium chloride 06 p1071 A67-17984

Niningerite composition and optical, physical and crystallographic properties 07 p1247 A67-19064

Physical properties of quenched binary alloys of titanium 07 p1206 A67-19281

Titanium alloy mechanical and physical characteristics, noting dependence on chemical and phase composition 07 p1206 A67-19285

Correlation of physical properties of transition elements with atomic electron structure, noting energetic stability of configurations 09 p1517 A67-21878

Grease lubricants for aerospace application, determining physical properties and testing them at 400 degrees F and under high vacuum [ASLE PAPER 66AM 3C2] 09 p1506 A67-22421

Electric, thermal and physical properties of pyrolytic carbides and nitrides of group

IV metals 11 p1804 A67-23903
Hall effect and electrical resistance of ZrC-NbC and TaC-HfC alloys at room temperature 11 p1804 A67-23904

Electronic structure and electrophysical properties of d-transition metal sulphides 12 p1986 A67-26096

Foundation of theory of physical dimensions 13 p2157 A67-26606

Nature of glassy state, reviewing nucleation, crystallization, chemical, physical, and electrical properties and transformation of glasses 13 p2143 A67-26696

Photoemission of semiconductor, theoretical treatment of phenomena, properties and production methods 14 p2363 A67-27748

Electron lens with hyperbolic field configuration designed to focus or modulate electron lenses, noting hyperbolic application to electron guns 14 p2276 A67-27768

Aluminum alloy systems physical and structural characteristics and phase diagrams 14 p2334 A67-27802

Alloying elements and impurities effects on aluminum-alloy systems properties including neutron absorption, temperature changes, electric conductivity, etc 14 p2335 A67-27805

Commercial aluminum casting alloys physical and mechanical properties 14 p2335 A67-27807

Physical properties of metals influence on friction, adhesion, wear and welding tendency in vacuum 14 p2324 A67-28000

Solid solution properties of niobium carbide-molybdenum carbide alloy, noting changes in electron structure 14 p2337 A67-28284

Temperature resistant elements and compounds for use above 3000 degrees F, considering melting points, atomic radii and densities 14 p2340 A67-28380

Polyphenyl ether physical, chemical and mechanical properties, noting experimental results and fluid performance in closed pump loops 14 p2341 A67-28953

Vapor cured resins for aerospace applications 15 p2506 A67-29544

Refractory material as component of silicate binder having stable optical and physical properties under simulated space conditions 15 p2506 A67-29547

Asbestos reinforced plastics evaluated for physical and optical properties, thermal vacuum and UV resistance 15 p2507 A67-29550

GaSB properties and perspective applications, noting junction formation, production processes, etc 15 p2536 A67-29700

Welding characteristics of aluminum alloys, noting influence of quenching temperature, quenching process delay and cooling velocity on weld tensile strength 15 p2503 A67-29781

Alloyed Ni-Be alloys properties, discussing influence of Mo, W, B, V and Co on heat resistance without impairing physical properties 15 p2504 A67-29974

High density moisture-proof noncrystalline family of gas generator propellants, surveying burning rates, physical properties and application 15 p2544 A67-29980

Alkali metal vapor and inert gas mixtures with alkali seeding radiation properties, noting nonequilibrium argon-krypton plasma parameter determination in electrical discharge 16 p2710 A67-30522

Physical properties of binary pulsed discharge plasma in helium and argon seeded with Cs and K vapor 16 p2711 A67-30525

Nonequilibrium plasma production via plasma electron heating with electric field induced in MHD generator 16 p2601 A67-30552

Ternary semiconductors, analyzing physical and physicochemical properties, noting synthesis and preparation of single crystals 16 p2725 A67-30801

Dynamic and physical properties of Kreutz family of sun-grazing comets suggesting collision mechanism for origin 16 p2751 A67-31464

Infrared reflectance and optical constants of tektites for origin mode, noting constituent dependence on geographic location 16 p2753 A67-31697

Molybdenum disulfide compacts pressurized by explosive forming, determining specific gravity, hardness,

compressive and tensile properties, etc 16 p2695 A67-31753

Extreme pressure /EP/ films from lubricants containing borate esters, studying structure and mode of action 16 p2683 A67-31756

Structure and substructure effect on thin film properties, discussing vacuum deposition mechanism of metals, alloys, dielectrics and semiconductors 17 p2920 A67-32888

Crystal growth, nucleation, supercooling, solidification, glass forming and kinetics of 1, 3, 5-tri-alpha-naphthylbenzene 17 p2809 A67-33255

Physical properties of semiconductors relation with energy and nature of interatomic bonds, discussing effect on elastic constant, thermodynamic functions, electric and dielectric properties 18 p3094 A67-33435

Dynamic theory of hybrid ionic-covalent /homopolar/ bonds applied to physical behavior of GaAs type crystals 18 p3094 A67-33436

Crystals for UV and IR optics, discussing solubility, hardness, melting, expansion coefficients and design 18 p3078 A67-33565

Matter density and other physical properties of Martian surface estimated from radio and IR observations 18 p3119 A67-33860

Plasma measuring methods relation to plasma properties noting photography, optics, particle analysis, etc 18 p3090 A67-34378

Book on coatings of high temperature materials covering properties and characteristics and coated refractory metals 19 p3244 A67-34956

Refractory metals physical, mechanical and chemical properties when coated with oxidation resistant coatings 19 p3244 A67-34958

Lower thermosphere physical properties, studying satellite drag for density profiles, composition, data comparison, etc 19 p3215 A67-35171

High modulus carbon fiber fracture path, orientation and crystallite size effects on physical properties 19 p3248 A67-35425

Physicochemical and mechanical properties of refractory materials at high temperature - Conference, Paris, June-July 1965 20 p3471 A67-36109

Synthetic lubricants noting chemical and physical properties of nonhydrocarbons, classes of synthetics, etc 20 p3455 A67-37264

Soap and nonsoap base greases physical and chemical nature, composition, characteristics and additives 20 p3455 A67-37265

Physical properties of thin layers of cadmium telluride-metal systems analyzed for metal concentration and temperature of base at time of deposition 20 p3513 A67-37448

Physical and chemical behavior of elements and chemical compounds, considering electron configurations, using condensed-state atom model 20 p3490 A67-37585

Physical properties of transition elements, alloys and compounds in terms of stable electron configurations, using Samsonov theory 20 p3490 A67-37586

InBi single crystal electrophysical properties, giving temperature dependences 20 p3514 A67-37605

Physical analysis of convective heat transfer in laminar and turbulent flow through ducts and boundary layers, deriving trailing functions by variational method 21 p3730 A67-37736

Aromatic poly-1, 3, 4-oxadiazole fiber preparation noting thermostability, property retention at high temperature and resistance to hydrolytic degradation 21 p3648 A67-37877

Low temperature effect on physical and mechanical properties of engineering materials and cryogenic fluids, discussing heat generation and removal at rubbing surfaces 21 p3633 A67-38141

Soviet papers on physical properties of ultrapure metals and semiconductors, stressing epitaxial silicon layers 21 p3681 A67-38357

Structural properties of Si anodic oxide layers studied by X-ray analysis, using Laue photograph method 21 p3681 A67-38360

Jupiter rotation variability used to understand internal physical processes, stressing variation of radio and Great Red Spot periods 21 p3710 A67-39002

Properties of liquid metals - Conference, Upton, New York, September 1966, Part 3 21 p3686 A67-39107

Niobium and tantalum nitrides physical properties including microhardness, electric and thermal conductivities, Hall coefficient and thermal EMF 22 p3861 A67-39917

Soviet book on present state of semiconductor technology covering theory, material properties and semiconductor devices 23 p3978 A67-40797

High density moisture-proof noncrystalline family of gas generator propellants, surveying burning rates, physical properties and application 24 p4207 A67-42921

PHYSICAL SCIENCE

Swedish space research organization, participating groups and experiments 19 p3321 A67-35302

PHYSICAL WORK

Heat metabolism in working men while isolated from environment by water-cooled suit and environmental chamber [ASME PAPER 66-WA/HT-45] 04 p0564 A67-15431

Subgravity traction simulation experiments to determine effects on metabolic rates during walking on treadmill 05 p0755 A67-16280

Absolute bed rest and recumbent exercise during bed rest effects on pulse rate response to submaximal work, cardiovascular functional capacity /maximal oxygen intake/, physical work capacity and orthostatic tolerance 05 p0755 A67-16283

Maximal muscular static force vs physical stress measurement for optimal work conditions 23 p3954 A67-41598

PHYSICS

SA ASTROPHYSICS

SA BIOPHYSICS

SA CLOUD PHYSICS

SA COMBUSTION PHYSICS

SA ELECTRONICS

SA GEOPHYSICS

SA LOW TEMPERATURE PHYSICS

SA MOLECULAR PHYSICS

SA NEUTRON PHYSICS

SA NUCLEAR PHYSICS

SA PLASMA PHYSICS

SA POLYMER PHYSICS

SA PSYCHOPHYSICS

SA RADIOPHYSICS

SA REACTOR PHYSICS

SA REENTRY PHYSICS

SA SOLAR PHYSICS

SA SOLID STATE PHYSICS

SA THEORETICAL PHYSICS

Evaluation of Einstein conclusion that moving body appears to be cool 03 p0466 A67-12847

Book on basic principles of physics of semiconductors and semiconductor devices including quantum theory, thermal properties of solid bodies, etc 07 p1231 A67-19301

Italian society of physics - Conference, Bologna, November 1965 11 p1818 A67-24102

Microcausality principle formulation in axiomatic manner using generalized functional space 13 p2155 A67-26385

Soviet papers on space physics problems 13 p2195 A67-26494

Soviet papers on physics of upper layers of atmosphere 13 p2111 A67-26667

Electronics and vacuum physics - Conference, Prague, September 1965 14 p2352 A67-27747

Fourier series solutions of boundary-value and mixed problems in mathematical physics by integrating partial differential equations 14 p2348 A67-28287

Physics of ferro- and antiferromagnetism - Conference, Sverdlovsk, USSR, July 1965 16 p2733 A67-31729

Soviet papers on mathematical physics covering solution of boundary value problems, structural analyses, etc 17 p2884 A67-32887

Soviet collection of articles on atmospheric physics 19 p3213 A67-34850

Computer theory and physics field relationship noting signal mechanics, geometry, logical networks, etc 19 p3202 A67-35606

Reports on progress in physics, volume 29, part II, covering type II superconductors,

origin of elements, plasma oscillations, etc 19 p3263 A67-35867

Progress in high temperature physics and chemistry, Volume 1, covering air opacity and state equation 20 p3485 A67-36928

Reports on progress in physics, Volume 30, Part I 22 p3837 A67-40071

PHYSIOCHEMISTRY

SA BIOCHEMISTRY

High temperature hardening and creation of highly heat resistant alloys of refractory metals 05 p0831 A67-17501

Ternary semiconductors, analyzing physical and physicochemical properties, noting synthesis and preparation of single crystals 16 p2725 A67-30801

Biochemical response pattern to combat flying stress of monitored carrier aircraft pilots 17 p2805 A67-31957

Negatively ionized ozone and diatomic oxygen concentration ratio determined from physicochemical processes for 10-60 km range 19 p3219 A67-35249

High temperature hardening and creation of highly heat resistant alloys of refractory metals 21 p3643 A67-38028

PHYSIOLOGICAL ACCELERATION

Space physiology acceleration problems including engineering aspects of impact absorption 13 p2059 A67-26760

Dynamics of pulse waves of intercranial pressure for transverse overloading accelerations 15 p2430 A67-30229

Acceleration problems in astronauts noting axis determination and effect on human body 20 p3371 A67-36822

Hemodynamic responses of conscious dogs exposed to various centrifugation levels and back angles to determine optimum angle for positioning astronauts 22 p3750 A67-39593

Survival times of rats studied from positive and negative acceleration test exposure in special centrifuge 22 p3753 A67-40540

Abdominal blood flow changes in anesthetized dogs during transverse acceleration 23 p3950 A67-41535

Cardiovascular acceleration-stress reactions during G acceleration of dogs, noting blood pressure, blood velocity and pressure waves 23 p3951 A67-41551

Vestibular organ acceleration while walking at lunar and earth gravity 23 p3953 A67-41584

Physiological response and acceleration tolerance in dynamic simulation via human centrifuge, noting symptoms occurrence frequency 23 p3953 A67-41590

Intracranial pressure in Macaca speciosa monkeys during controlled abrupt linear deceleration 23 p3954 A67-41596

PHYSIOLOGICAL FACTOR

Physiological effects of high altitude flights on human organism 12 p1903 A67-26164

Aortic insufficiency in flying personnel, discussing case histories and cardiovascular system 17 p2806 A67-31965

Physiological/psychotechnical selection of French cosmonauts with reference to ballistic, orbital and space flight 19 p3179 A67-35066

Spacecraft atmosphere selection covering physiological, engineering and fire criteria, evaluating oxygen diluent and recovery 22 p3755 A67-39889

Physical capabilities and work potential of man in terms of physiological elements and methodology 23 p3959 A67-41662

PHYSIOLOGICAL INDEX

Rate measurements determination and evaluation in analysis of space medical data 15 p2431 A67-29293

Automation problems in space-flight operative medical control, giving equations of changes in physiological indices 16 p2618 A67-30902

PHYSIOLOGICAL PHENOMENON

Mathematical model for otolith organs used to analyze human spatial orientation 16 p2610 A67-30753

PHYSIOLOGICAL RESPONSE

SA BIOLOGICAL EFFECT

SA PATHOLOGICAL EFFECT

Statistical guidelines for flight surgeon remotely monitoring body fluids of astronauts, determining when subject undergoes changes in serum values 01 p0015 A67-10951

Biomedical assessments of human circadian system, noting increase in subjective fatigue

and psychological and physiological performance 01 p0018 A67-10955
Upper torso exercises effect compared with torque maneuvers effect on oxygen metabolism under reduced gravity conditions 01 p0017 A67-10959
Biomedical data from U.S. manned space flight experience including cardiovascular and central nervous systems, blood composition changes, etc 01 p0016 A67-11394
Fractional g levels for reducing effects of conditioning to zero gravity on prolonged space flights 01 p0018 A67-11397
Manned spacecraft atmosphere selection, experimenting with 100 percent oxygen at 258 mm Hg, noting toxicity, toleration, substitution of helium for nitrogen, etc 02 p0187 A67-12319
Pharmacology in prolonged space flight noting increasing resistance of organism to extremal flight factors, use of pharmaceuticals during flight, etc 02 p0185 A67-12320
Prolonged autonomous existence of humans in space suits, discussing maintenance of heat balance by physiological perspiration 02 p0187 A67-12324
Reaction of human organism to time shifts experienced during flights of modern aircraft [DVL-611] 02 p0185 A67-12428
Animal study showing aversiveness of simulated gravity and importance of separating rotation effects from effects of G forces 02 p0189 A67-12633
Urinalysis assessment of physiological response of eight pilots to 18-hr flight in F-4C aircraft 03 p0364 A67-14287
Physiological responses of subjects in prolonged immersion to neck level, measuring losses of heat, fluid and electrolytes 03 p0364 A67-14294
Symptomatic responses of eight college females to high altitude exposure include headaches, drowsiness, fatigue and insomnia 03 p0365 A67-14298
Carotidogram recording of left ventricular ejection, noting application as diagnostic tool in heart physiology and in pathology 04 p0561 A67-14626
Biological effect of heavy particles, noting role of linear energy transfer and irreversible direct type effect 04 p0562 A67-14634
Long term effects of oxygen environment on rat colony at 210 mm Hg absolute showed no significant physiological changes and no difficulty in readaptation 05 p0755 A67-16285
Cupular function of man under acceleration, noting electroencephalographic results on caloric nystagmus under 1.2, 3 and 4 g and postrotational nystagmus 05 p0756 A67-16324
Spontaneous discharges from single units in cochlear nucleus after destruction of cochlea, noting results of animal study 06 p0952 A67-17847
Inhibitory effect of light from cool white fluorescent lamps on growth of yeast, alga and protozoa 06 p0952 A67-17872
Cardiovascular changes due to orthostasis, evaluating influence of intravascular instrumentation on orthostatic tolerance of normal men 06 p0953 A67-18776
Pre- and postflight medical examinations of Voskhod I cosmonauts 07 p1133 A67-19108
Tilt table response and blood volume changes in four males before and after 14-day bed rest 07 p1135 A67-19863
ECG measurement results on ascent in depressurized chamber, observing dislocation of electrical axis of heart due to diaphragm lift 08 p1287 A67-20643
Human performance on earth and in space noting depth perception, visual acuity, walking ability, reaction time, etc 08 p1289 A67-21068
Cardiovascular and respiratory reactions of cosmonauts during Voskhod II orbital flight 09 p1454 A67-22384
Speech distortion caused by respiration in helium-oxygen atmosphere, discussing standard and advanced correcting techniques 10 p1597 A67-23313
Cardiac output during rest and work determined via carbon dioxide method at 3800 m altitude 10 p1598 A67-23392
High altitude effect on work capacity, discussing bicycle ergometer test results on physiological response of human subjects 10 p1598 A67-23393

Changes in reproduction and growth of mice and rats under chronic centrifugation at various g force conditions 10 p1598 A67-23416
Backward, forward and transverse acceleration effects on cardiopulmonary systems of men and dogs 10 p1599 A67-23810
Heat stress effect on human renal function, measuring glomerular filtration rate, renal plasma flow, free water clearance and electrolyte excretion 10 p1599 A67-23811
Monomethylhydrazine effect on methemoglobin production in vitro and in vivo 10 p1599 A67-23812
Phagocytic activity and hepatic function following localized proton radiation to liver, discussing results of experiments performed on white rats 10 p1599 A67-23814
Dog study on microwave radiation and effect on response to X-ray irradiation 10 p1599 A67-23815
Graded dose gamma radiation effect on monkeys, noting change in number of white blood cells and occurrence of gastrointestinal disturbances 10 p1599 A67-23816
Hepatic effects of breathing pure oxygen for eight months upon rats, dogs and monkeys 10 p1600 A67-23818
Temporal characteristics of body temperature during high thermal stress, determining correlation between effective and rectal temperature 10 p1600 A67-23822
Complex measuring instrumentation effect upon tilt table response 10 p1602 A67-23823
Dog experiments, determining microwave radiation effects on physiological response 10 p1600 A67-23824
Cardiovascular and renal 24 hr synchronized and desynchronized circadian rhythm 11 p1747 A67-24785
Diurnal rhythm of cardiovascular responses to active orthostasis and Schneider test performance in function diagnostics of peripheral cycle regulation [DVL-620] 11 p1747 A67-25035
Aerospace clothing hygiene, discussing climate influence on protective garment selection and physiological responses of living organisms to obtain heat balance 12 p1902 A67-25176
Weightlessness and manned space flight medical data to date 12 p1902 A67-25727
Gastroenterology in space medicine and physiological basis of cosmonaut nutrition 13 p2058 A67-26752
Gas embolisms and gas bubble formation in tissue 13 p2059 A67-26849
Air embolism pathogenesis and therapy in terms of problem of treatment in overpressure [DVL-628] 13 p2059 A67-26850
Fourth-week syndrome in addition to normal medullary syndrome in DBA/2J mouse strain response to acute ionizing lethal irradiation 13 p2059 A67-26868
Physiological effects in baboon of prolonged decompressions simulating loss of cabin pressure 13 p2060 A67-26924
Independent effect of receptor adaptation level and pupil size on production of flashblindness by high intensity short-duration flashes 13 p2060 A67-26925
Effects of long term repeated short treatments of mice with hyperbaric oxygen on organ and body weights and hematologic and histologic development 13 p2060 A67-26926
Medical data on in-flight and postflight physiological performance to determine mans qualifications for long duration space flights 13 p2060 A67-27214
Graphical demonstration of human reaction to shock or vibration input in horizontal plane to study physiological functions of equilibration 13 p2064 A67-27274
Postmortem determination of pilot psychological state during aircraft collisions by examining sugar content of dead bodies 14 p2255 A67-28226
Miniature multichannel pulse-duration-modulated multiplex telemetry unit for medical monitoring of human subjects pulse, temperature, airflow, etc, under stress 14 p2259 A67-28688
Analysis of brain wave records from Gemini flight GT-VII by computations to be used in 30-day primate flight 15 p2425 A67-29104
Phase shifts in human circadian system

noting individual differences, performance deficit, physiological changes and dissociation from time zone displacements 15 p2425 A67-29108
Daily physiological rhythm changes associated with light intensity and color, noting body temperature oscillations vs light intensity, heart rate changes, etc 15 p2426 A67-29109
Human circadian rhythms in activity, body temperature and other physiological functions, discussing oscillator multiplicity, internal desynchronization and entrainment 15 p2428 A67-29110
Subjective responses to oscillation in yaw 15 p2427 A67-29269
Cardiovascular changes at onset of whole body, X-axis sinusoidal vibration in anesthetized mongrel dogs and unsedated humans 15 p2428 A67-29272
Urinary output patterns relationship to arterial pressure, pulse rate and parameters of hemoconcentration in study of homeostatic circulation regulation during prolonged gravitational stress 15 p2428 A67-29273
Prolonged recording from single vestibular units in frog during plane and space flight, significance and technique 15 p2430 A67-29281
Physiological reactions of man to effect of overload during space flight compared to results of laboratory /centrifuge/ tests 16 p2610 A67-30752
Hemodynamic modifications produced by orthostatism noting changes in cardiac frequency, arterial pressure and central blood volume produced 16 p2616 A67-30754
Physiological testing under simulated reduced gravity conditions with subject suspended and performing exercises on inclined treadmill 16 p2616 A67-30756
Physiological limits of adaptation of eye with respect to body noting increase of pressure in ophthalmic artery under different conditions of hypoxia 16 p2611 A67-30757
Mouse, rat and dog organism reaction to ionizing radiation, vibration and acceleration 16 p2611 A67-30765
Mutation of human tissue by cosmic radiation, discussing results of cell studies from male and female subjects 16 p2611 A67-30766
Effectiveness of therapeutic modalities upon mongrel dogs subjected to dysbarism by overcompression-decompression 16 p2611 A67-30770
Heat emission and equilibrium temperature of homothermal organism calculated using factors of surrounding medium 16 p2617 A67-30772
Weightlessness effect on human cardiovascular system noting mechanical forces, amount of work done to overcome hydrostatic pressure, etc 16 p2612 A67-30773
Prediction and measurement of metabolic energy cost for space suit system operation, noting procedure and test results 16 p2618 A67-30781
Cumulative effect of impact acceleration on physiological functions of rats, studying particularly lung lesions 16 p2612 A67-30904
Oxygen metabolism changes in muscular and brain tissues of animals exposed to prolonged transverse accelerations, examining oxygen consumption and body temperature 16 p2612 A67-30905
Hypoxia effect on cellular and humoral immunity of mice to bacterial infection 16 p2612 A67-30906
Physiological reaction of human body to applied stimuli, developing method evaluating metabolism 16 p2612 A67-30907
Physiological regeneration on cornea epithelium and intestines exposed to fractional irradiation with fission neutrons, studying mitotic index and chromosome aberrations content 16 p2613 A67-30909
Exposure to acceleration and prolonged confinement in bed studied for effects on functional state of human stomach 16 p2613 A67-30915
Maximum aerobic work correlation with anthropometric and spirometric parameters, studying ventilatory capacity coefficient 16 p2614 A67-31472
Acute hyperbaric oxygenation histological effects on pulmonary circulation of rabbits 16 p2614 A67-31473
Pilot self-medication causes and dangers,

classifying dangerous drugs and studying effects on pilot 16 p2614 A67-31474

Effect upon cardiovascular system of weightlessness simulated by immersion in brine 17 p2805 A67-31952

Stress-related and other physiological variables on jet aircraft pilots participating in storm penetration and perimeter flights 17 p2805 A67-31955

Biochemical response pattern to combat flying stress of monitored carrier aircraft pilots 17 p2805 A67-31957

Fundus oculi observation of retinal vessel caliber alteration during changes in arterial gas tensions 17 p2805 A67-31961

Biochemical reactions in human organism as indicator of cosmic ray variation, showing relationship between solar activity and erythrocytes in blood 17 p2934 A67-32099

Acid-base relation of blood and cerebrospinal fluid with respect to respiratory regulation studied in man at high altitude 17 p2806 A67-32333

Biopotential detection, recording and design noting electrocardiogram and electroencephalogram use to monitor weightlessness in manned space programs 17 p2807 A67-32666

Apollo mission launch noise and physiological effects on crew 18 p2996 A67-34718

Positive pressure breathing effects on inhibition of diuresis during water immersion 18 p2992 A67-34721

Human hair-root activity during short term deprivation of protein 19 p3177 A67-34954

Gemini program study to provide safe and biologically sound method of man qualifying for space exploration 19 p3177 A67-35208

Monkey psychomotor reactions during ballistic flight investigated noting alertness reduction during weightlessness 19 p3178 A67-35241

Monkey psychomotor reactions during ballistic flight, noting alertness reduction during weightlessness 19 p3181 A67-35466

Space environment utilization for biological and medical research, physiological studies and therapeutic purposes, discussing orbital hospital and ambulance launch vehicle 19 p3181 A67-35653

Vestibular inaptitude in atmospheric and space flight environment [AD-640908] 19 p3178 A67-35884

Human experiments to study somnolent and precollapto /collapto/ states when falling asleep and during prolonged standing tests 20 p3368 A67-36268

Effects of electric stimulation of human vestibular apparatus recorded by monosynaptic H-reflex technique 20 p3369 A67-36270

Micrometazoa as model systems for studying physiology of memory at cellular level, examining habituation and maze behavior 20 p3369 A67-36657

Weightlessness effect on human body noting brain hemodynamics, cardiovascular system, calcium metabolism, task performance, etc 20 p3369 A67-36668

Modification of rat sensitivity to rotation through vestibular end organ damage or previous vestibular experience, studying activity changes 20 p3371 A67-36818

Heat and exercise induced hypohydration effects upon physical performance of women, showing some deterioration in cardiovascular system 20 p3372 A67-37033

Plasma volume, red blood cell mass and erythrocyte survival determination before and after space flight 20 p3372 A67-37429

Improved response acquisition in deep hypothermia adapted rats 20 p3373 A67-37433

EEG and rhythmical tremor in outstretched upper extremities in man analyzed by autocorrelation and cross correlation 20 p3373 A67-37525

Correlation of airsickness in early flight training with subjective anxiety 21 p3575 A67-38086

Heat stress, skin and rectal temperatures, heat gain and water losses in Army pilots flying combat missions in Mohawk OV-1 aircraft in Vietnam 22 p3750 A67-39595

Lung changes resulting from prolonged exposure to 100 percent oxygen at 550 mm Hg suggest media erosion and evidence of hypertrophy and hyperplasia 22 p3751 A67-39601

Extreme flight factor effects on human

organism determined by simulation, noting physiological function level increase before stress increases resistance 22 p3752 A67-40533

Biomedical results for various human medical systems during weightlessness experiments of Gemini program, noting vestibular function and EVA 22 p3752 A67-40534

Middle aged pilot medical fitness for flying, noting age-accident statistics, changes in skill, performance, senses and responses 22 p3756 A67-40535

Adrenal gland reaction to different pressure breathing types by urine analysis 22 p3752 A67-40538

Cockpit environment thermal stress effect on psychological test performance and biomedical parameters 22 p3753 A67-40539

Rat adrenal gland responses to increased oxygen tension at ambient temperature, noting oxygen critical threshold partial pressure affecting survival time 23 p3950 A67-41538

High performance aircraft flight effect on blood glucose in fasting subjects noting no hypoglycemia tendency 23 p3950 A67-41550

Cardiovascular acceleration-stress reactions during G acceleration of dogs, noting blood pressure, blood velocity and pressure waves 23 p3951 A67-41551

Clineradiographic analysis of human visceral responses to short duration acceleration impact 23 p3951 A67-41553

Continuous EKG recording during free fall parachuting, discussing tachycardia as normal response 23 p3964 A67-41560

Acetazolamide effects in aiding altitude accommodation, examining action on blood and cerebrospinal fluid 23 p3951 A67-41566

Semicircular canal physiological response in cats recorded for case of parallel swing rotation, noting mechanical excitation mode of canal 23 p3952 A67-41576

Hematological criteria of chronic acceleration stress and adaptation 23 p3953 A67-41587

Physiological response and acceleration tolerance in dynamic simulation via human centrifuge, noting symptoms occurrence frequency 23 p3953 A67-41590

Chronic hypercapnia effects on pH level, Ca and P metabolism and electrolyte metabolism in normal sedentary man 23 p3955 A67-41605

Energy transfer effects on pathophysiological responses of guinea pigs and bradycardia response in monkeys under minus G impact 23 p3955 A67-41610

Ventilated wet suit /VWS/ for varying flight cockpit environment and emergency condition thermal protection, assessing physiological responses 23 p3967 A67-41614

Physiological responses to cold in men during extended period of sleep loss 23 p3955 A67-41615

Space suit atmosphere physiological suitability for prolonged moderate work, studying blood-gas parameter changes 23 p3955 A67-41617

Leg volume changes in response to lower body negative pressure due to blood redistribution 23 p3955 A67-41619

Thorax radiological changes associated with physiological and posture changes, discussing chest dynamics 23 p3956 A67-41625

Oxygen toxicity relation to nutrition, hormonal secretion and age factors, discussing experiments on rats 23 p3956 A67-41632

Renin secretion measurement for human adaptation to circulatory stress from G acceleration, discussing high plasma renin levels during acceleration 23 p3956 A67-41634

Oxygen role in cardiac rate in squirrel monkeys during acceleration stress on centrifuge 23 p3956 A67-41635

Fluorescence angiography technique to study human centrifugal acceleration effects on retinal circulation during blackout 23 p3957 A67-41639

Human response to low intensity long duration transverse acceleration, discussing increase in splanchnic blood flow during centrifugation and orthostatic intolerance 23 p3958 A67-41652

Increased oxygen tension causing increased free radical flux in rat kidney tissue akin to ionizing radiation exposure 23 p3958 A67-41654

Isolation effects in constant environment on cycles of physiological functions and performance levels of man 23 p3959 A67-41697

Cosmonaut physiological reactions during simulated space environment exposure outside Voskhod II spacecraft 24 p4113 A67-42054

Polydipsia elicited by synergistic action of saccharin and glucose solution 24 p4113 A67-42099

Visually controlled placing response tests for kittens reared without sight of limbs 24 p4113 A67-42221

Space flight emergency contingency planning for survival, evaluating physiological effects and remedial system effectiveness [AIAA PAPER 67-825] 24 p4116 A67-42972

PHYSIOLOGICAL TELEMETRY

Physiological functions of cosmonauts during flight of Voskhod, discussing measurement results of ECG, EEG, dynamography, etc 02 p0185 A67-11545

Physiological measurements of Soviet cosmonauts in Voskhod spacecraft, noting human performance characteristics and detection techniques 02 p0185 A67-11546

Physiological telemetry application in long space flights for medical examination and control during space flight 02 p0187 A67-12323

Physiological monitoring applied to man in space environment, emphasizing overall philosophy including need and results of monitoring [AIAA PAPER 66-928] 04 p0563 A67-14625

Telemetry applications to in-flight physiological measurements 09 p1457 A67-22461

Miniaturized multichannel multiplexed FM biotelemetry system designed to record physiological condition of pilot and test operational efficiency 14 p2256 A67-28210

Electrocardiogram amplifier-transmitter designed for long term heart rate monitoring on unrestrained subjects in orbiting laboratories 15 p2431 A67-29919

Special preprocessing circuit for cardiac beat recognition discriminates against noise artifacts in electrocardiogram 15 p2432 A67-29920

Physiological diagnostic information collection in prolonged space flight and data handling transmission systems 16 p2617 A67-30763

Physiological functions of cosmonauts during flight of Voskhod, discussing measurement results of ECG, EEG, dynamography, etc 16 p2614 A67-31611

Physiological measurements of Soviet cosmonauts in Voskhod spacecraft, noting human performance characteristics and detection techniques 16 p2614 A67-31612

Biotelemetry improvements in manned space flights, emphasizing bit rate reduction required for electrocardiogram data transmission to earth 17 p2807 A67-32900

Body temperature monitoring in external auditory meatus in pre-in-flight testing, showing correlation between sublingual and aural temperatures 18 p2995 A67-34709

Biological telemetry scientific classification system based on rules of logic law called division of concept 20 p3374 A67-36671

Chimpanzee mesenteric artery blood flow for various activities during 24 hr period monitored by radio telemetry 22 p3751 A67-39603

In-flight aeromedical monitoring of cardiorespiratory response of naval pilots during aircraft carrier combat operations, discussing physiological effects determination 23 p3963 A67-41541

Bioastronautics Laboratory Research Tool /BIO-ALERT/ as automatic biomedical monitoring system composed of digital computer, analog-digital converters and input-outputs 23 p3964 A67-41548

Biomedical safety monitoring instrumentation for Lunar Module oxygen filled internal environment simulator 23 p3969 A67-41640

Telemetry system for measuring body temperature and heart rate for physiological evaluation of space suits 23 p3969 A67-41651

Vibrophonocardiograph developed for use in shirt-sleeve flight environment, previous design miniaturized without sacrificing performance

characteristics 23 p3970 A67-41661

PHYSIOLOGY

SA DYSBARISM

SA ELECTROPHYSIOLOGY

SA ENDOCRINE SYSTEM

SA FLIGHT FATIGUE

SA GASTROINTESTINAL SYSTEM

SA HOMEOSTASIS

SA HUMAN BODY

SA METABOLISM

SA NEUROLOGY

SA NEUROPHYSIOLOGY

SA PSYCHOPHYSIOLOGY

SA RESPIRATORY PHYSIOLOGY

Physiological Support Division facility for training crew members of SR-71 aircraft 23 p3968 A67-41616

Equipment integration for Apollo Application Program /AAP/ physiological experiments, discussing design and dimensions [AIAA PAPER 67-846] 24 p4117 A67-42982

PIAGGIO-DOUGLAS PD-808 AIRCRAFT

Plaggio-Douglas PD-808, Italian executive jet emphasizing safety [AGARDGRAPH 95] 15 p2422 A67-30399

PICTURE

SA DISPLAY SYSTEM

SA MOTION PICTURE

PCM digital picture transmission for monochromatic still and motion pictures and color still pictures 02 p0208 A67-12167

Sequential operations in computer program for digital picture processing 03 p0375 A67-13560

Picture coding systems and selection of pre-and post-quantizing filters 11 p1791 A67-24711

PIEZOELECTRIC CRYSTAL

UHF ultrasonics, discussing generation and wave detection, progressive wave amplification, biological effects, power measurement, etc 03 p0468 A67-13546

Materials for energy transducers used in detection, generation or measurement of ultrasonic waves and materials for electrical filters 03 p0495 A67-13547

Bridge type piezoelectric filter with Zolotarev type attenuation characteristic 04 p0579 A67-14449

Piezoelectric grating /PEG/ dispersive device using ultrasonic propagation in prismatic quartz block 04 p0574 A67-15056

Thin film piezoelectric transducers properties used in microwave acoustic delay lines and phonon generators for analysis of phonon-phonon interactions in dielectric materials 04 p0621 A67-15116

Low loss phase modulator for optical signals, using piezoelectric effect 04 p0576 A67-15506

Electron-piezoelectric interaction giving rise to currents responsible for acoustoelectric effects, gain and nonlinear mixing 06 p1050 A67-18140

Optical phonons role in determining form of free carrier distribution function in semiconductors and nonohmic behavior of strongly piezoelectric crystals 06 p1065 A67-18952

Elastic wave and IR light interactions with moving high field domain in piezoelectric semiconductor, noting acoustic impedance 07 p1232 A67-19556

Elastic surface waves excitation method in quartz at high frequencies, noting absorption temperature dependence 11 p1848 A67-24835

Piezoelectric transducer electromechanical properties compared to electromagnetic actuator, noting fluid control applications 14 p2248 A67-28267

Current instabilities in GaAs for applied electric field along piezoelectric direction attributed to electron-phonon coupling, determining additional parameters from experimental data 14 p2374 A67-28983

Power output of pulse laser measured in terms of ultrasonic vibration intensity induced in piezocrystals by radiation 15 p2485 A67-29125

Measurement of laser frequency control characteristics of piezoelectric transducers, noting effect of mechanical structure supporting transducer on frequency control characteristics 15 p2502 A67-30426

Changes in length measured by tandem laser device investigating mirror separation modulation by piezoelectric materials 16 p2671 A67-30823

Design concept for piezoelectric resonator through mathematical formulation,

determining critical frequencies and electron drift rates 18 p3043 A67-33462

Piezoelectric microphone for measuring pulsed ultrasonic radiation intensity and energy distribution, discussing principles, operating conditions and construction of instrument 18 p3046 A67-33745

Miniature resonator consisting of piezoelectric cadmium sulphide transducer evaporated onto single-crystal quartz wafer 20 p3393 A67-36176

Anisotropy of piezothermal EMF in Si and Ge under uniaxial stress 20 p3511 A67-37147

Equivalent quadrupoles for analyzing ultrasonic systems using piezotransducer disks operating at any frequency 20 p3401 A67-37454

Piezoresistance effect measurement in PbTe single crystals, obtaining coefficients for principal valence band through hydrostatic and uniaxial stresses in several crystallographic directions 21 p3683 A67-38389

Three-and four-phonon processes in piezoelectric cadmium sulfide observed using ultrasonic amplifier confirm nonlinear theory of multiple wave interactions 22 p3854 A67-39246

IC emitter follower line driver with input filtering for PWM signal conditioning, solving onboard high impedance problems in drop tests with piezoelectric accelerometer 23 p4005 A67-41372

Temperature effect on zero shift of piezoelectric crystal accelerometers under shock loading using Hopkinson bar technique 23 p4006 A67-41376

PIEZOELECTRIC PRESSURE GAUGE

Internal wall pressure of obstacles in hypersonic wind tunnels with reflected shock waves measured by piezoelectric gauge system 01 p0005 A67-10259

Ionized impurities effect on current output from shock-loaded piezoelectric quartz disk 04 p0678 A67-15122

Equivalent circuit of piezoelectric quartz pressure transducer used with measuring circuit with small input resistance for solving gasdynamic problems 05 p0808 A67-17111

Ultrasonic flow meter for directly measuring average stream velocity using sing-around velocimeter with piezoelectric ceramics 10 p1656 A67-23079

Piezoelectric type accelerometer transverse sensitivity ratio /TSR/, discussing measurements of vibrations and rotations 12 p1943 A67-25703

Laboratory calibration of piezoelectric transducer used as micrometeoroid impact gauge 15 p2486 A67-29410

Piezoelectric pressure transducer, discussing design, material used and performance 16 p2677 A67-31427

Wall turbulent boundary layer pressure resolution by piezoelectric transducer, noting attenuation of frequency component with size and frequency dependence 20 p3422 A67-37002

Miniature transducers for shock tunnel instrumentation, noting compensating system to reduce spurious signals from pressure and skin friction acceleration 22 p3809 A67-40463

Variable gas pressure acting on turbine engine blades measured by piezoelectric sensors, discussing sensor structure and noise possibility 24 p4153 A67-42095

PIEZOELECTRICITY

HF conductivity, dispersion and temperature modulation of carrier waves and acoustic amplification in drifted semiconductor plasmas 03 p0496 A67-13558

Electromechanical hysteresis and relaxation effects in piezoelectric ceramics 03 p0498 A67-13706

Vannier-Mott excitons effect on ultrasound absorption in piezoelectric semiconductors 04 p0678 A67-15134

Deformation potential of valence band of indium antimonide, using piezoemission technique of shifting intrinsic recombination under uniaxial stress 06 p1062 A67-18932

Incremental stress effects in transistors at emitter-base junction due to piezoresistive and piezofunction effects 09 p1472 A67-21950

Vannier-Mott excitons effect on ultrasound absorption in piezoelectric semiconductors 12 p1978 A67-25158

Piezotransistor static characteristics approximated by exponential function of two variables 12 p1939 A67-25281

Magnetic field dependence of current oscillations in piezoelectric semiconductors 16 p2725 A67-30804

Controlled transient signal distortion by shock monitoring instrumentation circuits using piezoelectric accelerometers 23 p4007 A67-41382

Differential piezoelectric accelerometer charge system for monitoring in-flight jet engine vibrations 23 p4007 A67-41384

PIEZORESISTIVE DEVICE

Heat flux sensor using piezoresistive thermometer for sensing small temperature differentials, discussing design, analysis and test 01 p0069 A67-11020

Piezoresistive strain gauge accelerometers with subcritical damping and high overload capabilities 01 p0075 A67-11138

Miniaturized high shock package utilizing FM-modulated 19.8 megacycle transmitter and piezoresistive accelerometer for measuring deceleration profiles 02 p0242 A67-12011

Piezoresistive elements of germanium thin films 05 p0871 A67-17481

Piezoresistance measurement in p-type Ge as function of pressure and impurity concentration at 77 and 300 degrees K 07 p1233 A67-19644

Infinite plate consisting of monopolar semiconductor of given thickness under effect of electric field results in change in galvanomagnetic, piezoresistance and optical properties 08 p1367 A67-20416

Semiconductor piezoresistive strain gauges and application to compressor blade vibratory stresses measurement 12 p2014 A67-25416

Piezoresistive effect of homogeneous silicon diffused elements 13 p2175 A67-26658

PIG

S GUINEA PIG

PIGGYBACK SYSTEM

General utility spacecraft family, orbital bus and multiple orbit/payload launch missions for reducing unmanned space research and development costs [AIAA PAPER 67-637] 20 p3534 A67-37617

Multiple payload and multipurpose spacecraft evaluated for cost reduction in USAF space operations [AIAA PAPER 67-636] 20 p3535 A67-37621

Multiple payload mission planning for multiple and single earth orbits and apogee motor delivery, evaluating cost and performance 22 p3903 A67-39952

PIGMENT

SA RUTILE

Flaw detection methods using penetrating fluids, emphasizing fluorescent materials and pigments 13 p2122 A67-26255

Chromatographic accumulation of primary and secondary carotenoids in Spongiochloris typica over 8-week period 14 p2254 A67-28065

PILOT

SA ASTRONAUT

SA AUTOPILOT

SA JET PILOT

SA TEST PILOT

Military pilot escape, survival, search and rescue 05 p0752 A67-17102

PILOT ERROR

Correlation between heart rate, landing error and field of view for binocular and monocular sphere of vision of jet pilots 09 p1455 A67-21717

Safety in business aircraft operations based on available statistics noting need for thorough pilot training 14 p2245 A67-28320

General aviation accident investigation from medical and operational standpoint, concluding pilots poor judgement was cause of accident 18 p2996 A67-34724

Human Error Research and Analysis Program /HERAP/ for man-machine system, investigating pilot error and performance and aircraft accident prevention [AIAA PAPER 67-848] 24 p4117 A67-42984

PILOT PERFORMANCE

SA ASTRONAUT PERFORMANCE

Pilot experiment, recording simultaneously optical image position, atmospheric temperature fluctuations and wind direction 01 p0108 A67-10250

Radiotelemetric recordings of EEGs aviation pilots during long flight 01 p0017 A67-10962

Monograph on system philosophy of automatic learning systems in application to autopilots, discussing man-aircraft system cybernetics, human behavior, environmental

effects, etc 02 p0186 A67-12084
Combined linear and vibratory
accelerations effects on human body
dynamics and pilot performance 02 p0189 A67-12409
Experimental fixed and moving-base flight
simulator investigation of generalized
aircraft longitudinal pilot induced
oscillations 03 p0365 A67-12913
[AIAA PAPER 65-793] 03 p0365 A67-12913
Urinalysis assessment of physiological
response of eight pilots to 18-hr flight in F-
4C aircraft 03 p0364 A67-14287
Dose levels and hangover effect of
secobarbital on simulated pilotage
performance 03 p0366 A67-14291
Human reactions and attention shifts
during flight tracking tasks 04 p0562 A67-14544
Vertebral lesion in fighter pilot following
landing accident 04 p0561 A67-14632
Statistical analysis of high speed aircraft
piloting, including wing and tail surface
effects and pilot work load and
performance 04 p0653 A67-14894
Controllability limit of human pilot for
unstable second order system with positive
static stability analyzed by modified transfer
function and servomechanism theory 05 p0757 A67-17354
Extraterritorial extent of powers of
aircraft commander for maintaining safety
and order on board 07 p1269 A67-19519
Pilot-aircraft compatibility in landing
approach 07 p1136 A67-19888
Simulation of pursuit-evasion differential
game using variational method, comparing
performance of human pilot to optimal
pursuer 07 p1136 A67-20170
Queueing model of many-instrument visual
sampling 07 p1136 A67-20172
ECG measurement results on ascent in
depressurized chamber, observing dislocation
of electrical axis of heart due to diaphragm
lift 08 p1287 A67-20643
Integrated cockpit research in man-
machine relationship in aircraft 08 p1350 A67-20666
Sensory input overload effects on
performance of civil aviation pilots during
simulated instrument flights in Link AN
2550-1 trainer 09 p1455 A67-21726
Reaction time during voluntarily
controlled alveolar hyperventilation used to
study effects on psychomotor performance
of aircrew 09 p1453 A67-21728
Experiments showing occurrence of aero-
atelectasis in pilots exposed to high G
forces, breathing oxygen and using anti-G
suit 09 p1453 A67-21733
Gastrointestinal symptoms and drug use as
possible contributing causes of fatal crash of
race pilot 09 p1458 A67-21734
Telemetry applications to in-flight
physiological measurements 09 p1457 A67-22461
Carrier landing improvements in Fresnel
lens optical landing system, emphasizing
compensated-meatball stabilization
[AIAA PAPER 65-791] 09 p1441 A67-22494
Decompression sickness in high altitude
flying, discussing degrees of bends pain
among squadron members during five year
period 10 p1600 A67-23826
[SAM-TR-66-305] 10 p1600 A67-23826
Pathogenesis of focal neurological
dysbarism in pilots during altitude
decompression sickness 10 p1600 A67-23827
Divergent vertical helicopter oscillations
resulting from physical presence of pilot in
collective control loop 11 p1744 A67-24591
Turbulent atmosphere load effect on
gliders noting influence of piloting
techniques 13 p2052 A67-26484
Medical/human factors affecting pilots
during atmospheric turbulence 13 p2064 A67-27262
Visual flight simulation, detailing all-
weather operation requirements 13 p2091 A67-27267
Man-machine compatibility in very low
altitude flight determined by two-phase
controlled field experiments on obstruction
avoidance task 14 p2256 A67-27742
Miniaturized multichannel multiplexed FM
biotelemetry system designed to record
physiological condition of pilot and test
operational efficiency 14 p2256 A67-28210
Factors affecting human spatial orientation
system functioning during flights 14 p2254 A67-28211

Functional or reactive hypoglycemia as
potential cause of flight accidents, showing
alimentary behavior of pilot brings about
apparition of hypoglycemic phases 14 p2254 A67-28216
Flight simulator experiments test pilots
ability to disregard senses and trust only
flight control instruments 14 p2255 A67-28220
Temporary irritation by anti-g and change
in vestibular motor reflex action under
laboratory conditions 14 p2257 A67-28224
X-ray examination of arms of pilots killed
in aircraft collisions, determining from bone
injuries degree of control before
collision 14 p2255 A67-28227
Intermittent visual stimulus influence on
perceptual motor skills in aviation 14 p2258 A67-28668
Subjective responses to oscillation in
yaw 15 p2427 A67-29269
Training programs to improve airline pilot
performance, suggesting greater use of
flight simulators and pedagogy methods
[AIAA PAPER 67-387] 15 p2432 A67-30355
Pilot self-medication causes and dangers,
classifying dangerous drugs and studying
effects on pilot performance 16 p2614 A67-31474
Stress-related and other physiological
variables on jet aircraft pilots participating
in storm penetration and perimeter
flights 17 p2805 A67-31955
Cardiorespiratory functioning in flight
monitored on carrier pilots in
combat 17 p2805 A67-31956
Biochemical response pattern to combat
flying stress of monitored carrier aircraft
pilots 17 p2805 A67-31957
Acceleration stress effects on pilot
performance and dynamic response 17 p2808 A67-33176
Pilot describing function measurements in
multiloop control task to provide data for
multiloop pilot model 17 p2808 A67-33177
Controllability methods on VTOL
transporters, developing model of pilot
dynamic reaction to aircraft
machinery 18 p2993 A67-33457
Pilot medical examination frequency and
effect on safety 18 p2992 A67-34722
Medical complications of contact lenses
and aeromedical implications 18 p2993 A67-34723
Pilot performance in simulator training
during acute hypoxia noting effect on
altitude, engine power and directional
control 20 p3374 A67-36264
Visual display for aircraft, presenting
simplest visual picture compatible with
current pilot task 20 p3375 A67-36873
Scuba diving relation to development of
aviator decompression sickness, investigating
decompression time before flying 21 p3574 A67-38078
Radiological findings from pilots afflicted
with vertebral fractures from ejection
injuries 21 p3575 A67-38510
Heat stress, skin and rectal temperatures,
heat gain and water losses in Army pilots
flying combat missions in Mohawk OV-1
aircraft in Vietnam 22 p3750 A67-39595
Visual aspects of carrier landing,
discussing research program to evaluate
pilot ability to make critical visual
judgments 22 p3755 A67-39847
Devices to help pilot detection of aircraft
evaluated for systematic relationship
between detection functions under fixated
conditions and in visual search 22 p3755 A67-39848
Inverted pendulum and VTOL control
experiments with and without motion cues,
discussing various motion effects 22 p3755 A67-40087
Middle aged pilot medical fitness for
flying, noting age-accident statistics, changes
in skill, performance, senses and
responses 22 p3756 A67-40535
Sudden strong stimulus effects on pilot
simple visual reaction time and fatigued
muscle strength 22 p3756 A67-40537
Age limitations of flying personnel taking
into account physical condition and
professional capabilities 22 p3756 A67-40542
Laboratory psychophysiological efficiency
in flying personnel of various ages covering
pursuit reaction tests, serial motor activity
and optico-acoustic signal analysis 22 p3753 A67-40544
Speech audiometry for hearing loss

examinations of middle aged pilots 22 p3753 A67-40545
Pilot capability in low level high speed
flying analyzed for influence of roughness
fatigue, control improvements, vibration and
visual problems 23 p3963 A67-41068
Retinal angiomatosis and aircrew fitness
noting correction by photocoagulation 23 p3945 A67-41071
Aeromedical incidents among Canadian Air
Force pilots, using mailed questionnaire 23 p3963 A67-41540
In-flight aeromedical monitoring of
cardiorespiratory response of naval pilots
during aircraft carrier combat operations,
discussing physiological effects
determination 23 p3963 A67-41541
Flash blindness effects on pilot
performance simulating inadvertent exposure
to nuclear bursts of light by xenon gas
discharge tube 23 p3965 A67-41569
Gastroesophageal reflux measurements in
evaluation of hiatus hernia and chest pain in
fliers 23 p3954 A67-41599
Night and day carrier landing pilot
performance, noting altitude position
estimation inaccuracy as contribution to
higher accident rate 23 p3988 A67-41618
Relation of time between flights to
accident potential of pilots 23 p3970 A67-41696
PILOT SELECTION
Color vision testing criteria in analysis of
results from pseudo-isochromatic plate,
anomaloscope and signal lantern testing 07 p1135 A67-19865
Glucose loading effects on
electrocardiogram of pilot applicants
evaluated for injection before and after
diabetes test 21 p3573 A67-38068
Aerospace and Harvard PB word lists for
speech discrimination testing of aircrew
members while screening against possibility
of Meniere disease and vertigo 23 p3963 A67-41542
PILOT TRAINING
Pilot training, regulation, instrumentation
and airspace environment changes for
increased safety [AIAA PAPER 66-812] 01 p0008 A67-10032
T-38 pilot trainer with mandatory stability
control characteristics to meet current
supersonic aircraft requirements [AIAA PAPER 66-798] 01 p0009 A67-10536
Navy simulation techniques for pilot
training [ASME PAPER 66-WA/AV-3] 04 p0599 A67-15396
Platform with six degrees of freedom for
flight simulation in pilot training 09 p1483 A67-21555
Psychophysical and psychosocial factors as
causes for rejection of Italian Air Force
pilot trainees, discussing relationship
between pilot, instructor and physician 12 p1902 A67-25171
DC-9 training program using classroom
responder system and programmed-type
learning aids 13 p2064 A67-27261
Flight simulators for present and future
aircraft 13 p2090 A67-27263
Flight simulator computation methods
development 13 p2090 A67-27264
Flight simulator motion enhancement and
potential for flight crew training, examining
human vestibular system 13 p2064 A67-27268
Flight simulator acceptance and role in
pilot training and checking in UK 13 p2064 A67-27272
Astronaut training techniques applicability
to conventional aircraft pilots training,
discussing instruction and high fidelity
simulation devices 13 p2084 A67-27273
FAA test pilot training in intent and
administration of regulations 14 p2256 A67-27740
Required safety standards for selection of
commuter airlines and contracted
flying 14 p2245 A67-28318
In-flight simulation of fog for pilot
training noting heads-up optical viewing
system, daylight backscatter, photographic
method, etc [AIAA PAPER 67-386] 15 p2468 A67-30354
Training programs to improve airline pilot
performance, suggesting greater use of
flight simulators and pedagogy methods
[AIAA PAPER 67-387] 15 p2432 A67-30355
Pilot training for future commercial
transports, noting flight simulation devices
for safety and economic factors

- [AIAA PAPER 67-388] 15 p2432 A67-30356
Airline pilot recruitment, role, capability
and training 18 p2993 A67-34073
Pilot performance in simulator training
during acute hypoxia noting effect on
altitude, engine power and directional
control 20 p3374 A67-36264
Landing characteristics of SV-5P lifting
body vehicle analyzed using six degree of
freedom piloted simulation, noting gust
effect
[AIAA PAPER 67-574] 20 p3533 A67-37133
Noise reduction in residential areas near
landing strips using Tu-124 aircraft studied
with suggested takeoff and landing piloting
techniques 21 p3569 A67-38928
Salplanes with self-contained launching
apparatus noting minimum performance,
motor propulsion and auxiliary
equipment 22 p3744 A67-39303
Airsickness early in flight training
indicates high levels of anxiety and attrition
potentials and poor prognosis 23 p3963 A67-41544
Naval jet replacement pilot training
failures examined for significant
data 23 p3966 A67-41579
Parachute descent training for USAF
pilots using Para-Sail ascending
parachute 23 p3967 A67-41609

PILOTED AIRCRAFT

- Statistical analysis of high speed aircraft
piloting, including wing and tail surface
effects and pilot work load and
performance 04 p0653 A67-14894
Piloted flight simulator studies influence
on design of SST instruments, discussing
pitch indicator, landing and sonic boom
limitation display systems 13 p2154 A67-27269
SST ground and flight personnel training
program for system operation, discussing
expected role of piloted flight
simulator 13 p2091 A67-27270
Pilot and automatic control function
coordination in piloting and landing aircraft,
discussing precision problems, safety and
development of new processes 22 p3831 A67-39750

PILOTED CENTRIFUGE

- Vestibular, tactual and proprioceptive
information in judging Coriolis rotation and
attitudes during rotation and pitching on
piloted flight simulator 22 p3751 A67-39605

PINCH EFFECT

- Nuclear fusion, discussing magnetic
confinement methods of hot plasma shell
holding light nuclei 01 p0124 A67-10778
Pinch effect in containing fusion
reaction 03 p0481 A67-13733
Pinch effect in InSb degenerate plasma,
discussing electric conductivity and
recombination emission
spectra 06 p1049 A67-17879
Pinching of surface carriers toward center
of semiconductor produced by current
induced magnetic field 08 p1371 A67-21439
Electrodeless electromagnetic shock tube
with large discharge chamber for high
velocity shock waves, applying theta pinch
effect 11 p1773 A67-24592
Large-dimensional inverse pinch discharge
study of impulsive plasma acceleration, gas
dynamics and stability of unrestrained
current sheet
[AIAA PAPER 66-482] 14 p2356 A67-28123
Bounce model pinch stability, noting
plasma and field separation by thin surface,
with anisotropies in velocity distribution and
angular momentum 16 p2718 A67-31227
Pulsed high current arc in hydrogen
showing initial instability, discharge stability,
impurity content, pinch effect, decay,
etc 18 p3087 A67-34047
Electron beam passing through low
pressure gas generates plasma, computer
simulated beam trajectory studies explain
beam profile and pinch
effect 19 p3275 A67-35106
Pulsed-discharge-current interruption in
constricting aperture by pinch effect, loss of
ions, gas heating and oscillation
generation 19 p3278 A67-35127
Energy band pinch effect in laser-heated
GaAs, studying temperature effect on
radiative recombination
rate 20 p3460 A67-37106
Z-pinch in electron hole plasma observed
by microwave probe method, noting no
minimum current exists for
semiconductors 21 p3666 A67-38356

- Pinch effect in degenerate indium
antimonide plasma in longitudinal and
transverse electromagnetic
fields 21 p3666 A67-38369
Size effects in platelets of multivalley
bipolar semiconductors with long scattering
and electron-hole recombination times,
studying electric pinch
effect 23 p4042 A67-41292

PION

- High energy interaction of nucleons with
complex nuclei described by model of
cascade-type nucleon and pion multiplication
within nucleus 02 p0312 A67-12604
Ionization calorimeter photoemulsion
measurements at mountain altitudes,
determining formation mechanism of high
energy pions in primary cosmic
radiation 02 p0315 A67-12760
Ionization calorimeter measurements of
energy transmission by photons in cosmic
nuclear-active pion and nucleon interactions
with various nuclei 02 p0316 A67-12761
Nucleon interaction generating high
energy gamma rays, discussing photon and
energy spectra of electron photon cascade,
pion generation and gamma quantum
detection in atmospheric nuclear
interactions 02 p0316 A67-12763
Isobaric pions role in interaction between
nucleons and pions on one hand and nuclei
of air atoms on other 02 p0319 A67-12786
Self-consistent three-body calculation of
pion-nucleon scattering using off-energy
shell theory 04 p0660 A67-14858
Nucleon radius from pion-nucleon phase
shift, assuming nucleon is p-wave bound
state of pion and nucleon, using Gelfand-
Levitan formalism
[AIAA PAPER 67-213] 06 p1036 A67-18368
Frequency spectrum of P_1 2
micropulsation activity and relation to
planetary magnetic activity 13 p2109 A67-26327
Production of charged double pion in pi
plus-proton scattering, noting isobar model
failure to explain enhancement at 400
Mev 19 p3266 A67-36100
Ionization calorimeter photoemulsion
measurements at mountain altitudes,
determining formation mechanism of high
energy pions in primary cosmic
radiation 22 p3876 A67-40262
Ionization calorimeter measurements of
energy transmission by photons in cosmic
nuclear-active pion and nucleon interactions
with various nuclei 22 p3876 A67-40263
Nucleon interaction generating high
energy gamma rays, discussing photon and
energy spectra of electron photon cascade,
pion generation and gamma quantum
detection in atmospheric nuclear
interactions 22 p3876 A67-40265
Isobaric pions role in interaction between
nucleons and pions on one hand and nuclei
of air atoms on other 22 p3878 A67-40288
Proton-proton and pion and kaon elastic
scattering from protons at high energy,
deriving approximate formula for
differential cross section, noting nucleon
structure 24 p4193 A67-42855

PION BEAM

- Pionic and muonic K-series X-rays studied
by liquid He scintillation counter, obtaining
separation peaks 24 p4192 A67-42735
Isobar decay mechanism for high energy
pion generation in cosmic rays propagating
through atmosphere 24 p4218 A67-42841
Pion nucleon inelastic collisions at 17
Gev/c momentum, discussing proton pulse
spectra and ionization losses 24 p4192 A67-42853
Positive rho meson and doubly positive
nucleon-pion resonance generation in 2.34
Gev/c 24 p4193 A67-42856

PIONEER VI SPACE PROBE

- Solar wind ion concentration and velocity
measurements from Venus III and Pioneer
IV 13 p2195 A67-27343

PIONEER VII SPACE PROBE

- Pioneer VII plasma probe data indicating
geomagnetic wake at 1000 earth radii
downstream from earth 22 p3791 A67-39819

PIONEER SPACE PROBE

- Pioneer VI detector to measure degree of
anisotropy of cosmic radiation at various
energy ranges 09 p1500 A67-22427
Aspect system on Pioneer VI and VII
incorporates digital computer for accurate
time sector division of spin stabilized
vehicle 11 p1870 A67-24441

- Magnetic design of OGO and Pioneer solar
probe including data on instrumentation,
mechanical equipment, permanent magnets,
test methods, etc 16 p2757 A67-30637
Solar array as primary electrical power
source of Pioneer deep space probes,
comparing performance data with test and
design data 24 p4105 A67-42514

PIPE

SA TUBE

- Mississippi Test Facility gas metal-arc
welding of T-1 steel critical high pressure
piping systems for Saturn V launch
vehicle 03 p0430 A67-13691
Beading in thin walled pipes with localized
heating, noting stress deformation
state 07 p1192 A67-19752
Heat pipe, device with thermoconductivity
greater than solid conductors, based on
surface tension and latent heat of working
fluid 08 p1427 A67-21051
Tailpipe length effect on flame stability in
high velocity propane-air stream with bluff
body or reverse jet flame holders
[ASME PAPER 67-GT-4] 11 p1653 A67-24792
Condenser parameter effect on maximum
heat transport in heat pipes for nonradiative
and radiative cases 13 p2222 A67-26844
Plasma arc welding of pipes, studying
effects of various gas combinations on weld
characteristics 14 p2327 A67-28819
Parametric analysis of heat pipes, design,
operation principles and performance
capabilities 24 p4255 A67-42553

PIPEFLOW

- Empirical method predicting flexible hose
flow losses, with Fanning friction factor as
Reynolds number and internal hose
geometry function 22 p3785 A67-39971
Forced convective heat transfer in straight
pipe rotating around parallel axis with large
angular velocity 22 p3920 A67-40419
Heat pipe performance in zero gravity
field, discussing isothermal operation of
water heat pipe in earth
orbit 24 p4256 A67-42926

PIPELINE

- Elbow flow meters, comparing average
coefficients with theoretical
values 03 p0422 A67-13779
Aviation fuels and requirements that
refineries must meet 13 p2185 A67-26862
Arbitrary internal heat generation terms
in energy equation effect upon limiting
Nusselt number for heat transfer to pipeline
flow of non-Newtonian fluids
[AIChE PAPER 12] 20 p3552 A67-36828
Aircraft pipeline flanges manufacture by
compression permit direct connection of
sections into single main 21 p3637 A67-38924

PIRANI GAUGE

- Melting temperatures of ZrC-HfC, TaC-ZrC
and TaC-HfC compacts obtained via Pirani
method 09 p1518 A67-21879

PISTON

SA MAGNETIC PISTON

- Piston motion effect on flow uniformity in
hypersonic gun tunnel, using perforated
plate technique to prevent piston
fluctuation 05 p0791 A67-16430
Logic methods using conventional piston
valves applied to general
automation 08 p1282 A67-20470
Propagation of strong ionizing front at
arbitrary oblique angle relative to magnetic
field, determining limits to value of electric
field ahead of shock 17 p2908 A67-33114
Performance factors affecting size, shape
and operation of piston and bore including
hydraulic lock, viscous drag, oil
contamination, etc 20 p3366 A67-37367
Motion and thermodynamic conditions of
free piston ballistic compressor test gas
taking into account gas leakage, viscous
friction and heat losses 22 p3778 A67-39351

PISTON ENGINE

- Comparison of piston engine with turbojet
engine noting power-weight ratio, specific
fuel consumption, performance
characteristics, etc 03 p0502 A67-13005
Dust content of air flow created by piston
engine MI-1 and MI-4 helicopters in landing
and takeoff 11 p1744 A67-24530
Two-stroke cycle light aircraft engine with
respect to competitive power
plants 12 p1989 A67-25496
Lubricants for utility aircraft piston
engines, cost, availability, compatibility, etc
[SAE PAPER 670248] 12 p1989 A67-25502
System-effectiveness concept for turbine
and piston engine

- development 15 p2584 A67-30402
 Engine development and manufacture in Sweden 17 p2928 A67-32123
 Bird strike data on piston engine transport horizontal stabilizers summarized by bird weight, impact velocity, target-station distance and simulated and test load 22 p3746 A67-39845
- PISTON THEORY**
 Shock tube operation with free piston compression of driven gas, noting operating limitation 03 p0397 A67-13897
 Isentropic compression due to motion of heavy piston in gun tunnel noting nozzle throat effect on motion and stagnation pressure 11 p1773 A67-24577
- PITCH ATTITUDE**
 Pitching effect on aircraft gravity center during passage through gust, noting autopilot effect on tail assembly 09 p1440 A67-22473
 Manual altitude and attitude control effects on short-period handling quality requirements 19 p3175 A67-35974
 Peripheral jet GEM characteristics analysis by longitudinal static stability and dynamic pitching motion 22 p3745 A67-39837
- PITCH CONTROL**
 Self-adaptive system employing quick identification of parameters of aircraft short period pitch transfer 07 p1128 A67-19199
 Flight attitude control problems of manned lunar landing vehicles emphasizing pitch control [AIAA PAPER 67-239] 07 p1129 A67-20045
 Adaptation scheme applied to pitch axis control system of supersonic aircraft, using stability analysis for system design 09 p1440 A67-22387
 Piloted flight simulator studies influence on design of SST instruments, discussing pitch indicator, landing and sonic boom limitation display systems 13 p2154 A67-27269
 Mark 19 Sperry gyrocompass with SGN 4 inertial platform 14 p2322 A67-28989
 Earth-pointing satellite attitude control system using gravity gradient stabilization, deriving motion equations 15 p2564 A67-29329
 Suppression of oscillatory vertical force transmission from helicopter rotor to driving shaft using higher harmonic pitch angle inputs [AHS PAPER 129] 16 p2777 A67-31843
 Synthesis of closed loop system consisting of pitch control adaptive autopilot for changing flight conditions, using transient characteristics 18 p3075 A67-34282
 Linear segment pitch rate program for near optimum trajectory for rocket boosters 19 p3335 A67-35976
- PITCH CONTROLLER**
 Terrain following pulsed radar system without continuous scanning noting computer simulation, antenna and pitch control 11 p1752 A67-24259
- PITCHING MOMENT**
 Normal force and pitching moment values for interference on body, wing and overall body-wing obtained, using pressure distribution integration 04 p0545 A67-14439
 Span loading of swept wing which produces minimum induced drag with constraints on lift and pitching moment 06 p0937 A67-18010
 Simulated high altitude hypersonic cold wall testing of lifting bodies, measuring lift, drag and static pitching moment 06 p0943 A67-18847
 Nonlinear motion theory for axisymmetric sounding missiles or rockets with Magnus moments, showing application to near pitch-roll resonance 08 p1407 A67-20515
 Wing lift and pitching moment variation due to fin on supersonic aircraft 09 p1437 A67-22163
 Rate variation of aerodynamic parameters of pitching equation for aircraft, identifying them with linear plant model for simulation studies 15 p2420 A67-30340
 Drag coefficients used to evaluate normal force and pitching moment characteristics of revolving body at angle of attack 22 p3740 A67-39943
- PITOT-STATIC TUBE**
 Helicopter and VTOL vehicle low air speed measuring techniques and devices including pitot-static tube, hot-wire anemometer, sphere sensor and exotic techniques 01 p0073 A67-11122
- PITOT TUBE**
 Hemispheric pressure distributions, measuring effect of Mach number, hole size and angular position of hole on Pitot pressure 13 p2220 A67-27193
 Electric manometer using electrolytic fluid for low velocity measurements with Pitot tube 16 p2675 A67-31210
 Langley Hypersonic Nitrogen Facility flow evaluation covering pitot pressure survey of nozzle wall boundary layer, centerline and Mach number 21 p3607 A67-37777
 Turbulent skin friction in incompressible flow with heat transfer, determining Preston surface pitot tube applicability 23 p4004 A67-41341
- PITUITARY GLAND**
 Pituitary enzymes hydrolyzing aminoacyl arylamides and relation to peptidases 01 p0015 A67-10488
- PIVOT**
 AC and DC magnetic bearings efficient load support and development potentials [ASLE PREPRINT 67AM 6D-4] 14 p2325 A67-28788
 AC and DC magnetic bearings efficient load support and development potentials [ASLE PREPRINT 67AM 6D-4] 22 p3813 A67-40219
- PIVOTED WING**
 Pivot center position effect on aerodynamic characteristics of variable sweepback wings during rotation 03 p0351 A67-12994
 Wing pivoting design for supersonic aircraft adaptability to different flight conditions, noting experiments with F 111 16 p2590 A67-30839
 Performance requirements and design aspects of variable sweep aircraft, examining swing pivot systems 20 p3361 A67-36498
 US SST airframe prototype, surveying hardware developments, flight control, pivoting system, landing performance and pilot cabin [AIAA PAPER 67-750] 23 p3933 A67-40984
 Variable geometry in SST aircraft, discussing hardware, lift control system, compression inlet and full scale wing pivot [SAE PAPER 670878] 24 p4094 A67-42012
 Design and flying qualities of variable geometry aircraft, discussing wing pivot location and longitudinal stability [SAE PAPER 670879] 24 p4094 A67-42013
 Wing pivot joint and actuation system configurations for SST variable geometry design [SAE PAPER 670883] 24 p4160 A67-42017
 SST variable sweep wing actuation system and pivot bearing reliability [SAE PAPER 670884] 24 p4098 A67-42018
- PLAN POSITION INDICATOR /PPI/**
 Magnetic recording of various types of monopulse, PPI and MTI radar signals, with application to airborne data acquisition recorder and ground reproducer 02 p0196 A67-12004
 Visual presentation of data required for ATC task, noting possible traffic display and attributes 09 p1529 A67-22646
 Bowtie radar display effectiveness in target detection compared with conventional Plan Position Indicator /PPI/ [TR-750-7] 17 p2807 A67-32630
- PLANCK EQUATION**
 Atmospheric water vapor distribution estimated from satellite measurements, using Planck radiance and assuming temperature distribution to be given 02 p0239 A67-12364
 Black body radiation equation approximating Planck equation in intermediate region with optical pyrometry application 05 p0807 A67-18788
 Critical point thermodynamics, refuting criticism concerning Planck-Gibbs equation 11 p1882 A67-24036
 Short wave limit for plasma radiation emission of neon gas discharge analyzed by Kirchhoff-Planck relation 15 p2530 A67-29747
 Spectral coefficients of blackness in materials with low thermoconductivity determined by measuring radiation intensity and solving equations derived from Planck and Kirchhoff laws 18 p3048 A67-34056
 Solar abundance determination, discussing composition parameters and Planck gradient method 24 p4237 A67-42654
- PLANE**
 SA HALF-PLANE
- SA MONOPLANE**
 SA SURFACE
 Cosserat plane and shell theory development from considerations concerning equilibrium conditions with aid of introduced stress functions 07 p1263 A67-19885
 Plastic deformation theory applicable range for case of linear anisotropic consolidating medium 21 p3720 A67-38298
- PLANE WAVE**
 Optical harmonic generation and first order sum and difference frequencies in plane parallel crystal plate within framework of phenomenological theory 01 p0089 A67-10361
 Wave solutions for plane waves propagating in isotropic elastic solid using isentropic approximation 01 p0162 A67-10847
 Finite-amplitudinal plane wave propagation in elastic solids 02 p0338 A67-11792
 Negative lens property responsible for reconstruction of original scene in full three-dimensional reality 03 p0420 A67-13676
 Reflection and refraction of plane MHD waves at plane interface discontinuity of two semiminfinite homogeneous conducting fluids of different densities 03 p0480 A67-13727
 Diffraction of plane wave at sinusoidally stratified dielectric grating, using hologram analysis 03 p0423 A67-13905
 Plane electromagnetic wave diffraction at two parallel circular cylinders for TM and TE polarization 03 p0371 A67-13959
 Scattering of plane wave by grating of identical cylinder specialized for case in which individual elements of grating scatter isotropically 03 p0374 A67-14353
 Refraction of plane shock wave by interface between different gases, reducing motion equation to polynomial of degree 12 04 p0601 A67-14465
 Plane wave interaction with surface waves at plasma boundary 04 p0668 A67-15274
 Diffraction of plane harmonic horizontally polarized shear waves by parabolic cylinder, obtaining dynamic shear-stress concentration for parabolic notch and rigid parabolic insert [ASME PAPER 66-WA/APM-13] 04 p0713 A67-15405
 Coefficient of hydraulic resistance derived for plane flow of electrically conducting fluid in traveling magnetic field 04 p0670 A67-15534
 Group classification by Cartan method of equations of one-dimensional plane wave gas flow 04 p0611 A67-15982
 Stationary plane shock wave stability in arbitrary media, discussing error analysis 05 p0795 A67-17543
 Optical harmonic generation and first order sum and difference frequencies in plane parallel crystal plate within framework of phenomenological theory 06 p1009 A67-17619
 Short wave asymptotics of diffraction field at sphere for incident plane transverse waves 06 p1100 A67-18032
 Log amplitude covariance for horizontal and nonhorizontal propagation path of plane wave through turbulent atmosphere, noting refractive index effect 06 p1033 A67-18537
 Angular power pattern for circular aperture receiving plane wave perturbed by passage through turbulent atmosphere 06 p1033 A67-18538
 OPW calculation of six symmetry points in wurtzite Brillouin zone of CdS, using pseudopotential techniques 06 p1058 A67-18903
 Plane wave scattering by medium with strong fluctuations of refractive index, noting reentry condition 07 p1141 A67-19441
 Tangential magnetic field on earth surface excited by LF plane electromagnetic wave 07 p1142 A67-19449
 Electromagnetic plane wave diffraction on anisotropically conducting plane and shielding and reflecting activity of dense radial grating 07 p1143 A67-19589
 Plane wave growth associated with Cerenkov and cyclotron instabilities in plasma stream 08 p1358 A67-20893
 Gas ionizing shocks for plane flows with magnetic field lying in flow plane 08 p1358 A67-20895
 Nonlinear constant profile plane waves in cold Vlasov hydrogen plasma under influence of external magnetic field 08 p1359 A67-20896

Complex dielectric constant and EM plane wave propagation in flame plasma 08 p1359 A67-21045

Plane wave generation in metal plates by detonation of contact explosives, developing elastic-plastic deformation theory for finite stress-strain components 08 p1422 A67-21290

Diffraction of plane longitudinal wave in interior of elastic solid, where wave is harmonic in time and impinging on surface of penny shaped crack 09 p1573 A67-21863

Book on general electromagnetic fields represented by superposition of plane waves traveling in diverse directions 09 p1463 A67-21984

Monochromatic wave interaction with isotropic electron-plasma, determining field and surface wave generated on basis of Maxwell equations 09 p1464 A67-22012

Asymptotic law of propagation of plane detonation wave where perturbed motion behind wave transforms it to Chapman-Jouguet wave 09 p1489 A67-22218

Scattering of plane monochromatic sound wave by semilinear elastic pipe in moving medium, emphasizing axisymmetric oscillations 10 p1680 A67-23644

Plane electromagnetic wave diffraction by conducting half-plane embedded in uniaxial anisotropic medium 11 p1753 A67-24315

Geometrical optics approximation of plane electromagnetic wave reflection from ideally electrically conducting triaxial ellipsoid 11 p1754 A67-24986

Nonequilibrium MHD plasmas investigated for electrothermal instabilities noting effect of plane wave fluctuations 12 p1972 A67-25391

Gas dynamic stability of plane detonation wave propagating in ideal gas mixture, in terms of small perturbations that may result in surface bending and changes in thickness 12 p1930 A67-25965

Plane wave shielding effectiveness of thin films, using TEM mode 13 p2175 A67-26524

Plane shock wave in ideal gas characterized by infinitesimally thin discontinuity, determining width and distribution function 13 p2105 A67-27412

Expression for surface field components obtained for plane electromagnetic wave at nose-on incidence on semilinear cone 14 p2281 A67-28376

Group classification by Cartan method of equations of one-dimensional plane wave gas flow 14 p2305 A67-28483

Polarization and angle of arrival fluctuations for plane wave propagated through turbulent medium 16 p2625 A67-31344

Transient plane wave magnetic field attenuation through semilinear plate using simplified Laplace transfer function, noting infinite product form for LPTF 16 p2626 A67-31349

Electron-phonon interaction calculation for solid state transition metals justifying matrix element presented and using augmented plane wave 16 p2731 A67-31447

Diffraction of plane electromagnetic waves on compressible plasma cylinder analyzed, obtaining scattering cross sections 16 p2628 A67-31503

Plane wave disturbances in infinite rotating collisionless system for wave vector normal to axis of rotation [AD-653420] 16 p2753 A67-31700

Reflection coefficients of sharply bounded ionosphere for plane waves incident from arbitrary direction at magnetic equator 16 p2632 A67-31863

Plane wave scattering by finite circular cylinder treated by geometrical diffraction theory, obtaining formulas for radar cross section 17 p2816 A67-32789

Plane wave propagation in kinetic theory, noting Boltzmann equation and kinetic model 17 p2885 A67-32928

Asymptotic law of propagation of plane detonation wave where perturbed motion behind wave transforms it to Chapman-Jouguet wave 18 p3026 A67-33758

Beat frequency generation and multiplication and subsequent harmonic amplification in plasma-beam system, particular case of plane waves 18 p3087 A67-34037

Plane shock wave velocity measurement after interaction with obstacles in form of channelled diaphragms of various diameters, discussing stabilization 18 p3028 A67-34210

Scattering of plane monochromatic sound wave by semilinear elastic pipe in moving medium, emphasizing axisymmetric oscillations 18 p3080 A67-34413

Plane ionization wave propagation in uniform magnetic field compared with flame front expansion during slow burning 19 p3286 A67-35347

Infinitesimal driven plane wave characteristics in uniform plasma with finite electron drift velocity found, using Navier-Stokes and Poisson equations, energy conservation continuity and perfect gas law 19 p3290 A67-35376

Mode conversion in rectangular waveguides, describing results in terms of plane wave diffraction by grating 19 p3183 A67-35545

Wave field behind transmission grating illuminated by plane wave examined by Fourier spectrometry based on grating resonances 20 p3437 A67-36338

Electromagnetic plane wave diffraction on anisotropically conducting plane and shielding and reflecting activity of dense radial grating 20 p3384 A67-37326

Plane waves propagation in microelastic medium having only coupled stresses 20 p3542 A67-37681

Radiation of monofrequency antenna in compressible magnetoplasma expressing far field as sum of modal plane waves 20 p3388 A67-37701

Electromagnetic plane wave scattering cross section from plasma coated conducting cylinder using TE and TM modes of polarization with respect to cylinder axis 20 p3389 A67-37706

Laminar compressible boundary layer induced by plane shock wave passing over flat wall using empirical viscosity-temperature relation for Prandtl number 21 p3811 A67-37928

Plane wave approximation for dilatational mode response of thin hollow spherical shell embedded in elastic medium and subjected to asymmetric pressure wave 21 p3718 A67-38020

Reflection in water of plane shock waves from rigid wall 21 p3811 A67-38058

Standard equation method for normal incidence of plane monochromatic electromagnetic wave propagation in inhomogeneous anisotropic medium 21 p3579 A67-38111

Plane electromagnetic wave reflection from rough surface, calculating energy and polarization characteristics 21 p3580 A67-38115

Interaction between plane electromagnetic wave and separating boundary, considering electric field with component normal to boundary 21 p3581 A67-38292

Transient gas motions for various waves, analyzing motion equations and classifying integral curve fields 21 p3565 A67-38556

Boundary value problems of wave propagation in plane, investigating coverage, source distribution and velocity perturbations 21 p3615 A67-39093

Scattering of plane electromagnetic wave obliquely incident on surface of two coaxial disks investigated via separation of variables 22 p3758 A67-39306

HF plane waves diffraction on plane circular diaphragm solved by functional theoretic methods for integral equation for Fourier transform of screen covering 22 p3912 A67-39783

Plane electromagnetic wave reflection from ionization front, determining coefficient from finite thickness plasma layer and constant charged particle density 22 p3762 A67-40122

Hologram copying by Gabor holography of transparencies 23 p4002 A67-41268

Diffraction of H-polarized plane wave on metal grating with narrow slits 23 p3975 A67-41683

Plane shock wave disturbance development analysis by solving Cauchy problem, discussing low viscosity effect 24 p4141 A67-41931

PLANET

SA ALBEDO
SA EARTH
SA JUPITER /PLANET/
SA MARS /PLANET/
SA MERCURY /PLANET/
SA NEPTUNE
SA PLUTO /PLANET/

SA SATURN /PLANET/
SA URANUS
SA VENUS

Observations of 24 comets, 11 minor planets and Jupiter VIII, using computer 01 p0148 A67-10386

Communications of Lunar and Planetary Laboratory /University of Arizona/, Volume 4 /Numbers 64-69/ 05 p0896 A67-18716

Planetology and space mission planning - Conference, New York, November 1965 06 p1090 A67-18993

Gravitational field of any primary determined using observations of satellites in orbit about primary, noting numerical integration technique and special perturbation methods [AAS PAPER 66-109] 07 p1253 A67-19969

Moon and planets - Conference, Vienna, May 1966 18 p3120 A67-34134

Minor planets observational and computational results /1964/, discussing ephemeris volume 20 p3522 A67-36615

Minor planets position observations at Crimean Astrophysical Observatory during August and September 1964 20 p3522 A67-36620

Minor planets position observations at Crimean Astrophysical Observatory from October 1964 through March 1965 20 p3522 A67-36621

Soviet ephemeris of minor planets for 1968 covering orbital elements, opposition dates, time, etc 22 p3884 A67-39925

PLANETARY ATMOSPHERE
SA JUPITER ATMOSPHERE
SA MARS ATMOSPHERE
SA VENUS ATMOSPHERE

Composition and surface pressure of Martian atmosphere determined from photographic spectrum of Mars obtained at March 1965 opposition 02 p0323 A67-11695

Overlapping of bands of nitrogen oxide, CO and carbon dioxide in 4.5 micron region determined for inversion experiments 02 p0246 A67-12368

Outward flux and intensity of scattered radiation for top of Rayleigh atmosphere lying above smooth water surface that reflects radiation according to Fresnel law [AIAA PAPER 65-664] 03 p0411 A67-13044

Gaseous composition of unknown planetary atmosphere determined, using acoustic experiment combined with pressure and temperature data 03 p0509 A67-13215

Initial value formulation of Chandrasekhar problem for diffuse reflection of radiation from planetary atmosphere 03 p0462 A67-13903

Radiation equilibria in UV light on air, oxygen, carbon dioxide, etc, analyzed by bromine lamp in connection with studies of planetary atmospheres 03 p0513 A67-14088

Solar radiation effect on planetary atmosphere noting charged particle bombardment, dayglow phenomena, auroral emission, etc 04 p0696 A67-14699

Soviet papers on planetary atmospheric circulation and artificial earth satellites 04 p0651 A67-15467

Spectral study of Jupiter, Saturn and rings of Saturn, determining methane concentration in cloud layers 04 p0701 A67-15557

Radar observations of Venus at 3.8 cm noting low value of cross section, echo spectrum, polarization characteristics, absorption cross section and atmospheric attenuation 05 p0889 A67-16298

Planetary atmospheric absorption spectroscopy employing split-trajectory dual flyby mode [AIAA PAPER 67-121] 06 p1085 A67-18311

Atomic and molecular processes in upper atmospheres of Venus, Mars and Jupiter investigated by atmospheric models, presenting solar-planetary relationship 06 p1087 A67-18429

Radio occultation techniques for analysis of planetary atmospheres and surface topography by measuring perturbations to amplitude and frequency on radio links [AIAA PAPER 67-119] 06 p1087 A67-18454

Frost phenomena on Mars examined on basis of Martian wave of darkening, noting necessity of deliquescent salts to attract and retain water on surface 06 p1089 A67-18645

Structures of terrestrial and extraterrestrial atmospheres 06 p1091 A67-18997

Approximate formulas for determining

speed reduction, maximum deceleration and orbit modifications for ballistic vehicle that grazes atmosphere 08 p1394 A67-21106

Energy dissipation and other problems for alien planetary atmospheric entry at high speeds of interplanetary flight 08 p1394 A67-21155

Uranus and Neptune spectral absorptions compared with laboratory spectra obtained with very long optical paths indicate methane role in planetary absorption 08 p1397 A67-21213

Relationship between terrestrial and Jovian atmospheric circulations due to solar activity 08 p1398 A67-21215

IR observations for presence of ethane in atmospheres of Jupiter and Saturn reanalyzed and found consistent with previous results 08 p1398 A67-21218

Carbon dioxide study in Mercury atmosphere yields negative results from observations made with IR spectrometer and 61 inch reflector 09 p1565 A67-22016

Thermodynamic equilibrium composition of all combinations of C, H, O and N at average pressure and temperature calculated for atmospheres of earth, Venus, Mars, and Jupiter 09 p1566 A67-22236

Nongray model atmospheres of Jovian planets constructed for different relative concentrations of helium and diatomic hydrogen and various likely effective temperatures as chief sources of thermal opacity 09 p1567 A67-22237

Solution of angular distribution of outgoing thermal radiation from planetary atmosphere, using Chandrasekhar diffuse scattering and transmission functions 09 p1567 A67-22240

Free falling probe test during terminal descent for determining unknown planetary atmosphere profile from onboard measurements alone 10 p1629 A67-22768

Detecting planetary life from earth 11 p1747 A67-24063

Radar, radio astronomic and IR spectroscopic observations of Venus surface and atmosphere, examining general and surface data, chemical composition and atmospheric model 11 p1867 A67-24843

Planetary atmospheric composition study under ambient conditions using instrument involving very high Q Fabry-Perot microwave cavities 12 p1946 A67-25986

Molecular, continuum and line radiation of planetary atmospheres, comparing molecular band structure models with spectral measurements of CN violet band [AIAA PAPER 67-323] 12 p2037 A67-26038

Polarization properties of Mercury explained by surface only, so there is no polarimetric evidence for atmosphere on Mercury 12 p2010 A67-26244

Analytical expressions for multiply scattered light mean intensity and light source function in homogeneous planetary atmosphere derived using mathematical model 13 p2113 A67-26683

Discrete equilibrium temperatures of hypothetical planet with atmosphere and hydrosphere of one-component two-phase system under constant solar radiation 13 p2116 A67-27462

Spherically symmetrical planetary atmosphere brightness derivation using transport equation 14 p2313 A67-28766

Solar system planets characteristics, temperatures, atmospheres and internal structure 14 p2392 A67-28959

Venus brightness temperature and atmosphere and Mars atmosphere sounded by Mariner II space probe, noting data on Mars magnetic field 14 p2322 A67-28964

Earth magnetic field effect on ultralong radio wave propagation, considering directional effects from planetary inhomogeneities and reciprocity principle impairment 15 p2479 A67-30168

Multiple light scattering in inhomogeneous spherically symmetrical planetary atmosphere with exponentially varying attenuation coefficient 16 p2698 A67-31096

Two-layer model of Venusian atmosphere satisfying radioastronomic and radar self-radiation measurements 17 p2941 A67-32322

Oxygenic concentrations in primitive earth atmosphere, discussing Martian atmosphere composition 18 p3041 A67-34095

Visible brightness features in Mariner IV photographs of Mars interpreted as

clouds 18 p3123 A67-34149

Aerodynamic, thermodynamic, heat shield and structural design aspects of ballistic vehicle entering planetary atmosphere 19 p3332 A67-35315

Data representing monopole antenna voltage breakdown in simulated Mars and Venus atmospheres 19 p3197 A67-35829

Ascent and descent gravity turn trajectories of rocket in constant gravitational field, considering drag forces in motion equation [AIAA PAPER 67-596] 19 p3336 A67-35992

Analytical expressions for multiply scattered light, mean intensity and light source function in homogeneous planetary atmosphere derived using mathematical model 21 p3618 A67-38427

Planetary atmosphere radiation spectral distribution sounded with 4.3 micron carbon dioxide band to determine temperature profile 22 p3805 A67-40355

Planetary surface pressure and temperature of lower atmosphere determined from orbiting spacecraft with carbon dioxide laser 22 p3805 A67-40357

Extraterrestrial life detection studied from knowledge of major and trace components of atmospheres 23 p3944 A67-40999

Upper limit of carbon dioxide abundance in Mercury atmosphere 24 p4225 A67-41836

Earth-moon system origin assuming moon was formed from terrestrial material ejected from earth during rotational instability 24 p4230 A67-42325

Mariner space vehicles design evolution noting contribution to future space flights through measurement of atmospheric density of Mars 24 p4241 A67-42399

PLANETARY BASE

Proposed emplaced scientific station for lunar surface studies 15 p2553 A67-29300

PLANETARY CIRCULATIONS PROJECT

Stratospheric mean adiabatic vertical motion and temporal correlations with temperature, isobaric height, zonal/meridional wind and horizontal kinetic energy computed based on seasonal averages 19 p3224 A67-35529

PLANETARY CONFIGURATION

Neptunian planet-satellite system, discussing orbital motion of Triton 01 p0148 A67-10385

Forecasting length of solar cycle and maximum value of sunspot numbers, suggesting relation to joint tidal effect of Venus-Jupiter-earth 01 p0149 A67-10805

Interpretation of radar observations of Venus, Mercury and Mars with outline of direction of current radar astronomical research 07 p1246 A67-19053

Computing transits of outer planets /Jupiter to Pluto/ over solar disk, as seen from another outer planet 17 p2948 A67-33095

Martian atmosphere transparency and visibility of surface details in blue and UV light, showing dark and semitone areas intensity, etc 18 p3124 A67-34154

PLANETARY CONSTITUTION

Internal structure models for earth, Venus and Mars, discussing earth density distribution and seismic results 02 p0329 A67-12497

Mars constitution examined on assumption of similarity to earth, noting Emden equation and Lyttleton results 05 p0902 A67-17290

Chemical signatures from astronomical bodies, noting spectral results obtained from ground stations and orbiting spacecraft 06 p1092 A67-19014

Internal structure models for earth, Venus and Mars, discussing earth density distribution and seismic results 10 p1709 A67-23365

Nonrotating, hydrostatic models of geochemically likely planets calculated using solar elemental abundances and equations of state for cold materials 16 p2754 A67-31748

General theory of planets in connection with progress in space research 18 p3124 A67-34157

Internal and surface Martian geology synthesis, investigating parameters favoring organic growth and sites for exploration 19 p3323 A67-35334

Jupiter atmosphere, interior and surface properties, speculating on possibility of life in spite of presence of noxious

gases 21 p3703 A67-38191

Jupiter and Saturn models, giving planet constitution, heat balance and atmospheric composition 21 p3710 A67-39001

Jupiter internal structure investigated by observing visible surface and radio emission, discussing magnetic field origin and hydrodynamics of fluid regions 21 p3710 A67-39003

Planetary magnetic fields calculated from meteorite magnetic properties and assumptions about cores and crusts 21 p3711 A67-39042

Earth density/pressure relation and mantle and core mean atomic weight used to construct mass-mean density curve for planets 24 p4231 A67-42448

PLANETARY DISK

Radio emission from Jupiter, Saturn and Mercury noting disk temperatures [AD-653438] 05 p0892 A67-16409

Martian radius determined by measuring gravity field at known surface points [JPL-TR-32-1091] 09 p1569 A67-22682

Microwave radiometric measurements of planetary disk temperature of Venus, Mars, Jupiter and Saturn 11 p1869 A67-25094

Rotational velocity of Venus spots based on sidereal rotation measurements 13 p2198 A67-26588

Photoelectric measurement of planetary disk diameter and center-to-limb darkening 16 p2753 A67-31716

Photometric data on Mars opposition effect /nonlinear brightness surge at zero alpha phase angle/ noting phase curve steepness 24 p4226 A67-41838

PLANETARY ENTRY

Mars atmosphere entry probe configuration, aerodynamic characteristics, flow field, stability augmentation, instrumentation, thermal shielding, data handling and communications 01 p0156 A67-11424

Model of nonequilibrium properties of high temperature carbon dioxide and other gas mixtures in connection with studies for vehicles entering Martian atmosphere 01 p0008 A67-11436

Manned lifting entry vehicle capability, minimum weight, variable geometry, retractable landing engines, etc [AIAA PAPER 66-959] 02 p0332 A67-12287

Book on thermophysics and temperature control of spacecraft and entry vehicles 03 p0532 A67-13032

Lifting requirements of entry vehicles for near-earth planetary missions [AIAA PAPER 66-956] 03 p0520 A67-14140

Rotor entry vehicle systems /REVS/ concept based on lifting bodies L/D after entry with rotor needed only for improved landing [AIAA PAPER 67-203] 06 p0949 A67-18490

Optimum planetary approach of vehicle when direction of correcting pulses applied to trajectory plane is determined from maximum efficiency condition of pulse 07 p1247 A67-19093

Planetary entry vehicle development, discussing mission objectives, vehicle requirements, Voyager capsule, etc [AAS PAPER 66-57] 07 p1259 A67-19994

Flight dynamics of ballistic and lifting vehicle entries into planetary atmospheres of Mars, earth, Venus and Jupiter 08 p1410 A67-20623

RF bridge technique determining electric conductivity of plasma sheath around reentry vehicle 08 p1366 A67-21514

Martian entry condition analyzed as nonequilibrium flow field phenomenon, noting chemical kinetics and radiation behind shock wave in gas mixtures [AIAA PAPER 67-322] 12 p1930 A67-26037

Molecular, continuum and line radiation of planetary atmospheres, comparing molecular band structure models with spectral measurements of CN violet band [AIAA PAPER 67-323] 12 p2037 A67-26038

Total equilibrium shock layer radiation data for Martian entry body shapes at various angles of attack extrapolated to trajectory condition [AIAA PAPER 67-324] 12 p1894 A67-26039

Approach navigation accuracy and entry corridors for aerodynamic braking at Mars and Venus 13 p2212 A67-26837

Rotor entry vehicle system /REVS/ concept based on lifting bodies L/D after entry with rotor needed only for improved

landing
 [AIAA PAPER 67-203] 15 p2419 A67-29444
 Aerodynamic heating about vehicle
 entering atmosphere for corridor and
 guidance requirements analyzed on basis of
 Newton two-body problem 15 p2417 A67-30046
 Entry/Lander vehicle for Mars mission
 discussed in terms of gross payload, basic
 vehicle and preentry system 16 p2756 A67-30629
 Basic shock layer radiation data obtained
 in shock tube and free-flight ballistic range
 facilities applicable to Venus or Mars
 atmosphere entry 21 p3563 A67-37788
 Second order theory used to provide
 nearly exact solution for entry mechanics
 including solution of nonoscillating and
 oscillating trajectories [AIAA PAPER 66-488] 21 p3706 A67-38865
 Integral relations method for
 nonequilibrium hypersonic planetary entry,
 emphasizing flow fields and thermal
 environment determinations for blunt body
 vehicle configuration 22 p3740 A67-39936
 Spherical entry vehicle used to define
 planetary atmosphere structure and
 composition from dynamic response during
 entry, discussing aerodynamic
 characteristics 22 p3907 A67-40177

PLANETARY ENVIRONMENT
SA MARS ENVIRONMENT
 Environment, mission requirements and
 subsystem interfaces effect on space vehicle
 structure [SAE PAPER 660673] 01 p0153 A67-10580
 Quantitative estimation of liquid water
 content on Mars from thickness of snow
 blanket on planet polar cap 06 p1084 A67-18167
 Space mission planning in planetary
 environments, discussing methods and
 planetological parameters 06 p1093 A67-19035
 Sample acquisition from planetary surface
 by unmanned probes in life detection
 experiments [AAS PAPER 66-70] 07 p1189 A67-19999
 Russian and American practices and
 policies regarding planetary contamination in
 connection with COSPAR requirements 10 p1601 A67-23580
 Sterilization environment effects on
 structural systems design for interplanetary
 spacecraft 10 p1714 A67-23758
 Communications of lunar and planetary
 laboratory, Volume 5, University of
 Arizona 11 p1860 A67-24457
 Interplanetary transit and atmospheric
 entry of unmanned vehicle landing on Mars
 surface, with reference to heat shield
 technology [JPL-TR-32-1145] 12 p2034 A67-25715
 Solar system planets characteristics,
 temperatures, atmospheres and internal
 structure 14 p2392 A67-28959
 Saturn photograph analysis discussing
 interpretation of thin line on edge of ring
 system 14 p2393 A67-29029
 Planetary quarantine constraints, noting
 prevention of Martian atmosphere
 contamination 15 p2424 A67-29098
 Effects of spacecraft sterilization
 procedures and Mars dust environment on
 thermal control coatings 15 p2503 A67-29541
 Quantitative estimation of liquid water
 content on Mars from thickness of snow
 blanket on planet polar cap 16 p2742 A67-30511
 Nucleic acid molecule reproduction
 discussing probability of life development
 under favorable environmental
 circumstances 16 p2611 A67-30767
 Problem of manufacturing space vehicles
 with rigidly controlled cleanliness and
 biological contamination for missions to
 other planets 18 p2995 A67-34677
 Planetary and interplanetary environments
 based on experimental data and quantitative
 information, noting influence of sun in solar
 system mass 21 p3707 A67-38946
 Terrestrial environment guideline
 documents providing natural environment
 extremes, means and cycles for spacecraft
 development 22 p3829 A67-39927
 Jupiter environment, effects of huge mass,
 high rotation rate, temperature and
 dominant H and He atmosphere 22 p3887 A67-40141
 Program for preventing earth environment
 biological contamination by lunar
 material 23 p3961 A67-40845

PLANETARY EVOLUTION

IR observations of R Monocerotis
 preplanetary system, reporting on flux
 density and circumstellar dust 03 p0510 A67-13506
 Cosmological principles of interzonal
 couplings, noting cyclic and secular change,
 planetary evolution, terrestrial magnetism,
 etc 06 p0989 A67-19006
 Jovian atmosphere simulation with energy
 from corona discharge, producing simple
 organic molecules 07 p1246 A67-19057
 Geochemical studies of Wyoming
 Precambrian graywackes concerning
 composition of early and ancient North
 American crust 06 p1326 A67-21267
 Protoplanetary cloud and evolution, noting
 Hoyle rotatory nebula and other
 hypotheses 09 p1563 A67-21833
 Mercury abundance in various meteorite
 and rock types determined by neutron
 activation analysis, relating data to evolution
 of meteorites and earth 11 p1858 A67-24064
 Cosmochemical considerations, from
 thermodynamical viewpoint, of formation
 processes of earth, planets and
 meteorites 11 p1864 A67-24600
 UVB values and red shifts of quasars
 interpreted within steady state and
 Friedman cosmological models 14 p2392 A67-28965
 Pulsating gravitation, noting geological
 evidence such as ocean transgressions,
 regressions, climate variations, etc 17 p2841 A67-32211
 Thermal conductivity model for planetary
 igneous differentiation, discussing melting
 behavior as function of pressure and
 temperature 17 p2942 A67-32387
 Oxygenic concentrations in primitive earth
 atmosphere, discussing Martian atmosphere
 composition 18 p3041 A67-34095
 Possibility of common origin for comets
 Wolf I and Barnard 20 p3524 A67-36661
 Earth-moon system origin assuming moon
 was formed from terrestrial material ejected
 from earth during rotational
 instability 24 p4230 A67-42325
 Cooling rates for Widmanstätten pattern
 formation in iron meteorites used to obtain
 data on parent meteorite bodies 24 p4234 A67-42627
 Olivine and pyroxene composition
 distribution in type II carbonaceous
 chondrites, discussing metamorphic effects
 and gas-dust fractionation 24 p4237 A67-42651

PLANETARY EXPLORATION
SA MARS PROBE
 Manned geophysical observations from
 satellites as training ground for planetary
 research, especially Venus atmosphere 01 p0155 A67-11395
 Voyager project for planetary biological
 exploration 02 p0185 A67-11816
 Soviet program of planetary exploration
 with aid of automatic interplanetary stations,
 examining problems due to trajectory errors
 and communications breakdown 02 p0326 A67-12041
 Space station role in manned space flight
 noting mission goals, earth, moon and
 planet-oriented applications, etc 02 p0332 A67-12272
 [AIAA PAPER 66-906] System design of integrated automated
 laboratory payloads in scientific planetary
 research unmanned spacecraft 02 p0334 A67-12349
 Ground and flight spacecraft
 instrumentation for lunar and planetary
 exploration 03 p0420 A67-13378
 Solar electropropulsion developments for
 solar system exploration 03 p0513 A67-14097
 Laboratory payload concept of automated
 laboratories for planetary exploration, noting
 systems engineering advantages 04 p0706 A67-15237
 Interior structure of moon and planets
 studied by geophysical seismic
 methods 04 p0702 A67-15561
 Science subsystems for Jupiter flyby
 missions, discussing equipment selection,
 mission planning, spacecraft design and
 trajectory and constraints on vehicle
 configuration [AIAA PAPER 67-120] 06 p1084 A67-18287
 Planetary atmospheric absorption
 spectroscopy employing split-trajectory dual
 flyby mode [AIAA PAPER 67-121] 06 p1085 A67-18311
 Photographic mapping of Martian surface
 with electrically propelled solar-powered

photographic spacecraft placed into near
 polar orbit [AIAA PAPER 67-88] 06 p1096 A67-18438
 Terrestrial and planetary biospheres,
 tabulating probability values for
 matching 06 p0953 A67-19007
 Gravitational field signatures yield
 information about interior structure of
 planets 06 p1092 A67-19008
 Planetary exploration with radar, noting
 technical problems, advantages and
 results 06 p1092 A67-19012
 Geochemical differentiation in terrestrial
 environments, noting vertical planetary
 differentiation 06 p0999 A67-19015
 Well logging methods for study of
 composition of planetary near surface layers,
 noting electric, nuclear and acoustic
 measurement methods 06 p1092 A67-19016
 Nuclear or electric propulsion for
 planetary exploration, noting configuration
 and capabilities 06 p1098 A67-19019
 Saturn V launch vehicle, discussing
 payload-mass ratio, capabilities and
 modification possibilities 06 p1098 A67-19020
 Space communications, present and
 future 06 p0965 A67-19028
 Reliability in improving program quality
 and design decisions as in planetary
 exploration program 07 p1259 A67-19617
 Planned encounters with asteroids in
 manned missions to Mars for observational
 purposes, using computer program [AAS PAPER 66-124] 07 p1254 A67-19983
 Voyager type landers on Mars surface
 noting instrumentation, operation, reliability,
 etc [AAS PAPER 66-61] 07 p1259 A67-19997
 Trajectory design and computer programs
 for planetary mission analysis 08 p1384 A67-20617
 Saturn S-IVB Apollo systems application to
 planetary exploration, using extension of
 technology and hardware for lunar
 exploration 08 p1411 A67-21074
 Manned planetary mission possibilities
 stressing Mars exploration, noting trajectory
 planning, propulsion, crew requirements,
 etc 08 p1394 A67-21099
 Orbital reconnaissance of Mars in 1971
 using modified Lunar Orbiter spacecraft,
 noting photographic system, trajectory,
 launch system, etc 09 p1570 A67-21681
 Lunar resources for space and planetary
 exploration, discussing application of solar
 radiation, extraction of mineral resources
 from meteorites, etc 09 p1568 A67-22406
 Lifting entry vehicles requirements for
 near earth and planetary missions, noting
 four thermal protection systems 09 p1572 A67-22671
 Voyager project goals, orbital operations,
 capsule descent, navigational systems,
 etc 12 p2002 A67-25232
 Manned planetary exploration, Mercury
 and Gemini flight programs and projected
 goals of Apollo Applications Program 12 p2002 A67-25233
 International planetary organization with
 jurisdiction over activities on celestial
 bodies and lunar and planetary
 launches 12 p2042 A67-26136
 Evolutionary manned interplanetary
 exploration program with modular elements
 used for flyby, orbital capture and Mars
 landing, noting influence of Apollo
 program 13 p2199 A67-26827
 Planned encounters with asteroids in
 manned missions to Mars for observational
 purposes, using computer program [AAS PAPER 66-124] 13 p2209 A67-27537
 Planetary exploration Conference,
 Roquencourt, Seine-et-Oise, France,
 December 1966 14 p2391 A67-28958
 Launching of space probes and data
 obtained on radiation particles and magnetic
 fields in space 14 p2392 A67-28960
 Future planning of interplanetary voyages
 based on capabilities and economic
 advantages of classical propulsion, noting
 high escape velocity 14 p2392 A67-28961
 Propulsion systems in which propulsive
 fluid is accelerated to high speeds by
 electrical or electromagnetic
 processes 14 p2377 A67-28962
 Future manned planetary missions
 including flybys and landings, describing
 vehicle configurations and technological
 requirements [AAS PAPER 67-28] 15 p2562 A67-30103
 Space studies of Mars and Jupiter through

- cislunar and interplanetary rocket probes in near future
 [AAS PAPER 67-32] 15 p2562 A67-30105
 Spacecraft design for manned planetary landings noting mission characteristics, navigation requirements, crew housing, etc 16 p2756 A67-30625
 System design of automated laboratory and associated entry vehicle for unmanned Martian exploration 16 p2653 A67-30628
 Research into geological history of planetary bodies without atmosphere, discussing techniques for determining time of formation of layered ejecta units 16 p2747 A67-30988
 Rocket fuel production possibilities on moon surface and other planets for planetary explorations 16 p2655 A67-31008
 Voyager project goals, orbital operations, capsule descent, navigational systems, etc 16 p2751 A67-31487
 Nuclear propulsion for manned Mars expedition, discussing engine and launch optimization, computer simulation, performance, trip times, velocity, weight, etc [AIAA PAPER 67-510] 18 p3077 A67-33974
 Contribution of earth-made observations to direct planet exploration 18 p3121 A67-34136
 Planetary quarantine and biological search strategy, discussing Voyager-Mars mission configuration, sterilization, back-contamination and decisions 19 p3180 A67-35233
 Planetary quarantine problem for Martian survival of microorganisms investigated, using systems analysis 19 p3180 A67-35274
 Launch vehicle, payload size, velocity requirements, etc, for probes exploring solar system and near interstellar space 19 p3323 A67-35330
 Internal and surface Martian geology synthesis, investigating parameters favoring organic growth and sites for exploration 19 p3323 A67-35334
 Unmanned rough-landing survival capsules design considerations for potential planetary payloads 19 p3332 A67-35335
 Manned orbiting laboratories for exploring planets by remote sensing and planetary encounter missions compared to landing and flyby 19 p3332 A67-35336
 Legal aspects of use of satellites in exploiting earthbound or near-in natural resources 19 p3349 A67-35641
 Commercial aspects of exploitation of natural resources by satellite 19 p3349 A67-35642
 Growth of terrestrial microorganisms on Mars noting possibility of planetary contamination 19 p3178 A67-35896
 Scientist role in automated laboratory for remote biological exploration of planets [AIAA PAPER 67-632] 20 p3375 A67-37615
 Spacecraft design, solar powering, electric propulsion and side-looking radar for planetary surface observation mission on Mars or Venus [AIAA PAPER 67-712] 21 p3714 A67-38739
 Unmanned probe and launch vehicle selection for solar system exploration, considering tradeoffs in terms of reliability, cost, weight, experimental accuracy, etc 22 p3900 A67-39617
 Electric propulsion ion engine systems using solar power source for Mars and Jupiter exploratory unmanned spacecraft is adaptable to existing launch vehicles [AIAA PAPER 67-713] 22 p3868 A67-39844
 Saturn V launch vehicle and Apollo spacecraft hardware systems applied to unmanned exploration of Jupiter 22 p3887 A67-40138
 Optical technique with laser source for range measurements noting use of dispersion between two different light wavelengths 22 p3800 A67-40139
 TV camera reseau for engineering information on planetary missions and reducing geometric distortion [SMPT PAPER 102-39] 22 p3808 A67-40377
 Thermophysical research requirements for Venus Lander, Jupiter Entry Probe and Mercury Orbiter planetary exploration missions 24 p4227 A67-42041
- PLANETARY GRAVITATION**
 Planetary proximity influence on motion of planetoid, with application to solar influence on Venus as studied by Mariner II 02 p0321 A67-11495
 Long period features of motion of Trojan planets in vicinity of equilateral triangle configurations 06 p1079 A67-17764
 Comet P/Wolf I motion perturbations of six planets, searching ephermeris for perihelion in August 1967 11 p1868 A67-25085
 Spheroidal coordinate method for obtaining gravitational potential of oblate planet 15 p2580 A67-30042
 Planetary influences on sunspot formation and disappearance showing periodicity in Zurich relative daily sunspot number 17 p2943 A67-32439
 Gravitational capture of cosmic dust by sun and planets and evolution of circumterrestrial cloud 18 p3119 A67-33863
 Cometary astronomy problems from contemporary celestial mechanics viewpoint, considering short-period comets and orbital perturbations caused by Jupiter 20 p3524 A67-36658
 Statistical evidence of planetary and lunar modulation of geomagnetic activity 21 p3711 A67-39005
 Circular orbit stability in planetary axisymmetric gravitational and dipole magnetic fields 22 p3880 A67-39404
- PLANETARY-INTERPLANETARY PROGRAM**
 Space studies of Mars and Jupiter through cislunar and interplanetary rocket probes in near future [AAS PAPER 67-32] 15 p2562 A67-30105
- PLANETARY LANDING**
 SA MARS EXCURSION MODULE /MEM/
 Subsonic and supersonic parachutes for soft landing on Mars, discussing aerodynamic coefficients, descent rate, dynamic stability, inflation, porosity and wind effects, etc 04 p0551 A67-14574
 Sensing techniques for initiating parachute deployment on Mars lander vehicle [AIAA PAPER 67-202] 06 p0948 A67-18302
 Guided propulsive solution to Mars atmosphere-decelerated soft landing vehicle trajectory [AIAA PAPER 67-170] 06 p1029 A67-18508
 Approaching and soft landing on planet surface in absence of atmosphere, finding optimum acceleration vector control as function of generalized parameters 09 p1571 A67-21889
 Dynamic analysis and development of response histories and tradeoff study charts for spherical impact limiters for protecting hard landing planetary payloads 10 p1727 A67-23738
 Space programs and space politics, possible internal and international political effects of lunar or planetary landing 12 p2040 A67-25235
 Dynamic testing of crushable materials for planetary impact attenuation systems, noting Voyager and Ranger Lunar Capsule 12 p1956 A67-25731
 Rocket control with limited-power engine when approaching target 14 p2394 A67-28640
 Future manned planetary missions including flybys and landings, describing vehicle configurations and technological requirements [AAS PAPER 67-28] 15 p2562 A67-30103
 Multipurpose entry vehicle requirements for unmanned landings on bodies in solar system having tenuous atmospheres [AIAA PAPER 67-599] 19 p3336 A67-35995
 Subsonic and supersonic parachutes for soft landing on Mars, discussing aerodynamic coefficients, descent rate, dynamic stability, inflation, porosity and wind effects, etc 20 p3356 A67-36408
 Mars landing guidance requirements for unmanned lander after separation from interplanetary flyby space vehicle 21 p3655 A67-37783
 Computer analysis and simulation of Mars soft landing descent control system combining inertial and radar sensing techniques 22 p3898 A67-39177
 Unmanned probes designed to land on planetary surfaces to obtain temperature, atmospheric measurement and ground samples chemical analysis 22 p3900 A67-39613
- PLANETARY MAGNETIC FIELD**
 Planet Mercury magnetospheric scattering of solar-flare protons to earth, obtaining deflection angle [AIAA PAPER 67-150] 06 p1088 A67-18505
 Ashen light and magnetic field of Venus 17 p2948 A67-33096
 Interaction of planetary magnetic field with solar plasma studied using hypersonic analog, estimating energy transfer rate 17 p2951 A67-33208
- Magnetism and cosmos - Conference, University of Newcastle-upon-Tyne, England, April 1965 21 p3707 A67-38977
 Magnetic dipole moments of moon, Mars and Venus using space probes, discussing solar wind near-earth planetary field interaction measurements [JPL-TR-32-1059] 21 p3709 A67-38992
 Microwave radiations of Jupiter, deriving equivalent black body temperature, magnetic field data, radiation belts data and electron energy 21 p3710 A67-38995
 Decimeter radiation from Jupiter originating in synchrotron radiation of ultrarelativistic energy electrons in 1 gauss field 21 p3710 A67-38996
 Magnetic field rotation, satellite Io and interplanetary propagation effects accounting for time variation of Jupiter magnetic flux and polarization 21 p3710 A67-38998
 Jupiter internal structure investigated by observing visible surface and radio emission, discussing magnetic field origin and hydrodynamics of fluid regions 21 p3710 A67-39003
 Geomagnetic activity around conjunction and opposition of planets, noting decrease in years of low solar activity 21 p3711 A67-39004
 Planetary magnetic fields calculated from meteorite magnetic properties and assumptions about cores and crusts 21 p3711 A67-39042
 Circular orbit stability in planetary axisymmetric gravitational and dipole magnetic fields 22 p3880 A67-39404
 Stellar and planetary magnetic field formation theory based on concept of existing ionized turbulent mass flow on these celestial bodies 24 p4230 A67-42352
- PLANETARY MASS**
 Weight of moon, considering approaches of tides and force of attraction exerted by moon on element of earth 01 p0148 A67-10506
 Masses of moon and Venus and astronomical unit determined from Mariner II Doppler data, noting sources of error 05 p0895 A67-16575
 Arguments supporting IAU Executive Committee refusal to recommend changes in conventional values of principal planetary masses 05 p0900 A67-17081
 Estimated GM values of earth and moon, tracking station locations and lunar radii at impact points, from DSIF radio tracking data of Ranger Block III lunar flights [AAS PAPER 66-105] 07 p1253 A67-19965
 Cosmogenic hypotheses evaluation based on relation between oblateness, mass and number of satellites of planets of solar system 13 p2198 A67-26765
 Estimated GM values of earth and moon, tracking station locations and lunar radii at impact points, from DSIF radio tracking data of Ranger Block III lunar flights [AAS PAPER 66-105] 13 p2208 A67-27523
 Planetary masses, radii and orbital element and astronomic unit determinations from radar time delay and Doppler shift measurements 15 p2556 A67-29871
 Matter density and other physical properties of Martian surface estimated from radio and IR observations 18 p3119 A67-33860
 Mass and density of Pluto estimated from rotational impulse and by comparison with known mass and rotational impulse of another planet 18 p3135 A67-34544
 Motion theory of comet Wolf I during 1918-1925 revolution which included close approach to Jupiter in 1922 20 p3524 A67-36659
 Jupiter environment, effects of huge mass, high rotation rate, temperature and dominant H and He atmosphere 22 p3887 A67-40141
 Numerical integration of Eros orbital motion normals, obtaining earth-moon mass and various astronomical constants 23 p4061 A67-40621
 Angular momentum density vs mass log-log plot extended from planetary mass range to asteroids, noting support for constant period law 23 p4066 A67-41010
- PLANETARY MOTION**
 Rotation period of Jupiter determined by radio observations explaining cyclic drift 01 p0146 A67-10294
 Neptunian planet-satellite system, discussing orbital motion of

Triton 01 p0148 A67-10385
 Rotation rate and inclination of planetary axis determined from radiation incident on artificial satellite of planet 02 p0321 A67-11539
 Time delay measurements and radar echo determinations of planetary motions compared with IAU values 05 p0900 A67-17082
 Planet rotation and orbiting of satellite Io modulations effect on maximum RF of storms 05 p0904 A67-17408
 Mechanics of celestial bodies including problems on Newton gravitation law, motion equations, two-body problem, Kepler law, etc 06 p1030 A67-17772
 Unidentified satellite as explanation of abnormal perturbations in Saturn ring 11 p1866 A67-24770
 Orbits in Copenhagen problem asymptotic at L4 and genealogy 13 p2205 A67-27481
 Rotation rate and inclination of planetary axis determined from radiation incident on artificial satellite of planet 16 p2752 A67-31605
 Rotation and heating of planet Mercury, examining insolation and surface temperatures from coupling of orbital and rotational periods 17 p2940 A67-32210
 First order generalized planetary theory from Poisson form, deriving trigonometric expansion of disturbing functions, periodic inequalities, etc 18 p3120 A67-33865
 Radar studies of Venus noting values for rotation vector, latitudes and longitudes of several features and Earth influence on Venus rotation [JPL-TR-32-1081] 18 p3123 A67-34146
 Criticism of classical theory of Mercury rotation period equal to revolution around sun 18 p3125 A67-34191
 Hansen planetary theory representing position of disturbed planet as deviation in time and space from position of fictitious planet with Keplerian motion [AIAA PAPER 67-565] 19 p3328 A67-35961
 Jupiter rotation variability used to understand internal physical processes, stressing variation of radio and Great Red Spot periods 21 p3710 A67-39002
 Von Zepel method to eliminate short period terms in first order general planetary theory noting system transformation into canonical equations 22 p3881 A67-39514
 Venus rotation, discussing radar and optical and UV photography observations 23 p4063 A67-40800
 Apparent Jupiter rotation rate change from decametric emission probability histograms shown to differ from dynamic radiation spectra 23 p4065 A67-41002
 Angular momentum densities of planet-satellite systems, discussing earth-moon system and origin of celestial bodies 23 p4066 A67-41009
 Book on celestial mechanics covering Laplace-Newcombe method, Hill planet and lunar methods and periodic orbits methods using differential equations 23 p4069 A67-41429
 Motion equations for mean orbital and osculating elements of particle rotating in gravitational field of aspherical planet 24 p4228 A67-42274
 Periodic length of day /lod/ fluctuations, interplanetary torques and variations in earth rotation 24 p4229 A67-42313
 Book on Hamilton principle and physical systems covering planetary motion, rotating bodies, electromagnetic radiation, quantum theory, etc 24 p4189 A67-42406

PLANETARY NEBULA
 Models of reflection nebulae light for single scattering, pure or modified by internal nebular extinction, on spherical grains imitating dielectric or metallic particles 11 p1861 A67-24487
 Detectability of ion recombination free-free emission from H II regions 12 p2011 A67-26252
 Ionization structure of elements H, He, C, N, O, Ne in planetary nebulae computed for theoretically determined electron temperature and electron density variation 14 p2382 A67-27847
 Radio telescopic measurements of brighter planetary nebulae indicating majority are thermal radio sources 16 p2752 A67-31624
 Planetary nebulae origin, examining posthorizontal branch stars structure and evolution 20 p3527 A67-37272

Chemical history of Fe traced in nebular material assuming preplanetary particles were similar to those presently discarded by sun 23 p4068 A67-41360
 Planetary nebulae IR emission intensities, discussing radiative recombination, ionization equilibrium and fine structure level population 24 p4223 A67-41811
 IR nebula in Orion as protocluster with massive stars imbedded in opaque dust cloud, discussing collapse and lifetime 24 p4225 A67-41829
 IR line intensity of planetary nebula NGC 7027, noting presence of measurable continuum flux of stellar radiation 24 p4225 A67-41830

PLANETARY ORBIT
 Rotation rate and inclination of planetary axis determined from radiation incident on artificial satellite of planet 02 p0321 A67-11539
 Asteroid /1685-Toro/ discovered in 1948 and observed again in 1956 and 1964, noting semimajor axis equal to 1.3677 AU and period of sidereal revolution equal to 584.2 days 04 p0702 A67-15607
 Eckert-Brouwer orbit correction formula in general perturbations theory, expressed in rectangular coordinates and variation of astronomical elements, applied to planetary theory 05 p0904 A67-17391
 Resonance relation between orbits of Neptune and Pluto established by numerical integration 08 p1381 A67-20392
 Computer program for analytical development of planetary disturbing function 08 p1381 A67-20393
 Selection of constants defining reference orbit of planet and use in differential equations of motion 08 p1382 A67-20394
 Newton inverse square force for planets from invariant velocity components of Keplerian planetary motion by graphical model 10 p1711 A67-23791
 Spacecraft speed increment requirements for circular parking orbit about Mars and earth 12 p2003 A67-25741
 Horseshoe-shaped orbits in Jupiter-sun restricted problem, comparing Runge-Kutta and Steffensen integration methods 13 p2205 A67-27475
 Doubly symmetric orbits about collinear Lagrangian points, computing jacobians eigenvalues 13 p2205 A67-27482
 Generalization of Oepik theory of planetary bodies collision to include case where orbits of both colliding bodies are ellipses 14 p2384 A67-28055
 Rotation rate and inclination of planetary axis determined from radiation incident on artificial satellite of planet 16 p2752 A67-31605
 Radar determinations of astronomical unit and orbits, radii and rotation vectors of inner planets, proposing general relativity radar test 18 p3123 A67-34145
 Flight phase constraints effect on design of Voyager orbiter-capsule mission 20 p3532 A67-36564
 Corrected orbital data for 60 minor planets, giving osculating elements for asteroids 20 p3522 A67-36618
 Everhart comet and various minor planets positions through photographic observations at Tartu 20 p3522 A67-36622
 Differential coefficients of asteroids Gerda, Flora and Juno in heliocentric coordinate system including Jupiter and Saturn perturbations 20 p3523 A67-36627
 Shortest distance between two quasi-coplanar elliptical asteroid orbits, solving transcendental equations by consecutive approximation method 20 p3523 A67-36628
 Various minor planets positions from photographic observations at Crimean Astrophysical Observatory 20 p3523 A67-36630
 Equinox and equator corrections to FK3 system determined from meridian observations of Mars, Jupiter and minor planets 20 p3429 A67-36838
 Declinations of major and minor planets /1951-1959/ determined from meridian observations and reduced to FK3 system 20 p3524 A67-36839
 Janus /Saturn tenth satellite/ discovery on December 15, 1966, noting orbit in ring plane and period 20 p3527 A67-37399
 Nonzero cosmological constant effect /precise and trivial/, calculating perihelion precession from Schwarzschild exterior solution 22 p3889 A67-40382

PLANETARY ORIGIN
 Meteoritic origin from planetary disintegration 06 p1089 A67-18659
 Chemical composition and earth origin, with estimates of primordial abundances of elements in solar system 07 p1170 A67-19336
 Protoplanetary cloud and evolution, noting Hoyle rotatory nebula and other hypotheses 09 p1563 A67-21633
 Terrestrial origin hypothesis for tektites, moldavites and impact glass supported by krypton-argon and fission track measurements 11 p1866 A67-24693
 Cosmogonic hypotheses evaluation based on relation between oblateness, mass and number of satellites of planets of solar system 13 p2198 A67-26765
 Phobos and Deimos origin in equatorial circular orbits or asteroid capture and tidal modification 18 p3125 A67-34160
 Black magnetic spherules in Pleistocene and recent beach sands, investigating origin by electron microscopy 24 p4235 A67-42635

PLANETARY RADIATION
SA LUNAR RADIATION
 Radioisotope and radiation techniques for terrestrial and planetary gas and solid measurements 02 p0245 A67-12223
 Jovian decametric pulses compared with satellite and radio star scintillations in terrestrial ionosphere [RASSA PAPER 1-10-134] 03 p0373 A67-14245
 Mean values of methane wavelengths in Uranus spectrum measured for determination of atmospheric temperature 03 p0515 A67-14327
 Spectral types of decametric radiation bursts from Jupiter, noting classification based on duration or high resolution dynamic spectra 05 p0898 A67-16927
 Convective and radiative heat transfer to reentry vehicles at superorbital velocities [AIAA PAPER 66-106] 05 p0928 A67-17336
 Short duration pulses association with subsidiary B and C sources of Jovian decametric radiation 06 p1086 A67-18375
 Thermal radio emission from Mercury at 1.9 cm monitored by 140 ft radio telescope using tunnel diode radiometer 07 p1246 A67-19056
 Faraday rotation effects in spectral records of Jupiter decametric radiation 09 p1568 A67-22401
 Book on radioastronomical methods of antenna measurements covering physics of extraterrestrial sources and receiving equipment characteristics 12 p1915 A67-25842
 Earth albedo calculation using Pegasus I thermal data, discussing Rayleigh scattering, spacecraft position, atmospheric reflection effects, etc [AIAA PAPER 67-332] 12 p1938 A67-26046
 Geometrical model for calculation of solar heat fluxes reflected from planet onto plate 13 p2201 A67-27342
 Planetary radio emission measurements, noting no radio emission from Pluto 14 p2385 A67-28405
 Decametric radio noise data from Jupiter apparitions /1960-1964/ 14 p2389 A67-28838
 Jovian decametric emission of millisecond pulse variety analysis from observations of four apparitions 15 p2558 A67-30032
 Atmospheric temperature effect on latitudinal curve of cosmic ray intensity determined from radio probe observations 17 p2933 A67-32090
 L-pulses of Jupiter radiation, attributing 1-sec component of time structure on decametric emission to diffraction by solar wind inhomogeneities 17 p2944 A67-32643
 Relation between surface pressure and atmospheric brightness in optically thin Rayleigh scattering atmosphere, considering application to Mars 18 p3134 A67-34536
 Similarities between Jupiter decametric radiation and satellite induced ionospheric disturbances 20 p3521 A67-36308
 Soviet book on planetary physics covering Martian, Venusian and Mercurian atmospheres, Venusian surface temperature and Jovian radio emission 21 p3707 A67-38933
 21.2 cm spectra of Jupiter, Venus, Mars and Saturn noting mean effective brightness temperatures 21 p3709 A67-38993
 9.4 cm radiation from Jupiter and Saturn and 21.2 cm radiation from Saturn 21 p3709 A67-38994
 Microwave radiations of Jupiter, deriving equivalent black body temperature, magnetic field data, radiation belts data and electron

energy 21 p3710 A67-38995
 Declimeter radiation from Jupiter
 originating in synchrotron radiation of
 ultrarelativistic energy electrons in 1 gauss
 field 21 p3710 A67-38996
 Morphology of Jupiter decametric radio
 sources 21 p3710 A67-38997
 Magnetic field rotation, satellite Io and
 interplanetary propagation effects accounting
 for time variation of Jupiter magnetic flux
 and polarization 21 p3710 A67-38998
 Venus radiation spectrum in mm range
 from Venus atmosphere 22 p3886 A67-40120
 models 22 p3889 A67-40240
 Mercury radio emission observation
 yielding average brightness temperature and
 planetocentric phase angle 22 p3889 A67-40240
 Apparent Jupiter rotation rate change
 from decameter emission probability
 histograms shown to differ from dynamic
 radiation spectra 23 p4065 A67-41002
 Dependence of decametric radio emission
 from Jupiter on positions of Galilean
 satellites with respect to sun, earth and
 Jovian magnetic plane 23 p4069 A67-41362
PLANETARY SPACE FLIGHT
SA FLYBY MISSION
 Thermoradioisotope propulsion and
 integrated power application to cislunar and
 planetary space missions 01 p0155 A67-11413
 Planning of manned scientific planetary
 missions, distinguishing critical experiments,
 taxonomic knowledge and precursor
 knowledge 06 p1093 A67-19034
 Trajectory characteristics of high thrust
 Mars missions and effect on other aspects of
 mission planning 07 p1248 A67-19358
 Unmanned Jupiter space flights, discussing
 requirements for flyby, Orbiter and low
 thrust missions 07 p1249 A67-19570
 Escape of rocket vehicle from vicinity of
 planet, using tangential thrust 07 p1254 A67-19979
 Instrument integration for landing capsule
 payloads of planetary missions, considering
 functional operation, environmental
 constraints and interface definition
 [AIAA PAPER 66-59] 07 p1188 A67-19996
 Future space transportation techniques
 and mission applications in solar
 system 13 p2213 A67-27508
 Escape of rocket vehicle from vicinity of
 planet, using tangential thrust 13 p2209 A67-27534
 [AAS PAPER 66-120]
 Geometrical form for solar system escape
 criterion 17 p2940 A67-32075
 Vehicle mass requirements for optimal
 high and low thrust propulsion systems for
 manned and unmanned planetary
 missions 20 p3533 A67-37125
 Data return advantages of earth-Mars-earth
 flyby trajectories over more conventional
 Mars trajectories 20 p3530 A67-37626
 [AIAA PAPER 67-646]
 Manned planetary mission global network
 for continuous tracking, communication
 telemetry and TV transmission
 [AIAA PAPER 67-976] 24 p4125 A67-43052
PLANETARY SPACECRAFT
SA MARS SPACECRAFT
 Fabrication procedure for biologically
 clean planetary landing module for later
 sterilization 02 p0188 A67-12380
 Sensitivity of manned planetary spacecraft
 design to shield weight, onboard radiation
 and uncertainties in space environment
 radiation 07 p1258 A67-19376
 Trajectory design for spacecraft which
 returns in vicinity of earth after Mars
 encounter analyzed by patched conic model
 [AAS PAPER 66-126] 07 p1254 A67-19985
 Inertial sensors requirements for
 unmanned planetary
 missions 09 p1499 A67-22396
 Dynamic testing of crushable materials for
 planetary impact attenuation systems, noting
 Voyager and Ranger Lunar
 Capsule 12 p1956 A67-25731
 Simulation experiments to describe effects
 of measurement function nonlinearly and
 ambiguities when linear filters are applied
 in distant planet satellite orbit parameter
 estimation 14 p2347 A67-28130
PLANETARY SURFACE
SA MARS SURFACE
 VHF radar techniques for detecting and
 mapping subsurface discontinuities such as
 solid layering, rock interfaces and ore
 deposits in lunar and planetary
 surfaces 01 p0021 A67-10324

Sedimentologic process which comminutes,
 transports and deposits material by impact
 on planetary surfaces 02 p0235 A67-11451
 Spectral scans of Mars and region of moon
 in IR range obtained with 82-inch telescope
 reduced, using scans of moon and sun, to
 spectral reflectivity curve 02 p0319 A67-11454
 Volcanism triggered by meteoritic impact
 suggested from comparison of volcanic and
 impact data, noting terrestrial, lunar and
 Martian craters 02 p0319 A67-11455
 IR colorimetry of Martian bright and dark
 areas indicates correlations with limonite
 terrestrial rocks and volcanic
 ash 02 p0319 A67-11456
 Autonomous space navigation system using
 optical spatial filter techniques for
 recognition and tracking of planetary
 surfaces and star fields 02 p0264 A67-12316
 Mass distribution of meteoric bodies and
 relation to autocorrelation function of
 disintegrated planetary
 surface 02 p0329 A67-12495
 Reflective properties of natural surfaces,
 noting dependence on surface properties of
 total reflected energy, spectral distribution,
 polarization degree of radiation, etc
 [AIAA PAPER 65-665] 03 p0411 A67-13045
 Lunar and planetary surface elemental
 analysis technique by analysis of gamma rays
 resulting from inelastic scattering of
 neutrons 05 p0843 A67-16545
 Neutron activation analysis of Si, Fe, Al,
 Mg and O content of lunar and planetary
 surfaces 05 p0843 A67-16546
 Radio occultation techniques for analysis
 of planetary atmospheres and surface
 topography by measuring perturbations to
 amplitude and frequency on radio links
 [AIAA PAPER 67-119] 06 p1087 A67-18454
 Earth crust measurement techniques and
 use in studying other planetary
 lithospheres 06 p1091 A67-19001
 Middle and far IR spectra of silicate
 minerals for remote sensing of lunar or
 planetary surface
 composition 08 p1385 A67-20934
 Moon and planet surfaces analyzed based
 on thermal radiation for information on
 parameters of material of upper
 layer 08 p1390 A67-21024
 Mass distribution of meteoric bodies and
 relation to autocorrelation function of
 disintegrated planetary
 surface 10 p1709 A67-23363
 Neutron activation analysis for terrestrial
 and meteoritic rock major element
 abundance, noting possible application to
 extraterrestrial surface
 analysis 11 p1749 A67-23976
 Planetary mapping mission system
 requirements for photography, IR and radar
 imagery, radar reflectivity and spectroscopy
 with data analysis 11 p1859 A67-24438
 IR spectral techniques for satellite
 geodetic surveying, discussing spectral
 matching techniques for discriminating
 between different types of rocks
 [AIAA PAPER 67-284] 12 p1938 A67-26001
 Inconsistency in Martian surface pressure
 as calculated by Gray explained, using
 Leighton and Murray
 observations 14 p2389 A67-28842
 Cross section and angular scattering law
 for Venus and Mercury from delay and
 Doppler frequency shift radar echo
 measurements 15 p2556 A67-29870
 Venus and Mercury intrinsic rotation rates
 and surface radar reflectivity of former
 from radar echo
 measurements 15 p2556 A67-29872
 Moon surface origin and present surfaces
 of moon, Venus and Mars as determined
 from lunar photographs and data by flyby
 probes 18 p3121 A67-34135
 Jupiter atmosphere, interior and surface
 properties, speculating on possibility of life
 in spite of presence of noxious
 gases 21 p3703 A67-38191
 Spacecraft design, solar powering, electric
 propulsion and side-looking radar for
 planetary surface observation mission on
 Mars or Venus
 [AIAA PAPER 67-712] 21 p3714 A67-38739
 Radar type instrument for measuring
 reflection coefficients of planetary surfaces
 from unmanned
 spacecraft 22 p3795 A67-39159
 Incompatibility of microwave phase effects
 measurements in Mercury thermal emission

with simple model for thermal behavior of
 planet surface 24 p4226 A67-41837
 Tectonic activity on Venus compared with
 earth, discussing convection currents and
 temperature gradients in crust and
 mantle 24 p4227 A67-42222
PLANETARY TEMPERATURE
 Thermal radio emission from Mercury,
 Venus, Mars, Saturn and Uranus at various
 wavelengths, using radio telescope in
 Australia, determining emission
 spectrum 02 p0319 A67-11452
 IR brightness temperature of Uranus used
 to establish current lower limit at which
 brightness temperature of celestial object
 can be measured 02 p0324 A67-11773
 Boundaries and attenuating media effect
 on radiometric sounding of planetary
 atmospheres by remote sensing
 techniques 02 p0239 A67-12406
 Microwave radiometry application to
 navigation, thermonuclear diagnostics,
 astronomical temperature measurements,
 etc 03 p0367 A67-12805
 Interpretations of microwave emission
 from Venus through experiments in which
 anomalous signals have been observed in X-
 band from glow
 discharges 04 p0699 A67-14952
 Venus brightness temperature and
 polarization of integral radio emission at 3.75
 cm wavelength 04 p0702 A67-15566
 Surface temperature of
 Venus 05 p0886 A67-16029
 Martian topography influence on formation
 of temperature bright
 patches 06 p1088 A67-18644
 Microwave radiometric measurements of
 planetary disk temperature of Venus, Mars,
 Jupiter and Saturn 11 p1869 A67-25094
 Solar system planets characteristics,
 temperatures, atmospheres and internal
 structure 14 p2392 A67-28959
 Brightness temperature reduction of
 Venus at decimeter wavelengths determined
 from 49.1 cm
 measurements 16 p2749 A67-31409
 Radiative relaxation times for temperature
 perturbations in CO₂ with small water
 vapor admixture under conditions similar to
 Martian atmosphere, discussing dynamical
 phenomena 17 p2951 A67-33187
 Volcanic and tectonic activity on Venus
 inferred from high surface temperature,
 considering possible effect on atmosphere
 obscuration 17 p2951 A67-33232
 Venus surface temperature and microwave
 emission, discussing ionospheric model,
 greenhouse effect, microdischarge model,
 radio aurora, etc 18 p3135 A67-34543
 Solar wind velocity relationship to
 tropospheric temperature
 field 20 p3428 A67-36814
 21.2 cm spectra of Jupiter, Venus, Mars
 and Saturn noting mean effective brightness
 temperatures 21 p3709 A67-38993
 9.4 cm radiation from Jupiter and Saturn
 and 21.2 cm radiation from
 Saturn 21 p3709 A67-38994
 Microwave radiations of Jupiter, deriving
 equivalent black body temperature, magnetic
 field data, radiation belts data and electron
 energy 21 p3710 A67-38995
 Mercury radio emission observation
 yielding average brightness temperature and
 planetocentric phase angle
 relation 22 p3889 A67-40240
 Venus surface temperature measured
 using difference between optical and radar
 radii, cloud temperatures and adiabatic lapse
 rate 24 p4225 A67-41827
PLANFORM
SA RECTANGULAR PLANFORM
SA WING PLANFORM
 Structural, seal and sideboard design,
 propulsion and cavitation problems relevant
 to operational requirements of captured air
 bubble vehicle
 [AIAA PAPER 67-346] 14 p2245 A67-28729
 Cross sectional shape of magnetically
 balanced arc determined, noting elongation
 perpendicular to flow 17 p2906 A67-33033
PLANKTON
 Tektites presence in Australian sea
 sediments, suggesting relation between
 geomagnetic reversals and fossil plankton
 changes to cosmic bodies terrestrial
 intrusions 16 p2754 A67-31864
PLANNET PROGRAM
S DATA ACQUISITION

PLANNING

SA AIRPORT PLANNING
SA MANAGEMENT PLANNING
SA MISSION PLANNING
SA OPERATIONS RESEARCH
Changing role of technical writers and editors during next decade 20 p3556 A67-36587

PLANT /BIOL/

SA ALGAE
SA FUNGUS
SA ROOT
SA TRADESCANTIA
SA TREE
SA VASCULAR SYSTEM
SA VEGETATION
Point discharge from multiple points in irregular configuration, space-charge theory and plant discharge applications 01 p0107 A67-10114
Wheat seedlings grown so that coleoptile and early roots developed in moist air, noting organ orientation in relation to gravity 04 p0560 A67-14407
Killing and mutagenic efficiencies of heavy ionizing particles in *Arabidopsis thaliana* 06 p0953 A67-18379
Space flight effect on wheat seeds and plants grown from wheat seeds carried on board Vostok V and VI spacecraft 11 p1747 A67-24081
Electromechanical system for study of plant or organism growth and development in compensated gravitational fields 11 p1793 A67-24822
Biological clocks and cycles in man, lower animals and plants, discussing circadian rhythms 13 p2058 A67-26607
Potato radiation resistivity improvement in conditions of anoxia 13 p2058 A67-26755
Plants in low gravity environment simulated by 2 rpm clinostat with horizontal axis, studying growth direction and respiratory metabolism 15 p2426 A67-29114
Biological value of plant proteins for closed life-support system, studying diet effects on rats 16 p2612 A67-30908
Survival of desert algae at extremely low temperatures and diurnal freeze thaw cycles 23 p3945 A67-41346

PLASMA

SA ARGON PLASMA
SA BEAM-PLASMA AMPLIFIER
SA BLOOD PLASMA
SA CESIUM PLASMA
SA COLLISIONLESS PLASMA
SA CORE FLOW
SA COSMIC PLASMA
SA DEUTERIUM PLASMA
SA ELECTRON PLASMA
SA ELECTROSTATIC PLASMA
SA HELIUM PLASMA
SA HIGH TEMPERATURE PLASMA
SA HYDROGEN PLASMA
SA MAGNETOIONIC PLASMA
SA MAGNETOPLASMA
SA METALLIC PLASMA
SA NITROGEN PLASMA
SA NONEQUILIBRIUM PLASMA
SA NONUNIFORM PLASMA
SA PLASMA-ELECTROMAGNETIC INTERACTION
SA RAREFIED PLASMA
SA RELATIVISTIC PLASMA
SA ROTATING PLASMA
SA SOLAR PLASMA
SA THERMAL PLASMA

Time dependent light emission due to voltage breakdown in mesoplasma region in Si on Si diode surfaces 02 p0301 A67-12658
HF conductivity, dispersion and temperature modulation of carrier waves and acoustic amplification in drifted semiconductor plasmas 03 p0496 A67-13558
Electrostatic probes for collision dominated weakly ionized plasma noting mathematical formulation, density and V-A characteristics 09 p1539 A67-21782
HF plasma devices structural design, electrical parameters and power characteristics 09 p1547 A67-22322
Black body radiation, pressure and temperature dependences of equilibrium composition, enthalpy, specific heat and electron density of air-carbon plasmas 17 p2894 A67-32147

PLASMA ACCELERATION

Resonance conditions for maximum attainable induction acceleration of cylindrical plasma in space between two concentric glass tubes determined by solving

MHD equations 01 p0119 A67-10168
Current layer dynamics in flat electrode accelerator, relating plasma acceleration and polarization field 01 p0122 A67-10345
Landau damping in weakly inhomogeneous plasma related to Cerenkov radiation of accelerated electrons moving in external static field causing inhomogeneity 02 p0272 A67-11636
Interaction of plasma jets ejected from electrode spots with accelerating magnetic field as possible cause of electrode polarity effect on flat-electrode-type plasma acceleration 02 p0275 A67-12471
Theoretical possibilities of using electromagnetic forces for acceleration of plasmas /self-magnetic and Hall acceleration/ in case of axisymmetric electrode arrangement 04 p0687 A67-14559
Plasma acceleration and retardation by magnetic standing waves 04 p0688 A67-14564
Mass spectrometric study of energy distribution of ions of accelerated plasma produced by coaxial source 04 p0668 A67-15216
Thrust generation from neutral particle sputtering from solid target, noting advantages such as storage, operating life, etc 05 p0873 A67-16515
Electric propulsion research in foreign countries [AIAA PAPER 67-53] 06 p1075 A67-18494
Theoretical possibilities of using electromagnetic forces for acceleration of plasmas /self-magnetic and Hall acceleration/ in case of axisymmetric electrode arrangement 07 p1240 A67-19569
Acceleration of propellant in arcjet devices by thermal and self-magnetic forces, using various nozzle configurations 08 p1375 A67-20574
Statistical particle acceleration in turbulent plasma 08 p1358 A67-20861
Plasma ring acceleration produced by pulsed azimuthal electric field, noting magnetic field role in stabilization 11 p1828 A67-23893
Current layer dynamics in flat electrode accelerator, relating plasma acceleration and polarization field 11 p1843 A67-25018
Plasma acceleration across magnetic field in linear accelerator, calculating values from voltages at electrode ends 12 p1977 A67-28075
Plasma acceleration under combined axial magnetic and electric fields, noting experimental setup and results 14 p2353 A67-27750
MHD resonance acceleration of plasma clusters and shock waves, showing advantage for parallel or coaxial conductor systems 14 p2354 A67-27762
External magnetic field accelerating effect on constant-mass plasma clusters between parallel conductors 14 p2354 A67-27763
Large-dimensional inverse pinch discharge study of impulsive plasma acceleration, gas dynamics and stability of unrestrained current sheet [AIAA PAPER 66-482] 14 p2356 A67-28123
Soviet book on plasmoids covering coaxial plasma sources, magnetic field interaction and observation methods 15 p2524 A67-29243
Plasma acceleration in flat electrode plasma source simulated by ideally conducting bridge described electro-dynamically 15 p2525 A67-29249
Plasma flow layer, acceleration and other parameters investigated under several operation conditions in coaxial plasma gun 15 p2529 A67-29718
Plasma azimuthal inhomogeneity in homopolar system, noting Hall current and stationary plasma acceleration 15 p2529 A67-29723
Velocity limitations of accelerated plasma by momentum loss due to electrode impact of accelerated ions, proposing modified snowplow model 15 p2531 A67-30030
Mass spectrometric study of energy distribution of ions of accelerated plasma produced by coaxial source 15 p2532 A67-30264
Electric drive operating parameters and design, using exploding wire type device and electromagnetic apparatus for plasma production and acceleration 16 p2736 A67-30716
Collection of papers on charged particles

interaction with plasma, including gas discharge and plasma acceleration 16 p2716 A67-31175
Acceleration of plasma particles to high energies for case of interaction between plasma and stochastic field with harmonic-correlation time 16 p2718 A67-31192
Analytical plasma flow model for acceleration process in Hall current device, noting final velocity derivation, temperature, critical velocity, etc 16 p2719 A67-31237
Approximate solutions of spatial distributions of charged particles as gas discharge plasma obtained by two-point Jacobi expansion method 16 p2720 A67-31241
Soviet book on plasma physics covering magnetic traps, acceleration, radiation, etc 17 p2903 A67-32909
Plasma acceleration by SHF waves, worldwide research and results 17 p2904 A67-32915
Plasma behavior in shock tubes with parallel conductors, discussing shape of front and velocity dependence on pressure and gas composition 18 p3089 A67-34297
Plasma bunches-microwave interaction showing electron energy and plasma ions velocity increase 19 p3291 A67-35384
Hydrogen plasmoids produced by pulsed two-cascade injectors, using electron guns for plasma ionization and acceleration 19 p3297 A67-35597
Cathode phenomena in plasma thrusters with self-magnetic acceleration low mass-flow rates [DVL-631] 19 p3297 A67-35600
Model thruster designed and operated with argon and hydrogen for investigation of hybrid flow fields of plasma acceleration by thermal and magnetic forces [DVL-630] 19 p3297 A67-35601
Acceleration of plasma formed in electric explosion of foil in air atmosphere 20 p3502 A67-37604
Plasma acceleration by electromagnetic microwave discharge in static magnetic field gradient, discussing microwave-plasma energy transfer at electron cyclotron resonance [AIAA PAPER 67-660] 21 p3671 A67-38696
NI plasma acceleration in axisymmetric electric discharge by self-induced magnetic field, determining reaction force 22 p3844 A67-39356
Nuclear fusion control and relativistic high density matter acceleration, discussing amplification effect application to plasma theory, plasma RF confinement and acceleration 22 p3851 A67-39772
Electric propulsion research in foreign countries [AIAA PAPER 67-53] 24 p4208 A67-42902

PLASMA ACCELERATOR
Performance and characteristics of valve for pulsed gas injection into working volume of coaxial plasma accelerator 01 p0119 A67-10136
Numerical analysis showing dependence of vacuum plasma accelerator geometrical and electrical parameters on plasma acceleration kinematics 01 p0122 A67-10347
Electric conductivity, electrode temperature and potential distribution across channel in potassium seeded-argon atmospheric-pressure Faraday accelerator [AIAA PAPER 66-75] 01 p0014 A67-11177
Five calculations of plasma accelerators using quasi-one-dimensional and two-dimensional model for different nozzle shapes 02 p0274 A67-12337
Acceleration mechanism in plasma current layer forming when strong magnetic field moves at high speed into initially stationary field-free plasma 02 p0274 A67-12341
Repetitive plasma breakdown in flat electrode accelerator causing relatively low plasma velocity 02 p0275 A67-12472
Electrical propulsion of space vehicles using solar energy, electrostatic drive, drifting field plasma accelerator, etc 03 p0503 A67-13493
Harmonic response due to compressibility in traveling wave plasma devices, discussing magnetoacoustic resonances for case of cylindrical symmetry 03 p0485 A67-14051
Deuteron ion fluxes studied using plasma accelerator called Pleiade 04 p0672 A67-15647
Quasi-neutral charged particle bunches kinematics in flat electrode plasma accelerator 05 p0855 A67-16996
Diagnostic measurements in alkali plasma

- Hall accelerator /alpha/ including azimuth and axial velocity components, energy flux, total beam power, etc
[AIAA PAPER 87-46] 06 p1042 A67-18493
- Focused coaxial xenon gun to accelerate plasmas of high atomic weight with high power fluxes, measuring ablative and radiative flux at
boundaries 08 p1356 A67-20371
- Measuring apparatus for scalar and tensor plasma conductivity in AC MHD generators and accelerators 09 p1538 A67-21775
- Flow of ideal compressible electrically conducting fluid in traveling wave accelerator, using multiple coordinate method to approximate small perturbation solution 09 p1544 A67-21849
- Plasma in flat-electrode accelerator, examining optimum accelerator length associated with equilibrium between acceleration processes in plasma and diffusive scattering of
plasmoid 09 p1545 A67-22001
- Self-consistent field in HF plasma accelerator with static magnetic field gradient 10 p1683 A67-22852
- Numerical analysis showing dependence of vacuum plasma accelerator geometrical and electrical parameters on plasma acceleration kinematics 11 p1844 A67-25020
- Laser beam acceleration of inhomogeneous plasma by imparting high energies to oncoming ions 12 p1969 A67-25198
- Optimization of injection location in HF plasma accelerators 13 p2165 A67-26586
- Current density variation determination in plasma accelerated by traveling waves [ONERA-TP-472] 14 p2359 A67-28509
- Argon plasma accelerator producing diamagnetic discharge measured along axis for plasma properties 14 p2362 A67-29046
- Relativistic effects in HF plasma accelerators, noting decrease in transverse kinetic energy and axial velocity 15 p2527 A67-29475
- Magnetic moment of electron in HF plasma accelerator for case of negligible axial acceleration in resonance region 15 p2527 A67-29514
- Steady state plasma accelerators different from gas dynamic accelerators with Laval nozzles due to variety of waves, electric/magnetic fields, etc 17 p2898 A67-32185
- Axial electrostatic field forming in resonance zone of mixed structure noting ion entrainment, shock wave generation and motion of electrons 17 p2899 A67-32291
- Magnetoacoustic wave excitation and detection in rotating plasma accelerator, noting resonance and wave transition 19 p3298 A67-35746
- Electrode feed system for segmented-electrode MHD accelerator to avoid power supplies/switch gear 19 p3177 A67-35774
- Uniformly accelerated axisymmetric plasmoid isolation from pulsed accelerated walls in presence of external magnetic field, noting stable configuration 20 p3498 A67-36685
- Physical aspects of plasma accelerator using closed Hall currents, discussing equilibrium of forces and potential distribution 21 p3663 A67-37938
- Current sheet propagation transition to steady pattern in pulsed plasma accelerator, noting breakdown and current characteristics [AIAA PAPER 87-656] 21 p3689 A67-38692
- Tangential drag measurements at electrodes of arc in plasma accelerator, ion current partitioning at cathode and electrode damage 21 p3670 A67-38693
- Reversed polarity effect on propagating current sheet in coaxial plasma accelerator [AIAA PAPER 87-658] 21 p3671 A67-38694
- MPD plasma accelerator for spacecraft propulsion system, performance data and proposed acceleration mechanisms [AIAA PAPER 87-688] 21 p3693 A67-38719
- Valveless metal vapor feed system for use in pulsed plasma accelerators employing mercury as propellant [AIAA PAPER 87-738] 21 p3695 A67-38760
- Instrumentation systems for measuring thrust and electric power input of electromagnetic induction plasma thruster [AIAA PAPER 87-739] 21 p3695 A67-38761
- Synchronous orbit communication satellite electric thruster, considering space charge neutralized ion accelerator 23 p4049 A67-41428
- PLASMA ARC
- SA ARC CHAMBER
- Wave front scattering and refraction by laser spark studied by holograms of air plasma formed by giant ruby laser pulse 01 p0087 A67-10234
- Rotating plasma furnace and application to spheroidization of refractory powders, noting arc source 02 p0228 A67-11503
- Plasma arc tunnel tests show thermochemical heat of ablation of magnesia strongly dependent on stagnation enthalpy [AIAA PAPER 85-641] 03 p0449 A67-13061
- Field intensity probe measurements of potential distribution and I-V characteristics in AC arc plasma 03 p0475 A67-13087
- Electron temperature and concentration in DC plasma arc determined from Thomson scattering of laser radiation 03 p0437 A67-13209
- Plasma needle arc process for welding, brazing and cutting very thin metals for extremely low current work 03 p0430 A67-13690
- Battery power supply for split-ring plasma arcs operating as P hypersonic propulsion tunnel heaters 04 p0556 A67-15638
- Thermalization of cathodic electron flux by Langmuir oscillations in cesium arc plasma 04 p0673 A67-15971
- Rotating Langmuir probes for flow velocity distribution measurements in highly ionized supersonic low density MPD arc 05 p0851 A67-16466
- Continuous absorption cross section of argon from measurements of continuous emission of arc plasma in visible UV regions of spectrum and from temperature determination 05 p0854 A67-16988
- Critical mass flow rate existence for maximum thrust from MPD arc jet 06 p1075 A67-18866
- Current density distribution in MPD arc jet exhaust measured, using Hall effect sensors [AIAA PAPER 86-116] 08 p1375 A67-20573
- Thermal equilibrium method for calculating parameters of plasma arc in atmosphere of hydrogen, air and air containing 0.1 percent sodium vapor 09 p1546 A67-22315
- Energy characteristics of magnetically stabilized plasmatron effect on output power in crossed fields 09 p1547 A67-22316
- Temperature measurement methods in sulfur hexafluoride compared with reaction separation 10 p1684 A67-22892
- Electric field intensity distribution over length of plasmatron arc stabilized by longitudinal vortex air flow 11 p1843 A67-24972
- Arc rotation heat transfer effects in self-induced magnetic field plasma arc heaters used for aerodynamic tests 12 p2034 A67-25346
- Diagnostic techniques for atmospheric pressure arc plasmas, noting that integrated current density measurements are consistent with measured total arc current 12 p1973 A67-25393
- Multiple arc performance in 8000 kw plasma facility consisting of hyperthermal blowdown tunnel for ballistic flight simulation 12 p1974 A67-25404
- Cathode noise voltage in low current arc at atmospheric pressure as function of arc cathode surface state 14 p2354 A67-27764
- Weakly ionized argon plasma electrical conductivity in direct current arc determined, noting experimental equipment 16 p2710 A67-30523
- High pressure characteristics of helium and hydrogen pulsed arcs, noting formation of dense, completely ionized plasma 16 p2717 A67-31183
- Argon pulsed arcs produced at high pressures, considering emission absorption 16 p2717 A67-31184
- Various experiments explaining fundamental properties of probes used in measurements of plasma arc columns 17 p2896 A67-32166
- Composition, heat conduction and radiative energy transfer characteristics of hydrogen and argon plasmas produced by arc in cylindrical channel with cooled walls 17 p2897 A67-32172
- Stability conditions for gas stabilized DC electric arc in plasma-arc torch determined, using small perturbation technique schematic feed circuit 17 p2897 A67-32173
- Lithium plasma source current-voltage characteristics in vacuum, obtaining parameters valid for arcs burning under atmospheric pressure and nonzero magnetic fields 17 p2906 A67-33089
- Pulsed high current arc in hydrogen showing initial instability, discharge stability, impurity content, pinch effect, decay, etc 18 p3087 A67-34047
- Experimental data applicability for DC arcs in construction of AC plasmatrons 18 p3088 A67-34058
- Temperature and frequency response of argon arc continuum emission coefficient, explaining unexpected deviations 18 p3089 A67-34299
- Confined electric arc developed for gas-transport properties determination, noting measurement of flow pressure drop, radiative heat transfer, spectral temperature distribution, etc 18 p3091 A67-34731
- Stationary high density high temperature plasma production spectroscopic measurements, deducing arc radial temperature and density profiles from line and continuum intensities and line profiles 19 p3274 A67-35103
- Low voltage arc phenomena in cesium vapor investigated in connection with cesium-diode application as thermionic converter, calculating voltage-current characteristics 19 p3176 A67-35130
- Radial and axial temperature profiles of free-burning argon arc at various pressures, measuring continuum intensities [DVL-625] 19 p3278 A67-35135
- High pressure, high power argon arc studied using cascade apparatus, showing spectral line absorption increases and temperature decreases with increasing pressure 19 p3278 A67-35136
- Self-consistent model for cathode region of high pressure arc, considering free fall sheath connection, electron and ionization region and flaring contraction 19 p3278 A67-35137
- Self-consistent model for cathode region of high pressure arc, showing application to 200 amp arc in argon and boundary condition matching 19 p3279 A67-35138
- Radial pressure distribution in hydrogen arc located in axial magnetic field using Saha equation, determining temperatures and electron densities 19 p3279 A67-35139
- Water cooled copper anode operation compared to porous graphite transpiration cooled annular anode to study energy transfer in wall stabilized cascaded arc 19 p3279 A67-35141
- Temperature distribution in vortex cooled hydrogen arc obtained by emission and absorption coefficients in plasma source 19 p3279 A67-35142
- Energy balance of high current argon arc, showing main energy supply supported by cathodic plasma beam, measuring temperature decay and field 19 p3279 A67-35143
- Wall temperature distribution effect on transport coefficients determination from arc plasmas 19 p3280 A67-35144
- High pressure helium arc plasma behavior in cylindrical duct explained by theoretical model with different electron and heavy particle temperatures 19 p3280 A67-35145
- Energy balance of electric arcs in argon without and with superimposed gas flow investigated at various pressures [DVL-626] 19 p3280 A67-35146
- Conditions of stable burning of electric arc stabilized by gas stream in DC plasma arc torch, determining threshold current 19 p3281 A67-35150
- Average dwell times and velocities of Ba, Sr, La, Ti, Sn, Bi, Be, Zn, and Hg in arc plasma 19 p3281 A67-35155
- Temperature, electron density, and relative particle density radial distribution and mass separation effect in free burning DC arc 19 p3281 A67-35156
- Electric conductance exponential decay in column of wall stabilized nitrogen arc after current interruption 19 p3282 A67-35157
- Shock wave interaction with plasma arc discharge, investigating wave refraction, arc response to pressure and temperature pulses and aftershock flow field 19 p3294 A67-35407
- Absolute transition probabilities, Stark widths and shifts of S I and S II lines

determined experimentally 19 p3266 A67-36089

Plasma arc for high quality cutting and piercing of thick metals 20 p3456 A67-37694

Laser interferometric measurements of electron density in plasma arc discharge at atmospheric pressure 21 p3664 A67-38017

Electro-and permanent magnet configurations using different materials analyzed, determining lowest mass magnet system for MPD arcs [AIAA PAPER 67-686] 21 p3692 A67-38717

Tensile strength of charred ablation material under rapid heating conditions tested using plasma arc flow and miniaturized specimen 21 p3650 A67-38874

Steady flow ammonia MPD arc jet thruster propulsion performance, discussing test chamber pressure variation, thrust data and cooling systems [AIAA PAPER 67-690] 21 p3696 A67-38930

Trimming methods for Ti alloy materials including plasma arc cutting, band sawing, shearing, milling, nibbling and blanking 22 p3811 A67-39308

Electrical and spectral investigation of pulsed high pressure arc produced by capacitor bank discharge in helium and hydrogen 22 p3845 A67-39426

Apparatus for plasma investigation of pulsed arc discharge in high pressure argon 23 p4035 A67-41686

Axial component of electric field intensity in vortex stabilized arc measured by sectional channel and electrode spacing 24 p4195 A67-41940

Spectral lines diagrammed for temperature distribution in Ar plasma arc channel transverse emission with axial flow of working fluid 24 p4196 A67-42219

PLASMA ARC METAL SPRAYING

Spray coating particle flow rate dependence on plasma jet flow velocity, specific weight and particle size measured by high speed filming 24 p4159 A67-41961

PLASMA ARC WELDING

Plasma arc welding produces butt type joints in thick titanium aerospace structures [SAE PAPER 660646] 01 p0078 A67-10609

Plasma arc welding for fabricating 120-inch-diam D6AC steel rocket motor cases, comparing gas tungsten arc welds 01 p0080 A67-10944

Plasma arc welding for joining thick titanium, examining data for three common titanium alloys, three welding positions and process variables such as plasma gas composition and travel rates 01 p0081 A67-11039

Narrow welded joint, discussing advantages and limitations of narrow gap, electron beam and plasma arc techniques 04 p0627 A67-14805

Pulsed inert gas metal-arc welding technique for titanium 721, investigating arc characteristics in argon, argon/helium and helium 12 p1950 A67-25738

Plasma arc welding of pipes, studying effects of various gas combinations on weld characteristics 14 p2327 A67-28819

Plasma arc welding processes compared with TIG method for speed, cost quality, etc [ASME PAPER 67-DE-46] 14 p2328 A67-28879

Plasma arc process applied to stainless steel and titanium plate welding, discussing metallurgical and mechanical weld and deformation tests 20 p3456 A67-37542

PLASMA CHEMISTRY

Low temperature plasma - Conference, Moscow, July 1965 17 p2890 A67-32134

H, C, N, O, Cl, Ca and Al negative ion formation in plasma, noting role of continuous radiation, formation temperature and metastable and stable states 17 p2893 A67-32136

Ionization processes in hot products of combustion processes /flame gases/ as weak plasma media noting flame properties, mass spectroscopy, electron concentration, etc 17 p2967 A67-32140

Thermodynamic properties of plasmas in pressure and temperature equilibrium, showing evaluation accuracy to 4 percent 17 p2894 A67-32146

Partially ionized gases application to industry, stressing power units incorporating plasma converters, plasma electrolytic fuel elements and MHD generators 17 p2899 A67-32187

Chemical processes in low temperature plasmas, stressing nonequilibrium

characteristics, temperature and collision factors, ionization and particle excitation 17 p2809 A67-32188

Plasma technology in industry, discussing Polish-made plasma torch design and operation and plasmatron and spraying applications 17 p2865 A67-32189

PLASMA CLOUD

Ambipolar diffusion of plasma cloud imbedded in ionized gas with homogeneous magnetic field, assuming electric current is not vanishing 10 p1648 A67-23293

Antimatter and cosmology 11 p1858 A67-23994

Blast wave driven by solar flare ejecting plasma cloud proposed as origin of energy density increase causing sudden commencement of magnetic storm 15 p2476 A67-29625

Boundary form of freely expanding plasma cloud in magnetic field determined, assuming plasma pressure equal to external magnetic field pressure 16 p2706 A67-30457

Photographic recording of fast moving plasma clouds during pulsed discharges in rarefied gas using Topler apparatus 16 p2721 A67-31396

PLASMA COMPOSITION

Effective cooling of free electrons in plasma due to ambipolar diffusion and elastic collision with ions and neutrals 01 p0122 A67-10346

Effective cooling of free electrons in plasma due to ambipolar diffusion and elastic collision with ions and neutrals 11 p1843 A67-25019

Plasmas of gas state and of solid state compared, considering density, temperature, and anisotropic mass, noting wave propagation electric discharges and confinement phenomena plasmas of gas state and of solid state 12 p1980 A67-25202

Optical interferometry in plasma diagnostics, discussing degree of ionization, time dependent electron density distribution, etc 12 p1976 A67-26073

Ionization dependence of Na, K, Ca, Mg, Al, Fe and Si on arc temperature, noting correlations between temperature and electron concentration independent of plasma composition 12 p1977 A67-26108

Dispersion relation for linear three-component plasma, considering two extreme degrees of ionization 13 p2172 A67-27727

Hydrodynamic equations for electric field in steady collision-dominated three-component plasma 14 p2358 A67-28240

Seasonal variations and attenuation of ionospheric absorption, using A3 method 14 p2312 A67-28570

Structure of interplanetary plasma and magnetic field from long-period observations 14 p2362 A67-29047

Electron drift mobility and electron and ion temperatures difference in two-component plasma obtained from momentum and energy balance equations 16 p2706 A67-30450

Low temperature plasma production in combustion chamber for use in MHD generators, giving equations for plasma composition 17 p2833 A67-32167

Mass composition, contamination dynamics and jet structure of titanium plasma source 17 p2904 A67-32913

Plasmoid structure created by plasma injector and freely propagating in space, noting plasma composition, energy spectrum, electron temperature, density, etc 19 p3288 A67-35362

Theory of Langmuir probes in plasmas with negative ions, considering different ion concentrations and electron temperatures 19 p3296 A67-35587

Ionized gas properties for use in various microwave components to obtain amplification through electron beam plasma interaction 20 p3497 A67-36489

Classical nonisothermal two-component plasma correlation functions and pressure contribution from Coulomb interaction 20 p3502 A67-37603

Galilean invariance principle used to analyze system of multicomponent MHD equations to select reference system describing motions and transfer processes across magnetic field 24 p4197 A67-42351

PLASMA CONDUCTIVITY

Braking of conducting gas by transverse magnetic field in rectangular channel,

deriving one-dimensional channel flows 01 p0119 A67-10173

Supersonic MHD generator crisis possibility assuming quasi-one-dimensional noneat-conducting approximation at small Reynolds numbers and plasma scalar conductivity 01 p0011 A67-10177

Surface charge and impedance of plasma excited by incident electromagnetic waves 02 p0190 A67-11507

Self-focusing of laser beam in plasma, solving wave equation for slab and cylindrical beam configurations 02 p0252 A67-12089

Uniform velocity MHD channel flow of nonequilibrium plasma with tensor electroconductivity 02 p0275 A67-12552

Random phase approximation for plasma, establishing perturbed electron distribution in oscillating electric field 02 p0276 A67-12557

Conductivity of plasma accelerated by progressive waves, noting wall thermal absorption effect on electron temperature [ONERA-TP-424] 02 p0279 A67-12794

Plasma electric conductivity around 2000 degrees K measured, using double probe with interelectrode section of controllable length 03 p0478 A67-13603

Nonequilibrium conductivity of argon-cesium plasma 03 p0478 A67-13614

Cross section estimates for symmetric resonant charge exchange between ions differing by one electronic charge, noting effect on heat conduction in plasmas 03 p0484 A67-14038

Conductance theory for electrolytes and weakly ionized plasmas using pair distribution function in space in presence of short range forces 04 p0670 A67-15578

Effective diffusive scattering cross section of electrons in He and Ar plasma with K vapor additions and in pure K, based on DC plasma conductivity and microwave generator Q-factor 04 p0673 A67-15972

Plasma conductivity and temperature in theta pinch determined from magnetic field probe results 05 p0859 A67-17437

Convergence of Chapman-Enskog approximations to scalar electrical conductivity of some weakly ionized real gases 06 p1046 A67-18872

Correction of Fatkullin expressions for LF conductivities of homogeneous plasma in presence of electron-ion collisions in ionosphere 07 p1179 A67-19834

Induction method for measuring plasma conductivity 07 p1230 A67-20105

Self-charging of temperature independent radioactive ultrafine particles for MHD power generation 08 p1283 A67-20647

Complex dielectric constant and EM plane wave propagation in flame plasma 08 p1359 A67-21045

Measuring apparatus for scalar and tensor plasma conductivity in AC MHD generators and accelerators 09 p1538 A67-21775

Flow velocity, seeding ratio and electrical conductivity in seeded argon plasma, noting relation between plasma and MHD generator characteristics 09 p1539 A67-21780

Electrode conduction processes and segmented electrode-insulator ratio effects in MHD power generation experiments 09 p1539 A67-21785

Current-voltage characteristics of moving argon plasma, noting variation of plasma conductance with flush and filament electrodes 09 p1540 A67-21786

Shock tube studies of magnetically induced nonequilibrium ionization in potassium-seeded argon plasma, noting electrical conductivity, current density, wall potential, Soule dissipation and radiation loss 09 p1540 A67-21788

Measurements of conductivity, electron density and ionization rate of cesium in argon on alkali shock tube, describing MHD generator wind tunnel experiment 09 p1540 A67-21789

MHD flow of viscous conducting fluid jets and MHD flows with nonlinear temperature dependent conductivity 09 p1541 A67-21807

Numerical solutions for range of operating conditions in segmented linear MPD generators, using He-Cs working fluids 09 p1443 A67-21811

Electrical conductivity measurement of He 3 plasma induced by neutron irradiation 09 p1542 A67-21813

Conductivity of high density plasma of

MHD generator, noting quantum phenomena associated with overlapping electron wave functions 09 p1543 A67-21818

Approximation of electrical conductivity change in ideally conducting gas in turbulent MGD flow 09 p1544 A67-21860

Four-electrode device for measurement of electrical conductivity of shock ionized air 09 p1549 A67-22570

High resolution external probe for measuring electrical conductivity of argon plasma behind shock wave 10 p1684 A67-22963

Transient component in breakdown voltage of silicon p-n junction rectifiers in region of intermittent microplasma 10 p1612 A67-23375

Plasma thermoconductivity in general force fields, showing validity of Meador-Staton results in case of ambipolar diffusion and nonuniform total pressure 11 p1827 A67-23884

Ionized shock-nitrogen conductivity measured by four-electrode device 11 p1832 A67-24057

Plasma conductivity measurement based on Hall current and Hall voltage relation to electrical resistance 11 p1839 A67-24424

Electromagnetic wave scattering from plasmas calculated in context of physical optics, noting that radar cross section for plasmas with finite conductivity is polarization dependent 11 p1820 A67-24913

Conductivity of plasma capacitors in inhomogeneous plasma found to increase with frequency due to density gradient and resonance 12 p1969 A67-25194

Electromagnetic state theory applied to solar flares by analogy between ionized current-carrying plasma processes and solar flare conditions 12 p2001 A67-25224

Plasma conductivity in external electric fields calculated by LF longitudinal oscillation, using Boltzmann equation 12 p1970 A67-25249

Electric arc combustion stability in gas flow, noting relation to weakly ionized plasma conductivity 12 p2033 A67-25314

Cylindrical screened electrode for measuring temperature plasma conductivity in MGD generator 13 p2055 A67-26434

HF conductivity of weakly ionized plasma, establishing expression for Lorentz plasma conductivity 14 p2355 A67-27954

Arbitrary ionization ratio plasma conductivity in presence of constant and uniform magnetic field 14 p2355 A67-27955

Argon plasma thermal conductivity at atmospheric pressure and various temperatures determined in central zone of arc column 14 p2404 A67-28031

Surface charge and impedance of plasma excited by incident electromagnetic waves 14 p2261 A67-28071

Lorentzian scalar electrical conductivity as basis of mixture rules proposed for partially ionized gases in magnetic field to calculate tensor conductivity 15 p2523 A67-29218

Steady two-dimensional magnetic bottle in which moving, compressible and electrically conducting plasma is confined by horizontally aligned magnetic field 15 p2528 A67-29568

Microwave emission from magnetic-field-free electron hole plasma in p-type InSb at 77 degrees K 15 p2539 A67-29820

Nonequilibrium tensor conductivity in argon-potassium plasma under MHD generator conditions 16 p2709 A67-30514

Wall radiation, temperature, pressure and electric field strength effects on electric conductivity, electron density and ionization time of nonequilibrium He-Ce plasma 16 p2709 A67-30515

Electrical conductivity and electron energy balance in nonequilibrium plasma calculated over wide range of conditions on basis of ionization theory 16 p2709 A67-30516

Electron concentration and temperature, gas temperature, electrical field intensity and conductivity of Hg-Cs nonequilibrium plasma 16 p2709 A67-30517

Polyatomic gaseous impurity effect on electric conductivity of alkaline plasma from axial field and electron temperature measurements 16 p2710 A67-30520

Weakly ionized argon plasma electrical conductivity in direct current arc determined, noting experimental equipment 16 p2710 A67-30523

Electrical characteristics of low current arc discharge in magnetic field determining effect of nonequilibrium plasma on conductivity 16 p2710 A67-30524

Wall conductance of insulating gaps between electrode segments shown as cause of inferior performance of MHD generators 16 p2599 A67-30526

Ionization saturation and duct shape effects on losses near walls, including large Hall effects, regular current distribution, and plasma conductivity regularization 16 p2711 A67-30536

Pulsed discharge in transverse magnetic field noting relation between ionization instability and turbulent conductivity of nonequilibrium plasma 16 p2711 A67-30538

Effective conductivity tensor of nonhomogeneous plasma in homogeneous external magnetic field 16 p2711 A67-30539

Invariant solutions to nonlinear electromagnetic phenomena in dense plasma with nonequilibrium electric conductivity in variable magnetic field 16 p2712 A67-30543

Argon-potassium plasma electrical conductivity investigation showing that optimum increase in conductivity corresponds to optimum electrode length 16 p2602 A67-30560

Second order conductivity tensor of isotropic electron gas theory, using thermodynamic Green functions 16 p2713 A67-30803

Shock tube measurement of plasma electric conductivity, using Maxwell equation for quasi-steady state electromagnetic field 16 p2673 A67-31111

Effect of temperature dependence of plasma conductivity on magnetohydrodynamic channel flows 16 p2721 A67-31392

Electrical conductivity of plasma /produced in toroidal discharge chamber by injection method/ relation to electric field 16 p2721 A67-31483

Laminar flow of electrically-conducting fluid suddenly expanding in magnetic field calculated by approximate method 16 p2722 A67-31573

Low temperature plasma conductivity of combustion products, particularly of exhaust gases in duct of MHD oscillator 17 p2895 A67-32155

Thermal conductivity coefficient experimentally determined for argon plasma at atmospheric pressure and temperatures from 10,000 to 13,000 degrees K 17 p2895 A67-32157

Electrodeless probe, consisting of single-layer coil enclosed in insulating tube, for plasma conductivity measurements 17 p2854 A67-32164

Plasma conductivity measurement, applying Fishbeck nonperturbing method 17 p2896 A67-32165

Electric conductivity of flowing plasma, discussing boundary layer problem when measuring with immersed electrodes 17 p2900 A67-32343

Electrodeless device for currentless plasmoid generation noting flowing plasma conductivity, boundary layer phenomena and potential distribution 17 p2900 A67-32344

Nonexistence of critical current for pinching in electron-hole plasmas 18 p3098 A67-33523

Leakage current on insulating walls in MHD channel calculations, evaluating variable electrical conductivity in plasma boundary layer plasma boundary layer leakage current on insulating walls in MHD 18 p3088 A67-34061

Plasma electric conductivity around 2000 degrees K measured, using double probe with interelectrode section of controllable length 18 p3090 A67-34468

Nonequilibrium conductivity of argon-cesium plasma 18 p3091 A67-34479

One-dimensional electron plasma model, transport coefficient determination, Lorentz plasma conductivity measurement, decay rate, etc 18 p3092 A67-34748

Two-phase liquid metal MHD generators, appraising friction losses and conductivity limitations 19 p3175 A67-34802

Customary formulas for various effects including Thomson scattering, electron-ion, bremsstrahlung, etc, in context of plasma radiation theory 19 p3284 A67-35340

Convergence of solutions for AC and DC electric conductivity of plasma with

collisions 19 p3286 A67-35352

Homogeneous, fully ionized plasma HF conductivity computed using kinetic equation, showing application to two-temperature plasma 19 p3286 A67-35353

Thermal conductivity of nitrogen plasma in cascade arc, solving Elenbaas-Heller equation 19 p3287 A67-35358

Electric arc blowing in plasma of nonuniform conductivity and inclusion of effect in MHD flow 19 p3298 A67-35760

Transverse magnetic field retardation of flowing plasma in electromagnetic shock tube noting conductivity 20 p3496 A67-36214

Alfvén waves in ionized plasma of finite electrical conductivity, giving equations for semiphenomenological model 20 p3496 A67-36271

Viscosity, heat conduction and diffusion coefficients for two-temperature three-component plasma 20 p3500 A67-37049

Boundary conditions at dielectric-plasma interface 20 p3501 A67-37218

Plasma conductivity tensor in steady magnetic field in terms of electric field correlation using Kubo transport theory 20 p3503 A67-37692

MGD shock wave with conductivity jump, correlating wave boundary to gas parameter 21 p3664 A67-38238

Finite conductivity effect on two-dimensional plasma flow in coaxial channel solved numerically, obtaining steady state flow regime by build-up method 21 p3665 A67-38240

Energy transfer and electron conduction in nonequilibrium argon arc column at one atmosphere [AIAA PAPER 67-693] 21 p3672 A67-38722

Electrical conductivity of nitrogen plasma seeded with potassium, noting nonuniform temperature profile in flow [AIAA PAPER 67-716] 21 p3673 A67-38742

Neutralizer for large mercury thruster systems using hollow cathode forming plasma bridge neutralizer for large mercury thruster systems using hollow cathode forming plasma bridge [AIAA PAPER 67-671] 21 p3697 A67-38958

Spatial average plasma conductivity by RF impedance probes for cylindrical radially inhomogeneous plasma 22 p3844 A67-39366

Incompressible finite conductivity tearing instability in hard-core pinch with constant applied axial magnetic field 22 p3848 A67-39695

Ionized plasma electric conductivity calculation using Druyvesteyn and Maxwellian distribution for electrons and ions respectively 22 p3851 A67-39725

HF conductivity of partially ionized plasma in long wavelength limit, treating particle interactions by BBGKY and Boltzmann collision integral methods 23 p4031 A67-40888

Kinetic equation for steady state electron-ion system with electrons drifting under electric field, calculating HF resistivity drift velocity dependence 23 p4033 A67-40962

Accuracy of scalar electrical conductivity calculations of partially ionized plasma using third Chapman-Enskog approximation method 23 p4035 A67-41753

Plasma nonequilibrium electric conductivity in induced electric field investigated by MHD generator with Ar-K working fluid 24 p4196 A67-42209

Electrical conductivity of ionized plasma taking into account particle impenetrability, using Boltzmann and collision at distance integrals 24 p4198 A67-42662

PLASMA CONFINEMENT

Symmetric inductor with multipole magnetic field for stable plasma confinement, calculating input parameters 01 p0012 A67-10188

Nuclear fusion, discussing magnetic confinement methods of hot plasma shell holding light nuclei 01 p0124 A67-10778

Resonant cavity field containment of plasma 02 p0273 A67-12178

Distribution of charged particles of different energies escaping from magnetic trap in which spiral moving electron fluxes are created 02 p0274 A67-12459

Thermally ionized cesium plasma confinement investigated in magnetic mirror geometry, in terms of collisional diffusion and end plate ion recombination 02 p0276 A67-12560

Distortion of magnetic well in minimum-B system by plasma calculated, using

hydromagnetic equilibria equations 02 p0276 A67-12561

Electrolytic tank analog for magnetic field configurations in design of plasma containment device 02 p0279 A67-12693

Pinch effect in containing fusion reaction 03 p0481 A67-13733

Plasma components transmission from occluded-hydrogen titanium-washer source into mirror machine along curved field lines of magnetic cusp 03 p0485 A67-14048

Confinement times and density of deuterium plasma produced by ion cyclotron resonance heating in C stellarator 03 p0485 A67-14049

Kinetic theory of electromagnetic propagation in confined magnetoactive plasma 04 p0668 A67-15272

Ohm law in multicomponent nonisothermal plasmas derived as function of electric and magnetic fields and temperature and pressure gradients, using transport equation 05 p0857 A67-17422

Energy required to confine static shielded magnetic dipole field, immersed in highly conducting medium, by transient diamagnetic surface as function of dipole moment and disturbance field 06 p1030 A67-17658

Linear nonrelativistic motion of charged particle in field of traveling electromagnetic wave 06 p0975 A67-18087

Quasi-linear theory of loss cone instability of plasma confined in mirror type trap 08 p1359 A67-20899

Toroidal plasma containment, noting equilibrium theory consistency with first order orbit theory 08 p1364 A67-21395

Electron cloud equilibrium in toroidal magnetic and electric fields due to space and image charges 08 p1364 A67-21396

Excitation and damping of drift waves in stable regime of ionized plasma radially confined by axial magnetic field 09 p1550 A67-22679

Plasma confinement time in helium discharge determined by electron density and helium radiation intensity measurements 11 p1827 A67-23887

Computer simulation of anomalous diffusion, discussing scaling laws, quasi-steady state, plasma instabilities growth, steady diffusion, wall effects, etc 11 p1830 A67-24009

Magnetically confined cesium plasma analyzed under radial electric field, noting radial plasma loss rate 11 p1835 A67-24384

Cesium plasma confinement time measured in Q device by observing plasma density decay after atomic beam shut off 11 p1835 A67-24385

Plasma confinement by HF multipole electromagnetic field, noting role of potential accompanying rotating magnetic field 11 p1839 A67-24425

Magnetic field superposition technique for fast compression and long containment time of plasma in theta pinches 11 p1840 A67-24652

Calculations of plasma distributions and field configurations with particle containment and stability within particular framework 11 p1843 A67-24997

Plasmas of gas state and of solid state compared, considering density, temperature, and anisotropic mass, noting wave propagation electric discharges and confinement phenomena plasmas of gas state and of solid state compared, 12 p1980 A67-25202

Antisymmetric toroidal containment systems with line closure 12 p1970 A67-25251

Electron and ion temperature difference necessary to develop instability connected with loss cone of plasma with hot electrons placed in magnetic mirror trap 12 p1971 A67-25334

Combination scatter of electromagnetic waves by ion-acoustic oscillations in flat confined plasma layer with zero plasma density outside 12 p1974 A67-25447

Steady state properties of collisionless cylindrical injected plasma of zero temperature in presence of longitudinal magnetic field steady state properties of collisionless cylindrical injected plasma of zero temperature in 12 p1974 A67-25455

Stabilization of thermally ionized potassium plasma by applying shear to confining magnetic field 12 p1975 A67-25476

Thermal ionization for low temperature

plasma confined in magnetic field, examining magnetic field effect on ionization 12 p1975 A67-25757

Containment of transparent plasma produced by field of traveling wave in circular waveguide, noting plasma ion-current distribution 12 p1976 A67-26066

Electromagnetic wave diffraction by infinite set of parallel metallic plates, obtaining exact solution by Wiener-Hopf technique 15 p2435 A67-29191

Energetic plasma confined in magnetic mirrors shown to have little interaction with main plasma body 15 p2523 A67-29213

Density measurement of plasma discharge captured by magnetic field, considering linear and toroidal sections of collector 15 p2529 A67-29717

Boundary form of freely expanding plasma cloud in magnetic field determined, assuming plasma pressure equal to external magnetic field pressure 16 p2706 A67-30457

Magnetic bottles leakage in fusion reactors, describing differences between microinstabilities and MHD theories 16 p2724 A67-31865

Intense microwave radiation from high density plasma confined by magnetic mirror 17 p2894 A67-32145

Plasma injection into closed magnetic trap, studying effects of helical magnetic field on containment time, density and cross section distribution 17 p2903 A67-32910

Formation of high energy plasma in toroidal system by neutral atom injection, discussing differential equations 17 p2908 A67-33110

Density contour determination for magnetically confined plasma by energetic molecular ion beam probe of plasma and atomic ion measurement from collisional dissociation 17 p2910 A67-33356

Highly ionized two-fluid plasma confined magnetically analyzed for stability 18 p3086 A67-33986

Cesium plasma confinement time measurement in Q machine by plasma density decay observation 18 p3093 A67-34757

Drift instabilities and related phenomena in inhomogeneous plasma confined by strong magnetic fields 19 p3292 A67-35388

Ion cyclotron frequency wave generation in plasma confined in magnetic well for maximal density 19 p3295 A67-35419

Excitation temperature of low pressure magnetically confined argon plasma, using spectroscopic transition probability 20 p3499 A67-37028

Resonance phenomena in bounded magnetoplasma shown on basis of dispersion relation as due to formation of standing waves of electromagnetic waves 20 p3503 A67-37671

Electromagnetic wave pulses transmission through plasma boundary, studying boundary effects for broad and narrow frequency spectra 21 p3669 A67-38682

Combination scatter of electromagnetic waves by ion-acoustic oscillations in flat confined plasma layer with zero plasma density outside combination scatter of electromagnetic waves by ion-acoustic oscillations in flat confined plasma 21 p3674 A67-38821

Convective motion of low pressure plasma confined by strong magnetic field taking into account heat and mass transfer 21 p3675 A67-39014

Image radiance distribution of confined plasma in circular tubes noting absence of distortion 22 p3842 A67-39234

Rapid randomization phenomena in unstable plasma sac for Mach numbers close to unity attributed to electron interaction with trapped electroacoustic waves 22 p3844 A67-39357

Stabilizing effect of ion-ion collisions on collisional types of interchange instability, giving numerical solution of relevant normal mode equations 22 p3845 A67-39484

Temporary trapping device combining resonant perturbation and saddle point injection in Stormer potential configuration methods 22 p3849 A67-39697

Nuclear fusion control and relativistic high density matter acceleration, discussing amplification effect application to plasma theory, plasma RF confinement and acceleration 22 p3851 A67-39772

Dynamic equilibrium of Van Allen belts studied for self-consistency through

saturation of trapped plasma 22 p3871 A67-39799

Transverse field growth studied for generation of magnetic field in boundary layer by currents along magnetopause produced by tangential solar wind 22 p3871 A67-39801

PLASMA CYLINDER

Coaxial cylindrical plasma sheet motion and geomagnetic field/solar wind interaction 01 p0143 A67-10116

Multibeam microwave interferometer measurement of radial distribution of electron density in plasma cylinder 01 p0119 A67-10169

Effect of plasma outside cylindrical plasma column on dipole resonance, noting increased oscillation frequency and coupling of resonances 01 p0123 A67-10459

Electric field radial intensity distribution and charged particle density for positive plasma column between coaxial cylinders 01 p0125 A67-10924

Electromagnetic wave propagation along plasma column subjected to longitudinal magnetic field, calculating dispersion curves for two dipolar modes as function of wavelength and frequency 02 p0273 A67-12062

Resonances in low pressure mercury vapor discharge due to natural resonance modes of cylindrical plasmas 02 p0273 A67-12097

Radial electron density distribution in induced pulsed discharge from wave refraction in planes passing through and normal to plasma cylinder axis 02 p0278 A67-12624

Microwave radiation measurements from internal plasma resonance of positive column near electron cyclotron harmonic frequencies 03 p0476 A67-13355

Experimental results of microwave absorption by magnetoplasma indicate peaks result from excited electromagnetic wave propagation 03 p0476 A67-13357

Anomalous skin depths and magnetic probe measurement of oscillating magnetic field penetrating into plasma cylinder 03 p0477 A67-13534

Harmonic and anharmonic oscillations of cylindrical plasma with steady axial current 03 p0482 A67-13741

Infinite cylindrical antenna insulated from surrounding uniaxially anisotropic plasma by concentric cylindrical sheath of free space 03 p0384 A67-13849

Radiative modes of thin infinitely long circular plasma cylinder with dipolar azimuthal field variations 03 p0484 A67-14044

Interactions in low density plasma beams of electrostatic thrust engine exhaust, discussing neutralization, instabilities, plasma wind tunnel, etc 04 p0690 A67-15022

MHD stability of plasma cylinder in time dependent magnetic field 04 p0671 A67-15643

Cylindrically symmetric dynamic wall-stabilized plasma arc theory, considering detailed structure of column 06 p1040 A67-18123

Angular distribution of intensity and phase of electromagnetic wave scattered by cylindrical plasma column 06 p1041 A67-18138

Radiation enhancement and resonance scattering due to plasma sheath between spherical antenna and surrounding plasma layer 07 p1153 A67-19611

Equations for ionized positive plasma column of gas discharge between infinite dielectric planes under oblique magnetic field with component in direction of external electric field 08 p1358 A67-20849

Resonant frequencies of standing wave Bernstein modes propagating in magnetized homogeneous plasma columns and effects of anisotropy of unperturbed electron velocity and ambipolar-diffusional electric field 08 p1361 A67-21131

Langmuir probe experiments on electric and magnetic field, density and temperature profiles, I-V characteristic, etc, for rotating plasma in B-3 stellarator 08 p1361 A67-21137

Anomalous diffusion and radial density profile in positive column with longitudinal magnetic field 08 p1362 A67-21148

Transverse separation of rare gas-metal vapor mixture components in positive nonisothermal plasma column in plain-symmetric glow discharge 09 p1545 A67-21998

Plasma column and plasma beam of same radius situated in coaxial waveguide under magnetic field, obtaining dispersion equation 09 p1465 A67-22551

- Pressure rise in ionized He plasma cylinder due to Nernst effect 10 p1686 A67-23777
- Cross field diffusion coefficient measurement from volume loss properties of single ended Q device plasma column 11 p1830 A67-24005
- Stability of pulsating plasma cylinder contained by time dependent magnetic field described by MHD 11 p1832 A67-24154
- Electromagnetic wave diffraction on plasma cylinders calculated using wave equation and geometrical optics approximation 12 p1969 A67-25246
- Plasma column deviation from static state analyzed for time constants, considering conductivity and temperature change rates 12 p1973 A67-25394
- Axially flowing gas through arc discharge, examining effect on I-V characteristic and radial temperature distribution in arc column 12 p1975 A67-25751
- Stability of self-gravitating two-fluid infinite plasma cylinder model in axial magnetic field 13 p2163 A67-26285
- Radial electron density distribution in induced pulsed discharge from wave refraction in planes passing through and normal to plasma cylinder axis 13 p2171 A67-27380
- Phase shift between electron temperature, luminous intensity and electron density in stratified positive column of glow discharge 14 p2353 A67-27757
- Electron density variation, collision frequency and phase shift in standing striations in positive column 14 p2353 A67-27758
- Gravitational instabilities arising in plasma disk subjected to differential rotation in presence of magnetic field parallel to rotation axis 15 p2528 A67-29662
- Magnetic field finiteness effect on coordination between gyrotropic plasma waveguide and coaxial line 16 p2718 A67-31190
- Thermal plasma column instability concept applied to determine Kaufmann Criterion, calculating production coefficient, V-I characteristics, etc 16 p2719 A67-31229
- Millimeter wave resonant interferometer capable of measuring spatial distribution of electrons in low density transient plasma column subject to perturbation 16 p2675 A67-31263
- Incoherent scattering of plane electromagnetic waves on cylindrical plasma column with fluctuating charge-density 16 p2628 A67-31499
- Diffraction of plane electromagnetic waves on compressible plasma cylinder analyzed, obtaining scattering cross sections 16 p2628 A67-31503
- Mechanism of positive low pressure column in plasma of low electron density, studying steady state conditions of nonstratified inert gas discharges 17 p2907 A67-33103
- Radial hydromagnetic oscillation frequency of plasma cylinder, calculating g-factor and plasma mass 17 p2909 A67-33117
- Thermal radiation resonance of plasma cylinder in presence or absence of magnetic field 18 p3090 A67-34435
- Periodic spatial variations of parameters of positive column plasma in magnetic field along obstacle shadow due to electron wakes 19 p3273 A67-35093
- Positive column and striations of low pressure discharge of noble gas 19 p3273 A67-35097
- Discharge plasmas in hollow cathodes investigated using photography, showing mercury vapor and inert gas plasmas form homogeneous or laminar positive plasma columns 19 p3274 A67-35102
- Wave propagation and electron beam-plasma interaction in plasma column inside magnetic field, measuring plasma characteristics and spatial distribution 19 p3275 A67-35107
- Plasma column in magnetic field created by diffusion from low pressure pulsed discharge in hydrogen, with plasma density dependent on gas pumping speed 19 p3275 A67-35108
- RF plasma at electron cyclotron frequency produced with axially slotted metal cylinder 19 p3275 A67-35111
- Transverse forces acting on arbitrarily curved current carrying plasma cylinder in transverse magnetic field 19 p3281 A67-35151
- Column effects in arc interaction with transverse magnetic fields 19 p3281 A67-35152
- Cylindrical plasma column subjected to axial magnetic field measured for electric field oscillations by movable probe within ionized gas 19 p3288 A67-35374
- Microwave noise radiation and scattering from cylindrical plasma column, studying dissipative processes on emission spectrum 19 p3291 A67-35387
- Microwave refraction technique for determining electron density profiles in transient plasma column 19 p3295 A67-35517
- Inhomogeneous cylindrical plasma column oscillations with perturbations, finding density-independent mode 19 p3295 A67-35564
- Vortical stabilization of plasma column within radial electric field 20 p3500 A67-37062
- Electromagnetic plane wave scattering cross section from plasma coated conducting cylinder using TE and TM modes of polarization with respect to cylinder axis 20 p3389 A67-37706
- Motion of rotating plasma cylinder under gravity force assuming temperature time dependency 21 p3663 A67-37931
- Flute instability of maximally inhomogeneous rarefied plasma cylinder with thick transition layer amounting to two Larmor radii 21 p3667 A67-38371
- Electrostatic ion cyclotron waves excitation in plasma and ion heating due to cyclotron damping 21 p3667 A67-38407
- Particle distribution in infinite charged cylinder in plasma vicinity, showing plasma screening effect on potential 21 p3675 A67-39033
- Circular polarized magnetic field penetration into plasma cylinder noting penetration depth frequency dependence and MHD stability effect 22 p3848 A67-39508
- Microwave scattering cross section for turbulent weakly ionized plasma column, noting square root of mean square plasma density fluctuation limit for Born approximation 22 p3850 A67-39722
- Rapid scan spectrometer used to measure Stark broadened H lines in plasma column, determining electron density 23 p4032 A67-40957
- Fully ionized barium plasma column generating device, discussing spectroscopic measurements of ion motions, densities, temperatures and electron temperature 23 p4033 A67-41215
- Exact equation for potential oscillations of inhomogeneous plasma cylinder via Fourier transformations, discussing drift, cyclotron oscillations and flute instability 23 p4034 A67-41679
- Dense hydrogen plasma ohmic heating in quasi-stationary discharge without external magnetic field, obtaining stable impurity-free plasma column 24 p4195 A67-41939
- PLASMA DECAY**
- Microwave cavity measurement of recombination coefficient of decaying plasma obtained by gamma ray induced ionization of xenon 02 p0274 A67-12463
- Measurement of sticking coefficient for thermal electrons in oxygen and air, using microwave circuits 02 p0274 A67-12466
- Diffusion decay of discharge plasma with oscillating electrons in magnetic field 02 p0278 A67-12620
- Afterglow decay of number density and electron temperature of plasma with rare collisions between electrons and molecules 03 p0487 A67-14343
- Instability in hot electron plasma in mirror field occurring suddenly in quietly decaying plasma generated by high power microwave 04 p0663 A67-14621
- Stimulated emission of electromagnetic wave in decaying ionized plasma 05 p0855 A67-16998
- Hot electron plasma instability in magnetic mirror, discussing stabilization by cold plasma component and magnetic field line typing in conducting end plates 05 p0858 A67-17431
- Time dependence of electron density in afterglow of electrodeless discharge in hydrogen plasma measured, using microwave interferometer 07 p1229 A67-19682
- Microwave interferometer for measurement of effective recombination coefficient of decaying argon-cesium plasma with hot electrons at various argon pressures 09 p1542 A67-21817
- Decay kinetics of He plasma, examining pair collision, metastable atom diffusion coefficient and afterglow mechanism via spectroscopy 09 p1544 A67-21918
- Electric current flow in moving decaying plasma and plasma diagnostics, deriving nonlinear V-I characteristics 09 p1547 A67-22317
- Recombination processes determined from data of time dependence of spectral line intensities and number density in decay plasmas produced in neon and helium-neon mixtures 09 p1548 A67-22360
- Recombination processes in decaying helium plasmas as indicated by time dependence of spectral line intensities and ion number density 09 p1548 A67-22361
- Cesium plasma confinement time measured in Q device by observing plasma density decay after atomic beam shut off 11 p1835 A67-24385
- Diffusion decay of discharge plasma with oscillating electrons in magnetic field 13 p2170 A67-27376
- Decay kinetics of He plasma, examining pair collision, metastable atom diffusion coefficient and afterglow mechanism via spectroscopy 14 p2358 A67-28247
- Diffusion by microwave breakdown of weakly ionized helium plasma in metal chamber immersed in magnetic field 14 p2358 A67-28293
- Self-similar solutions for recombination plasma decay problem, considering plane and spherical symmetry 15 p2531 A67-30011
- Quasi-equilibrium number density of excited atoms and electronic transition rate in decaying optically-thick helium and hydrogen plasmas, considering Penning ionization 16 p2715 A67-31168
- Anomalous decay of discharge plasma with oscillating electrons in strong magnetic field, using diagrams 16 p2717 A67-31181
- Amplifying electromagnetic radiation in nonequilibrium decaying plasma of various degrees of ionization, taking into account kinetics 16 p2723 A67-31577
- Ionization decay in cesium vapor explained in terms of dissociative recombination and diffusion, showing strong dependence on vapor pressure 19 p3271 A67-35072
- Charge recombination coefficient of decaying He and Ar plasmas with Cs vapor additions at increased pressures 19 p3271 A67-35073
- Electron cyclotron resonance absorption of microwaves in oxygen magnetoplasma used to alter electron attachment and detachment rate coefficients 19 p3271 A67-35077
- Torsional Alfvén waves attenuation in decaying hydrogenous plasma 19 p3290 A67-35377
- Acoustic wave generation in weakly ionized plasma by fusion and damping of two ion-sound waves 20 p3501 A67-37291
- Self-similar solutions for recombination plasma decay problem, considering plane and spherical symmetry 20 p3502 A67-37536
- Hydrogen plasma discharge with hot electrons, investigating plasma decay and electron and plasma density 21 p3666 A67-38368
- Theta pinch energy loss determined and electron temperatures measured, discussing Poynting flux and plasma diamagnetism decay 22 p3849 A67-39696
- PLASMA DENSITY**
- Plasma density dependence of adiabatic motion of plasmoids in longitudinal magnetic field 01 p0122 A67-10351
- Inhomogeneity parameter over cross section of spectral line contour for case of Doppler distribution 01 p0125 A67-11046
- Three-mirror laser interferometer measuring electron densities in repetitively pulsed plasmas 02 p0241 A67-11875
- Decaying plasma density determined from high mode oscillations produced in magnetic trap with metallic chamber at 2000 to 6000 oe 02 p0274 A67-12464
- Criteria for cold plasma density necessary to stabilize grade B drift waves in finite length energetic plasmas 02 p0275 A67-12554
- Plasma density variation in toroidal gas discharge stabilized by weak longitudinal magnetic field 02 p0277 A67-12617
- Electron density measurement in shock

waves or plasma based on low power UHF wave attenuation 03 p0478 A67-13578

Plasma electron density as function of radius compared with ion cyclotron heating theory and stability criteria [AIAA PAPER 66-158] 04 p0664 A67-14823

Formation of magnetospheric plasma knee by combined action of magnetospheric convection and plasma escape from tail 04 p0693 A67-14964

Magnetic field effect on velocity of electron drift produced by electrical field in dense plasma 04 p0671 A67-15580

Radial distribution of plasma formed in simple mirror machines by quantum effect field ionization of fast neutral atoms 04 p0671 A67-15644

Luminous density distribution of decaying hydrogen plasma recorded by photoelectronic method 04 p0672 A67-15653

Electron collision rate and density calculations for He-Ne laser plasma 05 p0815 A67-16598

Plasma electron density range measurable by microwave extended by phase angle being expanded by impedance transformation 05 p0854 A67-16982

Plasma density, electron temperature and potential distribution measured across magnetic field, determining ion and electron-diffusion coefficients in plasma column 05 p0858 A67-17432

Pressure difference in cathode region of MPD accelerator as affected by plasma compression and magnetic field [AIAA PAPER 67-47] 06 p0951 A67-18466

Dynamics of ionized stellar winds noting anisotropic effect of stress tensors and densities, velocities and electrostatic potentials distributions [AIAA PAPER 67-146] 06 p1088 A67-18476

Stationary self-consistent plasma density distribution in field of strong electromagnet wave 06 p1045 A67-18779

Helium plasma density effect on results of spectroscopic electron temperature determination 07 p1228 A67-19514

Ionospheric plasma density determined by phase difference of incident waves on and reflected from plasma 07 p1173 A67-19701

Plasma spectrography in shock tube, determining charged particle concentration 08 p1358 A67-20853

Electron streaming instability of plasmas with zero order density gradients from variational analysis of Vlasov-and Maxwellian-plasma perturbation wave propagation 08 p1360 A67-21128

Anomalous diffusion and radial density profile in positive column with longitudinal magnetic field 08 p1362 A67-21148

Radial particle density profile in neon negative glow plasma in cylindrical discharge tube measured by double probe method 08 p1362 A67-21288

Plasma energy density, conductivity and temperature measurements at various pressures 08 p1362 A67-21303

Magnetic effect on injected plasma density and anomalous potential in semiconductor rods 09 p1552 A67-21761

Gas ionization by fast electron beam directed along waveguide leading to longitudinal distribution of secondary electron concentration 09 p1545 A67-22002

Convective type drift instability in collisional and collisionless regimes due to magnetic shear effects driven by density gradient 10 p1685 A67-23462

First integrals of motion to determine stationary distribution function of charged particles and self-consistent magnetic field of plasma 10 p1685 A67-23464

Higher fast ion density achieved by fast neutral particle injection into closed-line magnetic trap 10 p1686 A67-23466

Dependence of ion current from RF ion source on plasma density at boundary and longitudinal magnetic field intensity 10 p1687 A67-23794

Diffusion coefficient measurement based on relationship between correlation coefficient for density fluctuations and density coefficient 11 p1829 A67-24003

Electric field effect in Q machine with uniform end plate temperature, noting deviation from thermal equilibrium and increment in ion loss rate for certain range of particle densities 11 p1833 A67-24370

Effects related to ion cooling in Q device 11 p1833 A67-24371

Plasma turbulence and diffusion across magnetic field investigated by plasma instabilities in case of large amplitudes of oscillation measured by Langmuir probes 11 p1834 A67-24376

Highly ionized plasma with excitation and damping of density and temperature drift waves in stable regime 11 p1835 A67-24382

Diffusion of particles across magnetic lines in dense and quiescent plasma compared with Bohm and collisional values 11 p1835 A67-24383

Density measurements in Q-device by resonance fluorescence scattering, Langmuir probe and microwave methods compared, examining causes of discrepancy 11 p1838 A67-24405

Electrostatic probe techniques for low density thermally ionized plasmas 11 p1838 A67-24408

Plasma drift instability arising from initial nonuniformity in density and temperature 11 p1842 A67-24966

DC current density distribution in plasma electron gap obtained by simulation method 11 p1843 A67-24968

Plasma density dependence of adiabatic motion of plasmoids in longitudinal magnetic field 11 p1844 A67-25024

Rate equations for nonequilibrium excitation of neutral helium in plasmas of moderate density solved and compared with population densities 11 p1844 A67-25075

Magnetospheric model of Jupiter from numerical calculation of maximum number density of plasma 12 p2000 A67-25206

Langmuir probe and microwave transmission methods compared for plasma density measurement 12 p1939 A67-25256

High density one-component plasma radial distribution determination by Born-Green-Yvon integral 13 p2162 A67-26282

Surface density gradient and collision frequency effects on polarization of microwaves reflected from plasma surface 13 p2164 A67-26300

Cylindrical Langmuir probes examined in high density plasma flow 13 p2166 A67-26650

Electrically conductive self-similar gas flow in medium with given back pressure, assuming medium conductivity as function of temperature and density 13 p2169 A67-27307

Plasma density variation in toroidal gas discharge stabilized by weak longitudinal magnetic field 13 p2170 A67-27373

Radial variation of plasma electron density determined by surface wave resonances 14 p2355 A67-27829

Ion oscillations excitation by beam-plasma interaction near ion-plasma frequency, studying instability as function of magnetic field, plasma density and other parameters 14 p2360 A67-28553

Structure of interplanetary plasma and magnetic field from long-period observations 14 p2362 A67-29047

Transverse diffusion coefficient of collisionless plasma in magnetic field measured, using variations in radial plasma column density 14 p2363 A67-29067

Boltzmann kinetic equation solution for completely ionized plasma in magnetic field 14 p2363 A67-29071

Kinetic equation for plasma with electromagnetic interactions, using shielding approximation 15 p2519 A67-29209

Coaxial helium-plasma source with superimposed azimuthal magnetic field, noting plasmoid density increase with magnetic field, plasmoid velocity and experimental setup 15 p2526 A67-29254

Development of plasmoid density due to laser ionization measured using Fabry-Perot interferometer 15 p2527 A67-29474

Grid probe analysis of alkaline plasma, determining density, potential and energy distribution function 15 p2527 A67-29476

Stationary concentration of charged particles in plasma created by uniform and nonuniform SHF magnetic field in electron-cyclotron resonance state 15 p2529 A67-29716

Density measurement of plasma discharge captured by magnetic field, considering linear and toroidal sections of collector 15 p2529 A67-29717

Electron density and temperature in plasma measured, using self-focused laser beams 15 p2488 A67-29902

Time varying high density laser induced plasmas formed in high pressure gases studied using Mach-Zehnder

interferometer 15 p2488 A67-29903

Automatic recording and computer analysis of double probe measurements in plasma research, calculating electron temperature and plasma density 15 p2489 A67-30092

Pressure difference in cathode region of MPD accelerator as affected by plasma compression and magnetic field [AIAA PAPER 66-47] 15 p2531 A67-30205

Coulomb collisions effect on transverse wave along external magnetic field in dense plasma, noting damping of whistler mode and use of Fokker-Planck equation 16 p2713 A67-30608

Flute instability for inhomogeneous plasma equilibria in inhomogeneous magnetic fields of mirror machines, solving Vlasov and Poisson equations 16 p2714 A67-30875

Scattering method for observing plasma instability near electron gyrofrequency harmonics 16 p2715 A67-31062

Electrostatic wave propagating into region of decreasing electron density calculated using one-dimensional plasma with uniform electron density 16 p2715 A67-31063

High pressure characteristics of helium and hydrogen pulsed arcs, noting formation of dense, completely ionized plasma 16 p2717 A67-31183

Accelerated electrons effect on plasma in closed magnetic trap, measuring current flow, plasma density, X-ray/microwave radiation and light emission 16 p2717 A67-31186

Helium plasma electron temperature and density dependence, with/without magnetic field, on pinch discharge 16 p2718 A67-31187

Ionization, ion temperature and density dependence of cesium plasma on pressure of added rare gas 16 p2720 A67-31244

Electron wave resonances in bounded plasmas, examining application to average plasma density measurement 17 p2896 A67-32163

Charged particles with Alfvén velocities distribution in magnetosphere analyzed based on cold plasma density, emphasizing data ofOGO A 17 p2899 A67-32256

Spectroscopic observation of ion wings produced by plasma ion oscillations in laser produced plasma 17 p2901 A67-32368

Rapid earth electromagnetic field variations used for plasma concentration and magnetosphere radius determination 17 p2846 A67-32937

High altitude plasma-concentration diagnostics from magnetospheric oscillation spectra 17 p2846 A67-32940

Bohm criterion of boundary layer stability related to ambipolar sound generation in positive column plasma discharge, deriving plasma density ambipolar potential distribution 17 p2905 A67-32972

Wing slope techniques for analysis of Langmuir probe characteristics in low density plasma, using I-V characteristics and spherical and cylindrical geometries 17 p2906 A67-33054

Density contour determination for magnetically confined plasma by energetic molecular ion beam probe of plasma and atomic ion measurement from collisional dissociation 17 p2910 A67-33356

Frequency response of DC and AC currents flowing to RF resonance probe in quiescent cesium plasma, explaining measurements 18 p3044 A67-33713

Stationary self-consistent plasma density distribution in field of strong electromagnetic wave 18 p3086 A67-33720

Density redistribution of plasma electrons and ions caused by strong microwave field 18 p3087 A67-34040

Wind-driven plasma turbulence structure resolved by continuum ion probes at high Reynolds numbers, determining plasma density fluctuation from argon gas flow 18 p3030 A67-34743

Cesium plasma confinement time measurement in Q machine by plasma density decay observation 18 p3093 A67-34757

Thermally ionized cesium plasma produced containing negative Cl ions 19 p3272 A67-35084

Modified duoplasmatron in cusp fields to produce highly ionized and high density quiescent plasma, using DC discharge, noting helium plasma generation 19 p3274 A67-35104

Plasma column in magnetic field created by diffusion from low pressure pulsed

discharge in hydrogen, with plasma density dependent on gas pumping speed 19 p3275 A67-35108

Argon plasma ionization by oscillator supplying power near electron cyclotron resonance, measuring density variation 19 p3276 A67-35116

Plasma-density distribution produced in gas by tubular electron beam 19 p3278 A67-35128

High temperature plasma generation from dense plasma with moving metallic walls, evaluating electrical conductivity and energy breakdown periods 19 p3282 A67-35159

Plasmoid structure created by plasma injector and freely propagating in space, noting plasma composition, energy spectrum, electron temperature, density, etc 19 p3288 A67-35362

Plasma bunches-microwave interaction showing electron energy and plasma ions velocity increase 19 p3291 A67-35384

Plasma temperature and density measured behind luminous and preceding shock fronts in electromagnetic shock tube 19 p3293 A67-35399

Hot plasma corpuscular diagnostics methods, noting particle beam determination of hot plasma density, electron temperature and plasma electric fields 19 p3296 A67-35586

Density and temperature measurements of high temperature nitrogen plasma jet using schlieren photographic method 19 p3231 A67-35595

Holographic interferometry in fractional-fringe density plasmas, discussing sensitivity and advantages of combined method 19 p3232 A67-35691

Plasma microinstability theory, predicting dangerous instability above critical density, discussing applications to very high temperature plasma experiments 20 p3495 A67-36153

Magnetic cut-off system for plasma jet, with plasma flux reduction 20 p3497 A67-36679

Radial profiles of carrier density and energy in diffusion controlled plasma 20 p3501 A67-37239

Nonthermal plasma calculated from ratio of spectral line intensities of given ion 20 p3501 A67-37294

Parametric excitation in plasma located in oscillating electric field due to density gradient, showing predominance on electron-ion coupling 20 p3503 A67-37672

Electron temperature and density distributions for helium plasma produced in coaxial accelerator measured spectroscopically, checking thermal equilibrium assumption 21 p3661 A67-37752

Ion resonance probe for plasma density measurement using direct display method with frequency swept signal generator 21 p3627 A67-38258

Resonance spectrum of plasma column excited by SHF field investigated for nonlinear phenomena 21 p3666 A67-38354

FR-1 satellite-borne oxide cathode used to return to ground polarization current from ambient plasma 21 p3599 A67-38649

Plasma spatial electron density distribution from refraction of microwave beams with several frequency components 21 p3670 A67-38689

Variation method of microwave diagnostics of homogeneous plasma based on attenuation coefficient measurements, determining collision frequency and plasma density 21 p3675 A67-39032

Cooperative light scattering from density fluctuations in theta pinch plasmas, discussing peaks obtained 22 p3842 A67-39208

Turbulence effect on accuracy of microwave cut-off measurements of plasma density suggests electromagnetic wave scattering 22 p3845 A67-39430

Fluid model for magnetosphere shape, calculating flow velocity, density and temperature between shock and boundary 22 p3883 A67-39671

Hypersonic reentry plasma electron density measurement in free stream wake and shock layer using hotshot wind tunnel simulation 23 p3986 A67-40574

Shock wave produced optically-thin nonequilibrium plasmas studied using Rankine-Hugoniot calculations for properties, varying electron/ion temperature ratio [DVL-635] 24 p4194 A67-41860

Strongly enhanced radiation from antenna

surrounded by dielectric layer and plasma sheath, noting resonance at given operating frequency for certain plasma densities 24 p4121 A67-42266

PLASMA DIAGNOSTICS

Anisotropic magnetoplasma diagnostics using transient reflected polarized signals [AFCLR-67-0065] 03 p0371 A67-13865

Computer method analysis of electron temperature and density behavior on basis of glow discharge for plasma electron balance equation solution 14 p2353 A67-27755

Dispersion of proton whistlers in plasma in motion with respect to observer 14 p2379 A67-27933

Space-time description of dynamical phenomena in unbounded homogeneous linear medium, noting dispersion properties and wave structures in plasma 14 p2358 A67-28461

Macroscopic linear fluid model of plasma radiation and scattering restricted to bounded media, emphasizing physical interpretation of wave constituents 14 p2359 A67-28463

Numbers, flow velocities and temperatures of positive ions emitted by He and Ar plasmas pulsed into evacuated region by plasma gun determined by time-of-flight analysis 15 p2523 A67-29214

Soviet book on plasmoids covering coaxial plasma sources, magnetic field interaction and observation methods 15 p2524 A67-29243

Structure and magnetic field of plasmoids produced by conical induction source studied with probe-diagnostic method 15 p2526 A67-29255

Plasmoid structure, analyzing interdependence of plasmoid parameters along length 15 p2526 A67-29256

Active corpuscular plasma diagnostics method applied to hydrogen plasma study 15 p2526 A67-29257

Variable field Thomson mass spectrograph application to analysis of mass composition of plasmoids 15 p2526 A67-29258

Electron thermal diffusivity in room temperature neon afterglow plasma measured using Tonks-Dattner resonance, noting independence of electron density 15 p2532 A67-30381

Spectroscopic techniques for plasma parameter measurements in high temperature range, discussing methods employed and experimental setups 15 p2533 A67-30424

Calculating characteristics of cesium plasma in stationary state under electric field, considering excitation and ionization by inelastic electron collisions 16 p2713 A67-30868

Plasma probe diagnostic technique in shock tube, noting electron concentration, gas temperature and plasma potential from V-T characteristics 16 p2673 A67-31110

Thermodynamic characteristics and plasma parameters of lithium vapor in wide pressure and high temperature range 16 p2721 A67-31389

Vacuum chamber for plasma studies consisting of thin stainless steel shell strengthened by glass fiber reinforced plastic with epoxy compound as adhesive 16 p2676 A67-31397

Plasma concentration diagnostics by hydromagnetic probing method, determining concentration profile from latitude dependence of torsional vibrations 16 p2668 A67-31890

Microwave methods applied to plasma diagnostics restricted to steady state plasma 17 p2901 A67-32349

Nonlinear effects in collisionless plasma during interaction with strong HF field 17 p2905 A67-32920

High altitude plasma-concentration diagnostics from magnetospheric oscillation spectra 17 p2846 A67-32940

Michelson type carbon dioxide laser for AC discharge analysis, noting apparatus design and performance results 18 p3060 A67-34014

Diagnostic equations for electrostatic double probes for arbitrary ion Schmidt numbers 19 p3287 A67-34830

Nonlinear effects of laser radiation interaction with turbulent dense plasma, discussing wave propagation, plasma diagnostics, etc 19 p3291 A67-35385

Phenomena in ionized gases - Conference, Belgrade, Yugoslavia, August 1965, Volume

II 19 p3295 A67-35585

Hot plasma corpuscular diagnostics methods, noting particle beam determination of hot plasma density, electron temperature and plasma electric fields 19 p3296 A67-35586

Plasma electron density measurement method using beat frequencies between two dual frequency lasers 19 p3231 A67-35594

Oblique incidence millimeter wave technique using ray theory for measuring collisionless plasma electron density profile 20 p3496 A67-36311

Complex reflection coefficient for finite-width boundary used for plasma diagnostics in high electron-density range, discussing modeling errors 20 p3499 A67-36959

Plasma diagnostic measurement simulation, considering electromotive effect from satellite motion through geomagnetic field 20 p3418 A67-37428

Microwave methods of plasma diagnostics based on attenuation, reflection or refraction measurements compared to double probe density measuring technique 21 p3670 A67-38688

Diagnostic probe for low density plasma beam ion velocity distribution measurement in steady state and pulsed plasma exhausts [AIAA PAPER 67-706] 21 p3672 A67-38733

Plasma diagnostics using self-focused laser beams, determining electron density and temperature 21 p3673 A67-38734

Optical interferometer for refractive plasma diagnosis, noting Q-switched ruby laser and pulsed arc lamp 21 p3630 A67-38768

Variation method of microwave diagnostics of homogeneous plasma based on attenuation coefficient measurements, determining collision frequency and plasma density 21 p3675 A67-39032

Plasma jet front produced by coaxial gun studied using SHF diagnostics method 22 p3799 A67-39764

SHF phase meters used in plasma diagnostics classified to facilitate proper phase meter selection for specific application 24 p4154 A67-42218

Total head tube in combination with electrostatic probe used in supersonic plasma diagnostics, measuring plasma and shock wave front parameters 24 p4197 A67-42355

PLASMA DIFFUSION

Diffusion and lifetime of plasma charged particles in magnetic field covering instability, contraction, decay, recombination, etc 01 p0123 A67-10389

Plasma diffusional flow in toroidal axially symmetric discharge in presence of helical electric field and circular magnetic field 01 p0128 A67-11300

Diffusion of fully ionized plasma across magnetic field in computer model consisting of one thousand charged rods in two-dimensional motion 02 p0276 A67-12558

Lasers used to extend RF plasma diagnostic procedures to optical frequencies by interferometric and Thomson diffusion methods 03 p0477 A67-13474

Power and DC spectra for electron motion due to plasma heating and diffusion in static magnetic and transverse random electric field 03 p0485 A67-14046

Charged particle distribution in hollow cylinder shaped positive plasma column during diffusion and helical instability in longitudinal magnetic field 04 p0668 A67-15281

Electron beam excitation as possible explanation of relation between enhanced diffusion and HF oscillation in plasma 05 p0854 A67-16896

Microplasma effects arising in avalanche type breakdown in deep-seated large-area p-n junction in silicon 05 p0867 A67-17052

Arc diffusion measurements of electron temperature and density profile across magnetic field 05 p0858 A67-17433

Plasma half-space impedance for diffusive electron reflection from plasma vacuum boundary, noting damping decrement of surface electromagnetic wave, electric field Fourier components and absorption capacity 06 p1039 A67-18079

Ambipolar diffusion theory for describing diffusion of nonuniformities in ionosphere including F region 07 p1230 A67-19717

Time dependent behavior of diffusion of plasma inhomogeneities with or without particle drift 07 p1250 A67-19810

Ambipolar diffusion and drift of plasma of

added carriers in semiconductor in presence of magnetic field 08 p1369 A67-20900

Velocity space diffusion from weak collisionless plasma turbulence in magnetic field 08 p1360 A67-21123

LF wave frequency-and amplitude-dependent transverse anomalous diffusion coefficient in fully ionized magnetoplasma in Q-machine 08 p1360 A67-21125

Effective electron and ion diffusion coefficients measured for positive magnetic field gradients show reduced plasma diffusion 08 p1364 A67-21400

Plasma in flat-electrode accelerator, examining optimum accelerator length associated with equilibrium between acceleration processes in plasma and diffusive scattering of plasmoid 09 p1545 A67-22001

Diffusion coefficient measurement based on relationship between correlation coefficient for density fluctuations and density coefficient 11 p1829 A67-24003

Cross field diffusion coefficient measurement from volume loss properties of single ended Q device plasma column 11 p1830 A67-24005

Plasma diffusion across static magnetic fields in electrodeless E type RF discharges 11 p1830 A67-24008

Computer simulation of anomalous diffusion, discussing scaling laws, quasi-steady state, plasma instabilities growth, steady diffusion, wall effects, etc 11 p1830 A67-24009

Plasma stability, discussing flute and Kadomtsev instabilities and possibility of anomalous diffusion for confined steady state 11 p1831 A67-24011

Diffusion measurements in potassium magnetoplasmas based on volume plasma loss properties of variable length single-ended Q device 11 p1835 A67-24386

LF drift waves effect upon anomalous transverse diffusion in fully ionized magnetoplasma, noting wave amplitude 11 p1835 A67-24387

Electrostatic turbulence in low beta plasma and influence on diffusion across magnetic field, noting heating system for plates of Q device 11 p1789 A67-24413

Relativistic electron plasma diffusion, calculating dynamical friction and diffusion coefficient in Landau approximation 12 p1969 A67-25193

Drift effect on diffusion spreading of plasma inhomogeneities in magnetic field, deriving expression for Fourier component potential and magnetic field perturbations 12 p1933 A67-25546

Rate of resistive diffusion of hydromagnetic equilibrium computed using expansion near magnetic axis 13 p2164 A67-26296

Diffusion by microwave breakdown of weakly ionized helium plasma in metal chamber immersed in magnetic field 14 p2358 A67-28293

Generation of quiescent variable-parameter arc plasma in strong magnetic field 15 p2523 A67-29228

Microplasma effects arising in avalanche type breakdown in deep-seated large-area p-n junction in silicon 15 p2538 A67-29783

Self-similar solutions for recombination plasma decay problem, considering plane and spherical symmetry 15 p2531 A67-30011

Electron thermal diffusivity in room temperature neon afterglow plasma measured using Tonks-Dattner resonance, noting independence of electron density 15 p2532 A67-30381

Drift waves in fully ionized potassium magnetoplasma in single-ended Q machine, measuring effect on transverse diffusion coefficient 16 p2720 A67-31242

Instability and related anomalous diffusion of magnetized weakly ionized hydrogen plasma of RF discharge in cylindrical geometry 17 p2908 A67-33113

Negative glow diffusion model evaluated via generation function determined by discharge voltage and dependence of reduced length of cathode fall 18 p3085 A67-33668

Plasma column in magnetic field created by diffusion from low pressure pulsed discharge in hydrogen, with plasma density dependent on gas pumping speed 19 p3275 A67-35108

Thermodiffusion term in particle flux

equation, showing large electron temperature variation across low voltage arc plasma 19 p3279 A67-35140

Alkali-metal magnetoplasma properties related to enhanced diffusion, showing relationship to beam-plasma interaction 19 p3287 A67-35360

Viscosity, heat conduction and diffusion coefficients for two-temperature three-component plasma 20 p3500 A67-37049

Self-similar solutions for recombination plasma decay problem, considering plane and spherical symmetry 20 p3502 A67-37536

Asymptotic formulas for propagating discontinuity diffusion in magnetoplasma, considering discontinuity shape, diffusion and lifetime 21 p3621 A67-39020

Resonant particle diffusion of nonuniform plasma across magnetic field, calculating transport coefficients 22 p3848 A67-39687

Electron neutral heat transfer in plasmas, obtaining data on electron thermal diffusivity from pulsed heat flow experiments in helium afterglow 24 p4194 A67-41872

PLASMA DISCHARGE

SA TOROIDAL DISCHARGE

Channel model examination of output-dependent radius of spherical plasma discharge in thermal equilibrium 01 p0118 A67-10045

Weak longitudinal and transverse magnetic fields increase emf and optimum output voltage characteristics of thermionic diode introduced into autonomous mercury discharge plasma 01 p0034 A67-10135

Configurations of HF discharge plasma and dependence on gas pressure and annular electrode potential 01 p0122 A67-10348

Elementary processes in DC gas discharge plasma in helium, comparing measurements of population levels of excited states of atoms with calculated values 01 p0123 A67-10363

Temperature-dependent wave propagation in slightly inhomogeneous hot nonuniform plasma, examining positive column of mercury vapor discharge 02 p0193 A67-11782

Diffusion decay of discharge plasma with oscillating electrons in magnetic field 02 p0278 A67-12620

Discharge current, discharge voltage pressure and radius of discharge channel for discharge in water induced by tungsten filaments 03 p0476 A67-13210

Nonlinear theory of plasma instability in oscillating discharge, estimating oscillation energy and coefficient of turbulent diffusion 03 p0478 A67-13537

Propagation of nonaxisymmetric Alfvén waves in linear discharge tube filled with nonuniform plasma 03 p0485 A67-14045

Image converter observation of radial striated light filaments during gas breakdown and current sheath buildup in dense plasma focus coaxial discharge 03 p0486 A67-14055

Nonequilibrium plasma diagnostics of steady HF discharge in toroidal MHD plasma generator 04 p0553 A67-14580

Anomalous pulsed microwave emission at cyclotron frequency in partially ionized plasmas analysis extended to show that emission is not stationary with time 04 p0663 A67-14615

Electrical noises of plasma of steady state HF discharge in magnetic field discussed from standpoint of universal plasma instability 04 p0671 A67-15640

Helium mono and divalent ion electron recombination coefficient determined as function of electron density and temperature 04 p0672 A67-15774

Gas discharge in argon maintained within waveguide by microwave signal at cyclotron resonance, observing second harmonic radiation 05 p0850 A67-16046

Arc formation at metal surface in hydrogen plasma analyzed at various gas pressures, using Penning discharge, noting heat treatment effect on hydrogen 05 p0850 A67-16066

Formulas relating detector current to average UHF power obtained for positive plasma column and dark Faraday region of glow discharge 05 p0856 A67-17235

Plasma in Ar positive column DC discharge examined for wavelike perturbations about equilibrium, noting striation dispersion relation, density variations and electron

temperature 05 p0857 A67-17427

Elementary processes in DC gas discharge plasma in helium, comparing measurements of population levels of excited states of atoms with calculated values 06 p1038 A67-17621

Particle concentration and luminescence intensity correlation with electron cyclotron frequency in stationary SHF argon discharge in magnetic field 06 p1040 A67-18094

X-ray astronomy of discrete sources in or near galactic plane, noting likely X-ray production mechanism 06 p1092 A67-19009

Discharge plasma in He and argon with cesium and potassium vapor admixtures noting electric field, conductivity, electron temperature and emission spectrum 07 p1227 A67-19115

Field harmonics of HF plasma discharge taking nonlinear interaction into account 08 p1357 A67-20827

Scintillation analysis of hard X radiation from high power pulse discharges 08 p1357 A67-20846

Active component of voltage behavior in channel of helium pulse discharge measured, obtaining time dependence of channel resistance, input velocity and energy magnitude 08 p1357 A67-20848

Plasma spectrography in shock tube, determining charged particle concentration 08 p1358 A67-20853

Radial particle density profile in neon negative glow plasma in cylindrical discharge tube measured by double probe method 08 p1362 A67-21288

Microwave loss in reflex plasma discharge determined from microwave energy decay measurements 08 p1363 A67-21311

Amplification of RF wave in partially ionized gases with large Ramsauer effect in absence of magnetic field, due to negative absorption of stimulated bremsstrahlung 08 p1366 A67-21442

Pinch discharge cumulation by using stimulated emission generated in high temperature plasma of strong current pinch discharge 08 p1366 A67-21501

Direct current electrical discharge investigated in gas flow in magnetic field perpendicular to flow direction 09 p1542 A67-21816

Spectroscopic studies of plasma pulse discharge on hard electrodes in vacuum, determining excitation temperatures for various portions of jet 09 p1544 A67-21852

Collision of opposed supersonic jets in pulse discharges, noting formation of shock-constricted plasma regions between electrodes 09 p1544 A67-21855

Variation of phase constant and damping constant of SHF wave propagating in waveguide incorporating coaxial plasma-filled dielectric tube 09 p1473 A67-21999

Vortex stabilized electrodeless annular discharge in argon at atmospheric pressure, describing experimental equipment, procedure and results 09 p1547 A67-22319

Neutron emissions by noncylindrical discharges of revolution, noting high pressure and impurities favoring airtight magnetic piston 10 p1683 A67-22844

Vapor deposition of thin films by decomposition of metallic alcohols in luminescent discharge plasma 10 p1696 A67-23692

Plasma confinement time in helium discharge determined by electron density and helium radiation intensity measurements 11 p1827 A67-23887

Azimuthal modes of Kadomtsev plasma instability, describing subthreshold response spectra 11 p1829 A67-24001

Current distribution of magnetic field in plasma coaxial injector indicating dominant role of Hall effect in plasma acceleration 11 p1841 A67-24854

First azimuthally varying mode in mercury vapor plasma discharge, predicting growth of hose-like instability of electron beam 11 p1841 A67-24928

Configurations of HF discharge plasma and dependence on gas pressure and annular electrode potential 11 p1844 A67-25021

RF plasma torch coupling efficiency shown insensitive to input power and gas flow rate 12 p1976 A67-25925

High intensity runaway electron fluxes accelerated by external field in toroidal plasma discharge, noting pressure effect 13 p2162 A67-26270

Diffusion decay of discharge plasma with oscillating electrons in magnetic field 13 p2170 A67-27376

Pressure gradient in duoplasmatron ion source as function of parameters of discharge 14 p2359 A67-28512

Argon plasma accelerator producing diamagnetic discharge measured along axis for plasma properties 14 p2362 A67-29046

Density measurement of plasma discharge captured by magnetic field, considering linear and toroidal sections of collector 15 p2529 A67-29717

Physical properties of binary pulsed discharge plasma in helium and argon seeded with Cs and K 16 p2711 A67-30525

Pulsed discharge in transverse magnetic field noting relation between ionization instability and turbulent conductivity of nonequilibrium plasma 16 p2711 A67-30538

Drift instability of discharge plasma with oscillating electrons 16 p2717 A67-31180

Anomalous decay of discharge plasma with oscillating electrons in strong magnetic field, using diagrams 16 p2717 A67-31181

High pressure electrodeless discharge in pure Ne and Xe and mixture of Kr and Xe, detailing effect of steady state magnetic field on Xe plasmoid 16 p2717 A67-31185

Helium plasma electron temperature and density dependence, with/without magnetic field, on pinch discharge 16 p2718 A67-31187

Gas kinetic pressure measurement in high current rectilinear hydrogen-plasma discharge during electron heating 16 p2718 A67-31188

Approximate solutions of spatial distributions of charged particles as gas discharge plasma obtained by two-point Jacobi expansion method 16 p2720 A67-31241

Azimuthal motion of glow discharge plasma in space between two coaxial dielectric cylinders in crossed radial magnetic and axial electric fields 16 p2723 A67-31580

Optical properties of moon quantitatively compared with powder samples, bombarded with ions from hydrogen discharge plasma 16 p2753 A67-31744

HF electrodeless plasmatron working at atmospheric pressure, noting plasma discharge and temperature distribution characteristics, obtaining constricted plasma jet 17 p2897 A67-32175

Induced argon discharge shown to have shape of plasma filament, noting detachment from chamber walls 17 p2897 A67-32176

Geometric dimensional, plasma temperature and pressure effects on capillary discharge with evaporating wall /CDEW/ 17 p2897 A67-32177

Duoplasmatron ion source study with Langmuir probe, finding that pressure dependent discharge characteristics relate to magnetic field radial components 17 p2902 A67-32659

Bohm criterion of boundary layer stability related to ambipolar sound generation in positive column plasma discharge, deriving plasma density ambipolar potential distribution 17 p2905 A67-32972

Plasma resonances, deriving relations between coefficients for transmission, reflection and emission of microwaves and explaining collision-free discharge 17 p2907 A67-33105

Channel model examination of output-dependent radius of spherical plasma discharge in thermal equilibrium 17 p2910 A67-33323

Plasma time-dependent luminosity from pulsed discharge in vacuum, determining excitation temperature distribution and discharge spectral lines 18 p3087 A67-34049

High pressure vortical discharge in air and argon, solving differential equations for heat conduction and electromagnetic field by digital computer 18 p3088 A67-34062

Electron density radial distribution, neutral gas temperature and ionization-caused column contraction calculated for cylindrical discharge plasma in argon 18 p3089 A67-34298

Velocity distribution function in positive column plasma and implications for electron energy transfer mechanism on microscopic scale 19 p3267 A67-34948

Electron density decay curves in helium afterglows at high electron densities and gas pressure found controlled by recombination

loss process 19 p3270 A67-35071

Electron-atom collision cross-section in afterglow of pulsed cesium plasma as function of electron cyclotron absorption resonance and electron temperatures 19 p3271 A67-35076

Mercury-argon low pressure discharge initiation stressing positive column establishment, examining breakdown effects by spectrographic techniques 19 p3272 A67-35088

Periodic changes, using square-wave current modulation, between diffuse and highly constricted positive column in medium-pressure rare-gas discharges 19 p3274 A67-35101

Discharge plasmas in hollow cathodes investigated using photography, showing mercury vapor and inert gas plasmas form homogeneous or laminar positive plasma columns 19 p3274 A67-35102

Electron energy distribution and thermalization measurement in Langmuir mode discharge in plasmas, using electron energy spectrometer 19 p3274 A67-35105

Sinusoidal frequency oscillations in DC magnetron plasmas discharge, determining magnetic field, anode current and voltage and gas pressure dependence 19 p3277 A67-35124

DC discharge parameters solution using pressure theory with generation terms stressing one-and two-dimensional cases 19 p3277 A67-35126

Ohm law extended to electrical conduction of partially ionized plasmas and nonneutral ionized gases 19 p3287 A67-35356

High power microwave radiation from nonequilibrium plasma discharge near electron cyclotron frequency 19 p3291 A67-35386

Electron density behind shock front of discharge plasma measured using interferometer 19 p3290 A67-35395

Stream structure and bow waves in electromagnetic shock tube, establishing flow uniformity limitations through temperature and pressure measurements 19 p3294 A67-35404

Operation of ion source with cylindrical symmetry of crossed electric and magnetic fields 19 p3297 A67-35596

Pulsar circuit for studying large signal transient response in plasma lasers 20 p3445 A67-36530

Transient heating and cooling of current carriers in semiconductors and highly ionized plasma analyzed, using effective temperature method 20 p3513 A67-37438

Current distribution of magnetic field in plasma coaxial injector indicating dominant role of Hall effect in plasma acceleration 20 p3502 A67-37537

Singularities of two-fluid plasma equations, investigating compatibility and relation to boundary conditions 21 p3661 A67-37744

Steady state theory of low pressure plasma discharge column in axial magnetic field derived, using moments of Boltzmann equation 21 p3662 A67-37756

Plasma component velocity distribution and multiple plasmoid production indicated in spectrograms from high speed photography of coaxial injector discharge 21 p3664 A67-37939

Discharge plasma in He and argon with cesium and potassium vapor admixtures noting electric field, conductivity, electron temperature and emission spectrum 21 p3664 A67-38160

Complex structure elimination in shock wave region of T-tube, discussing discharge plasma, shock wave trajectories and photographic observation technique 21 p3612 A67-38257

Hydrogen plasma discharge with hot electrons, investigating plasma decay and electron and plasma density 21 p3666 A67-38368

Electron-temperature dependence of electron collision frequency in afterglow plasma 21 p3667 A67-38414

Spatial electron temperature distribution in electrodeless discharge, noting thermal conduction effect [AIAA PAPER 67-692] 21 p3672 A67-38721

Linear nonequilibrium MHD generator channel, studying discharge structure and stability and convective and Lorentz forces effects on electric characteristics [AIAA PAPER 67-718] 21 p3673 A67-38744

Electron temperature measurements of powerful pulsed plasma discharge using spectral line intensity 22 p3852 A67-39991

Electron density between shock front and discharge plasma in electromagnetic shock tube determined by interferometric technique, using guided waves 22 p3810 A67-40523

Platinum wire heating in sealed carbon dioxide laser results in catalyzing effect permitting high carbon dioxide concentration 23 p4011 A67-40784

Impedance of dipole antennas in isotropic He plasma measured at X band 23 p3979 A67-40833

Drop-across-reactance method found satisfactory for accurate current measurements in high voltage RF plasma discharges 23 p4001 A67-41224

Microwave plasma observed using spectroscopic and mass spectrometric techniques, discussing standing wave operation mode, emission and resonance lines 23 p4034 A67-41435

Ion optical system for extraction of dense ion beams from plasma discharges, studying beam forming characteristics via automatic trajectory tracer model 23 p4034 A67-41463

Energy distribution deviation of electrons emitted from plasma or solid via Maxwell distribution, deriving kinetic reflection coefficient in thermionic emission current expression 23 p4047 A67-41688

He-Ne gas mixture DC discharge electron temperature and concentration dependence on tube diameter, pressure and composition, using two-probe method 24 p4196 A67-42242

Plasma discharge instability effect on gas laser operation, discussing moving layers self-excitation and laser beam modulation 24 p4168 A67-42561

Plasma dynamics with HF theta pinch discharges confined in magnetic field 24 p4198 A67-42575

PLASMA DISPERSION

Scattered light spectrum in thetatron plasma, noting onset of ion wave instability 01 p0121 A67-10248

Inhomogeneity parameter for excited atom distributions and line width variations for dispersion contour of spectral line, noting dependency on frequency 01 p0125 A67-11045

Phenomenological approach to dispersion relation for hose instability of charged particle beam passing through plasma 02 p0272 A67-11525

Light modulation at hyperfine frequencies in optically pumped potassium vapor, noting detection techniques, optical absorption and dispersion 02 p0251 A67-11818

Instabilities and dispersion during electromagnetic wave excitation and propagation in weakly turbulent plasma 02 p0278 A67-12627

Landau damping in anisotropic electron plasma treated by kinetic dispersion equation 03 p0474 A67-12920

Warm plasma excitation by electric dipole 03 p0475 A67-13173

HF conductivity, dispersion and temperature modulation of carrier waves and acoustic amplification in drifted semiconductor plasmas 03 p0496 A67-13558

Wave propagation in rarefied two-component plasma situated in uniform constant magnetic field with finite Larmor radius 03 p0483 A67-13875

Dispersion relations and wave power of isotropic compressible lossy plasma slab bounded by free space and ground plane and excited by line sources 03 p0487 A67-14354

Dispersion equation for electromagnetic waves propagating in uniform plasma layer along boundary parallel to external magnetic field 04 p0667 A67-15207

Longitudinal and transverse waves transformation in nonuniform plasma 04 p0668 A67-15276

Ionospheric irregularities explained by gravitational field and positive electron density gradient joint effect on ionospheric region below electron distribution peak 05 p0760 A67-16002

Surface plasma wave dispersion in metals, noting method for solving Kulk equation 05 p0864 A67-16761

Dispersion nucleus of homogeneous nonmagnetic hot plasma and functional properties of plasma waves 06 p1039 A67-18048

Electromagnetic wave dispersion in semiconductor plasma waveguides for case of plane wave propagation normal to magnetic field vector 07 p1231 A67-19133

Electromagnetic-wave radiation peculiarities in homogeneous anisotropic dispersive magnetic plasma 08 p1294 A67-20821

Dispersion equation for whistler mode for velocity distribution with loss cone, discussing critical stability 08 p1324 A67-20894

Ion wave amplification in two-component plasma due to isothermal electron gas 08 p1365 A67-21414

Spectrum of ionic waves in plasma located in electrical field and interacting with charged particle beam, obtaining dispersion equation 09 p1544 A67-21846

Numerical integration of dispersion relation for electron beam in plasma 09 p1546 A67-22313

Plasma column and plasma beam of same radius situated in coaxial waveguide under magnetic field, obtaining dispersion equation 09 p1465 A67-22551

Dispersion relation for large amplitude circularly polarized plane wave propagation along magnetic field in hot collision-free plasma, considering distribution function 11 p1826 A67-23881

Summation of convergent series for cyclotron harmonic wave dispersion for numerical and analytic work 11 p1827 A67-23886

Hydromagnetic gradient waves theory extended to weakly ionized medium-density magnetized plasma of type expected in ionospheric E layer 11 p1783 A67-23923

Ion-ion collision and shear stabilizing effect on resistive drift mode, applying dispersion relation with BGK collision operator 11 p1834 A67-24374

Nonlinear wave processes in plasma in strong magnetic field, obtaining dispersion for fundamental and harmonic 11 p1836 A67-24392

Electron plasma wave propagation along cylindrical plasma column in magnetic field, calculating damping and dispersion curves 11 p1837 A67-24401

Random walks computer experiments on ensembles of random binary homogeneous velocity fields, using Eulerian and Lagrangian statistics 11 p1756 A67-24542

Ionic waves in plasma in electric field interacting with beam of charged particles at relaxation time, using dispersion equation 11 p1841 A67-24869

Instabilities and dispersion during electromagnetic wave excitation and propagation in weakly turbulent plasma 13 p2171 A67-27384

General dispersion relation for linear waves in multicomponent plasmas 13 p2172 A67-27726

Dispersion relation for linear three-component plasma, considering two extreme degrees of ionization 13 p2172 A67-27727

Dispersion of proton whistlers in plasma in motion with respect to observer 14 p2379 A67-27933

Dispersion relation for two-component model of collisionless nonrelativistic plasma with external magnetic field acting on system 14 p2356 A67-28201

Space-time description of dynamical phenomena in unbounded homogeneous linear medium, noting dispersion properties and wave structures in plasma 14 p2358 A67-28461

Source free solutions in ionized regions, discussing geometrical optics application to MGD with infinite conductivity 14 p2359 A67-28462

Motion and dispersion of inhomogeneity in unbounded plasma in magnetic and electric fields 14 p2359 A67-28504

Ion cyclotron resonance heating limitation in shallow magnetic beach explained by wave reflection 15 p2523 A67-29212

Dispersion relations of moving stratiations in rare gases, noting wave nature and dependence on discharge current 15 p2472 A67-29733

Oscillations of confined cylindrical plasma with hot electron current, obtaining dispersion relation for large Debye radius 15 p2531 A67-30072

Dispersion equation for electromagnetic waves propagating in uniform plasma layer

along boundary parallel to external magnetic field 15 p2532 A67-30255

Kelvin instability following velocity discontinuity in current-carrying cold collisionless plasmas under magnetic field, deriving dispersion relation and instability criteria from fluid equations 16 p2714 A67-30872

Field distribution in plasma waveguide at LF and large densities, noting dispersion properties of E and H waves 16 p2718 A67-31189

Asymptotic behavior of transient signal propagation in lossless, isotropic plasmas for stepmodulated sine wave input signal 16 p2627 A67-31351

Dispersion equations for long wavelength beam instability propagating through homogeneous plasma 17 p2895 A67-32160

Nonconvective instability for hot plasmas from poles colliding through negative wave numbers 17 p2899 A67-32276

Excitation and propagation of surface plasma waves along plasma column in noble gases, obtaining plasma dispersion curves 17 p2899 A67-32309

Stark effect in plasma, discussing theory, Lorentz symmetrical dispersion profile, atomic interaction, etc 17 p2901 A67-32404

L-pulses of Jupiter radiation, attributing 1-sec component of time structure on decametric emission to diffraction by solar wind inhomogeneities 17 p2944 A67-32643

Dispersion effect on shock wave structure in magnetoplasma, analyzing role of wave front inclination angle to magnetic field 18 p3084 A67-33525

Propagation and radiation problems in linear homogeneous dispersive anisotropic media in uniform motion solved using constitutive equation 18 p3001 A67-34198

Periodic changes, using square-wave current modulation, between diffuse and highly constricted positive column in medium-pressure rare-gas discharges 19 p3274 A67-35101

Plasma resonance in RF discharge excited with frequency higher than collision frequency, determining electron density 19 p3276 A67-35114

Media with cold homogeneous isotropic lossless plasma dispersion characteristics exhibiting no electromagnetic drag 19 p3298 A67-35828

Dispersion equation for electrodynamic boundary value problem of natural oscillations of cylindrical resonator with magnetoactive plasma 19 p3299 A67-36019

Dispersion equations and solution for transverse magnetic waves in parallel-plate waveguide partially filled with plasma slab, discussing existing modes 20 p3492 A67-36127

Dispersion relation for microinstabilities in finite plasma noting relation to particle motion 20 p3496 A67-36215

Auroral breakup relation to ring current interchange instability, studying dispersion relation effects 20 p3431 A67-37096

Surface plasma oscillations at optical frequencies detected by radiation from optical grating metal surface, measuring dispersion relation 20 p3514 A67-37569

Plasma wave propagation dispersion in sodium and potassium at cryogenic temperature using Landau-Fermi liquid theory 20 p3514 A67-37570

Ion cyclotron wave propagation in plasma, considering Larmor radius effects, quasi-static dispersion relation, phase velocity and cyclotron resonance 21 p3661 A67-37750

Dispersion equation of radioactive compressible nonviscous plasma with finite electric conductivity under gravitational and axial magnetic fields 21 p3663 A67-37918

Electrostatic ion cyclotron waves excitation in plasma and ion heating due to cyclotron damping 21 p3667 A67-38407

Dispersion equation for frequency dependence on wave amplitude propagated in plasma placed in constant magnetic field causing longitudinal oscillations 21 p3669 A67-38681

Dispersion equation for extraordinary and plasma waves propagating through magnetoplasma perpendicular to external magnetic field studied near lower hybrid frequency 22 p3844 A67-39419

Dispersion relation for wave propagation in electro-magneto-ionic medium under electric and magnetic fields obtained using Maxwell-Boltzmann-Vlasov equations,

discussing cut-off frequency 22 p3788 A67-39469

Unstable coupling between slow space charge mode of electron beam and lowest plasma electron band modes in finite geometry 22 p3847 A67-39643

Energy dissipation due to spatial dispersion proven identical to dissipation due to Landau damping for large waves 22 p3847 A67-39649

Maxwell-Euler equations reformulated into equivalent matrix integral equation, obtaining dispersion relation from integral equation kernel for compressible electron plasma 23 p3974 A67-41204

Dispersion equations for rectangular helix in presence of plasma 24 p4121 A67-42235

PLASMA DYNAMICS

Atomic energy levels in plasma, considering energy spectrum of hydrogen-like atom in plasma based on cut-off Coulomb potential model 06 p1039 A67-17881

Radio electronics, discussing quantum electronics, lasers, microwave devices and technology, plasma physics, etc 06 p0968 A67-18072

Low power MPD arc thruster design and performance with radiation cooled electromagnets and permanent magnets [AIAA PAPER 67-50] 06 p1074 A67-18436

Kinetic theory-plasma dynamics theory calculations of magnetospheric solar wind proton velocity distribution as function of particle speed 08 p1377 A67-21315

Optimum conditions for MHD power generation with Joulean dissipation derived from first and second law of thermodynamics 09 p1442 A67-21799

Approximation equations of thermodynamic data of air-carbon plasma with arbitrary carbon content in atomic region 10 p1732 A67-22919

Second order gyroviscous stress in collisionless plasma for LF propagation quasi-perpendicular to magnetic field, calculated by utilizing higher moments of Vlasov equation 10 p1685 A67-23331

Dynamics of fluids and plasmas - Conference, University of Maryland, October 1965 11 p1779 A67-24532

Stellar dynamics and galactic spiral structure analyzed using gas and plasma dynamics 11 p1863 A67-24534

Plasma physics basic principles, noting plasma dynamic behavior determination by electric and magnetic forces, plasma generation, etc 13 p2167 A67-27150

Current voltage characteristics of argon cesium plasma in inductive hydrodynamic shock tube 14 p2354 A67-27761

Plasma dynamics - AIAA and Northwestern University Conference, Evanston, August 1965 14 p2361 A67-29034

Lenard-Balescu kinetic equation solved by Chapman-Enskog method for transport coefficients of plasmas noting diminishing value 15 p2522 A67-29210

Anisotropic macroscopically neutral plasma excitations by arbitrary current described by potentials, noting electroacoustic wave propagation 15 p2527 A67-29482

Pressure attenuation of transverse fringe effect in flat linear induction pumps 16 p2723 A67-31582

Super-Alfvenic point or distance of effective corotation for loss of angular momentum in solar wind plasma 17 p2945 A67-32644

Plasmoid motion in longitudinal, transverse and two-dimensional multipole magnetic fields, investigating electric fields and plasmoid parameters 17 p2904 A67-32916

Electron concentration in turbulent boundary layer of weakly ionized plasma when injecting electrons through pores in wall 18 p3087 A67-34053

Vector wave functions for boundary value problems in compressible plasma for spherical geometry, noting Fourier series, acoustic wave, etc 18 p3090 A67-34382

Time and space development equations for longitudinal and transverse modes in Vlasov plasma 18 p3092 A67-34745

Collisionless electron plasma dynamics in one dimension, investigating nonlinear Vlasov equation for Landau damping and instability 18 p3092 A67-34747

Book on electrodynamics of plasmas covering analysis of collective properties of plasma based on classical and quantum-statistical mechanics 19 p3267 A67-34866

Plasma finite orbits instability due to plasma particle shift, discussing collision frequency role 19 p3267 A67-34896

LF acoustic/magnetoacoustic wave propagation in partially ionized plasmas studied within framework of macroscopic plasma dynamics, using dynamic adiabatic state equation 19 p3290 A67-35375

Magneto-fluid and plasma dynamics - Conference, New York, April 1965 20 p3493 A67-36142

Plasma kinetic theory, discussing BBGKY hierarchy, nonequilibrium processes and unstable plasma kinetic equations 20 p3495 A67-36154

Pressure transducers for use in high temperature and pressure gaseous detonation wave phenomena, discussing performance and application 20 p3443 A67-36514

Book on statistical theory of nonequilibrium processes in plasma, using microscopic equations to obtain two first moments of random functions 20 p3499 A67-36951

Counterstreaming ion electrostatic instability at cyclotron frequency to enhance trapping of injected ion beam 21 p3661 A67-37748

Plasma hydromagnetic jump conditions derived from two-fluid plasma model, discussing relevance to collisionless plasma shock 21 p3662 A67-37764

Low amplitude MHD shock wave attenuation, assuming high magnetic Reynolds numbers and small excitation zone width 21 p3665 A67-38239

MHD channel wall boundary layer equations for low temperature plasma, determining friction and heat transfer coefficients and leakage current 21 p3665 A67-38241

Energy indicators calculated for MHD channel flow with finite sectional electrodes and wide Hall parameter variations 21 p3665 A67-38242

Plasma rotation in MPD arc measured for electric and magnetic field distribution and current and electron density distribution [AIAA PAPER 67-655] 21 p3689 A67-38691

MPD Hall accelerator construction and operation using argon or helium propellants, measuring azimuthal velocities in plume [AIAA PAPER 67-672] 21 p3691 A67-38705

Anode heat transfer in MPD arc, discussing configurations and thrusters [AIAA PAPER 67-673] 21 p3691 A67-38706

Distributions of current, potential, electron density and pressure and ion velocity vector orientation in MPD arc, verifying electromagnetic effects presence [AIAA PAPER 67-676] 21 p3671 A67-38709

Strong blast waves and laser generated plasma dynamics in high pressure gas investigated using Mach-Zehnder interferometer and pressure probe measurements [AIAA PAPER 67-696] 21 p3672 A67-38725

Spacecraft-space plasma electric equilibrium, discussing active spacecraft configurations for control [AIAA PAPER 67-702] 21 p3714 A67-38729

Density, electric field and volt-ampere characteristics for spherical electrostatic Langmuir probe in collision plasma with weak ionization and recombination, using asymptotic method 21 p3672 A67-38732

[AIAA PAPER 67-705] 21 p3672 A67-38732

Electrostatic ion propulsion and KEMAN MPD thruster research in Germany [AIAA PAPER 67-724] 21 p3694 A67-38749

French research on electric propulsion dealing with plasma dynamics, discussing traveling wave accelerators, pulsed plasma guns, ion thrusters, etc [AIAA PAPER 67-740] 21 p3695 A67-38762

Steady flow ammonia MPD arc jet thruster propulsion performance, discussing test chamber pressure variation, thrust data and cooling systems [AIAA PAPER 67-690] 21 p3696 A67-38930

Plasma model kinetic equation, discussing collision operator approximating momentum and energy transfer rates 22 p3843 A67-39265

Dielectric susceptibility and ion density measurement for polarized hydrogen plasma moving through transverse magnetic field 22 p3845 A67-39424

Plasma stability in nonuniformly oriented magnetic field at guiding center limit 22 p3848 A67-39688

High beta plasmas in linear theta pinches and cusp compression devices, discussing various theta pinch and cusp experiments 22 p3851 A67-39983

Galactic plasma dynamics related to galactic magnetic field generation and topology, discussing agreement with Hoyle-Ireland model and Morris-Berg observations 22 p3854 A67-40503

Book on dynamics of rarefied gas, discussing kinetic theory, shock wave structure, Couette flow, gas flow between coaxial cylinders and plasma dynamics 23 p3989 A67-40873

Plasma dynamics with HF theta pinch discharges confined in magnetic field 24 p4198 A67-42575

Laser-irradiated plasma theoretical study indicating absorption enhancement in external magnetic field 24 p4199 A67-43104

PLASMA ELECTRODE

Potential distribution between graphite and metallic electrodes of MHD generator in nonstationary heat conditions under induced or applied electric field 01 p0011 A67-10176

Configurations of HF discharge plasma and dependence on gas pressure and annular electrode potential 01 p0122 A67-10348

Width and rate of propagation of plasma current layer along accelerating electrodes of plasma gun at initial phase of discharge 02 p0278 A67-12621

Electrode geometry effect on current and potential distributions in MPD arcs 06 p1074 A67-18335

Space charge and eddy currents in ionized gas flow in MHD channel determined, showing effect of cold electrode boundary layer on electrical performance 11 p1746 A67-24874

Configurations of HF discharge plasma and dependence on gas pressure and annular electrode potential 11 p1844 A67-25021

Electric current conduction between cold electrodes in shock-ionized air plasmas, noting current-voltage characteristics in flow behind shock wave 12 p1974 A67-25401

Plasma acceleration across magnetic field in linear accelerator, calculating values from voltages at electrode ends 12 p1977 A67-26075

Cylindrical screened electrode for measuring temperature plasma conductivity in MGD generator 13 p2055 A67-26434

Width and rate of propagation of plasma current layer along accelerating electrodes of plasma gun at initial phase of discharge 13 p2170 A67-27377

Plasma acceleration in flat electrode plasma source simulated by ideally conducting bridge described electrostatically 15 p2525 A67-29249

Wall conductance of insulating gaps between electrode segments shown as cause of inferior performance of MHD generators 16 p2599 A67-30526

Internal resistance, potential fall and current distribution for staggered electrode geometry in MHD generator of Faraday type 16 p2599 A67-30528

Current distribution in Faraday MHD generator measured with potassium resonance lines 16 p2599 A67-30529

Cleavage method to study pulsed pressure/energy content/ in dense gas-discharge hot plasma 16 p2714 A67-31037

Marshall plasma gun with titanium electrodes saturated with deuterium for filling magnetic collector 16 p2678 A67-31400

Electrode heating of arc burning in moving plasma in vacuum, giving setup, heat emission diagrams, etc 17 p2907 A67-33091

Electrode in low temperature air plasma containing potassium, investigating cathode potential drop, current density dependence, current-voltage characteristics, temperature, etc 18 p3088 A67-34054

Plasma behavior in shock tubes with parallel conductors, discussing shape of front and velocity dependence on pressure and gas composition 18 p3089 A67-34297

Space charge analyses applied to electron beam extractions from plasma cathodes, computing stability data for potential distributions and extracted current 20 p3495 A67-36168

Cold Cu electrode interaction with H plasma, measuring electrode I-V characteristics, interelectrode charge concentration, electron temperature, etc 22 p3846 A67-39505

PLASMA-ELECTROMAGNETIC INTERACTION

Combination scattering suffered by component, polarized parallel to electromagnetic wave incident on plasma cylinder, from Tonks-Dattner resonances excited by perpendicular component 01 p0020 A67-10148

Electromagnetic reflection and transmission coefficient maxima in bounded plasma slab 01 p0022 A67-10443

Reflection of vertically polarized exponentially varying electromagnetic waves by horizontally stratified magnetoplasma half-space 01 p0023 A67-10471

Cerenkov and cyclotron absorption of Alfvén and fast magnetoacoustic waves in plasma with gas-kinetic pressure in quasi-linear approximation 01 p0124 A67-10747

Surface charge and impedance of plasma excited by incident electromagnetic waves 02 p0190 A67-11507

Radio wave scattering and resonance scattering in wake of body moving in lower ionosphere plasma due to disturbance of electron concentration 02 p0192 A67-11657

Resonance absorption of electromagnetic power by weakly ionized gas produced in cylindrical discharge tube 02 p0273 A67-12184

Fast and slow electromagnetic wave propagation along annular plasma 02 p0204 A67-12187

Cross polarized component of radiation from spherical antenna produced by anisotropic plasma sheath 02 p0220 A67-12193

Kinetic theory for passage of electromagnetic wave through plasma layer in waveguide with metallic walls, assuming negligible transverse particle motion due to strong magnetic field 02 p0205 A67-12474

Stability of flute oscillations of rarefied plasma in constant electric field normal to magnetic field 02 p0278 A67-12619

Quasi-linear theory of plasma cyclotron instability for one-dimensional oscillation spectrum, noting energy of interaction with electromagnetic field, ion velocities, etc 03 p0475 A67-12933

Dispersion angle of radio waves in interplanetary plasma 03 p0368 A67-13279

Impedance of finite insulated antenna in cold plasma with perpendicular magnetic field 03 p0385 A67-13851

Laboratory-controlled nonlinear, nonresonant excitation of electron plasma oscillations with one transverse electromagnetic wave 03 p0485 A67-14052

Coherent interaction of two radio waves in plasma, generation of mutually-harmonic frequency wave and application to radio transmission in ionospheric F layer 03 p0372 A67-14091

Theoretical possibilities of using electromagnetic forces for acceleration of plasmas/self-magnetic and Hall acceleration/ in case of axisymmetric electrode arrangement 04 p0687 A67-14559

Three-wave interaction Hamiltonians describing nonlinear couplings of plasma oscillation with electromagnetic field derived by Bohm-Pines method 04 p0662 A67-14613

Interactions in low density plasma beams of electrostatic thrust engine exhaust, discussing neutralization, instabilities, plasma wind tunnel, etc 04 p0690 A67-15022

Plasma wave behavior in strong external magnetic field, discussing scattering at ions, wave transformations and nonlinear wave interactions 04 p0667 A67-15206

Plasma behavior in magnetic trap with opposite fields, noting Coulomb ion-ion collisions and proton charge reversal 04 p0667 A67-15211

Plane wave interaction with surface waves at plasma boundary 04 p0668 A67-15274

Bistatic radar cross section of underdense turbulent plasma measured at X-band and results compared with theoretical scattering model 05 p0760 A67-15999

Nonlinear instability of optical frequencies in partially ionized plasma, noting nonlinear frequency buildup for strong plasma waves 05 p0852 A67-16691

Small amplitude electromagnetic wave propagation in collisionless plasma with negative ions, noting bands and waves for various frequencies and polarizations 05 p0853 A67-16846

Radiation resistance and modes of oriented electric dipole in loss-free

- magnetoplasma 05 p0853 A67-16848
- Behavioral equations derived for caustic that envelops locally-plane cylindrical wave incident on plane surface of layered plasma wedge 05 p0765 A67-16962
- Book on electromagnetic wave emission, absorption and scattering processes in gaseous plasma 05 p0855 A67-17152
- Recognition and subsequent amplification of difference frequency in plasma-beam system with two electromagnetic waves propagating in opposite direction 05 p0766 A67-17170
- Nonlinear interaction of two electromagnetic waves in infinite cold magnetoactive plasma 05 p0766 A67-17230
- LF whistler mode of electromagnetic waves propagating at angle to magnetic field in model plasma 05 p0857 A67-17426
- Plasma expansion in magnetic field, showing dominating effect of initial outward momentum 05 p0858 A67-17428
- Statistical determination of correlation functions of plasma scattered coherent light 06 p1039 A67-17824
- Wave scattering in plasma in presence of transformation 06 p1045 A67-18785
- Electromagnetic and electroacoustic waves and scattering in compressible plasma 07 p1141 A67-19443
- Optical and acoustic waves and scattering in compressible plasma treated by ray optical method 07 p1141 A67-19444
- Input resistance of short filamental antenna in warm plasma according to kinetic theory and hydrodynamic equations 07 p1151 A67-19445
- Thin plasma effect on admittance of aperture antenna in infinite conducting plane for various modes 07 p1151 A67-19447
- Paramagnetic current formation due to volume resonator microwave field interaction with dense plasma subject to RF pressure and EPR in static magnetic field 07 p1228 A67-19512
- Theoretical possibilities of using electromagnetic forces for acceleration of plasmas /self-magnetic and Hall acceleration/ in case of axisymmetric electrode arrangement 07 p1240 A67-19569
- Radiation belts, energetic charged particle flux and trapped radiation in geomagnetic field as result of neutron albedo decay and plasma-magnetic field interactions 07 p1246 A67-20297
- Propagation difficulties and anomalies caused by characteristic plasma behavior in connection with space mission telecommunication 08 p1293 A67-20684
- Plasma sheath formation and effect on satellite interacting with geomagnetic field and ambient plasma 08 p1410 A67-20714
- Relativistic mechanism of electromagnetic wave scattering at velocity fluctuations and emission from plasma in external field 08 p1295 A67-20831
- Discrete spectrum of electromagnetic waves caused by excitation of dielectric layer on ideally conducting plane in homogeneous absorbing plasma 08 p1295 A67-20832
- Electrodynamic properties of homogeneous magnetoactive plasmas including wave propagation, excitation, scattering, etc 08 p1358 A67-20863
- Complex dielectric constant and EM plane wave propagation in flame plasma 08 p1359 A67-21045
- Ion beam excitation of drift waves in alkali plasma, discussing sinusoidal signal propagation characteristics, variations with beam velocity and with modulation frequency 08 p1361 A67-21135
- Energetic particle scattering by laboratory plasmas, deriving expressions for scattering coefficients in terms of electric field autocorrelation function 08 p1361 A67-21136
- Self-consistent field approximation to ion-beam-plasma boundary interaction noting effect on ion beam structure, boundary conditions and resulting current density 08 p1363 A67-21307
- Energy coupling among electron acoustic, ion acoustic and transverse electromagnetic waves at two-fluid plasma density discontinuity 08 p1364 A67-21397
- Transverse electromagnetic waves with constant phase velocity in fully ionized Vlasov plasmas 08 p1364 A67-21401
- Monochromatic wave interaction with isotropic electron-plasma, determining field and surface wave generated on basis of Maxwell equations 09 p1464 A67-22012
- Spectral analysis of interacting electromagnetic, plasma and spin waves in antiferromagnetic semiconductors and metals with easy-axis and plane type anisotropy 09 p1555 A67-22073
- Self-focusing laser beam in inhomogeneous plasma 09 p1515 A67-22276
- Admittance of circumferential gap in infinite cylindrical antenna covered by set of coaxial dielectric or plasma layers, noting excited metal cylinder 09 p1481 A67-22447
- Spectral densities of electromagnetic fields of thermal radiation in magnetoplasma as related to radiation resistance of immersed antenna 09 p1464 A67-22448
- Dispersion of mode couplings of wave propagation in waveguide containing plasma electron beam system 09 p1550 A67-22582
- Plasma magnetization under action of circularly polarized wave, noting inverse Faraday effect 10 p1683 A67-22853
- Wave propagation in hot plasma in cylindrical waveguide with arbitrary axial magnetic field, treating boundary value problem by perturbation expansion 11 p1826 A67-23874
- Electrostatic wave excitation growth in collisionless plasma interaction and simultaneous modification with electron beam studied for weakly unstable situations 11 p1826 A67-23875
- Nonlinearity caused by relativistic mass effect leading to radiation maxima of plasma excited by two pulses at electron gyrofrequency 11 p1827 A67-23889
- Flute instability in low beta plasma in presence of nonuniform electric field perpendicular to magnetic field 11 p1828 A67-23891
- Relativistic electron motion in mirror magnetic field interacting with axial electromagnetic wave calculated, comparing results with Seidl experiment 11 p1828 A67-23895
- Steady state plasma belt in dipole magnetic field, measuring spatial variation of density and temperature, electron spin, gyration, etc 11 p1828 A67-23940
- Current distribution and input admittance of infinitely long cylindrical antenna driven by slice generator and immersed in anisotropic plasma 11 p1761 A67-24284
- Low temperature alkali plasmas in magnetic fields in terms of collisional drift modes, determining steady state frequencies, amplitudes, etc 11 p1834 A67-24381
- Magnetically confined cesium plasma analyzed under radial electric field, noting radial plasma loss rate 11 p1835 A67-24384
- Nonlinear wave processes in plasma in strong magnetic field, obtaining dispersion for fundamental and harmonic 11 p1836 A67-24392
- Barium Q plasma device for optical diagnosis of oscillatory microinstabilities compared with Langmuir probe 11 p1838 A67-24406
- Enhanced plasma fluctuations produced by suprathermal electron effect on emission and scattering of electromagnetic waves, noting analogy with corona plasma 11 p1839 A67-24546
- Gyroviscosity of collisionless plasma in strong magnetic field, duality theorem and application to linear stability analysis 11 p1839 A67-24547
- Magnetic field effect on electromagnetic wave propagation through free carrier plasmas in semiconductors, considering Faraday configuration 11 p1840 A67-24663
- Ionic waves in plasma in electric field interacting with beam of charged particles at relaxation time, using dispersion equation 11 p1841 A67-24869
- Reflection and transmission of electromagnetic waves at interface between stationary isotropic medium and moving anisotropic medium 11 p1820 A67-24919
- Cylindrical wave propagation in rarefied plasma, examining effect of compression on internal plasma-magnetic field by external field 11 p1842 A67-24964
- Electron temperature vs plasma cell power input measured, determining electron energy loss factor for hot diatomic gases in electric field 12 p1973 A67-25398
- Plane wave propagation across thin stratified plasma sheaths, noting polarization and reflection [AIAA PAPER 66-481] 12 p1905 A67-25906
- Polarized harmonic electromagnetic wave propagation in plane stratified isotropic plasma of cold lossless electron gas, resolving inconsistency near resonance region 12 p1976 A67-25944
- Plasma acceleration across magnetic field in linear accelerator, calculating values from voltages at electrode ends 12 p1977 A67-26075
- Self-excitation regime associated with traveling magnetic field interaction with ionized gas flow 12 p1977 A67-26077
- RF sources imbedded in ionized plasma noting developments since 1963 12 p1908 A67-26162
- Plasma EM instability in magnetic mirror configuration, solving linearized Vlasov equation for dispersion relation of transverse EM waves 13 p2164 A67-26293
- Modulated electron beam interaction with plasma formed by beam causes ion heating to energies of hundreds of volts in magnetic mirror field 13 p2164 A67-26299
- Kinetic approximation of penetration of electric field into plasma layer situated in stationary magnetic field, determining plasma field 13 p2164 A67-26396
- Fast ions produced in interaction between escaping electrons and plasma 13 p2164 A67-26402
- Resonance scattering of electromagnetic waves on arbitrary rarefied plasma region with near zero intrinsic wave number relative to small perturbation 13 p2067 A67-26547
- Cerenkov and cyclotron absorption of Alfvén and fast magnetoacoustic waves in plasma with gas-kinetic pressure in quasi-linear approximation 13 p2166 A67-26776
- Plasma physics basic principles, noting plasma dynamic behavior determination by electric and magnetic forces, plasma generation, etc 13 p2167 A67-27150
- Stability of flute oscillation of rarefied plasma in constant electric field normal to magnetic field 13 p2170 A67-27375
- Integrals of motion-equations for charged particles in axisymmetric magnetic field derived using perturbation theory 14 p2353 A67-27752
- Cathode noise voltage in low current arc at atmospheric pressure as function of arc cathode surface state 14 p2354 A67-27764
- Plasma in diffusion regime situated in nonhomogeneous RF field with rotation symmetry 14 p2354 A67-27765
- HF conductivity of weakly ionized plasma, establishing expression for Lorentz plasma conductivity 14 p2355 A67-27954
- Surface charge and impedance of plasma excited by incident electromagnetic waves 14 p2261 A67-28071
- Electromagnetic wave propagation characteristics in solid plasmas without magnetic induction, showing dynamic Hall effect 14 p2366 A67-28473
- Spontaneous visible light emission due to laser action in carbon dioxide laser plasma, examining plasma current change with phase-lock technique 14 p2331 A67-28494
- Moment method treatment of collisionless plasma equilibria in confining magnetostatic fields, using Vlasov equation to determine distribution function of particles 14 p2360 A67-28554
- Equations describing forces of electromagnetic wave interaction with spherical plasmoid in free space 14 p2361 A67-28806
- Asymptotic solution of oblique waves in inhomogeneous vertically magnetized plasma 14 p2361 A67-28922
- Heating of magnetized hot diffuse plasma using difference-frequency signal generated from two HF transverse waves 15 p2521 A67-29188
- Kinetic equation for plasma with electromagnetic interactions, using shielding approximation 15 p2519 A67-29209
- Small nonpolarized plasmoids interacting with axisymmetric magnetic field, discussing penetration mechanism, equations of motion and magnetic moment 15 p2524 A67-29245
- Longitudinal deformation of plasmoid interacting with axisymmetric magnetic field, noting expansion in homogeneous region 15 p2525 A67-29246
- Radial deformation of premagnetized plasmoid interacting with increasing magnetic field 15 p2525 A67-29247

ONERA hot-shot wind tunnel flow stability and homogeneity and measurement of plasma electromagnetic field, skin friction, etc [ONERA-TP-447] 15 p2465 A67-29377

Steady two-dimensional magnetic bottle in which moving, compressible and electrically conducting plasma is confined by horizontally aligned magnetic field 15 p2528 A67-29568

Interaction between SHF field and created plasma in electron-cyclotron resonance state 15 p2529 A67-29715

Nonlinear instability of optical frequencies in partially ionized plasma, noting nonlinear frequency buildup for strong plasma waves 15 p2530 A67-29862

Reflection coefficient for electromagnetic wave in circular cylindrical shock tube incident on moving plasma calculated numerically 15 p2531 A67-29905

Plasma wave behavior in strong external magnetic field, discussing scattering at ions, wave transformations and nonlinear wave interactions 15 p2532 A67-30254

Plasma behavior in magnetic trap with opposite fields, noting Coulomb ion-ion collisions and proton charge reversal 15 p2532 A67-30259

Electrode-to-plasma conduction process effect on MHD generator performance, noting current saturation conditions and results 16 p2601 A67-30550

Radio wave scattering and resonance scattering in wake of body moving in lower ionosphere plasma due to disturbance of electron concentration 16 p2624 A67-31072

Acceleration of plasma particles to high energies for case of interaction between plasma and stochastic field with harmonic-correlation time 16 p2718 A67-31192

Electrostatic wave effect on anisotropic relativistic proton plasma in magnetic field, noting instability 16 p2739 A67-31234

Plasma anomalous resistive instability shown independent from microinstability and caused by poor conductivity parallel to magnetic lines 16 p2720 A67-31240

Interaction of incident H-wave with infinite conducting cylinder coated with inhomogeneous and anisotropic plasma sheath, noting far field pattern of scattered field 16 p2626 A67-31350

Excitation of high and low frequency electromagnetic waves in unbounded plasma by external currents, deriving wave excitation intensity expression 16 p2721 A67-31477

Particle theory analysis of electromagnetic and electrostatic instabilities due to anisotropic velocity distributions 16 p2722 A67-31560

Diamagnetic properties of plasma described by extended field equations suggest existence of steady state inductive power transfer between plasma and magnetic fields 17 p2898 A67-32178

Ruby laser light scattering by theta pinch plasma measured with Fabry-Perot spectrometer, noting cooperative density fluctuations superimposed on thermal density fluctuations 17 p2899 A67-32274

Nonlinear effects in collisionless plasma during interaction with strong HF field 17 p2905 A67-32920

Statistical particle acceleration mechanism in plasmas noting Cerenkov acceleration, particle state changes, wave generation, etc 17 p2905 A67-32921

Nonlinear interacting plasma wave equations derived by semiquantum analysis of wave-particle and wave-wave interactions 17 p2905 A67-32923

Voltage drop near electrode during plasma and electric field interaction in electrical discharge tube, giving plasma current-voltage curves 17 p2907 A67-33090

Trapped plasma build-up in magnetic field by ionization of injected atomic beam, noting ionization cross section parameters 17 p2908 A67-33115

Interaction of planetary magnetic field with solar plasma studied using hypersonic analog, estimating energy transfer rate 17 p2951 A67-33208

Coupling between neutral air motion and plasma transport in model F-2 layer, noting nonlinear diffusion equation, velocity profiles, etc 17 p2852 A67-33241

Density contour determination for magnetically confined plasma by energetic

molecular ion beam probe of plasma and atomic ion measurement from collisional dissociation 17 p2910 A67-33358

Thomson scattering of Q-switched ruby laser beam in shock wave plasma, determining electron densities, spectral distribution of scattered light, etc 18 p3084 A67-33649

Wave scattering in plasma in presence of transformation 18 p3086 A67-33727

LF waves induced by superimposed electric and magnetic fields in semiconductor plasma 18 p3102 A67-34442

Electromagnetic wave reflection and transmission by moving plasma medium as function of velocity 18 p3091 A67-34633

Interaction between electrostatic and guided electromagnetic wave, considering plasma wave amplification by pumping at microwave frequency 18 p3091 A67-34643

Wave propagation and electron beam-plasma interaction in plasma column inside magnetic field, measuring plasma characteristics and spatial distribution 19 p3275 A67-35107

Intense HF oscillations from plasma-beam interaction in cold cathodes PIG reflex discharge 19 p3275 A67-35109

RF plasma at electron cyclotron frequency produced with axially slotted metal cylinder 19 p3275 A67-35111

Gas ionization and plasma heating by high power microwaves using X-band and S-band frequency magnetrons 19 p3276 A67-35115

Spark perturbation of magnetic and electromagnetic fields, studying plasma-magnetic interaction and spark plasma characteristics 19 p3239 A67-35165

Radiation field interaction with particles in assemblage of electrons and atoms or ions using perturbation theory and Liouville equation 19 p3284 A67-35339

Customary formulas for various effects including Thomson scattering, electron-ion, bremsstrahlung, etc, in context of plasma radiation theory 19 p3284 A67-35340

Alkali-metal magnetoplasma properties related to enhanced diffusion, showing relationship to beam-plasma interaction 19 p3287 A67-35360

Chapman-Ferraro problem analyzed by impinging high speed hydrogen plasma stream against three-dimensional magnetic dipole, discussing boundary shape 19 p3288 A67-35366

Interaction of moving plasma with dipole magnetic field measured visually and with electric and magnetic probes 19 p3288 A67-35367

Intense runaway electron stream from wave-plasma interaction in magnetic field noting microwave radiation and disruption time 19 p3291 A67-35381

UHF wave interaction between plasma and electron stream in magnetic field noting convective instability 19 p3291 A67-35382

Plasma bunches-microwave interaction showing electron energy and plasma ions velocity increase 19 p3291 A67-35384

Nonlinear effects of laser radiation interaction with turbulent dense plasma, discussing wave propagation, plasma diagnostics, etc 19 p3291 A67-35385

Plasma-magnetic shock wave propagation in high pressure, partially ionized argon plasma 19 p3293 A67-35400

Electron distribution function of homogeneous imperfect Lorentz plasma disturbed by electric field 19 p3295 A67-35418

Nonparabolic conduction energy band in semiconductors produces electron plasma excitations of sum and difference frequencies under strong DC electric field 20 p3505 A67-36210

Transverse magnetic field retardation of flowing plasma in electromagnetic shock tube noting conductivity 20 p3496 A67-36214

Electric field produced by polarization in plasmod injected across field in closed system 20 p3497 A67-36681

Bounded plasma flux in magnetic field, considering plasma polarization on magnetic field boundary, noting flux deceleration 20 p3497 A67-36682

Electric vector expression of amplitude-modulated electromagnetic wave propagating in nonlinear dispersive medium 20 p3499 A67-36992

Microwave radiation from plasma beam interaction, measuring radiation intensity as

function of discharge current 21 p3668 A67-38416

NI plasma acceleration in axisymmetric electric discharge by self-induced magnetic field, determining reaction force 22 p3844 A67-39356

Steady state plasma in strong microwave electric field acting on electron component 22 p3845 A67-39431

Harmonic generation and turbulence-like spectrum from pulsed HF beam-plasma interaction, tabulating harmonic wave properties 22 p3847 A67-39615

Analog simulation of electromagnetic radiation from antenna of revolution in vacuum and plasma via networks, discussing rocket nose cone shapes 23 p3977 A67-40578

Charged particle gas interaction with EM field noting electron gas collective oscillations, EM wave propagation in anisotropic plasma and applications 23 p4037 A67-40759

Interaction between plasma stream and inhomogeneous field of electromagnetic wave studied for relation of plasma behavior to potential forces acting on charged particles 23 p4032 A67-40910

Variations in parameters of magnetized plasmods interacting in nonuniform fields determined by magnetic and electric probes 23 p4035 A67-41685

Dielectric function of semiconductor in external electric field, discussing effect on plasma frequency 24 p4201 A67-41979

Electromagnetic wave diffraction in magnetoactive plasma by conducting wedge using Laplace integral in rotating reference frame 24 p4123 A67-42706

PLASMA ENGINE

Low power MPD arc thruster design and performance with radiation cooled electromagnets and permanent magnets [AIAA PAPER 67-50] 06 p1074 A67-18436

German rocket prototype with mercury vapor plasma or xenon plasma engine, discussing design and performance 08 p1410 A67-20641

Plasma measurements in cesium electron bombardment ion engine indicate that reversed cathode-anode configuration improves radial ion distribution [AIAA PAPER 66-248] 10 p1698 A67-23121

Magnetically accelerating continuously operating plasma engine for spacecraft propulsion compared with electrothermal engine 11 p1855 A67-25100

Mercury fed plasma bridge neutralizers for in-flight operation of SERT II electron bombardment ion thruster [AIAA PAPER 67-670] 21 p3691 A67-38704

Rotating current spoke in MPD engine, existence and connection with exhaust fluctuations [AIAA PAPER 67-689] 21 p3693 A67-38720

Plasma Separator Thruster, advanced ion thruster design based on independent operation and optimization of plasma source and plasma extraction system [AIAA PAPER 66-598] 22 p3868 A67-40084

PLASMA FLOW

Space charge formation during flow of electric current in plasma moving under thermal emission of electrons 01 p0118 A67-10043

Cauchy problem of compressible conducting perfect fluid flowing under perturbation influence 01 p0121 A67-10257

Plasma effects in nozzle flow of hypersonic shock tunnel using air, obtaining electron density profile 01 p0126 A67-11442

Stability of counterstreaming flow of electrons and ions in heavily biased diodes theoretically studied by space charge wave and Nyquist analysis 02 p0214 A67-11883

Measurement of ion velocity distribution in plasma stream of pulsed coaxial accelerator agreeing with computation from momentum transfer and mass flow measurements 02 p0276 A67-12568

Motion of plasma through nonuniform transverse magnetic field, noting dependency of plasma motion solely on field intensity 02 p0278 A67-12623

Shape of magnetosphere of rectilinear flow in divergent plasma stream as function of plasma pressure 03 p0474 A67-12921

Lunar eclipse brightness variation relation to geomagnetic planetary index, showing that luminescence is in accord with rate of increase of plasma energy 03 p0509 A67-13165

Plasma streaming across magnetic field by

beam polarization studied by Vlasov equation 03 p0484 A67-14042

Plasma vortex filaments produced in pairs as shown by image converter photographs of interfaces between magnetic field and accelerated plasma 03 p0486 A67-14054

Supersonic conducting gas flow in coaxial channel in magnetic field formed by currents flowing over plasma 04 p0669 A67-15514

Geomagnetic and auroral storms provide information on interaction of solar plasma flows and magnetosphere 04 p0618 A67-15668

Stationary and reflected shock wave produced in moving argon plasma interacting with stationary magnetic field 05 p0850 A67-16067

Plasma stream translational energy transformation into random motion in connection with collisionless shock wave propagation along magnetic field 05 p0853 A67-16756

Parallel Couette and Poiseuille flows of multicomponent viscous plasma in presence of pressure gradient and electric field 05 p0854 A67-16894

Plasma flow velocity measurement in MHD channel using time-of-flight technique, noting experimental error 05 p0854 A67-16983

Source flow expansion of partially ionized gas into vacuum for predicting flow properties of low density free jet plasma expansions [AIAA PAPER 67-99] 06 p1041 A67-18281

MHD phenomena in open electric arc, determining role in formation of plasma configurations of arc 06 p1044 A67-18688

Plasma flow in plane MHD channel in absence of longitudinal thermal flux, considering temperature dependence of heat transfer and viscous energy dissipation coefficients 06 p1045 A67-18811

Book on MGD and plasma motion including ionized gas, plasma flows, Alfvén wave propagation, shock waves, plasma boundary layer, etc 07 p1230 A67-19727

Shock waves and periodic structures of supersonic plasma flows and effect on velocity of foremost luminous front 08 p1358 A67-20852

Geomagnetic storms due to solar flares statistically analyzed to obtain configuration of solar plasma flow generated by solar flares 08 p1377 A67-21360

Boundary value problem for Poisson-Vlasov equations resulting from interaction of conducting body and supersonic flow of rarefied plasma solved, using iterative method 08 p1363 A67-21368

Action of strong transverse magnetic field on supersonic current of ionized argon 09 p1540 A67-21787

Quasi-one-dimensional analysis of MGD, considering equations of continuity, state, current density, etc [AFOSR-67-1000] 09 p1540 A67-21792

Quasi-one-dimensional plasma motion in linear and radial Hall type MHD generator ducts 09 p1541 A67-21798

Hall effect in low temperature plasma in nonhomogeneous magnetic field, describing measuring device 09 p1541 A67-21803

Plasma flow in series type MHD generator duct, noting optimum flow conditions and quasi-one-dimensional model 09 p1443 A67-21805

Concentration waves excited by internal modulation of charged particle concentrations in cross section of plasma flow analyzed for various velocities of flow 09 p1544 A67-21851

Plasma flux shaping in setup consisting of air filled discharge chamber, electromagnet shock tube and vacuum 09 p1485 A67-22324

Variational problem for flow of plasma with variable electrical conductivity in channel of MHD generator solved, using Lagrange method of multipliers 10 p1684 A67-23023

Model of formation of magnetic bottle as result of interaction of drawn-out magnetic fields of solar origin, noting sunward flow of plasma 10 p1712 A67-23805

Plasma flows from normal and coaxial electrode contact points of arc and effect of external forces by schlieren photography 10 p1687 A67-23849

High velocity shock waves obtained by magnetic pressure and relaxation processes, using electromagnetic shock

tubes 11 p1832 A67-24034

Solar magnetic field in photosphere, discussing evolution through expanding solar wind plasma 11 p1863 A67-24548

Satellite measurement of magnetic fields in cislunar space and earth proximity, noting formation of confined geomagnetic field by continuous plasma flow from sun 11 p1863 A67-24549

Shock front parameters in plasma calculated from effective ratio of specific heats and adiabatic exponent 12 p1969 A67-25195

Hydrodynamic axial-symmetric model of plasma flow on sunward side of comet assuming cometary gas is ionized by solar UV radiation only 12 p1993 A67-25227

Large disk MHD generator studied for plasma properties and fluid mechanics, noting seed ionization effect on performance 12 p1972 A67-25386

Transient acoustical response of uniform flow to turbulence and noise in MHD generators 12 p1899 A67-25390

EMF induced in ionized gas across magnetic field measured for flow velocity determination 12 p1973 A67-25392

Plasma propagation theory of arc retrograde motion in transverse magnetic field 12 p1974 A67-25400

Braking of bodies moving in rarefied plasma 12 p1892 A67-25536

RF electromagnetic fields to control state of flowing thermal plasma 12 p1975 A67-25921

Self-excitation regime associated with traveling magnetic field interaction with ionized gas flow 12 p1977 A67-26077

Cylindrical Langmuir probes examined in high density plasma flow 13 p2166 A67-26650

Two-dimensional unsteady plasma flows in coaxial channel formed by two profile electrodes calculated in case of finite conductivity in presence of Hall effect 13 p2168 A67-27301

Nondissipative plasma flow past magnetized cylinder in absence of electromagnetic field, noting current force relation to distance between conductor and cylinder surface 13 p2168 A67-27303

Structure of electrostatic charge transported by pulsed plasma flow produced by coaxial source 13 p2168 A67-27306

MHD flow past sonic velocity in channel of constant cross section, discussing conditions for smooth acceleration 13 p2169 A67-27309

Motion of plasma through nonuniform transverse magnetic field, noting dependency of plasma motion solely on field intensity 13 p2170 A67-27379

Ion density concentration in magnetic-field-aligned rotating plasma columns/plasma eddies/ 13 p2171 A67-27433

Polytropic heat sources effect on ejection of stationary symmetrical plasma from sun 14 p2378 A67-27915

Local electrostatic potential for collisionless plasma flow derived, obtaining smooth solutions for self-consistent electron density distributions 14 p2356 A67-28202

Rarefied plasma/rapidly moving body interaction, discussing computational procedure and results 14 p2357 A67-28205

Collisionless plasma flow around conducting sphere in uniform magnetic field 14 p2357 A67-28206

Modified Thomson mass spectroscopy for visual observation of energy spectra of ion component of plasmoid 15 p2486 A67-29260

Plasma flow layer, acceleration and other parameters investigated under several operation conditions in coaxial plasma gun 15 p2529 A67-29718

Arc operation under nonsteady electrical inputs noting initial conditions, energy equation solution, temperature profiles, application of Green function for moving boundary problem, etc [AIAA PAPER 66-480] 15 p2531 A67-30204

Uniform flow ionization in MHD generators produced by electric arc investigated for preionized gas stream 16 p2712 A67-30547

Optimum Mach number for nonequilibrium helium-cesium plasma flow in MHD generator, explaining effect of deceleration temperature and internal efficiency level on optimum pressure 16 p2604 A67-30570

MHD effect in shock tube, studying EMF induced in motion of transverse

magnetoplasma 16 p2715 A67-31112

Analytical plasma flow model for acceleration process in Hall current device, noting final velocity derivation, temperature, critical velocity, etc 16 p2719 A67-31237

Attachment and detachment processes effect on plasma quenching by electronegative gases, showing usefulness of steady state nitrogen afterglow flow system 16 p2720 A67-31238

Three-dimensional structure of solar plasma flow generated by solar flares, noting geometric factors in geomagnetic storm intensity decrease 16 p2739 A67-31415

Cosmic plasma flow effect on cosmic radiation polarization, deriving difference between normal waves refractive indices in two-component medium 16 p2628 A67-31494

Self-similar motions in variable conducting fluid in strong magnetic field 16 p2724 A67-31782

Kinetic equation for chemical and electron processes in low temperature plasma flows 17 p2896 A67-32169

Refractive-index equation derived for electromagnetic wave propagation along static magnetic field in plasma motion direction, using relativistic transformations 17 p2812 A67-32304

Electric conductivity of flowing plasma, discussing boundary layer problem when measuring with immersed electrodes 17 p2900 A67-32343

Slipping instability of plasma flows, noting instability criteria for long and short wavelength oscillatory 17 p2905 A67-32925

Space charge formation during flow of electric current in plasma moving under thermal emission of electrons 17 p2910 A67-33321

Initial phase of expansion of two-component plasma into vacuum analyzed, using extension of Sedov homogeneous relative deformation method 18 p3084 A67-33423

Propagation and radiation of waves excited by electric dipole in dispersionless uniaxial moving medium 18 p3002 A67-34199

Nitrogen ion drift velocities in plasma jet flowing into vacuum chamber noting ion mobilities in parent and foreign gas 19 p3271 A67-35075

Flow of positive ions from negative glow plasma into cathode dark space determined, discussing ion current density results 19 p3273 A67-35099

Radial instreaming mass flow effect on cylindrically-symmetric arc with transpiration cooling, noting heat flux reduction 19 p3280 A67-35148

Explorer 33 plasma measurements, discussing plasma flow parameter calculation methods, including plasma models and magnetospheric shape and size 19 p3319 A67-35245

Chapman-Ferraro problem analyzed by impinging high speed hydrogen plasma stream against three-dimensional magnetic dipole, discussing boundary shape 19 p3288 A67-35366

Interaction of plasma stream with three-dimensional magnetic dipole field, discussing current distribution in cavity 19 p3221 A67-35368

Interplanetary magnetic field and plasma velocity variations observed during Mariner II flight 19 p3324 A67-35451

Langmuir probe collection of ions in low density plasma flows, with electron density agreeing with microwave data 19 p3297 A67-35591

Transverse magnetic field retardation of flowing plasma in electromagnetic shock tube noting conductivity 20 p3496 A67-36214

Abnormally early eastward auroral motion appearance in evening and associated magnetospheric plasma shell motion 20 p3426 A67-36294

Bounded plasma flux in magnetic field, considering plasma polarization on magnetic field boundary, noting flux deceleration 20 p3497 A67-36682

Plasmoid instability from inhomogeneous flow along magnetic field 20 p3498 A67-36693

Effect of energy redistribution between ion and electron components of plasma flow in nonuniform magnetic field, deriving relativistic and polarization corrections to classical theory 20 p3500 A67-37050

Flows superimposition on toroidal

hydromagnetic equilibrium, stressing stationary motion of plasma layers between neighboring magnetic surfaces 21 p3661 A67-37751

Finite conductivity effect on two-dimensional plasma flow in coaxial channel solved numerically, obtaining steady state flow regime by build-up 21 p3665 A67-38240

Collisionless shock wave existence in fully ionized plasma, noting shock wave internal structure 21 p3667 A67-38410

Tensor conductivity effect on continuum and collisionless MPD flows past slender bodies [AIAA PAPER 67-731] 21 p3674 A67-38755

Three-dimensional heat source influence on solar plasma flow contradicts Parker solar wind theory, based on gasdynamic acceleration 21 p3699 A67-39012

Convective motion of low pressure plasma confined by strong magnetic field taking into account heat and mass transfer 21 p3675 A67-39014

Inviscid compressible relativistic half-jet plasma flow stability, discussing disturbance equations and eigenvalues 22 p3850 A67-39705

Quasi-one-dimensional nonequilibrium argon plasma flow equation, discussing kinetic model with atom-atom and electron-atom impact ionization 22 p3850 A67-39708

Plasma flow and generation in CO comet due to electron-collisional ionization under influence of solar wind 22 p3885 A67-40081

Discontinuity conditions derived for nondissipative hydromagnetic shock surface flows, with jump relations from divergence form of MHD equations 22 p3854 A67-40317

Electrical conductivity or magnetic Reynolds number of shock produced plasma flow, discussing interaction between magnetic field and plasma 23 p4031 A67-40881

Space time distribution of cosmic rays as function of plasma efflux from sun, magnetic field intensity, topology and scale irregularities 23 p4059 A67-41133

Structure of quasi-steady-state MHD shock wave in plasma supersonic flow, analyzing width dependence magnetic field 24 p4195 A67-41937

One-dimensional plasma flow variables relations analyzed in crossed electric and magnetic fields with small magnetic Reynolds numbers 24 p4196 A67-42216

Total head tube in combination with electrostatic probe used in supersonic plasma diagnostics, measuring plasma and shock wave front parameters 24 p4197 A67-42355

Poynting vectors difference obtained by using convection and polarization current models of moving plasma in Minkowski theory 24 p4124 A67-42812

Steady electric power from Cs seeded Ar plasma in nonequilibrium ionization flowing at high speed through magnetic field 24 p4109 A67-42895

PLASMA FLUX MEASUREMENT

Jarrell-Ash model 75 spectrograph adapted for time resolved spectroscopy of transient plasma produced by exploding wire and shock waves 03 p0426 A67-14401

Shock wave structure in viscous heat conducting gas, deriving preservation law for irreversible energy flux, equation for velocity profile and expression for integral curve 04 p0604 A67-14747

Plasma flux interaction in magnetic multipole field, proving mutual polarization of interacting fluxes by photographic results 04 p0667 A67-15210

Plasma flux cut-off in uniform magnetic field by transverse electric 04 p0667 A67-15213

MHD approximation of solar plasma fluxes observed by Mariner II as free rotating jets 07 p1243 A67-19802

Summary of papers on plasma diagnostic techniques from Symposium on MHD Electrical Power Generation, Saltzburg, July 1966 09 p1538 A67-21774

Plasma flux interaction in magnetic multipole field, proving mutual polarization of interacting fluxes by photographic results 15 p2532 A67-30258

Plasma flux cut-off in uniform magnetic field by transverse electric 15 p2532 A67-30261

Plasma flux instability in inhomogeneous medium 18 p3090 A67-34434

PLASMA FREQUENCY

SA OSCILLATION FREQUENCY

Model for ionospheric drift measurements made by spaced receiver method when scattered wave has frequency above plasma frequency of scattering 03 p0407 A67-12831

Higher harmonics of anomalous cyclotron emission from partially ionized plasma ascribed to negative absorption 03 p0476 A67-13358

Operating possibility of axisymmetric electron beam so that plasma frequency will exceed electron cyclotron frequency of magnetic focusing field at some point or throughout beam 04 p0624 A67-15326

Boltzmann transfer equation consisting of DC electric field and two AC electric fields for nonlinear second harmonic generation and combination frequencies in homogeneous plasma 06 p1046 A67-18826

IR transmission measurements in single crystal thin film semiconductors, observing absorption band near plasma frequency 06 p1071 A67-18992

Radiation from linear resonant antenna in lossy compressible weakly ionized plasma and dependence on ratio of source to plasma frequency 07 p1227 A67-19428

Velocity spread on modulated electron beam of finite diameter analyzed as function of drive, drift length and perveance 08 p1362 A67-21298

Ionized medium effect on synchrotron emission spectra in solar corona proposed to account for LF cut-off in type IV radio bursts 08 p1402 A67-21464

Increment of constant HF electron flux in resonance probe determined for case of large constant potential, noting role of plasma 13 p2119 A67-26559

Current density combination frequency derived for homogeneous magnetoplasma due to alternating electric fields, considering distribution function isotropic and anisotropic parts 13 p2167 A67-26994

Antenna in interplanetary plasma, noting fluctuation noise in exosphere and radiation impedance when exposed to solar wind 14 p2279 A67-27856

Radiation from plasma films and columns nonlinearly excited by incident electromagnetic waves, showing predominance of radiation on scattering 14 p2356 A67-28153

Plasma produced transit time delay of reflected pulses for collisionless inhomogeneous plasma 17 p2810 A67-32070

Nonlinear incoherent light scattering from two frequency-differing coherent beams of electromagnetic radiation propagating in homogeneous plasma without magnetic field 17 p2901 A67-32354

Two peaks in emission from low pressure helium or neon discharge simulating plasma slab with second peak corresponding to plasma cut-off frequency 17 p2901 A67-32369

Nonlinear interaction between weakly ionized helium magnetoplasma produced by HF discharge and microwave field 17 p2903 A67-32676

Acceleration mechanisms of isolated plasma particles under effect of weak or strong field with frequency of order of Langmuir frequency of electron 17 p2905 A67-32922

Ionization frequency distribution in HF discharge produced by long single turn coil 19 p3276 A67-35118

Impedance measurements of RF discharge in single turn coil with superimposed static magnetic field, noting dependences and two resonances 19 p3276 A67-35119

High power microwave radiation from nonequilibrium plasma discharge near electron cyclotron 19 p3291 A67-35386

Guided waves on infinite cylindrical cavity in magnetolonic medium noting wave solutions, phase velocity, plasma frequencies, etc 20 p3383 A67-37107

Transient radiation of electric dipole in uniaxially anisotropic plasma examined for signal frequency greater and less than plasma frequency 20 p3388 A67-37704

Diffraction by cylinder in locally uniaxial medium with azimuthal optic axis, using Maxwell equation solution for plasma frequency 20 p3389 A67-37705

Reflection of incident right and left hand circularly polarized plane electromagnetic

waves from anisotropic helium afterglow plasma 20 p3389 A67-37707

Ion resonance effect in Langmuir probe exhibiting ion plasma frequency 21 p3663 A67-37765

Parametric excitation of electron plasma frequency derived using Boltzmann and Poisson equations 21 p3667 A67-38415

Dispersion equation for extraordinary and plasma waves propagating through magnetoplasma perpendicular to external magnetic field studied near lower hybrid frequency 22 p3844 A67-39419

Cyclotron harmonic resonances in plasma frequency conversion output due to harmonic interactions with incident waves 22 p3851 A67-39724

Energy dependent mobility in small signal analysis of waves in semiconductors 22 p3864 A67-40310

Ion wave propagation in weakly ionized gases 23 p4032 A67-40960

Rocket measurements with HF impedance probe for ionospheric electron density, discussing plasma gyro resonance frequency factors 23 p4003 A67-41321

Dielectric function of semiconductor in external electric field, discussing effect on plasma frequency 24 p4201 A67-41979

Proton gyrofrequency effect on antenna resonance at electron plasma frequency using Alouette II satellite 24 p4125 A67-43111

PLASMA GENERATION

Plasma electron density and formation determined, using Fabry-Perot resonator 02 p0275 A67-12469

Plasma production by conical electrode plasma gun studied by systematically changing gas loading 03 p0476 A67-13353

Expansion velocity of luminous front of plasma plume generated by giant pulse laser 03 p0478 A67-13573

High temperature single solid particle plasma generation by focused giant pulse Q-spooled ruby laser beam irradiation of LiH suspended in vacuum electric fields 03 p0485 A67-14047

Image converter observation of radial striated light filaments during gas breakdown and current sheath buildup in dense plasma focus coaxial discharge 03 p0486 A67-14055

Characteristics of different plasmas produced by nuclear explosions at high altitude on radar systems 04 p0569 A67-14506

Plasma formation by dissociation of diatomic hydrogen ions by Lorentz force 04 p0671 A67-15645

RF power oscillator for low pressure plasma production, noting work and grid coils and time and power controls 05 p0856 A67-17281

Glowing high voltage discharge produced with hollow anode in discharge gap of various configurations 06 p0968 A67-18093

Production and diagnostic measurement of deuterium, helium and neon plasmas, stressing electron and ion heating and cooling and attendant equilibration 06 p1041 A67-18147

Plasma formed by laser pulse on tungsten target, measuring radius, temperature and radiative properties, developing model 06 p1041 A67-18149

Electric properties of gas dynamic mirror formed in wake of shock wave front 07 p1227 A67-19118

Energy coupling measurement through electrodeless discharges in coaxial tubes, discussing parameters, dynamic processes, etc 08 p1338 A67-21291

Plasma source in which collimated photon beam generates plasma by single quantum photoionization of rarefied gas 09 p1549 A67-22426

Currents caused by light pressure on metal surface and in flare plasma when laser beam hits surface 10 p1664 A67-23333

Synthesized plasma ion beams by electron injection from hot filament noting electrostatic instabilities and growth rates corresponding to nonlinear regime 11 p1838 A67-24403

Porous W-Ta emitters as ion source for production of quiescent alkali plasmas of improved symmetry, reproducibility and uniformity 11 p1838 A67-24411

Quiescent cesium plasma production in thermal ionization chamber at high temperatures and low ionization level 11 p1838 A67-24412

Plasma production by ruby laser pulse irradiation of LiD investigated, results suggest collisionless electrostatic shock propagation at expanding plasma ball edge 11 p1840 A67-24561

Ion beam interaction with beam produced plasma, showing excitation of waves at electron plasma frequency 11 p1840 A67-24562

Gross behavior and properties of laboratory plasma generation with combined transverse and longitudinal ionizing currents parallel to magnetic field 11 p1845 A67-25098

Containment of transparent plasma produced by field of traveling wave in circular waveguide, noting plasma ion-current distribution 12 p1976 A67-26066

Current density combination frequency derived for homogeneous magnetoplasma due to alternating electric fields, considering distribution function isotropic and anisotropic parts 13 p2167 A67-26994

Time dependence of semiconductor enhanced reflectivity by pulsed argon ion laser based on thermally generated electron hole plasma 13 p2177 A67-27016

Charge exchange method for production of molecular beams, noting production of plasma by RF discharge and ion beam generation 14 p2316 A67-28190

Numbers, flow velocities and temperatures of positive ions emitted by He and Ar plasmas pulsed into evacuated region by plasma gun determined by time-of-flight analysis 15 p2523 A67-29214

Generation of quiescent variable-parameter arc plasma in strong magnetic field 15 p2523 A67-29228

Fast hydrogen ion generation in coaxial plasma source to determine point in gun chamber where fast particles arise 15 p2525 A67-29251

Electric field device to generate short plasmoids free from plasma contamination through contact with metal 15 p2526 A67-29259

Stationary concentration of charged particles in plasma created by uniform and nonuniform SHF magnetic field in electron-cyclotron resonance state 15 p2529 A67-29716

Nonequilibrium plasma production via plasma electron heating with electric field induced in MHD generator 16 p2601 A67-30552

High pressure characteristics of helium and hydrogen pulsed arcs, noting formation of dense, completely ionized plasma 16 p2717 A67-31183

Argon pulsed arcs produced at high pressures, considering emission absorption 16 p2717 A67-31184

Low temperature plasma production in combustion chamber for use in MHD generators, giving equations for plasma composition 17 p2833 A67-32167

Ionization of media, sterile plasma production, dense plasma heating and plasma trap falling, by laser emission 17 p2904 A67-32917

Formation of high energy plasma in toroidal system by neutral atom injection, discussing differential equations 17 p2908 A67-33110

Instrument for generation of thermal plasmas in direct current-arc discharges and expansion to walls of coaxial corotating cylinder 17 p2835 A67-33389

Structural dislocations effect on formation of microplasmas during avalanche breakdown of silicon p-n junction 18 p3099 A67-33698

Plasma produced by shock wave in low pressure gas measured for phase angle by microwave reflection probes 18 p3088 A67-34076

Laser driven plasma detonation waves in gases observed with Schlieren system, discussing shock wave growth 18 p3092 A67-34734

Ionization rate at higher electron densities in DC fields measured in toroidal discharge tube 19 p3272 A67-35078

Thermally ionized cesium plasma produced containing negative Cl ions 19 p3272 A67-35084

Plasma regime creation through boundary perturbations in low-pressure gas discharge, developing moving striations 19 p3273 A67-35096

Stationary high density high temperature plasma production spectroscopic measurements, deducing arc radial

temperature and density profiles from line and continuum intensities and line profiles 19 p3274 A67-35103

Modified duoplasmatron in cusp fields to produce highly ionized and high density quiescent plasma, using DC discharge, noting helium plasma generation 19 p3274 A67-35104

Electron beam passing through low pressure gas generates plasma, computer simulated beam trajectory studies explain beam profile and pinch effect 19 p3275 A67-35106

RF plasma at electron cyclotron frequency produced with axially slotted metal cylinder 19 p3275 A67-35111

Production and behavior of magnetically stabilized high density high temperature plasma, describing experiment 19 p3282 A67-35167

Beam-plasma interaction in magnetic field, studying microwave field distribution and emission 19 p3291 A67-35383

Hydrogen thermal ionization rate behind strong shock wave, considering nonadiabatic collisions and various relaxation mode interactions in shock speed 19 p3292 A67-35394

Galactic anisotropies observation, giving procedure for detecting periodicities and data on sidereal daily variation amplitude 19 p3315 A67-35484

Plasma production by ruby laser beam irradiation of lithium hydride particle, measuring electron temperatures 20 p3496 A67-36212

Electric properties of gas dynamic mirror formed in wake of shock wave front 21 p3664 A67-38163

Strong blast waves and laser generated plasma dynamics in high pressure gas investigated using Mach-Zehnder interferometer and pressure probe [AIAA PAPER 67-696] 21 p3672 A67-38725

RF induction heating and production of low pressure plasmas, discussing plasma electron density function [AIAA PAPER 67-732] 21 p3674 A67-38756

Plasma production by optical irradiation of gases and by solids, considering interaction of laser radiation with surfaces and irradiation of particles of solid material in vacuum [AIAA PAPER 66-174] 21 p3642 A67-38851

Temperature determination of wire explosion plasma from expansion and resistivity measurements, showing existence of two phases of electric arcs 22 p3847 A67-39644

Plasma flow and generation in CO comet due to electron-collisional ionization under influence of solar wind 22 p3885 A67-40081

Hot electron plasma production, discussing microwave power feeding across magnetic flux lines producing closed plasma shell structure 22 p3854 A67-40243

Ion energies in expanding plasma stream generated by intense giant pulse laser light in focus on solid LiD and LiH targets 23 p4033 A67-41152

Microwave production of plasma in trap at electron cyclotron resonance, investigating absorption and density 23 p4035 A67-41684

Multiphoton absorption in monatomic gases causing ionization of atom applied to plasma production by intense radiation from lasers 24 p4190 A67-42098

Impact ionization avalanche plasma production and instabilities in InSb at low temperatures, measuring current variation with electric field strength 24 p4204 A67-42344

Hypervelocity gas flows at high temperatures and pressures, discussing generation of dense plasmas at extreme temperature by implosion waves 24 p4092 A67-42753

PLASMA GENERATOR

SA MAGNETOHYDRODYNAMIC GENERATOR

Electron scattering cross section of argon and atomic oxygen measured, using microwave interferometer for analysis of plasma produced in shock tube 03 p0472 A67-13320

Electric arc stabilization mechanism for nonconducting gas flow in chamber of DC plasma generator 04 p0666 A67-15191

Electromagnetic field in induction type plasma generator in steady state, from Maxwell equations and heat conservation

equations 04 p0871 A67-15612

Heat transfer in plasma jet generators, considering electric arc types and thermal regime of electrodes 04 p0672 A67-15871

Minimum B magnetic field geometry for LF oscillations in Cs plasma of Topsy Q device 05 p0859 A67-17444

Plasma characteristics of partially dissociated and ionized air due to alpha emissions from radiolotope surface material 09 p1543 A67-21819

Three-phase AC plasmatrons designed to produce low temperature plasma 09 p1446 A67-22326

Potential distribution in emitter diode measured in single ended Q machine, using ribbon electron beam 11 p1764 A67-24373

Alkali metal plasma generator design and performance, noting characteristics of LF wave propagation parallel to magnetic field 11 p1837 A67-24396

Cylindrical screened electrode for measuring temperature plasma conductivity in MGD generator 13 p2055 A67-26434

Electron density and HF spectrum of beam generated plasma as function of gas pressure and injection parameter 14 p2352 A67-27749

Electrostatic stability of finite-length plasmas immersed in magnetic field studied on mathematical model, discussing experiments with plasma-generating machines 16 p2714 A67-30871

Physical/chemical characteristics of thermionic plasma noting equipment and technology involved 16 p2722 A67-31564

Arc burning mechanism of vortex-stabilized plasmatrons, noting effect of arc shunting on volt-ampere characteristics 17 p2897 A67-32171

Hall parameter instability and conductivity analysis applied to performance characteristics of subsonic flow generator 17 p2898 A67-32181

Synchronous and asynchronous idealized induction alternating current MGD generators 17 p2803 A67-32340

Titanium plasma source design features, performance, ion mean free path, energy spectrum and energy distribution 17 p2904 A67-32912

Mass composition, contamination dynamics and jet structure of titanium plasma source 17 p2904 A67-32913

Plasma sources of refractory ions classified according to methods of producing gas discharge 19 p3228 A67-34981

AMICON 8000 kw plasma facility for simulating reentry environments for material and thermodynamic tests 20 p3415 A67-36551

Argon arc plasma generator with film cooled anode for producing stable high temperature gas jet [ASME PAPER 67-HT-72] 20 p3498 A67-36752

Principles, design and operation of synthetic plasma source for studying space vehicle antennas over wide frequency band 21 p3664 A67-38214

Plasma production by pulsed laser irradiation of aluminum in space chamber vacuum 21 p3666 A67-38259

Plasma and sheath characteristics computation for alkali plasma devices involving contact ionization for ion production [AIAA PAPER 67-691] 22 p3868 A67-39843

Fully ionized barium plasma column generating device, discussing spectroscopic measurements of ion motions, densities, temperatures and electron temperature 23 p4033 A67-41215

PLASMA GUN

Plasma propulsion devices and phenomena responsible for energy losses, considering plasma gun and MPD arc jet 01 p0141 A67-11388

Channel flow interaction of plasma from coaxial plasma gun with transverse magnetic field 02 p0277 A67-12618

Width and rate of propagation of plasma current layer along accelerating electrodes of plasma gun at initial phase of discharge 02 p0278 A67-12621

Plasma production by conical electrode plasma gun studied by systematically changing gas loading 03 p0476 A67-13353

Electrical propulsion of space vehicles using solar energy, electrostatic drive, drifting field plasma accelerator, etc 03 p0503 A67-13493

Low inductance 50 kv spark gap with high voltage handling capacity and minimum jitter, for use in modified Bostick type plasma gun 03 p0486 A67-14095

Plasma ion gun with Pierce electrode 04 p0663 A67-14771

Conical induction plasma gun construction in strongly preionized regime and results of electrostatic probe measurements made with discharge camera 04 p0668 A67-15280

Short hydrogen plasmoid production by electromagnetic waves in decimeter range 05 p0855 A67-16997

Coaxial plasma gun performance in longitudinal magnetic field, noting conditions of generation of single plasmoid 06 p1039 A67-18084

Plasmoid structure produced by coaxial plasma gun with interchangeable polarity electrodes, noting experimental setup, particle velocity, density, energy, etc 06 p1040 A67-18085

Hydrogen density in coaxial plasma injector prior to application of high voltage to electrodes, noting experimental setup and results 06 p1040 A67-18086

Conical current sheet implosion forming of axial pinch in z-pinch plasma gun 07 p1230 A67-20257

Channel flow interaction of plasma from coaxial plasma gun with transverse magnetic field 13 p2170 A67-27374

Width and rate of propagation of plasma current layer along accelerating electrodes of plasma gun at initial phase of discharge 13 p2170 A67-27377

External magnetic field accelerating effect on constant-mass plasma clusters between parallel conductors 14 p2354 A67-27763

Numbers, flow velocities and temperatures of positive ions emitted by He and Ar plasmas pulsed into evacuated region by plasma gun determined by time-of-flight analysis 15 p2523 A67-29214

Current layer motion in coaxial plasma gun, measuring discharge current, electric and magnetic fields and ejected ions at gun outlet 15 p2525 A67-29250

Fast hydrogen ion generation in coaxial plasma source to determine point in gun chamber where fast particles arise 15 p2525 A67-29251

Coaxial plasma gun for plasmoids showing higher mean energy when gas admission is closer to plasma source 15 p2525 A67-29252

Coaxial plasma gun operating in longitudinal magnetic field, noting effect on plasmoid uniformity 15 p2525 A67-29253

Plasma flow layer, acceleration and other parameters investigated under several operation conditions in coaxial plasma gun 15 p2529 A67-29718

Nonlinear effects during titanium plasma source operation, investigating plasma nature and magnetic field effects on injector operation and plasma parameters 15 p2529 A67-29719

Gas stream discharge studied by using electromagnetic plasma gun to direct plasmoids toward beam 15 p2472 A67-29726

Marshall plasma gun with titanium electrodes saturated with deuterium for filling magnetic collector 16 p2676 A67-31400

Plasma technology in industry, discussing Polish-made plasma torch design and operation and plasmatron and spraying applications 17 p2865 A67-32189

HF electrostatic instability in low density plasma stream guided by magnetic field, discussing cause and anomalous loss of diamagnetism 17 p2907 A67-33106

Ionizing wave in plasma gun with crossed electric-magnetic fields, obtaining burning voltage of discharge and bias magnetic field ratios 19 p3277 A67-35123

Motion of plasmoids injected axially in two-dimensional multipolar magnetic field, studying losses 20 p3500 A67-37061

Plasmoid propagation at high pressures, emphasizing Bostick buttons performance compared to electromagnetic shock tube, describing button gun and photographic equipment 21 p3674 A67-38771

Thetatron gun plasma burst expanding freely in drift tube, discussing wall shorting effect inhibition method and measurements 22 p3846 A67-39485

Ar atomic beam produced by plasma burner measured for kinetic energy and Mach number 24 p4198 A67-42576

Measurement of time varying spectra of argon plasma in coaxial gun for two different gun geometries 24 p4198 A67-42730

PLASMA HEATING

HF heating of dense plasma by resonance excitation of cyclotron-type ion waves and fast magnetoacoustic waves 02 p0274 A67-12460

Spatial waveform of azimuthal electric field of Faraday shielded Stix coils for ion cyclotron resonance heating of plasma to thermonuclear temperatures 02 p0279 A67-12685

Energy relaxation as explanation of changes in electron density and temperature of helium plasma in upper hybrid resonant heating 03 p0477 A67-13360

Power and DC spectra for electron motion due to plasma heating and diffusion in static magnetic and transverse random electric field 03 p0485 A67-14046

Heating and scattering of plasma produced by giant laser pulse focused on solid target 03 p0486 A67-14194

Dissipative effects in converging cylindrical symmetric shock wave, considering ion and electron heat conductivity, ion viscosity and energy exchange 06 p0984 A67-18029

Electron-cyclotron heating of plasma via high power oscillator, noting experimental setup and characteristics 06 p1039 A67-18082

Skin heating effects on induction converters, noting magnetic field intensity and temperature as function of time and space 09 p1442 A67-21794

Electron cyclotron resonance heating of alkali plasmas by electromagnetic resonant absorption 11 p1838 A67-24407

Electrostatic turbulence in low beta plasma and influence on diffusion across magnetic field, noting heating system for plates of Q device 11 p1789 A67-24413

Hydrodynamic and overheating instability of nonisothermal plasma flux in crossed electric and magnetic fields in flat dielectric walled channel 11 p1842 A67-24950

Excitation of collisionless shock waves in low density plasma noting lifetime, discharge process, adiabatic contraction, etc 12 p1976 A67-26074

Modulated electron beam interaction with plasma formed by beam causes ion heating to energies of hundreds of volts in magnetic mirror field 13 p2164 A67-26299

Heating and scattering of plasma produced by giant laser pulse focused on solid target 14 p2360 A67-28539

Heating of magnetized hot diffuse plasma using difference-frequency signal generated from two HF transverse waves 15 p2521 A67-29188

Heating of ions in current carrying nonisothermal plasma deriving noise spectral density and electron and ion distribution functions 16 p2715 A67-31047

Electron heating by direct discharge during plasmoid interaction involving polarization 16 p2717 A67-31182

Acceleration of plasma particles to high energies for case of interaction between plasma and stochastic field with harmonic-correlation time 16 p2718 A67-31192

Interferometrically-measured ion temperatures compared to electron temperatures in pure barium and barium-cesium plasmas produced by contact ionization 16 p2720 A67-31243

Ionization of media, sterile plasma production, dense plasma heating and plasma trap falling, by laser emission 17 p2904 A67-32917

Laser heating of plasma situated in strong longitudinal magnetic field 18 p3060 A67-34041

Gas ionization and plasma heating by high power microwaves using X-band and S-band frequency magnetrons 19 p3276 A67-35115

High temperature plasma generation from dense plasma with moving metallic walls, evaluating electrical conductivity and energy breakdown periods 19 p3282 A67-35159

Thermodynamic model for laser induced gas discharges accounting for transmitted light attenuation, plasma heating, etc 19 p3239 A67-35163

Deuterium plasma heating by multiply charged hot impurity ions 19 p3287 A67-35357

Earth radiation belts nature and plasma activity in magnetosphere 19 p3315 A67-35485

Plasma furnace for treating refractory

products at high temperature to determine various oxides solidification temperature 19 p3299 A67-35900

Noncollisional ion heating from accelerations in microfields of turbulent plasma waves 20 p3497 A67-36531

Free convection of conducting fluid in coupled vertical channels for case of steady motion with lateral heating 20 p3500 A67-37051

Collisionless plasma heating by random magnetic fields, using simple betatron model 21 p3662 A67-37762

Eddy configuration plasma heated by induced currents, discussing electromagnetic radiation absorption 21 p3664 A67-38047

Soviet papers on HF properties of plasma including heating, stability, theory, electromagnetic wave scattering, etc 21 p3668 A67-38677

Efficiency of plasma heating by HF field with excited magnetosonic wave due to energy absorption 21 p3669 A67-38678

RF induction heating and production of low pressure plasmas, discussing plasma electron density function [AIAA PAPER 67-732] 21 p3674 A67-38756

Electron temperature spatial variation in late He afterglow due to standing wave microwave heating 22 p3844 A67-39353

Hot electron plasma production, discussing microwave power feeding across magnetic flux lines producing closed plasma shell structure 22 p3854 A67-40243

Dense hydrogen plasma ohmic heating in quasi-stationary discharge without external magnetic field, obtaining stable impurity-free plasma column 24 p4195 A67-41939

Anomalous electron heating rate in plasma region traversed by magnetic shock wave obtained by electron velocity distribution observation 24 p4198 A67-42736

PLASMA INSTABILITY

Electromagnetic oscillation excitation in plasma beam, analyzing cases of weak and strong external magnetic fields 01 p0122 A67-10349

Rotating flame resulting from instability of inhomogeneous plasma produced by arc discharge in magnetic field approaching critically 01 p0123 A67-10739

Effect of shifting radial electrical field sign on instability state of inhomogeneous plasma produced by arc discharge in equipotential volume 01 p0123 A67-10741

Type I solar radio bursts possibly caused by interaction of coronal electrons and finite-amplitude MHD pulses 01 p0146 A67-11278

D region equilibrium solution using absorption measurements, considering region as nonsteady plasma under special conditions 01 p0061 A67-11288

Ionospheric F-2 layer inhomogeneities attributed to plasma flute instability, using kinetic drift equations to describe plasma oscillations 02 p0236 A67-11669

Current instability of plasma injected into germanium, noting effect of strong electric field in presence of temperature gradient 02 p0297 A67-11833

Onset of electron oscillations in plasma with large velocity or temperature gradients 02 p0277 A67-12611

Finite ion Larmor radius in stabilizing rippling mode of Furth-Killen-Rosenbluth dissipative instabilities in plasma with finite resistance gradient 02 p0277 A67-12613

Rippling mode instabilities in positive helium discharge column at critical longitudinal magnetic field intensity 02 p0277 A67-12615

Instabilities and dispersion during electromagnetic wave excitation and propagation in weakly turbulent plasma 02 p0278 A67-12627

Quasi-linear theory of plasma cyclotron instability for one-dimensional oscillation spectrum, noting energy of interaction with electromagnetic field, ion velocities, etc 03 p0475 A67-12933

Hydrodynamic drift-dissipation instability of plasma with nonuniform temperature 03 p0476 A67-13296

Flute type instability of ideally conducting plasma in toroidal discharges with strong longitudinal magnetic field 03 p0476 A67-13343

Instabilities in drifting semiconductor plasma, noting dispersion curve and collision ionization for longitudinal

- oscillations 03 p0496 A67-13674
- Instability of gravitating slipstreams or mixed streams and cloud fragmentation of interstellar gas 03 p0511 A67-13877
- Instability of contrastreaming plasmas investigated by taking into account Coulomb collisions via Fokker-Planck coefficients in Boltzmann equation 04 p0662 A67-14519
- Semiconductor plasma slab subject to crossed electric and magnetic fields, examining plasma density wave instability caused by gradient in carrier density perpendicular to magnetic field 04 p0674 A67-14612
- Instability in hot electron plasma in mirror field occurring suddenly in quietly decaying plasma generated by high power microwave 04 p0663 A67-14621
- Hydrodynamic drift-dissipation instability of plasma with nonuniform temperature 04 p0663 A67-14721
- Conducting surface boundary effect on current plasma instability in terms of potential fluctuations 04 p0667 A67-15208
- Coaxial plasma source transition from high energy particle production to production of slow plasmoids, noting V-I characteristics and magnetic field 04 p0667 A67-15212
- Instability due to nonlinear coupling of electron plasma oscillation and ion acoustic oscillation to driving transverse field extended to longitudinal driving field 04 p0672 A67-15771
- Drift waves in finite pressure plasma, noting oscillation caused instabilities induced by Alfvén type and slow magnetoacoustic wave interaction 05 p0852 A67-16693
- Instability of electron hole plasma of semiconductor caused by nonlinear current-voltage characteristic 05 p0867 A67-17058
- Transverse wave instabilities in collisionless hydrogen plasmas under magnetic field 05 p0858 A67-17429
- Finite plasma pressure effect on interchange mode in finite Larmor radius weakly unstable regime 05 p0858 A67-17430
- Hot electron plasma instability in magnetic mirror, discussing stabilization by cold plasma component and magnetic field line typing in conducting end plates 05 p0858 A67-17431
- Nonlinear theory on effect of drifting cone plasma instability on particle drift from adiabatic trap 05 p0860 A67-17545
- Charged particle collisions effect on drift instability of low pressure plasma studied, using Landau collision integral as model collision integral 05 p0860 A67-17546
- Oscillations of inhomogeneous weakly ionized plasma situated in external electric and magnetic field, noting causes and conditions of plasma instability 06 p1039 A67-18080
- Plasma instability in HF electric and constant magnetic field for sufficiently low pressure 06 p1039 A67-18081
- Plasma stabilization mechanism for electron beam caused density variation, noting use of nonlinear effects 06 p1040 A67-18097
- Nonlinear instability of nonisothermal plasma in external electric field, determining ion-acoustic noise spectrum and time dependent variations in kinetic energy of plasma electrons and ions 06 p1045 A67-18801
- Plasma in HF electric field becoming kinetically unstable due to Cerenkov effect 06 p1045 A67-18803
- Plasma instabilities in solids noting developments in moving domains, nonlinear effects, Gunn effect, turbulence, etc 06 p1070 A67-18986
- Current and voltage measuring methods for impact ionization analysis including lag and avalanche time, peak fields, etc, noting instability 06 p1070 A67-18987
- Instability of inhomogeneous weakly ionized plasma in crossed electric and magnetic fields in quasi-approximation 07 p1228 A67-19508
- Plasma instabilities induced by charge convection across perturbing electric field and magnetic field 07 p1228 A67-19511
- Plasma instability in HF electric field perpendicular to given magnetic field under low pressures 08 p1357 A67-20847
- Plane wave growth associated with Cerenkov and cyclotron instabilities in plasma stream 08 p1358 A67-20893
- Quasi-linear theory of loss cone instability of plasma confined in mirror type trap 08 p1359 A67-20899
- Kinetic equation for unstable homogeneous plasma in uniform magnetic field when subjected to sudden uniform electric field 08 p1360 A67-21127
- Electron streaming instability of plasmas with zero order density gradients from variational analysis of Vlasov-and Maxwellian-plasma perturbation wave propagation 08 p1360 A67-21128
- Possible excitation of Kelvin-Helmholtz instability in rotating plasmas 08 p1362 A67-21145
- Generalized formulation of electrostatic oscillations and streaming instabilities in bounded and unbounded inhomogeneous Vlasov plasmas with transverse density gradients in strong axial magnetic field 08 p1363 A67-21305
- Transverse plasma instabilities as mechanism coupling motions of solar wind and cometary plasma, using thermal diffusion and conductivity transport coefficients to describe flow 08 p1401 A67-21367
- Stability of bumpy theta pinch plasma separated from vacuum by thin conducting surface 08 p1365 A67-21411
- Anomalous diffusion arising from drift instability in collision-free equilibrium plasma cylinder 08 p1366 A67-21440
- Anisotropic proton velocity distribution obtained from solar wind measurements on Pioneer VI spacecraft 08 p1378 A67-21475
- Excited atoms effect on nonequilibrium ionization of partially ionized plasma in direct energy conversion systems, using Klein effect 09 p1543 A67-21821
- Nonsteady state processes in nonequilibrium plasma with local collisions, using Boltzmann kinetic equation for application in MHD generators 09 p1543 A67-21823
- Plasma filament instability suppression by applying external magnetic field 09 p1545 A67-22069
- Nonlinear thermomagnetic wave theory and amplification in case of plasma instability 09 p1545 A67-22072
- Gardenhose instability for ultrarelativistic plasma in magnetic field, showing that instability criterion for particular non-Maxwellian distribution function is not met 09 p1546 A67-22229
- Magnetosonic wave effect on anisotropic relativistic plasma component, obtaining cosmic ray plasma instability when wave frequencies are less than electron cyclotron frequency 09 p1546 A67-22230
- Nonlinear effects produced by instability of nonpotential plasma waves in oscillating discharge, deriving wave kinetic equation 10 p1684 A67-22902
- Current instability in inhomogeneous plasma formed by drift and ion-acoustic waves with oscillation frequencies 10 p1685 A67-23461
- Convective type drift instability in collisional and collisionless regimes due to magnetic shear effects driven by density gradient 10 p1685 A67-23462
- Effect of ion collisions and other terms on resistive-g instability in plasmas 11 p1826 A67-23873
- Toroidal machine velocity space instabilities, rapidly saturating, with long time scale remaining 11 p1826 A67-23876
- Plasma parameter range for convective and absolute Harris instabilities, noting correlation with density 11 p1827 A67-23883
- Toroidal screw pinch equilibrium and stability in rapidly rising helical magnetic field, discussing experimental setup and results 11 p1827 A67-23888
- Electron plasma frequency instability, correlating coherent deceleration of electron beam with compression of interference pattern 11 p1827 A67-23890
- Flute instability in low beta plasma in presence of nonuniform electric field perpendicular to magnetic field 11 p1828 A67-23891
- Electrostatic oscillations excited in cylindrical plasma shell by electron beam, noting resultant instability 11 p1828 A67-23892
- Steady state plasma belt in dipole magnetic field, measuring spatial variation of density and temperature, electron spin, gyration, etc 11 p1828 A67-23940
- Plasma instability and anomalous transport - Conference, University of Miami, Coral Gables, May 1966 11 p1828 A67-23997
- Helical instability of positive plasma column in longitudinal magnetic field, using magnetic pickup coil 11 p1829 A67-23999
- Azimuthal modes of Kadomtsev plasma instability, describing subthreshold response spectra 11 p1829 A67-24001
- Flute instability in mirror confined plasmas assuming particle drift under external forces 11 p1830 A67-24004
- Cross field diffusion coefficient measurement from volume loss properties of single ended Q device plasma column 11 p1830 A67-24005
- Anomalous transport phenomena in ring discharge studied for instability and losses due to noise, using mc RF oscillator [AROD-6398-2] 11 p1831 A67-24010
- Plasma stability, discussing flute and Kadomtsev instabilities and possibility of anomalous diffusion for confined steady state 11 p1831 A67-24011
- Physical stabilization mechanism of helical instability of positive column in longitudinal magnetic field due to quasi-linear effects 11 p1831 A67-24012
- Plasma instability as obstacle to controlled nuclear fusion noting causes, effects, forbiddenness phenomenon, etc 11 p1831 A67-24016
- Nonisothermal alkali plasma collisional drift instability in radial electric field 11 p1834 A67-24380
- Low temperature alkali plasmas in magnetic fields in terms of collisional drift modes, determining steady state frequencies, amplitudes, etc 11 p1834 A67-24381
- Transition to turbulence in thermal plasma examined, using model based on coupled Van der Pol oscillators, noting noise spectrum rise 11 p1836 A67-24390
- Instabilities in DC electron beam/plasma experiment noting dependence on beam current, magnetic field strength, beam velocity and plasma density 11 p1837 A67-24400
- Barium Q plasma device for optical diagnosis of oscillatory microinstabilities compared with Langmuir probe 11 p1838 A67-24406
- First azimuthally varying mode in mercury vapor plasma discharge, predicting growth of hose-like instability of electron beam 11 p1841 A67-24928
- Hydrodynamic and overheating instability of nonisothermal plasma flux in crossed electric and magnetic fields in flat dielectric walled channel 11 p1842 A67-24950
- Plasma drift instability arising from initial nonuniformity in density and temperature 11 p1842 A67-24966
- LF loss cone instabilities of plasma in Taylor minimum-B configurations, discussing instability conditions and growth rate 12 p1969 A67-25199
- Negative-mass instability of cylindrical layer of relativistic electrons in geometrical configuration approximating Astron machine 12 p1970 A67-25254
- Electron and ion temperature difference necessary to develop instability connected with loss cone of plasma with hot electrons placed in magnetic mirror trap 12 p1971 A67-25334
- Plasma column deviation from static state analyzed for time constants, considering conductivity and temperature change rates 12 p1973 A67-25394
- Plasma acceleration across magnetic field in linear accelerator, calculating values from voltages at electrode ends 12 p1977 A67-26075
- Turbulent electrostatic shock in plasmas, discussing determination of structure by ion wave instabilities [SR-1] 13 p2162 A67-26281
- Electron-cyclotron wave instability in plasma noting dispersion relation, growth rate frequency, destabilizing effect of electrons, etc 13 p2163 A67-26286
- Elastic collisions in simulating one-dimensional plasma diodes on computer 13 p2164 A67-26294
- Plasma instabilities and controlled thermonuclear reactions 13 p2164 A67-26387
- Rotating flame resulting from instability of inhomogeneous plasma produced by arc

discharge in magnetic field approaching criticality 13 p2166 A67-26768
 Effect of shifting radial electrical field sign on instability state of inhomogeneous plasma produced by arc discharge in equipotential volume 13 p2166 A67-26770
 Onset of electron oscillations in plasma with large velocity or temperature gradients 13 p2170 A67-27367
 Finite ion Larmor radius in stabilizing rippling mode of Furth-Killen-Rosenbluth dissipative instabilities in plasma with finite resistance gradient 13 p2170 A67-27369
 Rippling mode instabilities in positive helium discharge column at critical longitudinal magnetic field 13 p2170 A67-27371
 Instabilities and dispersion during electromagnetic wave excitation and propagation in weakly turbulent plasma 13 p2171 A67-27384
 Silicon avalanche diode behavior for short duration surge current in reverse direction 13 p2084 A67-27576
 Flute type instability of ideally conducting plasma in toroidal discharges with strong longitudinal magnetic field 13 p2172 A67-27715
 Electrostatic waves in LF noise bands as cause of diffuse traces observed by Louette satellite ionospheric probe electrostatic waves in LF noise bands as cause of diffuse traces observed by Alouette satellite 14 p2312 A67-28518
 Ion oscillations excitation by beam-plasma interaction near ion-plasma frequency, studying instability as function of magnetic field, plasma density and other parameters 14 p2360 A67-28553
 Experimental detection and evaluation of plasma instabilities, discussing research state in connection with thermonuclear and cosmic problems 14 p2360 A67-28556
 Thermally ionized low density alkali-metal plasma for simulating controlled fusion processes, noting high particle losses and instability 14 p2362 A67-29038
 General resistive instabilities of self-pinched cylindrically symmetric beam of charged particles passing through ohmic plasma channel 15 p2522 A67-29198
 Recombination instability in plasma if temperature dependence is strong 15 p2522 A67-29208
 LF plasma instabilities indicated by Landau electron attenuation computation for short wavelengths 15 p2528 A67-29710
 Plasma drift instability in discharge with oscillating electrons, measuring plasma vibration spectrum 15 p2528 A67-29711
 Digital computer methods for calculating impulsive relaxation in unbalanced hydrogen plasma 15 p2529 A67-29713
 Influence of strong HF electrical fields on plasma instability originated in buildup of potential field oscillations 15 p2530 A67-29728
 Instability of electron hole plasma of semiconductor caused by nonlinear current-voltage characteristic 15 p2538 A67-29789
 Plasma characteristics and instability when plasma waves lead to current oscillations in bulk semiconductor 15 p2450 A67-29814
 Growth and damping rates of resistive instability in gaseous plasma in crossed fields determined from empirical observations 15 p2530 A67-29823
 Drift waves in finite pressure plasma, noting oscillation caused instabilities induced by Alfvén type and slow magnetoacoustic wave interaction 15 p2530 A67-29864
 Critical field dependence on pressure, tube radius and ion mass derived from ion-acoustic instability growth in low pressure RF discharge 15 p2531 A67-29904
 Conducting surface boundary effect on current plasma instability in terms of potential fluctuations 15 p2532 A67-30256
 Coaxial plasma source transition from high energy particle production to production of slow plasmoids, noting V-I characteristics and magnetic field distribution 15 p2532 A67-30260
 Kelvin instability following velocity discontinuity in current-carrying cold collisionless plasmas under magnetic field, deriving dispersion relation and instability criteria from fluid equations 16 p2714 A67-30872
 Stabilization of ion cyclotron plasma in mirror machines by energy spreading and application of high frequency electric

field 16 p2714 A67-30873
 Flute instability in mirror machines at very low plasma densities, using variational principle for stability criterion 16 p2714 A67-30876
 Collision plasma instability analysis based on MHD equations and ion motion along magnetic field 16 p2715 A67-31041
 Scattering method for observing plasma instability near electron gyrofrequency harmonics 16 p2715 A67-31062
 Ionospheric F-2 layer inhomogeneities attributed to plasma flute instability, using kinetic drift equations to describe plasma oscillations 16 p2865 A67-31084
 Parametric instability of infinitely wide periodically modulated electron beam with uniform cross section in terms of nonlinear theory of parametric excitation 16 p2716 A67-31178
 Quasi-linear theory of plasma cyclotron instability, analyzing transverse oscillations propagating along external magnetic field 16 p2717 A67-31179
 Drift instability of discharge plasma with oscillating electrons 16 p2717 A67-31180
 Drift instabilities in nonuniform collision-free plasma stabilized by magnetic shear noting longitudinal currents, electron and ion temperature gradients, etc 16 p2718 A67-31226
 Nonlinear instability, demonstrated for electron plasma waves driven toward instability by small ion beam but linearly stabilized by electron Landau damping 16 p2719 A67-31228
 Thermal plasma column instability concept applied to determine Kaufmann Criterion, calculating production coefficient, V-I characteristics, etc 16 p2719 A67-31229
 Electrostatic wave effect on anisotropic relativistic proton plasma in magnetic field, noting instability 16 p2739 A67-31234
 Plasma anomalous resistive instability shown independent from microinstability and caused by poor conductivity parallel to magnetic lines 16 p2720 A67-31240
 Origin of afternoon VHF radar echo from backscattering layer near auroral electrojet explained by plasma instability and perpendicular electric and magnetic fields 16 p2627 A67-31407
 Energy dissipation and transport coefficients temperature dependence effect on short wave perturbation development in magnetohydrodynamics 16 p2723 A67-31578
 Magnetic bottles leakage in fusion reactors, describing differences between microinstabilities and MHD theories 16 p2724 A67-31865
 Dispersion equations for long wavelength beam instability propagating through homogeneous plasma 17 p2895 A67-32160
 Nonconvective instability for hot plasmas from poles colliding through negative wave numbers 17 p2899 A67-32276
 Collisionless shock waves in plasmas with high beta parameter, discussing Alfvén wave turbulence, firehose instability, dissipation and structure 17 p2901 A67-32528
 Zero temperature cylindrical collisionless plasma in magnetic field studied for electrostatic instability, noting effect of radial velocities of electrons and ions 17 p2902 A67-32658
 Linear theory of collision-induced instability of partially ionized gases for waves propagating along external magnetic field 17 p2902 A67-32669
 Nonadiabatic theory for plasma behavior in strong electric field, discussing plasma instability conditions 17 p2905 A67-32924
 HF electrostatic instability in low density plasma stream guided by magnetic field, discussing cause and anomalous loss of diamagnetism 17 p2907 A67-33106
 Instability and related anomalous diffusion of magnetized weakly ionized hydrogen plasma of RF discharge in cylindrical geometry 17 p2908 A67-33113
 Fluctuating electric and magnetic fields due to plasma instabilities and stabilizing effect of mode coupling in collisionless plasma 17 p2909 A67-33229
 Auroral radar echo association with aurora, noting connection with two-stream plasma instability 17 p2852 A67-33244
 Propagation modes and instabilities of transverse disturbances in solid state plasmas 17 p2925 A67-33377
 Auroral backscatter theory and

relationship to instability concepts 18 p3038 A67-33618
 Cyclotron instabilities of two-component electron plasma 18 p3089 A67-34295
 Weakly ionized inhomogeneous plasma in crossed fields, discussing magnetic field strength effect on stability against perturbations 18 p3089 A67-34296
 Collision induced instability in semiconductor plasmas, noting system consisting of electrons and holes with transverse relative drift to static magnetic field 18 p3102 A67-34348
 Nonlinear instability of nonisothermal plasma in external electric field, determining ion-acoustic noise spectrum and time dependent variations in kinetic energy of plasma electrons and ions 18 p3090 A67-34420
 Plasma in HF electric field becoming kinetically unstable due to Cerenkov effect 18 p3090 A67-34422
 Plasma flux instability in inhomogeneous medium 18 p3090 A67-34434
 Macroscopic cross-field instability occurring in ionized plasma studied by computer, discussing wave interactions between Fourier modes 18 p3092 A67-34746
 Collisionless electrostatic shock in magnetized plasma in absence of initial magnetic field 18 p3092 A67-34749
 Particle trajectories analysis for drift instability mechanism, considering resonant and nonresonant particles 19 p3267 A67-34890
 Plasma finite orbits instability due to plasma particle shift, discussing collision frequency role 19 p3267 A67-34896
 Drift instabilities and related phenomena in inhomogeneous plasma confined by strong magnetic fields 19 p3292 A67-35388
 Stream instabilities in magnetized plasmas in presence of DC magnetic field, noting possibilities of growing waves 19 p3292 A67-35389
 Damping of high frequency waves in homogeneous fully ionized plasma with relative electron-ion drift calculated, using fokker-planck kinetic equation 19 p3292 A67-35391
 Diocotron effect in cylindrical charge layers analyzed, noting instability when layer thickness is less than critical, experimenting with plasma discharges 19 p3292 A67-35392
 Quiescent solar prominences general appearance described by theoretical model 19 p3324 A67-35436
 Damping effect of HF field on instabilities occurring in form of moving striations within plasma of gas laser 19 p3241 A67-35814
 Plasma oscillations, discussing kinetics, macroscopic and Vlasov equations, Landau damping and beam instabilities [AFOSR-66-2823] 19 p3299 A67-35871
 Inhomogeneous plasma oscillations, studying drift and flute instabilities and dielectric constant 20 p3492 A67-36130
 Plasma microinstability theory, predicting dangerous instability above critical density, discussing applications to very high temperature plasma 20 p3495 A67-36153
 Transport process instability theory, discussing collisionless plasma transport phenomena and relation to Ohm law 20 p3495 A67-36156
 Dispersion relation for microinstabilities in finite plasma noting relation to particle motion 20 p3496 A67-36215
 Inhomogeneous plasma instability from low pressure arc discharge in magnetic field 20 p3498 A67-36683
 Plasmoid instability from inhomogeneous flow along magnetic field 20 p3498 A67-36693
 Magnetospheric features, describing magnetic field distribution, electron and proton density, plasma instabilities, bow shock and solar wind 20 p3430 A67-36903
 Partial solutions of equations describing axisymmetric unstable motions of gravitating rarefied magnetoplasma 20 p3502 A67-37663
 Toroidal plasma instabilities analyzed, justifying use of two-dimensional slab models with varying gravitational field simulating magnetic lines curvature effect 21 p3661 A67-37747
 Two-stream instability calculations from phase-space boundary motion, using Vlasov equation in distribution function 21 p3662 A67-37763
 Stabilization conditions of isothermal

plasma drift in magnetic trap for comparable electron and ion temperatures 21 p3663 A67-37936

Flute instability of maximally inhomogeneous rarefied plasma cylinder with thick transition layer amounting to two Larmor radii 21 p3667 A67-38371

Drift instabilities of inhomogeneous plasma in HF electric field 21 p3667 A67-38374

Instability of plasma with anisotropic ion velocity distribution, deriving equations for temperature variations and magnetic field energy changes 21 p3669 A67-38680

Kaufman thruster with curved stainless steel accelerating-grid system, studying operation, efficiency, plasma instability, etc [AIAA PAPER 67-725] 21 p3694 A67-38750

Decay instability of steady state waves in plasma, considering Alfvén wave 21 p3674 A67-38803

ULF radiation in polar auroral zone explained via plasma beam instability, assessing perturbation of particle fluxes in magnetosphere 21 p3621 A67-39016

Ion wave dispersion relation in mercury vapor plasma, explaining cut-off frequency dependence on electron drift velocity 22 p3842 A67-39207

Rapid randomization phenomena in unstable plasma sac for Mach numbers close to unity attributed to electron interaction with trapped electroacoustic waves 22 p3844 A67-39357

Magnetic shear effects on density gradient drift instabilities in plasma with plasma pressure to magnetic pressure ratio larger than electron-ion mass ratio 22 p3845 A67-39483

Ion cyclotron instability potential and adiabatic compression of plasma in mirror machine, measuring plasma decay rate and potential 22 p3846 A67-39487

Unstable coupling between slow space charge mode of electron beam and lowest plasma electron band modes in finite geometry 22 p3847 A67-39643

Micropulsation pattern changes during magnetospheric transition from quiet to excited state, discussing influence of earth and long period and pearl-type pulsations 22 p3883 A67-39674

Kinetic equation for spatially uniform unstable plasma with collision term containing wave effect / plasmons / in system and Lenard-Balescu equation 22 p3848 A67-39690

Incompressible finite conductivity tearing instability in hard-core pinch with constant applied axial magnetic field 22 p3848 A67-39695

Quasi-linear perturbation expansion used to study evolution of localized disturbance in plasma 22 p3851 A67-39985

Cyclotron instability examined for plasma in magnetic mirror machines with anisotropic nonmonotonic ion distribution in velocity space 22 p3852 A67-39988

Stability of collisionless plasma with ions moving relative to electrons under electric field of ion cyclotron wave 22 p3852 A67-39989

Radial electron density profile and critical longitudinal magnetic field for helical current convective instability in hollow plasma column via Langmuir probe measurements 22 p3853 A67-40234

Turbulent plasma state and diffusion across magnetic field due to ion acoustic instability noting diffusion coefficient increment with instability excitation 23 p4032 A67-40905

Two-dimensional two-fluid nonlinear computer model applicable to low beta plasma interchange modes 23 p4033 A67-40995

Magnetogravitational instability of uniformly rotating compressible medium due to variable amplitude perturbations, stressing Jeans theory 23 p4033 A67-41019

Two-stream instability in plasma analyzed using magnetic field association with charged particle motion and boundary effects 23 p4034 A67-41450

Plasma potential oscillations in traps, discussing flute instabilities, cyclotron instabilities and resonance electron wave excitation 23 p4034 A67-41680

Impact ionization avalanche plasma production and instabilities in InSb at low temperatures, measuring current variation with electric field

strength 24 p4204 A67-42344

Plasma discharge instability effect on gas laser operation, discussing moving layers self-excitation and laser beam modulation 24 p4168 A67-42561

PLASMA JET

SA ARC JET

Laser, electron and plasma energy beam types and application to manufacturing technology 02 p0249 A67-12179

Interaction of plasma jets ejected from electrode spots with accelerating magnetic field as possible cause of electrode polarity effect on flat-electrode-type plasma acceleration 02 p0275 A67-12471

MHD stability of dense plasma jets flowing into transverse magnetic field, discussing effect of conductivity and Hall factor 03 p0477 A67-13462

Electron recombination in rapid cooling of magnetized plasma jet expanding into vacuum 03 p0488 A67-14195

Stability and steadiness of gas flow of argon plasma jet analyzed, using dual grating spectrograph 04 p0664 A67-14848

Photographic measurement of plasma jet velocity using time shift in brightness fluctuation 04 p0666 A67-15188

Aerodynamic detector measuring dynamic pressure distribution in laminar He jet heated by electric arc 05 p0850 A67-16035

Stallwood jet and DC arc in analysis of air contamination in inert gases 05 p0758 A67-16368

Self-absorption of radiation in high temperature plasma jet of hydrogen, argon and nitrogen 05 p0851 A67-16522

Spectroscopic measurement of temperature, electron density and conductivity in RF plasma torch 06 p1039 A67-17825

Treatment of steel with laser beam, obtaining precision holes without affecting microhardness of metal 06 p1008 A67-18234

Thermal fluxes in plasma jets produced by HF plasmatron in air 06 p1045 A67-18813

Nature of forces causing adhesion of coatings produced by plasma jet sputtering techniques 07 p1190 A67-19304

MHD approximation of solar plasma fluxes observed by Mariner II as free rotating jets 07 p1243 A67-19802

Evaporation process of particles in high temperature gas stream under nonadiabatic conditions 08 p1428 A67-21424

Plasma jet applications, emphasizing generation of high temperatures for refractory coatings in form of intermetallic compounds and cermets 09 p1545 A67-22172

Plasmatron jet with vertical arc stabilization of arc, correlating jet structure with nozzle geometry and electrode polarity 11 p1832 A67-24027

Supersonic rarefied argon plasma jet, determining pressure distribution, electron concentration and temperature 11 p1842 A67-24963

Hollow electrically conducting fluid jet stabilization in presence of uniform magnetic field 13 p2169 A67-27314

Electron recombination in rapid cooling of magnetized plasma jet expanding into vacuum 14 p2360 A67-28540

Viscosity and thermoconductivity values of partially ionized argon plasmas derived by investigating temperature decay and stream velocity distribution in argon plasma jet 15 p2531 A67-30203

Radiation spectra of plasma jets from IR to UV, determining electron density and argon excitation temperature, noting bremsstrahlung 17 p2893 A67-32144

Plasma jet electrical conductivity, using inductances with different diameters as measurement device 17 p2895 A67-32154

Ionization of low temperature supersonic plasma jets, noting kinetics of elementary processes, gas dynamic parameters and effects of combustion and alkali metal admixtures 17 p2896 A67-32170

HF electrodeless plasmatron working at atmospheric pressure, noting plasma discharge and temperature distribution characteristics, obtaining constricted plasma jet 17 p2897 A67-32175

Mass composition, contamination dynamics and jet structure of titanium plasma source 17 p2904 A67-32913

Plasma layer effect on antenna performance from wind tunnel studies, discussing antenna transmission and

breakdown in plasma jet flow 18 p3004 A67-34645

Nitrogen ion drift velocities in plasma jet flowing into vacuum chamber noting ion mobilities in parent and foreign gas 19 p3271 A67-35075

Supersonic free plasma jet with axial current, solving MGD equations for structure modifications due to self-magnetic forces 19 p3288 A67-35363

Density and temperature measurements of high temperature nitrogen plasma jet using schlieren photographic method 19 p3231 A67-35595

Trigatron spark gap using low voltage plasma jet as switch analyzed for properties, time lag and mechanisms 19 p3298 A67-35602

Ablation characteristics investigated using plasma jet wind tunnel, discussing effective heat of ablation and free stream stagnation enthalpy 20 p3544 A67-36640

Magnetic cut-off system for plasma jet, with plasma flux reduction 20 p3497 A67-36679

Propellants and propellant mixtures effects on MPD arc jet performance in test for ions and neutrals mixture acceleration to high velocity 21 p3688 A67-38715

[AIAA PAPER 67-684]

Spatial average plasma conductivity by RF impedance probes for cylindrical radially inhomogeneous plasma 22 p3844 A67-39366

Imbedded magnetic field stabilization effect on infinitely conducting inviscid compressible relativistic MGD half-jet 22 p3850 A67-39706

Plasma jet front produced by coaxial gun studied using SHF diagnostics method 22 p3799 A67-39764

High temperature turbulent jet gasdynamic behavior, discussing high temperature plasma jet experiments 23 p3989 A67-40728

Interaction between plasma stream and inhomogeneous field of electromagnetic wave studied for relation of plasma behavior to potential forces acting on charged particles 23 p4032 A67-40910

PLASMA JET SYNTHESIS

Nitrogen fluorides synthesis in nitrogen plasma jet intermixed with gaseous fluorides 02 p0190 A67-12235

Airframe heat protection for high performance sounding rockets, using plasma jet testing for leading edge design selection 08 p1425 A67-20528

Streaming thermal plasma /STP/ devices, discussing plasma jet synthesis of HCN from cold methane and thermal nitrogen plasma 21 p3578 A67-38393

Airframe heat protection for high performance sounding rockets, using plasma jet testing for leading edge design selection 24 p4256 A67-42914

PLASMA LAYER

Wave seepage through caustic surface in parabolic plasma layer 02 p0191 A67-11582

Acceleration mechanism in plasma current layer forming when strong magnetic field moves at high speed into initially stationary fluid-free plasma 02 p0274 A67-12341

Kinetic theory of electromagnetic wave propagation in layered plasma waveguide in strong magnetic field 05 p0761 A67-16341

Instability of current layer during plasma flux passage through local pinches of pulsed plasma accelerator 05 p0854 A67-16994

Quasi-neutral charged particle bunches kinematics in flat electrode plasma accelerator 05 p0855 A67-16996

Surface impedance of nonhomogeneous plasma with sharply varying parameters, noting skin effect and permittivity gradient 05 p0766 A67-17231

IMP-I satellite measurements of neutral sheet in geomagnetic tail noting dimensions, motion and parameters of sheet 07 p1244 A67-19922

Collective energy losses by plasmas in crystals caused by excitation of volume or surface plasmons 08 p1369 A67-20828

Combination scatter of electromagnetic waves by ion-acoustic oscillations in flat confined plasma layer with zero plasma density outside 12 p1974 A67-25447

Electrostatic polarization of cylindrical plasma layer in external static magnetic field, discussing transverse charged particle drift in crossed fields 13 p2168 A67-27305

Spectral line profile obtained by radiative transfer equation from radiation by dense,

- inhomogeneous plasma layer 16 p2715 A67-31064
Measured admittance of X-band waveguide radiating into dielectric and plasma layers compared with computed admittance figures 16 p2627 A67-31352
Plasma layer effect on antenna performance from wind tunnel studies, discussing antenna transmission and breakdown in plasma jet 18 p3004 A67-34645
Unsteady state of infinite plane layer of isotropic homogeneous plasma situated in steady electric field normal to layer 19 p3286 A67-35349
Dlocotron effect in cylindrical charge layers analyzed, noting instability when layer thickness is less than critical, experimenting with plasma discharges 19 p3292 A67-35392
Offset impedance sheet effect on admittance of slot antenna in conducting plane 19 p3197 A67-35823
Flows superimposition on toroidal hydromagnetic equilibrium, stressing stationary motion of plasma layers between neighboring magnetic surfaces 21 p3661 A67-37751
Kinetic theory of electromagnetic wave propagation in laminar plasma medium situated in steady HF or LF magnetic field normal to plasma layer 21 p3663 A67-37860
Interfaces 21 p3663 A67-37860
Electromagnetic wave propagation in plasma layer bounded by external constant magnetic field, using kinetic theory with Maxwell equations and distribution function 21 p3670 A67-38685
Asymptotic solution for planar electromagnetic wave diffraction on ideally conducting cylinder surrounded by inhomogeneous plasma layer 21 p3585 A67-38811
Combination scatter of electromagnetic waves by ion-acoustic oscillations in flat confined plasma layer with zero plasma density outside combination scatter of electromagnetic waves by ion-acoustic oscillations in flat confined plasma 21 p3674 A67-38821
Spherical electromagnetic wave refraction on heterogeneous parabolic plasma layer using beam optics 22 p3760 A67-39737
Kinetic theory of electromagnetic propagation through magnetoactive plasma, determining reflection, transmission and absorption coefficients and plasma field configuration 22 p3761 A67-39758
Plane electromagnetic wave reflection from ionization front, determining coefficient from finite thickness plasma layer and constant charged particle density 22 p3762 A67-40122
Electromagnetic propagation in plasma layer in magnetic field, determining absorption coefficient 22 p3762 A67-40123
Electromagnetic wave absorption and transformation in resonant layer of nonuniform plasma at oblique incidence 24 p4119 A67-42071
- PLASMA LIFETIME**
Plasma injected into magnetic trap with aid of conical theta pinch investigated to determine ion and electron energy, lifetime and charged particle concentration variation 04 p0668 A67-15279
Chandrasekhar dynamical friction theory for star in cluster adapted to Fokker-Plank electron in two-component plasma theory and including multiple encounters 10 p1711 A67-23790
- PLASMA LOSS**
Radial transport of cesium plasma governed by resistive diffusion as shown by stellarator experiments in which surface recombination losses within plasma volume were negligibly small 01 p0125 A67-10914
Plasma loss in single-ended Q device measured as function of magnetic field strength, obtaining diffusion coefficient directly 05 p0859 A67-17445
Collective energy losses by plasmas in crystals caused by excitation of volume or surface plasmons 08 p1369 A67-20828
End losses from linear theta pinch estimated from self-consistent calculation of structure of plasma and confining magnetic field 08 p1362 A67-21149
Velocity and current-driven universal instability of fluctuations in plasma of model C stellarator 08 p1365 A67-21406
- Anomalous losses in plasma confined in magnetic field, correlating loss process with tube dimensions, electron temperature, gas pressure and magnetic field 11 p1829 A67-24002
Anomalous transport phenomena in ring discharge studied for instability and losses due to noise, using mc RF oscillator [AROD-6398-2] 11 p1831 A67-24010
Magnetically confined cesium plasma analyzed under radial electric field, noting radial plasma loss rate 11 p1835 A67-24384
LF loss cone instabilities of plasma in Taylor minimum-B configurations, discussing instability conditions and growth rate 12 p1969 A67-25199
Radiation characteristics from electric dipole immersed in lossy anisotropic plasma taking into account collision effects 16 p2713 A67-30797
Energy losses of modulated azimuthal current in magnetoplasma, discussing specifically electron cyclotron resonance 16 p2716 A67-31177
Ambipolar potential-enhanced loss in magnetic trap reduced by potential difference in magnetic mirror throats dividing field 17 p2909 A67-33116
Motion of plasmoids injected axially in two-dimensional multipolar magnetic field, studying losses 20 p3500 A67-37061
- PLASMA OSCILLATION**
Combination scattering suffered by component, polarized parallel to electromagnetic wave incident on plasma cylinder, from Tonks-Dattner resonances excited by perpendicular component 01 p0020 A67-10148
Spectral energy density of turbulent plasma determined from spatial autocorrelation functions of electric fields of HF oscillations 01 p0121 A67-10235
Electromagnetic oscillation excitation in plasma beam, analyzing cases of weak and strong external magnetic fields 01 p0122 A67-10349
Langmuir probe method, obtaining exact results for small amplitude plasma oscillations 01 p0123 A67-10461
Coulomb collision damping on peculiar solutions for plasma oscillation equations 01 p0124 A67-10749
Simultaneous excitation of electron plasma and ion-acoustic oscillations, using single electromagnetic wave for plasma oscillation generation 01 p0125 A67-10913
Intrinsic electric field of rarefied ion-electron plasma in external magnetic field and plasma stability, noting use of Galerkin method to determine plasma layer slippage 01 p0126 A67-11299
Plasma electron and ion oscillations excitation by low voltage electron beams provide examples of turbulence 01 p0126 A67-11311
Born approximation theory of nonlinear scattering of microwaves from oscillating plasma column, noting diffraction patterns and frequency shifts 01 p0027 A67-11324
Absolute intensity and angular distribution of microwaves scattered from oscillating plasma column, noting diffraction patterns and frequency shifts 01 p0027 A67-11325
Ionospheric F-2 layer inhomogeneities attributed to plasma flute instability, using kinetic drift equations to describe plasma oscillations 02 p0236 A67-11669
Plasma oscillation properties, excitation and attenuation in films of various thickness, noting electron excitation 02 p0290 A67-11736
Oscillation spectra of plasma in quasi-steady state characterized by self-consistent distribution of plasma particles and turbulent pulsation 02 p0274 A67-12455
Ion motion effect on spectral region and energy density of Cerenkov excitation produced by charge moving in cold magnetoactive plasma 02 p0274 A67-12456
Oscillations of plasma composed of ions at rest and relativistic velocity electrons moving along external magnetic field analyzed in linear approximation 02 p0274 A67-12462
Three-dimensional eigenmodes for collisionless electronic Vlasov plasma imbedded in magnetic field in electrostatic approximation, noting plasma stability 02 p0275 A67-12553
Ion acoustic oscillations in collisionless region of fully ionized plasma excited by electric current 02 p0277 A67-12612
Stability of flute oscillations of rarefied plasma in constant electric field normal to magnetic field 02 p0278 A67-12619
Quasi-linear equations for inhomogeneous plasma in magnetic field applied to pumping of energy of Langmuir oscillations 03 p0475 A67-12936
Static theory of oscillations of relativistic plasma in uniform magnetic field 03 p0477 A67-13510
Small amplitude wave propagation in equilibrium plasma studied using collision model proposed by Bhatnagar, Gross and Krook 03 p0481 A67-13738
Relativistic plasma oscillations and two-stream instability treated by Boltzmann and Maxwell equations 03 p0482 A67-13739
Harmonic and anharmonic oscillations of cylindrical plasma with steady axial current 03 p0482 A67-13741
Laboratory-controlled nonlinear, nonresonant excitation of electron plasma oscillations with one transverse electromagnetic wave 03 p0485 A67-14052
Three-wave interaction Hamiltonians describing nonlinear couplings of plasma oscillation with electromagnetic field derived by Bohm-Pines method 04 p0662 A67-14613
Dispersion and damping of oscillations in Maxwellian plasmas with zero order density gradients examined, using Vlasov and Maxwell equations 04 p0665 A67-15103
Periodicity of plasma oscillation intensity spatial distribution upon electron beam excitation 04 p0666 A67-15181
Collisionless shock wave excitation in plasma, determining shock front thickness 04 p0666 A67-15187
Cyclotron ion wave interaction with HF plasma oscillations measured, using vacuum chamber and electron gun 04 p0667 A67-15209
Convective excitation of ionic oscillations in plasma by inhomogeneous electron beam as result of spatial gradient of distribution function 04 p0668 A67-15270
Convective effects role in exciting axisymmetric oscillations in plasma cylinder in magnetic field with aid of radius restricted electron beam 04 p0668 A67-15271
Transverse electromagnetic wave transformation into ion-acoustic plasma oscillations with formation of intermediate Langmuir electron wave 04 p0668 A67-15275
Oscillations of nonuniform plasma column 04 p0668 A67-15278
Instability due to nonlinear coupling of electron plasma oscillation and ion acoustic oscillation to driving transverse field extended to longitudinal driving field 04 p0672 A67-15771
Quasi-linear relaxation in unsteady states of noncollision plasma, noting electron beam distribution function and Langmuir plasma oscillations 05 p0852 A67-16696
Electron beam excitation as possible explanation of relation between enhanced diffusion and HF oscillation in plasma 05 p0854 A67-16896
LF oscillation 30 times greater than HF oscillation in plasma in magnetic field 05 p0854 A67-16897
HF plasma oscillations in planar diodes, noting boundary conditions in plasma electrode interspace 05 p0866 A67-16993
Nonlinear interaction between plasma oscillation normal modes in hydrodynamic approximation 05 p0858 A67-17434
Electrostatic ion cyclotron oscillations excitation by electrode immersed in plasma 05 p0859 A67-17435
Minimum B magnetic field geometry for LF oscillations in Cs plasma of Topsy Q device 05 p0859 A67-17444
Oscillation in finite plasma with two types of boundaries, showing dynamics of particles 05 p0859 A67-17448
LF electromagnetic field behavior in cold magnetoactive plasma near resonance layer, noting condition for energy absorption increase 06 p1039 A67-18078
Oscillations of inhomogeneous weakly ionized plasma situated in external electric and magnetic field, noting causes and conditions of plasma instability 06 p1039 A67-18080
Stabilization of hydrodynamic drift oscillations in rotating nonuniform cylindrical plasma 06 p1040 A67-18092
Solar radiation drift flares in decimeter range produced by ionic sound interaction

with plasma fluctuations 06 p1077 A67-18155
 Plasma interaction with cold homogeneous charged particle beam through dielectric interlayer of finite thickness 06 p1045 A67-18780
 Plasma in HF electric field becoming kinetically unstable due to Cerenkov effect 06 p1045 A67-18803
 Charged and neutral particles collision effect on LF oscillations in weakly ionized plasma in crossed electric and magnetic fields 06 p1046 A67-18827
 Electron plasma oscillations excited by two-beam instability and nonlinear coupling between them 06 p1046 A67-18828
 Generation of longitudinal plasma oscillation harmonics near electron cyclotron frequencies 06 p1046 A67-18831
 Parametric excitation of modes of infinite plasma by incident radiation using Vlasov equation, noting unstable oscillations for incident frequencies 07 p1228 A67-19502
 Paramagnetic current formation due to volume resonator microwave field interaction with dense plasma subject to RF pressure and EPR in static magnetic field 07 p1228 A67-19512
 Effect of longitudinal plasma oscillations excited by external electric field on plasma stability, deriving dispersion relations by using Vlasov equation 07 p1229 A67-19518
 LF resonance oscillations in cylindrical plasma column, considering ionization mechanism of Philips Ionization Gauge /PIG/ discharge 07 p1229 A67-19674
 Electromagnetic emission from growing plasma oscillations 07 p1230 A67-20146
 Plasma oscillations of electron shell of atom, discussing natural frequency, damping, probability and participation of plasmon in atomic reactions 08 p1355 A67-20860
 Frequency spectrum during UHF plasma oscillation excitation by monoenergetic primary electrons introduced into low pressure Hg discharge 08 p1358 A67-20869
 Landau type damping of plasma oscillations and Bernstein mode electrostatic propagation perpendicular to weak magnetic field 08 p1360 A67-21129
 Rotating helical perturbations in Penning discharge plasma accompanying LF oscillations enhance particle transport across magnetic field 08 p1362 A67-21146
 Generalized formulation of electrostatic oscillations and streaming instabilities in bounded and unbounded inhomogeneous Vlasov plasmas with transverse density gradients in strong axial magnetic field 08 p1363 A67-21305
 LF electron density microscopic fluctuations in bounded plasma examined by method having virtue of being exact at zero frequency 08 p1365 A67-21404
 Causality of steady state response of collisionless plasma model to applied external field 08 p1365 A67-21405
 Latitude dependent plasmasphere oscillations, providing toroidal and standing wave solutions for MHD equations 08 p1365 A67-21407
 Noise energy spectra created by wave-wave scattering of quasi-longitudinal waves in magnetoactive plasmas with different electron and ion temperatures 08 p1365 A67-21413
 Active region corona and type I bursts supposedly generated by plasma oscillations excited by electron beam 08 p1377 A67-21445
 Continuous transition from moving striation to helical oscillation in helium discharge plasma due to increase of applied magnetic field 09 p1536 A67-21570
 Steady state beam induced plasma parameters and behavior when affected by HF noise oscillations and effect on electron concentration in plasma 09 p1545 A67-21997
 Nonsymmetric oscillations in plasma in magnetic field arising from electron beam passage through plasma, deriving dispersion equation 09 p1545 A67-22003
 Electrostatic oscillations in dielectric, semiconductor and plasma in presence and absence of external magnetic field 09 p1555 A67-22011
 Beam-generated plasma oscillation frequency expansion due to temperature, field and density characteristics 09 p1546 A67-22282
 Microwave noise intensity emitted by electron plasma within framework of fluctuation theory 09 p1547 A67-22318

Magnetized plasma oscillations for arbitrary initial distributions of electrons and ions, obtaining dispersion equation in fifth degree 09 p1550 A67-22617
 Drift cyclotron oscillations of inhomogeneous collision plasma propagating across magnetic field, taking into account particle collisions with aid of Landau collision integral 10 p1686 A67-23595
 Electrostatic oscillations excited in cylindrical plasma shell by electron beam, noting resultant instability 11 p1828 A67-23892
 Negative ions in night ionosphere, discussing sub-ELF emission and excitation of ion acoustic oscillations in plasma by electron drifts 11 p1784 A67-23933
 Diurnally oscillating component of thermospheric east-west pressure acceleration at equator, noting balancing effect of viscous diffusion, ion distribution, etc 11 p1785 A67-23939
 Thermal plasma device /Q machine/ design objectives and proposed features, noting association with normal mode oscillations in gas laser 11 p1830 A67-24006
 Dispersion relation for LF oscillations in plasma with negative ions derived in three-fluid approximation 11 p1834 A67-24375
 Nonisothermal alkali plasma collisional drift instability in radial electric field 11 p1834 A67-24380
 Minimum B magnetic field geometry effect on spontaneous oscillations and anomalous cross field plasma transport in TOPSY Q device with uniform axial magnetic field 11 p1835 A67-24388
 Thermal dissipation of energy in ionized cesium plasma, obtaining plasma oscillation excitation which destroys electron drift motion 11 p1837 A67-24394
 Current flow through plasma sheath into magnetized plasma, noting negative resistance characteristics of sheath upon ion cyclotron frequency 11 p1837 A67-24397
 WKB /Wentzel-Kramers-Brillouin/ approximation to solve linearized Vlasov equation for oscillations of inhomogeneous one-dimensional plasma 11 p1838 A67-24404
 Barium Q plasma device for optical diagnosis of oscillatory microinstabilities compared with Langmuir probe 11 p1838 A67-24406
 Electrostatic separation probe to measure electronic velocity distribution function, showing evolution of distribution function relationship to plasma oscillation growth 11 p1789 A67-24409
 Undamped plasma oscillations in nonpolar semiconductors doped with impurities in external electric field, determining phase velocity 11 p1846 A67-24472
 Enhanced plasma fluctuations produced by suprathermal electron effect on emission and scattering of electromagnetic waves, noting analogy with corona plasma 11 p1839 A67-24546
 Interaction of plasma oscillation with electrons with positive distribution function, noting oscillation amplitude relation to function deformation 11 p1840 A67-24766
 Electrostatic oscillations in electron plasma, noting effect of external electric field on electron velocity distribution 11 p1848 A67-24868
 Magnetic effect and collision in damping of electron Langmuir oscillations 11 p1842 A67-24965
 Shunting process and associated fluctuations in plasmatron with vortex stabilized arc, noting anode spots 11 p1843 A67-24971
 Electromagnetic oscillation excitation in plasma beam, analyzing cases of weak and strong external magnetic fields 11 p1844 A67-25022
 Plasma conductivity in external electric fields calculated by LF longitudinal oscillation, using Boltzmann equation 12 p1970 A67-25249
 Spectrum of longitudinal plasma oscillations noting instability under resonance condition 12 p1970 A67-25255
 Electronegative plasma kc oscillations during glow discharge, measuring variations of frequency and longitudinal and radial intensity 12 p1970 A67-25281
 Nonequilibrium MHD plasmas investigated for electrothermal instabilities noting effect of plane wave

fluctuations 12 p1972 A67-25391
 Combination scatter of electromagnetic waves by ion-acoustic oscillations in flat confined plasma layer with zero plasma density outside 12 p1974 A67-25447
 Kinetic approximation of penetration of electric field into plasma layer situated in stationary magnetic field, determining plasma field 13 p2164 A67-26396
 Destruction of drift motion of electrons in quiescent cesium plasma by electron-plasma oscillations 13 p2166 A67-26731
 Coulomb collision damping on peculiar solutions for plasma oscillation equations 13 p2166 A67-26778
 UHF intensity-modulated light emanating from plasma observed with aid of photomultiplier 13 p2167 A67-27082
 Ion acoustic oscillations in collisionless region of fully ionized plasma excited by electric current 13 p2170 A67-27368
 Stability of flute oscillation of rarefied plasma in constant electric field normal to magnetic field 13 p2170 A67-27375
 Flute oscillations in bounded nonuniform plasmas and effect of incoherently precessing ions, noting variational methods and perturbation analysis 14 p2360 A67-28555
 Magnetactive plasma quasi-linear oscillations equations, determining damping decrements of plasma electric field components 14 p2361 A67-28753
 Turbulent state and diffusion of plasma during drift instability, noting increase with oscillation amplitude 14 p2363 A67-29068
 Heating of magnetized hot diffuse plasma using difference-frequency signal generated from two HF transverse waves 15 p2521 A67-29188
 Current damping, thermal expansion, radial oscillation, kinetic pressure and other dissipative processes effects on magnetic properties of plasmoids 15 p2524 A67-29244
 Plasma characteristics and instability when plasma waves lead to current oscillations in bulk semiconductor 15 p2450 A67-29814
 Quasi-linear relaxation in unsteady states of noncollision plasma, noting electron beam distribution function and Langmuir plasma oscillations 15 p2530 A67-29867
 Oscillations of confined cylindrical plasma with hot electron current, obtaining dispersion relation for large Debye radius 15 p2531 A67-30072
 Cyclotron ion wave interaction with HF plasma oscillations measured, using vacuum chamber and electron gun 15 p2532 A67-30257
 Effect of decomposition of Langmuir waves on interaction of electron beam with nonisothermal plasma 16 p2705 A67-30448
 Solar radiation drift flares in decimeter range produced by ionic sound interaction with plasma fluctuations 16 p2741 A67-30499
 Oscillation spectrum of weakly ionized plasma current flowing normal to applied magnetic field discussed and analyzed in linear approximation using MHD model 16 p2712 A67-30546
 Ionospheric F-2 layer inhomogeneities attributed to plasma flute instability, using kinetic drift equations to describe plasma oscillations 16 p2665 A67-31084
 Charged particle beam passage through plasma, detailing excitation of one-dimensional oscillation expanding perpendicularly to boundary of semiinfinite plasma 16 p2716 A67-31176
 Quasi-linear theory of plasma cyclotron instability, analyzing transverse oscillations propagating along external magnetic field 16 p2717 A67-31179
 Electron beam interaction with plasma analyzed using nonquasi-static plasma model 17 p2695 A67-32159
 Normal modes of hydromagnetic oscillations in rotating fluid sphere including ohmic dissipation, deriving dispersion relations 17 p2941 A67-32285
 Shock wave generation of electromagnetic radiation at magnetospheric boundary, discussing plasma oscillation excitation, plasma wave scattering, etc 17 p2846 A67-32935
 Longitudinal and transverse collective effects contribution to energy loss rate in relativistic isotropic plasma subject to external fields and particles 17 p2908 A67-33111
 Anomalous LF plasma oscillation by particles trapped in potential well behind

- satellite applied to ionospheric measurements 18 p3117 A67-33512
- Plasma interaction with cold homogeneous charged particle beam through dielectric interlayer of finite thickness 18 p3086 A67-33721
- Plasma in HF electric field becoming kinetically unstable due to Cerenkov effect 18 p3090 A67-34422
- Near earth and outer ionosphere plasma waves and oscillations in VLF and ELF bands 19 p3317 A67-34932
- Oscillations of electric arcs with superimposed gas flow in cylindrical nozzle and rectangular channel, determining critical Reynolds number [DVL-629] 19 p3280 A67-35147
- Cylindrical plasma column subjected to axial magnetic field measured for electric field oscillations by movable probe within ionized gas 19 p3288 A67-35374
- Intense runaway electron stream from wave-plasma interaction in magnetic field noting microwave radiation and disruption time 19 p3291 A67-35381
- Inhomogeneous cylindrical plasma column oscillations with perturbations, finding density-independent mode 19 p3295 A67-35564
- Electron energy spectrum, showing intensity maxima from surface plasma oscillations, noting thin films effect on surface losses 19 p3307 A67-35789
- Plasma oscillations, discussing kinetics, macroscopic and Vlasov equations, Landau damping and beam instabilities [AFOSR-66-2823] 19 p3299 A67-35871
- Dispersion equation for electrodynamic boundary value problem of natural oscillations of cylindrical resonator with magnetoactive plasma 19 p3299 A67-36019
- Linear electromagnetic oscillations in homogeneous plasma described by motion and Maxwell equations 20 p3492 A67-36129
- Inhomogeneous plasma oscillations, studying drift and flute instabilities and dielectric constant 20 p3492 A67-36130
- Weakly turbulent plasma theory, describing plasmon-particle interactions by quasi-linear theory 20 p3492 A67-36131
- Collective fluctuations in collisionless plasma, analyzing spectra fluctuations, particle distribution and wave scattering 20 p3493 A67-36139
- Longitudinal oscillations and Landau damping of electron plasma with fixed ion background, discussing initial and boundary value problems 20 p3494 A67-36150
- Charge density modulation from plasma-beam interaction 20 p3504 A67-36157
- Generalized formulas and stability criteria applied to higher order electrostatic oscillation modes in Vlasov plasmas, considering double-stream amplifier designs 20 p3495 A67-36169
- Dynamic response of nondegenerate electron hole plasma in semiconductor, obtaining frequency spectrum and Landau damping rate of plasma oscillation 20 p3499 A67-36945
- Acoustic wave generation in weakly ionized plasma by fusion and damping of two ion-sound waves 20 p3501 A67-37291
- Surface plasma oscillations at optical frequencies detected by radiation from optical grating metal surface, measuring dispersion relation 20 p3514 A67-37569
- Electron-plasma oscillation damping in hot collisional plasma with external uniform magnetic field investigated using Fokker-Planck equation 20 p3503 A67-37693
- Motion of rotating plasma cylinder under gravity force assuming temperature time dependency 21 p3663 A67-37931
- Oscillation of liquid sodium drop in dielectric medium in presence of constant magnetic field 21 p3665 A67-38245
- Stark effect spectral line broadening due to current or electron beam excitation of stochastic plasma 21 p3670 A67-38690
- Oscillations 21 p3670 A67-38690
- Combination scatter of electromagnetic waves by ion-acoustic oscillations in flat confined plasma layer with zero plasma density outside combination scatter of electromagnetic waves by ion-acoustic oscillations in flat confined plasma 21 p3674 A67-38821
- Plasma continuity equations, deriving oscillation frequency equations for LF oscillations in partially ionized gases 22 p3844 A67-39383
- Helical electromagnetic wave scattering and transformation during propagation in magnetoplasma, considering fluctuations 22 p3846 A67-39501
- 35 GHz second harmonic generation power and conversion efficiency in low pressure gas discharge, noting pressure and gas species variations 22 p3854 A67-40316
- Branch cut contribution to longitudinal electric field in relativistic Maxwell plasma using non-Laplace transformation procedure 22 p3854 A67-40319
- Exact equation for potential oscillations of inhomogeneous plasma cylinder via Fourier transformations, discussing drift, cyclotron oscillations and flute instability 23 p4034 A67-41679
- Electromagnetic wave fluctuations in semilinear plasmas, deriving correlation functions for electromagnetic parameters, considering surface waves 24 p4195 A67-42075
- Dispersion equations for rectangular helix in presence of plasma 24 p4121 A67-42235
- PLASMA-PARTICLE INTERACTION**
- Simultaneous excitation of electron plasma and ion-acoustic oscillations, using single electromagnetic wave for plasma oscillation generation 01 p0125 A67-10913
- Plasma electron and ion oscillations excitation by low voltage electron beams provide examples of turbulence 01 p0126 A67-11311
- Beam-plasma amplifier with input coupler as cavity and output coupling due to Cerenkov radiation 01 p0040 A67-11313
- Cerenkov radiation of beam-plasma system into dielectric, using mathematical model and mode coupling theory 01 p0040 A67-11314
- Cold beam plasma interaction theory for finite transverse dimensions and finite magnetic fields determined by computer solution of dispersion relations 02 p0272 A67-11884
- Injection of helical electron beams into magnetic mirror trap, examining plasma lifetime, density and electron and ion energies produced 02 p0274 A67-12457
- Effective capture of electrons in magnetic mirror trap with stationary field by pulse-type injection of helical electron beam 02 p0274 A67-12458
- Quasi-linear approximation of Cerenkov and cyclotron damping of electromagnetic waves in magnetoactive plasma, considering collisions of wave-absorbing resonance particles with plasma 03 p0475 A67-12934
- Solar wind-comet interaction simulation using plasma stream and carbon dioxide gas cloud sublimated from dry ice 03 p0506 A67-13575
- Partially ionized two-temperature plasma, deriving distribution function of first approximation associated with viscosity 04 p0668 A67-15186
- Cosmic ray isotropy mechanism, examining plasma beam instability and cosmic ray scattering at plasma turbulent pulsations 04 p0693 A67-15554
- Electron and ion acceleration by cosmic plasma waves, examining contribution of these processes to radiation belt formation 04 p0701 A67-15555
- Effective diffusive scattering cross section of electrons in He and Ar plasma with K vapor additions and in pure K, based on DC plasma conductivity and microwave generator Q-factor 04 p0873 A67-15972
- Cross section of proton production for molecular ion beams of hydrogen passing through lithium plasma 05 p0852 A67-16000
- Concentration and density distributions of particle flux near body moving in rarefied plasma 05 p0855 A67-17122
- Charged particle beam interaction with plasma, determining electron-ion temperatures and HF field 06 p1040 A67-18088
- Plasma interaction with cold homogeneous charged particle beam through dielectric interlayer of finite thickness 06 p1045 A67-18780
- Plasma instabilities induced by charge convection across perturbing electric field and magnetic field 07 p1228 A67-19511
- Solar wind magnetic field as medium for plasma-magnetosphere interaction 07 p1243 A67-19803
- Quasi-linear theory of ion beam instabilities of LF waves in plasma 07 p1230 A67-20145
- Electron-ion beam interaction with confined plasma in strong magnetic field, noting ion-sound excitation 08 p1358 A67-20857
- Equilibrium particle ionization effect on electron density of gas particle plasma 08 p1360 A67-21124
- Energetic particle scattering by laboratory plasmas, deriving expressions for scattering coefficients in terms of electric field autocorrelation function 08 p1361 A67-21136
- Kinetic equations for homogeneous electron gas derived to all orders in plasma parameter λ /reciprocal number of electrons per Debye sphere/ 08 p1363 A67-21394
- Atomic collisions, excitation transfer processes and energy level transition probabilities in plasma of gas lasers 09 p1513 A67-22067
- Beam-plasma interaction with transverse modulation, obtaining growth rates 09 p1546 A67-22280
- Beam-generated plasma oscillation frequency expansion due to temperature, field and density characteristics 09 p1546 A67-22282
- Gap excitation of waveguide loaded with plasma represented as charge-free medium with tensor dielectric constant 09 p1480 A67-22283
- Electron transport phenomena in thermionic converter plasmas, emphasizing electron-ion collisions to electron momentum transfer collision frequency 09 p1450 A67-22351
- First integrals of motion to determine stationary distribution function of charged particles and self-consistent magnetic field of plasma 10 p1885 A67-23464
- Higher fast ion density achieved by fast neutral particle injection into closed-line magnetic trap 10 p1686 A67-23466
- Ion beam interaction with beam produced plasma, showing excitation of waves at electron plasma frequency 11 p1840 A67-24562
- Electron beam plasma amplification measurements in interaction region by nonperturbing technique, measuring RF growth, phase velocity, etc 11 p1841 A67-24907
- Velocity space diffusion coefficient of electrons in thermal radiation field, using Hamilton-Jacobi theory 12 p1969 A67-25192
- Energetic particle interaction with hydromagnetic shock wave, noting case of particle in radiation belt 12 p1994 A67-25530
- Charged particle motion and penetration of magnetosphere in proximity of neutral point as result of solar wind-geomagnetic field interaction 12 p1975 A67-25643
- Lack of Cerenkov emission in isotropic plasma, presenting fast electron beam experiment for verification of theory 14 p2357 A67-28204
- Rarefied plasma/rapidly moving body interaction, discussing computational procedure and results 14 p2357 A67-28205
- Plasma-vehicle interaction, discussing charged particle motion about small vehicle in ionospheric orbit 14 p2357 A67-28209
- Ion oscillations excitation by beam-plasma interaction near ion-plasma frequency, studying instability as function of magnetic field, plasma density and other parameters 14 p2360 A67-28553
- General resistive instabilities of self-pinch cylindrically symmetric beam of charged particles passing through ohmic plasma channel 15 p2522 A67-29198
- Active corpuscular plasma diagnostics method applied to hydrogen plasma study 15 p2526 A67-29257
- Suprathermal electron production by quasi-cyclotron acceleration when interacting with monochromatic large amplitude electrostatic plasma wave 15 p2528 A67-29569
- Effect of decomposition of Langmuir waves on interaction of electron beam with nonisothermal plasma 16 p2705 A67-30448
- Collection of papers on charged particles interaction with plasma, including gas discharge and plasma acceleration 16 p2716 A67-31175
- Parametric instability of infinitely wide periodically modulated electron beam with uniform cross section in terms of nonlinear

theory of parametric excitation 16 p2716 A67-31178
 Electron heating by direct discharge during plasmoid interaction involving polarization 16 p2717 A67-31182
 Accelerated electrons effect on plasma in closed magnetic trap, measuring current flow, plasma density, X-ray/microwave radiation and light emission 16 p2717 A67-31186
 Nonlinear dependence of phase velocity on wave amplitude during electromagnetic propagation in plasma waveguide, describing test apparatus 16 p2718 A67-31191
 Plasma-particle distribution function in infinite system of alternating positive and negative electrodes, evaluating high-velocity neutron source effectiveness 16 p2718 A67-31193
 Electron beam interaction with plasma analyzed using nonquasi-static plasma model 17 p2895 A67-32159
 Parameter space partition in beam-plasma regime by determining lower limits of beam density yielding coherent and incoherent domains 17 p2902 A67-32674
 Acceleration mechanisms of isolated plasma particles under effect of weak or strong field with frequency of order of Langmuir frequency of electron 17 p2905 A67-32922
 Plasma interaction with cold homogeneous charged particle beam through dielectric interlayer of finite thickness 18 p3086 A67-33721
 Radiative heating of H and He containing suspension of solid particle absorbers, noting proportionality between gas particle dispersion decrease and energy absorption [AIAA PAPER 67-501] 18 p3158 A67-33965
 Interaction between ion and electron waves in plasma 18 p3089 A67-34186
 Comparison of experimental and theoretical results on electron beam produced mercury-vapor discharge 19 p3290 A67-35380
 Beam-plasma interaction in magnetic field, studying microwave field distribution and emission 19 p3291 A67-35383
 Geomagnetic micropulsation properties variation over last solar cycle and causes 19 p3325 A67-35486
 Cesium plasma created in diode equipped with Langmuir probe 19 p3296 A67-35588
 Weakly turbulent plasma theory, describing plasmon-particle interactions by quasi-linear theory 20 p3492 A67-36131
 Charge density modulation from plasma-beam interaction 20 p3504 A67-36157
 Dispersion relation for microinstabilities in finite plasma noting relation to particle motion 20 p3496 A67-36215
 Ionized gas properties for use in various microwave components to obtain amplification through electron beam plasma interaction 20 p3497 A67-36489
 Concentration and density distributions of particle flux near body moving in rarefied plasma 21 p3668 A67-38465
 Microwave amplification when electron beam passes through cesium plasma, noting noise figure dependence on tube pressure 21 p3668 A67-38605
 Stark effect spectral line broadening due to current or electron beam excitation of stochastic plasma 21 p3670 A67-38690
 Plasma production by optical irradiation of gases and by solids, considering interaction of laser radiation with surfaces and irradiation of particles of solid material in vacuum [AIAA PAPER 66-174] 21 p3642 A67-38851
 Ion and neutral particle interaction effects on F region winds, considering plasma forces 22 p3789 A67-39479
 Electron beam interaction with plasma investigated for spatial distribution of intensity and oscillation spectrum in stationary mode 23 p4032 A67-40904
 Relaxation of anisotropic plasmas based on Fokker-planck equation assuming elliptic distribution during process 24 p4198 A67-42440
PLASMA PERTURBATION
 Plasma electron and ion oscillations excitation by low voltage electron beams provide examples of turbulence 01 p0126 A67-11311
 Plasma kinetic theory calculation via

direct perturbation expansion of singular distribution for single system, comparing Dupree and Dawson-Nakayama version of BBGKY hierarchy 02 p0279 A67-12800
 Perturbation of electron density at large distances from body at high velocity in collisionless plasma under steady external magnetic field 03 p0475 A67-12939
 Criterion for deciding when effect of perturbation of electron-energy distribution in plasma by probe can be neglected 04 p0665 A67-15112
 Electrostatic polarization of plasma in applied electric field, excluding case for steady current flow 04 p0666 A67-15180
 Perturbation theory of ion concentration at great distances from body rapidly moving in collisionless plasma in constant magnetic field 05 p0855 A67-17139
 Perturbations caused by cylindrical field in plasma, obtaining electric field and electron and ion concentration dependences on distance 07 p1250 A67-19811
 Velocity and current-driven universal instability of fluctuations in plasma of model C stellerator 08 p1365 A67-21406
 Steady state beam induced plasma parameters and behavior when affected by HF noise oscillations and effect on electron concentration in plasma 09 p1545 A67-21997
 Perturbed zone stability of body immersed in equilibrium plasma during surface electron emission 10 p1683 A67-22782
 Perturbation theory developed to estimate magnetic surface stability against field irregularities, noting role of field resonances 10 p1686 A67-23468
 Hamilton-Jacobi solutions for Vlasov equation leading to nonsecular perturbation theory for macroscopic quantities 10 p1686 A67-23469
 Hydromagnetic gradient waves theory extended to weakly ionized medium-density magnetized plasma of type expected in ionospheric E layer 11 p1783 A67-23923
 Transient acoustical response of uniform flow to turbulence and noise in MHD generators 12 p1899 A67-25390
 Coupling of laser optical modes by intracavity time varying perturbation 13 p2125 A67-26407
 Finite ion Larmor radius effect on superposed fluid stability investigated for general perturbation direction, noting magnetically stabilized configurations, become overstable 13 p2167 A67-26993
 Resonant oscillation in Penning discharge when electron motion around plasma column perturbs plasma 14 p2355 A67-27828
 Screw instability in linear Hall accelerator 15 p2522 A67-29207
 Relativistic MHD shock wave stability in infinitely conducting plasma with magnetic field parallel to shock wave plane 15 p2523 A67-29216
 Vorticity generation by interaction of waves with plasma in magnetic field 15 p2524 A67-29231
 Electromagnetic surface wave propagation in plasma, studying oscillation spectra dependence on surface wave field amplitude 15 p2529 A67-29712
 Range of undistorted propagation of traveling disturbances, noting shape of altitude-frequency characteristics of ionosphere with parabolic electron density distribution 15 p2479 A67-30074
 Asymptotic stability of homogeneous system of partial differential equations in stratification wave theory, introducing source function for local plasma disturbance effect 17 p2907 A67-33101
 Vlasov equation for anisotropic electron plasma in external magnetic field solved by Laplace transform of density perturbation in initial value problem 17 p2907 A67-33104
 Boundary value problem for electrical potential and ion distribution function obeying Poisson-Vlasov equations when applied to rarefied plasma disturbance by supersonic body 17 p2909 A67-33205
 Plasma regime creation through boundary perturbations in low-pressure gas discharge, developing moving striations 19 p3273 A67-35096
 Spark perturbation of magnetic and electromagnetic fields, studying plasma-magnetic interaction and spark plasma characteristics 19 p3239 A67-35165
 Electromagnetic wave reflection by stratified magnetoplasma, obtaining formulas

providing perturbation effect on reflection coefficients 19 p3183 A67-35457
 Inhomogeneous cylindrical plasma column oscillations with perturbations, finding density-independent mode model 19 p3295 A67-35564
 Magnetic field line trajectories in toroidal stellarators, discussing rotational transforms on last closed surface and perturbation effects 21 p3662 A67-37753
 Perturbation theory of ion concentration at great distances from body rapidly moving in collisionless plasma in constant magnetic field 21 p3668 A67-38481
 Energy exchanges between plasma and excitation source sinusoidal in time and arbitrary in space 22 p3847 A67-39642
 Emissivity expressions and absorption coefficients developed for plasma particles interacting with electromagnetic field and at equilibrium 22 p3854 A67-40527
 Perturbed zone stability of body immersed in equilibrium plasma during surface electron emission 24 p4195 A67-42118
PLASMA PHYSICS
 SA CYCLOTRON RESONANCE
 SA LIOUVILLE EQUATION
 SA MAGNETOHYDRODYNAMICS
 SA MAGNETOHYDROSTATICS
 SA NUCLEAR PHYSICS
 SA THERMODYNAMICS
 Anisotropies and harmonics of homogeneous Lorentz plasma under electric field, using approximation method 01 p0121 A67-10230
 Channel flow interaction of plasma from coaxial plasma gun with transverse magnetic field 02 p0277 A67-12618
 Introductory text on electrical discharges in gases, emphasizing physical behavior of electrons and ions in ionized state 02 p0279 A67-12720
 Plasma diagnostics, comparing microwave toroidal resonator, cylindrical resonator and probe methods 03 p0477 A67-13466
 Lasers used to extend RF plasma diagnostic procedures to optical frequencies by interferometric and Thomson diffusion methods 03 p0477 A67-13474
 MHD and plasma physics and application to cosmic and geophysical phenomena 03 p0479 A67-13723
 Kinetic equations derived for plasma with particle interactions 03 p0481 A67-13735
 Kinetic plasma equations in form of Boltzmann equation or Fokker-Planck or Vlasov type of equations applied to astrophysics 03 p0481 A67-13736
 Anisotropic magnetoplasma diagnostics using transient reflected polarized signals [AFRL-67-0065] 03 p0371 A67-13865
 Kinetic model for three-component plasmas with ionization resulting from electron-neutral collisions 03 p0484 A67-14037
 Complex roots of dispersion relations involving transcendental analytic functions 03 p0486 A67-14056
 Multiparametric diagnostic technique for optically dense plasma 03 p0486 A67-14187
 Book on kinetic equations of gases and plasmas, with emphasis on theories which start from Liouville equation 04 p0660 A67-14581
 Nagoya University, Institute of Plasma Physics, Annual Review, April 1965-March 1966 04 p0662 A67-14590
 Approximations of electrodynamics of moving media 04 p0670 A67-15529
 Plasma observations in tail of terrestrial magnetosphere and circumlunar space by Luna X orbiter, using charged particle traps 05 p0875 A67-16054
 Explosive driven magnetic generator applied to investigate electric, optical and elastic properties of various substances, plasma physics and charged particle accelerator 05 p0786 A67-16365
 Optimum MHD generators using anisotropic plasma, discussing conducting-gas MHD flow, Hall effect, ion slip effect, etc 06 p0950 A67-18089
 Asymptotic kinetic equation for inhomogeneous plasma compared to results for initial value problem and Bogolubov method 06 p1042 A67-18572
 Monograph on MHD containing bibliography of Italian and foreign works 08 p1366 A67-21499
 Laser interferometry and photon scattering in high temperature plasma diagnostics 09 p1536 A67-21602

- Construction of model for chromospheric magnetic field over sunspot 09 p1563 A67-21628
- Supersonic flow velocity and density probe for direct measures of mass and momentum influx, noting solution of H-T diagram of argon and probe criteria 09 p1497 A67-21776
- Thermionic conversion - IEEE Specialist Conference, Houston, November 1966 09 p1446 A67-22330
- Ionosphere-stratosphere coupling and effect of atmospheric seasonal variations on plasma behavior 10 p1645 A67-23266
- Oriented velocity and temperature relaxation in Coulomb type plasma with particle velocities distributed according to Maxwellian law, evaluating Coulomb collisions effect on plasma components 10 p1685 A67-23410
- Convective type drift instability in collisional and collisionless regimes due to magnetic shear effects driven by density gradient 10 p1685 A67-23462
- Radial distribution function differential equation solution studied numerically and analytically for plasma parameters, using closure approximation 11 p1826 A67-23871
- Physics of quiescent plasmas - Conference Frascati, Italy, January 1967 11 p1832 A67-24367
- Quiescent plasma physics - Conference, Frascati, Italy, January 1967, Part 2 11 p1836 A67-24389
- Steady state properties of spheroidally symmetric static arcs with only conduction losses 12 p1970 A67-25290
- Plasma concentration diagnostics in exosphere from delay time of forward frequency as function of parameter of whistler trajectory 13 p2111 A67-26563
- Plasma physics basic principles, noting plasma dynamic behavior determination by electric and magnetic forces, plasma generation, etc 13 p2167 A67-27150
- Physics of plasmas, Volume 2, Weakly ionized gas, covering inelastic collision, free electron scattering, intermediary plasmas, etc 13 p2168 A67-27221
- Channel flow interaction of plasma from coaxial plasma gun with transverse magnetic field 13 p2170 A67-27374
- Spectroscopic measurements of plasma parameters in thermionic converters 13 p2056 A67-27385
- Magnetoquantum-electric effect in solid state plasmas based on displacement of centers of carrier cyclotron orbits 13 p2184 A67-27691
- Self-sustaining high temperature and electrically conducting gas layer formation observed in nonsteady interaction of compressible electrically conducting medium with magnetic field 14 p2355 A67-27839
- Local measurement of SHF electromagnetic field during plasma properties observation, using dipole antennas 15 p2485 A67-29124
- Book on mathematics of MHD which assumes that working fluid is Newtonian and obeys Ohm law in form appropriate to moving conductors 15 p2527 A67-29384
- References on heat and mass transfer 15 p2580 A67-29780
1967. SWIEECO record - IEEE Conference, Dallas, April 1967 15 p2450 A67-29901
- Mean absorption coefficient for optically thin plasma derived taking into account radiative losses, noting electron and ion temperature ratios 16 p2706 A67-30459
- Low temperature plasma - Conference, Moscow, July 1965 17 p2890 A67-32134
- Elementary processes in low temperature plasma 17 p2893 A67-32135
- Equilibrium thermodynamic and gas dynamic parameter calculation for low temperature plasma, using electromagnetic and diaphragm-type shock tubes 17 p2894 A67-32148
- Soviet book on plasma physics covering magnetic traps, acceleration, radiation, etc 17 p2903 A67-32909
- Plasma injection into closed magnetic trap, studying effects of helical magnetic field on containment time, density and cross section distribution 17 p2903 A67-32910
- Strong and weak magnetic field effects on qualitative characteristics of compressible media analyzed using Chaplygin-Sedov hodograph method 18 p3084 A67-33421
- Book on plasma physics covering plasma clouds in electromagnetic force field, kinetic equations, Boltzmann equation, etc 18 p3089 A67-34370
- Plasma measuring methods relation to plasma properties noting photography, optics, particle analysis, etc 18 p3090 A67-34378
- Holographic devices and principles, discussing application to plasma studies 19 p3228 A67-34949
- Spectral line resonance broadening using Griem theory, noting linear pressure dependence 19 p3272 A67-35085
- Penning cell discharge ignition in high vacuum magnetic field in terms of Townsend avalanche theory, with discharge-ignition curves 19 p3272 A67-35089
- Phenomena in ionized gases - Conference, Belgrade, Yugoslavia, August 1965, Volume 2, Plasma physics 19 p3282 A67-35338
- Plasma physics reviews, Volume 3 20 p3492 A67-36128
- Operators spectrum properties and corresponding singular eigenfunctions encountered in plasma problems, showing application to initial and boundary value problems 20 p3494 A67-36148
- Exact equation of state for two-dimensional plasma of equal positive and negative charged particles interacting by Coulomb potential 20 p3501 A67-37293
- Plasma observations in tail of terrestrial magnetosphere and circumlunar space by Luna X orbiter, using charged particle traps 21 p3697 A67-37841
- Soviet monograph on high speed measuring methods in gasdynamics and plasma physics, discussing high temperature plasma and shock wave production 21 p3625 A67-37964
- Convective electric arc stability and slanting in thermionic rail accelerator [AIAA PAPER 67-874] 21 p3671 A67-38707
- Conditioned distribution functions from BBGKY hierarchy distribution functions, with analogy to hydrodynamic approximation of Boltzmann distribution 21 p3675 A67-38931
- Plasma physics of thermionic converters, discussing simple physical models, I-V curve and converter operation region 22 p3747 A67-39342
- Magnetospheric free boundary representation synthesis problem, discussing relaxation solution, dipole moment and stream direction 22 p3854 A67-40347
- Plasma column and plasma-electron beam interaction properties by Langmuir and SHF probes noting resonance, coupling and microwave surface waves 24 p4194 A67-41911
- PLASMA PINCH**
- SA PINCH EFFECT
- SA THETA PINCH
- Magnetically compressed plasma as high intensity source of near UV and visible radiation experimentally studied in dynamic pinch 02 p0272 A67-11880
- Electrical pinch in elastically deformed germanium, examining redistribution of carriers across sample and current-voltage characteristics 04 p0675 A67-14922
- Instability of current layer during plasma flux passage through local pinches of pulsed plasma accelerator 05 p0854 A67-16994
- Faraday rotation measurement of trapped magnetic fields in theta pinch plasma, using gas laser beam 05 p0859 A67-17447
- Conical current sheet implosion forming of axial pinch in z-pinch plasma gun 07 p1230 A67-20257
- Pinch discharge cumulation by using stimulated emission generated in high temperature plasma of strong current pinch discharge 08 p1366 A67-21501
- Electron-hole plasma pinch instability in InSb on application of longitudinal magnetic fields shows change to helical rotating plasma 10 p1683 A67-22760
- Toroidal screw pinch equilibrium and stability in rapidly rising helical magnetic field, discussing experimental setup and results 11 p1827 A67-23888
- Plasma ring acceleration produced by pulsed azimuthal electric field, noting magnetic field role in stabilization 11 p1828 A67-23893
- Relaxation effects in initially non-Maxwellian high temperature theta pinch using Fokker-planck equation for particle velocity distribution function relaxation effects in initially non-Maxwellian 13 p2163 A67-26288
- Trapped magnetic field effect on hydrogen plasma parameters in theta pinch, noting density and temperature dependence on initial pressure 14 p2353 A67-27751
- Drift of theta pinch plasma due to asymmetry of magnetic field analyzed, using high speed photography 14 p2357 A67-28233
- Helium plasma electron temperature and density dependence, with/without magnetic field, on pinch discharge 16 p2718 A67-31187
- Bounce model pinch stability, noting plasma and field separation by thin surface, with anisotropies in velocity distribution and angular momentum 16 p2718 A67-31227
- Time dependent self-compressed pinch-discharge radiation characteristics in various gases analyzed photographically for luminescence distribution, spectral composition, etc 17 p2904 A67-32918
- Pinch radiation in quartz discharge chamber spectrographically studied for use as sources of short pulsed radiation with continuous spectrum 17 p2904 A67-32919
- Rotating field pinch dynamics in terms of temperature, pressure, plasma radius and magnetic field strength, noting energy transfer efficiency 17 p2908 A67-33108
- Magnetic field annihilation rate prediction in current pinches attributed to magnetic energy dissipation by ways other than ohmic losses 17 p2909 A67-33248
- Measurement of Doppler-broadened emission line width by Fabry-Perot interferometer to study ion temperature of pulsed plasma 17 p2862 A67-33292
- Nonexistence of critical current for pinching in electron-hole plasmas 18 p3098 A67-33523
- Electron beam passing through low pressure gas generates plasma, computer simulated beam trajectory studies explain beam profile and pinch effect 19 p3275 A67-35106
- Electron density time and location dependence in Z-pinch calculated from emission measurements 20 p3502 A67-37528
- Differential magnetic loop, density profile and gas laser interferometer measurements of beta, n and ion temperature in theta pinch operation 21 p3662 A67-37755
- Pinch-discharge source of ionizing plasmas for aerophysical investigations at high pressures, emphasizing stabilization and passage of AC current through vortex 21 p3675 A67-38912
- Cooperative light scattering from density fluctuations in theta pinch plasmas, discussing peaks obtained 22 p3842 A67-39208
- Thermonuclear origin of neutron emission in theta pinch plasma, determining ion temperature from scattering of ruby laser beam 22 p3843 A67-39244
- Incompressible finite conductivity tearing instability in hard-core pinch with constant applied axial magnetic field 22 p3848 A67-39695
- High beta plasmas in linear theta pinches and cusp compression devices, discussing various theta pinch and cusp experiments 22 p3851 A67-39983
- PLASMA POTENTIAL**
- Potential distribution between graphite and metallic electrodes of MHD generator in nonstationary heat conditions under induced or applied electric field 01 p0011 A67-10176
- Variation of floating potential formed between electrodes by injection of electronegative gas is logarithmic function of electron attachment coefficient on neutral particles 04 p0669 A67-15496
- Critical voltage of rotating plasma device in which confinement region surrounds ring shaped coil suspended by single rod 04 p0672 A67-15648
- Problems in using Langmuir probes in ionized medium for measuring electron and ion energy density, temperature and distribution 06 p1000 A67-17590
- Propellant injection through electrodes effect on potential distribution in MPD arc [AIAA PAPER 67-49] 06 p1074 A67-18435
- Potential distribution in electron-collisionless plasma in weak magnetic field 08 p1365 A67-21412
- Plasma potential and particle energies in cesium plasma measured by simultaneous observation of ion and electron energy spectra 09 p1548 A67-22338
- Bennett type RF spectrometer analysis of low pressure plasma discharge, noting

effusion current
determination 14 p2314 A67-27753
Excitation of potential LF electromagnetic waves in electron-hole plasma of solid body for negative volt-ampere characteristics of carrier current 15 p2537 A67-29702
Current flow patterns in cross connected MHD generator with four electrodes 18 p2987 A67-33704
Quantum statistics of high temperature plasma in thermodynamical balance, introducing effective potentials for partition function evaluation and calculating free energy 18 p3089 A67-34300
Electron temperature, concentration and potential distribution, measurement in moving striations by Langmuir probe method 19 p3273 A67-35095
Energy distribution functions for nearly normal glow discharge using two models and statistics 19 p3273 A67-35098
Negative ion accumulation in HF resonant discharges at low pressure and plasmoid formation 19 p3275 A67-35112
Slepián discharge /steady state DC crossed field discharge/, obtaining solutions for plasma velocity and potential to determine current-voltage characteristics 19 p3277 A67-35122
Cesium plasma created in diode equipped with Langmuir probe 19 p3296 A67-35588
Guiding center plasma theory /GCP/ stability, potential, Vlasov and motion equations, etc 20 p3494 A67-36152
Radial profiles of carrier density and energy in diffusion controlled plasma 20 p3501 A67-37239
Particle distribution in infinite charged cylinder in plasma vicinity, showing plasma screening effect on potential 21 p3675 A67-39033
Ion cyclotron instability potential and adiabatic compression of plasma in mirror machine, measuring plasma decay rate and potential 22 p3846 A67-39487
Plasma potential oscillations in traps, discussing flute instabilities, cyclotron instabilities and resonance electron wave excitation 23 p4034 A67-41680
Excitation of potential LF electromagnetic waves in electron-hole plasma of solid body for negative volt-ampere characteristics of carrier current 24 p4199 A67-41772
Plasma energy and heat transfer to surface with and without electric current, discussing various energy transfer models 24 p4197 A67-42331

PLASMA POWER SOURCE

Thermionic energy converter operation showing anomalous electron and ion currents in plasma mode, discussing heating power and emitter temperature 24 p4103 A67-42502

PLASMA PROBE

SA LANGMUIR PROBE

SA MICROWAVE PLASMA PROBE

Plasma probe measurement of distribution of electron concentration, temperature and space potential throughout entire interelectrode gap of thermoelectronic converters 01 p0012 A67-10353
One-trap probe measurement of ionospheric electron density, electron temperature, plasma space potential relative to vehicle potential of sounding rocket, mean ion mass, composition and temperature 01 p0064 A67-10565
Ionospheric electron density measurement by gyro plasma impedance probe 01 p0064 A67-10566
LF spectrum of density correlation function, obtaining diffusion coefficient of right order of magnitude using quiet plasma 01 p0124 A67-10911
Plasma probe for dense isothermal cesium plasma, noting electron concentration and temperatures, potential distribution, etc 02 p0184 A67-12467
Plasma probe in thermal emission converter with high cesium vapor, noting parameters of diffusion, electron concentration, etc 02 p0184 A67-12468
Waveguide interactometer measurement of plasma parameters 03 p0477 A67-13458
Plasma electric conductivity around 2000 degrees K measured, using double probe with interelectrode section of controllable length 03 p0478 A67-13603
Resonances of impedance of RF probe in low density plasma introduced by finite electron temperature 04 p0663 A67-14614
Positive ion current characteristics of

cylindrical probe in low density plasma stream, determining sheath thickness and speed ratio 04 p0663 A67-14766
V-I characteristics of stagnation point electrodes in lightly ionized atmospheric pressure plasma, calculating electric resistance from conductivity measurements 04 p0664 A67-14821
Electron cyclotron echo production from plasmas by repeated pulsing, developing theory based on electron neutral momentum transfer collisions 04 p0665 A67-15105
Laser action delay due to plasma-tube-surface decomposition resulting from bombardment by neon ions 04 p0633 A67-15110
Criterion for deciding when effect of perturbation of electron-energy distribution in plasma by probe can be neglected 04 p0665 A67-15112
Approximate analysis of electrostatic probe on reentry vehicle for electron density measurements in laminar boundary layer of continuum 04 p0705 A67-15231
Conical induction plasma gun construction in strongly preionized regime and results of electrostatic probe measurements made with discharge camera 04 p0668 A67-15280
Fields of two parallel wires immersed in plasma derived, obtaining formula for driving point impedance of probe 05 p0849 A67-16004
Electromagnetic waves produced by charge traveling at constant velocity in medium with convective instability 05 p0762 A67-16353
Mass spectrometry of plasma ionic constituents, identifying monatomic and polyatomic ionic species in gaseous plasma by isotopic techniques 05 p0851 A67-16381
Microwave interferometer reliability for plasma diagnostics in magnetic field 05 p0851 A67-16521
Upper atmospheric plasma measurements with impedance probe, determining gyro and hybrid resonance frequencies 05 p0798 A67-16861
Langmuir probe analysis when immersed in slightly ionized collision-dominated plasma, computing current-voltage characteristics and Poisson and diffusion equations 05 p0856 A67-17341
Water-cooled electrostatic probe capability of measuring local electron temperature, electron density, floating potential and saturation current ratio in dense plasmas [AIAA PAPER 66-73] 05 p0856 A67-17344
Spherical electrostatic probe in stationary plasma analyzed based on kinetic theory using Krook type model for collision integral formulation 05 p0857 A67-17423
Uncoupled form for plasma resonance probe in magnetic field obtained, using special coordinate transformation 06 p1041 A67-18145
Plasma induced interference signal in satellite VLF receiver originating with converter system and appearing only in daylight operation 06 p0964 A67-18569
Langmuir calorimetric probe to determine average energy per ion in tenuous plasma beam 06 p1076 A67-18879
Laser studies at RCA Victor Research Laboratories, Montreal, discussing spectroscopic, interferometric and plasma diagnostic research 07 p1194 A67-19082
Existence of maximum conductivity of ionized gas mixture as function of thermodynamic parameters 07 p1225 A67-19117
Diamagnetic probe measurements of kinetic pressure of plasma in magnetic field 07 p1228 A67-19513
Simple method for determining mean free path of primary electrons in plasma 07 p1229 A67-19515
Potential on hot body in plasma as function of surface temperature and plasma characteristics, considering case where photoemission is present 07 p1251 A67-19812
Shock wave propagation in plasma across magnetic field, solving problem via two-component hydrodynamic equation 08 p1358 A67-20858
Summary of papers on plasma diagnostic techniques from Symposium on MHD Electrical Power Generation, Salzburg, July 1966 09 p1538 A67-21774
Plasma diagnostics by microwave interferometry in MHD channel using open

waveguide, calculating field distribution and propagation characteristics 09 p1539 A67-21781
Probe measurements of intermediate and high pressure plasmas in cases where mean free path of particles is greater than probe dimension 09 p1539 A67-21783
Theory of electrostatic probes in high pressure plasma, discussing ionization and recombination phenomena, diffusion boundary layer, spherical probe, etc 09 p1539 A67-21784
Plasma mode work function measurement for studying thermionic emission from Hf, Th and Ti in Cs vapor at reservoir temperature of 414 degrees 09 p1450 A67-22353
Quasi-static theory of cylindrical impedance probe for magnetoplasma extended to include vacuum sheath effects 09 p1549 A67-22451
Dynamic pressures in helium and argon plasma jets in ambient atmosphere measured with sensitive probes 09 p1549 A67-22554
Plasma electron density determined from mutual impedance measurements obtained as function of frequency 09 p1501 A67-22561
High resolution external probe for measuring electrical conductivity of argon plasma behind shock wave 10 p1684 A67-22963
Ionospheric probes for measuring electron density in E region through detection of plasma resonances 10 p1656 A67-23285
Ionospheric electron density measurement by gyroplasma probe, using sweep frequency impedance technique 10 p1648 A67-23291
Plasma diagnostics using electrostatic probes under short mean free path conditions compared with microwave measurements 11 p1827 A67-23882
Langmuir probe and spectrometric electron temperature measurements in negative glow plasma compared, finding probe temperatures significantly higher 11 p1788 A67-23963
Level populations and energy loss rate of electrons during nonelastic collisions with impurity molecules in weakly ionized two-temperature plasma 11 p1831 A67-24019
Peak density in single ended Q machine described in agreement with equilibrium theory 11 p1833 A67-24368
Electrostatic probe techniques for low density thermally ionized plasmas 11 p1838 A67-24408
Polarized pyrometric probe applied to hot and dense plasmas, ascertaining particle energies and densities 11 p1789 A67-24410
Electrostatic probe and VHF microwave reflectometry study of nitrogen flow around models in hotshot wind tunnels, determining plasma sheath physical characteristics 11 p1839 A67-24445
Ion acceleration region demonstrated by coupling two HF magnetic field gradient accelerators 11 p1841 A67-24767
Electron beam plasma amplification measurements in interaction region by nonperturbing technique, measuring RF growth, phase velocity, etc 11 p1841 A67-24907
Plasma probe measurement of distribution of electron concentration, temperature and space potential throughout entire interelectrode gap of thermoelectronic converters 11 p1746 A67-25026
Ionospheric plasma resonances studied by four-electrode probe, calculating mutual impedance as function of orientation and excitation frequency 12 p1931 A67-25152
Langmuir probe and microwave transmission methods compared for plasma density measurement 12 p1939 A67-25256
Electronegative plasma kc oscillations during glow discharge, measuring variations of frequency and longitudinal and radial intensity 12 p1970 A67-25261
IMP-II and OGO-I measurements on plasma characteristics in transition region between solar wind and geomagnetic field 12 p1997 A67-25806
Design of rocketborne ionospheric plasma probe considering probe shape, location, payload, etc 12 p1937 A67-25838
Local magnetic field, ion density flow and electric field in plasma measured downstream of theta-pinch accelerator in presence of uniform guide field [AIAA PAPER 66-155] 12 p1975 A67-25895
Oscilloscope plotting of Langmuir probe

and double probe characteristics corresponding to time varying plasma properties 12 p1947 A67-26122

Intermediate and HF noise of probes immersed in gas discharges explained by space charge sheath and bulk plasma noises 12 p1948 A67-26226

Hydrogen plasma produced by coaxial gun located in magnetic mirror 13 p2163 A67-26291

Magnetic field intensification in plasmas determined from solution of MHD equations, noting formation of time independent fields 13 p2163 A67-26292

Uniformly valid asymptotic theory of collisionless electrostatic probes 13 p2118 A67-26298

Microwave interferometer with dielectric rods as waveguides for measuring electron density in small volume inside plasma 13 p2120 A67-26859

Structure and magnetic field of plasmoids produced by conical induction source studied with probe-diagnostic method 15 p2526 A67-29255

RF characteristics of spherical probe immersed in hot low-density plasma, using sheath model 15 p2528 A67-29564

Automatic recording and computer analysis of double probe measurements in plasma research, calculating electron temperature and plasma density 15 p2489 A67-30092

MHD power generation experiments with potassium seeded argon plasmas to study performance at Faraday and Hall parameters 16 p2601 A67-30554

Plasma probe diagnostic technique in shock tube, noting electron concentration, gas temperature and plasma potential from V-T characteristics 16 p2673 A67-31110

Electrodeless probe, consisting of single-layer coil enclosed in insulating tube, for plasma conductivity measurements 17 p2854 A67-32164

Various experiments explaining fundamental properties of probes used in measurements of plasma arc columns 17 p2896 A67-32166

Plasma behavior in laminar and turbulent hydrocarbon-air flames, discussing flame ionization, electron concentration and recombination, detonation wave ionization data, ignition, etc 17 p2968 A67-32168

Plasma electric conductivity around 2000 degrees K measured, using double probe with interelectrode section of controllable length 18 p3090 A67-34468

Alkaline-metal-plasma machine design, studying operating modes with electric probes 18 p3091 A67-34631

Diagnostic equations for electrostatic double probes for arbitrary ion Schmidt numbers 19 p3267 A67-34830

Electron distribution function in plasma determined using electrostatic separation probe 19 p3267 A67-34947

Flux, energy distribution and density of ions and electrons in magnetosphere plasma during solar activity period determined byOGO-C electrostatic probes 19 p3217 A67-35200

Electron density measurement in ionosphere-magnetosphere transition region using rocketborne gyroplasma swept frequency probe, discussing electron density profile and plasma medium 19 p3229 A67-35201

Ionospheric electron density profile microstructure studied by rocketborne gyroplasma probe discovering electron density irregularities 19 p3217 A67-35202

Cylindrical plasma column subjected to axial magnetic field measured for electric field oscillations by movable probe within ionized gas 19 p3288 A67-35374

Theory of Langmuir probes in plasmas with negative ions, considering different ion concentrations and electron temperatures 19 p3296 A67-35587

Cesium plasma diode investigated using ribbon electron beam probing technique, discussing stability of electric potential distribution modes 20 p3496 A67-36329

Pressure gauge for plasmas subjected to large dynamic electric and magnetic fields in accelerator channel of MHD wind tunnel 20 p3444 A67-36529

Second derivative of two-probe current measurement method for determining electron energy distribution in gas

discharge, noting low sensitivity to noise 20 p3498 A67-36687

Frequency characteristics of planar and spherical plasma resonance probes and RF impedance probe in magnetic field, considering equivalent electric circuit 20 p3503 A67-37670

Shock waves and related phenomena in shock tube investigated by streak interferometry and electrostatic probes, measuring plasma density and temperature 21 p3611 A67-37961

Existence of maximum conductivity of ionized gas mixture as function of thermodynamic parameters 21 p3659 A67-38162

HF resonance probes, giving theoretical results of nonzero electron plasma temperature effect and experimental results with plasma between plates of plane capacitor 21 p3626 A67-38220

Changes in electric resistance of ellipsoidal plasma probe in homogeneous magnetic field, deriving equations of potential and resistance 21 p3666 A67-38250

Ion resonance probe for plasma density measurement using direct display method with frequency swept signal 21 p3627 A67-38258

Probe for measuring three directional components of argon plasma magnetic field inside theta pinch conical coil, noting vortex structures [AIAA PAPER 67-659] 21 p3671 A67-38695

Parameter diagnostics of low temperature plasma in cesium diode, comparing probe measurements with transport equation solutions 22 p3845 A67-39425

Cesium plasma ionization in low voltage arc discharge, measuring electron ionization capacity, electron temperature and cesium ionization and excitation cross sections 22 p3847 A67-39510

Plasma electron and positive ion temperatures measurement using orbit magnetic analyzer probes 22 p3798 A67-39628

Double probe method for determining electron temperature and density variations in HF hydrogen plasma during second harmonic cyclotron resonance 22 p3848 A67-39650

Pioneer VII plasma probe data indicating geomagnetic wake at 1000 earth radii downstream from earth 22 p3791 A67-39819

Ionospheric plasma electron density profile and plasma resonance effects at base of magnetosphere measured by rocketborne gyro-plasma probe 22 p3793 A67-40043

Effective recombination coefficient in upper-E and F-1 layers at sunset from rocketborne gyroplasma probe measurements of electron density profile 22 p3793 A67-40044

Spectral and probe methods of plasma temperature measurement, discussing current-voltage characteristics 22 p3853 A67-40216

Hot Langmuir probe in Cs plasma studied for method of controlling current voltage characteristics 24 p4154 A67-42210

Resonance rectification effects for wire probe in magnetoplasma observed in terms of warm plasma perpendicular permittivity component 24 p4199 A67-43101

PLASMA PROPULSION

Plasma propulsion devices and phenomena responsible for energy losses, considering plasma gun and MPD arc jet 01 p0141 A67-11388

Rail-type plasma accelerator in creating ionized particles and electromagnetic field for spacecraft propulsion 03 p0477 A67-13509

Low specific impulse electric propulsion with plasma separator thruster that prevents surface recombination, drawback of Kaufman thruster 04 p0687 A67-14428

Electric drive operating parameters and design, using exploding wire type device and electromagnetic apparatus for plasma production and acceleration 16 p2736 A67-30716

Plasma propulsion for interplanetary flight, discussing optimization of specific impulse, weight distribution and flight path 17 p2928 A67-32226

Combustion rocket engines thermodynamic cycle and specific impulse values, considering motion equations and plasma engines 19 p3311 A67-35571

Solid propellant electric thruster /SPET/ using pulse plasma for spacecraft attitude

control and stationkeeping [AIAA PAPER 67-661] 21 p3690 A67-38697

Alkali plasma Hall accelerator /ALPHA/ thruster performance, discussing acceleration mechanisms and correlating data [AIAA PAPER 67-687] 21 p3692 A67-38718

PLASMA RADIATION

Radiation in Lorentzian moving anisotropic plasma 01 p0123 A67-10442

Bremsstrahlung, transient and plasma radiation as affected by surface properties of silver bombarded by electrons 02 p0291 A67-11737

Vaporization rate and diffusion of Cu, Mg and Cr in arc discharge plasma determined from curves of spectral-line emission energies 02 p0279 A67-12743

Intensity of light emitted by individual microplasmas of silicon p-n junctions increases with voltage to maximum and then decreases 03 p0491 A67-13176

Nondiffusive radiation transfer and ionization equilibrium of impurity in plasma 03 p0483 A67-13837

Bremsstrahlung emission from electron-electron collisions in plasma, obtaining spectra of longitudinal and transverse waves 03 p0484 A67-14043

Self-absorption of radiation in high temperature plasma jet of hydrogen, argon and nitrogen 05 p0851 A67-16522

Book on electromagnetic wave emission, absorption and scattering processes in gaseous plasma 05 p0855 A67-17152

Plasma formed by laser pulse on tungsten target, measuring radius, temperature and radiative properties, developing model 06 p1041 A67-18149

Radiation from linear resonant antenna in lossy compressible weakly ionized plasma and dependence on ratio of source to plasma frequency 07 p1227 A67-19428

Electromagnetic emission from growing plasma oscillations 07 p1230 A67-20146

Coherent radiation generation in electron-hole indium antimonide plasma, discussing emission spectrum 08 p1367 A67-20418

Scintillation analysis of hard X radiation from high power pulse discharges 08 p1357 A67-20846

Anomalous bremsstrahlung and cyclotron emission in partially ionized plasmas 08 p1366 A67-21441

Correlation radiometry examination of radiation emission in beam plasma discharge at harmonics of electron cyclotron frequency 09 p1536 A67-21601

Magnetic fields in solar corona, observing bursts with frequency splitting to determine correlation with plasma radiation theory 09 p1565 A67-21981

Interference filter of Fabry-Perot interferometer type for studying millimeter and submillimeter plasma radiation 09 p1545 A67-22000

Angular and frequency spectra of Cerenkov and cyclotron radiation from charged particle spiraling in cold magnetoplasma determined by Fourier transform method 09 p1562 A67-22228

Shock wave profile in shock tube at different distances from plasma source determined, using perforated sliding membrane 09 p1489 A67-22329

Perturbed zone stability of body immersed in equilibrium plasma during surface electron emission 10 p1683 A67-22782

Nonlinearity caused by relativistic mass effect leading to radiation maxima of plasma excited by two pulses at electron gyrofrequency 11 p1827 A67-23889

Approximate mode decomposition for treating boundary value problems for uniform compressible anisotropic plasma 11 p1753 A67-24307

Behavior of line source function of low density gas in presence of nonthermal velocity field, examining strong shock situation and differential velocity via ordered velocity structure 11 p1861 A67-24489

Measuring atomic radiation and collision cross section coefficients of plasmas 11 p1839 A67-24551

Spectroscopic methods for measuring plasma temperatures from 1000 to 10,000 degrees K, distinguishing optically thick and thin media 12 p1938 A67-25188

High temperature air plasma total radiant intensity measurements in shock tube [AIAA PAPER 67-311] 12 p2036 A67-26026

Plasma-radiation interaction represented by Compton effect, utilizing Boltzmann term developed according to powers of perturbation caused by electron motion 13 p2165 A67-26598

Nonequilibrium line radiation for generalized Lorentz profiles in spherical plasma of large optical thickness 13 p2166 A67-26728

Nondiffusive radiation transfer and ionization equilibrium of impurity in plasma 13 p2172 A67-27716

Cyclotron echo formation in rare gas and nitrogen afterglow plasma in presence of inhomogeneous magnetic field, stressing velocity-dependent collision frequency case 14 p2356 A67-28150

Radiation from plasma films and columns nonlinearly excited by incident electromagnetic waves, showing predominance of radiation on scattering 14 p2356 A67-28153

Macroscopic linear fluid model of plasma radiation and scattering restricted to bounded media, emphasizing physical interpretation of wave constituents 14 p2359 A67-28463

Magnetoplasma radiation by microwave pulse excitation at gyrofrequency harmonics, considering single particle approach 14 p2360 A67-28557

Short wave limit for plasma radiation emission of neon gas discharge analyzed by Kirchhoff-Planck relation 15 p2530 A67-29747

Plasma radiation analyzed by spectral line broadening theory as relaxation of excited atom, noting frequency dependent width and shift operators 15 p2532 A67-30380

Radiation characteristics from electric dipole immersed in lossy anisotropic plasma taking into account collision effects 16 p2713 A67-30797

Spectral line profile obtained by radiative transfer equation from radiation by dense, inhomogeneous plasma 16 p2715 A67-31064

Continuous spectrum emission from free-bound and free-free electron transitions into field of monatomic gas ion using shock tube 16 p2673 A67-31109

Measured admittance of X-band waveguide radiating into dielectric and plasma layers compared with computed admittance figures 16 p2627 A67-31352

Intense microwave radiation from high density plasma confined by magnetic mirror 17 p2894 A67-32145

Soviet book on plasma physics covering magnetic traps, acceleration, radiation, etc 17 p2903 A67-32909

Pinch radiation in quartz discharge chamber spectrographically studied for use as sources of short pulsed radiation with continuous spectrum 17 p2904 A67-32919

Energy and intensity density of radiation emitted by semiminfinite nonequilibrium electron plasma with non-Maxwellian particle distribution calculated, based on general fluctuation theory 19 p3267 A67-34902

Radiation field interaction with particles in assemblage of electrons and atoms or ions using perturbation theory and Liouville equation 19 p3284 A67-35339

Customary formulas for various effects including Thomson scattering, electron-ion, bremsstrahlung, etc, in context of plasma radiation theory 19 p3284 A67-35340

Reports on progress in physics, Volume 29, Part I, covering creep in metals and plasma spectroscopy 19 p3263 A67-35853

Plasma spectroscopy, discussing line profiles, local thermal equilibrium, methods of measuring number densities and temperatures 19 p3298 A67-35855

Recombination and bremsstrahlung continuum radiation measurements of atomic and ionic oxygen in plasma 19 p3299 A67-36093

Transient Stark and Zeeman spectral line shifts in plasma emission measured with multiple beam Fizeau interferometer, discussing instrument errors 20 p3439 A67-36351

Emission properties of vacuum spark plasma arising in production of high current electron beam 20 p3498 A67-36684

Wave transformation effect on inhomogeneous plasma radiation noise, applying results to stable plasma thermal radiation 20 p3498 A67-36691

Surface plasma oscillations at optical

frequencies detected by radiation from optical grating metal surface, measuring dispersion relation 20 p3514 A67-37569

Radiation of monofrequency antenna in compressible magnetoplasma expressing far field as sum of modal plane waves 20 p3388 A67-37701

Transient radiation of electric dipole in uniaxially anisotropic plasma examined for signal frequency greater and less than plasma frequency 20 p3388 A67-37704

Convex plasma thermal radiation at UHF, determining spectral composition using Fourier integrals 21 p3663 A67-37937

Resonance and noise microwave emission thresholds for InSb electron hole plasma subject to crossed electric and magnetic fields, noting Hall effect 21 p3683 A67-38403

Hard X-ray emission by hot electron plasma trapped in discharge tube due to magnetic field rise 21 p3667 A67-38413

Kinetic equations for electrons and photons in homogeneous plasma in strong magnetic field derived from Maxwell and classical motion equations 22 p3851 A67-39736

Helium RF discharge radiation temperature as magnetic field function measured, discussing enhanced diffusion role in radiation temperature determination 23 p4032 A67-40897

Light emission spots one to one correspondence with microplasmas in GaP p-n junctions 23 p4043 A67-41437

Perturbed zone stability of body immersed in equilibrium plasma during surface electron emission 24 p4195 A67-42118

PLASMA RESONANCE

Longitudinal electric field penetration into magnetoplasma layer in constant magnetic field 01 p0122 A67-10356

Resonances in low pressure mercury vapor discharge due to natural resonance modes of cylindrical plasmas 02 p0273 A67-12097

Poloidal hydromagnetic plasmaspheric resonance under conditions representative of inner magnetosphere 02 p0276 A67-12563

Parametric resonance in plasma situated in magnetic field noting oscillation, frequency stability, kinetic equations, electric field effect, etc 03 p0475 A67-12931

Microwave radiation measurements from internal plasma resonance of positive column near electron cyclotron harmonic frequencies 03 p0476 A67-13355

Resonances of impedance of RF probe in low density plasma introduced by finite electron temperature 04 p0663 A67-14614

Ion resonance in uniform plasma, analyzing behavior of RF resonance probe by comparing ion resonance with electron resonance 04 p0663 A67-14616

Oblique z-mode echoes in topside ionosphere between plasma and upper hybrid frequencies 04 p0614 A67-14956

Plasma resonance measurement from radio wave scattering in cylindrical tubes which simulate meteor trail models 04 p0700 A67-15226

Whistler recordings on thermal plasma motions and ionization density near magnetospheric knee, noting whistler attenuation VLF noise, ion effects, electron temperature, etc 05 p0795 A67-16011

Uncoupled form for plasma resonance probe in magnetic field obtained, using special coordinate transformation 06 p1041 A67-18145

Lower hybrid resonance /LHR/ noise bands occurrence patterns as function of latitude and time 06 p0964 A67-18567

IR transmission measurements in single crystal thin film semiconductors, observing absorption band near plasma frequency 06 p1071 A67-18992

Plasma ringing phenomena stimulated by Alouette I and other ionospheric probes at upper hybrid frequency and cyclotron frequency harmonics in near zero group velocity regions 07 p1179 A67-19916

Plasma resonance emission of thin Ag foils irradiated by light, noting intensity and direction of polarization 08 p1368 A67-20787

Resonance in plasma magnetized by radial magnetic field solved, obtaining MHD wave equation, noting relation to micropulsations 09 p1545 A67-22196

Electron density determination from plasma resonance measurements, using electric analogy for circuit 10 p1610 A67-22951

Ionospheric probes for measuring electron

density in E region through detection of plasma resonances 10 p1656 A67-23285

Plasma resonance absorption measurement in thin potassium foils, observing polarized light transmission at lambda 3270 10 p1691 A67-23478

Weak inhomogeneous plasma wave energy redistribution during quasi-normal oscillation expansion in resonance regions, noting electric analogy 11 p1842 A67-24953

Longitudinal electric field penetration into magnetoplasma layer in constant magnetic field 11 p1844 A67-25029

Parametric resonance excitation of Alfvén waves by small LF modulation of DC magnetic field imposed on ideal MHD plasma 11 p1844 A67-25062

Ionospheric plasma resonances studied by four-electrode probe, calculating mutual impedance as function of orientation and excitation frequency 12 p1931 A67-25152

MHD resonance acceleration of plasma clusters and shock waves, showing advantage for parallel or coaxial conductor systems 14 p2354 A67-27762

Radial variation of plasma electron density determined by surface wave resonances 14 p2355 A67-27829

Slotted-sphere antenna immersed in plasma measured for RF admittance 14 p2283 A67-28377

Magnetic moment of electron in HF plasma accelerator for case of negligible axial acceleration in resonance region 15 p2527 A67-29514

Plasma resonances, deriving relations between coefficients for transmission, reflection and emission of microwaves and explaining collision-free discharge 17 p2907 A67-33105

Thermal radiation resonance of plasma cylinder in presence or absence of magnetic field 18 p3090 A67-34435

Stimulated coherent emission at upper hybrid resonance frequency from magnetoplasma excited by microwave pulse 18 p3090 A67-34466

Weak turbulence theory for collisionless plasmas formulated in terms of test waves 18 p3092 A67-34744

Weakly ionized plasma and gyromagnetic resonances in helium low pressure HF electrodeless discharge in magnetic field 19 p3276 A67-35113

Plasma resonance in RF discharge excited with frequency higher than collision frequency, determining electron density 19 p3276 A67-35114

Parametric resonance in magnetosonic waves through analysis of perturbed particle trajectories in modulated plasma field, determining velocity time dependence 20 p3501 A67-37296

Highly asymmetric equation for MHD resonance of guided poloidal mode solved using dipole coordinates 20 p3502 A67-37427

Frequency characteristics of planar and spherical plasma resonance probes and RF impedance probe in magnetic field, considering equivalent electric circuit 20 p3503 A67-37670

Resonance phenomena in bounded magnetoplasma shown on basis of dispersion relation as due to formation of standing waves of electromagnetic waves 20 p3503 A67-37671

Electron-cyclotron harmonic resonances interactions in RFF excited electrodeless helium discharges, discussing magnetic field position measurement and plasma simulation 21 p3662 A67-37757

Ion resonance effect in Langmuir probe exhibiting ion plasma frequency 21 p3663 A67-37765

Comparison of classical approximations to free carrier absorption in semiconductors, using reflectivity minimum associated with plasma resonance as criteria 21 p3678 A67-38155

Resonance spectrum of plasma column excited by SHF field investigated for nonlinear phenomena 21 p3666 A67-38354

Micropulsation spectra /sonagrams/ indicating magnetosphere plasma resonances with recognizable modal pattern 21 p3619 A67-38513

Collisionless damping of temperature or secondary resonance spectrum of plasma column 22 p3845 A67-39482

Ionospheric plasma electron density profile and plasma resonance effects at base

of magnetosphere measured by rocketborne gyro-plasma probe 22 p3793 A67-40043
Kinetic model of Tonks-Dattner absorption resonances in plasma positive column providing plasma wave reflection mechanism 23 p4031 A67-40782
Secondary temperature resonances in magnetized plasma slab with nonsymmetric inhomogeneous density profile, noting spectrum degeneracy in symmetric nonuniform profile 23 p4034 A67-41359
Wave propagation in plasma with anisotropic pressure studied using modified Burgers equations, examining effect of collisions 24 p4197 A67-42260

PLASMA RING

Mercury flow in rotating torus with induction pump and magnetic field effect on flow studied for flow resistance 17 p2900 A67-32342

PLASMA SHEATH

Performance capabilities of Hall current accelerators determined from parameters influencing anode power loss [AIAA PAPER 66-184] 01 p0125 A67-11160
Ion extraction and plasma sheath formation in nitrogen discharge studied by quadrupole mass-spectrometric sampling probe, noting ion current ratio dependence on probe potential 02 p0272 A67-11889
Cross polarized component of radiation from spherical antenna produced by anisotropic plasma sheath 02 p0220 A67-12193
Impedance of finite insulated cylindrical antenna in cold plasma with longitudinal magnetic field 03 p0385 A67-13850
Positive ion current characteristics of cylindrical probe in low density plasma stream, determining sheath thickness and speed ratio 04 p0663 A67-14766
Plasma sheath simulation used to analyze effects of sheath discontinuities and inhomogeneities on slot antenna radiation pattern and input impedance 05 p0769 A67-16000
Collisionless theory of plasma sheath near infinite planar electrodes, developing new sheath model incorporating microscopic boundary conditions 05 p0857 A67-17424
Weakly ionized gas flows about electrically biased bodies under effects of compressibility and electron energy [AIAA PAPER 67-100] 06 p1042 A67-18471
Thin plasma effect on admittance of aperture antenna in infinite conducting plane for various modes 07 p1151 A67-19447
Radiation enhancement and resonance scattering due to plasma sheath between spherical antenna and surrounding plasma layer 07 p1153 A67-19611
Plasma sheath formation and effect on satellite interacting with geomagnetic field and ambient plasma 08 p1410 A67-20714
Steady state theory of discharge column, giving solutions to density and potential profiles for planar and cylindrical geometry 08 p1361 A67-21134
RF bridge technique determining electric conductivity of plasma sheath around reentry vehicle 08 p1366 A67-21514
Admittance of circumferential gap in infinite cylindrical antenna covered by set of coaxial dielectric or plasma layers, noting excited metal cylinder 09 p1481 A67-22447
Thin electrostatic sheath adjacent to body immersed in flowing weakly ionized continuum plasma analyzed for arbitrary Debye length mean free path ratios 11 p1825 A67-23868
Charge separation effects in Ferraro-Rosenbluth cold plasma sheath model; using relativistic treatment 11 p1825 A67-23869
Heat flow through Langmuir sheath in presence of electron emission and application to limitation of energy loss rate by thermal conduction 11 p1828 A67-23894
Transmission and reception properties of equatorial slot antenna on plasma clad reentry sphere 11 p1757 A67-23973
Radiation characteristics for slotted cylinder covered with magnetized inhomogeneous plasma sheath assuming parabolic electron density distribution 11 p1753 A67-24306
Current flow through plasma sheath into magnetized plasma, noting negative resistance characteristics of sheath upon ion cyclotron frequency 11 p1837 A67-24397
Electrostatic probe and VHF microwave reflectometry study of nitrogen flow around

models in hotshot wind tunnels, determining plasma sheath physical characteristics 11 p1839 A67-24445
Performance capabilities of Hall current accelerators determined from parameters influencing anode power loss [AIAA PAPER 66-201] 12 p1975 A67-25892
Plane wave propagation across thin stratified plasma sheaths, noting polarization and reflection [AIAA PAPER 66-481] 12 p1905 A67-25906
Behavior of RF sources embedded in plasma, determining antenna properties by configuration, current distribution and surrounding sheath properties 14 p2359 A67-28464
Simulation of magnetospheric effects for possible application to ionospheric probes 14 p2294 A67-29035
Radio blackout extent from simplified calculation of average sheath power loss for typical Apollo reentry trajectory 15 p2434 A67-29168
Inhomogeneous sheath effect on surface currents and scattering cross section of plasma-immersed cylinder in presence of electromagnetic and electrokinetic waves 15 p2521 A67-29192
RF characteristics of spherical probe immersed in hot low-density plasma, using sheath model 15 p2528 A67-29564
Interaction of incident H-wave with infinite conducting cylinder coated with inhomogeneous and anisotropic plasma sheath, noting far field pattern of scattered field 16 p2626 A67-31350
Plasma sheath detuning effect on small loaded dipole in free space investigated 16 p2627 A67-31367
HF magnetic fields for plasma sheath with perpendicularly superimposed static magnetic field and resonance excitation of electron cyclotron waves 19 p3276 A67-35117
Plasma-metal interface electric field intensity, deriving dimensionless formula from nonlinear second order differential equation 19 p3277 A67-35125
Stability of cesium Q-type machines analyzed for hot plasma-beam interactions in VLF range in sheath and in plasma 19 p3292 A67-35390
Effect of angular direct current magnetic field on radiation of slot antenna located on metal cylinder covered by plasma sheath 19 p3184 A67-35811
Theta pinch plasma sheath and fields time development for relaxing radial electric field 21 p3662 A67-37754
Radio telemetry links perturbations during ballistic missile reentry due to plasma from kinetic heating 21 p3581 A67-38228
Plasma and sheath characteristics computation for alkali plasma devices involving contact ionization for ion production [AIAA PAPER 67-691] 22 p3868 A67-39843
Kinetic collisionless plasma diode model stationary regimes, discussing sheath achievement density value dependence on temperature difference and trapped particle distribution 22 p3774 A67-40322
Radiation pattern, absorption and impedance measurements of conical antenna plasma sheath about dielectric coated metal cone excited by axial radiating slot 23 p3973 A67-40840
Strongly enhanced radiation from antenna surrounded by dielectric layer and plasma sheath, noting resonance at given operating frequency for certain plasma densities 24 p4121 A67-42266

PLASMA SLAB

Electromagnetic reflection and transmission coefficient maxima in bounded plasma slab 01 p0022 A67-10443
Electron oscillations of uniform plasma slab in presence of strong magnetic field, noting orthogonality condition of normal modes density gradients and profile and dispersion relation 03 p0482 A67-13747
Dispersion relations and wave power of isotropic compressible lossy plasma slab bounded by free space and ground plane and excited by line sources 03 p0487 A67-14354
Semiconductor plasma slab subject to crossed electric and magnetic fields, examining plasma density wave instability caused by gradient in carrier density perpendicular to magnetic field 04 p0674 A67-14612

Plasma sheet with enhanced energy density stretching across magnetotail as evidenced by Vela-IIB satellite observations 07 p1244 A67-19921
Nonlinear coupling between fast and slow waves of cold homogeneous plasma slab partially filling parallel plate waveguide 20 p3492 A67-36126
Plasma scale height errors from Alouette I topside sounder ionogram analysis 20 p3433 A67-37409
Secondary temperature resonances in magnetized plasma slab with nonsymmetric inhomogeneous density profile, noting spectrum degeneracy in symmetric nonuniform profile 23 p4034 A67-41359

PLASMA SOUND WAVE

Approximate calculation of speed of sound in plasma when enthalpy, density and pressures are known 02 p0276 A67-12567
Generation of oscillations in solar atmosphere by separate granules modeled by bottom zone of isothermal gravitating photospheric layer overlaid by hot corona 10 p1704 A67-22721
Antenna impedance dependence on excitation of acoustic waves by biconical dipoles encased in dielectric sphere immersed in warm plasma 11 p1769 A67-25030
Bohm criterion of boundary layer stability related to ambipolar sound generation in positive column plasma discharge, deriving plasma density ambipolar potential distribution 17 p2905 A67-32972
Flow stability in MHD generators after extracting significant electrical power from gas 18 p2967 A67-33705
Solitary pulse longitudinal waves existence in electron plasma related to trapped ions presence, studying ion pulse shape and oscillation stability 22 p3845 A67-39423

PLASMA SPECTRUM

Radiation sources from high temperature equilibrium air noting measurements, equipment and results [AIAA PAPER 67-95] 06 p1114 A67-18279
Plasma electron temperature determined from measured spectral line intensities 07 p1230 A67-20106
Plasma spectrography in shock tube, determining charged particle concentration 08 p1358 A67-20853
Argon-cesium plasma spectroscopy, describing equipment, ionization, conductivity, recombination, concentration, etc 09 p1538 A67-21779
Continuous spectra of atomic gases and low temperature plasma, analyzing photoionization cross section and electron transitions in neutral atom field 10 p1682 A67-23067
Spectrum of longitudinal plasma oscillations noting instability under resonance condition 12 p1970 A67-25255
Solar wind plasma properties, noting relation between positive ion component and interplanetary magnetic field as measured by Mariner II [JPL-TR-32-1107] 13 p2190 A67-26304
Stark-broadened isolated ion line agreement between theory and experiment obtained by Griem theory or by impact approximation of GBKO theory 15 p2520 A67-29678
Electron correlations influence on plasma-broadened Lyman alpha line 15 p2520 A67-29679
Plasma drift instability in discharge with oscillating electrons, measuring plasma vibration spectrum 15 p2528 A67-29711
Plasma spectrum, discussing electromagnetic oscillation damping on boundary of two media with different electrical properties 15 p2531 A67-30073
Exciting molecular emission spectra in cold plasma free of electrode-induced impurities by superhigh frequency source 16 p2704 A67-31478
Spectroscopic measurements of cold plasma charged particle concentrations, specifically spectral broadening due to Stark effect, forbidden-line intensities affected by internal electric fields and autoionization line intensities 17 p2896 A67-32161
Stark effect in plasma, discussing theory, Lorentz symmetrical dispersion profile, atomic interaction, etc 17 p2901 A67-32404
Argon, deuterium and air ionization at atmospheric pressure and lower by focused ruby laser radiation, analyzing plasma spectrum 19 p3239 A67-35166

Fluctuation spectrum in most stable state of turbulent plasma 20 p3496 A67-36213

Doppler widths from plasma UV lines using fast scan Michelson interferometer 20 p3438 A67-36343

Extremely fast varying and low intensity plasma emissions analyzed with reflection multichannel Fabry-Perot interferometer 20 p3439 A67-36352

Mathematical statistics methods for nonreabsorbed spectral line widths and shifts and optical density in plasma 20 p3471 A67-37601

Electron-ion three-body recombination rate in nonequilibrium dense nitrogen plasma measured spectroscopically [AIAA PAPER 67-703] 21 p3672 A67-38730

Measurement of time varying spectra of argon plasma in coaxial gun for two different gun geometries 24 p4198 A67-42730

PLASMA SPRAYING

SA FLAME SPRAYING

Boron fiber-reinforced aluminum composites fabrication by plasma spraying and tensile testing 03 p0444 A67-13431

Plasma spray gun as possible method of applying resin, ceramic and metallic bonded solid film lubricants [ASLE PREPRINT 67AM 7A-4] 14 p2326 A67-28792

Plasma technology in industry, discussing Polish-made plasma torch design and operation and plasmatron and spraying applications 17 p2865 A67-32189

Plasma sprayed alumina and beryllia dielectric coatings for heat sinks in electronic packaging, emphasizing heat dissipation from heat/generating components 21 p3650 A67-38849

PLASMA STABILITY

Plasma equilibrium in toroidal magnetic traps, discussing readjustment of small denominators in nondisturbance equation 01 p0123 A67-10508

Equilibrium of plasma excited by radio wave in low pressure gas in presence of magnetic field 01 p0124 A67-10811

Intrinsic electric field of rarefied ion-electron plasma in external magnetic field and plasma stability, noting use of Galerkin method to determine plasma layer slippage 01 p0126 A67-11299

Three-dimensional eigenmodes for collisionless electronic Vlasov plasma imbedded in magnetic field in electrostatic approximation, noting plasma stability 02 p0275 A67-12553

Criteria for cold plasma density necessary to stabilize grade B drift waves in finite length energetic plasmas 02 p0275 A67-12554

Unstable transverse waves in anisotropic multicomponent plasma, establishing stability criteria, noting role of electron distribution 02 p0276 A67-12562

Surface waves in current-carrying plasma filament of finite radius 02 p0277 A67-12614

Magnetohydrostatic equilibrium configurations of rotating plasma 03 p0475 A67-12923

Nonlinear theory of plasma instability in oscillating discharge, estimating oscillation energy and coefficient of turbulent diffusion 03 p0478 A67-13537

Plasma stability examined in terms of potential energy of system under all displacements 03 p0480 A67-13730

Surface charge distribution effect on stability of conducting fluid in presence of magnetic field 03 p0481 A67-13731

Charged particle distribution in hollow cylinder shaped positive plasma column during diffusion and helical instability in longitudinal magnetic field 04 p0668 A67-15281

Electrical noises of plasma of steady state HF discharge in magnetic field discussed from standpoint of universal plasma instability 04 p0671 A67-15640

Stability of spatially inhomogeneous current-carrying plasma in various frequency regions 04 p0671 A67-15641

MHD stability of plasma cylinder in time dependent magnetic field 04 p0671 A67-15643

Equilibrium concentrations for air water plasma at various temperatures tabulated for three densities, noting effect on electron concentration 05 p0850 A67-16131

Stabilization of hydrodynamic drift oscillations in rotating nonuniform cylindrical plasma 06 p1040 A67-18092

Plasma stability with randomly fluctuating

parameters for magnetic field with curved lines of force 06 p1045 A67-18790

Effect of longitudinal plasma oscillations excited by external electric field on plasma stability, deriving dispersion relations by using Vlasov equation 07 p1229 A67-19518

Bending effect of spectral lines in plasma created by rotating HF dipole in quasi-steady magnetic field 08 p1358 A67-20854

Resonant particle instabilities in uniform magnetic field of plasma waves propagating at arbitrary angle 08 p1359 A67-20897

Cyclotron resonance instability of ion cyclotron and magnetosonic waves propagating at angle to magnetic field in infinite uniform plasma 08 p1359 A67-20898

Combined Rayleigh-Taylor and Kelvin-Helmholtz instability for incompressible plasmas carrying uniform magnetic field including Hall current 08 p1359 A67-20902

Plasma with axially varying equilibrium quantities, examining stability in theta pinch configuration via energy principle 08 p1361 A67-21132

Newcomb entropy method extended to stability analysis of plasma in zero magnetic field 08 p1362 A67-21144

Self-consistent description of warm stationary plasma in uniformly sheared magnetic field, noting shear rate current flow 08 p1364 A67-21402

Electron plasma behavior and stability in presence of time dependent electric field 09 p1549 A67-22553

Vlasov equation for stationary distribution function of charged particles in plasma and self-consistent solution of Maxwell equations 10 p1685 A67-23463

Two-fluid theory for plasma stability, obtaining equation on velocity field perturbation by considering Ohm law, stress tensor with Larmor radius and viscosity from collisions 10 p1685 A67-23465

Stability of plasma toroidal configurations under effect of component of magnetic field curvature which lies within magnetic surface 10 p1686 A67-23467

Effect of varying magnetic field, vacuum and ion density at 27 MHz on properties of cylindrical argon plasma column, using capacitive and inductive coupling 10 p1686 A67-23504

Plasma stabilization by HF electromagnetic fields, noting mode spectrum spacing along sample axis and dependence on field strength 10 p1686 A67-23585

Plasma instabilities due to RF motion obtained by expanding fluid and electromagnetic wave equations in asymptotic series 11 p1825 A67-23870

Local potential variational method to study runaway stability of electrons in two-component plasma 11 p1826 A67-23872

Effect of low pressures on stability of plasma currents in closed hydromagnetic systems 11 p1826 A67-23877

Stabilization of current driven helical waves in weakly ionized plasmas by magnetic wells of finite but small depth 11 p1827 A67-23885

Plasma ring acceleration produced by pulsed azimuthal electric field, noting magnetic field role in stabilization 11 p1828 A67-23893

Plasma stability research program facilities for study of helical instabilities in cesium arc plasmas in axial, off-axis and other magnetic field configurations 11 p1829 A67-23998

Thermal plasma device /Q machine/ design objectives and proposed features, noting association with normal mode oscillations in gas laser 11 p1830 A67-24006

Magnetic field curvature effects on low temperature alkali metal plasma column stability 11 p1830 A67-24007

Outlook for controlled nuclear fusion process for industrial power generation, stressing plasma equilibrium preservation through magnetic trapping 11 p1831 A67-24015

One-dimensional flow through nozzle and stability of weakly ionized plasma with induced Hall current 11 p1832 A67-24155

Equilibrium and stability of K plasma with internal E field normal to confining magnetic field, noting wave propagation at ion momentum velocity 11 p1833 A67-24369

Ion-ion collision and shear stabilizing effect on resistive drift mode, applying dispersion relation with BGK collision

operator 11 p1834 A67-24374

Potassium plasma current instability, turbulence and diffusion across magnetic field for large amplitudes of oscillations treated as ionic sound waves 11 p1834 A67-24377

Collisionless instabilities in thermally ionized potassium plasma and effect of magnetic shear on oscillations and diffusion 11 p1834 A67-24378

Minimum B magnetic field geometry effect on spontaneous oscillations and anomalous cross field plasma transport in TOPSY Q device with uniform axial magnetic field 11 p1835 A67-24388

Synthesized plasma ion beams by electron injection from hot filament noting electrostatic instabilities and growth rates corresponding to nonlinear regime 11 p1838 A67-24403

Magnetic well stable to pure interchange instability and ballooning mode instability 11 p1839 A67-24544

Calculations of plasma distributions and field configurations with particle containment and stability within particular framework 11 p1843 A67-24997

Electromagnetic oscillation excitation in plasma beam, analyzing cases of weak and strong external magnetic fields 11 p1844 A67-25022

Plasma equilibrium in toroidal magnetic traps, discussing readjustment of small denominators in nondisturbance equation 11 p1844 A67-25071

Shock front parameters in plasma calculated from effective ratio of specific heats and adiabatic exponent 12 p1969 A67-25195

Mathematical theories applicable to excitation and ionization of atoms in plasmas at thermal equilibrium, determining electron density and temperature 12 p1968 A67-25432

Stabilization of thermally ionized potassium plasma by applying shear to confining magnetic field 12 p1975 A67-25476

Plasma equilibrium from gas discharge, role of electron concentration and contributions of excited atom transitions and quenching collisions 12 p1977 A67-26132

Relaxation of velocity distribution to equilibrium in electron plasma, showing linearized collision operator covers continuous spectrum of eigenvalues 12 p1977 A67-26176

Entropy functional characterization of equilibrium and stability properties of plasma configuration 12 p1977 A67-26227

Ion temperature gradients causing plasma instabilities when magnetic shear is present, deriving governing integral equation 13 p2162 A67-26284

Stability of self-gravitating two-fluid infinite plasma cylinder model in axial magnetic field 13 p2163 A67-26285

Nonuniform absorption of gyro-resonant microwave energy by electron gas used to produce helical configuration in magnetoplasmas 13 p2163 A67-26289

Oblique incidence of electromagnetic wave on plasma half-space 13 p2065 A67-26290

Pair correlations function in stable homogeneous plasma 13 p2164 A67-26295

Ionospheric fine structure, considering excitation of ion-acoustic waves by vertical gradients of density 13 p2109 A67-26329

Dynamics of weakly ionized gases analyzed using Liouville equation 13 p2167 A67-27003

Hollow electrically conducting fluid jet stabilization in presence of uniform magnetic field 13 p2169 A67-27314

Surface waves in current-carrying plasma filament of finite radius 13 p2170 A67-27370

Linearized Fokker-Planck kinetic equation, describing approach to equilibrium of test electrons injected into electron plasma in thermal equilibrium 14 p2356 A67-28203

Moment method treatment of collisionless plasma equilibria in confining magnetostatic fields, using Vlasov equation to determine distribution function of particles 14 p2360 A67-28554

Steady state velocity distribution in fully ionized plasma in DC electric field obtained through Bhatnagar-Gross-Krook equation 15 p2522 A67-29206

Screw instability in linear Hall accelerator 15 p2522 A67-29207

Relativistic MHD shock wave stability in infinitely conducting plasma with magnetic field parallel to shock wave

plane 15 p2523 A67-29216
 Gravitational instabilities arising in plasma disk subjected to differential rotation in presence of magnetic field parallel to rotation axis 15 p2528 A67-29662
 Spatially distributed automatic control system used in plasma plant stabilization 15 p2530 A67-29724
 Solution of Boltzmann and rate equations for electron distribution function and state populations in nonequilibrium MHD plasmas 16 p2710 A67-30519
 Current and potential distribution for thermally-stable plasma of Faraday-type segmented electrode MHD generator, taking into account nonequilibrium ionization 16 p2599 A67-30530
 Hot electron nonequilibrium plasma use in MHD generators, considering energy transfer, plasma stability, magnetogasdynamics, etc 16 p2601 A67-30545
 Electrostatic stability of finite-length plasmas immersed in magnetic field studied on mathematical model, discussing experiments with plasma-generating machines 16 p2714 A67-30871
 Flute instability for inhomogeneous plasma equilibria in inhomogeneous magnetic fields of mirror machines, solving Vlasov and Poisson equations 16 p2714 A67-30875
 Dispersion equation for stability of steady turbulent state obtained from perturbation theory and applied to drift cyclotron instability of plasma 16 p2719 A67-31230
 Temperature gradient effect on stability of inhomogeneous magnetically-confined plasma with frequent ion collisions 16 p2720 A67-31239
 Energy conservation in magnetohydrodynamics of plasmas, noting energy equation in 16 p2721 A67-31548
 Equilibrium deviation occurring in plasma with variable kinetic temperature due to radiation transport within plasma volume and outflow beyond limits of volume 16 p2723 A67-31787
 Stability conditions for gas stabilized DC electric arc in plasma-arc torch determined, using small perturbation technique schematic feed circuit 17 p2897 A67-32173
 Static equilibrium for two-dimensional toroidal plasma configurations with inner fields and purely meridional electric currents 17 p2903 A67-32709
 Particle motion and plasma equilibrium in helical magnetic field, discussing magnetic surface phenomena 17 p2904 A67-32914
 Slipping instability of plasma flows, noting instability criteria for long and short wavelength oscillatory 17 p2905 A67-32925
 Two-stream instability in semiconductor InSb plasmas, noting collision conditions, surface space charge, wave growth, etc 17 p2921 A67-33052
 Stabilized arc discharge characteristics using Elenbaas-Heller equation as basis for calculations 17 p2906 A67-33088
 Plasma stability with randomly fluctuating parameters for magnetic field with curved lines of force 18 p3086 A67-33732
 Highly ionized two-fluid plasma confined magnetically analyzed for 18 p3086 A67-33986
 Stable deflection of homogeneous plasma stream by linearly increasing transverse magnetic field, neglecting particle collisions 18 p3087 A67-34036
 Pulsed high current arc in hydrogen showing initial instability, discharge stability, impurity content, pinch effect, decay, etc 18 p3087 A67-34047
 Magnetic moment under short wave electrostatic perturbations 18 p3093 A67-34755
 Glow discharge positive column response to external perturbations, obtaining moving striations profile, structure and backward wave nature 19 p3273 A67-35094
 Production and behavior of magnetically stabilized high density high temperature plasma, describing 19 p3282 A67-35187
 Quantum-mechanical treatment of free-bound approximation for eigenstates and canonical partition function for plasma system in thermodynamic equilibrium 19 p3285 A67-35345
 Unsteady state of infinite plane layer of isotropic homogeneous plasma situated in

steady electric field normal to layer 19 p3286 A67-35349
 Stability of cesium Q-type machines analyzed for hot plasma-beam interactions in VLF range in sheath and in plasma 19 p3292 A67-35390
 Inhomogeneous plasma stability, considering wave drift oscillations expanding across external magnetic field and flute instability in noncompensating plasma 19 p3292 A67-35393
 Theory demonstrating stability of current sheets of different shapes in coaxial accelerators 19 p3294 A67-35406
 Entropy and free energy functionals for collisionless plasma at equilibrium in adiabatic magnetic field 19 p3298 A67-35731
 Helically symmetric MHD flow of compressible fluid in circular plasma cylinder, considering waves and stability 20 p3492 A67-36132
 Slightly resistive plasma stability analyzed by asymptotic methods, studying small perturbation growth rate 20 p3493 A67-36145
 Guiding center plasma theory /GCP/ stability, potential, Vlasov and motion equations, etc 20 p3494 A67-36152
 Plasma kinetic theory, discussing BBGKY hierarchy, nonequilibrium processes and unstable plasma kinetic equations 20 p3495 A67-36154
 Many-body system interaction with quasi-particle with assigned orbit, discussing applications to transport coefficient, plasma stability, etc 20 p3495 A67-36155
 Space charge analyses applied to electron beam extractions from plasma cathodes, computing stability data for potential distributions and extracted current 20 p3495 A67-36168
 Generalized formulas and stability criteria applied to higher order electrostatic oscillation modes in Vlasov plasmas, considering double-stream amplifier designs 20 p3495 A67-36169
 Uniformly accelerated axisymmetric plasmoid isolation from pulsed accelerated walls in presence of external magnetic field, noting stable configuration 20 p3498 A67-36685
 Wave transformation effect on inhomogeneous plasma radiation noise, applying results to stable plasma thermal radiation 20 p3498 A67-36691
 Plasma stability in combined magnetic fields investigated for oscillation frequencies 20 p3500 A67-37048
 Free convection of conducting fluid in coupled vertical channels for case of steady motion with lateral heating 20 p3500 A67-37051
 Vortical stabilization of plasma column within radial electric field 20 p3500 A67-37062
 LF and HF wave excitation in homogeneous plasma with external magnetic field, obtaining differential and integral wave intensities 20 p3501 A67-37142
 Counterstreaming ion electrostatic instability at cyclotron frequency to enhance trapping of injected ion beam 21 p3681 A67-37748
 Magnetic curvature effect on drift cyclotron instabilities, considering density gradients, Maxwell plasmas and resonance 21 p3681 A67-37749
 Soviet papers on HF properties of plasma including heating, stability, theory, electromagnetic wave scattering, etc 21 p3688 A67-38677
 Electromagnetic wave propagation in nonuniformly magnetized plasma with wave frequency near second electron cyclotron harmonic 22 p3843 A67-39263
 Malmberg-Wharton configuration electron plasma wave dispersion and damping 22 p3844 A67-39387
 Stabilizing effect of ion-ion collisions on collisional types of interchange instability, giving numerical solution of relevant normal mode equations 22 p3845 A67-39484
 Plasma stability in nonuniformly oriented magnetic field at guiding center limit 22 p3848 A67-39688
 Two particle correlation theory for static plasma from Poisson equation 22 p3848 A67-39689
 Numerical computations for resistive plasma drift instabilities in conducting cylinder, noting finite boundary conditions effect 22 p3848 A67-39693

Gravitational instability in anisotropic plasma including rotation effect 22 p3848 A67-39694
 Plasma stability investigated using constants of motion for solution of Vlasov equation 22 p3849 A67-39700
 Imbedded magnetic field stabilization effect on infinitely conducting inviscid compressible relativistic MGD half-jet 22 p3850 A67-39706
 Dynamic equilibrium of Van Allen belts studied for self-consistency through saturation of trapped plasma 22 p3871 A67-39799
 MHD stability in two-fluid model examined for condition where resistivity and electron inertia are neglected 22 p3851 A67-39984
 Linear magnetically trapped plasma stability theory described from MHD or quasi-fluid point of view 22 p3853 A67-40075
 Beta equals one theta pinch dynamic stabilization in all modes of m equal to or greater than one 23 p4031 A67-40793
 Quasi-linear relaxation dynamics of unstable distribution function for potential drift waves, deriving law governing average wave number time variation 23 p4032 A67-40911
 Temperature distribution measurements behind shock wave front in discharge tube with air and Ar indicate undisturbed thermodynamic equilibrium of plasmas 24 p4141 A67-41936
 Dense hydrogen plasma ohmic heating in quasi-stationary discharge without external magnetic field, obtaining stable impurity-free plasma column 24 p4195 A67-41939
PLASMA TEMPERATURE
 Microwave frequency measurements of radiation temperature of nitrogen afterglow plasma with Maxwellian electron velocity distributions 01 p0119 A67-10147
 Hall effect in low temperature plasma consisting of combustion products with admixture of KOH under variable sign magnetic field, demonstrating potential gradient existence 01 p0120 A67-10175
 Spectrographic method for measurement of temperature in plasma jets at atmospheric pressure, using amplification of beta line of hydrogen 01 p0124 A67-10773
 Temperature dependence of spectral line intensity emitted by thermal plasma 01 p0124 A67-10867
 Plasma electron temperature measured from soft X-ray bremsstrahlung absorption by beryllium foil 02 p0274 A67-12461
 Electron-ion recombination process due to electron collision in plasma with capture electrons transferred to ground level 03 p0474 A67-12853
 Nonequilibrium conductivity of argon-cesium plasma 03 p0478 A67-13614
 Temperature distribution in argon plasma jet with variable mass flow measured, using grating spectrometer [ASME PAPER 66-WA/HT-50] 04 p0669 A67-15434
 Energy transfer rate between electrons and ions in plasma, noting velocity dependence of Coulomb logarithm 04 p0672 A67-15775
 Viscosity and thermoconductivity of partially ionized argon plasma at atmospheric pressure measured, using equilibrium plasma jet 05 p0851 A67-16508
 Time resolved spectroscopic measurements of intensity and Stark width during decay of hydrogen plasma produced by ruby laser, determining electron density and temperature decay 05 p0852 A67-16653
 Electron density, optical thickness and temperature of ruby laser-induced carbon plasma 05 p0852 A67-16654
 Plasma conductivity and temperature in theta pinch determined from magnetic field probe results 05 p0859 A67-17437
 Radial temperature profile of magnetospheric plasma near equatorial plane observed by IMP 06 p0906 A67-18432
 Field aligned electron concentration profiles of equatorial anomaly, using parametric description for theoretical results 06 p0997 A67-18697
 Plasma energy density, conductivity and temperature measurements at various pressures 08 p1362 A67-21303
 Normal temperatures for optically thin plasma in state of local thermodynamic equilibrium

[DVL-644] 09 p1536 A67-21557
 Ionization and temperature measurement in MHD experiment, noting microwave interferometer response as electron density function and line reversal measurement 09 p1538 A67-21777
 Argon-cesium plasma spectroscopy, describing equipment, ionization, conductivity, recombination, concentration, etc 09 p1538 A67-21779
 Flow velocity, seeding ratio and electrical conductivity in seeded argon plasma, noting relation between plasma and MHD generator characteristics 09 p1539 A67-21780
 Law of mass action derivation of chemical equilibrium ionization of multitemperature system when electron and heavy particle temperature differ 09 p1544 A67-21858
 Modulation pyrometer measuring plasma temperature from spectral line intensity 09 p1499 A67-22328
 Larenz, two-line and calorimetric methods for plasma jet temperature measurements 11 p1793 A67-24825
 Plasmas of gas state and of solid state compared, considering density, temperature, and anisotropic mass, noting wave propagation electric discharges and confinement phenomena plasmas of gas state and of solid state compared, 12 p1980 A67-25202
 Electron transport coefficients and electron energy equation closed formulation for two-temperature plasma, considering elastic and nonelastic collisions 12 p1973 A67-25397
 Book on spectroscopic gas temperature measurement covering principles, radiometric and spectroscopic methods, instruments, applications to pyrometry, etc 12 p1940 A67-25431
 Electron concentration and temperature, gas temperature, electrical field intensity and conductivity of Hg-Cs nonequilibrium plasma 16 p2709 A67-30517
 Boundary layer equations for two-temperature plasma, showing distinction between electron and ion thermal boundary layer thickness 16 p2712 A67-30544
 Particle energy distribution in low temperature nonequilibrium plasma in diffusion approximation description 16 p2720 A67-31386
 Dynamic thermocouple for measuring plasma temperature up to 4000 degrees C, deriving relations for heating curve as function of time 17 p2854 A67-32162
 Temperature and/or velocity modulation of plasmas for generating MHD power 18 p3085 A67-33702
 Electrode and insulator behavior in experimental MHD generator electrically producing temperature modulation of gas stream 18 p2988 A67-33708
 Relationship between axial magnetic field necessary to extinguish oscillation from Brewster-angled laser and spontaneous intensity 18 p3061 A67-34200
 Electron density radial distribution, neutral gas temperature and ionization-caused column contraction calculated for cylindrical discharge plasma in argon 18 p3089 A67-34298
 Nonequilibrium conductivity of argon-cesium plasma 18 p3091 A67-34479
 Electron conductivities calculated for sodium-xenon and sodium-xenon-mercury plasmas assuming local thermal equilibrium, estimating plasma temperatures and electron number densities 19 p3278 A67-35134
 Significance of far field portion of plasma microfield 19 p3285 A67-35344
 Deuterium plasma heating by multiply charged hot impurity ions 19 p3287 A67-35357
 Plasma temperature and density measured behind luminous and preceding shock fronts in electromagnetic shock tube 19 p3293 A67-35399
 Viscosity, heat conduction and diffusion coefficients for two-temperature three-component plasma 20 p3500 A67-37049
 Electron temperature of shock-heated argon plasma determined by measuring microwave noise radiation and absorption 21 p3660 A67-37741
 MHD transformation of heat energy into electricity, discussing plasmatron applications and plasma velocity and temperature measurements in MHD generators 21 p3664 A67-38236
 Plasma electron and positive ion

temperatures measurement using orbit magnetic analyzer probes 22 p3798 A67-39628
 Temperature determination of wire explosion plasma from expansion and resistivity measurements, showing existence of two phases of electric arcs 22 p3847 A67-39644
 Particle and energy continuity equations derived and solved by computer method ion composition and plasma temperature measured by Explorer XXII particle and energy continuity equations derived and solved by computer method for ion composition 22 p3790 A67-39804
 Spectral and probe methods of plasma temperature measurement, discussing current-voltage characteristics 22 p3853 A67-40218
 Deuterium-tritium plasma temperature measurement using neutron detector, assuming Kerr cell ruby laser produced thermonuclear reaction heating in gas 23 p4031 A67-40892
 Shock wave produced optically-thin nonequilibrium plasmas studied using Rankine-Hugoniot calculations for properties, varying electron/ion temperature ratio [DVL-635] 24 p4194 A67-41880
 Electron scale heights from topside ionograms studied for radiation effects during quiet and disturbed conditions, noting relation to ionospheric plasma temperature 24 p4147 A67-42055

PLASMA THEORY

Electron velocity distribution equation extended to small wave numbers for electron-ion plasma 03 p0483 A67-13914
 Kinetic equation for homogeneous nongyrotropic magnetoplasma, discussing collective effects and errors in Sundaresan analysis 06 p1042 A67-18574
 Plasma transport properties, discussing application of ionization level as indicator for electric conductivity and viscosity 08 p1357 A67-20591
 MHD of flows with hot electrons in MHD ducts at low magnetic Reynolds numbers, emphasizing boundary layer and shock wave theory 09 p1541 A67-21797
 Spatial distribution of electrons and ions in neutral plasma, considering charge density 09 p1548 A67-22352
 Thermal equilibrium of quantum mechanical system composed of atom nuclei and electrons, using statistical method to eliminate divergence in sum of states of electron proton pair 09 p1550 A67-22864
 Skin effect in plasma theory for case of nonlocality of relation between current and electric field 15 p2522 A67-29211
 Kinetic equation for electron, ion and atom concentrations for Coulomb plasma taking into account inelastic processes 16 p2715 A67-31040
 Magnetic field finiteness effect on coordination between gyrotropic plasma waveguide and coaxial line 16 p2718 A67-31190
 DC discharge parameters solution using pressure theory with generation terms stressing one-and two-dimensional cases 19 p3277 A67-35126
 High pressure helium arc plasma behavior in cylindrical duct explained by theoretical model with different electron and heavy particle temperatures 19 p3280 A67-35145
 Guiding center plasma theory /GCP/ stability, potential, Vlasov and motion equations, etc 20 p3494 A67-36152
 Soviet papers on HF properties of plasma including heating, stability, theory, electromagnetic wave scattering, etc 21 p3668 A67-38677
 BBGKY hierarchy description of plasmas, with application to ionized particle charge distribution in external electric field 21 p3675 A67-38932
 Linear MPD channel theory with heavy component in uniform state evaluated for investigation of electrical conductivity phenomena 22 p3747 A67-39277
 Orthogonal transformation of neighboring quantum states into classical two-component plasmas, using WKB approximation 24 p4195 A67-42107

PLASMA TURBULENCE
 HF random phase transverse wave transmission through turbulent plasma generating scattered waves at combination frequencies 01 p0121 A67-10343
 Diagnostic measurement techniques for

statistical properties of ionized particles of equilibrium turbulent plasma, using electrostatic probe and high resolution microwave probe 02 p0275 A67-12550
 Perturbation theory for solving Vlasov equation for strong plasma turbulence, using statistical set of exact particle orbits 02 p0275 A67-12551
 Attenuation of uniform turbulent motion in incompressible fluid located in magnetic field 03 p0479 A67-13629
 Cosmic ray isotropy mechanism, examining plasma beam instability and cosmic ray scattering at plasma turbulent pulsations 04 p0693 A67-15554
 Bistatic radar cross section of underdense turbulent plasma measured at X-band and results compared with theoretical scattering model 05 p0760 A67-15999
 Fluctuation spectra of Cs and K plasmas produced by surface ionization in Q-3 device 05 p0859 A67-17443
 Instability of inhomogeneous weakly ionized plasma in crossed electric and magnetic fields in quasi-approximation 07 p1228 A67-19508
 Energy loss of charged particles during passage through weakly turbulent plasma in magnetic field with HF oscillations 08 p1357 A67-20844
 Generalized Gaussian distribution functional for weak plasma turbulence neglecting three-point correlation function 08 p1366 A67-21415
 Energy transfer spectra and Joule effect dissipation in decline of homogeneous turbulence in presence of uniform magnetic field with small Reynolds number 09 p1549 A67-22565
 Four-plasmon hydrodynamic equations describing weak turbulence spectrum in universal equilibrium region of plasma without magnetic field 10 p1886 A67-23597
 Stabilization of current driven helical waves in weakly ionized plasmas by magnetic wells of finite but small depth 11 p1827 A67-23885
 Plasma turbulence and diffusion across magnetic field investigated by plasma instabilities in case of large amplitudes of oscillation measured by Langmuir probes 11 p1834 A67-24376
 Potassium plasma current instability, turbulence and diffusion across magnetic field for large amplitudes of oscillations treated as ionic sound waves 11 p1834 A67-24377
 One-dimensional weak plasma turbulence, noting structure of spectra for various oscillation frequencies 11 p1837 A67-24393
 Electrostatic turbulence in low beta plasma and influence on diffusion across magnetic field, noting heating system for plates of Q device 11 p1789 A67-24413
 Kraichnan turbulence theory analyzed by computer calculated solutions with correlation and regression functions derived from experiment, shows good agreement with theory 11 p1780 A67-24539
 Random walks computer experiments on ensembles of random binary homogeneous velocity fields, using Eulerian and Lagrangian statistics 11 p1756 A67-24542
 Nonlinear mechanics of plasma-like distributed system studied with Q machine, noting mode locking 11 p1839 A67-24550
 HF random phase transverse wave transmission through turbulent plasma generating scattered waves at combination frequencies 11 p1843 A67-25016
 Stimulation of Jupiter radio emission by Io 12 p2000 A67-25204
 Turbulent state and diffusion of plasma during drift instability, noting increase with oscillation amplitude 14 p2363 A67-29068
 Generation of quiescent variable-parameter arc plasma in strong magnetic field 15 p2523 A67-29228
 Ion-acoustic interaction in weakly turbulent plasma deriving time variation of plasmon number 16 p2715 A67-31046
 Dispersion equation for stability of steady turbulent state obtained from perturbation theory and applied to drift cyclotron instability of plasma 16 p2719 A67-31230
 Turbulent plasma state from unstable, current driven drift waves, noting ion damping effect on amplitude of spectrum, density gradient, etc 16 p2719 A67-31231
 Superimposed electromotive force appearing in direction of magnetic field in

- presence of opposed spiral motion in turbulent field 17 p2842 A67-32341
- Collisionless shock waves in plasmas with high beta parameter, discussing Alfvén wave turbulence, firehose instability, dissipation and structure 17 p2901 A67-32528
- Statistical particle acceleration mechanism in plasmas noting Cerenkov acceleration, particle state changes, wave generation, etc 17 p2905 A67-32921
- Wake plasma turbulence of projectiles studied using electrostatic probe array 17 p2861 A67-33023
- Parametric coupling between ion and electron waves noting coefficients, growth rate amplification, etc 17 p2906 A67-33061
- Wind-driven plasma turbulence structure resolved by continuum ion probes at high Reynolds numbers, determining plasma density fluctuation from argon gas flow 18 p3030 A67-34743
- Weak turbulence theory for collisionless plasmas formulated in terms of test waves 18 p3092 A67-34744
- Periodic spatial variations of parameters of positive column plasma in magnetic field along obstacle shadow due to electron wakes 19 p3273 A67-35093
- Kinetic theory of transport processes in weakly turbulent plasma with and without magnetic field 19 p3286 A67-35351
- Electrical conductivity of weakly turbulent plasma calculated by behavior of electron distribution function 19 p3287 A67-35354
- Electron distribution function of homogeneous imperfect Lorentz plasma disturbed by electric field 19 p3295 A67-35418
- Validity range for weak turbulence theory in case of wave resonant interaction mechanism, treating Fokker-Planck and nonlinear optics approximations 19 p3298 A67-35792
- Weakly turbulent plasma theory, describing plasmon-particle interactions by quasi-linear theory 20 p3492 A67-36131
- Fluctuation spectrum in most stable state of turbulent plasma 20 p3496 A67-36213
- Noncollisional ion heating from accelerations in microfields of turbulent plasma waves 20 p3497 A67-36531
- Langmuir probe current in weakly ionized gas flow, studying correlation between hydrodynamical turbulence and pressure fluctuations 20 p3503 A67-37674
- Flows superimposition on toroidal hydromagnetic equilibrium, stressing stationary motion of plasma layers between neighboring magnetic surfaces 21 p3661 A67-37751
- Wave correlation evolution in uniformly turbulent weakly nonlinear systems 22 p3843 A67-39267
- Weakly turbulent spatially uniform ensemble of Vlasov plasmas, discussing time evolution of correlations due to collective interactions 22 p3849 A67-39701
- Thermal particles parallel velocity and transverse spatial diffusion coefficients found by studying test particle motion in weakly turbulent Vlasov magnetoplasma 22 p3849 A67-39702
- Approximate integrodifferential equations determining ensemble mean and covariance of particle distribution function of Vlasov plasma, discussing incompressible Navier-Stokes turbulence 22 p3850 A67-39703
- Microwave scattering cross section for turbulent weakly ionized plasma column, noting square root of mean square plasma density fluctuation limit for Born approximation 22 p3850 A67-39722
- Soviet papers on turbulent jets of air, plasma and real gas 23 p3988 A67-40727
- Turbulent plasma state and diffusion across magnetic field due to ion acoustic instability noting diffusion coefficient increment with instability excitation 23 p4032 A67-40905
- PLASMA WAVE**
- Diffraction of plane plasma wave in rectangular dielectric wedge, considering cases of E-wave and H-wave 01 p0020 A67-10139
- Self-focusing of transverse electromagnetic plane waves in magnetoplasma 02 p0191 A67-11571
- Photon interaction in plasma, determining energy density and collision frequency 02 p0272 A67-11583
- Oscillations observed from acoustical helium plasma wave in cylindrical hollow cathode attributed to radial shock wave initiated by energy pulse 02 p0273 A67-11899
- Inverse optimization for calculating refractive index and electrical resistivity of plasma in reentry and surface tension coefficient in ephedrodynamics 02 p0333 A67-12347
- Perturbation theory for solving Vlasov equation for strong plasma turbulence, using statistical set of exact particle orbits 02 p0275 A67-12551
- Plasma expansion wave propagation in vacuum after current cut-off 02 p0278 A67-12628
- Display method for investigating disturbance and wave propagation in discharge plasma 02 p0247 A67-12687
- Scattering of electromagnetic waves in plasma, noting effect of eddy current fluctuations 03 p0367 A67-12938
- Small amplitude wave propagation in incompressible conducting fluid 03 p0480 A67-13725
- Nonlinear hydromagnetic wave propagation in inviscid conducting compressible fluid 03 p0480 A67-13726
- Reflection and refraction of plane MHD waves at plane interface discontinuity of two semilinear homogeneous conducting fluids of different densities 03 p0480 A67-13727
- Propagation of coupled electromagnetic, electron-acoustic and ion-acoustic waves in horizontally stratified and magnetized electron-ion plasma 03 p0372 A67-13991
- Electron thermal conductivity of fully ionized Lorentz gas, determining energy transfer from Landau damping of plasma waves and collision parameters 03 p0484 A67-14039
- Spread-F occurrence dependency on F layer height variations with time, season and longitude and plasma wave generation near geomagnetic equator 03 p0415 A67-14115
- Stationary waves and nonstationary multibeam flows in plasma with arbitrary electron velocity distribution 03 p0486 A67-14198
- Transverse wave induced surface, compression and transverse waves in plasma, deriving expressions for amplitudes, phases and energies 04 p0663 A67-14744
- Entanglement effect of plasma and magnetic branches of oscillations in antiferromagnetic semiconductors on LF expanding plasma waves in strong electric fields 04 p0678 A67-15133
- Plasma wave behavior in strong external magnetic field, discussing scattering at ions, wave transformations and nonlinear wave interactions 04 p0667 A67-15206
- Differential equations describing wave transformation in weakly inhomogeneous plasma 04 p0668 A67-15217
- Kinetic theory of electromagnetic propagation in confined magnetoactive plasma 04 p0668 A67-15272
- Frequency range in which Vavilov-Cerenkov surface wave exists in plasma-vacuum boundary 04 p0668 A67-15273
- Coupled spin, electromagnetic and plasma waves in ferrites 04 p0686 A67-15973
- Wave interactions in spatially dispersive media 05 p0849 A67-16013
- Nonlinear instability of optical frequencies in partially ionized plasma, noting nonlinear frequency buildup for strong plasma waves 05 p0852 A67-16691
- Evolution of nonlinear perturbations in plasmas, noting physical meaning of self-similar solution based on Korteweg-de Vries equation 05 p0853 A67-16698
- Recognition and subsequent amplification of difference frequency in plasma-beam system with two electromagnetic waves propagating in opposite direction 05 p0766 A67-17170
- Steady oblique nonlinear waves in warm collision-free plasma 05 p0857 A67-17425
- Wave excitation in compressible partially ionized plasma by electromagnetic and acoustic/or mechanical sources, describing set of linearized hydrodynamic and Maxwell equations 05 p0859 A67-17436
- Nonlinear and quasi-linear transformation of HF waves in LF part of spectrum in inhomogeneous plasma 06 p1038 A67-17759
- Dispersion nucleus of homogeneous nonmagnetic hot plasma and functional properties of plasma waves 06 p1039 A67-18048
- Shock wave front structure in plasma, noting use of SHF diagnostics, electron concentration growth, etc 06 p0984 A67-18077
- Oscillations in stationary gas discharge, describing device for calculation of correlation function for electrical signals 07 p1227 A67-19120
- Radio wave emission due to shock wave propagation in magnetospheric boundary and electromagnetic scattering in plasma wave field 07 p1243 A67-19808
- Quasi-linear theory of ion beam instabilities of LF waves in plasma 07 p1230 A67-20145
- Nonlinear constant profile plane waves in cold Vlasov hydrogen plasma under influence of external magnetic field 08 p1359 A67-20896
- Fokker-Planck equation extended to small amplitude waves in uniform plasma 08 p1360 A67-21128
- Landau type damping of plasma oscillations and Bernstein mode electrostatic propagation perpendicular to weak magnetic field 08 p1360 A67-21129
- Excitation and propagation of Bernstein modes in nonuniform plasmas near electron cyclotron harmonics 08 p1361 A67-21130
- Ion beam excitation of drift waves in alkali plasma, discussing sinusoidal signal propagation characteristics, variations with beam velocity and with modulation frequency 08 p1361 A67-21135
- Treatments of drift wave velocities in Cs and K plasmas, noting radial electric field effect made negligible by reducing cathode temperature gradient 08 p1362 A67-21147
- Energy coupling among electron acoustic, ion acoustic and transverse electromagnetic waves at two-fluid plasma density discontinuity 08 p1364 A67-21397
- Nonlinear plasma wave equation in periodic solutions obtained by perturbation scheme 08 p1364 A67-21398
- Energy storage in plasma near upper hybrid resonance treated by macroscopic plasma model with nonlinear terms 08 p1364 A67-21399
- Landau damping and growth applied to electron plasma waves for Maxwellian velocity distribution in slab and cylindrical geometries 08 p1365 A67-21403
- Excitation of ion-acoustic waves in potassium-cesium plasma when passing current through it, finding natural frequencies of system when plasma is drifting along axis 09 p1544 A67-21853
- Fresnel formulas for transformation of transverse electromagnetic wave into longitudinal plasma wave at dielectric-plasma interface, using Laplace transforms 09 p1464 A67-21993
- Kinetics of nonuniform generation of longitudinal plasma waves by transverse wave beam with narrow spectrum, noting effect of magnetic field 09 p1545 A67-21995
- Wave propagation and noise in gas discharge at low pressure, noting luminescence fluctuations 09 p1545 A67-22220
- Sound propagation in partially ionized plasma, noting kinetic quadrature calculation results 10 p1683 A67-22783
- Excitation of electroacoustic lateral waves in compressible plasma by nonelectromagnetic source 10 p1683 A67-22865
- Nonlinear effects produced by instability of nonpotential plasma waves in oscillating discharge, deriving wave kinetic equation 10 p1684 A67-22902
- Low temperature alkali plasmas in strong magnetic fields interpreted in terms of collisional drift modes 10 p1684 A67-23073
- Current instability in inhomogeneous plasma formed by drift and ion-acoustic waves with oscillation frequencies 10 p1685 A67-23461
- Dispersion relation for large amplitude circularly polarized plane wave propagation along magnetic field in hot collision-free plasma, considering distribution function 11 p1826 A67-23881
- Stabilization of current driven helical waves in weakly ionized plasmas by magnetic wells of finite but small depth 11 p1827 A67-23885
- Relativistic solution to normal incidence on semilinear longitudinal drifting homogeneous temperate magnetoplasma,

obtaining reflected and transmitted waves 11 p1832 A67-24304

Cesium plasma measurements to determine steady state parameters and LF oscillation characteristics 11 p1834 A67-24379

LF drift waves effect upon anomalous transverse diffusion in fully ionized magnetoplasma, noting wave amplitude 11 p1835 A67-24387

Electron temperature variation induced effects and Landau damping of ion acoustic waves studied in quiescent discharge tube plasma 11 p1837 A67-24395

Connection between sub-ELF ionospheric emissions at night and high negative ion concentration, noting ion-acoustic wave excitation 11 p1787 A67-24399

Electron plasma wave propagation along cylindrical plasma column in magnetic field, calculating damping and dispersion curves 11 p1837 A67-24401

RF energy absorption by plasma column surrounded by periodic coupling structure, noting similarities with Landau damping and measurements of non-Maxwellian distributions 11 p1838 A67-24402

Ion beam interaction with beam produced plasma, showing excitation of waves at electron plasma frequency 11 p1840 A67-24562

Transverse diffusion of particle perpendicular to magnetic field by assembly of random Alfvén waves explains increase in electric field energy 11 p1840 A67-24753

Ionic waves in plasma in electric field interacting with beam of charged particles at relaxation time, using dispersion equation 11 p1841 A67-24869

Weak inhomogeneous plasma wave energy redistribution during quasi-normal oscillation expansion in resonance regions, noting electric analogy 11 p1842 A67-24953

Entanglement effect of plasma and magnetic branches of oscillations in antiferromagnetic semiconductors on LF expanding plasma waves in strong electric fields 12 p1978 A67-25157

Generation rate of secondary HF wave from resonant interaction of two longitudinal waves in cold beam-plasma under external magnetic field 12 p1970 A67-25250

Plasma models and methods used to study wave propagation phenomena, considering particle orbit, single species moment equations, velocity distribution function, etc 12 p1975 A67-25527

Modal wave solutions of isotropic plasma-filled parallel-plate waveguide examined, using cold and warm plasma models without collision 12 p1915 A67-25943

Earth bow plasma shock wave model with ion wave instabilities as principal shock structure [SR-2] 13 p2107 A67-26301

Magnetospheric regions of amplification of VLF emissions and micropulsations 13 p2115 A67-26858

Plasma expansion wave propagation in vacuum after current cut-off 13 p2171 A67-27386

General dispersion relation for linear waves in multicomponent plasmas 13 p2172 A67-27726

Linear waves in weakly ionized multicomponent plasmas investigated using dispersion relation 13 p2172 A67-27728

Small one-dimensional deviations of plasma parameters from equilibrium state, obtaining exact solution in form of inverse Laplace integral 14 p2353 A67-27754

Increase in mean electron energy shown to be factor leading to plasma stratification 14 p2353 A67-27756

One-dimensional plane shock wave propagation through hot dense plasmas under various energy and pressure conditions, noting magnetic field effect 14 p2356 A67-27957

Stationary waves and nonstationary multibeam flows in plasma with arbitrary electron velocity distribution 14 p2360 A67-28543

Correlation function and pressure change of slow waves in nonisothermal plasma 14 p2360 A67-28604

Plasma wave drift in stellarator helical magnetic field, deriving equations for wave developing conditions 14 p2361 A67-28762

Diffusive separation due to electrical coupling of ions and hot electrons and

effect on shock wave structure in plasmas 15 p2470 A67-29227

Frequency shift associated with nonlinear extraordinary wave in cold plasma calculated using Bogolubov method 15 p2524 A67-29230

Vorticity generation by interaction of waves with plasma in magnetic field 15 p2524 A67-29231

Superthermal electron production by quasi-cyclotron acceleration when interacting with monochromatic large amplitude electrostatic plasma wave 15 p2528 A67-29569

Electromagnetic surface wave propagation in plasma, studying oscillation spectra dependence on surface wave field amplitude 15 p2528 A67-29712

Short wave limit for plasma radiation emission of neon gas discharge analyzed by Kirchhoff-Planck relation 15 p2530 A67-29747

Nonlinear instability of optical frequencies in partially ionized plasma, noting nonlinear frequency buildup for strong plasma waves 15 p2530 A67-29862

Evolution of nonlinear perturbations in plasmas, noting physical meaning of self-similar solution based on Korteweg-de Vries equation 15 p2530 A67-29869

Nonlinear drift wave propagation arising from inhomogeneity transverse to magnetic field in plasma 15 p2531 A67-30187

Plasma wave behavior in strong external magnetic field, discussing scattering at ions, wave transformations and nonlinear wave interactions 15 p2532 A67-30254

Differential equations describing wave transformation in weakly inhomogeneous plasma 15 p2532 A67-30265

Ionization wave velocity in nonisothermal, low temperature plasma discussed, using generalized Ohm law, law of conservation of electron energy and SAHA equation 16 p2711 A67-30540

Nonlinear instability, demonstrated for electron plasma waves driven toward instability by small ion beam but linearly stabilized by electron Landau damping 16 p2719 A67-31228

Numerical analysis of structure of one-dimensional unsteady magnetic compression waves propagating into collisionless plasma, using motion equations 16 p2719 A67-31232

Drift waves in fully ionized potassium magnetoplasma in single-ended Q machine, measuring effect on transverse diffusion coefficient 16 p2720 A67-31242

Successive approximation method for asymptotic solution of waves in inhomogeneous gyrotronic plasma 16 p2627 A67-31366

Excitation of high and low frequency electromagnetic waves in unbounded plasma by external currents, deriving wave expression 16 p2721 A67-31477

Attenuation characteristics of longitudinal wave propagating in weakly inhomogeneous plasma, deriving expression for oscillations damping constant 16 p2628 A67-31498

Excitation and propagation of surface plasma waves along plasma column in noble gases, obtaining plasma dispersion curves 17 p2899 A67-32309

Nonlinear interacting plasma wave equations derived by semiquantum analysis of wave-particle and wave-wave interactions 17 p2905 A67-32923

Dispersion relations for coupled electromagnetic and longitudinal waves propagating along isotropic inhomogeneous cylindrical hot plasma column 17 p2908 A67-33107

Microwave and type IV solar bursts, examining gyrosynchrotron emission and various electron acceleration mechanisms 17 p2939 A67-33391

Wave propagation and noise in gas discharge at low pressure, noting luminescence fluctuations 18 p3086 A67-33764

Inhomogeneous hydrodynamic motion and thermal particle velocities effect on MHD wave propagation 18 p3086 A67-34034

Three-dimensional equation for wave propagation through inhomogeneous warm compressible plasma in inhomogeneous static magnetic field 18 p3088 A67-34071

Electromagnetic wave scattering from plasma wave analyzed using Vlasov equations for anisotropic plasma, applying formulas to boundary value problems 18 p3088 A67-34090

Interaction between ion and electron waves in plasma 18 p3089 A67-34186

LF waves induced by superimposed electric and magnetic fields in semiconductor plasma 18 p3102 A67-34442

Oblique, normal and transverse ionizing shock waves 18 p3092 A67-34733

Laser driven plasma detonation waves in gases observed with Schlieren system, discussing shock wave growth 18 p3092 A67-34734

Transverse and longitudinal waves in infinite nonrelativistic collisionless plasma, using Maxwell equation 18 p3093 A67-34750

Near earth and outer ionosphere plasma waves and oscillations in VLF and ELF bands 19 p3317 A67-34932

Rocket observation of ionospheric electron density using VLF doppler shift formula, determining wave polarization 19 p3215 A67-35180

Kinetic equation for inhomogeneous plasma in uniform external magnetic field, for application in studies of transport and high frequency wave phenomena 19 p3285 A67-35342

Experiments with thermally ionized cesium plasma in magnetic field with variable curvature 19 p3288 A67-35365

Microwave transmission through quiescent cesium plasma studied, noting apparatus for thermal ionization studies 19 p3288 A67-35370

Cyclotron harmonic wave propagation in warm magnetoplasmas predicted theoretically for perpendicular and oblique damping 19 p3288 A67-35371

Structure of shock waves in collision-free plasma at angle to external magnetic field studied by hydrodynamic equations 19 p3288 A67-35372

Cyclotron waves in collisionless plasma column, finding three distinct waves with resonances at/near electron cyclotron frequency 19 p3288 A67-35373

LF acoustic/magnetoacoustic wave propagation in partially ionized plasmas studied within framework of macroscopic plasma dynamics, using dynamic adiabatic state equation 19 p3290 A67-35375

Infinitesimal driven plane wave characteristics in uniform plasma with finite electron drift velocity found, using Navier-Stokes and Poisson equations, energy conservation continuity and perfect gas law 19 p3290 A67-35376

Phase velocity and attenuation of ionic plasma waves in weakly ionized gases measured in absence and presence of external magnetic fields 19 p3290 A67-35378

UHF wave interaction between plasma and electron stream in magnetic field noting convective instability 19 p3291 A67-35382

Stream instabilities in magnetotonic plasmas in presence of DC magnetic field, noting possibilities of growing waves 19 p3292 A67-35389

Damping of high frequency waves in homogeneous fully ionized plasma with relative electron-ion drift calculated, using fokker-planck kinetic equation 19 p3292 A67-35391

Inhomogeneous plasma stability, considering wave drift oscillations expanding across external magnetic field and flute instability in noncompensating plasma 19 p3292 A67-35393

Ion cyclotron frequency wave generation in plasma confined in magnetic well for maximal density 19 p3295 A67-35419

Longitudinal wave echo in collisionless electron plasma with Landau damping 19 p3295 A67-35534

Plasma wave influences on metal surface reflectivity investigated using Maxwell equation, calculating dielectric constant and conductivity 19 p3262 A67-35581

Electromagnetic radiation reflectivity on metal surface investigated using microscopic model to derive fields and boundary conditions 19 p3262 A67-35582

Wave propagation in anisotropic plasma in presence of electron density irregularities, noting Faraday effect 19 p3184 A67-35825

Nonlinear coupling between fast and slow waves of cold homogeneous plasma slab partially filling parallel plate waveguide 20 p3492 A67-36126

Linear electromagnetic oscillations in homogeneous plasma described by motion and Maxwell equations 20 p3492 A67-36129

Helically symmetric MHD flow of compressible fluid in circular plasma cylinder, considering waves and

- stability 20 p3492 A67-36132
- Plasma shock wave structure model, analyzing steady flow of electrically neutral fluid 20 p3493 A67-36144
- Quasi-linear plasma waves model, considering Vlasov approximation, deriving distribution functions and electric field equations solution 20 p3494 A67-36149
- Noncollisional ion heating from accelerations in microfields of turbulent plasma waves 20 p3497 A67-36531
- Plasma absorption of microwaves, noting 20 resonant maxima near harmonics of electron cyclotron frequency 20 p3498 A67-36692
- LF and HF wave excitation in homogeneous plasma with external magnetic field, obtaining differential and integral wave intensities 20 p3501 A67-37142
- Coupling coefficients for nonlinear interaction between two transverse waves and electron plasma wave in magnetic field 20 p3501 A67-37181
- Plasma wave propagation dispersion in sodium and potassium at cryogenic temperature using Landau-Fermi liquid theory 20 p3514 A67-37570
- Wave interactions in spatially dispersive media 20 p3502 A67-37590
- Classical nonisothermal two-component plasma correlation functions and pressure contribution from Coulomb interaction 20 p3502 A67-37603
- Oscillations in stationary gas discharge, describing device for calculation of correlation function for electrical signals 21 p3664 A67-38165
- Electrostatic ion cyclotron waves excitation in plasma and ion heating due to cyclotron damping 21 p3667 A67-38407
- Drift and ion acoustic waves and coupled waves in highly ionized dense plasma of finite ion temperature 21 p3667 A67-38412
- Dispersion equation for frequency dependence on wave amplitude propagated in plasma placed in constant magnetic field causing longitudinal oscillations 21 p3669 A67-38681
- Isolated longitudinal wave pulse amplitude and phase velocity dependence on trapped particle density in ion-electron and electron-positron plasmas 21 p3669 A67-38683
- Fast and slow magnetosonic wave propagation in plasma analyzed by Huygens principle 21 p3670 A67-38687
- Decay instability of steady state waves in plasma, considering Alfvén wave 21 p3674 A67-38803
- Alfvén, fast and slow magnetoacoustic and entropy hydromagnetic wave propagation in anisotropic collisionless magnetoplasma 22 p3843 A67-39268
- Malmberg-Wharton configuration electron plasma wave dispersion and damping 22 p3844 A67-39367
- Nonlinear theory of longitudinal plasma waves, formulating distribution function and Maxwell equation for electric field 22 p3845 A67-39421
- Dispersion characteristics of surface waves excited in infinitely long axially magnetized cold plasma by electric dipole 22 p3847 A67-39621
- X-ray diffusion from thermal agitation oscillations coupled with plasma waves in indium antimonide, discussing phonon-plasmon interactions and Hall effect measurements 22 p3859 A67-39652
- Steady state nonlinear Landau damping of electron plasma wave obtained from random phase approximation by balancing nonlinear and collision effects 22 p3848 A67-39691
- Electrostatic energy per degree of freedom of two-temperature plasma examined for validity of resonant approximations in ion wave region 22 p3852 A67-39986
- Laminar nonrelativistic finite amplitude hydromagnetic wave propagation in low temperature ionized plasma, using two-fluid model 22 p3852 A67-39990
- Standing waves in hot plasma traversed by quasi-neutral charged particle flux including numerical analysis of elongated wave occurrences 22 p3853 A67-40124
- Collisionless small and large amplitude electron plasma wave damping compared, showing small amplitude waves damp exponentially and large amplitude waves exhibit amplitude oscillations collisionless small and large amplitude
- electron 22 p3853 A67-40242
- Negative cyclotron resonance absorption due to electron elastic collisions with noble gas atoms, comparing results with kinetic plasma wave theory 22 p3842 A67-40346
- Elliptically polarized electromagnetic wave propagation in homogeneous infinite plasma, solving Vlasov equations of nonlinear theory by successive approximation 23 p4030 A67-40597
- Kinetic model of Tonks-Dattner absorption resonances in plasma positive column providing plasma wave reflection mechanism 23 p4031 A67-40782
- Rapid magnetic field variations observed in magnetosheath evaluated in terms of transverse modes of plasma wave propagation 23 p3995 A67-40804
- Transverse electric field generated by interaction of various longitudinal plasma waves in ion electron plasmas 23 p4033 A67-41151
- Wave propagation in random plasma medium with inhomogeneous parabolic electron density profile background for ionospheric propagation applications 23 p3974 A67-41199
- Plasma waves generation by transverse waves as function of phase relation of interaction 23 p4034 A67-41678
- Temporal and spatial echoes can occur in collision-free plasmas at various times for different wave number combinations and various positions for different frequency combinations 24 p4194 A67-41871
- Sound propagation in partially ionized plasma, noting kinetic coefficients and quadrature calculation results 24 p4195 A67-42119
- PLASMAGUIDE**
- Energy relation for acoustic propagation modes in hot electron plasma considered in application of Helmholtz theorem 01 p0123 A67-10441
- Modes of beam waveguide or beam waveguide resonator filled with axially magnetized plasma 02 p0213 A67-11619
- Magnetic field finiteness effect on effectiveness of gyrotronic plasma waveguide excitation by coaxial line of force 04 p0665 A67-15165
- Kinetic theory of electromagnetic wave propagation in layered plasma waveguide in strong magnetic field 05 p0781 A67-16341
- Reflection coefficients of plasma waveguide measured by determining wave modulation coefficients 06 p1039 A67-18083
- Plasma parameter determined from measurements of wave reflection coefficient in waveguide 06 p1041 A67-18187
- Electromagnetic wave dispersion in semiconductor plasma waveguides for case of plane wave propagation normal to magnetic field vector 07 p1231 A67-19133
- Symmetric wave propagation in cylindrical waveguide filled with inhomogeneous plasma, calculating phase velocities 07 p1158 A67-20242
- Discrete spectrum of electromagnetic waves caused by excitation of dielectric layer on ideally conducting plane in homogeneous absorbing plasma 08 p1295 A67-20832
- Plasma diagnostics by microwave interferometry in MHD channel using open waveguide, calculating field distribution and propagation characteristics 09 p1539 A67-21781
- Variation of phase constant and damping constant of SHF wave propagating in waveguide incorporating coaxial plasma-filled dielectric tube 09 p1473 A67-21999
- Gap excitation of waveguide loaded with plasma represented as charge-free medium with tensor dielectric constant 09 p1480 A67-22283
- Dispersion of mode couplings of wave propagation in waveguide containing plasma electron beam system 09 p1550 A67-22582
- Wave propagation in hot plasma in cylindrical waveguide with arbitrary axial magnetic field, treating boundary value problem by perturbation expansion 11 p1826 A67-23874
- Modal wave solutions of isotropic plasma-filled parallel-plate waveguide examined, using cold and warm plasma models without collision 12 p1915 A67-25943
- Microwave field distribution in waveguide partially filled with solid state plasma for application to isolator 13 p2076 A67-26521
- Magnetic field finiteness effect on effectiveness of gyrotronic plasma waveguide excitation by coaxial line of force 15 p2526 A67-29352
- Field distribution in plasma waveguide at LF and large densities, noting dispersion properties of E and H waves 16 p2718 A67-31189
- Magnetic field finiteness effect on coordination between gyrotronic plasma waveguide and coaxial line 16 p2718 A67-31190
- Nonlinear dependence of phase velocity on wave amplitude during electromagnetic propagation in plasma waveguide, describing test apparatus 16 p2718 A67-31191
- Magnetohydrodynamic wave dispersion theory at open end of sem infinite plasma waveguide closed by conducting diaphragm 16 p2722 A67-31574
- Coaxial and magnetohydrodynamic waveguide matching obtaining reflection coefficient of former and wave amplitude of latter 16 p2722 A67-31575
- Electromagnetic waves in isotropic laminar plasma waveguide 18 p3090 A67-34440
- Electric field due to double grid excitation in circular waveguide partially filled with warm homogeneous plasma in infinite magnetostatic fields 19 p3290 A67-35379
- Nonlinear coupling between fast and slow waves of cold homogeneous plasma slab partially filling parallel plate waveguide 20 p3492 A67-36126
- Thetatron gun plasma burst expanding freely in drift tube, discussing wall shorting effect inhibition method and measurements 22 p3846 A67-39485
- PLASMATRON**
- SA DUOPLASMATRON**
- Double-chamber plasmatron for low temperature gas discharge plasma investigations 06 p1038 A67-17745
- Thermal fluxes in plasma jets produced by HF plasmatron in air 06 p1045 A67-18813
- Energy characteristics of magnetically stabilized plasmatron effect on output power in crossed fields 09 p1547 A67-22318
- Three-phase AC plasmatrons designed to produce low temperature plasma 09 p1446 A67-22326
- Ion current from duo plasmatron ion source with expansion cuvette increased by superimposing weak magnetic induction in expansion zone and insulating cuvette walls 09 p1550 A67-22598
- Approximate similarity criterion for arc with self-adjusting length, burning in plasmatron with gas vortex stabilization, determined by shunting 11 p1843 A67-24969
- Convective heat transfer effect on plasmatron efficiency 11 p1843 A67-24970
- Shunting process and associated fluctuations in plasmatron with vortex stabilized arc, noting anode spots 11 p1843 A67-24971
- Volt-ampere and thermal characteristic of plasmatron with insert in electron gap 11 p1843 A67-24973
- Time-dependent mean-mass temperature of argon jet produced by arc plasmatron with powdered metal carbides injected into jet calculated using heat transfer equations 16 p2721 A67-31393
- HF electrodeless plasmatron working at atmospheric pressure, noting plasma discharge and temperature distribution characteristics, obtaining constricted plasma jet 17 p2897 A67-32175
- Plasma technology in industry, discussing Polish-made plasma torch design and operation and plasmatron and spraying applications 17 p2865 A67-32189
- High current arc operation characteristics in vortical-scheme plasmatron, determining current voltage characteristics 18 p3088 A67-34057
- Experimental data applicability for DC arcs in construction of AC plasmatrons 18 p3088 A67-34058
- MHD transformation of heat energy into electricity, discussing plasmatron applications and plasma velocity and temperature measurements in MHD generators 21 p3664 A67-38236
- Axial component of electric field intensity in vortex stabilized arc measured by sectional channel and electrode spacing 24 p4195 A67-41940

Net convective and radiative heat flow to electrodes of coaxial plasma generator may exceed heat flow from moving arc spot within arc burning region 24 p4098 A67-42250

PLASMOID

Plasma density dependence of adiabatic motion of plasmoids in longitudinal magnetic field 01 p0122 A67-10351

Short hydrogen plasmoid production by electromagnetic waves in decimeter range 05 p0855 A67-16997

Plasmoid structure produced by coaxial plasma gun with interchangeable polarity electrodes, noting experimental setup, particle velocity, density, energy, etc 06 p1040 A67-18085

Corrections for dielectric-constant tensor and conductivity tensor resulting from effect of electric field induced by plasmoid 07 p1229 A67-19517

Plasmoid density, electron temperature and radius variation during propagation through magnetic field, using electric and magnetic probes 09 p1545 A67-21996

Plasma in flat-electrode accelerator, examining optimum accelerator length associated with equilibrium between acceleration processes in plasma and diffusive scattering of plasmoid 09 p1545 A67-22001

Plasma density dependence of adiabatic motion of plasmoids in longitudinal magnetic field 11 p1844 A67-25024

Plasmoid generated by Q-switched neodymium-glass laser radiation focused on solid target, estimating plasma electron temperature 12 p1986 A67-26065

Soviet book on plasmoids covering coaxial plasma sources, magnetic field interaction and observation methods 15 p2524 A67-29243

Current damping, thermal expansion, radial oscillation, kinetic pressure and other dissipative processes effects on magnetic properties of plasmoids 15 p2524 A67-29244

Small nonpolarized plasmoids interacting with axisymmetric magnetic field, discussing penetration mechanism, equations of motion and magnetic moment 15 p2524 A67-29245

Longitudinal deformation of plasmoid interacting with axisymmetric magnetic field, noting expansion in homogeneous region 15 p2525 A67-29246

Radial deformation of premagnetized plasmoid interacting with increasing magnetic field 15 p2525 A67-29247

Plasmoid collisions in axisymmetric magnetic field studied spectrographically for energy density, radiative power, charged particle density, etc 15 p2525 A67-29248

Plasma acceleration in flat electrode plasma source simulated by ideally conducting bridge described electrostatically 15 p2525 A67-29249

Coaxial plasma gun for plasmoids showing higher mean energy when gas admission is closer to plasma source end 15 p2525 A67-29252

Coaxial plasma gun operating in longitudinal magnetic field, noting effect on plasmoid uniformity 15 p2525 A67-29253

Coaxial helium-plasma source with superimposed azimuthal magnetic field, noting plasmoid density increase with magnetic field, plasmoid velocity and experimental setup 15 p2526 A67-29254

Structure and magnetic field of plasmoids produced by conical induction source studied with probe-diagnostic method 15 p2526 A67-29255

Plasmoid structure, analyzing interdependence of plasmoid parameters along length 15 p2526 A67-29256

Variable field Thomson mass spectrograph application to analysis of mass composition of plasmoids 15 p2526 A67-29258

Electric field device to generate short plasmoids free from plasma contamination through contact with metal 15 p2526 A67-29259

Modified Thomson mass spectroscopy for visual observation of energy spectra of ion component of plasmoid 15 p2486 A67-29260

Development of plasmoid density due to laser ionization measured using Fabry-Perot interferometer 15 p2527 A67-29474

Gas stream discharge studied by using electromagnetic plasma gun to direct plasmoids toward beam 15 p2472 A67-29726

Electron heating by direct discharge during plasmoid interaction involving polarization 16 p2717 A67-31182

Electrodeless device for currentless plasmoid generation noting flowing plasma conductivity, boundary layer phenomena and potential distribution 17 p2900 A67-32344

Plasmoid motion in longitudinal, transverse and two-dimensional multipole magnetic fields, investigating electric fields and plasmoid parameters 17 p2904 A67-32916

Negative ion accumulation in HF resonant discharges at low pressure and plasmoid formation 19 p3275 A67-35112

Plasmoid structure created by plasma injector and freely propagating in space, noting plasma composition, energy spectrum, electron temperature, density, etc 19 p3288 A67-35362

Deuterium plasmoid structure, impurity distribution, passage through pulsed magnetic barrier and capture by longitudinal magnetic field with mirror geometry 19 p3288 A67-35364

Hydrogen plasmoids produced by pulsed two-cascade injectors, using electron guns for plasma ionization and acceleration 19 p3297 A67-35597

Field determination when produced by symmetrical plasmoid with time dependent current distribution traveling along cylindrical waveguide, using Wiener-Hopf method 20 p3497 A67-36680

Electric field produced by polarization in plasmoid injected across field in closed system 20 p3497 A67-36681

Uniformly accelerated axisymmetric plasmoid isolation from pulsed accelerated walls in presence of external magnetic field, noting stable configuration 20 p3498 A67-36685

Plasmoid instability from inhomogeneous flow along magnetic field 20 p3498 A67-36693

Motion of plasmoids injected axially in two-dimensional multipolar magnetic field, studying losses 20 p3500 A67-37061

Plasma component velocity distribution and multiple plasmoid production indicated in spectrograms from high speed photography of coaxial injector discharge 21 p3664 A67-37939

Plasmoid propagation at high pressures, emphasizing Bostick buttons performance compared to electromagnetic shock tube, describing button gun and photographic equipment 21 p3874 A67-38771

Pinch-discharge source of ionizing plasmoids for aerophysical investigations at high pressures, emphasizing stabilization and passage of AC current through vortex 21 p3875 A67-38912

Variations in parameters of magnetized plasmoids interacting in nonuniform fields determined by magnetic and electric probes 23 p4035 A67-41685

Interaction between broadening plasmoid and external magnetic field assuming time dependent conductivity and magnetic field as function of time 24 p4195 A67-41929

PLASMON

Pair production in irradiated semiconductors within framework of plasmon decay, considering variation of radiation ionization energies with band gap energy 06 p1063 A67-18935

Collective energy losses by plasmas in crystals caused by excitation of volume or surface plasmons 08 p1369 A67-20828

Interband transitions and plasmon excitation in calcium fluoride, discussing energy loss 09 p1558 A67-22585

Four-plasmon hydrodynamic equations describing weak turbulence spectrum in universal equilibrium region of plasma without magnetic field 10 p1686 A67-23597

Ion-acoustic interaction in weakly turbulent plasma deriving time variation of plasmon number 16 p2715 A67-31046

Weakly turbulent plasma theory, describing plasmon-particle interactions by quasi-linear theory 20 p3492 A67-36131

Electron energy loss calculations for nonnormal incidence in thin dielectric foil, with excitation probabilities and dispersion relations for bulk and surface plasmons 21 p3686 A67-39135

Kinetic equation for spatially uniform unstable plasma with collision term containing wave effect /plasmons/ in system and Lenard-Balescu equation 22 p3848 A67-39690

Light polarization and intensity for Raman scattering from plasmons and phonons in

GaAs 23 p4038 A67-40795

PLASTIC**SA REINFORCED PLASTIC**

High polymer rubber, plastic, and textile qualitative and quantitative properties, uses in space environment 13 p2143 A67-26698

PLASTIC ANISOTROPY

Anisotropy test examining failure behavior of aluminoborosilicate glass fibers under tensile and torsional loading [ACS PAPER 1-G-65F] 01 p0103 A67-10263

Soviet book on ideal plasticity theory covering basic assumptions, general theorems, Tresca yield condition, etc 11 p1875 A67-24511

Plastic strength of anisotropic rotating disks 13 p2125 A67-27737

Craggs propagating crack model extended to general elastic anisotropy deriving general theory for tensile or shear stress fracture propagation 16 p2770 A67-31291

Superplasticity resulting from high strain rate sensitivity observed in isothermal tension tests on several titanium and zirconium alloys 18 p3064 A67-34083

Fiber orientation and morphology effect on anisotropic tensile behavior of Al-Ni whisker reinforced aluminum, studying solidification rate, etc [ASTM PAPER 3] 18 p3067 A67-34569

PLASTIC COATING

Cyclic extension of elastic fiber with elastic-plastic coating when obeying Tresca yield condition 14 p2341 A67-29060

PLASTIC DEFORMATION**SA CRYSTAL STRUCTURE DEFECT**

Second phase interface influence on work-hardening behavior of aluminum-5 atomic percent silver alloy, examining substructure development and flow stress behavior 01 p0092 A67-10055

Deformation properties of polycrystalline and single crystal specimens of intermetallic compound NiAl studied as function of testing temperature and composition 01 p0092 A67-10059

Mechanical property and structural changes in titanium alloys subjected to high temperature thermomechanical treatment 01 p0095 A67-10641

Creep role in powder metallurgy sintering processes, considering plastic deformation, stresses and material transport mechanism 01 p0096 A67-10692

Plastic deformation including instability of circular membrane subject to hydrostatic pressure, obtaining stress-strain curve 01 p0161 A67-10776

Continuum theory of dislocations for polar elastic materials, each material point having three associated directors 01 p0162 A67-10848

Structural sensitivity of plastic properties of molybdenum alloys produced by electron beam fusion, investigating microstructure, failure in bending tests and grain fragmentation 01 p0101 A67-10936

Crystal orientation of grains during fatigue and plastic deformation analyzed on copper using X-ray diffraction, noting crystal behavior 02 p0254 A67-11467

Plastic zone expansion near circular hole in plate under pure shearing stress 02 p0337 A67-11845

Mg-Nd alloy structure development during plastic deformation at high temperature, noting lattice distortions and recrystallization process 02 p0255 A67-11868

Plastic deformation of indium and indium-thallium alloys, noting change of pure indium lattice to fcc with increase of thallium content 02 p0255 A67-11869

Mechanical properties of high polymer solid in terms of microbehavior as result of deformation and orientation, expressing anisotropic relaxation function as time dependent function 02 p0297 A67-11873

Elastoplastic equilibrium of thin arbitrary shells of revolution with finite deflection comparable to shell thickness 02 p0340 A67-12661

Thermal emf in plastic deformation of copper, considering effects of crystal lattice defects and lattice elastic distortions 02 p0301 A67-12740

Thermodynamics of metal cutting process, assuming plastic deformation accompanied by successive melting and solidification of metal area under deformation 03 p0427 A67-13192

Hardening during plastic deformation of steel samples under compression, deriving

stress-strain state in cutting process 03 p0427 A67-13193

Fibering of oxides by hot deformation in metal matrices of unalloyed columbium or tantalum, preparing composites by powder metallurgy 03 p0441 A67-13273

Beryllium wire reinforced epoxy-plastic composites in mechanical testing under various loadings 03 p0442 A67-13404

Griffith energy criterion and stress-strain environmental criterion for fractures in brittle cracked metallic plate 03 p0523 A67-13467

Plastic yielding effect on stress and deformation of edge notch subject to longitudinal shearing stress 03 p0523 A67-13469

Brittle fracture of Be tube under differential thermal contraction-induced plastic strain 03 p0445 A67-13470

Deformation and diffusion bonding of Al, Ti and stainless steel alloys, discussing surface condition, time, temperature, cold work, heat treatment and intermediate materials 03 p0430 A67-13692

Plastic strains in gas-turbine components under nonuniform cyclic heating, obtaining stress-strain relations 03 p0527 A67-14072

Torsion of infinite hollow cylinder with axially symmetric load, discussing deformations in terms of integral equations 03 p0529 A67-14164

Plastic deformation of isotropic tubular samples of steel, brass, copper and duralumin under complex loading at constant stress rate 03 p0530 A67-14169

Deformations and rupture criteria under cyclic loading using stress-strain diagram 03 p0531 A67-14361

Decay of K-state in Ni-Cr, Ni-Cr-Mo and Fe-Ni-Cr-Mo alloys studied in terms of electric conductivity during plastic deformation 04 p0635 A67-14429

Manson-Coffin relation for low cycle fatigue life derived from considerations of dynamical dislocation processes without specification of crack shape 04 p0707 A67-14512

Elastic-plastic continua with unstable elements obeying normality and convexity relations 04 p0708 A67-14622

Plastic deformation in titanium at low temperatures, noting prevalence of twinning and suitability as construction material in cryogenic technology 04 p0636 A67-14752

Stability of austenite in some Fe-Cr-Ni alloys under low temperature strain 04 p0636 A67-14753

Elastoplastic deformation of cylinder under torque and tensile stress based on stress stabilization in yield zones 04 p0708 A67-14796

Modes effect on plastic buckling of compressed cylindrical shells, considering deformation theory vs incremental theory 04 p0710 A67-14852

Distributions of screw dislocations in finite slab, examining crack extension with and without plasticity 04 p0716 A67-15798

Inelastic buckling of rib-cored orthotropic sandwich cylinders under external hydrostatic pressure, evaluating rigidity factor and Poisson ratio 04 p0719 A67-15936

Plastic deformation and aging effect on kinetics of beta phase decay, dispersion and alpha phase distribution of TC8 by optical and electron microscopy and measurements of hardness and mechanical properties in tension 04 p0640 A67-15976

Strains, slip lines and onset of cracks in thin chromium foils investigated by electron microscopy 04 p0640 A67-15977

Elastoplastic deformation of nonuniformly heated rotating disk determined to verify validity of theory under nonisothermal load 05 p0907 A67-16019

Stress-strain relationships in materials under high rate of torsional loading and torsional plastic wave propagation in long Cu tube 05 p0909 A67-16144

Elastoplastic calculation of turbine disks, considering cyclic plastic deformation 05 p0810 A67-16177

Stressed and deformed state of plastic disk under cyclic loading in variable temperature field, using increments method 05 p0810 A67-16178

Elastoplastic deformation of cylindrical shell under cyclic axisymmetric unsteady temperature field 05 p0912 A67-16182

Statistical dislocation theory of crystal brittle fracture seen as stochastic process with microcrack formation and propagation under plastic deformation 05 p0919 A67-16504

Diffraction grating technique for measuring dynamic plastic strain exceeding 4 percent deformation at high strain rates in variable intensity light source 05 p0920 A67-16824

Inertial force effect on propagation of plastic deformation in specimen under dynamic load 05 p0921 A67-16936

Small plastic deformation theory determination of elastoplastic stressed state of thin walled isotropic incompressible shell of revolution under axisymmetric power loads and nonuniform heating 05 p0922 A67-17177

Thrust chamber life estimation from calculable local heat flux and tube temperatures, using assumptions of elastic strain invariance and isotropic material properties 05 p0874 A67-17226

Fatigue crack growth in metal due to plastic deformation, predicting crack growth coefficient 05 p0924 A67-17333

Parity of components of stress functional in plasticity theory 05 p0925 A67-17477

Annealing temperatures effect on Young modulus, temperature coefficient and crystallographic texture of Fe-Ni-Ti alloys after deformation 05 p0831 A67-17485

Cold plastic deformation, rolling direction and annealing temperature effect on mechanical properties of sheet niobium at room and high temperature 05 p0831 A67-17504

Yield point and strain aging in tantalum, identifying interstitial atom in electron-beam melted tantalum after incremental plastic deformation 06 p1015 A67-17896

Plastic deformation of textured Ti alloy sheet examined, using tension testing along different directions and combined stress loading along principal axes of anisotropy 06 p1016 A67-17900

Plastic strains in thick cylindrical segment under mechanical and thermal loads [AIAA PAPER 67-113] 06 p1102 A67-18309

General solution of two-dimensional nonlinear problems of elastoplasticity using finite element method, piecewise linear load deflection relationship and computational algorithm [AIAA PAPER 67-144] 06 p1104 A67-18457

Plastic deformation under radial load determined, using plasticity equations that take into account Bauschinger effect 06 p1106 A67-18627

Strength of isotropic plates under bending by transverse loads in plastic range 06 p1108 A67-18660

Stress relaxation, creep and uniaxial elongation of polycrystals relationship as part of cumulative plastic deformation processes 06 p1109 A67-18809

Strain rate effects on low endurance fatigue noting constant frequency induced variations 07 p1261 A67-19059

Stability loss in thin walled plastic shell under tensile loading in plane stress conditions 07 p1261 A67-19190

Electron microscope study of plastic deformation mechanism of titanium alloy AT4 and fatigue strain mechanism in coarse grained specimens of alloy T-40 07 p1205 A67-19278

Surface and internal structural formation mechanism of metallic contact from plastic deformation of SAP type alloys under compression 07 p1208 A67-19303

Explosive loading and structural response measurement techniques for predicting large elastic-plastic dynamic and permanent deformations of shells under dynamic loading conditions 07 p1262 A67-19411

Deformation speed effect on structural changes in Ti, noting test results at 600 degrees C 07 p1209 A67-19735

Surface defects effect on mechanical properties of sheet metal under tension and bending, tracking brittle fracture to stress concentrators 07 p1263 A67-19751

Changes in microhardness, elastic modulus and shear orientation at boundary between plastic and plastic deformation in steel under tensile stress 07 p1210 A67-20011

Single niobium crystal deformation, discussing stress-strain curves, slippage, orientation and asymmetry of slip 07 p1211 A67-20164

Temperature dependence of relaxation-type ultrasound attenuation maxima in plastic deformation of molybdenum and niobium single crystals 08 p1367 A67-20419

Plastic deformation of diamonds due to differences in initial defect distribution examined by birefringence, X-ray topography and electron microscopy 08 p1346 A67-20795

Plastic flow peculiarities analysis based on X-ray diffraction effects obtained by deforming single crystal molybdenum of various orientations 08 p1342 A67-20809

Fracture initiation at low stress concentration, noting effect of energetic conditions and independence of plastic zone length from applied stress and defect length 08 p1421 A67-20955

Structural changes and changes in elastic properties of cold rolled Ti and Zr during precrystallization heating 08 p1342 A67-21003

Plane wave generation in metal plates by detonation of contact explosives, developing elastic-plastic deformation theory for finite stress-strain components 08 p1422 A67-21290

Simulation of stress-strain state of metal under elastoplastic deformation, based on models used in polarization-optical techniques, analyzing stresses in high polymers 08 p1423 A67-21330

Plastic strain distributions in polycrystalline austenitic stainless steel and titanium, using photoelastic coating 08 p1343 A67-21333

Plastic deformation and fracture of rotating turbine rotor model 09 p1502 A67-21554

Thermal buckling of prestressed cylindrical shells and rings where expansion coefficient of external layer is smaller [ONERA-TP-422] 09 p1574 A67-21848

Twinning and temperature effect in plastic deformation of titanium 09 p1518 A67-21965

Phenomenological process in thermal fatigue research, equipment, tests and evaluation 09 p1576 A67-22475

Plastic analysis of cylindrical shell deflections noting support against sliding, shell with clamped edges and with longitudinal force and membrane solution 10 p1715 A67-22922

Incremental elastic-plastic analysis of two-dimensional stress system by finite element method 10 p1719 A67-23456

Discrete element method for plastic analysis of complex built-up structures subjected to cyclic loading causing membrane stress and stress reversal 10 p1725 A67-23713

Nonlinear behavior of elastic structural systems, approximating displacement patterns, stress-strain ratios, post buckling behavior, etc 10 p1726 A67-23717

Elastic-plastic analysis showing relationship between tangent modulus and initial strain methods 10 p1726 A67-23718

Power flow formulas for white noise driven vibratory systems, estimating average oscillation amplitude and plastic strain accumulation rate 10 p1731 A67-23841

Temperature, strain rate and purity effects on alpha-titanium deformation yield and flow stresses, ascertaining thermal activation rate controlling mechanism 11 p1807 A67-24567

Dynamic effects on satellite motion of mechanical deformations in stabilizing system, deriving equations for rotational motion about center of inertia 11 p1870 A67-24674

Plastic zone about circular hole in infinite plate under uniform hydrostatic tension 11 p1879 A67-24887

Localized instantaneous plane heat sources position and strength determined using inert thermometers and time integrals of observed temperature transient 11 p1883 A67-24901

Nonuniform elastic unloading wave propagation into perfectly plastically deformed region, obtaining solution of displacement field 11 p1879 A67-24941

Strain hardening and softening of metals produced by cycles of plastic deformation explained in terms of Bauschinger effect 12 p2015 A67-25419

Elastic-plastic deformation around circular hole in plate under cyclic loading, recording strain distributions, development of plastic zone, etc 12 p2016 A67-25423

Vlasov engineering theory of equilibrium of shells used to study stress-strain state of

closed circular cylindrical shell loaded by internal pressure 12 p2028 A67-25632

Strengthening of sapphire single crystals by precipitates containing titanium 12 p1987 A67-26190

Material deformation, showing functional dependence of thermodynamic potential on state parameters in theory of plasticity, creep and relaxation 12 p1938 A67-26197

Crystal lattice defects as centers promoting dislocations during plastic deformation of ionic crystals 13 p2175 A67-26448

Dynamic and physical testing of metals, discussing yield point, plastic deformation and oscillation damping characteristics 13 p2215 A67-26452

Plastic deformation effect on resistivity and Hall effect of copper-palladium and gold-palladium alloys 13 p2133 A67-27005

Beryllium and other hexagonal metals mechanical properties compared under neutron irradiation, elucidating causes of beryllium embrittlement 13 p2135 A67-27102

Plastic deformation mechanisms of polycrystalline beryllium to analyze temperature dependence of critical shear in prismatic plane 13 p2138 A67-27121

Alloying elements effect on austenite hardening of high-nickel-content chromium-nickel steels during cold plastic deformation 13 p2142 A67-27285

X-ray analysis of size reduction of coherent scattering regions of metal deformed in ultrasonic field 13 p2124 A67-27627

Plastic strength of anisotropic rotating disks 13 p2125 A67-27737

Dynamic plastic buckling of thin strips, thin and moderately thick cylindrical shells and rods under longitudinal and radial impact and compression 14 p2397 A67-28088

Reciprocal theorem applied to linear and angular displacements due to creep or plastic strains in inelastic bodies 14 p2398 A67-28097

Plastic buckling of eccentrically stiffened circular cylindrical shells 14 p2399 A67-28121

Molybdenum polycrystal plastic strain rate in pre-yield region studied by successive stress relaxation method for dislocation density and mobility characteristics 14 p2337 A67-28230

Circular tube cross-sectional ovality in plastic bending 14 p2401 A67-28655

Iterative procedures for elastic, plastic and creep deformation of beams 14 p2339 A67-29003

Stress vs strain curves and slip systems in compression and tension of niobium single crystals 14 p2339 A67-29030

Effect of plastic deformation under compression on superconducting properties of Re single crystals 14 p2375 A67-29069

Classification of combined loadings in plasticity theory 15 p2576 A67-30146

Stress space theory and application to fatigue fracture theory, noting geometrical formulations for deformation and stress of body 16 p2768 A67-31277

Plastic accommodation in Mg O idealized as linear array of continuously distributed edge dislocations to study crack nucleation 16 p2775 A67-31326

High speed plastic deformation of bar studying relation of breaking strain vs tensile velocity and comparing values of former to static case 16 p2775 A67-31329

Metal-to-metal seal for separable joints /Bobbin seal/ utilizing elastic and plastic responses of seal structure and interface 17 p2864 A67-31993

Extension of plastic zone in direction of path of moving brittle crack, studying properties of plastic zone to crack length ratio 17 p2960 A67-32633

Etch pitting analysis of slips in Fe-Si bicrystals under plastic strains, noting effect of impingement of pure edge and pure screw slip bands 17 p2872 A67-32738

Evaluation of plasticity, durability and impact ductility of nonbrittle austenitic steel during high and low temperatures 17 p2873 A67-32767

Axisymmetric plastic buckling of axially compressed cylindrical shells initiated under increasing load 17 p2961 A67-32776

Hexagonal cobalt single crystals plastic deformation, determining stress, free enthalpy and volume activation, temperature and strain rate 17 p2873 A67-32815

Mass, momentum and energy conservation at wave fronts in coupled thermoplasticity, noting propagation velocities for isothermal/adiabatic discontinuities 17 p2964 A67-33134

Shell theory applied to anisotropy problem in axisymmetric cylindrical shells, illustrating shear deformation, twisting couple and circumferential displacement [ASME PAPER 67-APM-28] 17 p2965 A67-33155

Elastic-plastic rods theory using thermodynamical restrictions, examining straight rod motions 17 p2966 A67-33348

Plane plastic strain problem analyzed assuming absence of time effects and of intermediate principal stress 18 p3140 A67-33656

High-elongation foil strain gauges evaluation for measuring cyclic plastic strains, determining Poisson ratio 18 p3142 A67-33890

Plastic deformation of single crystals of vanadium by bending and compressing at 298 and 77 degrees K showed etching but no evidence of mechanical twinning 18 p3101 A67-34077

Flow stress of aluminum related to strain, strain rate and temperature, discussing compression testing machine and results 18 p3064 A67-34078

Strength characteristics of single crystals of nickel aluminide /gamma phase/, discussing temperature and orientation dependence of work hardening 18 p3064 A67-34079

Defect interaction and diffusion zone of short gold-silver couples 18 p3064 A67-34081

Spherical shape changes of droplet of viscous substance of high surface tension under variable external force and small deformation 18 p3028 A67-34220

Mechanical property and structural changes in titanium alloys subjected to high temperature thermomechanical treatment 18 p3066 A67-34405

Plastic deformation in titanium at low temperatures, noting prevalence of twinning and suitability as construction material in cryogenic technology 18 p3066 A67-34410

Stability of austenite in some Fe-Cr-Ni alloys under low temperature strain 18 p3066 A67-34411

Accumulated plastic deformation during sequence of isothermal and nonisothermal loading 19 p3242 A67-34887

Small elastic-plastic deformation /caused by internal pressure/ of thin walled tube clamped at one end to rigid support 19 p3341 A67-35715

Surface morphological changes of tantalum single crystals during plastic deformation, studying orientation dependence of yield stress in tension and compression 19 p3245 A67-35727

Thermal fatigue hysteresis loop shape variations for Coffin-type test samples, stressing temperature-cycle effect 19 p3343 A67-35820

Broadening of Debye-Scherrer line profiles and structure recovery studied in cold-worked Ti, Zr and Hf specimens by X-ray analysis 19 p3247 A67-35835

Friction data, elastoplastic deformation and surface geometry of rubbing surfaces 19 p3237 A67-35851

Fringe order estimation of principal stress difference in plastically deformed body shown useful for variable stress rate by calibration test in photorheological stress analysis 20 p3536 A67-36419

Thin walled structure bending in uniform temperature field, calculating stresses, deformations and creep 20 p3536 A67-36446

Critical plastic buckling of compressed spar flanges 20 p3537 A67-36842

High velocity metalworking /HVM/ techniques, applying transient pressure to specific workpiece area 20 p3454 A67-36886

Tungsten-molybdenum alloy heat-resistant properties noting vacuum testing and subjection to plastic deformation, with results related to molybdenum content and temperature 20 p3467 A67-36968

Screw dislocation distribution on intersecting planes using theoretical model to discuss errors 20 p3540 A67-37020

Crystal deformation and uniaxial failure under complex loading due to stress and temperature variations, applying physical state equation 20 p3540 A67-37057

Deformations and residual stresses in polycrystalline microstructures, using photoelastic coating method 20 p3540 A67-37059

Stress field on epitaxial dislocation line in weakly alloyed titanium, calculating energy of phase boundary and contribution of latter to plastic deformation 20 p3467 A67-37117

Hardening during deformation in stoichiometric nickel manganite alloy noting temperature effect, surface characteristics and electric resistance 20 p3467 A67-37118

Statistical dislocation theory of crystal brittle fracture seen as stochastic process with microcrack formation and propagation under plastic deformation 20 p3541 A67-37318

Hardenable thin walled cylindrical metal sample stress-strain state under cyclic thermal load, determining plastic deformation 21 p3716 A67-37910

Book on plasticity theory and application to solidity, discussing inelastic deformation, crystal physics, atomic grid structure mechanics, etc 21 p3718 A67-37966

Cold plastic deformation, rolling direction and annealing temperature effect on mechanical properties of sheet niobium at room and high temperature 21 p3644 A67-38032

Rapid deformation in tubular blank during expansion by pulsed loading studied by high speed motion picture photography 21 p3631 A67-38055

Characteristic method for determining stress field and plastic deformation mechanism during cutting, notching and punching processes 21 p3632 A67-38060

Stress-strain distribution in clamped membrane during stamping, deriving formulas for plastic deformation of metals 21 p3632 A67-38061

Plastic deformation theory applicable range for case of linear anisotropic consolidating medium 21 p3720 A67-38298

Pure plastic bending of sheet and strip at strains exceeding elastic limit analyzed by arbitrary stress-strain diagram 21 p3721 A67-38382

Metal mechanical properties determination during deformation by uniform ultrasonic loading 21 p3722 A67-38450

Book on inelastic shell theory and research covering field equations, viscous and plastic response, viscoelasticity, elastoplastic deformation, limit analysis, steady creep, etc 21 p3722 A67-38531

Plastic deformation of single-crystal Ni-Al investigated for temperature, orientation and strain-rate dependence of tensile flow 21 p3645 A67-38774

Triple layer cylindrical shells stability beyond elastic limit studied based on plastic deformations, loading principle and shallow shell theory 21 p3727 A67-38838

Plasticity stress-strain approximation for initial elastic behavior and incompressible state approach 21 p3728 A67-38880

Plastic deformation during metal cutting, deriving metal deformation, cutting tool stressed state and temperature as function of particle trajectories 21 p3637 A67-38923

Critical parameters of plane problem of transition of fluid into suspension, ignoring deformation of body up to point of limiting equilibrium 22 p3916 A67-39392

Kolter theorem generalized for examining unstable temperature field cyclic effects concerning progressive failure in elastoplastic bodies 22 p3910 A67-39453

Initial tension and compression effects on fatigue strength of aluminum alloy structures during plastic cold working 22 p3911 A67-39549

Structural sensitivity of plastic properties of molybdenum alloys produced by electron beam fusion, investigating microstructure, failure in bending tests and grain fragmentation 22 p3820 A67-39790

Metal projectiles plastic deformation impacting on rigid targets defined, obtaining computer code through direct analysis 22 p3914 A67-40182

Permanent deformation and interaction effects of rigid plastic clamped beam with constraints against axial displacements and subjected to transverse impulsive loading 23 p4072 A67-40606

Strain rate sensitivity and bending extension interaction in one degree of freedom deformation of clamped beam, considering vibration and load

duration 23 p4072 A67-40607
Permanent deformation of clamped plastic beam with central mass concentration subject to impulse 23 p4072 A67-40608
loading 23 p4072 A67-40608
Stress interaction in cumulative fatigue damage studied to predict remaining life of machine structures 23 p4074 A67-40650
Metal creep behavior under step function stress application including elastic and plastic deformation 23 p4018 A67-40717
Cleavage, plastic, creep, fatigue and other types of fracture noting initiation, propagation, mode, behavior, microstructure and appearance 23 p4019 A67-41033
Dislocation of aluminum during creep investigated for change in block structure 23 p4020 A67-41301
Positive effect of Zr on nickel plasticity, showing elimination of hot brittleness within wide range of 23 p4020 A67-41301
temperatures 24 p4169 A67-41922
Transmission electron microscopy for microstructure observations at growing fatigue crack tips in aluminum alloys, discussing plastic dislocation morphology and density 24 p4170 A67-41947
Microstructure of SGBF graphite under tensile and compressive stresses noting crack generation in layer planes [ACS PAPER 6-N-66F] 24 p4175 A67-42372
Hot working effects in octahedrite parent gamma phase, discussing spinel twinning and polycrystal assembly of gamma phase before kamacite precipitation 24 p4232 A67-42609
Dewrinkling and diffusion mass transport mechanisms in high temperature tensile and shear plastic deformation of pyrolytic carbons [JPL-TR-32-1137] 24 p4177 A67-42711
PLASTIC FILM
Optical incremental shaft resolver using plastic radial gratings 08 p1331 A67-20864
UV radiation effect on mechanical characteristics of polyethylene terephthalate film in vacuum and atmospheric pressure 13 p2184 A67-27624
Dielectric materials characteristics analysis to obtain flexible circuitry performance and selection factors, especially for flat cable [ASME PAPER 67-DE-52] 14 p2341 A67-28882
Solar radiation-balance measuring device using polyethylene film to give protection from wind effects 19 p3227 A67-34855
Slough characteristics measuring methods for clean packaging materials, considering Taber-Abraser, tumble-box and reciprocating-stylus method 23 p3986 A67-40847
PLASTIC FLOW
Plastic flow of axially symmetric notched bars pulled in tension, obtaining load factors 01 p0159 A67-10401
Solution of boundary value problems describing two-dimensional flow in plastic regions 01 p0165 A67-11304
Elastic-plastic solution for circular rigid inclusion in unidirectionally stressed flat plate of linearly strain-hardening material 02 p0336 A67-11633
Fiber strengthening theory, taking into account stress transfer between matrix and fiber in both elastic and plastic regions 03 p0449 A67-13257
Plastic behavior of simple solids in terms of atomistic processes, emphasizing high strength and ductility 03 p0442 A67-13303
Environmental effects on mechanical behavior of metals in vacuum and gases normally found in atmosphere, considering surface oxide layer 04 p0638 A67-14986
Flow characteristics of Fe single crystals and behavior of 04 p0640 A67-15793
imperfactions 04 p0640 A67-15793
Optimal plastic design of minimum cost structural beams with failure under given loads [ASME PAPER 66-WA/APM-22] 04 p0718 A67-15927
Differential equation derivation for creep analysis using plastic interaction curve and associated flow rule 05 p0917 A67-16299
Ultrahigh vacuum effects on flow and fracture behavior of 06 p1016 A67-17897
molybdenum 06 p1016 A67-17897
Plastic flow effects on MHD Couette flow in annular gap between two coaxial cylinders in radial magnetic field 06 p1044 A67-18680
Book on strength of materials covering energy density, plastic flow deformations,

friction heating and fracture mechanisms 08 p1414 A67-20307
Plastic flow peculiarities analysis based on X-ray diffraction effects obtained by deforming single crystal molybdenum of various orientations 08 p1342 A67-20809
Static and kinematic indeterminate states in three-dimensional plastic flow analyzed by replacing Haar-Karman yield conditions 10 p1716 A67-22932
Independent linearized solutions closely approximating Mises and Tresca /M-T/ limit loads in linear theory of plasticity for plane strain 10 p1718 A67-22933
Plastic flow and instability behavior of thin walled tubes of nickel-chrome steel subjected to constant ratio tensile stress 10 p1719 A67-23485
Rolling contact failure modes classification including wear, plastic flow, fatigue and bulk failure [ASLE PREPRINT 67AM 1C-3] 14 p2325 A67-28784
Analytic solution for finite radial expansion and consecutive unloading of circular hole in infinite elastic-plastic plate of initially varying thickness 17 p2966 A67-33347
Turbodynamo disk stress-strain state, with final deformations under unsteady operational conditions, noting plastic flow, continuity, tension, and disk equilibrium equations 19 p3234 A67-34880
Stream functions correctness for pressurized metals plastic flow by analyzing streamlines of various materials 21 p3637 A67-38926
Homogeneous isotropic elastoplastic thin flat plate under uniform unidirectional stress, studying plastic flow, fracture, distortion and slip plane inclination 22 p3915 A67-40220
Pressure sintered GaSb-GaAs alloys investigated for densification and thermoelectric properties 24 p4204 A67-42346
PLASTIC MATERIAL
Stress functional properties of plastic materials, discussing analyticity and continuity in terms of tensor analysis 02 p0336 A67-11630
Single crystal whisker composite methodology in plastics, metals and ceramics, emphasizing alignment and handling problems 03 p0453 A67-13410
Fiber reinforced metals 03 p0456 A67-13893
Load carrying capacity of thin plates of rigid perfectly plastic material with different tensile and compressive yield strength, using method of limit analysis 03 p0531 A67-14366
Nondestructive testing by oscillatory methods of viscoelastic properties of high molecular weight polymers as functions of frequency and temperature 04 p0641 A67-14587
Hypervelocity impact of polythene projectiles on seminfinitesimal aluminum targets at various obliquity angles, using RARDE gas launcher 04 p0710 A67-15003
Cryogenic temperature resistant plastics in space program, discussing insulation, adhesives, seals, gaskets and expulsion of cryogenic propellant in zero gravity environment [SAE PAPER 660638] 04 p0642 A67-15788
Thermoplasticity theory of hardening plastic material under nonuniform heating applied to various trajectories 05 p0911 A67-16175
Elastoplastic deformation of circular cylindrical shells of ideally plastic incompressible material under uniform supercritical hydrostatic pressure 05 p0922 A67-17176
Cosmic ray nuclei observed from satellites and balloons by nuclear emulsions in stacks of plastic sheets 06 p1076 A67-17641
Analytical solution, based on stress functions, for deflection of plastics sandwich beam under bending loads at center, agreeing with experimental results for short duration loading 09 p1579 A67-22812
Combining two or more nonmetallic substances noting applications of fiber reinforced, particulate filled and laminated composites 10 p1671 A67-23013
H-film /Kapton/ flexible circuits fabrication problems including tensile strength, pattern misregistration, delamination, embrittlement, etc 10 p1611 A67-23309

Yield surfaces for nonhomogeneous anisotropic shells of revolution under rotationally symmetric conditions of loading and support 10 p1719 A67-23544
Glass-fabric reinforced plastic shells fabrication and full scale structural evaluation 10 p1727 A67-23732
Soviet book on ideal plasticity theory covering basic assumptions, general theorems, Tresca yield condition, etc 11 p1875 A67-24511
Elastic-plastic body and elastic work hardening materials under static loading, using maximum principle for computing procedures 11 p1876 A67-24622
Plastic foam pattern technique for producing vibration and shock fixtures 12 p1949 A67-25687
Plastic molded transistors for hybrid integrated circuits, production and reliability 13 p2077 A67-26651
Thermodynamics of elastic materials using corollary of Clausius-Duhem inequality 13 p2224 A67-27145
Glass reinforced structural design fundamentals, discussing basic properties of filament materials, matrix material and composite materials [ASME PAPER 67-DE-16] 14 p2402 A67-28871
Thermal, mechanical stress and moisture resistance reliability tests of plastic encapsulated transistors 15 p2444 A67-29457
Similarity criteria for plastic behavior of polymers under combined effect of nonuniform temperature field and hydrostatic pressure 15 p2573 A67-29466
Silicones performance in high vacuum, temperature extremes and radiation environments of outer space, noting outgassing effect 15 p2508 A67-29557
Special plastics for low loss microwave transmission devices, describing electrical properties 15 p2508 A67-29930
Photographic spectra of ablating plastics in thermodynamic environments related to species and temperatures in boundary layers [AIAA PAPER 66-132] 15 p2582 A67-30206
Transparent plastic materials for aircraft application, noting glass developments and thermal stress conditions elimination 16 p2694 A67-30980
Creep properties of glass fiber reinforced plastics for long-term bearing structures, noting elastic strain, creep rate, etc 16 p2694 A67-31486
Printed circuit technology development survey showing refining processes and techniques 16 p2841 A67-31622
Fiberglass-reinforced thermoplastic production processes, discussing strength, rigidity, dimensional stability, etc 17 p2875 A67-31931
Dynamic response of rigid-plastic material ring subjected to arbitrarily distributed impulse load 17 p2959 A67-32412
General variational theorem for rigid perfectly plastic materials developed using Hill and Markov maximum plastic work principles, noting possible unified derivation of principles 18 p3143 A67-34006
Structural reinforced plastic composite materials for cryogenic temperature application evaluated noting tensile, compression, shear, flexural and bearing properties [ASTM PAPER 16] 18 p3070 A67-34577
Plastic based bearings, discussing polymer chemistry, use of fillers, incorporation into matrices of various resins, etc 20 p3455 A67-37266
Thermodynamic basis of plasticity, noting loading and unloading stress-strain relations 20 p3541 A67-37283
Hooke law type anisotropic fiberglass reinforced plastic, discussing elastic deformation and brittle fracture, using revised Mises ellipse equation 21 p3649 A67-37907
Crash and ballistic protection flight helmet with greater impact energy dissipating characteristics, noting laminated nylon fabric shell and polystyrene liner 21 p3577 A67-38075
External ear replica for acoustical testing noting sensing element, ear canal and eardrum impedance 21 p3577 A67-38148
Fatigue in fibers and plastics, use of cumulative extension testing and time dependent effects in fatigue tests 22 p3824 A67-39562
Reinforced plastic materials for light

aircraft wing structures, calculating torque strength 22 p3912 A67-39729

Plastics stability - Conference, Washington, D.C., September 1967 22 p3824 A67-39850

High temperature polyimide laminates for radomes and other supersonic aircraft components, discussing index flexural strength, dielectric constant and dissipation factor 22 p3825 A67-39853

Thermally stable polymers, discussing synthesis and testing on pilot plant and laboratory undeveloped stages 22 p3825 A67-39856

Environmental factors effect on stability of high performance polycarbonate 22 p3825 A67-39859

Guarded hot plate technique for measuring thermal conductivity of low conductivity materials at cryogenic temperatures 22 p3802 A67-40290

Bound functionals for limit analysis of plastic solids by variational method, discussing safety factor and sandwich structures 23 p4074 A67-40629

Internal light applied to opaque-faced edge-lighted plastic display panels [SAE PAPER 670196] 24 p4097 A67-41986

Reinforced plastics - Conference, Cleveland, October 1967 24 p4175 A67-42419

PLASTIC PROPELLANT

Raven solid propellant motor for Skylark noting design, ignition and plastic propellants burning properties 22 p3867 A67-39525

PLASTIC TAPE

Boron fiber reinforced epoxy matrix plastic composite for application to aircraft structures 10 p1723 A67-23697

PLASTIC YIELDING

Continuity gauge measurement of crack growth on flat and curved surfaces at cryogenic temperatures 01 p0102 A67-11028

Constant load creep test determination of creep ductility and dimensional instability of nickel at 500 and 525 degrees C 02 p0256 A67-12702

Rate controlling mechanism during yielding and flow of alpha-titanium below 0.4 times melting point 03 p0441 A67-13258

Indium antimonide specimens plastically bent to introduce excess of dislocations, examining dependence of lower yield stress for bending on direction of bend 03 p0498 A67-13870

Minimum weight structural designs for various types of behavior specifications including stiffness, elastic and plastic strength and stability 03 p0531 A67-14365

Biaxial fracture strength of textured titanium alloy for design of liquid fuel tankage 04 p0711 A67-15242

Plastic analysis of rib reinforced cylindrical shells using strain mapping method for Tresca yield conditions [ASME PAPER 66-WA/APM-14] 04 p0713 A67-15406

Structural change effects on plasticity and fracture characteristics on iron alloys with annealing 06 p1017 A67-18227

Dynamics of rigid plastic thin walled shells for short term constant high intensity load 12 p2025 A67-25607

Physical state of material analyzed using non-Riemannian plasticity theory 16 p2768 A67-31278

Plastic yielding near crack tip, noting general solution for deformation and stress distributions for various loads 16 p2769 A67-31288

Monography on plastic axisymmetric collapse of ring stiffened cylindrical shells under external hydrostatic pressure 18 p3140 A67-33432

Thermal fatigue of 18-8 and 13 Cr steels under transient cross-sectional temperature gradients, noting crack mechanics, tensile stresses, plastic strain range, etc 18 p3140 A67-33651

Strain distribution in aluminum filament reinforced metal, investigating matrix plastic behavior and residual stresses, etc [ASTM PAPER 8] 18 p3067 A67-34573

Resistance of ideal crystal studied for plastic yielding and brittle cracking, noting composite materials devised to resist both failures 20 p3469 A67-37248

Yielding behavior of materials and structures examined via one-dimensional models noting stress-strain relations 23 p4072 A67-40605

PLASTICITY**SA ELASTOPLASTICITY****SA VISCOPLASTICITY**

Book on dynamic strength, brittleness, plasticity and ductility of metals 05 p0907 A67-18031

Plasticity of cast molybdenum improved by vacuum-annealing at temperatures from 900 to 1200 degrees C 05 p0832 A67-17511

Hydrogen effect on high temperature plasticity failure and mechanical properties of titanium shown to be similar to that caused by strain 07 p1200 A67-19248

Alloying effect on elastic modulus, strength and plasticity of titanium in temperature range from 196 to 800 degrees 07 p1206 A67-19280

Strength of threaded joints compared under static and dynamic conditions 07 p1190 A67-19353

Active slip volume /active crystal length/ concept in plasticity theory and relation to temperature and strain rate 07 p1232 A67-19636

Spherical plastic shell theory and design methods 07 p1264 A67-20233

Plasticity and creep problems solution using conventional elastic optically active materials 08 p1423 A67-21331

Plasticity correction for single edge cracked specimen in uniaxial tension, estimating axial rigidity 10 p1717 A67-23016

Soviet book on ideal plasticity theory covering basic assumptions, general theorems, Tresca yield condition, etc 11 p1875 A67-24511

Static and kinematic formulation of plastic analysis of structures and duality in linear programming 11 p1876 A67-24623

Cyclic loading of thick tube with creep, plasticity and thermal effects 12 p2016 A67-25424

Rare earth metals effect on Neel temperature and plasticity of recrystallized chromium at 1200 degrees C in vacuum 13 p2131 A67-28450

Plastic behavior of zone refined and prestrained beryllium single crystals 13 p2137 A67-27111

Direct numerical method for finding optimal values of functionals and associated velocity fields in plastic limit analysis 13 p2219 A67-27153

Classification of combined loadings in plasticity theory 15 p2576 A67-30146

Plasticity and brittle fracture conditions combined for stability criteria derivation 18 p3144 A67-34174

Beryllium single crystal plasticity increased due to preprogrammed load 19 p3245 A67-35470

Plastic wave propagation in semilinear bar subjected to axially applied impact stress 20 p3536 A67-36416

Plasticity of cast molybdenum improved by vacuum-annealing at temperatures from 900 to 1200 degrees C 21 p3644 A67-38039

Additive elements studied for influence on morphology, nature and hot plasticity of sulfides in austenitic stainless steels 21 p3646 A67-39077

Plastics stability - Conference, Washington, D.C., September 1967 22 p3824 A67-39850

Soviet book on elasticity and plasticity covering perforated plates and shells and elastohereditary media 23 p4077 A67-40748

PLASTOMETER

Flow stress of aluminum related to strain, strain rate and temperature, discussing compression testing machine and results 18 p3064 A67-34078

PLATE

SA ANISOTROPIC PLATE

SA ANNULAR PLATE

SA BOILER PLATE

SA CANTILEVER PLATE

SA CIRCULAR PLATE

SA CORRUGATED PLATE

SA DISK

SA ELASTIC PLATE

SA END PLATE

SA FLAT PLATE

SA GOLD PLATE

SA METAL PLATE

SA ORTHOTROPIC PLATE

SA PARALLEL PLATE

SA PERFORATED PLATE

SA POROUS PLATE

SA RECTANGULAR PLATE**SA REINFORCED PLATE****SA SANDWICH PLATE****SA THIN PLATE**

Friction stress and flow rate for rarefied constant density gas flow past semilinear plate treated by approximate diffusion model 05 p0792 A67-16995

Vibratory energy dissipation of plates with riveted beams as induced by gas-pumping in structural joints 05 p0924 A67-17285

Boundary layer suction in two-component fluid flow around plate solved by method of partial averaging 06 p0985 A67-18204

Compression and tension of rod and plate with distribution of residual stresses such that deformation is partially plastic and elastic 06 p1107 A67-18633

Quasi-stationary regime during radiative-convective heating of infinite plate and cylinder, noting time dependent temperature variation 10 p1732 A67-23020

PLATE THEORY

Mechanics Conference, Ukrainian Academy of Sciences, Institute of Mechanics, Kiev, April 1966 01 p0157 A67-10214

Stability and free oscillations of three-layer plates of symmetrical structure with isotropic outer layers and light transversal isotropic filler and weakened by central rectangular cut-outs 01 p0158 A67-10219

Reinforcing round hole in isotropic plate by elastic gasket or thin multicomponent ring consisting of set of homogeneous component rings sweated together 01 p0158 A67-10222

Elastic wave propagation in heterogeneous plates, discussing various plate theories, frequency equations, transverse shear deformations, etc 01 p0160 A67-10407

Asymptotic method of refining classical theory of bending and stretching of plates by construction of two-dimensional equations for processes involved 01 p0163 A67-10996

Buckling tests on uniformly heated thin cylindrical shells, noting load and temperature effects 01 p0163 A67-11013

Stability of rectangular elastic orthotropic plates under distributed and concentrated loads, noting glass fiber reinforced plates 02 p0339 A67-12240

Soviet book on aircraft building and air fleet equipment, Number 6 02 p0339 A67-12436

Plane stressed state in plane contact problem of coupled plates under symmetrical load conditions 02 p0340 A67-12445

Forced periodic vibrations of homogeneous isotropic uniformly thick plate with free edges reduced to Fredholm integral equation 03 p0524 A67-13624

Minimum weight member sizes determination for structural design, considering trussed and stiffened plate structures 03 p0525 A67-13895

Deformation of rectangular slender webplates with boundary stiffeners flexible in plate plane under shear and compression 03 p0525 A67-13896

Elastic axisymmetric deformation of circular two-layer plate with closely spaced rod couplings compliant to radial shear 03 p0527 A67-14070

Torsional constraints in calculation of vibrational frequencies of compressor blade 03 p0528 A67-14081

Boundary bending conditions for anisotropic plates with free, hinged or rigidly clamped edge 03 p0531 A67-14200

Shape of meridian cross section, stressed state and deflection of circular plate of uniform strength loaded symmetrically 04 p0708 A67-14785

Maximum thermoelastic stress and deflection in plate or beam as function of cross sectional shape, temperature and end conditions [ASME PAPER 66-WA/APM-1] 04 p0714 A67-15428

Free and forced vibrations of viscoelastic plate with consideration of rotary inertia and shear deformation, noting rectangular plate 04 p0715 A67-15586

Ritz averaging method to determine free and forced vibratory response of beams and plates undergoing large amplitude steady state harmonic oscillations 04 p0715 A67-15659

Interference conductance between two plates during transient heat

- transfer 04 p0735 A67-15853
- Initial stress influence on frequency of three-dimensional vibrations of plates and rods 04 p0717 A67-15912
- Large elastoplastic deflection of simply supported plate subjected to uniform load, noting steel specimens 04 p0718 A67-15920
- Bending of plates under moment induced and internal stresses 05 p0907 A67-16016
- Elastoplastic deformation of nonuniformly heated rotating disk determined to verify validity of theory under nonisothermal load 05 p0907 A67-16019
- Tensile stress concentration near rhombic hole taking into account physical nonlinearity of aluminum brass 05 p0907 A67-16020
- Finite difference equation for biharmonic equation of plane 05 p0833 A67-16032
- Solution to external biharmonic problem for simply connected region bounded by Liapunov curve given in form of Fourier series and applied to elasticity 05 p0908 A67-16041
- Two jointed semilinear plates loaded by concentrated moment or doublet 05 p0914 A67-16217
- Approximate computer method solution to impact problem of elastoplastic wave reflection from flexible plates in resisting medium 05 p0919 A67-16495
- Acoustic field of random pressure pulsations into half-space behind infinite plate with arbitrary number of layers 05 p0846 A67-16708
- Moiré pattern method of determining fringes representing constant curvature of bent plates 05 p0921 A67-16827
- Linear theory of homogeneous anisotropic elastic shells and plates without considering Love-Kirchhoff assumptions 05 p0921 A67-16883
- Lagrange variational equation application to dynamic stability problems of plates in gas flow 05 p0923 A67-17188
- Smooth surface interpolation applied to finite element displacement analysis of rectangular plate 05 p0925 A67-17372
- Stability of elastic plates of arbitrary shape treated approximately 05 p0925 A67-17476
- Sandwich plate stability analysis by linear geometric and physical equations, for rigid and light cores 06 p1099 A67-17585
- Macroscopic brittle fracture theory for structural microheterogeneities effect on maximum macrostresses in plates with hyperbolic notches under tensile loads 06 p1100 A67-17950
- Quasi-steady aerodynamic and von Karman large deflection plate theory equations of nonlinear oscillations of fluttering plate for single mode subsonic and sonic or coupled mode supersonic oscillations [AIAA PAPER 67-13] 06 p1101 A67-18252
- Dynamic characteristics of distributed elastic structures in passive analog simulation, noting plate loading [AIAA PAPER 67-40] 06 p1102 A67-18334
- Finite rectangular plate under load solved by method involving Green function and Fourier sine transform 06 p1105 A67-18579
- Stress concentration in infinite incompressible plate with circular hole under bilateral tension analyzed, using variational method 06 p1107 A67-18634
- Strength of isotropic plates under bending by transverse loads in plastic range 06 p1108 A67-18660
- Buckling stability of compressed plate with transverse deflections, using energy method 06 p1109 A67-18747
- Stability of membrane solution in nonlinear plate and shell theory 07 p1263 A67-20032
- Equilibrium and elastic properties of triangular and parallelogram bending elements for plate and shell networks, discussing transition element and matrix force methods 08 p1417 A67-20553
- Mixed boundary value problem of flexure of elastic plate 08 p1422 A67-21201
- Aerodynamic forces on flexible plate embedded in right half-space undergoing arbitrary temporal and spatial motion 08 p1424 A67-21433
- Large deflection of asymmetrically layered plate, using parametric expansion techniques to extract system of differential equations governing scaling of stresses and displacement component for boundary conditions 09 p1574 A67-21756
- Deflection and bending moment coefficient for clamped skew plate under uniform pressure obtained, using double series satisfying boundary conditions for differential equation 09 p1575 A67-22165
- Sandwich plate problem involving subtraction to concentrated force of plate having filler flexural rigidity only, giving solution in form similar to that of thin isotropic plate 10 p1718 A67-22937
- Sandwich plate problem involving plate having filler flexibility only, giving solution via reciprocity theorem based on Rayleigh-Green equality in thin plate 10 p1718 A67-22938
- General instability and face wrinkling of sandwich plates with ideally orthotropic cores, deriving equations and boundary conditions [AIAA PAPER 66-138] 10 p1717 A67-23126
- Torsional stiffness of ribs effect on buckling strength of longitudinally stiffened plates compressed in direction of ribs 10 p1719 A67-23474
- Oscillations of plate in plane treated by finite difference method 10 p1721 A67-23645
- Supersonic motion of plate in two-component medium in two dimensions 10 p1628 A67-23647
- Exact solution of transverse shear deformation effect on axisymmetric large deflection of circular sandwich plates for different loading states and boundary conditions 10 p1728 A67-23762
- Computer program for solving bending of plates of any shape and with any variation in boundary conditions for static loading and transverse vibration 10 p1731 A67-23843
- Constrained layer damping mechanism for optimum performance of plates, beams and tubular structures, using viscoelastic material [ASME PAPER 67-VIBR-26] 11 p1872 A67-24184
- Linearization of hyperbolic equation for data analysis of stability of elastic column and plate structures, determining critical load 11 p1874 A67-24224
- Free oscillations of plates, strips, rods and cylinders subjected to arbitrary dynamic edge load 11 p1874 A67-24314
- Kantorovich method applied to approximate solution of nonlinear problems of heat conductivity theory of plate 11 p1883 A67-24323
- Acoustic field of random pressure pulsations into half-space behind infinite plate with arbitrary number of layers 11 p1820 A67-24930
- Stressed and strained state of infinite plate lying on elastic base weakened by finite number of arbitrarily located circular holes 11 p1879 A67-25053
- Flexural vibrations of plates studied by moiré method for nodes, antinodes, local amplitude and phase 12 p1966 A67-25293
- Theory of shells and plates - Conference, Baku, Azerbaidzhan SSR, September 1966 12 p2017 A67-25561
- Equivalent reinforcement and contour of symmetrically shaped hole corresponding to plate subjected to bilateral tension 12 p2019 A67-25564
- Wiener-Hopf and Aleksandrov methods solve plane and axisymmetric problems of equilibrium longitudinal cracks in thin plates with edges free of stresses 12 p2019 A67-25565
- Vlasov variational method application to stressed state of flexible plates and shells, linearizing partial differential equations by successive loadings 12 p2020 A67-25570
- Bending of three-layer plate freely supported along four edges in presence of variable surface heating 12 p2022 A67-25588
- Discrete analysis in plate and shell theory based on method of constructing difference equation, using strain energy of system 12 p2023 A67-25591
- Approximate solution of creep and relaxation problem for plates and shells subject to bending moments and tensile forces 12 p2025 A67-25610
- Plate bending by Reissner method and asymptotic method 12 p2026 A67-25616
- Geometrically nonlinear theory of elastic stability of anisotropic shells and linear stability of orthotropic plates, using differential equations 12 p2028 A67-25628
- Compression load stability of nonuniformly rigid plates within and beyond elasticity limits solved by combined Galerkin and finite difference methods 12 p2031 A67-25961
- Parametric self-excited vibrations of plates of finite length in plane supersonic flow, applying linearized potential flow theory, deriving frequency equations 13 p2218 A67-26804
- Stability of elastically clamped annular plate for nonuniform stress field 13 p2218 A67-26889
- Stability of nonlinearly elastic thin rectangular plates subject to compression 13 p2218 A67-26901
- Resistance and heat transfer of plate situated in turbulent MHD boundary layer in compressible fluid 13 p2169 A67-27312
- Deflection limits on plate-twisting test 14 p2399 A67-28102
- Infinite plate temperature field determined by approximate method when heat transfer coefficient is time dependent 14 p2407 A67-28647
- General method based on reciprocity theorem developed for problem solutions in elasticity theory 14 p2402 A67-28740
- Lateral heating and sublimation of arbitrary thick two-layer plate using thermal flux time-dependent on plate surface 14 p2408 A67-28802
- Thermal stresses in isotropic plate analyzed using Hankel transform, obtaining surface temperature for various cases 14 p2402 A67-28813
- Static deflection of parallelogram plates with clamped edges subjected to uniformly distributed pressure studied by energy method 15 p2573 A67-29312
- Linear theory of elastic Cosserat plate, noting bending theory which corresponds to bending of transversely isotropic three-dimensional plate 15 p2510 A67-29630
- Stability boundaries and critical frequencies for semilinearly elastically restrained plate determined at different boundary stiffnesses 15 p2575 A67-29858
- Unbounded laminar plate oscillations in bilateral potential ideal gas flow with uniform physical and mechanical parameters 15 p2575 A67-30009
- Refined plate bending theory taking into account edge effect 16 p2765 A67-31050
- Stress-strain state determination of nonlinear plate with circular holes, deriving boundary conditions and basic equations 16 p2766 A67-31147
- Transient plane wave magnetic field attenuation through semilinear plate using simplified Laplace transfer function, noting infinite product form for LPTF 16 p2626 A67-31349
- Buckling of compressed thin walled structural sections, noting design concepts and flat plate theories 17 p2957 A67-32025
- Shear buckling of thin walled structural sections, noting reinforcement methods including use of swedges 17 p2957 A67-32026
- Free convection oscillatory flow from horizontal plate having periodic temperature variations analyzed for LF and HF ranges 17 p2969 A67-32445
- Conducting plate backscatter minimization method by load adjusting of loop in front of plate, noting experimental verification 17 p2815 A67-32622
- Rectangular network analysis of displacement in disks and plates, developing differential equations and giving minimum conditions for potential energy 17 p2961 A67-32714
- Stress analysis of semilinear plate containing reinforced notch on one side under uniform tension 17 p2961 A67-32777
- Elastic plates linear theories for micropolar and director displacements, deriving plate equations by asymptotic expansion method 17 p2966 A67-33349
- Natural frequencies of vibration of supported sandwich plate [SESA PAPER 1175] 18 p3143 A67-33901
- Stress concentration in plates having average-depth cuts on both sides, determining applicability of infinitely shallow and deep cuts formulas 19 p3339 A67-34886
- Nonlinear approximation of thin elastic plane plates noting influence of elastic medium and strain tensor deformations 20 p3535 A67-36279
- Critical plastic buckling of compressed

spar flanges 20 p3537 A67-36642
Differential equations for stressed thin orthotropic plates of variable thickness derived and solved in cylindrical coordinates 20 p3539 A67-36919
Elastic and dynamic response of viscoelastic plate with finite thickness to rigid body impact 20 p3539 A67-36920
Unbounded laminar plate oscillations in bilateral potential ideal gas flow with uniform physical and mechanical parameters 20 p3542 A67-37539
Transverse deflection of rectangular plate with bitrapezoidal cross section subjected to uniform longitudinal curvature, comparing theory with experiment 21 p3722 A67-38436
Calculation method for mono-, two- and three-spar wings including membranes and plate, discussing stress formulas 21 p3722 A67-38525
Strain energy method for analyzing large deflections of trapezoidal plates with constant thickness and rigidly clamped edges under uniformly distributed load 21 p3725 A67-38794
Quasi-steady aerodynamic and von Karman large deflection plate theory equations of nonlinear oscillations of fluttering plate for single mode subsonic and sonic or coupled mode supersonic oscillations [AIAA PAPER 67-13] 21 p3727 A67-38870
Thin plate idealization to Hrennikoff lattice model framework for linear stiffness method analysis 21 p3728 A67-38877
Discrete method extension for bending stability problem in sectorial plates, obtaining algorithm for solutions of boundary conditions and external loads 21 p3729 A67-38907
Stress distribution on boundaries of two unequal circular holes in infinite plate determined by mapping region conformally onto annulus 21 p3730 A67-39086
Plate stability loss criterion for critical external load values without determining initial stresses applied to rectangular plate Sommerfeld problem 22 p3909 A67-39401
Rectangular plate with clamped edges studied for nonlinear cylindrical bending under uniform pressure 22 p3910 A67-39480
Viscoelastic behavior of laminated orthotropic plates, discussing single layer or homogeneous orthotropic viscoelastic plate problem 22 p3914 A67-40108
Thin circular elastic plate under uniform compressive thrust, with nonlinear boundary value problems involving partial differential equations for buckled states 22 p3916 A67-40525
Approximation method for finite element bending analysis of variable structural plates, giving linear equations defining nodal values 23 p4073 A67-40627
Thin plate strong bending generalized and smooth solutions existence 23 p4076 A67-40716
Shear modulus measurements in fiber-reinforced composites by plate-twisting test and torsion tube in terms of classical laminated plate and shell theory 23 p4021 A67-40738
Singular solutions for bending stresses in loaded infinite three-layer plate 23 p4079 A67-41415
Curved plate postbuckling behavior, deriving curved plate effective width formula 23 p4080 A67-41475
Curved plates tested under axial compression to prove curved plate buckling and postbuckling behavior formula, discussing stress distribution measurement 23 p4080 A67-41476
Optimal reinforcements of cuts in stressed plates, considering displacements and conditions in discrete points of contact contour 24 p4249 A67-42105

PLATELET
SA BLOOD GROUP
Coherent and noncoherent light emission in II-VI compounds, potential for laser applications in spectral region from 3200 to 7772 angstroms 11 p1801 A67-24735
CW operation of ultrathin CdSe platelet laser excited optically by HeNe laser 15 p2500 A67-29821
CdS single crystal platelet growing and treating technique, relating fluorescence emissions to growth conditions 22 p3778 A67-39359
In-plane and out-of-plane ferromagnetic resonance line widths in Ni single crystal

platelets noting cubic crystalline anisotropy at 25.92 GHz 22 p3864 A67-40245

PLATFORM
SA FLYING PLATFORM
SA INERTIAL PLATFORM
SA STABILIZED PLATFORM
Platform with six degrees of freedom for flight simulation in pilot training 09 p1483 A67-21555
Peripheral jet air cushion vehicle circular platform design, discussing dimensionless design parameter determination from operating height, translational speed and weight 22 p3745 A67-39726

PLATING
SA ELECTROPLATING
SA FINISH
SA FLAME PLATING
SA FLAME SPRAYING
SA NICKEL PLATING
Metallizing and plating techniques for printed circuit fabrication 08 p1334 A67-20744

PLATINUM
Surface roughness effect on spectral and total emittance of platinum, noting spatial distribution of polarized components [AIAA PAPER 67-320] 12 p1957 A67-26035
Linear bridge for use with platinum resistance temperature sensors 18 p3052 A67-34511

PLATINUM ALLOY
Activity of oxygen in liquid Fe-Pt alloy system, determining temperature and composition effect on equilibrium constant 02 p0256 A67-12708

PLATINUM COMPOUND
Semiconducting properties of platinum arsenide with pyrite-type crystal structure 03 p0488 A67-12926
Voltage fluctuations on Pt filament probes attributed to pressure variations 09 p1490 A67-22576

PLENUM CHAMBER
Gimballed jet engine development, noting application to V/STOL aircraft and design of plenum chamber burning engine 03 p0503 A67-13008
Perforated plenum technique for direct forced air cooling of electronic equipment inside rack enclosure 08 p1303 A67-21061
Book on analysis and design of pneumatic systems covering nozzle flow, transfer functions, root locus, plenum chambers, servoactuator, etc 18 p2988 A67-33754

PLOTTER
SA X-Y PLOTTER
Digital computer driven display system of electronic data and semiautomatic film plotters for rapid evaluation of aircraft carrier landing parameters 07 p1164 A67-19623
Computer graphic aids with applications of graph plotters, trace analyzers, cathode ray tubes, light pens, etc 13 p2073 A67-27188

PLOTTING
Automatic plotting of cloud information map on Setun digital computer from Tiros meteorological satellite data 04 p0652 A67-15471
Automatic carpet plotting applicability to reduction of wind tunnel data 08 p1278 A67-21530
Atmospheric trajectories of faint telescopic meteors observed by separate stations simultaneously and probability of plotting 16 p2751 A67-31461
Approximation method for plotting function of three independent variables 17 p2821 A67-32866
Distribution asteroids in space studied by computer analysis from selected plots of orbital elements 20 p3524 A67-36654
Three-dimensional surface projection method by computer plotting program applicable to surfaces with large amount of detail 24 p4125 A67-42430

PLOTTING INSTRUMENT
Plotting oriented graph of two-stage electronic circuit with cathode coupling 02 p0224 A67-11915
Correct method for affine transformation of model in processing of superwide angle photographs on autoradiograph 09 p1496 A67-21750
Circuit for plotting extremal values of cycle during analog computer simulation 23 p3976 A67-41339
Oscillating circuits with nonlinear active elements amplitude and phase frequency characteristics graphically plotted, noting effects on frequency

devices 24 p4136 A67-42191

PLUG
Plug contact configurations and characteristics 04 p0580 A67-14589

PLUME
SA JET PLUME
Convective mechanism in clear air, examining isolated plume by new model which differs from similarity model 04 p0648 A67-14647
Analysis of flame effects on measured electromagnetic propagation data for plume shape, plume electron density distribution and signal attenuation 19 p3344 A67-34819
Shock tube simulation of rocket exhaust plumes and effects on vehicles in space environment 24 p4253 A67-42029

PLUTO /PLANET/
Resonance relation between orbits of Neptune and Pluto established by numerical integration 08 p1381 A67-20392
Mass and density of Pluto estimated from rotational impulse and by comparison with known mass and rotational impulse of another planet 18 p3135 A67-34544

PLUTONIUM
Iodine isotope mass-yield distributions from spontaneous plutonium 242 fission, discussing heavy xenon isotopes from extinct plutonium 244 in meteorites 24 p4191 A67-42450

PLUTONIUM COMPOUND
Galactic and solar nucleosynthesis, determining formation of meteorites on basis of decay of nucleides Pu 244 and I 129 02 p0320 A67-11472

PLUTONIUM 238
High temperature Pu 238 heat source fuel capsule operable in space environment is applicable to thermoelectricity and Brayton cycle, discussing design and test program 24 p4185 A67-42536

PLUTONIUM 239
Pu 239 fueled fast spectrum nuclear reactor spacecraft power supply design for 1 kwe noting cost, control, heat transfer and optimization 24 p4185 A67-42538

PME EFFECT
S PHOTOELECTROMAGNETIC /PEM/ EFFECT

PNEUMATIC CIRCUIT
Single point charger design for A-7A aircraft fluid power accumulators 02 p0182 A67-11843
Pneumatic intermittent-action computers using linear controlled resistance 03 p0375 A67-13598
Pneumatic digital step optimizing device consisting of logic elements of ZPA system for process control 08 p1280 A67-20441
AND and EXCLUSIVE-OR passive elements based on interaction of two or more unbounded jets 08 p1280 A67-20443
Components and design improvement for FM and AM fluidic circuits 08 p1282 A67-20469
Performance of vortex diode, scroll diode and fluid flow rectifier 08 p1283 A67-20473
Pure fluid four bit binary comparator design and construction 08 p1283 A67-20474
Development of pneumatic logical elements and systems 13 p2056 A67-27239
Simulation of dynamic performance of pneumatic rebound-nozzle signal converters by analog computer 13 p2056 A67-27240
Pneumatic intermittent-action computers using linear controlled resistance 14 p2247 A67-27844
Static operating characteristics of diaphragm pneumatic logic device 14 p2275 A67-28347
High speed fluidic logic circuitry for pneumatic stepping motor 14 p2251 A67-28351
Electrical circuits for earth IR radiation emission measurements, describing apparatus and incorporated miniaturized pneumatic receiver 21 p3629 A67-38661

PNEUMATIC CONTROL
Pneumatic oscillator producing triangular waveforms of pressure vs time, using freely floating disk [ASME PAPER 66-WA/AUT-4] 04 p0555 A67-15388
Pneumatic transmission line model for use in fluidic control systems, noting nomographs determining gain-vs-frequency curves 05 p0753 A67-16237
Pneumatic grating for complete measuring system, considering fluidic techniques 08 p1330 A67-20439
Coanda device as pressure maintainer and

as switch or selector 08 p1281 A67-20453
 Optimal design of pneumatic control jet of fluid amplifier to obtain maximum logic gain 08 p1282 A67-20459
 Cartridge-pneumatic dual mode jet engine starter design and function, discussing energy conversion and handling of high pressure gas produced by starter cartridge [ASME PAPER 67-GT-49] 11 p1855 A67-24810
 Dynamic characteristics of pneumatic transmission lines in regulation loops noting parameters effects, calculation methods, etc 13 p2055 A67-26799
 Fluid state trigger logic element and bidirectional counter 16 p2609 A67-31663
 Pulse-length modulated pressure waves having zero quiescent pulse width, actuating floating flapper disk switching valves of pneumatic servomechanism 16 p2609 A67-31665
 Flight control power distribution systems for hypersonic aircraft, considering cooled and pulsating flow hydraulic, liquid metal, pneumatic and mechanical systems 17 p2800 A67-31970
 Plessey constant speed drive/starter /CSDS/ application to BAC 111 commercial transport, discussing dual 17 p2800 A67-31975
 Pneumatic power for attitude control of long-life orbiting satellite, considering parameters, mission objectives, etc 17 p2801 A67-31983
 Static and dynamic sealing concepts and materials for propellant feed systems and pneumatic and hydraulic control systems of liquid propellant rocket engines 17 p2864 A67-31990
 Fluidic breadboard version of rocket engine sequence control, describing pneumatic logic package and general limitations [AIAA PAPER 67-518] 18 p3114 A67-33981
 Feedback control system using pneumatic computing components and vibration isolators for automatic platform tilt stabilization, performance characteristics, etc [AIAA PAPER 67-548] 19 p3208 A67-35946
 Advanced high Mach number aircraft secondary power system requirements, discussing high pressure hydraulic systems and complex pneumatic positioning control systems 22 p3749 A67-40341
PNEUMATIC EQUIPMENT
 Aerodynamic characteristics of pneumatic elements with jet propulsion and Coanda effect 05 p0791 A67-16378
 Fluidic system design and fabrication method 06 p0950 A67-18063
 Fluidic test equipment for measuring rapidly varying fluid parameters and flow visualization 07 p1186 A67-19634
 Inputs and outputs of digital pneumatic jet components design for adaptation to standardized pressure range for use in installations 08 p1281 A67-20448
 Tire hydroplaning, noting lift force on planing surface and pressure distribution 09 p1441 A67-22492
 Pneumatic starting systems for gas turbine engines including energy sources, system components and arrangements [ASME PAPER 67-GT-15] 11 p1854 A67-24800
 Combined multishaker and gas flow tests as part of reliability test program for Saturn V, S-IC pneumatic systems 12 p1923 A67-25706
 Diaphragm element for digital logic requirements of data processing equipment, discussing functions and integrated circuit employed 14 p2274 A67-28346
 Book on analysis and design of pneumatic systems covering nozzle flow, transfer functions, root locus, plenum chambers, servomotor, etc 18 p2988 A67-33754
 Remote control pneumatic pressure test system for Saturn S-IC booster checkout with manual or automatic control, using computer 20 p3415 A67-36569
 Ablative material application to Apollo spacecraft for heat shielding using air injection guns 20 p3454 A67-36590
 Fluidic actuator for direct digital control, converting computer information into mechanical motion 23 p3942 A67-41710
PNEUMATICS
 Book on analysis and design of pneumatic systems covering nozzle flow, transfer functions, root locus, plenum chambers, servomotor, etc 18 p2988 A67-33754

PNEUMOGRAPHY

Miniaturized multichannel multiplexed FM biotelemetry system designed to record physiological condition of pilot and test operational efficiency 14 p2256 A67-28210

POCKEL EFFECT

SHF modulation techniques for laser radiation, covering Faraday, Kerr and Pockel effects, circular dichroism, etc 03 p0436 A67-13138
 Fluorescent emission of neodymium laser triggered by Pockels effect as function of population inversion 03 p0436 A67-13201
 Operation of synchronized neodymium laser time variable reflection /TVR/ oscillator, using single pockels cell to obtain Q-switching and cavity dumping 05 p0826 A67-17525
 Spatial coherence and shape of emission wave front of giant pulse from ruby laser with Pockels cell shutter 18 p3058 A67-33526
 Electric domains in high resistance GaAs single crystals, measuring electric field intensity with Pockels electro-optic effect noting surface state role 22 p3857 A67-39459

POGO

Axial vibration /pogo stick effect/ of Titan II, as Gemini launch vehicle, studied by analog computer simulation for instability influences 14 p2394 A67-28086
 Rubidium vapor magnetometer used for near earth orbiting spacecraft, instrumentation and in-flight performance 20 p3443 A67-36513

POHLHAUSEN SOLUTION

SA LAMINAR BOUNDARY LAYER
 SA VELOCITY DISTRIBUTION
 SA VISCOUS FLOW

Approximate method of treating three-dimensional laminar incompressible boundary layer equations when cross flow is small [ASME PAPER 66-WA/FE-34] 04 p0607 A67-15365

Von Karman-Pohlhausen boundary layer analysis of temperature and velocity profiles in inlet region between two parallel planes with relative motion and pressure gradient 04 p0729 A67-15808

POINCARÉ PROBLEM

Poincaré method applied to moon motion in vicinity of equilibrium configuration, using equations of linear variation 06 p1031 A67-17775

Higher order perturbations of elements in three-body problem determined using methods of Krylov-Bogolubov and Poincaré [AAS PAPER 66-99] 07 p1252 A67-19962

Long period effects in nearly commensurable cases of restricted three-body problem analyzed via Poincaré, isolating secular and critical terms of disturbing function 08 p1381 A67-20389

Nearly commensurable periods in restricted problem of three bodies, calculating long period variations in interior 2/1 case, noting solutions to Poincaré problem 08 p1381 A67-20391

Possible permutations producing cyclic permutations in theorems for component interactions in mechanical systems 14 p2349 A67-28745

Poincaré continuation method using simple pendulum problem, deriving elliptic functions as power series [AIAA PAPER 67-564] 19 p3250 A67-35960

Modified Poincaré method for studying nonlinear oscillations taking into account circumstances causing fictitious degeneration of system 22 p3836 A67-39393

POINT

S CRITICAL POINT
 S FIXED POINT
 S LATTICE POINT
 S MELTING POINT
 S MIRROR POINT
 S SINGULARITY /MATH/
 S STAGNATION POINT
 S TRANSITION POINT
 S YIELD POINT

POINT DEFECT

Metal resistivity change due to multiple point imperfections and lattice distortions, noting aggregate effect estimation from scattering power of isolated defects 05 p0830 A67-17190
 Time lag in thermal coefficient of resistivity of Ge whisker explained in terms of point defect diffusion 06 p1050 A67-18144
 DC resistivity due to electron scattering from vacancy, octahedral and tetrahedral interstitials in beryllium computed by

diffraction model concept of pseudopotentials in metal theory 07 p1209 A67-19643
 Oxygen precipitation consisting of point defects as explanation of structural changes of silicon single crystals during thermal treatment 08 p1370 A67-21205
 Threshold energy of formation and stable defect spatial distribution of silicon irradiated with electrons 15 p2542 A67-30250
 Defects in single crystal foils of compound bismuth telluride caused by irradiation with protons 17 p2921 A67-33050
 Dimensional changes of metals under simultaneous effects of thermal cycling and external load due to surplus point defects directional displacement 19 p3244 A67-34929
 Inhomogeneous elastic medium with nonlocal interaction, considering case of point defects and obtaining Green tensor 20 p3540 A67-37056
 Point defect concentration in GaAs determined from lattice constant 21 p3685 A67-38970
 Linear equations of motion of concentrated defect in elastic medium using variational principle 22 p3909 A67-39292

POINT ERROR

Confidence limits for pointing error of gimbaled sensor relative to off-gimbal reference, detailing sources of error and statistical properties 04 p0620 A67-14872
 Calibration of star tracker bias errors on OAO 17 p2955 A67-32479

POINT MATCHING METHOD

Point boundary value matching method calculation of current distribution in thin linear antenna 02 p0212 A67-11610

Point matching method, solving boundary value problem in uniform cylindrical waveguide with inserted conductor within conducting tube 02 p0193 A67-11781

Point matching solution developed for scattering by conducting bodies of arbitrary shape including circular and square wire loops, plates, spheres and hemispheres 03 p0370 A67-13855

Unidirectional fiber-reinforced composite under axial load, discussing power series along with point matching techniques for solving interface, matrix and filament stresses 20 p3474 A67-37268

POINT SOURCE

Point discharge from multiple points in irregular configuration, space-charge theory and plant discharge applications 01 p0107 A67-10114

Point separation dependence of starting voltages in two-point discharger 01 p0107 A67-10115

Radiation diffusion in gas analyzed by solving transport equation for homogeneous absorbing isotropically scattering spherical shell with point source in center 04 p0695 A67-14656

Detection of X-ray point sources from rocket and satellite experiments applied to astronomy 04 p0698 A67-14886

Average power patterns for various values of rms phase difference for points separated by aperture radius in turbulent atmosphere 09 p1462 A67-21610

Zero Reynolds limit of steady incompressible viscous fluid motion in sphere due to Landau source at center proved to be Stokes flow 09 p1487 A67-21665

Nonparaxial imaging, magnification and aberration properties in holography, examining point source object 09 p1496 A67-21707

Relativistic theory for interaction of electric point charge and magnetic dipole 09 p1580 A67-22549

Decomposition, in orthogonal universal vectors, of electromagnetic universal force created by point charge animated by universal velocity and acceleration 09 p1534 A67-22590

Ray solution for point source in medium with varying propagation constant determined, using Green function for scalar wave equation 11 p1751 A67-23969

Three-dimensional film plane hologram recording of object without external source reference beams 11 p1793 A67-24828

Coherent scattering of solar radiation in uniform isotropic medium containing point source surrounded by cavity 15 p2549 A67-29144

Image analysis by Fourier transformation into incoherent illumination, applied to point

source of light /star/ 16 p2671 A67-30863
 Model for radial and axial structure of geophysical vortices involving Boussinesq boundary-layer equations similarity solution in point heat source 16 p2778 A67-30949
 Point holograms, reconstituting wavefronts from high quality lenses and mirrors and use as optical elements for replacing lenses in optical systems 18 p3048 A67-34194
 Temperature field distribution and heat flux in thin narrow semiminfinite composite plate with moving point source 19 p3347 A67-36051
 Multielement correlation type arrays response to several point sources studied by extending spectral method 20 p3403 A67-37510
 Radio emission point sources fluctuations resulting from interplanetary plasma inhomogeneities observed at meter wavelength 20 p3529 A67-37514
 Electromagnetic point source in presence of planar interface between two anisotropic media, obtaining far fields through Fourier integral and ray optical calculation 20 p3388 A67-37703
 Directional characteristics in optical heterodyne detection processes including finite sources, bandwidth, random phase sources and rough surfaces 23 p4012 A67-40877
 Diffusion flame shape in wake of falling droplet taken as point source of fuel, limiting analysis to Lewis and Prandtl numbers unity 23 p4083 A67-41720
 Coherent scattering of solar radiation in uniform isotropic medium containing point source surrounded by cavity 24 p4222 A67-43067
POINT-TO-POINT COMMUNICATION
 Air traffic control system, discussing effect on business aircraft operations 14 p2347 A67-28317
POISEUILLE FLOW
 Continuum with director and constitutive equations for anisotropic fluids, obtaining solutions for simple shear, Poiseuille and Couette flows 01 p0053 A67-10849
 Stability of plane parallel flows in finite length tube at large Reynolds numbers, noting velocity profile 02 p0233 A67-11949
 Equation for laminar gas meter applied to flow coefficient derived from Hagen-Poiseuille relationship, noting effect of heat transfer, compressibility, etc, on meter performance 03 p0404 A67-13778
 Parallel Couette and Poiseuille flows of multicomponent viscous plasma in presence of pressure gradient and electric field 05 p0854 A67-16894
 Stability of plane Poiseuille flow between elastic boundaries 06 p0984 A67-18044
 Instability of plane Couette-Poiseuille flow of two superposed layers of different viscosities between two horizontal plates 08 p1321 A67-20709
 Plane Poiseuille flow calculations extended to Couette flow between coaxial circular cylinders, plotting flow velocity curves 09 p1490 A67-22595
 Linear stability of symmetrical parabolic flows of various types 13 p2092 A67-26276
 Variational method for linearized problems of rarefied gas dynamics applied to cylindrical Poiseuille flow and heat transfer from sphere, using BGK 13 p2101 A67-26966
 MHD flows in tubes in presence of longitudinal electric current 14 p2361 A67-28743
 Hydrodynamic stabilization of plane Poiseuille flow by modulating pressure gradient 15 p2470 A67-29332
 Electrohydrodynamic flow laminarization with tritium ionizer, obtaining Poiseuille flow stability 17 p2839 A67-32907
 Stability of plane parallel flows in finite length tube at large Reynolds numbers, noting velocity profile 17 p2841 A67-33266
 Behavior of finite-amplitude disturbances periodic in motion direction for plane parallel laminar flows studied, using partial differential equations 19 p3208 A67-35051
 Poiseuille flow of rarefied gases through cylindrical tube, solving integral equation, noting variational calculation of hydrodynamic velocity 21 p3609 A67-37738
 Numerical solution of Poiseuille flow with variable fluid properties, solving coupled momentum and energy equations [ASME PAPER 66-WA/FE-22] 23 p3989 A67-40930

Prandtl limit behavior near zero skin friction, with perturbation methods generalizing Poiseuille and Couette flows 24 p4142 A67-42170
 Three-dimensional disturbance after perturbation of supercritical Poiseuille flow between parallel planes treated by initial value method 24 p4144 A67-42562
 Mass efflux of Poiseuille flow over naturally permeable wall, discussing boundary layer effect 24 p4144 A67-42571
 Velocity profiles of non-Newtonian fluid /polyisobutylene solution/ in helical flow by flow visualization technique, discussing Poiseuille and viscometric flows 24 p4145 A67-42708
POISSONING
 S BERYLLIUM POISONING
 S CARBON TETRACHLORIDE POISONING
 S OXYGEN TOXICITY
POISSON DISTRIBUTION
 Binomial probability distribution applied to air battle analysis, discussing fire doctrines, attrition rates, weapon design classes and limitations of approach [AIAA PAPER 66-781] 01 p0169 A67-10527
 Reciprocal time domain analysis of RC networks, thin film networks and minority carrier devices 08 p1310 A67-20340
 Poisson statistics in distributions of coalescing cloud droplets analyzed using master functions 12 p1963 A67-25343
 Reliability analysis of active, standby and active-standby redundant system, discussing Poisson-binomial probability distribution function 13 p2123 A67-26828
 Sunspot decay and associated flare activity of coming minimum predicted, based on current cycle combined with sunspot lifetime and area 13 p2202 A67-27418
 Reliability statistics for repairable devices, proving Poisson distribution limitations and nonhomogeneous Poisson adequacy for analyzing stochastic processes 15 p2495 A67-30412
 First order generalized planetary theory from Poisson form, deriving trigonometric expansion of disturbing functions, periodic inequalities, etc 18 p3120 A67-33865
 Selection probability from multivariable normal populations in terms of noncentrality parameters 23 p4024 A67-41084
 Statistical significance of mathematical and logical foundations of information processing method applied to meteor stream 23 p4070 A67-41690
 Laser radiation model of superimposed coherent and incoherent radiation, determining statistics of photons 24 p4166 A67-41903
POISSON EQUATION
 Method giving bounds for difference quotients, up to second order, of discrete function 02 p0258 A67-11555
 Simple asymptotic formula for motion of simultaneous electric field and conductivity domains in semiconductors in terms of electrodynamics on basis of Poisson and continuity equations 04 p0877 A67-14936
 Variational analysis of Graetz problem of forced-convective laminar heat transfer in duct, for various cross sections and given wall temperature and temperature gradient 04 p0728 A67-15802
 Langmuir probe analysis when immersed in slightly ionized collision-dominated plasma, computing current-voltage characteristics and Poisson and diffusion equations 05 p0856 A67-17341
 Laws for aircraft control in terrain-following and formation-flight modes of operation, applying solution of Euler-Poisson equation 08 p1351 A67-20700
 Boundary value problem for Poisson-Vlasov equations resulting from interaction of conducting body and supersonic flow of rarefied plasma solved, using iterative method 08 p1363 A67-21368
 Iteration process by difference scheme for numerical solution to Dirichlet problem of two-dimensional Poisson equation 13 p2148 A67-27613
 Numerical solutions of Poisson and motion equations for electron gun design, examining truncation error via perturbation theory 14 p2287 A67-28677
 Computer solution for current density, continuity and Poisson equation to obtain electron density and electrostatic potential

in p-n junction 14 p2290 A67-28931
 Characteristics and mathematical model of junction field effect devices with small length-to-width ratios 15 p2446 A67-29638
 Flute instability for inhomogeneous plasma equilibria in inhomogeneous magnetic fields of mirror machines, solving Vlasov and Poisson equations 16 p2714 A67-30875
 Boundary value problem for electrical potential and ion distribution function obeying Poisson-Vlasov equations when applied to rarefied plasma disturbance by supersonic body 17 p2909 A67-33205
 Dirichlet problem solution for Poisson equation on rectangle with smooth boundary values, using higher order differences 19 p3249 A67-34794
 Higher order differences used in solution of Dirichlet problem for Poisson equation of rectangle 20 p3475 A67-36651
 Parametric excitation of electron plasma frequency derived using Boltzmann and Poisson equations 21 p3687 A67-38415
 Two particle correlation theory for static plasma from Poisson equation theory 22 p3848 A67-39689
 Interpolation of Poisson equation by method adjusting equations to insure existence of discrete solution 23 p4023 A67-40865
POISSON PROCESS
 Integral operators associated with Poisson transforms and operator H_{α} 05 p0835 A67-16733
POISSON RATIO
 SA AIRYS STRESS FUNCTION
 Tensile-instability mechanism concept determination of ultimate strength of most ductile materials under uniaxial or biaxial tension conditions [ASME PAPER 66-WA/MET-15] 04 p0712 A67-15378
 Exact and variational solutions to elastic wave propagation eigenvalue problem in constant Poisson ratio linear viscoelastic material 05 p0909 A67-16141
 Timoshenko beam equations modification necessary to account for normal pressure and Poisson ratio effects for application to thin walled circular tubes 14 p2403 A67-29013
 High-elongation foil strain gauges evaluation for measuring cyclic plastic strains, determining Poisson ratio 18 p3142 A67-33890
 Propagation of elastic waves through composite media studied with ultrasonic pulse technique, noting Poisson ratio, bulk modulus, etc 18 p3069 A67-34488
 Maximum stresses with changes in Poisson ratio for thin parallelogramic panels with nonlinear behavior 22 p3911 A67-39666
POLAND
 Research and facility of Institute of Fluid-Flow Machinery at Gdansk, Poland 06 p0981 A67-18823
 Polish space research noting satellite position observations, geodetic computations, meteorology, cosmic physics, magnetosphere, medicine and biology 19 p3321 A67-35296
POLAR AURORA
 Position of oval zone of polar aurora on earth nocturnal side on magnetically quiet days 02 p0236 A67-11663
 Existence of anomalously close radio reflections from sporadic ionization zone linked with polar aurora 02 p0193 A67-11674
 Rocket launching site in Sweden operated by ESRO for studies of polar auroras and polar cap absorption 03 p0395 A67-13498
 Emission spectra of nitrogen excited by electron beam of 0.1 to 20 keV and oxygen and air bombarded by 13-keV electrons 07 p1225 A67-19099
 Satellite observation of radiation belt and absorption of cosmic noise in polar aurora during magnetic storms of February 1964 07 p1243 A67-19683
 Pitch-angle distribution and differential energy spectrum of polar aurora protons penetrating earth 07 p1173 A67-19700
 Ionization structure of polar auroras from spatial distribution of radar-reflecting zones, taking into account magnetic field variations 07 p1174 A67-19710
 Polar auroras, considering types resulting from MHD wave heating of upper atmosphere, low energy particle penetration of atmosphere, etc 09 p1491 A67-21892
 Diurnal variations in arch azimuths of extended polar auroral formations

determined from diurnal winter observations 10 p1630 A67-22786
 IGY and IQSY auroral observations at Murmansk of frequency of occurrence of polar auroras in years of solar activity maxima and minima 10 p1630 A67-22787
 Polar auroras during minimum of solar activity cycle, winter 1963-64 and 1964-65 10 p1631 A67-22802
 Polar glow aurora, discussing optical emissions generated by solar cosmic ray protons and alpha particles, energy spectrum, atmospheric and ionospheric absorption effect, etc 10 p1637 A67-23190
 Electron and ion densities and temperatures measured by rockets in active auroras and correlated with directly measured ionizing flux 10 p1650 A67-23307
 Catalog of German polar aurora observations from 1882 to 1956 13 p2109 A67-26431
 ESRO I research satellite structural design test results for study of polar ionosphere, particularly auroras 13 p2211 A67-26583
 Polar aurora of September 13, 1957 and geomagnetic activity attributed to extraordinary solar flares 13 p2115 A67-27393
 Polar auroras statistically analyzed for relation between frequency of redness, solar activity and geomagnetic conditions 13 p2116 A67-27394
 Position of oval zone of polar aurora on earth nocturnal side on magnetically quiet days 16 p2665 A67-31078
 Existence of anomalously close radio reflections from sporadic ionization zone linked with polar aurora 16 p2624 A67-31089
 Coherency relation between quasi-periodic X-ray and optical pulsations in auroras 17 p2844 A67-32543
 Soviet book on polar auroras and night airglow 17 p2848 A67-32951
 Auroral belt dynamics including edge displacement rate, width, asymmetry of sides and relation to polar geomagnetic disturbances 17 p2850 A67-33184
 Rocket observations of energy spectra of auroral electrons 18 p3034 A67-33591
 Auroral rocket measurements of electron flux, electron and ion density, electron temperature and auroral brightness 18 p3034 A67-33593
 Simultaneous recording of rocket trajectory and rapid auroral variations using high sensitivity image orthicon TV system 18 p3034 A67-33594
 Electron measurements near weak aurora during rocket flight 18 p3034 A67-33595
 Polar cap auroras frequency patterns relationship to worldwide storms 18 p3037 A67-33611
 Polar auroral substorms, discussing mechanisms for dumping trapped particles 19 p3215 A67-35173
 Classification of main data on morphology and phenomenology of aurorae observed visually and with all-sky cameras during IGY 19 p3224 A67-35495
 Intense negative bays occurring in auroral zone in early evening hours explained by westward extension of polar electrojet 20 p3426 A67-36285
 Instantaneous distribution patterns for aurora on polar region, discussing geoelectric field role in internal structure of magnetosphere 20 p3430 A67-36906
 ULF radiation in polar auroral zone explained via plasma beam instability, assessing perturbation of particle fluxes in magnetosphere 21 p3621 A67-39016
 Intense negative bays occurring inside evening and midnight sectors of auroral zone during polar magnetic substorms 22 p3789 A67-39477
 Diurnal variations in arch azimuths of extended polar auroral formations determined from diurnal winter observations 24 p4149 A67-42122
 IGY and IQSY auroral observations at Murmansk of frequency of occurrence of polar auroras in years of solar activity maxima and minima 24 p4149 A67-42123
 Polar auroras during minimum of solar activity cycle, winter 1963-64 and 1964-65 24 p4150 A67-42139

POLAR CAP

Direct backscatter recordings from polar cap F-layer reflections used to predict communications 01 p0020 A67-10007
 Terrain information from high altitude side-looking radar imagery of Arctic

area 01 p0059 A67-10328
 Carbon dioxide condensation on Martian polar caps 04 p0694 A67-14494
 Ionospheric flux system of initial phase of geomagnetic storm of September 4, 1957 over polar cap 05 p0802 A67-17148
 High dispersion spectrograms of Mars examined for water vapor presence, results indicate amount depends on size of polar cap [JPL-TR-32-1048] 09 p1566 A67-22235
 Martian transient phenomena correlations among mass motion of water in atmosphere, polar cap growth and white cloud appearance frequency 11 p1862 A67-24501
 Riometer observations in polar caps of solar cosmic ray events during IQSY 12 p1993 A67-25228
 Mars polar cap size changes, color and visibility from observations in 1963 17 p2942 A67-32330
 Geomagnetic time and latitude distribution of magnetic disturbances at auroral and polar cap latitudes 18 p3032 A67-33583
 Low latitude neutron fluxes for PCN and quiet solar period, noting solar proton production of neutrons 20 p3519 A67-37406
 Evening sector polar magnetic substorm disturbance field morphology in transition region 21 p3616 A67-37998
 Ionospheric flux system of initial phase of geomagnetic storm of September 4, 1957 over polar cap 21 p3619 A67-38490
 Electron flux and energy spectrum measurements near polar cap investigated for diurnal intensity variations 22 p3872 A67-39802
 Temporal and spatial low energy solar proton intensity variations indicating interplanetary medium changes effects on magnetospheric configuration 22 p3873 A67-39813

POLAR CAP ABSORPTION

Solar flare mechanism, explaining absence of cosmic ray flares and occurrence of PCA events in years of sunspot minimum 03 p0506 A67-13651
 Sunspot cycle coronal Fe XIV 5303 angstrom radiation emission and type IV bursts in solar flares 03 p0507 A67-13811
 Seasonal PCA variations and type IV bursts associated with high energy proton injection into polar ionosphere 03 p0507 A67-13812
 PCA events during 1938-1955 detected from vertical incidence ionospheric soundings at high latitude, identifying some with proton flares 03 p0507 A67-13813
 Solar proton streams apparently synodic in solar rotation interval during maximum epoch of recent solar cycle as indicated by polar cap absorption events 03 p0507 A67-14116
 Recombination coefficient in D region determined by comparing electron density profile with ionization rate 06 p0995 A67-18073
 Quantitative estimation of liquid water content on Mars from thickness of snow blanket on planet polar cap 06 p1084 A67-18187
 Effects of AZA and PCA on radio wave propagation in Antarctic, noting reliability and radiation power requirements 07 p1143 A67-19692
 Radio wave absorption at high latitudes dependent on frequency, noting AZA and PCA are inversely proportional to powers of frequency 07 p1144 A67-19693
 Depression of low energy cosmic ray cut-offs relation to permanent geomagnetic tail using model calculation, explaining PCA midday recovery 07 p1245 A67-19927
 Geomagnetic disturbance and correlation with PCA in auroral zone on February 10, 1958 08 p1329 A67-21539
 Rapid and slow spreading absorption of cosmic rays over polar cap 10 p1699 A67-22790
 Properties of solar cosmic rays causing polar cap absorption measured with satellites 10 p1700 A67-23188
 Polar cap absorption with solar cosmic ray properties from balloons and relation to processes in terrestrial atmosphere 10 p1637 A67-23189
 Energetic solar particle effect on ionosphere, discussing signal phase, amplitude propagation and attenuation 10 p1637 A67-23192
 Polar based riometric observations of solar

cosmic ray events during IQSY 10 p1701 A67-23193
 Chemiluminescent radiation from interaction of nitric oxide with atmospheric ozone for PCA conditions [AFOSR-67-1379] 10 p1702 A67-23345
 Three stages of solar cosmic rays entry into polar cap atmosphere due to differential arrival of solar electrons, protons and alpha particles 11 p1855 A67-23925
 Forbush decreases associated with type IV burst flares, particularly in relation to PCA events, noting delay time and magnetic western boundary 12 p1992 A67-25129
 Solar proton and alpha particles entry into polar cap atmosphere 13 p2194 A67-27252
 Electron number density profiles and polar cap absorption of radio waves time history during weak solar cosmic ray event 14 p2380 A67-28042
 Quantitative estimation of liquid water content on Mars from thickness of snow blanket on planet polar cap 16 p2742 A67-30511
 Negative ion density and composition in lower ionosphere 16 p2665 A67-31019
 Low energy protons emitted by solar flare satellite observed inside and outside of magnetosphere, noting immediate access to polar caps 16 p2740 A67-31626
 Polar cap anomalous absorption effects from ionosphere and geomagnetic field studies, noting correlation with magnetic storms 17 p2846 A67-32936
 Polar cap absorption on July 1966, discussing solar flare, radio outburst, proton intensity, geomagnetic latitude, etc 19 p3313 A67-35214
 Two-ion D region model for polar cap absorption events 20 p3426 A67-36302
 Antarctic riometer observations of PCA event of February 1965 compared with satellite measurements of solar proton flux and spectrum during same event 22 p3872 A67-39803
 Rapid and slow spreading absorption of cosmic rays over polar cap 24 p4209 A67-42126

POLAR COORDINATE

Amplitude variations in earth free and forced polar motion indicate periodic solar activity and moon tidal forces influence 10 p1631 A67-22798
 Polar coordinate analysis of free oscillations of circular plates with loosely clamped edges under large deflections, obtaining Duffing equation 12 p2031 A67-25963
 Structures of solutions and expansion of radial heat equation with pole type data function 13 p2145 A67-26492
 Free vibrations of freely supported toroidal shell, noting elastic motion equations in terms of toroidal coordinates and boundary conditions applicable to polar motion 16 p2775 A67-31423
 Closed form regularized solutions in polar coordinates of two-body problem obtained and applied to restricted three-body problem 17 p2943 A67-32440
 Matrix generalization of polar coordinate transformation to second order matrix differential system 17 p2877 A67-32563
 Stress analysis by polar coordinate system of turbine disks produced in various wound-fiber configuration 19 p3234 A67-34873
 Long term global integrations of primitive meteorological equations for free surface model, using spherical polar coordinates 19 p3252 A67-35058
 Measuring methods for pole displacements and latitude variations, determining Universal Time from instantaneous pole coordinates, plotting polhody diagram 23 p3997 A67-41349
 Latitude variation and motion of instantaneous pole from astronomical stations during IGY, using differential method for coordinate system 23 p3997 A67-41350
 Amplitude variations in earth free and forced polar motion indicate periodic solar activity and moon tidal forces influence 24 p4149 A67-42134

POLAR GAS

Pressure induced monochromatic translational absorption coefficients for homopolar and nonpolar gases and gas mixtures, with application to molecular hydrogen 03 p0515 A67-14323

- Ordinary and dielectric second virial coefficients for dipolar gases calculated by off-center dipole model using series expansion 11 p1821 A67-23962
- Perceptron system for correcting average line position of open loop portion of control system, discussing pole interaction and self-organization 17 p2830 A67-33098
- Field-polar forces interaction effect on viscoelastic properties of polypropylene oxide, measuring dilatometric, modulus and damping constants [JPL-TR-32-1026] 24 p4174 A67-41806
- POLAR IONOSPHERE BEACON**
- S BEACON SATELLITE**
- POLAR METEOROLOGY**
- Fogle theory concerning possible latitudinal shift of noctilucent clouds, using cloud occurrence frequency 10 p1677 A67-23501
- Stratospheric temperatures in north and south polar regions shown to depend on land mass temperatures 15 p2475 A67-29579
- Whistler method detection of magnetospheric electric field associated with polar substorm 17 p2851 A67-33197
- Explorer XXII coherent frequency phase difference data for polar ionospheric integral electron density, discussing diurnal and seasonal variation 22 p3794 A67-40121
- POLAR NAVIGATION**
- Precise pole-to-pole navigation system without use of special grids or transverse computational modes 09 p1526 A67-21830
- POLAR ORBIT**
- Photographic mapping of Martian surface with electrically propelled solar-powered photographic spacecraft placed into near polar orbit [AIAA PAPER 67-88] 06 p1096 A67-18438
- High resolution density data from radar observations of low altitude polar orbiting satellites reveal longitudinal and geomagnetic variation, noting regression analysis 10 p1640 A67-23216
- Low energy proton precipitation measurements in austral and boreal auroral zones, using polar orbiting satellite 12 p1937 A67-25813
- Geomagnetic and gravitational field combined effects on magnetized satellite oscillations in plane of circular and elliptical polar orbits 21 p3713 A67-38590
- POLAR ORBITING GEOPHYSICAL OBSERVATORY /POGO/ S POGO**
- POLAR REGION**
- Quasi-stationary solar corpuscular fluxes, examining effect on atmospheric pressure in earth polar cap regions 01 p0061 A67-11279
- Slit size effect on magnetograph observations of solar magnetic field in near polar regions 06 p1082 A67-18015
- Atmospheric potential gradient near ground in polar region correlation with solar radio emission on 1000 mc 07 p1172 A67-19423
- Critical ionization frequencies in F-2 layer in near-polar region observed at Northern Hemisphere high latitude stations 07 p1179 A67-19832
- Thermal oscillations of polar night stratosphere and upward propagation 10 p1643 A67-23248
- Atmospheric potential gradient relation to solar activity at earth surface in polar region 14 p2306 A67-27884
- Electric current associated with polar magnetic substorms 14 p2313 A67-28573
- Early appearance of active aurora during geomagnetic storm caused by westward traveling surges along expanded oval 14 p2313 A67-28575
- Stratospheric temperatures in north and south polar regions shown to depend on land mass temperatures 15 p2475 A67-29579
- Polar magnetic disturbances accompanied by short period pulsations investigated with magnetogram for negative magnetic bay characteristics 17 p2847 A67-32943
- Winter and summer equivalent current systems of polar solar-diurnal variations studied from observations obtained during IGY 17 p2847 A67-32949
- Space time distribution of magnetic activity during IGY, noting elliptical region about magnetic pole characterized by increased activity 17 p2848 A67-32950
- Curves in polar plot representing auroral arcs over polar region organized in geomagnetic coordinate system and corrected by spherical harmonic terms 17 p2850 A67-33189
- Polar ionosphere by satellite-borne electron traps, measuring electron density, temperature, quasi-energetic electron flux, etc 19 p3215 A67-35174
- POLARIMETER**
- Apparatus for particulate smokes generation, control and sampling, noting combination with angular scanning spectropolarimeter 12 p1946 A67-25982
- Electronic polarimeter applied to Stokes parameter measurement of lunar surface, determining reflected light ellipticity 15 p2552 A67-29147
- Automatic photopolarimeter as pilot model for scans of planetary disks on fly-by missions 15 p2492 A67-30435
- Skylight polarimeter based on sequential detection of light transmitted by polarizers oriented at various angles 18 p3046 A67-33748
- Photoelectric polarimeter for measuring rotational, electro-optical and electrogratational effects and optical activity in ferroelectrics 21 p3631 A67-38969
- Electronic polarimeter applied to Stokes parameter measurement of lunar surface, determining reflected light ellipticity 24 p4239 A67-43070
- POLARIMETRY**
- Visual, photographic and photoelectric methods for comet polarimetry 05 p0890 A67-16334
- Wavelength dependence of polarization of IR star in Cygnus measured by far IR lead sulfide photopolarimeter 11 p1863 A67-24509
- Polarization properties of Mercury explained by surface only, so there is no polarimetric evidence for atmosphere on Mercury 12 p2010 A67-26244
- High time-resolution polarimeter observations of Jupiter decimeter radio bursts 14 p2388 A67-28836
- Polarimetric properties of simulated lunar surface, showing, polarization effect on particle size 16 p2754 A67-31749
- Optical polarimetric observations of quasi-stellar objects 19 p3331 A67-36083
- Earth surface influence on radiation polarimetry in vicinity of radio horizon 20 p3382 A67-36776
- POLARIS MISSILE**
- Functional analysis method application to reliability testing of Polaris missile 01 p0155 A67-11346
- Nondestructive testing /NDT/ developments noting radiography for quality control, ultrasonic, continuous wave, resonance and pulse echo methods and applications to Polaris program 04 p0706 A67-15263
- POLARISCOPE**
- Internally bonded polariscope incorporated into transparent model for three-dimensional photoviscoelastic material studies 03 p0531 A67-14364
- POLARIZABILITY**
- Energy densities of polar and antipolar arrays in barium titanate including nonlinear oxygen polarizability 21 p3683 A67-38406
- Electromagnetic wave focusing in nonlinear medium with small nonlinear polarizability 21 p3670 A67-38684
- POLARIZATION**
- SA CIRCULAR POLARIZATION**
- SA DEPOLARIZER**
- SA DIELECTRIC POLARIZATION**
- SA FERROMAGNETISM**
- SA MAGNETIC DOMAIN**
- SA OPTICAL POLARIZATION**
- SA PYROELECTRICITY**
- Polarization effects during radio wave scattering by cloud and precipitation particles, obtaining phase state from echo signal 01 p0109 A67-11249
- Energy spectra of avalanche electrons in copper, iron, aluminum and graphite determined by method of moments, considering polarization of medium and multiple scattering 02 p0316 A67-12768
- Slow polarization processes of barium titanate in weak field 03 p0497 A67-13702
- Plane electromagnetic wave diffraction at two parallel circular cylinders for TM and TE polarization 03 p0371 A67-13959
- Venus brightness temperature and polarization of integral radio emission at 3.75 cm wavelength 04 p0702 A67-15566
- Book on atmospheric absorption, diffusion and polarization of light and radioelectric radiation 06 p0998 A67-18718
- High altitude balloon-borne polarization measurements relevance in research program of radiation emerging from earth atmosphere 07 p1170 A67-19393
- Crystal symmetry, optical properties and ferroelectric polarization of barium titanate single crystals 07 p1234 A67-20096
- Variational principle for anisotropic and nonhomogeneous elasticity theory in terms of elastic polarization tensor 08 p1422 A67-20981
- Time variation of positional angle of polarization plane of radio sources due to Faraday rotation 08 p1388 A67-20987
- Polarization-optical method for investigation of stresses - All-Union Conference, Leningrad, June 1964 08 p1423 A67-21329
- Interstellar polarization with graphite grains covered with dirty ice mantles matched with entire range of observed interstellar extinction 09 p1569 A67-22439
- Measuring Hall effect in high specific resistance materials by using alternating magnetic field and DC current 10 p1691 A67-23502
- Polarization effects during radio wave scattering by cloud and precipitation particles, obtaining phase state from echo signal 11 p1815 A67-24120
- Spontaneous polarization and electric conductivity in fluorite single crystals doped with lime 12 p1980 A67-25182
- Surface density gradient and collision frequency effects on polarization of microwaves reflected from plasma surface 13 p2164 A67-26300
- Reflection coefficients for electromagnetic waves obliquely incident on sinusoidally stratified half-space 13 p2066 A67-26481
- Anomalous polarization of four cosmic OH lines predicted from states of polarization in OH maser amplifier 13 p2161 A67-27289
- Electron heating by direct discharge during plasmoid interaction involving polarization 16 p2717 A67-31182
- Satellite tracking simultaneous-lobing monopulse receiving system utilizing polarization diversity in coherent and noncoherent operational modes 18 p3020 A67-34110
- Rocket observation of ionospheric electron density using VLF doppler shift formula, determining wave polarization 19 p3215 A67-35180
- Electric field produced by polarization in plasmoid injected across field in closed system 20 p3497 A67-36681
- Bounded plasma flux in magnetic field, considering plasma polarization on magnetic field boundary, noting flux deceleration 20 p3497 A67-36682
- Polarizations of Pc 1 micropulsations intermittently recorded in Alaska with analysis of data for presence of right and left hand waves 22 p3793 A67-40078
- Energy spectra of avalanche electrons in copper, iron, aluminum and graphite determined by method of moments, considering polarization of medium and multiple scattering 22 p3877 A67-40270
- Poynting vectors difference obtained by using convection and polarization current models of moving plasma in Minkowski theory 24 p4124 A67-42812
- POLARIZATION CHARACTERISTICS**
- Combination scattering suffered by component, polarized parallel to electromagnetic wave incident on plasma cylinder, from Tonks-Dattner resonances excited by perpendicular component 01 p0020 A67-10148
- Radar backscatter return interpretation in identifying terrain phenomena and composition 01 p0059 A67-10330
- Null-free antenna radiation pattern shown to contain all axial ratios of elliptical polarization 02 p0211 A67-11598
- Polarization angle of linear feed antenna on polar mounted paraboloid relative to az-el coordinate system 02 p0212 A67-11611
- Electro-optical properties of paraelectric perovskites indicating origin in polarization 02 p0296 A67-11821
- Polarization pattern dependence on phase-amplitude distribution of field at microwave antenna aperture 02 p0214 A67-11905
- Collective excitations influence on polarization operator of superconductor with P-pairing 02 p0301 A67-12734
- Uniform electric field quadrupole

polarizabilities and shielding factors for S-state atoms and ions, demonstrating independence of factors from existence of field gradient 03 p0472 A67-13321

Nonrelativistic energies and mass polarization shifts of excited S states of lithium cation 03 p0472 A67-13323

Anisotropic magnetoplasma diagnostics using transient reflected polarized signals [AFCRL-67-0065] 03 p0371 A67-13865

Automatic recording equipment measuring polarization angle of Syncom III 137 mc/s radio signal and determination of ionospheric total electron content 03 p0415 A67-14110

Early Bird satellite measurement of ionospheric electron content by determining polarization twist of VHF radio signals [RASSA PAPER 1-10-130] 03 p0417 A67-14241

Variable polarization of magnetic star HD 71866 studied by observational program between January and April 1966 04 p0697 A67-14759

Cassegrain feed for 85-ft-diam antenna of planetary radar system noting operative conditions, polarization capabilities and performance data 04 p0596 A67-15048

Depolarization of fully polarized electromagnetic waves, obtaining degree of polarization 04 p0575 A67-15151

Electrostatic polarization of plasma in applied electric field, excluding case for steady current flow 04 p0668 A67-15180

Plasma flux interaction in magnetic multipole field, proving mutual polarization of interacting fluxes by photographic results 04 p0667 A67-15210

Change of polarization state of ray due to multiple internal reflections within many-sided reflectors 04 p0657 A67-15307

Polarization of light scattered from He-Ne laser beam, applying quantum theory to formula for depolarization ratio 04 p0634 A67-15624

Temperature stresses in plane elements by unsteady heat fields examined via polarization optical method 05 p0914 A67-16195

Radar observations of Venus at 3.8 cm noting low value of cross section, echo spectrum, polarization characteristics, absorption cross section and atmospheric attenuation 05 p0889 A67-16298

Combined probability density of axial coefficient and polarization angle of field scattered by target 05 p0784 A67-16905

Nonlinear medium anisotropy and saturation effects on orientation of polarization ellipse of gas laser mode 06 p1010 A67-17823

Polarization characteristics of ionized argon laser in magnetic field 06 p1011 A67-18542

Electromagnetic radiation at satellite-borne sensor, discussing spectral, spatial and temporal distributions of radiation energy intensity 06 p1006 A67-19010

Balloon-UV polarimetry using two different telescope-gondola systems 07 p1184 A67-19395

Control of polarization of radiation field of waveguide-slot antenna 07 p1153 A67-19598

Antenna orientation effect on polarization components of radio waves reflected from ionosphere, noting occurrence and properties of magnetotonic component of polarization 07 p1173 A67-19690

Phase variation dependence at receiver output on polarization of wave incident on antenna of phase measuring system 07 p1144 A67-19694

Time variation of preferential-polarization vector of pearl type oscillations during course of observations at Lovozero station, U.S.S.R. 07 p1174 A67-19711

Plasma resonance emission of thin Ag foils irradiated by light, noting intensity and direction of polarization 08 p1368 A67-20787

Geometric analysis of refractive index, absorption index and polarization characteristics of ionospheric radio waves 08 p1295 A67-21168

Isophotes of extended light sources in night sky, Stokes parameters, brightness and degree of polarization for Rayleigh-scattered light in earth atmosphere 08 p1328 A67-21243

Surface brightness and polarization state of zodiacal light measured from sounding rocket 08 p1326 A67-21244

Optical beam deflection method based on

polarization change of acoustically deflected light as compared to incident beam 09 p1510 A67-21574

Radio astronomical measurements within partial coherence theory showing coherence function relation to spectrum, brightness distribution and statistical electromagnetic fields polarization 09 p1460 A67-21585

Polarization of waves generated by annular laser resonators of triangular shape, obtaining directions of electric field vectors 09 p1512 A67-21923

Two-plate polarizer rendering worst cross polarization with arbitrary vane angles and differential phase shifts 09 p1474 A67-22089

Frequency stabilization of Zeeman laser, using intensity crossover region with cavity tuning between oscillations on two orthogonally circularly polarized axial modes 09 p1513 A67-22134

Plasma magnetization under action of circularly polarized wave, noting inverse Faraday effect 10 p1683 A67-22853

Inertialess polarization energy of charge interaction between neighboring lattice points in Ge crystal, using M-20 computer 10 p1695 A67-23657

Polarity patterns of interplanetary magnetic field observed by Mariner IV during solar rotations 11 p1857 A67-23942

Polarization characteristics of antenna measured, using stereographic projections of polarization sphere and various graphical methods 11 p1781 A67-24279

Natural remanent magnetization with normal polarity of lower lava flow in Olduvai Gorge, showing stability via thermal demagnetization 11 p1788 A67-24698

Confirmation of reality of Gilsa geomagnetic polarity event, discussing experimental techniques and results 11 p1788 A67-24700

Polarization properties of Mercury explained by surface only, so there is no polarimetric evidence for atmosphere on Mercury 12 p2010 A67-26244

Combined probability density of axial coefficient and polarization angle of field scattered by target 14 p2297 A67-28032

Polarization of waves generated by annular laser resonators of triangular shape, obtaining directions of electric field vectors 14 p2330 A67-28252

Mean flux density and polarization degree of radio emission from Jupiter in centimeter spectral range 14 p2389 A67-28837

Intensity and polarization of hydrogen Lyman alpha lines in day airglow as function of altitude for principal far UV emission 14 p2314 A67-28849

Depolarization of fully polarized electromagnetic waves, obtaining degree of polarization 15 p2435 A67-29338

Normal modes for solid state laser noting linear and elliptic polarization, resonant frequency and reflection loss 15 p2497 A67-29388

Polarization of complex wave form geomagnetic micropulsations of natural and artificial origin, using physical optics 15 p2476 A67-29620

Tables of Fresnel intensity reflectances from classical electrodynamics noting characteristics for amplitude minima, polarization maxima and 90 degrees phase difference [RE-TR-67-7] 15 p2518 A67-29769

Selective polarization filtering during hologram construction enhancing reconstructed image resolution and tonal range by eliminating specular reflection recording 15 p2488 A67-29818

Plasma flux interaction in magnetic multipole field, proving mutual polarization of interacting fluxes by photographic results 15 p2532 A67-30258

Magnesium fluoride double Rochon prism used as polarizer or analyzer in vacuum UV wavelengths 15 p2491 A67-30425

Combined probability density of axial coefficient and polarization angle of field scattered by target 16 p2823 A67-30881

Atmospheric radiation polarization characteristics, determining concentration and distribution of atmospheric scatterers 16 p2865 A67-30983

Earth electromagnetic field stable micropulsations/pearls/properties stressing apparent pearl polarization and polarization behavior 16 p2867 A67-31485

Cosmic plasma flow effect on cosmic

radiation polarization, deriving difference between normal waves refractive indices in two-component medium 16 p2628 A67-31494

Polarization characteristics of radio emission from rough lunar surface, analyzing averaging effects of antenna radiation pattern and surface roughness 16 p2628 A67-31495

Nonlinear laser theory to calculate amplitudes, frequencies and beat frequencies of circularly polarized modes in laser with axial magnetic field 16 p2886 A67-31562

Polarimetric properties of simulated lunar surface, showing polarization effect on particle size 16 p2754 A67-31749

Diurnal characteristics of geomagnetic micropulsations noting period, amplitude, continuity, time of occurrence, etc, proving existence of hydromagnetic waves generated at magnetosphere 17 p2841 A67-32212

Earth magnetic field micropulsation polarization properties at middle latitudes from three-component fluxmeter recordings 17 p2847 A67-32941

Polarization of periodic pearl-type oscillations of geomagnetic field at magnetically conjugate points 17 p2850 A67-32974

Spectral purity of Ebert type far IR grating spectrometer determined, noting experimental technique 17 p2863 A67-33300

Inertialess polarization energy of charge interaction between neighboring lattice points in Ge crystal, using M-20 computer 17 p2924 A67-33338

Polarization properties of single mode operating gas laser in small axial magnetic field with initial cavity anisotropy 17 p2870 A67-33368

Spectral brightness, reflectivity and polarization characteristics of clouds in IR band, measuring angular structure of underlying radiation field 18 p3073 A67-33563

Amplitude and polarization of radio pulse from extensive cosmic ray air shower indicating geomagnetic deflection mechanism of emission 18 p3116 A67-34196

Principal polarization radar cross sections as function of azimuth aspect angle for rectangular cylinder 19 p3183 A67-35518

Depolarization ratio of echo signals from point angle sources, using radar apparatus 20 p3384 A67-37237

Control of polarization of radiation field of waveguide-slot antenna emitter 20 p3401 A67-37337

Beta Lyrae intrinsic polarization amount and phase dependence in visual, blue and UV light observed, analyzing polarization curves 20 p3528 A67-37471

38 MHz solar burst duration, bandwidth, amplitude, number and polarization characteristics noting possible generating mechanisms 20 p3520 A67-37476

Plane electromagnetic wave reflection from rough surface, calculating energy and polarization characteristics 21 p3580 A67-38115

Reversed polarity effect on propagating current sheet in coaxial plasma accelerator [AIAA PAPER 67-658] 21 p3671 A67-38694

Photoelectric polarimeter for measuring rotational, electro-optical and electrogratational effects and optical activity in ferroelectrics 21 p3631 A67-38969

Coherent Raman amplification dynamics, considering pump depletion and coupling saturation and stimulated Raman scattering by polarization waves 22 p3816 A67-40318

O and B stars surveyed with 154 cm Catalina reflector show discrepancies from mean interstellar polarization-wavelength dependence near Orion 23 p4062 A67-40626

Circular and linear polarization of OH line radiation from NGC 6334 nebulae region using Parkes radio telescope 24 p4230 A67-42333

POLARIZED LIGHT

SA KERR EFFECT

Spectral polarimetry signature of terrestrial and planetary materials through remote sensing 01 p0059 A67-10331

Polarized light crystallization microanalysis for supercooled water droplets with additives applied to spherical single crystals of ice during droplet freezing 01 p0109 A67-11010

Irregularity of galactic magnetic field structure in vicinity of sun indicated by starlight polarization, interstellar cloud motion and Milky Way

photography 01 p0151 A67-11275
 Optical system consisting of polarized laser beams for monitoring missile attitude during early launch phase 04 p0619 A67-14505
 Observed interstellar polarization cannot be explained in terms of graphite-crystal color since polarization must increase monotonically from IR to UV 04 p0699 A67-14982
 Nonlinear optical reflection laws governing direction, polarization and intensity of second harmonic light generated in reflection 06 p1030 A67-17571
 Two-photon absorption spectrum of single crystal CdS, using polarized light and precise geometry 06 p1011 A67-18209
 Reflection and transmission of birefringent plates surrounded by semimfinite birefringent media with incident waves having polarized electric fields 06 p1033 A67-18544
 High power laser beam polarization direction effects on electron emission from Ag surface 06 p1012 A67-18759
 Microstructure interpretation of 5Al-2.5Sn titanium alloy, examining high optical magnification and polarized light illumination 08 p1340 A67-20365
 Photometric, polarimetric and IR study of lunar surface including polarization of moonlight, thermal measurements, lunar radar echo signals, etc 08 p1395 A67-21160
 Nonstationary thermoelastic stresses analyzed using photoelastic technique based on polarized light 08 p1423 A67-21334
 Self-focusing of elliptically polarized light resulting in formation of channels with linear polarization 08 p1340 A67-21503
 Plasma resonance absorption measurement in thin potassium foils, observing polarized light transmission at λ 3270 10 p1691 A67-23478
 Polarization phenomena in gas laser in presence of magnetic field 12 p1954 A67-26236
 Depolarization of linearly polarized EM waves backscattered from rough metals and inhomogeneous dielectrics with known statistical properties 13 p2158 A67-26878
 Holography preserving correspondence of polarization components in reconstructed image and in object 13 p2120 A67-26881
 Three-dimensional photoelasticity and determination of axes of birefringents and change in phase by scattering polarized light 13 p2219 A67-27092
 Line contours for Fe-I-6302.5 angstrom across sunspot in west solar limb measured simultaneously with magnetic field strengths and direction and Evershed velocity 15 p2554 A67-29460
 Visible continuous spectrum of comets rules out hypothesis of iron particles major role in scattering solar light 15 p2554 A67-29515
 Automatic photopolarimeter as pilot model for scans of planetary disks on fly-by missions 15 p2492 A67-30435
 Transverse and longitudinal waves in ultrasonic light modulators, noting superiority of transverse waves in polarization rotations 17 p2815 A67-32614
 Photo-induced microwave response of SbSI crystals to variations in reflection coefficient indicates photodielectric effect 17 p2915 A67-32675
 Laser beam slitting hologram production technique using polarization controller and birefringent prism 17 p2864 A67-33359
 Renormalization theory and Compton scattering of electron interacting with monochromatic LF polarized light beam 17 p2870 A67-33365
 Skylight polarimeter based on sequential detection of light transmitted by polarizers oriented at various angles 18 p3046 A67-33748
 Reflected light microscope for viewing unstained brain and ganglion cells 18 p2991 A67-34530
 Pulse width of ultrashort light pulses measured by Michelson type arrangement of nonlinear optics 20 p3456 A67-36172
 Light beam propagation in atomic vapor, with atoms undergoing magnetic resonance, describing electromagnetic wave polarization 20 p3458 A67-36435
 Two-port magnetoelastic delay performance obtained in YIG rod by injecting longitudinal elastic waves along axis 21 p3677 A67-38007
 Direction of sunspot magnetic force lines

at any point of solar surface by fringe analysis of light polarization 21 p3709 A67-38987
 Optically pumped vapor rotatory power as optical pumping experiment monitoring technique, discussing specific rotatory power and refractive index dependence on light frequency 22 p3816 A67-40320
 Light polarization and intensity for Raman scattering from plasmons and phonons in GaAs 23 p4038 A67-40795
 Two-photon absorption theory extension to include vibronic mixing between different electronic states using two-photon laser excitation of polycyclic atomic molecules 23 p4013 A67-40964
 Holography /phase-recording of diffracted wavelets/ for phase contrast and stroboscopy, interferometry in polarized light and 3-D photoelasticity 23 p3999 A67-41179
 Cesium vapor pumping by intensive polarized light used for studying Cs buffer gas collision influence on pumping cycle and Zeeman transitions effect on polarization 23 p4016 A67-41291
 Optical mixing process for study of polarized light in wedge shaped cells of Raman active medium 23 p4017 A67-41433
 Diffraction of H-polarized plane wave on metal grating with narrow slits 23 p3975 A67-41683
 Light propagation in electrically and magnetically anisotropic medium and diffraction by birefringent cylinder using coupled integrodifferential equations 24 p4119 A67-41889
 Electronic ellipsometer for measurement of very small changes in elliptically polarized light, discussing refractive index, Kerr effect and calibration 24 p4152 A67-41901
 Hologram technique using reference beam totally reflected from air-emulsion boundary of hologram plate permits close spacing 24 p4156 A67-42362

POLARIZED RADIATION

Origin of polarization of radiation from GaAs diodes, noting intensity dependence on current density and effect of anisotropic electron velocity distribution 01 p0034 A67-10090
 Current layer dynamics in flat electrode accelerator, relating plasma acceleration and polarization field 01 p0122 A67-10345
 Reflection of vertically polarized exponentially varying electromagnetic waves by horizontally stratified magnetoplasma half-space 01 p0023 A67-10471
 Far UV extinction curve and wavelength dependence of interstellar polarization by graphite grains 01 p0150 A67-10890
 Polarization measurements of distribution of ionized interstellar gas near galactic plane using two galactic region models 02 p0322 A67-11645
 Reflective properties of natural surfaces, noting dependence on surface properties of total reflected energy, spectral distribution, polarization degree of radiation, etc [AIAA PAPER 65-865] 03 p0411 A67-13045
 Depolarization of fully polarized electromagnetic waves, obtaining degree of polarization 04 p0575 A67-15151
 Polarization and directional variation effect on radiant heat transfer through long specular reflecting passages [ASME PAPER 66-WA/HT-32] 04 p0725 A67-15440
 Elliptically polarized wave reception by antenna, itself elliptically polarized, for use in interferometry problems, noting relation to complex vector 04 p0658 A67-15626
 Linear polarization of comet Na D-lines 05 p0891 A67-16406
 Elliptical polarization of Crab Nebula radiation possibly explained without synchrotron hypothesis by analyzing photoelectric observations of Stokes parameters 05 p0882 A67-16593
 Galactic depolarization of 21 cm wavelength radiation of extragalactic sources explained as function of distance traveled by radiation through halo 05 p0895 A67-16601
 Optimum wavelength and spectral bandwidth for measuring polarization of distributed cosmic RF radiation 05 p0768 A67-17228
 Tuning of lens and mirror antennas with circularly polarized radiation 05 p0766 A67-17239

Relation between optical and radio properties of quasars 06 p1086 A67-18374
 Electromagnetic diffraction at aperture, comparing three theories for case of partial polarized incident field 06 p1033 A67-18541
 Cross-polarization radiation of axisymmetric mirror antennas 08 p1305 A67-21277
 Radio spectrometer for polarization measurements of galactic emission in meter wave range 08 p1306 A67-21350
 Invariant properties of partially polarized electromagnetic waves analyzed in Poincare and Cayley-Klein models of hyperbolic space, using geometric constructions 09 p1460 A67-21588
 Mathematical analysis of polarization interferometry yielding polarization and brightness distribution of celestial radio sources [AFRL-67-0226] 09 p1470 A67-21608
 Scattering of circularly polarized electromagnetic wave in Coulomb field, noting coalescence of two-wave quanta into one quantum of double frequency 10 p1666 A67-23594
 Absolute gain measurements of vertically polarized HF test antennas over imperfect ground 11 p1761 A67-24278
 Degree of polarization and position angle measurements of linearly polarized components of galactic and extragalactic radio sources at short wavelength 11 p1861 A67-24486
 Polarization of cosmic OH 18-cm radiation 11 p1864 A67-24565
 Current layer dynamics in flat electrode accelerator, relating plasma acceleration and polarization field 11 p1843 A67-25018
 Nancy radiotelescope energy collection, illumination choice and development 12 p1914 A67-25310
 Possible polarization of X-ray bremsstrahlung of solar flares due to sharply anisotropic electron beams 13 p2191 A67-26383
 Polarization of cosmic X-ray produced by bremsstrahlung mechanism 13 p2191 A67-26713
 Polarization of extragalactic radiation sources and evidence of irregularities of magnetic field in our Galaxy 13 p2198 A67-26791
 Sporadic E layer scintillation effects on amplitude of 137 MHz radio waves from Early Bird 14 p2270 A67-28577
 Net polarization of celestial X-rays could lead to specification of source mechanism producing radiation 14 p2381 A67-28617
 Polarization and directional variation effect on radiant heat transfer through long specular reflecting passages [ASME PAPER 66-WA/HT-32] 15 p2579 A67-29319
 Depolarization of fully polarized electromagnetic waves, obtaining degree of polarization 15 p2435 A67-29338
 Radiation polarization in ruby laser with resonator shaped like rectangular parallelepiped 15 p2409 A67-29701
 Measurement of position of polarization plane of radiation emitted by neodymium-glass laser 15 p2499 A67-29758
 Semiconductor nonlinear polarizability at difference frequency calculated, considering exciton states alone and combined with band energy states 15 p2541 A67-30238
 Microwave spectrum and observation at 6 cm wavelength of Venus to determine total intensity and polarization of radiation 16 p2747 A67-30987
 Radio spectrometer for polarization measurements of galactic emission in meter wave range 17 p2822 A67-31946
 Refractive index variations, Coulomb scattering and time variation of shower front effects on coherent emission of polarized radio pulses from cosmic ray showers 18 p3116 A67-34197
 Circularly polarized radiation from Crab Nebula investigated from radio telescope observations at Arecibo 19 p3316 A67-35802
 Earth surface influence on radiation polarimetry in vicinity of radio horizon 20 p3382 A67-36776
 Radio emission polarization of Crab Nebula on February 1963 with Soviet radio telescope 20 p3529 A67-37516
 Interference method for measuring polarization of linearly polarized

- radiation 20 p3403 A67-37518
Bilateral metal grating effect on E and H polarized radiation from plane parallel layer noting intensity, energy density and reflection at interface with medium 21 p3638 A67-37865
FR-1 satellite-borne oxide cathode used to return to ground polarization current from ambient plasma 21 p3599 A67-38649
Possible polarization of X-ray bremsstrahlung of solar flares due to sharply anisotropic electron beams 21 p3698 A67-38817
Magnetic effect on polarization of resonance radiation in solar chromosphere 21 p3709 A67-38989
9.4 cm radiation from Jupiter and Saturn and 21.2 cm radiation from Saturn 21 p3709 A67-38994
Microwave radiations of Jupiter, deriving equivalent black body temperature, magnetic field data, radiation belts data and electron energy 21 p3710 A67-38995
Emission of axisymmetric parabolic antenna with antiphase field distribution at aperture, calculating radiation pattern of principal and cross polarization components of field 22 p3770 A67-39658
Depolarization problem and correlation method for cosmic radio emission polarization measurements in interstellar space 22 p3761 A67-39757
Solar type IV burst centimeter and decimeter polarization and spectral variabilities examined in helical electron stream cyclotron radiation hypothesis for solar corona model 23 p4050 A67-40776
Radiation polarization in ruby laser with resonator shaped like rectangular parallelepiped 24 p4166 A67-41771
Possible circular polarization of compact quasar radio and optical radiation, discussing astrophysical implications 24 p4226 A67-41884
- POLAROGRAPHY**
Analytical method, based on polarography, for measuring concentration of class of polymers in dilute aqueous solutions 15 p2433 A67-29676
Contamination detection by analytical instrumentation considering sampling, IR, atomic absorption spectrophotometer, gas chromatography, colorimetry and polarography 23 p3998 A67-40844
Inert gas effect on oxygen consumption in living tissue studied by polarographic and Warburg techniques 23 p3960 A67-41706
- POLE**
SA MAGNETIC DIPOLE
SA REGGE POLE
Oscillation discharge by reactive circuit elements in two-terminal line controlled by movable poles of circuit in complex plane 13 p2085 A67-27723
- POLISHED METAL**
Theoretical determination of polished metals emission factors, using model where emission depends on surface layer temperature and electric resistivity 14 p2407 A67-28558
- POLISHING**
SA ELECTROLYTIC POLISHING
Chemical polishing effects on sapphire whisker strength, obtaining correlation between fracture strength and whisker diameter 20 p3473 A67-36480
- POLLUTION**
S AIR POLLUTION
- POLYAMIDE**
SA NYLON
Temperature resistant aromatic ordered copolyamide fibers, obtaining tensile properties and radiation resistance 21 p3647 A67-37871
Fibers of ordered aromatic copolyamides, performance characteristics and resistance to degradation at high temperature 21 p3647 A67-37873
- POLYATOMIC GAS**
Thermoconductivity-temperature-diffusion coefficient relations for pure and mixed polyatomic gases 03 p0535 A67-13518
Chapman-Enskog method applied to kinetic equation describing evolution of singlet distribution function in dense gas of perfectly rough spheres 04 p0658 A67-15507
Models for collision processes and changes of degree of freedom in kinetic equation for polyatomic gases 08 p1323 A67-21386
Kinetic model equation for polyatomic gas with internal structure based on Wang Chang-Uhlenbeck equation 11 p1775 A67-23864
Thermal conductivity of binary gas mixtures, estimating conductivity at high temperatures 12 p2033 A67-25217
Book on ultrasonic wave absorption and dispersion in gases, liquids and solids, discussing physical mechanisms involved in sound absorption 12 p1867 A67-26157
Nonequilibrium effects in spherical free jet expansions of polyatomic gases and gas mixtures, obtaining moment equations for flow field development 13 p2104 A67-26983
Temperature dependence of thermodynamic functions of polyatomic gases at high temperatures 16 p2704 A67-31391
- POLYATOMIC MOLECULE**
Band and total emissivities estimation procedures for polyatomic molecules, discussing empirical emissivity charts and radiative exchange at local thermodynamic equilibrium 18 p3152 A67-33817
Rate constants and activation energy in bimolecular transfer reactions for halogen atoms 18 p3154 A67-33835
Calculation of vibration level populations of polyatomic molecules in electronic ground state 20 p3457 A67-36216
Electronic transitions optical saturations in polyatomic organic molecules with high intensity laser radiation, discussing relation to bleaching of dyes 22 p3817 A67-40487
- POLYBENZIMIDAZOLE**
Polybenzimidazole /PBI/ structural adhesives for bonding stainless steel, beryllium and titanium alloys 09 p1523 A67-22517
Mechanical properties of polybenzimidazole resin show suitability for metal-to-metal and sandwich composite adhesives and high and cryogenic temperatures 09 p1523 A67-22518
Structural modifications effect on PBI fiber critical properties, discussing strain-stress characteristics, target properties and crystallization 21 p3648 A67-37875
- POLYBUTADIENE**
Combustion characteristics and ballistic performance of dual layer propellant grains using polybutadiene/potassium perchlorate and polyurethane/ammonium perchlorate for end-burning type rocket motor 05 p0872 A67-16589
- POLYCARBONATE**
Environmental factors effect on stability of high performance polycarbonate 22 p3825 A67-39859
- POLYCARBUTENE**
X-band attenuation by rocket exhaust plume measured with AM/PM noise for various propellant systems 15 p2436 A67-29429
- POLYCRYSTAL**
Microprobe study of impurities in hot-pressed polycrystalline MgO compact and existence of significant grain boundary volume [JPL-TR-32-1015] 01 p0131 A67-10262
Nitrogen adsorption at room temperature on atomically clean polycrystalline rhodium, noting dependence of sticking coefficient upon surface coverage and temperature 02 p0257 A67-12728
Hardness, microhardness, electric resistance and toughness results tabulated for polycrystalline nonalloyed molybdenum 05 p0832 A67-17510
Absolute value of photoconductivity in polycrystalline high resistivity CdS and CdSe SHF field and experimental determination of barrier amplification factor and intercrystalline barrier height 08 p1370 A67-20997
Exponential sintering temperature dependence of conduction electrons density and attendant decrease of mobility due to ionized impurity scattering in cadmium oxide 10 p1691 A67-23503
Carbon action effect on tensile deformation in single and polycrystalline beryllium in terms of solutionized and precipitated states 13 p2137 A67-27112
Plastic deformation mechanisms of polycrystalline beryllium to analyze temperature dependence of critical shear in prismatic plane 13 p2138 A67-27121
Low pressure diffusion of carbon to nucleation sites and graphite growth in cubic morphology suggested as origin of cliftonite in meteorites 14 p2384 A67-28144
Barium titanate polycrystal dielectric constant aging, discussing 90 degree splitting in domain structure 14 p2364 A67-28228
Electric conductivity of p-Ga-Te polycrystals and single crystals in strong electric fields 14 p2375 A67-29085
High temperature diffusion of potassium in single crystal and polycrystalline molybdenum 15 p2504 A67-29972
Deformations and residual stresses in polycrystalline microstructures, using photoelastic coating method 20 p3540 A67-37059
Hardness, microhardness, electric resistance and toughness results tabulated for polycrystalline nonalloyed molybdenum 21 p3644 A67-38038
- POLYDOP**
S POLYSTYATION DOPPLER /POLYDOP/ TRACKING SYSTEM
- POLYESTER**
Cool burning smokeless propellants for gas generator applications and low signature missiles evaluated against criteria 15 p2544 A67-29981
Adhesive system for structural bonding of fiberglass reinforced polyester to itself and to metal 24 p4175 A67-42421
- POLYESTER RESIN**
Hardness of polyesters copolymerized with styrene, determining reticulation and temperature effects 05 p0759 A67-16787
Unsaturated polyester styrene, showing via gas chromatography and IR spectroscopy effect of reticulation on pyrolytic decomposition 05 p0759 A67-16788
UV radiation effect on mechanical characteristics of polyethylene terephthalate film in vacuum and atmospheric pressure 13 p2184 A67-27624
1, 3-diones and beta-ketoesters with cobalt for room temperature curing of unsaturated polyester resins by organic peroxide 24 p4175 A67-42420
- POLYETHYLENE**
Impact of cylindrical or spherical projectiles of dural and polyethylene at high velocities in seminfinite targets, analyzing crater shape and relation to kinetic energy 04 p0710 A67-15002
Rough surface recrystallization of heated polyethylene extended-chain crystals 04 p0566 A67-15201
Density, morphology and melting data on extended chain linear polyethylene and high molecular weight polymethylene crystallized from melt under high pressure 20 p3474 A67-37398
Cryogenic flexibility of single and multiple ply thin polymeric film tested for porosity, cycle life and film thickness relation 24 p4176 A67-42468
- POLYETHYLENE TEREPHTHALATE**
Crystallinity index measurements of poly(ethylene terephthalate) by X-ray diffractometric and differential scanning calorimetry index methods 04 p0641 A67-14527
UV radiation effect on mechanical characteristics of polyethylene terephthalate film in vacuum and atmospheric pressure 13 p2184 A67-27624
Cryogenic mechanical properties of poly(ethylene terephthalate) film studied for effects of stretch and heat set temperature and time 24 p4176 A67-42469
- POLYHEDRON**
Invariants of triangular shell element stiffness matrices associated with polyhedral deflection distribution, discussing effect of geometry [AIAA PAPER 67-114] 06 p1103 A67-18356
Class of problems of parametric linear programming of set of convex polyhedron having only target function coefficients dependent on parameter 07 p1219 A67-19167
Convex polyhedron theorem in determining whole set of optimal solutions in linear programming 11 p1814 A67-24979
- POLYISOBUTYLENE**
NBS polyisobutylene relaxation modulus and Rouse functions for torsional molecular vibrations and internal rotation in viscoelastic theory of amorphous polymers 08 p1346 A67-20878
Velocity profiles of non-Newtonian fluid /polyisobutylene solution/ in helical flow by flow visualization technique, discussing Poiseville and viscometric flows 24 p4145 A67-42708
- POLYMER**
SA BORON POLYMER
SA COPOLYMER

SA ORGANOMETALLIC POLYMER

SA VINYL POLYMER

Relation between acid-basic state and conductivity for polyaniline macromolecular semiconductors such as emaraldines 01 p0130 A67-10196

Ultrahigh vacuum installation using iongetter pumps for analysis of adhesion between plastics and metals in space environment 02 p0228 A67-11552

Mechanical properties of high polymer solid in terms of microbehavior as result of deformation and orientation, expressing anisotropic relaxation function as time dependent function 02 p0297 A67-11873

Nonlinear viscoelasticity theory for zone of rigid behavior of polymer materials 02 p0338 A67-12237

Spontaneous dielectric breakdown in Plexiglas sheets due to pulsed electrons with breakdown plane influenced by embedded metal foils 04 p0659 A67-15699

Specific degassing of high polymers placed in simulated space environment studied by residual gas analyzer 05 p0832 A67-16304

Length-temperature measurements for several polymers and mixtures for detection of transitions and determination of location and magnitude of expansion coefficient changes 06 p1019 A67-17851

Combustion and pyrolytic behavior of thermoplastic polymer spheres burning in quiescent atmospheres of air [AIAA PAPER 67-103] 06 p1114 A67-18283

Crack propagation in polymers and polymer type materials 06 p1106 A67-18626

Wear effects in polymer-metal joints under frictional loads 07 p1211 A67-19170

Reliability of nonlinearly elastic polymer components of structural elements exposed to random loads 07 p1261 A67-19171

Quantitative analysis of wear of metal-metal/polymer composite friction pairs as function of time and operational conditions 08 p1334 A67-20597

Photoelastic stress measurement techniques for birefringent high polymers extended to two- and three-dimensional linear viscoelasticity problems 08 p1420 A67-20887

Simulation of stress-strain state of metal under elastoplastic deformation, based on models used in polarization-optical techniques, analyzing stresses in high polymers 08 p1423 A67-21330

Long time mechanical and thermal stability of polymeric materials predicted from accelerated testing at increased temperature-time relations 10 p1672 A67-23743

High polymer rubber, plastic, and textile qualitative and quantitative properties, uses in space environment 13 p2143 A67-26698

Thermodynamic analysis of stress-strain relation for polymer type media 13 p2218 A67-26886

Similarity criteria for plastic behavior of polymers under combined effect of nonuniform temperature field and hydrostatic pressure 15 p2573 A67-29466

Friction and wear properties of resins and polymers with carbon fiber examined and compared for various amounts of fiber 16 p2694 A67-31021

Polymer fracture mechanism hypothesized as competition between localized hardening by molecular orientation and localized softening during deformation 18 p3068 A67-33488

Stress effects on structure of oriented crystallizing polymers, noting long periods changes due to displacement of crystallites in amorphous layers 18 p3068 A67-33489

Free radical formation correlated with breaking time and creep rate in solid polymers subject to crushing, breakdown and deformation 18 p3068 A67-33490

Polymeric materials in expulsion bladders for cryogenic liquids, describing fabrication, flexibility, permeability, storage, transfer, control factors, etc [AIAA PAPER 67-457] 18 p3069 A67-33931

Molecular theories for polymer elastic and viscoelastic properties near glass transition region [AIAA PAPER 67-488] 18 p3143 A67-33954

Spherical shape changes of droplet of viscous substance of high surface tension under variable external force and small deformation 18 p3028 A67-34220

Combustion rate and subsurface activity of

metallized burning polymers, stressing heat conduction role and applications to propellant combustion [CI PAPER 67-3] 19 p3344 A67-34998

Polymeric materials used for selected subsystems of Mariner IV space probe [JPL-TR-32-1031] 19 p3334 A67-35889

High strength glass damage, discussing protective polymer coating 20 p3473 A67-36159

Elastic and residual strains caused by friction load in polymer surface layers studied for dependence, slip rate and friction load duration 20 p3473 A67-36842

Low molecular weight polymer flow behavior variation with shear rate, shear stress and temperature 20 p3473 A67-36914

High tensile strength high elasticity modulus graphite fibers preparation from polymeric fibers for composite structures 21 p3649 A67-37884

Thermally stable polymers, discussing synthesis and testing on pilot plant and laboratory undeveloped stages 22 p3825 A67-39856

High performance engineering thermoplastic/Polymer 360/mechanical and electrical properties and environmental factors effects 22 p3825 A67-39858

Free energy of polymer solid consisting of entangled long chain molecules when deformed by elastic strain 22 p3826 A67-40201

Polymeric materials for extreme temperature emphasizing thermal stability 23 p4021 A67-41228

Plastics in aircraft and rocket parts construction noting silicon oils and solid polysiloxanes, discussing temperature resistance and rubber-elastic properties 23 p4021 A67-41400

Protocell origin, discussing radiation effects on polymers, proteinoid properties and already synthesized polymer stability 24 p4113 A67-42656

POLYMER CHEMISTRY

Water and internal acidity effect upon oligomeric polyanilines semiconductivity 01 p0130 A67-10197

Esterification rates of aliphatic carboxylic acids, acid terminated polybutadienes, etc, and steric environment in vicinity of acid groups 04 p0564 A67-14473

Unsaturated polyester styrene, showing via gas chromatography and IR spectroscopy effect of reticulation on pyrolytic decomposition 05 p0759 A67-16768

Hydrogen peroxide oxidation and ozonolysis of polymer type material in coal, kerosen and Orgueil meteorite 08 p1289 A67-21174

Adhesives development, discussing chemically and mechanically blocked reactant system and water based, hot melt, oil absorbent, heat resistant and low temperature adhesives 09 p1523 A67-22529

Catalytic effect of thermal polyanhydro-alpha-amino acids on hydrolysis of p-nitrophenylacetate, noting role of histidine residues 13 p2065 A67-26732

Treatise on adhesion and adhesives, Volume 1, Theory 14 p2340 A67-27793

Time dependent small-strain modulus of styrene-butadiene rubber, noting predictability from selected molecular parameters [AIAA PAPER 67-491] 18 p3143 A67-33956

Plastic based bearings, discussing polymer chemistry, use of fillers, incorporation into matrices of various resins, etc 20 p3455 A67-37266

Man-made organic polymer properties and characteristics, considering crystallization, cross-linking and polymeric chain stiffening for structural applications 20 p3474 A67-37713

Classification of 2-oxazolidones, examining preparation, physical chemistry, properties and polymerized derivatives 23 p3971 A67-41041

Field-polar forces interaction effect on viscoelastic properties of polypropylene oxide, measuring dilatometric, modulus and damping constants [JPL-TR-32-1026] 24 p4174 A67-41806

POLYMER PHYSICS

Solid propellant polymeric binder chemistry and high speed computer calculations of performance characteristics 08 p1373 A67-20875

NBS polyisobutylene relaxation modulus and Rouse functions for torsional molecular

vibrations and internal rotation in viscoelastic theory of amorphous polymers 08 p1346 A67-20878

Creep, stress relaxation and vibrational measurements, sinusoidal torsional forced oscillations and stress wave propagation in polymeric linear viscoelastic solids 08 p1419 A67-20885

Admissible configurations and diffusive motions of molecular chains on quadratic lattice narrow channels 08 p1356 A67-21299

Treatise on adhesion and adhesives, Volume 1, Theory 14 p2340 A67-27793

Analytical method, based on polarography, for measuring concentration of class of polymers in dilute aqueous solutions 15 p2433 A67-29676

Ionizing radiation effect on polymers used in electronics, producing temporary effects also found in mineral insulators like anodic tantalum oxide 17 p2917 A67-32841

Density, morphology and melting data on extended chain linear polyethylene and high molecular weight polymethylene crystallized from melt under high pressure 20 p3474 A67-37398

Fracture theory for amorphous high polymers below glass transition temperature, considering viscoelastic effects on structural defect stress concentration 22 p3824 A67-39740

Fiber reinforced plastic components for structural materials noting high temperature polymers 22 p3825 A67-39854

Change in brittle fracture work during combined impact and tensile load of polymer noting variation according to maximum law 23 p4072 A67-40595

POLYMERIZATION

Molecular weight sensitivity of thermoconductivity of polydimethylsiloxane and polyethyleneglycol 01 p0103 A67-10295

Nuclear magnetic resonance /NMR/ used to measure gelation times, rates of polymerization and nature of volatiles included in raw material resins 03 p0429 A67-13448

Dielectric properties applied determination of degree of reticulation of polymers during polymerization, noting losses due to free electrons and dipoles [ONERA-TP-476] 14 p2340 A67-27898

Ultrahigh molecular weight poly/ethylene terephthalate/ synthesized, studying catalyst, particle size, reaction temperature and time and carrier gas flow rate 24 p4176 A67-42487

N-vinyl carbazole reactions with anionic initiators, discussing radical anion and polymer formation and ESR spectra [JPL-TR-32-1126] 24 p4118 A67-42601

POLYMETHYL METHACRYLATE

Polymethylmethacrylate and polystyrene exposure to ruby and neodymium-glass laser radiation, noting appearance of EPR 01 p0086 A67-10075

Nonuniform temperature distribution effects on creep bending characteristics of linear viscoelastic columns of polymethyl methacrylate 01 p0160 A67-10560

Thermal conductivity variation of double-base solid propellants under acoustic irradiation compared with polymethyl methacrylate 15 p2545 A67-30199

Statistical probability of fractures in polymethylmethacrylate by laser radiation 20 p3473 A67-36161

POLYMORPHISM

Intermediate phases in alloys of Ti with Ir, Rh and Qs indicate possibility of polymorphism 13 p2131 A67-26472

Strain hardening of high temperature titanium multiphase solid solution by deformation and subsequent rapid cooling 15 p2504 A67-29971

POLYNOMIAL

SA HERMITIAN POLYNOMIAL

SA JACOBI POLYNOMIAL

SA LAME POLYNOMIAL

SA LEGENDRE POLYNOMIAL

Learning control system seeking optimum point of bimodal static characteristics by polynomial conjecture 01 p0048 A67-11236

Solution method for determinantal equation of matrix polynomial 02 p0258 A67-11799

Limiting conditions for polynomials orthonormal on unit circle for nonnegative summable 2-pi-periodic weight function 03 p0456 A67-12885

Approximation of functions of many variables by Bernstein polynomials, using

method based on conjugate operators 04 p0646 A67-15258

Criterion of completeness of system of polynomials in singly connected space 05 p0836 A67-17118

Sixth order polynomial calculation of axisymmetric laminar boundary layer of incompressible fluid removed by suction and arbitrary velocity 05 p0749 A67-17184

Collisionless aspects of strong shock wave structure as approximated by Boltzmann equation examined, using orthogonal polynomial expansion technique in velocity space 05 p0794 A67-17421

Stability criteria of Leonhard-Michailov and Nyquist for polynomial 06 p0973 A67-17626

Polynomials orthogonal with respect to contours, examining analytic function representation via Fourier series expansion of such polynomials 06 p1025 A67-18695

Approximate solutions for differential and integral equations in form of second order asymptotic polynomials 07 p1214 A67-19216

Intermediate value and simultaneous convergence obtained by sequence of polynomials for pair of functions on closed set E dense on norm z equals one 07 p1215 A67-19221

Simultaneous approximation of function and derivatives, ensuring uniqueness by imposing linear conditions on coefficients of polynomials 08 p1347 A67-20368

Maximum errors of polynomial approximations defined by interpolation and least squares method 08 p1349 A67-21262

Time varying weight functions effect on convergence of polynomial expansions of isotropic distribution 08 p1323 A67-21385

Analytic formulas for locating real and complex roots of polynomial equations up to and including seventh degree 08 p1350 A67-21536

Root squaring and subresistant /RSSR/ routine as root finder for polynomial equations with real coefficients 09 p1468 A67-22050

Polynomial approximation method for determining satellite orbits from large-time-interval trajectory measurements 11 p1858 A67-24066

Automatic technique of root location and determination of n th order polynomial equation using simple linear computing elements 11 p1756 A67-24639

Multiparameter data sorting technique for one-parameter information represented by simple distribution described by appropriate transformation coefficients 12 p1909 A67-25863

Cyclotomic numbers of order 18 with applications to difference sets 13 p2146 A67-28735

Variation diminishing spline approximation method of linear interpolation 13 p2147 A67-27468

Definition of solutions of problem that constitutes generalization of intrapolynomial problem and best approximation problem in normed space 13 p2148 A67-27471

Zeros of polynomials with real or complex coefficients determined, using steepest descent method in convergent procedure 13 p2148 A67-27496

Stable evaluation algorithm for polynomials, discussing minimal Newton forms, error estimation, etc 14 p2342 A67-28003

Linearization of oscillation differential equations containing even nonlinearities, using asymptotic polynomials 14 p2344 A67-28810

Strong approximation of continuously differentiated function by means of differentiated expressions of finite line matrix 14 p2345 A67-28940

Cauer polynomials forming procedure suitable for synthesis of LC ladder filters without mutual coupling, giving design procedure of Cauer filter network 15 p2452 A67-29935

Nonlinear decision surfaces determined by pattern-recognizing adaptive threshold device via generation of polynomial discriminant functions and computer programs 18 p3006 A67-34064

Structure of error curve when function is approximated in Chebyshev sense by polynomials 23 p4022 A67-40862

POLYPHENYL

Thermo-oxidative stability of polyphenylene resins in asbestos reinforced laminates 03 p0451 A67-13400

POLYPHENYL ETHER

Five-ball fatigue tester to investigate reduced pressure environment effect on rolling element fatigue life with polyphenyl ether [ASLE PREPRINT 67AM 8A-3] 14 p2326 A67-28795

Polyphenyl ether physical, chemical and mechanical properties, noting experimental results and fluid performance in closed pump loops 14 p2341 A67-28953

POLYPROPYLENE

Changes in giant molecule structure of polypropylene films under action of laser pulses analyzed by optical microscopy 07 p1211 A67-19169

POLYSTATION DOPPLER /POLYDOP/ TRACKING SYSTEM P

Earth-based navigation for two-spacecraft missions using analytical techniques for POLYDOP tracking data 13 p2155 A67-27526

POLYSTYRENE

Polymethylmethacrylate and polystyrene exposure to ruby and neodymium-glass laser radiation, noting appearance of EPR 01 p0088 A67-10075

Logarithmic dependence of energy losses on relativistic particle velocities in polystyrene films 01 p0125 A67-10926

Diffusion broadening in inelastic light scattering of cyclohexane-polystyrene near critical point for mixing 06 p1035 A67-17829

Intrinsic viscosity of linear homogeneous polystyrenes in decalin and toluene over large temperature ranges and molecular weights 10 p1602 A67-23384

Spectral emittance of melting or decomposing polystyrene determined, describing apparatus and experimental technique 20 p3446 A67-36663

POLYTETRAFLUOROETHYLENE

SA TEFLON

Rate dependent melting of polytetrafluoroethylene by differential thermal analysis, noting that amount of superheating is larger with higher molecular weight 04 p0641 A67-14528

EPR spectra of radicals formed during gamma irradiation of polytetrafluoroethylene 17 p2810 A67-33260

Decomposition of polytetrafluoroethylene in glow discharge studied using helium, helium plus oxygen or oxygen as carrier gas 18 p2998 A67-34369

Room temperature density-dose behavior of neutron and gamma irradiated polytetrafluoroethylene /PTFE/ noting crystallinity variations 23 p4021 A67-40781

Wear characteristics of polytetrafluoroethylene studied under various loading and sliding speeds in air and vacuum 23 p4009 A67-41062

POLYTROPIC PROCESS

Polytrope index for gas detonation products determined by velocity ratio for incident and reflected wave during collision of two detonation waves 05 p0927 A67-18999

Heat transfer effect in converging-diverging nozzle flow, considering polytropic process 08 p1278 A67-21526

Polytropic process of variations in state of system composed of gas and solid particles 12 p2033 A67-25317

Noether theorems describing continuum mechanics material applied to Hamiltonian principle for motion of piezotropic fluid or ideal gas undergoing polytropic process 13 p2105 A67-27397

Astronomical refraction in polytropic atmosphere adapted to automatic computers 13 p2152 A67-27484

Polytropic heat sources effect on ejection of stationary symmetrical plasma from sun 14 p2378 A67-27915

Polytrope structure from integrodifferential equation assuming metric, energy momentum tensor for static spherical symmetry and polytropic equation of state 21 p3658 A67-38615

Polytropic exponent along axis shown to approach adiabatic exponent at throat of convergent-divergent nozzle 22 p3742 A67-40112

Oscillations of polytropic and compressible cylinders investigated by small perturbation method noting separate mode of gravitational instability 22 p3896 A67-40526

One-dimensional steady MGD flow of polytropic gas with finite constant electric conductivity, noting flow patterns and oblique shock wave structure 24 p4198 A67-42707

POLYURETHANE

SA SYNTHETIC RESIN

Combustion characteristics and ballistic performance of dual layer propellant grains using polybutadiene/potassium perchlorate and polyurethane/ammonium perchlorate for end-burning type rocket motor 05 p0872 A67-16589

Vapor cured resins for aerospace applications 15 p2506 A67-29544

Compression tests with superimposed hydrostatic pressure to study rheological behavior of elastomer filled with granular potassium chloride [SESA PAPER 1224] 18 p3142 A67-33891

Compression tests with superimposed hydrostatic pressure to study rheological behavior of elastomer filled with granular potassium chloride 19 p3340 A67-35465

POLYURETHANE FOAM

Plastic foam pattern technique for producing vibration and shock fixtures 12 p1949 A67-25687

Long term cryogenic propellant storage in space, considering rigid open cell polyurethane foam as spacer in multilayer insulation system 24 p4254 A67-42480

POLYVINYL CHLORIDE

Klegecell G-300 mechanical and thermal properties tested for thermal insulation for cryogenic stage for liquid hydrogen on space vehicle 13 p2228 A67-27659

Chemical treatment reducing toxicity of polyvinyl chloride tapes used for insulating electric wires in space cabins 16 p2693 A67-30910

PONDEROMOTIVE FORCE

X and Z components of ponderomotive forces acting on conductive strip of finite width in EM field produced by unidirectional inductor 04 p0556 A67-15525

Effect of finite length of conducting body on ponderomotive forces acting on traveling magnetic field 04 p0670 A67-15526

Ponderomotive forces and geomagnetic westward drift in regard to MHD theory and earth core flows 13 p2114 A67-26855

Apparent forces of analytical mechanics for several cases of motion 19 p3261 A67-35049

PONTRYAGIN PRINCIPLE

SA REVERSE TIME

Deterministic optimal control, discussing Bellman dynamic programming method, Pontryagin maximum principle, orbital transfer, interplanetary guidance, etc 01 p0047 A67-11220

Optimization of control systems with nonlinear plants, using Pontryagin maximum principle 02 p0224 A67-11511

Navigation measurement optimization using Pontryagin maximum principle as necessary and sufficient condition to obtain smallest possible uncertainty 02 p0265 A67-12384

Optimal transfer of finite thrusting vehicle between circular coplanar orbits 02 p0330 A67-12719

General theory of variational problems of optimum control incorporating calculus of variations and Pontryagin maximum principle 04 p0647 A67-15981

Optimality conditions for nonlinear discrete systems, showing that at limit these conditions become Pontryagin maximum principle for continuous systems 05 p0782 A67-16320

Fixed time fuel-optimal controls computed by iterative procedure developed by Pontryagin principle 06 p1097 A67-18522

Pontryagin maximum principle for optimal control problem with constraints on control function 06 p0978 A67-18584

Optimality conditions of systems containing components with distributed parameters 07 p1159 A67-19138

Gyrostad transfer motion from initial stage to predicted orientation maneuver with minimum consumption, using Pontryagin method 07 p1184 A67-19149

Optimal control system having nonunique solution of Pontryagin equation and having separatrix between two strategies 07 p1160 A67-19203

Pontryagin maximum principle, discussing singular and nonsingular extremals

classification by numerical integration techniques 07 p1162 A67-20273

Extension of Pontryagin maximum principle to variable control region, using Hamilton equation 11 p1812 A67-24208

Satellite attitude control in elliptic orbit 11 p1869 A67-24337

Analog computer applied to solve two-point boundary value problem for fourth order optimal control problem with applied Pontryagin maximum principle 11 p1771 A67-24893

Time optimum control in n-dimensional linear dynamic system with constant coefficients determined by matrix method 13 p2087 A67-26619

Minimum of maximum overload in braking of vehicle in atmosphere, examining aerodynamic lift on basis of Pontryagin maximum principle 14 p2393 A67-27855

Book on variational calculus and integral equations, examining extremum conditions, Fredholm and Volterra integral equations, Pontryagin maximum principle, etc 16 p2696 A67-31200

Exact stability criteria for kinetics equations of coupled-core nuclear reactors, using Pontryagin theorem and models for time-distribution of coupling neutrons [ASME PAPER 66-WA/AUT-16] 17 p2882 A67-32015

Optimality conditions for nonlinear discrete systems, showing that at limit these conditions become Pontryagin maximum principle for continuous systems 18 p3017 A67-33871

Optimal control methods of Bellman and Pontryagin, discussing maximum rule and dynamic programming for optimization in presence of constraints 18 p3018 A67-34284

Book on optimal control covering theory and application of linear algebra, vector analysis, Euclidean space, Pontryagin principle, etc 18 p3018 A67-34758

Horizontal, solid, cantilever-beam profile with constant density, width and elasticity modulus determined, using Pontryagin principle 19 p3340 A67-35524

Pontryagin principle extension by mathematical formulation 19 p3204 A67-35904

Variational problem in optimal interaction systems with control constraints solved by dynamic programming and Pontryagin principle applications 20 p3407 A67-36440

Second order nonlinear optimal control system for various performance criteria using Pontryagin principle 20 p3410 A67-37252

Variational approach to error analysis in dynamic system computer simulation, applying maximum principle and Liapunov second method 21 p3588 A67-38180

Time optimal flight trajectories in planar and spatial pursuit problems with constraints on pursuer, using Pontryagin maximum principle 21 p3712 A67-39151

Optimal control problem with state variables subject to inequality conditions, deriving Pontryagin principle and differential equation 22 p3828 A67-39194

POODLE ROCKET ENGINE

POODLE low thrust radioactive propulsion technology, discussing operation, mission application, tests, capsule and thruster performance 05 p0843 A67-16551

SNAPOODLE isotope thruster/electric power unit, discussing thermal analyses, thruster and electrical performance and mission applications 05 p0753 A67-16552

Thermoelectric converter designed for operation with SNAPOODLE /hybrid radioisotope thruster/ electric generator/, discussing test results 24 p4184 A67-42507

POPULATION

Thermodynamics of electronic carrier populations in pure or doped dissociable binary semiconductor 01 p0130 A67-10198

Philadelphia International Airport facility planning based on forecasts, population and business growth, economic factors and historic trends 21 p3734 A67-38805

Selection probability from multivariable normal populations in terms of noncentrality parameters 23 p4024 A67-41084

POPULATION INVERSION

Approximate absolute values of pumping power, threshold power and critical excess population for ruby laser determined from relative flash tube intensity measurements 01 p0088 A67-10245

Elementary processes in DC gas discharge plasma in helium, comparing measurements of population levels of excited states of atoms with calculated values 01 p0123 A67-10363

Laser characteristics of narrow band type I solar radio burst and magnetic dipole transitions in split Zeeman sublevels of hydrogen atoms of solar corona in ground level 02 p0322 A67-11652

Temperature and stress dependence of electron lifetime in p-type Si-B and Ge-Zn between 1.5 and 4.2 degrees K 02 p0301 A67-12523

Fluorescent emission of neodymium laser triggered by Pockels effect as function of population inversion 03 p0436 A67-13201

Population inversion of upper laser level of carbon dioxide molecules, noting electron-molecule collision and effect of neon addition 03 p0437 A67-13297

Surface state density effect on electron mobility in Si inversion layer of MOS-FET 03 p0496 A67-13577

Spontaneous emission in inversely populated medium examined for uniform ruby rod laser with uniform pumping distribution 03 p0438 A67-14186

Temperature-composition relationship for Hall coefficient inversion point in Ti-doped Te single crystals 03 p0500 A67-14232

Radiation monopulse passage through amplifying and absorbing media having form of rods 03 p0374 A67-14329

Population inversion of upper laser level of carbon dioxide molecules, noting electron-molecule collision and effect of neon addition 04 p0631 A67-14722

Two-level resonator type laser using neutron-irradiated quartz single crystal with high recurrent inversion frequency 04 p0633 A67-15158

Population inversion variation during laser emission as shown by measurements of fluorescence intensity 04 p0634 A67-15497

Abrupt transmission change during ruby laser emission resulting from pumping with xenon flash lamp 04 p0634 A67-15649

Gas laser pumped microwave emission for producing controlled excited state population for RF spectroscopy of neon 05 p0817 A67-16638

Change in basic barrier relation for heterojunction compared to homojunction of wide gap emitter injection laser 05 p0825 A67-17097

Elementary processes in DC gas discharge plasma in helium, comparing measurements of population levels of excited states of atoms with calculated values 06 p1038 A67-17621

Giant pulse formation theory, measuring shape and duration of neodymium glass laser pulses for various values of inverse population 06 p1010 A67-17876

Effects of gain saturation by strong traveling fields in dilute laser media, noting atomic motion and line broadening 07 p1197 A67-20126

Helium-neon CW laser oscillation at 1.523 microns observed in high velocity gas flow system, using rapid mixing of metastable helium atoms with initially unexcited neon 09 p1510 A67-21568

Complete vibrational population inversion in molecular product of chemical reactions, finding stimulated emission 09 p1511 A67-21746

Population inversion of neon levels in He-Ne microwave discharge as affected by pressure and power scattered by unit discharge volume 09 p1512 A67-21924

Relaxation rate influence on power generation of gas laser and on magnitude of inverse population 10 p1684 A67-23335

Ruby laser output energy losses when passing from normal to passive Q-switched operation 11 p1800 A67-24241

Laser output pulse time dependence in acetone and nitrogen mixture, using indium antimonide detector 13 p2127 A67-27017

Population inversion of neon levels in He-Ne microwave discharge as affected by pressure and power scattered by unit discharge volume 14 p2330 A67-28253

Maser effect hypothesized as cause of 21 cm radiation in clouds of interstellar hydrogen in galactic corona 15 p2551 A67-29139

Lasing on Si II and Cl II lines in pulsed gaseous discharge, noting possible

mechanisms for achieving population inversion 15 p2496 A67-29178

Semiconductor laser output power varied by decreasing inverse population through heating electron-hole gas by intense optical radiation 15 p2496 A67-29236

Two-level resonator type laser using neutron-irradiated quartz single crystal with high recurrent inversion frequency 15 p2496 A67-29345

Gain of flowing carbon dioxide laser systems, noting extent of diameter dependence of gain, population variations, etc 15 p2497 A67-29390

Spectroscopic study of gas discharge parameters in argon ion lasers to determine level inversion mechanism in continuous or pulsed regime of generation 15 p2501 A67-30003

Laser characteristics of narrow band type I solar radio burst and magnetic dipole transitions in split Zeeman sublevels of hydrogen atoms of solar corona in ground level 16 p2747 A67-31067

Associated nonuniform electron-nucleus oscillations in ferromagnetic substances studied to determine feasibility of maser, using magnetic-reversal nuclear magnetic resonance 16 p2686 A67-31731

Line width vs optical thickness in pulsed argon-ion laser used to determine level population in plasma 17 p2867 A67-32452

Population of atomic levels by cascade, dielectric and three-body electronic recombination, discussing spontaneous transition, electron impact and RF spectra 17 p2947 A67-32762

Excited state and steady state populations in high pressure plasma with heavy particle collisional ionization and electron-ion recombination 17 p2909 A67-33228

Spectroscopic study of gas discharge parameters in argon ion lasers to determine level inversion mechanism in continuous or pulsed regime of generation 18 p3059 A67-33760

Depopulation of vibrational energy levels in fast chemical dissociation reactions 18 p2996 A67-33780

Diatom gas vibrational relaxation by master equation analysis, discussing quasi-steady state vibrational population distribution and transition probability increases 18 p3081 A67-33782

Emission equations describing radiation field amplitude and energy level populations of solid state laser with broad oscillation spectrum 18 p3061 A67-34388

Secondary ionization processes in mercury vapor, calculating relative populations of excited and metastable atoms per ion pair 19 p3265 A67-35090

Population inversion and spin-lattice relaxation effect on maser operation 19 p3304 A67-35547

Calculation of vibration level populations of polyatomic molecules in electronic ground state 20 p3457 A67-36216

Relaxation of carbon dioxide pulsed laser levels by collisions with hydrogen, showing gain dependence on hydrogen pressure 20 p3457 A67-36384

Ammonia inversion transition hyperfine structure for nitrogen 14 and 15 nuclear masses measured with two-cavity maser spectrometer 20 p3462 A67-37565

Laser population inversion using Fabrikant method, analyzing electron energy distribution in hollow cathode discharge 21 p3638 A67-37940

Rapid adiabatic cooling of gas systems for population inversion states 21 p3638 A67-37942

Electron temperature measurements of powerful pulsed plasma discharge using spectral line intensity 22 p3852 A67-39991

Giant pulse irradiation effect on ruby laser under oscillation quenching, amplification and characteristics changes in metastable state population 23 p4017 A67-41434

Ar II population inversion of 4s and 4p states in stationary arc discharge, measuring ionic and atomic spectral line shift, widths and intensities and emission power 24 p4196 A67-42245

Absorption characteristics for laser power stabilization using Rayleigh active material 24 p4187 A67-42360

Maser effect hypothesized as cause of 21 cm radiation in clouds of interstellar

- hydrogen in galactic corona 24 p4239 A67-43062
- POROSITY**
- SA BOUNDARY LAYER CONTROL
- SA FLUID INJECTION
- SA GAS INJECTION
- Porosity and particle size effects on magnetization curve of superconducting Nb sintered compacts with and without C added 12 p1978 A67-25139
- Stability of one-dimensional polyphase flow in porous medium studied using theory of servomechanisms 16 p2609 A67-31713
- Electron emission utilized in evaluating metal surface properties, particularly sintered material porosity 19 p3247 A67-35849
- Microwave use in measuring burning rate of solid propellant rocket motors and in detection of porosity in nonconducting materials 22 p3795 A67-39198
- POROUS BOUNDARY LAYER CONTROL**
- Integral energy equation for three-dimensional laminar boundary layer element on porous surface in presence of suction 11 p1783 A67-25052
- Approximation integral method for solution of coupled equations of heat and mass transfer in porous medium, discussing nonlinear and linear problems 20 p3553 A67-36938
- POROUS MATERIAL**
- Porous high efficiency predictable-pore-density tungsten ionizers for cesium ion engine 01 p0140 A67-10703
- Pressure distribution of porous self-lubricating bearing noting geometrical factors, dimensions, running speed, load, etc 01 p0079 A67-10708
- Powder metallurgical techniques for controlling porosity microstructures including powder selection, pore forming additives, compaction and sintering 01 p0100 A67-10723
- Two-layer model of lunar surface analyzed, using criteria of transparency to microwave radiation 02 p0324 A67-11700
- Materials for ablative cooling processes for rocket engines, noting structure and properties of porous and solid materials 02 p0306 A67-12791
- Metallurgical viewpoint of current status of porous refractory materials technology related to cesium contact ionizers 04 p0638 A67-15014
- Felted fibrous ceramic structures for thermal protection, fabricated by papermaking industry techniques, used for forming lightweight porous structures 04 p0642 A67-15452
- Relation between effective porosity and differential pressure of rigid steel and elastic nylon ribbon grids of various forms and porosities 06 p0944 A67-17630
- Compression and bending strength of porous materials prepared by sintering spheroidized powder refractory compounds increased by addition of cobalt chloride 07 p1208 A67-19307
- Flow field around porous wedge or cone immersed at zero angle of attack in uniform supersonic free stream when contact surface is straight 08 p1276 A67-20571
- Porous structures for ion engine application, discussing ionizer materials preparation, based on powder metallurgy and two-phase tungsten base alloy [AIAA PAPER 66-221] 08 p1341 A67-20576
- Permeability of porous materials of refractory compounds, determining experimentally relation between gas permeability, porosity and particle size 09 p1517 A67-21875
- Sintering of porous products of refractory compounds 10 p1687 A67-22827
- Porous W-Ta emitters as ion source for production of quiescent alkali plasmas of improved symmetry, reproducibility and uniformity 11 p1838 A67-24411
- Rate of formation of tungsten oxide in porous sample, noting increase in rate of oxidation due to porosity 11 p1809 A67-24915
- Pore formation, lifetime and microstructure of thin electrolytic metal films under load and high temperature at grain boundaries 12 p1955 A67-25448
- Fuel cell research noting gas porous electrodes, effect of geometry on performance and electrocatalysis 14 p2252 A67-29019
- Porous materials prepared from carbides, borides and silicides of refractory metals by oxidation reduction method, with simultaneous sintering of resulting active particles 16 p2683 A67-31596
- Cesium ion emission patterns from rear-fed porous refractory metals studied by thermal emission microscope 17 p2888 A67-33059
- Propellant injection through porous media, advantages, fluid flow nature, heat transfer, characteristics and uses [AIAA PAPER 67-463] 18 p3026 A67-33934
- Cesium vapor ionization on porous tungsten substrate creates gradients in surface atom concentrations diminishing ionization efficiency 20 p3487 A67-36170
- Bending strength dependence on porosity of sintered powdered glass beam 20 p3473 A67-36779
- Durability and electrical conductivity of metallic fiber materials noting influence of oxidation on properties 20 p3466 A67-36912
- Molecular flow mass spectrometer analysis of porous metal membranes for gases of different molecular weights 20 p3378 A67-37499
- Purification systems, filters and porous materials applications to liquids and gas systems associated with spacecraft, boosters and ground support equipment 21 p3570 A67-38103
- Steady motion of elastoviscous liquid through annulus between two coaxial right circular porous cylinders with suction and injection 21 p3613 A67-38411
- Pore formation, lifetime and microstructure of thin electrolytic metal films under load and high temperature at grain boundaries 21 p3646 A67-38827
- Body porosity effect on hypervelocity impact, computing pressure, velocity, density and specific internal energy profiles 22 p3912 A67-39748
- Porous cermet tubular element fire barriers of stainless steel powder for increased safety in gas flame processes, determining critical Peclet values 24 p4159 A67-41957
- Composite, reinforced and porous elastic body isotropic deformation, deriving macroscopic moduli, mean stress and strain values and dispersion 24 p4249 A67-42102
- POROUS PLATE**
- Heat-transfer coefficients and shearing stress in turbulent boundary layer along porous flat plate with uniform fluid injection 04 p0733 A67-15842
- Steady free convection in porous medium heated from below and accounting for end effects and mass discharge 06 p1113 A67-18127
- Differential equations for heat and mass transfer in laminar boundary layer of binary gas mixture flow past porous wet flat plate 14 p2242 A67-28307
- Counterflow diffusion flame in forward stagnation region of porous cylinder, detailing flame stability and velocity gradient 18 p3155 A67-33842
- Transpiration cooled porous surface in high temperature forced convection environment, applying transient energy balance with heat-transfer coefficient measurement [ASME PAPER 67-HT-27] 20 p3546 A67-36720
- Effect of initial flow turbulence on optimum suction of fluid from boundary layer of porous plate 24 p4143 A67-42282
- POROUS WALL**
- Uniform wall suction effect on inlet flow of porous cylindrical tube, noting laminar to turbulent transition 03 p0404 A67-13973
- Generalized Couette-type flow with variable viscosity in plane and annular channels, liquid being injected or sucked through porous surfaces 04 p0602 A67-14639
- Laminar flow through porous annulus with constant suction velocity at walls and swirl, using differential equations 16 p2662 A67-31551
- Wall suction rate effect on turbulent flow in cylindrical circular porous duct, measuring distributions of velocity, pressure, friction coefficient and Reynolds stresses 17 p2837 A67-32380
- Ignition conditions of pore walls in burning of porous charge, assuming ideal pores and same charge composition throughout system 17 p2974 A67-33142
- Flow of viscous incompressible conducting fluid in channel with porous walls 17 p2910 A67-33352
- Electron concentration in turbulent boundary layer of weakly ionized plasma when injecting electrons through pores in wall 18 p3087 A67-34053
- Parallel porous wall burner for studying premixed and diffusion flames in stagnation flows [CI PAPER 67-7] 19 p3345 A67-35002
- Temperature difference between solid and gas of transpiration cooled wall due to radiant heating [ASME PAPER 67-HT-29] 20 p3546 A67-36722
- Boundary layer theory applied to laminar flow with chemical reaction, considering coolant blown through porous wall and wall reaction with laminar boundary layer 20 p3424 A67-37345
- Partial differential equations solution in heat transfer between incompressible fluid and porous medium 22 p3917 A67-39640
- Mass efflux of Poiseuille flow over naturally permeable wall, discussing boundary layer effect 24 p4144 A67-42571
- PORPHYRIN**
- SA CHLOROPHYLL
- SA HEMOGLOBIN
- Interstellar material, emphasizing chemical characterization of dust by absorption spectroscopy 19 p3323 A67-35331
- PORABILITY**
- In-space hand-held electron beam welding gun design, testing and performance 20 p3454 A67-36575
- Ground vertical loop radio antenna for army use noting shape, performance, mobility, etc 20 p3399 A67-36884
- POSITION**
- S SOLAR POSITION
- POSITION ERROR**
- Hypersonic velocity effects on errors in vertical channel of inertial navigation system, particularly aboard artificial earth satellite 01 p0110 A67-10420
- Signal and clutter model of monopulse radar tracking errors 02 p0201 A67-12114
- Supersonic transport navigation system accuracy, reliability, directional measurement, inertial speed, etc 07 p1221 A67-19068
- Error due to multiple propagation in distance measurement by comparison of modulation phases on transmitted and reflected laser beam 07 p1186 A67-19068
- Evaluation of minimum-time courses for aircraft and inherent error 07 p1222 A67-19680
- Error model digital computer program applied to lunar surface hybrid navigation concepts, noting accuracy requirements from 1972 to 1985 08 p1351 A67-20675
- General mechanization in vehicular coordinates of gimballess inertial system for space navigation, obtaining equations for position errors and error damping method 08 p1351 A67-20698
- Statistical analysis of errors in angular measurement of distant objects due to gravitational scattering along light path 08 p1398 A67-21232
- Vehicle position determination using relationship between geographic and inertial coordinates, noting distinction between geodetic and geocentric latitudes and geocentric declination 11 p1786 A67-24353
- Astronomic data error effect on position of reference surface trigonometric net with regard to earth axis of rotation 11 p1787 A67-24593
- Meridian observation of Jupiter for planet position determination, analyzing discrepancies between ephemerides and observations, noting random error 11 p1868 A67-25087
- Error damping procedures for gimballess inertial navigational systems 16 p2701 A67-31268
- Inertial navigation horizontal position errors for medium L/D lifting body reentry vehicle using reference altitude for vertical channel stabilization 17 p2881 A67-32476
- Inertial tracker position error evolution, discussing equations and applicability to vehicle on ground or in circular orbit 17 p2882 A67-32725
- Astronomical determination of position on moon 18 p3120 A67-33864
- Radio astronomy sensitivity and resolution, discussing aperture synthesis and interferometric techniques for accurate position determinations 18 p3135 A67-34585

Satellite geodesy star catalog requirements, discussing accuracy of coordinates triangulation solution, criteria for homogeneity and extent of coverage, etc 18 p3043 A67-34586

First order perturbation solution for transition matrix relating errors at one point of two-body orbit to errors at later point 19 p3317 A67-34832

Hansen planetary theory representing position of disturbed planet as deviation in time and space from position of fictitious planet with Keplerian motion [AIAA PAPER 67-565] 19 p3328 A67-35961

Various minor planets positions from photographic observations at Crimean Astrophysical Observatory 20 p3523 A67-36630

Angular coordinates of pulsed incoherent scanning radar determined, comparing efficiency of direction finding by minimum rms error and maximum likelihood method 22 p3762 A67-39874

Flare positions relative to neutral line in longitudinal components of photospheric magnetic fields, stressing drift rate 23 p4060 A67-41231

POSITION INDICATOR

SA ALTIMETER

SA PLAN POSITION INDICATOR /PPI/

SA SEXTANT

SA SPACECRAFT POSITION INDICATOR

Inertial guidance platform as position sensor, discussing stabilizing gyro, pitch programmer and alignment 04 p0578 A67-15733

Aircraft position determined, using angle indications provided by vertical and directional gyro 07 p1189 A67-20151

Roll-angle indicators used for avoiding spatial disorientation during instrument flight 13 p2063 A67-26927

Performance characteristics of photodiodes with photoelectric cells as light-source position sensors 18 p3009 A67-33470

Radio astronomy sensitivity and resolution, discussing aperture synthesis and interferometric techniques for accurate position determinations 18 p3135 A67-34585

Automatic position determination for ships using active navigation satellite systems, discussing communications potential and safety 19 p3254 A67-35310

Aircraft position determination and surveillance requirements for ATC 19 p3256 A67-35860

Anharmonic method of photogrammetry rectification point by point, deriving positions from minimum control data 24 p4158 A67-42604

POSITION SERVO

Computer method for predicting servo positioner performance 05 p0753 A67-16235

POSITIONING

Satellite placing in synchronous orbit using ELDO PAS booster for telecommunications purposes 01 p0156 A67-11418

Optimal type of strategy of remote control and force sensitive and stable feedback presentation in master-slave manipulators with transmission delay 09 p1456 A67-22374

Limitation of radio position-finding with increased spacecraft distances, noting navigational methods from ground and spacecraft 11 p1817 A67-24707

Comparison of operator performance when using rotary selector, thumbwheel and digital pushbutton switches 15 p2430 A67-29135

Position determination of sonic points on head shock wave and blunt body surface in ballistics showing Mach number and gas type effects 16 p2593 A67-31132

Azimuth and zenith distance determined from simultaneous observations of topocentric coordinates of artificial satellite transformed into astronomical and geodetic quantities 20 p3428 A67-36483

Minor planets position observations at Crimean Astrophysical Observatory during August and September 1964 20 p3522 A67-36620

Minor planets position observations at Crimean Astrophysical Observatory from October 1964 through March 1965 20 p3522 A67-36621

Geometric satellite triangulation for position of fourth satellite, with position equations solved by least squares method and applied to geodetic satellites 20 p3429 A67-36890

POSITIONING EQUIPMENT

Apollo Guidance and Navigation System positioning by electrically torquing gyros, discussing error sources 01 p0073 A67-11115

Automatic directional-antenna position control system for ATS synchronous orbit spin-stabilized satellite 01 p0156 A67-11426

Configurations of hyperbolic position-fixing systems using synchronous satellites, showing Loran-like networks on earth resulting from these 09 p1526 A67-22393

Precise position and spectra of Scorpio X-ray source and location of two weaker sources in galactic plane, describing instrumentation used 12 p1995 A67-25761

POSITIVE FEEDBACK

S REGENERATION

POSITRON

Resonances in proton hydrogen and positron hydrogen scattering predicted at energies just below excitation thresholds 04 p0662 A67-15788

Solar flare microwave radio bursts, suggesting synchrotron radiation from relativistic positrons, calculating positron yield and synchrotron spectrum 20 p3519 A67-37101

POSITRON ANNIHILATION

Modified adiabatic scattering function applied to positron annihilation in helium 01 p0116 A67-10141

POST-BLAST NUCLEAR RADIATION

Artificial red aurora created in southern conjugate region by atmospheric nuclear burst 16 p2664 A67-30977

POSTURE

SA ORTHOSTATIC TOLERANCE

Tilt table response and plasma volume changes in experimental subjects evaluated before and after short term periods of deconditioning 17 p2805 A67-31953

Thorax radiological changes associated with physiological and posture changes, discussing chest dynamics 23 p3956 A67-41625

Conditioned falling reflex of analyzer systems effect on change of human posture and spatial position 24 p4114 A67-41848

POTABLE WATER

Potable water quality control and standards for aerospace systems 21 p3576 A67-38071

Hydrogen peroxide oxygen-water supply system as backup for long space flights noting storage tanks, catalytic reactor and heat exchanger 22 p3747 A67-39893

Chemical, physical, microbiological and radiological standards of aerospace system water potability 23 p3968 A67-41620

POTASSIUM

SA LIQUID POTASSIUM

Light modulation at hyperfine frequencies in optically pumped potassium vapor, noting detection techniques, optical absorption and dispersion 02 p0251 A67-11818

Neutron activation analysis applied to determination of Ar 40 and K 41 content of iron meteorites 02 p0326 A67-12045

Shock tube studies of magnetically induced nonequilibrium ionization in potassium-seeded argon plasma, noting electrical conductivity, current density, wall potential, Soule dissipation and radiation loss 09 p1540 A67-21788

Temperature dependence of saturated vapor pressure of sodium and potassium 09 p1579 A67-21857

Viscosity and thermoconductivity of vapors of sodium and potassium 09 p1579 A67-21865

Changes produced in urinary sodium, potassium, and calcium excretion in mice exposed to homogeneous magnetic field 10 p1600 A67-23819

Adiabatic flow of K vapor in supersaturated state noting supercooling and equilibrium through condensation jump 11 p1881 A67-24029

High temperature diffusion of potassium in single crystal and polycrystalline molybdenum 15 p2504 A67-29972

Electron emission and adsorption of potassium on tungsten single crystal faces, noting work function values 20 p3504 A67-36165

Film boiling of potassium on horizontal plate, discussing heat fluxes relationship to Berenson equation and heat transfer [AICHE PAPER 28] 20 p3552 A67-36832

Resonance electronic Raman effect and parametric induced anti-Stokes radiation in potassium vapor atoms 21 p3641 A67-38456

potassium vapor atoms 21 p3641 A67-38456

POTASSIUM ALLOY

Syringe injection system for seeding plasma with Na-K alloy in study of MHD power generation and propulsion 08 p1279 A67-20377

Plasma resonance absorption measurement in thin potassium foils, observing polarized light transmission at lambda 3270 10 p1691 A67-23478

Sodium-potassium alloy thermodynamic properties and ordering, with pairing model for configurational entropy loss 21 p3733 A67-39106

Index of refraction measurements near damage spots in KTN due to laser beam and electric field simultaneous presence 23 p4013 A67-40895

POTASSIUM BROMIDE

Heat of formation of KCl-KBr solid solutions and energy storage after proton irradiation 01 p0136 A67-11051

Fundamental absorption band structure of mixed KCl and KBr single crystals 05 p0872 A67-17493

Induced absorption in far IR by impurities and defects of single crystal of potassium bromide 09 p1557 A67-22571

Differential reaction cross section and internal excitation function from K and Br molecule crossed beam velocity analysis 11 p1750 A67-24991

POTASSIUM CHLORIDE

Heat of formation of KCl-KBr solid solutions and energy storage after proton irradiation 01 p0136 A67-11051

Dielectric behavior and point imperfections of high temperature KCl in microwave frequency range 02 p0299 A67-11896

Fundamental absorption band structure of mixed KCl and KBr single crystals 05 p0872 A67-17493

Third order elastic constant for NaCl and KCl single crystals by ultrasonic pulse techniques 07 p1238 A67-20218

POTASSIUM CHROMATE

Raman effect in solutions of potassium, sodium and ammonium dichromate and potassium dichromate single crystal 19 p3240 A67-35421

POTASSIUM COMPOUND

Zeeman field spatial orientation of paramagnetic spin-lattice relaxation for 2T2 states in rhombic symmetry, emphasizing application to Fe-doped potassium cobalticyanide and potassium ferricyanide 01 p0129 A67-10150

Far IR reflectivity of potassium tantalate analyzed as function of temperature, noting soft mode as temperature lowers towards Curie temperature far IR reflectivity of potassium tantalate 10 p1688 A67-22768

Preservation of viable microbes in anabolism in potassium salts determined improbable by failure to grow bacteria 15 p2427 A67-29118

Physical chemistry of potassium sulphate at high temperatures and use for MHD seeding 18 p3086 A67-33710

Second order Raman spectrum temperature dependence of strontium titanate and potassium tantalate 23 p4013 A67-40965

POTASSIUM IODIDE

Atmospheric ozone concentration measurement using potassium iodide method 16 p2676 A67-31376

POTASSIUM PERCHLORATE

Combustion characteristics and ballistic performance of dual layer propellant grains using polybutadiene/potassium perchlorate and polyurethane/ammonium perchlorate for end-burning type rocket motor 05 p0872 A67-16589

Aluminum fluoride effect on propagative ignition of fuel oxidant mixtures and on combustion between aluminum and oxygen 07 p1238 A67-19070

POTASSIUM PHOSPHATE

Ruby laser-induced effect of pulsed pressure on KDP crystal surface and thermal bulk effect on excitation of ultrasonic oscillation in crystal 08 p1337 A67-20417

Stimulated Raman effects in anisotropic crystal potassium dihydrogen phosphate with Stokes generations 11 p1800 A67-24243

Potassium dihydrogen phosphate inside laser cavity to achieve HF modulation 17 p2869 A67-33297

Scanning laser device using modified electro-optic display tube and potassium phosphate crystal mode selector 23 p4017 A67-41393

POTENTIAL

S CONTACT POTENTIAL
S COULOMB POTENTIAL
S ELECTRIC POTENTIAL
S GEOPOTENTIAL
S GRAVITATIONAL POTENTIAL
S IONIZATION POTENTIAL
S MORSE POTENTIAL
S PLASMA POTENTIAL
S VELOCITY POTENTIAL

POTENTIAL ENERGY

SA FROUDE NUMBER

Plasma stability examined in terms of potential energy of system under all displacements 03 p0480 A67-13730

Energy impulse vectors and kinetic moment tensor associated with body in gravitational field analyzed, using Brouwer theorem 04 p0658 A67-15494

Minimum potential energy principle and Rayleigh-Ritz method derivation of flutter equations for flat rectangular orthotropic panels 05 p0924 A67-17350

Second virial coefficient for atomic gas with divergent potential energy curves 07 p1225 A67-19122

Statistical basis for modified moment theory of elasticity that takes into account contribution of all deformation-tensor-component gradients to deformation energy 09 p1574 A67-21914

Stability of motions of satellite with rotor and cavity with liquid, reducing problem to solution of minimum change in potential energy of system 13 p2213 A67-27319

Potential model for helium-hydrogen interaction in thermal diffusion 13 p2161 A67-27729

Potentials occurring in excitation of highly ionized ions by electron impacts 15 p2520 A67-29527

Effective pair potential obtained for quantum electron gas to determine thermodynamic properties over large temperature and density range 15 p2533 A67-30383

Rectangular network analysis of displacement in disks and plates, developing differential equations and giving minimum conditions for potential energy 17 p2961 A67-32714

Mean internal potential for InSb lattice calculated, comparing empirical results with those obtained from Hartree and Thomas-Fermi-Dirac methods 18 p3095 A67-33442

Theory of available potential energy and rate of change and variational approach to atmospheric energetics 18 p3074 A67-34096

Long range first order interaction between two excited hydrogen atoms yielding perturbation energy matrix, discussing diagonalization process 18 p3083 A67-34517

Potential energy flux across isobaric surfaces in atmosphere indicates flux direction dependent on correlation sign between temperature and vertical velocity at surfaces 19 p3224 A67-35526

Performance characteristics in zero potential energy manual task, discussing work output 21 p3577 A67-38074

Thermodynamic stability conditions determined by potential functions of system potential at constant temperature and pressure 22 p3917 A67-39584

Potential energy release of stressed elastic body due to material removal and crack extension 22 p3911 A67-39679

Invariant form of strain-energy function of linearized elastic potential of isotropic thin shell using three-dimensional theory 24 p4249 A67-42156

POTENTIAL FIELD

Stability of steady state motions of solid body with one attached point located in potential force field 02 p0287 A67-11963

Field intensity probe measurements of potential distribution and I-V characteristics in AC arc plasma 03 p0475 A67-13087

Small oscillations of viscous incompressible fluid in container with free surface under action of potential force field 05 p0791 A67-16373

Strakhov method determination of optimum numerical filter for extraction of potential field signal from random noise background 05 p0767 A67-17390

Plasma density, electron temperature and

potential distribution measured across magnetic field, determining ion and electron-diffusion coefficients in plasma column 05 p0858 A67-17432

Field intensities and electron distribution function in hollow cathode, graphs show potential distribution along cathode axis 08 p1358 A67-20851

Semiconductor surface potential in ultrahigh vacuum and under controlled atmosphere 10 p1696 A67-23694

Local potential variational method to study runaway stability of electrons in two-component plasma 11 p1826 A67-23872

Quasi-static potential distribution in inhomogeneous volume conductor analyzed using Green theorem 11 p1746 A67-23991

Plasma confinement by HF multipole electromagnetic field, noting role of potential accompanying rotating magnetic field 11 p1839 A67-24425

Planar silicon transistors with improved performance and reliability due to metallic protection, noting low noise and surface potential stabilization 13 p2077 A67-26652

Earth gravitational potential field determined by satellite measurements, showing field in spherical harmonics form 13 p2116 A67-27395

Atomic collisions with negative ions, deriving transition matrices for resonance reactions and scatterings to analyze rearrangement process of associative electron detachment 14 p2350 A67-28149

Computational method for high altitude atmosphere density, orbital elements, drag coefficients and potentials from satellite displacement and velocity measurements 15 p2562 A67-30069

Internal resistance, potential fall and current distribution for staggered electrode geometry in MHD generator of Faraday type 16 p2599 A67-30528

Potential distribution and volt-ampere characteristics of ionized gas flows in ducts 16 p2713 A67-30598

Velocity potential near disturbance boundary for steady supersonic flow past body-and-wing model 17 p2790 A67-32403

Potential theory problems with potential distribution over surface solved by Tricomi equation 17 p2878 A67-32716

Gunther solution representation for stress fields noting tensor potential theorem, second order tensor fields, etc 17 p2964 A67-33136

Stability of steady state motions of solid body with one attached point located in potential force field 17 p2886 A67-33280

Ionizer with three-electrode electron gun, noting potential distribution between electrodes and ionization efficiency 18 p3080 A67-33722

Space-charge and potential distributions calculated for region between two plane electrodes of single collision model 19 p3265 A67-35129

Potential fields representation for electrostatic image tubes with curved cathodes, using analytic functions 19 p3194 A67-35544

Quasi-conical motion past wing-body lifting system, determining pressure distribution, potential expression and axial disturbance velocity 20 p3356 A67-36278

Cesium plasma diode investigated using ribbon electron beam probing technique, discussing stability of electric potential distribution modes 20 p3496 A67-36329

Potential field distribution in n-GaAs devices before and after switching indicate carrier generation in narrow region near anode 20 p3510 A67-36853

Particle paths in central force field derived through second order differential equation for inverse separation, noting perturbation potential 20 p3526 A67-37254

Physical aspects of plasma accelerator using closed Hall currents, discussing equilibrium of forces and potential distribution 21 p3663 A67-37938

Reflex klystron electron admittance dependence on potential distribution in repeller space, showing electrode structure and space charge effects 21 p3598 A67-38604

Distributions of current, potential, electron density and pressure and ion velocity vector orientation in MPD arc, verifying electromagnetic effects presence [AIAA PAPER 67-676] 21 p3871 A67-38709

Stationary state of collisionless plasma in magnetostatic and potential fields, deriving distribution functions and concentration formulas 22 p3842 A67-39243

DC potential solutions for low pressure Cs diode with zero slope at emitter noting stability, oscillations and instability for ion/electron ratios 23 p4031 A67-40886

Isothermal equilibrium of constant volume gas mixture under external mass forces field deriving from time independent potential 24 p4257 A67-43113

POTENTIAL FLOW

SA CARTAN SPACE

Conformal mapping of circle onto profile cascades with arbitrary parameters useful for exact computation of potential flow through cascade 01 p0005 A67-10277

Potential flow of ideal gas with acoustic surface coinciding with characteristic 01 p0053 A67-10999

Free streamline theory of two-dimensional separated potential flow past bluff body and formation of periodic vortex turbulent wake 02 p0178 A67-12233

Instability of nonlinear stationary oscillations of potential in electron-ion flows useful in distribution functions of ions and electrons 03 p0470 A67-12935

Von Karman-Pohlhausen boundary layer analysis of temperature and velocity profiles in inlet region between two parallel planes with relative motion and pressure gradient 04 p0729 A67-15808

Potential flow theory design of subsonic flow diffusers for centrifugal compressors, assuming compressible irrotational inviscid channel flow [ASME PAPER 66-WA/GT-9] 04 p0550 A67-15938

Propellant injection through electrodes effect on potential distribution in MPD arc [AIAA PAPER 67-49] 06 p1074 A67-18435

Nonlinear singularities method for calculating velocity distribution over thick wing of finite aspect ratio situated at zero angle of attack in incompressible frictionless potential flow 07 p1127 A67-19887

Unsteady aerodynamic field with application to panel flutter in low supersonic flow 08 p1418 A67-20608

Two-dimensional incompressible potential flow theory for airfoil design with prescribed velocity distribution over surface 09 p1437 A67-21740

Aerodynamic problem of steady potential flow and added mass in unsteady motion of idealized hemispherical parachute 09 p1438 A67-22485

Incompressible potential flow about arbitrary body shapes calculated, using singularity distribution over body surface computed as solution of integral equation 10 p1589 A67-22871

Supersonic motion of plate in two-component medium in two dimensions 10 p1628 A67-23647

Heat transfer from isothermal sphere to low Prandtl number fluid in steady and nonsteady potential flow compared with Stokes flow 11 p1882 A67-24119

Oscillation and stability of system of thin elastic shells in potential inviscid and incompressible fluid flow 12 p2023 A67-25589

Parametric self-excited vibrations of plates of finite length in plane supersonic flow, applying linearized potential flow theory, deriving frequency 13 p2218 A67-26804

Potential flow about two-dimensional hydrofoils with zero velocity boundary condition 13 p2095 A67-26910

Axially symmetric potential flow about slender body, noting source strength distribution and solution via integral equations 13 p2095 A67-26911

Unbounded laminar plate oscillations in bilateral potential ideal gas flow with uniform physical and mechanical parameters 15 p2575 A67-30009

Wing profile effect on thin wing aerodynamic characteristics approaching screen in incompressible fluid potential flow 18 p2981 A67-33412

Existence and stability of rectilinear translation motions of blunt body submerged in potential flow of incompressible fluid at rest at infinity 18 p3027 A67-34183

Potential flow stability of weightless incompressible fluid for specific flow geometries 18 p3028 A67-34219

Super-Alfvénic counterpart of transient sub-Alfvénic aligned-fields flow past airfoil 19 p3170 A67-35538

Potential delta well model for barrier in solid state tunneling 19 p3308 A67-36039

Perfect fluid theory analyzed from resistance viewpoint and compared with flow past material body when viscous, discussing potential flow 20 p3419 A67-36189

Two-dimensional potential flow through bend profile, obtaining streamlines and velocity distributions 20 p3356 A67-36533

Aerodynamic forces of harmonically oscillating cylindrical duct with supersonic internal flow within framework of potential flow theory 20 p3357 A67-37003

Unbounded laminar plate oscillations in bilateral potential ideal gas flow with uniform physical and mechanical parameters 20 p3542 A67-37539

Oscillation and stability of two irregular thin elastic cylindrical shells in potential flow of compressible fluid 21 p3720 A67-38296

Performance prediction of low solidity cascades from potential flow calculations 21 p3566 A67-39079

Incompressible potential flow about thick wing profiles and cascades for blade profiles with angular and round tapered trailing edges 23 p3929 A67-41254

POTENTIAL GRADIENT

Hall effect in low temperature plasma consisting of combustion products with admixture of KOH under variable sign magnetic field, demonstrating potential gradient existence 01 p0120 A67-10175

Radiosonde for measurement of electric potential gradient in atmosphere at high altitudes 01 p0068 A67-10870

Measurement and control of corona-generated noise in aircraft, noting charge rate during takeoff via potential gradient method 02 p0190 A67-11501

Potential difference variation in circuits consisting of diode, capacitance and active resistor 02 p0209 A67-11509

Plasma probe for dense isothermal cesium plasma, noting electron concentration and temperatures, potential distribution, etc 02 p0184 A67-12467

Uniform electric field quadrupole polarizabilities and shielding factors for S-state atoms and ions, demonstrating independence of factors from existence of field gradient 03 p0472 A67-13321

Atmospheric potential gradient near ground in polar region correlation with solar radio emission on 1000 mc 07 p1172 A67-19423

Magnetic effect on injected plasma density and anomalous potential in semiconductor rods 09 p1552 A67-21761

Device for measuring potential fluctuations in turbulent flow of distilled water 09 p1501 A67-22562

Solar eclipse effect on atmospheric potential gradients analyzed, noting negativity and variation pattern with five peaks 10 p1651 A67-23347

Reduced thermodynamic potentials of large classes of refractory metal carbides and nitrides 11 p1804 A67-23901

Dynamic Newtonian gravitational force gradient fields generator to calibrate response of dynamic gravitational gradient sensor 11 p1794 A67-24903

Drift field, field gradient and diffused impurity effects on minority carriers and quantum efficiency in silicon photocells 11 p1746 A67-24914

Atmospheric electricity conditions at ground level independent from auroras and potential gradients 11 p1857 A67-25031

Atmospheric potential gradient relation to solar activity at earth surface in polar region 14 p2306 A67-27884

Voltage gradient determination throughout two-dimensional electric field by electro-optic analog, noting applicability to boundary value problems satisfying Laplace equation 17 p2818 A67-32418

Formulas for potential temperatures derived from thermodynamic principles, considering four stages of reversible adiabatic transformation of humid air 17 p2844 A67-32566

Voltage drop near electrode during plasma and electric field interaction in electrical discharge tube, giving plasma current-voltage curves 17 p2907 A67-33090

Ambipolar potential-enhanced loss in magnetic trap reduced by potential difference in magnetic mirror throats dividing field 17 p2909 A67-33118

Electrode in low temperature air plasma containing potassium, investigating cathode potential drop, current density dependence, current-voltage characteristics, temperature, etc 18 p3088 A67-34054

Earth gravitational potential on geoid expressed by vertical and horizontal gradients for gravitational anomalies useful in earth figure determination 21 p3618 A67-38199

Magnetic field critical current density characteristics of Nb-Zr-Ti superconducting alloys, discussing peak effect and barrier height random distribution 23 p4044 A67-41451

Data analysis on electric potential gradient and air-to-earth current density 24 p4181 A67-41792

POTENTIAL PROBLEM

Vector potential representation of planar logarithmic spiral antenna field 03 p0378 A67-13285

Single layer potential solution to boundary value problems for heat equation in half-plane with one or two points of discontinuity in boundary conditions 03 p0459 A67-13590

Displacement potential for solutions of displacement equilibrium equations obtained by Mindlin for linear elastic medium where stresses are functions of strains and strain gradients 03 p0524 A67-13661

Virial theorem for electron plasma obtained by defining potential tensor and superpotential of electric field 03 p0482 A67-13746

Potential distribution and field dependence of electron velocity in bulk GaAs measured with point contact probe 03 p0499 A67-13985

Smoothness of thermal potential and existence of solution for second and third boundary value problems with directional derivative for parabolic equation 04 p0721 A67-14669

Conducting surface boundary effect on current plasma instability in terms of potential fluctuations 04 p0667 A67-15208

Concentration and density distributions of particle flux near body moving in rarefied plasma 05 p0855 A67-17122

Stability of flexible conductor in longitudinal magnetic field, using scalar potential to determine disturbed state 06 p1040 A67-18095

Nonlinear PDE for magnetostatic field with variable permeability in discontinuous medium solved with digital computer 07 p1132 A67-19795

Lunar landing problem, determining position, velocity and acceleration as functions of time from ignition to shutdown [AAS PAPER 66-121] 07 p1254 A67-19980

Boundary value problem for potentials in volume conductor based on Green theorem 08 p1288 A67-20601

Spatial variation of quasi-Fermi potentials in symmetrical step and linearly graded p-n junctions 09 p1556 A67-22201

Heat transfer in conducting and radiating gas analyzed, using governing equations reformulated as Lagrangian equations through introduction of potential 12 p2035 A67-25926

Lunar landing problem, determining position, velocity and acceleration as functions of time from ignition to shutdown [AAS PAPER 66-121] 13 p2209 A67-27535

Generalized potentials for medium energy inelastic nuclear scattering derived with projection operator method 14 p2350 A67-27789

Conducting surface boundary effect on current plasma instability in terms of potential fluctuations 15 p2532 A67-30256

Wave equation solution for potential of cylindrical Dirac pulse incident on reflecting half-plane 17 p2817 A67-33139

Concentration and density distributions of particle flux near body moving in rarefied plasma 21 p3668 A67-38485

Ground proximity effect on aerodynamic characteristics of slender wings by extension of slender body theory, solving potential function equation 23 p3930 A67-41310

POTENTIAL THEORY

Solutions for boundary value problems of

potential theory and elasticity theory for single cavity hyperboloids of revolution 02 p0338 A67-11955

Approximate solution of Gelfand-Levitan equation leading to localized bound-state wave function examined in S-matrix approach to first order energy shift 02 p0270 A67-12637

Equilibrium shape of earth, discussing space science discoveries and hydrostatic flattening mechanism 06 p0994 A67-17767

Inverse problems of potential theory analyzed for uniqueness of solution 06 p1023 A67-17861

Book on mixed boundary value problems in potential theory 06 p1024 A67-18427

Exact expression for thermodynamic potential in reversible-transformation continuums, for isothermic case of finite deformations of homogeneous and isotropic elastic bodies without inner constraints 06 p1119 A67-18583

Relation of magnetization of any homogeneous isotropic ellipsoid to local field and external applied magnetic field deduced from Maxwell equations and potential theory 07 p1234 A67-20127

Intermolecular forces in methyl chloride and benzene calculated using spherical shell central potential theory 07 p1138 A67-20191

Steady state theory of discharge column, giving solutions to density and potential profiles for planar and cylindrical geometry 08 p1361 A67-21134

Terrestrial behavior under action of time dependent periodic potential, treating earth as Maxwell body for shear processes 08 p1325 A67-21211

D'Alembert initial value problem for cylindrical waves, obtaining linearized potential equation for plane and symmetrically spherical case 09 p1488 A67-21932

Electric field in MHD channels in presence of near-electrode potential drop 11 p1840 A67-24671

Three-dimensional elastostatic problems for infinite solid with geometric discontinuities solved using potential functions 13 p2221 A67-27735

Solvability and methods of solution of boundary value problems noting uniqueness, potential theory application in solving polyharmonic equations and second-order equation 16 p2698 A67-31737

Potential theory problems with potential distribution over surface solved by Tricomi equation 17 p2878 A67-32716

Boundary value problem solution for three-dimensional layer in axisymmetric case 17 p2885 A67-32882

Solutions for boundary value problems of potential theory and elasticity theory for single cavity hyperboloids of revolution 17 p2966 A67-33272

Energy-momentum density and superpotentials in privileged frame of reference, giving results due to Einstein and Freud pseudotensors 19 p3281 A67-35048

Grid functions from nodal values on rectangular surface used to solve potential equation by finite difference method 19 p3342 A67-35717

Kinetic prediction theory for viscosity, thermal conductivity and diffusivity of binary liquid mixtures composed of molecules interacting with square-well potential 23 p4083 A67-41531

POTENTIOMETER

Linear equations solving methods on analog computers where system parameters are reproduced, using potentiometers and admittances 02 p0209 A67-12683

Dynamic behavior of potentiometer pressure transducers by direct experimental measurement of plan-phase diagrams to one-displacement-step response 08 p1312 A67-20768

Atmospheric long range spectral transmissivity measured by single beam photometer with recording potentiometer added to reduce beam noise 13 p2119 A67-26689

Space vehicle potentiometer, noting niobium diselenide lubricant and minimum frictional torque 14 p2325 A67-28770

Transverse-conduction photopotentiometer operating as functional energy converter, calculating resistive layer required for device operation 18 p3009 A67-33469

Simultaneous and independent

potentiostatic control of rotating ring and disk electrode and application to CuII/CuI/Cu system 20 p3446 A67-36655
Atmospheric long range spectral transmissivity measured by single beam photometer with recording potentiometer added to reduce beam noise 21 p3627 A67-38431
Phase delayed triggering of oscillographs using ring type potentiometer to produce phase displacements by mechanical rotation 22 p3799 A67-39754

POTENTIOMETRY

SA ELECTRIC CURRENT

Physicochemical processes in thin evaporated films studied in terms of emf of galvanic cell with film acting as electrode 02 p0290 A67-11735
Semiautomatic potentiometer measurement of nitrogen specific heat at small intervals, noting applicability of logarithmic law for other temperature ranges 03 p0532 A67-12929

POTTING COMPOUND

Optical coupling of photomultiplier tube to acrylic plastic using clear silicone pottting compound 24 p4158 A67-42700

POWDER

Diffuse spectral reflectance of optically thick cloud and powder layers composed of particles with strong IR resonance, noting effect of particle size [AIAA PAPER 65-667] 03 p0467 A67-13047
Powder admixtures influence on critical diameter of detonation of solid, continuous and macroscopically homogeneous explosive, noting inorganic admixtures role 04 p0723 A67-15197
Ignition of explosive powder by hot gas stream, with particular attention to heat transfer between substance and surrounding medium 06 p1112 A67-17956
Nonstationary combustion of powder under action of pressure pulse to determine temperature field variation and burning rate during transient process 06 p1112 A67-17957
Heat transfer through various silicate powders measured for lunar surface temperature studies, comparing theoretical results [AIAA PAPER 67-285] 12 p2035 A67-26002

POWDER METALLURGY

SA AUTOCLAVE PROCESS

SA SINTERING

Modern developments in powder metallurgy - International Conference, New York, June 1965, Volume I, Fundamentals and methods 01 p0096 A67-10691
Sintering mechanisms in powdered compacts of carbides, oxides and metals, examining grain growth, pore decrease and diffusion coefficients 01 p0096 A67-10694
Sintering of cobalt-nickel powder mixtures during formation of solid solutions, noting shrinkage and diffusion coefficients 01 p0096 A67-10695
Powder metallurgy - International Conference, New York, June 1965, Volume 2, Applications 01 p0097 A67-10696
Nickel-thoria powder produced by pressure hydrometallurgy techniques and dispersion-strengthened by compaction and rolling, noting tensile stress-rupture properties revealed by optical and electron microscopy 01 p0097 A67-10697
Sintered Ni-base heat resistant alloys, discussing composition-creep strength relation, grain size, prealloyed-powder production and thermal and structural shock properties 01 p0098 A67-10700
Gravity sintering and low pressure pressing of tungsten powders for economic production of large diameter W matrices 01 p0098 A67-10701
Modern developments in powder metallurgy - International Conference, New York, June 1965, Volume 3 01 p0099 A67-10706
Hot pressing of electrolytic grade CR beryllium, noting powder manufacturing process and quality control procedure 01 p0099 A67-10707
Powder metallurgy techniques for thermoelectric materials particularly lead telluride, germanium bismuth telluride and zinc antimonide 01 p0099 A67-10709
Sintered-metal friction materials from metallic and nonmetallic powders, noting composition 01 p0099 A67-10710
Powder metallurgy techniques and solid state reactions in alloy constitution research, examining advantages of sintering method

over modern melting methods 01 p0099 A67-10711

Powder metallurgy applications in space vehicle systems, discussing parts and materials actually used in successfully orbited spacecraft 01 p0100 A67-10712

Powder metallurgical techniques for controlling porosity microstructures including powder selection, pore forming additives, compaction and sintering 01 p0100 A67-10723

Compatibility and interaction characteristics of SiC and B fibers with metal matrices in composites prepared from powder metallurgy by hot pressing 03 p0444 A67-13430

Fiber reinforced composites with high strength high temperature resistance, using powder metallurgy and honeycomb structures 03 p0429 A67-13437

Cermets as substitutes for common carbon and alloyed steels, iron and nonferrous metals, discussing powdered metal technology and applications to structural materials 06 p1015 A67-17842

Particle microhardness and microbrittleness measured in powdered refractory compounds, noting relation to electron configuration 06 p1015 A67-17846

Hexagonal indexing of tungsten boride phase in reaction of boron with tungsten core, obtaining X-ray powder diffraction pattern 06 p1016 A67-17904

Surface and internal structural formation mechanism of metallic contact from plastic deformation of SAP type alloys under compression 07 p1208 A67-19303

Structural, physical and mechanical properties of hard alloys formed by sintering powdered VK 15 tungsten cobalt alloy with nonuniformly distributed carbide phase 07 p1208 A67-19305

Compression and bending strength of porous materials prepared by sintering spheroidized powder refractory compounds increased by addition of cobalt chloride 07 p1208 A67-19307

Porous structures for ion engine application, discussing ionizer materials preparation, based on powder metallurgy and two-phase tungsten base alloy [AIAA PAPER 66-221] 08 p1341 A67-20576

Metal working problems involving sheet metal, powder metallurgy, extrusion, nondestructive testing and concerning high strength, refractory and superalloys [SAE PAPER 670098] 09 p1509 A67-22540

Beryllium oxide occurrence, fabrication, properties and application 09 p1520 A67-22614

Activated sintering of beryllium 13 p2140 A67-27129

Microalloying beryllium for improved sintering characteristics and mechanical properties 13 p2140 A67-27130

Gas pressure bonding for hot isostatic pressing of beryllium powder into complex shapes 13 p2123 A67-27131

Mechanical properties of beryllium with emphasis on influence of anisotropy in forming and grain size in powder metallurgy 13 p2140 A67-27134

Aluminum powders and aluminum powder metallurgy products properties, discussing powder and particle applications in metallurgy 14 p2335 A67-27809

Heat resistance in air of dispersion hardened nickel alloys containing certain oxides prepared by powder metallurgy methods 14 p2336 A67-27867

Nb-N system diagram for five stable nitride phases, giving two reactions governing high temperature phase fields 14 p2337 A67-28419

Tungsten powder compacts impregnation technique by metallic halides solutions, obtaining even distribution of metal 14 p2338 A67-28614

Powder-metallurgical methods using mechanical filling, isostatic pressing and high vacuum-high temperature sintering for fabrication of airfoil turbine-blade blocks 17 p2865 A67-32821

Properties of pressed and sintered products of powder metallurgy, noting strength and ductility increase with increase in density 20 p3465 A67-36496

Slip casting of niobium carbide powders, noting effects of dispersed phase contents, pH variation and temperature on molding properties 20 p3466 A67-36909

Rate of diffusion and degree of density

during activated sintering of tungsten-molybdenum powders, noting influence of nickel additive 20 p3466 A67-36911

Particle microhardness and microbrittleness measured in powdered refractory compounds, noting relation to electron configuration 20 p3471 A67-37588

Aluminum magnesium alloys prepared by powder metallurgy and hot extrusion evaluated for tension, compression, impact, fatigue and creep 22 p3821 A67-40053

Composite materials development and application in powder metallurgy, considering laminated, fiber and particle reinforced materials 23 p4017 A67-40711

Pressure sintered GaSb-GaAs alloys investigated for densification and thermoelectric properties 24 p4204 A67-42346

POWDERED ALUMINUM

Aluminum particle combustion noting changes from preignition to burnout, flame structure, particle geometry, etc [WSCI PAPER 66-3] 22 p3919 A67-40224

POWDERED METAL

Two metal-powder sintered composites reinforced with metal fibers or fiberglass for increased tensile and impact strength at various temperatures 01 p0098 A67-10705

Aluminum and tungsten carbides formed from metal powders mixed with acetylene black and exposed to explosive shock 03 p0440 A67-12927

Aluminum powder damping of HF instability in solid propellant combustion in vortex burner 06 p1115 A67-18307

Fatigue of powder metal compositions, discussing data from rotating beam and reverse bending fatigue tests 10 p1667 A67-22702

Aluminum powder damping of HF instability in solid propellant combustion in vortex burner [AIAA PAPER 67-104] 21 p3732 A67-38860

TiC and ZrC powder properties after sintering investigated for linear growth rates vs temperature, obtaining sintering activation energy values 22 p3820 A67-39564

WC-NbC-Co alloys oxidation resistance in air studied by sintering powdered WC and NbC with Co, finding oxidation rate linear function of time 22 p3820 A67-39565

Spontaneous inflammability temperatures of Al, Mg and Al-Mg alloy powders measured noting moisture effect 22 p3919 A67-40325

POWER

S ENERGY

S FLUID POWER

S FORCE

S NUCLEAR POWER

S RESOLVING POWER

S SOLAR POWER SYSTEM

S THERMAL POWER

S THRUST POWER

POWER CONVERSION

SA ELECTRIC POWER CONVERSION

SA NUCLEAR POWER CONVERSION

SA TURBOELECTRIC CONVERSION

Power amplification/bandwidth product of active device as measure of rate at which power supply energy converts to signal energy, noting TWT role 01 p0032 A67-10011

EFM, interplay of electric fields with insulating fluids which cannot remain nonconductive at high temperatures, considering astronautics application 01 p0014 A67-11408

Maximum power transformed by nonlinear capacitance of semiconductor diode on closed p-n junction 02 p0210 A67-11510

Electric motor energized by microwaves in waveguides at S-band, investigating speed, torque and frequency characteristics 02 p0183 A67-12116

Closed Brayton cycle power conversion system development, discussing rotating components and single phase operating fluid [AIAA PAPER 66-889] 02 p0183 A67-12268

High temperature cobalt iron alloy for square loop and power transformer applications 05 p0864 A67-16833

Comparison of various electrostatic thrusters and proposed low pressure colloidal power converter for high payload lunar and planetary missions [AIAA PAPER 66-211] 05 p0874 A67-17216

Perfect thermodynamic vapor conversion and application to power conversion cycles 07 p1268 A67-19367

Flexible solar cell concept, discussing historical background, conceptual design and

future plans 07 p1132 A67-19877
 Pulse width modulation voltage regulator design for power conversion applications, considering interrelation of loop gain, switching frequency, etc 08 p1284 A67-20693
 Voltage transformation and power/energy utilization of radioisotopic thermoelectric generator source /RTG/ for space applications, analyzing components, inverter/converter circuits, etc 08 p1284 A67-20694
 DC-to-DC prime converter for anchored interplanetary monitoring platform spacecraft /AIMP/ transforming power from solar array into suitable level for instrumentation electronics 08 p1284 A67-20695
 Minimum volume conditions for MHD conversion duct with known upstream and downstream stagnation 09 p1443 A67-21800
 Varactor junction diode frequency multipliers emphasizing maximum conversion power and efficiency 10 p1609 A67-22836
 Single frequency light from argon FM laser with external lithium niobate modulator, discussing overall conversion efficiency and distortion reduction 10 p1664 A67-22906
 Two-phase liquid metal cycle MHD conversion, discussing thermodynamic aspect, hot gas system and possibility for use in spacecraft and ground power plants 12 p1896 A67-25121
 High density power converter using integrated circuits and thyristors, noting packaging 12 p1911 A67-25274
 Liquid metal MHD cycles with condensation by multistage injection of liquid 12 p1897 A67-25379
 Solar concentrator technology, discussing design requirements of space power conversion devices and manufacturing methods 13 p2055 A67-26826
 Maximum power transformed by nonlinear capacitance of semiconductor diode on closed p-n junction 14 p2283 A67-28073
 Power conversion circuits of Surveyor spacecraft including distribution system, battery charging and central regulator units 17 p2803 A67-32510
 Cycle and separator efficiencies and specific radiator area compared for liquid alkali metal-lithium MHD power generators 21 p3572 A67-38864
 Surveyor TV power conditioning circuit and product design, discussing weight saving features, reliability and magnetic housing 22 p3807 A67-40374
 Power conversion derivation in nonlinear resistive element in series with linear resistors 23 p3981 A67-41395
 Small scale Rankine cycle power conversion system using potassium working fluid under environmental, RF interference and ground performance tests 24 p4102 A67-42491
 SNAP-8, nuclear electric power-conversion system /PCS/ designed for operation in space, using liquid metals as working fluids 24 p4184 A67-42497
 Aerospace automatically activated electrochemical battery and DC-DC high voltage converter-regulator noting storage stability 24 p4108 A67-42541

POWER DENSITY

Determination of maximum number of nonzero elements in nonnegative matrix and first power for which maximum density is assumed 01 p0105 A67-10731
 Near field power density incident on eyes due to reflection from CW laser reduced by optical lens and shutter rearrangement 10 p1665 A67-23415
 Linear induction MHD generator with cryogenically cooled coil windings for alleviating large gap and short stator problems 12 p1898 A67-25380
 Solid fueled rocket powered MHD generators with high power densities 12 p1898 A67-25382
 Nonuniform distributed network problems solved by Lie algebras 12 p1919 A67-25979
 Nonlinear Bayes detector synthesized for Gaussian signal and noise fields using Wiener filters 12 p1919 A67-26087
 Generator parameters and thermal efficiencies optimization for gas-cooled MGD reactor system, studying temperature and partial-pressure relation to power density 16 p2604 A67-30571
 Nonsteady combustion MHD open cycle

generator improving power density by modulation of conductivity and particle velocity 16 p2607 A67-30595
 Maximum power density, maximum efficiency of diagonal wall generator, Faraday generators and Hall current generators compared 16 p2608 A67-30597
 Thermionic space power systems, examining solar, radioisotope and nuclear reactors as heat sources, discussing power density and electrode affinity 17 p2802 A67-32050
 Probability density function measurement, discussing turbulence problem, power spectral densities, Rice formula, inversion, etc 20 p3442 A67-36461
 Solar activity effect on distribution of source power of solar diurnal cosmic ray variation in relation to ecliptic plane 23 p4058 A67-41125
 Comparison of flat channel linear MHD induction generator analysis stressing gross power output in constant current and voltage modes 23 p3942 A67-41737
 Two-photon absorption in semiconductor laser in relation to upper limit of transmission power density 24 p4200 A67-41863
POWER EFFICIENCY
 Insulated gate FET tetrode with high drain breakdown potential 01 p0033 A67-10025
 Output power of frequency multiplier using varactor diode for given output voltage and terminal resistances at various harmonics 01 p0039 A67-10857
 Weight, efficiency and control requirements of subsystems of electric propulsion applied to Mars missions, selecting power-conditioning modules for ion propulsion engines [AIAA PAPER 66-501] 02 p0302 A67-11516
 Air cushion vehicle design, calculating annular nozzle, air channel optimum parameters, power capacity, aerodynamic characteristics, etc 02 p0179 A67-12437
 Klystron amplifier performance, noting increased efficiency by using double interaction in output circuit 02 p0222 A67-12531
 Comparison of piston engine with turbojet engine noting power-weight ratio, specific fuel consumption, performance characteristics, etc 03 p0502 A67-13005
 Pulsed gas discharge lasers noting required energy level for maximum efficiency, experimental techniques and results 05 p0819 A67-18650
 Traveling wave ruby laser as radar transmitter noting power gain, coherence, frequency shift and single mode of operation 05 p0819 A67-18657
 Direct-to-home TV broadcasting satellite system for upper UHF, describing stabilization, thermal control, antenna, power amplifier, etc [AIAA PAPER 66-309] 06 p1094 A67-17689
 Direct-to-home TV broadcasting satellite system for upper UHF, describing stabilization, thermal control, antenna, power amplifier, etc [AIAA PAPER 66-309] 06 p0964 A67-18414
 Mach and cavitation number effects in fluid dynamic elements and circuits such as operating pressure limit, power consumption and output 08 p1320 A67-20455
 Empiric design of taper for increasing efficiency of coupled cavity traveling wave tube 09 p1476 A67-22211
 Electronic conversion efficiency in gridless two-cavity klystrons for cylindrical and sheet beams 10 p1811 A67-23062
 Reversible and irreversible limitation of maximum power output from GaAs by thermal heating and surface damage 10 p1665 A67-23520
 Epitaxial GaAs Gunn effect oscillators, showing importance in high efficiency of preparation and method of contacting material and resonant cavity design 10 p1616 A67-23533
 Gunn effect devices high efficiency achievement, considering circuit and material from theoretical and experimental viewpoint 10 p1616 A67-23535
 GaAs semiconductor quantum generator heating during injection pulse, analyzing temperature effect on external quantum output and generator efficiency 10 p1666 A67-23568
 Longitudinal target defocusing effect on

solar reflector power parameters, noting energy redistribution phenomenon 12 p1896 A67-25323
 Linear induction MHD generator with cryogenically cooled coil windings for alleviating large gap and short stator problems 12 p1898 A67-25380
 Vidicon TV design modifications for spacecraft applications noting reduced power requirements, improvement of heaters, narrowing of bandwidth, etc [SMPTE PAPER 101-51] 12 p1914 A67-25471
 RF plasma torch coupling efficiency shown insensitive to input power and gas flow rate 12 p1976 A67-25925
 Micropower electronics noting effects of input capacitance and container and wiring capacitances on HF characteristics 12 p1917 A67-26206
 Satellite Telecommunications with Automatic Routing /STAR/ system modulation techniques, channel capacity and Start-Stop /SS/ operation 13 p2067 A67-26718
 Minimum power requirements of V/STOL aircraft 13 p2054 A67-27586
 Klystron amplifier performance, noting increased efficiency by using double interaction in output circuit 14 p2279 A67-28008
 Optimum pressure drop in compressed air driven turbine as function of initial pressure in air cylinder and turbine parameters 14 p2252 A67-28652
 Pulsed power output for microwave GaAs oscillator biased into avalanche, with diodes grown by liquid phase epitaxy 15 p2442 A67-29172
 Frequency doubler using two-diode varactor array to obtain double output power 15 p2442 A67-29176
 MHD generator with uniform rectangular duct, considering ion slip and Hall effect in case of two-dimensional flow 15 p2422 A67-29906
 Rhombic traveling wave antenna with feedback loop to utilize larger proportion of total power 17 p2824 A67-32313
 Organizational techniques and trade-offs for low power operation in spaceborne data processing systems 17 p2820 A67-32503
 Laser energy and power measurement, discussing radiation attenuation devices, measurement standards, etc 17 p2867 A67-32612
 Ambipolar potential-enhanced loss in magnetic trap reduced by potential difference in magnetic mirror throats dividing field 17 p2909 A67-33118
 Power consumption reduction problems in coded telemetry measurements for ESRO I and HEOS A satellites 21 p3584 A67-38864
 Arc jet power efficiencies tested in insulated tank, comparing deuterium with hydrogen [AIAA PAPER 67-677] 21 p3691 A67-38710
 Silicon avalanche oscillators under continuous operation at millimeter wavelengths, discussing efficiency and power densities 24 p4133 A67-42815

POWER GAIN
 Gain optimization for antenna arrays for determination of maximum expected gain and required excitations when finding random errors in amplitudes and phases of excitations 01 p0032 A67-10005
 Power amplification/bandwidth product of active device as measure of rate at which power supply energy converts to signal energy, noting TWT role 01 p0032 A67-10011
 Nonlinear attenuation or gain characteristics of Doppler-broadened atomic resonance involving levels with small splittings, noting mode coupling of gas laser 01 p0087 A67-10152
 Maximum power gain and admittance matrix for neutralized amplifier stages with three-terminal amplifier devices /electron tubes and transistors/ 01 p0035 A67-10432
 Closed loop gain of two-loop linear feedback system calculated, using computer 01 p0047 A67-11218
 Angular section errors effect on directive gain coefficient of parabolic antenna with automatic phasing 02 p0215 A67-11975
 Single crystal transistor with metallic base, noting frequency, V-I and power characteristics, radiation resistance, etc 02 p0221 A67-12530
 Parametric amplification of far IR in Te crystal pumped by carbon dioxide laser 03 p0437 A67-13572

Impedance matching conditions, gain nonlinearity and bistable mode instability in solid state parametric frequency converters 03 p0381 A67-13637

Tunnel-diode amplifier sensitivity gain due to negative resistance 03 p0382 A67-13668

Sharp cut-off nonlinear filter design with jump effect for rapid gain increase with small frequency increment 03 p0386 A67-13981

Single mode output power modulation analysis of saturation and gain of gas lasers and effects of excitation density modulation and resonator Q 04 p0633 A67-15111

Figure of merit as evaluation criterion for HF transistors, using unidirectional available power gain 04 p0585 A67-15501

Single mode output power modulation study of saturation and gain of gas laser 05 p0823 A67-16686

Amplifier using electro-optic junction modulator combined with photodetector, showing gain at microwave frequencies 05 p0774 A67-16822

Resonance cascade amplifier using additional AC resistance resulting in gain increase without band pass 06 p0972 A67-18900

X-band ruby maser design with liquid hydrogen cooling for high gain at low pumping power 07 p1194 A67-19131

Behavior of momentum effect jet interaction proportional amplifier using flow visualization on water table and large scale pneumatic model 08 p1282 A67-20460

Gain saturation effect on oscillating modes of optical masers 08 p1339 A67-21377

Blocking effect due to interference in parametric amplifier, discussing relation between gain and blocking frequency 10 p1609 A67-22834

Temperature effect on microwave-gain characteristics of bulk GaAs amplifier, interpreting results in terms of changing carrier concentration 10 p1612 A67-23371

Basic design differences illustrating paraboloidal reflector variations, noting factors contributing to or detracting from antenna efficiency 10 p1613 A67-23413

Effect of varying magnetic field, vacuum and ion density at 27 MHz on properties of cylindrical argon plasma column, using capacitive and inductive coupling 10 p1686 A67-23504

Surface conditions effects on silicon planar transistor current gain 11 p1759 A67-24139

Optical power gain characteristics of continuous wave carbon dioxide laser studied parametrically with single-pass amplifier 11 p1800 A67-24244

Compact nonresonant five-pass carbon dioxide laser amplifier structure giving small signal gains 11 p1800 A67-24245

Absolute gain measurements of vertically polarized HF test antennas over imperfect ground 11 p1761 A67-24278

Correction for gain computations based on pattern integration during translational motion of antenna 11 p1763 A67-24297

Superradiant transition in high gain pulsed laser 11 p1803 A67-24841

Mean power gain for diversity reception system with lobe switching 11 p1768 A67-24988

Single mode He-Ne laser, noting discontinuities in power output and inhomogeneous nature of gain curve 12 p1951 A67-25147

Slipstream propulsion theory, taking into account reacceleration which places power balance in proper perspective for efficiency gain 12 p1988 A67-25214

Power gain sensitivity of transistors with conjugate matched two-port amplifier 12 p1910 A67-25260

Hyperfrequency receiver noise temperature measurement, calculating gain stability influence 12 p1952 A67-25296

Parametric amplifiers of high gain stability for radio astronomy noting very low SNR and optimum noise temperature 12 p1912 A67-25298

Raman laser physics covering gain formula, stimulated and spontaneous scattering and cavities 12 p1953 A67-26124

Apollo spacecraft-earth two-way communications provided by vehicle-mounted variable gain antenna array, automatically

tracking ground-transmitted signals 13 p2068 A67-26802

Maximization of directive gain for circular and elliptical arrays 13 p2082 A67-27406

Single crystal transistor with metallic base, noting frequency, V-I and power characteristics, radiation resistance, etc 14 p2279 A67-28007

Transconductance and voltage gain of MOS/FET using hafnium dioxide 15 p2442 A67-29171

Gain of flowing carbon dioxide laser systems, noting extent of diameter dependence of gain, population variations, etc 15 p2497 A67-29390

Current gain and collector-base saturation current and breakdown voltage in aged silicon transistors 15 p2453 A67-30064

Radio gain between simple dipole antennas for single propagation paths, noting effect of resistance from imperfect ground 16 p2625 A67-31342

Cassegrain antenna gain and noise temperature with dual reflector system derived from feed pattern and system geometry 17 p2824 A67-32395

Antenna field strength measurement above 1 GHz, discussing formulas for high accuracy gain determination, multipath interference and antenna separation 17 p2815 A67-32609

Relationship between axial magnetic field necessary to extinguish oscillation from Brewster-angled laser and spontaneous intensity 18 p3061 A67-34200

Current distribution and element spacings for beam efficiency and gain optimization of antenna array 18 p3012 A67-34429

Relaxation of carbon dioxide pulsed laser levels by collisions with hydrogen, showing gain dependence on hydrogen pressure 20 p3457 A67-36384

Midband saturation characteristics of ammonia maser amplifier and variation of maser bandwidth with gain 20 p3458 A67-36431

Measurement of variation of formation time of Q-switched ruby laser as function of loop gain 20 p3458 A67-36432

Directional maximum gain of antennas with discrete propagation elements 20 p3398 A67-36775

Superradiant high gain pulsed lasers measured for single pass gain by comparing single pass and double pass radiation intensities 20 p3460 A67-36858

Radar moving target indicating filters performance, describing method for including target Doppler frequency statistics in gain probability 20 p3386 A67-37498

Digital program for stability-augmentation system-gain values yielding desired pole-zero locations for vehicle transfer functions of flight conditions 21 p3568 A67-38539

Low noise temperature traveling wave maser preamplifier for microwave reception, discussing design, applications and specific electron gain 21 p3641 A67-38640

High gain directional antenna networks for space communications 21 p3600 A67-38670

Sign of energy gain and direction of energy flow shown invariant under Lorentz transformation for two relatively moving systems possessing equal proper temperature 21 p3733 A67-39124

Neodymium-glass laser amplifier gain saturation investigation using laser driving signal, discussing Schulz-DuBois steady state theory and inversion density 22 p3813 A67-39349

Maximum efficiency at constant applied thermal power of thermoelectric generator noting power gain and materials employed 22 p3747 A67-39429

Magnetron type microwave amplifier gain increase, discussing electron beam interaction region M-type device gain calculations 22 p3770 A67-39654

Monolithic magnetic double-balanced modulator, comparing patterns from working sample with theoretical conversion gain 22 p3773 A67-39916

Active medium gain required in gas laser output power calculation obtained for intermediate case 22 p3816 A67-40128

Helix spurious mode effects on TW amplifier performance analyzed for methods of elimination 22 p3775 A67-40462

Electronic network analysis using topological techniques of signal flow graphs, flow graphs and k-trees 22 p3778 A67-40556

Design and performance of high gain

amplifier consisting of cadmium sulfide single crystal and thin film transducers 23 p3977 A67-40690

High gain wideband amplifier with rapid pulse trains, discussing silicon transistor response time, impedance, Q-factor and correction circuit 23 p3977 A67-40691

Simultaneous self-starting oscillations at unrelated frequencies in feedback loop containing one nonlinearity, calculating equivalent linear gain 23 p3984 A67-41157

Reactive optical information processing maximum efficiency from phase object in laser cavity, discussing modulation depth and power gain 23 p4002 A67-41270

Proportional characteristics and signal limiting capabilities of fluoric operational amplifier, discussing analog gain block performance 24 p4098 A67-41988

High gain phased array for satellite transmission using feedback to correct phase and amplitude parameters variations 24 p4124 A67-42816

Performance characteristics of active channel of insulated gate FET for application as high gain HF amplifier 24 p4133 A67-42824

Separate studies of power and collision broadening of gas laser transition showing proportional DC laser power to square of gain 24 p4169 A67-43103

POWER GENERATOR

Cryogenic techniques for space power generators based on superconductivity, discussing MHD converters 04 p0560 A67-15967

Program for radiol isotopic power on Nimbus B spacecraft provided by SNAP-19 generators 05 p0843 A67-16553

Role of negative ions in flames and of negative droplets in mercury vapor, noting use of isotopic tracer techniques and flame behavior as gaseous semiconductors 05 p0853 A67-16886

Electric thrusters and electric propulsion, examining overall efficiency as function of specific impulse 05 p0874 A67-16933

MHD application for power conversion and generation, discussing methods and efficiency 06 p1076 A67-19023

Book on theory of flow machines covering pumps, turbines, windmills, fluid dynamics, viscous flow fields, cascade flow, etc 08 p1321 A67-20758

Power output variation of solar Brayton space power plant with heat storage due to solid layer thermal resistance effects 09 p1442 A67-21698

MHD electrical power generation - Conference, Salzburg, July 1966, Volume I 09 p1536 A67-21773

Channel flow and power generation of MHD generator, stressing influence of nonequilibrium ionization 09 p1541 A67-21802

Point contact electrically formed semiconductor junction diodes, discussing harmonic generation by various material combinations 09 p1474 A67-22086

Electric power generating equipment for aircraft noting brushless rectifier AC generator, solid rotor AC generator and brushless DC generator 09 p1451 A67-22666

Aircraft DC electronic controls and generators for voltage regulation and system protection [SAE PAPER 670250] 11 p1745 A67-23983

Step-recovery action in transistor switch-off with current gain and reduction of load on driving source 13 p2078 A67-26784

Solid state semiconductor microwave power generator design, analyzing spurious oscillations rejection problem 13 p2081 A67-27204

Medium power millimeter wave klystron /Laddertron/ construction and characteristics 14 p2278 A67-27800

Mobile hydrogen generators for alkaline electrolyte cells and medium temperature fuel cells for autonomous hydrocarbon electricity units 14 p2253 A67-29021

Electrodeless MGD power generation during entry, using torque on magnet taken as rotating member of generator 15 p2422 A67-29443

Gunn effect as only solid state effect capable of producing high output power in microwave range in pulsed and continuous operation, noting physical nature 15 p2536 A67-29530

Microwave power generating semiconductor oscillators noting negative

resistance effect, construction of Gunn oscillator diode, etc 15 p2445 A67-29583

MHD power generation experiments with potassium seeded argon plasmas to study performance at Faraday and Hall parameters 16 p2601 A67-30554

MHD Brayton cycle power generation techniques, considering noble gases seeded with alkali metal vapors as working fluid 16 p2603 A67-30567

AC MHD power generator and turbine described noting working fluid flow 16 p2605 A67-30581

Direct and indirect converters emphasizing preconcentration of solar radiation, noting thermophotovoltaic generators of p-n type 16 p2608 A67-30713

Liquid-metal and plasma MHD systems for power generation in space environments, noting Rankine and Brayton cycles [JPL-TR-32-1129] 17 p2802 A67-32049

Experiments of internal impedance of MHD generator show wide range of working conditions as slowly varying function of applied current 17 p2802 A67-32182

Partially ionized gases application to industry, stressing power units incorporating plasma converters, plasma electrolytic fuel elements and MHD generators 17 p2899 A67-32187

Solar thermoelectric generator with cylindrical aluminum solar energy receiver using p and n type semiconductor materials and water cooled junctions 18 p2990 A67-34491

Gunn effect semiconductor oscillator for generating microwave power using GaAs 18 p3013 A67-34525

Closed-cycle generator using gasdynamic forces to transport charged particles against opposing electric field, noting enthalpy role 19 p3175 A67-34801

Book on energy conversion covering heat engines, power sources, solar energy, SNAP generators, etc 19 p3177 A67-35892

Lunar Orbiter power subsystem reliability tradeoff, methodology, performance prediction, etc 20 p3363 A67-36594

Thermionic conversion for space auxiliary power systems noting high reliability and longevity potential 20 p3364 A67-37019

Maximum efficiency at constant applied thermal power of thermoelectric generator noting power gain and materials employed 22 p3747 A67-39429

Energy exchanges between plasma and excitation source sinusoidal in time and arbitrary in space 22 p3847 A67-39642

Distributed power generation for radar and communications covering cost comparisons, antenna subsystems and reliability of solid state devices 22 p3761 A67-39861

Pulse generation method for high power modulators in Doppler radars studied, using step recovery diode to construct compression network 22 p3772 A67-39897

Direct solar to electric energy conversion using superconducting flux barrier, discussing superconductive phase change and magnetic properties 22 p3748 A67-40151

Nonmechanical electric power sources - Conference, Brighton, England, September 1966 22 p3748 A67-40226

Large model superconducting magnet for MHD central-station power generation, discussing performance and specifications 22 p3749 A67-40399

Solar arrays constructed of CdTe thin film solar cells are feasible and competitive if space sunlight conversion efficiency can be maintained at level greater than 6 percent 23 p3938 A67-41498

Solar cell array for LEM electric power system during lunar surface operation noting requirements and tradeoffs 23 p3939 A67-41510

Unipolar-bipolar transistor hybrids for stable temperature independent current generators, detailing circuit design 24 p4128 A67-41895

NASA radial flow turbine research related to Brayton cycle power generator, investigating size, Reynolds number and speed effects on efficiency and flow 24 p4102 A67-42489

SNAP-8 powered Brayton cycle system for large space stations noting components and overall design 24 p4102 A67-42490

Rotating boiler for high performance Rankine cycle power generator using water

as test fluid, obtaining heat-transfer coefficients 24 p4184 A67-42498

SET VIII Thermionic generator, evaluating operational and long term performance characteristics for space applications 24 p4103 A67-42499

Thermoelectric converter designed for operation with SNAPOODLE /hybrid radioisotope thruster/ electric generator/, discussing test results 24 p4184 A67-42507

Electro-fluid dynamic power generation, discussing Mach number, charged particle mobility, pressure level and radial space charge field effects on load characteristic and conversion ratio 24 p4107 A67-42527

Electrofluiddynamic /EFD/ power generator unipolar charge generation using corona discharge, noting pressure and geometry effects on ion currents and attractor voltage 24 p4107 A67-42528

Electrofluiddynamic /EFD/ power generator channel performance dependence on charge spreading for various geometries, noting stage efficiency and electric pressure 24 p4107 A67-42529

Chemical dynamic hydraulic power unit /HPU/ performance, weight and volume efficiencies, noting applications to solid and liquid propellants 24 p4107 A67-42531

Reentry vehicle solid propellant and liquid fuel compact turboalternator electric power system operating characteristics and performance 24 p4108 A67-42534

Random intact reentry and earth burial for radioisotope thermoelectric generators disposal without atmospheric contamination, evaluating design concepts for SNAP systems 24 p4241 A67-42559

High temperature strength and magnetic properties of cobalt-tungsten alloy for space power generator rotors 24 p4174 A67-42726

Advanced radioisotope thermoelectric generator /RTG/ system designs employing SiGe direct radiating power conversion subsystems 24 p4110 A67-42899

POWER-LIMITED VEHICLE

Optimum propulsion control law selection for limited motion capacity in mass accumulation regime determined, considering two-dimensional problem of vehicle motion 12 p1989 A67-25659

Optimal parameters of transfer function of low thrust power limited engines by approximate solution of differential equation 22 p3898 A67-39181

Flight optimization problems, considering spacecraft with energy storage and limited power engines 24 p4240 A67-42295

Spacecraft motion with limited power jet engine, applying simulation technique to determine operation modes for engine and control system 24 p4240 A67-42296

POWER LIMITER

SA OPTICAL POWER LIMITER

Second breakdown protection of Si power transistors by applying emitter resistances 02 p0222 A67-12654

Pulsed power technique and capacitive coupling between digital integrated circuits provide micropower redundant circuits with automatic error correction 07 p1155 A67-19844

Bulk reverse current in diffused Si power rectifiers, interpreting reverse characteristics in terms of thermal pair production 11 p1760 A67-24144

Coaxial and strip-line passive microwave components stressing design of hybrid junctions, microwave mixers, filters, etc 19 p3195 A67-35549

POWER PLANT

SA BY-PASS ENGINE

SA HEAT ENGINE

SA NUCLEAR POWER PLANT

Gas lubricated bearings used in Brayton cycle closed loop system turbomachinery, in design of two-shaft power plant [ASME PAPER 66-GT/CLC-9] 01 p0080 A67-10871

Two-phase flow and material attrition problems for Rankine cycle liquid metal power plants [ASME PAPER 66-GT/CLC-4] 01 p0014 A67-10872

Temperature and heat transfer conditions determination on rotating turbine wheel in jet power plant, using electric analogy 04 p0688 A67-14571

Design aspects of power plants for V/STOL aircraft, examining lift jets, thrust vectoring and lift fans

[ASME PAPER 67-GT-7] 11 p1744 A67-24795

Quantitative graphical method of screening working fluids for Rankine cycle power plants using single stage turbines at different levels of diameter and rpm [ASME PAPER 67-GT-12] 11 p1746 A67-24798

Two-stroke cycle light aircraft engine with respect to competitive power plants 12 p1989 A67-25496

ARGAS closed MHD loop noting technical, constructional details, intended research program and operational results 16 p2653 A67-30553

Unscheduled civil aircraft power plant diagnostic removals evaluated by metal detection, performance deterioration, vibration, oil consumption and nonoperational categories [SAE PAPER 670358] 17 p2930 A67-32997

Unscheduled civil aircraft power plant diagnostic removals evaluated by metal detection, performance deterioration, vibration, oil consumption and nonoperational categories [SAE PAPER 670358] 23 p4048 A67-40866

Design criteria for VTOL tactical aircraft power plant using turbojets for attack aircraft in support of land troops 23 p4049 A67-41044

Structural stability of welded joints of chromium steel used in power plant construction examined for structural stability 23 p4019 A67-41077

VFW/Flat joint project to develop single-seater fighter/reconnaissance aircraft noting structural design, power source and liftoff weight 23 p3934 A67-41255

Indirectly corrected gyro vertical used to determine vertical on power plant, considering random plant motion and gyroscopic drift 24 p4155 A67-42298

Inertial navigation system operation errors on moving power plant due to inaccurate initial data feeding into computer 24 p4182 A67-42300

Minimizing maximum control deviation problem reduced to motion equation numerical integration 24 p4188 A67-42301

Real gases examined for application as working fluid in Brayton cycle power plant, considering radiator area reduction to Rankine cycle 24 p4102 A67-42488

Organic Rankine cycle power system using monoisopropylbiphenyl /MIPB/ as working fluid noting advantages 24 p4103 A67-42494

Rankine cycle power plants using organic working fluids considered for near-term application 24 p4103 A67-42495

POWER REACTOR

Manned space mission requirements and application of space power technology to multipurpose space stations, noting operation of Pu-238 isotope/ Brayton cycle unit 17 p2953 A67-31979

POWER SERIES

One-dimensional refractive index distribution using power series expansions for refractive index and ray traces obtained from relation of inhomogeneities and interference pattern of Mach-Zehnder interferometer 03 p0423 A67-13908

Interpolation sets satisfying several conditions considered for application to integral functions with gap power series 03 p0461 A67-13941

Closed form for perturbation terms of linear Boltzmann equation 05 p0847 A67-17438

Fundamental frequency of natural oscillations of plate, using integrodifferential equations derived from elasticity theory in form of power series 06 p1108 A67-18662

Cylindrical shell stability under axial compression analyzed by generalized power series method, noting half-waves and critical load 07 p1262 A67-19345

Constructing formal integrals, in form of power series, of time independent Hamiltonian system near equilibrium point [AAS PAPER 66-102] 07 p1216 A67-19964

Power series technique applied to single edge notches in semifinite region in plane elasticity problems, using mapping function and Muskhelishvili theory 08 p1414 A67-20347

Stress distribution at tip of crack expanded as power series, noting relation of various terms to crack propagation 08 p1421 A67-20954

Tietjens function reexpressed as ratio of rapidly converging power series of complex argument and used in calculation of critical Reynolds numbers 08 p1322 A67-21138

Restricted problem of three bodies analyzed using Birkhoff variables and power series representing motion equations, obtaining coefficients for collision orbit 08 p1396 A67-21182

Isotropic scattering of radiation in finite two-dimensional atmosphere using integral equation, solved by power series 09 p1532 A67-21662

Analytic solution to blunt body problem in supersonic flow of ideal gas approximated, using power series [NOR REPORT 65-239] 10 p1593 A67-23454

Power series solutions of singular vibration problems converted to quotient of polynomials by transformation into continued fractions, using perturbation technique [ASME PAPER 67-VIBR-7] 11 p1872 A67-24167

Increasing modulus maximum of integral function relation to moduli of coefficients of power series 11 p1813 A67-24520

Series method of solving boundary value problems for nonlinear ordinary differential equations 11 p1814 A67-25050

New integral in restricted three-body problem expressed in terms of Delaunay variables 15 p2557 A67-29877

Analytic power series solution of nonrelativistic Schroedinger equation for two-electron atom, assuming fixed nucleus and singlet and triplet S states 15 p2520 A67-30158

Nontrivial real or complex solutions of nonlinear integral equations of Hammerstein type bifurcating from identically vanishing solution 16 p2695 A67-30858

Generalized power series method applied to compressed cylindrical shells stability analysis, giving formulas for direct shell designing 17 p2961 A67-32808

Instability zones for vibration equations system having periodic acceleration matrices, damping and spring forces 18 p3140 A67-33464

Computer integration of Faulkner-Skan equation in presence of normal and tangential flow velocity components on surface of body 18 p3024 A67-33538

Limiting values for remainder forms in Taylor series and error estimation procedures for power series approximations, including truncation error 18 p3072 A67-34398

Stability of equilibrium of holonomic system in critical cases by means of search for Liapunov functions, using power series 19 p3261 A67-35050

Poincare continuation method using simple pendulum problem, deriving elliptic functions as power series [AIAA PAPER 67-564] 19 p3250 A67-35960

Intermodulation interference effect on PCM/FM error rates studied using power series as mathematical model 20 p3380 A67-36563

Linear heat transfer problems inside equilateral region solved by integral transform series [ASME PAPER 67-HT-67] 20 p3550 A67-36748

Unidirectional fiber-reinforced composite under axial load, discussing power series along with point matching techniques for solving interface, matrix and filament stresses 20 p3474 A67-37268

Power series expansion of electron velocity distribution function, computing harmonic electric current densities in plasma 21 p3661 A67-37745

Asymptotic solution for class of integral equations of first kind with application to contact problem of infinite elastic cylinder 22 p3909 A67-39400

Validity of Liapunov first approximation theorems for motion stability when not satisfying power series terms 22 p3837 A67-39881

Procedure for expanding parameter in asymptotic power series of any order to investigate viscous compressible supersonic gas flow past blunt body 22 p3740 A67-40014

Air damping effect on structural fatigue failure evaluated mathematically as power function relating stress to number of cycles 22 p3915 A67-40405

Perturbation solution to one-dimensional nonadiabatic temperature distribution behind detached shocks taking into account absorption effects 23 p3992 A67-41738

HF and switching characteristics of junction transistors analyzed using power

series expansions 24 p4201 A67-41900

Elliptic integrals and numerical representation of power series to yield closed form approximation, presenting error as function of modulus 24 p4178 A67-42205

POWER SPECTRUM

Intensity dependent frequency shift in spectral output of monochromatic giant pulse lasers measured, using Fabry-Perot interferometer 01 p0088 A67-10251

Digital computer program for power spectral density analysis of vibration data, noting bandwidth variation with frequency [SAE PAPER 680715] 01 p0028 A67-10604

Red shifts and power outputs in quasars and radio galaxies 01 p0149 A67-10889

Statistical dependence effect of normal mode response of complex structures to random excitation 01 p0163 A67-11172

Q-active filter for narrow-band noise measurement in LF range 02 p0216 A67-12038

Incoherent scattering measurements of ionospheric power spectrum and autocorrelation function at geomagnetic equator to determine electron and ion temperatures, ion composition and ion density 03 p0408 A67-12834

Load factor estimation for flights in turbulent conditions by replacing exact transfer function with equivalent statistical model 03 p0351 A67-12997

Power spectral density /PSD/ methods applied to prediction of aircraft responses to continuous turbulence [AIAA PAPER 66-1000] 03 p0362 A67-14147

Velocity azimuth display technique analysis of wind parameters, noting fundamental limitations 04 p0648 A67-14674

Power spectrum of electromagnetic wave incoherently diffused by ionospheric electrons 04 p0571 A67-14896

Power spectrum of horizontal components of clear air turbulence in upper troposphere, examining influence of degenerating gravity waves on nature of turbulence spectra 05 p0837 A67-16486

Power spectrum improvement of multiple wave trains by concentrating power close to carrier frequency, noting constructive and destructive interference 06 p0963 A67-18401

Multiple scattering of light in turbulent atmosphere noting relation to refraction index and power spectra, using Born series solution to wave equation 06 p1033 A67-18536

Angular power pattern for circular aperture receiving plane wave perturbed by passage through turbulent atmosphere 06 p1033 A67-18538

Dynamic analysis of lunar surface vehicle including power spectral density terrain definition, vehicle velocity limiting criteria and nonlinear analysis of vehicle freedom to pitch, bounce and roll 07 p1163 A67-19369

Visual frequency analysis of geomagnetic micropulsation records with computed power spectra for four separate samples of data 07 p1171 A67-19421

Correlation functions and power spectra of stochastic processes with statistical structure defined by stationary Markov chains 07 p1217 A67-20196

Frequency response functions determined from correlation functions of force and response, using Bartlett triangular weighting function 08 p1353 A67-20592

Laser interferometric measurement of power spectral density of integrated particle density fluctuations in turbulent exhaust of sonic jet 08 p1337 A67-21142

Average power patterns for various values of rms phase difference for points separated by aperture radius in turbulent atmosphere 09 p1462 A67-21610

Power spectrum of irradiance for precessing cylinder computed as function of time for given value of phase angle 10 p1652 A67-22714

Qualitative vibration data reduction techniques for application to design problems, noting examples involving power spectra and probability-density functions 10 p1680 A67-23315

Photospheric brightness fluctuations recorded photoelectrically across solar disk center simultaneously for two regions of continuum, deriving autocorrelation functions and spatial power spectra 10 p1711 A67-23796

Ionospheric movement measurement with LF radio waves, using triangulation coupled with cross spectrum analysis of signal

fading 11 p1784 A67-23936

Atmosphere effects on laser beam propagation noting diameter, intensity amplitude and power dependence on transmitter and receiver aperture dimensions 11 p1801 A67-24665

Barometric pressure data analysis estimating autocovariance, using Fourier transform for spectral density calculation 11 p1816 A67-24840

Statistical performance confirmation of wideband random equalizer, emphasizing analysis technique, analyzer characteristics and power spectral density plot 12 p1942 A67-25692

Microwaves parametric amplification experiments in superconducting Josephson tunnel junctions, showing signal amplification as function of temperature, absorption dip of rutile resonator, etc 12 p1915 A67-25745

Power spectrum of horizontal components of clear air turbulence in upper troposphere, examining influence of degenerating gravity waves on nature of turbulence spectra 13 p2150 A67-26342

Digital real time spectral analysis with fast Fourier transform algorithm, using two special purpose computer configurations to estimate power spectrum 13 p2073 A67-27062

Radio measurements and standards for power, conductance, impedance and attenuation in upper frequency range 14 p2263 A67-28390

Power spectrum and difference frequency spectrum for energy exchange oscillations between three modes of He-Ne laser 14 p2331 A67-28603

Frequency spread in ionospheric radio propagation 14 p2273 A67-28712

Magnetic shielding properties of earth mantle obtained from power spectrum, deducing transfer function of mantle 14 p2314 A67-28887

Nonthermal X-ray radiation accompanying solar flares, comparing spectral power of synchrotron radiation, Compton radiation and bremsstrahlung as possible generation mechanisms 15 p2549 A67-29141

Quasi-biennial cycles in cosmic ray intensity 15 p2549 A67-29203

Clear air turbulence power spectra in free atmosphere near jet stream level, discussing CAT generation 15 p2513 A67-30058

Aircraft flutter testing using free-air turbulence as exciter 16 p2764 A67-30861

Output noise power spectrum properties of X-band ruby maser oscillator, noting frequency dependence on electromagnetic energy and cavity losses 16 p2685 A67-31055

Wind profile analysis from balloon sounding data, using Fourier series to filter out unwanted part of spectrum 16 p2668 A67-31742

All-electronic, ultra-fast scanning spectrometer utilizing image dissector for power spectral density function measurements of rapidly time varying optical emission 16 p2680 A67-31803

Statistical properties of wall pressure fluctuations in subsonic turbulent equilibrium boundary layer after transition from laminar flow 17 p2836 A67-32283

Power spectral density /PSD/ methods applied to prediction of aircraft responses to continuous turbulence [AIAA PAPER 66-1000] 17 p2797 A67-32582

Wave equations for disturbances in partly ionized gas due to current sources determined, using three-fluid model 17 p2906 A67-33056

Single laser pulse generation noting high peak power, subnanosecond time duration, optical cavity length, etc 17 p2869 A67-33063

Power spectrum of pulsating aurora measured at HF, noting relation to modulation mechanism in flux of primary particles 17 p2850 A67-33193

Frequency regions for Cerenkov radiation and power spectrum in collisionless magnetoplasma calculated using refractive index 18 p3090 A67-34428

Wind-driven plasma turbulence structure resolved by continuum ion probes at high Reynolds numbers, determining plasma density fluctuation from argon gas flow 18 p3030 A67-34743

Random vibration testing by multiple electrodynamic exciter technique, analyzing electromechanics and structural feedback 19 p3339 A67-34961

Power spectra and dissipation rate for vertical velocity fluctuations measured with sonic anemometers 19 p3251 A67-35056

Interplanetary magnetic field and plasma velocity variations observed during Mariner II flight 19 p3324 A67-35451

Probabilistic background of time series models which relate to spectral analysis and power spectrum and statistical inference for stationary stochastic processes 20 p3476 A67-36783

Radio parameter continuity between radio galaxies and quasars, plotting spectral indices against absolute spectral power 20 p3525 A67-36947

Nonstationary random process power spectral analysis, noting evolutionary power spectra estimation methods, local energy distribution, etc 20 p3485 A67-37004

He 3 ratio to He nuclei in cosmic rays, determining He nuclei path length in space, considering kinetic energy power spectrum 20 p3518 A67-37088

Cosmic ray diffusion in interplanetary magnetic field, examining statistical homogeneity and isotropy 20 p3520 A67-37473

Frequency limitations of PCM communication, determining PCM/PM and PCM/FM power spectra for hybrid modulation spectra calculations 21 p3584 A67-38652

Evaluation technique for correlation functions and power spectrum of randomly shaped pulse train using stationary point process 21 p3604 A67-38948

Harmonic generation and turbulence-like spectrum from pulsed HF beam-plasma interaction, tabulating harmonic wave properties 22 p3847 A67-39615

Rapid magnetic field variations observed in magnetosheath evaluated in terms of transverse modes of plasma wave propagation 23 p3995 A67-40804

Reduction and analysis of nonstationary missile flight vibration data, obtaining power spectral density 23 p4007 A67-41385

Wideband FM demodulation system providing good reception with smaller radio SNR through delayed signal 23 p3975 A67-41677

Nonthermal X-ray radiation accompanying solar flares, comparing spectral power of synchrotron radiation, Compton radiation and bremsstrahlung as possible generation mechanisms 24 p4222 A67-43064

POWER SUPPLY

SA AIRCRAFT POWER SOURCE

SA AUXILIARY POWER SOURCE

SA NUCLEAR-ELECTRIC POWER SUPPLY

SA PLASMA POWER SOURCE

SA SOLAR POWER SOURCE

SA SPACECRAFT POWER SUPPLY

Silicon power transistor use in power supply, line operated audio output, video amplifier and TV horizontal deflection high voltage circuits 01 p0038 A67-10761

Fuel cell as low voltage power source 02 p0183 A67-12102

Gyroscope rotor configuration using barium ferrite magnets and axial rotor magnetization 02 p0184 A67-12411

Nuclear power supplies for electrical propulsion including liquid metal reactor-potassium Rankine, Brayton, MHD power conversion and thermionic reactor [AIAA PAPER 66-1021] 03 p0363 A67-14153

Temperature stability of several types of modulated radiation sources employing GaAs diodes, examining current change with temperature change 03 p0388 A67-14271

F-111 type hydraulic power supply system design for supersonic aircraft using ground support equipment and military materials 05 p0752 A67-18159

Power source disturbance method for linear theory of flow past bodies 05 p0749 A67-17006

Circuits consisting of HF oscillator, kenotron heater, rectifier, etc, for low power HF voltage generator 05 p0780 A67-17499

High electric power production for short periods, anticipating magnetoaerodynamic power stage combined with conventional alternators 06 p0949 A67-17567

Power source for image converter tubes /ITC/ with regulated output voltage 06 p1004 A67-18393

Materials for large space power systems - Symposium, American Nuclear Society,

Washington, D.C., November 1965

Materials and fin tube geometry effects on ultimate size and mass of space radiator 07 p1223 A67-19459

Pulse width modulation voltage regulator design for power conversion applications, considering interrelation of loop gain, switching frequency, etc 08 p1284 A67-20693

PDM/FM high efficiency voltage regulator design, switching theory and regulation theory 08 p1286 A67-21030

Power supply design for avionics digital computer systems 08 p1286 A67-21031

Thermoelectric generator modules with Si-Ge alloys, discussing material preparation and generator fabrication 09 p1445 A67-22180

Theoretical and experimental basis of high performance Mg-air cells, discussing development and performance 09 p1445 A67-22187

LC smoothing filter in rectifier for pulse supply source stabilized by pulse width modulation 10 p1611 A67-22980

Interconnection of transmitters with no noninteracting elements reduces input traveling wave ratio of antenna arrays with power supply systems 13 p2080 A67-27033

Communication satellite program research 14 p2269 A67-28455

Temperature stability of several types of modulated radiation sources employing GaAs diodes, examining current change with temperature change 14 p2288 A67-28780

Military radar intercept calculator, discussing small size, low power supply, high performance and MOS memory 15 p2439 A67-29161

Fat cylindrical antenna admittance measured noting behavior similar to that of thin antenna admittances 15 p2454 A67-30137

Thyristor assemblies /dimmers/, for control of power supply, noting operation principles and examples cited 16 p2841 A67-31566

Open-cycle gas generator as power supply source for MHD generators, noting reduction of wall effects 17 p2802 A67-32179

Laser-energized explosive device /LEED/ for pyrotechnic device actuation noting power source, ruby laser, metallic fiber-optic conductor, missile design, etc 17 p2803 A67-32437

Early Bird and Intelsat commercial satellite communications system and associated ground stations noting design, power supply, control system, etc 18 p3136 A67-33545

Design considerations for reliable microwave power packs noting redundancy, independent module system and intrinsic reliability 18 p3010 A67-33665

Power source disturbance method for linear theory of flow past bodies 18 p2984 A67-34268

Flight measurement data retrieval on real time basis from worldwide range stations possible through Range Support Satellite system 20 p3531 A67-36470

Power semiconductor devices, emphasizing thyristors and silicon rectifier diodes applications 20 p3397 A67-36643

Multiple-winding choke design replacing separate inductors in filtering circuit and reducing power supply size and weight 20 p3399 A67-36862

Power supply family synthesized from series of modules evaluated for packaging design, treating module interconnection methods and optimum thermal characteristics 20 p3399 A67-36926

Thermal annealing of silicon solar cells with direct solar heating or electric storage methods to avoid radiation damage 20 p3364 A67-37129

Design and construction of power supply without hookup cables for manned lunar vehicle 21 p3571 A67-38337

Packaging design of modular power supplies for airborne computers 21 p3596 A67-38341

Ariel III satellite design, development, mechanisms, power supply and data handling systems 22 p3898 A67-39178

High power thyristor used with battery to operate pulse repeating sonar transducer 22 p3747 A67-39255

Unmanned 0.1 AU /ICARVS/ solar probe preliminary design, discussing thermal control and power supply problems unmanned 0.1 AU /ICARVS/ solar probe preliminary design, discussing thermal

control and power 22 p3906 A67-40152

Rankine cycle power plant for electric propulsion manned Mars mission analysis of system characteristics and mission duration effect 22 p3869 A67-40173

Power supply system consisting of two-piece coaxial cable and pulse transformer found to possess all characteristics for gas laser operation 22 p3817 A67-40414

Carcinotron hyperfrequency power oscillator with tube of same noise characteristics as control developed for space telecommunications 23 p3982 A67-41431

Cascaded and segmented thermoelectric module design, discussing SiGe and PbTe elements and performance 24 p4184 A67-42506

Large sun-oriented deployable solar array for OGO design, fabrication and flight performance 24 p4104 A67-42508

Multi-kilowatt photovoltaic power system design for manned earth orbital mission 24 p4104 A67-42511

POWER TRANSMISSION

Transmission power of dielectric waveguide 01 p0038 A67-10716

Solid state microwave telemetry transmitters, discussing power generation, stability, modulation /AM, PM and FM/, environmental effects and circuitry 02 p0216 A67-12008

Gear combination systemization providing ultraprecise ratios 04 p0627 A67-14708

Hydraulic power distribution system for flight control of F-111 aircraft 05 p0752 A67-16158

Ferromagnetic multilayer systems effect on SHF power transmission and variation of resonator parameter 08 p1368 A67-20606

Orion P-3 electrical power system changes effect on weapons system, noting power distribution and generation systems 09 p1452 A67-22677

Microwave oscillation-amplifying L-band platinotron tube to amplify peak power of radar transmitter 10 p1605 A67-23061

Supercritical speed helicopter power transmission shaft for rotor synchronizing, noting viscous damper for controlling shaft vibrations [ASME PAPER 67-VIBR-20] 11 p1796 A67-24179

Optimum illumination for maximum power transfer between two opposed rotationally symmetric antennas 11 p1762 A67-24291

Fracture line formation in glass specimen as result of laser beam focusing, noting refractive index variation 12 p1951 A67-25148

Electrical and electronics engineering - IEEE Conference, Jackson, Mississippi, April 1967 13 p2085 A67-26404

Two port power flow analysis using generalized scattering parameters 14 p2287 A67-28625

Microwave rocket propulsion through direct electromagnetic heating of gas and powered by wireless ground-transmitted microwaves 16 p2736 A67-30712

Flight control power distribution systems for hypersonic aircraft, considering cooled and pulsating flow hydraulic, liquid metal, pneumatic and mechanical systems 17 p2800 A67-31970

Axial gear differential /AGD/ design and selection for constant speed AC generator drive for aircraft engines 17 p2800 A67-31976

Roller traction drive unit for extremely quiet power transmission compared with planetary-gear drive [AIAA PAPER 67-429] 18 p3053 A67-33913

Scattering matrix method, determining power transfer between closely coupled antennas in complex environment 20 p3405 A67-37644

Topside ionospheric swept-frequency pulsed sounder onboard Alouette 2 satellite, discussing transmitter power, large range receiver and antenna array 21 p3583 A67-38636

Atmospheric absorption of carbon dioxide laser radiation calculation from laboratory absorption coefficient measurements, discussing effects on power transmission and communications 22 p3816 A67-40237

POYNTING THEOREM

Umov-Poynting theorem, Lorentz lemma, complex conjugate lemmas and quadratic relations for EM field intensity in electrodynamics of moving media 05 p0844 A67-16354

Radiation pressure of electromagnetic and

acoustic waves calculated from momentum of incident and scattered wave trains 05 p0846 A67-16583

Energy coupling among electron acoustic, ion acoustic and transverse electromagnetic waves at two-fluid plasma density discontinuity 08 p1364 A67-21397

Energy propagation and Poynting vector for electromagnetic wave propagation in tube of square cross section 13 p2070 A67-27207

Poynting vectors difference obtained by using convection and polarization current models of moving plasma in Minkowski theory 24 p4124 A67-42812

PPI
S PLAN POSITION INDICATOR /PPI/

PPM
S PULSE POSITION MODULATION /PPM/

PRACTICE
S MEMORY
S TRAINING

PRANDTL-MEYER EXPANSION
Nozzle wall shape design based on Mach waves generation appearing when supersonic gas expands about corner 03 p0352 A67-13818

Steady state relaxation hydrodynamic theory with generalized Prandtl-Meyer flows in nonequilibrium hydrodynamics [AFOSR-67-1992] 17 p2840 A67-33137

PRANDTL NUMBER
Forced-convective heat transfer in asymmetrically heated rectangular ducts as function of prandtl number, Reynolds number, aspect ratio and temperature difference 04 p0728 A67-15804

Convective heat transfer from bluff bodies analyzed, particularly small electrically heated cylinders at low Reynolds numbers, noting correlation with Nusselt and Prandtl numbers 04 p0732 A67-15831

Finite difference scheme for solving set of Prandtl equations for nonstationary flow of viscous incompressible fluid 10 p1628 A67-23672

Heat transfer from isothermal sphere to low Prandtl number fluid in steady and nonsteady potential flow compared with Stokes flow 11 p1882 A67-24119

Existence, uniqueness, stability and approximation of solutions of Prandtl system for nonstationary boundary layer 13 p2093 A67-26603

Nonlinear heat transfer between parallel plates, using ellipsoidal statistical model of Boltzmann equation 13 p2223 A67-26960

Effect of finite magnetic Prandtl number on hydromagnetic flow past thin airfoil 14 p2240 A67-28142

One-dimensional laminar MHD flow at hydrodynamic stabilization, discussing heat transfer, Hartmann flow, magnetic field, Prandtl number and Joule heating 14 p2358 A67-28283

Criterion expressions for Nusselt numbers of mass transfer in two-phase film system at high Prandtl numbers which describe physical properties of both phases 14 p2405 A67-28303

Air stream turbulence effect on local and macroscopic transport from cylinder, measuring thermal transfer and pressure coefficients at various Reynolds numbers 14 p2407 A67-28624

Laminar natural convection heat transfer between vertical plate and power-law fluid with high Prandtl number 16 p2780 A67-31553

Elliptic planform vertical submerged hydrofoils, determining circulation distribution over foil span at arbitrary Froude numbers 18 p3022 A67-33414

Steady two-dimensional laminar flow of incompressible viscous fluid, noting asymptotic convergence of velocity profile in Prandtl boundary layer 19 p3212 A67-36031

Laminar and turbulent free shear layers analysis unifying treatment of mixing layers, assessing Mach number, Prandtl number and temperature ratio effects on constant pressure mixing [ASME PAPER 67-HT-81] 20 p3551 A67-36759

Acoustic vibration effect on heterogeneous mass transfer at sphere surface in high Prandtl number liquids 20 p3554 A67-37068

Approximate solutions of Prandtl boundary layer problem for incompressible laminar flow derived, using Nagumo-Westphal theorem on parabolic differential operators. 21 p3583 A67-37888

Laminar compressible boundary layer

induced by plane shock wave passing over flat wall using empirical viscosity-temperature relation for Prandtl number 21 p3611 A67-37928

Finite difference scheme for solving set of Prandtl equations for nonstationary flow of viscous incompressible fluid 21 p3612 A67-38273

Heat transfer experiments with flat plate heated under constant heat flux, discussing wall temperature distribution, Prandtl number and Spalding function 22 p3918 A67-40041

Prandtl limit behavior near zero skin friction, with perturbation methods generalizing Poiseuille and Couette flows 24 p4142 A67-42170

Hydrodynamic separation using compatibility conditions for Prandtl steady boundary layer equations at zero skin friction point 24 p4142 A67-42172

Atomic Cs vapor experimental values for heat-transfer coefficient used to determine Cs atoms and molecules interaction potentials 24 p4253 A67-42211

Friction-drag and heat-transfer coefficients of plate in turbulent gas flow, estimating effect of turbulent Prandtl number 24 p4143 A67-42283

PRASEODYMIUM
Dielectric properties including permittivity, losses, polarization, impurity conduction and forbidden bandwidths of thin films of praseodymium, cerium and neodymium fluorides 08 p1370 A67-20995

Phonon spectrum of neodymium trichloride crystal lattice determined from polarized vibronic transition spectra and Zeeman effect of trivalent Pr and Nd impurity ions 22 p3840 A67-39434

PREAMPLIFIER
Low noise preamplifier traveling wave maser operated in closed cycle refrigerator for receiving Mariner IV picture transmissions 14 p2329 A67-27779

Functional maser consisting of amplifier, low noise header and superconducting magnet for use in ATS 20 p3459 A67-36595

Remote preamplifiers in multielement antenna arrays of radio telescopes operating at meter wavelengths, noting noise temperature effect 20 p3403 A67-37508

Low noise temperature traveling wave maser preamplifier for microwave reception, discussing design, applications and specific electron gain 21 p3641 A67-38640

PRECESSION
SA MOMENTUM PRECESSION
Precessional motion of corrected gyroscope as affected by viscous friction 01 p0084 A67-10421

Relativistic trajectory and orbital precession of spinning satellite under nonspherically symmetric gravitational field 05 p0906 A67-16849

Couple due to distant mass acting on nonspherical object determined, considering luni-solar precession and nutation variability 06 p1031 A67-17778

Power spectrum of irradiance for precessing cylinder computed as function of time for given value of phase angle 10 p1652 A67-22714

Angular precession and critical speed of two-bearing machines with overhung weight determined, considering shear deformation, gyroscopic moment and rotatory inertia [ASME PAPER 67-VIBR-19] 11 p1796 A67-24178

Motion of arbitrary gyrostabilizer in central Newtonian force field, applying Liapunov stability conditions for regular precession 11 p1791 A67-24683

Freely precessible gyroscope viscous fluid nutation damping response to translational and vibration accelerations near critical frequencies 12 p1942 A67-25679

Time dependent orientation of body fixed coordinate system relative to stars for spinning rigid torque-free body 13 p2154 A67-26816

Conservative systems motion stability, generalizing precession and nutation of gyroscope with respect to noncyclic coordinate 15 p2518 A67-29685

Precession theory of compensating gyroazimuth, discussing random disturbances reduction by introducing electric mismatch of both sensitive elements 16 p2670 A67-30467

Lunar core precession and coupling between assumed liquid core and moon mantle 16 p2754 A67-31746

MHD instability of sub-Alfvén equations for zonal flow outside diurnally oscillating boundary layer of precessing spheroid 20 p3494 A67-36147

Nonzero cosmological constant effect /precise and trivial/, calculating perihelion precession from Schwarzschild exterior solution 22 p3889 A67-40382

Lunar orbit precession due to quadrupole moment of sun arising from solar oblateness 23 p4066 A67-41014

Coupled earth core-mantle model for earth precessional torques, discussing precession energy dissipation and experiments on model 24 p4151 A67-42314

PRECIPITATION
SA ELECTRON PRECIPITATION
Maritime precipitation analyzed using radar data and satellite photographs of cloud cover 02 p0282 A67-12404

Prior cold reduction effect on precipitation and embrittlement of cobalt base alloy /L-605/ 04 p0639 A67-15457

Direct observation on precipitation and aging behavior in Cu-Ti alloys by transmission electron microscopy 11 p1809 A67-24948

Electron microscope observations on matrix precipitation in beryllium 13 p2136 A67-27106

Carbon influence on copper precipitation in dislocation free silicon single crystals with low oxygen, discussing growth mechanism and edge dislocation 21 p3686 A67-39136

PRECIPITATION HARDENING
Nickel-base superalloys hardened in part by precipitation of gamma phase examined by X-ray diffraction techniques 01 p0095 A67-10687

Mossbauer spectroscopy used to study precipitation reactions in 17-7 PH stainless steel and in 18Ni-8Co-5Mo maraging steel 02 p0256 A67-12705

Light and electron microscopy used with X-ray diffraction and X-ray fluorescence analysis to study effects of temperatures and stress on As-cast nickel-base superalloy 02 p0256 A67-12706

Hydrostatic pressure effect on dispersion of gamma prime phase in precipitation heat treatment of nickel-base superalloy 06 p1016 A67-17902

Nickel-chromium alloys with niobium in study of precipitation hardening and hardness 06 p1018 A67-18230

Mechanical properties of alloys in descriptive approach, noting data on precipitation hardening, plastic strain and creep 07 p1211 A67-20176

Heat treatment optimization for precipitation hardening superalloys, devising mathematical model for test sequence 07 p1192 A67-20249

Substructural strengthening of carbide precipitation hardened molybdenum alloy by swaging and wire drawing 11 p1805 A67-24108

Titanium and aluminum additions to cobalt-base alloys improve tensile and stress rupture properties and heat resistance 11 p1807 A67-24703

Cobalt alloys precipitation hardening behavior, oxidation, thermal shock resistance and stress rupture strength 11 p1808 A67-24704

Multipass welded Hastelloy joint age embrittlement from exposure in inert atmosphere at high temperature, stressing ductility, tensile and hardness tests 17 p2866 A67-33199

Coherent precipitation hardening theory treats yielding in nickel base alloy containing coherent stress-free ordered particles as dynamic process 18 p3064 A67-34080

Reversible contribution to flow stress in Ni-Al alloy analyzed by temperature change as function of tensile strain and precipitation hardening 18 p3065 A67-34383

Heat treatment practices for precipitation hardening steels noting use in missile and aerospace applications 21 p3634 A67-38178

Primary and secondary strengthening precipitates in 18Ni/250/Al, V and Ti maraging steels 22 p3822 A67-40059

Precipitation processes in Ta-Cr solid solutions investigated for temperature dependence and change in alloy properties

resulting from precipitation 23 p4018 A67-40712

Co effect on precipitation hardening in high strength stainless steels 23 p4018 A67-40871

PRECIPITATION PARTICLE MEASUREMENT

Polarization effects during radio wave scattering by cloud and precipitation particles, obtaining phase state from echo signal 01 p0109 A67-11249

Polarization effects during radio wave scattering by cloud and precipitation particles, obtaining phase state from echo signal 11 p1815 A67-24120

Periodicity of precipitation singularities and relation to period of comets and meteor streams 11 p1815 A67-24329

High energy particle precipitation into upper atmosphere at medium latitude after magnetic storms, dependence on season and latitude and correlation with geomagnetic pulsation enhancement 12 p1991 A67-25113

Coherent ordered precipitates formation in Ni-Cr-Al alloy, discussing spacing, shape and size of gamma prime particles as function of time 12 p1954 A67-25344

Low energy proton precipitation measurements in austral and boreal auroral zones, using polar orbiting satellite 12 p1937 A67-25813

Meteor stream relation to natural ice nuclei and precipitation 13 p2205 A67-27461

Correlation of measurements of precipitated electrons with ionospheric effects of winter anomaly in midlatitude D layer 14 p2310 A67-28043

Auroral particle precipitation, establishing latitude vs time pattern from gross statistical data on optical-and radio-auroral phenomena 17 p2850 A67-33191

VLF emission associated with aurora and particle precipitation, describing receiving equipment, types of emission and occurrence patterns 18 p3039 A67-33621

Atmospheric emissions and electron and proton precipitation latitude and diurnal variations measurements from satellite-borne photometric studies 18 p3039 A67-33623

Airborne precipitation collector, determining washed out radioactive particles from air between cloud base and surface by comparing surface and airborne samples 21 p3628 A67-38583

Auroral proton precipitation and hydrogen emissions 23 p3993 A67-40564

PREDICTION

S IMPACT PREDICTION

S LINEAR PREDICTION

S PERFORMANCE PREDICTION

PREDICTION RECORDING

Interference Prediction Model /IPM/ for RF interference study at satellite tracking stations 01 p0023 A67-10498

Man-made HF radio noise level measurement and prediction, discussing spectral and spatial distributions, soil/saltwater conductivity and receiver elevation effects, instrumentation and antennas 01 p0024 A67-10499

PREDICTION THEORY

Forecasting length of solar cycle and maximum value of sunspot numbers, suggesting relation to joint tidal effect of Venus-Jupiter-earth 01 p0149 A67-10805

Prediction method for system reliability in early proposal and feasibility phases of program 01 p0085 A67-11379

Adaptive technique determination of optimum operations for pure prediction of discrete time series with respect to mean square error cost 02 p0207 A67-12138

Prediction of turbulent boundary layer development in conical diffusers, using kinetic energy deficit equation 04 p0549 A67-15750

On-line digital computer used in optimizing control by prediction, including quadratic and steady state value 05 p0784 A67-16524

Minimum variance estimation and prediction theory for signal parameters in presence of noise 10 p1806 A67-23084

Two-dimensional nonsteady airflow in shaped duct prediction, using numerical method 12 p1928 A67-25357

Indeterminate recognition /game type/ and prediction systems 13 p2088 A67-27022

Reliability prediction with inadequate data in flight control systems, using nonelectric approach combining failure data with

judgment 18 p3058 A67-34699

Long term forecasts of proton flares 19 p3313 A67-35261

Solar-flare short and long term forecasting, discussing magnetic-field configurations and gradients 19 p3314 A67-35269

Biaxial buckling behavior of 45 degrees eccentric-stiffened waffle cylinders using prediction theory 19 p3341 A67-35525

Surface-temperature conditions in disks and gears stressing heat transfer coefficient and lubricated contact 19 p3237 A67-35840

temperature 19 p3237 A67-35840

Apollo gyro reliability covering Guidance, Navigation and Control systems, stressing failure mode prediction 19 p3259 A67-35984

Prognostic equation asymptotic solution for atmospheric pressure forecast 20 p3479 A67-36125

Book on stationary random processes, discussing prediction theory, interpolation, extrapolation, filtering, linear forecasting, etc 20 p3475 A67-36140

Prediction procedure for nonstationary stochastic processes with slow spectral density function variation with time 20 p3477 A67-36789

Stochastic models for forecasting seasonal and nonseasonal time series using iterative method 20 p3477 A67-36790

Prediction-comparison system for data compression, noting nonlinear error feedback and advantage of closed-loop predictor 20 p3412 A67-37497

Runge-Kutta integrations for all seasons by proceeding in blocks of N steps compared to predictor-corrector methods 21 p3652 A67-38173

Predictions from barotropic vorticity equation in spectral form analyzed for errors 21 p3654 A67-38575

Prediction of lunar surface temperature through digital computer program noting heat transfer equations 22 p3884 A67-39930

Analytical prediction of cryogenic propellant venting effects on orbital vehicle dynamic behavior, emphasizing vent thrusting and gas impingement 22 p3906 A67-40165

Model for compressible free jet with moving environment in core and developed region of exhaust plume 23 p3992 A67-41731

PREDICTOR

Adaptive data compression systems of predictor-comparator type 12 p1907 A67-25992

Data compression for analog signal transmission with smaller bandwidth requirement obtained from reduced signal redundancy and simulation of techniques 14 p2275 A67-28683

Predictor-corrector for solving ordinary differential equations, discussing influence of rounding-off errors on accuracy of solution 18 p3071 A67-34266

Predictor display instrument for optimal manual control, noting use in manned spacecraft missions and time factor 20 p3447 A67-36840

PREFLIGHT ANALYSIS

Feasibility of pure-fluid missile control system demonstrated by systems analyses, preflight tests and flight tests 07 p1257 A67-19360

PREFLIGHT OPERATION

Preflight testing of ATS-1 Thermal Coatings Experiment /TCE/, discussing cup designs, sensor and cup calibrations, etc [AIAA PAPER 87-333] 12 p2038 A67-26047

Computer applications in checkout of individual Saturn stages and in prelaunch checkout of complete Saturn vehicle 13 p2089 A67-28409

Rescue teams for manned testing in environmental chamber for Gemini spacecraft noting personnel, chamber and personal equipment, test operations and rescue function and drill 17 p2807 A67-32598

PRELAUNCH PROBLEM

Systems analysis applied to identification of Saturn V launch vehicle support system requirements and establishment of baseline logic for vehicle prelaunch processing simulation and systems optimization [AIAA PAPER 87-248] 07 p1165 A67-20066

Real time meteorological system providing prelaunch impact prediction for unguided high altitude rocket firings, noting computer program 08 p1314 A67-20543

Systems analysis applied to identification of Saturn V launch vehicle support system

requirements and establishment of baseline logic for vehicle prelaunch processing simulation and systems optimization [AIAA PAPER 87-248] 21 p3607 A67-37806

Real time meteorological system providing prelaunch impact prediction for unguided high altitude rocket firings, noting computer program 21 p3607 A67-37812

Launch vehicles of post-Saturn class noting requirements for launch facilities at Kennedy Space Center 21 p3608 A67-38808

PRELAUNCH TESTING

Digital computers connected by data link transmission system for prelaunch space vehicle checkout 01 p0050 A67-11031

Inspector role in prelaunch checkout of space system hardware 05 p0930 A67-17241

Optimal allocation of n test points within redundant digital system for prelaunch and in-flight spacecraft reliability estimate 08 p1300 A67-20637

Computer applications in checkout of individual Saturn stages and in prelaunch checkout of complete Saturn vehicle 13 p2089 A67-28409

Scientific instrument integration into Mariner IV spacecraft and prelaunch testing for flexible performance 18 p2757 A67-30640

Prelaunch checkout in 1970s, discussing vehicle subsystems, prelaunch requirements and operations and launch site technology 20 p3415 A67-36579

Prediction of Saturn V launch vehicle effectiveness during prelaunch phase using computer simulation [SMPTE PAPER 102-27] 22 p3908 A67-40371

PREMIXED FLAME

Flame noise in spherical volume of combustible gas confined within soap bubble and spark ignited, noting relation between radiated sound and flame movement and combustion 01 p0168 A67-11290

Air velocity and temperature, stabilizer size and blockage effects on fresh mixture entrainment in recirculation zone of bluff body stabilized flames 02 p0342 A67-12029

Quenching diameter of premixed fuel-oxidizer flames by volatile inhibitors, noting nature of oxidizers, particularly oxygen 02 p0342 A67-12031

Photometric measurements on deviations from equilibrium state in burnt gases of laminar premixed shielded flames at atmospheric pressure [AIAA PAPER 87-9] 06 p1072 A67-18345

One-dimensional steady laminar premixed flame characterized by matched asymptotic expansions 10 p1733 A67-23145

Role of electronically excited CH in formation of C3H3 ion and contribution to overall chemionization process 18 p3150 A67-33802

Collisional de-excitation rate or quenching of sodium in flat premixed laminar flames 18 p3150 A67-33803

Ionization and recombination processes of alkali metal ions in hydrogen-oxygen-nitrogen flames with hydrocarbon additives 18 p3107 A67-33806

Carbon monoxide and hydrogen flames ionization and electron temperatures with methane premixing 18 p3151 A67-33807

Carbon formation in oxygen premixed acetylene and benzene flames 18 p3151 A67-33808

Spectrophotometric study of multiple reaction zones of premixed trimethylaluminum-oxygen flames, emphasizing microstructure 18 p3109 A67-33840

Chemical structure of premixed flames of methane and perchloric acid vapor diluted with argon obtained in terms of composition, temperature and velocity profiles 18 p3109 A67-33841

Parallel porous wall burner for studying premixed and diffusion flames in stagnation flows [CI PAPER 87-7] 19 p3345 A67-35002

Chemiluminescence and chemionization in low pressure fuel-oxygen flames, measuring emission intensity of CH, carbon molecule and OH electronic bands 20 p3376 A67-37094

PRESERVATION

Preservation of viable microbes in anabiosis in potassium salts determined improbable by failure to grow bacteria 15 p2427 A67-29118

PRESSING

SA HOT PRESSING

Gravity sintering and low pressure

pressing of tungsten powders for economic production of large diameter W matrices 01 p0098 A67-10701

Microstructure and mechanical properties as functions of degree of deformation of pressed rods of Tsm2A alloy at 1300 degrees C 05 p0832 A67-17509

Soviet book on new elements in technology of pressworking 07 p1191 A67-19746

Microstructure and mechanical properties as functions of degree of deformation of pressed rods of Tsm2A alloy at 1300 degrees C 21 p3644 A67-38037

Volume strains in metals during pressworking and rolling 21 p3637 A67-38922

PRESSURE

SA ATMOSPHERIC PRESSURE

SA BASE PRESSURE

SA BLOOD PRESSURE

SA CHAMBER PRESSURE

SA CRITICAL PRESSURE

SA DYNAMIC PRESSURE

SA ELECTRON PRESSURE

SA FORCE

SA GAS PRESSURE

SA HIGH ALTITUDE PRESSURE

SA HYDROSTATIC PRESSURE

SA IMPACT PRESSURE

SA INLET PRESSURE

SA INTERNAL PRESSURE

SA INTRACRANIAL PRESSURE

SA ISOSTATIC PRESSURE

SA LIGHT PRESSURE

SA PARTIAL PRESSURE

SA RADIATION PRESSURE

SA STAGNATION PRESSURE

SA STATIC PRESSURE

SA STRAIN

SA SUPERCRITICAL PRESSURE

SA SURFACE PRESSURE

SA TRANSIENT PRESSURE

SA VAPOR PRESSURE

SA WALL PRESSURE

SA WATER PRESSURE

High pressure technology - AICE Symposium, Detroit, December 1966, Part 1 04 p0611 A67-15945

Inputs and outputs of digital pneumatic jet components design for adaptation to standardized pressure range for use in installations 08 p1281 A67-20448

PRESSURE APPARATUS

SA LOW PRESSURE CHAMBER

SA VAPOR PRESSURE APPARATUS

Ti-Mg alloy production under high pressure, noting existence of solid solution of one weight-percent Mg 03 p0441 A67-13255

Coanda device as pressure maintainer and as switch or selector 08 p1281 A67-20453

Static and dynamic performance of pancake vortex flow field and application to pressure amplification 14 p2248 A67-28272

Pressure Commutating System for propulsion research facility noting cost saving and allowance for pretest checkout 23 p3988 A67-41427

Apparatus for plasma investigation of pulsed arc discharge in high pressure argon 23 p4035 A67-41686

PRESSURE BREATHING

Book on positive pressure breathing as means for acceptable arterial oxygen tension at altitudes above 40,000 ft and effects of raised intrapulmonary pressure 08 p1288 A67-21500

Effects of breathing pure oxygen under pressure on autonomous regulatory systems /nervous, respiratory, circulatory/ of man 14 p2257 A67-28225

Positive pressure breathing effects on inhibition of diuresis during water immersion 18 p2992 A67-34721

Intrapulmonary pressures chosen during immersion in thermally neutral water, comparing transpharyngeal and transthoracic pressure gradients for various breathing devices 22 p3751 A67-39604

Adrenal gland reaction to different pressure breathing types by urine analysis 22 p3752 A67-40538

Inactivity and water immersion effects on fluid balance and tilt-table performance in dehydrated subjects, assessing vasopressin and positive pressure breathing effects 23 p3951 A67-41557

PRESSURE BROADENING

Quantitative intensity of weak carbon dioxide triad in 1 micron spectral region obtained, using pressure broadening techniques 06 p1031 A67-17870

Competitive and cascade coupling between transitions in CW water vapor laser 14 p2331 A67-28498

PRESSURE CHAMBER

Gas embolisms and gas bubble formation in tissue 13 p2059 A67-26849

Space simulation chamber for industry and research 14 p2292 A67-28063

Simulated acceleration and dynamic pressure environments generated by space vehicle flight ranging from weightlessness to impact from ground landing [AIAA PAPER 67-279] 15 p2465 A67-29425

Theory of supersonic gas ejector with cylindrical mixing chamber, discussing low and high pressure gas flow 20 p3358 A67-37085

PRESSURE COEFFICIENT

Two-dimensional shock induced separated flows in turbulent boundary layer, applying Crocco-Lee theory and calculating pressure rise coefficient 02 p0231 A67-11522

Total pressure losses in hypersonic wind tunnel with Eiffel chamber, calculating coefficient of pressure 04 p0546 A67-14780

Variation of total pressure loss coefficient with entry Mach number for conical diffusers, junction between parallel entry pipe and cone being sharp 04 p0549 A67-15748

Electrical resistance of manganin coil to 7 kbar and 200 degrees C, use as pressure indicator at elevated temperatures provided correction due to shift of resistance at different temperatures is made 08 p1353 A67-20373

Semiconductor-to-metal transitions in transition metal compounds 13 p2181 A67-27165

Interval size effect on minimum drag coefficients and optimum shapes of bodies of revolution determined from Newtonian impact theory 15 p2418 A67-29407

Minimum drag for slender body in hypersonic flow, assuming pressure coefficient is modified Newtonian and surface-averaged skin friction coefficient is constant 15 p2418 A67-29408

Slender two-dimensional wing lift-drag ratio at hypersonic speed maximized, assuming modified pressure coefficient 15 p2418 A67-29409

Atmospheric variations effects on cosmic radiation records from plastic scintillation monitors, calculating pressure coefficients 17 p2938 A67-32795

Barometric sensors insensitive to high winds 17 p2860 A67-32816

Aerodynamic characteristics of plane compressor cascades with high subsonic flow analyzed, noting application in determining flow deflection angle and pressure loss coefficient 20 p3358 A67-37079

Relation between incipient cavitation number and Reynolds number by combining bubble dynamics Rayleigh equation with cavitation number definition 22 p3787 A67-40176

PRESSURE DISTRIBUTION

SA SUPERSONIC PRESSURE DISTRIBUTION

Pressure and density of heat flux at surface of pointed or blunt nosed obstacle in divergent truncated cone of hypersonic nozzle 01 p0005 A67-10258

Pressure and stagnation temperature distribution in test chamber of blowdown hypersonic wind tunnel 01 p0049 A67-10558

Pressure distribution of porous self-lubricating bearing noting geometrical factors, dimensions, running speed, load, etc 01 p0079 A67-10708

Rarefaction parameter for planar bodies with sharp leading edge and tip defining hypersonic boundary of strong interaction regime 01 p0007 A67-11182

Pressure distribution in vicinity of wedge for separated turbulent flow analyzed, using modified Vasilu step solution 02 p0232 A67-11634

Approximate determination of sonic line and pressure distribution on surface of blunt body in supersonic and hypersonic flows 02 p0178 A67-12042

Leading edge blowing effects on pressure distribution of half-cone body with 75 degree sweep angle, obtaining normal and axial forces and pitching moments 02 p0178 A67-12225

Rutgers Axisymmetric Near-Wake Tunnel for testing turbulent supersonic base flow, temperatures and pressure distributions 02 p0230 A67-12361

Center of pressure stabilization for thin wing profile with downward deflected trailing edge, when placed in steady state flow of ideal incompressible fluid 02 p0179 A67-12438

Hypersonic flow past lower surface of slender delta wing for wide-range of angle of attack, determining velocity component, pressure and density distribution 03 p0350 A67-12874

Flexible wing analysis based on slender body theory, calculating wing profiles, pressure distribution as function of stress and lift force values 03 p0351 A67-12992

Nonlinear boundary value problem solution as applied to effect of uniformly distributed pressure and concentrated load on spherical dome 03 p0524 A67-13623

Normal force and pitching moment values for interference on body, wing and overall body-wing obtained, using pressure distribution integration 04 p0545 A67-14439

Ramjet external-combustion engine noting design of trailing edge, nomograms of pressure, temperature, thrust component, etc 04 p0688 A67-14578

Mercury device for analyzing pressure distribution, velocity profiles and resistance coefficients of turbulent flow in channels of linear induction pumps under traveling magnetic field 04 p0670 A67-15521

Aerodynamic detector measuring dynamic pressure distribution in laminar He jet heated by electric arc 05 p0850 A67-18035

Reynolds number effect on surface pressure distributions and boundary layer velocity profiles on three-quarter power law bodies of revolution in hypersonic flow 05 p0747 A67-16431

Time-dependent pressure distribution in parachute canopy during inflation measured by special transducers 06 p0945 A67-17631

Pressure distribution in externally pressurized bearings 06 p1007 A67-18060

Closed form solution methods for blast wave propagation in solid media assuming power law density profile [AIAA PAPER 67-141] 06 p1102 A67-18290

Supersonic flow over axisymmetric bodies with continuous or discontinuous slope solved via parametric differentiation [AIAA PAPER 67-5] 06 p0939 A67-18303

Integral representation for transonic flow about thick airfoils obtained from equations for two-dimensional inviscid flow and locally surface-orthogonal shock waves [AIAA PAPER 67-3] 06 p0939 A67-18331

Correlation of local heat transfer and friction coefficients for subsonic turbulent flow of air through high temperature annulus 06 p1117 A67-18386

Pressure distribution on rectangular wing with jet exhausting normally from lifting surface into uniform air stream [AIAA PAPER 67-1] 06 p0941 A67-18463

Approximate analysis of subsonic compressible flow in annular nozzle of short duct fan engines and inner wall curvature effect on pressure 06 p0944 A67-18871

Laminar boundary layer separation length data in hypersonic flow show strong Mach number dependence 06 p0992 A67-18878

Nonlinear singularities method for calculating velocity distribution over thick wing of finite aspect ratio situated at zero angle of attack in incompressible frictionless potential flow 07 p1127 A67-19887

Mean velocity and mean static pressure distribution on stability and space requirements of turbulent diffusion flames 08 p1425 A67-20304

Pressure distribution between lubricated rolling bearings, comparing static and dynamic stresses in cylindrical disks, noting film thickness 08 p1333 A67-20361

Wall pressure distribution in turbulent reattachment bubble calculated by splitting bubble into large number of small control volumes 08 p1320 A67-20451

Aerodynamic characteristics of flared bodies noting geometry, Reynolds number and boundary layer state effects on stability 08 p1275 A67-20499

Air loads on sounding rocket from distributed aerodynamics and pressure differential 08 p1276 A67-20501

Aeroelastic vehicle body loads computed by coupled system of digital computer programs 08 p1405 A67-20505

Linearized supersonic theory for favorable thickness distributions and drag reduction for wings in supersonic flow [AIAA PAPER 65-716] 08 p1276 A67-20559

Boundary layer development in throat region of converging-diverging nozzle, obtaining self-consistent solutions 08 p1277 A67-20589

Hypersonic rarefied gas flow past plate with sharp leading edge, determining rarefaction effect on induced pressure distribution and value 08 p1278 A67-20924

Viscosity effect on stability of plane flame front, showing destabilization from linearized equations of velocity and pressure disturbances 08 p1428 A67-21423

D'Alembert initial value problem for cylindrical waves, obtaining linearized potential equation for plane and symmetrically spherical case 09 p1488 A67-21932

Tire hydroplaning, noting lift force on planing surface and pressure distribution 09 p1441 A67-22492

Airflow past wing profile with leading edge slot blowing foreign gases, noting schlieren photographs of flow patterns and concentration distribution measurement 10 p1589 A67-22724

Aerodynamic design of swept wing-fuselage combination for cruising at transonic and supersonic speeds, noting pressure distribution role 10 p1589 A67-22872

Reynolds equation analysis for pressure distribution in gas bearing clearances by asymptotic solution 10 p1680 A67-23046

End-wall pressure distributions in confined vortex [JPL-TR-32-1099] 10 p1626 A67-23150

Falling sphere measurements of atmospheric density, noting temperature and density profiles, pressure distribution, etc 10 p1639 A67-23205

Interferometry analysis of stresses in plate due to pin 10 p1718 A67-23245

Load carrying capacity of plane and reinforced cylindrical shells clamped along edges and subjected to uniformly distributed internal pressure 10 p1720 A67-23600

Closed toroidal shell stability under effect of uniformly distributed external pressure 10 p1720 A67-23602

Pressure rise in ionized He plasma cylinder due to Nernst effect 10 p1686 A67-23777

Viscous flow around flat plate at various angles of incidences at high Mach number to evaluate shock wave intensity variation and wall pressure distribution 11 p1742 A67-24761

Supersonic rarefied argon plasma jet, determining pressure distribution, electron concentration and temperature 11 p1842 A67-24963

Approximate solution of equilibrium problem for shallow cylindrical shell of rational profile under pressure distribution from convex side 12 p2024 A67-25603

Shock wave diffraction and reflection problems on faces of angle situated in nonstationary gas flow 12 p1928 A67-25672

Static characteristics of radial gas dynamic bearing, using differential equation for pressure distribution 13 p2122 A67-26351

Potential flow about two-dimensional hydrofoils with zero velocity boundary condition 13 p2095 A67-26910

Turbulent mixing in plane nonisothermal jets, deriving solutions for velocity, temperature and pressure distribution 13 p2105 A67-27052

Hemispheric pressure distributions, measuring effect of Mach number, hole size and angular position of hole on Pitot pressure 13 p2220 A67-27193

Model with hydrostatic gas pressure distribution to interpret equivalent widths of atomic and ionic lines in spectra of umbrae 13 p2203 A67-27426

Static magnetic field effect on normal distribution of pressure, temperature and density in solar atmosphere, considering sunspots and velocity field effects [AFCLR-66-679] 13 p2204 A67-27435

Effect of Reynolds number on hypersonic flow of rarefied gas past sphere obtained from pressure distribution at surface 14 p2240 A67-27996

Automatic pressure stepping control and recycling system for use with Fabry-Perot interferometer 14 p2315 A67-28158

Time dependent pressure distribution and threshold acceleration for bubble formation in longitudinally vibrating flexible liquid filled cylinder [ASME PAPER 67-FE-1] 14 p2304 A67-28354

Two-dimensional curved diffuser design by comparison with flow regime and performance data, obtaining diffuser shape and pressure distribution criteria [ASME PAPER 67-FE-6] 14 p2242 A67-28358

Two-dimensional flow through bends with turning vanes, using Green theorem to obtain surface pressure distributions [ASME PAPER 67-FE-13] 14 p2304 A67-28362

Viscoseal operation in superlaminar flow regime noting pressure patterns, end effect, gas ingestion and sealing capacity 14 p2327 A67-28797

Two-dimensional expansion-deflection nozzle studied for internal pressure distribution and resultant thrust determination 14 p2244 A67-29050

Para-Foil models tested in wind tunnel and free flight for flight capability, L/D ratios, deployment, control and maneuverability, etc 14 p2246 A67-29054

Hypersonic decelerator deployment investigated for interactions between decelerator, connecting cable and wake of forebody it tails 14 p2244 A67-29055

Static deflection of parallelogram plates with clamped edges subjected to uniformly distributed pressure studied by energy method 15 p2573 A67-29312

Minimum drag for slender body in hypersonic flow, assuming pressure coefficient is modified Newtonian and surface-averaged skin friction coefficient is constant 15 p2416 A67-29408

Hypersonic trim angle of attack of lifting entry vehicles, correlating stagnation point values obtained from heat shield ablation and pressure distribution measurements 15 p2417 A67-29447

Pressure distributions and shock wave shapes on conical wings calculated by numerical solution of integral equations 16 p2589 A67-30619

Viscous, compressible fluid flow through narrow gap, noting compressibility effect on pressure distribution 16 p2661 A67-31420

Pressure distribution and convective heat flux at slender bodies of revolution surface, considering sphericity influence of free hypersonic flow 16 p2594 A67-31468

Decay and dispersion of disturbance pulse in fluid lines along pipe, considering velocity and pressure characteristics [ASME PAPER 66-WA/AUT-24] 17 p2835 A67-32017

Wall suction rate effect on turbulent flow in cylindrical circular porous duct, measuring distributions of velocity, pressure, friction coefficient and Reynolds stresses 17 p2837 A67-32380

Lift and drag coefficients of wing profile with elliptical pressure distribution calculated by approximate linearized theory 18 p3024 A67-33541

Pressure distribution in subsonic flow for vertical stabilizer calculated, using orthogonal function 18 p2982 A67-33655

Hydrogen-air reaction kinetics analyzed using standing wave normal shock, noting wall effects, ignition delay and recombination [AIAA PAPER 67-479] 18 p3157 A67-33948

Pressure-distribution estimation over entire forward face of blunt body at angle of attack 19 p3169 A67-34833

Aerodynamic forces pressure center on profile in plane rectilinear blade cascade 19 p3169 A67-34884

Radial pressure distribution in hydrogen arc located in axial magnetic field using Saha equation, determining temperatures and electron densities 19 p3279 A67-35139

Supersonic free plasma jet with axial current, solving MGD equations for structure modifications due to self-magnetic forces 19 p3288 A67-35363

Flow around thin delta wing under supersonic conditions, considering flow separation at leading edges 19 p3170 A67-35542

Boundary conditions of journal gas bearings lubrication, studying slots

effects 20 p3453 A67-36273

Quasi-conical motion past wing-body lifting system, determining pressure distribution, potential expression and axial disturbance velocity 20 p3356 A67-36278

50 degree semivertex angle sphere-cone Voyager configuration wind tunnel tested in dry nitrogen for aerodynamic characteristics, pressure and heat transfer distribution 20 p3356 A67-36562

Wind tunnel tests for load and pressure distributions on flat-top cylinders with thick boundary layer 20 p3421 A67-36781

Slender wing maximum lift-drag ratio at hypersonic speeds obtained assuming modified Newtonian pressure distribution and skin-friction drag 20 p3357 A67-36953

Lift-drag ratio attainable by slender flat-top body at supersonic speeds, considering Newtonian pressure distribution and constant skin friction 20 p3359 A67-37124

Surface pressure distribution on tube-lattice cluster with transverse gas flow to determine aerodynamic characteristics 20 p3359 A67-37306

Performance factors affecting size, shape and operation of piston and bore including hydraulic lock, viscous drag, oil contamination, etc 20 p3366 A67-37367

Air loads on sounding rocket from distributed aerodynamics and pressure differential 21 p3563 A67-37795

Molecular gas flow through cylindrical tube, using wall pressure distribution to measure pump speed 21 p3610 A67-37823

Incomplete expansion wave diffraction by corner, noting pressure discontinuity across boundary 21 p3564 A67-37929

Velocity and pressure distributions and free shape of conducting liquid in rotating circular cylinder under magnetic and electric fields 21 p3668 A67-38561

Conical shell of low aspect wing type, analyzing strength under distributed, high/low pressures on surface, deriving equations and formulas for stresses 21 p3724 A67-38779

Extent of lubricating film for which oil flow is plane, discussing lubricant compressibility, heat release, load capacity and pressure distribution 22 p3811 A67-39317

Velocity and pressure distributions and flow field for laminar incompressible source flow between two coaxial parallel disks rotating at different speeds 23 p3988 A67-40602

Shadow photography study of underexpanded nozzle ejected supersonic turbulent jet off-design behavior, discussing static pressure distribution, boundary layer and Mach number effect 23 p3928 A67-40732

Externally pressurized gas bearings examined for mechanism of series restrictors on pressure distribution, flow quantity and load capacity 23 p4010 A67-41064

Gas bearings with wide pockets investigated theoretically and experimentally for pressure distribution, flow quantity and load capacity 23 p4010 A67-41065

Energy transfer in sunspot model with vertical magnetic field, noting magnetic pressure distribution and magnetohydrostatic equations 24 p4226 A67-41966

Flexible membrane hydrostatic air bearing, determining membrane shape, pressure distribution and air gap by Navier-Stokes and membrane analogy equations [ASME PAPER 67-LUB-1] 24 p4162 A67-42668

Boundary layer theory in gas bearing lubrication problems, obtaining pressure asymptotic expansions for infinitely long slider squeeze-film bearing [ASME PAPER 67-LUB-7] 24 p4162 A67-42671

Squeeze film journal bearing load support capability, noting axial pressure distribution in finite case is considerably greater than infinite case [ASME PAPER 67-LUB-14] 24 p4163 A67-42675

Analysis divided into step and ridge regions used to obtain linearized PH solution to Reynolds equation, neglecting side leakage [ASME PAPER 67-LUB-17] 24 p4163 A67-42676

Film thickness, pressure distribution and load carrying capacity of loaded line contact in presence of viscoelastic lubricant noting

- high pressure spike
[ASME PAPER 67-LUB-23] 24 p4163 A67-42681
- PRESSURE DRAG**
Pressure losses and improved heat transfer in incompressible fluid flow through tubes containing twisted tapes 02 p0233 A67-12200
Minimum drag body with specified center of pressure 10 p1592 A67-23155
- PRESSURE DROP**
SA FRICTION PRESSURE DROP
Pressure drop correlation in developed, isothermal, laminar and turbulent flow in rectangular ducts 10 p1627 A67-23555
Incremental pressure drop in incompressible fluid laminar flow at entrance of rectilinear duct, using conformal mapping technique 12 p1930 A67-26166
Air embolism pathogenesis and therapy in terms of problem of treatment in overpressure [DVL-628] 13 p2059 A67-26850
Entrance region tube flow combined with rounded entrance flow meters to obtain theoretical solution relating flow rate, downstream pressure, pressure drop and temperature 13 p2120 A67-26932
Pressure drop study of near saturation Freon 11, noting flowing fluid quality condition for estimates 13 p2106 A67-27668
Fully developed velocity profile for prediction of hydrodynamic entrance lengths for ducts of arbitrary cross section [ASME PAPER 67-FE-4] 14 p2304 A67-28357
Frictional pressure drop for isothermal incompressible flow in isosceles triangular duct, with correlations for laminar and turbulent flow [ASME PAPER 67-FE-18] 14 p2243 A67-28365
Optimum pressure drop in compressed air driven turbine as function of initial pressure in air cylinder and turbine parameters 14 p2252 A67-28652
Critical region determination in viscous fluid flow using dye stream fuzziness or pressure drop discontinuity as measure of flow turbulence 14 p2305 A67-28801
Pressure loss measurements of compressible flow through gauzes with different porosity 14 p2305 A67-29009
Terminating solid propellant combustion by rapid drop in pressure 15 p2582 A67-29998
Depressurization behavior of human organism, noting endurance as flight duration and altitude function, and von Beckh chimpanzee absolute-vacuum experiments 16 p2615 A67-31766
Axial compressor inlet stator tests determining pressure loss relationship to geometric parameters 20 p3516 A67-37082
Pressure drop increase in choke eliminates axial compressor stage discontinuity caused by disrupted flow 20 p3358 A67-37083
Discharge line fluid conditions in cryogenic container with self-pressurized draining, using Bernoulli, continuity and general energy equations and fluid properties 22 p3784 A67-39968
- PRESSURE EFFECT**
Nonthermal radiation of Na in CO medium, analyzing temperature, pressure and composition variation effects of ambient 01 p0166 A67-10051
Cryogenic liquid level sensor consisting of diode heated by resistor 01 p0062 A67-10194
Physical and environmental effects on energy dissipation characteristics of balsa wood [SAE PAPER 660657] 01 p0103 A67-10616
Gas phase pyrolysis kinetics of tetranitromethane, noting pressure effect and rate equation of thermal decomposition 01 p0019 A67-10765
High intensity triboluminescence in europium tetrakis /dibenzoylmethide/-triethylammonium crystals under mechanical impact 01 p0019 A67-10897
Pressure coupled combustion dynamics of solid propellants analyzed as function of propellant variables, oscillation frequency and combustion pressure 01 p0143 A67-11448
Seasonal changes in cosmic ray intensity including barometric effect in neutron component, effect of earth seasonal position, etc 02 p0307 A67-11865
Inertia and pressure effects on energy potential of homogeneous and isotropic turbulence in weakly compressible medium 02 p0235 A67-12643
- Externally pressurized bearings treated as hydraulic closed loop servomechanism analyzed, using transfer functions [ASME PAPER 66-LUB-7] 03 p0431 A67-13759
Differential pressure flow meter for unsteady or transient fluid flow 03 p0422 A67-13775
Vibrational damping of externally pressurized orifice journal bearings undergoing free vibrations with and without shaft rotation 04 p0627 A67-14432
Connective heat transfer and viscous fluid friction at air pressure with high Reynolds numbers in cooled channels, noting coolant pressure effect 04 p0603 A67-14717
Pressure dependence of mean electron energy of plasma emerging from anode aperture of duoplasmatron ion source 04 p0663 A67-14768
Hydrogen oxidation noting explosive property as function of temperature, pressure, composition, etc 04 p0565 A67-15091
Average burn rate, average pressure relationships in solid rockets 04 p0724 A67-15250
Electron beam welding noting effects of pressure and vacuum 04 p0628 A67-15313
Combustion rate dependence on pressure in combustion process involving relaxation as induced by mechanical strength of fuels 04 p0726 A67-15593
Cosine series analysis of nonuniform internal pressure effect on crack extension in infinite body 04 p0718 A67-15797
Rapid depressurization transients effect on saturated pool boiling system from stainless steel surface 04 p0734 A67-15848
Vacuum deposition of thin films, noting importance of low pressure environment, with attention to diffusion and ion pumps 04 p0631 A67-15994
Elastoplastic axisymmetric stressed state of circular cylindrical shell under unsteady temperature field, internal pressure and axial force, using differential equation 05 p0912 A67-16181
Doppler and impact broadening of spectral lines and pressure effects on power output of gas laser 05 p0818 A67-16643
Enhanced lasing of high pressure He-Ne laser, commenting on delay time of light pulse emitting through walls of discharge tube from start of exciting pulse 05 p0823 A67-16687
Dynamic displacements of thin spherical shell buckling under uniform pressure 05 p0920 A67-16825
Exploding wire phenomena in air at atmospheric and reduced pressures 05 p0847 A67-17317
Flow pressure structures of supersonic flow over rearward facing step, showing pressure changes and Reynolds number role 05 p0750 A67-17339
Liquid droplet combustion at high pressures revealing effects of vapor source distribution on predicted burning time at supercritical pressures 05 p0929 A67-17359
Finite plasma pressure effect on interchange mode in finite Larmor radius weakly unstable regime 05 p0858 A67-17430
Experimental equipment for chemical reaction analysis in fluid systems based on study of partial oxidation of methane at high pressures 05 p0759 A67-17540
Relation between effective porosity and differential pressure of rigid steel and elastic nylon ribbon grids of various forms and porosities 06 p0944 A67-17630
Hydrostatic pressure effect on dispersion of gamma prime phase in precipitation heat treatment of nickel-base superalloy 06 p1016 A67-17902
Plasma instability in HF electric and constant magnetic field for sufficiently low pressure 06 p1039 A67-18081
Turbulence in reaction zone of detonating liquid explosives, noting pressure irregularities in and around shock wave front 06 p1113 A67-18143
Metastable form of C12 type calcium disilicide when under high temperature and pressure, noting X-ray diffraction powder patterns and superconductivity 06 p1051 A67-18372
Initial geometric and boundary condition imperfection effect on stability of shallow spherical shells under uniform pressure [AIAA PAPER 67-111] 06 p1104 A67-18453
Crack growth rate and measurements of temperature effect on low pressure fatigue of Al 06 p1019 A67-18561
Pressure dependence of output power of He-Ne laser on amplitude of periodic high voltage excitation pulses 06 p1012 A67-18784
Hydrostatic pressure effect on energy gap, carrier concentration and electron and hole mobilities of indium antimonide 07 p1231 A67-19061
Flammability limits of hydrogen-oxygen-nitrogen mixtures at low pressures 07 p1239 A67-19077
McDonnell Martian Environmental Simulation Facility, analyzing sand and dust storm behavior at low pressures 07 p1248 A67-19386
Gross hydrostatic pressure effect as related to foil and wire strain gauges 07 p1185 A67-19412
Pressure amplitude at resonance decreasing with increasing Mach number observed as effect of mean flow on wall damping of finite amplitude gas pulsations 07 p1168 A67-19576
Piezoresistance measurement in p-type Ge as function of pressure and impurity concentration at 77 and 300 degrees K 07 p1233 A67-19644
Photolysis of hydrazine vapor in vacuum UV, examining emission as function of pressure and photolysis time 07 p1138 A67-20190
Ruby laser-induced effect of pulsed pressure on KDP crystal surface and thermal bulk effect on excitation of ultrasonic oscillation in crystal 08 p1337 A67-20417
Stability of toroidal shell under uniform external pressure solved using series expansion, considering buckling modes 08 p1417 A67-20557
Plasma instability in HF electric field perpendicular to given magnetic field under low pressures 08 p1357 A67-20847
Active component of voltage behavior in channel of helium pulse discharge measured, obtaining time dependence of channel resistance, input velocity and energy magnitude 08 p1357 A67-20848
Device measuring uniaxial pressure effect on transmission factor of semiconductors in low absorption region 09 p1551 A67-21657
Rarefied gas flow dynamic behavior during reaction with gas measuring device mounted on moving plant 09 p1487 A67-21896
Probability of effervescence of superheated liquids as function of temperature and pressure, analyzing N-pentane and hexane under isobaric heating and reduced pressure 09 p1580 A67-21907
Spectral analysis of laser discharge in pure and impure He, obtaining spectra of spark at various pressures, determining electron concentration 09 p1512 A67-22010
Total and spectral reflectance of carbon dioxide cryodeposits on test vehicles and space simulator walls as function of deposit thickness, rate of formation, angle of incidence of light, etc 09 p1533 A67-22121
Low contamination space chamber design employing cryopanel array configurations with near unity sticking coefficients 09 p1485 A67-22122
Minimum N and O content in degassing determined from equilibrium pressures in Nb-O and Ta-O systems 09 p1518 A67-22125
Structures and materials for supersonic aircraft and space vehicles 09 p1576 A67-22429
Voltage fluctuations on Pt filament probes attributed to pressure variations 09 p1490 A67-22576
Heat losses in conductive and convective transfer through rarefied fluids investigated for dependence on temperature differences, static pressures, test geometries and fluids 10 p1731 A67-22725
Phonon lifetime variation effect on stimulated Brillouin and Raman scattering in gases by temperature, pressure and laser power variation and comparison with Stokes gain theories 10 p1662 A67-22758
Stability of radial motion of spherical gas bubble in incompressible inviscid fluid under external pressure 10 p1624 A67-23028
Pressure deflagration limit of high energy solid propellants increased to superatmospheric pressures by composition changes [AIAA PAPER 66-679] 10 p1696 A67-23131
Pressure dependence of nonmetalized

hybrid fuel regression rates in demonstrating major heat release reactions as heterogeneous or homogeneous 10 p1697 A67-23133

Currents caused by light pressure on metal surface and in flare plasma when laser beam hits surface 10 p1664 A67-23333

Free flight response of two panels subjected to turbulent pressure fluctuations at supersonic Mach numbers 10 p1719 A67-23558

Initial postbuckling behavior of spherical shell under external pressure determined using Koiter theory, analyzing effects of imperfections on buckling strength of structures 10 p1730 A67-23835

Effect of low pressures on stability of plasma currents in closed hydromagnetic systems 11 p1826 A67-23877

Helical instability of positive plasma column in longitudinal magnetic field, using magnetic pickup coil 11 p1829 A67-23999

Thermoconductivity of nitrosyl bromide at 290-900 degrees K and 200-600 torr measured by hot filament 11 p1881 A67-24022

Hydrostatic pressure effect on surface microstructure, dislocation substructure and stress-strain behavior of beryllium 11 p1805 A67-24110

Elastic response of circular cylinder under torsion 11 p1871 A67-24118

Efficiency of electroluminescent lamps, noting dependence on arsenic pressure and temperature during GaAs crystal growth 11 p1845 A67-24140

Heat and mass transfer during stationary adiabatic vaporization of water ethanol and carbon tetrachloride 11 p1882 A67-24319

Calculating method for parachute opening forces, system velocity, cloth pressure loading and filling time for horizontal and vertical deployment conditions 11 p1743 A67-24348

Effects related to ion cooling in Q device 11 p1833 A67-24371

Sco X-1 physical characteristics noting ionization, possible stellar wind and pressure equilibrium effects 11 p1862 A67-24506

Numerical and photoelastic solutions compared for uniform edge loading, obtaining pressure calibration by means of shear stress measurement 11 p1876 A67-24616

Solid state material analysis inducing controlled density variations and crystal structure changes via high pressure techniques 11 p1846 A67-24618

Gas pressure effect on electrical breakdown and field emission, discussing ion bombardment and whisker formation 11 p1820 A67-24921

X-ray analysis of lattice strain and crystallite size changes in tungsten carbide compressed at high pressure, noting annealing effect 11 p1809 A67-24949

Nonstationary gunpowder combustion at various pressures analyzed for combustion rate and surface temperature dependency on pressure and initial temperature 11 p1884 A67-24957

Monograph on theory of decompression sickness and application to diving tables, including calculation of critical size of localized bubbles formed from dissolved nonrespiration-involved gases in tissues [DVL-623] 11 p1748 A67-25036

MHD wave propagation in magnetoplasma-filled waveguide, discussing pressure, current inertia, resistivity, etc 12 p1969 A67-25247

Time variability of bearing clearance due to temperature and pressure treated by iterative-numerical calculation 12 p1949 A67-25330

Variational derivation of nonlinear equilibrium equations for three-layer conical shell with rigid incompressible filler under external pressure 12 p2025 A67-25609

Stability of cylindrical shell of oval cross section compressed along generatrix and under external pressure analyzed, using Laplace transforms 12 p2025 A67-25612

Rigid plastic cylindrical shell axisymmetrical deformations in terms of Tresca yield condition and gradient law when under load 12 p2026 A67-25618

Reinforced cylindrical shell stability under external pressure, considering irregular frame disposition effect 12 p2027 A67-25620

T-burner technique for determining acoustic pressure-and velocity-coupled

responses of solid propellants 12 p1988 A67-25910

High intensity runaway electron fluxes accelerated by external field in toroidal plasma discharge, noting pressure effect 13 p2162 A67-26270

Thermal accommodation coefficient of nitrogen and helium on nitrogen covered tungsten above room temperature 13 p2223 A67-26944

Beryllium corrosion in carbon dioxide under pressure at high temperatures 13 p2136 A67-27108

Curves of fusion and alpha-beta transformation of beryllium as function of pressure 13 p2137 A67-27110

Plastic flow in beryllium under fluid pressure at room temperature 13 p2139 A67-27123

Equilibrium states of buckled elastic rings under stress 13 p2219 A67-27147

Pressure effect on interband reflectivity spectra of germanium and related semiconductors 13 p2179 A67-27158

High pressure, uniaxial stress and temperature effects on GaAs electrical resistivity 13 p2180 A67-27159

Cohenite grains from iron meteorites studied by X-ray diffraction for establishing pressure scale, using solid state recrystallization 13 p2200 A67-27235

Pool boiling of methane over pressure range from 1 atm to critical pressure in both nucleate and stable film boiling regimes 13 p2229 A67-27667

Trapped magnetic field effect on hydrogen plasma parameters in theta pinch, noting density and temperature dependence on initial pressure 14 p2353 A67-27751

One-dimensional plane shock wave propagation through hot dense plasmas under various energy and pressure conditions, noting magnetic field effect 14 p2356 A67-27957

Stability of inhomogeneous anisotropic cylindrical shells containing elastic cores under pressure, axial load and torsion 14 p2399 A67-28119

Magnetic field, pressure and discharge current effects on saturation electron current of electrostatic probe used to measure magnetoplasma electron density 14 p2358 A67-28237

Automatic fluoric gain changer circuit for flight control systems counteracting Mach number and altitude pressure effects 14 p2251 A67-28352

Constant total pressure evaporation with heat reuse by built-in engine 14 p2407 A67-28623

Five-ball fatigue tester to investigate reduced pressure environment effect on rolling element fatigue life with polyphenyl ether [ASLE PREPRINT 67AM 8A-3] 14 p2326 A67-28795

Timoshenko beam equations modification necessary to account for normal pressure and Poisson ratio effects for application to thin walled circular tubes 14 p2403 A67-29013

Shock tube tests with cold argon and heated helium to determine heated driver gas effect on effect on shock tube performance 14 p2294 A67-29053

High altitude parachute systems test techniques for analysis of inflation, stability variations porosity, effects at low dynamic pressure, etc 15 p2419 A67-29433

Empirical correlation formulas for density and viscosity of equilibrium air, noting pressure variation at high enthalpies 15 p2579 A67-29436

Similarity criteria for plastic behavior of polymers under combined effect of nonuniform temperature field and hydrostatic pressure 15 p2573 A67-29466

Acoustic radiation of panels excited by random pressure fluctuation of turbulent boundary layer investigated, showing agreement with experiment 15 p2574 A67-29770

Polymorphism in IV-VI compounds induced by high pressure and thin film epitaxial growth 15 p2539 A67-29822

Critical field dependence on pressure, tube radius and ion mass derived from ion-acoustic instability growth in low pressure RF discharge 15 p2531 A67-29904

Combustion instability, transient burning during ignition and extinction by depressurization investigated in nonsteady

burning of solid propellants 15 p2580 A67-29984

Ignition response of solid propellants described with model including surface regression with verification of igniter flux and pressure effects 15 p2581 A67-29988

Changes in structure of gas detonation wave with changes in initial pressure 16 p2656 A67-30452

Localized uniaxial force effect on voltage-current relationship of gold-potassium tantalate Schottky barrier diodes, noting reversible changes 16 p2637 A67-31036

Seasonal changes in cosmic ray intensity including effect in neutron component, effect of earth seasonal position, etc 16 p2738 A67-31080

Design for light-gas gun with light piston by successive parameter computation of various parts 16 p2655 A67-31125

Ionization, ion temperature and density dependence of cesium plasma on pressure of added rare gas 16 p2720 A67-31244

High pressure hydrogen environment effects on mechanical properties of steels at high temperatures 16 p2689 A67-31327

Hydrostatic pressure effects on brittleness in Cr and yielding in center annealed iron specimen studying brittle-ductile transition of former 16 p2689 A67-31328

Twinning of copper, silver, iron, and gold alloys of beryllium pressurized in solid medium noting structural changes 16 p2690 A67-31371

Cesium impurities analyzed for behavior in thermionic converters, investigating equilibrium state as function of pressure and temperature 16 p2609 A67-31399

Physical exercise effect on oxygen consumption at decreased pressure 17 p2806 A67-31963

Volatile liquid pressurization as expulsion method for storable propellants noting in-flight refueling system design parameters 17 p2953 A67-31973

Thermodynamic properties of plasmas in pressure and temperature equilibrium, showing evaluation accuracy to 4 percent 17 p2894 A67-32146

Black body radiation, pressure and temperature dependences of equilibrium composition, enthalpy, specific heat and electron density of air-carbon plasmas 17 p2894 A67-32147

Geometric dimensional, plasma temperature and pressure effects on capillary discharge with evaporating wall /CDEW/ 17 p2897 A67-32177

Ventilatory mechanical system response to stepwise-increasing pressure stress studied with Laplace-Carson transform, giving characteristics of linear differential equation governing system 17 p2807 A67-32238

Nozzle and membrane effects on shock wave intensity in tube, showing graphically Mach number dependence upon initial pressure 17 p2837 A67-32345

High hydrostatic pressure effects on load cell using foil strain gauges and calibration for small uniaxial loads 17 p2855 A67-32393

Imperfections effect on buckling of complete electroformed spherical shells under uniform external pressure examined in rigid and soft testing systems 17 p2960 A67-32454

Duoplasmatron ion source study with Langmuir probe, finding that pressure dependent discharge characteristics relate to magnetic field radial components 17 p2902 A67-32659

Helium-neon laser generating simultaneously on two lines, showing pressure dependence and output radiation variation with discharge current 17 p2868 A67-32662

Differential depressions of iron I levels and red shifts of spectral lines under pressure, demonstrating error in assumed air refractive indices 17 p2886 A67-33162

Pressurization produced free dislocations effect on yielding and fracture in bcc metals 18 p3063 A67-33484

Spectral and recombination radiation intensity changes from indium phosphide diode under different uniaxial compressions 18 p3100 A67-33718

Pressure dependence of output power of He-Ne laser on amplitude of periodic high voltage excitation pulses 18 p3059 A67-33726

Ammonia-air combustion, flame speed needed to obtain optimum

performance 18 p3110 A67-33844
 General equation for explosion limits from unified thermal and chain theory, noting application to hydrogen and oxygen systems 18 p3156 A67-33849
 Compression tests with superimposed hydrostatic pressure to study rheological behavior of elastomer filled with granular potassium chloride [SESA PAPER 1224] 18 p3142 A67-33891
 Cesium viscosity coefficient over range of temperatures and pressures, assessing accuracy of results and collision integral values 18 p3087 A67-34050
 Aircraft front windshields, discussing thermal stability, clear vision maintenance, bird impact, atmospheric pressure effect, cabin pressure changes and tensile strength 18 p2986 A67-34099
 Ignition temperature and ignition delay of oxyhydrogen gas as function of pressure examined in shock wave tube, using Schlieren photography 18 p3160 A67-34261
 Plasma behavior in shock tubes with parallel conductors, discussing shape of front and velocity dependence on pressure and gas composition 18 p3089 A67-34297
 High pressure equations of state including electron gas correlation energy, giving density vs pressure curves for various elements 18 p3104 A67-34594
 Condensed phase thermal decomposition of ammonium perchlorate, studying pressure and additives effect on kinetics 19 p3309 A67-35003
 Pressure dependent surface reaction effects on acoustic response of composite solid propellants studied for various coatings 19 p3309 A67-35010
 Possibility of pressure destroying superconductivity in various metals, studying transition temperatures, critical pressures, etc 19 p3303 A67-35043
 Spectral line resonance broadening using Griem theory, noting linear pressure dependence 19 p3272 A67-35085
 DC discharge parameters solution using pressure theory with generation terms stressing one-and two-dimensional cases 19 p3277 A67-35126
 Retrograde motion of electric arc discharge at low pressure with transverse magnetic field, including cathode vaporization 19 p3281 A67-35153
 Shock wave interaction with plasma arc discharge, investigating wave refraction, arc response to pressure and temperature pulses and aftershock flow field 19 p3294 A67-35407
 Compression tests with superimposed hydrostatic pressure to study rheological behavior of elastomer filled with granular potassium chloride 19 p3340 A67-35465
 Plane incompressible wall jet ejected from slot into boundary layer in case of stationary and nonstationary external flow with and without pressure increase 20 p3420 A67-36277
 Axisymmetrical vibrations of cylindrical shell during HF internal pressure pulsations of gas flow containing uniformly distributed burning fuel droplets 20 p3536 A67-36445
 Elastic and residual strains caused by friction load in polymer surface layers studied for dependence, slip rate and friction load duration 20 p3473 A67-36842
 Equations of state of matter at high pressures and temperatures, discussing temperature density regions, theoretical calculations, etc 20 p3485 A67-36929
 Low pressure solid rocket motor design and application, noting advantages in high mass ratio performance and operational disadvantages 20 p3516 A67-37131
 Classical nonisothermal two-component plasma correlation functions and pressure contribution from Coulomb interaction 20 p3502 A67-37603
 Atmospheric absorption of gas laser radiation at two wavelengths noting dependence on gas pressure and amount of methane 20 p3463 A67-37668
 Attenuation cross section at Lyman alpha for Xe deviation from Beer law indicating diatomic Xe molecule formation 20 p3491 A67-37688
 Electric internal heater for heating helium driver gas to high temperature and pressure for shock tunnel experiments 21 p3806 A67-37770
 Linear melting curve of fayalite up to 40 kb determined, using piston cylinder and

thermocouples 21 p3617 A67-38190
 Pressure dependence of heat transfer by evaporation, obtaining parameters from dimensional analysis 21 p3732 A67-38499
 Plasmod propagation at high pressures, emphasizing Bostick buttons performance compared to electromagnetic shock tube, describing button gun and photographic equipment 21 p3674 A67-38771
 Stress analysis for rib-reinforced cylindrical shell subjected to rapidly varying pressure, calculating deflections and bending moments 21 p3725 A67-38790
 Aircraft construction techniques for terminating cables by pressure type connections, examining design factors 21 p3572 A67-39074
 Superconducting property of kappa phase in Bi-Sn alloy at high pressure, with determination of transition to superconducting state and temperature interval to keep stable 22 p3857 A67-39460
 Anomalous nonlinear preference for circular polarization in He-Ne laser noting variation with gas pressure 22 p3815 A67-39522
 Rapid decompression effect on lymph pressure of dog, discussing immediate and delayed rise phases 22 p3751 A67-39600
 Circumferential crack in pressurized cylindrical shell analyzed for extensional and bending components of stresses 22 p3911 A67-39678
 Gaseous ternary diffusion instabilities observed by ammonium chloride smoke technique, studying pressure and composition effects 22 p3917 A67-39713
 Similarity solutions for compressible laminar boundary layer, showing pressure and heat and mass transfer effects on wall temperature and shear stress 22 p3918 A67-39716
 Laminar boundary layer gas flows over slender bodies with massive blowing, discussing integral method solution and theoretical model including pressure effect 22 p3739 A67-39935
 Similarity parameters of gravity and pressure driven liquid discharge from propellant tanks obtained by dimensional analysis 22 p3785 A67-39969
 Reattachment of two-dimensional compressible air jets to planes, discussing pressure maximum and inlet Mach numbers 22 p3786 A67-40068
 35 GHz second harmonic generation power and conversion efficiency in low pressure gas discharge, noting pressure and gas species variations 22 p3854 A67-40316
 Curves for Hall effect logarithms, current carrier mobility and electric conductivity vs high pressure and temperature effects in InSb 22 p3864 A67-40323
 Nonlinear problems of parametric excitation of rings solved by equations, considering normally and centrally directed pressures 23 p4074 A67-40651
 Pressure effects on fatigue reported for Fe, Al and Ni wires subjected to oscillating strains, discussing several fatigue models 23 p4075 A67-40666
 Elastic equilibrium of jointed cylinder of elastic nonlinear resilient materials obtained by relations of two-dimensional nonlinear theory of elasticity 23 p4075 A67-40682
 Oxidation of ultrahigh purity Co at various oxygen pressures and at high temperatures 23 p4018 A67-40872
 Fermi pressure shifts of highly excited states of atoms in gaseous medium due to electron particle interactions, discussing scattering contributions 23 p4029 A67-40958
 Explorer 32 satellite atmospheric density experiment gas calibrations, comparing operation and pressure response of various ionization gauges 23 p4004 A67-41356
 Mass species abundance ratio of hydrogen ion beam from Oak Ridge type duoplasmatron ion source, discussing pressure dependent characteristics 23 p4034 A67-41436
 Treatment for relief of altitude decompression sickness for operations requiring extravehicular activity 23 p3960 A67-41702
 Periodic pressure fluctuations relation to structure and propagation of combustion front in solid propellant rockets, giving perturbation frequencies 24 p4252 A67-41798
 Rate resistance and reactivity in

hypothermal state to very low atmospheric pressure by hypercapnia-hypoxia exposure 24 p4111 A67-41849
 Variable gas pressure acting on turbine engine blades measured by piezoelectric sensors, discussing sensor structure and noise possibility 24 p4153 A67-42095
 Wave propagation in plasma with anisotropic pressure studied using modified Burgers equations, examining effect of collisions 24 p4197 A67-42260
 Air-oil separator for aircraft hydraulic system stops nose wheel shimmying, based on lowering pressure principle and using filter screen barrier 24 p4099 A67-42427
 Electro-fluid dynamic power generation, discussing Mach number, charged particle mobility, pressure level and radial space charge field effects on load characteristic and conversion ratio 24 p4107 A67-42527
 Microscopic and X-ray diffraction study of octahedrite shock history 24 p4234 A67-42631
 Fatigue crack initiation, comparing alpha brass and Al-Mg-Zn alloy, noting effect of increasing maximum pressure value in contact region [ASLE PAPER 67-LC-5] 24 p4174 A67-42744
 Synthetic molybdenum sulfide film examined for lubricating performance under extreme pressure conditions in air and immersed in fluids [ASLE PAPER 67-LC-15] 24 p4165 A67-42749
 Pressurized propellant tank system for rocket engine, discussing weight factors, propellant combinations and expellant gas pressure relations 24 p4241 A67-42754
 Attitude errors of inertially coupled gravity gradient satellite with solar radiation pressure as dominant disturbance, noting slot problems in stabilized package accommodating damper motion 24 p4241 A67-42904
PRESSURE FIELD
SA BALANCE EQUATION
 Pressure patterns, gas ingestion and sealing capacity of viscoelastic seals investigated using oil, water and liquid sodium as sealed fluids 03 p0428 A67-13226
 Vertical velocities in atmospheric front motions, noting pressure and temperature field distributions and application of computer to solve obtained equations 07 p1219 A67-19356
 Pulsating model of closed universe, noting ordinary matter time-dependent scalar field interaction and equation for nonvanishing pressure 11 p1868 A67-24867
 Wind and pressure fields diagnostic relations substituted for classical equation of stream function and solved as boundary value problem 13 p2149 A67-26273
 Wind tunnel tests of sonic boom phenomena, noting weak pressure field measurement, construction of extremely small models, boundary layer effects, etc [AIAA PAPER 66-765] 13 p2091 A67-27594
 Solar activity cycle effect on northern hemisphere pressure field solar activity cycle effect on Northern Hemisphere pressure field 13 p2117 A67-27632
 Far field pressure spectrum of sonic boom 13 p2055 A67-27703
 Various boundary layer parameters and transducer shape effect on Measurement error of random pressure field by finite size transducer 19 p3228 A67-34964
 Noise wave amplitude reduction method by suitable initial wind field adaptation to pressure field studied for applications to divergent barotropic model 19 p3253 A67-35530
 Heat transfer intensifying process experimented in wind tunnel by applying longitudinal/transverse pressure gradients through controlled flow pressure field 19 p3346 A67-35633
 Electromagnetic and pressure fields produced by current distributions in compressible magnetoplasmas determined using perturbation theory 20 p3496 A67-36312
 Velocity and pressure fields in viscous incompressible fluid flow in inlet of flat channel 20 p3423 A67-37066
 Steady flow field from turbulent boundary layer separation in front of forward facing step, discussing pressure field 21 p3613 A67-38853
 Isobaric mixing chamber configuration determination method for maintaining constant static pressure along flow during turbulent jet mixing 23 p3927 A67-40730

Second order nonlinear differential equation derived for pressure-time curve required for ideal solid propellant rocket motor 24 p4208 A67-42923

PRESSURE GAUGE

SA IONIZATION GAUGE

SA MANOMETER

SA MCLEOD GAUGE

SA PIEZOELECTRIC PRESSURE GAUGE
Role of space charge and discharge mechanism in gauge with cold cathode, noting electron sheath formation 05 p0809 A67-17494

Trigger discharge gauge compared with ionization gauge and partial pressure analyzer 06 p0950 A67-17749

Response of trigger discharge gauge, noting ion current component 06 p0950 A67-17750

Air gauge circuit analysis extended to fluidic restrictor circuits and complex resistor circuits, using Bernoulli and continuity equations 14 p2252 A67-28353

Pressure measuring apparatus for direct gas pressure measurements in millitorr ranges 17 p2855 A67-32351

Upper-atmosphere density determination methods, with comparison of orbital decay and instrument 18 p3041 A67-34254

Pressure gauge for plasmas subjected to large dynamic electric and magnetic fields in accelerator channel of MHD wind tunnel 20 p3444 A67-36529

Upper atmosphere density measurement systematic errors in orbiting pressure gauges by neglecting adsorption and desorption 20 p3450 A67-37103

Pressure gauge using acoustic techniques designed for gas pressure measurements, discussing limitations, sensitivity and experimental results 21 p3630 A67-38767

PRESSURE GRADIENT

Thermomolecular pressure differential in wide capillaries at low Knudsen numbers calculated, using irreversible thermodynamics 02 p0343 A67-12678

Hypersonic flow separation over simple geometries and aerodynamic controls, noting pressure gradients and heating-rate distributions [AIAA PAPER 65-753] 03 p0350 A67-12911

Effect of sudden change in magnetic field and/or pressure gradient on Hartmann flow, assuming stationary and nonconducting plates 03 p0482 A67-13745

Correlation scheme for mean velocity distributions in turbulent boundary layers developing in arbitrary adverse pressure gradients 04 p0601 A67-14459

Pressure variational law effect along boundary layer of flat plate on formation of turbulent spots measured via hot-wire technique 04 p0602 A67-14598

Free stream turbulence and pressure gradient effects on flat plate boundary layer velocity profiles and heat transfer [ASME PAPER 66-WA/HT-4] 04 p0608 A67-15448

Unsteady viscous fluid flow in MHD channel under action of pressure gradient solved for arbitrary load coefficient 04 p0669 A67-15519

Electron motion in gases in pressure range where electron mean free path is comparable to or less than chamber length, showing effect on ion currents 04 p0662 A67-15769

Von Karman-Pohlhausen boundary layer analysis of temperature and velocity profiles in inlet region between two parallel planes with relative motion and pressure gradient 04 p0729 A67-15808

Preston tube measurements of skin friction and velocity profiles in incompressible turbulent boundary layer, considering pressure gradient effects 04 p0609 A67-15818

Turbulent boundary layer calculation, considering compressible and incompressible flows with pressure gradients and heat transfer 04 p0610 A67-15908

Drift waves in finite pressure plasma, noting oscillation caused instabilities induced by Alfvén type and slow magnetoacoustic wave interaction 05 p0852 A67-16693

Parallel Couette and Poiseuille flows of multicomponent viscous plasma in presence of pressure gradient and electric field 05 p0854 A67-16694

Ohm law in multicomponent nonisothermal plasmas derived as function of electric and

magnetic fields and temperature and pressure gradients, using transport equation 05 p0857 A67-17422

Minimum structural response and acoustic radiation for panel excited by turbulent boundary layer 06 p0985 A67-18256

[AIAA PAPER 87-12] Convective heating in shoulder regions of flat-faced cylinder with large favorable pressure gradient 06 p1114 A67-18293

[AIAA PAPER 87-162] Wind tunnel study of boundary layer transition structure on ogive nose cylinders aligned parallel to flow 06 p0939 A67-18314

[AIAA PAPER 87-129] Static temperature-velocity distribution for zero pressure flat plate compressible turbulent boundary layer with heat transfer [AIAA PAPER 87-195] 06 p1116 A67-18362

Suction requirements for elimination of turbulent boundary layer separation in adverse pressure gradient, based on mixing rate hypothesis and von Karman momentum integral [AIAA PAPER 87-197] 06 p0988 A67-18442

Two-dimensional adiabatic laminar separated regions in supersonic flow, examining effects of blowing and suction at wall [AIAA PAPER 87-192] 06 p0988 A67-18459

Turbulent boundary layer properties for strong adverse pressure gradients, obtaining layer and displacement thickness, skin friction, heat transfer, etc [AIAA PAPER 87-196] 06 p0989 A67-18489

Magnification in profile drag of airfoil due to effect of pressure gradients on boundary layer downstream of isolated roughness element 06 p0990 A67-18748

Hypersonic boundary layer behavior in adverse pressure gradients used in designing high Mach number intake diffuser system 06 p0942 A67-18750

Transverse variation effects on accuracy of skin friction measurements determined via static hole pair 06 p1005 A67-18753

Friction coefficient of compressive gas flow growth when negative pressure gradients in channel reach very high levels 06 p0991 A67-18816

Laminar, transitional and turbulent boundary layer flows with adverse pressure gradient on axisymmetric blunted conical flared body at Mach 10 [AIAA PAPER 86-493] 06 p0943 A67-18844

Effect of fairing contraction into two-dimensional supersonic nozzle for wind tunnel, avoiding pressure gradients along walls unfavorable to boundary layer flow development 07 p1126 A67-19630

MGD lubrication, obtaining motion equation of gas in electric or magnetic fields, velocity distributions, pressure differential equations, etc 07 p1192 A67-20210

Velocity jump characteristics of boundary layer with gradient pressure for flows at inlet channel and in wake of symmetric and asymmetric bodies 07 p1169 A67-20223

Unsteady flow of rarefied gas under finite pressure gradient when starting from rest, varying gradient in time until steady flow is obtained 09 p1487 A67-18147

Pressure gradients effects on boundary layers grown on wall of wind tunnel, obtaining equilibrium boundary layers of Clauser type 09 p1489 A67-22415

Analytical expressions developed for prediction of partially wetted rotating disk pressure, gradient development and frictional drag for different flow regimes 10 p1659 A67-22708

Similar calculation of hypersonic laminar boundary layer characteristics in presence of pressure gradient, specifically heat transfer, skin friction and boundary layer thickness 10 p1592 A67-23141

Disturbance diffusion in incompressible zero pressure gradient flow 10 p1626 A67-23144

Main parameters of two-stage hydraulic amplifier-actuator system determined with aid of pressure and flow-rate amplification factors 10 p1597 A67-23321

Low density shear resistant ablators for lifting reentry vehicles 10 p1672 A67-23725

Laminar flow between parallel plates for arbitrary initial velocity distribution and time varying pressure gradient 10 p1629 A67-23842

Turbulent boundary layer phenomena, discussing parameters of production

processes, relation with instability, etc 11 p1776 A67-24043

Turbulent boundary layer development noting representation of velocity profiles, skin friction and eddy viscosity 11 p1776 A67-24044

Symmetrical jets and wakes in streaming flow with pressure gradient, noting time-mean profiles of particular pressure fields 11 p1741 A67-24047

Skewed turbulent boundary layers, noting absence of pressure gradient and shearing stress measurements in experiments and applicability of similarity defect equation 11 p1776 A67-24048

Electrical field in solar atmosphere caused by pressure gradient in case of partially ionized gas 12 p2000 A67-25133

Solutions to Falkner-Skan equation, making similarity solutions for pressure gradient parameter physically acceptable 12 p1893 A67-25935

Steady state model of solar wind flow in equatorial plane solved for radial and azimuthal motions, taking into account pressure gradient, magnetic field and gravitational effects 12 p2010 A67-26241

Wire screen roughnesses effect on turbulent boundary layer along flat plate without pressure gradient 13 p2093 A67-26529

Displacement and momentum loss thickness in boundary layer of rough flat plate at low velocities as function of wall roughness, pressure gradient, etc 13 p2095 A67-26809

Turbulent mixing at interface of two different density media under influence of pressure gradient, considering diffusion 13 p2105 A67-27411

Spectroscopic observation of sunspot structure, detailing sunspot model on basis of magnetic field and large scale motions interpretation 13 p2203 A67-27425

Sunspot magnetic field affecting convective energy transport so that resulting pressure gradient together with gravity force balances magnetic field force 13 p2204 A67-27436

Two-dimensional steady flow analysis in channels with variable cross sections under strong magnetic field action, calculating velocity distribution by series expansion 14 p2355 A67-27902

Planar incompressible free turbulent mixing with arbitrary velocity ratio and axial pressure gradient [ASME PAPER 87-FE-9] 14 p2304 A67-28359

Pressure gradient in duoplasmatron ion source as function of parameters of discharge 14 p2359 A67-28512

Natural boundary layer transition on ogive nose cylinders in zero and adverse pressure gradient analyzed for fluid dynamics, using smoke visualization 14 p2306 A67-29052

Two-dimensional wall jet effectiveness measurements and calculation procedures for injection conditions 15 p2468 A67-29128

Free stream turbulence and pressure gradient effects on flat plate boundary layer velocity profiles and heat transfer [ASME PAPER 66-WA/HT-4] 15 p2470 A67-29321

Hydrodynamic stabilization of plane Poiseuille flow by modulating pressure gradient 15 p2470 A67-29332

Drift waves in finite pressure plasma, noting oscillation caused instabilities induced by Alfvén type and slow magnetoacoustic wave interaction 15 p2530 A67-29864

Radial pressure gradients in clearance between two blade rims of axial turbomachine determined by introducing empirical function dependent on local twist exponent 15 p2417 A67-30144

Change in pressure losses in MHD generators channel, obtained from pressure gradient relation to flow rate of conducting fluid 16 p2705 A67-30449

Adiabatic gravitational collapse of spherically symmetrical distribution of matter, investigating nonvanishing internal pressure gradient, using Einstein field equation 16 p2746 A67-30865

Method of finite integral transforms as format for employment of incomplete eigenfunctions, discussing application of equilateral transform 17 p2876 A67-32423

Rotor system with blade angle reverse control noting blade-angle adjustment changes for achievement of higher flight speeds 18 p2985 A67-33460

Viscous fluid discharge from tubes of various cross sections under constant pressure gradient with longitudinal pulse along wall, noting short period stoppage 18 p3029 A67-34615

Turbulent boundary layer flow in conical supersonic nozzle, discussing convective heat transfer and adverse pressure gradient effect 19 p3169 A67-34814

Heat transfer intensifying process experimented in wind tunnel by applying longitudinal/transverse pressure gradients through controlled flow pressure 19 p3346 A67-35633

Incompressible turbulent boundary layers with arbitrary pressure gradients and divergent or convergent cross flows predicted by effective viscosity hypothesis 19 p3211 A67-35738

Gas-side heat transfer at high temperature combustor sonic points, discussing Reynolds number effect, boundary layer transitions, turbulence intensity, etc [AICHE PAPER 27] 20 p3552 A67-36831

Unsteady conducting fluid flow in MHD ducts with small magnetic Reynolds number and constant pressure 21 p3663 A67-37935

Turbulent MHD boundary layer in liquid with linear pressure gradient, discussing numerical integration, flow velocity and magnetic field 21 p3665 A67-38244

Combustion stability of powder in semiclosed volume, taking into account propellant surface temperature dependence on pressure and temperature gradient 21 p3732 A67-38526

Spherical symmetric problems in general relativity 21 p3707 A67-38962

Static reaction of radial gas dynamic bearing to journal axis angular displacement determined by splicing asymptotic solutions for low and high pressure levels 22 p3810 A67-39232

Intrapulmonary pressures chosen during immersion in thermally neutral water, comparing transpharyngeal and transthoracic pressure gradients for various breathing devices 22 p3751 A67-39604

Gravitational collapse model with pressure gradient and no energy flow, discussing spectral shift and mass radius relation 22 p3884 A67-39833

Incompressible laminar boundary layer flow on semiminfinite flat plate with impulsive motion solved using Meksyn steady pressure gradient boundary layer method 22 p3786 A67-40039

Two-dimensional adiabatic laminar separated regions in supersonic flow, examining effects of blowing and suction at wall [AIAA PAPER 87-192] 22 p3786 A67-40096

Apparatus for digital determination and storage of gas pressure variations, showing pressure curve diagram and numerical representation 22 p3804 A67-40328

Compressible laminar boundary layer in pressure gradient, analyzing suction on basis of momentum and thermal integral equations 22 p3788 A67-40421

Rotation and pressure gradient effects on gravitational instability of collapsing gas clouds, discussing subsequent fragmentation 22 p3893 A67-40501

Peristaltic viscous fluid motion through axisymmetric pipes and symmetrical channels produced by pressure gradients and cross section changes, using Stokes approximation 23 p3990 A67-41174

Second order boundary layer equations for hypersonic flow, noting interaction between pressure gradients 23 p3991 A67-41252

Convective heating in shoulder regions of flat-faced cylinder with large favorable pressure gradient [AIAA PAPER 87-162] 23 p3932 A67-41714

Compressible laminar boundary layer on infinite swept cylinder analyzed for effects of suction on spanwise profile 23 p3993 A67-41746

Boundary layer equation solution with constant pressure gradient restriction, discussing singularities 24 p4142 A67-42171

PRESSURE MEASUREMENT

SA IMPEDANCE MEASUREMENT

SA TONOMETRY

Equilibrium carbon monoxide pressures measured by torsion effusion studies of

reaction of graphite with hafnium and uranium dioxides at high temperatures 01 p0018 A67-10763

Pressure and density measurements of heat flux convected on sharp pointed cone placed in incidence in hypersonic flow 02 p0177 A67-11499

Angle of attack measurements of hypersonic reentry vehicle derived from flight test pressure data 02 p0178 A67-11942

General recursion formula for dynamic response of pressure measuring systems considered as series connection of tubes and volumes 03 p0418 A67-12998

Base pressure measurements on sharp and blunt 9 degree cones at Mach 3.50 to 9.20 04 p0547 A67-14851

Turning-arm apparatus operating in rarefied gas chamber and low pressure wind tunnel for drag measurements 04 p0596 A67-14993

Transfer function and input impedance of pressurized fluid piping system, using distributed parameters and block diagram feedback methods [ASME PAPER 66-WA/AUT-13] 04 p0555 A67-15416

Pressure, heat transfer and Pitot pressure profiles measured on wedges and cones at high Mach and Reynolds numbers in hypersonic tunnel 04 p0600 A67-15822

MacLeod and type U vacuumeters using liquid for pressure measurement 05 p0804 A67-16303

Reduced X-ray photoelectric current in modified Bayard-Alpert ion gauge for vacuum pressure measurements below 10 to minus tenth torr 05 p0805 A67-16462

Low pressure measurement with thermistors noting equipment and accuracy obtained 06 p1000 A67-17618

Diamagnetic probe measurements of kinetic pressure of plasma in magnetic field 07 p1228 A67-19513

High altitude supersonic isokinetic filter paper sampler for ALARR rocket, examining subsonic 3-D stagnation flow diffuser 08 p1276 A67-20500

Supersonic wind tunnel test providing static pressure measurements for use in cylinder flutter calculations 08 p1277 A67-20588

Book on airflow measurement techniques and flow meters 08 p1321 A67-20759

Micrometer U-tube manometers for medium vacuum measurements 08 p1332 A67-21493

Noise and pressure measurement in difficult conditions of vibrations and temperature for use in pressure-transducer design of jet and rocket systems 09 p1497 A67-21939

Hydrostatic pressure measurement by direct loading of semiconductor strain gauges 09 p1498 A67-22031

Elevation differences between Martian dark areas /maria/ and bright areas /deserts/, discussing surface pressure and temperature 10 p1706 A67-22957

Upper atmospheric wind, temperature and pressure variations measured using grenade launched Skylark sounding rockets 10 p1638 A67-23199

Pressure measurements on surface and in wake of circular cylinder at rest and in vortex excited oscillation at subcritical Reynolds numbers [ASME PAPER 87-VIBR-31] 11 p1777 A67-24189

Silicon semiconductor combustion pressure transducer for high temperature HF pressure measurements within liquid rocket motor chambers 11 p1792 A67-24820

Wafer thin button size sensor for differential pressure measurement across airfoils 11 p1795 A67-25061

Pressure on sharp-edged insulated flat plate in low density hypersonic flow, noting results and possible sources of error 14 p2241 A67-28164

Low density hypersonic wind tunnel, noting surface pressure and flow field measurements 14 p2293 A67-28166

Fluorid pressure, temperature and angular rate sensors for military and commercial applications [ASME PAPER 87-DE-12] 14 p2252 A67-28869

Rocketsonde and radiosonde temperature comparisons and evaluation of computed rocketsonde pressure and density 14 p2347 A67-28865

Pulmonary mechanics associated with oxygen toxicity and suggested physiological test for susceptibility to effects of oxygen 15 p2429 A67-29280

Flow velocity determination by cylindrical magnifying probe, measuring stagnation and wake pressures difference, noting magnifying factor variation under Reynolds number and stem and blockage effects 15 p2471 A67-29529

Dust remover using paper filters and wind tunnel with turbulence in cylindrical duct used for pressure determination 16 p2657 A67-30867

Rapidly varying high pressure measurement requirements, treating pressure transducer as seismic system and analyzing feed channel distortion 16 p2871 A67-31004

Pressure measurement at stagnation point of cylindrical missile with spherical nose cone during free flight in ballistic testing 16 p2593 A67-31123

Gas kinetic pressure measurement in high current rectilinear hydrogen-plasma discharge during electron heating 16 p2718 A67-31188

Slow oxidation of n-octane vapor /oxygen/ nitrogen mixtures at reduced pressures and temperatures 16 p2779 A67-31518

Pressure attenuation of transverse fringe effect in flat linear induction pumps 16 p2723 A67-31582

Pressure measuring instrumentation response requirements for computing decay rate in solid propellant termination systems 17 p2926 A67-32069

Density and pressure in real gas behind plane shock wave upon reflection from solid surface 17 p2836 A67-32072

Italian sensing devices for measuring temperature, pressure, acceleration, heat shield and vibration on ELDO satellite 17 p2854 A67-32227

Vacuumometer modification permitting direct pressure difference measurements in high and ultrahigh vacuum range 17 p2855 A67-32352

Vacuum system pressure measuring and monitoring by remote control methods as used in Gemini spacecraft test program 17 p2859 A67-32593

Instrumentation for space vacuum simulation used in testing operations, discussing pressure measurement requirements 17 p2860 A67-32594

Ionization effect on external pressure determination for high velocity gas flows past plates and shells with flutter 18 p2981 A67-33424

Physical and chemical wall effects on mechanism of combustion reaction in gases studied by introducing solids and measuring ignition pressure 18 p3155 A67-33847

Measurement within rocket exhaust plumes 18 p3051 A67-34507

Jet flow turbulence energy balance, measuring point-pressure/velocity correlations and spatial mean gradients, giving energy equation 19 p3170 A67-35412

Remote control pneumatic pressure test system for Saturn S-IC booster checkout with manual or automatic control, using computer 20 p3415 A67-36569

Aerospace technology and hardware transference to commercial and architectural testing, noting application to flow measurements, hydraulic acoustics and helium leak detection 20 p3416 A67-36698

Wall turbulent boundary layer pressure resolution by piezoelectric transducer, noting attenuation of frequency component with size and frequency dependence 20 p3422 A67-37002

Differential magnetic loop, density profile and gas laser interferometer measurements of beta, n and ion temperature in theta pinch operation 21 p3662 A67-37755

High altitude supersonic isokinetic filter paper sampler for ALARR rocket, examining subsonic 3-D stagnation flow diffuser 21 p3563 A67-37803

Electrostatic getter-ion pump performance, giving pumping speeds, pressure and starting characteristics, residual gas composition and operating life 21 p3624 A67-37822

Pressure measurement with McLeod type gauge in presence of saturated vapors condensed during compression 21 p3627 A67-38384

Pressure gauge using acoustic techniques designed for gas pressure measurements, discussing limitations, sensitivity and experimental results 21 p3630 A67-38767

Base pressure measurements on elliptic cones in supersonic flow with turbulent boundary layer as function of geometry 21 p3566 A67-39083

Gas dynamic self-regulation of supersonic nozzle consisting of cylindrical channel with central body, measuring nozzle inlet and static pressures 22 p3868 A67-39544

Temperature, pressure and density change effects free thermal conductivity gauge system for upper atmosphere pressure measurements 22 p3829 A67-40470

Wind tunnel pressure measurement installation, describing calibration bench and industrial testing 23 p3997 A67-40572

Book on vacuum engineering covering space vacuum simulation, pressure measurement, gas flow and load, vacuum systems and technology 23 p4028 A67-41353

Reentry vehicle surface pressure measurement, obtaining accuracy and reliability in stable high level pressure transducer 23 p4006 A67-41378

Diaphragm and piezoelectric pressure gauges for severe blast environment, discussing resonance, damping, heat shield and rise time 23 p4007 A67-41387

Human systolic and diastolic blood pressure measuring apparatus and method 23 p4008 A67-41424

Variable gas pressure acting on turbine engine blades measured by piezoelectric sensors, discussing sensor structure and noise possibility 24 p4153 A67-42095

Algebraic equations to predict time response to step input in free molecule, transition and continuum flow regimes 24 p4155 A67-42293

High speed internal flow past cone with large wall injection velocities, calculating pressure of outer flow using contact surface initial slope as parameter 24 p4092 A67-42398

PRESSURE OSCILLATION

Vibrations of elastic shells containing liquids 01 p0165 A67-11441

Mixing gaseous propellant injector, injection velocity and momentum flux ratio, combustion pressure and propellant combination effects on HF combustion pressure oscillations in rocket motor 02 p0302 A67-11940

Directed graphs application to calculation of forced pressure oscillations in hydraulic systems of flight vehicles and engines 04 p0557 A67-15886

Pressure variation in solid propellant rocket engine determined by digital computer in terms of propellant properties and engine design 07 p1239 A67-19351

Irrational fluctuations near turbulent boundary layer in Phillips theory and relation between one-and two-dimensional wave number spectra 08 p1320 A67-20705

Optimal control of elastic flight vehicles, describing axis oscillations by equations of beam with variable cross section 09 p1439 A67-22075

Pressure changes in cerebrospinal fluid in rhesus monkey cranial cavity with applied forces at abdominal wall 10 p1600 A67-23821

Vibratory type pressure oscillations in combustor with dual orifice fuel injection analyzed in gas turbine for possible elimination [ASME PAPER 67-GT-23] 11 p1854 A67-24804

Barometric pressure data analysis estimating autocovariance, using Fourier transform for spectral density calculation 11 p1816 A67-24840

Pressure oscillations induced by forced convection heating of dense hydrogen 13 p2107 A67-27670

Surface coupled heat release effect on oscillatory amplitude of pressure coupled response in solid propellant 15 p2544 A67-29983

Temperature and/or velocity modulation of plasmas for generating MHD power 18 p3085 A67-33702

Biennial oscillations effect on spring wind reversal in stratosphere and mesosphere, showing transition date dependence on geographical location and height 18 p3074 A67-34352

Pressure fluctuations beneath incompressible turbulent boundary layer with mass addition 18 p3030 A67-34742

Base bleed and initial boundary layer thickness effects on base pressure variations, calculating combining parameter for vehicle performance evaluation 19 p3172 A67-35779

Langmuir probe current in weakly ionized gas flow, studying correlation between hydrodynamical turbulence and pressure fluctuations 20 p3503 A67-37874

Pressure fluctuation onset conditions in jet engine combustion chambers with supersonic nozzles, discussing design factors effect on combustion process stability 21 p3896 A67-38909

Convective heat transfer between tube and airflow in tube for pulsating flow with pressure fluctuation frequency deviating from resonant frequency 23 p4082 A67-41285

PRESSURE PROBE

Turbulence measured by flow direction indicators used as pressure probes 01 p0076 A67-11192

Static pressure and velocity profiles of rotating flow with recirculation core in straight pipes determined by five-hole pressure probe [ASME PAPER 66-WA/FE-36] 04 p0607 A67-15367

Pressure sensor consisting of aluminum membrane for measuring pressure distribution in parachute canopy 06 p1002 A67-18021

Null-yaw and fixed direction multihole probes for aerodynamic measurements, describing calibration charts and error sources 12 p1940 A67-25352

Free molecular flow through circular orifice at high pressure ratios, discussing mass flux measurement methods 14 p2300 A67-28179

Pressure and temperature in orifice set in body located in free molecular flow, checking first moment of distribution function 14 p2302 A67-28198

Causes of ignition failure in solid-fuel rocket motors, obtaining simultaneously pressure and temperature data 15 p2543 A67-29773

Local mass flux and local impact pressure measurement in arc jet exhaust flow fields 17 p2861 A67-33029

Fluid dynamics effect on spontaneous pressure spikes in Apollo SPS thrust chamber, noting increased combustion instability, occurrence and mechanism of pops, etc [AIAA PAPER 67-513] 18 p3114 A67-33976

Leak detection methods in vacuum devices including compressed air, discharge tube, halogen tracers, radioactive krypton, pressure rebuild, etc 20 p3443 A67-36474

Pressure transducers for use in high temperature and pressure gaseous detonation wave phenomena, discussing performance and application 20 p3443 A67-36514

Static pressure probe nose derived from supersonic slender body theory and shaped for subsonic speeds 21 p3564 A67-36535

Strong blast waves and laser generated plasma dynamics in high pressure gas investigated using Mach-Zehnder interferometer and pressure probe measurements [AIAA PAPER 67-696] 21 p3672 A67-38725

PRESSURE PULSE

Nonstationary combustion of powder under action of pressure pulse to determine temperature field variation and burning rate during transient process 06 p1112 A67-17957

Pressure pulse and wall-to-jet heat transfer in discrete vortex zone of restrained gas jet in circular channel 06 p1118 A67-18550

Nuclear energy deposition effect on pressure pulse generation in fissioning gas flow through semilfinite cylindrical tube analyzed by method of characteristics 08 p1322 A67-21121

Matched pulses for two-layer laminates, discussing complete energy transfer to base and uniform momentum transfer 10 p1724 A67-23707

Physicochemistry of substances under impact compression, considering thermodynamic parameters, phase transformation and compressibility curves 11 p1749 A67-24324

Cleavage method to study pulsed pressure /energy content/ in dense gas-discharge hot plasma 16 p2714 A67-31037

Interaction of finite amplitude pressure pulse with combustion region at surface of burning solid propellant 18 p3108 A67-33830

Forced bending oscillations for three-layer cylindrical shell under pulsed internal pressure 19 p3338 A67-34878

Pressure pulse generator-peak amplitude detector system for dynamic calibration of pressure transducers 23 p4007 A67-41388

PRESSURE RATIO

Tabulated data on specific losses in flow systems 02 p0233 A67-11995

Oblique shock detection in conical nozzle with circular arc throat, noting measurement techniques 04 p0547 A67-14833

Magnitude of principal phase DR field of magnetic storm assuming plasma pressure remains constant or varies proportionally with magnetic pressure 05 p0884 A67-17132

Shock tunnel data on surface pressure resulting from hypersonic stream interaction with two transverse jets [AIAA PAPER 67-190] 06 p0939 A67-18299

Discharge characteristics of sharp and round edged orifices in transition regime noting variation of pressure ratio, magnitude of Knudsen and Reynolds numbers, etc 14 p2300 A67-28180

Impact stage of impacting jet amplifiers studied by interposing disk between two opposing coaxial jets, obtaining pressure gain 14 p2250 A67-28332

Shock tunnel data on surface pressure resulting from hypersonic stream interaction with two transverse jets 21 p3610 A67-37799

Magnitude of principal phase DR field of magnetic storm assuming plasma pressure remains constant or varies proportionally with magnetic pressure 21 p3698 A67-38475

Magnetic shear effects on density gradient drift instabilities in plasma with plasma pressure to magnetic pressure ratio larger than electron-ion mass ratio 22 p3845 A67-39483

PRESSURE RECORDER

Digital recording double Fabry-Perot spectrometer, discussing pressure difference control system 20 p3440 A67-36363

PRESSURE RECOVERY

Heat transfer and centrifugal force effects on hypersonic inlet boundary layer and pressure recovery [AIAA PAPER 65-805] 03 p0350 A67-12910

Total pressure losses in hypersonic wind tunnel with Eiffel chamber, calculating coefficient of pressure recovery 04 p0546 A67-14780

Unstalled two-dimensional diffusers performance prediction by method based on turbulent boundary layer integral theory [ASME PAPER 66-WA/FE-15] 04 p0548 A67-15351

Lip shock from separation edge of half-angle wedge and resultant static-pressure recovery distribution along wake [AIAA PAPER 67-29] 06 p0886 A67-18260

Pressure recovery increase in bistable fluid elements by stationary latching vortices 08 p1283 A67-20475

Rectangular and inverted wedge recompression step effect on recovery factor, heat-transfer coefficient, velocity profile and pressure distribution in open cavity flow [ASME PAPER 65-WA/HT-37] 08 p1278 A67-21320

Model tests on free jet scramjet facility configurations at high Mach numbers, obtaining data on bypass flow pressure recovery and diffusion 13 p2089 A67-26830

Optimum design of ring airfoil device for maintaining pressure recovery efficiency of conical diffuser 22 p3743 A67-40168

PRESSURE REGULATOR

Environmental control for high performance military aircraft covering air conditioning, temperature and pressure control and oxygen supply systems 21 p3572 A67-39136

Externally adjustable pressure regulation of Fabry-Perot interferometer, using device to measure cesium vapor spectral absorption in D-1 line 22 p3810 A67-40522

Blower compressors for high altitude pressure and climate regulation in commercial aircraft 24 p4109 A67-42708

PRESSURE RELIEF VALVE

Approximate solutions for nonlinear differential equations to study periodic motions for analysis of pressure relief

- system 20 p3366 A67-37369
- PRESSURE TRANSDUCER**
- Implementation of air data computers with solid state transducing and computing techniques 01 p0029 A67-10667
- Si semiconductor strain sensors and miniature pressure transducers for cryogenic pressure measurements 01 p0069 A67-11017
- Calibration of pressure transducers in liquid-hydrogen to liquid-helium temperature range, using cryogenic test setup 01 p0069 A67-11018
- Capacitive pressure transducer featuring exceptional sensitivity, hysteresis, resolution and repeatability, detailing sensing element and measuring circuit design 01 p0071 A67-11102
- Digital force-balance pressure transducer providing parallel binary output suitable for direct input to digital computer 01 p0075 A67-11135
- Variable-reluctance pressure transducer with pressure sensor assembly weight reduction for lightweight aerospace requirements 01 p0075 A67-11136
- VIM-1 vacuum gauge using inverse-magnetron type manometric transducer for measuring rarefied gas pressure 03 p0425 A67-14268
- Pneumatic oscillator producing triangular waveforms of pressure vs time, using freely floating disk [ASME PAPER 66-WA/AUT-4] 04 p0555 A67-15388
- Capacitor pressure sensor produced by furnace brazing molybdenum to itself and to zircon with pure copper and Cu-Au-Ni filler metals 04 p0630 A67-15460
- Sensors and signal conditioners, discussing operation and calibration of resistance thermometers, strain gauge pressure transducers and potentiometric transducers 04 p0626 A67-15731
- Liquid hydrogen pressure, temperature, flow and liquid level measuring techniques 05 p0807 A67-17019
- Time-dependent pressure distribution in parachute canopy during inflation measured by special transducers 06 p0945 A67-17631
- Dynamic behavior of potentiometer pressure transducers by direct experimental measurement of plan-phase diagrams to one-displacement-step response 08 p1312 A67-20768
- Fast response fluidic sensor for absolute pressure ratio operable in adverse temperature and vibration environment 08 p1332 A67-21286
- Environmentally induced stresses in encapsulated electronic modules measured using hydrostatically pressure-sensitive transducer, noting internal stress changes 08 p1306 A67-21418
- Noise and pressure measurement in difficult conditions of vibrations and temperature for use in pressure-transducer design of jet and rocket systems 09 p1497 A67-21939
- Hydrostatic pressure measurement by direct loading of semiconductor strain gauges 09 p1498 A67-22031
- Inductive sensor development for measurement of pressure, airspeed, altitude and acceleration during aircraft testing 09 p1501 A67-22465
- Spacecraft instrumentation, discussing selection criteria for signal conditioning, transducer sensors, photographic equipment, etc 10 p1655 A67-23000
- Silicon semiconductor combustion pressure transducer for high temperature HF pressure measurements within liquid rocket motor chambers 11 p1792 A67-24820
- Qualitative and quantitative prediction of corrosive environments effects on transducer performance [ASME PAPER 67-MET-14] 12 p1945 A67-25952
- VIM-1 vacuum gauge using inverse-magnetron type manometric transducer for measuring rarefied gas pressure 14 p2321 A67-28778
- Laboratory calibration of piezoelectric transducer used as micrometeoroid impact gauge 15 p2486 A67-29410
- Rapidly varying high pressure measurement requirements, treating pressure transducer as seismic system and analyzing feed channel distortion 16 p2671 A67-31004
- Piezoelectric pressure transducer, discussing design, material used and performance 16 p2677 A67-31427
- Ballistic range blast-traversal testing technique using scale models containing fast response FM telemetry system modulated by capacitance type pressure transducer [AIAA PAPER 66-777] 17 p2832 A67-32063
- Various boundary layer parameters and transducer shape effect on Measurement error of random pressure field by finite size transducer 19 p3228 A67-34964
- Pressure transducers for use in high temperature and pressure gaseous detonation wave phenomena, discussing performance and application 20 p3443 A67-36514
- Wall turbulent boundary layer pressure resolution by piezoelectric transducer, noting attenuation of frequency component with size and frequency dependence 20 p3422 A67-37002
- Tethered sonde for micrometeorological soundings of lower atmosphere noting pressure transducer, servoswitching system, thermistor, hygistor, data acquisition, etc 21 p3628 A67-38582
- Pressure transducer for speech articulation to detect minute changes in articulator gesture for possible application as control element 22 p3754 A67-39163
- Performance of electromechanical pressure transducers tested environmentally for static and dynamic temperature, steady acceleration and vibrational acceleration 22 p3809 A67-40464
- Reentry vehicle surface pressure measurement, obtaining accuracy and reliability in stable high level pressure transducer 23 p4006 A67-41378
- Diaphragm and piezoelectric pressure gauges for severe blast environment, discussing resonance, damping, heat shield and rise time 23 p4007 A67-41387
- Pressure pulse generator-peak amplitude detector system for dynamic calibration of pressure transducers 23 p4007 A67-41388
- PRESSURE TUBE**
- Natural frequencies and mode shapes of pressurized circular cylinders with flexible stringers and attached point-mass [AIAA PAPER 66-449] 14 p2399 A67-28120
- PRESSURE VESSEL**
- Storable propellant pressure vessel design for Titan launch vehicles and compatibility and stress-load-corrosion analysis [SAE PAPER 66-0677] 01 p0160 A67-10582
- Comparative efficiencies of thin wall aerospace pressure vessels, emphasizing primary structural weight 04 p0709 A67-14810
- Biaxial fracture strength of textured titanium alloy for design of liquid fuel tankage 04 p0711 A67-15242
- Optimum thin wall pressure vessels of anisotropic materials of monolithic and filamentary construction [ASME PAPER 66-APM-BB] 04 p0717 A67-15915
- Stress calculation comparison of computer data and photoelastic data for series of pressure vessels with hemispherical and torispherical heads [ASME PAPER 66-WA/PVP-5] 04 p0719 A67-15931
- Filament winding techniques and design for thin wall cylindrical pressure vessels 06 p1006 A67-17622
- Junction of several walls of revolution along parallel in axisymmetric vessel 06 p1105 A67-18588
- Oxygen pressure vessels for prototype BAC/Sud Concorde manufactured from stainless steel 06 p0952 A67-18734
- Literature review on effect of static fatigue on filament wound fiberglass internal pressure vessels, noting program to test and expand data 08 p1415 A67-20432
- Lower bound for limit pressure of cylindrical pressure vessel with unreinforced hole obtained by restricting stress directions of cylinder 08 p1421 A67-20921
- Pressure shell structures for space noting materials, machining, assembly, welding, testing, etc 10 p1661 A67-23731
- Pressure vessel design with ultrahigh strength steels, material strength variations, fracture toughness, minimum defect size and materials melting and fabrication practice [ASME PAPER 67-MET-18] 12 p2031 A67-25954
- Liquid venting concept for zero gravity environment by suppressing vapor generation with open loop refrigeration, using extracted liquid as working fluid 13 p2056 A67-27639
- Land recovery of launch vehicles, applying intersecting pressure vessel theory for shaping of tanks and hinged tail panels 15 p2569 A67-29852
- Plastic energy dissipation rate at onset of rapid crack growth for predicting biaxial fracture 16 p2775 A67-31324
- Filament overwrapped metallic cylindrical pressure vessels show greater efficiency ratio and buckling strength 17 p2958 A67-32054
- Gas temperature increase effect on thin walled container during prepressurization of high pressure blowdown systems [AIAA PAPER 67-443] 18 p3137 A67-33920
- Stress calculation comparison of computer data and photoelastic data for series of pressure vessels with hemispherical and torispherical heads [ASME PAPER 66-WA/PVP-5] 18 p3143 A67-34127
- Metal lined glass filament-wound pressure vessel performance at cryogenic temperatures, discussing fibers, resins and liners 18 p3067 A67-34578
- NERVA components including nozzle and associated hot gas bleed port, turbopump, control valve, pressure vessel and thermocouples 22 p3834 A67-40172
- Probable failure mode and minimum service life prediction for spacecraft pressure vessels using fracture mechanics analysis and fracture specimen test results [ASM PAPER C6-2.3] 23 p4079 A67-41408
- Methodology used to implement high reliability objectives for Surveyor pressure vessels, tabulating burst test results [ASM PAPER C6-2.1] 23 p4071 A67-41411
- Shear spun 300-grade maraging steel evaluated for pressure vessel applications, discussing fracture toughness [ASM PAPER C6-2.4] 23 p4020 A67-41412
- Corrosion and hydrogen embrittlement resistant nickel stainless maraging steel with bcc martensite crystal structure for pressure vessel applications 24 p4161 A67-42328
- Boron and graphite filament-resin composites tensile and interlaminar shear strengths and Al foil liner cyclic life in cryogenic pressure vessel tests 24 p4176 A67-42470
- PRESSURE WAVE**
- Book on propagation, reflection and superposition of shock waves in ideal gases based on theory of hyperbolic nonlinear PDEs 04 p0601 A67-14467
- Dynamic stresses at boundary of fluid filled cavity during passage of plane dilatational wave train 05 p0908 A67-16136
- Energy release effects on unsteady gas flow in explosion [AIAA PAPER 66-517] 13 p2106 A67-27582
- Cavitation correlation with sound pressure and vibration acceleration in closed circuit hydrodynamic tunnel, showing cavitation noise spectrum 14 p2295 A67-27870
- Infinitesimal pressure disturbance propagation in chemically reacting gas, deriving general equation for process, solution shows wavefront propagation at sound velocity [ASME PAPER 67-FE-2] 14 p2304 A67-28355
- Correlation function and pressure change of slow waves in nonisothermal plasma 14 p2360 A67-28604
- Pulse-length modulated pressure waves having zero quiescent pulse width, actuating floating flap disk switching valves of pneumatic servomechanism 16 p2609 A67-31665
- Soviet book on nonlinear problems of motion of compressible fluid with small disturbances, investigating pressure fronts, neighborhoods of wave fronts, etc 18 p3025 A67-33715
- Spherical gas bubble pulsations under pressure waves analyzed in compressible and incompressible fluids 20 p3422 A67-37065
- Plane wave approximation for dilatational mode response of thin hollow spherical shell embedded in elastic medium and subjected to asymmetric pressure wave 21 p3718 A67-38020
- Infrasonic wave anisotropic radiation from moving auroras analyzed using shock wave model, discussing sound propagation and ray tracing 24 p4147 A67-41882

PRESSURE WELDING

Percussive arc mode welding applicability to delicate components and butt type joints 12 p1948 A67-25269
Alloy effects in low pressure diffusion bonding of superalloys, presenting time, pressure, bond strength and temperature curves 17 p2866 A67-33200

PRESSURIZATION**SA FUEL TANK PRESSURIZATION SYSTEM**

Permanent joints for Agena pressure systems, discussing retention of pressurized gases in connector tubing system 17 p2801 A67-31984
Cryogenically stored helium pressurization system for LEM descent stage propulsion system, discussing weight advantages and liquid helium heat transfers 22 p3749 A67-40394

PRESSURIZED CABIN

Manned and unmanned spacecraft structures, discussing environmental and functional requirements, influence of vibration and pressurized gas containment [SAE PAPER 660672] 01 p0153 A67-10579
Human tolerance to changes in aircraft cabin pressurization 10 p1602 A67-23825
Small pressurized cabin design for light commercial aircraft including safe life vs fail-safe approaches, fatigue strength testing, etc [SAE PAPER 670259] 12 p2016 A67-25508

Instrumentation and fuel systems for turbocharged and/or pressurized aircraft, discussing vapor lock problem, hydrocarbon fuels and vapor pressure equipment [SAE PAPER 670262] 12 p1899 A67-25510
Pressurization of Mooney M22 aircraft by low cost exhaust-driven turbosupercharger based on diesel automotive unit [SAE PAPER 670267] 12 p1899 A67-25511

Possible decompression effects in supersonic transport cabin in terms of biomedical considerations for passenger safety 14 p2258 A67-28666
Cabin pressurization characteristics of USAF and commercial transport aircraft, stressing decompression sickness 21 p3577 A67-38081

Decompression tests, evaluating hazards of ejections and fatal injuries following window failure in small pressurized aircraft 23 p3965 A67-41575
Decompression tests for potential hazards of ejection or fatal head injuries in small pressurized aircraft 23 p3970 A67-41693

PRESSURIZED SUIT

Metabolic work requirement of man wearing pressure suit and associated biomechanical characteristics while locomoting on lunar gravity simulator 02 p0189 A67-12393
Reduced gravity, pressure suit and load effect on human self-locomotion on lunar surface [ASME PAPER 66-WA/BHF-6] 04 p0564 A67-15400

Evoked brain response to clicks as measure of vigilance tested in work-rest schedule and pressure suit-sleep experiments on man 09 p1452 A67-21721

Heat balance and ventilation of human body in pressure suit 09 p1455 A67-21731
Rigid articulated pressure suits, discussing design, construction and operation for low external pressure, mobility requirements, etc 16 p2618 A67-30779

Reduced gravity, pressure suit and load effect on human self-locomotion on lunar surface [ASME PAPER 66-WA/BHF-6] 17 p2807 A67-32814

Altitude chamber studies of passively pressurizing partial pressure suit for possible use by SST crew 23 p3969 A67-41647
Telemetry system for measuring body temperature and heart rate for physiological evaluation of space suits 23 p3969 A67-41651

PRESTON TUBE

Turbulent skin friction measurement with Preston tube, using similarity hypothesis for mean velocity profiles in turbulent flows 04 p0600 A67-14442

Preston tube measurements of skin friction and velocity profiles in incompressible turbulent boundary layer, considering pressure gradient effects 04 p0609 A67-15818

Preston tube in concentric annuli, discussing skin friction measurement in fully

developed turbulent flow 06 p0990 A67-18749

Local skin friction coefficient for turbulent boundary layers on smooth flat plates measured, using Preston tube 06 p0990 A67-18751

Turbulent skin friction in incompressible flow with heat transfer, determining Preston surface pitot tube applicability 23 p4004 A67-41341

PRESTRESSING

Shearing stress induced shock wave propagation in annealed aluminum under biaxial plastic prestresses [ASME PAPER 66-WA/APM-3] 05 p0909 A67-16143

Local buckling strength of high strength axially compressed maraging steel cylinders circumferentially prestressed with high strength epoxy-protected fiberglass filament windings 05 p0923 A67-17211

Biaxial prestressing in ceramic plates under nonuniform thermal stress for damage reduction study 20 p3538 A67-36778

Prestressing effects on stress-strain diagram of monodirectional transversely isotropic glass fiber reinforced plastic 21 p3650 A67-37911

PREVENTION**S ACCIDENT PREVENTION****S CORROSION PREVENTION****S FIRE PREVENTION****S ICE PREVENTION****PRIMARY COSMIC RADIATION****SA HEAVY COSMIC RAY PRIMARY**

Cosmic radiation data obtained by two gas-discharge counters installed in Luna X artificial satellite 01 p0145 A67-10906

Radiation types encountered and shielding used by Voskhod I and II manned spacecraft 02 p0308 A67-12321

Composition and energy spectra of primary cosmic radiation in low energy regions from observations of Mariner II and Explorer VII 02 p0310 A67-12582

Stratospheric measurements of electrons and gamma radiation in cosmic rays, using plastic scintillator and lead sheet supplemented Geiger counters 02 p0310 A67-12584

Spectrum of primary cosmic radiation determined for ultrahigh energies, based on international data on electron and meson air showers 02 p0311 A67-12588

Primary cosmic rays of superhigh energy using extensive air shower data, noting Geiger-Muller counters, scintillation counters and muon detector 02 p0311 A67-12589

Extensive atmospheric showers as means of gaining insight into energy spectrum and composition of primary cosmic radiation 02 p0312 A67-12603

Calorimetric measurement of ionization burst at 3200 m above sea level 02 p0315 A67-12758

Ionization calorimeter determination of effective cross section of high energy primary cosmic ray proton inelastic interaction with atmospheric atomic particles 02 p0315 A67-12759

Ionization calorimeter photoemulsion measurements at mountain altitudes, determining formation mechanism of high energy pions in primary cosmic radiation 02 p0315 A67-12760

Ionization calorimeter measurement of absorption of energy flux of primary cosmic radiation nuclear active component in iron 02 p0316 A67-12762

Extensive air shower characteristics related to energy spectrum, chemical composition and anisotropy of primary cosmic rays in superhigh energy range 02 p0318 A67-12778

Energy dependence of isotopic composition of primary helium nuclei, considering ionization loss, fragmentation and solar modulation 03 p0505 A67-12956

Extensive near-vertical air shower analysis at sea level for nucleon-air-nucleus and pion-air-nucleus interaction 03 p0506 A67-13517

Nuclear emulsion measurements of primary cosmic ray alpha particle flux over Hyderabad during high solar activity in 11-year cycle 03 p0506 A67-13720

Biological effect of heavy particles, noting role of linear energy transfer and irreversible direct type effect 04 p0562 A67-14634

Primary cosmic ray spectrum at high energies and spectra of gamma rays and muons in atmosphere 04 p0692 A67-14857

Primary cosmic radiation in interplanetary space, lunar surface albedo and soft particle fluxes in magnetosphere measured by Luna X orbiter 05 p0875 A67-16053

Temporal variations of nuclear flux of primary cosmic radiation of Elektron II and IV satellites, discussing Forbush effect in nuclear and neutron components 05 p0877 A67-16085

Direct energy spectrum measurements of primary cosmic radiation in wide energy range 05 p0877 A67-16086

Chemical composition of primary cosmic rays in moderate energy rigidity range with aid of satellite Proton I 05 p0877 A67-16088

High energy primary gamma quanta flux outside atmosphere estimated with aid of Proton I satellite 05 p0877 A67-16088

Electron intensity measurement in primary cosmic radiation by high altitude balloons carrying telescope made of two plastic scintillation counters 05 p0878 A67-16097

Change in intensity and forms of energy spectrum effects on accuracy of measuring values of meteorite preentry dimensions, weight and degree of ablation 05 p0887 A67-16099

Primary cosmic radiation intensity determined with help of nuclear particle tracks in moldavites and meteorites 05 p0887 A67-16100

Energy spectrum of secular variations of cosmic ray intensity in interplanetary space, using data from stratospheric measurements 05 p0879 A67-16104

Elektron satellite observations on primary cosmic radiation, noting correlation between intensity variation and neutron component intensity 05 p0880 A67-16109

Barometric effect of cosmic rays with allowance for changes in D/R/ primary spectrum and cut-off 05 p0884 A67-17136

High altitude solar X-ray burst and increase in ground level flux of heavy nuclei 07 p1242 A67-19113

Origin of fossil charged particle tracks in meteorites such as cosmic radiation, fission of U 238, meson jets, spallation recoils, etc 07 p1245 A67-19494

High energy primary electrons and universal body radiation 07 p1246 A67-20227

Proton I and II satellite instrumentation noting energy-charge spectrometer, gamma-quantum fluxmeter, equipment to determine chemical composition of charged cosmic ray particles, etc 08 p1376 A67-21001

Differential energy spectra and fluxes of charged splash and reentrant albedo proton measurement of cosmic radiation in various energy ranges 08 p1377 A67-21467

Proton II satellite measurements of intensity of nuclear component of primary cosmic radiation 09 p1561 A67-21897

High transmission Cerenkov spectrometer carried by proton I and II satellites to measure charges of primary cosmic ray nuclei high transmission Cerenkov spectrometer carried by Proton I and II satellites to measure 09 p1497 A67-21898

Directional telescope for measuring intensity and spectral composition of gamma rays in primary cosmic radiation 09 p1497 A67-21899

Energy spectrum of primary cosmic ray alpha particles measured by nuclear photographic emulsion, estimating geomagnetic cut-off energies 09 p1562 A67-22418

Large atmospheric jets with low muon content explained by presence of hypothetical primary cosmic photons with very high energies 09 p1562 A67-22558

Measurement of cosmic ray intensity by Zond III automatic space probe 10 p1701 A67-23230

Flux and energy spectra of primary cosmic X and gamma rays between 20 keV and 1 mev from balloon-rocket measurements 10 p1701 A67-23231

Diurnal variation of primary auroral electrons, average energy spectrum of 20-150 keV X-rays and time dependence of intensity and morphology 10 p1702 A67-23305

Primary cosmic ray proton and deuteron flux near geomagnetic equator determined by nuclear emulsion method 10 p1703 A67-23543

Electron component of primary cosmic radiation 11 p1856 A67-24104

Primary cosmic radiation abundance

measurements on iron and heavier nuclei, using Cerenkov counter on balloon flights 11 p1856 A67-24504

Cosmic ray measurements in interplanetary space and on moon noting intensity increase 12 p1992 A67-25123

Primary cosmic radiation investigated by Elektron II and IV satellites 12 p1998 A67-25827

Primary cosmic ray intensity and structure of air showers at high altitudes investigated by aircraft, balloons and sounding rockets 13 p2193 A67-27247

High energy muon flux in air showers at sea level determined, using semi-Monte Carlo method 13 p2195 A67-27579

Handbook of Physics, Volume 46/2, Cosmic radiation 14 p2379 A67-27960

Spectrum, intensity, and charge composition of primary cosmic radiation and relevance to origin and propagation of galactic radiation 14 p2379 A67-27963

Primary cosmic radiation composition effect on secondary emission, examining flux, spectra, nucleon interactions, proton component and neutrons 14 p2380 A67-27966

Mutagenic effects of primary cosmic radiation on bacteria 14 p2254 A67-28213

Primary cosmic ray electron flux and energy spectrum near solar minimum compared with nonthermal radio emission from high galactic latitudes 14 p2381 A67-28831

Cosmic ray mu-meson intensities at different altitudes at equator measured as function of zenith and azimuth, using scintillation counter telescope 15 p2549 A67-29184

Primary cosmic radiation and interaction in atmosphere studied during minimum solar activity by balloon flights to determine effect of latitude on secondary photons 15 p2550 A67-29533

Primary cosmic ray investigation by Proton I scientific space station concerning energy spectrum, chemical composition, galactic gamma ray and solar radiation hazard 16 p2737 A67-30647

Nucleon-nucleon collisions, analyzing pair production, electromagnetic cascade, secondary interactions, etc 16 p2703 A67-30965

Spectrometric system aboard Proton type satellite for analyzing energy and charge spectra of primary cosmic ray particles 17 p2854 A67-32245

Energy spectrum and composition of primary cosmic rays in high and superhigh energy range of Proton I and II satellites 17 p2935 A67-32246

Primary cosmic ray spectrum changes from differential response functions and specific yield functions of neutron monitors 17 p2938 A67-32533

Unexpected excess of primary cosmic ray helium nuclei flux value in nuclear photographic emulsions 17 p2939 A67-33237

Low energy H and He isotope detection in cosmic radiation at solar minima via balloon mounted scintillation counter 17 p2939 A67-33248

Spectral data on primary cosmic ray protons and helium nuclei analyzed, assuming solar cycle modulation due to diffusion-convection process 17 p2952 A67-33247

Cosmic ray and interplanetary medium and magnetic field studies in Bolivia 19 p3320 A67-35284

Extensive air showers due to extragalactic primary photons demonstrated, considering production process 19 p3316 A67-35796

Energy spectrum and production rates for secondary antiprotons from inelastic collisions of high energy galactic cosmic radiation with interstellar gas nuclei 19 p3316 A67-36098

Relative intensity contribution and time dependency of primary cosmic rays, splash albedo and reentrant albedo measured by polar orbiting satellite 20 p3517 A67-36306

Electrons energy spectrum stability dependence on spatial distribution of source, discussing cosmic ray generation 20 p3517 A67-36532

Cosmic ultrahigh-energy heavy nuclei and fragmentation products producing multiple mesons 20 p3518 A67-37092

Heavy nuclei intensity in primary cosmic rays, long term solar cycle modulation and time lag in various

phases 20 p3519 A67-37405

Primary cosmic radiation in interplanetary space, lunar surface albedo and soft particle fluxes in magnetosphere measured by Luna X orbiter 21 p3697 A67-37840

Barometric effect of cosmic rays with allowance for changes in D/R/ primary spectrum and cut-off 21 p3698 A67-38479

Antiproton production by primary cosmic ray collisions with atmospheric nuclei compared with interstellar gas 21 p3620 A67-38843

Penumbra influence on cosmic ray effective cut-off rigidity calculated, noting case of primary variations and constant magnetic field 21 p3699 A67-39017

Primary cosmic radiation electron component studies through differential energy spectrum observations, considering confinement regions and black body radiation at 3 degrees K 22 p3874 A67-40239

Calorimetric measurement of ionization burst at 3200 m above sea level 22 p3876 A67-40260

Ionization calorimeter determination of effective cross section of high energy primary cosmic ray proton inelastic interaction with atmospheric atomic particles 22 p3876 A67-40261

Ionization calorimeter photoemulsion measurements at mountain altitudes, determining formation mechanism of high energy pions in primary cosmic radiation 22 p3876 A67-40262

Ionization calorimeter measurement of absorption of energy flux of primary cosmic radiation nuclear active component in iron 22 p3842 A67-40264

Extensive air shower characteristics related to energy spectrum, chemical composition and anisotropy of primary cosmic rays in superhigh energy range 22 p3877 A67-40280

Charge spectrum of very heavy cosmic ray primaries studied from balloon observations in photographic emulsion detector for Texas atmosphere 23 p4050 A67-40676

Primary cosmic ray energy and jet CMS velocity estimations by three methods corrected by analyzing known energy interactions 23 p4051 A67-40913

Primary cosmic particles energy spectrum measurements onboard space station with ionization calorimeters and energy level discriminators 23 p4054 A67-41091

Primary cosmic rays with various charges measured for spectral energy with Cerenkov counter onboard space stations 23 p4054 A67-41093

Satellite and probe data analysis on ionizing component, primary cosmic rays and albedo particle flux intensity near atmospheric outer boundary 23 p4055 A67-41098

Solar cycle primary cosmic radiation variation above magnetosphere and radiation belts at stratosphere and surface, using neutron monitors and space vehicle measurements 23 p4055 A67-41101

Origin of heavy nuclei abundance in low energy primary cosmic ray flux, discussing association with quasi-stellar objects 24 p4209 A67-41874

Temporal variations of nuclear flux of primary cosmic radiation of Elektron II and IV satellites, discussing Forbush effect in nuclear and neutron components 24 p4212 A67-42761

Direct energy spectrum measurements of primary cosmic radiation in wide energy range 24 p4212 A67-42762

Chemical composition of primary cosmic rays in moderate energy rigidity range with aid of satellite Proton I 24 p4212 A67-42763

High energy primary gamma quanta flux outside atmosphere estimated with aid of Proton I satellite 24 p4212 A67-42764

Electron intensity measurement in primary cosmic radiation by high altitude balloons carrying telescope made of two plastic scintillation counters 24 p4213 A67-42773

Change in intensity and forms of energy spectrum effects on accuracy of measuring values of meteorite preentry dimensions, weight and degree of ablation 24 p4238 A67-42775

Primary cosmic radiation intensity determined with help of nuclear particle tracks in moldavites and meteorites 24 p4238 A67-42776

Energy spectrum of secular variations of cosmic ray intensity in interplanetary space, using data from stratospheric measurements 24 p4213 A67-42780

Elektron satellite observations on primary cosmic radiation, noting correlation between intensity variation and neutron component intensity 24 p4214 A67-42785

Primary cosmic ray particle chemical composition changes, explaining active particle energy spectra discrepancies between measurements and calculation 24 p4218 A67-42840

PRIMER

SA FINISH

Primer vector of fixed-time impulsive thrust trajectories [AIAA PAPER 67-54] 06 p1086 A67-18352

PRINCIPLE

S FERMAT PRINCIPLE

S HUYGEN PRINCIPLE

S INERTIA PRINCIPLE

S MAXIMUM PRINCIPLE

S MUSKHELISHVILI PRINCIPLE

S PONTRYAGIN PRINCIPLE

S SAINT VENANT PRINCIPLE

S VARIATIONAL PRINCIPLE

PRINTED CIRCUIT

Integrated ceramic printed and thin film circuitry in microelectronic technology 01 p0043 A67-11385

Computer and curve tracer method to generate photo masters for printed circuit microwave antennas, transmission lines and filters 03 p0383 A67-13790

Two types of slit-coupled strip transmission lines especially useful for realization of multisection components, using printed circuit techniques 04 p0592 A67-14862

PCM telemetry system for satellite test vehicle of ELDO program using transistorized printed circuit technology 06 p0957 A67-17613

Book on electronic component reliability noting effects of environmental conditions, possible faults, various circuits, wiring, transformers, etc 07 p1158 A67-20206

Printed circuits handbook covering fabrication, design, assembly, soldering, testing, etc 08 p1334 A67-20739

Design and layout of printed circuits 08 p1301 A67-20740

Copper clad phenolic paper, epoxy paper and epoxy glass laminates used as printed circuit base materials 08 p1334 A67-20741

Print-etch and negative-pattern image transfer techniques for fabrication 08 p1334 A67-20743

Metallizing and plating techniques for printed circuit fabrication 08 p1334 A67-20744

Etching techniques in fabrication of printed circuit boards 08 p1334 A67-20745

Multilayer laminating process in printed circuit wiring board design and production 08 p1335 A67-20746

Manual assembly process for small volume printed circuit board 08 p1335 A67-20747

Coating and embedding techniques for environmental protection of printed circuit assemblies 08 p1335 A67-20749

Printed circuit assembly testing, discussing preassembly component testing, test programming techniques, test facility requirements and economics 08 p1301 A67-20750

Printed circuit board manufacturing process assuring crack-free plated-through hole 08 p1304 A67-21190

Nondestructive testing techniques for multilayer printed wiring boards stressing axial transverse laminography and mutual coupling 09 p1502 A67-21867

Dielectric isolation techniques for elements of integrated circuit 10 p1610 A67-22971

H-film /Kapton/ flexible circuits fabrication problems including tensile strength, pattern misregistration, delamination, embrittlement, etc 10 p1611 A67-23309

Axial lead package and stack design of batch fabricated matrices to speed integrated circuit assembly 11 p1760 A67-24260

C-band traveling wave maser using printed circuit technology results in reduced structure size, perfect contact between structure and ruby, etc 11 p1801 A67-24727

Electronic packaging technique in thin film technology using flip-chip bonding and MTFI techniques 12 p1910 A67-25284

Interconnecting techniques for modules contained by printed circuit boards, noting usage of pin sockets and effect on maintainability and reliability 12 p1910 A67-25266

Silk screen techniques used for film circuitry implementation on integral sensor telemetry transmitter with standard components 12 p1911 A67-25272

Variability factors in fabrication of miniature printed glaze resistors and circuits evaluated to obtain optimal process control criteria 12 p1916 A67-25998

Computer-aided layout of minitstick artwork 12 p1950 A67-26130

High stability metal thin film resistors applied to thin film circuits, noting substrate properties and pattern design 12 p1918 A67-26209

Multilayer printed circuit board system for interconnecting microelectronic components noting application of X-ray, ultrasonic, beta-ray, etc to process control 16 p2681 A67-30478

Assembly of thick film microcircuit production facility detailing equipment, materials, marketing, etc 16 p2641 A67-31621

Printed circuit technology development survey showing refining processes and techniques 16 p2641 A67-31622

Reliability of multilayer printed wiring boards as interconnection device 16 p2642 A67-31726

Chemical milling technique for space vehicle chassis and circuitry production, noting similarity and differences with photoengraving and printed circuit techniques 16 p2683 A67-31739

Stencil screening methods for printing integrated circuit patterns for resistors, capacitors, etc, discussing automation possibilities 19 p3192 A67-35026

Printed circuit thermal design, discussing edge-to-center temperature gradient and circuit board models 21 p3594 A67-38330

Electrode with central heat sink used for joining flat-pack leads and copper tracks on printed circuit boards 21 p3635 A67-38624

Flat pack interconnection technique using hot gas soldering, discussing inspection and control requirements 21 p3635 A67-38626

IR for electronic circuit component diagnosis, discussing design criteria, quality control and acceptance testing 22 p3769 A67-39631

Solid state multilayer circuits preparation for use in microminiaturization, stressing advantages over printed circuits 22 p3774 A67-40327

Test procedure for Si microcircuit production consisting of bulk and junctions electric measurement, oxide thickness and junction position measurements 23 p3977 A67-40660

PRINTED RESISTOR

Variability factors in fabrication of miniature printed glaze resistors and circuits evaluated to obtain optimal process control criteria 12 p1916 A67-25998

Thin film integrated circuit, discussing development of large value resistors and capacitors 12 p1918 A67-26219

Variables in screen printing and firing processes for thick film resistors affecting reproducibility 16 p2641 A67-31620

PRISM

SA QUARTZ

Dynalens optical element characterized by variable-geometry fluid prism that deflects beam of light or electromagnetic energy 01 p0075 A67-11132

Ruby laser generation from two R lines by prismatic light dispersion in resonator 03 p0433 A67-13095

Laser mode selection by internal reflection prisms 10 p1662 A67-22742

Gaseous laser oscillations in Fabry-Perot resonator with corner-cube prism noting alignment characteristics 12 p1953 A67-25454

Appearance of extraordinary rays from double refraction in ruby laser crystals with polished rectangular prisms 20 p3507 A67-36330

Remote control of monochromator prism rotation using balanced-bridge system to regulate flow 20 p3451 A67-37308

Matrix method for analyzing systems of gimbaled mirrors, prisms and ray projectors 23 p4003 A67-41323

PRISMATIC BAR

Prismatic wideband directional couplers of

Brewster angle type, discussing basic theories, frequency characteristics, insertion loss and directivity 10 p1806 A67-23065

Plastic deformation mechanisms of polycrystalline beryllium to analyze temperature dependence of critical shear in prismatic plane 13 p2138 A67-27121

Homogeneous beam consisting of two isotropic bars with different elastic properties but identical cross sections studied for perimeters stress-strain state under torsion 20 p3535 A67-36122

Formulation of problem of elastoplastic torsion of rectangular or regular polygonal bar as variational problem 20 p3536 A67-36429

PRIVATE AIRCRAFT

Business jet aircraft engine design for increased service life, detailing turbine nozzles, bearings, rotors, etc [SAE PAPER 670234] 11 p1851 A67-23981

PRIVATE AVIATION

Air traffic control, navigation techniques, requirements and equipment for general aviation to end of century 19 p3258 A67-35861

Highway, ramp, terminal, runway and approach congestion problems for airports, suggesting separated general aviation airports and runways to alleviate big jet airports [AIAA PAPER 67-871] 24 p4139 A67-42992

PROBABILITY

SA DUFFING EQUATION

SA STATISTICAL PROBABILITY

SA TRANSITION PROBABILITY

Launch-on-time probability, showing dependence on initial countdown reliability and cumulative percentage of failures [AIAA PAPER 67-271] 07 p1260 A67-20080

Maximum probability criterion on output coordinates of system for selection of parameters of optimal nonlinear control system 20 p3408 A67-37042

Launch-on-time probability, showing dependence on initial countdown reliability and cumulative percentage of failures [AIAA PAPER 67-271] 21 p3712 A67-37808

PROBABILITY DENSITY

Approximation method for deriving expressions for small angle polydispersed indicatrix of gamma distribution of particles in light field 01 p0107 A67-10125

Radar imagery compilation of vegetation maps, noting extent of capabilities and results obtained 01 p0059 A67-10329

Statistical correlation theory of accuracy and error relationships of sensing element during parametric excitations caused by random vibrations 01 p0064 A67-10417

Fluctuation noise effects on phase-locked automatic frequency control system obtained using Markov processes, determining phase difference probability density and statistical characteristics 01 p0037 A67-10713

Test functions for testing location, scale and shape parameter hypotheses of Weibull distribution 01 p0107 A67-10931

Estimated amplitude of echo-signal for uniform, Rayleigh and a priori distribution of probability density of noise amplitudes 02 p0194 A67-11976

Theoretical approximations for probability densities of duration and interval between fades, assuming Rayleigh process characterizes fading 03 p0368 A67-13168

Probability density and distribution function of random function threshold overshooting 04 p0657 A67-14888

Two-dimensional characteristic function and probability-distribution density of random process which is phase modulated by normal noise 04 p0575 A67-15161

Conditional probability density of phase derivative of narrow-band normal noise determined for case when noise envelope is greater than electric field 04 p0575 A67-15162

Satellites in near-circular decaying polar orbits experience drag forces at equatorial latitudes greater than those at polar latitudes 04 p0706 A67-15233

First passage problems for lightly damped linear oscillator excited by white noise for two types of initial conditions and three types of barrier configurations 04 p0659 A67-15932

Probability density of oscillating system with piecewise-linear characteristic under action of exponentially correlated random force 05 p0844 A67-16014

Probabilistic displays and decision making effectiveness in situation with uncertain or failible information 05 p0757 A67-16308

Synthesis of stochastic optimal control for case of discrete input of feedback vector, noting dependency on coordinates characterizing probability density of plant vector 05 p0782 A67-16316

Output probability density distribution of stationary random noise containing regular signal components after mean squaring circuit 05 p0783 A67-16446

Combined probability density of axial coefficient and polarization angle of field scattered by target 05 p0764 A67-16905

Distribution function for probability density of random process at output of multiplier acted upon by envelopes consisting of Gaussian noise and pulse signal 05 p0767 A67-17397

Component, due to recombination-generation process, of overall noise from semiconductors under electric current, measuring probability densities by statistics 06 p0966 A67-17588

Iterative computation of a posteriori probability for M-ary nonsupervised adaptation 06 p0965 A67-17947

Curves of probability of detection vs signal to noise ratio for log-normal signals in Gaussian noise, considering correlated and uncorrelated signals 07 p1144 A67-19868

Error probability density distribution and selection of measurement accuracies and decision tolerances 08 p1336 A67-21057

Qualitative vibration data reduction techniques for application to design problems, noting examples involving power spectra and probability-density functions 10 p1680 A67-23315

Spatial variations in mean square response above lowest resonance frequency determined, using statistical analysis [ASME PAPER 67-VIBR-22] 11 p1872 A67-24181

Stochastic optimal control with noisy observations, obtaining Hamilton-Jacobi stochastic equation in function space [ASME PAPER 66-WA/FE-6] 11 p1770 A67-24276

Rain effects at random antenna elevation 11 p1753 A67-24303

Generalization of binary processes, discussing time domain and frequency domain analysis 11 p1813 A67-24312

Fokker-Planck-Kolmogoroff equations extended to cover conditional probability density functions of arbitrary random processes 12 p1961 A67-26082

Higher order time correlations, skewness, flatness and nonGaussian probability density distribution in turbulent field 13 p2092 A67-26278

Probability density functions for power from Rayleigh target 13 p2067 A67-26520

Monte Carlo calculation of kinetics of chemically reacting multicomponent gas for finite number of particles followed through random collision processes 13 p2102 A67-26971

Combined probability density of axial coefficient and polarization angle of field scattered by target 14 p2297 A67-28032

Upper atmospheric turbulence velocity probability density investigated in 90 to 110 km region 14 p2346 A67-28058

Two-dimensional characteristic function and probability-distribution density of random process which is phase modulated by normal noise 15 p2435 A67-29348

Conditional probability density of phase derivative of narrow-band normal noise determined for case when noise envelope is greater than electric field 15 p2435 A67-29349

Laser light photon counting statistics using probability density for laser light intensity 15 p2498 A67-29513

Combined probability density of axial coefficient and polarization angle of field scattered by target 16 p2623 A67-30881

One-dimensional probability distribution density of sum of pulsed and fluctuation noises 16 p2623 A67-31016

Curved mixing layer measured for probability density of turbulent velocities at several positions in curved mixing layer 16 p2660 A67-31219

Probability density and random distribution function derived from finite series for instantaneous voltage measurements of ideal multiplying

device 16 p2653 A67-31718
 Probability density function of ratio of two nonzero mean Gaussian random variables derived and applied to calibrated signal using noisy calibration levels 17 p2816 A67-32624
 Identification, coding and enumeration of distinguishable subnetwork configurations employing combinatorial analysis 18 p3016 A67-33496
 Synthesis of stochastic optimal control for case of discrete input of feedback vector, noting dependency on coordinates characterizing probability density of plant vector 18 p3016 A67-33867
 Optimal multidimensional systems for discriminating and detecting signals dependent on finite number of random parameters and combined with noise 19 p3185 A67-36097
 Probability density function measurement, discussing turbulence problem, power spectral densities, Rice formula, inversion, etc 20 p3442 A67-36461
 Probability of overlapping intercept by system of random intercepts and application to detection of flying objects in cloudy skies 20 p3477 A67-37036
 Scintillation depth measurement relationship with probability density of amplitude distribution 21 p3617 A67-38002
 Optimal nonlinear filtering, deriving differential equations for probability density or state vector for noise corrupted system 21 p3603 A67-38442
 Optimal reception of binary signals on background non-Gaussian noise determined by logarithm expansion for probability coefficient into Taylor series 24 p4122 A67-42377
PROBABILITY DISTRIBUTION
 Binomial probability distribution applied to air battle analysis, discussing fire doctrines, attrition rates, weapon design classes and limitations of approach [AIAA PAPER 66-781] 01 p0169 A67-10527
 Replacement policies for aircraft and missile parts that fail according to normal log-normal or Weibull continuous probability distribution 01 p0083 A67-11339
 Optimum /in Shannon sense/ truncated probability of signal for case of constant power and other conditions 02 p0194 A67-11908
 Nonlinear transformations of probability measures in functional spaces, noting application of random-process theory 02 p0259 A67-11922
 Stochastic process estimate of frequency and duration of weather events, using Monte Carlo simulation of probability distributions 02 p0261 A67-12079
 Clear line-of-sight through atmosphere determined, using probability estimates [AFRL-66-838] 02 p0262 A67-12080
 Automatic threshold control formulation and probability distribution of adaptive detection mode for matched and mismatched clutter model 02 p0203 A67-12139
 Compound statistical decision theory for pattern recognition based on Bayes conditional probability theory 02 p0208 A67-12164
 Noise rejection properties of threshold devices with storage circuit calculated on basis of intersection probability of fixed level by storage circuit output voltage 02 p0205 A67-12533
 Noise stability for wideband analog methods of information transmission based on analysis of probability distribution density, using normal rms error and anomalous error probability 03 p0369 A67-13581
 Meteor sighting probability and problem of actual number of meteors 03 p0511 A67-13815
 Exact solutions derived for problems of mathematical expectation and density distribution of maxima for two types of nonstationary random processes 03 p0461 A67-13948
 Statistical distribution of AM laser signal envelope upon passage through turbulent atmosphere 03 p0438 A67-13988
 Probability distribution of square of vertical wind velocity difference during unstable stratification 03 p0463 A67-14228
 Stochastic model of cratering and survival of craters on moon, discussing approximate diameter distribution of primary and

secondary craters 04 p0696 A67-14739
 Nonlinear recognition procedures, discussing probability distribution approximation by orthogonal expansion and by-product of low order conditional probabilities 04 p0578 A67-14800
 Minimum average conditional entropy for minimum probability of error in statistical decision theory 04 p0644 A67-14885
 Statistical topological analysis of electric measurement precision and accuracy 04 p0657 A67-14887
 Program selection for motion equations, parameters and control functions maximizing composite flight vehicle probability of delivering payload to given region 04 p0552 A67-15882
 Popov method for random parameter control system asymptotic stability in mean with respect to bounded perturbations 05 p0784 A67-16777
 Dead time corrections to photocount distributions using time interval probability density of counts, noting application to laser light 06 p1009 A67-17652
 Inertial guidance system accuracy and error sources, determining offset circular-or spherical-target error probabilities by approximate chi-square distribution 06 p1028 A67-17722
 Chernoff bound and tilted distribution argument for obtaining error probability bounds for binary signaling on slowly fading Rician channel [JPL-TR-32-1051] 06 p0961 A67-17943
 Converse of channel coding theorem, relating average probability of error to distortion measure of source sink pair 06 p0965 A67-17946
 Optimal one-dimensional truncated signal distribution ensuring optimal capacity or differential entropy 06 p0978 A67-18219
 Statistical analysis of aircraft accidents from 1938 to present 06 p0949 A67-18746
 Computer generation of error probability distribution for linear system response to random conditions 07 p1217 A67-20117
 Divergence and Bhattacharya distance measures in signal selection 09 p1459 A67-21580
 Random number generation by digital computer 09 p1468 A67-22052
 Statistical properties of superposition of coherent and incoherent electromagnetic fields studied in terms of coherent state formalism 10 p1667 A67-23778
 1/s line intensity distribution function for molecular spectra representation using growth curves calculated for Lorentz lines 11 p1822 A67-24416
 Multiple scattering and finite detector bandwidth effects on shape of absorption features in atmospheric scattering 11 p1862 A67-24502
 Probability distribution of square of vertical wind velocity difference during unstable stratification 12 p1963 A67-25484
 Spectrum, correlation and probability analysis of arbitrary waveforms 12 p1905 A67-25732
 Telemetry data processing problems noting error sources, probability distribution of counts in counting processes, sensor relay during motion in varying field, etc 12 p1905 A67-25779
 Stochastic differential equations for obtaining probability distribution of cosmic ray particles counted in given time interval sounding rocket detector 12 p1996 A67-25783
 Approximate formulas for information transmitted by discrete communication channel obtained by averaging tight and weaker bounds respectively from transition probability matrices 12 p1908 A67-26088
 Diffusion of protons and nuclei having elastic interactions at 27 GeV/c, using probability distribution for events outside Gaussian limit of multiple scattering 13 p2160 A67-26436
 Probability of ray position in beam waveguides 13 p2066 A67-26476
 Reliability analysis of active, standby and active-standby redundant system, discussing Poisson-binomial probability distribution function 13 p2123 A67-26828
 Nonequilibrium processes, analyzing required number of additional conditions and region of applicability of most probable distribution function, noting relation to Boltzmann equation 13 p2100 A67-26954
 Absorption probability for photons

traversing photon gases with different spectra 13 p2161 A67-27733
 Opacity of universe to high energy photons, estimating spectra and absorption probability 13 p2161 A67-27734
 Noise rejection properties of threshold devices with storage circuit calculated on basis of intersection probability of fixed level by storage circuit output voltage 14 p2261 A67-28010
 Stability, probability and reliability relationship presented together with statistical problems in structural stability 14 p2396 A67-28082
 Optimal structural design with failure probability constraints 14 p2399 A67-28122
 Efficiency criterion in form of probability of task completion estimated for dynamic systems with random parameters 15 p2455 A67-29121
 Sensitivity of cost functional in optimal control system with random variable parameters, noting system performance detection techniques 15 p2457 A67-29368
 Radiation hazard to man from solar proton events 15 p2429 A67-29450
 Hybrid computer calculation of instantaneous and peak amplitude probability distribution of random signal 15 p2440 A67-29774
 Book on optimization of stochastic systems noting probability distribution functions, random variables, Bayesian optimization convergence, linear and nonlinear system estimation, etc 15 p2459 A67-30024
 Stochastic model to structural fatigue, obtaining probability distribution for number of load repetitions necessary for fatigue failure 15 p2578 A67-30270
 Worst distribution analysis for statistical circuit design 15 p2455 A67-30406
 System reliability for single-time demand interval, calculating distribution function for time to system failure 15 p2495 A67-30413
 Statistical probability distribution for determining systematic errors of potentiometer multiplier by Monte Carlo method /static testing/ 16 p2633 A67-30464
 Carrier instability influence on noise immunity of discrete communication systems, with results presented graphically for uniform and normal random frequency distributions 16 p2620 A67-30477
 Optimal one-dimensional truncated signal distribution ensuring optimal capacity or differential entropy 16 p2643 A67-30485
 Probability distribution of number of photons and integrated intensity relation to normal and antinormal ordering of field operators in quantum optics 16 p2685 A67-30826
 Electromagnetic wave field probability distribution when scattering by medium with randomly varying refractive index 16 p2623 A67-30968
 Probability of perceiving meteor determined on basis of observation by independent counting method by group of observers 16 p2751 A67-31460
 Atmospheric trajectories of faint telescopic meteors observed by separate stations simultaneously and probability of plotting 16 p2751 A67-31461
 Continuous control process with random variable stopping time of known probability distribution, presenting optimal feedback control, trajectory and minimum cost 16 p2651 A67-31681
 Timing error and noisy phase reference joint effect on system performance of coded partially phase coherent reception 17 p2811 A67-32116
 Book on statistical models in engineering covering probability theory, random variables, frequency distributions, etc 17 p2876 A67-32236
 Dynamic system single- and multifrequency random oscillations described by differential-difference equations and solved through probability distribution 17 p2885 A67-32876
 Random errors in ultrasonic measurements, discussing Students distribution measurement repetition effect and rounding-off error evaluation 18 p3044 A67-33735
 Probability distribution of square of temperature difference between two points of turbulent flow measured by pulsation thermometer 18 p3026 A67-33757
 Ergodic properties of additive functionals of recurrent Markov

processes 18 p3071 A67-34182
 Emission statistics of nonresonant
 feedback laser produced by radiation
 scattering, showing fluctuations intensity,
 distribution function, etc 18 p3062 A67-34621
 Maximum entropy principle to derive
 reliability functions for creep failure modes
 of engineering materials at high
 temperatures, noting stress analysis,
 probability distribution,
 etc 18 p3145 A67-34675
 Probability function for turbulent velocity
 in duct flow determined from Doppler shift
 of scattered laser
 radiation 18 p3030 A67-34752
 Book on combinatorial methods in theory
 of stochastic processes covering ballot
 theorem, random variables, dam and storage
 processes, etc 19 p3250 A67-35572
 Minimax fuel requirement of aircraft
 angular stabilization for undetermined
 inertial moment probability
 distribution 19 p3202 A67-35887
 Probabilistic background of time series
 models which relate to spectral analysis and
 power spectrum and statistical inference for
 stationary stochastic
 processes 20 p3476 A67-36783
 Probability distribution errors effect in
 linear and planar impulse orbital transfers,
 considering angular orientation and
 impulsive velocity 20 p3527 A67-37259
 System reliability prediction and
 confidence limits for several component
 failure probability distributions, using Monte
 Carlo simulation on digital
 computer 20 p3455 A67-37314
 Lower bounds to minimum error
 probability for block
 discrete memoryless
 channels 22 p3764 A67-39296
 Error probability for binary signaling
 through multipath channel with receiver
 waveform comprising white Gaussian noise
 and time delayed frequency-shifted
 signal 24 p4121 A67-42341
 Escape probability of photon from
 homogeneous plane parallel medium,
 discussing coherent scattering process and
 integral equation 24 p4191 A67-42596

PROBABILITY THEORY
 Comparison of variances evaluated by
 Kolmogorov and Volterra techniques for
 phase locked loop subjected to white
 Gaussian input 01 p0044 A67-10480
 Book on noise and effect on
 communication covering random processes,
 fundamentals and spectra, nonlinear
 transformations /demodulation/, statistical
 theory of detection and information
 theory 01 p0024 A67-10725
 Markovian division process application for
 solving multicomponent preventive
 maintenance, work sampling and search
 theory problems 01 p0106 A67-10930
 Probabilistic structure of and
 establishment time for group synchronization
 in time-division-multiplex /binary code/
 transmission systems 01 p0027 A67-11238
 Reliability modeling utilizing conditional
 probability logic to simplify dependency and
 complex redundancy 01 p0083 A67-11353
 Problems in using probability theory by
 reliability engineers 01 p0084 A67-11355
 Limit theorems for sum of sequence of
 independent random
 variables 04 p0644 A67-14755
 Statistical parameters of linear antenna
 arrays after removal
 of emitters 04 p0583 A67-15149
 Probability estimation, discussing types,
 Bayesian method for binomial and
 multinomial distributions, sampling methods,
 etc 06 p1022 A67-17646
 Histogram construction via algebraic
 Monte Carlo method, determining
 simultaneous effect of several input
 statistical variables on output variable
 [AIAA PAPER 67-210] 06 p1024 A67-18326
 Soviet book on electronic properties of
 semiconductor solid solutions, noting
 relation between probability theory and
 ideal crystals theory 07 p1232 A67-19580
 Reliability in optimal control problems in
 terms of probability of faultless
 operation 07 p1162 A67-20027
 Inclusion probability of stochastic
 dynamical system shown to satisfy
 Kolmogoroff backward
 equation 08 p1308 A67-20323
 Monograph on applied methods of random

functions theory including stationary
 spectral theory, optimal dynamic systems,
 envelopes, etc 08 p1347 A67-20756
 Fracture of viscoelastic bodies, predicting
 statistical variability of rupture data for
 uniform and nonuniform excitation
 histories 08 p1421 A67-20913
 Book on probabilistic theory of structural
 dynamics, analyzing responses of structures
 to random vibrations 09 p1575 A67-21983
 Generalized maximum likelihood
 estimators with proof of asymptotic
 efficiency, considering Markov chain and
 stochastic difference
 equations 11 p1812 A67-24096
 Indeterminate recognition /game type/ and
 prediction systems 13 p2088 A67-27022
 Probability and payoff as factors
 influencing two-choice reaction
 time 15 p2427 A67-29134
 Statistical parameters of linear antenna
 arrays after removal
 of emitters 15 p2443 A67-29336
 Reliability assessment on incomplete and
 inaccurate field removal data, using
 reliability scoreboard 15 p2496 A67-30419
 Probability and prediction techniques
 related to maintainability discussed with
 application to early design, time constraints
 and maintenance goals 16 p2681 A67-30439
 Incorrect problems of mathematical
 physics examined and illustrated by classical
 Cauchy problem for Laplace
 equation 16 p2698 A67-31736
 Cosmic ray variation determination from
 single series of observations by methods of
 random process theory 17 p2935 A67-32108
 Book on statistical models in engineering
 covering probability theory, random
 variables, frequency distributions,
 etc 17 p2876 A67-32236
 Bounded solutions of boundary value
 problem with skew derivative studied by
 probability methods 17 p2878 A67-32737
 Integrodifferential equations for product
 surface area changes and grinding process
 development obtained by assuming
 proportionality between fracturing
 probability and particle
 size 19 p3236 A67-35725
 Book on probability in communication
 engineering covering probability theory,
 information and reliability theory, random
 processes and noise and random phasor
 sums 20 p3378 A67-36137
 Probability characteristics of oscillating
 satellite motion, considering random
 parameter scatter and atmospheric density
 variations, with expectation obtained by
 numerical integration 20 p3485 A67-36922
 Reliability criteria of systems with
 recovery, noting mean time to failure of
 system and mean time of system operation
 between failures 20 p3454 A67-37037
 Optimal system determined from
 maximum probability criteria of target
 hitting 20 p3410 A67-37226
 Book on optimal control theory covering
 Fourier and Laplace transforms, automatic
 control, mathematical theories,
 etc 21 p3602 A67-37829
 Glued metal joints properties analyzed
 from test results by method using theory of
 probability and statistical
 sample 21 p3716 A67-37950
 Discrete errors in continuous angle-
 modulation systems, considering conventional
 fidelity /SNR/ criterion and probabilistic
 theory 21 p3584 A67-38653
 Breakdown probability calculations to
 determine life span and reliability of
 structural components subjected to
 oscillations 22 p3908 A67-39284
 Error correcting codes for white Gaussian
 channel at low signal to noise ratio,
 discussing properties and performance
 criteria 23 p3984 A67-40752
 Fixed point probability row vector of
 regular or ergodic transition matrices
 simplified using generalized matrix inversion
 theory 23 p4023 A67-41032
 Correlation calculus applied in metrology,
 estimating correlation
 coefficient 23 p4008 A67-41397
 Multifrequency radar system performance,
 obtaining expression for detection
 probability as frequency number, false alarm
 probability and integrated pulse number
 function 24 p4122 A67-42408

PROBE
 S ELECTRON PROBE

S FLAME PROBE
 S IMPEDANCE PROBE
 S ION PROBE
 S LANGMUIR PROBE
 S LIGHT PROBE
 S LUNAR PROBE
 S MAGNETIC INDUCTION PROBE
 S MAGNETIC PROBE
 S MARS PROBE
 S METEOROLOGICAL PROBE
 S MICROWAVE PROBE
 S PLASMA PROBE
 S PRESSURE PROBE
 S RADIO PROBING
 S RESONANCE PROBE
 S SOLAR PROBE
 S SPACE PROBE
 S TEMPERATURE PROBE
 S VELOCITY PROBE
 S VENUS PROBE

PROBLEM
 S BOLZA PROBLEM
 S CANONICAL PROBLEM
 S CAUCHY PROBLEM
 S DIRICHLET PROBLEM
 S DUAL CONTROL PROBLEM
 S GOURSAT PROBLEM
 S INITIAL VALUE PROBLEM
 S ISOPERIMETRIC PROBLEM
 S MANY-BODY PROBLEM
 S NEUMANN PROBLEM
 S OPERATIONAL PROBLEM
 S POINCARE PROBLEM
 S POTENTIAL PROBLEM
 S PRELAUNCH PROBLEM
 S RIEMANN PROBLEM
 S SAINT VENANT FLEXURE PROBLEM
 S STURM-LIOUVILLE PROBLEM
 S THREE-BODY PROBLEM
 S TRAVELING SALESMAN PROBLEM
 S TWO-BODY PROBLEM
 S WEIERSTRASS PROBLEM

PROBLEM SOLVING
 Language and system design of numerical
 analysis problem solving system
 /NAPSS/ 02 p0206 A67-11803
 Problem solving under sequential and
 batch display conditions, noting effects of
 data density 02 p0186 A67-12231
 Cauchy problem of odd-order equations
 that are correct according to
 Petrovskii 03 p0459 A67-13644
 Four methods of solving elasticity theory
 contact problem and correlation of
 methods 05 p0923 A67-17180
 Book on methods of determining boundary
 conditions for unsteady state heat
 transfer 06 p1111 A67-17661
 Matrix and vector computational
 procedures for solution of partial and
 ordinary differential
 equations 06 p1022 A67-17788
 Solution properties and stability for
 system of nonlinear
 difference
 equations 09 p1524 A67-21926
 Convex polyhedron theorem in
 determining whole set of optimal solutions
 in linear programming 11 p1814 A67-24979
 Discrete rational approximation problem,
 procedure for solution 13 p2145 A67-26615
 Continuation in shooting methods for two-
 point boundary value
 problems 13 p2146 A67-27146
 Interval arithmetic methods used for error
 bounding in matrix calculations of linear
 equations 13 p2147 A67-27170
 Two LMS algorithms related to steepest
 descent method, obtaining generalized
 theorems 13 p2147 A67-27173
 Hankel transforms applied to generalized
 functions theory 13 p2148 A67-27470
 Definition of solutions of problem that
 constitutes generalization of infrapolynomial
 problem and best approximation problem in
 normed space 13 p2148 A67-27471
 Convergence of methods of tangential
 parabolas and hyperbolas used in nonlinear
 equation solution with nondifferentiable
 operators convergence of methods of
 tangential parabolas and hyperbolas used in
 nonlinear equation
 solution 13 p2149 A67-27619
 Nonlinear equation systems solved using
 parameters and varying them to original
 form while simultaneously tracing
 roots 14 p2342 A67-27975
 Oscillation pendulum equation solution
 properties, noting existence of certain
 bifurcation value of
 parameter 14 p2348 A67-28382
 Long wave type solutions for quasi-linear

elliptic equations, noting parameter lambda
for small nontrivial solutions
degeneration 14 p2343 A67-28386

Anisotropic macroscopically neutral plasma
excitations by arbitrary current described by
potentials, noting electroacoustic wave
propagation 15 p2527 A67-29482

Irreducible systems existence in class of
linear differential equations with quasi-
periodic coefficients having frequencies
represented by algebraic
numbers 15 p2510 A67-29629

Self-similar solutions for recombination
plasma decay problem, considering plane and
spherical symmetry 15 p2531 A67-30011

Technique based on dimensional analysis
for deriving set of dimensionless parameters
in problems involving large number of
variables, using matrix
calculations 15 p2518 A67-30078

Mathematical methods of nonlinear
programming, discussing convexity, quasi-
convexity, gradient, Taylor series and
quadratic approximations 17 p2818 A67-32425

Solving general integer programs,
investigating cutting methods, rounding
algorithm, branch and bound method and
partition method 17 p2819 A67-32427

Existence of solutions to differential
equations with multiple-valued right
side 18 p3070 A67-33554

Chebyshev approximation principle applied
to electronics problems, giving
algorithm 19 p3201 A67-34909

Natural torsional vibration frequency
calculation method, with frequency as
algebraic equations with real roots,
discussing example 19 p3341 A67-35711

Celestial mechanics, reviewing motion
observations, solution methods and
unresolved problems 20 p3522 A67-36623

Higher order differences used in solution
of Dirichlet problem for Poisson equation of
rectangle 20 p3475 A67-36651

Self-similar solutions for recombination
plasma decay problem, considering plane and
spherical symmetry 20 p3502 A67-37536

Moment-kinematic and moment-energetic
characteristics of servomotors applied to
point and functional problems of
servomechanisms in space 24 p4098 A67-42094

Penalty function approach for inequality
constrained optimal control
problems 24 p4135 A67-42180

Ad hoc exact solution techniques for
nonlinear partial differential equations
noting physical
applications 24 p4180 A67-43085

PROCEDURE
S OPTICAL CORRECTION PROCEDURE
PROCESS
S AUTOCALVE PROCESS
S BURNING PROCESS
S ERGODIC PROCESS
S IRREVERSIBLE PROCESS
S ISENTROPIC PROCESS
S ISOTHERMAL PROCESS
S MARKOV PROCESS
S N-STAGE PROCESS
S NUCLEATION PROCESS
S PERIODIC PROCESS
S POISSON PROCESS
S POLYTROPIC PROCESS
S RANDOM PROCESS
S STOCHASTIC PROCESS
PROCESSING
S DATA PROCESSING
S INFORMATION PROCESSING
S SIGNAL PROCESSING
PROCESSOR
S DATA PROCESSOR
PRODUCT DEVELOPMENT
Configuration management, method for
current and precise documentation which
attempts to assure customer and builder
that final hardware is what they agreed
on 04 p0739 A67-14424

Product identification and traceability
standards for space system quality assurance
program for NASA space
systems 05 p0930 A67-17251

Cost analysis for large scale development/
production programs
[AAS PAPER 66-148] 08 p1429 A67-20968

Operational reliability development
program, considering design, maintainability
and personnel subsystem 09 p1582 A67-22294

Management methods in military
equipment development to be used with
aircraft 11 p1885 A67-24655

Cost models for complex space programs,
analyzing data acquisition systems, computer
routines, etc 13 p2232 A67-27547

Cost analysis for large scale development/
production programs
[AAS PAPER 66-148] 13 p2232 A67-27549

Project initiation emphasizing market,
product /design, cost and timing/ and
resources to market 15 p2583 A67-29667

Defense procurement procedures and task
of project manager 15 p2583 A67-29668

Evaluating, reporting and improving on
quality performance of suppliers and
subcontractors of helicopter construction
firm 15 p2584 A67-30404

Supplier control and reliability, discussing
adequate input supply and output
monitoring 15 p2584 A67-30407

Materials engineering for electronic
hardware, discussing design, development
and construction, including tables on
metallic finishes, coatings for printed wiring,
etc 17 p2865 A67-33047

Operational computerized system for
automatic surveillance of reliability and
maintainability of spacecraft
hardware 18 p3021 A67-34701

PRODUCTION
S AIRCRAFT PRODUCTION
S ION PRODUCTION
S OXYGEN PRODUCTION
S PAIR PRODUCTION
S PARTICLE PRODUCTION
S PHOTOPRODUCTION
PRODUCTION ENGINEERING
British procurement procedures for
military aircraft noting cost estimate,
feasibility study, development contract and
production stages 02 p0343 A67-12242

Liquid hydrogen production techniques in
purification, ortho-para conversion and
refrigeration 05 p0789 A67-17017

Lasers and RCA 07 p1193 A67-19080

Production inaccuracy effects on
oscillation frequency characteristics of
turbomachine blades 07 p1261 A67-19134

Cost reduction and avoidance by value
engineering to yield lowest overall cost for
performance, reliability and maintainability
requirement 09 p1581 A67-22157

Mathematical analysis of electrochemical
machining phenomena, discussing behavior
predicting equations
[ASTME PAPER WES-7-09] 11 p1798 A67-24254

Producibility of aerospace products with
regard to machinability of aluminum alloy
[ASTME PAPER WES-7-29] 11 p1798 A67-24257

Soviet book on production of gas turbine
engines covering manufacturing methods,
automation of operations, tooling,
etc 11 p1798 A67-24516

Nuclear and engineering ceramics
Conference, Harwell, Berks., England,
October 1965 12 p1964 A67-25210

Mass production lines for monolithic
integrated circuits 12 p1916 A67-25995

Thin film integrated circuit technology,
discussing reliability, production, packaging,
components, etc 12 p1917 A67-26204

Thin film technology and
manufacturing 12 p1951 A67-26212

Standardization techniques for integrated
circuit production, particularly logic
circuits 12 p1918 A67-26215

Automatic production processes for
semiconductors 12 p1951 A67-26224

Statistical analysis of beryllium cross-
rolled sheet, hot pressed block and ring
rolled forgings 13 p2140 A67-27135

Vacuum equipment application in
semiconductor production 13 p2124 A67-27365

Microcellular techniques for fabricating
integrated circuit arrays 13 p2074 A67-27495

Systems approach as systematic
investigation of research, engineering and
management activities for technological or
sociological gain 13 p2231 A67-27513

Metal-semiconductor electric contacts for
GaAs bulk effect device noting uniformity,
linearity, usefulness, adaptability,
etc 13 p2183 A67-27567

Commercial forms of aluminum alloys,
production, applications and
marketing 14 p2336 A67-27812

Material processing in microelectronics
with laser beam noting solid state lasers,
power density, pulse frequency,
etc 15 p2493 A67-29682

Reliability, performance requirements and
environment in which system must
operate 15 p2583 A67-30128

Dollar consequence functions for producer
and consumer risks due to product faults
noting optimization 16 p2782 A67-31257

Assembly of thick film microcircuit
production facility detailing equipment,
materials, marketing, etc 16 p2641 A67-31621

Printed circuit technology development
survey showing refining processes and
techniques 16 p2641 A67-31622

Book on ultrasonic machining of
intractable materials covering basic
principles, vibrator design, machine tools,
technology, processes involved and
applications 17 p2865 A67-32200

Optimal control and convex programming,
discussing problem of admissible investment
program control for production
constraints 17 p2829 A67-32431

Materials engineering for electronic
hardware, discussing design, development
and construction, including tables on
metallic finishes, coatings for printed wiring,
etc 17 p2865 A67-33047

Production process of hermetically sealed
electronic package for aerospace
use 21 p3595 A67-38340

Component selection program for
equipment onboard FR-1 satellite covering
production facilities, qualifications, supply,
reliability, etc 21 p3572 A67-38676

Reliability in aircraft engines from start
of assembly to completion and
delivery 22 p3867 A67-39285

Densified carbon and graphite production
methods /carbon, metal and resin and
carbon with carbon impregnation/ for glass-
to-metal sealing jigs 24 p4174 A67-41913

Soviet metallurgical, chemical and
electrochemical studies and industrial
applications of titanium 24 p4169 A67-41918

Fastener and fastened joint technology
noting influence of hole preparation, surface
coating, thread lubricants and fit on fatigue
life 24 p4161 A67-42081

Zero gravity orbital manufacturing noting
free fall casting and blowing and zero
gravity surface tension casting and foaming,
discussing Serpentiator System engineering
[AIAA PAPER 67-842] 24 p4165 A67-42980

PROFILE
S AIRFOIL PROFILE
S ELECTRON DENSITY PROFILE
S SHOCK WAVE PROFILE
S TEMPERATURE PROFILE
S VELOCITY PROFILE
S WIND PROFILE
S WING PROFILE
PROGRAM
S APOLLO APPLICATIONS PROGRAM
/AAP/
S COMPILER PROGRAM
S COMPUTER PROGRAM
S GULLIVER PROGRAM
S HIGH ALTITUDE BALLOON
PROGRAM
S INSTRUMENTATION PROGRAM
S INTERSERVICE DATA EXCHANGE
PROGRAM /IDEP/
S LUNAR PROGRAM
S NASA PROGRAM
S NATIONAL LAUNCH VEHICLE
PROGRAM
S OPTICAL SATELLITE TRACKING
PROGRAM
S PLANETARY-INTERPLANETARY
PROGRAM
S ROCKET ENGINE ADVANCEMENT
PROGRAM
S SNAP PROGRAM
S SOLAR ENERGY THERMIONIC /SET/
PROGRAM
S SPACE PROGRAM
S SPACE TRAJECTORY PROGRAM
S SPACE VEHICLE CHECKOUT
PROGRAM
S TEST PROGRAM
S TOPSIDE PROGRAM
S UNIVERSITY PROGRAM
PROGRAM MANAGEMENT
Transportation and handling of large solid
rocket motors, considering program
management aspects
[SAE PAPER 660707] 01 p0169 A67-10623

DOD/NASA management practice program
ensuring identification, communication and
achievement of mission success requirement
[SAE PAPER 660729] 01 p0170 A67-10629

System reliability improvements based on

design and reliability experience producing increased success percentage of NASA systems from 62 to 87 percent 01 p0083 A67-11345

Reliability matrix analysis of AFSCM 375 management system 01 p0171 A67-11375

Integration of reliability, maintainability and other engineering disciplines, discussing objectives of program management [AIAA PAPER 66-859] 02 p0343 A67-12260

Space flight projects evaluation and development for long term meaningful space flight program 04 p0740 A67-14558

European Conference on Telecommunications by Satellites /CETS/, recommendations and patterns of cooperation 06 p1119 A67-17558

Management systems planning for control and information systems for Voyager project, with attention to work breakdown and scheduling [AAS PAPER 66-141] 08 p1429 A67-20966

Experiment selection process for specific flights in Apollo applications program /AAP/, using algorithms [AAS PAPER 66-142] 08 p1411 A67-20967

Cost analysis for large scale development/production programs [AAS PAPER 66-148] 08 p1429 A67-20968

Planning-Programming-Budgeting System /PPBS/ implementation by Federal agencies and relation to space activities [AAS PAPER 66-150] 08 p1430 A67-20970

F-111 fixed price contract management, discussing weapon system management, acquisition, controls and techniques to circumvent inherent problems [AAS PAPER 66-153] 08 p1430 A67-20971

NASA management and program trend line analysis [AAS PAPER 66-156] 08 p1430 A67-20973

Planned interdependency incentive method /PIIM/ for Gemini program at lowest cost and best performance [AAS PAPER 66-157] 08 p1430 A67-20974

Management aspects of design and development of Gemini spacecraft noting program organization, management techniques and personnel motivation [AAS PAPER 66-158] 08 p1430 A67-20975

Cost incentive contract effects on research and development 08 p1431 A67-21287

Program for satellite supported air traffic control 09 p1526 A67-21679

Research and development for better manufacturing emphasizing hydrothermal growth of ruby crystal 09 p1505 A67-22143

Implementation of NASA NPC 250-1 /Reliability Program Provisions for Space Systems Contractors/ as applied to Saturn V Mechanical Ground Support Equipment Program 09 p1582 A67-22292

Optimal control for investment program, obtaining solution through convex programming 10 p1620 A67-23426

Four alternative plans for future U.S. space programs 10 p1710 A67-23636

FAA development program for air traffic control, navigation and landing aids and airport capacity [SAE PAPER 670265] 11 p1885 A67-23988

Management of aerospace programs - AAS Conference, University of Missouri, November 1966 13 p2231 A67-27545

Experiment selection process for specific flights in Apollo applications program /AAP/, using algorithms [AAS PAPER 66-142] 13 p2214 A67-27548

Cost analysis for large scale development/production programs [AAS PAPER 66-148] 13 p2232 A67-27549

Planning-Programming-Budgeting System /PPBS/ implementation by Federal agencies and relation to space activities [AAS PAPER 66-150] 13 p2232 A67-27551

Management scheme for Apollo program 13 p2233 A67-27553

F-111 fixed price contract management, discussing weapon system management, acquisition, controls and techniques to circumvent inherent problems f-111 fixed price contract management, discussing weapon system management, acquisition, controls [AAS PAPER 66-153] 13 p2233 A67-27554

NASA management and program trend line analysis [AAS PAPER 66-156] 13 p2233 A67-27555

Planned interdependency incentive method /PIIM/ for Gemini program at lowest cost and best performance

[AAS PAPER 66-157] 13 p2233 A67-27558

Management aspects of design and development of Gemini spacecraft noting program organization, management techniques and personnel motivation [AAS PAPER 66-158] 13 p2233 A67-27559

Economics of military space launching systems 15 p2566 A67-29830

Management control system for technical, production, financial and contractual management of large scale or technical industry programs [AAS PAPER 67-153] 15 p2583 A67-29969

Applications of Program Evaluation and Review Technique /PERT/ in NASA 15 p2583 A67-30222

Critical Path Analysis /CPA/ system based on network techniques, coordinating separate development programs of ELDO member states 15 p2583 A67-30223

Maintainability prediction procedures applicable to systems and equipment as described in DOD handbook 16 p2781 A67-30442

Space project management noting job definition and organization for implementation and control 16 p2783 A67-31630

Controls Development /CODE/ program for proving design validity of B2707 SST flight control and hydraulic systems prior to flight 17 p2795 A67-32004

PERT /Program Evaluation and Review Technique/ planning method gives project management means for controlling project to accomplish task in shortest possible time 18 p3161 A67-33634

Relationship of management to reliability aspects during Athena program 18 p3138 A67-34651

Role in management of specification trees portraying interrelationship of requirement documents, specifications and standards applicable to particular program 18 p3162 A67-34671

Saturn V reliability analysis model used by management for predicting performance probabilities 18 p3138 A67-34684

Short haul air transportation potentials and problems, considering legislative, administrative and financial aspects of implementation and planning 19 p3347 A67-34971

Economic considerations of space operations noting cost identification, program planning, maximum utilization, etc 19 p3350 A67-35648

Management of aerospace programs, discussing budgeting and contracting procedures 19 p3350 A67-35879

Principal investigator task evaluation, discussing responsibility for instruments, prelaunch operation, operational program establishment, processing, analyzing and publishing of results [AIAA PAPER 67-630] 20 p3534 A67-37614

Multipurpose orbital bus-vehicle for alternate missions [AIAA PAPER 67-638] 20 p3534 A67-37618

Lessons from spacecraft industry experiences in 1960s and trends for 1970s, discussing subsystem performance experience, data acquisition, contracting, reliability, etc [AIAA PAPER 67-639] 20 p3557 A67-37622

Space electronic program management and requirement integration, discussing functional or matrix type organization and project organization 21 p3734 A67-38215

Test planning and decision making in environmental testing approached from program formulation involving resources and equipment, degree of simulation and optimum levels 22 p3781 A67-40402

Stationary satellite to provide educational TV to underdeveloped lands noting design, transmission terminals and safeguards against control and propaganda [AIAA PAPER 67-963] 24 p4260 A67-43042

PROGRAMMER

Autopilot programmer design for automatic guidance in approach and stabilization along course of aerial photography aircraft 03 p0465 A67-14284

Operational and circuit features of laboratory device built to simulate dynamic electrical output characteristics of programmable solar array in orbital flight 08 p1315 A67-20680

Automatic temperature programmed station for calibrating cryogenic sensors

[ISA PAPER 12-11-2-66] 11 p1795 A67-25060

High reliability sequence programmers for DIAMANT satellite booster switching functions 21 p3655 A67-38207

Lunar Orbiter flight programmer, electronic design, development, application and performance 21 p3601 A67-39062

Programmer for operational strength tests during aircraft construction 22 p3912 A67-39755

PROGRAMMING

SA CODING

SA COMPUTER PROGRAMMING

SA DYNAMIC PROGRAMMING

SA LANGUAGE PROGRAMMING

SA LINEAR PROGRAMMING

SA MULTIPROGRAMMING

SA NONLINEAR PROGRAMMING

SA ON-LINE PROGRAMMING

SA THRUST PROGRAMMING

Quadratic programming applied to design of digitally compensated sampled data control system 03 p0393 A67-13902

Book on geometric programming detailing theory of mathematical method for optimizing engineering design 09 p1469 A67-22435

Incipient cavitation calculation in hydrodynamics as example for applying quadratic programming to mechanical system subject to one-sided constraints 17 p2838 A67-32428

Optimal control and convex programming, discussing problem of admissible investment program control for production constraints 17 p2829 A67-32431

Automatic apparatus for flooding or spraying test specimens with liquid corrosive media according to predetermined program 21 p3715 A67-37827

Instructional broadcast satellites programming methods to reduce educational cost of students time without adding to technological cost [AIAA PAPER 67-787] 24 p4258 A67-42950

PROJECT

S APOLLO PROJECT

S BEACON PROJECT

S CENTAUR PROJECT

S FIRST PROJECT

S GEMINI PROJECT

S HARP PROJECT

S HAYSTACK PROJECT

S HIGH POWER PROJECT

S JUPITER PROJECT

S MERCURY PROJECT

S ORION PROJECT

S PERT PROJECT

S PLANETARY CIRCULATIONS PROJECT

S RANGER PROJECT

S REACTOR IN-FLIGHT TEST /RIFT/ PROJECT

S RESEARCH PROJECT

S ROCKET PROJECT

S ROVER PROJECT

S SPACE ELECTRIC ROCKET TEST /SERT/

S STAR FISH PROJECT

S STATISTICAL FORECASTING PROJECT

S SURVEYOR PROJECT

S SYNCHRONOUS COMMUNICATIONS SATELLITE PROJECT

S VELA PROJECT

S VOYAGER PROJECT

S WEST FORD PROJECT

PROJECTILE

SA HIGH ALTITUDE SOUNDING PROJECTILE /HASP/

SA HYPERVELOCITY PROJECTILE

SA MISSILE

Space-time correlation measurements in fluctuating turbulent wakes behind projectiles [AIAA PAPER 67-19] 06 p0940 A67-1843

Yaw force /Magnus/ of spinning projectile at angle of attack measured, using balance device in wind tunnel [AIAA PAPER 66-753] 14 p2292 A67-2813

Metal projectiles plastic deformation impacting on rigid targets defined, obtaining computer code through direct analysis 22 p3914 A67-4018

PROJECTILE CRATERING

Impact of cylindrical or spherical projectiles of dural and polyethylene at high velocities in semiminfinite targets, analyzing crater shape and relation to kinetic energy 04 p0710 A67-1500

- Hypervelocity impact of polythene projectiles on semilinear aluminum targets at various obliquity angles, using RARDE gas launcher 04 p0710 A67-15003
- Solid-solid impact at hypervelocities using flow equations, noting variations of impact velocity, projectile shape and density and state equation 04 p0710 A67-15004
- Momentum transfer during impact, penetration depth, crater form and mass loss at various velocities, using spherical aluminum projectiles and aluminum targets 04 p0710 A67-15005
- PROJECTILE PENETRATION**
- Effectiveness of meteoroid shielding from hypervelocity impact penetration and cratering 01 p0155 A67-11406
- Photooptical system for determining velocity of projectile after target penetration 09 p1502 A67-22823
- PROJECTION**
- SA LIGHT GAS PROJECTOR
- Earth azimuthal perspective projections /cosmographic projections/ in space photograph interpretation 03 p0419 A67-13264
- Viscous incompressible slow flow over circular arc wall projections or depressions with shear flow far from 06 p0992 A67-18887
- Generalized potentials for medium energy inelastic nuclear scattering derived with projection operator 14 p2350 A67-27789
- PROJECTIVE-DIFFERENTIAL GEOMETRY**
- Topology of three-dimensional integral surface projection of section of energy integral by third integral 08 p1380 A67-20382
- Probability of overlapping intercept by system of random intercepts and application to detection of flying objects in cloudy skies 20 p3477 A67-37036
- PROLATE SPHEROID FUNCTION**
- Time varying electromagnetic field pattern of prolate spheroid antenna with rotationally symmetric current distribution motion pictures generated by computer 11 p1758 A67-24115
- PROMINENCE**
- Amplification of solar dipolar magnetic field by differential rotation investigated, noting implications of Sporer law 10 p1705 A67-22895
- Homogeneity of solar prominences studied photographically in monochromatic light 14 p2382 A67-28941
- Association rate between solar surges and flares 17 p2938 A67-32820
- Dome formation in corona around prominence during February 1961 eclipse, describing observed features and proposing three-dimensional model 17 p2953 A67-33399
- Quiescent solar prominences general appearance described by theoretical model 19 p3324 A67-35436
- Gravitational model for chromosphere flarelike brightenings following disparities brusques, examining prominence and chromospheric characteristics 19 p3324 A67-35437
- Solar flare electron density determination by half-width method, discussing errors due to measurement and method 19 p3314 A67-35438
- Stable height to distance to supporting magnetic field origin ratio for prominences, noting agreement with Kippenhahn-Schluter model 20 p3528 A67-37469
- Solar prominence activation on March 25, 1967 observed with H-alpha visual patrol refracting telescope at Anacapri 23 p4060 A67-41234
- Mean intensity photospheric H-alpha radiation profile for prominences in solar corona, noting profile dependence on height, velocity and direction 24 p4209 A67-41965
- Decrement of Balmer line widths and H-alpha profiles when distributing fine components as function of radial velocity in optical prominences 24 p4232 A67-42595
- PRONY SERIES**
- Closed loop system with reference to different gyro stabilization loops present in modern space vehicle inertial measuring unit, using Prony exponential series curve fitting method as analytical tool 03 p0400 A67-14218
- PROPAGATION**
- SA COSMIC RAY PROPAGATION
- SA CRACK PROPAGATION
- SA DIFFRACTION PROPAGATION
- SA ELECTROMAGNETIC PROPAGATION
- SA FLAME PROPAGATION
- SA IONOSPHERIC PROPAGATION
- SA MULTIPATH PROPAGATION
- SA NOISE PROPAGATION
- SA RADIO PROPAGATION
- SA RADIO SIGNAL PROPAGATION
- SA SCATTER PROPAGATION
- SA SHOCK WAVE PROPAGATION
- SA SOUND PROPAGATION
- SA STRESS PROPAGATION
- SA TRANSEQUATORIAL PROPAGATION
- SA WAVE PROPAGATION
- Characteristics method applied to one-dimensional propagation problem, considering Massau grid and using partial differential equation 06 p0990 A67-18585
- PROPAGATION MODE**
- Energy relation for acoustic propagation modes in hot electron plasma considered in application of Helmholtz theorem 01 p0123 A67-10441
- Electromagnetic wave propagation in two waveguides with different cross section connected by long continuous slot 01 p0038 A67-10717
- Modes of beam waveguide or beam waveguide resonator filled with axially magnetized plasma 02 p0213 A67-11619
- Propagation characteristics of cylindrical waveguide partially filled with dielectric light modulation material 02 p0193 A67-11780
- Characteristic impedance of TEM mode transmission lines, extracting upper and lower bounds on finite difference solution of Laplace equation 02 p0194 A67-11784
- Radio wave propagation in multimode waveguides of arbitrary height, assuming ionosphere boundary to be perfectly reflecting 02 p0198 A67-12070
- Aperture admittance, material loading and higher order modes effect on rectangular cavity slot antenna design 02 p0218 A67-12098
- Poloideal hydromagnetic plasmaspheric resonance under conditions representative of inner magnetosphere 02 p0276 A67-12563
- Tuning techniques for waveguide band pass filters operating below cut-off frequency 03 p0387 A67-13994
- Theoretical curves for day and night time conditions for variation of peak frequency of radio atmospherics with distance computed from source spectrum and dominant propagation mode 03 p0415 A67-14117
- Transhorizon propagation modes from signals transmitted by orbiting radio beacon ionospheric satellite /ORBIT/, showing paths sustained by ionospheric ducts or usual hop modes [RASSA PAPER 1-10-146] 03 p0373 A67-14253
- TE modes propagation in rectangular waveguides containing two dielectric slabs, computing cut-off frequencies and propagation constants 04 p0570 A67-14860
- Transient analysis of TEM mode four-port microwave networks by flow graph techniques, with application to branch line coupler, phase shifter and ring hybrid 04 p0591 A67-14861
- Axiallysymmetric motions of Timoshenko type cylindrical shells composed of two elastic isotropic layers of different materials and thicknesses connected by perfect bond 04 p0717 A67-15909
- Radio Aurora and formation mechanism of ionospheric D and F regions, examining HF and VLF propagation via computer ray tracing, ionospheric storms and equatorial sporadic E layers 05 p0795 A67-18010
- Cut-off wavelength of lowest TE mode in rectangular waveguide having coaxial cylindrical conductor 05 p0773 A67-18511
- High magnetic field effect on interband semiconductor laser, particularly electromagnetic modes and coupling and threshold current 05 p0822 A67-18673
- Error due to multiple propagation in distance measurement by comparison of modulation phases on transmitted and reflected laser beam 07 p1188 A67-19606
- Symmetric wave propagation in cylindrical waveguide filled with inhomogeneous plasma, calculating phase velocities 07 p1158 A67-20242
- Landau type damping of plasma oscillations and Bernstein mode electrostatic propagation perpendicular to weak magnetic field 08 p1360 A67-21129
- Excitation and propagation of Bernstein modes in nonuniform plasmas near electron cyclotron harmonics 08 p1361 A67-21130
- Resonant frequencies of standing wave Bernstein modes propagating in magnetized homogeneous plasma columns and effects of anisotropy of unperturbed electron velocity and ambipolar-diffusional electric field 08 p1361 A67-21131
- LF gravitational-acoustic and internal gravity mode wave propagation in temperature-stratified photosphere-low chromosphere region and solar atmospheric resonant responses 08 p1399 A67-21236
- Propagation mode of one-dimensional HF finite acceleration pulses in nonlinear viscoelastic solids, stressing shock formation and propagation 09 p1573 A67-21547
- Meteor burst radio propagation channel clock synchronization experiment to determine frequency offset between two remotely located frequency standards 09 p1494 A67-21618
- Plasmod density, electron temperature and radius variation during propagation through magnetic field, using electric and magnetic probes 09 p1545 A67-21996
- Dispersion of mode couplings of wave propagation in waveguide containing plasma electron beam system 09 p1550 A67-22582
- Ionospheric thin layer stratifications and valley region analyzed by integrating propagation method and by impedance probe 10 p1648 A67-23290
- Measurement and theory of two modes in antenna apertures of magnitudes one to two wavelengths, obtaining field distribution 11 p1763 A67-24295
- Approximation method calculation of propagation constants of dielectric loaded TE wire-grid leaky wave antenna for near endfire radiation 11 p1763 A67-24296
- Approximate mode decomposition for treating boundary value problems for uniform compressible anisotropic plasma 11 p1753 A67-24307
- Transverse resonance method applied to slotted inhomogeneous circular waveguide with leaky wave mode propagation 11 p1766 A67-24690
- Primary illumination laws for parabolic reflector for maximum quality factor determined, considering multimode sources for cold antennas 12 p1913 A67-25307
- Phase measurements of VLF transmission over long distance transequatorial path 12 p1906 A67-25942
- Modal wave solutions of isotropic plasma-filled parallel-plate waveguide examined, using cold and warm plasma models without collision 12 p1915 A67-25943
- Two digital computer filing programs for determining ordinates of propagation curves of ground waves in visible region 13 p2070 A67-27202
- Waveguide structures for double beam leaky wave antennas 13 p2082 A67-27408
- Propagation constants of rectangular waveguide containing parallel sheets of finite conductivity using iterative computer program 13 p2083 A67-27443
- Microwave design techniques for calculating even and odd mode characteristic impedances of miniature microstrip transmission lines 13 p2071 A67-27445
- Atmospheric wind effects on guided propagation of VLF infrasonic waves over long distances, including variable wind and temperature profiles 13 p2117 A67-27702
- Radial variation of plasma electron density determined by surface wave resonances 14 p2355 A67-27829
- Higher harmonic components of tweaks as evidence of adequacy of waveguide mode theory of VLF propagation between earth and ionosphere 14 p2307 A67-27888
- Linear symmetric modes of propagation for viscous compressible liquid in rigid and elastic conduits analyzed using Navier-Stokes equations [ASME PAPER 67-FE-12] 14 p2304 A67-28361
- Propagation effects on distance, arrival angle and Doppler effect measurements with reference to tropospheric influence 14 p2284 A67-28400
- Oblique sounding of transequatorial path [AGARDOGRAPH 95] 15 p2438 A67-30298
- Distributed parameter concepts of propagation, reflection and characteristic termination applied to dynamic analysis and control of bending vibration 16 p2776 A67-31686
- Modal interference of VLF radio waves investigation from field strength data, noting

isotropic case 16 p2631 A67-31850
 Multimode propagation and mode conversion at sunrise and sunset lines explaining diurnal variations on vlf paths 16 p2631 A67-31852
 Normal modes of hydromagnetic oscillations in rotating fluid sphere including ohmic dissipation, deriving dispersion relations 17 p2941 A67-32285
 Propagation coefficients of leaky waveguide modes improved by corrections to radial line susceptance arising from uniform slot in wall of circular waveguide 17 p2812 A67-32317
 Propagation modes and instabilities of transverse disturbances in solid state plasmas 17 p2925 A67-33377
 Energy transport concentration around homogeneous lossless dielectric cylinder, calculating electric field strength distribution and limiting radius of several wave modes 18 p2999 A67-33529
 Characteristics of dielectric rod excited with dominant propagating mode 18 p3011 A67-34020
 Launching efficiency of PE-20 and PM-11 modes in dielectric-loaded trough waveguide excited by dielectric-loaded rectangular waveguide 19 p3194 A67-35514
 Earth-ionosphere whispering-gallery nature at VLF analyzed, using mode equation for idealized earth ionosphere model 19 p3184 A67-35827
 Higher order mode excitation by multipath propagation in deep fading of receiving horn-reflector antenna 20 p3385 A67-37355
 Torsional disturbance propagation in Gutenberg-Bullen earth model through spectral seismograms, discussing travel times and S wave amplitude [SR-16] 20 p3435 A67-37875
 Schumann Resonance frequencies, Q-factor and waveguide propagation constant derived at ELF for ionospheric profiles 21 p3579 A67-37993
 Electro-optic phase modulation of visible and IR light by p-n, p-i-n and metal semiconductor junctions and heterojunctions, noting propagation modes 21 p3684 A67-38453
 Propagation behavior analyzed for fundamental mode of parallel plate waveguide 21 p3597 A67-38566
 Parabolic cylindrical reflector beam waveguide, discussing conduction and diffraction losses of TE and TM modes 21 p3583 A67-38608
 Characteristic admittances of comb-type and undulating waveguide filters, considering diaphragm thickness and TE propagation mode 22 p3770 A67-39662
 Long period hydromagnetic propagation in theta model geomagnetic tail, deriving TM and TE modes equations 22 p3791 A67-39815
 Helix spurious mode effects on TW amplifier performance analyzed for methods of elimination 22 p3775 A67-40462
 Coupled electromagnetic whispering gallery modes in large dielectric cylinders, discussing circumferential phase velocity, boundary region and axial wave number 23 p3974 A67-41203
 Electromagnetic mode propagation in anisotropic dielectric p-n junction waveguide models noting Pockel effect of electric field on light 23 p3982 A67-41466

PROPAGATION VELOCITY

Unsteady interaction between blunt bodies and shock wave, comparing reflected shock wave velocity decrease for plane spherically blunted cylinders 01 p0008 A67-11294
 Material strength parameter /coupling modulus/ dependence on crack propagation velocity when accounting for rupture kinetics 03 p0529 A67-14166
 Space charge wave velocity in semiconductors, noting recombination type instability 04 p0676 A67-14928
 Propagation velocity and other characteristics of detonations in liquid mixtures of nitropropane 2 and nitric acid, noting relation to initial temperature and water content 04 p0728 A67-15495
 Relations between rates of propagation of constant pressure, density, etc, for one-dimensional MGD flows 08 p1357 A67-20585
 Parameters of supercompressed detonation wave in solid propellant system noting wavefront pressure, density and propagation rate dependence on displacement rate of interface 12 p1930 A67-26116
 Arc jet exhaust velocity compared with

propagation velocity of random light fluctuations 13 p2188 A67-26839
 Long spark formation in air under weakly focused laser radiation, deriving formula for mean propagation rate of spark beyond focal field 13 p2129 A67-27628
 Propagation rate of LF acoustic waves in low pressure glow discharge in nitrogen 14 p2354 A67-27759
 High frequency asymptotic behavior of wave field in two-dimensional diffraction problem on inhomogeneous cylinder of arbitrary cross section 16 p2628 A67-31505
 Extension of plastic zone in direction of path of moving brittle crack, studying properties of plastic zone to crack length ratio 17 p2960 A67-32633
 Propagation velocity of stable detonation wave in gaseous mixtures measured using Doppler effect resulting from reflection of electromagnetic wave from front of detonation wave 17 p2970 A67-32806
 Cylindrical expanding detonation waves in gas mixtures, studying detonability limits, propagation velocity and instability and vibratory phenomena 18 p3153 A67-33822
 Temperature field and electron concentration in electric arc moving along parallel electrodes in magnetic field, giving propagation rate, arc intensity, etc 18 p3087 A67-34046
 Finite propagation velocity in heat conduction, diffusion and viscous shear motion, studying assumptions of differential equation derivation 18 p3159 A67-34070
 Classification of small amplitude waves, surfaces of weak discontinuity and shock waves in ideal MHD medium obeying adiabatic state equation 19 p3294 A67-35409
 Gravitational waves, calculating velocity of propagation using perturbation method 19 p3262 A67-35708
 Stationary moving domains in hot electron semiconductors, obtaining criteria for soft and hard regimes of domain excitation 20 p3508 A67-36222
 Uniformly moving crack in infinite body, in antiplane strain, driven by loads in simultaneous travel 20 p3536 A67-36415
 Propagation rate of electromagnetic and gravity wave front in synchronous reference system in Riemann space 20 p3486 A67-37554
 Thermoelastic coupling effect on propagating discontinuities in stresses and particle velocities studied using characteristic method 21 p3715 A67-37893
 Wave propagation rate in elastoplastic bodies under completely plastic conditions, noting discontinuity magnitude 21 p3716 A67-37968
 Plasmoid propagation at high pressures, emphasizing Bostick buttons performance compared to electromagnetic shock tube, describing button gun and photographic equipment 21 p3874 A67-38771
 Long spark formation in air under weakly focused laser radiation, deriving formula for mean propagation rate of spark beyond focal field 21 p3642 A67-38824
 Nonself-similar energy diffusion of thermal radiation front for plane parallel geometry, giving series and parametric solutions 23 p4081 A67-40887
 Analysis of system described by heat equation where disturbance propagates with infinite speed as function of time 23 p4024 A67-41086
 Fatigue crack propagation in ultrahigh strength steels, noting rate sensitivity to moisture and plane strain fracture toughness 24 p4171 A67-41953

PROPANE

SA CYCLOPROPANE
 SA NITROPROPANE
 Propane gas system for satellite attitude control noting Skylark rocket 01 p0157 A67-11446
 Dissociation pressures of mixed gas hydrates predicted from data for hydrates of methane, propane and nitrogen with water 02 p0190 A67-12234
 Liquefied propane as fog dispersing agent 10 p1676 A67-22814
 Ion-molecule reactions in propane studied using mass and energy resolved ion beams in tandem mass spectrometer 17 p2810 A67-33264

PROPELLANT

SA BIPOPELLANT
 SA COLLOIDAL PROPELLANT
 SA COMPOSITE PROPELLANT

SA CRYOGENIC PROPELLANT
 SA DOUBLE BASE PROPELLANT
 SA EXPLOSIVE
 SA FUEL
 SA GAS PROPELLANT
 SA HIGH ENERGY PROPELLANT
 SA HYBRID PROPELLANT
 SA HYPERGOLIC PROPELLANT
 SA LIQUID PROPELLANT
 SA METAL PROPELLANT
 SA MONOPROPELLANT
 SA MULTIPROPELLANT
 SA PLASTIC PROPELLANT
 SA SOLID PROPELLANT
 SA STORABLE PROPELLANT
 Acceleration of propellant in arcjet devices by thermal and self-magnetic forces, using various nozzle configurations 08 p1375 A67-20574
 Rocket fuel production possibilities on moon surface and other planets for planetary explorations 16 p2655 A67-31008
 PROPELLANT ACTUATED DEVICE
 SA CARTRIDGE ACTUATED DEVICE
 SA THRUSTOR
 Lithium and ammonia MPD arc thrusters tests in low environmental pressure [AIAA PAPER 67-685] 21 p3692 A67-38716
 PROPELLANT ADDITIVE
 Metal fiber addition to basic propellant increases burning rate 05 p0872 A67-17215
 Aluminum powder damping of HF instability in solid propellant combustion in vortex burner 06 p1115 A67-18307
 GE T64 engine operation on emulsified fuel /JD1/, noting corrosion effects on fuel system components due to water additive [SAE PAPER 670369] 17 p2927 A67-33002
 Ionization and recombination processes of alkali metal ions in hydrogen-oxygen-nitrogen flames with hydrocarbon additives 18 p3107 A67-33806
 Condensed phase thermal decomposition of ammonium perchlorate, studying pressure and additives effect on kinetics 19 p3309 A67-35003
 Additives effect on ignition delay and pressure of hypergolic hydrazine-nitrogen tetroxide propellant systems 19 p3310 A67-35012
 Aluminum powder damping of HF instability in solid propellant combustion in vortex burner [AIAA PAPER 67-104] 21 p3732 A67-38860
 Fuel additives investigated for jet engine exhaust smoke elimination [SAE PAPER 670868] 24 p4206 A67-42006
 PROPELLANT BINDER
 Gel permeation chromatography for analytical fractionation of propellant binder prepolymers and separating and purifying labile binder ingredients 04 p0686 A67-14472
 Elastomer application in spacecraft launching, flight and reentry such as binder, sealant, base for adhesives, heat shielding, etc [ONERA-TP-407] 05 p0833 A67-16479
 Solid propellant polymeric binder chemistry and high speed computer calculations of performance characteristics 08 p1373 A67-20875
 PROPELLANT CHEMISTRY
 Imines reacting with difluoramine produce diazirines and other products having potential as missile propellant components 01 p0020 A67-11147
 Propellant preparation from extraterrestrial materials on moon and planets rather than transportation from earth as economical source of fuel for interplanetary manned traffic 04 p0695 A67-14555
 Calorimetric, titrimetric and gravimetric methods for determination of hexogen-octogen mixtures 05 p0872 A67-17153
 Jet propellant purity, safeguarding gas turbine fuel during production, transportation, storage and use 07 p1239 A67-18210
 Mechanics and chemistry of solid propellants - Symposium on Naval Structural Mechanics, Purdue University, April 1965 08 p1418 A67-20872
 Flame propagation effects and combustion chemistry of nitrate ester or double base solid propellants 08 p1374 A67-20877
 Thin film circular chromatography for determination of diphenylamine derivative products in propellant powders 13 p2185 A67-26425
 Chemistry and technology of explosives,

Volume 3, covering rocket propellants, mining explosives and smokeless powder manufacture 21 p3688 A67-37900

Ammonium perchlorate deflagration studied by flash pyrolysis and kinetic spectroscopy noting radical concentrations 22 p3867 A67-39639

Technical feasibility of rocket propellant combinations involving metal combustion and chemical heating of excess H 24 p4206 A67-42403

Chemical dynamic hydraulic power unit /HPU/ performance, weight and volume efficiencies, noting applications to solid and liquid propellants 24 p4107 A67-42531

Utilization of lunar geothermal emissions for rocket propellants and life support [AIAA PAPER 87-903] 24 p4165 A67-43011

PROPELLANT COMBUSTION

SA METAL COMBUSTION

SA SOLID PROPELLANT IGNITION

Ignition regularity criterion for solid propellant rocket engines, assuming ignition regularity controlled by heat transfer process between ignition source and propellant surface 01 p0139 A67-10524

Extension of analysis of unsteady state model for combustion of solid propellant to include nonlinearities of second order 01 p0141 A67-11158

Hybrid propellant burning rate determination using external gamma emission source 01 p0112 A67-11420

Steady state combustion analysis of solid propellant rocket motors extended by studying influence of grid sizes and number of steps used in numerical analysis 01 p0143 A67-11449

Steady state combustion model of mono- and double-base solid propellant with laminar flow 01 p0143 A67-11450

Equilibrium burning of spherical nongaseous fuel drop in slow convective hot-oxidant flow in thin flame 02 p0341 A67-11562

Mixing gaseous propellant injector, injection velocity and momentum flux ratio, combustion pressure and propellant combination effects on HF combustion pressure oscillations in rocket motor 02 p0302 A67-11940

Spin effects on rocket nozzle performance show higher combustion pressures and burning rates due to blockage of nozzle throat 02 p0303 A67-11947

Aerothermochemical analysis of solid propellant combustion 04 p0722 A67-14824

Combustion mechanism for boron-containing air-augmented propellant based on conductive, convective and radiant heat transfer between propellant and combustion products 04 p0687 A67-15814

Combustion characteristics and ballistic performance of dual layer propellant grains using polybutadiene/potassium perchlorate and polyurethane/ammonium perchlorate for end-burning type rocket motor 05 p0872 A67-16589

Solid propellant combustion research, discussing steady state combustion zone structure of propellants, composites, ignition, extinguishment and acoustic interaction [AIAA PAPER 87-87] 06 p1072 A67-18271

Techniques for study of metal combustion in rocketry including particle burning, bulk metal and metal vapor combustion and low temperature oxidation [AIAA PAPER 87-86] 06 p1072 A67-18437

Surface temperature of deflagrating ammonium perchlorate crystals calculated from crystal phase transition thickness [AIAA PAPER 87-68] 06 p1073 A67-18469

Ammonium perchlorate composite propellant deflagration studied by two burner analogs [AIAA PAPER 87-101] 06 p1073 A67-18472

Erosive burning of ammonium perchlorate solid propellants for combustion in turbulent boundary layer determined, using flat plate heat transfer correlation 07 p1238 A67-19069

Numerical calculation of critical hot spot thermal explosion conditions for plane slab, cylindrical and spherical symmetry 07 p1264 A67-19071

Isothermal kinetics and self-heating in binary mixtures of Mg and sodium nitrate as function of temperature and reactant composition 07 p1238 A67-19072

Solid propellant with heterogeneous surface reaction, noting agreement with

steady state and acoustic response properties of JPN propellant 07 p1239 A67-19074

Hypergolic propellant ignition experience during Project Sure Fire of Gemini program [AIAA PAPER 87-259] 07 p1241 A67-20046

Heterogeneous combustion in chemical propellant rocket chamber 07 p1239 A67-20116

Oscillatory burning of solid propellant studied using integral balance equation in solid gas interface, assuming Rayleigh criterion and sound wave 08 p1373 A67-20774

Transitional combustion phenomena in solid propellant rocket engines under unsteady conditions 08 p1373 A67-20781

Regression rates in transient regime of composite solid rocket propellant grains upon sudden opening of exhaust port 08 p1373 A67-20803

Flame propagation effects and combustion chemistry of nitrate ester or double base solid propellants 08 p1374 A67-20877

Optimal transfer of thrust limited vehicle between coplanar circular orbits 09 p1571 A67-21694

Cryogenic hydrogen-oxygen ignition with hydrogen-gas entrained Raney nickel as catalyst 09 p1579 A67-21706

Ignition of hydrogen-oxygen propellant combination by chlorine trifluoride 10 p1697 A67-23132

Pressure dependence of nonmetalized hybrid fuel regression rates in demonstrating major heat release reactions as heterogeneous or homogeneous 10 p1697 A67-23133

Volumetric loading factor expression derived for side burning solid propellant grains by imposing constraint on port channel flow Mach number 11 p1851 A67-24227

Head-end pressure deviation in slotted-tube solid propellant rocket motors with high loading densities and flexible thrust-time histories 11 p1852 A67-24352

Propellant composition influence on finite-amplitude axial wave mode instability in solid propellant rockets [AIAA PAPER 86-600] 12 p1988 A67-25909

Propellant characteristics under impaired combustion conditions, noting sufficiency of Chuiko-Margolin stability criteria 12 p2039 A67-26112

Model for solid rocket motor instability caused by chamber and propellant combustion characteristics, relating combustion and acoustic instabilities 14 p2404 A67-28113

Pyrotechnic actuation, discussing parameters, equipment and performance of explosive devices 15 p2543 A67-29304

Solid propulsion - ICRPG/AIAA Conference, Anaheim, June 1987 15 p2546 A67-29976

Burning rate vs pressure and other factors as function of composite solid propellant composition and oxidizer particle size distribution 15 p2580 A67-29985

Terminating solid propellant combustion by rapid drop in pressure 15 p2582 A67-29998

Solid propellant combustion research, discussing steady state combustion zone structure of propellants, composites, ignition, extinguishment and acoustic interaction [AIAA PAPER 87-87] 15 p2545 A67-30187

Pressure measuring instrumentation response requirements for computing decay rate in solid propellant termination systems 17 p2928 A67-32069

Hydrazine as single component fuel for gas generators and rocket engines, noting advantages and performance characteristics 18 p3106 A67-33459

Gas turbine environmental testing, measuring emulsified fuel flow, direct burning effects of JP-4 fuel on extended engine operation, etc [SAE PAPER 87-0367] 18 p3111 A67-33567

Composite ammonium perchlorate propellant temperature profile beneath burning surface, discussing main decomposition energy, heat sources, etc composite ammonium perchlorate propellant 18 p3107 A67-33811

Combustion mechanism of ammonium perchlorate propellants, discussing gasification, decomposition, pressures, binders, burning rates, temperatures, etc

etc 18 p3108 A67-33812

Deflagration of ammonium perchlorate studied using cleaved sections of large single crystals grown from water solution, discussing burning rate and combustion zone 18 p3108 A67-33814

Interaction of finite amplitude pressure pulse with combustion region at surface of burning solid propellant 18 p3108 A67-33830

Preignition phenomena in small Aerozine-50/nitrogen tetroxide pulsed rocket engines shown partly due to hydrazine nitrate accumulation [AIAA PAPER 87-516] 18 p3114 A67-33979

Calorimetric investigation of role of ballistic modifier in nitrocellulose propellants combustion [CI PAPER 87-1] 19 p3309 A67-34996

Combustion rate and subsurface activity of metallized burning polymers, stressing heat conduction role and applications to propellant combustion [CI PAPER 87-3] 19 p3344 A67-34998

Reaction mechanism between oxygen difluoride and diborane based on visual observation, gas composition and pressure-temperature relationships [CI PAPER 87-10] 19 p3309 A67-35005

Additives effect on ignition delay and pressure of hypergolic hydrazine-nitrogen tetroxide propellant systems 19 p3310 A67-35012

Surface-reaction effects on solid propellant acoustic-response functions characterizing transient combustion process 19 p3311 A67-35777

Combustion characteristics of hydrazine type propellants and resultant reactions in low thrust engines prior to ignition 21 p3687 A67-37798

Combustion stability of powder in semiclosed volume, taking into account propellant surface temperature dependence on pressure and temperature gradient 21 p3732 A67-38526

Liquid fuel polydisperse jet total combustion time curve determined based on droplet of fuel and medium parameters 21 p3732 A67-38528

Surface temperature of deflagrating ammonium perchlorate crystals calculated from crystal phase transition thickness [AIAA PAPER 87-68] 21 p3688 A67-38859

Dynamic ballistics of combustion termination by fluid injection in solid propellant motors, describing termination mechanisms 21 p3733 A67-38893

Erodibility of solid propellants subjected to rapid flow of gas past burning surface 22 p3867 A67-39538

Combustion in solid propellant rocket engines using mathematical model 22 p3867 A67-39539

Injector inlet conditions effects on combustion delay time in liquid bipropellant rocket engine, noting propellant atomization and droplet vaporization 22 p3868 A67-40161

Small perturbation analysis on mass conservation stability in solid propellant combustor, discussing parametric model 23 p4084 A67-41721

Catalyzed ignition of composite propellant fuels in presence of perchloric acid studied for acceleration of rate of acid decomposition 23 p4048 A67-41761

Periodic pressure fluctuations relation to structure and propagation of combustion front in solid propellant rockets, giving perturbation frequencies 24 p4252 A67-41798

Liquid rocket propellant combustion processes covering liquid phase mixing, vaporization, spray formation, atomization, gas-phase mixing and chemical reaction 24 p4256 A67-42720

PROPELLANT COMPOUND

Propellant composition variation for improving cooling characteristics of Surveyor vernier propulsion system [AIAA PAPER 86-827] 08 p1374 A67-21517

PROPELLANT DECOMPOSITION

Decomposition and stability of diphenylamine compounds in nitrocellulose powder, determining activation energies 15 p2543 A67-29889

Combustion mechanism of ammonium perchlorate propellants, discussing gasification, decomposition, pressures, binders, burning rates, temperatures, etc 18 p3108 A67-33812

PROPELLANT GRAIN

SA SOLID PROPELLANT

Elastic plate bending mechanical analog to two-dimensional thermoelastic problem, solving thermal stresses of solid propellant grain 95 p0917 A67-16417

Stress analysis of solid rocket engine propellant grains including linear viscoelasticity, thermal analysis and equilibrium, relaxation times, engine sizes, cooling, creep relaxation, etc 08 p1373 A67-20874

Static and dynamic combustion phenomena effects on grain structural design for solid propellant rocket engine 08 p1374 A67-20876

Solid rocket engine propellant grain structural dynamics including elastic and viscoelastic deformations, stress and shear vibration modes, natural frequency calculations, etc, using Fourier inversions and transforms 08 p1376 A67-20883

Experimental stress and strain analyses of solid propellant rocket engine grains under various loading conditions 08 p1419 A67-20886

Structural design of solid propellant rocket engine and failure, deformation and fracture of reinforced propellant grains 08 p1420 A67-20888

Failure mechanism of solid propellant grain and stress criteria for solid motor design and evaluation 08 p1374 A67-20891

Volumetric loading factor expression derived for side burning solid propellant grains by imposing constraint on port channel flow Mach number 11 p1851 A67-24227

High pressure hot gas solid propellant cartridge starter for aircraft turbine engine [ASME PAPER 67-GT-21] 11 p1854 A67-24803

Axial load deformation of grains with end-face limitation used in solid propellant engines 14 p2377 A67-28651

Statistical service life prediction based on propellant grain structural integrity for Minuteman third stage motor, noting grain stress analysis 15 p2547 A67-29996

Structures, charging into stage, thermal protection, ignition, and nozzles problems encountered in development of solid propellants 16 p2736 A67-31617

PROPELLANT MASS RATIO

Criteria for optimum liquid mixing for impinging jet injector elements, noting parameters for maximum efficiency 15 p2545 A67-29445

Propellants and propellant mixtures effects on MPD arc jet performance in test for ions and neutrals mixture acceleration to high velocity [AIAA PAPER 67-684] 21 p3688 A67-38715

PROPELLANT OXIDIZER

Liquid and solid rocket propellants, examining use of metals as fuels 14 p2376 A67-27877

Start characteristics of LM Ascent Engine determined by test series, noting effects of altitude variation, propellant lead time, temperature and valve slow-down [AIAA PAPER 67-522] 18 p3115 A67-33985

Hybrid rocket design combining flexibility of liquid fuel with simplicity and reliability of solid propellant rockets 20 p3516 A67-36487

Detonation properties in heterogeneous systems involving mixture of fuel with gaseous oxidant 20 p3551 A67-36815

Ring laser use for measuring gas flow on ground and fuel and oxidizer flow in rockets 22 p3800 A67-39892

Sampling bottle with valves and high pressure filter holder for fuel and oxidizer, by weighing bottle before and after sampling amount of fuel passing through filter can be calculated 23 p3998 A67-40849

PROPELLANT PROPERTY

Jet fuel lubricity noting poor performance due to polar compounds, improving lubricity by surface active additives 01 p0139 A67-10602

Propellant combinations evaluation for minimum weight of high energy propellant reaction control systems [AIAA PAPER 66-947] 02 p0304 A67-12281

Liquid oxygen and liquid hydrogen as propellants for rocket engines noting propulsor chamber, turbopump feed system and U.S. and French designs 05 p0874 A67-17014

High thrust fluorine engines and propellants 06 p1071 A67-17608

Chemical problems concerning specifications and use of nitrogen peroxide and unsymmetrical dimethyl hydrazine as

propellants 06 p1071 A67-17612

Propellant requirements for unmanned lunar and interplanetary soft landing vehicles presented with equations that couple injection, midcourse and terminal phases [AAS PAPER 66-129] 07 p1241 A67-19988

Thermodynamic processes influencing choice of rocket engine propellants 07 p1239 A67-20088

Compression strength and strain of solid propellants, noting internal loads developed during burning process 08 p1373 A67-20720

Mechanical properties of unfilled and filled elastomers 08 p1420 A67-20890

Jet fuel lubricity noting poor performance due to polar compounds, improving lubricity by surface active additives [SAE PAPER 660712] 12 p1988 A67-26163

Propellant requirements for unmanned lunar and interplanetary soft landing vehicles presented with equations that couple injection, midcourse and terminal phases [AAS PAPER 66-129] 13 p2214 A67-27540

Stratification similitude laws for liquid hydrogen determined and extrapolated to full size tanks from small tank data 13 p2186 A67-27643

Liquid and solid rocket propellants, examining use of metals as fuels 14 p2376 A67-27877

Book on motor fuels, performance and testing, including fuel source and nature, gasoline combustion, diesel, turbine fuels, etc 16 p2734 A67-30998

PROPELLANT SENSITIVITY

Approximation method for calculating self-ignition delay for monodisperse air-fuel mixtures 08 p1428 A67-21425

Qualitative and quantitative prediction of corrosive environments effects on transducer performance [ASME PAPER 67-MET-14] 12 p1945 A67-25952

PROPELLANT SPRAY

Charged particles generation by liquid subjected to high electric field for efficient bipolar microthruster [AIAA PAPER 67-728] 21 p3694 A67-38752

PROPELLANT STORABILITY

S STORABLE PROPELLANT

PROPELLANT STORAGE

Storable propellant pressure vessel design for Titan launch vehicles and compatibility and stress-load-corrosion analysis [SAE PAPER 660677] 01 p0160 A67-10582

Thrust generation from neutral particle sputtering from solid target, noting advantages such as storage, operating life, etc 05 p0873 A67-16515

Semilempirical description of stratification in wall heated containers of cryogenic fluids, noting decrease due to bottom heating 13 p2227 A67-27644

Two-phase cryogenic propellant storage under low gravity, discussing impact on vented and unvented vehicle design and performance 16 p2757 A67-30633

Volatile liquid pressurization as expulsion method for storable propellants noting in-flight refueling system design parameters 17 p2953 A67-31973

Gradient stabilization of cryogenic liquids in pendulum and sloshing motions, noting response to kinetic energy input, oscillation frequency period and stability criteria 17 p2836 A67-32053

Thermodynamic system for zero g venting, storage and transfer of cryogenic propellants, discussing heat exchanger 17 p2954 A67-32074

Propellant dependent inert weight for any propellant combination or venting condition for Mars mission 22 p3902 A67-39942

PROPELLANT TANK

SA FUEL TANK

SA ROCKET PROPELLANT TANK

SA STORAGE TANK

Design, development and main assemblies of third stage of ELDO satellite launcher 01 p0078 A67-10409

Dielectrophoretic propellant orientation systems design, noting electrode requirements and avoidance of electrohydrodynamic instabilities [AIAA PAPER 66-922] 02 p0301 A67-12275

Fluid management techniques for control in space of functions such as liquid expulsion, vapor venting, gauging and center-of-gravity control 04 p0553 A67-14427

Heat and mass transfer processes in rotationally symmetrical tank partially filled with liquid and subjected to external heating and acceleration in direction of longitudinal axis 04 p0720 A67-14577

Liquid-vapor interface in weightless environment noting dynamic behavior, configuration parameters and dependence on model size 04 p0605 A67-14988

Propellant flow in tanks at high and low accelerations simulated, using similarity parameters obtained from dimensional analysis and motion equations 04 p0598 A67-15243

Two-dimensional transient laminar natural convection heat transfer in partially filled liquid propellant tanks, solving vorticity and energy equations 04 p0731 A67-15826

Surveyor vernier propulsion system, discussing design of thrust chamber, propellant tank assemblies, functions of VPS, etc [AIAA PAPER 66-593] 08 p1413 A67-25156

Free and forced liquid sloshing motions in tank of arbitrary shape at low gravity environments analyzed, using Satterlee-Reynolds method 10 p1629 A67-23832

Cryogenic fluid behavior in passive storage tank as function of tank configuration, wall heating and acceleration 12 p2034 A67-25729

One-dimensional conduction model for predicting pressure variation of nonvented cryogenic propellant tanks in low gravity field [AIAA PAPER 67-338] 12 p2039 A67-26052

Fuel container design for space vehicles, discussing impact protection, reusability and long term cryogenic storage 13 p2212 A67-27218

Liquid venting concept for zero gravity environment by suppressing vapor generation with open loop refrigeration, using extracted liquid as working fluid 13 p2056 A67-27639

Low gravity liquid hydrogen tank venting, considering systems with heat exchange for space missions 13 p2057 A67-27640

Thermal performance of liquid hydrogen in horizontal hypersonic vehicle fuel tank 13 p2186 A67-27646

Very low heat background calorimeter design for heat-short experiments and checking analytical predictions for propellant tank insulation 13 p2228 A67-27658

Surface tension principles for propellant management devices, discussing static retention and dynamic control of spacecraft fuels 17 p2801 A67-31985

Long term cryogenic propellant storage in space, considering rigid open cell polyurethane foam as spacer in multilayer insulation system 24 p4254 A67-42480

Pressurized propellant tank system for rocket engine, discussing weight factors, propellant combinations and expellant gas pressure relations 24 p4241 A67-42754

PROPELLANT TESTING

SA ENGINE TESTING

Dynamic analysis of reaction control system/RCS/propellant feed network on lunar module using digital computers 01 p0142 A67-11435

T-burner tests for combustion stability evaluation of hydrazine diphosphate [AIAA PAPER 66-599] 04 p0723 A67-15246

Radiotracer propellant gauge for zero gravity space environmental conditions using radioactive krypton 85 gas 10 p1656 A67-23078

Fluorine compounds as propellants in upper stage propulsion units, discussing properties, suitability and performance 14 p2377 A67-28979

Starter cartridges for jet engines, discussing operational problems and mechanical design, igniter and propellant development, etc 15 p2423 A67-29982

Arc image ignition of solid propellants compared to conductive ignition, outlining corrective steps and deriving ignition time delay 15 p2581 A67-29987

Test program assessing propulsion performance of cryogenic and ambient temperature gaseous parahydrogen expanded through conical thrust nozzles 16 p2734 A67-30705

Concorde aircraft fuel, discussing fuel transfer, problem of boiling, in-flight environment simulation, payload/mass ratio, etc 16 p2734 A67-31809

Factors influencing rocket ignition

pressures and conditions leading to large ignition overpressures, estimating residual propellant in rocket combustor [AIAA PAPER 67-515] 18 p3114 A67-33978

Sensitivity of explosives to shock waves tested by device using water as intermediate layer 22 p3866 A67-39489

Propellant sloshing effect on vehicle dynamics under zero gravity conditions studied by programming motion equation into digital simulation of spacecraft, control and propellant 22 p3907 A67-40180

PROPELLANT TRANSFER

Surveyor throttleable liquid propellant rocket engine for operation on propellants saturated with dissolved liquid gas [AIAA PAPER 66-949] 02 p0304 A67-12283

Safety problems during loading and reduction of leakage hazards in management of liquid propellants including cavitation, oscillation and zero-g migration 04 p0703 A67-14604

Liquid hydrogen use in nuclear rocket testing, noting Kiwi reactor, Dewar system, transfer line, etc 05 p0789 A67-17013

Electron bombardment thrusters using liquid mercury cathodes noting lifetime, propellant and power efficiency, feed system, temperature limits, etc 13 p2188 A67-26822

Surveyor throttleable liquid propellant rocket engine for operation on propellants saturated with dissolved liquid gas [AIAA PAPER 66-949] 13 p2188 A67-26834

Volatile liquid pressurization as expulsion method for storable propellants noting in-flight refueling system design parameters 17 p2953 A67-31973

Thermodynamic system for zero g venting, storage and transfer of cryogenic propellants, discussing heat exchanger 17 p2954 A67-32074

Variable thickness insulation system for transport of hydrogen propellant into earth orbit for docking transfer to lunar and interplanetary mission vehicles [ASME PAPER 67-HT-50] 20 p3548 A67-36732

Cesium propellant systems utilizing surface tension to position and transfer liquid propellant in zero-g environment studied with high voltage electrical isolation methods [AIAA PAPER 67-681] 21 p3692 A67-38712

Earth orbital mission utilizing propellant transfer techniques based on fluid management under low gravity environment 22 p3906 A67-40163

PROPELLER

SA TILTED PROPELLER AXIS

VTOL aircraft with rotor or propeller lift systems for commercial transportation, discussing helicopter role in system development [AIAA PAPER 67-411] 15 p2422 A67-30378

Handley Page Jetstream power plant, propeller design, turboprop engine operation and control 22 p3868 A67-40131

PROPELLER BLADE

Curved flow effect on lift characteristics of blade using Scholz method, noting role of correction coefficient of lift curve slope and zero lift angle 05 p0791 A67-16427

Propeller-rotor whirl flutter and effect of hinged blades and flexible twisted blades 06 p1099 A67-17920

Flow field of finite bladed propeller in forward flight regime, analyzing harmonic content, noting fluctuating part of velocity component 06 p0937 A67-18004

Ice removal from solid nonmetallic aircraft propeller blade by nonsteady-state heating 14 p2405 A67-28305

Designing propeller blades with maximum aerodynamic efficiency by vortex theory, considering engine power, propeller diameter, forward velocity, etc 15 p2417 A67-30079

Dynamic stability of low disk loading propeller-rotors as function of various dimensionless parameters characterizing design [AHS PAPER 132] 18 p2777 A67-31846

Rotor system with blade angle reverse control noting blade-angle adjustment changes for achievement of higher flight speeds 18 p2985 A67-33460

Characteristics of cross flow fan determined as function of blade angle, diameter ratio of impeller and vortex position 18 p3025 A67-33650

Electrical analogy calculation of

incompressible and rotational axisymmetric flow around variable-circulation streamlined propeller 18 p3025 A67-33681

Blade airfoil sections two-dimensional aerodynamic characteristics studied in wind tunnel for aerodynamic optimization calculation of helicopter rotors 23 p3927 A67-40576

PROPELLER DRIVE

SA HELICOPTER PROPELLER DRIVE

Dead weight/service load ratio effect on propulsive efficiency and fuel consumption of large helicopters with mechanical, gearless or jet-propulsion drives 03 p0358 A67-12984

PROPELLER EFFICIENCY

Objection to marine propeller application to VTOL aircraft 02 p0182 A67-12427

PROPELLER SLIPSTREAM

Cessna tandem twin aerodynamics noting propeller slipstream variation effects, comparing front and rear engine operation [SAE PAPER 670243] 12 p1894 A67-25498

PROPERTY

S CHEMICAL PROPERTY

S DYNAMIC PROPERTY

S ELASTIC PROPERTY

S ELECTRIC PROPERTY

S MAGNETIC PROPERTY

S MECHANICAL PROPERTY

S OPTICAL PROPERTY

S PARTICLE PROPERTY

S PHYSICAL PROPERTY

S PROPELLANT PROPERTY

S SURFACE PROPERTY

S THERMAL PROPERTY

S THERMODYNAMIC PROPERTY

S THERMOPHYSICAL PROPERTY

S TRANSPORT PROPERTY

PROPORTIONAL CONTROL

Behavior of momentum effect jet interaction proportional amplifier using flow visualization on water table and large scale pneumatic model 08 p1282 A67-20460

PROPORTIONAL COUNTER

Fast and slow neutrons detected by proportional and scintillation counters 02 p0312 A67-12606

Gas proportional counter and scintillation telescope to search for quarks with unit and fraction charges in cosmic radiation at 3200 m altitude 02 p0316 A67-12767

Proportional counter spectrometer for solar soft X-ray spectrum study 20 p3448 A67-36960

Gas proportional counter and scintillation telescope to search for quarks with unit and fraction charges in cosmic radiation at 3200 m altitude 22 p3877 A67-40269

Cosmic X-ray sources spectra obtained by proportional counters and electronic systems on sounding rockets 23 p4001 A67-41222

PROPRIOCEPTION

SA SENSORY PERCEPTION

Cardiovascular deconditioning caused by microcirculatory changes which reduce proprioceptor sensory input of unanesthetized rat 09 p1452 A67-21714

Effects of display magnification, proprioceptive cues, displacement aiding, etc, on decreasing tracking error assessed, using heavy inertia tracking simulator 09 p1456 A67-22372

PROPULSION

SA CHEMICAL PROPULSION

SA ELECTRIC PROPULSION

SA ELECTROMAGNETIC PROPULSION

SA ELECTROSTATIC PROPULSION

SA HYBRID PROPULSION

SA IONIC PROPULSION

SA JET PROPULSION

SA LOW THRUST PROPULSION

SA NUCLEAR PROPULSION

SA PHOTONIC PROPULSION

SA PLASMA PROPULSION

SA SHIP PROPULSION

SA SOLAR PROPULSION

SA SPACECRAFT PROPULSION

SA THERMONUCLEAR PROPULSION

Differential equations and mathematical models for gas flows with chemical activity and radiative effects, particularly effects of reentry and propulsion 06 p0983 A67-17785

Propulsion and reentry - IAF Conference, Athens, September 1965, Volume 5 18 p2735 A67-30701

PROPULSION CALCULATION

Optimum performance of propulsion acceleration calculated by approximation method, noting earth-Mars transfer and Jupiter and Saturn

missions 16 p2760 A67-30735

Space probe rendezvous with Halley comet, considering use of planetary gravity field to modify trajectory [AIAA PAPER 67-614] 19 p3329 A67-36003

PROPULSION CONFIGURATION

SA INTERPLANETARY PROPULSION CONFIGURATION

V/STOL transport aircraft structural problems related to propulsion, associated acoustical, thermal and debris conditions and weight/cost effectiveness requirements [SAE PAPER 660668] 04 p0552 A67-15784

Kaufman mercury-ion thruster grid design, discussing radial slot configuration 24 p4208 A67-42929

PROPULSION SYSTEM

SA HOT CYCLE PROPULSION SYSTEM

SA ROCKET ENGINE

Liquid propulsion systems operating in space and resulting problems of phase transformation, noting plug formation and flow stoppage 01 p0055 A67-11386

Debugging of Emeraude propulsion system of Diamant launch vehicle, stressing problems with combustion chamber instabilities, vibrations, etc 01 p0155 A67-11389

Maneuvering propulsion problems for spacecraft attitude control 01 p0142 A67-11401

Propulsion systems including chemical, nuclear, etc, for manned interplanetary mission 01 p0142 A67-11402

Fluid mechanics of mixtures whose components are at large deviation from equilibrium with one another, considering propulsion system application 01 p0055 A67-11439

Turbine engine propulsion system development noting inlet temperatures, turbine-blade cooling methods, etc 02 p0302 A67-11817

Propulsion system selection considerations for Voyager spacecraft including Minuteman solid with liquid restartable midcourse, orbit trim system, LEM descent stage and transtage [AIAA PAPER 66-974] 02 p0305 A67-12296

Method for propulsion system selection, design and optimization on total space program cost effectiveness basis [AIAA PAPER 66-976] 02 p0305 A67-12298

Ripples in acceleration potential affect ion beam of electrostatic propulsion system by superimposing AC potential of 50 cps of variable amplitude on constant acceleration potential 02 p0306 A67-12790

By-pass propulsion systems development for V/STOL transports including aerothermodynamic aspects [AIAA PAPER 64-606] 03 p0502 A67-12902

Air augmented propulsion in liquid hydrogen-LOX rocket booster engines 03 p0504 A67-13873

Propulsion through drag interaction between magnetically-accelerated iron particle suspension and air [AIAA PAPER 66-926] 03 p0504 A67-14136

Propulsion system development for very high speed winged vehicles application 03 p0505 A67-14382

Propulsion systems for satellite attitude control, considering weight and thrust efficiency parameters 05 p0905 A67-18729

Optimization of single-shaft jet and two-shaft dual-flow engines for given flight conditions 06 p1073 A67-17806

Copy machining of thin walled propulsion duct pivot support tube used in Bell V/STOL aircraft 06 p1008 A67-18724

Advanced low thrust propulsion systems and propellants evaluation for stationkeeping and stability control of NASA Manned Orbital Research Laboratory [AIAA PAPER 66-226] 07 p1240 A67-19365

Air cushion vehicles propulsion noting various methods including air or water jets, air propellers, ducted air propellers, etc 07 p1128 A67-19535

Interplanetary trajectories for vehicles using high and low thrust propulsion systems, considering three two-body transfers and role of hyperbolic excess speeds [AAS PAPER 66-128] 07 p1241 A67-19887

Oxygen difluoride propellant system design and operational experience at Arnold Center [AIAA PAPER 67-279] 07 p1164 A67-20049

Testing of three individual propulsion

systems of lunar module space vehicle in preparation for man-rated flight service [AIAA PAPER 87-258] 07 p1166 A67-20073

Replacement of chemical launching rockets by advanced propulsion system, with particular reference to nuclear rocket 07 p1242 A67-20264

Liquid propellant utilization for sounding rockets 08 p1372 A67-20524

Ground test facilities for aircraft air breathing propulsion system development 08 p1315 A67-21063

Space systems performance, components and modes of operation, showing merits in terms of entire space program 08 p1431 A67-21108

Hypersonic air breathing engine, specifically scramjet, noting vehicle design, combustion system, nozzle, friction, etc 10 p1697 A67-22873

Book on propulsion systems covering gas-turbine engine, ramjet engine, chemical and electrical rockets, components, etc 10 p1698 A67-23689

Propulsion-lift system interrelationship in compound helicopter and design parameters affects performance vs speed such as disk loading, solidity and tip speed schedule [ASME PAPER 87-GT-18] 11 p1854 A67-24802

V/STOL aircraft gas turbine systems, discussing propulsion system configurations applied to fighter, fighter attack and transport cargo aircraft [ASME PAPER 87-GT-48] 11 p1744 A67-24809

Optimum propulsion control law selection for limited motion capacity in mass accumulation regime determined, considering two-dimensional problem of vehicle motion 12 p1989 A67-25659

Stirling cycle using dissociating gas 13 p2221 A67-26390

Small liquid propulsion systems testing in space environment simulator with high vacuum and low pumping capacity 13 p2089 A67-26840

Maximum payload for air-scooping low thrust space propulsion system 13 p2212 A67-26893

Propulsion by liquid-solid or hybrid rocket engines, performance and design 13 p2188 A67-27292

Space propulsion technology and mission capabilities in fiscal year 2001 13 p2189 A67-27502

Future cislunar transportation techniques for exploration and commercial application 13 p2213 A67-27507

Future space transportation techniques and mission applications in solar system 13 p2213 A67-27508

Interplanetary trajectories for vehicles using high and low thrust propulsion systems, considering three two-body transfers and role of hyperbolic excess speeds [AAS PAPER 66-128] 13 p2214 A67-27539

Propulsion systems for air cushion craft SKIP-I in marine environment [AIAA PAPER 66-731A] 13 p2054 A67-27593

Propulsion systems for booster rockets and space vehicles 14 p2377 A67-27875

Future planning of interplanetary voyages based on capabilities and economic advantages of classical propulsion, noting high escape velocity 14 p2392 A67-28961

Propulsion systems in which propulsive fluid is accelerated to high speeds by electrical or electromagnetic processes 14 p2377 A67-28962

Supersonic combustion simulation facility and duplicable static parameters for hydrogen fuel [AIAA PAPER 66-743] 15 p2465 A67-29437

Hot-water rocket design by dimensionless method, noting GRILLO rockets 15 p2567 A67-29840

Propulsion and vehicle systems for commercial exploitation of space, emphasizing transportation to and from earth orbit [AIAA PAPER 87-82] 15 p2570 A67-29949

Earth orbital transportation, proposing airline type system and composite nuclear-airbreathing engines for reusability with minimum refurbishment [AAS PAPER 87-84] 15 p2546 A67-29950

Solid propellants and motors for space exploration, comparing chemical and nonchemical propulsion systems 16 p2735 A67-30702

High pressure liquid propellant rocket

engines, noting high thrust, smaller engine dimensions, and combustion chamber cooling 16 p2735 A67-30704

Electric and photon propulsion systems in German-American research 16 p2736 A67-30710

Minimum-fuel transfers of moving body between infinitely close elliptical Keplerian orbits in central Newtonian field, considering propulsion system models 16 p2744 A67-30738

Turboprop lift fan concept for VTOL propulsion system, noting control capability, future potential, etc [AHS PAPER 115] 16 p2737 A67-31831

Effective engine protection system for CH-54A Flying Crane helicopter, consisting of an engine-inlet air-particle separator, noting Vietnam performance [AHS PAPER 117] 16 p2737 A67-31833

Reaction control system for spinning synchronous satellite noting selection criteria, tradeoff methods, etc 17 p2953 A67-31972

Surface tension principles for propellant management devices, discussing static retention and dynamic control of spacecraft fuels 17 p2801 A67-31985

Electrostatic ion engine timetable, noting contact ion and electron bombardment engines and application to NASA Applications Technology Satellite series 17 p2928 A67-32435

Integration of propulsion system into airframe of hypersonic cruise aircraft, discussing configurations, cooling and supersonic combustion 17 p2796 A67-32475

ADAM II /air deflection and modulation/propulsion system and application to long tube vertical propulsive wing aircraft configurations [SAE PAPER 87-0353] 17 p2929 A67-32993

Unscheduled civil aircraft power plant diagnostic removals evaluated by metal detection, performance deterioration, vibration, oil consumption and nonoperational categories [SAE PAPER 87-0358] 17 p2930 A67-32997

Systems thinking and systems management in rocket motor manufacture 18 p3111 A67-33638

Propulsion-oriented subsonic boundary layer combustion research, discussing turbulent and diffusion-limited conditions, radiant heat transfer, chemical kinetics and transient phenomena 18 p3150 A67-33800

Turbofan jet propulsion system reversed-thrust, discussing momentum net change, external drags, clamshell and annular targets and cascade reversers [AIAA PAPER 87-418] 18 p2982 A67-33905

Primary electric propulsion application to satellite and other space missions, considering auxiliary systems and experimental thruster systems [AIAA PAPER 87-426] 18 p3112 A67-33910

Phoebus 1B test /high-power-density reactors for space propulsion/ noting reactor design for fuel-element testing [AIAA PAPER 87-486] 18 p3076 A67-33952

Combined electric constant low thrust and chemical or nuclear high thrust space propulsion systems for interplanetary missions [AIAA PAPER 87-511] 18 p3114 A67-33975

Optical instrument for measurement and control of tube flares in connections in liquid propulsion systems 18 p3054 A67-34366

Propulsion sources for one-way unmanned subrelativistic interstellar probes, discussing interaction with deep space environment for vehicle control 19 p3322 A67-35316

Vostok launch vehicle design characteristics evaluated including performance, propellant weights, booster phase burning period, etc 19 p3334 A67-35843

High chamber-pressure propulsion systems and components captive testing, describing ground support system analysis, design and mechanisms 20 p3414 A67-36534

Space and high altitude simulation requirements for testing various rocket systems 20 p3415 A67-36544

Vapor phase decontamination for removing residual hypergolic propellants in Apollo propulsion system 20 p3516 A67-36578

Energy accumulator and constant power propulsion system for near-circular orbit space maneuvering, considering two-vehicle encounter 21 p3689 A67-37985

Clustered mercury electron bombardment ion engine system experiments showing feasibility, discussing components [AIAA PAPER 87-698] 21 p3693 A67-38727

Electrostatic ion propulsion and KEMAN MPD thruster research in Germany [AIAA PAPER 87-724] 21 p3694 A67-38749

Composite propulsion systems for aerospace missions, considering Mach range, specific impulse, oxygen source, design characteristics, capabilities and limitations 22 p3868 A67-39890

Cryogenically stored helium pressurization system for LEM descent stage propulsion system, discussing weight advantages and liquid helium heat transfers 22 p3749 A67-40394

Unscheduled civil aircraft power plant diagnostic removals evaluated by metal detection, performance deterioration, vibration, oil consumption and nonoperational categories [SAE PAPER 87-0358] 23 p4048 A67-40866

Wissenschaftliche Gesellschaft für Luft- und Raumfahrt, Annual Reports 1966 23 p3929 A67-41304

Parametric investigation of propulsion system effect on takeoff weight of VTOL subsonic ground combat aircraft 23 p3934 A67-41315

Turboramjet engine design for aerodynamic flight vehicles up to Mach number 6 23 p4049 A67-41318

SST engines design, combustion and thrust augmentation systems, engine controls and complications facing users [SAE PAPER 87-0865] 24 p4207 A67-42005

Solid propellant motors relative performance as related to intermediate payload missions, considering reusable liquid strap-on stages for post-Saturn payloads [DOUGLAS PAPER-4452] 24 p4240 A67-42388

Technical feasibility of rocket propellant combinations involving metal combustion and chemical heating of excess H 24 p4206 A67-42403

Booster for Skylark upper atmosphere research vehicle to increase altitude and reduce launching dispersion of single stage vehicle 24 p4206 A67-42580

Primary electric propulsion application to satellite and other space missions, considering auxiliary systems and experimental thruster systems [AIAA PAPER 87-426] 24 p4208 A67-42901

Rotor VTOL aircraft for future transport, noting rotor systems for low downwash velocity, minimum noise and low fuel consumption [AIAA PAPER 87-940] 24 p4097 A67-43030

PROPULSION SYSTEM PERFORMANCE

Electrothermal, electromagnetics and electrostatic propulsion system design principles, operation applications and performance characteristics 01 p0142 A67-11410

POODLE low thrust radioactive propulsion technology, discussing operation, mission application, tests, capsule and thruster performance 05 p0843 A67-16551

SNAPOODLE isotope thruster/electric power unit, discussing thermal analyses, thruster and electrical performance and mission applications 05 p0753 A67-16552

Nonconventional rocket propulsion systems performance and base environment characteristics evaluated, using separate cold flow and combustion models [AIAA PAPER 87-256] 07 p1241 A67-20072

Aerobee 350 sounding rocket for scientific use in heavy payload to moderate altitude performance region 08 p1404 A67-20496

German rocket prototype with mercury vapor plasma or xenon plasma engine, discussing design and performance 08 p1410 A67-20641

Turboramjet developed from Griffon aircraft capable of propelling hypersonic vehicles 09 p1559 A67-22003

Structural predictions of mean times between failures through maintenance activity for aircraft power systems 09 p1560 A67-22287

Reverse flow annular combustion system for TPE331 turboprop engine, noting fabrication and combustor efficiency [ASME PAPER 87-GT-25] 11 p1854 A67-24805

Test program assessing propulsion performance of cryogenic and ambient temperature gaseous parahydrogen expanded through conical thrust

nozzles 16 p2734 A67-30705
Liquid-bipropellant pressure-fed propulsion systems in lower thrust range and use for spacecraft maneuvering 16 p2736 A67-30707
Role of ground and flight simulation test facility on past, current and future developments in aerospace propulsion 16 p2654 A67-30709
Variational problem of maximum payload in mechanics of flights with limited propulsion power and energy storage unit 16 p2760 A67-30719
Potential advantages of hypersonic vehicles compatible with missions combining more than one cruise-flight regime, discussing gas dynamic heating for propulsion [SAE PAPER 670354] 17 p2798 A67-32994
Diagnostic devices for sensing performance deterioration and mechanical malfunctions in supersonic aircraft engines [SAE PAPER 670363] 17 p2930 A67-33000
Ejector ramjet and ducted rocket evaluation by analytical models for various flight trajectories, noting specific impulse improvement [AIAA PAPER 67-437] 18 p3112 A67-33915
Test facility for 5000 mw nuclear rocket propulsion modules, discussing effect on design and flight conditions duplication [AIAA PAPER 67-465] 18 p3020 A67-33936
Parametric analysis on hydrogen-fueled hypersonic aircraft for long range passenger transport missions and launch vehicle missions, noting propulsion system-airframe interactions [AIAA PAPER 67-493] 18 p2985 A67-33957
MIRA 150A variable thrust rocket engine applied to manned lunar exploration flying systems [AIAA PAPER 67-505] 18 p3113 A67-33969
Radioisotope heated hydrogen thrusters for propelling high energy upper stage, discussing performance, payload advantages and high energy kick stage [AIAA PAPER 67-509] 18 p3113 A67-33973
Northrop program for v/STOL aircraft including systems studies, propulsion, aerodynamics, flight control technology, performance characteristics and operation and testing northrop program for V/STOL aircraft including 18 p2987 A67-34708
Low thrust cold-gas reaction jets in vacuum studied for pulsed propulsive performance for use in spacecraft attitude control 19 p3310 A67-34805
Gun launched scramjet performance using various fuels, comparing weight and volume limitations effects 19 p3311 A67-34822
Strategy of holding higher performance rocket engines for critical missions analyzed statistically for increased payload 19 p3311 A67-34829
Guidance system requirements for unmanned Martian propulsive landing capsule [AIAA PAPER 67-619] 19 p3260 A67-36008
Cesium bombardment ion engine performance, giving starting circuit and automatic discharge power control system [AIAA PAPER 67-666] 21 p3690 A67-38700
MPD Hall accelerator construction and operation using argon or helium propellants, measuring azimuthal velocities in plume [AIAA PAPER 67-672] 21 p3691 A67-38705
Alkali plasma Hall accelerator /ALPHA/ thruster performance, discussing acceleration mechanisms and correlating data [AIAA PAPER 67-687] 21 p3692 A67-38718
Mercury electron bombardment thruster system performance as function of mass utilization and specific impulse, noting magnetic field shape and ion optical system design effects [AIAA PAPER 67-697] 21 p3693 A67-38726
Corona discharge propulsion system with space charge limited emission of negative ions, noting ion mobility performance and efficiency 21 p3696 A67-38856
Mass flow rate, viscosity and conductivity changes effects on single needle colloid thruster [AIAA PAPER 67-530] 21 p3696 A67-38957
Pulsed propulsive performance of low thrust subliming solid ammonium carbamate reaction jet, discussing transient response, apparatus, techniques, etc 21 p3697 A67-39152
Aerobee 350 sounding rocket for scientific use in heavy payload to moderate altitude performance region 22 p3904 A67-40090
Up-rated Saturn I first stage propulsion

system dynamic characteristics simulated by analog computer 22 p3869 A67-40169
Improvement of high performance liquid fuel rocket engine by optimization of liquid hydrogen /LOX/ propulsion mixtures 23 p4049 A67-41319
Pressure Commutating System for propulsion research facility noting cost saving and allowance for pretest checkout 23 p3988 A67-41427
Performance and feasibility of staged propulsion during terminal phase of Mars soft landing [AIAA PAPER 67-987] 24 p4246 A67-43059
PROPULSIVE EFFICIENCY
Resistojet design and fabrication, using hydrogen propellant and having 3-kw power input [AIAA PAPER 66-224] 02 p0302 A67-11937
Electric propulsion status of thruster performance, promises and potentialities [AIAA PAPER 66-1024] 03 p0504 A67-14155
Electrostatic propulsion using positive and negative ions, considering neutralization effects, thrust/surface and thrust/power ratios, etc 04 p0690 A67-15023
Electric thrusters and electric propulsion, examining overall efficiency as function of specific impulse 05 p0874 A67-16933
Slipstream propulsion theory, taking into account reacceleration which places power balance in proper perspective for efficiency gain 12 p1988 A67-25214
Electron bombardment ion thrusters with two accelerator-grid systems for producing ion beams in directions 180 or 90 degrees apart [AIAA PAPER 66-284] 12 p1990 A67-25891
Stirling cycle using dissociating gas 13 p2221 A67-26390
Gas turbine theory based on Coanda effect and turbine efficiency from fluid flow analysis of depressive blade-fitted turbines 20 p3515 A67-36274
Lithium and ammonia MPD arc thrusters tests in low environmental pressure [AIAA PAPER 67-685] 21 p3692 A67-38716
Space electric rocket test /SERT/ II thruster system, discussing flight worthiness and mercury bombardment discharges [AIAA PAPER 67-700] 21 p3693 A67-38728
Kaufman thruster with curved stainless steel accelerating-grid system, studying operation, efficiency, plasma instability, etc [AIAA PAPER 67-725] 21 p3694 A67-38750
Charged particles generation by liquid subjected to high electric field for efficient bipolar microthruster [AIAA PAPER 67-728] 21 p3694 A67-38752
Pulsed vacuum arc microthruster noting various performance data and advantages [AIAA PAPER 67-737] 21 p3695 A67-38759
Propulsion and time requirements for low gravity liquid settling obtained from known Bond number 22 p3869 A67-40171
Steady state matching of inlets, engines and exhaust nozzle for SST [AIAA PAPER 67-754] 23 p3928 A67-40988
PROPYLENE
S POLYPROPYLENE
PROPYLENE OXIDE
Field-polar forces interaction effect on viscoelastic properties of polypropylene oxide, measuring dilatometric, modulus and damping constants [JPL-TR-32-1026] 24 p4174 A67-41806
PROTECTION
SA ACCELERATION PROTECTION
SA CIRCUIT PROTECTION
SA EYE PROTECTION
SA INSULATION
SA METEOROID PROTECTION
SA RADIATION PROTECTION
SA THERMAL PROTECTION
SA VIBRATION PROTECTION
Puncture sealing of meteoroid penetration in spacecraft, giving mechanical and chemical methods and self-sealing tile inner shell process 22 p3913 A67-39885
PROTECTIVE CLOTHING
SA FLIGHT CLOTHING
SA SPACE SUIT
Relation between skin temperature and environmental air supply temperatures in fixed air-ventilated clothing assembly 02 p0188 A67-12346
Water cooled vest with insulated icebox and electric pump to reduce thermal strain and increase comfort for aircrew members in hot humid climates 05 p0756 A67-16284
Space suit design for mobility and

protection, comparing soft and rigid suits 07 p1137 A67-20271
Aerospace clothing hygiene, discussing climate influence on protective garment selection and physiological responses of living organisms to obtain heat balance 12 p1902 A67-25176
Hygiene of aerospace protective clothing, studying garments characteristics, disinfection and related skin diseases 16 p2619 A67-31476
Extremity cuffs or leotards effect in preventing or controlling cardiovascular deconditioning of bed rest 18 p2992 A67-34715
Reduction of microbial shedding from humans, comparing and evaluating clothing and surgical mask use 20 p3374 A67-36802
Soviet book on protective equipment for aviators and cosmonauts 21 p3576 A67-37934
Optimum cooling in ventilated impermeable clothing using ambient air over range of simulated physiological activity 23 p3967 A67-41604
Physiological protection by aviator flight suit overall when on raft in open sea after downing, noting circulating water effect 23 p3967 A67-41606
PROTECTIVE COATING
SA CLADDING
SA SPRAYED PROTECTIVE COATING
SA WATERPROOFING
Oxidation resistant thermal protection materials for 4000 degrees F high velocity air environment [SAE PAPER 660659] 01 p0094 A67-10617
Oxidation test and mechanical property data to determine suitability of columbium and tantalum alloys as thermal protective materials for use in multicycle earth reentry vehicles [SAE PAPER 660660] 01 p0094 A67-10618
Titanium shavings application preventing iron oxidation during heating 01 p0095 A67-10643
Corrosion detection of metal surface under protective coating, using beta radiation probe 02 p0245 A67-12218
Effect on protective coatings of launch pads of exhaust products, chamber pressure, nozzle diameter, etc, from aluminized solid propellant rocket motors [AIAA PAPER 66-972] 02 p0304 A67-12294
Paint film thickness of spacecraft coatings, effect on spectral directional reflectance and binormal transmittance in far IR [AIAA PAPER 65-653] 03 p0447 A67-13033
Reflectance and emittance properties of binary coatings in sintered or compacted powder form in terms of properties of pure components [AIAA PAPER 65-670] 03 p0448 A67-13038
Optical damage of spacecraft thermal control coatings in simulated space radiation environment of geomagnetically trapped particles [AIAA PAPER 65-646] 03 p0448 A67-13051
Spacecraft thermal control surface damage by solar wind bombardment in hydrogen and helium plasmas, with measurements of solar spectral reflectance and thermal emittance [AIAA PAPER 65-647] 03 p0448 A67-13052
Low energy proton effect on thermal control coatings [AIAA PAPER 65-648] 03 p0448 A67-13053
Proton and alpha particle effects on thermal properties of spacecraft and solar concentrator coating of anodic-coated aluminum, zinc oxide/ potassium silicate, etc [AIAA PAPER 65-649] 03 p0448 A67-13054
Ames emissivity experiment on OSO-II to measure thermal radiation properties of temperature control coatings exposed to space environment [AIAA PAPER 65-651] 03 p0448 A67-13056
SNAP-10A high emittance white coating, noting stability at 600 degrees F, irradiation and vacuum and mechanical vibration [AIAA PAPER 65-652] 03 p0448 A67-13057
Aircraft corrosion protection, discussing eloxation and electrophoretic deposition of multilayer synthetic resin coatings 04 p0636 A67-14576
Wear and compatibility of liquid metal bearing materials, including surface coatings and cemented refractory carbides, analyzed for Rankine cycle power plants [ASME PAPER 66-WA/LUB-3] 04 p0630 A67-15350
Spacecraft thermal control coatings based on optical properties, discussing stability,

environmental simulation in development, thermophototropic concepts, data retrieval and optical measurement techniques in ultrahigh vacuum 04 p0630 A67-15785

[SAE PAPER 680653] 04 p0630 A67-15785

Composite coatings provide temperature differences at surface of hot stamped blanks, thereby making it possible to control strain distribution over surface 04 p0630 A67-15901

Thermal shock testing of adhesive strength and crack resistance of turbine vane protective coating 08 p1006 A67-17610

Optimal thickness of protective action of crucible lining in smelting of titanium 07 p1200 A67-19250

Aircraft exfoliation corrosion, discussing methods for prevention in fastener holes 07 p1210 A67-20087

Coating and embedding techniques for environmental protection of printed circuit assemblies 08 p1335 A67-20749

Oxidation of tantalum coated with aluminum and aluminum-chromium alloys at high temperatures and various oxygen pressures, using X-ray diffraction, electron microscopy, etc 08 p1341 A67-20764

Nondestructive tests designed to increase reliability of coated specimens by elucidating failure mechanisms 09 p1519 A67-22303

Calorimetric measurement of source and broadband spectral absorptances of spacecraft thermal control coatings during exposure to UV in vacuum environment 09 p1534 A67-22452

Substrate metal hardness effect on performance of molybdenum disulfide films, noting wear rates 10 p1659 A67-22867

Material corrosion control techniques, considering initial structure design, coatings application and protective coatings specifications 11 p1773 A67-24940

Space environment simulation facility for thermal control coatings to study synergistic and healing effects 12 p1924 A67-25711

Light sources used for solar simulation testing in terms of operational characteristics and effect of different spectral irradiance characteristics on thermal control coatings 12 p1925 A67-25723

Gas turbine blade erosion from dust, discussing momentum separators and erosion-resistant coating 12 p1990 A67-25947

Semiconductor substrate photochemical processing and coating photoresistant techniques 12 p1916 A67-25996

Spacecraft thermal control coating experiments, discussing unreliability of degradation results due to failure to measure radiation properties, UV wavelength dependence and micrometeoroid damage [AIAA PAPER 67-329] 12 p2038 A67-26043

Thermal control coating degradation data from aluminum case containing four sensors aboard Pegasus spacecraft [AIAA PAPER 67-331] 12 p2038 A67-26045

Pre-flight testing of ATS-1 Thermal Coatings Experiment /TCE/, discussing cup designs, sensor and cup calibrations, etc [AIAA PAPER 67-333] 12 p2038 A67-26047

High energy particle and electromagnetic space radiation effects on thermal control coating, noting spectral absorptance for various conditions [AIAA PAPER 67-339] 12 p1959 A67-26053

Thermal control coating spectral sensitivity to UV induced degradation, noting rapidly increasing damage as incident radiation wavelength decreases [AIAA PAPER 67-340] 12 p1959 A67-26054

In situ measurements of diffuse hemispherical spectral reflectance of thermal control coatings irradiated in vacuo with various combinations [AIAA PAPER 67-342] 12 p1959 A67-26056

Low solar absorption surface coatings of aluminum, silver and silica with controlled emittance for spacecraft thermal control [AIAA PAPER 67-343] 12 p1959 A67-26057

UV stability of several white thermal control coatings spectrally characterized in vacuum for application to Lunar Orbiter project [AIAA PAPER 67-345] 12 p1959 A67-26059

Photoengraving and use as precision processing technique 12 p1951 A67-26213

Doping of aircraft and rockets 13 p2124 A67-27500

Low temperature engine suction line response to fluid exposed internal surface

coating, determining effects of varying flow rates 13 p2229 A67-27664

Formation of hydride zinc film on titanium activated for deposition of galvanic coating 14 p2336 A67-27868

Nickel protective coating on large parts through chemical reduction of nickel salt by sodium hypophosphite, discussing technological and economic aspects 14 p2324 A67-28609

Oxidation resistant-coated refractory alloy systems for use on reentry vehicles 15 p2466 A67-29537

Effects of spacecraft sterilization procedures and Mars dust environment on thermal control coatings 15 p2503 A67-29541

Absolute spectral reflectance measurement in solar region in vacuo for applications to thermal control coatings 15 p2487 A67-29542

Cladding effect on corrosion resistance and fatigue behavior of duralumin, noting role of alternating stresses in cladding layer 15 p2504 A67-29827

Spacecraft surface temperature-control coating requirements, selection and performance in prelaunch and space environments 16 p2757 A67-30634

Formation and degradation mechanisms of aluminide coatings on Ni-base superalloys, discussing experimental procedures 16 p2693 A67-31871

Effect on protective coatings of launch pads of exhaust products, chamber pressure, nozzle diameter, etc, from aluminized solid propellant rocket motors [AIAA PAPER 66-972] 17 p2928 A67-32064

Thermal control surface contamination due to rocket exhaust plumes and effects on solar absorptance and IR emittance of protective coatings 17 p2833 A67-32076

Titanium shavings application preventing iron oxidation during heating 18 p3066 A67-34407

Metal surface property improvement by thermal-spray coating noting flame plating 18 p3055 A67-34483

Soviet book on diffusion cladding of metals covering alloy surfaces diffusion saturation, glow discharge siliconizing of metals, vacuum siliconizing of refractory metals, etc 19 p3235 A67-34915

Wear, scaling and chemical resistance of carbide and boride diffusion coatings on refractory metals 19 p3243 A67-34921

Book on coatings of high temperature materials covering properties and characteristics and coated refractory metals 19 p3244 A67-34956

Methods of producing coatings based on metal-like high temperature materials 19 p3244 A67-34957

Refractory metals physical, mechanical and chemical properties when coated with oxidation resistant coatings 19 p3244 A67-34958

Fabrication, structure, possible failure and testing of coated refractory metals in applications for space 19 p3245 A67-34959

Interplanetary space environment effect on surface thermal radiative properties, noting results of exposure to simulated solar plasma, solar UV, solar wind, etc 19 p3249 A67-35748

Refractory metals and oxidation protection noting coating materials, application methods, etc 20 p3463 A67-36133

High strength glass damage, discussing protective polymer coating 20 p3473 A67-36159

Plasma arc deposition and gas pressure bonding technique for producing defect-free uniform iridium protective coatings for graphite reentry structures 20 p3465 A67-36607

Titanium susceptibility to corrosion, achieving protection by passive self-healing films forming on metal surface 20 p3466 A67-36638

Black and white surface coating materials exposed to simulated solar radiation in vacuum, noting deterioration of white coatings 21 p3650 A67-37960

Plasma sprayed alumina and beryllia dielectric coatings for heat sinks in electronic packaging, emphasizing heat dissipation from heat/generating components 21 p3650 A67-38849

Chromate conversion process applicable to IC interconnecting aluminization reveals defective areas under normal quality control

procedures 22 p3771 A67-39835

Hafnium-tantalum coated refractory metals investigated for use in high temperature rocket motors 22 p3821 A67-39891

Reentry vehicles heat protection design emphasizing composite material selection/development for coating within acceptable weight limitations 22 p3902 A67-39938

Factors affecting tensile ductility minimum behavior of silicide coated niobium alloys investigated in air for intermediate temperature range 22 p3821 A67-40052

High temperature materials assessed for properties needed for aerospace applications including metals, alloys, refractory fasteners, aluminide coats, ablative insulation and ceramic compositions 22 p3824 A67-40333

Chemical milling of aluminum alloy parts by dimensional etching, discussing protective coatings 23 p4009 A67-40641

Dielectric cover effect on resonant frequency of slots in rectangular waveguide, using Stevenson free space theory and plane-wave reflection coefficient 23 p3978 A67-40824

Performance of wide variety of exceptional metals studied for corrosion and temperature resistance characteristics in atomic power application 23 p4018 A67-40899

Barrier system for oxidation resistant protective coating for high temperatures protection of refractory coatings 23 p4018 A67-40900

Protective coatings of Ni and Co based superalloys for gas turbine engines, discussing microstructure, chemistry and phase composition [ASM PAPER C6-4.2] 23 p4020 A67-41405

Slurry coating applied to aerospace refractory metal component for oxidation protection [ASM PAPER C6-1.5] 23 p4020 A67-41407

Highly reflective coatings and interference filters for silicon solar cells on spinning spacecraft on near-sun mission 23 p3937 A67-41490

Martian sand and dust storms simulation and abrasive effects on spacecraft surface coatings, noting similarity with Earth deserts 24 p4227 A67-42038

Emittance and specific heat determination by transient thermal vacuum technique using coatings as function of temperature 24 p4153 A67-42039

Solar wind and UV exposure effects on spacecraft thermal control coatings, using in situ spectral reflectance measurements 24 p4174 A67-42040

Strength and oxidation tests evaluated for coated fasteners in extreme temperature use 24 p4160 A67-42078

Structural problems in high power solar photovoltaic arrays technology, discussing configuration, materials selection, thermal control coatings and tests results 24 p4251 A67-42897

Simulated solar absorptance of spacecraft thermal control coatings determined calorimetrically in vacuum at room and cryogenic temperatures 24 p4256 A67-42913

PROTEIN

SA CHLOROPHYLL

SA ENZYME

SA GELATIN

SA HEMOGLOBIN

SA PEPTIDE

SA SERUM

Estimation of changes in serum protein concentration under normal stress compared to human sera exposed to simulated altitude and aerospace flights 01 p0015 A67-10950

Tissue protein synthesis in hypodynamic rats studied with aid of carbon 14 and sulfur 35 tagged amino acids 13 p2059 A67-26759

Human hair-root activity during short term deprivation of protein 19 p3177 A67-34954

Simultaneous copolymerization of Leuchs anhydrides of 18 amino acids common to protein, discussing nutritional significance 20 p3377 A67-37597

Biological value of algal and soya proteins on four generations of white rats 24 p4111 A67-41847

PROTEIN METABOLISM

Effects of 1, 1, 3-tricyano-2-aminopropene /TCAP/ on incorporation of protein and nucleic acid precursors into frog nervous system in vitro 04 p0560 A67-14408

Protein synthesis reduced and turnover stimulated by valine in *P. saccharophila* in nongratuitous inducing

- conditions 13 p2058 A67-26584
Hydrazine effect, alone and with nicotinic acid, on oxygen consumption, respiratory quotient, carbohydrate pool and heat losses in rats studied using gradient calorimeter 18 p2992 A67-34714
Chlorella and Scenedesmus unicellular algae mixture tested for biological protein value in humans for possible food source 19 p3179 A67-35228
Human natural immunity with respect to substitution of Chlorella proteins for animal proteins, studying lysozyme activity in saliva and blood serum 20 p3368 A67-36269
Nucleic acid metabolism in Chinese hamster fibroblasts grown in vitro noting effects of concentrations of sodium azide 21 p3575 A67-38798
Determination of energy, water and protein requirements of man under simulated aerospace conditions 23 p3952 A67-41573
Monomethylhydrazine effects on metabolism and heat balance using various calorimetric methods 23 p3954 A67-41601
Particle electrophoresis technique for rapid clinical microorganism identification in blood elements, noting applications in serum protein analysis and antigen antibody reaction quantitation 23 p3956 A67-41628
- PROTEINOID**
Protecell origin, discussing radiation effects on polymers, proteinoid properties and already synthesized polymer stability 24 p4113 A67-42656
- PROBIOLOGY**
Protecell origin, discussing radiation effects on polymers, proteinoid properties and already synthesized polymer stability 24 p4113 A67-42656
- PROTON**
SA RECOIL PROTON
SA SOLAR PROTON
Integral intensity of charged particles diffusing through drift shells in earth magnetosphere with specific example for protons 02 p0306 A67-11550
Proton-I satellite measurement effective cross section of inelastic interaction of protons with carbon nuclei at extremely high energies 02 p0315 A67-12757
Low energy proton effect on thermal control coatings [AIAA PAPER 65-648] 03 p0448 A67-13053
Proton and alpha particle effects on thermal properties of spacecraft and solar concentrator coating of anodic-coated aluminum, zinc oxide/ potassium silicate, etc [AIAA PAPER 65-649] 03 p0448 A67-13054
Cross section of proton production for molecular ion beams of hydrogen passing through lithium plasma 05 p0852 A67-16600
Large deuterium isotope effect on fluorescence emission spectra and quantum yields observed in number of chromospheres that contain proton donor groups 05 p0758 A67-16701
Pitch-angle distribution and differential energy spectrum of polar aurora protons penetrating earth atmosphere 07 p1173 A67-19700
Longitude distribution of solar proton flares as function of recurrence period 08 p1377 A67-21248
Kinetic theory-plasma dynamics theory calculations of magnetospheric solar wind proton velocity distribution as function of particle speed 08 p1377 A67-21315
Differential energy spectra and fluxes of charged splash and reentrant albedo proton measurement of cosmic radiation in various energy ranges 08 p1377 A67-21487
Relativistic mass-velocity relationship in empirical verification involving data on electron-proton parameters 09 p1531 A67-21650
Primary cosmic ray proton and deuteron flux near geomagnetic equator determined by nuclear emulsion method 10 p1703 A67-23543
Differential spectrum of cosmic protons at various latitudes and years surveyed by balloons 11 p1855 A67-23932
Spectrometry of primary and solar protons at Skogar-Iceland using apparatus consisting of scintillation and Cerenkov counters 12 p1991 A67-25114
Sonagrams for micropulsations, computer simulated, using equations for cyclotron instability and quasi-linear diffusion of protons in bounded plasma 15 p2476 A67-29618
Integral intensity of charged particles diffusing through drift shells in earth magnetosphere with specific example for protons 16 p2740 A67-31616
Satellite-borne detection of decay protons as test of solar neutron observation 17 p2937 A67-32544
Proton mechanism of escape from earth magnetic field, analyzing charged particle in Alfvén wave field 20 p3520 A67-37667
Proton I satellite measurements of effective cross section of inelastic interaction of protons with carbon nuclei at extremely high energies 22 p3876 A67-40259
Plon nucleon inelastic collisions at 17 GeV/c momentum, discussing proton pulse spectra and ionization losses 24 p4192 A67-42853
- PROTON I SATELLITE**
Proton-I satellite measurement effective cross section of inelastic interaction of protons with carbon nuclei at extremely high energies 02 p0315 A67-12757
Direct energy spectrum measurements of primary cosmic radiation in wide energy range 05 p0877 A67-16086
Chemical composition of primary cosmic rays in moderate energy rigidity range with aid of satellite Proton I 05 p0877 A67-16087
High energy primary gamma quanta flux outside atmosphere estimated with aid of Proton I satellite 05 p0877 A67-16088
Captured proton intensity measurement in inner radiation belt in Brazilian anomaly, using satellites Proton I and II 05 p0878 A67-16089
Geographic position of cosmic ray equator from results of on board Proton I satellite measurements 05 p0878 A67-16090
High energy electron intensity measurement beyond atmosphere with aid of proton I and II satellites, showing capture by geomagnetic field 05 p0878 A67-16091
Proton I and II satellite instrumentation noting energy-charge spectrometer, gamma-quantum fluxmeter, equipment to determine chemical composition of charged cosmic ray particles, etc 08 p1376 A67-21001
Energy spectrum and composition of primary cosmic rays in high and superhigh energy range of Proton I and II satellites 17 p2935 A67-32248
Proton I satellite measurements of effective cross section of inelastic interaction of protons with carbon nuclei at extremely high energies 22 p3876 A67-40259
Proton space station design and onboard instruments used for high energy cosmic ray study 24 p4210 A67-42391
Direct energy spectrum measurements of primary cosmic radiation in wide energy range 24 p4212 A67-42762
Chemical composition of primary cosmic rays in moderate energy rigidity range with aid of satellite Proton I 24 p4212 A67-42763
High energy primary gamma quanta flux outside atmosphere estimated with aid of Proton I satellite 24 p4212 A67-42764
Captured proton intensity measurement in inner radiation belt in Brazilian anomaly, using satellites Proton I and II 24 p4212 A67-42765
Geographic position of cosmic ray equator from results of onboard Proton I satellite measurements 24 p4212 A67-42766
High energy electron intensity measurement beyond atmosphere with aid of proton I and II satellites, showing capture by geomagnetic field 24 p4213 A67-42767
- PROTON II SATELLITE**
Captured proton intensity measurement in inner radiation belt in Brazilian anomaly, using satellites Proton I and II 05 p0878 A67-16089
High energy electron intensity measurement beyond atmosphere with aid of proton I and II satellites, showing capture by geomagnetic field 05 p0878 A67-16091
Energy spectrum and composition of primary cosmic rays in high and superhigh energy range of Proton I and II satellites 17 p2935 A67-32248
Proton space station design and onboard instruments used for high energy cosmic ray study 24 p4210 A67-42391
Captured proton intensity measurement in inner radiation belt in Brazilian anomaly, using satellites Proton I and II 24 p4212 A67-42765
High energy electron intensity measurement beyond atmosphere with aid of proton I and II satellites, showing capture by geomagnetic field 24 p4213 A67-42767
- PROTON III SATELLITE**
Proton space station design and onboard instruments used for high energy cosmic ray study 24 p4210 A67-42391
- PROTON BEAM**
Low energy proton bombardment damage in thin film cadmium sulfide and in single crystal silicon with silicone coating 01 p0037 A67-10476
Angular and energy characteristics of proton beam in pulsed magnetic field, determining probability of proton-neutron charge exchange for proton in forward flight 02 p0271 A67-12753
Charge exchange of protons in alkali metal vapors with formation of highly excited hydrogen atoms, noting cross section, reaction mechanism, etc 08 p1358 A67-20855
Optical properties of thin aluminum and silver layers subjected to proton beam bombardment 14 p2373 A67-28855
Inelastic collisions of proton beam with carbon monoxide target molecules, determining ionization cross section and charge transfer 14 p2390 A67-28943
Adjustment and test of 300 Mev proton extraction system for NASA 600 Mev synchrocyclotron 20 p3413 A67-36182
Angular and energy characteristics of proton beam in pulsed magnetic field, determining probability of proton-neutron charge exchange for proton in forward flight 22 p3842 A67-40255
Resolution and geometrical factor determination for isotropic proton fluxes by using pencil beam and measurements over many angles and positions 23 p4001 A67-41225
Secondary particle pulse spectra and mean inelasticity coefficient dependence on particle multiplicity and primary proton energy in 20 GeV/c proton-proton interactions 24 p4193 A67-42854
Fast He nuclei from photoemulsion nuclear splitting induced by proton and antiproton bombardment 24 p4193 A67-42860
- PROTON BELT**
SA RADIATION BELT
Earth radiation belt, particle motion and magnetic cavity 01 p0143 A67-10254
Solar wind effect on cathode scattering of cosmic dust particles in earth proton belt and shortening of lifetime of captured particles 06 p1078 A67-18162
Time dependence of low energy proton belts noting spatial and differential energy distribution 08 p1378 A67-21470
Proton spectra and spatial distribution of energy protons on magnetic shells in earth radiation belts, using satellite data 10 p1702 A67-23300
Direct ionization and secondary excitation in proton auroras, noting magnitude of contribution by various processes 11 p1784 A67-23927
Van Allen belt proton measurements by pulse height analysis, using thin low-Z scintillator to minimize large angle electron scattering 11 p1856 A67-24014
Low energy proton and electron outer radiation belt satellite Cosmos 41 indicate capture and acceleration mechanism 12 p1997 A67-25810
Initial energy spectrum and flux of low energy protons responsible for luminescence of H in auroras 13 p2110 A67-26542
Equatorial measurement of intensity of protons with energies greater than 400 keV and electrons with energies greater than 2 MeV in outer radiation belt center in 1964 13 p2191 A67-26544
Solar wind effect on cathode scattering of cosmic dust particles in earth proton belt and shortening of lifetime of captured particles 16 p2737 A67-30506
Alpha particle proton ratio of geomagnetic field from data from charged-particle telescope on OGO 1 20 p3519 A67-37412
- PROTON DAMAGE**
Helium isotope formation in cosmic rays during light nuclei fragmentation due to high energy proton interaction 05 p0878 A67-16093
Annealing of proton radiation damage in silicon solar cells 07 p1237 A67-20143
Proton radiation effects on mirror reflectance in high vacuum at various temperatures, degradation by blistering

found to be highly temperature-dependent [AIAA PAPER 87-341] 12 p1957 A67-26055

Spacecraft thermal control coating damage in simulated space-bombardment conditions, using plasma bombardment techniques 14 p2293 A67-28138

High energy proton and electron damage on silicon junctions measured and compared with Van Allen belt radiation 20 p3507 A67-36237

Isochronal annealing effects on photovoltaic properties of n-on-p Si solar cells irradiated by energetic proton 23 p3940 A67-41518

High energy proton irradiation and annealing of n and p type Si, comparing proton and electron damage 23 p4047 A67-41519

Helium isotope formation in cosmic rays during light nuclei fragmentation due to high energy proton interaction 24 p4213 A67-42769

PROTON DENSITY

SA MAGNETOSPHERIC PROTON DENSITY

Low energy proton distribution in geomagnetic coordinates obtained from Elektron satellite measurements 05 p0880 A67-16108

Solar proton flux measurement with balloon-borne detectors in northern Scandinavia 05 p0882 A67-16740

Satellite measurement of low energy proton precipitation in auroral zone during magnetically quiet period 07 p1245 A67-19930

South Atlantic proton radiation anomaly measurements using rocket flown spectrometer, examining variation of counting rates with altitude 12 p1995 A67-25771

Interplanetary solar wind measurements during April 1965 geomagnetic storm using electrostatic analyzers on Vela satellite 13 p2189 A67-26303

Solar wind modulation of low energy galactic cosmic radiation, estimating primary source spectra, proton and helium fluxes 15 p2550 A67-29614

Structure and decay of artificial radiation belt produced by high altitude nuclear explosion 17 p2936 A67-32534

Antiproton abundance upper limit in low energy galactic cosmic radiation determined by exposing nuclear stack to residual atmosphere 20 p3518 A67-36872

Low energy proton flux increases in outer radiation belt during quiet magnetic activity and correlation with magnetic bay appearances 20 p3519 A67-37408

Balloon sounding data for atmospheric secondary and reentrant albedo proton intensity values, discussing empirical atmospheric secondary proton spectrum 23 p4051 A67-40810

Low energy proton distribution in geomagnetic coordinates obtained from Elektron satellite measurements 24 p4214 A67-42784

PROTON ENERGY

Cross sections for double electron capture by two 50-keV protons in single collisions with hydrogen and inert gas target 01 p0115 A67-10140

Rocket measurement of proton energy spectra and pitch angle distribution associated with auroral radio absorption, using solid state surface barrier detector 01 p0061 A67-11261

High energy proton from local radio sources, using telescopic system for Cerenkov effect detection of broad atmospheric showers 02 p0311 A67-12587

Rocket measurements of 1/2 to 4 mev trapped protons in near-equatorial magnetosphere [AFCL-66-865] 03 p0505 A67-12835

PCA events during 1938-1955 detected from vertical incidence ionospheric soundings at high latitude, identifying some with proton flares 03 p0507 A67-13813

Riometer data analysis results concerning cosmic ray event of April 18, 1965 04 p0693 A67-14973

Sun generated high and low energy protons analyzed, using semiconductor detectors during flights of interplanetary probes 06 p1077 A67-17841

Nitrogen and oxygen excitation by proton shocks, measuring emission cross sections of radiation and analyzing vibrational structure 06 p1037 A67-18706

Angular distribution of fast hydrogen atoms from exothermic reaction measured for various proton energies and scattering angles 07 p1225 A67-19495

Correlation of time variations of proton and electron intensity of outer radiation belt and dependence on geomagnetic environment 07 p1243 A67-19828

Proton energy spectrum obtained from nuclear emulsion measurements on Gemini IV and V missions 07 p1244 A67-19855

Trapped proton flux data from nuclear photographic emulsions 08 p1378 A67-21472

Elektron I and III earth satellite electron and proton energy distribution correlation with geomagnetic phenomena 12 p1996 A67-25804

Low energy proton precipitation measurements in austral and boreal auroral zones, using polar orbiting satellite 12 p1937 A67-25813

Solar wind bulk velocity studied via Vela 3A bow shock crossings, noting velocity decrease when entering magnetosheath 13 p2190 A67-26320

Solar corona broadening mechanism studied using microscopic model including kinetic equations, determining proton escape velocity from sun 13 p2194 A67-27340

Transmission energy characteristics of spherical plate electrostatic analyzers from external sources of electrons and protons 14 p2320 A67-28746

Charge transfer prediction by classical binary-encounter theory approximation and quantum mechanical approximation 15 p2519 A67-29331

Hypothesis attributing most energetic cosmic ray proton source to powerful radio galaxies noting pair production effect on cosmic ray sources 16 p2738 A67-30822

Low energy protons emitted by solar flare satellite observed inside and outside of magnetosphere, noting immediate access to polar caps 16 p2740 A67-31626

Energy spectrum and pitch-angle distribution of protons in auroras based on H-beta line profiles 17 p2938 A67-32982

Cross sections for electron capture by protons measured for various energies in nitrogen, argon and helium 17 p2889 A67-33227

Energetic proton flux measurements in magnetosphere using sounding rocket, discussing radial diffusion 20 p3518 A67-36898

Doubly differential cross section for ejected secondary electrons energy and angular distribution calculated from He by fast protons bombardment 22 p3839 A67-39201

Primary proton energy spectrum determination by particle energy measurements with ionization calorimeters and particle counters onboard space stations 23 p4054 A67-41092

Proton energy spectrum azimuthal asymmetry measured with telescopes using scintillation and Cerenkov counters 23 p4054 A67-41096

1 to 5 Mev solar proton emissions observed by increased counting rates on Venera II and III and Zond III interplanetary probes 23 p4056 A67-41112

Energetic protons from March 24, 1966 solar flare observed withOGO 1 satellite scintillation counter 23 p4060 A67-41233

Low energy cosmic ray proton flux as representative of interstellar medium, discussing electron density in neutral H I regions 24 p4208 A67-41833

Electron-resonance spikes on Alouette I ionograms observed for proton gyro-effects in topside ionosphere 24 p4148 A67-42062

High energy proton data from Telstar 1 satellite used to develop mathematical models of proton spatial distribution 24 p4210 A67-42334

Neutron and proton spectra anomalies from proton-nuclei interactions in 100 Mev region 24 p4192 A67-42731

PROTON IMPACT

Technique for making thin sulfur targets mounted on solid backings for purpose of proton capture 02 p0247 A67-12698

Ionization calorimeter determination of effective cross section of high energy primary cosmic ray proton inelastic interaction with atmospheric atomic particles 02 p0315 A67-12759

Auroral hydrogen emission measurements and indications of proton or electron

excitations 05 p0797 A67-16851

Electron capture cross section by protons in hydrogen atom obtained, using perturbed wave functions due to electric field 07 p1226 A67-19501

Effective excitation cross sections of helium simple levels under proton impacts 10 p1699 A67-22845

Proton I and II satellite measurement of effective cross sections of inelastic interactions between billion and trillion ev protons and carbon nuclei 17 p2935 A67-32247

Pearl period shift explained by model showing proton effect and limited spectrum MHD noise 17 p2847 A67-32946

Magnetic activity effect on position and characteristics of proton precipitation zone in aurora observed from Canada, noting temperatures and measurement methods used 18 p3037 A67-33612

Excitation cross sections for protons incident on atomic hydrogen calculated by nonadiabatic method 20 p3491 A67-37686

Ionization calorimeter determination of effective cross section of high energy primary cosmic ray proton inelastic interaction with atmospheric atomic particles 22 p3876 A67-40261

Capture, ionization and ionization captures in collisions of protons with argon atoms 23 p4030 A67-41687

Effective cross section of inelastic interaction between high energy protons and carbon nuclei monitored by Proton I and II 24 p4219 A67-42843

PROTON IRRADIATION

Kinetics of stored energy buildup in alkali halide crystals after proton irradiation, noting dependence on lattice energy of crystal 01 p0136 A67-11050

Heat of formation of KCl-KBr solid solutions and energy storage after proton irradiation 01 p0136 A67-11051

Nonuniform damage in silicon solar cells produced by proton irradiation 02 p0182 A67-11682

Glycogen accumulation in monkey and cat brain exposed to proton irradiation, discussing astrocytes function in carbohydrate metabolism 04 p0560 A67-14489

Increase in superconducting critical current density in diffusion layers of proton-irradiated niobium stannide and decrease at higher dosage 06 p1048 A67-17817

Biological effect on mice of bombardment by protons of 120 Mev 07 p1133 A67-19114

Evening micropulsation events with rising midfrequency characteristics, discussing possible source mechanisms 07 p1182 A67-19947

Electron and proton radiation effects on GaAs, CdS and CdTe thin film solar cells noting proton damage, estimates on cell life, etc 08 p1285 A67-20735

Spectrum of meteorite luminescence emission after irradiation with protons and UV radiation, using spectrophotometer 08 p1390 A67-21021

Lunar water sources, considering hydrous minerals, cold trapped volatile products of volcanic origin and dispersed hydrates 08 p1317 A67-21093

Phagocytic activity and hepatic functions following localized proton radiation to liver, discussing results of experiments performed on white rats 10 p1599 A67-23814

Remote aftereffect on hemopoietic tissues of mice under simultaneous irradiation and acceleration, using both X-rays and protons 13 p2057 A67-26458

Rhesus monkeys liver damage after irradiation by penetrating protons 14 p2254 A67-28064

Proton-irradiation darkening of rock powders, noting contamination, temperature effects and applications to solar wind darkening of moon [JPL-TR-32-1130] 16 p2753 A67-31743

Tritium diffusion from iron meteorites shortly after fall established by artificial proton irradiation 17 p2942 A67-32357

Degradation in silicon transistors due to particle bombardment analyzed, showing surface/ bulk recombination increase 17 p2917 A67-32845

Permanent displacement-induced effects in silicon semiconductor devices as function of radiation type and energy 17 p2917 A67-32847

Accelerated antimony diffusion in germanium due to excess vacancies from proton irradiation, determining migration

- energy and diffusion length of vacancies 17 p2919 A67-32862
- Defects in single crystal foils of compound bismuth telluride caused by irradiation with protons 17 p2921 A67-33050
- High kinetic energy electrons associated with solar flares, noting prompt and delayed types 17 p2940 A67-33401
- Influence of fast proton and electron irradiation on diffusion of substitution impurities in silicon 18 p3100 A67-33750
- Isochronal annealing of proton-irradiated silicon solar cells studied in vacuum over various temperature ranges 19 p3305 A67-35669
- High energy proton and electron damage on silicon junctions measured and compared with Van Allen belt radiation damage 20 p3507 A67-36237
- Silicon semiconductor alpha particle detector for spectrometry, noting radiation resistance for low energy proton bombardment 21 p3628 A67-38596
- Characteristics of geomagnetic crotches associated with proton flares, determining recombination coefficients and electron densities 23 p4050 A67-40871
- Hepatic hemorrhagic lesions produced by 32 and 55 Mev proton radiation in rhesus monkeys 23 p3944 A67-41017
- Isochronal annealing effects on photovoltaic properties of n-on-p Si solar cells irradiated by energetic proton 23 p3940 A67-41518
- High energy proton irradiation and annealing of n and p type Si, comparing proton and electron damage 23 p4047 A67-41519
- Acute and chronic cellular level effects of low energy proton irradiation in rat skin 23 p3957 A67-41644
- Pathological effects, including carcinogenesis following proton whole body irradiation in rats 23 p3958 A67-41645
- PROTON MAGNETIC RESONANCE**
- Proton gyrofrequency effect on antenna resonance at electron plasma frequency using Alouette II satellite 24 p4125 A67-43111
- PROTON PRECESSION**
- Proton precession magnetometer completely transistorized except for signal amplifier 05 p0807 A67-16712
- PROTON-PROTON REACTION**
- Secondary particle pulse spectra and mean inelasticity coefficient dependence on particle multiplicity and primary proton energy in 20 GeV/c proton-proton interactions 24 p4193 A67-42854
- Proton-proton and pion and kaon elastic scattering from protons at high energy, deriving approximate formula for differential cross section, noting nucleon structure 24 p4193 A67-42855
- PROTON PROTUBERANCE**
- Ionospheric irregularities following solar proton flare of July 1966 observed with Alouette topside sounders 19 p3312 A67-35178
- Solar X-ray emission associated with proton flare of July 1966 measured, plotted and described 19 p3313 A67-35218
- Long term forecasts of proton flares 19 p3313 A67-35261
- PROTON RESONANCE**
- Autocorrelation function of signal scattered incoherently from ionosphere, observing resonance at multiples of proton gyroperiod 21 p3578 A67-37758
- PROTON SCATTERING**
- Spectra of outgoing protons for various targets using scintillation counter, interpreting data by means of impulse-approximation calculation 02 p0269 A67-11862
- Red shift of magnetic zenith hydrogen line profiles and role of injection pitch-angle distribution of auroral protons 03 p0409 A67-12943
- Resonances in proton hydrogen and positron hydrogen scattering predicted at energies just below excitation thresholds 04 p0682 A67-15768
- Planet Mercury magnetospheric scattering of solar-flare protons to earth, obtaining deflection angle [AIAA PAPER 67-150] 06 p1088 A67-18505
- Anisotropic proton velocity distribution obtained from solar wind measurements on Pioneer VI spacecraft 08 p1378 A67-21475
- Proton mobility in ice when limited by lattice scattering calculated, using Boltzmann transport equation 13 p2160 A67-26991
- Inelastic differential scattering cross sections and angular distribution of Ni first-excited-state protons determined by distorted wave calculation 17 p2888 A67-32733
- PROTON TELESCOPE**
- High energy proton from local radio sources, using telescopic system for Cerenkov effect detection of broad atmospheric showers 02 p0311 A67-12587
- PROTOSTAR**
- Protoplanetary cloud and evolution, noting Hoyle rotatory nebula and other hypotheses 09 p1563 A67-21633
- Close binary protostellar system formation using model with stellar wind mass loss and primeval magnetic field 22 p3896 A67-40520
- PROTUBERANCE**
- SA PROTON PROTUBERANCE
- Solar flares, special features revealed by optical observations, classification, optical spectrum, shock waves and protuberances 01 p0144 A67-10771
- PSEUDORANDOM SIGNAL**
- All phases of pseudorandom sequence obtained by N-stage shift register generator 02 p0203 A67-12133
- Synthesis method for generating p-level pseudorandom signals derived from corresponding m-sequences, using standard binary logic elements 03 p0393 A67-13997
- Code-division-multiplex decentralized control system for communication satellites based on use of pseudorandom PM signals of wide bandwidth 06 p0959 A67-17672
- Artificial pseudorandom binary noise generation for flight testing and aircraft control systems and correlation function and frequency spectra of noise generators 08 p1279 A67-21005
- Noise immunity in binary detection and temporal shift measurement of pseudorandom amplitude keyed echo signal in multichannel system 24 p4120 A67-42233
- PSEUDOREA**
- Toxicity of radioprotective amino ethyl isothiuronium bromide from animal studies noting hazardous effects in human organism 22 p3753 A67-40546
- PSYCHIATRY**
- SA DEPERSONALIZATION
- SA MILITARY PSYCHIATRY
- Treatment of psychiatric diseases in ground staff and aircrew, discussing psychopharmacology in aeronautical medicine 23 p3967 A67-41603
- PSYCHOACOUSTICS**
- Laboratory psychophysiological efficiency in flying personnel of various ages covering pursuit reaction tests, serial motor activity and optico-acoustic signal analysis 22 p3753 A67-40544
- PSYCHOLOGICAL EFFECT**
- Sensory input overload effects on performance of civil aviation pilots during simulated instrument flights in Link AN 2550-1 trainer 09 p1455 A67-21726
- Secondary determiners of anticipatory physical stress threat as components of perceived proximity of unpleasant event 10 p1601 A67-23820
- Psychophysical and psychosocial factors as causes for rejection of Italian Air Force pilot trainees, discussing relationship between pilot, instructor and physician 12 p1902 A67-25171
- Space flight to Mars, discussing medical problems originating from changing gravitational fields, meteorite dangers, radiation and psychological considerations 13 p2061 A67-26338
- Postmortem determination of pilot psychological state during aircraft collisions by examining sugar content of dead bodies 14 p2255 A67-28226
- Human psychological reactions to space flight problems, investigating effects of weightlessness, immobility and confinement on cosmonaut health and ability 16 p2612 A67-30903
- Sensory discrimination, psychological and preference factors toward water reclaimed from urine, discussing identification from tap and distilled water, temperature and smoking effects 22 p3751 A67-39597
- Psychosomatic symptoms in student naval aviators 23 p3955 A67-41624
- Clinicopsychopathological method applied to analysis of hallucination, depersonalization and similar effects resulting from exposure to extremal factors from standpoint of space psychology 24 p4112 A67-41856
- PSYCHOLOGICAL FACTOR**
- Psychosociological problems of small isolated groups working under extreme conditions in lunar laboratory 02 p0185 A67-12374
- Psychology and space flight 09 p1454 A67-22056
- Research astronaut selection 13 p2062 A67-28763
- Physiological/psychotechnical selection of French cosmonauts with reference to ballistic, orbital and space flight 19 p3179 A67-35066
- PSYCHOLOGICAL INDEX**
- Rate measurements determination and evaluation in analysis of space medical data 15 p2431 A67-29293
- PSYCHOLOGICAL TESTING**
- Crew performance evaluation via behavioral and psychophysiological tests in Lunex II simulated lunar mobile laboratory 01 p0017 A67-11392
- Naming sequentially presented letters and words 06 p0954 A67-18533
- Reinforcing effect of informative stimulus that is not positive discriminative stimulus 11 p1748 A67-25065
- Perceptual motor-skills forgetting in simple printing task, attributing decrements to retroactive interferences 21 p3576 A67-39099
- Cockpit environment thermal stress effect on psychological test performance and biomedical parameters 22 p3753 A67-40539
- PSYCHOLOGY /GEN/**
- S FACTOR ANALYSIS
- S NEUROSCIENCE
- PSYCHOMETRICS**
- Second order personality factor analysis applied to air traffic control specialists 13 p2063 A67-26929
- PSYCHOMOTOR PERFORMANCE**
- SA REACTION TIME
- Effect of hypoxia on psychomotor behavior at simulated cabin altitudes of 5000 and 8000 ft 01 p0017 A67-10953
- Reaction time during voluntarily controlled alveolar hyperventilation used to study effects on psychomotor performance of aircrew 09 p1453 A67-21728
- Immobilization effects on electrical activity of brain and intellectual and perceptual motor processes 11 p1748 A67-25064
- Psychomotor adaptation to flight evaluated clinically, describing anxiety and other aviator symptoms in aerospace 17 p2806 A67-31964
- Monkey psychomotor reactions during ballistic flight investigated noting alertness reduction during weightlessness 19 p3178 A67-35241
- Monkey psychomotor reactions during ballistic flight, noting alertness reduction during weightlessness 19 p3181 A67-35466
- Human sensor-motor coordination testing in simulated weightlessness 20 p3368 A67-36263
- Tracking activity of human operator under effect of certain space flight factors, establishing relationship between control habits and level of hypoxia and hypercapnia 20 p3368 A67-36265
- Feedback changes effects on reaction time in stopping chronometer 22 p3756 A67-40536
- Light effects and aircraft safety studied for lightning strikes, noting temporary blindness and slowing of psychomotor reactions 23 p3945 A67-41069
- PSYCHOPHYSICS**
- Book on statistical decision theory and sensory processes in signal detection theory and psychophysics 07 p1136 A67-19726
- Approximate formulas for information transmitted by discrete communication channel obtained by averaging tight and weaker bounds respectively from transition probability matrices 12 p1908 A67-26088
- Nonphysical forces /human soul and personality/ analyzed to explain validity limits of laws of physics, discussing Descartes dualism, quantum mechanics, coincidences, determinism, etc 18 p3077 A67-33500
- PSYCHOPHYSIOLOGY**
- SA NEUROPHYSIOLOGY
- Adrenal cortical activity changes correlated with pathological emotional states 08 p0952 A67-17848
- Absolute threshold of cat optic nerves determined by inspection of poststimulus

time histograms, computed from responses of identical flashes of white light 10 p1598 A67-23581

Psychophysical and psychosocial factors as causes for rejection of Italian Air Force pilot trainees, discussing relationship between pilot, instructor and physician 12 p1902 A67-25171

Soviet space psychophysiology, discussing cosmonaut selection and medical control 13 p2058 A67-26751

Neutral buoyancy /water immersion/ technique for simulated space crewman performance, noting psychophysiological, man-machine and anthropomorphic parameters affecting space station design 15 p2431 A67-29282

Laboratory psychophysiological efficiency in flying personnel of various ages covering pursuit reaction tests, serial motor activity and optico-acoustic signal analysis 22 p3753 A67-40544

Pilot capability in low level high speed flying analyzed for influence of roughness fatigue, control improvements, vibration and visual problems 23 p3963 A67-41068

Psychosomatic symptoms in student naval aviators 23 p3955 A67-41624

Autogenous and exogenous suggestion applied to changing of psychophysiological state of human organism after exposure to prolonged bed rest 24 p4112 A67-41855

PTM

S PULSE TIME MODULATION /PTM/ PULLEY

Impact problem of passage of longitudinal and transverse waves arising in elastic infinite thread over sequence of absolutely smooth nonrotating pulleys 07 p1261 A67-19163

PULMONARY CIRCULATION

Physiologically inert gas continuous labelling of pulmonary circulation in one lung compartment and measurement of partial pressure of gas in arterial blood by gas chromatography 07 p1133 A67-19477

Book on positive pressure breathing as means for acceptable arterial oxygen tension at altitudes above 40,000 ft and effects of raised intrapulmonary pressure 08 p1288 A67-21500

Air embolism pathogenesis and therapy in terms of problem of treatment in overpressure [DVL-628] 13 p2059 A67-26850

Blood pressure changes and pulmonary edema in rat associated with hyperbaric oxygen 15 p2428 A67-29275

Acute hyperbaric oxygenation histological effects on pulmonary circulation of rabbits 16 p2614 A67-31473

Lung changes resulting from prolonged exposure to 100 percent oxygen at 550 mm Hg suggest media erosion and evidence of hypertrophy and hyperplasia 22 p3751 A67-39601

Pulmonary isotopic scanning technique in dog to assess embolism before and after lethal decompression 22 p3751 A67-39602

Arterial oxygen tension during acceleration recorded on anesthetized greyhounds using microelectrode and physiological gas analyzer 23 p3958 A67-41653

PULMONARY FUNCTION

SA LUNG

Dynamic pulmonary work of human males during muscular exertion at 2000 m and different barometric pressures 04 p0561 A67-14631

Absorptional atelectasis breathing oxygen at simulated altitude, discussing prevention by using inert gas 09 p1453 A67-21732

Experiments showing occurrence of aero-atelectasis in pilots exposed to high G forces, breathing oxygen and using anti-G suit 09 p1453 A67-21733

Theoretical lung with equal ventilation-perfusion ratio used to study determinants in inert gas elimination 21 p3575 A67-38515

Ventilation-perfusion inequality effects studied in inert gas elimination from lungs 21 p3575 A67-38516

Intrapulmonary pressures chosen during immersion in thermally neutral water, comparing transpharyngeal and transthoracic pressure gradients for various breathing devices 22 p3751 A67-39604

Radioisotopic color coded pulmonary lung scanning, diagnostic test in experimental decompression sickness 23 p3958 A67-41626

PULMONARY LESION

Anesthetized rabbits exposed to high explosive air shock waves in shock tube, examining changes of elastic properties of lungs of rabbits 03 p0364 A67-14292

Simulated high altitude effects on emphysematous blebs and bullae under reduced ambient barometric pressure 03 p0365 A67-14297

Proliferative pulmonary lesions in monkeys exposed to high concentrations of oxygen at 600 to 760 mm Hg pressure 15 p2428 A67-29276

Pulmonary mechanics associated with oxygen toxicity and suggested physiological test for susceptibility to effects of oxygen 15 p2429 A67-29280

PULSATING FLOW

Oscillation spectra of plasma in quasi-steady state characterized by self-consistent distribution of plasma particles and turbulent pulsation 02 p0274 A67-12455

Flow pulsation effect on error of flow measurement by means of steady flow formula, noting manometer design requirements 03 p0403 A67-13767

Engine test facility for measuring thrust and propellant flow in pulsating rockets 03 p0396 A67-13774

Flow meter for extremely low flow rates during steady state and pulse mode thruster operation 03 p0422 A67-13776

Erosion destruction mechanism in polycrystalline graphite, noting effect of gas flow over surfaces, flow pulsation frequency and generated aerodynamic loads 04 p0642 A67-15761

Enthalpy to work conversion in gas turbines using pulsating combustion chamber 05 p0873 A67-18743

Attenuation law of turbulent pulsations in viscous sublayer of turbulent boundary layer of incompressible fluid 06 p0982 A67-17741

Pressure amplitude at resonance decreasing with increasing Mach number observed as effect of mean flow on wall damping of finite amplitude gas pulsations 07 p1188 A67-19576

Heat transfer of pulsating liquid jet impinging on perpendicular flat surface and spreading laminarily 11 p1882 A67-24229

Changes in structure of gas detonation wave with changes in initial pressure 16 p2656 A67-30452

Viscous fluid discharge from tubes of various cross sections under constant pressure gradient with longitudinal pulse along wall, noting short period stoppage 18 p3029 A67-34615

Heat transfer for one- and two-dimensional pulsating incompressible laminar flow in circular tube with two thermal boundary conditions [ASME PAPER 67-HT-65] 20 p3550 A67-36747

Convective heat transfer between tube and airflow in tube for pulsating flow with pressure fluctuation frequency deviating from resonant frequency 23 p4082 A67-41285

Pulsed ion flow energy and mass spectra analyzer suitable for 1 to 3 msec duration and time variation over 10 msec 24 p4158 A67-42741

PULSE

SA ELECTRIC PULSE

SA GEOMAGNETIC PULSATION

Pulse shape formed during discharge of chain-type artificial line 01 p0038 A67-10719

Ideal incompressible liquid motion in rectangular container due to rectangular double and sinusoidal pulse 03 p0404 A67-13784

Thermal properties of semiconductor diode under steady and pulsed operation 05 p0772 A67-16448

Incidence of missed reply and garbled pulse trains and fruit interference effect determined in extraction of secondary radar plots 09 p1530 A67-22653

Circuit for discriminating neutrons, gammas and charged particles from each other in phoswich scintillator 12 p1945 A67-25857

Shape of extremely short pulses generated by helium-neon laser with mutual synchronization of intermodal beats achieved by Fabry-perot interferometer 15 p2500 A67-29760

Monte Carlo evaluation of linear and eigenvector-method for estimation of pulse transfer function of linear, time-invariant dynamic feedback system 16 p2653 A67-31695

Phase and amplitude characteristics of microwave amplifiers obtained from response to short input pulse 17 p2827 A67-32791

Deficiencies of pulse-parameter representation used for semiconductor diodes, discussing generalized parameter describing transient processes relaxation 18 p3009 A67-33474

PULSE AMPLITUDE

Transistorized logarithmic amplitude converter for recording pulses of radiation detector, automatic switching of conversion scale permits amplitude measurement 01 p0062 A67-10160

High temperature operation of diamond counters for nuclear particles 01 p0068 A67-10927

Narrow beam divergent Q-switched laser pulse generation, noting output characteristics and applications 01 p0091 A67-11024

Optimum reception criteria for double beam channels with fluctuating noise, signal phase and amplitude characteristics 02 p0205 A67-12532

Nanosecond pulse microwave breakdown in air 04 p0657 A67-15120

Ferroacoustic resonance in yttrium ferrite garnet crystals, noting effect of magnetic field on pulse amplitude 05 p0868 A67-17064

Giant pulse formation theory, measuring shape and duration of neodymium glass laser pulses for various values of inverse population 06 p1010 A67-17876

Propagation mode of one-dimensional HF finite acceleration pulses in nonlinear viscoelastic solids, stressing shock formation and propagation 09 p1573 A67-21547

Polarization characteristics of antenna measured, using stereographic projections of polarization sphere and various graphical methods 11 p1761 A67-24279

Electronic and ultrasonic principles defining pulse-echo high resolution and application to electronic and electroacoustic circuitry for testing aerospace structures 12 p1848 A67-25218

Digital and hybrid pulse analyzer designs for automatic measuring pulse characteristics digital and hybrid pulse analyzer designs for automatically measuring pulse characteristics 13 p2075 A67-26411

Pulse amplitude measurement from scintillation cosmic-ray counter 13 p2119 A67-26560

HF transistorized pulse analyzer with rise of 1 nsec and output voltages of more than 4 v designed for trigger pulses and traveling wave oscilloscope 13 p2082 A67-27400

Optimum reception criteria for double beam channels with fluctuating noise, signal phase and amplitude characteristics 14 p2261 A67-28009

Magnetoplasma radiation by microwave pulse excitation at gyrofrequency harmonics, considering single particle approach 14 p2360 A67-28557

Ferroacoustic resonance in yttrium ferrite garnet crystals; noting effect of magnetic field on pulse amplitude 15 p2538 A67-29795

Nanosecond baseband pulse rise time measurement, discussing real time and sampling oscillography, pulse comparison, basic instrumentation, etc 17 p2814 A67-32603

Point-by-point measurements of magnitude and phase of repetitive pulsed time functions using commerial equipment 19 p3182 A67-35031

Optical auroral pulsations in various frequency ranges analyzed using automatic zenith photometer 19 p3222 A67-35459

Memory-cell circuit employing Esaki diodes negative resistance characteristic, developing small memory pulse amplitude useful in minimizing cycle time 20 p3397 A67-36765

Injection locked pulsed magnetron in coherent echo detection system studied by observing echo pulses from acoustic delay medium 20 p3401 A67-37221

Ultrashort optical pulse propagation in two-level medium, describing pulse shapes by solving partial differential equation 20 p3461 A67-37286

Interference reduction potential of binomial type pulses 20 p3387 A67-37636

Fourier integral in terms of maximum harmonic amplitudes 20 p3406 A67-37656

Pulse magnitude and distribution due to energy release in liquid, on walls of shells

submerged in liquid, used to calculate loads 21 p3611 A67-38056

Statistical dependence between frequency and amplitude deviations of FM wave perturbed by white noise, describing amplitude-phase correlation FM demodulator 22 p3758 A67-39271

Solitary pulse longitudinal waves existence in electron plasma related to trapped ions presence, studying ion pulse shape and oscillation stability 22 p3845 A67-39423

Averaging method for studying system oscillations over infinite time interval subject to pulsed action 23 p4027 A67-40925

Pulse regenerative amplification in Q-switched argon-ion laser during buildup time to saturation 23 p4014 A67-41030

Pressure pulse generator-peak amplitude detector system for dynamic calibration of pressure transducers 23 p4007 A67-41388

PULSE AMPLITUDE MODULATION /PAM/

All-solid state airborne low level PAM multicoder that employs N-channel FETs for all analog switching functions of system 02 p0216 A67-12013

Effect of feedback capacity addition to M-ary PAM communication system perturbed by white Gaussian noise 02 p0204 A67-12170

Transfer function of pulse amplitude modulated sampled data control systems with element generating arbitrarily shaped pulses and first order element series connected with constant parameter elements 03 p0390 A67-13103

Transition to detonation in gaseous medium experimentally studied, based on self-sustained detonation front and adaptation of amplitude modulated giant pulse laser system 03 p0535 A67-13500

Telemetry systems, discussing PAM/FM/FM system, airborne equipment parts, ground support system and electronic testing procedures 04 p0577 A67-15728

Measuring harmonic AM frequency of bell-shaped videopulses train for modulation-to-repetition-frequency ratio greater than unity 07 p1139 A67-19227

Amplitude distortion as function of filter bandwidth for various generalized pulse shapes 07 p1157 A67-20090

Optimum linear receiver for noisy PAM system using criterion of mean square interference 11 p1752 A67-24134

Ionospheric dispersion of AM-FM artificial satellite signals noting distortion effects, synchronization and interference difficulties 13 p2070 A67-27197

Binary symmetrical channel noise effect on PCM picture quality compared with white Gaussian noise effect in PAM system 20 p3386 A67-37496

Most efficient use of voice band channel in digital data transmission by direct use of passband [IEEE PAPER 19-TP-67-1262] 23 p3972 A67-40741

Nonlinear sampled data system instability, discussing arbitrary single-valued nonlinearities and arbitrary modulation law /PAM, PWM or PFM/ 23 p3985 A67-41674

PULSE CODE MODULATION /PCM/

Optical modulator using electro-optic effect in lithium tantalate for PCM transmission systems operating at 224 megacycle bit rate 01 p0033 A67-10013

Ninety-eight-channel microelectronic PCM multiplexer-encoder design and development qualified to Apollo spacecraft environments 01 p0026 A67-10864

Binary detection probability for optical polarization modulation communication system using Gaussian approximation, noting signal to noise ratio 01 p0026 A67-10866

Decoder signaling system of Eldo satellite employing PCM telemetry channel, examining counters, shift registers, flip-flop circuit, etc 02 p0192 A67-11651

Evaluation of redundancy reduction algorithms to facilitate comparison in terms of performance by computer simulation, using real and synthesized data 02 p0197 A67-12015

Channel noise forces adaptive sampling system to operate at lower bit error probability than equivalent PCM system 02 p0197 A67-12016

Mean time analysis of PCM synchronization, noting pattern synchronization in presence of noise 02 p0197 A67-12020

Data quality assurance program for

telemetry ground station operations, noting frequency division and time division formats 02 p0198 A67-12023

PCM/TDM and influence of channel on signal determined, using mathematical model 02 p0202 A67-12130

PCM digital picture transmission for monochromatic still and motion pictures and color still pictures 02 p0208 A67-12167

Relation between sidelobe level and radar performance in clutter for nonresolvable difference between target and clutter Doppler 03 p0369 A67-13680

Stochastic analysis of energy spectrum of output signal of phase shift modulator in PCM systems 04 p0571 A67-14895

Automatic star trackers for long range aircraft navigation, discussing instrumentation methods and use of pulse code modulation for sensor design 04 p0655 A67-15661

PCM telemetry unit for Nimbus B spacecraft noting applications and performance 05 p0767 A67-17463

PCM telemetry system for satellite test vehicle of ELDO program using transistorized printed circuit technology 06 p0957 A67-17613

Communications requirements for manned deep space missions, using optical links, with PPM, PCM/PL and coherent reception for each link [AIAA PAPER 66-317] 06 p0961 A67-17706

Bit synchronization during transmission of heavily biased information on PCM data systems 06 p0963 A67-18110

Amplitude bounded noise and random measurement error smoothing, noting increased efficiency and possibility of narrow band application 06 p0975 A67-18217

Transmission methods, analyzing noise threshold, signal bunching, etc 07 p1141 A67-19339

Bias due to random bit errors that occur in PCM data during phases of operation of telemetry data processing system 07 p1145 A67-19874

Pulse sequences with good autocorrelation properties 10 p1608 A67-23330

PCM frame synchronization with self-varying threshold 11 p1764 A67-24434

Picture quality in PCM transmission of low resolution monochrome still pictures as affected by system parameter changes 11 p1791 A67-24712

Alternative modulation techniques for Satellite Telecommunications with Automatic Routing, considering start-stop operation with PCM-FDM system 13 p2068 A67-26720

Modulation and demodulation methods for multiplex telemetry, discussing PCM, PSK and SSB 14 p2271 A67-28682

Biorthogonal coded telemetry system for deep space applications, discussing construction and performance 14 p2271 A67-28695

Data handling system for 8-bit phase-coherent biorthogonal coded PCM telemeter 14 p2272 A67-28696

Pulse Doppler waveform coding, presenting technique of selecting pulse-period modulation codes requiring only computer calculations 15 p2437 A67-29934

Energy spectrum and correlation characteristics of PCM signal studied by Levin method, calculating correlation moments of code group symbols 16 p2620 A67-30478

Amplitude bounded noise and random measurement error smoothing, noting increased efficiency and possibility of narrow band application 16 p2642 A67-30483

First stage checkout techniques of satellite launcher, noting digital computer program from pulse-code-modulated telemetry 16 p2655 A67-30835

Troposcatter techniques reviewed proposing analog voice waveform conversion into digital form by delta modulation or PCM for upgrading present operational systems 16 p2628 A67-31492

Multidigit delta modulation system using individual optimized stages developed by successive approximation of message waveform 17 p2812 A67-32319

Threshold characteristics of systems for multistate orthogonal transmission of coded analog signals in communication systems 18 p3000 A67-34023

H-01 waveguide irregularities causing

transfer function fluctuation, calculating rms and relative distortion power from PCM signal 19 p3183 A67-35561

Intermodulation interference effect on PCM/FM error rates studied using power series as mathematical model 20 p3380 A67-36563

PCM telemetry system for ELDO program, discussing data acquisition and processing 20 p3392 A67-37162

Binary symmetrical channel noise effect on PCM picture quality compared with white Gaussian noise effect in PAM system 20 p3386 A67-37496

High reliability PCM digital telemetry system for onboard data transmission of analog and digital signals 21 p3583 A67-38635

Self-variable threshold method for synchronization code detection of PCM telemetry signal 21 p3583 A67-38641

PCM coder, programmer and analog switch of D-2 satellite, including systems characteristics and diagrams 21 p3599 A67-38647

Frequency limitations of PCM communication, determining PCM/PM and PCM/FM power spectra for hybrid modulation spectra 21 p3584 A67-38652

Bandwidth restriction effect on SNR in NRZ signal from PCM transmission system 21 p3584 A67-38667

Pulse code communication system for transmission of continuous random quantities 22 p3761 A67-39831

Microwave multichannel communication system using PCM, noting low power output requirement and suitability for digital data transmission 22 p3763 A67-40460

Broad bandwidth digital laser communication system utilizing pulse coded polarization modulation and binary detection including optical communication link and performance data 23 p3973 A67-41039

PULSE COMPRESSION

SA CODING

YIG dispersive delay line in ultrawide bandwidth pulse compression radar system 01 p0132 A67-10435

Doppler tolerant pulse train design, noting signal processing by delay line with fixed taps for significant changes in pulse spacing 01 p0023 A67-10464

Paired echo sidelobe produced by ripples of Fresnel spectrum in active linear compressed-pulse frequency modulation 01 p0027 A67-11328

Pulse compression radar system design and characteristics noting clutter, local oscillators and phase and amplitude measurement 04 p0572 A67-15032

Lumped electric circuit device producing dispersion for pulse compression system noting design 04 p0574 A67-15054

Dispersive network of apparatus producing dispersion in pulse compression system, noting role of relatively low center frequency 04 p0574 A67-15055

NRL lunar radar system applied to long term earth-moon distance measurements, using pulse compression for signal processing, noting high SNR 08 p1293 A67-20689

Pulse compression parallel channel technique for evaluating channel filter characteristics effect on compressed pulse form 11 p1754 A67-24648

Sidelobe reduction in phase-coded pulse compression radars solved by eliminating ripple of matched filter output with aid of weighting filter 12 p1908 A67-26092

Limitations in conventional radar compared to new multichannel radar with discontinuous pulse compression 13 p2070 A67-27203

Digital pulse compression radar receiver with digital-pulse compression advantages and disadvantages, noting target acquisition, range tracking and antenna scanning system 16 p2630 A67-31738

Ultrasonic correlating device for fabrication of pulse compression radar signals 18 p3002 A67-34227

Multichannel radar formula for discriminating power in distance corresponding to time resolution constant 18 p3002 A67-34228

Pulse compression in unmatched dispersive networks noting phase characteristic matched to signal received 20 p3379 A67-36380

Binary pulse compression codes generation with low periodic autocorrelation 20 p3386 A67-37493

Waveguide dispersive line use in FM pulse compression system outlined for high resolution in S-band radar 21 p3601 A67-39068

Pulse generation method for high power modulators in Doppler radars studied, using step recovery diode to construct compression network 22 p3772 A67-39897

Microwave pulse compression filter using dispersive characteristics of propagating magnetostatic spin waves in single crystal YIG rods 22 p3773 A67-39908

Optical characteristics of wideband pulse compression system using Brillouin scattering for compressing time duration of frequency swept pulses of acoustic wave 23 p4012 A67-40869

Laser pulse compression of RF signals using Bragg scattering produced in transparent solid by ultrasonic waves 24 p4188 A67-42368

RF pulse compression by chirped shear microwave sound in sapphire, inducing self-focusing of Bragg diffracted light 24 p4188 A67-42369

Book on radar signals covering FM pulse compression signals, waveform, Doppler shift, time factor, etc 24 p4122 A67-42425

PULSE DIFFRACTION

Wave equation solution for potential of cylindrical Dirac pulse incident on reflecting half-plane 17 p2817 A67-33139

Diffraction of stress pulse by spherical cavity embedded in infinite linear homogeneous isotropic elastic medium [ASME PAPER 87-APM-27] 17 p2965 A67-33154

Scattering amplitude of frequency spectrum components of isolated exponential acoustic pulse incident on hard sphere 21 p3657 A67-38057

Magnetic breakdown in metals covering one-electron theory, electronic motion, Bragg diffraction, de Hass-van Alphen effect, coupled orbits and HF oscillations 22 p3866 A67-40552

PULSE DURATION

Pulse length of collector current pulse, which causes secondary breakdown in transistors, measured at constant forward or reverse base current 02 p0223 A67-12657

Static characteristics of series connected tunnel diodes used in determining pulse duration and recovery time of driven multivibrator 03 p0377 A67-13236

Short triple electric and light pulse generation noting equipment design and performance 03 p0388 A67-14270

Short pulse Q-switched laser with variable pulse length 05 p0817 A67-16641

Pulse measurement of nanosecond intervals using time expansion chronometer 06 p1002 A67-18055

Apparatus producing voltage pulses in X-band magnetrons operating on pulse lengths of tens of nanoseconds 09 p1479 A67-22262

Matched pulses for two-layer laminates, discussing complete energy transfer to base and uniform momentum transfer 10 p1724 A67-23707

Empirical rules for shock spectrum, pulse and lead pellet interrelationship and implementation 12 p1967 A67-25686

Digital and hybrid pulse analyzer designs for automatic measuring pulse characteristics digital and hybrid pulse analyzer designs for automatically measuring pulse characteristics 13 p2075 A67-26411

Effect of semiconductor glass shield temperature on absorption coefficient, output energy, pulse duration and energy and peak power of ruby laser 14 p2332 A67-28857

Giant pulse time evolution influenced by pump-induced material inhomogeneities studied by analyzing laser rate equations 15 p2498 A67-29484

Generation of large pulses of extremely short duration in ruby laser by rotating mirror technique at lower frequencies 15 p2498 A67-29642

Argon pulsed arcs produced at high pressures, considering emission absorption 16 p2717 A67-31184

Quasi-continuous divalent dysprosium ion doped calcium fluoride laser with pyrotechnic excitation 16 p2686 A67-31484

Decay and dispersion of disturbance pulse in fluid lines along pipe, considering velocity

and pressure characteristics [ASME PAPER 86-WA/AUT-24] 17 p2835 A67-32017

Optically pumped alkali metal vapors orientation checking by light pulse method, noting relaxation curve 17 p2869 A67-32811

Single laser pulse generation noting high peak power, subnanosecond time duration, optical cavity length, etc 17 p2869 A67-33063

Instability in resonant amplifier and video pulse effect on amplifier resonant load during radio pulse formation 18 p3010 A67-33509

Systematic errors limiting velocity measurement accuracy of longitudinal ultrasonic waves when using pulse-delay methods, for application to ultrasonic equipment 18 p3044 A67-33734

Gallium phosphide diode-based laser generator of nanosecond light pulse sequence, noting simulation of scintillation counter photoelectric amplifiers, Cerenkov counters, etc 19 p3228 A67-34987

Low power pulsed reflex klystron used to produce hyperfrequency-wave trains for short time periods 19 p3193 A67-35416

Basic operating-time contribution to pulse behavior of diffused transistor components, introducing system function for semiconductor barrier-layer component 19 p3195 A67-35580

Effect of semiconductor glass shield temperature on absorption coefficient, output energy, pulse duration and energy and peak power of ruby laser 19 p3242 A67-36108

Two-photon photoconductivity in pulsed ruby laser excited cadmium sulfide, determining carrier density and density dependence on light intensity 20 p3456 A67-36164

Giant coherent light pulses generation by Q-switched laser, studying dynamics of generation and field distribution 21 p3640 A67-38373

Superconducting coils used for capacitors in pulsed operations to reduce size and weight of energy storage systems 22 p3747 A67-39900

Coherent optics technology, presenting effective black body temperature of six radiation sources and output and pulse duration of four laser sources 22 p3817 A67-40351

Formation of short ruby laser light pulse and repetition frequency control using mode locking with saturable absorbers 23 p4015 A67-41036

Very short pulse measurements by deriving delayed pulse from measured waveform, describing detector circuit 23 p3981 A67-41273

He-Ne laser pulse delay when excited in optical resonator noting dependence on gas pressures 24 p4167 A67-42207

Laser emission nonlinear effects for materials with internal induced absorption noting pulse elongation and spatial smoothing 24 p4168 A67-42370

PULSE DURATION MODULATION /PDM/

PDM/FM high efficiency voltage regulator design, switching theory and regulation theory 08 p1286 A67-21030

PULSE FREQUENCY MODULATION /PFM/

Microwave echoes in axially magnetized yttrium iron garnet cylinders following application of two pulses, with second twice frequency of first 02 p0297 A67-11874

Minimum time and fuel problems for PFM systems, deriving optimal control by heuristic argument 06 p0977 A67-18524

Pulsed RF slot antenna breakdown controlled by preionization and diffusion 11 p1758 A67-24128

Local and overall stability of nonlinear discrete system with variable modes consisting of linear filter preceded by impulse modulator 11 p1770 A67-24751

Nonlinear discrete system equivalence of integral pulse frequency modulation /ipfm/ feedback systems, discussing Lagrange stability criterion 16 p2652 A67-31685

Transistor overload in active region operated by large pulse trains, discussing thermal response and resistance and operational frequency intervals 17 p2827 A67-32784

Stability of nonlinear sampled data control systems, investigating pulse frequency modulation using Liapunov function 22 p3777 A67-39829

Nonlinear sampled data system instability, discussing arbitrary single-valued nonlinearities and arbitrary modulation law /PAM, PWM or PFM/ 23 p3985 A67-41674

Integral pulse FM effect on feedback control, obtaining stability of equivalent nonlinear discrete system 24 p4135 A67-42183

PULSE HEATING

Time and local temperature distribution in semiconductor under heating pulse 09 p1579 A67-21704

Differential negative conductivity in n-type GaAs, using microwave electron heating 14 p2369 A67-28595

Stacking faults in tungsten specimens heated rigidly for short time by electric discharge 20 p3464 A67-36224

Microwave sound generation by transient heating of material surface with laser pulses 20 p3457 A67-36386

Electron temperature measurements on powerful pulsed plasma discharge using spectral line intensity 22 p3852 A67-39997

Heat transfer from plate located on dielectric base to liquid helium in pulsed regime influencing kinetics of superconductivity in thin films 24 p4254 A67-42258

PULSE HEIGHT

CdTe properties evaluated through pulse height response of surface barrier devices to monoenergetic alpha particles normally incident to surface 08 p1356 A67-21308

Van Allen belt proton measurements by pulse height analysis, using thin low-Z scintillator to minimize large angle electron scattering 11 p1856 A67-24014

Quark fractional electronic charge in cosmic radiation determined through pulse height distribution 15 p2549 A67-29526

Digital to analog pulser system for integral and differential testing pulse height analyzers [JPL-TR-32-1049] 18 p3049 A67-34485

Multi-input photomultiplier pulse height photographic recording system using dual beam oscilloscope for cosmic ray experiments 20 p3444 A67-36525

Interference reduction potential of binomial type pulses 20 p3387 A67-37638

Two and three-pulse echo trains stimulated in magnetoplasma by repeated electron cyclotron frequency pulsing studied with single particle collision theory 23 p4031 A67-40883

Cosmic X-ray sources spectra obtained by proportional counters and electronic systems on sounding rockets 23 p4001 A67-41222

PULSE JET ENGINE

Design for throttling and pulsing operation of rocket engine, discussing test data [AIAA PAPER 87-506] 18 p3113 A67-33970

PULSE MODULATION

Pulse frequency multistable devices whose states differ, along with output voltage, by generated pulse rate 01 p0043 A67-10233

Oscillating limiter effect on message modulation for band pass filter with flat amplitude and linear phase characteristics in input signal frequency range 01 p0025 A67-10853

Pulsed laser Q-factor modulation using nonlinear resonator functions in absorbing medium 03 p0436 A67-13133

Tunnel diode combined with backward diode improves rate of response and pulse waveform in tunnel diode circuits 03 p0381 A67-13583

Bandwidth and distortion in pulse filters 03 p0389 A67-14303

Noise rejection of various types of modulation in data transmission with multiple noise 04 p0568 A67-14455

Asymptotic method of synthesizing FFM pulse signals from given autocorrelation function 04 p0575 A67-15161

Pulse front shaping with monostable tunnel-diode generator by successive triggering through storage inductance 04 p0586 A67-15677

Equation for dynamical behavior of laser solving case of deep modulation of output noting pulsation problems 05 p0820 A67-16666

Solid state pulse modulated 10 MHz/channel passband frequency switch design and reduction to microelectronic form 05 p0789 A67-17041

Expansion of free turbulent air jet controlled by given frequency from diaphragm pulsator 06 p0982 A67-17741

Conversion of frequency spectrum of

pulse-position-modulated signal passing through delay device and amplifier switched by input undelayed signal 07 p1139 A67-19229

Modulation devices for pulsed systems, discussing signal preparation and channel grouping for time multiplex systems 07 p1150 A67-19341

Pulse distortion in ionospheric plasma, discussing reflection from layer via geometrical optics and quadratic approximation 07 p1143 A67-19594

Three-dimensional correlation function for modulating bell shaped and rectangular radar probing pulses 09 p1463 A67-21961

Simultaneous stability and quality control of pulse regulation, discussing computation of sum of squares of difference 13 p2086 A67-26474

SNR and transmission error probability in pulse modulated optical communication 13 p2067 A67-26663

Effect of distortion on spectrum of pulse signal with linear frequency modulation 13 p2070 A67-27046

Sawtooth voltage oscillation of triangular shape for pulse width modulation pulse shapers 13 p2089 A67-27704

Pulse modulated data channel operation over parallel optical paths, noting advantages inherent in simple processing and control circuitry 14 p2272 A67-28699

Noise rejection of various types of modulation in data transmission with multiple noise 15 p2435 A67-29291

Asymptotic method of synthesizing FM pulse signals from given autocorrelation function 15 p2435 A67-29347

Pulse-length modulated pressure waves having zero quiescent pulse width, actuating floating flap disk switching valves of pneumatic servomechanism 16 p2609 A67-31665

Asynchronous pulse modulation systems developed using step and linear segment approximations of message waveforms 17 p2812 A67-32318

Coding system using pulse interval modulation and providing reduced quantizing noise in received message developed from decaying-step approximation of signal waveforms 17 p2813 A67-32320

Three-dimensional correlation function for modulating bell-shaped and rectangular radar probing pulses 20 p3383 A67-37191

Pulse distortion in ionospheric plasma, discussing reflection from layer via geometrical optics and quadratic approximation 20 p3384 A67-37334

Hydrogen integrator in pulsed mode of operation used to determine current pulse integrals 22 p3795 A67-39228

Pulse generation method for high power modulators in Doppler radars studied, using step recovery diode to construct compression network 22 p3772 A67-39897

PULSE MOTOR

Nuclear pulse propulsion, discussing principles of operation of contained and uncontained systems 06 p1030 A67-19025

PULSE POSITION MODULATION /PPM/

PPM-frequency time hopping for multichannel communication system to transmit digital data over tropospheric scatter path 02 p0202 A67-12131

Communications requirements for manned deep space missions, using optical links, with PPM, PCM/PL and coherent reception for each link 07 p1141 A67-19342

Stability and response time of quantified pulse-position modulation feedback control circuit consisting of nonlinear sampler and first order continuous part 22 p3776 A67-39647

PULSE RADAR

Frequency correlation of clutter by considering signal received by radar at time t after it has transmitted pulse 01 p0023 A67-10468

Pulse Doppler radar performance in presence of random fading to study ambiguity diagram and nature of variance with respect to Doppler frequency 04 p0653 A67-14876

Clutter suppression by complex weighting of coherent pulse train 04 p0570 A67-14878

Measurements by means of vertical beaming cloud pulsed radar operating

simultaneously on two wavelengths 04 p0573 A67-15036

Pulsed radar transmitter research in U.K., noting beam type microwave tubes, solid state switches, hydrogen thyatrons, etc 04 p0581 A67-15052

Radar data handling and display systems used with pulsed radars, detailing military type for use of weapons control officer 04 p0578 A67-15057

Pulse Doppler radar theory using Fourier transformation integrals applied to analysis of spectrum of all signals 06 p0957 A67-17592

Ionospheric sounding data obtained principally by ground-based ionosondes, topside sounders and incoherent backscatter systems 10 p1630 A67-22775

Principles, methods of operation, techniques and limitations of phase comparison position-determining CW and pulse type systems 10 p1605 A67-22996

Comparison of measurement accuracy for angular coordinates in radar systems by linear scanning and equal-signal zone methods 10 p1607 A67-23450

Terrain following pulsed radar system without continuous scanning noting computer simulation, antenna and pitch control 11 p1752 A67-24259

Distribution-free signal detection by multiple-resolution-element pulse radar, based on ranks of returns and having invariant false alarm rates 15 p2436 A67-29933

Digital pulse compression radar receiver with digital-pulse compression advantages and disadvantages, noting target acquisition, range tracking and antenna scanning system 16 p2630 A67-31738

Eldorado low altitude detection and short reaction time defense system, examining Doppler effect and Mirador pulse radar 17 p2816 A67-32751

Correlation detection for extracting reflected radar signal from noise 19 p3195 A67-35550

Pulse radar on Air Force Eastern Test Range, discussing precision, sensitivity, acquisition, signature and multiple target capability 20 p3381 A67-36581

PULSE RATE

SA CHRONOTRON

Laser producing two or three light pulses in sequence with interval between pulses mechanically controlled by optical wedge inserted into resonator 01 p0087 A67-10161

Current pause during circuit overloading accompanied by filament explosion 06 p1031 A67-17867

Background noise produced by high energy radiation incident on photomultiplier tube, stressing differences between tubes in number of small pulses produced 10 p1618 A67-23809

Radio pulse sequences selection according to carrier frequency by analyzing filter operation 14 p2261 A67-28278

Current dependent modes in pulsed avalanche diodes 15 p2442 A67-29174

Pseudorange sawtooth-pulse-reset controller design for satellite attitude control system 15 p2458 A67-29430

Pulse rebalance system in conjunction with pulse accumulator and comparator for precision velocity cut-off signals, presenting data and system characteristics 17 p2858 A67-32485

Electrodynamic transducer for liquid-borne ultrasonic pulse intensity measurements, considering limits, inductance and measuring system dimensions 18 p3043 A67-33463

Impact ionization in gallium arsenide through fast pulse experiment, noting conflict between theoretical and measured current-voltage characteristics 18 p3097 A67-33517

Thyratron circuit for generating high repetition rate high energy pulses, discussing design considerations and modifications 20 p3397 A67-36527

Passive Q-switching of carbon dioxide laser with cavity containing saturable absorber, noting peak power and pulse rate 20 p3460 A67-36854

Choke-coupled magnetic amplifiers and amplifiers with rotational magnetization, considering multicyle and single-cycle amplification 21 p3593 A67-38290

PULSE RATE /BIOL/

Absolute bed rest and recumbent exercise during bed rest effects on pulse

rate response to submaximal work, cardiovascular functional capacity /maximal oxygen intake/, physical work capacity and orthostatic tolerance 05 p0755 A67-16283

PULSE RECORDER

Transistorized logarithmic amplitude converter for recording pulses of radiation detector, automatic switching of conversion scale permits amplitude measurement 01 p0062 A67-10160

Semiconductor device measuring pulsed nanosecond currents produced in detectors by alpha particles 01 p0065 A67-10651

Binary tunnel diode scaler and factors essential for reliable operation 03 p0376 A67-14266

Timekeeping unit calibration, on basis of signals emitted by HBG transmitter, permitting measurement of state and performance of quartz oscillators 11 p1792 A67-24782

Automatic pulse digital analyzer design to measure simultaneously all-pulse parameters used for control of closed loop systems 13 p2078 A67-26801

Miniaturized no-moving-parts fluid pulse counter development for ordnance application 19 p3176 A67-34806

Ring circuit using glow-discharge thyatrons to combine functions of pulse indicator and pulse counter with decimal readings 19 p3228 A67-34990

Q-switched laser single pulse visual recording by oscillograph with storage tube/photodiode combination 22 p3817 A67-40415

PULSE TIME MODULATION /PTM/

Time expansion device for photomultiplier circuit for high pulse frequency using recording system, readout, thin film memory and simulation unit 01 p0029 A67-10662

Pulse-time modulation of first kind and block diagram of pulse time modulator studied for control system applications 15 p2455 A67-29122

Synthesis of radar ambiguity functions via burst-pulse time-frequency waveform coding, employing Bayesian statistical analysis 18 p3000 A67-34109

Onboard receiver-decoder control unit for ESRO I and II consisting essentially of four-state signal corresponding to time modulated pulses 21 p3581 A67-38201

PULSE TRANSMISSION SYSTEM

Doppler tolerant pulse train design, noting signal processing by delay line with fixed taps for significant changes in pulse spacing 01 p0023 A67-10464

Single self-mode-locked pulse selection from bleachable dye Q-switched Nd-doped glass laser 01 p0091 A67-10875

Probabilistic structure of and establishment time for group synchronization in time-division-multiplex /binary code/ transmission systems 01 p0027 A67-11238

Sunde channel model applied to Air Force tropo transmission test for calculating pulse error 02 p0202 A67-12129

Regularization method to minimize error in solving Wiener-Hopf integral equation to determine pulse transfer function 03 p0374 A67-13083

Longitudinal and shear wave velocities in polycrystalline sample of magnesium thorium alloy measured by pulse transmission technique as function of temperature [ASME PAPER 66-WA/MET-11] 04 p0639 A67-15375

Range safety and tracking systems, discussing C-band beacon, CW transponder and command-destruct receiver operation and testing 04 p0577 A67-15729

Parametric transformation of spectrum of video pulses in transmission line 05 p0762 A67-16359

Radar phase locking technique applied to magnetron radar, measuring transmitted pulse phase with respect to stalo running at magnetron frequency 05 p0780 A67-17521

Ultrasonic nondestructive inspection of adhesively bonded components, discussing pulse echo reflection, pulsed through transmission and sweep frequency coupling methods and scanning equipment 09 p1507 A67-22526

Transmission of large number of instrumentation channels over parallel pulse-modulated light beams, using electro-optical mosaic sources and detectors 11 p1764 A67-24444

Scattering and absorption of ultrashort

coherent radiation pulses passing through electron gas applied to ionosphere 17 p2812 A67-32312

Pulse rebalance system in conjunction with pulse accumulator and comparator for precision velocity cut-off signals, presenting data and system 17 p2858 A67-32485

Distributed Esaki diode pulse characteristics in solid state transmission circuit 21 p3599 A67-38609

Electromagnetic wave pulses transmission through plasma boundary, studying boundary effects for broad and narrow frequency spectra 21 p3669 A67-38682

Coded information transmission with reduced band emphasizing pulse prediction through redundancy, information quantity and delta signal 21 p3585 A67-38763

PULSE WIDTH

Phase locking of pulsed Gunn oscillators with 0.3 to 1 microsecond pulse widths in S-band 03 p0382 A67-13672

Picosecond laser pulse widths measurement by method using special symmetry properties of second harmonic generation at GaAs crystal surface 07 p1234 A67-20097

Monostable high speed pulse circuit using tunnel diode and transmission line, noting possibility of cascade connection without coupling elements between stages 10 p1609 A67-22773

Diffused base punchthrough avalanche transistor /PAT/ at high recurrence frequency having capacitance dependence of pulse width 10 p1609 A67-22839

High speed correlation technique to measure time development of width of ultrashort pulses generated by mode locked Nd trivalent ion glass laser 13 p2126 A67-27014

Passive reactive circuit conversion into circuit that shapes radio pulse with rectangular envelope 13 p2069 A67-27042

Fluidic pulse switching network hazards at high operating speeds, suggesting digital computer simulation to anticipate and rectify hazards before hardware fabrication 14 p2251 A67-28348

Mode-locked laser described in traveling light pulse terms, with saturable absorber, noting pulse width under steady state 16 p2686 A67-31808

Plasma produced transit time delay of reflected pulses for collisionless inhomogeneous plasma 17 p2810 A67-32070

Pulse width of ultrashort light pulses measured by Michelson type arrangement of nonlinear optics 20 p3456 A67-36172

Worm motion of domain walls in Permalloy films using Kerr magneto-optic apparatus under pulse drive with nanosecond rise time 22 p3860 A67-39901

PULSE WIDTH AMPLITUDE CONVERTER

Circuit design and performance to convert DC input voltage to pulse train with width proportional to input 19 p3197 A67-35702

PULSE WIDTH MODULATION /PWM/

Counting control methods for multistable elements containing nonlinear quadrupole with comb type amplitude characteristic, using short-term action on LF filter 01 p0044 A67-10497

Pulse amplitude range estimated for which PWM system is asymptotically stable, using method of Murphy and Wu 03 p0393 A67-13983

Stability criterion for PWM feedback systems containing one integrating element 03 p0393 A67-13984

Signal stabilization by linearization of time independent nonlinearities using extra signal and nonlinearity, noting role of pulse width modulation [ASME PAPER 66-WA/AUT-21] 04 p0592 A67-15392

Pulse width modulated series switch with input and output filtering for automatic impedance matching in DC circuits regardless of load or source characteristics 08 p1311 A67-20650

Pulse width modulation voltage regulator design for power conversion applications, considering interrelation of loop gain, switching frequency, etc 08 p1284 A67-20693

LC smoothing filter in rectifier for pulse supply source stabilized by pulse width modulation 10 p1611 A67-22980

Counting control methods for multistable elements containing nonlinear quadrupole

with comb type amplitude characteristic, using short term action on LF filter 10 p1621 A67-23619

Received signal degradation for coherent pulse transmission through rain scattering volume, calculating length and energy for various paths 11 p1752 A67-24285

Nonlinear theory of internally loss modulated laser including effect of arbitrary atomic line shape, saturation and mode pulling 13 p2127 A67-27084

Weak DC signals conversion into electric pulses by magnetic semiconductor pulse width modulator using AC generator 17 p2823 A67-32224

Pulse-width modulated control system optimization, with necessary conditions derived by variational calculus, and numerical solution to resulting boundary value problem 19 p3199 A67-34783

IC emitter follower line driver with input filtering for PWM signal conditioning, solving onboard high impedance problems in drop tests with piezoelectric accelerometer 23 p4005 A67-41372

Nonlinear sampled data system instability, discussing arbitrary single-valued nonlinearities and arbitrary modulation law /PAM, PWM or PFM/ 23 p3985 A67-41674

PULSED DOPPLER SYSTEM

Pulse Doppler waveform coding, presenting technique of selecting pulse-period modulation codes requiring only computer calculations 15 p2437 A67-29934

PULSED GENERATOR

Pulsed chronotron vernier for precise time expansion, discussing circuit configuration, operation and performance 01 p0067 A67-10658

Single cycle 1.72 mw pulse generator operating at 6 m wavelength 02 p0215 A67-11979

Combination flash photolysis-flash pyrolysis system with timing circuit, using Tektronix pulse generators and Ignitron circuit for firing spectroscopic lamp 02 p0247 A67-12689

Giant coherent light pulse generation by Q-factor modulated laser 03 p0433 A67-12941

Multistage thyatron generator for producing complex shaped pulses through rectifier control 03 p0388 A67-14267

Synchronous sequential multiphase pulse generator using unit distance cyclic code 07 p1162 A67-20199

Pulse generator for high power injection lasers at room temperature noting small size, cheapness, simplicity, and capability of switching several thousand amperes 08 p1337 A67-20372

Magnetothermoelastic mechanism of exploding wire effect under high intensity current surge in pulsed generator for hydrodynamic and magnetoelastic pumping 08 p1354 A67-21046

Stationary and transient processes in multiply stable pulsed element identified as autonomous system containing blocking generator, oscillatory circuit, detector and filter 09 p1473 A67-21959

Apparatus producing voltage pulses in X-band magnetrons operating on pulse lengths of tens of nanoseconds 09 p1479 A67-22262

Monograph on high power semiconductor-magnetic pulse generators, noting saturable inductors and silicon controlled rectifiers, circuit analysis, voltage regulator, etc 09 p1482 A67-22698

Solid fueled rocket powered MHD generators with high power densities 12 p1898 A67-25382

Contact-free controlled delay unit using shift register and clock-pulse generator for binary signals designed with wide range of time delay variation 13 p2088 A67-26798

Circuit for multifrequency ionospheric probing, with basic frequency scanning unit containing sawtooth pulse oscillator 14 p2315 A67-27949

Ultrashort light pulse generation by forcing oscillation modes, noting role played by dispersion of medium within resonator cavity 16 p2702 A67-31042

Pulse generator for semiconductor laser excitation, noting silicon controlled rectifiers and pulse shaping line 19 p3191 A67-34983

Thyatron circuit for generating high repetition rate high energy pulses, discussing design considerations and modifications 20 p3397 A67-36527

Stationary and transient processes in

multiply stable pulsed element identified as autonomous system containing blocking generator, oscillatory circuit, detector and filter 20 p3400 A67-37189

High power thyristor used with battery to operate pulse repeating sonar transducer 22 p3747 A67-39255

Multiple stimulated Brillouin scattering used for nanosecond high intensity pulse generation combining ruby laser with liquid cell and Fabry-Perot etalon 23 p4011 A67-40786

Explosion of ovoid copper wire conductors observed with pulsed X-rays noting effect of magnetic pressure 23 p4028 A67-41461

Space power system pulsed turbine concept using bipropellants, reviewing multistage and multiple pass reentry performance and operational characteristics 24 p4107 A67-42530

PULSED LASER

Laser producing two or three light pulses in sequence with interval between pulses mechanically controlled by optical wedge inserted into resonator 01 p0087 A67-10161

Q-switching of ruby laser using cell containing chloroaluminum phthalocyanine in chloronaphthalene to obtain giant pulses 01 p0089 A67-10448

Laser lines of pulsed discharge in iodine vapor 01 p0090 A67-10549

Molecular spectroscopy of illumination effects on cobalt activated ZnS exposed to ruby laser pulses 01 p0090 A67-10683

Intense pulse generation at 5300 angstroms by frequency doubling in Q-switched and glass laser and possibility of generating particular harmonics 01 p0090 A67-10759

Laser lines of pulsed discharge in iodine vapor 01 p0091 A67-11057

Organic glass disintegration induced by pulsed laser beams 02 p0257 A67-12241

Laser induced breakdown of complex organic molecules in vapor state, noting emission accompanied by formation of partially dissociated hot gas 02 p0252 A67-12451

Pumping of organic dyes in organic solvents, using pulsed ruby laser 02 p0253 A67-12515

Avalanche transistor pulser designed to drive GaAs radar-laser diode 03 p0376 A67-12964

Pulsed laser Q-factor modulation using nonlinear resonator functions in absorbing medium 03 p0436 A67-13135

Fluorescent emission of neodymium laser triggered by Pockels effect as function of population inversion 03 p0436 A67-13201

Mode characteristics of solid state lasers from analytical solution of conservative equation 03 p0437 A67-13208

Performance of two-photon laser operating in continuous wave mode, deriving formula for pulse frequency 03 p0437 A67-13292

Transition to detonation in gaseous medium experimentally studied, based on self-sustained detonation front and adaptation of amplitude modulated giant pulse laser system 03 p0535 A67-13500

Expansion velocity of luminous front of plasma plume generated by giant pulse laser 03 p0478 A67-13573

Coupling of pulse powers in TEM of up to 80 mw from He-Ne laser at 6328 angstroms 03 p0437 A67-13678

High temperature single solid particle plasma generation by focused giant pulse Q-spooled ruby laser beam irradiation of LiH suspended in vacuum electric fields 03 p0485 A67-14047

Performance characteristics for pulse type Ar laser with external interferential system of quasi-confocal spherical mirrors 03 p0438 A67-14188

Characteristics of pulsed laser action in He-Ne and He-Ar mixtures at pressures above 200 mm Hg 03 p0438 A67-14189

Temporal-spatial variation of cross sectional flux distribution of stimulated emission from Nd glass pulsed laser 03 p0439 A67-14280

Disintegration of alkali halide single crystals, polymers and glasses under laser radiation, noting parameters of disintegration region 03 p0439 A67-14367

Pulsed lasers as machine tools for material removal, noting tests on titanium, aluminum oxide, steel, etc 04 p0628 A67-15308

Laser pulse energy measurements with

- liquid absorption cell
calorimeter 04 p0624 A67-15456
- Vaporization of thin metallic films with focused laser beam, comparing theoretical and experimental results prepared by using pulsed high pressure helium-neon laser 04 p0630 A67-15478
- Short pulse Q-switched laser with variable pulse length 05 p0817 A67-16641
- Ruby laser with nonresonant feedback due to radiation scattering, showing use as optical frequency standard 05 p0818 A67-16642
- Pulsed gas discharge lasers noting required energy level for maximum efficiency, experimental techniques and results 05 p0819 A67-16650
- Divalence samarium ion doped calcium fluoride laser action at low temperatures obtained with giant pulse ruby laser excitation 05 p0820 A67-16661
- Equation for dynamical behavior of laser, solving case of deep modulation of output, noting pulsation problems 05 p0820 A67-16662
- Dysprosium doped calcium fluoride giant pulse laser with high repetition rate obtained, using DC pumping - xenon lamp 05 p0822 A67-16674
- Saturated absorption of color centers in glass self-Q-switched pulses, as in glass codoped with uranyl oxide and Nd ions 05 p0822 A67-16678
- Quenching of one pulsed ruby laser oscillation by another, noting coupled rate equations for steady state and transient behavior 05 p0823 A67-16682
- Tunable Raman laser obtained by electron mobility subjected to magnetic field, noting threshold pump power 05 p0823 A67-16684
- Enhanced lasing of high pressure He-Ne laser, commenting on delay time of light pulse emitting through walls of discharge tube from start of exciting pulse 05 p0823 A67-16687
- Stimulated emission in triplet system of nitrogen molecule produced by pulsed laser discharge, identifying lines and interpreting intensity distribution in rotational band spectrum 05 p0824 A67-16785
- Temperature field of active medium of pulsed laser using variational methods, considering two approximate solutions 05 p0825 A67-16935
- Transient behavior of He-Ne lasers under pulsed HF excitation, discussing rate equations representing atomic population density and photon density 05 p0825 A67-16980
- Nonlinear propagation of pulse signal in laser type traveling wave amplifier 05 p0825 A67-17232
- Periodic automodulation of radiation and possibility of generating giant pulses in three-level laser with inhomogeneously excited active medium 05 p0826 A67-17233
- Radiation transport in spectral lines as consecutive photon absorptions and emissions, discussing contemporary theories, approximation methods and applications spark shadow projections in air for giant pulse 06 p1010 A67-18090
- Extension of paper on saturable absorber giant pulse lasers to include effects of finite absorber lifetime on pulse parameters, noting pump role 06 p1011 A67-18148
- Plasma formed by laser pulse on tungsten target, measuring radius, temperature and radiative properties, developing model 06 p1041 A67-18149
- Treatment of steel with laser beam, obtaining precision holes without affecting microhardness of metal 06 p1008 A67-18234
- Semiconductor mirror for Q-factor modulation of laser resonator 06 p1012 A67-18789
- Cleavage and separation of dye-doped ice and paraffin instantaneously heated by laser pulse, measuring mechanical pulse at energy concentrations below vaporization heat 06 p1119 A67-18807
- Nanosecond pulse light sources used in free flight hypersonics for ballistic range measurements, noting less photographic blurring of motion 06 p0981 A67-18881
- Laser application to meteorology, discussing Rayleigh, aerosol and Raman scattering, system configuration and measurement problems 07 p1194 A67-19091
- Changes in giant molecule structure of polypropylene films under action of laser pulses analyzed by optical microscopy 07 p1211 A67-19169
- Traveling wave excitation of high power nitrogen and neon lasers with velocity matching that of stimulated emission 07 p1196 A67-20093
- Time behavior of pulsed water vapor laser, noting spiking from far IR emission lines 07 p1197 A67-20095
- Pulse generator for high power injection lasers at room temperature noting small size, cheapness, simplicity, and capability of switching several thousand amperes 08 p1337 A67-20372
- Selective imaging of objects in range using pulsed laser illuminator synchronized with Kerr cell camera, obtaining elimination of film exposure due to backscatter in turbid atmosphere 08 p1337 A67-20683
- Gas desorption following Q-switched laser beam bombardment of tungsten target in vacuum 08 p1338 A67-21310
- Calorimetric measurement of pulsed ruby laser output energy 09 p1510 A67-21615
- Envelope and phase velocities for laser pulse propagating in nonlinear dielectric with intensity dependent index of refraction 09 p1511 A67-21748
- Stimulated Brillouin scattering in liquids used for passive Q-switch applicable to visible and IR lasers 09 p1511 A67-21749
- Stimulated emission, absorption spectra and luminescence of neodymium-activated YAG crystals in pulsed laser 09 p1513 A67-22068
- Laser welding and machining - Seminar, Pennsylvania State University, June-July 1965 09 p1504 A67-22137
- Pulsed laser welding process, discussing wire-to-wire welds, sheet-to-sheet welds and circuit board weldings 09 p1504 A67-22139
- Laser as drilling and welding tool, noting industrial guidelines, pulse control techniques, micromachining, etc 09 p1504 A67-22140
- Laser as drilling tool 09 p1504 A67-22142
- Laser radiation effect on solids, noting laser properties, temperature rise, melting, vaporization and particle emission of materials 09 p1513 A67-22144
- Industrial laser application, giving background information on laser theory 09 p1505 A67-22145
- Welding of niobium and nickel alloys by high energy pulsed laser, noting weld joint 09 p1505 A67-22147
- Amplification and detection of high power TW laser pulses, noting superradiance limit 09 p1514 A67-22273
- Pulsed ruby laser rangefinder with high maximum repetition frequency and digital range readout for data acquisition for determining airborne target trajectories 09 p1465 A67-22622
- Duration and waveform of short single pulse emitted by injection semiconductor laser 09 p1516 A67-22659
- High power laser performance and material limitations, noting Q-switching with liquid cell 09 p1516 A67-22675
- Ruby laser cavity losses measurement by Fabry-Perot resonance 10 p1662 A67-22740
- Self-focusing processes of laser pulses in dissipative medium, analyzing temporal nonlinear aberrations connected with thermal effects 10 p1664 A67-23332
- High voltage pulsed electrodeless discharge in rare gas as light source for ruby and Nd glass laser excitation and observation of output characteristics 10 p1666 A67-23565
- Giant pulse generation range in transverse direction after Q-switching in ruby laser, examining resonator properties 10 p1666 A67-23584
- Pulsed ruby laser source for holography compared to He-Ne gas laser 10 p1657 A67-23625
- Field emission from sharply pointed CdS single crystals photon-enhanced by illumination from pulsed argon-ion laser 11 p1845 A67-24133
- Transient emission characteristics of pulsed argon ion laser, noting capillary discharge due to radiation trapping effect 11 p1801 A67-24649
- Superradiant transition in high gain pulsed laser 11 p1803 A67-24841
- Molecular spectroscopy of illumination effects on cobalt activated ZnS exposed to ruby laser pulses 11 p1804 A67-25072
- Pulsed ruby laser to obtain Fourier holograms in light reflected from diffusely scattering objects, discussing relaxation of resolving power of photographic emulsions 12 p1939 A67-25335
- Simple giant pulse ruby laser of high spectral brightness 12 p1953 A67-25984
- Time dependence of coherent emission wavelength shift of GaAs-P laser diodes during flat-topped current pulsation 13 p2125 A67-26513
- Pulsed UV laser using nitrogen noting synchronization characteristics, stability, peak power, etc 13 p2126 A67-26700
- Giant pulse operation of many-element laser with composite Q-switch consisting of spinning prism and saturable glass plate 13 p2126 A67-26729
- Discharge formation and propagation in He-Ne laser excited with pulsed RF voltage 13 p2126 A67-26730
- High speed correlation technique to measure time development of width of ultrashort pulses generated by mode locked Nd trivalent ion glass laser 13 p2126 A67-27014
- Time dependence of semiconductor enhanced reflectivity by pulsed argon ion laser based on thermally generated electron hole plasma 13 p2177 A67-27016
- Pulsed neon laser at 5401 angstroms 13 p2128 A67-27089
- Effectiveness of coupling between light source and active medium in optically pumped laser 13 p2128 A67-27230
- Amplitude, phase distribution and output beam characteristics in transverse modes of unstable optical cavities analyzed using pulsed gas laser 13 p2129 A67-27350
- Mode-locked laser traveling pulses proved experimentally to be 180 degree pulses 14 p2330 A67-28292
- Solid state lasers and pulsed ruby lasers for continuous and quasi-continuous operation, noting applications in micromachining 14 p2331 A67-28559
- Single frequency, far IR and high power gas laser design and manufacturing 14 p2333 A67-28970
- Pulsed laser beam induced elastic waves in metals, noting experimental techniques and role of radiation pressure in wave generation 14 p2374 A67-28987
- Power output of pulse laser measured in terms of ultrasonic vibration intensity induced in piezocrystals by radiation 15 p2485 A67-29125
- Magnetic field strength effects on pulse and CW operation of large diameter ionized gas lasers 15 p2496 A67-29173
- Stimulated emission from pulsed electrical discharge through helium with wavelength measured and transition identified with interferometer 15 p2497 A67-29395
- Transposition into holography of optical visualization methods by linking ultrahigh speed camera and solid state laser 15 p2487 A67-29481
- Giant pulse time evolution influenced by pump-induced material inhomogeneities studied by analyzing laser rate equations 15 p2498 A67-29484
- Double sapphire plate resonator to control multiple modes of commercial laser /Korad K-1Q/ without use of saturable dye 15 p2498 A67-29497
- Generation of large pulses of extremely short duration in ruby laser by rotating mirror technique at lower frequencies 15 p2498 A67-29642
- Time varying high density laser induced plasmas formed in high pressure gases studied using Mach-Zehnder interferometer 15 p2488 A67-29903
- Ultrashort light pulses, discussing laser modes, Q-switching pulse duration measurements, etc 16 p2686 A67-31741
- Airborne ground profiler using CW and pulsed lasers range finders discussing performance 16 p2679 A67-31798
- Periodic relaxation pulses caused by thermal resonance drift, studying diffraction loss and other effects on transverse modes in crystal lasers 17 p2867 A67-32362
- Line width vs optical thickness in pulsed argon-ion laser used to determine level population in plasma 17 p2867 A67-32452
- Frequency variation of ruby laser optically pumped by flash lamp, noting effect of phthalocyanine solution 17 p2868 A67-32705
- Saturable organic dye absorber giant pulse lasers in limit of large absorber cross

section, normalized initial inversion and relaxation time 17 p2869 A67-33055

Spatial coherence and shape of emission wave front of giant pulse from ruby laser with Pockels cell shutter 18 p3058 A67-33526

Semiconductor mirror for Q-factor modulation of laser resonator 18 p3059 A67-33731

External corrective system significantly decreased angular radiation divergence of single pulse laser, determining effect on focal spacing of corrective lens 18 p3061 A67-34042

Longitudinal magnetic field effect on radiation intensity of He-Ne laser operating in pulsed regime 18 p3061 A67-34043

Reentry vehicle heat shield materials thermal diffusivity measurements by flush method, using pulsed laser and xenon flash lamp 18 p3051 A67-34506

Laser pulse duration effect on photonuclear processes, as affected by matter-radiation interactions, observing ionization in gases and surface photoeffects 19 p3238 A67-34897

Two-channel single-pulse neodymium glass laser with 180 joule pulse, performance and optical features 19 p3239 A67-34986

Gallium phosphide diode-based laser generator of nanosecond light pulse sequence, noting simulation of scintillation counter photoelectric amplifiers, Cerenkov counters, etc 19 p3228 A67-34987

Pulsed injection laser radar for rendezvous and docking operations, giving results of test performance [AIAA PAPER 67-606] 19 p3259 A67-35997

Image reconstruction of diffusely reflecting objects using pulsed hologram technique 19 p3233 A67-36102

Rose bengal saturable filter for production of high peak power neodymium laser pulses by regeneration switching 20 p3457 A67-36175

Relaxation of carbon dioxide pulsed laser levels by collisions with hydrogen, showing gain dependence on hydrogen pressure 20 p3457 A67-36384

Sum generation of tunable two-frequency pulse output of gain-switched ruby laser 20 p3458 A67-36389

Photodiode holder design for ITT FW-114A high speed planar photodiode for monitoring giant pulse laser output 20 p3397 A67-36528

Superradiant high gain pulsed lasers measured for single pass gain by comparing single pass and double pass radiation intensities 20 p3460 A67-36858

Transitions in neutral spectra observed in near IR wavelength region in noble gases 20 p3460 A67-36859

Plasma production by pulsed laser irradiation of aluminum in space chamber vacuum 21 p3666 A67-38259

Temperature effect on Ni thermal diffusivity measured using ruby laser pulse 21 p3640 A67-38262

Giant coherent light pulses generation by Q-switched laser, studying dynamics of generation and field distribution 21 p3640 A67-38373

Laser welding and welding processes noting evolution as specialized tool to supplement present welding equipment 21 p3635 A67-38622

GaAs pulsed injection laser diode noting characteristics for room temperature operation 22 p3813 A67-39253

Operating and performance characteristics of helium-neon pulsed gas laser, discussing application to integrated microcircuits fabrication 22 p3813 A67-39333

Relaxation times of carbon dioxide vibrational levels and afterglow pulsed gain for nonflowing gas laser amplifiers 22 p3814 A67-39354

Steady laser oscillation by Maxwell equations, with allowance for diffusion effects, shows no qualitative changes in field distribution pattern 22 p3815 A67-39759

Rare gas isotopic analysis using ruby pulsed laser and mass spectrometer 22 p3816 A67-40241

Recovery time of carbon dioxide laser excited by electric pulse discharge noting heat conduction toward walls 23 p4011 A67-40692

Pulsed water vapor laser single wavelength operation using three diffraction gratings to make resonator frequency-selective 23 p4011 A67-40783

Transient interference studied for emission from pulsed ruby laser 23 p4012 A67-40883

Self-synchronization of axial modes of LF oscillations of laser giant pulse intensity with saturable filters 23 p4013 A67-40908

Pulse regenerative amplification in Q-switched argon-ion laser during buildup time to saturation 23 p4014 A67-41030

Temperature of metal surface irradiated by giant pulse laser beam by measuring energy of emitted thermal ions 23 p4015 A67-41035

Formation of short ruby laser light pulse and repetition frequency control using mode locking with saturable absorbers 23 p4015 A67-41036

Giant pulse ruby laser having tunable two-frequency output noting spectral measurements made with Fabry-Perot interferometer 23 p4015 A67-41038

Performance limits of laser rangefinder for design of all-weather terrestrial rangefinder, discussing echo signal, backscatter noise and TPG 23 p3999 A67-41040

Ion energies in expanding plasma stream generated by intense giant pulse laser light in focus on solid LiD and LiH targets 23 p4033 A67-41152

50 Hz ruby pulse laser emission, discussing power output, electromagnetic spectrum and transverse mode interaction 23 p4016 A67-41153

Emission of GaSb injection lasers in pulse regime, demonstrating existence of two staggered laser lines originating in diode regions 23 p4016 A67-41193

Energy detection of multipulse returns from optically rough target using Q-switched laser 23 p4016 A67-41265

Laser macrophotography for size distribution of particulate debris dispersed from ablating zirconium alloy specimen in hyperthermal wind tunnel ablation testing 23 p4006 A67-41380

Giant pulse irradiation effect on ruby laser under oscillation quenching, amplification and characteristics changes in metastable state population 23 p4017 A67-41434

Laser irradiation effect on semiconductor crystals surfaces using pulsed ruby laser 23 p4045 A67-41470

Optical Raman scattering from atmospheric oxygen and nitrogen via pulsed nitrogen UV laser light source, discussing spectral analysis of air scattering 24 p4147 A67-41883

Second optical harmonic generation of pulsed ruby laser emission in GaSe crystal suggesting only surface layer contribution to generation 24 p4167 A67-42074

Electrification of single crystals of semiconductor compounds of AlIBVI and AlIIBV type after exposure to ruby laser pulses 24 p4167 A67-42164

Thick walled carbon cone calorimeter in pulsed lasers used for calibration purposes, discussing error sources 24 p4154 A67-42174

He-Ne laser pulse delay when excited in optical resonator noting dependence on gas pressures 24 p4167 A67-42207

Absorption characteristics for laser power stabilization using Rayleigh active material 24 p4167 A67-42360

Two-photon absorption in alkali halide crystal via gas laser noting F center formation 24 p4167 A67-42361

Laser emission nonlinear effects for materials with internal induced absorption noting pulse elongation and spatial smoothing 24 p4168 A67-42370

Laser pulses producing local dissociation process in AlIIBV semiconductor compounds 24 p4168 A67-42725

PULSED RADIATION

Time resolving capabilities of RCA C-70045, 56 AVP and XP 1020 photomultipliers 01 p0067 A67-10659

Radio pulse pattern from EAS monitored at Yorkshire, England, observed on oscilloscope against galactic noise background 01 p0144 A67-10888

Fixed voltage, fixed energy and variable voltage variable energy pulsed neutron devices and applications in nuclear propulsion, radiation dosimetry, velocity measurements, etc 02 p0266 A67-12216

Optical frequency translation of pulses from mode locked laser, noting Doppler

shifts of large magnitude 02 p0253 A67-12506

Nitric oxide molecular laser obtained by dissociation of NO-Cl in pulsed electrical discharge 02 p0253 A67-12510

Microstructural analysis multiple electron-photon cascade resonance amplifier response to sine-square radio signal 03 p0376 A67-13091

Electron cyclotron echo production from plasmas by repeated pulsing, developing theory based on electron neutral momentum transfer collisions 04 p0665 A67-15105

Nuclear pulse propulsion activities of last decade and current research 06 p1030 A67-19026

Nonlinearity caused by relativistic mass effect leading to radiation maxima of plasma excited by two pulses at electron gyrofrequency 11 p1827 A67-23889

Physical and hydrodynamic processes induced in vaporizable solids by pulsed light radiation from sources using explosives 11 p1782 A67-24955

Balloon observations of large scale coherent pulsating electron precipitation events in auroral zone accompanied by geomagnetic continuous pulsations [AFOSR-67-1314] 12 p1931 A67-25112

Laser measurements and standards of energy, power, attenuation and frequency stability, using pulsed ruby and gas lasers as radiation source 14 p2319 A67-28392

Ultrashort light pulses, discussing laser modes, Q-switching pulse duration measurements, etc 16 p2686 A67-31741

Coherency relation between quasi-periodic X-ray and optical pulsations in auroras 17 p2844 A67-32543

Response of capacitors irradiated by pulses of transient nuclear radiation 17 p2828 A67-32863

Measurement of Doppler-broadened emission line width by Fabry-Perot interferometer to study ion temperature of pulsed plasma 17 p2862 A67-33292

Generation of giant pulses of coherent radiation by rotating-mirror technique and by passive Q-switch using cryptocyanine 17 p2871 A67-33390

Time-microscopy methods using laser flashlight, roentgen flashlight and rapid succession spark pulses in combination with stereo cameras 17 p2864 A67-33408

Piezoelectric microphone for measuring pulsed ultrasonic radiation intensity and energy distribution, discussing principles, operating conditions and construction of instrument 18 p3046 A67-33745

Plasma column in magnetic field created by diffusion from low pressure pulsed discharge in hydrogen, with plasma density dependent on gas pumping speed 19 p3275 A67-35108

Silicon transistors transient defect annealing from pulsed particle irradiation, stressing time factors 19 p3305 A67-35667

Giant pulse irradiation effect on ruby laser under oscillation quenching, amplification and characteristics changes in metastable state population 23 p4017 A67-41434

PUMP

SA AXIAL PUMP
SA CENTRIFUGAL PUMP
SA CONDENSATION PUMP
SA ELECTROMAGNETIC PUMP
SA FUEL PUMP
SA HEAT PUMP
SA HYDRAULIC PUMP
SA INJECTOR
SA ION PUMP
SA JET PUMP
SA MOLECULAR PUMP
SA TURBINE PUMP
SA TURBOPUMP
SA VACUUM PUMP

Metering and pumping equipment for test channel for high altitude permeability tests of parachute cloth, noting permeability of MIL-C-7350 B, type I fabric 02 p0182 A67-12789

Mercury device for analyzing pressure distribution, velocity profiles and resistance coefficients of turbulent flow in channels of linear induction pumps under traveling magnetic field 04 p0670 A67-15521

Relative external characteristics for calculation of maximum efficiency and minimum current supply of conduction pumps 04 p0556 A67-15527

Book on theory of flow machines covering

pumps, turbines, windmills, fluid dynamics, viscous flow fields, cascade flow, etc 08 p1321 A67-20758

Aircraft engine service life and reliability during series production, analyzing failure of parts 09 p1560 A67-22476

Frequency pattern analysis for liquid rocket pump fluid cavitation characteristics 21 p3613 A67-38437

PUMP IMPELLER

Cavitation damage in alkali metal pumps, noting damage resistance and material properties for application in space power systems 15 p2494 A67-30151

PUMPING

SA CRYOPUMPING

SA MAGNETIC PUMPING

SA OPTICAL PUMPING

Pump noise contribution to total noise of LF parametric converter, analyzing effect of magnitude of bridge out-of-balance voltage 01 p0032 A67-10002

Pump loop testing and operational evaluation of SST hydraulic fluids [SAE PAPER 660664] 01 p0103 A67-10572

Quasi-linear equations for inhomogeneous plasma in magnetic field applied to pumping of energy of Langmuir oscillations 03 p0475 A67-12936

Saturation effects studied by pumping speed measurements of diode and triode type getter ion pumps for He, molecular hydrogen and nitrogen at low pressures as function of time 08 p1333 A67-21494

Large and intermediate ultraclean vacuum chambers converted to sputter-ion and titanium sublimation pumping 12 p1921 A67-25691

Laser oscillation cessation with strong pumping, interpreting effect as consequence of line broadening due to pumping strokes 18 p3059 A67-33672

Interaction between electrostatic and guided electromagnetic wave, considering plasma wave amplification by pumping at microwave frequency 18 p3091 A67-34643

Molecular gas flow through cylindrical tube, using wall pressure distribution to measure pump speed 21 p3610 A67-37823

PUNCHED CARD

80-column punch card prototype for statistical generalization of cloud data from meteorological satellite 04 p0651 A67-15470

Punch card deck for serially completed upper wind observations as substitute for map scaling 09 p1525 A67-22691

PUPIL

Images reconstructed from multiple-exposure hologram separated by selecting appropriate-reconstructed pupil 15 p2487 A67-29500

PUPIL SIZE

Pupillary diametric size as indicator of load on human memory 05 p0756 A67-16587

Blockage of electrically evoked pupilodilation in cat by irradiating hypothalamus with cyclotron-accelerated alpha particles 10 p1598 A67-23394

Independent effect of receptor adaptation level and pupil size on production of flashblindness by high intensity short-duration flashes 13 p2060 A67-26925

PURIFICATION

SA AIR PURIFICATION

SA CLEANING

SA REFINING

SA STERILIZATION

SA WATER PURIFICATION

Continuous horizontal zone refining system for purification of organic compounds, inorganic salts, metals, etc 02 p0247 A67-12691

Niobium and tantalum purification from interstitial impurities by high vacuum annealing, noting effect on electric resistivity 07 p1210 A67-20112

Germanium tetrachloride purification process by radiochemical analysis and radioactive tracers investigated to determine possible simplification 18 p3104 A67-34600

Purification and properties of nicotine oxidase suggest metalloflavoprotein having riboflavin 5-phosphate 20 p3376 A67-37032

Purification systems, filters and porous materials applications to liquids and gas systems associated with spacecraft, boosters and ground support equipment 21 p3570 A67-38103

PURINE

S URANYL

PURITY

SA IMPURITY

Temperature and purity dependence of nuclear-spin relaxation time in type II superconductor gapless region and volume average of density states on Fermi surface 03 p0499 A67-13937

Carbon action effect on tensile deformation in single and polycrystalline beryllium in terms of solutionized and precipitated states 13 p2137 A67-27112

PURSUIT TRACKING

Simulation of pursuit-evasion differential game using variational method, comparing performance of human pilot to optimal pursuer 07 p1136 A67-20170

Minimax problem for pursuit problem of two linearly controlled objects describable by identical differential equations 11 p1812 A67-24145

Human operator performance in continuous pursuit tracking with advanced and delayed visual display 18 p2994 A67-34339

Time optimal flight trajectories in planar and spatial pursuit problems with constraints on pursuer, using Pontryagin maximum principle 21 p3712 A67-39151

Stochastic optimal control algorithm for pursuit process in problem of encounter of two cosmic objects 22 p3878 A67-39183

Factors in recovery from performance decrement, activation, inhibition and warm-up [NAVTRADEVCEIN-IH-72] 24 p4114 A67-41809

PUSH-PULL AMPLIFIER

Electrical design, mechanical fabrication and performance data of integrated broadband balanced transistor amplifier 17 p2825 A67-32599

PWM

S PULSE WIDTH MODULATION /PWM/ PYLON MOUNTING

Isolated nacelle design for high by-pass ratio turbofan engines, particularly pylon mounted engine 01 p0140 A67-10632

Tilt rotor VTOL aircraft stability, discussing results of wind tunnel tests on rotor-pylon behavior at different velocities [AIAA PAPER 67-17] 06 p0948 A67-18254

Helicopter rotor and pylon stability investigated through motion equation 14 p2246 A67-29048

PYRAMIDAL BODY

Hemisphere coverage by n planar phased arrays arranged in pyramids or pyramidal frustra solved by transformations leading to analytical solution 16 p2638 A67-31337

PYRANOMETER

U.S. Weather Bureau calibration of solar radiation pyranometer by means of 5000 watt tungsten filament lamp 03 p0419 A67-13076

Canadian calibration of solar radiation pyranometers 03 p0419 A67-13077

Integrating hemispherical system for creating indoor artificial diffusing sky used in calibrating meteorological pyranometers 03 p0419 A67-13078

Distillation process in spherical pyranometer studied for time constants and sensitivity in calibration until reaching balanced state 21 p3627 A67-38445

Integrating pyranometer operating on silicon photovoltaic solar cell for use by climatological stations and mesoscale networks 21 p3628 A67-38580

PYRIDINE NUCLEOTIDE

Molecular sizes of diphosphopyridine nucleotide linked dehydrogenases of representative animal, plant and microbial species 11 p1750 A67-24784

PYRIMIDINE

Hydrogen bonding of derivatives of guanosine and cytidine soluble in chloroform studied in IR, confirming geometrical specificity in two-stranded nucleic acids 02 p0190 A67-11585

Alteration in pyrimidine metabolism occurring after infection of E. coli with T-even bacteriophage 20 p3370 A67-36795

PYROELECTRICITY

SA DIPOLE MOMENT

Electromagnetic irradiation of pyroelectric hot spots and regional variation of response 02 p0299 A67-11893

Pyroelectrical effect in barium titanate ceramics used for weak thermal radiation recording 03 p0421 A67-13709

Q-switched carbon dioxide laser with

internal concave rotating mirror, discussing detection with pyroelectric thermal detector 09 p1511 A67-21769

Pyroelectric heat-transfer sensor performance compared with thin skin thermocouple heat sensors, noting discrepancy in measurement results in severe environment 11 p1790 A67-24453

Thin film thermal radiation detector noting construction, calibration, performance, error sources and advantages of pyroelectric over thin film gauges 11 p1790 A67-24454

Ultrasensitive miniature temperature sensor using pyroelectric material on gate of MOS transistor 13 p2119 A67-26517

Pure capacitance type IR radiation detector concept, comparing various materials as to pyroelectric effect [ACS PAPER 27E-66F] 20 p3459 A67-36644

Pyroelectric effect using single barium titanate crystals with liquid electrodes extending ferroelectric switching time measurements to low fields 24 p4203 A67-42090

PYROLYSIS

Combination flash photolysis-flash pyrolysis system with timing circuit, using Tektronix pulse generators and ignitron circuit for firing spectroscopic lamp 02 p0247 A67-12689

Flash pyrolytic technique applied to McFayden-Stevens reaction for various simple aliphatic aldehydes 04 p0565 A67-14524

Unsaturated polyester styrene, showing via gas chromatography and IR spectroscopy effect of reticulation on pyrolytic decomposition 05 p0759 A67-16768

Combustion and pyrolytic behavior of thermoplastic polymer spheres burning in quiescent atmospheres of air [AIAA PAPER 67-103] 06 p1114 A67-18283

High resolution gas chromatography combined with mass spectrometry applied to analysis of pyrolysis products of isoprene from 300 to 1000 degrees C 10 p1602 A67-22947

Very low pressure pyrolysis applied to combustion kinetics 18 p3149 A67-33787

Hydrocarbon pyrolysis and H/D substitution reaction rates, using single-pulse shock tube as chemical reactor 18 p2996 A67-33788

Photolysis and pyrolysis of nitromethane and methyl nitride using flash photolysis and kinetic spectroscopy 18 p3298 A67-34276

Pyrolysis gas chromatography method for life detection and chemical identification of microorganisms 20 p3378 A67-37500

Ammonium perchlorate deflagration studied by flash pyrolysis and kinetic spectroscopy noting radical concentrations 22 p3867 A67-39639

PYROLYTIC GRAPHITE

Autoradiographs of metal diffusion in pyrolytic graphite 02 p0257 A67-11898

Shear compliance of basal plane of hot worked pyrolytic graphite 05 p0833 A67-17331

Low pressure physical adsorption and electron microscope study of surface of annealed pyrolytic graphite, using flash filament technique 06 p1020 A67-17988

Reflectance of pyrolytic graphite and phenolic nylon chars for radiant heat rejection from nonablating heat shield 15 p2579 A67-29434

High tensile strength high elasticity modulus graphite fibers preparation from polymeric fibers for composite structures 21 p3649 A67-37884

Low dose reactor irradiation effect on temperature dependence of dynamic modulus and internal friction of as-deposited pyrolytic graphite 23 p4021 A67-41075

Dewrinkling and diffusion mass transport mechanisms in high temperature tensile and shear plastic deformation of pyrolytic carbons [JPL-TR-32-1137] 24 p4177 A67-42711

PYROLYTIC MATERIAL

SA ABLATING MATERIAL

Vapor flux of trichloromethylsilane affects morphology of pyrolytic deposits of silicon carbide 01 p0103 A67-10252

Reinforced pyrolyzed plastic composites for aerospace applications, noting high temperature stability and ease of utilization 03 p0443 A67-13415

Properties of pyrolytically produced boron fibers, noting strength decrease with temperature increase 06 p1016 A67-17903

Neutron induced dimensional changes in turbostratic carbons used as coatings on nuclear fuel particles, presenting densification curves 08 p1346 A67-21542

Electric, thermal and physical properties of pyrolytic carbides and nitrides of group IV metals 11 p1804 A67-23903

PYROMETER

S OPTICAL PYROMETER

S RADIATION PYROMETER

S THERMOCOUPLE PYROMETER

PYROTECHNICS

SA FLARE

Pyrotechnic shock testing, discussing equipment reliability and performance improvement, shock level reduction and applications

[SAE PAPER 660717] 01 p0139 A67-10606

Pyrotechnic actuation, discussing parameters, equipment and performance of explosive devices 15 p2543 A67-29304

Quasi-continuous divalent dysprosium ion doped calcium fluoride laser with pyrotechnic excitation 16 p2686 A67-31484

PYROXENE

SA SILICATE

Bununu meteorite /pyroxene-plagioclase achondrite/ composition and structure 09 p1564 A67-21736

Enstatite characteristics in enstatite achondrite meteorites, discussing mineralogy and composition 13 p2200 A67-27236

Lanthanide distribution between omphacite and Garnet, noting abundance ratios to whole rock of Japanese eclogite 24 p4151 A67-42449

PYRROLE

Pyrrolic compound formation by UV irradiation of delta-aminolevulinic acid 08 p1290 A67-21254

PYRUVIC ACID

Catalytic decarboxylation of oxaloacetic acid into pyruvic acid by thermally prepared poly-alpha-amino acids 13 p2065 A67-26589

P3V AIRCRAFT

S P-3 AIRCRAFT

Q**Q-FACTOR**

Optimization of sampled data systems with finite transient response time on basis of combined stochastically deterministic Q factors 01 p0043 A67-10202

Optimization of directive gain and SNR of arbitrary antenna array with or without constraint on array Q-factor 01 p0035 A67-10431

Low noise parametric self-resonance amplifiers with bandwidths, discussing use of high diode Q-factor 02 p0220 A67-12204

Ruby laser with liquid filter, considering relation between filter efficiency and absorption curve parameters when acting as Q-factor modulator 02 p0252 A67-12423

Synthesis of linear automatic control system with constant parameters for integral Q-factor, noting effect of small parameters on properties of optimum system 03 p0390 A67-13097

Pulsed laser Q-factor modulation using nonlinear resonator functions in absorbing medium 03 p0436 A67-13135

Spectral characteristics of two-photon optical excitation and light emission from CdSe semiconductor laser with modulated Q-factor 04 p0633 A67-15299

Phenomena accompanying geomagnetic field reversal, using measurements performed on samples of core Papagayo 3G 04 p0617 A67-15543

Effective diffusive scattering cross section of electrons in He and Ar plasma with K vapor additions and in pure K, based on DC plasma conductivity and microwave generator Q-factor 04 p0673 A67-15972

Radiation transport in spectral lines as consecutive photon absorptions and emissions, discussing contemporary theories, approximation methods and applications spark shadow projections in air for giant pulse 06 p1010 A67-18090

Semiconductor mirror for Q-factor modulation of laser resonator 06 p1012 A67-18789

Parallel equivalent circuit parameters and Q-factor of cylindrical cavity resonator in TM sub 010 mode 07 p1153 A67-19613

Laser mode-locking during resonator Q-factor modulation 09 p1513 A67-22065

High power laser performance and material limitations, noting Q-switching with liquid cell 09 p1516 A67-22675

Giant pulse generation range in transverse direction after Q-switching in ruby laser, examining resonator properties 10 p1666 A67-23584

Circuit Q of self-resonant coil of niobium stannide at RF low temperatures 11 p1767 A67-24726

Q parameter of hydrogen maser measurement by method of no clock structure modification and by inhomogeneous magnetic field method 11 p1802 A67-24754

Analytical representations of admittance matrix of transistors, describing methods of obtaining quality coefficients, equivalent circuit synthesis, etc 13 p2081 A67-27199

Microminiaturizable transistorized circuit for generating wide frequency range high Q inductances from semiconductor devices for integrated selective circuits 13 p2081 A67-27201

Effect of semiconductor glass shield temperature on absorption coefficient, output energy, pulse duration and energy and peak power of ruby laser 14 p2332 A67-28857

Superconducting microwave filters, discussing minimum insertion loss, loss dependence on various factors and effect of peak fields on maximum power 14 p2289 A67-28915

Laser radiation control techniques using saturation filter or negative feedback circuit with resonator Q-factor depending on radiation field power 15 p2499 A67-29722

Spherical dipole for Italian satellite, calculating radiation impedance and pattern, input admittance, efficiency, radiated field and antenna Q factor 17 p2826 A67-32780

Inductive characteristics of junction transistors, showing Q-factor increase achieved by using negative impedance produced by avalanche multiplication 18 p3009 A67-33479

Semiconductor mirror for Q-factor modulation of laser resonator 18 p3059 A67-33731

Digital filters with ICs boost Q without inductors 18 p3012 A67-34490

Resonance method for measuring microwave resonators Q-factor and its small variations 19 p3191 A67-34982

Automatic frequency-control system using superconducting resonator and reflex klystron 19 p3192 A67-34984

Amplification characteristics of multicavity masers, determining Q-factor using chain matrix A formalism 19 p3241 A67-36027

Effect of semiconductor glass shield temperature on absorption coefficient, output energy, pulse duration and energy and peak power of ruby laser 19 p3242 A67-36108

Schumann Resonance frequencies, Q-factor and waveguide propagation constant derived at ELF for ionospheric profiles 21 p3579 A67-37993

Analog treatment of digital telemetering signals using a priori information about transmission, noting Q-factor, storage and use of existing emissions 21 p3584 A67-38660

Collisionless damping of temperature or secondary resonance spectrum of plasma column 22 p3845 A67-39482

Photoconductivity in cadmium sulfide crystals induced by light from ruby laser with Q-factor modulation, showing photocurrent dependence on laser power 22 p3814 A67-39511

Transistorized LF LC filter with positive and negative feedback, analyzing circuit to increase Q-factor and narrow passband 22 p3772 A67-39869

Superconductors for high-Q microwave cavities construction, noting unloaded Q and resonant frequency measurements and surface properties 22 p3865 A67-40431

Niobium stannide for refrigerated RF preselectors for interference reduction in radio communications, stressing high Q factors 22 p3865 A67-40435

Logic gate with coupled integrated circuit transmitters 23 p3977 A67-40662

Analysis of laser with selective resonator indicating stimulated emission basic characteristics determined by active medium band shape and Q-factor 23 p4013 A67-40907

Q-SPOILING

Q-switching of ruby laser using cell containing chloroaluminum phthalocyanine in chloronaphthalene to obtain giant pulses 01 p0089 A67-10448

Single self-mode-locked pulse selection from bleachable dye Q-switched Nd-doped glass laser 01 p0091 A67-10875

Narrow beam divergent Q-switched laser pulse generation, noting output characteristics and applications 01 p0091 A67-11024

Q-spilling of ruby laser by optical pumping in intense inhomogeneous magnetic field with reduced gain 02 p0253 A67-12503

Fluorescent emission of neodymium laser triggered by Pockels effect as function of population inversion 03 p0436 A67-13201

Short pulse Q-switched laser with variable pulse length 05 p0817 A67-16641

Positive ion emission from tungsten surfaces laser irradiated studied, using time-of-flight spectrometer 05 p0819 A67-16651

Gas dynamic equations for determination of heating, vaporization and expansion of substance due to Q-switched laser radiated collimates onto surface of solids 05 p0819 A67-16652

Terminal level lifetime and fluorescence line of neodymium doped glass influence on dynamics and efficiency of Q-spilled laser 05 p0822 A67-16675

Q-switched ruby laser configuration with feedback control, noting frequency and instability correlation with theoretical results obtained from mathematical model 05 p0822 A67-16676

Saturated absorption of color centers in glass self-Q-switched pulses, as in glass codoped with uranyl oxide and Nd ions 05 p0822 A67-16678

Q-switched laser operation observed using liquid selenium mirror as reflector in ruby laser measuring reflectivity changes 05 p0822 A67-16679

Operation of synchronized neodymium laser time variable reflection /TVR/ oscillator, using single pockels cell to obtain Q-switching and cavity dumping 05 p0826 A67-17525

Stimulated Brillouin scattering in liquids used for passive Q-switch applicable to visible and IR lasers 09 p1511 A67-21749

Q-switched carbon dioxide laser with internal concave rotating mirror, discussing detection with pyroelectric thermal detector 09 p1511 A67-21769

Universal rotating mirrors for Q-switching neodymium glass laser 09 p1514 A67-22171

High speed correlation technique to measure time development of width of ultrashort pulses generated by mode locked Nd trivalent ion glass laser 13 p2126 A67-27014

Fabrication and operation of divalent dysprosium doped calcium fluoride laser, discussing magnetic field effects, Q-switching, cooling, etc 13 p2127 A67-27086

Rose bengal saturable filter for production of high peak power neodymium laser pulses by regeneration switching 20 p3457 A67-36175

Multiple stimulated Brillouin scattering from liquid within Q-switched ruby laser cavity, noting changes in pulse shape, output power and spectral characteristics 20 p3457 A67-36385

Spectroscopic investigations of emission under free generation and Q-switching conditions of mixed-fluoride crystal lasers 21 p3682 A67-38370

Neodymium doped YAG Q-spilled laser system for switching high voltage spark gap at 50 pps with nanosecond jitter 22 p3813 A67-39258

Q-switched laser use as light source for photographing droplets in spray containing fluorescent dye excited by second harmonic of ruby light 22 p3797 A67-39492

Q-switched laser single pulse visual recording by oscillograph with storage tube/photodiode combination 22 p3817 A67-40415

Giant pulse irradiation effect on ruby laser under oscillation quenching, amplification and characteristics changes in metastable state population 23 p4017 A67-41434

QSO

S QUASI-STELLAR RADIO SOURCE

/QSO/

QUADRANTID METEOR

Correlation between diurnal meteor activity and twilight emission of ionized calcium H and K lines confirmed by Quadrantides swarm observations 11 p1857 A67-24756

QUADRATIC EQUATION

Maximum problem solution with quadratic nonconcave objective functions and linear inequalities as constraints 04 p0644 A67-14772
Umov-Poynting theorem, Lorentz lemma, complex conjugate lemmas and quadratic relations for EM field intensity in electrodynamics of moving media 05 p0844 A67-16354

On-line digital computer used in optimizing control by prediction, including quadratic and steady state value 05 p0784 A67-16524

Extreme points of copositive quadratic forms constituting closed convex cone in Euclidean space 05 p0836 A67-17045

Model estimation programming to determine optimum design criteria for rocket propulsion system using estimating function, approximation solved by Lagrange method

[AIAA PAPER 67-208] 06 p1024 A67-18330

Acceleration of iteration process convergence when dividing polynomial by quadratic trinomial, approximating curves for remainder coefficients by straight lines 06 p1025 A67-18557

Quadratic control regulator problem with energy constraint analyzed, considering availability of limited control energy or as method of limiting maximum control amplitude 08 p1309 A67-20332

Five-variable extreme copositive quadratic forms, presenting previously unknown forms for application to inequality theory and block design analysis 08 p1348 A67-21154

Optimum reception problem of two zero mean Gaussian signals solved through comparison of quadratic form in observable waveform with predetermined threshold 11 p1760 A67-24235

Ionospheric index of solar activity obtained together with quadratic equation regression coefficients by minimizing standard error of F-2 layer critical frequency 14 p2311 A67-28375

Sampled data feedback control system using quadratic programming to determine optimum compensator 16 p2646 A67-31636
Ljapunov function from quadratic polynomial for n-order nonlinear differential equations 19 p3250 A67-34842

Thin elastic shell neutral equilibrium under axial compression and hydrostatic pressure, obtaining parametric terms for expressions by using quadratic functional 24 p4249 A67-42303

QUADRATURE

Quadrature solution method for bending of arbitrarily loaded thin slab whose circular edge is supported by elastic rod 01 p0158 A67-10223

Electronic technique producing quadrature signal from laser feedback interferometer 15 p2502 A67-30436

QUADRATURE APPROXIMATION

Erdos and Turan theory of fine and rough convergence of interpolation and quadrature processes 02 p0259 A67-11919

Single layer potential solution to boundary value problems for heat equation in half-plane with one or two points of discontinuity in boundary conditions 03 p0459 A67-13590

Membrane solution of spirally corrugated shell under axial and torsional loading determined from thin shell bending equations 06 p1110 A67-18856

General purpose quadrature method for numerical evaluation of specific definite integrals 09 p1524 A67-21834

Numerical quadrature methods of Romberg, Chebyshev and Monte Carlo, noting analytic function and program for machine evaluation 09 p1468 A67-22047

Interpolation between given data points by using spline functions 09 p1468 A67-22048

Unified method of numerical quadrature for integrands of certain complex analytic functions, obtaining asymptotic expansion of error functional 13 p2145 A67-26734

Mechanical quadrature theory and convergence problems 13 p2148 A67-27469

QUADRUPOLE

Temperature dependence of La-139 nuclear

quadrupole resonance in lanthanum fluoride 01 p0129 A67-10149

Counting control methods for multistable elements containing nonlinear quadrupole with comb type amplitude characteristic, using short-term action on LF filter 01 p0044 A67-10497

Uniform electric field quadrupole polarizabilities and shielding factors for S-state atoms and ions, demonstrating independence of factors from existence of field gradient 03 p0472 A67-13321

Exact vibrational matrix elements for molecular hydrogen and intensity of quadrupole rotation-vibration spectrum 03 p0515 A67-14324

Statistical properties of amplitude and phase of output signal of electron beam quadrupole amplifier with superposition of regular signal plus Gaussian noise at input 05 p0765 A67-17162

Quadrupole effects on gas diffusion, viscosity and thermal diffusion factors, computing collision integrals 06 p1038 A67-19046

Molecular quadrupole moments and shape parameters derived from viscosities and second virial coefficients 06 p1038 A67-19047

Two positive kinetic power waves coupled in interaction for DC pumped quadrupole amplifier having low noise and high efficiency 09 p1478 A67-22260

Counting control methods for multistable elements containing nonlinear quadrupole with comb type amplitude characteristic, using short term action on LF filter 10 p1621 A67-23619

Electric quadrupole-quadrupole and dipole-octupole forces contribution to dispersion energy for axially symmetric molecules, noting resonance frequencies 17 p2887 A67-32353

Charged particle beam guiding and focusing by helical magnetic multipole field for relativistic and nonrelativistic cases 17 p2908 A67-33112

Calculation of frequency characteristics of hydraulic main line sections with parameters varying continuously along length 20 p3363 A67-36444

QUADRUPOLE NETWORK

Optimal value of reactance of microwave parametric element 02 p0214 A67-11912

Stability analysis of spectrotron with external feedback based on time delay, inertia of nonlinear quadrupole and circuit phase shifts 03 p0377 A67-13092

Voltage generator consisting of quadrupole injectors where output voltage is complex function of previously chosen input voltages 03 p0392 A67-13450

Infinite magnetic quadrupole channel, discussing operations in complete transverse plane phase space via 4 x 4 matrix transformations 08 p1332 A67-21172

Definition, realizability and design of active gyrator, using two controlled current sources to obtain ideal impedance inverting characteristics 11 p1789 A67-24127

Theoretical realizability, design and stability of ideal gyrator with two operational amplifiers and resistance network 11 p1760 A67-24232

Wideband phase-leading quadrupoles with circuit breakers and effect on envelope of modulated signal 13 p2085 A67-27706

Gyrator type circuit which requires only three amplifiers and which, when terminated with capacitor, can replace ungrounded inductor 15 p2456 A67-29240

Equivalent quadrupoles for analyzing ultrasonic systems using piezotransducer disks operating at any frequency 20 p3401 A67-37454

Direct measurement of transfer curve slope of active quadrupole circuit to determine drain current and gate voltage of field effect transistors 22 p3773 A67-40305

Pump frequency reduction in Adler tubes, examining spatial harmonics of quadrupole structure field and suggesting use of cophase connection 24 p4130 A67-42240

QUALITATIVE ANALYSIS

Qualitative theory of second order dynamic systems in plane and on sphere covering trajectories, equilibrium states and boundary values 03 p0390 A67-13109

Small parameter method for rarefied gas dynamics problems using Boltzmann equation solution and kinetic equations 13 p2099 A67-26953

hierarchy

Characteristic for kernels of certain integral equations on semiaxis for determining solvability and number of possible solutions 14 p2344 A67-28809

Project initiation emphasizing market, product /design, cost and timing/ and resources to market product 15 p2583 A67-29667

Defense procurement procedures and task of project manager 15 p2583 A67-29668

Electronic circuit theoretical analysis noting nonlinear and qualitative processes 19 p3200 A67-34904

Book on stability of nonlinear mechanical systems covering qualitative methods, one degree of freedom systems, etc 24 p4188 A67-42375

Hazard studies and safety analyses qualitative method using checklist of possible mishaps and human errors [AIAA PAPER 67-935] 24 p4260 A67-43025

QUALITY

S FLYING QUALITY

S HANDLING QUALITY

QUALITY CONTROL

SA PRODUCT DEVELOPMENT

Hot pressing of electrolytic grade CR beryllium, noting powder manufacturing process and quality control procedure 01 p0099 A67-10707

Reliability Symposium, San Francisco, January 1966 01 p0081 A67-11332

Functional analysis method application to reliability testing of Polaris missile 01 p0155 A67-11346

Data and mission analysis in man-rating of Gemini launch vehicle 01 p0155 A67-11347

Reliable electronic design by suppression of adverse interactions among system levels 01 p0083 A67-11348

Integrated circuit reliability and nondestructive testing, noting component failure analysis, self-maintenance, network parameter determination, etc 02 p0224 A67-11526

History of selected reliability and maintainability committees and interested government agencies [AIAA PAPER 66-856] 02 p0343 A67-12259

Unreliability of mean-time-between-failures concept as standard quality measure for mechanical systems 02 p0249 A67-12426

Nuclear magnetic resonance /NMR/ used to measure gelation times, rates of polymerization and nature of volatiles included in raw material resins 03 p0429 A67-13448

Magnetic screening tests and use of parts sampling to control magnetic cleanliness for quality assurance 03 p0396 A67-13721

Nondestructive testing /NDT/ developments noting radiography for quality control, ultrasonic, continuous wave, resonance and pulse echo methods and applications to Polaris program 04 p0706 A67-15263

Ultrasonic reflectivity of liquid-solid interface used as indicator of near surface properties of solid in cold work, grain orientation, etc 04 p0621 A67-15264

Nucleonic quality gauging system for two-phase hydrogen pipeline 05 p0842 A67-16539

Nucleonic cryogenic quality meter design and development and fluid monitoring through hydrogen vent line on Saturn S-IVB stage under orbital conditions 05 p0842 A67-16540

Medical, design and operational aspects of quality requirements for reliability of man-rated space environment simulation chambers 05 p0788 A67-16621

American Society for Quality Control, Conference, New York, June 1966 05 p0812 A67-17240

NASA quality assurance program and NASA industry quality relationships, particularly for large space systems procurement 05 p0930 A67-17242

Quality control and internal combustion aircraft engine reliability from mechanical engineering viewpoint 05 p0812 A67-17243

Quality control program for establishing reliability critical items, emphasizing procurement, inspection and testing 05 p0812 A67-17244

Quality control around twin turboprop utility plane MU-2 at experimental stage 05 p0812 A67-17245

Quality evaluation review technique /QERT/ for management facilitation of program planning and scheduling, noting

time and cost estimation 05 p0930 A67-17246
 Product identification and traceability standards for space system quality assurance program for NASA space 05 p0930 A67-17251
 Integrated plan for reliability demonstration through safety margin testing 05 p0813 A67-17253
 Degradation analysis and variability measurement in reliability and quality control of component parts with application to Early Bird COMSAT satellite 05 p0813 A67-17257
 Nondestructive quality control testing, discussing thermoelectric, magnetic particle and fluorescent penetrant, ultrasonic and linear measurement methods 05 p0813 A67-17259
 Support of NASA quality requirements by Defense Contract Administration Services Regions 05 p0930 A67-17262
 Mechanized data system for quality and reliability control, noting performance characteristics and computer program 05 p0814 A67-17264
 Quality criteria in production flaw detection work, quantitatively estimating transition probability matrix and using error theory 06 p1007 A67-18104
 F-111 fixed price contract management, discussing weapon system management, acquisition, controls and techniques to circumvent inherent problems [AAS PAPER 66-153] 08 p1430 A67-20971
 Printed circuit board manufacturing process assuring crack-free plated-through hole 08 p1304 A67-21190
 Thermophysical parameters of semiconductors measured with same instrument set through pulse method, for quality control application 09 p1495 A67-21655
 Optimal control of variable structure system in presence of perturbation, discussing quality control and preservation of sliding plane 09 p1483 A67-22081
 Parameter control during vacuum deposition of electronic film circuits for obtaining acceptable tolerances 09 p1503 A67-22099
 Reliability management techniques for Projects Mercury, Gemini and F-4 Phantom II aircraft 09 p1582 A67-22288
 Failure reporting, analysis and correction on satellite programs, discussing system reliability 09 p1480 A67-22289
 Reliability criteria application to improvement of program and design decision quality during preliminary design 09 p1582 A67-22291
 Spacecraft electrical connector criteria to insure adequate quality for desired performance 09 p1480 A67-22295
 Parts reliability control by computer programs 09 p1583 A67-22307
 Yield strength and reliability of structural cluster welds determined using statistical analysis 09 p1506 A67-22308
 Interface between reliability cost and performance resulting from application of microelectronics to Sergeant Artillery Guided Missile Ground Electronics 09 p1572 A67-22309
 Reliability methodology in design and development stage, discussing component stresses, performance variation, etc 09 p1572 A67-22310
 Reliability of future space systems through adoption of complexity factor ratings 09 p1572 A67-22311
 Quality control system for adhesive bonding using Fokker bond tester ultrasonic resonance instrument 09 p1508 A67-22527
 Two-beam Mach-Zehnder and Michelson interferometers using coherence properties of lasers, construction and applications 10 p1652 A67-22709
 Structural and technological problems connected with miniature electromechanical filters 10 p1609 A67-22876
 X-ray image transformation, transmission and amplification directly into video signals for inspection of missile case walls and weldments 10 p1622 A67-22929
 X-radiographic nondestructive testing and inspection for quality control of electronic and electromechanical devices including printed circuits, encapsulated modules, thin films, etc 10 p1611 A67-23311
 Large part inspection via ultrasonic and eddy current techniques, discussing surface and discontinuity dimension

analysis 10 p1660 A67-23324
 Computer application to aerospace missions, discussing operation and equipment parameters, reliability, man-machine interaction, etc 11 p1756 A67-24248
 Gas turbine bucket alloy improvement via heat treatment, noting performance evaluation results from creep rupture tests [ASME PAPER 67-GT-55] 11 p1808 A67-24811
 Storage reliability for electronic systems in missiles, noting factors affecting failure rates after dormant storage 11 p1768 A67-25010
 Nondestructive testing methods noting applicability to flaw detection and quality control 12 p1948 A67-25138
 Satellite sealed subsystems individual leak rates in thermal-vacuum environment measured with mass spectrometer 12 p1921 A67-25690
 Large and intermediate ultraclean vacuum chambers converted to sputter-ion and titanium sublimation pumping 12 p1921 A67-25691
 Thin film integrated circuit, discussing development of large value resistors and capacitors 12 p1918 A67-26219
 Simultaneous stability and quality control of pulse regulation, discussing computation of sum of squares of difference 13 p2086 A67-26474
 Quality control in electron beam welding, discussing design, metallurgical aspects, etc 13 p2124 A67-27168
 F-111 fixed price contract management, discussing weapon system management, acquisition, controls and techniques to circumvent inherent problems f-111 fixed price contract management, discussing weapon system management, acquisition, controls [AAS PAPER 66-153] 13 p2233 A67-27554
 Metal-semiconductor electric contacts for GaAs bulk effect device noting uniformity, linearity, usefulness, adaptability, etc 13 p2183 A67-27567
 Aluminum welding techniques, evaluating various filler alloys and forms for welding ease and efficiency 14 p2323 A67-27819
 Methods for transformation of titanium alloys by forging or die stamping to meet particular requirements 14 p2324 A67-28630
 Computer partitioning for long term reliability in space, noting requirements for various phases of operation 15 p2439 A67-29306
 Strike aircraft design noting weapons compatibility, use of analytical and scale testing techniques, etc 15 p2418 A67-29396
 Apportioning system reliability requirements to various system components, using generalized failure mode and effects analysis for each equipment within system 15 p2492 A67-29605
 Spacecraft reliability requirements, discussing design parameters and performance standards 15 p2493 A67-29606
 Surveyor spacecraft reliability from test data, examining assessment outputs, basic definitions and mathematical models 15 p2493 A67-29608
 Electron tube requirements for space applications noting size, weight, environmental parameters, etc 15 p2447 A67-29752
 Prevention of burnout in high power linear beam traveling wave tubes by placing small negative electrode at end of collector opposite beam entrance 15 p2447 A67-29754
 Reliability, performance requirements and environment in which system must operate 15 p2583 A67-30128
 Hydraulic systems reliability and maintenance, designing corrective measures to eliminate fluid leakage [AIAA PAPER 67-403] 15 p2423 A67-30370
 American Society for Quality Control - Conference, Chicago, May-June 15 p2494 A67-30401
 System-effectiveness concept for turbine and piston engine development 15 p2584 A67-30402
 Reliability management under fixed-price contracts 15 p2584 A67-30403
 Evaluating, reporting and improving on quality performance of suppliers and subcontractors of helicopter construction firm 15 p2584 A67-30404
 Holography applications in quality assurance including checking jigs, fixtures, molds, vibration analysis,

etc 15 p2491 A67-30405
 Supplier control and reliability, discussing adequate input supply and output monitoring 15 p2584 A67-30407
 Circuit analysis by computer, noting programs for reliability and quality control 15 p2441 A67-30408
 System reliability study via detailed allocation method, selecting optimal solution in context of tradeoff analysis 15 p2512 A67-30409
 Systems approach for product and test equipment failure information reporting, including cause and corrective and preventive measures 15 p2584 A67-30410
 Laser interferometers for metrology applications, considering sources of error 15 p2501 A67-30411
 Reliability statistics for repairable devices, proving Poisson distribution limitations and nonhomogeneous Poisson adequacy for analyzing stochastic processes 15 p2495 A67-30412
 System reliability for single-time demand interval, calculating distribution function for time to system failure 15 p2495 A67-30413
 Engineering approach to nonelectrical reliability in design, stressing mechanical aspects 15 p2495 A67-30415
 Quality cost accounting and management decisions in performance of various functions 15 p2584 A67-30420
 Sampling plan for destructive testing, relating quality protection to cost 15 p2584 A67-30421
 Assurance and measurement of space vehicle alignment conforming to design requirements 15 p2496 A67-30422
 Lunar orbiter quality assurance program, emphasizing management, design, procurement, fabrication, quality control, etc 16 p2783 A67-31629
 Reliability through redundancy describing use of devices for averaging analog signals 16 p2649 A67-31667
 Weldable tube fittings, welding equipment and inspection methods for connecting tubing in aircraft and aerospace hydraulic systems 17 p2864 A67-32008
 Iterative on-line reliability calculation of automatically repaired space computer, noting reliability and performance 17 p2820 A67-32501
 Aerospace industry quality control requirements and specification, noting small business role 17 p2974 A67-32818
 Color contrast penetration method for crack detection in aircraft engines and motor car parts 18 p3045 A67-33739
 Welds qualification system based on radiographically determined macrostructure defectiveness, classifying defects according to size and distribution 18 p3053 A67-33742
 Reliability and maintainability - Conference, Cocoa Beach, Florida, July 1967, Volume 6 18 p3055 A67-34648
 Integrated reliability program for Scout launch vehicle in terms of design specification, review functions, malfunction reporting, failed parts analysis, quality control, standardization and certification 18 p3139 A67-34702
 Manual altitude and attitude control effects on short-period handling quality requirements 19 p3175 A67-35974
 Quality program planning criteria for NASA contracts involving NPC 200-3 20 p3556 A67-36602
 Potable water quality control and standards for aerospace systems 21 p3576 A67-38071
 IR monitoring technique to improve accuracy of welding inspection using voltage feedback to regulate output 21 p3634 A67-38620
 Quality control methods to ensure thin film circuitry integrity and reliability, showing need for better nondestructive testing techniques 21 p3635 A67-38623
 Quality assurance requirements for custom thin film circuit program covering functional reliability, environmental capabilities and latent defects detection 21 p3636 A67-38896
 Quality control organization of suppliers to provide reliability of structural component of spacecraft electronic systems 22 p3922 A67-39282
 Reliability in aircraft engines from start of assembly to completion and delivery 22 p3867 A67-39285
 IR for electronic circuit component

diagnosis, discussing design criteria, quality control and acceptance testing 22 p3769 A67-39631

Electronic parts degradations induced by assembling and packaging environments investigated for effects upon failure modes 22 p3771 A67-39834

Chromate conversion process applicable to IC interconnecting aluminization reveals defective areas under normal quality control procedures 22 p3771 A67-39835

Nondestructive inspection of composite structures in helicopter rotor blades, discussing structure, loading and quality control capability 22 p3812 A67-39857

Cryogenic thermoconductivity heat flow meter apparatus for felt, powder and block materials at atmospheric pressure 22 p3803 A67-40298

Theoretical and experimental research methods for engineering reliability operations 23 p4010 A67-41320

Shock testing to aid design analysis and for qualification and certification 23 p3987 A67-41414

QUALITY FACTOR

S Q-FACTOR

QUANTITATIVE ANALYSIS

Principal methods determining cosmic abundances of chemical elements, emphasizing quantitative spectral analysis of sun and fixed stars 03 p0510 A67-13538

Two-photon absorption in organic dyes for various wavelengths, extinction coefficients and concentrations 05 p0815 A67-16626

Quantitative analysis of wear of metal-metal/polymer composite friction pairs as function of time and operational conditions 08 p1334 A67-20597

Ge and Ga concentration in selected Fe meteorites used to determine quantization in terms of multiple parent body hypothesis and planetary fractionation processes 09 p1564 A67-21738

Quantitative graphical method of screening working fluids for Rankine cycle power plants using single stage turbines at different levels of diameter and rpm [ASME PAPER 67-GT-12] 11 p1746 A67-24798

Long term variation in magnitude of diurnal anisotropy of solar cosmic rays analyzed quantitatively by applying statistical techniques to recorded data 12 p1993 A67-25205

Chromatographic accumulation of primary and secondary carotenoids in *Spongiochloris typica* over 8-week period 14 p2254 A67-28065

Analysis of management methods applicable to aerospace industry, considering introduction of integrated information systems 15 p2583 A67-29669

Quantitative analysis of new mineral /gentnerite/ found in Odessa meteorite 20 p3529 A67-37526

Linear equation solving for gaseous mixture quantitative determination, based on combined cognitive system use of computing and programming devices 21 p3631 A67-39116

Binary and tetravalent signals quantitative comparison for noise sensitivity by computing transmission matrix during transmission via linear channel 22 p3761 A67-39787

S-process theory of heavy element formation in solar system confirmed by measuring neutron capture cross sections 24 p4224 A67-41817

Canon Diablo octahedrite quantitative chemical and modal mineralogical composition variations in rim and plain components 24 p4235 A67-42636

Interferometer employing diffraction grating investigated for applicability to quantitative study of gas dynamics 24 p4158 A67-42723

QUANTIZER

Time-space quantization of gravitational field by formalisms in general relativity theory 01 p0114 A67-10746

Quantization, sampling frequency and statistical scattering in correlation measurements 08 p1313 A67-21006

Output correlation function for N-step symmetric amplitude quantizer with summed sine wave and Gaussian noise input, noting approximations for low SNR 12 p1908 A67-26084

Time-space quantization of gravitational field by formalisms in general relativity theory 13 p2158 A67-26775

Quantizer optimal design for closed-loop

dynamic and open-loop static systems 15 p2456 A67-29364

Nonuniform error quantization effects on stability of feedback control systems, investigating limit cycles existence and giving optimum quantizer design procedure 17 p2829 A67-32016

QUANTUM AMPLIFIER

21-cm-wave radiospectrometer with quantum paramagnetic amplifier for investigating radio lines of hydrogen 02 p0241 A67-11638

Noises in quantum amplifier due to heat fluctuations and spontaneous emission of active microparticles, discussing negative temperature state 03 p0368 A67-13139

Soviet book on radio physics quantum amplifiers covering lasers, maser, paramagnetic resonance, etc 19 p3238 A67-34799

Solving Schroedinger equation with initial coherent radiation state 20 p3485 A67-36866

QUANTUM COUNTER

Nucleon interaction generating high energy gamma rays, discussing photon and energy spectra of electron photon cascade, pion generation and gamma quantum detection in atmospheric nuclear interactions 02 p0316 A67-12763

Nucleon interaction generating high energy gamma rays, discussing photon and energy spectra of electron photon cascade, pion generation and gamma quantum detection in atmospheric nuclear interactions 22 p3876 A67-40265

QUANTUM ELECTRODYNAMICS

SA FIELD THEORY

Soviet papers on quantum electronics 03 p0434 A67-13124

Quantum oscillation of transverse and longitudinal magnetothermal emf in n-type indium antimonide compared with oscillations of transverse and longitudinal magnetoresistance and Hall coefficient 04 p0680 A67-15288

Photodetachment probability for Cs and negative I due to simultaneous absorption of two ruby quanta 05 p0815 A67-16627

Bibliography on lasers covering modes, scattering mechanisms, quantum electrodynamics, matter-radiation interaction, plasma, holography and optics 06 p1010 A67-17890

RCA papers on laser research and engineering 07 p1193 A67-19079

Charged particles for lasing, discussing manufacture of argon laser 07 p1194 A67-19083

Frequency broadening of natural oscillations of optical resonator upon interaction with two-level atom in electromagnetic field 08 p1337 A67-20868

Quantum theory of optical coherence in twisted convolution formalism 08 p1354 A67-20871

Experimental verification of predictions of conventional quantum electrodynamics vacuum effects by Compton and other scattering techniques 09 p1534 A67-22021

Gas laser dynamic behavior, discussing internal modulation, mode locking, noise and perturbation modes 09 p1515 A67-22431

Self-locking of He-Ne lasers at various mirror separations by controlling oscillation frequency with intracavity modulator 09 p1516 A67-22432

Pressure scanned Fabry-Perot etalon for measuring ruby line widths at room temperature 10 p1662 A67-22741

Nonlinear excitation of electron plasmas in solids explained by mechanism of nonparabolic energy bands 10 p1689 A67-23075

Quantum efficiency of optimized GaAs diodes with Zn diffused in skin layer, noting dependence on junction depth 10 p1614 A67-23524

Systematic degradation of GaAs light emitter quantum efficiency, noting relation to current density 10 p1615 A67-23525

Frequency temperature dependence of longitudinal and transverse hypersonic wave absorption coefficients in quartz and artificial ruby crystal 10 p1693 A67-23582

Quantum oscillations of Nernst-Ettingshausen effect in indium arsenide 14 p2376 A67-29087

Close-coupling calculations of positions and widths of lowest-lying autoionizing D states in helium 16 p2704 A67-31167

Frequency and wavelength stabilization of

gas lasers, noting wavelength shifts due to gas pressure and gain variations 17 p2815 A67-32611

Probabilities for two-photon absorption processes induced by coherent and thermal light when acting on atomic system 17 p2870 A67-33317

Renormalization theory and Compton scattering of electron interacting with monochromatic LF polarized light beam 17 p2870 A67-33365

Optical parametric oscillator with ruby laser pumping, noting values of electro-optic and rotational tuning 18 p3059 A67-34011

Radiative effects in pair of spherical particles in radiation field produced by omnidirectional gravitational quanta 19 p3325 A67-35556

Magnetic properties of relativistic equilibrium plasma in magnetic field studied in Boltzmann and quantum cases, using thermodynamic functions 20 p3502 A67-37557

Book on laser systems covering quantum electronics, coherent radiation, modulation and spectral, distance, velocity and communication applications 22 p3814 A67-39445

QUANTUM GENERATOR

Mode characteristics of solid state lasers from analytical solution of conservative equation 03 p0437 A67-13208

I-V characteristic of GaAs diode with Fabry-Perot resonator, noting variations during amplification to generation transition 04 p0678 A67-15132

Superconducting tunnel diode for quantum generation and detection of incoherent phonons, discussing I-V characteristics 06 p1011 A67-18211

GaAs semiconductor quantum generator heating during injection pulse, analyzing temperature effect on external quantum output and generator efficiency 10 p1666 A67-23568

I-V characteristic of GaAs diode with Fabry-Perot resonator, noting variations during amplification to generation transition 12 p1951 A67-25156

Mixed crystals with fluoride base, investigating spectrum and time behavior of laser emission for operation below room temperature 16 p2725 A67-30809

Quantum efficiency in electroluminescent GaAs diodes, considering carrier concentration effect, electron injection ratio, photon absorption and radiative recombination 17 p2914 A67-32654

QUANTUM MECHANICAL GENERATOR

Laser radiation generation at indirect band transitions with free carrier participation in pure semiconductor 10 p1667 A67-23654

Equivalent classical source for weakly coupled quantum-mechanical source, estimating approximation extent 13 p2159 A67-27732

Laser radiation generation at indirect band transitions with free carrier participation in pure semiconductor 17 p2870 A67-33335

Laser light production and properties based on quantum mechanical equations, describing nonlinear interaction between radiation and matter 23 p4011 A67-40761

QUANTUM MECHANICS

SA FUNCTION SPACE

SA RELATIVITY THEORY

Perturbation theory and quantum mechanical applications - Seminar, University of Wisconsin, Madison, October 1965 02 p0270 A67-12721

Perturbation theory in molecular quantum physics using variational principles 02 p0270 A67-12722

Variational perturbation equations and time-independent Schroedinger equation for two-, three- and four-electron atoms 02 p0271 A67-12724

Atomic and molecular time-dependent quantum-mechanical perturbation theory with differential equation formulation within Hartree-Fock approximation 02 p0268 A67-12725

Stationary methods in continuous spectra perturbation theory of nonrelativistic quantum-mechanical scattering in Hilbert space 02 p0268 A67-12726

Quantum mechanical perturbation theory calculation of upper and lower bounds of energy eigenvalues using partitioning methods 02 p0269 A67-12727

Behavior of resonator quantum devices, using oscillating circuit with quasi-linear

negative conductance 03 p0379 A67-13293
Feynman space-time path formulation of nonrelativistic quantum mechanics applied to classical diffusion
problem 03 p0469 A67-13718
Lower bound electronic energy calculations for positive H, using methods of truncated Hamiltonians and of Temple and Kato 03 p0469 A67-13943
Hydrogen line intensity decrease in solar photosphere and chromosphere, noting agreement with Schroedinger equation results 03 p0512 A67-14004
Optical transitions and k conservation in crystalline solids explained in terms of localization of hole produced by excitation 04 p0674 A67-14526
Phase and amplitude fluctuation of gas and solid state lasers, accounting for noise caused by pumping, incoherent decay, lattice vibrations and atomic collisions 04 p0632 A67-14949
Transverse magnetoresistance of n-type InAs, noting temperature effect and correlation with quantum theory 04 p0681 A67-15293
Polarization of light scattered from He-Ne laser beam, applying quantum theory to formula for depolarization ratio 04 p0634 A67-15624
Radial distribution of plasma formed in simple mirror machines by quantum effect field ionization of fast neutral atoms 04 p0671 A67-15644
Magnetic field effect on transport equation, presenting relationship between classical Boltzmann equation and corresponding quantum mechanical formalism 04 p0659 A67-15773
Relaxation problem of two-level molecule in dense resonance medium 05 p0762 A67-16351
Radiative lifetimes of UV multiplets in Si, P, S, O, Ne 2 and Ar 2 measured via phase shift method, correcting for transition cascading 05 p0892 A67-16411
Semiconductor lasers noting strong field behavior and absorption coefficient for saturation 05 p0821 A67-16672
Collision induced dissociation of deuterium by argon and nitrogen examined with angular ion scattering apparatus, determining kinetic energy and angular distribution 05 p0848 A67-16834
Lower bound procedure in quantum mechanical energy equation eigenvalue problem by partitioning and bracketing Hilbert space 05 p0848 A67-16836
Relativistic interaction energies between atoms in degenerate states determined, using Breit-Pauli approximation 05 p0848 A67-16839
Structures of divalent and trivalent metals in terms of pseudopotentials and second order perturbation theory 05 p0869 A67-17189
Optical absorption due to direct intervalence band transitions in Ge, noting effect of lattice temperature 05 p0869 A67-17192
Landau level structure and transition matrix elements of InSb near Brillouin zone center during valence band cyclotron resonance 05 p0870 A67-17193
Second and third virial coefficient of quantum gas expressed in terms of two-particle scattering amplitude, starting from cluster expansion of partition function 05 p0849 A67-17316
Differential cross sections corresponding to excitation of seven states of residual nucleus in Al-Mg reaction at 20.9 Mev 05 p0849 A67-17381
Dead time corrections to photocount distributions using time interval probability density of counts, noting application to laser light 06 p1009 A67-17652
Stimulated two quantum radiation in optical range for transitions occurring between discrete levels of impurity crystals or free atoms 06 p1010 A67-17885
Electroluminescence, discussing semiconductor lasers with various excitation sources, luminescent efficiency, etc 06 p1010 A67-17889
Characteristic states of electromagnetic radiation field, using quantum mechanical theory of optical coherence 06 p1036 A67-18367
Interband magnetoabsorption of InSb, noting anomalies caused by enhanced polaron self-energy

effects 06 p1066 A67-18956
Electron-phonon interaction in semiconductors, considering three-phonon process and third order elastic constant 06 p1066 A67-18957
Transport properties of electrons in GaAs in connection with traveling domains of high electric field in material 06 p1066 A67-18959
Field and charge distribution in hot electron semiconductor, discussing drift and recombination 06 p1066 A67-18960
Nonlinearity 06 p1066 A67-18960
Nonlinear PDEs of two-valley model of Gunn effect materials, noting microscopic transport configurations 06 p1067 A67-18962
Quantum mechanical calculation of transport coefficients of gas of loaded spheres, obtaining scattering amplitudes and cross sections 06 p1038 A67-19045
Thermal excitation and de-excitation of alkali atoms in inert gas heat bath 07 p1265 A67-19075
Second virial coefficient for atomic gas with divergent potential energy curves 07 p1225 A67-19122
Quasi-particle ensemble theory applied to Fermi fluid, noting relation of thermodynamic properties to grand canonical ensemble 07 p1224 A67-19504
Point source detection using signals propagating in quantum field, in terms of correlation functions of thermal field fluctuations 07 p1142 A67-19585
Communication parameters associated with Martian flyby probes and with lander and manned vehicles 07 p1145 A67-19870
Temperature variation of spin-lattice relaxation time and spin-spin relaxation time in superconducting and normal states of vanadium compounds 07 p1236 A67-20139
Extended average energy approximation of first order perturbation wave function, proposing procedure for multidimensional problems 07 p1137 A67-20186
Intermolecular forces in methyl chloride and benzene calculated using spherical shell central potential theory 07 p1138 A67-20191
Charge exchange of protons in alkali metal vapors with formation of highly excited hydrogen atoms, noting cross section, reaction mechanism, etc 08 p1358 A67-20855
Theory of superconductivity on basis of phonon model for finite temperatures, comparing four-fermion/electron interaction with Bardeen hamiltonian model theory of superconductivity on basis of phonon 08 p1372 A67-21491
Quantum mechanical theory for IR absorption by excitons due to photolionization and intraband lattice scattering 09 p1552 A67-21670
Conductivity of high density plasma of MHD generator, noting quantum phenomena associated with overlapping electron wave functions 09 p1543 A67-21818
Correlation of physical properties of transition elements with atomic electron structure, noting energetic stability of configurations 09 p1517 A67-21878
Thermal equilibrium of quantum mechanical system composed of atom nuclei and electrons, using statistical method to eliminate divergence in sum of states of electron proton pair 09 p1550 A67-22664
Dielectronic recombination effect in hot dilute plasmas extended to energetically overlapping metastable levels involving matrix inversion in formal description 10 p1681 A67-22722
Quantum mechanical theory of interference between independent nonmonochromatic light beams using nonmonochromatic modes of radiation field 10 p1663 A67-22866
Rydberg series energy levels of oxygen molecule, comparing theoretical calculations with experimental results 10 p1681 A67-22887
Operator calculus, based on momentum operator choice, designed to take account of finite domain of wave functions in quantum mechanics 10 p1682 A67-23349
Explicit invariant forms of factor equations for factorization of secular equations by group 10 p1674 A67-23377
Relation between Slater screening constants and interchangeability of atomic orbitals 10 p1682 A67-23378
Molecular orbital electron charge density pictures, noting representation close to Hartree-Fock calculation

method 10 p1682 A67-23379
Quantum mechanical kinetic theory of gas loaded spheres to obtain limit of transport coefficients and relaxation time 10 p1682 A67-23383
Quantumstatistical thermodynamics with several temperatures for indivisible observation level 10 p1733 A67-23477
Effective cross sections of excitation of lower energy levels during electron collisions in alkaline metals, noting dependence of various levels on quantum number and atomic number 11 p1822 A67-24018
Quantum noise theory for lasers, obtaining rate equations and noise sources with moments appropriate to shot noise and amplitude spectrum 11 p1799 A67-24239
Dynamic correspondence between electromagnetism field density matrix and associated classical random problem, obtaining means of quantum operators through Fokker-Planck equation 11 p1799 A67-24240
Depression of superconducting transition temperature in narrow tin films, noting condition for maximum microwave enhancement of critical current 11 p1846 A67-24563
Phase shift analysis of nucleon-pion coupling, noting discrepancy between empirical and theoretical results 11 p1823 A67-24599
Drift field, field gradient and diffused impurity effects on minority carriers and quantum efficiency in silicon photocells 11 p1746 A67-24914
Spatial correlation and molecular properties in extended Hartree-Fock calculations, deriving first and second order density matrices for ground state of H, Li and F 11 p1824 A67-24993
Hamiltonian for free particle of arbitrary spin and mass formulated in terms of spin matrix polynomials, noting independence of expansion coefficients 11 p1824 A67-25074
Kinetic equation for electron gas in classical limit derived from quantum mechanical transport equation, using equilibrium analogy 11 p1844 A67-25076
Particle momentum distributions derived from relativistic quantum statistical mechanics 13 p2161 A67-27398
Second current saturation of nonohmic behavior in CdS single crystals caused by quantum mechanical interaction between drift electrons and acoustic phonons 14 p2365 A67-28239
Eigenvalue distribution in random Hermitian matrices, considering self-adjoint operators in N dimensional unitary space 14 p2343 A67-28501
Radio spectroscopy and quantum electronics - Conference, Poznan, Poland, April 1966 14 p2332 A67-28967
Lattice thermoconductivity noting local equilibrium hypothesis theory, thermal resistance mechanism, etc 14 p2374 A67-28981
Instrumentation using quantum effects in weakly coupled superconductors 14 p2375 A67-29043
Nonstationary disturbance effect on electron producing bound s-state during slow collision of atoms 14 p2352 A67-29073
Coherent resonant absorption and emission in IR and visible spectrum, discussing Lorentz oscillator and Dicke spin model of radiating molecule 15 p2519 A67-29190
Charge transfer prediction by classical binary-encounter theory approximation and quantum mechanical approximation 15 p2519 A67-29331
Master equation for statistical operator of laser mode leads to photon number distribution for arbitrary pumping 15 p2501 A67-30124
Two-photon recombination in semiconductors with degenerate electron-hole gas taking into account damping during interaction with phonons 15 p2542 A67-30244
Probability distribution of number of photons and integrated intensity relation to normal and antinormal ordering of field operators in quantum optics 16 p2685 A67-30826
Broadening of lines emitted by tunnel superconductor, noting unfeasibility of simultaneous amplitude-frequency prescription of Josephson current 16 p2728 A67-31044
Multiphonon relaxation in neodymium

doped lanthanum chloride, determining transition rates between stark levels with lifetime and quantum efficiency measurements 16 p2728 A67-31057

Static and dynamic behavior of weakly connected superconducting rings, noting methods of measurement and results 16 p2728 A67-31058

Conductivity, Hall effect and Seebeck coefficient measurements on single domain crystals of barium titanate 16 p2729 A67-31060

Resonances in wave mechanics and anomalous light dispersion, obtaining value of displacement 17 p2884 A67-32704

Short range intermolecular interaction of two ground state hydrogen molecules, using rigorous valence bond approach and population analysis 17 p2890 A67-33262

Coherent electromagnetic oscillation from voltage biasing of superconducting weak link producing coupled quantum oscillators 17 p2926 A67-33380

Nonphysical forces /human soul and personality/ analyzed to explain validity limits of laws of physics, discussing Descartes dualism, quantum mechanics, coincidences, determinism, etc 18 p3077 A67-33500

Quantum cosmology, discussing continuous fluid models as representations of early dense universe 18 p3117 A67-33515

Soviet book on lasers and nonlinear optics covering theory, physical processes and phenomena caused by strong electromagnetic laser radiation 19 p3238 A67-34800

Book on electrodynamics of plasmas covering analysis of collective properties of plasma based on classical and quantum-statistical mechanics 19 p3267 A67-34866

Quantum-mechanical treatment of free-bound approximation for eigenstates and canonical partition function for plasma system in thermodynamic equilibrium 19 p3285 A67-35345

Quantum mechanical transition time shown to be electron tunneling characteristic time 20 p3505 A67-36178

Fokker-Planck equation for distribution function over laser observable values derived from quantum-mechanical laser master equation by expanding statistical operator 20 p3461 A67-37182

Monograph on equilibrium statistical thermodynamics using quantum mechanics 20 p3554 A67-37271

Point source detection using signals propagating in quantum field, in terms of correlation functions of thermal field fluctuations 20 p3384 A67-37322

Quantum mechanical accounting for materials optical properties, considering electronic structure 20 p3515 A67-37717

Nonlinear generalization of Schrodinger equation describing hidden variables effect solved for spin-1/2 magnetic moment relaxing in constant magnetic field 21 p3658 A67-38845

Laser radiation photon number and amplitude fluctuations quantum mechanical calculation by deriving two coupled equations 22 p3815 A67-39784

Josephson effect and quantum coherence measurements in superconductors and superfluids, discussing perturbation theory and tunnel junctions interference effects 22 p3866 A67-40549

Thermodynamic properties of low temperature gaseous and liquid mixtures, discussing quantum effects in mixtures containing hydrogen isotopes and high density mixtures 22 p3921 A67-40553

Spectral dependence of enhanced quantum efficiency and overlap integrals in InSb semiconductors, calculating impact ionization and hot electrons thermalization 23 p4040 A67-41061

Statistical Newtonian mechanics and quantum physics, discussing classical, thermodynamical and biological time concepts 23 p4027 A67-41139

Internal quantum efficiency of red emitting GaP diodes noting low values due to nonradiative recombination 23 p4045 A67-41460

Population noise in semiconductor laser junctions calculated by quantum mechanical Langevin method 24 p4166 A67-41887

Electron emission models for evaluation of charge distribution and total energy of metal-gas interface, noting role of quantum

mechanical corrections 24 p4202 A67-42087

Orthogonal transformation of neighboring quantum states into classical two-component plasmas, using WKB approximation 24 p4195 A67-42107

QUANTUM NUMBER

SA ANGULAR MOMENTUM

Mean powers of r , sum rule and improved transition integrals computed for effective quantum number range up to 8.5, using Coulomb approximation wave functions 01 p0112 A67-10142

Quantum mechanical theory of microwave nonresonant absorption and dielectric and magnetic relaxation in gases 01 p0116 A67-10145

Quantum dimensional effects in bismuth films by tunnel spectroscopy, showing energy dependence of state density having form of step function 02 p0281 A67-11632

Quantum oscillations in magnetoresistance of n-type pure HgTe used to estimate electron effective mass and g value close to band edge 06 p1065 A67-18948

High energy electron ionization cross section for hydrogen, noting high quantum number correspondence to classical expression 19 p3266 A67-36090

Screened Coulomb potential solutions of Schrodinger equation using nonlinear method 19 p3266 A67-36091

QUANTUM THEORY

SA FIELD THEORY

SA SCHUMANN-RUNGE BAND SYSTEM

Electron impact induced transitions between principal quantum number levels in atomic hydrogen estimated via impact parameter method 01 p0124 A67-10780

Soviet papers on quantum electronics 03 p0434 A67-13124

Quantum effects in noise-free communication channels with infinite and limited pass bands in channels with noise, in quantum counters and coherent amplifiers 03 p0368 A67-13140

Quantum study of optical nonlinearities in absorbing materials, energy transfer between optical waves, laws of nonlinear reflection and coherence effects 04 p0657 A67-14881

Kinetic theory of quantum electron gas coupled to radiation field under uniform external magnetic field 04 p0672 A67-15770

Hypersonic excitations due to Brillouin scattering for case with Stokes feedback, deriving quantum equation of motion for creation of laser and Stokes modes and coupled acoustic mode 05 p0823 A67-16683

Landau quantization and removal of spin degeneracy effect on capacitance of p-n junction 06 p1065 A67-18951

Nonlinear galvanomagnetic effects due to hot electrons in n-type InSb in quantum limit 06 p1065 A67-18953

Book on basic principles of physics of semiconductors and semiconductor devices including quantum theory, thermal properties of solid bodies, etc 07 p1231 A67-19301

Single-and double-quantum photodetachment of negative ions, giving cross sections for electron elastic scattering 07 p1225 A67-19494

Quantum theory of electrical conductivity of semiconductors with nonstandard energy band 07 p1233 A67-19639

Undetermined coefficient method compared with confluent hypergeometric functions for solving first order perturbation equation for refractive index of He 11 p1813 A67-24787

Handbook of engineering sciences, Volume 1, Basic sciences 13 p2155 A67-26266

Optical double-quantum transition in which atom passes from one Zeeman sublevel to another by absorption and successive reemission of optical photons 13 p2127 A67-27079

Soviet papers on quantum field theory and hydrodynamics 13 p2105 A67-27410

Gas laser quantum theory, deriving motion equation for radiation-density matrix 14 p2332 A67-28716

Eigenstates of particle mixing matrices and relation to physical antiparticles 16 p2705 A67-31565

Nonlinear interacting plasma wave equations derived by semiquantum analysis of wave-particle and wave-wave interactions 17 p2905 A67-32923

Quantum formulas for optimal filtration of useful electromagnetic signal in noise

background based on maximum misinformation principle 18 p2999 A67-33533

Nature of gravity, discussing universal radiation of gravitation quanta, gravity velocity determination, effects on earth formation, etc 18 p3077 A67-33549

Free energy of N-particle system with far-reaching intramolecular interaction, using collective variables 18 p3085 A67-33670

Quantum statistics of high temperature plasma in thermodynamical balance, introducing effective potentials for partition function evaluation and calculating free energy 18 p3089 A67-34300

General quantum relativity theory in real universe with large radius and elementary particle structure 18 p3080 A67-34728

Quantum theory of laser having only single-mode oscillation and ignoring atomic motion and spatial variations in cavity mode 19 p3239 A67-35034

Multiquantum photoionization applied to laser-induced breakdown thresholds in cesium and rubidium vapors 19 p3241 A67-35810

Existence and stability conditions of several-quanta flux lines in type II superconductors 20 p3505 A67-36206

Lossless small-area Josephson junction analyzed from viewpoint of quantum dynamics, considering system of two superconducting plates 20 p3505 A67-36207

Electromagnetic properties of metal considered for strong quantization of electron states in magnetic field 20 p3464 A67-36224

Faster-than-light particles with spacelike four-momentum within special relativity theory, discussing quantum field theory rejection of objections 20 p3486 A67-37091

Quantum size effects in electric conductivity of thin films 21 p3678 A67-38099

Quantum transport theories for calculating multiple scattering in doped semiconductors 21 p3682 A67-38386

Quantum transport theories and multiple scattering in doped semiconductors evaluated for screened Coulomb potentials 21 p3682 A67-38387

Electron mobility in He, using irreversible quantum statistics theory to obtain momentum dependent relaxation time 22 p3840 A67-39210

Quantum theory of maser oscillator model consisting of radiation field mode interacting with 3-level atoms 22 p3814 A67-39436

Quantum damping theory formulated in coherent state representation, giving Green function solution to damped harmonic oscillator Fokker-Planck equation, noting density operator 22 p3817 A67-40486

Corrections for three results in asymptotic solution of nonideal Bose-Einstein particle system nonlinear integral equations 23 p4026 A67-40718

Laser and maser noise quantum theory emphasizing equations of motion and fluctuation problem, deriving density matrix equation 23 p4011 A67-40762

Book on Hamilton principle and physical systems covering planetary motion, rotating bodies, electromagnetic radiation, quantum theory, etc 24 p4189 A67-42406

QUARK

Charge composition of cosmic radiation, noting results for charges $1/3 e$ and $2/3 e$, experimental setup, etc 02 p0306 A67-11500

Flux measurement of particles with charges of one-third and two-thirds electron charge, reaching sea level with relativistic velocities 02 p0313 A67-12636

Gas proportional counter and scintillation telescope to search for quarks with unit and fraction charges in cosmic radiation at 3200 m altitude 02 p0316 A67-12767

Quarks in cosmic rays investigated using counter telescope 03 p0506 A67-13261

Identification of quark-atomic lines in solar spectrum 03 p0509 A67-13298

Quark confusion with electric-dipole transition in far UV solar spectrum 04 p0694 A67-14479

Identification of quark-atomic lines in solar spectrum 04 p0696 A67-14723

Cosmic ray analysis with Holborn scintillator stacks to determine existence of quarks 06 p1076 A67-17650

Quark radio wave line detection from quasars in galaxies with history of high intensity cosmic rays 08 p1400 A67-21246

Measurement of quark flux with $2/3$

charge of electron reaching sea level with relativistic velocities 11 p1823 A67-24598
 Mechanism for bounding quarks to atomic systems of low molecular weight 13 p2109 A67-26330
 Quark fractional electronic charge in cosmic radiation determined through pulse height distribution 15 p2549 A67-29526
 Hot model of universe supported by radioastronomical observations, estimating quark number density 15 p2555 A67-29640
 Gas proportional counter and scintillation telescope to search for quarks with unit and fraction charges in cosmic radiation at 3200 m altitude 22 p3877 A67-40269

QUARTZ

Spin-lattice relaxation time dependence on temperature and magnetic field in neutron-irradiated quartz with paramagnetic defects at helium temperature range 01 p0127 A67-10064
 Frequency stability of double beam ammonia laser with thermostatic quartz resonators on 3-2 line 01 p0088 A67-10247
 Quartz self-excited oscillator employing Hartley oscillator circuit 03 p0378 A67-13289
 Two-level resonator type laser using neutron-irradiated quartz single crystal with high recurrent inversion frequency 04 p0633 A67-15158
 Pulsed high energy ionizing radiation effects on behavior and output frequency of electronic quartz oscillator crystals 04 p0685 A67-15700
 FM in quartz oscillators, deriving nonlinear distortion and frequency deviation factors and analyzing effect of destabilizing factors 05 p0767 A67-17400
 Transmission of artificial quartz at room temperature, obtaining optical constants in far IR region 09 p1553 A67-21917
 Network analysis of frequency stability of quartz generators, showing possible reduction through additional HF cascades introduction into feedback loop 11 p1768 A67-24982
 Transmission of artificial quartz at room temperature, obtaining optical constants in far IR region 14 p2365 A67-28246
 Two-level resonator type laser using neutron-irradiated quartz single crystal with high recurrent inversion frequency 15 p2496 A67-29345
 Stimulated Raman scattering in IR active nontotally symmetric vibration of alpha quartz crystal, noting parametric oscillation 21 p3641 A67-38459
 Measuring device for frequency and resistance change measurements in quartz crystals due to temperature variations 21 p3601 A67-38975
 Optics for Queen Elizabeth II telescope noting design, tolerance, quartz mirror and test procedures 23 p4001 A67-41257
 Threshold power dependence on temperature and photoelasticity for stimulated Brillouin scattering in crystalline and fused quartz 24 p4204 A67-42365

QUARTZ TRANSDUCER

Equivalent circuit of piezoelectric quartz pressure transducer used with measuring circuit with small input resistance for solving gasdynamic problems 05 p0808 A67-17111
 Control-voltage transducer synthesis with variable capacitor compensation of quartz resonator frequency-temperature characteristics 08 p1306 A67-21280
 Loss in temperature compensation with varying frequency for quartz generators 11 p1757 A67-23909
 Miniature resonator consisting of piezoelectric cadmium sulphide transducer evaporated onto single-crystal quartz wafer 20 p3393 A67-36176
 Loss in temperature compensation with varying frequency for quartz generators 21 p3600 A67-38937
 Comparison calibration techniques for vibration transducers using quartz accelerometer 23 p4003 A67-41337

QUASAR

S QUASI-STELLAR RADIO SOURCE /QSO/

QUASI-STELLAR RADIO SOURCE /QSO/
 SA RADIO GALAXY
 Radio source counts interpretation in support of evolutionary cosmologies 01 p0147 A67-10358
 Red shifts and power outputs in quasars and radio galaxies 01 p0149 A67-10889

Statistical data on space density of bright elliptical galaxies, radio galaxies, quasars, noting relation between space density and age 02 p0322 A67-11685
 Red shifts and colors correlated for quasars leading to smoothed mean energy distribution and new values for K-correction 02 p0322 A67-11686
 Possible correlation between color indices of quasi-stellar radio sources and red shift 02 p0323 A67-11697
 Quasars history, properties and nature 02 p0326 A67-12046
 Quasar 3C-48 radio wave scattering by interplanetary plasma 03 p0509 A67-13204
 Inhomogeneities 03 p0511 A67-13652
 Spectrographic observation of quasi-stellar and Haro-Luyten objects, noting hydrogen absorption spectra and emission wavelengths 03 p0511 A67-13652
 Radio emission from blue stellar objects and radio galaxies, comparing upper flux densities with quasi-stellar radio source emission densities 03 p0512 A67-14002
 Red shifts and blue shifts relative frequency distribution for QSO 03 p0515 A67-14321
 Inverse Compton effect in causing energy loss of electrons in quasi-stellar objects 03 p0508 A67-14325
 Nature and theories of quasi-stellar radio sources and observation of red shift in spectra, examining possible gravitational or cosmological origin of shifts 03 p0516 A67-14337
 Quasi-stellar radio sources analysis including red shift, spectra, variability, etc, discussing possibility of local or cosmological objects 04 p0695 A67-14514
 Local model of quasi-stellar objects based on ejection by gravitational collapse 04 p0700 A67-15199
 Inverse Compton effect in models of quasi-stellar objects demonstrated to be independent of magnetic field 04 p0701 A67-15544
 Inverse Compton effect limits possible mean energy of relativistic electrons, thereby restricting quasar models 04 p0702 A67-15942
 Spectral indices of radio galaxies and quasi-stellar sources explained by relativistic electron injection into magnetic field by recurring blasts 05 p0891 A67-16400
 Variations in RF spectra of 3C 84, 3C 273, 3C 279 and other radio sources 05 p0891 A67-16401
 Correlation between position and red shift of quasars indicating anisotropic universe or galactic origin of quasars 05 p0898 A67-16887
 Quasi-stellar object red shift correlation with radio magnitude 05 p0898 A67-16923
 Inverse Compton effect in quasi-stellar source and relativistic electron distribution 05 p0898 A67-16924
 Angular sizes of quasi-stellar radio sources in extended interferometric survey 05 p0898 A67-16925
 Rising blue shift induced by acceleration in relativistically expanding objects and significance for intensity variations in quasars 05 p0898 A67-16926
 Quasar properties, discussing large red shift in star-like object associated with radio source 05 p0900 A67-17078
 Upper limits to high energy gamma flux from quasars 3C 147, 3C 196 and 3C 273 from Crab Nebula and from 53 Cam magnetic variable star 05 p0900 A67-17079
 Galactic explosions, radio galaxies and quasi-stellar radio sources theories, discussing role of large scale magnetic field 05 p0902 A67-17287
 Luminosity and density evolution hypotheses concerning distribution of flux densities of quasars, testing validity with Einstein-de Sitter model 05 p0903 A67-17328
 Absolute magnitudes of quasi-stellar radio sources, plotted against logarithms of red shifts, fall between two limits 06 p1086 A67-18373
 Relation between optical and radio properties of quasars 06 p1086 A67-18374
 Radio galaxy phenomena and quasars noting stellar evolution mechanism, energy generation and emission 07 p1246 A67-19055
 Quasar counting, red shift and brightness 07 p1249 A67-19661
 Gravitational red shifts in quasi-stellar objects 07 p1250 A67-19664
 Large scale quasar clusters in

inhomogeneous universe 07 p1250 A67-19665
 Anisotropic distribution of quasars with large red shift as effect of observational selection 07 p1250 A67-19666
 Radio observation of quasar CTA 102 at various frequencies from Arecibo for possible explanation of sinusoidal variation of flux density 08 p1397 A67-21186
 Radio telescope-spectrophotometric scanner investigation of continuous energy distribution of four quasars 08 p1398 A67-21230
 Spectrophotometric data correlations between color and red shifts of quasars 08 p1398 A67-21231
 Quark radio wave line detection from quasars in galaxies with history of high intensity cosmic rays 08 p1400 A67-21246
 Red shift relationship with ionization potential for absorption lines in quasi-stellar object 3C 191 08 p1400 A67-21251
 Spectrum of quasi-stellar source PHL 5200 with rapidly expanding envelope 08 p1400 A67-21253
 Red shift and absorption line of PKS 0237-23 09 p1587 A67-22242
 Absorption wavelengths of QSOs, noting relatively large red shifts 09 p1567 A67-22243
 Quasars, energy emission, high red shifts and relation to radio sources and visible stars 10 p1705 A67-22953
 Time variations in flux density of some quasi-stellar sources, discussing relationships with component age and thickness 10 p1705 A67-22955
 Coincidences in measured positions of absorption lines in spectra of quasi-stellar objects 11 p1862 A67-24507
 Quasi-stellar objects red shift and optical magnitude measurements, noting discrepancies with zero and nonzero cosmological constant 11 p1863 A67-24508
 Statistical verification of hypothesis explaining observed scintillations of light curve of quasi-stellar radio sources by explosions of supernovas 13 p2198 A67-26766
 Association of radio sources with peculiar galaxies in symmetrically distributed pairs 14 p2388 A67-28830
 Red shift determinations for quasi-stellar radio sources using spectrographic techniques 14 p2389 A67-28844
 Spectral energy distribution of source 3C 446 between August 17 and December 12, 1966 14 p2389 A67-28850
 Red shifts from absorption line spectra of quasi-stellar objects, discussing energy generation mechanism 14 p2390 A67-28851
 Suggestion of physical association of radio sources with stars in neighborhood as radio stars 14 p2391 A67-28945
 UVB values and red shifts of quasars interpreted within steady state and Friedman cosmological models 14 p2392 A67-28965
 Faint radio sources investigated for isotropy applying Scheuer statistical method rendering quasars local origin theory improbable 16 p2752 A67-31623
 Random amplitude fluctuations of quasi-stellar radio source from similarity between spectral-density distributions of observed and random-simulated luminosities 16 p2752 A67-31696
 Weak radio sources of small angular size studied by lunar occultation technique, using steerable telescope 17 p2943 A67-32634
 Millimeter radiation from 3C 273 17 p2944 A67-32635
 Interpretation of UVB measurements of quasi-stellar sources 17 p2944 A67-32637
 Quasar observations using interferometer baselines, noting regular fringes and small phase scintillation in Gaussian source model 17 p2947 A67-32760
 Quasi-stellar radio source optical spectrum observed, identifying spectral lines and determining red shift 18 p3118 A67-33854
 Mean density of cosmological matter determined from quasi-stellar sources observations, analyzing apparent-magnitude and red shift methods 18 p3119 A67-33856
 Radio astronomy sensitivity and resolution, discussing aperture synthesis and interferometric techniques for accurate position determinations 18 p3135 A67-34585
 Quasar regarded as early stage in formation of system like galaxy nucleus, using model 19 p3317 A67-34950

Minimum radius of line emitting regions in quasars estimation method, discussing origin problem 19 p3327 A67-35893

Absorption lines in quasi-stellar source analysis to obtain estimates of either particle density in absorbing region or distance between continuum source and absorber 19 p3330 A67-36082

Optical polarimetric observations of quasi-stellar objects 19 p3331 A67-36083

Differentiation between gravitational and cosmological components of quasars red shift by observational means 20 p3521 A67-36295

Relationship between radio galaxies and quasars, observing two sources of moderate distance, noting intense optical emission of limited intensity or duration 20 p3521 A67-36296

Statistical properties of optical variability of 3C 273 suggesting quasar nucleus as single body 20 p3521 A67-36297

Quasar sources studies set limits on possible density inhomogeneity magnitudes in universe by measuring cosmic microwave background isotropy and homogeneity 20 p3525 A67-36868

Radio parameter continuity between radio galaxies and quasars, plotting spectral indices against absolute spectral power 20 p3525 A67-36947

Quasars and radio galaxies characteristics contrasted, drawing conclusions about evolution using radio emission synchrotron hypothesis and consistent model 20 p3526 A67-37250

Quasi-stellar red shift assuming gravitational origin, deriving mass, radius and distance as function of flow density, linewidth and apparent diameter 20 p3531 A67-37683

Red shift magnitude relation for quasi-stellar objects 21 p3701 A67-37895

Relativity theory accounting for energy conservation properties in elementary particle interactions and small size and high energy emission of quasars 22 p3892 A67-40499

Unified theory for galaxy spiral formation and radio galaxy and quasar evolutionary dynamics, discussing galactic dipole magnetic field generation 22 p3893 A67-40504

Extragalactic radio sources interpreted as consistent evolutionary sequence, suggesting particle injection, relativistic gas expansion and intergalactic gas pressure equilibrium 23 p4069 A67-41361

Monograph on quasi-stellar objects including identification, line spectra, radio emission, continuum radiation, red shift and models 23 p4069 A67-41438

Absorption spectra of quasi-stellar objects /QSO/, suggesting origin in galaxies through which light passes on way to earth 23 p4069 A67-41442

Origin of heavy nuclei abundance in low energy primary cosmic ray flux, discussing association with quasi-stellar objects 24 p4209 A67-41874

Radio interferometric measurements of radio source diameters using 3074 km baseline 24 p4226 A67-41876

Possible circular polarization of compact quasar radio and optical radiation, discussing astrophysical implications 24 p4226 A67-41884

Novae and supernovae outbursts, suggesting mechanism which can account for both phenomena and for other problems concerned with quasi-stellar sources /quasars/ 24 p4231 A67-42451

QUATERNARY ALLOY
Probable upper limit of critical field for ternary and higher order ductile transition metal superconducting alloys 11 p1850 A67-24925

High oxygen Nb-Ti alloy solid solution critical superconducting current density and workability dependence on Th, Gd and Y solute content 23 p4036 A67-40705

QUATERNION
SA DYADIC
Dual quaternions in describing motions of offset unsymmetrical gyroscope [ASME PAPER 66-MECH-6] 08 p1332 A67-21316

Differential and Clifford matrix algebra relationship in relativity theory, generalizing Dirac and quaternion algebras to Riemann spaces 21 p3656 A67-37923

QUENCHING
SA FLAME QUENCHING

Amorphous whiskers from cobalt-gold alloy by quenching molten material through electron-beam heating and anvil-cooling device 01 p0135 A67-10895

Normal region distribution in superconducting solenoid measured after quenching by varying quenching current 01 p0137 A67-11065

Vacuum UV photolysis of solid ethane films, measuring product distributions, presenting evidence for quenching of excited ethane and ethylene 05 p0758 A67-16128

Auroral hydrogen line emission quenching by collisional ionization 05 p0804 A67-17413

Quenching rate effect on athermal stabilization of austenite steel 06 p1014 A67-17801

Quenching from alpha region and subsequent tempering effect on mechanical properties of titanium alloy VT5-1 07 p1200 A67-19249

Structure of system Ti-Mo-Cr-Fe-Al alloys when quenched from beta region, noting maximum hardness at aging temperatures 07 p1205 A67-19272

Physical properties of quenched binary alloys of titanium 07 p1206 A67-19281

Postquenching deformation effect on mechanical properties and creep resistance of aluminum alloys [ONERA-TP-423] 09 p1519 A67-22156

Quenching examination of phase equilibrium in system lead oxide-titanium oxide-zirconium oxide, determining isotherms lines, melting points, etc 12 p1986 A67-26188

Optical quenching of photoconductivity in silicon resulting from minority carrier capture by centers created by irradiation 13 p2173 A67-26358

Welding characteristics of aluminum alloys, noting influence of quenching temperature, quenching process delay and cooling velocity on weld tensile strength 15 p2503 A67-29781

Red luminescent band and photoconductivity in cadmium sulfide single crystal, discussing IR quenching of photocurrent 19 p3300 A67-34764

Delay time of quenching response and recovery in gallium arsenide injection laser 21 p3640 A67-38261

Optical quenching of photoconductivity in silicon resulting from minority carrier capture by centers by irradiation 21 p3679 A67-38315

Phase transformations in commercial titanium alloys compared for mechanical properties, emphasizing decomposition of metastable beta phases on quenching, aging or deformation 22 p3822 A67-40055

Quenched structures and precipitation in Al-Cu alloys with and without traces of Cd studied electromicroscopically, showing possible CD stabilizing effect 24 p4173 A67-42166

QUEUE
Queueing theory applied to phased array radar maintenance problems, specifically replacement and repair of transmitter and/or receiver modules 08 p1292 A67-20668

Reliability for redundant repairable systems using queueing theory, studying triplicate and similar/dissimilar subsystem systems 15 p2453 A67-30063

QUINOLINE BLUE
S CYANINE DYE

R

RABBIT
Anesthetized rabbits exposed to high explosive air shock waves in shock tube, examining changes of elastic properties of lungs of rabbits 03 p0364 A67-14292

RADAR
S COHERENT RADAR
S CONTINUOUS WAVE /CW/ RADAR
S DOPPLER RADAR
S LIDAR
S MONOPULSE RADAR
S MOVING TARGET INDICATOR /MTI/ RADAR
S OPTICAL RADAR
S PULSE RADAR
S SEARCH RADAR
S SECONDARY RADAR
S SIDE-LOOKING RADAR
S SURVEILLANCE RADAR

S TRACKING RADAR
S WEATHER RADAR
RADAR AIRCRAFT DETECTOR
Aircraft radio guidance system combining ILS and precision approach radar 04 p0653 A67-15042

RADAR ALTIMETER
Air traffic control radar beacon system with automatic altitude reporting system [SAE PAPER 670256] 12 p1941 A67-25506

Evaluation of satellite radar altimetry for geophysical and oceanographic measurement 16 p2742 A67-30688

Updated inertial navigation of continuously powered space vehicle during lunar landing mission, utilizing altimeter and Doppler radar 22 p3833 A67-40195

RADAR ANTENNA
SA DUPLEXER
Flying target detection and tracking with fixed antennas having radiation pattern scanning and multibeam characteristics 02 p0205 A67-12730

Machine design, capillary control selection, hydraulic circuitry and oil selection of two two-surface angular hydrostatic bearings used for azimuth turntable of radar antenna pedestals 03 p0431 A67-13749

Computer program to aid analysis of tracking radar towers and foundations 03 p0396 A67-13753

Reflected voltage provided by circulator for radar echo reduction, noting principle of antenna impedance loading 03 p0370 A67-13857

Treatment of surface of directional radar antenna with RF absorption material for sidelobe reduction 03 p0389 A67-14349

Helicopter main rotor blade used as scanning radar antenna 04 p0579 A67-14491

Side-looking airborne radar in which long antenna mounted along side of aircraft faces at right angles to flight path 04 p0573 A67-15039

Fast switching microwave phase shifters for high power array radars, describing drive control techniques 04 p0581 A67-15053

Simple secondary radar antenna with fan-shaped beam for monopulse operation 06 p0967 A67-17616

Radar antenna synthesis for optimum and suboptimum filtering of spatial signals according to mean square error minimization 07 p1158 A67-20238

Radar scan-antenna angle transmission over DC voltage in binary form for digital computer or display 11 p1760 A67-24269

Radar antenna synthesis for maximum SNR and minimum error dispersion in target bearing, reducing problem to filter synthesis 13 p2069 A67-27039

Size and shape of vertical polar diagrams of radars in situ measured using sun and other stars as signal sources 13 p2071 A67-27219

Radio stars as signal sources for accurate measurement of radar antennas vertical polar diagrams, describing solar noise technique disadvantages 15 p2436 A67-29645

Quantum paramagnetic amplifiers in USSR, discussing physical characteristics and operation of resonators in decimeter band, antenna systems for noise reduction, etc 16 p2623 A67-31024

Radiation pattern changes for helicopter antenna located in rotor blade as result of flight dynamics [AHS PAPER 109] 16 p2597 A67-31825

Modes of boresight shift in conical-scan and sequential-lobing types of amplitude sensitive angle-tracking antennas 17 p2814 A67-32523

External noise levels effect on angular accuracy of tracking radar pencil-beam antennas, emphasizing radome noise and dielectric coating characteristics 17 p2826 A67-32685

Dual-antenna AMTI radar ground clutter cancellation and signal enhancement 18 p3001 A67-34117

Efficient thermal design of steerable antennas, considering space-environmental requirements 22 p3750 A67-40409

Decision theory applied to angular resolution, deriving signal processing radar system beyond Rayleigh limits and target reliability 23 p3972 A67-40643

RADAR APPROACH CONTROL /RAPCON/
Atlanta advanced radar traffic control system with automatic alphanumeric field installation system and computerized

program for controlling aircraft approach 01 p0110 A67-10666

RADAR ASTRONOMY

Quantitative study of radar cross polarization factor D in order to obtain data on lunar surface roughness and dielectric properties 02 p0192 A67-11603

Radar mapping of lunar surface made with 10 ft beamwidth antenna at Arecibo, Puerto Rico 02 p0324 A67-11856

Planetary exploration with radar, noting technical problems, advantages and results 06 p0192 A67-19012

Interpretation of radar observations of Venus, Mercury and Mars with outline of direction of current radar astronomical research 07 p1246 A67-19053

Radar methods in lunar probing, discussing data obtained from surface soundings [AAS PAPER 66-186] 08 p1387 A67-20961

Radar observation of Mars, noting mean reflection coefficient for signals returned by near center disk sections 09 p1563 A67-21632

Orbit calculation of 12,500 meteors in earth vicinity based on radar observations of radiants and velocities 09 p1563 A67-21635

Radar measurements of Doppler spectra and power reflectivity of Mars interpreted as surface elevation differences between dark and bright areas 11 p1867 A67-24776

Two-dimensional aperture synthesis in lunar CW radar astronomy, showing measurement possibility for Fourier transform components of sky brightness distribution 14 p2385 A67-28442

Two-layer model of Venusian atmosphere satisfying radioastronomic and radar self-radiation measurements 17 p2941 A67-32322

Radar determinations of astronomical unit and orbits, radii and rotation vectors of inner planets, proposing general relativity radar test 18 p3123 A67-34145

RADAR ATTENUATION

Anechoic chamber characteristics, noting indoor antenna pattern measurements and transmission attenuation variations 16 p2640 A67-31364

Upper limits on liquid water content in Venus atmosphere 17 p2945 A67-32652

Degradation of moving clutter attenuation efficiency due to Doppler-frequency shift in MTI radar systems 23 p3972 A67-40642

RADAR BEACON

Digital data processing, transfer and display equipment applied to ATC terminal operations, using surveillance radars and radar beacons 08 p1351 A67-20677

Air traffic control system, discussing effect on business aircraft operations 14 p2347 A67-28317

RADAR BEAM

Fill factor of radar beams reflected from meteorological targets of various forms derived, taking antenna radiation pattern into account 01 p0025 A67-10790

Equations and curves defining pattern loss for fan-and pencil-beam arrays, discussing radar efficiency factor 06 p0968 A67-17964

Universal array of complementary-symmetry MOS transistors applied to missile and surface radar beam steering phase array storage unit 18 p3015 A67-34563

Multiplexed antenna array operating over certain frequency range through electric beam shifting 20 p3403 A67-37507

RADAR CLUTTER MAP

Frequency correlation of clutter by considering signal received by radar at time t after it has transmitted pulse 01 p0023 A67-10468

Theoretical approximations for probability densities of duration and interval between fades, assuming Rayleigh process characterizes fading phenomenon 03 p0368 A67-13168

Straight edge fence design for control of radar site environment from clutter return, pattern interference, tracking errors and high power hazard to personnel 03 p0396 A67-13853

RADAR CROSS SECTION

Short-pulse radio reflections to determine average scattering behavior of lunar surface at 23 cm wavelength 02 p0325 A67-11858

Radar cross section minimization on sphere using symmetrically attached wires 03 p0369 A67-13683

Radar scattering cross section for semiminfinite perfectly conducting blunted cones 03 p0370 A67-13854

Controlling radar cross section of long thin bodies by employing corrugated structures operating in nonpropagating mode 03 p0370 A67-13862

Spherical concentric geometry for designing absorber materials for application to curved surfaces determined by specular radar cross section 03 p0371 A67-13863

Radar cross sections, tracks and fluctuation spectra of grackles, pigeons and English sparrows 04 p0569 A67-14679

Bistatic radar cross section of underdense turbulent plasma measured at X-band and results compared with theoretical scattering model 05 p0760 A67-15999

Radar characteristics of lunar surface from Surveyor I spacecraft 08 p1386 A67-20941

Electromagnetic wave scattering from plasmas calculated in context of physical optics, noting that radar cross section for plasmas with finite conductivity is polarization dependent 11 p1820 A67-24913

Maintaining target track for nonmaneuvering targets approaching uniformly scanning search radar 13 p2068 A67-26782

Radar/backscatter/ cross section of wakes of vehicles in ionosphere, showing creation of mild electron depletion under broadside incidence conditions 14 p2261 A67-28125

Cross section and angular scattering law for Venus and Mercury from delay and Doppler frequency shift radar echo measurements 15 p2556 A67-29870

Plane wave scattering by finite circular cylinder treated by geometrical diffraction theory, obtaining formulas for radar cross section 17 p2816 A67-32789

Principal polarization radar cross sections as function of azimuth aspect angle for rectangular cylinder 19 p3183 A67-35518

Radar cross section measurement using standing wave method 19 p3184 A67-35826

Bistatic radar cross section of coherent-dot radar angel in convective thermal model 20 p3480 A67-36286

Time average of autocorrelation function measured by CW radar illuminating moon calculated without lunar surface properties knowledge 21 p3703 A67-38189

Simultaneous UV photographs and radar cross section measurements of Venus, discussing atmospheric motion and rotation 21 p3705 A67-38611

Radar cross section of Mars, discussing spectral analysis, echo delay and radar echoes from Jupiter 21 p3706 A67-38617

Cylindrical tube current distribution determined by digital computer solution of Fredholm integral equations 23 p3981 A67-41208

RADAR DATA

Magnetic recording of various types of monopulse, PPI and MTI radar signals, with application to airborne data acquisition recorder and ground reproducer 02 p0196 A67-12004

Radar data handling and display systems used with pulsed radars, detailing military type for use of weapons control officer 04 p0578 A67-15057

Conversion of frequency spectrum of pulse-position-modulated signal passing through delay device and amplifier switched by input undelayed signal 07 p1139 A67-19229

Wavelength dependence and aspect sensitivity of radar auroral echoes show Booker field-aligned scattering model inadequate 20 p3433 A67-37411

RADAR DETECTOR

Radar detection of tropopause and clear air turbulence 04 p0649 A67-14682

Optical range gated filter for detecting moving targets in clutter background, using laser beam for application to MTI radar 08 p1293 A67-20687

Moving-window detector for binary integration on quantized data, discussing possible application to multiple-range-element radar 12 p1916 A67-26079

Probability density functions for power from Rayleigh target 13 p2067 A67-26520

Distribution-free signal detection by multiple-resolution-element pulse radar, based on ranks of returns and having invariant false alarm rates 15 p2436 A67-29933

Eldorado low altitude detection and short reaction time defense system, examining Doppler effect and Mirador pulse radar 17 p2816 A67-32751

Digital simulation of clutter rejection MTI radars 20 p3388 A67-37651

80 km atmospheric backscattering enhancement detected by optical radar 22 p3759 A67-39558

RADAR DIRECTION FINDER

Marconi AD370 solid state automatic direction finder 05 p0839 A67-16579

Direction finding errors of method of instantaneous amplitude comparison in elliptically polarized antenna arrays 09 p1473 A67-21960

Microwave direction-finding receiver with digital output for blind aircraft landing and navigational uses 19 p3254 A67-35555

Direction finding errors of method of instantaneous amplitude comparison in elliptically polarized antenna arrays 20 p3400 A67-37190

Angular coordinates of pulsed incoherent scanning radar determined, comparing efficiency of direction finding by minimum rms error and maximum likelihood method 22 p3762 A67-39874

RADAR DISPLAY

SRT Daylight Display System for ATC in which radar video signals are passed through data processor 07 p1221 A67-19543

Direct view storage tubes for radar displays 09 p1528 A67-22628

Digital radar simulator capable of displaying 40 aircraft for air traffic control 09 p1528 A67-22632

High resolution 12 inch radar/synthetic display for air traffic control centers 09 p1465 A67-22640

Data acquisition, processing and display in computer based ATC system using radar with automatic position-reporting data link 15 p2515 A67-29941

Radar display layout for aircraft safety consisting of digital computer and CRT 15 p2468 A67-30129

Bowtie radar display effectiveness in target detection compared with conventional Plan Position Indicator /PPI/ [TR-750-7] 17 p2807 A67-32630

Book on fundamentals of display systems covering cathode ray tubes, color techniques, photographic and electromechanical systems, etc 20 p3435 A67-36135

Design characteristics of IBM 9020 system to provide automated aids for processing and updating flight information 23 p3976 A67-41057

RADAR ECHO

SA VENUS RADAR REFLECTION Frequencies of radar echoes from Mercury and Venus measured, for testing Doppler formula 01 p0026 A67-10920

Polarization effects during radio wave scattering by cloud and precipitation particles, obtaining phase state from echo signal 01 p0109 A67-11249

Radar observations of equatorial electrojet irregularities indicate reversal during nighttime of daylight westward traveling electrons stream 03 p0408 A67-12837

Reflected voltage provided by circulator for radar echo reduction, noting principle of antenna impedance 03 p0370 A67-13857

VHF backscatter observations of radio auroral radar echo occurrence at sunspot maximum associated with spirals in geomagnetic latitude and time, magnetic disturbance levels and season 03 p0513 A67-14113

Radar experiments of sun at 38 mc/s, presenting results on echo variation with sunspot number, coronal irregularities, etc 03 p0514 A67-14311

Mass distribution of meteoroid flux determined by relating frequency distribution of durations of radar echoes from meteor trails 03 p0516 A67-14348

24 hr history of radar angel activity at 3.2, 10.7 and 71.5 cm wavelengths 04 p0649 A67-14681

Doppler technique application to radar measurement of clear air target motion 04 p0569 A67-14684

Atmospheric turbulence compared with associated radar echoes, noting correlation coefficient for standard deviation of derived gust velocity with maximum radar reflectivity 04 p0649 A67-14687

Sunset peak in occurrence of F layer field-aligned echoes explained by Martyn amplification mechanism, estimating

ionization vertical velocities from electron number density 04 p0615 A67-14959

S-band pulse signal reflection from various grounds at vertical incidence 04 p0572 A67-15035

Propagation of clear air radar echoes in nonionized media and use in determining planetary surface and atmospheric structure 05 p0760 A67-16009

Radar observations of Venus at 3.8 cm noting low value of cross section, echo spectrum, polarization characteristics, absorption cross section and atmospheric attenuation 05 p0889 A67-16298

Time delay measurements and radar echo determinations of planetary motions compared with IAU values 05 p0900 A67-17082

Range determination with CW tracking radar controlling rms error, noting SNR role in holding target echo 06 p0957 A67-17593

Frequency effects in radar return from turbulent weakly ionized missile wakes, obtaining relationship between radar cross section and electron density distribution [AIAA PAPER 67-23] 06 p0963 A67-18258

Statistical properties of radar signals with internal coherence reflected from rough surfaces 07 p1139 A67-19223

Ionization structure of polar auroras from spatial distribution of radar-reflecting zones, taking into account magnetic field variations 07 p1174 A67-19710

NRL lunar radar system applied to long term earth-moon distance measurements, using pulse compression for signal processing, noting high SNR 08 p1293 A67-20689

East-West motion of auroras analyzed in Idaho using radar echoes, noting velocity, direction reversal, etc 10 p1651 A67-23344

Radar echoes from cloud-free atmosphere caused by turbulent pulsations of microwave refractive index 10 p1677 A67-23500

Polarization effects during radio wave scattering by cloud and precipitation particles, obtaining phase state from echo signal 11 p1815 A67-24120

Radar echo model from random collection of rotating dipole scatterers 11 p1764 A67-24435

Video mapping technique making possible radar moving target indication for permanent echoes only 12 p1909 A67-25128

Spectral characteristics of small scale refractive index fluctuations in troposphere using radar echoes 13 p2068 A67-26790

Lunar radar echoes depolarization studied via lunar surface backscattering characteristics at 23 cm wavelength 14 p2261 A67-28374

Clear atmosphere angels origin, clear air turbulence detection, radio propagation and atmospheric radar probing 14 p2264 A67-28395

Cross section and angular scattering law for Venus and Mercury from delay and Doppler frequency shift radar echo measurements 15 p2556 A67-29870

Planetary masses, radii and orbital element and astronomic unit determinations from radar time delay and Doppler shift measurements 15 p2556 A67-29871

VHF radar reflections from artificial earth satellites used to analyze amplitude scintillations in ionosphere [AGARDOGRAPH 95] 15 p2482 A67-30292

Radar observation of meteor echoes in upper atmosphere, particularly delonization of processes in meteor trains 16 p2749 A67-31251

Observed nonstationarity of low frequency radar echo envelope correlation with aircraft motion relative to receiver 16 p2625 A67-31273

Origin of afternoon VHF radar echo from backscattering layer near auroral electrojet explained by plasma instability and perpendicular electric fields 16 p2627 A67-31407

Auroral radar echo association with two-stream plasma instability 17 p2852 A67-33244

Influence of aurora on radio wave propagation 18 p3038 A67-33617

Passive electronics countermeasure device /chaff/ consisting of metal strips to produce radar echoes 18 p3001 A67-34118

Stratospheric aerosol concentrations observed by optical radar echoes compared with expected return from molecular

atmosphere to obtain vertical profile 18 p3042 A67-34493

Light deflection by solar gravity measuring method using radar interferometer 20 p3485 A67-36995

Radar and aircraft simultaneous clear air turbulence /CAT/ observations 20 p3481 A67-36996

Depolarization ratio of echo signals from point angel sources, using radar apparatus 20 p3384 A67-37237

Wavelength dependence and aspect sensitivity of radar auroral echoes show Booker field-aligned scattering model inadequate 20 p3433 A67-37411

Radar cross section of Mars, discussing spectral analysis, echo delay and radar echoes from Jupiter 21 p3706 A67-38617

Absolute radar echo duration dependence on meteoroid mass calculated for various velocities 24 p4228 A67-42268

RADAR EQUIPMENT

Transition zone anechoic chambers for field checkout, production and radiation testing of microwave antennas 03 p0397 A67-14102

Monolithic IC design of diodes and X-band microswitch transmission line fabricated on Si substrate 06 p0968 A67-18053

Three-dimensional chaff simulator to provide video inputs to operational radar equipment for exposing operators to jamming 08 p1314 A67-20656

Solderless-wrap lightweight interconnection board for Lunar Module landing radar, noting manufacturing details 16 p2642 A67-31919

Ultrasonic correlating device for fabrication of pulse compression radar signals 18 p3002 A67-34227

Target-tracking antenna design with primary feed system suitable for slewing of mobile radar equipment 22 p3760 A67-39592

RADAR FILTER

Waveform and filter design for acceptable performance in clutter environment 07 p1145 A67-19880

Frequency scanned filter in radar signal processing system designed to extract range and Doppler resolution, using properties of ambiguity function 09 p1466 A67-22695

Sidelobe reduction in phase-coded pulse compression radars solved by eliminating ripple of matched filter output with aid of weighting filter 12 p1908 A67-26092

Radar antenna synthesis for maximum SNR and minimum error dispersion in target bearing, reducing problem to filter synthesis 13 p2069 A67-27039

Radar moving target indicating filters performance, describing method for including target Doppler frequency statistics in gain probability 20 p3386 A67-37498

Coherent acceleration and velocity observation in real time /CAVORT/ analog radar signal processor for matched filtering pulse trains from radial accelerated targets 21 p3586 A67-38953

RADAR INSTRUMENTATION

Instrumentation radar characteristics, range equation for tracking performance, sensitivity, targets, systems performance evaluation, etc 10 p1605 A67-22994

Multifunction airborne radar instruments, discussing air to air, air to ground, shared aperture and combined systems, spoiled beam technique for ground mapping, etc 11 p1754 A67-25007

Moving-window detector for binary integration on quantized data, discussing possible application to multiple-range-element radar 12 p1916 A67-26079

Radar type instrument for measuring reflection coefficients of planetary surfaces from unmanned spacecraft 22 p3795 A67-39159

RADAR MAP

Radar backscatter return interpretation in identifying terrain phenomena and composition 01 p0059 A67-10330

Terrain relief appearance on aircraft radar determined from radar parallax and shadow parallax 02 p0239 A67-12539

Radar, IR and laser sensors production trends for airborne reconnaissance 15 p2485 A67-29163

Vegetation mapping from K-band radar imagery using image discrimination, enhancement, combination and sampling system 19 p3227 A67-34798

RADAR MEASUREMENT

VHF radar techniques for detecting and mapping subsurface discontinuities such as solid layering, rock interfaces and ore deposits in lunar and planetary surfaces 01 p0021 A67-10324

Radar measurement of vertical density profiles of clouds and precipitation 04 p0650 A67-14689

Radar measurements confirm West Ford dipoles reentered lower atmosphere in accord with predictions 04 p0618 A67-15941

Terrain backscattering characteristics at low grazing angles for X-and S-band 05 p0768 A67-17527

Low resolution side-looking radar application for geological studies, noting advantage over small scale aerial photography 06 p0994 A67-17833

Cloud melting zone, noting increased antenna temperature for radiation trapping between cloud layer and ground [AIAA PAPER 67-188] 06 p1026 A67-18491

Blind height effect in radar measurements of aircraft cruising speed treated by repetition frequency wobbling 07 p1139 A67-19228

ARSR Weather Surveillance System design, operation and performance 07 p1142 A67-19542

Measurement of attenuation of 8.6 mm wavelength radiation in rain, relation to rate of rainfall, using corner reflectors 07 p1146 A67-20201

Errors in R-meter measurement of velocity spread of meteorological targets resulting from radar frequency instabilities 10 p1676 A67-22816

East-West ionospheric wind component measured by CW meteor radar 10 p1644 A67-23253

Radar measurements of wind regime of meteor zone made by means of pulse-coherent method 13 p2110 A67-26552

Cloud height measurement by optical method compared with vertical radar procedure 13 p2152 A67-26866

Limitations in conventional radar compared to new multichannel radar with discontinuous pulse compression 13 p2070 A67-27203

Venus and Mercury intrinsic rotation rates and surface radar reflectivity of former from radar echo measurements 15 p2556 A67-29872

Pulse Doppler waveform coding, presenting technique of selecting pulse-period modulation codes requiring only computer calculations 15 p2437 A67-29934

Laser radar selenodesy for ground control selection of Apollo landing sites 16 p2623 A67-30982

Lunar radius facing earth determined from radar measurement data and lunar orbiters 19 p3319 A67-35263

Radar and aircraft simultaneous clear air turbulence /CAT/ observations 20 p3481 A67-36996

Radar station with antenna system for three target coordinates simultaneous measurements 21 p3582 A67-38498

Radar type instrument for measuring reflection coefficients of planetary surfaces from unmanned spacecraft 22 p3795 A67-39159

Ground based atmospheric and ionospheric particle temperature measurements, examining methods and thermosphere heat sources 22 p3870 A67-39676

Radar-derived results for midlatitude F-region densities and temperatures at sunspot minimum noting seasonal anomalies 22 p3793 A67-40080

Cloud melting zone, noting increased antenna temperature for radiation trapping between cloud layer and ground [AIAA PAPER 67-188] 23 p4025 A67-41747

Venus surface temperature measured using difference between optical and radar radii, cloud temperatures and adiabatic lapse rate 24 p4225 A67-41827

RADAR NAVIGATION

Radar techniques for detection tracking and navigation - AGARD Avionics Symposium, London, September 1964 04 p0571 A67-15028

RADAR OBSERVATION

Local geologic interpretation from intensity of radar return energy modified by illumination, surface roughness and object shape 01 p0058 A67-10310

Electron number density profile measurements of moderate and heavy sporadic E over Arecibo by incoherent backscatter technique 03 p0409 A67-12946

Radar observation of insects in free flight, noting backscatter and velocity measurement results [AFRL-67-0127] 03 p0371 A67-13916

Doppler technique application to radar measurement of clear air target motion 04 p0569 A67-14684

Radar and airborne instrumentation sampling of atmosphere, noting linked mode or one-one comparison between returned radar signal and meteorological probe 04 p0570 A67-14685

Power aspects of radar survey of limited earth surface regions 07 p1139 A67-19225

Orbit calculation of 12,500 meteors in earth vicinity based on radar observations of radiant and velocities 09 p1563 A67-21635

Absolute angular momentum of outflow winds and radar targets in hurricanes and typhoons 10 p1676 A67-22813

Radar evidence for atmospheric dust layers around 80 km altitude 13 p2109 A67-26333

Geometric and thermal height of shower and storm cells using radar observations 13 p2150 A67-26433

Ferrite-diode system with automatic gating of signal reflection used in radar wind velocity observations to reduce pulse interferences produced by meteor trails 13 p2197 A67-26505

Meteor distribution estimation attempted through radar observation, measuring kinetic energy level, velocity and electron distribution in meteor trails 13 p2197 A67-26507

Spatial distribution of auroral radio signal reflection centers based on radar observations 13 p2111 A67-26566

Tropospheric condition effect on near-ground ultrashort wave radio signal field-amplitude fluctuation, determining space-time correlation dependencies by radar observation 13 p2067 A67-26688

Bistatic CW radar observations of Venus conducted by U.S.S.R. and Great Britain during 1966 14 p2265 A67-28403

Soviet book on radio physics /1965-1966/ reviewing radio-astronomical observations and radar probing of Venus 15 p2553 A67-29241

Radar measurement of differential group delay to moon, showing large differences in total cislunar electron content above 1000 km in solar and antisolar directions 15 p2555 A67-29611

Titan IIIB launch vehicle spent stage I recovery experiment, evaluating feasibility of refurbishment and reuse 15 p2569 A67-29853

Radar observation of meteor echoes in upper atmosphere, particularly delonization of processes in meteor trails 16 p2749 A67-31251

Soviet book on meteors in earth atmosphere studied by radar discussing meteor trails, upper atmosphere winds, etc 16 p2754 A67-31866

Distribution of meteoritic matter in solar system determined, using radar observations and astronomical photography 17 p2941 A67-32321

Frothing-sloughing ablation concept explains density variations of cometary meteors obtained from photographic and radar observations 17 p2943 A67-32541

Injun III rocket orbital parameters determined by optical and radar observations to provide inclination values for studying upper atmosphere rotational speed 17 p2952 A67-33251

Radio and radar observations of Mercury, Venus and Mars 18 p3123 A67-34144

Radar studies of Venus noting values for rotation vector, latitudes and longitudes of several features and Earth influence on Venus rotation [JPL-TR-32-1081] 18 p3123 A67-34146

Future traffic control system for ensuring flight safety and automatic functioning by automatic radar observation and aircraft-movements control 19 p3255 A67-35806

Coronal heating extent placed at 1.6 solar radii by 38 MHz radar investigation studies, noting agreement with coronal density calculation 20 p3528 A67-37477

Tropospheric condition effect on near-

ground ultrashort wave radio signal field-amplitude fluctuation, determining space-time correlation dependencies by radar observation 21 p3582 A67-38430

Meteor activity radar observations and simultaneous ionosphere probe to establish relation between sporadic E layer ionization and sporadic meteors 21 p3623 A67-39040

Auroral ionization echoes observed simultaneously by separated VHF radar noting aspect sensitivity, time variation, correlation with visible aurora, etc 22 p3760 A67-39624

Microwave multiband spectral reconnaissance of earth and space vehicles using imaging radar on spacecraft 22 p3806 A67-40362

RADAR PHOTOGRAPHY

Radar echoes from cloud-free atmosphere caused by turbulent pulsations of microwave refractive index 10 p1677 A67-23500

RADAR RANGE

Compact flash X-ray systems for radiographic measurement of moving objects, radar ranging, atmospheric density, radiation effects, etc 02 p0245 A67-12215

Idealized radar range equation using narrow beam approximation of Probert-Jones 05 p0767 A67-17309

Radar range and Doppler effect simulation by stationary target outlining passive electronic countermeasure technique 07 p1146 A67-19882

Dynamic range of data processor /correlator/ associated with synthetic aperture mapping radar system, considering film grain noise 08 p1293 A67-20688

Frequency scanned filter in radar signal processing system designed to extract range and Doppler resolution, using properties of ambiguity function 09 p1466 A67-22695

Instrumentation radar characteristics, range equation for tracking performance, sensitivity, targets, systems performance evaluation, etc 10 p1605 A67-22994

Antenna radome subjected to aerodynamic heating investigated for effects on radar system operational range, analyzing antenna noise 18 p2999 A67-33510

RADAR RECEIVER

Ignitor-contributed noise deleterious effect on low noise radar receivers, noting influence of TR device inserted in front of receiver 10 p1611 A67-23329

Radar receiver as optimal filter and correlator, obtaining correlation and resulting ambiguity function 15 p2434 A67-29181

Digital pulse compression radar receiver with digital-pulse compression advantages and disadvantages, noting target acquisition, range tracking and antenna scanning system 16 p2630 A67-31738

Thin film circuits for narrow band radar receivers, discussing manufacture of inductors, capacitors and LC resonant circuits 21 p3589 A67-37917

Approximate method for evaluation of processing loss in delay line MTI receiver 22 p3758 A67-39211

RADAR RECEPTION

Weather information interpretation and utilization for air traffic control 04 p0650 A67-14688

Radar probe of clear atmosphere confirming detectability of birds, insects and irregularities in clear air refractivity 04 p0650 A67-15172

Synthesis of radar ambiguity functions via burst-pulse time-frequency waveform coding, employing Bayesian statistical analysis 18 p3000 A67-34109

RADAR REFLECTOR

Backscattering of centimeter waves from ruffled sea surface at small angles of slp 05 p0761 A67-16345

Sporadic E ionization and anomalous increase in rate of radar meteor counts during 1963 in mid-latitude European stations 07 p1172 A67-19424

Strong reflection from underlying surface effect on range-only radar measurements, deriving phase angle between side-and-carrier-frequency oscillation vectors 16 p2624 A67-31030

Laser ranging using reflectors proposed for investigating lunar motion and various lunar parameters 18 p3130 A67-34317

Bistatic radar cross section of coherent-dot radar angel in convective thermal model 20 p3480 A67-36286

Microwave multiband spectral reconnaissance of earth and space vehicles using imaging radar on spacecraft 22 p3806 A67-40362

RADAR RESOLUTION

Doppler tolerant pulse train design, noting signal processing by delay line with fixed taps for significant changes in pulse spacing 01 p0023 A67-10464

Relation between sidelobe level and radar performance in clutter for nonresolvable difference between target and clutter Doppler 03 p0369 A67-13680

Error in R-meter measurement of velocity spread of meteorological targets resulting from radar frequency instabilities 04 p0648 A67-14673

Optimum radar detection theory dealing with discrimination and resolution of one target from another and of target from noise and clutter 04 p0572 A67-15033

Radar target resolution and limits as function of environment, number of targets and size of delay Doppler space 04 p0572 A67-15034

High resolution radar correlometer measurement of spatial correlation radius of RF radiation scattered by disturbed ocean surface 08 p1294 A67-20819

Boundary value solutions for current density and radiation patterns in spiral excited sheath antennas in terms of Hankel function 09 p1482 A67-22696

Mathematical treatment of sequential detection and application to detection of radar targets 10 p1607 A67-23570

Radar resolution performance in moving target determined by cross section of desired target compared with combined cross section of all interfering targets 12 p1907 A67-26083

Distribution-free signal detection by multiple-resolution-element pulse radar, based on ranks of returns and having invariant false alarm rates 15 p2436 A67-29933

Decision theory applied to angular resolution, deriving signal processing radar system beyond Rayleigh limits and target reliability 23 p3972 A67-40643

Unresolvable targets producing single radar return estimation from slow amplitude fluctuation, discussing scattering cross section effects and computer simulation verification 23 p3974 A67-41198

RADAR SCANNING

Terrain information from high altitude side-looking radar imagery of Arctic area 01 p0059 A67-10328

Radar imagery compilation of vegetation maps, noting extent of capabilities and results obtained 01 p0059 A67-10329

Aircraft radio guidance system combining ILS and precision approach radar 04 p0653 A67-15042

Beam scanning and beam forming techniques for phased-array radar, noting frequency and phase scan methods 04 p0596 A67-15049

Electronic scanning of antenna beams, reducing feed complexity of large phased array by grouping of elements, tapering and array thinning 04 p0581 A67-15050

Radar scan-antenna angle transmission over DC voltage in binary form for digital computer or display 11 p1760 A67-24269

Reception of signals reflected from ionosphere in vertical radar probing, examining frequency-difference combinations 13 p2067 A67-26569

Maintaining target track for nonmaneuvering targets approaching uniformly scanning search radar 13 p2068 A67-26782

Spacecraft high aperture efficiency small scan communication antenna, noting radar installation 14 p2289 A67-28911

RADAR SCATTERING

Radar scatterometer remote sensing measurement of variation of radar scattering coefficient with angle, wavelength and polarization 01 p0021 A67-10317

Approximate general bistatic radar scattering relationships derived for finite length metal cylinder for transverse electric /TE/ and transverse magnetic /TM/ cases 02 p0192 A67-11623

Point matching solution developed for scattering by conducting bodies of arbitrary shape including circular and square wire loops, plates, spheres and

- p hemispheres 03 p0370 A67-13855
-
- Tracks of dot angels, insects and birds
-
- obtained by ultrasensitive multiwavelength
-
- radars 04 p0569 A67-14680
-
- Combined probability density of axial
-
- coefficient and polarization angle of field
-
- scattered by target 05 p0764 A67-16905
-
- Scattering by infinite cylinders of
-
- arbitrary cross section treated by method of
-
- finite difference 05 p0764 A67-16952
-
- Scatterometer measuring radar
-
- backscattering for prediction of terrain
-
- characteristics 08 p1293 A67-20682
-
- Combined probability density of axial
-
- coefficient and polarization angle of field
-
- scattered by target 14 p2297 A67-28032
-
- F region and magnetosphere observation
-
- by incoherent backscatter radar
-
- technique 14 p2265 A67-28410
-
- Combined probability density of axial
-
- coefficient and polarization angle of field
-
- scattered by target 16 p2623 A67-30881
-
- Microwave and acoustic frequency
-
- holography and possible application to target
-
- shape recognition and inverse scattering in
-
- radar 21 p3626 A67-38063
-
- Electromagnetic wave scattering by
-
- circular cylinder moving in free space,
-
- noting far field patterns and Doppler shift
-
- angular dependence 22 p3760 A67-39623
-
- Vector field theory of time dependent
-
- backscatter from distant slightly rough
-
- sphere for pulsed and sinusoidally steady
-
- state sources 23 p3974 A67-41200
-
- RADAR SIGNATURE**
-
- Correlation detection for extracting
-
- reflected radar signal from
-
- noise 19 p3195 A67-35550
-
- Color radar signal parameters display
-
- system using techniques based on
-
- mathematical application of Venn-Euler
-
- diagrams 19 p3231 A67-35624
-
- RADAR SYSTEM**
-
- YIG dispersive delay line in ultrawide
-
- bandwidth pulse compression radar
-
- system 01 p0132 A67-10435
-
- Boresight error in radar caused by effect
-
- of radome material and means to avoid
-
- it 02 p0215 A67-11973
-
- Mills cross arrays applied to radar
-
- systems, especially when target signals vary
-
- and great angular accuracy is
-
- needed 02 p0216 A67-12068
-
- Book on modulation, resolution and signal
-
- processing in radar, sonar and related
-
- systems 03 p0372 A67-14233
-
- Radar, range instrumentation and
-
- measurement systems 04 p0568 A67-14497
-
- Automatic checkout and monitoring of
-
- phased array radar
-
- system 04 p0595 A67-14500
-
- Characteristics of different plasmas
-
- produced by nuclear explosions at high
-
- altitude on radar systems 04 p0569 A67-14506
-
- Signal design and principle of vernier FM
-
- radar system to measure surface
-
- characteristics of small target at long
-
- distance and range 04 p0570 A67-14877
-
- Transmitter modulation choice for
-
- nonconventional radar system, taking into
-
- account scanning antenna modulation
-
- effects 04 p0572 A67-15029
-
- Pulse compression radar system design
-
- and characteristics noting clutter, local
-
- oscillators and phase and amplitude
-
- measurement 04 p0572 A67-15032
-
- Airborne Early Warning /AEW/ system
-
- designed to provide low altitude coverage in
-
- detection of enemy
-
- aircraft 04 p0573 A67-15040
-
- Automatic radar system for low level
-
- target detection, obtaining Doppler
-
- resolution and eliminating fixed atmospheric
-
- noise 04 p0573 A67-15043
-
- Ground station for space communications
-
- and radar and radio physics, noting use of
-
- Cassegrain antenna computer guided
-
- pointing control, plug-in equipment box,
-
- etc 04 p0596 A67-15047
-
- High power CW radar transmitter,
-
- discussing design parameters, development
-
- and performance
-
- characteristics 04 p0596 A67-15051
-
- Microwave and thermal vacuum testing to
-
- demonstrate design maturity of LEM
-
- rendezvous radar during simulated
-
- mission 04 p0576 A67-15397
-
- Stationary antenna arrays for target
-
- detection and tracking noting radiation
-
- patterns, radar systems,
-
- etc 04 p0654 A67-15538
-
- Radar phase locking technique applied to
-
- magnetron radar, measuring transmitted
-
- pulse phase with respect to stalo running at
-
- magnetron frequency 05 p0780 A67-17521
-
- Radar search and tracking system
-
- developments 06 p0957 A67-17584
-
- Apollo lunar module /LM/ rendezvous
-
- radar system and tracking
-
- device 06 p0962 A67-18056
-
- Power spectrum improvement of multiple
-
- wave trains by concentrating power close to
-
- carrier frequency, noting constructive and
-
- destructive interference 06 p0963 A67-18401
-
- Soviet papers on theory and technique of
-
- radar 07 p1138 A67-19222
-
- Wind compensation system at Kagoshima
-
- Space Center, University of Tokyo, consists
-
- of radar system for obtaining wind data and
-
- method for finding launch angle
-
- compensation 08 p1314 A67-20542
-
- Queueing theory applied to phased array
-
- radar maintenance problems, specifically
-
- replacement and repair of transmitter
-
- and/or receiver modules 08 p1292 A67-20668
-
- Thinned aperture computed lens /TACOL/
-
- of hard point demonstration array radar
-
- /HAPDAR/ phased array radar
-
- system 08 p1315 A67-20679
-
- Performance of wideband interferometers
-
- using interferometer ambiguity function for
-
- radar application 08 p1300 A67-20680
-
- Microelectronic radar intercept calculator
-
- /RIC/ for ground-controlled intercept
-
- capability when used with air search radar
-
- feeding information to PPI
-
- display 08 p1293 A67-20690
-
- Radar applications to ATC, pictorial
-
- display and role of paper flight strip,
-
- present and future 09 p1484 A67-21678
-
- Direct view storage tubes for radar
-
- displays 09 p1528 A67-22628
-
- Short range radar with 1 m resolution for
-
- FM-CW technique for vehicle guidance in
-
- fog, describing equipment 09 p1528 A67-22630
-
- Instrumentation radar characteristics,
-
- range equation for tracking performance,
-
- sensitivity, targets, systems performance
-
- evaluation, etc 10 p1605 A67-22994
-
- Comparison of measurement accuracy for
-
- angular coordinates in radar systems by
-
- linear scanning and equal-signal zone
-
- methods 10 p1607 A67-23450
-
- Terrain following pulsed radar system
-
- without continuous scanning noting
-
- computer simulation, antenna and pitch
-
- control 11 p1752 A67-24259
-
- Side-looking synthetic aperture radar
-
- systems 11 p1753 A67-24440
-
- Airborne weather radar for general
-
- aviation aircraft, considering transmitter
-
- power, wavelength, target area, reflectivity
-
- characteristics, instalational limitations, etc
-
- [SAE PAPER 870252] 12 p1905 A67-25503
-
- Normalization of effective coverage of
-
- bistatic radar with respect to maximum
-
- coverage of monostatic
-
- radar 12 p1908 A67-26223
-
- Book on new concepts in radars covering
-
- ideal reception, moving targets,
-
- autocorrelation, SNR, amplitude distribution,
-
- clutter, etc 13 p2071 A67-27224
-
- RCA papers on defense electronic
-
- products including search radar,
-
- superconductor devices, data and spacecraft
-
- communications, speech
-
- recognition 14 p2274 A67-28910
-
- Japanese weather radar facility featuring
-
- network relay equipment functioning in
-
- PPI/RHI mode, noting parabolic horn
-
- antenna 14 p2290 A67-28998
-
- German participation in solar eclipse
-
- campaign of ESRO, describing rockets and
-
- radar used 15 p2466 A67-29572
-
- Future radar developments noting range
-
- instrumentation deployment and
-
- employment, tracking, data acquisition radar
-
- sensors, changing cost patterns, etc
-
- [AIAA PAPER 87-55] 15 p2438 A67-30119
-
- Frequency shifting technique using
-
- auxiliary coil to produce magnetic field for
-
- masers in high power radar
-
- applications 15 p2439 A67-30392
-
- Immediate, delayed and cyclic maintenance
-
- policies for phased array radar
-
- systems 16 p2634 A67-30446
-
- Computer simulation model for cost
-
- effectiveness of built-in test equipment
-
- /BITE/ in airborne radar
-
- systems 17 p2833 A67-32491
-
- Cross polarization evaluation radio echo
-
- system /CERES/ concept for polarization
-
- component separation and echo
-
- depolarization evaluation 17 p2814 A67-32520
-
- Australian ATC radar network describing
-
- long range surveillance and control of
-
- neighboring airport 17 p2834 A67-32749
-
- Radar system using real-time on-line
-
- computer applied to adaptive control of
-
- beam direction and transmitter
-
- modulation 17 p2816 A67-32790
-
- Stochastic differential game with missile
-
- and radar, using linear theory in finding
-
- optimal strategies 18 p3075 A67-33495
-
- Antenna radome subjected to aerodynamic
-
- heating investigated for effects on radar
-
- system operational range, analyzing antenna
-
- noise 18 p2999 A67-33510
-
- Soviet book on digital processing of radar
-
- information covering signal processing,
-
- algorithms, discretization,
-
- etc 18 p3006 A67-33717
-
- Multichannel radar formula for
-
- discriminating power in distance
-
- corresponding to time resolution
-
- constant 18 p3002 A67-34228
-
- Microelectronics technology extended to
-
- microwave frequencies, considering
-
- development of solid state devices and
-
- ICs 18 p3015 A67-34562
-
- Characteristics of immediate, delayed and
-
- cyclic maintenance of phased planar array
-
- radar systems, considering outage availability
-
- effects 18 p3005 A67-34693
-
- Lunar landing module Doppler radar
-
- system in guidance navigation and control
-
- system, studying mathematical model
-
- performance 19 p3260 A67-36011
-
- Electronic system for measuring operator
-
- information retrieval in bisensory
-
- configuration, using video-record radar set
-
- and playback 20 p3419 A67-37639
-
- Mesoscale structure of atmospheric winds
-
- analyzed using data obtained from FPS-16
-
- radar/Jimsphere precision wind measuring
-
- system 21 p3655 A67-38576
-
- Waveguide dispersive line use in FM pulse
-
- compression system outlined for high
-
- resolution in S-band radar 21 p3601 A67-39068
-
- Distributed power generation for radar
-
- and communications covering cost
-
- comparisons, antenna subsystems and
-
- reliability of solid state
-
- devices 22 p3761 A67-39861
-
- Solid state and electron beam delay line
-
- features compared in optimal selection for
-
- radar system target
-
- simulation 23 p3982 A67-41503
-
- Multifrequency radar system performance,
-
- obtaining expression for detection
-
- probability as frequency number, false alarm
-
- probability and integrated pulse number
-
- function 24 p4122 A67-42408
-
- Book on radar signals covering FM pulse
-
- compression signals, waveform, Doppler
-
- shift, time factor, etc 24 p4122 A67-42425
-
- Earth science and resource studies with
-
- orbiting imaging radars onboard space
-
- vehicles
-
- [AIAA PAPER 87-767] 24 p4258 A67-42936
-
- RADAR TARGET**
-
- Signal and clutter model of monopulse
-
- radar tracking errors 02 p0201 A67-12114
-
- Complex indicated angle extension of
-
- monopulse normalized error signal used to
-
- locate unresolved targets 02 p0201 A67-12115
-
- Angular noise induced random error in
-
- direction finding as affected by target
-
- properties and sense
-
- finder 03 p0368 A67-13275
-
- Radar target clutter, fluctuation, echo
-
- level, direction error and noise in tracking
-
- system 03 p0372 A67-14093
-
- Radar techniques for detection tracking
-
- and navigation - AGARD Avionics
-
- Symposium, London, September
-
- 1964 04 p0571 A67-15028
-
- Special modulation and detection
-
- processes enable radar target to be analyzed
-
- into dimensions of time delay and Doppler
-
- shift simultaneously 04 p0699 A67-15031
-
- Combined probability density of axial
-
- coefficient and polarization angle of field
-
- scattered by target 05 p0764 A67-16905
-
- Optimum radar measurement of multiple
-
- target coordinates with unknown signal
-
- amplitudes and phases 05 p0765 A67-16960
-
- Continuous and discontinuous tracking of
-
- weapon system radar, discussing principles,
-
- characteristics, advantages and
-
- disadvantages 05 p0766 A67-17270
-
- FAA simulation systems for air traffic

control noting computer simulated radar target generation, display equipment, etc 08 p1315 A67-20678

Mathematical treatment of sequential detection and application to detection of radar targets 10 p1807 A67-23570

Probability density functions for power from Rayleigh target .3 p2067 A67-26520

Maintaining target track for nonmaneuvering targets approaching uniformly scanning search 13 p2068 A67-26782

Combined probability density of axial coefficient and polarization angle of field scattered by target 14 p2297 A67-28032

Military radar intercept calculator, discussing small size, low power supply, high performance and MOS memory 15 p2439 A67-29161

Combined probability density of axial coefficient and polarization angle of field scattered by target 16 p2623 A67-30881

Threshold value of SNR of radar system in target detection against reflecting background, deriving block diagram consisting of linear group, detector and integrator 17 p2816 A67-32684

Radar information automatic extraction by digital techniques, outlining information quantization, target detection and coordinate measurement principles 24 p4122 A67-42407

RADAR TRACKING

Radar cross sections, tracks and fluctuation spectra of grackles, pigeons and English sparrows 04 p0569 A67-14679

Radar techniques for detection tracking and navigation - AGARD Avionics Symposium, London, September 1964 04 p0571 A67-15028

Real time evaluation of radar signals processed by digital detector used in automatic target tracking 04 p0574 A67-15058

Tracking in air traffic control environment, noting differences with military environment and cooperative tracking methods 04 p0654 A67-15060

Terminal configuration with alphanumeric display and center-metroplex equipment for automation implementation in radar tracking data for expanding ATC 04 p0654 A67-15061

Trajectory determination from optical and radar data of spacecraft [JPL-TR-32-950] 08 p1384 A67-20621

Automatic tracking in aircraft identification and updating of flight prediction parameters for air traffic control 09 p1529 A67-22636

Stratospheric free air turbulence detection from slant-range FPS-16 radar tracked Jimsphere balloons 10 p1676 A67-22815

Instrumentation radar characteristics, range equation for tracking performance, sensitivity, targets, systems performance evaluation, etc 10 p1605 A67-22994

Book for amateurs on observing earth satellites including methods and discoveries about upper atmosphere and shape of earth 10 p1608 A67-23620

Performance errors analysis of navigation using inertial guidance and radar tracking 11 p1817 A67-24334

Laser applications to telemetry, radar, navigation, telecommunications, medicine, boring and welding 14 p2333 A67-28974

MSQ-1 radar system for rocket tracking used to measure distance, elevation and azimuth during May 20, 1966 solar eclipse 15 p2467 A67-29574

Radar, radio, photographic and visual satellite tracking methods 15 p2437 A67-30084

Satellite tracking, noting radio, radar and laser methods, and visual and photographic observations 16 p2630 A67-31765

Associative processors and application to automatic radar tracking and correlation, using digital computer 17 p2813 A67-32471

Altimeter using pulse repetition frequency /PRF/ tracking design with solid state X-band frequency source 17 p2859 A67-32522

Radar target designation tracking performance in simulated high speed low altitude aircraft, using closed loop analyses 17 p2830 A67-33181

Radio, radar and optical methods for close earth satellites tracking, advantages and limitations 18 p3003 A67-34235

Radio and radar tracking at Royal Radar Establishment at Malvern, discussing equipment, accuracy, alignment, performance, operation, drag and decay 18 p3048 A67-34239

Wind velocity and direction measurements by radar tracking of chaff /dipoles/ clouds 19 p3219 A67-36247

Analog and digital long range automatic radar tracking systems design characteristics and implementation by solid state components 20 p3379 A67-36244

Degree of isolation between radar tracking data and motion of ship determined, using frequency domain 20 p3415 A67-36555

Radar designation by computer and real time reentry tracking for future Apollo manned space flight 20 p3381 A67-36592

Two-terminal GaAs laser diode communication system noting laser driver component selection, system performance, construction, design and ranging and tracking applications 23 p3975 A67-41379

RADAR TRANSMISSION

Analog and digital wideband radar transmission and application to air traffic control 01 p0021 A67-10213

Pulsed radar transmitter research in U.K., noting beam type microwave tubes, solid state switches, hydrogen thyatrons, etc 04 p0581 A67-15052

Three-dimensional correlation function for modulating bell shaped and rectangular radar probing pulses 09 p1463 A67-21961

Radar information transmission using wideband microwave links and conventional display techniques 09 p1465 A67-22837

Microwave oscillation-amplifying L-band platinotron tube to amplify peak power of radar transmitter 10 p1605 A67-23061

Three-dimensional correlation function for modulating bell-shaped and rectangular radar probing pulses 20 p3383 A67-37191

RADIAL DISTRIBUTION

Multibeam microwave interferometer measurement of radial distribution of electron density in plasma cylinder 01 p0119 A67-10169

Electronic and molecular radial distribution functions for liquid carbon tetrafluoride using X-ray diffraction, determining orientational effects of carbon tetrachloride and temperature dependency 01 p0117 A67-10885

Radial distribution analysis of films of bismuth and gallium prepared by low temperature condensation for electron diffraction tests 01 p0137 A67-11060

Radial distribution analysis of films of Pb-12 percent Bi and beryllium in metastable phases prepared by low temperature condensation for electron diffraction tests 01 p0137 A67-11061

Radial extension of corpuscular flux from chromospheric flares and duration of earth immersion in flux 02 p0306 A67-11653

Radial electron density distribution in induced pulsed discharge from wave refraction in planes passing through and normal to plasma cylinder 02 p0278 A67-12624

Radial distribution of plasma formed in simple mirror machines by quantum effect field ionization of fast neutral atoms 04 p0671 A67-15644

Elastic cylindrical shell under arbitrary impulsive pressure distribution, discussing membrane and flexural stresses 05 p0909 A67-16139

Free hinged cylindrical shell problem with radial load on outer edge of cross section solved via linear differential equations 05 p0915 A67-16222

Iron and chromium films prepared at 4 degrees K analyzed by radial distribution, showing electron diffraction patterns of amorphous state 05 p0866 A67-16976

WKB approximation of quantum radial distribution function for neon intermolecular pair potential taking into account particle exchange effect 06 p1038 A67-19044

Argon, helium and nitrogen high temperature plasma compositions used to calculate radial temperature distribution 07 p1229 A67-19566

Forced torsional vibration of inhomogeneous hollow cylinder solved for radial variation of shear modulus and mass density 07 p1264 A67-20234

Anomalous diffusion and radial density profile in positive column with longitudinal magnetic field 08 p1362 A67-21148

Radial particle density profile in neon negative glow plasma in cylindrical discharge tube measured by double probe method 08 p1362 A67-21288

Radial distribution function differential equation solution studied numerically and analytically for plasma parameters, using closure approximation 11 p1826 A67-23871

Low temperature deposition of amorphous films of transition metals and alloys, noting atomic arrangement, comparing with case of metals condensed in crystalline state 12 p1982 A67-25451

Locally loaded orthotropic shells of revolution under radial concentrated forces 12 p2021 A67-25575

High density one-component plasma radial distribution determination by Born-Green-Yvon integral 13 p2162 A67-26282

Static characteristics of radial gas dynamic bearing, using differential equation for pressure distribution calculation 13 p2122 A67-26351

Radial electron density distribution in induced pulsed discharge from wave refraction in planes passing through and normal to plasma cylinder 13 p2171 A67-27380

Radial variation of plasma electron density determined by surface wave resonances 14 p2355 A67-27829

Effective pair potential obtained for quantum electron gas to determine thermodynamic properties over large temperature and density range 15 p2533 A67-30383

Radial extension of corpuscular flux from chromospheric flares and duration of earth immersion in flux 16 p2738 A67-31068

Electron density radial distribution, neutral gas temperature and ionization-caused column contraction calculated for cylindrical discharge plasma in argon 18 p3089 A67-34298

Positive column contraction in inert gas discharge, studying electron density and radiation intensity radial distribution and wall current 19 p3272 A67-35092

Radial pressure distribution in hydrogen arc located in axial magnetic field using Saha equation, determining temperatures and electron densities 19 p3279 A67-35139

Temperature, electron density, and relative particle density radial distribution and mass separation effect in free burning DC arc 19 p3281 A67-35156

Approximate electron radial functions for uniformly charged nucleus /UCN/ used in analyzing boron 12 and nitrogen 12 beta decay spectra 20 p3488 A67-36915

Energetic proton flux measurements in magnetosphere using sounding rocket, discussing radial diffusion 20 p3518 A67-36998

Radial profiles of carrier density and energy in diffusion controlled plasma 20 p3501 A67-37239

Radial distribution functions for liquid methanol and ethanol at room temperature, observing intermolecular hydrogen bonding 20 p3378 A67-37560

Structures of glow discharge and evaporated silicon oxide films determined by measuring intensity of electron wave scattering at large angles, describing measurement method 21 p3687 A67-39133

Suboptimal radial guidance scheme based on cubic time function of optimal trajectories radius vector modulus from simultaneous data analysis 22 p3830 A67-39164

Liquid He 4 ground state studied by variation method, deriving radial distribution function 22 p3835 A67-39301

Radial temperature distribution in high power argon arcs measured at atmospheric pressure and 5 atm for currents ranging from 200 to 500 amp 22 p3853 A67-40045

RADIAL FLOW

Unsteady adiabatic centrally symmetric radial flow of ideal fluid in general theory of relativity 01 p0114 A67-10987

Radial heat equation and Laplace transforms, discussing representations alternative to two solutions 03 p0460 A67-13811

Strain gauge method for determining stress concentration in radial flow impellers 04 p0708 A67-14537

Radial gap effect on effectiveness of turbine stage determined from gas leakage measurements by outlet cross section traversing techniques 04 p0690 A67-15895

Transverse magnetic field effect on laminar radial flow of incompressible fluid between closely spaced parallel plates

presenting graphs of pressure distribution 06 p1046 A67-18829

Steady state temperature distribution in disk with radial flow of electric current derived with and without heat transfer conditions 08 p1427 A67-20929

Self-aligning radial clearance seals, discussing design parameters, balance leakage and power loss as function of geometry 10 p1659 A67-22707

Radial flow of compressible fluids between disks solved through simpler form instead of numerical integration of differential equations 10 p1593 A67-23475

Irregularly spaced nozzle vanes effect upon blade vibration in radial flow gas turbine [ASME PAPER 67-VIBR-42] 11 p1797 A67-24195

Integral relation technique for approximate solution of dynamic and thermal expansion of laminar radial slot gas jets along plane wall 11 p1779 A67-24322

Radial flow of two-dimensional viscous conducting fluid in wedge shaped channel under magnetic field, reducing flow equation to differential equation 12 p1977 A67-26180

Heat leak and pressure decay for single phase cryogenic storage in nonequilibrium calculated for spherical tanks, using simplifying assumptions 13 p2227 A67-27641

Pneumatic angular rate sensor performance characteristics, solving boundary layer equations for radial flow 14 p2318 A67-28340

Radial mass flow effect on electric arcs, obtaining higher axis temperature and enthalpy densities 17 p2910 A67-33366

Centripetal radial blowing effect on flow and heat transfer in gap between rotating disk and wall, specifically effect of Reynolds number and dimensionless flow 20 p3357 A67-36794

Direct and inverse method of calculating rotating cascades with infinite number of blades and radial flow to enhance convergence 20 p3360 A67-37597

Viscous non-Newtonian fluid radial flow between circular disks solved, using model equation reduced to power law equation 21 p3612 A67-38381

Electromagnetically driven confined viscous vortex flow with high positive radial Reynolds numbers, solving energy equation for temperature distribution [AIAA PAPER 67-730] 21 p3674 A67-38754

Radial motions in small and young sunspots indicating different cooling processes than regular sunspots 21 p3707 A67-38964

Gruber method for radial flow impellers of greatly cambered forward curved blading, analyzing parameter variation effect on velocity distribution curves 21 p3614 A67-39053

Radial motion of spherical self-gravitating mass undergoing gravitational collapse or expansion using Einstein general relativity theory 22 p3892 A67-40495

Aerodynamic requirements for hovercraft and radial flow fans by adapting blade loading criteria for axial compressors 23 p3931 A67-41331

NASA radial flow turbine research related to Brayton cycle power generator, investigating size, Reynolds number and speed effects on efficiency and flow 24 p4102 A67-42489

RADIANT ENERGY

Radiant flux modulation using two lattices, for case of rectangular aperture with uniform flux distribution 01 p0022 A67-10423

Radiation calibration of heat flux sensors, comparing resistively heated filament and solar energy device 01 p0069 A67-11019

Herman and Gibbons conclusions on radiation energy concentration in ionized gas shown to be erroneous 03 p0411 A67-12961

Total normal emittance of various oxidation-resistant materials to very high temperatures in air determined, using special apparatus [AIAA PAPER 65-655] 03 p0447 A67-13035

Radiant energy transfer in absorbing medium with constant absorption coefficient 04 p0722 A67-14714

Sensitivity of dielectric rod terminal impedance to surface wave coupling when no resonance regions exist within energy-carrying cross section 07 p1158 A67-20299

Enhancement of fine detail in presence of

large radiance differences, noting radiance profiles and moon 10 p1653 A67-22746

Refractory and ablating polymeric reentry heat shield materials evaluated under high radiant fluxes, measuring surface temperature, recession rate, flux emittance, etc. refractory and ablating polymeric reentry heat 11 p1811 A67-24054

Dimensions effect on efficiency of radiant energy cells 11 p1745 A67-24437

Thin film thermal radiation detector noting construction, calibration, performance, error sources and advantages of pyroelectric over thin film gauges 11 p1790 A67-24454

High powered carbon arcs for solar simulation with increased radiant energy output 12 p1921 A67-25697

High temperature air plasma total radiant intensity measurements in shock tube [AIAA PAPER 67-311] 12 p2036 A67-26026

Radiant energy transfer below cloud cover in Venus atmosphere, noting greenhouse effect caused by atmosphere containing components capable of IR absorption 14 p2383 A67-27859

Solar gamma-ray flux in high energy region analyzed using OSO-I satellite 14 p2381 A67-28057

Plasmoid collisions in axisymmetric magnetic field studied spectrographically for energy density, radiative power, charged particle density, etc 15 p2525 A67-29248

Generating time series for amount of solar radiation falling on horizontal surface of unit area at top of atmosphere per unit time 15 p2477 A67-29628

Semiconductor thermoconductivity increase due to illumination on one face by radiated energy 19 p3304 A67-35461

Dimensions effect on efficiency of radiant energy cells 20 p3362 A67-36239

Characteristics method to determine radiative energy losses of supersonic gas flows past blunt cones 21 p3564 A67-38424

Gamma radiation energy direct conversion into electrical energy by electrochemical recombination of radiolysis products, proposing new sealed battery 22 p3748 A67-40199

Integrated intensities for thermal radiation heat transfer in nongray nonscattering gas approximated, deriving effective absorption coefficient 22 p3920 A67-40442

Energy transmitting characteristics and wall local energy absorption distribution of curved specular reflecting duct irradiated by collimated beam 23 p4028 A67-41271

Solar radiant energy attenuation by atmospheric ozone, deriving transmission function relation to ozone content 24 p4181 A67-41915

RADIANT HEATING

Radiant heating by inhomogeneous hot gases, determining spectral transmittances of inhomogeneous optical paths using Curtis-Godson approximation 02 p0342 A67-12050

Radiant heat influx to free atmospheric layers, atmospheric macrocirculation and time-corresponding geopotential field charts 03 p0463 A67-14226

Combustion mechanism for boron-containing air-augmented propellant based on conductive, convective and radiant heat transfer between propellant and combustion products 04 p0687 A67-15814

Composite coatings provide temperature differences at surface of hot stamped blanks, thereby making it possible to control strain distribution over surface 04 p0630 A67-15901

Gas dynamic equations for determination of heating, vaporization and expansion of substance due to Q-switched laser radiated collimates onto surface of solids 05 p0819 A67-16652

Vertical transport of latent and sensible heat of IR cooling and short wave heating 09 p1490 A67-21550

Radiant heat influx to free atmospheric layers, atmospheric macrocirculation and time-corresponding geopotential field charts 12 p1963 A67-25482

Arc-image furnace for direct gas heating at high temperature by concentrated radiation studies and efficient cavity-type receiver development 17 p2834 A67-32896

Fuel requirements for Concorde SST stressing flame luminosity, radiant heat, spontaneous ignition, fuel viscosity and

density 18 p3110 A67-34533

Temperature difference between solid and gas of transpiration cooled wall due to radiant heating [ASME PAPER 67-HT-29] 20 p3546 A67-36722

Radioisotope heating to provide ionizer temperatures in contact ion thrusters [AIAA PAPER 67-734] 21 p3695 A67-38757

Radiation heat transfer by flames to wire temperature sensor corrected by technique combining radiative input and catalytic activity 21 p3733 A67-38883

Unstable radiant heat interaction between two plane parallel infinite plates of finite thickness analyzed to determine thermal stabilization processes 24 p4254 A67-42257

RADIATION

SA ACOUSTIC RADIATION

SA ALPHA RADIATION

SA ATMOSPHERIC RADIATION

SA BACKGROUND RADIATION

SA BETA RADIATION

SA BLACK BODY RADIATION

SA CERENKOV RADIATION

SA COHERENT RADIATION

SA CONTINUUM RADIATION

SA CORPUSCULAR RADIATION

SA COSMIC RADIATION

SA CYCLOTRON RADIATION

SA DIFFUSE RADIATION

SA ELECTROMAGNETIC RADIATION

SA ELECTRON RADIATION

SA EXTRAGALACTIC RADIATION

SA GALACTIC RADIATION

SA GAMMA RADIATION

SA GRAVITATIONAL RADIATION

SA HARMONIC RADIATION

SA INCIDENT RAY

SA INFRARED RADIATION

SA INTERSTELLAR RADIATION

SA IONIZING RADIATION

SA IRRADIATION

SA LONG WAVE RADIATION

SA LUNAR RADIATION

SA MICROWAVE RADIATION

SA MONOCHROMATIC RADIATION

SA NONEQUILIBRIUM RADIATION

SA NUCLEAR RADIATION

SA PHOTON

SA PLANETARY RADIATION

SA PLASMA RADIATION

SA POLARIZED RADIATION

SA PULSED RADIATION

SA RADIO FREQUENCY RADIATION

SA REFLECTED RAY

SA REFRACTED RAY

SA SHORT WAVE RADIATION

SA SOLAR RADIATION

SA SPACE RADIATION

SA STELLAR RADIATION

SA STRATOSPHERE RADIATION

SA SYNCHROTRON RADIATION

SA TERRESTRIAL RADIATION

SA THERMAL RADIATION

SA TRAPPED RADIATION

SA TROPOSPHERIC RADIATION

SA ULTRASONIC RADIATION

SA ULTRAVIOLET RADIATION

SA VISIBLE RADIATION

SA VOLTERRA EQUATION

SA WAVE RADIATION

SA X-RAY

Frequency dependent two-photon absorption radiation-matter interaction and secondary harmonic generation in n-and p-type impurity semiconductors 03 p0435 A67-13126

Fracture mechanism of transparent crystals interacting with ruby laser beam 03 p0435 A67-13128

Antenna synthesis for wide band radiation reception using Fredholm integral equation 16 p2636 A67-30889

Condensation during heterogeneous combustion, discussing kinetics, radiation and gasdynamic heat release 18 p3149 A67-33798

RADIATION ABSORPTION

Radiation absorption by ionized hydrogen in plane of galaxy to explain brightness profiles for declination minus 37 degrees 02 p0307 A67-11688

Losses in ruby laser determined from data on variations in beam divergence angle and variations in lasing spot diameter 02 p0254 A67-12742

Sodium dayglow emission measurement by Zeeman photometer, presenting calculation of radiant energy absorption by sodium vapor in magnetic field 03 p0409 A67-12945

Absorptivity standard instrument to

investigate solar absorptance of four surfaces used for spacecraft temperature control for Mariner IV on Mars mission [AIAA PAPER 65-650] 03 p0448 A67-13055

Seasonal variation of morning and nighttime absorption of long waves 04 p0617 A67-15571

Radiative heat transfer and intensity distribution in one-dimensional absorbing isotropic scattering medium 04 p0737 A67-15862

Hydrogen atom excitation by Lyman alpha radiation absorption in electric field 05 p0848 A67-16795

Black ball radiation tables and radiative equilibrium temperatures computation 05 p0838 A67-17277

Twilight effects of solar ionizing radiation absorption, discussing ion production rates and fluorescence 05 p0885 A67-17410

Radiation transport theory and spatial radiative heat transfer in absorbing and isotropically scattering medium 06 p1118 A67-18552

Electric field induced IR absorption in GaAs p-n junction diodes 07 p1231 A67-19553

Quantum mechanical theory for IR absorption by excitons due to photolionization and intraband lattice scattering 09 p1552 A67-21670

Concentration of cesium in argon-cesium flow determined by total radiation absorption in resonance line of cesium 09 p1538 A67-21778

Radiation absorption and scattering by small spherical solid carbon particles in wavelength range 0.2 to 40 μ calculated by classical Mie theory [AIAA PAPER 66-134] 10 p1682 A67-23146

Ozone number densities in 30 to 75 km altitude determined at night by rocket measurements of lunar UV radiation absorption in various bands 10 p1638 A67-23203

Numerical solution methods of invariant imbedding equation for reflection function of spherical shell with absorption and isotropic multiple scattering 10 p1680 A67-23634

Wavelength selectivity in solar collector design, noting role of scatter in determining radiative properties of surfaces 11 p1817 A67-24052

Albedo upper and lower fluctuation bounds determined by astrophysical comparison and three other methods 12 p2003 A67-25684

Intergalactic radiation absorption and extragalactic sources contribution to LF background radiation 12 p1995 A67-25766

Heat capacity evaluation between 150 and minus 180 degrees C, using evaporated gold-black coating as primary standard [AIAA PAPER 67-303] 12 p1958 A67-26018

Metallic element concentrations in metals studied using atomic absorption spectrophotometry, noting chemical and bulk effect interferences 12 p1947 A67-26127

Neutral silicon photolionization cross sections for continuous UV absorption measured near ionization limits by shock tube technique 12 p1968 A67-26248

Temperature profile in stratosphere, noting contribution to heat budget by turbulent thermoconductivity and UV radiation absorption in ozone layer 13 p2113 A67-26677

Laser measurements and standards of energy, power, attenuation and frequency stability, using pulsed ruby and gas lasers as radiation source 14 p2319 A67-28392

Absorption of laser radiation in semiconductors and mechanisms of breakdown in process 15 p2537 A67-29704

Boundary layer problem concerned with effects of radiation absorption and emission for flow of high speed gas over flat plate [AIAA PAPER 66-521] 15 p2473 A67-30207

Heat transfer in stagnation-point laminar boundary layer with mass injection and absorption of incident radiation 16 p2658 A67-30941

Scattering and absorption of ultrashort coherent radiation pulses passing through electron gas applied to ionosphere 17 p2812 A67-32312

Argon plasma radiation emission and absorption measurement, determining transition probabilities 18 p3091 A67-34732

Absorption of total solar radiation using vertical profiles from balloon observations,

estimating attenuation due to aerosols 19 p3214 A67-34854

Absorption coefficients of radiation by water vapor and aerosols determined from atmospheric counter 19 p3251 A67-34858

Radiative processes in lower stratosphere and average monthly heating rates over all latitudes due to direct and reflected solar short wave radiation 19 p3226 A67-35922

Atmospheric radiation absorption measurements by radio-astronomy methods at wavelengths from 1.8 to 0.87 mm 19 p3185 A67-36014

High efficiency optical pumping system for crystal laser rods with application to CW output 20 p3461 A67-37290

Accurate determination of atmospheric gases spectral lines positions required for estimating atmospheric absorption coefficient of monochromatic laser radiation 20 p3462 A67-37559

Temperature dependence of far IR collision-induced absorption as probe of rare gas mixtures interatomic potentials 20 p3490 A67-37567

Atmospheric absorption of gas laser radiation at two wavelengths noting dependence on gas pressure and amount of methane 20 p3463 A67-37668

Thermophototropic model providing active thermal control in spacecraft surface functions as variable absorptance coating to compensate for solar irradiation changes 21 p3730 A67-37792

Eddy configuration plasma heated by induced currents, discussing electromagnetic radiation absorption 21 p3664 A67-38047

Radiating hydrogen two-dimensional equilibrium flow with variable absorption coefficient in axisymmetric nozzle analyzed in presence of gray radiation, examining transfer equation in diffusive approximation 22 p3785 A67-40013

Free-free radiation absorption from discrete radio sources calculated for various isotropic world models as red shift, electron density and temperature function 23 p4063 A67-40777

Radiation pattern, absorption and impedance measurements of conical antenna plasma sheath about dielectric coated metal cone excited by axial radiating slot 23 p3973 A67-40840

Absorptivity of medium, obtaining results for spectral quantities referred to given radiation frequency 23 p4083 A67-41288

Values 23 p4083 A67-41288

Absorption of laser radiation in semiconductors and mechanisms of breakdown in process 24 p4199 A67-41774

Nuclear cascade avalanche absorption in Fe analyzed by ionization calorimeter 24 p4219 A67-42850

RADIATION BELT

SA ARTIFICIAL RADIATION BELT

SA INNER RADIATION BELT

SA OUTER RADIATION BELT

SA PROTON BELT

SA TRAPPED RADIATION

SA VAN ALLEN BELT

Earth radiation belt, particle motion and magnetic cavity 01 p0143 A67-10254

Steady state of earth external radiation belt, considering high energy electrons, kinetic instability, anisotropy, etc 02 p0306 A67-11655

Photoelectric optical imaging system survival in earth radiation belt, noting noise level and total energy absorption 02 p0243 A67-12055

Location and radiation intensity variation in upper radiation belts determined, using scintillation counters aboard Cosmos satellites 02 p0311 A67-12598

Survey in satellite era of energetic particle radiations, plasmas and magnetic fields in space including solar wind, solar cosmic rays, etc 03 p0506 A67-13050

Electron and ion acceleration by cosmic plasma waves, examining contribution of these processes to radiation belt formation 04 p0701 A67-15555

Elektron I and II satellite measurements on outer radiation belt, noting geomagnetic field distortion and boundary dependence on magnetic perturbations 05 p0880 A67-16110

Change in cosmic ray cut-off rigidity caused by currents from trapped particle motion, according to Chapman-Akasofu

radiation belt model 05 p0880 A67-16111

Solar charged particles acceleration and propagation through interplanetary space, galactic cosmic ray origin, radiation belt structure, etc, analyzed from space data 05 p0883 A67-16877

Rocket sounding of intensity distribution of proton and electron fluxes at high altitudes, noting secondary particle emission from radiation belt 05 p0883 A67-16880

Magnitude of principal phase DR field of magnetic storm assuming plasma pressure remains constant or varies proportionally with magnetic pressure 05 p0884 A67-17132

Satellite observation of radiation belt and absorption of cosmic noise in polar aurora during magnetic storms of February 1964 07 p1243 A67-19683

Biological satellite research, discussing radiation effects on living organism as measured by Cosmos 110 07 p1136 A67-19867

Electron precipitation from outer radiation belt as cause of ionospheric disturbances, noting relation to time 07 p1245 A67-19928

Radiation belts, energetic charged particle flux and trapped radiation in geomagnetic field as result of neutron albedo decay and plasma-magnetic field interactions 07 p1246 A67-20297

ULF radio emission of upper atmosphere and other related geophysical phenomena, analyzing hsses, choruses and contribution to earth radiation belt 08 p1324 A67-20862

Auroral zone irregularity correlated with perturbations in outer radiation belt, noting simultaneous displacement of boundary zone of perturbations 10 p1699 A67-22784

Coulomb interaction influence upon electron distribution in radiation belts at low altitudes in magnetic anomaly region 10 p1702 A67-23299

Proton spectra and spatial distribution of energy protons on magnetic shells in earth radiation belts, using satellite data 10 p1702 A67-23300

Charge particle flux in earth radiation belt as observed by Cosmos XVII 11 p1856 A67-24074

Radial displacement of particles excited by solar-wind-induced current at boundary of and ring current within magnetosphere 12 p1994 A67-25531

Fast variations of electromagnetic field measured by satellites elektron I and II used as indication of state of radiation belts and magnetosphere of earth fast variations of electromagnetic field measured 12 p1994 A67-25537

Elektron I and III earth satellite electron and proton energy distribution correlation with geomagnetic phenomena 12 p1996 A67-25804

Electron-spectra, pitch angle distributions and total ionization measured throughout radiation belts by satellite magnetic spectrometer and integrating ionization chamber 12 p1997 A67-25807

Time variations of intensity in outer belt and near boundary deduced from Elektron I and II data, noting comparison with magnetic field variations 12 p1997 A67-25811

Elektron I and II satellite observational data on terrestrial radiation belt 12 p1998 A67-25816

Elektron II satellite charged particle flux measurements at distances up to 11.6 earth radii, using three-electrode charged particle trap 12 p1998 A67-25817

Cyclotron instability range in earth radiation belt analyzed taking into account wave absorption in atmosphere, using measurements of perturbation effects 14 p2378 A67-27916

Nonlinear theory of cyclotron instability of earth radiation belt covering time-dependent instability evolution, radiation belt stationary state, etc 14 p2379 A67-27930

High altitude dipole equivalence of geomagnetic field properties verified by satellite-detected electron belt investigation 14 p2308 A67-27932

Cosmic radiation protection during manned space flight, considering use of radiation warning devices and protective drugs 16 p2612 A67-30901

Steady state of earth external radiation belt, considering high energy electrons, kinetic instability, anisotropy, etc 16 p2738 A67-31070

Radiation protection during space flights, describing dangerous aspects of solar cosmic

rays and earth radiation belt 16 p2738 A67-31197

Position of outer radiation belt boundary as function of local time, discussing data from Elektron satellite scintillation counters 16 p2740 A67-31886

Rapid earth electromagnetic field variations used for plasma concentration and magnetosphere radius determination 17 p2846 A67-32937

Earth radiation belts nature and plasma activity in magnetosphere 19 p3315 A67-35485

Energetic electrons in Van Allen radiation belt through satellite measurements, giving intensity maps, energy spectra and pitch angle distributions 20 p3517 A67-36371

Magnitude of principal phase DR field of magnetic storm assuming plasma pressure remains constant or varies proportionally with magnetic pressure 21 p3698 A67-38475

Planet Jupiter research, noting unresolved questions of cosmology, interior structure and Great Red Spot 21 p3711 A67-39092

Auroral zone irregularity correlated with perturbations in outer radiation belt, noting simultaneous displacement of boundary zone of perturbations 24 p4209 A67-42120

Elektron I and II satellite measurements on outer radiation belt, noting geomagnetic field distortion and boundary dependence on magnetic perturbations 24 p4214 A67-42786

Change in cosmic ray cut-off rigidity caused by currents from trapped particle motion, according to Chapman-Akasofu radiation belt model 24 p4214 A67-42787

RADIATION CONTROL

SNAP-10A high emittance white coating, noting stability at 600 degrees F, irradiation and vacuum and mechanical vibration [AIAA PAPER 65-652] 03 p0448 A67-13057

Radiation equilibria in UV light on air, oxygen, carbon dioxide, etc, analyzed by bromine lamp in connection with studies of planetary atmospheres 03 p0513 A67-14088

Control of polarization of radiation field of waveguide-slot antenna emitter 07 p1153 A67-19598

Laser radiation control techniques using saturation filter or negative feedback circuit with resonator Q-factor depending on radiation field power 15 p2499 A67-29722

Control of polarization of radiation field of waveguide-slot antenna emitter 20 p3401 A67-37337

Magnetic annular arc /MAARC/ driven shock tube design, construction and performance, stressing radiation loss prevention 21 p3606 A67-37774

RADIATION COOLING

Anomalous cooling of moon surface during lunar eclipse explained possibly by lunar surface roughness in form of cracks and declivities at centimeter scale 02 p0320 A67-11460

Weight and cost comparative analysis of ablative and combined ablative/radiative heat shields for SV-5 and SV-32 lifting reentry vehicles [AIAA PAPER 66-990] 02 p0333 A67-12301

Approximate solution of problem of radiation cooling and unstable temperature field in solid bodies with internal heat source 03 p0535 A67-13118

Electron recombination in laser produced hydrogen discharge, noting temperature decay due to radiation, expansion cooling and electron loss 04 p0665 A67-15109

Transient temperature distribution in seminfinite solid, plate, cylinder and sphere subjected to heating or cooling thermal radiation 04 p0737 A67-15865

Radiation cooled reentry heat shield of graphitic surface over graphite felt insulation with receding surface [AIAA PAPER 67-153] 06 p1115 A67-18320

Low power MPD arc thruster design and performance with radiation cooled electromagnets and permanent magnets [AIAA PAPER 67-50] 06 p1074 A67-18436

Vertical transport of latent and sensible heat of IR cooling and short wave heating 09 p1490 A67-21550

IR flux for water vapor and flux divergence in atmosphere computed for rate of radiative cooling of atmosphere at coastal and continental stations 13 p2150 A67-26419

Weight and cost comparative analysis of ablative and combined ablative/radiative heat shields for SV-5 and SV-32 lifting reentry vehicles [AIAA PAPER 66-990] 15 p2564 A67-29421

Emission time history for red 6300 angstrom atmospheric emission from atomic oxygen produced by nuclear explosion 16 p2664 A67-30978

Long-wave radiation cooling effect in troposphere/stratosphere calculated based on vertical temperature and moisture profiles from nighttime probe 19 p3213 A67-34852

Transient temperature distribution of cylinder subject to radiation cooling, giving dimensionless computer-derived graphs [ASME PAPER 67-HT-71] 20 p3550 A67-36751

Optimal geometry of certain isolated heat-conducting circular fins cooled by radiation 20 p3554 A67-37067

Shock tube measurements of end-wall radiative heat transfer behind reflected shock waves in air, stressing radiative cooling and self-absorption effects [AIAA PAPER 67-695] 21 p3732 A67-38724

Radiative cooling and self-absorption effects on reflected shock flow field and end wall heat transfer studied using finite difference method 22 p3917 A67-39710

Coolant selection for radiative cooling circuit of space vehicles, considering flow rate, heat transfer rate, etc 24 p4253 A67-42217

RADIATION COUNTER

SA GEIGER COUNTER

SA IONIZATION COUNTER

SA SCINTILLATION COUNTER

Giant airshower recorder using liquid scintillators to record collision of cosmic rays with atmospheric nuclei 03 p0508 A67-14388

Energy spectra of galactic X-rays observed with three types of counters borne on sounding rockets 05 p0883 A67-16876

Directional telescope for measuring intensity and spectral composition of gamma rays in primary cosmic radiation 09 p1497 A67-21899

RADIATION DETECTOR

SA PARTICLE DETECTOR

SA SILICON RADIATION DETECTOR

Transistorized logarithmic amplitude converter for recording pulses of radiation detector, automatic switching of conversion scale permits amplitude measurement 01 p0062 A67-10160

Remote sensing techniques and data evaluation and processing in geography 01 p0058 A67-10308

Soviet and other papers on nuclear emission detectors, using electron-optical light amplifiers 01 p0069 A67-11006

Hybrid propellant burning rate determination using external gamma emission source 01 p0112 A67-11420

Requirements for radiation detection and measuring systems in aerospace environment, considering safety, design, circuit techniques, etc 02 p0220 A67-12208

Physical characteristics affecting detection efficiency of Geiger counters, proportional counters and ion chambers used in space measurements of particles 02 p0244 A67-12209

Physical and functional characteristics of contoured amplifying semiconductor radiation detectors for use in missile and satellite instrumentation 02 p0244 A67-12211

Distribution of cosmic rays on sphere and reception vector of radiation detector 05 p0884 A67-17121

Width of i band of p-i-n nuclear emission detector during Li ion drift through doped Si semiconductor detector 05 p0872 A67-17500

Sensors of electromagnetic radiation in UV, visible and IR ranges, noting improvement through automatic data processing 06 p1006 A67-19013

Balloon-borne sun seeker improvements through transistorized circuits and solid state switches 07 p1184 A67-19396

Pioneer VI detector to measure degree of anisotropy of cosmic radiation at various energy ranges 09 p1500 A67-22427

Potential sensitivity of energy radiation detectors, examining measurement error causes for radiation power of natural and artificial sources 10 p1607 A67-23589

Rise time in solid state detectors, considering equivalent circuit, plasma, time, etc 11 p1789 A67-24103

Thin film thermal radiation detector noting construction, calibration, performance, error sources and advantages of pyroelectric over thin film gauges 11 p1790 A67-24454

X-ray spectral distributions and fluxes in low kev range of five cosmic sources at low galactic latitude and longitude, noting effective temperature 11 p1856 A67-24505

Ionizing radiation in space, discussing detection techniques, devices, etc 11 p1791 A67-24619

Heterodyne detector of submillimeter radiation using CN maser as continuous wave source of coherent radiation 12 p1951 A67-25209

Three-channel particle spectrometer with semiconductor detectors and tunnel diode discriminators noting noise immunity, high signal level output, etc 12 p1944 A67-25853

Lithium drifted germanium detector with cylindrical annular shape permitting standardization of gamma spectroscopy techniques 12 p1945 A67-25861

Wideband-gap high atomic number semiconductor materials for high temperature counting radiation detectors 12 p1985 A67-25862

Thermal radiation emission detection from interplanetary dust, showing that zodiacal dust extends to within 4 solar radii of sun and confirming Poynting-Robertson effect 13 p2189 A67-26264

Maximum gravitational radiation detection range for binary stellar system analyzed by mechanically resonant antennas 15 p2563 A67-30162

Soviet and other papers on nuclear emission detector, using electron-optical light amplifiers 16 p2670 A67-30494

Vacuum UV radiation measurement from high temperature nitrogen, detecting radiation from shock layer of ballistic model 16 p2675 A67-31267

Strong X-ray source in vicinity of constellation Crux compared to SCO xr-1, findings suggest similar physical nature 17 p2937 A67-32761

Ionization mechanism of argon-permanent gas mixture in radioionization detector used for gas chromatography 19 p3226 A67-34797

Intensity and uniformity monitor for solar simulators using thermopile as detector 19 p3207 A67-34835

Lunar exploration by nuclear experiment, discussing instrument specifications for neutron gamma measurements 19 p3229 A67-35318

Cosmic ray intensity short-period variations investigated by high-counting rate detector indicating fluctuations related to geomagnetic cutoff rigidity periodic changes 19 p3315 A67-35537

Harmonic mixing and heterodyne detection of laser radiation 19 p3240 A67-35623

Pure capacitance type IR radiation detector concept, comparing various materials as to pyroelectric effect [ACS PAPER 27E-66F] 20 p3459 A67-36644

UV radiation detection using silicon carbide p-n junctions, showing wavelength increment at peak response and decreasing photovoltage with increasing temperature 21 p3591 A67-38156

Distribution of cosmic rays on sphere and reception vector of radiation detector 21 p3698 A67-38464

Silicon semiconductor alpha particle detector for spectrometry, noting radiation resistance for low energy proton bombardment 21 p3628 A67-38596

Solar proton and alpha radiation flux and spectral distribution measuring device on satellite HEOS A 21 p3629 A67-38665

Temporal periodicity of 10 cps observed in flux of auroral electrons by rocketborne radiation detectors 22 p3790 A67-39795

Ge/Li/ drifted gamma detector for 1/2 to 10 Mev range, measuring response deviation from linearity 23 p3998 A67-40819

Cosmic X-ray sources spectra obtained by proportional counters and electronic systems on sounding rockets 23 p4001 A67-41222

Solar and terrestrial thermal radiometer absolute calibration noting standards and methods 23 p4006 A67-41373

RADIATION DISTRIBUTION

Log periodic antennas operating in SHF bands having nonserrated radiation patterns 01 p0036 A67-10444

Geometrical factor and radiation pattern for single crystalline detectors and coaxial telescope 02 p0240 A67-11542

Radiation patterns and impedance plots of sleeve antenna over band with frequency ratio of 4 to 1 02 p0212 A67-11607

Approximation method for computation of radiation patterns from circular apertures and reflectors by single integration at wide angles and large Fresnel numbers 03 p0384 A67-13844

Temporal-spatial variation of cross sectional flux distribution of stimulated emission from Nd glass pulsed laser 03 p0439 A67-14280

Interferometric radio observations of Quiet Sun at 49 cm 04 p0694 A67-14486

Algorithm for statistical solution of radiant flux distribution in solar receivers with paraboloidal collectors 04 p0553 A67-14666

Stationary antenna arrays for target detection and tracking noting radiation patterns, radar systems, etc 04 p0654 A67-15538

Interchannel generation transfer and multichannel generation in laser with four unsplit levels, noting radiation density, temperature effect and variations in coefficients of losses 04 p0634 A67-15760

Flush cavity VOR antenna for DC-9 aircraft permitting omnidirectional radiation pattern characteristics 04 p0590 A67-15906

Fourier transform synthesis of aperture distributions producing sector beam patterns 04 p0590 A67-15907

Plasma sheath simulation used to analyze effects of sheath discontinuities and inhomogeneities on slot antenna radiation pattern and input impedance 05 p0769 A67-16000

Angular distribution of radiation at boundary of homogeneous diffusion sphere, with isotropic central point source calculated by Monte Carlo method 05 p0838 A67-16491

Distribution of cosmic rays on sphere and reception vector of radiation detector 05 p0884 A67-17121

Directional radiation pattern for circular arc antenna, using three-step method in which current distribution is treated as truncated Fourier series 07 p1152 A67-19550

Properties of real radiators and effects of mutual coupling between pairs noting impedance, pattern and polarization characteristics 07 p1154 A67-19782

Behavior of infinite arrays including radiation pattern approach yielding expressions for gain and periodic structure approach yielding input impedance variation with scan angle 07 p1154 A67-19783

Iterative solution for spherically symmetric mutual coherence function representing radiation propagating through statistically homogeneous and isotropic random medium 09 p1460 A67-21592

Isotropic scattering of radiation in finite two-dimensional atmosphere using integral equation, solved by power series 09 p1532 A67-21662

Solution of angular distribution of outgoing thermal radiation from planetary atmosphere, using Chandrasekhar diffuse scattering and transmission functions 09 p1567 A67-22240

Traveling wave V antenna, discussing parameter variation effect on radiation patterns 11 p1761 A67-24283

Measurement and theory of two modes in antenna apertures of magnitudes one to two wavelengths, obtaining field distribution 11 p1763 A67-24295

Approximation method calculation of propagation constants of dielectric loaded TE wire-grid leaky wave antenna for near endfire radiation 11 p1763 A67-24296

Far field radiation patterns of Advanced Antenna System presented by Surveyor I on lunar surface [JPL-TR-32-1079] 11 p1763 A67-24298

Measurement of radiation reflectively scattered from optical surfaces in far UV, noting role of overcoating with metal films 11 p1819 A67-24666

Optical configuration for long distance laser beam transmission determined from truncated Gaussian aperture distribution radiation patterns 11 p1754 A67-24724

Optimum antenna aperture distribution for finite line source and desired radiation pattern with given superdirective ratio upper boundary 11 p1768 A67-24943

Brightness distribution of radio emission over solar disk during solar activity minima determined from radioheliograms 12 p2001 A67-25226

Angular distribution of radiation at boundary of homogeneous diffusion sphere, with isotropic central point source calculated by Monte Carlo method 13 p2155 A67-26346

Radiation patterns of annular slots on conducting conical surface subjected to harmonic excitation 13 p2080 A67-27028

Range characteristics of antenna arrays composed of identical transmitters located along circumferential arc and producing pencil beam 13 p2080 A67-27027

Discrete recording of radiation patterns of antenna arrays 13 p2080 A67-27035

Normal distributions of various quantities related to radiation budgets of tropospheric column, earth surface and troposphere-earth system over Northern Hemisphere 13 p2116 A67-27458

Vertical distribution of heating rate by radiative processes over Northern Hemisphere presented in zonal cross sections 13 p2116 A67-27459

Synthesis of field distribution over aperture of antenna radiating maximum portion of power into given solid space angle 14 p2283 A67-28274

Method of radiation pattern synthesis for equally and unequally spaced arrays 14 p2285 A67-28451

Large antenna radiation from radio astronomy Explorer satellite determined on basis of antenna current distribution 14 p2286 A67-28507

Directivity factor of linear antenna array with Chebyshev radiation pattern 14 p2289 A67-28862

Angular distribution of laser radiation and variation in beam direction of stimulated radiation as function of misadjustment angle of resonator mirrors 15 p2500 A67-29759

Omnidirectional radiation pattern for S-band telemetry on rockets more than 1/2 ft in diameter by small electrical separation of antennas [AAS PAPER 67-51] 15 p2454 A67-30116

Scattering of surface wave incident upon junction of two semi-infinite planes joined together by step analyzed using Wiener-Hopf equation 16 p2626 A67-31348

Effect of random amplitude errors of continuous apertures on radiation pattern and gain 16 p2627 A67-31353

Variation of radiation pattern of array of two traveling-wave V-antennas and use as spacecraft antenna 16 p2639 A67-31360

Polarization characteristics of radio emission from rough lunar surface, analyzing averaging effects of antenna radiation pattern and surface roughness 16 p2628 A67-31495

Geometrical factor and radiation pattern for single crystalline detectors and coaxial telescope 16 p2677 A67-31608

Radiation pattern changes for helicopter antenna located in rotor blade as result of flight dynamics [AHS PAPER 109] 16 p2597 A67-31825

Light field distribution in optical resonator of Fabry-Perot type interferometer with nonparallel mirrors, using Airy function for localizing field concentration planes 17 p2853 A67-31925

Radiation properties of low-gain ring antenna on ground plane, showing by patterns effect of geometrical parameters and frequency 17 p2827 A67-32781

Rapid earth electromagnetic field variations used for plasma concentration and magnetosphere radius determination 17 p2846 A67-32937

Measurement of ensemble distribution of intensity fluctuations of laser radiation at threshold 18 p3098 A67-33522

Lagrange interpolation pattern synthesis technique using moment criterion for optimum pattern approximation by nonuniform antenna array 18 p3012 A67-34430

Inner zone electron intensity distribution model for solar activity minimum 19 p3219 A67-35238

Annular solar eclipse of May 20, 1966 visible at Bordeaux, noting active center on occultation curve 19 p3325 A67-35506

Sea level and stratosphere measurement of cosmic ray intensity latitude distribution, coupling coefficients and multiplicities 19 p3316 A67-35563

Squinted, sum and difference radiation patterns interrelationships for amplitude monopulse antennas with impedance

mismatch and mutual coupling between feeds 19 p3197 A67-35824

Chromium distribution in laser rubies with neutron activation 20 p3458 A67-36427

autoradiography 20 p3458 A67-36427

Transverse-mode distribution of emission intensity of solid state laser with plane mirrors 20 p3459 A67-36688

Angular divergence of gas-laser radiation as function of output power, analyzing interaction of angular modes 20 p3459 A67-36689

Blockage effects of centrally located sample on reflectance measurement by modified integrating sphere [ASME PAPER 67-HT-54] 20 p3447 A67-36736

Atmospheric energetics, discussing stratospheric-tropospheric energetics differences, atmospheric radiation balance distribution, meteorological satellite data, computer studies of atmospheric circulation, etc 20 p3429 A67-36895

Auroral transition radiation calculated from electron impact 20 p3433 A67-37420

Galactic cosmic ray density distribution anisotropy in solar system, discussing outward convection of cosmic rays by solar wind and inward diffusion model 20 p3520 A67-37474

Spaced antenna array radiation pattern frequency control analyzed for relationship between arrival angle and heterodyne frequency 20 p3402 A67-37506

Multiply-tuned antenna array operating over certain frequency range through electric beam shifting 20 p3403 A67-37507

Correlation type arrays resolving power noting role of averaging processes 20 p3403 A67-37509

Aperture antennas near field radiation patterns calculated by computer program based on semisimulated method 20 p3405 A67-37645

Distribution of cosmic rays on sphere and reception vector of radiation detector 21 p3698 A67-38464

Antenna array radiation pattern in isotropic linear medium by radiation pattern synthesis in moving medium 21 p3598 A67-38607

Crystal block structure and slip plane influence on laser radiation, discussing radiation energy distribution in space and divergence determination 21 p3642 A67-38968

Reception vectors for first and second spherical harmonics of cosmic ray distribution calculated for neutron monitor stations 21 p3699 A67-39018

Synthesis of nonuniformly spaced antenna arrays using lambda functions to reduce space factor and prescribed radiation pattern 21 p3602 A67-39071

Upper limit for condensation of fluctuations in primordial fireball determined by considering effects of radiative diffusion 21 p3711 A67-39120

Image radiance distribution of confined plasma in circular tubes noting absence of distortion 22 p3842 A67-39234

Sidelobe reduction by stepping E-plane field distribution on rectangular horn antenna aperture, finding values of geometrical parameters 22 p3767 A67-39273

Radiation pattern lobing structure elimination for recessed annular slot in coated metal cylinder 22 p3767 A67-39274

Target-tracking antenna design with primary feed system suitable for slewing of mobile radar equipment 22 p3760 A67-39592

Radiation pattern of linear antenna erected over tapered ground screen, noting system surface impedance variation 22 p3760 A67-39628

Radiation pattern of dielectric antenna using integral equations, noting differences between real antenna and idealized linear traveling wave antenna 22 p3770 A67-39656

Emission of axisymmetric parabolic antenna with antiphase field distribution at aperture, calculating radiation pattern of principal and cross polarization components of field 22 p3770 A67-39658

Radiation fluctuation of single mode continuously operating laser, deriving fluctuation spectral density and emission line intrinsic width 22 p3815 A67-39738

Impedance strip directional properties when excited through slot in metallic half-plane, noting case of reflector antenna with decreasing impedance 22 p3770 A67-39763

Odd value correlation coefficient and wave

amplitude fluctuation effects on mean radiation pattern and antenna amplification losses 23 p3977 A67-40599
 Bifilar complementary loaded helical antenna, determining radiation patterns, near field amplitudes and phase velocities 23 p3979 A67-40834
 Numerical results for source distribution estimation from external radiation field measurements, investigating transport processes in slab bounded by parallel planes 23 p4082 A67-40993
 Field of loop antenna with arbitrary current distribution located inside cylinder with arbitrary dielectric constant studied for effects on radiation pattern 23 p3982 A67-41666
 Surface wave propagation around sharp corners in single wire transmission lines, calculating and measuring radiation loss and pattern 24 p4119 A67-41971
 Mixed problems of antenna synthesis, solving approximately specified amplitude and phase radiation patterns and given antenna current amplitude or phase 24 p4129 A67-42228

RADIATION DOSE

Spacecraft shielding combinations for astronaut protection, comparing magnetic, electrostatic and passive methods on basis of dosage and mission duration 01 p0153 A67-10425
 Hazards to man on moon from flare-produced solar particle beams and galactic radiation, noting estimate for life shortening 02 p0189 A67-12394
 Space nuclear radiation dose rates in earth atmosphere with consideration of solar flare radiation variations 06 p1077 A67-18009
 Fourth-week syndrome in addition to normal medullary syndrome in DBA/2J mouse strain response to acute ionizing lethal irradiation 13 p2059 A67-26868
 Radiation doses measured by onboard dosimeters and those fastened to space suits of crews of Voskhod I and Voskhod II compared, noting radiation composition analysis by means of nuclear emulsions 14 p2256 A67-27863
 Radiation levels on Gemini IV flight including Van Allen belt and South Atlantic Anomaly 15 p2425 A67-29105
 Man-rated space-vehicle structural design considering space environment loads and material requirements, noting applicability of existing methods 16 p2756 A67-30630
 Ionizing radiation dosimetry for space pilots on short-and long-term space flights 16 p2617 A67-30764
 Cosmic radiation dose, estimating contributions due to mu meson and electron-photon cascade shower components 18 p2990 A67-33516
 Inner Van Allen belt proton dose rate and spectral charged particle environment profiles correlated, noting agreement with theoretical values 19 p3313 A67-35189
 Secondary dose equivalent model for calculating secondary proton and neutron doses determined, using random sampling techniques 20 p3482 A67-37551
 Monte Carlo method to determine derivatives of radiation doses in optimization of shape and composition of protective shields 21 p3577 A67-38425
 Room temperature density-dose behavior of neutron and gamma irradiated polytetrafluoroethylene /PTFE/ noting crystallinity variations 23 p4021 A67-40781
 Low dose reactor irradiation effect on temperature dependence of dynamic modulus and internal friction of as-deposited pyrolytic graphite 23 p4021 A67-41075
 Optically concentrated laser radiation beam properties using plane and spherical faced ruby resonators 23 p4016 A67-41322

RADIATION EFFECT

Polymethylmethacrylate and polystyrene exposure to ruby and neodymium-glass laser radiation, noting appearance of EPR 01 p0086 A67-10075
 Molecular spectroscopy of illumination effects on cobalt activated ZnS exposed to ruby laser pulses 01 p0090 A67-10683
 Damage rate deduced from room temperature conductivity measurements on n-and p-type floating zone silicon samples subject to electron irradiation at energies from 0.3 to 2.0 mev 01 p0133 A67-10752
 Peak effect in critical current of superconductors observed during deuteron

irradiation at low temperature 01 p0135 A67-10880
 X-ray irradiation effect on electrophysical properties of n-and p-type germanium, determining absorption coefficient 01 p0136 A67-11044
 Nonuniform damage in silicon solar cells produced by proton irradiation 02 p0182 A67-11682
 Photoelectric optical imaging system survival in earth radiation belt, noting noise level and total energy absorption 02 p0243 A67-12055
 Compact flash X-ray systems for radiographic measurement of moving objects, radar ranging, atmospheric density, radiation effects, etc 02 p0245 A67-12215
 Space radiation monitoring system aboard manned spacecraft to provide solutions to medical problems and safety of flight guidelines for mission control 02 p0188 A67-12387
 Secondary particle generation in satellite walls due to 0.1 to 20 bev pi-mesons and protons 02 p0312 A67-12610
 Neutron irradiation effect on twinning behavior and transition temperature of niobium-vanadium alloy 02 p0256 A67-12709
 Effect of electron irradiation on silicon solar cells constituting power generator aboard Diapason IA 03 p0362 A67-12897
 Bidirectional reflectance measurements to determine optical degradation induced by UV radiation [AIAA PAPER 65-672] 03 p0419 A67-13040
 Low energy proton effect on thermal control coatings [AIAA PAPER 65-648] 03 p0448 A67-13053
 Proton and alpha particle effects on thermal properties of spacecraft and solar concentrator coating of anodic-coated aluminum, zinc oxide/ potassium silicate, etc [AIAA PAPER 65-649] 03 p0448 A67-13054
 Neutron collision cross section and calculation of energy loss of displaced Si atoms to ionization 03 p0494 A67-13481
 Surface recombination velocity of thermally oxidized silicon structures exposed to X irradiation 03 p0496 A67-13677
 Thermally radiating and absorbing plane piston problem, obtaining zero order approximation in series expansion in density ratio across shock layer 03 p0405 A67-14029
 Radiation losses effects on temperature measurements with transparent sheathed thermometers 03 p0426 A67-14344
 Spacecraft environmental effects covering outgassing in high vacuum, deterioration of materials by evaporation, lubrication and changes in mechanical and electrical properties of plastics 04 p0704 A67-14995
 Threshold energy for electron radiation damage in Ag compared for liquid He and liquid Ni temperatures 04 p0638 A67-15115
 Book on nuclear radiation effects on electronic systems including radiation shielding, nuclear instrumentation systems and electronic design 04 p0583 A67-15267
 Gamma irradiation from Co 60 effect on indium antimonide, determining defect formation on dose and limiting position of Fermi level for n-and p-type material 04 p0680 A67-15283
 Nongray radiation effects on laminar boundary layer of absorbing gas over flat plate at low Eckert numbers [ASME PAPER 66-WA/HT-35] 04 p0724 A67-15428
 Isotope effects in gamma radiolysis at 77 degrees K of mixed water and deuterium oxide ice systems 04 p0658 A67-15508
 Nuclear and space radiation effects - IEEE Conference, Stanford University, July 1966 04 p0586 A67-15687
 Neutron energy deposition in silicon in ionization and elastic interactions calculated, noting effects of atomic recoils 04 p0684 A67-15688
 Displacement effects in n-and p-type silicon when exposed to energetic radiation, using electron spin resonance and galvanomagnetic techniques 04 p0684 A67-15689
 Defect impurity relation in electron damaged p-type silicon and electron irradiation effect on float zone n-type silicon 04 p0684 A67-15690
 Transient annealing following pulsed neutron exposure in silicon transistors and

solar cells as function of temperature and injection level 04 p0684 A67-15693
 Brittle fracture threshold of silicon, germanium and indium antimonide under pulsed electron irradiation 04 p0685 A67-15694
 Transient radiation effects induced in silicon irradiated by electron pulses measured, using resistivity transient response and Hall effect 04 p0685 A67-15695
 Transient response of transistor exposed to ionizing radiation environment determined, using lumped model technique 04 p0588 A67-15697
 Pulsed high energy ionizing radiation effects on behavior and output frequency of electronic quartz oscillator crystals 04 p0685 A67-15700
 Transient radiation effects on microcircuits 04 p0588 A67-15701
 Damage mechanism in semiconductors from space radiation and effects on various microcircuits 04 p0588 A67-15702
 Ionizing radiation effects on silicon planar bipolar transistors determine degradation mechanisms 04 p0588 A67-15707
 I-V characteristics shift and radiation hardening of Mos transistors for low ionizing dose level 04 p0589 A67-15714
 Space radiation effect on MOSFET and metal-silicon nitride-silicon devices, noting protective methods 04 p0589 A67-15715
 Transient gamma ray effect on thin film insulated gate FETs compared with FETs fabricated on silicon substrate 04 p0589 A67-15717
 Time-dependent response of polycrystalline cadmium selenide thin film transistor to transient high energy radiation 04 p0589 A67-15718
 Transient response of MOS transistors and integrated circuits to ionizing radiation 04 p0589 A67-15719
 Transient radiation response and permanent radiation damage in monolithic silicon-junction-transistorized integrated circuit 04 p0589 A67-15720
 Transient radiation response mechanisms in monolithic microcircuits using p-n junction isolation from substrate 04 p0589 A67-15721
 Thermal radiative property behavior of materials under elementary charged particle bombardment, determining effect of combined UV plus electron exposure and low energy proton bombardment 04 p0686 A67-15873
 Radiation effects on heat transfer and friction characteristics in natural and forced convection film boiling in boundary layer flows [ASME PAPER 66-WA/HT-8] 04 p0739 A67-15939
 Hugoniot-Rankine conditions, dissociation and ionization of hydrogen and nitrogen gas behind high speed shock wave and radiation effects 05 p0790 A67-16036
 Visual acuity decrement from laser lesion in fovea of stump tail macaque monkeys 05 p0756 A67-16287
 Damage in glass induced by linear absorption of laser radiation non-Q-spooled 05 p0824 A67-16794
 Basal plane contraction and annealing of degraphitized carbon examined via X-ray diffraction techniques 05 p0833 A67-16891
 Laser radiation effect on heating process and gas dynamic motion of finite transparent gas and motionless cold gas at vacuum interface 05 p0927 A67-17008
 Defects in silicon p-n solar cells with Li diffused N region produced by electron irradiation and spontaneously annealed at room temperature interpreted as Li ions 05 p0870 A67-17273
 Differential equations and mathematical models for gas flows with chemical activity and radiative effects, particularly effects of reentry and propulsion 06 p0983 A67-17785
 X-ray effect on conductivity, carrier concentration and mobility in Si crystals and Si p-n junction 06 p1048 A67-17855
 X and electron irradiation effect on current-voltage characteristics of p-n junctions in gallium arsenide 06 p1049 A67-17859
 Mathematical model for potential heating from gamma radiation source, determining transient temperature distribution for materials used in nuclear

rockets 06 p1116 A67-18363
 Space radiation effect on satellite design, noting guidelines for electronic equipment shielding 06 p1078 A67-18419
 Van Allen radiation belt simulation, obtaining accurate values for satellite and semiconductor lifetimes in orbit [AIAA PAPER 67-177] 06 p0981 A67-18510
 Physical characteristics of residual DNA in bacterial cells after degradation due to ionizing radiation 06 p0953 A67-18774
 Multiphoton ionization of krypton atom by ruby laser radiation 06 p1037 A67-18796
 Micro-and macrocrack formation in organic glass by focusing of laser beam 06 p1021 A67-18808
 Surface generation-recombination and channel effects on p-n junctions and transistors exposed to ionizing radiation 06 p1054 A67-18822
 Roentgen radiation effect on glycogen metabolism of rat brain 07 p1133 A67-19468
 Parametric excitation of modes of infinite plasma by incident radiation using Vlasov equation, noting unstable oscillations for incident frequencies 07 p1228 A67-19502
 Annealing of proton radiation damage in silicon solar cells 07 p1237 A67-20143
 Alkaline vapor refueling of solar thermionic converters, concept, development and tests 07 p1132 A67-20287
 Sensitivity of dielectric rod terminal impedance to surface wave coupling when no resonance regions exist within energy-carrying cross section 07 p1158 A67-20299
 Space environment effect on refractive optical systems, particularly solar radiation effect on optical properties of glass 08 p1330 A67-20644
 Electron and proton radiation effects on GaAs, CdS and CdTe thin film solar cells noting proton damage, estimates on cell life, etc 08 p1285 A67-20735
 Radiation noise effect on laser optical properties, noting density vs resonator characteristics, energy spectrum, etc 08 p1337 A67-20839
 Laser radiation effect on metals, noting disintegration mechanism, indentation formation and vapor 08 p1337 A67-20856
 Absorbed solar electromagnetic radiation effect on mean facial skin temperature 09 p1452 A67-21725
 Nondestructive testing techniques in radiation vulnerability analysis of electronic systems, noting ionization effects and permanent damage in semiconductors 09 p1471 A67-21868
 Laser radiation effect on solids, noting laser properties, temperature rise, melting, vaporization and particle emission of materials 09 p1513 A67-22144
 Silicon solar cell with drift fields of various widths and magnitudes, considering performance changes before and after radiation 10 p1596 A67-23161
 Radiation damage experiments for evaluation of silicon solar cell characteristics under simulated solar light 10 p1596 A67-23166
 Phagocytic activity and hepatic function following localized proton radiation to liver, discussing results of experiments performed on white rats 10 p1599 A67-23814
 Dog study on microwave radiation and effect on response to X-ray irradiation 10 p1599 A67-23815
 Dog experiments, determining microwave radiation effects on physiological response 10 p1600 A67-23824
 Nonequilibrium ionization and radiation effect on shock wave attenuation calculated using linearized theory 11 p1774 A67-23856
 DNA-agar annealing of residual DNA after degradation by ionizing radiation 11 p1746 A67-23919
 Fourier transform for exact solution of current distribution and input admittance of infinite cylindrical dielectric-coated antenna 11 p1757 A67-23972
 Molecular spectroscopy of illumination effects on cobalt activated ZnS exposed to ruby laser pulses 11 p1804 A67-25072
 Energy variation of two-body system due to gravitational radiation studied within framework of Minkowski theory 12 p1966 A67-25145
 Silicon crystals composition effect on solar cells reaction to irradiation by 4 mev electrons 12 p1896 A67-25150

Reduction of radiation effect on thermocouple in thermal vacuum testing by using fiberglass tape with aluminized mylar backing 12 p1943 A67-25695
 Radiation MGD, considering flow problems with thermal radiation and electromagnetic field effect 12 p1975 A67-25889
 Book on electron radiation damage in semiconductors and metals covering lattice defects, alloys, atom displacement, EPR testing, etc 12 p1986 A67-25890
 Multiple sample space UV simulation facility for in situ hemispherical spectral reflectance measurements [AIAA PAPER 67-312] 12 p1926 A67-26027
 Thermal control coating spectral sensitivity to UV induced degradation, noting rapidly increasing damage as incident radiation wavelength decreases [AIAA PAPER 67-340] 12 p1959 A67-26054
 Optical materials properties analyzed for UV induced degradation under vacuum conditions [AIAA PAPER 67-344] 12 p1959 A67-26058
 Anomalous shift in gate threshold voltage of high transconductance p-channel MOSFETs during exposure to space-like radiation 13 p2076 A67-26516
 Creep rupture, fatigue strength and brittle-ductile transition of aluminum as affected by nuclear radiation 13 p2133 A67-27090
 Defects in irradiated silicon, analyzing electron paramagnetic resonance and electron-nuclear double resonance of aluminum vacancy pair 13 p2180 A67-27161
 Military electronics equipment packaging, discussing integrated circuits, module board design, interconnectors, nuclear radiation effect, heat dissipation, power supply design and cooling 13 p2083 A67-27447
 UV radiation effect on mechanical characteristics of polyethylene terephthalate film in vacuum and atmospheric pressure 13 p2184 A67-27624
 Radiation effects on shear strength of several alloys at liquid hydrogen environment 13 p2143 A67-27678
 Bacteria survival and mutation in radiation environment on Voskhod I and II 14 p2254 A67-27864
 Rhesus monkeys liver damage after irradiation by penetrating protons 14 p2254 A67-28064
 Mutagenic effects of primary cosmic radiation on bacteria 14 p2254 A67-28213
 Cosmic radiation problems in space flights and in SST flights, examining biological effects, shielding methods, dosimetry and warning systems 14 p2255 A67-28217
 Radiobiological aspects of radiation safety in cosmic flights 14 p2255 A67-28222
 Nuclear radiation damage to circuit elements of missile FM/FM telemetry system, analyzing changes in electric characteristics 14 p2271 A67-28685
 Chronic acceleration and acute Co 60 whole body irradiation effects on rats, discussing weight to mass ratio 15 p2427 A67-29268
 Hypersonic stagnation point flow between strong shock wave and body involving radiation, conduction and dissociation 15 p2415 A67-29309
 Van Allen radiation belt simulation, obtaining accurate values for satellite and semiconductor lifetimes in orbit [AIAA PAPER 67-177] 15 p2465 A67-29446
 Simulated space effects on microelectronic device materials 15 p2466 A67-29549
 Thermal control materials for spacecraft, considering UV spectral distribution, radiation energy and flux, oxygen bleaching, etc 15 p2579 A67-29552
 Cobalt 60 gamma radiation effect on set of B-doped p-type silicon samples, giving radiation-induced defects. 16 p2724 A67-30472
 Mutation of human tissue by cosmic radiation, discussing results of cell studies from male and female subjects 16 p2611 A67-30766
 Overall profile of ophthalmic injury associated with ionizing and nonionizing electromagnetic radiation fields, based on human response to radiation exposure 16 p2611 A67-30769
 Spatial distribution of radiation damage in solids determined by spectral analysis of photovoltaic current of photovoltaic cell 16 p2726 A67-30815
 Characteristics of photovoltaic solar

converters, discussing drift field, wrap around and epitaxial webbed silicon cells, minimum film thickness and radiation damage 17 p2801 A67-32048
 H, C, N, O, Cl, Ca and Al negative ion formation in plasma, noting role of continuous radiation, formation temperature and metastable and stable states 17 p2893 A67-32136
 Interaction of radiation with solids - Conference, American University at Cairo, September 1966 17 p2913 A67-32371
 Semiconductor crystal structure defects caused by irradiation with energetic particles and photons 17 p2913 A67-32372
 Gamma ray radiation effects on laser glasses, noting ionization and atom displacements in lattice 17 p2867 A67-32374
 Recovery Stage III in neutron irradiated Al-Cu alloy, discussing vacancies and interstitials 17 p2873 A67-32743
 Effects of electric fields and configurations on thermal annealing and radiation hardening of MOSFETs 17 p2916 A67-32835
 Semiconductor device and transient ionizing radiation effects on monolithic integrated circuits 17 p2828 A67-32836
 Temperature, resistivity and injection level dependence of recombination processes in neutron irradiated silicon explained by two-level recombination model 17 p2916 A67-32837
 Electron radiation damage in CdSe crystals at cryogenic temperatures, noting electrical conductivity and cathodoluminescence properties before and during damage 17 p2916 A67-32838
 Radiation damage to satellite solar cells when shielded to various degrees, stressing silicon junction cells 17 p2804 A67-32840
 Ionizing radiation effect on polymers used in electronics, producing temporary effects also found in mineral insulators like anodic tantalum oxide 17 p2917 A67-32841
 Plane structure silicon transistors subjected to Co gamma radiation, considering electrical properties degradation to predict component survival probability 17 p2917 A67-32842
 Radiation effects on silicon transistor parameter behavior characteristics 17 p2917 A67-32843
 Silicon transistors obtained by diffusion studied for equivalence between radiations producing permanent degradation of transistor characteristics 17 p2917 A67-32844
 Degradation in silicon transistors due to particle bombardment analyzed, showing surface/ bulk recombination increase 17 p2917 A67-32845
 Neutron and Co gamma rays radiation effect on lithium drifted p-n silicon detectors 17 p2917 A67-32846
 N-and p-type silicon solar cells orientation and energy dependence of damage at room temperature under electron bombardment 17 p2918 A67-32848
 Fission-particle damage formation in semiconducting layer structures, using model based on thermal spike 17 p2918 A67-32849
 Electron bombardment effect on insulated-gate and junction-gate FETs and MOS IC indicates FET resistance to ionizing radiation 17 p2918 A67-32850
 First order prediction of equilibrium photocurrent in silicon switching diodes and radiation storage time in silicon low power planar and mesa transistors from electrical measurements 17 p2918 A67-32851
 MOST behavior under irradiation studied for defect creation and ionization, charge displacements and preexistent trap ionization 17 p2918 A67-32852
 Irradiated germanium observed for carrier concentration variations, using Hall coefficient measurements 17 p2918 A67-32853
 Electron paramagnetic resonance /EPR/ studies of interaction of irradiation-produced defects with impurities and other defects in silicon semiconductors 17 p2918 A67-32854
 Radiation-hardened semiconductor electronic circuit design, noting radiation environment existing in spacecraft nuclear generator vicinity 17 p2919 A67-32857
 Radiation effects on carrier recombination and mobility and on lifetime of semiconductor devices 17 p2919 A67-32858
 Disordered regions produced by fast neutron irradiation effect on semiconductor properties of silicon 17 p2919 A67-32859

Response of capacitors irradiated by pulses of transient nuclear radiation 17 p2828 A67-32863

Soviet book on study of defects of crystalline structure of metals and alloys including X-ray analysis of aluminum single crystals, radiation effects on niobium, etc 17 p2874 A67-32894

Neutron bombardment effect on niobium mechanical properties shown to depend on metal purity 17 p2874 A67-32898

Impurity effect on annealing behavior of irradiated silicon studied via isothermal annealing of minority carrier 17 p2921 A67-33051

Damage regions in Si, GaAs and InSb irradiated with monoenergetic neutrons determined, using electron microscopy 17 p2922 A67-33060

Radiation and weightlessness effect on human organism in space flights, discussing galactic cosmic, solar and Van Allen belt radiation 18 p3116 A67-33700

Explosion theory, reviewing chain and thermal theories, unification, fuel consumption effects, spatial distribution effects, etc 18 p3155 A67-33845

NERVA radiation effects tests at cryogenic temperatures 18 p3076 A67-33947

[AIAA PAPER 67-477] 18 p3076 A67-33947

Radiation power of He-Ne laser at 0.63, 1.15 and 3.39 microns, effect on electron concentration 18 p3060 A67-34038

Laser radiation effect on heating process and gas dynamic motion of finite transparent gas and motionless cold gas at vacuum interface 18 p3160 A67-34270

Radiation effects in metal-insulator-semiconductor /MIS/ devices, noting shift and shape change in characteristic curve 18 p3012 A67-34345

Multiphoton ionization of krypton atom by ruby laser radiation 18 p3083 A67-34415

Fast neutron irradiation effect on electrical conductivity and Hall effect in Zn doped n-type indium arsenide single crystals 19 p3301 A67-34771

Lubricant requirements for aircraft parts noting high and low temperature, radiation conditions, lubrication capability limits, etc 19 p3248 A67-34993

Lethal effect of solar UV radiations on dried Collipage T-1 exposed to space at sounding rocket altitudes 19 p3177 A67-35184

Terrestrial microorganism survival in space aboard Gemini satellite, discussing lethal effects of solar radiation 19 p3178 A67-35223

Ionospheric and stratospheric UV radiation effects on survival of microorganisms 19 p3178 A67-35271

Transmission decrease of various aqueous solutions under ruby laser irradiation 19 p3240 A67-35420

Radiative effects in pair of spherical particles in radiation field produced by omnidirectional gravitational quanta 19 p3325 A67-35556

Electron, X-ray and UV radiation effects on oxidized silicon surfaces and planar devices, noting space charge buildup 19 p3305 A67-35621

Silicon transistors transient defect annealing from pulsed particle irradiation, stressing time factors 19 p3305 A67-35667

Electromagnetic radiation, elementary particles and micrometeorites effects on earth satellites 19 p3327 A67-35672

Electronic structure of irradiation defects in ionic solids vacancies, interstitials and dislocations, explaining electronic relaxation 19 p3306 A67-35673

Radiation surface effects in semiconductor devices, noting positive space charge buildup in passivated device dielectric surface layer 19 p3306 A67-35674

Space environment effects on integrated circuits, discussing FET-MOS type 19 p3196 A67-35675

Mechanisms involved in damage in metal-insulator-semiconductor /MIS/ devices through exposure to nuclear radiation 19 p3306 A67-35676

Neutron irradiation effect on n-type and p-type semiconductors thermophysical parameters 19 p3307 A67-35874

Statistical probability of fractures in polymethylmethacrylate by laser radiation 20 p3473 A67-36161

High energy proton and electron damage on silicon junctions measured and compared

with Van Allen belt radiation damage 20 p3507 A67-36237

Radiation effects on MOS devices, analyzing electrical characteristics degradation mode and conduction threshold voltage variation 20 p3396 A67-36321

Girders examined from construction standpoint including damage tolerance, airworthiness, radiation, operational loads and reparability 20 p3360 A67-36454

Hardening technique for circuits using electrical shielding to withstand radiation effects of nuclear war 20 p3399 A67-36883

Cobalt 60 gamma radiation effect on MOS diodes fabricated on silicon substrates, noting surface state and oxide charge densities 20 p3510 A67-36961

Thermal annealing of silicon solar cells with direct solar heating or electric storage methods to avoid radiation damage 20 p3364 A67-37129

Low temperature and irradiation environment effects on mechanical properties of engineering materials 20 p3418 A67-37532

X-band propagation over rough earth when illuminated by radiation, studying scattering problems 20 p3388 A67-37647

Heat conductivity in materials ascribed to phonons, noting phonon radiation effects 20 p3515 A67-37715

Mathematical model for potential heating from gamma radiation source, determining transient temperature distribution for materials used in nuclear rockets 21 p3730 A67-37793

Black and white surface coating materials exposed to simulated solar radiation in vacuum, noting deterioration of white coatings 21 p3650 A67-37960

Radiation effect on MOS transistors in D-2 satellite telemetry coder 21 p3593 A67-38230

High energy electron radiation effects on silicon photocells deposited epitaxially on artificial satellite surface, discussing liberated carrier accumulation possibility 21 p3572 A67-38672

Viscous dissipation effect on heat transfer rates for laminar boundary layer flow of gray gas across flat plate 21 p3732 A67-38878

Laser thermal and radiation effect on metals, discussing mechanical damage 21 p3646 A67-39011

Nature of defects in InSb induced by gamma and X-ray irradiation, discussing recovery process 21 p3687 A67-39143

Junction potential measurement in irradiated tunnel diode showing no oscillation in any bias voltage 22 p3767 A67-39369

Radiation effects on bipolar transistors field effect devices and integrated circuits noting damage in degraded current gain, increased saturation voltages and leakage 22 p3772 A67-39863

Irradiation damage in germanium monitored by electric conductivity measurements, noting carrier population depletion by introducing acceptor levels into forbidden gap 22 p3862 A67-39997

Low temperature electron irradiation effects on undoped GaSb resulting in impurity conduction 22 p3862 A67-40000

Gamma irradiation effect on spinal cord timed differently, considering time factor in reactions of nervous system in guinea pigs 23 p3943 A67-40767

Laser induced damage reduction in lithium tantalate and niobate crystals, proposing mechanism to explain observed reduction 23 p4012 A67-40876

Maximum permissible energy density incident on retina determined for eye safety in viewing laser beam 23 p3962 A67-41052

Ionizing radiation effects on dark current and noise pulse spectrum of photomultiplier tubes used in balloon and satellite X-ray observations 23 p4000 A67-41216

Giant pulse irradiation effect on ruby laser under oscillation quenching, amplification and characteristics changes in metastable state population 23 p4017 A67-41434

Laser irradiation effect on semiconductor crystals surfaces using pulsed ruby laser 23 p4045 A67-41470

Photovoltaics - IEEE Conference, Cocoa beach, March 1967, Volume 3, Radiation and micrometeoroid effects on solar cells, lithium in silicon cells 23 p3940 A67-41516

High energy proton irradiation and

annealing of n and p type Si, comparing proton and electron damage 23 p4047 A67-41519

Li containing p-on-n and n-on-p Si cell degradation by bombardment noting carrier removal damage, annealing and radiation damage resistance 23 p3941 A67-41524

Li doped Si solar cell, studying irradiation damage, recovery effect, carrier removal, time dependency and annealing 23 p4047 A67-41525

Li doped Si solar cells noting fabrication, preradiation behavior, changes with temperature, recovery and I-V characteristics after irradiation 23 p3941 A67-41526

Psychophysical study of irradiation phenomena effects on target size perception by investigating luminance, fixation position and corrections 23 p3969 A67-41643

Constant voltage steps of AC Josephson effect observed in drop-form junctions exposed to radiation 24 p4200 A67-41864

Biosatellite II, mission objectives and planned experiments 24 p4240 A67-41897

Electron scale heights from topside ionograms studied for radiation effects during quiet and disturbed conditions, noting relation to ionospheric plasma temperature 24 p4147 A67-42055

Fast neutron radiation damage in narrow base p-n-p-n devices compared to one-dimensional theory, showing superiority to bipolar transistors 24 p4130 A67-42248

Preirradiated organism reaction to space flight acceleration studied in determination of admissible ionizing radiation dose 24 p4113 A67-42393

Protocell origin, discussing radiation effects on polymers, proteinoid properties and already synthesized polymer stability 24 p4113 A67-42656

Nuclear radiation damage to circuits noting Compton effect, ionization current effects, resistance drops, electron-hole pair formation, etc 24 p4132 A67-42702

Laser-irradiated plasma theoretical study indicating absorption enhancement in external magnetic field 24 p4199 A67-43104

Neutron irradiation effect on thermal conductivity of silicon at low temperature noting annealing stage 24 p4206 A67-43110

RADIATION EMISSION

Airborne surface temperature measurement relating surface appearances to radiation parameters 01 p0063 A67-10327

Meteor luminescence during atmospheric motion, obtaining radiation coefficient as function of cross sections of particle excitation and pulse transfer processes 01 p0151 A67-11287

Calorimetric apparatus for measurement of low temperature emittance of materials as function of temperature [AIAA PAPER 65-703] 03 p0418 A67-13037

Antenna with limited excitation region, discussing emitter design with prescribed radiation pattern and near field behavior 04 p0583 A67-15148

Simultaneous radiation of center-fed slotted rectangular waveguide array antenna for monopulse tracking radar 04 p0590 A67-15905

Spectrophotometry of Arend-Roland comet, estimating radiation from comet emission bands and continuous spectrum 05 p0891 A67-16338

Time-invariant Stokes, anti-Stokes and double emission processes in distributed traveling wave systems, calculating spatial EM field distribution and estimated conversion length 05 p0762 A67-16355

Radiative lifetimes of UV multiplets in Si, P, S, O, Ne 2 and Ar 2 measured via phase shift method, correcting for transition cascading 05 p0892 A67-16411

Stress effects of simple supports on radiation emission from turbulent flow near plane compliant surface, using acoustic equivalence to extended dipole system 05 p0748 A67-16813

Book on electromagnetic wave emission, absorption and scattering processes in gaseous plasma 05 p0855 A67-17152

Nitrogen and oxygen excitation by proton shocks, measuring emission cross sections of radiation and analyzing vibrational structure 06 p1037 A67-18706

Spectral analysis of emission of spatially separated spots in GaAs injection lasers 07 p1197 A67-20185

Radiation from equilibrium air over large temperature and density range 08 p1426 A67-20583

Radiation characteristics of current sources perpendicular to magnetostatic field for cylindrical column of free space surrounded by loss-free magnetotonic medium 08 p1357 A67-20715

Stimulated radiation from trivalent Nd ion doped barium crown glass fiber laser without resonator 08 p1337 A67-21203

Correlation radiometry examination of radiation emission in beam plasma discharge at harmonics of electron cyclotron frequency 09 p1536 A67-21601

Integral hemispherical and monochromatic radiative capacity of carbon compounds at high temperatures 09 p1497 A67-21877

Comet 1965 f /Ikeya-Seki/ interaction with solar corona produces no significant enhancement of emission at 2.2 m wavelength 10 p1706 A67-22958

Laser radiation generation at indirect band transitions with free carrier participation in pure semiconductor 10 p1667 A67-23654

Transient emission characteristics of pulsed argon ion laser, noting capillary discharge due to radiation trapping effect 11 p1801 A67-24649

Preparation and properties of electronic materials for radiative processes control - AIME Conference, Boston, August 1966 11 p1847 A67-24734

Weak cosmic ray burst relation to austral axis pole geomagnetic activity characteristics and propagation in interplanetary space of energetic solar cosmic rays 12 p1992 A67-25116

Thermophysical properties of heat-resistant solid solution of rhenium in tungsten produced by arc melting in vacuum 12 p1956 A67-25758

Intergalactic radiation absorption and extragalactic sources contribution to LF background radiation 12 p1995 A67-25766

Javelin rocket soundings with far UV scanning spectrometer, noting atomic hydrogen and oxygen radiation 12 p1934 A67-25787

Solar X-ray monitoring during IQSY 12 p1999 A67-25833

Thermal radiation emission detection from interplanetary dust, showing that zodiacal dust extends to within 4 solar radii of sun and confirming Poynting-Robertson effect 13 p2189 A67-26264

Total hemispherical emittance of transparent materials at low temperatures measured using calorimetry 13 p2159 A67-27356

Radiative heat exchange between surfaces of telescoped cylinders, determining angular radiation coefficients 14 p2406 A67-28308

Antenna with limited excitation region, discussing emitter design with prescribed radiation pattern and near field behavior 15 p2443 A67-29335

Decrease in degree of ionization of shock-heated argon resulting from radiative emission 15 p2527 A67-29563

Short wave limit for plasma radiation emission of neon gas discharge analyzed by Kirchhoff-Planck relation 15 p2530 A67-29747

Boundary layer problem concerned with effects of radiation absorption and emission for flow of high speed gas over flat plate [AIAA PAPER 66-521] 15 p2473 A67-30207

Cerenkov radiation due to point charge moving at uniform velocity parallel to magnetostatic field in unbounded magnetotonic medium 17 p2812 A67-32314

Microwave emission intensity from InSb, examining dependence on angle between DC electric and magnetic fields 17 p2914 A67-32615

Coherent radiation from cadmium sulfide single crystal excited by electron beam, noting transition nature in generation mode and spectral composition 17 p2915 A67-32660

Radiation kinetics of laser with resonator having lens system and low absorption nonlinear medium, showing time shift of kinetic curve 17 p2868 A67-32663

Lyman-alpha radiation emission from ion-target-gas collision measured for various projectile energies 17 p2889 A67-33224

Laser radiation generation at indirect band transitions with free carrier participation in pure semiconductor 17 p2870 A67-33335

Excitation and radiation of OH molecules and alkali metals in low pressure flames and

rocket exhausts 18 p3152 A67-33819

Optical radiation emission from rocket exhaust plumes, noting dependence on aerothermochemical properties, considering radiative transfer 18 p3152 A67-33821

Emission statistics of nonresonant feedback laser produced by radiation scattering, showing fluctuations intensity, distribution function, etc 18 p3062 A67-34621

Argon plasma radiation emission and absorption measurement, determining transition probabilities 18 p3091 A67-34732

Solar X-ray emission associated with proton flare of July 1966 measured, plotted and described 19 p3313 A67-35218

Stellar and solar atmosphere outermost layers structures, finding radiative equilibrium for massive stars 19 p3322 A67-35327

Spectral measurements of reflected solar and emitted thermal radiations from earth and clouds, using spectrometer with interference filter wedge 19 p3225 A67-35690

Effect of angular direct current magnetic field on radiation of slot antenna located on metal cylinder covered by plasma sheath 19 p3184 A67-35811

Metastable helium atom altitude distribution and 10830 angstrom radiation emission rate, discussing possible explanation of helium loss from atmosphere 20 p3427 A67-36310

Simultaneous absorption of two photons by transparent material at radiation frequency corresponding to only one photon 20 p3457 A67-36325

Wave transformation effect on inhomogeneous plasma radiation noise, applying results to stable plasma thermal radiation 20 p3498 A67-36691

Iterative solution for directional emissivities of two-dimensional semiminfinite slab of absorbing-scattering medium with gray isothermal dispersion [ASME PAPER 67-HT-12] 20 p3545 A67-36710

Gas local thermodynamic equilibrium effect on calculated thermal radiation emission [ASME PAPER 67-HT-51] 20 p3548 A67-36733

Lifetime decrease of metastable state of chromium ion in ruby and emerald due to temperature raise, showing radiative transition 21 p3676 A67-37816

Meander-line antenna operated under backfire conditions studied for electrical performance and radiation properties 21 p3597 A67-38397

Resonance and noise microwave emission thresholds for InSb electron hole plasma subject to crossed electric and magnetic fields, noting Hall effect 21 p3683 A67-38403

Ruby laser radiation frequency temperature dependence, observing narrow spectral width with Fabry-Perot interferometer 21 p3640 A67-38451

Resonance electronic Raman effect and parametric induced anti-Stokes radiation in potassium vapor atoms 21 p3641 A67-38456

Transient interference studied for emission from pulsed ruby laser 23 p4012 A67-40883

RADIATION EXPOSURE

Radiation stress effect on component reliability of electric circuits analyzed via mathematical statistics 02 p0210 A67-11527

Spallation produced Ar 40 in iron meteorites for determining cosmic ray exposure ages from radiogenic Ar 40 content 02 p0328 A67-12308

Glycogen accumulation in monkey and cat brain exposed to proton irradiation, discussing astrocytes function in carbohydrate metabolism 04 p0560 A67-14489

UV stability of several white thermal control coatings spectrally characterized in vacuum for application to Lunar Orbiter project [AIAA PAPER 67-345] 12 p1959 A67-26059

Rocket and balloon-borne exposure study of terrestrial microorganism survival in space 15 p2424 A67-29097

Micrometeoroid collection experiments flown on Gemini IX and Gemini XII analyzed, using optical and electron microscopy and mass spectrometry 19 p3339 A67-35196

RADIATION FIELD

Autocorrelation function of radiation electric field measurement from clipped correlation function and spacing estimation for optimally efficient SNR

determination 01 p0114 A67-10808

Symmetrical radiation feed patterns which are consequence of specified form of hybrid mode fields as disclosed by focal plane analysis 02 p0213 A67-11615

Reradiation pattern of Van Atta reflector consisting of half-wave dipoles 03 p0384 A67-13846

Estimated greatest permissible mirror misalignment, active medium inhomogeneity and extra-axial beam losses for artificial realization of very narrow radiation pattern in real laser 03 p0438 A67-14185

Kinetic theory of quantum electron gas coupled to radiation field under uniform external magnetic field 04 p0672 A67-15770

Accuracy and limit analysis of statistical distribution of EM radiation field by photoelectron counting distributions from photodetector for single mode laser near threshold 05 p0815 A67-16624

Multiphoton absorption processes, coherence of radiation fields and statistical properties of laser light 05 p0823 A67-16681

Radiation pattern of linear nonequidistant antenna array 05 p0775 A67-16964

Daytime profile of electron density in C and D layers of ionosphere from measurements of surface ultralong wave fields and atmospheric pressure profile 05 p0801 A67-17131

Characteristic states of electromagnetic radiation field, using quantum mechanical theory of optical coherence 06 p1036 A67-18367

Diathermy, derivation of equation relating monochromatic/integral radiation energy ratio of solid material of fluid heat emitter to temperature 07 p1211 A67-19130

Optical systems and holography in reconstruction of SHF antenna radiation patterns from field measurements in Fresnel zone 07 p1183 A67-19143

High altitude balloon-borne polarization measurements relevance in research program of radiation emerging from earth atmosphere 07 p1170 A67-19393

Retarded potentials and fields of oscillating electric dipole undergoing accelerated relativistic motions 10 p1679 A67-22730

Quantum mechanical theory of interference between independent nonmonochromatic light beams using nonmonochromatic modes of radiation field 10 p1663 A67-22866

Satellite-emitted short radio wave field intensity and ionospheric parameters 11 p1751 A67-24071

Statistical properties of coherent radiation noting correlation function, experiments on photon distribution, Bose-Einstein distribution, etc 11 p1799 A67-24106

Inclined log spiral antenna, noting back radiation reduction and frequency independence 11 p1763 A67-24294

Line source antenna radiation pattern computed from complex voltage patterns measured at various range lengths in near field 11 p1763 A67-24301

Possible thermal histories of intergalactic gas 11 p1860 A67-24485

Reflection coefficient of parabolic reflector antenna illuminated by horn radiator with sector shaped radiation pattern 11 p1767 A67-24716

Semirelativistic approximation of matter-radiation interaction 12 p1966 A67-25146

Velocity space diffusion coefficient of electrons in thermal radiation field, using Hamilton-Jacobi theory 12 p1969 A67-25192

Radiation field of monopole antenna hinged on spherical conducting support calculated with Green function technique 13 p2081 A67-27200

Electrostatic, induction and radiation field effects of lightning discharge on intensity spectrum of atmospheric source signals 14 p2346 A67-27880

Non-LTE line-transfer problem computational methods 14 p2351 A67-28994

Pseudo-isotropic radiation source as source with isotropic gain function and polarization depending on spatial direction 16 p2761 A67-30793

Radiation characteristics from electric dipole immersed in lossy anisotropic plasma taking into account collision effects 16 p2713 A67-30797

Unsteady heat transfer due to radiation of

two opaque bodies of finite dimensions, solving nonlinear Volterra integral equation with respect to net radiation density 16 p2779 A67-31208

Nagelberg formula locating Fresnel region phase center of aperture antennas examined by calculating phase patterns of radiation field 16 p2639 A67-31357

Spherical dipole for Italian satellite, calculating radiation impedance and pattern, input admittance, efficiency, radiated field and antenna Q factor 17 p2826 A67-32780

Optical systems and holography in reconstruction of SHF antenna radiation patterns from field measurements in Fresnel zone 17 p2861 A67-33222

Spectral brightness, reflectivity and polarization characteristics of clouds in IR band, measuring angular structure of underlying radiation field 18 p3073 A67-33563

Characteristics of dielectric rod excited with dominant propagating mode 18 p3011 A67-34020

Electromagnetic radiation from electric dipole moving with uniform relativistic velocity 18 p3000 A67-34022

Emission equations describing radiation field amplitude and energy level populations of solid state laser with broad oscillation spectrum 18 p3061 A67-34388

Spatial amplitude of field of ideally parallel laser beam focused by optical systems with spherical aberration 18 p3061 A67-34439

Radiation field interaction with particles in assemblage of electrons and atoms or ions using perturbation theory and Liouville equation 19 p3284 A67-35339

Radiative effects in pair of spherical particles in radiation field produced by omnidirectional gravitational quanta 19 p3325 A67-35556

Central data system for solar probe to map particle and radiation fields of solar corona 20 p3391 A67-36597

Short period seismic radiation patterns from underground nuclear explosions and small magnitude earthquakes, noting propagation characteristics [SR-1] 20 p3434 A67-37430

Fields with boundaries radiated by electric or magnetic current phased-line distributions, interpreting field constituents as geometric-optical and diffracted contributions 20 p3388 A67-37702

Electromagnetic point source in presence of planar interface between two anisotropic media, obtaining far fields through Fourier integral and ray optical calculation 20 p3388 A67-37703

Transient response and current distribution of thin vertical antenna coupled to pulse generator by electric network, determining radiation field 21 p3590 A67-38117

Daytime profile of electron density in C and D layers of ionosphere from measurements of surface ultralong wave fields and atmospheric pressure profile 21 p3619 A67-38474

Quantum theory of maser oscillator model consisting of radiation field mode interacting with 3-level atoms 22 p3814 A67-39436

Pencil-beam antenna with field distribution fluctuation determined for resolving power by mean square measuring of radiation pattern, detailing parabolic reflectors with rough surfaces 22 p3763 A67-40125

Radiation from infinite aperiodic array of parallel plate waveguides, using Wiener-Hopf technique for edge effect 23 p3978 A67-40825

Radiation pattern, absorption and impedance measurements of conical antenna plasma sheath about dielectric coated metal cone excited by axial radiating slot 23 p3973 A67-40840

Finite ground plane influence on raised electric dipole far field radiation pattern 23 p3980 A67-41202

Equilateral triangular stepped helical aerial observed characteristics including impedance variation, radiation patterns, axial ratio and velocity factor 24 p4128 A67-41970

Radiation field asymmetry and anomalous beam angle divergence of ruby lasers linked to dislocations in ruby crystals prepared by Verneuil method 24 p4166 A67-42070

Spatial coherence of radiation field across multimode He-Ne laser

beam 24 p4167 A67-42091

Functional equations in internal radiation field in finite inhomogeneous isotropically scattering atmosphere, using invariant embedding and Duhamel principle 24 p4189 A67-42597

Duhamel principle for internal radiation field in inhomogeneous finite atmosphere based on existence and uniqueness theorem for Milne integral equation 24 p4189 A67-42598

Divergence angles of helium-neon laser radiation, discussing resonator with spherical mirrors with unequal curvature radii 24 p4169 A67-42891

RADIATION FUNCTION

Radiation from dielectric antenna, noting erroneous radiation formula applications 17 p2824 A67-32308

Radiation conditions for derivatives of radiating functions, omitting prescribed asymptotic behavior 17 p2877 A67-32562

Raman spectra vibrational structure theory concerning crystal impurity centers, giving intensity distribution formulas and radiation model calculations 20 p3511 A67-37031

RADIATION HAZARD

Model describing effect of ionizing radiation on metal-oxide-silicon surfaces, showing relation to study of defect structure of silica 01 p0036 A67-10475

Hazards to man on moon from flare-produced solar particle beams and galactic radiation, noting estimate for life shortening 02 p0189 A67-12394

Protective shielding for astronauts from ionizing radiation from solar and galactic cosmic rays and radiation belts 03 p0365 A67-13539

Straight edge fence design for control of radar site environment from clutter return, pattern interference, tracking errors and high power hazard to personnel 03 p0396 A67-13853

Enzyme-isoenzyme changes in rhesus monkeys under gamma irradiation 07 p1134 A67-19860

Hazards of laser radiation, mechanisms, control and management 10 p1601 A67-23328

Radiation hazards and safety requirements for lunar and Mars manned space flights, discussing radiosensitivity, restoration and permissible doses 13 p2059 A67-26761

Extraterrestrial vestibular research in orientation of humans in space, noting possible disorders due to radiation and lack of protection 15 p2425 A67-29106

Radiation hazard to man from solar proton events 15 p2429 A67-29450

Radiation level on lunar surface noting degree of danger to astronaut, solar activity effect, creation of secondary emission, etc 16 p2737 A67-30782

Safety program for nuclear rocket engine testing, discussing role of cryogenics 20 p3482 A67-36565

Fluidics defined, giving uses in amplification, sensing, logic, switching and computation, noting reliability under extreme environmental and radiation conditions 20 p3364 A67-37171

Gas laser IR radiation hazards to eyes tested on rabbits indicates irreversible changes in cornea leading to impaired vision 20 p3375 A67-37276

Hepatic hemorrhagic lesions produced by 32 and 55 Mev proton radiation in rhesus monkeys 23 p3944 A67-41017

Radiobiological risk of SST flights from heavy ions of cosmic radiation, discussing methods of radiation detection 23 p3945 A67-41074

Galactic radiation hazard for long term space missions, discussing life shortening effect 23 p3953 A67-41583

Manned spacecraft space radiation monitoring system requirements and criteria to indicate biological response 23 p3966 A67-41589

Pathological effects, including carcinogenesis following proton whole body irradiation in rats 23 p3958 A67-41645

RADIATION INDICATOR

Radiation balance chart of earth atmosphere system for evaluation of radiation receivers on Nimbus II satellite 20 p3431 A67-36964

RADIATION INTENSITY

Nonthermal radiation of Na in CO medium, analyzing temperature, pressure and composition variation effects of

ambient 01 p0166 A67-10051

Stratospheric cosmic ray intensity, discussing Soviet measurements above Antarctica 02 p0310 A67-12573

Secular changes in stratospheric cosmic ray intensity from 1962 to 1964 02 p0311 A67-12595

Captured proton intensity measurement in inner radiation belt in Brazilian anomaly, using satellites Proton I and II 05 p0878 A67-16089

Change in intensity and forms of energy spectrum effects on accuracy of measuring values of meteorite preentry dimensions, weight and degree of ablation 05 p0887 A67-16099

Primary cosmic radiation intensity determined with help of nuclear particle tracks in moldavites and meteorites 05 p0887 A67-16100

Radiation intensity dependence for various spectral bands of diffused gallium arsenide p-n junctions on current density 05 p0861 A67-16391

Quasi-spiral nature of change in 27-day cosmic ray variation with solar activity shown by harmonic analysis 05 p0884 A67-17137

Quantitative intensity of weak carbon dioxide triad in 1 micron spectral region obtained, using pressure broadening techniques 06 p1031 A67-17870

Reciprocity principle of Equivalent Sun Hours /ESH/ as means of spacecraft material testing 06 p0980 A67-18365

Absolute intensity of radiation from center of solar disk at wavelengths between 3288 and 12,480 angstroms 06 p1089 A67-18710

Pair production in irradiated semiconductors within framework of plasmon decay, considering variation of radiation ionization energies with band gap energy 06 p1063 A67-18935

Thermal radiation intensity measurement from heating rate of Cu detector exposed to radiation 07 p1184 A67-19354

Statistical analysis of flare radiation intensity and brightness distribution of irregular and semiregular variables 07 p1248 A67-19486

Effects of AZA and PCA on radio wave propagation in Antarctica, noting reliability and radiation power requirements 07 p1143 A67-19692

Complex Doppler effect in dense cold magnetized plasma 08 p1357 A67-20818

Mercury emission intensity ratios in negative glow of Hg-hydrogen DC abnormal glow discharge 08 p1356 A67-21296

Vertical and horizontal variations of intensities of auroral OI and molecular nitrogen ion emissions 08 p1328 A67-21480

Proton II satellite measurements of intensity of nuclear component of primary cosmic radiation 09 p1561 A67-21897

Relationship between statistics of log amplitude and irradiance fluctuations due to atmospheric turbulence used to estimate effect of aperture in collecting scintillating light 10 p1603 A67-22711

Plasma confinement time in helium discharge determined by electron density and helium radiation intensity measurements 11 p1827 A67-23887

Polarized pyrometric probe applied to hot and dense plasmas, ascertaining particle energies and densities 11 p1789 A67-24410

Cosmic ray intensities under sea water and under rock 11 p1857 A67-24617

Shock tube study of oscillator strength of diatomic molecular carbon Swan bands 11 p1750 A67-25066

Cosmic ray secondary components yearly changes of intensity determined as function of earth heliolatitude 12 p1992 A67-25120

Cosmic ray measurements in interplanetary space and on moon noting intensity increase 12 p1992 A67-25123

Longitudinal target defocusing effect on solar reflector power parameters, noting energy redistribution phenomenon 12 p1896 A67-25323

Cosmic radiation intensity fluctuation in stratosphere, noting absence of explanation for anomaly 12 p1994 A67-25542

Electron and ion concentrations as function of solar radiation intensity and variation of ionospheric conditions, noting nitrous oxide/oxygen ion ratio 12 p1933 A67-25649

Oscillator strengths for extreme UV

resonance lines of ions in neon isoelectronic sequence calculated, based on single configurations in intermediate coupling 12 p1968 A67-26247

Vertical cut-off rigidities for specific locations of geophysical interest computed from trajectory tracing process 13 p2191 A67-26325

Laser gas-discharge tube /without resonator/ amplification relations, considering stimulating radiation, noting application as oscillator 14 p2328 A67-27771

Interplanetary electromagnetic field effects on cosmic ray intensity noting geomagnetism, modulation mechanisms and solar flare particle propagation 14 p2380 A67-27965

Behavior at infinity of specific intensity in plane-parallel atmosphere 14 p2391 A67-28946

Quasi-biennial cycles in cosmic ray intensity 15 p2549 A67-29203

Annual cosmic ray variations and changes in cosmic radiation intensity as function of earth heliollatitude 15 p2550 A67-30012

Microwave spectrum and observation at 6 cm wavelength of Venus to determine total intensity and polarization of radiation 16 p2747 A67-30987

Dependence of focusing property of aperture on coherence length of illuminating field in Fresnel diffraction from aperture 16 p2639 A67-31358

Solar-diurnal variations of neutron and muon components of cosmic rays based on IGY data, analyzing temperature effect 17 p2931 A67-32079

Cosmic ray intensity 11-year variation energy characteristics, discussing spectrum bending due to integral modulation in interplanetary space 17 p2932 A67-32083

Cosmic ray intensity, discussing modulation due to earth heliollatitude variation 17 p2932 A67-32086

Hysteresis phenomena in curves describing cosmic ray intensity dependence on number of sunspots 17 p2933 A67-32087

Atmospheric temperature effect on latitudinal curve of cosmic ray intensity determined from radio probe observations 17 p2933 A67-32090

Solar UV spectrum interpretation taking into account dielectronic recombination processes in ionization equilibrium computation, obtaining spectral lines intensities, abundances and atmospheric structure indications 17 p2941 A67-32235

Spectrophotometric observations used to construct empirical curve relating radiation intensity and magnetic field strength in sunspots 17 p2946 A67-32728

Photospheric mean alpha hydrogen radiation intensity profile computed for various heights above solar surface taking into account limb-darkening effect 17 p2946 A67-32729

Measurement of ensemble distribution of intensity fluctuations of laser radiation at threshold 18 p3098 A67-33522

Satellite tracking of cloud formation on earth shadow side, calculating outgoing radiation intensity under cloudless and cloudy sky 18 p3074 A67-33564

Piezoelectric microphone for measuring pulsed ultrasonic radiation intensity and energy distribution, discussing principles, operating conditions and construction of instrument 18 p3046 A67-33745

Longitudinal magnetic field effect on radiation intensity of He-Ne laser operating in pulsed regime 18 p3061 A67-34043

Radiation intensity and causes of radiation peak of nonequilibrium gas following strong shock waves 18 p3083 A67-34059

Penetrating radiation intensity on lunar surface and in space, evaluating counting rate, lunar surface radioactivity and radiation belts absence 18 p3122 A67-34143

Intensity and uniformity monitor for solar simulators using thermopile as detector 19 p3207 A67-34835

Energy and intensity density of radiation emitted by semilfinite nonequilibrium electron plasma with non-Maxwellian particle distribution calculated, based on general fluctuation theory 19 p3267 A67-34902

Corona temperature and logarithmic intensity gradients determined by pointwise three-color photoelectric photometry during solar eclipse 19 p3318 A67-35017

Positive column contraction in inert gas discharge, studying electron density and

radiation intensity radial distribution and wall current 19 p3272 A67-35092

Solar X-ray flare of July 1966 observed from satellite, giving curves describing energy flux, radiation intensity, etc 19 p3312 A67-35187

Spectral composition of earth IR radiation measured from satellites, giving radiation intensity and temperature distributions 19 p3219 A67-35253

Lunar rocks composition and radioactivity through satellite gamma-ray measurements indicating basaltic and ultrabasic composition 19 p3319 A67-35258

Absolute intensities of Lyman hydrogen alpha and beta lines used for interpretation of electron temperatures and density of emitting layers 19 p3325 A67-35464

Density gradient of cosmic radiation perpendicular to plane of ecliptic as cause of variations in amplitude and phase of solar diurnal variation 19 p3315 A67-35490

Underground cosmic ray intensity variation measurements to determine solar modulation processes 19 p3315 A67-35494

Cosmic ray intensity short-period variations investigated by high-counting rate detector indicating fluctuations related to geomagnetic cutoff rigidity periodic changes 19 p3315 A67-35537

Sea level and stratosphere measurement of cosmic ray intensity latitude distribution, coupling coefficients and multiplicities 19 p3316 A67-35563

Relative intensity contribution and time dependency of primary cosmic rays, splash albedo and reentrant albedo measured by polar orbiting satellite 20 p3517 A67-36306

Superradiant high gain pulsed lasers measured for single pass gain by comparing single pass and double pass radiation intensities 20 p3460 A67-36858

Optical metagalactic radiation measured by spacecraft photographic and photometric methods, reviewing Olbers paradox and night sky brightness measurements 20 p3526 A67-37127

Nonthermal plasma electron density calculated from ratio of spectral line intensities of given ion 20 p3501 A67-37294

Heavy nuclei intensity in primary cosmic rays, long term solar cycle modulation and time lag in various phases 20 p3519 A67-37405

Bilateral metal grating effect on E and H polarized radiation from plane parallel layer noting intensity, energy density and reflection at interface with medium 21 p3638 A67-37865

Maser output pulsations by varying active particles entering resonator through electric or magnetic field 21 p3638 A67-37941

Spectral analysis of intensity fluctuations of laser at threshold noting confirmation of time resolution in terms of weighted sum of exponential 21 p3640 A67-38355

Microwave radiation from plasma beam interaction, measuring radiation intensity as function of discharge current 21 p3668 A67-38416

Quasi-spiral nature of change in 27-day cosmic ray variation with solar activity shown by harmonic analysis 21 p3698 A67-38480

Flare X-ray emission period determined, noting maximum radio emission and optical intensity 21 p3699 A67-38965

Cause of cosmic radiation intensity increase before magnetic storms associated with Forbush effects 21 p3699 A67-39029

Extensive cosmic ray shower bremsstrahlung in RF and optical bands noting intensity and incoherency 22 p3870 A67-39517

Synchrotron radiation intensity of relativistic electron moving in anisotropic medium 22 p3851 A67-39735

Temporal and spatial low energy solar proton intensity variations indicating interplanetary medium changes effects on magnetospheric configuration 22 p3873 A67-39813

Total extraterrestrial and global solar radiation intensity and spectral distribution for designing radiation resistant satellites 22 p3874 A67-40031

Double sunspot cycle or 22-yr variation in cosmic ray diurnal variation phase, discussing streaming mechanisms 22 p3874 A67-40046

Laser detector using glow discharge tube

current changes to measure radiation intensity 23 p4012 A67-40894

Laser mode synchronization by electro-optical crystal dielectric constant modulation mounted inside resonator 23 p4013 A67-40903

Radiation intensity measurements in systems containing atomic oxygen and carbon monoxide by shock tube heating, deriving spectral intensity distribution for radiative combination 23 p4029 A67-40972

Cosmic ray regional variations in intensity and ionization magnitude and duration indicating heavy nucleus and low energy particle influx accompanying solar flares 23 p4055 A67-41100

Solar cycle primary cosmic radiation variation above magnetosphere and radiation belts at stratosphere and surface, using neutron monitors and space vehicle measurements 23 p4055 A67-41101

Interplanetary space cosmic ray intensity variation with time and distance from sun measured by Zond III and Venera II simultaneously 23 p4055 A67-41102

Galactic cosmic ray intensity measurements in stratosphere and at various atmospheric depths, studying secular variation energy spectra during solar cycle 23 p4055 A67-41103

Nuclear cosmic ray component intensity variation related to 27-day solar activity variation in Elektron II and IV analysis of modulating effect 23 p4055 A67-41104

Cosmic ray intensity solar cycle variations in terms of solar wind properties defined by solar activity characteristics parameters 23 p4056 A67-41106

Cosmic ray intensity variation mechanisms due to motion of solar system and quasi-radial interplanetary magnetic field 23 p4056 A67-41107

Cosmic ray intensity 27 day variations during low and high solar activity periods noting lower amplitude and softer spectrum 23 p4056 A67-41108

Cosmic ray intensity 19, 20 and 24 day quasi-periodic global variations in stratosphere related to solar activity variations, comparing amplitudes with Forbush effects 23 p4056 A67-41109

27-day cosmic ray intensity variations noting possible selective effects of active spots on solar hemispheres and plasma corpuscular fluxes structure 23 p4056 A67-41110

Heavy nuclei intensity during solar cosmic ray intensity increase accompanying chromospheric flares, proposing magnetic field dynamic dissipation acceleration mechanism for charged particles 23 p4056 A67-41113

Cosmic ray intensity increase in wake of chromospheric flares from stratospheric measurements 23 p4057 A67-41115

Neutron component intensity variation and particle generation on sun during chromospheric flares and electromagnetic radiation during solar activity cycle 23 p4057 A67-41116

Secular modulation of cosmic ray intensity in interplanetary space using Parker diffusion model 23 p4057 A67-41117

Solar diurnal variation and sudden changes in cosmic ray intensity from yearly neutron component data 23 p4058 A67-41123

Trapped radiation levels via AP1-5 and AE1-3 model environments noting long term effects 23 p4061 A67-41517

Mean intensity photospheric H-alpha radiation profile for prominences in solar corona, noting profile dependence on height, velocity and direction 24 p4209 A67-41965

Multiphoton absorption in monatomic gases causing ionization of atom applied to plasma production by intense radiation from lasers 24 p4190 A67-42098

Frequency and intensity of laser light analyzed for reaction of coupled optical resonator 24 p4168 A67-42574

Captured proton intensity measurement in inner radiation belt in Brazilian anomaly, using satellites Proton I and II 24 p4212 A67-42765

Change in intensity and forms of energy spectrum effects on accuracy of measuring values of meteorite preentry dimensions, weight and degree of ablation 24 p4238 A67-42775

Primary cosmic radiation intensity determined with help of nuclear particle tracks in moldavites and

- meteorites 24 p4238 A67-42776
- RADIATION LAW**
- S KIRCHHOFF LAW
- S QUANTUM THEORY
- S STEFAN-BOLTZMANN LAW
- RADIATION MEASUREMENT**
- SA PYRANOMETER
- Microwave frequency measurements of radiation temperature of nitrogen afterglow plasma with Maxwellian electron velocity distributions 01 p0119 A67-10147
- IR imagery application in locating anomalously hot earth in Yellowstone National Park 01 p0059 A67-10332
- Weather satellites, discussing photographic and radiation measuring equipment and automatic picture transmission 01 p0109 A67-10768
- Rotation rate and inclination of planetary axis determined from radiation incident on artificial satellite of planet 02 p0321 A67-11539
- Solar X-ray emission measurements with Geiger photon counters carried by Elektron II and IV satellites 02 p0240 A67-11544
- Radioisotope and radiation techniques for terrestrial and planetary gas- and solid measurements 02 p0245 A67-12223
- Paint film thickness of spacecraft coatings, effect on spectral directional reflectance and binormal transmittance in far IR [AIAA PAPER 65-653] 03 p0447 A67-13033
- U.S. Weather Bureau calibration of solar radiation pyranometer by means of 5000 watt tungsten filament lamp 03 p0419 A67-13076
- Canadian calibration of solar radiation pyranometers 03 p0419 A67-13077
- Silicon solar cell to measure solar radiation intensity, discussing effect of optical path length ratio and atmospheric constituents 03 p0419 A67-13079
- Microwave radiation measurements from internal plasma resonance of positive column near electron cyclotron harmonic frequencies 03 p0476 A67-13355
- Transition zone anechoic chambers for field checkout, production and radiation testing of microwave antennas 03 p0397 A67-14102
- Meteorological satellites noting necessity of radiation measurements 04 p0648 A67-14409
- Vertical intensity measurement of rigid gamma quanta at various atmospheric depths 05 p0879 A67-16098
- Solar UV and zodiacal light, emphasizing importance and merits of rocket and balloon observations 05 p0799 A67-16873
- Approximation of space wave plus complex wave using modified saddle point technique 05 p0766 A67-17297
- Radiosonde radiometer to measure long wave emission from earth and intervening atmosphere during night ascents 06 p1005 A67-18742
- Thermal radiation intensity measurement from heating rate of Cu detector exposed to radiation 07 p1184 A67-19354
- Atmospheric temperature profile to 30 km determined by balloon-borne grating spectrometer of radiance of earth between 2100 and 2700 reciprocal cm [JPL-TR-32-1080] 07 p1171 A67-19394
- Proton energy spectrum obtained from nuclear emulsion measurements on Gemini IV and V missions 07 p1244 A67-19855
- Time dependence of low energy proton belts noting spatial and differential energy distribution 08 p1378 A67-21470
- High transmission Cerenkov spectrometer carried by proton I and II satellites to measure charges of primary cosmic ray nuclei high transmission Cerenkov spectrometer carried by Proton I and II satellites to measure 09 p1497 A67-21898
- Soviet book on practical utilization of observational data from meteorological satellites covering radiation and cloud cover, emphasizing weather forming systems analysis, aerological and synoptical data comparisons, etc 10 p1876 A67-23017
- Electron synchrotron as source of extreme UV radiation noting 11 p1788 A67-23965
- Cosmic radiation measurements beyond radiation belts as observed by Cosmos XVII 11 p1856 A67-24075
- Radiometer system with photomultiplier tube for measuring absolute radiation from hypervelocity projectile flow fields 11 p1790 A67-24447
- Cosmic microwave background measurements along celestial equator, using Dicke radiometer to study anisotropy of cosmic black body radiation 11 p1864 A67-24564
- Cosmic ray intensities under sea water and under rock 11 p1857 A67-24617
- Spacecraft rotation effect on measurement of hydromagnetic radiation in solar wind 12 p1934 A67-25782
- Radiation pattern of irregular antennas, using digital computer and superimposition of components to determine composite pattern 12 p1915 A67-25974
- Total equilibrium shock layer radiation data for Martian entry body shapes at various angles of attack extrapolated to trajectory condition [AIAA PAPER 67-324] 12 p1894 A67-26039
- Singly ionized He measured for radiative lifetimes of various states using high energy atomic beam 13 p2160 A67-26880
- Receivers for measuring UV radiation in upper atmosphere and outer space 13 p2121 A67-27335
- IR radiation measurements by spectrometers flown on board stratospheric balloons, considering sky brightness, vertical distribution and thermal atmospheric emissions 14 p2313 A67-28768
- Electronic equipment used for IR radiation measurement during space experiment, describing thermal effect detectors [ONERA-TP-465] 15 p2486 A67-29382
- Spatial distribution of electrons and protons trapped by geomagnetic field and charged particle fluxes in interplanetary space 15 p2550 A67-29536
- Coated refractory metals thermal emittance measured at high temperatures for design of reentry vehicle under time-temperature-pressure profile 15 p2503 A67-29546
- Tiros satellites characteristics including ESSA I 15 p2565 A67-29762
- Book on radioisotope measurement applications in engineering covering nuclear radiation, gas detectors, scintillation, etc 15 p2516 A67-29900
- Graphite cloth and felt as resistance heating elements for calibration and simulation facilities, achieving fast changes in heat flux level without sacrificing power efficiency 15 p2490 A67-30153
- Artificial red aurora created in southern conjugate region by atmospheric nuclear burst 16 p2664 A67-30977
- Global and diffuse solar radiation measurements by Macerata observatory, noting Robitsch pyranographs, Moll thermopiles, and global radiation results 16 p2698 A67-31023
- Rotation rate and inclination of planetary axis determined from radiation incident on artificial satellite of planet 16 p2752 A67-31605
- Solar X-ray emission measurements with Geiger photon counters carried by Elektron II and IV satellites 16 p2677 A67-31610
- Statistical processing of satellite data on spectral distribution of outgoing radiation 16 p2668 A67-31887
- Solar X-ray fluxes measured by solar radiation satellite during IQSY, comparing X-rays and decimetric radio emission in 8-12 angstrom band 17 p2938 A67-33185
- LF gravitational waves radiated by electromagnetic field of moving bodies, discussing measurement problems 18 p3117 A67-33527
- Piezoelectric microphone for measuring pulsed ultrasonic radiation intensity and energy distribution, discussing principles, operating conditions and construction of instrument 18 p3046 A67-33745
- Transfer function use in outgoing IF radiation temperature measurement of vertical profile over Caspian Sea by airborne modulation radiometer 18 p3040 A67-34001
- Star occultation measurements accuracy for determining satellite orbit parameters, noting error sources 18 p3075 A67-34108
- IR imaging system with multiple target capability for measuring IR radiation emitted by missiles during launch, boost and reentry 18 p3052 A67-34532
- Solar radiation-balance measuring device using polyethylene film to give protection from wind effects 19 p3227 A67-34855
- Primary diffuse X-ray flux and spectrum found isotropic by balloon measurements made in three particular directions 19 p3313 A67-35244
- On-the-ground optical determination method of stratospheric aerosol particle numbers and sizes from ruby laser radiation measurement scattering 19 p3225 A67-35531
- Spectral measurements of reflected solar and emitted thermal radiations from earth and clouds, using spectrometer with interference filter wedge 19 p3225 A67-35690
- Atmospheric radiation absorption measurements by radio-astronomy methods at wavelengths from 1.8 to 0.87 mm 19 p3185 A67-36014
- Interference method for measuring polarization of linearly polarized radiation 20 p3403 A67-37518
- UV and X-ray background measurements by Venus 3 may lead to mean density estimation of matter in universe through determination of intergalactic medium density and thermal history 21 p3705 A67-38591
- Electrical circuits for earth IR radiation emission measurements, describing apparatus and incorporated miniaturized pneumatic receiver 21 p3629 A67-38661
- 9.4 cm radiation from Jupiter and Saturn and 21.2 cm radiation from Saturn 21 p3709 A67-38994
- Low latitude cosmic ray neutron monitor multiplicity distribution, discussing monitor geometry and latitude 22 p3874 A67-40047
- Intensities of cosmic ray produced deuterium and tritium in atmosphere measured from high altitude balloons 23 p3995 A67-40811
- Laser detector using glow discharge tube current changes to measure radiation intensity 23 p4012 A67-40894
- Numerical results for source distribution estimation from external radiation field measurements, investigating transport processes in slab bounded by parallel planes 23 p4082 A67-40993
- Cosmic ray intensity measurement data from Soviet 1966 expedition in Arctic Ocean 23 p4060 A67-41138
- Resolution and geometrical factor determination for isotropic proton fluxes by using pencil beam and measurements over many angles and positions 23 p4001 A67-41225
- Manned spacecraft space radiation monitoring system requirements and criteria to indicate biological response 23 p3966 A67-41589
- Radiation measurement from satellite, discussing observation of ozone absorption band 24 p4181 A67-42397
- Vertical intensity measurement of rigid gamma quanta at various atmospheric depths 24 p4213 A67-42774
- Actinometric measurements from aircraft of short wave radiation fluxes and radiation balance, determining absorption coefficient for clouds and true albedo 24 p4182 A67-42882
- RADIATION MEDICINE**
- Radioactive isotopes for aviation and space medicine, treating hemodynamic phenomena, metabolism, cytophysiological investigations and fluids distribution in organism 22 p3756 A67-40547
- RADIATION PRESSURE**
- SA LIGHT PRESSURE
- Radiation pressure of electromagnetic and acoustic waves calculated from momentum of incident and scattered wave trains 05 p0846 A67-16583
- Successive approximations determining radiation pressure effect on and disturbing function of motion equations of artificial satellite 06 p1081 A67-17787
- Solar radiation field interaction with flexible antenna as possible explanation of anomalous rapid spin decay of satellites [AIAA PAPER 67-39] 06 p1096 A67-18350
- Satellite perturbation by pressure of radiation reflected from earth 08 p1383 A67-20401
- Constant force effect on Keplerian orbit with reference to solar wind perturbation 08 p1383 A67-20402
- Exact theory of enclosed molecular radiometer using flow field solution from Wu-revised thermal transpiration theory in two cases 10 p1681 A67-22864
- Radiation pressure on vanes of rotary actuator of spacecraft radiation orientation

system 12 p2011 A67-25655
 Solar photon radiation reaction produced on body of satellite and utilized for satellite stationkeeping 13 p2213 A67-27489
 One-dimensional plane shock wave propagation through hot dense plasmas under various energy and pressure conditions, noting magnetic field effect 14 p2356 A67-27957
 Stability of interstellar gas to perturbations in gas pressure, magnetic field and cosmic ray pressure from hydromagnetic viewpoint taking rotation into account 14 p2388 A67-28832
 Pulsed laser beam induced elastic waves in metals, noting experimental techniques and role of radiation pressure in wave generation 14 p2374 A67-28987
 Helium-neon laser generating simultaneously on two lines, showing pressure dependence and output radiation variation with discharge current 17 p2868 A67-32662
 Very high satellite air drag acceleration studied by University of London Observatory, discussing solar radiation pressure acceleration 18 p3042 A67-34257
 Nonlinear resistance of multiple resonator arrays at incident sound high pressure levels 19 p3311 A67-34963
 Alouette I and Explorer XX /S-48/ spin behavior explained by solar heating of antennas and solar radiation pressure 21 p3712 A67-37784
 Ideal gas flow in spherically symmetric gravity field, considering radiant heat transfer and radiation pressure 22 p3880 A67-39407
 Solar radiation pressure perturbations on large planar reflector satellite orbit 22 p3903 A67-39953
 Solar radiation pressure utilization as propulsive force for space vehicles noting sun sail concept 23 p4071 A67-41345

RADIATION PROTECTION
 Protective shielding for astronauts from ionizing radiation from solar and galactic cosmic rays and radiation belts 03 p0365 A67-13539
 Radioactive contamination of high flying aircraft, discussing empirical observations and possible decontamination procedure 05 p0751 A67-16300
 Number transmission coefficients for isotropically incident electrons determined for spacecraft shield design [AIAA PAPER 66-511] 05 p0906 A67-17219
 Space radiation effect on satellite design, noting guidelines for electronic equipment shielding 06 p1078 A67-18419
 Biological effects of supersonic flight, discussing radiation at high altitudes and preventive measures 07 p1134 A67-19532
 Effects of radiation protective pharmacological agents /cystamine, serotonin AET, strychnine, etc/ on animals subjected to centrifugation, for application to astronauts 12 p1902 A67-25654
 Hermetically sealed semiconductor device tested for leaks with xenon 133 gas, determining radiation safety measures for personnel 14 p2324 A67-28280
 Cosmic radiation protection during manned space flight, considering use of radiation warning devices and protective drugs 16 p2612 A67-30901
 Radiation protection during space flights, describing dangerous aspects of solar cosmic rays and earth radiation belt 16 p2738 A67-31197
 Radioscopy for testing cast-steel parts, welding seams, etc, noting radiation protection, radioscope video control and information storage 18 p3045 A67-33737
 Safety program for nuclear rocket engine testing, discussing role of cryogenics 20 p3482 A67-36565
 Space electronic equipment design, considering incorporation of vibration, vacuum, micrometeoroid and radiation protection 21 p3591 A67-38209
 Monte Carlo method to determine derivatives of radiation doses in optimization of shape and composition of protective shields 21 p3577 A67-38425
 Radiation protection from cosmic rays during space flights, considering shielding, observation and warning, dosimetry and medical provisions 22 p3754 A67-39286
 Toxicity of radioprotective amino ethyl isothiolium bromide from animal studies

noting hazardous effects in human organism 22 p3753 A67-40546
 Laser experiment safety procedures for protection of personnel and persons not involved in laser work 23 p4015 A67-41054
 Sulfhydrylamine drugs effect for protection in rats exposed to high, low, sublethal, lethal and supralethal dose of X and gamma radiation 23 p3958 A67-41648
 Protective effect of substrates against ionizing radiation on enolase and lactic dehydrogenase [SAM-TR-66-264] 24 p4111 A67-41841

RADIATION PYROMETER
 Radiation techniques for surface temperature measurement, considering optical and radiation pyrometers, projection thermography and photographic techniques 01 p0062 A67-10274
 Polarized pyrometric probe applied to hot and dense plasmas, ascertaining particle energies and densities 11 p1789 A67-24410

RADIATION RESISTANCE
 Radiation resistance of silicon photoconverters onboard Elektron III satellite, noting protective coating 02 p0240 A67-11543
 High speed magnetic logic circuits for operation in nuclear radiation environment 02 p0219 A67-12161
 Lithium interaction with radium induced damage in silicon solar cells to produce center preserving minority carrier lifetime 04 p0556 A67-15703
 Structure of radiation resisted hypersonic shock in simple dissociating gas examined via quasi-equilibrium field for radiation field 06 p0993 A67-18893
 Spectral densities of electromagnetic fields of thermal radiation in magnetoplasma as related to radiation resistance of immersed antenna 09 p1464 A67-22448
 Potato radiation resistivity improvement in conditions of anoxia 13 p2058 A67-26755
 Antenna in interplanetary plasma, noting fluctuation noise in exosphere and radiation impedance when exposed to solar wind 14 p2279 A67-27856
 Current strip in cold magnetoplasma, noting radiation resistance of Hertzian dipole for large frequency ranges 15 p2521 A67-29185
 Mouse, rat and dog organism reaction to ionizing radiation, vibration and acceleration 16 p2611 A67-30765
 Radiation resistance of silicon photoconverters onboard Elektron III satellite, noting protective coating 16 p2677 A67-31609
 Silicon solar cells impurities, radiation resistance, fabrication, nonsilicon materials, development, etc 18 p2989 A67-34069
 Annealing under continuous irradiation in p-on-n silicon solar cells with lithium diffused in N region 19 p3306 A67-35671
 Temperature resistant aromatic ordered copolyamide fibers, obtaining tensile properties and radiation resistance 21 p3647 A67-37871
 Design procedure for production of radiation resistant NOR gate logic circuit 21 p3803 A67-38185
 Silicon semiconductor alpha particle detector for spectrometry, noting radiation resistance for low energy proton bombardment 21 p3628 A67-38596
 Silicon solar cells bombarded by energetic electrons for radiation resistance 21 p3571 A67-38648
 Total extraterrestrial and global solar radiation intensity and spectral distribution for designing radiation resistant satellites 22 p3874 A67-40031
 Li behavior in self-healing radiation resistant Si solar cells 23 p3941 A67-41522
 Li doped Si solar cell radiation resistance to high energy electrons, noting fabrication methods and annealing behavior differences 23 p3941 A67-41527
 Li doped p-plus/n solar cells optimum design and radiation resistance, noting concentration and room temperature annealing conditions 23 p3942 A67-41528
 Radiation resistance and reactance of thin film inductor in microwave integrated circuit determined using Fourier transform 24 p4128 A67-41924
 Radiation resistant silicon diode fast neutron monitors, discussing fission spectra and leakage currents in damaged diodes 24 p4183 A67-42473

Aerospace system power conditioning design optimization, treating efficiency, regulation, EMI, BITE, primary power, size, weight, radiation hardening and cost [AIAA PAPER 67-965] 24 p4110 A67-43057

RADIATION SHIELDING
 SA HEAT SHIELD
 SA SOLAR RADIATION SHIELD
 SA SPACECRAFT SHIELDING
 Radiation types encountered and shielding used by Voskhod I and II manned spacecraft 02 p0308 A67-12321
 Analogous studies of simultaneous conductive and radiative heat transfer across transparent laminar gas space, showing position of radiation shield between bounding surfaces 03 p0535 A67-13464
 Protective shielding for astronauts from ionizing radiation from solar and galactic cosmic rays and radiation belts 03 p0365 A67-13539
 Radionuclide production in lunar surface activated by solar proton with reference to radiation shielding and reflection 05 p0885 A67-17386
 Neutron exposure ages of meteorites, estimating amount of shielding which surrounds samples in space from Co-60 and Ar-39 activity data 06 p1082 A67-17871
 Lunar resources discussing exploitation methods for various forms of resources available 06 p1092 A67-19029
 Safety program for laser hazards, discussing eye and body protection 07 p1194 A67-19089
 Sensitivity of manned planetary spacecraft design to shield weight, onboard radiation and uncertainties in space environment radiation 07 p1258 A67-19376
 Invariant imbedding method applied to energy dependent neutron radiation penetration problems in thick and heterogeneous shields 11 p1817 A67-25063
 Shielding methods for electronic equipment packaging, considering magnetic, electromagnetic and RFI shielding in gamma and X-ray range 12 p1911 A67-25267
 Reduction of radiation effect on thermocouple in thermal vacuum testing by using fiberglass tape with aluminized mylar backing 12 p1943 A67-25695
 Radiation damage to satellite solar cells when shielded to various degrees, stressing silicon junction cells 17 p2804 A67-32840
 Monte Carlo method to determine derivatives of radiation doses in optimization of shape and composition of protective shields 21 p3577 A67-38425
 Radiation protection from cosmic rays during space flights, considering shielding, observation and warning, dosimetry and medical provisions 22 p3754 A67-39286
 Multiple-reflective metal foil structure with separating matrix transient thermal response, determining number of radiation shields for given thermal protection 22 p3919 A67-40115
 Shield-radiator weight tradeoffs to optimize K Rankine cycle space power plant heat source operating temperature, noting burnup 24 p4185 A67-42537
 SNAP-8 type reactors and shield subsystems for MORL and manned lunar base plants, discussing Rankine and thermoelectric power conversion systems 24 p4186 A67-42546
 Design integration of reactor, shielding and power conversion systems for manned earth orbital station 24 p4186 A67-42547

RADIATION SOURCE
 SA POINT SOURCE
 Radioisotope sources used for simulating space radiations, obtaining energy spectra by blending beta emitters 02 p0265 A67-12213
 Temperature stability of several types of modulated radiation sources employing GaAs diodes, examining current change with temperature change 03 p0388 A67-14271
 Possible models for X-ray source SCO-X-1, discussing conditions of gravitational confinement 04 p0694 A67-14484
 Calculation method for energetic photoelectric photometry system for tracing behind radiative source or for distance measurement 08 p1331 A67-21055
 Modified differential approximation for external radiation sources in radiation gas dynamics 10 p1733 A67-23113
 Optimum antenna aperture distribution for finite line source and desired radiation pattern with given superdirective ratio

upper boundary 11 p1768 A67-24943
Circular and rectangular radiation sources of large extent described by means of radiometric antennas 12 p1913 A67-25306
High directional gap antenna, considering radiation sources of equal energy located on concentric rings 12 p1914 A67-25311
Precise position and spectra of Scorpio X-ray source and location of two weaker sources in galactic plane, describing instrumentation used 12 p1995 A67-25761
Sco XR-1 source model corresponding to neutron star in state of accretion as possible explanation of X-ray emission power from source 13 p2189 A67-26262
X-ray source in Crab Nebula size and position, showing visible light distribution having common center within 15-inch precision of measurement and finite angular extent 13 p2189 A67-26263
Radioactive isotopes from cosmic ray action in atmosphere and nonatmospheric sources, discussing geophysical mixing and dispersion 14 p2380 A67-27967
Net polarization of celestial X-rays could lead to specification of source mechanism producing radiation 14 p2381 A67-28617
Temperature stability of several types of modulated radiation sources employing GaAs diodes, examining current change with temperature change 14 p2288 A67-28780
X-ray astronomy emphasizing interpretation of observational results and relationship to radio and optical astronomy and cosmic ray physics 15 p2551 A67-30224
Pseudo-isotropic radiation source as source with isotropic gain function and polarization depending on spatial direction 16 p2761 A67-30793
X-ray scanning of Cygnus region with large area proportional counters flown on attitude-controlled sounding rocket 17 p2937 A67-32648
Optical search of sky near X-ray positions of Cyg X-1 and Cyg X-2 for identification purposes 17 p2937 A67-32649
Strong X-ray source in vicinity of constellation Crux compared to SCO xr-1, findings suggest similar physical nature 17 p2937 A67-32761
Pinch radiation in quartz discharge chamber spectrographically studied for use as sources of short pulsed radiation with continuous spectrum 17 p2904 A67-32919
Compact black body source utilizing thermoelectric heat pumping for uniform and stable temperature control 17 p2862 A67-33288
Cloud-ion chamber stack to measure properties of interactions in light materials of high energy cosmic ray protons and pions 17 p2863 A67-33355
Flash X-ray source penetrates thick objects and records shadowgraphs directly on film 18 p3052 A67-34531
Secular behavior of optical properties of X-ray emitting object near Cygnus X-2 19 p3331 A67-36084
Cosmic radiation origin shown
Inconceivable in radio galaxies 19 p3316 A67-36088
Differentiation between gravitational and cosmological components of quasars red shift by observational means 20 p3521 A67-36295
Critical comments on Shklovsky model for newly identified X-ray source Sco XR-1 20 p3527 A67-37394
Cosmic X-ray sources in 20-180 kev energy range detected in balloon flights, giving energy spectra 20 p3520 A67-37475
Calculation method for energetic photoelectric photometry system for tracing behind radiative source or for distance measurement 22 p3797 A67-39417
Coherent optics technology, presenting effective black body temperature of six radiation sources and output and pulse duration of four laser sources 22 p3817 A67-40351
Integral equation derived to relate source function for spectral line formed by noncoherent resonance scattering to thermodynamics of radiating medium 22 p3896 A67-40529
Numerical results for source distribution estimation from external radiation field measurements, investigating transport processes in slab bounded by parallel planes 23 p4082 A67-40993

RADIATION SPECTRUM

Temperature dependence of spectral distribution of radiation, excitation and quantum output of green luminescence of cadmium sulfide films 03 p0433 A67-12889
Statistical effects during generation of second harmonic in optically transparent crystals, noting coefficient of correlation between harmonic and fundamental radiation power of solid state laser 03 p0467 A67-12928
High resolution equilibrium radiation spectra for shock layer of blunt bodies at reentry velocities and radiative recombination of N and O ions [AIAA PAPER 66-104] 04 p0546 A67-14816
Spectral characteristics of long term change of cosmic ray intensity during 1963-65 compared with Forbush decrease of September 1963 04 p0692 A67-14880
Solar corona and chromosphere activity observations at lunar observatory in gamma, X-ray and XUV regions 04 p0598 A67-15071
Recombination radiation from Ga-Sb p-n junctions, noting spectral composition as function of current density and impurity concentration 04 p0681 A67-15297
High cloud surface effect on satellite measurements of radiation temperature of stratosphere 05 p0802 A67-17376
Analogy between radiation angular spectrum reflected from rough surface and frequency spectrum of carrier burst related to radio propagation 06 p0957 A67-17579
Dynamics of narrowing effect of surface and spatial dispersing agents on radiation line of ruby laser with nonresonance feedback 06 p1012 A67-18797
Sum radiation frequency generation by ruby and neodymium lasers in KDP crystals 07 p1196 A67-19734
High energy solar cosmic ray spectrum during solar flare of February 23, 1956 07 p1243 A67-19805
Interference problems caused by spurious radio transmissions, analyzing radiation spectrum utilization 08 p1301 A67-20773
Angular and frequency spectra of Cerenkov and cyclotron radiation from charged particle spiraling in cold magnetoplasma determined by Fourier transform method 09 p1562 A67-22228
Heat radiation spectra of earth as measured by Cosmos satellites, comparing experimental and calculated results 10 p1637 A67-23194
Rocketborne photometer data analysis of night sky airglow and spectrum in 6300 angstrom region 11 p1786 A67-24072
Radiation characteristics for slotted cylinder covered with magnetized inhomogeneous plasma sheath assuming parabolic electron density distribution 11 p1753 A67-24306
Combination scatter of electromagnetic waves by ion-acoustic oscillations in flat confined plasma layer with zero plasma density outside 12 p1974 A67-25447
Recombination radiation spectra of InAs with different current carrier concentrations in initial material and different current densities 12 p1914 A67-25516
Charge spectrum of heavy cosmic ions of iron group in ionographic emulsions exposed in satellite 12 p1999 A67-25829
GaAs gas bombarded by fast electrons investigated for recombination radiation spectra, noting shift of edge emission maximum toward longer wavelengths 13 p2173 A67-26359
Multilaircraft measurements of cosmic ray spectrum and geomagnetic cut-off rigidity 13 p2193 A67-27246
Interaction between oppositely moving traveling waves in helium-neon laser with annular resonator 14 p2332 A67-28856
Model stellar atmosphere computations predict emergent radiation spectrum 14 p2392 A67-28993
Radiation by charged particle moving in spiral line between two adjacent dielectric surfaces, deriving equations for spectral density of radiation 15 p2520 A67-29714
Radiation spectra of plasma jets from IR to UV, determining electron density and argon excitation temperature, noting bremsstrahlung 17 p2893 A67-32144
Radiation from two optically coupled cavities of compound laser identical in time and spectral composition without tuning one cavity to other 17 p2868 A67-32661

Synchrotron radiation spectrum of self-absorbed radio sources for various electron distributions 17 p2947 A67-32755
Time dependent self-compressed pinch-discharge radiation characteristics in various gases analyzed photographically for luminescence distribution, spectral composition, etc 17 p2904 A67-32918
Pinch radiation in quartz discharge chamber spectrographically studied for use as sources of short pulsed radiation with continuous spectrum 17 p2904 A67-32919
Darkness of clouds of upper and middle levels in various spectral intervals and in thermal spectrum range 18 p3073 A67-33560
Spectral and recombination radiation intensity changes from indium phosphide diode under different uniaxial compressions 18 p3100 A67-33718
Radiation peak formation mechanism in spectral lines of nonequilibrium gas following passage of shock wave 18 p3083 A67-34060
Dynamics of narrowing effect of surface and spatial dispersing agents on radiation line of ruby laser with nonresonance feedback 18 p3061 A67-34416
Recombination radiation spectra of InAs with different current carrier concentrations in initial material and different current densities 18 p3012 A67-34447
Neodymium glass laser radiation investigation, using moving active body method, for spatial inhomogeneity of mode field in spectrum random structure 19 p3238 A67-34895
Interaction between oppositely moving traveling waves in helium-neon laser with annular resonator 19 p3242 A67-36107
Absorption spectra, spectral dependence of luminescence quantum output, glow curves and radiation spectra of color centers in ruby crystal 20 p3506 A67-36223
GaAs gas bombarded by fast electrons investigated for recombination radiation spectra, noting shift of edge emission maximum toward longer wavelengths 21 p3680 A67-38316
Combination scatter of electromagnetic waves by ion-acoustic oscillations in flat confined plasma layer with zero plasma density outside combination scatter of electromagnetic waves by ion-acoustic oscillations in flat confined plasma 21 p3674 A67-38821
Time dependency, anisotropy, propagation and spectral properties of cosmic radiation released by solar flares during sunspot activity 22 p3871 A67-39796
Venus radiation spectrum in mm range from Venus atmosphere models 22 p3886 A67-40120
Cosmic ray intensity 27 day variations during low and high solar activity periods noting lower amplitude and softer spectrum 23 p4056 A67-41108
High energy cosmic ray muon integral angular and integral spectrum below earth surface 24 p4222 A67-42877

RADIATION TOLERANCE

High energy electron bombardment of MIS capacitor with subsequent positive charge introduction into insulator investigated by C-V and G-V measurements 04 p0588 A67-15712
Hardening monolithic integrated circuits to transient ionizing radiation by controlling photocurrent and by evaluating fabrication processes 04 p0590 A67-15722
Terrestrial microorganisms survival in space, noting inactivation effect by solar radiation 19 p3178 A67-35221

RADIATION TRANSFER

Airborne double bolometer technique for deriving atmospheric water vapor profiles by solving radiative transfer equations 01 p0108 A67-10315
Intensity distribution of earth surface as seen at various altitudes above atmosphere due to Rayleigh scattering and diffused reflection from earth surface [AIAA PAPER 65-666] 03 p0411 A67-13046
Nondiffusive radiation transfer and ionization equilibrium of impurity in plasma 03 p0483 A67-13837
Fluid dynamic sources of radiation during atmospheric entry, considering equilibrium and nonequilibrium radiation, thermal radiation and relaxation processes in hypersonic flow 04 p0703 A67-14703
Radiation transfer effect on equilibrium temperature for laminar boundary layer flow

of absorbing-emitting gas over flat plate
[ASME PAPER 66-WA/HT-48]

04 p0739 A67-15940
Radiative transfer in inhomogeneous medium derived on basis of continuity equation for radiative energy density in coordinate space and group velocity space
05 p0761 A67-16340
Geometric model of radiative atmospheric space used in research on mean radiation temperature of space by
06 p1025 A67-17637
Nonlinear three-dimensional radiative transfer solved by method of self-consistent optical depths
07 p1248 A67-19485
Unsteady energy transfer in gray radiating gas during expansion at atmospheric pressure for arbitrary optical radius
08 p1323 A67-21391
Scattered particle intensity inside and outside finite medium determined from Maxwell and Schroedinger equations
09 p1531 A67-21631
General algorithm for solving atmospheric optics problem applicable to short wave radiation transfers of atmospheres with various light scattering, using Monte Carlo method
13 p2151 A67-26684
Nondiffusive radiation transfer and ionization equilibrium of impurity in plasma
13 p2172 A67-27716
Behavior at infinity of specific intensity in plane-parallel atmosphere
14 p2391 A67-28946
Radiation transport in spectral lines as photon absorptions and emissions, discussing contemporary theories, approximation methods and applications
17 p2893 A67-32143
Composition, heat conduction and radiative energy transfer characteristics of hydrogen and argon plasmas produced by arc in cylindrical channel with cooled walls
17 p2897 A67-32172
Local electronic energy balance formulation, including radiative transport effect in nonuniform seeded plasma, described by two-temperature model
17 p2906 A67-33010
Radiative transfer for electron scattering atmosphere, obtaining eigenfunctions of transport equations
17 p2950 A67-33164
Optical radiation emission from rocket exhaust plumes, noting dependence on aerothermochemical properties, considering radiative transfer
18 p3152 A67-33821
Thermal perturbations on fused silica primary mirror in orbiting space telescope, with numerical analysis of radiation transfer in telescope tube
18 p3046 A67-33880
Radiative transfer in heterogeneous scattering medium with Fresnel reflection at slab boundary interface, computing transmittance, reflectance and absorbance
[ASME PAPER 67-HT-19] 20 p3545 A67-36714
Atmospheric optics and radiation transfer covering sky brightness, solar insulation, earth radiance and albedo, etc
20 p3430 A67-36899
General algorithm for solving atmospheric optics problem applicable to short wave radiation transfers of atmospheres with various light scattering, using Monte Carlo method
21 p3618 A67-38428
Nonself-similar energy diffusion of thermal radiation front for plane parallel geometry, giving series and parametric solutions
23 p4081 A67-40887
Nonlinear radiation transport problem solution by reduction to linear, considering light resonant scattering in approximation of complete frequency mixing
23 p4051 A67-40909
Numerical results for source distribution estimation from external radiation field measurements, investigating transport processes in slab bounded by parallel planes
23 p4082 A67-40993
Statistical radiative transfer in turbulent atmosphere underlying region
23 p4068 A67-41281
Radiometer using black plate with radiation toward night sky balanced by IR radiation transfer in vacuum system
24 p4152 A67-41787
Light reflection and transmission by thick optical atmosphere according to phase function
24 p4147 A67-41819
Absorption of black body radiation by horizontal atmospheric layer, deriving expression of integral coefficient of atmospheric transparency
24 p4255 A67-42590

RADIATIVE HEAT TRANSFER

Book on radiative heat transfer between surfaces and participating media
01 p0166 A67-10378
Convective and radiative heat transfer in shock layer of hypersonic blunt body, noting asymptotic behavior of Navier-Stokes equation and energy transfer
01 p0188 A67-11421
Radiative energy loss from solar chromosphere and corona estimated in order to identify mechanical energy input mechanism
02 p0323 A67-11692
Spectral distribution of net radiance at boundary of nonisothermal gas applied to water vapor band
02 p0342 A67-12051
Thermal testing of critical systems module of meteoroid detection satellite without attaching sensor arrays
02 p0334 A67-12378
Radiant equilibrium temperature of opaque absorbing body relation to radiative temperature variations of
02 p0343 A67-12646
Radiant heat transfer from nongray surfaces with external radiation
[AIAA PAPER 66-21] 03 p0533 A67-13043
Perturbation solutions in differential analysis of radiation interactions with conduction and convection
03 p0378 A67-13288
Analogous studies of simultaneous conductive and radiative heat transfer across transparent laminar gas space, showing position of radiation shield between bounding surfaces
03 p0535 A67-13464
Radiative modes of thin infinitely long circular plasma cylinder with dipolar azimuthal field variations
03 p0484 A67-14044
Separating composite heat transfer into radiative and convective components
04 p0722 A67-14715
Temperature dependent thermal property models of lunar surface and radiative energy transport deduced from RF and IR observations
04 p0697 A67-14740
Linearized Couette flow problem in rarefied gas solved, using one-dimensional radiative heat transfer analogy
04 p0606 A67-15183
Radiative type heat shields using backface cooling in analysis, including thermal effects and structural heat short effects
[AIAA PAPER 66-507] 04 p0711 A67-15252
Polarization and directional variation effect on radiant heat transfer through long specular reflecting passages
[ASME PAPER 66-WA/HT-32] 04 p0725 A67-15440
Idempotent method solution of transport equations for radiative heat transfer in nonisothermal anisotropic scattering medium between two parallel plates
[ASME PAPER 66-WA/HT-28] 04 p0725 A67-15441
Radiative heat transfer and intensity distribution in one-dimensional absorbing isotropic scattering medium
04 p0737 A67-15862
Uniform flow of very high temperature radiating gas over semiinfinite flat plate
04 p0737 A67-15863
Equilibrium temperatures of mass transfer cooled walls in high speed flow of absorbing-emitting gas
04 p0737 A67-15864
Heat transfer to laminar flow of radiation absorbing-emitting fluid across isothermal plate
04 p0737 A67-15866
Transient temperature in slab insulated on one face and subjected to nonlinear thermal transfer at other face studied by perturbation technique
04 p0737 A67-15867
Interaction between radiation and conduction and resultant total heat flux increase in plane layer studied by differential method
04 p0738 A67-15868
Radiative heat exchange between specularly reflecting surfaces with direction dependent properties
04 p0738 A67-15869
Radiative heat transfer through openings of variable cross section, discussing temperature distribution and numerical results of right circular cone
04 p0738 A67-15870
Thermal design of Isis A spacecraft, noting possibility of passive thermal control and computer programmed multinode heat balance analysis
05 p0904 A67-16294
Convective and radiative heat transfers at stagnation point of hemisphere cylinder model immersed in high enthalpy partially ionized supersonic flow in plasma wind

tunnel
05 p0747 A67-16432
Convective and radiative heat transfer to reentry vehicles at superorbital velocities
[AIAA PAPER 66-106] 05 p0928 A67-17336
Velocity and temperature profiles of optically thick planar Couette flow, obtaining heat transfer rates for Rosseland mean absorption coefficient variation with temperature
05 p0793 A67-17343
Plane flow of radiating gas over semiinfinite flat plate, considering upstream effect when energy equation becomes elliptical
05 p0928 A67-17358
Time-independent radiative transfer through circular cylindrical medium, using numerical methods
06 p1111 A67-17874
Differential approximation applied to radiative transfer in various geometric configurations
06 p1113 A67-18116
Radiative heat exchange and equilibrium surface temperature in space environment
[AIAA PAPER 67-212] 06 p1115 A67-18328
Matrix equations approximating integral equations of radiative energy transfer
06 p1118 A67-18551
Radiation transport theory and spatial radiative heat transfer in absorbing and isotropically scattering medium
06 p1118 A67-18552
Temperature field of elements of thin shelled surfaces of satellites for radiant heat transfer
07 p1265 A67-19104
Inviscid hypersonic flow of radiating gray gas over sphere analyzed, noting temperature role in process
08 p1276 A67-20567
Rayleigh problem of compressible viscous heat-conducting radiating gray gas flow near flat plate set impulsively in motion in own plane
08 p1324 A67-21392
Analytical solution for determining inlet and outlet temperature for space radiator with heat rejection rate for steady state conditions and zero irradiation environment
08 p1429 A67-21511
Radiative heat transfer in interior of combustion chambers of solid propellant rockets
09 p1561 A67-22567
High speed photography of laser radiation damage to transparent materials and analysis of destruction mechanisms involved
09 p1516 A67-22660
Quasi-stationary regime during radiative-convective heating of infinite plate and cylinder, noting time dependent temperature variation
10 p1732 A67-23020
Optimal parameters of refrigerators with radiative regenerative gas cycle
10 p1596 A67-23022
Modified differential approximation for external radiation sources in radiation gas dynamics
10 p1733 A67-23113
Heat radiative flux divergences and equilibrium temperature distribution with altitude calculated for heat regime modeling radiative transfer conditions in stratosphere and mesosphere
10 p1647 A67-23275
Asymptotic analysis of radiative Rayleigh problem in flow of compressible viscous heat-conducting radiating gray gas extended to high plate Mach numbers
11 p1774 A67-23855
Transient radiative heat exchange on moon surface observed in 8 to 2 micron band during lunar eclipse, using model for quantitative comparisons transient radiative heat exchange on moon surface observed in 8 to 12 micron band during lunar
11 p1865 A67-24604
Radiation MGD, considering flow problems with thermal radiation and electromagnetic field effect
12 p1975 A67-25889
Heat transfer through various silicate powders measured for lunar surface temperature studies, comparing theoretical results
[AIAA PAPER 67-285] 12 p2035 A67-26002
Integral equations for radiative heat transfer inside solid whose solution leads to temperature-distance profile integral equations solution for radiative heat transfer inside solid leads to temperature-
[AIAA PAPER 67-287] 12 p2035 A67-26004
Closed form solution for determining total emissivity of metals and radiation conductivity of radiation shield for nongray metallic surfaces at low temperature
[AIAA PAPER 67-335] 12 p2038 A67-26049
Asymptotic and numerical solutions of Goulard integrodifferential equation describing hypersonic flow near stagnation

point past blunt bodies, allowing for radiative transfer effects 14 p2296 A67-27981

Radiative heat exchange between surfaces of telescoped cylinders, determining angular radiation coefficients 14 p2406 A67-28308

Two-way radiative heat transfer between surfaces and volumes of two bodies 14 p2406 A67-28309

Steady heat transfer through rib-reinforced wall of material with variable coefficient 14 p2407 A67-28646

Polarization and directional variation effect on radiant heat transfer through long specular reflecting passages [ASME PAPER 66-WA/HT-32] 15 p2579 A67-29319

Simulation of nonlinear radiant heat transfer for constant emitting heat source by circuit, using semiconductor and pentode 15 p2579 A67-29323

Equilibrium radiant heat transfer to bodies at hypersonic velocities in carbon dioxide atmosphere noting shock layer, shock standoff distance, shock velocity, etc 15 p2582 A67-30216

Mean absorption coefficient for optically thin plasma derived taking into account radiative losses, noting electron and ion temperature ratios 16 p2706 A67-30459

Equilibrium radiative transport properties of high temperature air coupled with aerodynamic flow field generated by planetary reentry vehicles 16 p2589 A67-30721

Structure of strong shock wave studied for simple models of nongray radiative transfer 16 p2658 A67-30938

Interaction of convection and radiation heat transfer in axisymmetric two-dimensional stagnation point low-speed flow of gray absorbing and emitting gas 16 p2591 A67-30939

Flow field and heat transfer in radiating stagnation-point shock layer of atmospheric-entry vehicles 16 p2591 A67-30940

Unsteady heat transfer due to radiation of two opaque bodies of finite dimensions, solving nonlinear Volterra integral equation with respect to net radiation 16 p2779 A67-31208

Sokolov method of averaging functional corrections for treatment of radiant interchange between surfaces 17 p2967 A67-32068

Neutron transport and radiative transfer analysis via generating function technique, confining analysis to one energy model 17 p2876 A67-32557

Radiative relaxation times for temperature perturbations in CO₂ with small water vapor admixture under conditions similar to Martian atmosphere, discussing dynamical phenomena 17 p2951 A67-33187

Propulsion-oriented subsonic boundary layer combustion research, discussing turbulent and diffusion-limited conditions, radiant heat transfer, chemical kinetics and transient phenomena 18 p3150 A67-33800

Radiative heating of H and He containing suspension of solid particle absorbers, noting proportionality between gas particle dispersion decrease and energy absorption [AIAA PAPER 67-501] 18 p3158 A67-33965

Atmospheric properties at high temperature, discussing atmosphere radiation influence on flow around reentry device and radiative heat transfer 18 p3159 A67-34126

Confined electric arc developed for gas-transport properties determination, noting measurement of flow pressure drop, radiative heat transfer, spectral temperature distribution, etc 18 p3091 A67-34731

Atmospheric heating due to radiative heat transfer of direct and earth-reflected solar rays calculated as function of moisture content 19 p3251 A67-34851

Atmospheric radiation balance studies via daytime balloon measurements, obtaining vertical profile curves for albedos, total and reflected radiation, etc 19 p3214 A67-34853

Atmospheric spectra and related quantities calculated, obtaining radiation spectral distribution by radiative transfer equation, comparing results with other studies 19 p3220 A67-35260

Adiabatic pulsations of inhomogeneous gaseous mass consisting of convective core and radiative envelope 19 p3261 A67-35502

Approximate method of solving integral equations of local radiation characteristics applied to numerical solution of specific problems of radiative heat

transfer 19 p3347 A67-35898

Radiant heat transfer computations from gray isothermal dispersions with isotropic scattering, using approximation methods and integrodifferential equation [ASME PAPER 67-HT-8] 20 p3544 A67-36706

Role of Rosseland approximation in convection-radiation interaction, considering flow of gray gas in laminar boundary layer [ASME PAPER 67-HT-9] 20 p3545 A67-36707

Iterative solution for directional emissivities of two-dimensional semiinfinite slab of absorbing-scattering medium with gray isothermal dispersion [ASME PAPER 67-HT-12] 20 p3545 A67-36710

Steady state heat transfer by simultaneous conduction and radiation through spherical shell [ASME PAPER 67-HT-20] 20 p3546 A67-36715

Radiative heat flux for free burning methanol and acetone flames of arbitrary size and geometry predicted, using transport equation [ASME PAPER 67-HT-47] 20 p3547 A67-36729

Spacecraft package temperature control by interior louver panel system, calculating net heat transfer [ASME PAPER 67-HT-64] 20 p3549 A67-36746

Transient temperature distribution of cylinder subject to radiation cooling, giving dimensionless computer-derived graphs [ASME PAPER 67-HT-71] 20 p3550 A67-36751

Steady state and transient temperature profiles for straight fins of trapezoidal profile with radiative heat transfer [ASME PAPER 67-HT-73] 20 p3550 A67-36753

Theoretical prediction of temperature profiles within heated cylinder and on surface to determine thermal conductivities at high temperature [AICHE PAPER 16] 20 p3552 A67-36829

Absorption coefficient of radiative transfer equation and high temperature air opacity 20 p3485 A67-36930

Heat transfer of gas between parallel plates including radiation and rarefaction effects treated, using kinetic theory 20 p3553 A67-36935

Volumetric absorption coefficient effect on Rosseland equilibrium radiative heat transfer and temperature profiles in optically thick fluid flowing past flat plate 20 p3553 A67-36936

Radiative heat transfer in nonisothermal nongray gas model, measuring absorption and emission in carbon dioxide and water gases [ASME PAPER 66-WA/HT-25] 20 p3555 A67-37607

Radiative flux and flux divergence for hot gas, considering spectral frequency, gas volume and spectral variation 21 p3730 A67-37825

Shock tube measurements of end-wall radiative heat transfer behind reflected shock waves in air, stressing radiative cooling and self-absorption effects [AIAA PAPER 67-695] 21 p3732 A67-38724

Radiation heat transfer by flames to wire temperature sensor corrected by technique combining radiative input and catalytic activity 21 p3733 A67-38883

Radiative heat loss effect on steady axisymmetric hypersonic flow past blunt body using gray gas approximation, with numerical solution for stagnation region 22 p3739 A67-39530

Radiative cooling and self-absorption effects on reflected shock flow field and end wall heat transfer studied using finite difference method 22 p3917 A67-39710

Radiative transfer in lunar surface diurnal heat flow, studying geometric model of porous medium 22 p3885 A67-39980

Carbon dioxide and water vapor band emissivities determination, discussing spectral absorption, radiative heat transfer and energy distribution 22 p3918 A67-40042

Higher lunar radio temperatures than IR measurements using temperature dependence of radiant energy transfer, considering thermal conductivity of lunar materials 22 p3886 A67-40119

Attenuation of plane sinusoidal acoustic waves due to electromagnetic radiative properties of carbon dioxide and water vapor bands 22 p3829 A67-40232

Radiative and convective heat transfer between solid body and heat generating medium in motion, calculating thermal conductivity 23 p4083 A67-41289

Thin foil heat flux sensor for radiative and convective heating rates over wide range and dynamic response, noting error mechanisms, calibration and accuracy 23 p4006 A67-41374

Radiative heat transfer in radiating and conducting media, calculating heat flux and temperature distribution for semisotropic model 23 p4083 A67-41718

Radiative heat transfer for light reflection and transmission by optically thick scatterers with three-term phase function, obtaining asymptotic formulas 24 p4147 A67-41820

Integral equation derived from Boltzmann equation for one-dimensional radiative heat transfer in plane layers of gray media 24 p4252 A67-41934

Temperature variations of satellite with radiatively coupled isothermal inner shell having heat source analyzed via perturbation method for differential equations 24 p4253 A67-42051

Net convective and radiative heat flow to electrodes of coaxial plasma generator may exceed heat flow from moving arc spot within arc burning region 24 p4098 A67-42250

Zonal method of determining radiative heat transfer between gray particle cloud and surrounding gray walls of enclosing system 24 p4253 A67-42252

Heat pipe dynamics analyzed for thermionic converter heat pipe radiator design criteria, discussing working fluid selection 24 p4104 A67-42503

Gaseous nuclear rocket engine propulsion, reviewing fluid mechanics, radiant heat transfer, transparent walls, nuclear criticality, coaxial flow reactor, etc [AIAA PAPER 67-783] 24 p4187 A67-42948

RADIATIVE RECOMBINATION

Photoconductivity resonances and recombination radiation in PbTe and InSb due to multiple photon interband transitions between Landau levels in high intensity magnetic fields 02 p0254 A67-12522

Room temperature recombination radiation induced by Lorentz field in InSb and ternary alloy of mercury, cadmium and tellurium under cross field conditions 03 p0496 A67-13675

High resolution equilibrium radiation spectra for shock layer of blunt bodies at reentry velocities and radiative recombination of N and O ions [AIAA PAPER 66-104] 04 p0546 A67-14816

Emission spectra and I-V characteristics of diffusion p-n junctions in InP and spontaneous radiative recombination in presence of small current 04 p0679 A67-15138

Radiative recombination in space charge layer of p-n junction in silicon carbide determined from I-V characteristics and capacitance 04 p0681 A67-15298

Auger effect radiative recombination of excitons bound to neutral donors of GaP and Si and generation of luminescent spectrum C line 04 p0682 A67-15463

Minority carrier lifetime dependence on injection level, obtaining recombination center parameters for neutron irradiated germanium, using photoconductivity 04 p0684 A67-15692

Radiation intensity dependence for various spectral bands of diffused gallium arsenide p-n junctions on current density 05 p0861 A67-16391

Radiative interband recombination in strong electric field of p-n junction, calculating radiation intensity as function of quantum energy and applied voltage 05 p0863 A67-16689

Shallow donor introduction in p-type GaAs laser results in increased efficiency of radiative recombination 05 p0826 A67-17280

Interaction between two high resistivity layers in Mn doped GaAs separated by region of bulk material 06 p1051 A67-18222

Optical transitions at isoelectronic traps in GaP and ZnTe, presenting fluorescent spectra 06 p1062 A67-18929

Recombination radiation of p-n junctions in GaAs with and without Fabry-Perot cavity, discussing nonequilibrium current carrier kinetics and I-V characteristics 06 p1063 A67-18934

Gunn effect in GaAs caused by field induced transfer of electrons from high to low conduction band valleys 06 p1067 A67-18961

Oxygen photochemical equilibrium above

150 km, assuming dominant role of radiative recombination above 120 km 07 p1178 A67-19814

Recombination radiation from GaAs p-n junctions with and without Fabry-Perot resonator, noting parameter dependence on current density 08 p1337 A67-20413

Recombination through exciton states in semiconductors compared to interband radiative recombination 09 p1554 A67-21974

Band-to-band radiative recombination in semiconductor groups IV, VI and III-V, presenting data on diamond, Si, Ge, Se and Te 09 p1558 A67-22601

Dielectronic recombination effect in hot dilute plasmas extended to energetically overlapping metastable levels involving matrix inversion in formal description 10 p1681 A67-22722

Semiconductor lasers for discrete outputs in broad spectral range determined by material characteristics, noting electronic applications 10 p1688 A67-22824

Nocturnal decline of ionospheric airglow 6300 angstrom line intensity due to diatomic oxygen ion-electron recombination 10 p1649 A67-23294

Radiative recombination processes in GaAs p-n junctions, noting correlation between temperature behavior and carrier transport mechanism 10 p1693 A67-23523

Emission spectra and I-V characteristics of diffusion p-n junctions in InP and spontaneous radiative recombination in presence of small current 12 p1979 A67-25161

Band-to-band radiative recombination in compounds of gallium and indium with phosphorus, arsenic and antimony 12 p1979 A67-25177

Recombination radiation spectra of InAs with different current carrier concentrations in initial material and different current densities 12 p1914 A67-25516

Stabilization of clusters of galaxies by ionized gas studied for recombination radiation 12 p2011 A67-26250

Radiative recombination through free carriers and localized states in silicon single crystals containing gamma-induced defects 13 p2172 A67-26357

GaAs gas bombarded by fast electrons investigated for recombination radiation spectra, noting shift of edge emission maximum toward longer wavelengths 13 p2173 A67-26359

Experimental apparatus for study of impact ionization and associated recombination radiation in semiconductors 13 p2168 A67-27228

N-type germanium doped with antimony and arsenic investigated for radiation recombination, noting energy spectrum and forbidden band changes 14 p2368 A67-28533

Processes influencing radiative decay in compound semiconductors 15 p2536 A67-29634

Effect of single-axis compression on radiative impurity recombination in arsenic- and gadolinium-doped germanium 15 p2537 A67-29705

Digital computer methods for calculating impulsive relaxation in unbalanced hydrogen plasma 15 p2529 A67-29713

Radiative interband recombination in strong electric field of p-n junction, calculating radiation intensity as function of quantum energy and applied voltage 15 p2539 A67-29859

Particle energy distribution in low temperature nonequilibrium plasma in diffusion approximation description 16 p2720 A67-31386

Radiative recombination mechanisms in photoluminescence of n-type InP, discussing emission bands 16 p2732 A67-31450

Gas pressure dependence of attachment and recombination coefficients for thermalized electrons in air and oxygen 17 p2893 A67-32139

Recombination through exciton states in semiconductors compared to interband radiative recombination 17 p2923 A67-33311

Spectral and recombination radiation intensity changes from indium phosphide diode under different uniaxial compressions 18 p3100 A67-33718

Hydrogen emission lines photoelectric measures in Ton 1542 indicates radiative recombination in upper levels and sharp intensity increase in red ascribed to nonthermal sources 18 p3120 A67-33997

Recombination radiation spectra of InAs

with different current carrier concentrations in initial material and different current densities 18 p3012 A67-34447

Effect of dislocations in GaAs single crystals on diffused p-n junctions structure and recombination radiation parameters 19 p3300 A67-34768

Electron-ion radiative recombination influence on time-dependent luminous intensity of various spectrum lines in cesium vapor 20 p3488 A67-36436

Energy band pinch effect in laser-heated GaAs, studying temperature effect on radiative recombination 20 p3460 A67-37106

Electroluminescent diodes emission efficiency factor for application to lasers 21 p3591 A67-38153

Radiative recombination through free carriers and localized states in silicon single crystals containing gamma-induced defects 21 p3679 A67-38314

GaAs gas bombarded by fast electrons investigated for recombination radiation spectra, noting shift of edge emission maximum toward longer wavelengths 21 p3680 A67-38316

Radiative recombination processes involving neutral donors and acceptors in silicon and germanium, describing extrinsic luminescence bands 22 p3862 A67-39998

N-type germanium doped with antimony and arsenic investigated for radiation recombination, noting energy spectrum and forbidden band changes 23 p4040 A67-40940

Radiation intensity measurements in systems containing atomic oxygen and carbon monoxide by shock tube heating, deriving spectral intensity distribution for radiative combination 23 p4029 A67-40972

Effect of single-axis compression on radiative impurity recombination in arsenic- and gadolinium-doped germanium 24 p4199 A67-41775

Planetary nebulae IR emission intensities, discussing radiative recombination, ionization equilibrium and fine structure level population 24 p4223 A67-41811

Ionization fronts stability, finding no instabilities for strong D type fronts 24 p4224 A67-41816

RADIATOR

SA CONDENSER RADIATOR

SA HEAT REJECTION DEVICE

SA SPACE RADIATOR

SA SPACECRAFT RADIATOR

Cassegrain monopulse feed system using end-fire polyrod radiators 15 p2451 A67-29925

RADICAL

S FREE RADICAL

RADIO

Radio science, Part 1, Radio standards and measurements, troposphere, ionosphere, magnetosphere and noise of terrestrial origin - Conference, Munich, September 1966 14 p2262 A67-28388

Receiving directional antenna effect on magnitude of frequency correlation in fluctuations of received radio emission 16 p2640 A67-31497

RADIO ALTIMETER

Instrumentation development making it possible to land safely under poor visibility conditions, goal being zero-zero landing 14 p2347 A67-28990

Method to extend operation range of FM altimeters, with block diagram of proposed system 16 p2676 A67-31274

RADIO ANTENNA

SA RHOMBIC ANTENNA

Statistical communication theory of antenna response to complex partially polarized nonisotropic random radio wave processes 02 p0191 A67-11588

System design analysis of Edwards high range UHF telemetry receiving station network, considering reliability, availability, design adequacy, antennas, initial and operating costs, etc 02 p0229 A67-12007

Long wave spacecraft antenna design, deployment and stabilization, noting environmental effects such as thermal expansion, solar pressure, etc [AIAA PAPER 66-848] 02 p0221 A67-12258

Haystack antenna used for satellite communications and celestial observation, noting digital computer for control system and data processing 05 p0790 A67-17517

Elastic deformation due to structural weight sustained by 22-meter parabolic reflector of RT-22 radio telescope of

U.S.S.R. Physics Institute 08 p1424 A67-21354

Elastic strains created in parabolic reflector /radio telescope antenna/ mounted on four supports by weight of structure in vertical position 08 p1424 A67-21355

Spaced antenna reception by quadratic addition of signals providing efficient operation at various statistical characteristics of radio channel 10 p1607 A67-23447

New antenna techniques for Hertzian radiometric cartography 12 p1913 A67-25305

Circular and rectangular radiation sources of large extent described by means of radiometric antennas 12 p1913 A67-25306

Signal processing in antennas with coupling elements between circuit and space fields 14 p2285 A67-28450

Parallel operation of same frequency transmitters on common antenna examining several designs 16 p2637 A67-31003

Antenna resolution by data processing noting limitations due to noise 16 p2639 A67-31339

Effect of random amplitude errors of continuous apertures on radiation pattern and gain 16 p2627 A67-31353

Soviet book on radio telescopes covering design and construction principles, structural considerations, astronomical data, antennas, parabolic reflectors, etc 17 p2831 A67-31534

Elastic deformation due to structural weight sustained by 22-meter parabolic reflector of RT-22 radio telescope of U.S.S.R. Physics Institute 17 p2956 A67-31950

Elastic strains created in parabolic reflector /radio telescope antenna/ mounted on four supports by weight of structure in vertical position 17 p2956 A67-31951

Stationary or long range space vehicle transmitting antennas remote alignment technique using received signal AM 18 p3016 A67-34596

Satellite attitude by onboard radio antennas method 21 p3583 A67-38637

Impedance strip directional properties when excited through slot in metallic half-plane, noting case of reflector antenna with decreasing impedance 22 p3770 A67-39763

Equivalent noise temperature of antennas located on earth surface, discussing cosmic, tropospheric and man-made noise classification 23 p3980 A67-41043

Differential departure from thermodynamic equilibrium and electron temperature in gaseous nebulae determined by observing RF emission lines 24 p4225 A67-41825

Electric and magnetic field measurement by energy density antenna applicable to reducing signal fading encountered on mobile radio transmission path 24 p4131 A67-42340

RADIO ASTRONOMY

Possible lunar surface vacuum layer structure from effective thermoconductivity coefficient based on radioastronomical data 02 p0322 A67-11567

Total atmospheric attenuation measurement at 3.2 Ghz due primarily to nonresonance absorption of molecular oxygen 02 p0237 A67-11855

Radio astronomical observation technique, eliminating tropospheric radiation noise fluctuation effects on telescope 02 p0198 A67-12033

Quasars history, properties and nature 02 p0326 A67-12046

High resolution LF observations of time stationary discrete sources and background continuum distribution, using two satellites in interferometric mode [AIAA PAPER 66-886] 02 p0221 A67-12265

Microwave radiometry application to navigation, thermonuclear diagnostics, astronomical temperature measurements, etc 03 p0367 A67-12805

1414 mc/sec observations of Jupiter using radio telescope and crystal mixer receiver with linearly polarized rotating feed horn 03 p0411 A67-13166

Radio astronomical and satellite studies of atmosphere - USAF Symposium, Boston, October 1965 03 p0415 A67-14234

Instrumentation and research potentialities of lunar radio astronomy observatory 04 p0598 A67-15069

Interferometer with compensated phase fluctuation applicable over entire wavelength range used in radio astronomy 04 p0621 A67-15166

Meteor train drift observation, describing apparatus and data processing used by Kharkov Polytechnic Institute 05 p0889 A67-16208

Radio emission from Jupiter, Saturn and Mercury noting disk temperatures [AD-653438] 05 p0892 A67-16409

Luminosity of galactic disk in 12.8 micron radiation, obtaining from volume integral stellar photon flux density and thermal radio emission rate 05 p0892 A67-16412

Mariner Venus 1967 space probe, obtaining atmospheric pressure density and refractive index from radio signal frequency, intensity and phase changes [AIAA PAPER 67-118] 06 p1085 A67-18310

Relation between optical and radio properties of quasars 06 p1086 A67-18374

Radio pulse coincidence with extensive air showers, noting consistency with Cerenkov radiation and charge separation in terrestrial magnetic field 07 p1242 A67-19619

Quasar counting, red shift and brightness 07 p1249 A67-19661

Observations of sun at Stanford on May 20, 1966 at 9.1 cm after annular eclipse in Greece and Turkey 07 p1251 A67-19914

LF galactic emissions, noting spiral arms and spherical halo on galactic hub, signal strength variation and terrestrial atmosphere role 08 p1385 A67-20866

Radio astronomical measurements within partial coherence theory showing coherence function relation to spectrum, brightness distribution and statistical electromagnetic fields polarization 09 p1460 A67-21585

Power pattern synthesized as product of two individual patterns produced from single linear array, obtaining formula for array element weighting coefficients 09 p1470 A67-21590

Angular sizes of radio sources at 6, 11, and 21 cm wavelengths, using Mark II radio telescope of Jodrell Bank 09 p1565 A67-21980

Mixed single and double sideband interferometer receiving system having phase processing and delay simplicity and multiple RF return cable 11 p1764 A67-24308

Anisotropy of coarse ionospheric inhomogeneities determined from measurements of irregular radioastronomic refraction 11 p1787 A67-24464

Radar, radio astronomic and IR spectroscopic observations of Venus surface and atmosphere, examining general and surface data, chemical composition and atmospheric model construction 11 p1867 A67-24843

Parametric amplifiers of high gain stability for radio astronomy noting very low SNR and optimum noise temperature 12 p1912 A67-25298

Receiver-antenna system in radio astronomy, discussing low noise, thermal signal reception and acquisition of information limited by internal or external noise 12 p1914 A67-25309

Book on radioastronomical methods of antenna measurements covering physics of extraterrestrial sources and receiving equipment characteristics 12 p1915 A67-25842

OH emission regions investigated using Millstone and Haystack antennas with interferometer, noting radio sources for base-line calibration and instrumental phase monitoring 12 p2009 A67-25972

Radio astronomical investigations of 18 cm ground state lambda doublet transition of OH suggest maser amplification of radiation takes place in interstellar medium 13 p2198 A67-26715

Jupiter decametric radiation analyzed with interferometer for manifestations of solar wind effects 14 p2385 A67-28404

Radio science, Part 2, Radio astronomy, radio waves and circuits and radio electronics - Conference, Munich, September 1966 14 p2266 A67-28428

Earth atmosphere effect on propagation of radio waves from space, image formation, phase stability, technical problems and multiaperture instruments 14 p2285 A67-28437

Stability in electronic equipment 14 p2285 A67-28438

On-line computers in radio astronomy for measuring radio source flux, position and width and for increasing Dicke radiometer sensitivity 14 p2275 A67-28439

Flux density absolute calibration of solar radio emission 14 p2385 A67-28440

Radio spectrographs for solar observation,

broadband and fine structure spectrography techniques and logarithmic amplifiers in receiver 14 p2386 A67-28443

Low noise amplifiers in radio astronomy 14 p2286 A67-28466

Suggestion of physical association of radio sources with stars in neighborhood as radio stars 14 p2391 A67-28945

Linear polarization of lunar radio emission observed using radio telescope 15 p2552 A67-29149

Soviet book on radio physics /1965-1966/ reviewing radio-astronomical observations and radar probing of Venus 15 p2553 A67-29241

Interferometer with compensated phase fluctuation applicable over entire wavelength range used in radio astronomy 15 p2436 A67-29353

Hot model of universe supported by radioastronomical observations, estimating quark number density 15 p2555 A67-29640

Phase lock techniques applied to microwave antenna arrays noting problems, advantages, properties, etc 15 p2451 A67-29922

Cambridge /England/ one-mile radiotelescope for study of extragalactic radio sources, discussing two-dimensional antenna synthesis method 15 p2467 A67-30027

X-ray astronomy emphasizing interpretation of observational results and relationship to radio and optical astronomy and cosmic ray physics 15 p2551 A67-30224

Antenna resolution by data processing noting limitations due to noise 16 p2639 A67-31339

Correcting feed for Arecibo ionospheric Observatory reflector noting antenna gain 16 p2639 A67-31359

Book on solar radio exploration covering electromagnetic radiation discovery, solar physics principles, solar radio activity and research instruments description 16 p2755 A67-31923

Soviet book on radio telescopes covering design and construction principles, structural considerations, astronomical data, antennas, parabolic reflectors, etc 17 p2831 A67-31934

Book on radio astronomy covering history and fundamentals, wave propagation, radio sources, antennas and receivers, Boltzmann law, etc 17 p2943 A67-32432

Millimeter radiation from 3C 273 17 p2944 A67-32635

Radio and radar observations of Mercury, Venus and Mars 18 p3123 A67-34144

Sun effective disk temperature from measurement of solar radiation during May 1966 eclipse 18 p3125 A67-34195

Radio astronomy sensitivity and resolution, discussing aperture synthesis and interferometric techniques for accurate position determinations 18 p3135 A67-34585

Venus and Mars atmosphere and surface studied by radio astronomy 19 p3317 A67-34796

Atmospheric radiation absorption measurements by radio-astronomy methods at wavelengths from 1.8 to 0.87 mm 19 p3185 A67-36014

Soviet papers on wideband cross-shaped radio telescope and radio astronomy studies 20 p3402 A67-37504

Amplification factor stabilization or variance of transistorized radio astronomy receivers, discussing circuit diagram, performance and reliability 20 p3403 A67-37517

Hydroxyl radical emission, hypotheses attempting to explain OH emission origin, including possible maser mechanism and interstellar communications 21 p3704 A67-38567

Jupiter rotation variability used to understand internal physical processes, stressing variation of radio and Great Red Spot periods 21 p3710 A67-39002

Jupiter internal structure investigated by observing visible surface and radio emission, discussing magnetic field origin and hydrodynamics of fluid regions 21 p3710 A67-39003

Mariner Venus*1967 space probe, obtaining atmospheric pressure density and refractive index from radio signal frequency, intensity and phase changes [AIAA PAPER 67-118] 22 p3886 A67-40094

Higher lunar radio temperatures than IR measurements using temperature dependence of radiant energy transfer,

considering thermal conductivity of lunar materials 22 p3886 A67-40119

Very large array /VLA/ of radio telescopes designed based on Ryle aperture synthesis principle, consisting of parabolic antennas and used for radio maps 23 p3978 A67-40798

Lunar crater utilization as LF radio astronomy parabolic reflector, noting electromagnetic characteristics [AIAA PAPER 67-904] 24 p4125 A67-43012

Linear polarization of lunar radio emission observed using radio telescope 24 p4239 A67-43072

RADIO ASTRONOMY EXPLORER /RAE/ SATELLITE

Variable ratio DC transformer regulator used in voltage boost configuration of power system in Radio Astronomy Explorer /RAE/ spacecraft, noting RF interference reduction 08 p1284 A67-20692

RADIO ATTENUATION

Atmospheric radio wave absorption coefficient and altitude determined and linked to effects of colliding paramagnetic oxygen molecules 01 p0022 A67-10391

Rocket measurement of proton energy spectra and pitch angle distribution associated with auroral radio absorption, using solid state surface barrier detector 01 p0061 A67-11261

Frequency dependence of enhanced absorption of cosmic radio emission during abrupt ionospheric disturbance 02 p0307 A67-11676

Attenuation of radio waves from Taurus A in interplanetary space and in space about sun 03 p0368 A67-13278

Field intensity of ultrashort radio waves in superrefraction 03 p0368 A67-13280

Treatment of surface of directional radar antenna with RF absorption material for sidelobe reduction 03 p0389 A67-14349

Enhancement factor and true absorption of VHF cosmic radio noise associated with solar flares 05 p0884 A67-16929

Noise injection and coherent detection to extend RF attenuation measurement range of series IF substitution 09 p1495 A67-21623

Height distributions of enhanced lower ionospheric ionization estimated from cosmic radio noise absorption 10 p1634 A67-23059

Winter anomaly of nondeviative ionospheric absorption of radio waves and relation to diurnal, seasonal, local and solar cycle variations 10 p1646 A67-23267

Amplification processes in parametrically regenerated circuit with simultaneous complex variation of capacitance and attenuation 10 p1607 A67-23446

Rain effects at random antenna elevation 11 p1753 A67-24303

Radio measurements and standards for power, conductance, impedance and attenuation in upper frequency range 14 p2263 A67-28390

Frequency dependence of enhanced absorption of cosmic radio emission during abrupt ionospheric disturbance 16 p2738 A67-31091

Effect of random amplitude errors of continuous apertures on radiation pattern and gain 16 p2827 A67-31353

Rainfall associated with atmospheric convective activity estimated by radio ray attenuation model 21 p3582 A67-38577

Ionospheric discontinuity dimensions determined from satellite signal findings at 20 and 40 mc correlating amplitudes 21 p3621 A67-39021

RADIO AURORA

VHF backscatter observations of radio auroral radar echo occurrence at sunspot maximum associated with spirals in geomagnetic latitude and time, magnetic disturbance levels and season 03 p0513 A67-14113

Radio Aurora and formation mechanism of ionospheric D and F regions, examining HF and VLF propagation via computer ray tracing, ionospheric storms and equatorial sporadic E layers 05 p0795 A67-16010

Auroral particle precipitation, establishing latitude vs time pattern from gross statistical data on optical-and radio-auroral phenomena 17 p2850 A67-33191

Static electric fields produced in magnetosphere and effects such as motion of visual and radio aurora and currents in ionosphere 18 p3035 A67-33600

Venus surface temperature and microwave

emission, discussing ionospheric model, greenhouse effect, microdischarge model, radio aurora, etc 18 p3135 A67-34543

Auroral ionization echoes observed simultaneously by separated VHF radar noting aspect sensitivity, time variation, correlation with visible aurora, etc 22 p3760 A67-39624

RADIO BEACON

Earth-based radio reference signal in obtaining attitude and pointing information for synchronous communications satellites 02 p0331 A67-12151

Amplitude fluctuations of VHF beacon of Early Bird synchronous satellite observed from stations in Italy and Massachusetts 10 p1640 A67-23233

Ionospheric electron content measured using passage of transit IVA radio beacon satellite across view field of observing station 12 p1935 A67-25797

Three-dimensional multielement transponder array designed to give directional replies toward source of interrogating signals 13 p2071 A67-27404

Earth-based radio reference signal in obtaining attitude and pointing information for synchronous communications satellites 18 p3137 A67-34113

RADIO BLACKOUT

Automatic scanning receiver for interference-free recording of solar flare effects and polar blackouts, using cosmic noise method 05 p0883 A67-16799

Auroral radio blackout correlation with magnetic dip pole motion 07 p1173 A67-19669

Radio blackout extent from simplified calculation of average sheath power loss for typical Apollo reentry 15 p2434 A67-29168

Water injection for alleviating reentry plasma sheath-induced communication blackout, analyzing spherical drop evaporation in free molecular flow 19 p3211 A67-35762

Radio telemetry links perturbations during ballistic missile reentry due to plasma from kinetic heating 21 p3581 A67-38228

RADIO BURST**SA SOLAR RADIO BURST**

Solar flares, discussing continuous electromagnetic radiation, hard X-ray radiation and microwave radio bursts 02 p0310 A67-12576

Alfven wave in outward corona as natural explanation of fast drift bursts 04 p0691 A67-14485

Temporal distribution of first and second harmonic of solar diurnal variation of cosmic rays after radio bursts of fourth type 05 p0881 A67-16116

Spectral types of decametric radiation bursts from Jupiter, noting classification based on duration or high resolution dynamic spectra 05 p0898 A67-16927

Type III solar radio bursts, noting association with noise storms and radio condensations 10 p1704 A67-22889

Radio burst produced by solar flare on August 28, 1966, analyzing flux increases as function of time and frequency 10 p1703 A67-23803

Short pearl type bursts as specific class of geomagnetic pulsation 13 p2110 A67-26454

High time-resolution polarimeter observations of Jupiter decameter radio bursts 14 p2388 A67-28836

Magnetospheric tail bursts of energetic electrons identified with auroral zone radiowave absorption 16 p2666 A67-31410

Instability in resonant amplifier and video pulse effect on amplifier resonant load during radio pulse formation 18 p3010 A67-33509

Statistical correlation of type III solar radio burst activity with coronal green line over solar cycle 19 p3316 A67-36029

Solar flare energetic X-ray events detected by onboard satellite ionization chambers, studying relationship to radio burst and space particle emission 23 p4060 A67-41232

Temporal distribution of first and second harmonics of solar diurnal variation of cosmic rays after radio bursts of fourth type 24 p4214 A67-42792

RADIO COMMUNICATION**SA DOUBLE-SIDEBAND RADIO COMMUNICATION****SA GROUND-AIR-GROUND COMMUNICATION**

Radio communications disruptions during magnetotonic disturbances in ionosphere at high latitudes during decreasing solar activity 02 p0193 A67-11660

Mechanical design and packaging of transceiver mounted in spacesuit helmet for intercommunication among astronauts and space vehicles 05 p0779 A67-17466

Antennas for HF radio communications integrated with shipboard structures 08 p1301 A67-20772

High power broadband traveling wave tube YH 1041 as transmitting tube for satellite radio communication, discussing mechanical layout and operational characteristics 08 p1307 A67-21446

VHF and UHF radio/telephone communication channels for air traffic control 09 p1465 A67-22633

Digital synthesis technique for automatic frequency search 10 p1604 A67-22970

Manned spaceflight RF radiation communications systems including voice, telemetry, tracking and ranging, up data and TV 12 p1907 A67-25993

Radio communications disruptions during magnetotonic disturbances in ionosphere at high latitudes during decreasing solar activity 16 p2624 A67-31075

Book on communication principles emphasizing digital radio communication system design, frequency and binary phase shift keying, filtering, fading, etc 16 p2624 A67-31254

Numerical calculation of self-focusing of axisymmetric electromagnetic-wave packets in nonabsorbing cubic isotropic media based on parabolic equation 16 p2628 A67-31504

Diversity-reception systems used in discontinuous radio communication, considering error probability and channel utilization factors 18 p3001 A67-34181

Telecommunication equipment reliability and maintenance costs reduction to increase availability, noting corrective method by transistorization 18 p3002 A67-34229

Short wave skip distance variation with reflection angles in multilayered ionosphere calculated from improved formula 20 p3382 A67-36763

Microwave multichannel communication system using PCM, noting low power output requirement and suitability for digital data transmission 22 p3763 A67-40460

Instructional broadcast satellites programming methods to reduce educational cost of students time without adding to technological cost [AIAA PAPER 67-787] 24 p4258 A67-42950

Medium range radio communication system using artificial ionosphere consisting of ion-electron cloud created by Cs-Al mixture explosion [AIAA PAPER 67-789] 24 p4152 A67-42952

RADIO DIRECTION FINDER

Direction finder accuracy optimization, considering automatic tracking of target angular coordinates 01 p0024 A67-10721

Octantal error of frequency band over which Adcock direction finder operates, noting observed and true bearing relation of arriving signal 01 p0027 A67-11327

Microwave direction-finding systems based on amplitude comparison for use with pulse or continuous wave signals, noting switching system 02 p0198 A67-12067

Earth-based radio reference signal in obtaining attitude and pointing information for synchronous communications satellites 02 p0331 A67-12151

Angular noise induced random error in direction finding as affected by target properties and sense 03 p0368 A67-13275

Short wave and very short wave direction finding from aircraft 03 p0465 A67-13394

Coefficient of mutual correlation of noises for two-antenna phase type direction finder 03 p0386 A67-13957

Equisignal zone technique for correlation-interference direction finder using commutable delay line 05 p0774 A67-16918

German papers on space research with satellites and space probes, Volume 2, Control, test stands and direction finding 07 p1260 A67-20266

Antenna aperture and array effect on characteristics and performance of radio direction finder 11 p1794 A67-25005

Design of broadband steerable Wullenweber antenna arrays allowing HF

element rings to be within LF rings 13 p2074 A67-26257

Statistical performance of wide aperture sampling linear array in HF direction finding 13 p2082 A67-27405

Equisignal zone technique for correlation-interference direction finder using commutable delay line 16 p2623 A67-30895

Earth-based radio reference signal in obtaining attitude and pointing information for synchronous communications satellites 18 p3137 A67-34113

Satellite orbit determination by measuring arrival angle of two transmitted waves with different frequencies 20 p3382 A67-36774

RADIO ECHO

International Satellites for Ionospheric Studies /ISIS/ program using radio sounders 01 p0057 A67-10293

Statistical properties of echoes from meteoric trails during forward scattering, determining diurnal variations for number, duration and fill factor of reflected signals 01 p0025 A67-10791

Radio wave reflection from ionosphere with perturbed electron density profile 02 p0192 A67-11618

Existence of anomalously close radio reflections from sporadic ionization zone linked with polar aurora 02 p0193 A67-11674

Microwave echoes in axially magnetized yttrium iron garnet cylinders following application of two pulses, with second twice frequency of first 02 p0297 A67-11874

Estimated amplitude of echo-signal for uniform, Rayleigh and a priori distribution of probability density of noise amplitudes 02 p0194 A67-11976

Statistical characteristics of meteor radio echoes in Geminides stream noting duration, amplitudes, intervals and ranges 05 p0889 A67-16205

Echo pulses in YIG crystal noting influence of lateral elastic HF signals 08 p1366 A67-20313

Ionospheric drift velocities observed by spaced receiver method compared with neutral winds from luminous rocket trails 10 p1643 A67-23252

Ionospheric radio wave absorption, noting inverse correlation between solar activity with stability of reflections from sporadic E layer 12 p1933 A67-25544

Spatial distribution of auroral radio signal reflection centers based on radar observations 13 p2111 A67-26566

Magnetospheric ion density measurement possibility from association of pulsating radio auroral echoes with sudden geomagnetic field fluctuations 14 p2313 A67-28574

*Angular spread of backscattered spread-F echoes compared with that associated with normal F region returns [AGARDOGRAPH 95] 15 p2480 A67-30278

Ionospheric movement detection using frequency swept sounder and rhombic antenna [AGARDOGRAPH 95] 15 p2484 A67-30301

Existence of anomalously close radio reflections from sporadic ionization zone linked with polar aurora 16 p2624 A67-31089

Cross polarization evaluation radio echo system /CERES/ concept for polarization component separation and echo depolarization evaluation 17 p2814 A67-32520

Hydromagnetic mechanism explaining pulsating radio auroral echoes accompanying sudden commencements, considering Wentzel resonant interaction 17 p2845 A67-32766

Contour maps of percentage occurrence of earth echoes observed on Alouette I ionograms, noting noise level 17 p2852 A67-33236

Autocorrelation functions for amplitude of multiple echoes of fading radio signals reflected from ionosphere 20 p3379 A67-36293

Vertical distribution of meteor showers obtained by measuring distribution in decay times of underdense radio echoes 20 p3521 A67-36303

RADIO ECHO OBSERVATION

Linear electron density measurement in meteor trains using radio echo observations of Geminides 1963 stream 05 p0889 A67-16206

Rocket observations of temperatures and winds in upper atmosphere, discussing physical interpretation of results 05 p0797 A67-16856

Conjugate ducting observation via fixed

- frequency topside-sounder satellite,
estimating electron concentration
difference 06 p0997 A67-18699
- Diurnal and seasonal variations in radio
echo observations from meteoric trains
during forward ultrashortwave
scattering 14 p2383 A67-27924
- RADIO ELECTRONICS**
- Book on circuitry for RF, AM and FM
electronic communication
systems 03 p0388 A67-14272
- Book on microwave engineering including
transmission lines, resonators, waveguides,
antennas, tubes, etc 04 p0583 A67-15269
- Radio measurement methods and
standards, reviewing progress in atomic and
quartz frequency standards, precision coaxial
connectors, etc 05 p0804 A67-16008
- Radio electronics, discussing quantum
electronics, lasers, microwave devices and
technology, plasma physics,
etc 06 p0968 A67-18072
- Soviet book on magnetic switching
elements in radio electronics covering
magnetic materials properties with
rectangular hysteresis, shift registers, logic
circuits, etc 11 p1765 A67-24515
- Electrothermal analogies for heat transfer
simulation by equivalent electrical
circuits 11 p1884 A67-25047
- RADIO EMISSION**
- SA THERMAL RADIO EMISSION**
- Rotation rate and inclination of planetary
axis determined from radiation incident on
artificial satellite of
planet 02 p0321 A67-11539
- Angular dimensions of radio sources from
interplanetary flickering in radio emission
intensity used to study structure of sun
supercorona at large
distances 02 p0322 A67-11684
- Total energy of slow particle radio
emission and real delta electron emission
determined in extensive air
showers 02 p0318 A67-12782
- Coherent radio emission of extensive air
showers determined from known threshold
energy of optical signal 02 p0318 A67-12783
- Instrument methods determining function
and density of length distribution of random
radio emissions 03 p0369 A67-13586
- Radio emission from blue stellar objects
and radio galaxies, comparing upper flux
densities with quasi-stellar radio source
emission densities 03 p0512 A67-14002
- Venus brightness temperature and
polarization of integral radio emission at 3.75
cm wavelength 04 p0702 A67-15566
- Nighttime magnetospheric auroral VLF
hiss generation by suprathermal particle
associated with coherent electron plasma
radio emission 04 p0618 A67-15686
- Radio emission intensity measurements in
interplanetary space at 20 to 210 kHz by
Zond II and III and Venera II
stations 05 p0887 A67-16060
- Radio interferometric observations of
decimeter emissions from planet
Jupiter 05 p0892 A67-16408
- Comparison of VLF emissions of two
conjugate stations, noting statistical results
for diurnal variation, magnetic activity, hiss,
etc 06 p0997 A67-18698
- Temperature of atmospheric radio
emission in decimeter range for elevation
angles from 1/2 to 10
degrees 07 p1142 A67-19586
- Radio wave emission due to shock wave
propagation in magnetospheric boundary and
electromagnetic scattering in plasma wave
field 07 p1243 A67-19808
- ULF radio emission of upper atmosphere
and other related geophysical phenomena,
analyzing hisses, choruses and contribution
to earth radiation belt 08 p1324 A67-20862
- Faraday rotation effects in spectral
records of Jupiter decametric
radiation 09 p1568 A67-22401
- Radio emission from cosmic ray showers
analyzed at Jodrell Bank, determining
effects of geomagnetic field and charge
separation 10 p1703 A67-23490
- Stimulation of Jupiter radio emission by
Io 12 p2000 A67-25204
- Brightness distribution of radio emission
over solar disk during solar activity minima
determined from
radioheliograms 12 p2001 A67-25226
- Lateral distribution of radio emission flux
of extensive air showers /EAS/ of cosmic
rays 12 p1940 A67-25337
- Evolutionary scheme of radio galaxies
based on radio luminosity vs volume
emissivity diagram, noting similarity and
parallelism between radio and X-ray
intensities 12 p2007 A67-25767
- Cosmic radio emission at 725 and 1525 kc
measured for intensity by direct
amplification receivers on Elektron II
satellite 12 p1995 A67-25769
- Satellites Europa, Ganymede, Callisto and
Amalthea show no effect on probability or
spectral character of decametric radio
emission of Jupiter 12 p2010 A67-26243
- Axial mode helical antenna radiation and
impedance improvement by using tapered
feeds and terminations 13 p2076 A67-26514
- Planetary radio emission measurements,
noting no radio emission from
Pluto 14 p2385 A67-28405
- Flux density absolute calibration of solar
radio emission 14 p2385 A67-28440
- Primary cosmic ray electron flux and
energy spectrum near solar minimum
compared with nonthermal radio emission
from high galactic
latitudes 14 p2381 A67-28831
- Solar radio emission spectroheliograms at
different millimeter wave
frequencies 14 p2388 A67-28834
- Mean flux density and polarization degree
of radio emission from Jupiter in centimeter
spectral range 14 p2389 A67-28837
- Dependence of angular dimensions of
discrete cosmic radio emission source on
radiation flux density and
frequency 15 p2549 A67-29140
- Lunar radio emission in 30 to 60 cm range,
showing mean radio temperature of moon as
225 degrees K and independence of
wavelength 15 p2552 A67-29148
- Linear polarization of lunar radio emission
observed using radio
telescope 15 p2552 A67-29149
- Jovian decametric emission of millisecond
pulse variety analysis from observations of
four apparitions 15 p2558 A67-30032
- Solar flares, analyzing X-ray emission,
radio emission and superposition of
ionospheric effect 16 p2739 A67-31459
- Polarization characteristics of radio
emission from rough lunar surface, analyzing
averaging effects of antenna radiation
pattern and surface
roughness 16 p2628 A67-31495
- Rotation rate and inclination of planetary
axis determined from radiation incident on
artificial satellite of
planet 16 p2752 A67-31605
- ULF radio emission properties
determination and relation to other
geophysical phenomena, noting experimental
equipment and correlation with auroral
activity 17 p2846 A67-32938
- ULF radio emission associated with
magnetic field disturbances, geomagnetic
pulsations, auroras and exospheric particle
acceleration 17 p2846 A67-32939
- Radio emission flux from local solar
sources relation to active solar regions
structure, based on radio-astronomical
observations 17 p2948 A67-32963
- Solar X-ray fluxes measured by solar
radiation satellite during IQSY, comparing
X-rays and decimetric radio emission in 8-12
angstrom band 17 p2938 A67-33185
- Attenuation of lunar microwave emission
measured by artificial moon method,
determining phase dependence of lunar
temperature 18 p3119 A67-33861
- Amplitude and polarization of radio pulse
from extensive cosmic ray air shower
indicating geomagnetic deflection mechanism
of emission 18 p3116 A67-34196
- Refractive index variations, Coulomb
scattering and time variation of shower
front effects on coherent emission of
polarized radio pulses from cosmic ray
showers 18 p3116 A67-34197
- Nonthermal radio emission from Jupiter
atmosphere, studying Io modulation
effect 19 p3317 A67-34933
- Atmospheric electric field as possible
cause of radio pulses from extensive air
showers 19 p3316 A67-35803
- Minimum radius of line emitting regions
in quasars estimation method, discussing
origin problem 19 p3327 A67-35893
- Quasars and radio galaxies characteristics
contrasted, drawing conclusions about
evolution using radio emission synchrotron
hypothesis and consistent
- model 20 p3526 A67-37250
- Temperature of atmospheric radio
emission in decimeter range for elevation
angles from 1/2 to 10
degrees 20 p3384 A67-37323
- Nonthermal radio emission from electric
discharges within Venus water
clouds 20 p3529 A67-37480
- Radio emission point sources fluctuations
resulting from interplanetary plasma
inhomogeneities observed at meter
wavelength 20 p3529 A67-37514
- Radio emission polarization of Crab Nebula
on February 1963 with Soviet radio
telescope 20 p3529 A67-37516
- Solar radio emission mechanism for spin
transitions of neutron beta decay electrons
in external magnetic field 20 p3520 A67-37522
- Radio emission intensity measurements in
interplanetary space at 20 to 210 kHz by
Zond II and III and Venera II
stations 21 p3701 A67-37847
- Flare X-ray emission period determined,
noting maximum radio emission and optical
intensity 21 p3699 A67-38965
- Morphology of Jupiter decametric radio
sources 21 p3710 A67-38997
- Magnetic field rotation, satellite Io and
interplanetary propagation effects accounting
for time variation of Jupiter magnetic flux
and polarization 21 p3710 A67-38998
- Depolarization problem and correlation
method for cosmic radio emission
polarization measurements in interstellar
space 22 p3761 A67-39757
- Satellite and ground observations of VLF
emissions, summarizing intensity, diurnal and
seasonal variation, emphasizing chorus and
hiss characteristics 22 p3794 A67-40083
- Mercury radio emission observation
yielding average brightness temperature and
planetocentric phase angle
relation 22 p3889 A67-40240
- Total energy of slow particle radio
emission and real delta electron emission
determined in extensive air
showers 22 p3878 A67-40284
- Coherent radio emission of extensive air
showers determined from known threshold
energy of optical signal 22 p3878 A67-40285
- UHF sferics detection system receiving
and display components for remote sensing
by satellite of convective cloud
development 22 p3806 A67-40358
- Dependence of decametric radio emission
from Jupiter on positions of Galilean
satellites with respect to sun, earth and
Jovian magnetic plane 23 p4069 A67-41362
- Monograph on quasi-stellar objects
including identification, line spectra, radio
emission, continuum radiation, red shift and
models 23 p4069 A67-41438
- Millisecond bursts in radio emission from
Jupiter not imposed by interplanetary
scintillation but by amplitude or frequency
variation in source 24 p4231 A67-42452
- Dependence of angular dimensions of
discrete cosmic radio emission source on
radiation flux density and
frequency 24 p4222 A67-43063
- Lunar radio emission in 30 to 60 cm range,
showing mean radio temperature of moon as
225 degrees K and independence of
wavelength 24 p4239 A67-43071
- Linear polarization of lunar radio emission
observed using radio
telescope 24 p4239 A67-43072
- RADIO EQUIPMENT**
- SA ULTRA-SHORT-WAVE RADIO
EQUIPMENT**
- SA VERY HIGH FREQUENCY RADIO
EQUIPMENT**
- Three representative microwave systems
of different transmitting capacity currently
in serial production 02 p0220 A67-12203
- Reflection amplifier design for use in
tunnel diode UHF radio
repeater 11 p1766 A67-24689
- Frequency generation and control for
radio systems - Conference, London, May
1967 15 p2444 A67-29580
- All-weather landing for civilian aircraft,
discussing equipment, terminology used and
low visibility flight
simulation 17 p2795 A67-32122
- Air Force rescue radio equipment
evolution, describing
models 17 p2814 A67-32516
- Instability in resonant amplifier and video
pulse effect on amplifier resonant load
during radio pulse

formation 18 p3010 A67-33509
 Telecommunication equipment reliability and maintenance costs reduction to increase availability, noting corrective method by transistorization 18 p3002 A67-34229
 Mathematical models of multichannel radio equipment in presence of noise, including guidance and coordinate measurement systems 19 p3185 A67-36095
 Onboard and ground radio-engineering system for stratospheric transport balloon noting telemetering, remote control and localization functions integrated in system 21 p3581 A67-38213
 Channel Evaluation and Call /CHEC/ system to improve air-ground-air communications by automatic selection of optimum channels 22 p3760 A67-39664

RADIO FILTER

Bandwidth and distortion in pulse filters 03 p0389 A67-14303
 Structural and technological problems connected with miniature electromechanical filters 10 p1609 A67-22876
 Radio pulse sequences selection according to carrier frequency by analyzing filter operation 14 p2261 A67-28278
 Noise model for simulating tropospheric turbulence effects on radio guidance and tracking range and angular measurements for optimum filter synthesis 21 p3587 A67-39147

RADIO FREQUENCY

SA FREQUENCY BAND

Fermi surface curvature of indium single crystals measured from RF size effect at reference point 01 p0133 A67-10742
 Microwave swept frequency measurements on RF transmission line systems and development of VSWR and insertion loss test set 01 p0039 A67-11038
 Phasing system using steered beam of coherent light for RF array 01 p0027 A67-11320
 Space communication maximum usable frequency and limitations imposed by atmospheric absorption 02 p0205 A67-12735
 Two frequency SHF tunnel diode trigger for automatic systems using frequency recorded information 03 p0378 A67-13245
 Ion resonance in uniform plasma, analyzing behavior of RF resonance probe by comparing ion resonance with electron resonance 04 p0663 A67-14616
 RF sputtering of insulators noting deposition rate, film properties, etc 04 p0631 A67-15993
 Variations in RF spectra of 3C 84, 3C 273, 3C 279 and other radio sources 05 p0891 A67-16401
 Gas laser pumped microwave emission for producing controlled excited state population for RF spectroscopy of neon 05 p0817 A67-16638
 RF power oscillator for low pressure plasma production, noting work and grid coils and time and power controls 05 p0856 A67-17281
 Planet rotation and orbiting of satellite Io modulations effect on maximum RF of storms 05 p0904 A67-17408
 Spectroscopic measurement of temperature, electron density and conductivity in RF plasma torch 06 p1039 A67-17825
 Paramagnetic current formation due to volume resonator microwave field interaction with dense plasma subject to RF pressure and EPR in static magnetic field 07 p1228 A67-19512
 Radio wave absorption at high latitudes dependent on frequency, noting AZA and PCA are inversely proportional to powers of frequency 07 p1144 A67-19693
 Control of RF hazard to electroexplosive devices 08 p1290 A67-20548
 Dual frequency VLF timing system for synchronization of remotely located clocks, noting WWVL radio carrier frequency, signal generator, etc 09 p1494 A67-21619
 Rocketborne RF mass spectrometers use in study of atmospheric composition at high altitudes, discussing sampling 09 p1491 A67-21895
 Dependence of ion current from RF ion source on plasma density at boundary and longitudinal magnetic field intensity 10 p1687 A67-23794
 Laser application to deep space communication noting advantages of optical frequencies for high rate transmission of

data 11 p1752 A67-24252
 Circuit Q of self-resonant coil of niobium stannide at RF low temperatures 11 p1767 A67-24726
 RF electromagnetic fields to control state of flowing thermal plasma 12 p1975 A67-25921
 RF sources imbedded in ionized plasma noting developments since 12 p1908 A67-26162
 P-i-n diode switches, discussing driving techniques for series and parallel biased switches, pulse leakage and RF turn-off delay minimization 12 p1917 A67-26194
 Holography applied to radio frequencies, noting recording technique with locally produced reference wave 13 p2119 A67-26518
 Discharge formation and propagation in He-Ne laser excited with pulsed RF voltage 13 p2126 A67-26730
 Fermi surface curvature of indium single crystals measured from RF size effect at reference point 13 p2176 A67-26771
 Plasma in diffusion regime situated in nonhomogeneous RF field with rotation symmetry 14 p2354 A67-27765
 Direct modulation of He-Ne laser with RF excitation, noting kinetic equations of transition processes 14 p2329 A67-27772
 Slotted-sphere antenna immersed in plasma measured for RF admittance 14 p2283 A67-28377
 Radio measurements and standards for power, conductance, impedance and attenuation in upper frequency range 14 p2263 A67-28390
 Device design for measurement of noise factor of RF transistor 14 p2286 A67-28587
 RF hardware implementation techniques utilizing devices illustrated in block diagrams 14 p2287 A67-28680
 RF design of communication satellite earth stations, discussing receiving, sensitivity parameters, etc 14 p2273 A67-28798
 Stark broadening of hydrogen lines of large principal quantum number for RF transitions by electron and ion impact approximation 14 p2389 A67-28839
 Troposphere and ionosphere effects on different frequency radio wave propagation for space communication [AAS PAPER 67-93] 15 p2437 A67-29953
 Automatic measurement of diurnal resonance frequency variations of earth/ionosphere cavity 15 p2489 A67-30071
 Low noise amplifier specifications for communication satellite earth station 16 p2635 A67-30473
 Radio gain between simple dipole antennas for single propagation paths, noting effect of resistance from imperfect ground 16 p2625 A67-31342
 Path diversity in millimeter waves propagation through rain for various frequency 16 p2625 A67-31343
 RF attenuation measurement methods and standards 17 p2815 A67-32607
 Voltage breakdown measurement in various gases at low pressures during simultaneous excitation by RF in superimposed DC field 17 p2902 A67-32672
 Phase and amplitude characteristics of microwave amplifiers obtained from response to short input pulse 17 p2827 A67-32791
 Instability and related anomalous diffusion of magnetized weakly ionized hydrogen plasma of RF discharge in cylindrical geometry 17 p2908 A67-33113
 Noise analysis in He-Ne laser during RF and DC excitation, noting relation between critical frequency and lifetime of metastable atom 18 p3058 A67-33648
 Frequency response of DC and AC currents flowing to RF resonance probe in quiescent cesium plasma, explaining measurements 18 p3044 A67-33713
 RF design of satellite communications ground stations, giving hardware data on receivers, transmitters, tracking systems, power amplifiers and reliability 18 p3003 A67-34349
 RC oscillators based on silicon n-p-n transistors for radio frequencies, analyzing active all-pass phase-shift circuit 19 p3191 A67-34946
 RF plasma at electron cyclotron frequency produced with axially slotted metal cylinder 19 p3275 A67-35111
 Optical subcarrier communications, noting use space-oriented missions and RF

techniques optical subcarrier communications, noting use in space-oriented missions and RF techniques 20 p3378 A67-36183
 Effect of electromagnetic field interaction with gravitational field calculated from satellite data, determining difference between frequencies 20 p3386 A67-37523
 Intermodulation due to nonlinearities in transistor amplifiers, discussing design guidelines for optimizing 20 p3404 A67-37634
 RF mixer and limiting IF models for RFI analysis of local oscillator control in FM-CW receivers, using digital computer simulation 20 p3405 A67-37649
 Nuclear fusion control and relativistic high density matter acceleration, discussing amplification effect application to plasma theory, plasma RF confinement and acceleration 22 p3851 A67-39772
 RF generation in VLF/LF thyristor transmitter for applications in long distance communications and navigation 22 p3771 A67-39842
 Niobium stannide for refrigerated RF preselectors for interference reduction in radio communications, stressing high Q factors 22 p3865 A67-40435
 RF size effects in plane parallel metal plate, discussing skin effect in magnetic fields, electron trajectories and spherical Fermi surface 22 p3866 A67-40551
 Deep-space communication capability spectral dependence analysis indicates optical transmissions would be several orders of magnitude poorer than RF technology 22 p3764 A67-40558
 Drop-across-reactance method found satisfactory for accurate current measurements in high voltage RF plasma discharges 23 p4001 A67-41224
 RF interference reduction by using choke blinder on feed horns of reflector type antennas 24 p4132 A67-42717

RADIO FREQUENCY DISCHARGE

SA ELECTRON EMISSION

Laser action delay due to plasma-tube-surface decomposition resulting from bombardment by neon ions 04 p0633 A67-15110
 Anomalous emission at electron cyclotron frequency in partially ionized plasmas 05 p0854 A67-16895
 Formative time lag for pulsed RF breakdown in dry air as function of gas pressure and power of slot antenna 07 p1153 A67-19607
 Population inversion of neon levels in He-Ne microwave discharge as affected by pressure and power scattered by unit discharge volume 09 p1512 A67-21924
 Plasma diffusion across static magnetic fields in electrodeless E type RF discharges 11 p1830 A67-24008
 Automatic cavity tuning of hydrogen masers to achieve frequency source of absolute accuracy over unlimited time periods 13 p2125 A67-26512
 Population inversion of neon levels in He-Ne microwave discharge as affected by pressure and power scattered by unit discharge volume 14 p2330 A67-28253
 Ion beam generation and applications, discussing duoplasmatron, RF source, contact ionization source and Penning discharge 15 p2488 A67-29756
 Plasma resonance in RF discharge excited with frequency higher than collision frequency, determining electron density 19 p3276 A67-35114
 Impedance measurements of RF discharge in single turn coil with superimposed static magnetic field, noting dependences and two resonances 19 p3276 A67-35119
 Magnetospheric discrete VLF emissions, discussing gyroresonance extension, resonant electron and emission frequency 23 p3995 A67-40802
 Helium RF discharge radiation temperature as magnetic field function measured, discussing enhanced diffusion role in radiation temperature determination 23 p4032 A67-40897

RADIO FREQUENCY HEATING

Transient effects of changes in applied radio frequency power to which latching ferrite phase shifters could be subjected in array applications 19 p3196 A67-35663
 RF induction heating and production of low pressure plasmas, discussing plasma electron density function

[AIAA PAPER 67-732] 21 p3674 A67-38756
RADIO FREQUENCY IMPEDANCE PROBE

Resonances of impedance of RF probe in low density plasma introduced by finite electron temperature 04 p0663 A67-14614
 RF characteristics of spherical probe immersed in hot low-density plasma, using sheath model 15 p2528 A67-29564
 Spatial average plasma conductivity by RF impedance probes for cylindrical radially inhomogeneous plasma 22 p3844 A67-39366
 Rocket measurements with HF impedance probe for ionospheric electron density, discussing plasma gyro resonance frequency factors 23 p4003 A67-41321

RADIO FREQUENCY MONITORING

Bit and message error rate dependence on variation of atmospheric noise statistical properties 02 p0203 A67-12165
 Telemetry design factors, discussing interference problems, antenna design, oscillator stability, preamplifiers, etc 03 p0372 A67-14120
 Book on electronic testing covering RF interference, tracking systems, receivers and transmitters, flight control equipment, digital computers, etc 04 p0577 A67-15726
 Far field localizer and glide path monitoring for ILS installations, noting spaced antennas system and receiver for detection of radio 07 p1222 A67-19653
 Lunar surface analysis via analysis of reflected signals from RF pulses 08 p1295 A67-21080
 Mean ionospheric height measurement from analysis of radio signals from beacon satellite 08 p1328 A67-21479
 RF bridge technique determining electric conductivity of plasma sheath around reentry vehicle 08 p1366 A67-21514
 Ground integrity monitor for category III ILS for use with automatically landing aircraft 09 p1529 A67-22644
 Comet 1965 f /Ikeya-Seki/ interaction with solar corona produces no significant enhancement of emission at 2.2 m wavelength 10 p1706 A67-22958
 Experimental transmissions for navigation system monitored over 8500 km path to determine phase variations of VLF signals, for use in design of radio navigation aid 15 p2515 A67-30134

RADIO FREQUENCY RADIATION

Coherent amplification of RF radiation in cosmic space 01 p0144 A67-10836
 High energy proton from local radio sources, using telescopic system for Cerenkov effect detection of broad atmospheric showers 02 p0311 A67-12587
 High resolution radar correlometer measurement of spatial correlation radius of RF radiation scattered by disturbed ocean surface 08 p1294 A67-20819
 Variation of radio brightness of synchrotron radiation from Van Allen belts as function of direction and frequency, using satellite receiver 11 p1855 A67-23944
 Method of radiation pattern synthesis for equally and unequally spaced arrays 14 p2285 A67-28451
 Behavior of RF sources embedded in plasma, determining antenna properties by configuration, current distribution and surrounding sheath 14 p2359 A67-28464
 Extensive cosmic ray shower bremsstrahlung in RF and optical bands noting intensity and 22 p3870 A67-39517
 Incoherency

RADIO FREQUENCY SHIELDING

Shielding methods for electronic equipment packaging, considering magnetic, electromagnetic and RFI shielding in gamma and X-ray range 12 p1911 A67-25267

RADIO GALAXY

Red shifts and power outputs in quasars and radio galaxies 01 p0149 A67-10889
 Statistical data on space density of bright elliptical galaxies, radio galaxies, quasars, noting relation between space density and age 02 p0322 A67-11685
 X-ray emission from radio galaxies as possible bremsstrahlung radiation of hot gas, noting Crab Nebula 02 p0308 A67-12482
 Statistical properties of newly identified radio galaxies, including monochromatic luminosity and linear extension distributions 03 p0512 A67-13878
 Intense radio emission from galaxies may be due to large scale explosions in galactic

nuclei, examining characteristics of synchrotron emission 03 p0516 A67-14335
 Upper limit to neutral atomic hydrogen density in halo regions of spiral galaxies 04 p0694 A67-14480
 Radio emission from 18 galaxies observed, noting accompaniment of optical spectrum emission and enhancement due to production of relativistic electrons in active nuclei 04 p0697 A67-14774
 Spectral indices of radio galaxies and quasi-stellar sources explained by relativistic electron injection into magnetic field by recurring blasts 05 p0891 A67-16400
 Galactic explosions, radio galaxies and quasi-stellar radio sources theories, discussing role of large scale magnetic field 05 p0902 A67-17287
 Radio galaxy phenomena and quasars noting stellar evolution mechanism, energy generation and emission 07 p1246 A67-19055
 X-ray emission from radio galaxies as possible bremsstrahlung radiation of hot gas, noting Crab Nebula 10 p1702 A67-23350
 Evolutionary scheme of radio galaxies based on radio luminosity vs volume emissivity diagram, noting similarity and parallelism between radio and X-ray intensities 12 p2007 A67-25767
 Polarization of extragalactic radiation sources and evidence of irregularities of magnetic field in our Galaxy 13 p2198 A67-26791
 Radio galactic X-ray emission noting possible cosmic radiation mechanism, history of X-ray astronomy, etc 14 p2381 A67-28427
 Association of radio sources with peculiar galaxies in symmetrically distributed pairs 14 p2388 A67-28830
 Suggestion of physical association of radio sources with stars in neighborhood as radio stars 14 p2391 A67-28945
 Hypothesis attributing most energetic cosmic ray proton source to powerful radio galaxies noting pair production effect on cosmic ray sources 16 p2738 A67-30822
 Origin of X radiation from radio galaxies Cygnus A and Virgo A, hypothesizing thermal radiation and bremsstrahlung 18 p3116 A67-33855
 Cosmic radiation origin shown inconceivable in radio galaxies 19 p3316 A67-36088
 Relationship between radio galaxies and quasars, observing two sources of moderate distance, noting intense optical emission of limited intensity or duration 20 p3521 A67-36296
 Radio parameter continuity between radio galaxies and quasars, plotting spectral indices against absolute spectral power 20 p3525 A67-36947
 Quasars and radio galaxies characteristics contrasted, drawing conclusions about evolution using radio emission synchrotron hypothesis and consistent model 20 p3526 A67-37250
 Red shifts of radio galaxies observed spectroscopically with 120-inch telescope, using prime focus and image tube 20 p3527 A67-37392
 Nonrandom optical red shift distribution of radio sources leading to uniform density over large volume 22 p3892 A67-40500
 Unified theory for galaxy spiral formation and radio galaxy and quasar evolutionary dynamics, discussing galactic dipole magnetic field generation 22 p3893 A67-40504
 Mean emissivity due to radio galaxies calculated, using assumption that total brightness temperature is uniform in universe 22 p3896 A67-40530

RADIO HORIZON
 Earth surface influence on radiation polarimetry in vicinity of radio horizon 20 p3382 A67-36776

RADIO INTERFERENCE
 Interference Prediction Model /IPM/ for RF interference study at satellite tracking stations 01 p0023 A67-10498
 HF conducted and radiated RF interference suppression by dielectric and magnetic absorption, pseudoresonant or interfacial loss and artificial skin effect 01 p0024 A67-10500
 Straight edge fence design for control of radar site environment from clutter return, pattern interference, tracking errors and high power hazard to personnel 03 p0396 A67-13853

Radar target clutter, fluctuation, echo level, direction error and noise in tracking system 03 p0372 A67-14093
 RF interference detection and elimination from communication systems noting signal, frequency and amplitude analysis techniques 04 p0577 A67-15730
 Equisignal zone technique for correlation-interference direction finder using commutable delay line 05 p0774 A67-16918
 Pulse interference inhibition in AM signals reception by nonlinear negative feedback loop in HF cascades of receiving device 05 p0785 A67-17471
 Selection of optimum ranging signal for jam resistant satellite communications system 06 p0959 A67-17671
 Errors by mutual interference in frequency-time coding in satellite communications systems, deriving expressions relating commissive and omissive error rates, simultaneous users per unit bandwidth, etc 06 p0961 A67-17696
 Plasma induced interference signal in satellite VLF receiver originating with converter system and appearing only in daylight operation 06 p0964 A67-18569
 Noise sources and characteristics, discussing incidental radio interference 06 p0965 A67-18834
 Variable ratio DC transformer regulator used in voltage boost configuration of power system in Radio Astronomy Explorer /RAE/ spacecraft, noting RF interference reduction 08 p1284 A67-20692
 Interference problems caused by spurious radio transmissions, analyzing radiation spectrum utilization 08 p1301 A67-20773
 VLF radio signal phase and amplitude interference observed on GBR-16.0 kc/s transmissions in November and December 1965 08 p1295 A67-20988
 Frequency sharing and compatibility of satellite and terrestrial radio relay systems design, discussing interference effects 09 p1464 A67-22411
 Blocking effect due to interference in parametric amplifier, discussing relation between gain and blocking frequency 10 p1609 A67-22834
 Protection of communications satellites data transmission against interplanetary interference sources and Van Allen belts 10 p1604 A67-22899
 Optimum filtration of signals in presence of arbitrary interference, using orthogonal function series 10 p1607 A67-23443
 Comparison of measurement accuracy for angular coordinates in radar systems by linear scanning and equal-signal zone methods 10 p1607 A67-23450
 Phase measurements of VLF transmission over long distance transequatorial path 12 p1906 A67-25942
 Ferrite-diode system with automatic gating of signal reflection used in radar wind velocity observations to reduce pulse interferences produced by meteor trails 13 p2197 A67-26505
 Equisignal zone technique for correlation-interference direction finder using commutable delay line 16 p2623 A67-30895
 Modal interference of VLF radio waves investigation from field strength data, noting isotropic case 16 p2631 A67-31850
 Intermodulation due to nonlinearities in transistor amplifiers, discussing design guidelines for optimizing 20 p3404 A67-37634
 Receiver performance related to signal and interference conditions for AM voice communication system analyzed for use in systems design 20 p3387 A67-37637
 Interference reduction potential of binomial type pulses 20 p3387 A67-37638
 Electromagnetic interference reduction between antennas on space vehicles 20 p3405 A67-37642
 RF mixer and limiting IF models for RFI analysis of local oscillator control in FM-CW receivers, using digital computer simulation 20 p3405 A67-37649
 Reduction of RF interference in reflection-type parametric amplifiers covering spurious responses, amplifier saturation, intermodulation and cross modulation 20 p3406 A67-37655
 Niobium stannide for refrigerated RF preselectors for interference reduction in radio communications, stressing high Q factors 22 p3865 A67-40435
 Power conversion derivation in nonlinear

resistive element in series with linear resistors 23 p3981 A67-41395

Harmonic analysis of half-wave dipole and director parallel to reflecting plane 24 p4132 A67-42715

RF interference reduction by using choke blinder on feed horns of reflector type antennas 24 p4132 A67-42717

Radio noise data compared for transmission lines, automotive traffic and RF stabilized arc welders 24 p4123 A67-42718

Frequency assignment for communications equipments mutual interference charts /MIC/ 24 p4123 A67-42719

RADIO INTERFEROMETER

Large-base radio interferometer system without radio relaying that independently records intermediate-frequency signals on each antenna and subsequently combines them 02 p0213 A67-11635

HF flight attitude indicator and forward and backward counting radio interferometer operating without rotating goniometer and phase locked oscillators 04 p0619 A67-14533

Integrated Trajectory System, measuring spatial positions, velocities, accelerations and scalar and vector miss distances for targets 04 p0654 A67-15045

Rotating interferometer measuring spread and coherence ratio of scattered radio wave 05 p0760 A67-15997

Radio interferometric observations of decimeter emissions from planet Jupiter 05 p0892 A67-16408

Traveling wave maser for radio astronomy interferometer noting superconducting magnet, dynamo and cryostat 07 p1197 A67-20115

Mathematical analysis of polarization interferometry yielding polarization and brightness distribution of celestial radio sources [AFRL-67-0226] 09 p1470 A67-21608

Coherent analog of compound intensity interferometer for measuring arbitrary distributions of incoherent radio sources, discussing simple and compound systems 09 p1493 A67-21609

Angular sizes of radio sources at 6, 11, and 21 cm wavelengths, using Mark II radio telescope of Jodrell Bank 09 p1565 A67-21980

Grating interferometer observation of slowly varying components of solar radio emission 10 p1711 A67-23802

Complex correlation function application to describe correlation between signals from two antennas of radio interferometer 11 p1762 A67-24287

Submillimeter-wave measurements for water-vapor detection from jet aircraft flying in stratosphere 13 p2114 A67-26795

Radio interferometer design with superlong base compensating for phase fluctuations 14 p2261 A67-28068

Long-baseline-interferometer observations of radio sources to ascertain angular dimensions of radio sources at LF 15 p2437 A67-30031

Phase-locked radio interferometer for satellite tracking 16 p2621 A67-30679

Radio interferometry method using precision clocks for earth rotation period measurement 18 p3043 A67-34528

Earth rotation measurement by radio interferometry, discussing rate changes in slowdown, Love number, etc 18 p3043 A67-34529

Radio interferometry at Dlane satellite tracking station, noting synchronous demodulation technique 21 p3587 A67-39052

Radio interferometric measurements of radio source diameters using 3074 km baseline 24 p4228 A67-41876

Two-antenna interferometer baseline observations and scanning interferometer characteristics, determining source coordinate and solar radiation center 24 p4129 A67-42227

RADIO METEOR

Near-earth meteor flux estimate through luminous efficiency and ionizing probability application to data on radio and photographic meteor fluxes 19 p3319 A67-35217

RADIO METEOROLOGY

Radar meteorology - AMS Conference, Oklahoma, October 1966 04 p0648 A67-14672

Errors in R-meter measurement of velocity spread of meteorological targets resulting from radar frequency instabilities 10 p1676 A67-22816

Radio refractive index irregularities in lower troposphere examined, using helicopter mounted spaced cavity refractometer 11 p1787 A67-24644

RADIO NAVIGATION

Synthesis of multichannel transponder for radio guidance and tracking station and associated parameters 02 p0264 A67-12355

Aircraft radio guidance system combining ILS and precision approach radar 04 p0653 A67-15042

Flight testing of radio navigation aids for civil aviation noting techniques, teleroscope and typical test 09 p1528 A67-22629

Antenna aperture and array effect on characteristics and performance of radio direction finder 11 p1794 A67-25005

Automatic exposure of longitudinal overlapping of aerial photographs solved by autonomous radio-navigation systems 15 p2485 A67-29137

VLF transmitter design criteria and characteristics for global time and navigation signal network 17 p2824 A67-32494

Soviet book on aircraft navigation covering theory, earth shape, map use, coordinate systems, instrumentation and aeronautical astronomy 19 p3254 A67-34894

Ground-based radio aids to navigation as represented by existing major systems 19 p3255 A67-35857

Kalman-Bucy filter for optimum radio inertial navigation, discussing a priori estimation 24 p4182 A67-42184

RADIO NOISE

Man-made HF radio noise level measurement and prediction, discussing spectral and spatial distributions, soil/saltwater conductivity and receiver elevation effects, instrumentation and antennas 01 p0024 A67-10499

Radiation absorption by ionized hydrogen in plane of galaxy to explain brightness profiles for declination minus 37 degrees 02 p0307 A67-11688

Frequency spectra of VLF hiss near auroral zone analyzed by Injun III satellite 04 p0614 A67-14958

Sunrise effect on atmospheric radio noise intensity, directional variations and formation of D region 04 p0618 A67-15575

Galactic emissions and LF and MF radio noises in ionosphere 05 p0898 A67-16867

Japanese sounding rocket measurements of intensity and frequency time variations in ionosphere to determine VLF radio noise 05 p0763 A67-16868

Hook whistler discovered in VLF radio noise data from Injun III satellite, noting time delay difference between components 05 p0799 A67-16888

Sidereal time recorder used with riometer for detection of radio noise absorption in ionosphere 08 p1329 A67-21489

Microwave noise intensity emitted by electron plasma within framework of fluctuation theory 09 p1547 A67-22318

Galactic radio noise intensity decrease correlated with decline in solar activity, calculating D and F region absorption 11 p1784 A67-23934

Anomalous transport phenomena in ring discharge studied for instability and losses due to noise, using mc RF oscillator [AROD-6398-2] 11 p1831 A67-24010

Electron component of primary cosmic radiation 11 p1856 A67-24104

Contribution of propagation factors in terrestrial atmosphere to noise received by antenna at hyperfrequencies 12 p1904 A67-25308

Receiver-antenna system in radio astronomy, discussing low noise, thermal signal reception and acquisition of information limited by internal or external noise 12 p1914 A67-25309

Diurnal cyclic intensity variations of atmospheric radio noise at stations widely spaced over globe 13 p2111 A67-26571

Relation between ionospheric no-echo conditions and absorption of cosmic radio noise measured using riometer, plotting diurnal variation values 13 p2114 A67-26794

Electrostatic, induction and radiation field effects of lightning discharge on intensity spectrum of atmospheric source signals 14 p2346 A67-27880

Radio noise spectrum on VLF bands in ionosphere observed by sounding rocket K-9M-19 14 p2307 A67-27886

Coding modulation and signal processing

noting algebraic coding and binary symmetric channel neglect, discussing coherent optical radiation in noise program 14 p2269 A67-28457

Decametric radio noise data from Jupiter apparitions /1960-1964/ 14 p2389 A67-28838

Signal-source noise mismatch and alignment in linear tripole amplifier networks 14 p2289 A67-28864

Carrier instability influence on noise immunity of discrete communication systems, with results presented graphically for uniform and normal random frequency distributions 16 p2620 A67-30477

Noise and HF input conductance measurement of double-injection germanium space-charge-limited diode, noting transit-time effect 16 p2637 A67-31034

Solar X-ray measurement with satellite noting radio noise flux, absorption in atmosphere and optical density changes 17 p2939 A67-33242

Eruption of solar flare of importance 2, describing evolution, associated optical and radio phenomena, structure of longitudinal magnetic field, etc 17 p2939 A67-33397

High kinetic energy electrons associated with solar flares, noting prompt and delayed types 17 p2940 A67-33401

Solar radio noise source position determined during occultation caused by partial solar eclipse of May 20, 1966 17 p2953 A67-33403

Noise theory for self-sustaining discharge verified for low frequencies, noting temperature dependence, silicon, etc 18 p3106 A67-34638

S-current intensity variation and 10.7 cm radio noise flux show agreement with Schmidt sunspot numbers 19 p3221 A67-35432

Earth-ionosphere whispering-gallery nature at VLF analyzed, using mode equation for idealized earth ionosphere model 19 p3184 A67-35827

Mathematical models of multichannel radio equipment in presence of noise, including guidance and coordinate measurement systems 19 p3185 A67-36095

VLF radio noise during auroral display studied by ground and rocketborne receivers, suggesting emissions triggered by high energy electron fluxes 20 p3428 A67-36374

Satellite and ground observations of VLF emissions, summarizing intensity, diurnal and seasonal variation, emphasizing chorus and hiss characteristics 22 p3794 A67-40083

Noise in polarized Si semiconductor avalanche junctions at RF and microwave frequencies noting determination of impact ionization parameters 23 p3980 A67-41189

Magnetic field intensity effect of sunspot group on source radio noise flux 24 p4209 A67-42136

RADIO OBSERVATION

Rotation period of Jupiter determined by radio observations explaining cyclic drift 01 p0146 A67-10294

Induced absorption coefficients in atmosphere model measured for calculation of Venus lower atmosphere properties from radio observations 03 p0394 A67-12949

Radio observations of Mercury, Venus and Mars, discussing concepts concerning planets physical condition 03 p0509 A67-13317

Radio observation of Cosmos satellites with flight path inclination angle of 65 and 51 degrees, discussing signal audibility, atmospheric density and ionospheric effects 03 p0518 A67-13540

Syncom III satellite measurement of time variation of total ionospheric electron content [RASSA PAPER 1-10-129] 03 p0417 A67-14240

Interferometric radio observations of Quiet Sun at 49 cm 04 p0694 A67-14486

Tiros VIII, Nimbus I and II and Essa II weather satellites and radio reception of observational results by German meteorological service APT receiver stations 05 p0904 A67-16028

Upper atmospheric turbulence measurements based on radiolocational observation of meteor trains 05 p0796 A67-16211

Radio occultation techniques for analysis of planetary atmospheres and surface topography by measuring perturbations to amplitude and frequency on radio links [AIAA PAPER 67-119] 06 p1087 A67-18454

Radio observation of quasar CTA 102 at

- various frequencies from Arecibo for possible explanation of sinusoidal variation of flux density 08 p1397 A67-21186
- Mars atmosphere and ionosphere analyzed by measuring effect on radio occultation of planet, determining shape, atmosphere density profile, diurnal variations, etc [JPL-TR-32-1157] 13 p2199 A67-26819
- Horizontal loop antenna for observation of whistler-like ELF radio waves between 3 and 60 c/s 14 p2306 A67-27885
- Atmospheric fine structure deduced from radio observation and from turbulence theory 14 p2311 A67-28396
- Goniometric measurements of two angles defining direction of incoming 30 MHz wave reflected by meteor streams, using radio link 14 p2390 A67-28900
- Long-baseline-interferometer observations of radio sources to ascertain angular dimensions of radio sources at LF 15 p2437 A67-30031
- Jovian decametric emission of millisecond pulse variety analysis from observations of four apparitions 15 p2558 A67-30032
- Radio observations of Mercury, Venus and Mars, discussing concepts concerning planets physical condition 16 p2741 A67-30493
- Digital technique for recording of step-frequency ionospheric soundings, obtaining maximum and lowest observed frequencies 16 p2625 A67-31340
- Book on solar radio exploration covering electromagnetic radiation discovery, solar physics principles, solar radio activity and research instruments 16 p2755 A67-31923
- Temperature effect on diurnal variation of hard cosmic ray component based on radio probe observations 17 p2933 A67-32089
- Atmospheric temperature effect on latitudinal curve of cosmic ray intensity determined from radio probe observations 17 p2933 A67-32090
- Matter density and other physical properties of Martian surface estimated from radio and IR observations 18 p3119 A67-33860
- Microwave radio observations of total sun eclipse made in Canada in 1963, discussing solar radio emission [AD-642463] 18 p3133 A67-34487
- Greek space research noting satellite optical tracking, solar photosphere and chromosphere, atmospheric electricity and solar eclipse measurements 19 p3320 A67-35292
- Transit drift-scan observations of radio sources using cornucopia horn reflector antenna 19 p3330 A67-36073
- Relationship between radio galaxies and quasars, observing two sources of moderate distance, noting intense optical emission of limited intensity or duration 20 p3521 A67-36296
- Radio source W49 and anomalous OH emission at radio wavelengths explained as OH formation in electronically excited state by two-body process 21 p3701 A67-37896
- F layer irregularities transverse scale measurements by two-frequency scintillation-ratio technique yielding 600-700 m scales in auroral zone 22 p3789 A67-39470
- Radio observations to estimate chromospheric parameters by measuring fluctuation correlation function of solar radio emission flux 22 p3886 A67-40127
- Apparent Jupiter rotation rate change from decametric emission probability histograms shown to differ from dynamic radiation spectra 23 p4065 A67-41002
- RADIO PROBING**
- Upper ionospheric electron density measurement by signals propagated between two parts of high altitude rocket 10 p1648 A67-23287
- Vertical component of gusts in upper atmosphere estimated from rotation rate of ascending radioprobe fan 12 p1964 A67-26165
- Radio probe to derive relations between ozone content of lower stratosphere and origin of air in layers 15 p2474 A67-29525
- RADIO PROPAGATION**
- SA IONOSPHERIC PROPAGATION**
- SA MAGNETOIONICS**
- Radio wave scattering propagation caused by geomagnetic field aligned irregularities 01 p0021 A67-10334
- Radio pulse pattern from EAS monitored at Yorkshire, England, observed on oscilloscope against galactic noise background 01 p0144 A67-10888
- Radio wave guiding along electron density discontinuity in magnetotonic exosphere, noting low dispersion modes 01 p0027 A67-11259
- Tropospheric and ionospheric models and parameter variations affecting satellite signal propagation, discussing refractive corrections 01 p0028 A67-11431
- Millimeter and centimeter radio wave propagation in near sea level tropospheric waveguides 02 p0191 A67-11569
- Wave seepage through caustic surface in parabolic plasma layer 02 p0191 A67-11582
- Engineering method of calculating Fresnel coefficients based on use of nomograms 02 p0266 A67-11910
- Atmospheric agitation effect on image of extended celestial light sources, showing importance in long-range tropospheric propagation of ultrashort radio wave 02 p0325 A67-11986
- Radio wave propagation in multimode waveguides of arbitrary height, assuming ionosphere boundary to be perfectly reflecting 02 p0198 A67-12070
- Radio star and satellite scintillations, discussing wave propagation through random media, interplanetary scintillations and ionospheric irregularities [RASSA PAPER 1-10-133] 03 p0372 A67-14244
- Ray tracing study of HF ducting propagation with satellites [RASSA PAPER 1-10-145] 03 p0373 A67-14252
- Radio propagation in microwave terrestrial model waveguide of variable surface impedance, using reciprocity theorem 04 p0570 A67-14865
- Angle-of-arrival measurements over troposcatter path by simultaneous reception in angle diversity, using antenna beams 05 p0760 A67-15998
- Radio propagation and ion effects in ionosphere and exosphere observed by spacecraft 05 p0763 A67-16866
- Longitudinal propagation of SLF electromagnetic waves through plane-laminar magnetoactive ionospheric plasma 05 p0765 A67-16955
- Analogy between radiation angular spectrum reflected from rough surface and frequency spectrum of carrier burst related to radio propagation 06 p0957 A67-17579
- Electromagnetic wave propagation around cylinder surrounded by nonmagnetic isotropic medium with dielectric constant function of radius, using conformal mapping 06 p0962 A67-18076
- Radio occultation techniques for analysis of planetary atmospheres and surface topography by measuring perturbations to amplitude and frequency on radio links [AIAA PAPER 67-119] 06 p1087 A67-18454
- HF limits for radio transmission calculated from oblique and vertical sweep frequency records over 2000 km north-south subauroral path 07 p1142 A67-19446
- Fluctuations in diurnal variations of ionization of F-2 layer interfering with radio wave propagation determined by series expansion 07 p1173 A67-19687
- Radio wave propagation in artificial ionized cloud in upper atmosphere determined, using geometrical optics 07 p1143 A67-19691
- Effects of AZA and PCA on radio wave propagation in Antarctic, noting reliability and radiation power requirements 07 p1143 A67-19692
- Propagation difficulties and anomalies caused by characteristic plasma behavior in connection with space mission telecommunication 08 p1293 A67-20684
- Meteor burst radio propagation channel clock synchronization experiment to determine frequency offset between two remotely located frequency standards 09 p1494 A67-21618
- Rectangular terminal block in rectangular waveguide and dispersion equation for surface wave propagating along waveguide 10 p1613 A67-23445
- Satellite emitted radio wave propagation mechanism based on radio wave paths in horizontally inhomogeneous spherically stratified ionosphere with variable electron density 11 p1751 A67-24070
- Solar wind modulation of far daytime field of extra-long radio waves in ionospheric C layer 12 p1933 A67-25549
- Radio propagation in inhomogeneous media with permittivity varying bilinearly with distance, noting model experiment 12 p1908 A67-26220
- Radio propagation influence on performance of azimuth channel of ILS defining characteristics of ILS signals relevant to monitor design 13 p2154 A67-26986
- Propagation measurements at 3.6 and 11 Gc/s over line-of-sight radio path 13 p2071 A67-27401
- HF power from transmitters in drop capsules of tube used for weightlessness experiments, utilizing Goubau transmission line to guide signals toward receiver 14 p2279 A67-27897
- Synthesized summary of reports on radio propagation in nonionized media, noting meteorological radar and precipitation effect 14 p2264 A67-28393
- Clear atmosphere angels origin, clear air turbulence detection, radio propagation and atmospheric radar probing 14 p2264 A67-28395
- Nuclear explosion effects on radio propagation, noting new ionization in ionosphere and radio signals generation 14 p2266 A67-28417
- Earth atmosphere effect on propagation of radio waves from space, image formation, phase stability, technical problems and multiperture instruments 14 p2285 A67-28437
- Frequency spread in ionospheric radio propagation 14 p2273 A67-28712
- Earth magnetic field effect on ultralong radio wave propagation, considering directional effects from planetary inhomogeneities and reciprocity principle impairment 15 p2479 A67-30168
- Spread-F and effects upon radiowave propagation and communication NATO/AGARD Conference, Copenhagen, August 1964
- [AGARDOGRAPH 95] 15 p2479 A67-30273
- Correlation of rainfall rate with attenuation at various frequencies of microwaves 16 p2625 A67-31341
- Path diversity in millimeter waves propagation through rain for various frequency 16 p2625 A67-31343
- Statistical correlation of microwave range variation and dispersion differential measurements over 25 km tropospheric path 16 p2627 A67-31363
- Calculation of Doppler shift of radio waves propagating through changing ionosphere by Fermat principle 16 p2629 A67-31516
- Frequency shifts on whistler mode signals from stabilized VLF transmitter from ionosphere and magnetosphere effects, noting electron density 16 p2631 A67-31856
- Reflection coefficients of sharply bounded ionosphere for plane waves incident from arbitrary direction at magnetic equator 16 p2632 A67-31863
- Influence of aurora on radio wave propagation 18 p3038 A67-33617
- High latitude disturbances influence on VLF propagation, showing high correlation with auroral absorption 18 p3004 A67-34426
- Ionospheric irregularity effect on lateral deviation of reflected radio waves from ionosphere, noting variation with solar activity 18 p3004 A67-34617
- Radio propagation of transmissions from stationary and near stationary satellites used to study anomalous atmospheric refraction at low angles of refraction 19 p3182 A67-35172
- Electromagnetic wave propagation in absorbing gyrotropic medium in terms of geometrical optics, considering applicability to radiowave propagation in upper atmosphere 19 p3185 A67-36015
- Radio wave propagation excitation of second harmonic in nonlinear periodically inhomogeneous communication line 19 p3185 A67-36020
- Chilbolton 25 m steerable antenna for radio wave propagation research 20 p3400 A67-37203
- Ionospheric radio wave theory using coupled vacuum modes with set of coupled wave equations 20 p3389 A67-37709
- Diurnal variation of earth-ionosphere cavity resonances and properties and propagation of ELF, ULF and MHD waves 20 p3390 A67-37727
- Soviet book on ionospheric geomagnetic disturbance prediction and short term radio propagation forecasting

service 21 p3616 A67-37933
 Long radio wave propagation in earth ionosphere waveguide channel, determining eigenvalues of boundary value problem from complex transcendental equation containing Bessel function 21 p3580 A67-38116
 Radio wave propagation in three-dimensional inhomogeneous magnetoactive ionosphere studied by geometrical optics method 21 p3582 A67-38592
 Electromagnetic waves passage through thin radio-transparent layer solved by asymptotic series 21 p3585 A67-38810
 Design studies for reliable long range ground-to-air communication, noting line of sight propagation and HF propagation not involving ionospheric reflections 23 p3972 A67-40742
 Radio wave field strengths received at Ahmedabad from Tashkent and solar X-ray emission effect, noting field strength increase with solar activity 23 p4051 A67-40915
 Magnetic and electric dipole antennas located above earth surface, deriving quasi-static electric and magnetic field components 23 p3981 A67-41210

RADIO RANGE

Construction of three-dimensional polygon intended as geodetic base for intercontinental geodetic connections, using radio rangefinder measurements and synchronous observations of artificial satellites 01 p0060 A67-10853
 Prediction of apparent elevation angle expected for object situated in troposphere at specified values of geometrical elevation angle height 02 p0199 A67-12083
 Construction of three-dimensional polygon intended as geodetic base for intercontinental geodetic connections, using radio rangefinder measurements and synchronous observations of artificial satellites 14 p2311 A67-28242
 Statistical correlation of microwave range variation and dispersion differential measurements over 25 km tropospheric path 16 p2627 A67-31363

RADIO RECEIVER

Receiver design for LF time signals on kilometric waves 02 p0190 A67-11481
 Telemetry receivers capture ratio effect on overall system accuracy, determining effect of IF filter characteristics 02 p0197 A67-12022
 Polarization-diversity telemetry receivers for combining FM/FM penetrometer data, noting signal fading 02 p0198 A67-12024
 Error probability of binary receivers for digital transmission over radio channels characterized by specular and selective fading components 02 p0203 A67-12166
 Electronic testing of transmitters and receivers noting AM and FM systems sensitivity, noise figures and image rejection 04 p0590 A67-15727
 Phase frequency characteristics of two- and three-circuit band pass filters used in radio receiving devices 08 p1305 A67-21279
 Optimum Bayes receiver for fading channels evaluated using Nakagami m-distribution 11 p1766 A67-24645
 Traveling wave maser in radiometry receiver 12 p1951 A67-25295
 Receiver-antenna system in radio astronomy, discussing low noise, thermal signal reception and acquisition of information limited by internal or external noise 12 p1914 A67-25309
 Spread spectrum for amplitude modulated transmitters and receivers 13 p2066 A67-26405
 Extended phase detector for phase-lock loop receivers 13 p2075 A67-26408
 Single-band radio transmitters and receivers and other types of advanced channel diversification and multiplex reception 14 p2273 A67-28861
 Magnetic tape simultaneous recording of radio atmospherics from broadband receivers and from waveform photographs, computing Fourier phase and pulse amplitude spectra 16 p2629 A67-31508
 Signal generator tuning to center frequency of narrow band receivers, noting test setup and procedure 17 p2827 A67-32800
 Microwave direction-finding receiver with digital output for blind aircraft landing and navigational uses 19 p3254 A67-35551
 Estimation of fluctuation sensitivity of measuring radio receiver modulated by

intermediate frequency 19 p3198 A67-36016
 amplifier 19 p3198 A67-36016
 Design and stability of wideband tunnel diode amplifiers for microwave radiolink receivers 20 p3395 A67-36248
 VLF radio wave tracking stations for ionospheric propagation investigation using atomic clock 20 p3386 A67-37481
 Amplification factor stabilization or variance of transistorized radio astronomy receivers, discussing circuit diagram, performance and reliability 20 p3403 A67-37517
 Noise generator for calibration of radio receiver working in 1-2.6 MHz range during rocket flight 21 p3592 A67-38221
 Carrier frequency measurement accuracy using panoramic radio receiver, discussing statistical estimate of errors using two different reading methods 22 p3772 A67-39871
 Balanced SHF transducer for microwave receiver input with separate signal and heterodyne lines coupled by directional bond openings, noting decoupled inputs 22 p3772 A67-39875

RADIO RECEPTION

Diffraction of angular spectrum of radio waves by phase changing screen 06 p0962 A67-17969
 Noise modulation effect on signal distortion by analyzing signal components in terms of noise parameters and of undistorted signal 07 p1147 A67-20240
 High directional gap antenna, considering radiation sources of equal energy located on concentric rings 12 p1914 A67-25311
 Design of broadband steerable Wullenweber antenna arrays allowing HF element rings to be within LF rings 13 p2074 A67-28257
 Optimum system for signal detection with single-band noise modulation during carrier suppression, noting receiving system 15 p2436 A67-29413
 Receiving directional antenna effect on magnitude of frequency correlation in fluctuations of received radio emission 16 p2640 A67-31497
 Soviet book on SHF radio receivers covering theoretical and engineering aspects of component design, control, signal detection, etc 17 p2822 A67-32020
 VLF radio reception anomalies explained by ephemeral natural satellite still in orbit, assuming reflections taking place near satellite perigee 21 p3582 A67-38514
 Random Gaussian signal with unknown mean value reception using adaptive systems 24 p4120 A67-42224

RADIO REFLECTION

Number of reverse signals reflected from F-2 layer during oblique reflection sounding 05 p0802 A67-17145
 Upper atmospheric turbulence and wind measurement by radio reflection from meteor tail 05 p0802 A67-17382
 Ionospheric absorption as indicator of particle flux below point of long radio wave reflection, noting relation to solar cosmic rays 09 p1561 A67-21844
 Ionization density as decisive factor in integral radio wave absorption increase accompanying increase in critical sporadic E layer frequency 10 p1631 A67-22807
 Terrain irregularity influences on radio wave propagation and reflection 14 p2264 A67-28398
 Vertical electron density profile method for determining altitude of lower boundary of ionosphere 17 p2842 A67-32383
 Anomalous magnetic field charts for heights in ionosphere useful for studying auroras spatial distribution and sporadic E layer distribution 17 p2847 A67-32948
 Reflection and scattering from lunar surface of meter radio waves emitted by lunar orbiter 17 p2948 A67-32976
 Bilateral metal grating effect on E and H polarized radiation from plane parallel layer noting intensity, energy density and reflection at interface with medium 21 p3638 A67-37865
 Number of reverse signals reflected from F-2 layer during oblique reflection sounding 21 p3619 A67-38487
 Ionization density as decisive factor in integral radio wave absorption increase accompanying increase in critical sporadic E layer frequency 24 p4150 A67-42144

RADIO RELAY

Radio relay systems with frequency, single

sideband and pulse phase modulation 07 p1141 A67-19342
 Ionospheric waveguide channels for long distance radio links below maximum of F-2 layer 13 p2071 A67-27328
 Electrical design, mechanical fabrication and performance data of integrated broadband balanced transistor amplifier 17 p2825 A67-32599

RADIO SCATTERING

Polarization effects during radio wave scattering by cloud and precipitation particles, obtaining phase state from echo signal 01 p0109 A67-11249
 Radio wave scattering and resonance scattering in wake of body moving in lower ionosphere plasma due to disturbance of electron concentration 02 p0192 A67-11657
 Quasar 3C-48 radio wave scattering by interplanetary plasma 03 p0509 A67-13204
 Dispersion angle of radio waves in interplanetary plasma 03 p0368 A67-13279
 Plasma resonance measurement from radio wave scattering in cylindrical tubes which simulate meteor trail models 04 p0700 A67-15226
 Book on atmospheric absorption, diffusion and polarization of light and radioelectric radiation 06 p0998 A67-18718
 Distribution of instantaneous value of amplitude of signal after scattering on meteor trails 07 p1250 A67-19721
 Increasing effective area of radio telescope antenna by decreasing scattering on struts 08 p1318 A67-21347
 Continuous phase binary FSK communications system operating over linear time-variant random parameter chaff scatter channel 09 p1462 A67-21604
 Distribution formula for unloaded prolate spheroidal receiving and scattering antenna 11 p1758 A67-23974
 Polarization effects during radio wave scattering by cloud and precipitation particles, obtaining phase state from echo signal 11 p1815 A67-24120
 Macroscopic neutral and ionized gas motions in ionospheric D and E layer interpreted from wind and radio wave scattering measurements 11 p1787 A67-24595
 Angular scattering of reflected radio waves from ionosphere, giving results of 300 cases 12 p1933 A67-25547
 Scattering angle of spherical radio waves on isotropic and radially elongated inhomogeneities of supercorona of sun 13 p2197 A67-26543
 Data processing of signal reception from Soviet satellites indicates radio signals scintillation caused by diffraction of waves from ionospheric nonuniformities 14 p2260 A67-27857
 General formulation and solution methods of electromagnetic wave diffraction and scattering problems 14 p2268 A67-28448
 Radio wave scattering and resonance scattering in wake of body moving in lower ionosphere plasma due to disturbance of electron concentration 16 p2624 A67-31072
 Radio ray divergence in ionosphere using computer techniques, noting ionospheric models and limitations 16 p2629 A67-31512
 Increasing effective area of radio telescope antenna by decreasing scattering on struts 17 p2831 A67-31943
 Reflection and scattering from lunar surface of meter radio waves emitted by lunar orbiter 17 p2948 A67-32976
 Ionospheric electron density profile microstructure studied by rocketborne gyroplasma probe discovering electron density irregularities 19 p3217 A67-35202
 Acoustic radio signal backscattering producing rippled signals, showing activity with broad ripple spectrum 19 p3185 A67-36018

RADIO SIGNAL

SA WHISTLER

Geomagnetic field effect on radio signal in oblique reflection sounding, noting differences between daylight and night measurements 02 p0193 A67-11662
 Elevation angle of arrival of ionospherically propagated HF radio signals determined with circular antenna arrays 02 p0217 A67-12088
 Microstructural analysis multiple electron-photon cascade resonance amplifier response to sine-square radio signal 03 p0376 A67-13091

Depolarization of fully polarized electromagnetic waves, obtaining degree of polarization 04 p0575 A67-15151

Book on asynchronous detection and reception of pulsed radio signals at HF and Shf against background of fluctuating noises 05 p0761 A67-16172

Optimal parameters of binary communication system using random coding and orthogonal radio signals with unknown phase 05 p0764 A67-16901

Correlator for determining envelope of autocorrelation function of wideband HF signal, using narrow band video amplifier 05 p0764 A67-16902

Factors governing amplitudes of reradiated signals from tall obstacles distorting VHF and UHF transmission 05 p0766 A67-17296

Radio pulses from air shower detection, noting correlation between shower arrival direction and antenna pattern and shower size and pulse frequency 06 p1076 A67-17554

Plasma induced interference signal in satellite VLF receiver originating with converter system and appearing only in daylight operation 06 p0964 A67-18569

Method for receiving radio signals against background of strong amplitude-modulated noise signal 06 p0965 A67-18898

Buildup effectiveness of sequence of quasi-coherent radio pulses by comb filter matched with ideally coherent signal 07 p1140 A67-19231

Adaptive antenna for ground reception of wideband RF signals in space communications systems 08 p1301 A67-20776

Five to fifty MHz direct reading phase meter with hundredth degree precision 09 p1494 A67-21620

Steady state dynamic properties of large spinning net-like antenna suitable for radio signal reception from space 10 p1727 A67-23753

Pulse compression parallel channel technique for evaluating channel filter characteristics effect on compressed pulse form 11 p1754 A67-24648

Tropospheric condition effect on near-ground ultrashort wave radio signal field-amplitude fluctuation, determining space-time correlation dependencies by radar observation 13 p2067 A67-26688

Radio whistlers occurrence relationship to solar and magnetic activities at various latitudes 14 p2265 A67-28413

Electron density perturbations caused by descending rocket in ionosphere studied by radio pulse signals 14 p2313 A67-28622

Depolarization of fully polarized electromagnetic waves, obtaining degree of polarization 15 p2435 A67-29338

F region irregularities studied by scintillation of radio signals from earth satellites [AGARDOGRAPH 95] 15 p2481 A67-30285

Measurements on scintillation observed on radio signals from Discoverer satellite, noting intensity increase with latitude and data on diurnal variation [AGARDOGRAPH 95] 15 p2483 A67-30293

Optimal parameters of binary communication system using random coding and orthogonal radio signals with unknown phase 16 p2622 A67-30877

Correlator for determining envelope of autocorrelation function of wideband HF signal, using narrow band video amplifier 16 p2622 A67-30878

Geomagnetic field effect on radio signal in oblique reflection sounding, noting differences between daylight and night measurements 16 p2624 A67-31077

Strength of radio signals incoherently scattered from ionosphere and distribution of ionospheric electron concentration 16 p2632 A67-31901

Coefficient characterizing stability of continuous radio signal reflections declining occurrence probability from sporadic ionospheric layer 16 p2669 A67-31907

Radio signals reflection by free radicals in ionosphere, observing predicted intensity and particle detection 17 p2817 A67-33233

Correlation function for random process energy spectrum at linear system output, obtaining expression of envelope distribution for radio signals 18 p2999 A67-33506

Radio occultation measurement of Martian atmosphere over two regions by Mariner IV space probe 18 p3123 A67-34151

Acoustic radio signal backscattering

producing rippled signals, showing activity with broad ripple spectrum 19 p3185 A67-36018

Scattered radio signals received during solar eclipse examined for indication of electron clouds masked by daytime high electron density 20 p3432 A67-37208

Tropospheric condition effect on near-ground ultrashort wave radio signal field-amplitude fluctuation, determining space-time correlation dependencies by radar observation 21 p3582 A67-38430

Seasonal and long term variations in duration of continuous radio signal reflections from sporadic E layer 21 p3623 A67-39038

Selective circuit with FM system and constant gain designed to determine radio whistler arrival direction as function of frequency 21 p3587 A67-39125

Short bursts of scintillation of satellite radio signals from S-66 satellite, discussing diurnal variation correlation with spread of occurrences 22 p3759 A67-39478

Isolated irregularities in auroral ionosphere studied by analyzing radio signals from rockets and Beacon satellite 22 p3760 A67-39627

Correlation between entropy of envelope fluctuation of UHF radio signal and corresponding thermodynamic stability of tropospheric common volume 24 p4124 A67-42810

Radio signals from clouds to yield information on cloud physics, using superheterodyne microwave receivers 24 p4124 A67-42883

RADIO SIGNAL ABSORPTION

Magnetometer predictions of geomagnetic disturbances and intense sporadic E layer occurrences at various sunspot cycle times in auroral zone and effects on VHF absorption 03 p0415 A67-14118

Raindrop and melting hailstone absorption, scattering and backscatter cross sections of millimeter waves in satellite communications and weather radars 04 p0577 A67-15685

Meteoritic dust particle effect on steady state distribution of electrons and ions in lower ionosphere, deriving expression for recombination coefficient from auroral radio absorption data 06 p0995 A67-18074

Diurnal and annual variation of absorption of short waves in ionosphere 13 p2066 A67-26486

Relation between ionospheric no-echo conditions and absorption of cosmic radio noise measured using riometer, plotting diurnal variation values 13 p2114 A67-26794

Correlation of measurements of precipitated electrons with ionospheric effects of winter anomaly in midlatitude D layer 14 p2310 A67-28043

Influence of spread-F upon apparent reflection coefficients of F region for HF radio waves [AGARDOGRAPH 95] 15 p2481 A67-30279

Vertical electron density profile method for determining altitude of lower boundary of ionosphere 17 p2842 A67-32383

Rocket exhaust jet plume effects on radio signal, calculating degradation by electromagnetic diffraction propagation 20 p3381 A67-36570

Block diagram and basic circuit for measuring ionospheric radio wave absorption 21 p3586 A67-39044

F-2 layer contribution to vertical radio wave absorption, using information about structure, electron and ion temperatures 22 p3789 A67-39472

RADIO SIGNAL PROPAGATION

Radio waves and information transmission, discussing antennas, waveguides, diffraction and scattering modulation theory, etc 06 p0962 A67-18071

Spread-F effects on WWV transequatorial propagation of HF radio waves 06 p0964 A67-18575

Scatter propagation due to geomagnetic field-aligned irregularities and calculation of scattering cross section 07 p1143 A67-19675

Maximum signal transfer theorem for radio wave transmission, scattering and subsequent detection 09 p1462 A67-21611

Short term and averaged characteristics of nonreciprocal HF ionospheric single and multipath propagation 11 p1762 A67-24286

Transverse resonance method applied to slotted inhomogeneous circular waveguide

with leaky wave mode propagation 11 p1766 A67-24690

Geographical location and optical path length effects upon fade margin required for desired propagation reliability of microwave signals 13 p2066 A67-26406

Spatial HF radio focusing caused by electron distribution between ionospheric layers, even in absence of horizontal density gradients 14 p2261 A67-28048

Nuclear explosion effects on radio propagation, noting new ionization in ionosphere and radio signals generation 14 p2266 A67-28417

Measurement errors of arrival direction of radio whistler caused by propagation in earth-ionosphere waveguide 15 p2436 A67-29480

Equipment used in rocketborne LF propagation experiment to measure electron distribution in D region of ionosphere 15 p2489 A67-30136

Differential Doppler effect on earth satellite radio signal and application to ionospheric electron density studies 16 p2627 A67-31463

Ionospheric irregularities field alignment responsible for radio signal fading analyzed, showing no evidence for relation to geomagnetic field 22 p3788 A67-39468

RADIO SOURCE

SA QUASI-STELLAR RADIO SOURCE /QSO/

Radio source counts interpretation in support of evolutionary cosmologies 01 p0147 A67-10358

Solar and stellar X-ray astronomy, noting Crab Nebula occultation experiment 01 p0144 A67-10900

Radio sources and background radiation survey at 38 mc/s, presenting contour maps of brightness temperature and list of flux densities 01 p0151 A67-10966

Angular dimensions of radio sources from interplanetary flickering in radio emission intensity used to study structure of sun supercorona at large distances 02 p0322 A67-11684

Nighttime F layer irregularities at equator responsible for scintillation of signals from radio sources and satellites 03 p0407 A67-12828

Maps of 2-cm brightness distribution of various radio sources including Taurus and Orion 03 p0511 A67-13796

Extraterrestrial radiation source spectrum determined by comparing main beam and sidelobe signal power received on suitable bandwidth 03 p0371 A67-13946

Absolute radio luminosity empirical relationship with surface brightness for extragalactic radio sources 03 p0515 A67-14320

Radio source MSH 21-23 observation during lunar occultation, using parabolic antenna and switched-type gain modulated receiver 03 p0515 A67-14326

Identification of strong extragalactic radio sources in declination zone zero to minus 20 degrees 04 p0697 A67-14773

Flux densities of 67 northern radio sources at 6 cm wavelength obtained, using CSIRO radio telescope 04 p0697 A67-14775

Weak radio sources observed with Cambridge one-mile telescope 04 p0698 A67-14808

Lunar occultation of celestial radio sources noting brightness distribution and spectral resolution 05 p0891 A67-16402

Number/flux density relation of radio sources in fourth Cambridge catalog 05 p0902 A67-17286

Clustering of radio sources analyzed using 4C catalog 05 p0902 A67-17289

Radio source diameter measurement through application of interplanetary scintillation, noting angular resolution 05 p0903 A67-17291

Radio sources and supernova theory of north polar Spur 05 p0903 A67-17292

Synchrotron nature of Sagittarius A central component radio spectrum and injection of relativistic cosmic particles 06 p1078 A67-18166

Short duration pulses association with subsidiary B and C sources of Jovian decametric radiation 06 p1086 A67-18375

Solar wind outside ecliptic plane studied, using radio sources scintillation 07 p1249 A67-19660

Enhanced interplanetary scintillations

associated with solar flares from radio sources survey 07 p1243 A67-19667

Time variation of positional angle of polarization plane of radio sources due to Faraday rotation 08 p1388 A67-20987

Technique for observation of 24 discrete radio emission sources at 9.6 cm in August and September 1961 and February through May 1962 08 p1401 A67-21351

Galactic radio sources noting disk model brightness distribution, relativistic particle energies, continuous particle acceleration and ratio between proton and electrical component of cosmic radiation 09 p1563 A67-21629

Radio source scintillations caused by electron density fluctuations extended to regime with large phase fluctuations, discussing autocorrelation function for any regime 09 p1565 A67-22222

Statistical quantities needed to fix scattering regime obtained from observations of radio scintillations, showing correlation length in electron density fluctuations 09 p1565 A67-22223

Interferometer radio observations of two lunar occultations of Crab Nebula 10 p1705 A67-22941

Quasars, energy emission, high red shifts and relation to radio sources and visible stars 10 p1705 A67-22953

Degree of polarization and position angle measurements of linearly polarized components of galactic and extragalactic radio sources at short wavelength 11 p1861 A67-24486

Extragalactic radio sources classified into five groups via radio magnitude and spectral index at 400 MHz 11 p1868 A67-25086

Cosmic x-ray sources identified using Geiger counters aboard rockets, noting clustering toward galactic disk 12 p1994 A67-25760

Pinhole X-ray photography of sun obtained during rocket flight, showing correlation of bright emitting regions on disk with calcium plages and radio emission sources 12 p2007 A67-25762

OH emission regions investigated using Millstone and Haystack antennas with interferometer, noting radio sources for base-line calibration and instrumental phase monitoring 12 p2009 A67-25972

RF sources imbedded in ionized plasma noting developments since 1963 12 p1908 A67-26162

Localization of radio source 3C 17 from moon occultations and identification with near galaxy 12 p2011 A67-26249

Magnetospheres of self-gravitating bodies with reference to radio sources and cosmic ray acceleration 12 p1999 A67-26251

Linear polarization of Crab Nebula, Cygnus A and other radio sources observed at wavelength of 21.3 cm, using radio telescope 13 p2198 A67-26714

Linear polarization of discrete radio sources at 6 cm wavelength 13 p2206 A67-27483

High resolution observations of sources of solar radio burst at 9.4 Gc/s, discussing bipolar structure of compulsive and long enduring bursts 14 p2383 A67-27883

Large scale nonrandom angular distribution of faint radio sources from drift records 14 p2383 A67-27958

Aperture efficiency of Parkes radio telescope reflector for declimeter and centimeter wavelengths obtained through celestial radio source 14 p2282 A67-28035

On-line computers in radio astronomy for measuring radio source flux, position and width and for increasing Dicke radiometer sensitivity 14 p2275 A67-28439

Flux density of variable radio sources with peculiar radio spectra 14 p2386 A67-28446

Association of radio sources with peculiar galaxies in symmetrically distributed pairs 14 p2388 A67-28830

Lunar occultations of two radio sources observed at various frequencies, estimating emersion time 14 p2389 A67-28841

Suggestion of physical association of radio sources with stars in neighborhood as radio stars 14 p2391 A67-28945

Origin of ultrarelativistic cosmic ray particles 14 p2382 A67-29028

Radio sources in declination ranges of minus 07 to 20 degrees and 40 to 80 degrees using Cambridge Interferometer at 178

mc 15 p2551 A67-29095

Dependence of angular dimensions of discrete cosmic radio emission source on radiation flux density and frequency 15 p2549 A67-29140

Cambridge /England/ one-mile radiotelescope for study of extragalactic radio sources, discussing two-dimensional antenna synthesis method 15 p2467 A67-30027

Long-baseline-interferometer observations of radio sources to ascertain angular dimensions of radio sources at LF 15 p2437 A67-30031

Observational evidence disproving cosmological steady state theory in favor of expanding universe 15 p2562 A67-30082

Synchrotron nature of Sagittarius A central component radio spectrum and injection of relativistic cosmic particles 16 p2737 A67-30510

Radio telescopic measurements of brighter planetary nebulae indicating majority are thermal radio sources 16 p2752 A67-31624

Technique for observation of 24 discrete radio emission sources at 9.6 cm in August and September 1961 and February through May 1962 17 p2940 A67-31947

Book on radio astronomy covering history and fundamentals, wave propagation, radio sources, antennas and receivers, Boltzmann law, etc 17 p2943 A67-32432

Weak radio sources of small angular size studied by lunar occultation technique, using steerable telescope 17 p2943 A67-32634

Photoelectric spectrophotometric study of emission line spectrum of quasi-stellar source 17 p2944 A67-32636

Synchrotron radiation spectrum of self-absorbed radio sources for various electron distributions 17 p2947 A67-32755

Solar radio noise source position determined during occultation caused by partial solar eclipse of May 20, 1966 17 p2953 A67-33403

Transit drift-scan observations of radio sources using cornucopia horn reflector antenna 19 p3330 A67-36073

Excitation of earth-ionosphere waveguide by VLF source for case of azimuth dependent properties of source and ionosphere 20 p3428 A67-36373

Upper limit of arc for hydroxyl /OH/ emission region associated with radio source W3, using Michelson interferometer consisting of two spaced radio telescope stations 20 p3523 A67-36648

Galactic radio source W49 at 3.4 mm, showing no additional components in spectrum with turnover points at various frequency ranges 20 p3527 A67-37393

Radio sources fluctuations due to inhomogeneities of solar supercorona and interplanetary plasma, studying solar wind and brightness distribution 20 p3520 A67-37513

Radio source W49 and anomalous OH emission at radio wavelengths explained as OH formation in electronically excited state by two-body process 21 p3701 A67-37896

Diameter and position of radio source 3C 132 determined by lunar occultation, confirming identification with red galaxy 21 p3706 A67-38616

Morphology of Jupiter decametric radio sources 21 p3710 A67-38997

High resolution interferometer data from radio source 3C 273 recorded at NASA deep space stations in Australia 21 p3712 A67-39122

Spectral index dependence on flux density and cosmological red shift, considering model universes populated with radio sources 23 p4062 A67-40634

Atmospheric opacity and extraterrestrial radio source intensity related by improved Taylor series technique using least squares method 23 p4062 A67-40733

[JPL-TR-32-1115] 23 p4062 A67-40733

Free-free radiation absorption from discrete radio sources calculated for various isotropic world models as red shift, electron density and temperature 23 p4063 A67-40777

X-ray survey of Virgo region revealing signals from radio sources 3C 273 and M 87 23 p4061 A67-41473

Relative radio source flux density at 8 GHz for various radio sources 24 p4224 A67-41824

Strong radio sources at 1415 MHz, discussing flux density measurements and

spectra of OQ208 source 24 p4225 A67-41831

Extended radio sources confinement through suggested dynamic process permitting intergalactic medium density deduction possibility 24 p4226 A67-41881

Magnetic field intensity effect of sunspot group on source radio noise flux 24 p4209 A67-42136

Radio evidence for two supernova remnants in Southern Milky Way and observations of shell type radio sources, considering shell model fitting problem 24 p4230 A67-42332

Dependence of angular dimensions of discrete cosmic radio emission source on radiation flux density and frequency 24 p4222 A67-43063

RADIO SPECTROSCOPY

21-cm-wave radiospectrometer with quantum paramagnetic amplifier for investigating radio lines of hydrogen 02 p0241 A67-11638

Statistical investigation of characteristics of chains of type I solar radio bursts including distribution with midfrequency, position on solar disk, lifetime, etc 03 p0508 A67-14359

Radio spectrometer for polarization measurements of galactic emission in meter wave range 08 p1306 A67-21350

Radar measurements of Doppler spectra and power reflectivity of Mars interpreted as surface elevation differences between dark and bright areas 11 p1867 A67-24776

Radio spectrographs for solar observation, broadband and fine structure spectrography techniques and logarithmic amplifiers use in receiver 14 p2386 A67-28443

Radio spectroscopy and quantum electronics - Conference, Poznan, Poland, April 1966 14 p2332 A67-28967

Radio spectrometer for polarization measurements of galactic emission in meter wave range 17 p2822 A67-31946

Red shifts of radio galaxies observed spectroscopically with 120-inch telescope, using prime focus and image tube 20 p3527 A67-37392

RADIO SPECTRUM

Lunar line waveguide parameters calculated for inner conductor displacement and ratio of radii 05 p0775 A67-16958

Antenna temperature in wings of line centered at 61.1506 GHz, comparing experimental and theoretical values on atmospheric oxygen 10 p1632 A67-22857

Evolution of radio spectral index of supernova remnants modeled to include synchrotron radiation energy distribution 11 p1859 A67-24114

MF and HF portions of radio spectrum relationship to communication systems, presenting amplitude and phase variation in conjunction with effects of fading, time and frequency spread and atmospheric noise [IEEE PAPER 19-CP-65-482] 11 p1755 A67-25080

Noise calculation in parametric amplifier using approximation method 12 p1913 A67-25300

Spread spectrum for amplitude modulated transmitters and receivers 13 p2066 A67-26405

Effect of distortion on spectrum of pulse signal with linear frequency modulation 13 p2070 A67-27046

Turbulent spectral density of radio refractive index in surface layer of atmosphere 14 p2262 A67-28379

Flux density of variable radio sources with peculiar radio spectra 14 p2386 A67-28446

Differential departure from thermodynamic equilibrium and electron temperature in gaseous nebulae determined by observing RF emission lines 24 p4225 A67-41825

RADIO STAR SIGNAL

Low noise receivers to achieve high sensitivity and accurate cross correlation measurement of antenna patterns, using radio star sources 02 p0213 A67-11617

Radio star and satellite scintillations, discussing wave propagation through random media, interplanetary scintillations and ionospheric irregularities [RASSA PAPER 1-10-133] 03 p0372 A67-14244

Jovian decametric pulses compared with satellite and radio star scintillations in terrestrial ionosphere [RASSA PAPER 1-10-134] 03 p0373 A67-14245

Bispectral analysis of electromagnetic wave diffraction by ionosphere, obtaining information on altitude and scale of irregularities 10 p1604 A67-22888

Latitudinal variations of ionospheric irregularities studied via synchronous and 1000 km satellites, noting Early Bird data, scintillation index graphs, radio star signals, etc 10 p1640 A67-23234

Degree of polarization and position angle measurements of linearly polarized components of galactic and extragalactic radio sources at short wavelength 11 p1861 A67-24486

Frequency dependence of radio star scintillations 15 p2555 A67-29621

Radio stars as signal sources for accurate measurement of radar antennas vertical polar diagrams, describing solar noise technique disadvantages 15 p2436 A67-29645

Geophysical model of radio star and satellite ionosphere amplitude scintillations at nonequatorial latitudes [AGARDOGRAPH 95] 15 p2482 A67-30286

Radio star fadeouts and radio propagation 15 p2563 A67-30287

Broadband radio star Cassiopeia A scintillations observed with swept frequency interferometer [AGARDOGRAPH 95] 15 p2563 A67-30288

Radio star Cassiopeia A scintillations and spread-F in auroral zone [AGARDOGRAPH 95] 15 p2482 A67-30289

Nature of nighttime F-layer irregularities responsible for scintillation of VHF signals received from radio stars and earth satellites [AGARDOGRAPH 95] 15 p2482 A67-30290

Standard scintillation index method for describing ionospheric effects, discussing power calibration, scaling, deviations, etc 19 p3220 A67-35256

RADIO TELEMETRY

Environmental, physical and practical limitations imposed on telemetry system performance when operating in UHF band 02 p0196 A67-12005

Performance and design characteristics of solid state microwave converters for converting VLF telemetry receivers to L-and S-bands 02 p0196 A67-12006

System design analysis of Edwards high range UHF telemetry receiving station network, considering reliability, availability, design adequacy, antennas, initial and operating costs, etc 02 p0229 A67-12007

Solid state microwave telemetry transmitters, discussing power generation, stability, modulation /AM, PM and FM/, environmental effects and circuitry 02 p0216 A67-12008

Book on principles of construction and theory of main elements and assemblies of analog radio telemetry systems with frequency and time channel separation 03 p0367 A67-13123

PCM telemetry unit for Nimbus B spacecraft noting applications and performance 05 p0767 A67-17463

Quantile system of data compression for space telemetry, discussing operation, efficiency and advantages [JPL-TR-32-772] 07 p1145 A67-19873

Fluctuating effective gain of rocket telemetry links determined from signal strength data of Black Brant sounding rockets 09 p1463 A67-21829

Book on range instrumentation covering optical, radar, support systems, etc 10 p1604 A67-22992

Transducers, transmission systems and display and implementation systems of radio telemetry and effect upon measurement 10 p1605 A67-22997

Solar X-ray data from satellite telemetry, comparing 8-20 angstrom flux with 10.7 cm radio flux 10 p1701 A67-23226

Telemetry transmitters using solid state wideband microwave voltage-controlled oscillators 11 p1753 A67-24442

Aircraft UHF radio system for distance measurements between airplane and two ground stations, noting onboard antenna 11 p1793 A67-24863

Telemetry data processing problems noting error sources, probability distribution of counts in counting processes, sensor relay during motion in varying field, etc 12 p1905 A67-25779

Solar X-ray soft component fluxes observed by satellite 12 p1999 A67-25835

Airborne radio telemetry equipment transmitting in-flight data to ground station for monitoring and analysis, using frequency- and time-division multiplexing 14 p2261 A67-28038

All solid state wideband telemetry transmitters realization by compact high-powered frequency multipliers 14 p2288 A67-28692

Biorthogonal coded telemetry system for deep space applications, discussing construction and performance 14 p2271 A67-28695

Data handling system for 8-bit phase-coherent biorthogonal coded PCM telemeter 14 p2272 A67-28696

Management role in making technical and administrative decisions regarding type of telemetry system required 14 p2272 A67-28698

Omnidirectional radiation pattern for S-band telemetry on rockets more than 1/2 ft in diameter by small electrical separation of antennas [AAS PAPER 67-51] 15 p2454 A67-30116

Design and construction principles of radio telemetry recording systems for gasdynamic observations in ballistic testing 16 p2624 A67-31124

Radio telemetry system for aerodynamic data acquisition from free-flight models in supersonic wind tunnels 16 p2675 A67-31259

Compatible integrated circuits using thin films on silicon for application in space telemetry systems 16 p2641 A67-31559

Predetection telemetry tape combiner 17 p2813 A67-32496

Electronic systems in Ariel III satellite detailing power distribution, storage control, telecommand, telemetry and data handling 17 p2827 A67-32822

Main characteristics of Saphir measurement system, definition of parameters to be measured and design problems 17 p2861 A67-33131

S-band telemetry data during spacecraft launch phases, discussing mission support problems 20 p3380 A67-36561

Biological telemetry scientific classification system based on rules of logic law called division of concept 20 p3374 A67-36671

Surveyor project composite telemetry processing system including signal processor, ground equipment, computer data program, etc 20 p3393 A67-37458

Telemetry antenna of instrument container of D-1 satellites 21 p3592 A67-38218

Radio telemetry links perturbations during ballistic missile reentry due to plasma from kinetic heating 21 p3581 A67-38228

Telemetry receiving station and remote control system for satellites and missiles, measuring Doppler effect, demodulation and diversity combiners 21 p3583 A67-38639

FM/PM and FM/FM radio telemetry in proportional and constant band covering regulation, SNR, noise threshold, etc 21 p3587 A67-39050

Chimpanzee mesenteric artery blood flow for various activities during 24 hr period monitored by radio telemetry 22 p3751 A67-39603

RADIO TELESCOPE

Operation of radio telescope at Cambridge using technique of synthesis to produce aperture one mile in diameter 02 p0322 A67-11584

Large multiplate steerable-beam antenna built by using independent reflectors that redirect energy from desired direction to focus 02 p0210 A67-11592

Constant phase local oscillator distributing signals for radio telescope, measuring phase length of transmission line 02 p0212 A67-11608

Radar mapping of lunar surface made with 10 ft beamwidth antenna at Arecibo, Puerto Rico 02 p0324 A67-11856

Instrument designed for rapid measurement of surface deformations of 210-ft radio telescope at Parkes, Australia 02 p0229 A67-12069

Orbiting radio telescope for cosmic radio wave frequency and amplitude detection 02 p0334 A67-12360

Thermal radio emission from Mercury at 1.9 cm monitored by 140 ft radio telescope using tunnel diode radiometer 07 p1246 A67-19056

Polarization and brightness temperature

distributions across lunar disk observed with Parkes radio telescope at various wavelengths 07 p1251 A67-19854

Radio telescope antenna gain losses due to surface irregularity atmospheric scattering and absorption 07 p1158 A67-20241

Pencil-beam radio telescope adjustment via methods of control of surface of optical telescopes 07 p1189 A67-20244

Soviet papers on radio telescopes 08 p1317 A67-21338

Radio telescope of cross shaped wideband antennas of parabolic cylinder type 08 p1318 A67-21339

Wideband feed for cross shaped antennas of parabolic cylinder type 08 p1306 A67-21340

Wideband feed with electrical scanning of radiation pattern for cross shaped radio telescope 08 p1306 A67-21341

Large radio telescope using short wave parabolic reflectors 08 p1318 A67-21342

Radio telescope antenna phase errors due to structural rigidity and fabrication accuracy 08 p1306 A67-21346

Increasing effective area of radio telescope antenna by decreasing scattering on struts 08 p1318 A67-21347

Sidelobes and amplification factors of narrow beam parabolic antennas in near zone 08 p1306 A67-21348

Radio telescope with spherical reflector and re-emitter placed in mirror focus 08 p1319 A67-21349

Elastic deformation due to structural weight sustained by 22-meter parabolic reflector of RT-22 radio telescope of U.S.S.R. Physics Institute 08 p1424 A67-21354

Illinois 400-ft radio telescope with compromised branching system and traveling wave system as transmission line 09 p1486 A67-22443

Structural design of large orbiting radio telescope employing structural flexibility rather than rigidity for dimensional accuracy 10 p1723 A67-23698

Short wavelength large steerable radio telescope design, considering wind, heat, gravity effects and economics 11 p1768 A67-24777

Nancay radiotelescope energy collection, illumination choice and development 12 p1914 A67-25310

Chromosphere observation at different millimeter radio wavelengths with 4.88-m-diam telescope establishing correlation between mm solar radiation and solar activities 13 p2206 A67-27488

Aperture efficiency of Parkes radio telescope reflector for decimeter and centimeter wavelengths obtained through celestial radio source 14 p2282 A67-28035

Bistatic CW radar observations of Venus conducted by U.S.S.R. and Great Britain during 1966 14 p2265 A67-28403

Radio science, Part 2, Radio astronomy, radio waves and circuits and radio electronics - Conference, Munich, September 1966 14 p2266 A67-28428

Design, principles and applications of optical stellar interferometer, gratings, aperture synthesis and pencil beam telescopes 14 p2284 A67-28429

Large parabolic radio astronomy antennas, discussing design and performance of current and next generation dishes 14 p2284 A67-28430

Noncircular and asymmetrical aperture radio telescopes, considering cylindrical paraboloid, Pulkova and Kraus type Nancay telescopes 14 p2284 A67-28431

Spherical reflector radio telescope design, performance and application, describing parameters of Tokyo, Lockheed, Nancay and Arecibo 14 p2284 A67-28432

One- and two-dimensional antenna synthesis for instruments of large resolving power and effective collecting area 14 p2284 A67-28433

Earth rotation synthesis using arrays of small antennas for better low declination sensitivity 14 p2284 A67-28434

Optimum spacing arrangement for 1100101 array of four antennas in straight line with spectral sensitivity in switched and unswitched cases 14 p2284 A67-28435

Y-shape, T-shape and hollow circle arrays, considering u-v plane coverage, number of antenna elements, etc 14 p2285 A67-28436

Large apertures and arrays for radio telescopes 14 p2285 A67-28449

Linear polarization of lunar radio emission observed using radio

telescope 15 p2552 A67-29149
 Astronomical radio telescope control, noting altazimuth and equatorial modes of operation, overall accuracy, etc 15 p2492 A67-29532
 Cambridge /England/ one-mile radiotelescope for study of extragalactic radio sources, discussing two-dimensional antenna synthesis method 15 p2467 A67-30027
 T-shaped radio telescope operating in decimeter range with electric beam control and frequency independent parameters 16 p2640 A67-31496
 Radio telescopic measurements of brighter planetary nebulae indicating majority are thermal radio sources 16 p2752 A67-31624
 Soviet book on radio telescopes covering design and construction principles, structural considerations, astronomical data, antennas, parabolic reflectors, etc 17 p2831 A67-31934
 Radio telescope of cross shaped wideband antennas of parabolic cylinder type 17 p2831 A67-31935
 Wideband feed for cross shaped antennas of parabolic cylinder type 17 p2822 A67-31936
 Wideband feed with electrical scanning of radiation pattern for cross shaped radio telescope 17 p2822 A67-31937
 Large radio telescope using short wave parabolic reflectors 17 p2831 A67-31938
 Radio telescope antenna phase errors due to structural rigidity and fabrication accuracy 17 p2822 A67-31942
 Increasing effective area of radio telescope antenna by decreasing scattering on struts 17 p2831 A67-31943
 Sidelobes and amplification factors of narrow beam parabolic antennas in near zone 17 p2822 A67-31944
 Radio telescope with spherical reflector and re-emitter placed in mirror focus 17 p2832 A67-31945
 Elastic deformation due to structural weight sustained by 22-meter parabolic reflector of RT-22 radio telescope of U.S.S.R. Physics Institute 17 p2956 A67-31950
 Low noise transistorized amplifier at 408 MHz for synthesis radiotelescope 17 p2827 A67-32785
 Antenna characteristics of Dwingeloo radio telescope, determining directivity, response pattern, ohmic loss, etc 18 p3008 A67-33433
 Two-mirror Nancy radiotelescope 19 p3193 A67-35462
 Circularly polarized radiation from Crab Nebula investigated from radio telescope observations at Arecibo 19 p3316 A67-35802
 Upper limit of arc for hydroxyl /OH/ emission region associated with radio source W3, using Michelson interferometer consisting of two spaced radio telescope stations 20 p3523 A67-36648
 Soviet papers on wideband cross-shaped radio telescope and radio astronomy studies 20 p3402 A67-37504
 Control system of mounting of cross-type radio telescope east-west line, discussing parabolic trusses 20 p3402 A67-37505
 Remote preamplifiers in multielement antenna arrays of radio telescopes operating at meter wavelengths, noting noise temperature effect 20 p3403 A67-37508
 Radio emission point sources fluctuations resulting from interplanetary plasma inhomogeneities observed at meter wavelength 20 p3529 A67-37514
 Radio emission polarization of Crab Nebula on February 1963 with Soviet radio telescope 20 p3529 A67-37516
 Wind perturbation effects on performance of radio telescope servosystems, giving method for determining optimal system parameters 20 p3403 A67-37519
 Very large array /VLA/ of radio telescopes designed based on Ryle aperture synthesis principle, consisting of parabolic antennas and used for radio maps 23 p3978 A67-40798
 Radio telescope design, considering sensitivity and resolving power, discussing classical optics and multiplicative antenna based telescope 23 p3980 A67-41081
 Circular and linear polarization of OH line radiation from NGC 6334 nebulae region using Parkes radio telescope 24 p4230 A67-42333
 Linear polarization of lunar radio emission observed using radio telescope 24 p4239 A67-43072
RADIO TRACKING
 Direction finder accuracy optimization,

considering automatic tracking of target angular coordinates 01 p0024 A67-10721
 Trajectories of artificial celestial bodies - Symposium, Paris, April 1965 05 p0893 A67-16554
 Masses of moon and Venus and astronomical unit determined from Mariner II Doppler data, noting sources of error 05 p0895 A67-16575
 Estimated GM values of earth and moon, tracking station locations and lunar radii at impact points, from DSIF radio tracking data of Ranger Block III lunar flights [AAS PAPER 66-105] 07 p1253 A67-19965
 Optical and radio orbit tracking facilities, analyzing data accuracy levels, minitrack functions, etc 09 p1464 A67-22055
 Book for amateurs on observing earth satellites including methods and discoveries about upper atmosphere and shape of earth 10 p1608 A67-23620
 Systematic local errors in radio leveling of aircraft for different scales and tracks, using aerial camera 13 p2118 A67-26482
 Estimated GM values of earth and moon, tracking station locations and lunar radii at impact points, from DSIF radio tracking data of Ranger Block III lunar flights [AAS PAPER 66-105] 13 p2208 A67-27523
 High accuracy radio guidance and tracking station, discussing relation between basic station parameters, error sources and associated error 14 p2260 A67-27972
 Radar, radio, photographic and visual satellite tracking methods 15 p2437 A67-30084
 Satellite tracking, noting radio, radar and laser methods, and visual and photographic observations 16 p2630 A67-31765
 Radio, radar and optical methods for close earth satellites tracking, advantages and limitations 18 p3003 A67-34235
 Radio and radar tracking at Royal Radar Establishment at Malvern, discussing equipment, accuracy, alignment, performance, operation, drag and decay 18 p3048 A67-34239
 Phase measuring equipment and instrumental performance of radio tracking station at Winkfield 18 p3048 A67-34240
 Sensitivity analysis method for poorly known model parameters and preliminary computer load requirements applied to radio tracking of space vehicles [ELDO-TM-F-5] 24 p4122 A67-42385
RADIO TRANSMISSION
SA SHORT WAVE RADIO TRANSMISSION
 Experimental aperture-to-medium coupling loss between one and two large antennas 02 p0213 A67-11620
 External ionosphere electron concentration measurement from data on Doppler shift variations in frequency of coherent radio signals from Cosmos and Elektron satellite 02 p0192 A67-11658
 Simulcast /simultaneous broadcasting technique/ has higher average signal power than one transmitter alone and low data rate 02 p0202 A67-12128
 Coherent interaction of two radio waves in plasma, generation of mutually-harmonic frequency wave and application to radio transmission in ionospheric F layer 03 p0372 A67-14091
 Automatic recording equipment measuring polarization angle of Syncom III 137 mc/s radio signal and determination of ionospheric total electron content 03 p0415 A67-14110
 Propagation of clear air radar echoes in nonionized media and use in determining planetary surface and atmospheric structure 05 p0760 A67-16009
 VHF and UHF communications between transoceanic commercial aircraft and ground stations by means of aeronautical communication satellites 06 p0961 A67-17701
 Interference problems caused by spurious radio transmissions, analyzing radiation spectrum utilization 08 p1301 A67-20773
 Computer method study of reflection and transmission coefficients in VLF range, noting effect of ionospheric D region electron density profiles 11 p1752 A67-24219
 Phase measurements of VLF transmission over long distance transequatorial path 12 p1906 A67-25942
 Passive reactive circuit conversion into circuit that shapes radio pulse with rectangular envelope 13 p2069 A67-27042

Clock synchronization with artificial satellites for precise time and frequency, comparing two-and one-way transmission and reception 14 p2263 A67-28391
 External ionosphere electron concentration measurement from data on Doppler shift variations in frequency of coherent radio signals from Cosmos and Elektron satellite 16 p2624 A67-31073
 Navigation system by measurement of Doppler shift in radio transmissions from satellite and equipment for measurement 16 p2701 A67-31272
 Policy decisions in space broadcasting, emphasizing range of possibilities allowed and limits imposed by technical factors 20 p3378 A67-36121
 Radio interior communication /RADIC/ system used in Apollo program, discussing future capabilities and advantages 20 p3380 A67-36559
 Instrument errors in HF radio rangefinder 20 p3446 A67-36632
 Transmission phenomenon of inhomogeneous electromagnetic wave in negative permittivity medium 23 p3975 A67-41480
 VLF transmissions during SIDs for compatibility with general form of theory of waveguide mode propagation 24 p4149 A67-42067
RADIO TRANSMITTER
 Solid state microwave telemetry transmitters, discussing power generation, stability, modulation /AM, PM and FM/, environmental effects and circuitry 02 p0216 A67-12008
 40 watt solid state UHF AM transmitter at 225.400 mc 02 p0219 A67-12111
 High power CW radar transmitter, discussing design parameters, development and performance characteristics 04 p0596 A67-15051
 TWT delivering CW power in L, S, C and X-band designed for space environment, considering size, weight and voltage and comparing klystrons, amplifiers, circuit design, etc 06 p0967 A67-17688
 Semiconductor devices in radio transmitters, examining operation of transistorized amplifiers and varactor multipliers in output stage 06 p0971 A67-18214
 Device for parallel combination of radio transmitters 08 p1294 A67-20777
 Transducers, transmission systems and display and implementation systems of radio telemetry and effect upon measurement 10 p1605 A67-22997
 Silk screen techniques used for film circuitry implementation on integral sensor telemetry-transmitter with standard components 12 p1911 A67-25272
 Spread spectrum for amplitude modulated transmitters and receivers 13 p2066 A67-26405
 Communication satellite program research 14 p2269 A67-28455
 Single-band radio transmitters and receivers and other types of advanced channel diversification and multiplex reception 14 p2273 A67-28861
 Semiconductor devices in radio transmitters, examining operation of transistorized amplifiers and varactor multipliers in output stage 16 p2635 A67-30480
 Satellite telemetry system transmitter optimization, noting error probability criterion, average power constraint, etc 16 p2622 A67-30693
 VLF transmitter design criteria and characteristics for global time and navigation signal network 17 p2824 A67-32494
 Instrument-landing system including microwave apparatus 19 p3255 A67-35867
 Satellite system with solid state transmitters with different frequencies in HF band for ionospheric guided propagation research 20 p3394 A67-36246
 Compact ionospheric station for six fixed frequencies, compared with automatic station 21 p3586 A67-39047
RADIO WAVE
SA COSMIC RADIO WAVE
SA GALACTIC RADIO WAVE
SA SOLAR RADIO WAVE
 Equilibrium of plasma excited by radio wave in low pressure gas in presence of magnetic field 01 p0124 A67-10811

Mitra three-receiver method improvement for measuring winds and diffraction of radioelectric waves in 03 p0406 A67-12819

Fading characteristics of radio waves reflected from sporadic E layer of ionosphere over magnetic equator 03 p0406 A67-12824

Spaced receiver method for measuring ground diffraction pattern of vertically reflected radio waves 03 p0407 A67-12830

Spaced antenna technique for determining drift and anisotropy of equatorial E and F region irregularities 03 p0407 A67-12833

Theoretical curves for day and night time conditions for variation of peak frequency of radio atmospherics with distance computed from source spectrum and dominant propagation mode 03 p0415 A67-14117

Fluctuation characteristics and spectrum of monochromatic radio waves when propagating in interplanetary medium 04 p0575 A67-15163

Whistler recordings on thermal plasma motions and ionization density near magnetospheric knee, noting whistler attenuation VLF noise, ion effects, electron temperature, etc 05 p0795 A67-16011

Atmospheric radio wave absorption at wavelengths ranging from 1.36 to 3.0 mm, determining absorption coefficients of molecular oxygen and water vapor 05 p0761 A67-16343

Daytime profile of electron density in C and D layers of ionosphere from measurements of surface ultralong wave fields and atmospheric pressure profile 05 p0801 A67-17131

Microradiowave absorption in air by water vapor dimers 06 p0963 A67-18206

Tabulation and plotting of VLF radio wave diurnal phase changes as function of frequency and path 07 p1142 A67-19450

Antenna orientation effect on polarization components of radio waves reflected from ionosphere, noting occurrence and properties of magnetotonic component of polarization 07 p1173 A67-19690

Phase variation dependence at receiver output on polarization of wave incident on antenna of phase measuring system 07 p1144 A67-19694

Absorption coefficient of water vapor in relative windows of transparency for millimeter and submillimeter radio waves 08 p1294 A67-20817

Lunar radio brightness distribution measured at various wavelengths, determining surface temperature decrease and dielectric constant 08 p1390 A67-21023

Geometric analysis of refractive index, absorption index and polarization characteristics of ionospheric radio waves 08 p1295 A67-21168

Amplification of RF wave in partially ionized gases with large Ramsauer effect in absence of magnetic field, due to negative absorption of stimulated bremsstrahlung 08 p1366 A67-21442

Deflection absorption of radio waves in ionosphere 09 p1491 A67-21845

Virtual heights and absorption of radio waves in ionosphere, discussing methods of computation 09 p1464 A67-22441

Ionospheric movement measurement with LF radio waves, using triangulation coupled with cross spectrum analysis of signal fading 11 p1784 A67-23936

Ionospheric electron density profile measurement via radio wave interaction technique, noting superiority of partial reflection method 11 p1785 A67-23946

Ionospheric absorption determination by measuring amplitudes of wave components of satellite transmission 11 p1786 A67-24059

Irregular refraction of radio waves by large ionospheric inhomogeneities elongated close to meridional direction 11 p1787 A67-24477

Scintillation characteristics of radio waves after passing through ionosphere 13 p2115 A67-26857

Doppler frequency changes of ionospheric propagating radio waves and relationship to geomagnetic variation 13 p2068 A67-26992

Distribution of radio brightness temperature over disk of Venus 13 p2200 A67-27333

Radio waves effect on ionospheric F layer, showing decrease in critical frequency and

disturbance of stationary electron and ion concentration 14 p2307 A67-27923

Terrain irregularity influences on radio wave propagation and reflection 14 p2264 A67-28398

Measurement of angular spectrum of radio waves from sources outside solar system 14 p2386 A67-28445

Sporadic E layer scintillation effects on amplitude of 137 MHz radio waves from Early Bird 14 p2270 A67-28577

Goniometric measurements of two angles defining direction of incoming 30 MHz wave reflected by meteor streams, using radio link 14 p2390 A67-28900

Fluctuation characteristics and spectrum of monochromatic radio waves when propagating in interplanetary medium 15 p2435 A67-29350

Troposphere and ionosphere effects on different frequency radio wave propagation for space communication [AAS PAPER 67-93] 15 p2437 A67-29953

Diffraction of HF radio waves by ionospheric layer containing field-aligned inhomogeneities [AGARDOGRAPH 95] 15 p2482 A67-30291

F scatter, flutter fading and maximum usable frequency phenomenology from HF radio propagation studies near equator 15 p2438 A67-30297

Ionospheric electron content as function of longitude and latitude calculated from Faraday fading of radio waves 16 p2627 A67-31362

Magnetic tape simultaneous recording of radio atmospherics from broadband receivers and from waveform photographs, computing Fourier phase and pulse amplitude spectra 16 p2629 A67-31508

Radio wave trapping and guiding along magnetic field lines by irregularities in electron density 16 p2667 A67-31513

Numerical analysis of ionospheric radio wave propagation, examining, attenuation polarization and power flow as function of electron density profiles 16 p2631 A67-31857

Changes of phase and signal amplitude of VLF radio waves during solar flares noting waveguide mode 16 p2632 A67-31859

Microradiowave absorption in air by water vapor dimers 17 p2817 A67-33219

Radio wave absorption associated with auroras 18 p3038 A67-33619

Small correlated amplitude and frequency fluctuations of stochastically-modulated radio waves 19 p3241 A67-36025

Ionospheric radio-wave absorption measurement by multiple and single echo techniques, applying vertical probing at fixed frequencies 20 p3378 A67-36124

Propagation characteristics of ELF electromagnetic waves investigated below anisotropic ionosphere, considering magnetic field 20 p3379 A67-36282

Light deflection by solar gravity measuring method using radar interferometer 20 p3485 A67-36995

Chilbolton 25 m steerable antenna for radio wave propagation research 20 p3400 A67-37203

VLF radio wave tracking stations for ionospheric propagation investigation using atomic clock 20 p3386 A67-37481

Gravitational radio wave frequency shift from satellite measurements, noting satellite-ground radio communication system 20 p3386 A67-37524

Scintillation depth measurement relationship with probability density of amplitude distribution 21 p3617 A67-38002

Daytime profile of electron density in C and D layers of ionosphere from measurements of surface ultralong wave fields and atmospheric pressure profile 21 p3619 A67-38474

Far tropospheric propagation of radio waves due to coherent scattering, explaining signal level dependence on distance and wavelength and signal fading 21 p3585 A67-38814

Launcher for trapped surface waves over ice-covered sea by ferrite loaded horn device 22 p3763 A67-40306

MF surface wave launching over earth, considering field strength at ground for given radiated power 22 p3763 A67-40315

Fading rate relation to ionospheric drift speed of radio waves, estimating size of irregularities 23 p3996 A67-41083

RADIO WAVE REFRACTION

Oscillations of vertical component of ionospheric refraction measured, using cliff radio interferometer and signals from satellites 01 p0022 A67-10390

Tropospheric and ionospheric models and parameter variations affecting satellite signal propagation, discussing refractive corrections 01 p0028 A67-11431

Radio data suggests dielectric constant variations in troposphere limited to discrete scale sizes [RASSA PAPER 1-10-141] 03 p0417 A67-14249

Sunset peak in occurrence of F layer field-aligned echoes explained by Martyn amplification mechanism, estimating ionization vertical velocities from electron number density 04 p0615 A67-14959

Frequency correlation of ionospheric radio waves in inhomogeneous thin layer medium and effect of irregular horizontal ionization gradients 07 p1144 A67-19836

Irregular refraction of radio waves caused by large scale electronic inhomogeneities in ionosphere 08 p1326 A67-21352

Radio refractive index irregularities in lower troposphere examined, using helicopter mounted spaced cavity refractometer 11 p1787 A67-24644

Doppler frequency shift for radio waves radiating coherently from satellite in ionosphere, considering electron concentration and angles of refraction 13 p2067 A67-26568

Turbulent spectral density of radio refractive index in surface layer of atmosphere 14 p2262 A67-28379

Irregular refraction of radio waves caused by large scale electronic inhomogeneities in ionosphere 17 p2841 A67-31948

Wave equation for electromagnetic wave propagation in randomly varying refractive index medium, noting focusing for radio waves in interplanetary plasma 20 p3386 A67-37521

Radio wave refraction and refraction-induced errors calculated in determination of artificial satellite trajectories 21 p3582 A67-38593

Plasma spatial electron density distribution from refraction of microwave beams with several frequency components 21 p3670 A67-38689

Spherical electromagnetic wave refraction on heterogeneous parabolic plasma layer using beam optics 22 p3760 A67-39737

Six-stage monogram for refraction of radio wave entering earth atmosphere in terms of meteorological conditions and wave elevation angle 23 p3975 A67-41212

RADIOACTIVE CONTAMINATION

Radioactive contamination of high flying aircraft, discussing empirical observations and possible decontamination procedure 05 p0751 A67-16300

Surface air radioactivity and ozone measurements in Antarctica reveal fission product yearly oscillation 20 p3429 A67-36871

Random intact reentry and earth burial for radioisotope thermoelectric generators disposal without atmospheric contamination, evaluating design concepts for SNAP systems 24 p4241 A67-42559

RADIOACTIVE DATING

Age determination of iron meteorites by comparing isotopic abundance of primordial potassium in inclusions with terrestrial standards 02 p0326 A67-12044

Spallation produced Ar 40 in iron meteorites for determining cosmic ray exposure ages from radiogenic Ar 40 content 02 p0326 A67-12308

Potassium-argon age of metal phase of Weekeroo Station iron meteorite 08 p1400 A67-21265

Radioactive krypton content in stone meteorites determined via mass spectrometry, deriving spall ratios and radiation ages 11 p1866 A67-24692

Meteorite age and related problems of cosmic chemistry 12 p1903 A67-25429

Xenon-iodine dating, sharp isochronism in chondrites 12 p2002 A67-25525

Techniques for determining cosmic ray age and stable and radioactive nuclide production rates in meteorites 14 p2380 A67-27968

Isotope fractionation processes and reproducibility of age of iron meteorites studied from cosmic ray exposure

ages 15 p2556 A67-29664
 Age determination of iron meteorite by Rb-Sr isotopic analyses of silicate inclusions, proving formation of younger solid objects in solar system 16 p2749 A67-31434
 Light and heavy rare gases content in St Severin meteorite and iron-enriched fractions 16 p2750 A67-31435
 Spallation and fissionogenic xenon and krypton content in Pasamonte achondrite as evidence for extinct radioactivity in meteorites 16 p2754 A67-31747
 Slow motion gamma spectrometry for measurement of sodium 24 abundance in Saint Severin meteorite, evaluating modes of formation 16 p2754 A67-31790
 Geomagnetic field intensity influence on atmospheric C-14 production, using two-reservoir model 21 p3620 A67-38981
 Strontium and rubidium 87 measurements on iron meteorite silicate inclusions, with age determination at 4.4 to 4.8 billion years 22 p3881 A67-39495
 Cosmogenic radioactivity in freshly fallen meteorites measured and compared to calculate terrestrial and exposure ages and spatial and time dependence 24 p4238 A67-42884

RADIOACTIVE DECAY

SA VECTOR CURRENT

Simulated radioactive decay experiment using random number generator or set of random numbers 01 p0112 A67-10826
 Absolute age of earth, heavy elements and meteorites determined by radioactive decay measurements, comparing present and initial ratios of uranium 235 and 238 02 p0329 A67-12496
 Measurement of half-life of 14.4 kev level of 57 Fe with scintillation detectors and digital timer 03 p0471 A67-13225
 Gas laser spectroscopic analysis of hyperfine structure, paramagnetic properties, radiative lifetimes and Doppler-broadened transition saturation behavior of excited states of Xe 129 04 p0661 A67-15462
 Absolute age of earth, heavy elements and meteorites determined by radioactive decay measurements, comparing present and initial ratios of uranium 235 and 238 10 p1709 A67-23364
 Zodiacal dust explained by radioactive Al 26 deposited in marine sediments and brought by micrometeorites exposed to solar protons 15 p2553 A67-29157
 Energy level behavior of metastable alkali atoms against autoionization and radiative decay 20 p3492 A67-37691
 Computer calculation of 1 Mev electron flux and irradiation degradation of solar cell I-V curves for charged particle environment 23 p3940 A67-41514

RADIOACTIVE ELEMENT

SA PLUTONIUM

Lunar gamma radiation intensity and spectral composition from Luna X data, deducing cosmic ray and radioactive decay origins 01 p0150 A67-10905
 Radiotracer propellant gauge for zero gravity space environmental conditions using radioactive krypton 85 10 p1656 A67-23078
 Lunar thermal history computed for different radioactive elements distribution 18 p3119 A67-33862
 Possibility of determining content of natural radioactive uranium, thorium and potassium in lunar rocks and of estimating chemical composition of rocks from cosmic ray induced radioactivity 18 p3122 A67-34142
 Lunar rocks composition and radioactivity through satellite gamma-ray measurements indicating basaltic and ultrabasic composition 19 p3319 A67-35258

RADIOACTIVE FALLOUT

Radioactivity, using Cs137 isotope as radioactive agent, in civilian Norwegian pilots 15 p2429 A67-29283

RADIOACTIVE ISOTOPE

SA ALUMINUM 26
 SA ARGON 40
 SA CESIUM 137
 SA COBALT 60
 SA HELIUM 3
 SA IRON 57
 SA PHOSPHORUS 32
 SA PLUTONIUM 238
 SA PLUTONIUM 239
 SA SODIUM 24
 SA STRONTIUM 90
 SA URANIUM 235

SA URANIUM 238

Diffusion parameters and solubility of Cd in InAs measured with aid of radioactive isotopes compared with diffusion coefficient measurement by p-n junction method 01 p0128 A67-10082
 Hartree-Fock-Slater calculation of internal conversion coefficients for magnetic multipoles for yttrium-87 with 0.05 or 0.15 mc-square gamma energy values 01 p0116 A67-10203
 Thermoradiolotope propulsion and integrated power application to cislunar and planetary space missions 01 p0155 A67-11413
 Galactic and solar nucleosynthesis, determining formation of meteorites on basis of decay of nucleides Pu 244 and I 129 02 p0320 A67-11472
 Emission, collection and analysis of radioactive rare gas xenon 133 as atmospheric tracer whose inert characteristics allow diffusion processes to be followed 02 p0237 A67-11854
 Radiolotopes for aerospace - symposium, Dayton, February 1966, Part 1, Advances and techniques 02 p0243 A67-12207
 Radiolotope sources used for simulating space radiations, obtaining energy spectra by blending beta emitters 02 p0285 A67-12213
 Kryptonate /radioactive source with Kr 85/ for temperature profiles of turbine blades, missile gas analysis, corrosion, oxidation, etc 02 p0285 A67-12214
 Gamma, bremsstrahlung and X-ray radiation limitations in aerospace application 02 p0286 A67-12217
 Transport jet engine inspection with radioactive isotopes, noting techniques and results 02 p0303 A67-12219
 Radiolotope tracers used to determine crack initiation and propagation characteristics in reinforced plastic composite materials, relating discontinuity growth to test conditions 02 p0249 A67-12222
 Electrical conductivity and Hall coefficient temperature dependence in pure and alloyed Te 03 p0492 A67-13344
 Rare earth trace element variations in anorthosite and quartz mangerite determined, using stable isotope dilution technique of analysis 03 p0513 A67-14006
 Specific radioactivity of Sb-124 and effect on diffusion of antimony in Sb-doped n-type Ge single crystals and Ga-doped p-type Ge single crystals 03 p0500 A67-14067
 Radiolotope application to spacecraft propulsion and integrated power noting potential sources, thruster design concepts and mission types 04 p0655 A67-14554
 Meteorite size prior to entering atmosphere, noting radius and use of isotope activity nomogram 04 p0702 A67-15751
 Space energy supply plant with nuclear energy sources, noting transformer design 04 p0558 A67-15958
 Radiolotope sources and nuclear reactors as energy sources for space vehicles 04 p0558 A67-15959
 Radionuclide generators with thermoelectric transformer for space application 04 p0559 A67-15960
 Radio nuclide generator using oxide of strontium 90 with thermionic converter, noting decaying characteristics 04 p0559 A67-15963
 Radioactive isotopes in iron meteorite used to determine cosmic ray origin and to study nuclear processes in early history of solar system 05 p0877 A67-16084
 Radiolotopes for aerospace - Symposium, Dayton, February 1966, Part 2, Systems and applications 05 p0840 A67-16526
 Feasibility of making continuous measurements of ablation of spacecraft heat shield by use of radiolotopes embedded in heat shield 05 p0841 A67-16529
 Radiolotopes for army aviation applications, stressing need for ballistic protection of crew members and critical components 05 p0841 A67-16534
 Operational spacecraft fuel gauging system based on application of radiolotope techniques 05 p0841 A67-16536
 Radiolotope and phosphor research and increased brightness of self-luminous devices 05 p0842 A67-16543
 Fission or radiolotopic nuclear radiation applied to laser pumping, discussing forms, sources, power, solid state and molecular gas lasers, energy transfer, optical fluorescence and cut-off phenomenon 05 p0814 A67-16547

Gulliver radiolotopic biochemical probe to detect extraterrestrial life 05 p0806 A67-16548

Radioactive clathrate technique to detect reactive gaseous contaminants in atmosphere in parts per million range 05 p0843 A67-16550
 POODLE low thrust radioactive propulsion technology, discussing operation, mission application, tests, capsule and thruster performance 05 p0843 A67-16551
 SNAPOODLE isotope thruster/electric power unit, discussing thermal analyses, thruster and electrical performance and mission applications 05 p0753 A67-16552
 Program for radiolotopic power on Nimbus B spacecraft provided by SNAP-19 generators 05 p0843 A67-16553
 Neutron produced phosphorus 32 measurement in Barwell and St. Severin meteorites 06 p1078 A67-17604
 Isotope effects on superconducting transition temperature of molybdenum boride and tungsten boride 06 p1047 A67-17642
 Radioactive tracer technique for measurement of yield and angular distribution of molybdenum sputtered by cesium ion beam 06 p1036 A67-18139
 Solid, liquid and gaseous core and radiolotope nuclear rocket engines, discussing thrust levels and other performance characteristics 06 p1030 A67-19024
 Voltage transformation and power/energy utilization of radiolotopic thermoelectric generator source /RTG/ for space applications, analyzing components, inverter/converter circuits, etc 08 p1284 A67-20694
 Diffusion parameters and solubility of Cd in InAs measured with aid of radioactive isotopes compared with diffusion coefficient measurement by p-n junction method 08 p1371 A67-21459
 Plasma characteristics of partially dissociated and ionized air due to alpha emissions from radiolotope surface material 09 p1543 A67-21819
 Isotope analysis of iron migration in Ni-Cd cells with pocket electrodes 09 p1458 A67-22178
 Evolution of radiocarbon concentration at low latitudes of Northern Hemisphere during past nine years explained by south equatorial maritime current 09 p1492 A67-22592
 Radiolotope applications to space science, discussing selection criteria for electric energy production and/or space propulsion 11 p1817 A67-24096
 Transition temperatures of Be compounds, noting evidence for strong coupling to Mo localized mode from observed isotope effect 11 p1846 A67-24582
 Cosmic ray spallation and special anomaly in achondrites 11 p1866 A67-24696
 Wideband-gap high atomic number semiconductor materials for high temperature counting radiation detectors 12 p1985 A67-25862
 Radiolotope application to spacecraft propulsion and integrated power noting potential sources, thruster design concepts and mission types 13 p2155 A67-26578
 Electrical conductivity and Hall coefficient temperature dependence in pure and alloyed Te 13 p2184 A67-27718
 Radioactive isotopes from cosmic ray action in atmosphere and nonatmospheric sources, discussing geophysical mixing and dispersion 14 p2380 A67-27967
 Radiolotope selection criteria for propulsion and auxiliary power generation in space 14 p2348 A67-27971
 Liquid scintillation counting method with sonic oscillations, noting decreased preparation time and increased counting efficiency 14 p2260 A67-28477
 Isotope fractionation processes and reproducibility of age of iron meteorites studied from cosmic ray exposure ages 15 p2556 A67-29664
 Book on radiolotope measurement applications in engineering covering nuclear radiation, gas detectors, scintillation, etc 15 p2516 A67-29900
 Nuclear reactor use in space environment as energy source for chemical synthesis and laser action [AAS PAPER 67-115] 15 p2558 A67-29962
 Carbon monoxide chemisorption on

- polycrystalline molybdenum studied by radiotracer, noting desorption at various temperatures as time function 15 p2434 A67-30099
- Thermionic space power systems, examining solar, radioisotope and nuclear reactors as heat sources, discussing power density and electrode affinity 17 p2802 A67-32050
- Testing for leak-proof encapsulation of semiconductor devices by use of krypton 85 as radioactive tracer gas 17 p2823 A67-32297
- Electrohydrodynamic flow laminarization with tritium ionizer, obtaining Poiseuille flow stability 17 p2839 A67-32907
- Carbon dioxide laser emission, discussing extension of wavelength range with carbon isotopes 17 p2869 A67-33062
- Performance of radioisotope heated ammonia thruster for spacecraft application [AIAA PAPER 67-425] 18 p3075 A67-33909
- Radioisotope heated hydrogen thrusters for propelling high energy upper stage, discussing performance, payload advantages and high energy kick stage [AIAA PAPER 67-509] 18 p3113 A67-33973
- Possibility of determining content of natural radioactive uranium, thorium and potassium in lunar rocks and of estimating chemical composition of rocks from cosmic ray induced radioactivity 18 p3122 A67-34142
- Germanium tetrachloride purification process by radiochemical analysis and radioactive tracers investigated to determine possible simplification 18 p3104 A67-34600
- Radioisotope heating to provide ionizer temperatures in contact ion thrusters [AIAA PAPER 67-734] 21 p3695 A67-38757
- Radioisotope heating for ionizer temperature of contact ionization thrusters for satellite attitude control and stationkeeping, studying power source mass saving [AIAA PAPER 67-735] 21 p3695 A67-38758
- Heterodiffusion of metallic impurities in body-centered phases of doped zirconium and titanium, determining diffusion coefficients via radioactive isotopes 22 p3820 A67-39823
- Radioactive isotopes for aviation and space medicine, treating hemodynamic phenomena, metabolism, cytophysiological investigations and fluids distribution in organism 22 p3756 A67-40547
- Positive isotope effect on superconducting transition temperature of alpha uranium 23 p4044 A67-41439
- Radioisotopic color coded pulmonary lung scanning, diagnostic test in experimental decompression sickness 23 p3956 A67-41626
- Iodine isotope mass-yield distributions from spontaneous plutonium 242 fission, discussing heavy xenon isotopes from extinct plutonium 244 in meteorites 24 p4191 A67-42450
- Systems optimization methodology to analyze radioisotope thermoelectric generators /RTG/ for spacecraft applications, discussing computer program 24 p4184 A67-42504
- Large long-life power supply system designed for earth orbiting spacecraft, discussing radioisotope interchangeability, controlled intact reentry, etc 24 p4184 A67-42505
- High temperature Pu 238 heat source fuel capsule operable in space environment is applicable to thermoelectricity and Brayton cycle, discussing design and test program 24 p4185 A67-42536
- Stirling, Brayton and Rankine dynamic cycles compatibility with isotope heat sources, emphasizing power system applications to long-duration earth orbital missions 24 p4185 A67-42542
- Galactic cosmic ray solar cycle and secular variations in bombardment of meteorites at average meteoroid solar distance and 1 AU from radioactive isotope ratios 24 p4210 A67-42622
- Rare earth and barium abundances in Ivory Coast tektites and rocks determined by isotope dilution 24 p4236 A67-42645
- Radioactive isotopes in iron meteorite used to determine cosmic ray origin and to study nuclear processes in early history of solar system 24 p4212 A67-42760
- Isotope ratios of fission and spallation xenon in meteorites from abundance data analysis by least squares method 24 p4238 A67-42886
- Advanced radioisotope thermoelectric generator /RTG/ system designs employing SiGe direct radiating power conversion subsystems 24 p4110 A67-42899
- RADIOACTIVE MATERIAL**
- Tissue protein synthesis in hypodynamic rats studied with aid of carbon 14 and sulfur 35 tagged amino acids 13 p2059 A67-26759
- Meteorology, goals and methods, prospects for effective utilization of satellites and new techniques 20 p3480 A67-36823
- Dispersion equation of radioactive compressible nonviscous plasma with finite electric conductivity under gravitational and axial magnetic fields 21 p3663 A67-37918
- Adsorption equilibrium data obtained at high pressure for methane and propane on silica gel using radioactive tracer pulsing 24 p4118 A67-42584
- RADIOACTIVE NUCLIDE**
- Existence of cosmic-ray-produced Mg-28 radionuclide in rain 04 p0692 A67-14495
- Short period radioactive nuclides induced by secondary neutron due to solar cosmic radiation in chondrites 11 p1858 A67-24058
- RADIOACTIVE PARTICLE**
- Self-charging of temperature independent radioactive ultrafine particles for MHD power generation 08 p1283 A67-20647
- Efficiency of fibrous filters for radioactive particles and small ions increased, using greater flow rate 09 p1562 A67-22683
- Airborne precipitation collector, determining washed out radioactive particles from air between cloud base and surface by comparing surface and airborne samples 21 p3628 A67-38583
- RADIOACTIVE WASTE**
- Random intact reentry and earth burial for radioisotope thermoelectric generators disposal without atmospheric contamination, evaluating design concepts for SNAP systems 24 p4241 A67-42559
- RADIOACTIVITY**
- S FISSION PRODUCT**
- RADIOBIOLOGY**
- Blockage of electrically evoked pupilodilation in cat by irradiating hypothalamus with cyclotron-accelerated alpha particles 10 p1598 A67-23394
- Radiobiological aspects of radiation safety in cosmic flights 14 p2255 A67-28222
- Radiobiological risk of SST flights from heavy ions of cosmic radiation, discussing methods of radiation detection 23 p3945 A67-41074
- Manned spacecraft space radiation monitoring system requirements and criteria to indicate biological response 23 p3966 A67-41589
- RADIOCHEMISTRY**
- Postirradiation radiochemical and spectrochemical analysis of short-cooled samples of SNAP-8 experimental reactor primary coolant 03 p0466 A67-13798
- Neutron activation analysis to determine trace elements in iron meteorites 14 p2391 A67-28947
- Germanium tetrachloride purification process by radiochemical analysis and radioactive tracers investigated to determine possible simplification 18 p3104 A67-34600
- RADIOGRAPHY**
- SA AUTORADIOGRAPHY**
- SA PHOTOGRAPHY**
- SA X-RAY PHOTOGRAPHY**
- Gamma and X-radiographic radioactive sources for nondestructive testing of hydrogenous materials such as rubber, adhesives and explosives in steel or other metal assemblies 02 p0249 A67-12220
- Radiographic analysis of thoracic cardiovascular rupture during abrupt deceleration associated with crashes [ARL-TR-67-17] 08 p1287 A67-20614
- X-radiographic nondestructive testing and inspection for quality control of electronic and electromechanical devices including printed circuits, encapsulated modules, thin films, etc 10 p1611 A67-23311
- Gamma flaw detectors for radiographic inspection 13 p2122 A67-26254
- Radioscopy for testing cast-steel parts, welding seams, etc, noting radiation protection, radioscope video control and information storage 18 p3045 A67-33737
- Welds qualification system based on radiographically determined macrostructure defectiveness, classifying defects according to size and distribution 18 p3053 A67-33742
- Aluminum welded joints investigated by radiographic and metallographic methods for bubbles and cracks 18 p3053 A67-33743
- Clineradiographic analysis of human visceral responses to short duration acceleration impact 23 p3951 A67-41553
- RADIOLOGY**
- Value of routine abdominal X-ray during aeromedical evaluation, noting number and significance of abnormalities detected 10 p1601 A67-23828
- Radiological findings from pilots afflicted with vertebral fractures from ejection injuries 21 p3575 A67-38510
- Thorax radiological changes associated with physiological and posture changes, discussing chest dynamics 23 p3956 A67-41625
- RADIOLYSIS**
- Hydroxyl radical formed by radiolysis of ice at 77 degrees K identified as center producing EPR lines 17 p2890 A67-33258
- RADIOMETER**
- SA DICKE TYPE RADIOMETER**
- SA MICROWAVE RADIOMETER**
- Anisotropy of reflected solar radiation from various surfaces as measured with aircraft-mounted radiometer 01 p0146 A67-10318
- Tunable airborne L-band radiometer designed to provide reliable operation over long period of time with minimum of operator adjustment 01 p0063 A67-10323
- Heat flux measurement with narrow view angle radiometers, discussing equipment design, performance characteristics and results 01 p0069 A67-11021
- Space applications research and development 01 p0152 A67-11430
- Eppley-JPL solar constant measurement experiment, noting 12-channel radiometer, filter wavelength limits and high altitude measurements 02 p0328 A67-12396
- Black ball radiation tables and radiative equilibrium temperatures computation 05 p0838 A67-17277
- Bias and random radiometersonde temperature errors effects in estimation of atmospheric downward, upward, net and equivalent IR irradiance 05 p0803 A67-17385
- Multichannel radiometer measurement of solar irradiance for realizing spacecraft radiative equilibrium 06 p1003 A67-18318
- [AIAA PAPER 67-147] 06 p1003 A67-18318
- Three-channel IR-UV rocket radiometer for onboard measurement of exhaust plumes under severe high altitude environmental conditions 06 p1005 A67-18714
- Radiosonde radiometer to measure long wave emission from earth and intervening atmosphere during night ascents 06 p1005 A67-18742
- Microwave feedback radiometers using electromechanical and all-electronic systems 07 p1155 A67-19875
- Absolutely calibrated radiometer for CW laser radiation in visible and near IR bands which relies on heat flow through standard thermal impedance 09 p1502 A67-22615
- Stabilized cross correlation radiometer for use at decametric wavelength, using two feedback loops controlling four noise diodes 11 p1762 A67-24288
- Temperature measurements of grassland, desert and water surfaces using IR radiometer found to compare favorably with miniature thermistors 13 p2117 A67-27606
- Scanning IR radiometer equipment to produce pictorial maps of lunar radiance patterns or of possible variations in lunar surface composition 15 p2492 A67-30434
- Sensitivity of radiometer operating in submillimeter range with multimode detector compared to crystal receiver equivalent noise temperature 16 p2677 A67-31501
- Millimeter wave passive radiometry noting design, capability, detectability and aerial reconnaissance 17 p2814 A67-32521
- Noise measurement covering principles, switching radiometer, sources, factors and temperature 17 p2814 A67-32604
- Transfer function use in outgoing IF radiation temperature measurement of vertical profile over Caspian Sea by airborne modulation radiometer 18 p3040 A67-34001
- Radiometric technique for absolute temperature measurement of microwave noise sources under field conditions 20 p3444 A67-36521
- Multichannel radiometer measurement of solar irradiance for realizing spacecraft radiative equilibrium 21 p3624 A67-37794

Solar and terrestrial thermal radiometer absolute calibration noting standards and methods 23 p4006 A67-41373
Radiometer using black plate with radiation toward night sky balanced by IR radiation transfer in vacuum system 24 p4152 A67-41787
Ground and water surface temperature measurements using IR radiometers onboard aircraft 24 p4181 A67-41789

RADIOMETRY

Tropospheric pressure-altitude data by satellite radiometric topography mapping, using oxygen absorption band centered at 5 mm 02 p0262 A67-12367
Quantitative expression of technique for observing 5-mm self-emission from oxygen of earth atmosphere to obtain vertical sense [RASSA PAPER 1-10-144] 03 p0418 A67-14251
Radiometric maps of brightness temperature contours on lunar disk from measurements of 3.3 mm wavelength thermal emission [JPL-TR-32-1058] 08 p1399 A67-21242

Correlation radiometry examination of radiation emission in beam plasma discharge at harmonics of electron cyclotron frequency 09 p1536 A67-21601
Exact theory of enclosed molecular radiometer using flow field solution from Wu-revised thermal transpiration theory in two cases 10 p1681 A67-22864
Extraterrestrial solar radiation simulation and total flux and spectral component measurement 11 p1772 A67-24053
Time course of blue-to-red light intensity ratio of visible solar spectrum during and after sunset 11 p1786 A67-24116

New antenna techniques for Hertzian radiometric cartography 12 p1913 A67-25305
Geochronology for earth and components using radiometric and thermoluminescence methods 12 p1903 A67-25428
Mars atmospheric composition determination by shock layer radiometry technique during probe experiment [AIAA PAPER 67-293] 12 p2009 A67-26009
Radiometric observations of total lunar eclipse of December 19, 1964 at wavelength of 3.3 mm indicate no significant temperature difference [JPL-TR-32-1097] 12 p2011 A67-26245

Millimeter waves in atmospheric research, discussing radar meteorology, radiometry, etc 13 p2072 A67-27493
Millimeter wave radiometry to study atmospheric properties, topographic relief, planets, medical and industrial research 14 p2265 A67-28402

S-10 and S-20 image orthicon tubes evaluated for radiometric measurements against reentry vehicles, considering radiometric response, resolution and calibration stability 20 p3452 A67-37311
Empirical orthogonal functions, determining vertical atmospheric temperature profiles from radiometric satellite measurements 22 p3828 A67-39325
Rocketborne UV radiometers for solar spectral intensity distribution, calculating irradiance and earth reflectivity 22 p3794 A67-40363

Earth upper atmosphere background radiance measured by UV radiometer carried on Air Force satellite 22 p3794 A67-40364
OH Meinel band, nitrogen dioxide continuum and O IS to ID transitions maxima altitudes in midlatitude night airglow emissions from rocket radiometer measurements 23 p3995 A67-40813

RADIOPHOSPHOR

Radioisotope and phosphor research and increased brightness of self-luminous devices 05 p0842 A67-16543
Temperature effect on diffusion coefficient of radioactive phosphorus in epitaxial Si layer 21 p3681 A67-38361

RADIOPHYSICS

Radiophysical measurement of small amplitude mechanical oscillations of self-oscillator by means of mechanical-electric converters and effects of natural line width on minimum amplitudes 05 p0805 A67-16357
Soviet book on random function theory application to statistical problems in radio physics 08 p1295 A67-21336
Soviet book on radio physics /1965-1966/ reviewing radio-astronomical observations and radar probing of Venus 15 p2553 A67-29241
Nonthermal radio emission from Jupiter

atmosphere, studying Io modulation 19 p3317 A67-34933

RADIOSENSITIVITY

Photomultipliers in DC output mode for extreme UV 10 p1653 A67-22737
Radiation hazards and safety requirements for lunar and Mars manned space flights, discussing radiosensitivity, restoration and permissible doses 13 p2059 A67-26761
Sensitivity of radiometer operating in submillimeter range with multimode detector compared to crystal receiver equivalent noise 16 p2677 A67-31501
Relationship between oxygen tension and radiosensitivity in complex biological system 17 p2806 A67-31962

RADIOSONDE

Radosonde for measurement of electric potential gradient in atmosphere at high altitudes 01 p0068 A67-10870
Boundaries and attenuating media effect on radiometric sounding of planetary atmospheres by remote sensing techniques 02 p0239 A67-12406
M-60 radosonde measurement reliability, comparing coupled pair subjected to same shocks and direct solar radiation 04 p0625 A67-15606
Bias and random radiometersonde temperature errors effects in estimation of atmospheric downward, upward, net and equivalent IR irradiance 05 p0803 A67-17385
Radosonde radiometer to measure long wave emission from earth and intervening atmosphere during night ascents 06 p1005 A67-18742

Atmospheric soundings made with A-60 radosonde compared with A-22 and RKZ 07 p1187 A67-17937
Digital /chirp/ radosonde for meteorological and earth satellite measurements employing pulse bursts from voltage controlled oscillator 10 p1655 A67-22823
Upper air turbulence gusts, describing vertical component test method using F type radosonde 10 p1676 A67-23085
Modified RK-1 radosonde circuit for stratospheric cosmic ray measurements 12 p1941 A67-25555

Automatic radosonde data processing system providing azimuth and elevation angles, temperature, humidity, etc 13 p2069 A67-27019
Clear air turbulence /CAT/ evaluated to alleviate effects on air traffic, noting forecasting techniques and in-flight and ground-based remote detectors 19 p3254 A67-35931

Tethered sonde for micrometeorological soundings of lower atmosphere noting pressure transducer, servoswitching system, thermistor, hygistor, data acquisition, etc 21 p3628 A67-38582

RADIOSONDE THERMISTOR

Rocketsonde and radosonde temperature comparisons and evaluation of computed rocketsonde pressure and density 14 p2347 A67-28885

RADOME

Large monolithic radome antenna fabrication 02 p0215 A67-11980
Angular errors in antennas with aerodynamic radome heating due to temperature variability 13 p2080 A67-27034
External noise levels effect on angular accuracy of tracking radar pencil-beam antennas, emphasizing radome noise and dielectric coating characteristics 17 p2826 A67-32685
Antenna radome subjected to aerodynamic heating investigated for effects on radar system operational range, analyzing antenna noise 18 p2999 A67-33510
Radant, integrated radome antenna system incorporating three trapezoidal-tooth log periodic radiating elements 18 p3016 A67-34598

RADOME MATERIAL

High temperature resistant materials for antennas on reentry and high performance aircraft 01 p0103 A67-10620
Boresight error in radar caused by effect of radome material and means to avoid it 02 p0215 A67-11973
High temperature polyimide laminates for radomes and other supersonic aircraft components, discussing index flexural strength, dielectric constant and dissipation factor 22 p3825 A67-39853

Radome antenna systems design utilizing dielectric structure applicable in aircraft, spacecraft and missile systems 22 p3775 A67-40468

RAE SATELLITE

S RADIO ASTRONOMY EXPLORER

/RAE/ SATELLITE

RAIL TRANSPORTATION

Vehicular traffic and rail transportation surveillance or coordination aids possibilities using earth orbiting satellite [AIAA PAPER 67-788] 24 p4242 A67-42951

RAIN

Existence of cosmic-ray-produced Mg-28 radionuclide in rain 04 p0692 A67-14495
Measurement of attenuation of 8.6 mm wavelength radiation in rain, relation to rate of rainfall, using corner reflectors 07 p1146 A67-20201
Received signal degradation for coherent pulse transmission through rain scattering volume, calculating length and energy for various paths 11 p1752 A67-24285
Rain effects at random antenna elevation 11 p1753 A67-24303
Periodicity of precipitation singularities and relation to period of comets and meteor streams 11 p1815 A67-24329
Geometric and thermal height of shower and storm cells using radar observations 13 p2150 A67-26433
Synthesized summary of reports on radio propagation in nonionized media, noting meteorological radar and precipitation effect 14 p2264 A67-28393
Millimeter wave attenuation measurement in rain using low height antennas 14 p2274 A67-28923
Correlation of rainfall rate with attenuation at various frequencies of microwaves 16 p2625 A67-31341
Path diversity in millimeter waves propagation through rain for various frequency 16 p2625 A67-31343
Absorption by atmospheric oxygen and rain of mm waves, using device permitting continuous frequency variation 18 p3002 A67-34230

SEMIPERMANENT REPELLANT FOR AIRCRAFT WINDSHIELDS TO OVERCOME EFFECT OF VISUAL ERRORS CAUSED BY RAIN ON WINDSHIELDS 08 p1279 A67-21042

RAIN REMOVAL SYSTEM

Semipermanent repellant for aircraft windshields to overcome effect of visual errors caused by rain on windshields 08 p1279 A67-21042

RAINDROP

Raindrop and melting hailstone absorption, scattering and backscatter cross sections of millimeter waves in satellite communications and weather radars 04 p0577 A67-15685
Radio signals from clouds to yield information on cloud physics, using superheterodyne microwave receivers 24 p4124 A67-42883

RAINSTORM

Rainfall associated with atmospheric convective activity estimated by radio ray attenuation model 21 p3582 A67-38577

RAMAN EFFECT

Stimulated Stokes emissions from Raman active media observed by using Q-switched ruby laser which emits multiple pulse in each shot 04 p0632 A67-14765
Stokes light generated in off-axis resonator for quantitative measurements of stimulated Raman effect in self-focusing materials 08 p1339 A67-21375
Stimulated inverse Raman effect, noting experimental laser setup and theory based on optical phonon emission 14 p2333 A67-28985

Raman effect in solutions of potassium, sodium and ammonium dichromate and potassium dichromate single crystal 19 p3240 A67-35421
Resonance electronic Raman effect and parametric induced anti-Stokes radiation in potassium vapor atoms 21 p3641 A67-38456
Stimulated Raman effects in calcite oscillator crystal, measuring gain index beta relative to Stokes wave 23 p4016 A67-41191
Optical mixing process for study of polarized light in wedge shaped cells of Raman active medium 23 p4017 A67-41433

RAMAN SCATTERING

Electronic Raman scattering by neutral Zn and Mg acceptors in GaP, energy level transitions and accompanying phonon wing 04 p0673 A67-14477
Wave interaction dynamics of far IR electromagnetic radiation generation by coherent molecular vibrations or phonons excited by stimulated Raman scattering and

- resonant phase matching
condition 04 p0657 A67-15113
- Sum and difference frequency mixing of visible and IR gas laser light in GaP at near reststrahl frequencies and relationship to spontaneous Raman scattering 04 p0682 A67-15464
- Polarization of light scattered from He-Ne laser beam, applying quantum theory to formula for depolarization ratio 04 p0634 A67-15624
- Properties of self-trapped light filaments noting stimulated Raman emission and creation, containment and termination mechanisms 05 p0818 A67-16648
- Tunable Raman laser obtained by electron mobility subjected to magnetic field, noting threshold pump power 05 p0823 A67-16684
- Two-phonon IR absorption and Raman scattering spectra to provide information about phonon spectra of crystals and phonon-electron interaction in filled valence bands 06 p1059 A67-18907
- Frequency doubling of light in ruby laser due to laser light interaction with corundum lattice, anti-Stokes-Raman scattering of laser light, etc 08 p1336 A67-20316
- Gallium arsenide laser pumped by Stokes component of induced Raman scattering in liquid nitrogen of Q-modulated ruby laser light 09 p1512 A67-21973
- Phonon lifetime variation effect on stimulated Brillouin and Raman scattering in gases by temperature, pressure and laser power variation and comparison with Stokes gain theories 10 p1662 A67-22758
- Stimulated Raman effects in anisotropic crystal potassium dihydrogen phosphate with Stokes generations 11 p1800 A67-24243
- Electronic Raman scattering from phosphorus donors and boron acceptor impurities in Si, noting importance of interband transitions 11 p1851 A67-24999
- Raman laser physics covering gain formula, stimulated and spontaneous scattering and cavities 12 p1953 A67-26124
- Coherent radiation frequency conversion and nonlinear optics methods, including stimulated Raman scattering and scattering 14 p2330 A67-28467
- Gallium arsenide laser pumped by Stokes component of induced Raman scattering in liquid nitrogen of Q-modulated ruby laser light 17 p2870 A67-33310
- Electric field enhanced Raman scattering and linear frequency shift of strontium titanate soft mode in random domain orientation and reorientation 18 p3098 A67-33520
- Laser bibliography V /July-December 1966/ covering giant-pulse techniques, Raman and Brillouin scattering, interaction effects, propagation, holography, etc laser bibliography V /July-December 1966/ 21 p3641 A67-38455
- Stimulated Raman scattering in IR active nontotally symmetric vibration of alpha quartz crystal, noting parametric oscillation 21 p3641 A67-38459
- Coherent Raman amplification dynamics, considering pump depletion and coupling saturation and stimulated Raman scattering by polarization waves 22 p3816 A67-40318
- Symmetry of phonons and rules of corresponding selection for IR absorption and Raman diffusion for two phonons 23 p4026 A67-40689
- IR absorption and Raman scattering spectra of diagonal cubic crystal structures 23 p4037 A67-40758
- Light polarization and intensity for Raman scattering from plasmons and phonons in GaAs 23 p4038 A67-40795
- Raman scattering for overdamped soft optic vibrational mode in barium titanate, giving temperature dependence of Raman spectrum 23 p4038 A67-40796
- Optical Raman scattering from atmospheric oxygen and nitrogen via pulsed nitrogen UV laser light source, discussing spectral analysis of air scattering 24 p4147 A67-41883
- RAMAN SPECTROSCOPY**
SA INFRARED SPECTROSCOPY
CW He-Ne laser compared with mercury arc source, obtaining Raman spectra of carbon tetrachloride by three methods of excitation 03 p0438 A67-13912
- Spectral resolution improvement by photoelectric Raman spectrometer with He-Ne laser excitation, noting results for carbon disulfide, carbon tetrachloride and azobenzene 09 p1492 A67-21561
- 800 mm and 1265 mm optical resonator He-Ne lasers, obtaining maximum output power and application as Raman spectroscopy light source 14 p2333 A67-28972
- RAMAN SPECTRUM**
Laser excited electronic Raman spectrum of trivalent Eu ion doped YGa garnet 01 p0091 A67-11084
- Second harmonic generations and mixings of Raman lines produced in cyclohexane, acetone, benzene and carbon disulfide, photographing first order Stokes radiation 02 p0252 A67-12052
- Lattice IR reflection and transmission spectra and Raman spectrum of monocrystalline and hot pressed pellets of ZnSe 06 p1059 A67-18909
- Spectrum of second order Raman lines in coupling of radiation and matter, using Green function 10 p1663 A67-22855
- Small scale trapping of laser beam and frequency shift in Raman radiations observed under various polarization conditions 16 p2684 A67-30607
- Photoelectric recording of Raman spectra excited by ruby laser 19 p3240 A67-35546
- Raman spectra vibrational structure theory concerning crystal impurity centers, giving intensity distribution formulas and radiation model calculations 20 p3511 A67-37031
- Second order Raman spectrum temperature dependence of strontium titanate and potassium tantalate 23 p4013 A67-40965
- IR vibrational and Raman spectra of thiophosphoryl trichloride, thiophosphoryl dichlorodifluoride, thiophosphoryl chlorodifluoride and thiophosphoryl trifluoride 23 p4041 A67-41242
- Semiconducting diamonds photoconductive response measured noting correlation with activation energy 23 p4044 A67-41454
- RAMJET ENGINE**
Combustion efficiency of supersonic ramjet, noting equations for chamber 01 p0141 A67-11149
- Impact-induced combustion in hypersonic ramjet engines, determining hypersonic fuel-air mixing from hydrogen concentration at Laval nozzle outlet [DVL-601] 03 p0503 A67-13014
- Generalized MGD equation for thrust in ramjet engine, with application to rocket engine and pulsed jet 03 p0503 A67-13086
- Ramjet external-combustion engine noting design of trailing edge, nomograms of pressure, temperature, thrust component, etc 04 p0688 A67-14578
- Flame stabilization by mechanical stabilizers in ramjet combustion chamber as function of temperature and pressure of fuel mixture 04 p0691 A67-15899
- Book on propulsion systems covering gas-turbine engine, ramjet engine, chemical and electrical rockets, components, etc 10 p1698 A67-23689
- Turboramjet engine transition phase noting problems in passing from turbojet to ramjet operation 12 p1988 A67-25185
- Materials requirements for aircraft turbojet and ramjet engines 13 p2187 A67-26694
- Fluidics applications to ramjet control systems incorporating sensing, logic and actuation functions to inlet duct, flow-air ratio and coolant control 17 p2927 A67-31981
- Wind tunnel ejector and hot water supply for ramjet power plant attitude test stand, noting synchronization of ejector with test section 17 p2834 A67-32817
- Supersonic combustor length and contours for optimum performance determined from one-dimensional pressure-area analysis 18 p3154 A67-33832
- Ejector ramjet and ducted rocket evaluation by analytical models for various flight trajectories, noting specific impulse improvement [AIAA PAPER 67-437] 18 p3112 A67-33915
- Supersonic combustion characteristics of hypersonic ramjet predicted by analytical method using constant-mass tube technique, discussing flow field properties [AIAA PAPER 67-494] 18 p2983 A67-33958
- Fluidic fuel control system for subsonic combustion ramjet engine, describing components, breadboard model and performance characteristics [AIAA PAPER 67-497] 18 p3113 A67-33961
- Flame stabilization with flame holders in supersonic flow, discussing improved combustion in ramjets at supersonic velocities 18 p3116 A67-34609
- Hypersonic flight programs, considering Air Force, Navy and NASA research programs on scramjets 20 p3517 A67-37447
- Physicochemical combustion of turbulent air-fuel mixture in straight flow combustion chambers, noting effects of various factors and intensification methods 22 p3921 A67-40448
- RAMP**
Mathematical models for loss measurements in thin Permalloy films with ramp drives 15 p2536 A67-29649
- RANDOM DISTRIBUTION**
Sweep random vibration test using narrow band random excitation with feedback control from variable gain stage 01 p0034 A67-10155
- Miscellaneous results connected with simple system alternating between two states, running or under repair 03 p0432 A67-13824
- Power and DC spectra for electron motion due to plasma heating and diffusion in static magnetic and transverse random electric field 03 p0485 A67-14046
- Multielement antenna scanning grid-phasing method having random function distribution at aperture 05 p0776 A67-17159
- Heat-transfer coefficients during dropwise condensation on randomly distributed nucleation sites analyzed through computer simulated model 08 p1426 A67-20925
- Electromagnetic wave scattering measurements using spheres moving randomly within slab region container, obtaining data for coherent phase, average intensity, etc 09 p1461 A67-21597
- Large scale structure of homogeneous turbulence generated at initial instant by distribution of random impulsive forces, noting statistical properties 09 p1490 A67-22417
- Large scale nonrandom angular distribution of faint radio sources from drift records 14 p2383 A67-27958
- N-type germanium doped with antimony and arsenic investigated for radiation recombination, noting energy spectrum and forbidden band changes 14 p2368 A67-28533
- Interpretation of tests for randomness of lunar craters, noting clustering and alignment 15 p2554 A67-29458
- Randomly distributed initial energy input effect on unbounded rotating barotropic atmosphere, noting energy density function as initial condition 15 p2478 A67-30056
- Probability density and random distribution function derived from finite series for instantaneous voltage measurements of ideal multiplying device 16 p2653 A67-31718
- Random processes from physical viewpoint, discussing random function, random noise properties, Gaussian distribution, digital analysis, Shannon sampling theorem, etc 20 p3483 A67-36459
- Distributed receiving system for optimal filtration of random field of space-distributed source 20 p3385 A67-37376
- N-type germanium doped with antimony and arsenic investigated for radiation recombination, noting energy spectrum and forbidden band changes 23 p4040 A67-40940
- Magnetic field critical current density characteristics of Nb-Zr-Ti superconducting alloys, discussing peak effect and barrier height random distribution 23 p4044 A67-41451
- RANDOM ERROR**
Gain optimization for antenna arrays for determination of maximum expected gain and required excitations when finding random errors in amplitudes and phases of excitations 01 p0032 A67-10005
- Angular noise induced random error in direction finding as affected by target properties and sense 03 p0368 A67-13275
- Different rotation bearings as method of reducing bearing friction and directional gyro errors from random disturbances 03 p0425 A67-14285
- Statistical linearization for minimization of mean square error between time derivatives for actual and model outputs for zero and

special memory
nonlinearities 04 p0591 A67-14420
Random tropospheric angle error
prediction in microwave observations of
Early Bird satellite 04 p0574 A67-15074
Amplitude bounded noise and random
measurement error smoothing, noting
increased efficiency and possibility of
narrow band application 06 p0975 A67-18217
Properties of antenna systems composed
of individual arrays noting effect of spatial
distribution, orientation,
etc 07 p1154 A67-19781
Bias due to random bit errors that occur
in PCM data during phases of operation of
telemetry data processing
system 07 p1145 A67-19874
Gaussian errors effects on antenna pattern
of any array of elements, describing errors
in terms of rms amplitude and phase errors
at each element 09 p1470 A67-21591
Random noise and measurement errors
limitation upon system identification in time
domain 15 p2463 A67-30332
Amplitude bounded noise and random
measurement error smoothing, noting
increased efficiency and possibility of
narrow band application 16 p2642 A67-30483
Gain maximization for arbitrary antenna
arrays with excitation amplitude and phase
and element positions are subjected to
random errors 16 p2638 A67-31336
Effect of random amplitude errors of
continuous apertures on radiation pattern
and gain 16 p2627 A67-31353
Error correction block encoding for high
speed HF digital data transmission
system 17 p2811 A67-32112
Random errors in ultrasonic
measurements, discussing Students
distribution measurement repetition effect
and rounding-off error
evaluation 18 p3044 A67-33735
Automatic control system for parameter
evaluation, reducing stochastic errors by
repeated measurements 18 p3017 A67-33991
Systematic and random error effects on
geodetic accuracy of results obtained by 3-
station laser telemetry 19 p3182 A67-35240
Integral equations for weight function of
optimum filter and correlation function of
random absolute error 20 p3408 A67-37040
Random error effect on directional gain of
sectional parabolic antenna with automatic
phasing, setting sections effectively by three
control points method 22 p3770 A67-39657

RANDOM LOAD
Arbitrary shallow shell under action of
space-time homogeneous random
load 01 p0163 A67-10995
Structural loading, discussing stationary
and nonstationary-random and severe loading
processes 01 p0163 A67-11014
Fatigue crack propagation under random
cyclic loading extended, obtaining zero-order
solution from mean crack
lengths 02 p0337 A67-11794
Structural fatigue-failure under
nonstationary random loading
processes 04 p0716 A67-15749
Probability density of oscillating system
with piecewise-linear characteristic under
action of exponentially correlated random
force 05 p0844 A67-16014
Automatic control system synthesis for
fatigue testing of structural elements under
random loads 06 p1101 A67-18239
Reliability of nonlinearly elastic polymer
components of structural elements exposed
to random loads 07 p1261 A67-19171
Design problems for hydraulic loading
circuit with random variation of loading with
time 09 p1451 A67-22472
Random-loading fatigue crack growth
behavior of airframe aluminum and titanium
alloys under sinusoidal, narrow band and
broad band random
loading 10 p1669 A67-23434
Dynamic snap-through of shallow arches
under stochastically varying transverse
loads 10 p1725 A67-23711
Energy techniques and matrix method for
computer programming of dynamic response
due to random and harmonic loading on
structural systems
[ASME PAPER 67-VIBR-56] 11 p1873 A67-24203
Astatic gyroscope accuracy dependence on
random fluctuations of dry friction moment
when under oscillatory motion of bearings,
giving correlation function of error

dispersion 11 p1794 A67-25044
Nonlinear oscillations of elastic plates
under simultaneous effect of harmonic and
random load 12 p2024 A67-25597
Fatigue process theory for general
broadband random loading, calculating mean
damage and survival
probability 15 p2576 A67-30084
Fatigue crack growth rates in metals
under random loading correlated to cyclic
load tests 16 p2774 A67-31320
Random thermoelastic stress concentration
near edge of circular cylindrical shell
determined using axisymmetric
formulation 21 p3718 A67-37979
Random load fatigue life and reliability via
fail-safe structural model, obtaining
statistical distribution of 2024-T4 aluminum
alloy bending strength 23 p4076 A67-40735

RANDOM NOISE
SA GAUSSIAN NOISE
Stochastic approximation theory to obtain
algorithms for recovery of functions, using
noisy measurements taken at randomly
selected points 01 p0028 A67-10450
Response of linear FM matched filter to
gated noise 01 p0037 A67-10484
Coherent echo modulation and detection
for binary data transmission, noting power
savings, time and frequency diversification
and communication 01 p0026 A67-10862
Error probabilities for partially coherent
diversity reception, noting linearized
receiver performance during random noise
output 01 p0026 A67-10863
Comparison of nonlinear and linear
filtration in sense of minimum of mean
square error of Markov process hidden in
noise 01 p0106 A67-10923
Dynamic programming recursive estimation
of modal trajectory for nonlinear non-
Gaussian noise and comparison with
Bayesian estimation and case of Gaussian
white noise 01 p0047 A67-11214
Passive detection of sonar target in
presence of Gaussian noise background with
unknown spectral
quantities 02 p0217 A67-12087
Spatially distributed system for optimal
filtration of useful signal in random noise
fields 03 p0391 A67-13181
Detectability criterion for signal received
against random noise
background 03 p0368 A67-13277
Equivalent noise current equations and
spontaneous fluctuations of leakage current
due to carrier generation in depletion layer
of reverse-biased junction
diode 03 p0379 A67-13479
Discrete gyroscopic servocontrol in
presence of multidimensional random noise,
ensuring optimal reproduction of input
signal 03 p0465 A67-14157
Gain adjustment of nonlinear time variant
control systems with random
inputs 05 p0783 A67-16444
Optimum switching function of relay
servosystem subjected to stationary Gaussian
random input found by perturbation
method 05 p0783 A67-16445
Output probability density distribution of
stationary random noise containing regular
signal components after mean squaring
circuit 05 p0783 A67-16446
Strakhov method determination of
optimum numerical filter for extraction of
potential field signal from random noise
background 05 p0767 A67-17390
Amplitude and phase detection for
determined signal with nonstationary
noise, using generalization of Levin
method 05 p0767 A67-17402
Optimal signal design for binary
communications systems using sequential
and nonsequential detection with
feedback 06 p0962 A67-17944
Filtering for nonlinear dynamical systems
with white Gaussian noise
processes 06 p1029 A67-18532
Artificial pseudorandom binary noise
generation for flight testing and aircraft
control systems and correlation function and
frequency spectra of noise
generators 08 p1279 A67-21005
Stochastic optimal control with noisy
observations, obtaining Hamilton-Jacobi
stochastic equation in function space
[ASME PAPER 66-WA/FE-6] 11 p1770 A67-24276
Cross correlation and statistical

dependence between envelope and
frequency deviation of sine wave plus
random noise, noting possible application to
frequency demodulation 11 p1753 A67-24646
Noise rejection of remote control
command information transmission in system
with comparison circuit, using error
detecting and correcting
codes 11 p1772 A67-25041
Discrete control gyroscopic servosystem
for tracing two-dimensional input signal
subjected to random noise
distortion 15 p2490 A67-30172
Predictive identification and fast moving
target recognition technique for adaptive
control and tracking
systems 15 p2463 A67-30330
Random noise and measurement errors
limitation upon system identification in time
domain 15 p2463 A67-30332
Cost function to evaluate quasi-optimal
amplitude meter for signal with random
initial phase on white noise background with
random correlation
function 16 p2623 A67-31015
One-dimensional probability distribution
density of sum of pulsed and fluctuation
noises 16 p2623 A67-31016
Digital computer simulations of
pseudorandom noise generators, determining
empirical sum distribution approximation of
binomial variable 18 p3006 A67-34066
Book on probability in communication
engineering covering probability theory,
information and reliability theory, random
processes and noise and random phasor
sums 20 p3378 A67-36137
Random processes from physical
viewpoint, discussing random function,
random noise properties, Gaussian
distribution, digital analysis, Shannon
sampling theorem, etc 20 p3483 A67-36459
Optimal detection of signals by spatially
distributed receiving system against random
noise background, using space-time signal
selection method 20 p3383 A67-37070
Mean error and optimal structures for
multidimensional extremal systems with
random noise obtained from steady
process 20 p3409 A67-37112
Dry friction servo system dynamics with
relay delay in random noise
case 20 p3451 A67-37152
Trajectory prediction for moving
stochastic systems 20 p3392 A67-37196
Three-dimensional hologram reconstruction
and image speckle, considering three-
dimensional boundary value
problem 20 p3451 A67-37309
Pulse code communication system for
transmission of continuous random
quantities 22 p3761 A67-39831

RANDOM NUMBER
Simulated radioactive decay experiment
using random number generator or set of
random numbers 01 p0112 A67-10826
Exodus method /modified Monte Carlo
method/ which does not use random
numbers and can be applied to any problem
admitting nodal network
[ASME PAPER 66-WA/HT-61] 04 p0646 A67-15436
Popov method for random parameter
control system asymptotic stability in mean
with respect to bounded
perturbations 05 p0784 A67-16777
Random number modeling on digital
computer 07 p1147 A67-19226
Random number generation by digital
computer 09 p1468 A67-22052
Solar cycle prediction based upon random
number technique, Fourier curve fits and
power spectra analysis 22 p3873 A67-39931

RANDOM PROCESS
SA MARKOV PROCESS
SA POISSON PROCESS
SA STOCHASTIC PROCESS
Convergence theorems for sequence of
expected values or random variables of
stochastic learning process with time-
dependent probabilities 01 p0104 A67-10280
Temperature, stress and displacement in
elastic bodies for random surface forces and
randomly distributed environmental
temperature 01 p0159 A67-10403
Stochastic approximation theory to obtain
algorithms for recovery of functions, using
noisy measurements taken at randomly
selected points 01 p0028 A67-10450
Kinetic equation describing microphysical
random condensation of cloud

droplets 01 p0109 A67-10684
 Book on noise and effect on communication covering random processes, fundamentals and spectra, nonlinear transformations /demodulation/, statistical theory of detection and information theory 01 p0024 A67-10725
 Infinitely divisible distributions of first passage times and hitting points in ordinary random walk solved by Bessel functions 01 p0106 A67-10735
 Limiting theorem for weak convergence of solutions of differential equations with random right hand part to Markov process 01 p0106 A67-10922
 Markovian division process application for solving multicomponent preventive maintenance, work sampling and search theory problems 01 p0106 A67-10930
 Electron density fluctuations in turbulent wake, using stochastic analysis and statistical averaging [AIAA PAPER 65-818] 01 p0007 A67-11168
 Statistical communication theory of antenna response to complex partially polarized nonisotropic random radio wave processes 02 p0191 A67-11588
 Statistical properties of estimation method for one-dimensional characteristic function of stationary ergodic random process 02 p0192 A67-11639
 Nonlinear transformations of probability measures in functional spaces, noting application of random-process theory 02 p0259 A67-11922
 Synthesis of optimum discrete control for eventual state of linear stochastic system, reducing problem to solution of Bellman functional equation 02 p0225 A67-11957
 Stability analysis of nonlinear stochastic systems in presence of random and Gaussian perturbations, determining validity of law of large numbers and amplified law of large numbers 02 p0267 A67-11958
 Stabilizability of class of linear stochastic systems 02 p0259 A67-12064
 Stochastic process estimate of frequency and duration of weather events, using Monte Carlo simulation of probability distributions 02 p0261 A67-12079
 Turbulent diffusion in nonuniform stratification atmosphere, obtaining vertical concentration profile by random walk method [AFRL-66-836] 02 p0262 A67-12081
 Scattering of partially coherent radiation by neutral molecules formulated as random process 02 p0201 A67-12096
 Digital simulation results for random approximation solutions of binary signal detection problems 02 p0204 A67-12169
 Algorithm for directed random search for minimum of function of n-variables 03 p0374 A67-13182
 Optimum terminal missile maneuver and evasion strategy with Gaussian process 03 p0465 A67-13267
 Instrument methods determining function and density of length distribution of random radio emissions 03 p0369 A67-13586
 Optimality principle in mean for optimum averaging of controls of stochastic systems 03 p0392 A67-13595
 Exact solutions derived for problems of mathematical expectation and density distribution of maxima for two types of nonstationary random processes 03 p0461 A67-13948
 Monte Carlo simulation provides realistic analysis of set of stochastic processes involved in flow within maintenance and logistics system 03 p0400 A67-14223
 Book on Monte Carlo method, method of statistical trials 03 p0462 A67-14256
 Stochastic model of cratering and survival of craters on moon, discussing approximate diameter distribution of primary and secondary craters 04 p0696 A67-14739
 Multiplicity theory of wide class of purely nondeterministic weakly stationary processes 04 p0644 A67-14754
 Stochastic analysis of energy spectrum of output signal of phase shift modulator in PCM systems 04 p0571 A67-14895
 Abruptly varying random processes with determinate deflection, discussing phase space in form of Banach space 04 p0646 A67-15260
 Fatigue crack propagation rates for aluminum cantilever beams in reversed bending under two-level constant amplitude

and random excitation, noting stress cycle effect [ASME PAPER 66-WA/MET-3] 04 p0639 A67-15343
 Function approximation from finite number of arbitrary points, using iteration methods 05 p0833 A67-16260
 Simulation of controlled diffusion-type Markov processes applied to two stochastic equations related to problem of misadjustment on analog computer 05 p0768 A67-16263
 Synthesis of stochastic optimal control for case of discrete input of feedback vector, noting dependency on coordinates characterizing probability density of plant vector 05 p0782 A67-16316
 Synthesis and control strategy of optimal final value linear system under random environment statistically considered, using Bellman dynamic programming 05 p0783 A67-16442
 Nonstationary response of closed loop control systems with random characteristics, noting statistical analysis of error response and conversion of random control system to constant parameter system 05 p0783 A67-16443
 Statistical dislocation theory of crystal brittle fracture seen as stochastic process with microcrack formation and propagation under plastic deformation 05 p0919 A67-16504
 Acoustic field of random pressure pulsations into half-space behind infinite plate with arbitrary number of layers 05 p0846 A67-16708
 Optimal parameters of binary communication system using random coding and orthogonal radio signals with unknown phase 05 p0764 A67-16901
 Matrix solution to free motion of point in randomly perturbed resisting medium in rotating aspherical geogravitational field 05 p0901 A67-17110
 Distribution function for probability density of random process at output of multiplier acted upon by envelopes consisting of Gaussian noise and pulse signal 05 p0767 A67-17397
 Liapunov theory of stochastic stability, discussing use to obtain information about random trajectories 06 p0974 A67-17931
 Optimal control of linear stochastic systems with complexity constraints applied to sampled data system 06 p0975 A67-17934
 Wave propagation in random medium, examining stochastic PDEs, solutions and method of regularization 06 p0132 A67-18101
 Charged particle excitation by random electromagnetic field, obtaining velocity distribution function via all-order perturbation method 06 p1040 A67-18102
 Level quantization effect in statistical analysis of closed loop digital automatic systems 06 p0976 A67-18406
 Dual control of plant with random amplification factor as Bayesian problem 06 p0976 A67-18408
 Optimization of stochastic dynamic system with noisy output 06 p0977 A67-18525
 Dynamics of spherical gyroscope considered as automatic control system operating in presence of random perturbation 06 p1006 A67-18791
 Digital computer simulation of nonstationary Gaussian processes using Gaussian white noise, with application to simulation of structural response, ground acceleration, velocity and displacement of earthquake 06 p1109 A67-18839
 Mean number of random process ejections over arbitrary time period at output of receiver with time and frequency selectivity 06 p0965 A67-18897
 Computer simulation of perceptron predicting result of cyclic process 07 p1147 A67-19150
 Cost function gradient estimation for optimum control of nonlinear stochastic systems 07 p1159 A67-19193
 Electronic generation of stochastic step processes defined by stationary Markov chains 07 p1162 A67-20195
 Correlation functions and power spectra of stochastic processes with statistical structure defined by stationary Markov chains 07 p1217 A67-20196
 Inclusion probability of stochastic dynamical system shown to satisfy Kolmogoroff backward equation 08 p1308 A67-20323

Stochastic input passage through class of nonlinear systems, developing functional relations between statistical properties 08 p1308 A67-20324
 Random deviation statistical analysis of acoustic and electromagnetic waves by comparatively large slope irregularities 08 p1294 A67-20820
 Repetitive analog computer for Monte Carlo method solution of linear stochastic programming problems 08 p1299 A67-21198
 Lunar crater depth distribution in stochastic model of formation, obliteration, filling and isostatic readjustment of craters 08 p1397 A67-21209
 Optimal control analysis of system behavior described by linear stochastic differential equations 08 p1313 A67-21325
 Behavioral analysis of stochastic automata in random media, discussing automata design with quasi-linear behavior and expedient behavior 08 p1313 A67-21327
 Wave propagation in random medium analyzed by solving stochastic wave equation with random function for refractive index coefficient and applied to laser beam 08 p1296 A67-21434
 Wave propagation through random and nonrandom medium, discussing relation of phenomena to coherence theory 09 p1460 A67-21586
 Stochastic waveguides containing media with constitutive parameters having random variations not necessarily small or statistically homogeneous [SR-2] 09 p1460 A67-21593
 Effect of weak random inhomogeneities on long distance wave propagation, calculating first two statistical moments 09 p1461 A67-21595
 Addenda to processes defined on finite Markov chain 09 p1524 A67-21660
 Stochastic approximation method for determining real number from observation of random variables 09 p1524 A67-21933
 Anomalies and irregularities in application of maximum probability method to stochastic processes 09 p1525 A67-22587
 Stochastic control problems, considering dynamic model selection for physical system under random perturbation 10 p1620 A67-23427
 Error of measurement of mean square value of fluctuation signals due to voltmeter calibration 10 p1607 A67-23451
 Stability of linear integro-differential equations for processes with distributed parameters 10 p1681 A67-23667
 Stochastic Markov model for transient amplitude variation in systems with damped free vibration compared with deterministic solution 10 p1724 A67-23709
 Number of intersections of level by Gaussian stochastic process 11 p1812 A67-24099
 Dynamic correspondence between electromagnetic field density matrix and associated classical random problem, obtaining means of quantum operators through Fokker-Planck equation 11 p1799 A67-24240
 Stochastic optimal control with noisy observations, obtaining Hamilton-Jacobi stochastic equation in function space [ASME PAPER 66-WA/FE-6] 11 p1770 A67-24276
 Generalization of binary processes, discussing time domain and frequency domain analysis 11 p1813 A67-24312
 Transverse diffusion of particle perpendicular to magnetic field by assembly of random Alfvén waves explains increase in electric field energy 11 p1840 A67-24753
 Random motion transport relation to heat propagation noting tensor characteristics, entropy effects and path dependence 11 p1819 A67-24757
 Acoustic field of random pressure pulsations into half-space behind infinite plate with arbitrary number of layers 11 p1820 A67-24930
 Noise calculation in parametric amplifier using approximation method 12 p1913 A67-25300
 Statistical estimates for Gaussian random processes shown to be asymptotically normal and efficient 12 p1960 A67-25312
 Stochastic thermoelastic time varying boundary effect in circular cylindrical shell 12 p2022 A67-25587
 Stochastic approximation as recursive

method for solving regression problems in communication engineering 12 p1907 A67-25989
 Fokker-Planck-Kolmogoroff equations extended to cover conditional probability density functions of arbitrary random processes 12 p1961 A67-26082
 Use of limiters for estimating signal to noise ratio 12 p1908 A67-26090
 Relation between correlation functions of stationary random input and output for linear discrete systems 13 p2144 A67-26430
 Random process generation methods using noise-voltage generators and electronic computers 13 p2088 A67-27023
 Normalization of mixture of pulse signal and noise by postdetector integration 13 p2069 A67-27044
 Dynamical equations for optimal nonlinear filtering and representation of conditional expectation as solution to stochastic differential equation 13 p2146 A67-27094
 Optimality principle in mean for optimum averaging of controls of stochastic systems 14 p2290 A67-27841
 Stationary property of random process approximating anomalous magnetic field, noting optimum filtering 14 p2309 A67-27946
 Dynamic stability of pin-ended column under different types of random axial loading 14 p2397 A67-28091
 Total number and number of distinct particles in equilibrium system of recurrent Markov processes 14 p2345 A67-28907
 Optimal control of random dynamical systems analyzed, using first order vector differential or difference equations 14 p2292 A67-29062
 Efficiency criterion in form of probability of task completion estimated for dynamic systems with random parameters 15 p2455 A67-29121
 Formulation and analysis of class of optimization problems based on contraction mappings in theory underlying dynamic programming 15 p2511 A67-29891
 Stochastic Liapunov function existence demonstrated for continuous strong Markov process with certain stochastic stability properties 15 p2458 A67-29898
 Book on optimization of stochastic systems noting probability distribution functions, random variables, Bayesian optimization convergence, linear and nonlinear system estimation, etc 15 p2459 A67-30024
 Derivation of moments of continuous stochastic system 15 p2459 A67-30131
 Interlocking plan for entire countdown checkout process by combining subsystems simulated as partially controlled stochastic process 15 p2441 A67-30166
 Subadditive functional expectations and inequality of variables 15 p2512 A67-30228
 Stochastic model to structural fatigue, obtaining probability distribution for number of load repetitions necessary for fatigue failure 15 p2578 A67-30270
 Control system identification for noise corrupted input/output data, using algorithmic approach and iteration procedure 15 p2461 A67-30320
 Invariant estimation of stochastic system parameters using autoregressive models to characterize linear plants of control systems 15 p2462 A67-30325
 Identification techniques with stochastic computers for advanced automatic control systems in form of learning machines 15 p2441 A67-30344
 Continuous estimation of frequency response of linear system directly from random input and output data measurements 15 p2465 A67-30345
 Reliability statistics for repairable devices, proving Poisson distribution limitations and nonhomogeneous Poisson adequacy for analyzing stochastic processes 15 p2495 A67-30412
 System reliability for single-time demand interval, calculating distribution function for time to system failure 15 p2495 A67-30413
 Random instability of nonlinear oscillations of dynamic system with time behavior described by equation 16 p2702 A67-30447
 Optimal parameters of binary communication system using random coding and orthogonal radio signals with unknown phase 16 p2622 A67-30877
 Probability that random function with known correlation function will not fall outside regions with given boundaries within

given time 16 p2696 A67-30920
 Optimal system determination for recognition and separation of useful signal combined with noise 16 p2643 A67-30923
 Nonlinearly 16 p2643 A67-30923
 Nonlinear automatic control systems with random processes studied using orthogonal polynomials with Hermitian series expansion 16 p2643 A67-30924
 Optimal nonlinear filter construction for steady-state random process correction using iterative method 16 p2636 A67-30925
 Behavior of quasi-linear stochastic differential equations with one degree of freedom subjected to effect of random periodic excitation 16 p2696 A67-31009
 Statistical probability for motion stability of nonlinear stochastic systems during time interval, discussing oscillation stability of pendulum with randomly oscillating bearing 16 p2703 A67-31145
 Numerical characteristics of random functions applied to aircraft load evaluation 16 p2596 A67-31152
 Acceleration of plasma particles to high energies for case of interaction between plasma and stochastic field with harmonic correlation time 16 p2718 A67-31192
 Fracture theory statistical models, static and stochastic approach 16 p2771 A67-31294
 Iterative solution methods for minimizing convex, differentiable function in Euclidean space 16 p2697 A67-31424
 Feedback from observations introduced into midcourse guidance correction program, showing optimal random feedback solution obtained for deterministic optimal feedback control problems 16 p2701 A67-31657
 Recursive procedures for determining relationships between random parameter of linear system and resulting output random variable 16 p2652 A67-31691
 Identification of continuous, nonlinear, time-dependent, single-input single-output systems represented by Volterra functional series model and stochastic approximation 16 p2653 A67-31694
 Random amplitude fluctuations of quasi-stellar radio source from similarity between spectral-density distributions of observed and random-simulated luminosities 16 p2752 A67-31696
 Cosmic ray variation analysis using theory of random processes 17 p2935 A67-32107
 Cosmic ray variation determination from single series of observations by methods of random process theory 17 p2935 A67-32108
 Hypothesis of convexity of economic function for generalizing problem of inequalities in nonlinear stochastic programming 17 p2819 A67-32428
 Bounded solutions of boundary value problem with skew derivative studied by probability methods 17 p2878 A67-32737
 Averaging principle applied to stochastic differential equations describing oscillatory system subject to white noise effects 17 p2885 A67-32878
 Linear continuous time stochastic optimal control process, obtaining optimum performance achievable as function of total effort at initiation of optimization period 17 p2830 A67-33012
 Linear temperature measuring system and automatic regulating system accuracy, investigating heat transfer with random input for recipients of various forms 17 p2973 A67-33074
 Sufficient conditions guaranteeing asymptotic stability of class of linear dynamic systems with bounded narrow band parametric excitation [ASME PAPER 67-APM-24] 17 p2830 A67-33152
 Synthesis of optimum discrete control for eventual state of linear stochastic system, reducing problem to solution of Bellman functional equation 17 p2831 A67-33274
 Stability analysis of nonlinear stochastic systems in presence of random and Gaussian perturbations, determining validity of law of large numbers and amplified law of large numbers 17 p2886 A67-33275
 Stochastic differential game with missile and radar, using linear theory in finding optimal strategies 18 p3075 A67-33495
 Learning in unknown stationary environment using stochastic approximation, discussing Bayesian interference, pattern recognition, automatic control and statistical communications 18 p3070 A67-33497

Correlation function for random process energy spectrum at linear system output, obtaining expression of envelope distribution for radio signals 18 p2999 A67-33506
 Synthesis of stochastic optimal control for case of discrete input of feedback vector, noting dependency on coordinates characterizing probability density of plant vector 18 p3016 A67-33867
 Signal and noise FM modulated random process characteristics determined by equation for correlation function, giving energy spectrum relationship of modulated process phase 18 p3001 A67-34177
 Wave scattering phenomenon on uneven surfaces 18 p3004 A67-34380
 Dynamics of spherical gyroscope considered as automatic control system operating in presence of random perturbation 18 p3049 A67-34456
 Exact dynamical equation derived for conditional density mode representing stochastic process 19 p3199 A67-34778
 Wave propagation and geometrical optics in random media, considering applications to solar corona heating by energy transfer, stellar scintillation and cosmic ray acceleration 19 p3261 A67-35507
 Book on combinatorial methods in theory of stochastic processes covering ballot theorem, random variables, dam and storage processes, etc 19 p3250 A67-35572
 Small correlated amplitude and frequency fluctuations of stochastically-modulated radio waves 19 p3241 A67-36025
 Quasi-spectrum concept applied to square matrix for study of class of stochastic matrices 19 p3251 A67-36049
 Parameter optimization by modified sequential random perturbation technique using hybrid computer, considering initial conditions and analog computer errors effect, for dynamic systems 19 p3188 A67-36058
 Sonic film memory for digital information storage, discussing block-oriented random access memory /BORAM/ 19 p3189 A67-36067
 Optimal multidimensional systems for discriminating and detecting signals dependent on finite number of random parameters and combined with noise 19 p3185 A67-36097
 Book on probability in communication engineering covering probability theory, information and reliability theory, random processes and noise and random phasor sums 20 p3378 A67-36137
 Book on stationary random processes, discussing prediction theory, interpolation, extrapolation, filtering, linear forecasting, etc 20 p3475 A67-36140
 Random processes from physical viewpoint, discussing random function, random noise properties, Gaussian distribution, digital analysis, Shannon sampling theorem, etc 20 p3483 A67-36459
 Probability density function measurement, discussing turbulence problem, power spectral densities, Rice formula, inversion, etc 20 p3442 A67-36461
 Probabilistic background of time series models which relate to spectral analysis and power spectrum and statistical inference for stationary stochastic processes 20 p3476 A67-36783
 Prediction procedure for nonstationary stochastic processes with slow spectral density function variation with time 20 p3477 A67-36789
 Book on statistical theory of nonequilibrium processes in plasma, using microscopic equations to obtain two first moments of random functions 20 p3499 A67-36951
 Nonstationary random process power spectral analysis, noting evolutionary power spectra estimation methods, local energy distribution, etc 20 p3485 A67-37004
 Computer programming method for analysis of complex systems 20 p3392 A67-37194
 Statistical dislocation theory of crystal brittle fracture seen as stochastic process with microcrack formation and propagation under plastic deformation 20 p3541 A67-37318
 Collisionless plasma heating by random magnetic fields using simple betatron model 21 p3662 A67-37762
 Stability of linear integro-differential equations for processes with distributed parameters 21 p3657 A67-38268

Evaluation technique for correlation functions and power spectrum of randomly shaped pulse train using stationary point process 21 p3604 A67-38948

Sample continuous second order martingale process, determining existence of limit of stochastic processes using approximation theorems 21 p3654 A67-38966

Stochastic optimal control algorithm for pursuit process in problem of encounter of two cosmic objects 22 p3878 A67-39183

Rapid randomization phenomena in unstable plasma sac for Mach numbers close to unity attributed to electron interaction with trapped electroacoustic waves 22 p3844 A67-39357

Dissociation and recombination of diatomic molecules by invert third bodies described by stochastic theory 22 p3756 A67-39386

Turbulence theory from local equilibrium breakdown macroscopic approach by imposing suitable conditions on correlation functions, discussing stochastic Navier-Stokes equations 22 p3782 A67-39500

Steady state nonlinear Landau damping of electron plasma wave obtained from random phase approximation by balancing nonlinear and collision effects 22 p3848 A67-39691

Repetitive analog computer for Monte Carlo method solution of linear stochastic programming problems 22 p3764 A67-39865

Asymmetry and peakedness variation from normal distribution of random process at output of linear filter matched with broadband PM and PPM signal 22 p3761 A67-39868

Book on continuous and scanning control systems optimization and random processes theory including numerical techniques, harmonic analysis and Gaussian transformation 22 p3777 A67-40070

Laser and maser noise quantum theory emphasizing equations of motion and fluctuation problem, deriving density matrix equation 23 p4011 A67-40762

Technique for simulating stochastic approximation methods for selection of properties to ensure predetermined output signal characteristics 23 p3976 A67-41340

Plasma waves generation by transverse waves as function of phase relation of interaction 23 p4034 A67-41678

Threshold discrimination for two unknown a priori probability signals against noise background, using stochastic approximation in algorithm 24 p4134 A67-41795

Design procedure for estimating state vector of discrete-time linear stochastic system with constrained memory estimator 24 p4135 A67-42185

Steady random process phase overshoot length distribution determined over given level as well as relationships for mean value and distribution 24 p4136 A67-42194

Indirectly corrected gyro vertical used to determine vertical on power plant, considering random plant motion and gyroscopic drift 24 p4155 A67-42298

Axis crossing intervals of sine wave plus noise 24 p4122 A67-42343

Automatic systems optimization, adaptation and learning 24 p4136 A67-42697

Book on stochastic approximation and nonlinear regression covering convergence, asymptotic methods, real time problem in presence of noise, etc 24 p4179 A67-42900

RANDOM SAMPLE

Time-normalized Fourier transform of sampling function of stationary random process as bounded nonstationary random function of frequency 02 p0224 A67-11901

Quantization, sampling frequency and statistical scattering in correlation measurements 08 p1313 A67-21006

Monte Carlo calculation of kinetics of chemically reacting multicomponent gas for finite number of particles followed through random collision processes 13 p2102 A67-26971

Adjoint simulation technique extended to signals consisting of continuous, sampled and multirate sampled systems with random inputs 16 p2652 A67-31684

Optimum estimation of linear dynamic systems with stochastic transition and output model matrices, independent from one sample point to next, with known mean and covariance 16 p2652 A67-31693

Program producing optimum structural design configurations when restrictions on

variables and aims of design are given as input data [AIAA PAPER 66-531] 17 p2960 A67-32577

Secondary dose equivalent model for calculating secondary proton and neutron doses determined, using random sampling techniques 20 p3482 A67-37551

Free and near-free molecular flow via cylindrical ducts using Monte Carlo method and high speed digital computer 22 p3784 A67-39946

RANDOM SIGNAL

SA PSEUDORANDOM SIGNAL

Upper bound of dynamic range for minimal probability of excluding randomly distributed signal 01 p0023 A67-10486

Solution of optimum filtering problems when input signals of automatic control system are described by different differential equations at successive time intervals 03 p0390 A67-13099

Amplitudes and phases of element weighting factors in linear processor determined in order to maximize SNR of array receiving random signal in noisy environment 03 p0385 A67-13860

Synthesis problem of optimum dynamic characteristics of multivariate linear control systems with random input signals 05 p0781 A67-16252

Optimum quadratic detection of sample vector from signal random process imbedded in Gaussian noise 05 p0765 A67-17041

Analyzer of characteristic function of random phase of quasi-harmonic signal using statistics 06 p0972 A67-18392

Adaptive lagging system with output following randomly varying signal with minimum mean square error 07 p1160 A67-19202

Pseudo-random binary signals as perturbation waveform in adaptive control 07 p1161 A67-19205

Effect of a priori known relation between random signal and noise voltages at output of two channels 07 p1143 A67-19593

Effective field for microwave breakdown for gas in external DC magnetic field and electric field valid for any stationary random signal 09 p1482 A67-21646

Dispersion of number of positive zeros as function of time for realization of quasi-harmonic random signal 11 p1754 A67-24985

Automatic frequency control for estimating random signal frequency when received against white noise background 13 p2069 A67-27037

Hybrid computer calculation of instantaneous and peak amplitude probability distribution of random signal 15 p2440 A67-29774

Random signal treatment by Monte Carlo method for cutting tool applications 16 p2643 A67-30922

Spectral density of stationary random signals corrupted by multiplicative noise 17 p2812 A67-32303

Soviet book on digital processing of radar information covering signal processing, algorithms, discretization, etc 18 p3006 A67-33717

Random pulse operation and random pulse machines structural requirements, with continuous variable dependent on certain sampling time 18 p3006 A67-34063

Linear minimum variance estimation for random signal with complex phase errors, considering signal processing and optical propagation 18 p3001 A67-34111

Receiving system for detecting binary random signals in white noise, determining correlation functions and error probability 18 p3001 A67-34180

Synthesis of optimal and quasi-optimal sampled data control systems applied to various order plants 18 p3017 A67-34281

Data reduction system noting magnetic tape data collection, data transfer, random data analyzer, system analysis with transfer function analysis, etc 20 p3442 A67-36460

Effect of a priori known relation between random signal and noise voltages at output of two channels 20 p3384 A67-37332

Approximate investigation of standard model reference adaptive systems with random input effects based on filtering properties of automatic control systems 23 p3985 A67-41675

Probability of signal detection and accuracy of measurement in fluctuating multichannel system

parameters 24 p4120 A67-42223

Random Gaussian signal with unknown mean value reception using adaptive systems 24 p4120 A67-42224

Aperture usage for random optical communication channel through turbulent atmosphere 24 p4124 A67-42814

Signal extraction and scattering of telluric currents studied for random sheets, semilinear medium and interface separating medium of different resistivities 24 p4152 A67-42885

RANDOM VARIABLE

Convergence theorems for sequence of expected values or random variables of stochastic learning process with time-dependent probabilities 01 p0104 A67-10280

Nonlinear Sturm-Liouville BVP with random forcing function 02 p0258 A67-11587

Steady state output ripple performance and sampling frequency choice for single and multirate direct digital control system with stochastic input 02 p0225 A67-12073

Pattern recognition preprocessing by similarity functionals, examining relationship between measurement, selection and feature definition 02 p0207 A67-12137

Asymptotic behavior of distribution of maximum for class of processes with independent increments 03 p0458 A67-13340

Axiomatic formulation for stationary point processes interpreted as ordered sequences of points randomly located on real line, noting relation to set theory 04 p0643 A67-14521

Limit theorems for sum of sequence of independent random variables 04 p0644 A67-14755

Two-dimensional characteristic function and probability-distribution density of random process which is phase modulated by normal noise 04 p0575 A67-15161

Doubling of frequency of light in nonlinear medium with random nonuniformities 05 p0762 A67-16348

Conwright-Longuet-Higgins-Rice theory on instantaneous maxima of stationary random variable for deriving instantaneous maximum gust ratio to mean wind speed 05 p0837 A67-16426

Plasma stability with randomly fluctuating parameters for magnetic field with curved lines of force 06 p1045 A67-18790

Sommerfeld effect in linear oscillating system with randomly variable natural frequency 07 p1261 A67-19140

Existence theorem for nth order linear stochastic ordinary differential equations 08 p1347 A67-20356

Monograph on applied methods of random functions theory including stationary spectral theory, optimal dynamic systems, envelopes, etc 08 p1347 A67-20756

Soviet book on random function theory application to statistical problems in radio physics 08 p1295 A67-21336

Nonlinear automatic control with random parameters, noting change of system operator as function of disturbances on system 11 p1770 A67-24211

Planar antenna array with randomly spaced elements experimentally investigated, using holey plate technique 11 p1761 A67-24282

Rain effects at random antenna elevation 11 p1753 A67-24303

Two uncorrelated Gaussian dependent random variables with non-Gaussian joint distribution may have any maximal correlation coefficient 12 p1960 A67-25313

Intensity fluctuations of waves diffracted by deeply modulated random phase screen 13 p2071 A67-27403

Entropy of sequence Y obtained from coded sequence of random variables X 14 p2292 A67-28935

Two-dimensional characteristic function and probability-distribution density of random process which is phase modulated by normal noise 15 p2435 A67-29348

Book on optimization of stochastic systems noting probability distribution functions, random variables, Bayesian optimization convergence, linear and nonlinear system estimation, etc 15 p2459 A67-30024

Technique based on Fokker-Planck equation for estimating statistics of randomly varying parameters in dynamic systems with known differential equation 15 p2461 A67-30323

Statistical dispersion methods for

identification of nonlinear controlled plants 15 p2462 A67-30324

Continuous control process with random variable stopping time of known probability distribution, presenting optimal feedback control, trajectory and minimum cost 16 p2651 A67-31681

Book on statistical models in engineering covering probability theory, random variables, frequency distributions, etc 17 p2876 A67-32236

Probability density function of ratio of two nonzero mean Gaussian random variables derived and applied to calibrated signal using noisy calibration levels 17 p2816 A67-32624

Sommerfeld effect in linear oscillating system with randomly variable natural frequency 17 p2965 A67-33217

Plasma stability with randomly fluctuating parameters for magnetic field with curved lines of force 18 p3086 A67-33732

Book on combinatorial methods in theory of stochastic processes covering ballot theorem, random variables, dam and storage processes, etc 19 p3250 A67-35572

Random variables generation in computer, explaining procedure for beta and chi-square variates and normal distribution 19 p3188 A67-36056

Probability of overlapping intercept by system of random intercepts and application to detection of flying objects in cloudy skies 20 p3477 A67-37036

Selection probability from multivariable normal populations in terms of noncentrality parameters 23 p4024 A67-41084

RANDOM VIBRATION

Statistical correlation theory of accuracy and error relationships of sensing element during parametric excitations caused by random vibrations 01 p0064 A67-10417

Statistical dependence effect of normal mode response of complex structures to random excitation 01 p0163 A67-11172

Transmission of random sound and vibration through double wall analyzed by general method applicable to acoustics and thermodynamics 03 p0468 A67-13214

Digital simulation of Gaussian random load forcing function and motion equations of nonlinear vibration of damped elastic beam 04 p0656 A67-14447

First passage problems for lightly damped linear oscillator excited by white noise for two types of initial conditions and three types of barrier configurations 04 p0659 A67-15932

Human body response to stationary and nonstationary vibration [ASME PAPER 66-WA/BHF-15] 04 p0564 A67-15937

Energy dissipation effect on vibrations of elastic element with one degree of freedom excited by steady state random Gaussian disturbance 05 p0923 A67-17182

Dynamic analysis of lunar surface vehicle including power spectral density terrain definition, vehicle velocity limiting criteria and nonlinear analysis of vehicle freedom to pitch, bounce and roll 07 p1163 A67-19369

Level and duration of sine wave tests, discussing rocket design proof via random vibration testing 08 p1402 A67-20477

Perturbation technique used to study random response of airplanes to effect of runway roughness 08 p1279 A67-20480

Dynamic properties of coupled systems derived from experimentally determined frequency response functions of component systems, noting cross correlation functions 09 p1573 A67-21752

Book on probabilistic theory of structural dynamics, analyzing responses of structures to random vibrations 09 p1575 A67-21983

Aerodynamic flow field past cascade of plane thin turbine blades subjected to small random vibrations [ONERA-TP-412] 09 p1439 A67-22588

Qualitative vibration data reduction techniques for application to design problems, noting examples involving power spectra and probability-density functions 10 p1680 A67-23315

Finite element approach for determining rms deflections and stresses in randomly acoustically excited complex aerospace elastic structures 10 p1724 A67-23710

Power flow formulas for white noise driven vibratory systems, estimating average oscillation amplitude and plastic strain

accumulation rate 10 p1731 A67-23841

Mean square asymptotic stability of linear system described by nth order equation with random coefficients 11 p1818 A67-24161

Statistical energy analysis for multimodal random vibration of complex system, discussing power flow, modal responses, kinetic energies, etc [ASME PAPER 67-VIBR-8] 11 p1872 A67-24168

Mode coupling effect on response of rigid body to random excitation analyzed, using two degree of freedom model [ASME PAPER 67-VIBR-36] 11 p1873 A67-24193

Nonlinear oscillations of elastic plates under simultaneous effect of harmonic and random load 12 p2024 A67-25597

Statistical performance confirmation of wideband random equalizer, emphasizing analysis technique, analyzer characteristics and power spectral density plot 12 p1942 A67-25692

Laboratory techniques for utilization of shock synthesizer/analyzer 12 p1942 A67-25693

Drift effects of rate gyro under random vibrations, noting doubled eigenfrequency 13 p2153 A67-26624

Random vibration testing of relays noting test equipment 13 p2085 A67-27699

Fokker-Planck-Kolmogorov method analysis of nonlinear systems described by stochastic partial differential equations 15 p2517 A67-29658

Precession theory of compensating gyroazimuth, discussing random disturbances reduction by introducing electric mismatch of both sensitive elements 16 p2670 A67-30467

Optimization for linear vibration isolators considering vibration clearance tradeoff for random base motion 16 p2703 A67-31642

Dynamic system single-and multifrequency random oscillations described by differential-difference equations and solved through probability distribution 17 p2885 A67-32876

Thin slightly curved profiles positioned at small angle of attack in subsonic gas flow and developing harmonic random vibrations studied for aerodynamic interference 17 p2792 A67-32903

Lapunov approach to obtain sufficient conditions for stability of parametrically excited random vibrational system [ASME PAPER 67-APM-9] 17 p2886 A67-33145

Continuous exposure to random vertical vibrations studied for effects on compensatory tracking performance, noting decrement by peak vibration acceleration power location 18 p2993 A67-34336

Random vibration testing by multiple electrodynamic exciter technique, analyzing electromechanics and structural feedback 19 p3339 A67-34961

Vibration effect on task performance evaluated from test series, using vibration simulator 19 p3181 A67-35557

Steady random natural frequency variation and subharmonic resonance, discussing periodic right hand side Duffing type equation describing system 22 p3836 A67-39405

Launch vehicle response in lateral vibration modes to nonstationary random transonic buffeting excitation 22 p3907 A67-40167

Measured acceleration time histories analyzed for automatic handling of recorded data, discussing advantage of amplitude distribution method 23 p3986 A67-40719

RANGE

SA BALLISTIC RANGE

SA FREQUENCY RANGE

SA LONG RANGE

SA MISSILE RANGE

SA RADAR RANGE

SA RADIO RANGE

SA REENTRY RANGE

SA SOUND RANGING

SA TEST RANGE

Propagation loss dependence in laser ranging systems on meteorological visibility and target-receiver range, noting inverse-square law confirmation 17 p2812 A67-32305

RANGE AND RANGE RATE TRACKING

SA GODDARD RANGE AND RATE SYSTEM

Doppler tracking systems as velocity measuring systems, including introduction

methods for necessary position knowledge, one-and two-way systems analyses, etc 10 p1605 A67-22995

Range characteristics of antenna arrays composed of identical transmitters located along circumferential arc and producing pencil beam 13 p2080 A67-27027

Potential requirements imposed upon ranges and networks by future unmanned reentry vehicles [AAS PAPER 67-35] 15 p2571 A67-30107

RANGE CONTROL

Burning, staging and thrust direction programs for range maximization of particle in planar motion under downward gravitational acceleration and linear drag 05 p0905 A67-16780

Range control system for lifting body reentry vehicles, using closed form prediction equations for longitudinal and lateral range control [AIAA PAPER 67-136] 06 p1095 A67-18316

Gold doped silicon diodes consisting of compressor and expander elements designed to eliminate impedance range control and linearity problems 24 p4130 A67-42335

RANGE ERROR

Mathematical tool for system design of pseudorandom coded ranging system used in space programs, noting failure probabilities 07 p1145 A67-19869

Instrumental accuracy of missile range instrumentation systems, discussing error sources, detection and correction 10 p1605 A67-23002

Simulation and error analysis of range-only location and tracking utilizing satellite system to obtain range measurements 15 p2514 A67-29597

Apollo ranging code with phase locked loop for bit synchronization, plotting SNR vs error probability and acquisition time 18 p3000 A67-34102

Logarithmic compression of digitally telemetered data for constant maximum percentage error throughout encoded range 18 p3006 A67-34115

RANGE INDICATOR

Geodetic electronic ranging system of satellites with Sequential Collation of Range /SECOR/ transponder 07 p1177 A67-19772

Airport glide slope visual range determination with single-ended transmissometer by measuring transmission between photosensitive detector and laser light source 23 p3999 A67-41027

Compact air-to-ground laser rangefinder onboard helicopter nose section 23 p3999 A67-41028

RANGE MEASUREMENT

SA AIRBORNE RANGE AND ORBIT DETERMINATION /AROD/

Range instrumentation developments for trajectory measurements including cinephotodolites and tracking radars, noting error sources, weapons systems problems, etc 04 p0568 A67-14436

Radar, range instrumentation and measurement systems 04 p0568 A67-14497

Nuclear radiation characteristics pertinent to propagation of signals for measurement of range and bearing 05 p0839 A67-16532

USAF Eastern Test Range, discussing telemetry, tracking, geodetic and time measurements 05 p0787 A67-16609

Range determination with CW tracking radar controlling rms error, noting SNR role in holding target echo 06 p0957 A67-17593

Range capability of gallium arsenide injection LIDAR against extended targets and corner reflectors under both negligible and high background radiation conditions 09 p1462 A67-21640

Book on range instrumentation covering optical, radar, support systems, etc 10 p1604 A67-22992

Principles, methods of operation, techniques and limitations of phase comparison position-determining CW and pulse type systems 10 p1605 A67-22996

Range instrumentation support systems, describing approaches to timing, firing and communications systems 10 p1605 A67-22998

Range instrumentation ships as major range subsystems, noting equipment used, accuracy and sources of errors 10 p1622 A67-22999

Satellite range measurements using laser in conjunction with photoelectric receiver and Baker-Nunn camera 10 p1606 A67-23182

Aircraft UHF radio system for distance

measurements between airplane and two ground stations, noting onboard antenna 11 p1793 A67-24863

Propagation effects on distance, arrival angle and Doppler effect measurements with reference to tropospheric influence 14 p2264 A67-28400

Simulation and error analysis of range-only location and tracking utilizing satellite system to obtain range measurements 15 p2514 A67-29597

Range instrumentation ships electronic capabilities, operation, electronic systems function, accuracy and future role [AAS PAPER 67-52] 15 p2468 A67-30117

Range of hypersonic gliders for various flight and reentry conditions, assuming small flight path angle and constant bank angle 16 p2595 A67-30963

Strong reflection from underlying surface effect on range-only radar measurements, deriving phase angle between side-and carrier-frequency oscillation vectors 16 p2624 A67-31030

Lasers for short-distance communication and space, ranging, and detection applications 16 p2685 A67-31195

Advanced range and orbit determination /AROD/ using airborne equipment to originate control and tracking signals by checking ground stations 16 p2701 A67-31491

Airborne ground profiler using CW and pulsed lasers range finders discussing performance 16 p2679 A67-31798

Flight measurement data retrieval on real time basis from worldwide range stations possible through Range Support Satellite system 20 p3531 A67-36470

Noise model for simulating tropospheric turbulence effects on radio guidance and tracking range and angular measurements for optimum filter synthesis 21 p3587 A67-39147

Optical technique with laser source for range measurements noting use of dispersion between two different light wavelengths 22 p3800 A67-40139

Energy detection of multipulse returns from optically rough target using Q-switched laser 23 p4016 A67-41265

RANGE SAFETY

Range safety and tracking systems, discussing C-band beacon, CW transponder and command-destruct receiver operation and testing 04 p0577 A67-15729

Wind variability effect on impact point of launch vehicle with reference to range safety at Western Test Range [AIAA PAPER 67-187] 06 p0980 A67-18323

Hazards in sounding rocket assembly and launch operations and safety techniques at NASA Wallops station noting storage, explosive control, ground safety, etc 08 p1314 A67-20547

Range sum Doppler system for early launch tracking system to get warnings of possible impact in neighborhood of critical installations [AAS PAPER 67-42] 15 p2437 A67-30111

Dynamical and statistical approach to range safety problems, noting impact-density function of space vehicle destruction at early launch stage [AAS PAPER 67-45] 15 p2572 A67-30113

Wind variability effect on impact point of launch vehicle with reference to range safety at Western Test Range 19 p3207 A67-34834

RANGEFINDING

SA OPTICAL RANGEFINDER

Scheme for switching from automatic target search to range tracking, finding error distribution of backup system 05 p0767 A67-17473

Instrument errors in HF radio rangefinder 20 p3446 A67-36632

RANGER III LUNAR PROBE

Maintainability system operating parallel with cruise-mode spacecraft attitude-control system, noting application to Ranger III spacecraft 16 p2763 A67-31646

RANGER VII LUNAR PROBE

Errors in estimates of lunar crater slope angles and surface roughness in Ranger VII and Ranger VIII pictures due to interpretation of dark areas as shadows [JPL-TR-32-994] 01 p0147 A67-10319

Interpretations of lunar crater erosion other than used by Jaffe from Ranger VII pictures 02 p0325 A67-11860

Communications of Lunar and Planetary

Laboratory /University of Arizona/, Volume 4, covering Ranger VII records 05 p0896 A67-16713

Ranger VII photographic interpretation and lunar surface structures 05 p0896 A67-16714

Ranger VII records in support of lunar maria being formed by material flow processes 05 p0896 A67-16715

Ranger VII telescopic observation of crater topography of Mare Cognitum 05 p0901 A67-17084

Lunar crater diameter-depth relationship from Ranger VII photographs 06 p1087 A67-18376

Crater forming processes on moon from Ranger VIII impact, ascertaining gravity scaling existence, noting relation to terrestrial soils 19 p3327 A67-35894

RANGER BLOCK III

Estimated GM values of earth and moon, tracking station locations and lunar radii at impact points, from DSIF radio tracking data of Ranger Block III lunar flights [AAS PAPER 66-105] 07 p1253 A67-19965

Estimated GM values of earth and moon, tracking station locations and lunar radii at impact points, from DSIF radio tracking data of Ranger Block III lunar flights [AAS PAPER 66-105] 13 p2208 A67-27523

Ranger Block III television system for lunar surface photography 16 p2620 A67-30643

RANGER LUNAR LANDING VEHICLE

Estimate of dynamical center from four lunar surface impact points determined by tracking Ranger probes from three earth-based stations 18 p3131 A67-34324

RANGER PROJECT

Ranger and Mariner spacecraft temperature control design, test and flight results 03 p0517 A67-13071

Size distribution of lunar craters from Ranger pictures show that frequency of crater occurrence is inversely proportional to square of diameter 05 p0903 A67-17293

Structure of lunar lithosphere using data from ground telescopes and Ranger photographs 06 p1092 A67-19004

Lower bounds for lunar surface strength obtained from data of Ranger and Luna spacecraft [JPL-TR-32-1068] 08 p1397 A67-21210

Depth of loose and loosely bonded material on lunar surface determined using Ranger VII, VIII and IX photographs 08 p1401 A67-21361

Selenological analysis of Ranger IX photographs examining origin and age of craters and mountain chains 10 p1705 A67-22898

Morphology of lunar craters from Ranger photographs, noting distribution and possible competing processes of crater formation and destruction 11 p1865 A67-24608

High volume data processing techniques applied to Ranger acoustic testing 12 p1924 A67-25713

Lunar surface and U.S. Ranger program significance and interpretation 18 p3121 A67-34137

Moon elevation profiles and lunar slopes determined by photometry and isodensitometric measurements of Ranger IX photographs 18 p3133 A67-34335

Lunar scar and ghost crater origin theories illustrated with Ranger 3-D slides 23 p4064 A67-40951

Lunar geology using probe data to distinguish impact and volcanic surface shaping processes [AIAA PAPER 67-862] 24 p4238 A67-42986

RANK TEST

Testing procedures for null hypothesis sensitive to ordered alternatives where at least one inequality is strict 21 p3650 A67-37780

RANKINE CYCLE

High temperature electrical material evaluation for Rankine cycle [SAE PAPER 66-0662] 01 p0094 A67-10571

Two-phase flow and material attrition problems for Rankine cycle liquid metal power plants [ASME PAPER 66-GT/CLC-4] 01 p0014 A67-10872

Rankine and Brayton cycles for spacecraft power generation, discussing operation principles, advantages and performance characteristics 01 p0112 A67-11428

Potassium metal Rankine cycle power system, testing turbines, bearings and seals,

potassium boiler and steam topping cycle analysis obtaining high heat-transfer coefficients [AIAA PAPER 66-1009] 02 p0184 A67-12307

Nuclear power supplies for electrical propulsion including liquid metal reactor-potassium Rankine, Brayton, MHD power conversion and thermionic reactor [AIAA PAPER 66-1021] 03 p0363 A67-14153

Rankine cycle power plant characteristics for electric propulsion manned Mars mission [AIAA PAPER 66-894] 03 p0504 A67-14274

Wear and compatibility of liquid metal bearing materials, including surface coatings and cemented refractory carbides, analyzed for Rankine cycle power plants [ASME PAPER 66-WA/LUB-3] 04 p0630 A67-15350

Materials technology presently available for advanced Rankine systems including nuclear fuels, refractory metal alloys, electrical materials and stainless steel 07 p1223 A67-19460

Li, Na, K, Rb and Cs vacuum tests as coolants and working fluids in high temperature compact space power plant 07 p1223 A67-19464

Electric propulsion for space exploration, discussing testing results on Rankine cycle power system [AIAA PAPER 66-890] 09 p1559 A67-21870

Gas turbine design, considering thermodynamic and physical properties of various Rankine-cycle working fluids [ASME PAPER 67-GT-6] 11 p1745 A67-24794

Quantitative graphical method of screening working fluids for Rankine cycle power plants using single stage turbines at different levels of diameter and rpm [ASME PAPER 67-GT-12] 11 p1746 A67-24798

Criteria for use of Rankine MHD systems in space 16 p2604 A67-30569

Liquid-metal and plasma MHD systems for power generation in space environments, noting Rankine and Brayton cycles [JPL-TR-32-1129] 17 p2802 A67-32049

Electric propulsion for space exploration, discussing testing results on Rankine cycle power system [AIAA PAPER 66-890] 17 p2928 A67-32051

Potassium metal Rankine cycle power system, testing turbines, bearings and seals [AIAA PAPER 66-10009] 17 p2802 A67-32052

Potassium Rankine cycle turboelectric space power system, emphasizing vapor film type of condensing radiator 20 p3364 A67-37018

Rankine cycle power plant for electric propulsion manned Mars mission analysis of system characteristics and mission duration effect 22 p3869 A67-40173

Small scale Rankine cycle power conversion system using potassium working fluid under environmental, RF interference and ground performance tests 24 p4102 A67-42491

Lithium-boiling potassium test facility to investigate transient and steady state characteristics of Rankine cycle system for application to spacecraft nuclear-electric propulsion 24 p4183 A67-42492

Organic Rankine cycle power system using monoisopropylbiphenyl /MIPB/ as working fluid noting advantages 24 p4103 A67-42494

Rankine cycle power plants using organic working fluids considered for near-term application 24 p4103 A67-42495

Rotating boiler for high performance Rankine cycle power generator using water as test fluid, obtaining heat-transfer coefficients 24 p4184 A67-42498

Shield-radiator weight tradeoffs to optimize K Rankine cycle space power plant heat source operating temperature, noting burnup 24 p4185 A67-42537

Stirling, Brayton and Rankine dynamic cycles compatibility with isotope heat sources, emphasizing power system applications to long-duration earth orbital missions 24 p4185 A67-42542

Integrated thermoelectric SNAP-8 Rankine power system for manned lunar base missions, studying man-system interactions effect on design criteria 24 p4185 A67-42544

Integrated design requirements of SNAP-8 Rankine power system for manned lunar base mission, discussing mission requirements and reactor shield system 24 p4185 A67-42545

Nuclear electric space power plant with Rankine cycle for plausible Mars manned

mission, discussing mission requirements and reactor elements 24 p4186 A67-42549

Alkali metal Rankine cycle space power system component and systems design 24 p4186 A67-42887

Lunar electric power systems transported by Saturn V noting Brayton cycle, Rankine cycle, solar cells and thermoelectric systems [AIAA PAPER 67-902] 24 p4110 A67-43010

RAPCON

S RADAR APPROACH CONTROL /RAPCON/

RARE EARTH

SA CERIUM

SA DYSPROSIUM

SA ERBIUM

SA EUROPIUM

SA GADOLINIUM

SA HOLMIUM

SA LANTHANIDE

SA LANTHANUM

SA NEODYMIUM

SA PRASEODYMIUM

SA SAMARIUM

Optical properties of thin metallic films relative to electronic structure in microcrystals 02 p0288 A67-11722

Rare earth trace element variations in anorthosite and quartz mangerite determined, using stable isotope dilution technique of analysis 03 p0513 A67-14006

Neodymium doped optical glasses for laser technology 05 p0824 A67-16855

Unfamiliar metals properties and potentialities from viewpoint of metallurgist 05 p0830 A67-17088

Meteoritic, solar and terrestrial rare earth distribution abundance in chondritic or ordinary stony meteorites 10 p1651 A67-23428

Optical and laser properties of trivalent Nd and Eu ion doped yttrium orthovanadate 11 p1847 A67-24739

Rare earth metal superconductive shielded magnetic lens for focusing high energy electrons 11 p1802 A67-24765

Laser emission temperature dependence resulting from variation in radiationless transfer of excitation in trivalent erbium and thulium 11 p1803 A67-24836

Rare earth metals effect on Neel temperature and plasticity of recrystallized chromium at 1200 degrees C in vacuum 13 p2131 A67-26450

Lanthanide partition coefficient for crystallization under calcium effect, noting inflectional pattern for inverse ionic radius variation 21 p3617 A67-38123

Rare earth elements distribution and component minerals in Bruderheim meteorite, using phase separation method 21 p3702 A67-38126

Charge compensation defects influence on UV excitation spectrum of rare earth doped crystals fluorescence 22 p3856 A67-39384

Microwave absorption phenomena observed in Tb, Dy, Ho and Er single crystals 23 p4036 A67-40710

Resonance transfer of energy as mechanism for quenching interaction between rare earth ions affecting fluorescent lifetime 23 p3971 A67-40974

Crystal structure of rare earth Co compounds prepared by levitation melting process investigated by X-ray 24 p4172 A67-41975

Lanthanide distribution between omphacite and Garnet, noting abundance ratios to whole rock of Japanese eclogite 24 p4151 A67-42449

Rare earth and barium abundances in Ivory Coast tektites and rocks determined by isotope dilution 24 p4236 A67-42645

Alkali, alkaline earth and rare earth elements distribution in chondrite component minerals 24 p4236 A67-42646

Photoexcited electroluminescence spectra of rare earth ions in cadmium fluoride semiconductor single crystal 24 p4205 A67-42893

RARE EARTH ALLOY

Ce and Pr effect on structure, hardness and mechanical properties of cast steel at 800 degrees C 07 p1199 A67-19242

Rare earth metal/manganese alloys analyzed by amalgam process 07 p1210 A67-20111

Exchange interaction between f-electrons and s-electrons in atomic shells of crystal lattice of rare earth metals, examining calculation methods for Hamiltonian of s-f exchange 16 p2733 A67-31730

Rare earth metals effect on mechanical properties of austenitic chromium steel at high temperatures 24 p4169 A67-41920

Exact calculation of indirect exchange interaction isotropic and nonisotropic terms in rare earth metals, with free electron model for conduction band 24 p4203 A67-42110

RARE EARTH COMPOUND

Four-linked rare earth chelate with sodium ion obtained with benzoylacetone and europium, analyzing molecular and ionic transitions by absorption and emission spectra 02 p0251 A67-11518

Vanadium charge compensator in laser calcium tungstate, determining vanadium positions via electron spin resonance 04 p0633 A67-15306

Rare earth compound and Ba abundances in Bununu howardite 07 p1249 A67-19537

Energy level structure of rare earth chelates, noting existence of isolated systems of optical electrons 09 p1512 A67-21921

Crystallization phase in Pbnm orthorhombic space group of yttrium manganite under pressure and high temperature 09 p1557 A67-22572

Laser generation through rare earth chelate solutions, requirements for working solutions and apparatus 10 p1664 A67-23068

Lanthanum germanide synthesis using arc furnace, noting chemical properties 13 p2131 A67-26470

Energy level structure of rare earth chelates, noting existence of isolated systems of optical electrons 14 p2330 A67-28250

Yttrium and gadolinium borides thermionic emission properties, noting inferiority to lanthanum hexaboride 15 p2534 A67-29358

Neodymium activated alpha-gagarinite crystal laser, noting ternary fluoride systems characterized by optical centers 15 p2496 A67-29360

Liquid lasers use of rare earth ions, chelate structures, selenium oxychloride, etc 15 p2501 A67-30086

IR lattice spectra of rare earth iron garnets noting absorption in low frequency bands and molecular weights 16 p2733 A67-31880

Electron paramagnetic resonance of trivalent rare earth-monovalent alkaline earth ion pairs in calcium fluoride 21 p3676 A67-37815

Phonon spectrum of neodymium trichloride crystal lattice determined from polarized vibronic transition spectra and Zeeman effect of trivalent Pr and Nd impurity ions 22 p3840 A67-39434

Absorption spectra of rare earth trichlorides with trivalent Pr, observing vibronic transitions noting assignments of phonon branches 22 p3840 A67-39435

RARE GAS

SA ARGON

SA HELIUM

SA KRYPTON

SA NEON

SA XENON

Cross sections for double electron capture by two 50-kev protons in single collisions with hydrogen and inert gas target 01 p0115 A67-10140

Decay cross section of pumped metastable He atoms in HeNe laser 01 p0090 A67-10511

Radiation from high energy level transitions excited in He-Ne laser during optical pumping with He lamp 01 p0090 A67-10513

Exciton and impurity states in Kr and Xe crystals and in rare-gas solids containing Xe impurity calculated by pseudopotential theory 02 p0281 A67-11490

Autoionization states and resonances in absorption spectra of rare gases 03 p0471 A67-13223

Krypton and xenon effect on dissociation rate of fluorine in presence of argon behind shock wave 04 p0567 A67-15951

Stallwood jet and DC arc in analysis of air contamination in inert gases 05 p0758 A67-16368

Amplitude of LF oscillations in He-Ne laser 05 p0825 A67-16948

Mass spectrometric observation of ions formed during shock wave heating of gaseous krypton and xenon at 3600 to 7800 degrees K 05 p0795 A67-17440

Momentum transfer accompanying ionizing impact of electrons against atoms of inert gases 06 p1037 A67-18426

Thermal excitation and de-excitation of alkali atoms in inert gas heat bath 07 p1265 A67-19075

Pitzer acentric factor relationship to Morse intermolecular potential function appears to hold only for normal fluids 07 p1138 A67-20193

Excitation cross section of states of Ne 2, Ar 2 and Kr 2 by electron collision 08 p1339 A67-21376

Absorptional atelectasis breathing oxygen at simulated altitude, discussing prevention by using inert gas 09 p1453 A67-21732

MHD generator using nonseeded inert gas as working fluid 09 p1444 A67-21812

Transverse separation of rare gas-metal vapor mixture components in positive nonisothermal plasma column in plain-symmetric glow discharge 09 p1545 A67-21998

Inert gas effect on performance characteristics of cesium thermionic converter, noting saturation current increase 09 p1444 A67-22008

Thermionic converter performance in presence of inert gases under conditions which avoid previous difficulties 09 p1448 A67-22339

Collision induced far IR absorption in rare gas mixtures with emission spectrum calculation 09 p1535 A67-22382

High voltage pulsed electrodeless discharge in rare gas as light source for ruby and Nd glass laser excitation and observation of output characteristics 10 p1666 A67-23565

Effects related to ion cooling in Q device 11 p1833 A67-24371

Hypersthene chondrite origin and history studied using noble gas content and shock and reheating by X-ray diffraction 11 p1865 A67-24602

Cesium thermionic diode parameters including added noble gas pressure effect for ignited mode performance prediction and optimization 12 p1896 A67-25262

Thermal accommodation of rare gases on clean metal surfaces, computing energy interaction with linear nearest-neighbor lattice 13 p2098 A67-26941

Thermal accommodation coefficient measurements with rare gases and metals and alkali metal sets 13 p2223 A67-26942

Thermal accommodation coefficient of rare gases on clean tungsten surfaces with gas temperature above room temperature 13 p2223 A67-26943

Noble gas molecular beam quasi-specular scattering from metal surfaces noting effects of beam incidence angle, molecular weight and gas temperature 13 p2099 A67-26949

Nogoya-type II carbonaceous chondrite noting cosmogenic, radiogenic and primordial noble gas components 14 p2390 A67-28890

Multiple ionization of rare gases analyzed in mass spectrometer with trapped ion source, noting energies of metastable levels 15 p2519 A67-29189

High temperature testing and evaluation of graphite helical-screw expanders and compressors for use with inert gas Brayton cycle 15 p2492 A67-29427

Dispersion relations of moving striations in rare gases, noting wave nature and dependence on discharge current 15 p2472 A67-29733

Laser output reduced by rare gas impurities in molecular neutral CO and nitrogen gas lasers 15 p2500 A67-29910

Condensation droplet growth in supersaturated vapor and inert carrier gas, noting thermal and diffusion effects 15 p2582 A67-30198

Atmospheric pressure discharges in inert gases seeded with alkali metal vapor, noting transition to low voltage high current discharge 16 p2709 A67-30513

Electron number density and number density of electronic states calculated from rate equations for noble gas seeded with alkali metal 16 p2710 A67-30518

Physical properties of binary pulsed discharge plasma in helium and argon seeded with Cs and K vapor 16 p2711 A67-30525

Experiments and design of low temperature seeded inert gas MHD power generator operating in nonthermal ionization mode 16 p2801 A67-30548

Large nonequilibrium MHD generator design and preliminary performance, emphasizing electrode-wall shorting phenomenon in channel 16 p2602 A67-30556

MHD Brayton cycle power generation techniques, considering noble gases seeded with alkali metal vapors as working fluid 16 p2603 A67-30567

High pressure electrodeless discharge in pure Ne and Xe and mixture of Kr and Xe, detailing effect of steady state magnetic field on Xe plasmoid 16 p2717 A67-31185

Temperature dependence of thermal diffusion factors in ternary system He-Ne-Kr by two-bulb method 16 p2661 A67-31223

Ionization, ion temperature and density dependence of cesium plasma on pressure of added rare gas 16 p2720 A67-31244

Light and heavy rare gases content in St Severin meteorite and iron-enriched fractions 16 p2750 A67-31435

Argon, krypton and xenon in chondrites noting constant abundance ratios and correlation of concentration to disequilibrium 16 p2750 A67-31436

El Taco meteorite samples analyzed for rare gas concentrations, comparing with rare gas data from Campo del Cielo and North Chile meteorites 16 p2750 A67-31439

Geometry of steady state annular electrodeless discharge in argon and xenon as function of discharge power, type of gas, gas pressure, etc 16 p2723 A67-31770

Ion-molecular reactions of hydrogen with inert gases caused by low energy electrons in low temperature plasmas, considering energy level populations, reaction cross sections, etc 17 p2808 A67-32141

Excitation and propagation of surface plasma waves along plasma column in noble gases, obtaining plasma dispersion curves 17 p2899 A67-32309

Concentration ratios of cosmic ray-produced isotopes of helium, neon and argon measured and effective irradiation hardening parameter calculated 17 p2942 A67-32358

Photoionization study of diatomic-ion formation in argon, krypton and xenon by collision process [AFRCL-66-785] 17 p2888 A67-32631

Mechanism of positive low pressure column in plasma of low electron density, studying steady state conditions of nonstratified inert gas discharges 17 p2907 A67-33103

Modified hot-wire thermal conductivity cell for measuring effects of finite length, pressure and temperature on heat transfer from wire in rare gases 17 p2863 A67-33357

Existence in alkali-metal-seeded rare gases of mode of nonequilibrium electric discharge with constricted positive column 17 p2910 A67-33385

Gas-borne suspensions of thermionically emitting particles as MHD working fluids 18 p3086 A67-33707

Spectra of noble gases in 4-micron region, using IR spectrometer equipped with cooled lead sulphide detector 18 p3082 A67-33876

Selective enhancement of molecular spectra of HD and diatomic deuterium in argon and krypton discharges 18 p3083 A67-34518

Primordial rare gases abundances in unequilibrated ordinary chondrites determined by mass spectrometry 19 p3317 A67-34912

Positive column contraction in inert gas discharge, studying electron density and radiation intensity radial distribution and wall current 19 p3272 A67-35092

Positive column and striations of low pressure discharge of noble gas 19 p3273 A67-35097

Periodic changes, using square-wave current modulation, between diffuse and highly constricted positive column in medium-pressure rare-gas discharges 19 p3274 A67-35101

Discharge plasmas in hollow cathodes investigated using photography, showing mercury vapor and inert gas plasmas form homogeneous or laminar positive plasma columns 19 p3274 A67-35102

Surface bombardment damage on molybdenum and tungsten crystals by inert gas ions 19 p3246 A67-35784

Transitions in neutral spectra observed in near IR wavelength region in noble gases 20 p3460 A67-36859

Temperature dependence of far IR

collision-induced absorption as probe of rare gas mixtures interatomic potentials 20 p3490 A67-37567

Optical third-harmonic generation in rare gases, comparing coefficients with Kerr effect coefficients 21 p3639 A67-37962

Abundance of stable isotopes of neon, argon, krypton and xenon in Costilla Peak iron meteorite, observing spallation components 21 p3702 A67-38124

Magnetic separations performed on Jodzie howardite, showing uniform primordial gas enrichment indicating covariant solar planetary components 21 p3704 A67-38503

Theoretical lung with equal ventilation-perfusion ratio used to study determinants in inert gas elimination 21 p3575 A67-38515

Ventilation-perfusion inequality effects studied in inert gas elimination from lungs 21 p3575 A67-38516

Electron impact ionization cross sections and rate coefficients for atoms and ions of Hg, rare gas and alkali metal groups 21 p3660 A67-39098

Rare gas isotopic analysis using ruby pulsed laser and mass spectrometer 22 p3816 A67-40241

Emission wavelength selection in multicolor-emission noble gas laser using linear polarization control device 23 p4014 A67-41025

Thermally activated inert gas ion injection into tungsten and gold to correlate energies associated with peaks in desorption spectrum 23 p4030 A67-41357

Weldability of Al when used in low temperature container construction noting shielding with rare gases 24 p4159 A67-41839

Total carbon content and primordial rare gases in chondrites 24 p4236 A67-42641

MPD energy conversion duct using heated inert gas working fluid, discussing Hall parameter operation and efficiency factors 24 p4109 A67-42898

RAREFACTION WAVE

Text describing physical phenomena and experimental apparatus for observing and measuring shock waves and detonations in gases 02 p0235 A67-12680

Low intensity shock wave transformation into rarefaction wave in nonconducting media in presence of external electric field 03 p0476 A67-13203

Monograph on shock tubes, weak and strong shock waves and rarefaction waves 07 p1169 A67-20205

Transonic gas flow past ducted bodies of revolution indicates shock wave asymptotic attenuation at infinity 14 p2296 A67-27989

Supersonic jet expelled from plane nozzle solved by characteristic method to determine family of rarefaction waves and nozzles 18 p2656 A67-30455

Experimental determination of compression and rarefaction shock waves structure causing high pressure phase formation and decay in potassium halides 23 p3989 A67-40906

RAREFIED GAS

Compressibility effects on rarefied gas flow in Rayleigh problem, using BGK model of Boltzmann equation 01 p0051 A67-10457

Rarefaction parameter for planar bodies with sharp leading edge and tip defining hypersonic boundary of strong interaction regime 01 p0007 A67-11182

Diffusion phenomena in rarefied gases treated, using Boltzmann equation expanded in Sonine Legendre polynomials in velocity space 02 p0234 A67-12544

Attenuation and dispersion of sound in nearly collisionless gases as function of sound-to-particle path ratio 02 p0235 A67-12565

Thermal creep in rarefied gas investigated using Boltzmann-Krook equation 03 p0402 A67-13359

Drag measurements of isolated lamellae and cylinders in rarefied gases with low velocity 03 p0404 A67-13972

VIM-1 vacuum gauge using inverse-magnetron type manometric transducer for measuring rarefied gas pressure 03 p0425 A67-14268

Heat transfer and equilibrium temperature of plate in supersonic flow of rarefied gas 04 p0546 A67-14783

Turning-arm apparatus operating in rarefied gas chamber and low pressure wind tunnel for drag measurements 04 p0596 A67-14993

Linearized Couette flow problem in rarefied gas solved, using one-dimensional radiative heat transfer analogy 04 p0606 A67-15183

Monte Carlo method analysis of rarefied gas heat transfer between parallel plates in terms of temperature, density and Knudsen number 04 p0728 A67-15807

Steady one-dimensional heat conduction in rarefied gas at rest analyzed from viewpoint of kinetic theory to determine existence or possible departure from Fourier law 05 p0925 A67-16272

Friction stress and flow rate for rarefied constant density gas flow past semiminfinite plate treated by approximate diffusion model 05 p0792 A67-16995

Diffusion-viscosity coupling in stationary flow of nitrous oxide-carbon dioxide mixture in case of Maxwellian intermolecular forces 05 p0794 A67-17380

Conductive heat transfer coefficient measurement from sphere to rarified gas mixtures over range of Knudsen numbers 06 p1117 A67-18388

Hypersonic rarefied gas flow past plate with sharp leading edge, determining rarefaction effect on induced pressure distribution and value 08 p1278 A67-20924

Boltzmann equation for rarefied gas flows between two parallel infinite plates for Maxwellian, hard sphere and BGK models 08 p1355 A67-21117

Discrete ordinate method for unsteady linearized Boltzmann Bhatnagar-Gross-Krook equation of rarefied gas flow 08 p1324 A67-21409

Rarefied gas flow dynamic behavior during reaction with gas measuring device mounted on moving plant 09 p1487 A67-21896

Rarefied gas flow past sphere studied by multibeam interferometry of density profile and shock structures 09 p1438 A67-22216

Plasma source in which collimated photon beam generates plasma by single quantum photoionization of rarefied gas 09 p1549 A67-22426

Heat losses in conductive and convective transfer through rarefied fluids investigated for dependence on temperature differences, static pressures, test geometries and fluids 10 p1731 A67-22725

Multiple wave interferometer application to determine parameters of rarefied gas flow past circular cylinder 10 p1625 A67-23043

Thirteen moment equation solved for problem of plane Couette flow by iteration scheme, showing functional dependence on Mach and Knudsen numbers 11 p1774 A67-23863

Heat flux in rarefied gas calculated via transport equations, noting validity of boundary temperature discontinuities 11 p1881 A67-24028

Quantitative fast response visualization technique for low density flow fields based on electron beam fluorescence probe 11 p1790 A67-24450

Pulsed inert gas metal-arc welding technique for titanium 721, investigating arc characteristics in argon, argon/helium and helium 12 p1950 A67-25738

Cylindrical Couette flow of rarefied monatomic gas calculated by double flow method 13 p2095 A67-26898

Rarefied multicomponent gas flow boundary conditions over subliming wall determined through Navier-Stokes approximation, noting distribution function of each component 13 p2105 A67-27054

Free stream variables from continuum effect followed experimentally into transition flow regime to investigate impact probe in rarefied hypersonic flows of diatomic gases 14 p2294 A67-27794

Aerodynamics survey emphasizing supersonic speed problems 14 p2239 A67-27874

VIM-1 vacuum gauge using inverse-magnetron type manometric transducer for measuring rarefied gas pressure 14 p2321 A67-28778

Boundary conditions for Navier-Stokes equations in rarefied monatomic gas with distribution function given a priori 15 p2470 A67-29234

Photographic recording of fast moving plasma clouds during pulsed discharges in rarefied gas using Topler apparatus 16 p2721 A67-31396

Rarefied gas supersonic flows studied in wind tunnel for aerothermal/aerodynamic characteristics 17 p2790 A67-32231

Rarefied gas flow past sphere studied by multibeam interferometry of density profile and shock structures 18 p2982 A67-33755

Mach and Reynolds numbers effect on rarefied supersonic gas flow pattern near forward stagnation point of blunt body, noting decrease in density 18 p3028 A67-34209

Hypersonic rarefied flow past sharp leading edge of flat plate noting incomplete compression phenomenon 19 p3171 A67-35735

Transient heat transfer through monatomic collisionless ideal gas enclosed between parallel walls analyzed for step change in one wall temperature [ASME PAPER 67-HT-53] 20 p3548 A67-36735

Stagnation-point flow of rarefied gas, using linearized BGK model of Boltzmann equation with small Mach number 20 p3425 A67-37673

Poiseuille flow of rarefied gases through cylindrical tube, solving integral equation, noting variational calculation of hydrodynamic velocity 21 p3609 A67-37738

Rarefied gas axisymmetric stagnation point flow, clarifying relationship between continuum and Knudsen layer flow 22 p3784 A67-39836

Monte Carlo method for molecular vacuum pump calculation, noting applicability to molecule-boundary and molecule-molecule collision conditions 22 p3785 A67-40012

Rarefied gas mixtures viscosity and heat conduction temperature dependence calculated, analyzing empirical relations 24 p4142 A67-42220

Hydrodynamic solution for shock wave parameters of monatomic gases assuming exponential molecular interaction potentials and absence of mass forces 24 p4142 A67-42271

First approximation analysis of rarefied hypersonic gas flow asymptotic properties near surface and front edge of thin plate, determining macroparameters 24 p4142 A67-42272

Soviet book on molecular flow in vessels covering mass balance, energy exchange, rarefied gas, etc 24 p4191 A67-42359

RAREFIED GAS DYNAMICS

Heat transfer and equilibrium temperature of heat conducting sharp cones in supersonic rarefied gas flow at zero angle of attack 01 p0007 A67-10977

Perturbations of gas-dynamic parameters behind shock wave front propagating from rarefied into dense gas with boundary between interfaces 01 p0053 A67-10984

Boltzmann equations in kinetic theory of rarefied gas dynamics [ONERA-TP-379] 01 p0054 A67-11092

Improved Monte Carlo method for calculating steady state monatomic rarefied-gas flows, using computer for calculating possibility of collision in given geometrical cell 01 p0055 A67-11292

Aerodynamic coefficients of symmetrical wing profiles and fuselages in rarefied gas calculated for free molecular flow 04 p0547 A67-14992

Plasma expansion in magnetic field, showing dominating effect of initial outward momentum 05 p0858 A67-17428

Mathematical analysis of gas flow equations and shock wave structure in rarefied gas dynamics 06 p0983 A67-17784

Unsteady flow of rarefied gas under finite pressure gradient when starting from rest, varying gradient in time until steady flow is obtained 09 p1487 A67-21847

Aerodynamic problems of low density high speed flow of rarefied gases past submerged body 10 p1623 A67-22874

Rarefied gas flow analyzed through transport equation in gas kinetics using bimodal two-stream distribution functions, with application to Couette flow 10 p1624 A67-22914

Rarefied gas motion instability, constructing general solution for effect of various force fields 11 p1782 A67-24688

Rarefied gas flow between parallel plates based on discrete ordinate method 13 p2092 A67-26277

Rarefied gas dynamics - Conference, Oxford University, July 1966, Volume I 13 p2096 A67-26934

Unified theory of gas-solid energy transfer

in perturbation approximation, examining physical principles 13 p2223 A67-26940

Spatial distribution of deuterium and hydrogen molecules and helium scatterer from /111/ plane of epitaxially grown silver 13 p2099 A67-26948

Kinetic theory and rarefied gas dynamics, discussing and analyzing Boltzmann equation 13 p2099 A67-26951

Diffusion phenomena of increasing mean free path with altitude in rarefied gas analyzed, incorporating gravitational field effect in Boltzmann equations 13 p2099 A67-26952

Small parameter method for rarefied gas dynamics problems using Boltzmann equation solution and kinetic equations hierarchy 13 p2099 A67-26953

Sound propagation in dilute monatomic gas confined in box and in unconfined rarefied monatomic gas assuming unidirectional perturbation of velocity distribution 13 p2100 A67-26955

Kinetic model with velocity dependent collision frequency applied to forced wave propagation in half-space and other unsteady problems 13 p2100 A67-26956

Generalized spatially uniform distribution functions for monatomic rarefied gas describing one-dimensional heat transfer in nonuniform flow 13 p2100 A67-26958

Couette flow and heat transfer of rarefied gas between parallel plates analyzed by Monte Carlo method 13 p2223 A67-26961

Drag coefficient for cylinder rotating in rarefied gas, comparing numerical method and approximate analytical solution 13 p2101 A67-26963

Two component equivalent of two-stream distribution function solution to plane Couette flow, studying nonlinear effects 13 p2101 A67-26965

Variational method for linearized problems of rarefied gas dynamics applied to cylindrical Poiseuille flow and heat transfer from sphere, using BGK 13 p2101 A67-26966

Monte Carlo approach to transition and free molecular flow problems having mass as well as thermal motion of molecules 13 p2101 A67-26967

Kinetic theory description of flow over right circular cylinder at low speed based on Lees moment method 13 p2102 A67-26969

Monte Carlo evaluation of Boltzmann collision integral for translational relaxation and plane steady shock problems 13 p2103 A67-26974

Accuracy of approximation solutions of Boltzmann equation for rarefied gas flow 13 p2104 A67-26979

Effect of Reynolds number on hypersonic flow of rarefied gas past sphere obtained from pressure distribution at surface 14 p2240 A67-27996

Boltzmann equation and deduced moment equations containing moments up to fourth order in arbitrary orthogonal curvilinear coordinates 14 p2297 A67-27998

Rarefied gas dynamics - conference, Oxford University, July 1966 14 p2298 A67-28160

Transitional rarefied flow regime noting drag on simple bodies, flows at sharp edges, lifting bodies, etc 14 p2299 A67-28161

Viscous hypersonic flow past leading edge of sharp flat plate analyzed, using Navier-Stokes equation and velocity slip and temperature jump wall boundary conditions 14 p2299 A67-28162

Continuum flow analysis for leading edge region of flat plate, using model based on hypersonic thin layer type of approximation 14 p2240 A67-28163

Flow field experiments for shock wave and boundary layer development on two-dimensional and axisymmetric bodies 14 p2241 A67-28168

Local flow field measurements of static temperature, density and local impact pressure of hypersonic rarefied flow over 10 degree cone 14 p2241 A67-28169

Thick laminar boundary layer effect on aerodynamic behavior of simple shapes in supersonic low density flow 14 p2241 A67-28170

Sphere drag coefficients measured using ultralightweight models launched from two-stage light-gas gun 14 p2242 A67-28172

Low density shock layer structure on cylinders at Mach 4 noting magnitude, location of disturbances, existence of shock

wave-like flows, recession of leading edge, etc 14 p2299 A67-28173

High Mach number low Reynolds number flow over two-dimensional circular cylinder obtaining surface pressure and heat transfer distributions 14 p2242 A67-28174

Hypersonic low density flow analysis with shock tunnel and electron beam densitometer, noting density profiles at various Mach and Knudsen numbers 14 p2300 A67-28176

Heat loss and recovery temperature of fine wires in transonic transitional flow regime, noting experimental and computational results 14 p2405 A67-28177

Wind tunnel heat transfer measurements from circular cylinders to transverse air flow, noting recovery factor as function of Knudsen number 14 p2405 A67-28178

Free molecular flow through circular orifice at high pressure ratios, discussing mass flux measurement methods 14 p2300 A67-28179

Molecular speed ratio in low density flows determined via stagnation point heat transfer and flat plate heat transfer measurements 14 p2301 A67-28182

Time of flight distribution measurement of weak molecular beam, noting limitations due to signal to noise ratio 14 p2316 A67-28185

Intensity and velocity distribution in molecular beams from nozzle sources, discussing physical processes responsible for formation 14 p2301 A67-28186

Electron beam analysis of skimmer influence on nozzle beam formation 14 p2301 A67-28187

Collimation of low density hypersonic jet from shock tube for atomic beam production, noting relation between beam intensity and velocity distribution 14 p2301 A67-28188

Kantrowitz-Grey molecular beam generator performance, noting high source pressure due to high pumping speed, background gas scattering, etc 14 p2316 A67-28189

Charge exchange method for production of molecular beams, noting production of plasma by RF discharge and ion beam generation 14 p2316 A67-28190

Molecular beam apparatus for determining momentum accommodation coefficients for neutral particle - surface interactions 14 p2316 A67-28192

Velocity distribution function measurement in rarefied gas flow, using principle based on time of flight of metastable molecules 14 p2316 A67-28193

Velocity distributions in surface scattered molecular beams, proposing broadband lock-in beam detection for signal to noise enhancement 14 p2317 A67-28195

First collision effects in rarefied high speed flows in low density wind tunnel, noting measurement techniques and apparatus used 14 p2317 A67-28197

Atomic oxygen density profiles obtained from radiation intensity resulting from nitric oxide reaction 14 p2293 A67-28199

Ionospheric aerodynamics, discussing flow field properties, satellite motion, flight characteristics, etc 14 p2242 A67-28200

Local electrostatic potential for collisionless plasma flow derived, obtaining smooth solutions for self-consistent electron density distributions 14 p2356 A67-28202

Lack of Cerenkov emission in isotropic plasma, presenting fast electron beam experiment for verification of theory 14 p2357 A67-28204

Rarefied plasma/rapidly moving body interaction, discussing computational procedure and results 14 p2357 A67-28205

Collisionless plasma flow around conducting sphere in uniform magnetic field 14 p2357 A67-28206

Plasma-vehicle interaction, discussing charged particle motion about small vehicle in ionospheric orbit 14 p2357 A67-28209

Solid film sublimation cooling effect in Couette gas flow simulating real rarefied gas flow heat transfer, for jet engine application 14 p2408 A67-28800

Heat transfer through rarefied gas between concentric circular cylinders and spheres, using Krook kinetic equation 15 p2579 A67-29570

Local gas density measurements, using large angle scattering from electron beam

passing through rarefied gas
flow 15 p2490 A67-30152

Rarefied gas flow interaction with sphere
analyzed using multiple wave interferometer,
noting transition region from continuous
medium to free molecular
flow 16 p2656 A67-30453

Rarefied gas flow density measurement by
determining changes in electron beam-
electron concentration while crossing
flow 16 p2673 A67-31107

Soviet book on rarefied gas dynamics
involving methods and approaches for
kinetic description of gas behavior,
emphasizing Boltzmann
equation 20 p3423 A67-37086

Drag measurements of cones in rarefied
flow regime extended to higher and lower
cone semivertex angles 21 p3565 A67-38884

Kramers problem for rarefied gas flow,
calculating slip coefficient for various
collision frequency models, noting only
slight model dependence 22 p3841 A67-39718

Book on dynamics of rarefied gas,
discussing kinetic theory, shock wave
structure, Couette flow, gas flow between
coaxial cylinders and plasma
dynamics 23 p3989 A67-40873

Electric power generation with closed
cycle MHD conversion fluid having gases
with high equilibrium conductivity,
discussing ionization and electrothermal
instability 24 p4099 A67-42416

RAREFIED PLASMA

Stability of flute oscillations of rarefied
plasma in constant electric field normal to
magnetic field 02 p0278 A67-12619

Wave propagation in rarefied two-
component plasma situated in uniform
constant magnetic field with finite Larmor
radius 03 p0483 A67-13875

Boundary layer structure between rarefied
plasma and magnetic field, detailing
mathematical formulation in relativistic
invariant form 04 p0665 A67-15179

Concentration and density distributions of
particle flux near body moving in rarefied
plasma 05 p0855 A67-17122

Charged particle distribution in wake of
fast moving body in rarefied
plasma 05 p0855 A67-17123

Quasi-MHD analysis of supersonic rarefied
plasma flow near magnetic
dipole 06 p1043 A67-18670

Cylindrical wave propagation in rarefied
plasma in presence of strong noncollision
dissipation 07 p1227 A67-19308

Two-dimensional model of magnetosphere
to find equilibrium boundary between
rarefied plasma and magnetic field of two-
dimensional dipole 10 p1649 A67-23297

Supersonic rarefied argon plasma jet,
determining pressure distribution, electron
concentration and
temperature 11 p1842 A67-24963

Braking of bodies moving in rarefied
plasma 12 p1892 A67-25536

Resonance scattering of electromagnetic
waves on arbitrary rarefied plasma region
with near zero intrinsic wave number
relative to small
perturbation 13 p2067 A67-26547

Stability of flute oscillation of rarefied
plasma in constant electric field normal to
magnetic field 13 p2170 A67-27375

Boundary layer in nozzle of arc-heated
wind tunnel, obtaining velocity, temperature
and density profiles 14 p2299 A67-28171

Self-consistent distribution theory of
charged particles and electric potential in
wake of conducting body moving rapidly in
rarefied plasma 14 p2357 A67-28208

Electrodynamic forces and torques on
charged bodies moving through rarefied and
partially ionized earth magnetosphere and
upper atmosphere 14 p2362 A67-29039

Finite-ion Larmor radius effect on wave
propagation in rarefied rotating plasma,
noting solar corona
application 15 p2533 A67-30396

Magnetoacoustic shock waves front in
rarefied plasma disintegration at high Mach
numbers as cause of increase in front wave
duration and width 16 p2714 A67-31039

Boundary layer structure between rarefied
plasma and magnetic field solved in
relativistic-invariant form 19 p3288 A67-35369

Energy dissipation of strong magnetosonic
waves in rarefied plasma, discussing
electrons ionizing collisions at wave
front 19 p3293 A67-35402

Partial solutions of equations describing
axisymmetric unstable motions of gravitating
rarefied magnetoplasma 20 p3502 A67-37663

Flute instability of maximally
inhomogeneous rarefied plasma cylinder with
thick transition layer amounting to two
Larmor radii 21 p3667 A67-38371

Concentration and density distributions of
particle flux near body moving in rarefied
plasma 21 p3668 A67-38465

Charged particle distribution in wake of
fast moving body in rarefied
plasma 21 p3668 A67-38466

Stable motion of rarefied plasma ions and
electrons in crossed electric and magnetic
fields 22 p3853 A67-40024

Galactic plasma dynamics related to
galactic magnetic field generation and
topology, discussing agreement with Hoyle-
Ireland model and Morris-Berg
observations 22 p3854 A67-40503

RAT

Extraction method for renin from rats
with bioassay simplified by using
microphonic method after injecting renin
extract into tail vein 01 p0015 A67-10412

Correlation of changes in serum enzyme
behavior in rats with pathological injuries
due to short transverse
decelerations 06 p0953 A67-17996

RATE

S BURNING RATE
S COLLISION RATE
S DECAY RATE
S DRIFT RATE
S EVAPORATION RATE
S HEART RATE
S LOADING RATE
S MASS FLOW RATE
S PULSE RATE
S RESPIRATORY RATE
S SIGNAL FADING RATE
S STRAIN RATE
S TIME MEASUREMENT
S VELOCITY

RATE METER

Motion rate of pendulum with two
antennas moving in electromagnetic field
with standing wave measured by correlation
meter 21 p3631 A67-39115

RATIO

S ASPECT RATIO
S FUEL-AIR RATIO
S HEMATOCRIT RATIO
S HUB-TIP RATIO
S LIFT-DRAG RATIO
S MASS RATIO
S POISSON RATIO
S PRESSURE RATIO
S PROPELLANT MASS RATIO
S SIGNAL TO NOISE RATIO
S STANDING WAVE RATIO
S THICKNESS RATIO
S THRUST-WEIGHT RATIO

RATIONAL FUNCTION

Partial fraction expansion in derivation of
inverse Laplace transform of rational
function with complex and/or repeated
poles 01 p0104 A67-10479

Rational approximation of generalized
Duffing equation, damped mass spring
oscillator equation and generalized second
order Riccati equation 04 p0647 A67-15660

Rational approximation method for
calculating supersonic axisymmetric flow of
perfect gas around given blunt
body 06 p0943 A67-18846

Recurrence relation for determining
asymptotic error constant of rational
function iterative methods for solving
equations 08 p1349 A67-21263

Chebyshev approximation for calculating
coefficients of rational
function 09 p1469 A67-22053

Discrete rational approximation problem,
procedure for solution 13 p2145 A67-26615

Generalization of two theorems proved by
Freud /1966/ concerning rational
approximation 14 p2345 A67-28939

Method for influence range determination
of stationary points of nonlinear recurrence
of order greater than one corresponding to
rational functions 19 p3205 A67-35913

RAVEN ROCKET

Raven solid propellant motor for Skylark
noting design, ignition and plastic
propellants burning
properties 22 p3867 A67-39525

RAY

S COSMIC RAY
S INCIDENT RAY

S RADIATION
S REFLECTED RAY
S REFRACTED RAY
S SOLAR COSMIC RAY
S X-RAY

RAY TRACING

Permittivity and permeability of smooth
convex body, using ray tracing technique for
vector fields 01 p0020 A67-10014

Tracing rays through hologram treated as
generalized case of tracing rays through
diffraction grating, determining local
diffracting power by geometry and
wavelength of beams 03 p0423 A67-13906

One-dimensional refractive index
distribution using power series expansions
for refractive index and ray traces obtained
from relation of inhomogeneities and
interference pattern of Mach-Zehnder
interferometer 03 p0423 A67-13908

Ray tracing study of HF ducting
propagation with satellites
[RASSA PAPER 1-10-145] 03 p0373 A67-14252

Geometrical light rays in lens-like media
and derivation of differential
equation 06 p1033 A67-18534

Rapid and accurate ray tracing algorithm
for horizontally stratified atmosphere, using
effective earth-radius
technique 09 p1464 A67-22450

Probability of ray position in beam
waveguides 13 p2066 A67-26476

Resonance for VLF waves by ionospheric
propagation using Haselgrove whistler ray
tracing method, interpreting path shape as
function of gradients 20 p3427 A67-36372

RAYLEIGH DISTRIBUTION

Optimum dynamic range centering for
Rayleigh distributed signal for case having
nonzero SNR by envelope detection
process 01 p0022 A67-10434

Rayleigh distribution function of envelope
of signal/noise mixture in n parallel
filter 04 p0568 A67-14453

Distribution function of modulus of
directivity characteristic of antenna grid
shown as modified Rayleigh
distribution 07 p1143 A67-19596

Rayleigh distribution function of envelope
of signal/noise mixture in n parallel
filter 15 p2435 A67-29290

Autocorrelation functions for amplitude of
multiple echoes of fading radio signals
reflected from ionosphere 20 p3379 A67-36293

Distribution function of modulus of
directivity characteristic of antenna grid
shown as modified Rayleigh
distribution 20 p3384 A67-37335

RAYLEIGH EQUATION

SA MATHIEU FUNCTION

Amplitudes of two-mass single-spring
system, using Rayleigh approach to
determination of
eigenfrequencies 01 p0159 A67-10282

Compressibility effects on rarefied gas
flow in Rayleigh problem, using BGK model
of Boltzmann equation 01 p0051 A67-10457

Rayleigh dissipation function and Lagrange
equations of nonlinear friction
forces 04 p0658 A67-15584

Load and friction torque of Rayleigh step
film scheme applied to journal bearing,
using Reynolds equation
[ASME PAPER 65-WA/LUB-2]
08 p1335 A67-20917

Theory of Rayleigh waves at surface of
elastic half-space, determining ratio of
horizontal to vertical component of
motion 13 p2156 A67-26602

Rayleigh problem in hydrodynamic
stability for two-dimensional parallel flow of
nonviscous incompressible
fluid 13 p2106 A67-27456

Rayleigh hypothesis applied to three-
dimensional rotationally symmetric flows
arising from rotating disk in rotating fluid
compared with steady
solutions 20 p3423 A67-37278

Acquisition phase of satellite with passive
magnetic attitude stabilization, discussing
programming difficulties and modified
Rayleigh model for German 625A-1
satellite 22 p3898 A67-39173

Rayleigh-Sommerfeld diffraction formula
to obtain imaging behavior of Gabor type
holograms of transparencies for
reconstructed wave forms with large
diffraction angles 22 p3835 A67-39241

Infinite horizontal fluid layer heated from
below /classical Rayleigh thermal stability
problem/ extended to fluid in rigid sphere

heated nonuniformly 22 p3918 A67-39715
 Relation between incipient cavitation number and Reynolds number by combining bubble dynamics Rayleigh equation with cavitation number 22 p3787 A67-40176
 Nonlinear differential equations solutions extended analytically by parameter substitution method applied to Rayleigh equation 23 p4023 A67-40926
 Longitudinal wall curvature effect on boundary layer flow stability and generalization of Rayleigh theorems for nonviscous instability 23 p3992 A67-41733
 Hydrodynamic stability of rotating flow with cylindrical free surface requiring Rayleigh criterion 24 p4144 A67-42568

RAYLEIGH FADING

Theoretical approximations for probability densities of duration and interval between fades, assuming Rayleigh process characterizes fading phenomenon 03 p0368 A67-13168
 Forced-erasure decoding of fading and nonfading channels compared with correlation and digital decoding 17 p2811 A67-32114
 Wideband troposcatter radio channel simulator exhibiting frequency flat or frequency selective fading over band greater than 10 MHz and centered at 70 MHz 20 p3385 A67-37354
 Film resolution limitation on hologram size, Rayleigh resolution and interference pattern recording 22 p3796 A67-39259

RAYLEIGH NUMBER

SA BUOYANCY

Analytic approximation method for thermal convection at large Rayleigh numbers 04 p0721 A67-14649
 Energy methods of subcritical convective instability theory and critical Rayleigh number dependence on Nusselt number 05 p0926 A67-16816
 Rayleigh thermal instability in horizontal circular cylinder, discussing two approximate methods for calculating upper bounds to critical Rayleigh number 05 p0929 A67-17415
 Cloudstreet formation by wind induced vorticity forces equal to buoyancy forces, noting Rayleigh number variation 08 p1350 A67-20951
 Linear theory solution of eigenvalue problem for natural convection in horizontal layers giving characteristic Rayleigh numbers for first ten modes 08 p1427 A67-21139
 Asymptotic analysis of radiative Rayleigh problem in flow of compressible viscous heat-conducting radiating gray gas extended to high plate Mach numbers 11 p1774 A67-23855
 Numerical technique for time dependent calculation of two incompressible fluids interaction to study viscous and inviscid Rayleigh-Taylor instability 11 p1774 A67-23859
 Priestley constant H of free convection temperature profile approaching atmospheric value for increasing Rayleigh number 13 p2151 A67-26737
 Numerical solution of initial and boundary value Rayleigh problems for nonlinear Krook equation at large wall velocities 13 p2102 A67-26968
 Rayleigh problem solution and accuracy and utility of discrete ordinate method for time dependent problems as applied to Couette flow problems 15 p2473 A67-30214
 Estimation of lower bounds to minimum Rayleigh number inducing state of convective motion in quasi-incompressible fluid with temperature gradient in body force direction 17 p2968 A67-32410
 Rayleigh number effect on importance of convective heat transfer in self-heating gaseous reactions checked against thermal ignition theory 18 p3156 A67-33852
 Wave number and Rayleigh numbers effect on stability of two-dimensional convection in layer heated from below 18 p3159 A67-34003
 Convection initiation Rayleigh number in closed cell and Nusselt number-Rayleigh number relation after convection initiation [ASME PAPER 67-HT-4] 20 p3544 A67-36703
 Heating rate and type effects on stationary fluids stability, noting dependence on critical Rayleigh number 20 p3553 A67-36848

RAYLEIGH-RITZ METHOD

SA VARIATIONAL PRINCIPLE

Nonrelativistic energies of several states of two-electron atoms by Rayleigh-Ritz expansions in independent variables chosen as natural coordinates 04 p0661 A67-15512
 Rayleigh-Ritz method for turbulent heat transfer in curvilinear channel and heat flux magnitudinal and directional effects on stability of isothermal flow in laminar boundary layer 04 p0610 A67-15900
 Minimum potential energy principle and Rayleigh-Ritz method derivation of flutter equations for flat rectangular orthotropic panels 05 p0924 A67-17350
 Free vibration analysis for ring and stringer stiffened cylindrical shell, using Rayleigh-Ritz technique [AIAA PAPER 67-71] 07 p1262 A67-19434
 Eigenvalues of five lowest lying states for three electron atomic systems obtained using conventional Rayleigh-Ritz variational method 07 p1226 A67-19500
 Bending of flexible tubes using variational calculus of Rayleigh-Ritz type 09 p1579 A67-22606
 Bounds for natural frequency eigenvalues of simply supported uniform beam with constant end load and uniformly distributed axial load 14 p2403 A67-29005
 Rayleigh-Ritz method used to predict elastic buckling of prolate spheroidal shells under hydrostatic pressure 17 p2963 A67-33017
 Propagation in rectangular waveguide solved for traveling wave maser design by Rayleigh-Ritz method reduced to matrix eigenvalue problem 17 p2828 A67-33086
 Thermal buckling of conical shells under circumferential temperature gradients analyzed using Rayleigh-Ritz method 19 p3343 A67-35772
 Simply-supported elliptic plate free vibration problem applying Rayleigh-Ritz technique to obtain fundamental frequencies 20 p3539 A67-37007
 Pointwise bounds for perturbed parabolic and elliptic equations using known bounds for corresponding strictly differential problems, noting Rayleigh-Ritz procedure 21 p3652 A67-38174
 Inequality for pointwise bounds of second initial boundary value problem for second order semilinear parabolic equation, noting Rayleigh-Ritz method 21 p3652 A67-38176
 Variational formulation and Rayleigh-Ritz method for nonequilibrium viscous incompressible flows, obtaining velocity and temperature distributions 22 p3788 A67-40422
 Lower bounds for eigenvalues of differential linear elliptical operator using Rayleigh-Ritz approximation extension 24 p4177 A67-42154

RAYLEIGH SCATTERING
 Outward flux and intensity of scattered radiation for top of Rayleigh atmosphere lying above smooth water surface that reflects radiation according to Fresnel law [AIAA PAPER 65-664] 03 p0411 A67-13044
 Intensity distribution of earth surface as seen at various altitudes above atmosphere due to Rayleigh scattering and diffused reflection from earth surface [AIAA PAPER 65-666] 03 p0411 A67-13046
 Theoretical approximations for probability densities of duration and interval between fades, assuming Rayleigh process characterizes fading phenomenon 03 p0368 A67-13168
 Terrestrial radiance in middle UV noting Rayleigh scattering, vertical distribution of air, oxygen and ozone, attenuation factors, etc 04 p0613 A67-14695
 High altitude atmospheric scattering of intense light from ruby laser beam interpreted principally in terms of Rayleigh scattering from atmospheric molecules 07 p1171 A67-19419
 Isophotes of extended light sources in night sky, Stokes parameters, brightness and degree of polarization for Rayleigh-scattered light in earth atmosphere 08 p1326 A67-21243
 Thermal conductivity of low temperature silicon and germanium irradiated by fast neutrons noting differences, additive thermal resistivity and possible scattering mechanisms 11 p1849 A67-24899
 Rayleigh scattering and Lambert ground reflection effect on solar energy absorbed by ozone in earth molecular atmosphere evaluated on basis of transfer

equation 12 p1932 A67-25341
 Hypersound propagation velocity in toluene cyclohexane, acetic acid, water, etc, determined at 6328 angstrom from He-Ne laser analysis of structure of Rayleigh scattering 12 p1953 A67-25446
 Earth albedo calculation using Pegasus I thermal data, discussing Rayleigh scattering, spacecraft position, atmospheric reflection effects, etc [AIAA PAPER 67-332] 12 p1938 A67-26046
 Book on new concepts in radars covering ideal reception, moving targets, autocorrelation, SNR, amplitude distribution, clutter, etc 13 p2071 A67-27224
 Atmospheric radiation polarization characteristics, determining concentration and distribution of atmospheric scatterers 16 p2665 A67-30983
 Coherent integral method applicable to scattering calculations for arbitrarily shaped dielectric bodies of low density [TR-67-114] 16 p2626 A67-31347
 Rocketborne spectrograph measurement of UV reflectivity of Venus and Jupiter, noting atmospheric Rayleigh scattering effects 18 p3123 A67-34147
 Relation between surface pressure and atmospheric brightness in optically thin Rayleigh scattering atmosphere, considering application to Mars 18 p3134 A67-34536
 Total atmospheric ozone from satellite measurements of solar UV reflected radiation determined, using atmospheric model with Rayleigh scattering 19 p3226 A67-35923
 Hypersound propagation velocity in toluene cyclohexane, acetic acid, water, etc, determined at 6328 angstrom from He-Ne laser analysis of structure of Rayleigh scattering 21 p3642 A67-38820
 Rayleigh scattered laser light technique for point measurements of time averaged neutral gas density in turbulent wake behind hypersonic velocity body 21 p3565 A67-38876
 70 to 450 km altitude atmospheric brightness at 5300 angstrom measured by rocket noting importance of aerosol component 21 p3623 A67-39043
 Correlation coefficient dependence on angular dispersion and ratio between antenna directivity and width of energy spectrum of waves scattered by troposphere 22 p3759 A67-39433
 Absorption characteristics for laser power stabilization using Rayleigh active material 24 p4167 A67-42360

RAYLEIGH WAVE
 Time harmonic Rayleigh wave attenuation in elastic half-space by surface impedance 03 p0371 A67-13945
 Theory of Rayleigh waves at surface of elastic half-space, determining ratio of horizontal to vertical component of motion 13 p2156 A67-26602
 Steady state vertical displacements at surface of elastic half-space due to Rayleigh waves from sonic boom, obtaining shock amplification factors 23 p4074 A67-40632

RC NETWORK
 Gyrator-RC filter synthesis procedure, noting open circuit voltage of network configuration 01 p0032 A67-10008
 Precision spectrum analyzer modification using RC network for analyzing filter applied to transient pulses for both Fourier and shock spectra 01 p0074 A67-11130
 All-pass RC filter network design for constant signal delay in LF systems, noting cascade phase characteristics 01 p0045 A67-11197
 Notch steepness of open circuit transfer function of loaded exponentially tapered RC notch filter 01 p0041 A67-11317
 Graphical method of analyzing nonlinear problems of fluidic circuits 02 p0182 A67-11775
 Ferrite-based microelements as quasi-resonant RC circuits 02 p0214 A67-11907
 MOS-FET amplifier RC network design 03 p0382 A67-13670
 Synthesis technique for RC network using two distributed RC elements, one negative impedance converter and one lumped capacitor 03 p0393 A67-13975
 Topology of thin film RC circuits fabricated by depositing metallic and dielectric films on insulating substrate 04 p0592 A67-15079
 RC active circuit under effect of amplifier

- finite input impedance, nonzero output impedance and nonzero source
05 p0785 A67-17299
- Inductive correction effect on single stage tunnel diode RC amplifier, noting increase of upper frequency limit and shortening of wave front buildup time
06 p0970 A67-18213
- Worst case gain sensitivity with zero phase sensitivity in active RC network
08 p1308 A67-20321
- Pole-zero sensitivity minimization with respect to active and passive elements in active RC circuit design
08 p1308 A67-20322
- Reciprocal time domain analysis of RC networks, thin film networks and minority carrier devices
08 p1310 A67-20340
- Operational and circuit features of laboratory device built to simulate dynamic electrical output characteristics of programmable solar array in orbital flight
08 p1315 A67-20660
- FM of RC generator by connecting parametric voltage transducer output to phase shift network and applying generated voltage to transducer input through matching network
09 p1496 A67-21692
- RC networks containing ferrite microcomponents, noting thermal stability
13 p2080 A67-27036
- RC network project for stabilization of tunnel diode, noting stability conditions, negative differential resistances, etc
14 p2283 A67-28041
- Properties of selective filter containing inhomogeneous semiconductor RC circuit with distributed parameters
14 p2291 A67-28275
- Asymmetric R and RC networks as electrical analogs for solving nonlinear equation of nonstationary thermal conductivity
14 p2274 A67-28315
- Linear lumped component three-terminal transformerless RC circuits analyzed using digital computers
14 p2291 A67-28459
- Thin film resistive and capacitive circuit design
14 p2287 A67-28611
- LF and HF single stage RC filters with steep frequency characteristic slope in transition region
14 p2289 A67-28863
- Second order optimal control system simulation by computer, describing method for generating time optimal controls
15 p2458 A67-29907
- Inductive correction effect on single stage tunnel diode RC amplifier, noting increase of upper frequency limit and shortening of wave front buildup time
16 p2635 A67-30479
- Thin film single-sideband demodulator using time-varying RC networks and containing extremely selective filter
17 p2825 A67-32600
- Computer method for determining time-frequency-domain response specifications of transversal linear wave filters, using thin film RC distributed networks
18 p3015 A67-34560
- Nonuniform RC lines with hypergeometric and spheroidal wave functions solutions, calculating driving point impedance
19 p3190 A67-34840
- Optimal design of RC lines distributed parameter systems using gradient technique and variational calculus
19 p3200 A67-34841
- RC oscillators based on silicon n-p-n transistors for radio frequencies, analyzing active all-pass phase-shift circuit
19 p3191 A67-34946
- Distributed RC parameters influence on Hall voltage magnitude in high resistivity semiconductors, explaining voltage decrease
20 p3513 A67-37452
- CR self-oscillation circuits, discriminating CR oscillators from astable, monostable and bistable multivibrators
21 p3604 A67-38601
- Switching behavior equations derived for FET with solutions applied to MOS and junction gate FET circuits
21 p3602 A67-39069
- RCC
- S RECOVERY CONTROL CENTER /RCC/
- RDF
- S RADAR DIRECTION FINDER
- S RADIO DIRECTION FINDER
- RDX
- S CYCLOTRIMETHYLENE TRINITRAMINE /RDX/
- REACTION
- S CHEMICAL REACTION
- S HUMAN REACTION
- S KINETICS
- S NUCLEAR REACTION
- S PROTON-PROTON REACTION
- S SURFACE REACTION
- S THERMONUCLEAR REACTION
- REACTION CONTROL
- Low thrust reaction control system utilizing solid propellant which sublimates into low molecular weight vapor, noting heat sources
01 p0142 A67-11407
- Dynamic analysis of reaction control system /RCS/ propellant feed network on lunar module using digital computers
01 p0142 A67-11435
- Temperature, valve and insulation criteria for designing low thrust subliming solid reaction systems
15 p2544 A67-29979
- Reaction control system for spinning synchronous satellite noting selection criteria, tradeoff methods, etc
17 p2953 A67-31972
- REACTION JET
- Shock tunnel data on surface pressure resulting from hypersonic stream interaction with two transverse jets
[AIAA PAPER 67-190] 06 p0939 A67-18299
- Time optimal position and velocity control of spinning vehicle with reaction jet
[AAS PAPER 66-115] 07 p1259 A67-19974
- Optimum stabilization of axisymmetric satellite by system of n reactive jets
14 p2393 A67-27854
- Shock tunnel data on surface pressure resulting from hypersonic stream interaction with two transverse jets
21 p3610 A67-37799
- Pulsed propulsive performance of low thrust subliming solid ammonium carbamate reaction jet, discussing transient response, apparatus, techniques, etc
21 p3697 A67-39152
- REACTION JET ATTITUDE CONTROL
- TECHNIQUE
- Satellite attitude control in elliptic orbit
11 p1869 A67-24337
- Low thrust cold-gas reaction jets in vacuum studied for pulsed propulsive performance for use in spacecraft attitude control
19 p3310 A67-34805
- REACTION TIME
- SA PERCEPTUAL SPEED
- SA PSYCHOMOTOR PERFORMANCE
- Effects of inhaled air ions on speed of response and attention level, heart and respiration rate and transepithelial DC potential of men
09 p1452 A67-21720
- Evoked brain response to clicks as measure of vigilance tested in work-rest schedule and pressure suit-sleep experiments on man
09 p1452 A67-21721
- Effect of image smear and dimension on target recognition measured on differently oriented, moved and remote Landolt C
09 p1455 A67-21723
- Reaction time during voluntarily controlled alveolar hyperventilation used to study effects on psychomotor performance of aircrew
09 p1453 A67-21728
- Vitreous silica and molten Al reaction, penetration rate of Al, reaction rate and effect of Bi and Sb on rates by lamellar compound formation
10 p1669 A67-23381
- Task load and type of underwater exposure effects on response time to signal light in visual periphery of novice divers
14 p2256 A67-28662
- Chemiluminescent reactions of atomic oxygen with carbonyl sulfide and hydrogen sulfide in flow system as function of reaction time and reactant concentrations
14 p2260 A67-28781
- Probability and payoff as factors influencing two-choice reaction time
15 p2427 A67-29134
- Comparison of operator performance when using rotary selector, thumbwheel and digital pushbutton switches
15 p2430 A67-29135
- Matrix formulation and resultant approximations as approach to nonlinear chemical reaction rate equations
15 p2434 A67-30023
- Eldorado low altitude detection and short reaction time defense system, examining Doppler effect and Mirador pulse radar
17 p2816 A67-32751
- Density induction times for shock wave induced exothermic reaction in lean mixtures of deuterium, hydrogen, ethylene and ethane with oxygen
18 p3081 A67-33792
- Post-induction kinetics in shock initiated hydrogen-oxygen reactions investigated by computer methods
18 p3153 A67-33823
- Current distribution and electron temperature profiles in nonequilibrium crossed field devices, considering nonuniformities, thermal diffusion, boundary layers and finite reaction rates effects
[AIAA PAPER 67-715] 21 p3673 A67-38741
- Digital temperature compensation and statistical filtering procedures for fast reaction alignment of inertial navigators
22 p3831 A67-39886
- Feedback changes effects on reaction time in stopping chronometer
22 p3756 A67-40536
- Sudden strong stimulus effects on pilot simple visual reaction time and fatigued muscle strength
22 p3756 A67-40537
- Intermittency hypothesis suggesting temporal integration of data processing of human central nervous system achieved through control of clock generating time points
23 p3944 A67-41020
- REACTION WHEEL
- Stabilite system, three-axis attitude control system utilizing single reaction wheel
06 p1094 A67-17681
- REACTOR
- SA ASTRON THERMONUCLEAR REACTOR
- SA CHEMICAL REACTOR
- SA FAST REACTOR
- SA GAS COOLED REACTOR /GCR/
- SA GAS REACTOR
- SA GASEOUS FISSION REACTOR
- SA KIWI B REACTOR
- SA KIWI ROCKET REACTOR
- SA LIQUID COOLED REACTOR
- SA LIQUID METAL COOLED REACTOR /LMCR/
- SA MATERIALS TESTING REACTOR
- SA PHOEBUS NUCLEAR REACTOR
- SA POWER REACTOR
- SA SPACE POWER UNIT REACTOR /SPUR/
- SA TEST REACTOR
- SA WATER MODERATED REACTOR
- Nuclear reactor use in space environment as energy source for chemical synthesis and laser action
[AAS PAPER 67-115] 15 p2558 A67-29962
- Preheated gas pulsed with shock waves studied for direct AC power production by MHD generator
16 p2603 A67-30564
- Mixing patterns and flow configurations in model for determining combustion performance in well-stirred reactor
18 p3154 A67-33833
- REACTOR CONTROL
- SA CONFINEMENT
- Testing of NRX/EST and NRX-A5 with emphasis on startup capability, engine control and high temperature operation
[AIAA PAPER 66-1004] 03 p0466 A67-14149
- Control of water moderated nuclear reactor using neutron absorbing helium 3 gas control elements
04 p0656 A67-15989
- Synthesis technique applying Liapunov theory for state vector tracking of nonlinear multivariable control systems illustrated by reactor control design
16 p2649 A67-31662
- Limiter circuits for NERVA reactor control, discussing design requirements and operation
24 p4183 A67-42472
- REACTOR CORE
- Fast and thermal reactors with thermionic converters in reactor core and nuclear system with converters outside core analyzed for power supply for space vehicles
04 p0559 A67-15964
- Multigroup diffusion theory analysis of gas-core /cavity/ nuclear rocket engine
08 p1352 A67-21196
- Critical volume of cylindrical reactors calculated using n-group diffusion theory
10 p1675 A67-23396
- Exact stability criteria for kinetics equations of coupled-core nuclear reactors, using Pontryagin theorem and models for time-distribution of coupling neutrons
[ASME PAPER 66-WA/AUT-16] 17 p2882 A67-32015
- REACTOR DESIGN
- Atomic power-supply system for space vehicles built in West Germany using sintered U-Y and U-Zr fuel elements
04 p0655 A67-14558
- Rates of surface chemical reactions in well-defined flow systems theoretically investigated by data reduction techniques and quantitative predictions
18 p2997 A67-33795
- Phoebus 1B test /high-power-density reactors for space propulsion/ noting reactor design for fuel-element testing

[AIAA PAPER 67-486] 18 p3076 A67-33952
Thermionic reactor with uranium diodes
core array, describing in-pile reactor uses,
arcjet, heat pipe and conceptual design
components
[AIAA PAPER 67-498] 18 p3076 A67-33962
Nuclear propulsion for aircraft, discussing
reactor compactness and shielding
techniques
[AIAA PAPER 67-508] 18 p3076 A67-33972
Integrated design requirements of SNAP-8
Rankine power system for manned lunar
base mission, discussing mission
requirements and reactor shield
system 24 p4185 A67-42545
SNAP-8 type reactors and shield
subsystems for MORL and manned lunar
base plants, discussing Rankine and
thermoelectric power conversion
systems 24 p4186 A67-42546
Design integration of reactor, shielding
and power conversion systems for manned
earth orbital station 24 p4186 A67-42547
Design requirements of reactor power
systems for manned earth orbital space
station 24 p4186 A67-42548

REACTOR FUEL

SA FISSION PRODUCT

SA FUEL ELEMENT

SA NUCLEAR FUEL

Mineral insulated thermocouple
applications in nuclear reactor, automobiles,
steel, concrete, plastics, textiles, ceramics
and heavy machinery 10 p1656 A67-23080
High pressure hydrogen atmosphere drop
calorimeter for SNAP reactor fuel specific
heat measurement, discussing calibration
problems 18 p3052 A67-34515
Pu 239 fueled fast spectrum nuclear
reactor spacecraft power supply design for 1
kwe noting cost, control, heat transfer and
optimization 24 p4185 A67-42538
Thermoelectric nuclear energy conversion
device operating inside reactor fuel element,
discussing conversion
efficiency 24 p4186 A67-42551

REACTOR IN-FLIGHT TEST /RIFT/

PROJECT

System for nuclear auxiliary power,
covering spaceflight test of SNAP-10A,
system testing, performance evaluation,
etc 16 p2701 A67-30638

REACTOR MATERIAL

SA NUCLEAR REACTOR MATERIAL

SNAP-8 reactor oscillating bearings to
provide low friction self-lubrication at 1150
degrees F
[ASLE PAPER 66AM 7A1] 08 p1335 A67-21034

REACTOR PHYSICS

Time analysis of Mossbauer spectrum
variation and isometric shift of source Te-
125m in PbTe absorber following neutron
irradiation in reactor 09 p1559 A67-22661

REACTOR TECHNOLOGY

Nuclear rocket propulsion development,
noting nuclear rocket engine test program
[AIAA PAPER 66-829] 03 p0466 A67-14124
Nuclear pulse propulsion activities of last
decade and current
research 06 p1030 A67-19026

Nuclear power and propulsion systems for
space applications, discussing present and
future technologies
[AAS PAPER 67-132] 15 p2516 A67-29967

NERVA program, reactor and nonnuclear
component development, full-scale testing,
engine program, facilities and materials
research

[AIAA PAPER 67-487] 18 p3076 A67-33953
Book on electromechanical, direct and
nuclear energy conversion covering
transducer design, nuclear structure,
photoelectric conversion, reactor theory,
thermionic conversion,
etc 22 p3749 A67-40329

READING MACHINE

Jackquard loom modification for
assembling read-only braided transformer
memories, describing self-contained
model 13 p2123 A67-26803

Pattern recognition machine construction
and design, using reading machine as
example 18 p3006 A67-34383

Associative memory system of persistent
current bit-cells using cryotrons in selection
and control network 21 p3587 A67-37955

READOUT

Linearized model of readout process in
image tubes incorporating progressive
erasure of stored image, noting increased

effects of erasure with increasing beam
modulation 03 p0426 A67-14396

Current stretch sensing for removing
limitations to usable density of cryotron
storage cells of random access
memories 11 p1765 A67-24625

All-glass electroluminescence readout panel
design with active areas integral part of
connector pin 11 p1766 A67-24628

Lunar Orbiter photographic system
readout for image conversion to video
signals

[SMPT PAPER 101-45] 12 p1940 A67-25463
Low cost accurate mechanical timers
[ASME PAPER 67-DE-39] 14 p2321 A67-28877

All-electronic, ultra-fast scanning
spectrometer utilizing image disector for
power spectral density function
measurements of rapidly time varying
optical emission 16 p2680 A67-31803

SNR performance of SEC vidicon image
storage tube at optimum and reduced
readout rates 22 p3773 A67-39961

REAGENT

S DIOXANE

REAL GAS

Apparent mass increase of sphere
accelerated from rest and before boundary
layer separation in cylinders of oil or water
[ASME PAPER 66-WA/UNT-6] 04 p0601 A67-14483

Convergence of Chapman-Enskog
approximations to scalar electrical
conductivity of some weakly ionized real
gases 06 p1046 A67-18872

Real gas effects on time required for
establishing detached bow shock in front of
cylinder 06 p0992 A67-18882

Calculation of weight flow and velocity for
real gas, obtaining correction
factor 11 p1779 A67-24355

Formation of compression shocks in
calorically ideal real gases with
thermodynamic relaxation analyzed in closed
form 13 p2094 A67-26636

Flow fields of inlets for real or perfect
gases determined through four methods for
application to supersonic and hypersonic
flight regimes

[AIAA PAPER 66-605] 13 p2050 A67-26831
Integral relation method analysis of
supersonic gas flow past blunt body of
revolution 17 p2791 A67-32679

Wave propagation in real gases,
considering one-dimensional time-dependent
disturbances semilinear in extent,
emphasizing matched asymptotic expansion
and coordinate stretching

methods 19 p3212 A67-35798
Kinetic thermodynamics applied to real
gas transport properties analysis by
generalization of mean-free-path
theory 20 p3543 A67-36185

Soviet papers on turbulent jets of air,
plasma and real gas 23 p3988 A67-40727

Real gas jet equations of motion, energy
and continuity derived, transformed and
solved for mixing region, discussing
approximate state equation
construction 23 p3989 A67-40729

Real gases examined for application as
working fluid in Brayton cycle power plant,
considering radiator area reduction to
Rankine cycle 24 p4102 A67-42488

Adiabatic constant formula which holds
for ideal and real gas derived, noting
application of thermodynamics and gas
dynamics formulas to real
gas 24 p4256 A67-42592

REAL TIME

Real time digital simulation of linear and
nonlinear control systems with large
sampling intervals, determining optimization
criterion by nonlinear multipoint boundary
value problem 01 p0045 A67-10674

Hybrid CDC 3200 digital computer
acquisition of response data from acoustic
and high force vibration
tests 01 p0029 A67-11025

Measurement systems control in rocket
engine testing via real-time surveillance,
computation, error correction and graphic
display 01 p0076 A67-11144

Real time digital simulation of stabilization
and control systems /SCS/ for manned
spacecraft noting transport delays, thruster
duration, etc 02 p0228 A67-11788

Univac 418 real time executive computer
design having storage speeds of 2 and 4
microseconds 02 p0206 A67-11806

Real time data transmission systems with

error detection, block retransmission
capabilities and buffer storage unit treated
as Markov process 02 p0194 A67-11810

Apollo launch data telemetry system
development from inception through
planning and into final hardware
implementation 02 p0195 A67-11997

Resolution of telemetering event
occurrence times with 1 and 2 microsecond
accuracy, considering real time systems,
delayed time systems and hybrid time
systems 02 p0197 A67-12012

Digital communications system evaluator
/DICOSE/ using stored program processor
coupled with communication channel arrays
to provide real time on-line
system 02 p0230 A67-12127

Wideband multipoint real time device
automatically calculating correlation
functions of acoustic
signals 04 p0620 A67-14890

Real time evaluation of radar signals
processed by digital detector used in
automatic target tracking 04 p0574 A67-15058

Data display for Real Time Telemetry
Data System /RTTDS/ 05 p0765 A67-17042

Automatic telemetry checkout station for
Saturn V systems using real time signal
digitizer and general purpose
computer 05 p0789 A67-17044

Man-computer graphics for computer aided
design 05 p0768 A67-17514

Real time approximation of continuous
system performance on digital computer
using difference equations obtained from
digitized transfer
function 05 p0768 A67-17518

Automatic telemetry checkout station for
Saturn V systems using real time signal
digitizer and general purpose
computer 06 p1089 A67-18861

Mechanized hybrid real time simulation
for Gemini crew to use in rendezvous
procedures

[AIAA PAPER 67-250] 07 p1166 A67-20068
Apollo spacecraft hybrid real time flight
simulation ensuring 40 msec sampling
interval

[AIAA PAPER 67-255] 07 p1166 A67-20071
Real time meteorological system providing
prelaunch impact prediction for unguided
high altitude rocket firings, noting computer
program 08 p1314 A67-20543

Dual redundancy digital computer for
improved reliability in real time processes
and control situations where fault results in
fatality or mission failure 08 p1298 A67-20638

Automatic real time data acquisition and
processing for ATS communications
experiments 08 p1298 A67-20669

Microelectronic radar intercept calculator
/RIC/ for ground-controlled intercept
capability when used with air search radar
feeding information to PPI
display 08 p1293 A67-20690

All-digital real time display system for
ground monitoring of manned space flight
including computers, software, output
devices, etc 09 p1483 A67-21677

Aircraft detection and in-flight tracking by
real time computers, assessing role in
missile and satellite
tracking 13 p2153 A67-26666

Digital real time spectral analysis with
fast Fourier transform algorithm, using two
special purpose computer configurations to
estimate power spectrum 13 p2073 A67-27062

Real time meteorological system for
ballistic high altitude multistage rocket
trajectory, computation and
prediction 13 p2091 A67-27610

Nonlinear imaging phenomena discussed in
connection with holography, describing
holographs permitting three-dimensional
magnification in real time 14 p2319 A67-28495

Processing satellite data at Goddard
Center noting Tiros IR data, cloud pictures
and Imp measurements 16 p2633 A67-30668

Nanosecond baseband pulse rise time
measurement, discussing real time and
sampling oscillography, pulse comparison,
basic instrumentation, etc 17 p2814 A67-32603

Real-time electrooptical spectrum
analyzers with coherent
detection 19 p3197 A67-35687

Real time Fourier transform synthesizer
for spectral distribution of
interferogram 20 p3437 A67-36341

Flight measurement data retrieval on real
time basis from worldwide range stations
possible through Range Support Satellite

- system 20 p3531 A67-36470
- Man-machine graphical communication device for real time monitoring with automated checkout 20 p3446 A67-36589
- Radar designation by computer and real time reentry tracking for future Apollo manned space flight 20 p3381 A67-36592
- Real time telemetry data system for Air Force Eastern Test Range 20 p3381 A67-36614
- Real time performance, ground control and data processing of Surveyor spacecraft during maneuvers [AIAA PAPER 67-644] 20 p3419 A67-37625
- Real time meteorological system providing prelaunch impact prediction for unguided high altitude rocket firings, noting computer program 21 p3607 A67-37812
- Optimum word length for signal simultaneous digital transmission in real time through single channel 21 p3581 A67-38179
- Satellite automatic telemetry data processing system, noting development of high speed computer for real time 21 p3588 A67-38638
- Coherent acceleration and velocity observation in real time /CAVORT/ analog radar signal processor for matched filtering pulse trains from radial accelerated targets 21 p3586 A67-38953
- Preliminary spacecraft concept for real time operational space environment monitoring system 22 p3901 A67-39928
- Solar X-ray emission below 20 angstroms made by Explorer XXX, discussing analog real time records and time resolution 23 p4050 A67-40805
- Mobile laser transceiver for atmospheric targets detection, discussing real time technique for determining atmospheric function 23 p4014 A67-41022
- Real time systems and applications 23 p3976 A67-41056
- Book on stochastic approximation and nonlinear regression covering convergence, asymptotic methods, real time problem in presence of noise, etc 24 p4179 A67-42900
- REAL VARIABLE**
- Real function interpolation method for synthesis of electric networks in time domain by sinusoidal exponential series 03 p0458 A67-13505
- Search for extremum of real function in presence of noise, using maximum principle 20 p3477 A67-37111
- REATTACHED FLOW**
- Turbulent reattachment of supersonic jet noting recompression region of flow, critical points and similarity law in evolution of wall pressures [ONERA-TP-326] 01 p0053 A67-11002
- Heat transfer in supersonic separated flow over two-dimensional backward-facing step found in entry enlargement region of supersonic parallel diffuser 04 p0546 A67-14640
- Heat transfer and pressure in laminar shock wave/boundary layer interaction corner flow at Mach 8 and 10 04 p0610 A67-15834
- Taylor series expansion of stream function, pressure and temperature about separation or reattachment points used to calculate incompressible closed streamline flows of unknown shape [AIAA PAPER 67-64] 06 p0989 A67-18468
- Incipient separation prediction in shock boundary layer interactions 06 p0992 A67-18874
- Switching time of turbulent reattachment fluid amplifier in large scale model and in theory 08 p1281 A67-20447
- Wall pressure distribution in turbulent reattachment bubble calculated by splitting bubble into large number of small control volumes 08 p1320 A67-20451
- Binary turbulent reattachment type fluid amplifier to control submerged jet of fluid 10 p1597 A67-23389
- Incompressible fluid flow in convergent nozzle with finite aspect ratio, predicting offset on nozzle flow and jet reattachment 14 p2303 A67-28334
- Control flow effect on power jet reattachment location and pressure in separation bubble enclosed by power jet for fluidic devices 14 p2250 A67-28336
- Reattachment of two-dimensional jet to adjacent plate assuming new hypothesis on path of dividing streamline 14 p2303 A67-28338
- Attachment distance for two-dimensional jet shown unaffected by presence or absence of second sidewall and nozzle aspect ratio 14 p2303 A67-28339
- Flow turning angle during two-dimensional turbulent supersonic reattachment to plane wall [ASME PAPER 67-FE-20] 14 p2305 A67-28367
- Jet reattachment for inclined walls at low Reynolds numbers and moderate nozzle aspect ratios [ASME PAPER 67-FE-25] 14 p2305 A67-28369
- Separated and reattaching flows emphasizing heat transfer considerations in calculations, especially in supersonic designs 17 p2790 A67-32448
- Mixing function parameter behavior in boundary layer separations by Crocco-Lees method, noting linearized Glick differential equations 17 p2840 A67-33031
- Reattachment of two-dimensional compressible air jets to planes, discussing pressure maximum and inlet Mach numbers 22 p3786 A67-40068
- RECEIVER**
- SA DELAY LOCK
- SA LOGARITHMIC RECEIVER
- SA MULTICHANNEL RECEIVER
- SA RADAR RECEIVER
- SA RADIO RECEIVER
- SA SINGLE-SIDEBAND RECEIVER
- SA SUPERHETERODYNE RECEIVER
- Microwave receiver with no separate local oscillator for plasma scattering experiments 06 p1000 A67-17617
- Plasma induced interference signal in satellite VLF receiver originating with converter system and appearing only in daylight operation 06 p0964 A67-18569
- Operational characteristics of receivers employing storages of nonquantized and quantized signals 06 p0965 A67-18895
- Mean number of random process ejections over arbitrary time period at output of receiver with time and frequency selectivity 06 p0965 A67-18897
- Low noise level microwave receivers - Conference, Paris, May 1966, Part 2 12 p1912 A67-25294
- Hyperfrequency receiver noise temperature measurement, calculating gain stability influence 12 p1952 A67-25296
- Receivers for measuring UV radiation in upper atmosphere and outer space 13 p2121 A67-27335
- Ultralow noise receiver configurations for cryogenically cooled microwave traveling wave masers and parametric amplifiers 14 p2260 A67-27776
- Flow processes and static and dynamic performance characteristics of axisymmetric fluid jet modulator and single receiver-diffuser studied 14 p2248 A67-28269
- Static and dynamic characteristics of interaction region for fluid jet and receiver-load system, examining stability conditions 14 p2248 A67-28270
- Sensitivity of radiometer operating in submillimeter range with multimode detector compared to crystal receiver equivalent noise 16 p2677 A67-31501
- Error probabilities of matched filter receiver operating in additive combination of impulsive and Gaussian noise 17 p2812 A67-32120
- Solar thermoelectric generator with cylindrical aluminum solar energy receiver using p and n type semiconductor materials and water cooled junctions 18 p2990 A67-34491
- Bicrystals use in optical receivers based on bicrystal interface 20 p3457 A67-36238
- TRKI-12 predetection receiver/recorder subsystem examined for performance characteristics 20 p3380 A67-36550
- Optimal wave path parameters determined by experimentally recorded pulsed signals processing, using least squares method 21 p3580 A67-38120
- RECEIVING SYSTEM**
- Noise factor of linear receiving systems in quantum and classical regions, noting role of dual push-pull amplifier and frequency converter 01 p0022 A67-10393
- System design analysis of Edwards high range UHF telemetry receiving station network, considering reliability, availability, design adequacy, antennas, initial and operating costs, etc 02 p0229 A67-12007
- Phase lock system used to receive and correctly utilize signals from distant transmitter 04 p0585 A67-15614
- Book on phase coherent communication principles based on statistical communication theory, discussing coherent receivers and analog and digital modulation systems 04 p0576 A67-15616
- Distribution formula for unloaded prolate spheroidal receiving and scattering antenna 11 p1758 A67-23974
- Optimum linear receiver for noisy PAM system using criterion of mean square interference 11 p1752 A67-24134
- Optimum reception problem of two zero mean Gaussian signals solved through comparison of quadratic form in observable waveform with predetermined threshold 11 p1760 A67-24235
- Mixed single and double sideband interferometer receiving system having phase processing and delay simplicity and multiple RF return cable 11 p1764 A67-24308
- Mean power gain for diversity reception system with lobe switching 11 p1768 A67-24988
- Rectangular guide receiver passband, estimating boundary effect, noting data characterizing interrelation of arrayed transmitters 13 p2069 A67-27032
- Liquid helium traveling wave maser amplifier for low noise ground station satellite communication receiver 14 p2329 A67-27777
- Low noise preamplifier traveling wave maser operated in closed cycle refrigerator for receiving Mariner IV picture transmissions 14 p2329 A67-27779
- Two-stage parametric amplifier system cooled to 20 degrees K, as low noise amplifier in receiving equipment for satellite communication 14 p2278 A67-27780
- Low noise receivers in transportable satellite communication ground terminals, discussing interrelationships between antenna, receiver and cryogenics 14 p2260 A67-27782
- Highly adaptive phase lock coherent receiving system fulfilling requirements of data and Doppler tracking receivers 14 p2271 A67-28691
- Optimum system for signal detection with single-band noise modulation during carrier suppression, noting receiving system 15 p2436 A67-29413
- Superlimiting phased-array receiving system in two-source environment 16 p2638 A67-31271
- Arc-image furnace for direct gas heating at high temperature by concentrated radiation studies and efficient cavity-type receiver development 17 p2834 A67-32696
- Design of receiver circuitry for IR surveillance system having high signal detectability 17 p2862 A67-33289
- VLF emission associated with aurora and particle precipitation, describing receiving equipment, types of emission and occurrence patterns 18 p3039 A67-33621
- Satellite tracking simultaneous-lobing monopulse receiving system utilizing polarization diversity in coherent and noncoherent operational modes 18 p3020 A67-34110
- Receiving system for detecting binary random signals in white noise, determining correlation functions and error probability 18 p3001 A67-34180
- Diversity-reception systems used in discontinuous radio communication, considering error probability and channel utilization factors 18 p3001 A67-34181
- Frequency modulated transmitter and receiver for audio high speed data transmission including discriminator for analyzing and distinguishing waveforms 20 p3379 A67-36247
- Optimal detection of signals by spatially distributed receiving system against random noise background, using space-time signal selection method 20 p3383 A67-37070
- Distributed receiving system for optimal filtration of random field of space-distributed source 20 p3385 A67-37376
- Soviet book on time-frequency remote control systems theory and design 20 p3412 A67-37632
- Receiver performance related to signal and interference conditions for AM voice communication system analyzed for use in

systems design 20 p3387 A67-37637
 KHz to GHz wide predetector bandwidth receiving system applicable to EMI evaluations of high data rate digital equipment 20 p3406 A67-37656
 Multistage receiver protector recovery period measurement, discussing nanosecond reaction time 21 p3589 A67-37819
 Telemetry receiving station and remote control system for satellites and missiles, measuring Doppler effect, demodulation and diversity combiners 21 p3583 A67-38639
 Receiving system for telemetering with orientable antenna error-measuring signal receiver and servo loops 21 p3599 A67-38645
 Parallel plate antenna for LF transmission and reception in conducting medium 22 p3773 A67-40307
 Wideband FM demodulation system providing good reception with smaller radio SNR through delayed signal 23 p3975 A67-41677
 Random Gaussian signal with unknown mean value reception using adaptive systems 24 p4120 A67-42224

RECEPTION
 S RADAR RECEPTION
 S RADIO RECEPTION
 S SIGNAL RECEPTION
 S TELEVISION RECEPTION

RECEPTOR
 S PHOTORECEPTOR

RECIPROCAL THEOREM
 Dynamic reciprocal theorem for sinusoidal oscillation of elastic medium treated as extension of static reciprocal theorem of Betti and Rayleigh, using continuum mechanics [ASME PAPER 65-WA/MD-21] 03 p0525 A67-13832
 Radio propagation in microwave terrestrial model waveguide of variable surface impedance, using reciprocity theorem 04 p0570 A67-14865
 Functional relation between mass, radius and angular velocity of earth, solar mass and corresponding lunar quantities shown via reciprocity principle 04 p0702 A67-15582
 Constitutive equations derived based on thermodynamics of irreversible processes and coupled thermoelasticity, formulating variational and reciprocity theorems 05 p0910 A67-16165
 Reciprocity principle of Equivalent Sun Hours /ESH/ as means of spacecraft material testing 06 p0980 A67-18365
 Validity of Onsager-Casimir reciprocal relations with theoretical framework of macroscopic nonequilibrium thermodynamics 07 p1268 A67-19574
 Sandwich plate problem involving plate having filler flexibility only, giving solution via reciprocity theorem based on Rayleigh-Green equality in thin plate theory 10 p1716 A67-22938
 Generalized reciprocity law relating behavior of elastic body and static and geometric boundary conditions 10 p1721 A67-23686
 Short term and averaged characteristics of nonreciprocal HF ionospheric single and multipath propagation paths 11 p1762 A67-24286
 Nonreciprocal characteristics of long distance HF ionospheric propagation path interpreted as interaction of waves with transmitting and receiving antennas 11 p1754 A67-24718
 Variational principles and reciprocity theorems for dynamic problems of elastic shell theory, particularly motion described by linear equations of Timoshenko type theory 12 p2019 A67-25563
 Reciprocal theorem applied to linear and angular displacements due to creep or plastic strains in inelastic bodies 14 p2398 A67-28097
 Diffraction field parts of slit aperture formed by two nonplanar screens satisfy variational principle 14 p2261 A67-28106
 General method based on reciprocity theorem developed for problem solutions in elasticity theory 14 p2402 A67-28740
 Virtual work principle shown equivalent to linear coupled thermoelasticity theory 19 p3342 A67-35763
 Reciprocal theorem in linearized theory of couple stresses for perfectly elastic nonhomogeneous anisotropic materials 20 p3540 A67-37281
 Generalized reciprocity law relating

behavior of elastic body and static and geometric boundary conditions 21 p3720 A67-38287
 Coupled micropolar thermoelasticity equations using strict motion invariance conditions, presenting reciprocity and variational theorems 24 p4251 A67-42659

RECIPROCATING ENGINE
 Torsional vibrations of reciprocating engine with allowance for vibration of second type treated by transfer-matrix method 10 p1720 A67-23577
 Growth and operational capabilities of turboprop and reciprocating engines [SAE PAPER 670236] 12 p1989 A67-25494

RECIRCULATIVE FLUID FLOW
 Air velocity and temperature, stabilizer size and blockage effects on fresh mixture entrainment in recirculation zone of bluff body stabilized flames 02 p0342 A67-12029
 Flow recirculation as affected by position and geometry of inducing obstacle 06 p0937 A67-17918
 Flow field model for laminar hypersonic near-wake in inviscid expansion, viscous sublayer and recirculating flow [AIAA PAPER 67-63] 06 p0940 A67-18353
 Viscous interaction theory for laminar supersonic near wake applied to calculation of recirculation region for range of flow conditions [AIAA PAPER 67-61] 06 p0941 A67-18467
 Exhaust gas recirculation for VTOL aircraft [AIAA PAPER 67-439] 18 p2985 A67-33916
 Recirculation zone in fluid mechanics experiments on cylindrical cavity simulating gas-core nuclear rocket as heavy gas reservoir, discussing flow patterns [AIAA PAPER 67-502] 18 p3076 A67-33966
 Heat pipe dynamics analyzed for thermionic converter heat pipe radiator design criteria, discussing working fluid selection 24 p4104 A67-42503

RECOGNITION
 SA CHARACTER RECOGNITION
 SA MACHINE RECOGNITION
 SA PATTERN RECOGNITION
 SA TARGET RECOGNITION
 Indeterminate recognition /game type/ and prediction systems 13 p2088 A67-27022

RECOIL PROTON
 Recoil proton detectors used for rocket measurements of fast neutron intensity above Fort Churchill, Canada, during 1964 and 1965 12 p1998 A67-25828
 Directional neutron spectrometer for events in which neutron is scattered by first scintillator into second 12 p1945 A67-25859
 Secondary neutron spectral data measured by proton recoil spectrometer from targets bombarded by 160 Mev protons 23 p4028 A67-40739

RECOMBINATION
 SA ATOMIC RECOMBINATION
 SA ELECTRON-ION RECOMBINATION
 SA ELECTRON RECOMBINATION
 SA HYDROGEN RECOMBINATION
 SA ION RECOMBINATION
 SA OXYGEN RECOMBINATION
 SA RADIATIVE RECOMBINATION
 Gamma radiation and fast neutron effects on dark resistance, photoconductivity, majority carrier mobility, recombination kinetics, etc, in CdS single crystal 01 p0128 A67-10086
 Analog computer ionization recombination parameters and balance equation of charged particles in F-2 layer 02 p0236 A67-11659
 Dissociative recombination rate of auroral ionization 02 p0236 A67-11661
 Electron beam scanning technique measurement of diffusion lengths in Si and GaP p-n junctions and recombination rate of dislocations in n-type Si 02 p0298 A67-11887
 Surface recombination velocity of thermally oxidized silicon structures exposed to X irradiation 03 p0496 A67-13677
 Ionization recombination mechanisms and density-time profiles for electric propulsion unit efflux 04 p0690 A67-15024
 Recombination waves appear in sample having ohmic contacts when drift velocity of carriers in constant electric field exceeds certain value 04 p0681 A67-15290
 Lifetime and recombination of excess carriers in silicon over seven orders of magnitude of injected carrier density 06 p0971 A67-18226
 Surface recombination velocities and diffusion lengths in GaAs determined by

variation of cathodoluminescence intensity with voltage of exciting electron beam 06 p1063 A67-18936
 Effect of surface recombination and parasitic capacitance on linear buildup of photoconductivity in semiconductors, noting germanium photoresistor 09 p1551 A67-21668
 Excitation-recombination statistics in semiconductors with donor and center interacting with both bands for given thermal disequilibrium, treating silicon 09 p1551 A67-21669
 Reduction or elimination of secondary asymmetry voltage in germanium Hall generators noting effect of surface recombination, temperature distribution stabilization, etc 12 p1939 A67-25278
 Photoconductivity kinetics and regeneration recombination noise spectrum of p-InSb crystals, showing association with hole capture, lifetime and alloying impurity 12 p1983 A67-25512
 Analog computer ionization recombination parameters and balance equation of charged particles in F-2 layer 16 p2665 A67-31074
 Dissociative recombination rate of auroral ionization 16 p2665 A67-31076
 Subthreshold electron irradiation effects on surface recombination properties of n- and p-type germanium and silicon crystals 17 p2916 A67-32834
 Temperature, resistivity and injection level dependence of recombination processes in neutron irradiated silicon explained by two-level recombination model 17 p2916 A67-32837
 Shock wave investigation of recombination in near-stoichiometric hydrogen-oxygen-argon mixtures at high temperatures 18 p2996 A67-33789
 Carbon monoxide and atomic oxygen recombination in expansion wave of single-pulse shock tube at high temperatures 18 p2997 A67-33790
 Photoconductivity kinetics and regeneration recombination noise spectrum of p-InSb crystals, showing association with hole capture, lifetime and alloying impurity 18 p3103 A67-34443
 Emission recombination in n-type Si single crystals irradiated with fast neutrons or gamma quanta 19 p3301 A67-34775
 Emission intensity dependence in CdS on laser excitation intensity for free and phonon-assisted exciton recombination at cryogenic temperature 20 p3461 A67-37295

RECOMBINATION COEFFICIENT
 Temperature dependence of lifetime of electrons and holes in GaAs, noting trapping effect of recombination centers and capture levels 01 p0128 A67-10091
 Three-body and wall recombination coefficients of atomic nitrogen, using electron spin resonance spectrometer for concentration measurements 01 p0117 A67-10883
 Radial transport of cesium plasma governed by resistive diffusion as shown by stellarator experiments in which surface recombination losses within plasma volume were negligibly small 01 p0125 A67-10914
 Two parallel carrier capture mechanisms at single recombination center in cadmium sulfide 01 p0138 A67-11298
 Microwave cavity measurement of recombination coefficient of decaying plasma obtained by gamma ray induced ionization of xenon 02 p0274 A67-12463
 Recombination processes in aluminum doped zinc telluride single crystals, determining distance of r-centers from C-band 02 p0300 A67-12478
 Temperature induced and optical quenching of emission recombination in gallium arsenide Be-doped electroluminescent diode 02 p0254 A67-12741
 Electron-ion recombination process due to electron collision in plasma with capture electrons transferred to ground level 03 p0474 A67-12853
 Autoionization mechanism role in formation of astrophysical spectra 03 p0509 A67-13217
 Anomalous variation in composition of lower ionospheric ion recombination coefficient as function of height, zenith angle and level of solar activity 03 p0411 A67-13346
 Space charge wave velocity in semiconductors, noting recombination type instability 04 p0676 A67-14928

Recombination coefficient measurement for He plasma during decay at high pressure in presence of K vapor admixture 04 p0667 A67-15215

Dissociative recombination coefficient of nitrosyl ion with electrons 04 p0567 A67-15765

Helium mono and divalent ion electron recombination coefficient determined as function of electron density and temperature 04 p0672 A67-15774

Current and frequency dependent differential resistance and diffusion capacity of junctions of p-n structures at high current densities 06 p1049 A67-17868

Pinch effect in InSb degenerate plasma, discussing electric conductivity and recombination emission spectra 06 p1049 A67-17879

Recombination coefficient in D region determined by comparing electron density profile with ionization rate 06 p0995 A67-18073

Meteoritic dust particle effect on steady state distribution of electrons and ions in lower ionosphere, deriving expression for recombination coefficient from auroral radio absorption data 06 p0995 A67-18074

Three-body collisional recombination coefficients calculated for cesium and argon atomic ions, assessing Gryzinski cross sections 06 p1036 A67-18151

Order of recombination coefficient in E layer determined, using ionospheric data 06 p0999 A67-18737

Recombination rate increase in F region following magnetic activity due to passage of atmospheric wave 07 p1171 A67-19418

Oxygen photochemical equilibrium above 150 km, assuming dominant role of radiative recombination above 120 km 07 p1178 A67-19814

Oxide film surface effect on electrophysical characteristics of Ge surface, noting potential changes and recombination rate 08 p1367 A67-20412

Ion-ion recombination coefficient corrections required because of nonuniform ion density and diffusion losses 08 p1355 A67-20718

Relaxation phenomena role in MHD generator using nonequilibrium ionization, noting collisional and radiative recombination mechanisms 09 p1542 A67-21815

Microwave interferometer for measurement of effective recombination coefficient of decaying argon-cesium plasma with hot electrons at various argon pressures 09 p1542 A67-21817

Electron-ion recombination behind shock waves in argon containing dilute lean mixtures of hydrocarbons and oxygen 09 p1457 A67-22024

Diatomic molecular ion composition and variation of effective recombination coefficient in ionosphere in terms of altitude, time of day, solar activity, temperature, etc 10 p1630 A67-22788

Electron-ion recombination coefficients for atmospheric ions determined in laboratory and compared with ionospheric analysis 10 p1682 A67-23261

Ion composition and effective recombination coefficient variation of ionosphere in study of X and UV radiation ionization of E layer 10 p1647 A67-23280

Electron and ion densities and temperatures measured by rockets in active auroras and correlated with directly measured ionizing flux 10 p1650 A67-23307

Active and reactive resistance components of p-n diodes with minimum distribution of steady state carrier concentration in base 13 p2182 A67-27282

Radiometric data on ionospheric absorption applied to determination of dissociative recombination coefficient, noting atmospheric ionization by fragment gamma-radiation 14 p2306 A67-27858

Nonlinear volt-ampere characteristic of photosensitive GaAs plus copper atoms in strong electric field 14 p2368 A67-28532

Semiconductor photoconductivity kinetics as affected by surface recombination, considering bi-and monopolar photoconductivity 14 p2372 A67-28756

Recombination instability in plasma if temperature dependence is strong 15 p2522 A67-29208

Temperature dependence of lifetime and

Hall coefficient in InSb, measuring lifetime by phase shift method, concluding that recombination centers are lattice defects 15 p2535 A67-29483

Recombination-regeneration formula for hole-electron pairs in randomly doped semiconductor materials 15 p2539 A67-29915

Self-similar solutions for recombination plasma decay problem, considering plane and spherical symmetry 15 p2531 A67-30011

Two-photon recombination in semiconductors with degenerate electron-hole gas taking into account damping during interaction with phonons 15 p2542 A67-30244

Recombination coefficient measurement for He plasma during decay at high pressure in presence of K vapor admixture 15 p2532 A67-30263

Diurnal variations asymmetry in critical frequency ratio of E layer for morning and evening values 16 p2668 A67-31895

Gas pressure dependence of attachment and recombination coefficients for thermalized electrons in air and oxygen 17 p2893 A67-32139

Quasi-particle recombination lifetimes in superconductors measured experimentally shown to differ from calculated lifetimes 17 p2913 A67-32370

Auroral rocket measurements of electron densities, ionization rates, particle energy fluxes, energy spectra, pitch angle distribution, etc 18 p3034 A67-33592

Experiments on equilibrium and nonequilibrium electrical conductivity of seeded combustion products and theory of nonequilibrium ionization and recombination 18 p3085 A67-33706

Ionization and recombination processes of alkali metal ions in hydrogen-oxygen-nitrogen flames with hydrocarbon additives 18 p3107 A67-33806

Effect of dislocations in GaAs single crystals on diffused p-n junctions structure and recombination radiation parameters 19 p3300 A67-34768

Reaction rate constants for gaseous chemical species at high temperatures [CI PAPER 67-11] 19 p3345 A67-35006

Electron density decay curves in helium afterglows at high electron densities and gas pressure found controlled by recombination loss process 19 p3270 A67-35071

Ionization decay in cesium vapor explained in terms of dissociative recombination and diffusion, showing strong dependence on vapor pressure 19 p3271 A67-35072

Charge recombination coefficient of decaying He and Ar plasmas with Cs vapor additions at increased pressures 19 p3271 A67-35073

Electron-ion radiative recombination influence on time-dependent luminous intensity of various spectrum lines in cesium vapor 20 p3488 A67-36436

Density and recombination coefficients of nonequilibrium carriers in Ge and GaAs as function of laser excitation intensity 20 p3513 A67-37437

Self-similar solutions for recombination plasma decay problem, considering plane and spherical symmetry 20 p3502 A67-37536

Dissociation and recombination of diatomic molecules by invert third bodies described by stochastic theory 22 p3756 A67-39386

Energy state of recombination level of thermally hardened silicon diode base, considering spatial lifetime of minority carriers 22 p3773 A67-39920

Effective recombination coefficient in upper-E and F-1 layers at sunset from rocketborne gyroplasma probe measurements of electron density profile 22 p3793 A67-40044

Gamma radiation energy direct conversion into electrical energy by electrochemical recombination of radiolysis products, proposing new sealed battery 22 p3748 A67-40199

Characteristics of geomagnetic crotchets associated with proton flares, determining recombination coefficients and electron densities 23 p4050 A67-40671

Nonlinear volt-ampere characteristic of photosensitive GaAs plus copper atoms in strong electric field 23 p4039 A67-40939

Diatomic molecular ion composition and variation of effective recombination coefficient in ionosphere in terms of altitude, time of day, solar activity, temperature, etc 24 p4149 A67-42124

Lifetimes of n-type Cd-Hg-Te alloy, showing Hall-Shockley-Read type recombination at low temperatures 24 p4205 A67-42664

RECONNAISSANCE

SA AERIAL RECONNAISSANCE

SA SURVEILLANCE

Aerial photographic techniques and equipment, noting use in reconnaissance and mapping 06 p1000 A67-17583

RECONNAISSANCE AIRCRAFT

Boundary layer control for improvement of lift at lower angles of attack by carrier-based supersonic aircraft [AIAA PAPER 65-751] 09 p1441 A67-22484

Sensors and sensor control devices for use in high speed low altitude reconnaissance aircraft 15 p2485 A67-29162

Target location systems functioning in daylight, darkness and under adverse weather conditions 17 p2814 A67-32507

RECORD-SETTING FLIGHT

23 world helicopter records established by YOJ-6A helicopter during 10 flights, noting details [AHS PAPER 125] 16 p2598 A67-31840

RECORDING INSTRUMENT

SA CABLE FORCE RECORDER

SA DATA RECORDER

SA ELECTRONIC RECORDING INSTRUMENT

SA FLIGHT LOAD RECORDER

SA FLIGHT RECORDER

SA MAGNETIC TAPE RECORDER

SA PHOTOGRAPHIC RECORDING INSTRUMENT

SA PLOTTING INSTRUMENT

SA PRESSURE RECORDER

SA PULSE RECORDER

SA TAPE RECORDER

SA VERY LOW FREQUENCY EMISSION RECORDER

SA WAVE RECORDER

SA WHISTLER RECORDER

Industrial F 115 photocompensation amplifiers for recording integral and reflected radiation aboard aircraft 01 p0062 A67-10127

Recording assembly for measurement of flexural and torsional moduli and internal friction at various frequencies and temperatures of small samples, using constant amplitude undamped oscillations 01 p0062 A67-10163

Piggyback twister /PBT/ magnetic memory for recording high impact data 02 p0242 A67-12019

Book on principles of construction and theory of main elements and assemblies of analog radio telemetry systems with frequency and time channel separation 03 p0367 A67-13123

Thermal high resolution recording using moving laser spot on metallic and organic thin films 05 p0815 A67-16586

DC amplifier with capacitive feedback as correcting device in recording currents while studying magnetoplasma generator 06 p0952 A67-18693

Astrospectrometer, instrument for recording high definition star spectra 07 p1186 A67-19425

Mesosphere ice point temperature, atomic oxygen concentration and total density measurement with heat recorder 10 p1656 A67-23207

Holography applied to radio frequencies, noting recording technique with locally produced reference wave 13 p2119 A67-26518

Minimum effective heights of ionospheric layers in continuous recording for study of ionization and disturbance 13 p2119 A67-26562

Recording of frequencies from 0 to 1000 Hz on low priced media 13 p2119 A67-26662

Spatially modulated laser recording parameters, emphasizing beam intensity ratio to signal beam, offset angle film transfer characteristic and recording wavelength 13 p2129 A67-27351

High resolution CRT for system designers to scan film or record photosensitive materials 15 p2447 A67-29734

Automatic recording and computer analysis of double probe measurements in plasma research, calculating electron temperature and plasma density 15 p2489 A67-30092

Multiparameter recording on DC-9 jet aircraft for advancing maintenance techniques, discussing use in engine, fire warning and air conditioning systems

performance
[AIAA PAPER 67-378] 15 p2420 A67-30349

Electronic equipment for generating delay times corresponding to missile velocity during optical recording by numerous sensors distributed along ballistic firing range 16 p2674 A67-31118

Design and construction principles of radio telemetry recording systems for gasdynamic observations in ballistic testing 16 p2624 A67-31124

Performance of fiber-optics coupled cascade image intensifier systems from standpoint of overall system noise, resolution, gain, contrast degradation and information rate capability 17 p2859 A67-32504

Instrument for processing and storing gas pressure data noting digital integrator, core storage unit and printer 19 p3230 A67-35565

Focused image holograms, amplitude-or phase-recorded, reconstructing sharp images by reflection from incoherent illumination 20 p3435 A67-36201

Digital recording double Fabry-Perot spectrometer, discussing pressure difference control system 20 p3440 A67-36363

TRKI-12 predetection receiver/recorder subsystem examined for performance characteristics 20 p3380 A67-36550

Recording and display programs illustrating relative capabilities of thermoplastic and direct electron beam on photographic film recording 20 p3449 A67-36984

Device for automatic recording of laser emission and of energy of pumping pulse 20 p3460 A67-37149

Cost effectiveness of digital and voice accident recorders in small fighter and military aircraft for low level missions, reconnaissance, flight testing and training 21 p3631 A67-39129

Design and operation of various recording instruments /speedobarographs/ for simultaneous measurements of aircraft altitude and speed 22 p3798 A67-39550

Polarizations of Pc 1 micropulsations intermittently recorded in Alaska with analysis of data for presence of right and left hand waves 22 p3793 A67-40078

Magnetoelectric device development to measure and register weak signals in digital form in converters of automatic control systems 22 p3809 A67-40475

Aircraft flyover noise recording system, considering calibration, weather tape recording and synchronization system equipment 23 p3999 A67-41145

Event recorder for in-flight measurements of missile heat-shield ablation 23 p4006 A67-41377

Lithium chloride impregnated balsa wood and surgically implanted electrodes for continuous heart rate recording over long periods of time 23 p3965 A67-41571

Solar magnetographs for defining strength and direction of magnetic field in solar atmosphere 24 p4223 A67-41769

Thermal development method used for observing and recording laser oscillations from output of nitrogen-carbon dioxide systems 24 p4166 A67-41908

Cosmic particle recording facility at Tskhra-Tskaro, giving data on free path of nuclear active particles in carbon with high energies 24 p4219 A67-42845

Electromagnetic showers in lead recorded with ionization calorimeter, discussing cascade curve 24 p4221 A67-42870

RECOVERABLE SPACE VEHICLE

Guided high altitude sounding rocket with paraglider recovery system that attains normal flight attitude upon atmospheric entry without control 04 p0703 A67-14547

Control and stabilization of thrust producing final stages of recoverable space vehicles during atmospheric reentry 04 p0652 A67-14557

Recoverable high altitude rocket space probe with paraglider 07 p1259 A67-19573

Multistage parachute recovery systems used for aerial delivery systems, escape from aircraft and recovery of spacecraft [AIAA PAPER 66-25] 08 p1413 A67-21513

European recoverable and reusable aerospace transporter 15 p2566 A67-29829

Near term reusable rocket launch vehicle concepts 15 p2566 A67-29831

Ballistic vs lifting body and winged recovery techniques for space launch vehicles, noting cost and operational capabilities 15 p2567 A67-29834

Fixed wing reusable horizontal landing boosters, comparing weight, cost, technical difficulty and availability 15 p2567 A67-29836

Integrated launch/reentry vehicle reusability via tip tank concept 15 p2567 A67-29837

French concept for aerospace transporter capable of horizontal takeoff from existing major airstrips 15 p2568 A67-29842

Partially reusable space vehicle systems examined and compared for operational costs, savings, feasibility, flexibility, simplification, etc 15 p2569 A67-29851

RECOVERY

SA BOOSTER RECOVERY

SA PRESSURE RECOVERY

SA SOFT RECOVERY

SA SPACECRAFT RECOVERY

SA SPINNING RECOVERY

SA VISUAL DISCRIMINATION RECOVERY

SA WATER RECOVERY

Range instrumentation ships electronic capabilities, operation, electronic systems function, accuracy and future role [AAS PAPER 67-52] 15 p2468 A67-30117

LW-3B escape system for low and medium performance V/STOL aircraft 17 p2794 A67-32000

Ultrasonic energy, used for removing microorganisms from various surfaces for enumeration, noting texture, pretreatment and heat effects on recovery efficiency 19 p3179 A67-34911

Low temperature transient creep behavior of polycrystalline aluminum investigated experimentally for recovery of surface layer stress 22 p3821 A67-40054

RECOVERY CONTROL CENTER /RCC/

Operational aspects and techniques of rocket payload recovery from sea and air noting recovery forces, aids, problem areas, location of recovery control, etc 08 p1409 A67-20546

RECOVERY DEVICE

Controlled recovery of payloads from high altitudes and at large glide distances, using Para-Foil 08 p1409 A67-20545

Space cryogenic propellant storage utilizing vent gas recovery noting storability spectrum plot 22 p3906 A67-40164

RECOVERY LAUNCH VEHICLE

Launch vehicle development in reusable and albreathing configurations 09 p1572 A67-22674

Navigation and guidance requirements of advanced single-stage-to-orbit reusable launch vehicle investigated to determine necessary modifications 20 p3481 A67-36576

RECOVERY PARACHUTE

Aerodynamic deceleration systems, discussing basic materials and fabrication techniques of BALLUTE program [AIAA PAPER 66-988] 02 p0181 A67-12299

Complex testing method for two-stage rocket probe recovery system with aid of two successively opening parachutes 03 p0518 A67-13397

Controlled recovery of payloads from high altitudes and at large glide distances, using Para-Foil 08 p1409 A67-20545

Low density wind tunnel enabling simulation of aerodynamic flows at high altitudes with rarefied air 17 p2835 A67-33132

RECOVERY TEMPERATURE

Variation of transition Reynolds number with wall to recovery temperature ratio at hypersonic speeds, comparing transition measurements with and without Pitot tube 04 p0604 A67-14836

Eckert reference temperature yields approximations for heat transfer, skin friction and recovery temperature in high speed laminar diatomic nitrogen and carbon dioxide boundary layers 11 p1883 A67-24576

RECOVERY ZONE

Effect of beryllium, boron, titanium, etc, additions on recovery and recrystallization processes in pure aluminum, using differential calorimetric techniques 04 p0637 A67-14910

Operational aspects and techniques of rocket payload recovery from sea and air noting recovery forces, aids, problem areas, location of recovery control, etc 08 p1409 A67-20546

Recovery site location importance in determining entry vehicle future requirements 21 p3607 A67-37804

RECRYSTALLIZATION

Degree of strain effect on kinetics of recrystallization of nickel and niobium monocrystals investigated by electron beam fusion in vacuum 01 p0101 A67-10940

Oxygen impurity effect on recrystallization temperature of annealed and rolled tantalum 02 p0255 A67-11866

Recovery and recrystallization of high purity warm-worked chromium sheet material 03 p0439 A67-12924

Laser beam-induced recrystallization of amorphous Ge semiconductor thin films prepared by thermal deposition on glass 03 p0498 A67-13839

Effect of beryllium, boron, titanium, etc, additions on recovery and recrystallization processes in pure aluminum, using differential calorimetric techniques 04 p0637 A67-14910

Rough surface recrystallization of heated polyethylene extended-chain crystals 04 p0566 A67-15201

Recrystallization and polygonization of pure and impure metals, noting role of vacancy supersaturation 05 p0830 A67-17311

Titanium, zirconium and hafnium effect on recrystallization temperature and strength of alloys of molybdenum with carbon 05 p0832 A67-17508

Manganese aluminide precipitation effect on primary recrystallization in metal systems, indicating softening processes in metals 06 p1015 A67-17810

Petrology and mineralogy of British Museum noncarbonaceous chondrites and relative abundance of primitive and recrystallized variants by isochemical recrystallization near 900 degrees C 07 p1249 A67-19538

Recrystallization of Ge and Si thin films and structural changes due to electron bombardment and thermal annealing 13 p2177 A67-27071

Cohenite grains from iron meteorites studied by X-ray diffraction for establishing pressure scale, using solid state recrystallization 13 p2200 A67-27235

Laser beam-induced recrystallization of amorphous Ge semiconductor thin films prepared by thermal deposition on glass 13 p2185 A67-27720

Thermal exposure effect on recrystallization and ductility of TZM molybdenum alloy sheet and foil 19 p3234 A67-34793

Tungsten sheets examined for recrystallization, grain growth and ductile-brittle transition temperature /DBTT/ as function of thermal treatment and grain size 20 p3467 A67-37119

Titanium, zirconium and hafnium effect on recrystallization temperature and strength of alloys of molybdenum with carbon 21 p3644 A67-38036

Chromium oxide addition effect on ruby recrystallization in carbonate and bicarbonate solutions under hydrothermal conditions, estimating chromic oxide solubility 21 p3685 A67-38971

Degree of strain effect on kinetics of recrystallization of nickel and niobium monocrystals investigated by electron beam fusion in vacuum 22 p3820 A67-39793

Softening and incipient recrystallization temperature of deformed niobium during annealing measured by X-ray analysis and mechanical properties 22 p3823 A67-40326

Achondrites and mesosiderites containing brecciated structures indicate magnetic differentiation, recrystallization, refragmentation and ejection from parent body 24 p4233 A67-42619

RECTANGULAR BEAM

Aerodynamic characteristics of rough cylinders, noting effect on head drag coefficient and Reynolds number 07 p1126 A67-19323

Cracked rectangular beam stress analysis, considering longitudinal shear and Saint-Venant torsion and flexure [ASME PAPER 67-APM-21] 17 p2964 A67-33150

Stress concentration of plane curved beams with uniform cross section determined from photoelastic experiments 20 p3540 A67-37210

Strain rate sensitivity and bending extension interaction in one degree of freedom deformation of clamped beam, considering vibration and load duration 23 p4072 A67-40607

Permanent deformation of clamped plastic beam with central mass concentration subject to impulse loading 23 p4072 A67-40608

RECTANGULAR GUIDE

Attenuation characteristics of unsupported resistive thin film applied to one face of dielectric vane in microwave attenuator 01 p0039 A67-10899

TE mode-selective coaxial directional coupler with coaxial primary line and rectangular waveguide as secondary line 02 p0214 A67-11650

Dispersion equations of ring delay circuit formed by bending diaphragmed rectangular waveguide in H plane 02 p0214 A67-11903

Dispersion equation for interaction of helical flux of relativistic electrons with wave field of rectangular guide 03 p0367 A67-13089

Slot couplings of rectangular single-mode waveguides analyzed by equivalent circuit and concentrated parameter methods 03 p0385 A67-13952

TE modes propagation in rectangular waveguides containing two dielectric slabs, computing cut-off frequencies and propagation constants 04 p0570 A67-14860

Simultaneous radiation of center-fed slotted rectangular waveguide array antenna for monopulse tracking radar 04 p0590 A67-15905

Cut-off wavelength of lowest TE mode in rectangular waveguide having coaxial cylindrical conductor 05 p0773 A67-16511

Wave diffraction in rectangular waveguides passing through double ribbon barriers 05 p0775 A67-16956

Numerical results of slot couplings of rectangular single mode waveguides as function of length, width, position and wavelength 05 p0775 A67-16957

Electromagnetic wave dispersion in semiconductor plasma waveguides for case of plane wave propagation normal to magnetic field vector 07 p1231 A67-19133

Galerkin-Ritz method application to Maxwell waveguide equations for calculation of propagation constant of rectangular guide with transverse ferrimagnetic core 07 p1152 A67-19590

Propagation coefficient of rectangular waveguide containing centrally placed semiconducting film 07 p1146 A67-20202

Variation of phase constant and damping constant of SHF wave propagating in waveguide incorporating coaxial plasma-filled dielectric tube 09 p1473 A67-21999

Controlled nonreciprocal microwave device using Faraday rotation in solid state plasma 09 p1474 A67-22090

Rectangular terminal block in rectangular waveguide and dispersion equation for surface wave propagating along waveguide 10 p1613 A67-23445

Pressure drop correlation in developed, isothermal, laminar and turbulent flow in rectangular ducts 10 p1627 A67-23555

Exact calculation of electrical performance of rectangular waveguide T-junction having arbitrary cross section used to find equivalent circuit 11 p1787 A67-24732

Rectangular to cylindrical waveguide transducer which couples dominant rectangular and cylindrical transverse electromagnetic modes 11 p1767 A67-24733

Dielectric constant of very low loss materials at mm wavelengths measured by oversized rectangular waveguide technique 11 p1792 A67-24764

Variational, quasi-static and integral equation analytic waveguide solutions, extending singular integral equation to homogeneous and inhomogeneous loaded waveguide junction 12 p1906 A67-25978

Cylindrical partially filled waveguides of rectangular cross section, formulating boundary value problem and characteristic equation 12 p1906 A67-25980

Field solution of TE sub k zero mode wave incidence on inductive iris in rectangular waveguide 13 p2066 A67-26475

Dispersion characteristics of annular resonator cavity based on waveguide of rectangular cross section 13 p2077 A67-26749

Rectangular guide receiver passband,

estimating boundary effect, noting data characterizing interrelation of arrayed transmitters 13 p2069 A67-27032

Propagation constants of rectangular waveguide containing parallel sheets of finite conductivity using iterative computer program 13 p2083 A67-27443

Mode correspondence between circular and square multimode tapered waveguide, noting similar behavior of coupling mechanism of waveguides 15 p2444 A67-29454

Rectangular light guides transfer energy from injection type semiconductor laser to laser with logic element 16 p2684 A67-30461

Laminar and turbulent MHD flows of liquid sodium in rectangular duct with conducting walls, determining wall and magnetohydraulic losses 16 p2712 A67-30573

Impedance and reflection coefficient measurement in uniconductor waveguide noting experimental techniques, coefficient standards, etc 17 p2815 A67-32606

Impedance wall validity range for microwave structure, discussing tunable filter 17 p2816 A67-32787

Propagation in rectangular waveguide solved for traveling wave maser design by Rayleigh-Ritz method reduced to matrix eigenvalue problem 17 p2828 A67-33086

Launching efficiency of PE-20 and PM-11 modes in dielectric-loaded trough waveguide excited by dielectric-loaded rectangular waveguide 19 p3194 A67-35514

Mode conversion in rectangular waveguides, describing results in terms of plane wave diffraction by grating 19 p3183 A67-35545

Discontinuity problem solution between unloaded rectangular waveguide and same waveguide completely loaded with transversely magnetized ferrite 20 p3380 A67-36381

Wave propagation in ferrite-filled rectangular waveguide with transverse magnetization 20 p3382 A67-36864

Galerkin-Ritz method application to Maxwell waveguide equations for calculation of propagation constant of rectangular guide with transverse ferrimagnetic core 20 p3401 A67-37327

Discontinuity problem between empty rectangular waveguide and one filled with transversely magnetized ferrite solved by introducing metal surface wave 22 p3758 A67-39272

Standing wave ratio and impedance measurement method for rectangular waveguides at microwave frequencies 22 p3767 A67-39371

Omnidirectional double slot array of thin X-band rectangular waveguides, noting design for slot conductance and power handling capacity 23 p3977 A67-40699

Dielectric cover effect on resonant frequency of slots in rectangular waveguide, using Stevenson free space theory and plane-wave reflection coefficient 23 p3978 A67-40824

Surface wave pole contribution to admittance of rectangular waveguide-fed slot into dielectric slab 23 p3979 A67-40829

Dominant mode field reflection at air-ferrite interface junction in anisotropic rectangular waveguide, deriving singular integral equations for discontinuity problem 23 p3973 A67-40880

Compensation method for longitudinal slot effects on propagation constant and characteristic impedance of rectangular waveguide used in standing wave meter 23 p4000 A67-41220

Propagation in periodically deformed circular and rectangular waveguides 24 p4121 A67-42287

RECTANGULAR PANEL

Minimum potential energy principle and Rayleigh-Ritz method derivation of flutter equations for flat rectangular orthotropic panels 05 p0924 A67-17350

Acoustic radiation of panels excited by random pressure fluctuation of turbulent boundary layer investigated, showing agreement with experiment 15 p2574 A67-29770

Buckling of longitudinally reinforced rectangular panel loaded by constant edge shear and longitudinal variable compression 16 p2763 A67-30792

Panels response to oscillating and to moving shock waves, discussing mode excitation, magnification factor, Bessel

function, etc 20 p3539 A67-37001

RECTANGULAR PLANFORM

Ideal incompressible liquid motion in rectangular container due to rectangular double and sinusoidal pulse excitation 03 p0404 A67-13784

RECTANGULAR PLATE

Stability and free oscillations of three-layer plates of symmetrical structure with isotropic outer layers and light transversal isotropic filler and weakened by central rectangular cut-outs 01 p0158 A67-10219

Deformation of rectangular slender webplates with boundary stiffeners flexible in plate plane under shear and compression 03 p0525 A67-13898

Orthogonal double series solutions of nonlinear deflections of thin rectangular plate 04 p0707 A67-14445

Concentrated tensile stresses induced by concentrated external loads applied to boundary of filament winding rectangular strip plate 05 p0914 A67-16216

Smooth surface interpolation applied to finite element displacement analysis of rectangular plate 05 p0925 A67-17372

Finite rectangular plate under load solved by method involving Green function and Fourier sine transform 06 p1105 A67-18579

Small oscillations and stability of hyperelastic incompressible rectangular strip under uniformly distributed biaxial load 06 p1111 A67-18892

Nonlinear flutter of simply supported rectangular plate under thermal compression in supersonic gas flow 09 p1574 A67-21915

Heated rectangular plate nonlinear free flexural vibration problem involving initial deflection, temperature change, etc 10 p1715 A67-22825

Vibration characteristics of two-layered plates of arbitrary thickness and differing materials, noting coupling effect between flexure and extension 10 p1718 A67-23140

Rectangular plate under periodic in-plane edge load investigated for transition mechanisms attendant to parametric vibrations [ASME PAPER 67-VIBR-5] 11 p1871 A67-24165

Bending under transverse load of isotropic plate with elastic base, using Ambartsumian theory of anisotropic plates 11 p1878 A67-24857

Approximate solution using finite difference method of bending of rectangular plate beyond elastic limit 11 p1879 A67-24886

Approximate method for determining free oscillation frequencies of hinged rectangular plate with variable thickness 12 p2021 A67-25574

Rectangular three-layer plate thermoelectric oscillations due to random pulses analyzed using series expansion 12 p2027 A67-25625

Elastoplastic equilibrium of rectangular compressible and incompressible plates under load concentrated near edge determined by elastic solutions and finite difference 12 p2031 A67-25960

Approximate method for solving bending problem of rectangular plates of nonuniform thickness under arbitrary external edge loading 12 p2031 A67-25962

Stability of nonlinearly elastic thin rectangular plates subject to compression 13 p2218 A67-26901

Numerical realization of partitioning method in case of rectangular plate bending with end loading, using bar scheme 15 p2576 A67-30180

Elastic stability of simply supported uniformly-thin rectangular plate under unequal compressive stresses at two opposite edges due to constant body force 15 p2577 A67-30218

Steady state heat flow and temperature fields in flat rectangular configurations with mixed boundary conditions 16 p2779 A67-31206

Forced transverse vibrations of sandwich plates of symmetrical structure 16 p2776 A67-31547

Galerkin method analysis of vibrations of clamped rectangular plates, using polynomial approximation 17 p2962 A67-32823

Critical compressive forces causing instability of rigidly-fastened rectangular plate determined by method of summary representations 17 p2962 A67-32871

Thermal stress concentration factors for rectangular flat plates penetrated by

holes 19 p3337 A67-34823
 Excess carrier distribution in inhomogeneous semiconductor rectangular plate under two illumination conditions 19 p3308 A67-36026
 Triangular finite element under plane stress analyzed using stiffness matrix, including in-plane concentrated moments and nodal rotation 20 p3538 A67-36676
 Transverse deflection of rectangular plate with bitrapezoidal cross section subjected to uniform longitudinal curvature, comparing theory with experiment 21 p3722 A67-38436
 Upper and lower bounds for frequencies of free vibration developed for uniform rectangular cantilever plates 21 p3730 A67-39094
 Plate stability loss criterion for critical external load values without determining initial stresses applied to rectangular plate Sommerfeld problem 22 p3909 A67-39401
 Rectangular plate with clamped edges studied for nonlinear cylindrical bending under uniform pressure 22 p3910 A67-39480
 Stiffness matrix for shallow rectangular shell element and application of finite element displacement method 23 p4073 A67-40628

RECTANGULAR WING
 Pressure distribution on rectangular wing with jet exhausting normally from lifting surface into uniform air stream [AIAA PAPER 67-1] 06 p0941 A67-18463
 Wind tunnel investigation of effect of ground level on static aerodynamic characteristics of sideslip for rectangular and delta wing with rudder assembly 07 p1126 A67-19886
 Nonlinear singularities method for calculating velocity distribution over thick wing of finite aspect ratio situated at zero angle of attack in incompressible frictionless potential flow 07 p1127 A67-19887
 Vortex wake and aerodynamic load distribution of slender rectangular wings 17 p2790 A67-32215

RECTIFIER
 SA AVALANCHE RECTIFIER
 SA GERMANIUM RECTIFIER
 SA IGNITRON
 SA SILICON CONTROL RECTIFIER /SCR/
 Weimer triode with contact rectifier for use as component of microminiature radio circuits, noting effect of contact rectification on current-voltage characteristics and amplifying power of such triodes 01 p0035 A67-10397
 Saturated transistor logic circuit using rectifier diodes to provide nonlinear current feedback from collector to base of transistor 01 p0038 A67-10817
 Ionization coefficient in selenium p-n step junction of rectifier cell 09 p1551 A67-21656
 LC smoothing filter in rectifier for pulse supply source stabilized by pulse width modulation 10 p1611 A67-22980
 Possibility of using p-i-n /p-n-n, n-p-p/ structure with heterojunctions for rectifier designed for ultrahigh current densities 13 p2174 A67-26366
 Full-wave rectifier using field effect transistor switches 13 p2078 A67-26780
 Electro-optical rectifier, types of materials generated, operational capability and lunar and aerial photographic application 14 p2321 A67-28828
 Statistical testing on digital computers for simulating current and voltage distribution in semiconductor rectifier circuits 15 p2439 A67-29416
 Differential resistance peaks of metal-semiconductor Schottky barrier rectifiers 19 p3198 A67-36042
 Current creep in selenium rectifier and effect on local conductivity channels in p-n junction of rectifier 20 p3508 A67-36403
 Possibility of using p-i-n /p-n-n, n-p-p/ structure with heterojunctions for rectifier designed for ultrahigh current densities 21 p3680 A67-38322
 Copper oxide and selenium semiconductor rectifiers as heat flux sensors, describing operation and thermal EMF 22 p3801 A67-40217

RECURSION FORMULA
 Dynamic programming recursive estimation of modal trajectory for nonlinear non-Gaussian noise and comparison with Bayesian estimation and case of Gaussian white noise 01 p0047 A67-12124

Energy spectra of avalanche electrons in copper, iron, aluminum and graphite determined by method of moments, considering polarization of medium and multiple scattering 02 p0316 A67-12768
 General recursion formula for dynamic response of pressure measuring systems considered as series connection of tubes and volumes 03 p0418 A67-12998
 Operational calculus for functions of one continuous and one discrete variable 05 p0834 A67-16725
 Nekrasov method application to construction of algorithm for small solutions to nonlinear integral equations, using recursion techniques 05 p0836 A67-17488
 Recurrence relation for determining asymptotic error constant of rational function iterative methods for solving equations 08 p1349 A67-21263
 Machine independent axiomatic theory of complexity of recursive functions 13 p2148 A67-27497
 Recursive formula for updating determinant of covariance matrix of state estimation error after incorporation of measurement 15 p2512 A67-30213
 Nontrivial real or complex solutions of nonlinear integral equations of Hammerstein type bifurcating from identically vanishing solution 16 p2695 A67-30858
 Extrapolation of time series with discrete Laguerre polynomials, deriving general recursion relation for expansion coefficients 16 p2697 A67-31418
 Optimum detection of Markov signals against noise background in case of discrete time 20 p3408 A67-37039
 Error divergence elimination in recursive minimum variance estimation of space vehicle trajectories 21 p3587 A67-39148
 Numerical recursion method for calculation of characteristic exponent of Mathieu differential equation 22 p3827 A67-39744
 Energy spectra of avalanche electrons in copper, iron, aluminum and graphite determined by method of moments, considering polarization of medium and multiple scattering 22 p3877 A67-40270
 Electron-photon shower creation probability by energetic particle, deriving recursion formulas 24 p4221 A67-42874

RED BLOOD CELL
S ERYTHROCYTE

RED SHIFT
 Red shifts and power outputs in quasars and radio galaxies 01 p0149 A67-10889
 Red shifts and colors correlated for quasars leading to smoothed mean energy distribution and new values for K-correction 02 p0322 A67-11686
 Possible correlation between color indices of quasi-stellar radio sources and red shift 02 p0323 A67-11697
 Red shift of magnetic zenith hydrogen line profiles and role of injection pitch-angle distribution of auroral protons 03 p0409 A67-12943
 Nature and theories of quasi-stellar radio sources and observation of red shift in spectra, examining possible gravitational or cosmological origin of shifts 03 p0516 A67-14337
 Quasi-stellar radio sources analysis including red shift, spectra, variability, etc, discussing possibility of local or cosmological objects 04 p0695 A67-14514
 Local model of quasi-stellar objects based on ejection by gravitational collapse 04 p0700 A67-15199
 Cosmological solutions of linear field theory, showing possible representation in form of hypersurface of second degree in five-dimensional affine space 05 p0897 A67-16773
 Correlation between position and red shift of quasars indicating anisotropic universe or galactic origin of quasars 05 p0898 A67-16887
 Quasi-stellar object red shift correlation with radio magnitude 05 p0898 A67-16923
 Quasar properties, discussing large red shift in star-like object associated with radio source 05 p0900 A67-17078
 Absolute magnitudes of quasi-stellar radio sources, plotted against logarithms of red shifts, fall between two limits 06 p1086 A67-18373
 Quasar counting, red shift and brightness 07 p1249 A67-19661
 Gravitational red shifts in quasi-stellar

objects 07 p1250 A67-19664
 Anisotropic distribution of quasars with large red shift as effect of observational selection 07 p1250 A67-19666
 Spectrophotometric data correlations between color and red shifts of quasars 08 p1398 A67-21231
 Statistical analysis of errors in angular measurement of distant objects due to gravitational scattering along light path 08 p1398 A67-21232
 Red shift relationship with ionization potential for absorption lines in quasi-stellar object 3C 191 08 p1400 A67-21251
 Red shift and absorption line of PKS 0237-23 09 p1567 A67-22242
 Absorption wavelengths of QSOs, noting relatively large red shifts 09 p1567 A67-22243
 Quasars, energy emission, high red shifts and relation to radio sources and visible stars 10 p1705 A67-22953
 Quasi-stellar objects red shift and optical magnitude measurements, noting discrepancies with zero and nonzero cosmological constant 11 p1863 A67-24508
 Extragalactic radio sources classified into five groups via radio magnitude and spectral index at 400 MHz 11 p1868 A67-25086
 Red shift determinations for quasi-stellar radio sources using spectrographic techniques 14 p2389 A67-28844
 Red shifts from absorption line spectra of quasi-stellar objects, discussing energy generation mechanism 14 p2390 A67-28851
 UVB values and red shifts of quasars interpreted within steady state and Friedman cosmological models 14 p2392 A67-28965
 Solar velocity with respect to distant galaxies estimated from red shift for nearby galaxies, noting cosmic microwave background 15 p2563 A67-30160
 Interpretation of UVB measurements of quasi-stellar sources 17 p2944 A67-32637
 Differential depressions of iron I levels and red shifts of spectral lines under pressure, demonstrating error in assumed air refractive indices 17 p2886 A67-33162
 Quasi-stellar radio source optical spectrum observed, identifying spectral lines and determining red shift 18 p3118 A67-33854
 Mean density of cosmological matter determined from quasi-stellar sources observations, analyzing apparent-magnitude and red shift methods 18 p3119 A67-33856
 Defects 18 p3119 A67-33856
 Differentiation between gravitational and cosmological components of quasars red shift by observational means 20 p3521 A67-36295
 Red shifts of radio galaxies observed spectroscopically with 120-inch telescope, using prime focus and image tube 20 p3527 A67-37392
 Quasi-stellar red shift assuming gravitational origin, deriving mass, radius and distance as function of flow density, linewidth and apparent diameter 20 p3531 A67-37683
 Red shift magnitude relation for quasi-stellar objects 21 p3701 A67-37895
 Nonrandom optical red shift distribution of radio sources leading to uniform density over large volume 22 p3892 A67-40500
 Spectral index dependence on flux density and cosmological red shift, considering model universes populated with radio sources 23 p4062 A67-40634
 Free-free radiation absorption from discrete radio sources calculated for various isotropic world models as red shift, electron density and temperature function 23 p4063 A67-40777
 Monograph on quasi-stellar objects including identification, line spectra, radio emission, continuum radiation, red shift and models 23 p4069 A67-41438
 Novae and supernovae outbursts, suggesting mechanism which can account for both phenomena and for other problems concerned with quasi-stellar sources /quasars/ 24 p4231 A67-42451

REDUCTION

SA DATA REDUCTION
 SA DRAG REDUCTION
 SA FRICTION REDUCTION
 SA PHOTOREDUCTION
 SA SIDELobe REDUCTION
 SA SPIN REDUCTION

- Reducibility and induction of set of ordinary differential equations in vicinity of smooth integral manifold 04 p0643 A67-14726
- Jordan form matrix algorithm of Wasow for reducing systems of first order ordinary differential equations with turning point 05 p0835 A67-16779
- Mean time between failures for repairable system in terms of MTBF and availability of constituent units by reducing reliability block diagram 15 p2453 A67-30062
- REDUNDANCY**
- Partial redundancy for improved reliability of computing machine [JPL-TR-32-1088] 07 p1153 A67-19604
- Dual redundancy digital computer for improved reliability in real time processes and control situations where fault results in fatality or mission failure 08 p1298 A67-20638
- Redundancy reduction methods for data compression, noting application to photographs of Tiro, Gemini and Ranger 09 p1470 A67-22676
- Reliability through redundancy describing use of devices for averaging analog signals 16 p2649 A67-31667
- REDUNDANCY ENCODING**
- Evaluation of redundancy reduction algorithms to facilitate comparison in terms of performance by computer simulation, using real and synthesized data 02 p0197 A67-12015
- Design, redundancy, reliability and tradeoffs for Launch Vehicle Digital Computer and Data Adapter /LVDC/LVDA/ for uprated Saturn I and V vehicles, noting logic circuit, memory, input/output, power supply 09 p1469 A67-22301
- Data compression for analog signal transmission with smaller bandwidth requirement obtained from reduced signal redundancy and simulation of techniques 14 p2275 A67-28683
- Redundancy reduction techniques and error correction coding of digital communication systems including waveform, pattern recognition, vocoding, etc 18 p3004 A67-34613
- Coded information transmission with reduced band emphasizing pulse prediction through redundancy, information quantity and delta signal 21 p3585 A67-38763
- Error control techniques covering parity check, longitudinal redundancy check and hamming and cyclic codes 22 p3776 A67-39372
- Video digital data compression technique, time-buffered coarse-fine /TBCF/, for redundancy reduction 24 p4123 A67-42806
- REDUNDANT STRUCTURE**
- Model ten-member redundant structure under constant-amplitude loads analyzed, determining statistical distribution of consecutive failures for fail safe design applications 10 p1718 A67-23432
- Redundancy reduction for conserving bandwidth and/or power in aerospace communication and telemetry 11 p1756 A67-24708
- Floating aperture predictor, zero order interpolator and fan interpolator for redundancy removal bandwidth compression 11 p1757 A67-24710
- Upper and lower bounds of survivorship function of redundant structure subjected to fatigue 16 p2774 A67-31319
- REDUNDANT SYSTEM**
- Modified long-term system reliability models for redundant systems, considering imperfect failure detection, repair and sparing 01 p0043 A67-11378
- Statistical procedures for analyzing test data to determine extent of dependence of failures in redundant components 05 p0813 A67-17256
- System reliability increased by introducing redundant elements or structural changes in elements 06 p1008 A67-18546
- Pulsed power technique and capacitive coupling between digital integrated circuits provide micropower redundant circuits with automatic error correction 07 p1155 A67-19844
- Optimal allocation of n test points within redundant digital system for prelaunch and in-flight spacecraft reliability estimate 08 p1300 A67-20637
- Adaptable large scale integrated military and space systems, discussing microelectronic circuit, logistics and dynamic redundancy 08 p1311 A67-20665
- Flexible flight plan processing system with high continuity of service, using differing degrees of redundancy and having comprehensive system monitoring and control facilities 09 p1531 A67-22656
- Logical redundancy technique based on failure-erasure circuitry for masking P-1 failures in P identical elements connected in parallel 09 p1470 A67-22668
- Reliability analysis of active, standby and active-standby redundant system, discussing Poisson-binomial probability distribution function 13 p2123 A67-26828
- Iterative numerical method for solving equations of single variable by using several approximations applied to parallel processing environment 13 p2148 A67-27487
- Variable data rate modem for digital signal transmission on HF radio circuits 14 p2272 A67-28705
- Reliability for redundant repairable systems using queueing theory, studying triplicate and similar/dissimilar subsystem systems 15 p2453 A67-30063
- Large scale integration of circuits studied for high yield, using concept of redundancy adjustment of probability 18 p3014 A67-34553
- Maintenance and support factors effects on systems availability described by mathematical models, giving applications in tradeoff studies 18 p3163 A67-34695
- Space systems reliability design problems, discussing estimation, weight-reliability tradeoffs, spare parts and redundancy 18 p3139 A67-34698
- Servo loop electronics reliability using continuous redundancy, integral self-test circuits, etc 19 p3191 A67-34847
- System reliability and effectiveness in manned and unmanned geological/geophysical space missions 19 p3332 A67-35323
- Application of redundancy in Saturn V guidance and control system to achieve desired reliability [AIAA PAPER 67-553] 19 p3257 A67-35950
- Effective guidance and control redundancy for spacecraft configurations and mission outcomes, discussing computer systems [AIAA PAPER 67-555] 19 p3257 A67-35952
- Series/parallel connection of redundant elements in thermopile shown to increase reliability of array over simple series of thermoelectric elements 20 p3363 A67-36958
- Transfluxor as self-repair unit of redundant automata 20 p3454 A67-37038
- Operational readiness of redundant system, deriving system readiness factor formula for operating and idle redundancy 20 p3451 A67-37158
- Optimum redundancy of multistage parallel systems using variational technique to maximize profit 20 p3556 A67-37316
- Spacecraft and space station reliability by orbital maintenance and extravehicular activity, comparing redundancy on system and cost effectiveness [AIAA PAPER 67-652] 20 p3535 A67-37629
- Ultrareliable six redundant sensor attitude reference system for Manned Orbital Laboratory /MOL/ with limited sparing capability 21 p3624 A67-37786
- System reliability increased by introducing redundant elements or structural changes in elements 22 p3812 A67-39745
- LF solid state equipment improves mission reliability through use of integrated molecular circuit and modular redundancy 22 p3771 A67-39840
- Spacecraft flight control and computerized systems, discussing redundant systems, integrated circuits and simulation for man-machine interaction and lack of response 22 p3908 A67-40336
- Missile and space support systems reliability, flight equipment and redundancy 22 p3781 A67-40342
- Planning and design of Voyager for future interplanetary flight, discussing RTG and spacecraft system redundancy 23 p4071 A67-40867
- Spacecraft power conditioning reliability using standby redundancy at functional component level and performance monitoring automatic failure detector 24 p4108 A67-42539
- Power conditioning subsystem failure detection provided by computer monitoring of performance, with signal for transfer to redundant unit [AIAA PAPER 67-983] 24 p4110 A67-43055
- Long term manned space mission system effectiveness and reliability through interchangeability and redundancy noting optimization, tradeoffs, maintenance and spares [AIAA PAPER 67-984] 24 p4166 A67-43056
- REENTRY**
- SA ATMOSPHERIC ENTRY
- SA HYPERBOLIC REENTRY
- SA HYPERSONIC REENTRY
- SA LIFTING REENTRY
- SA MANNED REENTRY
- SA SPACECRAFT REENTRY
- Propulsion and reentry - IAF Conference, Athens, September 1965, Volume 5 16 p2735 A67-30701
- REENTRY ANGLE**
- Range of hypersonic gliders for various flight and reentry conditions, assuming small flight path angle and constant bank angle 16 p2595 A67-30963
- REENTRY BODY**
- Thermal conductor of arbitrary shape, analogy with rectangular array of electrical resistance, detailing conformal transformation 01 p0167 A67-11015
- Integral relations method applied to separation of laminar boundary layer on cooled hypersonic reentry body 02 p0179 A67-12348
- Density gradient effect on development of turbulent wake of reentry object determined by studying wake of heated object at low speed 02 p0179 A67-12356
- Wind tunnel tests of lifting reentry body at Mach numbers up to 16.5 and at angles of attack up to 50 degrees 04 p0546 A67-14567
- Nuclear blast interaction with bow shock of reentry vehicle and effect on structural materials 12 p1929 A67-25730
- Thermal protection technique using resin fiber ablative materials for use on reentry bodies during ascent, emphasizing nozzle 21 p3731 A67-38377
- Roll-rate reversal dispersion effects of ballistic reentry body due to mass and aerodynamic asymmetries 22 p3742 A67-40117
- REENTRY COMMUNICATION**
- Plane wave propagation across thin stratified plasma sheaths, noting polarization and reflection [AIAA PAPER 66-481] 12 p1905 A67-25906
- Telemetry, tracking and command /TTC/ communications, emphasizing 1970 requirements for manned and unmanned earth-orbital, lunar and planetary missions 13 p2074 A67-27449
- Radio telemetry links perturbations during ballistic missile reentry due to plasma from kinetic heating 21 p3581 A67-38228
- REENTRY CONDITION**
- Minimum velocity increment for deboost from circular orbit as function of orbital altitude 01 p0153 A67-10429
- Reentry simulation, discussing aerodynamic and thermodynamic parameters, heat transfer and simulation accuracy 02 p0335 A67-12415
- Char generation and determination of thermal conductivity function under simulated entry heating conditions [AIAA PAPER 65-640] 03 p0534 A67-13060
- Exact transient temperature distribution in spherical region subjected to axisymmetric-reentry heat flux compared with one-dimensional theory [ASME PAPER 65-WA/HT-53] 03 p0537 A67-14014
- Critical heating conditions in hypersonic glider reentry 06 p1113 A67-17981
- Ablative material performance under high shear reentry condition, noting hyperthermal test of cones and wedges for heat shield design 10 p1734 A67-23722
- Multiple arc performance in 8000 kw plasma facility consisting of hyperthermal blowdown tunnel for ballistic flight simulation 12 p1974 A67-25404
- Aerothermodynamic testing of heat protective systems in arc tunnel 15 p2466 A67-29538
- Von Karman gas dynamics counterflow facility for simulating model high velocities and altitudes of reentry conditions 16 p2655 A67-31261
- Ablators for severe reentry environments evaluated from modifications of reference model constructed of epoxy resin with silica fiber and phenolic filler 22 p3826 A67-39887
- Dynamic destabilization for hypersonic flow around slender cone with severely blunt nose analyzed by blast wave

analogy 22 p3742 A67-40109
Hypersonic reentry plasma electron density measurement in free stream wake and shock layer using hotshot wind tunnel simulation 23 p3986 A67-40574
Reentry vehicle surface pressure measurement, obtaining accuracy and reliability in stable high level pressure transducer 23 p4006 A67-41378
Random intact reentry and earth burial for radioisotope thermoelectric generators disposal without atmospheric contamination, evaluating design concepts for SNAP systems 24 p4241 A67-42559

REENTRY EFFECT

Inverse optimization for calculating refractive index and electrical resistivity of plasma in reentry and surface tension coefficient in epihydrodynamics 02 p0333 A67-12347
High resolution equilibrium radiation spectra for shock layer of blunt bodies at reentry velocities and radiative recombination of N and O ions [AIAA PAPER 66-104] 04 p0546 A67-14816
Convective and radiative heat transfer to reentry vehicles at superorbital velocities [AIAA PAPER 66-106] 05 p0928 A67-17336
Differential equations and mathematical models for gas flows with chemical activity and radiative effects, particularly effects of reentry and propulsion 06 p0983 A67-17785
Refractory and ablating polymeric reentry heat shield materials evaluated under high radiant fluxes, measuring surface temperature, recession rate, flux emittance, etc refractory and ablating polymeric reentry heat 11 p1811 A67-24054
Transverse magnetic field interaction with laminar boundary layer on rotating cone during reentry, assessing effect on spin and controlling torques 12 p1892 A67-25385
Radio blackout extent from simplified calculation of average sheath power loss for typical Apollo reentry trajectory 15 p2434 A67-29168
Hypersonic reentry heating problems due to kinetic energy of space vehicle at reentry at orbital and escape velocity 17 p2970 A67-32828
AMICON 8000 kw plasma facility for simulating reentry environments for material and thermodynamic tests 20 p3415 A67-36551
Hot shot nitrogen gas source for pulsed MHD accelerator to provide lunar reentry 21 p3608 A67-38863
Roll-rate reversal dispersion effects of ballistic reentry body due to mass and aerodynamic asymmetries 22 p3742 A67-40117
Superorbital reentry environments, discussing materials, test environments, and heat factors 22 p3919 A67-40383
MGD reentry flow regimes analyzed, noting increased bow shock standoff distance and drag, comparing in-flight and laboratory simulation 24 p4199 A67-42920

REENTRY GLIDER

Phugoid trajectories of ballistic reentry of hypothetical glider into variable density atmosphere 05 p0847 A67-17009
Phugoid trajectories of ballistic reentry of hypothetical glider into variable density atmosphere 18 p3079 A67-34272

REENTRY GUIDANCE

Hybrid computer simulation of reentry guidance for lifting vehicle, noting compatibility of temperature rate flight control system with other vehicle controls 01 p0051 A67-11438
Reentry guidance by threshold network storage of precomputed optimum commands, using analogy of surface approximation problem in N plus one-dimensional space [AIAA PAPER 66-52] 11 p1869 A67-24338
Simulation evaluation of closed form lifting reentry guidance [AIAA PAPER 67-597] 19 p3259 A67-35993

REENTRY PHYSICS

Modeling of spacecraft performance during reentry /intact and disintegrated/ for evaluating spacecraft design through thermal and structural integrity tests 02 p0230 A67-12358
Viscous and bluntness induced pressures for flat plates, wedges, cylinders and cones at Mach 41 [AIAA PAPER 65-399] 04 p0546 A67-14815
Plane wave scattering by medium with strong fluctuations of refractive index, noting reentry condition 07 p1141 A67-19441
Optimum deorbit positioning on

planetocentric elliptic orbit for single impulse reentry treated by two coupled quartic polynomials 07 p1254 A67-19982
Flight dynamics of ballistic and lifting vehicle entries into planetary atmospheres of Mars, earth, Venus and Jupiter 08 p1410 A67-20623
Stable size and reaction of molten metal droplets with rarefied atmosphere as consequence of surface oxide film, treating beryllium 10 p1733 A67-23124
Convective and radiative heat transfer to entry vehicles protected by ablation heat shield, obtaining absorption coefficients [AIAA PAPER 67-327] 12 p2038 A67-26041
Optimum deorbit positioning on planetocentric elliptic orbit for single impulse reentry treated by two coupled quartic polynomials 13 p2209 A67-27536
Trends in technology for reusable launch vehicles 15 p2569 A67-29854
Theoretical and experimental work in flow field analysis has enhanced ability to predict aerodynamic heating in atmospheric entry 16 p2760 A67-30720
Calibration system for PRESS optical aircraft program utilizing portable collimators 16 p2679 A67-31796
Basic shock layer radiation data obtained in shock tube and free-flight ballistic range facilities applicable to Venus or Mars atmosphere entry 21 p3563 A67-37788
Second order theory used to provide nearly exact solution for entry mechanics including solution of nonoscillating and oscillating trajectories [AIAA PAPER 66-488] 21 p3706 A67-38865

REENTRY RANGE

Manned spacecraft design, discussing range hardware and software development and future entry vehicle programs [AAS PAPER 67-36] 15 p2571 A67-30108
High altitude hypersonic viscous flow degradation of L/D effects on entry vehicle lateral range capability 22 p3742 A67-40114

REENTRY SHIELD

SA HEAT SHIELD
Two fabric-reinforced plastics performance in reentry heating as function of zirconia powder, magnesia powder and Microbestos TX paper fillers [AIAA PAPER 67-154] 06 p1020 A67-18292
Graphite thermochemical response tested in simulated environment for use as thermal shield for hypersonic reentry vehicles [AIAA PAPER 65-643] 08 p1426 A67-20561
Materials, space vehicle structures and reentry research and development 13 p2213 A67-27503

REENTRY TRAJECTORY

Optimizing constant and variable parameter of minor circle solution for lateral maneuvering on spherical planet 02 p0333 A67-12335
Aerodynamic penetration and radius in drag and lift during atmospheric entry process 06 p1094 A67-18003
Trajectory control scheme effect on performance of lifting entry vehicles [AIAA PAPER 66-407] 07 p1257 A67-19362
Three-impulse orbital transfer from lunar orbits and earth reentry trajectory applications [AAS PAPER 66-134] 07 p1255 A67-19993
Thermal behavior of vehicle entering earth atmosphere at velocities approaching 15 km/sec 13 p2224 A67-27325
Three-impulse orbital transfer from lunar orbits and earth reentry trajectory applications [AAS PAPER 66-134] 13 p2210 A67-27544
Earth-moon and moon-earth trajectory parameters related to lunar orbit conditions for synthesizing lunar orbit trajectory 13 p2210 A67-27616
Modulation of L/D and bank angle to achieved heading, range and trajectory stabilization, using closed form equations 14 p2347 A67-28114
Magnetoaerodynamic drag and flight control available to vehicle entering earth atmosphere calculated, including induced magnetic fields effects and nonscalar conductivity 14 p2394 A67-29041
Reentry vehicle roll resonance criterion formulation for predicting roll conditions, noting vehicle configuration, aerodynamic and trajectory parameters, exoatmospheric vehicle attitude, etc 15 p2572 A67-30211

Precomputed approximation to weighting matrix in extended Kalman filter for ballistic reentry vehicle trajectories estimation 16 p2651 A67-31682
Airborne Astrographic Camera System using meteor orbit theory to observe reentry trajectory discussing data reduction theory and photo-optical instrumentation 16 p2679 A67-31795
Hypersonic reentries with thermal and structural integrity problems studied by Saphir rocket firings 17 p2955 A67-32376
Analog translational trajectory program replacing digital program for orbiting and reentry vehicles 19 p3190 A67-36070
Reentry trajectory optimization by repetitive computations of impulse response functions and state equations solution 19 p3190 A67-36072
Radar designation by computer and real time reentry tracking for future Apollo manned space flight 20 p3381 A67-36592
Trajectory optimization initial value problem, considering various conditions, methods of solution and reentry heating minimization 21 p3703 A67-38440
Closed form solution for two-dimensional reentry trajectories by transforming motion equations into Bernoulli with two arbitrary functions of inclination, considering constant gravitational field 22 p3881 A67-39526

REENTRY VEHICLE

SA FIRST PROJECT
SA HL-10 REENTRY VEHICLE
Oxidation test and mechanical property data to determine suitability of columbium and tantalum alloys as thermal protective materials for use in multicycle earth reentry vehicles [SAE PAPER 66-0660] 01 p0094 A67-10618
High temperature resistant materials for antennas on reentry and high performance aircraft 01 p1013 A67-10620
Winged lifting reentry hypersonic vehicles, discussing design, analysis, fabrication and testing of hot and cooled structures and materials [AIAA PAPER 65-367] 02 p0331 A67-11929
Angle of attack measurements of hypersonic reentry vehicle derived from flight test pressure data 02 p0178 A67-11942
Manned lifting entry vehicle capability, minimum weight, variable geometry, retractable landing engines, etc [AIAA PAPER 66-959] 02 p0332 A67-12287
Weight and cost comparative analysis of ablative and combined ablative/radiative heat shields for SV-5 and SV-32 lifting reentry vehicles [AIAA PAPER 66-990] 02 p0333 A67-12301
Modeling of spacecraft performance during reentry /intact and disintegrated/ for evaluating spacecraft design through thermal and structural integrity tests 02 p0230 A67-12358
Slender body theory application in obtaining aerodynamic stability derivatives for reentry vehicles via electrical analogy 03 p0354 A67-12918
Uncertainties in thermophysical properties of char-forming ablatives in intense convective and radiative heat transfer environments and effect on mathematical and physics models [AIAA PAPER 65-639] 03 p0534 A67-13059
Positions of Echo satellites during reentry stage observed at Aslago in 1964 03 p0509 A67-13105
Hollow-rib reinforced structure design from boron filament reinforced epoxy resin, describing fabrication equipment, techniques and test results 03 p0429 A67-13417
Elevated-temperature tensile testing of thin Rene 41, Hastelloy X and TD Nickel sheet 03 p0446 A67-13553
Manned lifting body flight test program, noting NASA M2-F2 and HL-10 and USAF SV-5P [AIAA PAPER 66-838] 03 p0519 A67-14127
Lifting reentry vehicles for achieving orbital plane changes by synergetic maneuvers [AIAA PAPER 66-960] 03 p0520 A67-14141
Structures, materials and thermal protection systems for future manned reentry vehicles, emphasizing crew compartment compatible materials [AIAA PAPER 66-987] 03 p0520 A67-14143
Prediction of subsonic base drag of hypersonic reentry vehicles [AIAA PAPER 66-991] 03 p0353 A67-14144

SUBJECT INDEX

Approximate analysis of electrostatic probe on reentry vehicle for electron density measurements in laminar boundary layer of continuum 04 p0705 A67-15231

Effects of reentry vehicle physical characteristics and trajectory constraints on variation of velocity-atmospheric density ambient value function 04 p0706 A67-15244

Lifting body reentry vehicle for return from orbit to continental U.S. 04 p0706 A67-15253

Onboard digital computer navigation, guidance and control of reentry and aerospace vehicles 06 p1028 A67-17922

Reentry trim angle of attack and lift-drag ratios from Gemini flights compared to wind tunnel data for aerodynamic studies [AIAA PAPER 67-166] 06 p0939 A67-18295

Aerodynamic performance characteristics of three entry vehicles designed for maximum L/D ratio of three and two at Mach 19 and Reynolds number 3,200,000 tested in 22-inch Langley helium tunnel [AIAA PAPER 67-138] 06 p0940 A67-18439

Heating restraints effect on aeroglide and aerocruise synergetic maneuver performance investigated for high lift-drag ratio vehicle [AIAA PAPER 67-169] 06 p1097 A67-18483

Steady roll resonance accompanied by large amplification of nonrolling trim angle, considering compound asymmetry such as lateral center of gravity offset [AIAA PAPER 67-137] 06 p1097 A67-18504

Lift-drag ratio, lift and drag coefficients and angle of attack effects on Gemini and Apollo reentry vehicles measured in shock tunnel under free flight conditions [AIAA PAPER 67-165] 06 p0941 A67-18507

Equilibrium air study extended to reentry speeds up to 70,000 fps, using transport and thermodynamic properties to examine stagnation point convective heat transfer including blowing rates 06 p0943 A67-18843

Control surface instabilities of lifting body configurations at very high speeds and with separated flows analyzed by wind tunnel tests for unsteady control surface load problems [AIAA PAPER 67-15] 07 p1258 A67-19430

Boron filament epoxy resin composites test program relative to mechanical design of reentry vehicle 08 p1345 A67-20424

Fabrication of complex hollow rib reinforced structures of wound boron filaments and anhydride cured epoxy resin for reentry vehicle application 08 p1345 A67-20435

RF bridge technique determining electric conductivity of plasma sheath around reentry vehicle 08 p1366 A67-21514

Wind tunnel model for analysis of autorotating rotors for reentry space vehicles tested at transonic and supersonic regimes 09 p1440 A67-22285

Shortcomings in complex reentry system design caused by human factors 09 p1456 A67-22290

Reentry vehicle heatshield materials including graphite, ablative reinforced plastics, etc 10 p1672 A67-23721

Low density shear resistant ablators for lifting reentry vehicles 10 p1672 A67-23725

Transmission and reception properties of equatorial slot antenna on plasma clad reentry sphere 11 p1757 A67-23973

Lifting reentry vehicles for achieving orbital plane changes by synergetic maneuvers [AIAA PAPER 66-960] 13 p2212 A67-26846

Blunt nosed reentry vehicle model with skewed magnetic field investigated in magnetoaerodynamic flow for possible bow shock distortion 14 p2244 A67-29049

Launcher for research and development on aerodynamic reentry 15 p2564 A67-29094

Tension string structure of high strength filaments for ultralightweight planetary entry vehicle 15 p2573 A67-29420

Weight and cost comparative analysis of ablative and combined ablative/radiative heat shields for SV-5 and SV-32 lifting reentry vehicles [AIAA PAPER 66-990] 15 p2564 A67-29421

Optimum entry vehicle design using aerobreaking for manned earth entry at hypersonic speeds, examining blunted conic, biconic and tetrahedral configurations [AIAA PAPER 66-489] 15 p2564 A67-29422

Ballistic reentry vehicle recovery via low

speed water impact or air snatch after vehicle has flown unperturbed trajectory down to altitude of maximum dynamic pressure 15 p2564 A67-29424

Nose bluntness effect on hypersonic unsteady aerodynamics of ablating flared or conical slender reentry vehicles 15 p2416 A67-29442

Oxidation resistant-coated refractory alloy systems for use on reentry vehicles 15 p2466 A67-29537

Coated refractory metals thermal emittance measured at high temperatures for design of reentry vehicle under time-temperature-pressure profile 15 p2503 A67-29546

Land recovery of launch vehicles, applying intersecting pressure vessel theory for shaping of tanks and hinged tail panels 15 p2569 A67-29852

Aerodynamic heating about vehicle entering atmosphere for corridor and guidance requirements analyzed on basis of Newton two-body problem 15 p2417 A67-30046

Potential requirements imposed upon ranges and networks by future unmanned reentry vehicles [AAS PAPER 67-35] 15 p2571 A67-30107

Manned spacecraft design, discussing range hardware and software development and future entry vehicle programs [AAS PAPER 67-36] 15 p2571 A67-30108

Reentry vehicle roll resonance criterion formulation for predicting roll conditions, noting vehicle configuration, aerodynamic and trajectory parameters, exoatmospheric vehicle attitude, etc 15 p2572 A67-30211

Synthesis of optimal linear control system coupled with vehicle configuration design technique for guidance parameters and temperature accumulation along optimum entry trajectories 16 p2758 A67-30660

Equilibrium radiative transport properties of high temperature air coupled with aerodynamic flow field generated by planetary reentry vehicles 16 p2589 A67-30721

Precomputed approximation to weighting matrix in extended Kalman filter for ballistic reentry vehicle trajectories estimation 16 p2651 A67-31682

Reentry trim angle of attack and lift-drag ratios from Gemini flights compared to wind tunnel data for aerodynamic studies [AIAA PAPER 67-166] 17 p2789 A67-32061

Cross sectional variation effects on velocity potential evaluated using slender body theory 17 p2789 A67-32067

Inertial navigation horizontal position errors for medium L/D lifting body reentry vehicle using reference altitude for vertical channel stabilization 17 p2881 A67-32476

Reentry vehicle heat shield materials thermal diffusivity measurements by flush method, using pulsed laser and xenon flash lamp 18 p3051 A67-34506

Lift-drag ratio, lift and drag coefficients and angle of attack effects on Gemini and Apollo reentry vehicles measured in shock tunnel under free flight conditions [AIAA PAPER 67-165] 19 p3169 A67-34818

Heating restraints effect on aeroglide and aerocruise synergetic maneuver performance investigated for high lift-drag ratio vehicle [AIAA PAPER 67-169] 19 p3332 A67-34831

Velocity and altitude at bottom of first plunge for reentry-vehicle pitch-plane maneuvers compared with digital simulation 20 p3532 A67-36577

Plasma arc deposition and gas pressure bonding technique for producing defect-free uniform iridium protective coatings for graphite reentry structures 20 p3465 A67-36607

S-10 and S-20 image orthicon tubes evaluated for radiometric measurements against reentry vehicles, considering radiometric response, resolution and calibration stability 20 p3452 A67-37311

Recovery site location importance in determining entry vehicle future requirements 21 p3607 A67-37804

Vaporizing solid or liquid underlayers for transpiration cooling of reentry vehicles, discussing advantages, handling, storage and self-regulating system 22 p3901 A67-39934

Reentry vehicles heat protection design emphasizing composite material selection/development for coating within acceptable weight limitations 22 p3902 A67-39938

Manned lifting reentry vehicle

optimization using Optimum Compromise between Conflicting Operational Factors /OCCOF/ computer 22 p3902 A67-39947

Reentry vehicle surface pressure measurement, obtaining accuracy and reliability in stable high level pressure transducer 23 p4006 A67-41378

Aerodynamic power and moment coefficients of space-transport configurations for hypersonic reentry and trajectory calculations 23 p3931 A67-41399

Reentry vehicle solid propellant and liquid fuel compact turboalternator electric power system operating characteristics and performance 24 p4108 A67-42534

Materials and structural concepts for design of entry systems, discussing environmental factors, reuse potential and high reliability [AIAA PAPER 67-805] 24 p4251 A67-42964

Reentry vehicle design characteristics and requirements for safe reentry of radioactive power sources, discussing heat protection systems [AIAA PAPER 67-966] 24 p4246 A67-43044

REFERENCE SYSTEM

SA INERTIAL REFERENCE SYSTEM

SA SPACE REFERENCE SYSTEM

Adaptive model reference systems without extremum search 07 p1160 A67-19198

Model reference control systems design using Liapunov synthesis technique 07 p1162 A67-20203

Synthetic target scenes generation technique by general purpose digital computer for early analytical evaluation of sensor concepts 11 p1791 A67-24456

Astronomic data error effect on position of reference surface trigonometric net with regard to earth axis of rotation 11 p1787 A67-24593

State space methods approach to model referenced adaptive control systems design using differential equations 11 p1771 A67-24894

Reduction of order technique pertaining to plant and reference model in controller design for linear plants transfer functions with zeros and slowly varying parameters 11 p1771 A67-24895

Longitudinal target defocusing effect on solar reflector power parameters, noting energy redistribution phenomenon 12 p1896 A67-25323

Holography applied to radio frequencies, noting recording technique with locally produced reference wave 13 p2119 A67-26518

Integration of Einstein gravitational equations implies that corpuscle be rigidly connected with particular Fermi space-time system of reference 13 p2158 A67-27298

No appreciable systematic differential motion between nearby neutral hydrogen and stars determined from measurement of relative velocity of former with respect to sun 17 p2943 A67-32443

Comparison of lunar limb profiles referred to system of reference points and limb region maps, giving data conversion formulas and map inaccuracies 17 p2949 A67-33124

Smithsonian Astrophysical Observatory Differential Orbit Improvement program for lunar orbits, with selenocentric reference system 18 p3132 A67-34327

Energy-momentum density and superpotentials in privileged frame of reference, giving results due to Einstein and Freud pseudotensors 19 p3261 A67-35048

Satellite orientation sensing and orbital gyrocompassing heading reference, examining effect of horizon sensor noise [AIAA PAPER 67-587] 19 p3258 A67-35983

Book on star trackers and systems design including technology, use for navigation and guidance, reference frames, error sources, atmospheric effects, etc 20 p3481 A67-36136

Azimuth and zenith distance determined from simultaneous observations of topocentric coordinates of artificial satellite transformed into astronomical and geodetic quantities 20 p3428 A67-36483

Propagation rate of electromagnetic and gravity wave front in synchronous reference system in Riemann space 20 p3486 A67-37554

Ultrareliable six redundant sensor attitude reference system for Manned Orbital Laboratory /MOL/ with limited sparring capability 21 p3624 A67-37786

Differential correction vectors for non-

Keplerian reference orbits, reexamining rotating ellipses in Hansen type intermediaries 21 p3705 A67-38612
 Generalized Lorentz transformation for inhomogeneous region in general relativity obtained by transformation leading to nearly straight system of reference 23 p4028 A67-41187
 Galilean invariance principle used to analyze system of multicomponent MHD equations to select reference system describing motions and transfer processes across magnetic field 24 p4197 A67-42351
 Hologram technique using reference beam totally reflected from air-emulsion boundary of hologram plate permits close spacing 24 p4156 A67-42362

REFINING

SA CLEANING

SA PURIFICATION

SA ZONE REFINING

Refining, forming and utilization of metals, discussing high pressure forming, vacuum degassing and superplasticity 03 p0440 A67-13198
 Iodide refining of vanadium, presenting internal friction and shear modulus curves for estimating interstitial impurity concentrations 19 p3243 A67-34924

REFLECTED RAY

Far IR reflection spectra of silicate mineral at room and liquid nitrogen temperatures [AIAA PAPER 65-668] 03 p0508 A67-13048
 Reflected light microscope for viewing unstained brain and ganglion cells 18 p2991 A67-34530
 Cloud measurements from Gemini 5 from reflected solar radiation spectra of oxygen A band region 22 p3807 A67-40369
 Dual beam bidirectional reflectance attachment permitting sample plane tilting in spectroscopic measurements 23 p4002 A67-41261
 Hologram technique using reference beam totally reflected from air-emulsion boundary of hologram plate permits close spacing 24 p4156 A67-42362

REFLECTED WAVE

Heat transfer to end wall of shock tube behind reflected shock wave in oxygen dissociated to varying degrees and at high temperatures 04 p0729 A67-15813
 Submillimeter wavelength electronic devices, examining development of lasers and reflected wave tubes with overlapping effective wave range 05 p0825 A67-17168
 Optimal signal transmission in detection system characterized by optimal linear filtration of reflected signal 06 p0963 A67-18216
 Ionospheric plasma density determined by phase difference of incident waves on and reflected from plasma 07 p1173 A67-19701
 Silicon oxide film thickness determined from intensity of reflected light 09 p1553 A67-21954
 Reflection of spherical shock wave from concentric spherical surface, using method of characteristics starting from initial boundary value problem 10 p1623 A67-22863
 Acoustic waves omnidirectional scattering by rough imperfectly reflecting surfaces analyzed using physical optics method 10 p1680 A67-23314
 Relativistic solution to normal incidence on semiinfinite longitudinally drifting homogeneous temperate magnetoplasma, obtaining reflected and transmitted waves 11 p1832 A67-24304
 Dynamic behavior model for gas shock wave motion and reflection in semiinfinite volume laterally bounded 11 p1782 A67-24954
 Conditions controlling shock wave reflection from duct end deflector plates, determining spacing of plates from pipe 12 p1928 A67-25356
 Parameters of gas behind incident and reflected shock waves calculated, using gas dynamic and chemical equilibrium equations for one-dimensional problem 12 p1930 A67-26134
 Asymptotic curve for single arbitrary reflection of atom from plane with weak surface roughness, calculating total momentum and energy fluxes 14 p2351 A67-28636
 Optimal signal transmission in detection system characterized by optimal linear filtration of reflected signal 16 p2620 A67-30482

Boundary layer effect on primary wave propagation and gas states behind reflected wave in shock tube with nozzle 17 p2837 A67-32346

Ionospheric irregularity effect on lateral deviation of reflected radio waves from ionosphere, noting variation with solar activity 18 p3004 A67-34617
 Interactions produced by shock wave running into magnetic field perpendicular to wave direction 19 p3294 A67-35405

Focused image holograms, amplitude-or phase-recorded, reconstructing sharp images by reflection from incoherent illumination 20 p3435 A67-36201
 Ethylene-oxygen reaction in shock waves, studying induction period and time dependency of mixture composition, ionization and chemiluminescence 20 p3376 A67-36232

White light reflection holography, discussing recording, reconstruction and color images 20 p3438 A67-36349

Ultrasonic and line reversal methods for measuring gas temperatures behind reflected shock waves 21 p3624 A67-37740
 Shock tube measurements of end-wall radiative heat transfer behind reflected shock waves in air, stressing radiative cooling and self-absorption effects [AIAA PAPER 67-695] 21 p3732 A67-38724
 Ionization gauge circuit for studies of solid explosives initiation by gaseous detonation waves and reflected wave trajectories in shock tunnels 21 p3630 A67-38770

Radiative cooling and self-absorption effects on reflected shock flow field and end wall heat transfer studied using finite difference method 22 p3917 A67-39710
 Re-reflected shock wave from convergent cylindrical channel, showing secondary shock wave overtaking primary wave 22 p3783 A67-39720

REFLECTING TELESCOPE

All-mirror Schmidt telescope system for space research providing easier switchover from photography to slitless spectroscopy 10 p1657 A67-23561
 Spectra broadening mechanism on reflector of Vilnius Observatory 18 p3044 A67-33659
 Optics for Queen Elizabeth II telescope noting design, tolerance, quartz mirror and test procedures 23 p4001 A67-41257

REFLECTION

S INFRARED REFLECTION
 S IONOSPHERIC REFLECTION
 S OPTICAL REFLECTIVITY
 S RADIO REFLECTION
 S SIGNAL REFLECTION
 S SOLAR RADAR REFLECTION
 S SPECTRAL REFLECTANCE
 S SPREAD REFLECTION
 S ULTRAVIOLET REFLECTION
 S WAVE REFLECTION

REFLECTION COEFFICIENT

Spectral reflectance coefficients for meadow grass, birch tree and lilac leaves, brick, sand, concrete and snow in region 0.7 to 0.5 microns 01 p0107 A67-10128
 Electromagnetic reflection and transmission coefficient maxima in bounded plasma slab 01 p0022 A67-10443
 Sound propagation in streaming air within tubes having changes of cross section and flow losses, discussing reflection coefficient dependence on flow velocity 01 p0114 A67-10819
 Mode transformation due to slightly tilted waveguide tube treated as boundary value problem 01 p0040 A67-11233
 Simulation of curvature in straight model earth-ionosphere waveguide, using planar structure loaded by inhomogeneous dielectric 01 p0040 A67-11310
 Geomagnetic field effect on radio signal in oblique reflection sounding, noting differences between daylight and night measurements 02 p0193 A67-11662
 Engineering method of calculating Fresnel coefficients based on use of nomograms 02 p0266 A67-11910
 Reflection coefficient of tapered waveguide determined via coupled mode theory, noting error estimation and design of reflectionless tapers 03 p0376 A67-12802
 Value and sign of phase jump taking place during light reflection from multilayer dielectric film 03 p0467 A67-12892
 Successive approximations for determining

direct and backward wave in inhomogeneous medium and consequently reflection coefficient and total field 03 p0467 A67-12893

Directional reflective coating consisting of cylindrical dielectric fibers oriented perpendicular to absorbing substrate [AIAA PAPER 65-871] 03 p0467 A67-13039
 Curvature effect on reflection coefficient of layered absorbers, examining backscattering from coated cylinder and sphere 03 p0370 A67-13852

Semiconductor character of mercury selenide determined by analyzing variation of band-edge effective mass as function of composition of HgSe-CdTe alloys 03 p0499 A67-13886

Passive core fiber laser does not remove completely need for optical quality in cladding material 05 p0821 A67-16666

One-dimensional inverse problem of scattering theory, noting differential equation reduction, determining traveling wave coefficient 05 p0765 A67-17158

Reflection coefficients of plasma waveguide measured by determining wave modulation coefficients 06 p1039 A67-18083

Value and sign of phase jump taking place during light reflection from multilayer dielectric film 06 p1034 A67-18770

Successive approximations for determining direct and backward wave in inhomogeneous medium and consequently reflection coefficient and total field 06 p1034 A67-18771
 Nonequilibrium effects on shock wave reflection coefficient 06 p0992 A67-18885

Coefficient of reflection of H-11 mode shock wave emitted from aperture of circular waveguide with infinite flange 08 p1302 A67-20825

Twofold phase modulation in meters of microwave reflection and transmission coefficients 08 p1295 A67-21276

Measuring techniques and limitations as related to small reflections in precision coaxial transmission line 09 p1495 A67-21624

Radar observation of Mars, noting mean reflection coefficient for signals returned by near center disk sections 09 p1563 A67-21632

Line profiles and equivalent widths for diffuse reflection of sunlight from model planetary atmosphere calculations, using invariant imbedding 10 p1710 A67-23635

Free electron density and effective collision frequency of ionized argon in wake of shock wave measured, using microwave probe methods 11 p1775 A67-24017

Computer method study of reflection and transmission coefficients in VLF range, noting effect of ionospheric D region electron density profiles 11 p1752 A67-24219

Impedance of strip antenna embedded in dielectric layer overlain by cold plasma, considering reflection coefficient and static magnetic field effect 11 p1763 A67-24305

Reflection coefficient of parabolic reflector antenna illuminated by horn radiator with sector shaped radiation pattern 11 p1767 A67-24716

Tin oxide films in microscopic quantities on glass and quartz substrates studied for transparency, reflectivity and roughness 12 p1982 A67-25324

Reflectance, transmittance and absorbance of muscovite type mica as function of thickness measured, using prism and grating spectrophotometers [AIAA PAPER 67-288] 12 p1958 A67-26005

Reflectance function for stainless steel with various surface roughnesses, comparing incident and reflected monochromatic fluxes of assigned directions [AIAA PAPER 67-321] 12 p1957 A67-26036

Reflection coefficients for electromagnetic waves obliquely incident on sinusoidally stratified half-space 13 p2066 A67-26481

Lambert diffuse reflection from general quadric surfaces 13 p2158 A67-26877

IR radiation detection by doped semiconductor with induced reflectivity variation 13 p2181 A67-27231

Reflection coefficient and separation of real and imaginary parts of optical index in nonmetal band-to-band transition model semiconductor 14 p2364 A67-27956

Reflection coefficient for electromagnetic waves incident at various angles on plane laminar medium of lunite 15 p2552 A67-29150

Electromagnetic wave diffraction by infinite set of parallel metallic plates, obtaining exact solution by Wiener-Hopf technique 15 p2435 A67-29191

- Normal modes for solid state laser noting linear and elliptic polarization, resonant frequency and reflection loss 15 p2497 A67-29388
- Reflectance of pyrolytic graphite and phenolic nylon chars for radiant heat rejection from nonablating heat shield 15 p2579 A67-29434
- Mitchelson interferometer with laser source analyzed for beam frequency and wavelength, refraction coefficient, etc 15 p2486 A67-29467
- Reflection coefficient for electromagnetic wave in circular cylindrical shock tube incident on moving plasma calculated numerically 15 p2531 A67-29905
- Influence of spread-F upon apparent reflection coefficients of F region for HF radio waves [AGARDOGRAPH 95] 15 p2481 A67-30279
- IR modulator utilizing field-induced free carrier absorption, with expressions for modulation index in terms of geometrical and physical properties of materials 15 p2491 A67-30428
- Geomagnetic field effect on radio signal in oblique reflection sounding, noting differences between daylight and night measurements 16 p2624 A67-31077
- Optical reflection spectra of GaS, GaSe, and GaTe single crystal semiconductors in electron volt band energy range 16 p2730 A67-31159
- Scattering of surface wave incident upon junction of two semi-infinite planes joined together by step analyzed using Wiener-Hopf equation 16 p2626 A67-31348
- Coaxial and magnetohydrodynamic waveguide matching obtaining reflection coefficient of former and wave amplitude of latter 16 p2722 A67-31575
- Reflection coefficients of sharply bounded ionosphere for plane waves incident from arbitrary direction at magnetic equator 16 p2632 A67-31863
- Reflectance and optical constants of evaporated iridium films measured in vacuum ultraviolet 16 p2733 A67-31878
- Plasma produced transit time delay of reflected pulses for collisionless inhomogeneous plasma 17 p2810 A67-32070
- Transmission coefficient associated with internal reflection from absorbing surface layer derived from reflection coefficient, noting relation to absorption 17 p2883 A67-32204
- Optical properties of Mg layers evaporated in ultrahigh vacuum, noting results of reflectivity measurements 17 p2913 A67-32292
- GaAs laser reflectance measurements of tactical landing terrain 17 p2858 A67-32483
- Impedance and reflection coefficient measurement in uniconductor waveguide noting experimental techniques, coefficient standards, etc 17 p2815 A67-32606
- Swept measurement techniques, discussing reflection coefficient and slotted line accuracy using signal flow graph 17 p2815 A67-32610
- Photo-induced microwave response of SbSI crystals to variations in reflection coefficient indicates photodielectric effect 17 p2915 A67-32675
- External mutual coupling of rectangular waveguide-slot emitters, deriving coefficient of reflection 17 p2826 A67-32683
- Frequency variation of ruby laser optically pumped by flash lamp, noting effect of phthalocyanine solution 17 p2868 A67-32705
- Nonuniform RC lines with hypergeometric and spheroidal wave functions solutions, calculating driving point impedance 19 p3190 A67-34840
- Electromagnetic wave reflection by stratified magnetoplasma, obtaining formulas providing perturbation effect on reflection coefficients 19 p3183 A67-35457
- Laser mirror transmissivity optimization in high power optical cavities noting reflection coefficient selection 19 p3241 A67-35701
- Squinted, sum and difference radiation patterns interrelationships for amplitude monopulse antennas with impedance mismatch and mutual coupling between feeds 19 p3197 A67-35824
- Ionospheric radio-wave absorption measurement by multiple and single echo techniques, applying vertical probing at fixed frequencies 20 p3378 A67-36124
- Excitation of earth-ionosphere waveguide by VLF source for case of azimuth dependent properties of source and ionosphere 20 p3428 A67-36373
- Fabry-Perot resonator with nonuniform reflectors, analyzing resonant modes amplitude/phase distribution and diffraction/reflection losses 20 p3447 A67-36767
- Complex reflection coefficient for finite-width boundary used for plasma diagnostics in high electron-density range, discussing modeling errors 20 p3499 A67-36959
- Density and recombination coefficients of nonequilibrium carriers in Ge and GaAs as function of laser excitation 20 p3513 A67-37437
- Reflection in water of plane shock waves from rigid wall 21 p3611 A67-38058
- Mitchelson interferometer with laser source analyzed for beam frequency and wavelength, refraction coefficient, etc 21 p3628 A67-38548
- Radar type instrument for measuring reflection coefficients of planetary surfaces from unmanned spacecraft 22 p3795 A67-39159
- Reflection coefficient for arbitrary lossy waveguide with large number of identical periodically positioned inhomogeneities determined by iteration 22 p3770 A67-39661
- Plane electromagnetic wave reflection from ionization front, determining coefficient from finite thickness plasma layer and constant charged particle density 22 p3762 A67-40122
- LiF freshly cleaved crystal reflectance spectrum between UV and 28 ev, computing dielectric response function and measuring gamma excitation band 23 p4038 A67-40774
- Electromagnetic pulse distortion during total internal reflection in stratified troposphere, discussing reflecting medium inhomogeneity effects on reflection coefficients 23 p3973 A67-40837
- Reflection coefficient determined for plane monochromatic electromagnetic wave incident on idealized laminar plane stratified jet stream, deriving Riccati type differential equation 23 p3974 A67-41201
- Energy distribution deviation of electrons emitted from plasma or solid via Maxwell distribution, deriving kinetic reflection coefficient in thermionic emission current expression 23 p4047 A67-41688
- Longitudinal mode generation in ruby laser emission operating in single pulse regime with resonant mirror reflector 24 p4169 A67-42894
- Reflection coefficient for electromagnetic waves incident at various angles on plane laminar medium of lunite 24 p4239 A67-43073
- REFLECTOMETER**
- Time domain reflectometry in reliability testing, detailing applications in checkout of electroexplosive devices with spark gap and cable validation equipment 01 p0084 A67-11361
- Vacuum integrating sphere for in situ spectral reflectance measurements of carbon dioxide cryodeposits from 0.5 to 10 microns [AIAA PAPER 67-298] 12 p1926 A67-26013
- Bidirectional spectrorreflectometer for reflectance of solid and powder samples [AIAA PAPER 67-313] 12 p1946 A67-26028
- Blockage effects of centrally located sample on reflectance measurement by modified integrating sphere [ASME PAPER 67-HT-54] 20 p3447 A67-36736
- Reflectometer based on goniometer design employing beam reversal and beam splitter for measuring exit beam intensity 20 p3448 A67-36955
- REFLECTOR**
- SA BEAM SPLITTER
- SA FRESNEL REFLECTOR
- SA MIRROR
- SA PARABOLIC REFLECTOR
- SA RADAR REFLECTOR
- SA SOLAR REFLECTOR
- Reflecting surface geometry calculated by reflection and scattering of light source 02 p0268 A67-12446
- Asymptotic evaluation for k approaching infinity of antenna field emerging from currents induced on surface of reflector with incident spherical wave 02 p0223 A67-12796
- Regenerative radiation from neon line in He-Ne laser, using spherical reflectors in resonator 03 p0434 A67-13096
- Monostatic scattered ultrasonic wave calculated as function of distance of reflector projection from source 03 p0369 A67-13551
- Arbitrary reflector array of Van Atta type analyzed for dipole elements 03 p0384 A67-13845
- Reradiation pattern of Van Atta reflector consisting of half-wave dipoles 03 p0384 A67-13846
- Relation between reflector surface shapes, heat collector and intensity of geometric concentration of parallel ray flux 04 p0553 A67-14665
- Synphase antenna with broadband active reflector 05 p0778 A67-17394
- Increasing effective area of radio telescope antenna by decreasing scattering on struts 08 p1318 A67-21347
- Radio telescope with spherical reflector and re-emitter placed in mirror focus 08 p1319 A67-21349
- Spherical reflector radio telescope design, performance and application, describing parameters of Tokyo, Lockheed, Nancay and Arecibo 14 p2284 A67-28432
- Helical antenna radiation characteristics under backfire operating conditions, noting improvement over endfire conditions 14 p2290 A67-29008
- Large aperture, low noise, steerable antennas for ground station commercial satellite communication networks 16 p2641 A67-31532
- Increasing effective area of radio telescope antenna by decreasing scattering on struts 17 p2831 A67-31943
- Radio telescope with spherical reflector and re-emitter placed in mirror focus 17 p2832 A67-31945
- Reflex klystron for 1.5 mm wavelength noting high current density cathodes, RF section simplification and better heat dissipation 22 p3768 A67-39493
- Moon-earth distance and moon-earth system astrometric parameters by laser ranging, describing artificial light reflector design 23 p4066 A67-41037
- REFLECTOR SATELLITE SYSTEM**
- Solar radiation increase using orbiting reflector satellite, discussing illumination capability [AAS PAPER 67-118] 15 p2570 A67-29964
- Solar radiation pressure perturbations on large planar reflector satellite orbit 22 p3903 A67-39953
- Orbiting reflector satellites, concepts, design, structural mechanizations and control [AIAA PAPER 67-786] 24 p4242 A67-42949
- REFLEX**
- S CAROTID SINUS REFLEX
- S CONDITIONED RESPONSE
- REFRACTED RAY**
- Transition functions occurring in diffraction theory of plane stratified medium with increasing refractive index 14 p2349 A67-29063
- Appearance of extraordinary rays from double refraction in ruby laser crystals with polished rectangular prisms 20 p3507 A67-36330
- Spherical electromagnetic wave refraction on heterogeneous parabolic plasma layer using beam optics 22 p3760 A67-39737
- REFRACTING TELESCOPE**
- Telescope optics techniques for compensation for lateral color aberration arising from atmospheric refraction, using modified Schupmann medial telescope 06 p1033 A67-18535
- Thermal perturbations on fused silica primary mirror in orbiting space telescope, with numerical analysis of radiation transfer in telescope tube 18 p3046 A67-33880
- Solar prominence activation on March 25, 1967 observed with H-alpha visual patrol refracting telescope at Anacapri 23 p4060 A67-41234
- REFRACTION**
- SA ABERRATION
- SA ATMOSPHERIC REFRACTION
- SA RADIO WAVE REFRACTION
- SA STELLAR REFRACTION
- Radial electron density distribution in induced pulsed discharge from wave refraction in planes passing through and normal to plasma cylinder axis 02 p0278 A67-12624
- Transverse wave behavior in reactive flow, analyzing refraction or reflection of acoustic waves at shock front, obtaining comparison

of behavior in corresponding real flows 03 p0405 A67-14026
 Mathematical methods for two classes of variational problems analogous to optical reflection and optical refraction in connection with rocket flight 10 p1678 A67-23425
 Radial electron density distribution in induced pulsed discharge from wave refraction in planes passing through and normal to plasma cylinder 13 p2171 A67-27380
 Mean flow refraction and temperature differences between mixing layer and outside fluid effect on HF component of jet noise 19 p3173 A67-34962

REFRACTIVE INDEX

Optical and magneto-optical phenomena in CdSnAs sub 2, discussing reflection and absorption spectrum, optical activity, double refraction, dielectric constant, etc 01 p0128 A67-10094
 Graphical calculation of wave refraction in dry atmosphere between 0.4 and 13 microns 01 p0108 A67-10129
 Optical characteristics, including refractive indices, of thin layer amorphous titanium oxide films 01 p0115 A67-11048
 Tropospheric and ionospheric models and parameter variations affecting satellite signal propagation, discussing refractive corrections 01 p0028 A67-11431
 Optical constants of silver solid solutions with gold addition, noting dependence of refractive index, absorption coefficient and conduction electrons on impurity concentration 02 p0255 A67-11870
 Fluctuations of refraction index of surface layers of atmosphere observed directly in daytime and parameters of fluctuation distribution 02 p0325 A67-11985
 Inverse optimization for calculating refractive index and electrical resistivity of plasma in reentry and surface tension coefficient in ephydrodynamics 02 p0333 A67-12347
 Ruby laser generation from two R lines by prismatic light dispersion in resonator 03 p0433 A67-13095
 Dispersion of refractive index of NO in fundamental vibration-rotation band 03 p0468 A67-13473
 Lasers used to extend RF plasma diagnostic procedures to optical frequencies by interferometric and Thomson diffusion methods 03 p0477 A67-13474
 Polarized radiation measurements of far IR absorption coefficient and refractive indices in lithium niobium oxide 03 p0496 A67-13571
 One-dimensional refractive index distribution using power series expansions for refractive index and ray traces obtained from relation of inhomogeneities and interference pattern of Mach-Zehnder interferometer 03 p0423 A67-13908
 Optical properties of evaporated barium films investigated at various wavelengths, using ultrahigh vacuum reflectometer 03 p0499 A67-13909
 Faraday fading rate of satellite signal as calculated from Appleton-Hartree formula for refraction index /without collision/ near transverse propagation [RASSA PAPER 1-10-127] 03 p0372 A67-14238
 Radio data suggests dielectric constant variations in troposphere limited to discrete scale sizes [RASSA PAPER 1-10-141] 03 p0417 A67-14249
 Random tropospheric angle error prediction in microwave observations of Early Bird satellite 04 p0574 A67-15074
 Electromagnetic wave propagation along confocal lens line for variable refractive index of ambient medium 04 p0575 A67-15150
 Radar probe of clear atmosphere confirming detectability of birds, insects and irregularities in clear air refractivity 04 p0650 A67-15172
 Seismic refraction measurements, computing statistics for depth to Moho, crustal thickness and upper mantle velocity for geographical and geological provinces 05 p0796 A67-16152
 Fluctuations of angle of incoming light waves from distributed source in atmosphere with turbulent pulsations of refractive index 05 p0761 A67-16346
 Self-focusing due to intensity dependent anomalous dispersion effect on electromagnetic radiation, emphasizing laser

radiation in saturated amplifying medium 05 p0819 A67-16649
 Frequency modulation of GaAs semiconductor laser by ultrasonic wave modulation of dielectric constant 05 p0821 A67-16671
 Density dependence of refractive index of air and phase and group refractive index as function of pressure, temperature and composition 05 p0838 A67-16783
 Thin film refractive index and thickness calculated by ellipsometry 05 p0847 A67-16796
 Self-focusing and self-trapping of intense light beams in nonlinear medium examined, using approximations of geometrical optics and accounting for diffraction effects 06 p1031 A67-17880
 Mariner Venus 1967 space probe, obtaining atmospheric pressure density and refractive index from radio signal frequency, intensity and phase changes [AIAA PAPER 67-118] 06 p1085 A67-18310
 Optical properties of interstellar grains, noting complex index of refraction as function of wavelength 06 p1087 A67-18410
 Geometrical light rays in lens-like media and derivation of differential equation 06 p1033 A67-18534
 Multiple scattering of light in turbulent atmosphere noting relation to refraction index and power spectra, using Born series solution to wave equation 06 p1033 A67-18536
 Log amplitude covariance for horizontal and nonhorizontal propagation path of plane wave through turbulent atmosphere, noting refractive index effect 06 p1033 A67-18537
 Plane wave scattering by medium with strong fluctuations of refractive index, noting reentry condition 07 p1141 A67-19441
 Electric field induced optical refractivity changes /Franz-Keldysh effect/ and nonlinear light scattering, light beam deflection and modulation in neutron-irradiated Si at 95 degrees K 07 p1231 A67-19487
 Gas lens focusing of light beams, using highly transparent gas with weakly varying refractive index to guide coherent transmission with small losses 07 p1188 A67-19789
 Light waves traveling backward and forward in very small filaments of optical material result in standing waves producing visible spatial beats, allowing detection of changes in refractive index 07 p1224 A67-19841
 Space environment effect on refractive optical systems, particularly solar radiation effect on optical properties of glass 08 p1330 A67-20644
 Geometric analysis of refractive index, absorption index and polarization characteristics of ionospheric radio waves 08 p1295 A67-21168
 Wave propagation in random medium analyzed by solving stochastic wave equation with random function for refractive index coefficient and applied to laser beam 08 p1296 A67-21434
 Ionized medium effect on synchrotron emission spectra in solar corona proposed to account for LF cut-off in type IV radio bursts 08 p1402 A67-21464
 Integral equation for propagation of second order correlation function assuming statistical independence of wave function and refractive index fluctuations 09 p1460 A67-21594
 Effect of weak random inhomogeneities on long distance wave propagation, calculating first two statistical moments 09 p1461 A67-21595
 Scattering of coherent and incoherent light compared, using CW He-Ne gas laser sources 09 p1510 A67-21600
 Envelope and phase velocities for laser pulse propagating in nonlinear dielectric with intensity dependent index of refraction 09 p1511 A67-21748
 Transmission of artificial quartz at room temperature, obtaining optical constants in far IR region 09 p1553 A67-21917
 Ionospheric absorption effects in D and E layers, noting refraction role and effective collision frequency 10 p1646 A67-23270
 Radar echoes from cloud-free atmosphere caused by turbulent pulsations of microwave refractive index 10 p1677 A67-23500
 Refractive index of microwave lenses made of ferrite material changed by varying DC magnetic field 11 p1752 A67-24125

Mutual coherence factor for plane electromagnetic wave propagating in stochastic locally homogeneous and isotropic medium of dielectric turbulence 11 p1818 A67-24415
 Irregular refraction of radio waves by large ionospheric inhomogeneities elongated close to meridional direction 11 p1787 A67-24477
 Models of reflection nebulae light for single scattering, pure or modified by internal nebular extinction, on spherical grains imitating dielectric or metallic particles 11 p1861 A67-24487
 Radio refractive index irregularities in lower troposphere examined, using helicopter mounted spaced cavity refractometer 11 p1787 A67-24644
 Multiply reflective laser detector diode design, showing internal reflection effect for trapping light in silicon due to large refractive index 11 p1802 A67-24737
 Undetermined coefficient method compared with confluent hypergeometric functions for solving first order perturbation equation for refractive index of He 11 p1813 A67-24787
 Plane electromagnetic wave reflection and refraction by sem infinite dielectric medium moving uniformly parallel to surface analyzed for arbitrary incidence plane orientation 11 p1820 A67-24909
 Fracture line formation in glass specimen as result of laser beam focusing, noting refractive index variation 12 p1951 A67-25148
 Reflectance, transmittance and absorptance of muscovite type mica as function of thickness measured, using prism and grating spectrophotometers [AIAA PAPER 67-288] 12 p1958 A67-26005
 Coulomb long range interaction effect on refractive index dependence on light frequency and on absorption lines shape of dipole active excitons 13 p2173 A67-26365
 Orographic factors effect on stratospheric pressure field, obtaining ascending vortical fluxes and heat input equations, discussing refractive index for atmospheric perturbations 13 p2112 A67-26672
 Transfer of large scale tropospheric perturbations into stratosphere analyzed using hydrodynamic model, noting role of atmospheric stratification, refractive index, etc 13 p2112 A67-26674
 Spectral characteristics of small scale refractive index fluctuations in troposphere using radar echoes 13 p2068 A67-26790
 Satellite and astronomical refraction determined from formulas for air refractive index determination 13 p2199 A67-26854
 Transmission of artificial quartz at room temperature, obtaining optical constants in far IR region 14 p2365 A67-28246
 Turbulent spectral density of radio refractive index in surface layer of atmosphere 14 p2262 A67-28379
 Tropospheric refractive index variation measurement technique 14 p2264 A67-28394
 Attenuation cross section and refractive index using collision theory, calculating resonance profiles of autoionizing lines based on scattering theory 14 p2351 A67-28811
 Optical properties of thin aluminum and silver layers subjected to proton beam bombardment 14 p2373 A67-28855
 Doppler effect application to solution of tracking problems with aid of artificial earth satellites 14 p2347 A67-28991
 Transition functions occurring in diffraction theory of plane stratified medium with increasing refractive index 14 p2349 A67-29063
 Reflection coefficient for electromagnetic waves incident at various angles on plane laminar medium of unit 15 p2552 A67-29150
 Electromagnetic wave propagation along confocal lens line for variable refractive index of ambient medium 15 p2435 A67-29337
 Region of air with slight variation in refractive index from surrounding air recorded by holographic technique 15 p2488 A67-29725
 Tables of Fresnel intensity reflectances from classical electrodynamics noting characteristics for amplitude minima, polarization maxima and 90 degrees phase difference [RE-TR-67-7] 15 p2518 A67-29769
 Magnesium fluoride double Rochon prism used as polarizer or analyzer in vacuum UV

wavelengths 15 p2491 A67-30425
Double exposure holographic formation of contour map over diffusely reflecting surface, using immersion method with liquids of different refractive indexes 16 p2670 A67-30612
Electromagnetic wave field probability distribution when scattering by medium with randomly varying refractive index 16 p2623 A67-30968
Refractive index dispersion of CdSe and CdTe crystals in visible and infrared spectral range at room temperature 16 p2732 A67-31481
Cosmic plasma flow effect on cosmic radiation polarization, deriving difference between normal waves refractive indices in two-component medium 16 p2628 A67-31494
Ellipsometer measurements to obtain estimates of refractive index and thickness of weakly absorbing isotropic, homogeneous slab 16 p2703 A67-31877
Reflectance and optical constants of evaporated iridium films measured in vacuum ultraviolet 16 p2733 A67-31878
Magnesium oxide and lithium fluoride in far UV, noting refractive and absorption indices 16 p2734 A67-31881
Refractive index of amorphous boron films determined from interference of transmission curves 16 p2734 A67-31884
Silicon oxide and nitride film thickness determined with interference technique, using spectrophotometer in UV and visible wavelength range 17 p2854 A67-32191
Refractive-index equation derived for electromagnetic wave propagation along static magnetic field in plasma motion direction, using relativistic transformations 17 p2812 A67-32304
Differential depressions of Iron I levels and red shifts of spectral lines under pressure, demonstrating error in assumed air refractive indices 17 p2886 A67-33162
Scattering theory for parameterization of absorption cross sections and refractivity for autoionizing spectral lines 18 p3082 A67-33878
Refractive index variations, Coulomb scattering and time variation of shower front effects on coherent emission of polarized radio pulses from cosmic ray showers 18 p3116 A67-34197
Frequency regions for Cerenkov radiation and power spectrum in collisionless magnetoplasma calculated using refractive index 18 p3090 A67-34428
Pump induced optical distortion in isotropic laser materials analyzed using Fermat principle, predicting ray refraction, beam divergence, etc 18 p3062 A67-34624
Pump radiation induced optical distortion in Nd-doped glass laser rods measured and compared to theory 18 p3062 A67-34625
Impurity effect on optical properties of interstellar graphite particles, examining wavelength dependence of absorption coefficient and refractive index of coals 19 p3323 A67-35423
Fluctuating light scattering cross section and Lorentz-Lorenz refractive index formula derived from microscopic equations 20 p3483 A67-36174
Tellurium nonlinear optical properties including absorption and refraction indices, discussing second harmonic radiation generation 20 p3507 A67-36324
Optical system using moire patterns to measure refractive index gradients in boundary layer, showing relation to temperature and density gradient [ASME PAPER 67-HT-3] 20 p3447 A67-36702
Algebraic equation for refractive index of arbitrarily directed oblique electromagnetic waves in compressible general magnetoplasma 20 p3499 A67-36944
Electromagnetic scattering from adsorbing spheres near resonances calculated from extinction efficiency factor and angular scattering function dependence on refractive index 21 p3656 A67-37856
Wave propagation in inhomogeneous half-space with refractive index depending on two coordinates analyzed, using parabolic equation method 21 p3580 A67-38114
Amplitude distributions of refractive index differences showing spikes superimposed on variations continuum due to water vapor clustering 21 p3617 A67-38187
Mariner Venus 1967 space probe, obtaining atmospheric pressure density and refractive index from radio signal frequency, intensity

and phase changes [AIAA PAPER 67-118] 22 p3886 A67-40094
Optically pumped vapor rotatory power as optical pumping experiment monitoring technique, discussing specific rotatory power and refractive index dependence on light frequency 22 p3816 A67-40320
Laser induced damage reduction in lithium tantalate and niobate crystals, proposing mechanism to explain observed reduction 23 p4012 A67-40876
Index of refraction measurements near damage spots in KTN due to laser beam and electric field simultaneous presence 23 p4013 A67-40895
Ar plasma refractive index measured at very high temperatures using gas laser 23 p4032 A67-40961
Stimulated Raman effects in calcite oscillator crystal, measuring gain index beta relative to Stokes wave 23 p4016 A67-41191
Light beam self-focusing, discussing electromagnetic interaction in nonlinear medium, refractive index dependence on wave intensity and geometrical optics 24 p4187 A67-41770
Graphical construction and electrical simulation for predetermining index and thickness of multilayer surfaces and filters 24 p4187 A67-41873
Electronic ellipsometer for measurement of very small changes in elliptically polarized light, discussing refractive index, Kerr effect and calibration 24 p4152 A67-41901
Optical measurement of atmospheric refractive index gradient showing approximate accuracy and simplicity for reasonably large gradients 24 p4188 A67-42093
Optical absorption, refractivity and electron scattering used to construct model dipole spectrum of molecular nitrogen and calculate dipole properties 24 p4190 A67-42096
ADP electro-optic crystal in laser emission control tested in beam deflection device and Michelson interferometer modulator, noting refractive index changes 24 p4187 A67-42239
Reflection coefficient for electromagnetic waves incident at various angles on plane laminar medium of unit 24 p4239 A67-43073
REFRACTOMETER
Microwave spaced-cavity refractometer for measuring small-scale variations of refractive index, wind speed, temperature, etc, in lower atmosphere 01 p0025 A67-10816
REFRACTORY ALLOY
Oxidation resistant thermal protection materials for 4000 degrees F high velocity air environment [SAE PAPER 660659] 01 p0094 A67-10617
Sintered Ni-base heat resistant alloys, discussing composition-creep strength relation, grain size, prealloyed-powder production and thermal and structural shock properties 01 p0098 A67-10700
Analytical model developed for using creep data at constant stress to predict creep behavior under linearly increasing stress 03 p0447 A67-13797
Continuous gas deposition of triniobium-tin alloy on moving refractory wire without reaction chamber contamination by by-products 03 p0500 A67-14065
Destruction of heat resistant alloys by repeated heating and cooling, deriving formulas which are applied to thermocyclic loads under conditions of stressed state 03 p0447 A67-14192
X-ray study of phase composition of refractory alloys carbide solid solutions noting hardness, electric resistance and elastic deformation energy of crystal lattice 04 p0638 A67-15205
Vacuum cup electrode in spectrographic analysis of solutions of refractory metal alloys 05 p0758 A67-16369
Refractory metal alloys rating on basis of weldability emphasizing metallurgical considerations, taking into account process control and welding as thermal process 05 p0830 A67-16829
Structure and certain properties of niobium-tantalum alloys containing tungsten and molybdenum show these alloying elements form continuous series of hard solutions 05 p0831 A67-17503
Cyclic load and temperature effects on creep behavior of Ni-base alloy Mar-M 200 between 1800 and 1900 degrees F 06 p1014 A67-17802

K-absorption spectrum of Ni as function of concentration of alloying elements and arrangement of atoms of alloying elements into Ni crystal lattice 06 p1017 A67-17952
Small additions of refractory elements effect on structure and properties of sheets of Al-Zn-Mg alloy in various states 07 p1201 A67-19254
Small additions of refractory elements effect on structure and properties of aluminum alloy castings containing Zn and Mg 07 p1201 A67-19255
Hall effect and electrical resistance of ZrC-NbC and TaC-HfC alloys at room temperature 11 p1804 A67-23904
Structural changes effect on creep resistance of heat resistant alloys 12 p1955 A67-25371
Continuous gas deposition of triniobium-tin alloy on moving refractory wire without reaction chamber contamination by by-products 13 p2185 A67-27721
Refractory carbides for high temperature applications, stressing use of metal-impregnated tantalum carbide [ONERA-TP-453] 15 p2502 A67-29378
Oxidation resistant-coated refractory alloy systems for use on reentry vehicles 15 p2466 A67-29537
Machinability of high strength steels, titanium alloys and refractory alloys, examining cutting and RF current induction for heat treatment 15 p2505 A67-30126
Refractory metal alloys tested in ultrahigh vacuum, measuring creep extension 16 p2690 A67-31524
Alloying principles for refractory metals based on softening mechanism, examining increased heat resistance of rhenium softened by recrystallization 16 p2691 A67-31589
Structure and certain properties of niobium-tantalum alloys containing tungsten and molybdenum show these alloying elements form continuous series of hard solutions 21 p3644 A67-38030
Soviet studies of Ni-and Fe-based heat resistant aging alloys and aircraft gas turbine technology 24 p4169 A67-41919
High temperature strength and magnetic properties of cobalt-tungsten alloy for space power generator rotors 24 p4174 A67-42726
REFRACTORY MATERIAL
SA CARBIDE
SA CERAMICS
SA CERMET
SA CORUNDUM
SA GLASS
Forming of refractory materials for rockets by explosive, magnetic and Dynapak forming and beam welding methods 01 p0079 A67-10638
Prolonged high temperature creep and endurance testing of refractory materials in vacuum or inert media 01 p0051 A67-11247
Rotating plasma furnace and application to spheroidization of refractory powders, noting arc source 02 p0228 A67-11503
Refractory ceramic and graphite fibers properties and strength in high temperature reinforcements 03 p0452 A67-13406
Reinforced pyrolyzed plastic composites for aerospace applications, noting high temperature stability and ease of utilization 03 p0443 A67-13415
Silicon carbide filament properties, fabrication and use as reinforcement of metal matrix composites, noting strength retention at high temperatures 03 p0445 A67-13439
High temperature reaction between refractory whiskers of silicon nitride and Al and Ni, observing results by electron microscopy 03 p0445 A67-13528
Nuclear rockets employing multiple exhaust nozzles, noting performance gain occurring because of high temperature capability of refractory nozzles [AIAA PAPER 66-925] 03 p0466 A67-14135
Metallurgical viewpoint of current status of porous refractory materials technology related to cesium contact ionizers 04 p0638 A67-15014
Wear and compatibility of liquid metal bearing materials, including surface coatings and cemented refractory carbides, analyzed for Rankine cycle power plants [ASME PAPER 66-WA/LUB-3] 04 p0630 A67-15350
Particle microhardness and microbrittleness measured in powdered

refractory compounds, noting relation to electron configuration 06 p1015 A67-17846

Thermal conductivity coefficients of refractory materials at high temperatures determined by measuring one-dimensional stationary thermal flux at single point 07 p1265 A67-19124

Thermostability of refractory materials and effects of high brittleness on thermal stress resistance of structural elements under single and multiple heat treatment and loads 07 p1198 A67-19128

Soviet book on high temperature strength of materials noting test stands, stresses, loads, applications to jet and rocket technologies, etc 07 p1208 A67-19299

Compression and bending strength of porous materials prepared by sintering spheroidized powder refractory compounds increased by addition of cobalt chloride 07 p1208 A67-19307

Refractory glass fibers composition, fiber forming characteristics, construction and operation 07 p1212 A67-20261

Testing machine for evaluating high temperature fabrics under dynamic loading and heating conditions 07 p1212 A67-20262

Manufacturing methods for continuous filament refractory fibers including extrusion and chemical vapor deposition 08 p1345 A67-20427

Electrochemical properties of solid refractory oxides for high temperature fuel cells 08 p1284 A67-20703

Permeability of porous materials of refractory compounds, determining experimentally relation between gas permeability, porosity and particle size 09 p1517 A67-21875

Plasma jet applications, emphasizing generation of high temperatures for refractory coatings in form of intermetallic compounds and cermets 09 p1545 A67-22172

Thermal conductivity coefficient of refractory materials at temperatures to 1600 degrees C 10 p1621 A67-22828

Behavior of metals, graphites and reinforced plastics for reentry nose cones tested, using rocket engine exhaust flame as heat source 10 p1698 A67-23480

Reentry vehicle heatshield materials including graphite, ablative reinforced plastics, etc 10 p1672 A67-23721

Refractory materials for hypersonic vehicle leading edges 10 p1670 A67-23723

Thermoconductivity of heat resistant materials during cooling at room temperature, using photopyrometer to record temperature gradients 11 p1789 A67-24021

Refractory and ablating polymeric reentry heat shield materials evaluated under high radiant fluxes, measuring surface temperature, recession rate, flux emittance, etc refractory and ablating polymeric reentry heat 11 p1811 A67-24054

Vacuum apparatus for testing flat and cylindrical specimens of high melting point materials for creep and long term strength 11 p1877 A67-24817

Hypereutectic carbides from carbide graphite alloys exhibiting high thermal shock resistance 11 p1809 A67-25004

High temperature behavior and testing techniques for refractory materials of different groups 12 p1939 A67-25321

Hot electrodes for open cycle MHD generators, noting refractory oxides 12 p1899 A67-25405

Book on engineering properties of ceramic materials covering high melting materials, physical, thermal and mechanical properties, thermal stress, oxidation, corrosion resistance, etc 12 p1960 A67-26201

Nondestructive determination of mechanical properties of refractory materials by ultrasonic and radiometric measurements 14 p2340 A67-28258

Operation, structure, performance and application of solid, molten and aqueous electrolyte fuel cells 14 p2253 A67-29023

Refractory material as component of silicate binder having stable optical and physical properties under simulated space conditions 15 p2506 A67-29547

Prediction of large rocket nozzle material performance using semiempirical technique, noting mathematical models for internal and external heat and mass transfer 15 p2547 A67-29993

Refractory materials thermal expansion at

elevated temperatures measured with apparatus consisting of optical comparator and controlled gradient vacuum furnace 16 p2677 A67-31542

Porous materials prepared from carbides, borides and silicides of refractory metals by oxidation reduction method, with simultaneous sintering of resulting active particles 16 p2683 A67-31596

Prolonged high temperature creep and endurance testing of refractory materials in vacuum or inert media 17 p2835 A67-33170

Densification and wear resistance of hot pressed pure and binary systems of diboride established with TaC and other refractory additives 17 p2875 A67-33407

Evaporation of thin films of high melting point materials by focused laser beam and reflectance and relative transmittance in vacuum UV 18 p3059 A67-33885

Knudsen cell used in mass spectrometry of the thermodynamics of refractory substances vaporization 19 p3242 A67-34864

Soviet book on high temperature nonmetallic thermocouples and sheaths covering thermal control automation of metallurgical processes, thermoelectric and refractory properties, electrodes, electromotive force, etc 19 p3227 A67-34922

Plasma sources of refractory ions classified according to methods of producing gas discharge 19 p3228 A67-34981

Plasma furnace for treating refractory products at high temperature to determine various oxides solidification temperature 19 p3299 A67-35900

Physicochemical and mechanical properties of refractory materials at high temperature - Conference, Paris, June-July 1965 20 p3471 A67-36109

Refractory properties and mechanical characteristics of graphites and carbons, discussing maximum compatibility temperature of graphite 20 p3472 A67-36110

Temperature effect on mechanical properties of solids with high melting point, with quasi-static hardness as strength measure at high temperatures 20 p3463 A67-36111

Ceramic material requirements for MHD generator electrodes and duct walls, discussing tests in alkali-seeded plasma 20 p3472 A67-36114

Refractory oxides solidification points measurement using optical-pyrometer method 20 p3472 A67-36118

Particle microhardness and microbrittleness measured in powdered refractory compounds, noting relation to electron configuration 20 p3471 A67-37588

Laboratory equipment for R and D on fibrous refractory materials 21 p3649 A67-37883

Continuous filament ceramic fibers via viscose process involving lattice forming, spinning, weaving and firing 21 p3649 A67-37885

Thermal conductivity coefficients of refractory materials at high temperatures determined by measuring one-dimensional stationary thermal flux at single point 21 p3731 A67-38168

Ceramics operating without protective atmospheres at ultrahigh temperatures, discussing tolerance formation, mechanical properties and working processes 21 p3650 A67-38194

Soviet book on high temperature materials for vacuum or inert gas industrial processes 21 p3645 A67-38600

Apparatus for refractory single crystal fusion growth at high temperature using arc melting 21 p3636 A67-38769

MX solids refractory character correlation with volatility at triple point, calculating bond energy according to formation enthalpy equation 24 p4173 A67-42084

REFRACTORY METAL

Space environmental effects on metallic and polymeric plastic structures including aluminum, magnesium, titanium, beryllium and stainless steel [SAE PAPER 660675] 01 p0094 A67-10581

Oxidation test and mechanical property data to determine suitability of columbium and tantalum alloys as thermal protective materials for use in multicycle earth reentry vehicles [SAE PAPER 660660] 01 p0094 A67-10618

Thermogravimetric analysis and electron microscopy of agglomeration and chemical

instability of submicron refractory dispersoids in tungsten 01 p0097 A67-10699

Powder metallurgy techniques and solid state reactions in alloy constitution research, examining advantages of sintering method over modern melting methods 01 p0099 A67-10711

Carbon diffusion in refractory metals with bcc lattice at temperatures of 1100 to 1600 degrees C, considering activation energy and frequency factor 01 p0101 A67-10937

Full temperature range electron and ion emission from polycrystalline surfaces of Nb, Mo, Ta, W, Re, Os and Ir in cesium vapor 02 p0269 A67-11878

Refractory metal chlorides reacted with methane and nitrogen in hydrogen jet to form carbides and nitrides 03 p0440 A67-12925

RF spark source mass spectrometer to detect and identify trace amounts of vapor molecular carbide species for refractory metal carbides 03 p0367 A67-13228

Stress-rupture data for refractory metals which yields linear relationship between Larson-Miller parameter and logarithm of applied stress 03 p0441 A67-13253

Fiberling of oxides by hot deformation in metal matrices of unalloyed columbium or tantalum, preparing composites by powder metallurgy 03 p0441 A67-13273

Ceramic material strength improvement by refractory metal fiber reinforcement, noting strontium zirconate-molybdenum systems 03 p0450 A67-13312

Refractory composites consisting of high strength high modulus filaments imbedded in vapor deposited refractory metals 03 p0444 A67-13433

Fiber reinforced composites with high strength high temperature resistance, using powder metallurgy and honeycomb structures 03 p0429 A67-13437

Vacuum processing in controlling contamination during joining of superalloy and refractory type metals 03 p0430 A67-13555

Refractory metal alloys mechanical properties, metallurgical behavior and applications 05 p0829 A67-16741

High temperature hardening and creation of highly heat resistant alloys of refractory metals 05 p0831 A67-17501

Temperature, admixtures, structural state and deformation rate on mechanical properties of refractory metals in niobium-tantalum and molybdenum-tungsten groups 05 p0831 A67-17502

Refractory metals and metal alloys analyzed regarding electron work function and threshold temperature for surface ionization in all-metal guard ring diode with directly heated wire [AIAA PAPER 66-223] 06 p1035 A67-18137

Materials technology presently available for advanced Rankine systems including nuclear fuels, refractory metal alloys, electrical materials and stainless steel 07 p1223 A67-19460

Interrelation between relaxation center in tungsten and molybdenum and high temperature internal friction background of spectrum 07 p1210 A67-20010

Oxidation of tantalum coated with aluminum and aluminum-chromium alloys at high temperatures and various oxygen pressures, using X-ray diffraction, electron microscopy, etc 08 p1341 A67-20764

Sintering of porous products of refractory compounds 10 p1667 A67-22827

Reduced thermodynamic potentials of large classes of refractory metal carbides and nitrides 11 p1804 A67-23901

Electronic computer usage to control temperature during creep and long term strength tests of heat resistant steels 11 p1877 A67-24818

Molybdenum and niobium effect on structure and physical properties of austenitic Cr-Mn steels with or without nickel 12 p1955 A67-25439

High temperature spectral directional hemispherical reflectance of refractory metals and ceramics measured with integrating sphere and He-Ne CW laser source [AIAA PAPER 67-300] 12 p2035 A67-26015

Temperature resistant elements and compounds for use above 3000 degrees F, considering melting points, atomic radii and densities 14 p2340 A67-28380

Polyhedral boundary precipitations of complex heat resistant nickel alloy in carbide phase caused by boron and cerium 14 p2338 A67-28674

Heat resistant stainless steel honeycomb cores for cylindrical applications, measuring energy absorption characteristics [ASME PAPER 67-DE-14] 14 p2402 A67-28870

Metal matrices reinforcement by whiskers demonstrating high strength at high temperatures [ASME PAPER 67-DE-35] 14 p2328 A67-28876

Coated refractory metals thermal emittance measured at high temperatures for design of reentry vehicle under time-temperature-pressure profile 15 p2503 A67-29546

High temperature superalloys for gas turbine applications noting alloys based on cobalt, iron, nickel and dispersion hardening 16 p2686 A67-30487

Refractory intermetallic compounds as high mobility semiconductors, noting crystal preparation and lowest carrier concentration obtained 16 p2725 A67-30806

Experiments on oxidation kinetics of refractory metals in undissociated and partly dissociated oxygen-chlorine mixtures 17 p2971 A67-33021

Cesium ion emission patterns from rear-fused porous refractory metals studied by thermal emission microscope 17 p2888 A67-33059

Nickel-base alloys refractory-melt reactions in vacuum induction melting investigated by measuring contact angles from photographs, noting carbon contact angles from photographs noting carbon effect 19 p3242 A67-34786

Soviet book on diffusion cladding of metals covering alloy surfaces diffusion saturation, glow discharge siliconizing of metals, vacuum siliconizing of refractory metals, etc 19 p3235 A67-34915

Glow-discharge siliconizing of refractory metals by unilow gas method in silicon tetrachloride vapor and hydrogen atmosphere 19 p3242 A67-34917

Vacuum siliconization of refractory metals in Mo-Si system noting thermodiffusion layers, vapor phase, chemical reaction, diffusion and temperature gradient 19 p3236 A67-34918

Wear, scaling and chemical resistance of carbide and boride diffusion coatings on refractory metals 19 p3243 A67-34921

Alloying volatile metals with refractory metals in Nb-Zn system, noting thermal analysis and microhardness determination 19 p3243 A67-34926

Apparatus for measuring metal/alloy hot hardness using indenter static impression and unilateral flattening 19 p3227 A67-34930

Book on coatings of high temperature materials covering properties and characteristics and coated refractory metals 19 p3244 A67-34956

Refractory metals physical, mechanical and chemical properties when coated with oxidation resistant coatings 19 p3244 A67-34958

Fabrication, structure, possible failure and testing of coated refractory metals in applications for space technology 19 p3245 A67-34959

Thermionic properties, surface ionization, atomic and ionic sublimation of Re, Mo, Ta and W 19 p3264 A67-35082

Traction test apparatus for vacuum and high temperature testing of refractory metals, with modifications for rupture and brittleness tests 20 p3463 A67-36112

Refractory metals and compounds vaporization study, using Knudsen effusion method and mass spectrometry for vapor tension and vaporization energy 20 p3463 A67-36116

Refractory metals and oxidation protection noting coating materials, application methods, etc 20 p3463 A67-36133

Materials of high vacuum technology, Volume 1, Metals and metalloids 20 p3463 A67-36134

Analytical procedures for oxygen, nitrogen and hydrogen determination in high melting metals 20 p3467 A67-37120

Refractory metals in aerospace applications, considering aerodynamic heating, melting resistance, liquid-metal corrosion, electrical superconductors, etc 20 p3469 A67-37342

High temperature hardening and creation of highly heat resistant alloys of refractory metals 21 p3643 A67-38028

Temperature, admixtures, structural state and deformation rate on mechanical properties of refractory metals in niobium-tantalum and molybdenum-tungsten groups 21 p3644 A67-38029

Fast production of semiconductor and refractory metals by reducing silicon tetrachloride and molybdenum trioxide with hydrogen in electric discharge 21 p3681 A67-38358

Physicochemical interactions between components of refractory metals solid solutions, determining metal alloying effects on system structure and high temperature durability 22 p3818 A67-39319

Phase and chemical compositions of structural components forming in iron-nickel-chromium alloys with aluminum and titanium content 22 p3820 A67-39788

Carbon diffusion in refractory metals with bcc lattice at temperatures of 1100 to 1600 degrees C, considering activation energy and frequency factor 22 p3820 A67-39791

Hafnium-tantalum coated refractory metals investigated for use in high temperature rocket motors 22 p3821 A67-39891

High temperature materials assessed for properties needed for aerospace applications including metals, alloys, refractory fasteners, aluminate coats, ablative insulation and ceramic compositions 22 p3824 A67-40333

Performance of wide variety of exceptional metals studied for corrosion and temperature resistance characteristics in atomic power application 23 p4018 A67-40899

Barrier system for oxidation resistant protective coating for high temperature protection of refractory coatings 23 p4018 A67-40900

Slurry coating applied to aerospace refractory metal component for oxidation protection [ASM PAPER C6-1.5] 23 p4020 A67-41407

Strength and oxidation tests evaluated for coated fasteners in extreme temperature use 24 p4160 A67-42078

Electron emission models for evaluation of charge distribution and total energy of metal-gas interface, noting role of quantum mechanical corrections 24 p4202 A67-42087

Stress-rupture properties of composites containing refractory metal fibers and nickel alloys evaluated at high temperatures 24 p4174 A67-42475

High temperature thermal insulation consisting of thin refractory metal foils separated by thin refractory oxide layers 24 p4103 A67-42501

Molybdenum sulfide solid lubricant oxidation characteristics analyzed by thermogravimetry [ASLE PAPER 67-LC-14] 24 p4165 A67-42748

REFRIGERATING EQUIPMENT

Thermoelectric /Peltier/ refrigeration technique for cooling complex electronic equipment in avionic weapon systems line replaceable units 05 p0754 A67-17454

Miniature cryogenic refrigeration systems design for masers and parametric amplifiers, investigating efficiency and contamination 14 p2277 A67-27775

Stirling type closed cycle cooling system for masers and other microwave electronic devices 14 p2278 A67-27784

Low temperature closed cycle refrigeration for electronics, with emphasis on relationship to system effectiveness 14 p2278 A67-27785

Lightweight liquid helium dewar for LEM program, with 870 liter capacity, 10 percent ullage and 1.5 percent boiloff per day 22 p3808 A67-40391

Cryosorption pumping of helium and hydrogen in high vacuum, describing refrigerated panels and space environment simulation application 22 p3838 A67-40396

REFRIGERATION

SA COOLING SYSTEM

SA CRYOGENICS

Air conditioning and refrigeration in air cargo industry 06 p0981 A67-18566

Pulse tube refrigeration heat pumping rates 13 p2229 A67-27680

Continuous flow cryostat system for open cycle cold fluid 14 p2404 A67-27786

REFRIGERATOR

Optimal parameters of refrigerators with

radiative regenerative gas cycle 10 p1596 A67-23022

Large helium refrigerators for very high speed cryopumping techniques required in space simulation facilities 12 p1924 A67-25716

Size and power requirements of liquid helium temperature refrigerators 13 p2057 A67-27679

Low noise preamplifier traveling wave maser operated in closed cycle refrigerator for receiving Mariner IV picture transmissions 14 p2329 A67-27779

REFUELING

Volatile liquid pressurization as expulsion method for storable propellants noting in-flight refueling system design parameters 17 p2953 A67-31973

REGENERATION

SA BIOREGENERATION

Regenerative radiation from neon line in He-Ne laser, using spherical reflectors in resonator 03 p0434 A67-13096

Tunnel diode superregenerative amplification and detection in linear regime and volt-ampere characteristics of diode 05 p0772 A67-16450

Thermal regeneration in power dissipating elements and effects on transistor circuit failures 06 p0971 A67-18245

Amplification processes in parametrically regenerated circuit with simultaneous complex variation of capacitance and attenuation 10 p1607 A67-23446

Photoconductivity kinetics and regeneration recombination noise spectrum of p-InSb crystals, showing association with hole capture, lifetime and alloying impurity 12 p1983 A67-25512

Photoconductivity kinetics and regeneration recombination noise spectrum of p-InSb crystals, showing association with hole capture, lifetime and alloying impurity 18 p3103 A67-34443

REGENERATIVE COOLING

Probe for total enthalpy measurements in arc jet exhausts 17 p2971 A67-33030

REGENERATIVE CYCLE

Subnanosecond time interval measurements with recirculating transmission line memory 02 p0243 A67-12092

Completely regenerative spacecraft life support systems, discussing loop closure techniques and possible conversion methods for metabolic wastes [AIAA PAPER 66-935] 02 p0187 A67-12278

Construction of lunar microcosm, considering recycling based on photosynthesis 02 p0185 A67-12313

Unsteady state analysis of heat transfer and energy transformation processes in closed cycle regenerative heat energy converters, using differential equations [AIAA PAPER 67-216] 06 p0951 A67-18329

Variable thermal capacity of gas mixture taken into account in calculation of heat regeneration in gas turbine cycles, using working bodies 07 p1266 A67-19181

Optimal parameters of refrigerators with radiative regenerative gas cycle 10 p1596 A67-23022

Spacecraft life support systems should ensure radiation protection, food, power supply, waste removal, etc 13 p2061 A67-26753

Parametric comparative study of helicopters powered with current-technology engines and advanced non-regenerative and regenerative twin-engine installations [AHS PAPER 119] 16 p2598 A67-31835

Molecular sieves using regenerable carbon dioxide solid adsorbents for spacecraft life support systems 20 p3374 A67-36611

Regenerative dual tandem cable servomotor design for use in manual and automatic spoiler control system of C-141 Star Lifter 20 p3366 A67-37550

Unsteady state analysis of heat transfer and energy transformation processes in closed cycle regenerative heat energy converters, using differential equations 21 p3689 A67-37791

Regenerable sorbent /GAT-O-SORB/ in granular form for carbon dioxide removal from air, discussing design and performance tests of laboratory prototype [SAE PAPER 670844] 24 p4115 A67-41997

REGENERATOR

Performance of thermal regenerators in which rapid flow cycling is accompanied by large pressure variations with time [ASME PAPER 66-WA/PID-1]

Oxygen regeneration life support system for multiple mission manned space flights evaluated with subsystem model [SAE PAPER 670849] 04 p0724 A67-15379 24 p4115 A67-42000

REGGE POLE

Algebra of factorized Regge pole residues applied to obtain relations between meson-baryon and baryon-baryon exchange processes 16 p2705 A67-31627

REGION

S FRESNEL REGION
S M-REGION
S POLAR REGION
S STAGNATION REGION

REGRESSION

Regression rates in transient regime of composite solid rocket propellant grains upon sudden opening of exhaust port 08 p1373 A67-20803

REGRESSION ANALYSIS

SA VARIANCE

Statistical analysis for pulsed flow measurement evaluation using correlation and regression techniques 03 p0403 A67-13777

Solid propellant regression rate in hybrid rocket motor examined via combustion process model, assuming homogeneous flow in central channel 05 p0874 A67-16766

Hybrid fuel regression rate, discussing oxydizer flow rate and burner pressure interdependence

[AIAA PAPER 66-113] 05 p0873 A67-17347

High resolution density data from radar observations of low altitude polar orbiting satellites reveal longitudinal and geomagnetic variation, noting regression analysis 10 p1640 A67-23216

Stochastic approximation as recursive method for solving regression problems in communication engineering 12 p1907 A67-25989

Ignition response of solid propellants described with model including surface regression with verification of igniter flux and pressure effects 15 p2581 A67-29988

Relationship between acceptance test and operational reliability studied by multiple regression analysis 18 p3138 A67-34668

Book on stochastic approximation and nonlinear regression covering convergence, asymptotic methods, real time problem in presence of noise, etc 24 p4179 A67-42900

REGRESSION COEFFICIENT

Sufficient conditions for asymptotic invariance of Bayes estimate of regression coefficient for nonstationary noise 10 p1619 A67-22952

Pressure dependence of nonmetalized hybrid fuel regression rates in demonstrating major heat release reactions as heterogeneous or homogeneous 10 p1697 A67-23133

Ionospheric index of solar activity obtained together with quadratic equation regression coefficients by minimizing standard error of F-2 layer critical frequency 14 p2311 A67-28375

Boundary layer combustion in hybrid rockets from simplified model comprising convective transport and chemical kinetic factors, analyzing fuel regression rate [AIAA PAPER 67-471] 18 p3157 A67-33941

Bayes estimate of regression coefficients in cost function selection in presence of unsteady noise 24 p4134 A67-41796

REGULATION

SA HEAT REGULATION

SA SPEED REGULATION

Aircraft noise regulation at Kennedy International Airport 13 p2053 A67-26538

Selection of two regularizing functions reduced to one by evaluating relations between them in restricted three-body problem 15 p2557 A67-29875

REGULATOR

SA FLOW REGULATOR

SA FREQUENCY REGULATOR

SA PRESSURE REGULATOR

SA ROBERTSHAW-FULTON REGULATOR

SA VOLTAGE REGULATOR

Annex circuits for regulating electrolyte grade, cell temperature, reactant supply, fluid circulation and generated electricity of unit cells grouped in batteries 14 p2253 A67-29024

Soviet book on photoelectric sensors in monitoring, control and regulation systems noting design principles, operational requirements, etc 18 p3011 A67-33716

REINFORCED MATERIAL

Two metal-powder sintered composites reinforced with metal fibers or fiberglass for increased tensile and impact strength at various temperatures 01 p0098 A67-10705

Whisker strength measurement methods, noting role in reinforcement of ductile metal matrices 01 p0163 A67-11152

Resistance of copper-tungsten fiber composites to repeated tension cycles 02 p0254 A67-11793

Strength characteristics of whisker crystals, microcrystals and macrocrystals influencing selection and use of composite reinforced materials 03 p0449 A67-13306

Mechanical characterization and structural perfection of alpha aluminum oxide wool whiskers in diameter range of 0.6 to 4.0 microns 03 p0449 A67-13307

Boron filaments for possible use as reinforcing phase in composite materials for aerospace structures 03 p0452 A67-13407

Single crystal fiber reinforced composites, discussing use of silicon carbide whisker as interstitial reinforcement 03 p0453 A67-13411

Potential payoffs of using high modulus filament reinforced composite materials in aerospace systems applications discussed in light of development programs 03 p0443 A67-13414

Hollow-rib reinforced structure design from boron filament reinforced epoxy resin, describing fabrication equipment, techniques and test results 03 p0429 A67-13417

Thermodynamic compatibility of B, SiC, BN, boron carbide and tin nitride with various metal matrices in fiber-reinforced composites 03 p0443 A67-13429

Boron fiber-reinforced aluminum composites fabrication by plasma spraying and tensile testing 03 p0444 A67-13431

Boron filaments for reinforcement of aluminum alloys used in turbomachinery 03 p0444 A67-13436

Fiber reinforced metal manufacture, discussing possible fiber-matrix combinations and high temperature applications 06 p1047 A67-17713

Factors affecting strength of whisker reinforced metals noting characteristics [ASME PAPER 66-MD-8] 06 p1015 A67-17835

Coated filaments effect in controlling composite microstructures for several metal-graphite and metal-boron systems [AIAA PAPER 67-175] 06 p1019 A67-18441

Mechanical properties of continuous carbon filament/graphite binder composite including tensile, compressive, flexure, fatigue and shear properties [AIAA PAPER 67-173] 06 p1021 A67-18509

Filament-metal matrix composite material research, considering reinforcement and binder 06 p1019 A67-18657

Tensile failure of whisker reinforced composites for loading in fiber direction 08 p1344 A67-20421

Structural design of solid propellant rocket engine and failure, deformation and fracture of reinforced propellant grains 08 p1420 A67-20888

Reinforcement of solid propellants and use of high strength wires and cylinders 08 p1374 A67-20889

Fiber reinforced materials for composite structures noting deformation of metals, ceramics and glasses 08 p1342 A67-20903

Mechanical behavior of fiber reinforced materials, discussing elastic properties, failure theories, stress analysis, fracture toughness, structural design, etc 08 p1342 A67-20904

Fiber reinforced composite material behavior examined from shear loading tests, using finite difference analysis for representative PDEs 08 p1420 A67-20908

Nickel composite with tungsten filament and aluminum oxide whiskers, noting parameters of tensile strength after annealing 08 p1342 A67-20909

Elastic moduli of composite with aligned continuous fibers derived from elastic properties of constituents 10 p1715 A67-22859

Fiber aspect ratio, residual stress state and geometry of multifiber arrays studied in terms of influence on local stress concentration and matrix reinforcement 10 p1671 A67-23705

Dynamic effective stiffness theory of layered and unidirectionally fiber reinforced composites, detailing field equations for

laminated composite 10 p1724 A67-23708

Glass fiber reinforced composite materials for aircraft engine, discussing construction of bearing and compressor casings [SAE PAPER 670333] 12 p1958 A67-25874

Metal matrix composite fatigue behavior in tension-tension loading as function of volume fraction 14 p2337 A67-28422

Steady heat transfer through rib-reinforced wall of material with variable coefficient 14 p2407 A67-28646

Glass reinforced structural design fundamentals, discussing basic properties of filament materials, matrix material and composite materials [ASME PAPER 67-DE-16] 14 p2402 A67-28871

Metal matrices reinforcement by whiskers demonstrating high strength at high temperatures [ASME PAPER 67-DE-35] 14 p2328 A67-28876

Friction and wear properties of resins and polymers with carbon fiber examined and compared for various amounts of fiber 16 p2694 A67-31021

Stress distribution in reinforced-material models consisting of isolated fiber embedded in brittle matrix analyzed by photoelastic technique 17 p2966 A67-33387

Sapphire whisker reinforced aluminum composites fabrication and evaluation [ASTM PAPER 2] 18 p3070 A67-34568

Fiber orientation and morphology effect on anisotropic tensile behavior of Al-Ni whisker reinforced aluminum, studying solidification rate, etc [ASTM PAPER 3] 18 p3067 A67-34569

Strain distribution in aluminum filament reinforced metal, investigating matrix plastic behavior and residual stresses, etc [ASTM PAPER 8] 18 p3067 A67-34573

Netting analysis of reinforced sheets for load envelopes which combine tension and shear, determining optimum fiber arrangements 21 p3729 A67-39082

Book on fiber reinforced materials covering theories, principles and experimental data noting stress distribution, fiber orientation effects, etc 22 p3820 A67-39590

Composite materials development and application in powder metallurgy, considering laminated, fiber and particle reinforced materials 23 p4017 A67-40711

Diagrams of specific strength of materials made of fibrous composites 24 p4246 A67-41921

REINFORCED PLASTIC

Energy dissipation and heating due to oscillation of polymers whose rheological properties are described by elastic heredity theory, considering homogeneous and reinforced plastics 01 p0102 A67-10220

Space environmental effects on metallic and polymeric plastic structures including aluminum, magnesium, titanium, beryllium and stainless steel [SAE PAPER 660675] 01 p0094 A67-10581

Radioactive tracers used to determine crack initiation and propagation characteristics in reinforced plastic composite materials, relating discontinuity growth to test conditions 02 p0249 A67-12222

Multidirectional reinforced epoxy plastics in testing mechanical response to stress 03 p0451 A67-13401

Reinforced pyrolyzed plastic composites for aerospace applications, noting high temperature stability and ease of utilization 03 p0443 A67-13415

Surface treatment and interface stability of boron filaments reinforcing plastic composite materials 03 p0455 A67-13428

Engineering estimates of transverse properties of unidirectional composites compared with conventional glass-reinforced plastics 03 p0522 A67-13443

Thermophysical properties of glass-fiber reinforced plastics for selecting optimum structural patterns when under axisymmetrical load 04 p0708 A67-14787

Plastic reinforced composites, weight savings, strength and thermal capability [SAE PAPER 660642] 04 p0642 A67-15786

Ground tests of 2.3-m-diam models of foldable foam-reinforced plastic paraboloidal mirrors for satellite energy supply system and optimization of optical characteristics 04 p0558 A67-15957

Organic composites reinforced with single crystal fibers manufactured, using

fiberization of whiskers 05 p0832 A67-16167
 Anisotropy effect on strength of unwoven glass fiber reinforced plastic, ascertaining nature of stressed state arising at high temperature 05 p0912 A67-16183
 Glass fiber reinforced plastics experience for preparing high precision models of complex shape, noting wind tunnel application 06 p1007 A67-18019
 Molded aircraft wheels of epoxy resin reinforced with noncontinuous glass filaments 06 p1007 A67-18026
 Anisotropic elastic constants and strength characteristics of fiberglass reinforced plastics during shear 06 p1020 A67-18099
 Two fabric-reinforced plastics performance in reentry heating as function of zirconia powder, magnesia powder and Microbestos TX paper fillers [AIAA PAPER 67-154] 06 p1020 A67-18292
 Mechanical and structural properties of three-dimensionally reinforced plastic, noting composite cylinder [AIAA PAPER 67-171] 06 p1020 A67-18296
 Boron fibers and reinforced plastic composites, noting mechanical and physical properties, application, 06 p1021 A67-18855
 Glass fiber reinforced parts for Boeing 737 noting fabrication, properties and applications 07 p1193 A67-20252
 Filamentary reinforced resin matrix composite materials for high specific strength and specific modulus necessary for aircraft structures 08 p1333 A67-20359
 Reinforced plastics - SPI Conference, Washington, D.C., January-February 1967 08 p1344 A67-20420
 Micromechanical failure mechanism of fiber reinforced plastics under tension, compression and shear 08 p1344 A67-20422
 Nuclear magnetic resonance and nuclear quadrupole resonance techniques for nondestructive testing of reinforced plastics for curing and internal stresses 08 p1345 A67-20425
 Inorganic continuous ceramic fibers production, properties and application 08 p1345 A67-20426
 Light aircraft design using fiberglass reinforced plastic primary structure for fibrous composite airframe 08 p1414 A67-20429
 Reinforced plastic facings as sandwich materials instead of metal skins noting cost effectiveness, weight efficiency and layout times 08 p1414 A67-20430
 Automatic rigidizing of expandable fabric impregnated space structures, detailing gelatin system 08 p1345 A67-20433
 Fabrication of complex hollow rib reinforced structures of wound boron filaments and anhydride cured epoxy resin for reentry vehicle application 08 p1345 A67-20435
 Fiber reinforced plastics, determining composite elastic constants in terms of elastic moduli and geometric parameters of constituents 08 p1346 A67-20910
 Ultrasonic inspecting technique for reinforced plastic components and adhesive bonds of solid propellant booster nozzles 10 p1659 A67-22930
 Uniaxial tensile strain rate on stability of soft reinforced plastics with two-component fibrous base 10 p1671 A67-23605
 Boron fiber reinforced epoxy matrix plastic composite for application to aircraft structures 10 p1723 A67-23697
 High modulus high strength reinforcements incorporated in epoxy matrix plastic composites for aerospace structural use 10 p1671 A67-23704
 Glass-fabric reinforced plastic shells fabrication and full scale structural evaluation 10 p1727 A67-23732
 Ablation study scheme enabling determination, for given environment and material, of ablation starting time and temperature distribution within mass of material 13 p2222 A67-26596
 High strength and high elastic modulus in resin-matrix composite structures of single-crystal whiskers [ASME PAPER 67-DE-9] 14 p2340 A67-28868
 Asbestos reinforced plastics evaluated for physical and optical properties, thermal-vacuum and UV resistance 15 p2507 A67-29550
 Reinforced plastics composites for jet lift engines 15 p2508 A67-29671

Vacuum chamber for plasma studies consisting of thin stainless steel shell strengthened by glass fiber reinforced plastic with epoxy compound as adhesive 16 p2676 A67-31397
 Creep properties of glass fiber reinforced plastics for long-term bearing structures, noting elastic strain, creep rate, etc 16 p2694 A67-31486
 Stresses in fiber-reinforced plate 16 p2776 A67-31544
 Fiberglass-reinforced thermoplastic production processes, discussing strength, rigidity, dimensional stability, etc 17 p2875 A67-31931
 Ultrasonic joining techniques for plastic welding, metal insertion, staking and reactivation of adhesives, emphasizing lock-seal process 19 p3233 A67-34791
 Correlation and analysis of ultrasonic test results in evaluating reinforced resin laminates 19 p3249 A67-35554
 Synthetics in aircraft and rocket construction, recommending duroplastics 20 p3473 A67-36453
 Ablation characteristics investigated using plasma jet wind tunnel, discussing effective heat of ablation and free stream stagnation enthalpy 20 p3544 A67-36640
 Vapor deposition-prepared continuous silicon carbide filaments for use as reinforcement in high strength oxidation-resistant structural plastic composite 21 p3648 A67-37881
 Fiber reinforced plastic composite strength and elastic modulus dependence on fiber properties, volume content, directional orientation and matrix load transfer properties 21 p3649 A67-37882
 Loading rate effect on unidirectional fiberglass reinforced plastics under tension, examining mechanical characteristics and determining tensile strength and elastic modulus 21 p3649 A67-37908
 Prestressing effects on stress-strain diagram of monodirectional transversely isotropic glass fiber reinforced plastic 21 p3650 A67-37911
 Composite technology emphasizing fiber-reinforced metal matrix composites, discussing filaments, plastics, ceramics, fabrication methods, etc 21 p3643 A67-37953
 Glass fiber reinforced plastics stress and strain, considering applications in structural design 21 p3650 A67-38519
 Reinforced plastic materials for light aircraft wing structures, calculating torque strength 22 p3912 A67-39729
 Fiber reinforced plastic components for structural materials noting high temperature polymers 22 p3825 A67-39854
 Performance reliability of reinforced plastics for structural load-bearing components using nondestructive testing, defining material-energy interactions 22 p3826 A67-39860
 Reinforced plastics, evaluating epoxy resin with glass fiber reinforcements for laminates, measuring tensile, compressive and flexural strengths [ASM PAPER C6-21.1] 23 p4022 A67-41403
 Reinforced plastics - Conference, Cleveland, October 1967 24 p4175 A67-42419
 Adhesive system for structural bonding of fiberglass reinforced polyester to itself and to metal 24 p4175 A67-42421
 Temperature, fiber compositions and matrix resin effects on flexural properties of unidirectionally reinforced short fiber composites 24 p4175 A67-42422
 Reinforced plastics pressed sheet materials series based on chrysotile asbestos fibers and thermoplastic resin combinations or thermoplastic and thermosetting resins 24 p4176 A67-42423
 Textile fabrication methods produce multidirectional materials, describing commercial use of 3-D materials 24 p4176 A67-42424

REINFORCED PLATE
 Thin plate reinforcement around holes in plane sheets subjected to stresses at infinity 10 p1719 A67-23472
 Equivalent reinforcement and contour of symmetrically shaped hole corresponding to plate subjected to bilateral tension 12 p2019 A67-25564
 Buckling of longitudinally reinforced rectangular panel loaded by constant edge shear and longitudinal variable compression 16 p2763 A67-30792

Stresses in fiber-reinforced plate 16 p2776 A67-31544
 Flexural rigidity of plates reinforced by parallel stiffeners for direction normal to stiffener orientation determined together with stresses induced by bending moment 17 p2959 A67-32408
 Stress analysis of semiminfinite plate containing reinforced notch on one side under uniform tension 17 p2961 A67-32777
 Optimal reinforcements of cuts in stressed plates, considering displacements and conditions in discrete points of contact contour 24 p4249 A67-42105

REINFORCED SHELL
 Buckling loads of reinforced cylindrical shells, discussing size and placement of stiffening members 03 p0521 A67-13019
 Load concentration effects on stability of rigidly reinforced strictly convex shell, determining upper critical load 03 p0526 A67-14063
 Axisymmetric deformation of cylindrical shell reinforced by frames located at arbitrary distance from each other and having different geometrical and elastic characteristics 03 p0530 A67-14171
 Plastic analysis of rib reinforced cylindrical shells using strain mapping method for Tresca yield conditions [ASME PAPER 66-WA/APM-14] 04 p0713 A67-15406
 Two contact problems involving cylindrical shells reinforced with elastic frames 04 p0717 A67-15889
 Stressed and strained state of reinforced cylindrical shell under nonuniform heating and compression, noting three solutions to buckling problem 05 p0913 A67-16190
 Instability of thin reinforced cylindrical shell clamped at both ends and energy method calculation of critical pressure 05 p0918 A67-16422
 Stress distribution at rigid ring-reinforced curvilinear hole in spherical shell 05 p0922 A67-17178
 Rib elasticity effect on stressed state of circular cylindrical shell with rectangular cut in torsion 06 p1107 A67-18632
 Free vibration analysis for ring and stringer stiffened cylindrical shell, using Rayleigh-Ritz technique [AIAA PAPER 67-71] 07 p1262 A67-19434
 Load carrying capacity of plane and reinforced cylindrical shells clamped along edges and subjected to uniformly distributed internal pressure 10 p1720 A67-23600
 Dynamic stability of cylindrical shell reinforced by thin walled rigid longitudinal ribs 10 p1721 A67-23604
 Asymptotic solution of typical bay in hydrostatically loaded ring-reinforced noncircular cylinder of finite length 10 p1729 A67-23766
 Instability of cylindrical shells stiffened with rings and stringers of nonuniform cross sections, noting load and weight savings 11 p1874 A67-24225
 Buckling test data for internal integral ring-stiffened aluminum cylinders under combinations of axisymmetrical axial load and external lateral pressure 11 p1875 A67-24611
 Tensometry method to study stress concentration around circular hole in orthotropic glass-fiber reinforced cylindrical shell 12 p2021 A67-25579
 Approximate theory for stress-strain state of thin cylindrical shell reinforced with elastic ribs having bending rigidity 12 p2022 A67-25584
 Deflection function of glass fiber reinforced circular cylindrical shells under axial supercritical compressive loading 12 p2023 A67-25590
 Reinforced cylindrical shell stability under external pressure, considering irregular frame disposition effect 12 p2027 A67-25620
 Rigidly reinforced conical shell stability under external load investigated for boundary conditions 12 p2027 A67-25622
 Laminated thin shell theory applied to calculation of elastic coefficients of fiber reinforced shells [AIAA PAPER 66-526] 12 p2030 A67-25914
 Lower and upper critical loads measured in process of axial compression of cylindrical shells of glass fiber reinforced resin 12 p2031 A67-25959
 Stress and stability of stringer-reinforced

circular cylindrical shell 13 p2218 A67-26892
 Load concentration effects on stability of rigidly reinforced strictly convex shell, determining upper critical load 13 p2221 A67-27722
 Stability of reinforced thin structurally-orthotropic cylindrical shell problem, discussing rib eccentricity, axial compression load, torsional load, etc 19 p3338 A67-34874
 Free axisymmetric oscillations of reinforced, closed, cylindrical circular shells, discussing natural frequencies and bending oscillations 19 p3338 A67-34877
 Limiting equilibrium of crosswise reinforced cylindrical shells of waffle type, allowing interaction between vertical and horizontal ribs 21 p3717 A67-37972
 Stress analysis of ribbed shell of revolution, noting case of open shell of zero Gaussian curvature with cyclic symmetrical stresses 21 p3718 A67-37980
 Stress analysis for rib-reinforced cylindrical shell subjected to rapidly varying pressure, calculating deflections and bending moments 21 p3725 A67-38790
 Elpatovskii method applied to axisymmetric deformation of two-layer cylindrical shell with helical glass fiber reinforcements, obtaining equations for stressed state 21 p3725 A67-38795
 Long cylindrical shell with externally loaded reinforcing ring, solving stress distributions and displacements 21 p3727 A67-38871
 Constrained torsion computation for multispar box with elastic diaphragms assuming applied stresses at end ribs 21 p3728 A67-38906

REINFORCEMENT
SA METAL REINFORCEMENT
 Shear buckling of thin walled structural sections, noting reinforcement methods including use of swedges 17 p2957 A67-32026

REINFORCEMENT RING
 Stress distribution in elastic anisotropic plate with row of elliptical holes reinforced by elastic rings 01 p0158 A67-10221
 Reinforcing round hole in isotropic plate by elastic gasket or thin multicomponent ring consisting of set of homogeneous component rings sweated together 01 p0158 A67-10222
 Second order variation of system potential energy of axially compressed circular cylindrical shell with ring-stiffened edges evaluated for purely inextensional deformation 02 p0339 A67-12345
 Stress concentration near elastic ring-reinforced hole in elongated nonlinear plate 02 p0341 A67-12665
 Hole-weakened spherical body represented by deformation of two spherical shells with reinforcing rings under uniform internal load beyond elastic limit 05 p0923 A67-17187
 Generalized Stodola iteration method for computer analysis of axisymmetric buckling of ring-stiffened orthotropic shells of revolution [AIAA PAPER 67-109] 06 p1103 A67-18339
 Prebuckling deformations, ring stiffeners and load eccentricity effect on buckling of stiffened cylinders 10 p1727 A67-23759
 Asymptotic solution of typical bay in hydrostatically loaded ring-reinforced noncircular cylinder of finite length 10 p1729 A67-23766
 Asymptotic expansion procedure applied to Donnell equations for cylindrical shell, obtaining solution for interaction of infinite cylinder reinforced by radially loaded ring [ASME PAPER 66-WA/APM-27] 10 p1730 A67-23839
 Ribbed circular cylindrical shell under axial compression, reducing problem to determination of deflection and stress functions 12 p2020 A67-25571
 Vibration characteristics and fundamental frequency of circular plate with arbitrary cross section reinforcing ring 13 p2216 A67-26534
 Influence coefficients for stresses at circular holes in shallow cylindrical shells with both flat and curved reinforcements [AIAA PAPER 67-365] 14 p2401 A67-28733
 Differential equation for axisymmetric deformation of thin circular cylindrical shell stiffened by circumferential rings and subjected to lateral and axial pressure 20 p3537 A67-36495
 Flexible ring reinforcing cylindrical shell under external load strength, considering

ring cross-sectional shape change effect on bending moment 21 p3724 A67-38783
 Long cylindrical shell with externally loaded reinforcing ring, solving stress distributions and displacements 21 p3727 A67-38871
 Nonlinear problems of parametric excitation of rings solved by equations, considering normally and centrally directed pressures 23 p4074 A67-40651
 Elastic buckling loads of shallow spherical shells supported by edge rings including nonlinear prebuckling effects 23 p4080 A67-41729

REINFORCING FIBER
 Tungsten composites strengthened by fibered or reacted additive 01 p0098 A67-10702
 Two metal-powder sintered composites reinforced with metal fibers or fiberglass for increased tensile and impact strength at various temperatures 01 p0098 A67-10705
 Metallurgical and geometrical factors affecting high temperature tensile properties of discontinuous tungsten fiber reinforced composites 03 p0441 A67-13272
 Strengthening mechanisms in metals and ceramics - Conference, Raquette Lake, N.Y., August 1965 03 p0441 A67-13302
 Advanced fibrous reinforced composites - Conference, San Diego, November 1966 03 p0450 A67-13399
 Graphite fiber reinforced epoxy resin matrix composites, determining mechanical properties 03 p0452 A67-13402
 Mechanical properties of silicon carbide filament reinforced epoxy resin composites fabricated by plying monolayer tapes into unidirectional and balanced bidirectional composites 03 p0452 A67-13403
 Carbonaceous fiber yarn reinforcements in epoxy-anhydride binder, noting moisture adsorption degradation of interlaminar shear values 03 p0452 A67-13405
 Refractory ceramic and graphite fibers properties and strength in high temperature reinforcements 03 p0452 A67-13406
 Fiber reinforced rotor blades, discussing composite material selection for research, mass balance, dynamic response tuning and material design 03 p0453 A67-13416
 Synthesis route to form continuous filaments of SiC, noting tensile strength, elastic modulus and density of product 03 p0454 A67-13422
 Structural carbon yarn for reinforcement of composite plastics 03 p0454 A67-13424
 Fiber formation and performance properties of carbon-silica fibers and use in plastic composites 03 p0454 A67-13425
 Surface treatment and interface stability of boron filaments reinforcing plastic composite materials 03 p0455 A67-13428
 Thermodynamic compatibility of B, SiC, BN, boron carbide and tin nitride with various metal matrices in fiber-reinforced composites 03 p0443 A67-13429
 Compatibility and interaction characteristics of SiC and B fibers with metal matrices in composites prepared from powder metallurgy by hot pressing 03 p0444 A67-13430
 Residual stress effect on stress-strain curve of uniaxial composite consisting of stainless steel wire and aluminum alloy matrix 03 p0444 A67-13432
 Fiber reinforced composites with high strength high temperature resistance, using powder metallurgy and honeycomb structures 03 p0429 A67-13437
 Silicon carbide filament properties, fabrication and use as reinforcement of metal matrix composites, noting strength retention at high temperatures 03 p0445 A67-13439
 Fiber reinforced metals 03 p0456 A67-13893
 Composite materials using whisker and short fiber reinforcements, discussing specific strength and specific moduli [SAE PAPER 660640] 04 p0842 A67-15787
 Fiber diameter, length and discontinuity effects on fatigue properties of fiber-reinforced metal 06 p1099 A67-17712
 Fiber reinforced metal manufacture, discussing possible fiber-matrix combinations and high temperature applications 06 p1047 A67-17713
 Electric resistivity and electroconductivity of copper composites reinforced with fibrous felts of tungsten 06 p1015 A67-17808

Molded aircraft wheels of epoxy resin reinforced with noncontinuous glass filaments 06 p1007 A67-18026
 Strengthening of eutectic composite fibrous wire and rod fabricated by hydrostatic extrusion [AIAA PAPER 67-172] 06 p1008 A67-18458
 Boron fibers and reinforced plastic composites, noting mechanical and physical properties, application, etc 06 p1021 A67-18855
 Fabrication, properties, deformation and fracture of silica fiber reinforced aluminum, noting effect of heat treatment and stress rupture 07 p1211 A67-20266
 Micromechanical failure mechanism of fiber reinforced plastics under tension compression and shear 08 p1344 A67-20422
 Inorganic continuous ceramic fibers production, properties and application 08 p1345 A67-20426
 Void effect on strength of filament reinforced composite materials 08 p1415 A67-20434
 Fiber reinforced materials for composite structures noting deformation of metals, ceramics and glasses 08 p1342 A67-20903
 Mechanical behavior of fiber reinforced materials, discussing elastic properties, failure theories, stress analysis, fracture toughness, structural design, etc 08 p1342 A67-20904
 Continuous filament reinforcement data, analyzing boron and silicon carbide for metal matrix applications [ASTME PAPER WES-7-75] 10 p1668 A67-23010
 Combining two or more nonmetallic substances noting applications of fiber reinforced, particulate filled and laminated composites 10 p1671 A67-23013
 Fiber reinforced composite materials, discussing high temperature behavior, strength/weight ratio, structural composition, fabrication, etc 11 p1805 A67-24221
 Book on composite materials covering theory of metal strengthening, dispersion, fiber strengthened materials, material potentials, etc 11 p1807 A67-24634
 Fiber reinforcement theory, considering strengthened metal behavior at elevated temperatures and under work hardening conditions 11 p1807 A67-24635
 Fiber strengthening processes, advantages and limitations of fiber for composite systems and incorporation in metal matrices 11 p1811 A67-24637
 High temperature polyimide unidirectionally reinforced with silica fiber, noting precuring process to avoid porosity and strength degradation 11 p1811 A67-24641
 Fiber reinforced metal coating by passing silica through molten aluminum, discussing freezing by radial conduction of heat into fiber 12 p1954 A67-25292
 Stresses and strains in dual element and fibrous to steady state creep load calculated by considering individual properties of constituent elements 12 p2031 A67-25953
 Nozzle ablations studied based on chemical mechanism, discussing pure on reinforced phenolic resin [ONERA-TP-475] 14 p2404 A67-27896
 Transverse normal loading of doubly periodic unidirectional elastic fiber reinforced infinite elastic matrix 14 p2398 A67-28098
 Thermal conductivities of unidirectional composite materials parallel and normal to filaments, using analogy to shear loading response 14 p2404 A67-28099
 Stress distribution in matrix of composite material for case of filler between one infinite and two displaced semifinite microfibers 14 p2398 A67-28100
 Metal matrices reinforcement by whiskers demonstrating high strength at high temperatures [ASME PAPER 67-DE-35] 14 p2328 A67-28876
 Cyclic extension of elastic fiber with elastic-plastic coating when obeying Tresca yield condition 14 p2341 A67-29060
 Reinforcing fiber orientation effect on elastic moduli of materials, noting results on long and finite fibers 15 p2576 A67-30178
 Friction and wear properties of resins and polymers with carbon fiber examined and compared for various amounts of fiber 16 p2694 A67-31021
 Stresses in fiber-reinforced

- plate 16 p2776 A67-31544
- Stress distribution in reinforced-material models consisting of isolated fiber embedded in brittle matrix analyzed by photoelastic technique 17 p2966 A67-33387
- Parameters governing high resistance of reinforced resins, stressing elastomechanical equilibrium at interface [ONERA-TP-468] 18 p3069 A67-34462
- Mechanical behavior of fiber-reinforced aluminum and effect on engineering application [ASTM PAPER 10] 18 p3070 A67-34575
- Tensile properties of fiber-reinforced metals, discussing failure at notch root 20 p3464 A67-36417
- Unidirectional fiber-reinforced composite under axial load, discussing power series along with point matching techniques for solving interface, matrix and filament stresses 20 p3474 A67-37268
- Radioactively labeled coupling agents adsorption on E-glass surfaces, noting continuous film formation with covalent bonding occurring at interface 20 p3474 A67-37269
- Metals, ceramics, glasses and polymers combined as composite materials, reviewing mechanical properties and considering applications to engineering design 20 p3475 A67-37714
- Vapor deposition-prepared continuous silicon carbide filaments for use as reinforcement in high strength oxidation-resistant structural plastic composite 21 p3648 A67-37881
- Fiber reinforced plastic composite strength and elastic modulus dependence on fiber properties, volume content, directional orientation and matrix load transfer properties 21 p3649 A67-37882
- High tensile strength high elasticity modulus graphite fibers preparation from polymeric fibers for composite structures 21 p3649 A67-37884
- Hooke law type anisotropic fiberglass reinforced plastic, discussing elastic deformation and brittle fracture, using revised Mises ellipse equation 21 p3649 A67-37907
- Electroplating for fabricating fibrous composite materials noting advantages of low temperatures and absence of mechanical working 22 p3819 A67-39560
- Book on fiber reinforced materials covering theories, principles and experimental data noting stress distribution, fiber orientation effects, etc 22 p3820 A67-39590
- Composite material mechanical characteristics, discussing organic polymeric materials application in wide temperature range 22 p3825 A67-39855
- Composite materials development and application in powder metallurgy, considering laminated, fiber and particle reinforced materials 23 p4017 A67-40711
- Shear modulus measurements in fiber-reinforced composites by plate-twisting test and torsion tube in terms of classical laminated plate and shell theory 23 p4021 A67-40738
- Suitability of finite element method for stresses in composite materials, examining single broken fiber in matrix 23 p4077 A67-41156
- Diagrams of specific strength of materials made of fibrous compositions 24 p4246 A67-41921
- Silicon carbide and B filament reinforced Ti alloy composites analyzed metallurgically and micromechanically, noting stress-strain behavior [SAE PAPER 670862] 24 p4172 A67-42004
- Boron and graphite filament-resin composites tensile and interlaminar shear strengths and Al foil liner cyclic life in cryogenic pressure vessel tests 24 p4176 A67-42470
- Interfiber distance and temperature effects on critical aspect ratio in fiber composites obtained from modified pull-out test 24 p4173 A67-42474
- REISSNER EQUATION**
- Nonlinear influence coefficient obtained by extension of Reissner nonlinear analysis to include uniform pressure loading over surface of spherical shell 01 p0164 A67-11178
- Reissner variational method stability analysis of small eccentricity nonlinearly elastic thin circular ring 03 p0531 A67-14230
- Reissner variational formulation of temperature distribution boundary value problem of axisymmetric thermal stresses in isotropic sandwich shells of revolution [AIAA PAPER 66-528] 12 p2030 A67-25917
- Refined plate bending theory taking into account edge effect 16 p2765 A67-31050
- Reissner differential equation simplified for problems involving small strains in thin shells of revolution due to symmetrical deflections 23 p4073 A67-40612
- RELATION**
- S STRESS-STRAIN-TIME RELATION**
- RELATIVISTIC EFFECT**
- Relativistic interaction energies between atoms in degenerate states determined, using Breit-Pauli approximation 05 p0848 A67-16839
- Two-flow equations for stationary relativistic electron cloud in self-consistent crossed fields 05 p0774 A67-16907
- Nonlinear equations of traveling wave tube solved approximately, taking account of relativistic effects 05 p0776 A67-17164
- Deriving Lagrangian for system of extended rotating bodies, noting contribution of relativistic corrections for kinetic energy of rotation 05 p0847 A67-17496
- Phenomenological metric method applied to four tests of general relativity in evaluation for nearly flat space with spherical symmetry 13 p2159 A67-27399
- Relativistic effect of atomic clocks, noting error and magnitude increase with experiment duration 14 p2348 A67-27866
- Mass dependence of behavior of stellar core undergoing gravitational collapse examined, using improved equation of state and mean free path for energy transfer 15 p2553 A67-29183
- Relativistic effects in HF plasma accelerators, noting decrease in transverse kinetic energy and axial velocity 15 p2527 A67-29475
- Two-flow equations for stationary relativistic electron cloud in self-consistent crossed fields 16 p2636 A67-30884
- Michelson interferometer and ring laser compared for measurement of relativistic rotational effects of earth 17 p2883 A67-32361
- Book on electrodynamics of moving media, deriving force distribution using Hamiltonian and virtual power principles in relativistic formulations 20 p3500 A67-37087
- Sign of energy gain and direction of energy flow shown invariant under Lorentz transformation for two relatively moving systems possessing equal proper temperature 21 p3733 A67-39124
- Tenuous high temperature plasma electromagnetic wave scattering, with relativistic corrections for scattered radiation spatial and spectral distribution 22 p3849 A67-39699
- Gravitational collapse model with pressure gradient and no energy flow, discussing spectral shift and mass radius relation 22 p3884 A67-39833
- Time reversible difference procedures including Lorentz and continuity equations, relativistic orbits and gyrocenter motion 23 p4027 A67-40996
- RELATIVISTIC PARTICLE**
- SA HAMILTON-JACOBI EQUATION**
- Logarithmic dependence of energy losses on relativistic particle velocities in polystyrene films 01 p0125 A67-10926
- Oscillations of plasma composed of ions at rest and relativistic velocity electrons moving along external magnetic field analyzed in linear approximation 02 p0274 A67-12462
- Galaxy M82, analyzing continuous optical magnetobremstrahlung and relativistic electrons 02 p0310 A67-12578
- Gas-filled Cerenkov radiation detector combined with solid detectors to measure charge and flux of relativistic cosmic rays 02 p0247 A67-12695
- High energy cosmic ray muons studied, using ionization calorimeter and hodoscope counters 02 p0317 A67-12770
- Superhigh energy particle accelerators and energy spectra of cosmic ray muons in electron photon cascades 02 p0317 A67-12772
- Absorption curve and energy spectrum of high energy muons 02 p0317 A67-12775
- Characteristics of relativistic electron precipitation events in and near auroral zone during day and night 03 p0410 A67-12957
- Dispersion equation for interaction of helical flux of relativistic electrons with wave field of rectangular guide 03 p0367 A67-13089
- Radio emission from 18 galaxies observed, noting accompaniment of optical spectrum emission and enhancement due to production of relativistic electrons in active nuclei 04 p0697 A67-14774
- Relativistic electron stream requirements to obtain self-magnetic confinement, noting 4 million volt pulsed electron field emission accelerator 04 p0624 A67-15325
- Metagalactic existence of type of hypothetical particles representing stable closed Einstein microcosms 04 p0702 A67-15757
- Relativistic photoelectric cross section for two electrons of K-shell computed, using numerical program 04 p0661 A67-15763
- Two-particle ring term for kinetic equation with Darwin interaction relationship to relativistic Landau equation 04 p0672 A67-15772
- Inverse Compton effect limits possible mean energy of relativistic electrons, thereby restricting quasar models 04 p0702 A67-15942
- Spectral indices of radio galaxies and quasi-stellar sources explained by relativistic electron injection into magnetic field by recurring blasts 05 p0891 A67-16400
- Diffuse omnidirectional inverse Compton and synchrotron X and gamma radiation from cosmic distributions of fast electrons and thermal photons 05 p0882 A67-16404
- Inverse Compton effect in quasi-stellar source and relativistic electron distribution 05 p0898 A67-16924
- Cosmic ray analysis with Holborn scintillator stacks to determine existence of quarks 06 p1076 A67-17650
- Synchrotron nature of Sagittarius A central component radio spectrum and injection of relativistic cosmic particles 06 p1078 A67-18166
- Galactic radio sources noting disk model brightness distribution, relativistic particle energies, continuous particle acceleration and ratio between proton and electrical component of cosmic radiation 09 p1563 A67-21629
- Solar flares as acceleration mechanisms for relativistic and subrelativistic particles 10 p1700 A67-23186
- Nonlinearity caused by relativistic mass effect leading to radiation maxima of plasma excited by two pulses at electron gyrofrequency 11 p1827 A67-23889
- Relativistic electron motion in mirror magnetic field interacting with axial electromagnetic wave calculated, comparing results with Seidl experiment 11 p1828 A67-23895
- Evolution of radio spectral index of supernova remnants modeled to include synchrotron radiation energy distribution 11 p1859 A67-24114
- Inhomogeneous gas of weakly coupled relativistic electrons, deriving kinetic equation for particle electromagnetic field system 11 p1782 A67-24781
- Variational principle extended to relativistic scalar hydrodynamics, deriving Hamilton equations 11 p1844 A67-25034
- Negative-mass instability of cylindrical layer of relativistic electrons in geometrical configuration approximating Astron machine 12 p1970 A67-25254
- Synchrotron radiation of relativistic electrons in magnetic field of dipole 12 p1994 A67-25535
- Relativistic-electron diffusion wave in outer radiation belt recorded by device mounted on Cosmos XLI satellite in high geomagnetic latitudes 13 p2191 A67-26545
- Energy of system of particles defined as related to active gravitational mass, or to inertial mass and passive gravitational mass respectively, in expanding universe 13 p2199 A67-27004
- Flux density of variable radio sources with peculiar radio spectra 14 p2386 A67-28446
- Origin of ultrarelativistic cosmic ray particles 14 p2382 A67-29028
- Motion equation for nonideal relativistic electron gas, reviewing hydrodynamics obtained from Landau equation 15 p2527 A67-29517
- Synchrotron nature of Sagittarius A central component radio spectrum and

injection of relativistic cosmic particles 16 p2737 A67-30510
 Energy dissipation by relativistic charged particle and magnetic field containing it shown to exceed initial energy 17 p2952 A67-33320
 General quantum relativity theory in real universe with large radius and elementary particle structure 18 p3080 A67-34728
 Relativistic Boltzmann collisionless equation solution in presence of certain external fields 19 p3266 A67-35710
 Decimeter radiation from Jupiter originating in synchrotron radiation of ultrarelativistic energy electrons in 1 gauss field 21 p3710 A67-38996
 Synchrotron radiation intensity of relativistic electron moving in anisotropic medium 22 p3851 A67-39735
 High energy cosmic ray muons investigated, using ionization calorimeter and hodoscope counters 22 p3877 A67-40272
 Superhigh energy particle accelerators and energy spectra of cosmic ray muons in electron photon cascades 22 p3877 A67-40274
 Absorption curve and energy spectrum of high energy muons 22 p3877 A67-40277
 Relativistic particles producing ionization bursts studied for energy spectrum recorded during operation of stack of ionization chambers alternating with lead and graphite layers 24 p4218 A67-42834

RELATIVISTIC PLASMA
 Radiation in Lorentzian moving anisotropic plasma 01 p0123 A67-10442
 System of equations derived governing behavior of ideal relativistic charged fluid by means of variational principle, through introduction of generalized Clebsch transform 02 p0273 A67-12195
 Static theory of oscillations of relativistic plasma in uniform magnetic field 03 p0477 A67-13510
 Relativistic plasma oscillations and two-stream instability treated by Boltzmann and Maxwell equations 03 p0482 A67-13739
 Relativistic mechanism of electromagnetic wave scattering at velocity fluctuations and emission from plasma in external field 08 p1295 A67-20831
 Gardenhose instability for ultrarelativistic plasma in magnetic field, showing that instability criterion for particular non-Maxwellian distribution function is not met 09 p1546 A67-22229
 Magnetosonic wave effect on anisotropic relativistic plasma component, obtaining cosmic ray plasma instability when wave frequencies are less than electron cyclotron frequency 09 p1546 A67-22230
 Charge separation effects in Ferraro-Rosenbluth cold plasma sheath model, using relativistic treatment 11 p1825 A67-23869
 Relativistic solution to normal incidence on semilinear longitudinal drifting homogeneous temperate magnetoplasma, obtaining reflected and transmitted waves 11 p1832 A67-24304
 Relativistic electron plasma diffusion, calculating dynamical friction and diffusion coefficient in Landau approximation 12 p1969 A67-25193
 Soviet papers on quantum fluid theory and hydrodynamics 13 p2105 A67-27410
 Relativistic velocity shock wave propagation in stellar high temperature high density plasmas with pair production, thermonuclear reactions and neutrino emissions 14 p2355 A67-27953
 Relativistic MHD shock wave stability in infinitely conducting plasma with magnetic field parallel to shock wave plane 15 p2523 A67-29216
 Electrostatic wave effect on anisotropic relativistic proton plasma in magnetic field, noting instability 16 p2739 A67-31234
 Refractive-index equation derived for electromagnetic wave propagation along static magnetic field in plasma motion direction, using relativistic transformations 17 p2812 A67-32304
 Longitudinal and transverse collective effects contribution to energy loss rate in relativistic isotropic plasma subject to external fields and particles 17 p2908 A67-33111
 Wave propagation velocity in relativistic fluids determined using new hydrodynamic equations 18 p3025 A67-33683
 Boundary layer structure between rarefied plasma and magnetic field solved in

relativistic-invariant form 19 p3288 A67-35369
 Magnetic properties of relativistic equilibrium plasma in magnetic field studied in Boltzmann and quantum cases, using thermodynamic functions 20 p3502 A67-37557
 Statistics and kinetic equations of plasma in opacity region taking into account relativistic effects 20 p3502 A67-37662
 Classical scalar plasma with relativistic Hartree equilibrium approximation for energy, entropy and state equation noting effect of linear perturbation 22 p3842 A67-39209
 Inviscid compressible relativistic half-jet plasma flow stability, discussing disturbance equations and eigenvalues 22 p3850 A67-39705
 Nuclear fusion control and relativistic high density matter acceleration, discussing amplification effect application to plasma theory, plasma RF confinement and acceleration 22 p3851 A67-39772
 Branch cut contribution to longitudinal electric field in relativistic Maxwell plasma using non-Laplace transformation procedure 22 p3854 A67-40319

RELATIVISTIC THEORY

Ideal fluid energy-momentum tensor derivation of Crocco-Vazsonyi equation for ideal fluid relativistic hydrodynamics, discussing continuity equation for specific entropy 19 p3210 A67-35707
 Relativistic mechanics of continuous media reviewed on basis of variable eigenmass dynamics, with criticism and rejection of various energy flux concept methods 19 p3263 A67-35833
 Relativistic magnetic hydrodynamics profile streamlining and hodograph transformation 21 p3664 A67-38237
 Inhomogeneity formation probability in initially homogeneous Friedmann universe inhomogeneity formation probability in initially homogeneous Friedman universe 22 p3891 A67-40493
 Oscillating relativistic universe model from Einstein field equations, discussing Friedmann model matter and velocity distribution, Hubble law and universe volume oscillating relativistic universe model from 22 p3892 A67-40496
 Bolometric magnitude, angular diameter and radioflux density of various world models and red shift values, calculating universe and horizon age 24 p4228 A67-42259
 Einstein field equations derived for thin spherical shell of charged dust falling on spherically symmetric field of massive charged body, considering bounce 24 p4189 A67-42599

RELATIVISTIC VELOCITY

Flux measurement of particles with charges of one-third and two-thirds electron charge, reaching sea level with relativistic velocities 02 p0313 A67-12636
 Red shifts and blue shifts relative frequency distribution for QSO 03 p0515 A67-14321
 Rising blue shift induced by acceleration in relativistically expanding objects and significance for intensity variations in quasars 05 p0898 A67-16926
 Visual aspects of transstellar space flight 12 p2009 A67-26233
 Inverse problem of relativistic motion of point of variable mass 13 p2159 A67-27362
 Electromagnetic radiation from electric dipole moving with uniform relativistic velocity 18 p3000 A67-34022
 Head-on collision between stars at high initial relative velocity, considering one-dimensional driven shock motion in inhomogeneous medium 20 p3525 A67-36943
 Particle mass not related to velocity with respect to other particles velocity explained in terms of relativistic uniformly accelerated motion 22 p3837 A67-39879
 Extragalactic radio sources interpreted as consistent evolutionary sequence, suggesting particle injection, relativistic gas expansion and intergalactic gas pressure equilibrium 23 p4069 A67-41361
 Novae and supernovae outbursts, suggesting mechanism which can account for both phenomena and for other problems concerned with quasi-stellar sources /quasars/ 24 p4231 A67-42451

RELATIVITY THEORY

SA FIELD THEORY
 SA SCHWARZSCHILD METRIC

Electromagnetic analysis of rotating fluid systems containing rigid and inhomogeneous

parts within fluid by introducing additional relativistic transformation of gravitational constant 01 p0113 A67-10470
 Time-space quantization of gravitational field by formalisms in general relativity theory 01 p0114 A67-10746
 Langevin reasoning, used to establish Einstein energy inertia formula from energy conservation principle, applied to heat transformation in special theory of relativity 01 p0166 A67-10772
 London moment of rotating superconductors and relation to Lense-Thirring fields of general relativity 01 p0134 A67-10811
 Infield method of introducing Lagrange variables in special relativity as applied to describe fluid system in general relativity 01 p0114 A67-10869
 Unsteady adiabatic centrally symmetric radial flow of ideal fluid in general theory of relativity 01 p0114 A67-10987
 General inequalities for regular relativistic fluid spheres, noting gravitational potential energy limit 02 p0266 A67-11696
 Translational motion of two rotating spherical symmetrical bodies in general relativity theory 02 p0268 A67-12490
 Intranuclear cascades of nucleon-nucleus interaction calculated on basis of Fermi gas model, using Monte Carlo method and three-dimensional relativistic kinematics 02 p0314 A67-12748
 Evaluation of Einstein conclusion that moving body appears to be cool 03 p0466 A67-12847
 High order frequency shift measurement and general relativity effect 03 p0466 A67-12848
 Matter tensor of generally relativistic perfect fluid derived from invariant integral by Marx variational principle 03 p0468 A67-13392
 Electromagnetic field of accelerating charge using Coulomb law, relativity transformation relations, charge conservation, Newton third law, etc 03 p0469 A67-13719
 Five-dimensional relativistic space, giving physical interpretation for Riemannian space with metric form 04 p0656 A67-14746
 Vector field C defined at each point of space-time when curvature is zero, leading to series of cosmological models that satisfy Hoyle relativistic equations 04 p0698 A67-14809
 Lorentz invariance of special relativistic thermodynamics equations in inertial frame of observer 04 p0658 A67-15610
 Special relativity theory mechanical and thermodynamics laws for continuum 04 p0659 A67-15795
 Special relativity theory of electromagnetic interactions with thermoelectric solids, thermoviscous liquids and EM materials in continuum 04 p0659 A67-15796
 Pulsating gravitational collapse from point of view of external observer, noting oscillation period and distortion of contraction expansion symmetry 05 p0896 A67-16692
 Cosmological solutions of linear field theory, showing possible representation in form of hypersurface of second degree in five-dimensional affine space 05 p0897 A67-16773
 Relativistic trajectory and orbital precession of spinning satellite under nonspherically symmetric gravitational field 05 p0906 A67-16849
 Kruskal space in general relativity and uniform accelerated rigid rod in special relativity show striking formal similarities 05 p0847 A67-16970
 Shock wave structure in steady state monatomic relativistic gas 05 p0793 A67-17112
 Structure of general relativity theory space examined, using analytic continuation of geodesic equations 06 p1031 A67-17883
 Perturbed motion of comet in medium of constant low density in solar Schwarzschild field, using quasi-Newton approximation, considering electromagnetic and gravitational fields 06 p1084 A67-18164
 Variational derivations of field equations for relativistic mechanical, EM and gravitational fields in space-time continuum 06 p1033 A67-18582
 Equations of pulsations of spherically symmetrical configurations in general

- relativity theory, considering oscillation frequency and instability of singular sphere 07 p1248 A67-19483
- Equivalent vector method for obtaining Lorentz transformations of special relativity shown to have apparent variants 08 p1347 A67-20366
- General theory of relativity, emphasizing works discussed at London and Tbilisi conferences on gravitation theory 08 p1354 A67-20859
- Dynamical effects of heat absorption or rejection on flow of electrically charged fluid considered within special relativity framework 08 p1426 A67-20923
- Deformed figures of Maclaurin spheroids from solving post-Newtonian hydrodynamic equations for uniformly rotating axisymmetric bodies 08 p1354 A67-21245
- Solar oblateness indication of solar quadrupole moment effect on Mercury perihelion procession solar oblateness indication of solar quadrupole moment effect on Mercury perihelion precession 08 p1354 A67-21429
- Energy and momentum localization of gravitational field by direct field measurements 09 p1531 A67-21559
- Static axisymmetric interior solution of Einstein field equations which matches smoothly to one of Weyl exterior solutions 09 p1531 A67-21639
- Relativistic mass-velocity relationship in empirical verification involving data on electron-proton parameters 09 p1531 A67-21650
- Cosmological principle and field equations used in analysis of Einstein, de Sitter, Friedmann and Hoyle-Narlikar models 09 p1563 A67-21652
- Existence of gravitational waves, analyzing feasibility of experimental verification 09 p1531 A67-21653
- Relativistic rotation of perigee of satellite determined from first integral of motion equation 09 p1563 A67-21658
- Antisymmetric tensor theory of gravitation in flat space-time with energy and momentum conserved 09 p1532 A67-21979
- Relativistic electrodynamics of moving medium, discussing Maxwell-Minkowski equations, Born equations, field vector transformations, etc 09 p1533 A67-22449
- Relativistic theory for interaction of electric point charge and magnetic dipole 09 p1580 A67-22549
- Continuous charge distribution with time oriented streamlines in Minkowski space-time 09 p1534 A67-22579
- Dynamics of continuous media, proposing new equation in which action modifying intrinsic mass has no effect on velocity 09 p1534 A67-22580
- Complex vectorial formalism in general relativity, discussing Riemann connection related to representation of Lorentz group by three-dimensional linear space 09 p1525 A67-22625
- Translational motion of two rotating spherical symmetrical bodies in general relativity theory 10 p1680 A67-23358
- Evaluating accuracy of substitute term in Einstein equation, noting inconsistency with zero and second law of thermodynamics 10 p1680 A67-23496
- Temperature of moving body in relativistic frame of reference 10 p1680 A67-23497
- Singularities of cosmological solutions of gravitational equations for space filled with matter 10 p1710 A67-23588
- Cold star relativistic collapse kinematics, noting equilibrium and collapse of point masses system interacting by gravitation only 11 p1858 A67-24013
- Gravitational instability from reformulation of Lifshitz relativistic theory for galaxy formation in expanding universe and comparison with Bonnor approach 11 p1859 A67-24121
- Brans-Dicke theory of gravitational scalar field effect on structure of neutron cold spherical stellar model analyzed and compared with relativity theory 11 p1864 A67-24596
- Parametrization of reduced problem of stationary axially symmetric gravity fields 11 p1819 A67-24597
- Relativity theory for solid media model design, deriving equations of state and closed system of differential equations based on variational principle 11 p1819 A67-24675
- Turbulence tensor within framework of hydrodynamic relativity, noting generalization of Weber equation 11 p1782 A67-24760
- M-dimensional interpretation of n-dimensional Einstein equation 12 p1966 A67-25143
- Light deflection by solar activity 12 p2002 A67-25540
- Homogeneous solutions of Einstein-Lichnerowicz equations for electrically charged fluid with infinite conductivity universes 12 p1962 A67-26178
- Primordial element formation, primordial magnetic fields and universe isotropy, showing correctness of big-bang relativistic theory, early anisotropy of universe, etc 12 p2010 A67-26240
- Electromagnetic field tensor created by point charge provided with universal velocity and acceleration is equal to outer product of universal vectors 13 p2156 A67-26594
- Time-space quantization of gravitational field by formalisms in general relativity theory 13 p2158 A67-26775
- Energy of system of particles defined as related to active gravitational mass, or to inertial mass and passive gravitational mass respectively, in expanding universe 13 p2199 A67-27004
- Integration of Einstein gravitational equations implies that corpuscle be rigidly connected with particular Fermi space-time system of reference 13 p2158 A67-27298
- Particle momentum distributions derived from relativistic quantum statistical mechanics 13 p2161 A67-27398
- Phenomenological metric method applied to four tests of general relativity in evaluation for nearly flat space with spherical symmetry 13 p2159 A67-27399
- Relativistic thermodynamics in case of equilibrium with stationary co-moving metric and constant pocket temperature, deriving relativistic Fourier law of heat conduction 14 p2404 A67-27951
- Shear-free flows of gravitating gas investigated on basis of Newtonian mechanics 14 p2348 A67-28580
- Computer programs for calculating curvature tensors and motion equations [JPL-TR-32-1122] 14 p2276 A67-28847
- Hydrodynamics of gravitating stellar system numerically calculated for nonrotating spherically symmetric case 14 p2393 A67-28997
- Possibility of constructing and launching artificial satellite free of terrestrial influence to verify relativity theory 15 p2565 A67-29743
- Pulsating gravitational collapse from point of view of external observer, noting oscillation period and distortion of contraction expansion symmetry 15 p2556 A67-29863
- Momentum and energy of gravitational waves in terms of relativity theory 15 p2518 A67-30005
- Models of spherically symmetric nonstatic processes, including relativistic collapse to Schwarzschild sphere, constructed by space-time metrics [JPL-TR-32-1136] 15 p2564 A67-30438
- Perturbed motion of comet in medium of constant low density in solar Schwarzschild field, using quasi-Newton approximation, considering electromagnetic and gravitational fields 16 p2741 A67-30508
- Three-body problem reduced to two-body problem in general relativity theory 16 p2745 A67-30747
- Gravitation equations different from Einstein derived from Lagrangian in general form corresponding to general relativity theory 16 p2702 A67-31045
- Cosmological model for universe based on astronomical observations and validity of Einstein theory and existing laws of physics 16 p2752 A67-31540
- Supernova explosion and collapse theory using relativistic hydrodynamics 16 p2752 A67-31541
- Gravitation and antigravitation, with relativity review, noting gravitational energy field 16 p2703 A67-31764
- Soviet book on flight vehicle navigation accuracy and reliability 17 p2881 A67-31933
- Kinetic model of matter for energy momentum tensor of general relativity, noting freedom of
- divergence 17 p2883 A67-32360
- Michelson interferometer and ring laser compared for measurement of relativistic rotational effects of earth 17 p2883 A67-32361
- Relativistic generalization of Bernoulli equation from three-dimensional vector analysis of acoustic and entropy waves 18 p3084 A67-33422
- Necessary and sufficient conditions for space-time curvature tensor and isotropic vector field associated with double 2-form to satisfy higher order field equations 18 p3078 A67-33689
- Congruences of geodesic rays of Einstein vacuum spaces 18 p3078 A67-33690
- Integrability 18 p3078 A67-33690
- Structure of curved space-time in which electromagnetic wave propagation takes place without tail 18 p3079 A67-33761
- Momentum and energy of gravitational waves in terms of relativity theory momentum and energy of gravitational waves in terms of relativity theory 18 p3079 A67-33763
- Relativistic transformation formula for thermodynamics, with correspondence between energy change of reference system and energy change of moving body 18 p3159 A67-34119
- Einstein gravitation theory relation to general and special relativity, space time, unified four-dimensional continuum metric and chronogeometric theories 18 p3079 A67-34133
- Radar determinations of astronomical unit and orbits, radii and rotation vectors of inner planets, proposing general relativity radar test 18 p3123 A67-34145
- Schwarzschild criterion for convective instability in general relativity extended to Einstein hydrostatics to formulate buoyancy principle with aid of initial value problem 18 p3133 A67-34375
- General quantum relativity theory in real universe with large radius and elementary particle structure 18 p3080 A67-34728
- Energy-momentum density and superpotentials in privileged frame of reference, giving results due to Einstein and Freud pseudotensors 19 p3261 A67-35048
- Theoretical assumptions determining static long range force sign between particles in general relativity and other theories 20 p3483 A67-36184
- Gravitational effects and cosmic phenomena reconciliation with Einstein relativity scalar-tensor theories 20 p3524 A67-36834
- Kerr metric as Einstein field equations solution, considering Synge g method as possible Kerr metric source 20 p3486 A67-37089
- Faster-than-light particles with spacelike four-momentum within special relativity theory, discussing quantum field theory rejection of objections 20 p3486 A67-37091
- Soviet book on electromagnetic and gravitational fields theory based on relativity theories 20 p3486 A67-37207
- Radial adiabatic motion of spheres of uniform density and isotropic pressure in general relativity, giving bounce occurrence conditions 20 p3486 A67-37273
- Relativistic elasticity, discussing solution of field equations in transient unidirectional motion 20 p3486 A67-37279
- Rotating observer relative to inertial observer in relativity 20 p3486 A67-37501
- Differential and Clifford matrix algebra relationship in relativity theory, generalizing Dirac and quaternion algebras to Riemann spaces 21 p3656 A67-37923
- Polytrope structure from integrodifferential equation assuming metric, energy momentum tensor for static spherical symmetry and polytropic equation of state 21 p3658 A67-38615
- Gravitation wave radiation rate from binary stars, using Brans-Dicke general relativity theory 21 p3706 A67-38842
- Spherical symmetric problems in general relativity 21 p3707 A67-38962
- Gravitation theory, general theory of relativity, field theory and gravitational interactions with elementary particles 22 p3879 A67-39294
- Imbedded magnetic field stabilization effect on infinitely conducting inviscid compressible relativistic MGD half-jet 22 p3850 A67-39706

Intranuclear cascades of nucleon-nucleus interaction calculated on basis of Fermi gas model, using Monte Carlo method and three-dimensional relativistic kinematics 22 p3876 A67-40250

Nonzero cosmological constant effect /precise and trivial/, calculating perihelion precession from Schwarzschild exterior solution 22 p3889 A67-40382

Radial motion of spherical self-gravitating mass undergoing gravitational collapse or expansion using Einstein general relativity theory 22 p3892 A67-40495

Relativity theory accounting for energy conservation properties in elementary particle interactions and small size and high energy emission of quasars 22 p3892 A67-40499

Principles developed for founding of unified field theory of gravitation and electromagnetism, with space-time geodesics as charged particle motion equation 23 p4026 A67-40659

Lunar orbit precession due to quadrupole moment of sun arising from solar oblateness 23 p4066 A67-41014

Wave propagation in wave optics transition to geometrical optics in general relativity theory using series expansion 23 p4027 A67-41146

Rigorously geodetic inertial motion of extended object in Einstein gravitational field, using relativistic hydrodynamics 23 p4027 A67-41148

Generalized Lorentz transformation for inhomogeneous region in general relativity obtained by transformation leading to nearly straight system of reference 23 p4028 A67-41187

Einstein special relativity theory disproof based on four clocks situation 24 p4187 A67-41879

Rebuttal of Dingle disproof of Einstein special relativity theory 24 p4187 A67-41880

Relativistic gravitational collapse, considering asymmetric nonrotating star collapse 24 p4226 A67-41885

Energy-mass equivalence and relativistic transformation formulas application to extended bodies 24 p4188 A67-41905

Validity of formula of relativistic heat transformation, discussing pressure concept definition 24 p4257 A67-43107

RELAXATION

SA BED REST

SA CHEMICAL RELAXATION

SA CROSS RELAXATION

SA MAGNETIC RELAXATION

SA SPIN-LATTICE RELAXATION

SA STRESS RELAXATION

SA VIBRATIONAL RELAXATION

Thermal radiation effect on sound propagation in gases treated on basis of relaxation of molecular degrees of freedom 01 p0114 A67-10840

Stability of solutions to general equations of steady state one-dimensional relaxed flow of perfect gas mixtures [ONERA-TP-360] 01 p0054 A67-11089

Mode switching in tunnel diode, noting change from relaxation to microwave oscillation mode 02 p0217 A67-12090

Oscillatory relaxation of heavy two-atom molecules during single-quantum energy transitions in light-gas medium 02 p0269 A67-12422

Kinetic relaxation equation with initial values for uniformly expanding or contracting gas and Maxwellian molecule problem 04 p0604 A67-14792

Excitation and relaxation mechanisms for closed molecular gas laser 05 p0816 A67-16631

Relaxation theory and eigenvalue theory for linearized collision integrals for mixtures of Maxwell fluid molecules 08 p1355 A67-21116

Dielectric relaxation of gases and sharp rise in microwave absorption coefficient in Cytherean atmosphere 08 p1401 A67-21372

Relaxation rate influence on power generation of gas laser and on magnitude of inverse population 10 p1664 A67-23335

Oriented velocity and temperature relaxation in Coulomb type plasma with particle velocities distributed according to Maxwellian law, evaluating Coulomb collisions effect on plasma components 10 p1685 A67-23410

Optically pumped Rb in collisions with Kr inducing relaxation, noting two different correlation times due to kinetic collisions

and metastable states present 23 p4012 A67-40792

RELAXATION METHOD

Magnetic field gradient relaxation mechanism by random excitation of transitions in F equals 1 level of ground state of hydrogen atoms in maser 05 p0817 A67-16635

Finite difference approximation of balance wind equation, discussing convergence of Liebmann relaxation process, Coriolis term and computer time economy 09 p1525 A67-21551

Relaxation resistance of metals determined from creep test results, comparing calculated and experimental results 11 p1877 A67-24816

Elasticity problems for bounded connected region consisting of finite number of rectangles solved by relaxation techniques 13 p2215 A67-26372

Ferromagnetic resonance relaxation process in thin films 13 p2179 A67-27142

Electron correlations influence on plasma-broadened Lyman alpha line 15 p2520 A67-29679

Successive overrelaxation iterative method for solving elliptic partial differential equations 16 p2695 A67-30830

Cascade flow in mixed flow pumps and turbines, solving boundary value problems for stream function by relaxation method 20 p3356 A67-36421

Flow due to rotating disk with center sink solved numerically by considering flow unsteady [ASME PAPER 67-FE-8] 20 p3425 A67-37599

Circular polarization in j equals 1 to j equals zero transition in gas laser shown due to different atomic relaxation processes rates 21 p3640 A67-38353

Magnetospheric free boundary representation synthesis problem, discussing relaxation solution, dipole moment and stream direction 22 p3854 A67-40347

Aerospace vehicle structure loading under structural integrity tests with simulated aerodynamic heating conditions, discussing computer relaxation solution for rod temperature distribution 24 p4172 A67-42036

RELAXATION TIME

Mechanical properties of high polymer solid in terms of microbehavior as result of deformation and orientation, expressing anisotropic relaxation function as time dependent function 02 p0297 A67-11873

Diatomic gas flow past blunt bodies, noting effect of oscillation and dissociation relaxation on mean energy 02 p0180 A67-12465

Measurement method for spin relaxation and longitudinal decay of optically pumped vapors in weak magnetic fields 02 p0248 A67-12699

Theory of influence of surface states on impedance of semiconductor-insulator interface, determining relaxation times which directly affect cut-off frequency of device 03 p0487 A67-12810

Light absorption by uranium glass in excited state, showing relaxation time relation to luminescence 03 p0436 A67-13141

Hertzian relaxation spectra of MOS structures showing existence of two absorption regions 03 p0493 A67-13453

Spin-lattice relaxation time of dirty type II superconductor alloys in mixed state in almost upper critical field 03 p0493 A67-13472

Temperature and purity dependence of nuclear-spin relaxation time in type II superconductor gapless region and volume average of density states on Fermi surface 03 p0499 A67-13937

One-dimensional steady state gas compression flow undergoing thermodynamic relaxation processes 03 p0405 A67-14258

Relaxation process leading to thermal equilibrium behind ionizing shock waves in argon analyzed, using optical techniques 04 p0601 A67-14458

Spin relaxation times of ground state of atomic cesium in aromatic gases measured using optical pumping, noting dependency on temperature 04 p0680 A67-14611

Phenomenological theory of longitudinal Hall effect in cubic crystals, assuming anisotropic dispersion law and tensorial relaxation time 04 p0681 A67-15291

Energy relaxation in electron beams with high charge density, anomalous shiftings and broadenings and symmetrizations of energy

distribution 04 p0623 A67-15324

Shear relaxation in liquids, criticizing Knollman, Miles and Hamamoto relaxation time distribution measurement method 05 p0758 A67-16133

Quasi-linear relaxation in unsteady states of noncollision plasma, noting electron beam distribution function and Langmuir plasma oscillations 05 p0852 A67-16696

Magnon phonon scattering relaxation time as function of temperature and wave vector, calculating thermal conductivity of YIG 05 p0869 A67-17191

Temperature dependence of three-phonon processes in solids noting application to Si, Ge, GaAs and InSb 05 p0870 A67-17198

Hypersonic flow past sphere by relaxing gas with internal degrees of freedom in nonequilibrium 06 p0935 A67-17731

Grain boundary relaxation in high purity fcc metal using LF torsion pendulum, noting tests for internal friction and creep at constant stress 06 p1016 A67-17899

Dissociational rate constants and vibrational relaxation times modifications, considering coupling of vibrational and dissociational nonequilibrium of expanding gas in nozzle [AIAA PAPER 66-520] 06 p0992 A67-18851

Cyclotron resonance in tellurium at submillimeter wavelengths, deducing relation time anisotropy 06 p1061 A67-18920

Electron spin resonance of impurities in semiconductors, with attention to shallow centers 06 p1061 A67-18922

Size effects in electroconductivity of semiconductors with several groups of carriers with large intergroup relaxation time 06 p1064 A67-18944

Relaxation time of electrons in pure germanium and silicon measured from line width of cyclotron resonance at liquid helium temperatures taking into account quantum limit 06 p1064 A67-18945

Spin lattice relaxation times of donor electrons in Si, noting electric field effect on relaxation rate 06 p1068 A67-18971

Rotational relaxation times for homonuclear diatomic molecules 06 p1037 A67-19043

Plasma electron temperature determined from measured spectral line intensities 07 p1230 A67-20106

Stress analysis of solid rocket engine propellant grains including linear viscoelasticity, thermal analysis and equilibrium, relaxation times, engine sizes, cooling, creep relaxation, etc 08 p1373 A67-20874

NBS polyisobutylene relaxation modulus and Rouse functions for torsional molecular vibrations and internal rotation in viscoelastic theory of amorphous polymers 08 p1346 A67-20878

Restrictions on relaxation moduli of anisotropic linear viscoelastic solid 08 p1419 A67-20880

Two energy gaps in superconducting compounds studied by NMR techniques 08 p1371 A67-21443

Quantum mechanical theory of fluctuation and relaxation in semiconductor lasers, using Langevin method to calculate noise in quasi-Fermi electron distribution 10 p1663 A67-22891

Quantum mechanical kinetic theory of gas loaded spheres to obtain limit of transport coefficients and relaxation time 10 p1682 A67-23383

Semiconductor conductivity in strong SHF electric fields, measuring dielectric constant and Fourier component 10 p1657 A67-23567

Phase shift as quantitative measure of relationship between surface convection and charge relaxation 11 p1825 A67-23862

Relaxation in space of electron velocity distribution due to electron-ion collisions, obtaining time independent solution 11 p1833 A67-24372

Frequency stabilization of power klystron used in spectrometer for relaxation time measurement 11 p1767 A67-24752

Ionic waves in plasma in electric field interacting with beam of charged particles at relaxation time, using dispersion equation 11 p1841 A67-24869

Relaxation processes behind shock wave in free stream partially dissociated and vibrationally excited by monitoring time history of radiative emission in shock tube [AIAA PAPER 66-519] 12 p1929 A67-25905

Relaxation time for spatially homogeneous electron gas calculated by direct numerical integration of linearized Fokker-Planck equation 13 p2164 A67-26297

Field effect kinetics on pure germanium surface, measuring surface conductivity relaxation time by compensation-bridge techniques 13 p2174 A67-26403

Formation of compression shocks in calorically ideal real gases with thermodynamic relaxation analyzed in closed form 13 p2094 A67-26636

Heat transfer for gas with internal degrees of freedom between parallel plates, noting temperature profiles and jumps 13 p2100 A67-26959

Discrete ordinate technique for nonlinear Boltzmann equation for hard sphere molecules, considering pseudoshock relaxation 13 p2102 A67-26973

Rotational energy diffusion in shock wave structure, examining magnitude of error in effective number of intermolecular collisions required for equilibrium 13 p2104 A67-26980

Activation energy of molecular relaxation processes in terms of areas under loss factor and reciprocal temperature curves 14 p2259 A67-28299

Method for analyzing single- and double thermal relaxation processes 15 p2580 A67-29771

Quasi-linear relaxation in unsteady states of noncollision plasma, noting electron beam distribution function and Langmuir plasma oscillations 15 p2530 A67-29867

Semibrittle crack propagation dynamical criterion, noting relaxation rate increase with time 16 p2772 A67-31305

Phonon drag part of thermoelectric power in metals formula, by assuming electron scattering description by relaxation time 16 p2731 A67-31445

Nonequilibrium flow relation to flow in thermal balance, describing irreversible processes in terms of entropy source field and relaxation resistance 16 p2662 A67-31467

Molecular nitrogen rotational relaxation time by probing of supersonic free jet 16 p2705 A67-31757

Periodic relaxation pulses caused by thermal resonance drift, studying diffraction loss and other effects on transverse modes in crystal lasers 17 p2867 A67-32362

Relaxation processes for oxygen in solid solution in niobium demonstrating clustering of atoms into groups [AD-642957] 17 p2871 A67-32628

Optically pumped alkali metal vapors orientation checking by light pulse method, noting relaxation curve 17 p2869 A67-32811

Saturable organic dye absorber giant pulse lasers in limit of large absorber cross section, normalized initial inversion and relaxation time 17 p2869 A67-33055

Steady state relaxation hydrodynamic theory with generalized Prandtl-Meyer flows in nonequilibrium hydrodynamics [AFOSR-67-1992] 17 p2840 A67-33137

Radiative relaxation times for temperature perturbations in CO 2 with small water vapor admixture under conditions similar to Martian atmosphere, discussing dynamical phenomena 17 p2951 A67-33187

Scalar gravitational fields in pulsating stars, calculating scalar wave radiation rate and star relaxation time 17 p2952 A67-33319

Deficiencies of pulse-parameter representation used for semiconductor diodes, discussing generalized parameter describing transient processes relaxation 18 p3009 A67-33474

Atomic oxygen effect on vibrational relaxation of oxygen in shock waves at high temperatures, using laser schlieren technique 18 p3081 A67-33784

Free carrier absorption coefficients in 6H and 15R silicon carbide, showing probable ellipsoids of revolution 18 p3102 A67-34279

Multiphonon orbit-lattice relaxation of lower lying excited states of Dy doped lanthanum chloride investigated, using IR fluorescence and quantum counter techniques 19 p3302 A67-35035

Ionizational relaxation and excitation behind shock waves, proposing solution for kinetic equation system 19 p3293 A67-35403

Population inversion and spin-lattice relaxation effect on maser operation 19 p3304 A67-35547

Noise spectral density measured at low temperature in sensitized GaAs, studying

relaxation time, temperature effect, etc 19 p3307 A67-35733

Nonequilibrium quasi-one-dimensional nozzle flows in limit when relaxation time is large compared with characteristic flow time 19 p3172 A67-35800

Spherical interferometers used in measuring time-resolved spectra of ruby laser relaxation oscillations 19 p3241 A67-35804

Transport phenomena in semiconducting thin films studied using transport equation, obtaining relaxation time relationship to semiconductor 20 p3506 A67-36217

Relaxation of carbon dioxide pulsed laser levels by collisions with hydrogen, showing gain dependence on hydrogen pressure 20 p3457 A67-36384

Internal rotational relaxation effect on attenuation of HF turbulent vortices during degeneration of turbulence in viscous weakly elastic fluid 20 p3422 A67-37053

Wave kinetics of free Alfvén oscillations using Lagrange function of collisionless plasma, calculating energy growth rate and relaxation times 21 p3667 A67-38372

Nonideal type II superconductors, discussing flux motion and density, pinning force, magnetization, hysteresis, relaxation and energy loss 21 p3683 A67-38402

Nuclear relaxation time measurement in superconducting niobium near upper critical field 21 p3684 A67-38563

Electron mobility in He, using irreversible quantum statistics theory to obtain momentum dependent relaxation time 22 p3840 A67-39210

Relaxation times of carbon dioxide vibrational levels and afterglow pulsed gain for nonflowing gas laser amplifiers 22 p3814 A67-39354

Relaxation toward Maxwell distribution function of classical gas with initial nonequilibrium distribution function as velocity modulus function 22 p3782 A67-39406

Two-body relaxation term in N-body self-gravitating gases of one and three dimensions and validity of Vlasov equation 22 p3894 A67-40508

Ti isotopes nuclear magnetic resonance in hexagonal Ti metal showing d-like conduction-electron states at Fermi level by spin-lattice relaxation time 24 p4203 A67-42109

Very long nuclear spin relaxation times in gaseous He by suppressing He surface interactions measured in highly spin polarized samples 24 p4191 A67-42247

Relaxation of anisotropic plasmas based on Fokker-planck equation assuming elliptic distribution during process 24 p4198 A67-42440

Shock wave reflection with vibrational relaxation times investigated by matching characteristics equation to shock wave equation 24 p4144 A67-42564

Frequency limitation of Gunn effect associated with relaxation time for intervalley electron scattering in small signal approximation 24 p4205 A67-42811

RELAY

SA RADIO RELAY

Partially invariant relay systems 03 p0389 A67-13085

Coordination of integral and relay components in algorithms for adjusting control coefficients in model-reference self-adaptive control systems described by differential equations 03 p0390 A67-13102

Patching method applied to nonlinear differential equation of forced oscillation of second order relay system with damping 03 p0393 A67-13901

Probability of tracking process for given level of fading in automatic control relay system 04 p0591 A67-14658

Noise effect on ideal relay element with lagging feedback analyzed using Kolmogoroff equations, comparing performance with ideal forcing element connected to linear amplifier 05 p0782 A67-16321

Optimum switching function of relay servosystem subjected to stationary Gaussian random input found by perturbation method 05 p0783 A67-16445

Periodic oscillation mode of time invariant feedback system containing relay determined, using state space approach 06 p0978 A67-18719

Multidimensional self-adaptive control system involving dynamics and disturbance,

employing relay extremum control 07 p1161 A67-19204

Relays, ICs and hybrid /two-chip/ driver circuit for Motorola Digital Test Command System /DTCS/ 08 p1303 A67-21028

Annual National Relay Conference, Oklahoma State University, April 1967 13 p2084 A67-27693

Organic contaminant effects on relay reliability, discussing materials, degassing and contamination 13 p2084 A67-27694

Radiographic screening of relays for detection of solder balls, broken leads, cracks, etc 13 p2084 A67-27695

Relay testing for Saturn program including vibration scan, radiographic inspection, etc 13 p2084 A67-27696

Relay failure in spacecraft subsystem analyzed via vibration testing 13 p2085 A67-27697

Reliability of electromechanical relays, discussing test equipment, data analysis, etc 13 p2085 A67-27698

Random vibration testing of relays noting test equipment 13 p2085 A67-27699

Time constants of fast photodetectors measured, using mercury wetted relay and epitaxial indium arsenide diode laser 18 p3046 A67-33746

Noise effect on ideal relay element with lagging feedback analyzed using Kolmogoroff equations, comparing performance with ideal forcing element connected to linear amplifier 18 p3017 A67-33873

Dry friction servo system dynamics with relay delay in random noise case 20 p3451 A67-37152

Dynamic characteristics of relay servo systems 20 p3410 A67-37233

Suboptimal controller generating linear combination of state coordinates shown to give optimal performance when using linear controller preceding relay 20 p3410 A67-37251

Multivariable linear system noninteracting control realized by relays sliding motions 22 p3777 A67-39839

RELAY II SATELLITE

Clock synchronization via communications satellite Relay II 09 p1494 A67-21617

RELAY SATELLITE

Satellite relay techniques providing paths for aircraft-ground communication over ocean used in ATC, noting repeater electronics 01 p0021 A67-10207

Lunar communication satellites, discussing satellite relay, libration, random and synchronous satellite design, lunar orbits, etc [AIAA PAPER 66-315] 06 p0961 A67-17705

Radiation damage to satellite solar cells when shielded to various degrees, stressing silicon junction cells 17 p2804 A67-32840

Deep space communication system data rate increase using relay satellite 20 p3380 A67-36542

RELIABILITY

SA AIRCRAFT RELIABILITY

SA CIRCUIT RELIABILITY

SA COMPONENT RELIABILITY

SA QUALITY CONTROL

SA SPACECRAFT RELIABILITY

SA STRUCTURAL RELIABILITY

SA SYSTEM FAILURE

Graphical estimation of reliability of test results 01 p0104 A67-10157

Administrative considerations in systems effectiveness programs [SAE PAPER 660731] 01 p0170 A67-10631

Reliability Symposium, San Francisco, January 1966 01 p0081 A67-11332

System effectiveness critical activities covering reliability, maintainability, quality, design guides, etc, for aerospace industry 01 p0170 A67-11333

Reliability estimation techniques adaptable to computer implementation for complex manned systems 01 p0031 A67-11338

Reliability modelling utilizing conditional probability logic to simplify dependency and complex redundancy 01 p0083 A67-11353

Resource allocation for maximum system reliability, noting weight allocation in spacecraft and Lagrange multiplier approach 01 p0084 A67-11354

Problems in using probability theory by reliability engineers 01 p0084 A67-11355

Reliability and maintainability demonstration at Rome Air Development Center, discussing test methods 01 p0084 A67-11360

Time domain reflectometry in reliability testing, detailing applications in checkout of electroexplosive devices with spark gap and cable validation equipment 01 p0084 A67-11361

Reliability and maintainability requirements and electronic systems division /AFSC/ application 01 p0042 A67-11368

Reliability testing improvement through developments in vacuum systems, vibration systems and triaxial shock testing 01 p0084 A67-11369

Sampling plans for identification of inadequate subsystems 01 p0084 A67-11370

System reliability evaluation and identification of inadequate subsystems, with application to two missile-borne guidance systems 01 p0111 A67-11371

Game theory of economic incentive payment reliability demonstration and prediction 01 p0171 A67-11374

Reliability matrix analysis of AFSCM 375 management system 01 p0171 A67-11375

Modified long-term system reliability models for redundant systems, considering imperfect failure detection, repair and sparing 01 p0043 A67-11378

Unified treatment of costs yields and reliability in semiconductor manufacture 01 p0171 A67-11380

Bayesian statistics applicability to reliability estimation and decision-making 01 p0085 A67-11381

Reliability optimization relation to program time and costs and schedule for cost reduction keeping time constant 01 p0085 A67-11384

Tape recorder design for spaceborne data storage using isoelectric drive principle of peripherally driving tape packs to obtain high reliability 02 p0242 A67-12018

Integration of reliability, maintainability and other engineering disciplines, discussing objectives of program management [AIAA PAPER 66-859] 02 p0343 A67-12260

Analytic method for measurement of value of increased reliability or maintainability, using maintenance float as criterion [AIAA PAPER 65-734] 03 p0426 A67-12917

Book on electronics reliability, calculation and design 03 p0377 A67-13232

Miscellaneous results connected with simple system alternating between two states, running or under repair 03 p0432 A67-13824

Analytical, test and coordinative methods in reliability problems in aerospace systems 04 p0627 A67-14579

Exponential smoothing for prediction of reliability growth having advantages of tracking data precisely while retaining in memory only few historical statistics 05 p0811 A67-16828

Acceptance vibration testing program costs, benefits and test control 05 p0813 A67-17248

Reliability assessment technique, discussing application of Bayesian statistics 05 p0906 A67-17250

Mathematical models properties analyzed for system reliability and maintainability, namely mission availability, discussing relationship to failure and action rate and time constraint 05 p0813 A67-17252

Integrated plan for reliability demonstration through safety margin testing 05 p0813 A67-17253

Relation between packaging design and cooling, vibration, RF interference and reliability of microelectronic systems used in space vehicles 05 p0779 A67-17467

Failure rates and modes for nonoperating electronic packages, presenting solutions for reliability problem 05 p0780 A67-17469

Reliability in optimal control problems in terms of probability of faultless operation 07 p1162 A67-20027

Dual redundancy digital computer for improved reliability in real time processes and control situations where fault results in fatality or mission failure 08 p1298 A67-20638

RCA Variable Instruction Computer /VIC/ for high reliability applications 08 p1298 A67-20639

Multithreading design of reliable aerospace computer, showing inverse proportionalities between speed capacity and reliability 08 p1298 A67-20667

Systematic approach using weight factor for apportioning mean corrective times of equipment based upon maintainability, usage

and reliability data 08 p1315 A67-20670

System design decisions through static and rotating magnetic memories reliability as applied to command and control systems 08 p1299 A67-20685

MORL system reliability analysis, discussing Monte Carlo simulation, major parameters, constraints, program contingencies, etc 08 p1411 A67-21073

High energy booster and upper stage combinations for space research, discussing mission capabilities, cost factors, reliability, etc 08 p1412 A67-21075

Failure-correction decoding in improving error-correction block codes, using reliability estimates of received digit 09 p1459 A67-21578

Reliability - Symposium, Washington, D.C., January 1967 09 p1581 A67-22286

Reliability management techniques for Projects Mercury, Gemini and F-4 Phantom II aircraft 09 p1582 A67-22288

Reliability criteria application to improvement of program and design decision quality during preliminary design 09 p1582 A67-22291

Optimizing reliability level in conceptual phase system to ultimately yield operational systems of desired capability, illustrating with C-130/C-141 transport aircraft study 09 p1582 A67-22293

Operational reliability development program, considering design, maintainability and personnel subsystem 09 p1582 A67-22294

Nondestructive testing in calculating inherent reliability and improving reliability of manufactured product 09 p1506 A67-22304

Yield strength and reliability of structural cluster welds determined using statistical analysis 09 p1506 A67-22308

Reliability of future space systems through adoption of complexity factor ratings 09 p1572 A67-22311

Estimated reliability impairment of space equipment due to shortings from particle impact 09 p1481 A67-22312

Reliability analysis of active, standby and active-standby redundant system, discussing Poisson-binomial probability distribution function 13 p1213 A67-26828

Annex circuits for regulating electrolyte grade, cell temperature, reactant supply, fluid circulation and generated electricity of unit cells grouped in batteries 14 p2253 A67-29024

Mobile telemetry ground station and maximum reliability procedures for rocket telemetry transmission system used in solar eclipse 15 p2467 A67-29575

Systems approach to reliability, integrating cost and performance and demonstrating tradeoff decisions 15 p2448 A67-29800

Mean time between failures for repairable system in terms of MTBF and availability of constituent units by reducing reliability block diagram 15 p2453 A67-30062

Reliability for redundant repairable systems using queueing theory, studying triplicate and similar/dissimilar subsystem systems 15 p2453 A67-30063

Reliability management under fixed-price contracts 15 p2584 A67-30403

Supplier control and reliability, discussing adequate input supply and output monitoring 15 p2584 A67-30407

Engineering approach to nonelectric reliability in design, stressing mechanical aspects 15 p2495 A67-30415

Reliability assessment on incomplete and inaccurate field removal data, using reliability scoreboard 15 p2496 A67-30419

System design for maximum reliability when gross weight of system is assigned or minimum weight when system reliability is designated 16 p2681 A67-30635

Soviet book on flight vehicle navigation accuracy and reliability 17 p2881 A67-31933

Reliability studies for optimization of aerospace systems and military engineering design and manufacture 18 p3053 A67-33637

Human factors and anthropotechnology in development of weapon systems 18 p2993 A67-33643

Design considerations for reliable microwave power packs noting redundancy, independent module system and intrinsic reliability 18 p3010 A67-33685

Microelectronic systems design problems and solutions, discussing system adaptability concept and influence on design methods and technology 18 p3015 A67-34561

Reliability demonstration during category II and III testing of missile and airborne radar fire control system, emphasizing coordination between factory and field 18 p3138 A67-34652

Air Force programs for development of effectiveness and reliability data analysis systems 18 p3007 A67-34658

Centralized parts and materials reliability information center /PRINCE/APIC/, explaining data storage and retrieval 18 p3007 A67-34659

Navy method for integrating all reliability data by Integrated Data Plan, discussing Interagency Data Exchange and Failure Rate Data programs 18 p3007 A67-34660

Nature and magnitude of differences between intrinsic and operational reliability and maintainability characteristics, suggesting reconciliation 18 p3057 A67-34661

Statistical method for demonstrating reliability of clustered liquid propellant rocket engines 18 p3116 A67-34662

Relationship between acceptance test and operational reliability studied by multiple regression analysis 18 p3138 A67-34668

Reliability prediction prospects for electronic products, considering factory-to-target progress and reliability factors 18 p3057 A67-34672

Development and application of Monte Carlo logistic simulation model for measuring system availability dependence on reliability, maintainability and logistic support 18 p3021 A67-34674

Problem of manufacturing space vehicles with rigidly controlled cleanliness and biological contamination for missions to other planets 18 p2995 A67-34677

Saturn V reliability analysis model used by management for predicting performance probabilities 18 p3138 A67-34684

Manned mission reliability and maintainability requirements in future systems 18 p2995 A67-34686

Characteristics of immediate, delayed and cyclic maintenance of phased planar array radar systems, considering outage availability effects 18 p3005 A67-34693

Ground system design approach integrating reliability and maintainability with performance requirements, using Saturn V simulation as example 18 p3139 A67-34694

Maintenance and support factors effects on systems availability described by mathematical models, giving applications in tradeoff studies 18 p3163 A67-34695

Reliability and maintainability case histories 18 p3005 A67-34696

Space systems reliability design problems, discussing estimation, weight-reliability tradeoffs, spare parts and redundancy 18 p3139 A67-34698

Reliability prediction with inadequate data in flight control systems, using nonelectric approach combining failure data with judgment 18 p3058 A67-34699

Integrated reliability program for Scout launch vehicle in terms of design specification, review functions, malfunction reporting, failed parts analysis, quality control, standardization and certification 18 p3139 A67-34702

Reliability, orbit achievement and control and increased power bandwidth as factors making communications satellites economically feasible 19 p3350 A67-35649

Book on probability in communication engineering covering probability theory, information and reliability theory, random processes and noise and random phasor sums 20 p3378 A67-36137

Reliability criteria of systems with recovery, noting mean time to failure of system and mean time of system operation between failures 20 p3454 A67-37037

Reliability engineering - Conference, Nuremberg, April 1967 22 p3921 A67-39279

Anthropotechnical reliability establishing methods considering ability of man to assimilate amount of information in unit of time 22 p3754 A67-39280

Theoretical and experimental research methods for engineering reliability operations 23 p4010 A67-41320

RELIEF MAP

Millimeter wave radiometry to study atmospheric properties, topographic relief, planets, medical and industrial

- research 14 p2265 A67-28402
Photometric methods for determination of lunar relief 18 p3132 A67-34328
- RELIEF VALVE**
S PRESSURE RELIEF VALVE
- REMOTE CONTROL**
Numerical solution of ordinary differential equations at remote terminal, commenting on integration in on-line mode 02 p0259 A67-11802
Open-shop remote computing terminal system using direct coupled system of IBM 7094 and 7040 computers for core-to-core transmission, discussing experience gained from using and managing it 02 p0206 A67-11805
Test information systems improved by coupling data sources to users through remote terminals connected directly to large time sharing computing systems 02 p0207 A67-12001
Operator reorientation of attitude of simulated remote maneuvering unit /RMU/ using on-off acceleration command control system 02 p0186 A67-12230
Meteorological experiments possible in manned earth orbital spacecraft with aid of remote sensing of electromagnetic radiation 02 p0239 A67-12379
Functioning period of remote control systems in sporadic data transmission determined, using mathematical methods of queueing theory 05 p0782 A67-16266
Satellite role in worldwide meteorology, discussing global observation, observation platforms, manned satellites, and remote sensing and data collection of satellite instrumentation 05 p0837 A67-16383
Saturn V mobile launch facility design, discussing vertical assembly of space vehicle on launch platform, transfer to launch pad, automatic checkout and remote control of launch operation 05 p0788 A67-16616
Unmanned remotely operated lunar surface Emplaced Scientific Station /ESS/ design and objectives as Apollo follow-on lunar missions [AIAA PAPER 67-117] 06 p0980 A67-18286
Lunar ground data for interpretation of AES orbital experiments such as electromagnetic radiation monitoring, photographic data evaluation, spectrography, etc 08 p1392 A67-21078
Optimal type of strategy of remote control and force sensitive and stable feedback presentation in master-slave manipulators with transmission delay 09 p1456 A67-22374
Kinematic analysis of deviation from aircraft-missile line for designing electronic missile firing simulator, with manual telecontrol comprising controlled precession gyroscope for last integration 09 p1486 A67-22419
Noise rejection of remote control command information transmission in system with comparison circuit, using error detecting and correcting codes 11 p1772 A67-25041
First order factors affecting driver ability to safely control typical lunar vehicle through simulated mission profile over representative terrain [SMPT PAPER 101-54] 12 p1920 A67-25469
Space exploration by automatic, manned and remote-controlled space flight systems, noting applications, limitations, transmission power and distance 14 p2256 A67-28036
Stage separation, fluid behavior, engine plumes characteristics, etc, of Saturn vehicle detected, using remote sensing techniques 14 p2320 A67-28700
Global ocean data acquisition by remote sensor operating from spacecraft for oceanographic studies 15 p2477 A67-29698
Handbook of telemetry and remote control considering position measuring, missile guidance, flight control, data processing, feedback information, communications, etc 16 p2633 A67-31916
DIALOG /computer implemented retrieval system/ capabilities, design, philosophy and performance 17 p2819 A67-32468
Vacuum system pressure measuring and monitoring by remote control methods as used in Gemini spacecraft test program 17 p2859 A67-32593
Number of feasible information networks with single channel redundancy for remote control of telemechanical system 18 p3016 A67-33572
- High altitude research rocket HF telemetering remote control signal receivers, antennas and earth station, discussing design and circuitry of transmitter antenna 19 p3193 A67-35061
Remote control pneumatic pressure test system for Saturn S-IC booster checkout with manual or automatic control, using computer 20 p3415 A67-36569
Remote control of monochromator prism rotation using balanced-bridge system to regulate flow 20 p3451 A67-37308
Remote preamplifiers in multielement antenna arrays of radio telescopes operating at meter wavelengths, noting noise temperature effect 20 p3403 A67-37508
Scientist role in automated laboratory for remote biological exploration of planets [AIAA PAPER 67-632] 20 p3375 A67-37615
Soviet book on time-frequency remote control systems theory and design 20 p3412 A67-37632
Telemetry receiving station and remote control system for satellites and missiles, measuring Doppler effect, demodulation and diversity combiners 21 p3583 A67-38639
Multispectral remote sensing techniques for agricultural surveys from orbiting satellites, discussing in-flight signal processing 22 p3806 A67-40367
Cylindrical solid state oxygen generators, discussing manual and remote electrical activation 23 p3968 A67-41621
Automatic crop surveys contribution to agricultural technology in developed and underdeveloped countries [AIAA PAPER 67-766] 24 p4258 A67-42935
Passive sensing techniques for remote monitoring of nonelectronic systems [AIAA PAPER 67-774] 24 p4158 A67-42942
Spaceborne computer-managed laboratory for experiments and instruments control in future space missions [AIAA PAPER 67-957] 24 p4140 A67-43040
- RENAL FUNCTION**
Extraction method for renin from rats with bioassay simplified by using microphonic method after injecting renin extract into tail vein 01 p0015 A67-10412
High gradient acceleration effect on human renal clearances of free water and creatinine following moderate water load 05 p0756 A67-16288
Cannulation of renal capsular lymphatics in anesthetized dogs, testing if lymph fluid can serve to assess tissue oxidation 06 p0952 A67-17853
Heat stress effect on human renal function, measuring glomerular filtration rate, renal plasma flow, free water clearance and electrolyte excretion 10 p1599 A67-23811
Vasopressin-aldoosterone interrelation in diuresis and antidiuresis to explain body fluid weight loss in astronauts during space travel 21 p3574 A67-38082
Na and water excretion, renal plasma flow and glomerular filtration rate lowered by lower body negative pressure /LBNP/, noting application to space flight weightlessness [SAM-TR-65-329] 24 p4110 A67-41801
- RENDEZVOUS**
SA EARTH-MARS RENDEZVOUS
SA EARTH ORBITAL RENDEZVOUS /EOR/
SA EULER-LAMBERT EQUATION
SA ORBITAL RENDEZVOUS
SA SATELLITE RENDEZVOUS
Rendezvous problem of ascent and injection into transfer orbit and terminal phase 06 p1082 A67-17790
Linear single input optimal cooperative rendezvous problem with quadratic performance index solved using variational calculus 15 p2458 A67-29909
Interception satellite thrust and steering optimization for pursuing maneuverable satellite, analyzing both evader and pursuer sides with differential game concept 24 p4182 A67-42908
- RENDEZVOUS GUIDANCE SYSTEM**
Difference equations of absolute motion applied to universal rendezvous guidance scheme 01 p0110 A67-10427
Satellite rendezvous guidance laws applicable to circular, near-circular and elliptical orbits, using Lagrangian formulas for position and velocity in two-body orbit 02 p0264 A67-12315
X-band Cassegrainian tracking antenna for space rendezvous position and rate information for navigation and guidance computations 04 p0569 A67-14502
Laser guidance system for rendezvous and docking providing data acquisition for guidance computer 04 p0655 A67-15663
Finite thrust explicit guidance law for nearly circular orbital rendezvous 05 p0906 A67-17208
Gemini rendezvous results, discussing equipment, maneuvers, docking, stationkeeping, orbital calculation, etc 06 p1098 A67-18649
Linear/Monte Carlo method performance evaluation of intercept/rendezvous guidance and navigation for advanced space missions 17 p2882 A67-32493
Adaptive terminal guidance scheme for circular orbit rendezvous to provide near optimal trajectory 22 p3832 A67-39964
Lunar rendezvous spacecraft guidance system performance for various initial conditions and instrument errors simulated by Monte Carlo computer program 22 p3832 A67-39965
Variable point guidance technique modifications verified by simulation containing representation of typical booster and upper stage configuration 24 p4182 A67-42907
- RENDEZVOUS SPACECRAFT**
Pulsed injection laser radar for rendezvous and docking operations, giving results of test performance [AIAA PAPER 67-606] 19 p3259 A67-35997
Mathematical model for studying liquid slosh effects on rendezvous dynamics by incorporating sloshing dynamics into vehicle motion equation 22 p3888 A67-40189
- RENDEZVOUS TRAJECTORY**
SA EARTH-MARS RENDEZVOUS TRAJECTORY
Quasi-optimum control law for minimum-time bounded acceleration rendezvous in plane 01 p0111 A67-11212
Graphic solution of Lambert time of flight equation for spacecraft correctional maneuvers with respect to initial velocity 01 p0152 A67-11399
Minimax rendezvous time of two linear uniform control plants, constructing optimal pursuit 02 p0225 A67-11956
Fixed time rendezvous by two-impulse transfer maneuver in statistical optimization [AIAA PAPER 67-57] 06 p1029 A67-18266
Rocket maneuvers for rendezvous with propulsionless target satellite in elliptic orbit 08 p1410 A67-20640
Rendezvous between coplanar circular orbits, comparing Hohmann transfer with simple bielliptic method 09 p1564 A67-21695
Pontryagin maximum principle application to solution of one-dimensional minimum time rendezvous problem for thrust limited rocket with initial and final mass specified 12 p2012 A67-25922
Minimax rendezvous time of two linear uniform control plants, constructing optimal pursuit 17 p2831 A67-33273
Lambert theorem used to find required trajectory to effect rendezvous in space 19 p3332 A67-34828
Time optimal flight trajectories in planar and spatial pursuit problems with constraints on pursuer, using Pontryagin maximum principle 21 p3712 A67-39151
Alternate mission modes for manned Mars exploration 22 p3886 A67-40136
Three-impulse interplanetary rendezvous trajectory as solution of time fixed multipulse space problem 22 p3887 A67-40137
Two-finite burns minimum fuel rendezvous problem using dual phase plane description, determining control law 22 p3888 A67-40147
- REPAIR**
SA SELF-REPAIRING SYSTEM
Queueing theory applied to phased array radar maintenance problems, specifically replacement and repair of transmitter and/or receiver modules 08 p1292 A67-20668
Mean time between failures for repairable system in terms of MTBF and availability of constituent units by reducing reliability block diagram 15 p2453 A67-30062
Reliability for redundant repairable systems using queueing theory, studying triplicate and similar/dissimilar subsystem systems 15 p2453 A67-30063
Rapid Evaluation System To Repair Equipment /RESTORE/ approach to technical manual preparation on digital

equipment 23 p4085 A67-40582

REPEATER

Satellite relay techniques providing paths for aircraft-ground communication over ocean used in ATC, noting repeater electronics 01 p0021 A67-10207

Dynamic behavior of electric angle drive unit in linear automatic control system, noting nonlinearities 02 p0227 A67-12197

Reflection amplifier design for use in tunnel diode UHF radio 11 p1766 A67-24689

repeater 16 p2629 A67-31530

Satellite relay to provide communication paths for aircraft-ground communication over ocean, considering system design for ATC using reflex 20 p3381 A67-36591

REPLACEMENT

Replacement policies for aircraft and missile parts that fall according to normal log-normal or Weibull continuous probability distribution 01 p0083 A67-11339

Operational reliability components in four military systems, analyzing replacement data by digital and computer type circuitry employing semiconductors 01 p0041 A67-11344

In-service reliability analysis in reducing maintenance costs and spares requirements 01 p0083 A67-11352

Logistics simulation modeling for optimizing spares mix needed for maintenance of airborne systems at minimum cost 23 p4085 A67-40590

REPRODUCTIVE SYSTEM

Spermatogenesis condition of experimental dogs after 22-day space flight and reproduction function in first offspring generation 20 p3367 A67-36257

REPTILE

SNAKE

RESEARCH

S HIGH TEMPERATURE RESEARCH

S NUCLEAR RESEARCH

S OPERATIONS RESEARCH

RESEARCH AIRCRAFT

Scientific research using C-135 aircraft for AEC atmospheric testing 13 p2090 A67-27257

Scientific research using NASA CV-990 aircraft 13 p2090 A67-27258

Mountain wave and air turbulence program using high altitude research aircraft measurements and stressing 24 p4181 A67-42275

CAT 24 p4181 A67-42275

Wing tip vortices behind DC-8 measured for maximum circumferential velocities by research aircraft 24 p4091 A67-42276

RESEARCH FACILITY

Nagoya University, Institute of Plasma Physics, Annual Review, April 1965-March 1966 04 p0682 A67-14590

Ground station for space communications and radar and radio physics, noting use of Cassegrain antenna computer guided pointing control, plug-in equipment box, etc 04 p0596 A67-15047

Geological and astronomical research - Lunar International Laboratory Symposium, Athens, September 1965 04 p0596 A67-15062

Research and system requirements for two-to-six-man lunar scientific laboratory to investigate lunar habitability 04 p0597 A67-15063

Lunar International Laboratory /LIL/ exploration and lunar physics program 04 p0597 A67-15065

Space age facilities - ASCE Conference, Cocoa Beach, Florida, November 1965 05 p0786 A67-16606

Aeronautical research facility in West Germany 06 p0981 A67-18754

Research and facility of Institute of Fluid-Flow Machinery at Gdansk, Poland 06 p0981 A67-18823

Plasma stability research program facilities for study of helical instabilities in cesium arc plasmas in axial, Ioffe and other magnetic field configurations 11 p1829 A67-23998

Aeronautical research in India, precision instrumentation design and production

development, facilities, rocket launching station, etc 11 p1885 A67-24653

Superconductive magnets at Lewis Research Center of 12 p1978 A67-25105

NASA Simulator design, discussing control information category and presenting representative fixed and moving base research simulators to describe display design and motion cue 13 p2091 A67-27271

Safety practices for high energy physics research equipment filled with liquid hydrogen or deuterium 13 p2092 A67-27649

Supersonic combustion simulation facility and duplicable static parameters for hydrogen fuel 15 p2465 A67-29437

[AIAA PAPER 66-743] 15 p2465 A67-29437

Engine development and manufacture in Sweden 17 p2928 A67-32123

Indonesian space center, describing radar and optical tracking systems, launch complex telemetry system, etc 19 p3207 A67-35234

Pakistan space research noting facilities, sounding rocket experiments and satellite-and ground-based observations 19 p3321 A67-35297

Development of Indian sources of aerospace metals evaluated, noting availability, potential, priority of materials and research facilities 20 p3484 A67-36187

High altitude variable Mach number test cell for testing intake system of Concorde aircraft Olympus 593 20 p3414 A67-36497

AMICON 8000 kw plasma facility for simulating reentry environments for material and thermodynamic tests 20 p3415 A67-36551

Chilbolton 25 m steerable antenna for radio wave propagation 20 p3400 A67-37203

research 20 p3400 A67-37203

JPL free piston shock tube design, calibration and performance 21 p3606 A67-37773

Langley Hypersonic Nitrogen Facility flow evaluation covering pitot pressure survey of nozzle wall boundary layer, centerline and Mach number 21 p3607 A67-37777

Pressure Commutating System for propulsion research facility noting cost saving and allowance for pretest checkout 23 p3988 A67-41427

Experimental facilities to test antimatter hypothesis of comets and meteoric swarms 23 p4069 A67-41689

Materials development and testing in orbiting laboratory noting zero gravity benefits [AIAA PAPER 67-815] 24 p4139 A67-42969

Boeing Huntsville Simulation Center emphasizing ALPINE system and Interim Time Sharing System /ITS/ [AIAA PAPER 67-896] 24 p4126 A67-43005

RESEARCH PROJECT

Criteria used by Government patent departments in screening and evaluating inventions for patent applications 07 p1269 A67-19467

Cost incentive contract effects on research and development 08 p1431 A67-21287

Satellite telecommunication techniques including demodulation, detection, microwave amplification, antennas, etc 17 p2813 A67-32400

Italian scientific research program during IQSY, with summarization of preliminary results 19 p3223 A67-35480

Space research experiments reliability requirements, considering structural components, project planning and measuring methods adaptation to ambient conditions 22 p3899 A67-39283

Augmentor-Wing research program for developing high lift devices to reduce takeoff/landing speeds of jet aircraft [AIAA PAPER 67-741] 24 p4094 A67-42804

NACA transition to NASA noting factors shaping development of government space research policy [AIAA PAPER 67-836] 24 p4259 A67-42977

Deep-Space Network /DSN/ planning, discussing support for lunar and planetary flight support and applied research applications [AIAA PAPER 67-975] 24 p4260 A67-43051

RESEARCH VEHICLE

Joint NASA-USAF lifting body flight test program and M2/F2, HL-10 and SV-5P research vehicles 06 p0947 A67-18197

Flight tests of two X-22A dual tandem rotatable ducted propeller V/STOL research aircraft 06 p0948 A67-18201

Research and operational results obtained with nonaerodynamic variable stability flying platform for examining problem associated with lunar landing 06 p0948 A67-18202

Ground and flight tests to evaluate lunar landing research vehicle fly-by-wire control system [AIAA PAPER 67-273] 07 p1129 A67-20048

Bell X-22A VTOL research vehicle, assessing mechanical and aerodynamic characteristics, variable stability and control system, etc 11 p1743 A67-24097

XH-51A compound research flight test program, discussing adaptation of rigid rotor concept 13 p2052 A67-26421

Instrument testing for 625 A1 research satellite with Nike-Apache BRD-A1 high altitude research rocket 13 p2119 A67-26581

Temperature control in design of ESRO I European research satellite design 13 p2222 A67-26582

Design requirements for commercial orbital space stations intended for weather forecasting, agricultural prediction and industrial research [AAS PAPER 67-113] 15 p2557 A67-29961

Integrated reliability program for Scout launch vehicle in terms of design specification, review functions, malfunction reporting, failed parts analysis, quality control, standardization and certification 18 p3139 A67-34702

Booster for Skylark upper atmosphere research vehicle to increase altitude and reduce launching dispersion of single stage vehicle 24 p4206 A67-42580

RESIDUAL GAS

Sensitivity increase in leak detector by using grid to eliminate residual gas from scattered ions 04 p0625 A67-15631

Specific degassing of high polymers placed in simulated space environment studied by residual gas analyzer 05 p0832 A67-16304

Flashed getters for production of ultrahigh vacuum, tantalum most promising based on residual gas analysis 08 p1354 A67-21496

Magnetic trap electron capture lifetime dependence on magnetic field determined by scattering by residual gas, noting adiabaticity parameter critical value 15 p2526 A67-29361

Antiproton abundance upper limit in low energy galactic cosmic radiation determined by exposing nuclear stack to residual atmosphere 20 p3518 A67-36872

Fast scanning 180 degree magnetic mass spectrometer for monitoring fast changes in residual gas compositions 20 p3448 A67-36875

Cold cathode ion source /CCIS/ quadrupole mass spectrometer for ultrahigh residual gas analysis 23 p4000 A67-41217

RESIDUAL STRESS

Residual stress effect on stress-strain curve of uniaxial composite consisting of stainless steel wire and aluminum alloy matrix 03 p0444 A67-13432

Hole-drilling method of measuring residual stresses in elastic materials determined by empirically derived relation between magnitudes of principle stresses and strain relaxation about hole 03 p0531 A67-13436

Compression and tension of rod and plate with distribution of residual stresses such that deformation is partially plastic and elastic 06 p1107 A67-18633

Stress induced velocity variations of longitudinal and shear ultrasonic waves in steel, Al and Cu, calculating third order elastic constant 08 p1415 A67-20481

X-ray diffraction techniques and apparatus for measuring residual stresses in metals [SAE PAPER 670151] 09 p1502 A67-21771

Tensile residual stress measurement in area of failure origin in helicopter rotor blade, using laboratory tests and X-ray analysis [SAE PAPER 670154] 09 p1502 A67-21772

Ablative properties of nylon-phenolic materials used in fabrication of composite heat shield with low residual stresses 09 p1523 A67-22506

Portable X-ray equipment for measuring residual stresses in welded rocket motor case, machined aluminum parts and titanium welds [SAE PAPER 670152] 09 p1509 A67-22542

X-ray diffraction residual stress measurements in aluminum alloy [SAE PAPER 670153] 09 p1509 A67-22543

Fiber aspect ratio, residual stress state

and geometry of multifiber arrays studied in terms of influence on local stress concentration and matrix reinforcement 10 p1671 A67-23705

Asymptotic elastoplastic condition of spherical shell weakened by circular hole and sustaining residual deflections 12 p2028 A67-25631

Strain distribution in aluminum filament reinforced metal, investigating matrix plastic behavior and residual stresses, etc [ASTM PAPER 8] 18 p3067 A67-34573

Axial residual stress determination in metal surface layers based on measuring strains 19 p3343 A67-35844

Ultrasonics as nondestructive means of measuring residual stresses 20 p3537 A67-36475

Deformations and residual stresses in polycrystalline microstructures, using photoelastic coating method 20 p3540 A67-37059

Resistance spot welding process, using heating, cooling and stress development data to compute internal behavior 20 p3456 A67-37697

Triaxial state of residual stresses in long solid or hollow axisymmetric longitudinally uniform cylinder measured by boring out cut off specimen, analyzing process 22 p3913 A67-40034

Cylinder residual stress measurement, discussing stress distribution from Sachs equations 22 p3913 A67-40035

RESIDUE

Algebra of factorized Regge pole residues applied to obtain relations between meson-baryon and baryon-baryon exchange processes 16 p2705 A67-31627

RESIN

SA EPOXY RESIN

SA PHENOL RESIN

SA PLASTIC

SA POLYESTER RESIN

SA SILICONE RESIN

SA SYNTHETIC RESIN

Solid organic filters using polymethyl siloxane resin as host material for 2000-3000 angstrom range 03 p0470 A67-14393

Load carrying capability of adhesive bonded studs, analyzing resin systems and flexible linears 09 p1507 A67-22502

Dielectric properties applied determination of degree of reticulation of polymers during polymerization, noting losses due to free electrons and dipoles

[ONERA-TP-476] 14 p2340 A67-27898

Parameters governing high resistance of reinforced resins, stressing elastomechanical equilibrium at interface

[ONERA-TP-468] 18 p3069 A67-34462

Densified carbon and graphite production methods /carbon, metal and resin and carbon with carbon impregnation/ for glass-to-metal sealing jigs 24 p4174 A67-41913

RESIN BONDING

High temperature effect on strength of solidified resins and resin based materials, determining loss of weight, density, compression strength, permittivity and electric conductivity 05 p0833 A67-17098

Structural adhesives bonding - Symposium, Stevens Institute of Technology, Hoboken, September 1965 09 p1521 A67-22499

Book on adhesive bonding Alcoa aluminum covering techniques, applications including aircraft and military uses, classifications, etc 13 p2143 A67-27177

Adhesive bonding techniques for aluminum, advantages, drawbacks, joint design and surface treatment before bonding 14 p2323 A67-27820

Solid lubricants including powders, solid dispersions, resin bonded dry film and soft metal films, discussing metal oxide lubricant effect on graphite 20 p3455 A67-37263

Adhesive and water resistance properties of epoxy resin for bonding tensometers and underwater sealing 21 p3650 A67-38919

RESISTANCE

SA CONTACT RESISTANCE

SA CORROSION RESISTANCE

SA CREEP RESISTANCE

SA ELECTRIC RESISTANCE

SA FLOW RESISTANCE

SA FRACTURE RESISTANCE

SA HEAT RESISTANCE

SA MAGNETORESISTANCE

SA OXIDATION RESISTANCE

SA RADIATION RESISTANCE

SA SKIN RESISTANCE

Matrix solution to free motion of point in randomly perturbed resisting medium in rotating aspherical geogravitational field 05 p0901 A67-17110

RESISTANCE COEFFICIENT

Mercury device for analyzing pressure distribution, velocity profiles and resistance coefficients of turbulent flow in channels of linear induction pumps under traveling magnetic field 04 p0670 A67-15521

Turbulent flow of mercury in flat channels plane perpendicular to magnetic field, noting reduction of flow resistance coefficient 06 p1044 A67-18678

Turbulent flow of electrically conducting fluid in pipe located in longitudinal magnetic field 06 p1044 A67-18689

Size and shape of roughness projections effect on resistance coefficient during turbulent pipe flow in transverse magnetic field 06 p1044 A67-18690

Resistance coefficient of circular cylinder and sphere in range of Reynolds and Stuart numbers 06 p1045 A67-18692

Signal-source noise mismatch and alignment in linear tripole amplifier networks 14 p2289 A67-28864

Longitudinal magnetic field effect on conducting fluid turbulent flow found limited to dissipation mechanism occurrence 18 p3028 A67-34215

Measurement of column resistance during recovery of rapidly interrupted low current wall stabilized DC arc 19 p3282 A67-35158

Hydraulic resistance coefficient of rotating tubes, taking into account centrifugal mass forces effect on flow inside tube 20 p3421 A67-36793

Magnetic field effect on resistance coefficient of mercury flow in circular pipe 20 p3501 A67-37304

Si semiconductor strain gauge thermal coefficient of resistance /TCR/ reduction by high energy electron irradiation 23 p4008 A67-41391

Change of conductivity with temperature measurements for stabilized amorphous bismuth films 24 p4200 A67-41866

RESISTANCE DEVICE

SA NEGATIVE RESISTANCE DEVICE

SA PIEZORESISTIVE DEVICE

Electric-resistance strain gauge measuring techniques at high temperatures 01 p0071 A67-11096

Tantalum thin film resistors for integrated circuits, noting manufacture and applications 14 p2280 A67-28015

Linear bridge for use with platinum resistance temperature sensors 18 p3052 A67-34511

Resistance spot welding process, using heating, cooling and stress development data to compute internal behavior 20 p3456 A67-37697

Power conversion derivation in nonlinear resistive element in series with linear resistors 23 p3981 A67-41395

Metal-fatigue failure indicator-predictor gauge by correlating resistance changes with fatigue damage [AIAA PAPER 67-794] 24 p4251 A67-42955

RESISTANCE HEATING

Radiation calibration of heat flux sensors, comparing resistively heated filament and solar energy device 01 p0069 A67-11019

Graphite cloth and felt as resistance heating elements for calibration and simulation facilities, achieving fast changes in heat flux level without sacrificing power efficiency 15 p2490 A67-30153

High vacuum enclosure problems solved by use of magnetic seal for joints of large valves and degassing by direct heating of wall surfaces 17 p2802 A67-32300

RESISTANCE THERMOMETER

SA BOLOMETER

Heat flux to SNAP reactor system models in hypersonic continuum flow measured in shock and hyperthermal wind tunnels, using thin film resistance thermometer 01 p0112 A67-11022

Meteorological instrumentation for measuring physical characteristics of atmosphere 04 p0649 A67-14686

Sensors and signal conditioners, discussing operation and calibration of resistance thermometers, strain gauge pressure transducers and potentiometric transducers 04 p0626 A67-15731

New thermal radiative flux gauge utilizing thin film resistance thermometer and short

duration test techniques 11 p1792 A67-24821

Thermistor theory and special applications 18 p3050 A67-34503

Stability tests on birdcage high temperature platinum resistance thermometer, presenting potential ratio bridge design 18 p3051 A67-34504

Gold resistance thermometers for measuring surface temperature of semitransparent materials 18 p3051 A67-34505

Measurement of rapidly varying temperatures of gas flows with resistance thermometers taking into account heat transfer between heat probe and holders 21 p3630 A67-38914

RESISTIVITY

SA PHOTORESISTIVITY

Resistivity and Hall effect oscillations in antimony doped n-type germanium crystals in metallic impurity conduction state 14 p2365 A67-28231

Flux observations in type II superconductors when changing magnetic field suddenly, with results used to deduce flux flow resistivity 16 p2730 A67-31169

Type II superconductor flux flow resistivity theories, introducing Nozières-Vinen extension 16 p2731 A67-31170

Field ion microscopy of Ni-Mo alloys 18 p3065 A67-33664

N-type InSb hot electron and nonohmic effects, noting low temperature and magnetic and electric field dependence of Hall coefficient and resistivity 21 p3683 A67-38405

Pseudopotential-structure factor relation for small wave vector applied to liquid alkali metal electric resistivities and temperatures 21 p3686 A67-39102

RESISTOJET ENGINE

Resistojet design and fabrication, using hydrogen propellant and having 3-kw power input [AIAA PAPER 66-224] 02 p0302 A67-11937

Resistojet and axisymmetric electromagnetic space propulsion thrusters 02 p0305 A67-12340

Single nozzle thermal storage resistojet thruster for low thrust satellite attitude and orbit control applications, noting design and performance [AIAA PAPER 67-662] 21 p3690 A67-38698

Design, fabrication and performance of 10-millipound resistojet operating on hydrogen or ammonia, describing heat exchanger and nozzle geometry 21 p3690 A67-38699

Resistojet control system for MORL analyzed for requirements and applications [AIAA PAPER 67-721] 21 p3714 A67-38747

Electric propulsion applied to satellite stationkeeping and attitude control, noting ion engine resistojet combination providing complete redundancy [AIAA PAPER 67-722] 21 p3697 A67-38961

RESISTOR

SA ATTENUATOR

SA PRINTED RESISTOR

SA TUNNEL RESISTOR

Linearity of MOS transistor as variable resistor improved by keeping substrate floating and connecting substrate to drain 01 p0036 A67-10439

High pinch-off voltage field effect transistor /FET/ for use as electronically variable resistor 01 p0036 A67-10474

Precision of thin film resistors and capacitors mounted on single base as affected by fabrication factors 03 p0491 A67-13242

Cr-SiO cermet material used in precision thin film resistors for monolithic integrated circuits 03 p0381 A67-13663

Integrated circuits with evaporated thin film conductors, resistors and capacitors 03 p0387 A67-13999

Three-resistor thin film network possessing minimum sensitivity to random variations in individual components compared with single thin film resistor with same terminal impedance 04 p0593 A67-15487

Planar and sandwich resistor structures in Si thin film integrated circuits 08 p1302 A67-20793

Electrical characteristics of thin film nickel-chromium resistors dependency on variation in processing parameters including source and film composition, deposition rate, etc 09 p1555 A67-22103

High stability metal thin film resistors applied to thin film circuits, noting

substrate properties and pattern design 12 p1918 A67-26209

Structure dependent electric properties of anodized and unanodized tantalum-tantalum oxide thin film resistors, discussing aging, heat treatment, etc 13 p2082 A67-27366

Thin film resistive and capacitive circuit design 14 p2287 A67-28611

Coevaporation of cermet resistor compounds investigated for resistance and stability 18 p3014 A67-34550

Thin film resistor used to improve performance of picosecond silicon integrated digital circuit with p-n junction isolation 18 p3014 A67-34551

Reliability evaluation of passive electronic components of ceramic and mica condensers and carbon resistors, including defects and stress analysis 21 p3571 A67-38671

Dielectric thin film negative resistors for oscillator circuits compared to multilayer p-n-p-n structures for output frequency voltage temperature dependence 22 p3769 A67-39576

Photoresistors thermal characteristics in automatic semiconductor control devices studied in steady and pulsed modes of operation, determining current-voltage characteristic and thermoresistance 22 p3801 A67-40214

Learning threshold element circuit employing electrochemical controllable resistors as weight factors 22 p3809 A67-40480

RESOLUTION

SA RADAR RESOLUTION

SA SPECTRAL RESOLUTION

Holographic resolution as affected by materials, installation vibration, hologram dimension and light source 01 p0063 A67-10355

Holograms with incoherent illumination, noting patterns produced and resolution parameters 01 p0070 A67-11081

Resolving power of circular-aperture antenna affected by plane turbulent layer between antenna and point of observation 02 p0210 A67-11570

Mass spectrometer resolution improved by variable focus at any arbitrary ion current through three-element unipotential lens 02 p0248 A67-12700

High resolution aerial photography, examining systems and techniques evolved over last two decades reaching level of 100 lines/mm [SMPT PREPRINT 100-10] 03 p0423 A67-13804

Radio source diameter measurement through application of interplanetary scintillation, noting angular resolution 05 p0903 A67-17291

Angular resolving power limitations for linear arrays of equispaced elements receiving EM or acoustic waves, in cases of mechanical rotation and electron beam scanning 06 p0966 A67-17576

Model predicting effects of finite hologram emulsion resolving power on field range recorded in hologram and resolution in reconstructed image 06 p1004 A67-18543

Amplifying elements ensuring required dynamic properties of resolving amplifier without calculating entire amplifier circuitry 10 p1611 A67-22983

Holographic resolution as affected by materials, installation vibration, hologram dimension and light source 11 p1794 A67-25028

Antenna resolution by data processing noting limitations due to noise 16 p2639 A67-31339

Noise removal and deconvolution techniques applied to resolution of beam collision experiments 17 p2886 A67-33261

Resolution improvement of earth-based lunar photography, discussing film speeds, emulsions, etc 18 p3049 A67-34332

RESOLVING POWER

Optical resolution, light intensity and true perspective effect on imaging characteristics and parallax and image brightness influence on display realism of visual simulation 11 p1749 A67-24629

Electronic and ultrasonic principles defining pulse-echo high resolution and application to electronic and electroacoustic circuitry for testing aerospace structures 12 p1948 A67-25218

Pulsed ruby laser to obtain Fourier holograms in light reflected from diffusely

scattering objects, discussing relaxation of resolving power of photographic emulsions 12 p1939 A67-25335

System using holography for character recognition according to Gabor proposals 13 p2118 A67-26258

One-and two-dimensional antenna synthesis for instruments of large resolving power and effective collecting area 14 p2284 A67-28433

Earth rotation synthesis using arrays of small antennas for better low declination sensitivity 14 p2284 A67-28434

Fine structure profiles of solar radio bursts observed with high time resolution 14 p2381 A67-28579

Performance of single lens objective for coronagraph noting resolution, scattered-light background brightness, etc 15 p2485 A67-29151

Electrodynamics applied to two-dimensional problem of determining resolution of images reproduced from ideally plane infinitely thin holograms 15 p2489 A67-30006

Spherical and chromatic aberrations, astigmatism and field error of catadioptric telescope, determining resolving power with various methods 17 p2855 A67-32327

Electrodynamics applied to two-dimensional problem of determining resolution of images reproduced from ideally plane infinitely thin holograms 18 p3046 A67-33767

Multichannel radar formula for discriminating power in distance corresponding to time resolution constant 18 p3002 A67-34228

Correlation type arrays resolving power noting role of averaging processes 20 p3403 A67-37509

Film resolution limitation on hologram size, Rayleigh resolution and interference pattern recording 22 p3796 A67-39259

Selected-area small angle electron diffraction using double-condenser electron microscope, noting high resolution power 22 p3798 A67-39561

Pencil-beam antenna with field distribution fluctuation determined for resolving power by mean square measuring of radiation pattern, detailing parabolic reflectors with rough surfaces 22 p3763 A67-40125

Laser interferometric velocity measurements of moving objects, discussing accuracy improvements by recorder resolution power increase and atmospheric and seismic disturbance 23 p3997 A67-40571

Threshold voltage for onset of image-spot blurring of field-ion microscope screen and function of tip temperature 23 p3998 A67-40896

Radio telescope design, considering sensitivity and resolving power, discussing classical optics and multiplicative antenna based telescope 23 p3980 A67-41081

TV system resolution improvement without bandwidth increase, discussing accuracy of random alphabetic characters 23 p3975 A67-41282

Performance of single lens objective for coronagraph noting resolution, scattered-light background brightness, etc 24 p4158 A67-43074

RESONANCE

SA CAVITY RESONANCE

SA CYCLOTRON RESONANCE

SA DOUBLE RESONANCE

SA FERROMAGNETIC RESONANCE

SA GROUND RESONANCE

SA MAGNETIC RESONANCE

SA MAGNETOSONIC RESONANCE

SA MECHANICAL RESONANCE

SA MESON-BARYON RESONANCE

SA MICROWAVE RESONANCE

SA OPTICAL RESONANCE

SA PLASMA RESONANCE

SA PROTON RESONANCE

SA RLC CIRCUIT

SA SPIN RESONANCE

Orbital 2-1 periodic resonance in neighborhood of equilateral equilibrium points of restricted problem 02 p0321 A67-11497

Quasi-stationary techniques for calculating energies and widths of resonances occurring in electron-atom and electron-molecule scattering 02 p0269 A67-12449

Von Zepel transformation solution small divisor problem arising from natural

frequencies of orbital resonance motion of 24-hr artificial satellite 03 p0457 A67-13162

Resonance phenomena associated with small divisor in third integral of orbital motion 03 p0457 A67-13164

LF high-Q resonances in mixed state of pure outgassed Ne 06 p1048 A67-17818

Stationary resonance solutions for rotating systems with one degree of freedom applied to satellite rotation problems 09 p1532 A67-21910

Oscillator strengths for extreme UV resonance lines of ions in neon isoelectronic sequence calculated, based on single configurations in intermediate coupling 12 p1968 A67-26247

Resonance line profiles for Ca II and Mg II in lower solar chromosphere, noting interlocking effect 19 p3325 A67-35504

Steady random natural frequency variation and subharmonic resonance, discussing periodic right hand side Duffing type equation describing system 22 p3836 A67-39405

RESONANCE CHARGE EXCHANGE

Numerical integration of averaged cross section for electron induced resonance charge exchange and ionization of accelerated beam of hydrogen atoms 02 p0278 A67-12629

Cross section estimates for symmetric resonant charge exchange between ions differing by one electronic charge, noting effect on heat conduction in plasmas 03 p0484 A67-14038

Numerical integration of averaged cross section for electron induced resonance charge exchange and ionization of accelerated beam of hydrogen atoms 13 p2171 A67-27387

Molecular nitrogen and oxygen ions colliding with atomic sodium examined in crossed-beam experiment for resonance charge transfers 16 p2705 A67-31758

Measurement of cesium and mercury ion-atom resonance charge exchange cross section [AIAA PAPER 67-682] 21 p3660 A67-38713

RESONANCE EFFECT

Resonance amplification of associated slightly attenuating electromagnetic and acoustic helicon waves by electron drift in semiconductors and semimetals 01 p0128 A67-10081

Effect of plasma outside cylindrical plasma column on dipole resonance, noting increased oscillation frequency and coupling of resonances 01 p0123 A67-10459

Frequency equation for purely radial vibrations of infinite isotropic composite hollow cylinder with two concentric elastic layers 01 p0162 A67-10818

Driving-point impedance and current for long resonant cylindrical antennas 02 p0212 A67-11605

Orbital resonance caused by tesseral harmonics, examining perturbations of synchronous satellite in eccentric orbits 02 p0328 A67-12400

Role of second order internal resonance in problem of stability of equilibrium of system neutral in linear approximation 03 p0467 A67-12860

Electromagnetic wave propagation along confocal lens line for variable refractive index of ambient medium 04 p0575 A67-15150

Orbital elements determination from reduced Baker-Nunn observations of satellites, noting disturbance by resonance effects of earth gravitational potential sectorial and tesseral harmonics 05 p0763 A67-16562

Double resonance effects extended to case of stimulated emission in excited states of neon, using gas laser in transverse DC magnetic field 05 p0818 A67-16645

Impact approximation of spectral line broadening by resonance and Van der Waals forces in air molecule electronic-vibrational systems 05 p0759 A67-16790

LF electromagnetic field behavior in cold magnetoactive plasma near resonance layer, noting condition for energy absorption increase 06 p1039 A67-18078

Maneuverable geodetic satellite for better determination of resonant harmonics in geopotential field [AIAA PAPER 67-122] 06 p1096 A67-18340

Transient stress-strain state of elastic system developing combination resonance analyzed, using approximate

method 06 p1106 A67-18621
 Resonance transition of hinged ponderable rod with nonlinear supports 06 p1109 A67-18666
 Dynamics of narrowing effect of surface and spatial dispersing agents on radiation line of ruby laser with nonresonance feedback 06 p1012 A67-18797
 S-D interaction in electronic band structure of transition metals represented by model Hamiltonian, treating copper band structure 07 p1238 A67-20217
 Induced radiation at high photon densities, noting applicability of perturbation theory to multiphoton resonance radiation of lasers 08 p1337 A67-20823
 LF gravitational-acoustic and internal gravity mode wave propagation in temperature-stratified photosphere-low chromosphere region and solar atmospheric resonant responses 08 p1399 A67-21236
 Resonant oscillations of artificial earth satellite with nearly repetitive path relative to rotating primary with longitudinally varying gravitational field 08 p1401 A67-21362
 Resonance amplification of associated slightly attenuating electromagnetic and acoustic helicon waves by electron drift in semiconductors and semimetals 08 p1371 A67-21458
 Concentration of cesium in argon-cesium flow determined by total radiation absorption in resonance line of cesium 09 p1538 A67-21778
 Perturbation theory developed to estimate magnetic surface stability against field irregularities, noting role of field resonances 10 p1686 A67-23468
 Erratic vibration peaks, recognized as variable acoustic resonance, during tests of jet engine compressors [ASME PAPER 67-VIBR-57] 11 p1852 A67-24204
 Ion acceleration by drift resonance caused by crossed magnetostatic and space charge electrostatic fields 11 p1841 A67-24768
 Generation rate of secondary HF wave from resonant interaction of two longitudinal waves in cold beam-plasma under external magnetic field 12 p1970 A67-25250
 Spectrum of longitudinal plasma oscillations noting instability under resonance condition 12 p1970 A67-25255
 Polarized harmonic electromagnetic wave propagation in plane stratified isotropic plasma of cold lossless electron gas, resolving inconsistency near resonance region 12 p1976 A67-25944
 Collision broadening cross sections and effect of resonant interactions on gas-laser transitions 12 p1953 A67-26196
 Optical double-quantum transition in which atom passes from one Zeeman sublevel to another by absorption and successive reemission of optical photons 13 p2127 A67-27079
 Elastic rod, string or torsional member under effect of accelerating axial load, solving differential equation of motion in fixed end condition 14 p2399 A67-28140
 Nonlinear harmonic generation in magnetoplasma using Boltzmann equation, noting sharp resonance peaks 14 p2358 A67-28236
 Attenuation cross section and refractive index using collision theory, calculating resonance profiles of autoionizing lines based on scattering theory 14 p2351 A67-28811
 Possibility of Cerenkov effect in superconductors established from electromagnetic oscillation spectrum, calculating wave resistance and resonance maxima positions 14 p2375 A67-29079
 Electromagnetic wave propagation along confocal lens line for variable refractive index of ambient medium 15 p2435 A67-29337
 Nonlinear oscillation theory for parametric resonance effect in gas lasers placed in stationary and variable magnetic field 15 p2498 A67-29468
 HeNe laser output measured as function of axial magnetic field strength 15 p2498 A67-29512
 Reentry vehicle roll resonance criterion formulation for predicting roll conditions, noting vehicle configuration, aerodynamic and trajectory parameters, exoatmospheric vehicle attitude, etc 15 p2572 A67-30211
 Resonance effects for satellites with

nominally constant ground track 16 p2744 A67-30731
 Invariant curves dissolution and nonapplicability of third integrals explained examining perturbation values and initial conditions and resonance phenomena 16 p2748 A67-31140
 Gamma ray schemes of resonances in silicon 29-phosphorus 30 reaction for resonant and bound levels of phosphorus 30 properties 16 p2705 A67-31922
 Axial electrostatic field forming in resonance zone of mixed structure noting ion entrainment, shock wave generation and motion of electrons 17 p2899 A67-32291
 Hydromagnetic mechanism explaining pulsating radio auroral echoes accompanying sudden commencements, considering Wenzel resonant interaction 17 p2845 A67-32766
 Resonant interactions between energetic trapped particles and transverse electromagnetic wave, suggesting geophysical applications and examining resonances suppression conditions 17 p2939 A67-33210
 Plastic resonance problem for longitudinal elastoplastic waves in finite bar solved, considering bodies with rigid unloading characteristics 18 p3140 A67-33465
 Gallium arsenide single crystal lattice dielectric constant measured noting broad resonance 18 p3101 A67-34010
 Resonance effect in low energy or low velocity Li-Hg total scattering cross section 18 p3082 A67-34031
 Resonance effects arising during sub-and supersonic waves expansion in aerodynamic cascade 18 p2984 A67-34216
 Dynamics of narrowing effect of surface and spatial dispersing agents on radiation line of ruby laser with nonresonance feedback 18 p3061 A67-34416
 Spectral line resonance broadening using Griem theory, noting linear pressure dependence 19 p3272 A67-35085
 Ionization-enhanced microwave resonant radiation from model rocket exhausts studied using Dicke type radiometer 20 p3543 A67-36233
 Resonant-transfer sampling technique stressing bandpass filtering design and time division multiplex 20 p3379 A67-36243
 Properties of steps appearing on volt-ampere characteristic of Josephson current in superconducting tunneling, noting nonlinear resonance effects 20 p3509 A67-36690
 Time delay of remote-resonance trace of polarized electromagnetic pulse propagating through topside ionosphere 20 p3527 A67-37403
 Ion resonance effect in Langmuir probe exhibiting ion plasma frequency 21 p3663 A67-37765
 Blue Streak launch vehicle control system, discussing destabilizing resonance effects, hydraulic system, propellant movement in tanks and testing 21 p3570 A67-38102
 Resonance spectrum of plasma column excited by SHF field investigated for nonlinear phenomena 21 p3666 A67-38354
 Angular divergence of solid state laser radiation for case of variable resonator and pump parameters 21 p3640 A67-38367
 Resonance electronic Raman effect and parametric induced anti-Stokes radiation in potassium vapor atoms 21 p3641 A67-38456
 Nonlinear oscillation theory for parametric resonance effect in gas lasers placed in stationary and variable magnetic field 21 p3641 A67-38549
 Laser emission mode splitting of CN laser, discussing wavelength to resonance length and Fabry-Perot interferometer permitting line splitting observation 23 p4012 A67-40893
 Resonance transfer of energy as mechanism for quenching interaction between rare earth ions affecting fluorescent lifetime 23 p3971 A67-40974
 G factor of holes in Ge and Si semiconductors computed in quasi-classical region noting dependence on hole moves relative to magnetic field 23 p4042 A67-41297
 Dispersion of surface waves propagating in elliptical and rounded flat helices, discussing resonance effects 24 p4121 A67-42236
 Strongly enhanced radiation from antenna surrounded by dielectric layer and plasma sheath, noting resonance at given operating frequency for certain plasma

densities 24 p4121 A67-42266
 Resonance rectification effects for wire probe in magnetoplasma observed in terms of warm plasma perpendicular permittivity component 24 p4199 A67-43101
RESONANCE PROBE
 Mechanical impedance of device moving in liquid at resonance, determining viscoelastic magnitudes of Newtonian and non-Newtonian liquids under different dynamic conditions 02 p0240 A67-11521
 Plasma diagnostics, comparing microwave toroidal resonator, cylindrical resonator and probe methods 03 p0477 A67-13466
 Ion resonance in uniform plasma, analyzing behavior of RF resonance probe by comparing ion resonance with electron resonance 04 p0663 A67-14616
 Relaxation problem of two-level molecule in dense resonance medium 05 p0762 A67-16351
 Mechanism of enhancement of Li resonance line in twilight airglow due to upper atmospheric thermonuclear explosions 06 p0998 A67-18705
 Convex programming procedure yielding algorithm for tuning out system from possible resonance zone 08 p1353 A67-20837
 Increment of constant HF electron flux in resonance probe determined for case of large constant potential, noting role of plasma 13 p2119 A67-26559
 Emission intensity and spatial distribution of fluorescence measured for transitions in He, noting resonance radiation absorption effect on 5016 angstrom light spread 14 p2317 A67-28196
 Frequency response of DC and AC currents flowing to RF resonance probe in quiescent cesium plasma, explaining measurements 18 p3044 A67-33713
 HF resonance probes, giving theoretical results of nonzero electron plasma temperature effect and experimental results with plasma between plates of plane capacitor 21 p3626 A67-38220
 Ion resonance probe for plasma density measurement using direct display method with frequency swept signal generator 21 p3627 A67-38258
RESONANCE SCATTERING
SA NEUTRON SCATTERING
 Radio wave scattering and resonance scattering in wake of body moving in lower ionosphere plasma due to disturbance of electron concentration 02 p0192 A67-11657
 Autoionization calculation describing scattering aspect of phenomenon 03 p0471 A67-13220
 Angular dependence of elastic scattering resonance structure in atomic hydrogen 04 p0660 A67-14946
 Resonances in proton hydrogen and positron hydrogen scattering predicted at energies just below excitation thresholds 04 p0662 A67-15768
 CW argon ion laser scattering in argon plasma, noting resonance and correlation between data and plasma properties 05 p0820 A67-16665
 Resonance scattering measurement from solar illuminated lunar atmospheric constituents 06 p1091 A67-18999
 Radiation enhancement and resonance scattering due to plasma sheath between spherical antenna and surrounding plasma layer 07 p1153 A67-19611
 Airglow resonant emission transfer in Doppler incoherent scattering medium with respect to optically thick atmosphere 10 p1634 A67-23050
 Existence of nucleon bound state in PIN channel investigated through nonperturbative S-matrix in absence of forces arising from inelastic states 11 p1822 A67-23978
 Density measurements in Q-device by resonance fluorescence scattering, Langmuir probe and microwave methods compared, examining causes of discrepancy 11 p1838 A67-24405
 Resonance scattering of electromagnetic waves on arbitrary rarefied plasma region with near zero intrinsic wave number relative to small perturbation 13 p2067 A67-26547
 Atomic collisions with negative ions, deriving transition matrices for resonance reactions and scatterings to analyze rearrangement process of associative electron detachment 14 p2350 A67-28149

Position and width of lowest elastic scattering resonances in three-body atomic system, showing resonance shape dependence upon observation angle and angular resolution 14 p2351 A67-28152

Radio wave scattering and resonance scattering in wake of body moving in lower ionosphere plasma due to disturbance of electron concentration 16 p2624 A67-31072

Chemical reactions fluorescent and resonant scattering, electron impact and photodissociation from sunlight upon atmosphere 18 p3036 A67-33602

Spectrum of bound and quasi-bound states of hydrogen-hydrogen scattering and resonance, using Schroedinger equation 18 p3084 A67-34523

Compound state resonances in molecular collisions, stressing scattering cross sections behavior for deuterium-xenon 19 p3266 A67-35881

Electromagnetic scattering from adsorbing spheres near resonances calculated from extinction efficiency factor and angular scattering function dependence on refractive index 21 p3656 A67-37856

Magnetic effect on polarization of resonance radiation in solar chromosphere 21 p3709 A67-38989

Static Green function for elastic electron scattering by hydrogen atoms, using integrodifferential equations to determine resonance energies 22 p3839 A67-39204

Sodium D lines in Comet Ikeya-Seki /1965 f/ near perihelion passage noting possible formation by resonance scattering at comet densities and temperatures 22 p3880 A67-39414

Integral equation derived to relate source function for spectral line formed by noncoherent resonance scattering to thermodynamics of radiating medium 22 p3896 A67-40529

Optically pumped Rb in collisions with Kr inducing relaxation, noting two different correlation times due to kinetic collisions and metastable states present 23 p4012 A67-40792

Nonlinear radiation transport problem solution by reduction to linear, considering light resonant scattering in approximation of complete frequency mixing 23 p4051 A67-40909

Compound state resonances in atom/molecule collisions below first excitation threshold energy 23 p4029 A67-40959

RESONANCE TESTING

Steady state regime and stability of two-photon laser, noting field dependence of intensity and duration of frequency pulse and resonance excitation curves 04 p0631 A67-14745

Dispersion and interaction impedance of slow wave structures from cold tests measured, using resonance methods 09 p1476 A67-22212

Elastic properties of tektites measured using resonant sphere technique 11 p1864 A67-24558

Resonance frequency shift analysis of autostabilized light modulator at microwave frequencies noting heat transfer, transition temperature, etc 20 p3459 A67-36503

RESONANT CAVITY

SA CAVITY RESONANCE

Resonant cavity field containment of plasma 02 p0273 A67-12178

Vacuum resonant-cavity dielectrometer for in situ measurements of complex permittivity in simulated space environment 04 p0625 A67-15708

Loss measurement for ruby laser resonant cavity, comparing thresholds for R sub 1 and R sub 2 line operation 05 p0819 A67-16655

Microwave cavity techniques to measure electron precursors in shock tube [AIAA PAPER 66-175] 05 p0856 A67-17342

Klystron with axisymmetric output cavity without conventional coupling loop or iris for obtaining minimum harmonic power output 05 p0780 A67-17534

Helicon effect in semiconductors measured by resonant cavity method 06 p1071 A67-18990

Resonant cavity technique for measurement of k/beta diagrams /dispersion relations/ of leaky wave structures 07 p1153 A67-19612

Effect of load mismatch on laser output, determining nonlinear dependence of

equivalent negative conductance as function of oscillation amplitude in laser resonator cavity 08 p1338 A67-21270

Small size CW He-Ne laser pumped by resonant cavity, examining current-voltage characteristics and current dependence of output power 09 p1513 A67-22170

Gunn diode self-pumped parametric oscillator, showing power derived from variation of domain capacity at second harmonic of oscillation frequency 09 p1479 A67-22267

Mode discrimination of laser cavity exploiting transmission characteristics of Fabry-Perot interferometer 10 p1663 A67-22835

Natural ELF electromagnetic noise properties during solar flare of July 7, 1966, considering radiation compression effects on earth-ionosphere cavity 10 p1700 A67-23057

Epitaxial GaAs Gunn effect oscillators, showing importance in high efficiency of preparation and method of contacting material and resonant cavity design 10 p1616 A67-23533

Atmospheric absorption problem solution, using cavity maser operating at 4 mm wavelength 12 p1952 A67-25297

Automatic cavity tuning of hydrogen masers to achieve frequency source of absolute accuracy over unlimited time periods 13 p2125 A67-26512

Ruby maser with two synchronous symmetrical quarter-wave-coupled cavities, noting frequency gain 13 p2128 A67-27227

Jet driven fluoric oscillator 14 p2251 A67-28344

ELF and micropulsations phenomena divided into earth-ionosphere cavity resonances and regular and irregular pulsations 14 p2266 A67-28415

Semiconductor laser generating oscillations in external cavity, finding Brewster window effective in suppressing modes within crystal 15 p2498 A67-29511

Multipactor suppression properties of Ti, Cr, V and Ta determined using special electromagnetic cavities 15 p2448 A67-29757

Spectral narrowing and tunability over wide spectral range demonstrated in solid/liquid dye lasers using diffraction gratings as cavity reflectors 15 p2500 A67-29817

Nonaxial oscillation modes in He-Ne laser interaction with spherical mirror resonator confocal cavity 16 p2685 A67-31038

Ultrashort light pulse generation by forcing oscillation modes, noting role played by dispersion of medium within resonator cavity 16 p2702 A67-31042

Electromagnetic fluctuation structure associated with resonance properties of earth-ionosphere bounded cavity 17 p2847 A67-32942

Amplification characteristics of multicavity masers, determining Q-factor using chain matrix A formalism 19 p3241 A67-36027

Superconducting diode behavior in resonant electromagnetic radiation field, studying current-voltage-magnetic field relationship 20 p3511 A67-37241

Bandwidths of reflex multicavity solid state masers containing active material in cavities 20 p3462 A67-37328

Three-photon combination process used to increase laser emission frequency, determining laser field strength 22 p3815 A67-39760

Resonant cavity electric field excitation placed in magnetic field near electron cyclotron frequency studied for expressions of self-excitation current 22 p3816 A67-40126

Laser output power determination technique by rotating plane parallel wafer in resonant cavity to vary value of total losses 22 p3817 A67-40412

Langmuir probes investigated by comparing measurements in ionized He afterglow by cylindrical double probes and by gated microwave radiometer and resonant cavity 24 p4197 A67-42261

RESONANT FREQUENCY

Two-frequency volume resonator with independent tuning within wide frequency band 02 p0214 A67-11911

Vibration of entire multifrequency system reduced to single frequency resonance when frequency passes through zero, illustrated with solar system 02 p0267 A67-11917

Ring trapped mode resonator for use in microwave filters, developing expressions

for unloaded Q and resonant frequency in transverse electric mode 02 p0217 A67-12091

Low noise parametric self-resonance amplifiers with bandwidths, discussing use of high diode Q-factor 02 p0220 A67-12204

Axisymmetric sloshing oscillations of liquid in U-tube type connected cylindrical tanks, obtaining velocity, pressure and wave height 03 p0522 A67-13213

Mechanical design of parabolic steerable antenna structure of 150-ft diam having superior accuracy and resonant frequency resulting from high stiffness-to-weight ratio 03 p0396 A67-13752

Computer program for automated design of hyperstatic truss structures under resonant frequency used in multisatellite Agena launcher 03 p0526 A67-13968

Harmonic response due to compressibility in traveling wave plasma devices, discussing magnetoacoustic resonances for case of cylindrical symmetry 03 p0485 A67-14051

Moiré method in determining dynamic response of thin membranes 03 p0531 A67-14362

Resonant frequency change of oscillatory circuit due to nonlinear capacitance of semiconductor diode used as amplitude detector 04 p0586 A67-15677

Accelerometer frequency response and quadratic lag function amplitude response curves and relation to resonant frequency 04 p0627 A67-15792

Omnidirectional slot antenna with two slots resonant at frequencies nearly octave apart and fed by single common waveguide 04 p0590 A67-15904

Pneumatic transmission line model for use in fluidic control systems, noting nomographs determining gain-vs-frequency curves 05 p0753 A67-16237

Ruby laser with nonresonant feedback due to radiation scattering, showing use as optical frequency standard 05 p0818 A67-16642

Acoustic wave propagation characteristics in solar chromosphere, discussing resonant frequencies 05 p0900 A67-17075

LF whistler mode of electromagnetic waves propagating at angle to magnetic field in modal plasma 05 p0857 A67-17426

Vibrational characteristics of inflatable wing model, determining resonant frequencies and mode shapes by using influence coefficients 06 p1100 A67-18002

Continuous high resolution measurement of solid propellant burning rate using resonant LC circuit [AIAA PAPER 67-69] 06 p1072 A67-18450

Diurnal variation of Schumann resonances explained by geometrical factors relating position of sources and observational point, noting propagation difference between EW and NS 06 p0998 A67-18707

Waveguide resonant-iris bandpass filter with very wide passband and stopbands that provide transmission and attenuation characteristics for use with microwave generators 07 p1151 A67-19426

Radiation from linear resonant antenna in lossy compressible weakly ionized plasma and dependence on ratio of source to plasma frequency 07 p1227 A67-19428

Parametric excitation of modes of infinite plasma by incident radiation using Vlasov equation, noting unstable oscillations for incident frequencies 07 p1228 A67-19502

Resonance-like characteristics of direct modulation of junction laser with bias current analyzed by rate equations 07 p1196 A67-19800

Resonant frequencies of standing wave Bernstein modes propagating in magnetized homogeneous plasma columns and effects of anisotropy of unperturbed electron velocity and ambipolar-diffusional electric field 08 p1361 A67-21131

Power reflection technique for high quality varactor diode characterization 08 p1304 A67-21221

Energy storage in plasma near upper hybrid resonance treated by macroscopic plasma model with nonlinear terms 08 p1364 A67-21399

Circuit load effects on microwave properties of Gunn diodes, discussing equivalent circuit and graphical analysis of quenched and inhibited modes of operation 09 p1479 A67-22268

Resonant frequencies compared with associated mode shapes of truncated conical

shells with both edges free 10 p1718 A67-23455

Wideband coupling filters with expressions for resonant frequencies, damping factors, etc 10 p1618 A67-23639

Frequency response, equation of motion, elastic restraint and structural flexibility of gyroscopic vibration absorber, noting antiresonant frequency functions [ASME PAPER 67-VIBR-13] 11 p1795 A67-24173

Spatial variations in mean square response above lowest resonance frequency determined, using statistical analysis [ASME PAPER 67-VIBR-22] 11 p1872 A67-24181

Instability zone of electrometer, noting relation to parametric resonance of needle and Hill equation form of needle motion 11 p1877 A67-24758

Temperature dependence of Youngs modulus of tantalum alloy determined together with free-free vibrations and resonance frequency 12 p1954 A67-25141

Natural frequencies of bladed disks calculated from 12 p2014 A67-25417

Receptances 12 p2014 A67-25417

Resonance properties of semiconductor with moving electrical domains, showing periodic variation with illumination 12 p1983 A67-25517

Accelerometer mountings evaluated covering attachment, calibration, resonance frequencies, tension-compression, bending, shear interface and cantilever effect 12 p1942 A67-25680

Resonant gate transistor permitting high-Q frequency selection to be incorporated into silicon integrated circuits 13 p2079 A67-26870

Ruby maser with two synchronous symmetrical quarter-wave-coupled cavities, noting frequency gain 13 p2128 A67-27227

HF localized and LF resonant impurity modes valence effect on energy gap and transition temperature in isotropic superconductors 14 p2370 A67-28720

Coherent resonant absorption and emission in IR and visible spectrum, discussing Lorentz oscillator and Dicke spin model of radiating molecule 15 p2519 A67-29190

Normal modes for solid state laser noting linear and elliptic polarization, resonant frequency and reflection loss 15 p2497 A67-29388

Laser emission under external signal, analyzing competition between amplification mode and parasitic generation arising at resonant frequency, noting signal role 15 p2498 A67-29469

Automatic measurement of diurnal resonance frequency variations of earth/ionosphere cavity 15 p2489 A67-30071

Gain-bandwidth product of parametric reflection amplifiers with line-type resonators 15 p2454 A67-30145

Librational and flexural resonances induced in satellite whose center of mass is moving in planar elliptic orbit 15 p2572 A67-30195

Design guides for efficiency, bandwidth and resonant frequency derived from slot antenna analysis, using variational methods 16 p2638 A67-31334

Conducting loop resonant size determination and geometrical shape effect on resonant size in anechoic chamber experiment 16 p2639 A67-31356

Continuous IR chemical maser action in carbon dioxide, using chemi-optical resonant pumping 17 p2866 A67-32275

Electric quadrupole-quadrupole and dipole-octupole forces contribution to dispersion energy for axially symmetric molecules, noting resonance frequencies 17 p2887 A67-32353

Fabry-Perot resonator free oscillations defined by complex frequency, obtaining diffraction loss and resonant frequency 17 p2868 A67-32668

Resonances in wave mechanics and anomalous light dispersion, obtaining value of displacement 17 p2884 A67-32704

Miniaturized cavity resonator, giving criterion for evaluation of resonant resonators 17 p2827 A67-32786

Oscillation mode in open-ended circular cylindrical microwave cavity resonant frequency computed by Laplace transform and Wiener-Hopf techniques 17 p2828 A67-33083

Cylindrical Fabry-Perot resonator, determining resonant modes by applying boundary conditions, noting eigenvalue and eigenfunction roles 18 p3060 A67-34024

Tunnel diode amplifier with single circuit, stability analysis and calculation of circuit parameters 18 p3011 A67-34179

Resonance properties of semiconductor with moving electrical domains, showing periodic variation with illumination intensity 18 p3103 A67-34448

Stimulated coherent emission at upper hybrid resonance frequency from magnetoplasma excited by microwave pulse 18 p3090 A67-34466

Capture probability at Venus resonant rotation rate implying fluid core similar to earth 18 p3136 A67-34587

Resonance absorption and zero-field nuclear spin relaxation in normal and superconducting aluminum, studying phase change 19 p3303 A67-35044

Penning ionization gauge discharge nonlinear response to VHF signals, discussing resonance behavior 19 p3275 A67-35110

Negative ion accumulation in HF resonant discharges at low pressure and plasmoid formation 19 p3275 A67-35112

Plasma resonance in RF discharge excited with frequency higher than collision frequency, determining electron density 19 p3276 A67-35114

Time variation of Doppler broadened resonance line profile determined by assuming complete frequency redistribution 19 p3329 A67-36030

Resonance for VLF waves by ionospheric propagation using Haselgrove whistler ray tracing method, interpreting path shape as function of gradients 20 p3427 A67-36372

Panels response to oscillating and to moving shock waves, discussing mode excitation, magnification factor, Bessel function, etc 20 p3539 A67-37001

Guided wave characteristics in infinite free space cylindrical cavity in magnetotonic medium noting resonance, transition, cut-off frequencies, phase velocity, etc 20 p3383 A67-37108

Frequency characteristics of planar and spherical plasma resonance probes and RF impedance probe in magnetic field, considering equivalent electric circuit 20 p3503 A67-37670

Fine structure of nitrogen 14 resonance in hydrazine analyzed for Zeeman effect 21 p3688 A67-38418

Laser emission under external signal, analyzing competition between amplification mode and parasitic generation arising at resonant frequency, noting signal role 21 p3641 A67-38550

Continuous high resolution measurement of solid propellant burning rate using resonant LC circuit [AIAA PAPER 67-69] 21 p3688 A67-38857

Resonance lines originating from autoionization energy levels far above ionization potential observed for highly ionized atoms of Na I isoelectronic sequence 22 p3840 A67-39237

Attitude continuous instability regions in parameter space and resonance frequency of spinning unsymmetrical satellite noting periodic processes 22 p3899 A67-39311

Dispersion characteristics of surface waves excited in infinitely long axially magnetized cold plasma by electric dipole 22 p3847 A67-39621

Electrically tunable low pass filter using Permalloy films near resonance 22 p3772 A67-39906

Dielectric cover effect on resonant frequency of slots in rectangular waveguide, using Stevenson free space theory and plane-wave reflection coefficient 23 p3978 A67-40824

Convective heat transfer between tube and airflow in tube for pulsating flow with pressure fluctuation frequency deviating from resonant frequency 23 p4082 A67-41285

Rocket measurements with HF impedance probe for ionospheric electron density, discussing plasma gyro resonance frequency factors 23 p4003 A67-41321

Electron-resonance spikes on Alouette I ionograms observed for proton gyro-effects in topside ionosphere 24 p4148 A67-42062

Proton gyrofrequency effect on antenna resonance at electron plasma frequency

using Alouette II satellite 24 p4125 A67-43111

RESONANT VIBRATION

SA Q-FACTOR

Matrix analysis of resonant vibration stability conditions 01 p0113 A67-10675

Stress amplitude of gas turbine blades vibrating in resonance 02 p0336 A67-11466

Forced oscillations of two-mass dynamic system with impact reaction 02 p0248 A67-11964

Resonance in nonlinear dissipative systems subjected to periodic stimulating force 05 p0847 A67-17486

Unidirectional vibration isolation systems, discussing viscous damping, Coulomb damping transmissibility and resonance characteristics [ASME PAPER 67-VIBR-21] 11 p1796 A67-24180

Irregularly spaced nozzle vanes effect upon blade vibration in radial flow gas turbine [ASME PAPER 67-VIBR-42] 11 p1797 A67-24195

Erratic vibration peaks, recognized as variable acoustic resonance, during tests of jet engine compressors [ASME PAPER 67-VIBR-57] 11 p1852 A67-24204

Free vibration and resonance of vibrating plate interacting with sound waves in surrounding air 11 p1874 A67-24228

Photoelastic coating technique for measuring stress distribution in blades vibrating in resonant modes 12 p2014 A67-25415

Dynamic vibration in aircraft power plant components, noting responsiveness of parts and fatigue life evaluation [SAE PAPER 670237] 12 p1989 A67-25495

Traveling waves onset in gas turbine bladed disks, considering resonant vibrations 12 p2033 A67-26231

Influence of strong HF electrical fields on plasma instability originated in buildup of potential field oscillations 15 p2530 A67-29728

Amplitude dependence of energy dissipation due to internal friction in metals and alloys of various lattice types under near-resonance loading vibrations 15 p2504 A67-29970

GaAs single crystals excited to stable longitudinal vibrations by supersonic absorption, determining resonance curve 17 p2914 A67-32401

Forced oscillations of two-mass dynamic system with impact reaction 17 p2866 A67-33281

Resonant vibrations in rotating blades with hinged joints analyzed for small and large damping values, determining damping coefficient 19 p3235 A67-34883

Automatic frequency-control system using superconducting resonator and reflex klystron 19 p3192 A67-34984

Nonlinear resonant coupling between damped and undamped vibrations for damping roll in TRAAC and elastic dumbbell satellites [AIAA PAPER 67-568] 19 p3329 A67-35964

Magnetron cut-off characteristics modification via altering electron cloud resonant properties by injecting positive ions in interaction space 20 p3489 A67-37105

Parametric resonance in near-canonical systems with critical frequencies and instability boundary domain formulas derived from Iakubovich results 21 p3657 A67-37989

Forced resonant nonlinear oscillation of liquid in cylindrical tank 22 p3787 A67-40192

RESONATOR

SA CAVITY RESONATOR

SA ELECTRON TUBE

SA MAGNETRON

SA MASER RESONATOR

SA MULTIMODE RESONATOR

SA OPTICAL RESONATOR

Expansion of E type symmetrical oscillations in axisymmetrical delay systems used in calculation of cylindrical resonators 01 p0035 A67-10394

Sum signal of output of system consisting of two detuned resonators and two amplitude detectors used for automatic measurement of signal frequencies 01 p0022 A67-10413

Cylindrical resonator for high precision measurements of sound absorption in oxygen 01 p0067 A67-10838

Modes of beam waveguide or beam

waveguide resonator filled with axially magnetized plasma 02 p0213 A67-11619

Sonic resonator for nondestructive testing of composite structure operating only from one accessible surface 02 p0250 A67-12630

Behavior of resonator quantum devices, using oscillating circuit with quasi-linear negative conductance 03 p0379 A67-13293

Ferrite materials for resonators of magnetostrictive transducers and filters used in transmission and reception of ultrasonic waves 03 p0420 A67-13548

Resonators use for higher sound attenuation in waveguide with sound absorbing cladding 06 p1032 A67-18397

Neodymium glass laser with spherical mirror resonator in stationary regime 06 p1012 A67-18783

Confocal resonator wave meter used to obtain frequency resolution of 10 MHz at 100 GHz 06 p0972 A67-18835

Direct-coupled confocal resonators used as band pass filters at mm wavelengths 08 p1305 A67-21229

Effect of degree of coupling between resonator system and load on generation zones and regenerative amplification of pulsed magnetron, noting characteristics 08 p1305 A67-21271

Book on open resonators and open waveguides 13 p2075 A67-26461

Boundary layer in low speed flow over dispersively coupled system of acoustic resonators, noting excitation by flexible wall of oscillations 16 p2660 A67-31214

Millimeter wave resonant interferometer capable of measuring spatial distribution of electrons in low density transient plasma column subject to perturbation 16 p2675 A67-31263

Resonant gate transistor used in integrated circuits as frequency selector element for tuning problems 16 p2642 A67-31724

Design concept for piezoelectric resonator through mathematical formulation, determining critical frequencies and electron drift rates 18 p3043 A67-33462

Coupling factor between microwave resonator and transmission line determined by oscillographic recording of microwave field 18 p3010 A67-33508

Electromagnetic field coupling action through holes in metal screen, noting hole polarizability calculation and hole equivalent dipoles effect on resonators 18 p2999 A67-33530

Soviet book on waveguide theory covering resonators, Maxwell equations role, eigenfunctions, etc 18 p3000 A67-33677

Neodymium glass laser with spherical mirror resonator in stationary regime 18 p3059 A67-33725

Nonlinear resistance of multiple resonator arrays at incident sound high pressure levels 19 p3311 A67-34963

Resonance method for measuring microwave resonators Q-factor and its small variations 19 p3191 A67-34982

Dispersion equation for electrodynamic boundary value problem of natural oscillations of cylindrical resonator with magnetoactive plasma 19 p3299 A67-36019

Miniature resonator consisting of piezoelectric cadmium sulphide transducer evaporated onto single-crystal quartz wafer 20 p3393 A67-36176

RESPIRATION

SA HIGH ALTITUDE BREATHING

SA INHALATION

SA OXYGEN METABOLISM

SA PRESSURE BREATHING

Nonphosphorylating respiration of mitochondria from brown adipose tissue of rats, providing example of electron transport 02 p0185 A67-12527

RESPIRATORY IMPEDANCE

Anesthetized rabbits exposed to high explosive air shock waves in shock tube, examining changes of elastic properties of lungs of rabbits 03 p0364 A67-14292

RESPIRATORY PHYSIOLOGY

Forces deforming rib cage during breathing efforts 07 p1133 A67-19480

Book on positive pressure breathing as means for acceptable arterial oxygen tension at altitudes above 40,000 ft and effects of raised intrapulmonary pressure 08 p1288 A67-21500

Adapted Mueller-Franz portable breath-powered respirometer utilizing scuba-gear

for measuring underwater metabolism 09 p1455 A67-21722

Human lung gas mixing efficiency estimated, using residual lung nitrogen content curve 11 p1747 A67-24626

Comparison of effect of various diluent gases in evoking flyer bends in simulated orbital flights 13 p2062 A67-26916

Emergency recompression procedures during space flight studied by exposure of chimpanzees to near vacuum 14 p2257 A67-28219

Plants in low gravity environment simulated by 2 rpm clinostat with horizontal axis, studying growth direction and respiratory metabolism 15 p2426 A67-29114

Pulmonary mechanics associated with oxygen toxicity and suggested physiological test for susceptibility to effects of oxygen 15 p2429 A67-29280

Acid-base relation of blood and cerebrospinal fluid with respect to respiratory regulation studied in man at high altitude 17 p2806 A67-32333

Treatment of hypoxia by determining primary site of oxygen tension attenuation in transfer from respiratory environment to cellular level 23 p3953 A67-41591

RESPIRATORY RATE

Ventilatory response to carbon dioxide stimulus at spontaneous and consciously regulated rebreathing rates 07 p1133 A67-19479

Effects of inhaled air ions on speed of response and attention level, heart and respiration rate and transepithelial DC potential of men 09 p1452 A67-21720

Circadian rhythms detection, estimating parameters by cosinor procedure for temporal morphology aspects 14 p2255 A67-28480

Cardiorespiratory functioning in flight monitored on carrier pilots in combat 17 p2805 A67-31956

RESPIRATORY SYSTEM**SA CARDIORESPIRATORY SYSTEM****SA LUNG**

Cardiovascular and respiratory reactions of cosmonauts during Voskhod II orbital flight 09 p1454 A67-22384

Air embolism pathogenesis and therapy in terms of problem of treatment in overpressure 13 p2059 A67-26850

Experiments for relief of astronauts from cardiovascular and respiratory distress during EVA 23 p3953 A67-41586

Physical capabilities and work potential of man in terms of physiological elements and methodology 23 p3959 A67-41662

Human respiratory system impedance simulator for dynamic testing of aircraft breathing equipment to detect possible instabilities 24 p4114 A67-41782

RESPONSE

S CONDITIONED RESPONSE

S DYNAMIC RESPONSE

S ELECTRODERMAL RESPONSE

S FREQUENCY RESPONSE

S HEMODYNAMIC RESPONSE

S MODAL RESPONSE

S PHYSIOLOGICAL RESPONSE

S TIME RESPONSE

S TRANSIENT RESPONSE

REST

S BED REST

S SLEEP

RESTRAINT

Stress-strain analysis of effects of rapid loading rate of restraint harness webbing, especially during air crash 08 p1289 A67-20613

Conical shell stability under hydrostatic pressure for various in-plane boundary conditions, stressing axial restraint effect 11 p1873 A67-24214

RETINA

Visual acuity decrement from laser lesion in fovea of stump tail macaque monkeys 05 p0756 A67-16287

Retinal photocoagulation using solid state laser 14 p2333 A67-28973

Fundus oculi observation of retinal vessel caliber alteration during changes in arterial gas tensions 17 p2805 A67-31961

Maximum permissible energy density incident on retina determined for eye safety in viewing laser beam 23 p3962 A67-41052

Retinal angiomatosis and aircrew fitness noting conglomeration by photocoagulation 23 p3945 A67-41071

Color photographic study of blackout during radial acceleration on human centrifuge, presenting evidence confirming central retinal arterial collapse 23 p3957 A67-41638

Fluorescence angiography technique to study human centrifugal acceleration effects on retinal circulation during blackout 23 p3957 A67-41639

RETINAL ADAPTATION

Model of retinal receptor incorporating various feedback control processes consistent with physiological and psychological evidence 01 p0044 A67-10465

Photochemical cells and site involved in visual adaptation, reporting electoretinogram data 06 p0953 A67-18643

RETINAL IMAGE

Existence of fovea in human retina explained by blood supply interference with steady and acute vision 02 p0184 A67-11473

Contrast transfer characteristics of n tiple models of retinal receptive fields as function of optical signal size or spatial frequency 05 p0757 A67-17303

Three-dimensional projections on cathode ray tube screens noting visual transformations linking retinal image to space scene 20 p3450 A67-36985

Retinal discrimination and visual acuity at different degrees of hypoxia by reading symbol E individually and combined, using oxygen-poor mixtures 21 p3575 A67-38507

RETINENE

Vitamins A and E deficiency effects on rats exposed to pure oxygen noting less weight gain and growth 23 p3952 A67-41568

RETRIEVAL**SA DATA RETRIEVAL****SA INFORMATION RETRIEVAL**

Continuous mechanical ladder for troop/cargo lowering and retrieval from CH-47 helicopter 17 p2804 A67-32518

Satellite retrieval system called Space Bola, employing passive/active grappling units depending on target vehicle dynamic characteristics 20 p3532 A67-36556

RETROCKET

Reliability considerations in spherical solid retrorockets for Gemini spacecraft system 02 p0305 A67-12351

Lunar surface erosion by rockets simulated in laboratory to study hazards of retrorocket landing on airless planetary bodies 12 p1922 A67-25701

RETURN-TO-EARTH PHASE

Minimum velocity increment for deboost from circular orbit as function of orbital altitude 01 p0153 A67-10429

REUSABLE SPACECRAFT

Reusable space vehicles role in overall space program, noting orbital missions in future and economic impact [AIAA PAPER 66-862] 02 p0343 A67-12261

Design evolution studies defining technological, operational and cost characteristics for reusable aerospace passenger transport 03 p0519 A67-13791

European recoverable and reusable aerospace transporter feasibility 15 p2566 A67-29829

Near term reusable rocket launch vehicle concepts 15 p2566 A67-29831

Earth-orbital transport systems noting configurations, cost, capabilities, operational requirements, etc 15 p2567 A67-29835

European aerospace transporter, fundamental concepts and development 15 p2556 A67-29838

British reusable booster concept

MUSTARD /multitask space transport and recovery device/ using rocket-propelled VTO lifting bodies, noting feasibility and development cost 15 p2568 A67-29843

Reusable low weight hypersonic glider /space rotor/ for space vehicle reentry and recovery 15 p2568 A67-29845

Space transportation systems, considering recovery facilities, reusable boosters, cost, etc 15 p2568 A67-29846

Flight data of X-15 research aircraft noting development, operation and economic aspects of performance 15 p2420 A67-29848

Reusable booster concept, economic justification, cost characteristics and management planning 15 p2569 A67-29850

Partially reusable space vehicle systems examined and compared for operational costs, savings, feasibility, flexibility, simplification, etc 15 p2569 A67-29851

Titan IIIB launch vehicle spent stage I recovery experiment, evaluating feasibility of refurbishment and reuse 15 p2569 A67-29853

Trends in technology for reusable launch vehicles 15 p2569 A67-29854

Flight control requirements of reusable launch vehicles 15 p2570 A67-29857

Spaceport facilities, technology and economics 15 p2467 A67-29943

Earth orbital transportation, proposing airline type system and composite nuclear-airbreathing engines for reusability with minimum refurbishment [AAS PAPER 67-84] 15 p2546 A67-29950

Impact of performance improvements and reuse on cost of space transportation, noting size, configuration, mission requirements and commercial possibilities 15 p2570 A67-29966

Reusable shuttle transportation system for lunar base logistics, estimating cost and performance [AIAA PAPER 67-874] 24 p4140 A67-42995

Booster recovery systems development, payload and operational costs evaluated using postulated space program [AIAA PAPER 67-909] 24 p4245 A67-43016

REVERSE TIME

SA PONTRYAGIN PRINCIPLE

Reversal of diode with delay between last direct pulse and first reversed pulse 01 p0035 A67-10399

P-type Au compensated Si diode with negative resistance, determining reversed conductivity recovery 11 p1768 A67-24861

Time reversible difference procedures including Lorentz and continuity equations, relativistic orbits and gyrocenter motion 23 p4027 A67-40996

REVERSED FLOW

Thrust reverser efficiency on high by-pass ratio turbofan engines [SAE PAPER 660736] 01 p0140 A67-10635

Ordinary differential equation in boundary layer theory of reversed flow 06 p1025 A67-18730

Incompressible Newtonian fluid applied to dynamic reversibility of flows, analyzing motion equation and possible integration of Navier-Stokes equation 11 p1778 A67-24273

Reverse flow annular combustion system for TPE331 turboprop engine, noting fabrication and combustor efficiency [ASME PAPER 67-GT-25] 11 p1854 A67-24805

Magnetic variation measurements at Addis Ababa indicate intermittent existence of inverse direction equatorial electrojet 15 p2478 A67-30070

Hysteretic superconductor, analyzing critical state and constrained reversibility relations in diamagnetic and temperature paths 17 p2912 A67-32269

Reverse transient in p-n-p triode when reverse pulse is applied to gate 21 p3598 A67-38573

REVERSER

S THRUST REVERSER

REYNOLDS EQUATION

SA LINEAR EQUATION

SA NAVIER-STOKES EQUATION

Analysis of additional terms in Reynolds flux equation when under unsteady conditions, using wind and temperature measurements, noting role in micrometeorology 02 p0238 A67-12077

Load and friction torque of Rayleigh step film scheme applied to journal bearing, using Reynolds equation [ASME PAPER 65-WA/LUB-2] 08 p1335 A67-20917

Reynolds equation analysis for pressure distribution in gas bearing clearances by asymptotic solution 10 p1660 A67-23046

Quasi-static analysis of nonsynchronous response effect of gas bearing pivoted pad design variables and application to operating machinery [ASME PAPER 67-VIBR-15] 11 p1796 A67-24175

Mean velocities, turbulence intensities, Reynold stresses and wall friction measurement in turbulent radial wall jet [ASME PAPER 67-APM-10] 17 p2838 A67-32419

Analysis divided into step and ridge regions used to obtain linearized PH solution to Reynolds equation, neglecting side leakage [ASME PAPER 67-LUB-17]

24 p4163 A67-42676

Semiimplicit numerical methods for time transient gas-lubrication Reynolds equation stressing numerical stability [ASME PAPER 67-LUB-18]

24 p4163 A67-42677

REYNOLDS NUMBER

SA CRITICAL REYNOLDS NUMBER

SA FROUDE NUMBER

Supersonic MHD generator crisis possibility assuming quasi-one-dimensional nonheat-conducting approximation at small Reynolds numbers and plasma scalar conductivity 01 p0011 A67-10177

Surface roughness effect on laminar MHD flow through rectangular duct, deriving relation between transition friction factor and Reynolds and Hartmann numbers 01 p0120 A67-10186

Effect of electrode tips of MHD generator and induced magnetic field on fluid flow in generator analyzed, using approximation method 01 p0121 A67-10227

Vortex strength in wake of circular cylinders and comparison of vortex velocity distribution with that of Hoffman and Joubert, using hot-wire anemometers at various Reynolds numbers 01 p0005 A67-10256

Hot wire measurement of tangential velocity and Reynolds stresses in spiral laminar-turbulent flow 01 p0054 A67-11163

Stability of plane parallel flows in finite length tube at large Reynolds numbers, noting velocity profile 02 p0233 A67-11949

Viscous incompressible flow past finite flat plate obtained under Oseen approximation for large and moderate Reynolds numbers, using Wiener-Hopf technique 02 p0234 A67-12546

Second order spectral tensor equations governing turbulence occurring in presence of uniform magnetic field at low magnetic Reynolds numbers 03 p0483 A67-13883

Heat and mass transfer from vertical plates boundary layer in convection at low Reynolds number by interferometry [ASME PAPER 65-WA/HT-39] 03 p0404 A67-14011

Series coefficients of flow stream functions for plane laminar flows of viscous incompressible fluids in channels and near corners at small Reynolds numbers 03 p0405 A67-14259

Certain dissipative mechanisms of homogeneous turbulence in presence of uniform magnetic field with small magnetic Reynolds number 04 p0662 A67-14414

Numerical analysis of unsteady viscous fluid flow past circular cylinder, noting effect of Reynolds number 04 p0602 A67-14617

Connective heat transfer and viscous fluid friction at air pressure with high Reynolds numbers in cooled channels, noting coolant pressure effect 04 p0603 A67-14717

Reynolds number assessment in analytical relations for convective heat transfer and viscous fluid friction 04 p0722 A67-14718

Variation of transition Reynolds number with wall to recovery temperature ratio at hypersonic speeds, comparing transition measurements with and without Pitot tube 04 p0604 A67-14836

Base pressure measurements on sharp and blunt 9 degree cones at Mach 3.50 to 9.20 04 p0547 A67-14851

Reynolds number and incidence angle effects on inducer cavitation in water [ASME PAPER 66-WA/FE-31] 04 p0607 A67-15363

Velocity profiles for infinite cylindrical journal bearing, using small eccentricity perturbation calculation and modified Reynolds number as parameter [ASME PAPER 66-WA/APM-17] 04 p0630 A67-15408

Magnetic Reynolds number determinations for inductive MHD generator and DC conductive MHD generator 04 p0670 A67-15533

Mass transfer and hydrodynamics of gas jet injection into liquid surface, deriving empirical equations for hollow truncated point formed around injection point 04 p0727 A67-15754

Forced-convective heat transfer in asymmetrically heated rectangular ducts as function of prandtl number, Reynolds number, aspect ratio and temperature difference 04 p0728 A67-15804

Convective heat transfer from bluff bodies

analyzed, particularly small electrically heated cylinders at low Reynolds numbers, noting correlation with Nusselt and Prandtl numbers 04 p0732 A67-15831

Turbulent subsonic gas jets, importance of Reynolds number and geometrical configuration of nozzle in determination of flow parameter 05 p0790 A67-16033

Flow pressure structures of supersonic flow over rearward facing step, showing pressure changes and Reynolds number role 05 p0750 A67-17339

Hydromagnetic compressible boundary layer flow past flat plate analyzed via von Karman integral method 05 p0794 A67-17361

Hot-wire anemometer measurements of transition in incompressible wake of cone at low Reynolds number 05 p0751 A67-17439

Fixed vertical plane surface effect on velocity of solid sphere in free fall in laminar region of incident viscous flow for various Reynolds numbers 06 p0983 A67-17928

Heat transfer for wall adjacent to region of turbulent separated flow 06 p0985 A67-18131

Flow field and stability of far wake of circular cylinders at hypersonic speeds, noting Reynolds number role [AIAA PAPER 67-32] 06 p0939 A67-18348

Vortex periodicity in wakes as function of Reynolds and Rossby numbers, solving nonlinear viscous Navier-Stokes equations [AIAA PAPER 67-34] 06 p0987 A67-18349

Transition from laminar to turbulent boundary layer flow at hypersonic Mach numbers, noting measurement techniques [AIAA PAPER 67-130] 06 p0989 A67-18474

Low magnetic Reynolds number two-dimensional and axisymmetric MHD flow of conducting ideal gas through supersonic nozzle 06 p1043 A67-18669

Turbulent MHD boundary layer flow of constant-electroconductivity incompressible fluid past dielectric plate in TM field, for small magnetic Reynolds numbers 06 p1043 A67-18672

Resistance coefficient of circular cylinder and sphere in range of Reynolds and Stuart numbers 06 p1045 A67-18692

Weakly dissipative fluid with schematized zone of strong gradients in perfect fluid formed by shock wave characterized by inversion of Reynolds number 06 p0990 A67-18726

Preston tube in concentric annuli, discussing skin friction measurement in fully developed turbulent flow 06 p0990 A67-18749

Fluid flow through parallel cylinders when flow incidence is lateral and Reynolds numbers are small, determining particles trajectories 06 p0991 A67-18819

Oscillating variables of flow past cylinder, calculating magnitude and frequency of lift 07 p1168 A67-19258

Aerodynamic characteristics of rough cylinders, noting effect on head drag coefficient and Reynolds number 07 p1126 A67-19323

MHD phenomena in vortex ring in conducting fluid, noting intensification of initial field at high Reynolds numbers and self-excitation 07 p1229 A67-19684

Laboratory hypersonic wake fluid mechanics transition data over range of Reynolds number structured into three laws of far and near wake and interpolation regime [AIAA PAPER 67-33] 08 p1275 A67-20379

Moving part vs nonmoving part elements, with reference to Reynolds effects 08 p1281 A67-20454

Reynolds number and ratio with Mach number as similarity parameters in fluidic devices with significant compressibility and viscosity 08 p1283 A67-20471

Flow field in turbulent far wake at high Mach and Reynolds numbers, obtaining solution of boundary layer equations 08 p1277 A67-20577

Spread of turbulent plane jet issuing into parallel moving air stream, noting Reynolds number variation 08 p1321 A67-20713

Tietjens function reexpressed as ratio of rapidly converging power series of complex argument and used in calculation of critical Reynolds numbers 08 p1322 A67-21138

Precursor wave velocity, electron density and current content in electromagnetically driven shock tube, using hydrogen and argon 08 p1363 A67-21380

Ascending spherical balloon motion

reduced by flight Reynolds number
 reduction from supercritical to subcritical
 values 08 p1278 A67-21529

Zero Reynolds limit of steady
 incompressible viscous fluid motion in
 sphere due to Landau source at center
 proved to be Stokes flow 09 p1487 A67-21665

MHD of flows with hot electrons in MHD
 ducts at low magnetic Reynolds numbers,
 emphasizing boundary layer and shock wave
 theory 09 p1541 A67-21797

Unstable motion of incompressible viscous
 fluid in interspace between concentric
 spheres 09 p1487 A67-21928

Air mass measurement during turbulent
 axial flow towards surface of rotating disk,
 noting entrainment rates for high and low
 Reynolds numbers 09 p1437 A67-22159

Energy transfer spectra and Joule effect
 dissipation in decline of homogeneous
 turbulence in presence of uniform magnetic
 field with small Reynolds
 number 09 p1549 A67-22565

Sealing coefficient of visco seal for
 laminar and turbulent flow, noting Reynolds
 number effect 10 p1659 A67-22706

Steady flow of viscous conducting fluid in
 pipe under magnetic field analyzed for
 relations among Hartmann number, Reynolds
 number, skin friction, wall conductivity,
 etc 10 p1687 A67-23833

Short method measurement of Reynolds
 stresses in turbulent flow, using constant
 current hot-wire
 anemometer 10 p1629 A67-23845

Numerical technique for time dependent
 calculation of two incompressible fluids
 interaction to study viscous and inviscid
 Rayleigh-Taylor instability 11 p1774 A67-23859

Local heat transfer in water flow in
 horizontal annular tube, estimating local
 longitudinal and circumferential variations in
 Nusselt number at tube wall as function of
 Reynolds and Rayleigh
 numbers 11 p1881 A67-24025

Solid body translational movement in
 viscous incompressible conductive flow in
 magnetic field solved for case of zero
 magnetic Reynolds
 number 11 p1832 A67-24055

Laminar heat transfer rate to two-
 dimensional blunt base in supersonic flow
 evaluated for varying Reynolds, flow and
 shock Mach numbers 11 p1882 A67-24222

Constant Reynolds number applied to data
 evaluation for turbulent jet flow in
 converging-diverging axisymmetric tube
 using free turbulent jet 11 p1742 A67-24272

Formal expansion schemes in predicting
 statistical properties of turbulent flows at
 high Reynolds numbers 11 p1780 A67-24540

Laminar turbulent transition of
 nonisothermal incompressible forced flows in
 pipes measured for several working fluids
 and temperatures, using Reynolds number as
 criterion 11 p1781 A67-24574

Transfer process effect on stability of
 plane flame front, deriving revised
 approximate solution for large finite
 Reynolds numbers 11 p1883 A67-24672

Motion of hollow body filled with viscous
 fluid at large Reynolds numbers,
 determining Zhukovskii potentials and
 examining small
 oscillations 11 p1782 A67-24673

Free plane jet compared with wall jet,
 noting more rapid lateral expansion of free
 jet 12 p1891 A67-25142

Navier-Stokes equations solved by finite
 difference methods at low Reynolds
 numbers for viscous flow around sphere,
 noting no flow separation 12 p1927 A67-25283

Explosively driven MHD generator,
 obtaining conversion efficiency dependence
 on magnetic Reynolds number, load-to-
 channel inductance ratio and
 magnetic/kinetic energies
 ratio 12 p1901 A67-25896

Friction factors and velocity profiles in
 turbulent flow of viscoelastic non-Newtonian
 fluid, noting correlation between frictional
 characteristics and Reynolds
 number 12 p1929 A67-25904

Transition sticking in wake of slender
 hypersonic cone as Reynolds number
 increases 12 p1893 A67-25927

Navier-Stokes asymptotic solutions for
 large Reynolds number flows, emphasizing
 incompressible axial flow past semiminfinite
 circular cylinders 12 p1930 A67-26179

Turbulent flow through concentric annuli,

measuring velocity profiles, finding
 maximum velocity radius different from
 value for laminar flow and dependent on
 Reynolds number 13 p2092 A67-26268

Viscous fluid flow stability in boundary
 layer on plate, applying perturbation
 method, calculating critical values of
 modified Reynolds
 numbers 13 p2105 A67-27051

Plane one-dimensional MHD flow in
 transverse magnetic field with magnetic
 Reynolds number equal to or greater than
 unity 13 p2169 A67-27311

Fluid turbulence effect on rate of heat
 transfer from spheres in vertical wind
 tunnel indicate turbulent Reynolds number
 as important parameter 13 p2225 A67-27466

Stability of multiple rows of vortices
 created behind tripping cylinders at low
 Reynolds number 14 p2294 A67-27795

Effect of Reynolds number on hypersonic
 flow of rarefied gas past sphere obtained
 from pressure distribution at
 surface 14 p2240 A67-27996

Wind tunnel heat transfer measurements
 from circular cylinders to transverse air
 flow, noting recovery factor as function of
 Knudsen number 14 p2405 A67-28178

Discharge characteristics of sharp and
 round edged orifices in transition regime
 noting variation of pressure ratio, magnitude
 of Knudsen and Reynolds numbers,
 etc 14 p2300 A67-28180

Jet reattachment for inclined walls at low
 Reynolds numbers and moderate nozzle
 aspect ratios
 [ASME PAPER 67-FE-25] 14 p2305 A67-28369

Combustion of pure liquid monopropellant
 droplet burning in own combustion products
 at low Reynolds numbers 14 p2376 A67-28552

Air stream turbulence effect on local and
 macroscopic transport from cylinder,
 measuring thermal transfer and pressure
 coefficients at various Reynolds
 numbers 14 p2407 A67-28624

Relationship between effectiveness of film
 cooling, free stream Reynolds number, slot
 Reynolds number and angle of
 injection 14 p2408 A67-28816

Aerodynamic flow deflection over convex
 curved surface noting occurrence of
 hysteresis 14 p2305 A67-28978

Current carrying incompressible viscous
 fluid past nonconducting sphere taking fluid
 inertia into account, noting eddy formation
 and flow separation 15 p2469 A67-29224

Single-fluid model accounting for behavior
 of MHD shock producing devices with
 unseparated shock and driving current
 sheet 15 p2528 A67-29565

Initially isotropic turbulence, characterized
 by three dimensionless numbers, suppressed
 by applying uniform magnetic
 field 15 p2471 A67-29656

Unsteady flow of inviscid, electrically
 conducting but thermally nonconducting gas
 at small magnetic Reynolds numbers in MHD
 generator channel unsteady flow of inviscid
 electrically conducting but thermally
 nonconducting gas at small
 magnetic 16 p2706 A67-30451

Current and potential distribution for
 thermally-stable plasma of Faraday-type
 segmented electrode MHD generator, taking
 into account nonequilibrium
 ionization 16 p2599 A67-30530

MHD flow of liquid mercury through
 circular pipes at high Hartmann and
 Reynolds numbers, plotting friction
 factors 16 p2712 A67-30576

Limits of applicability of methods based
 on one-dimensional model employing
 Reynolds analogy for gas flow in
 pipes 16 p2660 A67-31203

Low Reynolds number flow past heated
 cylinder studied for fluid properties
 variation and thermal and velocity slip
 presence at wall 16 p2779 A67-31216

Heat loss from wires in nitrogen, helium
 and mixtures measured at low Reynolds
 numbers, finding agreement with theory of
 Kassoy 16 p2779 A67-31217

Wall jet compared to plane free jet
 examining equilibrium conditions of velocity
 profile of fluctuation and mean flow
 determining stress 16 p2662 A67-31470

Mhd boundary layer at various Reynolds
 numbers and magnetic Reynolds number
 conditions mhd boundary layer at various
 Reynolds numbers and magnetic Reynolds

number conditions mhd boundary layer at
 various Reynolds numbers 16 p2722 A67-31569

Hypersonic magnetohydrodynamic flow
 over blunt bodies for small magnetic
 Reynolds number hypersonic
 magnetohydrodynamic flow over blunt
 bodies for small magnetic Reynolds number
 hypersonic magnetohydrodynamic flow over
 blunt 16 p2594 A67-31579

Steady flow in rectangular cavity with
 driving motion by uniform translation of one
 wall 17 p2836 A67-32279

Tangentially injected plane jet spreading
 in slipstream at various Reynolds numbers
 at jet inlet slot studied in wind tunnel for
 dynamic behavior 17 p2839 A67-32906

Law for velocity distribution through wall
 boundary layers derived from eddy viscosity
 model, considering turbulent shear variation
 and Reynolds number
 effect 17 p2839 A67-33008

Stability of plane parallel flows in finite
 length tube at large Reynolds numbers,
 noting velocity profile 17 p2841 A67-33266

Nonstationary drag coefficient for
 unsteady flow for large Reynolds numbers
 determined experimentally, using analog
 computer method 18 p3023 A67-33425

Probability distribution of square of
 temperature difference between two points
 of turbulent flow measured by pulsation
 thermometer 18 p3026 A67-33757

Mach and Reynolds numbers effect on
 rarefied supersonic gas flow pattern near
 forward stagnation point of blunt body,
 noting decrease in
 density 18 p3028 A67-34209

Channel flow transition to jet flow,
 discussing turbulence determination in flow
 boundary layer as Reynolds number
 function 18 p3028 A67-34218

Pressure fluctuations beneath
 incompressible turbulent boundary layer
 with mass addition 18 p3030 A67-34742

Transition in oscillating boundary layer
 flows studied for various parameters
 effect 19 p3209 A67-35413

Compressibility effects on airfoils during
 high subsonic and low speed stalls,
 considering Reynolds and Mach number
 effect 19 p3170 A67-35521

Local heat-transfer coefficients of turbine
 blades, evaluating local Nusselt number
 distribution, Reynolds numbers, and
 turbulent flow effects 20 p3515 A67-36451

Vibrational frequency and amplitude
 effects on heat transfer intensity from
 vibrating cylinder into circular channel at
 low Reynolds numbers 20 p3554 A67-37303

Flow pattern at low Reynolds numbers
 about airfoil cascade illustrated by hydrogen
 bubble flow-visualization
 technique 20 p3359 A67-37483

Reynolds stress in turbulent flow
 dependence on mean velocity field
 determined by rational sequence of
 approximations 21 p3609 A67-37734

High performance aerodynamic impulse
 facility with shock tunnel, expansion tube
 and accelerator for high velocity and high
 Reynolds number
 environment 21 p3605 A67-37768

Unsteady conducting fluid flow in MHD
 ducts with small magnetic Reynolds number
 and constant pressure
 gradients 21 p3663 A67-37935

Low amplitude MHD shock wave
 attenuation, assuming high magnetic
 Reynolds numbers and small excitation zone
 width 21 p3665 A67-38239

Boundary value problem describing
 conducting fluid motion in longitudinal
 magnetic field, considering magnetic
 Reynolds numbers, electric current density
 distribution and heat
 exchange 21 p3665 A67-38243

Electromagnetically driven confined
 viscous vortex flow with high positive radial
 Reynolds numbers, solving energy equation
 for temperature distribution
 [AIAA PAPER 67-730] 21 p3674 A67-38754

Empirical method predicting flexible hose
 flow losses, with Fanning friction factor as
 Reynolds number and internal hose
 geometry function 22 p3785 A67-39971

Sound and white noise effects on
 turbulent jet aerodynamic characteristics
 studied at several Reynolds
 numbers 22 p3785 A67-40019

Relation between incipient cavitation
 number and Reynolds number by combining

bubble dynamics Rayleigh equation with cavitation number 22 p3787 A67-40176
 definition 22 p3787 A67-40176
 Wake turbulence regimes for flows behind typical hypersonic bodies 22 p3743 A67-40222
 Laminar flow field between rotating turbine disks solved for low Reynolds number and partial admission 23 p3988 A67-40614
 flow 23 p3988 A67-40614
 Electrical conductivity or magnetic Reynolds number of shock produced plasma flow, discussing interaction between magnetic field and plasma flow 23 p4031 A67-40881
 Linear MHD flow characteristics variation with electric conductivity and gas flow rate changes, noting transverse magnetic flow variation with magnetic Reynolds number 23 p4033 A67-41284
 Reynolds number effect on slender high speed cones wake-neck geometry, obtaining measurements of location, diameter and closure angle 23 p3932 A67-41754
 Perturbation theory definitions and overlap theorem proved and applied to small Reynolds number flows 24 p4142 A67-42168
 Singular perturbation methods for two-dimensional lifting low Reynolds number flow 24 p4091 A67-42169
 Boundary layer electric current temperature, velocity and density profile calculation on nonconducting MGD channel wall assuming smaller magnetic Reynolds number than unity 24 p4196 A67-42212
 One-dimensional plasma flow variables relations analyzed in crossed electric and magnetic fields with small magnetic Reynolds numbers 24 p4196 A67-42216
 NASA radial flow turbine research related to Brayton cycle power generator, investigating size, Reynolds number and speed effects on efficiency and flow 24 p4102 A67-42489
REYNOLDS NUMBER EFFECT
 Reynolds number effects and initial conditions effects on development of free shear in mixing layer from constant area nozzle 02 p0231 A67-11559
 Reynolds number effect on surface pressure distributions and boundary layer velocity profiles on three-quarter power law bodies of revolution in hypersonic flow 05 p0747 A67-16431
 Shock tunnel heat transfer measurement and hypersonic viscous flow over pointed cones, particularly viscous-layer regime at low Reynolds numbers 06 p0943 A67-18845
 Jet deviation by curved convex wall and Reynolds number explained as effect of boundary layer separation 08 p1320 A67-20450
 Skin heating effects on induction converters, noting magnetic field intensity and temperature as function of time and space 09 p1442 A67-21794
 Hydrodynamic drawing together problem for aerosol particles oscillating in sonic field at small Reynolds numbers, showing optimal field frequency-approach velocity correspondence 10 p1627 A67-23643
 Acoustical and aerodynamic characteristics of full scale axial flow air compressor simulation in Freon closed loop system operation [ASME PAPER 67-GT-27] 11 p1742 A67-24806
 Nozzle thermocouple for low flow rate measurement of high temperature gases, discussing calibration curves and taking into account Reynolds number effect 13 p2121 A67-27464
 Flow velocity determination by cylindrical magnifying probe, measuring stagnation and wake pressures difference, noting magnifying factor variation under Reynolds number and stem and blockage effects 15 p2471 A67-29529
 Hydraulic research data concerning control valve sizing and arrangement, noting liquid and gas control-valve formulas with limitations, Reynolds number effect, etc 15 p2423 A67-30400
 Flow turbulence on leading edge of attachment line of swept wing studied in wind tunnel 16 p2589 A67-30618
 Firing range for investigating Reynolds number effect on flow around bodies having complex design at transonic and supersonic velocities 16 p2655 A67-31116
 Turbulent flow in circular cylindrical duct at various Reynolds numbers, analyzing fluctuations and mean value of velocity 16 p2663 A67-31702

Tip losses in two types of turbine straight-blade cascades at several Reynolds numbers, noting vibration effect on stage performance 18 p2983 A67-33999
 Hydrodynamic drawing together problem for aerosol particles oscillating in sonic field at small Reynolds numbers, showing optimal field frequency-approach velocity correspondence 18 p3029 A67-34412
 Wind-driven plasma turbulence structure resolved by continuum ion probes at high Reynolds numbers, determining plasma density fluctuation from argon gas flow 18 p3030 A67-34743
 Centripetal radial blowing effect on flow and heat transfer in gap between rotating disk and wall, specifically effect of Reynolds number and dimensionless flow 20 p3357 A67-36794
 Gas-side heat transfer at high temperature combustor sonic points, discussing Reynolds number effect, boundary layer transitions, turbulence intensity, etc [AICHE PAPER 27] 20 p3552 A67-36831
 Transitional and turbulent boundary layers on cold flat plate in hypersonic flow noting bluntness, Reynolds and Mach numbers effects 21 p3615 A67-39080
 Reynolds number effect on base pressure behind wedge in supersonic and hypersonic flow based on Chapman wake flow recompression model 23 p3930 A67-41308
RHENIUM
 Ultrahigh temperature thermocouple using pure and boron-doped pyrolytic graphite or tungsten and rhenium for operation in vibration and oxidation environment 01 p0076 A67-11139
 Nitrogen adsorption at room temperature on atomically clean polycrystalline rhenium, noting dependence of sticking coefficient upon surface coverage and temperature 02 p0257 A67-12728
 Solubility of carbon in Mo, Re and W determined by isothermal carburization method 03 p0439 A67-12845
 Corrosion tests of W-, Mo-, Rh-based materials for compatibility in lithium at 2500, 2800 and 3000 degrees F 07 p1208 A67-19466
 Output characteristics of electroetched rhenium surface, bare and cesiated work function and performance 09 p1447 A67-22332
 Thermionic converter life-test results and failure mechanisms noting braze failure, collector deposit, emitter warpage and separation and cesium reservoir leak 09 p1447 A67-22334
 Performance of thermionic converters, discussing voltage output, interelectrode spacing, rhenium-rhenium and rhenium-molybdenum electrode systems 09 p1449 A67-22343
 Work functions of monocrystalline and polycrystalline rhenium with electron emission current measured by copper collector 09 p1451 A67-22358
 Corrosion of rhenium in various acids and hydroxides is electrochemical in nature and determined by kinetics of anodic and cathodic processes 12 p1955 A67-25359
 Effect of plastic deformation under compression on superconducting properties of Re single crystals 14 p2375 A67-29069
 Expected change in output voltage when W/W-26Re thermocouple is exposed to thermal neutrons, causing Re atom transmutation to Os 15 p2535 A67-29489
 Thermionic properties, surface ionization, atomic and ionic sublimation of Re, Mo, Ta and W 19 p3264 A67-35082
 Re and Os abundances in various chondrites determined by neutron activation analysis, noting fractionation 24 p4235 A67-42637
RHENIUM ALLOY
 Low temperature magnetic properties of superconducting Mo-Re alloys in fine wire form 07 p1236 A67-20135
 Thermophysical properties of heat-resistant solid solution of rhenium in tungsten produced by arc melting in vacuum 12 p1956 A67-25758
 Alloying principles for refractory metals based on softening mechanism, examining increased heat resistance of rhenium softened by recrystallization 16 p2691 A67-31589
 Structures in Mo-Re and W-Re systems examined by X-ray powder techniques,

discussing occurrence of chromium oxide type structure 17 p2873 A67-32813
 Co 60-Re alloy in externally fueled thermionic system shown economically desirable for multi-kwt terrestrial or undersea applications 24 p4185 A67-42535
RHEOELECTRIC SIMULATION
 Voltage gradient determination throughout two-dimensional electric field by electro-optic analog, noting applicability to boundary value problems satisfying Laplace equation 17 p2818 A67-32418
 Flow coefficient of various nozzles discharging into unbounded atmosphere for wall pressure distribution of potential rotational flow, using rheoelectric tank 23 p3989 A67-41140
RHEOLOGY
 Hydrodynamic thermal explosion of stationary axisymmetric non-Newtonian fluid in infinitely long cylindrical tube 01 p0052 A67-10681
 Inverse operation for Jaumann derivative /Integration/ applied to rheological equations of state for viscoelastic fluids 06 p0991 A67-18777
 Chemistry and rheology of gelled fuels, noting structure, thickeners, etc 10 p1696 A67-22911
 Rheology - Modern developments in mechanics of continua - Conference, Syracuse University, August 1965 11 p1781 A67-24569
 Two-dimensional jet plane problem, considering rheological solution for applications to ground effect machines 11 p1781 A67-24571
 Hydrodynamic thermal explosion of stationary axisymmetric non-Newtonian fluid in infinitely long cylindrical tube 11 p1783 A67-25068
 Conducting Bingham plastic fluids considered as lubricants in rheostatic bearing in presence of constant magnetic field [ASME PAPER 67-LUBS-4] 16 p2682 A67-31382
 Nonlinear macroscopic rheological behavior of dilute suspensions of deformable spheres 17 p2887 A67-32280
 Compression tests with superimposed hydrostatic pressure to study rheological behavior of elastomer filled with granular potassium chloride 18 p3142 A67-33891
 Compression tests with superimposed hydrostatic pressure to study rheological behavior of elastomer filled with granular potassium chloride 19 p3340 A67-35465
 Fringe order estimation of principal stress difference in plastically deformed body shown useful for variable stress rate by calibration test in photorheological stress analysis 20 p3536 A67-36419
 Extent of lubricating film for which oil flow is plane, discussing lubricant compressibility, heat release, load capacity and pressure distribution 22 p3811 A67-39317
RHO-THETA SYSTEM
 TACAN off-track airborne navigation computer and suitable indicator provide nonradial straight course as aid to ATC 09 p1531 A67-22658
RHODIUM ALLOY
 Microstructural and X-ray analysis of intermediate phases of Ti-Ir and Ti-Rh intermetallic compounds, including microhardness and fusion point variations 07 p1204 A67-19263
RHOMBIC ANTENNA
 SA RADIO ANTENNA
 Ionospheric movement detection using frequency swept sounder and rhombic antenna [AGARDOGRAPH 95] 15 p2484 A67-30301
 Rhombic traveling wave antenna with feedback loop to utilize larger proportion of total power 17 p2824 A67-32313
RHYTHM
 S BIOLOGICAL RHYTHM
 S CIRCADIAN RHYTHM
RIB
 Forces deforming rib cage during breathing efforts 07 p1133 A67-19480
 Torsional stiffness of ribs effect on buckling strength of longitudinally stiffened plates compressed in direction of ribs 10 p1719 A67-23474
 Asymmetric stability loss of nonuniformly heated circular plate rib, determining elastic properties and critical temperature jump

- value 20 p3536 A67-36447
- RIBBON PARACHUTE**
- Nike rocket boosted 20-ft-diam ribbon parachute for deployment at dynamic pressures above 400 psf 13 p2054 A67-27598
- RIBOFLAVIN**
- Purification and properties of nicotine oxidase suggest metalloflavoprotein having riboflavin 5-phosphate 20 p3376 A67-37032
- RIBONUCLEIC ACID /RNA/**
- SA DEOXYRIBONUCLEIC ACID /DNA/
- Effects of 1, 1, 3-tricyano-2-aminopropene /TCAP/ on incorporation of protein and nucleic acid precursors into frog nervous system in vitro 04 p0560 A67-14408
- Thiobarbituric acid reacted substance reaction with ribonuclease may be possible source of age pigment 15 p2433 A67-29296
- Saccharomyces cerevisiae light particle fraction containing fatty acid synthetase analyzed by density gradient method 19 p3178 A67-35873
- Organic phosphate shown as inhibitory factor from B. stearothermophilus for attachment of amino acids to transfer RNA 20 p3370 A67-36798
- RNA fractions base composition and labelling kinetics in presence and absence of actinomycin for rapidly labelled RNA in rabbit bone marrow rich in erythroid cells 23 p3944 A67-40801
- RICCATI EQUATION**
- SA DUFFING EQUATION
- Rational approximation of generalized Duffing equation, damped mass spring oscillator equation and generalized second order Riccati equation 04 p0647 A67-15660
- Algorithm for computing matrix Riccati equation solution in optimization problems 19 p3249 A67-34781
- Reflection coefficient determined for plane monochromatic electromagnetic wave incident on idealized laminar plane stratified jet stream, deriving Riccati type differential equation 23 p3974 A67-41201
- RICHARDSON NUMBER**
- Atmospheric turbulence effect on quality of star images based on telescopic observations of stars shows pronounced correlation 02 p0261 A67-11989
- Relative dispersion of particle pairs in homogeneous turbulence using Lagrangian-history direct interaction closure approximation for convected scalar field, obtaining Richardson diffusion equation 03 p0405 A67-14031
- Clear air turbulence relation to various ranges of Richardson number, noting set of nomograms for number estimation 05 p0838 A67-16709
- Nomograms and tables for calculation of Richardson number in relation to forecasting of clear air turbulence 05 p0838 A67-16710
- Helmholtz velocity profile instability in atmosphere with unstable density gradient /negative Richardson number/ 08 p1323 A67-21388
- Saha-Langmuir formula applied to description of temperature dependence of positive ion current in surface ionization of silicon atoms, comparing work functions by methods using contact potential, thermionic emission and Richardson graphs 09 p1554 A67-22006
- Shear flow, determined by velocity and density profiles, is stable for small disturbances of all wavelengths and Richardson numbers, enumerating eigenvalues 14 p2295 A67-27904
- RICIAN FADING**
- Chernoff bound and tilted distribution argument for obtaining error probability bounds for binary signaling on slowly fading Rician channel [JPL-TR-32-1051] 06 p0961 A67-17943
- RIEMANN INTEGRAL**
- Convolution type integral equation solution via reduction to Riemann problem in class of generalized functions 16 p2698 A67-31735
- Nonlinear hyperbolic equation solution formulation based on Riemann invariants 18 p3072 A67-34288
- RIEMANN PROBLEM**
- Mathematical physics PDE problems solved by combined method using Fourier integral transform and theory of Riemann boundary value problem 03 p0459 A67-13589
- Boundary value problem and singular integral equation applied to automatic control theory 20 p3475 A67-36652

- Quasi-linear elliptic system of first order equations used for Riemann-Hilbert boundary value problem 21 p3651 A67-37930
- Ferromagnetic magnetization curve approximated for analytical solutions of boundary value problems in nonlinear electrodynamics, obtaining Riemann functions 22 p3836 A67-39420
- RIEMANN SPACE**
- Five-dimensional relativistic space, giving physical interpretation for Riemannian space with metric form 04 p0656 A67-14746
- Curvature tensor in definition of affine branch point induced by Riemann branch point on isotropic hypersurface 09 p1534 A67-22566
- Covariant decomposition of tensor and gravitational Cauchy problem in Riemann space 10 p1679 A67-22841
- Derivative components of unit tangent vectors to parametric curves of curvilinear coordinate system in general Riemann space 10 p1675 A67-23792
- Cosmological distortion effect incorporating incident magnetic type gravitational field parameter upper limits measured from galactic cluster photographs 11 p1860 A67-24484
- Asymptotic behavior of curvature tensor in certain asymptotically Euclidean Riemannian space-time 11 p1819 A67-24763
- M-dimensional interpretation of n-dimensional Einstein equation 12 p1966 A67-25143
- Accidental degeneracy of hydrogen atom levels using Schroedinger equation, deriving eigenfunctions 18 p3083 A67-34072
- Propagation rate of electromagnetic and gravity wave front in synchronous reference system in Riemann space 20 p3486 A67-37554
- Einstein vacuum equation solution interpretation for gravitation, space and time concepts, using vector fields oriented in time and Riemann tensorial equations 20 p3487 A67-37684
- Differential and Clifford matrix algebra relationship in relativity theory, generalizing Dirac and quaternion algebras to Riemann spaces 21 p3656 A67-37923
- Principles developed for founding of unified field theory of gravitation and electromagnetism, with space-time geodesics as charged particle motion equation 23 p0426 A67-40659
- Higher dimensional spaces and symmetries arising on gravitational fields 23 p4028 A67-41188
- RIFT PROJECT**
- S REACTOR IN-FLIGHT TEST /RIFT/ PROJECT
- RIGID BODY**
- Plastic flow of axially symmetric notched bars pulled in tension, obtaining load factors 01 p0159 A67-10401
- Discontinuous impact vibration absorber with small auxiliary mass sliding in slit of rigid body excited by sinusoidal oscillation 01 p0161 A67-10645
- B-52 structural response to random turbulence with various stability augmentation systems, noting rigid body motions, normal vibration modes and control surface rotations [AIAA PAPER 66-998] 02 p0181 A67-12302
- Existence and stability of equilibrium orientations of rigid body with gyrost at in nonuniform gravitational field 02 p0268 A67-12385
- Motions of asymmetrical rigid body subjected to no-power forces 03 p0468 A67-13349
- Diffraction of plane harmonic horizontally polarized shear waves by parabolic cylinder, obtaining dynamic shear-stress concentration for parabolic notch and rigid parabolic insert [ASME PAPER 66-WA/APM-13] 04 p0713 A67-15405
- Nonlinear equations for supercritical axisymmetric elastic deformation of circular cylindrical shell under longitudinal impact from rigid body 05 p0907 A67-16015
- Integral motion equations of rigid body with cavity partly filled with viscous incompressible fluid with free surface 05 p0921 A67-17005
- Motion analysis of elastic deformable body visualized as rigid frame and elastic particles 05 p0923 A67-17183
- Canonical transformation to investigate rotational motion of uniaxial orbiting rigid

- body influenced by gravity gradient torque [AIAA PAPER 67-125] 06 p1084 A67-18288
- Rotational motion of rigid sphere about z axis in elastic medium taking into account surface adhesion 07 p1223 A67-19219
- Dual quaternions in describing motions of offset unsymmetrical gyroscope [ASME PAPER 66-MECH-6] 08 p1332 A67-21316
- Liapunov stability of motion of heavy rigid body with fixed point moving along spherical surface 11 p1818 A67-24163
- Mode coupling effect on response of rigid body to random excitation analyzed, using two degree of freedom model [ASME PAPER 67-VIBR-36] 11 p1873 A67-24193
- Longitudinal impact of two reinforced cylindrical shells coupled to each other at ribs against solid body 12 p2025 A67-25611
- Rigid disk impact against ideal fluid surface in cylinder, deriving formula for impulse pressure at disk surface 12 p1928 A67-25669
- Compression load stability of nonuniformly rigid plates within and beyond elasticity limits solved by combined Galerkin and finite difference methods 12 p2031 A67-25961
- Time dependent orientation of body fixed coordinate system relative to stars for spinning rigid torque-free body 13 p2154 A67-26816
- Dynamic equations for interacting connected rigid bodies 13 p2212 A67-26838
- Elastic deformation effects on stability of rotating satellite composed of elastically connected rigid bodies 13 p2212 A67-26905
- Rigid lifting body movement transfer function derived from translational and angular velocity components transfer functions 14 p2393 A67-28061
- Theorems defining class of motions of system of mass points of given mass in Lobachevskii space 16 p2702 A67-31011
- Approximate calculation of coefficients in equation for perturbed motion of rigid body containing liquid 16 p2765 A67-31051
- Dynamic response of rigid-plastic material ring subjected to arbitrarily distributed impulse load 17 p2959 A67-32412
- Shells of revolution with curved elements noting rigid body displacements in analysis by matrix displacement method 17 p2963 A67-33042
- Applicability to elastic flight vehicle control system of two variants for realization of invariance conditions 17 p2882 A67-33097
- Integral motion equations of rigid body with cavity partly filled with viscous incompressible fluid with free surface 18 p3028 A67-34267
- Book on methods for applying principles of dynamics to engineering problems covering three-dimensional approach, free-body system and derivation of motion equations 18 p3080 A67-34566
- Inhomogeneous second order linear differential equation solution based on Lie formalism, presenting physical applications 19 p3250 A67-35891
- Surface pressure spatial correlation function for rigid infinitely long cylinder in three-dimensional diffuse sound field 20 p3537 A67-36646
- Thermally induced boundary layer flows in isothermal rigid body rotation 20 p3421 A67-36843
- Elastic and dynamic response of viscoelastic plate with finite thickness to rigid body impact 20 p3539 A67-36920
- Quasi-optimum three-axis attitude control law for minimum time of rigid body, noting gyroscopic cross axis coupling 22 p3899 A67-39190
- Permanent deformation and interaction effects of rigid plastic clamped beam with constraints against axial displacements and subjected to transverse impulsive loading 23 p4072 A67-40606
- RIGID MOUNTING**
- Lower critical load determination of elastic spherical shell with rigidly fastened edge 12 p2021 A67-25580
- Approximate theory for stress-strain state of thin cylindrical shell reinforced with elastic ribs having bending rigidity 12 p2022 A67-25584
- Stress-strain state of thin sandwich plate consisting of arbitrary number of elastic isotropic layers rigidly coupled to each

- other 12 p2024 A67-25602
- RIGID ROTOR**
- Flights tests of XH-51A compound helicopter, discussing rigid rotor concept and results of compound flight research program 07 p1130 A67-20075
- Parametric oscillations of counterbalanced rotors 13 p2216 A67-26628
- Gyro-controlled rigid rotor system performance, noting steady state and transient response to various excitation [AHS PAPER 131] 16 p2599 A67-31845
- Soviet papers on friction and wear in machinery covering elastorheology and equilibrium stability of rigid rotor 22 p3811 A67-39315
- Equilibrium stability of rigid rotor in aerodynamic bearings, determining lubricant effect on journal 22 p3811 A67-39316
- RIGID ROTOR HELICOPTER**
- XH-51A compound research flight test program, discussing adaptation of rigid rotor concept 13 p2052 A67-26421
- Gyrocontrolled rigid rotor system for helicopter high speed performance 21 p3567 A67-38015
- AH-56A Cheyenne compound aircraft weapon system and major subsystems, discussing fire control, navigation system and performance 21 p3568 A67-38133
- RIGID STRUCTURE**
- Interpretation of built-up areas in cities and industrial sites from aerial photographs 02 p0240 A67-11533
- Expandable and modular structures for support on manned space missions, reviewing inflatable, chemically rigidizable, unfurlable and elastic recovery structures 02 p0333 A67-12342
- Model analysis of radial oscillations of shaft with pounding of ball bearings 05 p0812 A67-17236
- Book on matrices for structural analysis, including elementary algebra and detailed arithmetic of matrix methods applied to structure theory 10 p1719 A67-23476
- Dynamic stability of cylindrical shell reinforced by thin walled rigid longitudinal ribs 10 p1721 A67-23604
- Dynamics of rigid plastic thin walled shells for short term constant high intensity load 12 p2025 A67-25607
- Infinite horizontal fluid layer heated from below /classical Rayleigh thermal stability problem/ extended to fluid in rigid sphere heated nonuniformly 22 p3918 A67-39715
- Stresses, bending moments and displacements of variable rigidity toroidal shell in steady temperature field derived assuming independent thermal expansion coefficient and physical constants 23 p4075 A67-40680
- RIGIDITY**
- SA MAGNETIC RIGIDITY
- SA POISSON RATIO
- SA STRUCTURAL RIGIDITY
- Flexibility and rigidity requirements imposed on vibration damping systems of optimized precision devices 06 p1106 A67-18618
- Rigidity of surface with flattened point proved by Cauchy-Riemann equations, considering case where contact of surface with tangential plane approaches infinity 16 p2698 A67-31912
- RING**
- SA CIRCLE
- SA LOOP
- SA PLASMA RING
- SA REINFORCEMENT RING
- SA VORTEX RING
- Paraformaldehyde hypothesis of IR spectrum of Saturn ring 03 p0509 A67-13167
- Reissner variational method stability analysis of small eccentricity nonlinearly elastic thin circular ring 03 p0531 A67-14230
- Continuation of norms given at subring of matrix ring 04 p0646 A67-15257
- Circular ring subjected to two diametrical, equal and opposite forces with results converted into stress-strain charts 04 p0715 A67-15603
- Dynamic elastic response of ring loaded transiently on both edges 04 p0718 A67-15921
- Orthogonal function energy method calculation of stress concentration in ring under impact loads distributed along inner and outer edges 05 p0918 A67-16420
- Finite difference method solution of motion equations for free vibrations of initially disturbed thin elastic rings 06 p1109 A67-18838
- Damping coefficients for rigid and flexible ring baffles for slosh suppression 15 p2470 A67-29438
- Thin elastic circular ring equilibrium stability in rigid cavity subjected to parallel loading, considering small ring separation region at buckling [ASME PAPER 67-APM-19] 17 p2958 A67-32406
- Dynamic response of rigid-plastic material ring subjected to arbitrarily distributed impulse load 17 p2959 A67-32412
- Nonlinear flexural vibrations of rings studied without assuming zero midplane strain 17 p2963 A67-33032
- RING CURRENT**
- Vector potential of magnetic field of any axisymmetric electric current distribution used to compute field of two model magnetospheric ring currents 04 p0617 A67-15535
- Aurora and ring current theory confirming role of hydromagnetic plasma flow and frozen-in field lines in geomagnetic storms 06 p0995 A67-17973
- Magnetospheric distortion during geomagnetic storm on September 30, 1961, examining Explorer XII satellite evidence on ring currents 07 p1180 A67-19924
- Ionospheric heating by Joule dissipation of main-phase ring current associated with asymmetry 07 p1181 A67-19934
- Radial displacement of particles excited by solar-wind-induced current at boundary of and ring current within magnetosphere 12 p1994 A67-25531
- Magnetic field of ring current on earth surface according to observations during IGY 13 p2111 A67-26557
- Geomagnetic ring current observations using Elektron II satellite, noting location, orientation and structural features 14 p2308 A67-27928
- Synoptic charting of high latitude geomagnetic field distribution during magnetic storm, discussing ring current behavior 14 p2309 A67-27942
- Decay of persistent currents in small ring-shaped superconductors due to detectable internal thermodynamic fluctuations 14 p2370 A67-28717
- Asymmetric proton injection into magnetosphere using Vlasov equation, with solution in terms of electric potential 16 p2666 A67-31403
- Magnetic diffusion effects in sunspot region assuming Schroeter value for electric conductivity 17 p2952 A67-33395
- Simultaneous AC and DC in ring-shaped hard superconductors, confirming critical AC and superimposed DC existence 18 p3098 A67-33521
- Ring circuit using glow-discharge thyristors to combine functions of pulse indicator and pulse counter with decimal readings 19 p3228 A67-34990
- Simultaneous and independent potentiostatic control of rotating ring and disk electrode and application to CuII/CuI/Cu system 20 p3446 A67-36655
- Auroral breakup relation to ring current interchange instability, studying dispersion relation effects 20 p3431 A67-37096
- Charged particles of extraterrestrial ring current during geomagnetic storms, with Ogo 3 measurements of proton and electron differential energy spectrums 20 p3432 A67-37401
- Solar emissions and magnetic storms and auroras, discussing ring current, solar flux and Van Allen belt energetic particle density 21 p3620 A67-38978
- Solar wind geomagnetic field interactions during disturbed conditions, discussing solar particle emissions, solar plasma activity, ring and ionospheric currents 22 p3870 A67-39672
- RING DISCHARGE**
- Ring laser rotation sensing system, evaluating accuracy limit for minimized inaccuracy of known sources of error 03 p0438 A67-13992
- Anomalous transport phenomena in ring discharge studied for instability and losses due to noise, using mc RF oscillator [AROD-6398-2] 11 p1831 A67-24010
- HF magnetic fields for plasma sheath with perpendicularly superimposed static magnetic field and resonance excitation of electron cyclotron waves 19 p3276 A67-35117
- Ionization frequency distribution in HF discharge produced by long single turn coil 19 p3276 A67-35118
- RING LASER**
- Ring laser inertial sensor for aerospace systems obtaining high accuracy angular resolution and mechanical simplicity 04 p0625 A67-15665
- Michelson interferometer and ring laser compared for measurement of relativistic rotational effects of earth 17 p2883 A67-32361
- Counter traveling wave regime stability in ring gas laser, studying effects of atomic collisions, isotopic state and wave coupling 19 p3239 A67-34898
- Ring laser use for measuring gas flow on ground and fuel and oxidizer flow in rockets 22 p3800 A67-39892
- RING STRUCTURE**
- Directive gain and impedance calculated for ring array of antennas that concentrate radiated power in plane of ring and are omnidirectional 02 p0211 A67-11595
- Differential moduli of differential spaces on ring or on differential solid with variable coefficients 03 p0458 A67-13460
- Large deformations of circular membrane attached to ring subjected to action of uniform load 04 p0708 A67-14795
- Astrobleme in Australia analyzed for origin of eruptive gas 10 p1706 A67-22956
- Buckling test data for internal integral ring-stiffened aluminum cylinders under combinations of axisymmetrical axial load and external lateral pressure 11 p1875 A67-24611
- X-ray laser resonator proposal involving three-dimensional puckered ring arrangement of crystals at Bragg angle, discussing polarization losses 13 p2126 A67-27012
- Dynamic buckling of ring constrained in rigid circular surface and subjected to transiently applied inertial loading 14 p2398 A67-28093
- Lunar crater classification by morphological types discussing ring structures 16 p2747 A67-30984
- Approximate solution of elastic buckling of radially constrained circular ring under uniformly distributed loading 22 p3908 A67-39287
- Optimum design of ring airfoil device for maintaining pressure recovery efficiency of conical diffuser 22 p3743 A67-40168
- Stiffness matrix of unsymmetric nodal ring element for matrix displacement analysis of rib stiffened conical shells 22 p3914 A67-40191
- RING WING**
- Force measurements and visual observations made in water tunnel on fully wetted and ventilated flows past family of conical ring wing hydrofoils having flat plate section geometry [ASME PAPER 66-WA/UNT-4] 04 p0608 A67-15383
- RIOMETER**
- Riometer data analysis results concerning cosmic ray event of April 18, 1965 04 p0693 A67-14973
- Sidereal time recorder used with riometer for detection of radio noise absorption in ionosphere 08 p1329 A67-21489
- Riometer observations in polar caps of solar cosmic ray events during IQSY 12 p1993 A67-25228
- RIOMETRY**
- Polar based riometric observations of solar cosmic ray events during IQSY 10 p1701 A67-23193
- Auroral X radiation, measured by balloon-installed X-ray spectrometer incorporating scintillation counter with high speed analyzer, correlated with ionospheric radioelectric absorption and solar magnetic field variations 10 p1702 A67-23304
- Riometric data on ionospheric absorption applied to determination of dissociative recombination coefficient, noting atmospheric ionization by fragment gamma-radiation 14 p2306 A67-27858
- RISK-TAKING**
- Statistical analysis of heart rates of Navy carrier pilots during bombing attacks compared with those for launch and landing 09 p1455 A67-21718
- Mission risk appraisal technique for identification and quantification of high risk areas for unmanned interplanetary

missions 18 p3163 A67-34682

RITZ AVERAGING METHOD

Book on numerical realization of variational methods, discussing Hilbert space elements, Ritz and Bubnov-Galerkin stability processes, spectral and nonlinear problems, etc 04 p0645 A67-15009

Ritz averaging method to determine free and forced vibratory response of beams and plates undergoing large amplitude steady state harmonic oscillations 04 p0715 A67-15659

Galerkin-Ritz method application to Maxwell waveguide equations for calculation of propagation constant of rectangular guide with transverse ferrimagnetic core 07 p1152 A67-19590

Convergence rate of approximate Ritz and Bubnov-Galerkin method in application to equations having solutions in form of linear combination of functions 08 p1349 A67-21200

Variational integration principles used to integrate wave and Fourier thermoconductivity equations, noting solution by Ritz method 14 p2408 A67-28803

Variational technique for temperature field determination in plane system with given heat distribution sources, based on Galerkin-Ritz method 17 p2972 A67-33069

Dynamic stability of beam columns undergoing weakly nonlinear vibrations studied using Ritz-Galerkin procedure 19 p3342 A67-35758

Galerkin-Ritz method application to Maxwell waveguide equations for calculation of propagation constant of rectangular guide with transverse ferrimagnetic core 20 p3401 A67-37327

Vibrations of turbine disks of variable thickness calculated by Ritz method, applying functions approximating actual thickness of disk 21 p3636 A67-38836

RIVET

Rivet type aircraft fasteners 05 p0810 A67-16232

RIVETED JOINT

Elastoplastic behavior of riveted joints subjected to pulsating and alternating stress and preliminary fatigue cycles 01 p0163 A67-11151

Fatigue strength of riveted joints as affected by material properties, rivet placement and fabrication method 03 p0521 A67-13023

Load carrying capability of adhesive bonded studs, analyzing resin systems and flexible liners 09 p1507 A67-22502

Semimonocoque aluminum alloy glider design features, recommending integral construction with metal bonding or combination metal bonding and riveting 18 p3054 A67-34374

Surface treatment of metal to ensure strength of bonded joints, discussing causes of aluminum-alloy corrosion during pickling 19 p3237 A67-35822

Fastener and fastened joint technology noting influence of hole preparation, surface coating, thread lubricants and fit on fatigue life 24 p4161 A67-42081

RL-10 ROCKET ENGINE

Strategy of holding higher performance rocket engines for critical missions analyzed statistically for increased payload 19 p3311 A67-34829

RLC CIRCUIT

SA LC CIRCUIT

Effects of parameters of series circuit on current pulse in active load, using computer to calculate series circuit 05 p0785 A67-17470

Passband narrowing due to coupling between passive oscillating system and active substance contained in resonator cavity represented by RLC circuit 05 p0780 A67-17474

Ignition systems for turbine engines, discussing low and high energy, semiconductor spark plugs, effects of electric constants on performance, etc 09 p1559 A67-21691

Computer simulation of GaAs Gunn diode in resonant circuit noting frequency, efficiency and load characteristics 10 p1612 A67-23370

Parametric coupling analyzed in electrical RLC circuit coupled with mechanical system through nonlinear inductance [ASME PAPER 67-VIBR-30] 11 p1797 A67-24188

Analog multiplier using p-n junction dynamic capacitance, noting decays in RC

circuit current 14 p2290 A67-28928

Electrodynamically coupled system consisting of RCL circuit, transformer and mechanical system analyzed by mathematical analogy and analog computer 15 p2440 A67-30081

Determination of limits of correct operation of comparison and decision circuits in Akima model band subdivision demodulator 18 p3002 A67-34222

Digital filters with ICs boost Q without inductors 18 p3012 A67-34490

Stability analysis of steady combination oscillations of single loop circuit, obtaining equations relating voltage harmonic of nonlinear capacitances 19 p3262 A67-35706

Capacitance reduction in active RC synthesis noting RLC, transfer functions, canonic sections, etc 20 p3409 A67-37109

Asymptotic approximations for analysis of nonlinear resonant circuits through differential equations, assuming oscillation processes similar to harmonic system processes 20 p3409 A67-37113

RLC NETWORK

Synthesis of networks incorporating semiuniform loss by transformation into networks with near ideal reactances 03 p0393 A67-13974

Synthesis method for immittance matrix with grounded unity gain amplifier /GUGA/ as only active element 03 p0393 A67-13979

Network analysis with state variables describing system stored energy 05 p0781 A67-16022

Topological analysis of local stability and instability of nonlinear periodic RLC network based on Liapunov theorems 08 p1308 A67-20320

Normal form and stability of coupled nonlinear RLC networks with possible interconnected elements of like type 10 p1618 A67-22703

Electric network analogy for square matrix inversion 14 p2292 A67-28902

Computer aided network sensitivity analysis 15 p2440 A67-29937

ROBERTSHAW-FULTON REGULATOR

Escape equipment, emphasizing Robertshaw helmet design to provide facial protection and retention of high Q conditions 14 p2256 A67-27744

ROCK

SA LAVA

SA METAMORPHISM

SA MINERAL

SA PETROLOGY

SA QUARTZ

SA SEDIMENTARY ROCK

Rare earth trace element variations in anorthosite and quartz mangerite determined, using stable isotope dilution technique of analysis 03 p0513 A67-14006

IR spectra of Mars bright areas compared with terrestrial rock, drawing conclusions regarding Mars mineralogy and detrital cover 05 p0896 A67-16717

Ultramafic rock content of Na, Mn, Cr, Sc and Co determined by neutron activation technique 07 p1183 A67-20142

Boulder size distribution in Luna IX surface photographs 09 p1570 A67-22692

Igneous rock suitability for determination of ancient geomagnetic field intensity, discussing theory, application and results 11 p1788 A67-24697

ROCKET

SA AEROBEE ROCKET

SA AGENA ROCKET

SA ARCAS ROCKET

SA ATHENA ROCKET

SA CONTROL ROCKET

SA ECHO I CARRIER ROCKET

SA HYBRID ROCKET

SA JAVELIN ROCKET

SA KAPPA ROCKET

SA LAMBDA ROCKET

SA METEOR I ROCKET

SA METEOROLOGICAL ROCKET

SA MICROROCKET

SA MISSILE

SA MULTISTAGE ROCKET

SA NIKE-APACHE ROCKET

SA NIKE-CAJUN ROCKET

SA NIKE ROCKET

SA NIKE-TOMAHAWK ROCKET

SA NUCLEAR ROCKET

SA PROPULSION SYSTEM

SA RAVEN ROCKET

SA RETROROCKET

SA RUBIS ROCKET

SA SINGLE-STAGE ROCKET

SA SKYLARK ROCKET

SA SOUNDING ROCKET

SA TWO-STAGE ROCKET

SA VERONIQUE ROCKET

Complex testing method for two-stage rocket probe recovery system with aid of two successively opening parachutes 03 p0518 A67-13397

Microwave rocket propulsion through direct electromagnetic heating of gas and powered by wireless ground-transmitted microwaves 16 p2736 A67-30712

ROCKET BOOSTER

Liquid propellant rocket engine development in France, Egypt and Germany 02 p0335 A67-12430

Air augmented propulsion in liquid hydrogen-LOX rocket booster engines 03 p0504 A67-13873

Time-invariant system of linear perturbation equations for error analyses of rocket boost inertial navigation systems 05 p0839 A67-17353

Composite aerospace transport for spacecraft launching, particularly French projects 06 p1094 A67-17993

Controlled booster stage BER for sounding rockets to reduce dispersion of impact points at low acceleration [ONERA-TP-442] 08 p1404 A67-20495

High energy booster and upper stage combinations for space research, discussing mission capabilities, cost factors, reliability, etc 08 p1412 A67-21075

Dynamics of booster rockets and spacecraft with cavities partially filled with liquid 08 p1412 A67-21113

Space flight technology developments, particularly for booster rockets and space vehicles 14 p2393 A67-27873

Propulsion systems for booster rockets and space vehicles 14 p2377 A67-27875

British reusable booster concept MUSTARD /multitunit space transport and recovery device/ using rocket-propelled VTO lifting bodies, noting feasibility and development cost reduction 15 p2568 A67-29843

Flow equations for convective heating associated with recirculating flow in clustered engine boosters for free viscous shear layer along exhaust jet boundary 16 p2591 A67-30942

Time optimal control of system with multiple control inputs and bounded phase coordinates for design of autopilot for booster 16 p2762 A67-31643

Linear segment pitch rate program for near optimum trajectory for rocket boosters 19 p3335 A67-35976

Steering equation derived from dynamic equation of velocity gain, as function of booster state for rocket vehicle ballistic trajectory [AIAA PAPER 67-595] 19 p3259 A67-35991

Up-rated Saturn V vehicles and intermediate payload Saturn vehicles, studying costs, flexibility, performance and boost-assist components 20 p3531 A67-36539

Controlled booster stage BER for sounding rockets to reduce dispersion of impact points at low acceleration 21 p3712 A67-37802

Z-transform and W-transform theory applied to dynamic compensation of linear sampled data control systems for attitude control of large booster 21 p3713 A67-38027

Controller design for booster gust alleviation, considering stochastic minimization problem solved by iteration yielding linear finite time controller with time-varying gains 22 p3897 A67-39162

Booster autopilot in bounded phase coordinates subject to disturbances, determining extremal control as function of time 22 p3833 A67-40149

P4 double test stand for ground testing third stage of ELDO launch vehicle 23 p3987 A67-41325

Booster for Skylark upper atmosphere research vehicle to increase altitude and reduce launching dispersion of single stage vehicle 24 p4206 A67-42580

Steering equation derived from dynamic equation of velocity gain as function of booster state for rocket vehicle ballistic trajectory [AIAA PAPER 67-595] 24 p4182 A67-42910

Space structure design cost effectiveness studies for materials and configurations [AIAA PAPER 67-808] 24 p4252 A67-42965

Apollo historical perspectives, background to U.S. man on moon decision in mid-1961, rocket booster development and space mobility [AIAA PAPER 67-839] 24 p4259 A67-42978

ROCKET CHAMBER

Thrust chamber life estimation from calculable local heat flux and tube temperatures, using assumptions of elastic strain invariance and isotropic material properties 05 p0874 A67-17226

HF combustion pressure oscillations in gaseous propellant rocket engines analyzed for stably burning combustor design concepts [ASME PAPER 67-VIBR-34] 11 p1851 A67-24191

Mixture ratio distribution effect on rocket thrust chamber performance 15 p2545 A67-29431

Propellant injection through porous media, advantages, fluid flow nature, heat transfer, characteristics and uses [AIAA PAPER 67-463] 18 p3026 A67-33934

Correlation between thrust chamber design parameters and combustion stability, noting stability increment with increasing injection velocity, droplet diameter and chamber pressure [AIAA PAPER 67-474] 18 p3113 A67-33944

Physical and chemical conditions in rocket combustion chamber during starting transients and steady operation described by mathematical model intended for parametric studies [AIAA PAPER 67-517] 18 p3158 A67-33980

Igniter performance in solid propellant rocket motors, examining mass discharge rate effect on chamber pressure transients [AIAA PAPER 66-680] 19 p3310 A67-34811

Optimum discharge chamber configuration of permanent magnet mercury-bombardment thruster for SERT II mission [AIAA PAPER 67-668] 21 p3691 A67-38702

ROCKET COMBUSTOR

Mixing, ignition and combustion in secondary combustor for air-augmented solid rockets with solid particles in primary stream [AIAA PAPER 67-481] 18 p3158 A67-33950

Factors influencing rocket ignition pressures and conditions leading to large ignition overpressures, estimating residual propellant in rocket combustor [AIAA PAPER 67-515] 18 p3114 A67-33978

ROCKET ENGINE

SA HYDRAZINE ENGINE /NIMPHE/
SA HYDROX ENGINE
SA LIQUID PROPELLANT ROCKET ENGINE
SA M-1 ROCKET ENGINE
SA NUCLEAR ENGINE FOR ROCKET VEHICLE /NERVA/
SA POODLE ROCKET ENGINE
SA RL-10 ROCKET ENGINE
SA SOLID PROPELLANT ROCKET ENGINE

Space vacuum simulation chambers for testing of ionic, plasma and other rocket engines 01 p0048 A67-10302

Estimated structural response to aeroacoustic pressure loading due to jet and rocket engines and boundary layer turbulence [SAE PAPER 660721] 01 p0010 A67-10625

Measurement systems control in rocket engine testing via real-time surveillance, computation, error correction and graphic display 01 p0076 A67-11144

Rocket propulsion for U.S. space program, considering early unmanned space exploration, manned Mercury flights, Gemini flights, etc 01 p0141 A67-11265

Dynamic analysis of reaction control system /RCS/ propellant feed network on lunar module using digital computers 01 p0142 A67-11435

Pressure coupled combustion dynamics of solid propellants analyzed as function of propellant variables, oscillation frequency and combustion pressure 01 p0143 A67-11448

Mixing gaseous propellant injector, injection velocity and momentum flux ratio, combustion pressure and propellant combination effects on HF combustion pressure oscillations in rocket motor 02 p0302 A67-11940

Nuclear propulsion systems development for U.S. space program 02 p0266 A67-12336

Mercury ion rocket propulsion system compared to cesium ion

system 02 p0305 A67-12338

Elastic structural vibrations of vehicle effect on position of engine thrust vectors with respect to undisturbed nonvibrating vehicle 02 p0335 A67-12732

Materials for ablative cooling processes for rocket engines, noting structure and properties of porous and solid materials 02 p0306 A67-12791

Chemical reaction kinetics and gas dynamics combined to analyze processes occurring in combustion chambers and nozzles of jet and rocket engines [DVL-602] 03 p0366 A67-12999

Optimization of high energy turbopump unit engine for ELDO-B carrier rocket, employing system specific impulse 03 p0503 A67-13013

Engine test facility for measuring thrust and propellant flow in pulsating rockets 03 p0396 A67-13774

Air augmented propulsion in liquid hydrogen-LOX rocket booster engines 03 p0504 A67-13873

High thrust fluorine engines and propellants 06 p1071 A67-17608

Subscale cold-flow rocket motor model used to determine effect of purely geometric variables on acoustic performance leading to axial mode combustion instability 06 p1075 A67-18853

Solid, liquid and gaseous core and radioisotope nuclear rocket engines, discussing thrust levels and other performance characteristics 06 p1030 A67-19024

Influence of relative thickness of elastic case on acoustic stability of radial modes in solid propellant rockets [AIAA PAPER 66-473] 07 p1240 A67-19370

Hypergolic propellant ignition experience during Project Sure Fire of Gemini program [AIAA PAPER 67-259] 07 p1241 A67-20046

Space simulator application to development of space rocket propulsion systems, examining test problems of low pressure space engines [AIAA PAPER 67-257] 07 p1164 A67-20052

German rocket prototype with mercury vapor plasma or xenon plasma engine, discussing design and performance 08 p1410 A67-20641

Film cooled rocket engine efficiency and effects of distribution of fuel mixing ratio and characteristic velocity on performance 09 p1559 A67-22094

Filamentary materials for wound structures, particularly rocket motor cases, noting fabrication equipment, physical properties, etc 11 p1811 A67-25008

T-burner technique for determining acoustic pressure and responses of solid propellants 12 p1988 A67-25910

Book on mechanics of low thrust space flight covering physical principles and generalized characteristics of engine systems, problems in optimization of space vehicles, etc 13 p2211 A67-28460

Combustion process monitoring in rocket engines [JPL-TR-32-1124] 13 p2188 A67-26848

Rocket control with limited-power engine when approaching target planet 14 p2394 A67-28640

Rocket nozzle effect on acoustic losses from model motor chambers oscillating in first longitudinal mode 15 p2546 A67-29992

Model for velocity coupled axial mode combustion instability in solid propellant rocket motors, noting computer studies 15 p2547 A67-29997

Solid propellants and motors for space exploration, comparing chemical and nonchemical propulsion systems 16 p2735 A67-30702

High energy liquid propellant boosters, noting design, performance characteristics and limitations 16 p2760 A67-30703

High pressure liquid propellant rocket engines, noting high thrust, smaller engine dimensions, and combustion chamber cooling 16 p2735 A67-30704

Thermodynamic evaluation of nuclear fuels, suggesting operation with deuterium-tritium and deuterium-helium mixture 16 p2702 A67-30718

Liquid fluorine closed flow loop and rocket engine test position design, construction and operation 17 p2832 A67-32012

Propulsion by solid/liquid or hybrid rocket motor 17 p2929 A67-32727

Hydrazine as single component fuel for gas generators and rocket engines, noting advantages and performance characteristics 18 p3106 A67-33459

Computer conversion of hydrodynamic data into simulated static test of deep-throttling bipropellant rocket engine, considering inert calibration techniques [AIAA PAPER 67-427] 18 p3112 A67-33911

Space pressure and temperature environment simulation facility for liquid rocket space-ignition reliability testing [AIAA PAPER 67-428] 18 p3112 A67-33912

Twin spool zero-NPSP /net positive suction pressure/ turbopump selected for NERVA rocket after assessing turbopump, engine, vehicle and mission related systems [AIAA PAPER 67-476] 18 p3075 A67-33946

Economical feasibility of open and closed cycle vortex-stabilized gaseous nuclear rocket engines, investigating vortex flow characteristics [AIAA PAPER 67-500] 18 p3076 A67-33964

Vacuum-ignition phenomena in Apollo rocket engine when oriented in upward-firing attitude [AIAA PAPER 67-514] 18 p3114 A67-33977

Preliminary phenomena in small Aerozine-50/nitrogen tetroxide pulsed rocket engines shown partly due to hydrazine nitrate accumulation [AIAA PAPER 67-516] 18 p3114 A67-33979

Descent engine for lunar module specifications and operational requirements covering throttling, firing duration, crushable nozzle skirt, etc [AIAA PAPER 67-521] 18 p3115 A67-33984

Ground technology program for nuclear rocket development, discussing NERVA and KIWI programs 18 p3077 A67-34706

Strategy of holding higher performance rocket engines for critical missions analyzed statistically for increased payload 19 p3311 A67-34829

Combustion rocket engines thermodynamic cycle and specific impulse values, considering motion equations and plasma engines 19 p3311 A67-35571

Safety program for nuclear rocket engine testing, discussing role of cryogenics 20 p3482 A67-36565

ELDO-A satellite launcher engine assembly and shell section production and testing 20 p3533 A67-37166

Hafnium-tantalum coated refractory metals investigated for use in high temperature rocket motors 22 p3821 A67-39891

Approximating method for predicting multiengine exhaust geometry and thermodynamic properties with single reference engine 22 p3902 A67-39940

Multiple exhaust nozzles for advanced nuclear rocket engines noting design and performance prediction procedures 22 p3834 A67-40160

Rocket engine cluster thrust and moment vectors analyzed statistically for thrust misalignment 22 p3869 A67-40170

Gaseous nuclear rocket engine propulsion, reviewing fluid mechanics, radiant heat transfer, transparent walls, nuclear criticality, coaxial flow reactor, etc [AIAA PAPER 67-783] 24 p4187 A67-42948

ROCKET ENGINE ADVANCEMENT PROGRAM

Solid propellant rocket motors reliability, discussing corrective action, retest, success probability, requirements, capability, simulation model, etc [AIAA PAPER 67-435] 18 p3112 A67-33914

ROCKET ENGINE CONTROL

Instrumentation and control /I and C/ system for ground test of Nerva propulsion system 03 p0395 A67-13384

Controls and control experimental program for nuclear rocket engine employing hot bleed cycle [AIAA PAPER 66-1005] 03 p0466 A67-14150

Extension of manual control to liquid rocket engine necessary to enable pilot to save primary mission or to change to planned secondary mission 04 p0703 A67-14426

Structural compliance induced cross axis coupling effect on gimballing system stability of rocket engine two-axis attitude TVC system [AIAA PAPER 67-42] 06 p1097 A67-18448

Thrust magnitude and restart control of

solid propellant motor by injection of fluorine and chlorine trifluoride 08 p1376 A67-21518

Closed form solution to three-dimensional rocket trajectory problem, considering flight velocity and acceleration laws for guidance design applications 10 p1709 A67-23484

Fluidic breadboard version of rocket engine sequence control, describing pneumatic logic package and general limitations [AIAA PAPER 67-518] 18 p3114 A67-33981

Structural compliance induced cross axis coupling effect on gimballing system stability of rocket engine two-axis attitude TVC system [AIAA PAPER 67-42] 24 p4242 A67-42909

ROCKET ENGINE DESIGN

Role of large solid propellant rocket motor in U.S. space program noting design, technology, testing, cost, thrust-vector control systems, etc 01 p0142 A67-11447

Compact rocket engine concept utilizing very small thrust units confined between and joined to plates, resulting in honeycomb structure [AIAA PAPER 66-924] 02 p0303 A67-12276

Heat sterilizable solid propellant motor designs for interplanetary missions, considering case-bonded spherical, case-bonded cylindrical, free-standing, internal burning and free-standing end burning [AIAA PAPER 66-973] 02 p0304 A67-12295

Performance, weight, design, flexibility, engine cycles and reliability of liquid propellant rocket engines used in NASA and USAF vehicles [AIAA PAPER 66-828] 03 p0504 A67-14123

Analytical solution to determine rocket design for maximum payload energy 04 p0706 A67-15240

Model estimation programming to determine optimum design criteria for rocket propulsion system using estimating function, approximation solved by Lagrange method [AIAA PAPER 67-208] 06 p1024 A67-18330

German papers on space research with satellites and space probes, Volume 1, Physical principles and methods of constructing carrier rockets 07 p1260 A67-20265

Solid and hybrid propulsion relationship to sounding rocket vehicle design and mission analysis, particularly application to synoptic meteorology 08 p1374 A67-20492

Solid propellant motor design for Black Brant VB sounding rocket 08 p1375 A67-20519

Sounding rocket disintegration studies to avoid falling mass hazards, noting design of pyrotechnic core in sandwich construction 08 p1407 A67-20520

Packaged liquid power plants for meteorological rockets, design and performance 08 p1408 A67-20523

Naval solid propellant rocket engine structural design, configurations, handling, storage and adaptation to environmental conditions 08 p1375 A67-20873

Nuclear rocket engine design for near-optimum vehicle performance for mission capability 08 p1412 A67-21107

Solid propellant rocket motor for third stage of satellite launcher, performance requirements and design 10 p1698 A67-23483

HF combustion pressure oscillations in gaseous propellant rocket engines analyzed for stably burning combustor design concepts [ASME PAPER 67-VIBR-34] 11 p1851 A67-24191

Soviet book on calculations of strength and vibrations of rocket engines 11 p1852 A67-24512

Vibration environment of liquid propellant rocket engines 12 p1989 A67-25704

Heat sterilizable solid propellant motor designs for interplanetary missions, considering case-bonded spherical, case-bonded cylindrical, free-standing, internal burning and free-standing end burning 13 p2188 A67-26833

Rocket cost dependence on weight and airframe resistance studied for design problem solutions 14 p2245 A67-28638

Compact rocket engine concept utilizing very small thrust units confined between and joined to plates, resulting in honeycomb structure [AIAA PAPER 66-924] 15 p2545 A67-29435

Hot-water rocket design by dimensionless

method, noting GRILLO rockets 15 p2567 A67-29840

Prediction of large rocket nozzle material performance using semiempirical technique, noting mathematical models for internal and external heat and mass transfer 15 p2547 A67-29993

Systems thinking and systems management in rocket motor manufacture 18 p3111 A67-33638

Ejector ramjet and ducted rocket evaluation by analytical models for various flight trajectories, noting specific impulse improvement [AIAA PAPER 67-437] 18 p3112 A67-33915

Rocket engine turbopump assembly test capability design, facilities, cryogenic systems, control requirements, computer simulation, activation and checkout [AIAA PAPER 67-441] 18 p3112 A67-33918

Micro-orifice injector rocket motors covering efficiency, nominal thrust, size, performance, cooling, design factors, etc [AIAA PAPER 67-462] 18 p3113 A67-33933

MIRA 150A variable thrust rocket engine applied to manned lunar exploration flying systems [AIAA PAPER 67-505] 18 p3113 A67-33969

Design for throttling and pulsing operation of rocket engine, discussing test data [AIAA PAPER 67-506] 18 p3113 A67-33970

Man-rating F-1 engine, noting capabilities and future plans [AIAA PAPER 67-519] 18 p3115 A67-33982

Solid propellant rocket motor-body shape as additional variable used to achieve given thrust-time program 18 p3115 A67-34361

LF oscillations built up in bipropellant rocket engine equipped with pressurized feeding system 19 p3311 A67-35052

Structural and systems design characteristics of British launch vehicle noting control and guidance system, flight development and test programs 19 p3333 A67-35841

Low pressure solid rocket motor design and application, noting advantages in high mass ratio performance and operational disadvantages 20 p3516 A67-37131

Cryogenic rocket upper stage structural design, fabrication and testing 22 p3899 A67-39533

Structural and mechanical design of Lunar Module Descent Engine, discussing component testing effect on development schedule 24 p4207 A67-42394

Cryogenic liquid propellant rocket engine technology and design [AIAA PAPER 67-978] 24 p4208 A67-43053

ROCKET ENGINE NOISE

Ideal incompressible liquid motion in rectangular container due to rectangular double and sinusoidal pulse excitation 03 p0404 A67-13784

Engine generated and in-flight noise environment problems of space vehicles analyzed, using theoretical methods and scale model wind tunnel tests 13 p2212 A67-27216

Rocket engine noise study in infrasonic range from launching pad ignition phase through flight phase, including ignition signals from upper stages 14 p2393 A67-28053

Apollo mission launch noise and physiological effects on crew 18 p2996 A67-34718

ROCKET EXHAUST

Theoretical analysis of heat transfer in solid propellant rocket exhaust plumes by use of temperature probe located in plume environment 01 p0071 A67-11101

Thermal and pressure effects of rocket exhaust impinging on flat plate surface at high vacuum [AIAA PAPER 66-46] 02 p0341 A67-11934

Spectral radiance of model rocket exhaust gases measured by rapid scanning spectrometer at simulated altitude [AIAA PAPER 67-10] 06 p1116 A67-18346

Three-channel IR-UV rocket radiometer for onboard measurement of exhaust plumes under severe high altitude environmental conditions 06 p1005 A67-18714

Mass spectrometric investigations of interaction of atmospheric ions with molecules of rocket gas release 10 p1640 A67-23215

Behavior of metals, graphites and reinforced plastics for reentry nose cones tested, using rocket engine exhaust flame as heat source 10 p1698 A67-23480

Wind tunnel test program for simulation of gas-particle rocket exhaust plume, separated flow around nozzle and base recirculation [AIAA PAPER 66-767] 11 p1773 A67-24351

Drag coefficient of particles in rocket nozzle 12 p1930 A67-25924

X-band attenuation by rocket exhaust plume measured with AM/PM noise for various propellant systems 15 p2436 A67-29429

Submerged nozzle for solid rockets, noting exhaust flow velocity and direction determination 15 p2547 A67-29994

Thermal control surface contamination due to rocket exhaust plumes and effects on solar absorptance and IR emittance of protective coatings 17 p2833 A67-32076

Excitation and radiation of OH molecules and alkali metals in low pressure flames and rocket exhausts 18 p3152 A67-33819

Mathematical model for thermal and chemi-ionization processes in turbulent nonequilibrium afterburning rocket exhausts plume, studying neutral and charged species distribution 18 p3152 A67-33820

Optical radiation emission from rocket exhaust plumes, noting dependence on aerothermochemical properties, considering radiative transfer 18 p3152 A67-33821

Measurement within rocket exhaust plumes 18 p3051 A67-34507

Spectral radiance of model rocket exhaust gases measured by rapid scanning spectrometer at simulated altitude [AIAA PAPER 67-10] 19 p3346 A67-35761

Ionization-enhanced microwave resonant radiation from model rocket exhausts studied using Dicke type radiometer 20 p3543 A67-36233

Rocket exhaust jet plume effects on radio signal, calculating degradation by electromagnetic diffraction propagation 20 p3381 A67-36570

Shock tube simulation of rocket exhaust plumes and effects on vehicles in space environment 24 p4253 A67-42029

ROCKET FIRING

Five-million pound load cell design and compression calibration at NBS 01 p0050 A67-11097

Heat transfer processes during ignition of solid propellant rockets, considering radiative and convective components [AIAA PAPER 66-66] 05 p0873 A67-17217

Elimination of rocket motor ignition by electrostatic initiation through development of electrically insensitive igniter and nonelectric stimulus transfer system 08 p1372 A67-20525

Real time meteorological system providing prelaunch impact prediction for unguided high altitude rocket firings, noting computer program 08 p1314 A67-20543

Hazards in sounding rocket assembly and launch operations and safety techniques at NASA Wallops station noting storage, explosive control, ground safety, etc 08 p1314 A67-20547

Mechanical impedance testing and analysis for spacecraft with single firing 08 p1422 A67-21285

Launch vehicle preparation and firing, discussing instrumentation, missile safety and range operations 10 p1622 A67-23001

Vacuum-ignition phenomena in Apollo rocket engine when oriented in upward-firing attitude [AIAA PAPER 67-514] 18 p3114 A67-33977

Rocket launchings of French ballistic program, discussing trajectory study techniques 18 p3020 A67-34379

Real time meteorological system providing prelaunch impact prediction for unguided high altitude rocket firings, noting computer program 21 p3607 A67-37812

ROCKET FLIGHT

Optimal rocket trajectories, discussing role and significance of intermediate thrust arcs of rocket extremals in vacuum 02 p0335 A67-12397

Dragon rocket probe, launch history and flight modifications 03 p0517 A67-13028

Data acquisition system for Blue Streak flight trials noting telemetry and radar and relation to trajectory, autopilot, structure, etc 04 p0568 A67-14438

High accuracy tracking system for measurement of missile and rocket trajectories during lift-off phase 05 p0762 A67-16530

Wind compensation system at Kagoshima Space Center, University of Tokyo, consists of radar system for obtaining wind data and method for finding launch angle compensation 08 p1314 A67-20542

Mathematical methods for two classes of variational problems analogous to optical reflection and optical refraction in connection with rocket flight 10 p1678 A67-23425

Closed form solution to three-dimensional rocket trajectory problem, considering flight velocity and acceleration laws for guidance design applications 10 p1709 A67-23484

Motion of point of variable mass in Newtonian central gravitational field 13 p2199 A67-26894

Thesa nose cones in supersonic flight, calculating aerodynamic coefficients from trajectory and flight phases 13 p2051 A67-27291

Real time meteorological system for ballistic high altitude multistage rocket trajectory, computation and prediction 13 p2091 A67-27610

Regularization method for maximum height ascent of rocket uniformly approximating control function by gradient projection method 13 p2149 A67-27618

Thrust vector controls for solid rockets, discussing liquid secondary injection, jet tabs, direct chamber bleed, omnialxial movable nozzle and lockseal 15 p2545 A67-29136

French Rubis rocket flight noting high altitude barium release experiment, high energy proton and electron measurements, etc 16 p2738 A67-31017

Simultaneous recording of rocket trajectory and rapid auroral variations using high sensitivity image orthicon TV system 18 p3034 A67-33594

Launching and ballistic flight of Rubis IV rocket, discussing scientific preparation and payload testing 24 p4241 A67-42573

ROCKET FUEL TANK

Pressurized propellant tank system for rocket engine, discussing weight factors, propellant combinations and expellant gas pressure relations 24 p4241 A67-42754

ROCKET INSTRUMENTATION

Mechanical construction of two types of Gerdien condenser rocket probes, noting instrumentation racks and inflatable parachutes for descent 03 p0518 A67-13368

Stabilized Skylark rocket using N-gas jet system, solar sensors and magnetometer to obtain three-axis control 08 p1408 A67-20537

Maksutov-Cassegrain type telescope for rocket mounting, design and performance 10 p1654 A67-22751

Aerobee rocket instrumentation for solar spectroscopy in soft X-ray region 10 p1712 A67-23804

Mobile telemetry ground station and maximum reliability procedures for rocket telemetry transmission system used in solar eclipse 15 p2467 A67-29575

Omnidirectional radiation pattern for S-band telemetry on rockets more than 1/2 ft in diameter by small electrical separation of antennas [AAS PAPER 67-51] 15 p2454 A67-30116

High resolution UV spectrograph with echelle, noting optical line-up for photographing H-Lyman alpha line at 1216 angstroms 16 p2680 A67-31875

Noise generator for calibration of radio receiver working in 1-2.6 MHz range during rocket flight 21 p3592 A67-38221

Gemini booster launch photographic recording with 50 cameras collecting engineering data and motion pictures of prelaunch, launch and postlaunch 22 p3807 A67-40372

Nuclear magnetometers for magnetospheric measurements from rockets 23 p3998 A67-40697

Rocket instrumentation and sensing techniques for collecting stratospheric wind and temperature data 23 p4025 A67-41445

Rocketsonde thermistor mount noting thin film configuration and long lead mount for heat dissipation 23 p4025 A67-41446

Soviet meteorological rocket observation and research, basic techniques and program results 23 p4025 A67-41447

Nuclear subsystem controls and instrumentation for NERVA noting automatic startup, override, power and temperature controller

testing 24 p4183 A67-42471

ROCKET LAUNCHING DEVICE

COSPAR manual on establishment of rocket launch facility 06 p0979 A67-17553

Air launched sounding rockets design, development and testing noting aerodynamic loading and surface, propulsion unit, cost effectiveness, etc 08 p1407 A67-20518

Mobile Aerobee Launch Facility /MALF/, noting applications to space science 08 p1314 A67-20544

Air breathing reusable rocket launchers for European development, comparing ramrocket and turboramjet propulsion 15 p2568 A67-29844

Electronic control system for triaxial control of geocentric satellite and second stage of CORALIE booster 21 p3656 A67-38231

European rockets characteristics and launch firing ranges, discussing rocket probes for near-earth and space environments 21 p3714 A67-39049

CNES rocket probe mobile launching unit for auroras, eclipses and Van Allen belt layer experiments 21 p3609 A67-39051

Hazards of rocket launching noting propellant toxicity, airborne fragmentation, inadvertent ignition and nuclear radiation 22 p3900 A67-39884

Ducted silo launchers transient pressures caused by rocket engine ignition and shutdown, treating wave propagation by one-dimensional theory 22 p3780 A67-40091

ROCKET MEASUREMENT

L-3 rocket observation of proton and electron fluxes at high altitudes, using solid state detectors 01 p0144 A67-10564

Pyrotechnic shock testing, discussing equipment reliability and performance improvement, shock level reduction and applications [SAE PAPER 660717] 01 p0139 A67-10606

Data acquisition techniques and system accuracies for static testing of solid propellant rocket engines 01 p0051 A67-11109

Rocket measurements of 1/2 to 4 mev trapped protons in near-equatorial magnetosphere [AFCLR-66-865] 03 p0505 A67-12835

Middle UV region of solar radiation, discussing rocket and balloon mounted spectrograph measurement results 04 p0695 A67-14691

Shock wave from release of gas at 230 km altitude indicated luminosity due to scattered sunlight and temperature of 743 degrees K 05 p0795 A67-16027

Rocket observations of temperatures and winds in upper atmosphere, discussing physical interpretation of results 05 p0797 A67-16856

Magnetic field observations by rockets and satellites 05 p0798 A67-16870

Solar UV and zodiacal light, emphasizing importance and merits of rocket and balloon observations 05 p0799 A67-16873

Rocket measurement of altitude dependence of flux intensity of solar vacuum UV radiation, using ionization chambers 05 p0799 A67-16874

Altitude variation of cosmic ray intensity in atmosphere, checking accuracy of flux data from rockets and satellites 05 p0883 A67-16879

Aerobee rockets measurement of sodium dayglow suggest equilibrium between sodium atoms and distribution of dust particles 07 p1180 A67-19917

Mean noon profile of mesospheric electron number density at 35 degrees S latitude preceding solar eclipse 08 p1378 A67-21483

Rocket measurement of quiet D-region electron number density profiles near sunrise 08 p1379 A67-21488

Echelle spectrograph for middle UV solar spectroscopy from rockets 10 p1653 A67-22735

Atmospheric scattering of solar flux in UV noting radiation transfer for airborne detector, air component absorption coefficient and spectra from rocket flight 10 p1629 A67-22736

Variation of inner scale of turbulence in upper atmosphere with height studied from density variations of alkaline clouds ejected by rockets 10 p1638 A67-23201

Rocket measurement of diurnal variation of ozone profiles above maximum concentration level 10 p1638 A67-23202

Solar cycle variations in atmospheric

density deduced from meteor observations and rocket measurements in mesopause and thermosphere 10 p1638 A67-23204

Aerobee rocket measurement in sampling of micrometeoroid debris during peak of Leonid meteor shower 10 p1707 A67-23237

Geophysical rocket determination of aerosol scattering coefficient variation from brightness values at 70-450 km heights 10 p1641 A67-23240

Measurements of positive ion composition of mesosphere and ionospheric D layer from rocket experiments 10 p1645 A67-23264

Model ionosphere with homogeneous isotropic turbulence investigated for values of kinematic viscosity and dissipation rate of turbulent energy determined from rocket measurements 10 p1646 A67-23273

Atomic ions of meteoric origin indicated as source of midlatitude E region in IQSY rocket measurement 10 p1648 A67-23289

Energy spectrum of primary electron flux and brightness of auroral light measured by rockets in active auroras used to derive electron production rate 10 p1650 A67-23306

Electron and ion densities and temperatures measured by rockets in active auroras and correlated with directly measured ionizing flux 10 p1650 A67-23307

Molecular oxygen densities in range 70-90 km determined by rocket measurements of atmospheric absorption of solar UV radiation in Southern Hemisphere 12 p1934 A67-25786

Recoll proton detectors used for rocket measurements of fast neutron intensity above Fort Churchill, Canada, during 1964 and 1965 12 p1998 A67-25828

Directional neutron detector using liquid scintillator for low mev energy range for rocket and satellite experiments 12 p1945 A67-25860

Latitudinal cross section of ionospheric current density profile of equatorial electrojet from rocketborne magnetometers 13 p2107 A67-26307

Lower E-region positive ion concentrations measured at time of declining solar activity by rocket installed mass spectrometer 14 p2310 A67-28049

Rocket and balloon-borne exposure study of terrestrial microorganism survival in space 15 p2424 A67-29097

Equipment used in rocketborne LF propagation experiment to measure electron distribution in D region of ionosphere 15 p2489 A67-30136

Flux, energy spectrum and angular anisotropy of auroral electrons analyzed from space vehicle 16 p2670 A67-30648

Water vapor and atomic oxygen concentration in mesosphere measured by meteorological rocket 16 p2665 A67-31097

Volume emission profile vs height of positively ionized nitrogen molecule first negative band at 4278 angstroms 16 p2666 A67-31408

Vertical electron temperature and concentration distribution up to 480 km at middle latitudes from rockets 17 p2842 A67-32253

Mesospheric wind components via rocket measurements of Northern and Southern Hemispheres, noting semiannual wind fluctuation near equator 18 p3030 A67-33552

Auroral rocket measurements of electron densities, ionization rates, particle energy fluxes, energy spectra, pitch angle distribution, etc 18 p3034 A67-33592

Auroral rocket measurements of electron flux, electron and ion density, electron temperature and auroral brightness 18 p3034 A67-33593

Electron measurements near weak aurora during rocket flight 18 p3034 A67-33595

Ionosphere collision frequencies and densities studied by rocket measurements of magnetic field of VLF wave radiated from ground 18 p3041 A67-34233

Rocket optical studies of daylight day-time auroras, discussing luminosity-height data of emission lines 19 p3214 A67-35168

Rocket observation of ionospheric electron density using VLF doppler shift formula, determining wave polarization 19 p3215 A67-35180

Density, temperature, water vapor and atomic oxygen concentration in mesosphere measured by heat method 19 p3216 A67-35183

Auroral absorption events, discussing bremsstrahlung X-rays spectrum, electron densities and temperatures measured with

rockets 19 p3312 A67-35188
 Effective collection time for collecting cosmic dust in altitude ranges of cosmic and terminal velocities of particles, using rockets 19 p3318 A67-35195
 Electron density measurement in ionosphere-magnetosphere transition region using rocketborne gyroplasma swept frequency probe, discussing electron density profile and plasma medium 19 p3229 A67-35201
 Ionospheric electron density profile microstructure studied by rocketborne gyroplasma probe discovering electron density irregularities 19 p3217 A67-35202
 Daytime ozone density distribution of mesospheric layer measured by using UV photometers in rockets 19 p3217 A67-35203
 Electron density and temperature, solar UV radiation and upper atmosphere neutral components measured using rockets 19 p3218 A67-35215
 Density, temperature and pressure profiles variations in upper atmosphere obtained from rocketborne experiments 19 p3218 A67-35219
 Upper ionospheric electron density profile variation with sunspot number controlled by temperature and ion composition as shown from rocket data 19 p3218 A67-35222
 Mesosphere and lower thermosphere density variations related to solar cycle obtained, using rocket grenades 19 p3219 A67-35231
 Ionospheric ion and electron densities and temperatures from rocket probes near geomagnetic equator 19 p3219 A67-35232
 Vertical distribution of diffuse sky light in stratosphere determined by rocket measurements, noting intensity peak in aerosol layer 19 p3221 A67-35273
 D-region positive ion density during solar eclipse of May, 1966 observed by cylindrical Langmuir probe onboard rocket 19 p3222 A67-35454
 Rocket and balloon studies of solar radiation, wind characteristics, equatorial electrojet and lower ionosphere electron density 19 p3223 A67-35474
 Rocket measurements above England, noting relation of temperature maximum at stratopause to mesospheric wind maximum 20 p3480 A67-36966
 70 to 450 km altitude atmospheric brightness at 5300 angstrom measured by rocket noting importance of aerosol component 21 p3623 A67-39043
 Far UV spectra of brighter stars in vicinity of epsilon Orionis photographed with objective spectrograph carried by rocket 22 p3882 A67-39555
 Ionospheric and magnetospheric temperature measurements using rockets and satellites including neutral particle, ion and electrons 22 p3871 A67-39677
 Ionospheric plasma electron density profile and plasma resonance effects at base of magnetosphere measured by rocketborne gyro-plasma probe 22 p3793 A67-40043
 Effective recombination coefficient in upper-E and F-1 layers at sunset from rocketborne gyroplasma probe measurements of electron density profile 22 p3793 A67-40044
 Rocketborne UV radiometers for solar spectral intensity distribution, calculating irradiance and earth reflectivity 22 p3794 A67-40363
 Stratospheric attenuation measurements in near UV during rocket flight compared with values computed for dust free atmosphere 23 p3993 A67-40677
 Nuclear magnetometers for magnetospheric measurements from rockets 23 p3998 A67-40697
 Rocket measurements with HF impedance probe for ionospheric electron density, discussing plasma gyro resonance frequency factors 23 p4003 A67-41321
 Rocket measurements in auroral zone, considering proton and electron intensities, energy spectra and angular distribution 24 p4209 A67-42262

ROCKET MOTOR CASE

Plasma arc welding for fabricating 120-inch-diam D6AC steel rocket motor cases, comparing gas tungsten arc welds 01 p0080 A67-10944
 Composite material application to solid fuel rocket motor cases, discussing performance characteristics, manufacturing

techniques, etc 09 p1578 A67-22513
 Solid motor case technology, evaluating materials, fabrication, segmented case joint design and cost comparisons for large rocket motors 10 p1661 A67-23703
 Design considerations in material selection for rocket motor cases, considering fracture toughness, ductile-failure resistance and buckling under flight loading [AIAA PAPER 66-630] 15 p2573 A67-29418

ROCKET NOSE CONE

Telemetering and programming equipment used by CERMA in nose cones of rockets containing cats and rats in state of weightlessness 03 p0366 A67-13928
 Nose selection and vehicle motion dynamics for second stage of two-stage sounding rocket system, discussing nose shapes effect on altitude performance, overall vehicle stability, bending moments, etc 08 p1406 A67-20513

Rigid body ejection dynamics of split-fairing system for four-stage Javelin sounding rocket under various parameter changes 08 p1408 A67-20536
 Analog simulation of electromagnetic radiation from antenna of revolution in vacuum and plasma via networks, discussing rocket nose cone shapes 23 p3977 A67-40578

ROCKET NOZZLE**SA JET NOZZLE**

Thermal analysis of thin wafer heat flux transducer backed by finite heat sink subjected to reentry and rocket-nozzle heat transfer environments 01 p0071 A67-11095

Ground surface erosion due to rocket breaking, calculating flow-induced force parameters 01 p0156 A67-11434

Spin effects on rocket nozzle performance show higher combustion pressures and burning rates due to blockage of nozzle throat 02 p0303 A67-11947

Swirling flow-induced spin effect on rocket nozzle performance 04 p0548 A67-15255

Electroanalog analysis of convective and conductive heat transfer and transient temperature field in solid propellant rocket nozzle head 07 p1268 A67-19568

Hydraulic analogy applied to axisymmetric nonideal compressible gas systems, considering water table simulation of axisymmetric rocket nozzle 08 p1324 A67-21519

Ultrasonic inspecting technique for reinforced plastic components and adhesive bonds of solid propellant booster nozzles 10 p1659 A67-22930

Variation problem solution in hypersonic gas dynamics, noting intake portion construction for body with minimum resistance for limited length and flat end 11 p1777 A67-24153

Burn-pond concept of test facility for disposing of hydrogen at high flow rates 13 p2092 A67-27652

Submerged nozzle for solid rockets, noting exhaust flow velocity and direction determination 15 p2547 A67-29994

Rocket nozzle design to reduce gas misalignment noting turning moment, nozzle geometry, cold gas tests, static and flight trials of motors, etc 15 p2547 A67-29995

Condensed phase particle growth in rocket nozzle by particle collision and coalescence [AIAA PAPER 66-639] 15 p2548 A67-30200

Boundary layer effect on thrust of small rocket engines with high expansion ratio nozzles 16 p2736 A67-30706

Structures, charging into stage, thermal protection, ignition, and nozzles problems encountered in development of solid propellants 16 p2736 A67-31617

Laminar boundary layer theory applied to heat transfer in low thrust rocket nozzles, checking with experimental wall temperature data [AIAA PAPER 67-447] 18 p3112 A67-33923

Particle mass spectrum development in rocket nozzle, assuming droplet growth by collision and agglomeration as dominant mechanism 20 p3516 A67-37130

Optimization analysis for axisymmetric rocket motor nozzle design based on assumptions for gas particle flow [AIAA PAPER 66-538] 21 p3565 A67-38875

Quasi-cylindrical approximation theory on swirling nozzle flow in relation to spin effect on rocket nozzle performance 22 p3742 A67-40118

Cryogenically cooled rocket nozzle thermal

fatigue analysis by thermal-cycle testing of specimens 22 p3834 A67-40183

Shock refraction effects due to velocity and temperature gradients in rocket nozzles investigated by studying leading shock in two-dimensional secondary fluid injection 23 p3992 A67-41740

ROCKET PHOTOGRAPHY

Rocketborne photometer data analysis of night sky airglow and spectrum in 6300 angstrom region 11 p1786 A67-24072

Pinhole X-ray photography of sun obtained during rocket flight, showing correlation of bright emitting regions on disk with calcium plages and radio emission sources 12 p2007 A67-25761

Photographic recording by shadow method for alignment of optical equipment in firing range used to determine aerodynamic characteristics of various missiles 16 p2674 A67-31117

Theodolitic device for measuring coordinates of center of gravity of photographed missile in flight 16 p2674 A67-31120

Height profile of atomic oxygen 6300 angstrom emission in night airglow determined by rocket photography 19 p3215 A67-35177

Fabry-Perot interferometer improvements for high resolution rocket photography of solar Fraunhofer spectrum 20 p3440 A67-36359

ROCKET PROJECT

Rocket probe design for studying physical structure, chemical composition and interaction with sun of Tuttle-Giacobini-Kresak comet 03 p0518 A67-13497

ROCKET PROPELLANT TANK

Engineering formulas to determine fuel reserve margins for fueling techniques and fuel consumption events due to incidental rocket design parameter scatter 17 p2954 A67-32241

ROCKET SLED

Maximal intensity inflight stress effects on human tolerance investigated, noting deceleration experiments 14 p2257 A67-28218

Wind tunnel data predicted vertical forces for rocket sleds compared with measurement on test track noting disagreement 22 p3780 A67-40095

ROCKET SOUNDING**SA SOUNDING ROCKET**

March 1964-March 1965 seasonal variations in density, pressure and temperature at Woomera, Australia, by falling sphere method 01 p0061 A67-11260

Rocket measurement of proton energy spectra and pitch angle distribution associated with auroral radio absorption, using solid state surface barrier detector 01 p0061 A67-11261

Location of X-ray source Sco X-1 determined by instrumented payload flown on stabilized Aerobee rocket 02 p0308 A67-11771

Liquid nitrogen cooled rocketborne telescope, measuring IR signals from diffuse and discrete astronomical sources 02 p0243 A67-12047

Monograph on rocket experiments for studies of D region ion concentration and emission from released chemicals in twilight and aurora 03 p0412 A67-13366

Ion concentration in D region, describing wind tunnel experiments to determine electrode configuration for Gerdien condenser rocket probe 03 p0412 A67-13367

Intensity of sodium D-lines and auroral nitrogen band produced by sodium trail in aurora measured by calibrated photometer 03 p0412 A67-13373

Artificial shock wave from TNT explosion in aurora, in attempt to determine effects on auroral emission and temperature 03 p0413 A67-13374

Rocket payload with weight of 9 lb for release of sodium and lithium in aurora for study of D-region ion concentration and emission 03 p0413 A67-13375

Rocket launching site in Sweden operated by ESRO for studies of polar auroras and polar cap absorption 03 p0395 A67-13498

Rocket measurement of secondary electron energy distribution in aurora, employing 180 degree electrostatic deflection analyzer 03 p0418 A67-14357

Design and instrumentation of Rubis research rocket payload for analysis of geomagnetic and electric

- fields 04 p0703 A67-14565
- Terrestrial radiance in middle UV noting Rayleigh scattering, vertical distribution of air, oxygen and ozone, attenuation factors, etc 04 p0613 A67-14695
- Detection of X-ray point sources from rocket and satellite experiments applied to astronomy 04 p0698 A67-14886
- Rocket sounding of unpredictable geophysical disturbances, preparations, countdown procedure and difficulties encountered 05 p0904 A67-16295
- Ionospheric charged particle density measurements during IQSY by sounding rocket 05 p0798 A67-16860
- Day and night airglow measurements by K and L rockets 05 p0798 A67-16863
- Upper atmospheric density and composition determined by means of solar radiation attenuation and day airglow fluorescence 05 p0798 A67-16864
- Emitting height of night airglow determined by rocketborne photoelectric equipment 05 p0798 A67-16865
- Japanese sounding rocket measurements of intensity and frequency time variations in ionosphere to determine VLF radio noise 05 p0763 A67-16868
- Kappa rocket sounding of ionospheric Sq-currents, using rubidium vapor magnetometer 05 p0799 A67-16871
- Energy spectra of galactic X-rays observed with three types of counters borne on sounding rockets 05 p0883 A67-16876
- Solar charged particles acceleration and propagation through interplanetary space, galactic cosmic ray origin, radiation belt structure, etc, analyzed from space data 05 p0883 A67-16877
- Rocket sounding of intensity distribution of proton and electron fluxes at high altitudes, noting secondary particle emission from radiation belt 05 p0883 A67-16880
- Rocket sounding of stratospheric circulation, noting relationship between minima in westerly zonal flow of 45-55 km stratopause layer and tropospheric cut-off lows 05 p0838 A67-17306
- Ionospheric electron density profiles determined by impedance probe and Doppler effect probe aboard rockets 06 p0993 A67-17595
- Upper atmospheric rocket sounding experiment during solar eclipse over Brazil, noting instrumentation and participating agencies 06 p0981 A67-18382
- Design and instrumentation of Rubis research rocket payload for analysis of geomagnetic and electric fields 07 p1258 A67-19572
- Book on structure of stratosphere and mesosphere noting rocket exploration results, synoptic observations, solar control over temperature variations, etc 07 p1172 A67-19603
- Ionospheric direct observation by sounding rockets during IQSY 07 p1186 A67-19677
- Diurnal and seasonal altitude variations of E and F layers analyzed for geomagnetic activity from rocket measurement of electron concentration 07 p1173 A67-19686
- Experimental Inter-American Meteorological Rocket Network /EXAMETNET/ for Southern Hemisphere research 08 p1350 A67-20549
- Gun-launched rockets for high performance sounding missions 08 p1409 A67-20550
- IR observations in one to seven micron region using astronomical telescope on Aerobee rocket above atmosphere 08 p1397 A67-21185
- Surface brightness and polarization state of zodiacal light measured from sounding rocket 08 p1326 A67-21244
- Thermal and momentum eddy diffusivities computed from wind profile and turbulence of rocket released chemical clouds 08 p1328 A67-21478
- Electron flux measurement during visible aurora, using high resolution rocketborne spectrometer 09 p1491 A67-22022
- Heat transfer equations for rocketborne stratospheric temperature sensor in form of spherical bead thermistor and experimental analysis of physical, thermodynamic and electrical characteristics of rocketsonde [AIAA PAPER 66-385] 10 p1632 A67-22819
- Ionospheric rocket sounding, measuring ion density and electron temperature between E and F layers 10 p1633 A67-22948
- Rocket observation of upper atmospheric winds noting wind shear, velocity, pressure, wind vector rotation, etc 10 p1638 A67-23198
- Upper atmospheric wind, temperature and pressure variations measured using grenade launched Skylark sounding rockets 10 p1638 A67-23199
- S-N wind components analyzed for diurnal and semidiurnal variations, noting results on amplitude and phase of components 10 p1638 A67-23200
- Ozone number densities in 30 to 75 km altitude determined at night by rocket measurements of lunar UV radiation absorption in various bands 10 p1638 A67-23203
- Falling sphere measurements of atmospheric density, noting temperature and density profiles, pressure distribution, etc 10 p1639 A67-23205
- Neutral particle densities of nitrogen, molecular and atomic oxygen and argon in upper atmosphere, noting density profile irregularities, diffusive separation altitude, etc 10 p1639 A67-23213
- LF ionospheric measurement of admittances of three orthogonal shock dipoles, noting impedance variation with respect to frequency attitude and voltage 10 p1648 A67-23286
- Upper ionospheric electron density measurement by signals propagated between two parts of high altitude rocket 10 p1648 A67-23287
- Nike-Cajun rocket investigation of equatorial D and E region parameters and effect on electrojet 10 p1648 A67-23288
- Neutral wind structure effects on ionospheric sporadic E layer variations, noting daytime evolution, nighttime characteristics and electron density profiles 11 p1783 A67-23924
- Aerobee rocket sounding of ionospheric sporadic E layer, noting abundance of metallic ions in layer and NO above and below 11 p1784 A67-23926
- Spectroscopic twilight airglow measurements for upper atmosphere interpreted using rocket flight data 11 p1786 A67-24263
- Aerobee rocket sounding of far UV spectra of six stars in Orion, extrapolating mass ejection from resonance absorption lines 11 p1861 A67-24488
- Tabulated localized cosmic X-ray sources and survey of rocket probe identifications 11 p1857 A67-24633
- Solar X-ray emission measurement below 25 angstroms using airborne Bragg spectrometers, with data reduced by computer 11 p1867 A67-24839
- Cosmic x-ray sources identified using Geiger counters aboard rockets, noting clustering toward galactic disk 12 p1994 A67-25760
- Javelin rocket soundings with far UV scanning spectrometer, noting atomic hydrogen and oxygen radiation 12 p1934 A67-25787
- Neutral upper atmosphere winds near equator, discussing sodium vapor rocket observation results 12 p1934 A67-25790
- Rocket observations of lowest ionosphere at sunrise and sunset 12 p1935 A67-25798
- Solar continuous spectrum observations indicating limb darkening around 2500 angstroms, using optical system mounted on Veronique rocket 12 p2007 A67-25820
- Solar studies in extreme UV using stabilized Skylark rockets, including data on chromospheric and coronal spectra and XUV spectroheliograms 12 p2008 A67-25826
- Atmospheric density, temperature and pressure profiles obtained in Florida and New Mexico using rockets 12 p1937 A67-25837
- Design of rocketborne ionospheric plasma probe considering probe shape, location, payload, etc 12 p1937 A67-25838
- Japanese rocket observations of upper atmospheric wind and temperatures in relation to new Cira model 12 p1937 A67-25841
- Temperature and wind fields in stratosphere obtained with rocket probes, noting diurnal and annual temperature variation differences for heights beyond 35 km 13 p2113 A67-26679
- Meteorological rocket measurement of wind patterns noting velocities, turbulences, stratospheric diffusion coefficients, etc 13 p2117 A67-27611
- Angular distribution of earth outgoing thermal radiation in IR region measured by geophysical rocket 14 p2306 A67-27860
- Rocketsonde and radiosonde temperature comparisons and evaluation of computed rocketsonde pressure and density 14 p2347 A67-28885
- Rocket soundings of electron angular distributions during auroral substorms, noting effects of anisotropy, intensity variations, etc 15 p2473 A67-29187
- German participation in solar eclipse campaign of ESRO, describing rockets and radar used 15 p2466 A67-29572
- Ionospheric electron density profiles obtained by dispersive Doppler from beacons on research rockets, noting inhomogeneities [AGARDOGRAPH 95] 15 p2483 A67-30296
- French Rubis rocket flight noting high altitude barium release experiment, high energy proton and electron measurements, etc 16 p2738 A67-31017
- Chromosphere and corona UV emission spectrum provided by sounding rocket using photographic recordings 16 p2752 A67-31625
- Evidence regarding possibility of midwinter stratospheric warmings in Southern Hemisphere 17 p2880 A67-32553
- Darkening of solar limb in UV spectral band observed through rocket sounding 17 p2945 A67-32647
- X-ray scanning of Cygnus region with large area proportional counters flown on attitude-controlled sounding rocket 17 p2937 A67-32648
- Rocket observations of energy spectra of auroral electrons 18 p3034 A67-33591
- Rocketborne spectrograph measurement of UV reflectivity of Venus and Jupiter, noting atmospheric Rayleigh scattering effects 18 p3123 A67-34147
- Mesospheric temperature possible relationship to occurrence of noctilucent clouds studied using rocket soundings 19 p3251 A67-34951
- Rocket observations of upper atmospheric winds, electron density, electron temperature, and neutral temperature in auroral region with Langmuir probes 19 p3214 A67-35169
- Rocket sounding of zodiacal light brightness at 4300, 5300 and 6000 angstroms 19 p3216 A67-35192
- Electron temperature observation in E region with Langmuir probes on Nike Apache rockets, discussing solar radiation effect 19 p3216 A67-35193
- Rocket sampling of noctilucent cloud particles in mesopause 19 p3216 A67-35194
- Fluctuations in stratospheric and mesospheric winds studied by meteorological sounding rockets, noting relation to solar activity 19 p3217 A67-35207
- Wind velocity and direction measurements by radar tracking of chaff /dipoles/ clouds 19 p3219 A67-35247
- Rocket observations of visible and UV dayglow including emission rates and electron density and temperature 19 p3221 A67-35277
- Early autumn stratospheric circulation of Southern Hemisphere investigated by meteorological rocket observations 19 p3253 A67-35920
- Temperature and wind profiles in stratosphere and mesosphere during winter and summer determined by grenade soundings, noting diurnal variations 19 p3226 A67-35924
- Diurnal variation investigated by rocket, discussing ionospheric electric currents and magnetosphere-ionosphere electric field 20 p3431 A67-36908
- Energetic proton flux measurements in magnetosphere using sounding rocket, discussing radial diffusion 20 p3518 A67-36998
- Correction technique validity determined by comparing parachute determined winds with chaff-determined wind profiles 21 p3654 A67-38186
- X-ray spectrum and location measurements of several cosmic X-ray sources, using rocketborne proportional counters 21 p3698 A67-38564
- Movable device for tracking rocket probes, discussing characteristics and requirements 21 p3608 A67-38673
- European rockets characteristics and launch firing ranges, discussing rocket probes for near-earth and space

environments 21 p3714 A67-39049
 Semiannual wind variation in equatorial stratosphere analyzed for origin from rocket sounding data 22 p3828 A67-39466
 Isolated irregularities in auroral ionosphere studied by analyzing radio signals from rockets and Beacon 22 p3760 A67-39627
 Contamination control program developed for investigation and elimination of contaminant particles from 1965 Leonid Meteor Shower micrometeoroids collected by rocket payload 23 p3986 A67-40850
 Cosmic X-ray sources spectra obtained by proportional counters and electronic systems on sounding rockets 23 p4001 A67-41222
 Auroral zone phenomena analyzed using rocketborne counters 23 p3997 A67-41333
 Soviet meteorological rocket observation and research, basic techniques and program results 23 p4025 A67-41447
 Ionospheric electron temperature and electron and ion density profiles from Japanese sounding rocket 23 p3997 A67-41478

ROCKET STEERING MOTOR

Hypersonic reentry, inertial guidance tests and construction of two-stage Diamant satellite launcher 15 p2571 A67-30089
 Steering equation derived from dynamic equation of velocity gain, as function of booster state for rocket vehicle ballistic trajectory [AIAA PAPER 67-595] 19 p3259 A67-35991
 Steering equation derived from dynamic equation of velocity gain as function of booster state for rocket vehicle ballistic trajectory [AIAA PAPER 67-595] 24 p4182 A67-42910

ROCKET TEST STATION

Steam generating technique for vacuum ejector system of high-altitude-simulating rocket test facility in West Germany [DVL-598] 03 p0394 A67-13030
 Vacuum simulation facility near Munich for testing third stage of ELDO rocket 03 p0394 A67-13031
 Arnold Center advanced ground test facilities for rocket and space vehicle environmental testing 05 p0788 A67-16617
 Facility for testing third stage of ELDO rocket, discussing high vacuum equipment in Ottobrunn laboratory 09 p1485 A67-22124
 Test facility for 5000 mw nuclear rocket propulsion modules, discussing effect on design and flight conditions duplication [AIAA PAPER 67-465] 18 p3020 A67-33936
 Space and high altitude simulation requirements for testing various rocket engine and propulsion systems 20 p3415 A67-36544
 Mississippi Test Facility /MTF/ of NASA noting rocket testing facilities, scientific laboratories and industrial complex 23 p3986 A67-40588
 Nuclear rocket propulsion development, hot test results, one breadboard engine configuration and flight stage planning [AIAA PAPER 67-981] 24 p4187 A67-43054

ROCKET THRUST

SA JET DAMPING
 Influence on stability of masses which are in relative motion with respect to projectile determined, noting engine thrust effect on attitude control system performance 03 p0517 A67-13027
 Impulsively thrusting rocket and bounded thrust rocket in relation to Newton law of motion, obtaining rigorous equation of motion 04 p0707 A67-15881
 Variational problem of rocket dynamics in homogeneous gravitational field in empty space reduced to differential equation system 05 p0904 A67-16049
 Rocket wind trajectory dispersion reduction by adjusting thrust-time curve without increasing total impulse 08 p1406 A67-20512
 Rocket engine thrust measuring system for accuracy analysis 08 p1375 A67-20779
 Propellant cost optimization using minimum characteristic velocity solutions for extra-atmospheric part of rocket ascent trajectory, emphasizing final elliptical orbit of arbitrary orientation 10 p1704 A67-22877
 Spatial trajectories of rocket under constant thrust in planetary field 11 p1869 A67-24082
 Pontryagin maximum principle application to solution of one-dimensional minimum time rendezvous problem for thrust limited rocket with initial and final mass

specified 12 p2012 A67-25922
 Mixture ratio distribution effect on rocket thrust chamber performance 15 p2545 A67-29431
 Micro-orifice injector rocket motors covering efficiency, nominal thrust, size, performance, cooling, design factors, etc [AIAA PAPER 67-462] 18 p3113 A67-33933
 Singular optimal control and attitude problem in rocket guidance [AIAA PAPER 67-582] 19 p3258 A67-35977
 Formulation of problem of guiding low thrust spacecraft back to nominal trajectory [AIAA PAPER 67-618] 19 p3260 A67-36007
 Variational problem of rocket dynamics in homogeneous gravitational field in empty space reduced to differential equation system 21 p3701 A67-37836
 Thrust history to produce maximum altitude for two-stage launch vehicle determined using simplifying assumptions and atmospheric drag 22 p3904 A67-40089
 Rocket engine cluster thrust and moment vectors analyzed statistically for thrust misalignment 22 p3869 A67-40170
 Velocity and path of vertical motion of constant thrust rocket in homogeneous gravitational field, giving hyperbolic acceleration expression as time function 24 p4241 A67-42578
 Erosion processes and outflow phenomena in ZnS rocket fuel, noting aluminum addition and gas leaks 24 p4206 A67-42579
 Rocket wind trajectory dispersion reduction by adjusting thrust-time curve without increasing total impulse 24 p4242 A67-42919

ROCKET VEHICLE**SA MULTISTAGE ROCKET VEHICLE**

Fabrication methods for aircraft, rockets and space vehicles including adhesives, sandwich and laminated structures, plastic fiberglass forms and explosion forming 01 p0078 A67-10304
 Explicit guidance law for minimum fuel horizontal translation with bounded control 06 p1090 A67-18867
 Recoverable high altitude rocket space probe with paraglider 07 p1259 A67-19573
 Escape of rocket vehicle from vicinity of planet, using tangential thrust [AAS PAPER 66-120] 07 p1254 A67-19979
 Sounding rocket vehicle technology - AIAA Conference, Williamsburg, February-March 1967 08 p1402 A67-20491
 Rocket vehicles for synoptic meteorology, evaluating vehicle concepts, performance characteristics and costs 08 p1404 A67-20497
 Balancing operations for rocket vehicles and payloads, defining terms, establishing relation between static and dynamic imbalance and flight vehicle motions, etc 08 p1408 A67-20535
 Escape of rocket vehicle from vicinity of planet, using tangential thrust [AAS PAPER 66-120] 13 p2209 A67-27534
 Motion equations of spin-stabilized rocket under thrust with jet damping, variable mass and momentum effects and all angular disturbances 19 p3334 A67-35938
 Onboard computer equations for rocket vehicle guidance to elliptical orbit, discussing iteration absence from computations and digital simulation results [AIAA PAPER 67-621] 19 p3260 A67-36010

ROD

Initial stress influence on frequency of three-dimensional vibrations of plates and rods 04 p0717 A67-15912
 Microstructure and mechanical properties as functions of degree of deformation of pressed rods of TsM2A alloy at 1300 degrees C 05 p0832 A67-17509
 Compression and tension of rod and plate with distribution of residual stresses such that deformation is partially plastic and elastic 06 p1107 A67-18633
 Rotation of thin walled elastoplastic tube of circular cross section after bending 06 p1107 A67-18635
 Resonance transition of hinged ponderable rod with nonlinear supports 06 p1109 A67-18666
 Aircraft hollow control rods with threaded joints noting compression and testing 07 p1192 A67-19753
 Stability of nonprismatic and nonhomogeneous rods under compressive tangential force, calculating critical force and corresponding

frequency 10 p1717 A67-22944
 Unloading wave expanding in elastoplastic rod determined by integration of differential equation in quadratures 10 p1721 A67-23685
 Systems constraints imposed on spacecraft utilizing long flexible rods with attached tip masses, specifically deployment and retraction problems 10 p1714 A67-23757
 Algorithms for operator partitioning method in reducing shell equations solution to calculation of solid intersecting rod systems 12 p2026 A67-25617
 Numerical solution of elastoplastic torsion of rods by method of local variations 12 p2029 A67-25667
 Natural frequencies of free longitudinal oscillations of circular rod with random parameters determined by modified Krylov-Bogoliubov asymptotic method 12 p2031 A67-25957
 Vibrational stress of clamped free rectangular rods of constant cross section under effect of instantaneous impulse 13 p2220 A67-27279
 Oscillation of rod in gas stream investigated for nonlinear factor effect on oscillations 14 p2243 A67-28639
 Thermal field of solid rod of uniform cross section and arbitrary profile with time dependent heat transfer 14 p2408 A67-28658
 Cross section central line algorithm developed and applied to torsional problems of rods with polyconal cross section 14 p2401 A67-28739
 Longitudinal bending and buckling of elastoplastic rods with allowance for creep 15 p2577 A67-30184
 Laser action of ruby and neodymium glass rods in case of axicon pumping 16 p2684 A67-30460
 Rod configuration determined optimum for gyro torquer controlled spinning space station subject to impulse disturbance 17 p2955 A67-32477
 Differential equations determining time-dependent torsional moment and stresses in thin walled rods in creep presence 17 p2821 A67-32830
 Transverse oscillations of elastic inhomogeneous rod with Youngs modulus varying along length, solved in Bessel functions infinite series 17 p2962 A67-32873
 Elastic-plastic rods theory using thermodynamical restrictions, examining straight rod motions 17 p2966 A67-33348
 Characteristics of dielectric rod excited with dominant propagating mode 18 p3011 A67-34020
 Stress-strain state of rod with end load and time variable load on other end, discussing forced and free oscillations 19 p3338 A67-34879
 Matrix method for calculating behavior of rod of constant cross section stressed by bending and stretching or compression loading 19 p3343 A67-35815
 Two-port magnetoelastic delay performance obtained in YIG rod by injecting longitudinal elastic waves along axis 21 p3677 A67-38007
 Microstructure and mechanical properties as functions of degree of deformation of pressed rods of TsM2A alloy at 1300 degrees C 21 p3644 A67-38037
 Unloading wave expanding in elastoplastic rod determined by integration of differential equation in quadratures 21 p3720 A67-38286
 Microwave pulse compression filter using dispersive characteristics of propagating magnetostatic spin waves in single crystal YIG rods 22 p3773 A67-39908

RODENT

S GUINEA PIG
 S RABBIT
 S RAT

ROLL CONTROL**SA MISSILE ROLL CONTROL**

Steady roll resonance accompanied by large amplification of nonrolling trim angle, considering compound asymmetry such as lateral center of gravity offset [AIAA PAPER 67-137] 06 p1097 A67-18504
 Dynamic flight characteristics of spin-stabilized sounding rockets during passage through atmosphere, emphasizing roll resonance and motions leading to roll lock-in and angle of attack 08 p1407 A67-20514
 Parameter management applied to roll rate control in ballistic missile target system /BMTS/ with fin

incidence 08 p1407 A67-20516
Wind tunnel investigation of dynamic instabilities in cruciform finned missiles due to rolling motion 08 p1413 A67-21531
Roll control techniques for model suspended in electromagnet system 10 p1623 A67-23471
Captured Air Bubble /CAB/ vehicle stability tests
[AIAA PAPER 67-349] 14 p2246 A67-28731
Mark 19 Sperry gyrocompass with SGN 4 inertial platform 14 p2322 A67-28989
Earth-pointing satellite attitude control system using gravity gradient stabilization, deriving motion equations 15 p2564 A67-29329
Canopus star sensor used for roll control of Mariner IV spacecraft 16 p2699 A67-30654
Automatic unique acquisition of Canopus for roll control of interplanetary spacecraft, discussing identification, discrimination and calibration
[AIAA PAPER 67-585] 19 p3258 A67-35980
Parameter management applied to roll rate control in ballistic missile target system /BMTS/ with fin incidence 21 p3712 A67-37801
Dynamic flight characteristics of spin-stabilized sounding rockets during passage through atmosphere, emphasizing roll resonance and motions leading to roll lock-in and angle of attack 24 p4242 A67-42917

ROLL FORMING
Roll fatigue tests of forged ZK60A-T5 magnesium and 2014-T6 aluminum wheels 10 p1661 A67-23439
Reentry vehicle roll resonance criterion formulation for predicting roll conditions, noting vehicle configuration, aerodynamic and trajectory parameters, exoatmospheric vehicle attitude, etc 15 p2572 A67-30211
Material point displacement velocity field of bending elements of sheet during profile shaping by roll forming, determining stress-strain condition 21 p3631 A67-38052
Volume strains in metals during pressworking and rolling 21 p3637 A67-38922

ROLLER BEARING
Materials for use as rolling-contact bearing lubricants in liquid hydrogen environment 01 p0077 A67-10119
Rolling-element bearings design and material processing for special conditions, noting stress and fatigue 01 p0079 A67-10726
Elastohydrodynamic lubrication in rolling bearings for avoiding oil-film breakdown in contact zone 01 p0079 A67-10728
Performance characteristics and bearing load-deflection equations of shaft supported by n roller bearings
[ASME PAPER 66-WA/LUB-4] 04 p0629 A67-15339
Literature in 1965 on lubrication and bearings covering friction and wear, boundary, metal working, gear and spline lubrication, rolling element bearings, etc [ASME PAPER 66-WA/LUB-8]
04 p0629 A67-15349
Book on roller bearings noting construction, operation and performance characteristics 06 p1008 A67-18837
Pressure distribution between lubricated rolling bearings, comparing static and dynamic stresses in cylindrical disks, noting film thickness 08 p1333 A67-20361
Monte Carlo simulation studies for fatigue data analysis of rolling-contact bearings, using Weibull equation
[ASLE PAPER 66AM 1B2] 08 p1336 A67-21038
Bearing selection for designers, considering available working types and load change during variable speed machine operation 21 p3633 A67-38145
Life tests of tapered roller bearings in mineral oils and synthetic fluids, demonstrating lubrication effect on contact fatigue crack propagation
[ASME PAPER 67-LUB-20] 24 p4163 A67-42678
Rolling element bearing fatigue life for cyclic race oscillation, analyzing variation with load, speed and oscillation amplitude via Weibull statistics
[ASME PAPER 67-LUB-22] 24 p4163 A67-42680
Film thickness, pressure distribution and load carrying capacity of loaded line contact in presence of viscoelastic lubricant noting high pressure spike
[ASME PAPER 67-LUB-23] 24 p4163 A67-42681

ROLLING

Cold plastic deformation, rolling direction and annealing temperature effect on mechanical properties of sheet niobium at room and high temperature 05 p0831 A67-17504
Precision rolling for fabrication of small gas turbine compressor blades for use in aircraft and stationary engines
[SAE PAPER 670095] 09 p1508 A67-22538
Critical rolling speed of aircraft tires calculated and experimentally verified 16 p2596 A67-31002
Lubrication and wear with reference to boundary lubrication, fluid and solid films, discussing dry and lubricated sliding and rolling theory 20 p3455 A67-37262
Cold plastic deformation, rolling direction and annealing temperature effect on mechanical properties of sheet niobium at room and high temperature 21 p3644 A67-38032
Hot rolling finishing temperature and cooling rate effects on aged 250 grade 18 Ni maraging steel fracture toughness 22 p3822 A67-40057

ROLLING CONTACT
Hollow rolling bearings for improved stress-fatigue and grain flow, noting welding problems 01 p0079 A67-10727
Rolling friction studies of intermetallic and zirconium oxide for control surface bearings for space reentry vehicle
[ASLE PAPER 66AM 5D4] 08 p1335 A67-21037
Material combination and hardness effect in rolling contact fatigue life of high speed tool steel, stainless steel and wear resistant materials 09 p1505 A67-22191
Metallurgical investigations by electron microscopy of rolling contact fatigue, elucidating mechanisms of failure due to shearing stress 12 p1954 A67-25329
Rolling contact failure modes classification including wear, plastic flow, fatigue and bulk failure
[ASLE PREPRINT 67AM 1C-3] 14 p2325 A67-28784
Hertz and Mindlin problems for fourth order paraboloids in contact generalized, minimizing microslips and annulus of slip
[ASME PAPER 67-APM-12] 15 p2505 A67-30149
Materials rolling contact fatigue strength measured by tester intended to serve as screening device
[ASME PAPER 67-LUBS-3] 16 p2676 A67-31381
Rolling friction with axial thrust analyzed for elastic cylinder, assuming Coulomb friction law and using integral equation 17 p2865 A67-32263
Hertz and Mindlin problems for fourth order paraboloids in contact generalized, minimizing microslips and annulus of slip
[ASME PAPER 67-APM-12] 17 p2871 A67-32411
Friction contact between semiconductor and rotating metal disk studied for sign shifts causing sharp temperature gradient producing thermal EMF 20 p3503 A67-36123
Contact region of glass ball rolling on viscoelastic plate at various velocities analyzed by interference microscope photography
[ASME PAPER 67-LUB-25] 24 p4176 A67-42683
Optical elastohydrodynamic system for evaluation of lubricants using interference pattern obtained from metal ball rolling against plate glass
[ASLE PAPER 67-LC-12] 24 p4164 A67-42747

ROLLING CONTACT BEARING
Stress patterns in lubricated rolling contact elements calculated from surface pressures and temperature
[ASME PAPER 66-LUB-16] 03 p0431 A67-13757
Lab techniques for studying unusual bearing failures, noting damage from water contaminated lubricant, pitting, etc 09 p1506 A67-22195
Hypothetical turbine driven power shaft bearing arrangement for logical analysis and practical approach to selection of optimum rolling bearings
[SAE PAPER 670060] 09 p1508 A67-22534
Nonlinear vibration damping functions for fluid film bearings
[SAE PAPER 670061] 09 p1508 A67-22535
Five-ball fatigue tester to investigate

reduced pressure environment effect on rolling element fatigue life with polyphenyl ether
[ASLE PREPRINT 67AM 8A-3] 14 p2326 A67-28795
Gyromotor vibration level variation causes and ball rotation regimes permitting stabilization 18 p3047 A67-33994
Low temperature effect on physical and mechanical properties of engineering materials and cryogenic fluids, discussing heat generation and removal at rubbing surfaces 21 p3633 A67-38141
Space environmental effect on lubricants and rolling element bearings, comparing evaporative losses of solid and liquid lubricants 21 p3633 A67-38143
Bearing selection for designers, considering available working types and load change during variable speed machine operation 21 p3633 A67-38145
High temperature lubricants for ball bearing applications, discussing bearing endurance and rolling-contact fatigue tests on synthetic paraffinic oil
[ASME PAPER 67-LUB-21] 24 p4163 A67-42679
Rolling element bearing fatigue life for cyclic race oscillation, analyzing variation with load, speed and oscillation amplitude via Weibull statistics
[ASME PAPER 67-LUB-22] 24 p4163 A67-42680

ROLLING MOMENT
Tailfin design effect on induced rolling moment characteristics of sounding rocket 08 p1405 A67-20503
Nonlinear motion theory for axisymmetric sounding missiles or rockets with Magnus moments, showing application to near pitch-roll resonance 08 p1407 A67-20515
Mathematical model used to determine influence of nonlinear induced roll moment and yawing moment on dynamic stability of cruciform tailed bomb 15 p2416 A67-29428
Dither and sinusoidal incidence variations effect on control wing hinge moments of transonic-supersonic rolling maneuvering guided missile
[AIAA PAPER 66-755] 17 p2789 A67-32062
Circulation control by blowing for gust insensitivity in stopped rotor aircraft application
[AIAA PAPER 67-747] 23 p3933 A67-40981

ROOM TEMPERATURE
Room temperature recombination radiation induced by Lorentz field in InSb and ternary alloy of mercury, cadmium and tellurium under cross field conditions 03 p0496 A67-13675
Electron microscope study of plastic deformation mechanism of titanium alloy AT4 and fatigue strain mechanism in coarse grained specimens of alloy T-40 07 p1205 A67-19278
Pressure scanned Fabry-Perot etalon for measuring ruby line widths at room temperature 10 p1662 A67-22741
Room temperature electroluminescence spectra of several materials with Ge, zinc blende and wurtzite structures by electrolyte technique 10 p1691 A67-23401
Hall effect and electrical resistance of ZrC-NbC and TaC-HfC alloys at room temperature 11 p1804 A67-23904
Thermoconductivity of heat resistant materials during cooling at room temperature, using photopyrometer to record temperature gradients 11 p1789 A67-24021
P-n junction fabrication in vapor phase grown GaAs-P alloys resulting in room temperature injection laser, thereby extending operation into visible spectrum 11 p1802 A67-24741
Laser activity from terbium trifluoroacetate in p-dioxane and acetonitrile at room temperature 11 p1803 A67-24833
Relative enthalpy and thermodynamic properties of beryllium aluminate from room temperature to melting point 15 p2508 A67-29764
Negative-resistance in evaporated silicon films at room and liquid-nitrogen temperatures believed due to double injection 16 p2728 A67-31035
Pulsed resistivity and Hall effect measurements of n-type GaAs in high electric fields at room temperature below microwave oscillation

threshold 16 p2731 A67-31449
N-and p-type silicon solar cells orientation and energy dependence of damage at room temperature under electron bombardment 17 p2918 A67-32848
Criticism of McCarroll statement on oxide formation on tungsten surface at room temperature 19 p3244 A67-34942
Models explaining long time delay between current-pulse application and generation of coherent oscillations in gallium arsenide junction lasers near room temperature 19 p3241 A67-36036
GaAs pulsed injection laser diode noting characteristics for room temperature operation 22 p3813 A67-39253
Room temperature density-dose behavior of neutron and gamma irradiated polytetrafluoroethylene /PTFE/ noting crystallinity variations 23 p4021 A67-40781
Numerically computed power outputs and efficiency of continuous room temperature ruby lasers in good agreement with theoretical model 23 p4017 A67-41465
1, 3-diones and beta-ketoesters with cobalt for room temperature curing of unsaturated polyester resins by organic peroxide 24 p4175 A67-42420

ROOT

Automatic technique of root location and determination of nth order polynomial equation using simple linear computing elements 11 p1756 A67-24639
Root trajectory theory use in automation schemes for analysis and synthesis of optimum control systems, outlining applications 13 p2085 A67-26394
Ordinary and time lag root locus diagram generating algorithm for adaptation to programming on digital computer 13 p2074 A67-27223
Loc types presented in Chang paper for systems with particular open-loop transfer function are only types possible for third order systems with no open-loop zeros regardless of nature of open-loop poles 15 p2457 A67-29375

ROOT-MEAN-SQUARE ERROR

Noise stability for wideband analog methods of information transmission based on analysis of probability distribution density, using normal rms error and anomalous error probability 03 p0369 A67-13581
Construction method for rms-optimal digital smoothing devices, noting case of astatic systems 05 p0782 A67-16268
Optimal filtration of nonlinear functional of Gaussian signal, obtaining expressions for kernels of optimal filter 05 p0782 A67-16317
Range determination with CW tracking radar controlling rms error, noting SNR role in holding target echo 06 p0957 A67-17593
Optimum transformation of linear system with minimal rms error from given point to fixed delta-environment of another given point 08 p1313 A67-21322
Gaussian errors effects on antenna pattern of any array of elements, describing errors in terms of rms amplitude and phase errors at each element 09 p1470 A67-21591
Adaptive data compression systems of predictor-comparator type 12 p1907 A67-25992
Inaccurate determination effect of input-signal characteristics on filtration quality, deriving equations for estimating upper limit of relative increase of rms filtration error 17 p2829 A67-32223
Optimal filtration of nonlinear functional of Gaussian signal, obtaining expressions for kernels of optimal filter 18 p3016 A67-33868
Residuals and rms residuals of control measurements made by Manchester Lunar Group members, showing reduced heights not affected by personal errors 18 p3132 A67-34331
Optimal discrete filter corresponding to given analog filter for minimum mean square error 19 p3199 A67-34782
H-01 waveguide irregularities causing transfer function fluctuation, calculating rms and relative distortion power from PCM signal 19 p3183 A67-35561
Noise effect on synthesis of discrete systems with and without feedback channel for transmitting continuous messages, using binary signal and criterion of minimum rms error 20 p3383 A67-37071

ROTARY DRIVE

Rotorcraft technology developments and possible improvements by

mid-1970s 11 p1744 A67-24589
Radiation pressure on vanes of rotary actuator of spacecraft radiation orientation system 12 p2011 A67-25655

ROTARY STABILITY

Existence and stability of uniform rotation of heavy blunt profile immersed in perfect incompressible irrotational fluid flow 05 p0792 A67-16595
Simplified resonance-amplitude analysis of unbalance vibration superimposed upon steady state eccentricity in aerodynamic bearings 09 p1509 A67-22613
Influence of internal friction on high speed rotor stability using motion equation, noting bearing support flexibility and damping role [ASME PAPER 67-VIBR-14] 11 p1795 A67-24174

Errors of real accelerometer and instability of rotation effect on accuracy of angular velocity measurements of aircraft motion 16 p2670 A67-30466
Dynamic imbalance of rotors determined and eliminated using angular oscillation and electrical erosion 16 p2681 A67-30469
Despun antenna system for satellite stabilized by rotation around axis perpendicular to orbital plane 21 p3591 A67-38204
Multirotor trochoidal engines external balancing problems, discussing cam distribution and shaft shape 21 p3696 A67-38910
Lunar origin related to earth rotational instability due to earth core formation 24 p4230 A67-42324
Earth-moon system origin assuming moon was formed from terrestrial material ejected from earth during rotational instability 24 p4230 A67-42325

ROTARY WING

Aeroelastic response problem of rotating wings in steady state flight solved by numerical method 06 p1099 A67-17917
Rotary wing decelerator for sonic and supersonic operation, noting components and potential application 17 p2796 A67-32517
Failure safety design of rotary wing aircraft, emphasizing airline type operation [SAE PAPER 670349] 17 p2798 A67-32991

ROTARY WING AIRCRAFT

SA AUTOGYRO
SA HELICOPTER
Comparative stability and control considerations for fixed wing and rotating wing aircraft 06 p0944 A67-17628
Requirements and disadvantages of proposed escape systems for fixed and rotary wing Army aircraft 17 p2794 A67-31998
Rotary wing role in short haul intercity transportation, comparing V/STOL and STOL advantages over fixed wing aircraft, noting need for compound helicopter 21 p3734 A67-38013
High speed helicopters and large transport capacity aircraft, discussing combination of rotors with wings and propeller drive, retractable blades and folding rotors 22 p3745 A67-39753
Hot cycle rotor/wing aircraft for high speed city-center transportation, estimating cost and performance [AIAA PAPER 67-770] 24 p4095 A67-42938

ROTATING BODY

Rotating gyroscope with conical cup on ball support, deriving expressions for moments of forces imposed by support 01 p0064 A67-10419
Magnetic field of M-element interaction with geomagnetic field as second possible cause of irregular fluctuations in velocity of earth diurnal rotation 02 p0237 A67-11678
Translational motion of two rotating spherical symmetrical bodies in general relativity theory 02 p0268 A67-12490
Rotating interferometer measuring spread and coherence ratio of scattered radio wave 05 p0760 A67-15997
Skewed boundary layers over body of revolution rotating in axial stream 05 p0747 A67-16218
Existence and stability of uniform rotation of heavy blunt profile immersed in perfect incompressible irrotational fluid flow 05 p0792 A67-16595
Deriving Lagrangian for system of extended rotating bodies, noting contribution of relativistic corrections for

kinetic energy of rotation 05 p0847 A67-17496
Free and forced oscillation of disks and right circular cylinders rotating in free stream, noting turbulent wake flow 06 p1101 A67-18136
Canonical transformation to investigate rotational motion of uniaxial orbiting rigid body influenced by gravity gradient torque [AIAA PAPER 67-125] 06 p1084 A67-18288
Rotation of thin walled elastoplastic tube of circular cross section after bending 06 p1107 A67-18635
Dynamo mechanism for formation of stellar magnetic field, considering effects of EM radiation emission and celestial body rotation 06 p1089 A67-18775
Flow of thin layer of liquid on surface of rotating body of revolution in moving system of coordinates connected with body 06 p0991 A67-18817
Rotational motion of rigid sphere about z axis in elastic medium taking into account surface adhesion 07 p1223 A67-19219
Spinning rocket attitude control technique including theory, system mechanization and performance 08 p1409 A67-20539
Bending effect of spectral lines in plasma created by rotating HF dipole in quasi-steady magnetic field 08 p1358 A67-20854
Deformed figures of Maclaurin spheroids from solving post-Newtonian hydrodynamic equations for uniformly rotating axisymmetric bodies 08 p1354 A67-21245
Stationary resonance solutions for rotating systems with one degree of freedom applied to satellite rotation problems 09 p1532 A67-21910
Translational motion of two rotating spherical symmetrical bodies in general relativity theory 10 p1680 A67-23358
Radar echo model from random collection of rotating dipole scatterers 11 p1764 A67-24435
Mass transfer rates for axisymmetrically rotating bodies, using diffusion controlled electrode reaction system 12 p2033 A67-25277
Finite rotation of body due to revolutions of internal flywheels determined assuming total kinetic moment of system is zero 12 p1966 A67-25655
Time dependent orientation of body fixed coordinate system relative to stars for spinning rigid torque-free body 13 p2154 A67-26816
Integration of boundary layer equations for axisymmetric body rotation in unbounded medium at rest 13 p2095 A67-26900
Nonrelativistic theory of rotating configurations in terms of gravitational potential, center mass density and variable angular velocity 14 p2382 A67-27833
Motion of solid body with rotating flywheels rotating at constant velocities relative to inertial space and body 15 p2493 A67-29686
Attitude stabilization and control system for rotationally symmetric gyroscopic body with two degrees of freedom 15 p2490 A67-30156
Free rotation of solid body analyzed using homogeneous canonical transformation 15 p2519 A67-30225
Magnetic field of M-element interaction with geomagnetic field as second possible cause of irregular fluctuations in velocity of earth diurnal rotation 16 p2665 A67-31093
Stationary flow in viscous fluid film on rotating body of revolution, using differential equations 17 p2836 A67-32261
Criticism of classical theory of Mercury rotation period equal to revolution around sun 18 p3125 A67-34191
Cassini second and third laws are independent of first law 18 p3128 A67-34303
Regularization of restricted three-body problem extended to case where three primaries of any mass revolve in circular orbits around common center of mass and fourth body of infinitesimal mass moves in their field 18 p3136 A67-34589
Solid body of variable mass with cavities filled with ideal incompressible fluid, analyzing differential equations of motion 18 p3080 A67-34604
Relative velocity effect on vaporization times and heat-transfer coefficients of water drops in Lelidenfrost film boiling on heated rotating wheel [AICHE PAPER 32] 20 p3552 A67-36833
Stress distribution in homogeneous

isotropic body under finite elastic deformation rotating with constant angular velocity 20 p3542 A67-37680
 Drag coefficients for random and planar tumbling satellites 21 p3563 A67-37809
 Combination paramagnetic resonance in mechanical system containing rotating body, giving procedure for approximate determination of oscillation amplitude and resonant zone boundaries 21 p3625 A67-37990
 Euler motion generalization of solid body, discussing inertial and kinetic moments 22 p3836 A67-39403
 Angle of attack determination from rotational body rates, formulating ordinary differential equations 22 p3741 A67-40093
 Flexural vibration of stiffened circular plates with respect to rotatory inertia, obtaining differential equation 23 p4073 A67-40613
 Book on Hamilton principle and physical systems covering planetary motion, rotating bodies, electromagnetic radiation, quantum theory, etc 24 p4189 A67-42406

ROTATING CONE

Three-dimensional boundary layer flow of incompressible second order viscous fluid near spinning cone 06 p0992 A67-18868
 Differential equations of motion for permanent rotation heavy gyro with fixed point 10 p1657 A67-23668
 Transverse magnetic field interaction with laminar boundary layer on rotating cone during reentry, assessing effect on spin and controlling torques 12 p1892 A67-25385
 Nonsimilar boundary layer flow and heat transfer of cone rotating in forced flow [ASME PAPER 65-WA/HT-31] 15 p2415 A67-29320
 Motion of gyroscope with conical cavity filled with ideal incompressible fluid describing rotating motion 15 p2518 A67-30171
 Differential equations of motion for permanent rotation heavy gyro with fixed point 21 p3627 A67-38269
 Mean flow and motion turbulence characteristics after separation from conical afterbody for various initial boundary layer thickness and convergence 23 p3927 A67-40631
 Incidence angle effects on wall heat flux in symmetry plane of cone of revolution in hypersonic regime, discussing wall pressure measurements 24 p4092 A67-42660

ROTATING CYLINDER

Harmonic generation in Taylor vortices between rotating cylinders, measuring amplitude of each harmonic, noting agreement with Davey 04 p0601 A67-14462
 Rotation and vibration of conducting circular cylinder in magnetic field, noting motion retardation due to induced electric current interaction with field 05 p0851 A67-16434
 Approximate solution of integral equations with aid of least squares for steady motions of viscous incompressible fluid in rotating cylinder 07 p1168 A67-19217
 Numerical solution for heat transfer to reversibly reacting gas in turbulent boundary on surface of rotating cylinder 07 p1268 A67-19575
 Cylindrical Couette flow of rarefied monatomic gas calculated by double flow method 13 p2095 A67-26898
 Drag coefficient for cylinder rotating in rarefied gas, comparing numerical method and approximate analytical solution 13 p2101 A67-26963
 Asymptotic theory for near-continuum gas flows applied to BGKW equation, deriving slip coefficient 13 p2101 A67-26964
 Temperature field of coaxial cylinders obtained as infinite series of Bessel and trigonometric functions 13 p2224 A67-27057
 Bifurcation of nonlinear operator equations to determine steady state axisymmetric homogeneous fluid flows between rotating cylinders 15 p2494 A67-29693
 Microscopic interpretation of generalized Helmholtz equation, considering particle in charged gas in adiabatic flow as rotating cylinder model 16 p2720 A67-31245
 Karman similarity hypothesis extended to cylindrical geometry to establish conditions for universal velocity similarity in fully turbulent rotating flows [ASME PAPER 67-APM-23] 17 p2838 A67-32416

Instrument for generation of thermal plasmas in direct current-arc discharges and expansion to walls of coaxial rotating cylinder 17 p2835 A67-33389
 Convective heat transfer in fluid between concentric cylinders with inner heated cylinder rotating and outer cooled cylinder stationary 20 p3543 A67-36422
 Oscillation stability of rotating cylindrical shell filled with ideal incompressible weightless fluid, determining instability region distribution 21 p3721 A67-38302
 Rigid cylinder two-dimensional motion in rotating incompressible fluid compared to motion in isotropic incompressible conducting medium under magnetic field 21 p3668 A67-38552
 Relative equilibrium of liquid cylinder investigated for uniform rotation in uniform axial electric field 22 p3787 A67-40135
 Taylor instability in circular Couette flow reexamined as eigenvalue problem noting suppression of geometry effect 23 p3988 A67-40601
 Temperature distribution in solid rotating cylinder exposed to solar radiation using Fourier series expansion 24 p4255 A67-42482
 Taylor vortices and turbulence in flow between eccentric rotating cylinders [ASME PAPER 67-LUB-12] 24 p4145 A67-42673

ROTATING DISK

Stresses in symmetrical three-layer circular disk rotating about own axis, with solutions in form of Fourier-Bessel integrals 01 p0080 A67-10777
 Heat transfer in viscous fluid flow in gap between permeable isothermal surface and rotating disk, solving energy equation 03 p0536 A67-13611
 Deformation of disk with nonsymmetric rim and hub 03 p0528 A67-14075
 Unsteady laminar flow of viscous incompressible fluid between two infinite parallel rotating disks with angular velocities varying with time 04 p0609 A67-15605
 Heat transfer in laminar source flow between stationary and rotating disk 04 p0729 A67-15812
 Elastoplastic deformation of nonuniformly heated rotating disk determined to verify validity of theory under nonisothermal load 05 p0907 A67-16019
 Inertial force effect on stress distribution around blade roots of turbine disk analyzed, using low Young modulus material and stroboscopy 05 p0811 A67-16602
 Free and forced oscillation of disks and right circular cylinders rotating in free stream, noting turbulent wake 06 p1101 A67-18136
 Principal mechanism of galactic structure based on stellar dynamics principles, discussing spiral pattern in presence of rotation and mathematical theory 08 p1379 A67-20353
 Plastic deformation and fracture of rotating turbine rotor 09 p1502 A67-21554
 Air mass measurement during turbulent axial flow towards surface of rotating disk, noting entrainment rates for high and low Reynolds numbers 09 p1437 A67-22159
 Analytical expressions developed for prediction of partially wetted rotating disk pressure, gradient development and frictional drag for different flow regimes 10 p1659 A67-22708
 Stroboscopic distortion during rotation of uniformly accelerated disk illuminated by light pulses 11 p1757 A67-23917
 Dissipative energy effect on laminar heat transfer from disk rotating in uniform forced stream 13 p2221 A67-26531
 Plastic strength of anisotropic rotating disks 13 p2125 A67-27737
 Gear materials and lubrication methods to satisfy high speed and temperature requirements in aerospace applications 14 p2334 A67-27791
 Flexural wave velocity-amplitude relation indicates possibility of stationary waves for fixed ratio of wave amplitude and spinning membrane angular velocity 14 p2403 A67-29016
 Finite displacements of solid body under effect of internal rotating flywheels and translational motion of masses 15 p2518 A67-30169
 Deformation and distribution of stresses in

rotating disk with variable thickness and temperature gradient 17 p2960 A67-32687
 Heat transfer due to flow of electrically conducting incompressible viscous fluid from rotating insulated disk under influence of axially oriented magnetic field 18 p3084 A67-33667
 Circular disk error magnitude determination by measuring rear-wall echo with angular probe 18 p3044 A67-33736
 Heat transfer in viscous fluid flow in gap between permeable isothermal surface and rotating disk, solving energy equation 18 p3161 A67-34476
 Turbodynamo disk stress-strain state, with final deformations under unsteady operational conditions, noting plastic flow, continuity, tension, and disk equilibrium equations 19 p3234 A67-34880
 Surface-temperature conditions in disks and gears stressing heat transfer coefficient and lubricated contact 19 p3237 A67-35840
 Friction contact between semiconductor and rotating metal disk studied for sign shifts causing sharp temperature gradient producing thermal EMF 20 p3503 A67-36123
 Centripetal radial blowing effect on flow and heat transfer in gap between rotating disk and wall, specifically effect of Reynolds number and dimensionless flow 20 p3357 A67-36794
 Rayleigh hypothesis applied to three-dimensional rotationally symmetric flows arising from rotating disk in rotating fluid compared with steady solutions 20 p3423 A67-37278
 Flow due to rotating disk with center sink solved numerically by considering flow unsteady [ASME PAPER 67-FE-8] 20 p3425 A67-37599
 Steady motion of electrically conducting viscous fluid due to slow rotation of thin dielectric disk inside housing immersed in magnetic field 21 p3665 A67-38247
 Stroboscopic distortion during rotation of uniformly accelerated disk illuminated by light pulses 21 p3601 A67-38945
 Durability of conical rotating disks having asymmetric profiles and arbitrarily varying thickness 22 p3812 A67-39534
 Electromagnetic forces effects on steady rotating motions of conducting viscous incompressible fluids via adjustable local boundary layer first order approximation 23 p4031 A67-40604
 Laminar flow field between rotating turbine disks solved for low Reynolds number and partial admission flow 23 p3988 A67-40614
 Frozen stress photoelastic technique used to determine hoop and radial stresses at hole boundaries for different flat disk configurations 23 p4077 A67-41154
 Lubricating action of electroplated gold on stainless steel examined under load by single rub block loaded against rotating disk [ASLE PAPER 67-LC-16] 24 p4165 A67-42750
 Limit diffusion flux on rotating ring electrode surface in turbulent regime, determining mass transfer constant 24 p4146 A67-43112

ROTATING ENVIRONMENT

Biochemical measures made as part of habitation experiment in which four subjects were exposed to rotation for 6 days 05 p0754 A67-16277
 Model for radial and axial structure of geophysical vortices involving Boussinesq boundary-layer equations similarity solution in point heat source 16 p2778 A67-30949
 Thermally induced boundary layer flows in isothermal rigid body rotation 20 p3421 A67-36843
 Antimotion sickness drugs and placebos effect on altering motion sickness susceptibility in Skyladder aircraft aerobatics and Slow Rotation Room dial test 21 p3574 A67-38083
 Jupiter environment, effects of huge mass, high rotation rate, temperature and dominant H and He atmosphere 22 p3887 A67-40141
 German Gyroscope Testing Laboratory noting revolving platform for simulating rotational velocities, signal testing and signal simulation 23 p4003 A67-41327
 Coriolis force effect on gross reach movements for instrument control consoles 23 p3956 A67-41630

ROTATING FLUID

Electromagnetic analysis of rotating fluid systems containing rigid and inhomogeneous parts within fluid by introducing additional relativistic transformation of gravitational constant 01 p0113 A67-10470

Rotating fluid dynamics with results derived from classical rules of vorticity, noting various types of waves 02 p0232 A67-11566

Flow of viscous fluid in closed cylindrical space under rotating surface solved by grid method appropriate for computers 03 p0401 A67-12871

Numerical determination of axisymmetric equilibrium shapes of interface between two nonmixing liquids uniformly rotating in vessel under weak centrifugal and capillary forces and zero gravity conditions 03 p0402 A67-12882

MHD equations, discussing dimensional and nondimensional parameters, modifications of Maxwell equations, vorticity and rate of circulation change in viscous flow, etc 03 p0480 A67-13724

Laboratory experiments on atmospheric simulation, mainly rapidly rotating fluids, with limitation to incompressible fluids 04 p0613 A67-14802

Static pressure and velocity profiles of rotating flow with recirculation core in straight pipes determined by five-hole pressure probe [ASME PAPER 66-WA/FE-36] 04 p0607 A67-15367

Stability of rotating liquid mass /e.g. earth/, following Jeans treatment of Jacobi ellipsoidal equilibrium configurations 06 p1080 A67-17768

MHD phenomena in vortex ring in conducting fluid, noting intensification of initial field at high Reynolds numbers and self-excitation 07 p1229 A67-19684

Axisymmetric thermal convection in rotating fluid annulus for various Peclet numbers, obtaining mean thermal structure and heat transfer 08 p1323 A67-21387

Motion induced by sources and sinks distributed along vertical boundary of rotating fluid, noting role of Ekman layers 09 p1489 A67-22416

Rotating Ekman boundary layer stability and transition for two-dimensional roll vortices superimposed upon basic boundary layer flow 11 p1781 A67-24543

Thermal convection in rotating fluid annulus analyzed using Navier-Stokes equations as initial value problem 12 p1963 A67-25339

Axisymmetric thermal convection flow in rotating fluid annulus 12 p1963 A67-25340

Linear theory for steady motions in rotating stratified fluid 19 p3209 A67-35410

Internal rotational relaxation effect on attenuation of HF turbulent vortices during degeneration of turbulence in viscous weakly elastic fluid 20 p3422 A67-37053

Rayleigh hypothesis applied to three-dimensional rotationally symmetric flows arising from rotating disk in rotating fluid compared with steady solutions 20 p3423 A67-37278

Velocity profiles of boundary layer of conducting fluid rotating over stationary dielectric disk of infinite radius in magnetic field 21 p3665 A67-38246

Rigid cylinder two-dimensional motion in rotating incompressible fluid compared to motion in isotropic incompressible conducting medium under magnetic field 21 p3668 A67-38552

Neutral carrier gas and slightly ionized plasma binary mixture model for nonhomogeneous seeding effects on rotating arc performance 21 p3674 A67-38885

Monograph on turbulent mixing of rotating jets in circular confined duct 21 p3615 A67-39128

Axisymmetric stationary gravitational field Einstein field equations in rigid uniformly rotating ideal fluid 23 p4028 A67-41149

Nonlinear steady motions produced by stable stratification in rapidly rotating fluid, discussing Ekman layers 23 p3990 A67-41170

ROTATING MACHINE

Closed Brayton cycle power conversion system development, discussing rotating components and single phase operating fluid [AIAA PAPER 66-889] 02 p0183 A67-12268

Temperature and heat transfer conditions

determination on rotating turbine wheel in jet power plant, using electric analogy 04 p0688 A67-14571

Stator whirl with rotors in bearing clearance noting jump and hysteresis phenomena [ASME PAPER 66-WA/MD-8] 04 p0629 A67-15346

Heat transfer and circulation data for rotating mixed convection thermosyphon geometry for application to cooling certain rotating components 04 p0731 A67-15828

Angular precession and critical speed of two-bearing machines with overhung weight determined, considering shear deformation, gyroscopic moment and rotatory inertia [ASME PAPER 67-VIBR-19] 11 p1796 A67-24178

Vibrational mode behavior of rotating gravitational mass sensors and sensor design to minimize nonideal effect of manufacturing and external disturbances 12 p1945 A67-25919

Parallelism between edges of aerial photographs and line of flight achieved by automatic rotation 16 p2671 A67-31031

Adhesives for bonding overlay materials to substrates for high speed hydrofoils, describing water tunnel and rotating arm tests 21 p3632 A67-38131

Rotating boiler for high performance Rankine cycle power generator using water as test fluid, obtaining heat-transfer coefficients 24 p4184 A67-42498

ROTATING MATTER

Rotation and pressure gradient effects on gravitational instability of collapsing gas clouds, discussing subsequent fragmentation 22 p3893 A67-40501

Galactic rotation effects on gaseous spiral arm stability for magnetic critical wavelength less than Jeans critical wavelength case 22 p3893 A67-40506

Mach principle manifestation in Jordan extended gravitation theory, calculating rotation of local inertial frame induced by rotating shell of mass 23 p4027 A67-41147

ROTATING MIRROR

Framing cameras of rotating mirror type, discussing optical principles used in American, British and Russian high speed cameras developed since original NACA camera 03 p0419 A67-13229

Time resolution dependence on ambient gas around rotating mirror in streak camera 03 p0424 A67-13915

Framing cameras of rotating mirror type, discussing optical principles used in American, British and Russian high speed cameras developed since original NACA camera 05 p0806 A67-16699

Photoexcited electron lifetimes measured in extrinsic germanium photoconductors using Doppler shift and rotating mirror square light pulse method 06 p1005 A67-18715

Universal rotating mirrors for Q-switching neodymium glass laser 09 p1514 A67-22171

Film transport methods and other factors relating to high speed frame cinematography 14 p2315 A67-27871

Special lighting equipment for high speed cinematography delivering high intensity light pulses in nanosecond range for use in shock wave and explosion filming 14 p2319 A67-28585

Generation of large pulses of extremely short duration in ruby laser by rotating mirror technique at lower frequencies 15 p2498 A67-29642

Rotating mirror streak cameras, noting development history and future needs 16 p2675 A67-31249

Generation of giant pulses of coherent radiation by rotating-mirror technique and by passive Q-switch using cryptocyanine 17 p2871 A67-33390

Matrix method for analyzing systems of gimbaled mirrors, prisms and ray projectors 23 p4003 A67-41323

ROTATING PLASMA

SA THETA PINCH

Rotating flame resulting from instability of inhomogeneous plasma produced by arc discharge in magnetic field approaching criticality 01 p0123 A67-10739

Magnetohydrostatic equilibrium configurations of rotating plasma 03 p0475 A67-12923

Ion velocity in rotating plasma treated by conservation equations of plasma

constituents 03 p0485 A67-14053

Free oscillations of rotating star with equal angular velocity 04 p0698 A67-14915

Critical voltage of rotating plasma device in which confinement region surrounds ring shaped coil suspended by single rod 04 p0672 A67-15648

Stabilization of hydrodynamic drift oscillations in rotating nonuniform cylindrical plasma 06 p1040 A67-18092

Langmuir probe experiments on electric and magnetic field, density and temperature profiles, I-V characteristic, etc, for rotating plasma in B-3 stellarator 08 p1361 A67-21137

Possible excitation of Kelvin-Helmholtz instability in rotating plasmas 08 p1362 A67-21145

Electron-hole plasma pinch instability in InSb on application of longitudinal magnetic fields shows change to helical rotating plasma 10 p1683 A67-22760

Torque on sun calculated from solar wind motion, taking rotation and magnetic field effects into consideration 11 p1857 A67-23931

Plasma confinement by HF multipole electromagnetic field, noting role of potential accompanying rotating magnetic field 11 p1839 A67-24425

Arc rotation heat transfer effects in self-induced magnetic field plasma arc heaters used for aerodynamic tests 12 p2034 A67-25346

Voltage-current characteristics measured by Fahleson alternate explanation, based on properties of Hartmann boundary layer in continuum type plasma 12 p1972 A67-25384

Hydrogen plasma produced by coaxial gun located in magnetic mirror 13 p2163 A67-26291

Rotating flame resulting from instability of inhomogeneous plasma produced by arc discharge in magnetic field approaching criticality 13 p2166 A67-26768

Ion density concentration in magnetic-field-aligned rotating plasma columns /plasma eddies/ 13 p2171 A67-27433

Diffusion due to ion-ion collisions between different ion species, stressing impurities diffusion in rotating plasmas 14 p2363 A67-29066

Gravitational instabilities arising in plasma disk subjected to differential rotation in presence of magnetic field parallel to rotation axis 15 p2528 A67-29662

Finite-ion Larmor radius effect on wave propagation in rarefied rotating plasma, noting solar corona application 15 p2533 A67-30396

Mercury flow in rotating torus with induction pump and magnetic field effect on flow studied for flow resistance 17 p2900 A67-32342

Rotating field pinch dynamics in terms of temperature, pressure, plasma radius and magnetic field strength, noting energy transfer efficiency 17 p2908 A67-33108

Model for distribution of thermal plasma in magnetosphere of Jupiter under assumption of corotation with planet 17 p2951 A67-33196

Rotational velocity and ion density profiles of plasma vortices by measuring radial electric field 19 p2388 A67-35361

Electromagnetic field energy absorption in cold rotating plasma, obtaining electric current density and plasma electric field relationship and cyclotron resonance 20 p3497 A67-36677

Motion of rotating plasma cylinder under gravity force assuming temperature time dependency 21 p3663 A67-37931

Plasma rotation effect on cyclotron resonance, noting electromagnetic field energy absorption 21 p3669 A67-38679

Plasma rotation in MPD arc measured for electric and magnetic field distribution and current and electron density distribution [AIAA PAPER 67-655] 21 p3689 A67-38691

Gravitational instability in anisotropic plasma including rotation effect 22 p3848 A67-39694

Magnetogravitational instability of uniformly rotating compressible medium due to variable amplitude perturbations, stressing Jeans theory 23 p4033 A67-41019

ROTATING SHAFT

Coupled flatwise and edgewise vibrations of beam rotating about one end 04 p0707 A67-14492

High speed drive for rotating shafts inside high vacuum chambers

[ASME PAPER 66-WA/PID-7]
04 p0628 A67-15330
Thin rod bending and twisting theory applied to critical speed of rotating shaft under axial loading and tangential torsion, using Galerkin approximation
[ASME PAPER 66-WA/MD-1]
04 p0629 A67-15348
Flexural-torsional vibration of rotating shaft with distributed parameters
07 p1264 A67-20104
Optical incremental shaft resolver using plastic radial gratings
08 p1331 A67-20864
Geometry variation effects on hydrodynamic bearing performance, noting locational dependence relative to pressure producing region
08 p1336 A67-21041
Imparting motion to system of two masses coupled by linear elastic shaft in infinite set of piecewise continuous loads, by variational method of influence
08 p1354 A67-21047
Gyroscopic moment effect on critical speeds of shaft-disk system mounted in short end bearings, obtaining frequency equations
[ASME PAPER 67-VIBR-9]
11 p1795 A67-24169
Unbalanced rotor deceleration through critical speed tested, considering maximum deflection increment and bending stress in rotor shaft
[ASME PAPER 67-VIBR-17]
11 p1796 A67-24176
Supercritical speed helicopter power transmission shaft for rotor synchronizing, noting viscous damper for controlling shaft vibrations
[ASME PAPER 67-VIBR-20]
11 p1796 A67-24179
Stability in whirl theory, considering internal damping role on motion of elastic shaft
11 p1798 A67-24316
General solution for motion equation of rotating shaft with changing angular velocity, noting transition through critical speed
12 p1949 A67-25408
Bearing mounted shaft-rotor system noting harmonic and stable whirl characteristics
12 p1949 A67-25409
Turbomachine rotating shaft and rotor systems critical speeds taking into account bearing support stiffness and clearances, noting vibration mode
12 p1949 A67-25410
Vibration in cylindrical shafts, noting high stresses due to low mechanical damping, existence of two natural frequencies, etc
12 p1949 A67-25411
Stability of prismatic shaft rotating with constant angular velocity as function of mass and setting point of rotating
16 p2766 A67-31151
Burst strength in high speed rotor in axial blower/gas turbine, noting effect of ductility and centrifugal force
17 p2961 A67-32688
Rotating device for transmitting motion through walls of ultrahigh vacuum chambers, using circular motion of bellows envelope and internal gearing
17 p2863 A67-33358
Inertial effects of rotor on synchronous motion of simply supported and cantilever arrangements of rotor shaft
20 p3453 A67-36500
Shape of line of deflection in systems subjected to flexural vibrations of rotating weightless shaft supporting eccentrically distributed mass points or
21 p3636 A67-38831
Optimal functional parameters of elastically damping turbine rotor bearing to determine critical velocities of
21 p3695 A67-38832
Amplitude of forced flexural vibrations of free rotating shaft under arbitrary load with dampers, taking into account viscous friction
21 p3726 A67-38834
Load carrying capacity of hydrostatic bearing having communicating chambers and operating with laminar flow of incompressible fluid, showing shaft vibration elimination
21 p3636 A67-38837
Heat transfer of fluid flow in annular channel with rotating shafts, deriving surface heat transfer estimation without axial flow
22 p3921 A67-40457

ROTATING SPHERE
Body of revolution bounded by sphere rolling on stationary sphere with force function of applied forces dependent on only one coordinate
02 p0267 A67-11960
Motion instability of liquid in interspace

between two rotating spheres when ratio of radii approaches 2
06 p0992 A67-18820
Electromagnetic induction in conducting sphere rotating in transverse field, extending results for steady state to unsteady rotation, determining magnetic moment
07 p1174 A67-19715
Time dependent viscous flow between two rotating spheres analyzed by extension of numerical methods
14 p2296 A67-27905
Behavior of perfect sphere rotating around axis and under no external force
16 p2677 A67-31715
Normal modes of hydromagnetic oscillations in rotating fluid sphere including ohmic dissipation, deriving dispersion relations
17 p2941 A67-32285
Body of revolution bounded by sphere rolling on stationary sphere with force function of applied forces dependent on only one coordinate
17 p2886 A67-33277
Incompressible hydromagnetic fluid oscillation in rotating spherical shell pervaded by strong toroidal and weak poloidal magnetic field for geomagnetic secular variation
21 p3621 A67-38983

ROTATING STALL
Aerodynamic theory of blade vibration, discussing compressibility effect, stalling and design
12 p2014 A67-25412
Onset delaying of rotating stall in axial flow compressors
22 p3744 A67-40563

ROTATING VEHICLE
Rotating artificial gravity system for manned orbital vehicles and stations requiring no expenditure of propulsive mass to attain full vehicle rotation
05 p0906 A67-17203
Elastic deformation effects on stability of rotating satellite composed of elastically connected rigid bodies
13 p2212 A67-26905
Two-channel control system for programmed roll of rapidly rotating carrier rocket, analyzing efficiency
22 p3898 A67-39175

ROTATION
SA AUTOROTATION
SA EARTH ROTATION
SA FARADAY ROTATION
SA GYRATION
SA LIQUID ROTATION
SA MOLECULAR ROTATION
SA SATELLITE ROTATION
SA SOLAR ROTATION
SA SOLID ROTATION
SA STELLAR ROTATION
SA TORQUE
Rotation period of Jupiter determined by radio observations explaining cyclic drift
01 p0146 A67-10294
Rotational temperatures measured in static low density air with electron beam probe
01 p0071 A67-11105
Audio frequency proportional to rotation rate of reentrant laser cavity system derived from single output beam
01 p0091 A67-11322
Dispersion of refractive index of NO in fundamental vibration-rotation band
03 p0468 A67-13473
Steady state rotations in perturbed autonomous systems
05 p0847 A67-17475
Laser interferometry application to detection of rotation in system by splitting light from source into two coherent beams
09 p1499 A67-22150
Energy functionals and universal integrals of motion for force field symmetric about axis of rotation
11 p1821 A67-25069
Calibration of vibrational transition of CO at various pressures to determine vibration-rotation wave numbers
13 p2160 A67-26600
Venus and Mercury intrinsic rotation rates and surface radar reflectivity of former from radar echo measurements
15 p2556 A67-29872
Remote control of monochromator prism rotation using balanced-bridge system to regulate flow
20 p3451 A67-37308
Rotation effect on growth of discontinuity across Alfvén wavefront, solving differential equations
21 p3662 A67-37761
Reconstructed image scanning by hologram rotation
21 p3624 A67-37852
Oscilloscope recording of mechanical rotation rate using semiconductor photoelectric effect
22 p3796 A67-39341

ROTATIONAL FLOW
MHD rotation of conducting viscoplastic fluid between two coaxial cylinders in crossed fields
01 p0120 A67-10180

Nonsteady state gas flows with small entropy gradients corresponding to supersonic flight
02 p0178 A67-11629
Supersonic flow past blunt body with convex corner calculated to establish sonic point on body
03 p0349 A67-12862
Gravitational and magnetogravitational stability of rotating fluid layers of uniform thickness under Coriolis force and magnetic field
03 p0482 A67-13744
High lift rotor design for jet propulsion VTOL aircraft
03 p0360 A67-13891
Free convective heat transfer between hot and cold rotating disks in laminar steady azimuthally symmetric flow in zero-gravity field
06 p1119 A67-18864
Suction-preserved steady state vortex sheet on surface of infinite porous circular cylinder in viscous MHD liquid suddenly rotated about axis
06 p1046 A67-18891
Ranque effect, based on model of two-dimensional vortex flow of viscous thermally conductive gas, explains radial temperature distribution
07 p1268 A67-19352
Turbulent fluctuations in rotationally symmetrical jet, obtaining velocity profiles from integration of motion equations
09 p1490 A67-22548
Device for analyzing propagation of nonrotating jet in rotating ambient flow, noting graphs for longitudinal and tangential velocity distributions
09 p1490 A67-22594
Inviscid two-dimensional flow using extension of Hele-Shaw analogy, noting axisymmetric, compressible and MHD cases
10 p1627 A67-23554
Symmetrical jets and wakes in streaming flow with pressure gradient, noting time-mean profiles of particular pressure fields
11 p1741 A67-24047
Rotational energy diffusion in shock wave structure, examining magnitude of error in effective number of intermolecular collisions required for equilibrium
13 p2104 A67-26980
Rotating vortex flow and transition phenomena in conical diffuser
[AIAA PAPER 66-426]
14 p2240 A67-28109
Three-dimensional rotational stagnation point flow solution noting surface curvature influence
17 p2789 A67-32039
Electrical analogy calculation of incompressible and rotational axisymmetric flow around variable-circulation streamlined propeller
18 p3025 A67-33681
Flow of steady compressible gas expressed in intrinsic relations to derive equations of rotational motions in Euclidean space
19 p3212 A67-35883
Boundary between stable operation of multistage axial flow compressor and rotational flow separation region, using variational condition
21 p3689 A67-38046
Concentration distribution time for heavy gas diffusing in light gas steady flow field
22 p3917 A67-39714
Forced convective heat transfer in straight pipe rotating around parallel axis with large angular velocity
22 p3920 A67-40419
Nonlinear hydrodynamic equation term effects on rotational fluid motion in galactic plane, discussing velocity perturbations and discontinuities
22 p3893 A67-40502
Velocity and pressure distributions and flow field for laminar incompressible source flow between two coaxial parallel disks rotating at different speeds
23 p3988 A67-40602
Strong traveling transverse acoustic modes generated by rotating gas jet in cylindrical cavity
23 p3993 A67-41763
Incompressible viscous fluid rotary turbulent flow microstructure between rotating cylinders, analyzing centrifugal force effects on turbulent heat transfer processes
24 p4142 A67-42214
Hydrodynamic stability of rotating flow with cylindrical free surface requiring Rayleigh criterion satisfaction
24 p4144 A67-42568

ROTOR

SA COMPRESSOR ROTOR
SA HELICOPTER ROTOR
SA LIFTING ROTOR
SA RIGID ROTOR
SA WING
Stress concentration in annular rotor with notch /or crack/ on inner surface, using integral equation
01 p0159 A67-10276
Existence and stability of equilibrium orientations of rigid body with gyrost at in

nonuniform gravitational field 02 p0268 A67-12385
 High lift rotor design for jet propulsion VTOL aircraft 03 p0360 A67-13891
 Optimum control of motion stability of solid body with fixed point, using gyrostabilizer rotors 06 p0134 A67-18617
 Magnetic field of cylindrical permanent magnet used as rotor of electromagnetic induction pump, determining induction components and permeances to fluxes 06 p0951 A67-18685
 Sign-discriminating field mill design using one rotor and one stator 16 p2671 A67-30972
 High temperature strength and magnetic properties of cobalt-tungsten alloy for space power generator rotors 24 p4174 A67-42726

ROTOR AERODYNAMICS

Moment of aerodynamic resistance calculated for gyromotors operating in H and He, examining laminar flow near rotor 01 p0064 A67-10418
 Predicting wake-induced nonuniform flow field in plane of rotor disk [AIAA PAPER 66-17] 03 p0354 A67-12909
 Design recommendations to offset greater momenta and sensitivity to gust winds of jointless helicopter rotor 03 p0359 A67-12986
 Helicopters, Design and Engineering, Book 1, Aerodynamics 04 p0551 A67-15286
 Flow recirculation as affected by position and geometry of inducing obstacle 06 p0937 A67-17918
 Hovercraft and rotorcraft, discussing design, construction, operation and future 06 p0949 A67-18744
 Book on rotor stability self-excited vibration and nonlinear resonances 07 p1263 A67-19631
 Wind tunnel model for analysis of autorotating rotors for reentry space vehicles tested at transonic and supersonic regimes 09 p1440 A67-22285
 Influence of internal friction on high speed rotor stability using motion equation, noting bearing support flexibility and damping role [ASME PAPER 67-VIBR-14] 11 p1795 A67-24174
 Radial gas turbine losses, obtaining rotor loss coefficients, discussing flow pattern for performance prediction 12 p1891 A67-25347
 Steady and dynamic loads on tandem rotor, controls and airframe flight tested with Army helicopter, using automatic data processing 13 p2054 A67-27596
 Book on aerodynamics of V/STOL aircraft emphasizing use of momentum and finite wing theories, considering deflection of trailing vortex system 14 p2243 A67-28678
 Numerical solution for angle-of-attack distribution, downwash and motion of high-speed helicopter rotor 16 p2590 A67-30930
 Circulation control by blowing for gust insensitivity in stopped rotor aircraft application [AIAA PAPER 67-747] 23 p3933 A67-40981

ROTOR AXIS

Suspension axes defects effect on gyro motion under base angular vibration analyzed, noting large gyro drift 14 p2320 A67-28741
 Gyroscope for stabilizing inertial navigation platform 14 p2322 A67-29010
 Maneuvering stability analysis of single rotor correctable gyrocompass with fluid torsional suspension of sensitive element 15 p2490 A67-30170

ROTOR BLADE

SA HINGED ROTOR BLADE
 Pseudoshocks in pipe flow in supersonic compressors represented as diffusion process, noting application in cascade and rotor configuration 03 p0352 A67-13011
 Fiber reinforced rotor blades, discussing composite material selection for research, mass balance, dynamic response tuning and material design 03 p0453 A67-13416
 Computational model for predicting unsteady aerodynamic loads of rotor blades divided into spanwise segments 04 p0545 A67-14490
 Helicopter main rotor blade used as scanning radar antenna 04 p0579 A67-14491
 Noncavitating water flow tests of three loaded axial flow pump rotor blades [ASME PAPER 66-WA/FE-24] 04 p0607 A67-15354
 Coupling of turbomachine blade vibrations through rotor or disk in causing variations

of natural frequencies and amplitudes [ASME PAPER 66-WA/GT-5] 04 p0711 A67-15360

Vibrational problems of rotor blades in axial turbomachinery [ASME PAPER 66-WA/GT-12] 04 p0712 A67-15362

Energy method analysis of flutter instabilities in turbojet engine rotors caused by interaction between unsteady air loading and coupled vibration modes [ASME PAPER 66-WA/GT-6] 04 p0713 A67-15384

Securing packets of reaction blades in turbine rotors and casings 05 p0811 A67-16841

Vortex-rotor disk interaction effect on helicopter rotor performance in forward flight 06 p0945 A67-17907

Hingeless-rotor structural loads and dynamics research 06 p1099 A67-17911

Periodic aerodynamic loading of helicopter rotor blades approximated by principles of potential flow aerodynamics 06 p0937 A67-17914

Propeller-rotor whirl flutter and effect of hinged blades and flexible twisted blades 06 p1099 A67-17920

Tilt rotor VTOL aircraft stability, discussing results of wind tunnel tests on rotor-pylon behavior at different velocities [AIAA PAPER 67-17] 06 p0948 A67-18254

Filamentary composite of boron and epoxy applied in design optimization of helicopter blade structure, considering filament orientation and stiffness [AIAA PAPER 67-176] 06 p1102 A67-18322

Aerodynamic characteristics of forced lead-lag rotor system, noting parameters of horizontal force, rolling and/or pitching moments 09 p1437 A67-21741

Aspect ratio effect on cascade performances, noting complex variation of boundary layer thickness and changes in axial velocity ratio 09 p1437 A67-21742

Graphical analysis of rotor flutter in hover using modified Theodorsen function 09 p1573 A67-21743

Tensile residual stress measurement in area of failure origin in helicopter rotor blade, using laboratory tests and X-ray analysis [SAE PAPER 670154] 09 p1502 A67-21772

Helicopter rotor blade service life substantiation through tests with rotor excitation panels inducing blade bending moments 10 p1622 A67-23431

Aeroelastic characteristics of stowed rotor system evaluated, considering aerodynamic excitations in forward flight, wind tunnel tests, etc 11 p1744 A67-24590

Relative eddy flows mechanism in mixed flow turbomachines 12 p1891 A67-25348

Three-dimensional flow in single stage axial flow fan rotor with prescribed and variable circulation along span 12 p1893 A67-25971

Linear aerodynamic theory of rotor blades for predicting lift distribution, considering wake vortex sheet distortion 13 p2051 A67-27589

Effect of blade row interference on cascade flutter investigated using semiautuator disk method 15 p2415 A67-29314

Powered flight rotor instabilities using analysis of second-order flap-lag coupling effects of torsionally rigid blades 16 p2595 A67-30927

Rotor-hovering performance-prediction with test data showing discrepancy increase with wake contraction, blade loading, tip Mach number and blades number [AHS PAPER 100] 16 p2594 A67-31817

Rotor blade stall, comparing power, flapping motion blade bending and vibratory hub shears for illustration [AHS PAPER 101] 16 p2595 A67-31818

Helicopter rotor at high Mach numbers, noting thin blade tips and compressibility effects and tests in wind tunnel [AHS PAPER 102] 16 p2595 A67-31819

Rotor blade compressibility effects on helicopter performance, describing flight test techniques and data analyses and comparing prediction and test results [AHS PAPER 103] 16 p2595 A67-31820

Aerodynamic loads and aeroelastic divergence characteristics on stopped rotor blades in flight [AHS PAPER 104] 16 p2595 A67-31821

Radiation pattern changes for helicopter

antenna located in rotor blade as result of flight dynamics [AHS PAPER 109] 16 p2597 A67-31825

Stall flutter instability of helicopter rotor blades analysis based on unsteady aerodynamic data [AHS PAPER 130] 16 p2777 A67-31844

BO 105 light helicopter design and characteristics noting plastic rotor blades, fuselage semimonocoque construction, etc 18 p2985 A67-33642

Energy method analysis of flutter instabilities in turbojet engine rotors caused by interaction between unsteady air loading and coupled vibration modes [ASME PAPER 66-WA/GT-6] 18 p3115 A67-34130

Circulation control rotor blades of circular or elliptical cross section for helicopters, VTOL and STOL and possible application to aircraft 18 p2987 A67-34707

Resonant vibrations in rotating blades with hinged joints analyzed for small and large damping values, determining damping coefficient 19 p3235 A67-34883

High lift coefficient production on helicopter rotor blades and application of circulation control by blowing 19 p3170 A67-35519

Three-dimensional flow in axial fan, consisting of rotor only, having finite number of blades, by method of isolated airfoil of finite span 19 p3171 A67-35712

Three-dimensional flow through rotor of single stage axial fan with prescribed spanwise variable circulation 19 p3171 A67-35714

Three-dimensional vortex flow inverse problem through axial fan solved using isolated airfoil method 19 p3171 A67-35723

Aerodynamic forces and pressure on wing model for Carafoli type MHT-C-04-10 profile characteristics, discussing applications to blade rotors 20 p3355 A67-36193

Rotor blade airload and dynamic response of large tandem rotor helicopter measured, using computer programs methods 20 p3536 A67-36462

Direct and inverse method of calculating rotating cascades with infinite number of blades and radial flow to enhance convergence 20 p3360 A67-37597

Lift reduction and increase of helicopter maximum speed by controlling optimum angle of attack of rotor blades over surface of revolution 22 p3744 A67-39548

Nondestructive inspection of composite structures in helicopter rotor blades, discussing structure, loading and quality control capability 22 p3812 A67-39857

Boundary layer control by suction at trailing edge to reduce profile drag of helicopter rotor blades 22 p3742 A67-40133

Helicopter maximum speed increase using rotor with controlled blade oscillation motion, studying flow velocity, distribution and asymmetry elimination 23 p3933 A67-40639

Coupling of turbomachine blade vibrations through rotor or disk in causing variations of natural frequencies and amplitudes [ASME PAPER 66-WA/GT-5] 24 p4251 A67-42461

Noncavitating water flow tests of three loaded axial flow pump rotor blades [ASME PAPER 66-WA/FE-24] 24 p4143 A67-42465

ROTOR DISK

Disk structural characteristics influence on rotors critical angular velocity 19 p3235 A67-34881

Spline friction effect on multiple disk brake and clutch packs, including torque and load variation and pressure distribution equations [ASME PAPER 67-LUB-26] 24 p4164 A67-42684

ROTOR GYROSCOPE

SA FLUID ROTOR GYROSCOPE
 Rodrigues-Hamilton and Cayley-Klein parameters used in applied theory of gyroscopes 01 p0068 A67-10989

Gyroscope rotor configuration using barium ferrite magnets and axial rotor magnetization 02 p0184 A67-12411

Gyro as force sensor in instrumentation systems, discussing types, testing and calibration procedures 04 p0628 A67-15732

Small helicopter flight test report, discussing testing procedures on 14 models

of one-man rotorcraft
[AIAA PAPER 67-264] 07 p1129 A67-20041
Frequency response, equation of motion,
elastic restraint and structural flexibility of
gyroscopic vibration absorber, noting
antiresonant frequency functions
[ASME PAPER 67-VIBR-13] 11 p1795 A67-24173
Sensor stability conditions for two rotor
gyrocompass on sea-going ship turning in
circle 13 p2118 A67-26373
Rotor bearing clearance effects on
whirling of gimbal-mounted
gyroscope 14 p2328 A67-29004
Gyroscope for stabilizing inertial
navigation platform 14 p2322 A67-29010
Motion equations of heavy symmetrical
gyroscope in gimbal suspension, noting
integrals of second 15 p2490 A67-30174
approximation 15 p2490 A67-30174
Stability of motion of symmetrical rotor
gyrostat about fixed point on rotating earth
18 p3078 A67-33555
Free-rotor gyros active damping evaluated
through experimental studies 19 p3233 A67-35986
Stationary motion stability of gyrostat
satellite in Newtonian force field, defining
body position in coordinate system 24 p4241 A67-42400

ROTOR LIFT
VTOL aircraft configurations features and
characteristics including helicopter,
compound, composite, tilt-wing, lift-fan,
lift/cruise and lift engine
[SAE PAPER 670686] 24 p4093 A67-41987

ROTOR SPEED
Helicopter rotor at high Mach numbers,
noting thin blade tips and compressibility
effects and tests in wind tunnel
[AHS PAPER 102] 16 p2595 A67-31819
Helicopter maximum speed increase by
generating supplementary forward thrust or
additional wings 22 p3744 A67-39540
Aircraft engine turbine structure effect on
blade tip clearance, analyzing clearance
variations as function of rotor angular
velocity 22 p3868 A67-39546
Lift reduction and increase of helicopter
maximum speed by controlling optimum
angle of attack of rotor blades over surface
of revolution 22 p3744 A67-39548
Helicopter maximum speed increase using
rotor with controlled blade oscillation
motion, studying flow velocity, distribution
and asymmetry elimination 23 p3933 A67-40639

ROTOR SYSTEM
Spring theory of ball bearing supporting
rotor and role in vibration analysis of
system 02 p0248 A67-11468
Imbalance of elastically deformed rotor
after starting only once with trial load,
noting role of oscillation modes of
rotor 03 p0528 A67-14078
Flights tests of XH-51A compound
helicopter, discussing rigid rotor concept
and results of compound flight research
program [AIAA PAPER 67-262] 07 p1130 A67-20075
Fluid film and rolling element bearings
effect on turbomachinery rotor dynamics
including critical speeds, imbalance
response, instability, turbulence, etc
[SAE PAPER 670059] 09 p1508 A67-22533
Helicopter design noting speed,
maneuverability, handling, carrying capacity
and disk loading 11 p1743 A67-23993
Unbalanced rotor deceleration through
critical speed tested, considering maximum
deflection increment and bending stress in
rotor shaft [ASME PAPER 67-VIBR-17] 11 p1796 A67-24176
Unbalance vibration of rotor analyzed for
application to rotor bearing system with
dynamic forces represented by spring and
damping coefficients [ASME PAPER 67-VIBR-27] 11 p1796 A67-24185
Rotor supported in fluid film journal
bearings, eliminating self-excited vibrations
through motion equation [ASME PAPER 67-VIBR-28] 11 p1797 A67-24186
Trapped fluid effect on high speed rotor
vibration, discussing asynchronous and
synchronous whirl for fully and partially
wetted cavities [ASME PAPER 67-VIBR-29] 11 p1797 A67-24187

Aeroelastic characteristics of stowed rotor
system evaluated, considering aerodynamic
excitations in forward flight, wind tunnel
tests, etc 11 p1744 A67-24590
High speed radial turbine rotor
temperature distribution measured for
pattern prediction of temperature 12 p1988 A67-25354
Bearing mounted shaft-rotor system noting
harmonic and stable whirl characteristics 12 p1949 A67-25409
Turbomachine rotating shaft and rotor
systems critical speeds taking into account
bearing support stiffness and clearances,
noting vibration mode 12 p1949 A67-25410
Single-rotor gyrocompass motion during
rocking, determining equilibrium point
displacement 12 p1941 A67-25662
Evaluation facility for rotor
containment/control devices [SAE PAPER 670332] 12 p1925 A67-25873
Three-dimensional flow in single stage
axial flow fan rotor with prescribed and
variable circulation along span 12 p1893 A67-25971
Stability of motions of satellite with rotor
and cavity with liquid, reducing problem to
solution of minimum change in potential
energy of system 13 p2213 A67-27319
Dynamic analysis of rotor motion of rigid
system in hovering state using complex
variables 13 p2054 A67-27588
Commercial rotor VTOL for economic
intercity transportation, discussing time-
frame and design requirements and
analyzing improvement factors [AIAA PAPER 67-410] 15 p2422 A67-30377
VTOL aircraft with rotor or propeller lift
systems for commercial transportation,
discussing helicopter role in system
development [AIAA PAPER 67-411] 15 p2422 A67-30378
Dynamic imbalance of rotors determined
and eliminated using angular oscillation and
electrical erosion techniques 16 p2681 A67-30469
Powered flight rotor instabilities using
analysis of second-order flap-lag coupling
effects of torsionally rigid blades 16 p2595 A67-30927
Aerodynamic loads and aeroelastic
divergence characteristics on stopped rotor
blades in flight [AHS PAPER 104] 16 p2595 A67-31821
Structural design, analysis and tests
pertaining to hot cycle rotor system used on
XV-9A aircraft [AHS PAPER 121] 16 p2598 A67-31836
Gyro-controlled rigid rotor system
performance, noting steady state and
transient response to various excitation
[AHS PAPER 131] 16 p2599 A67-31845
Effect of rotor control feedback loads of
two-bladed rotor system on helicopter
fuselage vibrations [AHS PAPER 133] 16 p2777 A67-31847
Rotor system with blade angle reverse
control noting blade-angle adjustment
changes for achievement of higher flight
speeds 18 p2985 A67-33460
Dynamic modeling of complex rotor
system to determine critical velocities,
noting influence of number of mass
concentrations on accuracy 21 p3689 A67-37951
Rotor bearing stability, describing
incompressible and compressible fluid film
bearings, calculating thresholds of
instability 21 p3632 A67-38136
Multirotor trochoidal engines external
balancing problems, discussing cam
distribution and shaft shape 21 p3696 A67-38910
Heat treatment effects on mechanical
properties of steel-forged gas turbine rotor
shafts, including microcracks formation and
growth and structural strength 22 p3819 A67-39323
Combat helicopters with reference to
Huey/Cobra noting stub wings, armor
protection, rotor and weapon systems 23 p3932 A67-40619
Gas bearing Brayton cycle turboalternator
rotor system stability and dynamic response
to electromagnet forces 24 p4102 A67-42487
Rotor VTOL aircraft for future transport
noting rotor systems for low downwash
velocity, minimum noise and low fuel
consumption [AIAA PAPER 67-940] 24 p4097 A67-43030

ROTORCRAFT HELICOPTER
SA TANDEM-ROTOR HELICOPTER
Rotorcraft technology developments and
possible improvements by mid-1970s 11 p1744 A67-24589
Structural reliability of fatigue loaded
rotorcraft estimated through S-N and
spectrum testing [AHS PAPER 123] 16 p2777 A67-31838

ROUGHNESS
SA SURFACE ROUGHNESS
Cloud vorticity effects on ocean
roughness, from Tiros autumnal
observations 04 p0651 A67-15469
Size and shape of roughness projections
effect on resistance coefficient during
turbulent pipe flow in transverse magnetic
field 06 p1044 A67-18690

ROUND-TRIP TRAJECTORY
Earth-Mars round-trip flight maximum
payload delivery variational problem,
determining optimum trajectories and
minimum flight time dependence on engine
parameters 17 p2941 A67-32240

ROVER PROJECT
Rover testing facilities of Nuclear Rocket
Development Station in Nevada
[AIAA PAPER 66-1003] 03 p0397 A67-14148
Project Rover liquid hydrogen
safety 13 p2092 A67-27650
NERVA engine development, discussing
NRX tests and Phoebus reactor tests for
high temperature and power
operation 20 p3482 A67-36571

ROVING
SA LUNAR ROVING VEHICLE /LRV/
Roving machine for impregnating glass
fibers with synthetic resins 06 p1007 A67-18023

ROYAL ZONE
S SUNSPOT

RUBBER
SA LATEX
SA SILICONE RUBBER
SA SYNTHETIC RUBBER
Elasticity parameters for finite static
deformations of rubber-like materials, noting
natural and latex rubber 01 p0161 A67-10797
Torsional creep measurements on natural
rubber vulcanizates cross linked to various
degrees complement studies on stress
relaxation behavior and dynamic mechanical
response 06 p1020 A67-17869
High polymer rubber, plastic, and textile
qualitative and quantitative properties, uses
in space environment 13 p2143 A67-26698
Strain-energy function of hyperelastic
material in terms of extension ratios, with
natural rubber as example 18 p3145 A67-34642
Free energy of polymer solid consisting of
entangled long chain molecules when
deformed by elastic strain 22 p3826 A67-40201

RUBIDIUM
Spin echo and free decay signals in
Rubidium optical pumping analyzed, using
pulse method and light modulation
technique 04 p0632 A67-14770
Crossed molecular beam kinetics of
reactive asymmetry of oriented methyl
iodide polar molecules reacting with
rubidium 06 p0955 A67-17831
General relations for amplification and
oscillation development in optically pumped
alkali vapor maser derived and applied to
rubidium 85 15 p2501 A67-30095
Rubidium vapor magnetometer used for
near earth orbiting spacecraft,
instrumentation and in-flight
performance 20 p3443 A67-36513
Small alternating magnetic field
modulation effects on sampled output of
rubidium magnetometer with frequency
counter 20 p3448 A67-36876
Chondrites solidification age measured via
rubidium-strontium pairs in component
minerals, using phase separation
method 21 p3702 A67-38125
Strontium and rubidium 87 measurements
on iron meteorite silicate inclusions, with
age determination at 4.4 to 4.8 billion
years 22 p3881 A67-39495
Optically pumped Rb in collisions with Kr
inducing relaxation, noting two different
correlation times due to kinetic collisions
and metastable states present 23 p4012 A67-40792

RUBIDIUM COMPOUND
Molecular beam electric resonance
/MBER/ spectrometer for hyperfine

structure of rubidium fluoride 11 p1821 A67-23961
 Rubidium nickel trifluoride transparent single crystal magnetic and optical properties analyzed, concluding compound is antiferromagnetic 12 p1984 A67-25747
 Atomic frequency standards based on rubidium gas cell approach, noting atomic clock types and applications 15 p2487 A67-29582
 Absolute reflectance of RbI and KI between 300 and 77 degrees K, noting spin orbit interaction effects and values of dielectric parameters 15 p2520 A67-29768
 Luminescence decay kinetics of trivalent Nd ions in antiferromagnetic Rb manganese fluoride, showing mechanism of transfer process of excitation energy of Mn ions 20 p3506 A67-36218

RUBIS ROCKET

Design and instrumentation of Rubis research rocket payload for analysis of geomagnetic and electric fields 04 p0703 A67-14565
 Design and instrumentation of Rubis research rocket payload for analysis of geomagnetic and electric fields 07 p1258 A67-19572
 French Rubis rocket flight noting high altitude barium release experiment, high energy proton and electron measurements, etc 16 p2738 A67-31017
 Launching and ballistic flight of Rubis IV rocket, discussing scientific preparation and payload testing 24 p4241 A67-42573

RUBY

Microwave mixing in paramagnetic crystal using traveling wave maser with ruby as mixer element, noting frequency conversion 01 p0086 A67-10003
 Nonemissive multiphonon transitions and quantum yield for ruby R line 03 p0433 A67-12852
 Chromium ion concentration and temperature effects on spin-lattice relaxation times in ruby at liquid He temperatures in zero magnetic field 05 p0817 A67-16637
 Energy transfer from single chromium ions to closely coupled pairs of chromium ions in ruby 05 p0862 A67-16659
 Ruby crystals grown by Czochralski technique using induction heated iridium crucible, noting laser oscillations in pulled crystals 05 p0866 A67-16975
 Adiabatic demagnetization of ruby to obtain cryogenic temperatures 06 p1047 A67-17760
 X-band ruby maser design with liquid hydrogen cooling for high gain at low pumping power 07 p1194 A67-19131
 Energy transfer from single chromium ions to closely coupled pairs of chromium ions in ruby 07 p1234 A67-20124
 Research and development for better manufacturing emphasizing hydrothermal growth of ruby crystal 09 p1505 A67-22143
 Nonexponential electron spin cross relaxation measurement in dilute ruby 17 p2924 A67-33369
 Optical methods used for study of ruby crystals uniformity, discussing Twyman interferometer design 18 p3098 A67-33576
 Chromium oxide addition effect on ruby recrystallization in carbonate and bicarbonate solutions under hydrothermal conditions, estimating chromic oxide solubility 21 p3685 A67-38971
 Czochralski ruby shows high inversion ratio when used as microwave maser material 24 p4205 A67-42813

RUBY LASER

Properties of uranyl-doped glass for application as saturable optical filter for use with lasers 01 p0032 A67-10009
 Polymethylmethacrylate and polystyrene exposure to ruby and neodymium-glass laser radiation, noting appearance of EPR 01 p0086 A67-10075
 CW laser using 3-inch ruby crystals with 15 percent mirror transmission, pumping power of double threshold value and 1.6 watt power output 01 p0088 A67-10244
 Approximate absolute values of pumping power, threshold power and critical excess population for ruby laser determined from relative flash tube intensity measurements 01 p0088 A67-10245
 Scattered light spectrum in thetatron plasma, noting onset of ion wave instability 01 p0121 A67-10248

Intensity dependent frequency shift in spectral output of monochromatic giant pulse lasers measured, using Fabry-Perot interferometer 01 p0088 A67-10251
 Q-switching of ruby laser using cell containing chloroaluminum phthalocyanine in chloronaphthalene to obtain giant pulses 01 p0089 A67-10448
 Molecular spectroscopy of illumination effects on cobalt activated ZnS exposed to ruby laser pulses 01 p0090 A67-10683
 Ruby laser with scattering induced feedback and absence of resonance type oscillations 01 p0090 A67-10740
 Coupling mechanism in passive Q-switching operation between filaments at different regions of ruby laser rod 01 p0090 A67-10813
 Narrow beam divergent Q-switched laser pulse generation, noting output characteristics and applications 01 p0091 A67-11024

Laser saturation of photoconductivity and determination of imperfection parameters in sensitive photoconductors such as single crystal of cadmium 02 p0251 A67-11879
 Output characteristics of half-wave mode Kerr cell ruby oscillator used as optical radar for clear air turbulence /CAT/ detection 02 p0198 A67-12053
 Ruby laser with liquid filter, considering relation between filter efficiency and absorption curve parameters when acting as Q-factor modulator 02 p0252 A67-12423

Self-focusing of ruby laser beam in NaCl crystals 02 p0252 A67-12481
 Q-spilling of ruby laser by optical pumping in intense inhomogeneous magnetic field with reduced gain 02 p0253 A67-12505
 Losses in ruby laser determined from data on variations in beam divergence angle and variations in lasing spot diameter 02 p0254 A67-12742
 Ruby laser pumping threshold energy, divergence angle and output power as affected by resonator length 03 p0433 A67-12855

Ruby laser frequency conversion technique by laser beam scattering and mixing of combined frequencies 03 p0433 A67-13094
 Ruby laser generation from two R lines by prismatic light dispersion in resonator 03 p0433 A67-13095
 Volume density of heat sources in ruby laser rod by numerical integration of pumping and absorption spectra 03 p0434 A67-13117
 Fracture mechanism of transparent crystals interacting with ruby laser beam 03 p0435 A67-13128

Linear phase distortions of plane resonator with tilted mirrors and effects on generation of stimulated emission in ruby crystal laser 03 p0435 A67-13130
 Luminescence in cadmium sulfide mixed crystals of widely varying composition in presence of excitation by ruby laser emission 03 p0436 A67-13153
 Spontaneous emission in inversely populated medium examined for uniform ruby rod laser with uniform pumping distribution 03 p0438 A67-14186
 Stimulated Stokes emissions from Raman active media observed by using Q-switched ruby laser which emits multiple pulse in each shot 04 p0632 A67-14765

Ruby laser as energy source for measuring thermophysical properties of materials via flash technique 04 p0623 A67-15305
 Modular liquid-cooled cylindrical ruby laser microwelder design and construction 04 p0628 A67-15310
 Multigigawatt oscillator-amplifier ruby laser system for high temperature plasma research [ASME PAPER 66-WA/ENER-2] 04 p0634 A67-15371

Population inversion variation during laser emission as shown by measurements of fluorescence intensity 04 p0634 A67-15497
 Abrupt transmission change during ruby laser emission resulting from pumping with xenon flash lamp 04 p0634 A67-15649

Degenerate stimulated four-photon interaction and four-wave parametric amplification observed in ruby laser and liquid cell arrangements 05 p0844 A67-16379
 Photodetachment probability for Cs and negative I due to simultaneous absorption of two ruby quanta 05 p0815 A67-16627
 Semiclassical and rate equations compared for determination of output power of steady state ruby laser 05 p0815 A67-16628

Ruby laser with nonresonant feedback due to radiation scattering, showing use as optical frequency standard 05 p0818 A67-16642
 Electron density, optical thickness and temperature of ruby laser-induced carbon plasma 05 p0852 A67-16654
 Loss measurement for ruby laser resonant cavity, comparing thresholds for R sub 1 and R sub 2 line operation 05 p0819 A67-16655
 Optically pumped ruby noting absorption and emission spectrum, transition stages and phonon terminated amplification 05 p0820 A67-16658
 Output spectra of Nd doped YAG and ruby lasers, determining mechanisms responsible for observed overall linewidths 05 p0820 A67-16660
 Q-switched ruby laser configuration with feedback control, noting frequency and instability correlation with theoretical results obtained from mathematical model 05 p0822 A67-16676
 Saturable optical absorption of light flux from high intensity Q-switched ruby laser 05 p0822 A67-16677
 Quenching of one pulsed ruby laser oscillation by another, noting coupled rate equations for steady state and transient behavior 05 p0823 A67-16682
 Optical heterodyne technique detecting stimulated Brillouin scattering, noting frequency shift demodulation arising from ruby laser light incidence on quartz crystal 05 p0823 A67-16688
 Holographic study of second harmonic wave emitted by ruby laser, examining influence of defects of spatial coherence of wave 05 p0808 A67-17322
 Ruby and neodymium glass lasers sum frequency generation using nonlinear electro-optical KDP crystal 06 p1009 A67-17754
 Semiconductor mirror for Q-factor modulation of laser resonator 06 p1012 A67-18789

Laser application to meteorology, discussing Rayleigh, aerosol and Raman scattering, system configuration and measurement problems 07 p1194 A67-19091

High altitude atmospheric scattering of intense light from ruby laser beam interpreted principally in terms of Rayleigh scattering from atmospheric molecules 07 p1171 A67-19419
 Sum radiation frequency generation by ruby and neodymium lasers in KDP crystals 07 p1196 A67-19734
 Wave interaction in saturable absorbers, noting hole burning in dye switched ruby laser 07 p1234 A67-20094
 Ruby laser mode locking and mode competition using RG-8 filter as passive modulator 07 p1197 A67-20147
 Ruby laser-induced effect of pulsed pressure on KDP crystal surface and thermal bulk effect on excitation of ultrasonic oscillation in crystal 08 p1337 A67-20417
 Ruby laser irradiation by similar laser situated at right angle to first results in radiation intensity reduction of irradiated laser 08 p1338 A67-21204
 Calorimetric measurement of pulsed ruby laser output energy 09 p1510 A67-21615
 Time dependent behavior of laser pumped ruby maser at low temperature 09 p1511 A67-21765
 Gallium arsenide laser pumped by Stokes component of induced Raman scattering in liquid nitrogen of Q-modulated ruby laser light 09 p1512 A67-21973
 Laser equipment for fusion welding of aerospace structural materials, examining ruby laser properties, flash tube and overall system 09 p1504 A67-22141
 Control of laser action, noting feedback theory conception and geometrical optics of laser modulation 09 p1513 A67-22146
 Ruby laser efficiency increase, using gamma irradiation 09 p1515 A67-22430
 Ruby laser cavity losses measurement by Fabry-Perot resonance 10 p1662 A67-22740
 Pressure scanned Fabry-Perot etalon for measuring ruby line widths at room temperature 10 p1662 A67-22741
 Flash spectroscopy apparatus with Q-switched ruby laser, discussing molecular electronic excitation 10 p1663 A67-22854
 Luminescence in cadmium sulfide mixed

- crystals of widely varying composition in presence of excitation by ruby laser emission 10 p1664 A67-23102
- Dependence of intrinsic noise temperature of ruby reflection maser on helium bath temperature and chromium trioxide doping, using circulator 10 p1665 A67-23505
- Frequency temperature dependence of longitudinal and transverse hypersonic wave absorption coefficients in quartz and artificial ruby crystal 10 p1693 A67-23582
- Giant pulse generation range in transverse direction after Q-switching in ruby laser, examining resonator properties 10 p1666 A67-23584
- Pulsed ruby laser source for holography compared to He-Ne gas laser 10 p1657 A67-23625
- Beam wavelength and laser intensity effect on attenuation in carbon disulfide induced by ruby laser indicate two-photon absorption 10 p1667 A67-23776
- Measuring method for beam divergence of Q-switched ruby laser rods 10 p1667 A67-23782
- Ruby maser operating with microrefrigerator at low temperature, noting broadband and bandwidth 11 p1800 A67-24467
- Molecular spectroscopy of illumination effects on cobalt activated ZnS exposed to ruby laser pulses 11 p1804 A67-25072
- Doped alkali-halogen-crystal color center origin and transformation at liquid N temperature using ruby laser, noting temporary bleaching 12 p1951 A67-25200
- Ruby laser generation spectrum width analyzed interferometrically as function of mirror spacing and pumping power 12 p1952 A67-25325
- Pulsed ruby laser to obtain Fourier holograms in light reflected from diffusely scattering objects, discussing relaxation of resolving power of photographic emulsions 12 p1939 A67-25335
- Emission spectrum of single and multicomponent ruby laser, observing decrease in number of modes during transition from solid to multielement instrument 12 p1952 A67-25436
- Premature generation breakdown in ruby laser, noting effect of additional media on pumping level/generation time ratio 12 p1953 A67-25445
- Lunar figure and orbit parameters measured by optical location method 12 p2002 A67-25647
- Oscillation effect on power and time characteristics of ruby laser output with variable threshold ratios of axial and inner radiation modes 13 p2125 A67-26398
- Time resolution amplification of flash spectroscopy apparatus equipped with switched laser 13 p2126 A67-26599
- Ruby laser with scattering induced feedback and absence of resonance type oscillations 13 p2126 A67-26769
- Spatial modulation in populations of optically pumped ruby investigated for possible application to analysis of space and time distribution of laser beam 13 p2126 A67-26860
- Ruby maser with two synchronous symmetrical quarter-wave-coupled cavities, noting frequency gain 13 p2128 A67-27227
- P-type GaAs laser excited by Q-switched ruby laser at liquid nitrogen temperature, noting spectral shift due to Burstein effect 14 p2329 A67-27831
- Laser measurements and standards of energy, power, attenuation and frequency stability, using pulsed ruby and gas lasers as radiation source 14 p2319 A67-28392
- CW solid state lasers, considering principal laser crystals 14 p2330 A67-28470
- Ruby laser with Fabry-Perot interferometer selector studied for wavelength and thermal stability control 14 p2332 A67-28759
- Trajectory systems, discussing atomic clock and laser based equipment design, operation and performance [ONERA-TP-446] 15 p2554 A67-29376
- Electron spin resonance measurement of ground state population in ruby rod during optical pumping 15 p2497 A67-29389
- Double sapphire plate resonator to control multiple modes of commercial laser /Korad K-1Q/ without use of saturable dye 15 p2498 A67-29497
- Gaussian and Lorentzian components separation in analyzing EPR spectrum in ruby, using variance techniques 15 p2536 A67-29499
- Generation of large pulses of extremely short duration in ruby laser by rotating mirror technique at lower frequencies 15 p2498 A67-29642
- Threshold temperature variation, output power and emission spectrum of short ruby crystals operated in quasi-continuous mode 15 p2498 A67-29665
- Radiation polarization in ruby laser with resonator shaped like rectangular parallelepiped 15 p2499 A67-29701
- Temperature measurement of ruby laser rods during pulsed pumping from birefringence dependence on temperature and resulting thermoelastic stresses 15 p2499 A67-29721
- Internal and coupling modulation and mode locking of continuous ruby laser 15 p2499 A67-29729
- Measurement of position of polarization plane of radiation emitted by neodymium-glass laser 15 p2499 A67-29758
- Angular distribution of laser radiation and variation in beam direction of stimulated radiation as function of misadjustment angle of resonator mirrors 15 p2500 A67-29759
- Output energy for ruby laser with parallel mirrors for varying excitation energies, pulse lengths, mirror reflectivities and losses due to absorption, scattering and reflection 15 p2502 A67-30427
- Direct lasing of conventional ruby rods requiring 200-joule xenon pump deriving energy from chemical reaction 15 p2502 A67-30437
- Laser action of ruby and neodymium glass rods in case of axicon pumping 16 p2684 A67-30460
- Laser beam study by interferometric technique using diverging spherical comparison wave noting interference patterns 16 p2685 A67-31032
- Output noise power spectrum properties of X-band ruby maser oscillator, noting frequency dependence on electromagnetic energy and cavity losses 16 p2685 A67-31055
- Ruby laser light scattering by theta pinch plasma measured with Fabry-Perot spectrometer, noting cooperative density fluctuations superimposed on thermal density fluctuations 17 p2899 A67-32274
- Spectroscopic observation of ion wings produced by plasma ion oscillations in laser produced plasma 17 p2901 A67-32368
- Confocal ruby laser mode structure analyzed for relation between mode number and spiking regularity, noting frequency hopping 17 p2867 A67-32402
- Gaseous chemical reaction dynamics analyzed with monochromatic laser light-induced photocatalysis 17 p2868 A67-32772
- Ruby laser radiation transmission by Crofon plastic fiber optics 17 p2870 A67-33302
- Gallium arsenide laser pumped by Stokes component of induced Raman scattering in liquid nitrogen of Q-modulated ruby laser light 17 p2870 A67-33310
- Generation of giant pulses of coherent radiation by rotating-mirror technique and by passive Q-switch using cryptocyanine 17 p2871 A67-33390
- Spatial coherence and shape of emission wave front of giant pulse from ruby laser with Pockels cell shutter 18 p3058 A67-33526
- Thomson scattering of Q-switched ruby laser beam in shock wave plasma, determining electron densities, spectral distribution of scattered light, etc 18 p3084 A67-33649
- Semiconductor mirror for Q-factor modulation of laser resonator 18 p3059 A67-33731
- Optical parametric oscillator with ruby laser pumping, noting values of electro-optic and rotational tuning 18 p3059 A67-34011
- Bipolar Ni-Cd cells for ruby lasers and power sources to yield high energy pulses for firing pyrotechnic devices 19 p3175 A67-34803
- Argon, deuterium and air ionization at atmospheric pressure and lower by focused ruby laser radiation, analyzing plasma spectrum 19 p3239 A67-35166
- Transmission decrease of various aqueous solutions under ruby laser irradiation 19 p3240 A67-35420
- Photoelectric recording of Raman spectra excited by ruby laser 19 p3240 A67-35546
- Spherical interferometers used in measuring time-resolved spectra of ruby laser relaxation oscillations 19 p3241 A67-35804
- Spectral-line narrowing in ruby laser during standing wave field displacement with respect to active center of ruby crystal 19 p3241 A67-36023
- Plasma production by ruby laser beam irradiation of lithium hydride particle, measuring electron temperatures 20 p3496 A67-36212
- Absorption spectra, spectral dependence of luminescence quantum output, glow curves and radiation spectra of color centers in ruby crystal 20 p3506 A67-36223
- Appearance of extraordinary rays from double refraction in ruby laser crystals with polished rectangular prisms 20 p3507 A67-36330
- Chromium distribution in laser rubies with neutron activation autoradiography 20 p3458 A67-36427
- Book on lasers and application to long distance terrestrial or space communications system 20 p3459 A67-36639
- Laser induced gas electrical breakdown theories, predicting high threshold field strengths invalidated by single mode, phase-locked and laser measurements 20 p3459 A67-36851
- Spectral variations resulting from thermal processes in crystals subjected to focused ruby laser beam 20 p3460 A67-37146
- Self-focusing of laser light pulses in ruby and leucosapphire crystals, noting different damage forms for fundamental and second harmonics 21 p3639 A67-38094
- Laser welding and welding processes noting evolution as specialized tool to supplement present welding equipment 21 p3635 A67-38622
- Optical interferometer for refractive plasma diagnosis, noting Q-switched ruby laser and pulsed arc lamp 21 p3630 A67-38768
- Premature generation breakdown in ruby laser, noting effect of additional media on pumping level/generation time ratio 21 p3642 A67-38819
- Crystal block structure and slip plane influence on laser radiation, discussing radiation energy distribution in space and divergence determination 21 p3642 A67-38968
- Photoconductivity in cadmium sulfide crystals induced by light from ruby laser with Q-factor modulation, showing photocurrent dependence on laser power 22 p3814 A67-39511
- IR laser rangefinder using neodymium doped rods, noting noise peak value and advantages over ruby laser 22 p3799 A67-39780
- Rare gas isotopic analysis using ruby pulsed laser and mass spectrometer 22 p3816 A67-40241
- Ruby rods in concentric spherical cavities observing spiking, mode structure and output energy distribution 22 p3817 A67-40485
- Giant pulse ruby laser having tunable two-frequency output noting spectral measurements made with Fabry-Perot interferometer 23 p4015 A67-41038
- 50 Hz ruby pulse laser emission, discussing power output, electromagnetic spectrum and transverse mode interaction 23 p4016 A67-41153
- Optically concentrated laser radiation beam properties using plane and spherical faced ruby resonators 23 p4016 A67-41322
- Giant pulse irradiation effect on ruby laser under oscillation quenching, amplification and characteristics changes in metastable state population 23 p4017 A67-41434
- Numerically computed power outputs and efficiency of continuous room temperature ruby lasers in good agreement with theoretical model 23 p4017 A67-41465
- Radiation polarization in ruby laser with resonator shaped like rectangular parallelepiped 24 p4166 A67-41771
- Radiation field asymmetry and anomalous beam angle divergence of ruby lasers linked to dislocations in ruby crystals prepared by Verneuil method 24 p4166 A67-42070
- Electrification of single crystals of semiconductor compounds of AIIIBVI and AIIIBV type after exposure to ruby laser pulses 24 p4167 A67-42164
- Longitudinal mode generation in ruby

laser emission operating in single pulse regime with resonant mirror reflector 24 p4169 A67-42894

RUDDER

Beryllium rudder and structures for F-4C aircraft, discussing weight factor, analysis, design, fabrication, ground tests and fail-safe flight test programs [SAE PAPER 680666] 01 p0094 A67-10574
Wind tunnel investigation of effect of ground level on static aerodynamic characteristics of sideslip for rectangular and delta wing with rudder assembly 07 p1126 A67-19886

RULE

S INSTRUMENT FLIGHT RULE /IFR/ S REGULATION

RUMANIA

Rumanian space research in meteorology, fluid mechanics, space medicine, etc 19 p3321 A67-35305

RUNGE-KUTTA INTEGRATION

Stability and error analysis of Runge-Kutta-Fehlberg numerical integration method 04 p0645 A67-14986
Multistep generalization of Runge-Kutta methods with four or five stages 07 p1218 A67-20198
Free parameters in third and fourth order pseudo-Runge-Kutta methods involving two points 07 p1218 A67-20215
Solutions of fifth order Runge-Kutta equations 08 p1347 A67-20369
Solid particle drag, convective heat transfer and ablation effects on structure of normal shock wave in nonreacting mixture of gas and ablating dust, using Runge-Kutta integration 08 p1427 A67-21120
Stability of fourth order Runge-Kutta method for solving differential equation 08 p1349 A67-21259
Numerical values of coefficients for four different implicit Runge-Kutta formulas 13 p2146 A67-26743
Horseshoe-shaped orbits in Jupiter-sun restricted problem, comparing Runge-Kutta and Steffensen integration methods 13 p2205 A67-27475
Perturbation theory methods as applied to first order differential equation 15 p2560 A67-30041
Runge-Kutta-Fehlberg method for systems of ordinary first and second order differential equations applied to numerical solution of many-body problem 15 p2561 A67-30052
Numerical solutions to differential equations governing earth electric field near surface obtained by Runge-Kutta method 16 p2664 A67-30974
Digital analog simulation program for IBM 7040 based on signal flow diagram, noting use of Runge-Kutta integration method 17 p2821 A67-32803
Runge-Kutta integrations for all seasons by proceeding in blocks of N steps compared to predictor-corrector methods 21 p3652 A67-38173
Runge-Kutta method applied to Fredholm type integrodifferential equations 21 p3653 A67-38421
Natural frequencies and shape of axisymmetric oscillations of thin spherical shell under initial stress calculated via boundary value problem, using computer method 21 p3725 A67-38791
Strength of synchronous rotation of moon in terms of upper and lower limits on rotational period, using Runge-Kutta integration 22 p3885 A67-39978

RUNWAY

SA LANDING AID
Airport traffic control tower instrument panel displaying continuously telemetered data on current weather conditions of runway complex 10 p1656 A67-23087
Roughness data and statistical analysis of off-runway landing areas in Canada, using aerial photography for profile measurement 10 p1622 A67-23388
Philadelphia air transportation, discussing runway construction program, passenger terminal, automated cargo handling, etc 21 p3608 A67-38804

RUNWAY CONDITION

Concrete pavement performance at ten civil airports, examining durability of surfaces, jointing subbase thickness and maintenance 02 p0229 A67-11841
Perturbation technique used to study random response of airplanes to effect of

runway roughness 08 p1279 A67-20480
Soft gravel and aerated concrete material of various sizes tested to safely decelerate aircraft overshooting runway during takeoff and landing 14 p2246 A67-28817
Aircraft flotation requirements, emphasizing surface strength reduction 17 p2832 A67-31986
Ground requirements for instrument landing systems noting approach lighting, runway marking, taxi guidance and blind navigation [AIAA PAPER 67-756] 23 p3933 A67-40989

RUNWAY LIGHT

Houston Intercontinental airport planning and development for supersonic jet, superjet and SST aircraft 22 p3779 A67-39374

RUPTURE

S FAILURE
S FATIGUE
S STRESS RUPTURE

RUTHENIUM

Luminescence from ruthenium complexes, investigating charge-transfer absorption bands 19 p3181 A67-35880

RUTILE

Chromium-doped rutile suitability as active material in solid state maser resonator 01 p0088 A67-10246
Electroabsorption measurements on rutile in clarifying band structure and dichroic nature at absorption edge 01 p0131 A67-10339
Quantum paramagnetic traveling wave amplifier using rutile with admixture of chromium and combined with magnet with superconducting coil 05 p0825 A67-17161
L-band rutile traveling wave maser, discussing slowing factor and inverted susceptibility 09 p1514 A67-22270
Rutile in meteorites, noting presence of titanium oxide as result of electron microprobe studies 14 p2386 A67-28476

RYAN MILITARY AIRCRAFT

S XC-142 AIRCRAFT

S

S-1A

S EXPLORER VII SATELLITE

S-3

S EXPLORER XII SATELLITE

S-3A

S EXPLORER XIV SATELLITE

S-6

S EXPLORER XVII SATELLITE

S-BAND

Ultralow-noise tunable S-band amplifier using TWM as second stage 01 p0034 A67-10106
Performance and design characteristics of solid state microwave converters for converting VLF telemetry receivers to L-and S-bands 02 p0196 A67-12006
Erectable antenna design for S-band communications between lunar surface and earth during lunar stay portion of Apollo mission 04 p0569 A67-14501
S-band direct phase modulator using varactor diodes with extremely linear phase characteristics 04 p0580 A67-14596
S-band pulse signal reflection from various grounds at vertical incidence 04 p0572 A67-15035
Terrain backscattering characteristics at low grazing angles for X-and S-band 05 p0768 A67-17527
S-band parametric amplifier pumped at J-band using balanced idler circuit with two varactor diodes incorporated in one encapsulation 06 p0966 A67-17580
Automatic phase sensor for waveguide combiner in S-band ground tracking and space communication network 07 p1149 A67-19051
High efficiency S-band monopulse focal point tracking feed, discussing aperture geometry design theory 08 p1300 A67-20654
Noise comparators and associated thermal standards to provide noise source calibration facilities at S-and X-bands 09 p1495 A67-21621
Electrostatically focused extended interaction S-band klystron amplifier using helical buncher resonators for interplanetary spaceborne communication systems 09 p1477 A67-22252
Noise measurements on pulsed four-cavity electrostatically focused S-band klystrons 09 p1477 A67-22253
S-band traveling wave phototube operating

with He-Ne laser noting performance, design and methods of operation 09 p1479 A67-22279
RF hardware implementation techniques utilizing devices illustrated in block diagrams 14 p2287 A67-28680
Omnidirectional radiation pattern for S-band telemetry on rockets more than 1/2 ft in diameter by small electrical separation of antennas [AAS PAPER 67-51] 15 p2454 A67-30116
S-band telemetry data during spacecraft launch phases, discussing mission support problems 20 p3380 A67-36561
Waveguide dispersive line use in FM pulse compression system outlined for high resolution in S-band radar 21 p3601 A67-39061
S-band rectangular digital phase shifter combining advantages of waveguide design with compactness of strip transmission line structure 22 p3773 A67-39909
S and X band ignitor design eliminating spike leakage variations in tracking radar tubes 24 p4131 A67-42350

S-MATRIX

S-matrix computations for quantum transitions, considering close coupling case of homonuclear diatomic molecular rotational excitation 21 p3659 A67-38005

S-N DIAGRAM

Aircraft reliability as function of fatigue life of welded joints noting static strength variation, S-N curve and multiple safety factor 09 p1506 A67-22471
Phenomenological process in thermal fatigue research, equipment, tests and evaluation 09 p1576 A67-22475
Fatigue of powder metal compositions, discussing data from rotating beam and reverse bending fatigue tests 10 p1667 A67-22702
Product reliability dependence on scatter extent determination in fatigue life, recommending testing in S-N diagram short life region 20 p3538 A67-36699

S-WAVE

Variational bound method applied to calculation of lower bounds on S-wave phase shifts for scattering of electrons by hydrogen atoms 07 p1226 A67-19499
Torsional disturbance propagation in Gutenberg-Bullen earth model through spectral seismograms, discussing travel times and S wave amplitude [SR-16] 20 p3435 A67-37675
Three-body problem application to nuclear reactions involving neutron, proton and heavy nucleus, parametrizing two-body interactions in terms of s-wave separable potentials 24 p4191 A67-42593

S-16

S OSO-I

S-27

S ALOUETTE I SATELLITE

S-48

S EXPLORER XX SATELLITE

S-49

S OGO-A

S-50

S OGO-C

S-52

S ARIEL II SATELLITE

S-53

S UK-E

S-55C

S EXPLORER XXIII SATELLITE

S-56A

S EXPLORER IX SATELLITE

S-74

S EXPLORER XVIII SATELLITE

S-99

S EXPLORER SATELLITE

SA 330 HELICOPTER

S SUD-AVIATION SA 330 HELICOPTER

SAAB 37 AIRCRAFT

Automatic test equipment for checkout and fault finding on Saab 37 Viggen 24 p4137 A67-41896

SACCHAROMYCES

Saccharomyces cerevisiae light particle fraction containing fatty acid synthetase analyzed by density gradient method 19 p3178 A67-35873
Enzyme activity of light and heavy crude ribosomal fractions in Saccharomyces cerevisiae indicating subcellular sites of lipid synthesis 21 p3573 A67-37919

SAFETY

SA AIRCRAFT SAFETY

SA FLIGHT SAFETY

SA HAZARD

SA INDUSTRIAL SAFETY

- SA RANGE SAFETY
Project Rover liquid hydrogen
safety 13 p2092 A67-27650
Rapid Availability of Information and Data
for Safety/RAIDS/ system as tool of system
safety engineering 18 p3007 A67-34703
- SAFETY DEVICE
Near field power density incident on eyes
due to reflection from CW laser reduced by
optical lens and shutter
rearrangement 10 p1665 A67-23415
Intrinsically safe and nonincendive
electrical installations for hazardous
environments 12 p1900 A67-25677
Electrostatic discharging systems for
helicopters, discussing earth field effect and
fail-safe concept
[AHS PAPER 107] 16 p2610 A67-31824
Helicopter cargo restraint system program
meeting prescribed operational and safety
requirements
[AHS PAPER 124] 16 p2598 A67-31839
Safety device to prevent overloading of
models and sensitive wire strain gauge
balance by aerodynamic forces during
starting and switching off in wind
tunnel 22 p3780 A67-39756
Safety control requirements in thermal-
vacuum testing involving protection against
electric equipment operation in pressure
range for glow discharge 22 p3782 A67-40404
Polyimide passenger smoke hood for
protection from smoke, toxic gases and
flame inhalation 23 p3968 A67-41623
- SAFETY FACTOR
Structural safety of Mercury and Gemini
vehicles, noting fail-safe and fracture
tolerant design
[SAE PAPER 660681] 01 p0154 A67-10585
Design strength calculation for materials
as function of reliability level and number
of components 04 p0627 A67-14705
Aircraft reliability as function of fatigue
life of welded joints noting static strength
variation, S-N curve and multiple safety
factor 09 p1506 A67-22471
Launch vehicle preparation and firing,
discussing instrumentation, missile safety
and range operations 10 p1622 A67-23001
Soviet book on calculations of strength
and vibrations of rocket
engines 11 p1852 A67-24512
Space vehicle hazard due to focusing of
meteor streams by earth in antiradiant
direction 12 p2002 A67-25656
Radiation hazards and safety requirements
for lunar and Mars manned space flights,
discussing radiosensitivity, restoration and
permissible doses 13 p2059 A67-26761
Book on safety of
structures 14 p2395 A67-28030
Book on cryogenic fluids covering safety
principles, design data, first aid and hazard
control procedures 15 p2543 A67-29233
Process control program including failure
mode and effects analysis, critical
characteristics determination, safety features
and test equipment
complexity 18 p3058 A67-34673
Risk assessment techniques for design,
fabrication and testing of complex
spacecraft noting component reliability,
Bayesian statistics, Monte Carlo technique,
etc 18 p3138 A67-34683
System safety management/engineering
procedures and techniques for safety
requirements application 18 p3163 A67-34691
Automatic position determination for ships
using active navigation satellite systems,
discussing communications potential and
safety 19 p3254 A67-35310
Orpheus program for space flight safety
using lifeboat rescue of astronauts on Apollo
and other manned
missions 20 p3532 A67-36572
Design, equipment and techniques of
electronic packaging in Titan III program,
stressing environmental levels and safety
factors 21 p3595 A67-38335
Bound functionals for limit analysis of
plastic solids by variational method,
discussing safety factor and sandwich
structures 23 p4074 A67-40629
Factors for SST safety and airworthiness
requirements, discussing environment,
engineering level, learning and flying quality
[AIAA PAPER 67-751] 23 p3933 A67-40985
Manned spacecraft recovery safety noting
operational testing of postlanding systems,
recovery support and retrieval procedures
for Apollo
- [AIAA PAPER 67-852] 24 p4243 A67-42985
Implementation of safety provisions in
manned systems
[AIAA PAPER 67-937] 24 p4096 A67-43027
- SAFETY HAZARD
Space launch facilities, discussing site
plan, zoning and development of John F.
Kennedy Space Center at Merritt
Island 02 p0228 A67-11838
Manned lunar launch area site selection
and planning, considering safety hazards,
spaceport zoning, instrumentation,
interference control, community relations,
etc 05 p0787 A67-16608
Safety program for laser hazards,
discussing eye and body
protection 07 p1194 A67-19089
Hazards in sounding rocket assembly and
launch operations and safety techniques at
NASA Wallops station noting storage,
explosive control, ground safety,
etc 08 p1314 A67-20547
Prevention system of short circuit in
vacuum chambers due to glow
discharges 10 p1622 A67-23316
Safety practices for high energy physics
research equipment filled with liquid
hydrogen or deuterium 13 p2092 A67-27649
Problems involved in ditching business
aircraft on ocean and subsequent
recovery 14 p2245 A67-28319
Electrical detonator characteristics and
safety precautions in handling and use,
noting untimely functioning and misfiring as
causes of accidents 17 p2927 A67-33093
Incident/accident information exchange
system for hazard information flow to safety
teams 18 p3163 A67-34692
Fault tree analysis concept development
for predicting possible undetected safety
hazards within complex missile
systems 19 p3331 A67-34827
Analysis of explosion hazards of large
solid motors, suggesting mathematical
approach in predicting blast damage
[CI PAPER 67-14] 19 p3309 A67-35008
Plasma microinstability theory, predicting
dangerous instability above critical density,
discussing applications to very high
temperature plasma
experiments 20 p3495 A67-36153
Instrumentation grounding at Cape
Kennedy, noting characteristics of ground
system used for safety and clean space
signals 20 p3398 A67-36837
Timing considerations in sequential fluid
power circuits design in terms of stray
delay concept and safety of asynchronous
circuit 20 p3365 A67-37362
Floating airports proposed as solution to
short haul air traffic problems in New
York 20 p3418 A67-37445
Flame mechanism experiments for solid
material surface, measuring flame velocity,
stressing space capsule fire hazard
minimization 22 p3904 A67-40110
Laser safety - Conference, London,
November 1966 23 p4015 A67-41049
Lasers in ophthalmology, discussing surgery
and hazards 23 p3962 A67-41051
Maximum permissible energy density
incident on retina determined for eye safety
in viewing laser beam 23 p3962 A67-41052
Safety of personnel from laser hazards
covering installation containment, operator
screening and eye
protection 23 p4015 A67-41053
Laser experiment safety procedures for
protection of personnel and persons not
involved in laser work 23 p4015 A67-41054
Aircraft/bird collision noting dispersion,
flock detection and windshield
protection 23 p3934 A67-41070
Decompression tests for potential hazards
of ejection or fatal head injuries in small
pressurized aircraft 23 p3970 A67-41693
Aircrew safety emphasizing prior to abort
aspects in detection of catastrophic failure
and initiation of abort sequence
[AIAA PAPER 67-934] 24 p4245 A67-43024
Hazard studies and safety analyses
qualitative method using checklist of
possible mishaps and human errors
[AIAA PAPER 67-935] 24 p4260 A67-43025
Mathematical model for identification and
control of systems safety in manned space
programs using Monte Carlo techniques
[AIAA PAPER 67-936] 24 p4245 A67-43026
Emergency oxygen supply systems for
aircraft, discussing simplicity,
standardization, safety, reliability and
maintenance
- [AIAA PAPER 67-965] 24 p4110 A67-43043
- SAGITTARIUS CONSTELLATION
Synchrotron nature of Sagittarius A
central component radio spectrum and
injection of relativistic cosmic
particles 06 p1078 A67-18166
Synchrotron nature of Sagittarius A
central component radio spectrum and
injection of relativistic cosmic
particles 16 p2737 A67-30510
- SAGNAC EFFECT
Electromagnetic sensing of absolute
rotation with self-oscillating laser version of
Sagnac interferometer 14 p2349 A67-28812
- SAHA EQUATION
Saha-Langmuir formula applied to
description of temperature dependence of
positive ion current in surface ionization of
silicon atoms, comparing work functions by
methods using contact potential, thermionic
emission and Richardson
graphs 09 p1554 A67-22006
Electron number density and number
density of electronic states calculated from
rate equations for noble gas seeded with
alkali metal 16 p2710 A67-30518
Ionization wave velocity in nonisothermal,
low temperature plasma discussed, using
generalized Ohm law, law of conservation of
electron energy and SAHA
equation 16 p2711 A67-30540
Correlation of measurement data on
electrical conductivity of nonequilibrium
plasma with impurities 17 p2895 A67-32153
Excited state and steady state populations
in high pressure plasma with heavy particle
collisional ionization and electron-ion
recombination 17 p2909 A67-33228
Radial pressure distribution in hydrogen
arc located in axial magnetic field using
Saha equation, determining temperatures
and electron densities 19 p3279 A67-35139
- SAIL
SA HYPERSONIC SAIL
Parachute descent training for USAF
pilots using Para-Sail ascending
parachute 23 p3967 A67-41609
- SAILPLANE
Open jet wind tunnel testing of Meteor
sailplane, examining aerodynamic merging of
wings, fuselage and
cockpit 01 p0006 A67-10970
Flexible sailplane designs allowing for
towing cable analyzed with analog computer
for gust loading 10 p1593 A67-23015
Dynamic response of sailplanes to
longitudinal maneuvers based on steady lift
coefficients on wing and
tails 16 p2596 A67-31465
Dynamic response of sailplanes to elevator
control in longitudinal maneuvers, discussing
load factors and tail loads as function of
aerodynamic and inertial
parameters 16 p2597 A67-31786
Sailplanes with self-contained launching
apparatus noting minimum performance,
motor propulsion and auxiliary
equipment 22 p3744 A67-39303
- SAINT ELMO FIRE
S CORONA DISCHARGE
SAINT VENANT FLEXURE PROBLEM
Optimal flexure solution for Saint Venant
problem in circular cylinder, using
Papkovich-Neuber stress functions
[ASME PAPER 66-WA/APM-19] 04 p0714 A67-15410
Cracked rectangular beam stress analysis,
considering longitudinal shear and Saint-
Venant torsion and flexure
[ASME PAPER 67-APM-21] 17 p2964 A67-33150
- SAINT VENANT PRINCIPLE
Saint Venant principle in linear and
nonlinear plane elasticity in two-dimensional
isotropic body 22 p3912 A67-39743
- SALICYLATE
S SODIUM SALICYLATE
SALT
SA CARBONATE
SA NITRATE
SA PHOSPHATE
SA SODIUM CHLORIDE
SA SULFATE
Preservation of viable microbes in
anabiosis in potassium salts determined
improbable by failure to grow
bacteria 15 p2427 A67-29118
- SAMARIUM
Divallence samarium ion doped calcium
fluoride laser action at low temperatures

obtained with giant pulse ruby laser excitation 05 p0820 A67-16661
Internal conversion electron spectrum for samarium 155 to europium 155 transmutation, noting multipolarities and new lines 16 p2733 A67-31706

SAMARIUM COMPOUND

Stark and Zeeman splitting in far IR spectra of erbium, dysprosium and samarium ethyl sulphate 04 p0686 A67-15778

SAMPLED DATA

Test functions for testing location, scale and shape parameter hypotheses of Weibull distribution 01 p0107 A67-10931
Data abbreviation application to actual range telemetry data recorded on magnetic tape, noting redundancy removal, processing time reduction, etc 02 p0197 A67-12017
Power spectra analysis based on method of computing weighting sequence whose frequency characteristics approximate one-third octave filter and applying coefficients recursively to digitized data 03 p0375 A67-13563

Radiation hardened sampled data recording system design, fabrication and testing incorporating parallel write-in, variable rate sampling and tunnel diode memory 04 p0625 A67-15709

Transfer function of linear system obtained from discrete values of input-output data 08 p1311 A67-20344

Interpolation errors visualization by spectrum of sampled data waveform 10 p1605 A67-23005

Sampled data control system analysis, determining gain margin in unsampled loops 13 p2086 A67-26416

Geomagnetic field analytical representation based on Cosmos 49 observational data 14 p2307 A67-27919

Multistage linear dynamic systems with sequentially correlated noise, evaluating filtering, prediction and smoothing procedures 19 p3206 A67-35941

SAMPLED DATA SYSTEM

Difference equations of nonlinear sampled data systems and resultant recurrence formula for system response calculation 01 p0043 A67-10201

Optimization of sampled data systems with finite transient response time on basis of combined stochastically deterministic Q factors 01 p0043 A67-10202

Stability of sampled data feedback systems with time-varying gain by restriction with memoryless element and nonanticipative linear time-invariant subsystem 01 p0048 A67-11226

Sufficient condition for absolute bounded-input-bounded-output stability for certain class of nonlinear sampled data feedback systems 02 p0224 A67-11586

Evaluation of redundancy reduction algorithms to facilitate comparison in terms of performance by computer simulation, using real and synthesized data 02 p0197 A67-12015

Channel noise forces adaptive sampling system to operate at lower bit error probability than equivalent PCM system 02 p0197 A67-12016

Steady state output ripple performance and sampling frequency choice for single and multirate direct digital control system with stochastic input 02 p0225 A67-12073

Transfer function of pulse amplitude modulated sampled data control systems with element generating arbitrarily shaped pulses and first order element series connected with constant parameter elements 03 p0390 A67-13103

Absolute stability criterion for nonlinear sampled data automatic systems 03 p0392 A67-13596

Quadratic programming applied to design of digitally compensated sampled data control system 03 p0393 A67-13902

Stability analysis of multiloop multirate sampled systems using identities expressing Laplace transforms of sampled signals in terms of shifted transforms of same signals sampled with smaller periods 04 p0591 A67-14825

Iterative method determination of output signal, impulse response and transfer function of variable parameter linear sampled data system 05 p0784 A67-16705

Optimal control of linear stochastic systems with complexity constraints applied to sampled data system 06 p0975 A67-17934

Optimal processes in sampled data control system 06 p0976 A67-18404

Time-weighted minimal energy control of nth order plant 06 p0977 A67-18531

Process parameter estimation and self-adaptive control, noting performance and spurious noise 07 p1159 A67-19195

Identification of unknown transfer function in nonlinear sampled data systems, using iterative method 08 p1310 A67-20336

Steady state trajectory and stability of nonlinear sampled data systems with constant sampling frequencies described by finite difference equations 08 p1312 A67-20755

Combined use of time-domain waveforms, detection probability and false alarm probability for selection of optimum sample period and quantization interval for detection of impulse waveforms 09 p1459 A67-21582

Synthesis of control device for one class of nonlinear sampled data systems, obtaining processes with minimum control time 09 p1483 A67-22082

Multiple sampled data systems with cyclically varying sampling rates, determining smoothing filters and periodic presampling filters 10 p1618 A67-22731

Nonlinear sampled system with parameters in functional dependence on sign of error at discrete instants of sampling 11 p1769 A67-24056

Aerospace computer hardware, discussing general purpose requirement on basis of various computer designs 11 p1755 A67-24247

Simulation of sampled data systems for pure servo delay by analog computer using potentiometer 12 p1919 A67-25203

Absolute stability criterion for nonlinear sampled data automatic systems 14 p2290 A67-27842

Postsampling exponential first order digital filter and application to data reduction for trend analysis and noisy phenomena 14 p2288 A67-28687

Liapunov function analysis applied to derivation of general stability criterion for control system 14 p2292 A67-28898

Sufficient condition providing nonlinear sampled system with set of initial conditions 15 p2458 A67-29473

Steady state and transient analysis of digital phase-locked loops 15 p2458 A67-29939

Sampled data feedback control system using quadratic programming to determine optimum compensator 16 p2646 A67-31636

Suboptimal, adaptive solutions to sampled data problem for quadratic performance index minimization by obtaining control law and sampling scheme 16 p2649 A67-31660

Random pulse operation and random pulse machines structural requirements, with continuous variable dependent on certain sampling time 18 p3006 A67-34063

Synthesis of optimal and quasi-optimal sampled data control systems applied to various order plants 18 p3017 A67-34281

X-transform for open/closed loop sampled data system with zero-order hold device 19 p3263 A67-35927

Z-transform and W-transform theory applied to dynamic compensation of linear sampled data control systems for attitude control of large booster 21 p3713 A67-38027

Output noise variance minimization, calculating smoothing coefficients for discrete time invariant filters used in sampled data systems 21 p3601 A67-38949

Transmission buffer overflow prevention in telemetry data compressors using adaptive queueing control 21 p3586 A67-38956

Stability of nonlinear sampled data control systems, investigating pulse frequency modulation using Liapunov function 22 p3777 A67-39829

Stability margins for hybrid continuous discrete data control systems, developing open loop transfer function 22 p3778 A67-40157

Nonlinear sampled data automatic control system optimization by statistical method 23 p3985 A67-41673

Nonlinear sampled data system instability, discussing arbitrary single-valued nonlinearities and arbitrary modulation law /PAM, PWM or PFM/ 23 p3985 A67-41674

Noninteraction and deadbeat response in linear sampled data multivariable systems

synthesis by state difference equation 24 p4134 A67-42027

SAMPLING**SA AIR SAMPLING****SA RANDOM SAMPLE**

Sampling plans for identification of inadequate subsystems 01 p0084 A67-11370

Truncation error bounds for sampling representations of band limited signals 04 p0570 A67-14871

Cartwright-Longuet-Higgins-Rice theory on instantaneous maxima of stationary random variable for deriving instantaneous maximum gust ratio to mean wind speed 05 p0837 A67-16426

Molecular beam technique for mass spectrometric sampling of high temperature systems at high atmospheric pressure [AIAA PAPER 67-37] 06 p0956 A67-18305

Apollo spacecraft hybrid real time flight simulation ensuring 40 msec sampling interval [AIAA PAPER 67-255] 07 p1166 A67-20071

Queueing model of many-instrument visual sampling 07 p1136 A67-20172

Relation among sampling theorem, Z transformation and time series method for applications to network analysis 07 p1146 A67-20194

Rocketborne RF mass spectrometers use in study of atmospheric composition at high altitudes, discussing sampling 09 p1491 A67-21895

Discrete continuous feedback control systems with signal dependent sampling constraints, analyzing sampling interval criteria 09 p1483 A67-22608

Sampling plan for destructive testing, relating quality protection to cost 15 p2584 A67-30421

Optimal control problem for nonlinear systems with constrained sample times 16 p2646 A67-31635

Adjoint simulation technique extended to signals consisting of continuous, sampled and multirate sampled systems with random inputs 16 p2652 A67-31684

Inertia and muscle tone level effects on intermittence sampling frequency in hand movement control system 17 p2808 A67-33180

Modified Monte Carlo procedure using partitioning method and stratified sampling 18 p3072 A67-34396

Collection, processing and return to earth of lunar specimens as part of Apollo program 19 p3328 A67-35929

Random processes from physical viewpoint, discussing random function, random noise properties, Gaussian distribution, digital analysis, Shannon sampling theorem, etc 20 p3483 A67-36459

Sampling interval criteria with nonlinear integrands in discrete-continuous feedback control systems, obtaining performance surfaces in object function-parameter space 24 p4134 A67-42024

SAMPLING DEVICE

Recording assembly for measurement of flexural and torsional moduli and internal friction at various frequencies and temperatures of small samples, using constant amplitude undamped oscillations 01 p0062 A67-10163

Ion extraction and plasma sheath formation in nitrogen discharge studied by quadrupole mass-spectrometric sampling probe, noting ion current ratio dependence on probe potential 02 p0272 A67-11889

Micrometeoroid sampling with Luster sounding rocket during Leonid meteor shower, detailing contamination control program 04 p0699 A67-14966

Soil mechanics surface sampler experiment for Surveyor 08 p1410 A67-20945

Graphical method for ascertaining acceptance number and size of sample in destructive and expensive testing 09 p1506 A67-22197

Glass filament wound interlaminar shear specimen design and instrumentation 11 p1875 A67-24614

Statistical performance of wide aperture sampling linear array in HF direction finding 13 p2082 A67-27405

Nanosecond baseband pulse rise time measurement, discussing real time and sampling oscillography, pulse comparison, basic instrumentation, etc 17 p2814 A67-32603

Extraterrestrial life detection methods compared, discussing sampling and method requirements 19 p3180 A67-35250

- Resonant-transfer sampling technique stressing bandpass filtering design and time division multiplex 20 p3379 A67-36243
- Small alternating magnetic field modulation effects on sampled output of rubidium magnetometer with frequency counter 20 p3448 A67-36876
- Improved filtration techniques for aircraft hydraulic systems, noting high pressure filter unit using paper-based element for ground service 20 p3418 A67-37169
- Need for increased sampling rates of particle counters to improve monitoring system performance for clean room sampling and leak testing of HEPA filters 23 p3961 A67-40843
- Contamination detection by analytical instrumentation considering sampling, IR, atomic absorption spectrophotometer, gas chromatography, colorimetry and polarography 23 p3998 A67-40844
- In-Line-Filter-Holder and Counter /ILFHC/ designed for high and low pressure systems to verify particulate cleanliness levels in modern fluid systems 23 p3935 A67-40846
- Sampling bottle with valves and high pressure filter holder for fuel and oxidizer, by weighing bottle before and after sampling amount of fuel passing through filter can be calculated 23 p3998 A67-40849
- Germ sampling at high altitudes using hydroaeroscopes attached to conventional aircraft 23 p3963 A67-41072
- Very short pulse measurements by deriving delayed pulse from measured waveform, describing detector circuit 23 p3981 A67-41273
- Surveyor III lunar surface sampler for picking, digging, scraping and transporting material, noting design and operation 23 p4005 A67-41370
- Depth sampler for testing dirt content of jet fuels, discussing settling effects 24 p4206 A67-42279
- SAN MARCO SATELLITE**
- San Marco satellite structural configuration for measurement of total force acting on satellite, electron content from satellite to earth and guided propagation 03 p0517 A67-12900
- Atmospheric density scale height and variation law at different heights obtained from San Marco satellite data 10 p1712 A67-23212
- San Marco project, joint effort of NASA and Italian Space Commission to launch satellite for atmospheric and ionospheric measurements 16 p2757 A67-30642
- Spherical dipole for Italian satellite, calculating radiation impedance and pattern, input admittance, efficiency, radiated field and antenna Q factor 17 p2826 A67-32780
- Italian space-research activities /1966-1967/, discussing San Marco 2 satellite project 19 p3321 A67-35295
- SANDWICH CONSTRUCTION**
- SA MULTILAYER STRUCTURE**
- Test methods for determination of shear and flexural properties of sandwich panels 01 p0164 A67-11269
- Semiconductor-metal-semiconductor structure with metal vapor deposited, analyzing voltage-current characteristics for amplifier technology 02 p0293 A67-11754
- Electric conductivity due to tunnel effect in aluminum-alumina-silver sandwich structures, determining potential barrier in alumina and absorption coefficient of hot electrons 02 p0295 A67-11762
- Tunnel-current measurements of sandwich configurations, determining metal/metal-oxide work function 02 p0295 A67-11764
- Insert size, shape and core undercut diameter and depth effect on insert tensile strength of honeycomb sandwich fasteners 02 p0248 A67-11943
- Compact rocket engine concept utilizing very small thrust units confined between and joined to plates, resulting in honeycomb structure [AIAA PAPER 66-924] 02 p0303 A67-12276
- Synthetic spherulites in plastic foam and synthetic tube segments in honeycomb form as fillers in sandwich construction 03 p0521 A67-13022
- Axially symmetric motion of elastic spherical sandwich shell, determining natural frequencies and effects of shear deformation, normal stress and rotatory inertia 03 p0522 A67-13212
- Free vibration of sandwich beams viscoelastic cores, examining equations of motion, natural boundary conditions and derivation of expressions for modal distribution of damping [ASME PAPER 66-WA/UNT-3] 04 p0713 A67-15382
- Inelastic buckling of rib-cored orthotropic sandwich cylinders under external hydrostatic pressure, evaluating rigidity factor and Poisson ratio effect 04 p0719 A67-15936
- Effects of 450 and 600 degrees F exposures on mechanical properties of glass-fiber polyimide resin sandwich panels to be used on large skin areas of SST aircraft [AIAA PAPER 67-174] 06 p1021 A67-18484
- Anisotropic sandwich constructions characteristics for orthotropic materials used for facings and cores, considering stiffness and buckling 06 p1108 A67-18655
- Temperature dependence for n-n epitaxial GaAs sandwich structures mounted on infinite half-plane of copper 07 p1155 A67-19797
- Light aircraft design using fiberglass reinforced plastic primary structure for fibrous composite 08 p1414 A67-20429
- Reinforced plastic facings as sandwich materials instead of metal skins noting cost effectiveness, weight efficiency and layup times 08 p1414 A67-20430
- Sounding rocket disintegration studies to avoid falling mass hazards, noting design of pyrotechnic core in sandwich construction 08 p1407 A67-20520
- Unsymmetric free vibrations of orthotropic sandwich shells of revolution treated by Rayleigh-Ritz technique 08 p1417 A67-20555
- Planar and sandwich resistor structures in SI thin film integrated circuits 08 p1302 A67-20793
- Creep measurement associated with adhesive bonding of aircraft structures, particularly creep of metal-metal lap joints and bonded sandwich structures creep measurement associated with adhesive bonding 09 p1522 A67-22505
- Single stage bonding of tapered aluminum honeycomb panels employing wrap-around skins and nonperforated core 09 p1507 A67-22507
- Graphite fibers as internal electrical resistance heat source for curing structural adhesives demonstrated in lap shears, larger area and sandwich construction 09 p1507 A67-22516
- Mechanical properties of polybenzimidazole resin show suitability for metal-to-metal and sandwich composite adhesives and high and cryogenic temperatures 09 p1523 A67-22518
- Analytical solution, based on stress functions, for deflection of plastics sandwich beam under bending loads at center, agreeing with experimental results for short duration loading 09 p1579 A67-22612
- General instability and face wrinkling of sandwich plates with ideally orthotropic cores, deriving equations and boundary conditions [AIAA PAPER 66-138] 10 p1717 A67-23126
- Antisymmetric stress-strain state of thin walled isotropic and anisotropic sandwich shells of revolution with meridian of arbitrary shape for complex boundary conditions 10 p1720 A67-23603
- Diffusion bonding of titanium sandwich structure for Saturn tank wall application 10 p1661 A67-23702
- Unified theory for bending and buckling of honeycomb type sandwich shell and linearized governing equations applied to axially compressed circular cylinder 10 p1728 A67-23761
- Composite loss factor and natural frequencies of vibrating beams composed of alternate layers of elastic and viscoelastic material [ASME PAPER 67-VIBR-6] 11 p1871 A67-24166
- Vibrational experiments with honeycomb type core sandwich beams on lowest natural frequency, node locations and damping, noting core shear flexibility [ASME PAPER 67-VIBR-11] 11 p1872 A67-24171
- InAs epitaxial layers grown on GaAs substrate investigated via sandwich method and electron diffraction 12 p1980 A67-25201
- Energy distribution of electron tunneling through metal-insulator-metal diode noting dependence on temperature, film thickness and voltage 12 p1982 A67-25449
- Elastic filler effect on thin cylindrical sandwich shell stability subjected to compression along generatrix 12 p2023 A67-25592
- Differential equation and boundary conditions for sandwich shells, noting bending resistance and shear deformation 13 p2219 A67-26906
- Compact rocket engine concept utilizing very small thrust units confined between and joined to plates, resulting in honeycomb structure [AIAA PAPER 66-924] 15 p2545 A67-29435
- Passage of hot electrons through metal film in semiconductor-metal-semiconductor system 15 p2541 A67-30239
- Ultrasonic wave amplification by supersonic flux of drift electrons in sandwich structure of piezoelectric dielectric and semiconductor 15 p2542 A67-30245
- Thermal stresses in three-layer cylindrical sandwich shell of finite length with rigid filler having temperature as function of radius only 16 p2765 A67-31049
- Fission-particle damage formation in semiconducting layer structures, using model based on thermal spike 17 p2918 A67-32849
- Dynamic stability of homogeneous and inhomogeneous sandwich columns with pinned ends under pulsating periodic loads governed by Mathieu equation 17 p2963 A67-33036
- Bond-layer compliances effect on flexural responses of sandwich beam, discussing homogeneous and composite beams, deformation equations, etc [ESA PAPER 1214] 18 p3142 A67-33895
- Thin films deposited onto substrates cooled to low temperatures investigated for transition temperature in structures of superconductor-dielectric-superconductor 18 p3101 A67-33989
- Prestressed-shell buckling, using Budianski-Kolter tensor nonlinear equilibrium equations by numerical analysis 19 p3343 A67-35778
- Buckling analysis of sandwich beams with elastic orthotropic cores under axial compression 20 p3537 A67-36641
- Polyt IV glider wing noting bonded aluminum sheet/honeycomb sandwich shell 22 p3811 A67-39302
- Axisymmetric vibrations of homogeneous and sandwich spherical shells obtained from generalized variational motion equations including thickness-shear deformation effect 23 p4075 A67-40667
- Honeycomb sandwich structures for aircraft and missile construction, discussing panel configurations 23 p4077 A67-41047
- Critical strain parameter concept for adhesive bond joints noting strength dependence on geometry and material elastic properties [SAE PAPER 670856] 24 p4160 A67-42003
- SANDWICH PLATE**
- Stability problems of sandwich plates, considering buckling and wrinkling 02 p0341 A67-12713
- Bending of orthotropic sandwich plates in differential equation derived based on variational method 04 p0709 A67-14844
- Dynamic response of cylindrical sandwich shell under axially symmetric moving ring load, considering steady state behavior 04 p0713 A67-15404
- Approximation in sandwich plate analysis obtained by various methods 04 p0717 A67-15913
- Transverse shear and edge condition effect on nonlinear vibration and dynamic buckling of homogeneous and sandwich plates 05 p0910 A67-16146
- Axisymmetric bending of circular sandwich plates with lightweight compressible filler subject to special transverse or local loads 05 p0922 A67-17175
- Sandwich plate stability analysis by linear geometric and physical equations, for rigid and light cores 06 p1099 A67-17585
- Governing equation for bending of multilayered sandwich elastic plates composed of n membranes developed by variational method 06 p1110 A67-18857
- Thermoelastic stressed state of sandwiched plate in temperature field 07 p1261 A67-19326
- Equations for nonstationary temperature

field of n-layer plate, noting convective heat transfer on free surface of plate 07 p1267 A67-19327

Shear modulus determination from free flexural vibrations of sandwich beams with steel facing, using filled elastomer as core 09 p1574 A67-21838

Sandwich plate problem involving subjection to concentrated force of plate having filler flexural rigidity only, giving solution in form similar to that of thin isotropic plate 10 p1716 A67-22937

Sandwich plate problem involving plate having filler flexibility only, giving solution via reciprocity theorem based on Rayleigh-Green equality in thin plate theory 10 p1716 A67-22938

Dynamic analysis of sandwich plate with clamped edges executing plane strain motions, using variational motion equation and Galerkin method 10 p1717 A67-23138

Deflection of free three-layer strip under impact, determining displacement function and bending oscillations 10 p1721 A67-23610

Glass-fabric reinforced plastic shells fabrication and full scale structural evaluation 10 p1727 A67-23732

Exact solution of transverse shear deformation effect on axisymmetric large deflection of circular sandwich plates for different loading states and boundary conditions 10 p1728 A67-23762

Bending theory for sandwich plates solved by Galerkin method assuming load distribution over upper and lower faces of plate 11 p1880 A67-25095

Stress-strain state of thin sandwich plate consisting of arbitrary number of elastic isotropic layers rigidly coupled to each other 12 p2024 A67-25602

Reissner variational formulation of temperature distribution boundary value problem of axisymmetric thermal stresses in isotropic sandwich shells of revolution [AIAA PAPER 66-528] 12 p2030 A67-25917

Natural transverse vibrations of sandwich plates with rigid and lightweight fillers, deriving stability equations from eigenvalue equivalent problem 14 p2402 A67-28901

Stability equation of multilayer sandwich plates with isotropic homogeneous facing layers and orthotropic homogeneous core layers 15 p2577 A67-30267

Large deflection bending of simply supported rectangular sandwich plates with isotropic core under uniform normal pressure, solving governing differential equations by digital computer 15 p2577 A67-30269

Forced transverse vibrations of sandwich plates of symmetrical structure 16 p2776 A67-31547

Natural frequencies of vibration of supported sandwich plate [SESA PAPER 1175] 18 p3143 A67-33901

Differential equations and potential for simply supported anisotropic sandwich plate under compression and shear stresses above buckling limit 19 p3341 A67-35575

Nonlinear bending theory of sandwich plates with orthotropic layers 19 p3342 A67-35716

Rectangular sandwich plates large deflection equations solved by successive approximation method 19 p3342 A67-35770

Thermal stresses in orthotropic sandwich plate solved by boundary value and stress distribution 20 p3541 A67-37298

Deflection of free three-layer strip under impact, determining displacement function bending oscillations 20 p3542 A67-37540

Two plates bounded by adhesive layer in plane stressed state, calculating system stability 21 p3719 A67-38050

Homogeneous and sandwich spherical caps and circular plate torsional frequency calculations based on sandwich and spherical shell equations 23 p4073 A67-40618

Bound functionals for limit analysis of plastic solids by variational method, discussing safety factor and sandwich structures 23 p4074 A67-40629

SANITATION

SA HYGIENE

SA POTABLE WATER

Long term space mission sanitation, personal hygiene and body cleansing to control microbe populations on body surface and teeth 23 p3967 A67-41611

SAPPHIRE

Temperature dependence of heat-pulse

propagation in sapphire at low temperature intervals, noting phonon mean free path 01 p0131 A67-10341

Microelectronic applications of silicon-on-sapphire /SOS/ and MOS-FET large scale arrays /LSA/ 02 p0219 A67-12108

Mechanical characterization and structural perfection of alpha aluminum oxide wool whiskers in diameter range of 0.6 to 4.0 microns 03 p0449 A67-13307

Electron beam float-zone melting process applied to dielectric compound aluminum trioxide to obtain sapphire crystals 04 p0628 A67-15320

Sessile drop technique to study effect of atmosphere and alloy additions of Ti and Cr on surface tension and contact angle of N on sapphire substrated at 1500 degrees C 08 p1343 A67-21543

Strengthening of sapphire single crystals by precipitates containing titanium 12 p1987 A67-26190

Donor surface states and bulk acceptor traps in silicon on sapphire films due to activation of absorbed impurities 21 p3677 A67-38012

Heteroepitaxial Si films grown on sapphire studied for current voltage relations, finding space charge limited current 23 p4038 A67-40785

SATAN

S SENSOR FOR AIRBORNE TERRAIN ANALYSIS /SATAN/

SATELLITE

SA ALOUETTE I SATELLITE

SA ALOUETTE SATELLITE

SA ANNA SATELLITE

SA APPLICATIONS TECHNOLOGY SATELLITE /ATS/

SA ARIEL II SATELLITE

SA ARIEL SATELLITE

SA BEACON SATELLITE

SA BIOSATELLITE

SA COMMUNICATIONS SATELLITE

SA COSMOS II SATELLITE

SA COSMOS III SATELLITE

SA COSMOS V SATELLITE

SA COSMOS XII SATELLITE

SA COSMOS XLI SATELLITE

SA COSMOS SATELLITE

SA D-1 SATELLITE

SA DODGE SATELLITE

SA EARLY BIRD SATELLITE

SA ECHO I SATELLITE

SA ECHO II SATELLITE

SA ECHO SATELLITE

SA ELDO SATELLITE

SA ELEKTRON SATELLITE

SA EQUATORIAL SATELLITE

SA ESRO I SATELLITE

SA ESRO II SATELLITE

SA ESSA SATELLITE

SA EVASIVE SATELLITE

SA EXPLORER IX SATELLITE

SA EXPLORER VII SATELLITE

SA EXPLORER XII SATELLITE

SA EXPLORER XIV SATELLITE

SA EXPLORER XVII SATELLITE

SA EXPLORER XVIII SATELLITE

SA EXPLORER XX SATELLITE

SA EXPLORER XXII SATELLITE

SA EXPLORER XXXIII SATELLITE

SA EXPLORER SATELLITE

SA FR-1 SATELLITE

SA GEODETIC SATELLITE

SA GEOPHYSICAL SATELLITE

SA GRAVITY GRADIENT SATELLITE

SA GREB 5 SATELLITE

SA INJUN III SATELLITE

SA INTESAT SATELLITE

SA ISIS-A

SA ISIS SATELLITE

SA LINCOLN EXPERIMENTAL SATELLITE /LES/

SA LUNAR SATELLITE

SA MANEUVERABLE SATELLITE

SA METEOROLOGICAL SATELLITE

SA NATURAL SATELLITE

SA NAVIGATION SATELLITE

SA NIMBUS SATELLITE

SA OGO-A

SA OGO-B

SA OGO-C

SA ORBITING RADIO BEACON

SA IONOSPHERIC SATELLITE

SA ORBITING SATELLITE

SA OV2 /ORBITING VEHICLE-2/

SA PASSIVE SATELLITE

SA PEGASUS SATELLITE

SA PROTON II SATELLITE

SA PROTON III SATELLITE

SA RADIO ASTRONOMY EXPLORER /RAE/ SATELLITE

SA REFLECTOR SATELLITE SYSTEM

SA RELAY SATELLITE

SA SAN MARCO SATELLITE

SA SCIENTIFIC SATELLITE

SA SOLAR RADIATION I SATELLITE

SA SPACE VEHICLE

SA SPUTNIK III SATELLITE

SA SYNCHRONOUS SATELLITE

SA TELSTAR SATELLITE

SA TIROS III SATELLITE

SA TIROS IV SATELLITE

SA TIROS VII SATELLITE

SA TIROS SATELLITE

SA TRAAC SATELLITE

SA TRANSIT IVA SATELLITE

SA TRANSIT SATELLITE

SA TWENTY-FOUR HOUR SATELLITE

Decoder signaling system of Eldo satellite employing PCM telemetry channel, examining counters, shift registers, flip-flop circuit, etc 02 p0192 A67-11655

Environment-simulation testing effectiveness for unmanned space systems 04 p0598 A67-15223

Satellite material problems in corrosion fatigue failure, vacuum degradation, etc 10 p1670 A67-23734

Geometry of lunar eclipse of earth satellite for shadow function as quart polynomial in cosine of true anomaly 11 p1859 A67-24355

Doppler effect application to solution of tracking problems with aid of artificial earth satellites 14 p2347 A67-28995

Spheroidal coordinate method for obtaining gravitational potential of oblate planet 15 p2560 A67-30044

F region irregularities studied by scintillation of radio signals from earth satellites [AGARDOGRAPH 95] 15 p2481 A67-30228

Geophysical model of radio star an satellite ionosphere amplitude scintillation at nonequatorial latitudes [AGARDOGRAPH 95] 15 p2482 A67-30228

VHF radar reflections from artificial earth satellites used to analyze amplitude scintillations in ionosphere [AGARDOGRAPH 95] 15 p2482 A67-30228

Illumination impinging on geocentric satellite during eclipse by earth 16 p2761 A67-30995

Artificial satellites lifetime in low altitude orbits, discussing atmospheric, geomagnetic solar and lunar factors 18 p3136 A67-33555

Shape of earth studied for irregularities other than flattening at poles as revealed by perturbation of artificial satellite orbits 22 p3792 A67-39885

SATELLITE ATTITUDE CONTROL

Geomagnetic stabilization of satellite initially torque-stabilized, deriving motion equation 01 p0153 A67-10211

Propane gas system for satellite attitude control noting Skylark rocket 01 p0157 A67-11444

Earth-based radio reference signal for obtaining attitude and pointing information for synchronous communications satellites 02 p0331 A67-12155

Human pilot dynamic characteristic effects on manual satellite attitude control system stability, using root locus analysis of mathematical models 02 p0186 A67-12223

Dynamics of spin-stabilized satellite with nonrigid extendible antennas, noting effect of terrestrial magnetic and gravitational field 02 p0333 A67-12303

Propulsion systems for satellite attitude control, considering weight and thrust efficiency parameters 05 p0905 A67-16722

Effect of man walking inside or outside satellite on attitude 05 p0906 A67-17202

Experimental and operational communication satellite, discussing attitude stabilization, automatic routing, etc 06 p1094 A67-18055

Attitude stability of spinning rigid symmetric satellite in elliptic orbit examined for motion about equilibrium position with spin axis normal to orbit plane [AIAA PAPER 67-124] 06 p1095 A67-18333

Planar librational stability boundaries for flexible satellite under solar heating influence, using phase space concept [AIAA PAPER 67-126] 06 p1095 A67-18333

Attitude control for sun-pointing scientific satellites, considering control loop, sensor and actuator control

torques 06 p1098 A67-18765

Linear and nonlinear attitude control law synthesis for spinning aerospace vehicles, including analog simulation for control designs based on frequency symmetry 07 p1257 A67-19359

Command laws for DC magnetic attitude control of spin-stabilized earth satellites by means of coil of axis parallel to spin, including effects of orbital eccentricity and magnetic dipole 07 p1257 A67-19361

Electric propulsion for satellite applications, noting cesium contact microthruster ion engine system [AIAA PAPER 67-80] 07 p1240 A67-19435

Satellite attitude control in elliptic orbit 11 p1869 A67-24337

Malkin theorem for satellite attitude control subjected to light pressure perturbation 11 p1870 A67-24723

Rate of satellite turn in elliptical orbit calculated by introducing nondimensional angle, deriving master curves, noting applicability to attitude control systems 12 p2000 A67-25124

Low thrust divergent flow cesium-on-tungsten contact ionization electrostatic thruster for satellite attitude control and stationkeeping missions [AIAA PAPER 66-569] 13 p2188 A67-26824

Design and optimal performance considerations on application of derived rate increment feedback to satellite attitude control systems in limit cycle and acquisition systems 13 p2212 A67-27297

Earth-pointing satellite attitude control system using gravity gradient stabilization, deriving motion equations 15 p2564 A67-29329

Pseudorate sawtooth-pulse-reset controller design for satellite attitude control system 15 p2458 A67-29430

Magnetic device design optimization for satellite attitude control, noting equations and charts 15 p2572 A67-30385

Flux-gate magnetometer device for determining attitude of satellite or rocket probe, considering magnet perturbation due to solar wind and solar storms 16 p2700 A67-30658

Fluoric solar attitude control device functioning as sensor and actuator, noting design principles and operation 17 p2954 A67-31982

Pneumatic power for attitude control of long-life orbiting satellite, considering parameters, mission objectives, etc 17 p2801 A67-31983

Attitude control system and actuator locations in flexible spinning toroidal manned space station 17 p2954 A67-32055

Active damping concept for gravity gradient satellite attitude control to reduce oscillation time constant, initial capture time and oscillation magnitude 17 p2954 A67-32073

Calibration of star tracker bias errors on OAO 17 p2955 A67-32479

Earth-based radio reference signal in obtaining attitude and pointing information for synchronous communications satellites 18 p3137 A67-34113

Attitude stability of spinning rigid symmetric satellite in elliptic orbit examined for motion about equilibrium position with spin axis normal to orbit plane 19 p3333 A67-35747

Attitude determination and hydrogen peroxide control system for spacecraft orientation in Syncom, Early Bird and ATS [AIAA PAPER 67-532] 19 p3334 A67-35934

Lunar Orbiter Attitude Control System design and space flight performance [AIAA PAPER 67-533] 19 p3334 A67-35935

Damped mass expulsion for space vehicle attitude control reducing propellant consumption and pulsing frequency [AIAA PAPER 67-535] 19 p3334 A67-35937

Strapdown star tracker for space vehicle attitude control, using scanning and error-signal determination method [AIAA PAPER 67-551] 19 p3233 A67-35948

Control moment gyro /CMG/ and use in space-vehicle attitude-control system, emphasizing control laws [AIAA PAPER 67-589] 19 p3336 A67-35985

Attitude control methods compared for use in rockets collecting data in UV region from various stars 20 p3531 A67-36411

Predictor display instrument for optimal manual control, noting use in manned spacecraft missions and time factor 20 p3447 A67-36840

Mathematical model describing magnetic damping in attitude control system of ESRO I satellite 21 p3878 A67-38216

Satellite stabilization in geomagnetic field by applying magnet to satellite axis and using damping elements of soft magnetic materials 21 p3713 A67-38375

Passive orientation of space vehicle toward sun by black and white coating, analyzing free oscillation about equilibrium 21 p3713 A67-38598

Satellite attitude by onboard radio antennas method 21 p3583 A67-38637

Solid propellant electric thruster /SPET/ using pulse plasma for spacecraft attitude control and stationkeeping [AIAA PAPER 67-661] 21 p3690 A67-38697

Single nozzle thermal storage resistojet thruster for low thrust satellite attitude and orbit control applications, noting design and performance [AIAA PAPER 67-682] 21 p3690 A67-38698

Satellite orbit adjustment, stationkeeping and attitude control of typical earth-and sun-synchronous satellites by electric propulsion systems [AIAA PAPER 67-719] 21 p3694 A67-38745

Multijet electrothermal systems for attitude control and stationkeeping of synchronous communications satellite [AIAA PAPER 67-723] 21 p3694 A67-38748

Radioisotope heating for ionizer temperature of contact ionization thrusters for satellite attitude control and stationkeeping, studying power source mass saving [AIAA PAPER 67-735] 21 p3695 A67-38758

Pulsed vacuum arc microthruster noting various performance data and advantages [AIAA PAPER 67-737] 21 p3695 A67-38759

Electric propulsion applied to satellite stationkeeping and attitude control, noting ion engine resistojet combination providing complete redundancy [AIAA PAPER 67-722] 21 p3697 A67-38961

Minimum variance simulation for satellite attitude determination reliability using magnetic and solar measurements 21 p3715 A67-39150

Fuel optimal control conditions in attitude correction of satellite in circular orbit determined using maximum principle, solving resulting boundary value problem 21 p3715 A67-39153

Single-axis time and fuel supoptimal /superior optimal/ control for spacecraft attitude control obtained via bang-bang manipulation of damping and jet commands 22 p3897 A67-39155

Triaxial attitude control stabilization for second-generation /TIROS/ meteorological satellite 22 p3897 A67-39156

Matrix method proposed for systems of linear differential equations governing satellite attitude control in elliptical orbits, considering integral criteria calculation 22 p3897 A67-39160

Satellite attitude stabilization using gimbaled star trackers, analyzing satellite and star tracker motion in terms of angular velocity 22 p3830 A67-39170

Linear servosystem parametric optimization and application to satellite attitude control, discussing selective and gradient methods 23 p4070 A67-40577

Ariel III satellite attitude determination using optical glint technique 24 p4240 A67-41877

Sun pointing attitude control acquisition by space vehicle with jet control system 24 p4182 A67-41974

Star tracker error signal processor for onboard current satellite attitude control over wide range of gimbal angles 24 p4154 A67-42175

Attitude errors of inertially coupled gravity gradient satellite with solar radiation pressure as dominant disturbance, noting slot problems in stabilized package accommodating damper motion 24 p4241 A67-42904

Stabilization and control techniques for future unmanned commercial space vehicles, emphasizing application of projected technological advances in instrumentation [AIAA PAPER 67-878] 24 p4244 A67-42997

SATELLITE ATTITUDE DISTURBANCE

Oscillatory motions of orbiting body around center of mass, noting stability of these librations if amplitude is always limited in time 01 p0153 A67-10411

Nonlinear resonance effect on attitude librations of undamped rigid gravity gradient stabilized satellite in circular Earth orbit 16 p2745 A67-30741

Attitude continuous instability regions in parameter space and resonance frequency of spinning unsymmetrical satellite noting periodic processes 22 p3899 A67-39311

SATELLITE COMMUNICATION

Two-stage parametric amplifier using GaAs cooled in closed cycle cryogenic refrigeration system applied to satellite communications 01 p0033 A67-10029

Ground station receiver for satellite communication which utilizes liquid-helium-cooled parametric amplifier at top producing extremely low noise temperature 01 p0023 A67-10469

Velocity aberration and atmospheric refraction pertaining to laser satellite communication experiments, obtaining equations for estimation of effects 02 p0198 A67-12054

Ray tracing study of HF ducting propagation with satellites [RASSA PAPER 1-10-145] 03 p0373 A67-14252

Satellite to satellite communications experiment simulation via digital computer, proving existence of whispering gallery propagation in lower ionosphere [RASSA PAPER 1-10-148] 03 p0373 A67-14255

NASA FM telemetry system for data acquisition and processing from Ariel satellites including methods for storage, transmission, handling, etc 04 p0568 A67-14437

Raindrop and melting hailstone absorption, scattering and backscatter cross sections of millimeter waves in satellite communications and weather radars 04 p0577 A67-15685

Haystack antenna used for satellite communications and celestial observation, noting digital computer for control system and data processing 05 p0790 A67-17517

Operative satellite applications including telecommunications, meteorology and radionavigation 06 p1093 A67-17555

International Consortium for Telecommunications by Satellites /Intelsat/, noting Comsat connections 06 p0956 A67-17556

European Conference on Telecommunications by Satellites /CETS/, recommendations and patterns of cooperation 06 p1119 A67-17558

Communications satellite systems technology, papers from AIAA Conference, Washington, D.C., May 1966 06 p0957 A67-17662

Effective radiated power, receiving sensitivity, bandwidth and nonlinear performance of Early Bird satellite 06 p0959 A67-17664

Performance of Early Bird communications satellite and associated ground stations 06 p0959 A67-17665

Selection of optimum ranging signal for jam resistant satellite communications system 06 p0959 A67-17671

Fading and multipath propagation mechanism for communication links involving satellites and aircraft with antenna beams, assuming fading models and estimating margins required for FSK teletype transmission 06 p0960 A67-17673

Satellite ground terminal design considerations using adaptive digital communications techniques, noting analog to digital conversion 06 p0960 A67-17675

Ground-based steerable paraboloid spherical reflector and multiplate type antennas, noting cost per unit area for unit wind speed of 30 mph and frequency of 1400 mc, performance, restrictions, etc [AIAA PAPER 66-324] 06 p0967 A67-17685

Errors by mutual interference in frequency-time coding in satellite communications systems, deriving expressions relating commissive and omissive error rates, simultaneous users per unit bandwidth, etc 06 p0961 A67-17696

Future pattern of communications satellite systems, reviewing world requirements for telephony, telex, TV and radio [AIAA PAPER 66-319] 06 p0961 A67-17709

Satellite communications system noting instrumentation, design criteria, frequency range, propagation aspects and suitable trajectories 07 p1141 A67-19344

Satellite-borne transmitter operating at 138 MHz 07 p1151 A67-19523

Complex and decision feedback systems for command channels in space communications 07 p1145 A67-19872

Mechanical and electrical performance requirements of satellite communications antenna using Cassegrain configuration, noting relation to design 07 p1157 A67-20092

Millimeter wave satellite communications, considering propagation, orbital and system design parameters, antenna pointing and satellite and ground equipment 08 p1292 A67-20671

Satellite communication network requirements and orbital characteristics 08 p1293 A67-20724

Sea station and satellite for long range communication with aircraft 08 p1294 A67-20778

High power broadband traveling wave tube YH 1041 as transmitting tube for satellite radio communication, discussing mechanical layout and operational characteristics 08 p1307 A67-21446

Satellite orbit effect on establishment of global communications network 08 p1296 A67-21505

Transmission methods in satellite communications and power level decrease by noise reduction 09 p1463 A67-21758

Multicavity klystrons and traveling wave tubes and use in ground stations 09 p1478 A67-22257

Transoceanic aircraft control and communication via satellite 09 p1466 A67-22641

Echo suppressor for reducing speech interference in telephone relaying by satellite 10 p1603 A67-22771

Total electron content calculated by measurement of Faraday and Doppler effects of satellites 10 p1604 A67-22987

Amplitude fluctuations of VHF beacon of Early Bird synchronous satellite observed from stations in Italy and Massachusetts 10 p1640 A67-23233

Ground station antenna steering system for satellite communication, noting design 11 p1758 A67-24061

Satellite-emitted short radio wave field intensity and ionospheric parameters 11 p1751 A67-24071

Rain effects at random antenna elevation 11 p1753 A67-24303

Low noise amplifiers at Fucino for reception from Early Bird satellite 12 p1913 A67-25301

Parabolic Cassegrain antenna with low noise temperature for space telecommunication station 12 p1913 A67-25304

OGO communication system design and flight test 12 p1907 A67-25994

Satellite telecommunications system, merits of single global system and legal aspects 12 p2042 A67-26140

Doppler frequency shift for radio waves radiating coherently from satellite in ionosphere, considering electron concentration and angles of refraction 13 p2067 A67-26568

Satellite Telecommunications with Automatic Routing /STAR/ system composition and operation, detailing signal relaying procedure 13 p2067 A67-26717

Satellite Telecommunications with Automatic Routing /STAR/ system modulation techniques, channel capacity and Start-Stop /SS/ operation 13 p2067 A67-26718

Satellite Telecommunications with Automatic Routing /STAR/ system transmission system operation and modulation techniques 13 p2068 A67-26719

Alternative modulation techniques for Satellite Telecommunications with Automatic Routing, considering start-stop operation with PCM-FDM system 13 p2068 A67-26720

Satellite telecommunication, with automatic routing noting switching concept and modulating methods 13 p2087 A67-26721

Satellite telecommunication with automatic routing noting switching 13 p2087 A67-26722

Liquid helium traveling wave maser amplifier for low noise ground station satellite communication 14 p2329 A67-27777

Cooling system for maser amplifier for ground station satellite communication 14 p2277 A67-27778

Two-stage parametric amplifier system cooled to 20 degrees K, as low noise amplifier in receiving equipment for satellite communication 14 p2278 A67-27780

Two-stage fixed-tuned parametric amplifier for satellite communications earth stations, considering circulator development and varactor 14 p2278 A67-27781

Low noise receivers in transportable satellite communication ground terminals, discussing interrelationships between antenna, receiver and cryogenics 14 p2260 A67-27782

Low temperature parametric amplifiers, discussing varactors, circulators and demands on cooling 14 p2278 A67-27783

World telecommunication satellite developments, service, requirements, technical and financial elements 14 p2270 A67-28583

Total electron content calculation by measuring Faraday and Doppler effects of satellites on reception frequency 14 p2270 A67-28607

Demand, applications and technology for future satellite communications covering transoceanic and military telecommunication, TV network, weather data, etc 14 p2274 A67-28912

Communication technology role in commercial utilization of space, considering spectrum utilization, economic benefits and satellite programs [AAS PAPER 67-78] 15 p2437 A67-29945

Business, government and possible home applications /including mail and education/ for electronic communications via satellites, discussing legal implications [AAS PAPER 67-91] 15 p2437 A67-29952

Proposed worldwide navigation, communication and traffic control system for all weather to guide aircraft and vessels, locate distressed vehicles and direct rescue operations at sea [AAS PAPER 67-102] 15 p2515 A67-29957

Multiple carrier measurements using TWT for application to satellite communications 15 p2438 A67-30140

Worldwide meteorological satellite system, operation, structure and functions 16 p2759 A67-30686

Satellite communication, noting satellite and ground terminal design performance criteria 16 p2622 A67-30689

Lunar communications using satellites in astrodynamical aspects of lunar orbital stability and effective communications zone 16 p2622 A67-30730

Satellite receiving and transmission antenna orientation effects obtained by Faraday rotation 16 p2628 A67-31507

Satellite relay to provide communication paths for aircraft-ground communication over ocean, considering system design for ATC using reflex repeater 16 p2629 A67-31530

Linear programming algorithm for optimizing channel assignments in satellite communication systems 17 p2810 A67-32111

Component selection of antenna steering system in satellite communication system, discussing tracking system characteristics and servo operation modes 17 p2833 A67-32190

European Satellite Telecommunication Conference /CETS/, discussing government participation, INTELSAT projects, European technical program and juridical and administrative operations 17 p2974 A67-32398

Satellite telecommunication techniques including demodulation, detection, microwave amplification, antennas, etc 17 p2813 A67-32400

Multiple laser communication design, considering links between ground stations and earth-synchronous satellite with single telescope and laser 17 p2813 A67-32495

Multipath effect measurement in propagation path at UHF frequencies from synchronous satellite to aircraft 17 p2816 A67-32626

Radiated power and frequency limitations of repeater in stationary satellite covering physical, legal and project viability limitations 18 p2999 A67-33657

RF design of satellite communications ground stations, giving hardware data on receivers, transmitters, tracking systems, power amplifiers and reliability 18 p3003 A67-34349

European heavy launching vehicle development potential and economy,

discussing communication satellites, thrust augmentation, zero stages, synchronous orbit, etc 18 p3137 A67-34353

Computer application to planning and operating simultaneous access European ground station network 18 p3003 A67-34355

Ground station for satellite communications in Italy covering TV transmission 19 p3207 A67-35568

International Telecommunications Satellite Consortium /INTELSAT/ organization 19 p3349 A67-35640

Modulation systems in satellite communications evaluated by criteria of baseband signal noise ratio, signal power, frequency band requirements, etc 20 p3383 A67-36956

Worldwide satellite communications requirements, financial aspects and projects 21 p3581 A67-38211

Satellite influence on microwave antenna design, discussing mount designs, multifunctional antenna feed systems, structural analysis and geometries for microwave antennas 21 p3593 A67-38233

Telemetry receiving station and remote control system for satellites and missiles, measuring Doppler effect, demodulation and diversity combiners 21 p3583 A67-38639

Nonline-of-sight communication with FR-1 satellite along magnetic field line of emitter, using VLF electromagnetic waves 21 p3584 A67-38656

Luna IX automatic station flight control complex, detailing communication, orientation and stabilization systems operation after separation from acceleration module 22 p3897 A67-39167

Short bursts of scintillation of satellite radio signals from S-66 satellite, discussing diurnal variation correlation with spread of occurrences 22 p3759 A67-39478

Weather effects on exposed and enclosed earth based satellite communications antenna systems, discussing performance characteristics under various meteorological conditions 22 p3763 A67-40408

Tracking ground station on Ascension Island to relay communication with Apollo spacecraft via INTELSAT II 23 p3986 A67-40706

SATELLITE CONFIGURATION

San Marco satellite structural configuration for measurement of total force acting on satellite, electron content from satellite to earth and guided propagation 03 p0517 A67-12900

Explorer type compared to Orbiting Observatory type satellites regarding weight, volume, reliability, data transmission, power, etc 12 p2012 A67-25785

SATELLITE CONTROL

Computer program providing ion thruster design criteria and power and weight requirements for specific satellite control mission [AIAA PAPER 66-498] 02 p0302 A67-11515

Ion propulsion systems development for near term mission, noting solar cell weight reduction [AIAA PAPER 66-1026] 03 p0504 A67-14275

Early Bird hydrogen peroxide control system maneuvers to place satellite into final stationary position 06 p1093 A67-17663

Code-division-multiplex decentralized control system for communication satellites based on use of pseudorandom PM signals of wide bandwidth 06 p0959 A67-17672

Parameters of satellite communication system control and scheduling function, emphasizing distinction between scheduling model and scheduling algorithm 06 p0961 A67-17699

Orbit position control based on solar pressure on plane sail structure and hollow thin-skinned lenticular shape of passive communications satellites [AIAA PAPER 66-313] 06 p1094 A67-17703

Testing facility and methods for FR-1 and D-1 satellite control 07 p1163 A67-19530

Feedback control system to position satellite in vicinity of unstable collinear libration point with application to lunar communication problem [AAS PAPER 66-132] 07 p1146 A67-19991

German papers on space research with satellites and space probes, Volume 2, Control, test stands and direction finding 07 p1260 A67-20266

Synchronous satellite communication systems including altitude and motion

effects, time delay, control system, antenna, etc 12 p1907 A67-25991

Computer program providing ion thruster design criteria and power and weight requirements for specific satellite control mission 13 p2188 A67-26825

[AIAA PAPER 66-498] Elastic deformation effects on stability of rotating satellite composed of elastically connected rigid bodies 13 p2212 A67-26905

Feedback control system to position satellite in vicinity of unstable collinear libration point applied to lunar communication problem 13 p2210 A67-27543

[AAS PAPER 66-132] Optimum stabilization of axisymmetric satellite by system of n reactive jets 14 p2393 A67-27854

Optimum control of earth satellites and space vehicles and stable solutions of orbits in orbital mechanics 14 p2393 A67-27879

Onboard receiver-decoder control unit for ESRO I and II consisting essentially of four-state signal corresponding to time modulated pulses 21 p3581 A67-38201

Satellite stabilization with respect to geomagnetic field obtained by applying moments of magnetic forces 21 p3713 A67-38589

Satellite-gyroscope asymptotic equilibrium positions obtained by general motion equation, calculating gravitational and aerodynamic moment 22 p3898 A67-39187

Synchronous orbit communication satellite electric thruster, considering space charge neutralized ion accelerator 23 p4049 A67-41428

Vehicular traffic and rail transportation surveillance or coordination aids possibilities using earth orbiting satellite [AIAA PAPER 67-788] 24 p4242 A67-42951

Geopolitical factors connected with navigation satellite operation and control [AIAA PAPER 67-960] 24 p4260 A67-43041

SATELLITE DESIGN

Matching reliability methods to real situations in system-assessment context 01 p0078 A67-10514

OGO experiments including earth atmosphere, magnetosphere, earth-sun system, etc 02 p0334 A67-12359

Thermal design method for Japanese scientific satellite L4S, based on skin temperature determination and correlation with inner compartments 02 p0335 A67-12392

FR-1 satellite design difficulties such as material selection, insulation of structure, making structure perfectly conducting, etc 03 p0518 A67-13601

Nuclear power systems for future communications satellites noting reactor, radioisotope, power system and thermoelectric power conversion equipment 06 p1029 A67-17687

Tiros satellite development and Tiros operational satellite /TOS/ system noting design, camera orientation, spin-rate control, etc 06 p1096 A67-18412

Space radiation effect on satellite design, noting guidelines for electronic equipment shielding 06 p1078 A67-18419

Temperature fluctuation of thin walled satellite passing periodically from sun to shade simulated by hybrid computer 07 p1257 A67-19375

DI satellite structure noting rigidity and shock absorbing properties 07 p1258 A67-19526

FR-1 satellite structure and fabrication 07 p1191 A67-19529

Satellite structure from Be-lockalloy, properties compared with Al and joining methods 07 p1192 A67-20251

German papers on space research with satellites and space probes, Volume 1, Physical principles and methods of constructing carrier rockets 07 p1260 A67-20265

UK-3 satellite electrical design and ground checkout equipment 09 p1484 A67-21828

Thermal design of navigational satellites, obtaining reduction in discrepancy between operational orbital temperatures and preflight calculations through thermal vacuum testing 09 p1572 A67-22062

Diademe satellites design including laser beam range determination reflectors for spatial geodesy, laser telemetry, etc 10 p1712 A67-22860

Pressure shell structures for space noting

materials, machining, assembly, welding, testing, etc 10 p1661 A67-23731

Albedo upper and lower fluctuation bounds determined by astrophysical comparison and three other methods 12 p2003 A67-25684

Satellite sealed subsystems individual leak rates in thermal-vacuum environment measured with mass spectrometer 12 p1921 A67-25690

Satellite size via experiment design, demonstrating advantages and drawbacks of small and large satellites 12 p2007 A67-25784

OGO communication system design and flight test 12 p1907 A67-25994

U.S. communication satellites design and transmission, including antenna types offering interference-free reception 13 p2066 A67-26334

Temperature control in design of ESRO I European research satellite 13 p2222 A67-26582

ESRO I research satellite structural design test results for study of polar ionosphere, particularly auroras 13 p2211 A67-26583

Possibility of constructing and launching artificial satellite free of terrestrial influence to verify relativity theory 15 p2565 A67-29743

Magnetic design of OGO and Pioneer solar probe including data on instrumentation, mechanical equipment, permanent magnets, test methods, etc 16 p2757 A67-30637

Nimbus I spacecraft overall characteristics, performance and major subsystems, particularly performance of meteorological sensors 16 p2759 A67-30690

Fundamental design features that have made synchronous communications satellites practical 16 p2759 A67-30690

Early Bird satellite technology including design parameters, structure, power supply, control system and test program 16 p2759 A67-30691

European television satellite design emphasizing coverage area, carrier frequency selection, etc 16 p2622 A67-30697

Communications satellite systems discussing launching, orbits economics, etc 16 p2760 A67-30700

Diapason satellite thermal control noting external energy exchange calculation, coating, in-space simulation tests, temperature measurements, etc 16 p2762 A67-31018

Lunar orbiter quality assurance program, emphasizing management, design, procurement, fabrication, quality control, etc 16 p2783 A67-31629

Configuration study for ELDO-PAS test satellite based on communications requirements 17 p2955 A67-32396

Future satellite regional and intercontinental telecommunication network, considering weight, classes, performance and orbital factors 17 p2813 A67-32397

Diamant satellite series, describing design and construction of Diapason and Diadem orbital satellites 17 p2956 A67-32746

Characteristics, operation, technology and reliability of telemetering systems for ESRO I, HEOS A, TD 1 and TD 2 including control factors and coding 17 p2816 A67-32747

Electronic systems in Ariel III satellite detailing power distribution, storage control, telecommand, telemetry and data handling 17 p2827 A67-32822

German Azur research satellite program design, instrumentation, payload, etc, and NASA role 18 p3162 A67-33640

Circuit for integral majority-voting logic elements intended for satellite design, analyzing reliability and performance 18 p3007 A67-34664

Specific features of French Diademe satellites noting payload stabilization, thermal control observation carried, instrumentation, etc 19 p3333 A67-35500

Early Bird satellite design features, orbital performance, use, COMSAT applications, etc 19 p3183 A67-35636

Satellite programs for Black Arrow launch vehicle, discussing functions, tasks, tests, etc 19 p3333 A67-35842

Influence of navigational requirements and technology on design of navigation-satellite system 19 p3256 A67-35862

Computer program for determining net thermal energy incident on satellite by computing projected surface area

[ASME PAPER 67-HT-56] 20 p3549 A67-36738

General purpose unmanned spacecraft and multimission applications satellite possibilities [AIAA PAPER 67-635] 20 p3534 A67-37620

Thermal design of electronic packaging of Nimbus satellite control system 21 p3594 A67-38328

Component selection program for equipment onboard FR-1 satellite covering production facilities, qualifications, supply, reliability, etc 21 p3572 A67-38676

Ariel III satellite design, development, mechanisms, power supply and data handling systems 22 p3898 A67-39178

Solar cell power systems design and control technique for use in satellite programs, specifically transit 3B and 4A, ionosphere Beacon satellite, etc 23 p3938 A67-41507

Solar cell power supply design to satisfy whole satellite, discussing power supply size and solar cell panel fabrication 23 p3939 A67-41508

Biosatellite II, mission objectives and planned experiments 24 p4240 A67-41897

Environmental control and life support system design for NASA Biosatellite program, discussing experimental results [SAE PAPER 670839] 24 p4114 A67-41995

Temperature variations of satellite with radiatively coupled isothermal inner shell having heat source analyzed via perturbation method for differential equations 24 p4253 A67-42051

ESRO II satellite project objectives, design, testing program and mission requirements 24 p4241 A67-42402

Solar cell/battery power systems for post-1975 satellites, discussing oriented thin film CdS solar cell array 24 p4105 A67-42515

Orbiting reflector satellites, concepts, design, structural mechanizations and control [AIAA PAPER 67-786] 24 p4242 A67-42949

Graphics system for space vehicle design and flight plan via light pen, trajectory computation and performance curve display on scope [AIAA PAPER 67-897] 24 p4126 A67-43006

Stationary satellite to provide educational TV to underdeveloped lands noting design, transmission terminals and safeguards against control and propaganda [AIAA PAPER 67-963] 24 p4260 A67-43042

SATELLITE DRAG

Motion of satellite inside resisting atmosphere 04 p0696 A67-14737

Induction drag of long cylindrical satellites and Alfvén waves emitted from them, determining potential and current distribution and effect on energy loss [AIAA PAPER 66-478] 04 p0704 A67-14829

Electric drag of satellites noting contribution of impinging ions 04 p0705 A67-14998

Satellites in near-circular decaying polar orbits experience drag forces at equatorial latitudes greater than those at polar latitudes 04 p0706 A67-15233

Upper atmospheric rotation speed reevaluated from satellite orbital inclination changes 05 p0803 A67-17412

Equations of motion for earth satellite indicate greater significance for atmospheric resistance than gravitational effect 06 p1083 A67-18040

Plasma sheath formation and effect on satellite interacting with geomagnetic field and ambient plasma 08 p1410 A67-20714

Shape and location of diurnal bulge in upper atmosphere, analyzing density and temperature distribution at high latitude from satellite drag data 10 p1639 A67-23208

Time delay between geomagnetic storm and corresponding maximum in atmospheric density obtained from satellite drag data 10 p1639 A67-23209

Atmospheric density determination from drag of eleven low altitude satellites, discussing correlation with geomagnetic activity and daily periodicity 11 p1784 A67-23937

Ionospheric aerodynamics, discussing flow field properties, satellite motion, flight characteristics, etc 14 p2242 A67-28200

Satellite drag analysis of atmospheric temperatures noting effects of UV, solar radiation and geomagnetic fluctuations 14 p2314 A67-29027

Semiannual exospheric density variation confirmed by satellite orbit

analysis 17 p2852 A67-33238
 Atmospheric density determination from satellite drag, noting effects of magnetic storms, diurnal and semiannual variations, solar activity, etc 18 p3041 A67-34253
 Geomagnetic activity effect derived from Explorer IX drag data, with atmospheric temperature as geomagnetic storm intensity function and atmospheric density increase 18 p3042 A67-34255
 Very high satellite air drag acceleration studied by University of London Observatory, discussing solar radiation pressure acceleration 18 p3042 A67-34257
 Upper atmosphere density, temperature and variation determined from satellite drag data, proposing thermosphere model 19 p3214 A67-34931
 Lower thermosphere physical properties, studying satellite drag for density profiles, composition, data comparison, etc 19 p3215 A67-35171
 Air density variations at heights near 150 km determined by analyzing satellite orbit changes, noting solar activity effect 19 p3215 A67-35181
 Upper atmosphere densities and scale heights from Soviet earth satellite drag data, noting diurnal variation 19 p3219 A67-35252
 Drag coefficients for random and planar tumbling satellites 21 p3563 A67-37809
SATELLITE GROUND SUPPORT NETWORK
 Weather effects on exposed and enclosed earth based satellite communications antenna systems, discussing performance characteristics under various meteorological conditions 22 p3763 A67-40408
SATELLITE GROUND TRACK
 Resonance effects for satellites with nominally constant ground track 16 p2744 A67-30731
SATELLITE GUIDANCE
 Three-stage Black Arrow satellite launcher, detailing guidance system used in first and second stages and system used to rotate third stage 03 p0519 A67-13929
SATELLITE INSTRUMENTATION
 Energetic particle monitoring satellites, discussing design and development of four IMP generations 01 p0156 A67-11415
 Electrical system design and integration in UK-3 scientific satellite, noting noise control for receiver 01 p0156 A67-11423
 Solar X-ray emission measurements with Geiger photon counters carried by Elektron II and IV satellites 02 p0240 A67-11544
 Shaped-beam pattern attitude-stabilized satellite communications antenna as improvement over conventional horn antenna 02 p0212 A67-11606
 Decoder signaling system of Eldo satellite employing PCM telemetry channel, examining counters, shift registers, flip-flop circuit, etc 02 p0192 A67-11651
 Wide range vibrating-reed Mariner II electrometer, describing components, performance characteristics and results 02 p0241 A67-11681
 Physical and functional characteristics of contoured amplifying semiconductor radiation detectors for use in missile and satellite instrumentation 02 p0244 A67-12211
 Operation and control of satellite equipment, discussing automatic, semiautomatic, human and telefactor /man-extension system/ methods [AIAA PAPER 66-918] 02 p0204 A67-12250
 Line scan TV for earth observation satellites noting camera design, coverage, systems effectiveness and performance results 02 p0335 A67-12398
 Calibration procedures for earth albedo experimental package of Orbiting Solar Observatory 02 p0246 A67-12401
 Effect of electron irradiation on silicon solar cells constituting power generator aboard Diapason IA 03 p0362 A67-12897
 Problems of temperature data from Explorer and Ariel II satellites including magnetometer failure, poor conduction, paint degradation, etc 03 p0518 A67-13074
 Cosmos 53 satellite radiation data using on board gas discharge 05 p0879 A67-16107
 Silicon integrated circuit data encoder for Isis A satellite particle counting experiment, noting design and construction 05 p0770 A67-16292
 Satellite role in worldwide meteorology, discussing global observation, observation

platforms, manned satellites, and remote sensing and data collection of satellite instrumentation 05 p0837 A67-16383
 ESRO II satellite project, describing systems and program management 05 p0905 A67-16728
 PCM telemetry unit for Nimbus B spacecraft noting applications and performance 05 p0767 A67-17463
 Data processing and control by spaceborne computer on instrumentation satellite used for analyzing space scientific properties, noting factors influencing system design 05 p0768 A67-17516
 TWT delivering CW power in L, S, C and X-band designed for space environment, considering size, weight and voltage and comparing klystrons, amplifiers, circuit design, etc 06 p0967 A67-17688
 [AIAA PAPER 66-308]
 Plasma induced interference signal in satellite VLF receiver originating with converter system and appearing only in daylight operation 06 p0984 A67-18569
 Oceanographic measurements with instrumented satellites, examining surface temperature surface waves, tides, albedo, heat flux and coordination of airborne and seaborne sensing systems 06 p0999 A67-19000
 OAO satellites for astronomical experiments, discussing planning and specific features 06 p1098 A67-19048
 Laser application to meteorology, discussing Rayleigh, aerosol and Raman scattering, system configuration and measurement problems 07 p1194 A67-19091
 Photomultiplier tubes for satellite instrumentation, discussing application as circuit components and star trackers 07 p1185 A67-19397
 Satellite camera of Potsdam Geodetic Institute 07 p1187 A67-19763
 Proton I and II satellite instrumentation noting energy-charge spectrometer, gamma-quantum fluxmeter, equipment to determine chemical composition of charged cosmic ray particles, etc 08 p1376 A67-21001
 Onboard device locating present and future orbital satellite position through microfilm map dependent on satellite motion equation 08 p1352 A67-21525
 Cosmos satellites physical research 09 p1570 A67-21654
 Solar cell system for UK-3 satellite, discussing design, material selection, development and fabrication 09 p1445 A67-22179
 Failure reporting, analysis and correction on satellite programs, discussing system reliability 09 p1480 A67-22289
 Pioneer VI detector to measure degree of anisotropy of cosmic radiation at various energy ranges 09 p1500 A67-22427
 Digital /chirp/ radiosonde for meteorological and earth satellite measurements employing pulse bursts from voltage controlled oscillator 10 p1655 A67-22823
 Diademe satellites design including laser beam range determination reflectors for spatial geodesy, laser telemetry, etc 10 p1712 A67-22860
 Multipurpose satellite computer for data processing 10 p1608 A67-22974
 Scattered Lyman alpha radiation in geocorona analyzed using satellite mounted equipment 10 p1706 A67-23223
 TV subsystem of Surveyor I, discussing operation-design constraints, camera configuration, video sequence, etc [SMPTE PAPER 101-43] 12 p1904 A67-25461
 Dual camera for Lunar Orbiter, design, performance and hardware modifications [SMPTE PAPER 101-47] 12 p1940 A67-25465
 High quality film processing in Lunar Orbiter spacecraft photo system, noting separate environmental control system [SMPTE PAPER 101-49] 12 p1941 A67-25467
 Satellite measurement of low energy electrons and protons in auroral regions, discussing use of instruments with variable energy electrostatic thresholds and postacceleration techniques 12 p1944 A67-25851
 Nuclear abundances of galactic and solar cosmic rays, discussing detector electronics system for measurement of particle energy spectrum 12 p1944 A67-25852
 Digitized spark chamber for gamma ray and charged particle experiments on balloons and satellites noting construction,

performance characteristics and results 12 p1944 A67-25854
 Channel multiplier instrument measuring low energy electron and proton auroral fluxes from polar orbiting satellites 12 p1944 A67-25855
 Directional neutron detector using liquid scintillator for low mev energy range for rocket and satellite experiments 12 p1945 A67-25860
 Microminiature circuits in space electronics 12 p1918 A67-26216
 Instrument testing for 625 A1 research satellite with Nike-Apache BRD-A1 high altitude research rocket 13 p2119 A67-26581
 Electric field meter /E-meter/ measurement of field strength at given point on spacecraft surface [AIAA PAPER 66-74] 13 p2120 A67-26835
 Space flight technology developments, particularly for booster rockets and space vehicles 14 p2393 A67-27873
 Large antenna radiation from radio astronomy Explorer satellite determined on basis of antenna current distribution 14 p2286 A67-28507
 High data rate storage for Nimbus B satellite noting signal processing, checkout and retrieval operations 14 p2276 A67-28918
 Military surveillance satellite for high resolution photography noting design, application and projected performance 15 p2564 A67-29400
 Thermal, mechanical and electrical design of stable quartz crystal oscillator used for Geos satellite to generate RF carriers and Doppler system timing signals 15 p2445 A67-29585
 French satellite FR-1 to be launched in late 1965 by NASA for ionospheric studies, noting instrumentation, data transmission, etc 16 p2757 A67-30641
 Semiquantitative evaluation of instrument requirements of solar probe as function of perihelion 16 p2758 A67-30644
 Probe for measuring energy transfer between satellite surface and upper atmosphere 16 p2670 A67-30646
 Satellite onboard multichannel systems for information processing, discussing construction, quick response memory and block diagrams 16 p2633 A67-30673
 Solar X-ray emission measurements with Geiger photon counters carried by Elektron II and IV satellites 16 p2677 A67-31610
 Batteries and fuel cells for space power systems, discussing Ni-Cd, Ag-Cd, Ag-Zn, Bacon cell, etc 17 p2801 A67-32047
 Schmidt satellite cameras to record trail from bearing and elevation fixed in relation to earth, detailing optical system of Royal Radar Establishment /RRE/ camera 18 p3048 A67-34237
 Structure of quasi-linear and wideband satellite transponders, discussing possible improvements 18 p3003 A67-34356
 Exhaust gases effect on satellites optical equipment calculated by determining propane attitude-control jet gas flow parameters 18 p3137 A67-34359
 Space research activities in Denmark /1966-1967/, discussing instrumentation design and development, experiments, etc 19 p3319 A67-35281
 Satellite programs for Black Arrow Launch vehicle, discussing functions, tasks, tests, etc 19 p3333 A67-35842
 High data rate storage system for Nimbus B tested by simulation 20 p3445 A67-36547
 Proportional counter spectrometer for solar soft X-ray spectrum study 20 p3448 A67-36960
 Principal investigator task evaluation, discussing responsibility for instruments, prelaunch operation, operational program establishment, processing, analyzing and publishing of results [AIAA PAPER 67-630] 20 p3534 A67-37614
 High reliability sequence programmers for DIAMANT satellite booster switching functions 21 p3655 A67-38207
 Traveling wave tube as hyperfrequency amplifier onboard satellites for reliable space communications 21 p3592 A67-38212
 ESRO I satellite electronic equipment design applied to aurora studies 21 p3713 A67-38217
 Telemetering antenna of instrument container of D-1 satellites 21 p3592 A67-38218
 Radiation effect on MOS transistors in D-2 satellite telemetry coder 21 p3593 A67-38230

Packaging of satellite plated wire memory components including memory plane stack, electronic circuit modules and interconnections 21 p3595 A67-38339

Penetration rates of thin aluminum foil sensors of Ariel II satellites compared with flux measured by microphone detectors in vicinity of earth 21 p3722 A67-38494

Satellite methods to determine absolute coordinates for geodetic points and to bridge continents 21 p3620 A67-38520

Satellite attitude by onboard radio antennas method 21 p3583 A67-38637

Satellite automatic telemetry data processing system, noting development of high speed computer for real time 21 p3588 A67-38638

PCM coder, programmer and analog switch of D-2 satellite, including systems characteristics and diagrams 21 p3599 A67-38647

FR-1 satellite-borne oxide cathode used to return to ground polarization current from ambient plasma 21 p3599 A67-38649

Junction field effect transistors for onboard satellite equipment, noting resistance to ionizing radiation 21 p3600 A67-38659

Sensors for acquisition and aiming of solar direction aboard D-2 satellite, discussing operating principles 21 p3629 A67-38666

Nomograph construction for earth pointing cameras, evaluating imaging system effectiveness as ground resolution and scale factor, plotting system performance characteristics 22 p3800 A67-40106

Multispectral remote sensing techniques for agricultural surveys from orbiting satellites, discussing in-flight signal processing 22 p3806 A67-40367

Explorer 32 satellite atmospheric density experiment gas calibrations, comparing operation and pressure response of various ionization gauges 23 p4004 A67-41356

Proton space station design and onboard instruments used for high energy cosmic ray study 24 p4210 A67-42391

Cosmos 53 satellite radiation data using onboard gas discharge counter 24 p4213 A67-42783

SATELLITE INTERCEPTOR

Comet mission study using space probes boosted by Atlas Agena and Atlas Centaur launch vehicles for interception from 1967 to 1975 16 p2745 A67-30750

Satellite retrieval system called Space Boia, employing passive/active grappling units depending on target vehicle dynamic characteristics 20 p3532 A67-36556

SATELLITE LAUNCHING

Design, development and main assemblies of third stage of ELDO satellite launcher 01 p0078 A67-10409

ELDO launching rockets for communications satellites 01 p0153 A67-10454

Solid propellant rocket motor for third stage of satellite launcher, performance requirements and design 10 p1698 A67-23483

Sun illumination time of artificial earth satellite moving in elliptical orbit 13 p2200 A67-27338

French space program /1966-1970/ techniques and installations for satellite launching and tracking 14 p2409 A67-28605

French installations for space research, describing laboratory work and industrial investments for satellite launching 14 p2320 A67-28606

Satellite launch vehicle performance analysis based on velocity requirements and gravity and drag losses for applications to booster configurations 14 p2394 A67-28701

Hypersonic reentry, inertial guidance tests and construction of two-stage Diamant satellite launcher 15 p2571 A67-30089

Satellite-launched artificial meteors discussing use, system concept, orbit considerations, cost, acceleration and separation 16 p2758 A67-30645

First stage checkout techniques of satellite launcher, noting digital computer program from pulse-code-modulated telemetry 16 p2655 A67-30835

Initial weight prediction of single and multistage launching vehicles by coordinating practical and theoretical aspects 16 p2762 A67-31490

Airborne camera system for high altitude photography of rocket and spacecraft vehicle launchings describing development 16 p2879 A67-31800

Projected series of satellite launchings by COMSAT, giving size and capacity comparisons with Early Bird technology 19 p3183 A67-35646

Chronological table of artificial satellites launched during 1966 including lifetimes, weights, dimensions and orbital details 20 p3531 A67-36307

Soviet space activity /1933-1967/ noting Sputnik, Venera I, Luna and Zond programs 23 p4086 A67-40919

AZUR project /first German satellite/ cooperation with NASA, testing, signal recording, etc 23 p4071 A67-41326

SATELLITE LIFETIME

Van Allen radiation belt simulation, obtaining accurate values for satellite and semiconductor lifetimes in orbit [AIAA PAPER 67-177] 06 p0981 A67-18510

Semiannual effect on satellite orbit decay, correlating with difference in latitude between perigee and subsolar point 07 p1251 A67-19850

Graphical method predicting orbital lifetime of satellite, considering oblate earth effects and long period fluctuations in atmospheric density [AAS PAPER 66-96] 07 p1252 A67-19960

Approximate method for predicting lunar satellite lifetimes and application to lunar orbit mission analysis [AAS PAPER 66-130] 07 p1255 A67-19989

Approximate determination of satellite lifetime by nomogram constructed on basis of known upper atmosphere density data 13 p2213 A67-27324

Graphical method predicting orbital lifetime of satellite, considering oblate earth effects and long period fluctuations in atmospheric density [AAS PAPER 66-96] 13 p2208 A67-27520

Approximate method for predicting lunar satellite lifetimes and application to lunar orbit mission analysis [AAS PAPER 66-130] 13 p2209 A67-27541

Van Allen radiation belt simulation, obtaining accurate values for satellite and semiconductor lifetimes in orbit [AIAA PAPER 67-177] 15 p2465 A67-29446

Artificial satellites lifetime in low altitude orbits, discussing atmospheric, geomagnetic, solar and lunar factors 18 p3136 A67-33550

Computer program for calculating optimal launch windows for orbiting satellites 19 p3190 A67-36071

Unmanned spacecraft reliability, discussing design requirements, testing, lifetimes, performance and ball bearing failures 20 p3532 A67-36573

Designs and performance of communications satellites, discussing long life, cooling, efficiency, larger future satellites, antennas and arrays 22 p3763 A67-40337

U.S. unmanned satellite program history, aims, success and failures 24 p4258 A67-42752

SATELLITE MANEUVER

Second order solutions to motion equations governing satellite rendezvous in elliptical orbit 12 p2012 A67-25931

Satellite maneuverability in orbit using hypothetical elliptical orbit to demonstrate formulas used 22 p3882 A67-39563

SATELLITE MEASUREMENT

Doppler-Flizeau frequency effect in ionospheric satellites measuring device based on wave refraction 01 p0057 A67-10233

Tiros VII satellite IR measurement data used to determine sea surface temperature gradients, examining problem of cloud cover 01 p0109 A67-10321

Interaction of solar wind and frozen-in magnetic field with geomagnetic field inside and outside magnetosphere, comparing theory with satellite measurements 02 p0320 A67-11461

External ionosphere electron concentration measurement from data on Doppler shift variations in frequency of coherent radio signals from Cosmos and Elektron satellite 02 p0192 A67-11658

Atmospheric water vapor distribution estimated from satellite measurements, using Planck radiance and assuming temperature distribution to be given 02 p0239 A67-12364

Thermal testing of critical systems module of meteoroid detection satellite without attaching sensor arrays 02 p0334 A67-12378

Weather satellite system determining worldwide occurrence and distributions of

thunderstorms and associated atmospheric effects 02 p0262 A67-12399

Low energy charged particle measurements, describing satellite mounted spherical electrostatic analyzer 02 p0310 A67-12571

Beacon satellite measurement of Faraday rotation and diurnal and seasonal variations of total electron content of ionosphere near Nairobi 03 p0406 A67-12825

San Marco satellite structural configuration for measurement of total force acting on satellite, electron content from satellite to earth and guided propagation 03 p0517 A67-12900

Latitude distribution of ozone at high altitudes, deduced from radiance of earth daylight atmosphere, measured with satellite-borne radiometer 03 p0410 A67-12948

400-kev electrons precipitation in auroral zone measured with solid state detector mounted on polar satellite 03 p0410 A67-12952

Galactic deuterium and energy spectrum above 20 mev per nucleon measured by IMP-III satellite near minimum solar activity 03 p0472 A67-13390

Six solutions for tesseral harmonic coefficients of geopotential from satellite determinations compared with gravimetry 03 p0414 A67-13933

Automatic recording equipment measuring polarization angle of Syncom III 137 mc/s radio signal and determination of ionospheric total electron content 03 p0415 A67-14110

Supersatellite technology and advantages of larger automaton craft including superweather, superremote sensor, superutility, supersurveillance and superscientific satellite systems 04 p0703 A67-14601

Nimbus II AVCS, APT, HRIR and MRIR sensory data analysis 04 p0613 A67-14801

Electron energy spectrum measured near equator by satellite mounted scintillator 04 p0614 A67-14950

Statistical properties of interplanetary magnetic field variations, charged particles propagation in solar system and photospheric processes analyzed, using Mariner II magnetometer 04 p0698 A67-14951

Spatial distribution of energetic electrons in geomagnetic tail by analyzing counting rates from solid state detector on IMP I satellite 04 p0692 A67-14953

Lunar IR emission and solar radiation reflected by moon in visible region measured by Luna X orbiter 05 p0886 A67-16052

Primary cosmic radiation in interplanetary space, lunar surface albedo and soft particle fluxes in magnetosphere measured by Luna X orbiter 05 p0875 A67-16053

Lunar gamma radiation measured by spectrometer on Luna X orbiter noting lunar rock radiation level, effect of cosmic rays, etc 05 p0887 A67-16055

High altitude vertical photoelectron distribution from electron concentration measurements by Cosmos V and IMP I and II 05 p0795 A67-16061

Captured proton intensity measurement in inner radiation belt in Brazilian anomaly, using satellites Proton I and II 05 p0878 A67-16089

Geographic position of cosmic ray equator from results of on board Proton I satellite measurements 05 p0878 A67-16090

High energy electron intensity measurement beyond atmosphere with aid of proton I and II satellites, showing capture by geomagnetic field 05 p0878 A67-16091

Low energy proton distribution in geomagnetic coordinates obtained from Elektron satellite measurements 05 p0880 A67-16108

Elektron satellite observations on primary cosmic radiation, noting correlation between intensity variation and neutron component intensity 05 p0880 A67-16109

Interplanetary space properties studied from IMP-I satellite data on cosmic ray variations 05 p0880 A67-16115

Geometric satellite triangulation system and relation to dynamical coordinate system 05 p0797 A67-16569

Differential Doppler measurements of satellite radio emissions for obtaining ionospheric electron content 05 p0764 A67-16930

High cloud surface effect on satellite measurements of radiation temperature of stratosphere 05 p0802 A67-17376

Sun generated high and low energy protons analyzed, using semiconductor detectors during flights of interplanetary probes 06 p1077 A67-17841

Artificial satellite UV photometry and polarimetry of galactic star clusters 06 p1077 A67-18065

Radio occultation techniques for analysis of planetary atmospheres and surface topography by measuring perturbations to amplitude and frequency on radio links [AIAA PAPER 67-119] 06 p1087 A67-18454

Electromagnetic radiation at satellite-borne sensor, discussing spectral, spatial and temporal distributions of radiation energy intensity 06 p1006 A67-19010

Biological satellite research, discussing radiation effects on living organism as measured by Cosmos 110 07 p1136 A67-19867

Vela II measurements of earth magnetopause and bow shock positions, showing relationship to magnetic disturbance index and thus also to solar wind velocity 07 p1180 A67-19920

IMP-I satellite measurements of neutral sheet in geomagnetic tail noting dimensions, motion and parameters of sheet. 07 p1244 A67-19922

Magnetospheric distortion during geomagnetic storm on September 30, 1961, examining Explorer XII satellite evidence on ring currents 07 p1180 A67-19924

Satellite measurement of low energy proton precipitation in auroral zone during magnetically quiet period 07 p1245 A67-19930

Penetrating radiation measurement on moon surface obtained by Luna IX spacecraft 08 p1385 A67-20841

Soviet lunar probe measurements of gamma spectrometry, magnetic and gravitational fields, corpuscular radiation intensity, etc 08 p1411 A67-20999

Lunar photography application to creation of selenographic coordinates enveloping near and far sides of moon 08 p1388 A67-21000

Upper atmosphere density determined from satellite braking 08 p1325 A67-21002

Measurements performed from Mariner type probe during intercept with comet complement measurements performed from ground-based astronomical observatories by direct sampling 08 p1393 A67-21098

Explorer XXXIII satellite magnetometric measurements of geomagnetic tail at distances beyond lunar orbit 08 p1402 A67-21468

Particle effects of interplanetary shock wave, noting discontinuous drop in solar proton intensities 08 p1378 A67-21469

Trapped proton flux data from nuclear photographic emulsions 08 p1378 A67-21472

Cosmic ray nuclei propagation in interstellar space and solar system examined from balloon, rocket and satellite soundings 08 p1378 A67-21473

Anisotropic proton velocity distribution obtained from solar wind measurements on Pioneer VI spacecraft 08 p1378 A67-21475

Mean ionospheric height measurement from analysis of radio signals from beacon satellite 08 p1328 A67-21479

Ion temperature profiles obtained from satellite measurements of dawn-dusk auroral zone orbits 08 p1329 A67-21482

Satellite observations of energetic trapped electrons, August 1964 08 p1379 A67-21484

Electron concentration in ionosphere by coherent frequency method, examining Cosmos XI and Elektron I satellite measurement errors 09 p1491 A67-21893

Proton II satellite measurements of intensity of nuclear component of primary cosmic radiation 09 p1561 A67-21897

High transmission Cerenkov spectrometer carried by proton I and II satellites to measure charges of primary cosmic ray nuclei high transmission Cerenkov spectrometer carried by Proton I and II satellites to measure 09 p1497 A67-21898

Satellite geodesy program at Smithsonian Astrophysical Observatory, with emphasis on twelve Baker-Nunn tracking stations 10 p1636 A67-23177

Direct method for determining space directions and adjustment of satellite triangulation net 10 p1637 A67-23181

Radiation data measured by Tiros IV satellite for determination of global

distribution of atmospheric water vapor 10 p1677 A67-23195

Latitudinal and seasonal variations in atmospheric densities during low solar activity obtained by inflatable air density satellites 10 p1639 A67-23211

Atmospheric density scale height and variation law at different heights obtained from San Marco satellite data 10 p1712 A67-23212

High resolution density data from radar observations of low altitude polar orbiting satellites reveal longitudinal and geomagnetic variation, noting regression analysis 10 p1640 A67-23216

Solar X-ray data from satellite telemetry, comparing 8-20 angstrom flux with 10.7 cm radio flux 10 p1701 A67-23226

Brightness of night glow measured in several spectral ranges by Cosmos 92 satellite-installed colorimeter 10 p1647 A67-23276

Airglow lines measured through photometers on OGO-II satellite, noting nadir and zenith airglow 10 p1660 A67-23278

UV solar radiation absorption in upper atmosphere determined from measurement of photoelectron currents emitted by planar metallic orthogonal photocathodes onboard Cosmos II satellite 10 p1647 A67-23282

Laminar composition structure and periodicity of variations with time in outer radiation belt investigated by solar radiation satellites 10 p1701 A67-23298

Proton spectra and spatial distribution of energy protons on magnetic shells in earth radiation belts, using satellite data 10 p1702 A67-23300

FR-I satellite data on VLF propagation in lower magnetosphere 10 p1649 A67-23301

Rotational speed of upper atmosphere determined from satellite measurements 10 p1652 A67-23493

Satellite measurement of upper atmospheric density variations due to geomagnetic disturbances, correlating time delay with geographic latitude 11 p1783 A67-23922

Variation of radio brightness of synchrotron radiation from Van Allen belts as function of direction and frequency, using satellite receiver 11 p1855 A67-23944

Ionospheric absorption determination by measuring amplitudes of wave components of satellite transmission 11 p1786 A67-24059

Satellite measurement of magnetic fields in cislunar space and earth proximity, noting formation of confined geomagnetic field by continuous plasma flow from sun 11 p1863 A67-24549

Structural and mechanical properties of lunar maria surface material derived from satellite and earth-based data 11 p1864 A67-24557

Riometer observations in polar caps of solar cosmic ray events during IQSY 12 p1993 A67-25228

Local electron concentration determination by dispersion method and satellite proved unreliable because of horizontal ionization gradient and ionospheric instability 12 p1932 A67-25539

Sputnik III data application to plotting of total magnetic field intensity chart above U.S.S.R., using spherical harmonic analysis 12 p1933 A67-25652

Albedo upper and lower fluctuation bounds determined by astrophysical comparison and three other methods 12 p2003 A67-25684

Polar orbiting satellite measurements correlating ionospheric irregularities with trapped and precipitated energetic particles in South American anomaly 12 p1996 A67-25776

Geomagnetic field measurements in Brazilian magnetic anomaly, using Alouette topside sounder satellite 12 p1933 A67-25777

Rocket and satellite measurements of electron and ion thermal structure of ionospheric F region 12 p1935 A67-25796

Inhomogeneous formations and disturbances of electron concentrations in outer ionosphere indicated by Doppler shift differences measured by Elektron I satellite 12 p1936 A67-25800

Relation between solar flare, X-rays and sudden ionospheric disturbances (SID) using satellite measurements 12 p1905 A67-25801

Earth magnetosphere at distances 7 to 11.7 earth radii obtained by Elektron satellites,

noting differences between measured and calculated field vector 12 p1936 A67-25803

IMP-II and OGO-I measurements on plasma characteristics in transition region between solar wind and geomagnetic field 12 p1997 A67-25806

Electron spectra, pitch angle distributions and total ionization measured throughout radiation belts by satellite magnetic spectrometer and integrating ionization chamber 12 p1997 A67-25807

Relation between electron and proton distributions and existence of electric fields in magnetosphere 12 p1936 A67-25808

Low energy proton and electron outer radiation belt satellite Cosmos 41 indicate capture and acceleration mechanism 12 p1997 A67-25810

Long period hydromagnetic waves in magnetosphere and coupling to solar wind studied by Explorer XIV 12 p1937 A67-25812

Elektron I and II satellite observational data on terrestrial radiation belt 12 p1998 A67-25816

Electron and proton fluxes at geocentric distance of 7 earth radii measured by charged particle traps on interplanetary station Zond 2 12 p1998 A67-25818

Preliminary results of magnetic field measurements in vicinity of magnetosphere and interplanetary space from Mariner IV 12 p2007 A67-25822

IR spectral techniques for satellite geodetic surveying, discussing spectral matching techniques for discriminating between different types of rocks [AIAA PAPER 67-284] 12 p1938 A67-26001

Albedo and earth-radiation measurements from OSO-II compared with other results, noting limb-brightening effect [AIAA PAPER 67-330] 12 p1938 A67-26044

Earth albedo calculation using Pegasus I thermal data, discussing Rayleigh scattering, spacecraft position, atmospheric reflection effects, etc [AIAA PAPER 67-332] 12 p1938 A67-26046

Satellite radiation data application to synoptic weather analysis including cloud pattern mapping, tropospheric relative humidity and vertical cloud structure inference 13 p2149 A67-26274

Satellite measurements of electron flux and electron energy spectra in inner radiation belt 13 p2191 A67-26324

Relativistic-electron diffusion wave in outer radiation belt recorded by device mounted on Cosmos XLI satellite in high geomagnetic latitudes 13 p2191 A67-26545

Solar and galactic particle spectra and composition measured with cosmic ray telescope mounted on satellite 13 p2193 A67-27249

Ionospheric ion temperature determination from variations in collector current of ion trap mounted on rotating satellite 13 p2115 A67-27330

Earth gravitational potential field determined by satellite measurements, showing field in spherical harmonics form 13 p2116 A67-27395

Angular, spectral and geographical distributions of outgoing fluxes of thermal radiation and earth albedo measured, using Cosmos satellite 14 p2306 A67-27861

Relativistic effect of atomic clocks, noting error and magnitude increase with experiment duration 14 p2348 A67-27866

Measurement of total number of electrons in ionosphere, horizontal gradients, equivalent height and vertical profile from recorded Elektron satellite signals 14 p2307 A67-27922

Unlikelihood of obtaining useful information on atmospheric composition from indirect sensing of scale heights by satellites 14 p2310 A67-27959

Long term measurement of trapped-electron environment in narrow region of space at lower edge of inner radiation belt 14 p2380 A67-28051

IMP II satellite measurements of magnetic fields in interplanetary space by onboard monoaxial fluxgate magnetometers 14 p2310 A67-28052

IR spectrum evaluation procedures and optical measurement as applied to atmosphere physics 14 p2311 A67-28401

Orbiter II lunar photography analysis, noting surface characteristics of Southern Hemisphere of moon 14 p2387 A67-28506

Omicron I satellite measurements of total

ionospheric electron content, comparing values at Houghton, Michigan, with others for different latitudes 15 p2474 A67-29193

Astronomical and satellite measurements of meteoroid environment of spacecraft in solar system 15 p2555 A67-29535

Time and frequency accuracies obtainable with geostationary satellites, noting measurement error sources 15 p2565 A67-29593

Radar measurement of differential group delay to moon, showing large differences in total cislunar electron content above 1000 km in solar and antisolar directions 15 p2555 A67-29611

Ionospheric electron content obtained as function of longitude and latitude, using satellite measurements of Faraday rotation 15 p2478 A67-29923

Geographical distribution of surface temperature of ground and/or clouds and mean relative humidity of upper troposphere 15 p2513 A67-30059

Computational method for high altitude atmosphere density, orbital elements, drag coefficients and potentials from satellite displacement and velocity measurements 15 p2562 A67-30069

Multichannel photometer for space applications requiring low weight and power, no moving parts and high sensitivity divided in four electrically and optically distinct quadrants 15 p2491 A67-30433

Flux, energy spectrum and angular anisotropy of auroral electrons analyzed from space vehicle 16 p2670 A67-30648

Evaluation of satellite radar altimetry for geophysical and oceanographic measurement 16 p2742 A67-30688

Atmospheric radiation polarization characteristics, determining concentration and distribution of atmospheric scatterers 16 p2665 A67-30983

External ionosphere electron concentration measurement from data on Doppler shift variations in frequency of coherent radio signals from Cosmos and Elektron satellite 16 p2624 A67-31073

Navigation system by measurement of Doppler shift in radio transmissions from satellite and equipment for measurement 16 p2701 A67-31272

Ionospheric electron content as function of longitude and latitude calculated from Faraday fading of radio waves 16 p2627 A67-31362

Radio wave trapping and guiding along magnetic field lines by irregularities in electron density 16 p2667 A67-31513

Lunar internal heat flow measured by infrared mapping of polar regions from orbiting satellites 16 p2754 A67-31750

Position of outer radiation belt boundary as function of local time, discussing data from Elektron satellite scintillation counters 16 p2740 A67-31886

Magnetic field measurement with Lunik x near lunar orbit noting magnitude, time behavior and existence of terrestrial magnetic tail 16 p2755 A67-31888

Magnetic field in moon proximity constructed from Lunik x satellite plasma and magnetic measurements 16 p2755 A67-31889

Proton I and II satellite measurement of effective cross sections of inelastic interactions between billion and trillion ev protons and carbon nuclei 17 p2935 A67-32247

Spectrometers onboard satellite, studying cosmic ray particle energy spectra and chemical composition 17 p2935 A67-32248

Energy spectrum of cosmic ray nuclei in helium through scandium range studied with Proton I and II satellites 17 p2935 A67-32249

Dust content in upper atmosphere of earth from satellite light absorption measurements 17 p2842 A67-32257

Interplanetary magnetic field data by Mariner II compared to ground-based standard magnetograms and micropulsation recordings for October 7, 1962 geomagnetic storm 17 p2844 A67-32540

Satellite-borne detection of decay protons as test of solar neutron observation 17 p2937 A67-32544

Tropospheric water vapor analysis via Tiros IV satellite, determining spatial and temporal temperature, humidity and mass variations 17 p2880 A67-32550

Space research effects on science and technology, noting fields of

application 17 p2974 A67-32771

Micrometeoritic cloud existence near earth refuted by satellite incidence-frequency measurements, describing satellite measuring devices 17 p2850 A67-32975

Solar X-ray fluxes measured by solar radiation satellite during IQSY, comparing X-rays and decimetric radio emission in 8-12 angstrom band 17 p2938 A67-33185

Solar X-ray measurement with satellite noting radio noise flux, absorption in atmosphere and optical density changes 17 p2939 A67-33242

Anomalous LF plasma oscillation by particles trapped in potential well behind satellite applied to ionospheric measurements 18 p3117 A67-33512

Error factors in cloud and underlying surface temperature determination from weather satellites in various spectral intervals 18 p3073 A67-33558

Auroral particle fluxes and effects from coordinated satellite-, aircraft- and ground-based measurements 18 p3034 A67-33590

Atmospheric emissions and electron and proton precipitation latitude and diurnal variations measurements from satellite-borne photometric studies 18 p3039 A67-33623

Moon spectrophotometric measurements from space probe compared with solar spectrum structure, calculating lunar albedo curve 18 p3122 A67-34140

Upper atmosphere diurnal and seasonal latitudinal variations satellite data, showing diurnal bulge migration with subsolar point, 2 PM bulge peak, etc 19 p3215 A67-35178

Zodiacal dust particle flux measurements from OGO 3 and Mariner IV spacecraft in cislunar and interplanetary space 19 p3318 A67-35185

Inner zone trapped electron flux measurements by satellite indicating natural environment emergence from Starfish remnants 19 p3216 A67-35186

Solar X-ray emission associated with proton flare of July 1966 measured, plotted and described 19 p3313 A67-35218

French laser telemetry network, noting Q-switched ruby laser, Doppler effect measurement and local spatial geodesy program 19 p3182 A67-35239

Explorer 33 plasma measurements, discussing plasma flow parameter calculation methods, including plasma models and magnetospheric shape and size 19 p3319 A67-35245

Spectral composition of earth IR radiation measured from satellites, giving radiation intensity and temperature distributions 19 p3219 A67-35253

Molecular and atomic ion concentration in earth upper atmosphere observed from low altitude satellite, discussing diurnal variation and solar effect 19 p3220 A67-35262

Lunar radius facing earth determined from radar measurement data and lunar orbiters 19 p3319 A67-35263

Automatic position determination for ships using active navigation satellite systems, discussing communications potential and safety 19 p3254 A67-35310

Solar x-ray spectral intensity distribution using atmospheric extinction of solar radiation as measured by satellites 19 p3314 A67-35441

Solar wind velocity and interplanetary magnetic field components obtained by IMP II related to geomagnetic field variation 19 p3222 A67-35473

Balloon and satellite measurements of 11-year solar modulation of low energy protons and helium nuclei in galactic cosmic rays 19 p3315 A67-35487

Specific features of French Diademe satellites noting payload stabilization, thermal control observation carried, instrumentation, etc 19 p3333 A67-35500

Satellite programs for Black Arrow launch vehicle, discussing functions, tasks, tests, etc 19 p3333 A67-35842

Total atmospheric ozone from satellite measurements of solar UV reflected radiation determined, using atmospheric model with Rayleigh scattering 19 p3226 A67-35923

Elliptic geocentric satellite orbit for measurements of magnetosphere-nearby space region, analyzing orbital lifetimes and perturbations 19 p3226 A67-36005

[AIAA PAPER 67-616] 19 p3226 A67-36005

Digital telemetry system for maximum

transmission efficiency of measurements performed on space vehicle 20 p3394 A67-36245

Relative intensity contribution and time dependency of primary cosmic rays, splash albedo and reentrant albedo measured by polar orbiting satellite 20 p3517 A67-36306

Energetic electrons in Van Allen radiation belt through satellite measurements, giving intensity maps, energy spectra and pitch angle distributions 20 p3517 A67-36371

Flight measurement data retrieval on real time basis from worldwide range stations possible through Range Support Satellite system 20 p3531 A67-36470

Electronic satellite position and motion measurement for satellite geodesy, with rapid data reduction, day-night capability and optical accuracy 20 p3383 A67-36889

Ionosphere information via rocket and satellite measurements covering ion temperatures and concentration, electron content variation, etc 20 p3430 A67-36907

Optical metagalactic radiation measured by spacecraft photographic and photometric methods, reviewing Olbers paradox and night sky brightness measurements 20 p3526 A67-37127

Charged particles of extraterrestrial ring current during geomagnetic storms, with Ogo 3 measurements of proton and electron differential energy spectrums 20 p3432 A67-37401

Effect of electromagnetic field interaction with gravitational field calculated from satellite data, determining difference between frequencies 20 p3386 A67-37523

Gravitational radio wave frequency shift from satellite measurements, noting satellite-ground radio communication system 20 p3386 A67-37524

Lunar IR emission and solar radiation reflected by moon in visible region measured by Luna X orbiter 21 p3701 A67-37839

Primary cosmic radiation in interplanetary space, lunar surface albedo and soft particle fluxes in magnetosphere measured by Luna X orbiter 21 p3697 A67-37840

Lunar gamma radiation measured by spectrometer on Luna X orbiter noting lunar rock radiation level, effect of cosmic rays, etc 21 p3701 A67-37842

High altitude vertical photoelectron distribution from electron concentration measurements by Cosmos V and IMP I and II 21 p3615 A67-37848

Power consumption reduction problems in coded telemetry measurements for ESRO I and HEOS A satellites 21 p3584 A67-38646

Solar proton and alpha radiation flux and spectral distribution measuring device on satellite HEOS A 21 p3629 A67-38665

Satellite-borne superheterodyne radiometer for measuring stratospheric temperature utilizing millimeter wave spectrum of molecular oxygen 21 p3584 A67-38669

Planetary magnetic fields calculated from meteorite magnetic properties and assumptions about cores and crusts 21 p3711 A67-39042

Empirical orthogonal functions, determining vertical atmospheric temperature profiles from radiometric satellite measurements 22 p3828 A67-39325

Antarctic riometer observations of PCA event of February 1965 compared with satellite measurements of solar proton flux and spectrum during same event 22 p3872 A67-39803

Payload integration process for space experimentation 22 p3922 A67-39982

UHF sferics detection system receiving and display components for remote sensing by satellite of convective cloud development 22 p3806 A67-40358

Ozone parameters determination from measurements of radiation backscattered by earth atmosphere 22 p3794 A67-40365

Satellite Infrared Spectrometer (SIRS)/ flown by balloon for cloud top and surface temperatures 22 p3829 A67-40370

Auroral proton precipitation and hydrogen emissions 23 p3993 A67-40564

Balloon sounding data for atmospheric secondary and reentrant albedo proton intensity values, discussing empirical atmospheric secondary proton spectrum 23 p4051 A67-40810

Primary cosmic particles energy spectrum

measurements onboard space station with ionization calorimeters and energy level discriminators 23 p4054 A67-41091

Primary proton energy spectrum determination by particle energy measurements with ionization calorimeters and particle counters onboard space stations 23 p4054 A67-41092

Primary cosmic rays with various charges measured for spectral energy with Cerenkov counter onboard space stations 23 p4054 A67-41093

Heavy and superheavy nuclei energy spectra studied from measurements by Cerenkov counter onboard space stations 23 p4054 A67-41094

Cosmic ray measurements during low geomagnetic activity using scintillation, gas discharge and semiconductor proton counters mounted on Cosmos satellite 23 p4055 A67-41099

Interplanetary space cosmic ray intensity variation with time and distance from sun measured by Zond III and Venera II simultaneously 23 p4055 A67-41102

1 to 5 Mev solar proton emissions observed by increased counting rates on Venera II and III and Zond III interplanetary probes 23 p4056 A67-41112

Explorer XXII amplitude recordings, analyzing duration, strength and frequency of ionospheric electron density horizontal gradients 23 p3974 A67-41177

Ionospheric composition and temperature for South Atlantic latitudes from scale height values obtained by Alouette I satellite 24 p4147 A67-42057

High energy proton data from Telstar I satellite used to develop mathematical models of proton spatial distribution 24 p4210 A67-42334

Radiation measurement from satellite, discussing observation of ozone absorption band 24 p4181 A67-42397

Captured proton intensity measurement in inner radiation belt in Brazilian anomaly, using satellites Proton I and II 24 p4212 A67-42765

Geographic position of cosmic ray equator from results of onboard Proton I satellite measurements 24 p4212 A67-42766

High energy electron intensity measurement beyond atmosphere with aid of proton I and II satellites, showing capture by geomagnetic field 24 p4213 A67-42767

Low energy proton distribution in geomagnetic coordinates obtained from Elektron satellite measurements 24 p4214 A67-42784

Elektron satellite observations on primary cosmic radiation, noting correlation between intensity variation and neutron component intensity 24 p4214 A67-42785

Interplanetary space properties studied from IMP-I satellite data on cosmic ray variations 24 p4214 A67-42791

SATELLITE NAVIGATION SYSTEM

Hypersonic velocity effects on errors in vertical channel of inertial navigation system, particularly aboard artificial earth satellite 01 p0110 A67-10420

AN/SRN-9 integral Doppler equipment for use with navigation satellites to determine ship position at sea 05 p0839 A67-17388

All-weather satellite navigation system using AN/SRN-9 Doppler data equipment 05 p0839 A67-17389

Program for satellite supported air traffic control 09 p1526 A67-21679

Configurations of hyperbolic position-fixing systems using synchronous satellites, showing Loran-like networks on earth resulting from these configurations 09 p1526 A67-22393

Gravitational satellite stabilization, star tracking, targets and sensors for orientation and inertial navigational instrumentation 14 p2347 A67-27878

Automatic satellite navigation and communication system for aircraft and ships using cooperating ground stations 16 p2700 A67-30695

Navigation system by measurement of Doppler shift in radio transmissions from satellite and equipment for measurement 16 p2701 A67-31272

Guidance, navigation and two phases of targeting of Saturn V lunar landing mission, analyzing launch, boost to orbit and iterative guidance 17 p2881 A67-32057

Navy Navigation Satellite System,

discussing naval and civilian application and improved gravitational field model 19 p3255 A67-35638

Worldwide navigation satellite system in next decade, studying economical, organizational, technological, operational and safety aspects 19 p3255 A67-35658

Influence of navigational requirements and technology on design of navigation-satellite system 19 p3256 A67-35862

Satellite navigation systems requirements including Loran, inertial navigation and Navy systems 23 p4025 A67-41363

SATELLITE NETWORK

Technical properties of Early Bird communications satellite noting launching, positioning, worldwide system establishment, etc 03 p0367 A67-12898

Lincoln Experimental Terminal /LET/ system, ground antenna, RF and signal processing equipment for communications via several satellites 06 p0959 A67-17669

Adaptive utilization of communication satellite systems optimizing dynamic traffic handling of combined ground and satellite communications complex, noting network configurations 06 p0959 A67-17670

Multiple-access worldwide satellite communication system for aircraft terminals with limited antenna gain and transmitter power 06 p0960 A67-17674

Data processing centers integration through ground and satellite telecommunications networks for global information network [AIAA PAPER 66-331] 06 p0961 A67-17700

Long range projections of demand for intercontinental communication satellite systems and use as basis for business decisions [AIAA PAPER 66-322] 06 p1120 A67-17708

European satellite triangulation network, discussing scientific, technical and organizational aspects 07 p1176 A67-19761

Satellite telecommunications system, merits of single global system and legal aspects 12 p2042 A67-26140

Global communications satellite networks and emerging customary law for outer space 12 p2043 A67-26143

International legal principles and cooperation requirements for worldwide radio and TV broadcasting by satellite telecommunications networks 12 p2043 A67-26144

Communication satellite techniques future development 13 p2070 A67-27151

Satellite telecommunication networks commercial, political and military implications 14 p2270 A67-28567

Early Bird project ground stations and launch-synchronizing operations, considering time delay on transmission performance 16 p2760 A67-30692

Future satellite regional and intercontinental telecommunication network, considering weight, classes, performance and orbital factors 17 p2813 A67-32397

Data and orbit analysis supporting Navy satellite Doppler system Tranet, discussing editing and archiving of Doppler data and orbital ephemerides 18 p3003 A67-34245

Worldwide satellite telecommunication system, economic and political implications and effects on CEPT 18 p3162 A67-34357

SATELLITE OBSERVATION

Satellite triangulation based on simultaneous observations from two stations defining space orientation of plane 01 p0055 A67-10037

Orbits, altitudes, viewing geometry, coverage and resolution pertinent to satellite observations of earth and atmosphere 01 p0147 A67-10325

NASA program involving orbiting satellite studies of natural and cultural resources 01 p0168 A67-10326

Cosmic radiation data obtained by two gas-discharge counters installed in Luna X artificial satellite 01 p0145 A67-10906

Manned geophysical observations from satellites as training ground for planetary research, especially Venus atmosphere 01 p0155 A67-11395

Rotation rate and inclination of planetary axis determined from radiation incident on artificial satellite of planet 02 p0321 A67-11539

Errors of IR-horizon pickups due to satellite determination of

vertical 02 p0240 A67-11541

High resolution LF observations of time stationary discrete sources and background continuum distribution, using two satellites in interferometric mode [AIAA PAPER 66-886] 02 p0221 A67-12265

Composition and energy spectra of primary cosmic radiation in low energy regions from observations of Mariner II and Explorer VII 02 p0310 A67-12582

Latitudinal effects on satellite beacon scintillations as observed from three stations [AFCRL-66-864] 03 p0406 A67-12820

Transverse magnetic disturbances at high altitudes in auroral region observed with magnetically oriented satellite 03 p0409 A67-12944

Satellite measurement of behavior of high latitude energetic electron trapping boundary, noting geomagnetic storm effects 03 p0410 A67-12951

Position finding techniques based on precise observations of satellite orbits for ATC purposes 03 p0465 A67-13025

Nature of lunar surface, discussing interpretations of Luna IX photographs by Jaffe and Kuiper 03 p0512 A67-13934

Radio astronomical and satellite studies of atmosphere - USAF Symposium, Boston, October 1965 03 p0415 A67-14234

Total electron content distribution over Europe in terms of geomagnetic activity, noting occurrence of scintillations [RASSA PAPER 1-10-125] 03 p0416 A67-14236

Latitudinal and diurnal variation of ionospheric electron content in auroral zone proximity [RASSA PAPER 1-10-126] 03 p0416 A67-14237

Explorer XXII satellite measurement of total electron content from observations of Faraday effect [RASSA PAPER 1-10-128] 03 p0372 A67-14239

Topside ionosphere over American continents, noting electron density and scale height distribution [RASSA PAPER 1-10-132] 03 p0417 A67-14243

ORBIS satellite experimental results, noting long range propagation at night and during sunrise [RASSA PAPER 1-10-147] 03 p0373 A67-14254

Frequency spectra of VLF hiss near auroral zone analyzed by Injun III satellite 04 p0614 A67-14958

Random tropospheric angle error prediction in microwave observations of Early Bird satellite 04 p0574 A67-15074

Plasma observations in tail of terrestrial magnetosphere and circumlunar space by Luna X orbiter, using charged particle traps 05 p0875 A67-16054

Structurally regular magnetic field in circumlunar space recorded by Luna X orbiter, noting variations in intensity and solar wind effect 05 p0887 A67-16056

Soviet rocket and satellite observation of meteoric dust from 1957 through 1966 05 p0887 A67-16057

Solid interplanetary matter in vicinity of moon observed by Luna X piezoelectric pickups attached to orbiter skin 05 p0887 A67-16058

Satellite orbital parameters determined from visual observations 05 p0894 A67-16559

Satellite trajectory determination through high accuracy observations, using short arcs 05 p0894 A67-16561

Orbital elements determination from reduced Baker-Nunn observations of satellites, noting disturbance by resonance effects of earth gravitational potential sectorial and tesseral harmonics 05 p0763 A67-16562

Magnetic field observations by rockets and satellites 05 p0798 A67-16870

Hook whistler discovered in VLF radio noise data from Injun III satellite, noting time delay difference between components 05 p0799 A67-16888

Cosmic ray intensity variations using gas discharge counters onboard Soviet satellites, noting Forbush effects 05 p0884 A67-17025

Geometrical methods for solving higher order geodetic problems from satellite observations including direction, position, coordinate, etc 05 p0800 A67-17031

Satellite observations determine average cloud cover over region 05 p0839 A67-17393

Stellar magnitude of 100 satellites 05 p0767 A67-17407

Cosmic ray nuclei observed from satellites and balloons by nuclear emulsions in stacks

- of plastic sheets 06 p1076 A67-17641
Oxygen A band near 7600 angstroms used by Gemini V astronauts to measure cloud top altitude, showing method of computing correction factor 06 p1026 A67-18563
Lower hybrid resonance /LHR/ noise bands occurrence patterns as function of latitude and time 06 p0964 A67-18567
Electron number density determined using interference pattern recorded by satellite ionograms at high latitudes 06 p0996 A67-18568
Field aligned electron concentration profiles of equatorial anomaly, using parametric description for theoretical results 06 p0997 A67-18697
Conjugate ducting observation via fixed frequency topside-sounder satellite, estimating electron concentration difference 06 p0997 A67-18699
Gravitational field signatures yield information about interior structure of planets 06 p1092 A67-19008
Physical pattern of high altitude fission cloud and motion of gamma and beta fission fragments captured by geomagnetic field and observed by Cosmos 07 p1242 A67-19102
Interplanetary gas, solar corpuscular activity and magnetic storms and zodiacal dust cloud from satellite observations during IQSY and use of cometary tail as plasma probe 07 p1248 A67-19333
Upper atmospheric neutral gas density determination from simultaneous satellite position measurements 07 p1172 A67-19626
Satellite observation of radiation belt and absorption of cosmic noise in polar aurora during magnetic storms of February 1964 07 p1243 A67-19683
Cooperative European geodetic observation of luminous objects at high altitude using Echo type satellite 07 p1176 A67-19762
Astrometric processing of synchronous photographic observations of Echo I satellite 07 p1144 A67-19769
Criticism of Ivanov assumption regarding IMP-I observation of lunar wake in solar wind by magnetic field and plasma measurements 07 p1243 A67-19829
Properties and velocity distribution functions observed by Vela III satellites 07 p1244 A67-19919
Plasma sheet with enhanced energy density stretching across magnetotail as evidenced by Vela-IIB satellite observations 07 p1244 A67-19921
Magnetopause structure and altitude from Explorer XII observations 07 p1180 A67-19925
Electron energy spectra analyzed in earth magnetosphere usingOGO 3, noting relation to radial distance 07 p1244 A67-19926
Atmospheric composition data from Explorer XVII satellite, obtaining expression for thermal diffusion factor of He 07 p1181 A67-19937
Limitations in tilted fluxgate magnetometer data from Explorer XVIII satellite due to ambient dynamic field effects 07 p1182 A67-19943
Zonal harmonics determination through satellite observations processed using computer program, noting necessity for increased number of satellites [AAS PAPER 66-91] 07 p1183 A67-19956
Gravitational field of any primary determined using observations of satellites in orbit about primary, noting numerical integration technique and special perturbation methods [AAS PAPER 66-109] 07 p1253 A67-19969
Small perturbation analysis of observed organized cloud convection for arbitrary unidirectional wind profile 08 p1350 A67-20950
Cosmic space exploration in U.S.S.R., discussing results obtained from Cosmos and Elektron earth satellites 08 p1394 A67-21110
High latitude increase in ionization of F layer correlating in space and time with auroral precipitation as shown by ionospheric electron number density data 08 p1328 A67-21481
Parameters of simultaneous amplitude phase modulation of periodic cosmic ray variations obtained from satellite observations 10 p1698 A67-22779
Theodolite Astro-2 observation of azimuth and position of moving satellite 10 p1655 A67-22985
Soviet book on practical utilization of observational data from meteorological satellites covering radiation and cloud cover, emphasizing weather forming systems analysis, aerological and synoptical data comparisons, etc 10 p1676 A67-23017
Properties of solar cosmic rays causing polar cap absorption measured with satellites 10 p1700 A67-23188
Heat radiation spectra of earth as measured by Cosmos satellites, comparing experimental and calculated results 10 p1637 A67-23194
IR transition zone between earth and space studied by gyro-stabilized satellite 10 p1637 A67-23196
Photometric measurements of eclipses of artificial solar satellite 1960 Eta 2 at sunrise and sunset in Lyman alpha and violet spectral range 10 p1706 A67-23221
Surveillance of solar activity based on optical observations of satellites 10 p1606 A67-23222
Ionospheric electron content calculated from beacon satellite data on Faraday rotation 10 p1641 A67-23235
Satellite measurement of ionospheric electron density, determining Faraday null times 10 p1641 A67-23236
Meteoritic matter investigation with Venus II and Zond III probes, discussing impact rate and distribution along flight path 10 p1708 A67-23241
Geomagnetic field values obtained fromOGO-2 satellite-mounted rubidium vapor magnetometer 10 p1641 A67-23244
Diurnal variation of difference between dipole and measured field for quiet magnetosphere from Elektron satellite data 10 p1649 A67-23296
Ion composition and natural electromagnetic emissions of VLF phenomena observed by Alouette I and II 10 p1649 A67-23303
Book for amateurs on observing earth satellites including methods and discoveries about upper atmosphere and shape of earth 10 p1608 A67-23620
Surveying earth resources from high flying aircraft and earth orbiting satellites 10 p1735 A67-23688
Cosmic radiation measurements beyond radiation belts as observed by Cosmos XVII 11 p1856 A67-24075
Atmospheric number density measured by attenuation of solar X-rays monitored when satellite passes from darkness to sunlight 11 p1857 A67-24605
Astronomical satellite for photoelectric spectrometry in UV region to measure stars of galactic clusters 12 p2002 A67-25460
Cosmic radio emission at 725 and 1525 kc measured for intensity by direct amplification receivers on Elektron II satellite 12 p1995 A67-25769
Atmospheric density distribution at altitudes from 200 to 300 km based on Soviet satellite observations during minimum solar activity 12 p1934 A67-25788
Seasonal variations of total electron content of ionosphere during sunspot minimum 12 p1935 A67-25795
Altitude-time distribution of electron concentration of outer ionosphere measured by coherent signals from Elektron I satellite 12 p1936 A67-25799
Inflation of magnetosphere near 8 earth radii in Southern Hemisphere using Explorer XIV satellite 12 p1936 A67-25805
Low energy particles detected close to equatorial plane of magnetosphere by satellites Elektron and Cosmos 12 p1997 A67-25811
Micrometeoritic particle condensation in vicinity of earth measured by Elektron II satellite 12 p2008 A67-25825
Charge spectrum of heavy cosmic ions of iron group in ionographic emulsions exposed in satellite 12 p1999 A67-25829
Solar X-ray soft component fluxes observed by satellite 12 p1999 A67-25835
Solar X-ray events observed by 1964-1-D satellite launched by U.S. Naval Research Laboratory in 1964 12 p1999 A67-25836
Molecular ion concentration around dawn-dusk auroral zone satellite orbit 13 p2108 A67-26315
Solar wind properties studied using Vela electrostatic analyzers, noting velocity ranges, proton temperature and ion density 13 p2190 A67-26319
Transient variations in magnetospheric boundary position 13 p2109 A67-26328
Solar flare electron propagation in interplanetary space 13 p2194 A67-27251
Energy spectra of solar wind ion fluxes outside magnetosphere measured using Venus 3 space vehicle 13 p2194 A67-27331
Geomagnetic field analytical representation based on Cosmos 49 observational data 14 p2307 A67-27919
Energy absorption profile and ionization rates for electron beam dependence on beam energy, altitude and atmospheric layer thickness and mass 14 p2379 A67-27921
Geomagnetic ring current observations using Elektron II satellite, noting location, orientation and structural features 14 p2308 A67-27928
High altitude dipole equivalence of geomagnetic field properties verified by satellite-detected electron belt investigation 14 p2308 A67-27932
Dispersion of proton whistlers in plasma in motion with respect to observer 14 p2379 A67-27933
Earth bow shock observations with Explorer XII satellite magnetometer 14 p2383 A67-28047
F region phenomena, discussing charged particles dynamics, equatorial and seasonal anomalies and nighttime F layer maintenance, using Alouette I data 14 p2312 A67-28409
VLF noise emissions originating in ionosphere and magnetosphere with reference to ground-based, rocket and satellite observations 14 p2265 A67-28414
French optical satellite observation network 14 p2270 A67-28589
Venus brightness temperature and atmosphere and Mars atmosphere sounded by Mariner II space probe, noting data on Mars magnetic field 14 p2322 A67-28964
Solar magnetic field origin and effects revealed by direct and satellite observations of photosphere, chromosphere, corona and earth neighborhood 15 p2554 A67-29531
Global response of topside ionosphere to magnetic disturbances at solar minimum studied from electron concentration measurements at 640 km 15 p2475 A67-29610
Dayside distortion of geomagnetic field by solar wind beyond 3.5 earth radii measured and compared with three magnetosphere models 15 p2475 A67-29612
Mean variations of total electron density with latitude and local time during winter obtained from dispersive Doppler investigations 15 p2477 A67-29666
Global ocean data acquisition by remote sensor operating from spacecraft for oceanographic studies 15 p2477 A67-29698
Tlros satellites characteristics including ESSA I 15 p2565 A67-29762
Environmental prediction using orbital sensors [AAS PAPER 67-104] 15 p2478 A67-29959
Satellite visibility calculation for individual ground stations of telemetry and tracking network as function of orbital injection parameters 15 p2561 A67-30047
Spaceport meteorology by satellite observation of earth atmosphere and cloud systems [AAS PAPER 67-47] 15 p2513 A67-30115
Measurements on scintillation observed on radio signals from Discoverer satellite, noting intensity increase with latitude and data on diurnal variation [AGARDOGRAPH 95] 15 p2483 A67-30293
Satellite scintillation in auroral zone depends on time of observation and on magnetic activity 15 p2483 A67-30294
Large-scale structure of F layer studied by observing Faraday rotation of satellite signals, noting irregularities in total electron content 15 p2483 A67-30295
Spherical coordinates near apogee of Cosmos 41 satellite determined with TV system and meniscus telescope 16 p2621 A67-30683
Research potential of manned earth orbiting spacecraft in meteorology 16 p2759 A67-30687
Comparison of lunar surface photography from space probes and ground-based observatories 16 p2671 A67-30990
Faraday rotation satellite observations at closely spaced frequencies, allowing electron content figure determination 16 p2629 A67-31514
Topside ionosphere irregularity studied by

Alouette I ionograms and ground based ionosonde records, noting spread-f occurrence topside ionosphere irregularity studied by Alouette I ionograms and ground based ionosonde 16 p2667 A67-31515

Rotation rate and inclination of planetary axis determined from radiation incident on artificial satellite of planet 16 p2752 A67-31605

Errors of IR-horizon pickups due to satellite determination of vertical 16 p2677 A67-31607

Low energy protons emitted by solar flare satellite observed inside and outside of magnetosphere, noting immediate access to polar caps 16 p2740 A67-31626

Statistical processing of satellite data on spectral distribution of outgoing radiation 16 p2668 A67-31887

Spectrometric system aboard Proton type satellite for analyzing energy and charge spectra of primary cosmic ray particles 17 p2854 A67-32245

Shock wave propagation in solar wind caused by tangential discontinuities and geomagnetic sudden storm commencement 17 p2936 A67-32530

Evidence regarding possibility of midwinter stratospheric warmings in Southern Hemisphere 17 p2880 A67-32553

Correlation of diameter of cirrus cloud shield and severity of thunderstorm complex 17 p2880 A67-32554

Soviet space effort and Cosmos satellites, deducing orbital parameters, transmission frequencies, launching time/place, nature of experiments, etc 17 p2956 A67-32724

Interplanetary sector structure observed by IMP-I satellite compared with photospheric magnetic field and plage structure observations 17 p2953 A67-33400

Satellite tracking of cloud formation on earth shadow side, calculating outgoing radiation intensity under cloudless and cloudy sky 18 p3074 A67-33564

Satellite technique for sounding atmospheric optical properties and height distribution of ozone and aerosols 18 p3040 A67-33853

Contribution of earth-made observations to direct planet exploration 18 p3121 A67-34136

Martian atmosphere circulation model from Mariner IV occultation experiment, studying lateral eddy viscosity, winds, surface temperature and stress 18 p3124 A67-34153

Development of kinetheodolites for satellite tracking 18 p3048 A67-34238

U.S. Navy Doppler geodetic Tranet system configuration and operation, discussing tropospheric and ionospheric refraction, timing and frequency errors 18 p3003 A67-34241

Luna IX and Luna X near moon, studying injection phase, orbit and landing phase from transmitted frequency observations 18 p3003 A67-34242

Low perigee satellite orbit determination by visual observation, comparing directional accuracy and orbital elements with Minitrack and Baker-Nunn 18 p3126 A67-34247

Echo I orbit determined from field-reduced Baker-Nunn observations 18 p3127 A67-34248

Effective geopotential at synchronous height determined using observations of Syncom satellites during free drift periods, noting longitude dependence 18 p3041 A67-34251

Variations in lunar gravitational field noting hydrostatic equilibrium state and relation to lunar topography 18 p3127 A67-34252

OGO-A satellite observations of hydromagnetic whistlers /pearls/ nature, showing linkage to magnetosphere 18 p3042 A67-34390

Ground instrumentation system for Mariner IV occultation experiment, using Doppler frequency perturbation method for Mars atmospheric parameters determination 18 p3049 A67-34498

Zonal gravity harmonics of moon from tracking data 18 p3135 A67-34539

Ionospheric irregularities following solar proton flare of July 1966 observed with Alouette topside sounders 19 p3312 A67-35176

Size-frequency distribution of particles and craters and optical, thermal, radio and other properties of lunar surface obtained from Surveyor I landing 19 p3318 A67-35179

Solar X-ray flare of July 1966 observed from satellite, giving curves describing energy flux, radiation intensity, etc 19 p3312 A67-35187

Solar X-ray spectra below 25 angstroms from crystal spectrometer mounted on solar pointer flown on satellite 19 p3318 A67-35198

Diurnal atmospheric density bulge shifts observed by Explorer, showing latitudinal-seasonal variation in helium concentration 19 p3218 A67-35226

Geos satellite observational technique in France 19 p3182 A67-35237

Tropospheric circulation observation through FR-2 satellite project, discussing instrumentation, ground stations, trajectory analysis, etc 19 p3332 A67-35243

Time variations of electron intensity in outer radiation belt observed by satellites, studying electron radial diffusion and drift velocity 19 p3313 A67-35257

Graphical method predicting latitudes where satellites in circular orbit are visible, in both Northern and Southern Hemispheres 19 p3182 A67-35268

Time dependency, anisotropy degree and spectral composition of cosmic radiation generated during July 1966 solar flares as observed by Pioneer VI 19 p3314 A67-35270

Space research activities in Czechoslovakia, discussing satellite observation, aerospace medicine, solar physics, etc 19 p3320 A67-35282

East Germany space research in satellite tracking, coupling processes, upper atmosphere, high energy particles, etc 19 p3321 A67-35294

Pakistan space research noting facilities, sounding rocket experiments and satellite-and ground-based observations 19 p3321 A67-35297

Spacecraft surveys of earth used for city growth observations, draw land-use maps, etc 19 p3221 A67-35324

Interplanetary magnetic field and plasma velocity variations observed during Mariner II flight 19 p3324 A67-35451

Interplanetary magnetic field variation properties and effects on solar cosmic rays determined through Mariner II recordings employed to develop model 19 p3314 A67-35452

Geomagnetic field boundary observations by Explorer XII 19 p3222 A67-35453

Legal aspects of use of satellites in exploiting earthbound or near-in natural resources 19 p3349 A67-35641

Commercial aspects of exploitation of natural resources by satellite 19 p3349 A67-35642

Survey satellite potential uses in vegetation resources and terrain analysis, emphasizing satellite photography 19 p3231 A67-35654

Satellites role in World Weather Watch /WWW/ program for weather analyses and forecasts 19 p3253 A67-35656

Miniature optically immersed thermistor bolometer arrays employed for earth atmospheric horizon scanning from orbiting vehicles 19 p3231 A67-35684

Satellite earth crashing time and place calculated, providing observation possibilities 19 p3184 A67-35831

Highly eccentric orbit satellite /HEOS/ for solar wind, cosmic ray and magnetic field data collection, noting design and mission program 20 p3531 A67-36412

Azimuth and zenith distance determined from simultaneous observations of topocentric coordinates of artificial satellite transformed into astronomical and geodetic quantities 20 p3428 A67-36483

Satellite observations made by two or more satellites simultaneously on interplanetary medium 20 p3521 A67-36501

Meteorology, goals and methods, prospects for effective utilization of satellites and new techniques 20 p3480 A67-36823

Artificial satellite motion determination of external earth gravity field compared with surface measurements, orbit theory, etc 20 p3432 A67-37205

Plasma scale height errors from Alouette I topside sounder ionogram analysis 20 p3433 A67-37409

Brightness and contrast study of noctilucent clouds in twilight layer indicating preferability of satellite observation 20 p3434 A67-37426

Inclination of quasi-geocentric coordinate

system from satellite observations 20 p3434 A67-37548

Plasma observations in tail of terrestrial magnetosphere and circumlunar space by Luna X orbiter, using charged particle traps 21 p3697 A67-37841

Structurally regular magnetic field in circumlunar space recorded by Luna X orbiter, noting variations in intensity and solar wind effect 21 p3701 A67-37843

Soviet rocket and satellite observation of meteoric dust /1957 through 1966/ 21 p3701 A67-37844

Solid interplanetary matter in vicinity of moon observed by Luna X piezoelectric pickups attached to orbiter skin 21 p3701 A67-37845

Space triangulation equalization method based on modified closing plane method, discussing error equations 21 p3618 A67-38196

Geometrical methods for solving higher order geodetic problems from satellite observations including direction, position, coordinate, etc 21 p3618 A67-38263

Solar atmosphere absorption of light nuclei generated on sun indicated by satellite observation of heavy nuclei cosmic ray flux and X-ray electron bremsstrahlung 21 p3698 A67-38595

Coherent acceleration and velocity observation in real time /CAVORT/ analog radar signal processor for matched filtering pulse trains from radial accelerated targets 21 p3586 A67-38953

Lunar surface geology from results of Ranger, Luna IX and Surveyor I missions for selection of manned lunar landing site 22 p3879 A67-39309

Seasonal and diurnal variations of trough and ionospheric electron content and slab thickness, using S-66 satellite observation 22 p3789 A67-39471

Interplanetary space properties from satellite observations, discussing solar wind, geomagnetic field, comet tail effects, coronal plasma kinetic properties, etc 22 p3883 A67-39668

Ionospheric observations using Elektron I and III satellites, discussing state of ionosphere, electron concentration variation, etc 22 p3760 A67-39734

Solar particle event of February 1965 observation with Mariner IV and Injun IV showing 70 degrees heliocentric longitudinal distribution in interplanetary space 22 p3872 A67-39811

Photographic research of small scale meteorological disturbances /cloud formations/ observed by Tiros satellites 22 p3829 A67-39972

Microwave multiband spectral reconnaissance of earth and space vehicles using imaging radar on spacecraft 22 p3806 A67-40362

Atmospheric density, temperature and composition altitude variation measured by satellite observation of laser backscatter Raman component 22 p3806 A67-40366

Determination of coordinates from satellite observations noting triangulation method and optical technique 23 p3994 A67-40700

Martian atmosphere component due to proton penetration into atmosphere from solar wind, suggesting radio occultation by Mars orbiter 23 p4063 A67-40799

Solar X-ray emission below 20 angstroms made by Explorer XXX, discussing analog real time records and time resolution 23 p4050 A67-40805

Growth and decay of geomagnetic storms of April 17-18, 1965 studied using data from 88 ground stations, Explorer XXVI and Vela satellites 23 p3995 A67-40814

Lunar soil cohesive and disruptive properties from Surveyor I data, discussing micrometeorite impacts, thermal fracturing, metal vapor deposition and atomic adhesion 23 p4064 A67-40949

Satellite and probe data analysis on ionizing component, primary cosmic rays and albedo particle flux intensity near atmospheric outer boundary 23 p4055 A67-41098

Storm behavior of topside ionosphere studied from electron concentration satellite data, discussing height and latitude effects 24 p4148 A67-42058

Spread ionization in topside of ionosphere from satellite observations 24 p4148 A67-42060

Electron-resonance spikes on Alouette I ionograms observed for proton gyro-effects in topside ionosphere 24 p4148 A67-42062

Diurnal variations of electron concentration in topside ionosphere studied at low and middle latitudes using satellite data, noting secondary nighttime maximum 24 p4148 A67-42064

Parameters of simultaneous amplitude phase modulation of periodic cosmic ray variations obtained from satellite observations 24 p4209 A67-42115

Satellites and balloons for earth surface observation surveyed by types noting operations concerning geodesy, weather, oceanography, vegetation and wildlife 24 p4150 A67-42201

Surveyor V scientific experiment, comparing lunar surface sampling with that in Surveyor III, noting resemblance to granular terrestrial soil 24 p4228 A67-42308

Forestry applications for remote sensing from earth orbiting vehicles for inventory and evaluation of resources [AIAA PAPER 67-765] 24 p4258 A67-42934

SATELLITE ORBIT

Effect of meridional wind on satellite orbit inclination 01 p0146 A67-10255

Orbital elements of satellite determined from three position coordinates and three velocity components 01 p0149 A67-10788

Odd zonal harmonics in terrestrial gravitational potential determined from 14 well distributed satellite orbits 02 p0235 A67-11475

Numerical study of Newtonian potential perturbation effects on satellite motion about planet 02 p0321 A67-11496

Satellite orbit calculation using cylindrical coordinates 02 p0321 A67-11547

Variant of analytical determination /in terms of osculating-orbit elements/ of moments of entry into and emergence from earth shadow of artificial satellite 02 p0321 A67-11548

Minimum initial velocity and corresponding orbital inclination of satellite in Keplerian motion 02 p0327 A67-12334

Near circular orbit of satellite in terrestrial gravitational field analyzed, using approximate solution of perturbed Kepler motion 02 p0327 A67-12373

Heliocentric earth orbit precursor satellite, noting position outside earth and moon gravitational fields, orbital stability for solar phenomena evaluation, etc 02 p0335 A67-12410

Lunar gravitational field determined from orbital motion of Luna X satellite 03 p0510 A67-13341

Kinetic moment in celestial mechanics, noting application to satellite orbit determination in terrestrial gravitational field 03 p0510 A67-13456

Radio observation of Cosmos satellites with flight path inclination angle of 65 and 51 degrees, discussing signal audibility, atmospheric density and ionospheric effects 03 p0518 A67-13540

Book of physics and mathematics as foundation for application of satellites to geodesy including spherical harmonics, matrices, orbital geometry, statistical implications and data analysis 04 p0611 A67-14466

Synchronous satellite orbits exploration, ground track plots show effects of varying orbit eccentricity and inclination 04 p0694 A67-14503

Relative motion of body about satellite in orbit, determining impulses which cause body to remain in satellite vicinity 04 p0706 A67-15249

Fine structure of gravitational field in neighborhood of earth orbiting vehicle, analyzing contributions to field from earth, moon, sun, etc 05 p0798 A67-16518

Trajectories of artificial celestial bodies - Symposium, Paris, April 1965 05 p0893 A67-16554

Satellite orbital parameters determined from visual observations 05 p0894 A67-16559

Satellite orbit major axis determination by using coincidence of time when satellite crosses plane of tracking station parallel with time of crossing topocentric celestial equator 05 p0894 A67-16560

Earth potential in ellipsoidal coordinates developed using Lane function 05 p0796 A67-16564

Effect of precession of earth axis of

rotation on satellite motion 05 p0894 A67-16565

Computational methods employed with Doppler observations and derivation of geodetic results 05 p0894 A67-16571

Lunar orbit characteristics and perturbations of Lunar Orbiter and Anchored IMP 05 p0895 A67-16576

Space flight problems in cislunar space, noting lunar probes, high apogee satellite specifications and orbital stability 05 p0897 A67-16732

Relativistic trajectory and orbital precession of spinning satellite under nonspherically symmetric gravitational field 05 p0906 A67-16849

Earth gravitational field parameters from near-surface satellite observations influenced by zonal and tesseral harmonics 05 p0800 A67-17080

External sources of geomagnetic field at F-2 layer altitude and effects on recurring-orbit satellites 05 p0800 A67-17119

Rotational speed of upper atmosphere obtained by measuring changes in orbital inclinations of satellites or movements of vapor trails 06 p0993 A67-17564

Effects of varying orbital parameters including number of satellites, orbit altitude, positioning, tracking accuracy, cost effectiveness, etc, on establishment and maintenance of communications satellite system 06 p1094 A67-17698

Items affecting information transmitted from payload landed on remote planet to earth via communications satellite including orbit, transmission policy and orbit injection error effect on communication capability [AIAA PAPER 66-314] 06 p1094 A67-17704

Geodetic error effect on time dependence of satellite tracking data received by ground station 06 p1080 A67-17769

Drag free motion of satellite of oblate planet determined by differential equation expressing planet gravitational potential as spherical harmonics 06 p1081 A67-17777

Successive approximations determining radiation pressure effect on and disturbing function of motion equations of artificial satellite 06 p1081 A67-17787

Maneuverable geodetic satellite for better determination of resonant harmonics in geopotential field [AIAA PAPER 67-122] 06 p1096 A67-18340

Satellite under perturbing acceleration having constant modulus and directed along normal to osculating plane of orbit, calculating rotation of orbital plane 06 p1088 A67-18620

Semiannual effect on satellite orbit decay, correlating with difference in latitude between perigee and sub-solar point 07 p1251 A67-19850

Modification of Encke perturbation method for computing satellite orbits, obtaining integration of motion equations [AAS PAPER 66-93] 07 p1252 A67-19957

Rigorous error bounds on position and velocity of satellite derived from Hamiltonian theory and von Zeipel method [AAS PAPER 66-94] 07 p1252 A67-19958

Satellite motion for all inclinations around oblate planet with potential including second and fourth zonal harmonics 08 p1382 A67-20398

Satellite orbit computation program with element representation based on drag-free perturbation theory coupled with differential correction procedure 08 p1383 A67-20403

Solution of motion equations for lunar satellites in near equatorial plane using transformation of variables 08 p1383 A67-20582

Coefficient of major axis of symmetry of spherical harmonic in satellite oscillations 08 p1383 A67-20587

Periodic solutions for restricted three-body problem 08 p1384 A67-20619

Satellite communication network requirements and orbital characteristics 08 p1293 A67-20724

Lunar gravitational field and effect on motion of lunar satellite 08 p1395 A67-21163

Ellipticities of moon for radial shift and rotation of unperturbed orbit of close satellite in plane of instantaneous motion 08 p1396 A67-21178

Satellite orbit effect on establishment of global communications network 08 p1296 A67-21505

Inclination variation with time of 24-hr

low inclination orbits perturbed by solar-lunar gravitation 08 p1402 A67-21508

Onboard device locating present and future orbital satellite position through microfilm map dependent on satellite motion equation 08 p1352 A67-21525

Orbital behavior and stationkeeping propulsion requirements for synchronous satellites, considering solar radiation and earth oblateness effects 09 p1571 A67-21697

Tabulated altitudes, periods and velocities for Martian satellites in circular parking orbits 09 p1564 A67-21716

Orbital disturbances of satellite produced by zonal harmonics of gravitational field 09 p1564 A67-21884

Orbit perturbations due to tesseral harmonics contained in series expansion of gravitational potential determined using computer program 09 p1467 A67-21885

Equations describing orbital plane rotation of satellites, noting analogy between equations for oscillations of mechanical system with one degree of freedom 09 p1564 A67-21887

Optimization in terms of energy expenditure of problem of interorbital one- and two-pulse satellite transfer in central gravitational field 09 p1564 A67-21888

Elliptic type orbit determination in generalized problem of two stationary centers by integration in quadratures of motion equations of satellite 09 p1565 A67-21902

Cable suspension of daughter satellite from parent satellite, examining synchronous rotation at less than synchronous altitude 10 p1712 A67-23148

Semianalytical solution of motion of satellite in lunar orbit, considering perturbations due to lunar and earth gravity and solar attraction 10 p1706 A67-23185

Polynomial approximation method for determining satellite orbits from large-time-interval trajectory measurements 11 p1858 A67-24066

Error accumulation in numerical integration of motion equation analyzed for circular satellite orbits 11 p1859 A67-24317

Asymptotic calculation of effect of small tangential thrust on satellite motion problem solved for satellite orbit in first and second approximation 11 p1870 A67-24684

Rate of satellite turn in elliptical orbit calculated by introducing nondimensional angle, deriving master curves, noting applicability to attitude control systems 12 p2000 A67-25124

Upper atmospheric density determination from data of satellite orbit evolution, noting effect of solar activity 12 p1932 A67-25533

High order tesseral harmonic effects on satellite orbit calculation 12 p2008 A67-25831

Molecular ion concentration around dawn-dusk auroral zone satellite orbit 13 p2108 A67-26315

Geocentric orbital elements determined from quasi-simultaneous direction observations to satellites 13 p2199 A67-26852

Satellite and astronomical refraction determined from formulas for air refractive index determination 13 p2199 A67-26854

Sun illumination time of artificial earth satellite moving in elliptical orbit 13 p2200 A67-27338

Maximum and minimum eclipse time of earth satellites with circular and elliptical orbits, considering dependence on argument of orbital perigee 13 p2201 A67-27339

Satellite orbit analysis and computer program for earth zonal harmonics determination, considering orbit elements and gravitational constants [AAS PAPER 66-91] 13 p2116 A67-27516

Modification of Encke perturbation method for computing satellite orbits, obtaining integration of motion equations [AAS PAPER 66-93] 13 p2207 A67-27517

Rigorous error bounds on position and velocity of satellite derived from Hamiltonian theory and von Zeipel method [AAS PAPER 66-94] 13 p2207 A67-27518

Orbit determination of stationary satellites through data analysis, noting perturbation effect and estimation of Early Bird satellite orbit 13 p2208 A67-27522

Lunar gravitational field determined from orbital motion of Luna X satellite 13 p2211 A67-27714

Space flight technology developments, particularly for booster rockets and space

vehicles 14 p2393 A67-27873
 Mathematical investigation of satellite motion in vicinity of critical inclination, analyzing singularity 14 p2384 A67-28077
 Approximate analytical solution for satellite circular orbits subjected to small tangential thrust or drag 14 p2384 A67-28117
 Simulation experiments to describe effects of measurement function nonlinearity and ambiguities when linear filters are applied in distant planet satellite orbit parameter estimation 14 p2347 A67-28130
 Topocentric velocity of artificial satellite determined by introducing two pairs of unitary vectors in orbital plane 15 p2556 A67-29745
 Artificial satellite radius vector determination examined for degree of accuracy, discussing geodetic applications 15 p2477 A67-29746
 Spheroidal coordinate method for obtaining gravitational potential of oblate planet 15 p2560 A67-30042
 Free molecular flow region, calculating drag on plate, sphere and general body, considering drag effect on satellite orbit 15 p2561 A67-30045
 Satellite visibility calculation for individual ground stations of telemetry and tracking network as function of orbital injection parameters 15 p2561 A67-30047
 Spinor algebra application to Fourier series transformation of spherical harmonics expansion representing earth gravitational potential at space location 15 p2561 A67-30055
 Accuracy of satellite orbit prediction for rendezvous mission related to ground-based tracking network sensors by digital computer simulation 15 p2441 A67-30165
 Librational and flexural resonances induced in satellite whose center of mass is moving in planar elliptic orbit 15 p2572 A67-30195
 Rotational analysis theorem concerning earth satellite motion about angular-momentum vector with respect to inertial reference frame 15 p2519 A67-30209
 Satellite-launched artificial meteors discussing use, system concept, orbit considerations, cost, acceleration and separation 16 p2758 A67-30645
 Spherical coordinates near apogee of Cosmos 41 satellite determined with TV system and meniscus telescope 16 p2621 A67-30683
 Communications satellite systems discussing launching, orbits economics, etc 16 p2760 A67-30700
 Asymptotic calculation of satellite orbit evolution in noncentral gravitational field of earth 16 p2743 A67-30724
 Orbits of artificial satellites for suitable variables, noting oblate shape of earth and air resistance 16 p2743 A67-30725
 Improvement of satellite elliptical orbits with small eccentricities using differential formulas 16 p2743 A67-30727
 Gravitational stabilization of satellites with respect to orbital system of coordinates 16 p2760 A67-30740
 Photometric theory of artificial satellite ellipse by earth with application to atmospheric study 16 p2745 A67-30746
 Geometric restraints on orbit about Mars noting trajectories of unmanned Mars exploration satellite, payload, orbit inclination, etc 16 p2745 A67-30748
 Secular and periodic perturbations of orbits of artificial satellites of earth and moon by attraction of external bodies 16 p2746 A67-30981
 Satellite orbit calculation using cylindrical coordinates 16 p2752 A67-31613
 Variant of analytical determination /in terms of osculating-orbit elements/ of moments of entry into and emergence from earth shadow of artificial satellite 16 p2752 A67-31614
 Motion of dynamically symmetric satellite under action of gravitational moments, discussing stability and nonlinear oscillations 17 p2955 A67-32243
 ELDO-PAS program principles, objectives, ground stages, orbital injection, etc 17 p2955 A67-32399
 Three-body problem of Jupiter satellites orbits under solar influence, computing initial elements, determining orbital stability and solving satellite motion equations 17 p2946 A67-32753

Heliocentric orbits of former Jupiter satellites, relating direct or retrograde satellite to heliocentric semimajor axis as asteroid 17 p2946 A67-32754
 Ascent of satellite of variable mass from elliptic orbit along spiral trajectories by low thrust 17 p2948 A67-33022
 Coefficients of odd zonal harmonics in terrestrial gravitation evaluated from orbital eccentricity analysis of artificial satellites 17 p2853 A67-33249
 Star occultation measurements accuracy for determining satellite orbit parameters, noting error sources 18 p3075 A67-34108
 Phobos and Deimos origin in equatorial circular orbits or asteroid capture and tidal modification 18 p3125 A67-34160
 Satellite orbit determination, observation, dynamical theory, perturbations, drag, computation, etc 18 p3126 A67-34243
 Orbit determination from Minitrack observations, discussing effects of ionospheric refraction, atmospheric drag and earth tesseral harmonics 18 p3126 A67-34244
 Data and orbit analysis supporting Navy satellite Doppler system Tranet, discussing editing and archiving of Doppler data and orbital ephemerides 18 p3003 A67-34245
 Balloon satellite orbital elements predicted in advance by computation of solar radiation, gravitational perturbations, etc 18 p3126 A67-34246
 Low perigee satellite orbit determination by visual observation, comparing directional accuracy and orbital elements with Minitrack and Baker-Nunn 18 p3126 A67-34247
 Satellite orbit perturbations in theories determining earth gravitational field, observing relation to departures from Keplerian ellipse 18 p3041 A67-34249
 Determination of Love number of earth from variations of orbital inclinations of satellites 18 p3041 A67-34250
 Air drag effect on six Cosmos satellites orbits having low perigee, discussing diurnal air density variation at 280 km height 18 p3042 A67-34256
 Satellite orbit perturbation analysis for lunar gravitational field determination using von Zeipel transformation 18 p3131 A67-34325
 Initial defense communications satellite program giving payload characteristics and orbit analysis of 15 military launchings 18 p3137 A67-34612
 Upper atmosphere rotational speed determined by analyzing changes in satellites orbital inclinations 19 p3216 A67-35182
 Exospheric density variation as related to solar activity determined from satellite orbits 19 p3217 A67-35211
 Graphical method predicting latitudes where satellites in circular orbit are visible, in both Northern and Southern Hemispheres 19 p3182 A67-35268
 Solar system bodies gravitational fields, discussing possibility of holding satellite in orbit 19 p3323 A67-35337
 Air density variation at 220 km altitude shown due to increased solar activity, from satellite orbit observation 19 p3222 A67-35458
 Elliptic geocentric satellite orbit for measurements of magnetosphere-nearby space region, analyzing orbital lifetimes and perturbations [AIAA PAPER 67-616] 19 p3226 A67-36005
 Highly eccentric orbit satellite /HEOS/ for solar wind, cosmic ray and magnetic field data collection, noting design and mission program 20 p3531 A67-36412
 Atmospheric drag influence on orbital elements of satellites having highly eccentric orbits 20 p3522 A67-36616
 Intersection points for satellite orbit and earth shadow /shadow equation/ solved for small eccentricities by iteration 20 p3523 A67-36624
 Artificial earth satellite orbital element accuracy, describing least squares method of choosing time intervals for reducing errors 20 p3523 A67-36625
 Shortest distance between two quasi-coplanar elliptical asteroid orbits, solving transcendental equations by consecutive approximation method 20 p3523 A67-36628
 Satellite orbit determination by measuring arrival angle of two transmitted waves with different frequencies 20 p3382 A67-36774
 Probability characteristics of osculating satellite motion, considering random

parameter scatter and atmospheric density variations, with expectation obtained by numerical integration 20 p3485 A67-36922
 Plasma diagnostic measurement simulation, considering electromotive effect from satellite motion through geomagnetic field 20 p3418 A67-37428
 Alouette I and Explorer XX /S-48/ spin behavior explained by solar heating of antennas and solar radiation pressure 21 p3712 A67-37784
 Lunar cartography using space vehicles, considering satellite orbits and information transmission 21 p3703 A67-38197
 Frequency bands and modulation methods for space communication system 21 p3581 A67-38235
 External sources of geomagnetic field at F-2 layer altitude and effects on recurring-orbit satellites 21 p3618 A67-38462
 Upper atmosphere angular velocity determined from changes in satellite orbital inclinations, noting increase with height 21 p3619 A67-38512
 VLF radio reception anomalies explained by ephemeral natural satellite still in orbit, assuming reflections taking place near satellite perigee 21 p3582 A67-38514
 Satellite with symmetry axis perpendicular to orbit analyzed for rotational motion, determining instability for eccentric orbit, noting gravitational effect 21 p3713 A67-38588
 Geomagnetic and gravitational field combined effects on magnetized satellite oscillations in plane of circular and elliptical polar orbits 21 p3713 A67-38590
 Radio wave refraction and refraction-induced errors calculated in determination of artificial satellite trajectories 21 p3582 A67-38593
 Differential correction vectors for non-Keplerian reference orbits, reexamining rotating ellipses in Hansen type intermediaries 21 p3705 A67-38612
 Satellite orbit adjustment, stationkeeping and attitude control of typical earth-and sun-synchronous satellites by electric propulsion systems [AIAA PAPER 67-719] 21 p3694 A67-38745
 Optical determination accuracy of satellite orbits, investigating orbit elements by Gaussian averaging calculation assuming elliptical orbit 22 p3830 A67-39161
 Position fix and range data techniques for preliminary orbit determination for lunar satellites, using least squares method for data smoothing 22 p3879 A67-39310
 Orbital element periodic variations for satellite motion about oblate planet with low and moderate eccentricity 22 p3880 A67-39313
 Circular orbit stability in planetary axisymmetric gravitational and dipole magnetic fields 22 p3880 A67-39404
 Doppler effect method application to satellites and space vehicles motion, giving formulas for satellite velocity, orbital shape and position 22 p3831 A67-39588
 Satellite motion in libration point vicinity, neglecting lunar eccentricity and solar perturbation, discussing lunar communication system utilizing libration point satellites 22 p3886 A67-40107
 Minimum fuel flight plans for injecting synchronous satellite into circular equatorial orbit, developing four methods 22 p3886 A67-40116
 Soviet book on motion of artificial satellites in earth gravitational field covering perturbation theory, force field, algorithms for calculations, etc 23 p4063 A67-40734
 Solar conversion/energy storage power systems for satellites in near earth orbits to provide continuous power supply 23 p3938 A67-41506
 Lunar gravitational fields based on Cassini and Euler rotation laws compared with solar, Saturnian and Jovian effects on Saturn and Jupiter satellites 24 p4229 A67-42311
 Gravity oriented satellite coupled librational motion in circular orbit analyzed for motion stability by numerical methods 24 p4231 A67-42384
 Terrestrial gravity anomalies influence on satellite orbits treated by analytical numerical integration 24 p4237 A67-42686
 Satellite rise and set time of distant primary and occultation interaction determined for case of Martian satellite 24 p4238 A67-42925

SATELLITE ORIENTATION

SA IMAGE DISSECTOR TUBE
Neptunian planet-satellite system,
discussing orbital motion of
Triton 01 p0148 A67-10385
Communications satellite orientation with
respect to earth, using structure mounted
electromagnetic actuator
coils 05 p0905 A67-16831
Direct-to-home TV broadcasting satellite
system for upper UHF, describing
stabilization, thermal control, antenna, power
amplifier, etc 06 p1094 A67-17689
[AIAA PAPER 66-309]
Direct-to-home TV broadcasting satellite
system for upper UHF, describing
stabilization, thermal control, antenna, power
amplifier, etc 06 p0964 A67-18414
[AIAA PAPER 66-309]
Graphical method for converting
geocentric satellite coordinates into
topocentric, determining azimuth, elevation
angle, etc 06 p0964 A67-18577
Simultaneity circles used in space geodesy
to obtain synchronous observation of trials
of satellites and determination of absolute
directions in space of lines joining tracking
stations 07 p1177 A67-19778
Calculation of geocentric position errors of
satellite obtained by nonsimultaneous
observations 07 p1177 A67-19779
Longitudinal and lateral axes orientation
of uniformly rotating or rapidly rotating
vehicle utilizing outputs from solar sensors
and lateral magnetometer 08 p1409 A67-20538
Optimization problem associated with fuel
consumption for control of satellite
orientation by means of active
system 09 p1571 A67-21696
Satellite orientation with respect to
velocity vector determined using attached
planar ion traps 09 p1571 A67-21890
Propellant cost optimization using
minimum characteristic velocity solutions for
extra-atmospheric part of rocket ascent
trajectory, emphasizing final elliptical orbit
of arbitrary orientation 10 p1704 A67-22877
Gyroscopic stabilization of relative
equilibrium of satellite 11 p1869 A67-24067
Dynamic effects on satellite motion of
mechanical deformations in stabilizing
system, deriving equations for rotational
motion about center of
inertia 11 p1870 A67-24674
Space vehicle orientation with respect to
rotating system of
coordinates 12 p2011 A67-25641
Low energy proton precipitation
measurements in austral and boreal auroral
zones, using polar orbiting
satellite 12 p1937 A67-25813
Solar photon radiation reaction produced
on body of satellite and utilized for satellite
stationkeeping 13 p2213 A67-27489
Gravity-gradient oriented satellite
stabilization by means of solar pressure
torques on adjustable
slats 14 p2395 A67-29051
Rapid acquisition of sun in solar energy
conversion systems based on momentum
exchange from rotating flywheels to
platform 15 p2423 A67-30130
Molniva type communication satellite,
discussing optimum orbital requirements for
maximum coverage, phasing,
etc 16 p2742 A67-30698
Attitude determination and hydrogen
peroxide control system for spacecraft
orientation in Syncom, Early Bird and ATS
[AIAA PAPER 67-532] 19 p3334 A67-35934
Satellite orientation sensing and orbital
gyrocompassing heading reference,
examining effect of horizon sensor noise
[AIAA PAPER 67-587] 19 p3258 A67-35983
Electron content measured using satellite
motion and position effects on Faraday
rotation 20 p3431 A67-37102
Luna IX automatic station flight control
complex, detailing communication,
orientation and stabilization systems
operation after separation from acceleration
module 22 p3897 A67-39167
Statistical method for determining satellite
orientation and rotation based on
differential motion equation
model 22 p3878 A67-39168
Flight control system for automatic
interplanetary stations /AIS/, comparing
Venera series orientation and correction
system to Mariner 22 p3898 A67-39185
systems

Active control of space vehicles
orientation, discussing optimal and rational
control and rotational motion braking
problems 22 p3899 A67-39189
Triaxial orbital orientation control
algorithm for space vehicle with incomplete
angular position
information 22 p3899 A67-39191
Variational calculus for optimal attitude
acquisition/stabilization controller synthesis
for spinning and nonspinning space
vehicles 22 p3904 A67-40105

SATELLITE PERTURBATION
SA ORBIT PERTURBATION

Encke special perturbation method of
integrating motion equations of near-earth
satellites modified to eliminate first-order
effects of earth
oblateness 01 p0148 A67-10383
Nominal trajectory in modified Encke
special perturbation method, using two-body
functions 01 p0148 A67-10384
Case of integrability of equations of
perturbed motion of satellite under action
of Newtonian force 01 p0151 A67-10994
Harmonic analysis of perturbed satellite
motion from exact solution for point motion
about two fixed centers
[ONERA TP-420] 02 p0320 A67-11494
Solar-lunar perturbation of 24-hour
satellite, independence of librational motion
and impossibility of
equilibrium 02 p0321 A67-11498
Flexible antenna effect on stability of
spin-stabilized satellite in viscous damped
oscillator model 02 p0330 A67-11927
Diurnal and latitudinal variation of
satellite scintillation during local summer at
low southern geomagnetic
latitudes 03 p0406 A67-12821
Ion thrust motors used to overcome solar-
lunar attraction, earth triaxiality, solar
pressure and other forces tending to
perturb satellite orbit or modify
orientation 04 p0705 A67-15027
Perturbations of satellite orbital elements
caused by pressure of solar radiation
reflected from earth 05 p0894 A67-16566
Radiation effect on satellite in presence of
partly diffuse and partly specular reflecting
body 05 p0905 A67-16567
Perturbed motion of satellite with small
orbital eccentricities 05 p0905 A67-16570
Estimation problems in determining even
zonal harmonics of external geopotential
from secular satellite motion, examining
least squares method
validity 05 p0797 A67-16573
Stability of planar librations of dumbbell
gravity gradient satellite in elliptic
orbit 05 p0901 A67-17104
Effect of man walking inside or outside of
satellite on attitude 05 p0906 A67-17205
Structural and librational dynamics of
satellite deploying flexible booms or
antennas
[AIAA PAPER 67-43] 06 p1095 A67-18264
Zonal and tesseral harmonic perturbations
of artificial satellite 08 p1382 A67-20399
Satellite motion with large inclination and
large eccentricity around planet and
perturbed by sun 08 p1382 A67-20400
Satellite perturbation by pressure of
radiation reflected from
earth 08 p1383 A67-20401
Constant force effect on Keplerian orbit
with reference to solar wind
perturbation 08 p1383 A67-20402
Lunar satellite motion under terrestrial
perturbations and lunar
potential 08 p1383 A67-20404
Control moment gyros for semipassive
damping of satellite librational
motion 08 p1330 A67-20586
Resonant oscillations of artificial earth
satellite with nearly repetitive path relative
to rotating primary with longitudinally
varying gravitational field 08 p1401 A67-21362
Proposal for computation of unknown
parts of gravitation field of earth from
successive satellite
passages 10 p1636 A67-23180
Motion and stability of spinning spring-
mass system in orbital plane with equation
linearization 10 p1710 A67-23752
Dynamic effects on satellite motion of
mechanical deformations in stabilizing
system, deriving equations for rotational
motion about center of
inertia 11 p1870 A67-24674
Malkin theorem for satellite attitude

control subjected to light pressure
perturbation 11 p1870 A67-24723
Angular momentum considerations for
stability of satellites with moving inner
masses 13 p2211 A67-26623
Stability of motions of satellite with rotor
and cavity with liquid, reducing problem to
solution of minimum change in potential
energy of system 13 p2213 A67-27319
Earth gravitational field eccentricity effect
on deviation of satellites from Kepler ellipse
orbits 13 p2200 A67-27322
Boundary value problem for differential
equations of perturbed satellite motion
assuming perturbing accelerations defined
by Vinti potential 13 p2200 A67-27323
Solar photon radiation reaction produced
on body of satellite and utilized for satellite
stationkeeping 13 p2213 A67-27489
Ionospheric satellite trail, noting relation
between length scales of medium properties
and scales determined by body
dimensions 14 p2302 A67-28207
Material elasticity effects on planar
librational motion of rigid satellite under
action of gravity
gradients 16 p2761 A67-30743
Secular and periodic perturbations of
orbits of artificial satellites of earth and
moon by attraction of external
bodies 16 p2746 A67-30981
Eccentricity change for satellite in
librational resonance shown periodic due to
gravity dependence on
longitude 19 p3220 A67-35254
Geostationary satellite stability in
presence of geopotential field zonal
harmonics, using Liapunov
theory 19 p3333 A67-35569
Lunar-solar gravitational perturbation of
satellite with sidereal day period, discussing
stability 20 p3523 A67-36626
Kinetic theory of ionospheric satellite
trail, discussing neutral and charged
components from BGK model equation
[AIAA PAPER 66-477] 21 p3706 A67-38862
Nonlinear differential equations describing
extensional motion of dumbbell satellite
solved on digital
computer 22 p3886 A67-40086

SATELLITE PHOTOGRAPHY

Nautical chart information extracted from
hyperaltitude color photographs obtained on
Gemini orbital flights IV, V and
VII 01 p0059 A67-10322
Interpretations of lunar crater erosion
other than used by Jaffe from Ranger VII
pictures 02 p0325 A67-11860
Stereo interpretation of Nimbus II
automatic picture transmission photography
for cloud patterns
[AFCR-66-805] 02 p0241 A67-11970
Table of names of formations on moon far
side identified by Zond III lunar orbiter
photographs 02 p0329 A67-12498
Positions of Echo satellites during reentry
stage observed at Asiago in
1964 03 p0509 A67-13105
Propellant preparation from
extraterrestrial materials on moon and
planets rather than transportation from
earth as economical source of fuel for
interplanetary manned
traffic 04 p0695 A67-14555
Satellite photographs received from APT
facility used in analysis of old occluded
depression structure, deducing jet stream
position and sea-ice
presence 04 p0650 A67-14868
Tiros VIII, Nimbus I and II and Essa II
weather satellites and radio reception of
observational results by German
meteorological service APT receiver
stations 05 p0904 A67-16028
Size distribution of lunar craters from
Ranger pictures show that frequency of
crater occurrence is inversely proportional
to square of diameter 05 p0903 A67-17293
Satellite three-dimensional triangulation
accuracy, discussing orientation of camera
axes and plate coordinates of satellite
images as error sources 06 p0994 A67-17717
Lunar crater diameter-depth relationship
from Ranger VII
photographs 06 p1087 A67-18376
Tiros satellite development and Tiros
operational satellite /TOS/ system noting
design, camera orientation, spin-rate control,
etc 06 p1096 A67-18412
Photographic mapping of Martian surface
with electrically propelled solar-powered

photographic spacecraft placed into near polar orbit
 [AIAA PAPER 67-88] 06 p1096 A67-18438
 Photographs taken by astronauts as part of Synoptic Terrain Photography Experiment including geological features such as Sonora Desert, Agua Blanca and Gulf of Aden 06 p0999 A67-19002
 Structure of lunar lithosphere using data from ground telescopes and Ranger photographs 06 p1092 A67-19004
 Graphical method by which small local users of meteorological satellite pictures can identify geographical position of features in image [AIAA PAPER 66-439] 07 p1184 A67-19373
 ANNA satellite geodesy experiments emphasizing operation of strobe light 07 p1176 A67-19766
 Geodetic linking of France and North Africa by synchronous photographs of Echo I satellite 07 p1176 A67-19767
 High precision artificial satellites photography experiment to measure astronomical bearings 07 p1144 A67-19768
 Astrometric processing of synchronous photographic observations of Echo I satellite 07 p1144 A67-19769
 TV pictures of Surveyor I compartment radiators taken on June 11 and July 12, 1966, discussing cause of some changes in dust locations 08 p1386 A67-20944
 Lunar surface topography analyzed using Ranger photographs, particularly texture of lunar maria such as ray craters, ridges, collapse depressions, etc 08 p1390 A67-21025
 Ranger photographs of lunar surface noting erosion and fragmentation by meteorite bombardment 08 p1390 A67-21026
 Relative depths of moon mountain rings and craters in region of Mare Nubium 08 p1390 A67-21027
 Pictures of moon taken by Ranger, Surveyor and Orbiter spacecraft analyzed for origin, history, libration, temperature and properties 08 p1401 A67-21428
 Surveyor system and camera design for photographic mission on Mars surface 09 p1570 A67-21680
 Orbital reconnaissance of Mars in 1971 using modified Lunar Orbiter spacecraft, noting photographic system, trajectory, launch system, etc 09 p1570 A67-21681
 Selenological analysis of Ranger IX photographs, examining origin and age of craters and mountain chains 10 p1705 A67-22898
 Photographing satellites, using optical system and image converter for determining coordinates 10 p1606 A67-23184
 Table of names of formations on moon far side identified by Zond III Lunar Orbiter photographs 10 p1709 A67-23366
 Cloud photographs obtained on board ATS-I satellite with camera equipped with reflecting telescope show feasibility of short-lived weather systems from synchronous altitude 10 p1657 A67-23367
 Film camera and video transmission system onboard Lunar Orbiter 10 p1657 A67-23624
 Planetary mapping mission system requirements for photography, IR and radar imagery, radar reflectivity and spectroscopy with data analysis techniques 11 p1859 A67-24438
 Lunar soil composition determined to be porous fine-grain moderately cohesive rock powder, from Surveyor I and Luna IX pictures 11 p1865 A67-24607
 Morphology of lunar craters from Ranger photographs, noting distribution and possible competing processes of crater formation and destruction 11 p1865 A67-24608
 Heavy cosmic ions recorded on ionographic emulsions exposed on polar satellite 12 p1999 A67-25830
 Nondeepening synoptic scale tropical disturbance showing dependence on in situ development and decay in upper troposphere 13 p2152 A67-27605
 Low noise preamplifier traveling wave maser operated in closed cycle refrigerator for receiving Mariner IV picture transmissions 14 p2329 A67-27779
 Panoramic photograph processing theory 14 p2318 A67-28372
 French optical satellite observation network 14 p2270 A67-28589
 Military surveillance satellite for high resolution photography noting design,

application and projected performance 15 p2564 A67-29400
 Variability in human estimation of total cloud cover data by satellite-photograph interpretation, noting use of Nimbus I photographs 17 p2880 A67-32555
 Lunar surface photographs taken by Luna IX and Surveyor I showing linear and circular ground features, rock blocks and dust 17 p2948 A67-33094
 Parametrization of photographs of cloud system by satellite TV cameras, discussing brightness problems via data processing 18 p3073 A67-33561
 Moon surface origin and present surfaces of moon, Venus and Mars as determined from lunar photographs and data by flyby probes 18 p3121 A67-34135
 Lunar surface and U.S. Ranger program significance and interpretation 18 p3121 A67-34137
 Analysis of lunar surface panoramas transmitted by automatic station Lunik IX after soft landing 18 p3122 A67-34138
 UV spectra of lunar surface photographed from Zond III automatic space probe 18 p3122 A67-34141
 Visible brightness features in Mariner IV photographs of Mars interpreted as clouds 18 p3123 A67-34149
 Survey satellite potential uses in vegetation resources and terrain analysis, emphasizing satellite photography 19 p3231 A67-35654
 Detection of mineral resources by orbiting satellite photography, using remote sensor techniques 19 p3225 A67-35655
 ATS-1 spin scan camera experiment for photographic recording of weather motions 20 p3446 A67-36610
 Surveyor I spacecraft location and identification on moon surface by photographs taken by Orbiter 20 p3524 A67-36649
 Optical data acquisition by NASA for National Geodetic Satellite Program flash photography 20 p3382 A67-36888
 Imaging systems of ground-viewing satellite, discussing TV, lasers, radar, etc 20 p3452 A67-37310
 Mountain lee waves, comparing wavelengths observed on satellite pictures with calculations assuming wind speed increase with height 21 p3655 A67-38578
 TIROS satellite program accomplishments since 1960, describing operational system, TOS ground-station network and ESSA satellites 22 p3899 A67-39608
 Estimated thickness of fragmental surface layer of Oceanus Procellarum from laboratory impact cratering studies 22 p3885 A67-39977
 Shock processes pertinent to lunar terrain fragmentation and lithification noting Surveyor and Lunar Orbiter pictures 23 p4064 A67-40948
 Lunar scar and ghost crater origin theories illustrated with Ranger 3-D slides 23 p4064 A67-40951
 Seleno-geological evidence for lunar surface properties from Surveyor I, discussing weathering products and volcanic genesis 23 p4064 A67-40952
 Ranger, Surveyor and Orbiter probe lunar surface photographic data, discussing lunar event distribution, lunar craters and maria distribution 23 p4065 A67-40953
 Similarity between Icelandic lava field photographs and Luna IX lunar surface photographs 23 p4065 A67-40954
 ATS-1 spin scan camera experiment for photographic recording of weather motions 24 p4156 A67-42405
 Brightness distortions quantitative determinations in digitized Tiros/ESSA satellite vidicon data to normalize scene to uniformly illuminated image 24 p4156 A67-42431
 Clouds over equatorial and tropical Pacific investigated by comparing photographs from Tiros satellites and jet aircraft 24 p4181 A67-42667
SATELLITE RENDEZVOUS
 Satellite rendezvous guidance laws applicable to circular, near-circular and elliptical orbits, using Lagrangian formulas for position and velocity in two-body orbit 02 p0264 A67-12315
SATELLITE ROTATION
 Earth oblateness effect on torque experienced in nonuniform geogravitational

field by satellite with unequal principal moments of inertia 01 p0154 A67-11184
 Passive spin propulsion of large flexible spherically shaped satellites by solar radiation field 05 p0905 A67-16568
 Quasi-steady state temperature distribution in thick walled spherical satellite under solar radiation 05 p0906 A67-17368
 Simulation of deployment dynamics of spinning spacecraft, discussing test methods emphasizing gravity compensating techniques [AIAA PAPER 67-207] 06 p0980 A67-18325
 Solar radiation field interaction with flexible antenna as possible explanation of anomalous rapid spin decay of satellites [AIAA PAPER 67-39] 06 p1096 A67-18350
 Inertial forces on straight light appendage used as antenna on artificial satellite 08 p1410 A67-20786
 Relativistic rotation of perigee of satellite determined from first integral of motion equation 09 p1563 A67-21658
 Equations describing orbital plane rotation of satellites, noting analogy between equations for oscillations of mechanical system with one degree of freedom 09 p1564 A67-21887
 Stationary resonance solutions for rotating systems with one degree of freedom applied to satellite rotation problems 09 p1532 A67-21910
 Apparatus for simulating spatial turn in artificial satellite and feasibility of developing turns in near-earth space by applying force perpendicular to orbital plane 09 p1484 A67-22095
 Cable suspension of daughter satellite from parent satellite, examining synchronous rotation at less than synchronous altitude 10 p1712 A67-23148
 Optimum stabilization problem for axisymmetric satellite, considering fuel consumption 12 p2011 A67-25639
 Spacecraft rotation effect on measurement of hydromagnetic radiation in solar wind 12 p1934 A67-25782
 Photometric studies of eclipses of Echo I and II satellites, noting period of rotation from luminosity curves and 180 degree phase shift 12 p2008 A67-25832
 Stability analysis of deformable space vehicle in torque free state noting gravitational effect, stability of spin motion, characteristic motion equations, etc 17 p2956 A67-32779
 Book on celestial mechanics presenting solution of artificial satellite motion in earth gravitational field, using Lagrange equations 17 p2950 A67-33166
 Gravitational and magnetic torque effects on rotational motion of asymmetric Pegasus satellite in circular orbit [AIAA PAPER 67-567] 19 p3335 A67-35963
 Satellite with symmetry axis perpendicular to orbit analyzed for rotational motion, determining instability for eccentric orbit, noting gravitational effect 21 p3713 A67-38588
 Statistical method for determining satellite orientation and rotation based on differential motion equation model 22 p3878 A67-39168
 Active control of space vehicles orientation, discussing optimal and rational control and rotational motion braking problems 22 p3899 A67-39189
 Strength of synchronous rotation of moon in terms of upper and lower limits on rotational period, using Runge-Kutta integration 22 p3885 A67-39978
 Stationary motion stability of gyrostat satellite in Newtonian force field, defining body position in coordinate system 24 p4241 A67-42400
SATELLITE TELEVISION
 Satellites for TV distribution and broadcasting system for Western Europe, considering increased antenna gain of ground station for minimum satellite energy consumption 01 p0027 A67-11417
 Broadcasting of TV by satellites, examining altitude effects, stationary satellite types, FM advantages, etc 06 p0956 A67-17560
 Interference ratios in space telecasting, considering methods of control for cochannel broadcasting 06 p0960 A67-17692
 Synchronous stationary satellite system for networking television and radio material to broadcast stations, noting frequency requirements and

constraints 06 p0961 A67-17697

Feasibility and potential uses of TV satellites for direct broadcast, considering shared use by government agencies [AAS PAPER 67-95] 15 p2570 A67-29955

European television satellite design emphasizing coverage area, carrier frequency selection, etc 16 p2822 A67-30697

Optical system for earth observation satellite with line-scan television for weather forecasting discussing photometry and fiber optics 16 p2679 A67-31797

Parametrization of photographs of cloud system by satellite TV cameras, discussing brightness problems via data processing 18 p3073 A67-33561

Satellite TV broadcasting systems with multiple independently controllable channels visualized after 1975 19 p3183 A67-35657

DODGE TV system for evaluating attitude control system in gravity gradient stabilization at synchronous altitude 20 p3452 A67-37571

DODGE satellite vidicon cameras and information processing system electronics design and performance 20 p3452 A67-37572

DODGE satellite TV cameras for black and white, plus color picture transmission with photometric analysis and camera optics 20 p3452 A67-37573

TV system with spark chamber detector for analysis and transmission of cosmic ray pictures to earth from satellites 21 p3599 A67-38655

Stationary satellite to provide educational TV to underdeveloped lands noting design, transmission terminals and safeguards against control and propaganda [AIAA PAPER 67-963] 24 p4260 A67-43042

SATELLITE TRACKING

SA OPTICAL SATELLITE TRACKING PROGRAM

Ionospheric studies using tracking beacon on Early Bird synchronous satellite, noting scintillations due to irregularities 03 p0407 A67-12832

Nonionized atmosphere effect on radial velocity measurement of satellite via Doppler-Fizeau method 03 p0369 A67-13530

Satellite orbit inclination, longitude of ascending node and nodal period obtained from synchronous observations 05 p0894 A67-16555

Preliminary analysis of INTEROBS program observations in Hungary, noting determination of changes in period of satellite 05 p0763 A67-16556

Simultaneous visual observation of satellite 1960 sigma 3, obtaining quasi-nodal period 05 p0763 A67-16557

Simultaneous visual tracking data reduction for satellite period 05 p0763 A67-16558

Density and temperature of upper atmosphere, satellite tracking, geodetic applications and long distance measurements, using laser output 06 p1008 A67-17591

PCM telemetry system for satellite test vehicle of ELDO program using transistorized printed circuit technology 06 p0957 A67-17613

U.S. Coast and Geodetic Survey satellite triangulation program based on optical tracking of passive satellites simultaneously from two or more mobile camera stations 07 p1176 A67-19764

BMK ballistic camera with equatorial and azimuthal mount for stellar geodetic satellite tracking and punch card controlled mono- and stereocomparators 07 p1188 A67-19773

Smithsonian observatory tracking network and geodetic results 07 p1177 A67-19774

Geodetic program of simultaneous measurement of equatorial topocentric coordinates of artificial satellites 07 p1177 A67-19775

Ballistic camera calibration method and triangulation of satellite position from camera observations 07 p1188 A67-19776

Optical and radio orbit tracking facilities, analyzing data accuracy levels, minitrack functions, etc 09 p1464 A67-22055

Lasers for tracking and geometric geodesy as used in Explorer and Geos satellite missions 10 p1664 A67-23071

Satellite range measurements using laser in conjunction with photoelectric receiver and Baker-Nunn camera 10 p1606 A67-23182

High resolution density data from radar observations of low altitude polar orbiting satellites reveal longitudinal and

geomagnetic variation, noting regression analysis 10 p1640 A67-23216

Laser applications to satellite tracking, orbit calculation and atmospheric studies 14 p2331 A67-28608

Doppler effect application to solution of tracking problems with aid of artificial earth satellites 14 p2347 A67-28991

Simulation and error analysis of range-only location and tracking utilizing satellite system to obtain range measurements 15 p2514 A67-29597

Satellite tracking of ghost balloons used for data collection on atmospheric circulation in troposphere and stratosphere [AAS PAPER 67-103] 15 p2420 A67-29958

Radar, radio, photographic and visual satellite tracking methods 15 p2437 A67-30084

Phase-locked radio interferometer for satellite tracking 16 p2621 A67-30679

Interferometric system of Diane satellite tracking stations permits high altitude tracking and measurements with larger solid angle 16 p2621 A67-30680

French interferometer for satellite tracking featuring antennas with single radiating element covering all useful space 16 p2621 A67-30681

Evaluation and calibration of missile and space tracking systems including test-by-test analysis, lofted rockets, self-calibrating systems, etc 16 p2621 A67-30682

Satellite tracking, noting radio, radar and laser methods, and visual and photographic observations 16 p2630 A67-31765

Airborne optical satellite tracking, discussing accuracy limitations and comparing to ground stations 16 p2630 A67-31799

Satellite tracking simultaneous-lobing monopulse receiving system utilizing polarization diversity in coherent and noncoherent operational modes 18 p3020 A67-34110

Orbital analysis - Conference, London, October 1966 18 p3125 A67-34234

Radio, radar and optical methods for close earth satellites tracking, advantages and limitations 18 p3003 A67-34235

Artificial satellites tracking by Smithsonian Astrophysical Observatory, discussing station locations, instrumentation, operation modes, interface and selection 18 p3003 A67-34236

Development of kinetheodolites for satellite tracking 18 p3048 A67-34238

Radio and radar tracking at Royal Radar Establishment at Malvern, discussing equipment, accuracy, alignment, performance, operation, drag and decay 18 p3048 A67-34239

Phase measuring equipment and instrumental performance of radio tracking station at Winkfield 18 p3048 A67-34240

Gravity data from lunar orbiter tracking, discussing Kepler element role 18 p3131 A67-34326

Soviet northern cosmodrome location determination from data obtained through radio/visual observation of Cosmos satellites 18 p3004 A67-34358

Tracking of GEOS-A satellite by Riga station, explaining negatives reduction 19 p3182 A67-35235

Geos satellite observational technique in France 19 p3182 A67-35237

Tracking station network organization, equipment and operations of National Center for Space Studies /CNES/ in France 19 p3207 A67-35242

Antares triaxial tracking camera noting mounting, electronic and optical systems and performance techniques 19 p3229 A67-35267

Space research activities in Finland /1966/, detailing satellite station 19 p3320 A67-35289

Cosmic space research activities in Hungary, discussing data recording, satellite tracking, etc 19 p3320 A67-35291

Polish space research noting satellite position observations, geodetic computations, meteorology, cosmic physics, magnetosphere, medicine and biology 19 p3321 A67-35296

Satellite earth crashing time and place calculated, providing observation possibilities 19 p3184 A67-35831

Data analysis and reduction studies for calibration of missile tracking systems using near earth satellite 20 p3381 A67-36604

Geometric satellite triangulation for position of fourth satellite, with position equations solved by least squares method

and applied to geodetic satellites 20 p3429 A67-36890

Continuous wave laser ground-space-ground experiment in conjunction with Explorer XXII satellite tracking 21 p3578 A67-37858

Synchronous detection for signal phase gap measurements and Diana type satellite tracking, discussing hypothetical carrier 21 p3583 A67-38644

Radio interferometry at Diane satellite tracking station, noting synchronous demodulation technique 21 p3587 A67-39052

SATELLITE TRACKING AND DATA ACQUISITION NETWORK

SA RANGE AND RANGE RATE TRACKING

Aircraft detection and in-flight tracking by real time computers, assessing role in missile and satellite tracking 13 p2153 A67-26666

NASA STADAN and Apollo network antenna systems, analyzing tracking antenna systems, command systems and operational problems 14 p2287 A67-26861

Onboard data systems selection and design and relation to ground networks [AAS PAPER 67-54] 15 p2440 A67-30118

Satellite tracking and data acquisition network of receiving stations /TRANET/ that acquires and processes Doppler frequency shift data 16 p2630 A67-31740

Reduction of dynamic data from geodetic satellites noting satellite tracking station position, gravitational potential, gravity coefficients, synchronous satellites, etc 20 p3429 A67-36891

Manned planetary mission global network for continuous tracking, communication telemetry and TV transmission [AIAA PAPER 67-976] 24 p4125 A67-43052

SATELLITE TRANSMISSION

Oscillations of vertical component of ionospheric refraction measured, using cliff radio interferometer and signals from satellites 01 p0022 A67-10390

Faraday fading rate of satellite signal as calculated from Appleton-Hartree formula for refraction index /without collision/ near transverse propagation [RASSA PAPER 1-10-127] 03 p0372 A67-14238

Electron cloud-like distribution in ionosphere shown from phase measurements of 162 and 324 mc emissions of Transit and Anna satellites [RASSA PAPER 1-10-135] 03 p0417 A67-14246

Transhorizon propagation modes from signals transmitted by orbiting radio beacon ionospheric satellite /ORBIS/, showing paths sustained by ionospheric ducts or usual hop modes [RASSA PAPER 1-10-146] 03 p0373 A67-14253

Installation for measuring Doppler effect of satellites, investigating limits, optimization, SNR and orbital parameter accuracy 06 p0979 A67-18018

Periodic frequency change in signals from Cosmos V possibly due to solar cell output fluctuations 06 p0964 A67-18766

Fast regular scintillation of VHF signals received from earth satellites distinguished from scintillation associated with irregular ionospheric diffracting phase screen, showing correlation with sporadic E layer 07 p1141 A67-19416

Doppler frequency measurements in satellite transmissions and use for geometric geodesy 07 p1144 A67-19771

Transmission characteristics of high power traveling wave tubes for satellite ground stations 09 p1478 A67-22258

Frequency sharing and compatibility of satellite and terrestrial radio relay systems design, discussing interference effects 09 p1464 A67-22411

Protection of communications satellites data transmission against interplanetary interference sources and Van Allen belts 10 p1604 A67-22899

Potential buildup on electron emitting ionospheric satellite, noting limitation on current emission by geomagnetic field 11 p1869 A67-23941

Satellite emitted radio wave propagation mechanism based on radio wave paths in horizontally inhomogeneous spherically stratified ionosphere with variable electron density 11 p1751 A67-24070

Use of onboard data processing for eliminating irrelevant information telemetered from satellite

experiment 12 p1909 A67-25780
 U.S. communication satellites design and transmission, including antenna types offering interference-free reception 13 p2066 A67-26334
 Direct TV reception from satellites, discussing cost of Yagi and parabolic antennas, noting output tube 13 p2066 A67-26336
 Charge and energy spectra of galactic cosmic rays during solar minimum from satellite and Skyhook balloon data 13 p2193 A67-27248
 Low noise preamplifier traveling wave maser operated in closed cycle refrigerator for receiving Mariner IV picture transmissions 14 p2329 A67-27779
 Data processing of signal reception from Soviet satellites indicates radio signals scintillation caused by diffraction of waves from ionospheric nonuniformities 14 p2260 A67-27857
 Clock synchronization with artificial satellites for precise time and frequency, comparing two-and one-way transmission and reception 14 p2263 A67-28391
 Sporadic E layer scintillation effects on amplitude of 137 MHz radio waves from Early Bird 14 p2270 A67-28577
 Ionospheric electron content variation across sunrise and sunset lines deduced from radio-beacon satellite transmissions 15 p2476 A67-29624
 Feasibility and potential uses of TV satellites for direct broadcast, considering shared use by government agencies [AAS PAPER 67-95] 15 p2570 A67-29955
 Processing satellite data at Goddard Center noting Tiros IR data, cloud pictures and lmp measurements 16 p2633 A67-30668
 Satellite telemetry system transmitter optimization, noting error probability criterion, average power constraint, etc 16 p2622 A67-30693
 Satellite receiving and transmission antenna orientation effects obtained by Faraday rotation measurements 16 p2628 A67-31507
 Wideband varactor upconverters for satellites use, emphasizing transmission characteristics and stability over wide temperature range 16 p2640 A67-31531
 French Diademe satellites power supply systems and planned laser experiments 17 p2941 A67-32232
 Perturbing factors in avionics communications noting drawbacks and advantages of satellite utilization, possible commercial applications, etc 17 p2813 A67-32498
 Radio propagation of transmissions from stationary and near stationary satellites used to study anomalous atmospheric refraction at low angles of 19 p3182 A67-35172
 Satellite TV broadcasting systems with multiple independently controllable channels visualized after 1975 19 p3183 A67-35657
 Satellite system with solid state transmitters with different frequencies in HF band for ionospheric guided propagation research 20 p3394 A67-36246
 Lunar cartography using space vehicles, considering satellite orbits and information transmission 21 p3703 A67-38197
 High stability quartz master oscillator for D-1 satellite transmitter control 21 p3591 A67-38206
 High reliability PCM digital telemetry system for onboard data transmission of analog and digital signals 21 p3583 A67-38635
 Ionospheric discontinuity dimensions determined from satellite signal fading at 20 and 40 mc correlating amplitudes 21 p3621 A67-39021
 Reception of ground based Loran transmissions by fixed-frequency topside sounder satellite 24 p4119 A67-42061
 High gain phased array for satellite transmission using feedback to correct phase and amplitude parameters variations 24 p4124 A67-42816
SATURATION
SA SUPERSATURATION
 Initial saturation voltage effects in alloy-type transistors at high injection levels 02 p0215 A67-11977
 Single mode output power modulation analysis of saturation and gain of gas lasers and effects of excitation density modulation and resonator Q

modulation 04 p0633 A67-15111
 Single mode output power modulation study of saturation and gain of gas laser 05 p0823 A67-16686
 Nonlinear medium anisotropy and saturation effects on orientation of polarization ellipse of gas laser mode 06 p1010 A67-17823
 Gain saturation effect on oscillating modes of optical masers 08 p1339 A67-21377
 Saturation effects studied by pumping speed measurements of diode and triode type getter ion pumps for He, molecular hydrogen and nitrogen at low pressures as function of time 08 p1333 A67-21494
 Compact nonresonant five-pass carbon dioxide laser amplifier structure giving small signal gains 11 p1800 A67-24245
 Saturation effect on phase shift of traveling wave masers and reflex type cavity masers 11 p1800 A67-24468
 Diffusion saturation of industrial iron, molybdenum, Kh18N9T steel and ZrS6-K alloy with powdered beryllium mixture 12 p1955 A67-25369
 True air life support system, describing concept for deriving fixed percentage binary gas from two steady state cryogenic liquids 13 p2064 A67-27638
 Temperature and carrier concentration effect on threshold electric field of current saturation and saturation drift velocity in gallium arsenide 14 p2364 A67-27826
 Liquid nuclei formation at condensation centers in atmosphere analyzed for various degrees of saturation 14 p2346 A67-27908
 Two-step saturation of pulsed current in CdS single crystals, noting electron bunching mechanism and volt-ampere characteristics 14 p2365 A67-28238
 Second current saturation of nonohmic behavior in CdS single crystals caused by quantum mechanical interaction between drift electrons and acoustic phonons 14 p2365 A67-28239
 Current saturation phenomena in junction-gate field effect transistor 15 p2446 A67-29637
 Numerical methods for calculating pseudoadiabatic characteristics of saturated air parcels 17 p2879 A67-32549
 Temperature effect on gas saturation in alpha and beta titanium alloys 18 p3065 A67-34292
 Diffusion saturation methods of alloy surfaces by metals and metaloids classified by physicochemical characteristics of active phase of diffusing element 19 p3242 A67-34916
 Traveling wave maser saturation and signal distortion, determining magnetic moment 21 p3642 A67-38813
 Lande factors of neon atoms subjected to magnetic field and multimode laser irradiation measured by observing resonant saturations in fluorescent light emitted 22 p3815 A67-39651
SATURN I /SA-5/ LAUNCH VEHICLE
 Optical and UHF Doppler /UDOP/ tracking for lift-off phase of Saturn SA-5 launch vehicle 03 p0368 A67-13383
SATURN I LAUNCH VEHICLE
 Matrix-Holzer method for predicting free vibration modes of clustered launch vehicles in bending applied to first eight modes of Saturn I model 02 p0337 A67-11931
 Up-rated Saturn I first stage propulsion system dynamic characteristics simulated by analog computer 22 p3869 A67-40169
SATURN IB LAUNCH VEHICLE
 Data system requirements for large space vehicles and flexible telemetry system design for all stages of Saturn IB and V vehicles 02 p0196 A67-12000
 Second generation Saturn vehicles, discussing anomalies discovered during flight tests, development, etc 02 p0331 A67-12255
 [AIAA PAPER 66-839]
 Diffusion bonding of titanium sandwich structure for Saturn tank wall application 10 p1661 A67-23702
 Saturn IB flight test loads, comparing measured and calculated bending moment, noting launch time wind profile 10 p1713 A67-23734
SATURN /PLANET/
 Paraformaldehyde hypothesis of IR spectrum of Saturn ring 03 p0509 A67-13167
 Molecular hydrogen features in spectra of Saturn and Uranus 04 p0696 A67-14738
 Spectral study of Jupiter, Saturn and rings

of Saturn, determining methane concentration in cloud layers 04 p0701 A67-15557
 IR observations for presence of ethane in atmospheres of Jupiter and Saturn reanalyzed and found consistent with previous results 08 p1398 A67-21218
 Saturn edgewise rings rapid fading and brightness variation on disk 10 p1710 A67-23564
 Unidentified satellite as explanation of abnormal perturbations in Saturn ring 11 p1866 A67-24770
 Saturn photograph analysis discussing interpretation of thin line on edge of ring system 14 p2393 A67-29029
 Janus /Saturn tenth satellite/ discovery on December 15, 1966, noting orbit in ring plane and period 20 p3527 A67-37399
 Evaporation of Saturn ice rings by UV and solar wind sputtering or by photosputtering in IR and proton bombardment 21 p3705 A67-38599
 21.2 cm spectra of Jupiter, Venus, Mars and Saturn noting mean effective brightness temperatures 21 p3709 A67-38993
 9.4 cm radiation from Jupiter and Saturn and 21.2 cm radiation from Saturn 21 p3709 A67-38994
 Jupiter and Saturn models, giving planet constitution, heat balance and atmospheric composition 21 p3710 A67-39001
SATURN V LAUNCH VEHICLE
 U.S. Saturn/Apollo moon program, considering Saturn V booster, Apollo spacecraft and Lunar Excursion Module 01 p0154 A67-11001
 Saturn V ground support instrumentation systems, emphasizing launcher umbilical tower /LUT/ 01 p0051 A67-11117
 Saturn V Mobile Launcher configuration, design and testing 02 p0228 A67-11840
 Data system requirements for large space vehicles and flexible telemetry system design for all stages of Saturn IB and V vehicles 02 p0196 A67-12000
 Ground testing, development of engines, stages and ground support equipment of Saturn V launch vehicle [AIAA PAPER 66-840] 02 p0331 A67-12256
 Mississippi Test Facility gas metal-arc welding of T-1 steel critical high pressure piping systems for Saturn V launch vehicle 03 p0430 A67-13691
 Integration, testing and launching of flight hardware for Apollo/Saturn V space vehicle at Kennedy Space Center [AIAA PAPER 66-837] 03 p0397 A67-14126
 Orbital space station design for permanent residence within earth-orbital payload capacity of Saturn V launch vehicle [AIAA PAPER 66-936] 03 p0520 A67-14138
 Compatibility of checkout systems for rockets and space vehicles, with application to Saturn V launch vehicle 03 p0399 A67-14209
 Vibration testing facilities for Apollo Saturn V launch vehicle, noting structural assemblies under dynamic testing 05 p0786 A67-16156
 Mobile launcher and crawler transporter facilities for Apollo/Saturn V launch exploration vehicle 05 p0787 A67-16611
 NASA Apollo-Saturn V Moon Project crawlerway construction for lunar launch complex 05 p0788 A67-16615
 Saturn V mobile launch facility design, discussing vertical assembly of space vehicle on launch platform, transfer to launch pad, automatic checkout and remote control of launch operation 05 p0788 A67-16616
 Automatic telemetry checkout station for Saturn V systems using real time signal digitizer and general purpose computer 05 p0789 A67-17044
 Digital computer simulation model implementation in prelaunch prediction of Saturn V launch vehicle system performance [AIAA PAPER 67-205] 06 p1096 A67-18344
 Automatic telemetry checkout station for Saturn V systems using real time signal digitizer and general purpose computer 06 p1089 A67-18861
 Saturn V launch vehicle, discussing payload-mass ratio, capabilities and modification possibilities 06 p1098 A67-19020
 Atmospheric density, winds and turbulence relative influence on Saturn V vehicle control system and structural bending moment response during Atlantic Missile Range ascent flight

[AIAA PAPER 66-341] 07 p1257 A67-19372
Mobile launch concept for Apollo/Saturn V lunar landing mission, discussing structural composition, functions and performance of launcher

[AIAA PAPER 67-247] 07 p1165 A67-20065
Systems analysis applied to identification of Saturn V launch vehicle support system requirements and establishment of baseline logic for vehicle prelaunch processing simulation and systems optimization

[AIAA PAPER 67-248] 07 p1165 A67-20066
Saturn V with maximum payload lunar landing stage for extended lunar exploration, noting LESA delivery modes

08 p1412 A67-21089
Umbilical carriers and quick-disconnect facilities of Saturn V ground support equipment noting location, ejecting methods, etc

09 p1484 A67-22038
Implementation of NASA NPC 250-1 /Reliability Program Provisions for Space Systems Contractors/ as applied to Saturn V Mechanical Ground Support Equipment Program

09 p1582 A67-22292
Cargo delivery to lunar surface using Apollo hardware and Saturn

09 p1486 A67-22403
Influence of explosive forming characteristics on springback based upon tests in forming of gore sections for Saturn V rocket

10 p1660 A67-23170
Lumped parameter analysis of liquid-filled shells with application to 1/10-scale Saturn V model

10 p1713 A67-23749
Combined multishaker and gas flow tests as part of reliability test program for Saturn V, S-1C pneumatic systems

12 p1923 A67-25706
Instrumentation and data acquisition system used in Saturn V dynamic test program for design of flight control system

12 p1923 A67-25709
Computer controlled dynamic test facility to provide data on flight characteristics of Apollo-Saturn V launch vehicle by measuring vibration amplitudes

14 p2293 A67-28593
Apollo/Saturn V vehicle launching site, assembly building and lunar flight

15 p2569 A67-29849
Vibro-acoustic test system for simulation of Saturn V dynamic launch environment on major space vehicle structures, discussing design and operation characteristics

17 p2832 A67-32005
Guidance, navigation and two phases of targeting of Saturn V lunar landing mission, analyzing launch, boost to orbit and iterative guidance

17 p2881 A67-32057
Man-rating F-1 engine, noting capabilities and future plans

[AIAA PAPER 67-519] 18 p3115 A67-33982
Saturn V reliability analysis model used by management for predicting performance probabilities

18 p3138 A67-34684
Digital computer simulation model Implementation in prelaunch prediction of Saturn V launch vehicle system performance

[AIAA PAPER 67-205] 19 p3331 A67-34807
Flight control system of Saturn V launch vehicle, discussing attitude/attitude-rate scheme, gain required and stability achieved

19 p3331 A67-34808
Application of redundancy in Saturn V guidance and control system to achieve desired reliability

[AIAA PAPER 67-553] 19 p3257 A67-35950
Reliability contribution of pilot using manual backup control for first stage of Saturn V tested using simulation

[AIAA PAPER 67-554] 19 p3335 A67-35951
Powered flight trajectory determination for Saturn V vehicles through computer method

[AIAA PAPER 67-547] 19 p3258 A67-35981
Adaptive control systems for stabilizing structural bending modes of Saturn V launch vehicle

[AIAA PAPER 67-591] 19 p3336 A67-35987
Computer simulation model for Saturn V launch vehicle system

20 p3414 A67-36536
Up-rated Saturn V vehicles and intermediate payload Saturn vehicles, studying costs, flexibility, performance and boost-assist components

20 p3531 A67-36539
Hydraulic support system for free flight simulation with Saturn V-Apollo vehicle, discussing stability requirements, upper bounds of system design, conversion from nonlinear to linear model,

etc

21 p3607 A67-37796
Systems analysis applied to identification of Saturn V launch vehicle support system requirements and establishment of baseline logic for vehicle prelaunch processing simulation and systems optimization

[AIAA PAPER 67-248] 21 p3607 A67-37806
Saturn V S-IVB stage propellant slosh amplification minimization at boost thrust termination analysis, simulating slosh wave motion by time varying nonlinear spring-mass model

22 p3903 A67-39970
Saturn V launch vehicle and Apollo spacecraft hardware systems applied to unmanned exploration of

22 p3887 A67-40138
Jupiter

Prediction of Saturn V launch vehicle effectiveness during prelaunch phase using computer simulation

[SMPT E PAPER 102-27] 22 p3908 A67-40371
Apollo Crawler System analyzed by computer simulation for dynamic interactions of transporter and umbilical tower

22 p3782 A67-40466
Lunar electric power systems transported by Saturn V noting Brayton cycle, Rankine cycle, solar cells and thermoelectric systems

[AIAA PAPER 67-902] 24 p4110 A67-43010
Saturn V payload capabilities uprating by building block approach using solid propellant rocket motor, noting cost factor and mission flexibility

[AIAA PAPER 67-907] 24 p4244 A67-43014
Lunar applications of spent Saturn V/S-IVB/IU stage concept, discussing payload capabilities

[AIAA PAPER 67-986] 24 p4246 A67-43058
SATURN LAUNCH VEHICLE
Saturn vehicles possible future applications to space

01 p0156 A67-11422
exploration

Computer design test program to automate checkout process of Saturn I and V space boosters gradually while retaining manual checkout

01 p0051 A67-11427
Auxiliary solid propellant motors in Saturn launch vehicle

[AIAA PAPER 66-946] 02 p0303 A67-12280
Path adaptive guidance modes for Saturn space vehicle, particularly Iterative Guidance Mode

02 p0264 A67-12318
Nondestructive testing /NDT/ of materials, components and systems for Saturn-Apollo program

02 p0250 A67-12631
Hydraulic gimbal system with closed loop design for orienting Saturn S-IVB engine

03 p0363 A67-13535
Factory-to-launch sequences of checkout in Saturn/Apollo program, examining present and planned levels of

03 p0399 A67-14207
automation

Chemical propellants in Apollo program, noting Saturn launch vehicle and spacecraft propulsion

05 p0874 A67-17016
Manned interplanetary flights before Mars landing, using Saturn-Apollo technology

06 p1092 A67-19031
Transonic wind tunnel studies of ground-wind loads on aeroelastic models of Saturn launch vehicle, investigating structural damping, wind velocity and azimuth angle

07 p1257 A67-19371
Optimization of Saturn vehicle, considering interaction of guidance, control and propellant utilization systems

[AAS PAPER 66-117] 07 p1222 A67-19975
Static firing ground testing of Saturn launch vehicle

[AIAA PAPER 67-234] 07 p1165 A67-20057
Ultrasonic techniques for nondestructive testing for Saturn honeycomb heat shields

07 p1192 A67-20166
Manned lunar exploration systems for Saturn-Apollo

08 p1393 A67-21091
Design, redundancy, reliability and tradeoffs for Launch Vehicle Digital Computer and Data Adapter /LVDC/LVDA/ for up-rated Saturn I and V vehicles, noting logic circuit, memory, input/output, power supply

09 p1469 A67-22301
Optimization of base thermal protection system for advanced Saturn II boosters employing strap-on solid propellant motors

10 p1735 A67-23729
Computer applications in checkout of individual Saturn stages and in prelaunch checkout of complete Saturn vehicle

13 p2089 A67-26409
Optimization of Saturn vehicle, considering interaction of guidance, control and propellant utilization systems

[AAS PAPER 66-117] 13 p2155 A67-27532
Relay testing for Saturn program including vibration scan, radiographic inspection, etc

13 p2084 A67-27696
Stability problems in control system of Saturn launch vehicles

14 p2393 A67-28085
Stage separation, fluid behavior, engine plumes characteristics, etc, of Saturn vehicle detected, using remote sensing techniques

14 p2320 A67-28700
Gemini-Apollo capability, Apollo application and proposed earth-orbital experiments, describing typical missions with illustrative experimental payloads

16 p2756 A67-30627
Operational capabilities of Saturn-Apollo space vehicle, discussing lunar missions

19 p3333 A67-35643
Digital computer test program for automatic checkout of Saturn launch vehicles allowing manual intervention

20 p3391 A67-36574
Automation techniques for stage checkout in Saturn program noting equipment, time factor, etc

20 p3417 A67-36975
Lunar mission simulators for Saturn-Apollo project noting optimal computer approach on flexibility, accuracy, cost, etc

20 p3418 A67-37482
Saturn computer design and fault simulation on IBM 7090

21 p3588 A67-38181
Secondary payload for Saturn launch vehicle evaluation according to experiment/mission effectiveness and compatibility by computer program methodology

22 p3903 A67-39950
Maintainability problems analyzed noting Apollo/Saturn program

23 p4070 A67-40581
Optimization of base thermal protection system for advanced Saturn II boosters employing strap-on solid propellant motors

24 p4256 A67-42915
SATURN S-IB STAGE
Motion equations for planar simulation of flexible Saturn IB launch vehicles under in-flight winds using Appell equation, noting sloshing mode

10 p1713 A67-23750
Saturn S-IB stage fuel system, studying LOX density fluctuations, heat transfer and boiling under various weather conditions

13 p2186 A67-27637
SATURN S-IC STAGE
Remote control pneumatic pressure test system for Saturn S-IC booster checkout with manual or automatic control, using computer

20 p3415 A67-36569
SATURN S-IVB STAGE
Automatic checkout system for factory checkout, acceptance firing and postfire checkout of Saturn S-IVB stage

03 p0395 A67-13381
Systems application in orbital launch operations

[AIAA PAPER 66-908] 03 p0519 A67-14132
Man-machine interface and automatic test operations in Saturn S-IVB system

03 p0398 A67-14204
Software configuration management by engineering methods, considering application to automatic support equipment /ASE/ for Saturn S-IVB stage

03 p0538 A67-14221
Nucleonic cryogenic quality meter design and development and fluid monitoring through hydrogen vent line on Saturn S-IVB stage under orbital conditions

05 p0842 A67-16540
Transportation of Douglas Saturn S-IVB stages to test and launch sites

05 p0787 A67-16610
Saturn S-IVB Apollo systems application to planetary exploration, using extension of technology and hardware for lunar exploration

08 p1411 A67-21074
Saturn IVB flight data evaluation, discussing heat transfer effect on fluid system as function of gravity changes

12 p2034 A67-25721
Contamination control in hydraulic system of Saturn S-IVB stage, noting five-fold approach to anticontamination procedure

20 p3363 A67-36801
Procedures, facilities and equipment used in contamination control of Saturn S-IVB stage hydraulic system

23 p3935 A67-40848
SC-5 AIRCRAFT
S SHORT SC-5 AIRCRAFT
SCALAR MAGNETIC FLUX
Measuring apparatus for scalar and tensor plasma conductivity in AC MHD generators and accelerators

09 p1538 A67-21775

Variational principle extended to relativistic scalar hydrodynamics, deriving Hamilton equations 11 p1844 A67-25034

Lagrangian for interaction of electric charge with field induced by scalar magnetic charge to determine electrical dipole moment 17 p2883 A67-32100

Time variation of magnetic flux distribution in type II superconductor under sinusoidal magnetic field, obtaining flux penetration rate, pinning forces and hysteresis loop 21 p3685 A67-39075

Classical scalar plasma with relativistic Hartree equilibrium approximation for energy, entropy and state equation noting effect of linear perturbation 22 p3842 A67-39209

Large angle flux reversal of Permalloy magnetic films investigated from experimental results of switching characteristics 22 p3860 A67-39903

SCALE

SA TIME SCALE

Updating application of aerial photographs to scale of map based on radio altimeter data 03 p0419 A67-13262

SCALE EFFECT

Titanium oxidation characteristics, determining activation energy of scale formation, oxygen absorption of base metal and total oxygen absorption 05 p0829 A67-16759

Scale grating with moire fringe effect, noting attachment to Zeiss 3030 coordinate measuring instrument 14 p2319 A67-28590

Diffusing plane turbulent free jet compared with correspondent wall jet velocity distribution and variation and length scales 20 p3360 A67-37492

Analog and digital computer methods for research and development of fluidic circuit components, discussing scaling effects 21 p3612 A67-38106

SCALE ERROR

Scale transfer for lunar photographs, using selenodetic controls with suitable point pattern 11 p1860 A67-24460

Lunar rotational constants determined from measurements on scaled and oriented photographs, using least squares analysis and rigorous formalism 11 p1860 A67-24462

Plasma scale height errors from Alouette I topside sounder ionogram analysis 20 p3433 A67-37409

SCALE HEIGHT

Unlikelihood of obtaining useful information on atmospheric composition from indirect sensing of scale heights by satellites 14 p2310 A67-27959

Upper atmosphere densities and scale heights from Soviet earth satellite drag data, noting diurnal variation 19 p3219 A67-35252

Vertical distribution of meteor showers obtained by measuring distribution in decay times of underdense radio echoes 20 p3521 A67-36303

Changes in topside ionosphere during large magnetic storm, studying electron density, slab thickness, scale height, etc 20 p3427 A67-36305

Plasma scale height errors from Alouette I topside sounder ionogram analysis 20 p3433 A67-37409

F layer irregularities transverse scale measurements by two-frequency scintillation-ratio technique yielding 600-700 m scales in auroral zone 22 p3789 A67-39470

Diurnal, latitudinal and seasonal variations of midlatitude topside ionosphere electron density profiles and plasma scale heights calculated from Alouette I ionograms 23 p3994 A67-40775

Electron scale heights from topside ionograms studied for radiation effects during quiet and disturbed conditions, noting relation to ionospheric plasma temperature 24 p4147 A67-42055

Ionospheric composition and temperature for South Atlantic latitudes from scale height values obtained by Alouette I satellite 24 p4147 A67-42057

SCALE MODEL

Thermal vacuum performance testing of scaled models as technique for reducing development costs of spacecraft 11 p1773 A67-24346

Articulated optical pickup system for scale model simulation providing pitch, roll and yaw motions and fixed perspective point 12 p1941 A67-25470

Engine generated and in-flight noise

environment problems of space vehicles analyzed, using theoretical methods and scale model wind tunnel tests 13 p2212 A67-27216

Thermal scaling for test models in heat transfer studies of bodies enveloped in large luminous flames [ASME PAPER 67-HT-60] 20 p3549 A67-36742

Articulated optical pickup system for scale model simulation providing pitch, roll and yaw motions and fixed perspective point 23 p3988 A67-41502

SCALING

Scaling of binary titanium alloys in carbon dioxide at high temperatures using kinetic, metallographic and electron probe microanalysis [AAS PAPER 66-190] 08 p1341 A67-20763

Inverse heat transfer problem in air flow past cylinder, calculating heat transfer coefficient and scaling functions 13 p2224 A67-27053

Wear, scaling and chemical resistance of carbide and boride diffusion coatings on refractory metals 19 p3243 A67-34921

Standard scintillation index method for describing ionospheric effects, discussing power calibration, scaling, deviations, etc 19 p3220 A67-35256

Crater forming processes on moon from Ranger VIII impact, ascertaining gravity scaling existence, noting relation to terrestrial soils 19 p3327 A67-35894

Scaling resistance of nickel and cobalt binary alloys investigated to determine heat resistance as function of composition 20 p3467 A67-37115

Scaled Unsöld approximation for Hartree-Fock function in perturbation expansion 23 p4030 A67-40977

SCALING LAW

Steady state kinetics and microstructures of simultaneous internal oxidation and external scale formation of Cb-Zr and Cb-Zr-Re alloys in pure oxygen at 1000 degrees C 05 p0828 A67-16471

Asymptotic solution for one-dimensional MHD generator scaling numerical values to obtain correct results for zero initial current and velocity 05 p0856 A67-17365

Steady oblique nonlinear waves in warm collision-free plasma 05 p0857 A67-17425

Scaling equations for wind tunnel simulation of trajectory of jettisoned stores from aircraft 06 p0979 A67-18006

Mars stopover mission with Venus swingby technique, discussing velocity requirements, trip times and initial mass in earth orbit [AIAA PAPER 67-27] 06 p1085 A67-18332

Reynolds number scaling theory for hypersonic ablation, deriving heat and mass transfer relationship [AIAA PAPER 67-155] 06 p1117 A67-18478

Scaling-law equation of state for gases in critical region 16 p2778 A67-31061

Mars stopover mission with Venus swingby technique, discussing velocity requirements, trip times and initial mass in earth orbit [AIAA PAPER 67-27] 17 p2940 A67-32059

Limits of application of binary scaling for hypersonic flight 19 p3212 A67-35769

Multiple scaling for analyzing flight vehicle performance and dynamic behavior [AIAA PAPER 67-560] 19 p3335 A67-35957

Thermal scaling for test models in heat transfer studies of bodies enveloped in large luminous flames [ASME PAPER 67-HT-60] 20 p3549 A67-36742

Scaling law derived from small angle scattering theory, interpreting data in spectroscopic manner to deduce potentials and interactions between electronic states 22 p3839 A67-39205

Low gravity slosh simulation parameters and scaling law used to extrapolate data to full scale spacecraft systems 24 p4141 A67-42032

Scaling laws and hydrodynamic model design techniques for high fidelity underwater simulation of zero and partial-g environments for manned space activities [AIAA PAPER 67-925] 24 p4140 A67-43021

SCANDIUM

Ultramafic rock content of Na, Mn, Cr, Sc and Co determined by neutron activation technique 07 p1183 A67-20142

SCANNING

SA FREQUENCY SCANNING

SA OPTICAL BEAM SCANNING

SA PANORAMIC SCANNING

SA RADAR SCANNING

Image scanning systems applied to filmed data processing 07 p1148 A67-19745

Behavior of infinite arrays including radiation pattern approach yielding expressions for gain and periodic structure approach yielding input impedance variation with scan angle 07 p1154 A67-19783

Optimal scanning problem variant with simple analytical solution, determining cessation moment 15 p2459 A67-30227

Scintillation and dynamic range problems mitigated for Fourier spectrometry by rapid scanning 20 p3438 A67-36342

Selective modulation spectrometry, discussing problem of spectrometry without slit 20 p3438 A67-36348

Array antenna directive pattern scanning utilizing difference in phase lead between heterodyne and converted signals at feeder 24 p4130 A67-42234

Linear and planar phased array antennas investigated for radiation impedance as function of scan variable 24 p4130 A67-42339

SCANNING DEVICE

SA HORIZON SCANNER

SA IMAGE TRANSDUCER

SA INFRARED SCANNER

Second breakdown in junction transistors examined, using scanning electron microscope 02 p0222 A67-12653

Flying target detection and tracking with fixed antennas having radiation pattern scanning and multibeam characteristics 02 p0205 A67-12730

High resolution mass spectra obtained from fast magnetic scans of gas chromatographic effluents 03 p0367 A67-13336

Helicopter main rotor blade used as scanning radar antenna 04 p0579 A67-14491

Internally scanned laser beam having high deflection rate produced by pulsed optical delay line 05 p0818 A67-16647

Automatic scanning receiver for interference-free recording of solar flare effects and polar blackouts, using cosmic noise method 05 p0883 A67-16799

Apollo TV scan conversion, discussing equipment and performance 06 p0964 A67-18413

Laser line-scanning photographic system, discussing possible extraterrestrial applications 06 p1006 A67-19011

Microwave scanning antennas, Volume 3, Array systems 07 p1151 A67-19544

Frequency and phase scanning for pencil-shaped beam antenna 07 p1152 A67-19546

Mutual coupling and edge effects in finite scanning arrays 07 p1154 A67-19784

Radio telescope-spectrophotometric scanner investigation of continuous energy distribution of four quasars 08 p1398 A67-21230

Electronic processes on semiconductor device surfaces analyzed using scanning light beam, for application to Si planar transistors 09 p1472 A67-21949

Ultrasonic nondestructive inspection of adhesively bonded components, discussing pulse echo reflection, pulsed through transmission and sweep frequency coupling methods and scanning equipment 09 p1507 A67-22526

Enlarged internal laser beam projecting high contrast images generated on photochromic plate within laser cavity 11 p1801 A67-24717

Determinants of electronically steerable antenna arrays 12 p1917 A67-26158

Scanning microscope for studying Si p-n junctions by electron or ion bombardment 13 p2120 A67-27069

Scanning electron microscope observations of p-n junctions using small periodic bias voltages 13 p2177 A67-27072

Star tracker using camera tube sensors and electronic scanning noting system errors reduction 13 p2154 A67-27491

Induced impedance dependence on scanning angle and array parameters calculated, analyzing edge effects 14 p2279 A67-28005

Automatic pressure stepping control and recycling system for use with Fabry-Perot interferometer 14 p2315 A67-28158

Complex organic compounds analysis by fast-electrical-scanning high resolution mass spectrometry and gas chromatography 14 p2259 A67-28425

High resolution CRT for system designers to scan film or record photosensitive materials 15 p2447 A67-29734

Broadband monopulse three-element tracking feeds for spherical Luneberg lens scanning antenna, discussing radiator design, radiation pattern and cross coupling between error channels 15 p2451 A67-29924

Segmented two-stage waveguide-slot scanning antennas with intersegment phase shifters connected in series in transmission line 16 p2637 A67-31026

All-electronic, ultra-fast scanning spectrometer utilizing image dissector for power spectral density function measurements of rapidly time varying optical emission 16 p2680 A67-31803

High resolution direct electron beam film scanner operable at 20 MHz, construction and performance 17 p2857 A67-32469

Electron beam and laser beam line scan recorders requirements, limits, applications and techniques 17 p2857 A67-32470

Rastering nanosecond laser sensitometer for materials responsive to short duration signals, discussing recording, sensitometric and measuring subsystem 17 p2858 A67-32482

Raster scan parameters influencing target identification in image recognition experiments using video display 17 p2859 A67-32508

CRT flying-spot-scanner spatial frequency response, determining film-plane modulation response to periodic sine/square wave 17 p2860 A67-32665

High speed methods of frame scanning in character output element with character point shaping on CRT screen 17 p2822 A67-33100

Photographic systems and photoelectric scanner for observation of solar annular eclipse 18 p3049 A67-34312

High resolution flying-spot scanner as input device for computer simulation of optical character-recognition systems 18 p3006 A67-34403

Optical and stereoscan microscope scanning combined with X-ray microanalysis used to investigate results on collection surfaces of space probes 19 p3339 A67-35197

Strapdown star tracker for space vehicle attitude control, using scanning and error-signal determination method [AIAA PAPER 67-551] 19 p3233 A67-35948

Pressure scanned Fabry-Perot interferometer for twilight sky and zodiacal light observations 20 p3440 A67-36361

Image dissector camera providing high resolving power, photometric fidelity and long life for use in meteorological satellite 20 p3445 A67-36541

Fast scanning 180 degree magnetic mass spectrometer for monitoring fast changes in residual gas compositions 20 p3448 A67-36875

Multiple scan correlator construction stressing flashing lamp system and rapid film processor 20 p3452 A67-37312

Automated system for growth and analysis of bacterial colonies using environmental chamber and computer controlled flying-spot scanner 20 p3453 A67-37598

Reconstructed image scanning by hologram rotation 21 p3624 A67-37852

Rapid scan spectrometer for carbon dioxide laser studies noting time dependent effects 21 p3641 A67-38460

Image tubes to obtain signal and noise solutions, determining Noise Equivalent Power /NEP/, Detectivity Star and Detective Quantum Efficiency 22 p3805 A67-40352

Airborne multiple scan interferometry for low temperature IR emission spectral distribution of minerals 22 p3807 A67-40368

Scanning electron microscope signal processing and application to electronic devices failures, processes variations, integrated circuits and thin film circuit continuity 22 p3774 A67-40411

Fabry-Perot interferometer for emission spectra time variations observed by employing electromechanical system to vary mirror motion speed 22 p3809 A67-40416

Integrated circuit for TV camera including photosensitive array and self-scanned solid state image sensor 23 p3998 A67-40868

Aperture system using moire fringe method to execute spectral scan for Fabry-Perot spectrometer 23 p4001 A67-41258

Scanning laser device using modified electro-optic display tube and potassium phosphate crystal mode selector 23 p4017 A67-41393

Radioisotopic color coded pulmonary lung scanning, diagnostic test in experimental

decompression sickness 23 p3956 A67-41626

Two-antenna interferometer baseline observations and scanning interferometer characteristics, determining source coordinate and solar radiation center 24 p4129 A67-42227

SCATTER PROPAGATION

Scatter propagation due to geomagnetic field-aligned irregularities and calculation of scattering cross section 07 p1143 A67-19675

Ionospheric electron and ion temperatures during 10.7 cm-solar radio flux activity, giving scatter diagrams 21 p3616 A67-38000

SCATTERING

SA ACOUSTIC SCATTERING

SA ATMOSPHERIC SCATTERING

SA BACKSCATTER

SA COHERENT SCATTERING

SA DIFFRACTION

SA ELASTIC SCATTERING

SA ELECTROMAGNETIC SCATTERING

SA ELECTRON SCATTERING

SA FEYNMAN DIAGRAM

SA FORWARD SCATTER

SA INCOHERENT SCATTERING

SA INELASTIC SCATTERING

SA ION SCATTERING

SA IONOSPHERIC F-SCATTER

SA LIGHT SCATTERING

SA LUNAR SCATTERING

SA MICROWAVE SCATTERING

SA NEUTRON SCATTERING

SA NUCLEAR SCATTERING

SA NUCLEON-NUCLEON SCATTERING

SA PROTON SCATTERING

SA RADIO SCATTERING

SA RAMAN SCATTERING

SA RAYLEIGH SCATTERING

SA RESONANCE SCATTERING

SA TRANSMITTANCE

SA TROPOSCATTER

SA WAVE SCATTERING

SA X-RAY SCATTERING

Stationary methods in continuous spectra perturbation theory of nonrelativistic quantum-mechanical scattering in Hilbert space 02 p0268 A67-12726

Solar neutrino-electron interaction and use of boron-cycle solar neutrino fluxes to determine existence of neutrino and antineutrino scattering effects 02 p0317 A67-12776

Scatterers identification by measuring separations between antenna grating lobes, signal direction and difference in levels of maxima and minima 03 p0370 A67-13856

Geometric-optics curvilinear coordinate system computation of scattered field of smooth bodies with sharp edge in terms of phase structure 07 p1143 A67-19588

Invariant imbedding and time dependent scattering processes including applications to particles moving in rod, radiative transfer in slab, photon diffusion and homogeneous diffusion processes 07 p1224 A67-20274

Variational bounds on eigenphase shifts in scattering theory obtained by SB and R approaches 08 p1355 A67-20865

Geometric-optics curvilinear coordinate system computation of scattered field of smooth bodies with sharp edge in terms of phase structure 20 p3384 A67-37325

Scattering from hard surface solved numerically assuming constant potentials, relating potential present values to retarded values and to incident field 21 p3658 A67-39058

Solar neutrino-electron interaction and use of boron-cycle solar neutrino fluxes to determine existence of neutrino and antineutrino scattering effects 22 p3877 A67-40278

SCATTERING AMPLITUDE

Close-coupling calculation of resonant structure of scattering amplitude of excited-state atoms and molecules in continuum 03 p0471 A67-13221

Scattering amplitude for multiple mixtures in Mossbauer effect determined, from which can be derived absorption cross section and complex refractive index 04 p0680 A67-14758

Second and third virial coefficient of quantum gas expressed in terms of two-particle scattering amplitude, starting from cluster expansion of partition function 05 p0849 A67-17316

Quantum mechanical calculation of transport coefficients of gas of loaded spheres, obtaining scattering amplitudes and

cross sections 06 p1038 A67-19045

Diffusion of protons and nuclei having elastic interactions at 27 GeV/c, using probability distribution for events outside Gaussian limit of multiple scattering 13 p2160 A67-26436

Spatial distribution of deuterium and hydrogen molecules and helium scatterer from /111/ plane of epitaxially grown silver 13 p2099 A67-26948

Beckmann theory on scattering applied to laser mirrors, predicting wavelength dependence of scattering profiles 13 p2129 A67-27348

Generalized potentials for medium energy inelastic nuclear scattering derived with projection operator method 14 p2350 A67-27789

Multiple scattering of electromagnetic waves by arbitrary configurations extended to three-dimensional vector case 15 p2435 A67-29197

Localized defects in semiconductors, using solid state scattering theory to calculate energies of bound states 15 p2534 A67-29325

Scattering amplitude of frequency spectrum components of isolated exponential acoustic pulse incident on hard sphere 21 p3657 A67-38057

Photonuclear interaction effect on large angle scattering of high energy muons 24 p4222 A67-42881

SCATTERING COEFFICIENT

Hall mobility, Seebeck and Nernst coefficients measured in temperature range from about 100 to 350 degrees K for scattering mechanisms of conduction electrons in n type CdS 03 p0493 A67-13351

Point matching solution developed for scattering by conducting bodies of arbitrary shape including circular and square wire loops, plates, spheres and hemispheres 03 p0370 A67-13855

Alkali ion scattering coefficient from tungsten single crystals surface and dependence on incidence angle 06 p1036 A67-18424

Energetic particle scattering by laboratory plasmas, deriving expressions for scattering coefficients in terms of electric field autocorrelation function 08 p1361 A67-21136

Geophysical rocket determination of aerosol scattering coefficient variation from brightness values at 70-450 km heights 10 p1641 A67-23240

Multiple air scattering in mesosphere as function of zenith distance of sun and brightness of twilight sky 11 p1785 A67-23957

Characteristics of open resonators, obtaining coupling and scattering coefficients 15 p2501 A67-30075

Phonon scattering at point defects theory found to disagree with experimental results on InSb-InTe 16 p2730 A67-31156

Scattering theory for parameterization of absorption cross sections and refractivity for autoionizing spectral lines 18 p3082 A67-33878

Altitude variation of air scattering coefficient determined from brightness profile measurements of haze at planet limb, using spacecraft photography 20 p3432 A67-37238

Optical system performance and atmosphere attenuation, analyzing absorption and scattering phenomena in terms of weather conditions 22 p3828 A67-39612

SCATTERING CROSS SECTION

Effective electron scattering cross section in helium and argon plasma with cesium vapor admixture measured by Langmuir probe theory 01 p0119 A67-10134

Impact expansions and interference patterns in atomic scattering theory for cases of forward scattering, backscatter, inversion problem and screened Coulomb potential approximation 01 p0112 A67-10143

Scattered light spectrum in thetatron plasma, noting onset of ion wave instability 01 p0121 A67-10248

Radio wave scattering propagation caused by geomagnetic field aligned irregularities 01 p0021 A67-10334

Differential cross section for excitation of helium electronic states by helium ions 01 p0116 A67-10337

Optical scattering cross sections for polydispersions of dielectric spheres, showing dependence on ratio of third to second moment of shape and size distribution function 01 p0115 A67-11077

Particle size measurements based on use

of optical mean scattering cross sections 01 p0070 A67-11078

Momentum loss rate by conduction electrons of polar semiconductors for known energy and momentum distribution 02 p0280 A67-11486

Approximate general bistatic radar scattering relationships derived for finite length metal cylinder for transverse electric /TE/ and transverse magnetic /TM/ cases 02 p0192 A67-11623

Spectra of outgoing protons for various targets using scintillation counter, interpreting data by means of impulse-approximation calculation 02 p0269 A67-11862

Quasi-stationary techniques for calculating energies and widths of resonances occurring in electron-atom and electron-molecule scattering 02 p0269 A67-12449

Proton-I satellite measurement effective cross section of inelastic interaction of protons with carbon nuclei at extremely high energies 02 p0315 A67-12757

Ionization calorimeter determination of effective cross section of high energy primary cosmic ray proton inelastic interaction with atmospheric atomic particles 02 p0315 A67-12759

Low energy electron-helium atom scattering, using formal optical potential in variational expression for scattering phase shifts 03 p0471 A67-13318

Low energy total and momentum-transfer scattering cross sections for electrons on He and Ar compared, using modified effective range formulas 03 p0471 A67-13319

Electron scattering cross section of argon and atomic oxygen measured, using microwave interferometer for analysis of plasma produced in shock tube 03 p0472 A67-13320

Potassium atom reactive scattering from oriented methyl iodine molecules, determining variation of chemical reactivity over molecular surface 03 p0367 A67-13524

Radar scattering cross section for semiminfinite perfectly conducting blunted cones 03 p0370 A67-13854

Photon scattering in three-dimensional semiminfinite medium for constant frequency and survival probability 04 p0695 A67-14655

Kinetic phenomena in impure ionic semiconductors of cubic symmetry, finding region for dominant scattering mechanism 04 p0675 A67-14923

Excitonic effects in interband absorption of semiconductors noting electron-hole interaction, Coulomb interaction energy maxima and minima and scattering cross sections 04 p0676 A67-14926

Angular dependence of elastic scattering resonance structure in atomic hydrogen 04 p0660 A67-14946

Plasma wave behavior in strong external magnetic field, discussing scattering at ions, wave transformations and nonlinear wave interactions 04 p0667 A67-15206

Raindrop and melting hailstone absorption, scattering and backscatter cross sections of millimeter waves in satellite communications and weather radars 04 p0577 A67-15685

Effective diffusive scattering cross section of electrons in He and Ar plasma with K vapor additions and in pure K, based on DC plasma conductivity and microwave generator Q-factor 04 p0673 A67-15972

Gas kinetic theory of negative ion collisional detachment, using elastic sphere model 05 p0844 A67-16003

Scattering cross section of electromagnetic waves by finite objects in compressible plasma in absence of DC magnetic field 05 p0853 A67-16802

Current carrier scattering mechanism in PbTe determined from ratio of electric conductivity and Wiedemann-Franz ratio 05 p0868 A67-17067

Necessary conditions for equilibrium of Maxwell-Boltzmann distribution using analyticity of S-matrix 05 p0849 A67-17115

Magnon phonon scattering relaxation time as function of temperature and wave vector, calculating thermal conductivity of YIG 05 p0869 A67-17191

Nozzle type molecular beam measuring distribution of speeds after scattering incident beam from solid surface 05 p0849 A67-17276

Optical phonon production, showing existence of electric field strength range at low temperature scattering in which phonon

emission results in electron stoppage 06 p1010 A67-17884

Highly spin polarized carriers for studying neutral impurity scattering in P doped silicon 06 p1063 A67-18937

Carrier-carrier scattering influence on Hall effect and on minority-majority carrier mobility in graphite 06 p1063 A67-18938

Electron mobility in AlSb, GaP and GaSb calculated by combining effects of optical polar and deformation potential scattering 06 p1067 A67-18964

Quantum mechanical calculation of transport coefficients of gas of loaded spheres, obtaining scattering amplitudes and cross sections 06 p1038 A67-19045

Laser application to meteorology, discussing Rayleigh, aerosol and Raman scattering, system configuration and measurement problems 07 p1194 A67-19091

High altitude atmospheric scattering of intense light from ruby laser beam interpreted principally in terms of Rayleigh scattering from atmospheric molecules 07 p1171 A67-19419

Angular distribution of fast hydrogen atoms from exothermic reaction measured for various proton energies and scattering angles 07 p1225 A67-19495

Cross sections for photodetachment of electron from negative atomic oxygen ion 07 p1225 A67-19497

Energy spectrum of inelastically scattered alpha particles from alpha particle helium 3 reaction 07 p1226 A67-19563

Scatter propagation due to geomagnetic field-aligned irregularities and calculation of scattering cross section 07 p1143 A67-19875

Scattering in semiconductors, calculating collision term in Boltzmann equation for acoustic modes and differential collision operator for isotropic part of distribution function 07 p1237 A67-20180

Electromagnetic wave scattering by rough surface computed by approximate method 07 p1147 A67-20237

Radio telescope antenna gain losses due to surface irregularity atmospheric scattering and absorption 07 p1158 A67-20241

Scatterometer measuring radar backscattering for prediction of terrain characteristics 08 p1293 A67-20682

Maximum signal transfer theorem for radio wave transmission, scattering and subsequent detection 09 p1462 A67-21611

Scattered particle intensity inside and outside finite medium determined from Maxwell and Schroedinger equations 09 p1531 A67-21631

Potential-well characteristics from energy dependence of glory extrema in total elastic scattering cross sections 09 p1535 A67-22028

Frequency redistribution function of noncoherently scattered radiation, noting effect on source functions of two-level atoms 11 p1823 A67-24490

Anomalous IR attenuation in fast neutron irradiated GaAs and CdTe arises through scattering and absorption by highly conducting spike zones 11 p1850 A67-24910

Differential reaction cross section and internal excitation function from K and Br molecule crossed beam velocity analysis 11 p1750 A67-24991

Angular scattering of reflected radio waves from ionosphere, giving results of 300 cases 12 p1933 A67-25547

Energy dependence of effective total cross sections of elastic scattering involving H and He atoms and H molecules 13 p2159 A67-26384

Collective scattering cross section and collective spectral extinction of Mie scattering with logarithmic Gaussian distributions 13 p2150 A67-26432

Three-dimensional hard spheres theory of gas atom scattering from solid surface noting velocity distribution, energy and momentum accommodation coefficients, etc 13 p2097 A67-26936

Velocity dependence of total scattering cross sections for atom-atom collisions measured in high energy range 13 p2161 A67-27361

Absolute cross sections and isomeric yield ratios for d,p reactions up to 15 mev in various metals 14 p2350 A67-27790

Position and width of lowest elastic scattering resonances in three-body atomic system, showing resonance shape dependence upon observation angle and

angular resolution 14 p2351 A67-28152

Macroscopic linear fluid model of plasma radiation and scattering restricted to bounded media, emphasizing physical interpretation of wave constituents 14 p2359 A67-28463

Absorption law for weak lines in semiminfinite homogeneous scattering atmosphere for isotropic scattering 14 p2314 A67-28848

Electron-electron scattering in field of monochromatic laser beam, noting resonances in effective Moller scattering cross section 14 p2334 A67-29078

Inhomogeneous sheath effect on surface currents and scattering cross section of plasma-immersed cylinder in presence of electromagnetic and electrokinetic waves 15 p2521 A67-29192

Temperature dependence of current carrier mobility in nickel and iron oxide, noting scattering due to magnetic field 15 p2533 A67-29315

Current carrier scattering mechanism in PbTe determined from ratio of electric conductivity and Wiedemann-Franz ratio 15 p2539 A67-29798

Local gas density measurements, using large angle scattering from electron beam passing through rarefied gas flow 15 p2490 A67-30152

Plasma wave behavior in strong external magnetic field, discussing scattering at ions, wave transformations and nonlinear wave interactions 15 p2532 A67-30254

Coherent integral method applicable to scattering calculations for arbitrarily shaped dielectric bodies of low density [TR-67-114] 16 p2626 A67-31347

Diffraction of plane electromagnetic waves on compressible plasma cylinder analyzed, obtaining scattering cross sections 16 p2628 A67-31503

Inelastic differential scattering cross sections and angular distribution of Ni first-excited-state protons determined by distorted wave calculation 17 p2888 A67-32733

He-He ground state and first excited state potentials obtained from differential scattering cross sections 17 p2889 A67-33257

Volume backscattering functions and optical extinction coefficients for visible and IR radiation and selected cloud models 17 p2817 A67-33293

Renormalizing approximate wave functions so that amplitude is correct by means of matrix, with applications to Born approximation 17 p2887 A67-33318

Resonance effect in low energy or low velocity Li-Hg total scattering cross section 18 p3082 A67-34031

Electromagnetic scattering by thin inhomogeneous circular cylinders, presenting numerical results for induced axial current and scattering cross section 18 p3004 A67-34431

Microwave noise radiation and scattering from cylindrical plasma column, studying dissipative processes on emission spectrum 19 p3291 A67-35387

Computational scheme for calculation of Mie cross sections of absorbing particles 19 p3184 A67-35688

Compound state resonances in molecular collisions, stressing scattering cross sections behavior for deuterium-xenon 19 p3266 A67-35881

High energy electron ionization cross section for hydrogen, noting high quantum number correspondence to classical expression 19 p3266 A67-36090

Fluctuating light scattering cross section and Lorentz-Lorenz refractive index formula derived from microscopic equations 20 p3483 A67-36174

Angular distribution of products in electron impact dissociation of hydrogen molecule calculated following Born approximation for scattering amplitude 20 p3487 A67-36231

Differential cross sections for inelastic large angle alpha particle scattering from unnatural parity states in Mg showing diffraction pattern 20 p3488 A67-36931

Absolute electron impact excitation cross section of 3914 angstrom band of positively ionized nitrogen molecule 20 p3450 A67-37104

Semiempirical electron impact cross sections for He from oscillator strengths, using Born approximation 20 p3489 A67-37416

Relative photon scattering cross sections

for He and Ne at Lyman alpha, describing measurement technique 20 p3489 A67-37431

Low energy electron scattering from hydrogen molecules in ground electronic and vibrational states, calculating rotational excitation cross section 20 p3491 A67-37687

Electromagnetic plane wave scattering cross section from plasma coated conducting cylinder using TE and TM modes of polarization with respect to cylinder axis 20 p3389 A67-37706

Peak energy dependence on atomic number in inelastic alpha particle scattering at 24.8 Mev by Ni 58, Cu, Ag, Ta and Au 21 p3659 A67-38401

Differential cross sections for elastic scattering of alpha particles by oxygen, giving angular distributions and resonances 21 p3659 A67-38517

Differential cross sections of elastic scattering of alpha particles by oxygen, measuring angular distributions 21 p3659 A67-38518

Energy dependence of effective total cross sections of elastic scattering involving H and He atoms and H 21 p3660 A67-38822

Maximum likelihood method used as criterion in processing optical images propagated through turbulent atmosphere 21 p3586 A67-38954

Integrals properties with respect to paraboloid and asymptotics of Born approximations in scattering theory for Schroedinger equation applied to parabola 22 p3835 A67-39307

Ion-molecule collision cross section determined from pressure broadening of ion cyclotron resonance lines at high electric field/pressure ratio 22 p3840 A67-39365

Mass spectrometric method for measuring double charge exchange cross sections of low energy positive ions, investigating current distribution 22 p3797 A67-39427

Helical electromagnetic wave scattering and transformation during propagation in magnetoplasma, considering fluctuations 22 p3846 A67-39501

Microwave scattering cross section for turbulent weakly ionized plasma column, noting square root of mean square plasma density fluctuation limit for Born approximation 22 p3850 A67-39722

Proton I satellite measurements of effective cross section of inelastic interaction of protons with carbon nuclei at extremely high energies 22 p3876 A67-40259

Ionization calorimeter determination of effective cross section of high energy primary cosmic ray proton inelastic interaction with atmospheric atomic particles 22 p3876 A67-40261

Scattering cross section reduction of metal core loaded dielectric circular cylinder using harmonic series expansion for resonance phenomena 23 p3979 A67-40830

Electromagnetic scattering from free-space impedance homogeneous spheres, discussing null production in backscattering cross section 23 p3973 A67-40882

Bond formation effect on electron scattering cross sections for molecular H, N and O 23 p4029 A67-40966

Unresolvable targets producing single radar return estimation from slow amplitude fluctuation, discussing scattering cross section effects and computer simulation verification 23 p3974 A67-41198

Cross section data for molecular oxygen and electron collision processes, discussing elastic scattering, attachment, rotational transitions and Born cross section 23 p4030 A67-41481

Angular distributions of elastic and inelastic alpha scattering from tellurium isotopes using Lewis cyclotron 24 p4192 A67-42732

Effective cross section of inelastic interaction between high energy protons and carbon nuclei monitored by Proton I and II 24 p4219 A67-42843

Cross section of inelastic interactions and free path between nuclear active cosmic particles and lead nuclei at high energies 24 p4219 A67-42844

Cross section of inelastic interaction between cosmic ray neutrons and carbon nuclei at energies of 100 Gev 24 p4219 A67-42848

Nuclear active cosmic ray particles and Fe atom nuclei inelastic interaction cross

section 24 p4219 A67-42849

High energy nucleon and pi-and K-mesons inelastic interaction cross sections from quasi-linear approximation of optical model 24 p4192 A67-42852

Proton-proton and pion and kaon elastic scattering from protons at high energy, deriving approximate formula for differential cross section, noting nucleon structure 24 p4193 A67-42855

SCATTERING FUNCTION

SA MIE SCATTERING FUNCTION

Modified adiabatic scattering function applied to positron annihilation in helium 01 p0116 A67-10141

Scattering of plane wave by grating of identical cylinder specialized for case in which individual elements of grating scatter isotropically 03 p0374 A67-14353

Metal resistivity change due to multiple point imperfections and lattice distortions, noting aggregate effect estimation from scattering power of isolated defects 05 p0830 A67-17190

Quantization, sampling frequency and statistical scattering in correlation measurements 08 p1313 A67-21006

Generalized potentials for medium energy inelastic nuclear scattering derived with projection operator 14 p2350 A67-27789

Scattering function derivation using lunar limb occultation of solar disk during partial eclipse 14 p2386 A67-28475

Scattering problem for partial difference equations with finite perturbation and inverse problem determining perturbation 17 p2817 A67-32885

Spectral data on primary cosmic ray protons and helium nuclei analyzed, assuming solar cycle modulation due to diffusion-convection process 17 p2952 A67-33247

Searchlight brightness measurements for vertical turbidity layer of troposphere using computing scattering functions 19 p3225 A67-35532

Electromagnetic scattering from adsorbing spheres near resonances calculated from extinction efficiency factor and angular scattering function dependence on refractive index 21 p3656 A67-37856

Scaling law derived from small angle scattering theory, interpreting data in spectroscopic manner to deduce potentials and interactions between electronic states 22 p3839 A67-39205

Cosmic ray fluctuations without imposing limitations on particle scattering, deriving expressions using three-dimensional cascade shower theory 22 p3873 A67-39880

Fermi pressure shifts of highly excited states of atoms in gaseous medium due to electron particle interactions, discussing scattering contributions 23 p4029 A67-40958

Strong electric field effects on parabolic energy band semiconductor magnetoresistance and Hall coefficients, discussing scattering mechanisms 24 p4202 A67-41982

Signal extraction and scattering of telluric currents studied for random sheets, seminfinitesimal medium and interface separating medium of different resistivities 24 p4152 A67-42885

SCATTERING MATRIX

Fundamental theorem for diode switches proved, using scattering matrix formulation permitting generalization of theorem to nonreciprocal structures 01 p0032 A67-10010

Matrices of scattering transmission wave and normed cascade parameters of linear passive 2/m plus m/ terminal networks 02 p0221 A67-12528

Scattering matrix properties of symmetrical octupoles 04 p0586 A67-15673

Scattering matrix coefficients and relation between transmission and reflection coefficients of three-port circulator 05 p0770 A67-16170

Finite scattering matrix for plane wave excited infinite array in relating array number and active element properties 07 p1151 A67-19442

Relation of scattering matrix, Riccati equation and boundary conditions 10 p1673 A67-22964

Scattering matrix equations for waveguide structure of varying surface impedance boundaries 11 p1751 A67-23968

Theory of nephelometric method for

measuring transparency and structure of atmospheric aerosols 13 p2151 A67-26685

Progress in linear circuit theory, discussing scattering matrices, broadband matching and distributed and mixed lumped networks 14 p2291 A67-28460

Two port power flow analysis using generalized scattering parameters 14 p2287 A67-28625

Attenuation cross section and refractive index using collision theory, calculating resonance profiles of autoionizing lines based on scattering theory 14 p2351 A67-28811

Restriction elimination in interchanges of reference impedances of scattering matrices 16 p2630 A67-31719

Renormalizing approximate wave functions so that amplitude is correct by means of matrix, with applications to Born approximation 17 p2887 A67-33318

Resonance methods for microwave measurement of scattering matrix of two-port reciprocal junction 18 p3002 A67-34223

Scattering and transmission parameter methods for semiconductor device measurement, discussing linear integrated circuit test requirement 19 p3191 A67-34944

Fluorescence spectrum of activating europium ion in lutetium oxide matrix and appearance in crystalline-field model 19 p3307 A67-35794

Scattering matrix method, determining power transfer between closely coupled antennas in complex environment 20 p3405 A67-37644

Anderson model Hamiltonian exchange character application to conduction electron Green function determination 22 p3861 A67-39994

Errors in measuring scattering patterns of arbitrary body in Fresnel region due to body/antenna finite distances and directivities 24 p4120 A67-42229

SCF

S SELF-CONSISTENT FIELD /SCF/ SCHEDULING

Airline strategy for domination of Northeast Corridor despite improvements in high speed ground transportation [AIAA PAPER 66-942] 03 p0361 A67-14021

Quality evaluation review technique /QERT/ for management facilitation of program planning and scheduling, noting time and cost estimation 05 p0930 A67-17246

Parameters of satellite communication system control and scheduling function, emphasizing distinction between scheduling model and scheduling algorithm 06 p0961 A67-17699

Computer applications to test scheduling problem against probabilistic demand in heuristic environment [AAS PAPER 67-46] 15 p2467 A67-30114

Retrofit accountability system requirements, environment, purpose and future applications 20 p3556 A67-36545

V/STOL aircraft scheduling for passenger demand and equipment mix, optimizing airline earnings with mathematical programming model [AIAA PAPER 67-801] 24 p4259 A67-42961

V/STOL airbus transportation system schedules, travel times and fares for Northeast Corridor generated by computer method [AIAA PAPER 67-972] 24 p4127 A67-43049

SCHLIEREN PHOTOGRAPHY

SA SHADOW PHOTOGRAPHY

Laser light source controlled by Kerr cell coupled with Z-type schlieren optical system to produce multiple flash photographs of detonation wave development 02 p0245 A67-12227

Lasers applied to photo-optical instrumentation problems, detailing schlieren systems, interferometry, high speed streak photography and transmissometer 02 p0245 A67-12243

Transition to detonation in gaseous medium experimentally studied, based on self-sustained detonation front and adaptation of amplitude modulated giant pulse laser system 03 p0535 A67-13500

Photographic techniques developed for photographing ballistic missiles and associated explosive reactions, including shadowgraph and schlieren techniques [SMPTE PREPRINT 100-59] 03 p0423 A67-13807

Sensitivity of optical system used in

schlieren setup in determining quality of recorded information 04 p0619 A67-14606

Local details of influence of vertical sound field on heat transfer from circular cylinder determined, using schlieren system 04 p0733 A67-15845

Schlieren and hot-wire anemometric observation of supersonic wakes in wind tunnel turbulent flows [ONERA-TP-417] 05 p0748 A67-16482

Schlieren techniques used in free flight range study of far wake of hypersonic cones [AIAA PAPER 67-31] 06 p0938 A67-18261

Gas lens focusing of light beams, using highly transparent gas with weakly varying refractive index to guide coherent transmission with small losses 07 p1188 A67-19789

Test of probes designed to determine direction of supersonic flows in wind tunnels, using schlieren photography 09 p1496 A67-21693

Plasma flows from normal and coaxial electrode contact points of arc and effect of external forces by schlieren photography 10 p1687 A67-23849

Quantitative schlieren interferometry, measuring thermal distributions near heated vertical plate and horizontal cylinder 11 p1791 A67-24668

Laser holography combined with schlieren techniques to measure ray deviations in optically inhomogeneous field of transient phenomenon 11 p1794 A67-24927

Flow visualization, discussing schlieren process in light of Toepler, fine focusing, microscopic, phase contrast and field absorption processes 14 p2315 A67-27974

Supersonic flow separation from corner of base compared to Stokes-type flow separation 14 p2240 A67-28111

Far wake behavior of hypersonic spheres analyzed using schlieren techniques 15 p2417 A67-30190

Schlieren techniques used in free flight range study of far wake of hypersonic cones [AIAA PAPER 67-31] 17 p2793 A67-33006

Atomic oxygen effect on vibrational relaxation of oxygen in shock waves at high temperatures, using laser schlieren technique 18 p3081 A67-33784

Detonative ignition induced by shock merging ahead of accelerating flame in hydrogen-oxygen mixture analyzed by stroboscopic laser-schlieren photography 18 p3153 A67-33826

Ignition temperature and ignition delay of oxyhydrogen gas as function of pressure examined in shock wave tube, using Schlieren photography 18 p3160 A67-34261

Laser driven plasma detonation waves in gases observed with Schlieren system, discussing shock wave growth 18 p3092 A67-34734

Density and temperature measurements of high temperature nitrogen plasma jet using schlieren photographic method 19 p3231 A67-35595

Sensitivity of single-mirror schlieren system, deriving expression relating film density change with angular light deflection 20 p3441 A67-36400

Color schlieren and high speed photography technique for transient flows in wind tunnels 20 p3445 A67-36537

Oxygen-hydrogen mixtures burning characteristics in shock wave tube, studying ignition processes with schlieren photographs 21 p3731 A67-38366

Laser macrophotography for size distribution of particulate debris dispersed from ablating zirconium alloy specimen in hyperthermal wind tunnel ablation testing 23 p4006 A67-41380

SCHMIDT CAMERA

Design and operation of all-reflecting Schmidt camera 14 p2319 A67-28562

Schmidt satellite cameras to record trail from bearing and elevation fixed in relation to earth, detailing optical system of Royal Radar Establishment /RRE/ camera 18 p3048 A67-34237

SCHMIDT METHOD

Llapunov-Schmidt method combined with topological method show secondary flows formed after stability loss 10 p1734 A67-23673

Llapunov-Schmidt method combined with topological method show secondary flows formed after stability loss 21 p3731 A67-38274

SCHMIDT NUMBER

Concentration profiles in fixed laminar

boundary layer with catalyst distribution on wall, discussing Schmidt number effect and approximations 18 p3159 A67-34161

Diagnostic equations for electrostatic double probes for arbitrary ion Schmidt numbers 19 p3267 A67-34830

S-current intensity variation and 10.7 cm radio noise flux show agreement with Schmidt sunspot numbers 19 p3221 A67-35432

SCHOTTKY EFFECT

Electron tunneling through space charge region of uniformly doped metal-semiconductor barriers calculated in effective-mass approximation 02 p0280 A67-11483

Single crystal transistor with metallic base, noting frequency, V-I and power characteristics, radiation resistance, etc 02 p0221 A67-12530

Electrochemical deposition of Schottky contacts of copper and gold on gallium arsenide 03 p0494 A67-13484

Schottky emission as rate limiting factor in thermal oxidation of metals 04 p0677 A67-14947

Schottky barrier photodiodes with antireflection coating on metal film for fast and efficient optical detectors 04 p0582 A67-15078

Electron transfer in thin film tantalum-tantalum oxide diodes, noting tunnel and Schottky emission 04 p0582 A67-15106

Fluctuation spectra of amplitude and frequency of reflex klystron oscillations excited by fluctuation noise /Schottky effect/ 04 p0583 A67-15169

Electric conduction through tantalum oxide thin films, showing dependence of V-I characteristics on tunneling and Schottky effect 05 p0862 A67-16525

Multiple contact Schottky barrier microwave diode, comparing operation with single diode in mixing and small and large signal detection 05 p0780 A67-17526

Low 1/f noise mixer diodes, comparing Schottky barrier diode with backward diode type 05 p0780 A67-17528

Schottky theory and electron affinity of semiconducting CdSe from DC I-V characteristics and work function of Au, Ag and Cu contacts with CdSe 07 p1231 A67-19491

Transient phenomena in reverse current and capacitance in gallium arsenide Schottky barrier diode in monochromatic light 09 p1471 A67-21762

GaAs Schottky diodes for integrated circuits, discussing fabrication, parameters and performance 10 p1615 A67-23527

Semiconductor devices for microcircuits, discussing MOS FET, metal base transistor, etc 12 p1918 A67-26206

Transient phenomena in capacitance and reverse current for n-type GaAs Schottky barrier diodes at different carrier concentrations 14 p2384 A67-27827

Single crystal transistor with metallic base, noting frequency, V-I and power characteristics, radiation resistance, etc 14 p2279 A67-28007

Fluctuation spectra of amplitude and frequency of reflex klystron oscillations excited by fluctuation noise /Schottky effect/ 15 p2444 A67-29355

Large dynamic range, high-burnout microwave varistor diode construction and planar technique for Schottky barrier diode array fabrication 16 p2642 A67-31723

Schottky approximate formula adaptation for abrupt junctions with asymmetric doping ratios 18 p3106 A67-34646

Differential resistance peaks of metal-semiconductor Schottky barrier rectifiers 19 p3198 A67-36042

Semiconductor metal diodes operation principles, emphasizing lack of minority carrier storage 20 p3509 A67-36491

Schottky tunneling measurements in GaAs with Au noting fine structure 22 p3861 A67-39996

Schottky photodiode narrow spectral response in Spicer absorption diffusion model shown to exist only in rapidly changing absorption coefficient region 23 p3981 A67-41272

SCHROEDINGER EQUATION

Approximate solution of Gelfand-Levitan equation leading to localized bound-state wave function examined in S-matrix approach to first order energy

shift 02 p0270 A67-12637

Variational perturbation equations and time-independent Schroedinger equation for two-, three- and four-electron atoms 02 p0271 A67-12724

Autoionization calculation describing scattering aspect of phenomenon 03 p0471 A67-13220

Lower bound electronic energy calculations for positive H, using methods of truncated Hamiltonians and of Temple and Kato 03 p0469 A67-13943

Hydrogen line intensity decrease in solar photosphere and chromosphere, noting agreement with Schroedinger equation results 03 p0512 A67-14004

Allowed and forbidden direct interband optical transitions in anisotropic semiconductors, using effective mass theory for exciton, solving Schroedinger equation 04 p0674 A67-14610

Self-conjugacy of semibounded Schroedinger operator 04 p0646 A67-15262

Impurity energy levels in semiconductors described by equivalent Schroedinger equation containing short range as well as conventional terms for long range Coulomb potential 07 p1230 A67-19060

Extended average energy approximation of first order perturbation wave function, proposing procedure for multidimensional problems 07 p1137 A67-20186

Steady state laser design, comparing balance method with method based on quasi-classical theory 07 p1197 A67-20245

Analytic properties of solutions to generalized axisymmetric Schroedinger equation 08 p1346 A67-20355

Scattered particle intensity inside and outside finite medium determined from Maxwell and Schroedinger equations 09 p1531 A67-21631

Analytic power series solution of nonrelativistic Schroedinger equation for two-electron atom, assuming fixed nucleus and singlet and triplet S states 15 p2520 A67-30158

Rapidly converging analytic solution by integral series of nonrelativistic Schroedinger equation for He atom 15 p2520 A67-30159

One-dimensional three-body problem, noting shell model for two particles and coordinate transformation 17 p2888 A67-32926

Wave surfaces of Einstein-Schroedinger theory and nonlinear electrodynamics brought together using antisymmetric tensor 18 p3078 A67-33688

Accidental degeneracy of hydrogen atom levels using Schroedinger equation, deriving eigenfunctions 18 p3083 A67-34072

Spectrum of bound and quasi-bound states of hydrogen-hydrogen scattering and resonance, using Schroedinger equation 18 p3084 A67-34523

Screened Coulomb potential solutions of Schroedinger equation using nonlinear method 19 p3266 A67-36091

German book on differential operators of mathematical physics covering Hilbert space h, Schroedinger spectral theory, etc 20 p3475 A67-36434

Solving Schroedinger equation with initial coherent radiation state 20 p3485 A67-36866

Variational approximation for ground state of perturbed Schroedinger equation with single variable wave function 20 p3479 A67-37600

Nonlinear generalization of Schroedinger equation describing hidden variables effect solved for spin-1/2 magnetic moment relaxing in constant magnetic field 21 p3658 A67-38845

Integrals properties with respect to paraboloid and asymptotics of Born approximations in scattering theory for Schroedinger equation applied to parabola 22 p3835 A67-39307

Perturbation theory for exchange forces using Brillouin and Schroedinger equations 24 p4194 A67-43115

SCHUMANN MODE

Schumann Resonance frequencies, Q-factor and waveguide propagation constant derived at ELF for ionospheric profiles 21 p3579 A67-37993

SCHUMANN-RUNGE BAND SYSTEM

Heat radiative flux divergences and equilibrium temperature distribution with altitude calculated for heat regime modeling radiative transfer conditions in stratosphere

and mesosphere 10 p1647 A67-23275

SCHWARZ-CHRISTOFFEL TRANSFORMATION

Schwarz transformation methods for electrical studies of MHD generators with tensor conductivity 16 p2600 A67-30535

SCHWARZSCHILD METRIC

Light propagation through Schwarzschild singular sphere, solving problem of visual image of emitting surface of gravitating sphere as seen by observer 03 p0467 A67-12932

Kruskal space in general relativity and uniform accelerated rigid rod in special relativity show striking formal similarities 05 p0847 A67-16970

Perturbed motion of comet in medium of constant low density in solar Schwarzschild field, using quasi-Newton approximation, considering electromagnetic and gravitational fields 06 p1084 A67-18164

Phenomenological metric method applied to four tests of general relativity in evaluation for nearly flat space with spherical symmetry 13 p2159 A67-27399

Models of spherically symmetric nonstatic processes, including relativistic collapse: to Schwarzschild sphere, constructed by space-time metrics [JPL-TR-32-1136] 15 p2564 A67-30438

Perturbed motion of comet in medium of constant low density in solar Schwarzschild field, using quasi-Newton approximation, considering electromagnetic and gravitational fields 16 p2741 A67-30508

Schwarzschild criterion for convective instability in general relativity extended to Einstein hydrostatics to formulate buoyancy principle with aid of initial value problem 18 p3133 A67-34375

Schwarzschild criterion validity, reducing initial value problem for hydrodynamic perturbation equation to time independent problem 18 p3029 A67-34737

Nonzero cosmological constant effect /precise and trivial/, calculating perihelion precession from Schwarzschild exterior solution 22 p3889 A67-40382

Relativistic gravitational collapse, considering asymmetric nonrotating star collapse 24 p4226 A67-41885

SCIENCE

SA ENVIRONMENTAL SCIENCE

SA LIFE SCIENCE

SA MATERIALS SCIENCE

SA NEUROSCIENCE

SA PHYSICAL SCIENCE

SA SPACE SCIENCE

German-English index of mathematical tables for science and technology 08 p1431 A67-21541

Scientific research using C-135 aircraft for AEC atmospheric testing 13 p2090 A67-27257

Technical obsolescence of engineers and scientists, considering knowledge explosion impact in terms of organizations and individuals [SAE PAPER 670833] 24 p4257 A67-41993

SCIENTIFIC SATELLITE

SA DODGE SATELLITE

Supersatellite technology and advantages of larger automaton craft including superweather, superremote sensor, superutility, supersurveillance and superscientific satellite systems 04 p0703 A67-14601

Temporal variations of intensities of electrons of various energy ranges trapped in outer radiation zone measured by research satellite Injun III 04 p0693 A67-14962

Oceanographic measurements with instrumented satellites, examining surface temperature surface waves, tides, albedo, heat flux and coordination of airborne and seaborne sensing systems 06 p0999 A67-19000

Primary cosmic ray investigation by Proton I scientific space station concerning energy spectrum, chemical composition, galactic gamma ray and solar radiation hazard 16 p2737 A67-30647

Satellite system with solid state transmitters with different frequencies in HF band for ionospheric guided propagation research 20 p3394 A67-36246

Central data system for solar probe to map particle and radiation fields of solar corona 20 p3391 A67-36597

Principal investigator task evaluation, discussing responsibility for instruments,

prelaunch operation, operational program establishment, processing, analyzing and publishing of results [AIAA PAPER 67-630] 20 p3534 A67-37614

Navigation satellites for information during movements of manned/unmanned terrestrial vehicles containing position determination, communications and weather relay service and scientific sensors 22 p3831 A67-39524

Lincoln experimental satellite program, discussing communications satellites applications 24 p4242 A67-42906

SCIENTIST

Research astronaut selection 13 p2062 A67-26763

Technical obsolescence of engineers and scientists, considering knowledge explosion impact in terms of organizations and individuals [SAE PAPER 670833] 24 p4257 A67-41993

SCINTILLATION

SA PHOSWICH SCINTILLATION

Photoelectric recording of scintillation of stellar images by function of nature of scintillation while carrying out observations 02 p0326 A67-11991

Latitudinal effects on satellite beacon scintillations as observed from three stations [AFCLR-66-864] 03 p0406 A67-12820

Diurnal and latitudinal variation of satellite scintillation during local summer at low southern geomagnetic latitudes 03 p0406 A67-12821

Nighttime F layer irregularities at equator responsible for scintillation of signals from radio sources and satellites 03 p0407 A67-12828

Ionospheric studies using tracking beacon on Early Bird synchronous satellite, noting scintillations due to irregularities 03 p0407 A67-12832

Radio star and satellite scintillations, discussing wave propagation through random media, interplanetary scintillations and ionospheric irregularities [RASSA PAPER 1-10-133] 03 p0372 A67-14244

Radio source diameter measurement through application of interplanetary scintillation, noting angular resolution 05 p0903 A67-17291

Scintillation analysis of hard X radiation from high power pulse discharges 08 p1357 A67-20846

Radio source scintillations caused by electron density fluctuations extended to regime with large phase fluctuations, discussing autocorrelation function for any regime 09 p1565 A67-22222

Statistical quantities needed to fix scattering regime obtained from observations of radio scintillations, showing correlation length in electron density fluctuations 09 p1565 A67-22223

Relationship between statistics of log amplitude and irradiance fluctuations due to atmospheric turbulence used to estimate effect of aperture in collecting scintillating light 10 p1603 A67-22711

Covariance of log amplitude fluctuations for propagation of spherical wave in turbulent medium over horizontal path to obtain phase structure function 10 p1678 A67-22712

Amplitude fluctuations of VHF beacon of Early Bird synchronous satellite observed from stations in Italy and Massachusetts 10 p1640 A67-23233

Latitudinal variations of ionospheric irregularities studied via synchronous and 1000 km satellites, noting Early Bird data, scintillation index graphs, radio star signals, etc 10 p1640 A67-23234

Statistical verification of hypothesis explaining observed scintillations of light curve of quasi-stellar radio sources by explosions of supernovas 13 p2198 A67-28766

Data processing of signal reception from Soviet satellites indicates radio signals scintillation caused by diffraction of waves from ionospheric nonuniformities 14 p2260 A67-27857

Measurement of angular spectrum of radio waves from sources outside solar system 14 p2386 A67-28445

Sporadic E layer scintillation effects on amplitude of 137 MHz radio waves from Early Bird 14 p2270 A67-28577

Frequency dependence of radio star scintillations 15 p2555 A67-29621

Statistical analysis of spread-F and

scintillation data in middle latitude noting diurnal and seasonal variations [AGARDOGRAPH 95] 15 p2481 A67-30284

F region irregularities studied by scintillation of radio signals from earth satellites [AGARDOGRAPH 95] 15 p2481 A67-30285

Geophysical model of radio star and satellite ionosphere amplitude scintillations at nonequatorial latitudes [AGARDOGRAPH 95] 15 p2482 A67-30286

Radio star fadeouts and radio propagation 15 p2563 A67-30287

Broadband radio star Cassiopeia A scintillations observed with swept frequency interferometer [AGARDOGRAPH 95] 15 p2563 A67-30288

Radio star Cassiopeia A scintillations and spread-F in auroral zone [AGARDOGRAPH 95] 15 p2482 A67-30289

Nature of nighttime F-layer irregularities responsible for scintillation of VHF signals received from radio stars and earth satellites [AGARDOGRAPH 95] 15 p2482 A67-30290

VHF radar reflections from artificial earth satellites used to analyze amplitude scintillations in ionosphere [AGARDOGRAPH 95] 15 p2482 A67-30292

Measurements on scintillation observed on radio signals from Discoverer satellite, noting intensity increase with latitude and data on diurnal variation [AGARDOGRAPH 95] 15 p2483 A67-30293

Satellite scintillation in auroral zone depends on time of observation and on magnetic activity 15 p2483 A67-30294

Atmosphere effect on laser beam scintillation measurements after propagating over 8 km path near ground for various collector sizes and environmental conditions 16 p2686 A67-31879

Quasar observations using interferometer baselines, noting regular fringes and small phase scintillation in Gaussian source model 17 p2947 A67-32760

Diurnal and seasonal variation of electron content and diurnal variation of slab thickness investigated, emphasizing relation between electron content and scintillation occurrence 17 p2850 A67-33190

Scintillation and dynamic range problems mitigated for Fourier spectrometry by rapid scanning 20 p3438 A67-36342

Scintillation of ground-to-space laser beam through atmospheric turbulence 20 p3383 A67-37023

Scintillation depth measurement relationship with probability density of amplitude distribution 21 p3617 A67-38002

Wind and cloudiness effects on terrestrial scintillation based on visual estimates and measurements 22 p3828 A67-39240

Short bursts of scintillation of satellite radio signals from S-66 satellite, discussing diurnal variation correlation with spread of occurrences 22 p3759 A67-39478

Atmospheric scintillation effects on optical data channel for application to laser radar noting SNR role 23 p3975 A67-41266

SCINTILLATION COUNTER

Time measurement with semiconductor device, noting parameter variation effect and experimental results 01 p0066 A67-10652

Semiconductor surface barrier Si n-type detector yielding fast resolution curve in alpha-gamma radiation coincidence experiment 01 p0066 A67-10657

Time resolving capabilities of RCA C-70045, 56 AVP and XP 1020 photomultipliers 01 p0067 A67-10659

Spectra of outgoing protons for various targets using scintillation counter, interpreting data by means of impulse-approximation calculation 02 p0269 A67-11862

Location and radiation intensity variation in upper radiation belts determined, using scintillation counters aboard Cosmos satellites 02 p0311 A67-12598

Fast and slow neutrons detected by proportional and scintillation counters 02 p0312 A67-12606

Apparatus for investigating nucleon reactions with approximate energy greater than 100,000 bev, including Cerenkov and scintillation counters and spark chambers 02 p0316 A67-12765

Measurement of half-life of 14.4 kev level of 57 Fe with scintillation detectors and digital timer 03 p0471 A67-13225

Electron intensity measurement in primary

cosmic radiation by high altitude balloons carrying telescope made of two plastic scintillation counters 05 p0878 A67-16097

Cosmic ray analysis with Holborn scintillator stacks to determine existence of quarks 06 p1076 A67-17650

Energy spectra of Tau X-1 and isotropic component of galactic X-rays, using rocketborne scintillation and GM counters 10 p1701 A67-23229

Van Allen belt proton measurements by pulse height analysis, using thin low-Z scintillator to minimize large angle electron scattering 11 p1856 A67-24014

Spectrometry of primary and solar protons at Skogar-Iceland using apparatus consisting of scintillation and Cerenkov counters 12 p1991 A67-25114

Upper limits to hard X-ray flux from quiet sun analyzed by balloon-borne scintillation detector measuring celestial sources 13 p2189 A67-26302

Solar wind measurements and small scale structure of interplanetary medium using scintillation technique 13 p2190 A67-26318

Pulse amplitude measurement from scintillation cosmic-ray counter 13 p2119 A67-26560

Liquid scintillation counting method with sonic oscillations, noting decreased preparation time and increased counting efficiency 14 p2260 A67-28477

Angular diameter of scintillating source 3C 279 determined from fluctuation spectrum width 14 p2389 A67-28843

Cosmic ray mu-meson intensities at different altitudes at equator measured as function of zenith and azimuth, using scintillation counter 15 p2549 A67-29184

Atmospheric electron energy spectrum in range 70-2000 mev measured, using scintillation telescope with gas Cerenkov detector and lead glass total energy spectrometer 15 p2475 A67-29615

Spark chambers and scintillation counters used to search for fractionally charged particles in cosmic rays near sea level 15 p2550 A67-29680

Position of outer radiation belt boundary as function of local time, discussing data from Elektron satellite scintillation counters 16 p2740 A67-31886

Atmospheric variations effects on cosmic radiation records from plastic scintillation monitors, calculating pressure coefficients 17 p2938 A67-32795

Low energy H and He isotope detection in cosmic radiation at solar minima via balloon mounted scintillation counter 17 p2939 A67-33246

Standard scintillation index method for describing ionospheric effects, discussing power calibration, scaling, deviations, etc 19 p3220 A67-35256

Apparatus for investigating nucleon reactions with approximate energy greater than 100,000 Bev, including Cerenkov and scintillation counters and spark chambers 22 p3876 A67-40267

Photon beam transmission measurement technique for determining bone mineral content in vivo 23 p3945 A67-41087

Proton energy spectrum azimuthal asymmetry measured with telescopes using scintillation and Cerenkov counters 23 p4054 A67-41096

Cosmic ray measurements during low geomagnetic activity using scintillation, gas discharge and semiconductor proton counters mounted on Cosmos satellite 23 p4055 A67-41099

Energetic protons from March 24, 1966 solar flare observed with OGO 1 satellite scintillation counter 23 p4060 A67-41233

High energy neutrino flux from atmosphere studied in South African gold mine using liquid scintillation detector 24 p4210 A67-42581

Plonic and muonic K-series X-rays studied by liquid He scintillation counter, obtaining separation peaks 24 p4192 A67-42735

Electron intensity measurement in primary cosmic radiation by high altitude balloons carrying telescope made of two plastic scintillation counters 24 p4213 A67-42773

SCINTILLATION SPECTROMETER

High transmission Cerenkov spectrometer carried by proton I and II satellites to measure 09 p1497 A67-21898

Auroral X radiation, measured by balloon-installed X-ray spectrometer incorporating scintillation counter with high speed analyzer, correlated with ionospheric radioelectric absorption and solar magnetic field variations 10 p1702 A67-23304

Versatile digital data handling system designed to accept and control output of space radiation scintillation spectrometer 12 p1909 A67-25864

Scintillation characteristics of radio waves after passing through ionosphere 13 p2115 A67-26857

Rapid assay for thymidylate synthetase as specific and sensitive measure of enzyme activity 14 p2260 A67-28479

F layer irregularities transverse scale measurements by two-frequency scintillation-ratio technique yielding 600-700 m scales in auroral zone 22 p3789 A67-39470

SCINTILLATOR

Giant airshower recorder using liquid scintillators to record collision of cosmic rays with atmospheric nuclei 03 p0508 A67-14388

Electron energy spectrum measured near equator by satellite mounted scintillator 04 p0614 A67-14950

Directional neutron spectrometer for events in which neutron is scattered by first scintillator into second 12 p1945 A67-25859

Directional neutron detector using liquid scintillator for low mev energy range for rocket and satellite experiments 12 p1945 A67-25860

Probes containing various scintillators for measuring electron energy spectrum at high altitude in cosmic ray flux 23 p4054 A67-41095

Electron photon cascades in lead scintillator devices investigated using Nagel Monte Carlo calculations for energies between 100 and 440 Mev 24 p4191 A67-42439

SCORPIO CONSTELLATION

Visual component identification of Sco X-1 X-ray source 01 p0151 A67-10963

Optical observation of brightest X-ray source in Scorpius, giving tabulated data as function of radius 05 p0892 A67-16414

Sco X-1 physical characteristics noting ionization, possible stellar wind and pressure equilibrium effects 11 p1862 A67-24506

Precise position and spectra of Scorpio X-ray source and location of two weaker sources in galactic plane, describing instrumentation used 12 p1995 A67-25781

Sco XR-1 source model corresponding to neutron star in state of accretion as possible explanation of X-ray emission power from source 13 p2189 A67-26262

Strong X-ray source in vicinity of constellation Crux compared to SCO xr-1, findings suggest similar physical nature 17 p2937 A67-32761

SCOUT LAUNCH VEHICLE

Integrated reliability program for Scout launch vehicle in terms of design specification, review functions, malfunction reporting, failed parts analysis, quality control, standardization and certification 18 p3139 A67-34702

SCR

S SILICON CONTROL RECTIFIER

/SCR/

SCRAM

S SUPERSONIC COMBUSTION RAMJET MISSILE /SCRAM/

SCRAMJET ENGINE

Supersonic combustion air breathing engines as propulsion systems for hypersonic vehicles [AIAA PAPER 66-826] 04 p0688 A67-14624

Supersonic combustion ramjet development 06 p1073 A67-17609

Scramjet testing with wave superheater hypersonic tunnel [AIAA PAPER 67-182] 06 p0980 A67-18343

Hypersonic air breathing engine, specifically scramjet, noting vehicle design, combustion system, nozzle, friction, etc 10 p1697 A67-22873

Scramjet performance analysis stressing construction problems and importance of fuel choice 11 p1853 A67-24748

Model tests on free jet scramjet facility configurations at jet Mach numbers, obtaining data on bypass flow pressure recovery and diffusion 13 p2089 A67-26830

Scramjet engine nozzle contours noting expansion-deflection, bell, plug and arbitrary annular nozzles, with optimum nozzle design and computer program for performance prediction [AIAA PAPER 67-453] 18 p2983 A67-33927

Gun launched scramjet performance using various fuels, comparing weight and volume limitations effects 19 p3311 A67-34822

Supersonic combustion simulation for hypersonic flight in relation to scramjet operation, discussing auto-ignition limits [CI PAPER 67-6] 19 p3344 A67-35001

Scramjet testing with wave superheater hypersonic tunnel [AIAA PAPER 67-182] 19 p3208 A67-35767

Hypersonic flight programs, considering Air Force, Navy and NASA research programs on scramjets 20 p3517 A67-37447

Wave superheater based on shock tube principles, discussing application in scramjet design 21 p3608 A67-38800

Composite propulsion systems for aerospace missions, considering Mach range, specific impulse, oxygen source, design characteristics, capabilities and limitations 22 p3868 A67-39890

SCREEN

Intensity fluctuations of waves diffracted by deeply modulated random phase screen 13 p2071 A67-27403

Electromagnetic field coupling action through holes in metal screen, noting hole polarizability calculation and hole equivalent dipoles effect on resonators 18 p2999 A67-33530

SCREEN EFFECT

Interferences between waves diffracted by circular screens or thin wires and coherent background provided by laser, producing rings or rectilinear fringes 01 p0087 A67-10231

Screen effect on cosmic ray intensity measurement by comparing data from various rocket and satellite soundings 02 p0307 A67-11668

Screening effect on Coulomb interaction, electron-ion recombination and surface neutralization 03 p0473 A67-13512

Screen and honeycomb effect on variation of skin friction in low speed wind tunnel, noting turbulent boundary layer growth 10 p1627 A67-23556

Effect of wide angle screened diffuser on turbulent velocity fluctuations [ASME PAPER 67-FE-23] 14 p2243 A67-28368

Screen effect on cosmic ray intensity measurement by comparing data from various rocket and satellite soundings 16 p2738 A67-31083

Screening frequency dependence on reflection cut-off frequency in sporadic E layer 20 p3428 A67-36762

SCREENING TECHNIQUE

Magnetic screening tests and use of parts sampling to control magnetic cleanliness for quality assurance 03 p0396 A67-13721

Straight edge fence design for control of radar site environment from clutter return, pattern interference, tracking errors and high power hazard to personnel 03 p0396 A67-13853

Screening to improve reliability of silicon integrated circuit, noting failure mode and mechanism 09 p1480 A67-22300

Quantitative graphical method of screening working fluids for Rankine cycle power plants using single stage turbines at different levels of diameter and rpm [ASME PAPER 67-GT-12] 11 p1746 A67-24798

Silk screen techniques used for film circuitry implementation on integral sensor telemetry transmitter with standard components 12 p1911 A67-25272

Cylindrical screened electrode for measuring temperature plasma conductivity in MGD generator 13 p2055 A67-26434

Radiographic screening of relays for detection of solder balls, broken leads, cracks, etc 13 p2084 A67-27695

Variables in screen printing and firing processes for thick film resistors affecting reproducibility 16 p2641 A67-31620

Airborne imagery screening using automatic target recognition device 17 p2859 A67-32509

Point charges interaction energy in semiconductor thin film 18 p3101 A67-34091

Optimum short term screen tests developed for integrated

circuits 18 p3018 A67-34649
Stencil screening methods for printing integrated circuit patterns for resistors, capacitors, etc, discussing automation possibilities 19 p3192 A67-35026
Screened Coulomb potential solutions of Schroedinger equation using nonlinear method 19 p3266 A67-36091

SCREW DISLOCATION
Dislocation structure in tantalum single crystals deformed in tension to various strains at 373 degrees K studied by transmission electron microscopy 01 p0092 A67-10057
Elastic interaction energies between edge and screw dislocations and tetragonal defects in anisotropic NaCl lattice 02 p0298 A67-11885
Stress field generation by screw dislocation pile-up at hard circular cylindrical inclusions obtained, using approximation of continuously distributed dislocations 04 p0707 A67-14403
Distributions of screw dislocations in finite slab, examining crack extension with and without plasticity 04 p0716 A67-15798
Thermally activated motion of screw dislocations in bcc metals 07 p1209 A67-19640
Dislocation theory of slip geometry and temperature dependence of flow stress in bcc metals 07 p1209 A67-19641
Energy factors of infinite straight dislocations and stresses of piecewise straight dislocation configurations expressed through Green functions of elasticity 08 p1418 A67-20798
Shear modulus effect on stress distribution of planar array of screw dislocations near bimetallic welded half-planes interface 11 p1804 A67-24107
Temperature dependence of bcc metals elastic limit at low temperature, assuming sessile-dissociated screw dislocations formation during microdeformation, stressing stacking fault energy 13 p2130 A67-26438
Screw dislocation and crack interaction when elastic field is independent of one of three Cartesian coordinates 16 p2764 A67-30993
Elastic interactions of cracks and dislocations of screw type in two-dimensional model 16 p2768 A67-31281
Si-Fe deformation in tension/compression noting orientation dependence of yield stress, slip band formation and direction of screw dislocations 17 p2872 A67-32741
Dislocation in field-ion micrograph analyzed by computer-simulated Ranganathan hypothesis using Moore shell model 19 p3266 A67-35603
Screw dislocation distribution on intersecting planes using theoretical model to discuss errors 20 p3540 A67-37020
Spontaneous decomposition of helical dislocations in metal crystal into row of pinched-off loops plus straight dislocation line 21 p3677 A67-38092

SEA
S OCEAN
S SUDDEN ENHANCEMENT OF ATMOSPHERICS /SEA/
SEA WATER
Tiro VII satellite IR measurement data used to determine sea surface temperature gradients, examining problem of cloud cover 01 p0109 A67-10321
Corrosive effects of chlorides in aqueous environment on pickled and anodized sheet beryllium 04 p0640 A67-15618
Continuous total immersion stress corrosion testing of beryllium in synthetic sea water, discussing relationship between time-to-failure and tensile stress 14 p2336 A67-28147
Ground and water surface temperature measurements using IR radiometers onboard aircraft 24 p4181 A67-41789
Military flight clothing tested in actual survival conditions for ability of subject to withstand moderate sea water environment [AIAA PAPER 67-968] 24 p4118 A67-43046

SEALANT
Pressure patterns, gas ingestion and sealing capacity of viscoelastic investigated using oil, water and liquid sodium as sealed fluids 03 p0428 A67-13226
Chemical, mechanical and chemical-mechanical self-sealant systems incorporated in spacecraft walls for micrometeoroid protection 10 p1673 A67-23748

SEALING
SA GASKET
SA HERMETIC SEAL
SA SELF-SEALING
Groove geometry effect on performance viscoelastic with sealed water in laminar and turbulent conditions [ASME PAPER 66-WA/FE-28] 04 p0630 A67-15356
High vacuum welding of cermet seals with titanium 04 p0630 A67-15632
Soft metal enclosed in higher-melting-point metal forming seal bakeable at temperatures above 500 degrees C 04 p0630 A67-15633
Cryogenic temperature resistant plastics in space program, discussing insulation, adhesives, seals, gaskets and expulsion of cryogenic propellant in zero gravity environment [SAE PAPER 660638] 04 p0642 A67-15788
Component design advances with fatigue tests on hydraulic tubes and outline of seal development 05 p0753 A67-18749
Aircraft equipment retrieval after long term storage for periods of up to 23 years under jungle, desert and arctic environment, discussing sealing and hydraulic systems [AIAA PAPER 67-185] 06 p0951 A67-18487
Cryogenic low pressure seal to seal aluminum or stainless steel flanges 08 p1336 A67-21498
Circumferential seal application and place in seal spectrum relative to gas turbines [SAE PAPER 670062] 09 p1508 A67-22536
Mechanical difficulties in designing shaft, bearing and seal systems for three high speed turbine engines [SAE PAPER 670064] 09 p1560 A67-22537
Seals, Reference Issue, Machine Design magazine, March 9, 1967 09 p1509 A67-22610
Leakage and optimum film thickness of gas lubricated high-pressure mainshaft seals for jet engine compressors 10 p1658 A67-22705
Sealing coefficient of visco seal for laminar and turbulent flow, noting Reynolds number effect 10 p1659 A67-22706
Resistance welds produced by butyl sealant prevent passive films formation on aluminum and magnesium alloys 12 p1948 A67-25287
Satellite sealed subsystems individual leak rates in thermal-vacuum environment measured with mass spectrometer 12 p1921 A67-25690
Hydrodynamic lubrication in face seals, discussing mechanism of fluid film, surface roughness, wear, leakage, thickness, temperature, pressure, etc [BHRA PAPER E5] 14 p2324 A67-27889
Structural, seal and sideboard design, propulsion and cavitation problems relevant to operational requirements of captured air bubble vehicle [AIAA PAPER 67-346] 14 p2245 A67-28729
Viscoelastic operation in superlaminar flow regime noting pressure patterns, end effect, gas ingestion and sealing capacity 14 p2327 A67-28797
Dynamic-seal technology in applications employing liquid metals, gas and standard organic fluids for ground, aerospace and space turbomachinery [ASME PAPER 67-DE-50] 14 p2328 A67-28881
Humidity, temperature, contamination and disconnection effects on gasket and grease seals for extended space mission computer connectors 15 p2442 A67-29182
Static and dynamic sealing concepts and materials for propellant feed systems and pneumatic and hydraulic control systems of liquid propellant rocket engines 17 p2864 A67-31990
Gland design variation effects in gaseous helium seal performance from O-ring permeation measurements at pressures up to 1000 psi 17 p2801 A67-31992
Metal-to-metal seal for separable joints /Bobbin seal/ utilizing elastic and plastic responses of seal structure and interface 17 p2864 A67-31993
High vacuum enclosure problems solved by use of magnetic seal for joints of large valves and degassing by direct heating of wall surfaces 17 p2802 A67-32300
Cermet sealing material dry-friction characteristics over wide sliding-speed range, discussing graphite and boron nitride lubricants 19 p3247 A67-35850
Book on vacuum sealing techniques

covering permanent seals, demountable seals, current transmission, design, materials, etc 19 p3238 A67-35925
Adhesive and water resistance properties of epoxy resin for bonding tensometers and underwater sealing 21 p3650 A67-38919
Vacuum jacketed cryogenic globe valve design providing tight sealing, low heat leak, low cool-down mass and high flow 23 p3936 A67-41426
Two-axis gimbal system for solar simulation spacecraft testing, demonstrating intermediate axis internal drive system and outer axis drive input 24 p4153 A67-42044
Groove geometry effect on performance viscoelastic with sealed water in laminar and turbulent conditions [ASME PAPER 66-WA/FE-28] 24 p4161 A67-42466

SEAPLANE
SA SHIN MEIWA UF-XS AIRCRAFT
Tilt and vertical float program of Naval Air Systems Command comprising four studies covering factors involved in any open ocean aircraft 03 p0354 A67-12901
UF-XS Japanese STOL seaplane used to investigate slow speed flying quality and hydrodynamic characteristics of PX-S aircraft 14 p2245 A67-27743

SEARCH RADAR
Error equation for accuracy of monopulse radar in search mode applied to monopulse radar systems, using logarithmic normalization 01 p0022 A67-10446
Search and acquisition problem to relate spacecraft radar parameters and mission parameters, illustrating optimization and emphasizing radar power aperture product 04 p0572 A67-15030
Radar search and tracking system developments 06 p0957 A67-17584
Maintaining target track for nonmaneuvering targets approaching uniformly scanning search radar 13 p2068 A67-26782
RCA papers on defense electronic products including search radar, superconductor devices, data and spacecraft communications, speech recognition 14 p2274 A67-28910
Military radar intercept calculator, discussing small size, low power supply, high performance and MOS memory 15 p2439 A67-29161

SEASONAL VARIATION
March 1964-March 1965 seasonal variations in density, pressure and temperature at Woomeera, Australia, by falling sphere method 01 p0061 A67-12680
Seasonal changes in cosmic ray intensity including barometric effect in neutron component, effect of earth seasonal position, etc 02 p0307 A67-11665
Temperature effect in neutron component of cosmic rays and seasonal changes in intensity affected by interplanetary magnetic field 02 p0307 A67-11666
Diurnal and seasonal variations of ionospheric turbidity 02 p0236 A67-11670
Beacon satellite measurement of Faraday rotation and diurnal and seasonal variations of total electron content of ionosphere near Nairobi 03 p0406 A67-12825
Monthly and seasonal variation of magnetic horizontal component in Eastern Africa on international quiet and disturbed days from February 1964 to January 1965 03 p0408 A67-12838
Seasonal PCA variations and type IV bursts associated with high energy proton injection into polar ionosphere 03 p0507 A67-13812
Carbon dioxide content in troposphere and lower stratosphere measured at various altitudes, showing seasonal variations 03 p0414 A67-14086
Time-dependent photochemical model for space-time variations of oxygen allotropes in 20 to 100 km layer 03 p0414 A67-14087
Seasonal atmospheric attenuation measurements at 3.27 cm wavelength indicate twice as much vertical attenuation in winter as in summer [RASSA PAPER 1-10-142] 03 p0417 A67-14250
Diurnal variations of ionospheric ion composition over Arecibo at various altitudes for solar minimum winter and summer conditions 04 p0614 A67-14955
Sporadic E layer behavior noting seasonal variations and duration 04 p0618 A67-15223
Seasonal and diurnal variations of

geomagnetic field in equatorial regions 04 p0616 A67-15224

Seasonal and solar-cyclic variations of nondeviate absorption in ionospheric D region 04 p0617 A67-15570

Seasonal variation of morning and nighttime absorption of long waves 04 p0617 A67-15571

Correction for characteristic number of E layer based on electron transport processes and seasonal variations 04 p0618 A67-15573

E layer stratification, fine structure and boundary accuracy in frequency measurements based on seasonal variations in solar activity 04 p0618 A67-15574

Seasonal changes in solar diurnal and semidiurnal variations of cosmic ray neutron component due to earth rotation axis and anisotropy sources 05 p0885 A67-17138

Temporal variations in values of variability characteristic of parameters of ionosphere cross sections below principal maximum 05 p0801 A67-17142

Seasonal variation in temperature in nighttime F region through analysis of emission intensity of oxygen red line and upper atmosphere structure 06 p0996 A67-18431

Horizontal variability of properties of model thermosphere with seasonal changes 06 p0996 A67-18564

Long range weather forecasting, discussing synoptic, statistical and physical approaches 06 p1027 A67-18604

Winter radio absorption anomaly at middle latitudes theory in terms of temperature and nitric oxide distributions in D region 07 p1171 A67-19415

Ten years ionospheric drift measurements in LF range 07 p1171 A67-19420

Cyclic curves of F-2 layer critical frequencies based on seasonal phase variations in solar cycle 07 p1179 A67-19833

Semiannual effect on satellite orbit decay, correlating with difference in latitude between perigee and subsolar point 07 p1251 A67-19850

Electron temperature and concentration at 1000 km altitude, obtaining resolution of two full diurnal cycles of ionospheric behavior 07 p1181 A67-19935

Seasonal observations of nocturnal ionospheric absorption, noting connection with structural state of sporadic E layer 09 p1491 A67-21930

Strong geomagnetic disturbances distribution in space and time analyzed for correlation of magnetic activity with auroral brightness 10 p1632 A67-22809

Magnetic field variation at high latitude from quiet days in summer of IGY based on calculations for winter 10 p1632 A67-22810

Seasonal-latitudinal variations in lower thermospheric density, temperature and composition 10 p1639 A67-23210

Ionosphere-stratosphere coupling and effect of atmospheric seasonal variations on plasma behavior 10 p1645 A67-23266

Winter anomaly of nondeviate ionospheric absorption of radio waves and relation to diurnal, seasonal, local and solar cycle variations 10 p1646 A67-23267

Vertical drift of charged particles effect on electron density profile as cause of seasonal variations in ionospheric absorption 10 p1646 A67-23269

Seasonal and annual variations of electron density in ionospheric F layer interpreted as changes in production rate and ionization loss caused by atmospheric composition variations from neutral atmosphere 10 p1647 A67-23274

Diurnal and seasonal variation of total columnar ionospheric electron content at magnetic equator analyzed, using Faraday rotation technique 10 p1651 A67-23341

Seasonal variations in ionospheric total electron content measured by observing Faraday rotation of linearly polarized wave from geostationary satellite Syncom III 10 p1651 A67-23346

Effect of variation of vertical air density profile on relative optical air mass for ARDC standard model atmosphere 1959 compared with measurements 10 p1652 A67-23622

Vertical distribution of ozone over Tallahassee, noting maximum and minimum density altitudes, seasonal variations, etc 11 p1787 A67-24555

Lunar influence on total electron content

of winter ionosphere at minimum solar activity 11 p1788 A67-24771

Barometric pressure data analysis estimating autocovariance, using Fourier transform for spectral density calculation 11 p1816 A67-24840

Seasonal variations of total electron content of ionosphere during sunspot minimum 12 p1935 A67-25795

Atmospheric temperature, pressure, density and wind measurements between 30 and 80 km by Skylark rocket at Woomera, Australia 12 p1937 A67-25840

Unstable diurnal and seasonal variation of ionization of F region of ionosphere during years of minimum solar activity over Ashkhabad 12 p1938 A67-26100

Diurnal and annual variation of absorption of short waves in ionosphere 13 p2066 A67-26486

Diurnal, annual and seasonal variations of high altitude turbulent motions in upper atmosphere through observation of meteor trails by coherent pulse method 13 p2110 A67-26506

Dependence of seasonal occurrence probability of F-zero layer on level of geomagnetic activity and ionospheric activity observed above 13 p2110 A67-26549

Ashkhabad 13 p2110 A67-26549

Seasonal variations in high latitude stratosphere and mesosphere 13 p2113 A67-26675

Variations of ionizing radiation of E layer, eliminating aeronomic effects by considering seasonal variations of ionization index 13 p2191 A67-26767

Meteor stream relation to natural ice nuclei and precipitation 13 p2205 A67-27461

Long term solar cycle and seasonal variation of whistler dispersion 14 p2307 A67-27887

Revised ionization-equilibrium equation to obtain criterion for presence of winter anomaly in E layer 14 p2307 A67-27912

Diurnal and seasonal variations in radio echo observations from meteoric trains during forward ultrashortwave scattering 14 p2383 A67-27924

Seasonal and diurnal variation of parameters of vertical electron density distribution 14 p2308 A67-27934

Ionospheric inhomogeneity winter drifts during periods of high and low solar activity 14 p2308 A67-27936

Seasonal and latitudinal magnetic activity variations in Northern Hemisphere, investigating time-space characteristics of K index 14 p2309 A67-27943

F region phenomena, discussing charged particles dynamics, equatorial and seasonal anomalies and nighttime F layer maintenance, using Alouette I data 14 p2312 A67-28409

Quiet sun current system effects on seasonal variations of critical frequency in E region, noting dependence on local time and latitude 14 p2312 A67-28569

Seasonal variations and attenuation of ionospheric absorption, using A3 method 14 p2312 A67-28570

Diurnal and seasonal variations in occurrence probability of screening and semitransparent types of sporadic E layer 15 p2474 A67-29387

Occurrence frequency of midlatitude blanketing sporadic E studied for seasonal, diurnal and latitudinal variations 15 p2476 A67-29622

Mean variations of total electron density with latitude and local time during winter obtained from dispersive Doppler investigations 15 p2477 A67-29666

Seasonal variations in position and intensity of equatorial electrojet and correlation of latter with sunspot number 15 p2478 A67-30061

Nuclear explosion effects on atmospheric pressure, electron density, and F-2 layer height, noting dependence on time, season, etc 15 p2478 A67-30067

Diurnal, seasonal and geographic variations of frequency of spread-F occurrence over Antarctica [AGARDOGRAPH 95] 15 p2481 A67-30282

Statistical analysis of spread-F and scintillation data in middle latitude noting diurnal and seasonal variations [AGARDOGRAPH 95] 15 p2481 A67-30284

Spread-F occurrence studied using hourly soundings near magnetic equator

[AGARDOGRAPH 95] 15 p2484 A67-30307

Morning effect on F region, noting seasonal variation of corresponding solar zenith angle and worldwide distribution of predawn minimum 16 p2664 A67-30976

Martian secular changes and dark area regeneration attributed to movement of sand, dust and wind caused by elevation and slope differences 16 p2747 A67-30989

Seasonal changes in cosmic ray intensity including effect in neutron component, effect of earth seasonal position, etc 16 p2738 A67-31080

Temperature effect in neutron component of cosmic rays and seasonal changes in intensity affected by interplanetary magnetic field 16 p2738 A67-31081

Diurnal and seasonal variation of ionospheric turbidity 16 p2665 A67-31085

Statistical correlation of latitude with time of maximum darkening of Mars dark areas, noting consistency of 2 models 16 p2749 A67-31401

Semitransparency range of sporadic E layer as solar radiation function, noting diurnal and seasonal variations 16 p2669 A67-31904

Relation between frequency distribution of sudden changes in cosmic ray intensity and solar-diurnal variation 17 p2932 A67-32082

Seasonal variations in afternoon and evening maxima of F-2 layer and dependence of temperature and frequency on minimum zenith angle of sun 17 p2842 A67-32384

Harmonic spectrum of variations in earth rotation, noting seasonal variation and effects of lunar tides 17 p2843 A67-32444

Pearl type oscillations studied by recording ground currents, discussing 24-hr and seasonal variations 17 p2847 A67-32944

Winter and summer equivalent current systems of polar solar-diurnal variations studied from observations obtained during IGY 17 p2847 A67-32949

Helium afterglow observation at high latitudes, determining He line intensity on IR spectrograph and giving time-dependent seasonal variations 17 p2849 A67-32959

Diurnal and seasonal variation of electron content and diurnal variation of slab thickness investigated, emphasizing relation between electron content and scintillation occurrence 17 p2850 A67-33190

Alpha diurnal and seasonal intensity variations in geocorona indicating hydrogen content build-up during night 17 p2851 A67-33202

Semiannual exospheric density variation confirmed by satellite orbit analysis 17 p2852 A67-33238

Nightglow emission structure and variation at airglow equator, discussing predawn and storm effects, intensity variations with solar cycle, OH bands, etc 18 p3036 A67-33607

Microbial numbers relation to phosphatase activity in soil, discussing seasonal variation, sterilization by irradiation and moisture content 18 p2991 A67-33660

Atmospheric ozone content compared for discrepancies between theoretical and experimental results for vertical, latitudinal and seasonal variations 19 p3214 A67-34856

Upper atmosphere diurnal and seasonal latitudinal variations satellite data, showing diurnal bulge migration with subsolar point, 2 PM bulge peak, etc 19 p3215 A67-35178

Diurnal atmospheric density bulge shifts observed by Explorer, showing latitudinal-seasonal variation in helium concentration 19 p3218 A67-35226

Seasonal variations in incidence of E-2 layer from 1960 through 1965 19 p3221 A67-35429

Air density variation at 220 km altitude shown due to increased solar activity, from satellite orbit observation 19 p3222 A67-35458

Hydrogen and hydroxyl emissions in nightglow 19 p3223 A67-35483

Stratospheric mean adiabatic vertical motion and temporal correlations with temperature, isobaric height, zonal/meridional wind and horizontal kinetic energy computed based on seasonal averages 19 p3224 A67-35529

Winter anomaly in ionospheric E-layer 19 p3225 A67-35617

Daily and seasonal changes in numbers, dimensions and shapes of micrometeoritic particles over period of two years, discussing origin 19 p3327 A67-35878

Daily magnetic variations over England, noting difference between values obtained for summer IQD and other days of year 20 p3429 A67-36870

Zonal winds studied by meridional sections from observations made during same months over several years 20 p3480 A67-36965

Lunar tide in E layer, diurnal/semidiurnal components and seasonal variation 21 p3616 A67-37997

Winter anomaly of ionospheric adsorption studied by field strength recordings 21 p3617 A67-38001

Temporal variations in values of variability characteristic of parameters of ionosphere cross sections below principal maximum 21 p3619 A67-38484

Geomagnetic activity around conjunction and opposition of planets, noting decrease in years of low solar activity 21 p3711 A67-39004

Planetary distribution of horizontal gradients of F-2 layer critical frequency and diurnal, seasonal and solar cycle variations 21 p3622 A67-39034

Seasonal and long term variations in duration of continuous radio signal reflections from sporadic -E layer 21 p3623 A67-39038

Seasonal changes in solar diurnal and semidiurnal variations of cosmic ray neutron component due to earth rotation axis and anisotropy sources 21 p3700 A67-39048

Photometric observation data on Jupiter atmospheric activity /1964-1965/ noting three-month periodic change 22 p3879 A67-39299

Seasonal and diurnal variations of trough and ionospheric electron content and slab thickness, using S-66 satellite observation 22 p3789 A67-39471

Radar-derived results for midlatitude F-region densities and temperatures at sunspot minimum noting seasonal anomalies 22 p3793 A67-40080

Satellite and ground observations of VLF emissions, summarizing intensity, diurnal and seasonal variation, emphasizing chorus and hiss characteristics 22 p3794 A67-40083

Diurnal, latitudinal and seasonal variations of midlatitude topside ionosphere electron density profiles and plasma scale heights calculated from Alouette I ionograms 23 p3994 A67-40775

Nighttime variation of ionospheric winds over Barbados via luminous trails measurements, obtaining steady state components for seasonal variations 23 p3995 A67-40807

Equatorial anomaly in F-2 layer of ionosphere, examining solar activity, seasonal variation relation to magnetic activity, lunar phase and heights 23 p3996 A67-41082

Biennial component of seasonal variation in earth rotation rate using time observation data, calculating stratospheric zonal wind effect 23 p3996 A67-41085

Equatorial electrojet currents studied from IGY data from South American stations 24 p4148 A67-42065

Strong geomagnetic disturbances distribution and time analyzed for correlation of magnetic activity with auroral brightness 24 p4150 A67-42146

Magnetic field variation at high latitude from quiet days in summer of IGY based on calculations for winter 24 p4150 A67-42147

SEAT

SA EJECTION SEAT

Dynamics of commercial aircraft seats with viscous dampers and elastic couplings during crash landing [ASME PAPER 66-WA/SAF-1] 04 p0551 A67-15329

SEAT BELT

Animal study of irreversible trauma in lateral impact when restrained only by aircraft lap seat belt 23 p3954 A67-41595

SECOBARBITAL

Dose levels and hangover effect of secobarbital on simulated pilotage performance 03 p0366 A67-14291

SECOND

S NANOSECOND

SECOND STAGE

ELDO missile second stage automatic control system, noting programming control sequences, analysis of measurement results, etc 03 p0502 A67-12899

Electronic control system for triaxial control of geocentric satellite and second

stage of CORALIE booster 21 p3656 A67-38231

Thor SLV upper stage 2 design, performance and cost 21 p3713 A67-38379

SECONDARY AIR

Mixing, ignition and combustion in secondary combustor for air-augmented solid rockets with solid particles in primary stream [AIAA PAPER 67-481] 18 p3158 A67-33950

Fuel burnout processes in inlet flow of secondary air stream to turbine combustion chamber determined by working mechanism in inlet section of chamber 22 p3869 A67-40453

Steady state matching of inlets, engines and exhaust nozzle for SST 23 p3928 A67-40988

SECONDARY EMISSION

Secondary electron emission investigated by transmission and backscatter experiments with thin films, noting maximum exit depth dependence on energy 02 p0290 A67-11733

Calculation of neutron generation by mu-mesons for various depths in earth 02 p0312 A67-12607

Second breakdown in junction transistors examined, using scanning electron microscope 02 p0222 A67-12653

Secondary breakdown characterization technique in Ge p-n-p alloyed junction transistors with open base condition 02 p0223 A67-12655

Text on high power electronics including cathodic losses in magnetrons, electrodynamic theory of grids, high frequency measurement, secondary electron emission and electromagnetic oscillations 03 p0379 A67-13301

Multipactor in T-R switch for improved recovery time 03 p0383 A67-13827

Rocket measurement of secondary electron energy distribution in aurora, employing 180 degree electrostatic deflection analyzer 03 p0418 A67-14357

Second order scattering effect on earth albedo calculations in middle UV, noting distribution functions and parameters used 04 p0613 A67-14696

Intensity of various secondary cosmic ray components in cut-off rigidity range from 0.3 to 10 Bev 05 p0881 A67-16124

X-ray diffraction study of crystallographic transistor defects causing secondary breakdown 07 p1156 A67-19896

Current mode second breakdown in epitaxial planar transistors, describing V-I behavior 07 p1156 A67-19897

Stability of various surfaces with respect to electron bombardment heating, noting influence of roughness on electron trapping 09 p1500 A67-22428

Direct ionization and secondary excitation in proton auroras, noting magnitude of contribution by various processes 11 p1784 A67-23927

Short period radioactive nuclides induced by secondary neutron due to solar cosmic radiation in chondrites 11 p1858 A67-24058

Cosmic ray secondary components yearly changes of intensity determined as function of earth heliolatitude 12 p1992 A67-25120

Radiation-induced electroconductivity and secondary emission in alkali halide single crystals under positive ion bombardment 13 p2177 A67-27073

Transverse-momentum distribution of secondaries from high energy nuclear interactions in accelerator energy region interpreted by statistical model 13 p2195 A67-27580

Primary cosmic radiation composition effect on secondary emission, examining flux, spectra, nucleon interactions, proton component and neutrons 14 p2380 A67-27966

Delta coefficient of secondary emission of monocystal of GaAs with various doping 14 p2367 A67-28516

Secondary electron detector for electronic microcircuits bombarded by electron beam used to observe potential distribution in junction breakdown 15 p2453 A67-30065

Circuit of automatic multichannel secondary particle recorder of SKL type for cosmic ray station, using azimuthal muon telescope and neutron supermonitor 17 p2854 A67-32098

Photon transmission delaying processes and secondary ionization growth time dependence on overvoltage in neon 19 p3284 A67-35086

Statistics of electron avalanche generating secondary effect at cathode through photon emission, obtaining excited molecule distribution 19 p3265 A67-35087

Factors influencing secondary electron emission produced by high energy molecular beam impact on metal surface 20 p3488 A67-36438

Doubly differential cross section for ejected secondary electrons energy and angular distribution calculated from He by fast protons 22 p3839 A67-39201

Intensity of various secondary cosmic ray components in cut-off rigidity range from 0.3 to 10 Bev 24 p4215 A67-42800

Secondary particles angular distribution in showers studied with cloud chamber, ionization calorimeter and counters to identify particles causing shower asymmetry and symmetry 24 p4217 A67-42829

Asymmetry in angular distribution of secondary particles in cosmic ray showers 24 p4218 A67-42838

SECONDARY FLOW

Secondary vorticity for compressible flow in centrifugal impeller, noting parameter effects on motion 03 p0402 A67-13337

Prediction theory for effect of shear flows on outlet angle in axial compressor cascades, taking into account effects of secondary flow, Bernoulli surface rotation and spanwise flow displacement 04 p0548 A67-15387

Inflow boundary layer effect on secondary flow at blade tips of circular cascade of reaction turbine, considering tip and gap losses 06 p0937 A67-17991

Free vortex decay above stationary boundary for varying viscosity, determining plate boundary layer solution for small nondimensional radial distances 06 p0985 A67-18135

Application limit of inviscid small perturbation theory to secondary flow in cascade, comparing experimental and calculated vortex strength 08 p1275 A67-20406

Entrance conditions and flow separation effect on rectangular diffuser performance, showing importance of secondary flows 10 p1627 A67-23557

Liapunov-Schmidt method combined with topological method show secondary flows formed after stability loss 10 p1734 A67-23673

Theory on secondary flows through axial compressor or turbine cascade 13 p2049 A67-26530

Heat transfer calculation to turbine blading in cascade in presence of secondary flow, considering flow velocity estimation, blade boundary layer and related heat transfer properties 13 p2225 A67-27465

Transverse secondary flow effects on laminar turbulent transition of free axisymmetric jet 14 p2303 A67-28328

Convective secondary flow in channel flow of quasi-incompressible fluid noting temperature gradient role [ASME PAPER 67-HT-28] 20 p3546 A67-36719

Acoustic vibration effect on heterogeneous mass transfer at sphere surface in high Prandtl number liquids 20 p3554 A67-37068

Liapunov-Schmidt method combined with topological method show secondary flows formed after stability loss 21 p3731 A67-38274

Forced convective heat transfer in straight pipe rotating around parallel axis with large angular velocity 22 p3920 A67-40419

SECONDARY HARMONIC GENERATION

Second harmonic generations and mixings of Raman lines produced in cyclohexane, acetone, benzene and carbon disulfide, photographing first order Stokes radiation 02 p0252 A67-12052

Frequency dependent two-photon absorption radiation-matter interaction and secondary harmonic generation in n-and p-type impurity semiconductors 03 p0435 A67-13126

Kinetic equation derivation from density matrix for case of quantum generation of secondary optical harmonic in laser cavity under various optical pumping conditions 03 p0435 A67-13127

Harmonic generation by travelling waves in nonlinear dispersive medium for quasi-monochromatic signals, obtaining correlation function and spectrum of second harmonic for Gaussian processes 04 p0657 A67-15146

Second harmonic generation of light by

focused laser beams in nonlinear crystals at exit surface 05 p0817 A67-16640

Holographic study of second harmonic wave emitted by ruby laser, examining influence of defects of spatial coherence of wave 05 p0808 A67-17322

Nonlinear optical reflection laws governing direction, polarization and intensity of second harmonic light generated in reflection 06 p1030 A67-17571

Nonlinear second harmonic generation of current density in inhomogeneous magnetoplasma and reflected electromagnetic wave from free space interface 06 p1046 A67-18825

Boltzmann transfer equation consisting of DC electric field and two AC electric fields for nonlinear second harmonic generation and combination frequencies in homogeneous plasma 06 p1046 A67-18826

Convective heat transfer in tube with gaseous heat carrier pulsating at frequency corresponding to second resonance harmonic 07 p1266 A67-19182

Cylindrical optics in converting laser emission into second harmonic in ADP and KDP crystals, obtaining high conversion efficiency 09 p1511 A67-21916

Second harmonic generation in liquid crystals, noting absence of effective center in molecular configuration 09 p1517 A67-22680

Laser variable output coupler, construction, performance and applications 10 p1662 A67-22753

Fluorescein family organic dyes exhibiting laser action when excited by ruby and neodymium second harmonics 12 p1953 A67-25748

Cylindrical optics in converting laser emission into second harmonic in ADP and KDP crystals, obtaining high conversion efficiency 14 p2329 A67-28245

Harmonic generation by traveling waves in nonlinear dispersive medium for quasi-monochromatic signals, obtaining correlation function and spectrum of second harmonic for Gaussian processes 15 p2517 A67-29333

Continuous second harmonic generation of 2572 angstrom argon II laser, noting optimum phase matching, power dependence on crystal temperature, etc 15 p2497 A67-29392

Sum generation of tunable two-frequency pulse output of gain-switched ruby laser 20 p3458 A67-36389

Electromagnetic wave propagation in nonuniformly magnetized plasma with wave frequency near second electron cyclotron harmonic 22 p3843 A67-39263

35 GHz second harmonic generation power and conversion efficiency in low pressure gas discharge, noting pressure and gas species variations 22 p3854 A67-40316

Second harmonic generation in Se and Te-Se using carbon dioxide laser, measuring nonlinear coefficients and synchronism direction 23 p4016 A67-41192

Second optical harmonic generation of pulsed ruby laser emission in GaSe crystal suggesting only surface layer contribution to generation 24 p4167 A67-42074

Second harmonic power generation associated with simultaneous application of DC fields and gas laser beams to narrow band gap semiconductor 24 p4168 A67-42364

SECONDARY INJECTION

Mass effect on blast wave equations of shock generation by secondary injection of fluid into hypersonic flow 01 p0141 A67-11179

Production of low energy cosmic ray electrons, investigating energy inputs to injected secondary electrons by possible low magnitude solar electric field and possible galactic Fermi acceleration 02 p0312 A67-12635

Film cooling by helium secondary flow injection into incompressible low speed airflow in turbulent boundary layer above flat plate 06 p1116 A67-18385

Fluid flow processes for secondary sonic jet injection into Mach 6 free stream, noting upstream flow into separated flow regions 12 p1893 A67-25934

Three-dimensional detached flow patterns forming near secondary jet injected into supersonic flow 18 p3027 A67-34207

SECONDARY RADAR

Simple secondary radar antenna with fan-shaped beam for monopulse operation 06 p0967 A67-17616

Secondary surveillance radar system design, discussing interrogator interference, decoding and display 09 p1530 A67-22648

Incidence of missed reply and garbled pulse trains and fruit interference effect determined in extraction of secondary radar plots 09 p1530 A67-22653

Secondary surveillance radar /SSR/ as principal sensor in future air traffic control service 09 p1466 A67-22657

SECRETION

Secretory activity of algal *Chlorella* cells effect on buffering characteristics of Tris or sodium citrate-citric acid suspending fluid 21 p3573 A67-37729

SECTION

S AIRFOIL SECTION

SECULAR PERTURBATION

Secular changes in stratospheric cosmic ray intensity from 1962 to 1964 02 p0311 A67-12595

Increase with latitude of Forbush effects and secular variations in cosmic ray intensity explained by worldwide data obtained with meson detectors 02 p0311 A67-12596

Secular variation of earth magnetic field 03 p0414 A67-13944

Frozen field estimation of surface flow of earth core and effects of secular change resulting from flow pattern nonuniformity 08 p1329 A67-21485

Difference assessment between secular and long period perturbations generated by similar initial conditions for celestial mechanics problems 09 p1563 A67-21637

Stability analysis of long period Trojan librations treated as short period oscillations about long period reference solution 11 p1866 A67-24774

Secular variations of geomagnetic field before our era studied by method using archaeological objects 12 p1933 A67-25554

Statistics and evolution of sunspots, discussing frequency, shape, long solar cycle and secular variation 13 p2202 A67-27417

Commensurability cases of asteroid and Jupiter within framework of secular perturbation theory 15 p2559 A67-30038

Secular and periodic perturbations of orbits of artificial satellites of earth and moon by attraction of external bodies 16 p2746 A67-30981

Martian secular changes and dark area regeneration attributed to movement of sand, dust and wind caused by elevation and slope differences 16 p2747 A67-30989

Normal modes of hydromagnetic oscillations in rotating fluid sphere including ohmic dissipation, deriving dispersion relations 17 p2941 A67-32285

Geomagnetic field secular variation forecasting method suggesting inclusion of anomalies 17 p2847 A67-32947

Secular behavior of optical properties of X-ray emitting object near Cygnus X-2 19 p3331 A67-36084

Lunar-solar gravitational perturbation of satellite with sidereal day period, discussing stability 20 p3523 A67-36626

Comet Wolf I orbit evolution over 400 years /1660-2060/, accounting for planetary perturbations and considering secular deceleration 20 p3524 A67-36660

Geomagnetic field configuration and time change using dipole vector, noting variation role 21 p3620 A67-38979

Geomagnetic field secular variation, with time explained by strength changes of BFD and nondipole field and drift 21 p3620 A67-38980

Incompressible hydromagnetic fluid oscillation in rotating spherical shell pervaded by strong toroidal and weak poloidal magnetic field for geomagnetic secular variation 21 p3621 A67-38983

Deep subterranean electric conductivity using 30-year cyclic geomagnetic field variation data 21 p3622 A67-39025

Earth core surface fluid velocity patterns and magnetic field secular change at earth surface for various epochs 23 p3996 A67-40815

Irregular earth rotation velocity variation analyzed by comparing universal time with atomic time 24 p4150 A67-42312

Time dependent gravitational constant theory, studying earth rotation secular acceleration 24 p4229 A67-42321

Lunar origin and earth-moon system, discussing dynamical requirements based on secular variation of some parameters 24 p4230 A67-42322

Galactic cosmic ray solar cycle and secular variations in bombardment of meteorites at average meteoroid solar distance and 1 AU from radioactive isotope ratios 24 p4210 A67-42622

Uniformization of asymptotic expansions, constructing counterterms by nesting increasing number of extensions for both secular and singular perturbation terms 24 p4190 A67-43094

SEDIMENT

Sedimentologic process which comminutes transports and deposits material by impact on planetary surfaces 02 p0235 A67-11451

Oils and shales from 3 million to 2.7 billion years old analyzed for hydrocarbon content, using gas chromatography and mass spectrometry 05 p0797 A67-16580

Optical rotation of lipids extracted from soils, sediments and Orgueil carbonaceous meteorite 08 p1289 A67-21173

Stable isotope distribution in carbonates 14 p2310 A67-27970

SEDIMENTARY ROCK

Sedimentary rock analysis for aliphatic hydrocarbons, discussing methods and results 10 p1709 A67-23488

Confirmation of reality of Gilsa geomagnetic polarity event, discussing experimental techniques and results 11 p1788 A67-24700

Mass spectrometric analysis of sedimentary rocks for Sr-Rb and Sr isotopic composition from Bosumtwi crater, Ghana 14 p2314 A67-28952

Zodiacal dust explained by radioactive Al 26 deposited in marine sediments and brought by micrometeorites exposed to solar protons 15 p2553 A67-29157

Chemical analysis of meteorite impact glass from separated areas across Henbury strewnfield 16 p2667 A67-31452

Terrestrial surface spectral IR emissivities determined in situ interferometrically, noting igneous and sedimentary rock composition and texture 22 p3805 A67-40354

Antimony abundance in meteorites, tektites and terrestrial rock by neutron activation analysis 24 p4236 A67-42647

SEEBECK COEFFICIENT

Anisotropy of electric resistivity, Seebeck and Hall coefficients and magnetoresistance of n-type single crystal ferric oxide /hematite/ containing tetravalent tin ion as impurity 02 p0299 A67-12085

Hall coefficient, electrical resistivity and Seebeck coefficient of p-type lead telluride measured, using two-valence band model 14 p2367 A67-28520

Conductivity, Hall effect and Seebeck coefficient measurements on single domain crystals of barium titanate 16 p2729 A67-31060

SEEBECK EFFECT

S PELTIER EFFECT

S THOMSON EFFECT

SEEDING

SA CLOUD SEEDING

Syringe injection system for seeding plasma with Na-K alloy in study of MHD power generation and propulsion 08 p1279 A67-20377

Third Chapman-Enskog approximation to tensor electrical conductivity of partially ionized gas applied to two conductivity mixture rules for atmospheric cesium seeded argon 12 p1975 A67-25893

Magnetically induced ionization in nonseeded helium and argon gas mixtures used to determine nonseeding operation of MHD generator in nonequilibrium ionization mode 16 p2711 A67-30542

Experiments and design of low temperature seeded inert gas MHD power generator operating in nonthermal ionization mode 16 p2601 A67-30548

Existence in alkali-metal-seeded rare gases of mode of nonequilibrium electric discharge with constricted positive column 17 p2910 A67-33385

Experiments on equilibrium and nonequilibrium electrical conductivity of seeded combustion products and theory of nonequilibrium ionization and recombination 18 p3085 A67-33706

Physical chemistry of potassium sulphate at high temperatures and use for MHD

- seeding 18 p3086 A67-33710
Current-voltage characteristics for double probe measured in seeded combustion products by low temperature surface emission 19 p3345 A67-35079
Temperature effect on seeding atom emission in argon plasma laminar jet 20 p3497 A67-36397
Electrical conductivity of nitrogen plasma seeded with potassium, noting nonuniform temperature profile in flow [AIAA PAPER 67-716] 21 p3673 A67-38742
Neutral carrier gas and slightly ionized plasma binary mixture model for nonhomogeneous seeding effects on rotating arc performance 21 p3674 A67-38885
- SEEKER**
S HOMING DEVICE
SEISMIC ENERGY
Mechanism for connection between seismic earth and solar activity on atmosphere and lithosphere of earth 13 p2111 A67-26556
Short period seismic radiation patterns from underground nuclear explosions and small magnitude earthquakes, noting propagation characteristics [SR-1] 20 p3434 A67-37430
- SEISMIC WAVE**
Seismic refraction measurements, computing statistics for depth to Moho, crustal thickness and upper mantle velocity for geographical and geological provinces 05 p0796 A67-16152
Seismic experimentation methods to be performed on moon, giving P and S wave travel time curves for models of lunar interior 08 p1387 A67-20963
Steady state wave propagation in homogeneous anisotropic media studied from near field behavior of Green matrix 13 p2158 A67-27179
Rapidly varying high pressure measurement requirements, treating pressure transducer as seismic system and analyzing feed channel distortion 16 p2671 A67-31004
Laboratory equipment protection from vibration environment, noting instrumentation and results 17 p2833 A67-32066
Conceptual design of active seismic experiment for lunar surface missions, analyzing communication approaches 19 p3323 A67-35328
Solar gravitational effect on earth seismic activity, showing relation between annual variations and earth-sun radius 19 p3221 A67-35430
- SEISMOGRAPH**
SA LUNAR SEISMOGRAPH
Vertical component seismograph for use in Surveyor lunar landing missions 08 p1411 A67-20947
- SEISMOLOGY**
Wave propagation in continents and adjacent shelf areas used for study of seismic crustal refraction and reflection measurements 01 p0060 A67-10502
Internal structure models for earth, Venus and Mars, discussing earth density distribution and seismic results 02 p0329 A67-12497
Internal structure models for earth, Venus and Mars, discussing earth density distribution and seismic results 10 p1709 A67-23365
Conceptual design of active seismic experiment for lunar surface missions, analyzing communication approaches 19 p3323 A67-35328
Green function for SH-line source in wedge-shaped medium with apex removed by circular cylinder, determining reflected and refracted fields 21 p3579 A67-37925
- SEISMOMETER**
Seismological equipment for space research applied to earthquake-resistant structural design 13 p2120 A67-27217
- SELECTION**
S PERSONNEL SELECTION
SELECTIVE FADING
Antenna height protection against microwave diffraction fading determined, using digital computer to evaluate residue series for grazing conditions 09 p1464 A67-22444
- SELENIDE**
SA CADMIUM SELENIDE
SA GALLIUM SELENIDE
SA LEAD SELENIDE
SA ZINC SELENIDE
- Electron diffraction structural studies of lead bismuth selenide 01 p0136 A67-11009
Crystal structure of alpha-and beta-indium selenide semiconductor 03 p0493 A67-13361
Temperature dependence of electrical properties of alpha-indium selenide n-type semiconductor single crystals 03 p0493 A67-13362
Electric conductivity of AsSeGe-AsSGe glasses 06 p1052 A67-18611
Impurity effects on electroconductivity of vitreous AsSe 06 p1053 A67-18612
- SELENIUM**
Pure selenium conductivity, thermal emf and Hall effect 01 p0138 A67-11297
Q-switched laser operation observed using liquid selenium mirror as reflector in ruby laser measuring reflectivity changes 05 p0822 A67-16679
Ionization coefficient in selenium p-n step junction of rectifier cell 09 p1551 A67-21656
Band-to-band radiative recombination in semiconductor groups IV, VI and III-V, presenting data on diamond, Si, Ge, Se and Te 09 p1558 A67-22601
Fast neutron activation cross sections of Se and Fe measured, noting subshell closure effect and isomer ratio 11 p1822 A67-23979
Gamma decay of Se 73 and Se 81 isomeric pairs with half-lives, energies and decay schemes 11 p1822 A67-23980
Theory of small signal current transients applied to study of electron trapping in amorphous selenium 20 p3509 A67-36507
Second harmonic generation in Se and Te-Se using carbon dioxide laser, measuring nonlinear coefficients and synchronism direction 23 p4016 A67-41192
- SELENIUM COMPOUND**
Impurity effects on nucleation of Se vapor onto Pyrex glass noting degree of critical supersaturation, production of phase with nonequilibrium structure, etc 11 p1821 A67-24992
Thermal capacity of gallium and thallium selenides 13 p2174 A67-26367
Liquid lasers use of rare earth ions, chelate structures, selenium oxochloride, etc 15 p2501 A67-30086
Thermal capacity of gallium and thallium selenides 21 p3680 A67-38323
- SELENOGRAPHY**
SA LUNAR GEOLOGY
SA LUNAR MAP
SA LUNAR SURFACE
SA LUNAR TOPOGRAPHY
Lunar photography application to creation of selenographic coordinates enveloping near and far sides of moon 08 p1388 A67-21000
Book on moon in space age covering lunar motion around gravity center, nature of lunar soil, lunar satellite perturbations, etc 08 p1395 A67-21156
Observation methods for determination of moon shape including libration effect, local topography and determination of apparent contour 08 p1395 A67-21159
Selenographic measurement including stereoscopic photography, crater wall heights and slopes, peak illumination limit methods, etc 08 p1396 A67-21166
Composition and internal structure of moon and related research tasks of first lunar laboratory 09 p1568 A67-22409
Catalog for interpretation of objects in eastern sector of far side of moon 11 p1867 A67-24844
Error analysis shows laser-radar method improves accuracy of astronomical parameters of earth-moon system, taking into account physical libration 13 p2200 A67-27327
Soviet book on moon figure and motion covering coordinate systems, surface features positions, rotational parameters, etc 17 p2948 A67-33118
Catalog of selenocentric rectangular coordinates, selenographic longitudes and latitudes and absolute altitudes of lunar surface features 17 p2949 A67-33119
Moon rotational parameters determined by refractometric observations of craters position angles, tabulating selenographic and topocentric coordinates, reference system conversion corrections, etc 17 p2949 A67-33121
Earth to lunar ground points measurement by lasers, describing experimental set-up, transmitting and receiving apparatus, etc 18 p3130 A67-34316
- Lunar Planetary Laboratory selenodetic measurement precision and comparison with contemporary selenodetic triangulations 18 p3131 A67-34323
Lunar data covering mass, shape, dimensions, earth-moon relations, orbits, selenography, etc 20 p3530 A67-37549
Seleno-geological evidence for lunar surface properties from Surveyor I, discussing weathering products and volcanic genesis 23 p4064 A67-40952
Absolute coordinates of 910 lunar features determined by stereoscopic method 23 p4065 A67-41005
Lunar Orbiter II lunar surface photographs noting Copernicus H and Copernicus crater interior peak cluster 23 p4066 A67-41012
Cauchy domes in Mare Tranquillitatis, deriving relief pictures with photometry 23 p4066 A67-41013
- SELENOLOGY**
Geocentric initial conditions for motion of bodies leaving moon surface after initial instantaneous thrust 01 p0148 A67-10387
Lunar International Laboratory /LIL/ exploration and lunar physics program 04 p0597 A67-15065
Book on moon covering motion of moon and dynamics of earth-moon system, internal constitution, topography, radiation and surface structure 06 p1087 A67-18428
Lunar observation in wavelength range one to three mm, noting brightness temperature drop during total eclipse, obtaining dielectric constant 08 p1390 A67-21022
Photometric, polarimetric and IR study of lunar surface including polarization of moonlight, thermal measurements, lunar radar echo signals, etc 08 p1395 A67-21160
Selenological analysis of Ranger IX photographs, examining origin and age of craters and mountain chains 10 p1705 A67-22898
Astronomical determination of position on moon 18 p3120 A67-33864
Measure of moon - Conference, Manchester University, England, May-June 1966 18 p3127 A67-34301
Selenodetic measurement methods, considering point coordinates determination on lunar surface near limb or center, including moon profile studies during solar eclipse 18 p3129 A67-34309
Selenodetic evaluation of 11 selected original photographic plates from 1894-1909 Paris Observatory collection of lunar photographs 18 p3129 A67-34311
Selenodesy, determining gravitational constant-lunar mass product, lunar gravitational field variation, physical librations, inertial moments, lunar tides, lunar radius, etc 20 p3525 A67-36893
- SELF-ADAPTIVE SYSTEM**
SA ADAPTIVE CONTROL
Channel noise forces adaptive sampling system to operate at lower bit error probability than equivalent PCM system 02 p0197 A67-12016
Linearized motion equation of self-adaptive systems with stabilized frequency characteristics, considering effect of control and noise signals in basic control loop 03 p0390 A67-13101
Coordination of integral and relay components in algorithms for adjusting control coefficients in model-reference self-adaptive control systems described by differential equations 03 p0390 A67-13102
Monograph on self-adaptive servocontrol systems, discussing transfer function optimization, frequency filter structure, noise problems, etc 03 p0393 A67-13715
Self-organizing approach to structure adaptation in pattern recognition applied to handwritten numerals, spoken vowels and EEGs 04 p0578 A67-14797
Stability region of complex linear self-conjugate systems of differential equations containing skew-Hermitian matrix 04 p0647 A67-15980
Multiparameter self-adaptive control by pole-zero cancellation with simple structure and fast response 05 p0783 A67-16523
Amplitude effect reduced on performance of nonlinear circuits by using shunt circuit, pseudolinear laws, and negative resistances, reviewing self-adaptive systems 05 p0785 A67-17271
Dynamics of self-adaptive systems with

stabilized frequency characteristics 06 p0976 A67-18405

Self-adaptive control systems theory - IFAC Symposium, Teddington, Middx., England, September 1965 07 p1159 A67-19192

Adaptive functions of man in vehicle control systems 07 p1221 A67-19194

Process parameter estimation and self-adaptive control, noting performance and spurious noise 07 p1159 A67-19195

contamination 07 p1159 A67-19195

Self-adaptive system employing quick identification of parameters of aircraft short period pitch transfer function 07 p1128 A67-19199

Nonlinear self-adjusting system with linear prediction analyzed by digital computer 07 p1160 A67-19200

Synthesis methods for structures equivalent to self-adjusting systems for plants with variable parameters 07 p1160 A67-19201

Adaptive lagging system with output following randomly varying signal with minimum mean square error 07 p1160 A67-19202

Multidimensional self-adaptive control system involving dynamics and disturbance, employing relay extremum control 07 p1161 A67-19204

Pseudo-random binary signals as perturbation waveform in adaptive control 07 p1161 A67-19205

Self-adjusting control systems with models, reviewing basic theoretical problems of analysis and synthesis 08 p1313 A67-21328

Optimum control and prediction in designing self-adjusting controllers for linear systems with correlated disturbances 10 p1618 A67-22732

PCM frame synchronization with self-varying threshold detector 11 p1764 A67-24434

Approximate similarity criterion for arc with self-adjusting length, burning in plasmatron with gas vortex stabilization, determined by shunting 11 p1843 A67-24969

Automatic control systems classification for ordinary systems in relation to self-adaptive systems 13 p2088 A67-26800

Self-adjustable orthogonal digital filters for system identification and optimization 13 p2088 A67-27409

Influence of different stresses on sugar content changes of blood and stabilization at another level as adaptation result of organism 14 p2255 A67-28221

Step-by-step self-adaptive algorithm for selective systems with automatic control 15 p2455 A67-29123

Discrete interval binary-noise perturbation signal application for identification and compensation of three-variable self-adaptive flight control system 15 p2572 A67-30319

Adjustment uniqueness in defining dynamic characteristics with help of self-adjusting model 15 p2464 A67-30339

Effectiveness for automatic control systems estimated by comparing performance with ideally functioning systems 16 p2643 A67-30919

Efficiency of using self-adjustment with respect to input signal in automatic control systems, estimating gain and stability 20 p3409 A67-37198

Discrete self-adaptive servosystem with nonstationary random useful and noise signals applied to input 20 p3409 A67-37199

Self-adaptive multidimensional continuous servosystem 20 p3412 A67-37379

Essential additional operator, essential transformed system and cross correlation function methods for self-adjusting circuit design, considering sign of gradient component 21 p3604 A67-39110

Single channel self-adaptive servosystem synthesized for optimal tracking of diffusion type signal with drift 23 p3983 A67-40598

SELF-CONSISTENT FIELD /SCF/

Boundary layer structure between rarefied plasma and magnetic field, detailing mathematical formulation in relativistic invariant form 04 p0665 A67-15179

Lamb self-consistent theory and rate equation approximation study of magnetic depolarization of vapor and polarization of monomode gas laser in magnetic field 05 p0818 A67-16644

Two-flow equations for stationary relativistic electron cloud in self-consistent crossed fields 05 p0774 A67-16907

Self-consistent field approach to nonstationary time dependent turbulence 05 p0794 A67-17417

Free energy of spatially homogeneous phase in approximation of self-consistent field for application to fluids and gases 07 p1168 A67-19186

Self-consistent field approximation to ion-beam-plasma boundary interaction noting effect on ion beam structure, boundary conditions and resulting current density 08 p1363 A67-21307

Book on superconductivity of metals and alloys including fundamental properties, condensed state, analysis of Landau-Ginsburg equations, magnetic field effects, etc 10 p1690 A67-23160

Vlasov equation for stationary distribution function of charged particles in plasma and self-consistent solution of Maxwell equations 10 p1685 A67-23463

Spin-projected unrestricted self-consistent field /SCF/ methods for spin density calculations used to determine hyperfine coupling constants 13 p2160 A67-26540

Two-flow equations for stationary relativistic electron cloud in self-consistent crossed fields 16 p2636 A67-30884

Self-consistent model for cathode region of high pressure arc, considering free fall sheath connection, electron and ionization region and flaring contraction 19 p3278 A67-35137

Self-consistent model for cathode region of high pressure arc, showing application to 200 amp arc in argon and boundary condition matching 19 p3279 A67-35138

Spin restricted, unrestricted, projected unrestricted and extended SCF wave functions energies compared, discussing calculation method for spin extended SCF functions 20 p3483 A67-36230

Dynamic response of nondegenerate electron hole plasma in semiconductor, obtaining frequency spectrum and Landau damping rate of plasma oscillation 20 p3499 A67-36945

Total energy of beryllium hydride molecule analyzed, using difference between SCF energies and single determinant wave function 20 p3377 A67-37139

Total energy of beryllium hydride molecule as sum of SCF, correlation and relativistic energy and SCF error by LCAO-MO method 24 p4118 A67-41926

SELF-DIFFUSION

Interdiffusion of niobium and molybdenum over 1400-2300 degrees C range using diffusion couples, determining activation energy values 01 p0100 A67-10767

Self-diffusion coefficients of simple liquids as predicted by Rice-Allnatt theory, noting friction coefficient and correlation function 06 p1035 A67-17989

Niobium self-diffusion in alloys with tungsten, showing dependence on specimen composition 13 p2141 A67-27283

SELF-ERECTING ANTENNA

Variation of radiation pattern of array of two travelling-wave V-antennas and use as spacecraft antenna 16 p2639 A67-31360

SELF-EXCITATION

Single mode approximation of parametric excitation and self-excitation of oscillations in Fabry-Perot resonator filled with nonlinear dispersive medium 02 p0251 A67-11575

Linear theory of self-excitation of oscillations in semiconductors in presence of large current density inhomogeneity 03 p0489 A67-13147

AC MHD generator with liquid metal working fluid operating under self-excitation conditions 06 p0951 A67-18683

Transient self-excitation in autonomous electromechanical system consisting of pump and MHD generator 06 p0952 A67-18686

Analysis of uncontrolled synchronized self-excited oscillator 08 p1302 A67-20829

Self-excited oscillations of nonlinear servosystems examined, applying expression for generalized transmittance of nth order system 10 p1818 A67-22851

Linear theory of self-excitation of oscillations in semiconductors in presence of large current density inhomogeneity 10 p1689 A67-23096

Self-excited liquid metal MHD induction generator 12 p1897 A67-25378

Self-excitation regime associated with travelling magnetic field interaction with

ionized gas flow 12 p1977 A67-26077

Self-excited systems sensitivity function maximum value attained via time dependency on natural frequency and damping factor only 13 p2216 A67-26627

Large combustion-driven, self-excited Faraday-type MHD generator having multi-or single-circuit net power output, discussing design 16 p2608 A67-30596

One-component nonviscous nonheatconducting perfect gas in container with gaseous adsorption at boundary, noting acoustic oscillation instability for certain frequency disturbances 22 p3836 A67-39719

Analysis of laser with selective resonator indicating stimulated emission basic characteristics determined by active medium band shape and Q-factor curve 23 p4013 A67-40907

Geomagnetic dynamo laboratory model self-excitation conditions determined from solutions of electrodynamic equations, diagramming magnetic field and current distribution 24 p4231 A67-42353

SELF-INDUCED VIBRATION

Parametric self-excited vibrations of plates of finite length in plane supersonic flow, applying linearized potential flow theory, deriving frequency equations 13 p2218 A67-26804

Self-excited vibration of cylindrical shell in coaxial rigid cylindrical duct with gas flowing past 13 p2218 A67-26806

SELF-IONIZATION

Autolionization mechanism role in formation of astrophysical spectra 03 p0509 A67-13217

Autolionization calculation describing scattering aspect of phenomenon 03 p0471 A67-13220

Autolionization effects in UV absorption spectra of hot atomic gases 03 p0471 A67-13222

Autolionization states and resonances in absorption spectra of rare gases 03 p0471 A67-13223

Collisional excitation of Si ion from ground state to autolionization levels at coronal temperatures 07 p1256 A67-20168

Dielectronic recombination effect in hot dilute plasmas extended to energetically overlapping metastable levels involving matrix inversion in formal description 10 p1681 A67-22722

Spectroscopic measurements of cold plasma charged particle concentrations, specifically spectral broadening due to Stark effect, forbidden-line intensities affected by internal electric fields and autolionization line intensities 17 p2896 A67-32161

Rydberg series in extreme UV observed in absorption spectrum of helium-nitrogen discharges and active nitrogen [AFRCL-66-835] 17 p2888 A67-32629

Dielectronic recombination and autolionization included in ionization formula for solar corona 17 p2952 A67-33392

SELF-LUBRICATING MATERIAL

Pressure distribution of porous self-lubricating bearing noting geometrical factors, dimensions, running speed, load, etc 01 p0079 A67-10708

Self-lubricating properties of composites of porous nickel and nickel-chromium alloy impregnated with barium fluoride-calcium fluoride eutectic [ASLE PAPER 66AM 1C2] 08 p1335 A67-21035

Filament wound sleeve seal impregnated with solid lubricants dissipates heat in rubbing contact zone and provides wear characteristics for use in air compressor [ASLE PREPRINT 67AM 7A-3] 14 p2326 A67-28791

Solid self-lubricating materials mechanically strong and resisting oxidation for high temperature air applications, examining friction-wear characteristics 16 p2683 A67-31752

SELF-LUMINOUS BODY

SA ELECTROLUMINESCENCE

Radioisotope and phosphor research and increased brightness of self-luminous devices 05 p0842 A67-16543

Position determination for mobile luminous objects in sky by triangulation, using ballistic photographic chambers in positions pinpointed by star sightings 07 p1188 A67-19770

SELF-MANEUVERING UNIT

SA SPACE SELF-MANEUVERING UNIT /SMU/

Extravehicular space maneuvering units, manned and unmanned, in satellite laboratory systems, describing space flight requirements and systems 16 p2615 A67-30631

SELF-OSCILLATION

Periodic regimes in two-channel automatic systems with nonlinear element in single channel part of loop, showing cross connections effect on auto-oscillations 01 p0023 A67-10494

Analog computer solution to autonomous systems with one degree of freedom capable of self-excited oscillation or excited by external periodic force 02 p0209 A67-12712

Automatic system auto-oscillations when transmission coefficient of nonlinear part of system depends on amplitude and frequency of input signal 05 p0782 A67-16323

Radiophysical measurement of small amplitude mechanical oscillations of self-oscillator by means of mechanical-electric converters and effects of natural line width on minimum amplitudes 05 p0805 A67-16357

Time structure and amplitude self-modulation of emission from GaAs injection laser observed, using electron-optical converter 06 p1009 A67-17756

Periodic regimes in two-channel automatic systems with nonlinear element in single channel part of loop, showing cross connections effect on auto-oscillations 10 p1608 A67-23616

Combustion chamber model for self-oscillating thermoacoustic system initiated by stimulation effect of acoustic shock 11 p1884 A67-24958

Electromagnetic sensing of absolute rotation with self-oscillating laser version of Sagnac interferometer 14 p2349 A67-28812

Automatic system auto-oscillations when transmission coefficient of nonlinear part of system depends on amplitude and frequency of input signal 18 p3017 A67-33875

Input signal level for stability loss or self-oscillations automatic control in system, using analysis for nonlinear systems with forced vibrations 20 p3408 A67-37041

Extremal systems having auto-oscillating optimizers and controlled plants, investigating performance improvement by complex modification of input signal 20 p3409 A67-37110

CR self-oscillation circuits, discriminating CR oscillators from astable, monostable and bistable multivibrators 21 p3604 A67-38601

Self-oscillations of axial compressor blades, taking into account variation in natural frequency of flexural vibrations between blades 21 p3727 A67-38835

Dynamics of single channel extremal systems having plants in linear and nonlinear elements and control units in form of self-oscillating type optimizer 22 p3777 A67-39777

SELF-PROPELLED VEHICLE

Sailplanes with self-contained launching apparatus noting minimum performance, motor propulsion and auxiliary equipment 22 p3744 A67-39303

SELF-REPAIRING SYSTEM

Adaptable large scale integrated military and space systems, discussing microelectronic circuit, logistics and dynamic redundancy 08 p1311 A67-20665

Integral fuel tank maintenance, summarizing tank-sealant repair data 09 p1442 A67-22678

Transfluxor as self-repair unit of redundant automata 20 p3454 A67-37038

SELF-SEALING

Dynamic-seal technology in applications employing liquid metals, gas and standard organic fluids for ground, aerospace and space turbomachinery [ASME PAPER 87-DE-50] 14 p2328 A67-28881

Puncture sealing of meteoroid penetration in spacecraft, giving mechanical and chemical methods and self-sealing tile inner shell process 22 p3913 A67-39885

SELF-SUSTAINED EMISSION

Noise theory for self-sustaining discharge verified for low frequencies, noting temperature dependence, silicon, etc 18 p3106 A67-34638

SEMICIRCULAR CANAL

Vestibular tests of caloric irrigations and mild angular accelerations of semicircular

canals of professional figure

skaters 03 p0364 A67-14288

Caloric nystagmus in man clarified by test in weightless phase of parabolic flight 15 p2428 A67-29277

Semicircular canal physiological response in cats recorded for case of parallel swing rotation, noting mechanical excitation mode of canal 23 p3952 A67-41576

Decerebrate cat experiments for semicircular canal response to rotational stimulation 23 p3956 A67-41633

SEMICONDUCTOR

SA EXCITON

SA INTERMETALLICS

SA JUNCTION TRANSISTOR

SA METAL OXIDE SEMICONDUCTOR

/MOS/

SA N-TYPE SEMICONDUCTOR

SA ORGANIC SEMICONDUCTOR

SA P-I-N DIODE

SA P-TYPE SEMICONDUCTOR

Zone melting peculiarities for two-component system where semiconductor is ring-shaped or straight 01 p0127 A67-10074

Localized electron states of semiconductor surface due to lattice defects, determining excited state, ground state and bonding energies 01 p0128 A67-10078

Resonance amplification of associated slightly attenuating electromagnetic and acoustic helicon waves by electron drift in semiconductors and semimetals 01 p0128 A67-10081

Superconductivity of nondegenerate semiconductor thin films, dependence on current carrier concentration, impurity level positions and film thickness 01 p0128 A67-10084

State density for highly doped semiconductor in magnetic field, obtaining results at near Fermi level energies and at bottom of conduction band 01 p0128 A67-10096

Efficiency criterion for semiconductors, using equations for flux density of electric current and energy for isotropic semiconductor in absence of magnetic field 01 p0129 A67-10103

Relation between acid-basic state and conductivity for polyaniline macromolecular semiconductors such as emeraldines 01 p0130 A67-10196

Water and internal acidity effect upon oligomeric polyanilines semiconductivity 01 p0130 A67-10197

Thermodynamics of electronic carrier populations in pure or doped dissociable binary semiconductor 01 p0130 A67-10198

Generation of current oscillations by electroacoustic effects in semiconducting cadmium sulfide 01 p0130 A67-10199

Gunn effect noting negative bulk conductivity, creation of external negative conductance and zones with different field intensities in semiconductor crystals 01 p0130 A67-10253

Photon modulation of tunnel emission produced by IR irradiation of thin film semiconductor sandwich of aluminum-aluminum trioxide-tellurium-gold 01 p0131 A67-10369

Temperature dependence of optical phonon mean free paths and mean energy loss per collision predict avalanche multiplication and voltage breakdown of Si and Ge p-n junctions 01 p0132 A67-10374

Magnetic susceptibility studies show semiconductor to metal transition in titanium pentoxide and titanium trioxide, clarifying electronic nature of phase transition 01 p0132 A67-10376

Traveling wave amplification by interaction of drifting carriers in semiconductors with external slow wave circuit 01 p0132 A67-10377

Oscillations associated with S type current controlled negative resistance in seminsulator gallium arsenide samples, examining LF instability 01 p0133 A67-10473

Electrical and optical properties of solid solutions formed by beta manganese and chromium dioxide within wide composition range, showing magnetic semiconductor behavior 01 p0134 A67-10755

Complex band structure properties in diamond type crystals, discussing symmetry of various surface states with and without spin-orbit coupling 01 p0134 A67-10786

Equivalent series resistance of semiconductor region of varactor diodes at

UHF determined, using series resonance method 01 p0038 A67-10815

Current transmission through semiconductors with impurities, calculating V-I characteristics at high temperatures during acceptor level creation 01 p0135 A67-10925

Neumann problems of Laplace equation with nonhomogeneous boundary conditions in theory of probe measurements of parameters of semiconductor films 01 p0136 A67-10997

Unified treatment of costs yields and reliability in semiconductor manufacture 01 p0171 A67-11380

Relaxation effect in electrical conductivity of semiconductors and metals, taking into account scattering by ionized impurities and Debye cloud polarization 02 p0280 A67-11480

Momentum loss rate by conduction electrons of polar semiconductors for known energy and momentum distribution 02 p0280 A67-11486

Oscillatory semiconductor photoconductivity dependence on photon energy periodic in longitudinal-optical phonon energy treated by Boltzmann equation, noting elastic scattering 02 p0280 A67-11488

Shallow impurity states in semiconductor described by Green function method, considering effective-mass equation corrections 02 p0281 A67-11491

Epitaxy of semiconductor on insulating monocrystalline base of corundum, noting electronic characteristics of silicon layers 02 p0294 A67-11755

Semiconducting properties of lead telluride thin films, analyzing electron transport phenomena 02 p0294 A67-11756

Thermodynamics of epitaxial growth of GaAs-Ge heterojunctions in closed tube process 02 p0296 A67-11767

Distribution function and electron mobility in polar semiconductors for nonparabolic dispersion law 02 p0296 A67-11825

Ferromagnetic semiconductors with exchange interaction due to conduction electrons 02 p0296 A67-11826

Electron-hole conductivity effect on temperature variations of Hall coefficient and Nernst-Ettingshausen effect in semiconductor 02 p0296 A67-11829

Thermal emf and electric conductivity in solid and liquid semiconducting copper-antimony-ditelluride 02 p0297 A67-11846

Negative resistance and current density in double-injection filaments in seminsulating Si 02 p0298 A67-11886

Gunn effect semiconductors and contact preparation techniques, noting excitation of oscillations and amplification characteristics in GHz range 02 p0220 A67-12198

Current carrier concentration and dynamic coefficients for nondegenerated and highly degenerated Fermi gases subject to nonparabolic isotropic laws of dispersion 02 p0300 A67-12475

Resistivity, temperature coefficient of resistivity and Hall coefficient as function of bismuth film thickness, showing that size quantization of films leads to semiconductor metals 02 p0300 A67-12509

Optical nonlinearities due to conduction band electrons in InAs, InSb, GaAs and PbTe studied, using Q-switched carbon dioxide laser radiation 02 p0254 A67-12524

Optical mixing due to conduction band electrons in semiconductor 02 p0254 A67-12525

Transition time dependence between avalanche and second breakdown on input power to p-n silicon junction, noting thermal effects in semiconductors 02 p0222 A67-12650

Theory of influence of surface states on impedance of semiconductor-insulator interface, determining relaxation times which directly affect cut-off frequency of device 03 p0487 A67-12810

Electrical properties of GaSe-layer-semiconductor single crystals used to determine scattering mechanisms of charge carriers, depth of impurity centers, effective mass and forbidden gap 03 p0488 A67-12816

Semiconducting properties of platinum arsenide with pyrite-type crystal structure 03 p0488 A67-12926

Optical properties of semiconductors by measuring spectral emittance of transparent and opaque solids and measurements on materials used in IR optics

[AIAA PAPER 65-654] 03 p0418 A67-13034
Frequency dependent two-photon
absorption radiation-matter interaction and
secondary harmonic generation in n-and p-
type impurity 03 p0435 A67-13126
semiconductors
Thermoelectric current effect on stability
of electric current and charge distribution
in semiconductors 03 p0489 A67-13144
Linear theory of self-excitation of
oscillations in semiconductors in presence of
large current density
inhomogeneity 03 p0489 A67-13147
Theory of second sound in semiconductors
caused by long wave phonons interacting
with current carriers in absence of external
field 03 p0490 A67-13152
Theoretical semiconductor
electroconductivity dependence on
intensities of strong electric and magnetic
fields 03 p0490 A67-13158
Electron processes at semiconductor
surface in presence of chemisorption, noting
conductivity and impurity 03 p0492 A67-13315
Metal-semiconductor surface barrier and
prediction using concepts of covalent and
ionic crystals 03 p0494 A67-13475
Majority carrier current flow in metal-
semiconductor barriers according to theory
incorporating Schottky diffusion theory and
Bethe thermionic emission 03 p0494 A67-13476
theory
Lattice vibration spectra and energies of
two-phonon summation bands and
reststrahlen bands in gallium arsenide
phosphide single crystals 03 p0495 A67-13514
HF conductivity, dispersion and
temperature modulation of carrier waves
and acoustic amplification in drifted
semiconductor plasmas 03 p0496 A67-13558
Heats of adsorption of hydrogen and
oxygen on semiconductors of zinc blende
type calculated, using Clausius-Clapeyron
and Bering-Serpinski equations 03 p0496 A67-13646
Visible and X-ray photoelectric emissions
in layers of Se-As-Tl intrinsic semiconductor
films in vacuum 03 p0498 A67-13838
Laser beam-induced recrystallization of
amorphous Ge semiconductor thin films
prepared by thermal deposition on
glass 03 p0498 A67-13839
Diffusion coefficient for electroactive
impurity in semiconductor based on current
carrier concentration variations during
successive removal of surface
layers 03 p0498 A67-13841
Semiconductor character of mercury
selenide determined by analyzing variation
of band-edge effective mass as function of
composition of HgSe-CdTe alloys 03 p0499 A67-13886
GaAs epitaxial layer ultrasonic wave
transducers fabricated from seminsulator
material, for generation of longitudinal
waves 03 p0426 A67-14302
Free current carrier formation in
molecular crystal, examining dependence of
photoconductivity on magnetic field
intensity 03 p0501 A67-14369
Damped oscillations and velocity of sound
waves in semiconductors and metals in
presence of strong magnetic
field 03 p0501 A67-14370
Semiconductor photoconductivity
dependence on external radiation frequency,
examining electron-phonon
interaction 03 p0502 A67-14374
Donor electron IR absorption coefficients
in semiconductors in 3-10 micron range used
to study wavelength
dependence 04 p0674 A67-14608
Allowed and forbidden direct interband
optical transitions in anisotropic
semiconductors, using effective mass theory
for exciton, solving Schrodinger
equation 04 p0674 A67-14610
Semiconductor plasma slab subject to
crossed electric and magnetic fields,
examining plasma density wave instability
caused by gradient in carrier density
perpendicular to magnetic
field 04 p0674 A67-14612
Lattice thermal conductivity of disordered
alloys of ternary compound semiconductors
Cu₂/Sn, Ge/Se/S₃, /Ag, Pb, Sb/Te₂ and
/Ag, Sn, Sb/Te₂ 04 p0675 A67-14760
Simple asymptotic formula for motion of
simultaneous electric field and conductivity
domains in semiconductors in terms of

electrodynamics on basis of Poisson and
continuity equations 04 p0677 A67-14936
Entanglement effect of plasma and
magnetic branches of oscillations in
antiferromagnetic semiconductors on LF
expanding plasma waves in strong electric
fields 04 p0678 A67-15133
Vannier-Mott excitons effect on ultrasound
absorption in piezoelectric
semiconductors 04 p0678 A67-15134
Light absorption and photolionization of
shallow impurity levels in semiconductors
during acoustic phonon
scattering 04 p0678 A67-15135
Dimensional effect in electric conductivity
of semiconductors during heating of electric
field when electron energy relaxation length
exceeds mean free path 04 p0679 A67-15137
Gamma irradiation from Co 60 effect on
indium antimonide, determining defect
formation on dose and limiting position of
Fermi level for n-and p-type
material 04 p0680 A67-15283
Photomechanical effect in germanium,
noting dependence of mechanical properties
on quantity of impurity
concentration 04 p0680 A67-15285
Field and charge density distributions in
semiconductor with hot electrons, showing
domain movement type oscillations due to
stationary wave
propagation 04 p0680 A67-15286
Electron energy spectrum for alloyed
semiconductors, determining state densities
via Thomas-Fermi statistical
method 04 p0681 A67-15296
Resistivity, dielectric constant and
junction depth changes in semiconductor
materials by exposure to electron
beam 04 p0681 A67-15314
Brittle fracture threshold of silicon,
germanium and indium antimonide under
pulsed electron
irradiation 04 p0685 A67-15694
Damage mechanism in semiconductors
from space radiation and effects on various
microcircuits 04 p0588 A67-15702
Anomalous photovoltaic effect in
semiconductor Ge, Si, CdTe and GaAs thin
films due to photodiffusion and
microtransitions 04 p0685 A67-15758
Surface photoelectromotive force in GaAs
type semiconductors with short duration
minority carriers 04 p0686 A67-15969
Electron diffraction patterns for GaP
semiconducting thin films deposited on
indium oxide substrates, determining
structure as function of film
thickness 04 p0686 A67-15970
Energy spectrum of semiconductor
compounds with chalcopyrite structure
analyzed, using perturbation theory, noting
changes resulting from crystalline and spin-
orbital interactions 05 p0861 A67-16393
Electric field effect on donors diffusion
into intrinsic
semiconductor 05 p0861 A67-16397
Excess carrier lifetime in semiconductors
by measuring photoconductive phase shift of
spreading resistance under point
contact 05 p0861 A67-16501
Dember effect, bulk photovoltaic effect
and current density in illuminated
inhomogeneous
semiconductor 05 p0863 A67-16702
Internal electric field effect on
simultaneous diffusion of donors and
acceptors in semiconductors, considering
case of indium and antimony diffusing into
germanium 05 p0867 A67-17051
Anisotropic semiconductor in hot electron
theory, deriving volt-ampere
characteristics 05 p0867 A67-17053
Instability of electron hole plasma of
semiconductor caused by nonlinear current-
voltage characteristic 05 p0867 A67-17058
Stability of state of semiconductors with
absolute negative
conductivity 05 p0868 A67-17059
Unfamiliar metals properties and
potentialities from viewpoint of
metallurgist 05 p0830 A67-17088
Band structure and conduction phenomena
in semiconductors of groups III-V,
particularly in GaAs, noting signal
instabilities and Gunn
effect 05 p0871 A67-17325
Component, due to recombination-
generation process, of overall noise from
semiconductors under electric current,
measuring probability densities by

statistics 06 p0966 A67-17588
Semiconductor surface photovoltage under
small signal conditions, when quasi-
equilibrium approximation will be valid in
space charge layer 06 p1047 A67-17600
Electron cooling in polar semiconductor by
application of electric
field 06 p1048 A67-17816
Cadmium selenide arsenide single crystals
obtained free of cracks, using synthesis
method 06 p1048 A67-17840
Small signal MIS capacitance vs bias
characteristics measured over wide range of
biases and sweep speeds 06 p1002 A67-17979
Device for measurement of photocurrent
noise spectra in semiconductors at 1 cps to
5 kc 06 p0970 A67-18194
Injected carrier flow in seminsulator
containing deep impurity
gradient 06 p1051 A67-18221
Auger mechanism of recombination of
electron emission from semiconductors and
dielectrics 06 p1051 A67-18222
Hot electron emission from polar
semiconductors with nonparabolic dispersion
law, specifically qualitative effect of
nonparabolicity and field on electron
emission 06 p1052 A67-18423
Electric conductivity of vitreous As-Se
semiconductor 06 p1053 A67-18614
Cooling requirements for intrinsic
photoconductive IR detector, comparing
theory and experiment 06 p1005 A67-18713
Vibrating capacitor type device for
measuring semiconductor contact potential
and changes due to illumination or ambient
atmosphere 06 p1005 A67-18728
Semiconductor physics - Conference,
Kyoto, September 1966 06 p1054 A67-18901
Experimental evidence of conduction band
of semiconducting strontium
titanate 06 p1059 A67-18906
Lattice IR reflection and transmission
spectra and Raman spectrum of
monocrystalline and hot pressed pellets of
ZnSe 06 p1059 A67-18909
Local mode absorption bands for Al
impurities in InSb and for P impurities in
GaAs at various temperatures, using grating
spectroscopy 06 p1059 A67-18910
Linear and nonlinear magneto-optical
phenomena in semiconductors, examining
line and level broadening, cyclotron
resonance with lasers, etc 06 p1060 A67-18916
Exciton and oscillatory magnetoabsorption
spectra in layer type semiconductors in high
magnetic fields 06 p1060 A67-18917
Electron spin resonance of impurities in
semiconductors, with attention to shallow
centers 06 p1061 A67-18922
Impurity band tails in degenerate
semiconductors, showing relation between
decay in density of states and screening
density 06 p1061 A67-18923
Magnetic field strength effects on excited
acceptor states of semiconducting diamond
determined, using Zeeman splittings of main
excited lines 06 p1062 A67-18927
Pair production in irradiated
semiconductors within framework of
plasmon decay, considering variation of
radiation ionization energies with band gap
energy 06 p1063 A67-18935
Size effects in electroconductivity of
semiconductors with several groups of
carriers with large intergroup relaxation
time 06 p1064 A67-18944
Optical phonons role in determining form
of free carrier distribution function in
semiconductors and nonohmic behavior of
strongly piezoelectric
crystals 06 p1065 A67-18952
Band structures of group V semimetals
and IV-VI semiconductors analyzed using
tunneling, noting data on band edge
energies 06 p1069 A67-18975
Superconductivity in degenerate
semiconductors, applying Bardeen-Cooper-
Schrieffer theory, calculating electron-
electron interaction 06 p1069 A67-18979
Oscillations in conductivity of electron-
hole plasma in semiconductors due to
nonlinearity of volt-ampere
characteristics 06 p1070 A67-18988
Helicon effect in semiconductors measured
by resonant cavity
method 06 p1071 A67-18990
Deformation potential effect on helicon-
phonon interaction in multivalley
semiconductor 06 p1071 A67-18991
IR transmission measurements in single

crystal thin film semiconductors, observing absorption band near plasma frequency 06 p1071 A67-18992

Impurity energy levels in semiconductors described by equivalent Schrodinger equation containing short range as well as conventional terms for long range Coulomb potential 07 p1230 A67-19060

Electromagnetic wave dispersion in semiconductor plasma waveguides for case of plane wave propagation normal to magnetic field vector 07 p1231 A67-19133

State density of strongly alloyed semiconductor in external constant electric field 07 p1149 A67-19188

Shottky theory and electron affinity of semiconducting CdSe from DC I-V characteristics and work function of Au, Ag and Cu contacts with CdSe 07 p1231 A67-19491

Soviet book on electronic properties of semiconductor solid solutions, noting relation between probability theory and ideal crystals theory 07 p1232 A67-19580

Quantum theory of electrical conductivity of semiconductors with nonstandard energy band 07 p1233 A67-19639

Three-component semiconducting compound corresponding to stoichiometry of mercury thallium sulphide, noting properties 07 p1233 A67-19650

Excitation of probe near semiconductor 07 p1154 A67-19790

Semiconductor dislocation noting velocities and effect on transport properties 07 p1237 A67-20162

Temperature effect on equilibrium carrier concentrations and intrinsic lattice defects in semiconductor with self-activated conductivity, considering cuprous oxide 07 p1237 A67-20177

Scattering in semiconductors, calculating collision term in Boltzmann equation for acoustic modes and differential collision operator for isotropic part of distribution function 07 p1237 A67-20180

Semiconducting properties of ferroelectrics estimating free carrier densities in n and p regions and distributions over plate thickness semiconducting properties of ferroelectrics, estimating free carrier densities in n and p 08 p1367 A67-20314

Semiconductor loaded E plane T waveguide junction spectrometer for microwave measurement of transport parameters in semiconductors 08 p1329 A67-20375

Distribution of capacitive photo-emf over surface of semiconductor determined by measuring value created by scanning surface of sample with narrow modulated-light beam 08 p1367 A67-20415

Infinite plate consisting of monopolar semiconductor of given thickness under effect of electric field results in change in galvanomagnetic, piezoresistance and optical properties 08 p1367 A67-20416

Microwave third harmonic generation in homogeneous semiconductors at low temperatures, noting ionized impurity scattering effect 08 p1368 A67-20701

Semiconductor thin film properties for photovoltaic cell applications 08 p1368 A67-20727

Book on IR spectroscopy covering molecular spectroscopy, lattice vibrations, semiconductor electronic effects, IR detectors, far IR, etc book on IR spectroscopy covering molecular spectroscopy, lattice vibrations, semiconductor 08 p1353 A67-20762

Ambipolar diffusion and drift of plasma of added carriers in semiconductor in presence of magnetic field 08 p1369 A67-20900

Comparison of integrated microcircuits deposited on semiconductor and insulating substrates, noting vacuum deposition techniques 08 p1302 A67-20918

Integrated semiconductor circuits and thin film hybrid circuits on insulating substrate developed in Europe for linear circuits 08 p1302 A67-20919

Electroconductivity variations in CdS and CdSe single crystals with SHF electric field strength, intensity of bias lighting and temperature in minus 70 to plus 70 degrees C interval 08 p1370 A67-20996

Pinching of surface carriers toward center of semiconductor produced by current induced magnetic field 08 p1371 A67-21439

Resonance amplification of associated slightly attenuating electromagnetic and acoustic helicon waves by electron drift in semiconductors and semimetals 08 p1371 A67-21458

Thermophysical parameters of semiconductors measured with same instrument set through pulse method, for quality control application 09 p1495 A67-21655

Device measuring uniaxial pressure effect on transmission factor of semiconductors in low absorption region 09 p1551 A67-21657

Effect of surface recombination and parasitic capacitance on linear buildup of photoconductivity in semiconductors, noting germanium photoresistor 09 p1551 A67-21668

Excitation-recombination statistics in semiconductors with donor and center interacting with both bands for given thermal disequilibrium, treating silicon 09 p1551 A67-21669

Electron temperature variation in polar indium antimonide with dominant optical scattering 09 p1552 A67-21672

Time and local temperature distribution in semiconductor under heating pulse 09 p1579 A67-21700

Magnetic effect on injected plasma density and anomalous potential in semiconductor rods 09 p1552 A67-21761

Nondestructive testing techniques in radiation vulnerability analysis of electronic systems, noting ionization effects and permanent damage in semiconductors 09 p1471 A67-21868

Average diffusion coefficient and apparent effective charges of components of alloys of Ti-S system 09 p1553 A67-21906

Thermoconductivity values as function of temperature for semiconductors, noting effect of doping, alloying, etc 09 p1553 A67-21943

Fluctuation levels and induced photoconductivity in vitreous semiconductor thallium selenide and arsenic telluride mixture 09 p1553 A67-21969

Nernst-Ettingshausen coefficient calculated for scattering at short duration potential, at impurity ions and at acoustic oscillations 09 p1554 A67-21970

Impact ionization in ionic semiconductors for arbitrary temperatures and electric field intensities 09 p1554 A67-21971

Electron beam excitation of longitudinal transverse waves in ionic semiconductors, obtaining amplitude increments and frequencies 09 p1554 A67-21978

Systems with toroidal magnetic field increasing toward periphery, considering method using skin effect of semiconductors 09 p1545 A67-22005

Electrostatic oscillations in dielectric, semiconductor and plasma in presence and absence of external magnetic field 09 p1555 A67-22011

Spectral analysis of interacting electromagnetic, plasma and spin waves in antiferromagnetic semiconductors and metals with easy-axis and plane type anisotropy 09 p1555 A67-22073

Domain formation process during passage of current through multivalley semiconductor when electron intervalley scattering drift length exceeds diffusion length 09 p1555 A67-22074

Pressure dependence of thermoconductivity of gases measured using thermoelectric power of semiconductor 09 p1499 A67-22424

Propagation of bounded domain with strong electric field in semiconductor with negative differential conductivity 09 p1557 A67-22558

Single crystal thin semiconducting films prepared by short distance evaporation diffusion under isothermal conditions 09 p1557 A67-22573

Band-to-band radiative recombination in semiconductor groups IV, VI and III-V, presenting data on diamond, Si, Ge, Se and Te 09 p1558 A67-22601

Free carrier electro-magneto-optical phenomenon in semiconductors, noting conductivity tensor, Faraday effect, Derr effect and Voigt effect 09 p1558 A67-22602

Monte Carlo calculations of impurity band states in degenerate semiconductor 09 p1558 A67-22618

Time analysis of Mossbauer spectrum variation and isometric shift of source Te-125m in PbTe absorber following neutron

irradiation in reactor 09 p1559 A67-22661

Thermoelectric current effect on stability of electric current and charge distribution in semiconductors 10 p1689 A67-23094

Linear theory of self-excitation of oscillations in semiconductors in presence of large current density inhomogeneity 10 p1689 A67-23096

Theory of second sound in semiconductors caused by long wave phonons interacting with current carriers in absence of external field 10 p1690 A67-23101

Theoretical semiconductor electroconductivity dependence on intensities of strong electric and magnetic fields 10 p1690 A67-23106

Room temperature electroluminescence spectra of several materials with Ge, zinc blende and wurtzite structures by electrolyte technique 10 p1691 A67-23401

Gallium arsenide - International Symposium, Reading, Berks., England, September 1966 10 p1613 A67-23509

Absorption coefficient of light in semiconductors in crossed electric and magnetic fields, examining conditions for Franz-Keldysh effect occurring in magnetic field 10 p1693 A67-23590

Nonlinear dependence of current in electric field in thin semiconductor film in quantizing magnetic field 10 p1694 A67-23591

Electromagnetic propagation in semiconductor with account of nonlinear effects such as skin effects arising from electron heating by field 10 p1694 A67-23592

Static Jahn-Teller effect on impurity centers in semiconductors, discussing nature and magnitude of splitting of ground state 10 p1694 A67-23593

Multiple-photon radiative transitions in strongly doped semiconductor, noting state density 10 p1694 A67-23652

Multiquantum electron transfers within conductivity band of semiconductors accompanied by emission or absorption of acoustic phonon, calculating absorption coefficient of electromagnetic emission 10 p1695 A67-23658

Perturbation theory applied to study of electron states and interband optical transfers in strong electric fields of semiconductors 10 p1695 A67-23659

Magnetic resistance and Hall effect dependence on external electric field in semiconductors, noting difference for parabolic and nonparabolic law of carrier dispersion 10 p1695 A67-23661

Conductivity of almost intrinsic infinite p-n junction semiconductor, noting volume charge effect on behavior of junction 10 p1695 A67-23662

Metal-beryllium oxide bond for semiconductors noting mechanical and electrical strength, thermal conductivity and refractivity 10 p1696 A67-23691

Semiconductor surface potential in ultrahigh vacuum and under controlled atmosphere 10 p1696 A67-23694

Structure, conductivity and Hall effect of electron bombardment evaporated silicon films on sapphire substrates, noting deposition temperature source doping effectiveness 11 p1845 A67-24141

Optical transmission and electrical properties of complementary metallic meshes fabricated by formation of complement of agglomerated thin films 11 p1845 A67-24142

Undamped plasma oscillations in nonpolar semiconductors doped with impurities in external electric field, determining phase velocity 11 p1846 A67-24472

Analytical expression for steady state rate of electric domain movement in semiconductors in terms of electric field distribution at domain center 11 p1846 A67-24482

Temperature effects in wave propagation on drifting carriers in semiconductors 11 p1847 A67-24720

Galvano- and thermomagnetic phenomena in semiconductors analyzed using transient method, noting extraneous EMF influence on Hall effect 11 p1792 A67-24814

Anomalous IR attenuation in fast neutron irradiated GaAs and CdTe arises through scattering and absorption by highly conducting spike zones 11 p1850 A67-24910

Short circuit current measuring technique and results of electron diffusion lengths in diffused p type and holes in uniformly

doped n type GaAs 11 p1850 A67-24912
 Temperature dependence of thermal conductivity and phonon and electron components in solid and liquid n-and p-type semiconductors 11 p1851 A67-24975
 Entanglement effect of plasma and magnetic branches of oscillations in antiferromagnetic semiconductors on LF expanding plasma waves in strong electric fields 12 p1978 A67-25157
 Vannier-Mott excitons effect on ultrasound absorption in piezoelectric semiconductors 12 p1978 A67-25158
 Light absorption and photolization of shallow impurity levels in semiconductors during acoustic phonon scattering 12 p1978 A67-25159
 Dimensional effect in electric conductivity of semiconductors during heating of electric field when electron energy relaxation length exceeds mean free path 12 p1979 A67-25160
 AC conductivity of glass semiconductor measured over various frequency and temperature ranges, noting activation energy 12 p1980 A67-25181
 Tin oxide films in microscopic quantities on glass and quartz substrates studied for transparency, reflectivity and roughness 12 p1982 A67-25324
 Magnetic ordering effect on electrical properties of antiferromagnetic semiconductor MnTe indicate temperature anomaly above 440 degrees K 12 p1982 A67-25326
 Electrical resistance of semiconducting diamond measured by pulse method 12 p1939 A67-25332
 Resonance properties of semiconductor with moving electrical domains, showing periodic variation with illumination intensity 12 p1983 A67-25517
 Wideband-gap high atomic number semiconductor materials for high temperature counting radiation detectors 12 p1985 A67-25862
 Book on electron radiation damage in semiconductors and metals covering lattice defects, alloys, atom displacement, EPR testing, etc 12 p1986 A67-25890
 Microwave methods for electric resistivity measurements of semiconductor materials, noting application to GaAs 12 p1916 A67-25999
 Semiconductor integrated circuits, discussing hybrid, multichip and beam-lead methods in digital and linear circuit applications 12 p1917 A67-26203
 Reliability and cost analysis of semiconductor integrated circuit and vapor deposited thin film IC, discussing failures and defects 12 p1918 A67-26207
 Crystal growing technology for application to semiconductor production noting methods, impurity control, etc 12 p1950 A67-26211
 Bonding and packaging techniques in production of semiconductor integrated circuits, discussing chip, lead and thermopressure bonding methods 12 p1951 A67-26214
 Propagation characteristics in waveguide loaded with cylindrical semiconductor rod, calculating electric field distribution 12 p1918 A67-26222
 Automatic production processes for semiconductors 12 p1951 A67-26224
 Density of energy levels in amorphous semiconductors induced by local fluctuations in atomic arrangement 13 p2172 A67-26353
 Current carrier concentration gradient in InSb, investigating effect on transverse reluctance coefficient and Hall effect dependence on magnetic field intensity 13 p2173 A67-26360
 Current carrier concentration distribution in semiconductor with intrinsic anisotropy created by strong electric field 13 p2173 A67-26362
 Exciton molecule formation in semiconductors in case of large radius exciton, determining dissociation energy and temperature 13 p2173 A67-26363
 Anomalous photovoltages in CdSe and CdS thin layers 13 p2175 A67-26429
 Light-emitting semiconductors and solid state lasers using various electron-exciting mechanisms 13 p2176 A67-26810
 Local magnetic moment derivation methods using magnetoresistivity data, estimating concentration and temperature dependence 13 p2177 A67-26990
 Time dependence of semiconductor

enhanced reflectivity by pulsed argon ion laser based on thermally generated electron hole plasma 13 p2177 A67-27016
 Pressure effect on interband reflectivity spectra of germanium and related semiconductors 13 p2179 A67-27158
 General model for semiconductor-to-metal transition 13 p2180 A67-27163
 Metal-to-semiconductor transition measurements of hydrostatic pressure shift and uniaxial stress of temperature 13 p2180 A67-27164
 Semiconductor-to-metal transitions in transition metal compounds 13 p2181 A67-27165
 Band structure of spinel-type semiconductors calculation, applying model potential to nearly free electron model 13 p2181 A67-27166
 Experimental apparatus for study of impact ionization and associated recombination radiation in semiconductors 13 p2168 A67-27228
 IR radiation detection by doped semiconductor with induced reflectivity variation 13 p2181 A67-27231
 Effect of mutual entrainment of electrons and phonons on Wiedemann-Franz law for semiconductors, calculating thermoconductivity 13 p2181 A67-27280
 Vacuum equipment application in semiconductor production 13 p2124 A67-27365
 Book on chemical bond in semiconductors and solids, evaluating strength and determining effect on properties of substances 13 p2182 A67-27486
 Hot carrier DC conduction in elemental semiconductors germanium and silicon 13 p2183 A67-27568
 Current-voltage characteristics of germanium-silicon isotype heterojunctions with regard to capacitance and photoelectric measurements 13 p2183 A67-27569
 Average heat of atomization in correlating composition and temperature limits of stability of NaCl type structure among IV-VI compound semiconductors 13 p2184 A67-27570
 Fabrication of small geometry planar bipolar transistors by using electron beam 13 p2084 A67-27574
 Chemical influence of holes and electrons on dislocation velocity in semiconductors 13 p2184 A67-27692
 Visible and X-ray photoelectric emissions in layers of Se-As-Tl intrinsic semiconductor films in vacuum 13 p2184 A67-27719
 Laser beam-induced recrystallization of amorphous Ge semiconductor thin films prepared by thermal deposition on glass 13 p2185 A67-27720
 Photoemission of semiconductor, theoretical treatment of phenomena, properties and production methods 14 p2363 A67-27748
 Semiconductor conductivity measurement from propagation irregularities of SHF electromagnetic waves in medium containing semiconductor 14 p2364 A67-27836
 Reflection coefficient and separation of real and imaginary parts of optical index in nonmetal band-to-band transition model semiconductor 14 p2364 A67-27956
 Semiconductor integrated circuit slices interconnection processes, using gas laser for thermal micromachining 14 p2281 A67-28023
 Properties of selective filter containing inhomogeneous semiconductor RC circuit with distributed parameters 14 p2291 A67-28275
 Apparatus for determining impurity distribution in semiconductor structure 14 p2317 A67-28281
 Galvano and thermomagnetic effects in semiconductors determined by using Hall effect, resistance variations in magnetic field and Nernst-Ettingshausen transverse effect 14 p2365 A67-28314
 Microwave spectroscopy of organic semiconductors, examining EPR of chemical bonds in energy transfer 14 p2366 A67-28505
 Faraday effect in semiconductors in cylindrical waveguides analyzed using numerical calculation 14 p2270 A67-28522
 Equation describing electron transfer between semiconductor surface bands and space bands, applying Fermi concept 14 p2371 A67-28754
 Semiconductor photoconductivity kinetics as affected by surface recombination, considering bi-and monopolar

photoconductivity 14 p2372 A67-28756
 Optical absorption coefficient due to conduction electrons in nondegenerate semiconductors derived using Plakida method, noting light scattering 14 p2372 A67-28808
 Variable composition samples method for preparation of lead telluride semiconductor films by vacuum deposition 14 p2372 A67-28823
 Critical frequency dependence of pi-4 type semiconductor triodes on emitter current or injection level 14 p2289 A67-28824
 Zn-Sb intermetallic compounds preparation for single crystals in semiconductor phase 14 p2372 A67-28826
 Effect of semiconductor glass shield temperature on absorption coefficient, output energy, pulse duration and energy and peak power of ruby laser 14 p2332 A67-28857
 EPR applied to investigation of various semiconductors containing iron, and Mn at liquid nitrogen temperature 14 p2373 A67-28968
 Thermal lattice conductivity at high temperatures in compound semiconductors, linking dilatation coefficient of molecular theory to ionic nature of interatomic bonds 14 p2374 A67-28984
 Electron mobility and temperature due to electric field in polar semiconductor investigated assuming displaced Maxwellian velocity distribution 14 p2375 A67-29065
 Space-charge-wave growth and differential negative resistance conditions in two-valley semiconductors obtained from impedance 15 p2442 A67-29179
 Steady state one-dimensional carrier distribution in depth for electron beam excitation of semiconductors computed, including diffusion and surface recombination 15 p2442 A67-29180
 Phase shift lifetime of excess carriers in semiconductors under sinusoidal injection, showing decrease as injection frequency increases 15 p2533 A67-29264
 Simulation of nonlinear radiant heat transfer for constant emitting heat source by circuit, using semiconductor and pentode 15 p2579 A67-29323
 Localized defects in semiconductors, using solid state scattering theory to calculate energies of bound states 15 p2534 A67-29325
 Current-voltage characteristic determination for n-InSb Corbino disk, noting capacitance and internal resistance current source at cryogenic temperature 15 p2534 A67-29359
 Electrical properties of degenerate intrinsic semiconductor noting spherical energy surfaces, parabolic density of states, acoustic phonon scattering, etc 15 p2535 A67-29487
 P-n semiconductor junction widening due to impurity diffusion and drift, noting first order differential equations describing space-charge width variation with time 15 p2535 A67-29488
 Electrically active centers distribution in Zn and Te implantations into GaAs 15 p2536 A67-29495
 Mass analysis of ion beams from low voltage spark ion source for ion-implantation doping of semiconductors 15 p2536 A67-29496
 Hole mobility produced by single pulses of electrons in films of polyvinyl acetate semiconductors with sputtered gold electrodes, determining relation between film conductivity and mobility 15 p2537 A67-29703
 Absorption of laser radiation in semiconductors and mechanisms of breakdown in process 15 p2537 A67-29704
 Internal electric field effect on simultaneous diffusion of donors and acceptors in semiconductors, considering case of indium and antimony diffusing into germanium 15 p2537 A67-29782
 Anisotropic semiconductor in hot electron theory, deriving volt-ampere characteristics 15 p2538 A67-29784
 Instability of electron hole plasma of semiconductor caused by nonlinear current-voltage characteristic 15 p2538 A67-29789
 Stability of state of semiconductors with absolute negative conductivity 15 p2538 A67-29790
 Measurement methods for determining semiconductor surface properties stressing Garrett and Brattain

calculations 15 p2449 A67-29810
 Polymorphism in IV-VI compounds induced by high pressure and thin film epitaxial growth 15 p2539 A67-29822
 Recombination-regeneration formula for hole-electron pairs in randomly doped semiconductor materials 15 p2539 A67-29915
 Semiconductor nonlinear polarizability at difference frequency calculated, considering exciton states alone and combined with band energy states 15 p2541 A67-30238
 Difference leveling between electron and hole concentrations near junction by compensating charges of donors and acceptors with semiconductor space charges 15 p2542 A67-30242
 Origin of forced oscillation in space-charge density of free current carriers in semiconductors ascribed to periodic generation of carriers 15 p2542 A67-30243
 Electron temperature reduction possibility in individual valleys of multivalley semiconductors, based on energy-balance equation in electron-temperature approximation 15 p2542 A67-30246
 Isochronous and isothermal annealing of indium antimonide irradiated by X-rays and gamma rays, studying changes in current-carrier concentration 15 p2542 A67-30247
 Low temperature conductivity of semiconductors in electric and magnetic fields analyzed, noting electron-photon interactions and photon heating 15 p2542 A67-30248
 Charge curves for germanium and silicon surface obtained by field effect measurements, noting nature and mechanism of effect 15 p2542 A67-30249
 Electron processes at semiconductor surface in presence of chemisorption, noting conductivity and impurity distribution 16 p2724 A67-30491
 Infrared lattice vibration spectra of II-VI compounds analyzed by Drude dispersion, obtaining transverse-optical-mode frequency 16 p2724 A67-30603
 Ternary semiconductors, analyzing physical and physicochemical properties, noting synthesis and preparation of single crystals 16 p2725 A67-30801
 Magnetic field dependence of current oscillations in piezoelectric semiconductors 16 p2725 A67-30804
 Electron emission current density for semiconductors for all conditions between limits of thermionic and field emission 16 p2725 A67-30805
 Refractory intermetallic compounds as high mobility semiconductors, noting crystal preparation and lowest carrier concentration obtained 16 p2725 A67-30806
 Exact solutions for spatial distribution of potential within space-charge region of non-degenerate semiconductor in contact with metal 16 p2727 A67-30850
 Collection of articles on complex semiconductors investigating conductivity, thermal, electrical and other properties, and preparation methods 16 p2729 A67-31154
 Electric and thermal conductivity and Hall effect in solid solution of complex semiconductors noting temperature dependence 16 p2729 A67-31155
 Phonon scattering at point defects theory found to disagree with experimental results on InSb-InTe 16 p2730 A67-31156
 Double-walled cryostat with copper holder for probe measurements of temperature dependence of semiconductor galvanomagnetic effects 16 p2730 A67-31158
 Optical reflection spectra of GaS, GaSe, and GaTe single crystal semiconductors in electron volt band energy range 16 p2730 A67-31159
 Impurity concentration and temperature dependence of reverse current in indium antimonide diodes, determining components 16 p2637 A67-31162
 Book on microelectronics in U.S. covering semiconductor and thin film integrated circuits, hybrid circuits, fabrication, applications, etc 16 p2637 A67-31255
 Thermal conductivity of group of molten and solid chalcogenides at various temperatures, estimating heat transfer mechanism role 16 p2731 A67-31388
 Frequency tripling of electromagnetism waves passing through hot electron gas in semiconductors, deriving third harmonic amplitude for helical wave 16 p2628 A67-31500

Heat transfer in cryogenic range, noting heat flux measurements, use of semiconductors, etc 16 p2780 A67-31533
 Admissible film thickness in probe measurements of electrical conductivity of semiconductor samples 17 p2910 A67-31928
 Transmission coefficient associated with internal reflection from absorbing surface layer derived from reflection coefficient, noting relation to 17 p2883 A67-32204
 Stoichiometric composition effect on semiconducting properties of gamma iron telluride at high temperature phase 17 p2911 A67-32220
 Semiconductor field development, discussing component reliability and miniaturization 17 p2823 A67-32299
 Semiconductor crystal structure defects caused by irradiation with energetic particles and photons 17 p2913 A67-32372
 Book on effects of hot electrons associated with carrier concentration in semiconductors at very low temperatures 17 p2914 A67-32378
 Kronig-Penney model for electron potential in crystal adapted to semiconductor, discussing cubic lattice 17 p2914 A67-32386
 Traveling wave amplification by interaction of drifting carriers in semiconductors with external slow wave circuit 17 p2826 A67-32656
 Impurity atoms and defects distributions in Si and Ge bombarded by different ions of medial energies calculated by Monte Carlo method 17 p2916 A67-32839
 Fission-particle damage formation in semiconducting layer structures, using model based on thermal spike 17 p2918 A67-32849
 Structure of Ge-Sn thin films vacuum deposited on glass substrates analyzed by electron diffraction methods 17 p2920 A67-32891
 Abnormally high photostresses in semiconductor films under monochromatic light studied, using angular dependence observation technique 17 p2921 A67-32970
 Cadmium selenide arsenide single crystals obtained free of cracks, using synthesis method 17 p2922 A67-33218
 Fluctuation levels and induced photoconductivity in vitreous semiconductor thallium selenide and arsenic telluride mixture 17 p2923 A67-33306
 Nernst-Ettingshausen coefficient calculated for scattering at short duration potential, at impurity ions and at acoustic oscillations 17 p2923 A67-33307
 Impact ionization in ionic semiconductors for arbitrary temperatures and electric field intensities 17 p2923 A67-33308
 Electron beam excitation of longitudinal transverse waves in ionic semiconductors, obtaining amplitude increments and frequencies 17 p2923 A67-33315
 Multiple-photon radiative transitions in strongly doped semiconductor, noting state density 17 p2923 A67-33333
 Multiquantum electron transfers within conductivity band of semiconductors accompanied by emission or absorption of acoustic phonon, calculating absorption coefficient of electromagnetism emission 17 p2924 A67-33339
 Perturbation theory applied to study of electron states and interband optical transfers in strong electric fields of semiconductors 17 p2924 A67-33340
 Magnetic resistance and Hall effect dependence on external electric field in semiconductors, noting difference for parabolic and nonparabolic law of carrier dispersion 17 p2924 A67-33342
 Conductivity of almost intrinsic infinite p-n junction semiconductor, noting volume charge effect on behavior of junction 17 p2924 A67-33343
 Soviet book on thermodynamic study of chemical bond in semiconductors 18 p3093 A67-33434
 Physical properties of semiconductors relation with energy and nature of interatomic bonds, discussing effect on elastic constant, thermodynamic functions, electric and dielectric properties 18 p3094 A67-33435
 Elastic moduli, bond parameters and effective ion charges for wurtzite and sphalerite binary crystal lattices 18 p3094 A67-33437

Pauling empirical equation relating thermal effect of reaction to negative ionization potential of solid substances 18 p3094 A67-33438
 X-ray K spectra of phosphorus absorption and emission in indium, gallium and boron phosphide semiconductors and red phosphorus 18 p3095 A67-33440
 Covalent bonds found more prevalent than ionic bonds in X-ray spectral study of Al and Sb in A-III B-V type semiconductor compounds 18 p3095 A67-33443
 Free energy, heat and entropy of formation of several semiconductors by measuring EMF 18 p3095 A67-33445
 Solubility of impurities in semiconductors and mechanism for deviation from stoichiometry 18 p3096 A67-33449
 Changes in InSb, GaSb and Te crystal lattice structure and chemical bonds investigated for effects on thermoelectricity, thermal EMF and microhardness 18 p3096 A67-33451
 Thermal and elastic properties of ternary diamond-like semiconductor compounds, determining ultrasonic wave propagation rates 18 p3096 A67-33452
 Current-voltage characteristic of metal semiconductor point contact, taking into account rectifying effect of junction gap and majority and minority current carrier 18 p3097 A67-33476
 Paramagnetic and electrical properties of organic polyvinyl-acetate-based semiconductor films irradiated with electrons before and after heating 18 p3099 A67-33694
 Excitement of slow and fast recombination waves in semiconductors with mutually independent current-carrier concentrations and lifetime 18 p3099 A67-33696
 Operator for spin-phonon interaction between conduction electrons and polarization-induced longitudinal oscillations of semiconductor lattice 18 p3099 A67-33697
 Ground-state splitting in semiconductor double acceptors 18 p3099 A67-33699
 Thermal processes role in thin semiconducting and dielectric films, discussing current-voltage characteristics, thermal inertia, etc 18 p3100 A67-33766
 Soviet book on production of homogeneous semiconductor crystals, discussing nonuniformities in structural composition 18 p3100 A67-33773
 Mechanisms of atomic recombination at surfaces analyzed, considering behavior of insulators and semiconductor oxides 18 p2997 A67-33794
 Point charges interaction energy in semiconductor thin film 18 p3101 A67-34091
 Hamiltonian equations and Fourier transformations applied to free electron and gap motions in doped semiconductor 18 p3002 A67-34231
 LF waves induced by superimposed electric and magnetic fields in semiconductor plasma 18 p3102 A67-34442
 Resonance properties of semiconductor with moving electrical domains, showing periodic variation with illumination intensity 18 p3103 A67-34448
 Glass semiconductor threshold switches application in memory-addressing circuits, decoding matrices and current dividers 18 p3012 A67-34489
 Gunn effect semiconductor oscillator for generating microwave power using GaAs 18 p3013 A67-34525
 Friedel sum rule applied to semiconductors, discussing Born approximation role 18 p3104 A67-34591
 Thin semiconductor layers, studying surface conductivity variation with semiconductor thickness and surface band curvature 19 p3299 A67-34759
 Light absorption of single-band semiconductor calculated from wave function of electron-hole pairs located near charged impurities, obtaining pair lifetime 19 p3300 A67-34767
 Nonuniform stationary states of current in semiconductors having S-shaped current-voltage characteristics 19 p3301 A67-34900
 Semiconductor galvanothermoelectric characteristics analyzed using all-metal device 19 p3228 A67-34989
 Semiconductor thermoconductivity increase due to illumination on one face by radiated energy 19 p3304 A67-35461

Excess carrier distribution in inhomogeneous semiconducting rectangular plate under two illumination conditions 19 p3308 A67-36026

Voltage breakdown in undoped and chromium doped semiconducting GaAs 19 p3308 A67-36040

Determining resistivity and Hall coefficient using four point contacts placed on Hall plate isotropic uniformly thick two-dimensional sheet with perpendicular magnetic field 19 p3308 A67-36041

Effect of semiconductor glass shield temperature on absorption coefficient, output energy, pulse duration and energy and peak power of ruby laser 19 p3242 A67-36108

Semiconductor surface electromagnetic oscillations excitation in presence of strong electric and magnetic fields, obtaining damping and dispersion law 20 p3504 A67-36163

Nonparabolic conduction energy band in semiconductors produces electron plasma excitations of sum and difference frequencies under strong DC electric field 20 p3505 A67-36210

Transport phenomena in semiconducting thin films studied using transport equation, obtaining relaxation time relationship to semiconductor 20 p3506 A67-36217

Nonohmic electrical conduction of semiconducting thin films in strong electric fields analyzed using electron temperature approximation 20 p3506 A67-36219

Stationary moving domains in hot electron semiconductors, obtaining criteria for soft and hard regimes of domain excitation 20 p3506 A67-36222

Temperature dependence of electrical conductivity in organic semiconductors, examining compounds during transition from solid to liquid state 20 p3508 A67-36404

Screened electron-phonon interaction effect on mobility of conduction electrons in semiconductors at low temperatures 20 p3509 A67-36433

Silicon semiconductor strain-gauge techniques applied to transducer design noting small light units, high sensitivity, silicon integrated circuits, reliability, etc 20 p3442 A67-36458

Millimeter wave reflectance for semiconductor panel, air space and metal reflector arranged planarly, discussing reflectance variation with conductivity and complete absorption 20 p3510 A67-37025

Electric conductivity of surface space charge layers in semiconductors, solving Boltzmann equation and determining current density and carrier mobility 20 p3511 A67-37144

Differential equations governing steady state current flow in semiconductors computed, considering variations as function of distance, hole and electron densities, etc 20 p3400 A67-37216

Ternary semiconductor composition found through valence equation 20 p3512 A67-37243

Excess carrier lifetime in semiconductors by measuring photoconductive phase shift of spreading resistance under point contact 20 p3512 A67-37317

Superconducting critical temperature of sandwich of two semiconducting films in contact 20 p3512 A67-37434

Transient heating and cooling of current carriers in semiconductors and highly ionized plasma analyzed, using effective temperature method 20 p3513 A67-37438

Thermal EMF in semiconductors with electric fields caused by hot carriers, showing energy relaxation of high energy electrons 20 p3513 A67-37451

Distributed RC parameters influence on Hall voltage magnitude in high resistivity semiconductors, explaining voltage decrease 20 p3513 A67-37452

Surface potential of semiconducting gallium arsenide through temperature dependence measurements of transverse conductivity of clamped contact 21 p3676 A67-37869

Negative differential conductivity in semiconductor in acoustic instability mode and connection with sound amplification and number of electron traps 21 p3678 A67-38097

Carrier spatial redistribution under magnetic field effect of current in semiconducting crystal with intrinsic conductivity noting I-V curve

shape 21 p3678 A67-38098

Density of energy levels in amorphous semiconductors induced by local fluctuations in atomic arrangement 21 p3679 A67-38310

Current carrier concentration gradient in InSb, investigating effect on transverse reluctance coefficient and Hall effect dependence on magnetic field intensity 21 p3680 A67-38317

Current carrier concentration distribution in semiconductor with intrinsic anisotropy created by strong electric field 21 p3680 A67-38319

Exciton molecule formation in semiconductors in case of large radius exciton, determining dissociation energy and temperature 21 p3680 A67-38320

Negative differential conductivity in viscous semiconductor with stationary sound wave propagating under sound amplification conditions 21 p3681 A67-38352

Soviet papers on physical properties of ultrapure metals and semiconductors, stressing epitaxial silicon layers 21 p3681 A67-38357

Fast production of semiconductor and refractory metals by reducing silicon tetrachloride and molybdenum trioxide with hydrogen in electric discharge 21 p3681 A67-38358

Oxygen concentration in silicon semiconductors, discussing oxygen properties and effects on carrier lifetime, surface etching and dislocations 21 p3682 A67-38363

Book on electrical properties of semiconductor surfaces covering space charge layer theory, solid state theory, etc 21 p3682 A67-38365

Microscopic theory of zero-bias magnetic tunneling anomalies covering weak and strong coupling limits in p-n semiconductors and tunnel junctions 21 p3682 A67-38385

Quantum transport theories and multiple scattering in doped semiconductors evaluated for screened Coulomb potentials 21 p3682 A67-38387

Impurity crystal-field spectra in II-VI and III-V compound semiconductors used to predict unexplored systems spectra impurity crystal-field spectra in II-VI and III-V compound semiconductors used to predict 21 p3682 A67-38388

Soviet book on physicochemical principles of semiconductor alloying covering chemical bonds, crystal structure, binary systems, etc 21 p3684 A67-38433

AlN single crystal thermostable semiconductor optical/electrical properties, measuring space-charge-limited current and photocurrent 21 p3684 A67-38522

High magnification microscopes for semiconductor research noting advantages of illumination system and light sources 21 p3630 A67-38895

Failure mechanisms in semiconductor components under thermomechanical and electrical stresses for D2 satellite application 21 p3601 A67-39061

Electrical conductivity temperature dependence, Hall coefficient, current carrier mobility, melting point and density data for single crystal of AIIIV type electrical conductivity temperature dependence, 21 p3687 A67-39144

Photoconductivity measurements for chromium doped seminsulating gallium arsenide, discussing response peak and possible mechanisms 22 p3855 A67-39348

Soviet book on semiconductor electrochemistry covering space charge layer structure, semiconductor corrosion, etc 22 p3856 A67-39413

Current carrier mobility, Hall effect and magnetoresistance in semiconductors with nonuniform ion distribution 22 p3858 A67-39507

Magnetic element impurity effects on semiconductor resistivity, calculating spin dependent scattering of free carriers 22 p3859 A67-39625

Electron energy band structure of semiconductor films determined by analysis of structural symmetry of germanium and silicon samples 22 p3861 A67-39919

Posistors barium titanate, lead titanate and potassium compound semiconductor and ferroelectric properties analyses indicating closely interrelated properties 22 p3801 A67-40215

Semiconducting alloys of gallium

investigated by photometric method using gallium and xylene orange 22 p3804 A67-40299

High temperature microhardness of semiconductors determined by method measuring indentation diagonals of cooled single crystal specimens 22 p3804 A67-40302

Energy dependent mobility in small signal analysis of waves in semiconductors 22 p3864 A67-40310

Electronic transport in graded band gap semiconductor heterojunctions without space charges, using method based on intraband transitions between complete Hamiltonian eigenstates 22 p3864 A67-40381

New semiconductor compounds derived by cross substitution of group IV semiconductors, giving thermal properties and phase diagrams 23 p4036 A67-40720

G factor of holes in Ge and Si semiconductors computed in quasi-classical region noting dependence on hole moves relative to magnetic field 23 p4042 A67-41297

High temperature thermal EMF and electrical conductivity in intense electric field for semiconductors with low charge carrier mobility 23 p4043 A67-41299

Laser irradiation effect on semiconductor crystals surfaces using pulsed ruby laser 23 p4045 A67-41470

Electromechanical and photomechanical effects on microhardness in semiconductors 23 p4045 A67-41472

Lifetime gradient and Dember photovoltages in n and p type germanium and silicon semiconductors 23 p4045 A67-41483

Lattice heat capacities, Debye temperatures, heat capacity, free formation energy and thermodynamic functions of groups II-IV semiconductors 23 p4047 A67-41533

Hole mobility produced by single pulses of electrons in films of polyvinyl acetate semiconductors with sputtered gold electrodes, determining relation between film conductivity and mobility 24 p4199 A67-41773

Absorption of laser radiation in semiconductors and mechanisms of breakdown in process 24 p4199 A67-41774

Dielectric function of semiconductor in external electric field, discussing effect on plasma frequency 24 p4201 A67-41979

Spectral response of p-n semiconductor heterojunction, considering absorption effects and photocurrent loss 24 p4202 A67-41981

Strong electric field effects on parabolic energy band semiconductor magnetoresistance and Hall coefficients, discussing scattering mechanisms 24 p4202 A67-41982

Free carrier effect on higher harmonic generation in semiconductors from nonlinear Boltzmann equation 24 p4202 A67-41985

Electrification of single crystals of semiconductor compounds of AIIIVI and AIIIBV type after exposure to ruby laser pulses 24 p4187 A67-42164

Phonon assisted magnetoabsorption in direct band semiconductors 24 p4203 A67-42267

Second harmonic power generation associated with simultaneous application of DC fields and gas laser beams to narrow band gap semiconductors 24 p4168 A67-42364

Phenomena between evaporated metal and semiconductor surface affecting potential barrier by metal electrons extraction potential and semiconductor fast state concentration 24 p4204 A67-42410

Laser pulses producing local dissociation process in AIIIBV semiconductor compounds 24 p4168 A67-42725

Photoexcited electroluminescence spectra of rare earth ions in cadmium fluoride semiconductor single crystal 24 p4205 A67-42893

SEMICONDUCTOR DEVICE

SA DIFFERENTIAL AMPLIFIER

SA ELECTRON TUBE

SA PARAMETRIC DIODE

Impedance measurement of silver bonded Ge diode at X band and in mm wave region, improving performance by usage in breakdown region 01 p0033 A67-10028

Exact solution, using Laplace transform, for problem of transient characteristic of semiconductor diode, challenging Nosov view 01 p0035 A67-10398

Ferroelectric field effect device having

drain current gate voltage characteristic
reproducing hysteresis character of
ferroelectric gate
insulator 01 p0036 A67-10463
High speed nuclear electronics
Colloquium, Polytechnic Institute and
Nuclear Study Center, Grenoble, France,
February 1966 01 p0065 A67-10649
Charge collection velocity in
semiconductor particle energy detector
expressed in terms of electron and hole
motion and induced charges 01 p0065 A67-10650
Semiconductor device measuring pulsed
nanosecond currents produced in detectors
by alpha particles 01 p0065 A67-10651
Counting errors and amplitude spectra
distortion in detectors for statistical
characteristics of information contained in
signals 01 p0066 A67-10653
Circuit design measuring travel time
required by low energy particle of varying
mass 01 p0066 A67-10654
Semiconductor surface barrier Si n-type
detector yielding fast resolution curve in
alpha-gamma radiation coincidence
experiment 01 p0066 A67-10657
Pulsed chronotron vernier for precise time
expansion, discussing circuit configuration,
operation and performance 01 p0067 A67-10658
Binary compound transistors, calculating
parameters using T-shaped equivalent
circuits 01 p0038 A67-10828
Si semiconductor strain sensors and
miniature pressure transducers for cryogenic
pressure measurements 01 p0069 A67-11017
X-ray radiation effect on p-n junctions of
germanium diodes, noting changes in V-I
characteristics 01 p0136 A67-11047
Semiconductor integrated circuit negative
feedback amplifier design with high
response characteristics for carrier terminal
equipment application 01 p0040 A67-11241
Checking ohmic back contact on
semiconductor wafers before fabrication of
diode, using four-point probe 01 p0077 A67-11315
Modulation phase lag in causing
overheating of semiconductor diodes as
frequency of rectified voltage increases 02 p0209 A67-11508
Switching and dynamic characteristics of
germanium peak diodes used as AM
devices 02 p0210 A67-11531
Low noise figure 94 gc gallium arsenide
mixer diode for minimum crystal noise ratio
and minimum package parasitics 02 p0213 A67-11649
Semiconductor-metal-semiconductor
structure with metal vapor deposited,
analyzing voltage-current characteristics for
amplifier technology 02 p0293 A67-11754
Abnormal diffusion of base dopant
impurities in shallow double-diffused
structures in silicon, noting cooperative
diffusion in enhanced or retarded
penetration of base region 02 p0298 A67-11877
Semiconductor heterojunction properties
of epitaxial single crystal layer of GaAs
grown on Ge substrate 02 p0299 A67-11895
Three representative microwave systems
of different transmitting capacity currently
in serial production 02 p0220 A67-12203
Physical and functional characteristics of
contoured amplifying semiconductor
radiation detectors for use in missile and
satellite instrumentation 02 p0244 A67-12211
Surface barrier diffused-junction lithium-
compensated silicon and lithium-compensated
germanium particle detectors for aerospace
application 02 p0245 A67-12212
Switching from transmission direction to
barrier direction in junction diode at high
injection levels 02 p0223 A67-12677
Noise level and noise voltage
measurements and noise frequency spectra
of passive semiconductor resistors,
thermistors, Ge rectifying diode and
logarithmic diode 02 p0223 A67-12797
Fluctuations and broadening of energy-loss
spectrum of charged particles passing
through semiconductor detectors 03 p0491 A67-13224
V-I characteristics of low voltage
transistors 03 p0377 A67-13237
Equivalent circuit for four-layer dinistor
with frequency independent elements,
noting dependence of network elements on
dinistor parameters 03 p0377 A67-13238

Dinistor trigger circuits with counting
input, discussing flip-flop circuits 03 p0377 A67-13239
Forward voltage characteristics of
thyristors in fired state, depending on
injection level for high current density 03 p0380 A67-13482
Nonuniform p-type base width effect on
forward switching voltage of diffused
alloyed thyristor devices, comparing
empirical and theoretical values 03 p0380 A67-13483
Spectral intensity of short-circuited noise
current of space-charge-limited solid state
diodes 03 p0380 A67-13486
Rectification and detection characteristics
of space-charge-limited solid state diode at
VHF 03 p0380 A67-13488
Method for intermodulation output
spectrum generation in semiconductor diode
junction 03 p0381 A67-13664
Temperature stability of several types of
modulated radiation sources employing GaAs
diodes, examining current change with
temperature change 03 p0388 A67-14271
Avalanching transit time diode, noting
dynamic resistance mechanism of formation
and linear and nonlinear diode
behavior 04 p0583 A67-15154
Book on digital transistor circuits in
semiconductor devices based on Boolean
algebra and logical and switching circuit
principles 04 p0622 A67-15268
Recombination waves appear in sample
having ohmic contacts when drift velocity of
carriers in constant electric field exceeds
certain value 04 p0681 A67-15290
Nonohmic contacts, metal semiconductor
point contact and soldered contact instead
of p-n junctions used to measure diffusion
length for minority carriers 04 p0584 A67-15481
Resonant frequency change of oscillatory
circuit due to nonlinear capacitance of
semiconductor diode used as amplitude
detector 04 p0586 A67-15677
Book on semiconductor devices with
negative resistance having decreasing section
in volt-ampere characteristics 05 p0770 A67-16171
Beam lead sealed junction technology for
planar processes, noting preparation and
application 05 p0770 A67-16238
Planar integrated circuit technology and
beam lead sealed junctions, noting
fabrication techniques, performance and
applications 05 p0770 A67-16240
Book on semiconductor devices including
thermal processes and microwave frequency
conversion in semiconductor diodes 05 p0771 A67-16447
Thermal properties of semiconductor
diode under steady and pulsed
operation 05 p0772 A67-16448
Matrix analysis of small signal microwave
frequency conversion based on linear
operation of semiconductor diode 05 p0772 A67-16449
Electron energy quantization phenomenon
in thin film studied by using dielectric
barrier sandwiched between semiconductor
films of same conductivity type 05 p0865 A67-16966
Width of l band of p-l-n nuclear emission
detector during Li ion drift through doped
Si semiconductor detector 05 p0872 A67-17500
Spectra of unlocked driven semiconductor
oscillators observed with millimeter wave
reflex klystrons, noting gradual controllable
frequency pulling 05 p0780 A67-17522
Multiple contact Schottky barrier
microwave diode, comparing operation with
single diode in mixing and small and large
signal detection 05 p0780 A67-17528
Sun generated high and low energy
protons analyzed, using semiconductor
detectors during flights of interplanetary
probes 06 p1077 A67-17841
Monolithic IC design of diodes and X-band
microswitch transmission line fabricated on
Si substrate 06 p0968 A67-18053
Steady state thermal conditions in
semiconductor thermoelectric cooling
device 06 p1113 A67-18180
Method for observing thermal field of
semiconductor device using temperature
dependence of zinc sulfide phosphor 06 p0970 A67-18193
Semiconductor devices in radio
transmitters, examining operation of
transistorized amplifiers and varactor

multipliers in output stage 06 p0971 A67-18214
Reliability and temperature stability of
metals used for contacts and
interconnections on semiconductor
devices 06 p0971 A67-18246
Semiconductor heterojunctions noting
preparation, properties, measurement and
results 06 p1053 A67-18756
Surface generation-recombination and
channel effects on p-n junctions and
transistors exposed to ionizing
radiation 06 p1054 A67-18822
Emission spectrum of GaP diodes analyzed
as function of current and
temperature 06 p1062 A67-18931
Book on basic principles of physics of
semiconductors and semiconductor devices
including quantum theory, thermal
properties of solid bodies, etc 07 p1231 A67-19301
Soviet book on junction processes in pulse
type semiconductor diodes 07 p1150 A67-19302
Soviet papers on electromagnetic and
semiconductor devices in conversion
technology 07 p1150 A67-19316
Gallium arsenide planar technology using
starting material obtained by vapor growth,
noting doped silicon dioxide
technique 07 p1155 A67-19889
Energy dependence of semiconductor
devices with respect to secondary
breakdown explained on basis of transient
thermal resistance 07 p1156 A67-19895
Image analyzer tube for IR TV based on
phenomenon of accumulation at
semiconductor junctions 07 p1189 A67-20158
Propagation coefficient of rectangular
waveguide containing centrally placed
semiconducting film 07 p1146 A67-20202
Semiconducting compounds for thin film
photovoltaic devices using GaAs crystals,
considering absorption coefficient 08 p1284 A67-20725
Electron and proton radiation effects on
GaAs, CdS and CdTe thin film solar cells
noting proton damage, estimates on cell life,
etc 08 p1285 A67-20735
Semiconductor integrated circuits,
discussing fabrication processes, component
characteristics and electrical isolation
methods 08 p1301 A67-20788
Thin film and semiconductor integrated
circuits, discussing functional flexibility,
fabrication by microengraving, isolation and
computer fabrication 08 p1301 A67-20791
Capacitance voltage and V-I characteristics
of four-layer p-n-nu-n semiconductor diode
structures 08 p1303 A67-21054
Semiconductor-insulator-semiconductor
structure as negative resistance, noting V-I
characteristics under various
conditions 08 p1370 A67-21292
GaAs p-n-l-n diode as light activated
switch, noting electrical and optical
properties 08 p1306 A67-21295
Continuous waves from synchronized
pulsed bulk GaAs oscillators operating in
microwave region 09 p1471 A67-21645
Ignition systems for turbine engines,
discussing low and high energy,
semiconductor spark plugs, effects of
electric constants on performance, etc 09 p1559 A67-21691
Electronic processes on semiconductor
device surfaces analyzed using scanning light
beam, for application to Si planar
transistors 09 p1472 A67-21949
Hydrostatic pressure measurement by
direct loading of semiconductor strain
gauges 09 p1498 A67-22031
Planar technique for germanium, outlining
manufacture of planar transistor based on
amplifier 09 p1555 A67-22037
Electronic carrier transport in
semiconductor films, stressing active thin
film devices and typical behavior 09 p1555 A67-22111
Thin films of indium antimonide for active
devices grown by various methods including
atomic mixing, flash evaporation,
etc 09 p1474 A67-22112
Gunn effect devices including lab results,
design, materials, frequency variation,
etc 09 p1556 A67-22173
Microwave and optical generation and
amplification - International Conference,
Cambridge, England, September
1966 09 p1476 A67-22251
Trace element concentration in iron

meteorites determined using lithium drifted Ge semiconductor 09 p1569 A67-22686

Monograph on high power semiconductor-magnetic pulse generators, noting saturable inductors and silicon controlled rectifiers, circuit analysis, voltage regulator, etc 09 p1482 A67-22698

Photon modulated tunneling in Te-Al oxide-Al structures, noting increased spectral response and detection range 10 p1689 A67-22907

Functional properties of semiconductor devices and integrated circuits, considering network design 10 p1610 A67-22976

Electron mobility and lifetime variations effects on drift field in silicon junction devices 10 p1612 A67-23374

Tunneling assisted photon absorption process /Franz-Keldysh effect/ in semiconductor junctions studied, using differential photocurrent response 10 p1691 A67-23402

Binary compound transistors, calculating parameters using T-shaped equivalent circuits 10 p1613 A67-23459

Metal GaAs diodes as frequency changers, discussing fabrication, performance characteristics and parameters 10 p1615 A67-23528

Rise time in solid state detectors, considering equivalent circuit, plasma, time, etc 11 p1789 A67-24103

V-I characteristics of In and Ge structures with negative resistance, noting effect of four-layer substructures 11 p1765 A67-24474

Diffusion effect on hole mobility in base of semiconductor device with p-n-p-n structure 11 p1765 A67-24480

GaAs semiconductor diodes for thermometric measurements in low and intermediate ranges, showing temperature dependence of injected current on emitter to collector voltage 11 p1766 A67-24650

Preparation and properties of III-V compounds for radiative processes, discussing epitaxial deposition of GaAs into semi-insulating substrate for array of devices 11 p1847 A67-24736

Specific resistance of semiconductor plates measured by change in effective loss component of toroidal coil 11 p1792 A67-24812

Specific resistance of epitaxial layers on low resistance substrates measured, using opposing probe method 11 p1792 A67-24813

Silicon semiconductor combustion pressure transducer for high temperature HF pressure measurements within liquid rocket motor chambers 11 p1792 A67-24820

Electrostatic oscillations in electron plasma, noting effect of external electric field on electron velocity distribution 11 p1848 A67-24868

Semiconductor junction devices analyzed for diffusion and electric field currents in bulk regions 11 p1849 A67-24904

Semiconductor diode light sources, discussing phenomenon of p-n junction luminescence and potential application in optical displays and data transmission 12 p1979 A67-25169

Testing instrument for determination of lead wire mechanical properties and bond strengths within semiconductor devices 12 p1911 A67-25270

Semiconductor piezoresistive strain gauges and application to compressor blade vibratory stresses measurement 12 p2014 A67-25416

Recombination radiation spectra of InAs with different current carrier concentrations in initial material and different current densities 12 p1914 A67-25516

Semiconductor substrate photochemical processing and coating photoresistant techniques 12 p1916 A67-25996

Explanation of anomalies of experimental static current-voltage characteristics of GaAs tunnel diode oscillators 12 p1917 A67-26098

Semiconductor devices for microcircuits, discussing MOS FET, metal base transistor, etc 12 p1918 A67-26208

Ultrasensitive miniature temperature sensor using pyroelectric material on gate of MOS transistor 13 p2119 A67-26517

Planar silicon transistors with improved performance and reliability due to metallic protection, noting low noise and surface potential stabilization 13 p2077 A67-26652

Semiconductor diffusion by entrainment of

impurity in gas phase 13 p2176 A67-26657

Semiconductor device fabrication and operation, analyzing silicon, germanium, silicon carbide, InSb and GaAs 13 p2176 A67-26693

Nonequilibrium states in metal-to-semiconductor junction resulting from emission of high energy holes and hot free electrons in same 13 p2176 A67-26861

Model for shifts in gate turn-on voltage of insulated-gate field effect devices induced by ionizing radiation 13 p2079 A67-26871

Book on MOSFET covering device theory, characteristics and usage in discrete and integrated circuit form and application to practical circuit design 13 p2079 A67-26997

Solid state semiconductor microwave power generator design, analyzing spurious oscillations rejection 13 p2081 A67-27204

Operation and electrical characteristics of bulk negative resistance semiconductor devices 13 p2183 A67-27562

Metal-semiconductor electric contacts for GaAs bulk effect device noting uniformity, linearity, usefulness, adaptability, etc 13 p2183 A67-27567

Modulation phase lag in causing overheating of semiconductor diodes as frequency of rectified voltage increases 14 p2283 A67-28072

Hermetically sealed semiconductor device tested for leaks with xenon 133 gas, determining radiation safety measures for personnel 14 p2324 A67-28280

Temperature stability of several types of modulated radiation sources employing GaAs diodes, examining current change with temperature change 14 p2288 A67-28780

DC operation of FET at liquid helium temperature noting transfer and drain characteristics similar to those at room temperature 14 p2290 A67-28926

Equivalent circuit model for solid state junction devices with single energy level defect centers including transient properties 15 p2456 A67-29170

Avalanching transit time diode, noting dynamic resistance mechanism of formation and linear and nonlinear diode behavior 15 p2443 A67-29341

Fast warmup crystal oscillator, noting advantages and applications in equipment requiring low power consumption and frequency stability 15 p2445 A67-29584

Processes influencing radiative decay in compound semiconductors 15 p2536 A67-29634

Substrate resistivity effect on threshold of surface inversion in MOS system, deriving expression for threshold voltage vs impurity concentration 15 p2446 A67-29638

Semiconductor device measurements and test methods - Conference, Budapest, April 1967 15 p2448 A67-29789

Test methods and measurements of semiconductor devices - Conference, Budapest, April 1967, Part 2 15 p2449 A67-29809

High speed automatic testing of semiconductor devices, discussing wafers and integrated circuits 15 p2449 A67-29812

Electron beam probing of semiconductor materials and devices 15 p2450 A67-29813

Plasma characteristics and instability when plasma waves lead to current oscillations in bulk semiconductor 15 p2450 A67-29814

Hybrid microwave integrated circuits, discussing use of planar and passivated chip devices 15 p2452 A67-29929

Criteria for optimized avalanche photodiode design and for best semiconductor material choice based on carrier multiplication 15 p2453 A67-30015

Parametric negative resistance range and impedance matrix element values of microwave Read avalanche diode 15 p2453 A67-30016

Secondary electron detector for electronic microcircuits bombarded by electron beam used to observe potential distribution in junction breakdown 15 p2453 A67-30065

Cathode sputtering, evaporation and anodic oxidation for thin film deposition in integrated circuit technology 15 p2453 A67-30066

Ultrasonic wave amplification by supersonic flux of drift electrons in sandwich structure of piezoelectric dielectric and semiconductor 15 p2542 A67-30245

Current distribution parallel connected semiconductor triodes based on approximate transfer characteristics of diodes 16 p2634 A67-30462

Effect of capture levels on current-voltage characteristic of semiconductor p-n diode with ohmic back contact 16 p2635 A67-30471

Semiconductor devices in radio transmitters, examining operation of transistorized amplifiers and varactor multipliers in output stage 16 p2635 A67-30480

Hall effect in semiconducting electrode MHD generators, noting Joule heating losses, nonlinear electrical conductivity, etc 16 p2600 A67-30533

Nonuniform base width effects on h-parameters of junction transistor 16 p2635 A67-30795

I-V curve related to state densities on both sides of n-p junction of tunneling system 16 p2725 A67-30808

Thyristor assemblies /dimmers/, for control of power supply, noting operation principles and examples cited 16 p2641 A67-31566

Flip-component technology discussing bonding of flip chips and face bonding of semiconductor devices 16 p2642 A67-31727

Small signal current gain of p-n-p-n section of four-layer Si structure as function of current, noting effect of base width, minority carrier lifetime and doping level 17 p2911 A67-32193

Stress effect on electric properties of p-n junction of semiconductor diodes and means of control 17 p2912 A67-32252

Transverse and longitudinal electron effective masses for wurtzite type crystals 17 p2913 A67-32273

Testing for leak-proof encapsulation of semiconductor devices by use of krypton 85 as radioactive tracer gas 17 p2823 A67-32297

Semiconductor-metal potential barriers for semiconductor devices obtained by silicon dioxide and silicon local sputtering in argon discharge 17 p2916 A67-32809

Semiconductor device and transient ionizing radiation effects on monolithic integrated circuits 17 p2828 A67-32836

Permanent displacement-induced effects in silicon semiconductor devices as function of radiation type and energy 17 p2917 A67-32847

First order prediction of equilibrium photocurrent in silicon switching diodes and radiation storage time in silicon low power planar and mesa transistors from electrical measurements 17 p2918 A67-32851

Electron paramagnetic resonance /EPR/ studies of interaction of irradiation-produced defects with impurities and other defects in silicon semiconductors 17 p2918 A67-32854

Radiation-hardened semiconductor electronic circuit design, noting radiation environment existing in spacecraft nuclear generator vicinity 17 p2919 A67-32857

Radiation effects on carrier recombination and mobility and on lifetime of semiconductor devices 17 p2919 A67-32858

Frequency spectra of excess noise in semiconductor devices due to characteristics fluctuations after applying signal 17 p2828 A67-33383

Epitaxial deposition of silicon on silicon substrates, discussing vapor and vacuum deposition, impurity distributions, layer thickness, etc 18 p3097 A67-33456

Soviet book on semiconductor technology and microelectronics covering photoelectric functional converters, junction characteristics, etc 18 p3008 A67-33467

Photoelectric functional converters application to semiconductor microelectronics and optoelectronic circuits 18 p3008 A67-33468

Niobium alloy semiconductor structures with nonlinear negative resistance, giving volt-ampere characteristics 18 p3009 A67-33472

Deficiencies of pulse-parameter representation used for semiconductor diodes, discussing generalized parameter describing transient processes relaxation 18 p3009 A67-33474

Thermal stabilization of inverse current of p-n junction by additional gate for minority carriers extraction 18 p3009 A67-33478

Semiconductor strain gauge theory, application and installation 18 p3047 A67-33893

Open circuit voltage, short circuit current and maximum power for silicon solar cells

- at low temperatures 18 p2989 A67-34101
- Semiconductor surface thermocouples, determining heat-transfer rates associated with wind tunnel testing 18 p3048 A67-34103
- Radiation effects in metal-insulator-semiconductor /MIS/ devices, noting shift and shape change in characteristic curve 18 p3012 A67-34345
- Collision induced instability in semiconductor plasmas, noting system consisting of electrons and holes with transverse relative drift to static magnetic field 18 p3102 A67-34348
- Recombination radiation spectra of InAs with different current carrier concentrations in initial material and different current densities 18 p3012 A67-34447
- Solar thermoelectric generator with cylindrical aluminum solar energy receiver using p and n type semiconductor materials and water cooled junctions 18 p2990 A67-34491
- Slow response of cadmium selenide thin film transistors related to trapping levels in insulator 18 p3015 A67-34557
- Scattering and transmission parameter methods for semiconductor device measurement, discussing linear integrated circuit test requirement 19 p3191 A67-34944
- Diffusion and epitaxial equipment controlling doping level in semiconductor integrated circuits, discussing fabrication materials and techniques 19 p3236 A67-35019
- Microwave photon interaction with superconducting tunneling currents measured in aluminum-indium junctions, extended to tin-lead junctions, discussing phase shift 19 p3303 A67-35046
- Electron, X-ray and UV radiation effects on oxidized silicon surfaces and planar devices, noting space charge buildup 19 p3305 A67-35621
- Radiation surface effects in semiconductor devices, noting positive space charge buildup in passivated device dielectric surface layer 19 p3306 A67-35674
- Mechanisms involved in damage in metal-insulator-semiconductor /MIS/ devices through exposure to nuclear radiation 19 p3306 A67-35676
- Differential resistance peaks of metal-semiconductor Schottky barrier rectifiers 19 p3198 A67-36042
- Materials technology expansion in electronics industry, discussing complete equipment components processed on semiconductor slices and large scale integrated electronics 19 p3198 A67-36054
- System/semiconductor interface with complex integrated circuits, examining different designs 19 p3199 A67-36055
- Semiconductor negative resistance devices to achieve analog to digital conversion 20 p3390 A67-36252
- MOS devices electrical characteristics controlled by physical parameters studied for approximate relations between loads, potentials and surface fields 20 p3507 A67-36319
- Simultaneous absorption of two photons by transparent material at radiation frequency corresponding to only one photon 20 p3457 A67-36325
- Hall constant of semiconductors noting dependence on specimen size, film and current electrode parameters 20 p3508 A67-36406
- Semiconductor metal diodes operation principles, emphasizing lack of minority carrier storage 20 p3509 A67-36491
- Power semiconductor devices, emphasizing thyristors and silicon rectifier diodes applications 20 p3397 A67-36643
- Potential field distribution in n-GaAs devices before and after switching indicate carrier generation in narrow region near anode 20 p3510 A67-36853
- Operation of Hall generator with variable thickness active layer 20 p3401 A67-37220
- Continuous DC EMF in semiconductor with symmetrical nonlinear conductivity analyzed in variable AC waveguide magnetic field 20 p3513 A67-37449
- Time dependent variations in parameters of junction semiconductors investigated for stability 20 p3401 A67-37450
- Soviet book on electronic and semiconductor devices of servosystems, examining theoretical principles, computational methods, design principles, analog and digital computers, etc 20 p3406 A67-37700
- Small signal interaction impedance of bulk semiconductor amplifier with nonuniform doping profile, noting two-dimensional representation 21 p3588 A67-37818
- Field effect devices noting insulated gate transistor, thin single crystal silicon film deposition on sapphire single crystal, etc 21 p3590 A67-38064
- Charge instability problems in metal-nitride-semiconductors /MNS/ solved by using thin silicon dioxide layer between silicon nitride film and substrate 21 p3678 A67-38151
- P-n-p-n triode turn-off characteristics showing forward biased center junction, establishing general turn-off criterion 21 p3591 A67-38154
- Comparison of classical approximations to free carrier absorption in semiconductors, using reflectivity minimum associated with plasma resonance as criteria 21 p3678 A67-38155
- Gunn effect applied to GaAs crystals for use as diodes, discussing current-voltage characteristics 21 p3684 A67-38444
- Propagation behavior analyzed for fundamental mode of parallel plate waveguide 21 p3597 A67-38566
- P-n junction devices static behavior assuming Van Roosbroeck differential equations in bulk and transition regions 21 p3598 A67-38571
- Silicon semiconductor alpha particle detector for spectrometry, noting radiation resistance for low energy proton bombardment 21 p3628 A67-38596
- Semiconductor detector for information on charged particles of cosmic radiation, studying characteristics of instrument 21 p3629 A67-38664
- Limitations imposed on performance of large area p-n junctions by quality of silicon material, discussing defect-free processing techniques 22 p3766 A67-39247
- Second breakdown in semiconductor devices, discussing measurement methods and techniques, development, breakdown mode and safe operating conditions 22 p3766 A67-39248
- Protection of equipment and systems using semiconductor devices by suppression of voltage transients 22 p3766 A67-39250
- Basic equation derived for I-V characteristics of p-n-p-n device with graphical solution for related p-n junctions 22 p3766 A67-39251
- Oscilloscope recording of mechanical rotation rate using semiconductor photoelectric effect 22 p3796 A67-39341
- Conduction electron ground state and anomalous magnetic moment in antiferromagnetic semiconductor, considering magnetic polaron 22 p3857 A67-39462
- Soviet papers on semiconductor technology and microelectronics 22 p3768 A67-39567
- Current-voltage characteristics of semiconductor diode with spheroidal contact 22 p3769 A67-39571
- LF noise spectrum of p-n junction using arbitrary pulse duration distribution functions 22 p3858 A67-39573
- Semiconductor device noise theory emphasizing junction diodes, bipolar transistors and field effect transistors 22 p3770 A67-39773
- Radiation effects on bipolar transistors field effect devices and integrated circuits noting damage in degraded current gain, increased saturation voltages and leakage 22 p3772 A67-39863
- Photoresistors thermal characteristics in automatic semiconductor control devices studied in steady and pulsed modes of operation, determining current-voltage characteristic and thermoresistance 22 p3801 A67-40214
- Copper oxide and selenium semiconductor rectifiers as heat flux sensors, describing operation and thermal EMF 22 p3801 A67-40217
- Dynamic behavior of accumulation layer and efficiency of Gunn effect semiconductors in limited space charge mode of operation 22 p3864 A67-40314
- Soviet book on present state of semiconductor technology covering theory, material properties and semiconductor devices 23 p3978 A67-40797
- Oscillator diode in limited space charge accumulation oscillation mode, obtaining maximum DC to RF conversion efficiency for sine wave excitation for n-GaAs 23 p3979 A67-40875
- Field induced photoelectron emission /FPE/ from Si surface barrier diodes, discussing FPE measurement using xenon arc lamp and grating monochromator 23 p3980 A67-40890
- Schottky photodiode narrow spectral response in Spicer absorption diffusion model shown to exist only in rapidly changing absorption coefficient region 23 p3981 A67-41272
- Molecular sieves as casings filter for semiconductor devices, discussing stabilization of electrical parameters and absorptive capacity of synthetic zeolites 23 p4042 A67-41274
- Property changes of semiconductor materials during processing, discussing photoelectric methods, resistivity derivative, recombination parameters and mechanical stresses 23 p4043 A67-41364
- Structural defects in Ge and Si alloyed semiconductor junction devices caused by improper technological processing, noting microscopic photographs 23 p4043 A67-41365
- Integral Si stress sensor with transverse and shear piezoresistance sensitivity, noting design and fabrication 23 p4005 A67-41371
- Si semiconductor strain gauge thermal coefficient of resistance /TCR/ reduction by high energy electron irradiation 23 p4008 A67-41391
- Laser applications in welding and machining thin film and semiconductor integrated circuits 23 p3983 A67-41765
- Fast neutron radiation damage in narrow base p-n-p-n devices compared to one-dimensional theory, showing superiority to bipolar transistors 24 p4130 A67-42248
- ## SEMICONDUCTOR LASER
- Semiconductor laser array structure with common n-type substrate and individual contacts to p-layer for higher optical power output 01 p0086 A67-10023
- Indium phosphide based semiconductor laser amplification, loss factor and radiation pattern 01 p0086 A67-10065
- Threshold and power characteristics of gallium arsenide diode laser operating in pulsed regime 01 p0086 A67-10066
- Surface effect on temperature, I-V and watt-ampere characteristics of p-n junction semiconductor injection laser diode as coherent light source 01 p0087 A67-10077
- Volt-ampere characteristics and other properties of GaAs lasers with tellurium and Zn-doped epitaxial p-n junction 01 p0087 A67-10080
- Current injection effect on time delay of GaAs laser radiation 01 p0087 A67-10083
- Minimum spectral line width, threshold current density, radiation-peak displacement and possible recombination mechanism for GaSb laser diode p-n junctions in coherent radiation 01 p0087 A67-10085
- Indium arsenic antimonide single crystals in p-n junction laser 01 p0087 A67-10087
- Coherent emission of indium arsenide phosphide p-n junction 01 p0087 A67-10101
- Time variation in intensity of light emitted from CW GaAs laser diodes 01 p0088 A67-10243
- Flashlight /Incoherent/ pumping of visible and IR, InSb and CdS-CdSe lasers 01 p0089 A67-10447
- Continuous coherent radiation of GaAs semiconductor laser with epitaxial p-n junction at ambient temperature of 77 degrees K 01 p0090 A67-10548
- Optical pumping with diode laser into Fabry-Perot resonator face of thin highly-absorbing semiconductor, noting variable mode spacing including single mode output 01 p0091 A67-10879
- Continuous coherent radiation of GaAs semiconductor laser with epitaxial p-n junction at ambient temperature of 77 degrees K 01 p0091 A67-11056
- Simultaneous derivation of optical gain factor and loss per unit length of series of solution grown diffused GaAs injection laser 01 p0138 A67-11072
- Laser based on excitation of gallium phosphorus arsenide solid solution by beam of fast electrons 02 p0251 A67-11824
- Laser type regime of semiconductor having radiation induced by impurity band transitions of current carriers 03 p0436 A67-13137

Threshold current density dependency on photon energy in gallium arsenide laser diodes 03 p0379 A67-13480

Light absorption by free current carriers role in kinetic equations of semiconductor laser/radiation system 03 p0439 A67-14376

I-V characteristic of GaAs diode with Fabry-Perot resonator, noting variations during amplification to generation transition 04 p0678 A67-15132

Spectral characteristics of two-photon optical excitation and light emission from CdSe semiconductor laser with modulated Q-factor 04 p0633 A67-15299

Surface aspects of thermal degradation of GaAs p-n junction lasers and tunnel diodes 04 p0585 A67-15620

Performance of GaAs semiconductor laser with resonator, noting dependence of forbidden zone width and absorption coefficient on free carrier concentration and incident photon energy 04 p0634 A67-15759

Optical coupling using gallium arsenide laser for variation of frequency of diode emission through small change in current density 05 p0814 A67-16390

Semiconductor lasers and fast IR detectors, discussing InAs, InSb and three types of mercury cadmium telluride detectors 05 p0821 A67-16668

Semiconductor lasers with radiating mirrors developed by excitation, using electron beam and neodymium laser glass radiation 05 p0821 A67-16669

Frequency modulation of GaAs semiconductor laser by ultrasonic wave modulation of dielectric constant 05 p0821 A67-16671

Semiconductor lasers noting strong field behavior and absorption coefficient for saturation 05 p0821 A67-16672

High magnetic field effect on interband semiconductor laser, particularly electromagnetic modes and coupling and threshold current conditions 05 p0822 A67-16673

Indium arsenide diode laser fabrication using liquid phase epitaxy, noting quantum efficiency 05 p0825 A67-17096

Change in basic barrier relation for heterojunction compared to homojunction of wide gap emitter injection laser 05 p0825 A67-17097

Shallow donor introduction in p-type GaAs laser results in increased efficiency of radiative recombination 05 p0826 A67-17280

Time structure and amplitude self-modulation of emission from GaAs injection laser observed, using electron-optical converter 06 p1009 A67-17756

Electroluminescence, discussing semiconductor lasers with various excitation sources, luminescent efficiency, etc 06 p1010 A67-17889

Radio electronics, discussing quantum electronics, lasers, microwave devices and technology, plasma physics, etc 06 p0968 A67-18072

Temperature dependence of threshold current in injection lasers in continuous operation under liquid nitrogen cooling 06 p1012 A67-18788

Semiconductor mirror for Q-factor modulation of laser 06 p1012 A67-18789

Interband electron absorption and dispersion during one- and two-photon processes in semiconductors subjected to electromagnetic field, noting laser applications 06 p1054 A67-18798

Semiconductor lasers using single and double photon optical excitation 06 p1013 A67-18930

Lasers and RCA 07 p1193 A67-19080

GaAs room temperature laser diode application to communication and radar systems 07 p1194 A67-19086

Gallium arsenide laser output increase due to aluminum evaporated coating on silicon dioxide used as reflective coating 07 p1196 A67-19794

Resonance-like characteristics of direct modulation of junction laser with bias current analyzed by rate equations 07 p1196 A67-19800

Spectral analysis of emission of spatially separated spots in GaAs injection lasers 07 p1197 A67-20185

Pulse generator for high power injection lasers at room temperature noting small size, cheapness, simplicity, and capability of

switching several thousand amperes 08 p1337 A67-20372

Coherent radiation generation in electron-hole indium antimonide plasma, discussing emission spectrum 08 p1367 A67-20418

Optical and electrical properties of epitaxial and diffused GaAs injection lasers noting spectral characteristics, optical gain, current distribution, etc 08 p1338 A67-21289

Indium phosphide based semiconductor laser amplification, loss factor and radiation pattern 08 p1339 A67-21448

Threshold and power characteristics of gallium arsenide diode laser operating in pulsed regime 08 p1339 A67-21449

Surface effect on temperature, I-V and watt-ampere characteristics of p-n junction semiconductor injection laser diode as coherent light source 08 p1339 A67-21455

Volt-ampere characteristics and other properties of GaAs lasers with tellurium and Zn-doped epitaxial p-n junction 08 p1340 A67-21457

Current injection effect on time delay of GaAs laser radiation 08 p1340 A67-21460

Range capability of gallium arsenide injection LIDAR against extended targets and corner reflectors under both negligible and high background radiation conditions 09 p1462 A67-21640

Avalanche transistors circuit generating high current fast risetime pulses suitable for driving injection lasers 09 p1510 A67-21642

Gallium arsenide laser pumped by Stokes component of induced Raman scattering in liquid nitrogen of Q-modulated ruby laser light 09 p1512 A67-21973

Crystal orientation effect on epitaxial growth gallium arsenide crystals for smooth laser junction 09 p1515 A67-22275

Output and emission spectra of p-n junction diodes analyzed in connection with laser effect in GaSb 09 p1516 A67-22600

Duration and waveform of short single pulse emitted by injection semiconductor laser 09 p1516 A67-22659

Wave equation solution yielding steady absorption coefficient for laser diode 09 p1516 A67-22663

Design characteristics and operation of continuous neodymium laser 09 p1516 A67-22665

Semiconductor lasers for discrete outputs in broad spectral range determined by material characteristics, noting electronic applications 10 p1688 A67-22824

Quantum mechanical theory of fluctuation and relaxation in semiconductor lasers, using Langevin method to calculate noise in quasi-Fermi electron distribution 10 p1663 A67-22891

Photon absorption coefficients measured in active and passive regions of electron-beam-pumped semiconductor laser 10 p1664 A67-22909

High power operation of semiconductor lasers, noting differential equation of field distribution along junction 10 p1665 A67-23519

Reversible and irreversible limitation of maximum power output from GaAs by thermal heating and surface damage 10 p1665 A67-23520

GaAs laser diodes in pulse operation at liquid nitrogen temperature, comparing reflection and diffraction losses with absorption losses 10 p1666 A67-23521

Distribution of injected carrier densities in strongly forward biased laser junctions 10 p1666 A67-23522

GaAs semiconductor quantum generator heating during injection pulse, analyzing temperature effect on external quantum output and generator efficiency 10 p1666 A67-23568

Steady state field distribution of semiconductor laser with nonuniform excitation pumped by electron 10 p1666 A67-23648

Laser emission at band-band transitions in impurity semiconductor without conservation of quasi-momentum 10 p1666 A67-23653

Laser radiation generation at indirect band transitions with free carrier participation in pure semiconductor 10 p1667 A67-23654

Stimulated emission in GaSb injection lasers with steep flat p-n junction, noting dependence of luminescence intensity on current density 10 p1667 A67-23665

Coherent and noncoherent light emission in II-VI compounds, potential for laser

applications in spectral region from 3200 to 7772 angstroms 11 p1801 A67-24735

P-n junction fabrication in vapor phase grown GaAs-P alloys resulting in room temperature injection laser, thereby extending operation into visible spectrum 11 p1802 A67-24741

Heat resistance of GaAs laser diodes from 77 to 300 degrees K, showing relationship to thermal conductivity 11 p1802 A67-24744

GaAs laser diode noting peak optical power, spectra and role of individual diodes in stack operation 11 p1802 A67-24745

Room temperature laser threshold reduction and stimulated emission delay in GaAs diffused junction diodes 11 p1803 A67-24911

I-V characteristic of GaAs diode with Fabry-Perot resonator, noting variations during amplification to generation transition 12 p1951 A67-25156

Time dependence of coherent emission wavelength shift of GaAs-P laser diodes during flat-topped current pulsation 13 p1215 A67-26513

Effect of multiple zinc diffusions on threshold and CW output power of semiconductor laser 13 p1215 A67-26522

Fabrication and operation of divalent dysprosium doped calcium fluoride laser, discussing magnetic field effects, Q-switching, cooling, etc 13 p1217 A67-27086

Interference effects in far field patterns of semiconductor diode lasers 13 p1218 A67-27288

P-type GaAs laser excited by Q-switched ruby laser at liquid nitrogen temperature, noting spectral shift due to Burstein effect 14 p2329 A67-27831

Laser transition absorption cross section at room temperature for neodymium ion in yttrium-aluminum garnet determined by two methods 14 p2331 A67-28713

Semiconductor laser output power varied by decreasing inverse population through heating electron-hole gas by intense optical radiation 15 p2496 A67-29236

Semiconductor laser generating oscillations in external cavity, finding Brewster window effective in suppressing modes within crystal 15 p2498 A67-29511

Direct experimental verification of frequency modulating semiconductor injection laser using ultrasonic waves 15 p2499 A67-29731

IR modulator utilizing field-induced free carrier absorption, with expressions for modulation index in terms of geometrical and physical properties of materials 15 p2491 A67-30428

Rectangular light guides transfer energy from injection type semiconductor laser to laser with logic element 16 p2684 A67-30461

Delay time between current pulse and light emission of GaAs laser diodes, noting nonlinearity between current and delay time 17 p2824 A67-32316

GaAs laser reflectance measurements of tactical landing terrain samples 17 p2858 A67-32483

Gallium arsenide laser pumped by Stokes component of induced Raman scattering in liquid nitrogen of Q-modulated ruby laser light 17 p2870 A67-33310

Steady state field distribution of semiconductor laser with nonuniform excitation pumped by electron 17 p2870 A67-33329

Laser emission at band-band transitions in impurity semiconductor without conservation of quasi-momentum 17 p2870 A67-33334

Laser radiation generation at indirect band transitions with free carrier participation in pure semiconductor 17 p2870 A67-33335

Stimulated emission in GaSb injection lasers with steep flat p-n junction, noting dependence of luminescence intensity on current density 17 p2870 A67-33346

Temperature dependence of threshold current in injection lasers in continuous operation under liquid nitrogen cooling 18 p3059 A67-33730

Semiconductor mirror for Q-factor modulation of laser resonator 18 p3059 A67-33731

Numerical solution of electromagnetic wave equations for semiconductor junction laser using McWhorter model 18 p3060 A67-34019

Interband electron absorption and dispersion during one- and two-photon

processes in semiconductors subjected to electromagnetic field, noting laser applications 18 p3102 A67-34417

Photon generation threshold energy temperature dependence for gallium-arsenic epitaxial injection lasers 19 p3238 A67-34773

Threshold current density dependency on photon energy in diffused and epitaxial p-n junction GaAs injection lasers 19 p3238 A67-34774

Pulse generator for semiconductor laser excitation, noting silicon controlled rectifiers and pulse shaping line 19 p3191 A67-34983

Gallium phosphide diode-based laser generator of nanosecond light pulse sequence, noting simulation of scintillation counter photoelectric amplifiers, Cerenkov counters, etc 19 p3228 A67-34987

IR spectroscopy by variable wavelength semiconductor lasers 20 p3439 A67-36354

Book on lasers and application to long distance terrestrial or space communications system 20 p3459 A67-36639

Semiconductor laser light field amplitude equation of van der Pol oscillator derived and shown valid for optical band-to-band transitions 20 p3461 A67-37184

Zinc telluride laser generation by electron-beam excitation noting high threshold values 21 p3641 A67-38458

GaAs pulsed injection laser diode noting characteristics for room temperature operation 22 p3813 A67-39253

Coherent emission observation in indium phosphide excited by injection laser at 77 degrees K 22 p3814 A67-39461

Optical system models based on gallium-arsenide laser techniques for SNR measurements 23 p4014 A67-41026

Emission of GaSb injection lasers in pulse regime, demonstrating existence of two staggered laser lines originating in diode regions 23 p4016 A67-41193

Two-terminal GaAs laser diode communication system noting laser driver component selection, system performance, construction, design and ranging and tracking applications 23 p3975 A67-41379

Two-photon absorption in semiconductor laser in relation to upper limit of transmission power 24 p4200 A67-41863

Population noise in semiconductor laser junctions calculated by quantum mechanical Langevin method 24 p4166 A67-41887

SENSATION

S TACTILE SENSATION

SENSING

SA HORIZON SENSING

SA LATITUDE SENSING

SA LONGITUDE SENSING

Remote sensing of environment - USAF and USN Symposium, University of Michigan, Ann Arbor, April 1966 01 p0057 A67-10307

Meteorological experiments possible in manned earth orbital spacecraft with aid of remote sensing of electromagnetic radiation 02 p0239 A67-12379

Statistical problems in use of EM data for remote sensing of geological attributes of lithosphere-atmosphere interface 05 p0803 A67-17387

Oceanographic measurements with instrumented satellites, examining surface temperature surface waves, tides, albedo, heat flux and coordination of airborne and seaborne sensing systems 06 p0999 A67-19000

Current stretch sensing for removing limitations to usable density of cryotron storage cells of random access memories 11 p1765 A67-24625

Manned orbiting laboratories for exploring planets by remote sensing and planetary encounter missions compared to landing and flyby 19 p3332 A67-35336

Motion equation derivation permitting analysis of gyrosystems mounted on fixed or moving plants, determining instrumental errors 22 p3795 A67-39230

Electromagnetic sensing of earth from satellites - Conference, University of Florida, November 1965 22 p3804 A67-40350

Forestry applications for remote sensing from earth orbiting vehicles for inventory and evaluation of resources [AIAA PAPER 67-765] 24 p4258 A67-42934

Passive sensing techniques for remote monitoring of nonelectronic systems [AIAA PAPER 67-774] 24 p4158 A67-42942

SENSITIVITY

SA IMPACT SENSITIVITY

SA NOTCH SENSITIVITY

SA PROPELLANT SENSITIVITY

SA RADIOSENSITIVITY

SA SHOCK SENSITIVITY

Stability and sensitivity requirements considered simultaneously in control system design, minimizing time domain sensitivity index and incorporating transient response characteristics 01 p0047 A67-11217

Sensitivity analysis of VTOL aircraft control in vertical-horizontal transition 03 p0358 A67-12982

Invariance and sensitivity theories applied to automatic control system design 03 p0391 A67-13186

Tunnel-diode amplifier sensitivity gain due to negative resistance variation 03 p0382 A67-13668

Digital computer-aided circuit sensitivity analysis using symbols, with example of band pass filter analysis 04 p0578 A67-15088

Sensitivity increase in leak detector by using grid to eliminate residual gas from scattered ions 04 p0625 A67-15631

Light sensitivity of diffused Si phototransistor and of system of two cascade coupled phototransistors 05 p0770 A67-16169

Control of adaptive systems using sensitivity coefficients and logic circuits 08 p1308 A67-20318

Worst case gain sensitivity with zero phase sensitivity in active RC network 08 p1308 A67-20321

Pole-zero sensitivity minimization with respect to active and passive elements in active RC circuit design 08 p1308 A67-20322

Sensitivity models in terms of influence of time variation in given part on behavior of whole system 08 p1309 A67-20325

Optimal control for linear system with respect to performance functional which includes trajectory sensitivity 08 p1309 A67-20327

Sensitivity of index of performances to variations in plant parameter for open and closed loop optimal control with one or two degrees of freedom 08 p1309 A67-20328

Multiparameter sensitivity index for control systems noting synthesis method for minimization of sensitivity 08 p1309 A67-20329

Potential sensitivity of energy radiation detectors, examining measurement error causes for radiation power of natural and artificial sources 10 p1607 A67-23589

Power gain sensitivity of transistors with conjugate matched two-port amplifier 12 p1910 A67-25260

Alternate approach for spacecraft design sensitivities treating vehicle design variables as special control variables 13 p2054 A67-27600

Earth rotation synthesis using arrays of small antennas for better low declination sensitivity 14 p2284 A67-28434

Optimum spacing arrangement for 1100101 array of four antennas in straight line with spectral sensitivity in switched and unswitched cases 14 p2284 A67-28435

Computer aided network sensitivity analysis 15 p2440 A67-29937

Sensitivity tests required to verify nonnormality in sample population, studied by computer simulation techniques 16 p2634 A67-31525

Sensitivity analysis application to nonlinear system modeling and compensation noting minimization procedure parameter determination and performance index 16 p2650 A67-31674

Equipment for processing data giving optimum performances of Doppler radar 17 p2816 A67-32750

Hypersensitization procedure for spectroscopic plates, minimizing nonuniformities of plate fog by use of stop bath 18 p3047 A67-33883

Sensitivity coefficients through flowgraphic representation of network function, discussing algorithmic computer program 19 p3200 A67-34846

Various boundary layer parameters and transducer shape effect on Measurement error of random pressure field by finite size transducer 19 p3228 A67-34964

Functional sensitivity to cavitation of hydroflood cascade, solving Fredholm type integral equations 20 p3419 A67-36188

Plant parameter uncertainties sensitivity constraint for optimal linear control synthesis, discussing Wiener-Hopf equation condition 21 p3602 A67-38026

Sensitivity of film with and without image intensifier compared, using emulsion densities as function of number of incident quanta 22 p3796 A67-39278

Optimum sensitivities of control function with respect to vehicle parameter changes and state variables without using finite differences 22 p3833 A67-40159

Distributive systems interaction between feedback and sensitivity noting parameter variations effects on external characteristics 23 p3983 A67-40644

Sensitivity analysis of linear differential-difference equations with hereditary influences 24 p4134 A67-42026

Photoelectromagnetic detector spectral sensitivity, magnetoresistance and time constants with optically polished thin elements fabricated from Ge, InAs, GaSb and InSb single crystals 24 p4154 A67-42243

Sensitivity analysis method for poorly known model parameters and preliminary computer load requirements applied to radio tracking of space vehicles [ELDO-TM-F-5] 24 p4122 A67-42385

Tunnel diode low level detection characteristics under various bias conditions, discussing sensitivity performance and stability characteristics 24 p4131 A67-42444

SENSOR

SA GUIDANCE SENSOR

SA IMAGE VELOCITY SENSOR

SA OPTICAL SENSOR

SA OXYGEN SENSOR

SA SOLAR SENSOR

SA SPACECRAFT SENSOR

Statistical correlation theory of accuracy and error relationships of sensing element during parametric excitations caused by random vibrations 01 p0064 A67-10417

Heat flux sensor using piezoresistive thermometer for sensing small temperature differentials, discussing design, analysis and test 01 p0069 A67-11020

Liquid metal level measurements using thermocouple type probes as tank sensors, noting usage of electrical resistance of probe sheath 01 p0070 A67-11027

Capacitive pressure transducer featuring exceptional sensitivity, hysteresis, resolution and repeatability, detailing sensing element and measuring circuit design 01 p0071 A67-11102

Helicopter and VTOL vehicle low air speed measuring techniques and devices including pitot-static tube, hot-wire anemometer, sphere sensor and exotic techniques 01 p0073 A67-11122

White Sands Missile Range instrumentation modernization program, discussing advanced range testing, reporting and control /ARTRAC/ system, telemetry and electronic and optical sensors 02 p0229 A67-12003

Test arrangement and statistical data analysis for remote sensing of local flow instabilities and turbulence 03 p0422 A67-13773

Confidence limits for pointing error of gimbaled sensor relative to off-gimbal reference, detailing sources of error and statistical properties 04 p0620 A67-14872

Temperature perturbations produced by internal sensors embedded parallel to heated surface of low conductivity material [ASME PAPER 66-WA/HT-8] 04 p0724 A67-15427

Capacitor pressure sensor produced by furnace brazing molybdenum to itself and to zircon with pure copper and Cu-Au-Ni filler metals 04 p0630 A67-15460

Ring laser inertial sensor for aerospace systems obtaining high accuracy angular resolution and mechanical simplicity 04 p0625 A67-15665

HF analog microcircuits in sensors for information transmission systems, noting problems of precision and high power 05 p0776 A67-17039

Fluid amplifiers and sensors for jet-engine control systems 06 p0949 A67-17611

Differential inductive sensor with correcting windings for monitoring and measuring various nonelectric quantities and processes 06 p1003 A67-18173

Bi-metallic sensing elements calculation method employed by Russian Scientific

Research Institute of Hydrometeorological Instrument Design 07 p1187 A67-19738
Thermobimetallic sensing elements tested by compensation method 07 p1187 A67-19740
Angular acceleration sensor for control system stabilization using MHD principles, obtaining transfer function 08 p1331 A67-20697
Shock and vibration sensors, discussing types for measuring strain, displacement, acceleration, velocity, pressure, etc 10 p1656 A67-23081
Synthetic target scenes generation technique by general purpose digital computer for early analytical evaluation of sensor concepts 11 p1791 A67-24456
Dynamic Newtonian gravitational force gradient fields generator to calibrate response of dynamic gravitational gradient sensor 11 p1794 A67-24903
Wafer thin button size sensor for differential pressure measurement across airfoils 11 p1795 A67-25061
Vibrational mode behavior of rotating gravitational mass sensors and sensor design to minimize nonideal effect of manufacturing and external disturbances 12 p1945 A67-25919
Sensor stability conditions for two rotor gyrocompass on sea-going ship turning in circle 13 p2118 A67-26373
Remote sensing of surface and cloud temperatures using 899 cm spectral interval 13 p2152 A67-27355
Sensor beam, scan mode and perinadir nadir angle determination for Tiros IR data using simplified graph method 13 p2117 A67-27612
Infrasonic and hydromagnetic wave propagation in atmosphere and ionosphere measured by array of underwater and acoustic sensors 13 p2122 A67-27701
Pneumatic angular rate sensor performance characteristics, solving boundary layer equations for radial flow 14 p2318 A67-28340
Flueric pressure, temperature and angular rate sensors for military and commercial applications [ASME PAPER 67-DE-12] 14 p2252 A67-28869
Sensors and sensor control devices for use in high speed low altitude reconnaissance aircraft 15 p2485 A67-29162
Linear signal multiplier using thermally stable InSb, InAs or GaAs sensors with Hall effect voltage linearly dependent on control current 15 p2444 A67-29386
Vibrophonocardiographic techniques for monitoring cardiac dynamics in flight environment 17 p2806 A67-31954
Italian sensing devices for measuring temperature, pressure, acceleration, heat shield and vibration on ELDO satellite 17 p2854 A67-32227
Barometric sensors insensitive to high winds 17 p2860 A67-32816
Diagnostic devices for sensing performance deterioration and mechanical malfunctions in supersonic aircraft engines [SAE PAPER 670363] 17 p2930 A67-33000
Soviet book on photoelectric sensors in monitoring, control and regulation systems noting design principles, operational requirements, etc 18 p3011 A67-33716
Strain and strain-rate sensor for measurements under dynamic conditions and without physical contact with deformation field being sensed 18 p3141 A67-33888
Temperature sensing device development for temperature ranges from cryogenic to ambient 18 p3051 A67-34510
Linear bridge for use with platinum resistance temperature sensors 18 p3052 A67-34511
Sensors used in cosmic dust experiments studied for response to microparticle hypervelocity impacts, noting relationship to velocity 19 p3229 A67-35210
Systems approach combining human experience and logic with computer technology to implement navigation management function 19 p3254 A67-35313
Book on electronic sensing devices covering physical-chemical-electronic effects in solids, liquids, gases, etc 19 p3230 A67-35533
Gravimetry, discussing absolute determinations, navigation, NBS measurements, etc 20 p3448 A67-36894
Sensors and display systems covering fiber optics, sensing of parameters for built-in

equipment and passive monitors, passive chemical vapor/gas detection, etc 20 p3449 A67-36980
Nondestructive testing of electronic circuits with fiber optic scintillators, vidicon data sampling and pattern recognition displays, discussing TV data handling 20 p3449 A67-36982
Direct fluidic sensors for fluid control circuitry design, discussing aerosonic and acoustic flow and obstacle sensing 21 p3625 A67-37958
High sensitivity inductive transducer using ferrite rings for measuring nutational oscillations of gyroscopic instruments 21 p3630 A67-38917
Absolute and relative vibration measurement in aeronautical engineering, describing sensing units for vibration amplitude, rate and acceleration determinations 22 p3798 A67-39545
Copper oxide and selenium semiconductor rectifiers as heat flux sensors, describing operation and thermal 22 p3801 A67-40217
Microwave and mm radiometric sensor for passive satellite reconnaissance of earth atmosphere and terrain thermal noise 22 p3805 A67-40353
Hydraulic angular acceleration sensor motion equation obtained by kinetostatic method 22 p3809 A67-40477
Gravity gradiometer digital computer program for simulated rotating gravitational mass sensor and gradient contour mapping 23 p4000 A67-41218
Oscillating mass flow characteristics in modified Moore variometer configuration for step, triangular and infrasonic functions 23 p4000 A67-41221
SENSOR FOR AIRBORNE TERRAIN ANALYSIS /SATAN/
Multispectral remote sensing techniques for agricultural surveys from orbiting satellites, discussing in-flight signal processing 22 p3806 A67-40367
SENSORIMOTOR PERFORMANCE
S PSYCHOMOTOR PERFORMANCE
SENSORY DEPRIVATION
SA CONFINEMENT
Immobilization effects on electrical activity of brain and intellectual and perceptual motor processes 11 p1748 A67-25064
Task load and type of underwater exposure effects on response time to signal light in visual periphery of novice divers 14 p2256 A67-28662
Tracking activity of human operator under effect of certain space flight factors, establishing relationship between control habits and level of hypoxia and hypercapnia 20 p3368 A67-36265
Sensory deprivation in space medicine, discussing irritation spectrum leading to pathological changes in psychic processes of test subjects 24 p4111 A67-41842
SENSORY DISCRIMINATION
SA BRIGHTNESS DISCRIMINATION
Hearing discrimination in hyperbaric air explained by fact that increased ambient pressure causes disturbances of sound conduction 09 p1453 A67-21729
Diffusion model of perceptual memory process when observer compares two consecutive stimuli, noting visual and auditory discrimination 21 p3576 A67-39097
Sensory discrimination, psychological and preference factors toward water reclaimed from urine, discussing identification from tap and distilled water, temperature and smoking effects 22 p3751 A67-39597
SENSORY FEEDBACK
Cardiovascular deconditioning caused by microcirculatory changes which reduce proprioceptor sensory input of unanesthetized rat 09 p1452 A67-21714
Feedback changes effects on reaction time in stopping chronometer 22 p3756 A67-40536
SENSORY PERCEPTION
SA KINESTHESIS
SA PROPRIOCEPTION
Sensory information necessary for size-weight illusion 03 p0363 A67-12850
Human perception of airflow resistance and perception thresholds under various conditions 07 p1133 A67-19478
Book on statistical decision theory and sensory processes in signal detection theory and psychophysics 07 p1136 A67-19726
Human sensor-motor coordination testing

in simulated weightlessness 20 p3368 A67-36263
SENSORY STIMULATION
Diffusion model of perceptual memory process when observer compares two consecutive stimuli, noting visual and auditory discrimination 21 p3576 A67-39097
Sudden strong stimulus effects on pilot simple visual reaction time and fatigued muscle strength 22 p3756 A67-40537
Decerebrate cat experiments for semicircular canal response to rotational stimulation 23 p3956 A67-41633
Involuntary vestibularly driven head movements in man during rotational simulation 23 p3959 A67-41659
SEPARATED FLOW
Pressure distribution in vicinity of wedge for separated turbulent flow analyzed, using modified Vasiliiu step solution 02 p0232 A67-11634
Free streamline theory of two-dimensional separated potential flow past bluff body and formation of periodic vortex turbulent wake 02 p0178 A67-12233
Shear layer and internal flow arising from turbulent boundary layer separation and heat transfer over cavity 02 p0179 A67-12344
Viscous shear flow past two-dimensional cavity of infinite depth by use of Stokes approximation, emphasizing flow pattern near dividing streamline 03 p0402 A67-13356
Heat transfer in supersonic separated flow over two-dimensional backward-facing step found in entry enlargement region of supersonic parallel diffuser 04 p0546 A67-14640
Heat-transfer coefficient measurements in separated flow regions in heated duct with circumferential grooves, ribs and enlargements, by visual flow techniques 04 p0729 A67-15810
Taylor series expansion of stream function, pressure and temperature about separation or reattachment points used to calculate incompressible closed streamline flows of unknown shape [AIAA PAPER 67-64] 06 p0989 A67-18468
Boundary layer theory of heat exchange in vortex region of separated flow past cylinder 06 p1119 A67-18821
Incipient separation prediction in shock boundary layer interactions 06 p0992 A67-18874
Ranque effect, based on model of two-dimensional vortex flow of viscous thermoconductive gas, explains radial temperature distribution 07 p1268 A67-19352
Fluid flow processes for secondary sonic jet injection into Mach 6 free stream, noting upstream flow into separated flow regions 12 p1893 A67-25934
Hydraulic analog for qualitative analysis of flow field of expansion-deflection nozzle 14 p2297 A67-28136
Dynamic phenomena in diurnal variation of cosmic rays used to determine width and existence of separate flows in interplanetary medium 16 p2740 A67-31898
Separated and reattaching flows emphasizing heat transfer considerations in calculations, especially in supersonic designs 17 p2790 A67-32448
Separation streamline for massive blowing in free stream for model injected into arc tunnel flow [AIAA PAPER 66-457] 17 p2839 A67-33007
Heat transfer in region of separated flow over two-dimensional rectangular cavity facing oncoming turbulent boundary layer [ASME PAPER 67-HT-14] 20 p3545 A67-36711
Compressor blade flutter stability in separating flow with external perturbations analyzed, using digital computer 20 p3517 A67-37488
Flared afterbody aerodynamic characteristic predictions for aircraft stability at high Mach numbers, discussing turbulent separation 24 p4093 A67-42924
SEPARATION
SA BOUNDARY LAYER SEPARATION
SA CHARGE SEPARATION
SA DESORPTION
SA EXTRACTION
SA FLOW SEPARATION
SA SPACING
SA STAGE SEPARATION
Transverse separation of rare gas-metal vapor mixture components in positive nonisothermal plasma column in plain-symmetric glow discharge 09 p1545 A67-21998

Generalized formulation of code separation incorporating general assumptions concerning nature of channel distortion 17 p2830 A67-32827
Temperature, electron density, and relative particle density radial distribution and mass separation effect in free burning DC arc 19 p3281 A67-35156

SEPARATOR

SA FILTER

Carbonation Cell System for removing carbon dioxide from space cabin atmosphere using electrochemical process 23 p3965 A67-41578
Air-oil separator for aircraft hydraulic system stops nose wheel shimmying, based on lowering pressure principle and using filter screen barrier 24 p4099 A67-42427

SEQUENCE

S MODE SEQUENCE

SEQUENTIAL ANALYSIS

Pathcount and coding matrices for sequence time encoding and decoding for data compression 01 p0028 A67-10022
Closed loop realization of optimum control law superior to open loop implementation for linear system not asymptotically stable or subject to random disturbances 01 p0048 A67-11225
Structural design optimization by nonlinear programming noting Sequential Unconstrained Minimization Technique, use of variable metric, Powell direct search method, etc 02 p0209 A67-12711
Bessel function applications of two Sonin theorem formulations compared for range of applicability 07 p1215 A67-19472
Computation of optimal estimators synthesis reduced through partitioning of system state vector 11 p1764 A67-24443
Variational procedure for sequential decoding scheme with mean error probability dependence on code limitation approximately same as for optimal decoding 19 p3185 A67-36096
Nonlinear sequential estimation problem from noisy measurement data using nonstatistical least squares formulation, obtaining approximate solution to two-point boundary value problem 20 p3410 A67-37319
Sequential decoding algorithm with memoryless channel, obtaining lower bound to distribution of computation and limiting factor [JPL-TR-32-1121] 20 p3412 A67-37494
Reynolds stress in turbulent flow dependence on mean velocity field determined by rational sequence of approximations 21 p3609 A67-37734
Generation of arbitrary binary sequence with integrated circuits, describing logic circuit by means of circuit algebra 21 p3590 A67-37946
Spacecraft trajectory parameter estimation, discussing various time-varying error components 21 p3705 A67-38587
Optimal control problem solving by Legendre polynomial expansions and relating function sequence correspondence approximated by finite nonlinear programming 23 p3983 A67-40647
Biochemical model for long term sequential memory in nervous system, introducing network serving as clock to maintain temporal order of stored events 24 p4116 A67-42698

SEQUENTIAL CONTROL

Sequential suboptimal adaptive control of nonlinear systems, considering generation of optimum closed-loop control for startup dynamics of nuclear reactor 02 p0226 A67-12156
Asynchronous control of information transmission in networks consisting of independent sequential circuits 07 p1161 A67-19884
Fluid circuits used in drilling sequence control, detailing ring counter, binary counting stage and comparator 08 p1281 A67-20458
Gradient acceleration technique for solving optimal systems with unbounded control 11 p1771 A67-24896
Digital sequencing systems containing error-detecting and -correcting properties 16 p2647 A67-31647
Fluidic breadboard version of rocket engine sequence control, describing pneumatic logic package and general limitations [AIAA PAPER 67-518] 18 p3114 A67-33981

Multistage linear dynamic systems with sequentially correlated noise, evaluating filtering, prediction and smoothing procedures 19 p3206 A67-35941
Timing considerations in sequential fluid power circuits design in terms of stray delay concept and safety of asynchronous circuit 20 p3365 A67-37362
High reliability sequence programmers for DIAMANT satellite booster switching functions 21 p3655 A67-38207

SEQUENTIAL DETECTION

Multichannel sequential detection in case of reception through independent multiple channels with noise 05 p0765 A67-16953
Mathematical treatment of sequential detection and application to detection of radar targets 10 p1607 A67-23570
Power advantage of optimum system achieved with suboptimum feedback function for sequential binary detection system 14 p2292 A67-28707
Skylight polarimeter based on sequential detection of light transmitted by polarizers oriented at various angles 18 p3046 A67-33748
Reliable efficient communication channel utilization by use of sequential decoding 20 p3384 A67-37348
Deep space communication system using sequential decoding, binary phase-shift keying and 8-level quantized decisions 20 p3384 A67-37349
Sequential circuits design possessing distinguishing sequences and with very short fault detection experiments 21 p3588 A67-38183
Orthogonal signaling in sequential decision feedback on communication over additive white Gaussian noise channel, obtaining expression for error probability 22 p3775 A67-39295

SEQUENTIAL MACHINE

Monograph on internal state assignment problems in sequential machine circuit synthesis 07 p1147 A67-19208
Synchronous sequential multiphase pulse generator using unit distance cyclic code 07 p1162 A67-20199
Compact encoding of stationary Markov sources 12 p1919 A67-26085
Distinct state assignments for synchronous sequential machines, with modification of Dolotta-McCluskey algorithm 13 p2073 A67-27066
Internal states minimization of sequential machines by developing algorithm 19 p3200 A67-34844
Sequential circuits design possessing distinguishing sequences and with very short fault detection experiments 21 p3588 A67-38183
Asynchronous finite state sequential nonlinear controller synthesis with few flip-flops for dynamic space vehicle systems [AIAA PAPER 67-988] 24 p4127 A67-43060

SERGEANT MISSILE

Interface between reliability cost and performance resulting from application of microelectronics to Sergeant Artillery Guided Missile Ground Electronics 09 p1572 A67-22309

SERIES

S BALMER SERIES
S COSINE SERIES
S FOURIER-BESSEL SERIES
S FOURIER SERIES
S LEGENDRE FUNCTION SERIES
S MACLAURIN SERIES
S POWER SERIES
S PRONY SERIES
S SINE SERIES
S TIME SERIES

SERIES EXPANSION

SA CHEBYSHEV APPROXIMATION
SA FUNCTIONAL ANALYSIS
Impact expansions and interference patterns in atomic scattering theory for cases of forward scattering, backscatter, inversion problem and screened Coulomb potential approximation 01 p0112 A67-10143
Marguerre-Vlasov equations accuracy analysis based on equations for thin walled shallow shells derived, using series expansion 01 p0159 A67-10275
Levi-Civita regularized equations of elliptic motion of particle influenced by massive primary and perturbed by smaller primary, Part I, Trigonometric series solution 01 p0147 A67-10379
Partial fraction expansion in derivation of inverse Laplace transform of rational

function with complex and/or repeated poles 01 p0104 A67-10479
Differential equation solution by separation of multiplicative derivative, by perturbation method, by reduction to Volterra equation and by integral series 01 p0107 A67-11250
Cut-off frequency of diffusion transistor calculated, using series expansion for current transport factor 03 p0382 A67-13685
Digital computer calculation of trigonometric series expansions arising in solid mechanics problems 03 p0524 A67-13788
One-dimensional refractive index distribution using power series expansions for refractive index and ray traces obtained from relation of inhomogeneities and interference pattern of Mach-Zehnder interferometer 03 p0423 A67-13908
Thermally radiating and absorbing plane piston problem, obtaining zero order approximation in series expansion in density ratio across shock layer 03 p0405 A67-14029
Convergence of eigenfunction series expansion of nonself-conjugate boundary value problem in complex variables 03 p0461 A67-14060
Orthogonal double series solutions of nonlinear deflections of thin rectangular plate 04 p0707 A67-14445
Two proofs for Cauchy inequality between arithmetical and geometrical means of set of nonnegative numbers 04 p0643 A67-14728
Asymptotic simplification of self-adjoint differential equations with parameter 04 p0647 A67-15741
Infinite series and finite difference solutions of elastic response of thin walled spherical shell to axisymmetric transient blast loading [ASME PAPER 66-APM-EE] 04 p0718 A67-15918
Menshov theorem of enhanced C-properties applied to Walsh series convergence 05 p0835 A67-17003
Fourier series approximation of functions with structural properties differing with segments of domain of definition 05 p0836 A67-17107
Two variable expansion procedure for approximate asymptotic solution to nonlinear differential equation 06 p1022 A67-17789
Taylor series expansion of stream function, pressure and temperature about separation or reattachment points used to calculate incompressible closed streamline flows of unknown shape [AIAA PAPER 67-64] 06 p0989 A67-18468
Control system synthesis based on approximation principle using transfer function expansion in MacLaurin series 06 p0978 A67-18559
Lagrange theorem for series expansion with remainder for weak function whose argument satisfies implicit relation 06 p1025 A67-18731
Fluctuations in diurnal variations of ionization of F-2 layer interfering with radio wave propagation determined by series expansion 07 p1173 A67-19687
Stability of toroidal shell under uniform external pressure solved using series expansion, considering buckling modes 08 p1417 A67-20557
Time varying weight functions effect on convergence of polynomial expansions of isotropic distribution functions 08 p1323 A67-21385
Orbit perturbations due to tesseral harmonics contained in series expansion of gravitational potential determined using computer program 09 p1467 A67-21885
Proof that Tandoni theorem gives best estimate for convergence rates of orthogonal series 09 p1524 A67-21911
London superconductors in local approximation, obtaining solution to equation in form of gradient expansions 09 p1556 A67-22221
Plane problem of rigid die penetration into elastic medium solved, using divergent series form 10 p1721 A67-23671
Method of images series solution converging rapidly for simply supported Euler-Bernoulli beam with high velocity moving concentrated load 10 p1730 A67-23837
Plasma instabilities due to RF motion obtained by expanding fluid and electromagnetic wave equations in asymptotic series 11 p1825 A67-23870
Optimum representation of signals with

limited spectrum by truncated Kotelnikov series for discrete correctors 11 p1769 A67-23906

Ordinary and dielectric second virial coefficients for dipolar gases calculated by off-center dipole model using series expansion 11 p1821 A67-23962

Dual integral equation and dual series analysis and application to mixed boundary value problems in elasticity, hydrodynamics and electrostatics 11 p1812 A67-24150

Double shutter drift tube for measuring electron drift velocities and momentum transfer cross sections in methane, ethane, ethylene, etc 11 p1824 A67-24994

Series method of solving boundary value problems for nonlinear ordinary differential equations 11 p1814 A67-25050

Rectangular three-layer plate thermoelastic oscillations due to random pulses analyzed using series expansion 12 p2027 A67-25625

Multiparameter data sorting technique for one-parameter information represented by simple distribution described by appropriate transformation coefficients 12 p1909 A67-25863

Structures of solutions and expansion of radial heat equation with pole type data function 13 p2145 A67-26492

Newtonian analogues of trigonometric and exponential functions studied by series 13 p2146 A67-26851

Shock structure calculations by modified Grad orthogonal expansion method, noting problems of singularity 13 p2103 A67-26976

Plane conducting fluid-into-fluid jet in presence of transverse magnetic field, examining series expansion of stream function 13 p2169 A67-27317

Maclaurin series expansion representation of generalized heat equation 13 p2147 A67-27454

Extension of Zygmund approximation series to two dimensions, noting periodic function role 14 p2345 A67-28938

New integral in restricted three-body problem expressed in terms of Delaunay variables 15 p2557 A67-29877

Exact solution of three-dimensional problem to derive algorithm for development of applied theories of improved accuracy for circular cylindrical shell 15 p2576 A67-30179

Intermodulation distortion due to nonlinear elements in transistors analyzed using Volterra series representation 15 p2455 A67-30386

Nonlinear automatic control systems with random processes studied using orthogonal polynomials with Hermitian series expansion 16 p2643 A67-30924

General formula for homogeneous second-order differential equation by Lie series, noting computer application 17 p2876 A67-32045

Conservative series-parallel approximations to study systems models for reliability analysis and display 17 p2865 A67-32585

Series solution for end effect in seminfinite transversely isotropic cylinders, noting elastic analysis 17 p2962 A67-33014

London superconductors in local approximation, obtaining solution to equation in form of gradient expansions 18 p3100 A67-33765

Heat transfer in steady axisymmetric MHD flow near stagnation point, with series solutions for velocity, magnetic field and temperature 18 p3161 A67-34381

Elastic potential used to study Green and Neumann tensors through series expansion for Dirichlet problem 19 p3341 A67-35541

Power series expansion of electron velocity distribution function, computing harmonic electric current densities in plasma 21 p3661 A67-37745

Stress analysis of closed cylindrical shell under concentrated loading at free edge, solving differential equation by expanding functions into Fourier series 21 p3718 A67-37982

Plane problem of rigid die penetration into elastic medium solved, using divergent series form 21 p3719 A67-38272

HF noise spectrum of drain and gate currents of junction FET computed from current series expansion 21 p3597 A67-38569

Electromagnetic waves passage through thin radio-transparent layer solved by asymptotic series 21 p3585 A67-38810

Second order weak interaction expansion

for hypersonic flow past adiabatic flat plate, obtaining expressions for static pressure, displacement thickness and skin friction 21 p3586 A67-38892

Optimum representation of signals with limited spectrum by truncated Kotelnikov series for discrete correctors 21 p3604 A67-38934

Arbitrary function expansion into series of functions involved in plane elasticity problem with Fourier series form satisfying boundary conditions 22 p3909 A67-39397

Scattering cross section reduction of metal core loaded dielectric circular cylinder using harmonic series expansion for resonance phenomena 23 p3979 A67-40830

Wave propagation in wave optics transition to geometrical optics in general relativity theory using series expansion 23 p4027 A67-41146

Electronic system reliability statistical estimates obtained from test results of components using series expansion 23 p3982 A67-41669

HF and switching characteristics of junction transistors analyzed using power series expansions 24 p4201 A67-41900

Temperature distribution in solid rotating cylinder exposed to solar radiation using Fourier series expansion 24 p4255 A67-42482

SERT
S SPACE ELECTRIC ROCKET TEST /SERT/

SERUM
SA PROTEIN
Estimation of changes in serum protein concentration under normal stress compared to human sera exposed to simulated altitude and aerospace flights 01 p0015 A67-10950
GUT, GPT, MDH, LDH, SDH and aldolase serum enzyme activity in dogs subjected to moderate impact 06 p0953 A67-17997

SERVICE
S METEOROLOGICAL SERVICE

SERVICE MODULE
SA COMMAND MODULE
Apollo command and service modules simulation [AIAA PAPER 67-231] 07 p1260 A67-20050
Queueing theory applied to phased array radar maintenance problems, specifically replacement and repair of transmitter and/or receiver modules 08 p1292 A67-20668
Explosive-actuated cutting mechanism for severing electrical service lines connecting Apollo command module to service module and lunar module to spacecraft-LM adapter [ASME PAPER 67-DE-33] 14 p2394 A67-28874
Acceptance checkout equipment spacecraft for centralized control and LEM and CSM systems testing 20 p3391 A67-36976

SERVO LOOP
Microwave feedback radiometers using electromechanical and all-electronic systems 07 p1155 A67-19875
Self-excited oscillations of nonlinear servosystems examined, applying expression for generalized transmittance of nth order system 10 p1618 A67-22851
Servo loop electronics reliability using continuous redundancy, integral self-test circuits, etc 19 p3191 A67-34847
Receiving system for telemetering with orientable antenna error-measuring signal receiver and servo loops 21 p3599 A67-38645
Monograph on frequency stabilization of LF oscillator by servo method, showing improved SNR of 21 p3587 A67-39126
Discrete methods for control network implementation using integrated circuitry to reduce inertial navigation systems complexity 22 p3800 A67-40184

SERVOACTUATOR
F-111 wing sweep actuator with irreversible Acme-thread jackscrew driven by hydraulic servomotor 05 p0752 A67-18157
Horizontal tail two-stage hydraulic servoactuator for F-111 horizontal stabilizer control 05 p0752 A67-18160
F-111 aircraft wing spoilers controlled by hydraulic servoactuators 05 p0753 A67-18162
Multiplex electrohydraulic actuators development, noting fault detection and feedback signals to prevent output drift 05 p0754 A67-18752
Automatic flight control development for general aviation, discussing fluidics, electropneumatic servoactuator and microelectronics [SAE PAPER 670255] 12 p1895 A67-25505

Pulse-length modulated pressure waves having zero quiescent pulse width, actuating floating flapper disk switching valves of pneumatic servomechanism 16 p2609 A67-31665

Regenerative dual tandem cable servoactuator design for use in manual and automatic spoiler control system of C-141 Star Lifter 20 p3366 A67-37550

Hydraulic servodrive with supply source, control valve, actuator and feedback components analyzed for stability, deriving motion equations 21 p3570 A67-38048

SERVOAMPLIFIER
Linear amplitude characteristics in synthesis of instrumental servosystems with saturated components such as amplifiers 11 p1794 A67-25040
Dynamics of electrohydraulic servomechanism /transducer-amplifier/ for transforming signals into forces for displacing spacecraft control mechanism, examining motion equations 23 p3935 A67-40637

SERVOCONTROL
Servo control system selection for air-launched missile with Homing guidance system, reviewing four major designs of torque-proportional hardware 02 p0182 A67-11842
Informal automaton simulating certain processes of information processing by human brain controlled by servosystems 03 p0365 A67-13084
Monograph on self-adaptive servocontrol systems, discussing transfer function optimization, frequency filter structure, noise problems, etc 03 p0393 A67-13715
Gas squeeze film stiffness and damping torques on circular disk oscillating about diameter [ASME PAPER 66-LUB-4] 03 p0432 A67-13762
Force /or torque/ electrohydraulic servocontrols, considering transfer function, compatibility conditions and hydraulic perturbation 07 p1132 A67-20113
Simulator studies of MOL tracking experiments 08 p1317 A67-21105
Manipulators for astronauts using anthropomorphic mechanical hands and arms controlled by bilateral servo system in exoskeletal master 11 p1749 A67-25011
Mechanical cascade toroidal servo flight control system tested using simulator [SAE PAPER 670269] 12 p1895 A67-25867
Discrete control gyroscopic servosystem for tracing two-dimensional input signal subjected to random noise distortion 15 p2490 A67-30172
Component selection of antenna steering system in satellite communication system, discussing tracking system characteristics and servo operation modes 17 p2833 A67-32190
Spectrometer with two servocontrolled Fabry-Perot interferometers 20 p3441 A67-36364
High chamber-pressure propulsion systems and components captive testing, describing ground support system analysis, design and mechanisms 20 p3414 A67-36534
Self-adaptive multidimensional continuous servocontrol system 20 p3412 A67-37379
Linear servosystem parametric optimization and application to satellite attitude control, discussing selective and gradient methods 23 p4070 A67-40577

SERVOMECHANISM
SA ACTUATOR
Instrument, force and motion servos in cockpit simulation in large aerospace flight simulators, using DC analog voltages 03 p0395 A67-13386
Externally pressurized bearings treated as hydraulic closed loop servomechanism analyzed, using transfer functions [ASME PAPER 66-LUB-7] 03 p0431 A67-13759
Static and dynamic properties of servomechanical transducers for nonelectrical signals with help of electrical signals 04 p0618 A67-14412
Time slope relation to frequency bandwidth extended to less particular input 04 p0591 A67-14516
Closed loop LaCoste and Romberg gravimeter servo system operating at sensitivity approach thermal fluctuation limits 05 p0809 A67-17392
Numerical handling of data in statistical

study of servomechanism, noting circuitry and random function 06 p0966 A67-17586

Balloon-borne sun seeker improvements through transistorized circuits and solid state switches 07 p1184 A67-19396

Maximal error estimation arising from delay in output functions of servomechanisms provided bandwidth, maximum oscillation and slope are known 08 p1286 A67-20780

Book on modern analytical design of instrument servomechanism noting computer programming, optimization, amplifier saturation, gear stiffness, etc 08 p1332 A67-21171

Pressure feedback in electrohydraulic servomechanisms for high inertia loads to increase stability, using dynamic analysis and differential equations 09 p1442 A67-21687

Inequality to derive error estimation of performance of automatic pulse servosystem inside interval of discreteness 11 p1772 A67-25039

Fluid bulk modulus and density effect on typical hydraulic servomechanism [ASME PAPER 67-FE-19] 14 p2252 A67-28366

Three-step nonlinear analysis procedure for nonlinear stability for position-control servomechanical system applications 15 p2459 A67-30143

Electronic technique producing quadrature signal from laser feedback interferometer 15 p2502 A67-30436

Linearized differential equations for invariant servodrive with hydraulic actuator controlled by throttle slide valve 16 p2609 A67-31378

Dynamics of electromechanical metering servosystems calculated by harmonic linearization method 16 p2644 A67-31380

Stability of one-dimensional polyphase flow in porous medium studied using theory of servomechanisms 16 p2609 A67-31713

Equation derived for accurate approximation of viscous friction coefficient in spool and nozzle-flapper preamplifier stages of electrohydraulic servovalve 16 p2610 A67-31915

Transfer functions in electrohydraulic servo systems through feedback instability properties, discussing root locus theory and typical servomechanism properties 17 p2830 A67-32932

Uniqueness of response of nonlinear continuous servosystem subjected to any signal 18 p3017 A67-34185

Dry friction servo system dynamics with relay delay in random noise case 20 p3451 A67-37152

Activity of Satellite Servo System and Electronic Division of San Giorgio in aerospace field 20 p3400 A67-37163

Approximating probability characteristics of mismatch for steady mode of operation of astatic servosystem with modulation 20 p3409 A67-37201

Dynamic characteristics of relay servo systems 20 p3410 A67-37233

Wind perturbation effects on performance of radio telescope servosystems, giving method for determining optimal system parameters 20 p3403 A67-37519

Soviet book on electronic and semiconductor devices of servosystems, examining theoretical principles, computational methods, design principles, analog and digital computers, etc 20 p3406 A67-37700

Closed loop stepping motor as mechanical memory and time optimal control and digital servomechanism applications 21 p3570 A67-37787

Hydraulic servodrive with supply source, control valve, actuator and feedback components analyzed for stability, deriving motion equations 21 p3570 A67-38048

Linear oscillator forced motion subjected to harmonic AM perturbations studied for servomechanisms 21 p3658 A67-38554

Single channel self-adaptive servosystem synthesized for optimal tracking of diffusion type signal with drift 23 p3983 A67-40598

Moment-kinematic and moment-energetic characteristics of servomotors applied to point and functional problems of servomechanisms in space 24 p4098 A67-42094

Hydraulic failure detection system in Titan booster servo injector module featuring anticipation and correction of servomodular failure 24 p4099 A67-42426

SERVOMOTOR

Altitude control for VTOL aircraft facilitates control of hovering flight, noting construction, operation principles and performance 03 p0363 A67-12981

Jaeger electromagnetic powder coupler characteristics and space application 07 p1131 A67-19525

Linear servomotor for high speed rectilinear response 08 p1286 A67-20992

Small size cylindrical gear reduction system design for servomotors of synchro systems in electronic equipment 11 p1745 A67-24553

Linearized differential equations for invariant servodrive with hydraulic actuator controlled by throttle slide valve 16 p2609 A67-31378

Elimination of electrical transients in high performance sleeve induction motors for missile guidance control systems 16 p2609 A67-31664

Extravehicular activity /EVA/ simulator for zero gravity environment using servodrive and computer control 17 p2832 A67-31994

Moment-kinematic and moment-energetic characteristics of servomotors applied to point and functional problems of servomechanisms in space 24 p4098 A67-42094

SERVOSTABILITY CONTROL

Soviet book on theory of inertial navigation, autonomous systems 11 p1817 A67-24513

SET PROGRAM

S SOLAR ENERGY THERMIONIC /SET/ PROGRAM

SET THEORY

Dispersion method of spontaneous subdivision of image space into compact sets /images/ 03 p0374 A67-13081

Unsolubility of recognition of linear context-free language, searching for algorithm and generalizing to metalinear languages 03 p0375 A67-13562

Interpolation sets satisfying several conditions considered for application to integral functions with gap power series 03 p0461 A67-13941

Continuous single-value mapping of straight line segment in partially ordered system of attracting sets 03 p0461 A67-14061

Axiomatic formulation for stationary point processes interpreted as ordered sequences of points randomly located on real line, noting relation to set theory 04 p0643 A67-14521

Fundamental theorems on ordinals in inner models of set theory 04 p0646 A67-15608

Tame subsets of spheres in Euclidean-3 space, showing tameness of closed subset F of 2-sphere S 07 p1215 A67-19507

Ljapunov theorem extension to onto mappings in compact sets 10 p1673 A67-22850

Cyclotomic numbers of order 18 with applications to difference sets 13 p2146 A67-26735

Attainable sets and generalized geodesic spheres, noting set properties and meaning of conjugate points 13 p2088 A67-27096

Closure and convexity of attainable control sets in finite and infinite dimensions, noting Ljapunov theorem 20 p3408 A67-37075

Book on optimal control theory covering Fourier and Laplace transforms, automatic control, mathematical theories, etc 21 p3602 A67-37829

SEXTANT

Gemini VII star sightings analyzed, using hand-held space sextant in Gemini VI, discussing effect of bias, timing angle measurement and trajectory errors 13 p2154 A67-26817

Hand-held sextant capability in in-flight spacecraft navigation measurements [AIAA PAPER 67-775] 24 p4183 A67-42943

SFERICS

UHF sferics detection system receiving and display components for remote sensing by satellite of convective cloud development 22 p3806 A67-40358

Radio signals from clouds to yield information on cloud physics, using superheterodyne microwave receivers 24 p4124 A67-42883

SHADOW

SA LUNAR SHADOW

SA UMBRA

Gaussian noise model of shadowing effect

on wave backscatter from one-dimensional random rough surface 02 p0192 A67-11602

Apollo thermal control systems and concepts, discussing self-shadowing 02 p0334 A67-12390

Intersection points for satellite orbit and earth shadow /shadow equation/ solved for small eccentricities by iteration method 20 p3523 A67-36624

SHADOW PHOTOGRAPHY

Laser light source controlled by Kerr cell coupled with Z-type schlieren optical system to produce multiple flash photographs of detonation wave development 02 p0245 A67-12227

Photographic techniques developed for photographing ballistic missiles and associated explosive reactions, including shadowgraph and schlieren techniques [SMPTE PREPRINT 100-59] 03 p0423 A67-13807

Radiation transport in spectral lines as consecutive photon absorptions and emissions, discussing contemporary theories, approximation methods and applications spark shadow projections in air for giant pulse 06 p1010 A67-18090

Synchronized shadow photochronographic investigation of wire explosion shock waves in air 09 p1532 A67-22064

Monochromatic photographs through filters for observation of shading variation in intensity of solar emission between center and edge of solar disk 14 p2387 A67-28517

Shadow method analysis of shock wave interaction with fixed bodies in shock tube at small and medium supersonic Mach numbers 16 p2673 A67-31105

Photographic recording by shadow method for alignment of optical equipment in firing range used to determine aerodynamic characteristics of various missiles 16 p2674 A67-31117

Residuals and rms residuals of control measurements made by Manchester Lunar Group members, showing reduced heights not affected by personal errors 18 p3132 A67-34331

Lunar charting for selenocentric coordinates from densitometric analysis and altitude measurements, using photometric methods and Isodensitracer 18 p3049 A67-34333

Flash X-ray source penetrates thick objects and records shadowgraphs directly on film 18 p3052 A67-34531

Shadow photometer conversion to various interferometer types for studying inhomogeneous three-dimensional fluid flows in transparent media 19 p3228 A67-34985

Microsphere ablation in free-flight range observed by laser photography, giving shadowgraphs with density contour map 19 p3346 A67-35757

Shadow photography study of underexpanded nozzle ejected supersonic turbulent jet off-design behavior, discussing static pressure distribution, boundary layer and Mach number effect 23 p3928 A67-40732

SHADOWGRAPH

Statistical characteristics of high speed turbulent wake boundaries [AIAA PAPER 65-808] 01 p0007 A67-11165

Asymmetric interaction of supersonic vehicle intercepted with oblique shock wave [AIAA PAPER 67-180] 06 p0989 A67-18486

Laser photography, discussing equipment used and shadowgraphs obtained in free flight range 08 p1330 A67-20595

Shadowgraphic and interferometric investigation of transversely impinging two-dimensional jet flows 14 p2303 A67-28325

Flash X-ray source penetrates thick objects and records shadowgraphs directly on film 18 p3052 A67-34531

Microsphere ablation in free-flight range observed by laser photography, giving shadowgraphs with density contour map 19 p3346 A67-35757

SHAFT

SA ROTATING SHAFT

Monograph on higher modes of critical speed of shafts with elastic clamping moment at bearings 02 p0250 A67-12710

Elastic-plastic torsion of shafts with hyperbolic notches solved for Ramberg-Osgood and bilinear stress-strain curve 04 p0627 A67-14977

Performance characteristics and bearing load-deflection equations of shaft supported by n roller bearings

[ASME PAPER 66-WA/LUB-4]

Model analysis of radial oscillations of shaft with pounding of ball bearings 05 p0812 A67-17236
 Motion equations for free vibrations of shaft mounted on ball bearings 07 p1191 A67-19355
 Mechanical difficulties in designing shaft, bearing and seal systems for three high speed turbine engines 09 p1560 A67-22537 [SAE PAPER 670064]
 Contact stresses and deformations between circular cylindrical shafts and sleeves obtained by numerical method, considering contact with and without friction 18 p3054 A67-34263

SHALLOW SHELL EQUATION

Marguerre-Vlasov equations accuracy analysis based on equations for thin walled shallow shells derived, using series expansion 01 p0159 A67-10275
 Arbitrary shallow shell under action of space-time homogeneous random load 01 p0163 A67-10995
 Forced small axisymmetric oscillations of elastic right circular cylinder with end plates in form of shallow spherical shell filled with heavy ideal fluid 03 p0530 A67-14174
 Stress state of cylindrical cantilever shell under action of concentrated normal force applied to free edge 04 p0708 A67-14784
 Shallow spherical shells with uniform and/or point loads in prebuckled or postbuckled configuration treated by approximate solution [ASME PAPER 66-WA/APM-21]

Point load on thin shallow elliptic paraboloid with singular solutions expressed as power series 04 p0719 A67-15934
 General critical stressed state of strictly convex convex shell under arbitrary load distributed over edge 04 p0719 A67-15983

Eigenfunction expansion solution for axisymmetric vibrations of shallow spherical shell with concentrated mass 05 p0910 A67-16147
 Bending problem of isotropic shallow helical cantilever shell under distributed normal load 05 p0915 A67-16220
 Free hinged cylindrical shell problem with radial load on outer edge of cross section solved via linear differential equations 05 p0915 A67-16222

Approximate method for solving elastic equilibrium problems of shallow shells with holes, using computer algorithm 05 p0916 A67-16224
 Axisymmetric deformation of shallow shells of revolution, noting membrane solutions 05 p0917 A67-16245
 Initial geometric and boundary condition imperfection effect on stability of shallow spherical shells under uniform pressure [AIAA PAPER 67-111] 06 p1104 A67-18453
 Snap-through buckling of open bimetallic shallow spherical shell under uniform temperature field 06 p1105 A67-18590

Displacement formulations of first order linear thin elastic shell equations in terms of stress resultant and middle surface, using modified Kirchhoff hypothesis 08 p1417 A67-20551

Partial differential equations for displacement and stress functions of shallow shells expressed as Bessel functions 09 p1573 A67-21664
 Generalization of Gaussian arbitrary constant sign curvature to shallow shells by introducing corrections in Lauricella-Sherman potentials 09 p1575 A67-21927
 Dynamic snap-through of shallow arches under stochastically varying transverse loads 10 p1725 A67-23711

Concentration of force and moments near circular holes in shells of revolution with large elastic displacements 11 p1878 A67-24879
 Stress concentration near holes in perturbed shallow shells of revolution 11 p1878 A67-24880

Stress concentration calculated at holes in shallow shells subjected to finite deformation via iteration method 12 p2023 A67-25594
 Approximate solution of equilibrium problem for shallow cylindrical shell of rational profile under pressure distribution from convex side 12 p2024 A67-25603

Oscillation frequency and frequency density distribution equations derived for thin elastic shells of revolution clamped along two parallels, using differential equations 12 p2027 A67-25627

Resolvent equations of shallow multilayer shells of regular structure to solve problems involving calculations of strength, stability and oscillations 12 p2029 A67-25668

Dynamic response of clamped shallow thin elastic spherical shells under time dependent loads 12 p2030 A67-25915 [AIAA PAPER 66-446]

Dynamic snap-through buckling of shallow spherical caps of elastic material 12 p2030 A67-25923

Temperature field in plates and shallow shells with internal heat sources noting solutions for various boundary conditions 13 p2224 A67-27056

General critical stressed state of strictly convex shell under arbitrary load distributed over edge 14 p2400 A67-28492

Triple layer cylindrical shells stability beyond elastic limit studied based on plastic deformations, loading principle and shallow shell theory 21 p3727 A67-38838

Displacement and stress distribution in shallow spherical shell under concentrated loads including normal force, tangential force and bending moment 21 p3730 A67-39087

Shallow spherical shell dynamic stability under variable moment load 22 p3911 A67-39683

Homogeneous and sandwich spherical caps axisymmetric vibration natural frequencies solved approximately, noting application to shallow and spherical shell problems 23 p4073 A67-40617

Stiffness matrix for shallow rectangular shell element and application of finite element displacement method 23 p4073 A67-40628

Discrete stress analysis method for shallow shells of double curvature and rectangular planform with various end conditions 23 p4075 A67-40679

Shallow spherical shell stress and displacement distribution calculated by integral equation 24 p4249 A67-42104

SHANNON-WIENER MEASURE

Shannon expression of information entropy measure and average uncertainty 02 p0203 A67-12168

Entropy of sequence Y obtained from coded sequence of random variables X 14 p2292 A67-28935

SHAPE

S EARTH SHAPE

S LINE SHAPE

S MODE SHAPE

S PLANFORM

SHAPED CHARGE

Low temperature effects on detonation velocity and other explosive parameters for linear shaped charge systems 13 p2230 A67-27686

SHARP LEADING EDGE

Transitional rarefied flow regime noting drag on simple bodies, flows at sharp edges, lifting bodies, etc 14 p2299 A67-28161

Viscous hypersonic flow past leading edge of sharp flat plate analyzed, using Navier-Stokes equation and velocity slip and temperature jump wall boundary conditions 14 p2299 A67-28162

Continuum flow analysis for leading edge region of flat plate, using model based on hypersonic thin layer type of approximation 14 p2240 A67-28163

Pressure on sharp-edged insulated flat plate in low density hypersonic flow, noting results and possible sources of error 14 p2241 A67-28164

Flow field measurement near sharp leading edge of cooled flat plate parallel to low density hypersonic stream 14 p2241 A67-28165

Numerical solutions of hypersonic sharp leading edge flows, with full time-dependent Navier-Stokes equations 18 p2984 A67-34739

Hypersonic rarefied flow past sharp leading edge of flat plate noting incomplete compression phenomenon 19 p3171 A67-35735

SHEAR CREEP

Angular precession and critical speed of two-bearing machines with overhung weight determined, considering shear deformation, gyroscopic moment and rotatory inertia

[ASME PAPER 67-VIBR-19]

11 p1796 A67-24178

SHEAR DISTURBANCE

Steady state response of viscoelastic cylindrical shells to moving loads, obtaining exact solution with correction for shear deformation and rotatory inertia effects via Fourier transforms 03 p0522 A67-13211

Shear relaxation in liquids, criticizing Knollman, Miles and Hamamoto relaxation time distribution measurement method 05 p0758 A67-16133

Shell theory applied to anisotropy problem in axisymmetric cylindrical shells, illustrating shear deformation, twisting couple and circumferential displacement [ASME PAPER 67-APM-28]

Axial shear wave radial propagation in nonhomogeneous elastic medium under axisymmetric loading solved by Laplace transform and characteristics method 21 p3719 A67-38146

Magnetic shear effects on density gradient drift instabilities in plasma with plasma pressure to magnetic pressure ratio larger than electron-ion mass ratio 22 p3845 A67-39483

SHEAR FATIGUE

Diffraction of plane harmonic polarized shear waves by half-plane crack extending under antiplane strain [ASME PAPER 66-WA/APM-18]

04 p0714 A67-15409

SHEAR FLOW

Knudsen layer in steady shear flow with temperature gradient along infinite flat wall 01 p0052 A67-10460

Boundary layer flow having periodically distributed suction over permeable surface 01 p0052 A67-10794

Continuum with director and constitutive equations for anisotropic fluids, obtaining solutions for simple shear, Poiseuille and Couette flows 01 p0053 A67-10849

Observed differences between lateral transport rates of heat and chemical species and of momentum in turbulent free shear flows accounted for by model [AIAA PAPER 65-810] 01 p0054 A67-11167

Reynolds number effects and initial conditions effects on development of free shear in mixing layer from constant area nozzle 02 p0231 A67-11559

Internal gravity-shear waves in troposphere for two-and three-layer model of air density and horizontal velocity, noting phase velocities 02 p0238 A67-12190

Amplitude of perturbations about each interface in internal gravity-shear waves in troposphere according to three-layer model 02 p0239 A67-12191

Viscous shear flow past two-dimensional cavity of infinite depth by use of Stokes approximation, emphasizing flow pattern near dividing streamline 03 p0402 A67-13356

Turbulent lubrication analysis in fluid film theory and turbulent shear flow, with application to bearings [ASME PAPER 66-LUB-12]

Effects of horizontal shear and aspect ratio change on baroclinic instability in rotating annulus heated differentially 03 p0463 A67-13932

Prediction theory for effect of shear flows on outlet angle in axial compressor cascades, taking into account effects of secondary flow, Bernoulli surface rotation and spanwise flow displacement 04 p0548 A67-15387

Relative diffusion of liquid particles in turbulent flow with shear, deriving formulas 05 p0837 A67-16490

Laminar shearing flows breakdown for second order viscoelastic fluids in channels of critical width 05 p0792 A67-16724

Projectile wake turbulence measurements using hot-wire anemometer 05 p0750 A67-17346

Transient response of Couette shear flow to step function change in blowing velocity across channel 05 p0751 A67-17420

Reynolds stress maintenance by components of turbulent shear flow, noting jet mixing layer 06 p0985 A67-18133

Minimum structural response and acoustic radiation for panel excited by turbulent boundary layer [AIAA PAPER 67-12] 06 p0985 A67-18256

Numerical analysis of free boundary problem inviscid incompressible fluid flow of

- impinging jet and two-dimensional Joukowski airfoil in sheared wind tunnel flow [AIAA PAPER 87-217] 06 p0988 A67-18460
- Viscous incompressible slow flow over circular arc wall projections or depressions with shear flow far from projection 06 p0992 A67-18887
- Similarity law for wall region of turbulent boundary layers in compressible flow, discussing Coles theory 08 p1320 A67-20565
- Shear flow generation by flat plate grid with added turbulence generator and roughened floor in wind tunnel 09 p1483 A67-21566
- Compressible nonswirling rotational flows through ducts with varying hub radii 09 p1489 A67-22161
- Atmospheric tides, shorter period gravity waves and shear waves 10 p1643 A67-23249
- Similarity laws for jet noise and shear flow instability as suggested by experiments 10 p1628 A67-23830
- Supersonic shear flow over cavity investigated, constructing velocity and shear stress coefficient profiles satisfying boundary conditions 11 p1778 A67-24218
- Free turbulent shear flows and bound turbulent shear layer flows 12 p1928 A67-25355
- Relative diffusion of liquid particles in turbulent flow with shear, deriving formulas 13 p2093 A67-26345
- Shear flow, determined by velocity and density profiles, is stable for small disturbances of all wavelengths and Richardson numbers, enumerating eigenvalues 14 p2295 A67-27904
- Numerical analysis of boundary layer separation effect on evolution of wake, noting sensitivity to initial velocity profile 14 p2297 A67-28129
- Hydrodynamic stabilization of plane Poiseuille flow by modulating pressure gradient 15 p2470 A67-29332
- Nose bluntness effect on hypersonic conical aerodynamics of ablating flared or conical slender reentry vehicles 15 p2416 A67-29442
- Ductile fracture depending on stress/strain history and material element rotation relative to stress/strain axes proposed for asymmetrically notched specimens 16 p2770 A67-31293
- Nonlinear macroscopic rheological behavior of dilute suspensions of deformable spheres 17 p2887 A67-32280
- Law for velocity distribution through wall boundary layers derived from eddy viscosity model, considering turbulent shear variation and Reynolds number effect 17 p2839 A67-33008
- Stratified shear flow instability examined through two classical models 19 p3210 A67-35611
- Approximate solution to heat transfer coefficient on flat plate in linear shearing flow [ASME PAPER 67-HT-46] 20 p3547 A67-36728
- Heat and mass transfer conditions in ablation of shear thinning and thickening fluids investigated at stagnation point [ASME PAPER 67-HT-78] 20 p3551 A67-36756
- Waveguide model for turbulent shear flow, calculating streamwise dependence of cross-power spectral density using Orr-Sommerfeld equation 22 p3782 A67-39529
- Turbulence onset from small eddies in shear flow analyzed by nonlinear approach 23 p3990 A67-41173
- Two-dimensional incompressible flow near airfoil trailing edge treated by inviscid flow model, with constant vorticity inducing velocity field causing flow retardation 23 p3928 A67-41245
- Exponential vertical flow shear effect on induced drag of elliptically loaded lifting line 23 p3932 A67-41735
- Lifting line theory for blade cascade in subsonic shear flow, noting compressibility effect dependence on harmonic mean upstream Mach number 24 p4091 A67-42204
- SHEAR LAYER**
SA CHAPMAN SHEAR LAYER
Turbulence in free shear layer in mixing region of circular jet, comparing statistical characteristics of mathematical and physical models [AIAA PAPER 65-805] 01 p0054 A67-11164
- Instability and transition to turbulence in separated shear layer produced by laminar boundary layer separation from rearward-facing step, noting periodic spanwise structure 02 p0232 A67-11563
- Shear layer and internal flow arising from turbulent boundary layer separation and heat transfer over cavity 02 p0179 A67-12344
- Approximate theory for development of steady two-dimensional turbulent free mixing shear layers from initial velocity profile, including effects of compressibility and heat transfer [ASME PAPER 66-WA/FE-17] 04 p0606 A67-15352
- Vibration characteristics of two-layered plates of arbitrary thickness and differing materials, noting coupling effect between flexure and extension 10 p1718 A67-23140
- Glass filament wound interlaminar shear specimen design and instrumentation 11 p1875 A67-24614
- Flow equations for convective heating associated with recirculating flow in clustered engine boosters for free viscous shear layer along exhaust jet boundary 16 p2591 A67-30942
- Local turbulent properties of shear layer derived from covariance of two crossed perpendicular beams of radiation 17 p2855 A67-32282
- Laminar and turbulent free shear layers analysis unifying treatment of mixing layers, assessing Mach number, Prandtl number and temperature ratio effects on constant pressure mixing [ASME PAPER 67-HT-81] 20 p3551 A67-36759
- Book on parallel laminar flow stability covering channel and pipe flows, jets, wakes, free shear and boundary layers 22 p3783 A67-39632
- SHEAR STRAIN**
Timoshenko beam theory equations and shear coefficient formula derived from three-dimensional elasticity theory [ASME PAPER 66-APM-C] 04 p0717 A67-15916
- Fiber reinforced composite material behavior examined from shear loading tests, using finite difference analysis for representative PDEs 08 p1420 A67-20908
- Strength of laminar composites, discussing application of statistical theory to determine parameters 08 p1346 A67-20915
- Exact solution of transverse shear deformation effect on axisymmetric large deflection of circular sandwich plates for different loading states and boundary conditions 10 p1728 A67-23762
- Reissner variational formulation of temperature distribution boundary value problem of axisymmetric thermal stresses in isotropic sandwich shells of revolution [AIAA PAPER 66-528] 12 p2030 A67-25917
- Ductile fracture with rotation under shear and normal stresses, noting relationship between fracture strain and stress state for given inclusion content [ASME PAPER 67-MET-9] 12 p1956 A67-25950
- Pneumatic angular rate sensor performance characteristics, solving boundary layer equations for radial flow 14 p2318 A67-28340
- Yielding effects in stress corrosion cracking in susceptible alloys 18 p3063 A67-33487
- Axisymmetric vibrations of homogeneous and sandwich spherical shells obtained from generalized variational motion equations including thickness-shear deformation effect 23 p4075 A67-40667
- SHEAR STRENGTH**
Interatomic force model calculation of shear and tensile strengths, predicting stress-strain curves for crystal structures 03 p0495 A67-13532
- Titanium alloy forging tests covering notched tension, compression, shear, bearing, fracture toughness and smooth and axial fatigue 03 p0446 A67-13552
- Niobium-aluminum alloys elasticity, shear cubic compressibility modul, Poisson ratio, characteristic temperature and crystal lattice structure 04 p0635 A67-14431
- Cadmium sulfide film transducers for shear mode with various insertion losses, noting effect of uniformity in oblique c axes orientations 04 p0621 A67-15126
- Compression, shear and bending strengths of tubular synthetic products as materials for aircraft structural component 04 p0715 A67-15539
- Shear compliance of basal plane of hot worked pyrolytic graphite 05 p0833 A67-17331
- Anisotropic elastic constants and strength characteristics of fiberglass reinforced plastics during shear 06 p1020 A67-18099
- Stress distribution in unidirectional multifiber composite under external and residual shrinkage loads expressed via displacement potentials 08 p1420 A67-20912
- Shear modulus determination from free flexural vibrations of sandwich beams with steel facing, using filled elastomer as core 09 p1574 A67-21838
- Shear strength of various joint designs measured, using steel adherends and rubbery adhesives to isolate factors affecting shear stress 09 p1577 A67-22503
- Carbon fiber composite, noting incorporation into epoxy resin and inverse correlation of shear strength with fiber modulus 10 p1671 A67-23495
- Ablative material performance under high shear reentry condition, noting hyperthermal test of cones and wedges for heat shield design 10 p1734 A67-23722
- Low density shear resistant ablators for lifting reentry vehicles 10 p1672 A67-23725
- Glass filament wound interlaminar shear specimen design and instrumentation 11 p1875 A67-24614
- Radiation effects on shear strength of several alloys at liquid hydrogen environment 13 p2143 A67-27678
- Deflection limits on plate-twisting test 14 p2399 A67-28102
- Treating bending-torsion problem of straight beam using Trefftz definition of shear center 15 p2572 A67-29311
- Elastic properties of hardened Ti alloys discussed for behavior of elastic and shear modul vs annealing temperature 16 p2687 A67-30848
- Shear-spinning technique for manufacturing molybdenum alloy missile nose tips 18 p3054 A67-34365
- Shear modulus measurements in fiber-reinforced composites by plate-twisting test and torsion tube in terms of classical laminated plate and shell theory 23 p4021 A67-40738
- SHEARING STRESS**
SA MANGLER TRANSFORMATION
Steady state flows without external forces becoming parallel in thermodynamic equilibrium at distance from body, noting relations between drag, shear, heat transfer, entropy, etc 01 p0005 A67-10281
- Elastic wave propagation in heterogeneous plates, discussing various plate theories, frequency equations, transverse shear deformations, etc 01 p0160 A67-10407
- Amplitude-dependent internal friction and defect structures in aluminum, measuring critical alternating shearing stress by bridge-circuit method 01 p0101 A67-10845
- Plastic zone expansion near circular hole in plate under pure shearing stress 02 p0337 A67-11845
- Axially symmetric motion of elastic spherical sandwich shell, determining natural frequencies and effects of shear deformation, normal stress and rotatory inertia 03 p0522 A67-13212
- Fiber strengthening theory, taking into account stress transfer between matrix and fiber in both elastic and plastic regions 03 p0449 A67-13257
- Plastic yielding effect on stress and deformation of edge notch subject to longitudinal shearing stress 03 p0523 A67-13469
- Stress patterns in lubricated rolling contact elements calculated from surface pressures and temperature [ASME PAPER 66-LUB-16] 03 p0431 A67-13757
- Apparent mass increase of sphere accelerated from rest and before boundary layer separation in cylinders of oil or water [ASME PAPER 66-WA/UNT-6] 04 p0601 A67-14483
- Shearing stress failure theory for high cycle fatigue employing rotating principal stress axes and nonsynchronous stresses [ASME PAPER 66-WA/MET-9] 04 p0712 A67-15374
- Diffraction of plane harmonic horizontally polarized shear waves by parabolic cylinder, obtaining dynamic shear-stress concentration for parabolic notch and rigid parabolic insert [ASME PAPER 66-WA/APM-13] 04 p0713 A67-15405

Temperature-vorticity analogy validity in laminar turbulent flows extended to compressible fluids, noting temperature relation to shear stress 04 p0727 A67-15680
 Mixing length flow theory of turbulent incompressible flow integral diffusion model extended for boundary layer, channel and Couette flows 04 p0609 A67-15811
 Wall shearing stress and heat transfer measurements through turbulent boundary layer on heated flat plate in accelerating and decelerating airflow 04 p0731 A67-15819
 Differential equations for local interfacial and wall shear stresses for one-dimensional annular two-phase flow 04 p0735 A67-15857
 Three-dimensional stress distribution around elliptical crack under arbitrary shear loading, discussing Griffith-Irwin fracture theory [ASME PAPER 66-APM-N]

04 p0718 A67-15926
 Shearing stress induced shock wave propagation in annealed aluminum under biaxial plastic prestresses [ASME PAPER 66-WA/APM-3]

05 p0909 A67-16143
 Transverse shear and edge condition effect on nonlinear vibration and dynamic buckling of homogeneous and sandwich plates 05 p0910 A67-16146

Upper and lower bounds of transverse vibrational frequencies of variable cross section cantilever bars, considering transverse shear and rotary inertia effects 05 p0910 A67-16151

Dislocation mechanisms for prismatic and basal slip in Ti at low temperatures, measuring critical shearing stress and temperature dependence of activation volume 05 p0828 A67-16467

Reynolds stress maintenance by components of turbulent shear flow, noting jet mixing layer 06 p0985 A67-18133

Characteristic method analysis of linear system of dynamic cylindrical equation for axisymmetric motion, including rotary inertia and shear correction factor [AIAA PAPER 67-79] 06 p1104 A67-18497

Local skin friction coefficient for turbulent boundary layers on smooth flat plates measured, using Preston tube 06 p0990 A67-18751

Changes in microhardness, elastic modulus and shear orientation at boundary between plastic and plastic deformation in steel under tensile stress 07 p1210 A67-20011

Strain rate dependence of critical shear stress in cadmium single crystals used in activation energy determination 07 p1234 A67-20109

Single niobium crystal deformation, discussing stress-strain curves, slippage, orientation and asymmetry of slip 07 p1211 A67-20164

Forced torsional vibration of inhomogeneous hollow cylinder solved for radial variation of shear modulus and mass density 07 p1264 A67-20234

Shear deformation and rotary inertia effects on modal data of nonuniform beam, with complex behavior defined by ordinary differential equations 08 p1416 A67-20533

Craggs propagating crack model for isotropic solid extended for general elastic anisotropy, obtaining propagation theory under tensile or shear stress 08 p1421 A67-20952

Self-consistent description of warm stationary plasma in uniformly sheared magnetic field, noting shear rate current flow 08 p1364 A67-21402

Asymptotic and particular solutions of conical shells subjected to lateral normal loads, discussing membrane forces, bending effects and boundary conditions for moments and shearing force 09 p1573 A67-21754

Large deflection of asymmetrically layered plate, using parametric expansion techniques to extract system of differential equations governing scaling of stresses and displacement component for boundary conditions 09 p1574 A67-21758

Unsteady incompressible flow of viscous electrically conducting fluid near stagnation point, determining skin friction and heat transfer at wall 09 p1544 A67-21934

Dynamic plane shear of incompressible viscoelastic material with temperature dependent viscosity determined, using electric transmission line

analog 09 p1533 A67-22152
 Film thicknesses in elastohydrodynamic lubrication by silicone fluids obtained from oscillatory shear related to continuous shear 09 p1506 A67-22193

Shear strength of various joint designs measured, using steel adherends and rubbery adhesives to isolate factors affecting shear stress 09 p1577 A67-22503

Yield surfaces for nonhomogeneous anisotropic shells of revolution under rotationally symmetric conditions of loading and support 10 p1719 A67-23544

Bassali theory to calculate bending, twisting moments and shearing forces for thin elastic plates under transverse flexure for structural design 10 p1720 A67-23569

Fracture criterion from application of energy principle to elastic plastic crack model, showing positive nature of energy change during propagation 10 p1730 A67-23829

Turbulent boundary layer phenomena, discussing parameters of production processes, relation with instability, etc 11 p1776 A67-24043

Turbulent boundary layer on smooth flat wall, measuring skin friction, turbulence intensity, shearing stress, transverse integral scale, etc 11 p1776 A67-24045

Skewed turbulent boundary layers, noting absence of pressure gradient and shearing stress measurements in experiments and applicability of similarity defect equation 11 p1776 A67-24048

Shear modulus effect on stress distribution of planar array of screw dislocations near bimetallic welded half-planes interface 11 p1804 A67-24107

Constant Reynolds number applied to data evaluation for turbulent jet flow in converging-diverging axisymmetric tube using free turbulent jet 11 p1742 A67-24272

Collisionless instabilities in thermally ionized potassium plasma and effect of magnetic shear on oscillations and diffusion 11 p1834 A67-24378

Numerical and photoelastic solutions compared for uniform edge loading, obtaining pressure calibration by means of shear stress measurement 11 p1878 A67-24616

Shear modulus magnitude effect on stress concentration at circular hole in cylindrical shell for various ratios of Youngs moduli 11 p1878 A67-24881

Metallurgical investigations by electron microscopy of rolling contact fatigue, elucidating mechanisms of failure due to shearing stress 12 p1954 A67-25329

Ductile fracture with rotation under shear and normal stresses, noting relationship between fracture strain and stress state for given inclusion content [ASME PAPER 67-MET-9]

12 p1956 A67-25950
 Ductility of beryllium samples subjected to compression at temperatures ranging from 300 to 600 degrees C, discussing slip effects 13 p2137 A67-27113

Flow of conducting incompressible viscous fluid near accelerated plate under parallel plate and magnetic field, noting velocity profiles and stress role 14 p2361 A67-28814

Mean diameter/wall thickness optimum ratio and corresponding maximum shear stress for thin walled cylinder under uniform pressure and radial heat transfer 15 p2574 A67-29528

Turbulent energy equation converted into differential equation for boundary layer development calculation 15 p2472 A67-29657

Prandtl shear stress theory applied to similarity models of free turbulence 16 p2657 A67-30857

Westergaard method of crack analysis extended for crack problems within infinite medium with cracks under applied loads at infinity 16 p2785 A67-30995

Shear buckling of thin walled structural sections, noting reinforcement methods including use of swedges 17 p2957 A67-32026

Stability of cantilevered elastic bar with end under compressive follower force, noting shear deformation, rotational inertia and internal damping forces 17 p2959 A67-32420

Cracked rectangular beam stress analysis, considering longitudinal shear and Saint-Venant torsion and flexure [ASME PAPER 67-APM-21]

17 p2964 A67-33150
 Monatomic step patterns on /100/ cleavage and tensile crack faces of NaCl crystals originate from dislocation processes of crack tip released by shear stress distribution 18 p3097 A67-33482

Shear stress distribution and dislocation processes at moving crack tips in ionic crystals 18 p3097 A67-33483
 Maximum shear stress dependence on composite materials microstructure, noting filler and binder role 18 p3069 A67-34170

Differential equations and potential for simply supported anisotropic sandwich plate under compression and shear stresses above buckling limit 19 p3341 A67-35575

Stability condition for inhomogeneous elastic body subjected to internal stresses 20 p3535 A67-36392

Circumferential displacement and shearing stresses in out-of-plane elasticity problem for solid torus 20 p3538 A67-36672

Low molecular weight polymer flow behavior variation with shear rate, shear stress and temperature 20 p3473 A67-36914

Stress-strain relationships for single layer used to obtain stress distribution in orthotropic laminates subjected to axial and shear stresses [ASME PAPER 66-WA/RP-5]

20 p3542 A67-37611
 Netting analysis of reinforced sheets for load envelopes which combine tension and shear, determining optimum fiber arrangements 21 p3729 A67-39082

Surface active lubricant influence on internal stresses in sign variable slippage case, discussing chemisorption, wear resistance and stress distribution 22 p3810 A67-39219

Trimming methods for Ti alloy materials including plasma arc cutting, band sawing, shearing, milling, nibbling and blanking 22 p3811 A67-39308

Similarity solutions for compressible laminar boundary layer, showing pressure and heat and mass transfer effects on wall temperature and shear stress 22 p3918 A67-39716

Ablators for severe reentry environments evaluated from modifications of reference model constructed of epoxy resin with silica fiber and phenolic filler 22 p3826 A67-39887

Cylindrical thin walled open section structures heated nonuniformly, calculating various elastic parameters, torsion properties and shearing stress 22 p3916 A67-40450

Numerical data for plane thermal stresses in isotropic elastic square plate bounded by edge stiffeners and under symmetric temperature distributions 23 p4073 A67-40611

Infinitesimal dislocation theory applied to materials with cracks and cylindrical hole, straight boundary between bonded materials and cylindrical insert subject to antiplane shearing stress 23 p4078 A67-41165

Turbulence structure of equilibrium boundary layers, discussing shear stress, thickness, eddy motion and intensity spectra 23 p3990 A67-41168

Heat transfer, skin friction and shearing stress from similar solutions to compressible laminar boundary layer equations for flow over flat plate 23 p4082 A67-41246

Tensile to shear transition behavior of fatigue crack fronts during cycling of sheet materials, noting correlation of shear with crack stress intensities 24 p4170 A67-41950

17 p2964 A67-33150
 Monatomic step patterns on /100/ cleavage and tensile crack faces of NaCl crystals originate from dislocation processes of crack tip released by shear stress distribution 18 p3097 A67-33482
 Shear stress distribution and dislocation processes at moving crack tips in ionic crystals 18 p3097 A67-33483
 Maximum shear stress dependence on composite materials microstructure, noting filler and binder role 18 p3069 A67-34170
 Differential equations and potential for simply supported anisotropic sandwich plate under compression and shear stresses above buckling limit 19 p3341 A67-35575
 Stability condition for inhomogeneous elastic body subjected to internal stresses 20 p3535 A67-36392
 Circumferential displacement and shearing stresses in out-of-plane elasticity problem for solid torus 20 p3538 A67-36672
 Low molecular weight polymer flow behavior variation with shear rate, shear stress and temperature 20 p3473 A67-36914
 Stress-strain relationships for single layer used to obtain stress distribution in orthotropic laminates subjected to axial and shear stresses [ASME PAPER 66-WA/RP-5]

20 p3542 A67-37611
 Netting analysis of reinforced sheets for load envelopes which combine tension and shear, determining optimum fiber arrangements 21 p3729 A67-39082

Surface active lubricant influence on internal stresses in sign variable slippage case, discussing chemisorption, wear resistance and stress distribution 22 p3810 A67-39219

Trimming methods for Ti alloy materials including plasma arc cutting, band sawing, shearing, milling, nibbling and blanking 22 p3811 A67-39308

Similarity solutions for compressible laminar boundary layer, showing pressure and heat and mass transfer effects on wall temperature and shear stress 22 p3918 A67-39716

Ablators for severe reentry environments evaluated from modifications of reference model constructed of epoxy resin with silica fiber and phenolic filler 22 p3826 A67-39887

Cylindrical thin walled open section structures heated nonuniformly, calculating various elastic parameters, torsion properties and shearing stress 22 p3916 A67-40450

Numerical data for plane thermal stresses in isotropic elastic square plate bounded by edge stiffeners and under symmetric temperature distributions 23 p4073 A67-40611

Infinitesimal dislocation theory applied to materials with cracks and cylindrical hole, straight boundary between bonded materials and cylindrical insert subject to antiplane shearing stress 23 p4078 A67-41165

Turbulence structure of equilibrium boundary layers, discussing shear stress, thickness, eddy motion and intensity spectra 23 p3990 A67-41168

Heat transfer, skin friction and shearing stress from similar solutions to compressible laminar boundary layer equations for flow over flat plate 23 p4082 A67-41246

Tensile to shear transition behavior of fatigue crack fronts during cycling of sheet materials, noting correlation of shear with crack stress intensities 24 p4170 A67-41950

24 p4170 A67-41950
 SHEATH
 S PLASMA SHEATH
 SHEET

S CURRENT SHEET
 S ELASTIC SHEET
 S FOIL
 S PANEL
 S PLATE
 S VORTEX SHEET
 SHEET METAL

Elastoplastic behavior of riveted joints subjected to pulsating and alternating stress and preliminary fatigue cycles 01 p0163 A67-11151

Tensile plastic instability in axisymmetric deformation of sheet metals 04 p0710 A67-14976

Fatigue crack propagation in sheet metal, noting usefulness of McClintock formula 05 p0924 A67-17332

Cold plastic deformation, rolling direction and annealing temperature effect on mechanical properties of sheet niobium at

room and high temperature 05 p0831 A67-17504
 Small additions of refractory elements effect on structure and properties of sheets of Al-Zn-Mg alloy in various states 07 p1201 A67-19254
 Integrally formed compression panel efficiencies compared with other aerospace panel concepts 10 p1729 A67-23769
 Hot pressing technique for aluminum sheet and stainless steel wire to produce composite high tensile strength plate 12 p1954 A67-25289
 Fracture toughness of 7075-T6 and -T651 sheet, plate and multilayered adhesive bonded panels, showing independence of thickness and number of layers [ASME PAPER 67-MET-4] 12 p1956 A67-25948
 Effect of V, Zr, and Y additions on mechanical properties of 1 mm sheet molybdenum 13 p2130 A67-26392
 Properties of fabricated ingot beryllium sheet selectively alloyed with copper to obtain improved strength 13 p2139 A67-27125
 Mechanical properties of beryllium-aluminum alloy sheet with improved fabricability 13 p2140 A67-27128
 Structural evaluation of sheet beryllium fabricated by three different methods 13 p2140 A67-27136
 Low noise SiFe sheet development and application, considering effects on magnetic properties 13 p2178 A67-27139
 Texture strengthening and fracture toughness of titanium alloy sheets biaxial stress fields at room and cryogenic temperatures 13 p2142 A67-27442
 Heat flux requirements for cutting low-plasticity metal sheets on lathe, noting thermal effect 14 p2325 A67-28654
 Silicon and phosphorus role in crack formation in manually welded high temperature resistant steel plate 18 p3063 A67-33673
 Electron fractographic techniques for failure analysis, examining fracture direction, differentiation between hydrogen embrittlement and stress corrosion in steels and cyclic stress 18 p3145 A67-34581
 Cold plastic deformation, rolling direction and annealing temperature effect on mechanical properties of sheet niobium at room and high temperature 21 p3644 A67-38032
 Material point displacement velocity field of bending elements of sheet during profile shaping by roll forming, determining stress-strain condition 21 p3631 A67-38052
 Elastic stability of three-layer cylindrical shell filled with corrugated metallic sheets under combined loads, deriving linear equations 21 p3724 A67-38786
 Electron beams applied during pressworking of sheet materials to provide temperatures favorable to microstructure defect healing 21 p3637 A67-38927
 Creep properties of sheet materials in SST environment for selection of optimal airframe materials 22 p3818 A67-39225
 Bainite beta to alpha transformation in titanium-oxygen system, using high temperature metallography techniques 22 p3821 A67-39825
 Tensile properties and notch toughness of aluminum alloy sheet and welded joints evaluated at room and subzero temperatures 23 p4020 A67-41348
 Fatigue crack propagation rate in sheet specimens under various loadings simulating rivet forces 24 p4247 A67-41944

SHELL
 S ANISOTROPIC SHELL
 S ATMOSPHERIC SHELL
 S CIRCULAR SHELL
 S CONICAL SHELL
 S CORRUGATED SHELL
 S CYLINDRICAL SHELL
 S ELASTIC SHELL
 S HEMISPHERICAL SHELL
 S K-SHELL
 S LIQUID-FILLED SHELL
 S METAL SHELL
 S ORTHOTROPIC SHELL
 S REINFORCED SHELL
 S SPHERICAL SHELL
 S THIN WALLED SHELL
 S TOROIDAL SHELL

SHELL STABILITY
 SA BUCKLING

Eigenfrequencies of flexural vibrations of circular cylindrical shells calculated by various methods and compared with measured values 01 p0162 A67-10839
 Nonlinear equations of shell equilibrium, considering slew, elongation and shear 01 p0162 A67-10903
 Arbitrary shallow shell under action of space-time homogeneous random load 01 p0163 A67-10995
 Nonlinear influence coefficient obtained by extension of Reissner nonlinear analysis to include uniform pressure loading over surface of spherical shell 01 p0164 A67-11178
 Loading rate effect on critical behavior of cylindrical shell responses 01 p0164 A67-11187
 Stability equation of elastic bodies subjected to body and pressure forces derived using virtual work principle, noting specialization to thin shells 01 p0165 A67-11307
 Toroidal shell of circular cross section free of bending under uniform normal hydrostatic pressure 02 p0336 A67-11589
 HF response of shell-type structures to buffeting aerodynamic environment [AIAA PAPER 66-81] 02 p0337 A67-11930
 Elastoplastic equilibrium of thin arbitrary shells of revolution with finite deflection comparable to shell thickness 02 p0340 A67-12661
 Stress-strain calculations for thin walled axisymmetric shells with arbitrarily shaped midplane based on second order theory 03 p0521 A67-13018
 Buckling loads of reinforced cylindrical shells, discussing size and placement of stiffening members 03 p0521 A67-13019
 Stability of thin walled conical shells under axially symmetric loading determined from nonlinear shell theory 03 p0521 A67-13020
 Load concentration effects on stability of rigidly reinforced strictly convex shell, determining upper critical load 03 p0526 A67-14063
 Soviet book on strength and dynamics of aircraft engines 03 p0526 A67-14068
 Strength of cylindrical shells under local radial loads and circumferential bending moments conveyed by reinforcing elements 03 p0527 A67-14069
 Strength of cylindrical shell deformed under radial temperature field 03 p0527 A67-14073
 Thin shells and stability in aerospace structures [AIAA PAPER 66-1022] 03 p0529 A67-14154
 Modification of Potter method of Gaussian elimination for solving eigenvalue problems of buckling and free vibrations of shells of revolution 04 p0656 A67-14839
 Variable thickness tension shell in nonlinear membrane analysis 04 p0709 A67-14843
 Modes effect on plastic buckling of compressed cylindrical shells, considering deformation theory vs incremental theory 04 p0710 A67-14852
 Vibration tests of hemispherical shell with free edge and constant thickness, exploring dynamic behavior through analytical methods 04 p0714 A67-15425
 Inversion of eccentricity effect in stiffened cylindrical shells buckling under external pressure 04 p0716 A67-15746
 Point load on thin shallow elliptic paraboloid with singular solutions expressed as power series 04 p0719 A67-15934
 Inelastic buckling of rib-cored orthotropic sandwich cylinders under external hydrostatic pressure, evaluating rigidity factor and Poisson ratio effect 04 p0719 A67-15936
 Eigenfunction expansion solution for axisymmetric vibrations of shallow spherical shell with concentrated mass 05 p0910 A67-16147
 Dynamic stability of coaxial cylindrical shells in nonuniform temperature field under uniformly distributed axial compression load 05 p0913 A67-16189
 Stressed and strained state of reinforced cylindrical shell under nonuniform heating and compression, noting three solutions to buckling problem 05 p0913 A67-16190
 Conical shell stability during axial compression and internal pressure under conditions of heating, noting reduction of critical load 05 p0913 A67-16192
 Deflection of centrally loaded thin circular

elastic plates on equally spaced point supports 05 p0917 A67-16366
 Instability of thin reinforced cylindrical shell clamped at both ends and energy method calculation of critical pressure 05 p0918 A67-16422
 Initial equilibrium state stability of multilayer orthotropic circular cylindrical shell based on anisotropic shell theory 05 p0919 A67-16585
 Axial flow dynamics of flexible slender cylindrical body immersed in fluid, emphasizing flow velocity, frictional forces, buckling and oscillatory instabilities 05 p0920 A67-16815
 Initial postbuckling behavior of double curvature shell segments under several loading conditions determined, using Koiter theory 05 p0921 A67-16885
 Supercritical deformation energy of thin elastic shell with clamped edge 05 p0921 A67-16940
 Linear buckling of circular cylindrical shells under asymmetric axial compressive stress distributions 05 p0922 A67-17103
 Approximate Vlasov equation for local stability of zero-moment shells of positive Gaussian curvature under arbitrary multiparameter subcritical load 05 p0923 A67-17186
 Matrix displacement approach to discrete element structural analysis for thin shell instability, emphasizing determination of membrane force distribution 05 p0925 A67-17352
 Kollmann theory on critical rpm of hollow shells of revolution containing liquid, explaining unstable oscillations appearance in supercritical region 06 p1100 A67-17992
 Finite difference method stability analysis of deformed eccentrically stiffened shells of revolution, accounting for finite prebuckling rotations [AIAA PAPER 67-110] 06 p1101 A67-18285
 Buckling of truncated conical shells due to directional thermal loadings [AIAA PAPER 67-112] 06 p1103 A67-18355
 Frequency response of pressurized torus shell held free or rigidly [AIAA PAPER 67-73] 06 p1104 A67-18470
 Vibration mode of conical shells measured, showing variation with conical angle and circumferential wave number 06 p1105 A67-18591
 Stability of truncated conical thin shells under torsional load 06 p1105 A67-18592
 Truncated conical shell stability under axial compression loads applied parallel to axis rather than along generatrix 06 p1105 A67-18593
 Stability of circular cylindrical shell in supersonic nonviscous conducting gas flow with unperturbed velocity and under magnetic field 06 p1106 A67-18622
 Logarithmic particular solutions of nonhomogeneous equation of cyclic deformation of shallow conical shell under nonuniform heating 06 p1109 A67-18664
 Shape of interaction curve for axial compression vs torsional buckling of conical shells 06 p1110 A67-18858
 Statistical analysis discrepancy in physical experimental values of buckling pressures of spherical shells 06 p1111 A67-18876
 Temperature field of elements of thin shelled surfaces of satellites for radiant heat transfer 07 p1265 A67-19104
 Stability loss in thin walled plastic shell under tensile loading in plane stress conditions 07 p1261 A67-19190
 Cylindrical shell stability under axial compression analyzed by generalized power series method, noting half-waves and critical load 07 p1262 A67-19345
 Thermal stresses in thin walled open spherical shell of constant thickness 07 p1262 A67-19348
 Explosive loading and structural response measurement techniques for predicting large elastic-plastic dynamic and permanent deformations of shells under dynamic loading conditions 07 p1262 A67-19411
 Small twist superposed on nonuniform large extensions in circular sheet with small hole 07 p1263 A67-19730
 Spherical plastic shell theory and design methods 07 p1264 A67-20233
 Remedies for deficiencies in approximations near transition point in asymptotic methods used for estimates of solutions to differential equations governing

axisymmetric vibrations of thin elastic shells 08 p1414 A67-20346

Imperfection sensitivity of eccentrically axial and ring stiffened cylindrical shells under axial compression and hydrostatic pressure 08 p1417 A67-20552

Unsymmetric free vibrations of orthotropic sandwich shells of revolution treated by Rayleigh-Ritz technique 08 p1417 A67-20555

Stability of toroidal shell under uniform external pressure solved using series expansion, considering buckling modes 08 p1417 A67-20557

Thermal buckling of prestressed cylindrical shells and rings where expansion coefficient of external layer is smaller [ONERA-TP-422] 09 p1574 A67-21848

Buckle pattern representation for isotropic cylinder rendering results of critical stress and role of buckle pattern upon ratio of critical stress 09 p1575 A67-22164

Thin shells and stability in aerospace structures [AIAA PAPER 66-1022] 10 p1715 A67-22767

Quasi-static problems of isotropic viscoelastic shells subjected to external loading and steady temperature field 10 p1717 A67-22943

Bending of viscoelastic cylindrical shell resting on viscoelastic base with monodirectional characteristic 10 p1717 A67-22945

Inextensional buckling of thin conical shell under axial compression [AIAA PAPER 66-125] 10 p1717 A67-23129

Plastic flow and instability behavior of thin walled tubes of nickel-chrome steel subjected to constant ratio tensile stress 10 p1719 A67-23485

Closed toroidal shell stability under effect of uniformly distributed external pressure 10 p1720 A67-23602

Dynamic stability of cylindrical shell reinforced by thin walled rigid longitudinal ribs 10 p1721 A67-23604

Straightforward method consistent with virtual work principle for accelerating convergence to exact solution in shell analysis by matrix displacement method 10 p1725 A67-23714

Finite element displacement method extended to bifurcation buckling of shells of revolution under axisymmetric loading 10 p1725 A67-23715

Structural design of stiffened cylindrical shells, discussing minimum weight, prevention of buckling modes, etc 10 p1726 A67-23719

Prebuckling deformations, ring stiffeners and load eccentricity effect on buckling of stiffened cylinders 10 p1727 A67-23759

Critical axial compression buckling loads of orthotropic cylinders having stiffening patterns analyzed, considering three instability failure modes 10 p1728 A67-23760

Unified theory for bending and buckling of honeycomb type sandwich shell and linearized governing equations applied to axially compressed circular cylinder shells 10 p1728 A67-23761

Applicability of Southwell plot to interpretation of test data from instability studies of shell bodies, based on modified Donnell equations 10 p1728 A67-23763

Bifurcation phenomena in spherical shells under concentrated and ring loads taking into account finite prebuckling deformation 10 p1728 A67-23764

Invariant stress and deformation functions for doubly curved shells, noting reduction of equilibrium equations and surface strain-displacement relations into compatibility equation 10 p1730 A67-23834

Initial postbuckling behavior of spherical shell under external pressure determined using Koiter theory, analyzing effects of imperfections on buckling strength of structures 10 p1730 A67-23835

Nonlinear membrane equations for extremely thin shell of revolution of very deformable material, assuming large displacements, rotations and strains 10 p1730 A67-23836

Deformation of laminated shell structures under axisymmetric loading, deriving differential equation by considering boundary conditions at both ends 10 p1731 A67-23846

Stability analysis of symmetrically loaded thin walled spherical shell, noting

construction of asymptotic expansion, error estimation and application of elasticity theory 11 p1871 A67-24152

Conical shell stability under hydrostatic pressure for various in-plane boundary conditions, stressing axial restraint effect 11 p1873 A67-24214

Instability of cylindrical shells stiffened with rings and stringers of nonuniform cross sections, noting load and weight savings 11 p1874 A67-24225

Buckling test data for internal integral ring-stiffened aluminum cylinders under combinations of axisymmetrical axial load and external lateral pressure 11 p1875 A67-24611

Torsional buckling stress of orthotropic cylindrical shells with high order terms due to internal pressure rise 11 p1876 A67-24701

Cylindrical shell stability under external pressure, presenting critical load value and nature of undulation 11 p1880 A67-25054

Nonlinear equations of shell equilibrium, considering slew, elongation and shear 11 p1880 A67-25073

Approximate solution of Novozhilov equilibrium equation for noncircular cylindrical shells by small parameter method 12 p1919 A67-25562

Closed cylindrical shell stability under combined bending and axial compression taking into account original arbitrary imperfection of shell form 12 p2020 A67-25567

Ribbed circular cylindrical shell under axial compression, reducing problem to determination of deflection and stress functions 12 p2020 A67-25571

Cylindrical shell stability under external radial load noting stress-strain states, critical load, etc 12 p2020 A67-25572

Cylindrical shell stability under nonuniform load, noting critical load dependence on subtending angle 12 p2020 A67-25573

Equilibrium equations of Vlasov engineering moment theory of shells of variable curvature 12 p2021 A67-25577

Oscillations and stability of cylindrical shell in conducting gas flow in presence of magnetic field 12 p2021 A67-25581

Stress-strain state of cylindrical shell analyzed based on elasticity theory, noting boundary value problem 12 p2022 A67-25583

Oscillation and stability of system of thin elastic shells in potential inviscid and incompressible fluid flow 12 p2023 A67-25589

Deflection function of glass fiber reinforced circular cylindrical shells under axial supercritical compressive loading 12 p2023 A67-25590

Elastic filler effect on thin cylindrical sandwich shell stability subjected to compression along generatrix 12 p2023 A67-25592

Three-layer shell with lightweight filler under creep studied for initial forms of equilibrium 12 p2024 A67-25598

Stress-strain state of thin cylindrical shell under effect of local forces 12 p2024 A67-25601

Nonlinear equations of thin shell theory, especially equilibrium equations, taking into account displacements, elongations and shear, noting linearization in stability problems 12 p2025 A67-25605

Dynamics of rigid plastic thin walled shells for short term constant high intensity load 12 p2025 A67-25607

Displacements, stresses and moments in orthotropic and bimetallic cylindrical shells under radial concentrated forces determined via computer method 12 p2025 A67-25608

Variational derivation of nonlinear equilibrium equations for three-layer conical shell with rigid incompressible filler under external pressure 12 p2025 A67-25609

Stability of cylindrical shell of oval cross section compressed along generatrix and under external pressure analyzed, using Laplace transforms 12 p2025 A67-25612

Critical stresses of compressed three-layer cylindrical shell of asymmetrical structure in presence of variable temperature 12 p2026 A67-25614

Axisymmetrical deformation and static instability region of circular cylindrical shell under longitudinal compressive load 12 p2026 A67-25615

Rigid plastic cylindrical shell axisymmetrical deformations in terms of

Tresca yield condition and gradient law when under load 12 p2026 A67-25618

Initial imperfection effects on free oscillation frequencies of cylindrical shell under static axial load 12 p2026 A67-25619

Reinforced cylindrical shell stability under external pressure, considering irregular frame disposition effect 12 p2027 A67-25620

Variational methods solutions for thin shell deformation mechanics 12 p2027 A67-25621

Rigidly reinforced conical shell stability under external load investigated for boundary conditions 12 p2027 A67-25622

Equation for relation between critical stresses of cylindrical shell loading and minimum natural-oscillation frequency of unloaded shell 12 p2027 A67-25623

Asymptotic method of integrating differential equations applied to analysis of axisymmetrical oscillations of thin elastic LF shells of revolution 12 p2027 A67-25624

Natural oscillation frequency of multilayer shells of revolution with nonsymmetrical structure containing rigid filler and subjected to transverse load 12 p2027 A67-25626

Geometrically nonlinear theory of elastic stability of anisotropic shells and linear stability of orthotropic plates, using differential equations 12 p2028 A67-25628

Large deformations of zero moment orthotropic shells of revolution under action of inertial loads caused by centrifugal acceleration of shells 12 p2028 A67-25629

Asymptotic elastoplastic condition of spherical shell weakened by circular hole and sustaining residual deflections 12 p2028 A67-25631

Vlasov engineering theory of equilibrium of shells used to study stress-strain state of closed circular cylindrical shell loaded by internal pressure 12 p2028 A67-25632

Shallow conical shell stability acted upon by external hydrostatic pressure 12 p2028 A67-25635

Resolvent equations of shallow multilayer shells of regular structure to solve problems involving calculations of strength, stability and oscillations 12 p2029 A67-25668

Asymptotic integration technique for small axisymmetrical oscillations of thin walled elastic shell of revolution for case of double reversal point 12 p2029 A67-25675

Effect of axisymmetric impact against water on shallow clamped aluminum spherical shell-type caps 12 p2030 A67-25937

Buckling of thin walled circular cylindrical shells under external pressure treated by Sanders theory 12 p2030 A67-25940

Axisymmetrical stability loss problem in thin walled cylindrical shell with continuous elastic filler 12 p2031 A67-25958

Lower critical load for deformation of cylindrical shell in torsion and hinged along edges 13 p2215 A67-26376

Goldenveizer technique to determine stability loss by shells of negative Gaussian curvature 13 p2218 A67-26891

Stress and stability of stringer-reinforced circular cylindrical shell 13 p2218 A67-26892

Flutter and dynamic stability of closed thin walled elastic cylindrical shell filled with liquid 13 p2219 A67-26903

Stability loss in steel cylindrical shells under axial compression for case of elastic and plastic strains 13 p2219 A67-26904

Differential equation and boundary conditions for sandwich shells, noting bending resistance and shear deformation 13 p2219 A67-26906

Load concentration effects on stability of rigidly reinforced strictly convex shell, determining upper critical load 13 p2221 A67-27722

Interaction between buckling and flutter of circular cylindrical shell subjected to axial compression and placed in axial supersonic flow 14 p2398 A67-28092

Dynamic buckling of ring constrained in rigid circular surface and subjected to transiently applied inertial loading 14 p2398 A67-28093

Stabilizing effects of viscoelastic cores on response of long circular cylindrical shells subjected to time dependent axial loads 14 p2399 A67-28118

Stability of inhomogeneous anisotropic cylindrical shells containing elastic cores under pressure, axial load and

- torsion 14 p2399 A67-28119
- Supercritical deformation energy of thin elastic shell with clamped edge 14 p2400 A67-28493
- Anisotropic circular cylindrical shell stability under linear axial stress and internal pressure 14 p2400 A67-28642
- Vlasov variational method applied to circular cylindrical shell design for local loading 14 p2400 A67-28643
- Cylindrical shell stability under circumferential band load effect applied to freely supported edge 14 p2401 A67-28645
- Cylindrical shell stability under longitudinal impact, examining buckling processes with high speed motion picture camera 14 p2401 A67-28736
- Cylindrical elastic shell under axial compression studied for stability loss, considering large axial strains 14 p2401 A67-28737
- First order finite difference numerical analysis of thin elastic orthotropic and inhomogeneous cylindrical shells with small deformations from external forces 15 p2574 A67-29471
- Displacement equations of prestressed thin bending-resistant shells 15 p2574 A67-29699
- Double curvature influence on rigidity of shell of revolution analyzed for surface loading and cross sectional linear loading, using Fourier series 16 p2766 A67-31149
- Stiffener eccentricity effect on critical load in cylindrical shells under axial compression 17 p2961 A67-32775
- Generalized power series method applied to compressed cylindrical shells stability analysis, giving formulas for direct shell designing 17 p2961 A67-32808
- Finite difference method stability analysis of deformed eccentrically stiffened shells of revolution, accounting for finite prebuckling rotations [AIAA PAPER 67-110] 17 p2963 A67-33015
- Orthotropic circular cylindrical shell of elastic material instability under combined torsion and hydrostatic pressure investigated for simply supported and clamped ends 17 p2963 A67-33016
- Shell theory applied to anisotropy problem in axisymmetric cylindrical shells, illustrating shear deformation, twisting couple and circumferential displacement [ASME PAPER 67-APM-28] 17 p2965 A67-33155
- Stability of cylindrical shells under torsion 18 p3144 A67-34171
- Graphic representation of Mises formula for stability analysis of cylindrical shell, discussing critical pressure and time and labor saving 19 p3338 A67-34875
- Quasi-static equilibrium of truncated conical shell of revolution discussed in terms of zero-moment theory, when under cyclic load 19 p3341 A67-35631
- Small elastic-plastic deformation /caused by internal pressure/ of thin walled tube clamped at one end to rigid support 19 p3341 A67-35715
- Stiffness matrix of thin flat triangular elements of nonzero Gaussian curvature derived by reducing geometrical idealization errors 19 p3342 A67-35750
- Prestressed-shell buckling, using Budianski-Koiter tensor nonlinear equilibrium equations by numerical analysis 19 p3343 A67-35778
- Differential equation for axisymmetric deformation of thin circular cylindrical shell stiffened by circumferential rings and subjected to lateral and axial pressure 20 p3537 A67-36495
- Second boundary value problem for differential equation of elastic equilibrium of shallow cylindrical shell 20 p3543 A67-37721
- Limiting equilibrium of crosswise reinforced cylindrical shells of waffle type, allowing interaction between vertical and horizontal ribs 21 p3717 A67-37972
- Hydrodynamic pressure on elastic cylindrical shell from acoustic shock wave, using higher order asymptotic approximations 21 p3717 A67-37973
- Circular cylindrical shell buckling mode and upper critical load under external transverse pressure, considering dynamic edge effect on shell stability 21 p3717 A67-37975
- Truncated elastic shell of revolution stability under tensile stress 21 p3718 A67-37978
- Shell curvature variation parameter noting influence on equilibrium equations and error in equations of strain compatibility 21 p3718 A67-37981
- Shell of revolution stability under axial compressive loading with changes in curvature due to initial imperfections effects 21 p3719 A67-38053
- Oscillation and stability of two irregular thin elastic cylindrical shells in potential flow of compressible fluid 21 p3720 A67-38296
- Dynamic instability of longitudinal oscillations of cylindrical shell charged with ideal fluid established by approximate reduction of nonlinear equations 21 p3720 A67-38297
- Nonlinear equilibrium equation system derived for shells of revolution, considering shell stability 21 p3721 A67-38304
- Elastic spherical shell stability under thermal stresses from abrupt temperature change at shell equator solved, using Fredholm integral equation 21 p3721 A67-38308
- Cylindrical shell deflection by radial concentrated force, using digital computer for stability analysis 21 p3721 A67-38309
- Eccentrically stiffened cylinders instability under axial compression, lateral or hydrostatic pressure and torsion 21 p3722 A67-38545
- Ten thin walled cylindrical shells under internal load investigated for bending stability, comparing experimental and analytical results 21 p3724 A67-38785
- Panel flutter analysis of hinged closed circular cylindrical shell in supersonic gas flow, considering axial compression and structural damping 21 p3725 A67-38788
- Ideal incompressible fluid axisymmetrical oscillations in elastic cylindrical shell, determining normal modes and natural frequencies of shell and fluid 21 p3613 A67-38789
- Stress analysis for rib-reinforced cylindrical shell subjected to rapidly varying pressure, calculating deflections and bending moments 21 p3725 A67-38790
- Natural frequencies and shape of axisymmetric oscillations of thin spherical shell under initial stress calculated via boundary value problem, using computer method 21 p3725 A67-38791
- Elpatovskii method applied to axisymmetric deformation of two-layer cylindrical shell with helical glass fiber reinforcements, obtaining equations for stressed state 21 p3725 A67-38795
- Critical compression stresses in cylindrical panel with clamped lateral edges and free longitudinal edge 21 p3726 A67-38796
- Calculated stressed state of short thin walled shells under transverse loads and torsional moments 21 p3726 A67-38797
- Triple layer cylindrical shells stability beyond elastic limit studied based on plastic deformations, loading principle and shallow shell theory 21 p3727 A67-38838
- Three layer cylindrical shell stability in elastic and inelastic domains under separate and joint loads, considering filler layer deformation 21 p3727 A67-38840
- Buckling of truncated conical shells due to directional thermal loadings [AIAA PAPER 67-112] 21 p3728 A67-38873
- Unloaded thin walled spherical shell rigidly hinged along edge noting existence of nontrivial form of equilibrium and negative lower critical load 22 p3910 A67-39402
- Ring finite element analysis for shells of revolution improved by extending polynomials representing displacements 22 p3911 A67-39499
- Shallow spherical shell dynamic stability under variable moment load 22 p3911 A67-39683
- Cracked cylindrical shell stress-strain state under symmetric load, discussing shell curvature effect and integral equation solution 22 p3911 A67-39684
- Elastically filled imperfect closed cylindrical shell stability, showing initial configuration defect effects on critical load relation to filler rigidity 22 p3912 A67-39685
- Buckling loads in orthotropic circular cylindrical shells under simultaneous longitudinal and external peripheral pressure stresses 22 p3912 A67-39752
- Reissner differential equation simplified for problems involving small strains in thin shells of revolution due to symmetrical deflections 23 p4073 A67-40612
- Bifurcation phenomena in spherical shells under concentrated and ring loads taking into account finite prebuckling deformation 23 p4080 A67-41728
- Elastic buckling loads of shallow spherical shells supported by edge rings including nonlinear prebuckling effects 23 p4080 A67-41729
- Stress functions for truncated conical shell buckling under uniform static pressure 23 p4081 A67-41760
- Shallow spherical shell stress and displacement distribution calculated by integral equation 24 p4249 A67-42104
- Thin elastic shell neutral equilibrium under axial compression and hydrostatic pressure, obtaining parametric terms for expressions by using quadratic functional 24 p4249 A67-42303
- Thin elastic shell nonlinear buckling theories, studying circular cylinder and truncated cone cases 24 p4252 A67-43096
- ### SHELL THEORY
- MHD effects during motion of dielectric shell in electrolyte in presence of external magnetic field 01 p0120 A67-10185
- Hollow rolling bearings for improved stress-fatigue and grain flow, noting welding problems 01 p0079 A67-10727
- Solutions to equations of multilayer anisotropic shells represented in terms of resolving function for high order equation 01 p0162 A67-10985
- Shell theory results compared with results obtained by asymptotic integration of three-dimensional equations of elasticity theory and error correction methods 01 p0163 A67-10986
- Vibration modes and relative frequencies of shells stiffened by angularly equidistant stringers, using Vlasov theory of circular cylindrical shells 01 p0163 A67-11148
- Computation by approximate methods of stress resultants for shell of revolution under distributed externally applied load 01 p0164 A67-11185
- Shells of revolution analyzed under symmetric and antisymmetric loading by matrix displacement method 01 p0164 A67-11191
- Yield surfaces for nonhomogeneous shells of revolution 03 p0523 A67-13501
- Elasticity and shell theory solutions for long circular cylindrical shells compared by numerical analysis 04 p0709 A67-14811
- Fatigue life of thin walled shells with inside pressure and outside support during axial motion [ASME PAPER 66-WA/MET-13] 04 p0712 A67-15377
- Plastic analysis of rib reinforced cylindrical shells using strain mapping method for Tresca yield conditions [ASME PAPER 66-WA/APM-14] 04 p0713 A67-15406
- Nonlinear elastic thin shell theory in parallel approach based on Kirchhoff hypothesis 04 p0715 A67-15585
- Axisymmetric motions of Timoshenko type cylindrical shells composed of two elastic isotropic layers of different materials and thicknesses connected by perfect bond 04 p0717 A67-15909
- Soviet monograph on dynamics and durability of machines 05 p0915 A67-16219
- Bending problem of isotropic shallow helical cantilever shell under distributed normal load 05 p0915 A67-16220
- Stressed state in rotationally symmetric shell assuming ideally rigid plastic, determining yield condition in terms of stress resultants 05 p0917 A67-16244
- Steady state creep stress in shells under uniform internal pressure derived, using transition theory of Seth 05 p0920 A67-16722
- Linear theory of homogeneous anisotropic elastic shells and plates without considering Love-Kirchhoff assumptions 05 p0921 A67-16883
- Small plastic deformation theory determination of elastoplastic stressed state of thin walled isotropic incompressible shell of revolution under axisymmetric power loads and nonuniform heating 05 p0922 A67-17177
- Stress-strain relations of linear theory of shells extended to corresponding inversion

with more complex results 06 p1100 A67-18111

Linear shell theory for nonlinear transverse coupled vibrations of partially filled circular cylindrical elastic tank [AIAA PAPER 67-74] 06 p1101 A67-18272

Supersonic flutter of thin walled circular cylindrical shells under compressive loading, comparing theory and experiment [AIAA PAPER 67-77] 06 p1103 A67-18354

Taylor theorem test as tool for determining completeness and convergence properties of finite element displacement functions, showing application to axisymmetric shell and conductive heat transfer [AIAA PAPER 67-143] 06 p1103 A67-18440

Analytical and empirical results on shell panel flutter boundaries compared, using nonlinear Donnell theory and linear piston theory approximation [AIAA PAPER 67-78] 06 p1104 A67-18452

Vibrational characteristics of composite shells, noting effects of circular joint connecting two components [AIAA PAPER 67-72] 06 p1104 A67-18496

Characteristic method analysis of linear system of dynamic cylindrical equation for axisymmetric motion, including rotary inertia and shear correction factor [AIAA PAPER 67-79] 06 p1104 A67-18497

Snap-through buckling of open bimetallic shallow spherical shell under uniform temperature field 06 p1105 A67-18590

Forming closed contour shells by straining with expandable punch 07 p1191 A67-19750

Cosserat plane and shell theory development from considerations concerning equilibrium conditions with aid of introduced stress functions 07 p1263 A67-19885

Stability of membrane solution in nonlinear plate and shell theory 07 p1263 A67-20032

Displacement formulations of first order linear thin elastic shell equations in terms of stress resultant and middle surface, using modified Kirchhoff hypothesis 08 p1417 A67-20551

Equilibrium and elastic properties of triangular and parallelogram bending elements for plate and shell networks, discussing transition element and matrix force methods 08 p1417 A67-20553

Shell structures solved numerically, using network of partial panels 08 p1417 A67-20556

One-dimensional adiabatic equilibration of plate with starting temperature compared with nonadiabatic equilibration and exoatmospheric cooling of cylindrical metallic and plastic shells 08 p1429 A67-21527

Straightforward method consistent with virtual work principle for accelerating convergence to exact solution in shell analysis by matrix displacement method 10 p1725 A67-23714

Linear motion equations including effects of transverse shear deformation and rotary inertia derived for thin elastic isotropic conical shells of revolution 10 p1729 A67-23767

Shells of revolution having arbitrary stiffness distribution of loads and temperatures 10 p1730 A67-23771

Basic equations for shells with circular parallel sections including shells of revolution 10 p1731 A67-23844

Fast neutron activation cross sections of Se and Fe measured, noting subshell closure effect and isomer ratio 11 p1822 A67-23979

Bending strain in linear shell theory, noting surface differential geometry and rotation vector and tensor [ASCE PAPER 268] 11 p1874 A67-24430

Nonlinear membrane theory for thin elastic inflatable shells during pressurization phase 11 p1875 A67-24432

Variational principle for elastic thin shells and panels of arbitrary shape and load conditions 11 p1876 A67-24624

Variational principle as basis for dynamics of elastic shell theory, discussing motion described by Timoshenko type equation 11 p1877 A67-24853

Stress distribution in hole weakened shells of negative Gaussian curvature, noting linear nature of distribution and propagation direction of perturbation 11 p1879 A67-24888

Theory of shells and plates - Conference, Baku, Azerbaidzhan SSR, September 1966 12 p2017 A67-25561

Approximate solution of Novozhilov equilibrium equation for noncircular cylindrical shells by small parameter method 12 p2019 A67-25562

Variational principles and reciprocity theorems for dynamic problems of elastic shell theory, particularly motion described by linear equations of Timoshenko type theory 12 p2019 A67-25563

Approximate solutions for boundary value problems of cylindrical shells of arbitrary geometry 12 p2021 A67-25576

Equilibrium equations of Vlasov engineering moment theory of shells of variable curvature 12 p2021 A67-25577

Discrete analysis in plate and shell theory based on method of constructing difference equation, using strain energy of system 12 p2023 A67-25591

Thermoplasticity problem for circular cylindrical shell subjected to arbitrary axisymmetric heating and loading 12 p2023 A67-25593

Infinite systems of equations for multiply connected finite regions in shells obtained by extending solutions for stressed state in infinite multiply connected regions 12 p2024 A67-25600

Nonlinear equations of thin shell theory, especially equilibrium equations, taking into account displacements, elongations and shear, noting linearization in stability problems 12 p2025 A67-25605

Longitudinal impact of two reinforced cylindrical shells coupled to each other at ribs against solid body 12 p2025 A67-25611

Algorithms for operator partitioning method in reducing shell equations solution to calculation of solid intersecting rod systems 12 p2026 A67-25617

Variational methods solutions for thin shell deformation mechanics 12 p2027 A67-25621

Geometrically nonlinear theory of elastic stability of anisotropic shells and linear stability of orthotropic plates, using differential equations 12 p2028 A67-25628

Asymptotic methods of obtaining refined solutions for zero moment equations of concentrated loads applied to shells with Gaussian curvature 12 p2028 A67-25630

Vlasov engineering theory of equilibrium of shells used to study stress-strain state of closed circular cylindrical shell loaded by internal pressure 12 p2028 A67-25632

Equilibrium equations modified in nonlinear theory of thin walled elastic shells 12 p2028 A67-25634

Asymptotic integration of elasticity theory equations applied to two-dimensional dynamic theory for cylindrical shells 12 p2029 A67-25636

Shells of revolution under axisymmetric loading analyzed within ideally plastic shell theory, examining mathematical difficulties of shell carrying capacity 12 p2029 A67-25637

Dynamic response of clamped shallow thin elastic spherical shells under time dependent loads [AIAA PAPER 68-446] 12 p2030 A67-25915

Vibrational characteristics of composite shells, noting effects of circular joint connecting two components [AIAA PAPER 67-72] 12 p2030 A67-25916

Stressed state of conical shell with circular hole subject to tension and torsion 13 p2218 A67-26888

Testing techniques for electroformed thin shells noting tensile properties determination 13 p2219 A67-27184

General method based on reciprocity theorem developed for problem solutions in elasticity theory 14 p2402 A67-28740

Exact solution of three-dimensional problem to derive algorithm for development of applied theories of improved accuracy for circular cylindrical shell 15 p2576 A67-30179

Holzer method extended to analysis of free vibration of spherical shells, solving boundary value problem as set of initial value problems until all boundary conditions can be satisfied 15 p2577 A67-30193

Transversally isotropic cylindrical shell under periodically spaced axisymmetric band loads, comparing expressions derived for stresses and displacements by elasticity and shell theories 15 p2578 A67-30271

Noncircular cylindrical shell of orthotropic material under distributed load numerically analyzed by shell theory 15 p2578 A67-30272

Deflections and stresses of paraboloidal shells of revolutions under gravity loads for applications to paraboloidal reflector antenna construction 16 p2763 A67-30678

Boundary conditions for thin shells and physical meaning analyzed according to Kirchhoff-Love theory 16 p2764 A67-30862

Stresses due to external forces and moments acting on elastic nonradial circular cylindrical nozzle attached to spherical shell 17 p2959 A67-32409

Zero-moment stressed state in shells of revolution under concentrated loading described by p-analytic functions 17 p2962 A67-32875

Shells of revolution with curved elements noting rigid body displacements in analysis by matrix displacement method 17 p2963 A67-33042

Shells of revolution produced by fiber-wound distributing internal and boundary stresses uniformly over fiber contours 19 p3337 A67-34871

Fiber shells of revolution under compression loads analyzed for use in pressurized balloons 19 p3338 A67-34872

Resolving equations of linear theory of isotropic viscoelastic shells subject to external load and steady temperature field 19 p3340 A67-35508

Stresses acting in oblique cross sections of composite shells computed in reference to different orientations 19 p3342 A67-35719

Zero moment elliptical paraboloidal translational shell under uniformly distributed load, reducing solution to Dirichlet problem 20 p3539 A67-36924

Variational principle as basis for dynamics of elastic shell theory, discussing motion described by Timoshenko type equation 20 p3542 A67-37541

Stress analysis of ribbed shell of revolution, noting case of open shell of zero Gaussian curvature with cyclic symmetrical stresses 21 p3718 A67-37980

Boundary value solutions by approximate method for variable thickness and rigidity shells using equilibrium equations 21 p3718 A67-37983

Shells and solid wall systems with/without symmetrical cross section, considering construction, stress-strain and calculation procedures 21 p3722 A67-38524

Calculation method for mono-, two- and three-spar wings including membranes and plate, discussing stress formulas 21 p3722 A67-38525

Book on inelastic shell theory and research covering field equations, viscous and plastic response, viscoelasticity, elastoplastic deformation, limit analysis, steady creep, etc 21 p3722 A67-38531

Linear shell theory for nonlinear transverse coupled vibrations of partially filled circular cylindrical elastic tank [AIAA PAPER 67-74] 21 p3727 A67-38866

Supersonic flutter of thin walled circular cylindrical shells under compressive loading, comparing theory and experiment [AIAA PAPER 67-77] 21 p3727 A67-38869

Approximate shell theory for unrestricted elastic deformation, discussing treatment of motion equations 22 p3909 A67-39293

Hypergeometric functions studied for solution of problems on elastic equilibrium of circular plates and shells of revolution 22 p3909 A67-39398

Hot electron plasma production, discussing microwave power feeding across magnetic flux lines producing closed plasma shell structure 22 p3854 A67-40243

Homogeneous and sandwich spherical caps axisymmetric vibration natural frequencies solved approximately, noting application to shallow and spherical shell problems 23 p4073 A67-40617

Homogeneous and sandwich spherical caps and circular plate torsional frequency calculations based on sandwich and spherical shell equations 23 p4073 A67-40618

Stiffness matrix for shallow rectangular shell element and application of finite element displacement method 23 p4073 A67-40628

Validity range of Flugge bending and Donnell theories established by comparing results with elasticity theory based results 23 p4074 A67-40630

Shear modulus measurements in fiber-reinforced composites by plate-twisting test and torsion tube in terms of classical

laminated plate and shell theory 23 p4021 A67-40738

Soviet book on elasticity and plasticity covering perforated plates and shells and elastohereditary media mechanics 23 p4077 A67-40748

Elastic bending of thin shells and plates perforated with holes in various arrays, calculating stress distribution and concentration 23 p4077 A67-40749

Book on nonlinear theory of thin shells covering deformation and stress state, surface kinetics, momentum conservation, etc 24 p4246 A67-41800

Dynamic boundary conditions for Kirchhoff constrained shell, obtaining symbolic scalar relationship for shell mechanics 24 p4249 A67-42152

Invariant form of strain-energy function of linearized elastic potential of isotropic thin shell using three-dimensional theory 24 p4249 A67-42156

SHELTER

S HANGAR

S LUNAR SHELTER

S SURVIVAL

SHIELDING

SA ATTENUATOR

SA ELECTROMAGNETIC SHIELDING

SA ELECTROSTATIC SHIELDING

SA HEAT SHIELD

SA MAGNETIC SHIELDING

SA NUCLEAR SHIELDING

SA RADIATION SHIELDING

SA RADIO FREQUENCY SHIELDING

SA REENTRY SHIELD

SA SPACECRAFT SHIELDING

SA WINDSHIELD

Uniform electric field quadrupole polarizabilities and shielding factors for S-state atoms and ions, demonstrating independence of factors from existence of field gradient 03 p0472 A67-13321

SHIFT

SA FREQUENCY SHIFT

SA FREQUENCY-SHIFT KEYING

SA ISOTOPE SHIFT

SA PHASE SHIFT

SA RED SHIFT

SA STELLAR DOPPLER SHIFT

SA THRESHOLD SHIFT

Pearl period shift explained by model showing proton effect and limited spectrum MHD noise 17 p2847 A67-32946

SHIFT REGISTER

All phases of pseudorandom sequence obtained by N-stage shift register generator 02 p0203 A67-12133

Tunnel diode circuits for fast digital circuits, noting shift generator and comparator generator 06 p0970 A67-18203

Soviet book on magnetic switching elements in radio electronics covering magnetic materials properties with rectangular hysteresis, shift registers, logic circuits, etc 11 p1765 A67-24515

Two-cycle shift register calculated, using magnetic element with rectangular hysteresis loop without shunting diode 11 p1769 A67-25042

Contact-free controlled delay unit using shift register and clock-pulse generator for binary signals designed with wide range of time delay variation 13 p2088 A67-26798

Digital real time spectral analysis with fast Fourier transform algorithm, using two special purpose computer configurations to estimate power spectrum 13 p2073 A67-27062

Operation and design principles of 200 MHz counter/shift register, noting integrated circuit fabrication techniques 17 p2824 A67-32306

Book on shift register sequence theory, discussing applications in communications, computers and switching theory 19 p3187 A67-35832

SHIN MEIWA UF-XS AIRCRAFT

UF-XS Japanese STOL seaplane used to investigate slow speed flying quality and hydrodynamic characteristics of PX-S aircraft 14 p2245 A67-27743

SHIP

SA HYDROFOIL

SA HYDROFOIL BOAT

Launching missiles safely from advanced marine systems 10 p1621 A67-22769

Sensor stability conditions for two rotor gyrocompass on sea-going ship turning in circle 13 p2118 A67-26373

Navigation satellites of next decade, discussing services for air and sea

intercontinental transportation vehicles [AAS PAPER 67-101] 15 p2570 A67-29956

Range instrumentation ships electronic capabilities, operation, electronic systems function, accuracy and future role [AAS PAPER 67-52] 15 p2468 A67-30117

Degree of isolation between radar tracking data and motion of ship determined, using frequency domain 20 p3415 A67-36555

SHIP PROPULSION

Objection to marine propeller application to VTOL aircraft 02 p0182 A67-12427

Structural, seal and sideboard design, propulsion and cavitation problems relevant to operational requirements of captured air bubble vehicle [AIAA PAPER 67-346] 14 p2245 A67-28729

SHOCK

SA BOW SHOCK

SA HYDRAULIC SHOCK

SA HYPERSONIC SHOCK

SA IMPACT

SA THERMAL SHOCK

Shock and vibration test specifications, contrasting approaches requiring exact duplication of environment with those simulating damaging characteristics 06 p0981 A67-18366

X-ray diffraction and metallographic investigation show iron meteorites shock at pressures of at least 130 kbar 10 p1705 A67-22954

SHOCK ABSORBER

Vibration shielding and shock absorbing systems design noting control function 03 p0530 A67-14180

Lunar surface mechanical properties at Surveyor landing site according to telemetry data and photographs 08 p1386 A67-20942

Dynamic analysis and development of response histories and tradeoff study charts for spherical impact limiters for protecting hard landing planetary payloads 10 p1727 A67-23738

Mechanical shock filter for isolating accelerometer during high g-level shock testing 11 p1799 A67-24824

Dynamic testing of crushable materials for planetary impact attenuation systems, noting Voyager and Ranger Lunar Capsule 12 p1956 A67-25731

Selection of angular rigidity of shock absorbing system of gyroscopic device 15 p2490 A67-30173

Wheel acceleration influence on landing gear operation at touchdown, noting effect on shock absorption system and elastic deformation of supporting legs 21 p3566 A67-37949

Short range FM transmitter-receiver system for shock measurements required to optimize shock absorber design 21 p3581 A67-38395

Optimal shock absorbers synthesis, showing reduction to variational problem and equations for one degree of freedom mass 22 p3776 A67-39394

SHOCK DISCONTINUITY

Time dependent computational method for three-dimensional blunt body flow fields traveling at supersonic speed including shock points, sphere cones and ellipsoid [AIAA PAPER 67-222] 06 p0941 A67-18461

Incipient separation prediction in shock boundary layer interactions 06 p0992 A67-18874

Real gas effects on time required for establishing detached bow shock in front of cylinder 06 p0992 A67-18882

Plane viscous problem of gas motion through weak straight line discontinuity of acceleration, noting formation of boundary layer 11 p1742 A67-24687

New MZI technique for detecting fringe shift across discontinuity as in shock tube or in shock tunnel flow 12 p1926 A67-25938

Normal shock relations in adiabatic constant area ducts used to connect properties on two sides of shock in steady one-dimensional flow 15 p2470 A67-29441

Single-fluid model accounting for behavior of MHD shock producing devices with unseparated shock and driving current sheet 15 p2528 A67-29565

Formula for pressure vs flow deflection at hypersonic speeds, useful in studies involving pressure on inclined surfaces 15 p2472 A67-29675

Microwave experimental technique for continuous velocity measurement of shock and contact discontinuities bounding air

plasma generated in cylindrical hypersonic shock tube 18 p3020 A67-34105

Classification of small amplitude waves, surfaces of weak discontinuity and shock waves in ideal MHD medium obeying adiabatic state equation 19 p3294 A67-35409

Time dependent computational method for three-dimensional blunt body flow fields traveling at supersonic speed including shock points, sphere cones and ellipsoid [AIAA PAPER 67-222] 19 p3171 A67-35736

Plasma hydromagnetic jump conditions derived from two-fluid plasma model, discussing relevance to collisionless plasma shock 21 p3662 A67-37764

Discontinuity conditions derived for nondissipative hydromagnetic shock surface flows, with jump relations from divergence form of MHD equations 22 p3854 A67-40317

Elastic wave problems involving one space variable solved by hyperbolic partial differential equations 23 p4072 A67-40610

Continuous shock wave profile found in MHD fluid where Whitham condition for wave profile discontinuity is satisfied 24 p4143 A67-42356

SHOCK FRONT

Luminescence front interaction with transverse magnetic field in electrodynamic shock tube 02 p0274 A67-12416

Transverse wave behavior in reactive flow, analyzing refraction or reflection of acoustic waves at shock front, obtaining comparison of behavior in corresponding real flows 03 p0405 A67-14026

Turbulent spots and wall roughness effects in shock tube boundary layer transition, noting stable region behind shock 08 p1322 A67-21382

Sound wave generation by columnar-starting vortex passing through reflected plane shock front analyzed, revealing alternate compression-rarefaction nature 10 p1625 A67-23117

Shock front parameters in plasma calculated from effective ratio of specific heats and adiabatic exponent 12 p1969 A67-25195

Luminous front in electric shock tube having coaxial gun without current crowbaring measured by phototransistors 14 p2355 A67-27823

Magnetoacoustic shock waves front in rarefied plasma disintegration at high Mach numbers as cause of increase in front wave duration and width 16 p2714 A67-31039

Two-dimensional inviscid flow pattern of gas behind shock front in neighborhood of stagnation point of cylindrical body acting as magnetic field source 16 p2723 A67-31581

Propagation velocity of stable detonation wave in gaseous mixtures measured using Doppler effect resulting from reflection of electromagnetic wave from front of detonation wave 17 p2970 A67-32806

Propagation of strong ionizing front at arbitrary oblique angle relative to magnetic field, determining limits to value of electric field ahead of shock 17 p2908 A67-33114

Hydrodynamic structure of exothermic reaction zone behind one-dimensional shock fronts in gaseous detonation studied by optical method 18 p3153 A67-33827

Supersonic fluid flow past elliptical and circular conical bodies at large angles of attack, using straight line method 18 p2984 A67-34211

Shock waves generated electromagnetically in T-tube studied with Mach-Zehnder interferometer 19 p3208 A67-35396

Plasma temperature and density measured behind luminous and preceding shock fronts in electromagnetic shock tube 19 p3293 A67-35399

Precursor waves in electromagnetically driven shock tube explained by considering tube as electromagnetic transmission line [AIAA PAPER 67-694] 21 p3613 A67-38723

Wave-like behavior of precursor electron density front in electromagnetic shock tubes explained via transmission line model 22 p3850 A67-39711

Discontinuity conditions derived for nondissipative hydromagnetic shock surface flows, with jump relations from divergence form of MHD equations 22 p3854 A67-40317

Electron density between shock front and discharge plasma in electromagnetic shock tube determined by interferometric technique, using guided waves 22 p3810 A67-40523

Plane shock wave disturbance development analysis by solving Cauchy problem, discussing low viscosity effect 24 p4141 A67-41931

Total head tube in combination with electrostatic probe used in supersonic plasma diagnostics, measuring plasma and shock wave front parameters 24 p4197 A67-42355

SHOCK HEATING

SA WAVE SUPERHEATER

Hypershen chondrite origin and history studied using noble gas content and shock and reheating by X-ray diffraction 11 p1865 A67-24602

Decrease in degree of ionization of shock-heated argon resulting from radiative emission 15 p2527 A67-29563

Nitric oxide production reaction rate measured in shock-heated air at high temperatures, with nitric oxide concentration determined by IR emission 18 p2997 A67-33791

Chain branching during induction period of hydrogen-oxygen reaction studied by shock heating 18 p2998 A67-34519

Oblique, normal and transverse ionizing shock waves 18 p3092 A67-34733

Initial ionization processes in shock heated argon consisting of atom-atom collisions followed by electron-atom processes 19 p3293 A67-35397

Electronic relaxation of shock-heated nonequilibrium argon plasma flow in microscopic-macroscopic treatment 19 p3298 A67-35745

Electron temperature of shock-heated argon plasma determined by measuring microwave noise radiation and absorption 21 p3660 A67-37741

Mach number effect on electron temperature structure of partially ionized monatomic and diatomic gas shocks 21 p3610 A67-37760

Radiation intensity measurements in systems containing atomic oxygen and carbon monoxide by shock tube heating, deriving spectral intensity distribution for radiative combination 23 p4029 A67-40972

Chemical analysis of glass bombs from Ries crater area investigated for textural differences due to shock melting and cooling rates 24 p4233 A67-42621

Microscopic and X-ray diffraction study of octahedrite shock history 24 p4234 A67-42631

SHOCK LAYER

Convective and radiative heat transfer in shock layer of hypersonic blunt body, noting asymptotic behavior of Navier-Stokes equation and energy transfer 01 p0168 A67-11421

Thermally radiating and absorbing plane piston problem, obtaining zero order approximation in series expansion in density ratio across shock layer 03 p0405 A67-14029

Separation points occurring in Newtonian theory of hypersonic flow locally treated by modifying shock layer equations, thus verifying free layer theory 04 p0545 A67-14463

High resolution equilibrium radiation spectra for shock layer of blunt bodies at reentry velocities and radiative recombination of N and O ions [AIAA PAPER 66-104] 04 p0546 A67-14816

Heat emission from compression shock layer about meteors in thermodynamic equilibrium 05 p0903 A67-17313

Continuum viscous nonequilibrium flow partial differential equations in thin shock layer 05 p0750 A67-17335

Subsonic drag rise for airfoil determined by limit line analysis in hodograph plane [AIAA PAPER 67-4] 06 p0938 A67-18248

Lip shock from separation edge of half-angle wedge and resultant static-pressure recovery distribution along wake [AIAA PAPER 67-29] 06 p0986 A67-18260

Book on inviscid hypersonic flow theory including nonequilibrium effects, flows on blunt bodies, shock layer, conical flows, etc 07 p1127 A67-20204

Inviscid hypersonic flow over plane power law bodies where blast theory applies as first approximation, determining shape and pressure distribution 08 p1277 A67-20708

Wall temperature effect on behavior of hypersonic stagnation region shock layer in incipient merged, layer flow, obtaining enthalpy function profile 08 p1278 A67-20928

Temperature measurement in hypersonic

gun tunnel, using modified line reversal two-beam optical pyrometer with measurements in shock layer at front of cylinder 09 p1486 A67-22413

Thin shock layer stagnation region analysis in hypersonic flow, emphasizing lateral asymmetry for planar and perturbed axisymmetrical cases 10 p1624 A67-22936

Calculation method for concentrated forces arising at intersection line of two surfaces due to interaction of shock layers, based on Newton law 10 p1590 A67-23035

Symmetrical equilibrium flow past blunt body at superorbital reentry conditions calculated by integrating motion equations across shock layer 10 p1591 A67-23109

Magnetoaerodynamic flow relations for axisymmetric blunt bodies with shock layers in shifting equilibrium 10 p1591 A67-23114

Mars atmospheric composition determination by shock layer radiometry technique during probe experiment [AIAA PAPER 67-293] 12 p2009 A67-26009

Total equilibrium shock layer radiation data for Martian entry body shapes at various angles of attack extrapolated to trajectory condition 12 p1894 A67-26039

Subsonic drag rise for airfoil determined by limit line analysis in hodograph plane [AIAA PAPER 67-4] 13 p2051 A67-27599

Low density shock layer structure on cylinders at Mach 4 noting magnitude, location of disturbances, existence of shock wave-like flows, recession of leading edge, etc 14 p2299 A67-28173

Finite difference method for treating head-on axisymmetric interactions of blast wave and shock layer in nose region of high speed blunt body 15 p2416 A67-29432

Equilibrium radiant heat transfer to bodies at hypersonic velocities in carbon dioxide atmosphere noting shock layer, shock standoff distance, shock velocity, etc 15 p2582 A67-30216

Stagnation region foreign gas injection in low Reynolds number hypersonic shock layer flow 16 p2591 A67-30936

Flow field and heat transfer in radiating stagnation-point shock layer of atmospheric-entry vehicles 16 p2591 A67-30940

Nonequilibrium air dissociation and ionization in stagnation region of blunt body investigated in merged layer regime 16 p2592 A67-30955

Vacuum UV radiation measurement from high temperature nitrogen, detecting radiation from shock layer of ballistic model 16 p2675 A67-31267

Shock and boundary layers about blunted two-dimensional slender bodies in hypersonic flow [AIAA PAPER 67-451] 18 p2982 A67-33925

Limits of application of binary scaling for hypersonic flight 19 p3212 A67-35769

Basic shock layer radiation data obtained in shock tube and free-flight ballistic range facilities applicable to Venus or Mars atmosphere entry 21 p3563 A67-37788

Inviscid hypersonic flow field between barrel shock and free boundary for source flow representing high altitude jet exhaust 22 p3739 A67-39410

Surface mass transfer effects on viscous hypersonic shock layer of blunt body including suction and injection of air into air 22 p3743 A67-40417

Hypersonic reentry plasma electron density measurement in free stream wake and shock layer using hotshot wind tunnel simulation 23 p3986 A67-40574

Shock curvature and flow variable gradients at tip of pointed axisymmetric body in nonequilibrium flow, solving linear differential equations and singularity 23 p3928 A67-41176

Perturbation solution to one-dimensional nonadiabatic temperature distribution behind detached shocks taking into account absorption effects 23 p3992 A67-41738

Shock refraction effects due to velocity and temperature gradients in rocket nozzles investigated by studying leading shock in two-dimensional secondary fluid 23 p3992 A67-41740

SHOCK LOAD

Thermodynamics of shock compression of metals 04 p0637 A67-14975

Ionized impurities effect on current output from shock-loaded piezoelectric quartz disk 04 p0678 A67-15122

Temperature effect on zero shift of piezoelectric crystal accelerometers under shock loading using Hopkinson bar technique 23 p4006 A67-41376

SHOCK MEASURING APPARATUS

Oblique shock detection in conical nozzle with circular arc throat, noting measurement techniques 04 p0547 A67-14833

Four-electrode device for measurement of electrical conductivity of shock ionized air 09 p1549 A67-22570

Shock and vibration sensors, discussing types for measuring strain, displacement, acceleration, velocity, pressure, etc 10 p1656 A67-23081

Instrumentation for ballistic pendulum shock accelerometer calibrator provides readout and display of peak amplitudes 12 p1943 A67-25708

Shock-on-shock effects explored in aerodynamic test facility combining blowdown wind tunnel and shock wave generator 13 p2091 A67-27490

Shock measurement discussing Fourier spectrum, vibrating reed gauge, analog and digital techniques, etc 16 p2671 A67-31022

Simultaneous measurement of many aerodynamic, electrical and electromagnetic parameters in test time interval of several hundred microseconds of MHD augmented shock tunnel 16 p2656 A67-31262

Microwave experimental technique for continuous velocity measurement of shock and contact discontinuities bounding air plasma generated in cylindrical hypersonic shock tube 18 p3020 A67-34105

Short range FM transmitter-receiver system for shock measurements required to optimize shock absorber design 21 p3581 A67-38395

Calibration of shock accelerometers, discussing velocity change and impact force methods with specific examples of systems in use 23 p4003 A67-41335

Comparison calibration of rectilinear vibration and shock pickups 23 p4004 A67-41338

Design of gasdynamic shock tube described with measuring apparatus developed for studying ionized gas flows in magnetic field 24 p4139 A67-42357

SHOCK SENSITIVITY

Graphical techniques in determining circuit-board resistance to shock and vibration 01 p0034 A67-10159

Optimum telemetry system characteristics for shock, vibration and acoustic measurements and data bandwidth sufficiency 02 p0196 A67-12009

Magnetic delay line vibration isolation system as heart of airborne special purpose computer in USN E-2A early warning aircraft 05 p0779 A67-17458

Buckling isolator system for carrier aircraft landing and catapult shock environment allowing use of available clearance for dynamic deflection 05 p0814 A67-17459

Sensitivity of single-mirror schlieren system, deriving expression relating film density change with angular light deflection 20 p3441 A67-36400

Brittle-ductile materials thermal shock characteristics explained by strains and elastic energy, noting ductile materials withstand more strains before failure 20 p3538 A67-36673

Sensitivity of explosives to shock waves tested by device using water as intermediate layer 22 p3866 A67-39489

SHOCK SPECTRUM

SA VIBRATIONAL SPECTRUM

Precision spectrum analyzer modification using RC network for analyzing filter applied to transient pulses for both Fourier and shock spectra 01 p0074 A67-11130

Shock spectrum synthesis and analysis as environmental test technique compared with time function shock testing 12 p2030 A67-25681

Empirical rules for shock spectrum, pulse and lead pellet interrelationship and implementation 12 p1967 A67-25686

Laboratory techniques for utilization of shock synthesizer/analyzer 12 p1942 A67-25693

Short duration shock machine 12 p1923 A67-25707

Operational requirements for modern space environment test laboratory covering thermal vacuum, shock, vibration and

- combined testing 22 p3781 A67-40401
Fourier transformation theory for shock
and vibration data analysis, discussing
programming considerations and
computational efficiency 24 p4248 A67-42011
[SAE PAPER 670874]
- SHOCK TESTING MACHINE**
Reliability testing improvement through
developments in vacuum systems, vibration
systems and triaxial shock
testing 01 p0084 A67-11369
Mechanical shock filter for isolating
accelerometer during high g-level shock
testing 11 p1799 A67-24824
Empirical rules for shock spectrum, pulse
and lead pellet interrelationship and
implementation 12 p1967 A67-25686
Laboratory techniques for utilization of
shock
synthesizer/analyzer 12 p1942 A67-25693
Short duration shock
machine 12 p1923 A67-25707
Shock-on-shock effects explored in
aerodynamic test facility combining
blowdown wind tunnel and shock wave
generator 13 p2091 A67-27490
Environmental simulation for aerospace
vehicle, discussing vibration, shock and high
temperature testing and space and nuclear
radiation simulation 22 p3781 A67-40343
Controlled transient signal distortion by
shock monitoring instrumentation circuits
using piezoelectric
accelerometers 23 p4007 A67-41382
Shock testing to aid design analysis and
for qualification and
certification 23 p3987 A67-41414
- SHOCK TUNNEL**
SA ELECTROMAGNETIC SHOCK TUBE
SA MAGNETIC ANNULAR SHOCK
TUBE /MAST/
SA WAVE SUPERHEATER
Internal wall pressure of obstacles in
hypersonic wind tunnels with reflected
shock waves measured by piezoelectric
gauge system 01 p0005 A67-10259
Shock tube measurement of dissociation
energy of NH radical in reflected shocks
through nitrogen-hydrogen-krypton and
ammonia-krypton
mixtures 01 p0117 A67-10787
Heat flux to SNAP reactor system models
in hypersonic continuum flow measured in
shock and hyperthermal wind tunnels, using
thin film resistance
thermometer 01 p0112 A67-11022
Heat flux measurement in very short
flows in short arc wind tunnels and shock
tubes 01 p0168 A67-11091
Plasma effects in nozzle flow of
hypersonic shock tunnel using arc, obtaining
electron density profile 01 p0126 A67-11442
Shock tunnel study of effects of nose
bluntness, angle of attack and boundary
layer cooling on transition at Mach number
5.5
[AIAA PAPER 66-495] 02 p0177 A67-11514
Shock wave attenuation due to boundary
layer effect calculated from initial pressure
conditions in shock tube 02 p0235 A67-12564
Twyman-Green arrangement of
interferometer with narrow laser beam and
twin photomultipliers, examining strong
shocks in argon in 15.2 cm shock
tube 02 p0247 A67-12688
Electron scattering cross section of argon
and atomic oxygen measured, using
microwave interferometer for analysis of
plasma produced in shock
tube 03 p0472 A67-13320
Shock tube operation with free piston
compression of driven gas, noting operating
limitation 03 p0397 A67-13897
Shock tube flow nonuniformity analyzed
where shock and contact surface have
maximum separation, applying results to
turbulent and laminar boundary layer for
heat transfer studies 03 p0397 A67-14027
DVL free piston shock tunnel and
measuring systems of three-component
balance based on use of strain
gauges 04 p0546 A67-14575
Gas flow with accelerated contact surface
and attenuated shock wave as example of
gas flow not explainable by ideal one-
dimensional theory 04 p0604 A67-14782
7-ft-diam shock tube for transonic and
supersonic aerodynamic
testing 04 p0598 A67-15254
Heat transfer to end wall of shock tube
behind reflected shock wave in oxygen
dissociated to varying degrees and at high
temperatures 04 p0729 A67-15813
Energy input requirements of electric
shock tube determined from empirical I-V
relations at electrodes 05 p0786 A67-16248
Shanlavsik multiply ionized gas model for
theoretical calculation of thermodynamic
equilibrium parameters of shock
tube 05 p0790 A67-16249
Shock wave attenuation in shock tube in
Mach 4 to 7 range, noting equipment used
and results 05 p0791 A67-16433
Tetrafluoroethylene dissociation in
nitrogen behind shock waves and
thermoequilibrium constants studied, using
shock tube and optical absorption
spectroscopy 05 p0759 A67-16840
Atmospheric argon effect on hypersonic
stagnation point convective heat transfer,
using arc-heated shock tube simulating flight
velocities up to 34,000 fps
[AIAA PAPER 66-29] 05 p0928 A67-17337
Microwave cavity techniques to measure
electron precursors in shock tube
[AIAA PAPER 66-175] 05 p0856 A67-17342
Radiation sources from high temperature
equilibrium air noting measurements,
equipment and results 06 p1114 A67-18279
Lift-drag ratio, lift and drag coefficients
and angle of attack effects on Gemini and
Apollo reentry vehicles measured in shock
tunnel under free flight conditions
[AIAA PAPER 67-185] 06 p0941 A67-18507
Shock tunnel heat transfer measurement
and hypersonic viscous flow over pointed
cones, particularly viscous-layer regime at
low Reynolds numbers 06 p0943 A67-18845
Shock wave tubes and wind tunnels for
momentary generation of steady air flows
for aerodynamic investigations at high
supersonic velocities 07 p1127 A67-20121
Monograph on shock tubes, weak and
strong shock waves and rarefaction
waves 07 p1169 A67-20205
Equilibrium air total radiation mechanism,
vacuum UV radiation and relation to
hypervelocity entry studied, using shock
tube blunt model test flow
[AIAA PAPER 66-103] 08 p1426 A67-20569
Shocked gas flow duration in small
diameter shock tubes at low initial
pressures 08 p1321 A67-21119
Solid particle drag, convective heat
transfer and ablation effects on structure of
normal shock wave in nonreacting mixture
of gas and ablating dust, using Runge-Kutta
integration 08 p1427 A67-21120
Precursor wave velocity, electron density
and current content in electromagnetically
driven shock tube, using hydrogen and
argon 08 p1363 A67-21380
Electrode conduction processes and
segmented electrode-insulator ratio effects
in MHD power generation
experiments 09 p1539 A67-21785
Action of strong transverse magnetic field
on supersonic current of ionized
argon 09 p1540 A67-21787
Shock tube studies of magnetically
induced nonequilibrium ionization in
potassium-seeded argon plasma, noting
electrical conductivity, current density, wall
potential, Soule dissipation and radiation
loss 09 p1540 A67-21788
Measurements of conductivity, electron
density and ionization rate of cesium in
argon on alkali shock tube, describing MHD
generator wind tunnel
experiment 09 p1540 A67-21789
Electric conductivity and kinetic energy in
seeded and unseeded airflow MHD
experiments in hypersonic shock tunnels for
aerospace applications 09 p1542 A67-21809
Uniform shock driven by gaseous
detonation induced by exploding wire in
single-diaphragm shock
tube 10 p1625 A67-23137
Gas flow and shock wave velocity
distribution in diaphragmed shock tube
photographically analyzed at various opening
rates 10 p1626 A67-23407
Quick change high vacuum window and
heat transfer gauge installation for shock
tubes 10 p1658 A67-23789
Ionized shock-nitrogen conductivity
measured by four-electrode
device 11 p1832 A67-24057
Electron number densities measured
behind shock wave in pressure-driven shock
tube by microwave resonant cavity
technique and by electrostatic quasi-
Langmuir probe 11 p1790 A67-24451
Thin film thermal radiation detector
noting construction, calibration,
performance, error sources and advantages
of pyroelectric over thin film
gauges 11 p1790 A67-24454
Isentropic compression due to motion of
heavy piston in gun tunnel noting nozzle
throat effect on motion and stagnation
pressure 11 p1773 A67-24577
Electrodeless electromagnetic shock tube
with large discharge chamber for high
velocity shock waves, applying theta pinch
effect 11 p1773 A67-24592
Gas state equation determination from
trajectory analysis of piston in hypersonic
wind tunnel 11 p1782 A67-24759
Shock tube study of oscillator strength of
diatomic molecular carbon Swan
bands 11 p1750 A67-25066
Constant density theory leads to analytical
forms for current-voltage characteristics and
electrical resistance associated with shock
tube sidewall electrostatic probe
problem 12 p1925 A67-25902
New MZI technique for detecting fringe
shift across discontinuity as in shock tube
or in shock tunnel flow 12 p1926 A67-25938
High temperature air plasma total radiant
intensity measurements in shock tube
[AIAA PAPER 67-311] 12 p2036 A67-26026
Chapman-Jouget theorem for MHD
detonation in shock tube blocked by
stationary perfectly conducting surface,
noting relation to magnetoacoustic
wave 12 p1976 A67-26071
Shock tube analysis of oscillation
relaxation in iodine between 1000 and 3800
degrees K 12 p1930 A67-26115
Hypersonic gun tunnel design and
performance up to 1000
atm 12 p1926 A67-26129
System for rupturing diaphragms in single
pulse shock tube, noting time decay
role 13 p2090 A67-27060
Hypersonic low density flow analysis with
shock tunnel and electron beam
densitometer, noting density profiles at
various Mach and Knudsen
numbers 14 p2300 A67-28176
Time varying magnetic field in shock tube,
analyzing electric current diffusion
layer 14 p2358 A67-28234
Driver chamber for very high
temperatures obtained with ceramic liner
for arc driven shock tube, reducing
contamination and cooling of driver
gas 14 p2293 A67-28749
Performance of low energy-density electric
shock tube in helium 14 p2293 A67-28752
Shock tube tests with cold argon and
heated helium to determine heated driver
gas effect on effect on shock tube
performance 14 p2294 A67-29053
Shock tube performance of Langmuir
probe suitable for ballistic range
applications, noting low pressure turbulent
wakes 15 p2490 A67-30212
Collection of papers on aerophysical
studies of supersonic flows covering shock
tube experiments, gas density,
interferometer and photographic
measurements, etc 16 p2672 A67-31101
Shock tube analysis of time dependent
formation of supersonic flow near blunt
bodies 16 p2592 A67-31102
Rarefied gas flow density measurement by
determining changes in electron beam-
electron concentration while crossing
flow 16 p2673 A67-31107
Continuous spectrum emission from free-
bound and free-free electron transitions into
field of monatomic gas ion using shock
tube 16 p2673 A67-31109
Plasma probe diagnostic technique in
shock tube, noting electron concentration,
gas temperature and plasma potential from
V-T characteristics 16 p2673 A67-31110
Shock tube measurement of plasma
electric conductivity, using Maxwell equation
for quasi-steady state electromagnetic
field 16 p2673 A67-31111
MHD effect in shock tube, studying EMF
induced in motion of transverse
magnetoplasma 16 p2715 A67-31112
Von Karman gas dynamics counterflow
facility for simulating model high velocities
and altitudes of reentry
conditions 16 p2655 A67-31261

Simultaneous measurement of many aerodynamic, electrical and electromagnetic parameters in test time interval of several hundred microseconds of MHD augmented shock tunnel 16 p2856 A67-31262

Magnetically driven shock tube as tool for aerodynamic studies of high velocity high enthalpy flows 16 p2594 A67-31265

Equilibrium thermodynamic and gas dynamic parameter calculation for low temperature plasma, using electromagnetic and diaphragm-type shock tubes 17 p2894 A67-32148

Magneto-Fanno flow shock tube experiments to determine one-dimensional MGD interactions between partially ionized gas flow and external magnetic field 17 p2898 A67-32183

Flow velocity measurement in shock tube using electronic Bascule Bootstrap type installation 17 p2855 A67-32287

Short duration shock tube molecular beam in helium and oxygen, giving test arrangement and data 17 p2835 A67-33361

Combustion processes studied by shock tubes, discussing experimental techniques of combustion science, high temperature measurement by spectrum line reversal method, etc 18 p3019 A67-33779

Shock wave investigation of recombination in near-stoichiometric hydrogen-oxygen-argon mixtures at high temperatures 18 p2996 A67-33789

Measurements of induction period, ammonia consumption rate after induction and radiation from electronically excited OH radicals in ammonia-oxygen reaction 18 p3155 A67-33836

Ignition kinetics of carbon monoxide-oxygen reaction 18 p3155 A67-33846

Ignition temperature and ignition delay of oxyhydrogen gas as function of pressure examined in shock wave tube, using Schlieren photography 18 p3160 A67-34261

Plasma behavior in shock tubes with parallel conductors, discussing shape of front and velocity dependence on pressure and gas composition 18 p3089 A67-34297

Lift-drag ratio, lift and drag coefficients and angle of attack effects on Gemini and Apollo reentry vehicles measured in shock tunnel under free flight conditions [AIAA PAPER 67-165] 19 p3169 A67-34818

Shock tube experiments conducted on mixtures of fine solid particles and gases 20 p3414 A67-36516

Compressible boundary layer-inviscid flow interactions in entrance region of internal flows, including shock tube boundary layer and effects of mass injection or suction [ASME PAPER 67-HT-2] 20 p3421 A67-36701

High performance aerodynamic impulse facility with shock tunnel, expansion tube and accelerator for high velocity and high Reynolds number environment 21 p3605 A67-37768

Performance of hydrogen driven shock tube investigated for usefulness, considering shock wave attenuation and helium driver performance 21 p3605 A67-37769

Electric internal heater for heating helium driver gas to high temperature and pressure for shock tunnel experiments 21 p3606 A67-37770

Two-dimensional turbulent mixing of supersonic reacting and nonreacting gases studied with square shock tube 21 p3606 A67-37772

JPL free piston shock tube design, calibration and performance 21 p3606 A67-37773

Shock waves and related phenomena in shock tube investigated by streak interferometry and electrostatic probes, measuring plasma density and temperature 21 p3611 A67-37961

Complex structure elimination in shock wave region of T-tube, discussing discharge plasma, shock wave trajectories and photographic observation technique 21 p3612 A67-38257

Oxygen-hydrogen mixtures burning characteristics in shock wave tube, studying ignition processes with schlieren photographs 21 p3731 A67-38366

Shock tube measurements of end-wall radiative heat transfer behind reflected shock waves in air, stressing radiative cooling and self-absorption effects [AIAA PAPER 67-695] 21 p3732 A67-38724

Ionization gauge circuit for studies of solid explosives initiation by gaseous detonation waves and reflected wave trajectories in shock tunnels 21 p3630 A67-38770

Wave superheater based on shock tube principles, discussing application in scramjet design 21 p3608 A67-38800

Drag measurements of cones in rarefied flow regime extended to higher and lower cone semivertex angles 21 p3565 A67-38884

Limiting driven conditions corresponding to optimum expansion and low density shock tube flow for overexpanded nozzle 21 p3609 A67-38886

Miniature transducers for shock tunnel instrumentation, noting compensating system to reduce spurious signals from pressure and skin friction 22 p3809 A67-40463

Lobb expression derived for optimum shock tube length, obtaining correct value 23 p3988 A67-41756

Shock tube simulation of rocket exhaust plumes and effects on vehicles in space environment 24 p4253 A67-42029

Heat transfer to end wall of shock tube after shock wave reflection through steep temperature gradient analyzed using variational method 24 p4257 A67-43092

SHOCK WAVE

SA CHEMICAL RELAXATION

SA NORMAL SHOCK WAVE

SA NOVA OUTBURST

SA OBLIQUE SHOCK WAVE

Solar flares, special features revealed by optical observations, classification, optical spectrum, shock waves and protuberances 01 p0144 A67-10771

Dynamic response of simple beam and rectangular plate under traveling shock wave at supersonic speed, using Fourier transforms 01 p0161 A67-10775

Equations for nonlinear wave propagation in incompressible heat-conducting elastic material, noting propagation of shocks in isotropic material 01 p0162 A67-10846

Recurrent cosmic-ray modulation phenomena with Forbush decrease characteristics correlated with M-region magnetic storms, concluding that each series results from shock wave solar initiated 01 p0145 A67-10919

Three-dimensional supersonic gas flow with shock waves around flat wing analyzed, using integral relations method 01 p0007 A67-10981

Nonlinear MHD waves, examining hyperbolic systems of quasi-linear PDEs, simple wave and flow theory 01 p0126 A67-11252

Shock wave in half-space filled with ideal gas in linear approximation 02 p0233 A67-11969

Forward and backward wave striations in constricted positive column of high pressure argon discharge 02 p0273 A67-12188

Structure of shock wave in monatomic gas analysis using orthogonal polynomial solution of Boltzmann equation, noting Mott-Smith distribution function 02 p0234 A67-12541

Shock wave structure in binary mixture, using Mott-Smith distribution postulating flow velocity and temperature of subsonic mode as position 02 p0234 A67-12542

Text describing physical phenomena and experimental apparatus for observing and measuring shock waves and detonations in gases 02 p0235 A67-12680

Calculating shock wave separation and relaxation velocities for supersonic airflow past sphere 03 p0349 A67-12863

Plane adiabatic flow of ideal gas behind separated shock wave for uniform supersonic symmetrical flow past smooth profile 03 p0349 A67-12873

Two-dimensional nonvortical shock-wave gas flow through Laval nozzle 03 p0350 A67-12886

Hypersonic flow of air past circular cylinder with nonequilibrium oxygen dissociation, including dissociation of free stream 03 p0351 A67-13000

Pseudoshocks in pipe flow in supersonic compressors represented as diffusion process, noting application in cascade and rotor configuration 03 p0352 A67-13011

Low intensity shock wave transformation into rarefaction wave in nonconducting media in presence of external electric

field 03 p0476 A67-13203

Electron density measurement in shock waves or plasma based on low power UHF wave attenuation 03 p0478 A67-13578

Asymptotic representation of solutions for boundary layers near weak shock waves in conical flows 03 p0352 A67-13631

State variables of shock induced states, analyzing calculations based on assumption of either constant volume or pressure from structural point of view 03 p0403 A67-13717

Nonlinear hydromagnetic wave propagation in inviscid conducting compressible fluid 03 p0480 A67-13726

Phenomena preceding shock waves in argon, evaluating electron density profile and UV brightness of plasma 03 p0483 A67-13885

Diffusion theory of vibration-dissociation coupling used to analyze transient effects in dissociation reactions behind shock waves 03 p0474 A67-14025

Air ionization rate behind high speed shock waves, determining electron density from IR emission 03 p0405 A67-14028

One-dimensional steady state gas compression flow undergoing thermodynamic relaxation processes 03 p0405 A67-14258

Relaxation process leading to thermal equilibrium behind ionizing shock waves in argon analyzed, using optical techniques 04 p0601 A67-14458

Refraction of plane shock wave by interface between different gases, reducing motion equation to polynomial of degree 12 04 p0601 A67-14465

Book on propagation, reflection and superposition of shock waves in ideal gases based on theory of hyperbolic nonlinear PDEs 04 p0601 A67-14467

Shock wave structure in viscous heat conducting gas, deriving preservation law for irreversible energy flux, equation for velocity profile and expression for integral curve 04 p0604 A67-14747

Hypersonic behavior of helium flow past highly blunt bodies, noting drag and shape of shock wave 04 p0546 A67-14779

Gas flow with accelerated contact surface and attenuated shock wave as example of gas flow not explainable by ideal one-dimensional theory 04 p0604 A67-14782

Steady blunt body problem solution via time-dependent technique, performing computation in shock layer 04 p0546 A67-14818

Sudden expansion or compression effect on momentum thickness change in turbulent boundary layer calculated, using parameter of velocity layer profile 04 p0604 A67-14840

Velocity distribution in shock wave, emphasizing heat transmission, longitudinal viscosity friction and relaxation 04 p0605 A67-14984

Collisionless shock wave excitation in plasma, determining shock front thickness 04 p0666 A67-15187

Structure of MHD shock wave taking into account ionization process 04 p0669 A67-15517

Heat transfer and pressure in laminar shock wave/boundary layer interaction corner flow at Mach 8 and 10 04 p0610 A67-15834

Krypton and xenon effect on dissociation rate of fluorine in presence of argon behind shock wave 04 p0567 A67-15951

Shock wave from release of gas at 230 km altitude indicated luminosity due to scattered sunlight and temperature of 743 degrees K 05 p0795 A67-16027

Hugoniot-Rankine conditions, dissociation and ionization of hydrogen and nitrogen gas behind high speed shock wave and radiation effects 05 p0790 A67-16036

Book on aerodynamics in relation to rocket and aviation technology including shock waves, rarefaction flow, heat transfer, skin friction, etc 05 p0747 A67-16173

Numerical algorithm for supersonic gas flow past blunt bodies with shock wave separation, using Dorodnitsyn method of integral correlation 05 p0791 A67-16374

One-dimensional self-similar motion of relaxing gas, noting ODEs of process and gas dynamic parameters of flow field 05 p0791 A67-16376

MHD and ionizing shock waves and conservation laws 05 p0851 A67-16416

Tetrafluoroethylene dissociation in nitrogen behind shock waves and

thermoequilibrium constants studied, using shock tube and optical absorption spectroscopy 05 p0759 A67-16840

Shock wave structure in steady state monatomic relativistic gas 05 p0793 A67-17112

Terminal shock-boundary layer interaction on slender cone-cylinder payloads at supersonic speeds and resulting flow separation

[AIAA PAPER 66-471] 05 p0924 A67-17213

Projectile wake turbulence measurements using hot-wire anemometer 05 p0750 A67-17346

Collisionless aspects of strong shock wave structure as approximated by Boltzmann equation examined, using orthogonal polynomial expansion technique in velocity space 05 p0794 A67-17421

Mass spectrometric observation of ions formed during shock wave heating of gaseous krypton and xenon at 3600 to 7800 degrees K 05 p0795 A67-17440

Impact of supersonic jet against surface 05 p0795 A67-17479

Stationary plane shock wave stability in arbitrary media, discussing error analysis 05 p0795 A67-17543

Difference scheme for calculating one-dimensional steady and unsteady Navier-Stokes equations for compressible gas flows 06 p0982 A67-17727

Hypersonic flow in compressed layer between tapered blunt leading edge of wing and internal shock wave forming in front when nonuniform flow moves past, considering expansion plane 06 p0936 A67-17733

Hypersonic laminar boundary layer on blunt cones, considering external flow vorticity caused by curved shock wave, calculating gas-enthalpy profile 06 p0936 A67-17734

Plane vortex flow in vicinity of orthogonality point of sound line to velocity vector 06 p0936 A67-17738

Mathematical analysis of gas flow equations and shock wave structure in rarefied gas dynamics 06 p0983 A67-17784

Electron temperatures and concentrations of charged particles behind strong shock wave in air measured noting techniques, maximal values and accuracy 06 p0983 A67-17878

Unsteady radial expansion of polytropic gaseous sphere in own gravitational field, using hydrodynamical equations and model limited by shock wave 06 p1083 A67-18064

Shock wave front structure in plasma, noting use of SHF diagnostics, electron concentration growth, etc 06 p0984 A67-18077

Turbulence in reaction zone of detonating liquid explosives, noting pressure irregularities in and around shock wave front 06 p1113 A67-18143

Trace fluorocarbon effect on vibrational relaxation in nitrogen shock waves studied by UV spectrophotometric technique 06 p0955 A67-18251

Shock induced supersonic combustion of fuel-air mixtures used to obtain induction time, evaluating kinetic data and effect of small contamination levels

[AIAA PAPER 67-105] 06 p1114 A67-18284

Supersonic flow over axisymmetric bodies with continuous or discontinuous slope solved via parametric differentiation

[AIAA PAPER 67-5] 06 p0939 A67-18303

Integral representation for transonic flow about thick airfoils obtained from equations for two-dimensional inviscid flow and locally surface-orthogonal shock waves

[AIAA PAPER 67-3] 06 p0939 A67-18331

Heat transfer to catalytic and noncatalytic surfaces on sharp flat plate in shock tube gas flow for checking various laminar boundary layer theories

[AIAA PAPER 67-163] 06 p0989 A67-18481

Ion density profiles and ionization rate in air behind high speed shock waves

[AIAA PAPER 67-94] 06 p1037 A67-18502

Three-dimensional internal flows in intakes and exhaust nozzles computed by combined characteristics and finite difference method

[AIAA PAPER 67-224] 06 p0942 A67-18516

Weakly dissipative fluid with schematized zone of strong gradients in perfect fluid formed by shock wave characterized by inversion of Reynolds number 06 p0990 A67-18726

Hypersonic boundary layer behavior in

adverse pressure gradients used in designing high Mach number intake diffuser system 06 p0942 A67-18750

Artificial heat conduction mechanism, introducing viscosity term into momentum and energy equations to account for shock discontinuities in flow problems 06 p0992 A67-18830

Radiation effect on hydrodynamic shock wave parameter distribution for bodies entering dense atmospheric layers at supersonic velocities 07 p1125 A67-19110

Electric properties of gas dynamic mirror formed in wake of shock wave front 07 p1227 A67-19118

Shock wave incident on unknown free boundary surface calculated in spatial method of characteristics 07 p1125 A67-19141

Exothermal reaction zone in one-dimensional shock wave in argon diluted oxygen-hydrogen and methane-oxygen mixtures 07 p1287 A67-19309

Effect of Mach number and specific heat ratio on distance of shock wave from end face of circular cylinder in axisymmetric flow 07 p1126 A67-19347

Shock waves in interplanetary medium caused by sudden expansion of solar corona following flare

[AFOSR-66-2638] 07 p1251 A67-19848

Monograph on shock tubes, weak and strong shock waves and rarefaction waves 07 p1169 A67-20205

Surface pressure, heat transfer coefficient, wave structure and shock disturbances of inviscid supersonic flow field along corner of intersecting wedges

[AIAA PAPER 66-128] 08 p1276 A67-20564

Shock wave strengthening by area convergence with viscous correction

[JPL-TR-32-1067] 08 p1321 A67-20707

Coefficient of reflection of H-11 mode shock wave emitted from aperture of circular waveguide with infinite flange 08 p1302 A67-20825

Shock waves and periodic structures of supersonic plasma flows and effect on velocity of foremost luminous front 08 p1358 A67-20852

Gas ionizing shocks for plane flows with magnetic field lying in flow plane 08 p1358 A67-20895

Shock wave formation due to heat addition to one-dimensional flow of ideal inviscid conducting monatomic compressible fluid under transverse magnetic field 08 p1359 A67-20980

Mott-Smith type moment method and restricted variational principle determinations of shock structure 08 p1355 A67-21141

Energy coupling measurement through electrodeless discharges in coaxial tubes, discussing parameters, dynamic processes, etc 08 p1338 A67-21291

Normal ionizing shocks propagating through hydrogen in sub-Alfvénic and trans-Alfvénic regimes in coaxial electromagnetic shock tube 08 p1363 A67-21381

Initial and boundary value problems in compressible fluid flow with moving boundaries governed by Navier-Stokes equation 08 p1322 A67-21384

Particle effects of interplanetary shock wave, noting discontinuous drop in solar proton intensities 08 p1378 A67-21469

MHD of flows with hot electrons in MHD ducts at low magnetic Reynolds numbers, emphasizing boundary layer and shock wave theory 09 p1541 A67-21797

Electron-ion recombination behind shock waves in argon containing dilute lean mixtures of hydrocarbons and oxygen 09 p1457 A67-22024

Rarefied gas flow past sphere studied by multibeam interferometry of density profile and shock structures 09 p1438 A67-22216

Effect of straightening section of airfoil contour on local supersonic flow, noting deformation of sonic line or characteristics 09 p1438 A67-22217

Shock wave profile in shock tube at different distances from plasma source determined, using perforated sliding membrane 09 p1489 A67-22329

Cabin noise in aircraft, discussing measurement techniques for sonic boom, shock wave intensity, etc 09 p1440 A67-22467

Reflection of spherical shock wave from concentric spherical surface, using method of characteristics starting from initial

boundary value problem 10 p1623 A67-22863

Starting phenomenon on reversed nozzle and multishock types of supersonic intakes 10 p1590 A67-22918

Double concurrent waves in one-dimensional nonstationary problems with discontinuous limit conditions 10 p1624 A67-22923

High resolution external probe for measuring electrical conductivity of argon plasma behind shock wave 10 p1684 A67-22963

Plane shock formed by steepening of continuous wave into shock in atmosphere having exponentially decreasing density 10 p1624 A67-22969

Flow pattern in front of cylinder mounted on plate at Mach 3 in wind tunnel, noting supersonic region between cylinder surface and shock wave 10 p1590 A67-23025

Three-dimensional flow in supersonic stream in symmetry plane of region of shock boundary layer interaction in front of obstacle mounted on plate, noting penetration in separation region 10 p1590 A67-23026

Shock and detonation waves in strong localized explosion in combustible gas mixture solved approximately 10 p1733 A67-23040

Inviscid flow characterized by annular elliptical region between shock wave and ducted body calculated by integral relation method, noting contraction coefficient values 10 p1591 A67-23045

Hydromagnetic shock wave intensity decrease in nonuniform magnetosphere treated by Chisnell-Whitham method 10 p1634 A67-23053

Numerical calculations of blast waves by standard and Hartree techniques compared with analytical results and application of Richardson extrapolation method 10 p1625 A67-23110

Effects of fast expansion and consequent lip shock at shoulder of supersonic base or downstream-facing step, suggesting alleviation by shoulder modification 10 p1592 A67-23156

Gas flow and shock wave velocity distribution in diaphragmed shock tube photographically analyzed at various opening rates 10 p1626 A67-23407

Inviscid axisymmetric radiating flow over blunt body, analyzing paraboloidal shock wave thermal radiation effects on temperature, density, velocity, etc 10 p1592 A67-23453

Parameters and shock wave characteristics of Tunguska explosion, postulating reaction mechanism 10 p1710 A67-23611

Existence and stability of solutions for equations of stationary thermal explosion in bounded container 10 p1734 A67-23679

Irregular refraction of plane shock wave by hot gas wedge, analyzing relation to Mach number values 11 p1775 A67-23878

Shock wave structure theory using Navier-Stokes character of shock wings and measured thickness, noting dependence on number density 11 p1775 A67-23879

Free electron density and effective collision frequency of ionized argon in wake of shock wave measured, using microwave probe methods 11 p1775 A67-24017

High velocity shock waves obtained by magnetic pressure and relaxation processes, using electromagnetic shock tubes 11 p1832 A67-24034

Pioneer I observations of geomagnetic field, discussing amplitude and polarization of oblique pulses, existence of collisionless oblique magnetic shock waves, soft electron acceleration, etc 11 p1786 A67-24078

Conditions at head shock wave in viscous hypersonic flow past blunt body for study of boundary layer separation 11 p1741 A67-24157

Viscous flow around flat plate at various angles of incidences at high Mach number to evaluate shock wave intensity variation and wall pressure distribution 11 p1742 A67-24761

Magnetofluid dynamics - AIAA Selected Reprint Series, Volume II 11 p1841 A67-24946

Decomposition rates of hydrogen halides examined behind incident shock waves between 2800 to 4600 degrees K, using IR techniques 11 p1750 A67-24995

Microexplosion by optical breakdown of air in focus of laser beam, analyzing volume of concentrated plasma by measuring external magnetic field

- perturbation 12 p1952 A67-25336
- Electric current conduction between cold electrodes in shock-ionized air plasmas, noting current-voltage characteristics in flow behind shock wave 12 p1974 A67-25401
- Equations in hodograph plane obtained for two-dimensional polytropic gas flow in presence of shock waves 12 p1892 A67-25443
- Oscillations of cylindrical shell containing compressible gas perturbed by heat induced shock wave 12 p2023 A67-25595
- Shock wave diffraction and reflection problems on faces of angle situated in nonstationary gas flow 12 p1928 A67-25672
- Nonstationary gas jet stream formation following shock wave outflowing from nozzle, obtaining calculation method 12 p1929 A67-25674
- Empirical rules for shock spectrum, pulse and lead pellet interrelationship and implementation 12 p1967 A67-25686
- Thermal electrode boundary layer for shock wave ionized air ohmic heating in discharge chamber, noting Joule heat consumption effect 12 p1975 A67-25894
- Relaxation processes behind shock wave in free stream partially dissociated and vibrationally excited by monitoring time history of radiative emission in shock tube [AIAA PAPER 66-519] 12 p1929 A67-25905
- Martian entry condition analyzed as nonequilibrium flow field phenomenon, noting chemical kinetics and radiation behind shock wave in gas mixtures [AIAA PAPER 67-322] 12 p1930 A67-26037
- Excitation of collisionless shock waves in low density plasma noting lifetime, discharge process, adiabatic contraction, etc 12 p1976 A67-26074
- Shock wave compression effect on low carbon steels, noting hardness-explosive correlation 12 p1957 A67-26117
- Soviet book on physical optics 12 p1967 A67-26131
- Parameters of gas behind incident and reflected shock waves calculated, using gas dynamic and chemical equilibrium equations for one-dimensional problem 12 p1930 A67-26134
- Temperature and density measurements in supersonic free jets of nitrogen and shock waves 13 p2093 A67-26279
- Earth bow plasma shock wave model with ion wave instabilities as principal shock structure [SR-2] 13 p2107 A67-26301
- Formation of compression shocks in calorically ideal real gases with thermodynamic relaxation analyzed in closed form 13 p2094 A67-26636
- Boltzmann equation and statistical properties for two-dimensional gas, analyzing integral iteration for shock wave flow 13 p2103 A67-26975
- Shock structure calculations by modified Grad orthogonal expansion method, noting problems of singularity 13 p2103 A67-26976
- Collisional parameters in kinetic model equations for binary gas mixtures, treating shock structure in weakly ionized argon 13 p2103 A67-26977
- Shock wave structure according to Krook model and Boltzmann collision integral 13 p2103 A67-26978
- Rotational energy diffusion in shock wave structure, examining magnitude of error in effective number of intermolecular collisions required for equilibrium 13 p2104 A67-26980
- Distribution function structure in gas kinetic flows as given by BGK model in plane weak shock in monatomic gas 13 p2104 A67-26981
- Soviet papers on quantum field theory and hydrodynamics 13 p2105 A67-27410
- Refraction and reflection of shock waves from interface between media having different densities 13 p2105 A67-27414
- Current voltage characteristics of argon cesium plasma in inductive hydrodynamic shock tube 14 p2354 A67-27761
- MHD resonance acceleration of plasma clusters and shock waves, showing advantage for parallel or coaxial conductor systems 14 p2354 A67-27762
- Nonlinear differential equation for shock wave of several circular arc airfoils integrated to give shock wave location 14 p2239 A67-27797
- Gas flow at high speed out of solid or liquid surface accompanied by heat transfer investigated for boundary shock wave occurrence 14 p2296 A67-27906
- Flow visualization, discussing schlieren process in light of Toepler, fine focusing, microscopic, phase contrast and field absorption processes 14 p2315 A67-27974
- Plane-parallel transonic flow with direct shock wave analyzed for case where Tricomi equation replaces Chaplygin equation 14 p2297 A67-27990
- Stable implosion initiation through converging detonation wave, discussing experimental techniques and results 14 p2293 A67-28141
- Two-dimensional supersonic fluid amplifier flow characteristics analyzed numerically by digital computer 14 p2250 A67-28333
- Source free solutions in ionized regions, discussing geometrical optics application to MGD with infinite conductivity 14 p2359 A67-28462
- Numerical evaluation of voltage and polarity variation induced by electron conductivity changes created by longitudinal phonon pressure caused by shock wave 14 p2367 A67-28514
- Special lighting equipment for high speed cinematography delivering high intensity light pulses in nanosecond range for use in shock wave and explosion filming 14 p2319 A67-28585
- Magnetosphere, turbulent transition region and shock wave characteristics and dimensions examined with regard to possible active or passive interaction with moon 14 p2388 A67-28619
- Parameter determination for flow field in space between shock wave of nonviscous supersonic gas flow and thin spherically blunt cone 14 p2243 A67-28659
- Equation of state for Debye continuum governing nonlinear propagation of perturbations terminating in shock wave at distance 14 p2374 A67-28982
- Axisymmetric blunt bodies shock standoff distances in hypersonic flow determined by numerical and analytic methods 14 p2244 A67-29056
- Heating of chromosphere above sunspot due to magnetoacoustic waves which develop into weak shock waves 15 p2551 A67-29142
- Relativistic MHD shock wave stability in infinitely conducting plasma with magnetic field parallel to shock wave plane 15 p2523 A67-29216
- Shock structure in diatomic gas described using Mott-Smith bimodal distribution function, including relaxation effects 15 p2469 A67-29217
- Solution for shock wave of bimodal distribution using Bhatnagar-Gross-Krook models, noting symmetry property destruction and recovery by using modified BGK model 15 p2470 A67-29226
- Diffusive separation due to electrical coupling of ions and hot electrons and effect on shock wave structure in plasmas 15 p2470 A67-29227
- Hypersonic stagnation point flow between strong shock wave and body involving radiation, conduction and dissociation 15 p2415 A67-29309
- Gas-ionizing shock wave with zero electrical conductivity of gas in front of shock wave and infinite conductivity behind 15 p2470 A67-29310
- Shock wave shapes around spherical and cylindrical-nosed bodies, assuming hyperbolic profile asymptotic to freestream Mach angle or attached shock angle 15 p2417 A67-29448
- Nozzle type similarity solution to axisymmetric viscous transonic equation, describing shock wave development at nozzle throat 15 p2417 A67-29654
- Energy accumulation of spherical and cylindrical shock waves in inhomogeneous gas 15 p2472 A67-29694
- Emissive power of air measured by determining charged particle distribution behind spark discharge generating shock wave in plasma 15 p2530 A67-29861
- Fundamental relations for normal shock wave behavior in compressible fluid for classical and hydromagnetic cases 15 p2473 A67-30226
- Preheated gas pulsed with shock waves studied for direct AC power production by MHD generator 16 p2603 A67-30564
- Pressure distributions and shock wave shapes on conical wings calculated by numerical solution of integral equations 16 p2589 A67-30619
- Discontinuities of shock adiabats and multivaluedness of compressions, noting similarity to Bancroft condition 16 p2659 A67-31043
- Shadow method analysis of shock wave interaction with fixed bodies in shock tube at small and medium supersonic Mach numbers 16 p2673 A67-31105
- Concentration profile of normal and excited mercury atoms in shock wave front and wake, noting gas density and electron concentration profiles 16 p2673 A67-31108
- High speed spark photography with electronic equipment, describing generating and control units and optical techniques for shock wave observation 16 p2674 A67-31127
- Photoelectric method measuring separation of head shock wave from supersonically-moving body, detailing equipment design and operation 16 p2674 A67-31128
- Mach number effect on location of head shock wave and flow stability at slightly supersonic velocities for various body shapes 16 p2593 A67-31129
- Shock-wave separation dependence on bluntness degree, Mach number and gas type during supersonic motion of ellipsoids of revolution 16 p2675 A67-31130
- Shape dependence of detached shock wave in supersonic gas flow of blunt-nosed models on Mach number, heat capacity and bluntness ratio 16 p2593 A67-31131
- Position determination of sonic points on head shock wave and blunt body surface in ballistics showing Mach number and gas type effects 16 p2593 A67-31132
- Sound velocities in granular ammonium perchlorate and potassium chloride, discussing chemical reaction of shocks 16 p2734 A67-31521
- Plane shock wave reflected from heat-conducting wall analyzed by method of matched asymptotic expansions 16 p2662 A67-31555
- Downstream flow of shock waves created by wing section moving at speed of sound 16 p2594 A67-31712
- Energy distribution of shock wave created by wire explosion and electrical discharge in air, studying attenuation, dimensional effects and energy conversion efficiency 17 p2883 A67-31927
- Density and pressure in real gas behind plane shock wave upon reflection from solid surface 17 p2836 A67-32072
- Voltage induced by magnetic field using shock tube with high velocity ionized argon flow 17 p2898 A67-32184
- Axial electrostatic field forming in resonance zone of mixed structure noting ion entrainment, shock wave generation and motion of electrons 17 p2899 A67-32291
- Electrodeless device for currentless plasmoid generation noting flowing plasma conductivity, boundary layer phenomena and potential distribution 17 p2900 A67-32344
- Nozzle and membrane effects on shock wave intensity in tube, showing graphically Mach number dependence upon initial pressure 17 p2837 A67-32345
- Intensity and specific heat ratio effects for laminar compressible boundary layers arising behind traveling shock waves 17 p2837 A67-32347
- Motion of shocks through chromosphere under guidance of magnetic fields 17 p2944 A67-32642
- Shock wave generation of electromagnetic radiation at magnetospheric boundary, discussing plasma oscillation excitation, plasma wave scattering, etc 17 p2846 A67-32935
- Lobb empirical relation applied to method for computing flow past blunt body when predicting sphere shock standoff distance 17 p2793 A67-33026
- Trace fluorocarbon effect on vibrational relaxation in nitrogen shock waves studied by UV spectrophotometric technique [AIAA PAPER 67-11] 17 p2809 A67-33035
- Separation shock near base of conical bodies at hypersonic speeds noting inflections in bow shock shape 17 p2793 A67-33044
- Shock wave incident on unknown free boundary surface calculated in spatial method of characteristics 17 p2840 A67-33213
- Shock wave in half-space filled with ideal gas in linear approximation 17 p2841 A67-33286
- Dispersion effect on shock wave structure

- in magnetoplasma, analyzing role of wave front inclination angle to magnetic field 18 p3084 A67-33525
- Thomson scattering of Q-switched ruby laser beam in shock wave plasma, determining electron densities, spectral distribution of scattered light, etc 18 p3084 A67-33649
- Rarefied gas flow past sphere studied by multibeam interferometry of density profile and shock structures 18 p2982 A67-33755
- Effect of straightening section of airfoil contour on local supersonic flow, noting deformation of sonic line or characteristics 18 p2982 A67-33756
- Atomic oxygen effect on vibrational relaxation of oxygen in shock waves at high temperatures, using laser schlieren technique 18 p3081 A67-33784
- Density induction times for shock wave induced exothermic reaction in lean mixtures of deuterium, hydrogen, ethylene and ethane with oxygen 18 p3081 A67-33792
- Post-induction kinetics in shock initiated hydrogen-oxygen reactions investigated by computer methods 18 p3153 A67-33823
- Radiation intensity and causes of radiation peak of nonequilibrium gas following strong shock waves 18 p3083 A67-34059
- Plasma produced by shock wave in low pressure gas measured for phase angle by microwave reflection probes 18 p3088 A67-34076
- Integral curves of two-dimensional shock and detonation waves in gas with varying density 18 p3028 A67-34273
- Laser driven plasma detonation waves in gases observed with Schlieren system, discussing shock wave growth 18 p3092 A67-34734
- Collisionless electrostatic shock in magnetized plasma in absence of initial magnetic field 18 p3092 A67-34749
- Shock thickness for monatomic Maxwell molecule gas calculated using conservation and moment equations 18 p3030 A67-34753
- Vibrational and/or chemical relaxation effects behind various shock waves in hypersonic air streams determined for equilibrium and nonequilibrium conditions 19 p3169 A67-34813
- Shock waves and spectrographic properties of emitted light during high energy linear discharge in ionized gaseous filament 19 p3176 A67-35133
- Interaction of plasma stream with three-dimensional magnetic dipole field, discussing current distribution in cavity 19 p3221 A67-35368
- Hydrogen thermal ionization rate behind strong shock wave, considering nonadiabatic collisions and various relaxation mode interactions in shock speed range 19 p3292 A67-35394
- Shock waves generated electromagnetically in T-tube studied with Mach-Zehnder interferometer 19 p3208 A67-35396
- Electron density and collision rate of shock produced plasma measured with X-band microwave reflection probe 19 p3293 A67-35398
- Air ionization behind shock wave front, estimating free electron concentration, ionization time and collision frequency 19 p3293 A67-35401
- Ionizational relaxation and excitation behind shock waves, proposing solution for kinetic equation system 19 p3293 A67-35403
- Classification of small amplitude waves, surfaces of weak discontinuity and shock waves in ideal MHD medium obeying adiabatic state equation 19 p3294 A67-35409
- Collapsing shocks and detonation waves gasdynamic problem, evaluating perturbations due to counterpressure and to heat release 19 p3209 A67-35411
- Magnetospheric boundary and standing shock wave for earth scaled down to apply to Mars 19 p3324 A67-35442
- Ionized gas flow past cylinder and sphere, determining ionization and dissociation effect on displaced shock wave form 19 p3170 A67-35449
- Flat plate continuum Langmuir probe ion density measurements, analyzing boundary layer and sheath of supersonic flow behind shock wave 19 p3296 A67-35590
- Inviscid hypersonic flow in stagnation region of circular cylinder with detached shock wave, considering real-gas effects 19 p3171 A67-35713
- Inviscid hypersonic axisymmetric flow over cylinder and sphere near stagnation point, including dissociation and detached shock wave 19 p3171 A67-35722
- Heat transfer to catalytic and noncatalytic surfaces on sharp flat plate in shock tube gas flow for checking various laminar boundary layer theories 19 p3211 A67-35739
- Vibrational excitation effects on shock wave behavior calculated analytically by linearizing problem 19 p3212 A67-35773
- Hydromagnetic shock waves in dissipative plasma, considering nonevolutionary normal shock break-up and switch-on shock stability 20 p3493 A67-36143
- Plasma shock wave structure model, analyzing steady flow of electrically neutral fluid 20 p3493 A67-36144
- Gas flow around wing in presence of moving shock wave with variable gas parameters noting wave equation, velocity potential, etc 20 p3355 A67-36191
- Ethylene-oxygen reaction in shock waves, studying induction period and time dependency of mixture composition, ionization and chemiluminescence 20 p3376 A67-36232
- Generalized Mott-Smith functions for shock wave structure in binary mixtures, relative diffusion velocity obtained and compared with Diakov solution 20 p3421 A67-36678
- Head-on collision between stars at high initial relative velocity, considering one-dimensional driven shock motion in inhomogeneous medium 20 p3525 A67-36943
- Coronal heating extent placed at 1.6 solar radii by 38 MHz radar investigation studies, noting agreement with coronal density calculation 20 p3528 A67-37477
- Parameters and shock wave characteristics of Tunguska explosion, postulating reaction mechanism 20 p3530 A67-37535
- Rott approximate method applied to steady compressible laminar boundary layer on unyawed seminfinitesimal solid circular cone with attached shock wave 20 p3360 A67-37595
- Ultrasonic and line reversal methods for measuring gas temperatures behind reflected shock waves 21 p3624 A67-37740
- Incident and reflected shocks from laminar and turbulent boundary layers measured over various Mach numbers 21 p3610 A67-37771
- Growth of laminar compressible boundary layer with stationary origin on uniformly moving flat plate, noting analogy to shock induced flow 21 p3611 A67-37927
- Laminar compressible boundary layer induced by plane shock wave passing over flat wall using empirical viscosity-temperature relation for Prandtl number 21 p3611 A67-37928
- Shock waves and related phenomena in shock tube investigated by streak interferometry and electrostatic probes, measuring plasma density and temperature 21 p3611 A67-37961
- Hydrodynamic pressure on elastic cylindrical shell from acoustic shock wave, using higher order asymptotic approximations 21 p3717 A67-37973
- Reflection in water of plane shock waves from rigid wall 21 p3611 A67-38058
- Electric properties of gas dynamic mirror formed in wake of shock wave front 21 p3664 A67-38163
- MGD shock wave with conductivity jump, correlating wave boundary to gas parameter 21 p3664 A67-38238
- Complex structure elimination in shock wave region of T-tube, discussing discharge plasma, shock wave trajectories and photographic observation technique 21 p3612 A67-38257
- Existence and stability of solutions for equations of stationary thermal explosion in bounded container 21 p3731 A67-38280
- Collisionless shock wave existence in fully ionized plasma, noting shock wave internal structure 21 p3667 A67-38410
- Solution methods for Cauchy problem and ideal unstable gas motion in cylindrical and spherical symmetry, discussing shock wave occurrence 21 p3565 A67-38562
- Strong blast waves and laser generated plasma dynamics in high pressure gas investigated using Mach-Zehnder interferometer and pressure probe [AIAA PAPER 67-696] 21 p3672 A67-38725
- Ionization gauge circuit for studies of solid explosives initiation by gaseous detonation waves and reflected wave trajectories in shock tunnels 21 p3630 A67-38770
- Equations in hodograph plane obtained for two-dimensional polytropic gas flow in presence of shock waves 21 p3613 A67-38816
- Shock induced supersonic combustion of fuel-air mixtures used to obtain induction time, evaluating kinetic data and effect of small contamination levels [AIAA PAPER 67-182] 21 p3732 A67-38858
- Supersonic blunt body problem noting sonic point singularity for reformulated integral relations 21 p3614 A67-38879
- Finite discontinuity jump conditions for plasma in strong magnetic field determined by approximation and Maxwell equation, noting possible application to satellite data 22 p3843 A67-39269
- UV absorption of ammonia at high temperatures behind shock waves, discussing NH radical formation from shock tube ammonia decomposition 22 p3756 A67-39442
- Radiative cooling and self-absorption effects on reflected shock flow field and end wall heat transfer studied using finite difference method 22 p3917 A67-39710
- Shock wave thickness in hydrogen gas as function of shock speed and postshock plasma mean free path 22 p3783 A67-39723
- Momentum equation examined by curvature of streamlines downstream from shock wave 22 p3783 A67-39727
- V-shaped wings with plane sides and sharp edges investigated for aerodynamic properties, deriving equations for flow parameters at Mach 6 22 p3741 A67-40016
- Supersonic flow over flat and axisymmetric blunt bodies, discussing shock wave position, adiabatic index, surface pressure distribution and body geometric parameters 22 p3741 A67-40026
- Atomic and molecular chemophysical processes in shock waves derived from high temperature thermal energy transfer including instrumentation, relaxation, ionization and spectroscopy 22 p3786 A67-40074
- Low velocity detonations /LVD/ of liquid explosives indicate shape and container material and presence of witness plate affect initiation 23 p4081 A67-40635
- Electrical conductivity or magnetic Reynolds number of shock produced plasma flow, discussing interaction between magnetic field and plasma flow 23 p4031 A67-40881
- Experimental determination of compression and rarefaction shock waves structure causing high pressure phase formation and decay in potassium halides 23 p3989 A67-40906
- Hypersonic wave rider flow and aerodynamic problems, discussing shaping, leading edge cooling and supersonic combustion propulsion 23 p3929 A67-41251
- Propagation of signals in transmission lines with distributed capacitance and conductance for nonlinear parameters 23 p3982 A67-41396
- Conformal mapping method for overcoming difficulties caused by limiting line in computing flow field about blunt body supporting paraboloidal shock wave 23 p3932 A67-41730
- Shock waves and boundary layer structure near tip of slender cone in rarefied hypersonic flow, discussing surface pressure peaks 23 p3932 A67-41762
- Shock wave produced optically-thin nonequilibrium plasmas studied using Rankine-Hugoniot calculations for properties, varying electron/ion temperature ratio [DVL-635] 24 p4194 A67-41860
- Temperature distribution measurements behind shock wave front in discharge tube with air and Ar indicate undisturbed thermodynamic equilibrium of plasmas 24 p4141 A67-41936
- Structure of quasi-steady-state MHD shock wave in plasma supersonic flow, analyzing width dependence magnetic field 24 p4195 A67-41937
- Kinetic behavior of electrons in air plasmas containing electrophilic gases studied with microwaves behind reflected shock waves 24 p4196 A67-42196
- Hydrodynamic solution for shock wave parameters of monatomic gases assuming

- exponential molecular interaction potentials and absence of mass 24 p4142 A67-42271
- Interferometer crossed with spectrograph used for electron concentration investigation in ionized argon behind shock waves propagating at high Mach numbers 24 p4197 A67-42358
- Shock wave reflection with vibrational relaxation times investigated by matching characteristics equation to shock wave equation 24 p4144 A67-42564
- Hypervelocity gas flows at high temperatures and pressures, discussing generation of dense plasmas at extreme temperature by implosion waves 24 p4092 A67-42753
- Heating of chromosphere above sunspot due to magnetoacoustic waves which develop into weak shock waves 24 p4239 A67-43065
- Heat transfer to end wall of shock tube after shock wave reflection through steep temperature gradient analyzed using variational method 24 p4257 A67-43092
- ### SHOCK WAVE ATTENUATION
- Shock wave attenuation due to boundary layer effect calculated from initial pressure conditions in shock tube 02 p0235 A67-12564
- Sonic boom decay and aural response in relation to SST configuration constraints and flight performance characteristics [AIAA PAPER 66-941] 03 p0361 A67-14139
- Nonequilibrium ionization and radiation effect on shock wave attenuation calculated using linearized theory 11 p1774 A67-23856
- Strong plane shock attenuation from impact studied with numerical method of characteristics for one-dimensional unsteady flow, showing late-stage equivalence 11 p1820 A67-24905
- Transonic gas flow past ducted bodies of revolution indicates shock wave asymptotic attenuation at infinity 14 p2296 A67-27989
- Performance of hydrogen driven shock tube investigated for usefulness, considering shock wave attenuation and helium driver performance 21 p3605 A67-37769
- Low amplitude MHD shock wave attenuation, assuming high magnetic Reynolds numbers and small excitation zone width 21 p3665 A67-38239
- ### SHOCK WAVE CONTROL
- Pyrotechnic shock testing, discussing equipment reliability and performance improvement, shock level reduction and applications [SAE PAPER 660717] 01 p0139 A67-10606
- Methods to minimize sonic boom ground exposure, considering aircraft design and maneuverability as function of altitude 09 p1439 A67-21942
- Conditions controlling shock wave reflection from duct end deflector plates, determining spacing of plates from pipe 12 p1928 A67-25356
- Perfect frictionless supersonic MHD gas flow model for shock wave control, noting nozzle geometry 18 p3088 A67-34123
- ### SHOCK WAVE GENERATOR
- Mass effect on blast wave equations of shock generation by secondary injection of fluid into hypersonic flow 01 p0141 A67-11179
- Shock wave formation due to nonlinear vibrations in tube containing fluid subjected to transverse magnetic field with plane heater at midsection and externally supplied energy 02 p0273 A67-12058
- Electroless electromagnetic shock tube with large discharge chamber for high velocity shock waves, applying theta pinch effect 11 p1773 A67-24592
- Shock-on-shock effects explored in aerodynamic test facility combining blowdown wind tunnel and shock wave generator 13 p2091 A67-27490
- Performance of hydrogen driven shock tube investigated for usefulness, considering shock wave attenuation and helium driver performance 21 p3605 A67-37769
- Soviet monograph on high speed measuring methods in gasdynamics and plasma physics, discussing high temperature plasma and shock wave production 21 p3625 A67-37964
- Quiet condition solar wind geomagnetic field interaction measurements, discussing solar plasma and bow shock wave generation 22 p3870 A67-39670
- Helium argon mixture shock wave density profile measurements, discussing shock wave production in flow field at supersonic nozzle exit 22 p3783 A67-39709
- Inexpensive high vacuum high voltage feedthrough used in conical shock driver system for plasma research 22 p3774 A67-40348
- Diaphragm and piezoelectric pressure gauges for severe blast environment, discussing resonance, damping, heat shield and rise time 23 p4007 A67-41387
- ### SHOCK WAVE INTERACTION
- Three-dimensional boundary layer and inviscid hypersonic flow interaction on infinitely thin triangular wing 01 p0007 A67-10982
- Shock-shock interactions for slender cone in theory and experiment 01 p0055 A67-11183
- Proposed modification of Wetzel model of direct ionization by primary continuum in light of recent steady state precursor electron density measurements ahead of Ar shocks 01 p0118 A67-11193
- Unsteady interaction between blunt bodies and shock wave, comparing reflected shock wave velocity decrease for plane spherically blunted cylinders 01 p0008 A67-11294
- Stationary and reflected shock wave produced in moving argon plasma interacting with stationary magnetic field 05 p0850 A67-16067
- Flow pressure structures of supersonic flow over rearward facing step, showing pressure changes and Reynolds number role 05 p0750 A67-17339
- Three-dimensional flows with Mach interaction between shock waves, drawing conclusions on possible types of interference between wing and wall 06 p0936 A67-17736
- Dissipative effects in converging cylindrical symmetric shock wave, considering ion and electron heat conductivity, ion viscosity and energy exchange 06 p0984 A67-18029
- Application of short wave theory to regime of regular interaction between weak shock waves 06 p0984 A67-18045
- Asymmetric interaction of supersonic vehicle intercepted with oblique shock wave [AIAA PAPER 67-180] 06 p0989 A67-18486
- Incipient separation prediction in shock boundary layer interactions 06 p0992 A67-18874
- Nonequilibrium effects on shock wave reflection coefficient 06 p0992 A67-18885
- Interaction of two cylindrical jets of uniform flow as far downstream as possible impinging at included angle of 60 degrees 06 p0944 A67-18888
- Three-dimensional plane shock wave intersection in space, noting parameter range for which two solutions exist 07 p1169 A67-20036
- Impossibility of three confluent shocks in two-dimensional irrotational flow proved independently of state equation 08 p1322 A67-21383
- Approximate closed form solutions for supersonic separated and reattaching laminar flow problem with boundary layer/shock wave interaction 10 p1591 A67-23115
- Dissipation of magnetic fields at neutral lines in two-dimensional field with two intersecting shocks 11 p1862 A67-24498
- Chemical kinetic processes in gasdynamic shock wave interactions, especially vibration in four-center transition states 11 p1773 A67-24535
- Nuclear blast interaction with bow shock of reentry vehicle and effect on structural materials 12 p1929 A67-25730
- Three-dimensional gas flow in region of incidence of shock wave on cylinder situated in high supersonic flow 14 p2297 A67-27995
- High intensity heat flux formation during heat transfer on steel cylinder in region of incident shock wave in supersonic flow 18 p3027 A67-34206
- Plane shock wave velocity measurement after interaction with obstacles in form of channeled diaphragms of various diameters, discussing stabilization 18 p3028 A67-34210
- Interaction of first and second shocks of blast-bow wave in double-driver shock tube, examining stagnation point pressure prediction methods 19 p3206 A67-34812
- Interactions produced by shock wave running into magnetic field perpendicular to wave direction 19 p3294 A67-35405
- Shock wave interaction with plasma arc discharge, investigating wave refraction, arc response to pressure and temperature pulses and aftershock flow field 19 p3294 A67-35407
- Oblique interaction between supersonic vehicle in free flight and plane shock wave simulated, noting large unbalanced force 21 p3607 A67-37776
- Second order weak interaction expansion for hypersonic flow past adiabatic flat plate, obtaining expressions for static pressure, displacement thickness and skin friction 21 p3566 A67-38892
- Upstream influence ahead of weak uniformly moving shock or expansion wave incident on plane wall boundary layer 21 p3615 A67-39089
- ### SHOCK WAVE LUMINESCENCE
- Luminescence front interaction with transverse magnetic field in electrodynamic shock tube 02 p0274 A67-12416
- Diffusive separation of helium-argon mixtures in underexpanded free jets and normal shock waves studied by electron beam 02 p0234 A67-12543
- Convective heat transfer in radiating gas, examining boundary layer equations and boundary conditions involving luminescence 03 p0532 A67-12866
- Brightness temperature of shock waves dependence on wave amplitude in xenon and air at high temperature 05 p0795 A67-17544
- Radiometer system with photomultiplier tube for measuring absolute radiation from hypervelocity projectile flow fields 11 p1790 A67-24447
- ### SHOCK WAVE PROFILE
- Approximate determination of sonic line and pressure distribution on surface of blunt body in supersonic and hypersonic flows 02 p0178 A67-12042
- Perfect fluid model for observed phenomena of plane transonic flow past given profile with attached shock wave, starting with lemma on possible hodograph configuration 07 p1128 A67-20282
- Nonlinear heat transfer between parallel plates, using ellipsoidal statistical model of Boltzmann equation 13 p2223 A67-26960
- Plane shock wave in ideal gas characterized by infinitesimally thin discontinuity, determining width and distribution function 13 p2105 A67-27412
- Shock wave structure in air at supersonic and hypersonic velocities studied by electron-beam density method 14 p2297 A67-27997
- Electron beam density survey in low density hypersonic flow field over sharp flat plate, noting results in outer and inner part of shock layer 14 p2241 A67-28167
- Flow field experiments for shock wave and boundary layer development on two-dimensional and axisymmetric bodies 14 p2241 A67-28168
- Structure of strong shock wave studied for simple models of nongray radiative transfer 16 p2658 A67-30938
- Hypersonic gas flow past slender body, obtaining pressure coefficient and shock wave curvature by linearizing differential equations involving stream function 17 p2791 A67-32868
- Diffraction shock wave profile for various corner angles and wall shock Mach numbers, comparing experimental and theoretical results 20 p3422 A67-36847
- Shock structure in kinetic theory of gases, solving Krook model of Boltzmann equation with small perturbation technique 22 p3782 A67-39196
- Continuous shock wave profile found in MHD fluid where Whitham condition for wave profile discontinuity is satisfied 24 p4143 A67-42356
- ### SHOCK WAVE PROPAGATION
- Perturbations of gas-dynamic parameters behind shock wave front propagating from rarefied into dense gas with boundary between interfaces distorted 01 p0053 A67-10984
- Artificial shock wave from TNT explosion in aurora, in attempt to determine effects on auroral emission and temperature 03 p0413 A67-13374
- Shock wave propagation in gas-dust medium, examining motion and velocities of gas and dust at distance approaching infinity 04 p0701 A67-15556
- Shearing stress induced shock wave propagation in annealed aluminum under biaxial plastic prestresses [ASME PAPER 66-WA/APM-3] 05 p0909 A67-16143
- Shock wave attenuation in shock tube in

Mach 4 to 7 range, noting equipment used and results 05 p0791 A67-16433

Plasma stream translational energy transformation into random motion in connection with collisionless shock wave propagation along magnetic field 05 p0853 A67-16756

Plane, cylindrical and spherical shock propagation from point source explosion in gas with counterpressure 05 p0793 A67-17099

Sound-ranging technique for locating supersonic missiles 05 p0766 A67-17282

Smear camera used to measure detonation front velocity of explosive or propellant 06 p1001 A67-17793

Soviet book on electromagnetic shock waves associated with not-very-high powers, using Maxwell-Lorentz equations 06 p1031 A67-17949

Mass velocity profile measured using electromagnetic device to record emf changes in metal probe embedded in nitromethane flow 06 p1112 A67-17953

Base pressure behind supersonic vehicle, calculating existence conditions for wake solutions and location of stable and unstable singularities [AIAA PAPER 67-60] 06 p0986 A67-18269

Closed form solution methods for blast wave propagation in solid media assuming power law density profile [AIAA PAPER 67-141] 06 p1102 A67-18290

Radio wave emission due to shock wave propagation in magnetospheric boundary and electromagnetic scattering in plasma wave field 07 p1243 A67-19808

Formation and expansion of electromagnetic shock waves in communication lines, using ferroelectric crystals 08 p1295 A67-20824

Shock wave propagation in plasma across magnetic field, solving problem via two-component hydrodynamic equation 08 p1358 A67-20858

Rocket measurements of small scale structure of ionization profile and wind speed fluctuations, propagation of gravity shock waves and stratification in upper atmosphere 08 p1325 A67-20986

Propagation mode of one-dimensional HF finite acceleration pulses in nonlinear viscoelastic solids, stressing shock formation and propagation 09 p1573 A67-21547

Free charged particles interaction with each other and neutral atoms in highly excited states effect on thermodynamic and gas dynamic parameters of shock wave propagating in cesium vapor, taking into account energy losses due to radiation 09 p1540 A67-21791

Synchronized shadow photochronographic investigation of wire explosion shock waves in air 09 p1532 A67-22064

Asymptotic law of propagation of plane detonation wave where perturbed motion behind wave transforms it to Chapman-Jouguet wave 09 p1489 A67-22218

One-dimensional steady solutions for shock wave propagation in class of nonlinear viscoelastic materials deduced from stated balance laws and representation theorem for compressive and expansive motions 09 p1576 A67-22410

Flow of ideal gas behind shock wave of finite amplitude analyzed, based on equation for one-dimensional adiabatic motion 10 p1624 A67-23033

Numerical calculations of nonlinear behavior of MHD shock waves in dissipative medium 11 p1825 A67-23854

Two-dimensional steady MHD flow with resolution of neutral sheets into intermediate and slow waves 11 p1862 A67-24499

Plasma production by ruby laser pulse irradiation of LiD investigated, results suggest collisionless electrostatic shock propagation at expanding plasma ball edge 11 p1840 A67-24561

Dynamic behavior model for gas shock wave motion and reflection in semilinear volume laterally bounded 11 p1782 A67-24954

Shock wave propagation in cylindrical tube, comparing theoretical and experimental results concerning light front, pressure and magnetic field 13 p2094 A67-26641

Similarity solutions derived for describing propagation of strong compression shock in transversely expanding gas 13 p2094 A67-26643

Buildup of waves to shocks and subsequent weak shock wave propagation 13 p2166 A67-26647

Relativistic velocity shock wave propagation in stellar high temperature high density plasmas with pair production, thermonuclear reactions and neutrino emissions 14 p2355 A67-27953

One-dimensional plane shock wave propagation through hot dense plasmas under various energy and pressure conditions, noting magnetic field effect 14 p2356 A67-27957

Plane shock wave propagation in inviscid perfect gas colliding with right angle obstacle, determining flow in perturbed region 14 p2296 A67-27979

Plasma wind tunnel facility for producing steady flow high conductivity collisionless plasma simulating solar wind interaction with magnetosphere 14 p2294 A67-29036

Approximate solution for interaction of shock wave moving in one dimension with sudden increase in cross sectional area 14 p2306 A67-29061

Approximate expression derivation for calculating propagation rate of strong shock wave in inhomogeneous cosmic medium 15 p2552 A67-29146

Behavior of electromagnetically accelerated shock waves investigated by Mach-Zehnder interferometer 15 p2488 A67-29663

Reflection coefficient for electromagnetic wave in circular cylindrical shock tube incident on moving plasma calculated numerically 15 p2531 A67-29905

Argon and nitrogen flows past sphere at low supersonic velocities analyzing formation of bow shock wave 16 p2592 A67-31103

Argon and nitrogen shock wave damping along tube in absence of effects of oscillation excitation, gas dissociation, ionization and emission 16 p2659 A67-31104

Shock wave velocity measurement using photoelectric, piezoelectric ionization and continuous scanning methods 16 p2673 A67-31106

Two-dimensional viscous fluid flow with formulation and solution of weak shock reflection problems by numerical method 16 p2662 A67-31534

Boundary layer effect on primary wave propagation and gas states behind reflected wave in shock tube with nozzle 17 p2837 A67-32346

Collisionless shock waves in plasmas with high beta parameter, discussing Alfvén wave turbulence, firehose instability, dissipation and structure 17 p2901 A67-32528

Shock wave propagation in solar wind caused by tangential discontinuities and geomagnetic sudden storm commencement 17 p2936 A67-32530

Propagation of strong ionizing front at arbitrary oblique angle relative to magnetic field, determining limits to value of electric field ahead of shock 17 p2908 A67-33114

Asymptotic law of propagation of plane detonation wave where perturbed motion behind wave transforms it to Chapman-Jouguet wave 18 p3026 A67-33758

Detonative ignition induced by shock merging ahead of accelerating flame in hydrogen-oxygen mixture analyzed by stroboscopic laser-schlieren photography 18 p3153 A67-33826

Radiation peak formation mechanism in spectral lines of nonequilibrium gas following passage of shock wave 18 p3083 A67-34060

Thermonuclear reactions occurring in supernova shock wave propagating through stellar envelope 18 p3136 A67-34726

Structure of shock waves in collision-free plasma at angle to external magnetic field studied by hydrodynamic equations 19 p3288 A67-35372

Electron density behind shock front of discharge plasma measured using interferometer 19 p3230 A67-35395

Plasma-magnetic shock wave propagation in high pressure, partially ionized argon plasma 19 p3293 A67-35400

Electric and magnetic field measurements in collisionless shock wave propagating through highly ionized magnetized plasma 19 p3294 A67-35408

Spark discharge generated blast wave application to shock on shock simulation, free-stream sound speed determination and

hypervelocity flow measurements [AIAA PAPER 66-763] 19 p3208 A67-35753

Panels response to oscillating and to moving shock waves, discussing mode excitation, magnification factor, Bessel function, etc 20 p3539 A67-37001

Incident step shock wave propagation through convergent channel containing explosive gaseous mixture, discussing detonation initiation 20 p3423 A67-37095

Growth and attenuation of acceleration waves and higher order waves derived from nonlinear fluid theory with internal state variables 21 p3610 A67-37739

Laval nozzles performance under off-design conditions, noting shock wave formation in region of supersonic velocity 21 p3564 A67-38420

Sonic boom and factors influencing shock wave propagation during straight horizontal supersonic flight 22 p3744 A67-39547

Propagation anomalies of atmospheric acoustic signals of nuclear explosions due to nonlinearities and refraction effects 22 p3790 A67-39645

Re-reflected shock wave from convergent cylindrical channel, showing secondary shock wave overtaking primary wave 22 p3783 A67-39720

Perturbed region behind diffracting shock wave on plane-walled convex corners at supersonic speed 23 p3990 A67-41172

Hypersonic aerodynamics, discussing tunnel testing, inviscid flows, airfoil shapes, real gas effect, shock wave theory and boundary layers 23 p3930 A67-41307

Imploding shocks and detonations propagation investigated by similarity solution extended to early imploding processes, using Oshima quasi-similar approximation 23 p3992 A67-41722

Density variation in shock tube across nonstationary shock wave separating from nitrogen gas fluorescence excited by fast electron beam 24 p4145 A67-42663

Anomalous electron heating rate in plasma region traversed by magnetic shock wave obtained by electron velocity distribution observation 24 p4198 A67-42736

Approximate expression derivation for calculating propagation rate of strong shock wave in inhomogeneous cosmic medium 24 p4239 A67-43069

SHORT CIRCUIT

Operation of coupled mutually loaded tunnel diodes, considering short circuit mode 09 p1473 A67-21963

Integral short circuit current of solar converters determined from spectral distribution of solar radiation energy, using simulator and SiO photocell films 09 p1451 A67-22531

Prevention system of short circuit in vacuum chambers due to glow discharges 10 p1622 A67-23316

Short circuit current measuring technique and results of electron diffusion lengths in diffused p type and holes in uniformly doped n type GaAs 11 p1850 A67-24912

Transistor failure analyses by measuring electric parameters, repeating production phases on opened transistors, destructive testing and defect production by extreme artificial stress 15 p2449 A67-29811

Electrical detonator characteristics and safety precautions in handling and use, noting untimely functioning and misfiring as causes of accidents 17 p2927 A67-33093

Isochronal annealing of short-circuit current of electron irradiated silicon solar cells 19 p3305 A67-35668

Operation of coupled mutually loaded tunnel diodes, considering short circuit mode 20 p3400 A67-37193

Short circuit photocurrent of avalanche photodiode, determining frequency response and multiplication effect on bandwidth 22 p3767 A67-39362

Tetatron gun plasma burst expanding freely in drift tube, discussing wall shorting effect inhibition method and measurements 22 p3846 A67-39485

Rise rate dependence of transition current of superconducting solenoids on presence of electrical short circuit 23 p4045 A67-41457

SHORT SC-5 AIRCRAFT

Drag problems of Belfast aircraft solved by modifications developed in wind tunnel program 24 p4092 A67-42443

SHORT WAVE RADIATION

Experimental verification of calculation of

- short wave radiation fluxes in real atmosphere from model 01 p0108 A67-10128
- Short and ultrashort wave power amplifiers using Soviet transistors 05 p0773 A67-16457
- Application of short wave theory to regime of regular interaction between weak shock waves 06 p0984 A67-18045
- Ionospheric propagation index for short term prediction of short wave propagation 07 p1248 A67-19409
- Angular intensity distribution of short wave radiation measured by automatic stratospheric balloons 07 p1220 A67-19453
- Short wavelength large steerable radio telescope design, considering wind, heat, gravity effects and economics 11 p1768 A67-24777
- Noise on short waves including terrestrial, extraterrestrial, radio sources, etc 12 p1904 A67-25303
- Diurnal and annual variation of absorption of short waves in ionosphere 13 p2066 A67-26486
- Linear polarization of discrete radio sources at 6 cm wavelength 13 p2206 A67-27483
- Atmospheric radiation balance studies via daytime balloon measurements, obtaining vertical profile curves for albedos, total and reflected radiation, etc 19 p3214 A67-34853
- Short wave spectrometer for measuring total and scattered sky radiation, spectral brightness and fluxes of direct and reflected solar radiation 19 p3227 A67-34860
- Radiative processes in lower stratosphere and average monthly heating rates over all latitudes due to direct and reflected solar short wave radiation absorption 19 p3226 A67-35922
- Similarities between Jupiter decametric radiation and satellite induced ionospheric disturbances 20 p3521 A67-36308
- ## SHORT WAVE RADIO TRANSMISSION
- Short wave radio links, discussing frequency converters, spectrum oscillators, transmitters, etc 07 p1150 A67-19343
- Signal intensity along short wave path calculated by method based on dead zone existence and geometrical optics 10 p1603 A67-22793
- Satellite-emitted short radio wave field intensity and ionospheric parameters 11 p1751 A67-24071
- Single-band radio transmitters and receivers and other types of advanced channel diversification and multiplex reception 14 p2273 A67-28861
- Short wave skip distance variation with reflection angles in multilayered ionosphere calculated from improved formula 20 p3382 A67-36763
- Signal intensity along short wave path calculated by method based on dead zone existence and geometrical optics 24 p4120 A67-42129
- ## SHOT NOISE
- Thermal, excess and shot noise in transducers, examining CW signal generator method for measuring average noise factor 01 p0039 A67-11196
- Equivalent circuit for field effect transistor, considering amplifying characteristics of component, noting use of thermal and shot noise 06 p0966 A67-17589
- Quantum noise theory for lasers, obtaining rate equations and noise sources with moments appropriate to shot noise and amplitude spectrum 11 p1799 A67-24239
- Cathode noise voltage in low current arc at atmospheric pressure as function of arc cathode surface state 14 p2354 A67-27764
- Noise and dark current reduction in photomultiplier tubes by magnetic defocusing [SRCC-43] 19 p3193 A67-35314
- ## SHOWER
- SA COSMIC RAY SHOWER
- SA METEOR SHOWER
- Geometric and thermal height of shower and storm cells using radar observations 13 p2150 A67-26433
- ## SHRINKAGE
- Sintering of cobalt-nickel powder mixtures during formation of solid solutions, noting shrinkage and diffusion coefficients 01 p0096 A67-10695
- Shrinkage process in zirconium diboride during sintering, noting variation with length of isothermal processing 03 p0456 A67-14191
- Emulsion shrinkage effect on hologram image space 17 p2863 A67-33303
- ## SHROUD
- Cryopumps incorporated into liquid N shrouds for small space simulation chambers 12 p1900 A67-25710
- ## SHROUDED BODY
- Shrouds for space vehicles, discussing advantages of Al and Mg as materials and longitudinally split and over-nose type covers 11 p1870 A67-25006
- Cooldown of shrouded spherical vessels in liquid nitrogen, determining smallest tank-shroud gap compatibility with rapid cooldown 13 p2229 A67-27666
- ## SHROUDED TURBINE
- Dynamic rubber wheel model to supplement digital computer analysis for prediction of frequencies, mode shapes and stress distributions of vibrating rotor stages [ASME PAPER 66-WA/GT-8] 04 p0712 A67-15364
- ## SHUNT
- Shunting of input current into collector region of planar triode 03 p0386 A67-13963
- One-dimensional linear approximation of effects of magnetic and electric shunting of linear inductor edges on constant velocity MHD channel flow 04 p0556 A67-15524
- Sample standard resistor combination to shunt pulsed currents used to study superconducting-to-normal transition in short wire samples 08 p1367 A67-20378
- ## SHUTTER
- SA CAMERA SHUTTER
- High speed electromagnetically driven shutter 10 p1658 A67-23786
- Shutter type thermal control system design for Nimbus spacecraft [AIAA PAPER 67-309] 12 p2012 A67-26024
- Improved dipole shutter, optical transparency for protection against high intensity flashes 23 p3965 A67-41565
- ## SICKNESS
- S ALTITUDE SICKNESS
- S DECOMPRESSION SICKNESS
- S DISEASE
- S MOTION SICKNESS
- ## SID
- S SUDDEN IONOSPHERIC DISTURBANCE /SID/
- ## SIDE-LOOKING RADAR
- Terrain information from high altitude side-looking radar imagery of Arctic area 01 p0059 A67-10328
- Coherent optical systems for processing data collected by sidelooking synthetic aperture radars 01 p0022 A67-10430
- Side-looking airborne radar in which long antenna mounted along side of aircraft faces at right angles to flight path 04 p0573 A67-15039
- Low resolution side-looking radar application for geological studies, noting advantage over small scale aerial photography 06 p0994 A67-17833
- Radar, IR and laser sensors production trends for airborne reconnaissance 15 p2485 A67-29163
- ## SIDEBAND
- SA DOUBLE-SIDEBAND RADIO COMMUNICATION
- SA SINGLE-SIDEBAND DEMODULATION
- SA SINGLE-SIDEBAND MODULATION
- SA SINGLE-SIDEBAND RECEIVER
- Compatible double sideband/single sideband/constant bandwidth FM telemetry system for wideband data 02 p0197 A67-12010
- Vestigial sideband FM mode combined with three-level coding for data transmission at 4800 bauds 02 p0201 A67-12119
- Upper sideband effect in parametric amplifier on positive conductance and negative resistance of circuits, deriving noise figure expression 06 p0966 A67-17575
- ## SIDELobe REDUCTION
- Paired echo sidelobe produced by ripples of Fresnel spectrum in active linear compressed-pulse frequency modulation 01 p0027 A67-11328
- Choke slots or corrugated structure in walls of horn antenna for reducing sidelobe and backlobe level by controlling illumination of E-plane edge 02 p0211 A67-11601
- Statistical analysis of sidelobe region of offset-feed parabolic reflector 03 p0382 A67-13673
- Treatment of surface of directional radar antenna with RF absorption material for sidelobe reduction 03 p0389 A67-14349
- Pulse Doppler radar performance in presence of random fading to study ambiguity diagram and nature of variance with respect to Doppler frequency 04 p0653 A67-14876
- Parabolic reflector with shields protecting feed from extraneous radio waves 08 p1318 A67-21343
- Sidelobe reduction in phase-coded pulse compression radars solved by eliminating ripple of matched filter output with aid of weighting filter 12 p1908 A67-26092
- Helix-conical circularly polarized antenna performance analyzed, noting increased gain and lower sidelobe level 13 p2076 A67-26515
- Parabolic reflector with shields protecting feed from extraneous radio waves 17 p2822 A67-31939
- Waveguide dispersive line use in FM pulse compression system outlined for high resolution in S-band radar 21 p3601 A67-39068
- Sidelobe reduction by stepping E-plane field distribution on rectangular horn antenna aperture, finding values of geometrical parameters 22 p3767 A67-39273
- Impedance strip directional properties when excited through slot in metallic half-plane, noting case of reflector antenna with decreasing impedance 22 p3770 A67-39763
- Antenna linear array design with limited amplitude tapering, showing desirable pattern characteristics in partially uniform array 23 p3978 A67-40827
- Harmonic analysis of half-wave dipole and director parallel to reflecting plane 24 p4132 A67-42715
- ## SIDESLIP
- Wind tunnel investigation of effect of ground level on static aerodynamic characteristics of sideslip for rectangular and delta wing with rudder assembly 07 p1126 A67-19886
- Captured Air Bubble /CAB/ vehicle stability tests [AIAA PAPER 67-349] 14 p2246 A67-28731
- ## SIEVE
- S MOLECULAR SIEVE
- ## SIGHT
- S VISION
- ## SIGHT LINE
- Helmet mounted sight as operational element in quick reaction boresighting system, using static and moving targets, obtaining field test data 09 p1456 A67-22371
- Motions of chromospheric fine structure in weak plage analyzed, using time resolved H-alpha spectra for estimating line-of-sight velocities of objects 12 p2001 A67-25222
- Simplified fire control system for helicopters, noting helmet sight, error source corrections and sighting and tracking convenience 22 p3755 A67-39849
- ## SIGNAL
- S CHIRP SIGNAL
- S ERROR SIGNAL
- S FLARE
- S MAGNETIC SIGNAL
- S OPTICAL SIGNAL
- S RADIO SIGNAL
- S RADIO STAR SIGNAL
- S RANDOM SIGNAL
- S TIME SIGNAL
- S VISUAL SIGNAL
- ## SIGNAL ANALYSIS
- Counting errors and amplitude spectra distortion in detectors for statistical characteristics of information contained in signals 01 p0066 A67-10653
- Phase cancellation of sinusoidal signals in presence of Gaussian noise for comparison and threshold decision schemes 01 p0025 A67-10860
- Signal conditioning variable resistance transducer excited by constant current power supply 01 p0071 A67-11099
- Ballistic integrator features and overall capacities, noting integration start-stop and peak detection 01 p0076 A67-11146
- Signal-space quantization and bandwidth compression examined, using theory of mappings of signal spaces with Riemann matrices 01 p0027 A67-11239
- Equations for small signal sinusoidal operation of intrinsic field effect transistor, considering physical principles of operation of device 02 p0216 A67-12071
- Signal suppression in ferrite frequency selective limiters evaluated using parametric subharmonic generator model 02 p0217 A67-12093
- Voice-bandwidth communication link

analyzer /CLA/ system for making measurements on communication link, using periodic pulse stream with suitable spectral filtering 02 p0203 A67-12134

Input impedances calculated for parametric up-converters, examining overall signal behavior 02 p0220 A67-12205

Synthesis of phase synchronization system providing maximum level filtering of external fluctuation noise, using generalized integral criterion 03 p0393 A67-13949

Activity criterion determination of boundary between active region and saturation region in transistor, using Ebers and Moll large signal equations 03 p0386 A67-13980

Amplitude and phase of weak signals at low signal to noise ratio, using parametric oscillators for signal phase quantization 04 p0620 A67-14748

Truncation error bounds for sampling representations of band limited signals 04 p0570 A67-14871

Asymptotic method of synthesizing FM pulse signals from given autocorrelation function 04 p0575 A67-15160

RF interference detection and elimination from communication systems noting signal, frequency and amplitude analysis techniques 04 p0577 A67-15730

Frequency fluctuations of laser field determined by measuring cross correlation function at two points 05 p0815 A67-16625

Oblique probe data applied to determination of minimum group path of signal for parabolic model of ionosphere 05 p0801 A67-17130

Pulse Doppler radar theory using Fourier transformation integrals applied to analysis of spectrum of all signals 06 p0957 A67-17592

Signal design problem of optimal waveforms for transmission through phase incoherent channel 06 p0962 A67-17945

Optimal one-dimensional truncated signal distribution ensuring optimal capacity or differential entropy 06 p0976 A67-18219

Output signal of switched amplifier with arbitrary input signal analyzed, using Fourier series 07 p1154 A67-19656

Probability of signal acquisition by phase locked oscillator system operating in frequency search mode, determining maximum admissible search rate without noise 08 p1295 A67-21275

Digital communications on pseudonoise tracking link using sequence inversion modulation, noting bit error probability 09 p1459 A67-21581

Average power patterns for various values of rms phase difference for points separated by aperture radius in turbulent atmosphere 09 p1462 A67-21610

Fluctuating effective gain of rocket telemetry links determined from signal strength data of Black Brant sounding rockets 09 p1463 A67-21829

Spectra and joint correlation function for PSK signal modulation 10 p1604 A67-22979

Minimum variance estimation and prediction theory for signal parameters in presence of noise 10 p1606 A67-23084

Amplitude spectra of complex signals with known autocorrelation functions 10 p1607 A67-23458

Complex correlation function application to describe correlation between signals from two antennas of radio interferometer 11 p1762 A67-24287

Independent control of angular location of independent zeros of directional pattern for linear array 11 p1762 A67-24290

Adaptive data compression techniques, principles and advantages 11 p1758 A67-24709

Relay testing under operational voltages and currents, discussing timing circuits and sequencing and computer inputs outputs 12 p1922 A67-25698

Static and dynamic behavior of large pulsed signal behavior of n-type MOSFET below and in constriction /pinch/ region 13 p2076 A67-26487

Asymptotic method of synthesizing FM pulse signals from given autocorrelation function 15 p2435 A67-29347

Energy spectrum and correlation characteristics of PCM signal studied by Levin method, calculating correlation moments of code group symbols 16 p2620 A67-30478

Optimal one-dimensional truncated signal distribution ensuring optimal capacity or

differential entropy 16 p2643 A67-30485

Small signal power conservation in space charge waves of multivelocity electron beam with rectangular velocity distribution 16 p2703 A67-30796

Wideband communication systems, detailing sequenced and parallel complex signals concept 16 p2624 A67-31025

Asymptotic behavior of transient signal propagation in lossless, isotropic plasmas for stepmodulated sine wave input signal 16 p2627 A67-31351

Adjoint simulation technique extended to signals consisting of continuous, sampled and multirate sampled systems with random inputs 16 p2652 A67-31684

Airborne field strength measurements in NPM antipode region noting variation with inverse square root of distance over sections of antipodal area 16 p2631 A67-31855

Changes of phase and signal amplitude of VLF radio waves during solar flares noting waveguide mode characteristics 16 p2632 A67-31859

Inaccurate determination effect of input-signal characteristics on filtration quality, deriving equations for estimating upper limit of relative increase of rms filtration error 17 p2829 A67-32223

Single circuit parametron with pulsed balance-modulated pumping voltage, showing existence of two independent subharmonic components 18 p3005 A67-33503

Fourier analysis of amplifier commutated capacitor type integrator output signal 18 p3011 A67-34107

Construction and uniqueness of time optimal control of multidimensional linear system with constraints on control signal amplitudes and rates 18 p3017 A67-34280

Large-signal analysis for varactor frequency upconverter under overdriven conditions, obtaining equations for varactor charge, current and voltage 20 p3396 A67-36510

Pulsar circuit for studying large signal transient response in plasma lasers 20 p3445 A67-36530

Oblique probe data applied to determination of minimum group path of signal for parabolic model of ionosphere 21 p3618 A67-38473

Hard limiter effect on test signal phase angle, considering single and two interfering signals 21 p3586 A67-38955

Test signal techniques for measurement and video monitoring used in ORTF network 22 p3796 A67-39233

Number of degrees of freedom for observation of motion of steady signal from uncontrolled plant 22 p3836 A67-39775

Equations for mode analysis in multichannel extremal control systems with harmonic probe signals, discussing synthesis of optimizers and phase shift automatic compensation 22 p3777 A67-39864

Energy dependent mobility in small signal analysis of waves in semiconductors 22 p3864 A67-40310

Slegman maximum signal theorem for coherent scattering detection, estimating attenuation through scattering medium 23 p3973 A67-40835

Technique for simulating stochastic approximation methods for selection of properties to ensure predetermined output signal characteristics 23 p3976 A67-41340

Internal combustion engine vibration signals application to automatic fault diagnosis, discussing engine instrumentation and signal analysis [SAE PAPER 870872] 24 p4207 A67-42009

SIGNAL ANALYZER

Space bandwidth signal spectral analysis using multichannel optical system and two-dimensional optical system with increased frequency resolution 02 p0243 A67-12049

Analyzer of characteristic function of random phase of quasi-harmonic signal using statistics 06 p0972 A67-18392

Image analyzer tube for IR TV based on phenomenon of accumulation at semiconductor junctions 07 p1189 A67-20158

Optimum representation of signals with limited spectrum by truncated Kotelnikov series for discrete correctors 11 p1769 A67-23906

Twelve-channel parallel action noise spectrum analyzer for LF noise measurement, using transistorized negative feedback amplifier 11 p1769 A67-25038

Statistical performance confirmation of wideband random equalizer, emphasizing analysis technique, analyzer characteristics and power spectral density plot 12 p1942 A67-25692

Versatile digital data handling system designed to accept and control output of space radiation scintillation spectrometer 12 p1909 A67-25864

Special purpose analog computer for analyzing wideband signals in two parts of network, with automatically plotting and coupling factor as function of frequency 13 p2089 A67-26410

Digital and hybrid pulse analyzer designs for automatic measuring pulse characteristics digital and hybrid pulse analyzer designs for automatically measuring pulse characteristics 13 p2075 A67-26411

Automatic pulse digital analyzer design to measure simultaneously all-pulse parameters used for control of closed loop systems 13 p2078 A67-26801

Predetection telemetry tape combiner 17 p2813 A67-32496

Optimum representation of signals with limited spectrum by truncated Kotelnikov series for discrete correctors 21 p3604 A67-38934

SIGNAL DETECTION

Statistical description of signal filtration 01 p0043 A67-10237

Optimum dynamic range centering for Rayleigh distributed signal for case having nonzero SNR by envelope detection process 01 p0022 A67-10434

Upper bound of dynamic range for minimal probability of excluding randomly distributed signal 01 p0023 A67-10486

Statistical properties of input signals and effect on structure of optimal binary system of signal reception 01 p0024 A67-10722

Book on noise and effect on communication covering random processes, fundamentals and spectra, nonlinear transformations /demodulation/, statistical theory of detection and information theory 01 p0024 A67-10725

Binary detection probability for optical polarization modulation communication system using Gaussian approximation, noting signal to noise ratio 01 p0026 A67-10866

Passive detection of sonar target in presence of Gaussian noise background with unknown spectral quantities 02 p0217 A67-12087

Digital simulation results for random approximation solutions of binary signal detection problems 02 p0204 A67-12169

Detectability criterion for signal received against random noise background 03 p0368 A67-13277

Optimum radar detection theory dealing with discrimination and resolution of one target from another and of target from noise and clutter 04 p0572 A67-15033

Book on asynchronous detection and reception of pulsed radio signals at HF and Shf against background of fluctuating noises 05 p0761 A67-16172

Radiophysical measurement of small amplitude mechanical oscillations of self-oscillator by means of mechanical-electric converters and effects of natural line width on minimum amplitudes 05 p0805 A67-16357

Tunnel diode superregenerative amplification and detection in linear regime and volt-ampere characteristics of diode 05 p0772 A67-16450

Approximate minimax detection of vector signal in Gaussian noise 05 p0834 A67-16493

Phase separation and synchronization during separation of AM signals with overlapping frequency spectra 05 p0764 A67-16903

Two-step procedure for high energy signal detection against noise background, based on statistical probability 05 p0765 A67-16954

Optimum quadratic detection of sample vector from signal random process imbedded in Gaussian noise 05 p0765 A67-17041

Strakhov method determination of optimum numerical filter for extraction of potential field signal from random noise background 05 p0767 A67-17390

Amplitude and phase detection for determined signal with nonstationary noise, using generalization of Levin method 05 p0767 A67-17402

Multiple contact Schottky barrier microwave diode, comparing operation with

single diode in mixing and small and large signal detection 05 p0780 A67-17526

Information criteria for threshold setting in simple binary hypothesis tests 06 p0962 A67-17948

Backward diode fabrication and properties for SHF detection, noting germanium diode 06 p0969 A67-18120

Electronic analog detection and separation of oscillations slightly differing in amplitude 06 p1109 A67-18667

Effectiveness of signal detection methods compared, using ratio-processed output value criterion 07 p1139 A67-19224

Heterodyne and photon counting receivers compared for optical communications 07 p1185 A67-19398

Point source detection using signals propagating in quantum field, in terms of correlation functions of thermal field fluctuations 07 p1142 A67-19585

Effect of a priori known relation between random signal and noise voltages at output of two channels 07 p1143 A67-19593

Book on statistical decision theory and sensory processes in signal detection theory and psychophysics 07 p1136 A67-19726

Curves of probability of detection vs signal to noise ratio for log-normal signals in Gaussian noise, considering correlated and uncorrelated signals 07 p1144 A67-19868

U.S. and U.S.S.R. search for extraterrestrial civilizations [AAS PAPER 66-78] 07 p1255 A67-20001

Combined use of time-domain waveforms, detection probability and false alarm probability for selection of optimum sample period and quantization interval for detection of impulse waveforms 09 p1459 A67-21582

Narrowband optical heterodyne detection, describing InAs photodiode arrangement 10 p1654 A67-22752

Digital synthesis technique for automatic frequency search 10 p1604 A67-22970

Detectability of coherent optical signals against incoherent Gaussian background noise radiation in heterodyne receiver with laser local oscillator 11 p1800 A67-24419

Signal duration effect on detection in presence of masking noise by human auditory system, using electric analogy for testing purposes 12 p1903 A67-26126

Energy detection of unknown deterministic signal in white Gaussian noise by energy measuring device 13 p2067 A67-26510

Size and shape of vertical polar diagrams of radars in situ measured using sun and other stars as signal sources 13 p2071 A67-27219

Auditory vigilance task, assessing effects on performance of signal detection value, miss or false detection cost and set size from which signals were drawn 14 p2258 A67-28664

Optimum system for signal detection with single-band noise modulation during carrier suppression, noting receiving system 15 p2436 A67-29413

Pulse measuring system for observing structure of pulsed signals in rectangular phase-time coordinates 15 p2444 A67-29414

Distribution-free signal detection by multiple-resolution-element pulse radar, based on ranks of returns and having invariant false alarm rates 15 p2436 A67-29933

Matched-filter systems waveform dependence investigated for signal detection in nonstationary clutter 15 p2438 A67-30135

Fat cylindrical antenna admittance measured noting behavior similar to that of thin antenna admittances 15 p2454 A67-30137

Phase separation and synchronization during separation of AM signals with overlapping frequency spectra 16 p2622 A67-30879

Small signal current gain of p-n-p-n section of four-layer Si structure as function of current, noting effect of base width, minority carrier lifetime and doping level 17 p2911 A67-32193

Space-charge-limited dielectric diode with quadratic I-V characteristics, noting shallow trap effects on detection properties 17 p2823 A67-32199

Design of receiver circuitry for IR surveillance system having high signal detectability 17 p2862 A67-33289

Repeating incoherent pulsed signal

detection problem in Gaussian noise studied by binary integration method assuming ideal control criteria 18 p2999 A67-33505

Quantum formulas for optimal filtration of useful electromagnetic signal in noise background based on maximum misinformation principle 18 p2999 A67-33533

Dual-antenna AMTI radar ground clutter cancellation and signal enhancement 18 p3001 A67-34117

Receiving system for detecting binary random signals in white noise, determining correlation functions and error probability 18 p3001 A67-34180

Polarity reversal with DC bias in hot-carrier microwave diode 19 p3198 A67-36038

Optimal multidimensional systems for discriminating and detecting signals dependent on finite number of random parameters and combined with noise 19 p3185 A67-36097

Low intensity photoelectric signal detection by Fabry-Perot spectrometer using SNR enhancing method 20 p3439 A67-36356

Sofar bomb signature identification by separation of desired signal from multipath signals with digital computer 20 p3484 A67-36558

Lasers for wideband planetary communication, describing heterodyne receiver and transmitter designs 20 p3381 A67-36566

Optimal signal selection on background of steady additive noise in realistic communications system 20 p3382 A67-36777

Influence on hits and false alarms of response and signal events on preceding trial 20 p3372 A67-36962

Optimum detection of Markov signals against noise background in case of discrete time 20 p3408 A67-37039

Optimal detection of signals by spatially distributed receiving system against random noise background, using space-time signal selection method 20 p3383 A67-37070

Point source detection using signals propagating in quantum field, in terms of correlation functions of thermal field fluctuations 20 p3384 A67-37322

Effect of a priori known relation between random signal and noise voltages at output of two channels 20 p3384 A67-37332

Adaptive unknown-waveform pulse signal detector algorithm construction method 20 p3384 A67-37333

Asymptotic relative efficiency of mixed statistical threshold tests with Gaussian samples 20 p3412 A67-37495

Minimum detectable signal and frequency response of mercury-doped germanium detector, measuring response time and SNR through optical heterodyne techniques 21 p3590 A67-38009

Synchronous detection for signal phase gap measurements and Diana type satellite tracking, discussing hypothetical carrier 21 p3583 A67-38644

Fredholm equation solution and minimax theory for p-dimensional vector signal detection against p-dimensional Gaussian noise background 22 p3762 A67-39876

Single channel self-adaptive servosystem synthesized for optimal tracking of diffusion type signal with drift 23 p3983 A67-40598

Modulation transfer functions of various solar recording films using interference device, giving detectability threshold of two-dimensional emulsion patterns 23 p4001 A67-41237

X-ray survey of Virgo region revealing signals from radio sources 3C 273 and M 87 23 p4061 A67-41473

Probability of signal detection and accuracy of measurement in fluctuating multichannel system 24 p4120 A67-42223

Noise immunity in binary detection and temporal shift measurement of pseudorandom amplitude keyed echo signal in multichannel system 24 p4120 A67-42233

SIGNAL DETECTOR

InSb submillimeter detector as mixer in superheterodyne receiver shows performance two orders less than ideal receiver 01 p0036 A67-10440

Noise-rejection characteristics of signal detector based on zero counting of random process 02 p0194 A67-11902

Power signal to noise ratios for coherent and noncoherent optical detection, for optimization of optical

systems 02 p0243 A67-12056

Reflex klystron operation modes such as phase locked amplifier, regenerative amplifier, detector and mixer 03 p0387 A67-14101

Quadratic detector with diodes, based on linear interpolation of parabola 04 p0581 A67-14891

Resonant frequency change of oscillatory circuit due to nonlinear capacitance of semiconductor diode used as amplitude detector 04 p0586 A67-15677

Determining theoretical minimum signal that can be detected by optical detection system noting dependence on integration time, noise, etc [SMPTE PAPER 101-91] 12 p1905 A67-25475

Nonlinear Bayes detector synthesized for Gaussian signal and noise fields using Wiener filters 12 p1919 A67-26087

Set of curves relating statistical properties of envelope detector output to SNR of CW signal in narrow band Gaussian noise at input 13 p2070 A67-27154

Optical detectors for images and selected radiation signals using Bendix Channeltron multiplier, describing types, properties and applications 17 p2858 A67-32480

Threshold value of SNR of radar system in target detection against reflecting background, deriving block diagram consisting of linear group, detector and integrator 17 p2816 A67-32684

Linear correlation-detection transducer arrays for directional noise field signals, giving N-element coherent detector performance in propagating and turbulent boundary layer 22 p3801 A67-40233

Very short pulse measurements by deriving delayed pulse from measured waveform, describing detector circuit 23 p3981 A67-41273

Optical signal detector performance, deriving outlet electron distribution function 24 p4166 A67-41797

SIGNAL DISCRIMINATOR

High performance LF wideband discriminators with negative voltage feedback 01 p0040 A67-11316

Noise rejection properties of time discrimination method of pulsed signals improved by using exponential rather than selecting function 02 p0194 A67-11909

Frequency shift keyed /FSK/ digital signal detection using FM discriminators, predicting error rates for several sequences 02 p0201 A67-12118

High speed analog-digital converter with fast response time of discriminator obtained by error correction 04 p0593 A67-15636

Sensors and signal conditioners, discussing operation and calibration of resistance thermometers, strain gauge pressure transducers and potentiometric transducers 04 p0626 A67-15731

Error signal generation method to control laser frequency of laser oscillator 08 p1339 A67-21378

Divergence and Bhattacharyya distance measures in signal selection 09 p1459 A67-21580

Spectral differentiation and hologram filtering in reducing optical signal comparison to signal correlation 09 p1497 A67-21826

Differential frequency discriminators under combined action of signal and noise 11 p1750 A67-23913

Circuit for discriminating neutrons, gammas and charged particles from each other in phoswich scintillator 12 p1945 A67-25857

Power amplifier with discrimination of even harmonics in anode circuit and rectangular excitation pulses 13 p2077 A67-26748

Microelectronic frequency discrimination techniques based on analyzing whole functional block and searching for circuit configurations 14 p2282 A67-28024

Reducing disturbances of certain form to zero by generating modified form of test signal to be applied to cross correlator 15 p2461 A67-30322

Sign-discriminating field mill design using one rotor and one stator 16 p2671 A67-30972

Discriminator for fine automatic frequency control of reflex-klystron by error signal 19 p3228 A67-34991

Optimal multidimensional systems for

discriminating and detecting signals dependent on finite number of random parameters and combined with noise 19 p3185 A67-36097

Influence on hits and false alarms of response and signal events on preceding trial 20 p3372 A67-36962

Visual noise induction methods investigated at seven noise levels, discussing pattern comparisons by 46 subjects 20 p3372 A67-37000

Optimum multichannel system utilization for receiving regular signal against background noise 20 p3384 A67-37197

Synthesis of control systems with minimum complexity, noting application to filter discrimination of nonstationary signals 20 p3409 A67-37223

Frequency shift keyed (FSK) digital signal detection using FM discriminators, predicting error rates for several sequences 20 p3385 A67-37351

Differential frequency discriminators under combined action of signal and noise 21 p3585 A67-38941

SIGNAL DISTORTION

Nonlinear distortion of envelope of amplitude modulated signal in selective HF channel 01 p0020 A67-10200

Nonlinear distortions in parallel and series tunnel diode voltage amplifiers 03 p0377 A67-13235

Signal distortion arising from nonlinear /parabolic/ transconductance voltage characteristics of MOS /metal oxide silicon/ transistor determined experimentally by distortion measurement techniques 03 p0388 A67-14183

Bandwidth and distortion in pulse filters 03 p0389 A67-14303

Signal distortion introduced by series-fed array compensated in presence of noise by prefilter and postfilter 04 p0570 A67-14874

Mean and mean square directivity factor of antenna array in presence of phase and amplitude distortions 04 p0583 A67-15164

Calculation method for distortion of envelope of pulses during reflection from inhomogeneous ionospheric plasma during topside sounding 05 p0765 A67-17125

FM in quartz oscillators, deriving nonlinear distortion and frequency deviation factors and analyzing effect of destabilizing factors 05 p0767 A67-17400

Optimal threshold level resulting in minimum residual probability of distortion in transmission of pulse coded signals in systems with information feedback 06 p0975 A67-18218

Small signal nonlinear amplitude distortion and phase shift measurement in TWT 07 p1151 A67-19427

Pulse distortion in ionospheric plasma, discussing reflection from layer via geometrical optics and quadratic approximation 07 p1143 A67-19594

Amplitude distortion as function of filter bandwidth for various generalized pulse shapes 07 p1157 A67-20090

Noise modulation effect on signal distortion by analyzing signal components in terms of noise parameters and of undistorted signal 07 p1147 A67-20240

Waveform independent condition for transmission coefficient in linear time-independent transmission system to provide upper limit to signal distortion 10 p1620 A67-23572

Delay equalization in UHF range by allpass networks with symmetric three-conductor transmission lines 11 p1760 A67-24231

Atmospheric distortion effect on signal reception by large dimensional antennas, obtaining numerical estimates for various parameters 11 p1753 A67-24439

Degradation factors in speech channels of multiple access communications satellites 11 p1754 A67-24719

Conditions for minimum nonlinear distortion in power amplification of single band signal 11 p1772 A67-24983

Radar resolution performance in moving target determined by cross section of desired target compared with combined cross section of all interfering targets 12 p1907 A67-26083

Restoration of distorted signals for linear and nonlinear process 13 p2088 A67-27021

Effect of distortion on spectrum of pulse signal with linear frequency

modulation 13 p2070 A67-27046

Intermodulation noise calculated for case of distortion variable in any way with frequency 13 p2070 A67-27195

Ionospheric dispersion of AM-FM artificial satellite signals noting distortion effects, synchronization and interference difficulties 13 p2070 A67-27197

Asymptotic behavior of parameter-dependent nonlinear functional equations arising in signal reconstruction study 13 p2147 A67-27451

Intermodulation distortion of phase-locked loop demodulator as influenced by system parameters 14 p2273 A67-28708

Mean and mean square directivity factor of antenna array in presence of phase and amplitude distortions 15 p2443 A67-29351

Discrete control gyroscopic servosystem for tracing two-dimensional input signal subjected to random noise 15 p2490 A67-30172

Intermodulation distortion due to nonlinear elements in transistors analyzed using Volterra series representation 15 p2455 A67-30386

Optimal threshold level resulting in minimum residual probability of distortion in transmission of pulse coded signals in systems with information feedback 16 p2642 A67-30484

Correlation reception of wideband signals from ionospheric inhomogeneities, considering effectiveness for signal distortion discrimination 16 p2632 A67-31909

Generalized formulation of code separation incorporating general assumptions concerning nature of channel distortion 17 p2830 A67-32827

Woodward ambiguity function extended to broadband signals including Doppler distortions of modulation function 18 p3001 A67-34114

H-01 waveguide irregularities causing transfer function fluctuation, calculating rms and relative distortion power from PCM signal 19 p3183 A67-35561

Instrumentation grounding at Cape Kennedy, noting characteristics of ground system used for safety and clean space signals 20 p3398 A67-36837

Pulse distortion in ionospheric plasma, discussing reflection from layer via geometrical optics and quadratic approximation 20 p3384 A67-37334

Calculation method for distortion of envelope of pulses during reflection from inhomogeneous ionospheric plasma 21 p3582 A67-38468

Travelling wave maser saturation and signal distortion, determining magnetic moment 21 p3642 A67-38813

MOS-FET signal distortion avoided by taking into account turn-on voltage dependence on source bias 21 p3600 A67-38847

Contact continuity, intermediate resistance consistency and passing signal distortion of current collector with slip rings and brushes of various metals 21 p3572 A67-38916

Phase locked automatic frequency control regulated phase distortion effects on radar signal mean peak power at matched receiver filter output 22 p3781 A67-39762

Mathematical model for linear memory arrays cross coupling problems, discussing signal distortion due to common mode capacitance effect 22 p3765 A67-39912

TV camera reseau for engineering information on planetary missions and reducing geometric distortion [SMPTÉ PAPER 102-39] 22 p3808 A67-40377

Modulated signal nonlinear distortions from AC system resulting from system components nonlinearities 22 p3763 A67-40478

Controlled transient signal distortion by shock monitoring instrumentation circuits using piezoelectric accelerometers 23 p4007 A67-41382

SIGNAL ENCODING

Speech commands in control systems, discussing operation of bandpass, formant, scanning, harmonic and correlation voice coders 01 p0016 A67-10823

SIGNAL FADING

SA DIFFRACTION PATTERN

Method of coherent addition of signals to calculate noise resistance of diversity reception 01 p0024 A67-10718

Differentially coherent phase-shift keying system analyzed under wide range of signal

and noise conditions 01 p0025 A67-10861

Error probabilities for partially coherent diversity reception, noting linearized receiver performance during random noise output 01 p0026 A67-10863

Polarization-diversity telemetry receivers for combining FM/FM penetrometer data, noting signal fading 02 p0198 A67-12024

Fading characteristics of radio waves reflected from sporadic E layer of ionosphere over magnetic equator 03 p0406 A67-12824

Spaced receiver method for measuring ground diffraction pattern of vertically reflected radio waves 03 p0407 A67-12830

Theoretical approximations for probability densities of duration and interval between fades, assuming Rayleigh process characterizes fading phenomenon 03 p0368 A67-13168

Target homing of tracking systems receiving signal packages only in absence of fading 04 p0591 A67-14659

Spin echo and free decay signals in Rubidium optical pumping analyzed, using pulse method and light modulation technique 04 p0632 A67-14770

Electron beam evaporation of silicon dioxide producing storage layers for automatic picture transmission vidicon, analyzing causes of signal loss after short operating time in flight tubes 04 p0623 A67-15315

Periodic frequency change in signals from Cosmos V possibly due to solar cell output fluctuations 06 p0964 A67-18766

Fast regular scintillation of VHF signals received from earth satellites distinguished from scintillation associated with irregular ionospheric diffracting phase screen, showing correlation with sporadic E layer 07 p1141 A67-19416

Ionization density as decisive factor in integral radio wave absorption increase accompanying increase in critical sporadic E layer frequency 10 p1631 A67-22807

Ionospheric movement measurement with LF radio waves, using triangulation coupled with cross spectrum analysis of signal fading 11 p1784 A67-23936

Long period fading of VLF atmospherics, attributing origin to ionospheric propagation characteristics induced by geomagnetic activity 11 p1785 A67-23947

Received signal degradation for coherent pulse transmission through rain scattering volume, calculating length and energy for various paths 11 p1752 A67-24285

Optimum Bayes receiver for fading channels evaluated using Nakagami m-distribution 11 p1766 A67-24645

MF and HF portions of radio spectrum relationship to communication systems, presenting amplitude and phase variation in conjunction with effects of fading, time and frequency spread and atmospheric noise [IEEE PAPER 19-CP-65-482] 11 p1755 A67-25080

Geographical location and optical path length effects upon fade margin required for desired propagation reliability of microwave signals 13 p2066 A67-26406

Propagation measurements at 3.6 and 11 Gc/s over line-of-sight radio path 13 p2071 A67-27401

Data analysis from oblique incidence soundings during spread-F conditions [AGARDOGRAPH 95] 15 p2481 A67-30280

Radio star fadeouts and radio propagation 15 p2563 A67-30287

F scatter, flutter fading and maximum usable frequency phenomenology from HF radio propagation studies near equator 15 p2438 A67-30297

Attenuation of natural hydromagnetic waves /Pc1/ in ionosphere, noting amplitude reduction and particle distribution in magnetosphere 17 p2843 A67-32536

Diurnal and seasonal variation of electron content and diurnal variation of slab thickness investigated, emphasizing relation between electron content and scintillation occurrence 17 p2850 A67-33190

Satellite tracking simultaneous-lobing monopulse receiving system utilizing polarization diversity in coherent and noncoherent operational modes 18 p3020 A67-34110

Diversity-reception systems used in discontinuous radio communication, considering error probability and channel

utilization factors 18 p3001 A67-34181
 Radio propagation of transmissions from stationary and near stationary satellites used to study anomalous atmospheric refraction at low angles of 19 p3182 A67-35172
 Autocorrelation functions for amplitude of multiple echoes of fading radio signals reflected from ionosphere 20 p3379 A67-36293
 Higher order mode excitation by multipath propagation in deep fading of receiving horn-reflector antenna 20 p3385 A67-37355
 Doppler frequency measurement error due to short fading relative to time constant of automatic phase control loop 21 p3584 A67-38674
 Far tropospheric propagation of radio waves due to coherent scattering, explaining signal level dependence on distance and wavelength and signal fading 21 p3585 A67-38814
 Ionospheric discontinuity dimensions determined from satellite signal fadings at 20 and 40 mc correlating amplitudes 21 p3621 A67-39021
 Ionospheric irregularities field alignment responsible for radio signal fading analyzed, showing no evidence for relation to geomagnetic field 22 p3788 A67-39468
 Fading rate relation to ionospheric drift speed of radio waves, estimating size of irregularities 23 p3996 A67-41083
 Ionization density as decisive factor in integral radio wave absorption increase accompanying increase in critical sporadic E layer frequency 24 p4150 A67-42144
 Electric and magnetic field measurement by energy density antenna applicable to reducing signal fading encountered on mobile radio transmission path 24 p4131 A67-42340

SIGNAL FADING RATE

Communication relay to aircraft by satellite, discussing wave propagation characteristics, standing wave pattern, signal fading rates, etc 02 p0205 A67-12306
 Faraday fading rate of satellite signal as calculated from Appleton-Hartree formula for refraction index /without collision/ near transverse propagation [RASSA PAPER 1-10-127] 03 p0372 A67-14238
 Faraday rotation data from Explorer XXII, determining atmospheric electron content for magnetic field aligned ionization layer location and occurrence 23 p3996 A67-40818

SIGNAL FLOW GRAPH

Swept measurement techniques, discussing reflection coefficient and slotted line accuracy using signal flow graph 17 p2815 A67-32610
 Digital analog simulation program for IBM 7040 based on signal flow diagram, noting use of Runge-Kutta integration method 17 p2821 A67-32803
 Electronic network analysis using topological techniques of signal flow graphs, flow graphs and k-trees 22 p3778 A67-40556

SIGNAL GENERATOR

Thermal, excess and shot noise in transducers, examining CW signal generator method for measuring average noise factor 01 p0039 A67-11196
 Single cycle 1.72 mw pulse generator operating at 6 m wavelength 02 p0215 A67-11979
 All phases of pseudorandom sequence obtained by N-stage shift register generator 02 p0203 A67-12133
 HF electromagnetic angular displacement signal generator for use in gyro guidance systems 02 p0220 A67-12224
 Threshold of parametric oscillator system with idler modes in same frequency spacing as laser pump source 05 p0824 A67-16823
 Navigation system test by phase shifter, noting signal generator which simulates omnirange systems 07 p1155 A67-19839
 Fluidic binary full-adder configurations performance for subtraction function required to generate error signal in closed loop control system 08 p1280 A67-20444
 Error signal generation method to control laser frequency of laser oscillator 08 p1339 A67-21378
 LF test generator producing ramp output for phase shift detection in electronic systems at different input voltages 08 p1307 A67-21537
 Dual frequency VLF timing system for synchronization of remotely located clocks, noting WWVL radio carrier frequency, signal

generator, etc 09 p1494 A67-21619
 Loss in temperature compensation with varying frequency for quartz generators 11 p1757 A67-23909
 Dynamic Newtonian gravitational force gradient fields generator to calibrate response of dynamic gravitational gradient sensor 11 p1794 A67-24903
 Fluidic temperature sensor using frequency beating technique for generating analog pressure signal proportional to frequency differences 14 p2318 A67-28345
 Thermal, mechanical and electrical design of stable quartz crystal oscillator used for Geos satellite to generate RF carriers and Doppler system timing signals 15 p2445 A67-29585
 Weak DC signals conversion into electric pulses by magnetic semiconductor pulse width modulator using AC generator 17 p2823 A67-32224
 Signal generator tuning to center frequency of narrow band receivers, noting test setup and procedure 17 p2827 A67-32800
 Ultrasonic correlating device for fabrication of pulse compression radar signals 18 p3002 A67-34227
 Noise generator for calibration of radio receiver working in 1-2.6 MHz range during rocket flight 21 p3592 A67-38221
 Ion resonance probe for plasma density measurement using direct display method with frequency swept signal generator 21 p3627 A67-38258
 Loss in temperature compensation with varying frequency for quartz generators 21 p3600 A67-38937
 Plasma jet front produced by coaxial gun studied using SHF diagnostics method 22 p3799 A67-39764
 Speedy generation of space flight guidance command signals and comparative analysis of operational schemes for generating guidance signals 22 p3832 A67-40145
 Series and parallel pulse forming feed networks for generating microwave signals, comparing output parameters and limitations 22 p3774 A67-40444
 Book on radar signals covering FM pulse compression signals, waveform, Doppler shift, time factor, etc 24 p4122 A67-42425

SIGNAL MEASUREMENT
SA ELECTRONIC SIGNAL
MEASUREMENT

Optimum nonlinear inertialess conversion of signals from several devices, taking into account unreliability in operation 01 p0043 A67-10238
 Sum signal of output of system consisting of two detuned resonators and two amplitude detectors used for automatic measurement of signal frequencies 01 p0022 A67-10413
 Octantal error of frequency band over which Adcock direction finder operates, noting observed and true bearing relation of arriving signal 01 p0027 A67-11327
 Spectral analysis of pulsed signal reflected from ionospheric F-2 layer 02 p0193 A67-11872
 Optimum radar measurement of multiple target coordinates with unknown signal amplitudes and phases 05 p0765 A67-16960
 Centering accuracy, off-course sensitivity, mean modulation depth and relative tone phase of ILS signal measurement improved by phase locked detection technique 06 p0957 A67-17577
 Confocal resonator wave meter used to obtain frequency resolution of 10 MHz at 100 GHz 06 p0972 A67-18835
 Small signal nonlinear amplitude distortion and phase shift measurement in TWT 07 p1151 A67-19427
 Technique for observation of 24 discrete radio emission sources at 9.6 cm in August and September 1961 and February through May 1962 08 p1401 A67-21351
 Precision power measurements of spacecraft CW signal level with microwave noise standards, noting Mariner IV application [JPL-TR-32-1070] 09 p1495 A67-21622
 Noise injection and coherent detection to extend RF attenuation measurement range of series IF substitution 09 p1495 A67-21623
 Arbitrarily doped four-terminal field effect transistors /large and small signal models/ 09 p1475 A67-22199
 Signal and noise response of Ge avalanche photodiodes noting design, fabrication, LF

photomultiplication and static V-I characteristics 09 p1475 A67-22200
 Signal intensity along short wave path calculated by method based on dead zone existence and geometrical optics 10 p1603 A67-22793
 Autodyne design and operational principles for EPR in weak fields, using coaxial resonator 11 p1793 A67-24865
 Measurement errors of arrival direction of radio whistler caused by propagation in earth-ionosphere waveguide 15 p2436 A67-29480
 Spectral analysis of pulsed signal reflected from ionospheric F-2 layer 16 p2624 A67-31087
 Technique for observation of 24 discrete radio emission sources at 9.6 cm in August and September 1961 and February through May 1962 17 p2940 A67-31947
 Shock wave argon ionization in constant magnetic field, showing attenuation decrease of microwave signal in plasma and modulus change curves 18 p3087 A67-34045
 Point-by-point measurements of magnitude and phase of repetitive pulsed time functions using commercial equipment 19 p3182 A67-35031
 Superconducting parametric amplifier for measurements of small DC voltages in low impedance circuits 22 p3866 A67-40441
 Very short pulse measurements by deriving delayed pulse from measured waveform, describing detector circuit 23 p3981 A67-41273
 Signal intensity along short wave path calculated by method based on dead zone existence and geometrical optics 24 p4120 A67-42129

SIGNAL MIXING

Microwave mixer point contact diode with X-band intermediate frequency for good value of conversion loss 01 p0036 A67-10438
 Avalanche transit time diode used as sideband translator and combination local oscillator-mixer at X-band 03 p0381 A67-13666
 Sum and difference frequency mixing of visible and IR gas laser light in GaP at near reststrahl frequencies and relationship to spontaneous Raman scattering 04 p0682 A67-15464
 Three equivalent circuits of transistor mixer 05 p0784 A67-16943
 Statistical properties of envelope of signal-noise mixture with random angular modulation 05 p0765 A67-16961
 Intermodulation rejection in mixers, discussing performance characteristics of various combinations 08 p1304 A67-21223
 Fringe counting in laser interferometers and phase quadrature signals for bidirectional counting at good efficiency without mechanical or optical complications 09 p1493 A67-21613
 Doppler frequency-measuring tracking system in which tracking filter or retuned heterodyne is used for definition of signal with unknown frequency 10 p1607 A67-23452
 Feedback realization of continuous-time optimal filter, with application in redundant signal mixing 16 p2643 A67-31269
 Superlimiting phased-array receiving system in two-source environment 16 p2638 A67-31271
 Harmonic mixing and heterodyne detection of laser radiation 19 p3240 A67-35623
 Microwave mixing with weakly coupled Josephson superconducting diodes, discussing Fourier components 22 p3865 A67-40439
 Optical mixing of two low level signals in atomic states of He-Ne laser noting amplitude modulation of visible laser output 23 p4012 A67-40891

SIGNAL NOISE

Estimated amplitude of echo-signal for uniform, Rayleigh and a priori distribution of probability density of noise amplitudes 02 p0194 A67-11974
 Channel noise forces adaptive sampling system to operate at lower bit error probability than equivalent PCM system 02 p0197 A67-12016
 Coefficient of mutual correlation of noises for two-antenna phase type direction finder 03 p0386 A67-13957
 Thermodynamic equilibrium of binary channel with noise at fixed temperature 03 p0372 A67-14057
 Optimum AM reception in presence of interference signal and fluctuating

- noise 04 p0568 A67-14451
Rayleigh distribution function of envelope of signal/noise mixture in n parallel filter 04 p0568 A67-14453
Optimal filtration of noise from useful signal based on statistical information and minimax principle 04 p0591 A67-14636
Signal distortion introduced by series-fed array compensated in presence of noise by prefilter and postfilter 04 p0570 A67-14874
Approximation method determining follow-up failure conditions for nonlinear automatic systems in presence of control and noise signals 05 p0781 A67-16255
Statistical properties of envelope of signal-noise mixture with random angular modulation 05 p0765 A67-16961
Statistical properties of amplitude and phase of output signal of electron beam quadrupole amplifier with superposition of regular signal plus Gaussian noise at input 05 p0765 A67-17162
Simultaneous estimate of delay time and drift of carrier frequency during nonoptimum reception against correlated noise background 05 p0766 A67-17166
Stationarity conditions for FM oscillations with noise modulated frequency 05 p0766 A67-17167
Electromagnetic noise effect on aircraft examined, using fuselage mounted monitoring antennas 05 p0768 A67-17533
Upper sideband effect in parametric amplifier on positive conductance and negative resistance of circuits, deriving noise figure expression 06 p0966 A67-17575
Lower hybrid resonance /LHR/ noise bands occurrence patterns as function of latitude and time 06 p0964 A67-18567
Method for receiving radio signals against background of strong amplitude-modulated noise signal 06 p0965 A67-18898
Effectiveness of signal detection methods compared, using ratio-processed output value criterion 07 p1139 A67-19224
Electric signal transmission noting shape, properties, types, time dependency and use of Fourier transforms in calculations 07 p1141 A67-19338
Data smoothing, signal processing and exact minimum mean square error procedures 07 p1218 A67-20267
Dynamic range of data processor /correlator/ associated with synthetic aperture mapping radar system, considering film grain noise 08 p1293 A67-20688
Reliability of phase manipulated signal transmission with transient processes in channels and additive white noise 09 p1463 A67-21962
Gas laser dynamic behavior, discussing internal modulation, mode locking, noise and perturbation modes 09 p1515 A67-22431
Echo suppressor for reducing speech interference in telephone relaying by satellite 10 p1603 A67-22771
Mathematical treatment of sequential detection and application to detection of radar targets 10 p1607 A67-23570
Optimization techniques for linear matched filters to obtain maximum signal to noise ratio for certain signal waveforms 10 p1621 A67-23573
Lock-on band determination for inertial system of phase automatic frequency control in presence of fluctuation noises 11 p1750 A67-23910
Field statistics of linear in-phase antenna array in presence of periodically correlated phase errors 11 p1757 A67-23912
Differential frequency discriminators under combined action of signal and noise 11 p1750 A67-23913
Threshold region of FM signals having carrier modulated by Gaussian baseband signal 11 p1752 A67-24124
Optimum reception problem of two zero mean Gaussian signals solved through comparison of quadratic form in observable waveform with predetermined threshold 11 p1760 A67-24235
Stabilized cross correlation radiometer for use at decametric wavelength, using two feedback loops controlling four noise diodes 11 p1762 A67-24288
Normalization of mixture of pulse signal and noise by postdetector integration 13 p2069 A67-27044
Statistics of fluctuation processes occurring at outputs of filter/discriminator/integrator system acted upon by wideband noise 14 p2283 A67-28279
Signal-source noise mismatch and alignment in linear tripole amplifier networks 14 p2289 A67-28864
Optimum AM reception in presence of interference signal and fluctuating noise 15 p2435 A67-29288
Rayleigh distribution function of envelope of signal/noise mixture in n parallel filter 15 p2435 A67-29290
Carrier instability influence on noise immunity of discrete communication systems, with results presented graphically for uniform and normal random frequency distributions 16 p2620 A67-30477
Algorithm for statistical estimation of nonlinear function of signal containing noise 16 p2643 A67-30921
Optimal system determination for recognition and separation of useful signal combined with noise 16 p2643 A67-30923
Superlimiting phased-array receiving system in two-source environment 16 p2638 A67-31271
Spectral density of stationary random signals corrupted by multiplicative noise 17 p2812 A67-32303
Frequency spectra of excess noise in semiconductor devices due to characteristics fluctuations after applying signal 17 p2828 A67-33383
Signal and noise FM modulated random process characteristics determined by equation for correlation function, giving energy spectrum relationship of modulated process phase 18 p3001 A67-34177
Human controller as adaptive low pass filter to track signal contaminated with noise 18 p2994 A67-34340
Visual noise induction methods investigated at seven noise levels, discussing pattern comparisons by 46 subjects 20 p3372 A67-37000
Noise effect on synthesis of discrete systems with and without feedback channel for transmitting continuous messages, using binary signal and criterion of minimum rms error 20 p3383 A67-37071
Reliability of phase manipulated signal transmission with transient processes in channels and additive white noise 20 p3383 A67-37192
Noisy signal improvement through compact instrument, giving circuit and operational aspects and applications in ionospheric research 21 p3582 A67-38396
Lock-on band determination for inertial system of phase automatic frequency control in presence of fluctuation noises 21 p3585 A67-38938
Field statistics of linear in-phase antenna array in presence of periodically correlated phase errors 21 p3600 A67-38940
Differential frequency discriminators under combined action of signal and noise 21 p3585 A67-38941
Energy detection of multipulse returns from optically rough target using Q-switched laser 23 p4016 A67-41265
Optimal output effect for spatial temporal processing of signals in presence of multiplicative and additive signal fluctuations 24 p4120 A67-42232
- SIGNAL PROCESSING**
Doppler tolerant pulse train design, noting signal processing by delay line with fixed taps for significant changes in pulse spacing 01 p0023 A67-10464
Output autocorrelation function and spectral density of CW and FM signals passed through TWT 01 p0025 A67-10858
Oscillating limiter effect on message modulation for band pass filter with flat amplitude and linear phase characteristics in input signal frequency range 01 p0025 A67-10859
Coherent echo modulation and detection for binary data transmission, noting power savings, time and frequency diversification and communication stability 01 p0026 A67-10862
Varactor diode series resistance loss responsible for bandwidth loss in parametric delay lines used for signal processing 01 p0027 A67-11323
Time division multiplexing system for LF bioelectric signals, noting operation parameters and modes 02 p0216 A67-12075
National Electronics Conference, Chicago, October 1966 02 p0199 A67-12086
Adaptive visual signal preprocessor with quantized weights 02 p0207 A67-12140
Relation between sidelobe level and radar performance in clutter for nonresolvable difference between target and clutter Doppler 03 p0369 A67-13680
Statistical theory for optimum direction-finding system for space-time signal processing against wideband fluctuation noise background 03 p0371 A67-13947
Statistical distribution of AM laser signal envelope upon passage through turbulent atmosphere 03 p0438 A67-13988
Discrete gyroscopic servocontrol in presence of multidimensional random noise, ensuring optimal reproduction of input signal 03 p0465 A67-14157
Book on modulation, resolution and signal processing in radar, sonar and related systems 03 p0372 A67-14233
System Utilizing Signal-processing for Automatic Navigation, for moving vehicles, using time delays and frequency multiplication 04 p0653 A67-14870
Clutter suppression by complex weighting of coherent pulse train 04 p0570 A67-14878
Continuous wave radar application for obtaining velocity and range information on single targets at large distances 04 p0574 A67-15046
Beam scanning and beam forming techniques for phased-array radar, noting frequency and phase scan methods 04 p0596 A67-15049
Real time evaluation of radar signals processed by digital detector used in automatic target tracking 04 p0574 A67-15058
Laser application to radar signal processing and communications equipment 04 p0576 A67-15303
Telemetry systems, discussing PAM/FM/FM system, airborne equipment parts, ground support system and electronic testing procedures 04 p0577 A67-15728
Automatic telemetry checkout station for Saturn V systems using real time signal digitizer and general purpose computer 05 p0789 A67-17044
Small signal suppression and third order intermodulation products of ferrite frequency-selective limiters 05 p0780 A67-17532
Optimal Wiener values of filter parameters in phase-lock loop, noting possibility of improved performance despite deviations 06 p0973 A67-17615
Lincoln Experimental Terminal /LET/ system, ground antenna, RF and signal processing equipment for communications via several satellites 06 p0959 A67-17669
Chernoff bound and tilted distribution argument for obtaining error probability bounds for binary signaling on slowly fading Rician channel 06 p0961 A67-17943
Optimal signal design for binary communications systems using sequential and nonsequential detection with feedback 06 p0962 A67-17944
FM feedback system for lunar orbiter signal demodulation, discussing system composition and performance 06 p0975 A67-18108
Amplitude bounded noise and random measurement error smoothing, noting increased efficiency and possibility of narrow band application 06 p0975 A67-18217
Power spectrum improvement of multiple wave trains by concentrating power close to carrier frequency, noting constructive and destructive interference 06 p0963 A67-18401
Noise suppression on adaptive identification control systems, using series model 06 p0978 A67-18560
Sign codes and patterns of state variables for finding all possible responses in linear third order closed loop feedback control system 06 p0978 A67-18721
Exact expression for transient response for step modulated carrier signal obtained, using parallel plate waveguide 06 p0964 A67-18767
Automatic telemetry checkout station for Saturn V systems using real time signal digitizer and general purpose computer 06 p1089 A67-18861
Threshold SNR loss of coherent radar in reception of partially coherent packages, noting graph plotting 07 p1139 A67-19230
Passage of pulsed coherent useful and noise signals through two-channel time

discriminator 07 p1140 A67-19237
 Transmission methods, analyzing noise threshold, signal bunching, etc 07 p1141 A67-19339
 Modulation devices for pulsed systems, discussing signal preparation and channel grouping for time multiplex systems 07 p1150 A67-19341
 Image scanning systems applied to filmed data processing 07 p1148 A67-19745
 Cancellation of unwanted spectral components in FM multivibrator system by generating cancelling component in square law device 07 p1145 A67-19871
 Phase compensation technique for signals received at widely spaced antennas and processed at central location 07 p1155 A67-19876
 Radar antenna synthesis for optimum and suboptimum filtering of spatial signals according to mean square error minimization 07 p1158 A67-20238
 Data smoothing, signal processing and exact minimum mean square error procedures 07 p1218 A67-20267
 IR spectroscopy using Michelson interferometer coupled with computer and wave analyzer 07 p1190 A67-20272
 Inputs and outputs of digital pneumatic jet components design for adaptation to standardized pressure range for use in installations 08 p1281 A67-20448
 Equalization and cancellation model of binaural unmasking applied to data on interaural just-noticeable differences 08 p1290 A67-20482
 NRL lunar radar system applied to long term earth-moon distance measurements, using pulse compression for signal processing, noting high SNR 08 p1293 A67-20689
 Analysis of uncontrolled synchronized self-excited oscillator 08 p1302 A67-20829
 Average far field intensity patterns of antennas calculated for quasi-monochromatic space-time stationary signals 09 p1470 A67-21607
 Data handling systems, describing apparatus for processing of analog time varying signals in computer 09 p1501 A67-22466
 Frequency scanned filter in radar signal processing system designed to extract range and Doppler resolution, using properties of ambiguity function 09 p1466 A67-22695
 Spacecraft instrumentation, discussing selection criteria for signal conditioning, transducer sensors, photographic equipment, etc 10 p1655 A67-23000
 Optimum filtration of signals in presence of arbitrary interference, using orthogonal function series 10 p1607 A67-23443
 Reduction of peak factor in FM system design leading to reduction of thermal noise and increase in spectrum truncation distortion 11 p1752 A67-24123
 Waveguide dispersion effect on radiation pattern and directivity of series-fed linear arrays 11 p1762 A67-24289
 Radio system passband increase and multichannel intercorrelation signal processing for increasing noise rejection for limited analysis time 11 p1772 A67-24984
 Ground based conversion of Lunar Orbiter II video signals into photographic images, describing reconstruction electronics, signal processor, etc 12 p1940 A67-25466
 Three-channel particle spectrometer with semiconductor detectors and tunnel diode discriminators noting noise immunity, high signal level output, etc 12 p1944 A67-25853
 Contact-free controlled delay unit using shift register and clock-pulse generator for binary signals designed with wide range of time delay variation 13 p2088 A67-26798
 Error reduction in signal reconstitution represented by segment of band-limited function 13 p2069 A67-27040
 Signal processing in antennas with coupling elements between circuit and space fields 14 p2285 A67-28450
 Functional-analytic techniques providing understanding of some nonlinear circuits action on input to output signal production 14 p2291 A67-28453
 Coding modulation and signal processing noting algebraic coding and binary symmetric channel neglect, discussing coherent optical radiation in noise program 14 p2269 A67-28457
 Pulse modulated data channel operation

over parallel optical paths, noting advantages inherent in simple processing and control circuitry 14 p2272 A67-28699
 High data rate storage for Nimbus B satellite noting signal processing, checkout and retrieval operations 14 p2276 A67-28918
 Fluid sphere gyroscope designed for extreme shock, vibration, temperature and overrate, examining signal processing, design parameters, etc 14 p2322 A67-29081
 Approximate solution to nonlinear problem of pull-in range of phase locked loops, noting filter configurations and methods of analysis 15 p2446 A67-29589
 Ultrasonic devices for coherent optical systems, discussing CdS transducers, laser scanners and microwave signal processing 15 p2500 A67-29912
 Control system identification and loop stability limit, noting dominant components of time functions and classification of substitute functions 15 p2461 A67-30317
 Discrete interval binary-noise perturbation signal application for identification and compensation of three-variable self-adaptive flight control system 15 p2572 A67-30319
 Amplitude bounded noise and random measurement error smoothing, noting increased efficiency and possibility of narrow band application 16 p2642 A67-30483
 Signal phase acquisition techniques for arrays of large aperture steerable antennas discussing SNR role 16 p2638 A67-31264
 Necessity of incremental phase shift during IF time delay steering of antenna array main beam 16 p2639 A67-31354
 Piezoelectric pressure transducer, discussing design, material used and performance 16 p2677 A67-31427
 Reliability through redundancy describing use of devices for averaging analog signals 16 p2649 A67-31667
 Finite dimensional approximations of optimal nonlinear filters for class of large-noise, nonlinear, continuous-time problems 16 p2651 A67-31680
 Optimum filtering and control of randomly-sampled linear and nonlinear systems with Gaussian or non-Gaussian statistics, synthesizing generalized Kalman filter 16 p2651 A67-31683
 Perturbing factors in avionics communications noting drawbacks and advantages of satellite utilization, possible commercial applications, etc 17 p2813 A67-32498
 Soviet book on digital processing of radar information covering signal processing, algorithms, discretization, etc 18 p3006 A67-33717
 Synthesis of radar ambiguity functions via burst-pulse time-frequency waveform coding, employing Bayesian statistical analysis 18 p3000 A67-34109
 Linear minimum variance estimation for random signal with complex phase errors, considering signal processing and optical propagation 18 p3001 A67-34111
 Nonrecurring phenomena analysis and detection describing optimum criteria recording and data processing facility 19 p3230 A67-35329
 Real-time electrooptical spectrum analyzers with coherent detection 19 p3197 A67-35687
 Synthesis of specific type of automatic microprogramming systems using complex microcommand signals conditioned by functional-blocks 19 p3190 A67-36094
 Nonstationary correlation analysis using correlator in which bandwidths of two filters resolve errors 20 p3484 A67-36695
 Extremal systems having auto-oscillating optimizers and controlled plants, investigating performance improvement by complex modification of input signal 20 p3409 A67-37110
 Efficiency of using self-adjustment with respect to input signal in automatic control systems, estimating gain and stability 20 p3409 A67-37198
 Surveyor project composite telemetry processing system including signal processor, ground equipment, computer data program, etc 20 p3393 A67-37458
 Optimal wave path parameters determined by experimentally recorded pulsed signals processing, using least squares method 21 p3580 A67-38120
 Electronic circuit packaging in Apollo

lunar module signal conditioning equipment 21 p3635 A67-38628
 Exoionospheric communications system with ideal matched filter and signal processing at transmitter for increased range and secure coding possibilities 21 p3586 A67-38952
 Coherent acceleration and velocity observation in real time /CAVORT/ analog radar signal processor for matched filtering pulse trains from radial accelerated targets 21 p3586 A67-38953
 Approximate method for evaluation of processing loss in delay line MTI receiver 22 p3758 A67-39211
 Lower ionospheric drift studied from signal recordings from distant medium wave broadcasting stations 22 p3788 A67-39467
 Phase locked automatic frequency control regulated phase distortion effects on radar signal mean peak power at matched receiver filter output 22 p3761 A67-39762
 Angular coordinates of pulsed incoherent scanning radar determined, comparing efficiency of direction finding by minimum rms error and maximum likelihood method 22 p3762 A67-39874
 Multispectral remote sensing techniques for agricultural surveys from orbiting satellites, discussing in-flight signal processing 22 p3806 A67-40367
 Surveyor TV system signal processing and transmission, analyzing performance and computer simulation of some effects [SMPT PAPER 102-41] 22 p3808 A67-40379
 Scanning electron microscope signal processing and application to electronic devices failures, processes variations, integrated circuits and thin film circuit continuity 22 p3774 A67-40411
 Chromel-alumel thermocouple for high enthalpy gas flow temperature measurement, discussing design and measurement accuracy 23 p4081 A67-40569
 Decision theory applied to angular resolution, deriving signal processing radar system beyond Rayleigh limits and target reliability 23 p3972 A67-40643
 Star tracker error signal processor for onboard current satellite attitude control over wide range of gimbal angles 24 p4154 A67-42175
 Optimal output effect for spatial temporal processing of signals in presence of multiplicative and additive signal fluctuations 24 p4120 A67-42232
 Array antenna directive pattern scanning utilizing difference in phase lead between heterodyne and converted signals at feeder 24 p4130 A67-42234
 Signal processing and control computer system for materials research noting use in viscoelastic studies of crystalline polymers 24 p4126 A67-42930

SIGNAL RECEPTION
SA RADAR RECEPTION
SA RADIO RECEPTION
SA TELEVISION RECEPTION
 Cost effective error control for coded or M-ary signal reception 01 p0023 A67-10485
 Terminology of phase-difference modulated signal reception, noting coherent, correlation and autocorrelation methods 01 p0025 A67-10830
 Reception antenna of ONERA weightlessness laboratory in form of surface waveguide [ONERA-TP-374] 01 p0039 A67-11004
 Receiver design for LF time signals on kilometric waves 02 p0190 A67-11481
 Microwave direction-finding systems based on amplitude comparison for use with pulse or continuous wave signals, noting switching system 02 p0198 A67-12067
 Time limited receiver signals design for minimizing error probability under energy and frequency constraints 02 p0204 A67-12171
 Optimum reception criteria for double beam channels with fluctuating noise, signal phase and amplitude characteristics 02 p0205 A67-12532
 Optimum signal reception against non-Gaussian noise background in presence of white Gaussian noise 03 p0368 A67-13274
 Radio location by coherent light with quantum structure 03 p0368 A67-13283
 Nonionized atmosphere effect on radial velocity measurement of satellite via Doppler-Flzeau method 03 p0369 A67-13530
 Approximate method of computing attitude of sounding rockets from

- magnetometer data 03 p0519 A67-13782
- Extraterrestrial radiation source spectrum determined by comparing main beam and sidelobe signal power received on suitable bandwidth 03 p0371 A67-13946
- Optimum AM reception in presence of interference signal and fluctuating noise 04 p0568 A67-14451
- Mathematical model for adaptive signal preprocessor, noting eye adaptation to changes in signal intensity and bandwidth 04 p0563 A67-14799
- Phase lock system used to receive and correctly utilize signals from distant transmitter 04 p0585 A67-15614
- Book on asynchronous detection and reception of pulsed radio signals at HF and Shf against background of fluctuating noises 05 p0761 A67-16172
- Optimal reception of narrow band signals emerging from photomultiplier 05 p0764 A67-16913
- Multichannel sequential detection in case of reception through independent multiple channels with noise 05 p0765 A67-16953
- Recognition of fading signals transmitted by channels with unknown parameters, considering optimum reception technique based on arbitrary law 05 p0767 A67-17399
- Pulse interference inhibition in AM signals reception by nonlinear negative feedback loop in HF cascades of receiving device 05 p0785 A67-17471
- Operational characteristics of receivers employing storages of nonquantized and quantized signals 06 p0965 A67-18895
- Method for receiving radio signals against background of strong amplitude-modulated noise signal 06 p0965 A67-18898
- Electric signal transmission noting shape, properties, types, time dependency and use of Fourier transforms in calculations 07 p1141 A67-19338
- SRT Daylight Display System for ATC in which radar video signals are passed through data processor 07 p1221 A67-19543
- Adaptive antenna for ground reception of wideband RF signals in space communications systems 08 p1301 A67-20776
- Reliability of phase manipulated signal transmission with transient processes in channels and additive white noise 09 p1463 A67-21962
- X-ray image transformation, transmission and amplification directly into video signals for inspection of missile case walls and weldments 10 p1622 A67-22929
- Threshold signals and optimal modulation parameters of analog methods of transmitting information under conditions of ideal reception 10 p1604 A67-22984
- Spaced antenna reception by quadratic addition of signals providing efficient operation at various statistical characteristics of radio channel 10 p1607 A67-23447
- Discrete signal optimal reception based on analysis of signal noise mixture 10 p1607 A67-23457
- Terminology of phase-difference modulated signal reception noting coherent, correlation and autocorrelation methods 10 p1607 A67-23460
- Steady state dynamic properties of large spinning net-like antenna suitable for radio signal reception from space 10 p1727 A67-23753
- Optimal reception of signal transmitted through channel with randomly varying parameters, measuring amplitude and phase 11 p1751 A67-23914
- Ionospheric electron density distribution investigated by ground reception of satellite signals from Elektron I 11 p1786 A67-24073
- Optimum reception problem of two zero mean Gaussian signals solved through comparison of quadratic form in observable waveform with predetermined threshold 11 p1760 A67-24235
- Received signal degradation for coherent pulse transmission through rain scattering volume, calculating length and energy for various paths 11 p1752 A67-24285
- Atmospheric distortion effect on signal reception by large dimensional antennas, obtaining numerical estimates for various parameters 11 p1753 A67-24439
- Atmosphere effects on laser beam propagation noting diameter, intensity amplitude and power dependence on transmitter and receiver aperture dimensions 11 p1801 A67-24665
- Timekeeping unit calibration, on basis of signals emitted by HBG transmitter, permitting measurement of state and performance of quartz oscillators 11 p1792 A67-24782
- Receiver-antenna system in radio astronomy, discussing low noise, thermal signal reception and acquisition of information limited by internal or external noise 12 p1914 A67-25309
- Reception of signals reflected from ionosphere in vertical radar probing, examining frequency-difference combinations 13 p2067 A67-26569
- Radio propagation influence on performance of azimuth channel of ILS defining characteristics of ILS signals relevant to monitor design 13 p2154 A67-26986
- Automatic frequency control for estimating random signal frequency when received against whitenoise background 13 p2069 A67-27037
- Book on new concepts in radars covering ideal reception, moving targets, autocorrelation, SNR, amplitude distribution, clutter, etc 13 p2071 A67-27224
- Irregular fields effect on aperture reception characteristics 13 p2071 A67-27402
- Data processing of signal reception from Soviet satellites indicates radio signals scintillation caused by diffraction of waves from ionospheric nonuniformities 14 p2260 A67-27857
- Optimum reception criteria for double beam channels with fluctuating noise, signal phase and amplitude characteristics 14 p2261 A67-28009
- Total electron content calculation by measuring Faraday and Doppler effects of satellites on reception frequency 14 p2270 A67-28607
- Error rate expression for canonic binary receivers, evaluating performance of incoherent detection 14 p2272 A67-28706
- Optimum AM reception in presence of interference signal and fluctuating noise 15 p2435 A67-29288
- Optimal reception of narrow band signals emerging from photomultiplier 16 p2623 A67-30890
- Invariant operating regime of optimum threshold receiver during binary signal reception 16 p2624 A67-31029
- Correlation reception of wideband signals from ionospheric inhomogeneities, considering effectiveness for signal distortion discrimination 16 p2632 A67-31909
- Reduced noise rejection regions in receiver of PSK telemetry signals in narrow band concentrated noise, using phase and polarity comparison methods 18 p3000 A67-34085
- Second, third and fourth order phase locked loops performance characteristics compared for optimum selection, calculating integrated square error and peak error 18 p3001 A67-34116
- High altitude research rocket HF telemetering remote control signal receivers, antennas and earth station, discussing design and circuitry of transmitter antenna 19 p3193 A67-35061
- Reliability of phase manipulated signal transmission with transient processes in channels and additive white noise 20 p3383 A67-37192
- Soviet book on time-frequency remote control systems theory and design 20 p3412 A67-37632
- Solar radio spectrograph using broadband logarithmic antenna, considering receiver operation and frequency range 21 p3627 A67-38497
- Receiving system for telemetering with orientable antenna error-measuring signal receiver and servo loops 21 p3599 A67-38645
- Optimal reception of signal transmitted through channel with randomly varying parameters, measuring amplitude and phase 21 p3585 A67-38942
- Balanced SHF transducer for microwave receiver input with separate signal and heterodyne lines coupled by directional bond openings, noting decoupled inputs 22 p3772 A67-39875
- Threshold discrimination for two unknown a priori probability signals against noise background, using stochastic approximation in algorithm 24 p4134 A67-41795
- Reception of ground based Loran transmissions by fixed-frequency topside sounder satellite 24 p4119 A67-42061
- Random Gaussian signal with unknown mean value reception using adaptive systems 24 p4120 A67-42224
- Error probability for binary signaling through multipath channel with receiver waveform comprising white Gaussian noise and time delayed frequency-shifted signal 24 p4121 A67-42341
- Optimal reception of binary signals on background non-Gaussian noise determined by logarithm expansion for probability coefficient into Taylor series 24 p4122 A67-42377
- SIGNAL REFLECTION**
- Scatterers identification by measuring separations between antenna grating lobes, signal direction and difference in levels of maxima and minima 03 p0370 A67-13856
- Anisotropic magnetoplasma diagnostics using transient reflected polarized signals [AFCRRL-67-0065] 03 p0371 A67-13865
- Ionospheric sporadic E layer propagation characteristics and signal strength calculation, noting decrease in antenna gain when using highly directional antennas 04 p0576 A67-15503
- Radar observations of Venus at 23 cm noting flight time and Doppler shift measurements of reflected signals 05 p0889 A67-16297
- Combined probability density of axial coefficient and polarization angle of field scattered by target 05 p0764 A67-16905
- Calculation method for distortion of envelope of pulses during reflection from inhomogeneous ionospheric plasma during topside sounding 05 p0765 A67-17125
- Lunar surface analysis via analysis of reflected signals from RF pulses 08 p1295 A67-21080
- Microwave reflection from region with nonuniform hydrometeor for case where dimensions vary greatly and relation to wavelength is arbitrary 11 p1754 A67-24981
- Ferrite-diode system with automatic gating of signal reflection used in radar wind velocity observations to reduce pulse interferences produced by meteor trails 13 p2197 A67-26505
- Statistical properties of phase and amplitude fluctuations during total reflection of waves from ionospheric layer 13 p2067 A67-26551
- Signal spectral characteristics when reflected from rough surface exposed to monochromatic and frequency modulated oscillations from moving airborne emitter 13 p2154 A67-27038
- Combined probability density of axial coefficient and polarization angle of field scattered by target 14 p2297 A67-28032
- Combined probability density of axial coefficient and polarization angle of field scattered by target 16 p2623 A67-30881
- Coefficient characterizing stability of continuous radio signal reflections declining occurrence probability from sporadic ionospheric layer 16 p2669 A67-31907
- Modes of boresight shift in conical-scan and sequential-lobing types of amplitude sensitive angle-tracking antennas 17 p2814 A67-32523
- Correlation detection for extracting reflected radar signal from noise 19 p3195 A67-35550
- Calculation method for distortion of envelope of pulses during reflection from inhomogeneous ionospheric plasma 21 p3582 A67-38468
- SIGNAL STABILIZATION**
- Pulse amplitude range estimated for which PWM system is asymptotically stable, using method of Murphy and Wu 03 p0393 A67-13983
- Signal stabilization by linearization of time independent nonlinearities using extra signal and nonlinearity, noting role of pulse width modulation [ASME PAPER 66-WA/AUT-21] 04 p0592 A67-15392
- Signal stabilization of memory type nonlinearity, using dual input describing function to determine effect of external sinusoidal signal on system limit cycles [ASME PAPER 66-WA/AUT-1] 04 p0593 A67-15421
- Adaptive feedback paths of adaptive aircraft control system in small signal

stability analysis 11 p1772 A67-25081
 Input signal level for stability loss or self-oscillations automatic control in system, using analysis for nonlinear systems with forced vibrations 20 p3408 A67-37041

SIGNAL TO NOISE RATIO
 Optimization of directive gain and SNR of arbitrary antenna array with or without constraint on array Q-factor 01 p0035 A67-10431
 Optimum dynamic range centering for Rayleigh distributed signal for case having nonzero SNR by envelope detection process 01 p0022 A67-10434
 Fluctuation noise effects on phase-locked automatic frequency control system obtained using Markov processes, determining phase difference probability density and statistical characteristics 01 p0037 A67-10713
 Autocorrelation function of radiation electric field measurement from clipped correlation function and spacing estimation for optimally efficient SNR determination 01 p0114 A67-10808
 Phase cancellation of sinusoidal signals in presence of Gaussian noise for comparison and threshold decision schemes 01 p0025 A67-10860
 Differentially coherent phase-shift keying system analyzed under wide range of signal and noise conditions 01 p0025 A67-10861
 Error probabilities for partially coherent diversity reception, noting linearized receiver performance during random noise output 01 p0026 A67-10863
 Model distribution for phase error in second-order phase locked loop used to complement analytical model in signal to noise region [JPL-TR-32-1017] 01 p0026 A67-10865
 Geomagnetic field effect on radio signal in oblique reflection sounding, noting differences between daylight and night measurements 02 p0193 A67-11662
 AGC and noise controlled dual-channel optimal ratio predetection combiners, examining design and performance by studying diversity combining techniques 02 p0198 A67-12025
 Power signal to noise ratios for coherent and noncoherent optical detection, for optimization of optical systems 02 p0243 A67-12056
 Attenuation of background noise and exterior static through use of low impedance links and use of light loading in transistorized assemblies 03 p0379 A67-13389
 Limiting SNR determines, for given initial detuning, probability close to unity of phase jumps in phase locked AFC system 03 p0380 A67-13580
 Noise reduction in FM receivers with negative frequency feedback by reducing IF bandwidth 03 p0381 A67-13662
 Amplitudes and phases of element weighting factors in linear processor determined in order to maximize SNR of array receiving random signal in noisy environment 03 p0385 A67-13860
 Antenna aperture size effect on tropospheric phase-of-arrival fluctuations determined by theoretical considerations of atmospheric turbulence 03 p0385 A67-13864
 Amplitude and phase of weak signals at low signal to noise ratio, using parametric oscillators for signal phase quantization 04 p0620 A67-14748
 Turbulence as producer of noise in proportional fluid amplifiers, considering signal and noise at receiver entrance in terms of stagnation pressure 04 p0557 A67-15919
 Frequency fluctuations of laser field determined by measuring cross correlation function at two points 05 p0815 A67-16625
 Linear system providing maximum signal to noise ratio for given parameters of correlation function of incoming quasi-harmonic signal mixed with white noise 05 p0767 A67-17396
 Adaptive decoding technique for analyzing information-carrying signals in order to control signal to noise ratio during transmission time of single compound signal 05 p0768 A67-17401
 Design technique for inertial navigation instruments makes it possible to package within instrument electronics necessary to control and operate each of its facilities 05 p0779 A67-17464
 Range determination with CW tracking

radar controlling rms error, noting SNR role in holding target echo 06 p0957 A67-17593
 Chernoff bound and tilted distribution argument for obtaining error probability bounds for binary signaling on slowly fading Rician channel 06 p0961 A67-17943
 [JPL-TR-32-1051]
 Installation for measuring Doppler effect of satellites, investigating limits, optimization, SNR and orbital parameter accuracy 06 p0979 A67-18018
 Threshold reduction in phase locked loop by retarding phase of return signal from voltage controlled oscillator to phase detector 06 p0969 A67-18109
 Supersensitive laser light detector for wideband receivers to approach theoretical SNR limit set by noise in signal 07 p1194 A67-19085
 Threshold SNR loss of coherent radar in reception of partially coherent packages, noting graph plotting 07 p1139 A67-19230
 Modulation devices for pulsed systems, discussing signal preparation and channel grouping for time multiplex systems 07 p1150 A67-19341
 Effect of a priori known relation between random signal and noise voltages at output of two channels 07 p1143 A67-19593
 Signal to noise ratio of optical-heterodyne detection system as affected by atmospheric distortion of optical wave front 07 p1144 A67-19786
 Curves of probability of detection vs signal to noise ratio for log-normal signals in Gaussian noise, considering correlated and uncorrelated signals 07 p1144 A67-19868
 CW interference and white noise effect on second order phase lock loop, using reciprocal of loop mean square phase error as index of performance 07 p1161 A67-19878
 Quality of optical images and physical receivers including both curve of modulation transfer and noise 07 p1146 A67-20155
 Noise and signal fluctuation effects on angle tracking radar with amplitude comparison system 07 p1147 A67-20239
 NRL lunar radar system applied to long term earth-moon distance measurements, using pulse compression for signal processing, noting high SNR 08 p1293 A67-20689
 Threshold value lowering in synchronous demodulation, determining output SNR as function of input SNR 08 p1294 A67-20771
 Background limit to sensitivity of point to point optical communication obtained through signal to noise ratio of optical point detectors under BLIP condition 09 p1462 A67-21641
 Comparison of electron tubes, transistors and FET noise figures as function of source impedance of generator 10 p1610 A67-22924
 Threshold signals and optimal modulation parameters of analog methods of transmitting information under conditions of ideal reception 10 p1604 A67-22984
 Discrete signal optimal reception based on analysis of signal noise mixture 10 p1607 A67-23457
 Detectability of coherent optical signals against incoherent Gaussian background noise radiation in heterodyne receiver with laser local oscillator 11 p1800 A67-24419
 Performance characteristics of photosensors and limitation by statistical fluctuation in absorption rate of light quanta in primary photoprocess 11 p1766 A67-24627
 Radio system passband increase and multichannel intercorrelation signal processing for increasing noise rejection for limited analysis time 11 p1772 A67-24984
 Dispersion of number of positive zeros as function of time for realization of quasi-harmonic random signal 11 p1754 A67-24985
 Parametric amplifiers of high gain stability for radio astronomy noting very low SNR and optimum noise temperature 12 p1912 A67-25298
 Output correlation function for N-step symmetric amplitude quantizer with summed sine wave and Gaussian noise input, noting approximations for low SNR 12 p1908 A67-26084
 Use of limiters for estimating signal to noise ratio 12 p1908 A67-26090
 Signal to noise ratios of transistorized constant current and constant temperature hot-wire anemometers 12 p1947 A67-26121
 System using holography for character recognition according to Gabor

proposals 13 p2118 A67-26258
 Spread spectrum for amplitude modulated transmitters and receivers 13 p2066 A67-26405
 Time resolution amplification of flash spectroscopy apparatus equipped with switched laser 13 p2126 A67-26599
 SNR and transmission error probability in pulse modulated optical communication 13 p2067 A67-26663
 Radar antenna synthesis for maximum SNR and minimum error dispersion in target bearing, reducing problem to filter synthesis 13 p2069 A67-27039
 Accuracy of SNR measurement as function of noise power and signal parameter 13 p2070 A67-27045
 Set of curves relating statistical properties of envelope detector output to SNR of CW signal in narrow band Gaussian noise at input 13 p2070 A67-27154
 Light sensitive arrays based on photodiodes combined with MOS devices analyzed for use of image, pattern detection and other applications 14 p2282 A67-28026
 Time of flight distribution measurement of weak molecular beam, noting limitations due to signal to noise ratio 14 p2316 A67-28185
 Velocity distributions in surface scattered molecular beams, proposing broadband lock-in beam detection for signal to noise enhancement 14 p2317 A67-28195
 Nomogram to predict SNR for certain laser setups 14 p2330 A67-28289
 Signal processing in antennas with coupling elements between circuit and space fields 14 p2285 A67-28450
 Communication problems connected with deep space transmissions of interplanetary distances range 14 p2268 A67-28454
 Discriminator threshold and SNR above threshold response when demodulating FM signal undergoing selective fading 14 p2273 A67-28711
 Distribution-free signal detection by multiple-resolution-element pulse radar, based on ranks of returns and having invariant false alarm rates 15 p2436 A67-29933
 Avalanche photodiode model with guard-ring for active area 15 p2452 A67-30014
 Multicolor image reconstruction from holograms behaving as planar diffraction gratings, excluding crosstalk images formation 15 p2491 A67-30431
 Cost function to evaluate quasi-optimal amplitude meter for signal with random initial phase on white noise background with random correlation function 16 p2623 A67-31015
 Geomagnetic field effect on radio signal in oblique reflection sounding, noting differences between daylight and night measurements 16 p2624 A67-31077
 Signal phase acquisition techniques for arrays of large aperture steerable antennas discussing SNR role 16 p2638 A67-31264
 Monte Carlo evaluation of linear and eigenvector-method for estimation of pulse transfer function of linear, time-invariant dynamic feedback system 16 p2653 A67-31695
 Atmospheric modulation noise in optical heterodyne receiver, deriving signal power variance and mean-square frequency spread from propagation statistics for wave structure function 16 p2630 A67-31807
 Timing error and noisy phase reference joint effect on system performance of coded partially phase coherent reception 17 p2811 A67-32116
 Error probabilities of matched filter receiver operating in additive combination of impulsive and Gaussian noise 17 p2812 A67-32120
 System for information transmission over optical path using microwave subcarrier, noting satisfactory SNR 17 p2812 A67-32237
 High resolution direct electron beam film scanner operable at 20 MHz, construction and performance 17 p2857 A67-32469
 Threshold value of SNR of radar system in target detection against reflecting background, deriving block diagram consisting of linear group, detector and integrator 17 p2816 A67-32684
 Design of receiver circuitry for IR surveillance system having high signal detectability 17 p2862 A67-33289
 Design criteria for narrow optical

passband filters used in reception of nonparallel modulated monochromatic radiation 17 p2862 A67-33291

Automatic AM control noting proportionate variation of carrier level to signal volume 18 p2998 A67-33502

Threshold characteristics of systems for multistate orthogonal transmission of coded analog signals in communication systems 18 p3000 A67-34023

Apollo ranging code with phase locked loop for bit synchronization, plotting SNR vs error probability and acquisition time 18 p3000 A67-34102

Unlock behavior of second order phase locked loop with and without interfering carriers 18 p3018 A67-34346

Enhancement of signal to noise ratio of turbulence measurements by cross correlation and heat transfer transducer 18 p3050 A67-34499

Voltage amplitude limiting for improving stability of correlation detector of electronic cross correlation systems, noting variation of SNR 18 p3012 A67-34524

Correlation detection for extracting reflected radar signal from noise 19 p3195 A67-35550

FM signals demodulation and negative feedback modulation, deriving signal to noise ratio and noise spectrum formulas 19 p3183 A67-35562

Enhancement of faint photographic spectra using signal averaging digital computer 19 p3232 A67-35698

Fourier spectroscopy problems including source noise effects on interferogram modulation and maximum SNR attainable in spectrum estimated from given interferogram 20 p3437 A67-36336

Low intensity photoelectric signal detection by Fabry-Perot spectrometer using SNR enhancing method 20 p3439 A67-36356

Fabry-Perot interferometer with magnetostrictive scanning and SNR improves system for solar physics and airglow observations 20 p3440 A67-36360

Spectrometer SNR improvement without affecting resolution by using larger inlet and outlet slit openings 20 p3441 A67-36365

Pulse compression in unmatched dispersive networks noting phase characteristic matched to signal received 20 p3379 A67-36380

Postdetection maximal ratio diversity combiners, discussing signal to noise enhancement 20 p3397 A67-36583

Optimal signal selection on background of steady additive noise in realistic communications system 20 p3382 A67-36777

Signal model with white noise fitted to time series, discussing signal proportion estimation methods 20 p3476 A67-36788

Modulation systems in satellite communications evaluated by criteria of baseband signal noise ratio, signal power, frequency band requirements, etc 20 p3383 A67-36956

Discrete self-adaptive servosystem with nonstationary random useful and noise signals applied to input 20 p3409 A67-37199

Effect of a priori known relation between random signal and noise voltages at output of two channels 20 p3384 A67-37332

Bandpass hard limiter intermodulation with low input signal to noise ratio 20 p3385 A67-37356

Signal to noise ratio for optical solar spectra, describing low noise level spectrometer 21 p3624 A67-37730

Minimum detectable signal and frequency response of mercury-doped germanium detector, measuring response time and SNR through optical heterodyne techniques 21 p3590 A67-38009

Discrete errors in continuous angle-modulation systems, considering conventional fidelity /SNR/ criterion and probabilistic theory 21 p3584 A67-38653

Bandwidth restriction effect on SNR in NRZ signal from PCM transmission system 21 p3584 A67-38667

FM/PM and FM/FM radio telemetry in proportional and constant band covering regulation, SNR, noise threshold, etc 21 p3587 A67-39050

Monograph on frequency stabilization of LF oscillator by servo method, showing improved SNR of passband 21 p3587 A67-39126

Statistical dependence between frequency

and amplitude deviations of FM wave perturbed by white noise, describing amplitude-phase correlation FM demodulator 22 p3758 A67-39271

Pulse code communication system for transmission of continuous random quantities 22 p3761 A67-39831

Output SNR dependence on difference between input signal and natural frequencies for quasi-optimal linear filters, noting improvement for mismatched input 22 p3761 A67-39867

SNR performance of SEC vidicon image storage tube at optimum and reduced readout rates 22 p3773 A67-39961

Linear correlation-detection transducer arrays for directional noise field signals, giving N-element coherent detector performance in propagating and turbulent boundary layer 22 p3801 A67-40233

Image tubes to obtain signal and noise solutions, determining Noise Equivalent Power /NEP/, Detectivity Star and Detective Quantum Efficiency 22 p3805 A67-40352

Error correcting codes for white Gaussian channel at low signal to noise ratio, discussing properties and performance criteria 23 p3984 A67-40752

Optical system models based on gallium-arsenide laser techniques for SNR measurements 23 p4014 A67-41026

Atmospheric scintillation effects on optical data channel for application to laser radar noting SNR role 23 p3975 A67-41266

Wideband FM demodulation system providing good reception with smaller radio SNR through delayed signal 23 p3975 A67-41677

Proportional characteristics and signal limiting capabilities of fluoric operational amplifier, discussing analog gain block performance 24 p4098 A67-41988

Multiple speed data transmission precoding by changing data rate and overall channel characteristics simultaneously 24 p4121 A67-42342

Proactive inhibition, recency and limited channel capacity under acoustic stress 24 p4116 A67-42701

SIGNAL TRANSMISSION

HF random phase transverse wave transmission through turbulent plasma generating scattered waves at combination frequencies 01 p0121 A67-10343

Oscillations of vertical component of ionospheric refraction measured, using cliff radio interferometer and signals from satellites 01 p0022 A67-10390

Electromagnetic reflection and transmission coefficient maxima in bounded plasma slab 01 p0022 A67-10443

Trigger circuits for generating sharply defined rectangular waves phase locked to repetitive signal 01 p0036 A67-10451

Direction finder accuracy optimization, considering automatic tracking of target angular coordinates 01 p0024 A67-10721

Functional integration analysis of exponential behavior of nonlinear feedback control systems 01 p0047 A67-11211

Integrated circuit eliminating pilot tones in digital data by simultaneously phase modulating binary data and bit-timing signals on carrier 02 p0194 A67-11797

Optimum /ln Shannon sense/ truncated probability of signal for case of constant power and other conditions 02 p0194 A67-11908

Simulcast /simultaneous broadcasting technique/ has higher average signal power than one transmitter alone and low data rate 02 p0202 A67-12128

PCM/TDM and influence of channel on signal determined, using mathematical model 02 p0202 A67-12130

Transhorizon propagation modes from signals transmitted by orbiting radio beacon ionospheric satellite /ORBIS/, showing paths sustained by ionospheric ducts or usual hop modes [RASSA PAPER 1-10-146] 03 p0373 A67-14253

ORBIS satellite experimental results, noting long range propagation at night and during sunrise [RASSA PAPER 1-10-147] 03 p0373 A67-14254

Radiation monopulse passage through amplifying and absorbing media having form of rods 03 p0374 A67-14329

Transmitter modulation choice for nonconventional radar system, taking into account scanning antenna modulation

effects 04 p0572 A67-15029

Automatic system auto-oscillations when transmission coefficient of nonlinear part of system depends on amplitude and frequency of input signal 05 p0782 A67-16323

Factors governing amplitudes of reradiated signals from tall obstacles distorting VHF and UHF transmission 05 p0766 A67-17296

Adaptive decoding technique for analyzing information-carrying signals in order to control signal to noise ratio during transmission time of single compound signal 05 p0768 A67-17401

Interference ratios in space telecasting, considering methods of control for cochannel broadcasting 06 p0960 A67-17692

Signal design problem of optimal waveforms for transmission through phase incoherent channel 06 p0962 A67-17945

Optimal signal transmission in detection system characterized by optimal linear filtration of reflected signal 06 p0963 A67-18216

Unsteady aerodynamic forces on thin wing oscillating in transonic flow, discussing acoustic ray paths and signal transmission times [AIAA PAPER 67-16] 06 p0943 A67-18841

Signal delay transmission on several frequencies from solar orbiting spacecraft to terrestrial receiver used for continuous coronal electron density profile 06 p1091 A67-18996

German book on transmission of communications including transmission methods and shapes, signals, radio relays, terminal devices, etc 07 p1140 A67-19337

Electric signal transmission noting shape, properties, types, time dependency and use of Fourier transforms in calculations 07 p1141 A67-19338

Long distance propagation of ultrashort radio waves by ionospheric scattering in subpolar region, noting graphs of signal level changes 07 p1144 A67-19707

Continuous phase binary FSK communications system operating over linear time-variant random parameter chaff scatter channel 09 p1462 A67-21604

Maximum signal transfer theorem for radio wave transmission, scattering and subsequent detection 09 p1462 A67-21611

Decimeter wave propagation over large distance indicates signal propagation does not follow great circle 09 p1492 A67-22593

Changes in electron concentration in lower ionosphere with temperature dependent effective recombination coefficient during transmission of pulse radio signals 10 p1630 A67-22791

Pulse sequences with good autocorrelation properties 10 p1608 A67-23330

Time variable linear transmission systems with arbitrary initial state in case of abruptly varying periodic or nonperiodic system parameters and input signal analyzed, using Laplace transform 10 p1608 A67-23638

Optimum representation of signals with limited spectrum by truncated Kotelnikov series for discrete correctors 11 p1769 A67-23906

Optimal reception of signal transmitted through channel with randomly varying parameters, measuring amplitude and phase 11 p1751 A67-23914

Image transmission by two-dimensional contour coding using edge point coordinates studied by computer simulation 11 p1791 A67-24713

HF random phase transverse wave transmission through turbulent plasma generating scattered waves at combination frequencies 11 p1843 A67-25016

Error probability for transmission of M orthogonal equally probable equal-energy signals over partially coherent channel 12 p1908 A67-26091

Laser communication system for black and white tv signal transmission noting focusing, noise level and light modulation laser communication system for black and white TV signal transmission noting focusing, noise 13 p2068 A67-26724

Behavior in atmosphere of laser beam modulated for black and white TV signal transmission 13 p2068 A67-26725

Apollo spacecraft-earth two-way communications provided by vehicle-mounted variable gain antenna array, automatically tracking ground-transmitted signals 13 p2068 A67-26802

Automatic signal gain control system under constraints, determining time constants for signal filtering 13 p2088 A67-27041

Three-dimensional multielement transponder array designed to give directional replies toward source of interrogating signals 13 p2071 A67-27404

High Noise Immunity Logic Family /HNIL/ digital switching microcircuits for long distance signal transmission operating at high voltage 14 p2282 A67-28028

Design of simple circuit for high speed transmission gating of analog signals with fast switching diode and small overshoot 14 p2287 A67-28686

Multiple format telemetry programmer design using control signals 14 p2275 A67-28689

Laser emission under external signal, analyzing competition between amplification mode and parasitic generation arising at resonant frequency, noting signal role 15 p2498 A67-29469

Navigation satellites of next decade, discussing services for air and sea intercontinental transportation vehicles [AAS PAPER 67-101] 15 p2570 A67-29956

Experimental transmissions for navigation system monitored over 8500 km path to determine phase variations of VLF signals, for use in design of radio navigation aid 15 p2515 A67-30134

Static and dynamic parameter estimation of nonlinear transfer elements from step responses 15 p2463 A67-30331

Optimal signal transmission in detection system characterized by optimal linear filtration of reflected signal 16 p2620 A67-30482

TV signal transmission over gas laser light beam with ADP crystal at 7GHz modulating frequency 16 p2684 A67-30610

Signal field energy distribution optimization ensuring minimum error dispersion during digital information transmission through channels with noise fluctuations 16 p2623 A67-31014

Book on communication principles emphasizing digital radio communication system design, frequency and binary phase shift keying, filtering, fading, etc 16 p2624 A67-31254

Radar waveforms for suppression of extended clutter, discussing confinement of matched filter response in delay and Doppler or ambiguity function 16 p2625 A67-31270

Vlf transequatorial wave propagation, noting phase cycle slipping during sunrise transition 16 p2630 A67-31848

Periodic field strength variations during, sunrise on vlf signals in long path propagation noting amplitude minima and stepwise phase increase 16 p2630 A67-31849

Sunrise variations of phase and amplitude of vlf signals over single long path interpreted as interference between waveguide modes 16 p2631 A67-31851

Multimode propagation and mode conversion at sunrise and sunset lines explaining diurnal variations on vlf paths 16 p2631 A67-31852

Frequency shifts on whistler mode signals from stabilized VLF transmitter from ionosphere and magnetosphere effects, noting electron density 16 p2631 A67-31856

Oblique incidence ionospheric reflections, from phase and amplitude variations of Loran-C pulse signals, noting lower ionosphere two-layer formation 16 p2632 A67-31862

Digital error performance of transportable troposcatter facility evaluated as function of path length 17 p2811 A67-32118

Generalized formulation of code separation incorporating general assumptions concerning nature of channel distortion 17 p2830 A67-32827

Feedback-signal lag and channel discreteness effect on rate of information transmission over Gaussian channel with feedback during symbolized coding 18 p2999 A67-33531

Automatic system auto-oscillations when transmission coefficient of nonlinear part of system depends on amplitude and frequency of input signal 18 p3017 A67-33875

Threshold characteristics of systems for multistate orthogonal transmission of coded analog signals in communication

systems 18 p3000 A67-34023

Uniqueness of response of nonlinear continuous servosystem subjected to any signal 18 p3017 A67-34185

Stationary or long range space vehicle transmitting antennas remote alignment technique using received signal AM 18 p3016 A67-34596

Penning ionization gauge discharge nonlinear response to VHF signals, discussing resonance behavior 19 p3275 A67-35110

Tracking of GEOS-A satellite by Riga station, explaining negatives reduction 19 p3182 A67-35235

Input-to-output amplitude and phase modulation characteristics derived for multicavity klystron 19 p3197 A67-35809

CW transmission measured for carrier and modulation phase, examining carrier phase perturbations due to mode interference CW transmission measured for carrier and modulation phase, examining carrier phase 20 p3379 A67-36292

Large-signal analysis for varactor frequency upconverter under overdriven conditions, obtaining equations for varactor charge, current and voltage 20 p3396 A67-36510

Modulation systems in satellite communications evaluated by criteria of baseband signal noise ratio, signal power, frequency band requirements, etc 20 p3383 A67-36956

Scattered radio signals received during solar eclipse examined for indication of electron clouds masked by daytime high electron density 20 p3432 A67-37208

Transient radiation of electric dipole in uniaxially anisotropic plasma examined for signal frequency greater and less than plasma frequency 20 p3388 A67-37704

Displacement detector operating on Hall effect basis with differential magnetic circuit, including displacement transmitters with unified output 21 p3626 A67-38159

Optimum word length for signal simultaneous digital transmission in real time through single channel 21 p3581 A67-38179

Laser emission under external signal, analyzing competition between amplification mode and parasitic generation arising at resonant frequency, noting signal role 21 p3641 A67-38550

High reliability PCM digital telemetry system for onboard data transmission of analog and digital signals 21 p3583 A67-38635

Analog treatment of digital telemetering signals using a priori information about transmission, noting Q-factor, storage and use of existing emissions 21 p3584 A67-38660

Bandwidth restriction effect on SNR in NRZ signal from PCM transmission system 21 p3584 A67-38667

Optimum representation of signals with limited spectrum by truncated Kotelnikov series for discrete correctors 21 p3604 A67-38934

Optimal reception of signal transmitted through channel with randomly varying parameters, measuring amplitude and phase 21 p3585 A67-38942

Solid state photosensitive devices combining p-n diodes and MOS circuitry noting application in electrical readout, image and pattern detection 22 p3796 A67-39332

Binary and tetravalent signals quantitative comparison for noise sensitivity by computing transmission matrix during transmission via linear channel 22 p3761 A67-39787

Pulse code communication system for transmission of continuous random quantities 22 p3761 A67-39831

Terminal guidance problem involving optimal control for deviations in systems with transport lag 22 p3833 A67-40158

Multimode monopulse feed system optimum aperture distribution determination, obtaining maximum rate of signal change on axis 22 p3763 A67-40313

Surveyor TV system signal processing and transmission, analyzing performance and computer simulation of some effects [SMPTE PAPER 102-41] 22 p3808 A67-40379

Modulated signal nonlinear distortions from AC system resulting from system

components nonlinearities 22 p3763 A67-40478

Modulator-demodulator device using phase shifts between signals in successive time intervals to speed handling of data in HF band 22 p3764 A67-40557

Design studies for reliable long range ground-to-air communication, noting line of sight propagation and HF propagation not involving ionospheric reflections 23 p3972 A67-40742

Propagation of signals in transmission lines with distributed capacitance and conductance for nonlinear parameters 23 p3982 A67-41396

Changes in electron concentration in lower ionosphere with temperature dependent effective recombination coefficient during transmission of pulse radio signals 24 p4149 A67-42127

Recording methods error probability burning code message transmission with start-stop distortion ensuring authenticity by short pulses or integral method 24 p4122 A67-42376

Double signal modulation used to increase authenticity of information transmission in binary systems having resolving feedback 24 p4122 A67-42378

Errorless code transmission in specific nonbinary cyclic channels, describing effective decoding process 24 p4136 A67-42409

SIGNATURE

S MISSILE SIGNATURE

S RADAR SIGNATURE

SIKORSKY MILITARY HELICOPTER

S CH-53 HELICOPTER

SIKORSKY S-65 HELICOPTER

S CH-53 HELICOPTER

SILANE

Radioactively labeled coupling agents adsorption on E-glass surfaces, noting continuous film formation with covalent bonding occurring at interface 20 p3474 A67-37269

SILICA GLASS

Vitreous silica and molten Al reaction, penetration rate of Al, reaction rate and effect of Bi and Sb on rates by lamellar compound formation 10 p1669 A67-23381

High temperature vapor fractionation of silicate glass related to variations of oxygen isotopes in tektites 15 p2564 A67-30394

Chemical analysis of meteorite impact glass from separated areas across Henbury strewnfield 16 p2667 A67-31452

Fundamentals of silicon integrated device technology, Volume 1, Oxidation, diffusion and epitaxy 18 p3096 A67-33453

Oxide films on silicon, discussing silica glass properties, junction formation, surface protection/passivation, device structures and oxidation techniques 18 p3096 A67-33454

Strength of single crystals, amorphous materials and other brittle materials lacking grain boundaries, noting loading rate dependence 18 p3069 A67-33491

Bending strength dependence on porosity of sintered powdered glass beam 20 p3473 A67-36779

Optical glass selection for design of double-lens objective for IR region of spectrum, considering aberrations 20 p3451 A67-37157

Polished glass substrates for thin film microcircuits, analyzing surface resistivity and optical transmittance changes due to heat treatment 23 p4043 A67-41366

SILICATE

SA PYROXENE

Iron-rich silicates significance in Mezo-Madagascar chondrite [AFCLR-67-0012] 07 p1256 A67-20013

Middle and far IR spectra of silicate minerals for remote sensing of lunar or planetary surface composition 08 p1385 A67-20934

Composition of Marthas Vineyard and selected Georgia tektites mutually related to silica-rich basaltites 09 p1569 A67-22687

UV reflectance measurements of granitic, gabbroic and serpentine rocks used to identify lunar silicates 09 p1569 A67-22689

Observations with birefringent interferometer and photoelectric spectrophotometer of Martian surface materials composition, noting strong band at 3.1 micron suggesting hydrated minerals 11 p1865 A67-24603

Heat transfer through various silicate powders measured for lunar surface

- temperature studies, comparing theoretical results
[AIAA PAPER 67-285] 12 p02035 A67-26002
Preferred shape orientation of olivine crystals in porphyritic chondrules suggesting drawing from larger magma
bodies 16 p2619 A67-30986
Tektite composition considered from results of high temperature vapor fractionation of silicates 24 p4237 A67-42649
- SILICIDE**
Titanium silicide preparation by simultaneous hydrogen reduction of silicon tetrachloride-titanium tetrachloride mixtures at 1200 degrees C 01 p0093 A67-10292
Hall effect and fine structure of X-ray fluorescence and absorption K spectrum of vanadium in silicides 01 p0101 A67-10935
X-ray microstructural and chemical analysis of sintering of zirconium diboride-molybdenum disilicide
alloys 01 p0102 A67-11242
Energy gap of vanadium silicide measured by tunneling technique based on proximity effect 03 p0492 A67-13327
X-ray, microstructural and chemical analysis of sintering of zirconium diboride-molybdenum disilicide
alloys 17 p2875 A67-33167
Methods of producing coatings based on metal-like high temperature materials 19 p3244 A67-34957
- SILICON**
Surface charge after annealing of aluminum-silicon dioxide-silicon structures in inert atmospheres, analyzing effect of applied electric field 01 p0032 A67-10004
Diffusion coefficient of lithium in p-type silicon determined by method using electrophotographic developing agents 01 p0127 A67-10061
Variable effect of external electrical field on IR photoconductivity of thin n-and p-type silicon samples with low bulk impurity contents 01 p0128 A67-10076
Dislocation-free silicon web crystal growth controlling supercooling and resistivities, noting elastic strains 01 p0131 A67-10367
Epitaxial temperature for Si films vacuum deposited on silicon as function of substrate crystallographic orientation observed by low energy electron diffraction patterns 01 p0132 A67-10372
Double crystal spectrometer measurement of X-ray Compton and thermal scattering accompanying Bragg reflection from Si and Ge single crystals 01 p0132 A67-10456
Low energy proton bombardment damage in thin film cadmium sulfide and in single crystal silicon with silicone coating 01 p0037 A67-10476
Resistivity and Hall coefficient measurement of n-and p-type gold-diffused silicon over wide temperature range 01 p0134 A67-10754
Nearest neighbor electron scattering in silicon, showing existence of diffuse rings association with Kikuchi pattern 01 p0135 A67-10877
Si single crystal lattice parameter measurement using double-diffraction effect 01 p0135 A67-10894
Si semiconductor strain sensors and miniature pressure transducers for cryogenic pressure measurements 01 p0069 A67-11017
Silicon-tantalum oxide system prepared by reactive sputtering, noting characteristics of MOS diode of system 01 p0137 A67-11071
External electron emission measurement from polished n-germanium and n-silicon surfaces 02 p0296 A67-11830
High resistivity silicon single crystals, discussing carrier lifetime, photoconductivity and recombination levels 02 p0297 A67-11832
Negative resistance and current density in double-injection filaments in seminsulating Si 02 p0298 A67-11886
Electron beam scanning technique measurement of diffusion lengths in Si and GaP p-n junctions and recombination rate of dislocations in n-type Si 02 p0298 A67-11887
Deep-level localized current oscillations in n-type silicon crystal 02 p0298 A67-11892
Microelectronic applications of silicon-on-sapphire /SOS/ and MOS-FET large scale arrays /LSA/ 02 p0219 A67-12108
Electron microscopy analysis of microinhomogeneities in commercial Si used in preparation of p-n junction devices 02 p0257 A67-12434
Dependence of conductivity on microhardness of p-doped n-type silicon, examining effect of gamma radiation 02 p0300 A67-12477
Isolation-diffusion of phosphorus in silicon with low surface concentration, with applicability to preparation of integrated solid state circuits 02 p0223 A67-12736
Phosphorus-diffusion method in silicon with thin phosphorus containing layer used to produce working area of planar strain gauges 02 p0248 A67-12737
Energy and wave functions of singly charged donor impurity centers in silicon and germanium 03 p0488 A67-12857
Shallow donor potential in silicon 03 p0493 A67-13363
Neutron collision cross section and calculation of energy loss of displaced Si atoms to ionization 03 p0494 A67-13481
Epitaxial growth and control of low-resistivity n-type silicon layers on p-type boron-doped substrates 03 p0494 A67-13485
Surface recombination velocity of thermally oxidized silicon structures exposed to X irradiation 03 p0496 A67-13677
Carrier mobility and concentration in epitaxial silicon layers obtained by vacuum sublimation 03 p0498 A67-13869
Integrated circuit fabrication on silicon single crystals 03 p0387 A67-14000
Emissive power of germanium and silicon with various surface finishes in temperature range from 700 to 1200 degrees K 04 p0674 A67-14719
IR transmission microscopy and X-ray microanalysis of anomalous etching on surface of Si single crystals grown in Ar gas 04 p0675 A67-14769
Maximum concentrations estimation for solidus of germanium and silicon solid solutions in retrograde melting 04 p0677 A67-14943
Nonsinusoidal periodic oscillations observed in high resistivity n-type silicon compensated by zinc and phosphorus 04 p0679 A67-15142
Uniaxial compression effect on two jump conductivity processes occurring in p-type silicon 04 p0679 A67-15145
Dislocation-induced relaxation in silicon single crystals by measuring internal friction and Young's modulus at temperatures from 77 to 300 degrees K 04 p0681 A67-15294
Auger effect radiative recombination of excitons bound to neutral donors of GaP and Si and generation of luminescent spectrum C line 04 p0682 A67-15463
Force constants and local mode frequencies for vibrations of interstitial lithium positive ion in Si crystal, using covalent orbital bond model 04 p0683 A67-15609
Neutron energy deposition in silicon in ionization and elastic interactions calculated, noting effects of atomic recoils 04 p0684 A67-15688
Neutron induced degradation of carrier lifetime in n-and p-type silicon containing oxygen and dopant 04 p0684 A67-15691
Transient radiation effects induced in silicon irradiated by electron pulses measured, using resistivity transient response and Hall effect 04 p0685 A67-15695
Lithium interaction with radium induced damage in silicon solar cells to produce center preserving minority carrier lifetime 04 p0556 A67-15703
Substructure of aluminum monocrystals in relation to silicon content 05 p0827 A67-16075
Dislocation structure of crystals with diamond type lattice analysis made possible by growing silicon monocrystals along growth axis 05 p0860 A67-16076
Dislocation reaction in crystals with diamond type structure analyzed on silicon grown by Czochralski method along /100/ axis 05 p0860 A67-16077
High resolution X-ray diffraction topography of dislocation structure of Si crystal 05 p0860 A67-16078
Electron spin resonance in phosphorus-doped silicon at various temperature ranges 05 p0861 A67-16499
Silicon electrical properties at low temperatures and various carrier concentrations, noting impurity 05 p0861 A67-16502
Polygonization in silicon single crystal by chemical etching, determining activation energy, noting dependence on annealing temperature 05 p0862 A67-16503
Dislocation loops by gold diffusion into silicon crystals analyzed, using X-ray diffraction topography and optical microscopy 05 p0866 A67-16974
Local variations in spacing and orientation of lattice plane in silicon single crystal, measuring angular positions of diffraction peak by double crystal spectrometer 05 p0866 A67-16977
Microplasma effects arising in avalanche type breakdown in deep-seated large-area p-n junction in silicon 05 p0867 A67-17052
EPR spectral shape and width as affected by phosphor concentration, degree of boron compensation and temperature in strongly doped n-silicon 05 p0867 A67-17055
Defects in silicon p-n solar cells with Li diffused N region produced by electron irradiation and spontaneously annealed at room temperature interpreted as Li ions 05 p0870 A67-17273
Impurity IR photoconductivity of silicon surface doped with gold 05 p0871 A67-17491
Photoconductivity of silicon alloyed with gold and zinc at various temperatures 05 p0871 A67-17492
Energy spectrum of levels appearing in silicon single crystals irradiated by integral fluxes of fast electrons, neutrons and gamma quanta 05 p0872 A67-17547
X-ray effect on conductivity, carrier concentration and mobility in Si crystals and Si p-n junction 06 p1048 A67-17855
Optical scattering dependence on heat treatment of monocrystalline silicon containing nitrogen 06 p1050 A67-18183
Lifetime and recombination of excess carriers in silicon over seven orders of magnitude of injected carrier density 06 p0971 A67-18226
Paired defect production rate in silicon created in single electron scattering event 06 p1053 A67-18711
Impurity centers arising from sulfur in silicon identified, using IR absorption technique and uniaxial stress effect 06 p1061 A67-18924
Ground state energies of P, As and Sb donors in Si taking account of dielectric screening of donor potential 06 p1061 A67-18925
Highly spin polarized carriers for studying neutral impurity scattering in P doped silicon 06 p1063 A67-18937
Electron scattering by neutralized acceptors investigated in Ge and Si through cyclotron resonance 06 p1063 A67-18939
Oscillatory magnetoconductance in inverted surfaces of p-type silicon 06 p1063 A67-18940
Relaxation time of electrons in pure germanium and silicon measured from line width of cyclotron resonance at liquid helium temperatures taking into account quantum limit 06 p1064 A67-18945
Far IR resonant absorption in n-type silicon analyzed, considering donor-pair conduction dominant mechanism 06 p1068 A67-18974
Electric field induced optical refractivity changes /Franz-Keldysh effect/ and nonlinear light scattering, light beam deflection and modulation in neutron-irradiated Si at 95 degrees K 07 p1231 A67-19487
Collisional excitation of Si ion from ground state to autoionization levels at coronal temperatures 07 p1256 A67-20168
Photoionization cross section of negatively charged in atoms in n-type silicon from comparison of intrinsic photoconductivity with impurity photoconductivity 08 p1367 A67-20410
Oxygen precipitation consisting of point defects as explanation of structural changes of silicon single crystals during thermal treatment 08 p1370 A67-21205
Diffusion coefficient of lithium in p-type silicon determined by method using electrophotographic developing agents 08 p1371 A67-21447
Lattice constant of thin silicon specimens determined using electron diffraction techniques 09 p1553 A67-21881
Saha-Langmuir formula applied to description of temperature dependence of positive ion current in surface ionization of silicon atoms, comparing work functions by methods using contact potential, thermionic

- emission and Richardson graphs 09 p1554 A67-22006
- Relation in silicon between annealing rates, residual damage and defect concentrations, noting link to activation energy increase 09 p1557 A67-22420
- Band-to-band radiative recombination in semiconductor groups IV, VI and III-V, presenting data on diamond, Si, Ge, Se and Te 09 p1558 A67-22601
- Radiation damage experiments for evaluation of silicon solar cell characteristics under simulated solar light 10 p1596 A67-23166
- Carrier drift velocity measurements in silicon at high electric fields, using time-of-flight technique 10 p1690 A67-23167
- Fast neutron irradiated p-type silicon single crystals electric and photoelectric properties 10 p1691 A67-23404
- Electron capture coefficient of A-centers in silicon at helium temperatures 10 p1694 A67-23649
- Anisotropic properties of acoustic electron scattering in Si samples in 8 mm wavelength and liquid nitrogen temperature 10 p1695 A67-23664
- Space-charge-limited currents in p-type silicon noting I-V characteristics, theoretical values agreement, Hall coefficient measurements correlation, etc 11 p1845 A67-24135
- Vacuum UV wavelength standards and energy levels in first silicon spectrum from low pressure source 11 p1822 A67-24417
- Noise spectral distribution and instability in germanium and silicon photodiodes 11 p1765 A67-24473
- P-type Au compensated Si diode with negative resistance, determining reversed conductivity recovery time 11 p1768 A67-24861
- Thermal conductivity of low temperature silicon and germanium irradiated by fast neutrons noting differences, additive thermal resistivity and possible scattering mechanisms 11 p1849 A67-24899
- Edge dislocations effect on electrical noise in n-type silicon analyzed and results compared with Shockley-Read model 11 p1849 A67-24906
- Electronic Raman scattering from phosphorus donors and boron acceptor impurities in Si, noting importance of interband transitions 11 p1851 A67-24999
- Silicon crystals composition effect on solar cells reaction to irradiation by 4 mev electrons 12 p1896 A67-25150
- Nonsinusoidal periodic oscillations observed in high resistivity n-type silicon compensated by zinc and phosphorus 12 p1979 A67-25165
- Uniaxial compression effect on two jump conductivity processes occurring in p-type silicon 12 p1979 A67-25168
- Electrical and photovoltaic properties of PbS-Si heterodides 12 p1980 A67-25180
- P atoms distribution in doped surface layer of silicon photoconverter for various thermomdiffusion conditions exhibiting typical concentration curves 12 p1982 A67-25322
- P-and n-type silicon spectral emissivity measured at several temperatures and wavelengths for carrier concentrations and direct current resistivities [AIAA PAPER 67-302] 12 p1958 A67-26017
- Neutral silicon photolization cross sections for continuous UV absorption measured near ionization limits by shock tube technique 12 p1968 A67-26248
- Nonlinear effects in steady state volt-ampere characteristics of zinc compensated n-type silicon single crystals 13 p2172 A67-26356
- Radiative recombination through free carriers and localized states in silicon single crystals containing gamma-induced defects 13 p2172 A67-26357
- Optical quenching of photoconductivity in silicon resulting from minority carrier capture by centers created by irradiation 13 p2173 A67-26358
- Fundamental absorption edge of silicon heavily doped with boron, arsenic, phosphorus or antimony 13 p2173 A67-26361
- High resistivity regions in silicon exposed to photon bombardment 13 p2173 A67-26364
- Piezoresistive effect of homogeneous silicon diffused elements 13 p2175 A67-26656
- Temperature dependence of small signal AC field effect kinetics in silicon within 170-300 K, considering majority carriers and one energy level theory 13 p2176 A67-28708
- Thin silicon solar cells for large flexible arrays having low specific mass and radiation resistance 13 p2055 A67-26716
- Temperature dependence of energy levels of shallow donor impurities in silicon, noting electron-phonon interaction 13 p2176 A67-26987
- Recrystallization of Ge and Si thin films and structural changes due to electron bombardment and thermal annealing 13 p2177 A67-27071
- Defects in irradiated silicon, analyzing electron paramagnetic resonance and electron-nuclear double resonance of aluminum vacancy pair 13 p2180 A67-27161
- Orbach spin lattice relaxation of shallow donors in silicon 13 p2180 A67-27162
- Current-voltage characteristics of germanium-silicon isotype heterojunctions with regard to capacitance and photoelectric measurements 13 p2183 A67-27569
- Evaporated silicon thin-film transistors operating by field effect conductivity modulation of n-type inversion layer at p-type film surface 13 p2083 A67-27573
- Silicon photocells at high luminous flux concentrations, noting increase in multiplicity of power with series resistance 13 p2056 A67-27622
- Electrical and energy performance of high efficiency GaAs solar cells compared to silicon photocells, discussing temperature effect and p-n junction depth 13 p2056 A67-27623
- Resistivity and magnetoresistance for metallic impurity conduction in phosphorus doped silicon at low temperature with various donor concentrations 14 p2365 A67-28232
- Ionization threshold energy of electrons and holes in silicon 14 p2368 A67-28535
- P-type silicon IR photoconductivity burst in nonequilibrium field effect 14 p2368 A67-28536
- Silicon surface purified by argon ion bombardment and annealing, studying field effect kinetics 14 p2372 A67-28755
- Forward conduction characteristics of contacts between gold n-type silicon measured at different temperatures 14 p2373 A67-28925
- DC operation of FET at liquid helium temperature noting transfer and drain characteristics similar to those at room temperature 14 p2290 A67-28926
- EPR applied to investigation of various semiconductors containing iron, and Mn at liquid nitrogen temperature 14 p2373 A67-28968
- Solar energy conversion into electric power by GaAs and Si cells analyzed, using photovoltaic cell theory 15 p2536 A67-29503
- Microplasma effects arising in avalanche type breakdown in deep-seated large-area p-n junction in silicon 15 p2538 A67-29783
- EPR spectral shape and width as affected by phosphor concentration, degree of boron compensation and temperature in strongly doped n-silicon 15 p2538 A67-29786
- Temperature homogenization effect on structure of industrial aluminum, determining mechanical properties dependency on Fe/Si ratio 15 p2504 A67-29975
- Cathode sputtering, evaporation and anodic oxidation for thin film deposition in integrated circuit technology 15 p2453 A67-30066
- Fast neutron bombardment and temperature effects on conductivity, photoconductivity and resistivity of Si single crystals, determining energy levels of defects 15 p2541 A67-30236
- Conductivity and Hall effect in analysis of temperature dependence of current carrier concentration and mobility in silicon, explaining ionization energy 15 p2541 A67-30240
- Charge curves for germanium and silicon surface obtained by field effect measurements, noting nature and mechanism of effect 15 p2542 A67-30249
- Threshold energy of formation and stable defect spatial distribution of silicon irradiated with electrons 15 p2542 A67-30250
- Minority carrier lifetime in p-silicon, analyzed varying temperature and injection level and studying recombination 16 p2725 A67-30807
- Spatial distribution of radiation damage in solids determined by spectral analysis of photovoltaic current of photovoltaic cell 16 p2726 A67-30815
- Light attenuation measurement in chilled silicon noting attenuation increase with incident intensity 16 p2685 A67-30870
- Compatible integrated circuits using thin films on silicon for application in space telemetry systems 16 p2641 A67-31559
- Characteristics of photovoltaic solar converters, discussing drift field, wrap around and epitaxial webbed silicon cells, minimum film thickness and radiation damage 17 p2801 A67-32048
- Si-Fe deformation in tension/compression noting orientation dependence of yield stress, slip band formation and direction of screw dislocations 17 p2872 A67-32741
- Subthreshold electron irradiation effects on surface recombination properties of n-and p-type germanium and silicon crystals 17 p2916 A67-32834
- First order prediction of equilibrium photocurrent in silicon switching diodes and radiation storage time in silicon low power planar and mesa transistors from electrical measurements 17 p2918 A67-32851
- Low temperature thermal conductivity measurement of fast-neutron-irradiated silicon and germanium, showing difference between bombardment induced scattering in two materials 17 p2919 A67-32855
- Disordered regions produced by fast neutron irradiation effect on semiconductor properties of silicon 17 p2919 A67-32859
- Silicon photoconductivity measurements after electron irradiation at cryogenic temperature 17 p2920 A67-32864
- Impurity effect on annealing behavior of irradiated silicon studied via isothermal annealing of minority carrier lifetime 17 p2921 A67-33051
- Electron capture coefficient of A-centers in silicon at helium temperatures 17 p2923 A67-33330
- Anisotropic properties of acoustic electron scattering in Si samples in 8 mm wavelength and liquid nitrogen temperature 17 p2924 A67-33345
- Fourier series applied to X-ray investigation of potential and electron density distribution in silicon lattice to study chemical bonds 18 p3094 A67-33439
- Fundamentals of silicon integrated device technology, Volume 1, Oxidation, diffusion and epitaxy 18 p3096 A67-33453
- Oxide films on silicon, discussing silica glass properties, junction formation, surface protection/passivation, device structures and oxidation techniques 18 p3096 A67-33454
- Impurity diffusion role in silicon device technology, discussing error function distribution 18 p3096 A67-33455
- Epitaxial deposition of silicon on silicon substrates, discussing vapor and vacuum deposition, impurity distributions, layer thickness, etc 18 p3097 A67-33456
- Phonon spectrum of Si calculated by Monte Carlo method, determining Si thermodynamic functions 18 p3098 A67-33629
- Influence of fast proton and electron irradiation on diffusion of substitution impurities in silicon 18 p3100 A67-33750
- Silicon solar cells impurities, radiation resistance, fabrication, nonsilicon materials, development, etc 18 p2989 A67-34069
- Silicon surface depth damage determination technique, with confirmation by Sirtl etching, oxidation and epitaxial deposition 18 p3103 A67-34565
- Au and P doped n-type Si, noting formation of p-type surface layer of increasing thickness when heat treated 19 p3299 A67-34761
- Emission recombination in n-type Si single crystals irradiated with fast neutrons or gamma quanta 19 p3301 A67-34775
- Vacuum siliconization of refractory metals in Mo-Si system noting thermomdiffusion layers, vapor phase, chemical reaction, diffusion and temperature gradient 19 p3236 A67-34918
- Dissolution of single crystal silicon by aqueous solutions of hydrofluoric acid and chromium oxide studied as function of etchant composition 19 p3301 A67-34934
- Processes and instrumentation for forming contacts on microelectronics devices 19 p3236 A67-35022

- Electron, X-ray and UV radiation effects on oxidized silicon surfaces and planar devices, noting space charge buildup 19 p3305 A67-35621
- Isochronal annealing of short-circuit current of electron irradiated silicon solar cells 19 p3305 A67-35668
- Isochronal annealing of proton-irradiated silicon solar cells studied in vacuum over various temperature ranges 19 p3305 A67-35669
- Annealing under continuous irradiation in p-on-n silicon solar cells with lithium diffused in N region 19 p3306 A67-35671
- Conductivity profiles investigated as function of ion energy, total flux and annealing schedule, when implanting boron into silicon 19 p3307 A67-35812
- Simultaneous diffusion of gallium and arsenic in silicon from gallium arsenide source, obtaining profiles at various temperatures 19 p3308 A67-36035
- Effect of irradiation of silicon by fast neutrons on switching time of alloy diode synthesized on silicon base 20 p3508 A67-36402
- Germanium films crystallization when deposited by evaporation on silicon single crystals studied by optical microscopy and electron diffraction 20 p3509 A67-36473
- Layer removal techniques with Hall effect and sheet resistivity measurements indicate carrier concentrations exceeding thermal equilibrium solubility for antimony implants into silicon 20 p3510 A67-36856
- Si optical and electrical properties and energy levels with Mg as donor impurity 20 p3510 A67-36916
- Inverse layer effect on p-type silicon MOS structure surface, examining deviation from equilibrium space charge theory 20 p3511 A67-37141
- Anisotropy of piezothermal EMF in Si and Ge under uniaxial stress 20 p3511 A67-37147
- Nonlinear effects in steady state volt-ampere characteristics of zinc compensated n-type silicon single crystals 21 p3679 A67-38313
- Radiative recombination through free carriers and localized states in silicon single crystals containing gamma-induced defects 21 p3679 A67-38314
- Optical quenching of photoconductivity in silicon resulting from minority carrier capture by centers by irradiation 21 p3679 A67-38315
- Fundamental absorption edge of silicon heavily doped with boron, arsenic, phosphorus or antimony 21 p3680 A67-38318
- High resistivity regions in silicon exposed to photon bombardment 21 p3680 A67-38321
- Silicon semiconductor alpha particle detector for spectrometry, noting radiation resistance for low energy proton bombardment 21 p3682 A67-38596
- High energy electron radiation effects on silicon photocells deposited epitaxially on artificial satellite surface, discussing liberated carrier accumulation possibility 21 p3572 A67-38672
- Hall effect measurements on heat treated and quenched p-type silicon crystals, noting donor centers appearance due to vacancy cluster 21 p3687 A67-39138
- Ground state and four lowest optically excited states of shallow donor in Si calculated using isotropic effective mass 22 p3854 A67-39245
- Vacancy concentration in dislocation enhanced diffusion model as explanation of phosphorus and boron anomalous diffusion in silicon 22 p3855 A67-39346
- Anomalous phosphorus diffusion in Si at high surface concentrations explained by excess vacancy generation at edge jogs on gliding dislocations 22 p3855 A67-39347
- Al impurity redistribution near Si semiconductor surface subjected to high temperature oxidation 22 p3857 A67-39502
- Silicon AC strain gauges performance investigated by employing oriented p-Si crystals operating in static and dynamic modes 22 p3798 A67-39569
- Energy state of recombination level of thermally hardened silicon diode base, considering spatial lifetime of minority carriers 22 p3773 A67-39920
- Test procedure for Si microcircuit production consisting of bulk and junctions electric measurement, oxide thickness and junction position
- measurements 23 p3977 A67-40660
- Na and K introduced into Si by diffusion from thin layer of alkali metal and during electrolysis of molten alkali halogenides 23 p4037 A67-40721
- Space charge limited /SCL/ hole current in Si noting mobility, capacitance, current density, I-V characteristics and double injection 23 p4038 A67-40878
- Ionization threshold energy of electrons and holes in silicon 23 p4040 A67-40942
- P-type silicon IR photoconductivity burst in nonequilibrium field effect 23 p4040 A67-40943
- Si and S ion oscillator strengths for resonance lines in solar spectrum, discussing spin-spin and spin-other orbit interactions 23 p4067 A67-41235
- Defects in surface layer of silicon crystals during deep diffusion of phosphorus studied by X-ray diffraction 23 p4042 A67-41295
- Dislocation structure of tension deformed Si samples investigated by electron microscopy 23 p4042 A67-41296
- Si and Cd solar cell arrays compared using rigid frame Si solar cell concept 23 p3938 A67-41497
- Isochronal annealing effects on photovoltaic properties of n-on-p Si solar cells irradiated by energetic proton 23 p3940 A67-41518
- Li interactions with complex damage clusters produced by neutrons in Si solar cells, discussing annealing, radiation hardening and energy dependence 23 p3940 A67-41520
- Simulated micrometeoroid bombardment effect on n/p Si and CdS solar cells performance 23 p3941 A67-41521
- Li behavior in self-healing radiation resistant Si solar cells 23 p3941 A67-41522
- Spontaneous annealing models of lithium-diffused Si solar cells, discussing defect compensation and metastable defect formation 23 p3941 A67-41523
- Li containing p-on-n and n-on-p Si cell degradation by bombardment noting carrier removal damage, annealing and radiation damage resistance 23 p3941 A67-41524
- Li doped Si solar cell, studying irradiation damage, recovery effect, carrier removal, time dependency and annealing 23 p4047 A67-41525
- Li doped Si solar cells noting fabrication, preradiation behavior, changes with temperature, recovery and I-V characteristics after irradiation 23 p3941 A67-41526
- Li doped Si solar cell radiation resistance to high energy electrons, noting fabrication methods and annealing behavior differences 23 p3941 A67-41527
- Deposited Al layer thickness on Si determined using X-ray spectrometric technique 24 p4200 A67-41803
- Silicon abundances in chondrules from different chondrites by neutron activation analysis 24 p4236 A67-42644
- Neutron irradiation effect on thermal conductivity of silicon at low temperature noting annealing stage 24 p4206 A67-43110
- SILICON ALLOY**
- Thermoelectric generator modules with Si-Ge alloys, discussing material preparation and generator fabrication 09 p1445 A67-22180
- Operational economy of dip brazing method of joining aluminum and reliability of ultrasonic printout procedures for inspection of assemblies 10 p1660 A67-23007
- SILICON CARBIDE**
- Peculiarities of Hall curves of n-type alpha silicon carbide, noting concentration of conduction electrons related to temperature 01 p0129 A67-10102
- Vapor flux of trichloromethylsilane affects morphology of pyrolytic deposits of silicon carbide 01 p0103 A67-10252
- Silicon carbide generation by pyrolysis of gas mixtures on tungsten wires, using X-ray diffraction to analyze structure 01 p0103 A67-10688
- Nucleation of epitaxial SiC on Si surfaces 02 p0299 A67-11894
- Mechanical properties of silicon carbide filament reinforced epoxy resin composites fabricated by plying monolayer tapes into unidirectional and balanced bidirectional composites 03 p0452 A67-13403
- Single crystal fiber reinforced composites, discussing use of silicon carbide whisker as interstitial reinforcement 03 p0453 A67-13411
- Synthesis route to form continuous filaments of SiC, noting tensile strength, elastic modulus and density of product 03 p0454 A67-13422
- Boron-modified SiC continuous filament fabrication by vapor deposition on hot W wire substrate and tensile testing 03 p0454 A67-13423
- Compatibility and interaction characteristics of SiC and B fibers with metal matrices in composites prepared from powder metallurgy by hot pressing 03 p0444 A67-13430
- Coatings of nickel, chromium and Cu on SiC and aluminum oxide whiskers by electroforming and metalizing, using electron microscope techniques 03 p0444 A67-13434
- Silicon carbide filament properties, fabrication and use as reinforcement of metal matrix composites, noting strength retention at high temperatures 03 p0445 A67-13439
- Enthalpy measurement for self-binding silicon carbide at high temperatures 03 p0446 A67-13609
- Epitaxial growth of SiC film on silicon substrate and electron diffraction analysis of crystal structure 04 p0675 A67-14762
- Negative differential resistances and inductive effects in alpha-modified SiC p-n junction diodes 04 p0679 A67-15136
- Photoconductivity and negative resistance caused by carrier lifetime change in response to change in injection level in SiC p-n junctions 04 p0680 A67-15156
- Radiative recombination in space charge layer of p-n junction in silicon carbide determined from I-V characteristics and capacitance 04 p0681 A67-15298
- Temperature effect on impact ionization coefficient in SiC semiconductor p-n junctions with reversed current in strong electric field 05 p0865 A67-16916
- Electron mobility measurements in n-type SiC polytypes noting temperature dependence 08 p1370 A67-21294
- Continuous filament reinforcement data, analyzing boron and silicon carbide for metal matrix applications [ASTME PAPER WES-7-75] 10 p1668 A67-23010
- Superfine structure of EPR spectrum of nitrogen in silicon carbide as function of nitrogen concentration and sample temperature 10 p1694 A67-23650
- High modulus high strength reinforcements incorporated in epoxy matrix plastic composites for aerospace structural use 10 p1671 A67-23704
- Characteristics of electroluminescent p-n junctions prepared on base of beryllium-doped silicon carbide 14 p2367 A67-28524
- Photoconductivity and negative resistance caused by carrier lifetime change in response to change in injection level in SiC p-n junctions 15 p2534 A67-29343
- Energy dependence on wave vector in valence band of diamond, Si, Ge and SiC, obtaining Coulomb and resonance integrals 15 p2541 A67-30237
- Temperature effect on impact ionization coefficient in SiC semiconductor p-n junctions with reversed current in strong electric field 16 p2727 A67-30893
- Superfine structure of EPR spectrum of nitrogen in silicon carbide as function of nitrogen concentration and sample temperature 17 p2923 A67-33331
- Measuring IR Faraday rotation and Hall effect in 6H and 15R polytypes of silicon carbide 18 p3102 A67-34278
- Free carrier absorption coefficients in 6H and 15R silicon carbide, showing probable ellipsoids of revolution 18 p3102 A67-34279
- Enthalpy measurement for self-binding silicon carbide at high temperatures 18 p3066 A67-34474
- Vapor deposition-prepared continuous silicon carbide filaments for use as reinforcement in high strength oxidation-resistant structural plastic composite 21 p3648 A67-37881
- Epitaxial growth of aluminum nitride on silicon carbide studied for influence of substrate temperature on perfection of crystal deposit 23 p4037 A67-40722
- Characteristics of electroluminescent p-n junctions prepared on base of beryllium-doped silicon carbide 23 p4039 A67-40931

SILICON COMPOUND

- SA SILANE
SA SILICATE
SA SILICIDE
- Far IR reflection spectra of silicate mineral at room and liquid nitrogen temperatures
[AIAA PAPER 65-668] 03 p0508 A67-13048
- High temperature reaction between refractory whiskers of silicon nitride and Al and Ni, observing results by electron microscopy 03 p0445 A67-13528
- Niobium and tantalum oxides from decomposition of zircon-pyrophor concentrate by silicon 04 p0637 A67-14941
- Elastic and inelastic lattice strain at oxide window edges determined from imperfections of n and p type 08 p1370 A67-21297
- Conductance-and capacitance-voltage curves of MOS capacitors analyzed for temperature dependence of inversion layer frequency response in n-type silicon 11 p1846 A67-24234
- Barrier height between tungsten silicide films and n-type silicon base determined, using photoelectric response measurements 11 p1850 A67-24924
- Lasing on Si II and Cl II lines in pulsed gaseous discharge, noting possible mechanisms for achieving population inversion 15 p2496 A67-29178
- Silicon oxide and nitride film thickness determined with interference technique, using spectrophotometer in UV and visible wavelength range 17 p2854 A67-32191
- Semiconductor-metal potential barriers for semiconductor devices obtained by silicon dioxide and silicon local sputtering in argon discharge 17 p2916 A67-32809
- Carbon silica reaction during erosion of silica-phenolic composites noting silica removal mechanisms 17 p2809 A67-33034
- Oxygen concentration in silicon semiconductors, discussing oxygen properties and effects on carrier lifetime, surface etching and dislocations 21 p3682 A67-38363
- Impurity effect on solubility of another impurity in p-n silicon tunnel diodes studied by measuring current-voltage characteristics 21 p3682 A67-38364
- Radiative recombination processes involving neutral donors and acceptors in silicon and germanium, describing extrinsic luminescence bands 22 p3862 A67-39998
- Molecular sieves as casings filler for semiconductor devices, discussing stabilization of electrical parameters and absorptive capacity of synthetic zeolites 23 p4042 A67-41274
- SILICON CONTROL RECTIFIER /SCR/**
- Maximum alloying temperature and cooling rate of p-n junctions effect on volt-ampere characteristics of silicon diode and minority carrier lifetime 01 p0039 A67-11053
- Forward voltage characteristics of thyristors in fired state, depending on injection level for high current density 03 p0380 A67-13482
- Gamma radiation effect on SCR correlated with electron radiation encountered by spacecraft 04 p0590 A67-15725
- Monograph on high power semiconductor-magnetic pulse generators, noting saturable inductors and silicon controlled rectifiers, circuit analysis, voltage regulator, etc 09 p1482 A67-22698
- Pulse generator for semiconductor laser excitation, noting silicon controlled rectifiers and pulse shaping line 19 p3191 A67-34963
- Distributed power generation for radar and communications covering cost comparisons, antenna subsystems and reliability of solid state devices 22 p3761 A67-39861
- SILICON FILM**
- Topographic X-ray analysis of deformation in tension of silicon crystal 03 p0493 A67-13452
- Thin film silicon-on-sapphire deep depletion MOS transistors 09 p1475 A67-22203
- Structure, conductivity and Hall effect of electron bombardment evaporated silicon films on sapphire substrates, noting deposition temperature source doping effectiveness 11 p1845 A67-24141
- Coating of titanium with aluminum and silicon by immersion of titanium samples in molten aluminum or in aluminum/silicon melts 12 p1955 A67-25360

- Space-charge limited ionic currents in MOS structure oxide film, noting relationship between interface ion trapping rate and SCL currents 15 p2539 A67-29825
- Negative-resistance in evaporated silicon films at room and liquid-nitrogen temperatures believed due to double injection 16 p2728 A67-31035
- Tunneling characteristics of metal-oxide-silicon semiconductors, observing band structure and interface-state densities influences 19 p3308 A67-36045
- Donor surface states and bulk acceptor traps in silicon on sapphire films due to activation of absorbed impurities 21 p3677 A67-38012
- Field effect devices noting insulated gate transistor, thin single crystal silicon film deposition on sapphire single crystal, etc 21 p3590 A67-38064
- Soviet papers on physical properties of ultrapure metals and semiconductors, stressing epitaxial silicon layers 21 p3681 A67-38357
- Nature, distribution and causes of structural imperfections and dislocations in epitaxial Si layers with base layer orientation /111/ 21 p3681 A67-38359
- Structural properties of Si anodic oxide layers studied by X-ray analysis, using Laue photograph method 21 p3681 A67-38360
- Temperature effect on diffusion coefficient of radioactive phosphorus in epitaxial Si layer 21 p3681 A67-38361
- Phosphorus concentration influence on epitaxial silicon layers growth and electrical characteristics 21 p3681 A67-38362
- Electron energy band structure of semiconductor films determined by analysis of structural symmetry of germanium and silicon samples 22 p3861 A67-39919
- Epitaxial silicon layers grown by electron microscopy with small quantities of gold, discussing possible growth mechanisms 23 p4036 A67-40656
- Heteroepitaxial Si films grown on sapphire studied for current voltage relations, finding space charge limited current 23 p4038 A67-40785
- Implantation process for thin silicon solar cell fabrication, discussing leakage losses and efficiency 23 p4046 A67-41488
- Thin silicon, dendritic and cadmium sulfide solar cells technology and large-area lightweight arrays 23 p3939 A67-41512
- Single crystal silicon films on insulating substrates, discussing preparation methods and chemical and structural perfection for use in field effect and bipolar devices 24 p4202 A67-42089
- SILICON JUNCTION**
- Stacking faults in steam-oxidized silicon wafers annealed in vacuum at 800, 1000 and 1200 degrees C observed by chemical etching and transmission electron microscopy 01 p0126 A67-10052
- Locked oscillation of silicon p-n junction avalanche diodes in 50 to 140 GHz range 01 p0035 A67-10436
- Junction perfection in coherent microwave oscillation in avalanching p-n silicon diodes 01 p0036 A67-10449
- Space-charge layer effect on volt-ampere characteristics of multilayer diffusion structures in silicon 02 p0281 A67-11504
- Radiation resistance of silicon photoconverters onboard Elektron III satellite, noting protective coating 02 p0240 A67-11543
- Impurity concentration and electric field distribution determined in drift region of silicon p-n detectors from capacity as function of reverse voltage 02 p0296 A67-11823
- Abnormal diffusion of base dopant impurities in shallow double-diffused structures in silicon, noting cooperative diffusion in enhanced or retarded penetration of base region 02 p0298 A67-11877
- Implantation of Cs and Na ions into p-type silicon, effect on hot electron emission from p-n junction 02 p0299 A67-11897
- Transition time dependence between avalanche and second breakdown on input power to p-n silicon junction, noting thermal effects in semiconductors 02 p0222 A67-12650
- Time dependent light emission due to voltage breakdown in mesoplasma region in Si on Si diode surfaces 02 p0301 A67-12658

- DC parametric device in which capacitance variation of silicon p-n junctions due to input signal causes FM 03 p0377 A67-13106
- Intensity of light emitted by individual microplasmas of silicon p-n junctions increases with voltage to maximum and then decreases 03 p0491 A67-13176
- Temperature effect on electron emission and stability of p-n junction using silicon and silicon carbide 03 p0494 A67-13487
- Temperature sensor controller in form of linear monolithic integrated silicon device 04 p0619 A67-14595
- Electrical parameters of Polish-developed silicon varactors 04 p0581 A67-14920
- Scanning electron microscope used as conductive probe to measure depletion layer widening in silicon diode as function of applied voltage 04 p0584 A67-15483
- Scanning electron microscope used in emissive mode to quantitatively measure depletion layer widening in silicon mesa diode 04 p0584 A67-15484
- Noise spectra of double base diode for case of uniform field in base and comparison with experimental noise measurements 04 p0585 A67-15619
- Equilibrium photocurrents in silicon switching diodes from nondestructively measured electrical parameters 04 p0588 A67-15698
- Transient radiation response and permanent radiation damage in monolithic silicon-junction-transistorized integrated circuit 04 p0589 A67-15720
- Diffusion and melting techniques used to determine effect of Ni, W, Ti and Ta impurities on lifetime of minority carriers in n-base of silicon p-n junctions 05 p0865 A67-16967
- Silicon p-n junction avalanche breakdown voltages obtained from formula for ionization coefficient 05 p0869 A67-17090
- Bias voltage dependence of capacitance in n-type silicon p-n junctions with voltage breakdown 05 p0869 A67-17171
- Ambient medium temperature effects on microplasma phenomena and on breakdown voltage of silicon p-n junction 06 p1050 A67-17895
- Monolithic IC design of diodes and X-band microswitch transmission line fabricated on Si substrate 06 p0968 A67-18053
- Silicon-gallium phosphide heterojunction fabricated by epitaxial deposition, presenting V-I characteristics and energy band diagrams 06 p1051 A67-18223
- Models for second breakdown, considering localized high temperatures in crystals and voltage drop mechanisms 07 p1156 A67-19894
- Delay time of avalanche discharge in silicon p-n junction as function of overvoltage 07 p1238 A67-20256
- Photovoltaic emf of silicon solar cell illuminated by ruby laser 08 p1285 A67-20732
- Mechanical stresses in silicon single crystal containing p-pi junction and ohmic contact measured by photoelastic method, determining birefringence 08 p1423 A67-21332
- Junction curvature effect on avalanche breakdown for abrupt junctions in silicon 09 p1471 A67-21945
- Stress-dependence of Si p-n junctions with dense generation-recombination centers, showing that shifts in bias I-V characteristics are due to bandgap changes 09 p1553 A67-21947
- Avalanche breakdown voltages of diffused silicon p-n junction calculated, using impact ionization rates 09 p1556 A67-22205
- Cut-off frequency, breakdown voltage and capacitance calculations for diffused junctions in thin epitaxial silicon layer for microwave diode design 09 p1556 A67-22206
- Large area 200-v planar voltage-variable capacitance diodes 09 p1475 A67-22207
- Optical signal modulation to measure noise figure at UHF of photoparametric amplifier, using silicon mesa diode as both photodetector and varactor diode 09 p1476 A67-22208
- Silicon solar cell with drift fields of various widths and magnitudes, considering performance changes before and after radiation 10 p1596 A67-23161
- Ion implantation technique for production of n-on-p silicon solar cells applied to dendritic material 10 p1596 A67-23162
- Mobile charge carrier velocity measurements in silicon at high field strengths 10 p1690 A67-23168

Electron mobility and lifetime variations effects on drift field in silicon junction devices 10 p1612 A67-23374

Transient component in breakdown voltage of silicon p-n junction rectifiers in region of intermittent microplasma conduction 10 p1612 A67-23375

Volt-ampere characteristics of diffused silicon n-n junctions with negative resistance analyzed, noting preparation technique 11 p1768 A67-24859

Temperature dependence of volt-ampere characteristics of silicon space charge limited diode compared with ordinary diodes 12 p1914 A67-25459

Volt-ampere characteristics effect on thickness of contact materials of some heterojunctions and band structures obtained by epitaxial deposition 12 p1983 A67-25515

Hall EMF measurement in base of negative resistance silicon diode 12 p1917 A67-26097

IR surface photoconductivity of silicon as function of surface potential and current carrier parameters 13 p2174 A67-26397

Si avalanche diode with p-n-n mesa structure, noting high efficiency and high power output at UHF 13 p2076 A67-26519

Stroboscopic electron mirror microscope observations of Si p-n junctions in pulsed regime 13 p2120 A67-27070

Micrometeoroid damage of n-p silicon and CdS solar cells 13 p2056 A67-27440

Silicon avalanche diode behavior for short duration surge current in reverse direction 13 p2084 A67-27576

Stress effect on minority carrier mobility and concentration in germanium and silicon p-n junctions under uniaxial compression 14 p2364 A67-27825

Origin of excessive reverse current in silicon p-n junction, discussing surface layer channel formation 14 p2283 A67-28040

Criteria for optimized avalanche photodiode design and for best semiconductor material choice based on carrier multiplication process 15 p2453 A67-30015

Possible degradation effects produced in uncovered and covered N/P silicon solar cells by simulated micrometeoroid exposure 15 p2423 A67-30219

Reactive characteristics of diffused p-n junctions in p-and n-silicon at high injection levels and in strong electric fields 16 p2726 A67-30817

Radiation resistance of silicon photoconverters onboard Elektron III satellite, noting protective coating 16 p2677 A67-31609

Surface leakage current and reverse current flow in silicon p-n junction diode affected by positive ion bombardment and oxygen adsorption 17 p2911 A67-32202

Radiation damage to satellite solar cells when shielded to various degrees, stressing silicon junction cells 17 p2804 A67-32840

Current-voltage characteristics of clamped metal/p-silicon diodes 18 p3009 A67-33475

Au, Zn or Ni doped silicon diodes studied for current distribution over base cross section with negative resistance 18 p3010 A67-33577

Structural dislocations effect on formation of microplasmas during avalanche breakdown of silicon p-n junction 18 p3099 A67-33698

Volt-ampere characteristics effect on thickness of contact materials of some heterojunctions and band structures obtained by epitaxial deposition 18 p3103 A67-34446

Thin film resistor used to improve performance of picosecond silicon integrated digital circuit with p-n junction isolation 18 p3014 A67-34551

Time dependence of avalanche in silicon junctions including effects of different ionization rates and velocities of charge carriers 18 p3105 A67-34828

Pulsed operation of large-area silicon p-n junction avalanche diode oscillators for microwave frequencies 19 p3196 A67-35627

High energy proton and electron damage on silicon junctions measured and compared with Van Allen belt radiation damage 20 p3507 A67-36237

Silicon semiconductor strain-gauge techniques applied to transducer design noting small light units, high sensitivity, silicon integrated circuits, reliability,

etc 20 p3442 A67-36458

Controlled differential negative resistance silicon junction diodes with cadmium alloyed base 20 p3397 A67-36696

UV radiation detection using silicon carbide p-n junctions, showing wavelength increment at peak response and decreasing photovoltage with increasing temperature 21 p3591 A67-38156

Performance prediction calculations for double junction n-p-n silicon solar cells, discussing simplified model limits and space radiation environment 21 p3571 A67-38232

Back collection of charge due to ionizing alpha or beta particles by silicon p-n junction detector with space charge width less than range 22 p3797 A67-39345

Microminiaturization problems associated with design and preparation of solid state Si microdiode matrices 22 p3769 A67-39580

Microminiaturized matrix preparation using welded and diffused Si diodes assembled in two groups of perpendicular metal strips 22 p3769 A67-39581

Current oscillations in Co-doped Si p-I-n diode devices noting SCL I-V characteristics 23 p3978 A67-40788

Noise in polarized Si semiconductor avalanche junctions at RF and microwave frequencies noting determination of impact ionization parameters 23 p3980 A67-41189

Structural defects in Ge and Si alloyed semiconductor junction devices caused by improper technological processing, noting microscopic photographs 23 p4043 A67-41365

P-I-n structures obtained from p-type Si by Li drift studied for carriers collection efficiency and potential path distributions 23 p4044 A67-41456

High energy proton irradiation and annealing of n and p type Si, comparing proton and electron damage 23 p4047 A67-41519

Gold doped silicon diodes consisting of compressor and expander elements designed to eliminate impedance range control and linearity problems 24 p4130 A67-42335

Logarithmic nature of I-V characteristics of silicon junction diodes for design of analog multiplier with differential operational amplifier 24 p4131 A67-42478

Silicon avalanche oscillators under continuous operation at millimeter wavelengths, discussing efficiency and power densities 24 p4133 A67-42815

Read type and avalanche type oscillations in silicon varactor diodes, noting parasitic series resistance and electric field peak effects 24 p4133 A67-42820

SILICON NITRIDE

Silicon nitride deposition on metal coated substrates for studying resistivity, breakdown strength and other electrical properties of thin dielectric films 15 p2540 A67-29932

GaAs epitaxial layer in transistors with silicon nitride insulator surpasses silicon MOS device in power gain, frequency response and temperature range 15 p2455 A67-30391

Charge instability problems in metal-nitride-semiconductors /MNS/ solved by using thin silicon dioxide layer between silicon nitride film and substrate 21 p3678 A67-38151

Metal-silicon nitride-silicon /MNS/ capacitor charge storage variation with temperature and time 22 p3767 A67-39257

SILICON OXIDE

Optical transmittance of fused silica at elevated temperatures, showing shift in UV to IR absorption with increasing temperature 01 p0138 A67-11074

Properties of Si-Si interface subjected to thermal oxidation in dry and wet oxidizing gases, thermal decomposition of ethyltriethoxysilane and vacuum evaporation of SiO and quartz 02 p0293 A67-11751

Electronic interactions in silicon-silicon dioxide system lead to various distributions of electric charges 02 p0293 A67-11752

Thermally grown silicon dioxide and resulting silicon-silicon dioxide interface, noting potential difference effect on n-type inversion layer 02 p0293 A67-11753

MOS capacitance measurements combined with neutron activation analysis, showing positive charge increase at oxidized silicon surfaces by sodium presence 02 p0300 A67-12518

Transmittance increase of silicon film

when illuminated by silicon dioxide layer in long wave IR spectrum 03 p0488 A67-12891

Local diffusion of Ga into Sb-doped Ge samples from Ga-doped silicon dioxide films prepared in specially designed vacuum ampoule 03 p0491 A67-13175

Loss angle tangent of film capacitors with rectangular Al films and dielectric silicon monoxide interlayer 03 p0378 A67-13243

Fiber formation and performance properties of carbon-silica fibers and use in plastic composites 03 p0454 A67-13425

Cr-SiO cermet material used in precision thin film resistors for monolithic integrated circuits 03 p0381 A67-13663

Properties of silicon dioxide-silicon system, examining oxidation process and electrical properties of metal oxide silicon /MOS/ structure 03 p0500 A67-14181

Electron beam evaporation of silicon dioxide producing storage layers for automatic picture transmission vidicon, analyzing causes of signal loss after short operating time in flight tubes 04 p0623 A67-15315

Conductivity changes in thin layer of silicon oxide induced by electron beam of scanning electron microscope 04 p0682 A67-15318

HF acid vapor technique for room temperature etching of photolithographic stage of planar silicon dioxide device 04 p0682 A67-15488

Variation of elastic constants of molten silica at high temperatures measured, using pulse method 04 p0683 A67-15499

Energy distribution of surface states at steam-grown silicon-silicon dioxide interfaces determined by LF differential capacitance measurements of MOS structures 04 p0683 A67-15622

Photoemission of electrons from conduction and valence bands of n-type degenerate Si into thermally grown silicon dioxide layers 05 p0870 A67-17195

Transmittance increase of silicon film when illuminated by silicon dioxide layer in long wave IR spectrum 06 p1054 A67-18769

Illumination effect on capacitance of metal-SiO-Si system with various biases 07 p1152 A67-19591

Gallium arsenide laser output increase due to aluminum evaporated coating on silicon dioxide used as reflective coating 07 p1196 A67-19794

Positive charge drift induced by hydrogen heating in silicon dioxide film on MOS transistor 09 p1552 A67-21763

Silicon oxide film thickness determined from intensity of reflected light 09 p1553 A67-21954

Evaporated thin film capacitor from silicon oxide, noting electron diffraction patterns and IR adsorption peaks 09 p1555 A67-22102

Thin film capacitor dielectrics of silicon oxides and various metal oxides, noting influence on vacuum deposited compounds 12 p1918 A67-26210

Photoengraving and use as precision processing technique 12 p1951 A67-26213

Charge motion on outer silicon oxide surface of MOS structure, estimating surface resistance and dependency on humidity and other factors 13 p2176 A67-26707

Molecule dissociation in meteoric trains, discussing coordinate system to determine cross sections for dissociation of magnesium and silicon oxides 14 p2383 A67-27945

Advances in microelectronics, emphasizing role of MOS transistors 14 p2285 A67-28458

Chemical deposition of dielectrics for thin film circuits and components 14 p2369 A67-28612

Slowly decaying broad maximum of parallel conductance explained by tunneling for surface states near Si-silicon oxide interface 18 p3101 A67-34018

Illumination effect on capacitance of metal-SiO-Si system with various biases 20 p3401 A67-37330

Oxidized silicon surface properties affected by diffused oxygen and gold, finding parasitic n-type layer formations and positive surface charge production 21 p3678 A67-38149

Structures of glow discharge and evaporated silicon oxide films determined by measuring intensity of electron wave scattering at large angles, describing measurement method 21 p3687 A67-39139

Limitations imposed on performance of

large area p-n junctions by quality of silicon material, discussing defect-free processing techniques 22 p3766 A67-39247

Avalanche breakdown voltage in Si planar p-n junctions studied for relation to impurity gradient 22 p3766 A67-39256

Mass spectrometric analysis of electrolyte degradation during electrolysis in sulfuric acid silica gel cell for oxygen recovery 23 p3970 A67-41705

CdS single crystal film trap energy spectrum studied with thermo-stimulated currents /TSC/ noting effect of SiO layer 24 p4203 A67-42246

Adsorption equilibrium data obtained at high pressure for methane and propane on silica gel using radioactive tracer pulsing 24 p4118 A67-42584

SILICON RADIATION DETECTOR

Silicon solar cell to measure solar radiation intensity, discussing effect of optical path length ratio and atmospheric constituents 03 p0419 A67-13079

Silicon surface barrier detector beta gauge for density measurements in liquid hydrogen 05 p0842 A67-16541

Transient characteristics of doped silicon diodes with negative resistance, determining electron lifetime vs current, noting space charge role 13 p2076 A67-26489

Cobalt 60 gamma radiation effect on set of B-doped p-type silicon samples, giving radiation-induced defects. 16 p2724 A67-30472

Neutron and Co gamma rays radiation effect on lithium drifted p-n silicon detectors 17 p2917 A67-32846

Superconducting magnet spectrometer using lithium drifted silicon detectors for measurement of electron spectra 20 p3444 A67-36523

Radiation resistant silicon diode fast neutron monitors, discussing fission spectra and leakage currents in damaged diodes 24 p4183 A67-42473

SILICON TETRACHLORIDE

Glow-discharge silicizing of refractory metals by unilow gas method in silicon tetrachloride vapor and hydrogen atmosphere 19 p3242 A67-34917

Fast production of semiconductor and refractory metals by reducing silicon tetrachloride and molybdenum trioxide with hydrogen in electric discharge 21 p3681 A67-38358

SILICON TRANSISTOR

Silicon power transistor use in power supply, line operated audio output, video amplifier and TV horizontal deflection high voltage circuits 01 p0038 A67-10761

Second breakdown and hot spot formation in simplified HF silicon power transistor with interdigitated comb emitter structure 02 p0222 A67-12649

Second breakdown protection of Si power transistors by applying emitter resistances 02 p0222 A67-12654

Aluminum-titanium dioxide-silicon varactor equivalent circuit, noting measurement of parameters 03 p0377 A67-13240

Signal distortion arising from nonlinear /parabolic/ transconductance voltage characteristics of MOS /metal oxide silicon/ transistor determined experimentally by distortion measurement techniques 03 p0388 A67-14183

Failure mechanisms in silicon transistors deduced from step stress tests 04 p0584 A67-15482

Transient annealing following pulsed neutron exposure in silicon transistors and solar cells as function of temperature and injection level 04 p0684 A67-15693

Electron induced ionization and displacement damage in n-p-n and p-n-p transistors at medium and low powers 04 p0588 A67-15706

Ionizing radiation effects on silicon planar bipolar transistors determine degradation mechanisms 04 p0588 A67-15707

Insulated gate field effect transistors with silicon dioxide and silicon nitride insulation under electron irradiation, noting gate turn-on voltage reduction and source-drain leakage elimination 04 p0588 A67-15713

Instability effect in n-channel silicon MOS transistors bombarded with ionizing radiation 04 p0589 A67-15716

Light sensitivity of diffused Si phototransistor and of system of two cascade coupled phototransistors 05 p0770 A67-16169

Beam lead sealed junction technology for planar processes, noting preparation and application 05 p0770 A67-16238

Switching process for silicon p-n-p structures, deriving relations for delay and response times and transient period as function of parameters 05 p0865 A67-16911

Phase locked oscillations of silicon avalanche diodes noting hysterisis 05 p0775 A67-16984

Impurity concentration profiles in silicon epitaxial wafer determined, using MOS capacitors 05 p0866 A67-16985

V-I characteristics and turnover phenomenon in Si devices in relation to second breakdown in transistors 07 p1156 A67-19898

Current constriction in p-n junction under thermal breakdown, deriving expressions for terminal voltage and radius of constriction 07 p1157 A67-19901

Self-healing electric breakdown in MOS structures noting magnitude duration, temperature and propagation characteristics 07 p1157 A67-19904

Logical design and fabrication of Si integrated circuit 08 p1301 A67-20792

Effects of dry and wet preoxidation on characteristics of MOS transistor using silicon 09 p1552 A67-21768

Electronic processes on semiconductor device surfaces analyzed using scanning light beam, for application to Si planar transistors 09 p1472 A67-21949

Flicker noise characterization in silicon planar transistor 09 p1474 A67-22041

Screening to improve reliability of silicon integrated circuit, noting failure mode and mechanism 09 p1480 A67-22300

Comparison of electron tubes, transistors and FET noise figures as function of source impedance of generator 10 p1610 A67-22924

Processing techniques for integrated microwave circuits using silicon-on-sapphire /SOS/ transistors for high frequency power outputs 10 p1610 A67-22972

Surface conditions effects on silicon planar transistor current gain 11 p1759 A67-24139

Volt-ampere characteristics of diffused silicon n-n junctions with negative resistance analyzed, noting preparation technique 11 p1768 A67-24859

Substrate doping, source bias and bulk contact effect upon DC characteristics of silicon MOS transistors 12 p1916 A67-26068

Planar silicon transistors with improved performance and reliability due to metallic protection, noting low noise and surface potential stabilization 13 p2077 A67-26652

Lateral bipolar n-p-n transistors fabricated using heteroepitaxial films of silicon on sapphire 13 p2078 A67-26779

Silicon space charge limited triode considered as analog transistor noting I-V characteristics, current proportionality, voltage amplification and noise performance 13 p2083 A67-27571

Multichannel field effect transistor theory and experiment 15 p2446 A67-29635

Current gain and collector-base saturation current and breakdown voltage in aged silicon transistors 15 p2453 A67-30064

Switching process for silicon p-n-p structures, deriving relations for delay and response times and transient period as function of parameters 16 p2727 A67-30888

Silicon negative-resistance junction diodes, studying n-p-n structure and diode characteristics dependence on light, temperature, voltage and frequency 16 p2636 A67-30898

Temperature, resistivity and injection level dependence of recombination processes in neutron irradiated silicon explained by two-level recombination model 17 p2916 A67-32837

Plane structure silicon transistors subjected to Co gamma radiation, considering electrical properties degradation to predict component survival probability 17 p2917 A67-32842

Radiation effects on silicon transistor parameter behavior characteristics 17 p2917 A67-32843

Silicon transistors obtained by diffusion studied for equivalence between radiations producing permanent degradation of transistor characteristics 17 p2917 A67-32844

Degradation in silicon transistors due to particle bombardment analyzed, showing

surface/ bulk recombination increase 17 p2917 A67-32845

Permanent displacement-induced effects in silicon semiconductor devices as function of radiation type and energy 17 p2917 A67-32847

Electron paramagnetic resonance /EPR/ studies of interaction of irradiation-produced defects with impurities and other defects in silicon semiconductors 17 p2918 A67-32854

Structure of wafer type point-contact diodes 18 p3011 A67-34021

RC oscillators based on silicon n-p-n transistors for radio frequencies, analyzing active all-pass phase-shift circuit 19 p3191 A67-34946

MOS and silicon transistors for design of logarithmic amplifiers for space instrumentation 19 p3194 A67-35463

Silicon transistors transient defect annealing from pulsed particle irradiation, stressing time factors 19 p3305 A67-35667

HF transistor design principles, considering current technology 20 p3396 A67-36493

Static electricity as potential reliability problem in electronic equipment production, noting transistor failure 20 p3397 A67-36608

Cobalt 60 gamma radiation effect on MOS diodes fabricated on silicon substrates, noting surface state and oxide charge densities 20 p3510 A67-36961

MOS transistors surface properties and leakage current affected by gold, showing positive charge production 21 p3678 A67-38150

Radiation effect on MOS transistors in D-2 satellite telemetry coder 21 p3593 A67-38230

Base region thickness, minority carrier lifetime and impurity concentration effects on conduction characteristics of silicon diodes and thyristors 21 p3597 A67-38523

Concentric ring junction to prevent surface breakdown in planar p-n junctions 22 p3766 A67-39252

Recombination centers in silicon transistor emitter-base junctions causing anomalous base current component studied via temperature dependence of forward characteristics 22 p3770 A67-39732

SILICONE

Lubrication and bearing problems in space environment, noting molybdenum disulfide and silicones 05 p0811 A67-16932

Film thicknesses in elastohydrodynamic lubrication by silicone fluids obtained from oscillatory shear related to continuous shear 09 p1506 A67-22193

Vacuum chamber contaminants, discussing silicone pumping fluid from diffusion pumped systems 24 p4138 A67-42035

SILICONE RESIN

Silicones performance in high vacuum, temperature extremes and radiation environments of outer space, noting outgassing effect 15 p2508 A67-29557

Highly purified silicone junction coating resins and silicone molding compound for microelectronic packaging 18 p3069 A67-34564

SILICONE RUBBER

Adhesives development, discussing chemically and mechanically blocked reactant system and water based, hot melt, oil absorbent, heat resistant and low temperature adhesives 09 p1523 A67-22529

SILOXANE

Solid organic filters using polymethyl siloxane resin as host material for 2000-3000 angstrom range 03 p0470 A67-14393

SILVER

Bremsstrahlung, transient and plasma radiation as affected by surface properties of silver bombarded by electrons 02 p0291 A67-11737

Effects of order-disorder state and film thickness on structure and electric conductivity of evaporated nickel, titanium and silver films 02 p0292 A67-11745

Structural and magnetic properties of /111/ films of permalloy produced epitaxially on epitaxial /111/ Ag on mica 04 p0676 A67-14931

Threshold energy for electron radiation damage in Ag compared for liquid He and liquid Ni temperatures 04 p0638 A67-15115

K-shell ionization cross sections of silver, tin and gold from electron bombardment 04 p0661 A67-15762

Metallographic, X-ray and electron microscopie studies of dislocation substructure and fatigue life extension in bending-fatigued Al and Ag

crystals 06 p1013 A67-17798
 High power laser beam polarization direction effects on electron emission from Ag surface 06 p1012 A67-18759
 Anisotropic resistivity of dislocations produced by deformation measured in high purity Au, Ag and Cu single crystals 07 p1209 A67-19638
 Plasma resonance emission of thin Ag foils irradiated by light, noting intensity and direction of polarization 08 p1368 A67-20787
 Single crystal film structure of fcc metals evaporated in ultrahigh vacuum onto alkali halide surfaces cleaved in air and in situ 09 p1552 A67-21671
 Equality conditions for gold and silver electrode zero charge and transient peak potentials by pH and anion effects, using scraped electrodes 10 p1602 A67-23158
 Bi and Ag nucleation on evaporated substrates studied as function of substrate temperature and impinging flux using electron microscopy 23 p4044 A67-41455
SILVER ALLOY
 High temperature steady state creep rate analysis of pure Ag and internally ionized Ag-Mg alloys 06 p1014 A67-17805
 Catalytic performance of silver alloys as oxygen electrodes of low temperature fuel cells 09 p1458 A67-22181
 Silver-gold and silver-germanium alloys tested for Fermi surface changes with alloying, using thermoelectric power measurements 16 p2731 A67-31448
SILVER-CADMIUM BATTERY
 Sealed silver-cadmium batteries meeting space requirements, discussing high energy plates, cell design and packaging 22 p3749 A67-40230
SILVER CHLORIDE
 Possible stabilization of AgCl crystals against solar radiation effects by addition of Cu, Ni, Zn, Cs, S or Hg 04 p0685 A67-15752
 Vibrational energy levels leading to laser oscillation in UV, noting process using Lyman discharge 21 p3638 A67-37855
SILVER COMPOUND
 Optical constants of silver solid solutions with gold addition, noting dependence of refractive index, absorption coefficient and conduction electrons on impurity concentration 02 p0255 A67-11870
 Thermochromic materials application in display devices 05 p0860 A67-16307
 Chemical stability of silver graphite, molybdenum disulfide, zinc oxide, boron nitride, muscovite and phlogopite mica solid lubricants 10 p1659 A67-22829
SILVER IODIDE
 Continuous automatic and portable instrument for ice nuclei detection and counting 10 p1654 A67-22818
SILVER OXIDE-ZINC BATTERY
S ZINC-SILVER OXIDE BATTERY
SILVER-ZINC BATTERY
 Reliability of silver zinc battery using mathematical model 09 p1446 A67-22297
 Mathematical model for predicting temperature and life of silver-zinc battery system in spacecraft [AIAA PAPER 67-334] 12 p1901 A67-26048
 Zinc penetration through regenerated cellulose membrane separators shown to be growth mechanism in silver-zinc cell 22 p3758 A67-40227
SIMILARITY HYPOTHESIS
 Pattern recognition preprocessing by similarity functionals, examining relationship between measurement, selection and feature definition 02 p0207 A67-12137
 Determining dependences of criteria for metal cutting processes from studies of thermal effects 03 p0428 A67-13195
 Turbulent skin friction measurement with Preston tube, using similarity hypothesis for mean velocity profiles in turbulent flows 04 p0600 A67-14442
 Convective mechanism in clear air, examining isolated plume by new model which differs from similarity model 04 p0648 A67-14647
 Thermal similarity study of models in space environmental chambers for deducing characteristics of typical space vehicle element [AIAA PAPER 66-460] 04 p0724 A67-15247
 Kruskal space in general relativity and uniform accelerated rigid rod in special relativity show striking formal similarities 05 p0847 A67-16970
 Similarity theory applied to electron

processes in p-n junctions 06 p1048 A67-17854
 Two-cell solution to vorticity equations in unstably stratified atmosphere 06 p1026 A67-18565
 Similarity relationships for study of transient and steady state thermal displacements, strains and stresses between model and prototype 07 p1262 A67-19413
 Disturbance diffusion in incompressible zero pressure gradient flow 10 p1626 A67-23144
 Similarity laws for jet noise and shear flow instability as suggested by experiments 10 p1628 A67-23830
 Skewed turbulent boundary layers, noting absence of pressure gradient and shearing stress measurements in experiments and applicability of similarity defect equation 11 p1776 A67-24048
 Approximate similarity criterion for arc with self-adjusting length, burning in plasmatron with gas vortex stabilization, determined by shunting 11 p1843 A67-24969
 Similarity solutions derived for describing propagation of strong compression shock in transversely expanding gas 13 p2094 A67-26643
 Atmospheric boundary layer dynamics models, similarity hypothesis and theories 13 p2151 A67-26687
 Similarity solutions for two-dimensional unsteady compressible boundary layer equations using group theoretic methods 14 p2297 A67-28135
 Soviet atmospheric turbulence studies considering microstructure, wave propagation in turbulent atmosphere, turbulent exchange in atmospheric ground layers, etc 14 p2346 A67-28763
 Similarity solution to laminar boundary layer heat transfer from monatomic gas to cooled wall with no applied electric or magnetic fields 15 p2523 A67-29219
 [JPL-TR-32-1143]
 Similarity criteria for plastic behavior of polymers under combined effect of nonuniform temperature field and hydrostatic pressure 15 p2573 A67-29466
 Similarity parameters for gas generators obtained from equations governing gas-stream ejection 15 p2423 A67-30080
 High altitude jet structure for two-dimensional and axisymmetric cases with very large exit/ambient pressure ratio 15 p2418 A67-30208
 Flat plate, simultaneous heat and mass transfer for Newtonian fluids in free convection analyzed, using group theory 15 p2582 A67-30217
 Prandtl shear stress theory applied to similarity models of free turbulence 16 p2657 A67-30857
 Model for radial and axial structure of geophysical vortices involving Boussinesq boundary-layer equations similarity solution in point heat source 16 p2778 A67-30949
 Velocity profile of vortex region formed downstream of step-shaped wall calculated, assuming flow is turbulent, using similarity hypothesis 16 p2662 A67-31469
 Karman similarity hypothesis extended to cylindrical geometry to establish conditions for universal velocity similarity in fully turbulent rotating flows [ASME PAPER 67-APM-23] 17 p2838 A67-32416
 Book on similarity theory applications to heat and mass transfer in moving medium 17 p2970 A67-32464
 Cone and disk laminar flows of power-law fluids similarity solution by Navier-Stokes equation 17 p2793 A67-33040
 Least squares method for heat problems and approximate similarity law covering orthogonal expansions and compatibility between contradictory requirements 18 p3071 A67-33752
 Temperature convection and vertical velocity fluctuations measured and compared with similarity theory of free convection and laboratory heated plates 19 p3252 A67-35059
 Ionized gas flow past cylinder and sphere, determining ionization and dissociation effect on displaced shock wave form 19 p3170 A67-35449
 Langevin similarity theorem applied to ballistic perturbation theory, deriving formulation containing temperature gradient, descent acceleration and kinetic height parameters 19 p3326 A67-35578

Ram effect similarity criteria determination from partial differential equation system noting composite similarity, simulation possibilities, continuity equation, etc 20 p3419 A67-36190
 Hypersonic weak-interaction similarity solutions for viscous heat-conducting compressible flow past flat plate, using Navier-Stokes equations 20 p3357 A67-36849
 Motion equations of incompressible nonisothermal fluid jet studied by closed similarity solutions, obtaining temperature distributions 20 p3423 A67-37209
 Dimensional analysis method for determining similarity criteria for MHD processes in liquid metals and alloys 21 p3665 A67-38248
 Atmospheric boundary layer dynamics models, similarity hypothesis and theories 21 p3654 A67-38429
 Similarity solutions for compressible laminar boundary layer, showing pressure and heat and mass transfer effects on wall temperature and shear stress 22 p3918 A67-39716
 Similarity parameters of gravity and pressure driven liquid discharge from propellant tanks obtained by dimensional analysis 22 p3785 A67-39969
 Dynamic impossibility of free stream velocity distributions admitting similarity solutions, calculating laminar boundary layers 23 p3992 A67-41741
 Similarity analysis of partial differential equations, discussing free parameter analysis, variables separation method, group theory approach and dimensional analysis 24 p4180 A67-43082
SIMILARITY NUMBER
 Similarity constant variation method of aircraft design 04 p0552 A67-15892
SIMILITUDE LAW
 Turbulent reattachment of supersonic jet noting recompression region of flow, critical points and similarity law in evolution of wall pressures [ONERA-TP-326] 01 p0053 A67-11002
 Measurement techniques used in wind tunnel and free atmosphere parachute tests 06 p0979 A67-18017
 Similarity law for wall region of turbulent boundary layers in compressible flow, discussing Coles theory 08 p1320 A67-20565
 Stratification similitude laws for liquid hydrogen determined and extrapolated to full size tanks from small tank data 13 p2186 A67-27643
SIMULATED ALTITUDE
 Estimation of changes in serum protein concentration under normal stress compared to human sera exposed to simulated altitude and aerospace flights 01 p0015 A67-10950
SIMULATED EMISSION
 IR emission measurement of lunar-like materials during simulated eclipse, noting dependence on time [AIAA PAPER 67-290] 12 p2009 A67-26007
 Simulated micrometeoroid bombardment effect on n/p Si and CdS solar cells performance 23 p3941 A67-41521
SIMULATION
 SA ACOUSTIC SIMULATION
 SA ALTITUDE SIMULATION
 SA ANALOG SIMULATION
 SA BIOSIMULATION
 SA COMPUTER SIMULATION
 SA DIGITAL SIMULATION
 SA ENVIRONMENT SIMULATION
 SA FLIGHT SIMULATION
 SA LANDING SIMULATION
 SA RHEOELECTRICAL SIMULATION
 SA SOLAR SIMULATION
 SA SPACE CABIN SIMULATION
 SA SPACE SIMULATION
 SA TARGET SIMULATION
 SA THERMAL SIMULATION
 SA WAR GAME
 SA WEIGHTLESSNESS SIMULATION
 Monte Carlo techniques use of random numbers, noting Buffon needle problem, Laplace equation, number generation and radar target detection simulation 01 p0104 A67-10158
 Simulated radioactive decay experiment using random number generator or set of random numbers 01 p0112 A67-10826
 Monte Carlo simulation studies for fatigue data analysis of rolling-contact bearings, using Weibull equation [ASLE PAPER 66AM 1B2] 08 p1336 A67-21038

Simulation of stress-strain state of metal under elastoplastic deformation, based on models used in polarization-optical techniques, analyzing stresses in high polymers 08 p1423 A67-21330

Geomagnetic field influence on cosmic rays simulated by electron beam and terrella situated in vacuum tank 13 p2192 A67-27243

Simulation and training - Conference, New York, April 1967 13 p2063 A67-27259

Data compression for analog signal transmission with smaller bandwidth requirement obtained from reduced signal redundancy and simulation of techniques 14 p2275 A67-28683

Thermally ionized low density alkali-metal plasma for simulating controlled fusion processes, noting high particle losses and instability 14 p2362 A67-29038

Ionization fluctuations due to interaction between shower particles and absorbing component of ionization calorimeter and effect on accuracy of energy measurement 17 p2855 A67-32250

Unsteady heat conduction and transfers by electrical simulation methods, determining temperature field in canonical metal bodies 17 p2973 A67-33082

Development and application of Monte Carlo logistic simulation model for measuring system availability dependence on reliability, maintainability and logistic support 18 p3021 A67-34674

Exhaust manifold design for two-cycle diesel engine with turbosupercharger using physical simulation, discussing simulation criteria for gasdynamic processes 21 p3696 A67-38908

Gas laser simulation technique to facilitate teaching of laser physics 22 p3816 A67-39923

Logistics simulation modeling for optimizing spares mix needed for maintenance of airborne systems at minimum cost 23 p4085 A67-40590

Foundation apparent weight during force controlled vibration test simulated electronically 23 p3987 A67-41383

SIMULATOR

SA COCKPIT SIMULATOR

SA CONTROL SIMULATOR

SA EXHAUST SIMULATOR

SA FLIGHT SIMULATOR

SA HIGH VACUUM ORBITAL SIMULATOR /HIVOS/

SA MISSILE SIMULATOR

SA ORBITAL SIMULATOR

SA SOLAR SIMULATOR

SA SPACE CABIN SIMULATOR

SA SPACE SIMULATOR

SA TEST FACILITY

SA VIBRATION SIMULATOR

MNT-VZ-V device for simulating electromagnetic field in radio waveguides by induced current method 06 p1001 A67-17937

Digital computer use to provide controllable display of star field for use with spacecraft simulator for optical sightings [AIAA PAPER 67-254] 07 p1149 A67-20051

Vertical vee gyro damping system for gravity gradient satellite, considering scaling, inertia, time and torque factors and viscosity change effects 12 p1920 A67-25122

Method of implementing training problems for site simulator in simulated system training 13 p2090 A67-27233

Simulator design, discussing control information category and presenting representative fixed and moving base research simulators to describe display design and motion cue effects 13 p2091 A67-27271

MNT-VZ-V device for simulating electromagnetic field in radio waveguides by induced current method 18 p3046 A67-33774

Vibration effect on task performance evaluated from test series, using vibration simulator 19 p3181 A67-35557

Electron beam probe for determination of local gas parameters in reentry simulation 20 p3445 A67-36588

Wideband troposcatter radio channel simulator exhibiting frequency flat or frequency selective fading over band greater than 10 MHz and centered at 70 MHz 20 p3385 A67-37354

Motion simulator with spherical self-regulating gas bearing for testing attitude control, analyzing turbine and tilting momentum 22 p3778 A67-39165

SIMULATOR TRAINING

SA PILOT TRAINING

Visual or environmental factors which affect usefulness of training simulator experimentally studied, examining problems of measuring transfer of training 02 p0186 A67-12072

Motion reproduction, analyzing control systems, dynamic fidelity, voltage command, etc [AIAA PAPER 67-252] 07 p1166 A67-20070

DC-9 training program using classroom responder system and programmed-type learning aids 13 p2064 A67-27261

Extravehicular activity /EVA/ simulator for zero gravity environment using servodrive and computer control 17 p2832 A67-31994

Mission simulator for manned space flight support used for real time training 20 p3414 A67-36538

Lunar mission simulators for Saturn-Apollo project noting optimal computer approach on flexibility, accuracy, cost, etc 20 p3418 A67-37482

Motion reproduction, analyzing control systems, dynamic fidelity, voltage command, etc 21 p3608 A67-38540

SIMULTANEOUS LINEAR EQUATION

Analog computer solution of simultaneous systems of linear algebraic equations, based on modified Gauss-Zeidel method 01 p0105 A67-10542

Linear equation system with coefficient matrix of multiple diagonal bands solved by direct method, reducing numerical solution error 20 p3478 A67-36675

SINE SERIES

Real function interpolation method for synthesis of electric networks in time domain by sinusoidal exponential series 03 p0458 A67-13505

SINE WAVE

Phase cancellation of sinusoidal signals in presence of Gaussian noise for comparison and threshold decision schemes 01 p0025 A67-10860

Microstructural analysis multiple electron-photon cascade resonance amplifier response to sine-square radio signal 03 p0376 A67-13091

Level and duration of sine wave tests, discussing rocket design proof via random vibration testing 08 p1402 A67-20477

Cross correlation and statistical dependence between envelope and frequency deviation of sine wave plus random noise, noting possible application to frequency demodulation 11 p1753 A67-24646

Output correlation function for N-step symmetric amplitude quantizer with summed sine wave and Gaussian noise input, noting approximations for low SNR 12 p1908 A67-26084

CRT flying-spot-scanner spatial frequency response, determining film-plane modulation response to periodic sine/square wave 17 p2860 A67-32665

Sine wave tracking, studying operator manual control performance 17 p2808 A67-33179

Digital frequency synthesizers analysis and synthesis, considering clocked-pulse and sine-wave systems to obtain guidelines for DFS system designs 21 p3601 A67-38974

Oscillator diode in limited space charge accumulation oscillation mode, obtaining maximum DC to RF conversion efficiency for sine wave excitation for n-GaAs 23 p3979 A67-40875

Axial crossing intervals of sine wave plus noise 24 p4122 A67-42343

SINGLE CRYSTAL

Dislocation structure in tantalum single crystals deformed in tension to various strains at 373 degrees K studied by transmission electron microscopy 01 p0092 A67-10057

Room temperature microstrain behavior of zone-refined single crystal beryllium examined as function of prestrain 01 p0092 A67-10058

Deformation properties of polycrystalline and single crystal specimens of intermetallic compound NiAl studied as function of testing temperature and composition 01 p0092 A67-10059

Gamma radiation and fast neutron effects on dark resistance, photoconductivity, majority carrier mobility, recombination kinetics, etc, in CdS single

crystal 01 p0128 A67-10086

Indium arsenic antimonide single crystals in p-n junction laser 01 p0087 A67-10087

Superconducting transition temperature and critical field curve for pure Ga single crystals 01 p0130 A67-10153

Low energy electron diffraction study of interaction of thin deposit of amorphous boron with tungsten single crystal surfaces 01 p0093 A67-10205

Hall coefficient tensor in single crystals of titanium measured at room temperature as function of crystallographic orientation in magnetic field 01 p0132 A67-10375

Field electron emission measurements for determination of work function of single crystal /110/ planes of tungsten 01 p0135 A67-10878

Si single crystal lattice parameter measurement using double-diffraction effect 01 p0135 A67-10894

Induction heating contributions to solid state technology including zone refining and zone leveling, growth of metallic and nonmetallic single crystals, thin film production and epitaxial growth 01 p0080 A67-10972

Interaction of crystalline film of one substance growing on surface of second substance, examining influence on film structure 02 p0286 A67-11708

Optical transmission and transition in semiconductor single crystals of various unit cells, considering bismuth tellurium sulfide 02 p0289 A67-11725

Current-voltage characteristics peculiarities of fine cadmium sulfide single crystals with nonohmic contacts 02 p0296 A67-11831

Experimental setup for determining acoustic parameters of solids as media for ultrasound propagation 02 p0241 A67-11851

Structural orientation, purity and perfection of molybdenum single crystals grown by zonal electron-beam melting process 02 p0255 A67-11867

Proton irradiation effect on Hall coefficient, resistivity and magnetoresistance of p-type bismuth telluride single crystals 02 p0298 A67-11882

Semiconductor heterojunction properties of epitaxial single crystal layer of GaAs grown on Ge substrate 02 p0299 A67-11895

Optical absorption spectra of hexagonal red HgS single crystals at self-absorption edge at temperatures from 20.4 to 310 degrees K 02 p0300 A67-12476

Recombination processes in aluminum doped zinc telluride single crystals, determining distance of r-centers from C-band 02 p0300 A67-12478

Single crystal transistor with metallic base, noting frequency, V-I and power characteristics, radiation resistance, etc 02 p0221 A67-12530

Short wave length series of edge emission of cadmium sulfide single crystals at temperatures between 18 and 150 degrees K 03 p0488 A67-12813

Electrical properties of GaSe-layer-semiconductor single crystals used to determine scattering mechanisms of charge carriers, depth of impurity centers, effective mass and forbidden gap 03 p0488 A67-12816

Gallium arsenide crystal properties for use in optical filter 03 p0488 A67-12858

Microhardness of n-type InSb single crystals and crack formation near indentation area 03 p0489 A67-13093

Mechanical pressure effect on polarization processes in barium titanate single crystals and barium titanate-zinc oxide solid solutions 03 p0489 A67-13145

Cadmium selenide single crystals subjected to gas discharge saturation of current-voltage characteristic, noting section with negative differential resistance 03 p0489 A67-13146

Steady state photoconductivity and photomagnetic effect in single crystals of n-type GaAs with various carrier concentrations 03 p0490 A67-13151

Electron-hole pair separation energy in CdS single crystal during 5 to 50 keV electron bombardment 03 p0490 A67-13160

Optical or inertial electron mass dependence on N-concentration in IR spectrum of n-type GaAs monocrystal with S, Se and Te impurities 03 p0490 A67-13161

Single crystal fiber reinforced composites, discussing use of silicon carbide whisker as

interstitial reinforcement 03 p0453 A67-13411
 Lattice vibration spectra and energies of two-phonon summation bands and reststrahlen bands in gallium arsenide phosphide single crystals 03 p0495 A67-13514
 Directional solidification and single-crystal casting for jet engine turbine blades 03 p0429 A67-13541
 Barium titanate single crystals at infrared frequencies investigated for polarization, effective permittivity and coercive field 03 p0497 A67-13697
 Reversing permittivity of barium titanate single crystals measured, using lithium chloride solution for electrodes 03 p0497 A67-13698
 Permittivity of barium titanate single crystals with laminar domain structure 03 p0497 A67-13699
 Polarization and domain structure of barium titanate single crystals with double hysteresis loop 03 p0497 A67-13700
 Specific radioactivity of Sb-124 and effect on diffusion of antimony in Sb-doped n-type Ge single crystals and Ga-doped p-type Ge single crystals 03 p0500 A67-14067
 Energy gap anisotropy effects in pure single crystal superconductors investigated by factorable BCS-like model for effective electron-electron matrix element 04 p0673 A67-14518
 X-ray anomalous transmission used in analysis of gallium arsenide crystal perfection with various dislocation densities, determining ratios of anomalous absorption coefficient 04 p0674 A67-14620
 Hall effect and transport properties of single crystals of iodine measured by alternating current technique, using field effect transistors 04 p0675 A67-14757
 Loops and spirals on freshly cleaved surfaces of laboratory grown single crystals of NaCl thermally etched by placing them in muffle furnace on platinum lid 04 p0675 A67-14761
 IR transmission microscopy and X-ray microanalysis of anomalous etching on surface of Si single crystals grown in Ar gas 04 p0675 A67-14769
 Electrical conductivity of p-GaSe single crystals in strong electric fields 04 p0676 A67-14929
 Transmission spectra of GaS, GaSe, InSe and TlSe single crystals obtained at 300 degrees K by means of IR spectrometer 04 p0676 A67-14932
 Interband Faraday effect in Cd-Te single crystals 04 p0676 A67-14933
 Dielectric permittivity of barium titanate monocrystals with anisotropic stratified domain structure 04 p0678 A67-15131
 Open circuit voltage and short circuit current capability of solar energy converter photoelement made of single crystal n-type indium phosphide 04 p0679 A67-15141
 Dislocation-induced relaxation in silicon single crystals by measuring internal friction and Young's modulus at temperatures from 77 to 300 degrees K 04 p0681 A67-15294
 Flow characteristics of Fe single crystals and behavior of imperfections 04 p0640 A67-15793
 Substructure of aluminum monocrystals in relation to silicon content 05 p0827 A67-16075
 Dislocation structure of crystals with diamond type lattice analysis made possible by growing silicon monocrystals along growth axis 05 p0860 A67-16076
 Electron beam zonal fusion growth of Mo, W and Ta single crystals without using crucible 05 p0827 A67-16079
 Electron beam zonal vacuum fusion growth of Mo-Nb alloy single crystals 05 p0827 A67-16080
 Growth condition effect on perfection of single crystals of niobium examined, using X-ray diffraction techniques 05 p0828 A67-16470
 Polygonization in silicon single crystal by chemical etching, determining activation energy, noting dependence on annealing temperature 05 p0862 A67-16503
 Heat treatment conversion of large grain n-type indium antimonide single crystals and twin crystals into p-type samples 05 p0862 A67-16507
 Crystal structure defects and electroconductivity variations in CdS single crystals in oxygen ambient and effects of various surface treatments 05 p0862 A67-16605

Thermoelectric powers and conductivities of vanadium dioxide whiskers measured from 273 to 335 degrees 05 p0864 A67-16698
 Temperature dependence of electrical and galvanomagnetic properties of single crystal InSb dendrites 05 p0869 A67-17092
 Fundamental absorption band structure of mixed KCl and KBr single crystals 05 p0872 A67-17493
 Energy spectrum of levels appearing in silicon single crystals irradiated by integral fluxes of fast electrons, neutrons and gamma quanta 05 p0872 A67-17547
 Optical method observations of phase transition of ferroelectric monocrystal SbSi 06 p1047 A67-17758
 Metal single crystal use in structural design of stress resisting devices 06 p1013 A67-17795
 Cadmium selenide arsenide single crystals obtained free of cracks, using synthesis method 06 p1048 A67-17840
 X-ray Debye temperature thermal variation measurements of pure nickel and chromium 06 p1015 A67-17850
 Two-photon absorption spectrum of single crystal CdS, using polarized light and precise geometry 06 p1011 A67-18209
 Alkali ion scattering coefficient from tungsten single crystals surface and dependence on incidence angle 06 p1036 A67-18424
 Hall effect and magnetoresistance effect measured on p- and n-CdSb single crystals above 77 degrees K and magnetic fields up to 7500 gauss 06 p1054 A67-18824
 Far IR lattice bands in n-type indium antimonide single crystal 06 p1059 A67-18908
 Anisotropic resistivity of dislocations produced by deformation measured in high purity Au, Ag and Cu single crystals 07 p1209 A67-19638
 Crystal symmetry, optical properties and ferroelectric polarization of barium titanate single crystals 07 p1234 A67-20096
 Third order elastic constant for NaCl and KCl single crystals by ultrasonic pulse techniques 07 p1238 A67-20218
 Reverse magnetization and energy of anisotropy of single crystal ferromagnetic films 08 p1368 A67-20607
 Electroconductivity variations in CdS and CdSe single crystals with SHF electric field strength, intensity of bias lighting and temperature in minus 70 to plus 70 degrees C interval 08 p1370 A67-20996
 Mechanical stresses in silicon single crystal containing p-pi junction and ohmic contact measured by photoelastic method, determining birefringence 08 p1423 A67-21332
 Anisotropy of electronic metal work functions for zero and high electric fields perpendicular to surface measured by field emission and thermionic techniques 09 p1450 A67-22356
 Induced absorption in far IR by impurities and defects of single crystal of potassium bromide 09 p1557 A67-22571
 Single crystal thin semiconducting films prepared by short distance evaporation diffusion under isothermal conditions 09 p1557 A67-22573
 Pulsed oscillations of microwave Gunn effect oscillator in n-type single crystal GaAs 10 p1609 A67-22838
 Cadmium selenide single crystals subjected to gas discharge saturation of current-voltage characteristic, noting section with negative differential resistance 10 p1689 A67-23095
 Steady state photoconductivity and photomagnetic effect in single crystals of n-type GaAs with various carrier concentrations 10 p1690 A67-23100
 Electron-hole pair separation energy in CdS single crystal during 5 to 50 kev electron bombardment 10 p1690 A67-23107
 Optical or inertial electron mass dependence on N-concentration in IR spectrum of n-type GaAs monocrystal with S, Se and Te impurities 10 p1690 A67-23108
 Fast neutron irradiated p-type silicon single crystals electric and photoelectric properties 10 p1691 A67-23404
 Eutectics use in composite material by growing single crystal whiskers aligned inside matrix 10 p1669 A67-23637
 Thermoelectronic properties of pure and barium-film coated face of tungsten single crystal thermoelectronic properties of pure

and barium-film coated face of tungsten single crystal 10 p1694 A67-23646
 Noise in space charge limited current in CdS single crystal at low injection level 10 p1696 A67-23772
 Field emission from sharply pointed CdS single crystals photon-enhanced by illumination from pulsed argon-ion laser 11 p1845 A67-24133
 Anodic behavior of GaAs single crystals at increased current densities in alkaline and acidic solutions, discussing etch tunnels 11 p1848 A67-24743
 Surface hole photoconductivity for pressed metal anode CdS ohmic cathode system, noting spectral distribution dependency on crystal heat treatment and air humidity 11 p1849 A67-24871
 Temperature dependence of elastic constants of molybdenum single crystals measured, using thin rod resonance techniques 11 p1809 A67-24908
 Stress and temperature dependence of motion of edge dislocations in nickel single crystals 11 p1809 A67-24920
 Synthetic pink-ruby crystal demagnetization characteristics when employed as coolant in cryostat, noting temperature dependence 11 p1851 A67-25033
 Mechanical properties of zone melt molybdenum single crystals as affected by orientation and gas impurities 11 p1810 A67-25092
 Beryllium single crystal dislocation and twinning induced by compression deformation 11 p1810 A67-25093
 Silicon crystals composition effect on solar cells reaction to irradiation by 4 mev electrons 12 p1896 A67-25150
 Dielectric permittivity of barium titanate monocrystals with anisotropic stratified domain structure 12 p1978 A67-25155
 Open circuit voltage and short circuit current capability of solar energy converter photoelement made of single crystal n-type indium phosphide 12 p1979 A67-25164
 Spontaneous polarization and electric conductivity in fluorite single crystals doped with lime 12 p1980 A67-25182
 Electric conductivity of calcium fluorite single crystals doped with uranium dioxide 12 p1980 A67-25183
 Rubidium nickel trifluoride transparent single crystal magnetic and optical properties analyzed, concluding compound is antiferromagnetic 12 p1984 A67-25747
 Strengthening of sapphire single crystals by precipitates containing titanium 12 p1987 A67-26190
 Crystal growing technology for application to semiconductor production noting methods, impurity control, etc 12 p1950 A67-26211
 Stimulation of photosensitivity of cadmium sulfide single crystals by chemical etching 13 p2174 A67-26401
 Radiation-induced electroconductivity and secondary emission in alkali halide single crystals under positive ion bombardment 13 p2177 A67-27073
 Plastic behavior of zone refined and prestrained beryllium single crystals 13 p2137 A67-27111
 Carbon action effect on tensile deformation in single and polycrystalline beryllium in terms of solutionized and precipitated states 13 p2137 A67-27112
 Electron microscope study of cold working and tempering of beryllium single crystals 13 p2138 A67-27117
 Single crystal transistor with metallic base, noting frequency, V-I and power characteristics, radiation resistance, etc 14 p2279 A67-28007
 HF photoconductive phase responses in single crystal n-type indium arsenide, deriving carrier lifetimes 14 p2364 A67-28104
 CdSb single crystals doped with Au at liquid helium temperature studied for temperature dependence and Hall effect 14 p2372 A67-28757
 Zn-Sb intermetallic compounds preparation for single crystals in semiconductor phase 14 p2372 A67-28826
 High strength and high elastic modulus in resin-matrix composite structures of single-crystal whiskers 14 p2340 A67-28868
 Stress vs strain curves and slip systems in compression and tension of niobium single crystals 14 p2339 A67-29030
 Electron microscope study of dislocation

structures in deformed niobium single crystals 14 p2339 A67-29031

Copper phthalocyanine single crystal measurements for electric, thermoelectric and galvanomagnetic properties 14 p2376 A67-29086

Temperature dependence of complex permittivity and spontaneous polarization of SbSI single-crystal whiskers in phase transformation region 15 p2537 A67-29707

High temperature diffusion of potassium in single crystal and polycrystalline molybdenum 15 p2504 A67-29972

Electric and thermoelectric effects in single crystals of zinc-cadmium-antimony solid solution, measuring electrical conductivity, Hall constant and thermoelectric power 15 p2540 A67-30029

Temperature dependent noise spectra of InSb single crystals, noting deep energy level and impurity energy level 15 p2541 A67-30235

Ternary semiconductors, analyzing physical and physicochemical properties, noting synthesis and preparation of single crystals 16 p2725 A67-30801

Hall effect measurement in single crystal of arsenic at liquid helium temperatures in magnetic fields noting quantum oscillations 16 p2727 A67-30820

Collection of articles on complex semiconductors investigating conductivity, thermal, electrical and other properties, and preparation methods 16 p2729 A67-31154

Optical reflection spectra of GaS, GaSe, and GaTe single crystal semiconductors in electron volt band energy range 16 p2730 A67-31159

High purity single crystal molybdenum electrical resistivity dependence on deformation 16 p2689 A67-31370

Interface alloy technique for heterojunctions between GaAs and InSb single-crystal heterojunctions shown by X-ray analysis 17 p2911 A67-32196

Superhyperfine interactions in electron-spin-resonance spectrum of substitutional gadolinium 3 impurity in calcium fluoride single crystals under applied stress 17 p2913 A67-32367

GaAs single crystals excited to stable longitudinal vibrations by supersonic absorption, determining resonance curve 17 p2914 A67-32401

Coherent radiation from cadmium sulfide single crystal excited by electron beam, noting transition nature in generation mode and spectral composition 17 p2915 A67-32660

Soviet book on study of defects of crystalline structure of metals and alloys including X-ray analysis of aluminum single crystals, radiation effects on niobium, etc 17 p2874 A67-32894

X-ray spectral analysis of bent aluminum single crystals with crystallographic plane parallel to reflecting surface of crystal 17 p2874 A67-32895

Cadmium selenide arsenide single crystals obtained free of cracks, using synthesis method 17 p2922 A67-33218

Hydroxyl radical formed by radiolysis of ice at 77 degrees K identified as center producing EPR lines 17 p2890 A67-33258

Skin effect in type II superconductor, observing flux penetration into single crystal cylinder immersed in LF alternating magnetic field 17 p2926 A67-33381

Impurity diffusion role in silicon device technology, discussing error function distribution 18 p3096 A67-33455

Tensometric properties of silicon whiskers and acicular single crystals studied under static and dynamic loads, estimating suitability as strain gauge 18 p3097 A67-33473

Strength of single crystals, amorphous materials and other brittle materials lacking grain boundaries, noting loading rate dependence 18 p3069 A67-33491

Optical methods used for study of ruby crystals uniformly, discussing Twyman interferometer design 18 p3098 A67-33576

Deflagration of ammonium perchlorate studied using cleaved sections of large single crystals grown from water solution, discussing burning rate and combustion zone 18 p3108 A67-33814

Gallium arsenide single crystal lattice dielectric constant measured noting broad resonance 18 p3101 A67-34010

Plastic deformation of single crystals of

vanadium by bending and compressing at 298 and 77 degrees K showed etching but no evidence of mechanical twinning 18 p3101 A67-34077

Single gallium arsenide crystals sputtered by normally incident low energy argon ions in mass spectrometer source 18 p3106 A67-34639

Effect of dislocations in GaAs single crystals on diffused p-n junctions structure and recombination radiation parameters 19 p3300 A67-34768

Emission recombination in n-type Si single crystals irradiated with fast neutrons or gamma quanta 19 p3301 A67-34775

Dissolution of single crystal silicon by aqueous solutions of hydrofluoric acid and chromium oxide studied as function of etchant composition 19 p3301 A67-34934

Beryllium single crystal plasticity increased due to preprogrammed load 19 p3245 A67-35470

Irradiation effect on minority carrier lifetime for p-n junction devices in epitaxial film and single crystal forms 19 p3306 A67-35670

Surface morphological changes of tantalum single crystals during plastic deformation, studying orientation dependence of yield stress in tension and compression 19 p3245 A67-35727

Fractional order peaks in low energy electron diffraction /LEED/ patterns from single crystal metal surfaces 19 p3246 A67-35783

Etch pitting and electron microscopy used for tungsten single crystals dislocation density measurements at different strain levels 19 p3248 A67-36028

Photomagnetic effect and kinetic photoconductivity in cadmium sulfide single crystals, determining lifetime and mobility of nonequilibrium holes 20 p3504 A67-36158

Stolzite and scheelite single crystal dielectric constant 20 p3505 A67-36179

Neodymium doped calcium tungstate single crystals synthesized, obtaining continuous laser action 20 p3458 A67-36494

Magnesium oxide single crystal electronic spectrum obtained from reflectance spectra, observing large plasma peak in energy loss function 20 p3509 A67-36508

Nickel-base single crystal superalloy tensile and creep properties, comparing single and multiple slip orientations 20 p3470 A67-37387

Density, morphology and melting data on extended chain linear polyethylene and high molecular weight polymethylene crystallized from melt under high pressure 20 p3474 A67-37398

Elastic bending vibrations amplitude and frequency effects on current oscillations in CdS single crystals 20 p3514 A67-37463

InBi single crystal electrophysical properties, giving temperature dependences 20 p3514 A67-37605

Intrinsic and impurity photoconductivity kinetics over wide temperature and illumination range of p-type indium sulfide single crystals obtained by zone melting 21 p3676 A67-37859

Impurities compensated p-type cadmium antimonide single crystals, determining Hall effect temperature dependence and specific resistance 21 p3676 A67-37868

Single crystals of lithium-meta-niobate evaluated for nonlinear optical quality, using gas laser and interferometer 21 p3677 A67-38010

Lattice relation of cuprous sulfide formed on CdS single crystal noting precisely similar orientation 21 p3677 A67-38011

Field ion images from single crystals of titanium carbide, noting development of two crystallographic regions 21 p3645 A67-38093

Odd and even photomagnetic effect oscillations in InSb, measuring EMF at low temperatures and strong fields 21 p3677 A67-38095

Piezoresistance effect measurement in PbTe single crystals, obtaining coefficients for principal valence band through hydrostatic and uniaxial stresses in several crystallographic directions 21 p3683 A67-38389

AlN single crystal thermostable semiconductor optical/electrical properties, measuring space-charge-limited current and photocurrent 21 p3684 A67-38522

Plastic deformation of single-crystal Ni-Al investigated for temperature, orientation and

strain-rate dependence of tensile flow 21 p3645 A67-38774

Electrical conductivity temperature dependence, Hall coefficient, current carrier mobility, melting point and density data for single crystal of AIBIV type electrical conductivity temperature dependence, 21 p3687 A67-39144

CdS single crystal platelet growing and treating technique, relating fluorescence emissions to growth conditions 22 p3778 A67-39359

Electron beam detectors employing CdS single crystals, considering procedure for obtaining crystals characterized by high sensitivity to electron fluxes 22 p3798 A67-39568

X-ray analysis of hydrate of diethylamine three-dimensional crystal structure, determining bond distances and angles 22 p3757 A67-39634

Ultrasonic wave absorption in high purity gallium single crystals in magnetic field, observing large magnitude geometric oscillations at cryogenic temperature 22 p3859 A67-39653

Microwave pulse compression filter using dispersive characteristics of propagating magnetostatic spin waves in single crystal YIG rods 22 p3773 A67-39908

Time dependent relation between coloring and spontaneous conductivity increase in barium titanate single crystals by strong electric field 22 p3861 A67-39918

Temperature dependence and electro-optic coefficients in lithium niobate single crystal measured, noting relationship in paraelectric perovskites 22 p3863 A67-40235

High temperature microhardness of semiconductors determined by method measuring indentation diagonals of cooled single crystal specimens 22 p3804 A67-40302

Anisotropic energy gap measurements in niobium single crystals by tunneling 22 p3865 A67-40440

Design and performance of high gain amplifier consisting of cadmium sulfide single crystal and thin film transducers 23 p3977 A67-40690

Microwave absorption phenomena observed in Tb, Dy, Ho and Er single crystals 23 p4036 A67-40710

Evaporated metallic contacts to conducting strontium titanate single crystals measured for electric properties evaporated metallic contacts to conducting strontium titanate single crystals measured for 23 p4038 A67-40874

Stimulated emission and spectroscopic investigations of double lanthanum-sodium molybdate single crystals with neodymium impurities, considering applicability in lasers 23 p4039 A67-40901

Ice single crystal growth rate in supercooled water explained on basis of combined heat dissipation mechanism and molecular growth kinetics 23 p4024 A67-40973

EPR spectrum of divalent Mn ion impurity in CdTe single crystals noting concentration dependence, ion distribution and interaction nature 23 p4042 A67-41294

Vapor growth of single crystal heterojunctions of GaAs on Ge or InAs on GaAs using iodine process in closed tube system 23 p4043 A67-41432

Temperature dependence of complex permittivity and spontaneous polarization of SbSI single-crystal whiskers in phase transformation region 24 p4199 A67-41777

Electron beam retarding potential method to measure work function changes resulting from Cs, oxygen and hydrogen adsorption on /110/ Ta single crystal 24 p4201 A67-41892

Linear defects imaging in single crystals by interpreting anomalous behavior of propagating X-rays ascribed to structural defects 24 p4202 A67-42072

Single crystal silicon films on insulating substrates, discussing preparation methods and chemical and structural perfection for use in field effect and bipolar devices 24 p4202 A67-42089

Pyroelectric effect using single barium titanate crystals with liquid electrodes extending ferroelectric switching time measurements to low fields 24 p4203 A67-42090

Maximum Corbino magnetoresistivity in indium antimonide single crystals, investigating impurity concentration and layer distribution 24 p4203 A67-42208

SINGLE-PHASE FLOW

Single-phase and two-phase cavitating flow regime performance of liquid propellant rocket engine turbopump inducers [ASME PAPER 66-WA/FE-23]

04 p0554 A67-15353

Heat transfer - AICE International Conference, Chicago, August 1966, Volume 1, Single phase forced convection

04 p0727 A67-15800

Heat transfer - AICE International Conference, Chicago, August 1966, Volume 3, Single phase, mass transfer and vibrations

04 p0732 A67-15837

Test program for induction coupled MHD generator using liquid sodium as working fluid, noting equivalent single phase circuit for electrical characteristics

12 p1897 A67-25376

Single-phase and two-phase cavitating flow regime performance of liquid propellant rocket engine turbopump inducers [ASME PAPER 66-WA/FE-23]

24 p4143 A67-42464

SINGLE-SIDEBAND DEMODULATION

Modulation and demodulation methods for multiplex telemetry, discussing PCM, PSK and SSB

14 p2271 A67-28682

Thin film single-sideband demodulator using time-varying RC networks and containing extremely selective filter

17 p2825 A67-32600

SINGLE-SIDEBAND MODULATION

Radio relay systems with frequency, single sideband and pulse phase modulation

07 p1141 A67-19342

Ideal SSB modulation theory, discussing DSB Laplace transform formalism, noting Butterworth filters for channel contaminants reduction

19 p3181 A67-34848

SINGLE-SIDEBAND RECEIVER

Mixed single and double sideband interferometer receiving system having phase processing and delay simplicity and multiple RF return cable

11 p1764 A67-24308

Monolithic circuits for RF communications systems

14 p2282 A67-28027

SINGLE-STAGE ROCKET

Initial weight prediction of single and multistage launching vehicles by coordinating practical and theoretical aspects

16 p2782 A67-31490

Navigation and guidance requirements of advanced single-stage-to-orbit reusable launch vehicle investigated to determine necessary modifications

20 p3481 A67-36576

Multistage rocket advantages compared to single stage rocket with respect to attainment of characteristic velocity

20 p3534 A67-37297

SINGULAR INTEGRAL EQUATION

Approximate solutions for integral equations with Hilbert kernel and degenerate nucleus

02 p0258 A67-11625

Integrable function representation by double singular integral at generalized Lebesgue point

03 p0461 A67-14107

Advances in microwaves, Volume 1, covering stanford accelerator design, directional couplers, waveguide singular integral equations, Lie algebras, microwave network application, etc advances in microwaves, Volume 1,

12 p1906 A67-25975

Variational, quasi-static and integral equation analytic waveguide solutions, extending singular integral equation to homogeneous and inhomogeneous loaded waveguide junction

12 p1906 A67-25978

Mutually adjoint boundary value problems for linear systems of first order equations of composite type with two independent variables

14 p2344 A67-28670

Numerical solutions of multidimensional singular integral equations in problems of hydrodynamics

18 p3024 A67-33537

Integral equation solution of hydrodynamic problem through computer program

18 p3024 A67-33543

Operators spectrum properties and corresponding singular eigenfunctions encountered in plasma problems, showing application to initial and boundary value problems

20 p3494 A67-36148

Noether theory for system of singular integral equations with Carleman shift and complex conjugate unknowns as applied to boundary value problem

21 p3653 A67-38399

Dominant mode field reflection at air-ferrite interface junction in anisotropic rectangular waveguide, deriving singular

integral equations for discontinuity problem 23 p3973 A67-40880

SINGULARITY /MATH/

Fundamental solutions to certain singular partial differential equations with constant coefficients, using Bessel iteration operator and Fourier-Bessel

01 p0105 A67-10676

Swirling axisymmetric radial jet flow of conducting fluid in presence of axial magnetic field, citing conditions for singularity in two-dimensional

01 p0124 A67-10800

Singularity in motion equations of closed loop optimal guidance systems

01 p0111 A67-11224

Space-time singularities and Einstein equations

01 p0151 A67-11291

Qualitative dynamic stability analysis of motion equations with two zeros and trajectories near singular

03 p0467 A67-12887

Necessary conditions from second variation, via transformed accessory minimum problem, for class of singular Bolza problems, including singular optimal control problems

04 p0594 A67-15879

Approximation for low thrust trajectory without singularity at escape and having correct behavior up to and beyond escape, using motion equation

05 p0903 A67-17363

Convergence rate of method of gradients relationship to singularity of second variation operator in optimal programming problems

06 p0975 A67-17935

Base pressure behind supersonic vehicle, calculating existence conditions for wake solutions and location of stable and unstable singularities

[AIAA PAPER 67-60]

06 p0986 A67-18269

Regularization of motion equations in computation of vehicle trajectory going near singularity

[AIAA PAPER 67-26]

06 p1087 A67-18464

Nonlinear singularities method for calculating velocity distribution over thick wing of finite aspect ratio situated at zero angle of attack in incompressible frictionless potential flow

07 p1127 A67-19887

Oseen flow past semiinfinite plate and vertical force formulated by integral equations solved for drag and lifting singularities distribution, using Wiener-Hopf technique

08 p1319 A67-20350

Incompressible potential flow about arbitrary body shapes calculated, using singularity distribution over body surface computed as solution of integral equation

10 p1589 A67-22871

Singularities of cosmological solutions of gravitational equations for space filled with matter

10 p1710 A67-23588

Matched asymptotic expansion for singular pressure loading behavior for oscillating wings or control surface

10 p1593 A67-23712

Power series solutions of singular vibration problems converted to quotient of polynomials by transformation into continued fractions, using perturbation technique

[ASME PAPER 67-VIBR-7]

11 p1872 A67-24167

Galerkin method applied to approximation of periodic solution of system of singular differential equations

11 p1819 A67-24762

Singularities causing numerical instabilities used in steady gas dynamic Cauchy problem solution, exemplifying with supersonic blunt body

12 p1893 A67-25932

Auxiliary singularity-carrier-curve theorems derived for blade profile design calculations

12 p1893 A67-25970

Unified method of numerical quadrature for integrands of certain complex analytic functions, obtaining asymptotic expansion of error functional

13 p2145 A67-26734

Shock structure calculations by modified Grad orthogonal expansion method, noting problems of singularity

13 p2103 A67-26976

Mathematical investigation of satellite motion in vicinity of critical inclination, analyzing singularity

14 p2384 A67-28077

Singular point topological classification and analytical criteria relating singular points to generalized Liapunov-Krasovskii functions

14 p2342 A67-28381

Selection of two regularizing functions reduced to one by evaluating relations between them in restricted three-body problem

15 p2557 A67-29875

Regularization of motion equations in computation of vehicle trajectory near singularity [AIAA PAPER 67-26]

17 p2948 A67-33039

Singularities due to concentrated couples in infinite linear elastic isotropic Cosserat continuum, noting dissimilar singular solutions

17 p2964 A67-33141

Singularity carrier auxiliary curves for design of straight cascades of slightly curved bladings

20 p3360 A67-37596

Singularities of two-fluid plasma equations, investigating compatibility and relation to boundary conditions

21 p3661 A67-37744

Generalized Legendre-Clebsch condition applied to singular arc trajectory solutions of state and adjoint equations for optimal control

21 p3602 A67-38023

Necessary and sufficient conditions for linear system response to input vector with limited amplitude and slope, noting singular case existence

21 p3603 A67-38175

Occurrence of singularities in cosmology, giving testable condition implying existence of singularity assuming causality

21 p3703 A67-38493

Parallel conducting flow along insulating pipe under applied magnetic field, elucidating singularities of Hartmann boundary layers

21 p3668 A67-38495

Characterization of eigenvalues of singular nonself-adjoint differential operator of second order

21 p3653 A67-38557

Supersonic blunt body problem noting sonic point singularity for reformulated integral relations

21 p3614 A67-38879

Spherical symmetric problems in general relativity

21 p3707 A67-38962

Position of real singular point of solution function of differential equation of Prandtl boundary layer theory

21 p3615 A67-39096

Pole shifting methods for differential amplifiers noting comparisons, singularities, alternative techniques and schematic diagrams of cascade stages

22 p3771 A67-39862

Solution of linear system of equations with singularity and stable with respect to small changes in matrix elements

23 p4023 A67-41048

Shock curvature and flow variable gradients at tip of pointed axisymmetric body in nonequilibrium flow, solving linear differential equations and singularity

23 p3928 A67-41176

Boundary layer equation solution with constant pressure gradient restriction, discussing singularities

24 p4142 A67-42171

SINK

SA HEAT SINK

Molecular sink for simulated testing of spacecraft components noting vessel construction, vacuum pump system, molecular trap array, etc

18 p3019 A67-33547

Flow due to rotating disk with center sink solved numerically by considering flow unsteady

20 p3425 A67-37599

SINTERED ALUMINUM POWDER

Sintering of crystalline oxides through volume diffusion, noting sintering rates

01 p0096 A67-10693

Surface and internal structural formation mechanism of metallic contact from plastic deformation of SAP type alloys under compression

07 p1208 A67-19303

SINTERING

Creep role in powder metallurgy sintering processes, considering plastic deformation, stresses and material transport mechanism

01 p0096 A67-10692

Sintering mechanisms in powdered compacts of carbides, oxides and metals, examining grain growth, pore decrease and diffusion coefficients

01 p0096 A67-10694

Sintering of cobalt-nickel powder mixtures during formation of solid solutions, noting shrinkage and diffusion coefficients

01 p0096 A67-10695

Sintered Ni-base heat resistant alloys, discussing composition-creep strength relation, grain size, prealloyed-powder production and thermal and structural shock properties

01 p0098 A67-10700

Gravity sintering and low pressure pressing of tungsten powders for economic production of large diameter W matrices

01 p0098 A67-10701

Titanium diboride densification at high pressure and high temperature, noting grain

growth 01 p0098 A67-10704
Powder metallurgy techniques for thermoelectric materials particularly lead telluride, germanium bismuth telluride and zinc antimonide 01 p0099 A67-10709
Sintered-metal friction materials from metallic and nonmetallic powders, noting composition 01 p0099 A67-10710
Powder metallurgy techniques and solid state reactions in alloy constitution research, examining advantages of sintering method over modern melting methods 01 p0099 A67-10711
X-ray microstructural and chemical analysis of sintering of zirconium diboride-molybdenum disilicide alloys 01 p0102 A67-11242
Heating unit of device for testing small samples of sintered materials for thermal fatigue 03 p0420 A67-13545
Shrinkage process in zirconium diboride during sintering, noting variation with length of isothermal processing 03 p0456 A67-14191
Vacuum effect on sintering temperature, describing measuring apparatus and results 06 p1006 A67-17559
Carbon content effects on properties of WC-TiC-Co alloys vacuum sintered 06 p1017 A67-17968
Structural, physical and mechanical properties of hard alloys formed by sintering powdered VK 15 tungsten cobalt alloy with nonuniformly distributed carbide phase 07 p1208 A67-19305
Compression and bending strength of porous materials prepared by sintering spheroidized powder refractory compounds increased by addition of cobalt chloride 07 p1208 A67-19307
Sintering of porous products of refractory compounds 10 p1667 A67-22827
Exponential sintering temperature dependence of conduction electrons density and attendant decrease of mobility due to ionized impurity scattering in cadmium oxide 10 p1691 A67-23503
Porosity and particle size effects on magnetization curve of superconducting Nb sintered compacts with and without C added 12 p1978 A67-25139
Activated sintering of beryllium 13 p2140 A67-27129
Microalloying beryllium for improved sintering characteristics and mechanical properties 13 p2140 A67-27130
Compaction pressure and sintering temperature effect on initiation and propagation of cracks during bend testing of Ni and Mo specimens 16 p2691 A67-31586
Porous materials prepared from carbides, borides and silicides of refractory metals by oxidation reduction method, with simultaneous sintering of resulting active particles 16 p2683 A67-31596
Dispersed aluminum oxides effect on size of nickel grains in sintered or extruded nickel-aluminum oxide cermets, studying compressive strength dependence 17 p2871 A67-31924
Powder-metallurgical methods using mechanical filing, isostatic pressing and high vacuum-high temperature sintering for fabrication of airfoil turbine-blade blocks 17 p2865 A67-32821
X-ray, microstructural and chemical analysis of sintering of zirconium diboride-molybdenum disilicide alloys 17 p2875 A67-33167
Surface, volume and grain-boundary diffusion role in metal sintering process, discussing theoretical equations 19 p3247 A67-35836
Properties of pressed and sintered products of powder metallurgy, noting strength and ductility increase with increase in density 20 p3465 A67-36496
Bending strength dependence on porosity of sintered powdered glass beam 20 p3473 A67-36779
Influence of palladium additives and sintering temperature on tungsten molding noting shrinkage, density, microhardness, durability and microstructure 20 p3466 A67-36910
Rate of diffusion and degree of density during activated sintering of tungsten-molybdenum powders, noting influence of nickel additive 20 p3466 A67-36911
TiC and ZrC powder properties after sintering investigated for linear growth rates

vs temperature, obtaining sintering activation energy values 22 p3820 A67-39564
WC-NbC-Co alloys oxidation resistance in air studied by sintering powdered WC and NbC with Co, finding oxidation rate linear function of time 22 p3820 A67-39565
Cementite formation during sintering in cermet compositions with titanium carbide base and steel or iron binder noting CO role 24 p4171 A67-41960
SINUS
S CAROTID SINUS REFLEX
SINUSOID
Discontinuous impact vibration absorber with small auxiliary mass sliding in slit of rigid body excited by sinusoidal oscillation 01 p0181 A67-10645
Book on network theory of negative-resistance tunnel diode linear and nonlinear sinusoidal circuits and application to amplifiers 03 p0383 A67-13817
Harmonic components of current of HF transistor under sinusoidal excitation, using piecewise parabolic approximation 05 p0772 A67-16456
Pulsed sinusoidal bridge for simultaneous measurement of volt-capacitance and volt-ampere characteristics of relaxing p-n junction barriers 08 p1303 A67-20998
Permanent states of Van der Pol equation in forced sinusoidal state using first harmonic theory which relies on amplitudes of response 23 p4026 A67-40688
SITE
S LANDING SITE
S LAUNCH SITE
SIZE
S BODY SIZE /BIOL/
S DROP SIZE
S PARTICLE SIZE
S PUPIL SIZE
SIZE PERCEPTION
Size effects in electroconductivity of semiconductors with several groups of carriers with large intergroup relaxation time 06 p1064 A67-18944
Effect of image smear and dimension on target recognition measured on differently oriented, moved and remote Landolt C 09 p1455 A67-21723
SKELETON
S BONE
S RIB
SKID LANDING
Skidding accident reduction investigated for runway and highway safety noting worn tires, smooth surface texture, locked wheels and pilot technique 19 p3173 A67-35930
SKIMMER
Electron beam analysis of skimmed influence on nozzle beam formation 14 p2301 A67-28187
SKIN
SA STRUCTURAL MATERIAL
Skin stringer panel rows natural frequencies and normal modes predicted by transfer matrix method 20 p3539 A67-37008
SKIN /BIOL/
SA TACTILE DISCRIMINATION
Cutaneous sensitivity communications, discussing information situations, applications and subsystems 09 p1456 A67-22375
Stereoisomers of sulfur containing amino acids effect on local skin protection in X-irradiated mice 18 p2992 A67-34716
Potential contamination of equipment by primate passenger during 30-day earth orbit, studying skin, body particulate matter and indigenous microflora 23 p3944 A67-40856
Long term space mission sanitation, personal hygiene and body cleansing to control microbe populations on body surface and teeth 23 p3967 A67-41611
Acute and chronic cellular level effects of low energy proton irradiation in rat skin 23 p3957 A67-41644
Pathological effects, including carcinogenesis following proton whole body irradiation in rats 23 p3958 A67-41645
SKIN FRICTION
Skin effect association with anisotropy of medium in solid mechanics, analyzing surface instability, internal buckling and surface wave propagation 01 p0113 A67-10406
Injection from half-plane located in steady viscous flow in Oseen approximation, noting skin friction 01 p0052 A67-10793
Boundary layer effect on lift and drag characteristics of hypersonic lifting bodies 03 p0351 A67-12991

Coolant injection in turbulent boundary layer for protection of surfaces from effects of high temperature and high energy gas flows 03 p0536 A67-13526
Turbulent skin friction measurement with Preston tube, using similarity hypothesis for mean velocity profiles in turbulent flows 04 p0600 A67-14442
Exponentially decaying solution of Hartree as limiting solution for Falkner-Skan equation 04 p0604 A67-14830
Linearized Couette flow problem in rarefied gas solved, using one-dimensional radiative heat transfer analogy 04 p0606 A67-15183
Heat transfer and skin friction rates increase in gas-liquid droplet suspension system flowing over circular cylinder formulated by laminar boundary layer theory 04 p0725 A67-15439
Preston tube measurements of skin friction and velocity profiles in incompressible turbulent boundary layer, considering pressure gradient effects 04 p0609 A67-15818
Unsteady incompressible laminar forced convection around stagnation point due to arbitrary timewise-variant free stream velocity, considering skin friction and heat transfer 04 p0610 A67-15830
Heat-transfer coefficients and shearing stress in turbulent boundary layer along porous flat plate with uniform fluid injection 04 p0733 A67-15842
Radiation effects on heat transfer and friction characteristics in natural and forced convection film boiling in boundary layer flows [ASME PAPER 66-WA/HT-6] 04 p0739 A67-15939
Transverse curvature effect on axisymmetric compressible laminar boundary layer flow, obtaining asymptotic solutions for skin friction and heat transfer 05 p0791 A67-16509
Two-phase flow of gas over harmonically oscillating flat plate expressed in laminar boundary layer terms, presenting liquid film thickness, heat transfer rate, skin friction, etc 05 p0793 A67-17338
Turbulent boundary layer characteristics of compliant surfaces, using hot-wire anemometer to measure velocity profiles, Reynolds stresses and skin friction [AIAA PAPER 67-128] 06 p0987 A67-18336
Skin friction under mass injection on porous flat plate in supersonic turbulent flow [AIAA PAPER 67-194] 06 p0987 A67-18341
Turbulent boundary layer properties for strong adverse pressure gradients, obtaining layer and displacement thickness, skin friction, heat transfer, etc [AIAA PAPER 67-196] 06 p0989 A67-18489
Turbulent flow of mercury in flat channels plane perpendicular to magnetic field, noting reduction of flow resistance coefficient 06 p1044 A67-18678
Preston tube in concentric annuli, discussing skin friction measurement in fully developed turbulent flow 06 p0990 A67-18749
Local skin friction coefficient for turbulent boundary layers on smooth flat plates measured, using Preston tube 06 p0990 A67-18751
Transverse variation effects on accuracy of skin friction measurements determined via static hole pair 06 p1005 A67-18753
Correlation number for calculation of skin friction and heat transfer for laminar compressible boundary layer flow with arbitrary pressure gradient, using von Karman momentum integral 06 p0992 A67-18862
Boundary layer development in throat region of converging-diverging nozzle, obtaining self-consistent solutions 08 p1277 A67-20589
Turbulence effects on laminar skin friction and heat transfer from plates and circular cylinders in incompressible flow, using two low turbulence wind tunnels 08 p1427 A67-21118
Unsteady incompressible flow of viscous electrically conducting fluid near stagnation point, determining skin friction and heat transfer at wall 09 p1544 A67-21934
Similar calculation of hypersonic laminar boundary layer characteristics in presence of pressure gradient, specifically heat transfer, skin friction and boundary layer

- thickness 10 p1592 A67-23141
Screen and honeycomb effect on variation of skin friction in low speed wind tunnel, noting turbulent boundary layer growth 10 p1627 A67-23556
Steady flow of viscous conducting fluid in pipe under magnetic field analyzed for relations among Hartmann number, Reynolds number, skin friction, wall conductivity, etc 10 p1687 A67-23833
Turbulent boundary layer development noting representation of velocity profiles, skin friction and eddy viscosity 11 p1776 A67-24044
Turbulent boundary layer on smooth flat wall, measuring skin friction, turbulence intensity, shearing stress, transverse integral scale, etc 11 p1776 A67-24045
Eckert reference temperature yields approximations for heat transfer, skin friction and recovery temperature in high speed laminar diatomic nitrogen and carbon dioxide boundary layers 11 p1883 A67-24576
Heat transfer and skin friction increase for gas stream with liquid-droplet suspension flowing over blunt-nosed body near stagnation point 14 p2405 A67-28126
Heat transfer and skin friction rates increase in gas-liquid droplet suspension system flowing over circular cylinder formulated by laminar boundary layer theory [ASME PAPER 66-WA/HT-33] 15 p2579 A67-29322
Analytical method, based on polarography, for measuring concentration of class of polymers in dilute aqueous solutions 15 p2433 A67-29676
Theory and supporting experimental results on application of small heated film for skin friction measurements in laminar and turbulent boundary layers 16 p2659 A67-30950
Lateral convex curvature and helium surface injection effect on turbulent wall boundary layer characteristics and skin friction 16 p2659 A67-30952
Turbulent channel flow of mercury in presence of uniform transverse magnetic field deducing skin friction coefficient 16 p2661 A67-31224
Turbulent channel flow of electrically conducting fluid in presence of magnetic field obtaining skin friction coefficient and velocity profiles 16 p2661 A67-31225
Transverse curvature effect on axisymmetric compressible laminar boundary layer flow, obtaining asymptotic solutions for skin friction and heat transfer 16 p2662 A67-31600
Three-dimensional laminar boundary layer flow, calculating skin friction and velocity profiles 17 p2790 A67-32284
Compressible laminar spanwise boundary layer on yawed infinite cylinder with disturbed suction calculated using momentum equation 19 p3342 A67-35724
Steady two-dimensional laminar flow of incompressible viscous fluid, noting asymptotic convergence of velocity profile in Prandtl boundary layer 19 p3212 A67-36031
Lift-drag ratio attainable by slender flat-top body at supersonic speeds, considering Newtonian pressure distribution and constant skin friction 20 p3359 A67-37124
Approximate solutions of Prandtl boundary layer problem for incompressible laminar flow derived, using Nagumo-Westphal theorem on parabolic differential operators 21 p3563 A67-37888
Second order weak interaction expansion for hypersonic flow past adiabatic flat plate, obtaining expressions for static pressure, displacement thickness and skin friction 21 p3566 A67-38892
Aircraft skin friction balance components for hostile environments noting system design 22 p3795 A67-39188
Miniature transducers for shock tunnel instrumentation, noting compensating system to reduce spurious signals from pressure and skin friction 22 p3809 A67-40463
Heat transfer, skin friction and shearing stress from similar solutions to compressible laminar boundary layer equations for flow over flat plate 23 p4082 A67-41246
Turbulent skin friction in incompressible flow with heat transfer, determining Preston surface pitot tube applicability 23 p4004 A67-41341
Skin friction under mass injection on porous flat plate in supersonic turbulent flow [AIAA PAPER 67-194] 23 p3991 A67-41713
Transverse curvature parameter in hypersonic flow regime for modifying effects on velocity profile slope, skin friction and heat transfer rate 23 p3993 A67-41755
Prandtl limit behavior near zero skin friction, with perturbation methods generalizing Poiseuille and Couette flows 24 p4142 A67-42170
Hydrodynamic separation using compatibility conditions for Prandtl steady boundary layer equations at zero skin friction point 24 p4142 A67-42172
SKIN FRICTION DRAG
Skin friction drag of constant property turbulent boundary layer with uniform injection, corrections of experimental law-of-wall and velocity-defect law concepts 10 p1625 A67-23111
Transition delay and skin friction drag reduction by considering boundary layer flow over flexible aerodynamic surface [AIAA PAPER 66-430] 13 p2106 A67-27585
Skin friction drag coefficient at supersonic-hypersonic speeds as function of transition on delta wing 13 p2051 A67-27597
Interaction between buckling and flutter of circular cylindrical shell subjected to axial compression and placed in axial supersonic flow 14 p2398 A67-28092
Minimum drag for slender body in hypersonic flow, assuming pressure coefficient is modified Newtonian and surface-averaged skin friction coefficient is constant 15 p2416 A67-29408
SKIN RESISTANCE
Effects of 450 and 600 degrees F exposures on mechanical properties of glass-fiber polyimide resin sandwich panels to be used on large skin areas of SST aircraft [AIAA PAPER 67-174] 06 p1021 A67-18484
Skin effect in type II superconductor, observing flux penetration into single crystal cylinder immersed in LF alternating magnetic field 17 p2926 A67-33381
Read type and avalanche type oscillations in silicon varactor diodes, noting parasitic series resistance and electric field peak effects 24 p4133 A67-42820
SKIN TEMPERATURE
Thermal design method for Japanese scientific satellite L4S, based on skin temperature determination and correlation with inner compartments 02 p0335 A67-12392
Skin heating effects on induction converters, noting magnetic field intensity and temperature as function of time and space 09 p1442 A67-21794
Pyroelectric heat-transfer sensor performance compared with thin skin thermocouple heat sensors, noting discrepancy in measurement results in severe environment 11 p1790 A67-24453
Flight test skin temperatures of supersonic aircraft compared with theoretical results, explaining measurement discrepancies 14 p2243 A67-28977
Wing shape and size selection for hypersonic velocities formulated as extremum problem of drag, aerodynamic property, temperature and coolant consumption for given wing volume 22 p3741 A67-40015
SKIN TEMPERATURE /BIOL/
SA TEMPERATURE CONTROL
Relation between skin temperature and environmental air supply temperatures in fixed air-ventilated clothing assembly 02 p0188 A67-12346
Absorbed solar electromagnetic radiation effect on mean facial skin temperature 09 p1452 A67-21725
Experiments on undercooling and overcooling with liquid cooling garments, noting correct cooling defined by narrow biothermal response band 23 p3970 A67-41655
SKY
S NIGHT SKY
SKY BRIGHTNESS
SA AIRGLOW
Maps of 2-cm brightness distribution of various radio sources including Taurus and Orion 03 p0511 A67-13796
Large star fields outside earth atmosphere, using wide-angled photoelectric photometer for simultaneous UV and visible spectrum measurements of sky brightness 04 p0700 A67-15073
Solar eclipse of May 20, 1966, first and fourth contact times, sky brightness and temperature and photographic records 05 p0897 A67-16731
Multiple scattering effect on brightness of twilight sky, noting changes in spectral composition due to radiation absorbing effect of ozone and height variation of multiple layer 07 p1219 A67-19148
Isophotes of extended light sources in night sky, Stokes parameters, brightness and degree of polarization for Rayleigh-scattered light in earth atmosphere 08 p1326 A67-21243
Surface brightness and polarization state of zodiacal light measured from sounding rocket 08 p1326 A67-21244
Daytime sky brightness relationship to atmospheric anisotropic light scattering 09 p1491 A67-21638
Brightness of night glow measured in several spectral ranges by Cosmos 92 satellite-installed colorimeter 10 p1647 A67-23276
Energy spectrum of primary electron flux and brightness of auroral light measured by rockets in active auroras used to derive electron production rate 10 p1650 A67-23306
Absorption and brightness temperature variations of atmosphere on basis of statistical characteristics of vertical temperature and humidity structures 11 p1785 A67-23956
Multiple air scattering in mesosphere as function of zenith distance of sun and brightness of twilight sky 11 p1785 A67-23957
Large antenna radiation from radio astronomy Explorer satellite determined on basis of antenna current distribution 14 p2286 A67-28507
IR radiation measurements by spectrometers flown on board stratospheric balloons, considering sky brightness, vertical distribution and thermal atmospheric emissions 14 p2313 A67-28768
Sky brightness temperature measurements at various millimeter wavelengths for possible isotropic electromagnetic emission in universe 17 p2935 A67-32230
Night airglow brightness spatial distribution observed by photoelectric photometry in 5893 angstrom band, including isophotes charts and emission-inhomogeneity drift histogram 17 p2848 A67-32953
Optical observations of daytime aurorae by means of atomic-oxygen-emission interferometry 17 p2852 A67-33212
Skiyglot polarimeter based on sequential detection of light transmitted by polarizers oriented at various angles 18 p3046 A67-33748
Short wave spectrometer for measuring total and scattered sky radiation, spectral brightness and fluxes of direct and reflected solar radiation 19 p3227 A67-34860
Rocket sounding of zodiacal light brightness at 4300, 5300 and 6000 angstroms 19 p3216 A67-35192
Vertical distribution of diffuse sky light in stratosphere determined by rocket measurements, noting intensity peak in aerosol layer 19 p3221 A67-35273
Searchlight brightness measurements for vertical turbidity layer of troposphere using computing scattering functions 19 p3225 A67-35532
Upper atmosphere optical properties determined by simultaneous twilight balloon and ground measurements, establishing twilight sky luminance ratios to solar luminance 20 p3427 A67-36369
Atmospheric optics and radiation transfer covering sky brightness, solar insulation, earth radiance and albedo, etc 20 p3430 A67-36899
Brightness and contrast study of noctilucent clouds in twilight layer indicating preferability of satellite observation 20 p3434 A67-37426
Radio sources fluctuations due to inhomogeneities of solar supercorona and interplanetary plasma, studying solar wind and brightness distribution 20 p3520 A67-37513
Spacecraft optical environment, considering sky luminance, spacecraft corona, spacecraft scattered light and glare sources 21 p3713 A67-38568
Discovery position plotting of various long period comets, showing tendency to cluster near sun in morning sky, orbit distribution and estimated probabilities 21 p3705 A67-38614

70 to 450 km altitude atmospheric brightness at 5300 angstrom measured by rocket noting importance of aerosol component 21 p3623 A67-39043

Zodiacal light and interplanetary dust, discussing brightness, polarization, color, spectrum and dust cloud about earth 22 p3794 A67-40426

Mean emissivity due to radio galaxies calculated, using assumption that total brightness temperature is uniform in universe 22 p3896 A67-40530

SKY RADIATION
S PYRANOMETER
SKY WAVE
 HF skywave propagation computer model for interference prediction 20 p3387 A67-37646

LF downcoming sky wave phase calculation method, discussing complex integral representation for resultant field 23 p3973 A67-40838

SKYCRANE HELICOPTER
S CH-54 HELICOPTER
SKYDROL
S ESTER
S PHOSPHATE
SKYLARK ROCKET
 Propane gas system for satellite attitude control noting Skylark rocket 01 p0157 A67-11446

Shock wave from release of gas at 230 km altitude indicated luminosity due to scattered sunlight and temperature of 743 degrees K 05 p0795 A67-16027

Skylark rocket attitude in free space determined from solar and magnetic sensor data used in least squares method 08 p1406 A67-20508

Stabilized Skylark rocket using N-gas jet system, solar sensors and magnetometer to obtain three-axis control 08 p1408 A67-20537

Upper atmospheric wind, temperature and pressure variations measured using grenade launched Skylark sounding rockets 10 p1638 A67-23199

LF ionospheric measurement of admittances of three orthogonal shock dipoles, noting impedance variation with respect to frequency attitude and voltage 10 p1648 A67-23286

Solar studies in extreme UV using stabilized Skylark rockets, including data on chromospheric and coronal spectra and XUV spectroheliograms 12 p2008 A67-25826

Atmospheric temperature, pressure, density and wind measurements between 30 and 80 km by Skylark rocket at Woomera, Australia 12 p1937 A67-25840

Raven solid propellant motor for Skylark noting design, ignition and plastic propellants burning 22 p3867 A67-39525

Booster for Skylark upper atmosphere research vehicle to increase altitude and reduce launching dispersion of single stage vehicle 24 p4206 A67-42580

SLAB
 Distributions of screw dislocations in finite slab, examining crack extension with and without plasticity 04 p0716 A67-15798

Bending of circular and elliptical slabs clamped along contours under loads described by certain algebraic polynomials 15 p2573 A67-29465

Diurnal and seasonal variation of electron content and diurnal variation of slab thickness investigated, emphasizing relation between electron content and scintillation occurrence 17 p2850 A67-33190

Iterative solution for directional emissivities of two-dimensional semiinfinite slab of absorbing-scattering medium with gray isothermal dispersion [ASME PAPER 67-HT-12] 20 p3545 A67-36710

SLAG
 Phase composition of titanium containing slag formed during alloying of stainless steel with titanium, noting titanium oxidation 16 p2687 A67-30842

SLED
S ROCKET SLED
SLEEP
 EEG of pilot during orbital flight on Gemini VII used to study sleep cycles 01 p0015 A67-10954

Evoked brain response to clicks as measure of vigilance tested in work-rest schedule and pressure sleep experiments on man 09 p1452 A67-21721

EEG baselines covering wide range of

states of wakefulness and sleep in astronaut candidates estimated by computation and pattern recognition techniques 13 p2062 A67-26921

Sleep characteristics during simulated space flight noting influence of noise, angular accelerations and isolation 16 p2613 A67-30913

SLEEP DEPRIVATION
SA WAKEFULNESS
 Human experiments to study somnolent and precollapoid /collapoid/ states when falling asleep and during prolonged standing tests 20 p3368 A67-36268

Physiological responses to cold in men during extended period of sleep loss 23 p3955 A67-41615

SLEEVE
 Contact stresses and deformations between circular cylindrical shafts and sleeves obtained by numerical method, considering contact with and without friction 18 p3054 A67-34263

SLENDER BODY
 Pressure and density of heat flux at surface of pointed or blunt nosed obstacle in divergent truncated cone of hypersonic nozzle 01 p0005 A67-10258

Heat transfer and equilibrium temperature of heat conducting sharp cones in supersonic rarefied gas flow at zero angle of attack 01 p0007 A67-10977

Shock-shock interactions for slender cone in theory and experiment 01 p0055 A67-11183

Approximate method for calculating parallel flow past slender bodies of noncircular cross section 02 p0177 A67-11517

Instability and transition of wake behind axisymmetric slender body with sound-induced velocity fluctuation amplification 02 p0177 A67-11560

Nonsteady state gas flows with small entropy gradients corresponding to supersonic flight conditions 02 p0178 A67-11629

Hypersonic flow past lower surface of slender delta wing for wide-range of angle of attack, determining velocity component, pressure and density distribution 03 p0350 A67-12874

Slender body theory application in obtaining aerodynamic stability derivatives for reentry vehicles via electrical analogy 03 p0354 A67-12918

Flexible wing analysis based on slender body theory, calculating wing profiles, pressure distribution as function of stress and lift force values 03 p0351 A67-12992

Optimum shaped-bodies of maximum lift-to-drag ratio in hypersonic flow for modified Newtonian pressure distribution and constant skin friction 04 p0546 A67-14817

Three-dimensional flow separation over structures with various geometric configurations, calculating limiting streamlines for subsonic laminar boundary layer conditions 05 p0747 A67-16293

Axial flow dynamics of flexible slender cylindrical body immersed in fluid, emphasizing flow velocity, frictional forces, buckling and oscillatory instabilities 05 p0920 A67-16815

Spence integrodifferential equation for flow around slender slightly curved profile with jet at trailing edge 05 p0749 A67-16842

Terminal shock-boundary layer interaction on slender cone-cylinder payloads at supersonic speeds and resulting flow separation [AIAA PAPER 66-471] 05 p0924 A67-17213

Explosion analogy in flows past slender blunt bodies, noting accuracy improvement by placing explosion center ahead of origin 06 p0936 A67-17732

Dynamic characteristics of variable mass slender elastic body, solving vector differential equations [AIAA PAPER 67-41] 06 p1095 A67-18263

Linearized long wave diffraction theory of supersonic inviscid flow past slender circular cylindrical bodies and thin wings 06 p0942 A67-18729

Turbulent wake of slender body analyzed to include dominant mode of laminar diffusion, deriving solution for linear electron chemistry 06 p0943 A67-18870

Aerodynamic effect of volume addition to high lift to drag wing-body ratio at Mach 6 07 p1126 A67-19382

Boundary value problem for electrostatic field external to slender axisymmetric

conductor 08 p1413 A67-21301

Minimum drag body with specified center of pressure 10 p1592 A67-23155

Inviscid flow theory in internal aerodynamics, discussing irrotational, secondary and flow past thin airfoils and slender bodies 11 p1776 A67-24049

Fluid dynamic fields from hypersonic flow around slender bodies, using extension of Vallander tangent cone method for zero angle of attack 11 p1741 A67-24091

Legendre polynomial form of slender body motion in spherical coordinate systems generalized for axially symmetric harmonic functions in three dimensions with validity for Helmholtz equation 11 p1812 A67-24310

Drag coefficients of hypersonic optimum bodies at nonoptimum Mach numbers 12 p1892 A67-25744

Shape effects on hypersonic slender body wake geometry and transition distance 13 p2050 A67-26832

Axially symmetric potential flow about slender body, noting source strength distribution and solution via integral equations 13 p2095 A67-26911

Sufficiency proofs for problem of optimum transversal contour of slender conical body 13 p2051 A67-27457

Flow field experiments for shock wave and boundary layer development on two-dimensional and axisymmetric bodies 14 p2241 A67-28168

Vortex flow about wings, fins and fuselages of slender aircraft and missiles analyzed using small water tunnel 15 p2465 A67-29399

Interval size effect on minimum drag coefficients and optimum shapes of bodies of revolution determined from Newtonian impact theory 15 p2416 A67-29407

Minimum drag for slender body in hypersonic flow, assuming pressure coefficient is modified Newtonian and surface-averaged skin friction coefficient is constant 15 p2416 A67-29408

Pressure distribution and convective heat flux at slender bodies of revolution surface, considering sphericity influence of free hypersonic flow 16 p2594 A67-31468

Cross sectional variation effects on velocity potential evaluated using slender body theory 17 p2789 A67-32067

Cross sectional shape and thickness ratio variation effect on maximum high lift/drag ratio examined, using flat-topped conical bodies 17 p2789 A67-32071

Hypersonic gas flow past slender body, obtaining pressure coefficient and shock wave curvature by linearizing differential equations involving stream function 17 p2791 A67-32868

Dynamic characteristics of variable mass slender elastic body, solving vector differential equations [AIAA PAPER 67-41] 17 p2956 A67-33013

Shock and boundary layers about blunted two-dimensional slender bodies in hypersonic flow [AIAA PAPER 67-451] 18 p2982 A67-33925

Lift penetration and growth effects on space vehicle response based on slender body theory 19 p3337 A67-35999

Lift-drag ratio attainable by slender flat-top body at supersonic speeds, considering Newtonian pressure distribution and constant skin friction 20 p3359 A67-37124

Static pressure probe nose derived from supersonic slender body theory and shaped for subsonic speeds 21 p3564 A67-38535

Tensor conductivity effect on continuum and collisionless MPD flows past slender bodies [AIAA PAPER 67-731] 21 p3674 A67-38755

Laminar boundary layer gas flows over slender bodies with massive blowing, discussing integral method solution and theoretical model including pressure effect 22 p3739 A67-39935

Electrostatic and magnetostatic potentials for slender bodies of revolution in axially symmetric external fields 23 p4026 A67-40753

Ground proximity effect on aerodynamic characteristics of slender wings by extension of slender body theory, solving potential function equation 23 p3930 A67-41310

Integral solution for massive blowing on slender hypersonic wedges and cones in laminar flow, assuming homogeneous nonreacting perfect gas mixtures 23 p3932 A67-41743

Earth and planetary atmosphere entry problems for blunt nosed slender vehicles noting aerodynamics, stability, heating, ablation and interaction of effects [AIAA PAPER 67-803] 24 p4243 A67-42963

SLENDER CONE

Aerothermochemical eddy diffusion model for predicting rapid wake ionization decay behind hypersonic slender clean cone obtained in free flight ballistic range [AIAA PAPER 67-21] 06 p0938 A67-18257

Shock tunnel heat transfer measurement and hypersonic viscous flow over pointed cones, particularly viscous-layer regime at low Reynolds numbers 06 p0943 A67-18845

Parameterization of minimum-drag slender pointed cone situated in viscous hypersonic gas flow 13 p2050 A67-26882

Nose bluntness effect on hypersonic unsteady aerodynamics of ablating flared or conical slender reentry vehicles 15 p2416 A67-29442

Dynamic destabilization for hypersonic flow around slender cone with severely blunt nose analyzed by blast wave analogy 22 p3742 A67-40109

Asymptotic perturbation of hypersonic flow over blunt slender cones and wedges showing oscillatory nature 23 p3931 A67-41665

Reynolds number effect on slender high speed cones wake-neck geometry, obtaining measurements of location, diameter and closure angle 23 p3932 A67-41754

Shock waves and boundary layer structure near tip of slender cone in rarefied hypersonic flow, discussing surface pressure peaks 23 p3932 A67-41762

SLENDER WING

Aerodynamics of slender wings executing simple harmonic oscillations and having leading edge separation 03 p0352 A67-13894

Slender wing basic shape for adaptation to fuselage of circular cross section [ONERA-TP-425] 05 p0748 A67-16762

Linearized supersonic theory for favorable thickness distributions and drag reduction for wings in supersonic flow [AIAA PAPER 65-716] 08 p1276 A67-20559

Handling criteria for basic stability and control characteristics of slender wing and V/STOL aircraft 13 p2053 A67-27192

Vortex breakdown effects on lift, drag and pitching moment coefficients of slender sharp-edged delta wings with different aspect ratios 13 p2050 A67-27194

Slender two-dimensional wing lift-drag ratio at hypersonic speed maximized, assuming modified pressure coefficient 15 p2416 A67-29409

Three-dimensional slender wings of maximum lift/drag ratio in hypersonic flow studied by variational calculus under several lift and volume 16 p2592 A67-30964

Vortex wake and aerodynamic load distribution of slender rectangular wings 17 p2790 A67-32215

Approximation solution of three-dimensional problems associated with slender wing motion in transonic gas flow with perturbations 18 p2981 A67-33535

Slender wing maximum lift-drag ratio at hypersonic speeds obtained assuming modified Newtonian pressure distribution and skin-friction drag 20 p3357 A67-36953

Ground proximity effect on aerodynamic characteristics of slender wings by extension of slender body theory, solving potential function equation 23 p3930 A67-41310

SLIDING CONTACT

Sliding contact wear under very dry high altitude or space conditions due to lack of contact film prevented by using chemical compounds like graphite or lithium carbonate 02 p0221 A67-12435

Sliding electrical contact material for ultrahigh vacuum with 300 amp/sq inch current density, 425 in/min sliding velocity and 10 psi brush pressure 11 p1805 A67-24345

Alloys, cermets and ceramics used in bearing applications at 600 to 2000 degrees F, noting significance of oxides 14 p2324 A67-28001

Hertz and Mindlin problems for fourth order paraboloids in contact generalized, minimizing microslips and annulus of slip [ASME PAPER 67-APM-12] 15 p2505 A67-30149

Hertz and Mindlin problems for fourth order paraboloids in contact generalized, minimizing microslips and annulus of slip

[ASME PAPER 67-APM-12] 17 p2871 A67-32411

Contact stresses and deformations between circular cylindrical shafts and sleeves obtained by numerical method, considering contact with and without friction 18 p3054 A67-34263

Lubrication and wear with reference to boundary lubrication, fluid and solid films, discussing dry and lubricated sliding and rolling theory 20 p3455 A67-37262

Highly elastic materials temperature dependence of contact area and sliding friction forces affected by elastic modulus decrease with temperature under load 23 p4021 A67-40596

Wear characteristics of polytetrafluoroethylene studied under various loading and sliding speeds in air and vacuum 23 p4009 A67-41062

SLIDING FRICTION

Sliding friction characteristics in vacuum of single and polycrystalline aluminum oxide in contact and with various metals 03 p0428 A67-13231

Partial cone crack formation in brittle material loaded with sliding spherical indenter 18 p3144 A67-34275

Metallurgical aspects of nitrided component application in unmanned satellite drive systems to remedy sliding wear and increase reliability 18 p3058 A67-34676

Sliding friction between spherical steel rider and gold-plated steel flat measured for varied loading, steel combinations and gold film thicknesses 19 p3237 A67-35837

Sliding friction characteristics in vacuum of single and polycrystalline aluminum oxide in contact and with various metals 19 p3237 A67-35838

Cermet sealing material dry-friction characteristics over wide sliding-speed range, discussing graphite and boron nitride lubricants 19 p3247 A67-35850

Lubrication and wear problems of surfaces of solid materials noting influence of contact area, adhesion, speed, etc. on friction 21 p3633 A67-38139

Lubrication and wear in high vacuum, considering inability to maintain oxide films, evaporation of lubricants, heat transfer and sliding friction 21 p3633 A67-38142

Surface active lubricant influence on internal stresses in sign variable slippage case, discussing chemisorption, wear resistance and stress 22 p3810 A67-39219

SLIP

SA SIDESLIP

Backscattering of centimeter waves from ruffled sea surface at small angles of slip 05 p0761 A67-16345

Slip and change in displacement vector in elastoplastic boundary value problems 05 p0918 A67-16424

Active slip volume /active crystal length/ concept in plasticity theory and relation to temperature and strain rate 07 p1232 A67-19636

Ductility of beryllium samples subjected to compression at temperatures ranging from 300 to 600 degrees C, discussing slip effects 13 p2137 A67-27113

Activation energy and volume of prismatic slip in beryllium 13 p2138 A67-27115

Hertz and Mindlin problems for fourth order paraboloids in contact generalized, minimizing microslips and annulus of slip [ASME PAPER 67-APM-12] 15 p2505 A67-30149

Cross slip and slip character related to fatigue, brittle fracture and strain hardening in crystal solids 16 p2772 A67-31299

Hertz and Mindlin problems for fourth order paraboloids in contact generalized, minimizing microslips and annulus of slip [ASME PAPER 67-APM-12] 17 p2871 A67-32411

Temperature and composition effect on ductility transitions, yield stress and dislocation pinning strength in iron base alloys due to change in slip 18 p3063 A67-33485

Aluminum alloy examined for dislocation arrangements and susceptibility to intergranular stress corrosion cracking, using electron microscopy 18 p3063 A67-34000

Surface morphological changes of tantalum single crystals during plastic deformation, studying orientation dependence of yield stress in tension and

compression 19 p3245 A67-35727

Interaction between environment, oxide layer and surface slip formation in aluminum during cyclic bending 19 p3247 A67-35788

Acoustic radio signal backscattering producing rippled signals, showing activity with broad ripple spectrum 19 p3185 A67-36018

Plastic deformation of single-crystal Ni-Al investigated for temperature, orientation and strain-rate dependence of tensile flow 21 p3645 A67-38774

Slip factors for centrifugal impellers, presenting empirical expression and correction for range and number of blade angles [ASME PAPER 66-WA/FE-18] 24 p4143 A67-42463

SLIP BAND

Dislocation theory of slip geometry and temperature dependence of flow stress in bcc metals 07 p1209 A67-19641

Discontinuous yield phenomena for slip band dislocations, when frictional stress that hinders dislocation motion undergoes static or dynamic drop 11 p1807 A67-24568

Reversed speed effect and grain boundary diffusion as explanations of discrepancy of activation energy values for strain aging under fatigue or simple stress conditions 12 p2013 A67-25284

Etch pitting analysis of slips in Fe-Si bicrystals under plastic strains, noting effect of impingement of pure edge and pure screw slip bands 17 p2872 A67-32738

Si-Fe deformation in tension/compression noting orientation dependence of yield stress, slip band formation and direction of screw dislocations 17 p2872 A67-32741

Slip band length in plate with circular hole determined in terms of linear theory of elasticity 19 p3344 A67-35848

SLIP FLOW

Relative eddy flows mechanism in mixed flow turbomachines 12 p1891 A67-25348

Rotating blades cascade performance in mixed flow turbomachines, noting flow characteristics and slip factors 12 p1892 A67-25350

Drag coefficient for cylinder rotating in rarefied gas, comparing numerical method and approximate analytical solution 13 p2101 A67-26963

Velocity distribution function of re-emitted molecules effect on slip flow boundary conditions 13 p2102 A67-26970

Slip flow of incompressible viscous fluid past permeable infinite plate during fluid seepage into main homogeneous outer flow 18 p3023 A67-33419

Particle mass spectrum development in rocket nozzle, assuming droplet growth by collision and agglomeration as dominant mechanism 20 p3516 A67-37130

Fringing effects on electric efficiency variation with slip for cylindrical induction MHD device operable as accelerator, generator or Joule heater [AIAA PAPER 67-714] 21 p3673 A67-38740

Kramers problem for rarefied gas flow, calculating slip coefficient for various collision frequency models, noting only slight model dependence 22 p3841 A67-39718

Cyclic stress-strain in annealed and cold worked fcc polycrystalline metals and alloys studied for hardening and softening by transmission electron microscopy 22 p3821 A67-40033

Dislocation structure of tension deformed SI samples investigated by electron microscopy 23 p4042 A67-41296

SLIPSTREAM

SA PROPELLER SLIPSTREAM

Instability of gravitating slipstreams or mixed streams and cloud fragmentation of interstellar gas 03 p0511 A67-13877

Slipstream propulsion theory, taking into account reacceleration which places power balance in proper perspective for efficiency gain 12 p1988 A67-25214

Tangentially injected plane jet spreading in slipstream at various Reynolds numbers at jet inlet slot studied in wind tunnel for dynamic behavior 17 p2839 A67-32906

SLOPE

SA GLIDE SLOPE

SA INCLINATION

Martian secular changes and dark area regeneration attributed to movement of sand, dust and wind caused by elevation and slope differences 16 p2747 A67-30989

Effect of deviation of inlet fluid temperature change from step change on maximum slopes of transient response curves
[ASME PAPER 67-HT-79] 20 p3551 A67-36757

Anabatic winds caused by solar heating of slope, investigating flow patterns useful for soaring purposes 24 p4181 A67-42022

SLOSHING
S LIQUID SLOSHING

SLOT
Wave diffraction in rectangular waveguides passing through double ribbon barriers 05 p0775 A67-16956

Numerical results of slot couplings of rectangular single mode waveguides as function of length, width, position and wavelength 05 p0775 A67-16957

Elastic deformation of unbounded transversely isotropic body with internal plane circular slot under slot surface load 11 p1876 A67-24681

RF plasma at electron cyclotron frequency produced with axially slotted metal cylinder 19 p3275 A67-35111

Compensation method for longitudinal slot effects on propagation constant and characteristic impedance of rectangular waveguide used in standing wave meter 23 p4000 A67-41220

SLOT ANTENNA
Planar slot array with four independent beams, discussing special design problems and effect of dimensional tolerances on port isolation 02 p0211 A67-11594

Symmetrical radiation feed patterns which are consequence of specified form of hybrid mode fields as disclosed by focal plane analysis 02 p0213 A67-11615

Aperture admittance, material loading and higher order modes effect on rectangular cavity slot antenna design 02 p0218 A67-12098

Waveguide-slot antenna design, considering interaction of radiators on principal wave 03 p0385 A67-13951

Slot couplings of rectangular single-mode waveguides analyzed by equivalent circuit and concentrated parameter methods 03 p0385 A67-13952

Slot filters for H waves in circular waveguide 03 p0386 A67-13960

Broadening of frequency bandwidth of slot array antenna by adopting center fed method 04 p0585 A67-15505

Omnidirectional slot antenna with two slots resonant at frequencies nearly octave apart and fed by single common waveguide 04 p0590 A67-15904

Simultaneous radiation of center-fed slotted rectangular waveguide array antenna for monopulse tracking radar 04 p0590 A67-15905

Flush cavity VOR antenna for DC-9 aircraft permitting omnidirectional radiation pattern characteristics 04 p0590 A67-15906

Plasma sheath simulation used to analyze effects of sheath discontinuities and inhomogeneities on slot antenna radiation pattern and input impedance 05 p0769 A67-16000

Input admittance of slot antenna after RF voltage breakdown 05 p0775 A67-16947

Control of polarization of radiation field of waveguide-slot antenna emitter 07 p1153 A67-19598

Formative time lag for pulsed RF breakdown in dry air as function of gas pressure and power of slot antenna 07 p1153 A67-19607

Transmission and reception properties of equatorial slot antenna on plasma clad reentry sphere 11 p1757 A67-23973

Segmented two-stage waveguide-slot scanning antennas with intersegment phase shifters connected in series in transmission line 16 p2637 A67-31026

Design guides for efficiency, bandwidth and resonant frequency derived from slot antenna analysis, using variational methods 16 p2638 A67-31334

External mutual coupling of rectangular waveguide-slot emitters, deriving coefficient of reflection 17 p2826 A67-32683

Mutual admittance of slot antennas measured for free space and ionized environment by different techniques 19 p3194 A67-35516

Effect of angular direct current magnetic field on radiation of slot antenna located on metal cylinder covered by plasma sheath 19 p3184 A67-35811

Offset impedance sheet effect on admittance of slot antenna in conducting plane 19 p3197 A67-35823

Control of polarization of radiation field of waveguide-slot antenna emitter 20 p3401 A67-37337

Radiation pattern lobing structure elimination for recessed annular slot in coated metal cylinder 22 p3767 A67-39274

Dielectric cover effect on resonant frequency of slots in rectangular waveguide, using Stevenson free space theory and plane-wave reflection coefficient 23 p3978 A67-40824

Radiation pattern, absorption and impedance measurements of conical antenna plasma sheath about dielectric coated metal cone excited by axial radiating slot 23 p3973 A67-40840

Diffraction of H-polarized plane wave on metal grating with narrow slits 23 p3975 A67-41683

Mutual admittance of infinite conducting slot antennas covered by dielectric layer and impedance sheet, noting losses effects on waveguide modes 24 p4133 A67-42818

SLOTTED ANTENNA
Helicopter main rotor blade used as scanning radar antenna 04 p0579 A67-14491

Electrical properties of slotted waveguide bridge section based on symmetric terminal network theory and classical thermodynamical methods 04 p0582 A67-15147

Pulsed RF slot antenna breakdown controlled by preionization and diffusion 11 p1758 A67-24126

Transmission line approach for determining input admittance of slotted antenna array covered by dielectric sheet 11 p1762 A67-24293

Radiation characteristics for slotted cylinder covered with magnetized inhomogeneous plasma sheath assuming parabolic electron density distribution 11 p1753 A67-24306

Transverse resonance method applied to slotted inhomogeneous circular waveguide with leaky wave mode propagation 11 p1766 A67-24690

Slotted inhomogeneous waveguide propagation behavior investigated, using transverse equivalent network 11 p1766 A67-24691

Radiation patterns of annular slots on conducting conical surface subjected to harmonic excitation 13 p2080 A67-27026

Waveguide structures for double beam leaky wave antennas 13 p2082 A67-27408

Slotted-sphere antenna immersed in plasma measured for RF admittance 14 p2283 A67-28377

Electrical properties of slotted waveguide bridge section based on symmetric terminal network theory and classical thermodynamical methods 15 p2443 A67-29334

Propagation coefficients of leaky waveguide modes improved by corrections to radial line susceptance arising from uniform slot in wall of circular waveguide 17 p2812 A67-32317

Equivalent circuit of two-port antennae with application to magic-T systems 18 p3013 A67-34527

Radome antenna systems design utilizing dielectric structure applicable in aircraft, spacecraft and missile systems 22 p3775 A67-40468

Omnidirectional double slot array of thin X-band rectangular waveguides, noting design for slot conductance and power handling capacity 23 p3977 A67-40699

SLOTTED WIND TUNNEL
Lateral efflux from flow along wall into suction slot computed by conformal mapping contraction coefficient 10 p1627 A67-23559

Wind tunnel studies of heat shield over plane surface with film cooling during injection through two tangential slots 11 p1884 A67-25055

SLOW NEUTRON
Detection of slow neutrons escaping from atmosphere by counters filled with boron fluoride onboard high altitude balloons 02 p0312 A67-12599

Fast and slow neutrons detected by proportional and scintillation counters 02 p0312 A67-12606

Atmospheric slow neutron flux measurement in energy range from thermal to 100 ev carried out with sounding balloons from 1960 to 1962 05 p0885 A67-17140

Atmospheric slow neutron flux measurement in energy range from thermal to 100 ev carried out with sounding balloons from 1960 to 1962 21 p3698 A67-38482

SLURRY
S COLLOID
S EMULSION

SM-A
S SAN MARCO SATELLITE

SMALL PERTURBATION FLOW
Small-perturbation hover dynamics motion equations, characteristic modes, stability derivatives and dimensional analysis [SAE PAPER 660576] 01 p0010 A67-10570

Small amplitude wave propagation in equilibrium plasma studied using collision model proposed by Bhatnagar, Gross and Krook 03 p0481 A67-13738

Small amplitude wave propagation in ionized high temperature gas embedded in uniform magnetic field with Hall current 03 p0482 A67-13742

Transonic airfoil problem solved via differentiation of airfoil thickness ratio by infinitesimal perturbation method [AIAA PAPER 66-90] 08 p1276 A67-20563

Small perturbation analysis of observed organized cloud convection for arbitrary unidirectional wind 08 p1350 A67-20950

Lagrange and Euler representations of particle shapes and vortex theorems in hydrodynamic flow 13 p2094 A67-26644

One-dimensional small signal linear model of fluid transmission line using finite lumped parameter elements and Navier-Stokes equations 14 p2247 A67-28265

Lighthill uniformization technique applied to singular perturbation problems using Lagrange expansion 14 p2346 A67-29059

Oscillations of polytropic and compressible cylinders investigated by small perturbation method noting separate mode of gravitational instability 22 p3896 A67-40526

SMEETING
Optimal thickness of protective action of crucible lining in smelting of titanium 07 p1200 A67-19250

SMOKE
Apparatus for particulate smokes generation, control and sampling, noting combination with angular scanning spectropolarimeter 12 p1946 A67-25982

Smoke generator control and performance for flow visualization applications [JPL-TR-32-1117] 14 p2293 A67-28751

Fuel additives investigated for jet engine exhaust smoke elimination [SAE PAPER 670866] 24 p4206 A67-42006

SMOKE TRAIL
Cool burning smokeless propellants for gas generator applications and low signature missiles evaluated against criteria 15 p2544 A67-29981

Transverse wave structure in detonations investigated using smoked-foil technique in gas mixtures, showing dependence on tube geometry and heat capacity 18 p3153 A67-33828

Mesosphere winds and turbulence observed by forming aluminum oxide smoke trails 18 p3043 A67-34496

Gaseous ternary diffusion instabilities observed by ammonium chloride smoke technique, studying pressure and composition effects 22 p3917 A67-39713

SMOOTHING
SA DATA SMOOTHING
SA POLISHING
Smooth surface interpolation applied to finite element displacement analysis of rectangular plate 05 p0925 A67-17372

Smoothing filter with output controlled parallel transistors, discussing empirical and experimental formulas and approximate circuit calculation 06 p0971 A67-18215

Smoothing filter with output controlled parallel transistors, discussing empirical and experimental formulas and approximate circuit calculation 16 p2635 A67-30481

Filter and error-covariance equations developed for optimal fixed-point smoothing for continuous linear systems 16 p2648 A67-31652

Uniqueness theorem for Cauchy problem, elliptic equations with double characteristics derived by imposing smoothness condition 20 p3475 A67-36456

Output noise variance minimization, calculating smoothing coefficients for discrete time invariant filters used in

sampled data systems 21 p3601 A67-38949
Laser emission nonlinear effects for materials with internal induced absorption noting pulse elongation and spatial smoothing 24 p4168 A67-42370

SMS
S SYNCHRONOUS METEOROLOGICAL SATELLITE /SMS/

SMU
S SPACE SELF-MANEUVERING UNIT /SMU/

SNAKE
Glands in two sea snakes located in oral area compared, identified and proved not to be salt glands 21 p3573 A67-37898

SNAP-8
Postirradiation radiochemical and spectrochemical analysis of short-cooled samples of SNAP-8 experimental reactor primary coolant 03 p0466 A67-13798
SNAP-8 reactor oscillating bearings to provide low friction self-lubrication at 1150 degrees F [ASLE PAPER 66AM 7A1] 08 p1335 A67-21034
Orbiting Energy Depot, discussing fuel regeneration and resupply to enable use of fuel cells combined with nuclear power as main onboard power 22 p3902 A67-39948
SNAP-8 powered Brayton cycle system for large space stations noting components and overall design 24 p4102 A67-42490
SNAP-8, nuclear electric power-conversion system /PCS/ designed for operation in space, using liquid metals as working fluids 24 p4184 A67-42497
Integrated thermoelectric SNAP-8 Rankine power system for manned lunar base missions, studying man-system interactions effect on design criteria 24 p4185 A67-42544
Integrated design requirements of SNAP-8 Rankine power system for manned lunar base mission, discussing mission requirements and reactor shield system 24 p4185 A67-42545
SNAP-8 type reactors and shield subsystems for MORL and manned lunar base plants, discussing Rankine and thermoelectric power conversion systems 24 p4186 A67-42546

SNAP PROGRAM
Heat flux to SNAP reactor system models in hypersonic continuum flow measured in shock and hyperthermal wind tunnels, using thin film resistance thermometer 01 p0112 A67-11022
Thermoelectric generators, discussing design capabilities of SNAP series and thermoelectric materials 07 p1131 A67-19191
SNAP-10A and SNAP-8, discussing reactor thermoelectric space power program 08 p1352 A67-21052
Nuclear power and propulsion systems for space applications, discussing present and future technologies [AAS PAPER 67-132] 15 p2516 A67-29967
System for nuclear auxiliary power, covering spaceflight test of SNAP-10A, system testing, performance evaluation, etc 16 p2701 A67-30638
High pressure hydrogen atmosphere drop calorimeter for SNAP reactor fuel specific heat measurement, discussing calibration problems 18 p3052 A67-34515
Thermoelectric converter designed for operation with SNAPOODLE /hybrid radioisotope thruster/ electric generator/, discussing test results 24 p4184 A67-42507

SNAP-10A
SNAP-10A high emittance white coating, noting stability at 600 degrees F, irradiation and vacuum and mechanical vibration [AIAA PAPER 65-652] 03 p0448 A67-13057
SNAP-10A flight test instrumentation performance, discussing exceptions 08 p1330 A67-20655
SNAP-10A design, ground test and flight test 10 p1678 A67-23853
Data handling and reduction evolution for SNAP-10A from manual methods to completely electronic and computerized flight test telemetry 20 p3482 A67-36957

SNAP-19
Program for radioisotopic power on Nimbus B spacecraft provided by SNAP-19 generators 05 p0843 A67-16553

SNAP-27
Beryllium braze joining for light stiff components noting structural examples and fabrication techniques, with reference to Apollo SNAP-27 radiator housing

[SAE PAPER 670805] 24 p4159 A67-41991

SOAP
Soap and nonsoap base greases physical and chemical nature, composition, characteristics and additives 20 p3455 A67-37265

SOCIAL FACTOR
Psychosociological problems of small isolated groups working under extreme conditions in lunar laboratory 02 p0185 A67-12374
Model for social system for extended-duration spaceship crews subject to isolation, confinement and/or stress 03 p0366 A67-14293
Global examination of growth of aircraft noise nuisance in vicinity of airports, determining index of community nuisance 05 p0751 A67-16385
Global examination of growth of aircraft noise nuisance in vicinity of airports, determining index of community nuisance 09 p1439 A67-21702
Medical factors involving ATC information displays 13 p2064 A67-27564
Airport economics application to new airports, considering social implications, cost, profit and land value [SAE PAPER 670356] 17 p2974 A67-32995
Intelsat and communications satellites economic, political and social consequences, UN General Assembly Resolutions and use of satellite facilities for distribution of TV transmissions to broadcasting stations 18 p3162 A67-34354
Individual caged mice susceptibility found greater than groups to toxic effect of d-amphetamine [AFOSR-66-1883] 19 p3178 A67-35885
Frequency bands and modulation methods for space communication system 21 p3581 A67-38235

SOCIAL ISOLATION
Isolation of Acinetobacter anitratus from subject and room area during spacecraft environmental tests 21 p3573 A67-38072
Isolation effects in constant environment on cycles of physiological functions and performance levels of man 23 p3959 A67-41697

SOCIOLOGY
Network-diagram methods theory, discussing CPM, PERT, MPM, noting applications to technology and sociology 16 p2783 A67-31631

SODIUM
SA ALKALI METAL
SA LIQUID SODIUM
MOS capacitance measurements combined with neutron activation analysis, showing positive charge increase at oxidized silicon surfaces by sodium presence 02 p0300 A67-12518
Artificial sodium cloud in twilight produced by French rocket studied, using auroral spectrophotometer and cameras 03 p0412 A67-13370
Artificial cloud produced in twilight over Wallops Island by payload containing sodium azide and lithium azide 03 p0412 A67-13371
Emission from sodium trail released from rocketborne vaporizer in height range 85 to 165 km during aurora of brightness IBC II 03 p0412 A67-13372
Rocket payload with weight of 9 lb for release of sodium and lithium in aurora for study of D-region ion concentration and emission 03 p0413 A67-13375
Free convective heat transfer measurements of sodium boiling on surface of horizontal tube 04 p0736 A67-15860
Boiling Na free-and forced-convective heat transfer rates, surface temperature and pool-boiling heat-transfer coefficient measurements 04 p0737 A67-15861
Ultramafic rock content of Na, Mn, Cr, Sc and Co determined by neutron activation technique 07 p1183 A67-20142
Viscosity and thermoconductivity of vapors of sodium and potassium 09 p1579 A67-21865
Characteristic optical density and equilibrium of alkyl-sodium and aromatic hydrocarbons as function of temperature and wavelengths, correlating electron affinity with enthalpy values 09 p1458 A67-22214
Free sodium atom distribution in upper atmosphere related to diurnal and nocturnal variation 10 p1645 A67-23262
Space correlation of main emission lines for night sky emission spectra and altitude distribution of sodium

luminescence 10 p1647 A67-23279
Changes produced in urinary sodium, potassium, and calcium excretion in mice exposed to homogeneous magnetic field 10 p1600 A67-23819
Cross correlation /by superposed epoch method/ between upper atmospheric sodium and stratospheric warmings at high latitude 13 p2110 A67-26441
Sodium effect on dwell time and transport rates of various elements using DC arc, stressing spectral consequences 17 p2888 A67-32377
Collisional de-excitation rate or quenching of sodium in flat premixed laminar flames 18 p3150 A67-33803
Quantitative method for determining sodium in gas turbine fuels by direct spectral analysis of unashed fuel samples 21 p3688 A67-38016
Na and water excretion, renal plasma flow and glomerular filtration rate lowered by lower body negative pressure /LBNP/, noting application to space flight weightlessness [SAM-TR-65-329] 24 p4110 A67-41801

SODIUM ALLOY
Syringe injection system for seeding plasma with Na-K alloy in study of MHD power generation and propulsion 08 p1279 A67-20377
Premelting of predetermined sites in sodium-potassium alloys studied by transmission UV microscopy 14 p2339 A67-29032
Sodium-potassium alloy thermodynamic properties and ordering, with pairing model for configurational entropy loss 21 p3733 A67-39106

SODIUM AZIDE
Nucleic acid metabolism in Chinese hamster fibroblasts grown in vitro noting effects of concentrations of sodium azide 21 p3575 A67-38798

SODIUM BROMIDE
Gradient-elastic tensor of ions in sodium chloride and sodium bromide crystals determined from effects of static elastic strain on nuclear magnetic resonance 02 p0280 A67-11485

SODIUM CHLORIDE
Gradient-elastic tensor of ions in sodium chloride and sodium bromide crystals determined from effects of static elastic strain on nuclear magnetic resonance 02 p0280 A67-11485
Epitaxial deposition of Van Arkel zirconium on sodium chloride and calcium fluoride cleavages at various temperatures 02 p0286 A67-11711
Elastic interaction energies between edge and screw dislocations and tetragonal defects in anisotropic NaCl lattice 02 p0298 A67-11885
Self-focusing of ruby laser beam in NaCl crystals 02 p0252 A67-12481
Third order elastic constant for NaCl and KCl single crystals by ultrasonic pulse techniques 07 p1238 A67-20218
Electrical conductivity measurements of NaCl as function of particle size and temperature used to study subsurface diffusion 12 p1987 A67-26191

SODIUM COMPOUND
Nickel protective coating on large parts through chemical reduction of nickel salt by sodium hypophosphite, discussing technological and economic aspects 14 p2324 A67-28609
Raman effect in solutions of potassium, sodium and ammonium dichromate and potassium dichromate single crystal 19 p3240 A67-35421

SODIUM D-LINE
Sodium dayglow emission measurement by Zeeman photometer, presenting calculation of radiant energy absorption by sodium vapor in magnetic field 03 p0409 A67-12945
Linear polarization of comet Na D-lines 05 p0891 A67-16406
Central intensities and profiles of sodium D lines in solar spectrum, discussing atomic and photospheric data 10 p1704 A67-22885
Free atomic sodium distribution in daytime upper atmosphere, noting thin layer formation and radiative transfer theory 15 p2475 A67-29616
Brightening observed near D-2 line of sodium I on July 28, 1966 17 p2939 A67-33396
Sodium D lines in Comet Ikeya-Seki /1965 f/ near perihelion passage noting possible

formation by resonance scattering at comet densities and temperatures 22 p3880 A67-39414

SODIUM IODIDE

Electron conduction band structure of NaI crystals, using Hartree-Fock-Slater modified equation 03 p0495 A67-13513

Thermionic and electrical sorption properties of tungsten in alkali iodide vapors at high pressure 17 p2887 A67-32201

SODIUM NITRATE

Isothermal kinetics and self-heating in binary mixtures of Mg and sodium nitrate as function of temperature and reactant composition 07 p1238 A67-19072

SODIUM SALICYLATE

UV sensitivity increase in sodium salicylate photomultiplier combination 07 p1185 A67-19405

SODIUM VAPOR

Intensity of sodium D-lines and auroral nitrogen band produced by sodium trail in aurora measured by calibrated photometer 03 p0412 A67-13373

Upper atmospheric wind measurement by artificial cloud method which releases sodium at twilight and trimethyl aluminum at night 05 p0798 A67-16858

Upper atmospheric wind measurements derived from ~ vapor trail soundings 06 p1025 A67-17594

Aerobee rockets measurement of sodium dayglow suggest equilibrium between sodium atoms and distribution of dust particles 07 p1180 A67-19917

Temperature dependence of saturated vapor pressure of sodium and potassium 09 p1579 A67-21857

Low temperature alkali plasmas in strong magnetic fields interpreted in terms of collisional drift modes 10 p1684 A67-23073

Electron conductivities calculated for sodium-xenon and sodium-xenon-mercury plasmas assuming local thermal equilibrium, estimating plasma temperatures and electron number densities 19 p3278 A67-35134

Sodium cloud between 85 and 110 km shows turbulent phenomena stratification exists and disappears with upward propagation of movements due to energy decreases 20 p3427 A67-36367

Optical pumping of sodium vapor with deuterium light, discussing optical transparency in excited state mixing cross sections 21 p3639 A67-38018

Ionization potentials of clustered sodium atoms measured, describing experiment involving mass spectrometry 21 p3660 A67-39109

SODIUM 24

Slow motion gamma spectrometry for measurement of sodium 24 abundance in Saint Severin meteorite, evaluating modes of formation 16 p2754 A67-31790

SOFT LANDING**SA LUNAR LANDING**

Terminal descent design for unmanned vehicle soft lunar landing in Surveyor project [AIAA PAPER 64-644] 02 p0263 A67-11923

Subsonic and supersonic parachutes for soft landing on Mars, discussing aerodynamic coefficients, descent rate, dynamic stability, inflation, porosity and wind effects, etc 04 p0551 A67-14574

Soft landing problems for unmanned Mars entry noting parachute system, descent time, sensing system constraints, extreme wind environment, etc 04 p0706 A67-15236

Guided propulsive solution to Mars atmosphere-decelerated soft landing vehicle trajectory [AIAA PAPER 67-170] 06 p1029 A67-18508

Soft landing of manned spacecraft on lunar surface 07 p1258 A67-19429

Chemical analysis of lunar surface composition by instruments on board soft landing probes 07 p1186 A67-19571

Propellant requirements for unmanned lunar and interplanetary soft landing vehicles presented with equations that couple injection, midcourse and terminal phases [AAS PAPER 66-129] 07 p1241 A67-19988

Approaching and soft landing on planet surface in absence of atmosphere, finding optimum acceleration vector control as function of generalized parameters 09 p1571 A67-21889

Reliability effect on design of lunar soft landing spacecraft /Surveyor/, Syncoms I, II

and III, Applications Technology Satellites, Early Bird and four Intelsat IIs 09 p1582 A67-22302

Propellant requirements for unmanned lunar and interplanetary soft landing vehicles presented with equations that couple injection, midcourse and terminal phases [AAS PAPER 66-129] 13 p2214 A67-27540

Terminal guidance concept for soft and accurate lunar landing of unmanned spacecraft [AIAA PAPER 67-594] 19 p3259 A67-35990

Subsonic and supersonic parachutes for soft landing on Mars, discussing aerodynamic coefficients, descent rate, dynamic stability, inflation, porosity and wind effects, etc 20 p3356 A67-36408

Spacecraft in lunar exploration by type and properties, emphasizing soft landing and orbiting mooncraft 20 p3526 A67-37249

Computer analysis and simulation of Mars soft landing descent control system combining inertial and radar sensing techniques 22 p3898 A67-39177

Performance and feasibility of staged propulsion during terminal phase of Mars soft landing [AIAA PAPER 67-987] 24 p4246 A67-43059

SOFT RECOVERY

In-flight escape of helicopter personnel using Navy fuselage capsule, describing devices for recovery, protection and survival 17 p2794 A67-31999

SOIL**SA LUNAR SOIL****SA MINERAL**

Soil mechanics surface sampler experiment for Surveyor 08 p1410 A67-20945

Optical rotation of lipids extracted from soils, sediments and Orgueuil carbonaceous meteorite 08 p1289 A67-21173

Response of fungi to diurnal temperature extremes, describing soil, simulated Martian temperature regime and fungi growth 09 p1454 A67-21991

Fluorimetric technique for phosphatase activity in soil based on beta-naphthol release from sodium-beta-naphthylphosphate 14 p2254 A67-28067

Ecological patterns of microorganisms in desert soils 15 p2426 A67-29112

Microbial numbers relation to phosphatase activity in soil, discussing seasonal variation, sterilization by irradiation and moisture content 18 p2991 A67-33660

Pedoscope use in soil microbiological studies including ecology, infection susceptibility, etc 19 p3179 A67-35205

Transiently loaded foundation on soil designed using graphical phase-plane analysis, considering soil stiffness and damping effect [AIAA PAPER 67-550] 19 p3208 A67-35947

SOLAR ABSORBER

Surface blistering of metals due to low energy hydrogen ion bombardment, determining solar absorptance change in gold-plated specimens 08 p1343 A67-21520

Spacecraft surface temperature-control coating requirements, selection and performance in prelaunch and space environments 16 p2757 A67-30634

Simulated solar absorptance of spacecraft thermal control coatings determined calorimetrically in vacuum at room and cryogenic temperatures 24 p4256 A67-42913

SOLAR ACTIVITY**SA PROMINENCE****SA SPICULE****SA SUNSPOT**

Radio whistler occurrence in nighttime and daytime during maximum and minimum solar activity 01 p0057 A67-10261

Profile and fine structure of diurnal variation of cosmic ray intensity during high and low solar activity 01 p0144 A67-10810

Cosmic radiation data obtained by two gas-discharge counters installed in Luna X artificial satellite 01 p0145 A67-10906

Recurrent cosmic-ray modulation phenomena with Forbush decrease characteristics correlated with M-region magnetic storms, concluding that each series results from shock wave solar initiated 01 p0145 A67-10919

Solar prominences, proton flares and chromospheric flares in intensity of corona and solar radio emission and sunspots, noting maxima during eleven-year solar activity cycle 01 p0146 A67-11281

Heliocentric earth orbit precursor satellite, noting position outside earth and moon gravitational fields, orbital stability for solar phenomena evaluation, etc 02 p0335 A67-12410

Stellar diurnal variation determined during reduced solar activity from crossed-telescope and neutron monitor data 02 p0311 A67-12594

Energy spectrum of variations in cosmic ray intensity and changes in spectrum with decreasing solar activity calculated for additional particle flux 02 p0311 A67-12597

27-day changes in solar diurnal variation from 1957 to 1958 based on neutron component data, noting modulation of cosmic ray anisotropy 02 p0312 A67-12600

Babcock theory of solar activity, quiet sun and 11-year magnetic cycle 02 p0330 A67-12639

F region ionization equatorial anomaly during two periods of minimum sunspot activity in 1965 03 p0407 A67-12827

Anomalous variation in composition of lower ionospheric ion recombination coefficient as function of height, zenith angle and level of solar activity 03 p0411 A67-13346

Zodiacal light brightness variation during solar activity cycle 03 p0413 A67-13454

Zodiacal light and solar activity, examining results of visual observations and photometric measurements for correlation between phenomena 03 p0413 A67-13455

Relative sunspot numbers and variations within each cycle and from cycle to cycle 03 p0511 A67-13809

Explorer XXII satellite measurement of total electron content from Faraday rotation recordings, noting correlation with solar activity above 80 solar flux units [RASSA PAPER 1-10-124] 03 p0416 A67-14235

Diurnal variations of ionospheric ion composition over Arecibo at various altitudes for solar minimum winter and summer conditions 04 p0614 A67-14955

Solar corona and chromosphere activity observations at lunar observatory in gamma, X-ray and XUV regions 04 p0598 A67-15071

E layer stratification, fine structure and boundary accuracy in frequency measurements based on seasonal variations in solar activity 04 p0618 A67-15574

Secular modulation of galactic cosmic rays in interplanetary space as function of solar activity 05 p0877 A67-16083

Space and time characteristics of electron fluxes penetrating into terrestrial atmosphere in auroral zone, based on riometer measurements 05 p0879 A67-16101

Intensity of ionizing and neutron component of cosmic rays, noting correlation for sporadic cyclic variations and solar activity cycles 05 p0879 A67-16103

Solar cosmic ray generation during chromospheric flares, noting increased neutron intensity 05 p0880 A67-16112

Temporal distribution of first and second harmonic of solar diurnal variation of cosmic rays after radio bursts of fourth type 05 p0881 A67-16116

Variation of seasonal diurnal distribution of sudden changes in cosmic ray neutron component intensity related to solar activity changes 05 p0881 A67-16118

Solar diurnal variation of cosmic ray neutron component in Antarctic during minimum activity period, using harmonic analysis 05 p0881 A67-16119

Amplitude of 27-day cosmic ray modulation in relation to solar and geomagnetic activities 05 p0881 A67-16122

Cosmic radiation directional intensity during solar activity minimum, noting altitude dependence of charged particle photon flux 05 p0883 A67-16878

Solar hydrogen convection zone interaction with photosphere restricted to relation of convection theory to granulation and supergranulation 05 p0899 A67-17070

Diffusion reflections during cycle of solar activity, showing frequency changes according to increase in solar activity 05 p0800 A67-17127

Specific type of geomagnetic pulsations corresponding to solar corpuscular radiation, noting flux geometry and intensity variations 05 p0884 A67-17134

Quasi-spiral nature of change in 27-day cosmic ray variation with solar activity shown by harmonic analysis 05 p0884 A67-17137

Seasonal changes in solar diurnal and semidiurnal variations of cosmic ray neutron component due to earth rotation axis and anisotropy sources 05 p0885 A67-17138

Temporal variations in values of variability characteristic of parameters of ionosphere cross sections below principal maximum 05 p0801 A67-17142

Changeability laws in quiet solar diurnal magnetic variations in 1964 and relation to state of ionosphere resulting from dynamo effect 05 p0802 A67-17147

Rotation of vector of solar diurnal variation in intensity of cosmic radiation neutron component during solar activity minimum 05 p0885 A67-17497

Low energy heavy nuclei analyzed by slicing emulsion in connection with solar activity studies 06 p1076 A67-17634

Sun generated high and low energy protons analyzed, using semiconductor detectors during flights of interplanetary probes 06 p1077 A67-17841

Loss coefficient and vertical transport velocity for nighttime F region during solar activity 06 p0995 A67-17971

Upper atmospheric condition noting solar activity effect, synoptic meteorology, etc 06 p1027 A67-18607

Stormer height measurements of aurora, analyzing height distribution at various geomagnetic latitudes, noting relation to solar activity 06 p0997 A67-18694

Soviet book on comets covering photometric and spectral studies, solar activity, structural elements, characteristics tables and bibliography 07 p1247 A67-19300

Interplanetary gas, solar corpuscular activity and magnetic storms and zodiacal dust cloud from satellite observations during IQSY and use of cometary tail as plasma probe 07 p1248 A67-19333

Ionospheric propagation index for short term prediction of short wave propagation 07 p1248 A67-19409

Atmospheric potential gradient near ground in polar region correlation with solar radio emission on 1000 mc 07 p1172 A67-19423

Book on structure of stratosphere and mesosphere noting rocket exploration results, synoptic observations, solar control over temperature variations, etc 07 p1172 A67-19603

Longitudinal variations of characteristics of F-1 layer compared for periods of high and low solar activity 07 p1173 A67-19688

Solar causes of geomagnetic storm with sudden or gradual commencement 07 p1175 A67-19720

Electron density variation, solar activity and geomagnetic storm effects on ionospheric F-region theory 07 p1177 A67-19785

Estimation of ion formation rate at various altitudes in ionosphere and zenith angles during low and high solar activity periods 07 p1178 A67-19830

Definition and computation of daily solar flare activity index 07 p1251 A67-19945

Relationship between terrestrial and Jovian atmospheric circulations due to solar activity 08 p1398 A67-21215

Active region corona and type I bursts supposedly generated by plasma oscillations excited by electron beam 08 p1377 A67-21445

Hydrogen, He and ionized Ca lines in chromospheric spicules, noting large scale motion in spicule interior indicated by line width expansion and peculiarities in shape of line contours 09 p1563 A67-21627

Cosmic ray intensity variation detection with respect to sidereal time on basis of simultaneous amplitude phase modulation 10 p1698 A67-22780

Intensity gradient of galactic cosmic rays, analyzing modulation induced by solar activity 10 p1699 A67-22801

Polar auroras during minimum of solar activity cycle, winter 1963-64 and 1964-65 10 p1631 A67-22802

Cosmic ray nucleonic component in Antarctic zone measured by neutron monitor, standardized and related to solar activity 10 p1699 A67-22862

Latitudinal and seasonal variations in atmospheric densities during low solar activity obtained by inflatable air density satellites 10 p1639 A67-23211

Surveillance of solar activity based on optical observations of

satellites 10 p1606 A67-23222

Eleven year solar activity cycle noting presence of two maxima 10 p1711 A67-23801

Galactic radio noise intensity decrease correlated with decline in solar activity, calculating D and F region absorption 11 p1784 A67-23934

Polar bright surges at limb, showing frequency and parameters of occurrence 11 p1882 A67-24496

Solar flare data computerized, reducing reported values of importance and area to standard scales, considering universal time and day 11 p1856 A67-24497

Lunar influence on total electron content of winter ionosphere at minimum solar activity 11 p1788 A67-24771

Type IV bursts and associated active regions 12 p1993 A67-25131

Comet Encke tail variation and apparent correlation with solar activity 12 p2000 A67-25137

Spectral analysis of geomagnetic pulsations from 0.5 to 100 sec in period for quiet sun condition 12 p1932 A67-25189

Brightness distribution of radio emission over solar disk during solar activity minima determined from radioheliograms 12 p2001 A67-25226

Ionospheric radio wave absorption, noting inverse correlation between solar activity with stability of reflections from sporadic E layer 12 p1933 A67-25544

Solar activity dependence of sporadic E layer, noting cyclic variation in characteristics from 1957 to 1964 12 p1933 A67-25545

Solar activity and irregular variations in earth rotational rate 12 p1933 A67-25553

Seasonal variations of total electron content of ionosphere during sunspot minimum 12 p1935 A67-25795

Solar X-ray monitoring during IQSY 12 p1999 A67-25833

Unstable diurnal and seasonal variation of ionization of F region of ionosphere during years of minimum solar activity over Ashkhabad 12 p1938 A67-26100

Solar activity relationship to terrestrial magnetic and associated auroral, ionospheric and cosmic ray effects 13 p2109 A67-26418

Solar cosmic ray events characteristics for solar minimum vs solar maximum 13 p2194 A67-27253

Preferential acceleration of heavy nuclei on sun compared with ionizing power of primary particles 13 p2195 A67-27341

Geomagnetic induction arrow direction determined from quiet solar activity variations 13 p2116 A67-27396

Sunspot decay and associated flare activity of coming minimum predicted, based on current cycle combined with sunspot lifetime and area 13 p2202 A67-27418

Departures of maxima of solar activity from parabolic law 13 p2202 A67-27420

Chromosphere observation at different millimeter radio wavelengths with 4.88-m diam telescope establishing correlation between mm solar radiation and solar activities 13 p2206 A67-27488

Atmospheric potential gradient relation to solar activity at earth surface in polar region 14 p2306 A67-27884

Electron production time variations in D layer during solar activity 14 p2378 A67-27909

Limiting frequencies median values suggested as suitable characteristics of relation between solar activity and sporadic E layer behavior 14 p2307 A67-27913

Micropulsations of earth electromagnetic field relation to disturbed diurnal solar variation 14 p2308 A67-27925

Ionospheric inhomogeneity winter drifts during periods of high and low solar activity 14 p2308 A67-27936

Lower E-region positive ion concentrations measured at time of declining solar activity by rocket installed mass spectrometer 14 p2310 A67-28049

Ionospheric index of solar activity obtained together with quadratic equation regression coefficients by minimizing standard error of F-2 layer critical frequency 14 p2311 A67-28375

Radio whistlers occurrence relationship to solar and magnetic activities at various latitudes 14 p2265 A67-28413

Profiles of cores of Ca II H and K lines in solar spectrum during maximum and

minimum activity period 14 p2387 A67-28561

Relation between number of photospheric granules and Wolf sunspot number 14 p2387 A67-28582

Atmospheric warming over Central Europe related to low solar and magnetic activity 14 p2313 A67-28621

Wideband solar-burst spectrum analyzer noting antenna design and operation 14 p2382 A67-28966

Weighted mean latitudes of sunspots of new cycle during years of minimum solar activity, determining period 15 p2552 A67-29145

Primary cosmic radiation and interaction in atmosphere studied during minimum solar activity by balloon flights to determine effect of latitude on secondary photons 15 p2550 A67-29533

Pc-1 micropulsations, noting harmonic curve for diurnal variations and effect of magnetic and solar activity 15 p2476 A67-29619

Radiation level on lunar surface noting degree of danger to astronaut, solar activity effect, creation of secondary emission, etc 16 p2737 A67-30782

Relationship between variations of critical frequencies of sporadic E layer and solar activity cycle 16 p2669 A67-31903

Drift data harmonic analysis correlation between solar quiet diurnal variation and ionospheric drift 16 p2669 A67-31908

Diurnal variation of hard component near minimum solar activity, emphasizing temperature effects 17 p2932 A67-32080

Statistical analysis of solar-diurnal and semidiurnal variations of cosmic ray neutron component with respect to geomagnetic field perturbations 17 p2932 A67-32081

Relation between frequency distribution of sudden changes in cosmic ray intensity and solar-diurnal variation 17 p2932 A67-32082

27-day cycle variation in various noncosmic ray electromagnetic complex phenomena 17 p2932 A67-32084

Biochemical reactions in human organism as indicator of cosmic ray variation, showing relationship between solar activity and erythrocytes in blood 17 p2934 A67-32099

New lower upper limit on solar neutron flux at energies greater than 60 mev for emission during quiet times 17 p2936 A67-32532

Luminosity variations of comet 1963 III related to solar and geomagnetic disturbances caused by corpuscular solar particles 17 p2946 A67-32730

Hydrogen distribution in upper atmosphere and geocorona, relating H-alpha emission increase to solar activity decrease 17 p2849 A67-32961

Solar diurnal wave from underground muon detectors and relationship to solar activity over 11-year cycle, noting phase changes 18 p3116 A67-33514

Atmospheric density determination from satellite drag, noting effects of magnetic storms, diurnal and semiannual variations, solar activity, etc 18 p3041 A67-34253

Flux, energy distribution and density of ions and electrons in magnetosphere plasma during solar activity period determined byOGO-C electrostatic probes 19 p3217 A67-35200

Fluctuations in stratospheric and mesospheric winds studied by meteorological sounding rockets, noting relation to solar activity 19 p3217 A67-35207

Exospheric density variation as related to solar activity determined from satellite orbits 19 p3217 A67-35211

Inner zone electron intensity distribution model for solar activity minimum 19 p3219 A67-35238

Synoptical and monitoring projects for solar activity, interplanetary space, magnetosphere, ionosphere, aeronomy, etc 19 p3223 A67-35475

IQSY geophysical work in Greece, examining geomagnetism, aurora, ionosphere, airglow, solar activity, etc 19 p3223 A67-35478

IQSY program in U.S.S.R. /1964-1966/ including meteorology, aurora studies, solar activity, etc 19 p3223 A67-35482

Density gradient of cosmic radiation perpendicular to plane of ecliptic as cause of variations in amplitude and phase of solar diurnal variation 19 p3315 A67-35490

Interplanetary space magnetic clouds velocity and spatial distribution obtained

from cosmic ray modulation data, noting relation to solar activity 19 p3325 A67-35493

National IQSY research programs /1964-1965/ 19 p3325 A67-35497

Canadian program for IQSY including aurora studies, solar observation, space research, etc 19 p3324 A67-35498

Statistical correlation of type III solar radio burst activity with coronal green line over solar cycle 19 p3316 A67-36029

Cross-spectrum analysis in meteorology, considering property fluxes and time series, discussing turbulent energy flux, solar activity, etc 20 p3480 A67-36786

Periodic fluctuations of cosmic ray diurnal variation statistically studied, using neutron and meson component data 20 p3518 A67-36993

Correlating lunar eclipse brightness, solar activity and corona ellipticity data 20 p3528 A67-37462

Stable height to distance to supporting magnetic field origin ratio for prominences, noting agreement with Kippenhahn-Schluter model 20 p3528 A67-37469

Astronomical research /1965/ noting New Zealand observatory, telescopes in Chile, Hawaii and China, solar activity, planet studies, etc 21 p3700 A67-37830

Ionospheric electron and ion temperatures during 10.7 cm-solar radio flux activity, giving scatter diagrams 21 p3616 A67-38000

Ionospheric conductivities, electric currents and field height variations in equatorial electrojet region calculated from model, including solar activity 21 p3617 A67-38066

Diffusion reflections during cycle of solar activity showing frequency changes according to increase in solar activity 21 p3618 A67-38470

Specific type of geomagnetic pulsations corresponding to solar corpuscular radiation, noting flux geometry and intensity variations 21 p3698 A67-38477

Quasi-spiral nature of change in 27-day cosmic ray variation with solar activity shown by harmonic analysis 21 p3698 A67-38480

Temporal variations in values of variability characteristic of parameters of ionosphere cross sections below principal maximum 21 p3619 A67-38484

Changeability laws in quiet solar diurnal magnetic variations in 1964 and relation to state of ionosphere resulting from dynamo effect 21 p3619 A67-38489

Sunspot cycles rise time and periodic variation probable values 21 p3704 A67-38511

ESRO V satellite-borne solar-proton spectrometry experiment to study proton and alpha particle energy spectra emitted during solar activity 21 p3629 A67-38663

Radial motions in small and young sunspots indicating different cooling processes than regular sunspots 21 p3707 A67-38964

Solar magnetic fields, discussing Zeeman effect, solar activity regularity and filamentary current in force-free magnetic fields 21 p3709 A67-38990

Geomagnetic activity around conjunction and opposition of planets, noting decrease in years of low solar activity 21 p3711 A67-39004

Solar disturbance variations of geomagnetic field dependence on solar activity indicates interplanetary magnetic field activity 21 p3623 A67-39041

Seasonal changes in solar diurnal and semidiurnal variations of cosmic ray neutron component due to earth rotation axis and anisotropy sources 21 p3700 A67-39048

Mean solar activity curves for 11-year and 80-year cycles from 1698 to 1964 reveal significant difference between two cycles 22 p3889 A67-40303

Solar X-ray emission below 20 angstroms made by Explorer XXX, discussing analog real time records and time resolution 23 p4050 A67-40805

Radio wave field strengths received at Ahmedabad from Tashkent and solar X-ray emission effect, noting field strength increase with solar activity 23 p4051 A67-40915

Equatorial anomaly in F-2 layer of ionosphere, examining solar activity, seasonal variation relation to magnetic activity, lunar phase and heights 23 p3996 A67-41082

Low energy cosmic ray measurements during solar activity minimum suggesting changes in cosmic ray composition due to solar wind 23 p4054 A67-41097

Neutron component intensity variation and particle generation on sun during chromospheric flares and electromagnetic radiation during solar activity cycle 23 p4057 A67-41116

Forbush effects variations during solar activity cycle using hard cosmic ray component data 23 p4057 A67-41118

Solar activity cycle effect on cosmic ray anisotropy diurnal variation 23 p4057 A67-41120

Diurnal variation in cosmic ray anisotropy from observations during solar activity minimum, giving amplitudes and phases distribution 23 p4058 A67-41122

Atmospheric temperature effect on cosmic ray hard component diurnal variation in high latitude regions, discussing anomalous diurnal variation 23 p4058 A67-41127

Solar active formations relation to annual cosmic ray variations, discussing spot group, chromospheric flares and calcium flocculi area distributions 23 p4059 A67-41132

Solar prominence activation on March 25, 1967 observed with H-alpha visual patrol refracting telescope at Anacapri 23 p4060 A67-41234

Cosmic ray intensity variation detection with respect to sidereal time on basis of simultaneous amplitude, phase modulation 24 p4209 A67-42116

Intensity gradient of galactic cosmic rays, analyzing modulation induced by solar activity 24 p4209 A67-42138

Polar auroras during minimum of solar activity cycle, winter 1963-64 and 1964-65 24 p4150 A67-42139

Secular modulation of galactic cosmic rays in interplanetary space as function of solar activity 24 p4212 A67-42759

Space and time characteristics of electron fluxes penetrating into terrestrial atmosphere in auroral zone based on riometer measurements 24 p4213 A67-42777

Intensity of ionizing and neutron component of cosmic rays, noting correlation for sporadic cyclic variations and solar activity cycles 24 p4213 A67-42779

Solar cosmic ray generation during chromospheric flares noting increased neutron intensity 24 p4214 A67-42788

Temporal distribution of first and second harmonics of solar diurnal variation of cosmic rays after radio bursts of fourth type 24 p4214 A67-42792

Variation of seasonal diurnal distribution of sudden changes in cosmic ray neutron component intensity related to solar activity changes 24 p4214 A67-42794

Solar diurnal variation of cosmic ray neutron component in Antarctic during minimum activity period, using harmonic analysis 24 p4214 A67-42795

Amplitude of 27-day cosmic ray modulation in relation to solar and geomagnetic activities 24 p4214 A67-42798

Weighted mean latitudes of sunspots of new cycle during years of minimum solar activity, determining 24 p4239 A67-43068

SOLAR ACTIVITY EFFECT

Solar activity and polar migrations role in origin and evolution of terrestrial life during Eocambrian and subsequent geological epochs 01 p0149 A67-10756

Quasi-stationary solar corpuscular fluxes, examining effect on atmospheric pressure in earth polar cap regions 01 p0061 A67-11279

Distribution of solar-tropospheric disturbances over earth surface, based on simultaneous observations of 103 U.S.S.R. stations 01 p0061 A67-11280

Temporal variations in velocity of westward drift of nondipole geomagnetic field and negative correlation with solar activity 02 p0237 A67-11679

Systematic measurement of ionospheric absorption at vertical incidence made by pulse reflection method at frequencies in range 2-3 mc. at Colombo, Ceylon 03 p0406 A67-12822

Diurnal variations in F layer at Ibadan exhibit peak before noon during sunspot maximum and after noon during sunspot minimum 03 p0407 A67-12826

Cosmic radiation intensity measurement using automatic interplanetary stations with

on board Geiger counters 05 p0879 A67-16106

Solar perturbation effect on motion near collinear earth-moon libration points [ATAA PAPER 67-24] 06 p1084 A67-18259

Small two-dimensional oscillations in XY plane for isothermal magnetosphere in uniform gravitational field, postulating Boltzmann equilibrium density distribution 07 p1173 A67-19699

Parametric analysis of stability of reflection from sporadic E layer during 11-year solar cycle 07 p1174 A67-19704

Cyclic variations in maximum electron concentration of F-2 layer with solar activity explained by upper atmosphere temperature variations 07 p1178 A67-19818

Dependence of electron concentration in F-1 layer on zenith angle of sun 07 p1178 A67-19820

Solar modulation of galactic protons and He nuclei during last solar cycle analyzed according to Parker theory 07 p1244 A67-19913

Geomagnetic, auroral, ionospheric and cosmic ray perturbations interdependence and relationship with solar activity 07 p1183 A67-20174

IGY and IQSY auroral observations at Murmansk of frequency of occurrence of polar auroras in years of solar activity maxima and minima 10 p1630 A67-22787

Amplitude variations in earth free and forced polar motion indicate periodic solar activity and moon tidal forces influence 10 p1631 A67-22798

Cosmic ray measurements in interplanetary space and on moon noting intensity increase 12 p1992 A67-25123

Light deflection by solar activity 12 p2002 A67-25540

Atmospheric density distribution at altitudes from 200 to 300 km based on Soviet satellite observations during minimum solar activity 12 p1934 A67-25788

Solar activity effect on brightness and polarization of zodiacal light 13 p2109 A67-26332

Mechanism for connection between seismic earth and solar activity on atmosphere and lithosphere of earth 13 p2111 A67-26556

Earth aerospace thermodynamic properties from 100 to 100,000 km alt predicted, considering diurnal and extreme solar activity variations for engineering applications 13 p2114 A67-26821

Ionospheric structure and micropulsations of geomagnetic field correlated, studying magnetodynamic wave damping and solar activity effects 13 p2114 A67-26856

Cosmic noise intensity at 25 MHz noting nighttime variation dependence on solar activity 13 p2201 A67-27392

Polar aurora of September 13, 1957 and geomagnetic activity attributed to extraordinary solar flares 13 p2115 A67-27393

Polar auroras statistically analyzed for relation between frequency of redness, solar activity and geomagnetic conditions 13 p2116 A67-27394

Solar activity cycle effect on northern hemisphere pressure field solar activity cycle effect on Northern Hemisphere pressure field 13 p2117 A67-27632

Interplanetary electromagnetic field effects on cosmic ray intensity noting geomagnetism, modulation mechanisms and solar flare particle propagation 14 p2380 A67-27965

Quiet sun current system effects on seasonal variations of critical frequency in E region, noting dependence on local time and latitude 14 p2312 A67-28569

Equatorial electrojet width and intensity analyzed with ground level magnetic field measurements from Peru and Nigeria 14 p2312 A67-28572

Electric current associated with polar magnetic substorms 14 p2313 A67-28573

Global response of topside ionosphere to magnetic disturbances at solar minimum studied from electron concentration measurements at 640 km 15 p2475 A67-29610

Seasonal variations in position and intensity of equatorial electrojet and correlation of latter with sunspot number 15 p2478 A67-30061

Flux-gate magnetometer device for determining attitude of satellite or rocket probe, considering magnet perturbation due to solar wind and storms 16 p2700 A67-30658

Temporal variations in velocity of westward drift of nondipole geomagnetic field and negative correlation with solar activity 16 p2665 A67-31094

Correlation of monthly and nightly green line 5577 Angstroms /OI/ airglow intensity with sunspot number and 10.7 cm flux 16 p2749 A67-31404

Search for solar M-regions complicated by velocity decrease near active sun, considering corpuscular streams as enhanced solar wind 16 p2749 A67-31414

Ionospheric irregularity effect on lateral deviation of reflected radio waves from ionosphere, noting variation with solar activity 18 p3004 A67-34617

Air density variations at heights near 150 km determined by analyzing satellite orbit changes, noting solar activity effect 19 p3215 A67-35181

Isolated solar events effects on neutral and charged earth atmosphere studied in West Germany during IQSY 19 p3223 A67-35479

Reception vectors for first and second spherical harmonics of cosmic ray distribution calculated for neutron monitor stations 21 p3699 A67-39018

Spicules and inhomogeneities in corona and interplanetary plasma compared assuming mutual relationship spicules and inhomogeneities in corona and interplanetary plasma compared assuming mutual 21 p3711 A67-39028

Planetary distribution of horizontal gradients of F-2 layer critical frequency and diurnal, seasonal and solar cycle variations 21 p3822 A67-39034

F-2 layer critical frequencies variation with solar activity, evaluating criteria for unperturbed state based on magnetically inactive days 21 p3822 A67-39035

Ionospheric F-1 layer critical frequency at sunspot minimum and maximum, discussing critical frequency diurnal variation 22 p3789 A67-39476

Solar cycle primary cosmic radiation variation above magnetosphere and radiation belts at stratosphere and surface, using neutron monitors and space vehicle measurements 23 p4055 A67-41101

Nuclear cosmic ray component intensity variation related to 27-day solar activity variation in Elektron II and IV analysis of modulating effect 23 p4055 A67-41104

Cosmic ray intensity variation mechanisms due to motion of solar system and quadrilateral interplanetary magnetic field 23 p4056 A67-41107

Cosmic ray intensity 27 day variations during low and high solar activity periods noting lower amplitude and softer spectrum 23 p4056 A67-41108

Cosmic ray intensity 19, 20 and 24 day quasi-periodic global variations in stratosphere related to solar activity variations, comparing amplitudes with Forbush effects 23 p4056 A67-41109

Solar activity effect on distribution of source power of solar diurnal cosmic ray variation in relation to ecliptic plane 23 p4058 A67-41125

IGY and IQSY auroral observations at Murransk of frequency of occurrence of polar auroras in years of solar activity maxima and minima 24 p4149 A67-42123

Amplitude variations in earth free and forced polar motion indicate periodic solar activity and moon tidal forces influence 24 p4149 A67-42134

Cosmic radiation intensity measurement using automatic interplanetary stations with onboard Geiger counters 24 p4213 A67-42782

SOLAR ATMOSPHERE

SA CHROMOSPHERE

SA CORONA

SA PHOTOSPHERE

Irregularities in fine structure of solar atmosphere with respect to radio emissions, electron density, temperature and flux density 01 p0150 A67-10891

Diffusion and dissociation of CO molecules in solar atmosphere 01 p0151 A67-11284

Solar content of carbon isotope 13 obtained by examining solar atmosphere at center of disk 02 p0324 A67-11770

Book on solar atmosphere with emphasis on chromospheric network and surface topography 03 p0515 A67-14331

Solar atmospheric circulation and fields 05 p0891 A67-16363

Observational techniques and detection of solar turbulence by local Doppler shifts of Fraunhofer lines 05 p0899 A67-17069

Three-dimensional oscillatory motions generation and propagation in solar atmosphere 05 p0900 A67-17074

Acoustic wave propagation characteristics in solar chromosphere, discussing resonant frequencies 05 p0900 A67-17075

Solar atmosphere structure over sunspots studied from radio emission data 06 p1083 A67-18153

Energy balance equations for solar atmosphere, considering hydromagnetic and thermodynamic processes, noting turbulent eddy effects 06 p1089 A67-18738

LF gravitational-acoustic and internal gravity mode wave propagation in temperature-stratified photosphere-low chromosphere region and solar atmospheric resonant responses 08 p1399 A67-21236

Emission of particles, causing geomagnetic storms, without accompanying radio effects 11 p1787 A67-24594

Electrical field in solar atmosphere caused by pressure gradient in case of partially ionized gas 12 p2000 A67-25133

Compton effect produced by thermal photons on relativistic electrons in solar atmosphere 12 p2002 A67-25528

Sunspot phenomenon covering formation, penumbra, spot umbra, magnetic field, interpretation, radiative deficit in umbra and penumbra, energy flux through Evershed stream, etc 13 p2202 A67-27416

Sunspot groups and chromospheric features associated with magnetic fields of active region in light of supergranular structure of solar atmosphere 13 p2204 A67-27434

Static magnetic field effect on normal distribution of pressure, temperature and density in solar atmosphere, considering sunspots and velocity field effects [AFCR-66-679] 13 p2204 A67-27435

Solar flux density absolute microwave spectra 14 p2385 A67-28441

Solar magnetic field origin and effects revealed by direct and satellite observations of photosphere, chromosphere, corona and earth neighborhood 15 p2554 A67-29531

Solar atmosphere structure over sunspots studied from radio emission data 16 p2741 A67-30497

He abundance in sun suggests He stellar nucleosynthesis was responsible for increase in He abundance in interstellar gas between formation of sun and present 17 p2947 A67-32763

Microwave and type IV solar bursts, examining gyrosynchrotron emission and various electron acceleration mechanisms 17 p2939 A67-33391

Lower thermal boundary layer of solar convection zone within framework of mixing length theory 18 p3133 A67-34378

Stellar and solar atmosphere outermost layers structures, finding radiative equilibrium for massive stars 19 p3322 A67-35327

Velocity fields in solar atmosphere observed with magnetograph, studying magnetic field effect on oscillations amplitude and frequency 19 p3324 A67-35434

Solar supercorona observations using three-base interferometer with correlation radiometer, discussing concentration ellipses, supercoronal inhomogeneities and interference fringe modulation index 20 p3529 A67-37515

Solar atmosphere absorption of light nuclei generated on sun indicated by satellite observation of heavy nuclei cosmic ray flux and X-ray electron bremsstrahlung 21 p3698 A67-38595

Fast electrons formation mechanism during flares ascribed to fast proton deceleration in flare region rather than high energy particle ionization 21 p3699 A67-39013

Spectral line wavelengths of solar violet bands of carbon /isotope/ nitride and hydride molecules, determining solar abundance ratios 22 p3889 A67-40207

Solar hydrogen convection zone mean stratification derived from mixing length theory, discussing zone structure dependence on temperature and density dependence of opacity 23 p4068 A67-41278

Rapid temperature increase due to lower photosphere turbulence generation of mechanical waves, discussing gravity wave

generation and acoustic noise 23 p4068 A67-41280

Static tufted magnetic field perturbing effect on solar atmosphere small scale structure, noting pressure, density and temperature changes 24 p4222 A67-41767

[SR-15] 24 p4222 A67-41767

Magnetic changes in solar atmosphere, discussing current-free field configurations using solar magnetograms and photospheric field effect 24 p4222 A67-41768

Solar magnetographs for defining strength and direction of magnetic field in solar atmosphere 24 p4223 A67-41769

Lithium content of T Tauri stars shown to exceed ionization of Li in solar atmosphere 24 p4227 A67-42161

Solar abundance determination, discussing composition parameters and Planck gradient method 24 p4237 A67-42654

SOLAR CELL

Low energy proton bombardment damage in thin film cadmium sulfide and in single crystal silicon with silicone coating 01 p0037 A67-10476

Photovoltaic effect application to conversion of solar radiation to electrical energy, presenting pictorial explanation of solar cell 01 p0013 A67-10553

Radiation resistance of silicon photoconverters onboard Elektron III satellite, noting protective coating 02 p0240 A67-11543

Nonuniform damage in silicon solar cells produced by proton irradiation 02 p0182 A67-11682

Solar cell power systems for electric propulsion, considering methods of generating, controlling and conditioning onboard electric power [AIAA PAPER 66-891] 02 p0183 A67-12269

Effect of electron irradiation on silicon solar cells constituting power generator aboard Diapason IA satellite 03 p0362 A67-12897

Proton and alpha particle effects on thermal properties of spacecraft and solar concentrator coating of anodic-coated aluminum, zinc oxide/ potassium silicate, etc [AIAA PAPER 65-649] 03 p0448 A67-13054

CdS thin film solar cells history, design, fabrication and performance 04 p0553 A67-14474

Bulk minority carrier lifetime measured directly in solar cell by measuring short circuit current decay constant which is dependent on cell thickness and carrier type 04 p0554 A67-15128

Optimum gridline spacing for photovoltaic cells operating at high solar fluxes, noting maximum power point efficiency dependence on cell and geometric parameters and solar flux level [ASME PAPER 66-WA/SOL-1] 04 p0555 A67-15381

Lithium interaction with radium induced damage in silicon solar cells to produce center preserving minority carrier lifetime 04 p0556 A67-15703

Solar cell development and characteristics of Si, GaAs, CdS and CdTe types 04 p0558 A67-15955

Design of solar cells as satellite power supply sources 04 p0558 A67-15956

Defects in silicon p-n solar cells with Li diffused N region produced by electron irradiation and spontaneously annealed at room temperature interpreted as Li ions 05 p0870 A67-17273

Solar array output protection against individual cell failures, considering effects of paralleling 06 p0951 A67-18420

Periodic frequency change in signals from Cosmos V possibly due to solar cell output fluctuations 06 p0964 A67-18766

Flexible solar cell concept, discussing historical background, conceptual design and future plans 07 p1132 A67-19877

Annealing of proton radiation damage in silicon solar cells 07 p1237 A67-20143

Manufacturing process and life testing of bismuth telluride alloy based flat plate thermoelectric solar cells for near earth orbits 08 p1283 A67-20648

Adaptive power conditioning for optimal power transfer from solar cell array to load regardless of environment, impedance or volt-ampere characteristics 08 p1284 A67-20651

Solar cell model of CdS on copper sulfide 08 p1285 A67-20729

Copper telluride-cadmium telluride thin film heterojunction fabrication and characteristics for solar cell applications 08 p1285 A67-20730

Solar photovoltaic cell properties and preparation using thin films of copper and cadmium telluride 08 p1285 A67-20731

Electron and proton radiation effects on GaAs, CdS and CdTe thin film solar cells noting proton damage, estimates on cell life, etc 08 p1285 A67-20735

Thin film CdS and CdTe solar cells compared for space applications 08 p1285 A67-20736

Solar cell system for UK-3 satellite, discussing design, material selection, development and fabrication 09 p1445 A67-22179

Silicon solar cell with drift fields of various widths and magnitudes, considering performance changes before and after radiation 10 p1596 A67-23161

Ion implantation technique for production of n-on-p silicon solar cells applied to dendritic material 10 p1596 A67-23162

Humidity and simulated space environment effect on various cadmium-sulfide thin film solar cells, noting degradation rates 10 p1596 A67-23163

CdS solar cell model noting spectral response, V-I characteristic and temperature variation 10 p1596 A67-23164

Vapor deposited GaAs thin film solar cells for application to solar power systems 10 p1596 A67-23165

Radiation damage experiments for evaluation of silicon solar cell characteristics under simulated solar light 10 p1596 A67-23166

Material considerations in establishing failure mechanism of Nimbus solar array drive 10 p1713 A67-23741

Silicon crystals composition effect on solar cells reaction to irradiation by 4 mev electrons 12 p1896 A67-25150

Thin silicon solar cells for large flexible arrays having low specific mass and radiation resistance 13 p2055 A67-26716

Micrometeoroid damage of n-p silicon and CdS solar cells 13 p2056 A67-27440

Electrical and energy performance of high efficiency GaAs solar cells compared to silicon photocells, discussing temperature effect and p-n junction depth 13 p2056 A67-27623

Possible degradation effects produced in uncovered and covered N/P silicon solar cells by simulated micrometeoroid exposure 15 p2423 A67-30219

Radiation resistance of silicon photoconverters onboard Elektron III satellite, noting protective coating 16 p2677 A67-31609

Characteristics of photovoltaic solar converters, discussing drift field, wrap around and epitaxial webbed silicon cells, minimum film thickness and radiation damage 17 p2801 A67-32048

Radiation damage to satellite solar cells when shielded to various degrees, stressing silicon junction cells 17 p2804 A67-32840

N-and p-type silicon solar cells orientation and energy dependence of damage at room temperature under electron bombardment 17 p2918 A67-32848

Silicon solar cells impurities, radiation resistance, fabrication, nonsilicon materials, development, etc 18 p2989 A67-34069

Open circuit voltage, short circuit current and maximum power for silicon solar cells at low temperatures 18 p2989 A67-34101

Optimum grid line spacing for photovoltaic cells operating at high solar fluxes, noting maximum power point efficiency dependence on cell and geometric parameters and solar flux level [ASME PAPER 66-WA/SOL-1] 18 p2989 A67-34129

Germanium photovoltaic cells as solar conversion devices [ONERA-TP-478] 18 p2990 A67-34464

Electrical characteristics of GaAs p-n diffusion junctions used as solar cells 19 p3300 A67-34769

Isochronal annealing of short-circuit current of electron irradiated silicon solar cells 19 p3305 A67-35688

Isochronal annealing of proton-irradiated silicon solar cells studied in vacuum over various temperature ranges 19 p3305 A67-35689

Annealing under continuous irradiation in p-on-n silicon solar cells with lithium diffused in N region 19 p3306 A67-35671

Equivalent resistance circuit of solar cell taking into account all sources of linear resistance 19 p3177 A67-36037

Parametric comparison between tracking with solar cell arrays and nontracking systems with respect to space power supplies 20 p3363 A67-36585

Lunar Orbiter power subsystem reliability tradeoff, methodology, performance prediction, etc 20 p3363 A67-36594

Thermal annealing of silicon solar cells with direct solar heating or electric storage methods to avoid radiation damage 20 p3364 A67-37129

Thin film cadmium telluride solar cells, discussing efficiencies and photoelectric properties of junction 21 p3679 A67-38224

Performance prediction calculations for double junction n-p-n silicon solar cells, discussing simplified model limits and space radiation environment 21 p3571 A67-38232

Integrating pyranometer operating on silicon photovoltaic solar cell for use by climatological stations and mesoscale networks 21 p3628 A67-38580

Silicon solar cells bombarded by energetic electrons for radiation resistance 21 p3571 A67-38648

High energy electron radiation effects on silicon photocells deposited epitaxially on artificial satellite surface, discussing liberated carrier accumulation possibility 21 p3572 A67-38672

Solar probe mission planning, evaluating high temperature electronics capability and high flux GaAs solar cell efficiency 22 p3903 A67-39956

CdS solar cell model, discussing p-n junction, CdS and copper sulfide properties and microscopic junction formation and behavior 23 p4046 A67-41486

Implantation process for thin silicon solar cell fabrication, discussing leakage losses and efficiency 23 p4046 A67-41488

Decreasing thickness and temperature variation effects on solar cell performance 23 p3937 A67-41489

Highly reflective coatings and interference filters for silicon solar cells on spinning spacecraft on near-sun mission 23 p3937 A67-41490

Solar cell integral covers, discussing solar simulation, vacuum and thermal tests, performance characteristics, etc 23 p3937 A67-41491

High voltage solar cell made by integrated circuit processes noting fabrication and electrical characteristics 23 p3937 A67-41492

Thin film GaAs solar cell fabrication and operating characteristics, describing two-cell types 23 p4046 A67-41493

Clevite thin film CdS solar cell fabricated with two different substrate structures noting design changes, improvements and performance characteristics 23 p3937 A67-41494

CdTe thin film solar cell, examining spectral response, sputtered Pt photovoltaic barrier-forming method and integrated array fabrication 23 p4046 A67-41495

Environmental testing of thin film solar cells, studying long term thermal cycling effect on CdS solar cell 23 p3937 A67-41496

Si and Cd solar cell arrays compared using rigid frame Si solar cell concept 23 p3938 A67-41497

Solar arrays constructed of CdTe thin film solar cells are feasible and competitive if space sunlight conversion efficiency can be maintained at level greater than 6 percent 23 p3938 A67-41498

Photovoltaics - IEEE conference, Cocoa Beach, Florida, March 1967, Volume 2, Spacecraft power systems, solar cell mathematical model 23 p3938 A67-41505

Solar cell power systems design and control technique for use in satellite programs, specifically transit 3B and 4A, ionosphere Beacon satellite, etc 23 p3938 A67-41507

Solar cell power supply design to satisfy whole satellite, discussing power supply size and solar cell panel fabrication 23 p3939 A67-41508

Solar cell array for LEM electric power system during lunar surface operation noting requirements and tradeoffs 23 p3939 A67-41510

Flexible integrated deployable solar cell array design, environmental testing and performance prediction 23 p3939 A67-41511

Thin silicon, dendritic and cadmium sulfide solar cells technology and large-area lightweight arrays 23 p3939 A67-41512

Improvement 23 p3939 A67-41512

Computer program for predicting silicon solar cell current-voltage characteristics as function of incident solar intensity and cell temperature over heliocentric distances 23 p3939 A67-41513

Computer calculation of 1 Mev electron flux and irradiation degradation of solar cell I-V curves for charged particle environment 23 p3940 A67-41514

Solar cell array model constrained at four points, with computer simulating V-I characteristics for environmental temperature and illumination intensity effects 23 p3940 A67-41515

Isochronal annealing effects on photovoltaic properties of n-on-p Si solar cells irradiated by energetic proton 23 p3940 A67-41518

Li interactions with complex damage clusters produced by neutrons in Si solar cells, discussing annealing, radiation hardening and energy dependence 23 p3940 A67-41520

Simulated micrometeoroid bombardment effect on n/p Si and CdS solar cells performance 23 p3941 A67-41521

Li behavior in self-healing radiation resistant Si solar cells 23 p3941 A67-41522

Spontaneous annealing models of lithium-diffused Si solar cells, discussing defect compensation and metastable defect formation 23 p3941 A67-41523

Li containing p-on-n and n-on-p Si cell degradation by bombardment noting carrier removal damage, annealing and radiation damage resistance 23 p3941 A67-41524

Li doped Si solar cell, studying irradiation damage, recovery effect, carrier removal, time dependency and annealing 23 p4047 A67-41525

Li doped Si solar cells noting fabrication, preradiation behavior, changes with temperature, recovery and I-V characteristics after irradiation 23 p3941 A67-41526

Li doped Si solar cell radiation resistance to high energy electrons, noting fabrication methods and annealing behavior differences 23 p3941 A67-41527

Li doped p-plus/n solar cells optimum design and radiation resistance, noting concentration and room temperature annealing conditions 23 p3942 A67-41528

Solid state electrochemical solar cell using various anode metals and charge transfer complexes as cathodes, noting I-V characteristics and discharge curves [JPL-TR-32-1116] 24 p4097 A67-41804

Distributive circuit element model for computation of optimum gridding of solar cells 24 p4098 A67-42086

Large sun-oriented deployable solar array for OGO design, fabrication and flight performance 24 p4104 A67-42508

Multifaceted solar array performance determination 24 p4104 A67-42509

Solar cell array design techniques for temperature extremes induced by space environment, discussing orbital flight requirements 24 p4104 A67-42510

Electrical design of large lightweight solar array for electric propulsion type Mars-bound spacecraft, discussing magnetic effects and power losses 24 p4104 A67-42512

Characteristics of high energy electron radiation and temperature and effect on N/P silicon solar cells 24 p4105 A67-42513

Solar array as primary electrical power source of Pioneer deep space probes, comparing performance data with test and design data 24 p4105 A67-42514

Solar cell/battery power systems for post-1975 satellites, discussing oriented thin film CdS solar cell array 24 p4105 A67-42515

Large area solar array design for photovoltaic system for manned space systems based on orbital perturbations and mechanical and thermal environment considerations 24 p4105 A67-42516

Orbit-and sun-oriented solar cell concepts compared, discussing aerodynamic drag penalties 24 p4105 A67-42517

Solar cell array flight systems, discussing flight experience, design and fabrication

history 24 p4105 A67-42518
 Spacecraft structural criteria for
 lightweight photovoltaic solar arrays
 development, discussing Mariner type panel
 designs and power-to-weight
 ratios 24 p4108 A67-42557
 Solar cell submodule fabrication and
 design for Mariner and Surveyor spacecraft,
 describing automatic conveyor soldering
 oven 24 p4109 A67-42558
 Large lightweight rigid multi-kilowatt solar
 arrays, discussing substrate construction,
 design and testing 24 p4109 A67-42560
 Structural problems in high power solar
 photovoltaic arrays technology, discussing
 configuration, materials selection, thermal
 control coatings and tests
 results 24 p4251 A67-42897
 Lunar electric power systems transported
 by Saturn V noting Brayton cycle, Rankine
 cycle, solar cells and thermoelectric systems
 [AIAA PAPER 67-902] 24 p4110 A67-43010

SOLAR CHROMOSPHERE
S CHROMOSPHERE
SOLAR COLLECTOR
SA CONCENTRATOR
 Effect of concentrator orientation with
 respect to sun on solar energy converter
 performance 09 p1451 A67-22532
 Wavelength selectivity in solar collector
 design, noting role of scatter in determining
 radiative properties of
 surfaces 11 p1817 A67-24052
 Proton radiation effects on mirror
 reflectance in high vacuum at various
 temperatures, degradation by blistering
 found to be highly temperature-dependent
 [AIAA PAPER 67-341] 12 p1957 A67-26055
 Solar concentrator technology, discussing
 design requirements of space power
 conversion devices and manufacturing
 methods 13 p2055 A67-26826
 Coordinated laboratory and flight test
 program, determining stability of solar
 concentrator reflective surfaces in orbital
 environment 17 p2832 A67-32060

SOLAR CONSTANT
 Solar constant and sunspot relationship
 interpreted by solar radio flux effect on
 lower ionosphere density 12 p1932 A67-25342

SOLAR CONVERTER
 Open circuit voltage and short circuit
 current capability of solar energy converter
 photoelement made of single crystal n-type
 indium phosphide 04 p0679 A67-15141
 Emitter material, emitter treatment,
 collector lateral area and interelectrode and
 lateral spacing effects on solar converter
 performance 09 p1449 A67-22345
 Integral short circuit current of solar
 converters determined from spectral
 distribution of solar radiation energy, using
 simulator and SiO photocell
 films 09 p1451 A67-22531
 Effect of concentrator orientation with
 respect to sun on solar energy converter
 performance 09 p1451 A67-22532
 Open circuit voltage and short circuit
 current capability of solar energy converter
 photoelement made of single crystal n-type
 indium phosphide 12 p1979 A67-25164
 Direct solar to electric energy conversion
 using superconducting flux barrier,
 discussing superconductive phase change and
 magnetic properties 22 p3748 A67-40151

SOLAR CORONA
S CORONA
SOLAR COSMIC RAY
 Luna X shielded gas-discharge counter
 data on soft corpuscular radiation, noting
 solar contribution to magnetospheric
 tail 01 p0145 A67-10907
 Solar cosmic ray generation, discussing
 proton energy spectrum analysis and wave
 propagation in interplanetary
 space 02 p0310 A67-12572
 Solar particles zones of incidence during
 maximum and minimum solar
 activity 02 p0310 A67-12574
 Cosmic rays from solar flare and
 interplanetary space properties, covering
 particle scattering and magnetic field
 induced one-dimensional particle
 diffusion 02 p0310 A67-12575
 Changes in solar cosmic ray and
 geomagnetic field intensities during
 magnetic storms accompanied by decrease in
 galactic cosmic ray intensity, using moving
 averages method 02 p0311 A67-12593
 Protective shielding for astronauts from
 ionizing radiation from solar and galactic

cosmic rays and radiation
 belts 03 p0365 A67-13539
 Photometric cross section of nonradial
 coronal structure in 5303 angstrom line
 following proton flares with cosmic,
 subcosmic and corpuscular
 emissions 03 p0507 A67-13810
 Stratospheric recordings of solar cosmic
 rays from chromospheric flares, calculating
 and comparing diffusion coefficient of
 cosmic rays and energy spectrum of solar
 protons 07 p1243 A67-19698
 High energy solar cosmic ray spectrum
 during solar flare of February 23,
 1956 07 p1243 A67-19805
 Ionospheric absorption as indicator of
 particle flux below point of long radio wave
 reflection, noting relation to solar cosmic
 rays 09 p1561 A67-21844
 Cosmic ray nucleonic component in
 Antarctic zone measured by neutron
 monitor, standardized and related to solar
 activity 10 p1699 A67-22862
 Solar cosmic ray event characteristics
 1962-1966, solar minimum vs solar
 maximum 10 p1700 A67-23187
 Properties of solar cosmic rays causing
 polar cap absorption measured with
 satellites 10 p1700 A67-23188
 Polar cap absorption with solar cosmic ray
 properties from balloons and relation to
 processes in terrestrial
 atmosphere 10 p1637 A67-23189
 Polar glow aurora, discussing optical
 emissions generated by solar cosmic ray
 protons and alpha particles, energy
 spectrum, atmospheric and ionospheric
 absorption effect, etc 10 p1637 A67-23190
 Polar based riometric observations of solar
 cosmic ray events during
 IQSY 10 p1701 A67-23193
 Measurement of cosmic ray intensity by
 Zond III automatic
 probe 10 p1701 A67-23230
 Three stages of solar cosmic rays entry
 into polar cap atmosphere due to
 differential arrival of solar electrons,
 protons and alpha
 particles 11 p1855 A67-23925
 Solar cosmic ray diffusion coefficient
 dependence on cosmic ray energy and
 distance to sun studied via solar
 flares 12 p1991 A67-25111
 Weak cosmic ray burst relation to austral
 axis pole geomagnetic activity characteristics
 and propagation in interplanetary space of
 energetic solar cosmic
 rays 12 p1992 A67-25116
 Riometer observations in polar caps of
 solar cosmic ray events during
 IQSY 12 p1993 A67-25228
 Interstellar gas dynamics suggests that
 energy density of galactic cosmic rays places
 firm upper limit on undetermined constant
 of solar modulation 13 p2189 A67-26265
 Solar proton and alpha particles entry into
 polar cap atmosphere 13 p2194 A67-27252
 Solar cosmic ray events characteristics for
 solar minimum vs solar
 maximum 13 p2194 A67-27253
 Electron number density profiles and
 polar cap absorption of radio waves time
 history during weak solar cosmic ray
 event 14 p2380 A67-28042
 Spectrographic observations of late stages
 of limb flare by achromatic
 coronagraph 14 p2381 A67-28835
 Radiation protection during space flights,
 describing dangerous aspects of solar cosmic
 rays and earth radiation
 belt 16 p2738 A67-31197
 Diffusion coefficient dependence on solar
 particle energy and distance from sun noting
 time variation 16 p2740 A67-31892
 Solar cosmic radiation, discussing effect
 on geomagnetic storm 16 p2740 A67-31899
 Statistical correlation between phase and
 amplitude in first harmonic solar-diurnal
 variation of neutron component, noting
 longitude effect 17 p2931 A67-32078
 Solar-diurnal variations of neutron and
 muon components of cosmic rays based on
 IGY data, analyzing temperature
 effect 17 p2931 A67-32079
 Solar cosmic ray generation, discussing
 chromospheric eruptions, spectra, chemical
 and nuclear composition, particle
 acceleration, etc 17 p2934 A67-32095
 Solar cosmic ray observations, discussing
 emission spectrum, interplanetary particle
 distribution, diffusion coefficient, magnetic

field strength, space-time distribution,
 etc 17 p2934 A67-32096
 Energy transport, cosmic ray particle
 storage and triggering mechanism in solar
 flares, considering relation with stellar
 flares 17 p2939 A67-33398
 Cosmic ray and interplanetary medium and
 magnetic field studies in
 Bolivia 19 p3320 A67-35284
 Interplanetary magnetic field variation
 properties and effects on solar cosmic rays
 determined through Mariner II recordings
 employed to develop
 model 19 p3314 A67-35452
 Solar atmosphere absorption of light
 nuclei generated on sun indicated by
 satellite observation of heavy nuclei cosmic
 ray flux and X-ray electron
 bremsstrahlung 21 p3698 A67-38595
 Mathematical model for solution of
 anisotropic diffusion equations of solar
 cosmic ray propagation 22 p3872 A67-39809
 Numerical program integrating motion
 equation of charged particles from realistic
 geomagnetic field model, with trajectory
 calculations for solar cosmic
 rays 22 p3872 A67-39810
 Solar particle event of February 1965
 observation with Mariner IV and Injun IV
 showing 70 degrees heliocentric longitudinal
 distribution in interplanetary
 space 22 p3872 A67-39811
 Cosmic ray yearly variation during solar
 activity cycle, discussing flare and
 acceleration mechanisms, stable coronal
 condensation and sunspot magnetic
 field 22 p3874 A67-40045
 Solar cosmic ray multiple neutron
 production increase on January 28, 1967
 from Antarctica cosmic ray neutron monitor
 measurements 22 p3874 A67-40048
 Heavy nuclei intensity during solar cosmic
 ray intensity increase accompanying
 chromospheric flares, proposing magnetic
 field dynamic dissipation acceleration
 mechanism for charged
 particles 23 p4056 A67-41113
 Solar diurnal variation and sudden changes
 in cosmic ray intensity from yearly neutron
 component data 23 p4058 A67-41123
 Solar activity effect on distribution of
 source power of solar diurnal cosmic ray
 variation in relation to ecliptic
 plane 23 p4058 A67-41125
 Solar and galactic low energy cosmic ray
 nuclear ionizing and interaction effects on
 meteorite surface isotopic composition,
 estimating particle fluxes 24 p4210 A67-42634

SOLAR CYCLE
SA SUNSPOT
 Tables of observational data on flattening,
 integrated brightness, brightness distribution
 and polarization of white
 corona 01 p0150 A67-10933
 Mechanism of solar activity cycle,
 examining relation of stability threshold of
 disintegration of solar magnetic belt into
 separate cells 01 p0146 A67-11282
 Radio communications disruptions during
 magnetotonic disturbances in ionosphere at
 high latitudes during decreasing solar
 activity 02 p0193 A67-11660
 Eleven year solar cycle, with emphasis on
 existence of two maxima 03 p0506 A67-13316
 Nuclear emulsion measurements of
 primary cosmic ray alpha particle flux over
 Hyderabad during high solar activity in 11-
 year cycle 03 p0506 A67-13720
 Sunspot magnetic field and effect on solar
 cycles, noting wave propagation in inviscid
 conducting fluid 03 p0511 A67-13740
 Annual variation of quiet sun radio
 emission during solar cycle, noting daily
 mean values of flux at different
 frequencies 03 p0513 A67-14005
 Recurrent variations of cosmic radiation
 during solar cycle 04 p0691 A67-14417
 Seasonal and solar-cyclic variations of
 nondeviate absorption in ionospheric D
 region 04 p0617 A67-15570
 Hysteresis effect on cosmic ray intensity
 of solar cycle variations 07 p1242 A67-19620
 Electrical conductivity of earth interior
 from data concerning annual geomagnetic
 variations for all years of solar
 cycle 07 p1178 A67-19826
 Trapped proton flux data from nuclear
 photographic emulsions 08 p1378 A67-21472
 Large-scale structure of solar magnetic
 field during declining and minimum phases
 of solar cycle and effect on interplanetary

magnetic field 10 p1700 A67-23055
 Solar cycle variations in atmospheric density deduced from meteor observations and rocket measurements in mesopause and thermosphere 10 p1638 A67-23204
 High altitude atmospheric models, discussing Harris-Priester and Nicolet theories 10 p1640 A67-23217
 Winter anomaly of nondeviative ionospheric absorption of radio waves and relation to diurnal, seasonal, local and solar cycle variations 10 p1646 A67-23267
 Eleven year solar activity cycle noting presence of two maxima 10 p1711 A67-23801
 Solar wind region magnitude, scattering transport path of particles and spectral variation of magnetic inhomogeneities analyzed on basis of 11-year cosmic ray cycle 11 p1855 A67-23930
 Geomagnetic disturbances dependence on interplanetary magnetic field sector structure and incident solar ion current at and near minimum of solar cycle 11 p1786 A67-24331
 Forecasting geomagnetic storms and disturbances from solar observations 12 p1931 A67-25110
 Solar wind particle propagation and scattering path in interplanetary space according to data of 11-yr cosmic ray variations 12 p1991 A67-25115
 Long term variation in magnitude of diurnal anisotropy of solar cosmic rays analyzed quantitatively by applying statistical techniques to recorded data 12 p1993 A67-25205
 Position of anomalous radio absorption in ionosphere during various phases of solar activity cycle 12 p1933 A67-25550
 Galactic cosmic ray intensity depression by convective region and by surrounding static barrier of expanding corona 13 p1291 A67-26323
 Diurnal variations in sporadic E layer parameters during solar cycle based on Moscow observations 13 p2111 A67-26570
 Solar cosmic ray events characteristics for solar minimum vs solar maximum 13 p2194 A67-27253
 Statistics and evolution of sunspots, discussing frequency, shape, long solar cycle and secular variation 13 p2202 A67-27417
 Sunspot decay and associated flare activity of coming minimum predicted, based on current cycle combined with sunspot lifetime and area 13 p2202 A67-27418
 Primary cosmic ray electron flux and energy spectrum near solar minimum compared with nonthermal radio emission from high galactic latitudes 14 p2381 A67-28831
 Radiation hazard to man from solar proton events 15 p2429 A67-29450
 Eleven-year solar cycle, with emphasis on existence of two maxima 16 p2737 A67-30492
 Radio communications disruptions during magnetolonic disturbances in ionosphere at high latitudes during decreasing solar activity 16 p2624 A67-31075
 Solar flares causing Forbush effect, determining relevant parameters, variations with solar cycle and mutual relations 16 p2739 A67-31457
 Soviet book on cosmic rays including solar-diurnal, 11-year and 27-day variations, temperature effect, geomagnetic field effect, etc 17 p2930 A67-32077
 Cosmic ray intensity 11-year variation energy characteristics, discussing spectrum bending due to integral modulation in interplanetary space 17 p2932 A67-32083
 Association rate between solar surges and flares 17 p2938 A67-32820
 Nature of Pcl oscillations in solar cycle, discussing frequency spectra of data obtained 17 p2847 A67-32945
 Cosmic ray motion in interplanetary electromagnetic field for isotropic/anisotropic diffusion situations presented by convective diffusion models assuming spherical symmetry for solar cavity 17 p2938 A67-33188
 Spectral data on primary cosmic ray protons and helium nuclei analyzed, assuming solar cycle modulation due to diffusion-convection process 17 p2952 A67-33247
 Solar diurnal wave from underground muon detectors and relationship to solar activity over 11-year cycle, noting phase

changes 18 p3116 A67-33514
 Nightglow emission structure and variation at airglow equator, discussing predawn and storm effects, intensity variations with solar cycle, OH bands, etc 18 p3036 A67-33607
 Storm-time change and average electron density profile of polar topside ionosphere at sunspot minimum 19 p3218 A67-35230
 Mesosphere and lower thermosphere density variations related to solar cycle obtained, using rocket grenades 19 p3219 A67-35231
 Long term forecasts of proton flares 19 p3313 A67-35261
 Geomagnetic micropulsation properties variation over last solar cycle and causes 19 p3325 A67-35486
 Balloon and satellite measurements of 11-year solar modulation of low energy protons and helium nuclei in galactic cosmic rays 19 p3315 A67-35487
 Statistical correlation of type III solar radio burst activity with coronal green line over solar cycle 19 p3316 A67-36029
 Phase relationship between solar activity changes and changes in solar wind parameters over 11-year cycle 20 p3519 A67-37395
 Heavy nuclei intensity in primary cosmic rays, long term solar cycle modulation and time lag in various phases 20 p3519 A67-37405
 F-2 layer critical frequencies variation with solar activity, evaluating criteria for unperturbed state based on magnetically inactive days 21 p3622 A67-39035
 Empirical model of sunspot activity within solar cycle limits indicating separate consideration of magnetic field generation and spot formation 22 p3879 A67-39300
 Outer Van Allen radiation zone intensity maximum position dependence on electron energy and magnetic activity, noting relation to diffusion theory 22 p3870 A67-39620
 Solar cycle prediction based upon random number technique, Fourier curve fits and power spectra analysis 22 p3873 A67-39931
 Cosmic ray diurnal anisotropy component annual means variation with two solar cycles 23 p4051 A67-40817
 Solar cycle primary cosmic radiation variation above magnetosphere and radiation belts at stratosphere and surface, using neutron monitors and space vehicle measurements 23 p4055 A67-41101
 Galactic cosmic ray intensity measurements in stratosphere and at various atmospheric depths, studying secular variation energy spectra during solar cycle 23 p4055 A67-41103
 Cosmic ray intensity solar cycle variations in terms of solar wind properties defined by solar activity characteristics 23 p4056 A67-41106
 Cosmic ray intensity variation mechanisms due to motion of solar system and quasi-radial interplanetary magnetic field 23 p4056 A67-41107
 Galactic cosmic ray solar cycle and secular variations in bombardment of meteorites at average meteoroid solar distance and 1 AU from radioactive isotope ratios 24 p4210 A67-42622

SOLAR ECLIPSE

Radio spectrum of active region near east limb of Sun determined from July 20, 1963 eclipse [AFCRL-66-839] 01 p0148 A67-10388
 Solar eclipse effects on geomagnetic field, suggesting geomagnetic observations at low latitudes 03 p0408 A67-12839
 Eclipse observation from moon and cislunar space 04 p0700 A67-15070
 Solar eclipse of May 20, 1966, first and fourth contact times, sky brightness and temperature and photographic records 05 p0897 A67-16731
 DFL mobile telemetry ground station participation in solar eclipse expedition of ESRO in Greece 06 p0980 A67-18020
 Upper atmospheric rocket sounding experiment during solar eclipse over Brazil, noting instrumentation and participating agencies 06 p0981 A67-18382
 November 12, 1966 total eclipse observation from aircraft flying in moon shadow, describing instrumentation and results 06 p1004 A67-18383
 Local temperature drops at central line of annular solar eclipse of May 20,

1966 06 p1028 A67-19049
 Matrix techniques for finding geomagnetic field strength in solar ecliptic coordinate system 07 p1170 A67-19111
 Observations of sun at Stanford on May 20, 1966 at 9.1 cm after annular eclipse in Greece and Turkey 07 p1251 A67-19914
 Solar eclipse study program in Argentina 07 p1260 A67-20226
 Coronal observations during solar eclipse in Bolivia, discussing equipment used and results 08 p1391 A67-21044
 Mean noon profile of mesospheric electron number density at 35 degrees S latitude preceding solar eclipse 08 p1378 A67-21483
 F layer changes during solar eclipse observed at equatorial station, obtaining values for effective electron loss coefficients 10 p1651 A67-23340
 Electron density variation from photochemical rates in equatorial F layer during October 1959 solar eclipse 10 p1651 A67-23342
 Solar eclipse effect on atmospheric potential gradients analyzed, noting negativity and variation pattern with five peaks 10 p1651 A67-23347
 Solar temperatures from observations of July 1963 eclipse with horn antenna in left and right circular polarization, noting magnetization 11 p1867 A67-24779
 Image and other techniques to measure and reduce stray and scattered light in sunspot photometry, emphasizing possibility of using partial solar eclipse 13 p2203 A67-27424
 Scattering function derivation using lunar limb occultation of solar disk during partial eclipse 14 p2386 A67-28475
 Solar corona temperature from intensity gradients measured during total eclipse of May 30, 1965 14 p2387 A67-28564
 German participation in solar eclipse campaign of ESRO, describing rockets and radar used 15 p2466 A67-29572
 Chromospheric solar radiation measured during solar eclipse with UV monochromator, using electromagnetic radiation photomultipliers 15 p2565 A67-29573
 MSQ-1 radar system for rocket tracking used to measure distance, elevation and azimuth during May 20, 1966 solar eclipse 15 p2467 A67-29574
 Mobile telemetry ground station and maximum reliability procedures for rocket telemetry transmission system used in solar eclipse 15 p2467 A67-29575
 Shutter speed and illumination data for cinematographic documentation of total solar eclipse 15 p2555 A67-29576
 Airborne photographic instrumentation system for photometric observation of total solar eclipse, noting automatic tracking system 16 p2678 A67-31794
 Coronal condensation analysis observed photographically during total solar eclipse, finding good correspondence of loop system spatial trajectories to force line configurations 17 p2945 A67-32690
 Dome formation in corona around prominence during February 1961 eclipse, describing observed features and proposing three-dimensional model 17 p2953 A67-33399
 Solar radio noise source position determined during occultation caused by partial solar eclipse of May 20, 1966 17 p2953 A67-33403
 Sun effective disk temperature from measurement of solar radiation during May 1966 eclipse 18 p3125 A67-34195
 Selenodetic measurement methods, considering point coordinates determination on lunar surface near limb or center, including moon profile studies during solar eclipse 18 p3129 A67-34309
 Photographic systems and photoelectric scanner for observation of solar annular eclipse 18 p3049 A67-34312
 Photometric determination of moon limb shape during annular solar eclipse, using rotating prisms 18 p3129 A67-34313
 Lunar profile deviations from circle determined from annular solar eclipses, discussing measurement techniques 18 p3130 A67-34314
 Microwave radio observations of total sun eclipse made in Canada in 1963, discussing solar radio emission [AD-642463] 18 p3133 A67-34487
 Corona temperature and logarithmic intensity gradients determined by pointwise

three-color photoelectric photometry during solar eclipse 19 p3318 A67-35017

Stratosphere and mesosphere wind and temperature measurements, noting additional cosmic radiation measurements during 1966 solar eclipse in Argentina 19 p3320 A67-35287

Greek space research noting satellite optical tracking, solar photosphere and chromosphere, atmospheric electricity and solar eclipse 19 p3320 A67-35292

D-region positive ion density during solar eclipse of May, 1966 observed by cylindrical Langmuir probe onboard rocket 19 p3222 A67-35454

Annular solar eclipse of May 20, 1966 visible at Bordeaux, noting active center on occultation curve 19 p3325 A67-35506

Nitrogen and oxygen dayglow emissions observed during total solar eclipse of May 1965, studying emission/continuum intensity ratio 20 p3427 A67-36368

Scattered radio signals received during solar eclipse examined for indication of electron clouds masked by daytime high electron density 20 p3432 A67-37208

Instrumentation for observing limb darkening of solar continuum during annular eclipse of May 1966 20 p3529 A67-37502

Solar spectral line center-to-limb variations during solar eclipse of May 20, 1966 20 p3453 A67-37682

Ionospheric pulse absorption study of measurements taken in Bulgaria during solar eclipse of May 1966 21 p3616 A67-37995

Observation of annular solar eclipse of 1966 from Madrid, noting photographs application for occulted region chord measurements 22 p3888 A67-40200

Coronal line spectra of 1952 total solar eclipse, noting emitted energies and isothermic coronal region 22 p3889 A67-40206

Wavelengths and intensities of IR coronal lines of silicon and magnesium ions from airborne total solar eclipse observations 24 p4224 A67-41822

Solar eclipse effects on topside ionosphere electron concentration, noting decrease for magnetic quiet conditions 24 p4148 A67-42059

Soviet noneclipse coronagraph structure, tracking system and artificial eclipse mechanism 24 p4154 A67-42111

Horizontal telescope used for solar corona photography during total eclipse /1966/, determining radii passing through solar magnetic poles 24 p4227 A67-42153

Solar corona spectra during total eclipse /1966/ using polaroid camera 24 p4154 A67-42157

SOLAR EFFECT

Planetary proximity influence on motion of planetoid, with application to solar influence on Venus as studied by Mariner II 02 p0321 A67-11495

Structurally regular magnetic field in circumlunar space recorded by Luna X orbiter, noting variations in intensity and solar wind effect 05 p0887 A67-16056

Large ground antenna performance with solar noise jamming 05 p0780 A67-17524

Atmospheric Sciences Laboratory proposed under Apollo applications program [AIAA PAPER 67-186] 06 p1088 A67-18488

Orbital behavior and stationkeeping propulsion requirements for synchronous satellites, considering solar radiation and earth oblateness effects 09 p1571 A67-21697

IR images of lunar crater Tycho during lunar night provide evidence that thermal anomaly is produced by solar rather than internal heat 09 p1565 A67-22013

Semiannual variations of magnetic activity 10 p1630 A67-22796

Geomagnetic micropulsation excitation by solar wind flow around magnetosphere, noting surface wave propagation 10 p1699 A67-22797

Solar flares as acceleration mechanisms for relativistic and subrelativistic particles 10 p1700 A67-23186

Geomagnetic and solar control of ionization at 1000 km determined from electron density data obtained from Alouette satellite 10 p1650 A67-23339

F layer changes during solar eclipse observed at equatorial station, obtaining values for effective electron loss coefficients 10 p1651 A67-23340

Electron density variation from photochemical rates in equatorial F layer during October 1959 solar

eclipse 10 p1651 A67-23342

Solar eclipse effect on atmospheric potential gradients analyzed, noting negativity and variation pattern with five peaks 10 p1651 A67-23347

Forecasting geomagnetic storms and disturbances from solar observations 12 p1931 A67-25110

Nighttime ionosphere maintained by downward flux of electrons from protonosphere as shown by columnar electron contents measurements, noting decay rate 13 p2107 A67-26305

Sporadic E backscatter noting two peaks in activity, motion, temporal component parameters and cause 13 p2107 A67-26306

Sun illumination time of artificial earth satellite moving in elliptical orbit 13 p2200 A67-27338

Jupiter decametric radiation analyzed with interferometer for manifestations of solar wind effects 14 p2385 A67-28404

Gravity-gradient oriented satellite stabilization by means of solar pressure torques on adjustable slats 14 p2395 A67-29051

Partial correlation coefficients between ionospheric, solar and geomagnetic parameters and spread-F occurrence probability [AGARDGRAPH 95] 15 p2481 A67-30283

Expulsion of ions from comets toward sun examined for source, dissociation and ionization of parent particles, velocity, etc 16 p2746 A67-30979

Rotational time scale and analytical representation by single formula for earth rotation variation 16 p2750 A67-31443

Solar cosmic radiation, discussing effect on geomagnetic storm 16 p2740 A67-31899

Cosmic ray intensity, discussing modulation due to earth heliographic variation 17 p2932 A67-32086

Three-body problem of Jupiter satellites orbits under solar influence, computing initial elements, determining orbital stability and solving satellite motion equations 17 p2946 A67-32753

Model of dust distribution in interplanetary space accounting for solar effects 17 p2947 A67-32758

Balloon satellite orbital elements predicted in advance by computation of solar radiation, gravitational perturbations, etc 18 p3126 A67-34246

Upper atmosphere diurnal and seasonal latitudinal variations satellite data, showing diurnal bulge migration with subsolar point, 2 PM bulge peak, etc 19 p3215 A67-35178

Exospheric density variation as related to solar activity determined from satellite orbits 19 p3217 A67-35211

Developments in upper atmosphere research noting atmospheric density, temperature, diurnal variations, solar and geomagnetic activity effects, etc 19 p3218 A67-35225

Molecular and atomic ion concentration in earth upper atmosphere observed from low altitude satellite, discussing diurnal variation and solar effect 19 p3220 A67-35262

Air density variation at 220 km altitude shown due to increased solar activity, from satellite orbit observation 19 p3222 A67-35458

Underground cosmic ray intensity variation measurements to determine solar modulation processes 19 p3315 A67-35494

Electron component observation in studying solar modulation of galactic cosmic rays, discussing Parker model and Gloeckler-Jokipii model 19 p3315 A67-35496

Alouette I and Explorer XX /S-48/ spin behavior explained by solar heating of antennas and solar radiation pressure 21 p3712 A67-37784

Structurally regular magnetic field in circumlunar space recorded by Luna X orbiter, noting variations in intensity and solar wind effect 21 p3701 A67-37843

Luminance of lunar surface site predicted by direct solar and earth reflected illumination together with local albedo variations 22 p3887 A67-40143

Lunar orbit precession due to quadrupole moment of sun arising from solar oblateness 23 p4066 A67-41014

Solar eclipse effects on topside ionosphere electron concentration, noting decrease for magnetic quiet conditions 24 p4148 A67-42059

Semiannual variations of magnetic activity 24 p4149 A67-42132

Geomagnetic micropulsation excitation by solar wind flow around magnetosphere, noting surface wave propagation 24 p4209 A67-42133

SOLAR ENERGY

Electrical propulsion of space vehicles using solar energy, electrostatic drive, drifting field plasma accelerator, etc 03 p0503 A67-13493

Mediterranean cooperation on solar energy use - General Spring Session, University of Marseille, May 1966 07 p1132 A67-20285

Storage of solar electric energy by electrolysis of water, separate storage and subsequent recombination of gases by fuel cells 07 p1132 A67-20288

Solar energy role in lunar water production, evaluating efficiency of collector-absorber systems 08 p1317 A67-21094

Rayleigh scattering and Lambert ground reflection effect on solar energy absorbed by ozone in earth molecular atmosphere evaluated on basis of transfer equation 12 p1932 A67-25341

Parabolic reflectors providing auxiliary solar energy for space stations and spacecraft, manufacturing and testing procedures 13 p2211 A67-26335

Power supply and transformation equipment in satellites, discussing batteries, fuel cells, nuclear reactors and solar energy 14 p2252 A67-28566

Solar energy conversion into electric power by GaAs and Si cells analyzed, using photovoltaic cell theory 15 p2536 A67-29503

Local transportation in commercial space operations, extravehicular activity evolution and space environment characteristics utilization [AAS PAPER 67-116] 15 p2432 A67-29963

Rapid acquisition of sun in solar energy conversion systems based on momentum exchange from rotating flywheels to platform 15 p2423 A67-30130

Dayglow emissions observation by ground-based instruments indicate atmospheric response to concurrent input of solar energy 18 p3033 A67-33586

Conversion of solar-thermal to electrical energy by capacitance-change pumping of thermoelectric thin films, noting space environmental chamber tests 24 p4108 A67-42555

SOLAR ENERGY ABSORPTION FILM

Solar absorptance and thermal emittance of aluminum coated with vacuum deposited films of aluminum oxide of various thicknesses [ATAA PAPER 65-656] 03 p0448 A67-13036

SOLAR ENERGY THERMIONIC /SET/ PROGRAM

Alkaline vapor refueling of solar thermionic converters, concept, development and tests 07 p1132 A67-20287

SET VIII Thermionic generator, evaluating operational and long term performance characteristics for space applications 24 p4103 A67-42499

SOLAR FACULAE

Spectral equivalent linewidths of four solar faculae and adjacent undisturbed photosphere sections 01 p0151 A67-11285

Photoelectric measurements of continuum intensity differences and concave grating spectra of faculae and undisturbed photosphere 14 p2378 A67-27846

Radial motions in small and young sunspots indicating different cooling processes than regular sunspots 21 p3707 A67-38964

SOLAR FLARE

SA SUNSPOT

Solar flares, special features revealed by optical observations, classification, optical spectrum, shock waves and protuberances 01 p0144 A67-10771

Intensity observation of ELF electromagnetic field integral and SEA phenomena caused by solar flare-induced SID 01 p0060 A67-11240

Radial extension of corpuscular flux from chromospheric flares and duration of earth immersion in flux 02 p0306 A67-11653

Spectrophotometric study of hydrogen alpha, beta, gamma, epsilon and hydrogen and K spectral lines of chromospheric flare of August 21, 1959 02 p0308 A67-11850

Powerful X-ray flare on sun detected by high altitude rocket, noting high energy electrons in superchromospheric

- layer 02 p0308 A67-11974
- Origin of geomagnetic field, attributing paleomagnetic inversions to electromagnetic induction effects produced by solar corpuscular eruptions 02 p0326 A67-12063
- Radiation types encountered and shielding used by Voskhod I and II manned spacecraft 02 p0308 A67-12321
- Solar particles zones of incidence during maximum and minimum solar activity 02 p0310 A67-12574
- Solar flares, discussing continuous electromagnetic radiation, hard X-ray radiation and microwave radio bursts 02 p0310 A67-12576
- Relation between Forbush decreases and chromospheric flares, obtaining longitudinal distributions before and after onset, using statistics 02 p0311 A67-12592
- Solar flare mechanism, explaining absence of cosmic ray flares and occurrence of PCA events in years of sunspot minimum 03 p0506 A67-13651
- Photometric cross section of nonradial coronal structure in 5303 angstrom line following proton flares with cosmic, subcosmic and corpuscular emissions 03 p0507 A67-13810
- Sunspot cycle coronal Fe XIV 5303 angstrom radiation emission and type IV bursts in solar flares 03 p0507 A67-13811
- Seasonal PCA variations and type IV bursts associated with high energy proton injection into polar ionosphere 03 p0507 A67-13812
- PCA events during 1938-1955 detected from vertical incidence ionospheric soundings at high latitude, identifying some with proton flares 03 p0507 A67-13813
- Forbush effect relation to location of large solar flares, noting association of magnetic bottles with phenomena 03 p0507 A67-14003
- Sudden cosmic noise absorption and X-ray flares noting peak, nature of decay and theoretical and experimental values [RASSA PAPER 1-10-139] 03 p0373 A67-14247
- Thermal and nonthermal cosmic radio sources explained by short circuit breakdown of predischarged field initiated by breakdown to thermally ionized arc discharge 04 p0691 A67-14433
- Tritium production in atmosphere by galactic cosmic rays, by solar flare accelerated particles and accretion from sun 04 p0613 A67-14855
- Solar cosmic ray generation during chromospheric flares, noting increased neutron intensity 05 p0880 A67-16112
- Spectrophotometric results for H-alpha and K line contours of August 21, 1959 chromospheric flare 05 p0892 A67-16496
- H-alpha, H-beta, H-gamma, H-epsilon, H-8, H-11, H-12 and H-13 line emission of June 25, 1960 chromospheric flare 05 p0893 A67-16497
- Solar flare of August 28, 1966 associated with sunspot group which crossed sun face at 7 degrees N 05 p0882 A67-16577
- Solar proton flux measurement with balloon-borne detectors in northern Scandinavia 05 p0882 A67-16740
- Automatic scanning receiver for interference-free recording of solar flare effects and polar blackouts, using cosmic noise method 05 p0883 A67-16799
- Proton flares and types of spot groups in 11-year cycle, discussing time-latitude occurrence combined with emissions of cosmic and subcosmic radiation 05 p0883 A67-16808
- Enhancement factor and true absorption of VHF cosmic radio noise associated with solar flares 05 p0884 A67-16929
- Solar chromosphere and corona activities during flare, noting UV radiation, echelette spectrum, radio wave, X-ray and fast particle emission 05 p0885 A67-17266
- Energetic neutrons relationship to subsolar flare 06 p1076 A67-17602
- Space nuclear radiation dose rates in earth atmosphere with consideration of solar flare radiation variations 06 p1077 A67-18009
- Motion and asymmetry of emission lines of chromospheric flares with small plasmoid distribution 06 p1077 A67-18156
- Planet Mercury magnetospheric scattering of solar-flare protons to earth, obtaining deflection angle [AIAA PAPER 67-150] 06 p1088 A67-18505
- Spectrophotometric study of H, K and He spectral line characteristics of chromospheric flare of June 25, 1960 07 p1247 A67-19166
- Enhanced interplanetary scintillations associated with solar flares from radio sources survey 07 p1243 A67-19667
- High energy solar cosmic ray spectrum during solar flare of February 23, 1956 07 p1243 A67-19805
- Shock waves in interplanetary medium caused by sudden expansion of solar corona following flare [AFOSR-66-2838] 07 p1251 A67-19848
- Definition and computation of daily solar flare activity index 07 p1251 A67-19945
- Apparent area as basis for solar flare importance, noting dependence on position 08 p1376 A67-21237
- Longitude distribution of solar proton flares as function of recurrence period 08 p1377 A67-21248
- Geomagnetic storms due to solar flares statistically analyzed to obtain configuration of solar plasma flow generated by solar flares 08 p1377 A67-21360
- Ionograms of chromospheric eruptions with eruptive filament of December 1965, obtaining morphological data and determining radiation frequency range 09 p1561 A67-21842
- Rise and decay times of spike burst during type IV event of February 5, 1965, noting electron stream velocities and coronal temperature 09 p1562 A67-22233
- Electric fields due to electron-plasma and ion-acoustic waves associated with sunspot magnetic field variation as main cause of electron acceleration in solar flares 10 p1700 A67-23056
- Natural ELF electromagnetic noise properties during solar flare of July 7, 1966, considering radiation compression effects on earth-ionosphere cavity 10 p1700 A67-23057
- Solar flares as acceleration mechanisms for relativistic and subrelativistic particles 10 p1700 A67-23186
- Flare spray on west solar limb on July 11, 1966, noting radial polarization effects suggesting Thompson scattering as source of continuous spectrum 10 p1703 A67-23798
- H-alpha and white light cinematograms of September 1963 flare/sunspot group and radio, ionospheric and magnetic field data 10 p1703 A67-23799
- Radio burst produced by solar flare on August 28, 1966, analyzing flux increases as function of time and frequency 10 p1703 A67-23803
- Model of formation of magnetic bottle as result of interaction of drawn-out magnetic fields of solar origin, noting sunward flow of plasma 10 p1712 A67-23805
- Solar flare data computerized, reducing reported values of importance and area to standard scales, considering universal time and day 11 p1856 A67-24497
- Emission of particles, causing geomagnetic storms, without accompanying radio effects 11 p1787 A67-24594
- Sunspot groups configuration preceding and following formation of type IV radio burst flares 12 p1992 A67-25130
- Electromagnetic state theory applied to solar flares by analogy between ionized current-carrying plasma processes and solar flare conditions 12 p2001 A67-25224
- Detection of solar flare effect during severe geomagnetic disturbances from ionospheric flare effects 12 p1993 A67-25363
- Relation between solar flare, X-rays and sudden ionospheric disturbances /SID/ using satellite measurements 12 p1905 A67-25801
- Possible polarization of X-ray bremsstrahlung of solar flares due to sharply anisotropic electron beams 13 p2191 A67-26383
- Solar flare electron propagation in interplanetary space 13 p2194 A67-27251
- Polar aurora of September 13, 1957 and geomagnetic activity attributed to extraordinary solar flares 13 p2115 A67-27393
- Interplanetary electromagnetic field effects on cosmic ray intensity noting geomagnetism, modulation mechanisms and solar flare particle propagation 14 p2380 A67-27965
- Solar flare observation with monochromatic heliograph at Mitaka 14 p2384 A67-28095
- Spectrographic observations of late stages of limb flare by achromatic coronagraph 14 p2381 A67-28835
- Nonthermal X-ray radiation accompanying solar flares, comparing spectral power of synchrotron radiation, Compton radiation and bremsstrahlung as possible generation mechanisms 15 p2549 A67-29141
- Blast wave driven by solar flare ejecting plasma cloud proposed as origin of energy density increase causing sudden commencement of magnetic storm 15 p2476 A67-29625
- Motion and asymmetry of emission lines of chromospheric flares with small plasmoid distribution 16 p2737 A67-30500
- Radial extension of corpuscular flux from chromospheric flares and duration of earth immersion in flux 16 p2738 A67-31068
- Three-dimensional structure of solar plasma flow generated by solar flares, noting geometric factors in geomagnetic storm intensity decrease 16 p2739 A67-31415
- Solar flares causing Forbush effect, determining relevant parameters, variations with solar cycle and mutual relations 16 p2739 A67-31457
- Forbush effect causing solar flares not originating from same active solar region, discussing long connection to sun and interlocking 16 p2739 A67-31458
- Solar flares, analyzing X-ray emission, radio emission and superposition of ionospheric effect 16 p2739 A67-31459
- Low energy protons emitted by solar flare satellite observed inside and outside of magnetosphere, noting immediate access to polar caps 16 p2740 A67-31626
- Changes of phase and signal amplitude of VLF radio waves during solar flares noting waveguide mode characteristics 16 p2632 A67-31859
- Solar flare effect on electron production and electron density in lower ionosphere 17 p2936 A67-32382
- Association rate between solar surges and flares 17 p2938 A67-32820
- Brightening observed near D-2 line of sodium I on July 28, 1966 17 p2939 A67-33396
- Eruption of solar flare of importance 2, describing evolution, associated optical and radio phenomena, structure of longitudinal magnetic field, etc 17 p2939 A67-33397
- Energy transport, cosmic ray particle storage and triggering mechanism in solar flares, considering relation with stellar flares 17 p2939 A67-33398
- High kinetic energy electrons associated with solar flares, noting prompt and delayed types 17 p2940 A67-33401
- Ionospheric irregularities following solar proton flare of July 1966 observed with Alouette topside sounders 19 p3312 A67-35176
- Solar X-ray flare of July 1966 observed from satellite, giving curves describing energy flux, radiation intensity, etc 19 p3312 A67-35187
- Polar cap absorption on July 1966, discussing solar flare, radio outburst, proton intensity, geomagnetic latitude, etc 19 p3313 A67-35214
- Solar X-ray emission associated with proton flare of July 1966 measured, plotted and described 19 p3313 A67-35218
- Long term forecasts of proton flares 19 p3313 A67-35261
- Solar-flare short and long term forecasting, discussing magnetic-field configurations and gradients 19 p3314 A67-35269
- Time dependency, anisotropy degree and spectral composition of cosmic radiation generated during July 1966 solar flares as observed by Pioneer VI 19 p3314 A67-35270
- Gravitational model for chromosphere flarelike brightenings following dispartitions brusques, examining prominence and chromospheric characteristics 19 p3324 A67-35437
- Solar flare electron density determination by half-width method, discussing errors due to measurement and method 19 p3314 A67-35438
- Solar flare electron density measurements using half-width method, noting variations with height, development and area 19 p3314 A67-35439
- Flare of September 20, 1966 morphology and mechanism, discussing observations, narrowing of spectral line, etc 19 p3314 A67-35440
- Italian scientific research program during IQSY, with summarization of preliminary

results. 19 p3223 A67-35480
Particle acceleration in solar flares and relative abundance of various nuclei among energetic solar particles 19 p3315 A67-35492
Aurora events of July 1958 attributed to solar flare from study of solar and geomagnetic data 19 p3225 A67-35618
Satellite observations made by two or more satellites simultaneously on interplanetary medium 20 p3521 A67-36501
Foreshortening law for apparent area of flare derived using statistical method 20 p3518 A67-36841
Solar flare microwave radio bursts, suggesting synchrotron radiation from relativistic positrons, calculating positron yield and synchrotron spectrum 20 p3519 A67-37101
Solar X-ray emission line spectrum from 1.3 to 20 angstroms in solar flares identified as Fe XXVI through Fe XX transitions 20 p3519 A67-37396
Low latitude neutron fluxes for PCN and quiet solar period, noting solar proton production of neutrons 20 p3519 A67-37406
Possible polarization of X-ray bremsstrahlung of solar flares due to sharply anisotropic electron beams 21 p3698 A67-38817
Flare X-ray emission period determined, noting maximum radio emission and optical intensity 21 p3699 A67-38965
Evidence for relationship between solar flares and magnetic fields explained by neutral point type model, considering smaller flares 21 p3699 A67-38988
Fast electrons formation mechanism during flares ascribed to fast proton deceleration in flare region rather than high energy particle ionization 21 p3699 A67-39013
Solar RF radiation in mm wavelength evaluated for information on solar flare activity 22 p3882 A67-39591
Time dependency, anisotropy, propagation and spectral properties of cosmic radiation released by solar flares during sunspot activity 22 p3871 A67-39796
Intense fluxes of charged particles associated with disturbances in interplanetary medium during 1966 22 p3871 A67-39797
Cosmic ray propagation processes studied from measurement of anisotropic character of cosmic radiation 22 p3871 A67-39798
/1965-1966/
Solar flare occurrences probability, designating two-year period centered on sunspot minimum as safe time zone for vehicles on missions to Mars and Venus 22 p3873 A67-39929
Solar cycle prediction based upon random number technique, Fourier curve fits and power spectra analysis 22 p3873 A67-39931
Cosmic ray yearly variation during solar activity cycle, discussing flare and acceleration mechanisms, stable coronal condensation and sunspot magnetic field 22 p3874 A67-40045
Geomagnetic crotchets of solar flares based on materials analysis recorded at Hurlerovo, discussing time factors and characteristics 23 p4049 A67-40670
Characteristics of geomagnetic crotchets associated with proton flares, determining recombination coefficients and electron densities 23 p4050 A67-40671
Cosmic ray regional variations in intensity and ionization magnitude and duration indicating heavy nucleus and low energy particle influx accompanying solar flares 23 p4055 A67-41100
Heavy nuclei intensity during solar cosmic ray intensity increase accompanying chromospheric flares, proposing magnetic field dynamic dissipation acceleration mechanism for charged particles 23 p4056 A67-41113
Cosmic ray intensity increase in wake of chromospheric flares from stratospheric measurements 23 p4057 A67-41115
Neutron component intensity variation and particle generation on sun during chromospheric flares and electromagnetic radiation during solar activity cycle 23 p4057 A67-41116
Flare positions relative to neutral line in longitudinal components of photospheric magnetic fields, stressing drift rate 23 p4060 A67-41231
Solar flare energetic X-ray events detected by onboard satellite ionization

chambers, studying relationship to radio burst and space particle emission 23 p4060 A67-41232
Energetic protons from March 24, 1966 solar flare observed with OGO 1 satellite scintillation counter 23 p4060 A67-41233
Solar cosmic ray generation during chromospheric flares noting increased neutron intensity 24 p4214 A67-42788
Nonthermal X-ray radiation accompanying solar flares, comparing spectral power of synchrotron radiation, Compton radiation and bremsstrahlung as possible generation mechanisms 24 p4222 A67-43064
SOLAR FLUX
F-2 layer ion-atom interchange coefficients, ion-neutral diffusion coefficient and flux of solar ionizing radiation, comparing ionospheric data 01 p0056 A67-10108
Solar autoionization line profiles for Al I in rocket UV spectrum 02 p0323 A67-11699
Thermal emittance and reflectance of diffuse-bottomed specular-walled groove in solar radiant-flux environment [AIAA PAPER 66-459] 02 p0342 A67-11939
Eppley-JPL solar constant measurement experiment, noting 12-channel radiometer, filter wavelength limits and high altitude measurements 02 p0328 A67-12396
Solar neutrino-electron interaction and use of boron-cycle solar neutrino fluxes to determine existence of neutrino and antineutrino scattering effects 02 p0317 A67-12776
Penetration of flows into stable layer below solar hydrogen convection zone based on detailed model of sun 04 p0694 A67-14470
Specific type of geomagnetic pulsations corresponding to solar corpuscular radiation, noting flux geometry and intensity variations 05 p0884 A67-17134
Quasi-stationary gas emission from active solar regions and relation to recurrent geomagnetic disturbances 06 p1077 A67-18152
Atmospheric scattering of solar flux in UV noting radiation transfer for airborne detector, air component absorption coefficient and spectra from rocket flight 10 p1629 A67-22736
Energetic solar particle effect on ionosphere, discussing signal phase, amplitude propagation and attenuation 10 p1637 A67-23192
Atmospheric attenuation at millimeter wavelength measured noting correlation with weather conditions and solar flux effect 11 p1751 A67-23971
Lyman alpha emission from sun near solar minimum 11 p1862 A67-24503
Solar X-ray soft component fluxes observed by satellite 12 p1999 A67-25835
Solar X-ray events observed by 1964-1-D satellite launched by U.S. Naval Research Laboratory in 1964 12 p1999 A67-25836
Sudden cosmic noise absorption correlated with solar microwave flux to establish daily mean value 13 p2190 A67-26311
Solar gamma-ray flux in high energy region analyzed using OSO-I satellite 14 p2381 A67-28057
Flux density absolute calibration of solar radio emission 14 p2385 A67-28440
Solar flux density absolute microwave spectra 14 p2385 A67-28441
Quasi-stationary gas emission from active solar regions and relation to recurrent geomagnetic disturbances 16 p2737 A67-30496
Radio emission flux from local solar sources relation to active solar regions structure, based on radio-astronomical observations 17 p2948 A67-32969
Specific type of geomagnetic pulsations corresponding to solar corpuscular radiation, noting flux geometry and intensity variations 21 p3698 A67-38477
Antarctic riometer observations of PCA event of February 1965 compared with satellite measurements of solar proton flux and spectrum during same event 22 p3872 A67-39803
Solar neutrino-electron interaction and use of boron-cycle solar neutrino fluxes to determine existence of neutrino and antineutrino scattering effects 22 p3877 A67-40278
27-day cosmic ray intensity variations noting possible selective effects of active spots on solar hemispheres and plasma corpuscular fluxes 23 p4056 A67-41110
structure

SOLAR GENERATOR
Solar thermoelectric flat plate generator application to auxiliary power systems for incident solar fluxes from 130 to 1000 watts/square ft 08 p1286 A67-20737
Solar thermoelectric generator with cylindrical aluminum solar energy receiver using p and n type semiconductor materials and water cooled junctions 18 p2990 A67-34491
SOLAR GRANULATION
S PHOTOSPHERE
SOLAR GRAVITATIONAL EFFECT
Solar-lunar perturbation of 24-hour satellite, independence of librational motion and impossibility of equilibrium 02 p0321 A67-11498
Satellite motion with large inclination and large eccentricity around planet and perturbed by sun 08 p1382 A67-20400
Inclination variation with time of 24-hr low inclination orbits perturbed by solar-lunar gravitation 08 p1402 A67-21508
Gravitational capture of cosmic dust by sun and planets and evolution of circumterrestrial cloud 18 p3119 A67-33863
Deformations of earth crust produced by known forces of luni-solar and surface types 18 p3040 A67-34093
Solar gravitational effect on earth seismic activity, showing relation between annual variations and earth-sun radius 19 p3221 A67-35430
Lunar-solar gravitational perturbation of satellite with sidereal day period, discussing stability 20 p3523 A67-36626
Light deflection by solar gravity measuring method using radar interferometer 20 p3485 A67-36995
Solar oblateness and Mercury perihelion advance, showing turbulent viscosity forces acting on photospheric meridional currents as possible distortion cause 21 p3701 A67-37963
SOLAR HEAT
Neutrino flux recording for temperature determination of sun interior, discussing thermonuclear reactions 01 p0152 A67-11301
Planar librational stability boundaries for flexible satellite under solar heating influence, using phase space concept [AIAA PAPER 67-126] 06 p1095 A67-18313
Solar radiation field interaction with flexible antenna as possible explanation of anomalous rapid spin decay of satellites [AIAA PAPER 67-39] 06 p1096 A67-18350
IR images of lunar crater Tycho during lunar night provide evidence that thermal anomaly is produced by solar rather than internal heat 09 p1565 A67-22013
Helium 3 anomaly in octahedrites and low spallogenic tritium content in freshly fallen iron meteorites caused by tritium loss due to solar heating in space 11 p1866 A67-24694
Inertial guidance and navigation systems and components testing facility 1100 feet underground [AIAA PAPER 67-538] 19 p3208 A67-35940
Thermal annealing of silicon solar cells with direct solar heating or electric storage methods to avoid radiation damage 20 p3364 A67-37129
Coronal heating extent placed at 1.6 solar radii by 38 MHz radar investigation studies, noting agreement with coronal density calculation 20 p3528 A67-37477
Radiometric determination of absorption by earth atmosphere and solar brightness temperature at 5.65 mm frequency 22 p3897 A67-40560
Energy distribution of photometric spectra in solar UV continuum in 1550 to 2100 angstrom range, discussing radiation temperature decrease 24 p4225 A67-41835
Anabatic winds caused by solar heating of slope, investigating flow patterns useful for soaring purposes 24 p4181 A67-42022
SOLAR HEAT FLOW
Coronal temperature-gradient regions analyzed, using data of Lyot and corona condensation spectrum 06 p1083 A67-18154
Solar cycle variations in atmospheric density deduced from meteor observations and rocket measurements in mesopause and thermosphere 10 p1638 A67-23204
Geometrical model for calculation of solar heat fluxes reflected from planet onto plate 13 p2201 A67-27342
Heating of chromosphere above sunspot due to magnetoacoustic waves which develop into weak shock waves 15 p2551 A67-29142

Coronal temperature-gradient regions analyzed, using data of Lyot and corona condensation spectrum 16 p2741 A67-30498
Heating of chromosphere above sunspot due to magnetoacoustic waves which develop into weak shock waves 24 p4239 A67-43065

SOLAR INSTRUMENT

Absorptivity standard instrument to investigate solar absorptance of four surfaces used for spacecraft temperature control for Mariner IV on Mars mission [AIAA PAPER 65-650] 03 p0448 A67-13055
Book on solar radio exploration covering electromagnetic radiation discovery, solar physics principles, solar radio activity and research instruments

description 16 p2755 A67-31923
Solar spectral line center-to-limb variations during solar eclipse of May 20, 1966 20 p3453 A67-37682

Modulation transfer functions of various solar recording films using interference device, giving detectability threshold of two-dimensional emulsion patterns 23 p4001 A67-41237

SOLAR LONGITUDE

Solar-flare short and long term forecasting, discussing magnetic-field configurations and gradients 19 p3314 A67-35269

SOLAR MAGNETIC FIELD

Mechanism of solar activity cycle, examining relation of stability threshold of disintegration of solar magnetic belt into separate cells 01 p0146 A67-11282

MHD wave generation in sunspots, examining depth of solar magnetic layer that affects magnetic convection 01 p0151 A67-11283

Interaction of solar wind and frozen-in magnetic field with geomagnetic field inside and outside magnetosphere, comparing theory with satellite measurements 02 p0320 A67-11461

Data and theories on solar and stellar magnetic fields, including techniques for analyzing extraterrestrial magnetic phenomena 02 p0322 A67-11683

Anisotropic distributions of suprathermal electrons as explanation of observed line splitting for type II solar radio outburst and indirect determination of coronal magnetic fields 02 p0307 A67-11691

Sunspot magnetic field structure in model constructed from solution of boundary problem for semispace 02 p0329 A67-12489

Babcock theory of solar activity, quiet sun and 11-year magnetic cycle 02 p0330 A67-12639

Sunspot magnetic field and effect on solar cycles, noting wave propagation in inviscid conducting fluid 03 p0511 A67-13740

Magnetic fields at various depths of solar atmosphere measured by Crimean Astrophysical Observatory double magnetograph 04 p0701 A67-15551

Spoerer and Gleissberg laws for Babcock and Tuominen models of solar activity concerning migration in heliographic latitude of sunspot area and role of solar magnetic field 05 p0897 A67-16809

Slit size effect on magnetograph observations of solar magnetic field in near polar regions 06 p1082 A67-18015

Oblong shape and Alfvén waves of looped expanding coronal prominence 06 p1078 A67-18157

Average latitudinal drift of sunspots and migration of magnetic fields on sun 06 p1089 A67-18708

Construction of model for chromospheric magnetic field over sunspot 09 p1563 A67-21628

Magnetic fields in solar corona, observing bursts with frequency splitting to determine correlation with plasma radiation theory 09 p1565 A67-21981

Type II and IV solar radio bursts analyzed, determining nature and geoeffectiveness of causing agents 10 p1698 A67-22776

Amplification of solar dipolar magnetic field by differential rotation investigated, noting implications of Spörer law 10 p1705 A67-22895

Large-scale structure of solar magnetic field during declining and minimum phases of solar cycle and effect on interplanetary magnetic field 10 p1700 A67-23055

Sunspot magnetic field structure in model constructed from solution of boundary

problem for semispace 10 p1708 A67-23357

Solar magnetic field in photosphere, discussing evolution through expanding solar wind plasma 11 p1863 A67-24548

Solar temperatures from observations of July 1963 eclipse with horn antenna in left and right circular polarization, noting magnetization 11 p1867 A67-24779

Forbush decreases associated with type IV burst flares, particularly in relation to PCA events, noting delay time and magnetic western boundary 12 p1992 A67-25129

High velocity particles and slower corpuscles penetration into lower ionosphere occurring after solar flare explained by Sweet mechanism 12 p1993 A67-25134

Distribution and intensity of solar magnetic fields gained from spectrograms, noting correspondence between magnetic field and Ca-K line emission 12 p2001 A67-25219

Neutral /zero/ points and geometry of solar magnetic fields 12 p2002 A67-25534

Solar wind interaction with solar dipole magnetic field in coupled hydrodynamic and hydromagnetic equations 12 p2008 A67-25920

[AIAA PAPER 66-509] Zeeman effect in measuring magnetic fields of sun and stars, noting apparatus 12 p2010 A67-26235

Steady state model of solar wind flow in equatorial plane solved for radial and azimuthal motions, taking into account pressure gradient, magnetic field and gravitational effects 12 p2010 A67-26241

Sunspot phenomenon covering formation, penumbra, spot umbra, magnetic field, interpretation, radiative deficit in umbra and penumbra, energy flux through Evershed stream, etc 13 p2202 A67-27416

Magnetic field amplification within sunspot groups, considering convective zone and viscosity 13 p2202 A67-27419

Line formation in sunspots taking into account magnetic field which greatly changes line profile, presenting transfer equations and solutions 13 p2204 A67-27431

Sunspot magnetic field affecting convective energy transport so that resulting pressure gradient together with gravity force balances magnetic field force 13 p2204 A67-27436

Photoelectric measurements of continuum intensity differences and concave grating spectra of faculae and undisturbed photosphere 14 p2378 A67-27846

Current diagram plotting by graphical integration method for diurnal solar magnetic variations in especially quiet days 14 p2309 A67-27939

Photographs of sunspots analyzed to obtain magnetic field strength data 14 p2384 A67-28076

Method for complete observation of magnetic field structure in sunspots 14 p2390 A67-28942

Solar magnetic field origin and effects revealed by direct and satellite observations of photosphere, chromosphere, corona and earth neighborhood 15 p2554 A67-29531

Oblong shape and Alfvén waves of looped expanding coronal prominence 16 p2737 A67-30501

Interplanetary sector structure observed by IMP-I satellite compared with photospheric magnetic field and plage structure observations 17 p2953 A67-33400

Small scale magnetic fields observed in photosphere explained by sunspots made invisible by lateral heat influx 17 p2953 A67-33404

Quiescent solar prominences general appearance described by theoretical model 19 p3324 A67-35436

Solar magnetic fields studied by measuring Fraunhofer line shifts with circular-polarization analyzer, showing relationship to gravity center displacement 19 p3325 A67-35505

Theory, similar to Babcock solar magnetic field theory, explaining magnetic stars variability 19 p3328 A67-35933

Stable height to distance to supporting magnetic field origin ratio for prominences, noting agreement with Kippenhahn-Schluter model 20 p3528 A67-37469

Solar magnetic field existence evidenced by transverse fields in sunspots, field vector spatial distribution around sunspots and granular pattern inside sunspots 21 p3708 A67-38966

Direction of sunspot magnetic force lines at any point of solar surface by fringe analysis of light polarization ellipse 21 p3709 A67-38987

Magnetic effect on polarization of resonance radiation in solar chromosphere 21 p3709 A67-38989

Solar magnetic fields, discussing Zeeman effect, solar activity regularity and filamentary current in force-free magnetic fields 21 p3709 A67-38990

Turbulent convective eddies effect on solar concentrated magnetic fields, plotting force lines 21 p3709 A67-38991

Cosmic rays interaction with solar and terrestrial magnetic fields, noting interplanetary plasma flows and solar activity 21 p3699 A67-39006

Cosmic ray yearly variation during solar activity cycle, discussing flare and acceleration mechanisms, stable coronal condensation and sunspot magnetic field 22 p3874 A67-40045

Solar system environment, discussing solar magnetic field, flare flux and energy spectrum, interplanetary plasma and radiation, asteroids, meteoroids and comets 22 p3889 A67-40407

Static tufted magnetic field perturbing effect on solar atmosphere small scale structure, noting pressure, density and temperature changes [SR-15] 24 p4222 A67-41767

Magnetic changes in solar atmosphere, discussing current-free field configurations using solar magnetograms and photospheric field effect 24 p4222 A67-41768

Solar magnetographs for defining strength and direction of magnetic field in solar atmosphere 24 p4223 A67-41769

Type II and IV solar radio bursts analyzed, determining nature and geoeffectiveness of causing agents 24 p4209 A67-42112

SOLAR NEBULA

Protoplanetary cloud and evolution, noting Hoyle rotatory nebula and other hypotheses 09 p1563 A67-21633

Condensation path of cooling gas of solar composition calculated considering barriers to homogeneous nucleation of condensed phase 16 p2751 A67-31454

Abundance of volatile elements in meteorites, comparing chondrite decrease for evidence of fractionations in solar nebula 20 p3526 A67-37173

Gravitational torque mechanism for radial outward angular momentum transport in solar nebula 24 p4223 A67-41790

Circular and linear polarization of OH line radiation from NGC 6334 nebulae region using Parkes radio telescope 24 p4230 A67-42333

Olivine and pyroxene composition distribution in type II carbonaceous chondrites, discussing metamorphic effects and gas-dust fractionation 24 p4237 A67-42651

SOLAR NOISE

Size and shape of vertical polar diagrams of radars in situ measured using sun and other stars as signal sources 13 p2071 A67-27219

Radio stars as signal sources for accurate measurement of radar antennas vertical polar diagrams, describing solar noise technique disadvantages 15 p2436 A67-29645

East-west parabolic reflector array for design of high resolution multielement interferometer for solar noise observations 17 p2864 A67-33402

38 MHz solar burst duration, bandwidth, amplitude, number and polarization characteristics noting possible generating mechanisms 20 p3520 A67-37476

SOLAR OBSERVATORY**SA OSO**

Manned planetary exploration, Mercury and Gemini flight programs and projected goals of Apollo Applications Program 12 p2002 A67-25233

Solar flare observation with monochromatic heliograph at Mitaka 14 p2384 A67-28095

U.S. research program for IQSY 1964-1965 covering solar synoptic observations, zodiacal light, comet tails, atmosphere, etc 19 p3224 A67-35501

Pointing control system /PCS/ for Apollo Telescope Mount /ATM/ for solar observations [AIAA PAPER 67-534] 19 p3334 A67-35936

Proportional counter spectrometer for solar soft X-ray spectrum study 20 p3448 A67-36960

SOLAR PHOTOSPHERE
S PHOTOSPHERE
SOLAR PHYSICS

Geophysical and heliophysical characteristics for enhanced cosmic radiation intensity during magnetic storm in February 1959 05 p0885 A67-17498

Evolution of sun and planets 06 p1091 A67-18995

Solar physics and MHD model of sun 07 p1247 A67-19331

Monograph on physics of solar corona including history, observational methods, data analysis, coronal gas, magnetic fields, temperature, density and radiative processes 07 p1251 A67-19838

Solar-terrestrial physics - Conference, Belgrade, August-September 1966 12 p1990 A67-25106

Nuclear spectroscopy and solar neutrino astrophysics 16 p2753 A67-31734

Book on solar radio exploration covering electromagnetic radiation discovery, solar physics principles, solar radio activity and research instruments description 16 p2755 A67-31923

Solar physics and hydrodynamics - Conference, Tatranska Lomnica, Czechoslovakia, October 1964 18 p3118 A67-33749

Corona observation within one solar radius of photosphere, identifying emission lines and explaining continuous spectrum and Fraunhofer lines reduced depth 19 p3318 A67-35055

UK contribution to IQSY in meteorology, geomagnetism, airglow observations, etc 19 p3223 A67-35476

Fabry-Perot interferometer with magnetostriptive scanning and SNR improves system for solar physics and airglow observations 20 p3440 A67-36360

Foreshortening law for apparent area of flare derived using statistical method 20 p3518 A67-36841

Solar-terrestrial physics and magnetosphere - Conference, Belgrade, August-September 1966 22 p3882 A67-39667

SOLAR PLASMA

Wide range vibrating-reed Mariner II electrometer, describing components, performance characteristics and results 02 p0241 A67-11681

Intensity and energy distribution of solar plasma determined by mass spectrometers which can separate hydrogen and helium components of plasma stream 02 p0247 A67-12692

Geomagnetic and auroral storms provide information on interaction of solar plasma flows and magnetosphere 04 p0618 A67-15668

Aurora and ring current theory confirming role of hydromagnetic plasma flow and frozen-in field lines in geomagnetic storms 06 p0995 A67-17973

Solar wind magnetic field as medium for plasma-magnetosphere interaction 07 p1243 A67-19803

Interplanetary magnetic field and plasma effect on geomagnetic activity during quiet sun conditions 07 p1251 A67-19912

Geomagnetic storms due to solar flares statistically analyzed to obtain configuration of solar plasma flow generated by solar flares 08 p1377 A67-21360

Interplanetary and Martian vicinity data from Mariner IV solar plasma experiment 10 p1707 A67-23228

Hydromagnetic wave propagation and energy transfer in stratified isothermal plasma embedded in parallel uniform gravity and magnetic fields 11 p1868 A67-25083

IMP-II and OGO-I measurements on plasma characteristics in transition region between solar wind and geomagnetic field 12 p1997 A67-25806

Super-Alfvénic point or distance of effective corotation for loss of angular momentum in solar wind 17 p2945 A67-32644

Interaction of planetary magnetic field with solar plasma studied using hypersonic analog, estimating energy transfer rate 17 p2951 A67-33208

Steady state model of system consisting of solar corona and interplanetary plasma, noting plasma efflux from sun 20 p3529 A67-37520

Three-dimensional heat source influence on solar plasma flow contradicts Parker solar wind theory, based on gasdynamic acceleration 21 p3699 A67-39012

Quiet condition solar wind geomagnetic field interaction measurements, discussing solar plasma and bow shock wave generation 22 p3870 A67-39670

Solar wind geomagnetic field interactions during disturbed conditions, discussing solar particle emissions, solar plasma activity, ring and ionospheric currents 22 p3870 A67-39672

27-day cosmic ray intensity variations noting possible selective effects of active spots on solar hemispheres and plasma corpuscular fluxes 23 p4056 A67-41110

Space time distribution of cosmic rays as function of plasma efflux from sun, magnetic field intensity, topology and scale irregularities 23 p4059 A67-41133

SOLAR POSITION

Numerical integration of solar orbit in model of galactic system 02 p0330 A67-12714

Ionospheric absorption variation with solar zenith angle measured with continuous wave recording 04 p0576 A67-15634

Balloon-borne sun seeker improvements through transistorized circuits and solid state switches 07 p1184 A67-19396

Morning effect on F region, noting seasonal variation of corresponding solar zenith angle and worldwide distribution of predawn minimum 16 p2664 A67-30976

U.S.S.R. astronomical almanac for 1970 21 p3703 A67-38200

SOLAR POWER SOURCE

Fluoride solar attitude control device functioning as sensor and actuator, noting design principles and operation 17 p2954 A67-31982

Solar photovoltaic cell design for lower temperature operation, noting application to near-sun missions 21 p3570 A67-37789

High payload electric propulsion spacecraft powered by solar array for multiple interplanetary missions [AIAA PAPER 67-711] 21 p3714 A67-38738

Electric propulsion ion engine systems using solar power source for Mars and Jupiter exploratory unmanned spacecraft is adaptable to existing launch vehicles [AIAA PAPER 67-713] 22 p3868 A67-39844

SOLAR POWER SYSTEM

Rankine and Brayton cycles for spacecraft power generation, discussing operation principles, advantages and performance characteristics 01 p0112 A67-11428

Solar electropulsion developments for solar system exploration 03 p0513 A67-14097

Relation between reflector surface shapes, heat collector and intensity of geometric concentration of parallel ray flux 04 p0553 A67-14665

Algorithm for statistical solution of radiant flux distribution in solar receivers with paraboloidal collectors 04 p0553 A67-14666

Photographic mapping of Martian surface with electrically propelled solar-powered photographic spacecraft placed into near polar orbit [AIAA PAPER 67-88] 06 p1096 A67-18438

Thermodynamic cycle for solar power systems using hexafluorobenzene as working fluid, discussing efficiency and radiator area 07 p1131 A67-19366

Characteristics of single circuit space power installation with thermoelectric converter noting capacity, temperature and heat transfer 10 p1596 A67-23019

Vapor deposited GaAs thin film solar cells for application to solar power systems 10 p1596 A67-23165

Dynamic control study for solar mirror aboard spacecraft using breadboard apparatus and computer simulation method 11 p1745 A67-24274

Structural analysis and design of large area solar array, noting factors such as temperature distribution, dynamics, internal loads, permissible weight, etc 17 p2954 A67-31980

Primary electric propulsion systems for deep space missions with reference to SERT II program and compatibility with other spacecraft programs [AIAA PAPER 67-424] 18 p3111 A67-33908

In situ study of comets by solar electric propulsion spacecraft, analyzing mission characteristics 19 p3323 A67-35333

Trajectory optimization, performance and other factors in analysis of low thrust solar electric propulsion Jupiter flyby mission [AIAA PAPER 67-710] 21 p3706 A67-38737

Spacecraft design, solar powering, electric propulsion and side-looking radar for planetary surface observation mission on Mars or Venus 21 p3714 A67-38739

Graphic optimization technique for mass reduction in solar powered ion propulsion system with acceptable reliability constraint [AIAA PAPER 67-701] 21 p3697 A67-38960

Solar conversion/energy storage power systems for satellites in near earth orbits to provide continuous power supply 23 p3938 A67-41506

Solar cell power supply design to satisfy whole satellite, discussing power supply size and solar cell panel fabrication 23 p3939 A67-41508

Flight performance and power system design of Mariner IV Mars probe 23 p3939 A67-41509

Optimization of electric energy storage for solar thermal space power systems 24 p4108 A67-42543

SOLAR PROBE

Suitability of Saturn IB/Centaur and Atlas/Centaur launched solar-electric propulsion vehicles for performing 0.1-AU solar probe mission [AIAA PAPER 66-496] 11 p1852 A67-24343

Satellite size via experiment design, demonstrating advantages and drawbacks of small and large satellites 12 p2007 A67-25784

Semiquantitative evaluation of instrument requirements of solar probe as function of perihelion 16 p2758 A67-30644

Central data system for solar probe to map particle and radiation fields of solar corona 20 p3391 A67-36597

Solar probe mission planning, evaluating high temperature electronics capability and high flux GaAs solar cell efficiency 22 p3903 A67-39956

Unmanned 0.1 AU /icarvus/ solar probe preliminary design, discussing thermal control and power supply problems unmanned 0.1 AU /ICARVUS/ solar probe preliminary design, discussing thermal control and power 22 p3906 A67-40152

Thermal testing techniques for solar probe spacecraft using analytical and experimental models 24 p4139 A67-42043

SOLAR PROMINENCE

SOLAR PROPULSION

Solar and nuclear-electric propulsion thrusters including ion engines, plasma engines, arc jets, resistojets, etc [AIAA PAPER 66-830] 02 p0303 A67-12253

Resistojets and axisymmetric electromagnetic space propulsion thrusters 02 p0305 A67-12340

Solar electric spacecraft performance in specific Mars orbiter-lander mission evaluated, using characteristic length concept 06 p1074 A67-18276

Feasibility design study of solar powered ion propulsion system for interplanetary spacecraft [AIAA PAPER 66-214] 07 p1240 A67-19364

Optimum weight ratio for space vehicle with solar energy operated engine, noting dependence on distance from sun, trajectory optimization, etc 09 p1571 A67-21886

Solar-electric powered vehicle trajectory optimization using variational calculus, assuming general forms for efficiency and solar power variation [AIAA PAPER 67-583] 19 p3329 A67-35978

Low thrust Jupiter flyby mission analysis for interplanetary vehicles with solar electric propulsion [AIAA PAPER 67-708] 21 p3706 A67-38735

Solar electric propulsion for space missions, evaluating modularized ion propulsion systems to determine effect of electric isolation on system reliability, weight, etc [AIAA PAPER 67-699] 21 p3697 A67-38959

SOLAR PROTON

Proton induced hydroxyl formation on lunar surface simulated by bombarding glass, chemically similar to silicate minerals, with high energy protons [AFCLR-66-795] 02 p0324 A67-11857

Solar cosmic ray generation, discussing proton energy spectrum analysis and wave propagation in interplanetary

space 02 p0310 A67-12572

Seasonal PCA variations and type IV bursts associated with high energy proton injection into polar ionosphere 03 p0507 A67-13812

Solar proton streams apparently synodic in solar rotation interval during maximum epoch of recent solar cycle as indicated by polar cap absorption events 03 p0507 A67-14116

Continuous flux of solar protons entering earth atmosphere important in energy balance of ionosphere and sun [RASSA PAPER 1-10-140] 03 p0417 A67-14248

Role of solar photon and corpuscular radiation in dissociation and ionization of water molecules in cometary atmospheres 05 p0888 A67-16203

Radionuclide production in lunar surface activated by solar proton with reference to radiation shielding and reflection 05 p0885 A67-17386

Stratospheric recordings of solar cosmic rays from chromospheric flares, calculating and comparing diffusion coefficient of cosmic rays and energy spectrum of solar protons 07 p1243 A67-19698

High energy solar proton propagation in interplanetary magnetic field by Fokker-Planck equation 07 p1243 A67-19806

Particle effects of interplanetary shock wave, noting discontinuous drop in solar proton intensities 08 p1378 A67-21469

Solar proton and alpha particles entry into polar cap atmosphere 13 p2194 A67-27252

Radiation hazard to man from solar proton events 15 p2429 A67-29450

Solar proton diffusion data for model of quiescent interplanetary medium 17 p2937 A67-32539

Satellite-borne detection of decay protons as test of solar neutron observation 17 p2937 A67-32544

Energy spectrum and pitch-angle distribution of protons in auroras based on H-beta line profiles 17 p2938 A67-32962

Solar proton flux measurement by balloon on July 7, 1966 in northern Scandinavia, with differential proton flux calculated for several energies 19 p3312 A67-35175

Low latitude neutron fluxes for PCN and quiet solar period, noting solar proton production of neutrons 20 p3519 A67-37406

Solar proton and alpha radiation flux and spectral distribution measuring device on satellite HEOS A 21 p3629 A67-38665

Antarctic riometer observations of PCA event of February 1965 compared with satellite measurements of solar proton flux and spectrum during same event 22 p3872 A67-39803

Solar particle event of February 1965 observation with Mariner IV and Injun IV showing 70 degrees heliocentric longitudinal distribution in interplanetary space 22 p3872 A67-39811

Solar proton event /February 1965/, time history of low energy protons was more complex than that of higher energy particles 22 p3872 A67-39812

Temporal and spatial low energy solar proton intensity variations indicating interplanetary medium changes effects on magnetospheric configuration 22 p3873 A67-39813

Martian atmosphere component due to proton penetration into atmosphere from solar wind, suggesting radio occultation by Mars orbiter 23 p4063 A67-40799

1 to 5 Mev solar proton emissions observed by increased counting rates on Venera II and III and Zond III interplanetary probes 23 p4056 A67-41112

SOLAR RADAR REFLECTION

Radar experiments of sun at 38 mc/s, presenting results on echo variation with sunspot number, coronal irregularities, etc 03 p0514 A67-14311

SOLAR RADIATION

Long term variation in relations of solar indices to E and F region character figures interpreted without assuming changes in solar radiation 01 p0056 A67-10110

Anisotropy of reflected solar radiation from various surfaces as measured with aircraft-mounted radiometer 01 p0146 A67-10318

Hazards to man on moon from flare-produced solar particle beams and galactic radiation, noting estimate for life shortening 02 p0189 A67-12394

Electron concentration in metallic emission regions in chromosphere 02 p0328 A67-12485

Profile difference of two IR hydrogen lines in facula and in photosphere 02 p0308 A67-12488

U.S. Weather Bureau calibration of solar radiation pyranometer by means of 5000 watt tungsten filament lamp 03 p0419 A67-13076

Canadian calibration of solar radiation pyranometers 03 p0419 A67-13077

Silicon solar cell to measure solar radiation intensity, discussing effect of optical path length ratio and atmospheric constituents 03 p0419 A67-13079

Glass in refractive space optics, discussing UV solarization and athermalization [SMPTE PREPRINT 100-34] 03 p0469 A67-13808

Meteorological satellites noting necessity of radiation measurements 04 p0648 A67-14409

Middle UV region of solar radiation, discussing rocket and balloon mounted spectrograph measurement results 04 p0695 A67-14691

Atmospheric ozone in middle UV spectral region, noting vertical distribution, destruction by solar radiation, lifetime below layer in photochemical equilibrium, etc 04 p0612 A67-14694

Horizon studies for monochromatic radiation following Lambert-Beer law of transmission, noting Chapman theory on exponential distribution of atmospheric constituent of absorption 04 p0613 A67-14697

Solar radiation effect on planetary atmosphere noting charged particle bombardment, dayglow phenomena, auroral emission, etc 04 p0696 A67-14699

M-60 radisonde measurement reliability, comparing coupled pair subjected to same shocks and direct solar radiation 04 p0625 A67-15606

Lunar IR emission and solar radiation reflected by moon in visible region measured by Luna X orbiter 05 p0886 A67-16052

Perturbations of satellite orbital elements caused by pressure of solar radiation reflected from earth 05 p0894 A67-16566

Radiation effect on satellite in presence of partly diffuse and partly specular reflecting body 05 p0905 A67-16567

Passive spin propulsion of large flexible spherically shaped satellites by solar radiation field 05 p0905 A67-16568

Upper atmospheric density and composition determined by means of solar radiation attenuation and day airglow fluorescence 05 p0798 A67-16864

Solar UV and zodiacal light, emphasizing importance and merits of rocket and balloon observations 05 p0799 A67-16873

Rocket measurement of altitude dependence of flux intensity of solar vacuum UV radiation, using ionization chambers 05 p0799 A67-16874

Critical frequencies of F-2 and E layers in ionosphere relation to total daily influx of solar wave radiation into earth atmosphere 05 p0800 A67-17128

Solar radiation integrator, discussing design, composition and performance characteristics 05 p0808 A67-17310

Quasi-steady state temperature distribution in thick walled spherical satellite under solar radiation 05 p0906 A67-17368

Twilight effects of solar ionizing radiation absorption, discussing ion production rates and fluorescence 05 p0885 A67-17410

Motion and asymmetry of emission lines of chromospheric flares with small plasmoid distribution 06 p1077 A67-18156

Multichannel radiometer measurement of solar irradiance for realizing spacecraft radiative equilibrium [AIAA PAPER 67-147] 06 p1003 A67-18318

Solar radiation field interaction with flexible antenna as possible explanation of anomalous rapid spin decay of satellites [AIAA PAPER 67-39] 06 p1096 A67-18350

Reciprocity principle of Equivalent Sun Hours /ESH/ as means of spacecraft material testing 06 p0980 A67-18365

Book on atmospheric absorption, diffusion and polarization of light and radioelectric radiation 06 p0998 A67-18718

Direct solar radiation up to 30 km and

stratification of attenuation components in stratosphere, noting aerosol extinction properties in free atmosphere 07 p1170 A67-19390

Techniques for calculating vertical distribution of atmospheric ozone from intensity of solar UV radiation at various altitudes 07 p1172 A67-19456

Cosmos LXI spectrophotometric measurements of atmosphere-reflected UV radiation spectra 07 p1178 A67-19801

Solar UV reflection and scattering from earth atmosphere, use in determining total concentration and vertical distribution of ozone 07 p1178 A67-19815

E layer ionization and characteristic number as affected by solar X radiation in 44-60 angstrom range 07 p1178 A67-19822

Relation between solar radiation and electron concentration up to F layer analyzed in winter and summer 07 p1179 A67-19831

Space environment effect on refractive optical systems, particularly solar radiation effect on optical properties of glass 08 p1330 A67-20644

Color phenomena on moon 08 p1396 A67-21165

Solar environment and aerodynamic drag effect on deflection of structural booms in space [AIAA PAPER 66-502] 08 p1413 A67-21512

Absorbed solar electromagnetic radiation effect on mean facial skin temperature 09 p1452 A67-21725

Lunar resources for space and planetary exploration, discussing application of solar radiation, extraction of mineral resources from meteorites, etc 09 p1568 A67-22406

Integral short circuit current of solar converters determined from spectral distribution of solar radiation energy, using simulator and SiO photocell films 09 p1451 A67-22531

High resolution density data from radar observations of low altitude polar orbiting satellites reveal longitudinal and geomagnetic variation, noting regression analysis 10 p1640 A67-23216

Cosmos 65 spectrophotometric measurements of atmosphere-reflected UV radiation spectra 10 p1647 A67-23277

UV solar radiation absorption in upper atmosphere determined from measurement of photoelectron currents emitted by planar metallic orthogonal photocathodes onboard Cosmos II satellite 10 p1647 A67-23282

Electron concentration in metallic emission regions in chromosphere 10 p1708 A67-23353

Profile difference of two IR hydrogen lines in facula and in photosphere 10 p1702 A67-23356

Line profiles and equivalent widths for diffuse reflection of sunlight from model planetary atmosphere calculations, using invariant imbedding 10 p1710 A67-23635

Chromospheric background intensity difference between equatorial and polar regions of sun 10 p1711 A67-23800

Partial coherence functions to investigate contribution of solar radiation and gravitational tide in causing geomagnetic variations /ionospheric tides/ 11 p1785 A67-23938

Short period radioactive nuclides induced by secondary neutron due to solar cosmic radiation in chondrites 11 p1858 A67-24058

Solar K-line intensity and emission area at various phases of sunspot cycle 11 p1861 A67-24493

Photographic technique for obtaining solar image in rays of Lyman alpha line spectrum, using quartz crystal 11 p1793 A67-24862

Relative solar abundance for O, Si and Fe determined from intensities of far UV emission lines of solar corona 12 p2001 A67-25225

Brightness distribution of radio emission over solar disk during solar activity minima determined from radioheliograms 12 p2001 A67-25226

Hydrodynamic axial-symmetric model of plasma flow on sunward side of comet assuming cometary gas is ionized by solar UV radiation only 12 p1993 A67-25227

Solar constant and sunspot relationship interpreted by solar radio flux effect on lower ionosphere density 12 p1932 A67-25342

Electron and ion concentrations as function of solar radiation intensity and

variation of ionospheric conditions, noting nitrous oxide/oxygen ion 12 p1933 A67-25649

Pinhole X-ray photography of sun obtained during rocket flight, showing correlation of bright emitting regions on disk with calcium plages and radio emission 12 p2007 A67-25762

Molecular oxygen densities in range 70-90 km determined by rocket measurements of atmospheric absorption of solar UV radiation in Southern Hemisphere 12 p1934 A67-25786

Thermal coordinate analysis of lunar IR scan data for directional effects caused by surface geometry, illumination and sensor angle [AIAA PAPER 67-291] 12 p2009 A67-26008

Heat capacity evaluation between 150 and minus 180 degrees C, using evaporated gold-black coating as primary standard [AIAA PAPER 67-303] 12 p1958 A67-26018

Nighttime ionosphere maintained by downward flux of electrons from protonosphere as shown by columnar electron contents measurements, noting decay rate 13 p2107 A67-26305

Anomalous absorption and scattering in global and diffuse radiation measurements during cloudless summer 13 p2113 A67-26739

Solar cosmic ray interaction with earth ionosphere and resultant cosmic radio noise absorption 13 p2194 A67-27254

Discrete equilibrium temperatures of hypothetical planet with atmosphere and hydrosphere of one-component two-phase system under constant solar radiation 13 p2116 A67-27462

Chromosphere observation at different millimeter radio wavelengths with 4.88-m-diam telescope establishing correlation between mm solar radiation and solar activities 13 p2206 A67-27488

Solar photon radiation reaction produced on body of satellite and utilized for satellite stationkeeping 13 p2213 A67-27489

Heat balance in rocketsonde semiconductor thermometers, noting dissipation constant dependence on altitude and solar radiation 13 p2117 A67-27608

Accelerated method for spectral calculation of optical parameters of solar radiation 13 p2211 A67-27625

Solar radiation passage through earth atmosphere in triplet lines O I, considering molecular hydrogen absorption and brightness distribution of radiation 14 p2378 A67-27862

Additional electron production in lower D layer due to solar radiation penetration 14 p2378 A67-27910

Flux density absolute calibration of solar radio emission 14 p2385 A67-28440

Monochromatic photographs through filters for observation of shading variation in intensity of solar emission between center and edge of solar disk 14 p2387 A67-28517

Satellite drag analysis of atmospheric temperatures noting effects of UV, solar radiation and geomagnetic fluctuations 14 p2314 A67-29027

Coherent scattering of solar radiation in uniform isotropic medium containing point source surrounded by cavity 15 p2549 A67-29144

Geomagnetic pulsations and auroral activity, using magnetosphere simplified model 15 p2474 A67-29505

Large space simulation chamber for studying low temperature, absolute vacuum and solar radiation effects 15 p2466 A67-29571

Generating time series for amount of solar radiation falling on horizontal surface of unit area at top of atmosphere per unit time 15 p2477 A67-29628

Solar radiation increase using orbiting reflector satellite, discussing illumination capability [AAS PAPER 67-118] 15 p2570 A67-29964

Motion and asymmetry of emission lines of chromospheric flares with small plasmoid distribution 16 p2737 A67-30500

Primary cosmic ray investigation by Proton I scientific space station concerning energy spectrum, chemical composition, galactic gamma ray and solar radiation hazard 16 p2737 A67-30647

Direct and indirect converters emphasizing preconcentration of solar radiation, noting thermophotovoltaic generators of p-i-n

type 16 p2608 A67-30713

Space environment factors effects on living organism including changing gravity, high vacuums and solar radiation 16 p2614 A67-31000

Global and diffuse solar radiation measurements by Macerata observatory, noting Robitsch pyranographs, Moll thermopiles, and global radiation results 16 p2698 A67-31023

Semitransparency range of sporadic E layer as solar radiation function, noting diurnal and seasonal variations 16 p2669 A67-31904

Cross section of Helium 3 reaction calculated for possible solar neutrino source 16 p2741 A67-31921

Thermionic space power systems, examining solar, radioisotope and nuclear reactors as heat sources, discussing power density and electrode affinity 17 p2802 A67-32050

Galactic and solar ray behavior equations, with cosmic ray drift velocity and diffusion tensor determined for interstellar space in anisotropic-diffusion approximation 17 p2935 A67-32109

New lower upper limit on solar neutron flux at energies greater than 60 mev for emission during quiet times 17 p2936 A67-32532

Measurement of solar extreme UV radiation atmospheric attenuation to establish daytime variations in upper atmosphere composition 17 p2843 A67-32535

Photographic high atmosphere observations of hydroxyl and helium emission bands, determining solar UV radiation and electron flux 17 p2849 A67-32960

Radio emission flux from local solar sources relation to active solar regions structure, based on radio-astronomical observations 17 p2948 A67-32969

Diurnal variations of ionospheric ion/electron temperatures predicted assuming solar UV radiation heating, collisional cooling and heat transport by conduction 17 p2850 A67-33192

Artificial satellites lifetime in low altitude orbits, discussing atmospheric, geomagnetic, solar and lunar factors 18 p3136 A67-33550

Atmospheric aerosol internal changes, studying atmospheric transparency for direct solar radiation 18 p3073 A67-33562

Sun effective disk temperature from measurement of solar radiation during May 1966 eclipse 18 p3125 A67-34195

Very high satellite air drag acceleration studied by University of London Observatory, discussing solar radiation pressure acceleration 18 p3042 A67-34257

Graphical integration method for calculating optical characteristics of materials used in solar radiation spectral measurements 18 p2990 A67-34492

Atmospheric heating due to radiative heat transfer of direct and earth-reflected solar rays calculated as function of moisture content 19 p3251 A67-34851

Absorption of total solar radiation using vertical profiles from balloon observations, estimating attenuation due to aerosols 19 p3214 A67-34854

Solar radiation-balance measuring device using polyethylene film to give protection from wind effects 19 p3227 A67-34855

Short wave spectrometer for measuring total and scattered sky radiation, spectral brightness and fluxes of direct and reflected solar radiation 19 p3227 A67-34860

Electron temperature observation in E region with Langmuir probes on Nike Apache rockets, discussing solar radiation effect 19 p3216 A67-35193

Polar cap absorption on July 1966, discussing solar flare, radio outburst, proton intensity, geomagnetic latitude, etc 19 p3313 A67-35214

Electron density and temperature, solar UV radiation and upper atmosphere neutral components measured using rockets 19 p3218 A67-35215

Terrestrial microorganisms survival in space, noting inactivation effect by solar radiation 19 p3178 A67-35221

Terrestrial microorganism survival in space aboard Gemini satellite, discussing lethal effects of solar radiation 19 p3178 A67-35223

Ground based solar electromagnetic

radiation environment studies in visible and radio windows 19 p3323 A67-35332

Rocket and balloon studies of solar radiation, wind characteristics, equatorial electrojet and lower ionosphere electron density 19 p3223 A67-35474

Spectral measurements of reflected solar and emitted thermal radiations from earth and clouds, using spectrometer with interference filter wedge 19 p3225 A67-35690

Balloon-borne diffusing system designed to measure absorption of minor atmospheric constituents, as sun set and passed below horizon 19 p3232 A67-35697

Interplanetary space environment effect on surface thermal radiative properties, noting results of exposure to simulated solar plasma, solar UV, solar wind, etc 19 p3249 A67-35748

Radiative processes in lower stratosphere and average monthly heating rates over all latitudes due to direct and reflected solar short wave radiation absorption 19 p3226 A67-35922

Upper atmosphere optical properties determined by simultaneous twilight balloon and ground measurements, establishing twilight sky luminance ratios to solar luminance 20 p3427 A67-36369

Meteorology, goals and methods, prospects for effective utilization of satellites and new techniques 20 p3480 A67-36823

Stratosphere and mesosphere, discussing energetics, energy transfer, ionospheric currents, magnetic fields, atmospheric trace components, solar UV radiation measurements, etc 20 p3430 A67-36897

Proportional counter spectrometer for solar soft X-ray spectrum study 20 p3448 A67-36960

Radiation balance chart of earth atmosphere system for evaluation of radiation receivers on Nimbus II satellite 20 p3431 A67-36964

Dayglow photoelectron excitation rate from electron energy loss calculations, with energy transfer functions calculated from photoelectrons produced by UV solar radiation 20 p3434 A67-37421

Thermophototropic model providing active thermal control in spacecraft surface functions as variable absorptance coating to compensate for solar irradiation changes 21 p3730 A67-37792

Multichannel radiometer measurement of solar irradiance for realizing spacecraft radiative equilibrium 21 p3624 A67-37794

Lunar IR emission and solar radiation reflected by moon in visible region measured by Luna X orbiter 21 p3701 A67-37839

Black and white surface coating materials exposed to simulated solar radiation in vacuum, noting deterioration of white coatings 21 p3650 A67-37960

Critical frequencies of F-2 and E layers in ionosphere relation to total daily influx of solar wave radiation into earth atmosphere 21 p3618 A67-38471

Thermophile radiation receiver utilizing detector comprised of fuel cells in series studied for application to actinometry 21 p3628 A67-38530

Solar emissions and magnetic storms and auroras, discussing ring current, solar flux and Van Allen belt energetic particle density 21 p3620 A67-38978

Solar radiation pressure perturbations on large planar reflector satellite orbit 22 p3903 A67-39953

Total extraterrestrial and global solar radiation intensity and spectral distribution for designing radiation resistant satellites 22 p3874 A67-40031

Cloud measurements from Gemini 5 from reflected solar radiation spectra of oxygen A band region 22 p3807 A67-40369

Earth shine illuminated lunar surface TV picture taking by modifying Surveyor equipment to provide light integration [SMPT PAPER 102-40] 22 p3808 A67-40378

Lunar surface luminance transient enhancement noting photoabsorbing color center formation, increased reflectivity and photoluminescence, photoionization and photoemission 23 p4065 A67-41004

Solar neutrino astrophysics, universal neutrino sea, high energy neutrinos, neutrino detectors, stellar energy production, solar thermometry and gravitational constant time

variation 23 p4056 A67-41111
 Solar neutron observations with boron fluoride counter on OSO-1, discussing absence of diurnal variation 23 p4061 A67-41236
 Solar radiation pressure utilization as propulsive force for space vehicles noting sun sail concept 23 p4071 A67-41345
 Solar and terrestrial thermal radiometer absolute calibration noting standards and methods 23 p4006 A67-41373
 Aircraft cockpit and surface temperatures after solar radiation exposure in desert, showing inadequacies of meteorological data for thermal stress predictions 23 p3935 A67-41593
 Solar radiant energy attenuation by atmospheric ozone, deriving transmission function relation to ozone content 24 p4181 A67-41915
 Two-antenna interferometer baseline observations and scanning interferometer characteristics, determining source coordinate and solar radiation center 24 p4129 A67-42227
 Temperature distribution in solid rotating cylinder exposed to solar radiation using Fourier series expansion 24 p4255 A67-42482
 Solar neutrino observation, considering inverse nuclear beta decay and elastic scattering by orbital electrons 24 p4210 A67-42583
 Attitude errors of inertially coupled gravity gradient satellite with solar radiation pressure as dominant disturbance, noting slot problems in stabilized package accommodating damper motion 24 p4241 A67-42904
 Coherent scattering of solar radiation in uniform isotropic medium containing point source surrounded by cavity 24 p4222 A67-43067
SOLAR RADIATION I SATELLITE
 Solar X-ray fluxes measured by solar radiation satellite during IQSY, comparing X-rays and decimeter radio emission in 8-12 angstrom band 17 p2938 A67-33185
SOLAR RADIATION OBSERVATION
 Balloon observation of upper limits of solar gamma rays for spectral ranges 20-200 kev and 1-10 mev 04 p0693 A67-14974
 Atmospheric sounding of twilight phenomena in upper layers, solar ray illumination techniques and solar ray color spectral variation 04 p0617 A67-15475
 Symmetry of time axis and solar observations, offering counterworld alternative to Stannard 06 p1079 A67-17605
 Photometry of coronal emission line 5303 angstrom on Mt. Lomnický Štít 10 p1705 A67-22897
 Comet 1965 f /Ikeya-Seki/ interaction with solar corona produces no significant enhancement of emission at 2.2 m wavelength 10 p1706 A67-22958
 Atmospheric dust content estimation, using solar radiation depletion by particulate matter and separating attenuation by gases and water vapor 10 p1700 A67-23086
 Solar temperatures from observations of July 1963 eclipse with horn antenna in left and right circular polarization, noting magnetization 11 p1867 A67-24779
 Upper limits to hard X-ray flux from quiet sun analyzed by balloon-borne scintillation detector measuring celestial sources 13 p2189 A67-26302
 East-west parabolic reflector array for design of high resolution multielement interferometer for solar noise observations 17 p2864 A67-33402
 Twilight observations for 80-100 km region, noting orthohelium measurements for solar radiation and dust and alkali-metal concentrations for D-region ionic constitution 18 p3035 A67-33601
 Space research in West Germany noting ionospheric physics, magnetosphere and solar and cosmic radiation 19 p3321 A67-35293
 Solar x-ray spectral intensity distribution using atmospheric extinction of solar radiation as measured by satellites 19 p3314 A67-35441
 Argentina 1964-1965 IQSY program emphasizing aerology, solar radiation, ozone concentration, geomagnetism, etc 19 p3224 A67-35499
 Hydrogen emission by sun offers no unique interpretation for Lyman alpha profile 21 p3700 A67-37733
 X-ray emissions from coronal condensation

regions studied with pinhole camera, obtaining intensity profiles along intense X-ray regions 24 p4224 A67-41821
SOLAR RADIATION SHIELD
 Possible stabilization of AgCl crystals against solar radiation effects by addition of Cu, Ni, Zn, Cs, S or Hg 04 p0685 A67-15752
SOLAR RADIO BURST
 Time varying energy distribution of high energy electrons producing solar microwave impulsive bursts and X-ray bursts by emission of gyrosynchrotron radiation 01 p0145 A67-11145
 Type I solar radio bursts possibly caused by interaction of coronal electrons and finite-amplitude MHD pulses 01 p0146 A67-11278
 Laser characteristics of narrow band type I solar radio burst and magnetic dipole transitions in split Zeeman sublevels of hydrogen atoms of solar corona in ground level 02 p0322 A67-11652
 Anisotropic distributions of suprathermal electrons as explanation of observed line splitting for type II solar radio outburst and indirect determination of coronal magnetic fields 02 p0307 A67-11691
 Sunspot cycle coronal Fe XIV 5303 angstrom radiation emission and type IV bursts in solar flares 03 p0507 A67-13811
 Seasonal PCA variations and type IV bursts associated with high energy proton injection into polar ionosphere 03 p0507 A67-13812
 Annual variation of quiet sun radio emission during solar cycle, noting daily mean values of flux at different frequencies 03 p0513 A67-14005
 Statistical investigation of characteristics of chains of type I solar radio bursts including distribution with midfrequency, position on solar disk, lifetime, etc 03 p0508 A67-14359
 Solar radio burst analysis from spectral diagrams noting sudden beginning, precursory activity and succession of isolated peaks and islands 04 p0692 A67-14588
 Solar proton flux measurement with balloon-borne detectors in northern Scandinavia 05 p0882 A67-16740
 Solar radiation drift flares in decimeter range produced by ionic sound interaction with plasma fluctuations 06 p1077 A67-18155
 Origin of solar type I noise storm radiation seen in cyclotron radiation from electron streams gyrating in spot field configurations in corona 07 p1244 A67-19852
 Solar radio noise storm model, determining intensities for various frequency separations 07 p1256 A67-20169
 Active region corona and type I bursts supposedly generated by plasma oscillations excited by electron beam 08 p1377 A67-21445
 Rise and decay times of spike burst during type IV event of February 5, 1965, noting electron stream velocities and coronal temperature 09 p1562 A67-22233
 Type II and IV solar radio bursts analyzed, determining nature and geoeffectiveness of causing agents 10 p1698 A67-22776
 Type III solar radioburst characteristics determined using sweep frequency interferometer 10 p1699 A67-22886
 Type III solar radio bursts, noting association with noise storms and radio condensations 10 p1704 A67-22889
 H-alpha and white light cinematograms of September 1963 flare/sunspot group and radio, ionospheric and magnetic field data 10 p1703 A67-23799
 Grating interferometer observation of slowly varying components of solar radio emission 10 p1711 A67-23802
 Enhanced plasma fluctuations produced by suprathermal electron effect on emission and scattering of electromagnetic waves, noting analogy with corona plasma 11 p1839 A67-24546
 Emission of particles, causing geomagnetic storms, without accompanying radio effects 11 p1787 A67-24594
 Forbush decreases associated with type IV burst flares, particularly in relation to PCA events, noting delay time and magnetic western boundary 12 p1992 A67-25129
 Sunspot groups configuration preceding and following formation of type IV radio burst flares 12 p1992 A67-25130
 Type IV bursts and associated active regions 12 p1993 A67-25131

Statistical analysis of solar dm radio bursts in frequency range 536-2000 mc/s 12 p1993 A67-25132
 High resolution observations of sources of solar radio burst at 9.4 Gc/s, discussing bipolar structure of compulsive and long enduring bursts 14 p2383 A67-27883
 Fine structure profiles of solar radio bursts observed with high time resolution 14 p2381 A67-28579
 Wideband solar-burst spectrum analyzer noting antenna design and operation 14 p2382 A67-28966
 Solar radiation drift flares in decimeter range produced by ionic sound interaction with plasma fluctuations 16 p2741 A67-30499
 Laser characteristics of narrow band type I solar radio burst and magnetic dipole transitions in split Zeeman sublevels of hydrogen atoms of solar corona in ground level 16 p2747 A67-31067
 Microwave and type IV solar bursts, examining gyrosynchrotron emission and various electron acceleration mechanisms 17 p2939 A67-33391
 Type II solar radio bursts observed by Zond III space probe 18 p3119 A67-33859
 Polar cap absorption on July 1966, discussing solar flare, radio outburst, proton intensity, geomagnetic latitude, etc 19 p3313 A67-35214
 Solar flare microwave radio bursts, suggesting synchrotron radiation from relativistic positrons, calculating positron yield and synchrotron spectrum 20 p3519 A67-37101
 38 MHz solar burst duration, bandwidth, amplitude, number and polarization characteristics noting possible generating mechanisms 20 p3520 A67-37476
 Ionospheric electron and ion temperatures during 10.7 cm-solar radio flux activity, giving scatter diagrams 21 p3616 A67-38000
 Radio observations to estimate chromospheric parameters by measuring fluctuation correlation function of solar radio emission flux 22 p3886 A67-40127
 Solar type IV burst centimeter and decimeter polarization and spectral variabilities examined in helical electron stream cyclotron radiation hypothesis for solar corona model 23 p4050 A67-40776
 Type II and IV solar radio bursts analyzed, determining nature and geoeffectiveness of causing agents 24 p4209 A67-42112
SOLAR RADIO WAVE
 Solar atmosphere structure over sunspots studied from radio emission data 06 p1083 A67-18153
 Atmospheric potential gradient near ground in polar region correlation with solar radio emission on 1000 mc 07 p1172 A67-19423
 Maps of two-dimensional radio brightness distribution on solar disk at wavelength of 8 mm 08 p1401 A67-21353
 Solar radio emission spectroheliograms at different millimeter wave frequencies 14 p2388 A67-28834
 Solar atmosphere structure over sunspots studied from radio emission data 16 p2741 A67-30497
 Book on solar radio exploration covering electromagnetic radiation discovery, solar physics principles, solar radio activity and research instruments description 16 p2755 A67-31923
 Maps of two-dimensional radio brightness distribution on solar disk at wavelength of 8 mm 17 p2940 A67-31949
 Microwave radio observations of total sun eclipse made in Canada in 1963, discussing solar radio emission [AD-642463] 18 p3133 A67-34487
 Solar radio emission mechanism for spin transitions of neutron beta decay electrons in external magnetic field 20 p3520 A67-37522
 Solar RF radiation in mm wavelength evaluated for information on solar flare activity 22 p3882 A67-39591
SOLAR REFLECTOR
 Solar coronal reflection and occultation of 38 mc/sec galactic radio energy, using Taurus A and galactic equatorial continuum as occulted sources 05 p0891 A67-16403
 Longitudinal target defocusing effect on solar reflector power parameters, noting energy redistribution phenomenon 12 p1896 A67-25323

SOLAR ROTATION

Longitudinal proper motion of sunspot groups shown to be function of size and relative extension in longitude [AFCL-66-801] 01 p0149 A67-10804

Solar proton streams apparently synodic in solar rotation interval during maximum epoch of recent solar cycle as indicated by polar cap absorption events 03 p0507 A67-14116

Solar rotation, coronal self-gravitational attraction and interplanetary magnetic fields effect on solar wind, presenting linearized hydrodynamic equations 03 p0508 A67-14313

East-west asymmetry of sunspots attributed to simultaneous action of rotation of sun, increase in sunspot area and sphericity of sun 04 p0699 A67-14980

Solar oblateness indication of solar quadrupole moment effect on Mercury perihelion precession solar oblateness indication of solar quadrupole moment effect on Mercury perihelion precession 08 p1354 A67-21429

Amplification of solar dipolar magnetic field by differential rotation investigated, noting implications of Sporer law 10 p1705 A67-22895

Polarity patterns of interplanetary magnetic field observed by Mariner IV during solar rotations 11 p1857 A67-23942

Variability of integrated K-line emission studied during one solar rotation 12 p2001 A67-25223

Rapid rotation of solar interior 12 p1994 A67-25526

27-day cycle variation in various noncosmic ray electromagnetic complex phenomena 17 p2932 A67-32084

Surface stress effect on oblateness of sun and surface stress distribution, noting latitude dependence of angular velocity 17 p2940 A67-32207

Solar spin-down problem, noting oblateness effect on perihelion precession of Mercury 17 p2940 A67-32208

Super-Alfvenic point or distance of effective corotation for loss of angular momentum in solar wind 17 p2945 A67-32644

Ekman pumping in solar core noting slow meridional-current distribution in spinning core determined by energy balance 24 p4225 A67-41834

SOLAR SENSOR

Radiation calibration of heat flux sensors, comparing resistively heated filament and solar energy device 01 p0069 A67-11019

Spacecraft attitude sensor types, principles and future development 03 p0465 A67-14100

Attitude control for sun-pointing scientific satellites, considering control loop, sun sensor and actuator control torques 06 p1098 A67-18765

Balloon-borne sun seeker improvements through transistorized circuits and solid state switches 07 p1184 A67-19396

Stabilized Skylark rocket using N-gas jet system, solar sensors and magnetometer to obtain three-axis control 08 p1408 A67-20537

Longitudinal and lateral axes orientation of uniformly rotating or rapidly rotating vehicle utilizing outputs from solar sensors and lateral magnetometer 08 p1409 A67-20538

Gyroless Solar Pointing Aerobee Rocket Control System /SPARCS/ using no inertial platform and having solid state circuitry 08 p1409 A67-20540

Control signal generator and output characteristics of angular position and velocity sensors used in single-axis sun-oriented system of Vostok spacecraft 12 p1964 A67-25642

Attitude control methods compared for use in rockets collecting data in UV region from various stars 20 p3531 A67-36411

Sensors for acquisition and aiming of solar direction aboard D-2 satellite, discussing operating principles 21 p3629 A67-38666

Gyroless Solar Pointing Aerobee Rocket Control System /SPARCS/ using no inertial platform and having solid state circuitry 24 p4242 A67-42905

SOLAR SIMULATION

Thermally scaled model space station subjected to steady state and cyclical transient solar environments [AIAA PAPER 65-658] 03 p0534 A67-13063

Half-scale thermal model of Mariner IV spacecraft tested in simulated solar

environment [AIAA PAPER 66-23] 03 p0517 A67-13066

Undulatory radiation in space and simulation in space test chambers 03 p0395 A67-13495

Solar simulation tests on UK-3 satellite, evaluating thermal environment and sorting out interface problems between spacecraft and test chamber 09 p1486 A67-22434

Radiation damage experiments for evaluation of silicon solar cell characteristics under simulated solar light 10 p1596 A67-23166

Extraterrestrial solar radiation simulation and total flux and spectral component measurement 11 p1772 A67-24053

High powered carbon arcs for solar simulation with increased radiant energy output 12 p1921 A67-25697

In-space visual environment simulation, discussing photometric and geometric requirements, solar illumination characteristics and effects on human performance 12 p1922 A67-25700

Light sources used for solar simulation testing in terms of operational characteristics and effect of different spectral irradiance characteristics on thermal control coatings 12 p1925 A67-25723

Copper anode lamp for solar simulation facilities, discussing effect on arc brightness and anode loading of magnetic fields, gas mixtures, pressure, etc 12 p1925 A67-25734

Space vehicle thermal testing in cold vacuum chambers with and without solar simulation [AIAA PAPER 67-306] 12 p1926 A67-26021

Space simulation chamber for industry and research 14 p2292 A67-28063

Solar simulation, comparing techniques for reproducing space thermal radiation environment with sun characteristics 16 p2654 A67-30674

Space environment simulator of CNES in France describing reproduction of low pressure atmosphere, heat sink, solar and planetary radiation, etc 16 p2654 A67-30675

Arc-image furnace for direct gas heating at high temperature by concentrated radiation studies and efficient cavity-type receiver development 17 p2834 A67-32696

Solar cell integral covers, discussing solar simulation, vacuum and thermal tests, performance characteristics, etc 23 p3937 A67-41491

Two-axis gimbal system for solar simulation spacecraft testing, demonstrating intermediate axis internal drive system and outer axis drive input 24 p4153 A67-42044

SOLAR SIMULATOR

UV technology, discussing radiation sources, photodetectors, filters, polarizers, reflective coatings, etc 04 p0619 A67-14704

Simulator solar incidence factors for thermal analysis of imperfectly collimated radiation [AIAA PAPER 66-458] 07 p1268 A67-19374

Operational and circuit features of laboratory device built to simulate dynamic electrical output characteristics of programmable solar array in orbital flight 08 p1315 A67-20660

S-4A solar simulator consisting of hexagonal array of 19 interreflector modules 12 p1922 A67-25699

JPL solar simulator design, fabrication and performance 12 p1925 A67-25733

Modular xenon solar simulator for large area solar simulation, discussing source, transfer optical system and Cassegrain module, including fill-in optics 12 p1925 A67-25735

Vacuum simulation developments and trends, noting solar simulator hardware advances with cryogenic systems 17 p2834 A67-32597

Intensity and uniformity monitor for solar simulators using thermopile as detector 19 p3207 A67-34835

Optimum solar simulator and design of thermal vacuum chamber around it 24 p4138 A67-42042

Boeing 20-ft solar simulator alignment, calibration, cleanliness, optical system, xenon light sources and vacuum system 24 p4139 A67-42045

SOLAR SPECTROGRAPH

Echelle spectrograph for middle UV solar spectroscopy from rockets 10 p1653 A67-22735

Photoelectric observation of Fraunhofer

line profiles by high dispersion solar spectrograph 13 p2198 A67-26706

Radio spectrographs for solar observation, broadband and fine structure spectrography techniques and logarithmic amplifiers use in receiver 14 p2386 A67-28443

Performance of single lens objective for coronagraph noting resolution, scattered-light background brightness, etc 15 p2485 A67-29151

High resolution spectra of Venus and Jupiter using image intensifier and solar spectrograph, measuring abundances in planetary atmospheres 20 p3521 A67-36309

Solar radio spectrograph using broadband logarithmic antenna, considering receiver operation and frequency range 21 p3627 A67-38497

Lyot-coronagraph with 53 cm lens, grating spectrograph, 12.6 cm solar disk image at spectrograph slit and one angstrom per mm dispersion 23 p4001 A67-41238

Performance of single lens objective for coronagraph noting resolution, scattered-light background brightness, etc 24 p4158 A67-43074

SOLAR SPECTRUM

Radio spectrum of active region near east limb of Sun determined from July 20, 1963 eclipse [AFCL-66-839] 01 p0148 A67-10388

Limb intensity profiles at center of hydrogen alpha calculated for several simple models of absorption coefficient at line center, showing abrupt changes in gradient 02 p0323 A67-11693

Line emission of hydrogen alpha limb spectra beyond continuum limb analyzed to yield data about height of formation in solar chromosphere [AFCL-66-834] 02 p0323 A67-11694

Solar autoionization line profiles for Al I in rocket UV spectrum 02 p0323 A67-11699

Continuum brightness fluctuations and equivalent line widths in sunspot penumbral spectrum 02 p0330 A67-12715

Identification of quark-atomic lines in solar spectrum 03 p0509 A67-13298

Quark confusion with electric-dipole transition in far UV solar spectrum 04 p0694 A67-14479

Book on middle UV science and technology 04 p0612 A67-14690

Identification of quark-atomic lines in solar spectrum 04 p0696 A67-14723

Identification of diatomic H bands in large sunspot spectrum 04 p0698 A67-14916

Balloon observation of upper limits of solar gamma rays for spectral ranges 20-200 kev and 1-10 mev 04 p0693 A67-14974

Fourier transform used in correction of instrument contour error when observing solar spectral line profile 04 p0624 A67-15564

Hydrogen line profile in Paschen series of solar spectrum, taking into account Stark effect and line broadening 04 p0702 A67-15567

Differential residual displacements of Fraunhofer lines in solar spectrum 05 p0901 A67-17116

O-to-Fe ratio determined in active solar corona from intensity ratio of O-8 to Fe-17 lines and in quiet corona from O-7 to Fe-14 ratio 06 p1083 A67-18068

November 12, 1966 total eclipse observation from aircraft flying in moon shadow, describing instrumentation and results 06 p1004 A67-18383

Absolute intensity of radiation from center of solar disk at wavelengths between 3288 and 12,480 angstroms 06 p1089 A67-18710

Oscillator strength of atomic and ionic lines, normalization of NBS gf values and solar abundances of alkali metals 07 p1256 A67-20167

Solar wavelength measurements for approximately 14 bands of CO fourth positive group in solar rocket UV spectrum 08 p1399 A67-21235

Equivalent width of weak solar line at lambda 8668 angstroms as CN 08 p1400 A67-21247

Center limb variation of H-and K-lines of Ca-2 08 p1401 A67-21444

Rotational temperatures of CO molecule oscillation-rotational bands in solar atmosphere refute assumed temperature nonuniformities 09 p1563 A67-21626

Hydrogen, He and ionized Ca lines in chromospheric spicules, noting large scale motion in spicule interior indicated by line

width expansion and peculiarities in shape of line contours 09 p1563 A67-21627

Solar spectrum reexamination determining lower limit for C12/C13 isotopic abundance ratio in photosphere [AFRL-67-0480] 09 p1566 A67-22231

Spectrum of quiet sun between 30 and 128 angstroms analyzed in November 1965, using rocketborne grating monochromator with Geiger detector 09 p1566 A67-22232

Horizontal motions of solar granulation toward supergranulation from data of granule coordinates and velocities 10 p1704 A67-22723

Near IR atmospheric absorption over 25-km horizontal path at sea level 10 p1629 A67-22744

Maksutov-Cassegrain type telescope for rocket mounting, design and performance 10 p1654 A67-22751

Central intensities and profiles of sodium D lines in solar spectrum, discussing atomic and photospheric data 10 p1704 A67-22885

Extreme UV emission, discussing chromospheric coarse mottling and network characteristics of He II 304 10 p1707 A67-23224

Rocket photography of sun and spectrum in EUV and soft X-ray regions 10 p1707 A67-23225

Fresnel microzone plates for X-ray images of sun 10 p1707 A67-23232

Amplitude distributions of solar photospheric fluctuations 10 p1711 A67-23795

Photospheric brightness fluctuations recorded photoelectrically across solar disk center simultaneously for two regions of continuum, deriving autocorrelation functions and spatial power spectra 10 p1711 A67-23796

Source function, distribution function, damping constant, etc., determined from high resolution Fraunhofer line profiles in solar or stellar spectra 10 p1711 A67-23797

Flare spray on west solar limb on July 11, 1966, noting radial polarization effects suggesting Thompson scattering as source of continuous spectrum 10 p1703 A67-23798

Chromospheric background intensity difference between equatorial and polar regions of sun 10 p1711 A67-23800

Homogeneous solar photosphere and lower chromosphere model in hydrostatic and local thermodynamic equilibrium, reproducing continuous and line spectrum 11 p1858 A67-24112

Generalized integro-exponential weighting functions allow accurate computations of Fraunhofer lines in solar /intensity/ and stellar /flux/ spectra 11 p1859 A67-24113

Time course of blue-to-red light intensity ratio of visible solar spectrum during and after sunset 11 p1786 A67-24116

Center-to-limb variations for continuum, faint iron lines and core of strong Fraunhofer lines measured along polar and equatorial diameters of solar disk 11 p1861 A67-24492

Atomic beam resonance spectrophotometer used with solar telescope to observe solar line oscillation 11 p1861 A67-24494

Polar bright surges at limb, showing frequency and parameters of occurrence 11 p1862 A67-24496

Solar X-ray emission measurement below 25 angstroms using airborne Bragg spectrometers, with data reduced by computer 11 p1867 A67-24839

Photoelectric recorder in solar tower used to investigate two new lines in solar spectrum 11 p1868 A67-24848

Distribution and intensity of solar magnetic fields gained from spectrograms, noting correspondence between magnetic field and Ca-K line emission sources 12 p2001 A67-25219

Motions of chromospheric fine structure in weak plage analyzed, using time resolved H-alpha spectra for estimating line-of-sight velocities of objects 12 p2001 A67-25222

Variability of integrated K-line emission studied during one solar rotation 12 p2001 A67-25223

Copper anode lamp for solar simulation facilities, discussing effect on arc brightness and anode loading of magnetic fields, gas mixtures, pressure, etc 12 p1925 A67-25734

Pinhole X-ray photography of sun obtained during rocket flight, showing correlation of bright emitting regions on disk with calcium plages and radio emission

sources 12 p2007 A67-25762

Solar continuous spectrum observations indicating limb darkening around 2500 angstroms, using optical system mounted on Veronique rocket 12 p2007 A67-25820

Solar studies in extreme UV using stabilized Skylark rockets, including data on chromospheric and coronal spectra and XUV spectroheliograms 12 p2008 A67-25826

Photoelectric observation of Fraunhofer line profiles by high dispersion solar spectrograph 13 p2198 A67-26706

Solar and galactic particle spectra and composition measured with cosmic ray telescope mounted on satellite 13 p2193 A67-27249

Rocket photography of sun and spectrum in EUV and soft X-ray regions 13 p2200 A67-27334

Molecular spectra of sunspots and solar disk 13 p2203 A67-27428

Identification of forbidden nitrogen IR multiplet in Fraunhofer spectrum 14 p2382 A67-27848

Solar flux density absolute microwave spectra 14 p2385 A67-28441

Profiles of cores of Ca II H and K lines in solar spectrum during maximum and minimum activity period 14 p2387 A67-28561

Photoelectric solar spectroscopy at Nice Observatory, discussing suitability of location and results 14 p2387 A67-28592

Nitrogen presence in solar material, using measurements of high resolution spectrophotometric record of Fraunhofer spectrum [AFRL-67-0479] 15 p2554 A67-29516

Atmospheric ozone vertical distribution, discussing optical measurement method 16 p2876 A67-31375

Solar spectrum observations in oxygen regions, describing prism-grating spectrometer, photoelectric recording and scan-averaging by digital computer [AFRL-67-0478] 16 p2749 A67-31417

High resolution UV spectrograph with echelle, noting optical line-up for photographing H-Lyman alpha line at 1216 angstroms 16 p2680 A67-31875

Solar UV spectrum interpretation taking into account dielectronic recombination processes in ionization equilibrium computation, obtaining spectral lines intensities, abundances and atmospheric structure indications 17 p2941 A67-32235

Excitation temperatures of electron levels of CH molecule in photosphere 17 p2941 A67-32326

Darkening of solar limb in UV spectral band observed through rocket sounding 17 p2945 A67-32647

Solar X-ray spectrum observed by rocket carried Bragg crystal spectrometers and pinhole cameras array 17 p2937 A67-32650

Forbidden nitrogen I lines in IR solar spectrum, computing oscillation frequencies, nitrogen abundance and equivalent widths, comparing predictions to observational results 17 p2948 A67-32819

Corona observation within one solar radius of photosphere, identifying emission lines and explaining continuous spectrum and Fraunhofer lines reduced depth 19 p3318 A67-35055

Solar identifications for forbidden carbon I lines in solar spectrum 19 p3324 A67-35435

Spectral analysis of K alpha type X-ray transitions in solar atmosphere and laboratory plasma 19 p3331 A67-36086

Lead abundance in sun computed from measurement of Pb lines equivalent widths 19 p3331 A67-36087

Balloon-borne Michelson interferometer for far IR solar spectrometry 20 p3438 A67-36344

Fabry-Perot interferometer improvements for high resolution rocket photography of solar Fraunhofer spectrum 20 p3440 A67-36359

Proportional counter spectrometer for solar soft X-ray spectrum study 20 p3448 A67-36960

Extreme UV solar spectrum, reviewing echelle spectrum, soft X-rays and coronal emission 20 p3528 A67-37467

Solar spectral line center-to-limb variations during solar eclipse of May 20, 1966 20 p3453 A67-37682

Signal to noise ratio for optical solar spectra, describing low noise level

spectrometer 21 p3624 A67-37730

Line broadening by collision damping, explaining solar and stellar curves of growth 21 p3700 A67-37731

Spectral irradiances determined by conventional prism monochromator and by system employing narrow bandpass interference filters 21 p3656 A67-37850

Spectral line wavelengths of solar violet bands of carbon /isotope/ nitride and hydride molecules, determining solar abundance ratios 22 p3889 A67-40207

Rocketborne UV radiometers for solar spectral intensity distribution, calculating irradiance and earth reflectivity 22 p3794 A67-40363

Zodiacal light and interplanetary dust, discussing brightness, polarization, color, spectrum and dust cloud about earth 22 p3794 A67-40426

Si and S ion oscillator strengths for resonance lines in solar spectrum, discussing spin-spin and spin-other orbit interactions 23 p4067 A67-41235

Energy distribution of photometric spectra in solar UV continuum in 1550 to 2100 angstrom range, discussing radiation temperature decrease 24 p4225 A67-41835

IR C atom multiplet in solar spectrum at 10,700 angstroms, noting C abundance dependence on convective velocities and deviations from black body function and local thermodynamic equilibrium 24 p4237 A67-42655

SOLAR STORM

Solar disturbance variations of geomagnetic field dependence on solar activity indicates interplanetary magnetic field activity 21 p3623 A67-39041

SOLAR STREAM

Double sunspot cycle or 22-yr variation in cosmic ray diurnal variation phase, discussing streaming mechanisms 22 p3874 A67-40046

SOLAR SYSTEM

SA ASTEROID

SA GALAXY

SA PLANET

Thermal radio emission from Mercury, Venus, Mars, Saturn and Uranus at various wavelengths, using radio telescope in Australia, determining emission spectrum 02 p0319 A67-11452

Functional relation between mass, radius and angular velocity of earth, solar mass and corresponding lunar quantities shown via reciprocity principle 04 p0702 A67-15582

Zond III interplanetary probe lunar surface photographs analyzed, considering asymmetry of moon, far side and relation of moon to solar system 05 p0887 A67-16059

Radioactive isotopes in iron meteorite used to determine cosmic ray origin and to study nuclear processes in early history of solar system 05 p0877 A67-16084

Halley comet head diameter change determined by converting propane and ethylene molecules in photon and corpuscular radiation field of sun 05 p0888 A67-16202

Correlation of meteoroid environments in solar system, analyzing meteor mass measurement results, hypervelocity impact and solar electromagnetic radiation effects [AIAA PAPER 67-151] 06 p1085 A67-18319

Interplanetary gas, solar corpuscular activity and magnetic storms and zodiacal dust cloud from satellite observations during IQSY and use of cometary tail as plasma probe 07 p1248 A67-19333

Chemical composition and earth origin, with estimates of primordial abundances of elements in solar system 07 p1170 A67-19336

Solar system geometric effect in diurnal, annual and semiannual cosmic ray variations 07 p1243 A67-19607

Solar and stellar systems orbit theory - IAU Symposium, Salonika, Greece, August 1964 08 p1379 A67-20380

Mission requirements for unmanned exploration of solar system including energy and flight time, noting thrust vs ballistic vehicles 08 p1393 A67-21096

Energy dissipation and other problems for alien planetary atmospheric entry at high speeds of interplanetary flight 08 p1394 A67-21155

Internal lunar structure considered from direct measurements and extrapolation of data on constitution of solar system bodies and meteorites 08 p1395 A67-21161

Evolution of low mass stars, differences between solar system planets and black dwarfs and rotational angular momentum of G, K and M dwarfs 08 p1398 A67-21217

Cosmic ray nuclei propagation in interstellar space and solar system examined from balloon, rocket and satellite soundings 08 p1378 A67-21473

Cosmic ray effects on solar system and on galactic scale, discussing energy spectrum, particle diffusion and motion, solar wind, etc 09 p1562 A67-22530

Asymmetric distribution of asteroids in heliocentric latitude and longitude 10 p1705 A67-22894

Solar oblateness effect on quadrupole moment and on perihelion of Mercury 10 p1709 A67-23487

Planetary system abundance for stellar system mass near solar mass determined from mass/angular momentum diagram 11 p1865 A67-24610

Earth rotational and orbital motions interrelated by Lofitslanski theorem for turbulent fluid motion 12 p1932 A67-25190

Voyager project goals, orbital operations, capsule descent, navigational systems, etc 12 p2002 A67-25232

International planetary organization with jurisdiction over activities on celestial bodies and lunar and planetary launches 12 p2042 A67-26136

Cosmogony of celestial bodies, discussing orbital data, asteroid collisions and existence of distant comet cloud 13 p2195 A67-26466

Cosmogonic hypotheses evaluation based on relation between oblateness, mass and number of satellites of planets of solar system 13 p2198 A67-26765

Future space transportation techniques and mission applications in solar system 13 p2213 A67-27508

Velocity requirements for scientific probe vehicles in direct flight and planetary swingby modes of operation throughout solar system 14 p2387 A67-28618

Solar system planets characteristics, temperatures, atmospheres and internal structure 14 p2392 A67-28959

Information on early history of solar system material obtained for neutron buildup processes of heavy element synthesis in stars 15 p2519 A67-29156

Future interplanetary unmanned space missions, examining velocity requirements and launch vehicle and payload sizes necessary for scientific investigation of solar system [AIAA PAPER 67-29] 15 p2562 A67-30104

Rocket fuel production possibilities on moon surface and other planets for planetary explorations 16 p2655 A67-31008

Age determination of iron meteorite by Rb-Sr isotopic analyses of silicate inclusions, proving formation of younger solid objects in solar system 16 p2749 A67-31434

Voyager project goals, orbital operations, capsule descent, navigational systems, etc 16 p2751 A67-31487

Geometrical form for solar system escape criterion 17 p2940 A67-32075

Cosmic ray variations methodology, considering solar system geometry, interstellar cosmic ray gradient, phase and amplitude modulation, etc 17 p2934 A67-32103

Distribution of meteoritic matter in solar system determined, using radar observations and astronomical photography 17 p2941 A67-32321

Book on red giants and white dwarfs covering stellar evolution, planets and life, solar system origin, etc 18 p3117 A67-33430

General theory of planets in connection with progress in space research 18 p3124 A67-34157

Bulgarian research in spectroscopy, solar system, ionosphere, gravitation equations, astrophysics, etc 19 p3320 A67-35283

Launch vehicle, payload size, velocity requirements, etc, for probes exploring solar system and near interstellar space 19 p3323 A67-35330

Solar system bodies gravitational fields, discussing possibility of holding satellite in orbit 19 p3323 A67-35337

Multipurpose entry vehicle requirements for unmanned landings on bodies in solar system having tenuous atmospheres [AIAA PAPER 67-599] 19 p3336 A67-35995

Multiplanet mission for Jupiter, Saturn, Uranus and Neptune, using swingby

technique for probe launched in late 1970s [AIAA PAPER 67-613] 19 p3329 A67-36002

Galactic cosmic ray density distribution anisotropy in solar system, discussing outward convection of cosmic rays by solar wind and inward diffusion 20 p3520 A67-37474

Space program in 1970s, discussing solar system exploration, investigation of universe, practical applications of space and development of technology [AIAA PAPER 67-626] 20 p3530 A67-37613

Zond III interplanetary probe lunar surface photographs analyzed, considering asymmetry of moon, far side and relation of moon to solar system 21 p3701 A67-37846

U.S.S.R. astronomical almanac for 1970 21 p3703 A67-38200

Planetary and interplanetary environments based on experimental data and quantitative information, noting influence of sun in solar system mass 21 p3707 A67-38946

Unmanned probe and launch vehicle selection for solar system exploration, considering tradeoffs in terms of reliability, cost, weight, experimental accuracy, etc 22 p3900 A67-39617

Solar system environment, discussing solar magnetic field, flare flux and energy spectrum, interplanetary plasma and radiation, asteroids, meteoroids and comets 22 p3889 A67-40407

Solar system resonances emphasizing nongravitational forces in resonance formation and asteroid collision formation of Kirkwood gaps 23 p4062 A67-40623

U.S. exploration of solar system with unmanned spacecraft 23 p4086 A67-40920

Cosmic ray anisotropy in solar system, considering diurnal variation in terms of anisotropic diffusion 23 p4058 A67-41121

Sidereal diurnal cosmic ray variation caused by modulation in solar system, discussing variations in coordinate systems 23 p4059 A67-41129

Chemical history of Fe traced in nebular material assuming preplanetary particles were similar to those presently discarded by sun 23 p4068 A67-41360

Correlation of meteoroid environments in solar system, analyzing meteor mass measurement results, hypervelocity impact and solar electromagnetic radiation effects [AIAA PAPER 67-151] 23 p4070 A67-41719

S-process theory of heavy element formation in solar system confirmed by measuring neutron capture cross sections 24 p4224 A67-41817

Radioactive isotopes in iron meteorite used to determine cosmic ray origin and to study nuclear processes in early history of solar system 24 p4212 A67-42760

SOLAR VELOCITY

Solar velocity with respect to distant galaxies estimated from red shift for nearby galaxies, noting cosmic microwave background 15 p2563 A67-30160

No appreciable systematic differential motion between nearby neutral hydrogen and stars determined from measurement of relative velocity of former with respect to sun 17 p2943 A67-32443

SOLAR WIND

SA M-REGION

SA STELLAR WIND

Coaxial cylindrical plasma sheet motion and geomagnetic field/solar wind interaction 01 p0143 A67-10116

Charged particle traps installed in Luna X providing evidence for moon passing through tail of earth magnetosphere, noting effect of solar wind 01 p0145 A67-10908

Interaction of solar wind and frozen-in magnetic field with geomagnetic field inside and outside magnetosphere, comparing theory with satellite measurements 02 p0320 A67-11461

Radial extension of corpuscular flux from chromospheric flares and duration of earth immersion in flux 02 p0306 A67-11653

Origin of geomagnetic field, attributing paleomagnetic inversions to electromagnetic induction effects produced by solar corpuscular eruptions 02 p0326 A67-12063

Solar dynamics, with emphasis on solar wind interaction with magnetosphere of earth [AFCRL-66-867] 02 p0326 A67-12246

Properties of solar and geophysical phenomena analyzed, concluding that magnetic field of corpuscular fluxes has

forceless structure 02 p0311 A67-12590

Shape of magnetosphere of rectilinear flow in divergent plasma stream as function of plasma pressure 03 p0474 A67-12921

Solar wind-magnetosphere system simulation, testing hypothesis that observed convective pattern is established by earth rotation 03 p0506 A67-12959

Survey in satellite era of energetic particle radiations, plasmas and magnetic fields in space including solar wind, solar cosmic rays, etc 03 p0506 A67-13050

Spacecraft thermal control surface damage by solar wind bombardment in hydrogen and helium plasmas, with measurements of solar spectral reflectance and thermal emittance [AIAA PAPER 65-647] 03 p0448 A67-13052

Solar wind-comet interaction simulation using plasma stream and carbon dioxide gas cloud sublimated from dry ice 03 p0506 A67-13575

Solar rotation, coronal self-gravitational attraction and interplanetary magnetic fields effect on solar wind, presenting linearized hydrodynamic equations 03 p0508 A67-14313

Formation of magnetospheric plasma knee by combined action of magnetospheric convection and plasma escape from tail 04 p0693 A67-14964

Lunar and cislunar observation of interplanetary medium including lunar magnetic field, solar wind, existence of collisionless shock wave, gegenschein, zodiacal light and recovery of interplanetary particles 04 p0700 A67-15072

Solar wind flow past comet, obtaining minimum radius of comet source 04 p0693 A67-15563

Energy spectrum of secular variations of cosmic ray intensity in interplanetary space, using data from stratospheric measurements 05 p0879 A67-16104

Solar wind plasma penetration into geomagnetic field under effects of drift in crossed electric-geomagnetic fields 05 p0884 A67-17120

Solar corpuscular streams effect on magnetospheric loop and on earth rotational velocity 05 p0801 A67-17135

Solar plasma intrusion into model magnetosphere 05 p0859 A67-17441

Unsteady radial expansion of polytropic gaseous sphere in own gravitational field, using hydrodynamical equations and model limited by shock wave 06 p1083 A67-18064

Solar wind effect on cathode scattering of cosmic dust particles in earth proton belt and shortening of lifetime of captured particles 06 p1078 A67-18162

Interplanetary gas, solar corpuscular activity and magnetic storms and zodiacal dust cloud from satellite observations during IQSY and use of cometary tail as plasma probe 07 p1248 A67-19333

Solar wind outside ecliptic plane studied, using radio sources scintillation 07 p1249 A67-19660

Geomagnetic activity and solar corpuscular fluxes forecasting by Bednarova-Novakova method 07 p1175 A67-19719

MHD approximation of solar plasma fluxes observed by Mariner II as free rotating jets 07 p1243 A67-19802

Solar wind magnetic field as medium for plasma-magnetosphere interaction 07 p1243 A67-19803

Solar wind parameter variation, magnetosphere flux interaction and dependence of geomagnetic storm on magnetospheric conditions and geomagnetic field increase 07 p1243 A67-19804

Solar corpuscular stream magnetic field effect on change in orientation of geomagnetic field related to change in stream geoeffectiveness 07 p1243 A67-19827

Criticism of Ivanov assumption regarding IMP-I observation of lunar wake in solar wind by magnetic field and plasma measurements 07 p1243 A67-19829

Interplanetary magnetic field and plasma effect on geomagnetic activity during quiet sun conditions 07 p1251 A67-19912

Properties and velocity distribution functions observed by Vela III satellites 07 p1244 A67-19919

Vela II measurements of earth magnetopause and bow shock positions, showing relationship to magnetic disturbance index and thus also to solar wind velocity 07 p1180 A67-19920

Transient lunar brightening, discussing

- attempted correlation with solar wind activity 07 p1256 A67-20160
- Constant force effect on Keplerian orbit with reference to solar wind perturbation 08 p1383 A67-20402
- Quasi-shock structure in collision free plasma in magnetic field and comparison with bow shock on solar wind near earth 08 p1359 A67-20901
- Lunar water sources, considering hydrous minerals, cold trapped volatile products of volcanic origin and dispersed hydrates 08 p1317 A67-21093
- Cometary tails relationship to interplanetary gas properties and solar wind velocities deduced from observation of type I ionic cometary tails 08 p1399 A67-21238
- Solar corona and interplanetary gas corotation with sun and effects of solar wind, considering poloidal magnetic field of rotating star 08 p1399 A67-21239
- Kinetic theory-plasma dynamics theory calculations of magnetospheric solar wind proton velocity distribution as function of particle speed 08 p1377 A67-21315
- Transverse plasma instabilities as mechanism coupling motions of solar wind and cometary plasma, using thermal diffusion and conductivity transport coefficients to describe flow 08 p1401 A67-21367
- Anisotropic proton velocity distribution obtained from solar wind measurements on Pioneer VI spacecraft 08 p1378 A67-21475
- Low ionosphere with suitable selected track for absorption observation as indicator of galactic cosmic rays modulation by solar wind 09 p1561 A67-21843
- Cosmic ray protons and helium nuclei intensity measured as function of energy or magnetic rigidity, determining particle intensity gradient under equilibrium conditions for diffusion 09 p1562 A67-22241
- Motion of structures in coma and tail of Morehouse comet compared with hydrodynamic model interaction between solar wind and cometary plasma 10 p1704 A67-22720
- Field buildup during sudden commencement of magnetic storms in magnetosphere determined from MHD wave and solar wind pressure measurements 10 p1630 A67-22777
- Geomagnetic micropulsation excitation by solar wind flow around magnetosphere, noting surface wave propagation 10 p1699 A67-22797
- Background noise curve of geomagnetic variations, attributing minimum spectral energy on ground to existence of permanent static solar wind component 10 p1632 A67-22856
- Physics of aurora as magnetospheric and cosmic phenomena 10 p1633 A67-22986
- Two-dimensional model of magnetosphere to find equilibrium boundary between rarefied plasma and magnetic field of two-dimensional dipole 10 p1649 A67-23297
- Interplanetary magnetic field effect on hydrodynamic supersonic expansion of solar corona noting solar wind velocity, nonradial flow, wave motion, etc 10 p1709 A67-23546
- Solar wind region magnitude, scattering transport path of particles and spectral variation of magnetic inhomogeneities analyzed on basis of 11-year cosmic ray cycle 11 p1855 A67-23930
- Torque on sun calculated from solar wind motion, taking rotation and magnetic field effects into consideration 11 p1857 A67-23931
- Solar corona and occurrence of solar wind and influence on evolution of red giant star 11 p1858 A67-24095
- Geomagnetic disturbances dependence on interplanetary magnetic field sector structure and incident solar ion current at and near minimum of solar cycle 11 p1786 A67-24331
- Solar magnetic field in photosphere, discussing evolution through expanding solar wind plasma 11 p1863 A67-24548
- Satellite measurement of magnetic fields in cislunar space and earth proximity, noting formation of confined geomagnetic field by continuous plasma flow from sun 11 p1863 A67-24549
- Solar wind trapping in solids using ion bombardment of aluminum foils at various energies and temperatures 11 p1825 A67-25079
- Collective effects and centrifugal instability from charged solar wind particle injected into earth magnetosphere near neutral point 12 p1991 A67-25109
- Solar wind particle propagation and scattering path in interplanetary space according to data of 11-yr cosmic ray variations 12 p1991 A67-25115
- Hydrodynamic axial-symmetric model of plasma flow on sunward side of comet assuming cometary gas is ionized by solar UV radiation only 12 p1993 A67-25227
- Rapid rotation of solar interior 12 p1994 A67-25526
- Solar wind modulation of far daytime field of extra-long radio waves in ionospheric C layer 12 p1933 A67-25549
- Charged particle motion and penetration of magnetosphere in proximity of neutral point as result of solar wind-geomagnetic field interaction 12 p1975 A67-25643
- Spacecraft rotation effect on measurement of hydromagnetic radiation in solar wind 12 p1934 A67-25782
- IMP-I earth satellite magnetic field measurement experimental results including solar wind flow effects 12 p1936 A67-25802
- Inflation of magnetosphere near 8 earth radii in Southern Hemisphere using Explorer XIV satellite 12 p1936 A67-25805
- Electron and proton fluxes at geocentric distance of 7 earth radii measured by charged particle traps on interplanetary station Zond 2 12 p1998 A67-25818
- Solar corpuscular stream magnetic field theoretical model including hydromagnetic stability conditions and undisturbed solar wind 12 p1998 A67-25821
- Solar wind interaction with solar dipole magnetic field in coupled hydrodynamic and hydromagnetic equations [AIAA PAPER 66-509] 12 p2008 A67-25920
- Interplanetary medium including solar wind, geomagnetosphere and observation instruments 12 p2009 A67-26173
- Steady state model of solar wind flow in equatorial plane solved for radial and azimuthal motions, taking into account pressure gradient, magnetic field and gravitational effects 12 p2010 A67-26241
- Interplanetary solar wind measurements during April 1965 geomagnetic storm using electrostatic analyzers on Vela satellite 13 p2189 A67-26303
- Solar wind plasma properties, noting relation between positive ion component and interplanetary magnetic field as measured by Mariner II [JPL-TR-32-1107] 13 p2190 A67-26304
- Solar wind structure model, proposing surface granularities correlation with modulation at source of wind 13 p2190 A67-26313
- Solar wind measurements and small scale structure of interplanetary medium using scintillation technique 13 p2190 A67-26318
- Solar wind properties studied using Vela electrostatic analyzers, noting velocity ranges, proton temperature and ion density 13 p2190 A67-26319
- Solar wind bulk velocity studied via Vela 3A bow shock crossings, noting velocity decrease when entering magnetosheath 13 p2190 A67-26320
- Dependence of diurnal cosmic ray variations on angle which is proportional to shortest distance from earth to axis of corpuscular stream 13 p2191 A67-26546
- Energy spectra of solar wind ion fluxes outside magnetosphere measured using Venus 3 space vehicle 13 p2194 A67-27331
- Solar corona broadening mechanism studied using microscopic model including kinetic equations, determining proton escape velocity from sun 13 p2194 A67-27340
- Solar wind ion concentration and velocity measurements from Venus III and Pioneer IV 13 p2195 A67-27343
- Antenna in interplanetary plasma, noting fluctuation noise in exosphere and radiation impedance when exposed to solar wind 14 p2279 A67-27856
- Polytropic heat sources effect on ejection of stationary symmetrical plasma from sun 14 p2378 A67-27915
- Magnetosphere rotation problem in presence of solar wind analyzed for auroral particle acceleration, noting perturbing field of induced electric current 14 p2307 A67-27917
- Equilibrium of magnetic field confined by impact pressure of beam of ions for general direction of incidence of beam 14 p2310 A67-28046
- Spacecraft thermal control coating damage in simulated space-bombardment conditions, using plasma bombardment techniques 14 p2293 A67-28138
- Jupiter decametric radiation analyzed with interferometer for manifestations of solar wind effects 14 p2385 A67-28404
- ELF and micropulsations phenomena divided into earth-ionosphere cavity resonances and regular and irregular pulsations 14 p2266 A67-28415
- Catalog tabulating 1600 comet tail orientation observations 14 p2386 A67-28481
- Plasma wind tunnel facility for producing steady flow high conductivity collisionless plasma simulating solar wind interaction with magnetosphere 14 p2294 A67-29036
- Solar magnetic field origin and effects revealed by direct and satellite observations of photosphere, chromosphere, corona and earth neighborhood 15 p2554 A67-29531
- Dayside distortion of geomagnetic field by solar wind beyond 3.5 earth radii measured and compared with three magnetosphere models 15 p2475 A67-29612
- Solitary waves, discussing electron and ion acceleration and transfer mechanism of solar wind ion kinetic energy to electrons 15 p2475 A67-29613
- Solar wind modulation of low energy galactic cosmic radiation, estimating primary source spectra, proton and helium fluxes 15 p2550 A67-29614
- Solar wind effect on cathode scattering of cosmic dust particles in earth proton belt and shortening of lifetime of captured particles 16 p2737 A67-30506
- Radial extension of corpuscular flux from chromospheric flares and duration of earth immersion in flux 16 p2738 A67-31068
- Search for solar M-regions complicated by velocity decrease near active sun, considering corpuscular streams as enhanced solar wind 16 p2749 A67-31414
- Proton-irradiation darkening of rock powders, noting contamination, temperature effects and applications to solar wind darkening of moon [JPL-TR-32-1130] 16 p2753 A67-31743
- Optical properties of moon quantitatively compared with powder samples, bombarded with ions from hydrogen discharge plasma 16 p2753 A67-31744
- Electron microprobe analysis of quartz and alumina darkening upon solar wind ion bombardment, noting existence of iron, tungsten and carbon in samples 16 p2753 A67-31745
- Effective volume of asymmetric solar wind shown to be independent of primary cosmic radiation energy, noting role of 27-day variation 17 p2932 A67-32085
- Shock wave propagation in solar wind caused by tangential discontinuities and geomagnetic sudden storm commencement 17 p2936 A67-32530
- L-pulses of Jupiter radiation, attributing 1-sec component of time structure on decametric emission to diffraction by solar wind inhomogeneities 17 p2944 A67-32643
- Super-Alfvénic point or distance of effective corotation for loss of angular momentum in solar wind plasma 17 p2945 A67-32644
- Magnetosphere and auroral phenomena including Van Allen radiation zones, satellite telemetry, solar wind fluctuations and cyclotron resonance phenomenon 17 p2844 A67-32664
- Nature of trapping regions, using spherical harmonic expansion for magnetic field created by currents on geomagnetic cavity surface 17 p2938 A67-33207
- Interaction of planetary magnetic field with solar plasma studied using hypersonic analog, estimating energy transfer rate 17 p2951 A67-33208
- Solar wind perturbation of uncharged interplanetary dust particle orbits, calculating particle lifetime 17 p2951 A67-33234
- Auroral and polar magnetic substorms related to magnetic field lines reconnection in magnetosphere tail 18 p3117 A67-33615
- Airglow and auroral phenomena, discussing ideal coordinate system, electric fields, morphology, solar wind-magnetosphere interactions, and particle precipitation 18 p3039 A67-33625

- Magnetospheric boundary and standing shock wave for earth scaled down to apply to Mars 19 p3324 A67-35442
- Solar wind velocity and interplanetary magnetic field components obtained by IMP II related to geomagnetic field variation 19 p3222 A67-35473
- Statistical correlation of type III solar radio burst activity with coronal green line over solar cycle 19 p3316 A67-36029
- Highly eccentric orbit satellite /HEOS/ for solar wind, cosmic ray and magnetic field data collection, noting design and mission program 20 p3531 A67-36412
- Proton velocity distribution in solar wind flow around magnetosphere 20 p3518 A67-36653
- Solar wind velocity relationship to tropospheric temperature field 20 p3428 A67-36814
- Geomagnetic variations discussing attempts to explain 27-day recurrence tendency and to relate solar wind and magnetic indices 20 p3430 A67-36902
- Magnetospheric features, describing magnetic field distribution, electron and proton density, plasma instabilities, bow shock and solar wind 20 p3430 A67-36903
- Phase relationship between solar activity changes and changes in solar wind parameters over 11-year cycle 20 p3519 A67-37395
- Magnetosheath observations by Vela 3 at 18 earth radii, discussing substructure, shock crossings and pulsations 20 p3433 A67-37410
- Perturbation scheme deriving geomagnetic Euler potentials applied to magnetospheric model with solar wind effect 20 p3434 A67-37423
- Radio sources fluctuations due to inhomogeneities of solar supercorona and interplanetary plasma, studying solar wind and brightness distribution 20 p3520 A67-37513
- Solar wind plasma penetration into geomagnetic field under effects of drift in crossed electric-geomagnetic fields 21 p3698 A67-38463
- Solar corpuscular streams effect on magnetospheric loop and on earth rotational velocity 21 p3619 A67-38478
- Evaporation of Saturn ice rings by UV and solar wind sputtering or by photosputtering in IR and proton bombardment 21 p3705 A67-38599
- Magnetic dipole moments of moon, Mars and Venus using space probes, discussing solar wind near-earth planetary field interaction measurements [JPL-TR-32-1059] 21 p3709 A67-38992
- Three-dimensional heat source influence on solar plasma flow contradicts Parker solar wind theory, based on gasdynamic acceleration 21 p3699 A67-39012
- Interplanetary space properties from satellite observations, discussing solar wind, geomagnetic field, comet tail effects, coronal plasma kinetic properties, etc 22 p3883 A67-39668
- Solar wind general dynamical theory, discussing interplanetary space condition determined by coronal expansion 22 p3883 A67-39669
- Quiet condition solar wind geomagnetic field interaction measurements, discussing solar plasma and bow shock wave generation 22 p3870 A67-39670
- Solar wind geomagnetic field interactions during disturbed conditions, discussing solar particle emissions, solar plasma activity, ring and ionospheric currents 22 p3870 A67-39672
- Magnetospheric energetic charged particles interrelations, discussing electron and proton energy spectra, particle population domains, trapped radiation and solar wind kinetic energy 22 p3870 A67-39673
- Auroras /ordinary and type with forbidden emission of atomic oxygen/, examining wind-aurora relation 22 p3790 A67-39675
- Transverse field growth studied for generation of magnetic field in boundary layer by currents along magnetopause produced by tangential solar wind 22 p3871 A67-39801
- Pioneer VII plasma probe data indicating geomagnetic wake at 1000 earth radii downstream from earth 22 p3791 A67-39819
- Magnetospheric open split tail topology noting stability of geometry in all solar wind and interplanetary medium conditions 22 p3792 A67-39820
- Energy changes between solar wind and cosmic rays, discussing particle motion description by Fokker-Planck differential equation 22 p3874 A67-40079
- Plasma flow and generation in CO comet due to electron-collisional ionization under influence of solar wind 22 p3885 A67-40081
- Low energy cosmic ray measurements during solar activity minimum suggesting changes in cosmic ray composition due to solar wind 23 p4054 A67-41097
- Drift equation supplemented by collision terms for describing interplanetary regular magnetic field and solar wind velocity fluctuation effects on cosmic ray propagation 23 p4056 A67-41105
- Cosmic ray intensity solar cycle variations in terms of solar wind properties defined by solar activity characteristics parameters 23 p4056 A67-41106
- Streaming and spatial gradient equations of cosmic ray particles in interplanetary medium model, discussing Fokker-Planck equation and heliocentric field modulation 24 p4208 A67-41832
- Solar wind and UV exposure effects on spacecraft thermal control coatings, using in situ spectral reflectance measurements 24 p4174 A67-42040
- Field buildup during sudden commencement of magnetic storms in magnetosphere determined from MHD wave and solar wind pressure measurements 24 p4149 A67-42113
- Geomagnetic micropulsation excitation by solar wind flow around magnetosphere, noting surface wave propagation 24 p4209 A67-42133
- Energy spectrum of secular variations of cosmic ray intensity in interplanetary space, using data from stratospheric measurements 24 p4213 A67-42780
- SOLAR X-RAY**
- Solar and stellar X-ray astronomy, noting Crab Nebula occultation experiment 01 p0144 A67-10900
- Time varying energy distribution of high energy electrons producing solar microwave impulsive bursts and X-ray bursts by emission of gyrosynchrotron radiation 01 p0145 A67-11145
- Solar X-ray emission measurements with Geiger photon counters carried by Elektron II and IV satellites 02 p0240 A67-11544
- Powerful X-ray flare on sun detected by high altitude rocket, noting high energy electrons in superchromospheric layer 02 p0308 A67-11974
- Sudden cosmic noise absorption and X-ray flares noting peak, nature of decay and theoretical and experimental values [RASSA PAPER 1-10-139] 03 p0373 A67-14247
- Solar X-ray emission centers photographed by Veronique rocket 04 p0698 A67-14917
- High altitude solar X-ray burst and increase in ground level flux of heavy nuclei 07 p1242 A67-19113
- Solar X-ray data from satellite telemetry, comparing 8-20 angstrom flux with 10.7 cm radio flux 10 p1701 A67-23226
- Solar X-ray spectrum of Tousey analyzed using criteria of abundance of elements of Pottasch 10 p1707 A67-23227
- Aerobee rocket instrumentation for solar spectroscopy in soft X-ray region 10 p1712 A67-23804
- Atmospheric number density measured by attenuation of solar X-rays monitored when satellite passes from darkness to sunlight 11 p1857 A67-24605
- Relation between solar flare, X-rays and sudden ionospheric disturbances /SID/ using satellite measurements 12 p1905 A67-25801
- Solar X-ray monitoring during IQSY 12 p1999 A67-25833
- Solar X-ray soft component fluxes observed by satellite 12 p1999 A67-25835
- Solar X-ray events observed by 1964-1-D satellite launched by U.S. Naval Research Laboratory in 1964 12 p1999 A67-25836
- Nonthermal X-ray radiation accompanying solar flares, comparing spectral power of synchrotron radiation, Compton radiation and bremsstrahlung as possible generation mechanisms 15 p2549 A67-29141
- Solar X-ray flux for wavelength less than five angstroms measured, noting extreme variations in spectral slope and intensity 16 p2739 A67-31411
- Solar flares, analyzing X-ray emission, radio emission and superposition of ionospheric effect 16 p2739 A67-31459
- Solar X-ray emission measurements with Geiger photon counters carried by Elektron II and IV satellites 16 p2677 A67-31610
- Solar flare effect on electron production and electron density in lower ionosphere 17 p2936 A67-32382
- Solar X-ray spectrum observed by rocket carried Bragg crystal spectrometers and pinhole cameras array 17 p2937 A67-32650
- Solar X-ray fluxes measured by solar radiation satellite during IQSY, comparing X-rays and decimetric radio emission in 8-12 angstrom band 17 p2938 A67-33185
- Solar X-ray measurement with satellite noting radio noise flux, absorption in atmosphere and optical density changes 17 p2939 A67-33242
- Solar X-ray flare of July 1966 observed from satellite, giving curves describing energy flux, radiation intensity, etc 19 p3312 A67-35187
- Solar X-ray spectra below 25 angstroms from crystal spectrometer mounted on solar pointer flown on satellite 19 p3318 A67-35198
- Solar X-ray emission associated with proton flare of July 1966 measured, plotted and described 19 p3313 A67-35218
- Solar x-ray spectral intensity distribution using atmospheric extinction of solar radiation as measured by satellites 19 p3314 A67-35441
- Solar X-ray emission line spectrum from 1.3 to 20 angstroms in solar flares identified as Fe XXVI through Fe XX transitions 20 p3519 A67-37396
- Extreme UV solar spectrum, reviewing echelle spectrum, soft X-rays and coronal emission 20 p3528 A67-37467
- Solar atmosphere absorption of light nuclei generated on sun indicated by satellite observation of heavy nuclei cosmic ray flux and X-ray electron bremsstrahlung 21 p3698 A67-38595
- Solar X-ray emission below 20 angstroms made by Explorer XXX, discussing analog real time records and time resolution 23 p4050 A67-40805
- Radio wave field strengths received at Ahmedabad from Tashkent and solar X-ray emission effect, noting field strength increase with solar activity decrease 23 p4051 A67-40915
- Solar flare energetic X-ray events detected by onboard satellite ionization chambers, studying relationship to radio burst and space particle emission 23 p4060 A67-41232
- X-ray emissions from coronal condensation regions studied with pinhole camera, obtaining intensity profiles along intense X-ray regions 24 p4224 A67-41821
- Nonthermal X-ray radiation accompanying solar flares, comparing spectral power of synchrotron radiation, Compton radiation and bremsstrahlung as possible generation mechanisms 24 p4222 A67-43064
- SOLDER**
- Microscopic solder slivers as cause of malfunction in high density etched circuit boards having close conductor spacings 03 p0389 A67-14279
- SOLDERED JOINT**
- Solar cell submodule fabrication and design for Mariner and Surveyor spacecraft, describing automatic conveyor soldering oven 24 p4109 A67-42558
- SOLDERING**
- Solderability of 15 CDV 6 25 mm thick steel using argon arc and electric arc, noting mechanical properties of resulting alloy 01 p0078 A67-10270
- Flat pack interconnection technique using hot gas soldering, discussing inspection and control requirements 21 p3635 A67-38626
- SOLENOID**
- SA COIL
- Normal region distribution in superconducting solenoid measured after quenching by varying quenching current 01 p0137 A67-11065
- Inductance, flow current and external magnetic field effects caused by diamagnetism of superconducting solenoid winding 06 p1051 A67-18207
- Superconducting solenoid producing oscillatory magnetic fields having peak to peak amplitudes, noting niobium-zirconium wire performance 14 p2288 A67-28747
- Magnet consisting of superconductive solenoid of niobium-zirconium wire with

- ferromagnetic insertions 15 p2422 A67-29127
Variational technique involving Lagrange function representation of Grad magnetohydrostatic equation extended to symmetrical solenoid field 15 p2530 A67-29727
Inductance, flow current and external magnetic field effects caused by diamagnetism of superconducting solenoid winding 17 p2922 A67-33221
Electric field of AC solenoid of finite length in Hall conducting medium 18 p2990 A67-34500
Book on generation of high magnetic fields, discussing solenoids, cooling systems, superconducting and pulsed coils, etc 20 p3483 A67-36452
Rise rate dependence of transition current of superconducting solenoids on presence of electrical short circuit 23 p4045 A67-41457
- SOLID LUBRICANT**
Liquid solid film lubrication of hydrodynamic bearings, including effects of solid particles in liquid base lubricant 01 p0077 A67-10122
Antifrictional properties of mica and boron nitride for use instead of graphite as solid lubricant in cermet packing materials 01 p0081 A67-11246
Heavy metal derivative solid lubricants, properties and application [ASLE PAPER 66AM 2B3] 04 p0627 A67-14707
Chemical stability of silver graphite, molybdenum disulfide, zinc oxide, boron nitride, muscovite and phlogopite mica solid lubricants 10 p1659 A67-22829
Substrate metal hardness effect on performance of molybdenum disulfide films, noting wear rates 10 p1659 A67-22867
Solid lubricants frictional behavior in press-fit tests, measuring sliding speed, load and surface roughness as function of time [ASLE PREPRINT 67AM 5A-2] 14 p2325 A67-28786
Test methods to determine wear coefficients and design calculations for solid film lubricants, covering wide temperature range [ASLE PREPRINT 67AM 5A-5] 14 p2325 A67-28787
Polyimide bonded solid lubricants development [ASLE PREPRINT 67AM 7A-1] 14 p2326 A67-28789
Wear life improvement of ceramic bonded solid film lubricant by compression and artificial filling of film voids [ASLE PREPRINT 67AM 7A-2] 14 p2326 A67-28790
Filament wound sleeve seal impregnated with solid lubricants dissipates heat in rubbing contact zone and provides wear characteristics for use in air compressor [ASLE PREPRINT 67AM 7A-3] 14 p2326 A67-28791
Plasma spray gun as possible method of applying resin, ceramic and metallic bonded solid film lubricants [ASLE PREPRINT 67AM 7A-4] 14 p2326 A67-28792
Influence of surface roughness and humidity on endurance of rubbed films of various lamellar solids on steel 16 p2681 A67-30853
Variation of friction and wear of solid lubricant film with thickness particle based on junction and wear particle size 16 p2683 A67-31751
Molybdenum disulfide compacts pressurized by explosive forming, determining specific gravity, hardness, compressive and tensile properties, etc 16 p2695 A67-31753
Strength and durability in friction tests of soft, vacuum deposited, thin-metal gold film lubricants, noting dependence on film-substrate interface 16 p2684 A67-31816
Antifrictional properties of mica and boron nitride for use instead of graphite as solid lubricant in cermet packing materials 17 p2866 A67-33169
Polyimide bonded solid lubricants development 19 p3233 A67-34790
Lubrication and wear with reference to boundary lubrication, fluid and solid films, discussing dry and lubricated sliding and rolling theory 20 p3455 A67-37262
Solid lubricants including powders, solid dispersions, resin bonded dry film and soft metal films, discussing metal oxide lubricant effect on graphite 20 p3455 A67-37263
Space environmental effect on lubricants and rolling element bearings, comparing evaporative losses of solid and liquid lubricants 21 p3633 A67-38143
Chemical interactions in formation of oxidation resistant solid lubricant composites of tungsten diselenide-gallium alloys for use in ball bearing systems [ASLE PAPER 67-LC-6] 24 p4164 A67-42745
Molybdenum sulfide solid lubricant oxidation characteristics analyzed by thermogravimetry [ASLE PAPER 67-LC-14] 24 p4165 A67-42748
Worm gear lubrication with bonded solid film lubricants, discussing efficiency and wear life test apparatus [ASLE PAPER 67-LC-18] 24 p4165 A67-42751
- SOLID PHASE**
Thermal emf and electric conductivity in solid and liquid semiconducting copper-antimony-ditelluride 02 p0297 A67-11846
High temperature effect on strength of solidified resins and resin based materials, determining loss of weight, density, compression strength, permittivity and electric conductivity 05 p0833 A67-17098
Eutectic alloys of heavy metal phases with InP compound analyzed, noting phase orientation parallel to solidification direction 09 p1552 A67-21880
Structure, composition and morphology of carbide phases of nickel superalloy 13 p2131 A67-26573
Gas condensation near comet nucleus as source of formation of entire dust component of comet coma 15 p2552 A67-29153
Surface-reaction effects on solid propellant acoustic-response functions characterizing transient combustion process 19 p3311 A67-35777
Semiconductivity of molybdenum-oxygen systems, analyzing solid phase effect on solution mechanism 20 p3510 A67-36816
Germanium distribution in metallic phases of various iron meteorites by electron probe microanalysis 22 p3885 A67-39976
Hot working effects in octahedrite parent gamma phase, discussing spinel twinning and polycrystal assembly of gamma phase before kamacite precipitation 24 p4232 A67-42609
Gas condensation near comet nucleus as source of formation of entire dust component of comet coma 24 p4239 A67-43076
- SOLID PROPELLANT**
SA COMPOSITE PROPELLANT
SA CYCLOTETRAMETHYLENE TRINITRAMINE /RDX/
SA DOUBLE BASE PROPELLANT
SA PROPELLANT GRAIN
Mechanical constitutive theory and methods of stress analysis for physically nonlinear solid propellants [AIAA PAPER 66-124] 01 p0139 A67-11155
Extension of analysis of unsteady state model for combustion of solid propellant to include nonlinearities of second order 01 p0141 A67-11158
Low thrust reaction control system utilizing solid propellant which sublimates into low molecular weight vapor, noting heat sources 01 p0142 A67-11407
Pressure coupled combustion dynamics of solid propellants analyzed as function of propellant variables, oscillation frequency and combustion pressure 01 p0143 A67-11448
Steady state combustion model of mono- and double-base solid propellant with laminar flow 01 p0143 A67-11450
Transient temperature and mass evolution from solid propellants during pressure decays 04 p0687 A67-14835
Solid propellant regression rate in hybrid rocket motor examined via combustion process model, assuming homogeneous flow in central channel 05 p0874 A67-16766
Solid propellant burning rate, combustion gas influx, tube geometry and propellant and tube thermophysical properties [AIAA PAPER 67-102] 06 p1074 A67-18282
Aluminum powder damping of HF instability in solid propellant combustion in vortex burner 06 p1115 A67-18307
Continuous high resolution measurement of solid propellant burning rate using resonant LC circuit [AIAA PAPER 67-69] 06 p1072 A67-18450
Combustion dynamics of solid propellants in LF range, discussing equipment and results [AIAA PAPER 67-70] 06 p1073 A67-18451
Specific impulse and thrust coefficient performance as function of flight Mach number and altitude for air augmented solid propellant propulsion vehicle using supersonic combustion [AIAA PAPER 67-226] 06 p1097 A67-18517
Erosive burning of ammonium perchlorate solid propellants for combustion in turbulent boundary layer determined, using flat plate heat transfer correlation 07 p1238 A67-19069
Solid propellant with heterogeneous surface reaction, noting agreement with steady state and acoustic response properties of JPN propellant 07 p1239 A67-19074
Thermodynamic processes influencing choice of rocket engine propellants 07 p1239 A67-20088
Ballistic propellant combustion alteration and thermal effects due to dynamic spinning observed on solid propellant sounding rockets 08 p1408 A67-20522
Initial solid propellant temperature effect on constant pressure burning rate based on granular diffusion flame model /GDFM/ 08 p1375 A67-20581
Surface effects for solid propellant combustion, discussing flame profile and instability, surface burning mechanism, temperature distribution, etc 08 p1373 A67-20642
Compression strength and strain of solid propellants, noting internal loads developed during burning process 08 p1373 A67-20720
Oscillatory burning of solid propellant studied using integral balance equation in solid gas interface, assuming Rayleigh criterion and sound wave criterion 08 p1373 A67-20774
Ablation rate of hybrid rocket solid propellants in two-dimensional engine simulated chamber 08 p1373 A67-20804
Mechanics and chemistry of solid propellants - Symposium on Naval Structural Mechanics, Purdue University, April 1965 08 p1418 A67-20872
Solid propellant polymeric binder chemistry and high speed computer calculations of performance characteristics 08 p1373 A67-20875
Flame propagation effects and combustion chemistry of nitrate ester or double base solid propellants 08 p1374 A67-20877
Nonlinear continuum mechanics of viscoelastic materials with application to solid propellants 08 p1419 A67-20879
Reinforcement of solid propellants and use of high strength wires and cylinders 08 p1374 A67-20889
Mechanical properties of unfilled and filled elastomers 08 p1420 A67-20890
Failure mechanism of solid propellant grain and stress criteria for solid motor design and evaluation 08 p1374 A67-20891
Filler effects on deformation and rupture of amorphous gum elastomers with various molecular structures, noting failure envelopes [JPL-TR-32-922] 08 p1420 A67-20892
Structural adhesives bonding - Symposium, Stevens Institute of Technology, Hoboken, September 1965 09 p1521 A67-22499
Pressure deflagration limit of high energy solid propellants increased to superatmospheric pressures by composition changes [AIAA PAPER 66-679] 10 p1696 A67-23131
Mechanism of decomposition of ammonium perchlorate in accord with experimental fact 10 p1697 A67-23157
Volumetric loading factor expression derived for side burning solid propellant grains by imposing constraint on port channel flow Mach number 11 p1851 A67-24227
High pressure hot gas solid propellant cartridge starter for aircraft turbine engine [ASME PAPER 67-GT-21] 11 p1854 A67-24803
T-burner technique for determining acoustic pressure and velocity-coupled responses of solid propellants 12 p1988 A67-25910
Powder and solid propellant combustion, discussing heterogeneous and homogeneous systems, characteristics of foam, fizz and flame zones, etc 12 p1988 A67-26110
Parameters of supercompressed detonation wave in solid propellant system noting wavefront pressure, density and propagation

rate dependence on displacement rate of interface 12 p1930 A67-26116

Propulsion systems for booster rockets and space vehicles 14 p2377 A67-27875

Liquid and solid rocket propellants, examining use of metals as fuels 14 p2376 A67-27877

Low cost rocket launch vehicles for various payload capacities 15 p2566 A67-29832

Solid propulsion - ICRPG/AIAA Conference, Anaheim, June 1967 15 p2546 A67-29976

Mechanical response of highly filled elastomer in complex triaxial tensile stress field, demonstrating dewetting effect, need for more testing, etc 15 p2575 A67-29978

Cool burning smokeless propellants for gas generator applications and low signature missiles evaluated against criteria 15 p2544 A67-29981

Surface coupled heat release effect on oscillatory amplitude of pressure coupled response in solid propellant 15 p2544 A67-29983

Burning rate vs pressure and other factors as function of composite solid propellant composition and oxidizer particle size distribution 15 p2580 A67-29985

Kinetics and energetics of condensed phase thermal decomposition reactions of ammonium perchlorate composite propellants analyzed, using differential scanning calorimetry 15 p2544 A67-29989

Combustion characteristics of crystalline oxidizers noting materials used, experiments performed and results 15 p2581 A67-29990

Parameters determining magnitude of acceleration effect on burning rate increase of aluminized and nonaluminized composite solid propellants 15 p2581 A67-29991

Statistical service life prediction based on propellant grain structural integrity for Minuteman third stage motor, noting grain stress analysis 15 p2547 A67-29996

Model for velocity coupled axial mode combustion instability in solid propellant rocket motors, noting computer studies 15 p2547 A67-29997

Terminating solid propellant combustion by rapid drop in pressure 15 p2582 A67-29998

Defonation characteristics evaluation of solid-composite propellant, noting hazards study program /Project SOPHY/ and critical geometry theory 15 p2544 A67-29999

Thermal conductivity variation of double-base solid propellants under acoustic irradiation compared with polymethyl methacrylate 15 p2545 A67-30199

Solid propellants and motors for space exploration, comparing chemical and nonchemical propulsion systems 16 p2735 A67-30702

Pressure measuring instrumentation response requirements for computing decay rate in solid propellant termination systems 17 p2926 A67-32069

Preignition phase of solid propellant burning, determining concentration of volatilized species as function of surface temperature 17 p2927 A67-33028

Interaction of finite amplitude pressure pulse with combustion region at surface of burning solid propellant 18 p3108 A67-33830

Metallized and nonmetallized composite solid propellant burning rates, analyzing effects of acceleration, noting agglomeration and nonnormal conditions [AIAA PAPER 67-470] 18 p3157 A67-33940

Swirl effect on nozzle flow applied to solid propellant nozzles assuming irrotational flow so that tangential velocity field has free vortex characteristics 19 p3311 A67-34826

Solid-propellant combustion instability models describing combustion zone dynamics applied to acoustic and nonacoustic instability in low frequency regime [CI PAPER 67-13] 19 p3311 A67-35007

Pressure dependent surface reaction effects on acoustic response of composite solid propellants studied for various coatings 19 p3309 A67-35010

Surface-reaction effects on solid propellant acoustic-response functions characterizing transient combustion process 19 p3311 A67-35777

Hybrid rocket design combining flexibility of liquid fuel with simplicity and reliability of solid propellant 20 p3516 A67-36487

Acoustic vibrations during solid-fuel

combustion, studying acoustic energy increase rate and development 20 p3551 A67-36817

Combustion stability of powder in semiclosed volume, taking into account propellant surface temperature dependence on pressure and temperature gradient 21 p3732 A67-38526

Solid propellant electric thruster /SPET/ using pulse plasma for spacecraft attitude control and stationkeeping [AIAA PAPER 67-661] 21 p3690 A67-38697

Continuous high resolution measurement of solid propellant burning rate using resonant LC circuit [AIAA PAPER 67-69] 21 p3688 A67-38857

Aluminum powder damping of HF instability in solid propellant combustion in vortex burner [AIAA PAPER 67-104] 21 p3732 A67-38860

Pulsed propulsive performance of low thrust subliming solid ammonium carbamate reaction jet, discussing transient response, apparatus, techniques, etc 21 p3697 A67-39152

Raven solid propellant motor for Skylark noting design, ignition and plastic propellants burning properties 22 p3867 A67-39525

Erodibility of solid propellants subjected to rapid flow of gas past burning surface 22 p3867 A67-39538

Solid propellant space propulsion technology covering developments in missiles, launch vehicles, fabrication and range of application 22 p3869 A67-40334

Small perturbation analysis on mass conservation stability in solid propellant combustor, discussing parametric model 23 p4084 A67-41721

Solid propellant burning rate, combustion gas influx, tube geometry and propellant and tube thermophysical properties 23 p4084 A67-41723

Chemical dynamic hydraulic power unit /HPU/ performance, weight and volume efficiencies, noting applications to solid and liquid propellants 24 p4107 A67-42531

Reentry vehicle solid propellant and liquid fuel compact turboalternator electric power system operating characteristics and performance 24 p4108 A67-42534

SOLID PROPELLANT IGNITION

Ignition regularity criterion for solid propellant rocket engines, assuming ignition regularity controlled by heat transfer process between ignition source and propellant surface 01 p0139 A67-10524

Aerothermochemical analysis of solid propellant combustion 04 p0722 A67-14824

Heat transfer processes during ignition of solid propellant rockets, considering radiative and convective components. [AIAA PAPER 66-66] 05 p0873 A67-17217

Solid propellant combustion research, discussing steady state combustion zone structure of propellants, composites, ignition, extinguishment and acoustic interaction [AIAA PAPER 67-67] 06 p1072 A67-18271

Flame spreading velocity over surface of igniting solid rocket propellants as function of atmospheric pressure and chemistry and specimen surface condition 06 p1073 A67-18852

Gaseous ammonia composite solid propellant ignition upon contact with oxidizing vapors such as perchloric acid vapor 06 p1073 A67-18869

Aluminum fluoride effect on propagative ignition of fuel oxidant mixtures and on combustion between aluminum and oxygen 07 p1238 A67-19070

Solid propellant highly restartable electric trigger microthruster, noting triggering electrode and feed system 11 p1746 A67-25013

Combustion instability, transient burning during ignition and extinction by depressurization investigated in nonsteady burning of solid propellants 15 p2580 A67-29984

Arc image ignition of solid propellants compared to conductive ignition, outlining corrective steps and deriving ignition time delay 15 p2581 A67-29987

Ignition response of solid propellants described with model including surface regression with verification of igniter flux and pressure effects 15 p2581 A67-29988

Solid propellant combustion research, discussing steady state combustion zone

structure of propellants, composites, ignition, extinguishment and acoustic interaction [AIAA PAPER 67-67] 15 p2545 A67-30187

Prediction of solid propellant hot-gas ignition based on preignition transient convective heat transfer model [AIAA PAPER 66-67] 15 p2582 A67-30196

Structures, charging into stage, thermal protection, ignition, and nozzles problems encountered in development of solid propellants 16 p2736 A67-31617

Aluminum particle combustion in solid rocket grains, noting drop formation mechanism and droplet combustion analysis [ONERA-TP-486] 17 p2926 A67-32697

Ammonium perchlorate solid propellant ignition characteristics recording preignition surface exotherms 17 p2927 A67-33027

Effect of copper chromite, carbon and other potential catalysts on thermal decomposition and ignition of ammonium perchlorate 18 p3108 A67-33813

Mixing, ignition and combustion in secondary combustor for air-augmented solid rockets with solid particles in primary stream [AIAA PAPER 67-481] 18 p3158 A67-33950

Igniter performance in solid propellant rocket motors, examining mass discharge rate effect on chamber pressure transients [AIAA PAPER 66-680] 19 p3310 A67-34811

Flame spreading over igniting solid propellant surface in high pressure oxygen-inert environment 19 p3344 A67-34999

Solution for coupled system of parabolic partial differential equations describing reactants diffusion and heat conduction in gas phase 23 p4048 A67-41764

SOLID PROPELLANT ROCKET ENGINE

SA ATHENA ROCKET

Transportation and handling of large solid rocket motors, considering program management aspects [SAE PAPER 660707] 01 p0169 A67-10623

Theoretical analysis of heat transfer in solid propellant rocket exhaust plumes by use of temperature probe located in plume environment 01 p0071 A67-11101

Data acquisition techniques and system accuracies for static testing of solid propellant rocket engines 01 p0051 A67-11109

Digital data processing consideration in acquisition-reduction system engineering with reference to solid rocket engine testing 01 p0030 A67-11110

Transducers role in problems associated with accurate and precise measurements during static firing tests of solid propellant motors 01 p0073 A67-11111

Solid propellant electrical thrusters for spacecraft attitude and trajectory control 01 p0142 A67-11433

Role of large solid propellant rocket motor in U.S. space program noting design, technology, testing, cost, thrust-vector control systems, etc 01 p0142 A67-11447

Steady state combustion analysis of solid propellant rocket motors extended by studying influence of grid sizes and number of steps used in numerical analysis 01 p0143 A67-11449

Spin effects on rocket nozzle performance show higher combustion pressures and burning rates due to blockage of nozzle throat 02 p0303 A67-11947

Auxiliary solid propellant motors in Saturn launch vehicle [AIAA PAPER 66-946] 02 p0303 A67-12280

Solid booster thrust decay control for payload or upper stage separation, noting inert slivers with auxiliary retrorockets as separation control [AIAA PAPER 66-971] 02 p0304 A67-12293

Effect on protective coatings of launch pads of exhaust products, chamber pressure, nozzle diameter, etc, from aluminized solid propellant rocket motors [AIAA PAPER 66-972] 02 p0304 A67-12294

Heat sterilizable solid propellant motor designs for interplanetary missions, considering case-bonded spherical, case-bonded cylindrical, free-standing, internal burning and free-standing end burning [AIAA PAPER 66-973] 02 p0304 A67-12295

Reliability considerations in spherical solid retrorockets for Gemini spacecraft system 02 p0305 A67-12351

Solid propellant rocket motor capabilities for space flights, noting specific impulse on density basis 02 p0305 A67-12352

Average burn rate, average pressure relationships in solid rockets 04 p0724 A67-15250

Ignition pressure transient in solid rocket motors, examining chamber filling interval, flame propagation, heat transfer correlation, burning area, etc 05 p0873 A67-16513

Thrust generation from neutral particle sputtering from solid target, noting advantages such as storage, operating life, etc 05 p0873 A67-16515

Combustion characteristics and ballistic performance of dual layer propellant grains using polybutadiene/potassium perchlorate and polyurethane/ammonium perchlorate for end-burning type rocket motor 05 p0872 A67-16589

Nozzle submergence loss in solid propellant rocket engine, correlating loss percentage of specific impulse with dimensionless groups 05 p0875 A67-17366

Dynamic characteristics of variable mass slender elastic body, solving vector differential equations [AIAA PAPER 67-41] 06 p1095 A67-18263

Pressure variation in solid propellant rocket engine determined by digital computer in terms of propellant properties and engine design 07 p1239 A67-19351

Influence of relative thickness of elastic case on acoustic stability of radial modes in solid propellant rockets [AIAA PAPER 66-473] 07 p1240 A67-19370

Diamant solid propellant booster development 07 p1240 A67-19521

Electroanalogue analysis of convective and conductive heat transfer and transient temperature field in solid propellant rocket nozzle head 07 p1268 A67-19568

Optimized equipment systems design studies for handling and transportation of large solid fuel rocket motors [AIAA PAPER 67-266] 07 p1164 A67-20047

Design criteria for NASA test facility for firings of 20 inch diameter solid rocket motors [AIAA PAPER 67-236] 07 p1241 A67-20059

Exhaust cloud diffusion from solid rocket motors correlated with measurable meteorological variables [AIAA PAPER 67-280] 07 p1221 A67-20084

Solid and hybrid propulsion relationship to sounding rocket vehicle design and mission analysis, particularly application to synoptic meteorology 08 p1374 A67-20492

Feasibility and design study of unguided solar orbital launch vehicle 08 p1404 A67-20493

Solid propellant motor design for Black Brant VB sounding rocket 08 p1375 A67-20519

Transitional combustion phenomena in solid propellant rocket engines under unsteady conditions 08 p1373 A67-20781

Naval solid propellant rocket engine structural design, configurations, handling, storage and adaptation to environmental conditions 08 p1375 A67-20873

Stress analysis of solid rocket engine propellant grains including linear viscoelasticity, thermal analysis and equilibrium, relaxation times, engine sizes, cooling, creep relaxation, etc 08 p1373 A67-20874

Static and dynamic combustion phenomena effects on grain structural design for solid propellant rocket engine 08 p1374 A67-20876

Solid rocket engine propellant grain structural dynamics including elastic and viscoelastic deformations, stress and shear vibration modes, natural frequency calculations, etc, using Fourier inversions and transforms 08 p1376 A67-20883

Experimental stress and strain analyses of solid propellant rocket engine grains under various loading conditions 08 p1419 A67-20886

Structural design of solid propellant rocket engine and failure, deformation and fracture of reinforced propellant grains 08 p1420 A67-20888

Thrust magnitude and restart control of solid propellant motor by injection of fluorine and chlorine trifluoride 08 p1376 A67-21518

Bonding of rigid insulation to case of solid propellant rocket motor, considering fabrication, operation and storage requirements 09 p1578 A67-22512

Composite material application to solid fuel rocket motor cases, discussing performance characteristics, manufacturing techniques, etc 09 p1578 A67-22513

Adhesive bonding of solid propellants in rocket motors, emphasizing propellant liner interface and bonding at 09 p1578 A67-22514

Thermal IR inspection technique for bond flaw inspection in simulated solid propellant rocket engines 09 p1508 A67-22528

Radiative heat transfer in interior of combustion chambers of solid propellant rockets 09 p1561 A67-22567

Solid propellant rocket motor for third stage of satellite launcher, performance requirements and design 10 p1698 A67-23483

Optimization of base thermal protection system for advanced Saturn II boosters employing strap-on solid propellant motors 10 p1735 A67-23729

Head-end pressure deviation in slotted-tube solid propellant rocket motors with high loading densities and flexible thrust-time histories 11 p1852 A67-24352

Solid fueled rocket powered MHD generators with high power densities 12 p1898 A67-25382

Propellant composition influence on finite-amplitude axial wave mode instability in solid propellant rockets [AIAA PAPER 66-600] 12 p1988 A67-25909

Heat sterilizable solid propellant motor designs for interplanetary missions, considering case-bonded spherical, case-bonded cylindrical, free-standing, internal burning and free-standing end burning 13 p2188 A67-26833

Short duration technique providing simulation of thermodynamic properties and composition of exhaust products of liquid and solid propellant rocket engines [AIAA PAPER 66-760] 13 p2090 A67-26843

Model for solid rocket motor instability caused by chamber and propellant combustion characteristics, relating combustion and acoustic instabilities 14 p2404 A67-28113

Thrust vector controls for solid rockets, discussing liquid secondary injection, jet tabs, direct chamber bleed, omnaxial movable nozzle and lockseal 15 p2545 A67-29136

Causes of ignition failure in solid-fuel rocket motors, obtaining simultaneously pressure and temperature data 15 p2543 A67-29773

Combustion stability in solid propellant rockets, reviewing Soviet T-sub s and Q models 15 p2581 A67-29986

Submerged nozzle for solid rockets, noting exhaust flow velocity and direction determination 15 p2547 A67-29994

System requirements effect on ballistic and hardware design of cast double-base solid propellant rocket motors 15 p2548 A67-30000

Saphir test vehicle, two-stage guided and controlled rocket 15 p2571 A67-30090

Third 260-inch diameter solid propellant rocket engine test firing 15 p2548 A67-30150

Effect on protective coatings of launch pads of exhaust products, chamber pressure, nozzle diameter, etc, from aluminized solid propellant rocket motors [AIAA PAPER 66-972] 17 p2928 A67-32064

Propulsion by solid/liquid or hybrid rocket motor 17 p2929 A67-32727

Dynamic characteristics of variable mass slender elastic body, solving vector differential equations [AIAA PAPER 67-41] 17 p2956 A67-33013

Rocket chamber pressure influence on particle size measurements of heterogeneous combustion products of solid propellants containing aluminum 18 p3109 A67-33839

Solid propellant rocket motors reliability, discussing corrective action, retest, success probability, requirements, capability, simulation model, etc [AIAA PAPER 67-435] 18 p3112 A67-33914

Solid propellant engines treated for constant missile volume and mass 18 p3137 A67-34360

Solid propellant rocket motor-body shape as additional variable used to achieve given thrust-time program 18 p3115 A67-34361

Analysis of explosion hazards of large solid motors, suggesting mathematical approach in predicting blast damage [CI PAPER 67-14] 19 p3309 A67-35008

Solid propellant gas generator power systems for normal and emergency space operations 20 p3533 A67-36601

Solid propellant stages development from

experience acquired in France to future large space projects 20 p3516 A67-36878

Low pressure solid rocket motor design and application, noting advantages in high mass ratio performance and operational disadvantages 20 p3516 A67-37131

Dynamic ballistics of combustion termination by fluid injection in solid propellant motors, describing termination mechanisms 21 p3733 A67-38893

Microwave use in measuring burning rate of solid propellant rocket motors and in detection of porosity in nonconducting materials 22 p3795 A67-39196

Combustion in solid propellant rocket engines using mathematical model 22 p3867 A67-39539

Base flow characteristics and thermal environment of launch vehicles with strap-on solid rocket motors 22 p3902 A67-39939

Periodic pressure fluctuations relation to structure and propagation of combustion front in solid propellant rockets, giving perturbation frequencies 24 p4252 A67-41798

Solid propellant motors relative performance as related to intermediate payload missions, considering reusable liquid strap-on stages for post-Saturn payloads [DOUGLAS PAPER-4452] 24 p4240 A67-42388

Optimization of base thermal protection system for advanced Saturn II boosters employing strap-on solid propellant motors 24 p4256 A67-42915

Second order nonlinear differential equation derived for pressure-time curve required for ideal solid propellant rocket motor 24 p4208 A67-42923

Saturn V payload capabilities uprating by building block approach using solid propellant rocket motor, noting cost factor and mission flexibility [AIAA PAPER 67-907] 24 p4244 A67-43014

SOLID ROTATION

Finite displacements of solid body under effect of internal rotating flywheels and translational motion of masses 15 p2518 A67-30169

SOLID SOLUTION

Electron resonance and magnetic properties of solid solution in bismuth ferrite and barium titanate system, obtaining phase diagram 01 p0127 A67-10063

Band structure of spectra of gallium phosphide, gallium arsenide and solid solutions determined by optical reflection techniques 01 p0086 A67-10067

Diffusion parameters and solubility of Cd in InAs measured with aid of radioactive isotopes compared with diffusion coefficient measurement by p-n junction method 01 p0128 A67-10082

Work function of solid solutions of tungsten with molybdenum and tantalum explained by surface adsorption effects 01 p0093 A67-10092

Sintering of cobalt-nickel powder mixtures during formation of solid solutions, noting shrinkage and diffusion coefficients 01 p0096 A67-10695

Electrical and optical properties of solid solutions formed by beta manganese and chromium dioxide within wide composition range, showing magnetic semiconductor behavior 01 p0134 A67-10755

Heat of formation of KCl-KBr solid solutions and energy storage after proton irradiation 01 p0136 A67-11051

Formation conditions for yttrium boride-lanthanum boride solid solution by reduction of Y and La oxides in vacuum 01 p0138 A67-11244

Laser based on excitation of gallium phosphorus arsenide solid solution by beam of fast electrons 02 p0251 A67-11824

Structural changes during early stages of decomposition of oversaturated solid solution of titanium in cobalt, noting secondary diffusive reflection 02 p0255 A67-11865

Optical constants of silver solid solutions with gold addition, noting dependence of refractive index, absorption coefficient and conduction electrons on impurity concentration 02 p0255 A67-11870

Three-component diffusion theory applied to calculation of three-component metallic solid solutions, examining interstitial and substitutional systems with different boundary conditions 02 p0256 A67-12707

Diffusion effect on thermal stresses in neighborhood of macrodefects in solid

solution resulting in time dependent change of stress-strain state 03 p0521 A67-13121

Mechanical pressure effect on polarization processes in barium titanate single crystals and barium titanate-zinc oxide solid solutions 03 p0489 A67-13145

Ti-Mg alloy production under high pressure, noting existence of solid solution of one weight-percent Mg 03 p0441 A67-13255

X-ray and thermal analyses and phase diagram of titanium chromide-tantalum chromide-niobium chromide solid solution at high temperatures 03 p0447 A67-13640

Ferroelectric properties and morphotropic phase boundary in phase diagram of ternary system of compounds of lead, titanium and nickel 03 p0498 A67-13704

Kinetics of degassing of tantalum-nitrogen solid solutions by annealing in high vacuum at various high temperatures 04 p0637 A67-14909

Maximum concentrations estimation for solidus of germanium and silicon solid solutions in retrograde melting 04 p0677 A67-14943

X-ray analysis of Nb-Ni-Al solid solutions, noting solubility of Nb and construction of phase diagram 04 p0638 A67-15204

X-ray study of phase composition of refractory alloys carbide solid solutions noting hardness, electric resistance and elastic deformation energy of crystal lattice 04 p0638 A67-15205

Tantalum interaction with nitrogen and air show retardation of grain growth 05 p0832 A67-17507

K-absorption spectrum of Ni as function of concentration of alloying elements and arrangement of atoms of alloying elements into Ni crystal lattice 06 p1017 A67-17952

Solubility limit of Fe in close-packed hexagonal alpha-Ti noting temperature dependence and superconductivity 06 p1051 A67-18370

Temperature dependence of thermal emf, electrical conductivity, current carrier mobility and thermal conductivity of GeTe-GeSe solid solution 07 p1231 A67-19164

Physicochemical properties of Ti-AlO solid solutions 07 p1203 A67-19260

Titanium carbide-molybdenum carbide interaction and structure of resulting Ti-Mo-C 07 p1203 A67-19261

Phase diagrams of various titanium-phosphorus compounds and mixtures with up to 45 atomic percent P and microstructural characteristics of Ti-P alloys 07 p1203 A67-19262

Phase equilibrium and physicochemical properties of titanium aluminide-titanium stannide-zirconium quasi-ternary alloy 07 p1204 A67-19264

Chemical and crystal structural analysis of solid solution of titanium chromide and zirconium chromide metalides 07 p1204 A67-19265

Heats of solution and formation of Ti-Al alloys in region of alpha-solid solution determined, using calorimetry 07 p1204 A67-19268

Structure of system Ti-Mo-Cr-Fe-Al alloys when quenched from beta region, noting maximum hardness at aging temperatures 07 p1205 A67-19272

Ternary system Ti-Al-V alloys analyzed using thermal, microstructural, etc, methods, plotting solidus surface in crystallization region of beta-solid solution 07 p1205 A67-19273

Dielectric properties of complete solid solutions with perovskite structures in barium titanate-barium stannate and barium titanate-barium ferrotantalate systems 07 p1231 A67-19489

Soviet book on electronic properties of semiconductor solid solutions, noting relation between probability theory and ideal crystals theory 07 p1232 A67-19580

Kinetics of two-phase decomposition of solid solution of magnesium-aluminum alloy using X-ray analysis, noting grain orientation and size 08 p1342 A67-20810

Specific heat and magnetic susceptibility of yttrium solid solutions with magnetic impurities of Gd 08 p1369 A67-20870

Phase state of thin layers of vapor deposited InTe with 50-60 percent Te 08 p1369 A67-20994

Temperature dependent variations in Hall coefficient of indium and indium-rich alloys with Pb, Cd, Ti and Hg 08 p1371 A67-21438

Band structure of spectra of gallium phosphide, gallium arsenide and solid solutions determined by optical reflection techniques 08 p1339 A67-21450

Diffusion parameters and solubility of Cd in InAs measured with aid of radioactive isotopes compared with diffusion coefficient measurement by p-n junction method 08 p1371 A67-21459

Double valence band and thermoelectric properties of lead telluride-tin telluride solutions 10 p1688 A67-22848

Solid solubility of boron in graphite as function of temperature and nature of solution from density and lattice constants 12 p1960 A67-26189

Model for concentrated interstitial solid solutions applied to carbon solution in gamma iron 13 p2131 A67-26574

Interaction between phases of nickel aluminum-nickel titanium pseudobinary system, determining concentration dependence of properties of system 13 p2142 A67-27286

Solid solution properties of niobium carbide-molybdenum carbide alloy, noting changes in electron structure 14 p2337 A67-28284

Strain hardening of high temperature titanium multiphase solid solution by deformation and subsequent rapid cooling 15 p2504 A67-29971

Electric and thermoelectric effects in single crystals of zinc-cadmium-antimony solid solution, measuring electrical conductivity, Hall constant and thermoelectric power 15 p2540 A67-30029

GeTe solid solutions reviewed considering thermal EMF, temperature dependence and current carrier mobility 16 p2730 A67-31164

Electrical conductivity and Hall effect of indium arsenide solid solutions, noting temperature dependence and hole mobility 16 p2732 A67-31480

Solid solutions of titanium, tungsten, chromium prepared by carbidization of mixtures in hydrogen medium and obtained as fine-grained carbide powders 16 p2691 A67-31587

Melting point and microhardness of carbon-saturated TiC-VC solid solutions, noting temperature of eutectic of TiC-VC with graphite 16 p2691 A67-31588

Magnetic, electric and SHF properties of oxides and solid solutions of bivalent europium from 1.6 to 300 degrees K 16 p2733 A67-31732

Relaxation processes for oxygen in solid solution in niobium demonstrating clustering of atoms into groups [AD-642957] 17 p2871 A67-32628

X-ray and thermal analyses and phase diagram of titanium chromide-tantalum chromide-niobium chromide solid solution at high temperatures 17 p2875 A67-33173

Mean values of characteristic temperatures and dynamic displacements of ions for lattice of solid substitution solutions of zinc telluride-cadmium telluride system 18 p3095 A67-33446

Energy band structure of crystals of groups IV, III-V and II-VI and magnesium silicide type crystals 18 p3095 A67-33448

InSb-InAs solid solution thin films absorption spectra, noting band structure, temperature change and Hall EMF reduction 18 p3096 A67-33450

Temperature and composition effect on ductility transitions, yield stress and dislocation pinning strength in iron base alloys due to change in slp 18 p3063 A67-33485

Changes in experimental relationship between preexponential factor in diffusion equation and activation energy for solid solutions 19 p3243 A67-34928

Particle growth during coalescence of fine phases of metallic alloys 19 p3245 A67-35469

Copper and its solid solutions retarding force profiles studied for explanation of Cottrell-Stokes law deviation 20 p3464 A67-36220

Semiconductivity of molybdenum-oxygen systems, analyzing solid phase effect on solution mechanism 20 p3510 A67-36816

Chromium activities in binary Cr-Ti solid solutions measured by Knudsen effusion technique, noting deviations from Raoult law and free energy 20 p3469 A67-37384

Tantalum interaction with nitrogen and air

show retardation of grain growth 21 p3644 A67-38035

Relation between electric conductivity and Hall coefficient in solid solutions, determining sample composition and temperature for forbidden band width concentration dependence 21 p3684 A67-38449

Indium antimonide-indium arsenide solid solution carrier mobility related to sample composition and temperature, measuring Hall coefficient and electrical conductivity 21 p3684 A67-38452

Physicochemical interactions between components of refractory metals solid solutions, determining metal alloying effects on system structure and high temperature durability 22 p3818 A67-39319

Aluminum magnesium alloys prepared by powder metallurgy and hot extrusion evaluated for tension, compression, impact, fatigue and creep 22 p3821 A67-40053

Interstitial oxygen solubility in niobium using X-ray diffraction, micrographic and thermal techniques, discussing lattice structure 22 p3823 A67-40209

Lattice parameter of bcc Nb-Hf alloy with interstitial solid solution of oxygen 22 p3823 A67-40210

Oxygen interstitial solid solubility in niobium, noting decrease with addition of tungsten and molybdenum 22 p3823 A67-40211

High oxygen Nb-Ti alloy solid solution critical superconducting current density and workability dependence on Th, Gd and Y solute content 23 p4036 A67-40705

Precipitation processes in Ta-Cr solid solutions investigated for temperature dependence and change in alloy properties resulting from precipitation 23 p4018 A67-40712

Equilibrium phases in annealed NiCrTiAlW alloy using optical and electron microscopy and X-ray analysis 23 p4019 A67-41078

Interstitial solid solubility of N in Nb and Nb binary alloys containing Hf, Mo and W as function of pressure and temperature 24 p4172 A67-41976

Hf, Mo and W influence on maximum interstitial solid solubility of N in Nb rich ternary systems 24 p4172 A67-41977

SOLID STATE

Soviet book on solid state chemistry and electroconductivity of chemical systems 06 p1052 A67-18608

Nonlinear PDEs of two-valley model of Gunn effect materials, noting microscopic transport configurations 06 p1067 A67-18962

Hall effect in hopping region of Si and Ge attributed to residual thermal and impact ionization 06 p1067 A67-18966

Plasma instabilities in solids noting developments in moving domains, nonlinear effects, Gunn effect, turbulence, etc 06 p1070 A67-18986

Electromagnetic wave dispersion in semiconductor plasma waveguides for case of plane wave propagation normal to magnetic field vector 07 p1231 A67-19133

Plasmas of gas state and of solid state compared, considering density, temperature, and anisotropic mass, noting wave propagation electric discharges and confinement phenomena plasmas of gas state and of solid state 12 p1980 A67-25202

Microwave power coupling from waveguide to helicon mode in doped indium antimonide by placing aluminium oxide cones on semiconductor surface 12 p1986 A67-26160

Solid state technology limitation, discussing obsolescence within framework of digital application 13 p2183 A67-27561

Electron-phonon interaction calculation for solid state transition metals justifying matrix element presented and using augmented plane wave 16 p2731 A67-31447

Potential delta well model for barrier in solid state tunneling 19 p3308 A67-36039

Microwave delay-line techniques using YIG crystal, examining solid state dispersion characteristics 20 p3507 A67-36241

Book on electrical properties of semiconductor surfaces covering space charge layer theory, solid state theory, etc 21 p3682 A67-38365

Solid state and electron beam delay line features compared in optimal selection for radar system target simulation 23 p3982 A67-41503

Solid chemical state O for spacecraft

noting advantages over liquid and high pressure gas, discussing storage, handling, losses, shelf life, availability and containers 23 p3967 A67-41608

Ultrahigh molecular weight poly(ethylene terephthalate)/ synthesized, studying catalyst, particle size, reaction temperature and time and carrier gas flow rate 24 p4176 A67-42467

SOLID STATE DEVICE

SA DIFFERENTIAL AMPLIFIER

SA LASER

SA MASER

SA PARAMETRIC DIODE

SA SEMICONDUCTOR DEVICE

Solid state inductive element with magnetoresistance used for increase of Q 01 p0032 A67-10006

Diffusely transmitting integrating sphere with solid state photodiode used in laser output measurement 01 p0089 A67-10445

L-3 rocket observation of proton and electron fluxes at high altitudes, using solid state detectors 01 p0144 A67-10564

Induction heating contributions to solid state technology including zone refining and zone leveling, growth of metallic and nonmetallic single crystals, thin film production and epitaxial growth 01 p0080 A67-10972

Energy spectra and abundances of elements He through Si of galactic cosmic ray above 20 mev per nucleon in nuclear charge range between 2 and 26 02 p0307 A67-11687

Surface origin of LF noise power spectrum demonstrated via silicon MOS field effect structures 02 p0296 A67-11820

Solid state microwave telemetry transmitters, discussing power generation, stability, modulation /AM, PM and FM/, environmental effects and circuitry 02 p0216 A67-12008

Solid state high power LF and VLF telemetry transmitters, considering power amplifier design, RF output network, cooling systems, etc 02 p0218 A67-12106

40 watt solid state UHF AM transmitter at 225-400 mc 02 p0219 A67-12111

Isolation-diffusion of phosphorus in silicon with low surface concentration, with applicability to preparation of integrated solid state circuits 02 p0223 A67-12736

400-kev electrons precipitation in auroral zone measured with solid state detector mounted on polar satellite 03 p0410 A67-12952

Characteristics and performance of two solid state devices, using FM principle for measurements of low currents, suitable for space vehicles 03 p0377 A67-13107

Internal modulation and heterodyning in construction of highly linear large-deviation VHF solid state FM oscillator /FMO/ 03 p0381 A67-13636

Impedance matching conditions, gain nonlinearity and bistable mode instability in solid state parametric frequency converters 03 p0381 A67-13637

Acoustic propagation for solid state microwave delay line, discussing generation and propagation of phonon signals in passive media providing fixed delays 04 p0580 A67-14607

Pulsed radar transmitter research in U.K., noting beam type microwave tubes, solid state switches, hydrogen thyatrons, etc 04 p0581 A67-15052

Digital computer driven electroluminescent solid state vertical scale indicator design, development and fabrication emphasizing size, weight, power, reliability and display readability 05 p0805 A67-16310

Solid state diode matrix display using gallium phosphide light sources to investigate use as data recording device 05 p0771 A67-16313

Marconi AD370 solid state automatic direction finder 05 p0839 A67-16579

Rocket sounding of intensity distribution of proton and electron fluxes at high altitudes, noting secondary particle emission from radiation belt 05 p0883 A67-16880

Solid state pulse modulated 10 MHz/channel passband frequency switch design and reduction to microelectronic form 05 p0789 A67-17043

Analog/hybrid computer design, noting inclusion of solid state and integrated circuits for reliability cost reduction and speed 05 p0769 A67-17519

Thermal noise limitation in space-charge-

limited solid state diodes and triodes 06 p0971 A67-18224

Semiconductor heterojunctions noting preparation, properties, measurement and results 06 p1053 A67-18756

Balloon-borne sun seeker improvements through transistorized circuits and solid state switches 07 p1184 A67-19396

Temperature dependence of paramagnetic resonance spectral shifts in chromium-doped titanium oxide crystal of cross relaxation rutile maser 07 p1196 A67-19676

Transconductance limitation in FET devices obtained through changes in Shockley theory, noting behavior and design of solid state devices 08 p1300 A67-20335

Solid state microwave square law detectors, comparing threshold response for unit video bandwidth using Noise Equivalent Power /NEP/ concept 08 p1304 A67-21220

Thermal noise in space-charge-limited solid state diodes, showing equivalence of noise resistance with DC resistance 09 p1472 A67-21951

Short aging test results on GaAs diodes, noting surface changes and dependence of nonradiative excess current component on device perimeter 09 p1472 A67-21952

Controlled nonreciprocal microwave device using Faraday rotation in solid state plasma 09 p1474 A67-22090

Mosaic of photosensors for solid state imaging, discussing electro-optical conversion, structure and characteristics 09 p1476 A67-22209

Microwave and optical generation and amplification - International Conference, Cambridge, England, September 1966 09 p1476 A67-22251

Solution regrowth technology of electroluminescent devices noting reduced threshold current densities, external quantum efficiency and adaptation to planar technology 10 p1665 A67-23518

Rise time in solid state detectors, considering equivalent circuit, plasma, time, etc 11 p1789 A67-24103

Telemetry transmitters using solid state wideband microwave voltage-controlled oscillators 11 p1753 A67-24442

Ionizing radiation in space, discussing detection techniques, devices, etc 11 p1791 A67-24619

Equation for solid state differential amplifier-circuit configuration effect on overall system accuracy and performance 11 p1768 A67-24823

High input impedance obtained with junction transistors, discussing circuit design for different frequency modulators, FET properties and applications 13 p2077 A67-26661

Solid state semiconductor microwave power generator design, analyzing spurious oscillations rejection problem 13 p2081 A67-27204

Two-stage parametric amplifier system cooled to 20 degrees K, as low noise amplifier in receiving equipment for satellite communication 14 p2278 A67-27780

Constant temperature hot-wire anemometer circuit using solid state amplifiers, obtaining frequency response expression 14 p2315 A67-28159

RF hardware implementation techniques utilizing devices illustrated in block diagrams 14 p2287 A67-28680

Performance of electron tube and solid state devices in microwave region, comparing low noise amplifier devices 14 p2289 A67-28913

Equivalent circuit model for solid state junction devices with single energy level defect centers including transient properties 15 p2456 A67-29170

Gunn effect as only solid state effect capable of producing high output power in microwave range in pulsed and continuous operation, noting physical nature 15 p2536 A67-29530

Processes influencing radiative decay in compound semiconductors 15 p2536 A67-29634

Book on large signal transistor circuits covering device physics and equivalent circuits 15 p2454 A67-30233

Solid state microwave delay lines noting advantages, operation principles, fixed variable construction, etc 16 p2637 A67-31196

GaAs injection lamp efficiency correlated with presence of trapping levels, noting experimental technique and

results 17 p2911 A67-32192

Solid state switching applied to aircraft electric systems noting design, performance and contactless switching concept 17 p2825 A67-32513

Solid state protection and control device characteristics noting thermal, thermal magnetic and magnetic circuit breakers for circuit protection 17 p2825 A67-32514

Altimeter using pulse repetition frequency /PRF/ tracking design with solid state X-band frequency source 17 p2859 A67-32522

Superheterodyne receiver operating in K-band having solid state low noise characteristics 18 p3011 A67-34068

Microelectronics technology extended microwave frequencies, considering development of solid state devices and ICs 18 p3015 A67-34582

Solid state microwave device technology concerning generators, low noise and control devices, discussing computerized technique for circuit analysis and design 18 p3015 A67-34595

Solid state pulsed carrier IF-AGC system design for microwave receivers noting input network, video circuit, AGC loop gain, etc 18 p3016 A67-34597

Electrical characteristics of degenerate n-type germanium diode with gold or indium as metallic element 18 p3105 A67-34635

Circuit theory - Conference, Purdue University, May 1967 19 p3200 A67-34838

Flowgraph models of thermal and electrical parameters interaction in solid state devices, examining performance characteristics, system stability, etc 19 p3191 A67-34845

Techniques for achieving contaminant-free sealed package of solid state active devices 19 p3236 A67-35024

Lunar exploration by nuclear experiment, discussing instrument specifications for neutron gamma measurements 19 p3229 A67-35318

MOS and silicon transistors for design of logarithmic amplifiers for space instrumentation 19 p3194 A67-35463

Book on electronic sensing devices covering physical-chemical-electronic effects in solids, liquids, gases, etc 19 p3230 A67-35533

C-band solid state YIG serrodyne theory and operation, outlining phase velocity modulation of magnetostatic modes 19 p3196 A67-35661

Solid state devices operational characteristics from applications in transmission technology 20 p3394 A67-36242

Analog and digital long range automatic radar tracking systems design characteristics and implementation by solid state components 20 p3379 A67-36244

Satellite system with solid state transmitters with different frequencies in HF band for ionospheric guided propagation research 20 p3394 A67-36246

Design and characteristics of solid state UHF transmitters and receivers applicable in color TV systems 20 p3395 A67-36249

Bandwidths of reflex multicavity solid state masers containing active material in cavities 20 p3462 A67-37328

Design and operation of three-cavity solid state ruby maser 20 p3462 A67-37329

Field effect devices noting insulated gate transistor, thin single crystal silicon film deposition on sapphire single crystal, etc 21 p3590 A67-38064

Ionospheric ion and electron densities by Langmuir probes, stressing solid state logarithmic amplifier for spatial electrometry 21 p3592 A67-38223

Distributed Esaki diode pulse characteristics in solid state transmission circuit 21 p3599 A67-38609

Cathodoluminescence device for rapid identification of phase assemblages in solid state reaction system magnesium oxide/magnesium silicate 21 p3630 A67-38845

Solid state photosensitive devices combining p-n diodes and MOS circuitry noting application in electrical readout, image and pattern detection 22 p3796 A67-39332

Microminiaturization problems associated with design and preparation of solid state Si microdiode matrices 22 p3769 A67-39580

LF solid state equipment improves mission reliability through use of integrated

molecular circuit and modular redundancy 22 p3771 A67-39840
Solid state linear digital amplifier with external modulation using high operating efficiency of transistors as saturated switching elements 22 p3771 A67-39841
Distributed power generation for radar and communications covering cost comparisons, antenna subsystems and reliability of solid state devices 22 p3761 A67-39861
Solid state multilayer circuits preparation for use in microminiaturization, stressing advantages over printed circuits 22 p3774 A67-40327
Power systems for long duration missions including photovoltaic solar energy, thermoelectric, Brayton cycle and thermionic conversion systems, discussing solid state components 22 p3749 A67-40339
Cylindrical solid state oxygen generators, discussing manual and remote electrical activation 23 p3968 A67-41621
Solid state electrochemical solar cell using various anode metals and charge transfer complexes as cathodes, noting I-V characteristics and discharge curves - [JPL-TR-32-1116] 24 p4097 A67-41804

SOLID STATE LASER
Generating mode number in solid state lasers using traveling wave and standing wave 01 p0086 A67-10069
Intense pulse generation at 5300 angstroms by frequency doubling in Q-switched and glass laser and possibility of generating particular harmonics 01 p0090 A67-10759
Radiation of giant pulses of superluminescence by highly excited active medium of Nd glass with rapid cut-in of amplification 01 p0091 A67-10837
Possible oscillation modes in cylindrical solid state laser and dependence of pumping threshold, output power and divergence angle on resonator length 03 p0435 A67-13129
Emission losses in solid state laser resonator calculated for Nd glass laser 03 p0435 A67-13133
Mode characteristics of solid state lasers from analytical solution of conservative equation 03 p0437 A67-13208
Phase and amplitude fluctuation of gas and solid state lasers, accounting for noise caused by pumping, incoherent decay, lattice vibrations and atomic collisions 04 p0632 A67-14949
Neodymium-glass laser using spontaneous amplified emission in nonresonant system to obtain high brightness output pulse 04 p0633 A67-15100
Fission or radioisotopic nuclear radiation applied to laser pumping, discussing forms, sources, power, solid state and molecular gas lasers, energy transfer, optical fluorescence and cut-off phenomenon 05 p0814 A67-16547
Neodymium doped optical glasses for laser technology 05 p0824 A67-16855
Ruby and neodymium glass lasers sum frequency generation using nonlinear electro-optical KDP crystal 06 p1009 A67-17754
Neodymium glass laser time characteristics and spectral changes during conversion to traveling wave laser 06 p1012 A67-18782
Neodymium glass laser with spherical mirror resonator in stationary regime 06 p1012 A67-18783
RCA papers on laser research and engineering 07 p1193 A67-19079
YAG solid state laser system, discussing output, theoretical limits, performance characteristics, etc 07 p1194 A67-19084
Steady state laser design, comparing balance method with method based on quasi-classical theory 07 p1197 A67-20245
Radiation noise effect on laser optical properties, noting density vs resonator characteristics, energy spectrum, etc 08 p1337 A67-20839
Generating mode number in solid state lasers using traveling wave and standing wave 08 p1339 A67-21452
Injection luminescence and photoluminescence spectra of epitaxial heterojunctions in GaP-GaAs system 09 p1554 A67-21975
Universal rotating mirrors for Q-switching neodymium glass laser 09 p1514 A67-22171
Laser mode selection by internal reflection prisms 10 p1662 A67-22742
Hazards of laser radiation, mechanisms, control and management 10 p1601 A67-23328

Coupling of laser optical modes by intracavity time varying perturbation 13 p2125 A67-26407
Light-emitting semiconductors and solid state lasers using various electron-exciting mechanisms 13 p2176 A67-26810
CW solid state lasers, considering principal laser crystals 14 p2330 A67-28470
Solid state lasers and pulsed ruby lasers for continuous and quasi-continuous operation, noting applications in micromachining 14 p2331 A67-28559
Retinal photocoagulation using solid state laser 14 p2333 A67-28973
Normal modes for solid state laser noting linear and elliptic polarization, resonant frequency and reflection loss 15 p2497 A67-29388
Mixed crystals with fluoride base, investigating spectrum and time behavior of laser emission for operation below room temperature 16 p2725 A67-30809
Absorption, fluorescence and laser emission spectra of triply ionized neodymium yttrium in compound below room temperature 16 p2726 A67-30810
Periodic relaxation pulses caused by thermal resonance drift, studying diffraction loss and other effects on transverse modes in crystal lasers 17 p2867 A67-32362
Laser research and development in France and applications to holography, metrology and gyros 17 p2868 A67-32745
Injection luminescence and photoluminescence spectra of epitaxial heterojunctions in GaP-GaAs system 17 p2923 A67-33312
Temperature gradient in steady state thermally operated solid state lasers, calculating end face curvatures and light paths for resonator mode correction 18 p3059 A67-33714
Neodymium glass laser time characteristics and spectral changes during conversion to traveling wave laser 18 p3059 A67-33724
Neodymium glass laser with spherical mirror resonator in stationary regime 18 p3059 A67-33725
Emission equations describing radiation field amplitude and energy level populations of solid state laser with broad oscillation spectrum 18 p3061 A67-34388
Spectral characteristics of solid state laser with large angular divergence of light, showing contribution from degenerate modes 19 p3239 A67-34903
Two-channel single-pulse neodymium glass laser with 180 joule pulse, performance and optical features 19 p3239 A67-34986
Models explaining long time delay between current-pulse application and generation of coherent oscillations in gallium arsenide junction lasers near room temperature 19 p3241 A67-36036
Neodymium doped calcium tungstate single crystals synthesized, obtaining continuous laser action 20 p3458 A67-36494
Transverse-mode distribution of emission intensity of solid state laser with plane mirrors 20 p3459 A67-36688
Solid state laser theory and technology, describing media, pumping sources, illuminators, component elements, etc 20 p3462 A67-37547
Delay time of quenching response and recovery in gallium arsenide injection laser 21 p3640 A67-38261
Angular divergence of solid state laser radiation for case of variable resonator and pump parameters 21 p3640 A67-38367
Spectroscopic investigations of emission under free generation and Q-switching conditions of mixed-fluoride crystal lasers 21 p3682 A67-38370
Neodymium-glass laser amplifier gain saturation investigation using laser driving signal, discussing Schulz-DuBois steady state theory and inversion 22 p3813 A67-39349
Solid state laser with mode selection within active medium ensures beam collimation in one plane, noting use in second-harmonic generation and parametric frequency conversion 22 p3814 A67-39458
Ruby and neodymium-glass lasers light emission mixing, noting created wave frequency is sum of two initial wave frequencies 22 p3815 A67-39765
IR laser rangefinder using neodymium doped rods, noting noise peak value and

advantages over ruby laser 22 p3799 A67-39780
Lasers as light source in optical telemetry, discussing laser radiation, solid state and gas lasers and critical parameters 22 p3800 A67-39981
IR Q-switched neodymium glass laser rangefinder performance and advantages 23 p3999 A67-41029
Efficiency of optical system of solid state laser with cathode luminescence pumping 24 p4169 A67-42892

SOLID STATE PHYSICS
SA HOLE MOBILITY
Spontaneous and induced coherent radiation from indium antimonide electron-hole plasma 01 p0087 A67-10088
Shallow impurity states in semiconductor described by Green function method, considering effective-mass equation corrections 02 p0281 A67-11491
Josephson tunnel effect in semiconductors 05 p0860 A67-16360
Semiconductor physics - Conference, Kyoto, September 1966 06 p1054 A67-18901
Book on organic semiconductors emphasizing physical methods, organic chemicals and solid state theory 08 p1372 A67-21506
Solid state physics - Conference, Kiev, June 1965 09 p1580 A67-21903
Paramagnetic Knight shift in metals and semiconductors as affected by temperature and magnetic and electric field intensity 09 p1554 A67-21972
Recombination through exciton states in semiconductors compared to interband radiative recombination 09 p1554 A67-21974
Solid state material analysis inducing controlled density variations and crystal structure changes via high pressure techniques 11 p1846 A67-24618
Interband magneto-optical phenomena involving linear single photon absorption and dispersion in semiconductors and semimetals 11 p1847 A67-24662
Spatial distribution of radiation damage in solids determined by spectral analysis of photovoltaic current of photovoltaic cell 16 p2726 A67-30815
Superconducting transitions of three metastable states of Ga 17 p2915 A67-32707
Paramagnetic Knight shift in metals and semiconductors as affected by temperature and magnetic and electric field intensity 17 p2923 A67-33309
Recombination through exciton states in semiconductors compared to interband radiative recombination 17 p2923 A67-33311
Schottky approximate formula adaptation for abrupt junctions with asymmetric doping ratios 18 p3106 A67-34646
Red luminescent band and photoconductivity in cadmium sulfide single crystal, discussing IR quenching of photocurrent 19 p3300 A67-34764
Stationary moving domains in hot electron semiconductors, obtaining criteria for soft and hard regimes of domain excitation 20 p3506 A67-36222
Physical electronics formulas tabulated, with solid state physics variables dimensionally coded and resultant nondimensional products cataloged, using computer routine 20 p3506 A67-36235
Dynamic response of nondegenerate electron hole plasma in semiconductor, obtaining frequency spectrum and Landau damping rate of plasma oscillation 20 p3499 A67-36945
Book on transistor electrical characteristics, discussing transistor model correspondence with real transistors, temperature variation effects, etc 20 p3399 A67-37010
Surface superconductivity of cylindrical niobium samples, discussing microscopic surface roughness and approximate character of theory 21 p3685 A67-38802
Liquid metal properties - Conference, Upton, New York, September 1966, Part 2 21 p3686 A67-39103
Soviet book on semiconductor electrochemistry covering space charge layer structure, semiconductor corrosion, etc 22 p3856 A67-39413
Physics of superconducting devices - Conference, University of Virginia, April 1967 22 p3864 A67-40430
Dynamical processes in solid state optics - Conference, Oslo, Japan, August-September

- 1966, Part 1 23 p4037 A67-40756
 FORTRAN program for B number
 computation applied to solid state
 physics 23 p3977 A67-41458
 Phonon annihilation during decay of two
 metastable fluorescent states of ionized Ba
 compound 24 p4205 A67-42737

SOLID SURFACE

- Quasi-stationary heat transfer equations
 and maximum possible heat-transfer
 coefficient for solid surface moving in very
 fluid rotating boiling medium 06 p1118 A67-18549
 Physical and hydrodynamic processes
 induced in vaporizable solids by pulsed light
 radiation from sources using explosives
 11 p1782 A67-24955
 Collapse of isolated spherical vapor-air
 cavitation pocket moving toward solid
 surface in incompressible fluid medium
 12 p1927 A67-25320
 Gas flow at high speed out of solid or
 liquid surface accompanied by heat transfer
 investigated for boundary shock wave
 occurrence 14 p2296 A67-27906
 Thermal slip rate of gas near solid surface
 determined by measuring gas-flow
 distribution function according to Bhatnagar,
 Gross and Krook 15 p2582 A67-30390
 Flapped finite-span wing lift, center-of-
 pressure and hinge moment moving near
 solid wall determined as functions of flap
 length, rotation angle, etc 17 p2792 A67-32902
 Heat transfer between gas flows and solid
 /carbon/ surfaces, considering chemical
 reactions 24 p4252 A67-41935

SOLID SUSPENSION

SA COLLOID

- Suspension axes defects effect on gyro
 motion under base angular vibration
 analyzed, noting large gyro
 drift 14 p2320 A67-28741
 Motion of small solid particles suspended
 in steady isotropic and locally uniform
 turbulent gas flow 18 p3025 A67-33626
 Gas-borne suspensions of thermionically
 emitting particles as MHD working
 fluids 18 p3086 A67-33707
 Shock tube experiments conducted on
 mixtures of fine solid particles and
 gases 20 p3414 A67-36516
 Preformed micron and submicron-sized
 solid particles for colloidal propulsion,
 investigating particle feeding and charging
 [AIAA PAPER 67-727] 21 p3688 A67-38751
 Steady flow extremum principles for
 incompressible viscous fluid generalized to
 liquid flow containing suspended solid
 bodies and drops of another
 liquid 24 p4144 A67-42567

SOLIDIFICATION

- Controlled solidification in casting, ingot-
 making and other processes including
 composites and highly undercooled
 melts 03 p0442 A67-13305
 Unidirectional solidification of eutectics
 for production of composite materials,
 avoiding problems with whiskers, interfacial
 bonding, matrix distribution,
 etc 03 p0444 A67-13435
 Directional solidification and single-crystal
 casting for jet engine turbine
 blades 03 p0429 A67-13541
 Crystal growth, nucleation, supercooling,
 solidification, glass forming and kinetics of
 1, 3, 5-tri-alpha-naphthylbenzene
 17 p2809 A67-33255
 Fiber orientation and morphology effect
 on anisotropic tensile behavior of Al-Ni
 whisker reinforced aluminum, studying
 solidification rate, etc 18 p3067 A67-34569
 Plasma furnace for treating refractory
 products at high temperature to determine
 various oxides solidification
 temperature 19 p3299 A67-35900
 Refractory oxides solidification points
 measurement using optical-pyrometer
 method 20 p3472 A67-38118
 Unidirectionally solidified eutectic alloys
 noting materials preparations for
 thermoelectric, magnetic, optical and
 electronic applications 20 p3469 A67-37359
 Unidirectional solidification of cast nickel-
 base superalloys, effect on creep behavior,
 stress-rupture properties and thermal shock
 resistance 20 p3469 A67-37383

SOLIDS

SA INFINITE SOLID

- Finite-amplitudinal plane wave propagation
 in elastic solids 02 p0336 A67-11792

- Mechanical properties of high polymer
 solid in terms of microbehavior as result of
 deformation and orientation, expressing
 anisotropic relaxation function as time
 dependent function 02 p0297 A67-11873
 Materials for ablative cooling processes for
 rocket engines, noting structure and
 properties of porous and solid
 materials 02 p0306 A67-12791
 Plastic behavior of simple solids in terms
 of atomistic processes, emphasizing high
 strength and ductility 03 p0442 A67-13303
 Elastic modulus, Youngs modulus and
 Poisson ratio for solids containing foreign
 inclusions imbedded in matrix
 03 p0524 A67-13785
 Finite deformations of elastic oriented
 solid with Cosserat trihedrons taken as
 initial schema 03 p0526 A67-13971
 Mean surface temperature-time solution of
 heat absorbed by semifinite solids
 [ASME PAPER 66-WA/HT-58]
 04 p0725 A67-15437

- Stresses in solids moving during loading,
 using velocity vector and strain rate tensor
 as variables for instantaneous state of body
 motion 05 p0914 A67-16194

- Temperature distribution effect on
 roughness of contacting surfaces of two
 juxtaposed solid materials 05 p0926 A67-16596
 Mathematical studies of mechanics of
 solids in Rumania, noting use of matrices,
 Fourier expansions, stresses, shock waves,
 etc 05 p0920 A67-16797

- Closed form solution methods for blast
 wave propagation in solid media assuming
 power law density profile
 [AIAA PAPER 67-141] 06 p1102 A67-18290

- Optimum control of motion stability of
 solid body with fixed point, using
 gyro stabilizer rotors 06 p1034 A67-18617
 Liapunov function for motion stability of
 solid body on earth surface having fixed
 point and internal gyro 06 p1004 A67-18619
 Qualitative and quantitative descriptions
 of penetration of solids by high power
 density electron beams in welding,
 calculating penetration vs welding velocity
 and current curves 06 p1008 A67-18696

- Diathermy, derivation of equation relating
 monochromatic/integral radiation energy
 ratio of solid material of fluid heat emitter
 to temperature 07 p1211 A67-19130

- Propagation mode of one-dimensional HF
 finite acceleration pulses in nonlinear
 viscoelastic solids, stressing shock formation
 and propagation 09 p1573 A67-21547

- Solid body translational movement in
 viscous incompressible conductive flow in
 magnetic field solved for case of zero
 magnetic Reynolds
 number 11 p1832 A67-24055

- Crystalline solids deformation
 Conference, Ottawa, August 1966, Part
 1 11 p1806 A67-24566

- Asymptotic solutions for free and forced
 oscillations of solid having cavity filled with
 viscous fluid, considering several degrees of
 freedom and arbitrary cavity
 shapes 12 p2029 A67-25657

- Integral equations for radiative heat
 transfer inside solid whose solution leads to
 temperature-distance profile integral
 equations solution for radiative heat transfer
 inside solid leads to temperature.
 [AIAA PAPER 67-287] 12 p2035 A67-26004

- Far IR electronic transitions in pure and
 doped solids 13 p2178 A67-27085

- Book on chemical bond in semiconductors
 and solids, evaluating strength and
 determining effect on properties of
 substances 13 p2182 A67-27486

- Analytic properties of finite-band models
 in solids as generalization of Kohn
 procedure 15 p2534 A67-29324

- Interaction of radiation with solids -
 Conference, American University at Cairo,
 September 1966 17 p2913 A67-32371

- Unsteady heat transfer between solid body
 and surrounding fluid flow, using convective
 fluid heat transfer and body
 thermoconductivity
 equations 17 p2972 A67-33071

- Pauling empirical equation relating
 thermal effect of reaction to negative
 ionization potential of solid
 substances 18 p3094 A67-33438

- Transient heat conduction in
 inhomogeneous solids with periodic
 temperature boundary conditions, using
 Keller perturbation

- method 18 p3159 A67-34007
 Hertzian fracture of brittle solid under
 spherical indenter, discussing path and
 stability crack in nonuniformly directed
 stress field 18 p3144 A67-34274
 Inertial motion of solid body in space of
 constant curvature, obtaining solution to
 differential equation 18 p3079 A67-34372
 Linear equation for micropolar elastic
 solids deformation, including radial
 displacements with axial and radial
 symmetries 20 p3540 A67-37021
 Parameters for motion of flight vehicle as
 solid body and for elastic
 deformations 20 p3482 A67-37381
 Temperature distributions and heat
 generation in viscoelastic isotropic solid
 resulting from mechanical deformations
 determined by energy
 equation 21 p3715 A67-37894
 Book on plasticity theory and application
 to solidity, discussing inelastic deformation,
 crystal physics, atomic grid structure
 mechanics, etc 21 p3716 A67-37966
 Radiative and convective heat transfer
 between solid body and heat generating
 medium in motion, calculating thermal
 conductivity 23 p4083 A67-41289

SOLUBILITY

- Solubility of carbon in Mo, Re and W
 determined by isothermal carburization
 method 03 p0439 A67-12845

- Solubility limit of Fe in close-packed
 hexagonal alpha-Ti noting temperature
 dependence and
 superconductivity 06 p1051 A67-18370

- Limited mutual solubility of gases above
 critical point of least volatile
 component 06 p1116 A67-18381

- Oxygen solubility in fused carbonates and
 corrosion behavior of Ag and Cu oxide, air
 and carbon dioxide cathodes in molten
 carbonate fuel cells 09 p1458 A67-22182

- Diffusion, solubility and electrical behavior
 of lithium in gallium
 antimonide 16 p2726 A67-30811

- Solubility of impurities in semiconductors
 and mechanism for deviation from
 stoichiometry 18 p3096 A67-33449

- Layer removal techniques with Hall effect
 and sheet resistivity measurements indicate
 carrier concentrations exceeding thermal
 equilibrium solubility for antimony implants
 into silicon 20 p3510 A67-36856

- Chromium oxide addition effect on ruby
 recrystallization in carbonate and
 bicarbonate solutions under hydrothermal
 conditions, estimating chromic oxide
 solubility 21 p3685 A67-38971

- Na and K introduced into Si by diffusion
 from thin layer of alkali metal and during
 electrolysis of molten alkali
 halogenides 23 p4037 A67-40721

- Solubility of niobium carbide in gamma
 iron determined from experiments using Fe-
 Nb alloy in equilibrium with hydrogen-
 methane mixtures 24 p4173 A67-42348

SOLUTION

SA ITERATIVE SOLUTION

SA POHLHAUSEN SOLUTION

SA PROBLEM SOLVING

SA SOLID SOLUTION

- Short and long range redistribution of
 solute in weld fusion zones of alloy systems
 through data from electron microprobe
 analyses 05 p0811 A67-16830

- Transmission decrease of various aqueous
 solutions under ruby laser
 irradiation 19 p3240 A67-35420

SOLUTION HEAT

SA SPECIFIC HEAT

- Heats of solution and formation of Ti-Al
 alloys in region of alpha-solid solution
 determined, using
 calorimetry 07 p1204 A67-19268

SOLVENT

- Pumping of organic dyes in organic
 solvents, using pulsed ruby
 laser 02 p0253 A67-12515

SOMMERFELD APPROXIMATION

- Sommerfeld effect in linear oscillating
 system with randomly variable natural
 frequency 07 p1261 A67-19140

- Sommerfeld effect in linear oscillating
 system with randomly variable natural
 frequency 17 p2965 A67-33217

- Rayleigh-Sommerfeld diffraction formula
 to obtain imaging behavior of Gabor type
 holograms of transparencies for
 reconstructed wave forms with large
 diffraction angles 22 p3835 A67-39241

SONAR

Book on modulation, resolution and signal processing in radar, sonar and related systems 03 p0372 A67-14233

SONDE

S RADIOSONDE

SONIC ANEMOMETER

Power spectra and dissipation rate for vertical velocity fluctuations measured with sonic anemometers 19 p3251 A67-35056

SONIC BOOM

Near field and far field sonic boom signature of supersonic transport, noting structural response 03 p0360 A67-13921

Sonic boom decay and aural response in relation to SST configuration constraints and flight performance characteristics [AIAA PAPER 66-941] 03 p0361 A67-14139

SST sonic boom acceptance by public and problems of control 04 p0551 A67-14623

Property damage caused by sonic booms, discussing recovery of damages under Federal Tort Claims Act 05 p0930 A67-16772

Potential damage to structural elements caused by sonic booms determined by considering effect of gap between beam and supports [AIAA PAPER 67-14] 06 p1101 A67-18253

Methods to minimize sonic boom ground exposure, considering aircraft design and maneuverability as function of altitude 09 p1439 A67-21942

Sonic boom measurements for supersonic aircraft, discussing techniques and results 09 p1440 A67-22457

Cabin noise in aircraft, discussing measurement techniques for sonic boom, shock wave intensity, etc 09 p1440 A67-22467

Lower bounds for sonic boom intensity from slender aircraft flying straight and level at supersonic speeds 10 p1594 A67-23470

Near field and far field sonic boom signature of supersonic transport, noting structural response 11 p1743 A67-24038

Sonic booms attributed to subsonic flight 12 p1895 A67-25936

Wind tunnel tests of sonic boom phenomena, noting weak pressure field measurement, construction of extremely small models, boundary layer effects, etc [AIAA PAPER 66-765] 13 p2091 A67-27594

Far field pressure spectrum of sonic boom 13 p2055 A67-27703

Sonic boom effect on structural behavior 15 p2573 A67-29401

Meteorological conditions, acoustic phenomena and fireballs associated with meteorite fall at Barwell, England 15 p2562 A67-30083

Supersonic boom, discussing aerodynamic field of aircraft, sonic ray characteristics and noise suppression 16 p2589 A67-30832

Subjective evaluation of relative annoyance of sonic booms, explosions and jet aircraft noise 18 p2986 A67-34393

Sonic boom and subsonic aircraft noise test results 21 p3569 A67-39118

Concorde SST economics noting short/medium haul characteristics, flight times, sonic boom problems, load factor, etc 22 p3744 A67-39339

Sonic boom and factors influencing shock wave propagation during straight horizontal supersonic flight 22 p3744 A67-39547

Future improvements in aeronautical field covering noise control, centralization, TV communication, ultimate speed, sonic boom and nuclear cargo aircraft 22 p3746 A67-39846

Boeing SST competition, cost, operation, design, airport noise and sonic boom 22 p3746 A67-39882

Steady state vertical displacements at surface of elastic half-space due to Rayleigh waves from sonic boom, obtaining shock amplification factors 23 p4074 A67-40632

SONIC FLOW

Electron-piezoelectric interaction giving rise to currents responsible for acoustoelectric effects, gain and nonlinear mixing 06 p1050 A67-18140

Compressibility factors of gases determined by using sonic velocity measurements, providing reliable representations of equations of state 07 p1168 A67-19577

Axisymmetric vortex flow in neighborhood of point having sonic line orthogonal to velocity vector 10 p1624 A67-23034

Linearized theory for unsteady flow about bodies of revolution in sonic stream 16 p2589 A67-30790

stream 16 p2589 A67-30790

SONIC NOZZLE

Rocket nozzle effect on acoustic losses from model motor chambers oscillating in first longitudinal mode 15 p2546 A67-29992

SONIC SPEED

SA SUBSONIC SPEED

MHD flow past sonic velocity in channel of constant cross section, discussing conditions for smooth acceleration 13 p2169 A67-27309

Position determination of sonic points on head shock wave and blunt body surface in ballistics showing Mach number and gas type effects 16 p2593 A67-31132

Thermodynamic characteristics and plasma parameters of lithium vapor in wide pressure and high temperature range 16 p2721 A67-31389

Rotary wing decelerator for sonic and supersonic operation, noting components and potential application areas 17 p2796 A67-32517

SONOGRAM METHOD

Sonoholograms, techniques and information content 04 p0625 A67-15678

Polarizations of Pc 1 micropulsations intermittently recorded in Alaska with analysis of data for presence of right and left hand waves 22 p3793 A67-40078

SORPTION

SA ABSORPTION

SA ADSORPTION

SA CHEMISORPTION

SA CRYOSORPTION

SA DESORPTION

Sorption process for determining sticking probability of molecules on surface of sorbents, diffusion coefficient of molecules through sorbents and adsorption isotherms 09 p1533 A67-22115

SOUND

S ACOUSTICS

S UNDERWATER SOUND

SOUND AMPLIFICATION

Resonance amplification of associated slightly attenuating electromagnetic and acoustic helicon waves by electron drift in semiconductors and semimetals 01 p0128 A67-10081

HF conductivity, dispersion and temperature modulation of carrier waves and acoustic amplification in drifted semiconductor plasmas 03 p0496 A67-13558

Resonance amplification of associated slightly attenuating electromagnetic and acoustic helicon waves by electron drift in semiconductors and semimetals 08 p1371 A67-21458

Acoustic vibrations during solid-fuel combustion, studying acoustic energy increase rate and development 20 p3551 A67-36817

Negative differential conductivity in semiconductor in acoustic instability mode and connection with sound amplification and number of electron traps 21 p3678 A67-38097

Negative differential conductivity in viscous semiconductor with stationary sound wave propagating under sound amplification conditions 21 p3681 A67-38352

SOUND DETECTOR

High intensity acoustic test facility for electronic packages and structures 12 p1924 A67-25718

Rocket engine noise study in infrasonic range from launching pad ignition phase through flight phase, including ignition signals from upper stages 14 p2393 A67-28053

SOUND FIELD

Inertia and pressure effects on energy potential of homogeneous and isotropic turbulence in weakly compressible medium 02 p0235 A67-12643

Sound field of vibrating circular plates and membranes 05 p0924 A67-17283

Hydrodynamic drawing together problem for aerosol particles oscillating in sonic field at small Reynolds numbers, showing optimal field frequency-approach velocity correspondence 10 p1627 A67-23643

Combustion of liquid fuel droplet in sound field, noting rate dependence on sound parameters 15 p2580 A67-29778

Behavior of high speed, coherent, turbulent liquid jet in planar, standing, transverse acoustic field 16 p2658 A67-30945

Laminar flow with forced convection heat transfer in parallel plate channel under influence of intense, longitudinal, resonant acoustic field 16 p2778 A67-30947

Hydrodynamic drawing together problem for aerosol particles oscillating in sonic field at small Reynolds numbers, showing optimal field frequency-approach velocity correspondence 18 p3029 A67-34412

Surface pressure spatial correlation function for rigid infinitely long cylinder in three-dimensional diffuse sound field 20 p3537 A67-36646

SOUND INTENSITY

SA NOISE INTENSITY

Aircraft noise measurement evaluation and control, discussing monitoring and mapping 04 p0551 A67-14591

Human response to comparative sounds from aircraft and objective measurement of reference sound, determining acceptable noise levels 09 p1456 A67-21940

Acoustic problems from SST and multimillion pound thrust launch vehicles studied at Eastern Test Range, using Launch Acoustics Measuring System /LAMS/ 20 p3415 A67-36593

Noise measurement and instrumentation used 21 p3630 A67-38900

Sound and white noise effects on turbulent jet aerodynamic characteristics studied at several Reynolds numbers 22 p3785 A67-40019

Design and operation of loudness level meter /8051A/ which uses analog switching circuits 22 p3810 A67-40561

SOUND MEASUREMENT

Cylindrical resonator for high precision measurements of sound absorption in oxygen 01 p0067 A67-10838

Sonic analysis for determining performance and mechanical integrity of turbine engines by using phase-locked filter and frequency ratio generator 01 p0076 A67-11141

Low accuracy of interferometric measurement of coefficient of ultrasound absorption in gas 06 p1004 A67-18395

Ultrasonic thermometry in solids and gases at elevated temperatures 18 p3051 A67-34509

Nonlinear resistance of multiple resonator arrays at incident sound high pressure levels 19 p3311 A67-34963

Sonic boom and factors influencing shock wave propagation during straight horizontal supersonic flight 22 p3744 A67-39547

Design and operation of loudness level meter /8051A/ which uses analog switching circuits 22 p3810 A67-40561

SOUND PROPAGATION

Energy relation for acoustic propagation modes in hot electron plasma considered in application of Helmholtz theorem 01 p0123 A67-10441

Boundary value problem solution for sound generated at oscillating wall, propagating into half-space, for linear Boltzmann equation with general cut-off molecular potential 01 p0114 A67-10736

Sound propagation in streaming air within tubes having changes of cross section and flow losses, discussing reflection coefficient dependence on flow velocity 01 p0114 A67-10819

Thermal radiation effect on sound propagation in gases treated on basis of relaxation of molecular degrees of freedom 01 p0114 A67-10840

Two sound-absorption maxima in liquid nitrogen tetroxide resulting from relaxation of dissociation equilibrium 01 p0019 A67-10841

Attenuation and dispersion of sound in nearly collisionless gases as function of sound-to-particle path ratio 02 p0235 A67-12565

Acoustic propagation for solid state microwave delay line, discussing generation and propagation of phonon signals in passive media providing fixed delays 04 p0580 A67-14607

Sonic boom measurements for supersonic aircraft, discussing techniques and results 09 p1440 A67-22457

Sound propagation in partially ionized plasma, noting kinetic quadrature calculation results 10 p1683 A67-22783

Book on ultrasonic wave absorption and dispersion in gases, liquids and solids, discussing physical mechanisms involved in sound absorption 12 p1967 A67-26157

Sound propagation in dilute monatomic gas confined in box and in unconfined rarefied monatomic gas assuming unidirectional

perturbation of velocity distribution 13 p2100 A67-26955

Steady state forced sound propagation in semiminfinite gas induced by oscillating plane piston reflecting particles with Maxwellian distribution 13 p2100 A67-26957

Method for analyzing single and double thermal relaxation processes 15 p2580 A67-29771

Sofar bomb signature identification by separation of desired signal from multipath signals with digital computer 20 p3484 A67-36558

Negative differential conductivity in viscous semiconductor with stationary sound wave propagating under sound amplification conditions 21 p3681 A67-38352

Dispersion relations for elastic wave propagation in lamellar composite materials obtained with averaged elastic constants 21 p3729 A67-39056

Propagation anomalies of atmospheric acoustic signals of nuclear explosions due to nonlinearities and refraction effects 22 p3790 A67-39645

Infrasonic wave anisotropic radiation from moving auroras analyzed using shock wave model, discussing sound propagation and ray tracing 24 p4147 A67-41882

Sound propagation in partially ionized plasma, noting kinetic coefficients and quadrature calculation results 24 p4195 A67-42119

SOUND RANGING

Sound-ranging technique for locating supersonic missiles 05 p0766 A67-17282

SOUND TRANSMISSION

Transmission of random sound and vibration through double wall analyzed by general method applicable to acoustics and thermodynamics 03 p0468 A67-13214

Acoustic waveform procession to auditory centers of brain, discussing transformations used by animals 09 p1454 A67-21686

Optimal wave path parameters determined by experimentally recorded pulsed signals processing, using least squares method 21 p3580 A67-38120

SOUND VELOCITY

Approximate calculation of speed of sound in plasma when enthalpy, density and pressures are known 02 p0276 A67-12567

Hugoniot equation of state of alkali metals, using technique based on isentropic sound speed measurement at room temperature 06 p1032 A67-18141

Deformation of surface of removable wave front discontinuity in acoustically anisotropic medium with variable sound velocity 06 p1032 A67-18396

Hypersound propagation velocity in toluene cyclohexane, acetic acid, water, etc, determined at 6328 angstrom from He-Ne laser analysis of structure of Rayleigh scattering 12 p1953 A67-25446

Hypersonic sound velocity dispersion in liquids of low viscosity analyzed using Mandelstam-Brillouin components 12 p1967 A67-26133

Infinitesimal pressure disturbance propagation in chemically reacting gas, deriving general equation for process, solution shows wavefront propagation at sound velocity [ASME PAPER 67-FE-2] 14 p2304 A67-28355

Method for analyzing single and double thermal relaxation processes 15 p2580 A67-29771

Temperature and transport properties of helium and argon at high temperatures from ultrasonic determination of sound velocity and sound absorption 15 p2580 A67-29882

Sound velocities in granular ammonium perchlorate and potassium chloride, discussing chemical reaction of shocks 16 p2734 A67-31521

Temperature dependence of sound velocity in liquid helium at saturation vapor pressure and cryogenic temperatures 17 p2886 A67-33231

Ultrasonic thermometry in solids and gases at elevated temperatures 18 p3051 A67-34509

Spark discharge generated blast wave application to shock on shock simulation, free-stream sound speed determination and hypervelocity flow measurements [AIAA PAPER 66-763] 19 p3208 A67-35753

Velocity of sound in liquids measurement using ultrasonic interferometry and laser diffraction spectra 21 p3630 A67-38772

Hypersound propagation velocity in toluene cyclohexane, acetic acid, water, etc, determined at 6328 angstrom from He-Ne laser analysis of structure of Rayleigh scattering 21 p3642 A67-38820

SOUND WAVE

SA ELECTROACOUSTIC WAVE

SA PLASMA SOUND WAVE

Lethal effects of high intensity airborne sound and ultrasound and irradiation time on *Bacillus Subtilis* for applications to spacecraft sterilization 01 p0016 A67-10881

Phasing system using steered beam of coherent light for RF array 01 p0027 A67-11320

Oscillations observed from acoustical helium plasma wave in cylindrical hollow cathode attributed to radial shock wave initiated by energy pulse 02 p0273 A67-11899

Continuously variable optical delay line using acoustic waves to diffract and frequency shift portion of argon ion laser beam 02 p0253 A67-12517

Transverse wave behavior in reactive flow, analyzing refraction or reflection of acoustic waves at shock front, obtaining comparison of behavior in corresponding real flows 03 p0405 A67-14026

Acoustic wave energy absorption by superconductors in intermediate state 03 p0502 A67-14377

Lethal effect of high intensity sonic and ultrasonic waves on spores of *Bacillus subtilis* var. niger ATCC 9372 04 p0562 A67-14520

Velocity measurements at various temperatures made with zinc sulfide thin film longitudinal acoustic wave transducers, used on germanium 04 p0621 A67-15127

Transverse electromagnetic wave transformation into ion-acoustic plasma oscillations with formation of intermediate Langmuir electron wave 04 p0668 A67-15275

Radiation pressure of electromagnetic and acoustic waves calculated from momentum of incident and scattered wave trains 05 p0846 A67-16583

Approximate calculation of local characteristics of sound waves into liquid and gaseous media 05 p0846 A67-16707

Aerodynamic generation of noise in stellar convection zones, solving inhomogeneous wave equation when assuming isothermal disturbance 05 p0899 A67-17073

Acoustic wave propagation characteristics in solar chromosphere, discussing resonant frequencies 05 p0900 A67-17075

Deformation of Fraunhofer line linked to sound waves in solar disk 05 p0900 A67-17076

Wave excitation in compressible partially ionized plasma by electromagnetic and acoustic /or mechanical/ sources, describing set of linearized hydrodynamic and Maxwell equations 05 p0859 A67-17436

Electron-piezoelectric interaction giving rise to currents responsible for acoustoelectric effects, gain and nonlinear mixing 06 p1050 A67-18140

Sound diffraction by semiminfinite elastic plate in moving medium 06 p1032 A67-18398

Boundary layer thickness in air measured in presence of sound field, determining flow velocity distribution in layer 06 p0988 A67-18400

LF gravitational-acoustic and internal gravity mode wave propagation in temperature-stratified photosphere-low chromosphere region and solar atmospheric resonant responses 08 p1399 A67-21236

Optical beam deflection method based on polarization change of acoustically deflected light as compared to incident beam 09 p1510 A67-21574

Excitation of ion-acoustic waves in potassium-cesium plasma when passing current through it, finding natural frequencies of system when plasma is drifting along axis 09 p1544 A67-21853

Acoustic waves amplification in CdS crystal by electron-phonon interaction 09 p1558 A67-22591

Electric fields due to electron-plasma and ion-acoustic waves associated with sunspot magnetic field variation as main cause of electron acceleration in solar flares 10 p1700 A67-23056

Sound wave generation by columnar-starting vortex passing through reflected plane shock front analyzed, revealing alternate compression-rarefaction nature 10 p1625 A67-23117

Scattering of plane monochromatic sound wave by semiminfinite elastic pipe in moving medium, emphasizing axisymmetric oscillations 10 p1680 A67-23644

Free vibration and resonance of vibrating plate interacting with sound waves in surrounding air 11 p1874 A67-24228

Potassium plasma current instability, turbulence and diffusion across magnetic field for large amplitudes of oscillations treated as ionic sound waves 11 p1834 A67-24377

Electron temperature variation induced effects and Landau damping of ion acoustic waves studied in quiescent discharge tube plasma 11 p1837 A67-24395

Approximate calculation of local characteristics of turbulence developing during intense injection of sound waves into liquid and gaseous media 11 p1820 A67-24929

Transient acoustical response of uniform flow to turbulence and noise in MHD generators 12 p1899 A67-25390

Ionospheric fine structure, considering excitation of ion-acoustic waves by vertical gradients of density 13 p2109 A67-26329

Infrasonic and hydromagnetic wave propagation in atmosphere and ionosphere measured by array of underwater and acoustic sensors 13 p2122 A67-27701

Propagation rate of LF acoustic waves in low pressure glow discharge in nitrogen 14 p2354 A67-27759

Model thermospheres, studying ducted traveling acoustic gravity waves originating in ionosphere 14 p2310 A67-28054

Radiants associated with sonic, magnetosonic and Alfvén waves and definition in terms of distribution of delta operator of infinitesimal discontinuity 14 p2359 A67-28511

Optical reconstruction from sampled holograms made with sound waves 14 p2320 A67-28602

Longitudinal acoustic wave attenuation in superconducting aluminum measured, verifying acoustic attenuation predictions 14 p2373 A67-28858

Tunnel current modulation by acoustic wave in superconductors 15 p2537 A67-29708

Optical image reconstruction from sampled hologram using wavefront reconstruction technique 15 p2488 A67-29819

Supersonic boom, discussing aerodynamic field of aircraft, sonic ray characteristics and noise suppression 16 p2589 A67-30832

Acoustic wave attenuation coefficients for small gap superconductors, noting electromagnetic absorption and collisional drag as cause 16 p2729 A67-31059

Propagation of shear acoustic waves traveling parallel to magnetic field along symmetry direction in metal crystal 16 p2731 A67-31446

Acoustic wave mode in weakly ionized gas analyzed, noting charge separation and electroacoustic effects 17 p2909 A67-33230

Relativistic generalization of Bernoulli equation from three-dimensional vector analysis of acoustic and entropy waves 18 p3084 A67-33422

HF response of local burning rate in laminar diffusion flames subjected to transverse sound waves in free stream 18 p3108 A67-33831

Influence of dissipation of acoustic waves on temperature rise in chromosphere 18 p3125 A67-34192

Nonvolatile block-oriented random access memory /BORAM/ combining thin magnetic films and scanning strain waves 18 p3012 A67-34347

Scattering of plane monochromatic sound wave by semiminfinite elastic pipe in moving medium, emphasizing axisymmetric oscillations 18 p3080 A67-34413

Mean flow refraction and temperature differences between mixing layer and outside fluid effect on HF component of jet noise 19 p3173 A67-34962

Soviet book on wave propagation in turbulent atmosphere covering geometric optics of electromagnetic and acoustic wave scattering and propagation, etc 19 p3182 A67-35206

Microwave sound generation by transient heating of material surface with laser pulses 20 p3457 A67-36386

Acoustic wave generation in weakly ionized plasma by fusion and damping of two ion-sound waves 20 p3501 A67-37291

Electromagnetic and acoustic waves diffraction at smooth convex body of arbitrary shape, solving field equations 21 p3579 A67-38108

Drift and ion acoustic waves and coupled waves in highly ionized dense plasma of finite ion temperature 21 p3667 A67-38412

Acoustic ion waves phase velocity and attenuation constant measurements verify predicted dependence on ion mass, with attenuation due to ion-neutral collisions 21 p3675 A67-39054

Ducted acoustic gravity wave propagation in isothermal atmosphere, obtaining dispersion relations ducted modes and surface wave in incompressible medium 21 p3623 A67-39057

One-component nonviscous nonheatconducting perfect gas in container with gaseous adsorption at boundary, noting acoustic oscillation instability for certain frequency disturbances 22 p3836 A67-39719

Optical characteristics of wideband pulse compression system using Brillouin scattering for compressing time duration of frequency swept pulses of acoustic wave 23 p4012 A67-40869

Rapid temperature increase due to lower photosphere turbulence generation of mechanical waves, discussing gravity wave generation and acoustic noise 23 p4068 A67-41280

Tunnel current modulation by acoustic wave in superconductors 24 p4200 A67-41778

RF pulse compression by chirped shear microwave sound in sapphire, inducing self-focusing of Bragg diffracted light 24 p4188 A67-42369

SOUNDING

S BALLOON SOUNDING

S IONOSPHERIC SOUNDING

S RADIOSONDE

S ROCKET SOUNDING

SOUNDING ROCKET

SA AEROBEE ROCKET

SA JAVELIN ROCKET

SA KAPPA ROCKET

SA METEOROLOGICAL ROCKET

SA NIKE-APACHE ROCKET

SA NIKE-CAJUN ROCKET

SA NIKE ROCKET

SA RAVEN ROCKET

SA ROCKET SOUNDING

Rotating vane electric field meter system flown on Nike-Cajun sounding rocket to determine electrostatic potential on vehicle throughout flight 01 p0074 A67-11126

Approximate method of computing attitude of sounding rockets from magnetometer data 03 p0519 A67-13782

Guided high altitude sounding rocket with paraglider recovery system that attains normal flight attitude upon atmospheric entry without control maneuvers 04 p0703 A67-14547

Micrometeoroid sampling with Luster sounding rocket during Leonid meteor shower, detailing contamination control program 04 p0699 A67-14966

Transient variation of ionospheric dynamo current systems obtained from sounding rocket measurements of geomagnetic field activities 05 p0797 A67-16582

Optimum thrust programming for sounding rocket extended by reducing state to single variable to obtain sufficient conditions for specific extremal solution 05 p0906 A67-17225

Radio-controlled reusable sounding rocket design characteristics, trajectory analysis, drag and lift, reentry stress control system, guidance, stabilization, etc 06 p1098 A67-18763

HARP program objectives 06 p1098 A67-19021

Sounding rocket vehicle technology - AIAA Conference, Williamsburg, February-March 1967 08 p1402 A67-20491

Solid and hybrid propulsion relationship to sounding rocket vehicle design and mission analysis, particularly application to synoptic meteorology 08 p1374 A67-20492

Payload-apogee altitude performance, static stability and dynamic motions of Tomahawk vehicle analyzed for ability to meet 100 km sounding rocket requirement 08 p1404 A67-20494

Controlled booster stage BER for sounding rockets to reduce dispersion of impact points at low acceleration [ONERA-TP-442] 08 p1404 A67-20495

Aerobee 350 sounding rocket for scientific

use in heavy payload to moderate altitude performance region 08 p1404 A67-20496

Aerodynamics of sounding rockets, discussing stabilization by fins, conical flares, etc 08 p1275 A67-20498

Air loads on sounding rocket from distributed aerodynamics and pressure differential 08 p1276 A67-20501

Extra-atmospheric coning motions of Tomahawk sounding rocket caused by dynamic instability after motor burnout 08 p1405 A67-20502

Tailfin design effect on induced rolling moment characteristics of sounding rocket 08 p1405 A67-20503

Fin-flare combination for stabilizing upper stage of Black Brant IV two-stage sounding rocket 08 p1405 A67-20504

Aeroelastic vehicle body loads computed by coupled system of digital computer programs 08 p1405 A67-20505

Tip-off motion due to separation of stages or payload by multispring separation system with guided plungers 08 p1405 A67-20506

Spin rate effect on stability and transient response of vehicle treated by root locus technique 08 p1405 A67-20507

Skylark rocket attitude in free space determined from solar and magnetic sensor data used in least squares method 08 p1406 A67-20508

Error in application of WKB method to linearized postburnout equation of motion of sounding rocket 08 p1406 A67-20510

Nose selection and vehicle motion dynamics for second stage of two-stage sounding rocket system, discussing nose shapes effect on altitude performance, overall vehicle stability, bending moments, etc 08 p1406 A67-20513

Dynamic flight characteristics of spin-stabilized sounding rockets during passage through atmosphere, emphasizing roll resonance and motions leading to roll lock-in and angle of attack 08 p1407 A67-20514

Nonlinear motion theory for axisymmetric sounding missiles or rockets with Magnus moments, showing application to near pitch-roll resonance 08 p1407 A67-20515

Aerodynamic stability coefficients determined from sounding rocket flight data, using computer program for numerically integrating six degrees of freedom motion equations 08 p1407 A67-20517

Air launched sounding rockets design, development and testing noting aerodynamic loading and surface, propulsion unit, cost effectiveness, etc 08 p1407 A67-20518

Solid propellant motor design for Black Brant VB sounding rocket 08 p1375 A67-20519

Sounding rocket disintegration studies to avoid falling mass hazards, noting design of pyrotechnic core in sandwich construction 08 p1407 A67-20520

Frangible sounding rocket vehicle and explosive fragmentation system, determination of impact kinetic energy of fragments and flight tests results 08 p1407 A67-20521

Ballistic propellant combustion alternation and thermal effects due to dynamic spinning observed on solid propellant sounding rockets 08 p1408 A67-20522

Liquid propellant utilization for sounding rockets 08 p1372 A67-20524

Terrier two-stage sounding rocket design, fabrication, flight testing and performance characteristics 08 p1408 A67-20527

Airframe heat protection for high performance sounding rockets, using plasma jet testing for leading edge design selection 08 p1425 A67-20528

Black Brant III sounding rocket analyzed via mathematical model to predict temperature distribution in ablation material 08 p1425 A67-20531

Black Brant sounding rocket fin design, discussing flight characteristics, engine selection criteria and stability parameters 08 p1416 A67-20532

Nike-Tomahawk rocket aeroelastic behavior, noting occurrence of large extra-atmospheric coning angles 08 p1418 A67-20534

Spinning rocket attitude control technique including theory, system mechanization and performance 08 p1409 A67-20539

Gyroless Solar Pointing Aerobee Rocket Control System /SPARCS/ using no inertial platform and having solid state circuitry 08 p1409 A67-20540

COTIR wind weighting technique to reduce impact dispersion of sounding rockets 08 p1313 A67-20541

Hazards in sounding rocket assembly and launch operations and safety techniques at NASA Wallops station noting storage, explosive control, ground safety, etc 08 p1314 A67-20547

Vector electric field and particle intensity measurements from sounding rocket launched into visible aurora 08 p1329 A67-21486

Fluctuating effective gain of rocket telemetry links determined from signal strength data of Black Brant sounding rockets 09 p1463 A67-21829

Spectrum of quiet sun between 30 and 128 angstroms analyzed in November 1965, using rocketborne grating monochromator with Geiger detector 09 p1566 A67-22232

Energy spectra of Tau X-1 and isotropic component of galactic X-rays, using rocketborne scintillation and GM counters 10 p1701 A67-23229

Rocket probe measurements indicate existence of maximum ion concentration in stratosphere and lower ion concentration at equator than at midlatitudes 10 p1648 A67-23284

Lyman alpha emission from sun near solar minimum 11 p1862 A67-24503

Rocket probe measurements indicate existence of maximum ion concentration in stratosphere and lower ion concentration at equator than at midlatitudes 12 p1933 A67-25650

Circulation patterns in upper atmosphere, using sounding rockets from Indian equatorial station during monsoon and winter periods 12 p1935 A67-25791

R/D on water launched space probes, discussing operation, applications and results 12 p2012 A67-25839

Primary cosmic ray intensity and structure of air showers at high altitudes investigated by aircraft, balloons and sounding rockets 13 p2193 A67-27247

Radio noise spectrum on VLF bands in ionosphere observed by sounding rocket K-9M-19 14 p2307 A67-27886

Atomic oxygen density profiles obtained from radiation intensity resulting from nitric oxide reaction 14 p2293 A67-28199

Satellite launch vehicle performance analysis based on velocity requirements and gravity and drag losses for applications to booster configurations 14 p2394 A67-28701

Frangible sounding rocket vehicle and explosive fragmentation system, determination of impact kinetic energy of fragments and flight tests results 15 p2565 A67-29449

Free atomic sodium distribution in daytime upper atmosphere, noting thin layer formation and radiative transfer theory 15 p2475 A67-29616

Peak altitude of multistage sounding rocket vertical trajectory in vacuum determined by dimensionless graphs 16 p2762 A67-31247

Space-time wind variability for forecasting from near ground surface sampling for unguided rocket impact prediction 17 p2880 A67-32551

Pulsations in electron intensities in postbreakup aurora, noting possibility of distant processes affecting electrons 17 p2844 A67-32765

COTIR wind weighting technique to reduce impact dispersion of sounding rockets 19 p3207 A67-34837

High altitude research rocket HF telemetering remote control signal receivers, antennas and earth station, discussing design and circuitry of transmitter antenna 19 p3193 A67-35061

Canadian space research, detailing sounding rocket and satellite launchings 19 p3320 A67-35288

Pakistan space research noting facilities, sounding rocket experiments and satellite- and ground-based observations 19 p3321 A67-35297

Attitude control methods compared for use in rockets collecting data in UV region from various stars 20 p3531 A67-36411

Micrometeorite flux rate for Leonid shower measured with Luster sounding rocket collecting surface 20 p3528 A67-37424

Air loads on sounding rocket from distributed aerodynamics and pressure

differential 21 p3563 A67-37795
Controlled booster stage BER for sounding rockets to reduce dispersion of impact points at low acceleration 21 p3712 A67-37802
Black Brant sounding rocket fin design, discussing flight characteristics, engine selection criteria and stability parameters 21 p3712 A67-37807
Measuring assembly containing logarithmic-response electrometric amplifiers for sounding rockets 21 p3592 A67-38222
Profile of night sky hydrogen Lyman alpha emission line determined using data from rocketborne hydrogen-filled filter tube 22 p3790 A67-39805
Charged particle /ion/ collection rates using supersonic atmospheric sounding rocket with electrode at stagnation point, noting electric field effect 22 p3791 A67-39818
Thrust history to produce maximum altitude for two-stage launch vehicle determined using simplifying assumptions and atmospheric drag 22 p3904 A67-40089
Aerobee 350 sounding rocket for scientific use in heavy payload to moderate altitude performance region 22 p3904 A67-40090
Ionospheric observation using Japanese sounding rocket, discussing electron density profile, ion density and electron temperature measurements 24 p4150 A67-42151
Gyroless Solar Pointing Aerobee Rocket Control System /SPARCS/ using no inertial platform and having solid state circuitry 24 p4242 A67-42905
Nike-Tomahawk rocket aeroelastic behavior, noting occurrence of large extra-atmospheric coning angles 24 p4242 A67-42912
Airframe heat protection for high performance sounding rockets, using plasma jet testing for leading edge design selection 24 p4256 A67-42914
Dynamic flight characteristics of spin-stabilized sounding rockets during passage through atmosphere, emphasizing roll resonance and motions leading to roll lock-in and angle of attack 24 p4242 A67-42917

SOURCE

S COHERENT SOURCE
S ELECTRON SOURCE
S ENERGY SOURCE
S HEAT SOURCE
S ION SOURCE
S LIGHT SOURCE
S NEUTRON SOURCE
S POWER SUPPLY
S RADIATION SOURCE
S RADIO SOURCE

SOUTH AMERICA

S ARGENTINA
S BRAZIL
S MEXICO

SOUTHERN HEMISPHERE

Experimental Inter-American Meteorological Rocket Network /EXAMETNET/ for Southern Hemisphere research 08 p1350 A67-20549
Geomagnetic field anomalies in Southern Hemisphere and effects on cosmic rays, geomagnetically trapped radiation and ionosphere 12 p1933 A67-25770
Airglow and enhanced penetrating electromagnetic radiation in southern radiation anomaly observed with scintillation crystal during aircraft flight 12 p1996 A67-25775
Molecular oxygen densities in range 70-90 km determined by rocket measurements of atmospheric absorption of solar UV radiation in Southern Hemisphere 12 p1934 A67-25786
Inflation of magnetosphere near 8 earth radii in Southern Hemisphere using Explorer XIV satellite 12 p1936 A67-25805
Optical astronomy opportunities in cosmology, stressing need for additional telescopes located in Southern Hemisphere 15 p2563 A67-30393
Time and space distribution of anomalous ionization in ionospheric F-2 layer above Southern Hemisphere, noting maximums of ionization distribution 16 p2668 A67-31893
Evidence regarding possibility of midwinter stratospheric warmings in Southern Hemisphere 17 p2880 A67-32553
Trajectory analysis of EOLE meteorological balloons flights in troposphere over Southern Hemisphere 19 p3332 A67-35276
Early autumn stratospheric circulation of Southern Hemisphere investigated by

meteorological rocket observations 19 p3253 A67-35920
Annual and diurnal variations of geomagnetic anomaly in Australasian Zone during sunspot minimum, stressing role in transequatorial propagation of VHF radio signals 22 p3759 A67-39473
SPACE
S BANACH SPACE
S CARTAN SPACE
S CISLUNAR SPACE
S DEEP SPACE
S EUCLIDEAN SPACE
S FARADAY DARK SPACE
S FREE SPACE
S FUNCTION SPACE
S HALF-SPACE
S HILBERT SPACE
S HYPERBOLIC SPACE
S INTERPLANETARY SPACE
S INTERSTELLAR SPACE
S ORLICZ SPACE
S RIEMANN SPACE
S VECTOR SPACE
SPACE BIOLOGY
S BIOASTRONAUTICS
S EXTRATERRESTRIAL LIFE
SPACE CABIN ATMOSPHERE
SA CLOSED ECOLOGICAL SYSTEM
Manned spacecraft atmosphere selection, experimenting with 100 percent oxygen at 258 mm Hg, noting toxicity, toleration, substitution of helium for nitrogen, etc 02 p0187 A67-12319
Gas-off products from space cabin materials determined by continuous recording instruments, gas chromatography and IR analysis 02 p0189 A67-12388
Selection of space cabin atmospheres including pressure, fire and blast hazard, humidity and temperature control, etc 11 p1748 A67-24262
Normalization of noise produced by life support systems in spaceship cabins during prolonged flights 16 p2617 A67-30762
Multifunctional chemical compounds development for use as air revitalization materials 16 p2618 A67-30778
Spacecraft atmosphere selection covering physiological, engineering and fire criteria, evaluating oxygen diluent and recovery 22 p3755 A67-39889
Reactions of animals exposed to pure oxygen space cabin atmosphere for 235 days, noting no systematic toxicity 23 p3952 A67-41574
Carbonation Cell System for removing carbon dioxide from space cabin atmosphere using electrochemical process 23 p3965 A67-41578
Solid chemical state O for spacecraft noting advantages over liquid and high pressure gas, discussing storage, handling, losses, shelf life, availability and containers 23 p3967 A67-41608
Space suit atmosphere physiological suitability for prolonged moderate work, studying blood-gas parameter changes 23 p3955 A67-41617
Space cabin simulator tests in helium-oxygen mixtures at various total pressures and ratios of oxygen to diluent 23 p3969 A67-41646
Oxygen regeneration life support system for multiple mission manned space flights evaluated with subsystem model [SAE PAPER 670849] 24 p4115 A67-42000
Space cabin atmosphere relation to environmental and operational variables, discussing effect of hypoxia and hypercapnia on spacecrew and mission safety [AIAA PAPER 67-855] 24 p4117 A67-42999
SPACE CABIN SIMULATION
Simultaneous simulation of space and thermal conditions of spacecraft [ASME PAPER 66-WA/HT-29] 04 p0599 A67-15443
Mechanized hybrid real time simulation for Gemini crew to use in rendezvous procedures [AIAA PAPER 67-250] 07 p1166 A67-20068
Comparison of effect of various diluent gases in evoking flyer bends in simulated orbital flights 13 p2062 A67-26916
Contaminant control in space cabins by systematic screening of materials and supplies used, noting significance of test temperature 21 p3577 A67-38077
Space cabin environmental changes studied for susceptibility of mice to viral infection 21 p3574 A67-38080

Microbial interaction factors determined between men and environment in closed systems 23 p3962 A67-40858
SPACE CABIN SIMULATOR
Low contamination space chamber design employing cryopanel array configurations with near unity sticking coefficients 09 p1485 A67-22122
NASA and USAF experiment on mans contribution to trace contaminants in space cabin simulator at 760 mm of Hg 15 p2430 A67-29278
Space suit support loop for use within manned space cabin simulator 20 p3374 A67-36548
Thermal comfort zone test for helium-oxygen and nitrogen-oxygen atmospheric mixture for 18-day continuous manned run 22 p3754 A67-39599
Contaminant concentration due to human habitation of space cabin simulator at 258 mm Hg and oxygen atmosphere environment 23 p3964 A67-41559
Open cycle air evaporation urine processing system recovering potable water in space cabin simulator, discussing wick evaporator 23 p3969 A67-41631
Space cabin simulator tests in helium-oxygen mixtures at various total pressures and ratios of oxygen to diluent 23 p3969 A67-41646
SPACE CAPSULE
SA SPACECRAFT
Design, construction and operation of vacuum chamber space simulator for testing Gemini space capsule 01 p0049 A67-10303
Emergency Global Rescue, Escape and Survival System /EGRESS/ to protect space crew in emergencies encountered in earth-orbital operations 05 p0906 A67-17204
Flame mechanism experiments for solid material surface, measuring flame velocity, stressing space capsule fire hazard minimization 22 p3904 A67-40110
SPACE CHARGE
Space charge formation during flow of electric current in plasma moving under thermal emission of electrons 01 p0118 A67-10043
Point discharge from multiple points in irregular configuration, space-charge theory and plant discharge applications 01 p0107 A67-10114
Microwave negative conductance due to traveling space charge waves in n-type GaAs 01 p0133 A67-10487
Electron tunneling through space charge region of uniformly doped metal-semiconductor barriers calculated in effective-mass approximation 02 p0280 A67-11483
Space-charge layer effect on volt-ampere characteristics of multilayer diffusion structures in silicon 02 p0281 A67-11504
Surface charge and impedance of plasma excited by incident electromagnetic waves 02 p0190 A67-11507
Stability of counterstreaming flow of electrons and ions in heavily biased diodes theoretically studied by space charge wave and Nyquist analysis 02 p0214 A67-11883
Cesium ion beam generation by accelerating cesium in space charge sheath located between ionizer and plasma filled region [AIAA PAPER 66-927] 02 p0303 A67-12251
Stability of flute oscillations of rarefied plasma in constant electric field normal to magnetic field 02 p0278 A67-12619
Spectral intensity of short-circuited noise current of space-charge-limited solid state diodes 03 p0380 A67-13486
Rectification and detection characteristics of space-charge-limited solid state diode at VHF 03 p0380 A67-13488
Space charge fields of planar magnetron calculated taking account of effect of conducting planes of cathode and anode 03 p0385 A67-13954
Growing space charge wave phenomenon due to collision coupling in warm compressible dissipative electron plasma in uniform motion 03 p0483 A67-13995
Damped oscillations and velocity of sound waves in semiconductors and metals in presence of strong magnetic field 03 p0501 A67-14370
Space charge wave velocity in semiconductors, noting recombination type instability 04 p0676 A67-14928
Small signal theory of space charge

limited unipolar diodes, calculating impedance and negative conductance 04 p0582 A67-15097

Space charge limited unipolar nonstationary currents in solid, calculating nonsteady modes in plane parallel electrode structure due to carrier injection into gap 04 p0680 A67-15155

Laminar electrohydrodynamic flow in plane diffusor, taking into account molecular diffusion of space charge 04 p0668 A67-15277

Radiative recombination in space charge layer of p-n junction in silicon carbide determined from I-V characteristics and capacitance 04 p0681 A67-15298

Generation of dense electron beams of energy half-width including tightly collimated beams of very low energy, space charge effects in deflectors, etc 04 p0623 A67-15323

Noise figure of low noise to TWT obtained by calculating equivalent noise impedance stage by stage 05 p0773 A67-16510

Two-flow equations for stationary relativistic electron cloud in self-consistent crossed fields 05 p0774 A67-16907

Graphical data concerning drifting beams as possibility for calculation of reduction coefficient of space charge field of electron beams moving in periodic electrostatic fields 05 p0764 A67-16908

Instabilities and scattering in space charge focused low voltage electron beams in absence of magnetic field 05 p0849 A67-17449

Role of space charge and discharge mechanism in gauge with cold cathode, noting electron sheath formation 05 p0809 A67-17494

Semiconductor surface photovoltage under small signal conditions, when quasi-equilibrium approximation will be valid in space charge layer 06 p1047 A67-17600

Thermal noise limitation in space-charge-limited solid state diodes and triodes 06 p0971 A67-18224

Magnetic field effect on space charge neutralization in thin beam approximation [AIAA PAPER 67-83] 06 p1041 A67-18275

Ion extractor system for electrostatic thrusters designed, using salient features of digital computer and electrolytic tank analog methods 06 p1075 A67-18877

Conductivity changes in flash evaporated p-GaAs films caused by field effect and optical and thermal excitation at temperatures about 100 degrees K 07 p1232 A67-19564

Avalanche characteristics and failure mechanisms in junction diodes, showing negative resistance regions due to space charge effect of carriers 07 p1156 A67-19899

Electron space-charge neutralization in design of thermionic /heat-to-electricity/ converters 08 p1286 A67-21177

Trap-free space-charge-limited current produced by space charge injection in oxygen doped n-GaAs crystals at low temperature 09 p1552 A67-21767

Thermal noise in space-charge-limited solid state diodes, showing equivalence of noise resistance with DC 09 p1472 A67-21951

Spatial distribution of electrons and ions in neutral plasma, considering charge density 09 p1548 A67-22352

Mobile charge carrier velocity measurements in silicon at high field strengths 10 p1690 A67-23168

Space charge conductance and electron drift velocity measurements for avalanching p-n diode 10 p1611 A67-23169

Noise in space charge limited current in CdS single crystal at low injection level 10 p1696 A67-23772

Space-charge-limited currents in p-type silicon noting I-V characteristics, theoretical values agreement, Hall coefficient measurements correlation, etc 11 p1845 A67-24135

Magnetically confined helical electron beams formed by two-anode electron guns, considering effect of space charge 11 p1764 A67-24466

Harmonic power at TWT taking into account effect of space charge on electron beam bunching 11 p1765 A67-24478

Channel transistor characteristics for impurity distribution taking into account space charge penetration into gate 11 p1765 A67-24481

Analytical expression for steady state rate

of electric domain movement in semiconductors in terms of electric field distribution at domain center 11 p1846 A67-24482

High power pulsed microwave generation in gallium arsenide diode when operated at X-band frequencies 11 p1767 A67-24721

Ion acceleration by drift resonance caused by crossed magnetostatic and space charge electrostatic fields 11 p1841 A67-24768

Space charge and eddy currents in ionized gas flow in MHD channel determined, showing effect of cold electrode boundary layer on electrical performance 11 p1746 A67-24874

Temperature dependence of volt-ampere characteristics of silicon space charge limited diode compared with ordinary diodes 12 p1914 A67-25459

Intermediate and HF noise of probes immersed in gas discharges explained by space charge sheath and bulk plasma noises 12 p1948 A67-26226

Transient characteristics of doped silicon diodes with negative resistance, determining electron lifetime vs current, noting space charge role 13 p2076 A67-26489

Electric field distribution in p region, space charge layer and n region of p-n abrupt junction germanium diode at room temperature 13 p2078 A67-26788

Nondissipative plasma flow past magnetized cylinder in absence of electromagnetic field, noting current force relation to distance between conductor and cylinder surface 13 p2168 A67-27303

Stability of flute oscillation of rarefied plasma in constant electric field normal to magnetic field 13 p2170 A67-27375

Silicon space charge limited triode considered as analog transistor noting I-V characteristics, current proportionality, voltage amplification and noise performance 13 p2083 A67-27571

Current-voltage characteristics of cadmium sulfide crystal diodes with indium and gold cathodes 13 p2085 A67-27731

Surface charge and impedance of plasma excited by incident electromagnetic waves 14 p2261 A67-28071

HF negative resistance in dielectric diodes with high density of shallow traps taking into account transit time 14 p2367 A67-28521

Interband states in vicinity of metallurgical junction, deriving formula for depletion layer capacitance of abrupt junctions with interface states 14 p2373 A67-28929

Space-charge-wave growth and differential negative resistance conditions in two-valley semiconductors obtained from impedance 15 p2442 A67-29179

Space charge limited unipolar nonstationary currents in solid, calculating nonsteady modes in plane parallel electrode structure due to carrier injection into gap 15 p2534 A67-29342

P-n semiconductor junction widening due to impurity diffusion and drift, noting first order differential equations describing space-charge width variation with time 15 p2535 A67-29488

Barrier-layer FET frequency behavior solved, deriving inner transistor quadrupole parameters by way of boundary value problem 15 p2447 A67-29644

Space charge varactor compared to p-n junction varactor, noting applications 15 p2449 A67-29804

Space-charge limited ionic currents in MOS structure oxide film, noting relationship between interface ion trapping rate and SCL currents 15 p2539 A67-29825

Difference leveling between electron and hole concentrations near junction by compensating charges of donors and acceptors with semiconductor space charges 15 p2542 A67-30242

Origin of forced oscillation in space-charge density of free current carriers in semiconductors ascribed to periodic generation of carriers 15 p2542 A67-30243

Noise suppression in p-n junction biased in direction of current, noting effect of space charge on current fluctuation 15 p2543 A67-30252

Small signal power conservation in space charge waves of multivelocity electron beam with rectangular velocity distribution 16 p2703 A67-30796

Exact solutions for spatial distribution of

potential within space-charge region of non-degenerate semiconductor in contact with metal 16 p2727 A67-30850

Two-flow equations for stationary relativistic electron cloud in self-consistent crossed fields 16 p2636 A67-30884

Graphical data concerning drifting beams as possibility for calculation of reduction coefficient of space charge field of electron beams moving in periodic electrostatic fields 16 p2636 A67-30885

Noise and HF input conductance measurement of double-injection germanium space-charge-limited diode, noting transit-time effect 16 p2637 A67-31034

One-dimensional charged particle flow in bounded system, particularly overlapping steady state zero-temperature flow approximation solutions, noting instabilities 16 p2704 A67-31233

Space-charge-limited dielectric diode with quadratic I-V characteristics, noting shallow trap effects on detection properties 17 p2823 A67-32199

Cesium-vapor vacuum diode for thermionic conversion stressing role of electrode homogeneity, space charge and transport phenomena 17 p2823 A67-32222

Transistor current-voltage characteristics when controlled by space-charge and transit-time effects, obtaining large negative conductances at HF 17 p2824 A67-32302

GaAs diodes measured for capacitance at 77 degrees K, noting change due to traps photoexcited in space charge layer 17 p2914 A67-32655

Two-stream instability in semiconductor InSb plasmas, noting collision conditions, surface space charge, wave growth, etc 17 p2921 A67-33052

Space charge formation during flow of electric current in plasma moving under thermal emission of electrons 17 p2910 A67-33321

Space charge limited currents in copper phthalocyanine thin films measured as function of voltage, temperature, thickness and illumination 18 p3104 A67-34626

Space-charge and potential distributions calculated for region between two plane electrodes of single collision model 19 p3265 A67-35129

Electron, X-ray and UV radiation effects on oxidized silicon surfaces and planar devices, noting space charge buildup 19 p3305 A67-35621

Radiation surface effects in semiconductor devices, noting positive space charge buildup in passivated device dielectric surface layer 19 p3306 A67-35674

Dispersion equations for two types of transverse interaction tubes analyzed numerically in presence of strong space charge 19 p3198 A67-36022

Gold-doped silicon diode space charge and oscillation effect, discussing deviation from Ohm law at lowest voltages 19 p3198 A67-36043

Depletion layer capacitance of p-n step junction with inclusion of effect of spillover charge as function of voltage 20 p3504 A67-36167

Space charge analyses applied to electron beam extractions from plasma cathodes, computing stability data for potential distributions and extracted current 20 p3495 A67-36168

Electron space-charge and nonzero beam-coupling impedance effects on TWT, considering weakly saturated state 20 p3395 A67-36313

Time-dependent current flow equations solved for insulator with traps if injected space charge produces negligible perturbation on external electric field 20 p3509 A67-36506

Inverse layer effect on p-type silicon MOS structure surface, examining deviation from equilibrium space charge theory 20 p3511 A67-37141

Electric conductivity of surface space charge layers in semiconductors, solving Boltzmann equation and determining current density and carrier mobility 20 p3511 A67-37144

Germanium conductivity dependence on surface and space charges in transverse magnetic field 21 p3676 A67-37862

P-n-p diode volt-ampere characteristic qualitative calculation, analyzing device negative resistance with avalanche

- multiplication 21 p3593 A67-38289
 Diode volt-ampere characteristics, considering space charge in base barrier layer and rear contact oxide film, noting vertical section appearing on direct branch 21 p3593 A67-38291
 Book on electrical properties of semiconductor surfaces covering space charge layer theory, solid state theory, etc 21 p3682 A67-38365
 AlN single crystal thermostable semiconductor optical/electrical properties, measuring space-charge-limited current and photocurrent 21 p3684 A67-38522
 Reflex klystron electron admittance dependence on potential distribution in repeller space, showing electrode structure and space charge effects 21 p3598 A67-38604
 Corona discharge propulsion system with space charge limited emission of negative ions, noting ion mobility performance and efficiency 21 p3696 A67-38856
 Soviet book on semiconductor electrochemistry covering space charge layer structure, semiconductor corrosion, etc 22 p3856 A67-39413
 Unstable coupling between slow space charge mode of electron beam and lowest plasma electron band modes in finite geometry 22 p3847 A67-39643
 Gunn effect, describing electron transfer, domain propagation and space charge instabilities in GaAs 22 p3841 A67-40073
 Dynamic behavior of accumulation layer and efficiency of Gunn effect semiconductors in limited space charge mode of operation 22 p3864 A67-40314
 Electronic transport in graded band gap semiconductor heterojunctions without space charges, using method based on intraband transitions between complete Hamiltonian eigenstates 22 p3864 A67-40381
 Heteroepitaxial Si films grown on sapphire studied for current voltage relations, finding space charge limited current 23 p4038 A67-40785
 Current oscillations in Co-doped Si p-i-n diode devices noting SCL I-V characteristics 23 p3978 A67-40788
 Oscillator diode in limited space charge accumulation oscillation mode, obtaining maximum DC to RF conversion efficiency for sine wave excitation for n-GaAs 23 p3979 A67-40875
 Space charge limited /SCL/ hole current in Si noting mobility, capacitance, current density, I-V characteristics and double injection 23 p4038 A67-40878
 Cesium ion beam generation by accelerating cesium in space charge sheath located between ionizer and plasma filled region [AIAA PAPER 66-927] 23 p4049 A67-41736
 Space charge effect on potential barrier in field emission, obtaining expression for work function increase using electrical image method 24 p4201 A67-41894
 Electrode configurations producing various intense charged particle beams, deriving algorithm applicable to three-dimensional problems 24 p4153 A67-41928
 Space charge layers on surfaces of lead sulfide photoconducting film noting Hall coefficients 24 p4204 A67-42363
 Electro-fluid dynamic power generation, discussing Mach number, charged particle mobility, pressure level and radial space charge field effects on load characteristic and conversion ratio 24 p4107 A67-42527
 Complex wave propagation and coupling in inhomogeneous media, discussing WKB type amplitude coefficients and electromagnetic and space charge waves 24 p4123 A67-42657
- SPACE COMMUNICATION**
SA INTERPLANETARY COMMUNICATION
 Communications subsystem providing S-band link between LEM and earth and VHF link between LEM and Command Module 02 p0205 A67-12273
 Space communication maximum usable frequency and limitations imposed by atmospheric absorption 02 p0205 A67-12735
 Negative lens property responsible for reconstruction of original scene in full three-dimensional reality 03 p0420 A67-13676
 Radar, range instrumentation and measurement systems 04 p0568 A67-14497
 Microwave data link system development for deep space communication 04 p0568 A67-14499
- Erectable antenna design for S-band communications between lunar surface and earth during lunar stay portion of Apollo mission 04 p0569 A67-14501
 System design analysis of laser methods of deep space communication, examining local heterodyne system /LHS/, direct detection system /DDS/ and transmitted reference system 06 p0957 A67-17635
 Communications requirements for manned deep space missions, using optical links, with PPM, PCM/PL and coherent reception for each link [AIAA PAPER 66-317] 06 p0961 A67-17706
 RCA papers on spacecraft and space systems 06 p0963 A67-18411
 Space communications, present and future 06 p0965 A67-19028
 Automatic phase sensor for waveguide combiner in S-band ground tracking and space communication 07 p1149 A67-19051
 Communication parameters associated with Martian flyby probes and with lander and manned vehicles 07 p1145 A67-19870
 Verbal communication intelligibility in man-rated altitude simulator with nitrogen or helium added to oxygen atmosphere 08 p1287 A67-20484
 Propagation difficulties and anomalies caused by characteristic plasma behavior in connection with space mission telecommunication 08 p1293 A67-20684
 Adaptive antenna for ground reception of wideband RF signals in space communications systems 08 p1301 A67-20776
 Space communications between points on earth by space vehicles and between earth and space vehicles 08 p1294 A67-20783
 Gemini ground support system extension to cover Apollo program, stressing launch complex, deep space tracking, S-band linkage, communications satellite, etc 08 p1317 A67-21281
 Blocking effect due to interference in parametric amplifier, discussing relation between gain and blocking frequency 10 p1609 A67-22834
 Steady state dynamic properties of large spinning net-like antenna suitable for radio signal reception from space 10 p1727 A67-23753
 Pseudocolor technique, noting applicability to TV data presentation from space vehicles 11 p1789 A67-24250
 Laser application to deep space communication noting advantages of optical frequencies for high rate transmission of data 11 p1752 A67-24252
 Redundancy reduction for conserving bandwidth and/or power in aerospace communication and telemetry 11 p1756 A67-24708
 Parallel data decoding with high transmission rates close to channel capacity for space telemetry systems design 12 p1909 A67-25781
 Apollo spacecraft-earth two-way communications provided by vehicle-mounted variable gain antenna array, automatically tracking ground-transmitted signals 13 p2068 A67-26802
 Telemetry, tracking and command /TTC/ communications, emphasizing 1970 requirements for manned and unmanned earth-orbital, lunar and planetary missions 13 p2074 A67-27449
 Past and future development in communication, components and guidance for space application 13 p2072 A67-27504
 Design of simple circuit for high speed transmission gating of analog signals with fast switching diode and small overshoot 14 p2287 A67-28686
 Biorthogonal coded telemetry system for deep space applications, discussing construction and performance 14 p2271 A67-28695
 Modulation indexes for two-channel phase coherent communication system determining data rate yielding predetermined bit-error probability [JPL-TR-32-1118] 14 p2273 A67-28709
 Microwaves and laser links for spacecraft-earth communications noting limitations by external noise effects, atmospheric turbulence, fabrication tolerances, etc 14 p2273 A67-28799
 RCA papers on defense electronic products including search radar, superconductor devices, data and spacecraft communications, speech recognition 14 p2274 A67-28910
 Radio blackout extent from simplified calculation of average sheath power loss for typical Apollo reentry trajectory 15 p2434 A67-29168
 Troposphere and ionosphere effects on different frequency radio wave propagation for space communication [AAS PAPER 67-93] 15 p2437 A67-29953
 Communication with and by space vehicles at ghz frequencies, using atmospheric windows [AAS PAPER 67-94] 15 p2478 A67-29954
 Graphical technique for phase-modulated deep-space communications links resulting in optimum power division between carrier and sine and square-wave carriers 16 p2625 A67-31258
 Compatible integrated circuits using thin films on silicon for application in space telemetry systems 16 p2641 A67-31559
 Policy decisions in space broadcasting, emphasizing range of possibilities allowed and limits imposed by technical factors 20 p3378 A67-36121
 Deep space communication system data rate increase using relay satellite 20 p3380 A67-36542
 Radio interior communication /RADIC/ system used in Apollo program, discussing future capabilities and advantages 20 p3380 A67-36559
 Book on lasers and application to long distance terrestrial or space communications system 20 p3459 A67-36639
 Scintillation of ground-to-space laser beam through atmospheric turbulence 20 p3383 A67-37023
 Deep space communication system using sequential decoding, binary phase-shift keying and 8-level quantized decisions 20 p3384 A67-37349
 Design and performance of frequency multiplexed phase-modulated communication systems 20 p3385 A67-37353
 Integrated MOS-FET analog gate for pointing and logic of space telemetry switch 21 p3592 A67-38227
 Frequency bands and modulation methods for space communication system 21 p3581 A67-38235
 Frequency limitations of PCM communication, determining PCM/PM and PCM/FM power spectra for hybrid modulation spectra calculations 21 p3584 A67-38652
 High gain directional antenna networks for space communications 21 p3600 A67-38670
 Data compression and error control coding in space telemetry analyzed, using performance measures similar to distortion function 21 p3586 A67-38950
 Exolonspheric communications system with ideal matched filter and signal processing at transmitter for increased range and secure coding possibilities 21 p3586 A67-38952
 Deep-space communication capability spectral dependence analysis indicates optical transmissions would be several orders of magnitude poorer than RF technology 22 p3764 A67-40558
 Carcinotron hyperfrequency power oscillator with tube of same noise characteristics as control developed for space telecommunications 23 p3982 A67-41431
 System parameters of linear time-variant space communication channels from input-output viewpoint, measuring correlation functions and Doppler spread 24 p4123 A67-42476
 Manned planetary mission global network for continuous tracking, communication telemetry and TV transmission [AIAA PAPER 67-976] 24 p4125 A67-43052
- SPACE DEBRIS**
 Electron microscope and microprobe measurements of luster flight samples, nondispersing particle size distribution and nondispersive chemical analysis 10 p1707 A67-23238
 Legal problems of salvage and removal of man-made objects from outer space 12 p2043 A67-26147
 Salvage and removal problems of man-made objects from outer space, stressing need for international procedures and standards 20 p3556 A67-36484
- SPACE DENSITY**
SA ATMOSPHERIC DENSITY

- Statistical data on space density of bright elliptical galaxies, radio galaxies, quasars, noting relation between space density and age 02 p0322 A67-11685
- Quantum cosmology, discussing continuous fluid models as representations of early dense universe 18 p3117 A67-33515
- Extended radio sources confinement through suggested dynamic process permitting intergalactic medium density deduction possibility 24 p4226 A67-41881
- Space distribution function of Knudsen gas in closed volume investigated using gas model noting dependence of time 24 p4190 A67-41902
- SPACE ELECTRIC ROCKET TEST /SERT/**
- Optimum discharge chamber configuration of permanent magnet mercury-bombardment thruster for SERT II mission [AIAA PAPER 67-668] 21 p3691 A67-38702
- Mercury fed plasma bridge neutralizers for in-flight operation of SERT II electron bombardment ion thruster [AIAA PAPER 67-670] 21 p3691 A67-38704
- Space electric rocket test /SERT/ II thruster system, discussing flight worthiness and mercury bombardment discharges [AIAA PAPER 67-700] 21 p3693 A67-38728
- SPACE ENVIRONMENT**
- SA EXTRATERRESTRIAL ENVIRONMENT**
- Space environmental effects on metallic and polymeric plastic structures including aluminum, magnesium, titanium, beryllium and stainless steel [SAE PAPER 660675] 01 p0094 A67-10581
- Changing environmental condition effects on spacecraft structure from launch through orbit to entry and recovery [SAE PAPER 660680] 01 p0154 A67-10584
- Fluid power support equipment for space vehicles outside earth atmosphere, based on earth environment effect on various systems [SAE PAPER 660708] 01 p0013 A67-10600
- Ultrahigh vacuum installation using iongetter pumps for analysis of adhesion between plastics and metals in space environment 02 p0228 A67-11552
- Sliding contact wear under very dry high altitude or space conditions due to lack of contact film prevented by using chemical compounds like graphite or lithium carbonate 02 p0221 A67-12435
- Aerospace requirements for bearings and lubricants in natural environments 02 p0250 A67-12454
- Interstellar and intergalactic gas, dust and magnetic fields 02 p0330 A67-12579
- Ames emissivity experiment on OSO-II to measure thermal radiation properties of temperature control coatings exposed to space environment [AIAA PAPER 65-651] 03 p0448 A67-13056
- Spacecraft environmental effects covering outgassing in high vacuum, deterioration of materials by evaporation, lubrication and changes in mechanical and electrical properties of plastics 04 p0704 A67-14995
- Vacuum resonant-cavity dielectricmeter for in situ measurements of complex permittivity in simulated space environment 04 p0625 A67-15708
- Specific degassing of high polymers placed in simulated space environment studied by residual gas analyzer 05 p0832 A67-16304
- Near-earth meteoroid flux measurements for spacecraft design [AIAA PAPER 67-152] 06 p1085 A67-18291
- Radiative heat exchange and equilibrium surface temperature in space environment [AIAA PAPER 67-212] 06 p1115 A67-18328
- Structural adhesives for fabricating large one-piece hemispherical bulkheads, noting effect of radiation and high vacuum 09 p1578 A67-22523
- Satellite material problems in corrosion, fatigue failure, vacuum degradation, etc 10 p1670 A67-23740
- IES conference, Washington, D.C., April 1967, Volume 2, covering space and earth environments, shock and vibration, instrumentation and acoustics IES Conference, Washington, D.C., April 1967, Volume 2, covering space and earth environments, 12 p1922 A67-25705
- Space environment simulation facility for thermal control coatings to study synergistic and healing effects 12 p1924 A67-25711
- Thermal radiation characteristics of spacecraft temperature control louvers in solar space environment, discussing specular reflection [AIAA PAPER 67-307] 12 p2036 A67-26022
- High polymer rubber, plastic, and textile qualitative and quantitative properties, uses in space environment 13 p2143 A67-26698
- Space flight factors effect on mutability, survival rate and dynamics of cells of inactive cultures of chlorella on board Cosmos 110 13 p2060 A67-27336
- Interplanetary space environment effects on spacecraft optical equipment noting thermal design [JPL-TR-32-1098] 13 p2144 A67-27358
- Simulation of magnetospheric effects for possible application to ionospheric probes 14 p2294 A67-29035
- Environmental conditions effect on engineering systems, considering vibration, climatic, pressure, radiation, corrosion, dust penetration, etc 15 p2492 A67-29502
- Effects of space environment on materials - Conference, St. Louis, April 1967 15 p2505 A67-29534
- Astronomical and satellite measurements of meteoroid environment of spacecraft in solar system 15 p2555 A67-29535
- Design, mission and environment considered as criteria in material selection for use in spacecraft 15 p2502 A67-29539
- Space environmental effects on filled elastomers, nylon parachute material and adhesion of metals 15 p2506 A67-29540
- Effects of spacecraft sterilization procedures and Mars dust environment on thermal control coatings 15 p2503 A67-29541
- Silicones performance in high vacuum, temperature extremes and radiation environments of outer space, noting outgassing effect 15 p2508 A67-29557
- Microelectronics practice and possible use of space for fabrication [AAS PAPER 67-79] 15 p2452 A67-29946
- Nuclear reactor use in space environment as energy source for chemical synthesis and laser action [AAS PAPER 67-115] 15 p2558 A67-29962
- Local transportation in commercial space operations, extravehicular activity evolution and space environment characteristics utilization [AAS PAPER 67-116] 15 p2432 A67-29963
- Solar simulation, comparing techniques for reproducing space thermal radiation environment with sun characteristics 16 p2654 A67-30674
- Space environment simulator of CNES in France describing reproduction of low pressure atmosphere, heat sink, solar and planetary radiation, etc 16 p2654 A67-30675
- Space environment factors effects on living organism including changing gravity, high vacuums and solar radiation 16 p2614 A67-31000
- Medicophysiological aspects of NASA program stressing cardiovascular, muscular and osseous problems 16 p2614 A67-31538
- Depressurization behavior of human organism, noting endurance as flight duration and altitude function, and von Beckh chimpanzee absolute-vacuum experiments 16 p2615 A67-31766
- Liquid-metal and plasma MHD systems for power generation in space environments, noting Rankine and Brayton cycles [JPL-TR-32-1129] 17 p2802 A67-32049
- Coordinated laboratory and flight test program, determining stability of solar concentrator reflective surfaces in orbital environment 17 p2832 A67-32060
- Characteristics, operation, technology and reliability of telemetering systems for ESRO I, HEOS A, TD 1 and TD 2 including control factors and coding 17 p2816 A67-32747
- Molecular sink for simulated testing of spacecraft components noting vessel construction, vacuum pump system, molecular trap array, etc 18 p3019 A67-33547
- Control and measurement of temperatures of Mariner IV 18 p3052 A67-34514
- Gemini program study to provide safe and biologically sound method of man qualifying for space exploration 19 p3177 A67-35208
- Terrestrial microorganisms survival in space, noting inactivation effect by solar radiation 19 p3178 A67-35221
- Propulsion sources for one-way unmanned subrelativistic interstellar probes, discussing interaction with deep space environment for vehicle control 19 p3322 A67-35316
- Ground based solar electromagnetic radiation environment studies in visible and radio windows 19 p3323 A67-35332
- Space environment utilization for biological and medical research, physiological studies and therapeutic purposes, discussing orbital hospital and ambulance launch vehicle 19 p3181 A67-35653
- Electromagnetic radiation, elementary particles and micrometeorites effects on earth satellites 19 p3327 A67-35672
- Space environment effects on integrated circuits, discussing FET-MOS type 19 p3196 A67-35675
- Vestibular inaptitude in atmospheric and space flight environment [AD-640908] 19 p3178 A67-35884
- Design, fabrication and testing to enable optical systems to resist space environmental degradation 20 p3445 A67-36568
- In-space hand-held electron beam welding gun design, testing and performance 20 p3454 A67-36575
- Space environmental effect on lubricants and rolling element bearings, comparing evaporative losses of solid and liquid lubricants 21 p3633 A67-38143
- Space electronic equipment design, considering incorporation of vibration, vacuum, micrometeoroid and radiation protection 21 p3591 A67-38209
- Spacecraft optical environment, considering sky luminance, spacecraft corona, spacecraft scattered light and glare sources 21 p3713 A67-38568
- Frequency stability of molecular beam laser in space environment during prolonged continuous and repeatedly interrupted operation 21 p3582 A67-38594
- Bacillus brevis var. G-B survival ratio dependence on space flight factors, noting no induction of dissociation products nor appearance of auxotrophic mutants 21 p3577 A67-38597
- Spacecraft-space plasma electric equilibrium, discussing active spacecraft configurations for control [AIAA PAPER 67-702] 21 p3714 A67-38729
- European rockets characteristics and launch firing ranges, discussing rocket probes for near-earth and space environments 21 p3714 A67-39049
- Preliminary spacecraft concept for real time operational space environment monitoring system 22 p3901 A67-39928
- Mapping of fluctuation field of space and earth environment by electromagnetic techniques 22 p3884 A67-39949
- Sealed silver-cadmium batteries meeting space requirements, discussing high energy plates, cell design and packaging 22 p3749 A67-40230
- Safety control requirements in thermal-vacuum testing involving protection against electric equipment operation in pressure range for glow discharge 22 p3782 A67-40404
- Efficient thermal design of steerable antennas, considering space-environmental requirements 22 p3750 A67-40409
- Astronauts and astronaut support personnel training requirements 23 p3960 A67-40594
- High emittance coatings radiation characteristics investigated for space applications, considering thickness effect on high temperature emittance and space environment effect at moderate temperatures [ASM PAPER C6-4.3] 23 p4020 A67-41404
- Psychophysical study of irradiation phenomena effects on target size perception by investigating luminance, fixation position and corrections 23 p3969 A67-41643
- Indigenous microflora as determined in men undergoing simulated space conditions, considering microbic shock postulated on long term missions 23 p3958 A67-41656
- Manned testing of EVA equipment in simulated space environment, emphasizing crewman ingress and egress and mission objectives 24 p4115 A67-42049
- Space genetics, discussing space environment exposure of experimental animals as cause of mutations, hereditary damage, etc 24 p4113 A67-42053
- Cosmonaut physiological reactions during simulated space environment exposure outside Voskhod II spacecraft 24 p4113 A67-42054
- Solar cell array design techniques for temperature extremes induced by space environment, discussing orbital flight

- requirements 24 p4104 A67-42510
 High temperature Pu 238 heat source fuel capsule operable in space environment is applicable to thermoelectricity and Brayton cycle, discussing design and test program 24 p4185 A67-42536
 Voyager thermal insulation requirements noting tests of vapor deposited Au on Mylar and Kapton [AIAA PAPER 67-777] 24 p4257 A67-42945
 Orbital research hospital design for utilizing zero and low gravity therapeutic value in treating physiological conditions [AIAA PAPER 67-833] 24 p4243 A67-42976
- SPACE ENVIRONMENTAL LUBRICATION**
 System design and lubricating materials for spacecraft lubrication 02 p0250 A67-12453
 Lubrication and bearing problems in space environment, noting molybdenum disulfide and silicones 05 p0811 A67-16932
 Grease lubricants for aerospace application, determining physical properties and testing them at 400 degrees F and under high vacuum [ASLE PAPER 66AM 3C2] 09 p1506 A67-22421
 Lubricant requirements for aircraft parts noting high and low temperature, radiation conditions, lubrication capability limits, etc 19 p3248 A67-34993
- SPACE ERECTABLE STRUCTURE**
 Erectable antenna design for S-band communications between lunar surface and earth during lunar stay portion of Apollo mission 04 p0569 A67-14501
 Theoretical derivation of self-extension velocities of storable tubular extendible member /STEM/ 06 p1008 A67-18594
 Automatic rigidizing of expandable fabric impregnated space structures, detailing gelatin system 08 p1345 A67-20433
- SPACE EXPLORATION**
SA LUNAR EXPLORATION
 Saturn vehicles possible future applications to space exploration 01 p0156 A67-11422
 UN activity concerning agreement in space problem 04 p0740 A67-14549
 Space age facilities - ASCE Conference, Cocoa Beach, Florida, November 1965 05 p0786 A67-16606
 Planning of manned scientific planetary missions, distinguishing critical experiments, taxonomic knowledge and precursor knowledge 06 p1093 A67-19034
 Space mission planning in planetary environments, discussing methods and planetological parameters 06 p1093 A67-19035
 Biological significance of space effort including colonization and adaptation of man to extraterrestrial habitats 06 p0954 A67-19040
 Post Apollo space exploration - AAS Meeting, Chicago, May 1965 08 p1391 A67-21064
 Apollo extension systems, discussing current space technology and accomplishments 08 p1391 A67-21066
 Human performance on earth and in space noting depth perception, visual acuity, walking ability, reaction time, etc 08 p1289 A67-21068
 Space astronomy program development, discussing manned orbital observatory concept and instrumentation 08 p1392 A67-21071
 High energy booster and upper stage combinations for space research, discussing mission capabilities, cost factors, reliability, etc 08 p1412 A67-21075
 Apollo spacecraft, discussing performance of Command and Service Module with typical payloads 08 p1412 A67-21077
 Lunar surface analysis via analysis of reflected signals from RF pulses 08 p1295 A67-21080
 Post Apollo space exploration - AAS Meeting, Chicago, May 1965 08 p1392 A67-21087
 Solar energy role in lunar water production, evaluating efficiency of collector-absorber systems 08 p1317 A67-21094
 Mission requirements for unmanned exploration of solar system including energy and flight time, noting thrust vs ballistic vehicles 08 p1393 A67-21096
 Cosmic space exploration in U.S.S.R., discussing results obtained from Cosmos and Elektron earth satellites 08 p1394 A67-21110
 Direct method for determining space directions and adjustment of satellite triangulation net 10 p1637 A67-23181
 Scattered Lyman alpha radiation in geocorona analyzed using satellite mounted equipment 10 p1706 A67-23223
 Four alternative plans for future U.S. space programs 10 p1710 A67-23636
 Economic, technological and sociological impact of projected manned and unmanned space flights 12 p2040 A67-25234
 R/D on water launched space probes, discussing operation, applications and results 12 p2012 A67-25839
 Legal status of heavenly bodies 12 p2042 A67-26139
 Resolutions of Institute of International Law and UN give state international responsibility for space activity 12 p2043 A67-26145
 Political ramifications of lunar landings, noting UN resolution concerning national possession of moon 13 p2230 A67-26339
 Commercial possibilities in space exploration programs, considering transportation and fuel costs 13 p2231 A67-27512
 Space exploration by automatic, manned and remote-controlled space flight systems, noting applications, limitations, transmission power and distance effects 14 p2256 A67-28036
 French installations for space research, describing laboratory work and industrial investments for satellite launching 14 p2320 A67-28606
 Hardware and life-support systems on submarines and space vehicles, discussing oxygen supply, temperature-humidity control, etc [AIAA PAPER 67-364] 14 p2259 A67-28732
 Navigation and guidance functions performed in typical space-exploration mission 14 p2347 A67-28963
 Design requirements for commercial orbital space stations intended for weather forecasting, agricultural prediction and industrial research [AAS PAPER 67-113] 15 p2557 A67-29961
 Project High Altitude Research Program /HARP/ directed toward use of guns for scientific probing of upper atmosphere [AIAA PAPER 67-38] 15 p2467 A67-30110
 Solid propellants and motors for space exploration, comparing chemical and nonchemical propulsion systems 16 p2735 A67-30702
 High energy liquid propellant boosters, noting design, performance characteristics and limitations 16 p2760 A67-30703
 Comet missions, discussing spacecraft exploration criteria for short period and long period first-apparition comets 16 p2745 A67-30749
 Lunar pogo stick, discussing velocities, horizontal and vertical displacements and weight estimates of man-carrying vehicle 17 p2832 A67-32065
 Book on Japans activities in space exploration including 1966-1967 programs 17 p1316 A67-34618
 Structure and properties of glass-ceramics noting applications to space and oceanographic exploration 20 p3473 A67-36596
 Space program in 1970s, discussing solar system exploration, investigation of universe, practical applications of space and development of technology [AIAA PAPER 67-626] 20 p3530 A67-37613
 U.S. space flight affairs and decisions /1957-1967/ 23 p4086 A67-40918
 Soviet space activity /1933-1967/ noting Sputnik, Venera I, Luna and Zond programs 23 p4086 A67-40919
 U.S. exploration of solar system with unmanned spacecraft 23 p4086 A67-40920
 NASA space program planning and proposed progress in 1970s 23 p4086 A67-40921
- SPACE FLIGHT**
SA INTERPLANETARY FLIGHT
SA INTERSTELLAR TRAVEL
SA ONE-WAY SPACE FLIGHT
SA PLANETARY SPACE FLIGHT
 Fractional g levels for reducing effects of conditioning to zero gravity on prolonged space flights 01 p0018 A67-11397
 Direct ballistic gravity-assisted ballistic and nuclear electric low thrust flight modes for interplanetary exploration 02 p0327 A67-12366
 Space flight projects evaluation and development for long term meaningful space flight program 04 p0740 A67-14550
 Fluid dynamic aspects of space flight NATO-AGARD Specialists Meeting, Marseille, April 1964, Volume 1 04 p0805 A67-14981
 Space flight problems in cis-lunar space, noting lunar probes, high apogee satellite specifications and orbital stability 05 p0897 A67-16731
 Centaur electronic packages for space flight thermal and radiative environmental control 05 p0778 A67-17451
 Missions of Gemini VI through X covering rendezvous, docking, thermal overloading, translation maneuver, etc 06 p1094 A67-18191
 Digital simulation program for system design of long-duration space station of MORL type [AIAA PAPER 67-206] 06 p0981 A67-18512
 Optimal parameter problem of controlled dynamic systems, considering antagonism between designer and nature, applying results to space flight mechanics 06 p1088 A67-18610
 Interstellar flight justification by science fiction writer 06 p1120 A67-19041
 Dynamic characteristics of human operator in tracking system under spaceflight conditions onboard Voskhod II spacecraft dynamic characteristics of human operator in tracking system under space flight conditions 07 p1135 A67-19100
 German contribution to space flight and aerospace technology in international community 07 p1269 A67-19562
 Unmanned Jupiter space flights, discussing requirements for flyby, Orbiter and low thrust missions 07 p1249 A67-19570
 Recent developments in space flight mechanics - Conference, Berkeley, December 1965 08 p1384 A67-20616
 Orientation and navigation in space-time 11 p1820 A67-24936
 Economic, technological and sociological impact of projected manned and unmanned space flights 12 p2040 A67-25234
 Space flight to Mars, discussing medical problems originating from changing gravitational fields, meteorite dangers, radiation and psychological considerations 13 p2061 A67-26338
 Book on mechanics of low thrust space flight covering physical principles and generalized characteristics of engine systems, problems in optimization of space vehicles, etc 13 p2211 A67-26460
 Technical and economical possibilities of fast interplanetary space flight systems 13 p2211 A67-26577
 Medical data on in-flight and postflight physiological performance to determine mans qualifications for long duration space flights 13 p2060 A67-27214
 Space propulsion technology and mission capabilities in fiscal year 2001 13 p2189 A67-27502
 Interstellar space travel evaluation 13 p2206 A67-27509
 AAS Space Flight Mechanics Specialists Conference, University of Denver, July 1966 13 p2206 A67-27515
 Space flight technology developments, particularly for booster rockets and space vehicles 14 p2393 A67-27873
 Factors affecting human spatial orientation system functioning during flights 14 p2254 A67-28211
 Cosmic radiation problems in space flights and in SST flights, examining biological effects, shielding methods, dosimetry and warning systems 14 p2255 A67-28217
 Emergency recompression procedures during space flight studied by exposure of chimpanzees to near vacuum 14 p2257 A67-28219
 Analysis of brain wave records from Gemini flight GT-VII by computations to be used in 30-day primate flight 15 p2425 A67-29104
 Advanced vision research for extended space flight 15 p2430 A67-29274
 Propulsion and vehicle systems for commercial exploitation of space, emphasizing transportation to and from earth orbit [AIAA PAPER 67-82] 15 p2570 A67-29949
 Earth orbital transportation, proposing airline type system and composite nuclear-airbreathing engines for reusability with minimum refurbishment

[AAS PAPER 67-84] 15 p2546 A67-29950
Space tourism potential, cost estimate of equipment, management, etc

[AAS PAPER 67-127] 15 p2558 A67-29965
Commercial space utilization considering space transportation cost as fundamental factor

[AAS PAPER 67-134] 15 p2571 A67-29968
Extravehicular space maneuvering units, manned and unmanned, in satellite laboratory systems, describing space flight requirements and systems

configuration 16 p2615 A67-30631
Correctional maneuver changing space vehicle position on planet approach, assuming flight velocity pulsation during correction 16 p2758 A67-30661
Sleep characteristics during simulated space flight noting influence of noise, angular accelerations and isolation 16 p2613 A67-30913
Radiation protection during space flights, describing dangerous aspects of solar cosmic rays and earth radiation belt 16 p2738 A67-31197
Ultraviolet camera lenses for space flight use discussing techniques for testing and evaluating performance 16 p2680 A67-31805
Combined electric constant low thrust and chemical or nuclear high thrust space propulsion systems for interplanetary missions

[AIAA PAPER 67-511] 18 p3114 A67-33975
Biological problems in prolonged space voyages including oxygen replacement, water supply and food 19 p3179 A67-35209
Economics related to practical extraction of logistics and water from moon, nearby planets and asteroids 19 p3327 A67-35652
Spermatogenesis condition of experimental dogs after 22-day space flight and reproduction function in first offspring generation 20 p3367 A67-36257
Ionizing radiation received by biological tissue during space flights measured by nuclear-emulsion technique 20 p3368 A67-36260
German Institute for Air and Space Travel, 1966 Annual Report 20 p3418 A67-37313
Spacecraft optical environment, considering sky luminance, spacecraft corona, spacecraft scattered light and glare sources 21 p3713 A67-38568
Variational method used to obtain extremal flight conditions, considering flights between circular orbits and planets close to each other 21 p3705 A67-38585
Quality control organization of suppliers to provide reliability of structural component of spacecraft electronic systems 22 p3922 A67-39282
Radiation protection from cosmic rays during space flights, considering shielding, observation and warning, dosimetry and medical provisions 22 p3754 A67-39286
German capability of competing in space travel with other nations 22 p3922 A67-39532
Mission flight profile, considering thrust failure prior to attaining orbital speed, analyzing instantaneous impact point /IIP/ 22 p3831 A67-39610
Hydrogen peroxide oxygen-water supply system as backup for long space flights noting storage tanks, catalytic reactor and heat exchanger 22 p3747 A67-39893
NERVA components including nozzle and associated hot gas bleed port, turbopump, control valve, pressure vessel and thermocouples 22 p3834 A67-40172
Evolution of U.S. space program since inception and future manned and unmanned exploration 23 p4086 A67-40917
Wissenschaftliche Gesellschaft für Luft- und Raumfahrt, Annual Reports 1966 23 p3929 A67-41304
Treatment for relief of altitude decompression sickness for operations requiring extravehicular activity 23 p3960 A67-41702
Mariner space vehicles design evolution noting contribution to future space flights through measurement of atmospheric density of Mars 24 p4241 A67-42399
Reusable shuttle transportation system for lunar base logistics, estimating cost and performance

[AIAA PAPER 67-874] 24 p4140 A67-42995
Launch time prediction with mathematical appendix

[AIAA PAPER 67-906] 24 p4244 A67-43013
SPACE FLIGHT FEEDING
SA DIET
Cosmonauts diets on short, intermediate and long space flights, with suggestions and concepts of onboard natural-food production 20 p3374 A67-36253
Microbic shock in human organism during prolonged space flight due to intestinal tract flora variation from food consumption lacking variety 22 p3750 A67-39334
Food, water and oxygen regeneration and reclamation techniques for long duration space flights, considering carbon dioxide removal, water reclamation from urine and contamination control 22 p3755 A67-40340

SPACE FLIGHT STRESS
SA MANNED SPACE FLIGHT
Space flight acceleration, vibration and ionizing radiation effects on body functions, oxidizing metabolism of central nervous system and fission processes of hemopoietic tissues 01 p0015 A67-10336
Estimation of changes in serum protein concentration under normal stress compared to human sera exposed to simulated altitude and aerospace flights 01 p0015 A67-10950
Biomedical data from U.S. manned space flight experience including cardiovascular and central nervous systems, blood composition changes, etc 01 p0016 A67-11394
Heat, noise, vibration and acceleration simulation to determine beneficial effects of boost and reentry stresses on humans 03 p0366 A67-14389
Chromosome configuration and mitosis impairment in micropores Tradescantia paludosa due to space flight effects of Voskhod I 07 p1133 A67-19109
Medical tests of spacemen Beliaev and Lenov during training and orbital flight 11 p1748 A67-24080
Space flight effect on wheat seeds and plants grown from wheat seeds carried on board Vostok V and VI 11 p1747 A67-24081
Space physiology acceleration problems including engineering aspects of impact absorption 13 p2059 A67-26760
Space flight factors effect on mutability, survival rate and dynamics of cells of inactive cultures of chlorella on board Cosmos 110 13 p2060 A67-27336
Lowering of psychic tone, absentmindedness and vigilance decline during astronaut weightlessness on long space flights 15 p2425 A67-29103
Physiological reactions of man to effect of overload during space flight compared to results of laboratory /centrifuge/ tests 16 p2610 A67-30752
Tracking activity of human operator under effect of certain space flight factors, establishing relationship between control habits and level of hypoxia and hypercapnia 20 p3368 A67-36265
Extreme flight factor effects on human organism determined by simulation, noting physiological function level increase before stress increases resistance 22 p3752 A67-40533
Sensory deprivation in space medicine, discussing irritation spectrum leading to pathological changes in psychic processes of test subjects 24 p4111 A67-41842
Nervous and humoral mechanisms of extralabyrinthine effects on vegetative disturbances during space flight factors 24 p4111 A67-41843

SPACE FOOD
Food quality design for Gemini and Apollo space programs 05 p0757 A67-17261
Potato radiation resistivity improvement in conditions of anoxia 13 p2058 A67-26755
Biological problems in prolonged space voyages including oxygen replacement, water supply and food 19 p3179 A67-35209
Chlorella and Scenedesmus unicellular algae mixture tested for biological protein value in humans for possible food source 19 p3179 A67-35228
Cosmonauts diets on short, intermediate and long space flights, with suggestions and concepts of onboard natural-food production 20 p3374 A67-36253
Determination of energy, water and protein requirements of man under simulated aerospace conditions 23 p3952 A67-41573
Biological value of algal and soya proteins

on four generations of white rats 24 p4111 A67-41847

SPACE GLIDER
Glider takeoff using tow winch, emphasizing flight path and aerodynamic loads and forces 24 p4093 A67-41917

SPACE LABORATORY
System design of integrated automated laboratory payloads in scientific planetary research unmanned spacecraft 02 p0334 A67-12349
Fluid dynamics, structures and operations research and development at Netherlands National Aerospace Laboratory 02 p0231 A67-12640
Laboratory payload concept of automated laboratories for planetary exploration, noting systems engineering advantages 04 p0706 A67-15237
Extravehicular space maneuvering units, manned and unmanned, in satellite laboratory systems, describing space flight requirements and systems configuration 16 p2615 A67-30631
Spacecraft computer managed laboratory /CML/ for flexible decision making in space missions of 1970s 20 p3393 A67-37624
[AIAA PAPER 67-643] 20 p3393 A67-37624
Space simulator growth problems, discussing advantages of orbiting space laboratories 24 p4243 A67-42968
[AIAA PAPER 67-814] 24 p4243 A67-42968
Spaceborne computer-managed laboratory for experiments and instruments control in future space missions 24 p4140 A67-43040

SPACE LAW
Legal analysis of subject of national control over natural planetary bodies 01 p0170 A67-10928
International space control agency needed for 1970s 02 p0343 A67-11815
Soviet book on space and problem of world peace 03 p0538 A67-13200
International law and peaceful uses of outer space 04 p0740 A67-15990
Rule on exhaustion of local remedies and liability for damages inflicted by space vehicles 04 p0740 A67-15991
Communications satellites, legal analysis and prognosis 06 p1120 A67-17711
Space programs and space politics, possible internal and international political effects of lunar or planetary landing 12 p2040 A67-25235
International outer space law - IAF Conference, Madrid, October 1966 12 p2041 A67-26135
International planetary organization with jurisdiction over activities on celestial bodies and lunar and planetary launches 12 p2042 A67-26136
Principles and general standards on rights and responsibilities in lunar exploration 12 p2042 A67-26137
Lawful concept of heavenly bodies 12 p2042 A67-26138
Legal status of heavenly bodies 12 p2042 A67-26139
Satellite telecommunications system, merits of single global system and legal aspects 12 p2042 A67-26140
Communications satellites within framework of space law, noting relation of commercial treaties to communication systems 12 p2042 A67-26141
Legal problems of space research connected with telecommunication and meteorological activity 12 p2042 A67-26142
Global communications satellite networks and emerging customary law for outer space 12 p2043 A67-26143
International legal principles and cooperation requirements for worldwide radio and TV broadcasting by satellite telecommunications 12 p2043 A67-26144
Resolutions of Institute of International Law and UN give state international responsibility for space activity 12 p2043 A67-26145
Legal status of space objects according to different criteria noting international rights, obligations and jurisdiction 12 p2043 A67-26146
Legal problems of salvage and removal of man-made objects from outer space 12 p2043 A67-26147
Legal status of space vehicles, nationality /unilateral decisions/ vs internationality /multinational operation/ 12 p2043 A67-26148

Juridical regime of craft and space installations 12 p2043 A67-26149

Nomenclature applicable to juridical norms regulating outer atmosphere and space activities 12 p2043 A67-26150

Peaceful utilization concept in international cosmic law in relation to UN resolutions and ambiguity 12 p2044 A67-26152

Legal and political aspects of international meteorological data collection and distribution system, including use of satellites 12 p2044 A67-26153

U.S. and U.S.S.R. in space science and technology, noting limited progress in legal management, control, use and equitable division of space 12 p2044 A67-26154

Legal forms of international cooperation of U.S.S.R. in peaceful exploration of outer space, discussing bilateral and multilateral agreements between government and nongovernment organizations 12 p2044 A67-26155

Political ramifications of lunar landings, noting UN resolution concerning national possession of moon 13 p2230 A67-26339

Formal foundation of law of outer space 13 p2230 A67-27098

Business, government and possible home applications /including mail and education/ for electronic communications via satellites, discussing legal implications [AAS PAPER 67-91] 15 p2437 A67-29952

Space law education 16 p2782 A67-30789

International aspects of space applications and political, legal and economic problems involved 19 p3349 A67-35639

Legal aspects of use of satellites in exploiting earthbound or near-in natural resources 19 p3349 A67-35641

Salvage and removal problems of man-made objects from outer space, stressing need for international procedures and standards 20 p3556 A67-36484

Legal problems associated with telecommunications and meteorological satellites and with launching and retrieval of manned spacecraft 24 p4257 A67-42387

Outer Space Treaty by 82 nations evaluated, emphasizing nature of task facing each nation in developing own methods for compliance 24 p4257 A67-42389

Geopolitical factors connected with navigation satellite operation and control [AIAA PAPER 67-960] 24 p4260 A67-43041

SPACE LOGISTICS

Space support, discussing functions during planning phases, constraints, systems engineering approach and integration of subsystems into unified scheme [SAE PAPER 660688] 01 p0049 A67-10592

Integrated logistics system capable of supporting earth orbital operations and sufficiently flexible for demanding applications of space and lunar operations [AIAA PAPER 66-864] 02 p0331 A67-12262

Space rescue capability and proposed concepts to achieve it [AIAA PAPER 66-905] 02 p0332 A67-12271

Effects of space station logistic requirements on design of spacecraft configurations with various hypersonic lift/drag ratios, comparing payload, cost, etc [AIAA PAPER 66-958] 02 p0332 A67-12286

National space inventory of launch vehicles, spacecraft, space station studies, facilities and projected modifications evaluated for USAF low earth orbital logistics [AIAA PAPER 66-866] 03 p0519 A67-14017

Titan III system capability for space support and logistics, discussing parameters of assessment 08 p1412 A67-21076

LEM Truck concept based on Apollo hardware, delivering payloads for increase of lunar staytime and radius of operations 08 p1316 A67-21084

Manned Orbital Research Laboratory /MORL/ design and utilization 08 p1414 A67-21545

Economics related to practical extraction of logistics and water from moon, nearby planets and asteroids 19 p3327 A67-35652

Logistics in 1970s - Conference, Washington, D.C., September 1967 23 p4084 A67-40579

Earth orbital integrated logistics system extendable to space and lunar operations, considering technical and economic feasibility 23 p4061 A67-40592

Astronauts and astronaut support personnel training

requirements 23 p3960 A67-40594

SPACE MAINTENANCE

Maintainability, reliability and operational flexibility of manned orbital space station [AIAA PAPER 66-933] 02 p0331 A67-12252

Maintenance, assembly and construction in space, discussing environmental effects such as zero gravity, radiation, high vacuum and meteoroids 05 p0902 A67-17247

Maintenance, assembly and construction in space, discussing environmental effects such as zero gravity, radiation, high vacuum and meteoroids 16 p2741 A67-30445

Apollo Applications Program objectives, discussing revisitation and reuse of hardware left in orbit, in-flight maintenance for long duration space missions, etc 18 p2994 A67-34657

MARCEP mathematical and mission simulation models to evaluate parameters affecting maintainability of long duration manned space flights 18 p3138 A67-34688

Sterile lock and split-seam techniques for sterile insertion and repair of spacecraft 19 p3180 A67-35259

Spacecraft and space station reliability by orbital maintenance and extravehicular activity, comparing redundancy on system and cost effectiveness [AIAA PAPER 67-652] 20 p3535 A67-37629

Human engineering performance data for equipment design for manned space systems, discussing zero gravity maintenance and repair [AIAA PAPER 67-653] 20 p3375 A67-37630

Spacecraft equipment in-space maintainability design criteria 23 p4070 A67-40591

Earth orbital integrated logistics system extendable to space and lunar operations, considering technical and economic feasibility 23 p4061 A67-40592

Computerized microfilm or magnetic tape production for manned space station maintenance documentation 23 p4071 A67-40593

Part and component cleanliness maintenance for hydraulic systems, liquid propellants and spacecraft interiors, noting protective methods [SAE PAPER 670825] 24 p4159 A67-41989

Long term manned space mission system effectiveness and reliability through interchangeability and redundancy noting optimization, tradeoffs, maintenance and spares [AIAA PAPER 67-984] 24 p4166 A67-43056

SPACE MECHANICS

AAS Space Flight Mechanics Specialist Conference, University of Denver, July 1966 13 p2206 A67-27515

Geometrical form for solar system escape criterion 17 p2940 A67-32075

Inertial motion of solid body in space of constant curvature, obtaining solution to differential equation 18 p3079 A67-34372

Book on mechanics of controlled body including control system realization, motion programming, dynamic error assessment and three-dimensional problems 20 p3482 A67-37459

Method for determining physical interactions in system of bodies with arbitrary perturbations, using vector form equation 21 p3657 A67-37987

Book on astronautics covering rocket theory, celestial mechanics and space problems 21 p3703 A67-38434

Solar system resonances emphasizing nongravitational forces in resonance formation and asteroid collision formation of Kirkwood gaps 23 p4062 A67-40623

General Pythagorean three-body problem solved completely using numerical method 23 p4062 A67-40624

Jacobi high energy ellipsoid orbits in barred spirals valid at galactic time scales 23 p4063 A67-40898

Solution to Burrau three-body problem including historical and scientific background 24 p4232 A67-42605

SPACE MISSION

Comparison of performance of atom-ion and colloidal thruster systems for orbital transfers, noting influence of various parameters on mission capabilities 04 p0688 A67-14560

Trajectory modes for manned and unmanned missions to Mercury, 1980-2000 [AIAA PAPER 67-28] 06 p1086 A67-18333

Planetology and space mission planning -

Conference, New York, November 1965 06 p1090 A67-18993

Gimballed unitized stellar reference inertial platform for space missions, noting optical lobing technique 08 p1331 A67-20699

Voyager project, orbital operations, objectives for 1971, etc 08 p1412 A67-21097

Measurements performed from Mariner type probe during intercept with comet complement measurements performed from ground-based astronomical observatories by direct sampling 08 p1393 A67-21098

Interplanetary trajectory design, considering energy and duration of mission, arrival velocity at target and earth, use of Hohmann transfer orbit, trajectory maps, etc 08 p1401 A67-21282

Psychology and space flight 09 p1454 A67-22056

Earth-based navigation for two-spacecraft missions using analytical techniques for POLYDOP tracking data 13 p2155 A67-27526

Conservation of cryogenic propellants on long duration space missions by reliquefaction of vapor 13 p2091 A67-27636

Hydrodynamic gas spin bearing gyroscope design for long duration space missions 14 p2322 A67-29084

Humidity, temperature, contamination and disconnection effects on gasket and grease seals for extended space mission computer connectors 15 p2442 A67-29182

Space rescue mission planning and targeting by computer 15 p2555 A67-29609

Display/control system of Mission Control Center, Houston, operation and performance 15 p2467 A67-29736

Nuclear power and propulsion systems for space applications, discussing present and future technologies [AAS PAPER 67-132] 15 p2516 A67-29967

Future lunar surface missions, defining adequate spacecraft configurations by applying technology and hardware developed on Apollo Lunar Module program [AIAA PAPER 67-27] 15 p2571 A67-30102

Future interplanetary unmanned space missions, examining velocity requirements and launch vehicle and payload sizes necessary for scientific investigation of solar system [AIAA PAPER 67-29] 15 p2562 A67-30104

Automatic photopolarimeter as pilot model for scans of planetary disks on fly-by missions 15 p2492 A67-30435

Photo-optical instrumentation for biosatellite 30-day orbiting primate mission discussing adverse environmental effects and other constraints regarding requirements 16 p2680 A67-31806

Manned space mission requirements and application of space power technology to multipurpose space stations, noting operation of Pu-238 isotope/Brayton cycle unit 17 p2953 A67-31979

Linear/Monte Carlo method performance evaluation of intercept/rendezvous guidance and navigation for advanced space missions 17 p2882 A67-32493

Primary electric propulsion application to satellite and other space missions, considering auxiliary systems and experimental thruster systems [AIAA PAPER 67-426] 18 p3112 A67-33910

Problem areas within cryogenic chemical and nuclear propulsion systems for space missions, noting available technology and limitations [AIAA PAPER 67-454] 18 p3110 A67-33928

Telecommunication system for lunar, planetary and deep space flight mission control and data acquisition 19 p3207 A67-35224

Lunar orbiter missions goals and design, spacecraft construction and equipment and examination of lunar surface photographs 19 p3319 A67-35268

Method for assigning numerical value to space scientific payload effectiveness toward satisfying mission goals 19 p3322 A67-35319

System reliability and effectiveness in manned and unmanned geological/geophysical space missions 19 p3332 A67-35323

In situ study of comets by solar electric propulsion spacecraft, analyzing mission characteristics 19 p3323 A67-35333

Manned orbiting laboratories for exploring planets by remote sensing and planetary encounter missions compared to landing and

flyby 19 p3332 A67-35336
Operational capabilities of Saturn-Apollo
space vehicle, discussing lunar
missions 19 p3333 A67-35643
Research areas in future NASA program
covering materials, energy conversion,
guidance, instrumentation,
etc 19 p3349 A67-35645
Multipurpose entry vehicle requirements
for unmanned landings on bodies in solar
system having tenuous atmospheres
[AIAA PAPER 67-599] 19 p3336 A67-35995
Multiplanet mission for Jupiter, Saturn,
Uranus and Neptune, using swingby
technique for probe launched in late 1970s
[AIAA PAPER 67-613] 19 p3329 A67-36002
Optical subcarrier communications, noting
use space-oriented missions and RF
techniques optical subcarrier
communications, noting use in space-oriented
missions and RF 20 p3378 A67-36183
Comparison of performance of atom-ion
and colloidal thruster systems for orbital
transfers, noting influence of various
parameters on mission
capabilities 20 p3515 A67-36407
Solid propellant gas generator power
systems for normal and emergency space
operations 20 p3533 A67-36601
Multipurpose orbital bus-vehicle for
alternate missions [AIAA PAPER 67-638] 20 p3534 A67-37618
Spacecraft computer managed laboratory
/CML/ for flexible decision making in space
missions of 1970s [AIAA PAPER 67-643] 20 p3393 A67-37624
Trajectory modes for manned and
unmanned missions to Mercury,
1980-2000 21 p3700 A67-37782
Space vehicle tracking noting significance
of accuracy and rapidity in determination of
position, velocity and
acceleration 21 p3583 A67-38642
High payload electric propulsion spacecraft
powered by solar array for multiple
interplanetary missions [AIAA PAPER 67-711] 21 p3714 A67-38738
Solar electric propulsion for space
missions, evaluating modularized ion
propulsion systems to determine effect of
electric isolation on system reliability,
weight, etc [AIAA PAPER 67-699] 21 p3697 A67-38959
Solar flare occurrences probability,
designating two-year period centered on
sunspot minimum as safe time zone for
vehicles on missions to Mars and
Venus 22 p3873 A67-39929
Multiple payload mission planning for
multiple and single earth orbits and apogee
motor delivery, evaluating cost and
performance 22 p3903 A67-39952
Highly reflective coatings and interference
filters for silicon solar cells on spinning
spacecraft on near-sun
mission 23 p3937 A67-41490
Galactic radiation hazard for long term
space missions, discussing life shortening
effect 23 p3953 A67-41583
Thermophysical research requirements for
Venus Lander, Jupiter Entry Probe and
Mercury Orbiter planetary exploration
missions 24 p4227 A67-42041
Stirling, Brayton and Rankine dynamic
cycles compatibility with isotope heat
sources, emphasizing power system
applications to long-duration earth orbital
missions 24 p4185 A67-42542
Nuclear electric space power plant with
Rankine cycle for plausible Mars manned
mission, discussing mission requirements and
reactor elements 24 p4186 A67-42549
Primary electric propulsion application to
satellite and other space missions,
considering auxiliary systems and
experimental thruster systems [AIAA PAPER 67-426] 24 p4208 A67-42901
Water immersion simulation, studying
astronaut performance characteristics in
Gemini and proposed Apollo missions
[AIAA PAPER 67-773] 24 p4116 A67-42941
Apollo manned Lunar Module /LM/ earth
orbital development missions, reviewing key
subsystems and technical problems
[AIAA PAPER 67-863] 24 p4244 A67-42987
U.S. launch operations techniques
emphasizing launch site testing prior to
launch [AIAA PAPER 67-889] 24 p4140 A67-43002
R and D deep space communication

system planning methodology for comparing
laser, IR and mm wave possibilities,
analyzing tradeoff and optimizations
[AIAA PAPER 67-973] 24 p4260 A67-43050
SPACE NAVIGATION
SA ASTRONAUTICS
SA INTERPLANETARY NAVIGATION
Recursive space navigation applied to
navigating in near orbit of planet by
measuring directions to known
landmarks 01 p0110 A67-11157
Autonomous space navigation system using
optical spatial filter techniques for
recognition and tracking of planetary
surfaces and star fields 02 p0264 A67-12316
Human space navigation in vicinity of
earth and in and out of solar
system 04 p0695 A67-14517
Onboard guidance scheme as backup to
earth-based orbit determination techniques
and for approach navigation and orbit
correction in planetary capture
maneuver 04 p0654 A67-15234
General mechanization in vehicular
coordinates of gimballess inertial system for
space navigation, obtaining equations for
position errors and error damping
method 08 p1351 A67-20698
Cislunar navigation assuming availability of
power for making changes in attitude,
velocity and direction, considering factors
affecting space navigator 08 p1351 A67-21100
Maximum data recovery from
interplanetary reconnaissance probe by
returning vehicle to earth vicinity, using
space velocity meter as navigation
instrument 08 p1332 A67-21102
Visibility of point sources approaching or
receding from high luminance source in
apparent frontal plane 08 p1351 A67-21103
Limitation of radio position-finding with
increased spacecraft distances, noting
navigational methods from ground and
spacecraft 11 p1817 A67-24707
Space station operations in navigation and
tracking, communication coverage, abort
recovery, etc 12 p2012 A67-25743
Space activities effect on International
Civil Aviation Organization including
navigational problems, aircraft
communication, meteorological data and
technological advances 12 p2043 A67-26151
Visual aspects of transstellar space
flight 12 p2009 A67-26233
Gravitational satellite stabilization, star
tracking, targets and sensors for orientation
and inertial navigational
instrumentation 14 p2347 A67-27878
Optimum control of earth satellites and
space vehicles and stable solutions of orbits
in orbital mechanics 14 p2393 A67-27879
Linearized manual space navigation
incorporating redundant measurements to
compensate for instrumentation
inaccuracies 14 p2347 A67-28128
General purpose digital computer for
airborne and spaceborne guidance and
navigation systems 14 p2275 A67-28684
Navigation and guidance functions
performed in typical space-exploration
mission 14 p2347 A67-28963
Orbiting navigation with compensation for
periodic errors, using modified Kalman
filtering technique 15 p2513 A67-29595
Principle of recursive
navigation 16 p2700 A67-30656
Advanced range and orbit determination
/AROD/ using airborne equipment to
originate control and tracking signals by
checking ground stations 16 p2701 A67-31491
Autonomous landmark tracking by
holography for space
navigation 17 p2881 A67-32436
Deflected laser beam use in TV,
machining, photo etching, space navigation
and data storage 19 p3239 A67-35060
Deep space navigation and guidance
technology, emphasizing simplification of
onboard navigation procedures 19 p3255 A67-35856
Software aspects of space navigation
including computer programming, mission
planning, error analysis and reliability
realization 19 p3187 A67-35858
Strapdown inertial reference and
navigation system initial alignment utilizing
coordinate-transformation matrix computer
[AIAA PAPER 67-556] 19 p3257 A67-35953
Initial-convergence examination of Kalman
filter for various autonomous navigation
modes

[AIAA PAPER 67-623] 19 p3260 A67-36012
Energy accumulator and constant power
propulsion system for near-circular orbit
space maneuvering, considering two-vehicle
encounter 21 p3689 A67-37985
Rocket control using analog computers,
determining thrust vectors for
trajectory 21 p3655 A67-38208
Autonomous solution to orbital navigation
problem yielding direct measure of orbital
parameters 22 p3830 A67-39179
Doppler effect method application to
satellites and space vehicles motion, giving
formulas for satellite velocity, orbital shape
and position 22 p3831 A67-39588
Speedy generation of space flight guidance
command signals and comparative analysis of
operational schemes for generating guidance
signals 22 p3832 A67-40145
Optimal filtering theory for horizon sensor
data processing for orbital navigation,
examining statistical
characteristics 22 p3834 A67-40196
Hand-held sextant capability in in-flight
spacecraft navigation measurements -
[AIAA PAPER 67-775] 24 p4183 A67-42943
SPACE ORIENTATION
Satellite triangulation based on
simultaneous observations from two stations
defining space orientation of
plane 01 p0055 A67-10037
Information model for manual control of
astronaut motion and space orientation in
free space 02 p0188 A67-12330
Inertial system using gyros and
accelerometers, determining autonomously
plant curvilinear coordinates and plant space
orientation parameter 03 p0465 A67-13617
Spacecraft orientation during
interplanetary flights, using system
employing two rigidly connected telescopes,
one aimed at sun and other aimed at
stars 11 p1751 A67-24084
Time dependent orientation of body fixed
coordinate system relative to stars for
spinning rigid torque-free
body 13 p2154 A67-26816
Catalog tabulating 1600 comet tail
orientation observations 14 p2386 A67-28481
Extraterrestrial vestibular research in
orientation of humans in space, noting
possible disorders due to radiation and lack
of protection 15 p2425 A67-29106
Passive orientation of space vehicle
toward sun by black and white coating,
analyzing free oscillation about
equilibrium 21 p3713 A67-38598
SPACE PHOTOGRAPHY
SA ASTRONOMICAL PHOTOGRAPHY
Cloud cover space photography by
Voskhod I and Voskhod II to determine
spatial structure of clouds of various types
and fields of brightness 01 p0110 A67-11429
Ultimate sensitivity of space camera
imaging devices with particular reference to
slow scan vidicon 02 p0245 A67-12245
Earth azimuthal perspective projections
/cosmographic projections/ in space
photograph interpretation 03 p0419 A67-13264
Panoramic facsimile camera for unmanned
space operation providing 360 degrees IR
and visible spectrum imagery
[SMPT PREPRINT 100-40] 03 p0423 A67-13806
Photometric analysis of twilight halo
photographs by Vostok VI
spacecraft 03 p0415 A67-14227
Meteorological studies from manned
spacecraft, discussing interpretation of cloud
pictures and optical inhomogeneity of
troposphere and
stratosphere 07 p1221 A67-20008
NASA earth orbital photographic
experiments planned for 1967-1969 as
supplement to Mercury and Gemini
efforts 12 p1940 A67-25433
Photometric analysis of twilight halo
photographs by Vostok VI
spacecraft 12 p1932 A67-25483
Aerial and space photography for
forestry 14 p2321 A67-28827
Potentialities of space cartographic
systems evaluated for geometric map
accuracy and economic aspects
[AAS PAPER 67-106] 15 p2478 A67-29960
Mariner IV photographs of Mars,
discussing mission objectives, functioning of
camera system and interpretation of
pictures 18 p3123 A67-34150
Meteorological satellite program results,
discussing Tiros satellites cloud pictures,

- storm warning, etc 19 p3253 A67-35637
 Altitude variation of air scattering coefficient determined from brightness profile measurements of haze at planet limb, using spacecraft 20 p3432 A67-37238
 Analog and digital data processes for interplanetary photoscience with reference to Mariner Mars flyby mission, discussing telemetric transmission and SNR [IEEE PAPER 19-TP-66-1134] 23 p3998 A67-40740
 Lunar Orbiter design, development, testing and space flight 24 p4241 A67-42404
- SPACE POWER UNIT REACTOR /SPUR/**
 Shield-radiator weight tradeoffs to optimize K Rankine cycle space power plant heat source operating temperature, noting burnup 24 p4185 A67-42537
- SPACE PROBE**
 SA DUMBBELL SPACE PROBE
 SA MARINER II SPACE PROBE
 SA MARINER IV SPACE PROBE
 SA MARINER SPACE PROBE
 SA MARS PROBE
 SA PIONEER VI SPACE PROBE
 SA PIONEER VII SPACE PROBE
 SA PIONEER SPACE PROBE
 SA SOLAR PROBE
 SA VENUS PROBE
 SA ZOND II SPACE PROBE
 SA ZOND III SPACE PROBE
 Alpha Centauri probe and sun-orbiting concentrator to power probe 01 p0155 A67-11403
 Tape recorder design for spaceborne data storage using isoelectric drive principle of peripherally driving tape packs to obtain high reliability 02 p2424 A67-12018
 Unmanned spacecraft systems design for deep space probes, examining flyby and orbiter missions, attitude stabilization, etc [AIAA PAPER 66-887] 02 p0331 A67-12266
 Low energy charged particle measurements, describing satellite mounted spherical electrostatic analyzer 02 p0310 A67-12571
 Velocity requirements for orbital transfer and selection criteria for comet missions from 1967 to 1986 03 p0510 A67-13491
 Scientific program and instrumentation of comet probe 03 p0510 A67-13496
 Five-comet probe mission, discussing velocity requirements for launch from earth orbit, cometary brightness, weight requirements and possible carrier rockets 04 p0695 A67-14532
 Space probe launching conditions for accurate cometary orbit 05 p0895 A67-16574
 Near-earth cosmic dust cloud and data obtained from satellite, rocket and ground measurement 06 p1083 A67-18161
 Recoverable high altitude rocket space probe with paraglider 07 p1259 A67-19573
 German papers on space research with satellites and space probes, Volume 1, Physical principles and methods of constructing carrier rockets 07 p1260 A67-20265
 German papers on space research with satellites and space probes, Volume 2, Control, test stands and direction finding 07 p1260 A67-20266
 Self-contained midcourse guidance system with space velocity meter /SVM/ used in returning probe to earth vicinity for data retrieval and orbit control 08 p1331 A67-21101
 Tabulated localized cosmic X-ray sources and survey of rocket probe identifications 11 p1857 A67-24633
 Cosmic ray measurements in interplanetary space and on moon noting intensity increase 12 p1992 A67-25123
 Magnetic and plasma observations of Explorer X and Mariner II confirmed that interplanetary shock waves give rise to sudden storm commencements magnetic and plasma observations of Explorer X 12 p2008 A67-25823
 Interplanetary medium including solar wind, geomagnetosphere and observation instruments 12 p2009 A67-26173
 Solar activity effect on brightness and polarization of zodiacal light 13 p2109 A67-26332
 Velocity requirements for scientific probe vehicles in direct flight and planetary swingly modes of operation throughout solar system 14 p2387 A67-28618
 RF hardware implementation techniques utilizing devices illustrated in block diagrams 14 p2287 A67-28680
 Launching of space probes and data obtained on radiation particles and magnetic fields in space 14 p2392 A67-28960
 Simulation of magnetospheric effects for possible application to ionospheric probes 14 p2294 A67-29035
 Near-earth cosmic dust cloud and data obtained from satellite, rocket and ground measurement 16 p2741 A67-30505
 Development, design and test operation of attitude control system of space probe with mission duration of 7 minutes [ONERA-TP-271] 16 p2758 A67-30653
 Comet mission study using space probes boosted by Atlas Agena and Atlas Centaur launch vehicles for interception from 1967 to 1975 16 p2745 A67-30750
 Comparison of lunar surface photography from space probes and ground-based observatories 16 p2671 A67-30990
 Moon surface origin and present surfaces of moon, Venus and Mars as determined from lunar photographs and data by flyby probes 18 p3121 A67-34135
 Optical and stereoscan microscope scanning combined with X-ray microanalysis used to investigate results on collection surfaces of space probes 19 p3339 A67-35197
 Day-and nighttime electron and ion density profiles in lower ionosphere deduced from blunt probe theory and measurements 19 p3218 A67-35213
 Asteroid belt study with spin-stabilized flyby probes 19 p3322 A67-35317
 Space probe rendezvous with Halley comet, considering use of planetary gravity field to modify trajectory [AIAA PAPER 67-614] 19 p3329 A67-36003
 Weightlessness state in atmosphere and vacuum applied to satellites and space probes, noting effects on passengers and equipment 20 p3418 A67-37260
 Small and large orbiting observatory satellites compared for operational needs, interference problems, scheduling and multisampling of space phenomena [AIAA PAPER 67-634] 20 p3534 A67-37616
 Unmanned spacecraft systems design for deep space probes, examining flyby and orbiter missions, attitude stabilization, etc 21 p3712 A67-37781
 Electrometer and varactor devices for onboard low current measurements in space probes 21 p3599 A67-38634
 Magnetic dipole moments of moon, Mars and Venus using space probes, discussing solar wind near-earth planetary field interaction measurements [JPL-TR-32-1059] 21 p3709 A67-38992
 CNES rocket probe mobile launching unit for auroras, eclipses and Van Allen belt layer experiments 21 p3609 A67-39051
 Unmanned probe and launch vehicle selection for solar system exploration, considering tradeoffs in terms of reliability, cost, weight, experimental accuracy, etc 22 p3900 A67-39617
- SPACE PROGRAM**
 SA EUROPEAN SPACE PROGRAM
 SA NASA PROGRAM
 SA U.S.S.R. SPACE PROGRAM
 Rocket propulsion for U.S. space program, considering early unmanned space exploration, manned Mercury flights, Gemini flights, etc 01 p0141 A67-11265
 Reusable space vehicles role in overall space program, noting orbital missions in future and economic impact [AIAA PAPER 66-862] 02 p0343 A67-12261
 Method for propulsion system selection, design and optimization on total space program cost effectiveness basis [AIAA PAPER 66-976] 02 p0305 A67-12298
 Nuclear propulsion systems development for U.S. space program 02 p0266 A67-12336
 Gemini manned space flight program 02 p0327 A67-12363
 Space flight projects evaluation and development for long term meaningful space flight program 04 p0740 A67-14556
 Coding method for transmitting digital data over IRIG-FM/FM telemetry system applied to German-American high altitude/space flight program 04 p0569 A67-14572
 Program for radioisotopic power on Nimbus B spacecraft provided by SNAP-19 generators 05 p0843 A67-16553
 COSPAR manual on establishment of rocket launch facility 06 p0979 A67-17553
 Applied mathematics of space program fluid mechanics and aerodynamics 06 p0983 A67-17783
 Planetary transportation model application to space program planning 06 p1093 A67-19032
 Specification and evaluation of space projects and programs, noting model construction and planning 06 p1093 A67-19033
 Economics of U.S. space program, effect on overall economy, research, geographical regions, manpower, etc 06 p1120 A67-19038
 Biological significance of space effort including colonization and adaptation of man to extraterrestrial habitats 06 p0954 A67-19040
 Unmanned spacecraft program costs estimation through empirical studies of past and current NASA programs [AAS PAPER 66-149] 08 p1429 A67-20969
 Planning-Programming-Budgeting System /PPBS/ implementation by Federal agencies and relation to space activities [AAS PAPER 66-150] 08 p1430 A67-20970
 Manned planetary mission possibilities stressing Mars exploration, noting trajectory planning, propulsion, crew requirements, etc 08 p1394 A67-21099
 Space systems performance, components and modes of operation, showing merits in terms of entire space program 08 p1431 A67-21108
 Economic impact of defense and space programs 10 p1735 A67-23629
 Space programs and space politics, possible internal and international political effects of lunar or planetary landing 12 p2040 A67-25235
 Evolutionary manned interplanetary exploration program with modular elements used for flyby, orbital capture and Mars landing, noting influence of Apollo program 13 p2199 A67-26827
 Commercial possibilities in space exploration programs, considering transportation and fuel costs 13 p2231 A67-27512
 Management of aerospace programs - AAS Conference, University of Missouri, November 1966 13 p2231 A67-27545
 Manned interplanetary program planning, suggesting basic parameters for manned trip to Mars and Venus 13 p2210 A67-27546
 Cost models for complex space programs, analyzing data acquisition systems, computer routines, etc 13 p2232 A67-27547
 Unmanned spacecraft program costs estimation through empirical studies of past and current NASA programs [AAS PAPER 66-149] 13 p2232 A67-27550
 Planning-Programming-Budgeting System /PPBS/ implementation by Federal agencies and relation to space activities [AAS PAPER 66-150] 13 p2232 A67-27551
 Communication satellite program research 14 p2269 A67-28455
 Future planning of interplanetary voyages based on capabilities and economic advantages of classical propulsion, noting high escape velocity 14 p2392 A67-28961
 Economics of military space launching systems 15 p2566 A67-29830
 Management control system for technical production, financial and contractual management of large scale or technical industry programs [AAS PAPER 67-153] 15 p2583 A67-29963
 Launch operations requirements for future space programs [AAS PAPER 67-37] 15 p2467 A67-30109
 Support requirements for future manned space programs [AAS PAPER 67-56] 15 p2562 A67-30120
 Space project management noting job definition and organization for implementation and control 16 p2783 A67-31630
 Book on Japans activities in space exploration including 1966-1967 programs 17 p1316 A67-34615
 Manpower planning concept assuring personnel availability for space missions 18 p3162 A67-34677
 Indonesian space center, describing radar and optical tracking systems, launch complex telemetry system, etc 19 p3207 A67-35234
 Space research in Brazil, discussing rocket launching facility, meteorological experiments, X-ray astronomy, satellite observations, etc 19 p3320 A67-35285

- Australian space research, discussing support to Apollo and U.S. manned space flight programs, ionospheric observations, satellite information, etc 19 p3320 A67-35286
- Canadian space research, detailing sounding rocket and satellite launches 19 p3320 A67-35288
- Mexican space research activities noting studies in meteorology, aeronomy, solar radiation, communications, tracking, astronomy and geomagnetism 19 p3321 A67-35298
- Japanese national report on space research to COSPAR 19 p3321 A67-35300
- Swedish space research organization, participating groups and experiments 19 p3321 A67-35302
- Spanish space research activities, describing organization, facilities, participating institutions and training programs 19 p3321 A67-35303
- South African space research, describing ground-based observations and tracking stations 19 p3321 A67-35304
- United Kingdom space research activities since May 1966, noting facilities, ground-based studies and rocket and satellite tracking experiments 19 p3322 A67-35306
- Canadian program for IQSY including aurora studies, solar observation, space research, etc 19 p3322 A67-35498
- Practical space applications - Conference, San Diego, February 1966 19 p3326 A67-35634
- Application satellite program, discussing meteorological and communications satellites, noting ESSA 1, Syncom, etc 19 p3333 A67-35635
- International aspects of space applications and political, legal and economic problems involved 19 p3349 A67-35639
- Space program applications for environmental sciences and operations including oceanography, seismology, wind direction, etc 19 p3253 A67-35647
- Economic considerations of space operations noting cost identification, program planning, maximum utilization, etc 19 p3350 A67-35648
- Space utilization by joint venture approach, discussing communications, ocean studies, etc 19 p3350 A67-35651
- Management of aerospace programs, discussing budgeting and contracting procedures 19 p3350 A67-35679
- Design, construction and procedure changes in Apollo following fire of January 1967 19 p3334 A67-35928
- Satellite retrieval system called Space Bola, employing passive/active grappling units depending on target vehicle dynamic characteristics 20 p3532 A67-36556
- Solid propellant stages development from experience acquired in France to future large space projects 20 p3516 A67-36878
- Space program in 1970s, discussing solar system exploration, investigation of universe, practical applications of space and development of technology [AIAA PAPER 67-626] 20 p3530 A67-37613
- National space program planning viewpoint of Executive Branch of Federal Government [AIAA PAPER 67-628] 20 p3556 A67-37619
- Trends in contracting that will influence spacecraft design and development in 1970s [AIAA PAPER 67-641] 20 p3557 A67-37623
- Purification systems, filters and porous materials applications to liquids and gas systems associated with spacecraft, boosters and ground support equipment 21 p3570 A67-38103
- Space electronic program management and requirement integration, discussing functional or matrix type organization and project organization 21 p3734 A67-38215
- Three-impulse interplanetary rendezvous trajectory as solution of time fixed multipulse space problem 22 p3887 A67-40137
- Progress in various space programs noting NASA role 23 p4086 A67-40668
- Evolution of U.S. space program since inception and future manned and unmanned exploration 23 p4086 A67-40917
- INTELSAT I communications satellite, discussing communications gear design and U.S. domestic satellite program 23 p4086 A67-41430
- U.S. unmanned satellite program history, aims, success and failures 24 p4258 A67-42752
- Cost estimating techniques for military and NASA programs, comparing spacecraft resource forecasting with expenditure estimates [AIAA PAPER 67-809] 24 p4259 A67-42966
- Booster recovery systems development, payload and operational costs evaluated using postulated space program [AIAA PAPER 67-909] 24 p4245 A67-43016
- Man in space programs, examining costs and benefits [AIAA PAPER 67-927] 24 p4117 A67-43023
- Hazard studies and safety analyses qualitative method using checklist of possible mishaps and human errors [AIAA PAPER 67-935] 24 p4260 A67-43025
- Onboard computer-based checkout simulator system to assist astronauts in monitoring data requirements of future space programs [AIAA PAPER 67-951] 24 p4127 A67-43035
- Onboard checkout system /OCS/ impact on space station program [AIAA PAPER 67-953] 24 p4245 A67-43037
- SPACE RADIATION**
- SA EXTRAGALACTIC RADIATION
- SA GAMMA RADIATION
- SA INTERSTELLAR RADIATION
- SA PRIMARY COSMIC RADIATION
- Coherent amplification of RF radiation in cosmic space 01 p0144 A67-10836
- Physical characteristics affecting detection efficiency of Geiger counters, proportional counters and ion chambers used in space measurements of particles 02 p0244 A67-12209
- Radioisotope sources used for simulating space radiations, obtaining energy spectra by blending beta emitters 02 p0265 A67-12213
- Space radiation monitoring system aboard manned spacecraft to provide solutions to medical problems and safety of flight guidelines for mission control 02 p0188 A67-12387
- Planetary distribution and interpretation of abrupt increases in cosmic ray intensity observed during periods of maximum solar activity but not related to visible solar phenomena 02 p0312 A67-12602
- Dispersion angle of radio waves in interplanetary plasma 03 p0368 A67-13279
- Nuclear and space radiation effects - IEEE Conference, Stanford University, July 1966 04 p0586 A67-15687
- Damage mechanism in semiconductors from space radiation and effects on various microcircuits 04 p0588 A67-15702
- Fluxgate magnetometer for OGO-E spacecraft in observing MHD waves and magnetic field structures in space 04 p0626 A67-15724
- Thermal radiative property behavior of materials under elementary charged particle bombardment, determining effect of combined UV plus electron exposure and low energy proton bombardment 04 p0686 A67-15873
- Cosmic ray origin and space plasmas 05 p0882 A67-16362
- Space electric field measurement techniques 06 p0993 A67-17582
- Space radiation effect on satellite design, noting guidelines for electronic equipment shielding 06 p1078 A67-18419
- Sensitivity of manned planetary spacecraft design to shield weight, onboard radiation and uncertainties in space environment radiation 07 p1258 A67-19376
- Dead time instability effect on neutron monitor performance 10 p1699 A67-22799
- Extraterrestrial solar radiation simulation and total flux and spectral component measurement 11 p1772 A67-24053
- Cosmic radiation measurements beyond radiation belts as observed by Cosmos XVII 11 p1856 A67-24075
- Book on radioastronomical methods of antenna measurements covering physics of extraterrestrial sources and receiving equipment characteristics 12 p1915 A67-25842
- Versatile digital data handling system designed to accept and control output of space radiation scintillation spectrometer 12 p1909 A67-25864
- High energy particle and electromagnetic space radiation effects on thermal control coating, noting spectral absorbance for various conditions [AIAA PAPER 67-339] 12 p1959 A67-26053
- Vertical cut-off rigidities for specific locations of geophysical interest computed from trajectory tracing process 13 p2191 A67-26325
- Anomalous shift in gate threshold voltage of high transconductance p-channel MOSFETs during exposure to space-like radiation 13 p2076 A67-26516
- Receivers for measuring UV radiation in upper atmosphere and outer space 13 p2121 A67-27335
- Rocket and balloon-borne exposure study of terrestrial microorganism survival in space 15 p2424 A67-29097
- Spatial distribution of electrons and protons trapped by geomagnetic field and charged particle fluxes in interplanetary space 15 p2550 A67-29536
- Long-baseline-interferometer observations of radio sources to ascertain angular dimensions of radio sources at LF 15 p2437 A67-30031
- Variation of radiation pattern of array of two traveling-wave V-antennas and use as spacecraft antenna 16 p2639 A67-31360
- Temperature effect measurement of neutron cosmic ray component, noting results of Chicago and Hobart geophysical stations 17 p2933 A67-32088
- Underground cosmic ray intensity variation measurements to determine solar modulation processes 19 p3315 A67-35494
- Annealing under continuous irradiation in p-on-n silicon solar cells with lithium diffused in N region 19 p3306 A67-35671
- Thermal annealing of silicon solar cells with direct solar heating or electric storage methods to avoid radiation damage 20 p3364 A67-37129
- Performance prediction calculations for double junction n-p-n silicon solar cells, discussing simplified model limits and space radiation environment 21 p3571 A67-38232
- Total extraterrestrial and global solar radiation intensity and spectral distribution for designing radiation resistant satellites 22 p3874 A67-40031
- Solar system environment, discussing solar magnetic field, flare flux and energy spectrum, interplanetary plasma and radiation, asteroids, meteoroids and comets 22 p3889 A67-40407
- Atmospheric opacity and extraterrestrial radio source intensity related by improved Taylor series technique using least squares method [JPL-TR-32-1115] 23 p4062 A67-40733
- Reentrant cosmic ray albedo intensity, considering nuclear interaction and trajectory spiraling 23 p4050 A67-40808
- Differentiation between true variation amplitude and statistical instrument error, deriving diurnal variation amplitude and phase distribution 23 p4059 A67-41131
- Manned spacecraft space radiation monitoring system requirements and criteria to indicate biological response 23 p3966 A67-41589
- Electron transport theory for energy below 10 Mev, reviewing interactions, scattering, thick targets, complex geometry and penetration in space environment [UCC/DSSD-287] 24 p4190 A67-41805
- Radio interferometric measurements of radio source diameters using 3074 km baseline 24 p4226 A67-41876
- Dead time instability effect on neutron monitor performance 24 p4209 A67-42135
- Preirradiated organism reaction to space flight acceleration studied in determination of admissible ionizing radiation dose 24 p4113 A67-42393
- Cosmic ray physics - All-Union Conference, Alma-Ata, Kazakh SSR, October 1966 24 p4215 A67-42826
- Effective lambda and sigma hyperons and K-meson production cross section dependence on target element atomic weight during cosmic rays interaction with various nuclei 24 p4220 A67-42851
- Search for neutral particles other than muons with high penetration capability from heavy mass or passivity at 40 mwe depth 24 p4220 A67-42866
- Energy flux fluctuation of nuclear active component in extensive air shower stem for given fixed muon and electron numbers 24 p4220 A67-42867
- Electromagnetic showers in lead recorded with ionization calorimeter, discussing cascade curve 24 p4221 A67-42870
- Electron-photon shower creation probability by energetic particle, deriving

recursion formulas 24 p4221 A67-42874
 Penetrating component of high energy cosmic rays below ground measured for intensity 24 p4221 A67-42876
 Hard component penetration of cosmic rays investigated by ionization calorimeter and hodoscope counters 24 p4222 A67-42878

SPACE RADIATOR

Directional reflective coating consisting of cylindrical dielectric fibers oriented perpendicular to absorbing substrate [AIAA PAPER 65-671] 03 p0467 A67-13039
 Materials and fin tube geometry effects on ultimate size and mass of space radiator 07 p1223 A67-19461
 Brazed graphite-stainless steel composites for tube-to-armor joints of high temperature graphite space radiators 07 p1223 A67-19462
 Analytical solution for determining inlet and outlet temperature for space radiator with heat rejection rate for steady state conditions and zero irradiation environment 08 p1429 A67-21511
 Potassium Rankine cycle turboelectric space power system, emphasizing vapor fin type of condensing radiator 20 p3364 A67-37018
 Automatic control of Block II Apollo ECS space radiator system, deriving linearized control equations for subsystem 22 p3916 A67-39174
 Moebius strip self-irradiation coefficient calculated as function of relative width or area of strip 23 p4083 A67-41287
 Beryllium braze joining for light stiff components noting structural examples and fabrication techniques, with reference to Apollo SNAP-27 radiator housing [SAE PAPER 670805] 24 p4159 A67-41991

SPACE REFERENCE SYSTEM

Gimballed unitized stellar reference inertial platform for space missions, noting optical lobing technique 08 p1331 A67-20699
 Satellite geodesy star catalog requirements, discussing accuracy of coordinates triangulation solution, criteria for homogeneity and extent of coverage, etc 18 p3043 A67-34586

SPACE RENDEZVOUS MANEUVER

X-band Cassegrainian tracking antenna for space rendezvous position and rate information for navigation and guidance computations 04 p0569 A67-14502
 Optimal maneuvers for space rendezvous between earth satellite and propelled vehicle on circular orbits, studying fuel consumption and rendezvous time 16 p2758 A67-30652
 Gemini guidance and control, discussing design, ground monitoring, launch and flight guidance, spacecraft instrumentation, maneuvering, etc 16 p2700 A67-30659

SPACE SCIENCE

Space research and astronautics, importance to science and European economy 01 p0168 A67-10268
 Atomic interactions and space physics - Symposium, Goddard Space Flight Center, Greenbelt, Maryland, August 1965 03 p0470 A67-13216
 Data processing and control by spaceborne computer on instrumentation satellite used for analyzing space scientific properties, noting factors influencing system design 05 p0768 A67-17516
 Space mathematics - Seminar, Cornell University, July-August 1963, Part 2 06 p1079 A67-17761
 Space mathematics - Seminar, Cornell University, July-August 1963, Part 1 06 p1080 A67-17771
 Space mathematics - Seminar, Cornell University, July-August 1963, Part 3 06 p0983 A67-17782
 Unmanned remotely operated lunar surface Emplaced Scientific Station /ESS/ design and objectives as Apollo follow-on lunar missions [AIAA PAPER 67-117] 06 p0980 A67-18286
 Interstellar flight justification by science fiction writer 06 p1120 A67-19041
 German papers on space research with satellites and space probes, Volume 1, Physical principles and methods of constructing carrier rockets 07 p1260 A67-20265
 German papers on space research with satellites and space probes, Volume 2, Control, test stands and direction finding 07 p1260 A67-20266
 Mobile Aerobee Launch Facility /MALF/,

noting applications to space science 08 p1314 A67-20544
 Space research - Symposium, Vienna, May 1966, Volume 2 10 p1634 A67-23176
 Space research - COSPAR International Symposium, Vienna, May 1966, Volume 1 10 p1841 A67-23246
 All-mirror Schmidt telescope system for space research providing easier switchover from photography to slitless spectroscopy 10 p1657 A67-23561
 Radioisotope applications to space science, discussing selection criteria for electric energy production and/or space propulsion 11 p1817 A67-24096
 Cosmic ray and space research through direct measurement of particles, radiation, magnetosphere, etc 11 p1856 A67-24105
 Low cost time delay and multiple programmer for space research 12 p1909 A67-25230
 Economic, technological and sociological impact of projected manned and unmanned space flights 12 p2040 A67-25234
 Space research - Conference, Mar del Plata, Argentina, May 1965 12 p2003 A67-25759
 Interplanetary medium including solar wind, geomagnetosphere and observation instruments 12 p2009 A67-26173
 Soviet papers on space physics problems 13 p2195 A67-26494
 Soviet space psychophysiology, discussing cosmonaut selection and medical control 13 p2058 A67-26751
 Seismological equipment for space research applied to earthquake-resistant structural design 13 p2120 A67-27217
 Astronomical year-report, 1965, including bibliographies and works on instruments, position astronomy, interplanetary objects, quasars, etc 13 p2200 A67-27225
 Space age in fiscal year 2001 - AAS Conference, Washington, D.C., March 1966 13 p2230 A67-27501
 Life sciences in fiscal year 2001, advanced concepts with emphasis on neurophysiological and behavioral problems 13 p2061 A67-27505
 Space astronomy utilizing gains made by space science and stressing X-ray astronomy 13 p2206 A67-27510
 Life sciences and space research - Conference, Vienna, May 1966 15 p2423 A67-29096
 Free-running circadian oscillations noting nature of driving oscillation, physiology of circadian organization and relation to manned space flight 15 p2425 A67-29107
 Space systems design course for fourth- and fifth-year students at MIT noting departmental, industrial and governmental cooperation 16 p2781 A67-30784
 Space systems engineering course, noting unmanned Mars exploration vehicle project and world weather system 16 p2782 A67-30785
 Lunar core precession and coupling between assumed liquid core and moon mantle 16 p2754 A67-31746
 Neutrino occurrence in universe noting postcreation and relic neutrinos, energy density, relic neutrino concentration, cosmic ray-neutrino interaction, etc 17 p2940 A67-32102
 Space research effects on science and technology, noting fields of application 17 p2974 A67-32771
 Moon and planets - Conference, Vienna, May 1966 18 p3120 A67-34134
 General theory of planets in connection with progress in space research 18 p3124 A67-34157
 Intelsat and communications satellites economic, political and social consequences, UN General Assembly Resolutions and use of satellite facilities for distribution of TV transmissions to broadcasting stations 18 p3162 A67-34354
 French space program research on ionospheric plasma, wave emissions, wind velocity, etc 19 p3320 A67-35290
 Space research organizational structure in Netherlands noting programs and experiments 19 p3321 A67-35299
 United Kingdom space research activities since May 1966, noting facilities, ground-based studies and rocket and satellite tracking experiments 19 p3322 A67-35306
 U.S. space research program /1966/, national organization, international

participation, space vehicle research and experiments related to future programs 19 p3322 A67-35300
 Soviet national report to COSPAR summarizing findings in upper atmosphere on lunar surface and outer space from 1966 to 1966 19 p3322 A67-35300
 International aspects of space applications and political, legal and economic problems involved 19 p3349 A67-35631
 Switched Proton Electron Channeltron Spectrometer /SPECs/ developed for measurement of charged particles in space 20 p3443 A67-36511
 Occurrence of singularities in cosmology giving testable condition implying existence of singularity assuming causality 21 p3703 A67-38491
 Pure magnetic integrated logic circuit for space research, noting improvement or speed factor 21 p3588 A67-38672
 Soviet book on planetary physics covering Martian, Venusian and Mercurian atmospheres, Venusian surface temperature and Jovian radio emission 21 p3707 A67-38933
 Planet Jupiter research, noting unresolved questions of cosmology, interior structure and Great Red Spot 21 p3711 A67-39092
 Missiles and aerospace vehicles sciences AAS Conference, Huntsville, Alabama, December 1966, Volume 1 22 p3900 A67-39926
 Missiles and aerospace vehicles sciences Conference, Huntsville, Alabama, December 1966, Volume 2 22 p3904 A67-40134
 NACA transition to NASA noting factors shaping development of government space research policy [AIAA PAPER 67-836] 24 p4259 A67-42977
SPACE SELF-MANEUVERING UNIT /SMU/
 Role, mobility, maneuvering, tools and techniques of future astronaut engaged in doing mechanical work 04 p0563 A67-14603
 Simulation testing of modular maneuvering unit for stabilized and unthethered maneuvers in free space 07 p1163 A67-19379
SPACE SIMULATION
SA ENVIRONMENT SIMULATION
 Environmental simulation techniques to supplement facility capabilities for environmental test program of Lunar Excursion Module /LEM/ [SAE PAPER 660682] 01 p0049 A67-10587
 Environmental structural testing capabilities for orbital and space vehicles [SAE PAPER 660685] 01 p0154 A67-10589
 Effects of various diets and simulated space conditions on human waste and water consumption applied to life support system development 02 p0188 A67-12339
 Lunar landing type or Doppler radar system evaluated by space dynamic simulation testing, using helicopter and various types of terrain 02 p0205 A67-12412
 Steady state and transient full-scale, half-scale and quarter-scale thermal models in simulated space environment [AIAA PAPER 65-659] 03 p0534 A67-13064
 Solar wind-comet interaction simulation using plasma stream and carbon dioxide gas cloud sublimated from dry ice 03 p0506 A67-13575
 Directory of RCA environmental test facilities 03 p0396 A67-13635
 Aerospace vehicle simulation concept defined, examining relation to major problem areas of checkout 03 p0399 A67-14210
 Low temperature technology and space flight 04 p0720 A67-14538
 Cryogenic pumping capability of liquid helium cooled plate in supersonic flow field at simulated high altitude 04 p0606 A67-14999
 Space environment simulation testing as essential part of contemporary space flight development programs [AIAA PAPER 65-474] 04 p0598 A67-15229
 Piloted space flight simulation at Langley Research Center [ASME PAPER 66-WA/AV-2] 04 p0599 A67-15295
 Microwave and thermal vacuum testing to demonstrate design maturity of LEM rendezvous radar during simulated mission 04 p0576 A67-15397
 Simultaneous simulation of space and thermal conditions of spacecraft [ASME PAPER 66-WA/HT-29] 04 p0599 A67-15443
 Van Allen radiation belt simulation, obtaining accurate values for satellite and semiconductor lifetimes in orbit

- AIAA PAPER 67-177] 06 p0981 A67-18510
Space environment simulation noting
various testing facilities for space
equipment 07 p1163 A67-19534
Apollo command and service modules
simulation
AIAA PAPER 67-231] 07 p1260 A67-20050
Effect on human performance of variations
from true values in simulation of
extraterrestrial visual environment
AIAA PAPER 67-251] 07 p1166 A67-20069
Building block visual simulation facility
using new generation and display techniques
combined with TV model image
generation 08 p1314 A67-20659
German space simulation chamber,
discussing influences of cryogenic panel and
solar simulation on vacuum
system 09 p1485 A67-22123
Design, tests, operation and limitations of
Apollo man-rated environmental control
system simulation
chamber 11 p1748 A67-24340
Thermal vacuum performance testing of
scaled models as technique for reducing
development costs of
spacecraft 11 p1773 A67-24346
Vacuum or low pressure contamination
removal from space simulation chamber,
using bakeout with externally and internally
supplied heat 11 p1773 A67-24976
Large and intermediate ultraclean vacuum
chambers converted to sputter-ion and
titanium sublimation
pumping 12 p1921 A67-25691
In-space visual environment simulation,
discussing photometric and geometric
requirements, solar illumination
characteristics and effects on human
performance 12 p1922 A67-25700
Cryopumps incorporated into liquid N
shrouds for small space simulation
chambers 12 p1900 A67-25710
Large helium refrigerators for very high
speed cryopumping techniques required in
space simulation facilities 12 p1924 A67-25716
Multiple sample space UV simulation
facility for in situ hemispherical spectral
reflectance measurements
[AIAA PAPER 67-312] 12 p1926 A67-26027
Man rating requirements of space
environment simulation laboratory consisting
of two large chambers with floors which can
be cooled by liquid nitrogen down to 92
degrees K 13 p2090 A67-26841
Gears evaluation testing under vacuum
chamber space simulation
[ASLE PAPER 66AM-7A4] 13 p2123 A67-27099
Spacecraft thermal control coating damage
in simulated space-bombardment conditions,
using plasma bombardment
techniques 14 p2293 A67-28138
Plasma wind tunnel facility for producing
steady flow high conductivity collisionless
plasma simulating solar wind interaction
with magnetosphere 14 p2294 A67-29036
Neutral buoyancy /water immersion/
technique for simulated space crewman
performance, noting psychophysiological,
man-machine and anthropomorphic
parameters affecting space station
design 15 p2431 A67-29282
Van Allen radiation belt simulation,
obtaining accurate values for satellite and
semiconductor lifetimes in orbit
[AIAA PAPER 67-177] 15 p2465 A67-29446
Apparatus for direct weight loss recording
of space materials 15 p2466 A67-29543
Refractory material as component of
silicate binder having stable optical and
physical properties under simulated space
conditions 15 p2506 A67-29547
Simulated space effects on microelectronic
device materials 15 p2466 A67-29549
Large space simulation chamber for
studying low temperature, absolute vacuum
and solar radiation effects 15 p2466 A67-29571
Sleep characteristics during simulated
space flight noting influence of noise,
angular accelerations and
isolation 16 p2613 A67-30913
Instrumentation for space vacuum
simulation used in testing operations,
discussing pressure measurement
requirements 17 p2860 A67-32594
Space simulation using cryogenic
adsorption pumping 17 p2884 A67-32595
Vacuum simulation developments and
trends, noting solar
advances with cryogenic
systems 17 p2834 A67-32597
Space pressure and temperature
environment simulation facility for liquid
rocket space-ignition reliability testing
[AIAA PAPER 67-428] 18 p3112 A67-33912
Blaxial satellite motion simulator for large
space-simulation chamber, discussing
temperature and pressure
simulation 18 p3021 A67-34611
Space and high altitude simulation
requirements for testing various rocket
engine and propulsion
systems 20 p3415 A67-36544
Thermocouple surface temperature
measurement errors in space simulation
chambers due to heat conduction and
radiation of wires
[ASME PAPER 67-HT-57] 20 p3447 A67-36739
Microbial interaction in closed system by
simulating space flight conditions, noting
degree of crowding effect on
buildup 21 p3577 A67-38899
Environmental simulation for aerospace
vehicle, discussing vibration, shock and high
temperature testing and space and nuclear
radiation simulation 22 p3781 A67-40343
Cryosorption pumping of helium and
hydrogen in high vacuum, describing
refrigerated panels and space environment
simulation application 22 p3838 A67-40396
RCA papers on environmental
sciences 22 p3781 A67-40400
Operational requirements for modern
space environment test laboratory covering
thermal vacuum, shock, vibration and
combined testing 22 p3781 A67-40401
Test planning and decision making in
environmental testing approached from
program formulation involving resources and
equipment, degree of simulation and
optimum levels 22 p3781 A67-40402
Extreme flight factor effects on human
organism determined by simulation, noting
physiological function level increase before
stress increases
resistance 22 p3752 A67-40533
Book on vacuum engineering covering
space vacuum simulation, pressure
measurement, gas flow and load, vacuum
systems and technology 23 p4028 A67-41353
Physiological measurements in obtaining
energy expenditure and workloads during
simulated lunar surface
mission 23 p3959 A67-41657
Space simulation - Conference,
Philadelphia, September
1967 24 p4137 A67-42028
Shock tube simulation of rocket exhaust
plumes and effects on vehicles in space
environment 24 p4253 A67-42029
Adhesive qualities of lunar soil simulated
by rock comminuted in ultrahigh
vacuum 24 p4227 A67-42034
Vacuum chamber contaminants, discussing
silicone pumping fluid from diffusion
pumped systems 24 p4138 A67-42035
Two-axis gimbal system for solar
simulation spacecraft testing, demonstrating
intermediate axis internal drive system and
outer axis drive input 24 p4153 A67-42044
Variable point guidance technique
modifications verified by simulation
containing representation of typical booster
and upper stage
configuration 24 p4182 A67-42907
SPACE SIMULATOR
Space vacuum simulation chambers for
testing of ionic, plasma and other rocket
engines 01 p0048 A67-10302
Design, construction and operation of
vacuum chamber space simulator for testing
Gemini space capsule 01 p0049 A67-10303
Large space environmental simulation
chamber design problems arising due to
man-rated feature 05 p0788 A67-16618
Arnold Engineering Development Center,
discussing aircraft and space vehicle
environmental simulation and
testing 05 p0788 A67-16619
Medical, design and operational aspects of
quality requirements for reliability of man-
rated space environment simulation
chambers 05 p0788 A67-16621
Space environment simulator for analysis
of spacecraft material reliability during long-
duration space mission 07 p1163 A67-19384
Low pressure low-temperature ignition of
hypergolic propellants, particularly
hydrazine-nitrogen tetroxide systems, in
space environment simulator and conclusions
on gas phase reactions 07 p1163 A67-19385
Space simulator application to
development of space rocket propulsion
systems, examining test problems of low
pressure space engines
[AIAA PAPER 67-257] 07 p1164 A67-20052
Nonuniform molecular density, pumping
power and gas temperature distribution in
evacuated space simulator 09 p1503 A67-22118
Man-rated space simulation facility,
emphasizing checkout and qualification of
systems 12 p1921 A67-25689
Space simulation using contamination-free
test facilities combining several cryogenic
techniques to produce all cryogenic
system 12 p1924 A67-25717
Small liquid propulsion systems testing in
space environment simulator with high
vacuum and low pumping
capacity 13 p2089 A67-26840
Space simulation chamber for industry and
research 14 p2292 A67-28063
Simulated acceleration and dynamic
pressure environments generated by space
vehicle flight ranging from weightlessness to
impact from ground landing
[AIAA PAPER 67-279] 15 p2465 A67-29425
Electronic checkout, environmental
qualification and integration of OGO by
spacecraft simulator and performance
analysis system 16 p2654 A67-30639
Space environment simulator of CNES in
France describing reproduction of low
pressure atmosphere, heat sink, solar and
planetary radiation, etc 16 p2654 A67-30675
Air-bearing facility for Lunar Orbiter
attitude control system testing minimizing
external disturbances in platform, platform
mass deflection and room thermal
currents 16 p2655 A67-31260
Manrating of space environment
simulators, emphasizing integration of
physical facility requirements and operation
procedure to provide
safety 17 p2807 A67-31960
Thermal control surface contamination due
to rocket exhaust plumes and effects on
solar absorptance and IR emittance of
protective coatings 17 p2833 A67-32076
Space magnetic environment simulation
coil facility for spacecraft testing by
mapping magnetic fields 24 p4138 A67-42030
Optimum solar simulator and design of
thermal vacuum chamber around
it 24 p4138 A67-42042
Space simulator growth problems,
discussing advantages of orbiting space
laboratories
[AIAA PAPER 67-814] 24 p4243 A67-42968
SPACE STATION
SA MANNED ORBITAL LABORATORY
/MOL/
SA MANNED ORBITAL RESEARCH
LABORATORY /MORL/
SA ORBITAL SPACE STATION
Lunar orbiter command and telemetry
data handling system at deep space
stations 02 p0194 A67-11808
Soviet program of planetary exploration
with aid of automatic interplanetary stations,
examining problems due to trajectory errors
and communications
breakdown 02 p0326 A67-12041
Space station role in manned space flight
noting mission goals, earth, moon and
planet-oriented applications, etc
[AIAA PAPER 66-906] 02 p0332 A67-12272
Effects of space station logistic
requirements on design of spacecraft
configurations with various hypersonic
lift/drag ratios, comparing payload, cost, etc
[AIAA PAPER 66-958] 02 p0332 A67-12286
Thermally scaled model space station
subjected to steady state and cyclical
transient solar environments
[AIAA PAPER 65-658] 03 p0534 A67-13063
Orbital space station design for permanent
residence within earth-orbital payload
capacity of Saturn V launch vehicle
[AIAA PAPER 66-936] 03 p0520 A67-14138
Manned Orbital Research Laboratory
design and flight control
characteristics 09 p1572 A67-22672
Large orbital observatories design for
permanent residence, noting atmospheric
control and vehicle
stabilization 09 p1572 A67-22673
Cryogenic computers in space based on
phenomenon of
superconductivity 10 p1608 A67-22770
Legal status of space objects according to

different criteria noting international rights, obligations and 12 p2043 A67-26146

jurisdiction 12 p2043 A67-26146

Parabolic reflectors providing auxiliary solar energy for space stations and spacecraft, manufacturing and testing procedures 13 p2211 A67-26335

Neutral buoyancy /water immersion/ technique for simulated space crewman performance, noting psychophysiological, man-machine and anthropomorphic parameters affecting space station design 15 p2431 A67-29282

Spaceport meteorology by satellite observation of earth atmosphere and cloud systems [AAS PAPER 67-47] 15 p2513 A67-30115

Manned orbital research laboratory /MORL/ examining experimental program, design, mission definition, logistics, cost 16 p2756 A67-30623

Attitude control system and actuator locations in flexible spinning toroidal manned space station 17 p2954 A67-32055

Rod configuration determined optimum for gyro torquer controlled spinning space station subject to impulse disturbance 17 p2955 A67-32477

Spacecraft and space station reliability by orbital maintenance and extravehicular activity, comparing redundancy on system and cost effectiveness [AIAA PAPER 67-652] 20 p3535 A67-37629

Operational and cost-influencing characteristics of low orbit space operations compared from manned orbital base and earth base [AIAA PAPER 67-654] 20 p3530 A67-37631

Computerized microfilm or magnetic tape production for manned space station maintenance documentation 23 p4071 A67-40593

Primary cosmic particles energy spectrum measurements onboard space station with ionization calorimeters and energy level discriminators 23 p4054 A67-41091

Feasibility of short radius centrifuge incorporation in space station, testing radius effects on operator performance of tasks 23 p3965 A67-41567

Optimum stabilization system for manned space station with asymptotic damping of initial angular momentum 24 p4240 A67-42088

SNAP-8 powered Brayton cycle system for large space stations noting components and overall design 24 p4102 A67-42490

Parametric analysis and system optimization of nuclear reactor heated Brayton cycle space power plants, discussing turbomachinery performance and shielding weight factors 24 p4186 A67-42550

Orbital research hospital design for utilizing zero and low gravity therapeutic value in treating physiological conditions [AIAA PAPER 67-833] 24 p4243 A67-42976

Commercial earth orbital manned space station power system requirements, estimating operational and logistical costs for isotope and reactor designs [AIAA PAPER 67-879] 24 p4187 A67-42998

Docking mechanisms for spacecraft systems noting hard vs soft and in-line vs off-set systems [AIAA PAPER 67-908] 24 p4244 A67-43015

Onboard checkout system /OCS/ impact on space station program [AIAA PAPER 67-953] 24 p4245 A67-43037

Long term manned space mission system effectiveness and reliability through interchangeability and redundancy noting optimization, tradeoffs, maintenance and spares [AIAA PAPER 67-984] 24 p4166 A67-43056

SPACE STORAGE

Space cryogenic propellant storage utilizing vent gas recovery noting storability spectrum plot 22 p3906 A67-40164

SPACE SUIT

SA PRESSURIZED SUIT

Prolonged autonomous existence of humans in space suits, discussing maintenance of heat balance by physiological perspiration 02 p0187 A67-12324

Passive heat transfer system for metabolic heat removal in extravehicular activity suit 03 p0364 A67-14295

Integrated space suit, suit loop and backpack system for intravehicular operation on interplanetary missions 04 p0563 A67-15235

Water cooled vest with insulated icebox

and electric pump to reduce thermal strain and increase comfort for aircrew members in hot humid climates 05 p0756 A67-18284

Mechanical design and packaging of transceiver mounted in spacesuit helmet for intercommunication among astronauts and space vehicles 05 p0779 A67-17466

Space suit design for mobility and protection, comparing soft and rigid suits 07 p1137 A67-20271

Radiation doses measured by onboard dosimeters and those fastened to space suits of crews of Voskhod I and Voskhod II compared, noting radiation composition analysis by means of nuclear emulsions 14 p2256 A67-27863

Hemodynamic modifications produced by orthostatism noting changes in cardiac frequency, arterial pressure and central blood volume produced 16 p2616 A67-30754

Prediction and measurement of metabolic energy cost for space suit system operation, noting procedure and test results 16 p2618 A67-30781

Space suit support loop for use within manned space cabin 20 p3374 A67-36548

Soviet book on protective equipment for aviators and cosmonauts 21 p3576 A67-37934

Energy expenditure in space suits studied for controlled cooling during high work rates 23 p3965 A67-41562

Space suit atmosphere physiological suitability for prolonged moderate work, studying blood-gas parameter changes 23 p3955 A67-41617

Telemetry system for measuring body temperature and heart rate for physiological evaluation of space suits 23 p3969 A67-41651

SPACE SURVEILLANCE SYSTEM

Military surveillance satellite for high resolution photography noting design, application and projected performance 15 p2564 A67-29400

Spacecraft surveys of earth used for city growth observations, draw land-use maps, etc 19 p3221 A67-35324

SPACE SYSTEMS ENGINEERING

Space support, discussing functions during planning phases, constraints, systems engineering approach and integration of subplans into unified scheme [SAE PAPER 660688] 01 p0049 A67-10592

Medical, design and operational aspects of quality requirements for reliability of manned space environment simulation chambers 05 p0788 A67-16621

NASA quality assurance program and NASA industry quality relationships, particularly for large space systems procurement 05 p0930 A67-17242

Apollo extension systems, discussing current space technology and accomplishments 08 p1391 A67-21066

Reliability of future space systems through adoption of complexity factor ratings 09 p1572 A67-22311

European aerospace transporter feasibility and worth 15 p2567 A67-29839

Space systems design course for fourth- and fifth-year students at MIT noting departmental, industrial and governmental cooperation 16 p2781 A67-30784

Space systems engineering course, noting unmanned Mars exploration vehicle project and world weather system 16 p2782 A67-30785

Bioastronautics role in population explosion and technological evolution problems, noting biocybernetics, and aerospace systems 16 p2782 A67-30787

Paracone emergency escape system for rescuing space crews from orbits at hypersonic velocities 17 p2794 A67-32001

Manned mission reliability and maintainability requirements in future systems 18 p2995 A67-34686

Human engineering research to aid system designers to optimize man's role as control element in space systems 18 p2995 A67-34687

Space systems reliability design problems, discussing estimation, weight-reliability tradeoffs, spare parts and redundancy 18 p3139 A67-34698

Active parotin preparation to lower serum calcium levels, Ca excretion and possibly prevent decalcification, for applicability to potential system engineering 18 p2991 A67-34712

Human engineering performance data for

equipment design for manned space systems, discussing zero gravity maintenance and repair [AIAA PAPER 67-653] 20 p3375 A67-37630

Reliability engineering - Conference, Nuremberg, April 1967 22 p3921 A67-39279

SPACE TEMPERATURE

Biaxial satellite motion simulator for large space-simulation chamber, discussing temperature and pressure simulation 18 p3021 A67-34611

Strength and oxidation tests evaluated for coated fasteners in extreme temperature use 24 p4160 A67-42078

SPACE-TIME CONTINUUM

Time-space quantization of gravitation, field by formalisms in general relativity, theory 01 p0114 A67-10746

Space-time singularities and Einstein equations 01 p0151 A67-11291

Vector field C defined at each point of space-time when curvature is zero, leading to series of cosmological models that satisfy Hoyle relativistic equations 04 p0698 A67-14809

Mach principle as consequence of de Sitter universe filled with Dirac dust 05 p0847 A67-16803

Variational derivations of field equations for relativistic mechanical, EM and gravitational fields in space-time continuum 06 p1033 A67-18582

Antisymmetric tensor theory of gravitation in flat space-time with energy and momentum conserved 09 p1532 A67-21979

Continuous charge distribution with time-oriented streamlines in Minkowski space-time 09 p1534 A67-22579

Dynamics of continuous media, proposing new equation in which action modifying intrinsic mass has no effect on velocity 09 p1534 A67-22580

Electromagnetic field tensor created by point charge provided with universal velocity and acceleration is equal to outer product of universal vectors 13 p2156 A67-26594

Time-space quantization of gravitational field by formalisms in general relativity theory 13 p2156 A67-26775

Dyadic formalism to prove Herglotz-Noether theorem for flat manifolds [JPL-TR-32-1125] 17 p2879 A67-32929

Space-time properties of hydroxyl emission observed by spectrophotoelectrometry, giving diagrams of periodic variations and measurement errors 17 p2848 A67-32954

Einstein gravitation theory relation to general and special relativity, space-time, unified four-dimensional continuum metric and chronogeometric theories 18 p3079 A67-34133

SPACE-TIME FUNCTION

Arbitrary shallow shell under action of space-time homogeneous random load 01 p0163 A67-10995

Analog device for measuring coefficient of space-time signal correlations and applications to statistical mechanics of turbulent fluids and random noise 01 p0054 A67-11090

Feynman space-time path formulation of nonrelativistic quantum mechanics applied to classical diffusion problem 03 p0469 A67-13718

Space and time characteristics of electron fluxes penetrating into terrestrial atmosphere in auroral zone, based on riometer measurements 05 p0879 A67-16101

Space-time correlations of turbulent field measured by grid using high speed computer 11 p1780 A67-24541

Interdisciplinary perspectives of time - Conference, New York, January 1966 11 p1820 A67-24935

Orientation and navigation in space-time 11 p1820 A67-24936

Space-time cross correlation function for antennas generalized by complex antenna-height function 12 p1917 A67-26089

Tropospheric condition effect on near-ground ultrashort wave radio signal field-amplitude fluctuation, determining space-time correlation dependencies by radar observation 13 p2067 A67-26688

Book on space-time relations of stellar positions on celestial sphere, detailing long focus astrometry, emphasizing mathematical principles 13 p2199 A67-26933

Integration of Einstein gravitational

equations implies that corpuscle be rigidly connected with particular Fermi space-time system of reference 13 p2158 A67-27298

Seasonal and latitudinal magnetic activity variations in Northern Hemisphere, investigating time-space characteristics of K index 14 p2309 A67-27943

Space-time description of dynamical phenomena in unbounded homogeneous linear medium, noting dispersion properties and wave structures in 14 p2358 A67-28461

Space-time region division method for reducing nonlinear heat conduction to subordinate linear multilayer system problems, assuming stationary time characteristics and coordinates 14 p2408 A67-28804

Space-time distribution of heavy penetrating particles in extensive air showers, applying scale transformation properties of distribution to integration over primary particle spectrum 15 p2550 A67-29749

Drag coefficient of moving body during ballistic tests calculated from given space-time dependence 16 p2592 A67-31121

Time and space distribution of anomalous ionization in ionospheric F-2 layer above Southern Hemisphere, noting maximums of ionization distribution 16 p2668 A67-31893

Solar cosmic ray observations, discussing emission spectrum, interplanetary particle distribution, diffusion coefficient, magnetic field strength, space-time distribution, etc 17 p2934 A67-32096

Statistical properties of wall pressure fluctuations in subsonic turbulent equilibrium boundary layer after transition from laminar flow 17 p2836 A67-32283

Classification of main data on morphology and phenomenology of aurorae observed visually and with all-sky cameras during IGY 19 p3224 A67-35495

Time-growing instability existences in distributed parametric media using dispersion relation 19 p3195 A67-35620

Relativistic Boltzmann collisionless equation solution in presence of certain external fields 19 p3266 A67-35710

Gravitational theory with all curvilinear coordinate systems and space-time avoided illustrated by applying method to Dirac field case 20 p3484 A67-36836

Rotating observer relative to inertial observer in relativity 20 p3486 A67-37501

Tropospheric condition effect on near-ground ultrashort wave radio signal field-amplitude fluctuation, determining space-time correlation dependencies by radar observation 21 p3582 A67-38430

Optimal output effect for spatial temporal processing of signals in presence of multiplicative and additive signal fluctuations 24 p4120 A67-42232

Space and time characteristics of electron fluxes penetrating into terrestrial atmosphere in auroral zone based on riometer measurements 24 p4213 A67-42777

PACE-TIME METRIC

SA CARTAN SPACE

SA SCHWARZSCHILD METRIC

Five-dimensional relativistic space, giving physical interpretation for Riemannian space with metric form 04 p0656 A67-14746

Homogeneous anisotropic cosmological model with magnetic field for solution of Einstein gravitational and Maxwell equations in space filled with ideal matter 04 p0702 A67-15984

Kruskal space in general relativity and uniform accelerated rigid rod in special relativity show striking formal similarities 05 p0847 A67-16970

Structure of general relativity theory space examined, using analytic continuation of geodesic equations 06 p1031 A67-17883

Static axisymmetric interior solution of Einstein field equations which matches smoothly to one of Weyl exterior solutions 09 p1531 A67-21639

Cosmological distortion effect incorporating incident magnetic type gravitational field parameter upper limits measured from galactic cluster photographs 11 p1860 A67-24484

Parametrization of reduced problem of stationary axially symmetric gravity fields 11 p1819 A67-24597

Asymptotic behavior of curvature tensor in certain asymptotically Euclidean Riemannian space-time

manifold 11 p1819 A67-24763

Phenomenological metric method applied to four tests of general relativity in evaluation for nearly flat space with spherical symmetry 13 p2159 A67-27399

Homogeneous anisotropic cosmological model with magnetic field for solution of Einstein gravitational equations and Maxwell equations in space filled with ideal matter 14 p2386 A67-28485

Models of spherically symmetric nonstatic processes, including relativistic collapse to Schwarzschild sphere, constructed by space-time metrics [JPL-TR-32-1136] 15 p2564 A67-30438

Theorems defining class of motions of system of mass points of given mass in Lobachevskii space 16 p2702 A67-31011

Space time distribution of magnetic activity during IGY, noting elliptical region about magnetic pole characterized by increased activity 17 p2848 A67-32950

Line element not precluding peculiar motions or assuming isotropy and homogeneity of mass distribution of universe, considering kinematical consequences 18 p3117 A67-33427

Necessary and sufficient conditions for space-time curvature tensor and isotropic vector field associated with double 2-form to satisfy higher order field equations 18 p3078 A67-33689

Structure of curved space-time in which electromagnetic wave propagation takes place without tail formation 18 p3079 A67-33761

More general form of metric for explicitly solving field equations of Hoyle-Narlikar conformal theory of gravitation 21 p3657 A67-37924

Nonzero cosmological constant effect /precise and trivial/, calculating perihelion precession from Schwarzschild exterior solution 22 p3889 A67-40382

Principles developed for founding of unified field theory of gravitation and electromagnetism, with space-time geodesics as charged particle motion equation 23 p4026 A67-40659

Space time distribution of cosmic rays as function of plasma efflux from sun, magnetic field intensity, topology and scale irregularities 23 p4059 A67-41133

Wave propagation in wave optics transition to geometrical optics in general relativity theory using series expansion 23 p4027 A67-41146

Gravitational collapse considering space time diagrams and curvature of space, suggesting crushing body less than critical size 24 p4228 A67-42309

SPACE TOOL

Role, mobility, maneuvering, tools and techniques of future astronaut engaged in doing mechanical work 04 p0563 A67-14603

Telefactor system in control of space operations, describing master-slave manipulator servomechanism with TV network and electronic communication link 13 p2063 A67-27213

SPACE TRAJECTORY PROGRAM

Extremal space trajectories problems of one-impulse flights and two-impulse orbital transfers in central gravitational field 20 p3522 A67-36617

SPACE VEHICLE

SA EXTRAVEHICULAR OPERATION

SA RECOVERABLE SPACE VEHICLE

SA SATELLITE

Structural safety of Mercury and Gemini vehicles, noting fail-safe and fracture tolerant design [SAE PAPER 660681] 01 p0154 A67-10585

High speed photographic equipment, analyzing gun launching of vehicles in upper atmosphere and design of protection system against space vehicle failure due to meteorites 01 p0068 A67-10968

Arnold Center advanced ground test facilities for rocket and space vehicle environmental testing 05 p0788 A67-16617

Composite aerospace transport for spacecraft launching, particularly French projects 06 p1094 A67-17993

Parameter optimization procedure in three degree of freedom trajectory simulation computer program for multistage vehicles [AAS PAPER 66-111] 07 p1253 A67-19970

Planetary entry vehicle development, discussing mission objectives, vehicle requirements, Voyager capsule, etc

[AAS PAPER 66-57] 07 p1259 A67-19994

Mission requirements for unmanned exploration of solar system including energy and flight time, noting thrusted vs ballistic vehicles 08 p1393 A67-21096

Optimum weight ratio for space vehicle with solar energy operated engine, noting dependence on distance from sun, trajectory optimization, etc 09 p1571 A67-21886

Clean room techniques for Apollo/Saturn Instrument Unit, noting that environmental and guidance systems parts must be supercleaned to qualify for man-rated space vehicle 11 p1773 A67-24938

Verification of thermal mathematical model for artificial satellite using thermal vacuum chamber, noting error analysis [AIAA PAPER 67-304] 12 p2036 A67-26019

Legal status of space vehicles, nationality /unilateral decisions/ vs internationality /multinational operation/ 12 p2043 A67-26148

Juridical regime of craft and space installations 12 p2043 A67-26149

Engine generated and in-flight noise environment problems of space vehicles analyzed, using theoretical methods and scale model wind tunnel tests 13 p2212 A67-27216

Parameter optimization procedure in three degree of freedom trajectory simulation computer program for multistage vehicles [AAS PAPER 66-111] 13 p2214 A67-27527

Hardware and life-support systems on submarines and space vehicles, discussing oxygen supply, temperature-humidity control, etc [AIAA PAPER 67-364] 14 p2259 A67-28732

Entry/Lander vehicle for Mars mission discussed in terms of gross payload, basic vehicle and preentry system 16 p2756 A67-30629

Man-rated space-vehicle structural design considering space environment loads and material requirements, noting applicability of existing methods 16 p2756 A67-30630

Supporting equipment for space vehicles - Conference, Athens, September 1965, supporting equipment for space vehicles - IAF Conference, Athens, September 1965, Volume 3 16 p2620 A67-30667

Space vehicle automatic control considering order execution from guidance system and vehicle stabilization around its center of gravity 16 p2700 A67-30798

Saphir g space vehicle guidance systems consisting of inertial center and computer 16 p2701 A67-30800

Linear programming algorithm for optimizing life support systems of space vehicles in terms of minimum weight/efficiency ratio 17 p2807 A67-32254

Inertial tracker position error evolution, discussing equations and applicability to vehicle on ground or in circular orbit 17 p2882 A67-32725

Stationary or long range space vehicle transmitting antennas remote alignment technique using received signal AM 18 p3016 A67-34596

Tropospheric circulation observation through FR-2 satellite project, discussing instrumentation, ground stations, trajectory analysis, etc 19 p3332 A67-35243

Synthesis of single cycle of natural metabolic processes to be used as basis of space-vehicle self-sufficient life support systems 20 p3368 A67-36262

Electromagnetic interference reduction between antennas on space vehicles 20 p3405 A67-37642

Space vehicle tracking noting significance of accuracy and rapidly in determination of position, velocity and acceleration 21 p3583 A67-38642

Accurate geodetic altitude and sublatitude of low altitude space vehicle 22 p3879 A67-39312

Turboramjet engine design for aerodynamic flight vehicles up to Mach number 6 23 p4049 A67-41318

Shock tube simulation of rocket exhaust plumes and effects on vehicles in space environment 24 p4253 A67-42029

Coolant selection for radiative cooling circuit of space vehicles, considering flow rate, heat transfer rate, etc 24 p4253 A67-42217

Sensitivity analysis method for poorly known model parameters and preliminary computer load requirements applied to radio tracking of space vehicles

- [ELDO-TM-F-5] 24 p4122 A67-42385
Dynamic response of large flexible space systems subjected to motion inputs and arbitrary force, analyzing joined Timoshenko beams 24 p4240 A67-42395
- SPACE VEHICLE CHECKOUT PROGRAM**
Monitoring events occurring during testing of space vehicle by data compression techniques and time shared computer-controlled checkout system [SAE PAPER 660696] 01 p0049 A67-10593
Digital computers connected by data link transmission system for prelaunch space vehicle checkout 01 p0050 A67-11031
Computer design test program to automate checkout process of Saturn I and V space boosters gradually while retaining manual checkout 01 p0051 A67-11427
Automatic checkout equipment for prelaunch use, describing packaging technique 05 p0789 A67-17461
Space vehicle thermal testing in cold vacuum chambers with and without solar simulation [AIAA PAPER 67-306] 12 p1926 A67-26021
Computer applications in checkout of individual Saturn stages and in prelaunch checkout of complete Saturn vehicle 13 p2089 A67-26409
Assurance and measurement of space vehicle alignment conforming to design requirements 15 p2496 A67-30422
Electronic checkout, environmental qualification and integration of OGO by spacecraft simulator and performance analysis system 16 p2654 A67-30639
Ground installations for development, qualification and checkout testing of Apollo space vehicle 16 p2654 A67-30676
Space vehicle checkout procedure application to near-future transport aircraft, noting NASA sponsored advances [SAE PAPER 670337] 17 p2835 A67-32987
Prelaunch checkout in 1970s, discussing vehicle subsystems, prelaunch requirements and operations and launch site technology 20 p3415 A67-36579
Automatic satellite-checkout system for use under simulated space environment and stress conditions 22 p3778 A67-39192
Writing and use of ground checkout procedures in Apollo program using computer-assisted editing, publishing and information retrieval 23 p3976 A67-41055
- SPACE VEHICLE CONTROL**
Closed loop control system for space vehicle guidance, formulating efficient steering algorithm 01 p0154 A67-11156
Mayer technique in calculus of variation for constrained error coefficient criterion function for missile trajectory optimization in aerospace guidance and control 02 p0265 A67-12389
Control and stabilization of thrust producing final stages of recoverable space vehicles during atmospheric reentry 04 p0652 A67-14557
Transverse magnetic field interaction with laminar boundary layer on rotating cone during reentry, assessing effect on spin and controlling torques 12 p1892 A67-25385
Space vehicle flight control with minimum total characteristic velocity, determining optimum points for applying correcting acceleration 13 p2213 A67-27320
Minimum of maximum overload in braking of vehicle in atmosphere, examining aerodynamic lift on basis of Pontryagin maximum principle 14 p2393 A67-27855
Optimum control of earth satellites and space vehicles and stable solutions of orbits in orbital mechanics 14 p2393 A67-27879
Fuel optimum guidance law to achieve required velocity 16 p2700 A67-30655
Correctional maneuver changing space vehicle position on planet approach, assuming flight velocity pulsation during correction 16 p2758 A67-30661
Space vehicle optimal control, studying maximum principle application, developing numerical algorithms of dynamic programming type and describing variational problems 16 p2742 A67-30664
Control moment gyro /CMG/ and use in space-vehicle attitude-control system, emphasizing control laws [AIAA PAPER 67-589] 19 p3336 A67-35985
Luna IX automatic station flight control complex, detailing communication, orientation and stabilization systems operation after separation from acceleration
- module 22 p3897 A67-39167
Automatic check system for investigation of dynamic characteristics of stabilization system for carrier and space vehicle, noting system reliability 22 p3830 A67-39172
Two-channel control system for programmed roll of rapidly rotating carrier rocket, analyzing efficiency 22 p3898 A67-39175
Flight control system for automatic interplanetary stations /AIS/, comparing Venera series orientation and correction system to Mariner systems 22 p3898 A67-39185
Active control of space vehicles orientation, discussing optimal and rational control and rotational motion braking problems 22 p3899 A67-39189
Triaxial orbital orientation control algorithm for space vehicle with incomplete angular position information 22 p3899 A67-39191
Suboptimal feedback solution to guidance and control in minimum time and fuel for low thrust orbital transfer 22 p3832 A67-40146
Optimum sensitivities of control function with respect to vehicle parameter changes and state variables without using finite differences 22 p3833 A67-40159
- SPACECRAFT**
SA APOLLO SPACECRAFT
SA EUROPEAN I SPACECRAFT
SA FERRY SPACECRAFT
SA GEMINI SPACECRAFT
SA HYDROGEN OXYGEN /HOPE/ SPACECRAFT
SA INTERPLANETARY SPACECRAFT
SA LUNAR SPACECRAFT
SA MANEUVERABLE SPACECRAFT
SA MANNED SPACECRAFT
SA MARS SPACECRAFT
SA MILITARY SPACECRAFT
SA PLANETARY SPACECRAFT
SA REENTRY VEHICLE
SA RENDEZVOUS SPACECRAFT
SA REUSABLE SPACECRAFT
SA SATELLITE
SA SURVEYOR I SPACECRAFT
SA SURVEYOR III SPACECRAFT
SA SURVEYOR SPACECRAFT
SA UNMANNED SPACECRAFT
SA VOSTOK SPACECRAFT
RCA papers on spacecraft and space systems 06 p0963 A67-18411
Juridical regime of craft and space installations 12 p2043 A67-26149
- SPACECRAFT COMMUNICATION**
SA DEEP SPACE NETWORK /DSN/
Space station operations in navigation and tracking, communication coverage, abort recovery, etc 12 p2012 A67-25743
Spacecraft high aperture efficiency small scan communication antenna, noting radar installation 14 p2289 A67-28911
Applications Technology Satellite /ATS/ emphasizing communications facilities, repeater, antenna array, etc 16 p2760 A67-30694
- SPACECRAFT COMMUNICATIONS SYSTEM**
Surveyor telecommunications system from standpoint of actual subsystem implementation and performance, detailing reliability, flexibility, redundancy and data transmission modes 02 p0196 A67-11998
Long wave spacecraft antenna design, deployment and stabilization, noting environmental effects such as thermal expansion, solar pressure, etc [AIAA PAPER 66-848] 02 p0221 A67-12258
Precision power measurements of spacecraft CW signal level with microwave noise standards, noting Mariner IV application [JPL-TR-32-1070] 09 p1495 A67-21622
RF communication converter miniaturization and packaging techniques 12 p1911 A67-25271
Communication with and by space vehicles at ghz frequencies, using atmospheric windows [AAS PAPER 67-94] 15 p2478 A67-29954
Spacecraft and ground equipment of Lunar Orbiter telecommunications system 17 p2811 A67-32119
- SPACECRAFT COMPONENT**
Thermal control of Nimbus spacecraft by utilizing semipassive and passive thermal control elements to maintain temperature of overall spacecraft, subsystems and components 02 p0335 A67-12391

- Surface tension and equilibrium surfaces in weightless liquids, with application to spacecraft systems design 03 p0404 A67-13890
Spacecraft plumbing systems, discussing tubing materials and types of joints 07 p1192 A67-20247
Solid rocket components exposure to elevated temperatures, hard vacuum and UV radiation during space flight and reentry 15 p2507 A67-29548
Molecular sink for simulated testing of spacecraft components noting vessel construction, vacuum pump system, molecular trap array, etc 18 p3019 A67-33547
Steady thermal strains measurement in aero and industrial turbine and engine components, discussing fine wire behavior bonding agent, performance, requirements, etc 18 p3143 A67-33900
Metallurgical aspects of nitrided component application in unmanned satellite drive systems to remedy sliding wear and increase reliability 18 p3058 A67-34676
Giant forging press for aircraft and aerospace components 21 p3634 A67-38198
Component selection program for equipment onboard FR-1 satellite covering production facilities, qualifications, supply, reliability, etc 21 p3572 A67-38676
Probable failure mode and minimum service life prediction for spacecraft pressure vessels using fracture mechanics analysis and fracture specimen test results [ASM PAPER C6-2.3] 23 p4079 A67-41408
Alkali metal Rankine cycle space power system component and systems design 24 p4186 A67-42887
- SPACECRAFT CONFIGURATION**
Structural design and temperature control influence on configuration of Mariner space probes 01 p0156 A67-11440
Second generation Saturn vehicles, discussing anomalies discovered during flight tests, development, etc [AIAA PAPER 66-839] 02 p0331 A67-12255
Manned lifting entry vehicle capability, minimum weight, variable geometry, retractable landing engines, etc [AIAA PAPER 66-959] 02 p0332 A67-12287
Simulation of deployment dynamics of spinning spacecraft, discussing test methods emphasizing gravity compensating techniques [AIAA PAPER 67-207] 06 p0980 A67-18325
Aerodynamic characteristics of Mars probe/lander configurations consisting of blunted cone, shell and spherical segment analyzed at various Mach numbers on ballistic range [AIAA PAPER 67-167] 06 p0941 A67-18482
Ballistic vs lifting body and winged recovery techniques for space launch vehicles, noting cost and operational capabilities 15 p2567 A67-29834
Earth-orbital transport systems noting configurations, cost, capabilities, operational requirements, etc 15 p2567 A67-29835
Integrated launch/reentry vehicle reusability via tip tank concept 15 p2567 A67-29837
European aerospace transporter, fundamental concepts and development 15 p2556 A67-29838
Space tourism potential, cost estimate of equipment, management, etc [AAS PAPER 67-127] 15 p2558 A67-29965
Reentry vehicle roll resonance criterion formulation for predicting roll conditions, noting vehicle configuration, aerodynamic and trajectory parameters, exoatmospheric vehicle attitude, etc 15 p2572 A67-30211
Rod configuration determined optimum for gyro torquer controlled spinning space station subject to impulse disturbance 17 p2955 A67-32477
Aerodynamic characteristics of Mars probe/lander configurations consisting of blunted cone, shell and spherical segment analyzed at various Mach numbers on ballistic range [AIAA PAPER 67-167] 19 p3169 A67-34816
Effective guidance and control redundancy for spacecraft configurations and mission outcomes, discussing computer systems [AIAA PAPER 67-555] 19 p3257 A67-35952
Multiple payload and multipurpose spacecraft evaluated for cost reduction in USAF space operations [AIAA PAPER 67-636] 20 p3535 A67-37621
Spacecraft-space plasma electric equilibrium, discussing active spacecraft configurations for control

[AIAA PAPER 67-702] 21 p3714 A67-38729
Europa I third stage attitude control
system design, discussing various model
configurations and overall
simulation 22 p3897 A67-39171
Preliminary spacecraft concept for real
time operational space environment
monitoring system 22 p3901 A67-39928
Aerodynamic power and moment
coefficients of space-transport configurations
for hypersonic reentry and trajectory
calculations 23 p3931 A67-41399
SPACECRAFT CONSTRUCTION MATERIAL
Fabrication methods for aircraft, rockets
and space vehicles including adhesives,
sandwich and laminated structures, plastic
fiberglass forms and explosion
forming 01 p0078 A67-10304
Powder metallurgy applications in space
vehicle systems, discussing parts and
materials actually used in successfully
orbited spacecraft 01 p0100 A67-10712
Gas-off products from space cabin
materials determined by continuous
recording instruments, gas chromatography
and IR analysis 02 p0189 A67-12388
Magnesium alloys in aircraft and space
vehicle construction, discussing production,
processing and properties 04 p0638 A67-14983
Spacecraft environmental effects covering
outgassing in high vacuum, deterioration of
materials by evaporation, lubrication and
changes in mechanical and electrical
properties of plastics 04 p0704 A67-14995
Ablative materials for thermal insulation
of space vehicles, considering tungsten,
tantalum, niobium, etc, as backing
metals 04 p0726 A67-15536
Reciprocity principle of Equivalent Sun
Hours /ESH/ as means of spacecraft
material testing 06 p0980 A67-18365
Flame-sprayed ceramic coating in space
technology, examining solid atomization or
Rokide process 06 p1021 A67-18764
Construction of lunar landing module with
high reliability and low
weight 07 p1260 A67-20246
Satellite structure from Be-locks alloy,
properties compared with Al and joining
methods 07 p1192 A67-20251
Spacecraft metal-metal composites
consisting of continuous filaments in metal
matrix 08 p1343 A67-21523
Structures and materials for supersonic
aircraft and space
vehicles 09 p1576 A67-22429
Structural adhesives for fabricating large
one-piece hemispherical bulkheads, noting
effect of radiation and high
vacuum 09 p1578 A67-22523
Satellite material problems in corrosion,
fatigue failure, vacuum degradation,
etc 10 p1670 A67-23740
Spacecraft thermal joint conduction study
covering surface conditions, external
pressure, use of various fillers and parent
materials and vacuum environment
[AIAA PAPER 67-316] 12 p2037 A67-26031
Materials, space vehicle structures and
reentry research and
development 13 p2213 A67-27503
Design, mission and environment
considered as criteria in material selection
for use in spacecraft 15 p2502 A67-29539
Thermal control materials for spacecraft,
considering UV spectral distribution,
radiation energy and flux, oxygen bleaching,
etc 15 p2579 A67-29552
Organic dielectric materials for spacecraft,
selection and evaluation 15 p2508 A67-29556
Acceptance criteria of space materials,
discussing materials for
surveyor 15 p2508 A67-29559
Adhesives for nuclear powered spacecraft
tested for pressure, temperature and
radiation effects 15 p2508 A67-29560
Cost reduction of space vehicle structures
and materials 15 p2575 A67-29948
Composite material with titanium strength-
weight ratio and aluminum safety for
aerospace vehicle construction
[ASTM PAPER 15] 18 p3067 A67-34576
Polymeric materials used for selected
subsystems of Mariner IV space probe
[JPL-TR-32-1031] 19 p3334 A67-35889
Integrated nondestructive testing for
determining weld integrity of space
vehicles 20 p3454 A67-36586
Book on inspection, construction,
operation, maintenance and repair of aircraft

and aerospace vehicles including metal, steel
frames, wood structures and high
temperature structural
material 22 p3811 A67-39441
Beryllium braze joining for light stiff
components noting structural examples and
fabrication techniques, with reference to
Apollo SNAP-27 radiator housing
[SAE PAPER 670805] 24 p4159 A67-41991
Materials and structural concepts for
design of entry systems, discussing
environmental factors, reuse potential and
high reliability
[AIAA PAPER 67-805] 24 p4251 A67-42964
SPACECRAFT CONTAMINATION
Decontamination techniques and
sterilization environment, discussing
compatibility with components and hardware
of lunar orbiting
spacecraft 02 p0249 A67-12386
Postulates on microbial hazards of
astronauts in prolonged isolation based on
studies with animals with locked
flora 05 p0755 A67-16281
Low contamination space chamber design
employing cryopanel array configurations
with near unity sticking
coefficients 09 p1485 A67-22122
Reassessment of COSPAR
recommendations concerning planetary
quarantine and spacecraft sterilization,
particularly for Martian
environment 10 p1601 A67-23579
Russian and American practices and
policies regarding planetary contamination in
connection with COSPAR
requirements 10 p1601 A67-23580
Space simulation using contamination-free
test facilities combining several cryogenic
techniques to produce all cryogenic
system 12 p1924 A67-25717
Planetary quarantine constraints, noting
prevention of Martian atmosphere
contamination 15 p2424 A67-29098
Spacecraft sterilization for microflora and
microorganisms using dry heat for
instruments, liquid straining and gas for
surfaces 15 p2430 A67-29100
Low barometric pressure, high carbon
dioxide concentration and water availability
on simulated Mars environment related to
survival and growth of bacillus
cereus 15 p2426 A67-29111
Materials evaluation and selection for
compatibility with manned spacecraft
environment 15 p2507 A67-29551
Chemical treatment reducing toxicity of
polyvinyl chloride tapes used for insulating
electric wires in space
cabins 16 p2693 A67-30910
Planetary quarantine and biological search
strategy, discussing Voyager-Mars mission
configuration, sterilization, back-
contamination and
decisions 19 p3180 A67-35233
Planetary quarantine problem for Martian
survival of microorganisms investigated,
using systems analysis 19 p3180 A67-35274
Contaminant control in space cabins by
systematic screening of materials and
supplies used, noting significance of test
temperature 21 p3577 A67-38077
Food, water and oxygen regeneration and
reclamation techniques for long duration
space flights, considering carbon dioxide
removal, water reclamation from urine and
contamination control 22 p3755 A67-40340
Procedures, facilities and equipment used
in contamination control of Saturn S-IVB
stage hydraulic system 23 p3935 A67-40848
Comparative microbial contamination
levels in clean rooms used for assembly and
test of lunar spacecraft 23 p3961 A67-40851
Assessment of microbial contamination on
surfaces of space hardware by
ultrasounds 23 p3962 A67-40852
Numerical estimation of microbial
contamination on surfaces of spacecraft
using swab samples, environmental settling
strips and air samples 23 p3962 A67-40853
Potential contamination of equipment by
primate passenger during 30-day earth orbit,
studying skin, body particulate matter and
indigenous microflora 23 p3944 A67-40856
Contamination control for Titan IIIB
program, discussing MAPS, membrane filter
technique, environment cleanliness control
and particulate spectra 23 p3938 A67-41499
Contaminant concentration due to human
habitation of space cabin simulator at 258
mm Hg and oxygen atmosphere

environment 23 p3964 A67-41559
Manned spacecraft water supply microbial
contamination detection using firefly
bioluminescent reaction 23 p3968 A67-41627
Fecal waste management unit for life
support simulator or aerospace flights
[SAE PAPER 670852] 24 p4115 A67-42001
SPACECRAFT CONTROL
Flight control problems and techniques in
space age 01 p0153 A67-10267
Maneuvering propulsion problems for
spacecraft attitude
control 01 p0142 A67-11401
Solid propellant electrical thrusters for
spacecraft attitude and trajectory
control 01 p0142 A67-11433
Spacecraft attitude control using rotation
about single inertially fixed axis to change
vehicle orientation 01 p0157 A67-11445
Real time digital simulation of stabilization
and control systems /SCS/ for manned
spacecraft noting transport delays, thruster
duration, etc 02 p0228 A67-11788
Design balances, tradeoffs and approaches
to system design of various types of
transistor-magnetic logic for aerospace
timing 02 p0216 A67-12014
Optimum control of antenna pointing
direction and space vehicle height subject to
random disturbance 02 p0219 A67-12147
Inertia stabilized attitude control system
for space vehicle, noting selection of
compensating network
parameters 02 p0331 A67-12160
Surveyor throttleable liquid propellant
rocket engine for operation on propellants
saturated with dissolved liquid gas
[AIAA PAPER 66-949] 02 p0304 A67-12283
Vapor replacement in propellant feed duct
with subcooled liquid to meet engine
starting requirement of space vehicle parked
in orbit
[AIAA PAPER 66-975] 02 p0305 A67-12297
Book on thermophysics and temperature
control of spacecraft and entry
vehicles 03 p0532 A67-13032
Spacecraft thermal control design
problems including insulation, interface
conductances, testing, weight penalties,
etc 03 p0517 A67-13073
Spacecraft attitude
principles and future
development 03 p0465 A67-14100
Spacecraft extravehicular control and
display system 05 p0788 A67-16968
Time optimal position and velocity control
of spinning vehicle with reaction jet
[AAS PAPER 66-115] 07 p1259 A67-19974
Digital computer use to provide
controllable display of star field for use
with spacecraft simulator for optical
sightings
[AIAA PAPER 67-254] 07 p1149 A67-20051
Earth-based mission control system of
Lunar Orbiter I
[AIAA PAPER 67-278] 07 p1260 A67-20082
Cislunar navigation assuming availability of
power for making changes in attitude,
velocity and direction, considering factors
affecting space navigator 08 p1351 A67-21100
Passive separation system for APL
spacecraft providing despin, solar blade
unfolding, yaw of injection rocket, battery
elimination, etc 09 p1571 A67-22061
Fluid amplifiers based on Coanda effect,
digital and analog pure-fluid devices,
applications to spacecraft control,
gyrocontrol, etc 10 p1595 A67-22975
Ion thruster, including mercury feed
system and shielded neutralizer, designed
and tested for spacecraft station keeping
and attitude control
[AIAA PAPER 66-247] 10 p1698 A67-23120
Low thrust engine spacecraft control
during boost phase, independent of velocity
vector determination, by stabilizing
osculating orbit plane relative to
planetocentric coordinate
system 11 p1869 A67-24068
Thermal radiation characteristics of
spacecraft temperature control louvers in
solar space environment, discussing specular
reflection
[AIAA PAPER 67-307] 12 p2036 A67-26022
Spacecraft thermal control coating
experiments, discussing unreliability of
degradation results due to failure to
measure radiation properties, UV wavelength
dependence and micrometeoroid damage
[AIAA PAPER 67-329] 12 p2038 A67-26043
Thermal control coating spectral

- sensitivity to UV induced degradation, noting rapidly increasing damage as incident radiation wavelength decreases [AIAA PAPER 67-340] 12 p1959 A67-26054
- Simulation results of adaptive tracking filter application to stabilization of structural bending modes of SI-B launch vehicle 13 p2212 A67-26818
- Surveyor throttleable liquid propellant rocket engine for operation on propellants saturated with dissolved liquid gas [AIAA PAPER 66-949] 13 p2188 A67-26834
- Multistage rocket motion optimization in uniform gravitational field formulated as coupled variational problem 13 p2213 A67-27321
- Control moment gyro as attitude control actuator for spacecraft, noting advantages over other momentum transfer systems 15 p2486 A67-29307
- Navigational technique for manned interplanetary missions, noting resemblance to traditional nautical technique 15 p2514 A67-29598
- Steering laws synthesis for explicit guidance, noting generalization and solution of closed loop equations 15 p2514 A67-29603
- Software tools for certifying operational flight programs 15 p2440 A67-29604
- Rotating spacecraft attitude changes due to energy dissipation from angular deformation treated by modal method 15 p2572 A67-30201
- Space vehicle automatic control considering order execution from guidance system and vehicle stabilization around its center of gravity 16 p2700 A67-30798
- Maintainability system operating parallel with cruise-mode spacecraft attitude-control system, noting application to Ranger III spacecraft 16 p2763 A67-31646
- Control and measurement of temperatures of Mariner IV 18 p3052 A67-34514
- Human engineering research to aid system designers to optimize man's role as control element in space systems 18 p2995 A67-34687
- Mathematical model of rigid, long space-body spinning at constant rate about symmetry axis for optimal attitude control calculations 19 p3331 A67-34777
- Flight control system of Saturn V launch vehicle, discussing attitude/attitude-rate scheme, gain required and stability achieved 19 p3331 A67-34808
- Propulsion sources for one-way unmanned subrelativistic interstellar probes, discussing interaction with deep space environment for vehicle control 19 p3322 A67-35316
- Spacecraft package temperature control by interior louver panel system, calculating net heat transfer [ASME PAPER 67-HT-64] 20 p3549 A67-36746
- Apollo program automatic checkout equipment, examining computer controlled checkout concept for Apollo spacecraft 20 p3417 A67-36974
- Thermophototropic model providing active thermal control in spacecraft surface functions as variable absorbance coating to compensate for solar irradiation changes 21 p3730 A67-37792
- Apollo lunar landing mission strategy development concerning guidance, control and landing and propulsion systems 22 p3897 A67-39166
- Digital computers in spacecraft control complexes analyzed for design specifics, determining processors composition 22 p3764 A67-39169
- Test and control planning concepts for space travel projects, considering third stage of booster rocket Europa 22 p3921 A67-39281
- Spacecraft flight control and computerized systems, discussing redundant systems, integrated circuits and simulation for man-machine interaction and lack of response 22 p3908 A67-40336
- Dynamics of electrohydraulic servomechanism /transducer-amplifier/ for transforming signals into forces for displacing spacecraft control mechanism, examining motion equations 23 p3935 A67-40637
- Liquid coolant space radiator system for manned spacecraft thermal control, investigating design and transient performance [SAE PAPER 670838] 24 p4252 A67-41994
- vehicles, noting fail-safe and fracture tolerant design [SAE PAPER 660681] 01 p0154 A67-10585
- Winged lifting reentry hypersonic vehicles, discussing design, analysis, fabrication and testing of hot and cooled structures and materials [AIAA PAPER 65-367] 02 p0331 A67-11929
- Manned Orbital Research Laboratory /MORL/ design studies stressing stabilization and control and electric power subsystems, water supply, etc [AIAA PAPER 66-932] 02 p0332 A67-12277
- Effects of space station logistic requirements on design of spacecraft configurations with various hypersonic lift/drag ratios, comparing payload, cost, etc [AIAA PAPER 66-958] 02 p0332 A67-12286
- Maneuvering-range constraints effects on lifting-vehicle design parameters as velocity increments, propellant consumption, heating rates and acceleration tolerance [AIAA PAPER 66-961] 02 p0332 A67-12288
- Propulsion system selection considerations for Voyager spacecraft including Minuteman solid with liquid restartable midcourse, orbit trim system, LEM descent stage and transtage [AIAA PAPER 66-974] 02 p0305 A67-12296
- Modeling of spacecraft performance during reentry /intact and disintegrated/ for evaluating spacecraft design through thermal and structural integrity tests 02 p0230 A67-12358
- Optimal design configuration for third stage of European launching vehicle 02 p0334 A67-12376
- Temperature control of orbital Titan III-C transtage space booster, noting thermal design, configuration and materials test program support 02 p0335 A67-12395
- Ranger and Mariner spacecraft temperature control design, test and flight results 03 p0517 A67-13071
- Spacecraft thermal design problems including computer programs, thermal control coatings, testing, etc 03 p0517 A67-13072
- Spacecraft thermal control design problems including insulation, interface conductances, testing, weight penalties, etc 03 p0517 A67-13073
- Design evolution studies defining technological, operational and cost characteristics for reusable aerospace passenger transport 03 p0519 A67-13791
- Design techniques for advanced flight structures providing statistical assessment of environmental loads, forecasts of high performance material response and higher reliability design criteria 04 p0707 A67-14423
- Mathematical theory of dimensional analysis and similitude, application to spacecraft thermal design and experimental results 05 p0926 A67-16514
- Atmospheric turbulence effects on statistical design and analysis of space vehicles [AIAA PAPER 67-134] 06 p1096 A67-18359
- Digital computer analysis of mission parameters governing spacecraft thermal characteristics including ablation effects, radioisotope generator systems, etc 06 p0966 A67-18417
- Comparison between Monte Carlo and PERT models, noting PERT errors and Monte Carlo simulation for Voyager spacecraft development [AIAA PAPER 67-209] 06 p1097 A67-18513
- Sensitivity of manned planetary spacecraft design to shield weight, onboard radiation and uncertainties in space environment radiation 07 p1258 A67-19376
- Voyager type landers on Mars surface noting instrumentation, operation, reliability, etc [AAS PAPER 66-61] 07 p1259 A67-19997
- Post Apollo space flight technology, discussing recoverable and reusable booster rockets, spacecraft, life support systems, etc 08 p1391 A67-21065
- Saturn S-IVB Apollo systems application to planetary exploration, using extension of technology and hardware for lunar exploration 08 p1411 A67-21074
- Manned Orbital Research Laboratory /MORL/ design and utilization 08 p1414 A67-21545
- Orbital reconnaissance of Mars in 1971 using modified Lunar Orbiter spacecraft, noting photographic system, trajectory, launch system, etc 09 p1570 A67-21681
- Reliability criteria application to improvement of program and design decision quality during preliminary design 09 p1582 A67-22291
- Reliability effect on design of lunar soft landing spacecraft /Surveyor/, Syncoms I, II and III, Applications Technology Satellites, Early Bird and four Intelsat IIs 09 p1582 A67-22302
- OAO structure for measuring absolute stellar energy in UV region 10 p1712 A67-22991
- Meteoroid protection system designs for optimum orbital space laboratories and manned interplanetary spacecraft 10 p1713 A67-23700
- System design of Voyager-class Mars Probe/ Lander, considering selections of entry aeroshell, landed capsule and descent and postimpact instrumentation 10 p1714 A67-23756
- ESSA meteorological satellite system noting mission requirements, design and performance [SMPTE PAPER 101-56] 12 p2011 A67-25472
- Mass properties determination on aerospace balancing systems 12 p1925 A67-25724
- Dynamic testing of crushable materials for planetary impact attenuation systems, noting Voyager and Ranger Lunar Capsule 12 p1956 A67-25731
- Shutter type thermal control system design for Nimbus spacecraft [AIAA PAPER 67-309] 12 p2012 A67-26024
- Maneuvering-range constraints effects on lifting-vehicle design parameters as velocity increments, propellant consumption, heating rates and acceleration tolerance 13 p2212 A67-26829
- Fuel container design for space vehicles, discussing impact protection, reusability and long term cryogenic storage 13 p2212 A67-27218
- Interplanetary space environment effects on spacecraft optical equipment noting thermal design [JPL-TR-32-1098] 13 p2144 A67-27358
- Alternate approach for spacecraft design sensitivities treating vehicle design variables as special control variables 13 p2054 A67-27600
- Optimum entry vehicle design using aerobreaking for manned earth entry at hyperbolic speeds, examining blunted conic, biconic and tetrahedral configurations [AIAA PAPER 66-489] 15 p2564 A67-29422
- Design, mission and environment considered as criteria in material selection for use in spacecraft 15 p2502 A67-29539
- Spacecraft reliability requirements, discussing design parameters and performance standards 15 p2493 A67-29606
- Spacecraft system performance vs component reliability, discussing practical aspects of software tools for management purposes 15 p2493 A67-29607
- Advanced space vehicle planning analyzed from economic approach to decision making, noting cost decrease with time 15 p2566 A67-29833
- Space transportation systems; considering recovery facilities, reusable boosters, cost, etc 15 p2568 A67-29846
- Structural technologies applicable to future large launch vehicles 15 p2569 A67-29855
- Aerodynamic lift in future space vehicle design and implications for testing [AAS PAPER 67-34] 15 p2571 A67-30106
- Manned spacecraft design, discussing range hardware and software development and future entry vehicle programs [AAS PAPER 67-36] 15 p2571 A67-30108
- Assurance and measurement of space vehicle alignment conforming to design requirements 15 p2496 A67-30422
- Spacecraft systems, International Astronautical Congress, Athens, September 1965, Volume 1 spacecraft systems - IAF Conference, Athens, September 1965, Volume 1 16 p2755 A67-30622
- Spacecraft design for manned planetary landings noting mission characteristics, navigation requirements, crew housing, etc 16 p2756 A67-30625
- System design of automated laboratory and associated entry vehicle for unmanned Martian exploration 16 p2653 A67-30628
- Entry/Lander vehicle for Mars mission

SUBJECT INDEX

SPACECRAFT ENVIRONMENT

- discussed in terms of gross payload, basic vehicle and preentry system 16 p2756 A67-30629
- Thermodynamic system design in Biosatellite program noting mission and spacecraft 16 p2757 A67-30632
- Two-phase cryogenic propellant storage under low gravity, discussing impact on vented and unvented vehicle design and performance 16 p2757 A67-30633
- Bellaev description of 17-orbit flight of Voskhod II including spacecraft design and control, life support system and walk-in-space 16 p2816 A67-30758
- Aerothermodynamics for Apollo spacecraft design and results of flight tests 16 p2761 A67-30935
- Lilapnov-derived fixed gain flight control system design to fulfill response requirements over wide range of parametric variations 16 p2763 A67-31644
- Subcooled liquid and slush hydrogen fuels effects on space vehicle design and performance, discussing propulsion, insulation, pressurization, venting, management, etc [AIAA PAPER 67-467] 18 p3137 A67-33937
- Flight failures in complex, unmanned spacecraft systematically studied for Voyager spacecraft design, discussing component failure, design deficiencies and space environment 18 p3138 A67-34656
- Lunar orbiter missions goals and design, spacecraft construction and equipment and examination of lunar surface photographs 19 p3319 A67-35266
- Unmanned rough-landing survival capsules design considerations for potential planetary payloads 19 p3332 A67-35335
- Vostok launch vehicle design characteristics evaluated including performance, propellant weights, booster phase burning period, etc 19 p3334 A67-35843
- Design, construction and procedure changes in Apollo following fire of January 1967 19 p3334 A67-35928
- Lunar Orbiter Attitude Control System design and space flight performance [AIAA PAPER 67-533] 19 p3334 A67-35935
- Spacecraft performance, operation and design optimization solved by variational analysis [AIAA PAPER 67-557] 19 p3174 A67-35954
- Flight phase constraints effect on design of Voyager orbiter-capsule mission 20 p3532 A67-36564
- Coil and dipole systems for magnetic testing of large spacecraft 20 p3415 A67-36612
- Optimization for selection of optical coating patterns of external surfaces of spacecraft for temperature control [ASME PAPER 67-HT-55] 20 p3548 A67-36737
- ELDO-A satellite launcher engine assembly and shell section production and testing 20 p3533 A67-37166
- General purpose unmanned spacecraft and multimission applications satellite possibilities [AIAA PAPER 67-635] 20 p3534 A67-37620
- Trends in contracting that will influence spacecraft design and development in 1970s [AIAA PAPER 67-641] 20 p3557 A67-37623
- Spacecraft design, solar powering, electric propulsion and side-looking radar for planetary surface observation mission on Mars or Venus [AIAA PAPER 67-712] 21 p3714 A67-38739
- Lunar Module rendezvous with Command and Service Modules in lunar orbit, discussing thrusting-maneuver schedule 21 p3714 A67-39145
- Cryogenic rocket upper stage structural design, fabrication and testing 22 p3899 A67-39533
- Terrestrial environment guideline documents providing natural environment extremes, means and cycles for spacecraft development 22 p3829 A67-39927
- Reentry vehicles heat protection design emphasizing composite material selection/development for coating within acceptable weight limitations 22 p3902 A67-39938
- Spacecraft equipment in-space maintainability design criteria 23 p4070 A67-40591
- Heat transfer equations with combined conduction and radiation noting application to spacecraft problems 23 p4082 A67-40997
- Thermal radiation properties measurement for materials in spacecraft design, discussing apparatus, instruments, techniques, devices and methods 23 p4083 A67-41368
- Flight performance and power system design of Mariner IV Mars probe 23 p3939 A67-41509
- Physicochemical techniques for gas separation emphasizing pulsed gas chromatography for carbon dioxide removal in spacecraft 23 p3964 A67-41555
- Vehicle volume and design criteria for manned lunar roving vehicles investigated by evaluating subjects performance under prolonged simulated lunar environment 23 p3970 A67-41658
- Dynamic mass transfer equation for design parameters of regenerable absorption beds for carbon dioxide removal in spacecraft life support system [SAE PAPER 670842] 24 p4115 A67-41996
- Proton space station design and onboard instruments used for high energy cosmic ray study 24 p4210 A67-42391
- Mariner space vehicles design evolution noting contribution to future space flights through measurement of atmospheric density of Mars 24 p4241 A67-42399
- Lunar Orbiter design, development, testing and space flight 24 p4241 A67-42404
- Large sun-oriented deployable solar array for OGO design, fabrication and flight performance 24 p4104 A67-42508
- Space structure design cost effectiveness studies for materials and configurations [AIAA PAPER 67-808] 24 p4252 A67-42965
- Orbital research hospital design for utilizing zero and low gravity therapeutic value in treating physiological conditions [AIAA PAPER 67-833] 24 p4243 A67-42976
- Computer-aided design of space systems, discussing design morphology and process [AIAA PAPER 67-956] 24 p4127 A67-43039
- Reentry vehicle design characteristics and requirements for safe reentry of radioactive power sources, discussing heat protection systems [AIAA PAPER 67-966] 24 p4246 A67-43044
- Long term manned space mission system effectiveness and reliability through interchangeability and redundancy noting optimization, tradeoffs, maintenance and spares [AIAA PAPER 67-984] 24 p4166 A67-43056
- ### SPACECRAFT DOCKING
- ### S DOCKING
- ### SPACECRAFT ELECTRONIC EQUIPMENT
- Onboard checkout system capable of meeting requirements for advanced space missions [SAE PAPER 660461] 01 p0153 A67-10568
- Transducer measuring water quantity in water storage tanks of LEM under zero g conditions 01 p0073 A67-11114
- Vibrating-piston electrostatic field sensor for Gemini program, examining design improvements including unity-feedback preamplifier, noise reduction devices, etc 01 p0074 A67-11127
- Agema Gemini electric charge monitor measures static charge difference between orbiting space vehicles 01 p0074 A67-11128
- Characteristics and performance of two solid state devices, using FM principle for measurements of low currents, suitable for space vehicles 03 p0377 A67-13107
- Onboard checkout equipment design requirements, considering hardware and software for manned spacecraft flight 03 p0399 A67-14212
- Relation between packaging design and cooling, vibration, RF interference and reliability of microelectronic systems used in space vehicles 05 p0779 A67-17467
- Increased oscillation stability and efficiency of traveling wave tubes for global satellite communications systems 06 p0967 A67-17883
- TV camera to be used by Apollo astronauts noting integrated circuits, optical system, light intensifier, etc 09 p1499 A67-22175
- Estimated reliability impairment of space equipment due to shortings from particle impact 09 p1481 A67-22312
- Variable-duty-cycle spacecraft power switching circuit design giving high efficiency crewman illumination control of reticle within optical alignment 10 p1597 A67-23308
- Wire-connected electronic packaging module system providing change capability, design flexibility, arrangement freedom and volumetric efficiency 12 p1912 A67-25275
- Relay failure in spacecraft subsystem analyzed via vibration testing 13 p2085 A67-27697
- Design concepts for stored program data acquisition system in spacecraft applications 14 p2275 A67-28690
- Space vehicle potentiometer, noting niobium diselenide lubricant and minimum frictional torque 14 p2325 A67-28770
- Humidity, temperature, contamination and disconnection effects on gasket and grease seals for extended space mission computer connectors 15 p2442 A67-29182
- Microelectronics practice and possible use of space for fabrication [AAS PAPER 67-79] 15 p2452 A67-29946
- Automatic photopolarimeter as pilot model for scans of planetary disks on fly-by missions 15 p2492 A67-30435
- Satellite communication, noting satellite and ground terminal design performance criteria 16 p2622 A67-30689
- Chemical milling technique for space vehicle chassis and circuitry production, noting similarity and differences with photoengraving and printed circuit techniques 16 p2683 A67-31739
- Solderless-wrap lightweight interconnection board for Lunar Module landing radar, noting manufacturing details 16 p2642 A67-31919
- Organizational techniques and trade-offs for low power operation in spaceborne data processing systems 17 p2820 A67-32503
- Power conversion circuits of Surveyor spacecraft including distribution system, battery charging and central regulator units 17 p2803 A67-32510
- Geocentric trajectories for particles of single class 18 p3016 A67-34666
- Acceptance checkout equipment spacecraft for centralized control and LEM and CSM systems testing 20 p3391 A67-36976
- Activity of Satellite Servo System and Electronic Division of San Giorgio in aerospace field 20 p3400 A67-37163
- Heat transfer analysis using Mach-Zehnder interferometer with laser light source for applications to spacecraft electronics 21 p3731 A67-37959
- Space electronic equipment design, considering incorporation of vibration, vacuum, micrometeoroid and radiation protection 21 p3591 A67-38209
- ESRO I satellite electronic equipment design applied to aurora studies 21 p3713 A67-38217
- Cabling material problems associated with military standard connectors for space vehicles, discussing reliability, fabrication, assembly and design 21 p3595 A67-38334
- Soviet book on microminiaturized aerospace digital computers noting production problems, reliability, electronics, storage units and foreign computers 21 p3588 A67-38765
- Lunar Orbiter flight programmer, electronic design, development, application and performance 21 p3601 A67-39062
- Quality control organization of suppliers to provide reliability of structural component of spacecraft electronic systems 22 p3922 A67-39282
- Highly reflective coatings and interference filters for silicon solar cells on spinning spacecraft on near-sun mission 23 p3937 A67-41490
- Solar cell submodule fabrication and design for Mariner and Surveyor spacecraft, describing automatic conveyor soldering oven 24 p4109 A67-42558
- ### SPACECRAFT ENVIRONMENT
- ### SA CLOSED ECOLOGICAL SYSTEM
- Gamma radiation effect on SCR correlated with electron radiation encountered by spacecraft 04 p0590 A67-15725
- Interplanetary transit and atmospheric entry of unmanned vehicle landing on Mars surface, with reference to heat shield technology [JPL-TR-32-1145] 12 p2034 A67-25715
- Heat pipes and vapor chambers for thermal control of spacecraft, noting design and application [AIAA PAPER 67-310] 12 p2036 A67-26025
- Low solar absorption surface coatings of aluminum, silver and silica with controlled emittance for spacecraft thermal control [AIAA PAPER 67-343] 12 p1959 A67-26057
- Spacecraft life support systems should

ensure radiation protection, food, power supply, waste removal, etc 13 p2061 A67-26753

Spacecraft habitability, discussing chemical and bacteriological changes, air contamination and biological compatibility for crew selection 13 p2061 A67-26754

Optimization of man-machine environmental interface problems in framework of large-scale and long-term space operations [AAS PAPER 67-80] 15 p2432 A67-29947

Life in spacecraft, International Astronautical Congress, Athens, Greece, September 1965 life in spacecraft - IAF Conference, Athens, September 1965, Volume 7 16 p2615 A67-30751

Hemodynamic modifications produced by orthostatism noting changes in cardiac frequency, arterial pressure and central blood volume produced 16 p2616 A67-30754

Manned flight simulators suitable to space research, discussing types, phases of development, operational and performance features, etc 16 p2654 A67-30761

Spacecraft cabin atmosphere, comparing pure oxygen with two-gas atmosphere 16 p2617 A67-30776

Multifunctional chemical compounds development for use as air revitalization materials 16 p2618 A67-30778

Helium-oxygen environment relation to biological-thermal requirements of spacecrew 20 p3374 A67-36582

Isolation of *Acinetobacter anitratus* from subject and room area during spacecraft environmental tests 21 p3573 A67-38072

Spacecraft optical environment, considering sky luminance, spacecraft corona, spacecraft scattered light and glare sources 21 p3713 A67-38568

Thermal comfort zone test for helium-oxygen and nitrogen-oxygen atmospheric mixture for 18-day continuous manned run 22 p3754 A67-39599

Space magnetic environment simulation coll facility for spacecraft testing by mapping magnetic fields 24 p4138 A67-42030

Space cabin atmosphere relation to environmental and operational variables, discussing effect of hypoxia and hypercapnia on spacecrew and mission safety [AIAA PAPER 67-855] 24 p4117 A67-42999

SPACECRAFT GUIDANCE

Path adaptive guidance modes for Saturn space vehicle, particularly Iterative Guidance Mode 02 p0264 A67-12318

Mathematical technique of midcourse guidance for spin stabilized interplanetary spacecraft, specifically computer simulation for flight to Jupiter 02 p0264 A67-12369

Orbital guidance and rendezvous in inverse square central force field using perturbation method, considering elliptical and circular orbits [AIAA PAPER 67-55] 06 p1028 A67-18265

Diamant program research and development in servomotor, first stage engine and structural vibration 07 p1131 A67-19520

Man-machine simulations for Apollo navigation, guidance and control system [AIAA PAPER 67-242] 07 p1136 A67-20063

MARCO 4418 binary computer for strapdown guidance system in LEM/AGS 08 p1297 A67-20627

Rocket maneuvers for rendezvous with propulsionless target satellite in elliptic orbit 08 p1410 A67-20640

Manual calculation and navigation of spacecraft orbiting near planets 08 p1352 A67-21112

Airborne guidance computations using prescribed-H-method, representing two-body motion in inertial space, presenting equations for target hitting, circular orbit, etc 08 p1352 A67-21532

Soviet book on IR and optical devices for vehicle guidance and homing covering light propagation, radiation from targets, airborne missile homing systems, etc 11 p1791 A67-24514

Spacecraft guidance problem, examining general and one specific solution using boundary value problem and correction function 13 p2153 A67-26620

Modulation of L/D and bank angle to achieved heading, range and trajectory stabilization, using closed form equations 14 p2347 A67-28114

Linearized manual space navigation incorporating redundant measurements to compensate for instrumentation inaccuracies 14 p2347 A67-28128

Nongeometric derivation of solution equations for cotangential orbital transfer 14 p2384 A67-28134

Surveyor guidance program for midcourse and terminal information, noting redundancy in design, decision making telecommunications, etc 15 p2514 A67-29599

Spaceborne programming language for Surveyor guidance, discussing impact on flight software development 15 p2439 A67-29600

Gemini guidance and control, discussing design, ground monitoring, launch and flight guidance, spacecraft instrumentation, maneuvering, etc 16 p2700 A67-30659

Closed loop simulation of movement of center of gravity and optimum guidance laws for space vehicles by analog computer techniques 16 p2700 A67-30662

Guidance, navigation and two phases of targeting of Saturn V lunar landing mission, analyzing launch, boost to orbit and iterative guidance 17 p2881 A67-32057

Iterative guidance mode with application to three-dimensional upper stage vacuum flight 17 p2881 A67-32058

LEM-CSM analysis, elastic bending and propellant sloshing 17 p2955 A67-32478

Conventional guidance-problem parameters and basic parameters applicable to Surveyor in relation to accuracy of lunar landing 19 p3257 A67-35943

Design of time-shared multiformat display medium to improve guidance and control displays in manned spacecraft [AIAA PAPER 67-552] 19 p3257 A67-35949

Effective guidance and control redundancy for spacecraft configurations and mission outcomes, discussing computer systems [AIAA PAPER 67-555] 19 p3257 A67-35952

Singular optimal control and attitude problem in rocket guidance [AIAA PAPER 67-582] 19 p3258 A67-35977

Formulation of problem of guiding low thrust spacecraft back to nominal trajectory [AIAA PAPER 67-618] 19 p3260 A67-36007

Mars landing guidance requirements for unmanned lander after separation from interplanetary flyby space vehicle 21 p3655 A67-37783

Suboptimal radial guidance scheme based on cubic time function of optimal trajectories radius vector modulus from simultaneous data 22 p3830 A67-39164

Man-machine design for Apollo spacecraft navigation, guidance and control systems 22 p3830 A67-39180

Adaptive terminal guidance scheme for circular orbit rendezvous to provide near optimal trajectory 22 p3832 A67-39964

Lunar rendezvous spacecraft guidance system performance for various initial conditions and instrument errors simulated by Monte Carlo computer program 22 p3832 A67-39965

Nonstationary second order linear differential equation for near time optimal space vehicle guidance system design solved by linear transform 22 p3832 A67-39966

Speedy generation of space flight guidance command signals and comparative analysis of operational schemes for generating guidance signals 22 p3832 A67-40145

Hand-held sextant capability in in-flight spacecraft navigation measurements [AIAA PAPER 67-775] 24 p4183 A67-42943

SPACECRAFT INSTRUMENTATION

ISA National Aerospace Instrumentation Symposium, Philadelphia, May 1966 01 p0072 A67-11108

Space applications research and development 01 p0152 A67-11430

Apollo X-ray astronomy experiment, noting instrumentation techniques employed and advantages [AIAA PAPER 66-888] 02 p0246 A67-12267

Aerospace instrumentation - ISA National Symposium, Los Angeles, October 1965 03 p0395 A67-13377

Ground and flight spacecraft instrumentation for lunar and planetary exploration 03 p0420 A67-13378

Spinning-image coded X-ray star camera, based on image coding, permitting reconstruction of two-dimensional image

[AIAA PAPER 66-850] 03 p0424 A67-1401

Apollo lunar surface experiments package /ALSEP/ of scientific instruments and supporting subsystems 03 p0397 A67-1413

[AIAA PAPER 66-919] 03 p0397 A67-1413

Digital computer driven electroluminescent solid state vertical scale indicator design development and fabrication emphasizing size, weight, power, reliability and display readability 05 p0805 A67-1631

Apollo computer design mechanical packaging, implementing heat and vibration model to conduct thermal vibration and sealing tests 05 p0814 A67-1746

Apollo guidance and navigation computer holding fixed program with diverse and flexible applications 05 p0809 A67-1755

Science subsystems for Jupiter flyby missions, discussing equipment selection mission planning, spacecraft design and trajectory and constraints on vehicle configuration [AIAA PAPER 67-120] 06 p1084 A67-1828

Diamant mechanical subsystems and programmer 07 p1258 A67-1952

Chemical analysis of lunar surface composition by instruments on board soft landing probes 07 p1186 A67-1957

Instrument integration for landing capsule payloads of planetary missions, considering functional operation, environmental constraints and interface definition [AIAA PAPER 66-59] 07 p1188 A67-1999

Data transmission capabilities of Mariner probes and landing capsules [AAS PAPER 66-62] 07 p1146 A67-19999

Gemini rendezvous experience, describing flight test cycles, type of maneuvers needed ground and onboard support systems, etc [AIAA PAPER 67-272] 07 p1260 A67-2008

Soil mechanics surface sampler experiment for Surveyor 08 p1410 A67-2094

Mariner IV spacecraft modification for Venus mission, discussing extent of changes 09 p1571 A67-2168

Optical instrumentation for missile and space vehicle testing 10 p1655 A67-2299

Spacecraft instrumentation, discussing selection criteria for signal conditioning transducer sensors, photographic equipment etc 10 p1655 A67-2300

Aerospace computer hardware, discussing general purpose requirement on basis of various computer designs 11 p1755 A67-2424

Aspect system on Pioneer VI and VII incorporates digital computer for accurate time sector division of spin stabilized vehicle 11 p1870 A67-2444

Manipulators for astronauts - using anthropomorphic mechanical hands and arm-controlled by bilateral servo system in exoskeletal master 11 p1749 A67-2501

Lunar Orbiter photographic system design including film processing, image conversion relay, reconstitution, performance, characteristics, etc [SMPTE PAPER 101-46] 12 p1940 A67-2546

Vidcon TV design modifications for spacecraft applications noting reduced power requirements, improvement of heaters narrowing of bandwidth, etc [SMPTE PAPER 101-51] 12 p1914 A67-2547

Instrumentation and data acquisition system used in Saturn V dynamic test program for design of flight control system 12 p1923 A67-2570

Data processing and reduction on board spacecraft and on ground using generalized information system 12 p1909 A67-2586

Interplanetary space environment effect on spacecraft optical equipment noting thermal design [JPL-TR-32-1098] 13 p2144 A67-2735

Management role in making technical and administrative decisions regarding type of telemetry system required 14 p2272 A67-2865

Stage separation, fluid behavior, engine plumes characteristics, etc, of Saturn vehicle detected, using remote sensing techniques 14 p2320 A67-2870

Microwaves and laser links for spacecraft earth communications noting limitations by external noise effects, atmospheric turbulence, fabrication tolerances, etc 14 p2273 A67-2878

Proposed emplaced scientific station for lunar surface studies 15 p2553 A67-2930

Computer partitioning for long term reliability in space, noting requirements for

various phases of operation 15 p2439 A67-29306
 Spinning-image coded X-ray star camera, based on image coding, permitting reconstruction of two-dimensional image [AIAA PAPER 66-850] 15 p2486 A67-29440
 Electrodeless MGD power generation during entry, using torque on magnet taken as rotating member of generator 15 p2422 A67-29443
 Lunar module onboard guidance equipment design, noting operational strategies, control systems, etc 15 p2514 A67-29601
 Scientific instrument integration into Mariner IV spacecraft and prelaunch testing for flexible performance 16 p2757 A67-30640
 Computational limitations of onboard orbiting computers such as fixed point arithmetic, limited word length and solution techniques 17 p2881 A67-32056
 MOS and silicon transistors for design of logarithmic amplifiers for space instrumentation 19 p3194 A67-35463
 Examination of ability of man to determine drift angle of spacecraft with optical sight [AIAA PAPER 67-624] 19 p3337 A67-36013
 Apollo Manned Spacecraft Program systems design requirements, emphasizing instrumentation system and Phase I spacecraft 20 p3443 A67-36469
 Spacecraft computers role on advanced manned missions 20 p3391 A67-36549
 Gemini spacecraft antennas performance during reentry into ionized medium, discussing electron concentration profiles, nonearth atmosphere extrapolation and antenna breakdown effect 21 p3591 A67-38210
 Principles, design and operation of synthetic plasma source for studying space vehicle antennas over wide frequency band 21 p3664 A67-38214
 Guidance and navigation sensors and systems, discussing spacecraft facilitated by microelectronics, computer technology, optimal filtering and gyroscopic sensor design 22 p3834 A67-40335

SPACECRAFT LANDING
 Surveyor vernier propulsion system, discussing design of thrust chamber, propellant tank assemblies, functions of VPS, etc [AIAA PAPER 66-593] 08 p1413 A67-21516
 Spacecraft landing systems technology, materials and hardware, model impact testing and para-sail landing rocket program 15 p2570 A67-29856
 Conventional guidance-problem parameters and basic parameters applicable to Surveyor in relation to accuracy of lunar landing 19 p3257 A67-35943
 Guidance system requirements for unmanned Martian propulsive landing capsule [AIAA PAPER 67-619] 19 p3260 A67-36008

SPACECRAFT MANEUVER
SA STATIONKEEPING
 Linearly-approximated characteristics of maneuvers correcting near-planet positions of spacecraft with pulsed flight velocity characteristics 02 p0321 A67-11536
 Analytic solution in terms of modified Bessel functions of synergetic turn in exponential atmosphere, using spacecraft engines only for drag cancellation and orbit trimming [AIAA PAPER 66-487] 02 p0331 A67-11938
 Mariner IV midcourse 50-lb thrust pressure-controlled monopropellant hydrazine propellant system, predicting impulse and velocity error as function of burn time [AIAA PAPER 66-948] 02 p0304 A67-12282
 Maneuvering-range constraints effects on lifting-vehicle design parameters as velocity increments, propellant consumption, heating rates and acceleration tolerance [AIAA PAPER 66-961] 02 p0332 A67-12288
 Heating restraints effect on aeroglide and aerocruise synergetic maneuver performance investigated for high lift-drag ratio vehicle [AIAA PAPER 67-169] 06 p1097 A67-18483
 Transfer from elliptical orbit to coplanar hyperbolic asymptote treated in terms of limited classes of one-and two-impulse maneuvers [AAS PAPER 66-127] 07 p1255 A67-19986
 Expressions showing possibilities to change independently all orbital elements of spacecraft by means of small continuous

thrusts achieved through electric propulsion 08 p1413 A67-21365
 Spatial-turn simulator using rocking device rotating under effect of internal forces 10 p1655 A67-22840
 Maneuvering-range constraints effects on lifting-vehicle design parameters as velocity increments, propellant consumption, heating rates and acceleration tolerance 13 p2212 A67-26829
 Optimum utilization of aerodynamic forces in aircraft maneuvers 13 p2213 A67-27326
 Temperature, valve and insulation criteria for designing low thrust subliming solid reaction systems 15 p2544 A67-29979
 Liquid-bipropellant pressure-fed propulsion systems in lower thrust range and use for spacecraft maneuvering 16 p2736 A67-30707
 Determining control functions and choosing parameters governing transfer of dynamic system from initial to final state 16 p2744 A67-30732
 Linearly-approximated characteristics of maneuvers correcting near-planet positions of spacecraft with pulsed flight velocity characteristics 16 p2752 A67-31602
 Heating restraints effect on aeroglide and aerocruise synergetic maneuver performance investigated for high lift-drag ratio vehicle [AIAA PAPER 67-169] 19 p3332 A67-34831
 Aerocruise maneuver for optimizing orbital plane change with respect to cruise speed 20 p3532 A67-36552
 Mariner IV midcourse 50-lb thrust pressure-controlled monopropellant hydrazine propellant system, predicting impulse and velocity error as function of burn time 21 p3712 A67-37797
 Energy accumulator and constant power propulsion system for near-circular orbit space maneuvering, considering two-vehicle encounter 21 p3689 A67-37985

SPACECRAFT MECHANISM LUBRICATION
 Lubricant selection for lunar missions and manned spacecraft based on compatibility with oxygen-rich environment, propellant, anodic coatings and sliding friction behavior in vacuum [ASLE PAPER 66AM-7A2] 13 p2123 A67-27100
 Space vehicle lubrication methods, noting design and construction of test apparatus 15 p2492 A67-29558

SPACECRAFT MODEL
 Half-scale thermal model of Mariner IV spacecraft tested in simulated solar environment [AIAA PAPER 66-23] 03 p0517 A67-13066
 Thermal vacuum performance testing of scaled models as technique for reducing development costs of spacecraft 11 p1773 A67-24346
 Thermal modeling applicability to steady state and transient conditions, considering material property changes with temperature [AIAA PAPER 67-305] 12 p2036 A67-26020
 Shape effects on hypersonic slender body wake geometry and transition 13 p2050 A67-26832
 Launcher for research and development on aerodynamic reentry 15 p2564 A67-29094
 Mathematical model of rigid, long space-body spinning at constant rate about symmetry axis for optimal attitude control calculations 19 p3331 A67-34777
 Ablators for severe reentry environments evaluated from modifications of reference model constructed of epoxy resin with silica fiber and phenolic filler 22 p3826 A67-39887
 Optimum tapers determined for circular and rectangular ties, comparing resultant flexural stiffness with untapered supports 22 p3914 A67-40066
 Light gas gun model launching technique with advantages of aerodynamic and mechanical methods of sabot stripping 23 p3988 A67-41751
 Thermal testing techniques for solar probe spacecraft using analytical and experimental models 24 p4139 A67-42043

SPACECRAFT MODULE
 Apollo spacecraft, discussing performance of Command and Service Module with typical payloads 08 p1412 A67-21077
 British reusable booster concept MUSTARD/multiunit space transport and recovery device/ using rocket-propelled VTO lifting bodies, noting feasibility and development cost 15 p2568 A67-29843

SPACECRAFT MOTION
 Particle deflection techniques for determining electrostatic field strengths, detailing application to surface field strengths for isolated spacecraft 01 p0074 A67-11129
 Astrodynamical perturbation theory in which perturbed space-vehicle motion is described in terms of osculating hodograph applied to lunar landing [AIAA PAPER 67-25] 06 p1085 A67-18304
 Two generalized matrix forms of linear estimates for spaceship motion derived, based on maximum probability criterion 07 p1247 A67-19096
 Optimum control of space vehicle motion along binormal to circular reference orbit for minimum fuel consumption criterion 17 p2955 A67-32255
 Biaxial satellite motion simulator for large space-simulation chamber, discussing temperature and pressure simulation 18 p3021 A67-34611
 Optimal control for nonlinear dynamic systems with/without invariant properties investigated for departures from optimal motion 21 p3656 A67-38586
 Satellite attitude stabilization using gimballed star trackers, analyzing satellite and star tracker motion in terms of angular velocity 22 p3830 A67-39170
 Doppler effect method application to satellites and space vehicles motion, giving formulas for satellite velocity, orbital shape and position 22 p3831 A67-39588
 Flight optimization problems, considering spacecraft with energy storage and limited power engines 24 p4240 A67-42295
 Spacecraft motion with limited power jet engine, applying simulation technique to determine operation modes for engine and control system 24 p4240 A67-42296

SPACECRAFT ORBIT
 Mission design, operations planning and flight preparation for manned orbital space missions [AIAA PAPER 66-904] 03 p0519 A67-14131
 Stability of points of equilibrium in restricted problem as influenced by perturbations of Coriolis force 11 p1866 A67-24773
 Nonlinear correction method for determining orbital parameters of space vehicle, using residuals and least squares technique 14 p2384 A67-28127
 Flight phase constraints effect on design of Voyager orbiter-capsule mission 20 p3532 A67-36564
 Spacecraft ephemeris, orbit compatibility and scheduling in AAP mission experiments 22 p3885 A67-39959

SPACECRAFT ORBITAL RENDEZVOUS
 Orbital guidance and rendezvous in inverse square central force field using perturbation method, considering elliptical and circular orbits [AIAA PAPER 67-55] 06 p1028 A67-18265
 Gemini rendezvous results, discussing equipment, maneuvers, docking, stationkeeping, orbital calculation, etc 06 p1098 A67-18649

SPACECRAFT PERFORMANCE
 Automated spacecraft flights and cost /1965 to September 1966/, discussing Voyager, Jupiter probe, technology satellite, synchronous meteorological satellite and voice/TV broadcast satellite 05 p0904 A67-16384
 Aerospacecraft, reusable self-contained man-rated vehicle, noting economy, propulsion system and possible configurations 06 p1098 A67-19022
 Thermal design of navigational satellites, obtaining reduction in discrepancy between operational orbital temperatures and preflight calculations through thermal vacuum testing 09 p1572 A67-22062
 Alternate approach for spacecraft design sensitivities treating vehicle design variables as special control variables 13 p2054 A67-27600
 Impact of performance improvements and reuse on cost of space transportation, noting size, configuration, mission requirements and commercial possibilities [AAS PAPER 67-130] 15 p2570 A67-29966
 Electronic checkout, environmental qualification and integration of OGO by spacecraft simulator and performance analysis system 16 p2654 A67-30639
 Peak altitude of multistage sounding

rocket vertical trajectory in vacuum determined by dimensionless graphs 16 p2762 A67-31247

Base bleed and initial boundary layer thickness effects on base pressure variations, calculating combining parameter for vehicle performance evaluation 19 p3172 A67-35779

Lunar Orbiter Attitude Control System design and space flight performance [AIAA PAPER 67-533] 19 p3334 A67-35935

Spacecraft performance, operation and design optimization solved by variational analysis [AIAA PAPER 67-557] 19 p3174 A67-35954

Surveyor spacecraft star sensor calibration and spaceborne performance 19 p3233 A67-35982

Real time performance, ground control and data processing of Surveyor spacecraft during maneuvers [AIAA PAPER 67-644] 20 p3419 A67-37625

Design, fabrication and performance of 10-millipound resistojet operating on hydrogen or ammonia, describing heat exchanger and nozzle geometry [AIAA PAPER 67-664] 21 p3690 A67-38699

Flight performance and power system design of Mariner IV Mars probe 23 p3939 A67-41509

SPACECRAFT POSITION INDICATOR

Onboard device locating present and future orbital satellite position through microfilm map dependent on satellite motion equation 08 p1352 A67-21525

Positional coordinates of spacecraft determined by algorithm, using distance from three predetermined points as found by rangefinders 11 p1816 A67-24083

Limitation of radio position-finding with increased spacecraft distances, noting navigational methods from ground and spacecraft 11 p1817 A67-24707

Correlation position device for autonomous orbital navigation system 20 p3481 A67-36553

SPACECRAFT POWER SUPPLY

Thermoradiolotope propulsion and integrated power application to cislunar and planetary space missions 01 p0155 A67-11413

Rankine and Brayton cycles for spacecraft power generation, discussing operation principles, advantages and performance characteristics 01 p0112 A67-11428

Solar cell power systems for electric propulsion, considering methods of generating, controlling and conditioning onboard electric power [AIAA PAPER 66-891] 02 p0183 A67-12269

Manned Orbital Research Laboratory /MORL/ design studies stressing stabilization and control and electric power subsystems, water supply, etc [AIAA PAPER 66-932] 02 p0332 A67-12277

Electrochemical power components meeting extreme requirements of space applications, used in commercial market [AIAA PAPER 66-1012] 02 p0184 A67-12305

Space vehicle power supply systems using thermionic reactors, noting power distribution in fission zone, cooling, shielding, etc 04 p0553 A67-14551

Radiolotope application to spacecraft propulsion and integrated power noting potential sources, thruster design concepts and mission types 04 p0655 A67-14554

Atomic power-supply system for space vehicles built in West Germany using sintered U-Y and U-Zr fuel elements 04 p0655 A67-14558

Electrostatic generators for space power, describing single capacitor, constant oblique field and brushless types [AIAA PAPER 64-450] 04 p0554 A67-15251

Energy supply in space - Symposium, Stuttgart, West Germany, December 1965 04 p0557 A67-15953

Design of solar cells as satellite power supply sources 04 p0558 A67-15956

Ground tests of 2.3-m-diam models of foldable foam-reinforced plastic paraboloidal mirrors for satellite energy supply system and optimization of optical characteristics 04 p0558 A67-15957

Radiolotope sources and nuclear reactors as energy sources for space vehicles 04 p0558 A67-15959

Fast and thermal reactors with thermionic converters in reactor core and nuclear system with converters outside core analyzed for power supply for space vehicles 04 p0559 A67-15964

Liquid metal MHD converter with multistage thermodynamic drive for use as power source in space vehicles as alternative to thermionic converter 04 p0559 A67-15965

Space satellite power converter-regulator design for minimum magnetic disturbance 05 p0754 A67-17462

Megawatt ion-propulsion power conditioning system design for manned interplanetary missions, noting payload-mass ratio problems, advantages, etc [AIAA PAPER 67-52] 06 p1075 A67-18449

Nimbus power supply subsystems 1960-1969, discussing regulation techniques, battery and maximum power point tracking 08 p1283 A67-20649

Variable ratio DC transformer regulator used in voltage boost configuration of power system in Radio Astronomy Explorer /RAE/ spacecraft, noting RF interference reduction 08 p1284 A67-20692

Voltage transformation and power/energy utilization of radiolotope thermoelectric generator source /RTG/ for space applications, analyzing components, inverter/converter circuits, etc 08 p1284 A67-20694

DC-to-DC prime converter for anchored interplanetary monitoring platform spacecraft /AIMP/ transforming power from solar array into suitable level for instrumentation electronics 08 p1284 A67-20695

Electric propulsion for space exploration, discussing testing results on Rankine cycle power system [AIAA PAPER 66-890] 09 p1559 A67-21870

Solar cell system for UK-3 satellite, discussing design, material selection, development and fabrication 09 p1445 A67-22179

Variable-duty-cycle spacecraft power switching circuit design giving high efficiency crewman illumination control of reticle within optical alignment 10 p1597 A67-23308

Dynamic control study for solar mirror aboard spacecraft using breadboard apparatus and computer simulation method 11 p1745 A67-24274

Suitability of Saturn IB/Centaur and Atlas/Centaur launched solar-electric propulsion vehicles for performing 0.1-AU solar probe mission [AIAA PAPER 66-496] 11 p1852 A67-24343

Mathematical model for predicting temperature and life of silver-zinc battery system in spacecraft [AIAA PAPER 67-334] 12 p1901 A67-26048

Radiolotope application to spacecraft propulsion and integrated power noting potential sources, thruster design concepts and mission types 13 p2155 A67-26578

Thin silicon solar cells for large flexible arrays having low specific mass and radiation resistance 13 p2055 A67-26716

Solar concentrator technology, discussing design requirements of space power conversion devices and manufacturing methods 13 p2055 A67-26826

Energy supply and energy converters in satellites and space vehicles 14 p2247 A67-27876

Power supply and transformation equipment in satellites, discussing batteries, fuel cells, nuclear reactors and solar energy 14 p2252 A67-28566

Direct energy conversion techniques in generating electric power in space for future astronautic systems 14 p2253 A67-29044

Electron tube requirements for space applications noting size, weight, environmental parameters, etc 15 p2447 A67-29752

High temperature high power gas diodes and thyatrons for large nuclear electrical space power systems, noting parameters of design and performance 15 p2448 A67-29755

Cavitation damage in alkali metal pumps, noting damage resistance and material properties for application in space power systems 15 p2494 A67-30151

Criteria for use of Rankine MHD systems in space 16 p2604 A67-30569

System for nuclear auxiliary power, covering spaceflight test of SNAP-10A, system testing, performance evaluation, etc 16 p2701 A67-30638

Variational problem of maximum payload

in mechanics of flights with limited propulsion power and energy storage unit 16 p2760 A67-30719

Batteries and fuel cells for space power systems, discussing Ni-Cd, Ag-Cd, Ag-Zn, Bacon cell, etc 17 p2801 A67-32047

Electric propulsion for space exploration, discussing testing results on Rankine cycle power system [AIAA PAPER 66-890] 17 p2928 A67-32051

French Diademe satellites power supply systems and planned laser experiments 17 p2941 A67-32232

Nuclear reactors for space propulsion and onboard power supply, including conversion systems 18 p3075 A67-33655

Performance of radiolotope heated ammonia thruster for spacecraft application [AIAA PAPER 67-425] 18 p3075 A67-33909

Parametric comparison between tracking with solar cell arrays and nontracking systems with respect to space power supplies 20 p3363 A67-36585

Solid propellant gas generator power systems for normal and emergency space operations 20 p3533 A67-36601

Hydrogen-oxygen fuel cell for spacecraft power system 20 p3363 A67-37011

Electric power plant survey for space application, noting Rankine and Brayton cycles 20 p3364 A67-37917

Thermionic conversion for space auxiliary power systems noting high reliability and longevity potential 20 p3364 A67-37019

Orbiting Energy Depot, discussing fuel regeneration and resupply to enable use of fuel cells combined with nuclear power as main onboard power 22 p3902 A67-39948

Nonmechanical electric power sources - Conference, Brighton, England, September 1966 22 p3748 A67-40226

Power systems for long duration missions including photovoltaic solar energy, thermoelectric, Brayton cycle and thermionic conversion systems, discussing solid state components 22 p3749 A67-40339

Photovoltaics - IEEE conference, Cocoa Beach, Florida, March 1967, Volume 2, Spacecraft power systems, solar cell mathematical model 23 p3938 A67-41505

Solar conversion/energy storage power systems for satellites in near earth orbits to provide continuous power supply 23 p3938 A67-41506

Solar cell power systems design and control technique for use in satellite programs, specifically transit 3B and 4A, ionosphere Beacon satellite, etc 23 p3938 A67-41507

Solar cell power supply design to satisfy whole satellite, discussing power supply size and solar cell panel fabrication 23 p3939 A67-41508

Solar cell array for LEM electric power system during lunar surface operation noting requirements and tradeoffs 23 p3939 A67-41510

Real gases examined for application as working fluid in Brayton cycle power plant, considering radiator area reduction to Rankine cycle 24 p4102 A67-42488

Criterion for minimum weight Carnot limited space power systems 24 p4103 A67-42496

Systems optimization methodology to analyze radiolotope thermoelectric generators /RTG/ for spacecraft applications, discussing computer program 24 p4184 A67-42504

Large long-life power supply system designed for earth orbiting spacecraft, discussing radiolotope interchangeability, controlled intact reentry, etc 24 p4184 A67-42505

Multi-kilowatt photovoltaic power system design for manned earth orbital mission 24 p4104 A67-42511

Solar array as primary electrical power source of Pioneer deep space probes, comparing performance data with test and design data 24 p4105 A67-42514

Solar cell/battery power systems for post-1975 satellites, discussing oriented thin film CdS solar cell array 24 p4105 A67-42515

Solar cell array flight systems, discussing flight experience, design and fabrication history 24 p4105 A67-42518

Sealed heat sterilizable high impact resistant battery for space missions, grafting acrylic acid and polyethylene by irradiation for separator 24 p4106 A67-42521

Orbiting space vehicle secondary battery size and weight optimization based on cycle life and discharge depth 24 p4106 A67-42522

Apollo fuel cell power system transient temperature and voltage response characteristics predicted by analytic model 24 p4106 A67-42523

Space power system pulsed turbine concept using bipropellants, reviewing multistage and multiple pass reentry performance and operational characteristics 24 p4107 A67-42530

Pu 239 fueled fast spectrum nuclear reactor spacecraft power supply design for 1 kwe noting cost, control, heat transfer and optimization 24 p4185 A67-42538

Spacecraft power conditioning reliability using standby redundancy at functional component level and performance monitoring automatic failure detector 24 p4108 A67-42539

Analysis of satellite power systems for maximum utilization of power 24 p4108 A67-42540

Stirling, Brayton and Rankine dynamic cycles compatibility with isotope heat sources, emphasizing power system applications to long-duration earth orbital missions 24 p4185 A67-42542

Optimization of electric energy storage for solar thermal space power systems 24 p4108 A67-42543

High temperature strength and magnetic properties of cobalt-tungsten alloy for space power generator rotors 24 p4174 A67-42726

Alkali metal Rankine cycle space power system component and systems design 24 p4186 A67-42887

Commercial earth orbital manned space station power system requirements, estimating operational and logistical costs for isotope and reactor designs [AIAA PAPER 67-879] 24 p4187 A67-42998

Power conditioning subsystem failure detection provided by computer monitoring of performance, with signal for transfer to redundant unit 24 p4110 A67-43055

Aerospace system power conditioning design optimization, treating efficiency, regulation, EMI, BITE, primary power, size, weight, radiation hardening and cost [AIAA PAPER 67-985] 24 p4110 A67-43057

SPACECRAFT PROPULSION

SA ROCKET ENGINE

Rocket propulsion for U.S. space program, considering early unmanned space exploration, manned Mercury flights, Gemini flights, etc 01 p0141 A67-11265

Resource allocation for maximum system reliability, noting weight allocation in spacecraft and Lagrange multiplier approach 01 p0084 A67-11354

Electrothermal, electromagnetics and electrostatic propulsion system design principles, operation applications and performance characteristics 01 p0142 A67-11410

Propulsion system selection considerations for Voyager spacecraft including Minuteman solid with liquid restartable midcourse, orbit trim system, LEM descent stage and transtage [AIAA PAPER 66-974] 02 p0305 A67-12296

Solid propellant rocket motor capabilities for space flights, noting specific impulse on density basis 02 p0305 A67-12352

Electrical propulsion of space vehicles using solar energy, electrostatic drive, drifting field plasma accelerator, etc 03 p0503 A67-13493

Rail-type plasma accelerator in creating ionized particles and electromagnetic field for spacecraft propulsion 03 p0477 A67-13509

Electric propulsion role in auxiliary and primary spacecraft propulsion [AIAA PAPER 66-1025] 03 p0504 A67-14156

Rankine cycle power plant characteristics for electric propulsion manned Mars mission [AIAA PAPER 66-894] 03 p0504 A67-14274

Ion propulsion systems development for near term mission, noting solar cell weight reduction [AIAA PAPER 66-1026] 03 p0504 A67-14275

Integration of life support system and propulsion system for manned interplanetary space missions 04 p0563 A67-15245

Staustrahlrohr experiments in thermodynamic acceleration process for liquid metal of MHD converter for space vehicle propulsion 04 p0560 A67-15966

Chemical propellants in Apollo program, noting Saturn launch vehicle and spacecraft propulsion 05 p0874 A67-17016

Design, operational characteristics and testing of ion engine for spacecraft propulsion, considering mission analysis, orbit parameters and spacecraft orientation [AIAA PAPER 67-87] 06 p1074 A67-18342

Electric propulsion unit using electron cyclotron resonance plasma thruster for spacecraft 06 p1074 A67-18418

Nuclear or electric propulsion for planetary exploration, noting configuration and capabilities 06 p1098 A67-19019

Fusion propulsion for interstellar missions, examining requirements for detection of extra solar life 06 p1076 A67-19027

Marx model for interstellar travel in vehicle propelled by terrestrial laser beam 08 p1376 A67-20989

SNAP-10A and SNAP-8, discussing reactor thermoelectric space power program 08 p1352 A67-21052

Radioisotope applications to space science, discussing selection criteria for electric energy production and/or space propulsion 11 p1817 A67-24096

Geomagnetic thruster, noting superiority over electric or chemical propulsion for thrust durations of more than few weeks 11 p1855 A67-25009

Magnetically accelerating continuously operating plasma engine for spacecraft propulsion compared with electrothermal engine 11 p1855 A67-25100

Maximum payload for air-scooping low thrust space propulsion system 13 p2212 A67-26893

Radioisotope selection criteria for propulsion and auxiliary power generation in space 14 p2348 A67-27971

Electric and photon propulsion systems in German-American research 16 p2736 A67-30710

Spaceflight application of cryogenic techniques including cooling magnets, noise reduction in parametric amplifiers and quantum-electronic, superconductive and IR sensing devices 16 p2702 A67-30717

Reaction control system for spinning synchronous satellite noting selection criteria, tradeoff methods, etc 17 p2953 A67-31972

Plasma propulsion for interplanetary flight, discussing optimization of specific impulse, weight distribution and flight path 17 p2928 A67-32226

Development of liquid hydrogen-oxygen propulsion stage in France, discussing structure, thermal isolation, storage, etc 18 p3111 A67-33653

Primary electric propulsion systems for deep space missions with reference to SERT II program and compatibility with other spacecraft programs [AIAA PAPER 67-424] 18 p3111 A67-33908

Primary electric propulsion application to satellite and other space missions, considering auxiliary systems and experimental thruster systems [AIAA PAPER 67-426] 18 p3112 A67-33910

Subcooled liquid and slush hydrogen fuels effects on space vehicle design and performance, discussing propulsion, insulation, pressurization, venting, management, etc [AIAA PAPER 67-467] 18 p3137 A67-33937

Phoebus 1B test /high-power-density reactors for space propulsion/ noting reactor design for fuel-element testing [AIAA PAPER 67-486] 18 p3076 A67-33952

Liquid hydrogen pumping for Phoebus reactor, discussing feed systems, nozzles, configurations, design, testing, etc [AIAA PAPER 67-478] 18 p3077 A67-34402

Single nozzle thermal storage resistojet thruster for low thrust satellite attitude and orbit control applications, noting design and performance [AIAA PAPER 67-662] 21 p3690 A67-38698

MPD plasma accelerator for spacecraft propulsion system, performance data and proposed acceleration mechanisms [AIAA PAPER 67-688] 21 p3693 A67-38719

High payload electric propulsion spacecraft powered by solar array for multiple interplanetary missions [AIAA PAPER 67-711] 21 p3714 A67-38738

Thrust, power and performance requirements for synchronous satellite simulated for evaluating ion propulsion

feasibility [AIAA PAPER 67-720] 21 p3694 A67-38746

Solid propellant space propulsion technology covering developments in missiles, launch vehicles, fabrication and range of application 22 p3869 A67-40334

Solar radiation pressure utilization as propulsive force for space vehicles noting sun sail concept 23 p4071 A67-41345

SET VIII Thermionic generator, evaluating operational and long term performance characteristics for space applications 24 p4103 A67-42499

Primary electric propulsion application to satellite and other space missions, considering auxiliary systems and experimental thruster systems [AIAA PAPER 67-426] 24 p4208 A67-42901

SPACECRAFT RADIATOR

Proton and alpha particle effects on thermal properties of spacecraft and solar concentrator coating of anodic-coated aluminum, zinc oxide/ potassium silicate, etc [AIAA PAPER 65-649] 03 p0448 A67-13054

Variable geometry entry spacecraft making secondary use of extendable wings in space as antenna and as radiators 20 p3532 A67-36560

Liquid coolant space radiator system for manned spacecraft thermal control, investigating design and transient performance [SAE PAPER 670838] 24 p4252 A67-41994

SPACECRAFT RECOVERY

Rogallo wing aerodynamic characteristics compared for various wing configurations and Mach numbers for possible application to spacecraft recovery 11 p1869 A67-24093

Ballistic reentry vehicle recovery via low speed water impact or air snatch after vehicle has flown unperturbed trajectory down to altitude of maximum dynamic pressure 15 p2564 A67-29424

Load prediction method necessitated by minimum weight and volume requirements for spacecraft recovery system, considering nonuniform opening of parachutes in cluster 17 p2797 A67-32578

Flare and landing performance of glide vehicles with low lift-drag ratio, noting aerodynamic characteristics effect [AIAA PAPER 67-575] 19 p3335 A67-35970

Recovery site location importance in determining entry vehicle future requirements 21 p3607 A67-37804

Manned spacecraft recovery safety noting operational testing of postlanding systems, recovery support and retrieval procedures for Apollo [AIAA PAPER 67-852] 24 p4243 A67-42985

SPACECRAFT REENTRY

Aerodynamic deceleration systems, discussing basic materials and fabrication techniques of BALLUTE program [AIAA PAPER 66-988] 02 p0181 A67-12299

Combustion reactions during spacecraft reentry, noting degradation of heat shields composed of hydro-and fluorocarbon compounds 05 p0928 A67-17334

Reusable low weight hypersonic glider /space rotor/ for space vehicle reentry and recovery 15 p2568 A67-29845

Hypersonic reentry heating problems due to kinetic energy of space vehicle at reentry at orbital and escape velocity 17 p2970 A67-32828

Radar designation by computer and real time reentry tracking for future Apollo manned space flight 20 p3381 A67-36592

Superorbital reentry environments, discussing materials, test environments and heat factors 22 p3919 A67-40383

SPACECRAFT RELIABILITY

Data and mission analysis in man-rating of Gemini launch vehicle 01 p0155 A67-11347

NASA program for microelectronic circuit and space vehicle reliability 01 p0042 A67-11364

Reliability considerations in spherical solid retrorockets for Gemini spacecraft system 02 p0305 A67-12351

Voyager spacecraft guidance and control system analysis, examining systems design requirements, problems of redundancy implementation for critical functions and gyro system 02 p0285 A67-12381

Space vehicle vs ground systems reliability [SAE PAPER 660691] 04 p0740 A67-15790

Space environment simulator for analysis of spacecraft material reliability during long-duration space mission 07 p1163 A67-19384

Reliability in improving program quality and design decisions as in planetary exploration program 07 p1259 A67-19617

Spacecraft failures noting iron concentration, poor machining, nitriding and anisotropy as causes 07 p1193 A67-20253

Optimal allocation of n test points within redundant digital system for prelaunch and in-flight spacecraft reliability estimate 08 p1300 A67-20637

Reliability effect on design of lunar soft landing spacecraft /Surveyor/, Syncoms I, II and III, Applications Technology Satellites, Early Bird and four Intelsat IIs 09 p1582 A67-22302

Interplanetary flight reliability problem treated by availability concept in terms of function, duty cycle and subsequent reliability 11 p1869 A67-24339

Clean room techniques for Apollo/Saturn Instrument Unit, noting that environmental and guidance systems parts must be supercleaned to qualify for man-rated space vehicle 11 p1773 A67-24938

Nonhardware aspects of space navigation - Conference, Los Angeles, March 1967 15 p2513 A67-29594

Spacecraft reliability requirements, discussing design parameters and performance standards 15 p2493 A67-29606

Surveyor spacecraft reliability from test data, examining assessment outputs, basic definitions and mathematical models 15 p2493 A67-29608

Methodology for numerically defining international magnitude of space rescue requirements 16 p2781 A67-30771

Solid propellant rocket motors reliability, discussing corrective action, retest, success probability, requirements, capability, simulation model, etc 18 p3112 A67-33914

[AIAA PAPER 67-435] 18 p3112 A67-33914

Man-rating F-1 engine, noting capabilities and future plans [AIAA PAPER 67-519] 18 p3115 A67-33982

Reliability prediction, modeling and analysis activities in Apollo program 18 p3139 A67-34697

Software aspects of space navigation including computer programming, mission planning, error analysis and reliability realization 19 p3187 A67-35858

Application of redundancy in Saturn V guidance and control system to achieve desired reliability [AIAA PAPER 67-553] 19 p3257 A67-35950

Reliability contribution of pilot using manual backup control for first stage of Saturn V tested using simulation [AIAA PAPER 67-554] 19 p3335 A67-35951

Apollo gyro reliability covering Guidance, Navigation and Control systems, stressing failure mode prediction 19 p3259 A67-35984

Unmanned spacecraft reliability, discussing design requirements, testing, lifetimes, performance and ball bearing failures 20 p3532 A67-38573

Spacecraft and space station reliability by orbital maintenance and extravehicular activity, comparing redundancy on system and cost effectiveness [AIAA PAPER 67-652] 20 p3535 A67-37629

Automatic check system for investigation of dynamic characteristics of stabilization system for carrier and space vehicle, noting system reliability 22 p3830 A67-39172

Quality control organization of suppliers to provide reliability of structural component of spacecraft electronic systems 22 p3922 A67-39282

Missile and space support systems reliability, flight equipment and redundancy 22 p3781 A67-40342

Prediction of Saturn V launch vehicle effectiveness during prelaunch phase using computer simulation [SMPE PAPER 102-27] 22 p3908 A67-40371

Methodology used to implement high reliability objectives for Surveyor pressure vessels, tabulating burst test results [ASM PAPER C6-2.1] 23 p4071 A67-41411

Two-axis gimbal system for solar simulation spacecraft testing, demonstrating intermediate axis internal drive system and outer axis drive input 24 p4153 A67-42044

Spacecraft power conditioning reliability using standby redundancy at functional component level and performance monitoring automatic failure 24 p4108 A67-42539

Sterilization effect on functional reliability

of interplanetary spacecraft systems and reliability of mission success, considering internally sterile electronic piece parts [AIAA PAPER 67-776] 24 p4116 A67-42944

Spacecraft long life and reliability, examining mechanical and electronic equipment margin testing problem [AIAA PAPER 67-880] 24 p4244 A67-43000

Vehicle flight readiness review, technique for assuring maximum probability of mission success [AIAA PAPER 67-888] 24 p4140 A67-43001

Time factor in onboard checkout and in-flight maintenance of manned spacecraft, discussing mission events and man-machine interaction [AIAA PAPER 67-950] 24 p4245 A67-43034

SPACECRAFT RENDEZVOUS

Time-optimal rendezvous in three dimensions with bounds on thrust and propellant, comparing various methods 02 p0330 A67-11924

Evasive guidance and maneuvering during terminal phase of co-orbital rendezvous 02 p0330 A67-11926

Soviet book on IR and optical devices for vehicle guidance and homing covering light propagation, radiation from targets, airborne missile homing systems, etc 11 p1791 A67-24514

Second order solutions to motion equations governing satellite rendezvous in elliptical orbit 12 p2012 A67-25931

Rendezvous between spacecraft and target flying in elliptic orbit of arbitrary eccentricity solved, using new approach [AIAA PAPER 66-537] 14 p2394 A67-28115

Continuous nonlinear feedback law for controlling thrust direction to produce minimum time spacecraft rendezvous with nonmaneuvering target 16 p2758 A67-30651

SPACECRAFT SENSOR

Space applications research and development 01 p0152 A67-11430

Gemini carbon dioxide sensor for monitoring in closed loop breathing system useful for many gas measurements 05 p0806 A67-16549

Space technology developments for World Weather Watch, discussing satellites role in weather forecasting, meteorological sensor and instrumentation 10 p1677 A67-23369

Space vehicle orientation with respect to rotating system of coordinates 12 p2011 A67-25641

Control signal generator and output characteristics of angular position and velocity sensors used in single-axis sun-oriented system of Vostok spacecraft 12 p1964 A67-25642

Stage separation, fluid behavior, engine plumes characteristics, etc, of Saturn vehicle detected, using remote sensing techniques 14 p2320 A67-28700

Canopus star sensor used for roll control of Mariner IV spacecraft 16 p2699 A67-30654

Nimbus I spacecraft overall characteristics, performance and major subsystems, particularly performance of meteorological sensors 16 p2759 A67-30685

Temperature gradient and thermal effects on ceramic transducer sensors used on spacecraft for cosmic dust experiments 19 p3229 A67-35170

Commercial aspects of exploitation of natural resources by satellite 19 p3349 A67-35642

Surveyor spacecraft star sensor calibration and spaceborne performance 19 p3233 A67-35982

Self-contained and vehicle integrated on-board checkout systems, considering controller-evaluator and sensors 20 p3449 A67-36979

Ultrareliable six redundant sensor attitude reference system for Manned Orbital Laboratory /MOL/ with limited sparing capability 21 p3624 A67-37786

Electromagnetic sensing of earth from satellites - Conference, University of Florida, November 1965 22 p3804 A67-40350

Planetary surface pressure and temperature of lower atmosphere determined from orbiting spacecraft with carbon dioxide laser 22 p3805 A67-40357

UHF sferic detection system receiving and display components for remote sensing by satellite of convective cloud development 22 p3806 A67-40358

Atmospheric temperature profile to 75 km by remote sounding, using satellite

measurement of molecular oxygen resonance line at 5 mm 22 p3806 A67-40360

Earth upper atmosphere background radiance measured by UV radiometer carried on Air Force satellite 22 p3794 A67-40364

Multichannel image data handling and processing system using multispectral analysis for remote agricultural sensing and surveying from aerospace platforms 24 p4157 A67-42435

SPACECRAFT SHIELDING

SA HEAT SHIELD

SA RADIATION SHIELDING

Spacecraft shielding combinations for astronaut protection, comparing magnetic, electrostatic and passive methods on basis of dosage and mission duration 01 p0153 A67-10425

Two superlight ablative compositions /SLA-741 and SLA-561/ developed for Mars Lander thermal protection, examining superiority to conventional low density charring ablators [SAE PAPER 660654] 01 p0103 A67-10614

Aerodynamic, thermodynamic and structural design aspects of flight capsule entering low density Mars atmosphere from orbit 01 p0156 A67-11432

Optical damage of spacecraft thermal control coatings in simulated space radiation environment of geomagnetically trapped particles [AIAA PAPER 65-646] 03 p0448 A67-13051

Spacecraft thermal control surface damage by solar wind bombardment in hydrogen and helium plasmas, with measurements of solar spectral reflectance and thermal emittance [AIAA PAPER 65-647] 03 p0448 A67-13052

Multilayer insulation system materials and design data for use on spacecraft in temperature range from 300 to 800 degrees K [AIAA PAPER 65-663] 03 p0534 A67-13069

Spacecraft thermal control coatings based on optical properties, discussing stability, environmental simulation in development, thermophototropic concepts, data retrieval and optical measurement techniques in ultrahigh vacuum [SAE PAPER 660653] 04 p0630 A67-15785

Number transmission coefficients for isotropically incident electrons determined for spacecraft shield design [AIAA PAPER 66-511] 05 p0906 A67-17219

Multichannel radiometer measurement of solar irradiance for realizing spacecraft radiative equilibrium [AIAA PAPER 67-147] 06 p1003 A67-18318

Local radiation equilibrium temperatures in semigray enclosures, with reference to thermal design of spacecraft [AIAA PAPER 67-211] 06 p1115 A67-18327

Proton energy spectrum obtained from nuclear emission measurements on Gemini IV and V missions 07 p1244 A67-19855

Calorimetric measurement of source and broadband spectral absorptances of spacecraft thermal control coatings during exposure to UV in vacuum environment 09 p1534 A67-22452

Material properties effect on design of reentry vehicle heat shield 10 p1734 A67-23726

Chemical, mechanical and chemical-mechanical self-sealant systems incorporated in spacecraft walls for micrometeoroid protection 10 p1673 A67-23748

Shrouds for space vehicles, discussing advantages of Al and Mg as materials and longitudinally split and over-nose type covers 11 p1870 A67-25006

Space vehicle hazard due to focusing of meteor streams by earth in antiradiant direction 12 p2002 A67-25656

Interplanetary transit and atmospheric entry of unmanned vehicle landing on Mars surface, with reference to heat shield technology [JPL-TR-32-1145] 12 p2034 A67-25715

Multiple sample space UV simulation facility for in situ hemispherical spectral reflectance measurements [AIAA PAPER 67-312] 12 p1926 A67-26027

Spacecraft thermal control coating damage in simulated space-bombardment conditions, using plasma bombardment techniques 14 p2293 A67-28138

Designing methods for meteoroid impact emphasizing minimum weight shield arrangement [ASME PAPER 67-DE-45] 14 p2402 A67-28878

Astronomical and satellite measurements of meteoroid environment of spacecraft in solar system 15 p2555 A67-29535

Spacecraft surface temperature-control coating requirements, selection and performance in prelaunch and space environments 16 p2757 A67-30634

Local radiation equilibrium temperatures in semigray enclosures, with reference to thermal design of spacecraft [AIAA PAPER 67-211] 19 p3344 A67-34820

Multichannel radiometer measurement of solar irradiance for realizing spacecraft radiative equilibrium 21 p3624 A67-37794

Solar flare occurrences probability, designating two-year period centered on sunspot minimum as safe time zone for vehicles on missions to Mars and Venus 22 p3873 A67-39929

Martian sand and dust storms simulation and abrasive effects on spacecraft surface coatings, noting similarity with Earth deserts 24 p4227 A67-42038

Solar wind and UV exposure effects on spacecraft thermal control coatings, using in situ spectral reflectance measurements 24 p4174 A67-42040

Simulated solar absorptance of spacecraft thermal control coatings determined calorimetrically in vacuum at room and cryogenic temperatures 24 p4256 A67-42913

Leakage rate due to meteoroid penetration of single and multiple hulled spacecraft, discussing effect on internal pressure 24 p4251 A67-42928

SPACECRAFT STABILITY

Geomagnetic stabilization of satellite initially torque-stabilized, deriving motion equation 01 p0153 A67-10210

Flight experience of earth-orbiting gravity gradient stabilization systems 02 p0334 A67-12362

Equilibrium positions of synchronous equatorial satellite situated in directions of extremum positions of radius of equatorial section of synchronous geoid 02 p0327 A67-12370

Control and stabilization of thrust producing final stages of recoverable space vehicles during atmospheric reentry 04 p0652 A67-14557

Combined effect of aerodynamic and gravity torques on stability of motion of passive satellites investigated by Liapunov direct method 04 p0704 A67-14827

Synchronous orbit stationkeeping techniques, examining thrust control requirements of spin-stabilized spacecraft 06 p1094 A67-17679

Requirements for gravity gradient stabilization of medium and synchronous altitude communication satellite systems using zero gain antennas, noting stabilization accuracy, stationkeeping effects, etc 06 p1094 A67-17680

Stabilite system, three-axis attitude control system utilizing single reaction wheel 06 p1094 A67-17681

Planar librational stability boundaries for flexible satellite under solar heating influence, using phase space concept [AIAA PAPER 67-126] 06 p1095 A67-18313

Tailfin design effect on induced rolling moment characteristics of sounding rocket 08 p1405 A67-20503

Fin-flare combination for stabilizing upper stage of Black Brant IV two-stage sounding rocket 08 p1405 A67-20504

Tip-off motion due to separation of stages or payload by multispring separation system with guided plungers 08 p1405 A67-20506

Dynamics of booster rockets and spacecraft with cavities partially filled with liquid 08 p1412 A67-21113

Optimal gain settings for atmospheric turbulence in 407 atmosphere wind profiles [AIAA PAPER 66-484] 08 p1413 A67-21509

Lumped parameter analysis of liquid-filled shells with application to 1/10-scale Saturn V model 10 p1713 A67-23749

Systems constraints imposed on spacecraft utilizing long flexible rods with attached tip masses, specifically deployment and retraction problems 10 p1714 A67-23757

Annealing effect on damping rods for magnetic field stabilized satellites 12 p2011 A67-25212

Optimum stabilization problem for axisymmetric satellite, considering fuel consumption 12 p2011 A67-25639

Gravity-gradient oriented satellite

stabilization by means of solar pressure torques on adjustable slats 14 p2395 A67-29051

Gravity gradient stabilization systems for orientation of spacecraft and for damping of associated librations 16 p2758 A67-30663

Gravitational stabilization of satellites with respect to orbital system of coordinates 16 p2760 A67-30740

Elastic components influence on attitude stability of motion of spinning satellite 16 p2761 A67-30742

Space vehicle automatic control considering order execution from guidance system and vehicle stabilization around its center of gravity 16 p2700 A67-30798

Despun antenna system for satellite stabilized by rotation around axis perpendicular to orbital plane 21 p3591 A67-38204

Automatic check system for investigation of dynamic characteristics of stabilization system for carrier and space vehicle, noting system reliability 22 p3830 A67-39172

Stabilization and control techniques for future unmanned commercial space vehicles, emphasizing application of projected technological advances in instrumentation [AIAA PAPER 67-878] 24 p4244 A67-42997

SPACECRAFT STERILIZATION

Lethal effects of high intensity airborne sound and ultrasound and irradiation time on *Bacillus Subtilis* for applications to spacecraft sterilization 01 p0016 A67-10881

System engineering techniques applied to analysis of spacecraft sterilization objectives and available technology 02 p0188 A67-11928

Heat sterilizable solid propellant motor designs for interplanetary missions, considering case-bonded spherical, case-bonded cylindrical, free-standing, internal burning and free-standing end burning [AIAA PAPER 66-973] 02 p0304 A67-12295

Fabrication procedure for biologically clean planetary landing module for later sterilization 02 p0188 A67-12380

Hardware design and production problems in launch and at separation for minimizing earth bacteria biocontamination Martian lander 04 p0562 A67-14425

Electronic component reliability as affected by thermal doses and ethylene oxide gas used in spacecraft sterilization 04 p0563 A67-15239

Electronic part sterilization program using ethylene tetroxide gas 07 p1136 A67-19618

Luciferase denaturation prevention using vacuum and molecular sieve during sterilization temperature exposure 10 p1597 A67-22928

Reassessment of COSPAR recommendations concerning planetary quarantine and spacecraft sterilization, particularly for Martian environment 10 p1601 A67-23579

Sterilization environment effects on structural systems design for interplanetary spacecraft 10 p1714 A67-23758

Heat sterilization of activated carbon at 135 degrees C for 24 hr or 165 degrees C for 3 hr for application to spacecraft 11 p1749 A67-24788

Heat sterilization in microelectronic assemblies 12 p1914 A67-25683

Heat sterilizable solid propellant motor designs for interplanetary missions, considering case-bonded spherical, case-bonded cylindrical, free-standing, internal burning and free-standing end burning 13 p2188 A67-26833

Biological and engineering problems in spacecraft sterilization, noting heat treatment 15 p2430 A67-29099

Spacecraft sterilization for microflora and microorganisms using dry heat for instruments, liquid straining and gas for surfaces 15 p2430 A67-29100

Ethylene oxide and methyl bromide mixture for spacecraft sterilization, discussing penetrating power, effect on components and packing and toxicity 15 p2430 A67-29101

Effects of spacecraft sterilization procedures and Mars dust environment on thermal control coatings 15 p2503 A67-29541

Nonmetallic materials for unmanned spacecraft 15 p2507 A67-29553

Problem of manufacturing space vehicles with rigidly controlled cleanliness and biological contamination for missions to other planets 18 p2995 A67-34677

Antimicrobial properties for various spacecraft materials, discussing impregnation methods for bactericides and two-stage sterilization 19 p3179 A67-35229

Sterile lock and split-seam techniques for sterile insertion and repair of spacecraft 19 p3180 A67-35259

Analytical model for microbial population survival times during heat sterilization studied for spacecraft applications, considering environment and exposure time 19 p3180 A67-35264

Sterilization of spacecraft tape recorder, noting component design for individual sterilization compatibility 19 p3230 A67-35583

Spacecraft preparation and sterilization methods including heat treatment, chemical agents, etc 20 p3375 A67-36804

Microelectronic performance degradation resistance under thermal sterilization cycling conditions 21 p3596 A67-38344

Contamination control Conference, Washington, D.C., May 1967 23 p3961 A67-40842

Supercleaning processes for Lunar Orbiter calling for personnel training, clean room garments, chemical cleaners, special packaging and inspection for particulate contamination 23 p3962 A67-40854

Sterilization effect on functional reliability of interplanetary spacecraft systems and reliability of mission success, considering internally sterile electronic piece parts [AIAA PAPER 67-778] 24 p4116 A67-42944

SPACECRAFT STRUCTURE

Manned and unmanned spacecraft structures, discussing environmental and functional requirements, influence of vibration and pressurized gas containment [SAE PAPER 660672] 01 p0153 A67-10579

Environment, mission requirements and subsystem interfaces effect on space vehicle structure [SAE PAPER 660673] 01 p0153 A67-10580

Space environmental effects on metallic and polymeric plastic structures including aluminum, magnesium, titanium, beryllium and stainless steel [SAE PAPER 660675] 01 p0094 A67-10581

Changing environmental condition effects on spacecraft structure from launch through orbit to entry and recovery [SAE PAPER 660680] 01 p0154 A67-10584

Environmental structural testing capabilities for orbital and space vehicles [SAE PAPER 660685] 01 p0154 A67-10589

Expandable and modular structures for support on manned space missions, reviewing inflatable, chemically rigidizable, unfurlable and elastic recovery structures 02 p0333 A67-12342

Beryllium properties and treatment for use in manned space flight noting thermal stress resistance, toxicity, honeycomb structures, etc 04 p0635 A67-14563

Impact physics and meteoroid population, with particular reference to space flight problems and research in high velocity impact 04 p0705 A67-15000

Impact resistance of spacecraft structures indicate performance criterion effect on final structural configuration and importance of hypervelocity of realistic hypervelocity test specimens 04 p0705 A67-15001

Optimal temperature control design using IBM 7094 digital computer program for thermal environment simulation of stabilized multisurfaced earth-orbiting spacecraft structure [ASME PAPER 66-WA/HT-44] 04 p0724 A67-15430

Structural dynamics of Gemini program, discussing environmental prediction, component testing, docking system, stability, etc 05 p0924 A67-17212

Inertial forces on straight light appendage used as antenna on artificial satellite 08 p1410 A67-20786

Pressure shell structures for space noting materials, machining, assembly, welding, testing, etc 10 p1661 A67-23731

High volume data processing techniques applied to Ranger acoustic testing 12 p1924 A67-25713

Tension string structure of high strength filaments for ultralightweight planetary entry vehicle 15 p2573 A67-29420

Cost reduction of space vehicle structures and materials [AAS PAPER 67-81] 15 p2575 A67-29948

Man-rated space-vehicle structural design

considering space environment loads and material requirements, noting applicability of existing methods 16 p2756 A67-30630

Puncture sealing of meteoroid penetration in spacecraft, giving mechanical and chemical methods and self-sealing tile inner shell process 22 p3913 A67-39885

Analytical prediction of cryogenic propellant venting effects on orbital vehicle dynamic behavior, emphasizing vent thrusting and gas 22 p3906 A67-40165

Impingement 22 p3906 A67-40165

Mission profiles involving new materials for missile and space structures reviewed for progress in computer applications 22 p3915 A67-40330

Fatigue crack research effect on structural design of flight vehicle structures, discussing temperature effects, multiaxial strain effects and fatigue crack growth equations 24 p4247 A67-41942

Low gravity slosh simulation parameters and scaling law used to extrapolate data to full scale spacecraft systems 24 p4141 A67-42032

Aerospace vehicle structure loading under structural integrity tests with simulated aerodynamic heating conditions, discussing computer relaxation solution for rod temperature distribution 24 p4172 A67-42036

Spacecraft structural criteria for lightweight photovoltaic solar arrays development, discussing Mariner type panel designs and power-to-weight ratios 24 p4108 A67-42557

Space structure design cost effectiveness studies for materials and configurations [AIAA PAPER 67-808] 24 p4252 A67-42965

SPACECRAFT TELEVISION

Digital and analog TV transmission from spacecraft compared, noting data compression and development of hybrid system 06 p0964 A67-18415

TV pictures of Surveyor I compartment radiators taken on June 11 and July 12, 1966, discussing cause of some changes in dust locations 08 p1386 A67-20944

Mosaic construction and image analysis for Surveyor TV pictures 08 p1333 A67-21504

Scan converter for Apollo TV performing time base conversion with destructive readout storage element and flicker correction with magnetic disk [SMPTE PAPER 101-53] 12 p1904 A67-25468

Manned spaceflight RF radiation communications systems including voice, telemetry, tracking and ranging, up data and TV 12 p1907 A67-25993

World-educational space-telecasting technical and operational problems 16 p2622 A67-30696

Spaceborne fiber optics TV system emphasizing image enhanced flexible front end optical assembly 20 p3445 A67-36554

TV in lunar environment, discussing development and performance of instrument used during Surveyor I mission 21 p3629 A67-38658

Environmental, thermal and foreign particle effects on Surveyor vidicon performance and expected tube life [SMPTE PAPER 102-32] 22 p3807 A67-40373

Surveyor TV power conditioning circuit and product design, discussing weight saving features, reliability and magnetic housing 22 p3807 A67-40374

Surveyor TV system calibration, determining transfer functions for various parameters 22 p3807 A67-40376

TV camera reseau for engineering information on planetary missions and reducing geometric distortion [SMPTE PAPER 102-39] 22 p3808 A67-40377

Earth shine illuminated lunar surface TV picture taking by modifying Surveyor equipment to provide light integration [SMPTE PAPER 102-40] 22 p3808 A67-40378

Surveyor TV system signal processing and transmission, analyzing performance and computer simulation of some effects [SMPTE PAPER 102-41] 22 p3808 A67-40379

SPACECRAFT TRACKING

Accuracy of real-time tracking of space vehicles using radar or L-shaped interferometer 01 p0110 A67-10266

Dynamic characteristics of human operator in tracking system under spaceflight conditions onboard Voskhod II spacecraft dynamic characteristics of human operator in tracking system under space flight conditions 07 p1135 A67-19106

Mathematical tool for system design of pseudorandom coded ranging system used in space programs, noting failure probabilities 07 p1145 A67-19869

Limitation of radio position-finding with increased spacecraft distances, noting navigational methods from ground and spacecraft 11 p1817 A67-24707

Manned spaceflight RF radiation communications systems including voice, telemetry, tracking and ranging, up data and TV 12 p1907 A67-25993

Analog computer use in design of automatic steering control system of Apollo station ships for precision geographical track-keeping 16 p2701 A67-31659

Electromagnetic compatibility operational problems aboard Apollo spacecraft tracking ship 20 p3387 A67-37641

Space vehicle tracking noting significance of accuracy and rapidity in determination of position, velocity and acceleration 21 p3583 A67-38642

Movable device for tracking rocket probes, discussing characteristics and requirements 21 p3608 A67-38673

Decoupled shifting memory filter method for radio tracking of space vehicles flight 21 p3587 A67-39146

Manned planetary mission global network for continuous tracking, communication telemetry and TV transmission [AIAA PAPER 67-976] 24 p4125 A67-43052

SPACECRAFT TRAJECTORY

Nominal trajectory in modified Encke special perturbation method, using two-body functions 01 p0148 A67-10384

Gravity loss in motion of body propelled from vicinity of planet into space trajectory 04 p0695 A67-14515

Statistical mechanics applied to statistically occurring disturbance in flight mechanics 04 p0703 A67-14550

Book on variational problems in flight dynamics of winged aircraft and space vehicles 04 p0705 A67-15007

Space probe launching conditions for accurate cometary orbit 05 p0895 A67-16574

Regularization of motion equations in computation of vehicle trajectory going near singularity [AIAA PAPER 67-26] 06 p1087 A67-18464

Optimum planetary approach of vehicle when direction of correcting pulses applied to trajectory plane is determined from maximum efficiency condition of pulse 07 p1247 A67-19093

Trajectory characteristics of high thrust Mars missions and effect on other aspects of mission planning 07 p1248 A67-19358

Trajectory design for spacecraft which returns in vicinity of earth after Mars encounter analyzed by patched conic model [AAS PAPER 66-126] 07 p1254 A67-19985

Trajectory determination from optical and radar data of spacecraft [JPL-TR-32-950] 08 p1384 A67-20621

Flight trajectories to moon, Venus and Mars 08 p1394 A67-21115

Mariner IV trajectory analysis and importance of flight-path selection in construction of basic mission profile [AIAA PAPER 65-516] 08 p1413 A67-21507

Laser rangefinder limit for rocket, balloon or satellite trajectory, noting effects of various parameters related to source, receiver, etc [ONERA-TP-460] 10 p1663 A67-22881

Minimum fuel impulses for space trajectories under influence of gravitational and propulsive forces 10 p1678 A67-23424

Spatial trajectories of rocket under constant thrust in planetary field 11 p1869 A67-24082

Trajectory measurement errors for powered spacecraft using matrix analysis [AIAA PAPER 64-650] 11 p1817 A67-24335

Spacecraft speed increment requirements for circular parking orbit about Mars and earth 12 p2003 A67-25741

Space trajectory analysis of nuclear-electric propelled vehicle 13 p2199 A67-27169

Algorithm construction for processing of telemetry data in determination of space vehicle trajectories, applying dynamic filtering method 14 p2382 A67-27853

Kalman filter divergence control, noting analytical and empirical modification methods 14 p2347 A67-28116

Geometrical form for solar system escape criterion 17 p2940 A67-32075

Ascent of satellite of variable mass from elliptic orbit along spiral trajectories by low thrust 17 p2948 A67-33022

Regularization of motion equations in computation of vehicle trajectory near singularity 17 p2948 A67-33039

[AIAA PAPER 67-26] 17 p2948 A67-33039

Optimal payload lifting and nonlifting trajectories of winged boost-launch vehicle [AIAA PAPER 67-558] 19 p3335 A67-35955

Powered flight trajectory determination for Saturn V vehicles through computer method 19 p3258 A67-35981

[AIAA PAPER 67-547] 19 p3258 A67-35981

Spacecraft trajectory parameter estimation, discussing various time-varying error components 21 p3705 A67-38587

Radio interferometry at Diane satellite tracking station, noting synchronous demodulation technique 21 p3587 A67-39052

Optimal flexible strategies for pulsed correction of close-to-nominal space vehicle trajectory, using fuel reserve limitation criterion 22 p3878 A67-39186

SPACECREW

Model for social system for extended-duration spaceship crews subject to isolation, confinement and/or stress 03 p0366 A67-14293

Visual observations of earth, sea and sky made by astronauts and cosmonauts during space flights 09 p1569 A67-22604

Gemini experiments program, examining crew integration, mission planning and prelaunch operations 10 p1713 A67-23243

Research astronaut selection 13 p2062 A67-26763

Prophylaxis for negative effect of hypokinesia on human cardiovascular system 13 p2059 A67-26764

Ionizing radiation dosimetry for space pilots on short-and long-term space flights 16 p2617 A67-30764

Prolonged space flight effects on crew members health concerning crew selection test methods 16 p2813 A67-30911

Trends in digital flight simulation for training 17 p2833 A67-32489

Manpower planning concept assuring personnel availability for space missions 18 p3162 A67-34679

Physiological/psychotechnical selection of French cosmonauts with reference to ballistic, orbital and space flight 19 p3179 A67-35066

Drugs for protection and stimulation of biological functions of spacecrews, noting experimental results on transverse-acceleration resistance of animals 20 p3367 A67-36254

Helium-oxygen environment relation to biological-thermal requirements of spacecrew 20 p3374 A67-36582

Aerospace nursing, present applications and future implications 23 p3968 A67-41622

Space cabin atmosphere relation to environmental and operational variables, discussing effect of hypoxia and hypercapnia on spacecrew and mission safety [AIAA PAPER 67-855] 24 p4117 A67-42999

SPACING

SA SEPARATION

Autocorrelation function of radiation electric field measurement from clipped correlation function and spacing estimation for optimally efficient SNR determination 01 p0114 A67-10808

Approximation theory of optimum performance of nonuniformly spaced arrays 02 p0212 A67-11613

Fiber spacing and array geometry effect on modulus of composites of laminate configurations used in aerospace structures 10 p1729 A67-23768

Planar antenna array with randomly spaced elements experimentally investigated, using holey plate technique 11 p1761 A67-24282

Optimum spacing arrangement for 1100101 array of four antennas in straight line with spectral sensitivity in switched and unswitched cases 14 p2284 A67-28435

Wave interference and radiation tunneling phenomena influences on thermal radiation energy transfer between two separated solid dielectrics, noting spacing effect [ASME PAPER 67-HT-21] 20 p3546 A67-36716

SPAIN

Spanish space research activities, describing organization, facilities, participating institutions and training

- programs 19 p3321 A67-35303
- SPALLING**
- S NUCLEAR REACTION**
- SPAN**
- S LIFESPAN**
- S WING SPAN**
- SPAN LOADING**
- Span loading of swept wing which produces minimum induced drag with constraints on lift and pitching moment 06 p0937 A67-18010
- SPARK**
- Radiation transport in spectral lines as consecutive photon absorptions and emissions, discussing contemporary theories, approximation methods and applications spark shadow projections in air for giant pulse 06 p1010 A67-18090
- SPARK CHAMBER**
- Ionizing accompaniment of near 170 bev nucleons at 2000 m altitude recorded by spark chamber /Geiger counter/ ionization chamber apparatus 02 p0312 A67-12609
- Apparatus for investigating nucleon reactions with approximate energy greater than 100,000 bev, including Cerenkov and scintillation counters and spark chambers 02 p0316 A67-12765
- Muon flux measurement with aid of spark chamber at depth of 20 mwe used for spatial distribution near axis of extensive air showers 02 p0318 A67-12780
- Multiplate spark chamber as linear high energy electron and photon detector 03 p0425 A67-14264
- Spark counter for recording fission fragments in presence of high intensity alpha radiation 06 p1001 A67-17936
- High altitude balloon flights with gamma ray spark chamber for search of cosmic gamma ray source in Cygnus 06 p1078 A67-18212
- Ionizing radiation in space, discussing detection techniques, devices, etc 11 p1791 A67-24619
- Digitized spark chamber for gamma ray and charged particle experiments on balloons and satellites noting construction, performance characteristics and results 12 p1944 A67-25854
- Multiplate spark chamber as linear high energy electron and photon detector 14 p2321 A67-28776
- Spark chamber telescope observations on cosmic ray neutral primary sources 14 p2381 A67-28846
- Spark chambers and scintillation counters used to search for fractionally charged particles in cosmic rays near sea level 15 p2550 A67-29680
- TV system with spark chamber detector for analysis and transmission of cosmic ray pictures to earth from satellites 21 p3599 A67-38655
- Apparatus for investigating nucleon reactions with approximate energy greater than 100,000 Bev, including Cerenkov and scintillation counters and spark chambers 22 p3876 A67-40267
- Muon flux measurement with aid of spark chamber at depth of 20 mwe used for spatial distribution near axis of extensive air showers 22 p3877 A67-40282
- Low inductance three-electrode spark source for vacuum UV generating high degree ionization spectra 23 p4000 A67-41214
- SPARK DISCHARGE**
- Operational alpha counting characteristics for point plane counter in air working in corona streamer mode 02 p0241 A67-11680
- Spectrochemical analysis of solid specimen from vapor formed by laser beam and excited by spark discharge 05 p0824 A67-16786
- Generation of series limit continua with aid of sliding sparks for absolute measurements in vacuum UV, observing bremsstrahlung 13 p2155 A67-26271
- Long spark formation in air under weakly focused laser radiation, deriving formula for mean propagation rate of spark beyond focal field 13 p2129 A67-27628
- Nitrogen, oxygen and hydrogen determined by spark-source mass spectrography, noting reduction of instrument blank levels 15 p2433 A67-29403
- Emissive power of air measured by determining charged particle distribution behind spark discharge generating shock wave in plasma 15 p2530 A67-29861
- Ozone generator and calibrator, noting design principles, operation performance and results 16 p2676 A67-31374
- Spark produced in cell containing argon when concentrating laser beam in small volume, calculating temperature distribution 17 p2869 A67-32804
- Spark perturbation of magnetic and electromagnetic fields, studying plasma-magnetic interaction and spark plasma characteristics 19 p3239 A67-35165
- Spark discharge generated blast wave application to shock on shock simulation, free-stream sound speed determination and hypervelocity flow measurements [AIAA PAPER 66-763] 19 p3208 A67-35753
- Emission properties of vacuum spark plasma arising in production of high current electron beam 20 p3498 A67-36684
- Grazing incidence spectrometer and low inductance spark source used for energy level identification in various elements 20 p3378 A67-37468
- Long spark formation in air under weakly focused laser radiation, deriving formula for mean propagation rate of spark beyond focal field 21 p3642 A67-38824
- SPARK EROSION MACHINING**
- Book on nontraditional machining processes covering process parameters, shape and materials applications, tooling, chemical removal, etc 14 p2328 A67-28893
- SPARK GAP**
- SA DIELECTRICS**
- Time domain reflectometry in reliability testing, detailing applications in checkout of electroexplosive devices with spark gap and cable validation equipment connection 01 p0084 A67-11361
- Low inductance 50 kv spark gap with high voltage handling capacity and minimum jitter, for use in modified Bostick type plasma gun 03 p0486 A67-14095
- Short triple electric and light pulse generation noting equipment design and performance 03 p0388 A67-14270
- Trigatron spark gap using low voltage plasma jet as switch analyzed for properties, time lag and mechanisms 19 p3298 A67-35602
- Neodymium doped YAG Q-spoiled laser system for switching high voltage spark gap at 50 pps with nanosecond jitter 22 p3813 A67-39258
- SPARK IGNITION**
- Flame noise in spherical volume of combustible gas confined within soap bubble and spark ignited, noting relation between radiated sound and flame movement and combustion 01 p0168 A67-11290
- Thermodynamic parameters of combustible mixture and ignition system characteristics effect on energy of spark ignition of homogeneous gaseous mixture 03 p0535 A67-13396
- Stable Implosion Initiation through converging detonation wave, discussing experimental techniques and results 14 p2293 A67-28141
- Ignition temperature and ignition delay of oxyhydrogen gas as function of pressure examined in shock wave tube, using Schlieren photography 18 p3160 A67-34261
- SPARK PHOTOGRAPHY**
- Laser spark holography with time resolution 06 p1006 A67-18786
- High speed spark photography with electronic equipment, describing generating and control units and optical techniques for shock wave observation 16 p2674 A67-31127
- Time-microscopy methods using laser flashlight, roentgen flashlight and rapid succession spark pulses in combination with stereo cameras 17 p2864 A67-33408
- Laser spark holography with time resolution 18 p3044 A67-33728
- SPATIAL DEPENDENCY**
- Plasma stabilization by HF electromagnetic fields, noting mode spectrum spacing along sample axis and dependence on field strength 10 p1886 A67-23585
- Temporal and spatial low energy solar proton intensity variations indicating interplanetary medium changes effects on magnetospheric configuration 22 p3873 A67-39813
- Energetic outer radiation belt electron spectra spatial and time variations 22 p3873 A67-39822
- SPATIAL DISTRIBUTION**
- Spatial and angular particle distributions in muon-generated electron photon cascade, using spark chamber muon detectors 02 p0317 A67-12774
- Muon flux measurement with aid of spark chamber at depth of 20 mwe used for spatial distribution near axis of extensive air showers 02 p0318 A67-12780
- Distribution of electromagnetic fields, density of forces and Joule losses with higher spatial harmonics in asymmetric type of MHD induction generator allowing for conducting walls 03 p0475 A67-13178
- Spatially distributed system for optimal filtration of useful signal in random noise fields 03 p0391 A67-13181
- Influence of polarized atoms diffusion on spatial distribution of optically oriented atoms 03 p0437 A67-13388
- Two spatial distributions transformed simultaneously with single lens heterodyning Fourier transform of spatial spectra 03 p0423 A67-13904
- Ray tracing study of HF ducting propagation with satellites [RASSA PAPER 1-10-145] 03 p0373 A67-14252
- Spatial distribution of energetic electrons in geomagnetic tail by analyzing counting rates from solid state detector on IMP 1 satellite 04 p0692 A67-14953
- Periodicity of plasma oscillation intensity spatial distribution upon electron beam excitation 04 p0666 A67-15181
- Modes in spatial distribution of neutron density within cosmic ray neutron monitor, each mode having distinct lifetime, using diffusion theory 04 p0661 A67-15615
- Brightness and spatial luminosity distribution in comet heads analyzed for steady and variable emissive processes 05 p0891 A67-16339
- Time-invariant Stokes, anti-Stokes and double emission processes in distributed traveling wave systems, calculating spatial EM field distribution and estimated conversion length 05 p0762 A67-16355
- Subcritical convective instability, discussing effects of internal heat generation and spatial variation of gravity field on onset of thermal convection 05 p0926 A67-16817
- Local variations in spacing and orientation of lattice plane in silicon single crystal, measuring angular positions of diffraction peak by double crystal spectrometer 05 p0866 A67-16977
- Propellant injection through electrodes effect on potential distribution in MPD arc [AIAA PAPER 67-49] 06 p1074 A67-18435
- Energy balance equations for solar atmosphere, considering hydromagnetic and thermodynamic processes, noting turbulent eddy effects 06 p1089 A67-18738
- Dynamics of narrowing effect of surface and spatial dispersing agents on radiation line of ruby laser with nonresonance feedback 06 p1012 A67-18797
- Ionization structure of polar auroras from spatial distribution of radar-reflecting zones, taking into account magnetic field variations 07 p1174 A67-19710
- Properties of antenna systems composed of individual arrays noting effect of spatial distribution, orientation, etc 07 p1154 A67-19781
- Low spatial frequency white light hologram production on Diazo materials 09 p1493 A67-21572
- Power pattern synthesized as product of two individual patterns produced from single linear array, obtaining formula for array element weighting 09 p1470 A67-21590
- Coherent electromagnetic wave analysis using spectral density function in terms of wave vector 09 p1462 A67-21605
- Approximation method to general solutions yielding coherence tensors of electromagnetic waves excited by source distribution with known coherence properties 09 p1462 A67-21606
- Electric arc behavior in argon gas flowing through magnetic field, measuring flow velocity, electron temperature, spatial distribution, etc 09 p1543 A67-21824
- Spatial dispersion of viscosity coefficients of liquids near critical point 09 p1487 A67-21904
- Spatial distribution of electrons and ions in neutral plasma, considering charge density 09 p1548 A67-22352
- Properties of solar cosmic rays causing polar cap absorption measured with satellites 10 p1700 A67-23188

Proton spectra and spatial distribution of energy protons on magnetic shells in earth radiation belts, using satellite data 10 p1702 A67-23300

Distribution of injected carrier densities in strongly forward biased laser junctions 10 p1666 A67-23522

Spatial variations in mean square response above lowest resonance frequency determined, using statistical analysis [ASME PAPER 67-VIBR-22] 11 p1872 A67-24181

Nonlinear mechanics of plasma-like distributed system studied with Q machine, noting mode locking 11 p1839 A67-24550

Morphology of lunar craters from Ranger photographs, noting distribution and possible competing processes of crater formation and destruction 11 p1865 A67-24608

Spatial correlation and molecular properties in extended Hartree-Fock calculations, deriving first and second order density matrices for ground state of H, Li and F 11 p1824 A67-24993

Surface roughness effect on spectral and total emittance of platinum, noting spatial distribution of polarized components [AIAA PAPER 67-320] 12 p1957 A67-26035

Spatial distribution of auroral radio signal reflection centers based on radar observations 13 p2111 A67-26566

Two-velocity spatial correlation coefficients and lengths measured for wall jets 13 p2049 A67-26590

Spatial modulation in populations of optically pumped ruby investigated for possible application to analysis of space and time distribution of laser beam 13 p2126 A67-26860

Spatial distribution of deuterium and hydrogen molecules and helium scatterer from /111/ plane of epitaxially grown silver 13 p2099 A67-26948

Generalized spatially uniform distribution functions for monatomic rarefied gas describing one-dimensional heat transfer in nonuniform flow 13 p2100 A67-26958

Interplanetary particle diffusion model analysis in terms of energy, position in space, direction and time 13 p2193 A67-27250

Emission intensity and spatial distribution of fluorescence measured for transitions in He, noting resonance radiation absorption effect on 5016 angstrom light spread 14 p2317 A67-28196

Magnetactive plasma quasi-linear oscillations equations, determining damping decrements of plasma electric field components 14 p2361 A67-28753

Steady state one-dimensional carrier distribution in depth for electron beam excitation of semiconductors computed, including diffusion and surface recombination 15 p2442 A67-29180

Spatial distribution of electrons and protons trapped by geomagnetic field and charged particle fluxes in interplanetary space 15 p2550 A67-29536

Spatially distributed automatic control system used in plasma plant stabilization 15 p2530 A67-29724

Threshold energy of formation and stable defect spatial distribution of silicon irradiated with electrons 15 p2542 A67-30250

Spatial distribution of radiation damage in solids determined by spectral analysis of photovoltaic current of photovoltaic cell 16 p2726 A67-30815

Exact solutions for spatial distribution of potential within space-charge region of non-degenerate semiconductor in contact with metal 16 p2727 A67-30850

Approximate solutions of spatial distributions of charged particles as gas discharge plasma obtained by two-point Jacobi expansion method 16 p2720 A67-31241

Millimeter wave resonant interferometer capable of measuring spatial distribution of electrons in low density transient plasma column subject to perturbation 16 p2675 A67-31263

Effect of defects distribution on behavior of steel structures analyzed for plastically relaxed model of slit 16 p2768 A67-31282

Fracture theory statistical models, static and stochastic approach 16 p2771 A67-31294

Electron velocity distribution function in nonequilibrium plasma having spatial distribution governed by electron-electron and inelastic collisions 16 p2723 A67-31768

Dynamic response of rigid-plastic material

ring subjected to arbitrarily distributed impulse load 17 p2959 A67-32412

Anomalous magnetic field charts for heights in ionosphere useful for studying auroras spatial distribution and sporadic E layer distribution 17 p2847 A67-32948

Drift azimuths, sizes and displacements of spatial inhomogeneities in oxygen atom emission at 5577 angstroms during night airglow 17 p2848 A67-32952

Night airglow brightness spatial distribution observed by photoelectric photometry in 5893 angstrom band, including isophotes charts and emission-inhomogeneity drift histogram 17 p2848 A67-32953

Perspective and path length effects on determination of spatial distribution of auroral luminosity from optical observations 17 p2851 A67-33206

Explosion theory, reviewing chain and thermal theories unification, fuel consumption effects, spatial distribution effects, etc 18 p3155 A67-33845

Dynamics of narrowing effect of surface and spatial dispersing agents on radiation line of ruby laser with nonresonance feedback 18 p3061 A67-34416

Local condensation in early stage of universe suggested from observation of spatial inhomogeneity of cosmic black-body radiation 19 p3312 A67-34893

Wave propagation and electron beam-plasma interaction in plasma column inside magnetic field, measuring plasma characteristics and spatial distribution 19 p3275 A67-35107

Observational consequences of geocentric dust cloud whose particles are concentrated toward plane of ecliptic and which contribute to zodiacal light 19 p3222 A67-35460

Interplanetary space magnetic clouds velocity and spatial distribution obtained from cosmic ray modulation data, noting relation to solar activity 19 p3325 A67-35493

Corrective image deconvolution of smearing caused by extended instrument functions in optical imaging possible by holographic Fourier transform division 20 p3435 A67-36204

Electrons energy spectrum stability dependence on spatial distribution of source, discussing cosmic ray generation 20 p3517 A67-36532

Distribution asteroids in space studied by computer analysis from selected plots of orbital elements 20 p3524 A67-36654

Optimal detection of signals by spatially distributed receiving system against random noise background, using space-time signal selection method 20 p3383 A67-37070

Distributed receiving system for optimal filtration of random field of space-distributed source 20 p3385 A67-37376

Carrier spatial redistribution under magnetic field effect of current in semiconducting crystal with intrinsic conductivity noting I-V curve shape 21 p3678 A67-38098

Plasma spatial electron density distribution from refraction of microwave beams with several frequency components 21 p3670 A67-38689

Spatial electron temperature distribution in electrodeless discharge, noting thermal conduction effect [AIAA PAPER 67-692] 21 p3672 A67-38721

Solar magnetic field existence evidenced by transverse fields in sunspots, field vector spatial distribution around sunspots and granular pattern inside sunspots 21 p3708 A67-38986

Electron temperature spatial variation in late He afterglow due to standing wave microwave heating 22 p3844 A67-39353

Auroral ionization echoes observed simultaneously by separated VHF radar noting aspect sensitivity, time variation, correlation with visible aurora, etc 22 p3760 A67-39624

Tenuous high temperature plasma electromagnet wave scattering, with relativistic corrections for scattered radiation spatial and spectral distribution 22 p3849 A67-39699

Spatial and angular particle distributions in muon-generated electron photon cascade, using spark chamber muon detectors 22 p3877 A67-40276

Muon flux measurement with aid of spark chamber at depth of 20 mwe used for

spatial distribution near axis of extensive air showers 22 p3877 A67-40282

Electron beam interaction with plasma investigated for spatial distribution of intensity and oscillation spectrum in stationary mode 23 p4032 A67-40904

Cosmic ray variations over celestial sphere investigated by matrices applied to distribution model 23 p4059 A67-41134

High energy proton data from Telstar 1 satellite used to develop mathematical models of proton spatial distribution 24 p4210 A67-42334

Cosmogenic radioactivity in freshly fallen meteorites measured and compared to calculate terrestrial and exposure ages and spatial and time dependence 24 p4238 A67-42884

SPATIAL FILTERING

SA IMAGE VELOCITY SENSOR

Perturbation theory analysis of spatial dispersion effects on frequency addition in crystals 03 p0434 A67-13125

Noise-rejecting spatial filters in signal pattern recognition 03 p0368 A67-13276

Autonomous landmark tracking by holography for space navigation 17 p2881 A67-32436

Optical system devised to alter relative harmonic coefficients and eliminating ringing effects for photographs represented in two-dimensional Fourier series applied to lunar photography 18 p3047 A67-33998

Computer program for handling of transform between spatial coordinate representation and spatial frequency representation of image 18 p3007 A67-34599

Image velocity sensing technique applying moving reticle scanners, with time-dependent correlation function analyzed by frequency discriminator 19 p3231 A67-35689

Coherent light applications in holography and spatial filtering including Fourier transform holography and pattern recognition 20 p3457 A67-36333

Phase objects observation method using spatial filtering and Hilbert transform 20 p3458 A67-36388

Spatial filtering for altering relative harmonic coefficients in two-dimensional Fourier integral representation of astronomical photographs eliminates ringing effects 23 p3997 A67-40625

Image processing by computer generated binary filters 24 p4156 A67-42432

Spatial filters for code translation and image sharpening produced by holograph in reasonably good approximation 24 p4159 A67-43097

SPATIAL ISOTROPY

Pseudo-isotropic radiation source as source with isotropic gain function and polarization depending on spatial direction 16 p2761 A67-30793

Neodymium glass laser radiation investigation, using moving active body method, for spatial inhomogeneity of mode field in spectrum random structure 19 p3238 A67-34895

SPATIAL ORIENTATION

Zeeman field spatial orientation of paramagnetic spin-lattice relaxation for $2T_2$ states in rhombic symmetry, emphasizing application to Fe-doped potassium cobalticyanide and potassium ferricyanide 01 p0129 A67-10150

Epitaxial temperature for Si films vacuum deposited on silicon as function of substrate crystallographic orientation observed by low energy electron diffraction patterns 01 p0132 A67-10372

Hall coefficient tensor in single crystals of titanium measured at room temperature as function of crystallographic orientation in magnetic field 01 p0132 A67-10375

Damage rate deduced from room temperature conductivity measurements on n-and p-type floating zone silicon samples subject to electron irradiation at energies from 0.3 to 2.0 mev 01 p0133 A67-10752

Working equations for dimensions and orientation of impinging propellant sheets in liquid rocket engine injectors 02 p0182 A67-11946

Wheat seedlings grown so that coleoptile and early roots developed in moist air, noting organ orientation in relation to gravity 04 p0560 A67-14407

Orientation dependence of surface charge on anodized indium antimonide from MOS capacitance measurements 05 p0869 A67-17093

Optimal conditions of thermostability of anisotropic spherical ferrite microwave resonator with various orientations 07 p1153 A67-19597

Crystal symmetry, optical properties and ferroelectric polarization of barium titanate single crystals 07 p1234 A67-20096

Qualitative and quantitative methods for correlating preferred crystallographic orientation with biaxial strengths of titanium alloys 08 p1340 A67-20363

Two-impulse torquing scheme for reorienting spin axis of asymmetric spinning vehicle 08 p1413 A67-21510

Dissipative wave propagation in linearized compressible MHD flow, constructing solution for arbitrary values of dimensionless parameters and field orientation 11 p1825 A67-23867

Coherent ordered precipitates formation in Ni-Cr-Al alloy, discussing spacing, shape and size of gamma prime particles as function of time 12 p1954 A67-25344

Roll-angle indicators used for avoiding spatial disorientation during instrument flight 13 p2063 A67-26927

Factors affecting human spatial orientation system functioning during flights 14 p2254 A67-28211

Three-photo orientation solution to analytic aerotriangulation problem, investigating mathematical concepts and computer programming methods 15 p2486 A67-29298

Analytical reduction of panoramic and strip photography to equivalent frame photography 15 p2486 A67-29299

Mathematical model for otolith organs used to analyze human spatial orientation 16 p2610 A67-30753

Preferred shape orientation of olivine crystals in porphyritic chondrules suggesting drawing from larger magma bodies 16 p2619 A67-30986

Polymer fracture mechanism hypothesized as competition between localized hardening by molecular orientation and localized softening during deformation 18 p3068 A67-33488

Surface morphological changes of tantalum single crystals during plastic deformation, studying orientation dependence of yield stress in tension and compression 19 p3245 A67-35727

Optimal conditions of thermostability of anisotropic spherical ferrite microwave resonator with various orientations 20 p3401 A67-37336

Latitude relation of cuprous sulfide formed on CdS single crystal noting precisely similar orientation 21 p3677 A67-38011

Nature, distribution and causes of structural imperfections and dislocations in epitaxial Si layers with base layer orientation //11/ 21 p3681 A67-38359

Self-decoration effect in thermally etched polycrystalline lithium ferrite, discussing geometric symmetry relation to crystallographic surface orientation 22 p3855 A67-39344

Single crystal silicon films on insulating substrates, discussing preparation methods and chemical and structural perfection for use in field effect and bipolar devices 24 p4202 A67-42089

SPATIAL PERCEPTION

Gemini inflight experiments on space perception via measurements of ocular counterrolling as test of otolith function 13 p2062 A67-26920

Skilled response organization, discussing stimulus coherence, tracking task, spatial and temporal coherence, secondary task, sequence length and task coding 14 p2254 A67-28034

Conditioned falling reflex of analyzer systems effect on change of human posture and spatial position 24 p4114 A67-41848

SPECIFIC HEAT

SA FORMATION HEAT

SA SOLUTION HEAT

SA VAPORIZATION HEAT

Tabulated data on specific losses in flow systems 02 p0233 A67-11995

Semiautomatic potentiometer measurement of nitrogen specific heat at small intervals, noting applicability of logarithmic law for other temperature ranges 03 p0532 A67-12929

Thermodynamic approach to flow phenomena based on temperature dependence of specific

heat 03 p0537 A67-14304

Extreme variations of electronic effective mass with temperature cannot lead to satisfactory explanation of specific heat anomaly in superconducting lead 04 p0676 A67-14934

Transient method for simultaneously determining thermal conductivity and specific heat, utilizing finite difference and statistical procedure called nonlinear estimation 04 p0734 A67-15851

Increase in low temperature specific heat and change in electronic density of states of boronated graphite 05 p0833 A67-17197

Effect of Mach number and specific heat ratio on distance of shock wave from end face of circular cylinder in axisymmetric flow 07 p1126 A67-19347

Pauli-paramagnetic superconductivity in Ti-16 at. percent Mo from specific heat measurements 07 p1235 A67-20130

Specific heat and magnetic susceptibility of yttrium solid solutions with magnetic impurities of Gd 08 p1369 A67-20870

Thermal diffusivity and specific heat of molybdenum at high temperatures measured, using variable heating in induction furnace 09 p1517 A67-21866

Inverse problem of unsteady heat conduction equation for unbounded hollow cylinder, determining specific heat 11 p1882 A67-24031

Thermal expansion coefficient of ferromagnetic thin films compared with bulky samples by electronographic technique 12 p1939 A67-25242

Particle density and material functions of gases of random composition, calculating values without regard to reaction dissociation 15 p2543 A67-29090

Method for analyzing single and double thermal relaxation processes 15 p2580 A67-29771

Drag coefficient of sphere at supersonic velocities dependence on specific heat ratio of argon, air, carbon dioxide and freon 16 p2593 A67-31122

Intensity and specific heat ratio effects for laminar compressible boundary layers arising behind traveling shock waves 17 p2837 A67-32347

Thermal properties of anomalous superconductors, considering specific heat jump to normal state and thermal conductivity behavior 17 p2914 A67-32453

Temperature dependency of specific heat of titanium base alloys 17 p2873 A67-32770

High pressure hydrogen atmosphere drop calorimeter for SNAP reactor fuel specific heat measurement, discussing calibration problems 18 p3052 A67-34515

Specific heat of superconductors containing paramagnetic impurities calculated, noting effect of ordering impurity spins 19 p3303 A67-35045

Collapsing shocks and detonation waves gasdynamic problem, evaluating perturbations due to counterpressure and to heat release 19 p3209 A67-35411

Insulating foams at liquid hydrogen temperature, describing methods for measuring thermoconductivity, specific heat and density 19 p3346 A67-35587

Entropy and specific heat of superconductor in mixed state calculated using cellular model of vortex 21 p3680 A67-38349

Computer program charts for investigation of effect of temperature dependent thermal conductivity on transient temperature distribution of heated materials 22 p3916 A67-39481

Base pressure behind circular projection in Laval nozzles, measuring dependence on specific heat ratio at different Mach numbers by varying gas 22 p3741 A67-40021

Emittance and specific heat determination by transient thermal vacuum technique using coatings as function of temperature 24 p4153 A67-42039

SPECIFIC IMPULSE

Mariner IV midcourse 50-lb thrust pressure-controlled monopropellant hydrazine propellant system, predicting impulse and velocity error as function of burn time [AIAA PAPER 66-948] 02 p0304 A67-12282

Solid propellant rocket motor capabilities for space flights, noting specific impulse on density basis 02 p0305 A67-12352

Lift-drag ratio, specific impulse, aspect

ratio and weight of payload and power plant considered for STOL aircraft 03 p0358 A67-12980

Optimization of high energy turbopump unit engine for ELDO-B carrier rocket, employing system specific impulse 03 p0503 A67-13013

POODLE low thrust radioactive propulsion technology, discussing operation, mission application, tests, capsule and thruster performance 05 p0843 A67-16551

Electric thrusters and electric propulsion, examining overall efficiency as function of specific impulse 05 p0874 A67-16933

Nozzle submergence loss in solid propellant rocket engine, correlating loss percentage of specific impulse with dimensionless groups 05 p0875 A67-17366

Thermodynamic limits on specific work and specific impulse of adiabatic chemical engines and nuclear engines [AIAA PAPER 67-227] 06 p1029 A67-18445

Specific impulse and thrust coefficient performance as function of flight Mach number and altitude for air augmented solid propellant propulsion vehicle using supersonic combustion [AIAA PAPER 67-226] 06 p1097 A67-18517

Geomagnetic thruster, noting superiority over electric or chemical propulsion for thrust durations of more than few weeks 11 p1855 A67-25009

Mixture ratio distribution effect on rocket thrust chamber performance 15 p2545 A67-29431

Launch vehicle performance and engineering trade-off, considering mass fraction, weight reduction, specific impulse, losses and stage selection 16 p2762 A67-31489

Plasma propulsion for interplanetary flight, discussing optimization of specific impulse, weight distribution and flight path 17 p2928 A67-32226

Design and performance characteristics of electrothermal microthrust systems for spacecraft functions [AIAA PAPER 67-423] 18 p2988 A67-33907

Ejector ramjet and ducted rocket evaluation by analytical models for various flight trajectories, noting specific impulse improvement [AIAA PAPER 67-437] 18 p3112 A67-33915

Solid propellant engines treated for constant missile volume and mass 18 p3137 A67-34360

Combustion rocket engines thermodynamic cycle and specific impulse values, considering motion equations and plasma engines 19 p3311 A67-35571

Mariner IV midcourse 50-lb thrust pressure-controlled monopropellant hydrazine propellant system, predicting impulse and velocity error as function of burn time 21 p3712 A67-37797

Mercury electron bombardment thruster system performance as function of mass utilization and specific impulse, noting magnetic field shape and ion optical system design effects [AIAA PAPER 67-697] 21 p3693 A67-38726

Pulsed vacuum arc microthruster noting various performance data and advantages [AIAA PAPER 67-737] 21 p3695 A67-38759

Composite propulsion systems for aerospace missions, considering Mach range, specific impulse, oxygen source, design characteristics, capabilities and limitations 22 p3868 A67-39890

Cryogenic liquid propellant rocket engine technology and design [AIAA PAPER 67-978] 24 p4208 A67-43053

SPECTRAL ABSORPTION

S ABSORPTION SPECTRUM

SPECTRAL ANALYSIS

Scattered light spectrum in tetatron plasma, noting onset of ion wave instability 01 p0121 A67-10248

Digital computer program for power spectral density analysis of vibration data, noting bandwidth variation with frequency [SAE PAPER 660715] 01 p0028 A67-10604

Neutron spectrometric measurements, discussing starting time determination and conversion of travel time into amplitude spectrum 01 p0066 A67-10656

Precision spectrum analyzer modification using RC network for analyzing filter applied to transient pulses for both Fourier and shock spectra 01 p0074 A67-11130

Spectral analysis of pulsed signal reflected from ionospheric F-2

layer 02 p0193 A67-11672

Space bandwidth signal spectral analysis using multichannel optical system and two-dimensional optical system with increased frequency resolution 02 p0243 A67-12049

Electron spin resonance with trigonal and orthorhombic symmetry in cerium oxide doped calcium fluoride 03 p0492 A67-13328

Principal methods determining cosmic abundances of chemical elements, emphasizing quantitative spectral analysis of sun and fixed stars 03 p0510 A67-13538

Power spectra analysis based on method of computing weighting sequence whose frequency characteristics approximate one-third octave filter and applying coefficients recursively to digitized data 03 p0375 A67-13563

Fe spectrum energy levels for various subshell configurations, calculating oscillator strengths and transition probabilities 03 p0511 A67-13649

Postirradiation radiochemical and spectrochemical analysis of short-cooled samples of SNAP-8 experimental reactor primary coolant 03 p0466 A67-13798

Lower bound electronic energy calculations for positive H, using methods of truncated Hamiltonians and of Temple and Kato 03 p0469 A67-13943

Spectral analysis of HF oscillations with phase modulated fluctuation as functions of phase dispersion and spectral form of modulating fluctuations 03 p0393 A67-13950

Solar radio burst analysis from spectral diagrams noting sudden beginning, precursory activity and succession of isolated peaks and islands 04 p0692 A67-14588

Electron recombination in laser produced hydrogen discharge, noting temperature decay due to radiation, expansion cooling and electron loss 04 p0665 A67-15109

Spectrochemical analysis of solid specimen from vapor formed by laser beam and excited by spark 05 p0824 A67-16786

Basal plane contraction and annealing of degraphitized carbon examined via X-ray diffraction techniques 05 p0833 A67-16891

Spectra of unlocked driven semiconductor oscillators observed with millimeter wave reflex klystrons, noting gradual controllable frequency pulling 05 p0780 A67-17522

Spectrum signature data applied to interference analysis, noting data truncation 05 p0781 A67-17538

Transition probabilities for S I multiplets measured from arc spectra running through sulphuryl chloride liquid vortex 06 p1038 A67-17656

Spectroscopic measurement of temperature, electron density and conductivity in RF plasma torch 06 p1039 A67-17825

Quantitative intensity of weak carbon dioxide triad in 1 micron spectral region obtained, using pressure broadening techniques 06 p1031 A67-17870

Mechanism of enhancement of Li resonance line in twilight airglow due to upper atmospheric thermonuclear explosions 06 p0998 A67-18705

Metastable exciton states of cadmium and lead iodide obtained from fundamental reflectivity spectra 06 p1060 A67-18915

Optical transitions at isoelectronic traps in GaP and ZnTe, presenting fluorescent spectra 06 p1062 A67-18929

Electron spin resonance in P-doped Si at liquid He temperature, noting effects of P concentration, impurity scattering, etc 06 p1068 A67-18973

Spectral sensitivity and temperature characteristics of light generated pairs of photoelectric converters 07 p1131 A67-19105

Criteria for accuracy of line intensity and mean absorption coefficient measurements 07 p1185 A67-19404

Vertical incidence CW Doppler phase path sounder spectral analysis of ionospheric motions and irregularities due to atmospheric wave propagation into ionosphere from below 07 p1182 A67-19952

Molecular association in Na, K and Cs vapors, noting existence of dimer and tetramer molecules 08 p1355 A67-21033

Lunar ground data for interpretation of AES orbital experiments such as electromagnetic radiation monitoring, photographic data evaluation, spectrography, etc 08 p1392 A67-21078

Lunar surface analysis via analysis of reflected signals from RF pulses 08 p1295 A67-21080

Multispectral photography for AES missions, describing lunar color studies [AFCLR-66-796] 08 p1331 A67-21081

Upper atmospheric temperature measurement by analysis of AIO spectra 08 p1327 A67-21370

X-ray structural and spectral analysis of changes in lattice constant, linear expansion coefficient and K-absorption edge of iron and manganese in ferrite with spinel structure 08 p1372 A67-21492

Coherent electromagnetic wave analysis using spectral density function in terms of wave vector 09 p1462 A67-21605

Electric arc behavior in argon gas flowing through magnetic field, measuring flow velocity, electron temperature, spatial distribution, etc 09 p1543 A67-21824

Spectral analysis of laser discharge in pure and impure He, obtaining spectra of spark at various pressures, determining electron concentration 09 p1512 A67-22010

Spectral analysis of interacting electromagnetic, plasma and spin waves in antiferromagnetic semiconductors and metals with easy-axis and plane type anisotropy 09 p1555 A67-22073

Fluctuations in measurements of hurricane clouds, determining frequency domains for dominant mode of activity via variance spectrum analysis 10 p1676 A67-22817

Hydrogen line profiles in model atmospheres using quasi-static approximation for electrons and ions 10 p1704 A67-22883

Contribution of quasi-static electrons to broadening of hydrogen 2 line profile 10 p1704 A67-22884

Central intensities and profiles of sodium D lines in solar spectrum, discussing atomic and photospheric data 10 p1704 A67-22885

Bispectral analysis of electromagnetic wave diffraction by ionosphere, obtaining information on altitude and scale of irregularities 10 p1604 A67-22888

Scattered Lyman alpha radiation in geocorona analyzed using satellite mounted equipment 10 p1706 A67-23223

Occurrence of collisions between ionized and neutral particles based on analysis of spectrum diffused by E region 10 p1646 A67-23268

Time resolution spectroscopy applied to electron recombination in H plasma due to azimuthal pinch 11 p1841 A67-24769

Spectroscopic methods for measuring plasma temperatures from 1000 to 10,000 degrees K, distinguishing optically thick and thin media 12 p1938 A67-25188

Spectral analysis of geomagnetic pulsations from 0.5 to 100 sec in period for quiet sun condition 12 p1932 A67-25189

Mathematical theories applicable to excitation and ionization of atoms in plasmas at thermal equilibrium, determining electron density and temperature 12 p1968 A67-25432

Shock spectrum synthesis and analysis as environmental test technique compared with time function shock testing 12 p2030 A67-25681

Spectrum, correlation and probability analysis of arbitrary waveforms 12 p1905 A67-25732

Hyperfine structure and modified Zeeman effect in trivalent holmium in hexagonal lanthanum trichloride 12 p1987 A67-26237

Alpha particle spectral analysis in various lithium compounds 13 p2159 A67-26435

Developments in techniques of meteor spectral observations 13 p2197 A67-26503

Regularity properties in temporal variable of solutions of n-dimensional Navier-Stokes system, using various interpolation methods 13 p2145 A67-26604

Condensation spectrum evolution of cloud droplets 13 p2151 A67-26690

Spectral characteristics of small scale refractive index fluctuations in troposphere using radar echoes 13 p2068 A67-26790

Signal spectral characteristics when reflected from rough surface exposed to monochromatic and frequency modulated oscillations from moving airborne emitter 13 p2154 A67-27038

Digital real time spectral analysis with fast Fourier transform algorithm, using two special purpose computer configurations to estimate power spectrum 13 p2073 A67-27062

Solar flux density absolute microwave spectra 14 p2385 A67-28441

Slit width effect on accuracy of equivalent width measurements, noting results with 10 angstrom/mm plates 14 p2319 A67-28591

Transmission energy characteristics of spherical plate electrostatic analyzers from external sources of electrons and protons 14 p2320 A67-28746

Ni XIX, Cu XX and Zn XXI spectra observation using vacuum spark chamber 14 p2389 A67-28840

Optical constants of ionic crystals at low temperatures determined from reflection spectra, noting correlation between absorption coefficient, magnitude and phonon difference processes 14 p2374 A67-28986

Book on problems of optics covering emission, absorption, diffraction, dispersion, etc 14 p2349 A67-29006

Compatibility of some spectral functions with Helsenberg theory in axisymmetric turbulence and in equilibrium range [ONERA-TP-461] 15 p2470 A67-29381

Gaussian and Lorentzian components separation in analyzing EPR spectrum in ruby, using variance techniques 15 p2536 A67-29499

Spectral analysis of pulsed signal reflected from ionospheric F-2 layer 16 p2624 A67-31087

Solar X-ray flux for wavelength less than five angstroms measured, noting extreme variations in spectral slope and intensity 16 p2739 A67-31411

Ruby laser light scattering by theta pinch plasma measured with Fabry-Perot spectrometer, noting cooperative density fluctuations superimposed on thermal density fluctuations 17 p2899 A67-32274

Confocal ruby laser mode structure analyzed for relation between mode number and spiking regularity, noting frequency hopping 17 p2867 A67-32402

Long term gyro drift rate evaluation involving time series detrending and autoregression, pericodogram, autocorrelation, spectral density and mathematical model analysis 17 p2858 A67-32486

Millimeter radiation from 3C 273 17 p2944 A67-32635

Comet 1963 III spectrometric observations showing important continuous spectrum of comet, spectrum wavelengths identification, etc 17 p2946 A67-32731

Elemental composition effect on electron excited fluorescence of serpentines determined by spectral examination with electron microprobe 17 p2852 A67-33239

Spectral data on primary cosmic ray protons and helium nuclei analyzed, assuming solar cycle modulation due to diffusion-convection process 17 p2952 A67-33247

EPR spectra of radicals formed during gamma irradiation of polytetrafluoroethylene 17 p2810 A67-33260

Aircraft measurements of clouds in spectral range from 8 to 12 microns, determining albedo for stratified clouds 18 p3073 A67-33559

Darkness of clouds of upper and middle levels in various spectral intervals and in thermal spectrum range 18 p3073 A67-33560

Upper atmosphere observation at twilight, considering broad spectral regions and emission lines 18 p3033 A67-33585

Spectral data and energy level diagrams from magnetic and electric field passage through barium cloud 18 p3036 A67-33606

Phonon spectrum of Si calculated by Monte Carlo method, determining Si thermodynamic functions 18 p3098 A67-33629

Spectra of noble gases in 4-micron region, using IR spectrometer equipped with cooled lead sulphide detector 18 p3082 A67-33876

Graphical integration method for calculating optical characteristics of materials used in solar radiation spectral measurements 18 p2990 A67-34492

Spectrum of bound and quasi-bound states of hydrogen-hydrogen scattering and resonance, using Schroedinger equation 18 p3084 A67-34523

Soviet and foreign studies of atmospheric oxygen by optical and spectral methods 19 p3214 A67-34857

Impurities in high-purity niobium determined chemically and spectroscopically 19 p3243 A67-34927

Corona observation within one solar radius of photosphere, identifying emission lines and explaining continuous spectrum and Fraunhofer lines reduced depth 19 p3318 A67-35055

Argon, deuterium and air ionization at atmospheric pressure and lower by focused ruby laser radiation, analyzing plasma spectrum 19 p3239 A67-35166

Inner Van Allen belt proton dose rate and spectral charged particle environment profiles correlated, noting agreement with theoretical values 19 p3313 A67-35189

Time dependency, anisotropy degree and spectral composition of cosmic radiation generated during July 1966 solar flares as observed by Pioneer VI 19 p3314 A67-35270

Monochromator for measuring spectral distribution of laser light scattered by high temperature plasmas 19 p3230 A67-35593

Frequency amplitude spectra of atmospherics from multiple stroke lightning, showing shift to VLF 20 p3480 A67-36290

Auroral zone diurnal tidal effect studied by high resolution spectrum analysis, noting large diurnal conductivity variation giving rise to lunar auroral electrojet 20 p3521 A67-36298

High resolution spectra of Venus and Jupiter using image intensifier and solar spectrograph, measuring abundances in planetary atmospheres 20 p3521 A67-36309

SIMAC spectrograph, discussing brightness, speed, etc. of electronic camera and photographic plate 20 p3439 A67-36350

Multiple stimulated Brillouin scattering from liquid within Q-switched ruby laser cavity, noting changes in pulse shape, output power and spectral characteristics 20 p3457 A67-36385

Spectral analysis of time series - Conference, University of Wisconsin, October 1966 20 p3476 A67-36782

Probabilistic background of time series models which relate to spectral analysis and power spectrum and statistical inference for stationary stochastic processes 20 p3476 A67-36783

Numerical spectrum analysis procedures, discussing fast Fourier transform techniques, classical spectrum windows and complex demodulation process for time series studies 20 p3476 A67-36784

Cross-spectral method application problems in feedback system analysis, identification and linear time invariant system 20 p3407 A67-36785

Cross-spectrum analysis in meteorology, considering property fluxes and time series, discussing turbulent energy flux, solar activity, etc 20 p3480 A67-36786

Bias in coherency estimation resulting from phase changes 20 p3476 A67-36787

Prediction procedure for nonstationary stochastic processes with slow spectral density function variation with time 20 p3477 A67-36789

Approximate electron radial functions for uniformly charged nucleus /UCN/ used in analyzing boron 12 and nitrogen 12 beta decay spectra 20 p3488 A67-36915

Nonstationary random process power spectral analysis, noting evolutionary power spectra estimation methods, local energy distribution, etc 20 p3485 A67-37004

Spectral variations resulting from thermal processes in crystals subjected to focused ruby laser beam 20 p3460 A67-37146

Dynamic spectrum of long-period geomagnetic pulsations noting Pc range characteristics 20 p3433 A67-37413

Grazing incidence spectrometer and low inductance spark source used for energy level identification in various elements 20 p3378 A67-37468

Multielement correlation type arrays response to several point sources studied by extending spectral method 20 p3403 A67-37510

Interference reduction potential of binomial type pulses 20 p3387 A67-37638

Torsional disturbance propagation in Gutenberg-Bullen earth model through spectral seismograms, discussing travel times and S wave amplitude [SR-16] 20 p3435 A67-37675

Radiative flux and flux divergence for hot gas, considering spectral frequency, gas volume and spectral variation 21 p3730 A67-37825

Quantitative method for determining sodium in gas turbine fuels by direct spectral analysis of unashed fuel samples 21 p3688 A67-38016

Spectral analysis of intensity fluctuations of laser at threshold noting confirmation of time resolution in terms of weighted sum of exponential 21 p3640 A67-38355

Impurity crystal-field spectra in II-VI and III-V compound semiconductors used to predict unexplored systems spectra impurity crystal-field spectra in II-VI and III-V compound semiconductors used to predict 21 p3682 A67-38388

Condensation spectrum evolution of cloud droplets 21 p3654 A67-38432

Frequency pattern analysis for liquid rocket pump fluid cavitation characteristics 21 p3613 A67-38437

Micropulsation spectra /sonograms/ indicating magnetosphere plasma resonances with recognizable modal pattern 21 p3619 A67-38513

Predictions from barotropic vorticity equation in spectral form analyzed for errors 21 p3654 A67-38575

Radar cross section of Mars, discussing spectral analysis, echo delay and radar echoes from Jupiter 21 p3706 A67-38617

Separation of geomagnetic field into anomalous and normal components, analyzing spectral relation 21 p3622 A67-39024

High sensitivity information storage filter for spectrum analysis 21 p3601 A67-39067

Cooperative light scattering from density fluctuations in theta pinch plasmas, discussing peaks obtained 22 p3842 A67-39208

ELF waveforms spectral estimation at discrete frequencies of each polarity used for statistical comparison of mean spectra show normal distribution 22 p3789 A67-39474

LF noise spectrum of p-n junction using arbitrary pulse duration distribution functions 22 p3858 A67-39573

Solar cycle prediction based upon random number technique, Fourier curve fits and power spectra analysis 22 p3873 A67-39931

Spectral and probe methods of plasma temperature measurement, discussing current-voltage characteristics 22 p3853 A67-40216

Cloud measurements from Gemini 5 from reflected solar radiation spectra of oxygen A band region 22 p3807 A67-40369

Spectral index dependence on flux density and cosmological red shift, considering model universes populated with radio sources 23 p4062 A67-40634

Spectroscopic analysis of iron meteoroid radiation by emission growth curve method covering temperature factors and atom and electron concentrations 23 p4062 A67-40674

Intrinsic modes of spherical mirror resonators, noting parameters identifying beams generated by such resonators 23 p3998 A67-40709

Geomagnetic field structure determination by method used to divide geomagnetic field observed along limited magnetic profile derived from mathematical apparatus of correlation analysis 23 p3994 A67-40715

Giant pulse ruby laser having tunable two-frequency output noting spectral measurements made with Fabry-Perot interferometer 23 p4015 A67-41038

50 Hz ruby pulse laser emission, discussing power output, electromagnetic spectrum and transverse mode interaction 23 p4016 A67-41153

Turbulence structure of equilibrium boundary layers, discussing shear stress, thickness, eddy motion and intensity spectra 23 p3990 A67-41168

Least squares deconvolution technique for reducing Fabry-Perot spectrometer data to Voigt profiles 23 p4002 A67-41262

Hakenmethode theory and experimental technique, presenting basic arrangement for hook formation in crossed interferometer-spectrometer system 23 p4002 A67-41264

Strong radio sources at 1415 MHz, discussing flux density measurements and spectra of OQ208 source 24 p4225 A67-41831

Visual criteria for stellar spectral classification of Cordoba Observatory Atlas 24 p4227 A67-41967

Optical absorption, refractivity and electron scattering used to construct model dipole spectrum of molecular nitrogen and calculate dipole properties 24 p4190 A67-42096

FM oscillations spectrum component amplitude formula for multiple frequency modulation using Bessel function 24 p4122 A67-42379

Atmospheric spectral analysis of planets and stars by using computer, telescope and interferometer system 24 p4232 A67-42572

Photoexcited electroluminescence spectra of rare earth ions in cadmium fluoride semiconductor single crystal 24 p4205 A67-42893

Data handling capabilities of periodic time function for given bandwidth using Fourier series in sinusoidal spectrum analysis 24 p4124 A67-42931

Electron tunneling into superconductors to investigate pressure induced energy shifts in Pb phonon spectrum 24 p4206 A67-43100

SPECTRAL BAND

Spectral distribution of net radiance at boundary of nonisothermal gas applied to water vapor band 02 p0342 A67-12051

Frequency spectrum of micropulsations analysis from records taken at station near geomagnetic equator 03 p0410 A67-12954

Radiation intensity dependence for various spectral bands of diffused gallium arsenide p-n junctions on current density 05 p0861 A67-16391

Oxygen A band near 7600 angstroms used by Gemini V astronauts to measure cloud top altitude, showing method of computing correction factor 06 p1026 A67-18563

Far IR lattice bands in n-type indium antimonide single crystal 06 p1059 A67-18908

Passage of pulsed coherent useful and noise signals through two-channel time discriminator 07 p1140 A67-19237

Spectral properties of Nd doped yttrium vanadate grown from melt, noting reduced Stark splitting leading to laser action 07 p1195 A67-19559

Cancellation of unwanted spectral components in FM multivibrator system by generating cancelling component in square law device 07 p1145 A67-19871

Transient radiative heat exchange on moon surface observed in 8 to 2 micron band during lunar eclipse, using model for quantitative comparisons transient radiative heat exchange on moon surface observed in 8 to 12 micron band during lunar 11 p1865 A67-24604

Molecular, continuum and line radiation of planetary atmospheres, comparing molecular band structure models with spectral measurements of CN violet band [ATAA PAPER 67-323] 12 p2037 A67-26038

Calibration of vibrational transition of CO at various pressures to determine vibration-rotation wave numbers 13 p2160 A67-26600

Spectral narrowing and tunability over wide spectral range demonstrated in solid/liquid dye lasers using diffraction gratings as cavity reflectors 15 p2500 A67-29817

Statistical band model used to compute spectral emissivity in carbon dioxide micronband as function of pressure, optical path and temperature 15 p2521 A67-30429

Darkening of solar limb in UV spectral band observed through rocket sounding 17 p2945 A67-32647

Night airglow brightness spatial distribution observed by photoelectric photometry in 5893 angstrom band, including isophotes charts and emission-inhomogeneity drift histogram 17 p2848 A67-32953

Upper limit in flux density of intergalactic gas UV radiation measured from interplanetary satellite, showing temperature effect 18 p3116 A67-33524

Point-by-point measurements of magnitude and phase of repetitive pulsed time functions using commercial equipment 19 p3182 A67-35031

Statistical band model applied to NO fundamental vibration band, discussing transmittance measurements and validity of linear region criterion 19 p3266 A67-35681

Spectral transmittance of mixture of carbon monoxide and nitrous oxide for overlapping absorption bands 19 p3266 A67-35696

Flat-top pulse waveform with high transmission efficiency, confined spectra and good electromagnetic compatibility 20 p3388 A67-37654

Camera for multispectral color aerial photography noting four-band interpretation on companion viewer and application to

- target acquisition problems 22 p3797 A67-39451
- Carbon dioxide and water vapor band emissivities determination, discussing spectral absorption, radiative heat transfer and energy distribution 22 p3918 A67-40042
- Molecular band spectra of CN emission assuming Gaussian rotational line profile 23 p4030 A67-41695
- ### SPECTRAL EMISSION
- LF spectrum of density correlation function, obtaining diffusion coefficient of right order of magnitude using quiet plasma 01 p0124 A67-10911
- Radiant heating by inhomogeneous hot gases, determining spectral transmittances of inhomogeneous optical paths using Curtis-Godson approximation 02 p0342 A67-12050
- Short wave length series of edge emission of calcium sulfide single crystals at temperatures between 18 and 150 degrees K 03 p0488 A67-12813
- Optical properties of semiconductors by measuring spectral emittance of transparent and opaque solids and measurements on materials used in IR optics [AIAA PAPER 65-654] 03 p0418 A67-13034
- Spectral emittance of metallic and nonmetallic materials, discussing surface roughness effects [AIAA PAPER 65-675] 03 p0467 A67-13042
- Emissive power of germanium and silicon with various surface finishes in temperature range from 700 to 1200 degrees K 04 p0674 A67-14719
- Spectral response of short circuit photocurrent of niobium pentoxide metal diodes 04 p0582 A67-15125
- Temperature and doping level effect on conduction band edge of n-type semiconductors, noting doublet shifts resulting in narrower forbidden energy gaps 04 p0681 A67-15292
- H-alpha, H-beta, H-gamma, H-epsilon, H-8, H-11, H-12 and H-13 line emission of June 25, 1960 chromospheric flare 05 p0893 A67-16497
- Spectral radiance of low current graphite arc anode determined, using high accuracy spectroradiometer 05 p0846 A67-16787
- Spectral emissivity of Ti from 1100 degrees K to melting point 05 p0831 A67-17318
- Pinch effect in InSb degenerate plasma, discussing electric conductivity and recombination emission spectra 06 p1049 A67-17879
- Spectral radiance of model rocket exhaust gases measured by rapid scanning spectrometer at simulated altitude [AIAA PAPER 67-10] 06 p1116 A67-18346
- Modulation pyrometer measuring plasma temperature from spectral line intensity 09 p1499 A67-22328
- Photon modulated tunneling in Te-Al oxide-Al structures, noting increased spectral response and detection range 10 p1689 A67-22907
- Distribution and intensity of solar magnetic fields gained from spectrograms, noting correspondence between magnetic field and Ca-K line emission sources 12 p2001 A67-25219
- Photoemission study of electronic structure of CdTe, considering two strong reflectivity peaks in optical reflectivity spectrum [AFRL-67-0405] 12 p1983 A67-25478
- High temperature spectral directional hemispherical reflectance of refractory metals and ceramics measured with integrating sphere and He-Ne CW laser source [AIAA PAPER 67-300] 12 p2035 A67-26015
- P-and n-type silicon spectral emissivity measured at several temperatures and wavelengths for carrier concentrations and direct current resistivities [AIAA PAPER 67-302] 12 p1958 A67-26017
- Visible and near IR spectral reflectance and emittance at high temperature of ablation chars, carbon and graphite [AIAA PAPER 67-326] 12 p2037 A67-26040
- Closed form solution for determining total emissivity of metals and radiation conductivity of radiation shield for nongray metallic surfaces at low temperature [AIAA PAPER 67-335] 12 p2038 A67-26049
- Comparison of computed and experimental spectral transmissions through haze 13 p2152 A67-27357
- Angular, spectral and geographical distributions of outgoing fluxes of thermal radiation and earth albedo measured, using Cosmos satellite 14 p2306 A67-27861
- Neodymium activated alpha-gagarinite crystal laser, noting ternary fluoride systems characterized by optical centers 15 p2496 A67-29360
- Statistical band model used to compute spectral emissivity in carbon dioxide micronband as function of pressure, optical path and temperature 15 p2521 A67-30429
- Color indices of visible meteors observed by naked eye and through color filters noting brightness dependence and meteor train distribution 16 p2751 A67-31462
- Exciting molecular emission spectra in cold plasma free of electrode-induced impurities by superhigh frequency source 16 p2704 A67-31478
- Diffusion coefficient dependence on solar particle energy and distance from sun noting time variation 16 p2740 A67-31892
- Many-element lasers spiking emission for Fabry-Perot and confocal geometry, including time resolved spectroscopy and far and near field patterns 17 p2870 A67-33298
- Spectral coefficients of blackness in materials with low thermoconductivity determined by measuring radiation intensity and solving equations derived from Planck and Kirchhoff laws 18 p3048 A67-34056
- Short wave spectrometer for measuring total and scattered sky radiation, spectral brightness and fluxes of direct and reflected solar radiation 19 p3227 A67-34860
- Spectral brightness of metal chelate liquid fuel-air flames [CI PAPER 67-2] 19 p3309 A67-34997
- Spectral radiance of model rocket exhaust gases measured by rapid scanning spectrometer at simulated altitude [AIAA PAPER 67-10] 19 p3346 A67-35761
- Fundamental intensity error in Fourier spectroscopy noting requirement that interferograms be inverted by Fourier transformation 20 p3437 A67-36337
- Near IR grating spectrometer converted to multiplex instrument by adding encoding disk in spectrum plane 20 p3437 A67-36339
- Spectral emittance of melting or decomposing polystyrene determined, describing apparatus and experimental technique 20 p3446 A67-36663
- Spectral irradiances determined by conventional prism monochromator and by system employing narrow bandpass interference filters 21 p3656 A67-37850
- Photographically recorded spectra for absolute intensity processed by computer program, providing digitally recorded densities on magnetic tape 21 p3624 A67-37851
- Terrestrial surface spectral IR emissivities determined in situ interferometrically, noting igneous and sedimentary rock composition and texture 22 p3805 A67-40354
- Thermal radiation properties measurement for materials in spacecraft design, discussing apparatus, instruments, techniques, devices and methods 23 p4083 A67-41368
- ### SPECTRAL ENERGY DISTRIBUTION
- Spectral energy density of turbulent plasma determined from spatial autocorrelation functions of electric fields of HF oscillations 01 p0121 A67-10235
- Spectral distribution of relative quantum yield of photoluminescence in polycrystalline cadmium sulfide films 01 p0133 A67-10510
- Output autocorrelation function and spectral density of CW and FM signals passed through TWT 01 p0025 A67-10858
- Spectral density measurement of relative fluctuations of current amplification factor common-base transistor circuit 02 p0213 A67-11646
- Red shifts and colors correlated for quasars leading to smoothed mean energy distribution and new values for K-correction 02 p0322 A67-11686
- Luminescent intensity and spectral energy distribution determined for exciton luminescence of anthracene crystals for spontaneous and stimulated emission 03 p0436 A67-13136
- ESRO II satellite structural design, testing and material selection noting functions, vibration testing results, etc 03 p0518 A67-13600
- Current voltage characteristics of Cd-GaSe-Bi diode structure, rectification coefficient, activation energy and photocurrent spectral distribution 04 p0676 A67-14930
- Vertical profiles of horizontal wind in lower ionosphere treated by spectral energy density estimates [AFRL-67-0054] 04 p0615 A67-14970
- Intensity distribution in rotational structure of molecular spectra bands upon excitation by ion impacts 06 p1035 A67-17877
- Oscillation spectral density of SHF oscillators measured, using frequency phase self-tuning system to eliminate LF component of phase fluctuations 08 p1302 A67-20833
- MHD equations for spectral energy tensors of weak homogeneous magnetoturbulent field and derivation of asymptotic decay law by method of steepest descent 08 p1359 A67-21122
- Radio telescope-spectrophotometric scanner investigation of continuous energy distribution of four quasars 08 p1398 A67-21230
- Spectrophotometric data correlations between color and red shifts of quasars 08 p1398 A67-21231
- Integral short circuit current of solar converters determined from spectral distribution of solar radiation energy, using simulator and SiO photocell films 09 p1451 A67-22531
- X-ray spectral distributions and fluxes in low keV range of five cosmic sources at low galactic latitude and longitude, noting effective temperature 11 p1856 A67-24505
- Barometric pressure data analysis estimating autocovariance, using Fourier transform for spectral density calculation 11 p1816 A67-24840
- Surface hole photoconductivity for pressed metal anode CdS ohmic cathode system, noting spectral distribution dependency on crystal heat treatment and air humidity 11 p1849 A67-24871
- Reverberation chamber for high intensity acoustic testing of specimen subjected to directionally predetermined spectral distribution of acoustic energy field 12 p1924 A67-25712
- Non-LTE line-transfer problem computational methods 14 p2351 A67-28994
- Heating of ions in current carrying nonisothermal plasma deriving noise spectral density and electron and ion distribution functions 16 p2715 A67-31047
- Abel integral inverter discussing design, construction and performance of analog computer for solution of Abel integral equation 16 p2634 A67-31428
- Random amplitude fluctuations of quasi-stellar radio source from similarity between spectral-density distributions of observed and random-simulated luminosities 16 p2752 A67-31696
- Laser scattering from gas particles and diffuse surfaces, noting difference in intensity of speckle patterns formed 16 p2686 A67-31882
- Statistical processing of satellite data on spectral distribution of outgoing radiation 16 p2668 A67-31887
- Spectral density of stationary random signals corrupted by multiplicative noise 17 p2812 A67-32303
- Performance of matched filtering system related to degree of displacement for uniform and nonuniform spectral densities 17 p2862 A67-33295
- Thomson scattering of Q-switched ruby laser beam in shock wave plasma, determining electron densities, spectral distribution of scattered light, etc 18 p3084 A67-33649
- IR spectrophotometer developed for airborne study of spectral energy distribution in atmospheric self-radiation 19 p3227 A67-34859
- Atmospheric spectra and related quantities calculated, obtaining radiation spectral distribution by radiative transfer equation, comparing results with other studies 19 p3220 A67-35260
- Solar x-ray spectral intensity distribution using atmospheric extinction of solar radiation as measured by satellites 19 p3314 A67-35441
- Spectrometer SNR improvement without affecting resolution by using larger inlet and outlet slit openings 20 p3441 A67-36365
- Probability density function measurement, discussing turbulence problem, power

spectral densities, Rice formula, inversion, etc 20 p3442 A67-36461

Gas local thermodynamic equilibrium effect on calculated thermal radiation emission [ASME PAPER 67-HT-51] 20 p3548 A67-36733

Raman spectra vibrational structure theory concerning crystal impurity centers, giving intensity distribution formulas and radiation model calculations 20 p3511 A67-37031

Visual image description with aid of spectral power redistribution functions, discussing input arrangement in TV recognition system 21 p3605 A67-39114

Waveguide model for turbulent shear flow, calculating streamwise dependence of cross-power spectral density using Orr-Sommerfeld equation 22 p3782 A67-39529

Tenuous high temperature plasma electromagnetic wave scattering, with relativistic corrections for scattered radiation spatial and spectral distribution 22 p3849 A67-39699

Total to selective interstellar absorption ratio, with improved values calculated for six-star group, considering spectral energy distribution and color excesses 22 p3883 A67-39767

Total extraterrestrial and global solar radiation intensity and spectral distribution for designing radiation resistant satellites 22 p3874 A67-40031

Planetary atmosphere radiation spectral distribution sounded with 4.3 micron carbon dioxide band to determine temperature profile 22 p3805 A67-40355

Radiation intensity measurements in systems containing atomic oxygen and carbon monoxide by shock tube heating, deriving spectral intensity distribution for radiative combination 23 p4029 A67-40972

Primary cosmic rays with various charges measured for spectral energy with Cerenkov counter onboard space stations 23 p4054 A67-41093

Channel bandwidth assignment determination using prescribed fraction of total radiated power of system contained in channel, discussing spectral distribution 24 p4123 A67-42714

SPECTRAL LINE

SA SODIUM D-LINE

Laser lines of pulsed discharge in iodine vapor 01 p0090 A67-10549

Intensities of L, M and N X-ray spectra for wavelengths in region from 2 to 85 angstroms 01 p0116 A67-10690

Inhomogeneity parameter for excited atom distributions and line width variations for dispersion contour of spectral line, noting dependency on frequency 01 p0125 A67-11045

Inhomogeneity parameter over cross section of spectral line contour for case of Doppler distribution 01 p0125 A67-11046

Laser lines of pulsed discharge in iodine vapor 01 p0091 A67-11057

Numerical method to obtain emission coefficients from emitted spectral intensities for asymmetrical plasma sources such as atomic spectral argon line 01 p0115 A67-11073

Spectrophotometric study of hydrogen alpha, beta, gamma, epsilon and hydrogen and K spectral lines of chromospheric flare of August 21, 1959 02 p0308 A67-11850

Rotational intensity distribution of vacuum UV absorption spectrum bands of carbon monoxide arising through mixing of D state with neighboring states 02 p0269 A67-12450

Identification of quark-atomic lines in solar spectrum 03 p0509 A67-13298

Atomic and molecular absorption and emission in middle UV region of electromagnetic spectrum, noting energy levels, electronic transitions and oscillator strengths 04 p0660 A67-14692

Identification of quark-atomic lines in solar spectrum 04 p0696 A67-14723

Fourier transform used in correction of instrument contour error when observing solar spectral line profile 04 p0624 A67-15564

Intensity of characteristic spectral lines of Si, Al and Mg of lunar surface rock made fluorescent by solar X-rays determined from Luna X measurements 05 p0886 A67-16051

Electron spin resonance in phosphorus-doped silicon at various temperature ranges 05 p0861 A67-16499

Nitrogen wavelengths obtained from precision measurements of various nitrogen lines, using vacuum UV spectrograph 05 p0846 A67-16781

Spectrum of glow during gas phase reaction of germanium tetrahydride with atomic oxygen, observing new bands of D-X system 06 p0955 A67-17655

Motion and asymmetry of emission lines of chromospheric flares with small plasmoid distribution 06 p1077 A67-18156

Continuous absorber effect on spectral line reversal gas phase temperature measurement [AIAA PAPER 67-108] 06 p1004 A67-18503

Error due to electron thermal energy fluctuations in mean electron temperature measurement by line intensity ratio 06 p1042 A67-18540

Spectrophotometric study of H, K and He spectral line characteristics of chromospheric flare of June 25, 1960 07 p1247 A67-19166

Relative intensities and cascade transition ratio in CW Ar II laser near 4103.9 angstroms 07 p1195 A67-19560

Axial magnetic field effect on Ne-He laser power output operating in regime of simultaneous generation of 3.39 and 0.6328 micron lines 07 p1196 A67-19601

X-ray line broadening in deformed magnesium by Fourier analysis of line shapes and analysis of line widths, noting lattice distortion 07 p1210 A67-20108

Bending effect of spectral lines in plasma created by rotating HF dipole in quasi-steady magnetic field 08 p1358 A67-20854

Red shift relationship with ionization potential for absorption lines in quasi-stellar object 3C 191 08 p1400 A67-21251

Intensity and shape of spectral lines of excited hydrogen in radio range 08 p1356 A67-21345

Center limb variation of H-and K-lines of Ca-2 08 p1401 A67-21444

Normal temperatures for optically thin plasma in state of local thermodynamic equilibrium [DVL-644] 09 p1536 A67-21557

Spectrum of quiet sun between 30 and 128 angstroms analyzed in November 1965, using rocketborne grating monochromator with Geiger detector 09 p1566 A67-22232

Apparent rotation of spectral lines as viewed through holograms, obtaining equations for angular change of image position 10 p1653 A67-22717

Line profiles and equivalent widths for diffuse reflection of sunlight from model planetary atmosphere calculations, using invariant imbedding 10 p1710 A67-23635

Source function, distribution function, damping constant, etc, determined from high resolution Fraunhofer line profiles in solar or stellar spectra 10 p1711 A67-23797

1/s line intensity distribution function for molecular spectra representation using growth curves calculated for Lorentz lines 11 p1822 A67-24416

Center-to-limb variations for continuum, faint iron lines and core of strong Fraunhofer lines measured along polar and equatorial diameters of solar disk 11 p1861 A67-24492

Atomic beam resonance spectrophotometer used with solar telescope to observe solar line oscillation 11 p1861 A67-24494

Venus atmosphere spectra obtained by Michelson interferometer, finding HCl lines consistent with 2-mm Amagat of gas [JPL-TR-32-1106] 11 p1863 A67-24510

Calculation of thermal excitation function and optimum temperature and pressure of atom and ion spectral line shift in two-component plasma 11 p1840 A67-24580

Observations with birefringent interferometer and photoelectric spectrophotometer of Martian surface materials composition, noting strong band at 3.1 micron suggesting hydrated minerals 11 p1865 A67-24603

Correlation between diurnal meteor activity and twilight emission of ionized calcium H and K lines confirmed by Quadrantides swarm observations 11 p1857 A67-24756

Photoelectric recorder in solar tower used to investigate two new lines in solar spectrum 11 p1868 A67-24848

Central tuning dip in power output of continuous wave submillimeter molecular laser to measure radiative lifetime and collision line broadening 11 p1803 A67-24932

Distribution and intensity of solar magnetic fields gained from spectrograms,

noting correspondence between magnetic field and Ca-K line emission sources 12 p2001 A67-25219

Variability of integrated K-line emission studied during one solar rotation 12 p2001 A67-25223

Relative solar abundance for O, Si and Fe determined from intensities of far UV emission lines of solar corona 12 p2001 A67-25225

Ionization dependence of Na, K, Ca, Mg, Al, Fe and Si on arc temperature, noting correlations between temperature and electron concentration independent of plasma composition 12 p1977 A67-26108

Pulsed neon laser at 5401 angstroms 13 p1218 A67-27089

Anomalous polarization of four cosmic OH lines predicted from states of polarization in OH maser amplifier 13 p1261 A67-27289

Remote sensing of surface and cloud temperatures using 899 cm spectral interval 13 p1252 A67-27355

Hot and cold component model of sunspot umbrae derived from observation of continuous and line spectra 13 p2203 A67-27427

Line formation in sunspots taking into account magnetic field which greatly changes line profile, presenting transfer equations and solutions 13 p2204 A67-27431

Photoelectric scanning observations of night airglow for two spectral lines of OI 14 p2306 A67-27788

Solar radiation passage through earth atmosphere in triplet lines O I, considering molecular hydrogen absorption and brightness distribution of radiation 14 p2378 A67-27862

Velocity distribution function of gas measured with laser, noting relation to frequency variation of absorption coefficient across spectral line 14 p2317 A67-28194

Profiles of cores of Ca II H and K lines in solar spectrum during maximum and minimum activity period 14 p2387 A67-28561

Ni XIX, Cu XX and Zn XXI spectra observation using vacuum spark chamber 14 p2389 A67-28840

Spectroscopic methods applied to plasma electron temperature and density measurements 14 p2322 A67-29045

Stark-broadened isolated ion line agreement between theory and experiment obtained by Griem theory or by impact approximation of GBKO theory 15 p2520 A67-29678

Motion and asymmetry of emission lines of chromospheric flares with small plasmoid distribution 16 p2737 A67-30500

Spectral linewidth and shift of Ti I lines produced by neutral argon atoms analyzed using high pressure arc as light source 16 p2703 A67-30665

Spectral line profile obtained by radiative transfer equation from radiation by dense, inhomogeneous plasma layer 16 p2715 A67-31064

Solar spectrum observations in oxygen regions, describing prism-grating spectrometer, photoelectric recording and scan-averaging by digital computer [AFCLR-67-0478] 16 p2749 A67-31417

Intensity and shape of spectral lines of excited hydrogen in radio range 17 p2887 A67-31941

Radiation transport in spectral lines as photon absorptions and emissions, discussing contemporary theories, approximation methods and applications 17 p2893 A67-32143

Spectroscopic observation of ion wings produced by plasma ion oscillations in laser produced plasma 17 p2901 A67-32368

Sodium effect on dwell time and transport rates of various elements using DC arc, stressing spectral consequences 17 p2888 A67-32377

Stark effect in plasma, discussing theory, Lorentz symmetrical dispersion profile, atomic interaction, etc 17 p2901 A67-32404

Differential depressions of iron I levels and red shifts of spectral lines under pressure, demonstrating error in assumed air refractive indices 17 p2886 A67-33162

Elliptical patterns on emission lines of argon plasma jets attributed to antihalation backing during hypersensitization of film 17 p2863 A67-33305

Sigma components of line split in young sunspots magnetic fields measured with spectrocomparator, showing broadening of

iron line in intergranular space 17 p2952 A67-33394
 Brightening observed near D-2 line of sodium I on July 28, 1966 17 p2939 A67-33396
 Nightglow emission structure and variation at airglow equator, discussing predawn and storm effects, intensity variations with solar cycle, OH bands, etc 18 p3036 A67-33607
 Airglow emission analysis from low altitude observations, discussing temporal and spatial variations 18 p3037 A67-33608
 Kinetic temperature measurements of 5577 angstrom line night airglow with Fabry-Perot interferometer, discussing nightly mean temperatures 18 p3037 A67-33609
 High latitude night sky emissions observed by photographic spectrography, examining oxygen, nitrogen and hydrogen lines 18 p3037 A67-33610
 Combustion processes studied by shock tubes, discussing experimental techniques of combustion science, high temperature measurement by spectrum line reversal method, etc 18 p3019 A67-33779
 Quasi-stellar radio source optical spectrum observed, identifying spectral lines and determining red shift 18 p3118 A67-33854
 Scattering theory for parameterization of absorption cross sections and refractivity for autoionizing spectral lines 18 p3082 A67-33878
 Fabry-Perot interferometric observation of spectral line to investigate ionization rate of electrical discharge used for argon ion laser 18 p3061 A67-34044
 Plasma time-dependent luminosity from pulsed discharge in vacuum, determining excitation temperature distribution and discharge spectral lines 18 p3087 A67-34049
 Photosynthesis of nitrosoformaldehyde and identification of spectrum consisting of diffuse band 18 p2998 A67-34277
 High pressure, high power argon arc studied using cascade apparatus, showing spectral line absorption increases and temperature decreases with increasing pressure 19 p3278 A67-35136
 Rocket optical studies of daylit day-time auroras, discussing luminosity-height data of emission lines 19 p3214 A67-35168
 Flare of September 20, 1966 morphology and mechanism, discussing observations, narrowing of spectral line, etc 19 p3314 A67-35440
 Resonance line profiles for Ca II and Mg II in lower solar chromosphere, noting interlocking effect 19 p3325 A67-35504
 Diffuse reflected and transmitted spectral line profile calculations for uniform noncoherently scattering media 19 p3183 A67-35555
 Minimum radius of line emitting regions in quasars estimation method, discussing origin problem 19 p3327 A67-35893
 Time variation of Doppler broadened resonance line profile determined by assuming complete frequency redistribution 19 p3329 A67-36030
 Spectral analysis of K alpha type X-ray transitions in solar atmosphere and laboratory plasma 19 p3331 A67-36086
 Transient Stark and Zeeman spectral line shifts in plasma emission measured with multiple beam Flzeau interferometer, discussing instrument errors 20 p3439 A67-36351
 Extremely fast varying and low intensity plasma emissions analyzed with reflection multichannel Fabry-Perot interferometer 20 p3439 A67-36352
 Nitrogen and oxygen dayglow emissions observed during total solar eclipse of May 1965, studying emission/continuum intensity ratio 20 p3427 A67-36368
 Far IR CN laser action shown due to HCN molecule, explaining intense spectral lines around 337 microns 20 p3458 A67-36391
 Upper limit of arc for hydroxyl /OH/ emission region associated with radio source W3, using Michelson interferometer consisting of two spaced radio telescope stations 20 p3523 A67-36648
 Transitions in neutral spectra observed in near IR wavelength region in noble gases 20 p3460 A67-36859
 Nonthermal plasma electron density calculated from ratio of spectral line intensities of given ion 20 p3501 A67-37294
 Axial magnetic field effect on Ne-He laser power output operating in regime of simultaneous generation of 3.39 and 0.6328 micron lines 20 p3462 A67-37340

Solar X-ray emission line spectrum from 1.3 to 20 angstroms in solar flares identified as Fe XXVI through Fe XX transitions 20 p3519 A67-37396
 Highly ionized S, Cl, Ar and K resonance lines recorded, noting application for coronal Ca ions 20 p3528 A67-37478
 Accurate determination of atmospheric gases spectral lines positions required for estimating atmospheric absorption coefficient of monochromatic laser radiation 20 p3462 A67-37559
 Solar spectral line center-to-limb variations during solar eclipse of May 20, 1966 20 p3453 A67-37682
 Line broadening by collision damping, explaining solar and stellar curves of growth 21 p3700 A67-37731
 Ultrasonic and line reversal methods for measuring gas temperatures behind reflected shock waves 21 p3624 A67-37740
 Intensity of characteristic spectral lines of Si, Al and Mg of lunar surface rock made fluorescent by solar X-rays determined from Luna X measurements 21 p3701 A67-37838
 Resonance lines originating from autoionization energy levels far above ionization potential observed for highly ionized atoms of Na I isoelectronic sequence 22 p3840 A67-39237
 Spectral line changes caused by Rydberg constant shift detectable by observing very distant galaxies, discussing gravitational and cosmological theory 22 p3882 A67-39616
 Electron temperature measurements of powerful pulsed plasma discharge using spectral line intensity 22 p3852 A67-39991
 Spectral line wavelengths of solar violet bands of carbon /isotope/ nitride and hydride molecules, determining solar abundance ratios 22 p3889 A67-40207
 Laser lines observation in Freon-He mixtures in CW gas discharge 22 p3817 A67-40489
 Externally adjustable pressure regulation of Fabry-Perot interferometer, using device to measure cesium vapor spectral absorption in D-1 line 22 p3810 A67-40522
 Integral equation derived to relate source function for spectral line formed by noncoherent resonance scattering to thermodynamics of radiating medium 22 p3896 A67-40529
 Velocity field around sunspots from H-alpha line spectra observations 23 p4067 A67-41239
 K-line spectra from sunspots, discussing K-3 absorption line presence 23 p4067 A67-41241
 Wavelengths and intensities of IR coronal lines of silicon and magnesium ions from airborne total solar eclipse observations 24 p4224 A67-41822
 Differential departure from thermodynamic equilibrium and electron temperature in gaseous nebulae determined by observing RF emission lines 24 p4225 A67-41825
 IR line intensity of planetary nebula NGC 7027, noting presence of measurable continuum flux of stellar radiation 24 p4225 A67-41830
 Absolute frequency measurements on continuous wave hydrogen cyanide submillimeter laser lines 24 p4166 A67-41861
 Spectral lines diagrammed for temperature distribution in Ar plasma arc channel transverse emission with axial flow of working fluid 24 p4196 A67-42219
 Ar II population inversion of 4s and 4p states in stationary arc discharge, measuring ionic and atomic spectral line shift, widths and intensities and emission power 24 p4196 A67-42245
 Photochemical study of propyne with 2062-A iodine line 24 p4118 A67-42327
 Solar abundance determination, discussing composition parameters and Planck gradient method 24 p4237 A67-42654

SPECTRAL LINE WIDTH

Minimum spectral line width, threshold current density, radiation-peak displacement and possible recombination mechanism for GaSb laser diode p-n junctions in coherent radiation 01 p0087 A67-10085
 Spectral equivalent linewidths of four solar faculae and adjacent undisturbed photosphere sections 01 p0151 A67-11285
 Continuum brightness fluctuations and equivalent line widths in sunspot penumbral

spectrum 02 p0330 A67-12715
 Tunable dispersion resonator and broadening of laser emission spectral range to obtain operating frequency other than fundamental 03 p0435 A67-13131
 Effect of Doppler and impact line broadening of spectral characteristics of gas laser, noting standing monochromatic wave saturation 03 p0439 A67-14197
 Hydrogen line profile in Paschen series of solar spectrum, taking into account Stark effect and line broadening 04 p0702 A67-15567
 Width of spectral absorption line of water vapor at lambda equals 0.92 mm measured with aid of monochromatic radiation source and radiometer with thermal indicator 05 p0761 A67-16342
 Generalized Callen-Welton theorem applied to calculation of maser oscillations in amplification and generation regimes, determining noise spectral energy and spectral line width 05 p0762 A67-16350
 Gas laser pumped microwave emission for producing controlled excited state population for RF spectroscopy of neon 05 p0817 A67-16638
 Doppler and impact broadening of spectral lines and pressure effects on power output of gas laser 05 p0818 A67-16643
 Time resolved spectroscopic measurements of intensity and Stark width during decay of hydrogen plasma produced by ruby laser, determining electron density and temperature decay 05 p0852 A67-16653
 Output spectra of Nd doped YAG and ruby lasers, determining mechanisms responsible for observed overall linewidths 05 p0820 A67-16660
 Impact approximation of spectral line broadening by resonance and Van der Waals forces in air molecule electronic-vibrational systems 05 p0759 A67-16790
 Wavelength dependence of spectrum of laser beams traversing atmosphere 05 p0763 A67-16793
 EPR spectral shape and width as affected by phosphor concentration, degree of boron compensation and temperature in strongly doped n-silicon 05 p0867 A67-17055
 Doppler profiles of nocturnal green line /5577 angstroms/ nonthermal emission resulting from molecular oxygen ion dissociative recombination [AFRL-67-0443] 05 p0803 A67-17411
 Time structure and amplitude self-modulation of emission from GaAs injection laser observed, using electron-optical converter 06 p1009 A67-17756
 High power carbon dioxide laser heterodyne detection of beats and linewidth measurements 06 p1010 A67-17891
 Fabry-Perot interferometers with electronic determination of Doppler line widths, discussing effect of hyperfine and isotopic structure 07 p1185 A67-19399
 Absorption laws for spectral-line broadening due to propagation of intense monochromatic radiation through dielectric medium 08 p1294 A67-20816
 Asymmetric broadening of H-beta Balmer line in hydrogen doped argon plasma arc 09 p1536 A67-21562
 Approximation method to general solutions yielding coherence tensors of electromagnetic waves excited by source distribution with known coherence properties 09 p1462 A67-21606
 Hydrogen, He and ionized Ca lines in chromospheric spicules, noting large scale motion in spicule interior indicated by line width expansion and peculiarities in shape of line contours 09 p1563 A67-21627
 Self-broadening coefficients of spectral lines of absorbing atmospheric gases measured in comparison with line broadening effects of nitrogen 10 p1678 A67-22715
 Ruby laser generation spectrum width analyzed interferometrically as function of mirror spacing and pumping power 12 p1952 A67-25325
 Spectroscopic observation of sunspot structure, detailing sunspot model on basis of magnetic field and large scale motions interpretation 13 p2203 A67-27425
 Model with hydrostatic gas pressure distribution to interpret equivalent widths of atomic and ionic lines in spectra of umbrae 13 p2203 A67-27426
 Gain narrowing and saturation broadening

of Doppler broadened neon line in Zeeman scanned laser amplifier 13 p2129 A67-27485

Electromagnetic radiation equilibrium in gas lasers, studying effect of cavity length variations on linewidth 14 p2329 A67-27952

Effect of Doppler and impact line broadening of spectral characteristics of gas laser, noting standing monochromatic wave saturation 14 p2331 A67-28542

EPR spectral shape and width as affected by phosphor concentration, degree of boron compensation and temperature in strongly doped n-silicon 15 p2538 A67-29786

Plasma radiation analyzed by spectral line broadening theory as relaxation of excited atom, noting frequency dependent width and shift operators 15 p2532 A67-30380

Spectroscopic measurements of cold plasma charged particle concentrations, specifically spectral broadening due to Stark effect, forbidden-line intensities affected by internal electric fields and autoionization line intensities 17 p2896 A67-32161

Line width vs optical thickness in pulsed argon-ion laser used to determine level population in plasma 17 p2867 A67-32452

Distinction between macro-and microturbulence in solar photosphere studied from line profiles 17 p2944 A67-32641

Forbidden nitrogen I lines in IR solar spectrum, computing oscillation frequencies, nitrogen abundance and equivalent widths, comparing predictions to observational results 17 p2948 A67-32819

Exact expression for line profile of stigmatic spectrograph without vignetting, noting results with foil-excited ions as light source 18 p3082 A67-33877

Spectral line resonance broadening using Griem theory, noting linear pressure dependence 19 p3272 A67-35085

Broadening of Debye-Scherrer line profiles and structure recovery studied in cold-worked Ti, Zr and Hf specimens by X-ray analysis 19 p3247 A67-35835

Lead abundance in sun computed from measurement of Pb lines equivalent widths 19 p3331 A67-36087

Absolute transition probabilities, Stark widths and shifts of S I and S II lines determined experimentally 19 p3266 A67-36089

Line profiles and Stark widths of singly ionized carbon and calcium atoms measured using plasma source 19 p3299 A67-36092

Doppler widths from plasma UV lines using fast scan Michelson interferometer 20 p3438 A67-36343

Molecular oxygen absorption line equivalent widths measurement at 5 mm wavelength obtained from model atmosphere to determine earth atmospheric temperature 20 p3427 A67-36370

Glow-broadening rate dependence on initial pressure and discharge voltage in shock tube containing hydrogen plasma, studying charge distribution variations 20 p3501 A67-37145

Atmospheric pressure at cloud top and hydrogen abundance in Jupiter atmosphere determined by analyzing methane spectral line widths 20 p3529 A67-37479

Mathematical statistics methods for nonreabsorbed spectral line widths and shifts and optical density in plasma 20 p3471 A67-37601

Ruby laser radiation frequency temperature dependence, observing narrow spectral width with Fabry-Perot interferometer 21 p3640 A67-38451

Stark effect spectral line broadening due to current or electron beam excitation of stochastic plasma 21 p3670 A67-38690

Ion-molecule collision cross section determined from pressure broadening of ion cyclotron resonance lines at high electric field/pressure ratio 22 p3840 A67-39365

Atmospheric ground layer water vapor absorption of 183.31 GHz electromagnetic wave 22 p3759 A67-39506

Transition temperature, Knight shift and NMR line width variation in V-Au compounds as function of atomic ordering 22 p3858 A67-39520

Radiation fluctuation of single mode continuously operating laser, deriving fluctuation spectral density and emission line intrinsic width 22 p3815 A67-39738

In-plane and out-of-plane ferromagnetic resonance line widths in Ni single crystal

platelets noting cubic crystalline anisotropy at 25.92 GHz 22 p3864 A67-40245

Millidegree noise thermometry based on linewidth of Josephson radiation 22 p3865 A67-40436

Equivalent widths of line spectrum analyzed by modification of Milne-Eddington growth procedure curve 22 p3896 A67-40528

Spectrum line observation of decay transition of structure of gas laser 23 p4016 A67-41324

Decrement of Balmer line widths and H-alpha profiles when distributing fine components as function of radial velocity in optical prominences 24 p4232 A67-42595

SPECTRAL NOISE

Millidegree noise thermometry based on linewidth of Josephson radiation 22 p3865 A67-40436

SPECTRAL REFLECTANCE

Spectral reflectance coefficients for meadow grass, birch tree and lilac leaves, brick, sand, concrete and snow in region 0.7 to 0.5 microns 01 p0107 A67-10126

Reflectance and emittance properties of binary coatings in sintered or compacted powder form in terms of properties of pure components [AIAA PAPER 65-670] 03 p0448 A67-13038

Bidirectional reflectance measurements to determine optical degradation induced by UV radiation [AIAA PAPER 65-672] 03 p0419 A67-13040

Reflective properties of natural surfaces, noting dependence on surface properties of total reflected energy, spectral distribution, polarization degree of radiation, etc [AIAA PAPER 65-665] 03 p0411 A67-13045

Low energy proton effect on thermal control coatings [AIAA PAPER 65-648] 03 p0448 A67-13053

Room temperature reflectance spectra of GaAs, GaP and typical alloys in energy range 2.5 to 20 eV and 2.5 and 6 eV at liquid nitrogen temperature 03 p0501 A67-14355

Room temperature measurements determining mean slope and peak-to-valley height influences on bidirectional spectral reflectance of V-grooved surfaces 03 p0426 A67-14398

Polarization and directional variation effect on radiant heat transfer through long specular reflecting passages [ASME PAPER 66-WA/HT-32] 04 p0725 A67-15440

Total and spectral reflectance of carbon dioxide cryodeposits on test vehicles and space simulator walls as function of deposit thickness, rate of formation, angle of incidence of light, etc 09 p1533 A67-22121

Vacuum integrating sphere for in situ spectral reflectance measurements of carbon dioxide cryodeposits from 0.5 to 10 microns [AIAA PAPER 67-298] 12 p1926 A67-26013

High temperature spectral directional hemispherical reflectance of refractory metals and ceramics measured with integrating sphere and He-Ne CW laser source [AIAA PAPER 67-300] 12 p2035 A67-26015

Bidirectional spectrophotometer for reflectance of solid and powder samples [AIAA PAPER 67-313] 12 p1946 A67-26028

Reflectance function for stainless steel with various surface roughnesses, comparing incident and reflected monochromatic fluxes of assigned directions [AIAA PAPER 67-321] 12 p1957 A67-26036

Visible and near IR spectral reflectance and emittance at high temperature of ablation chars, carbon and graphite [AIAA PAPER 67-326] 12 p2037 A67-26040

In situ measurements of diffuse hemispherical spectral reflectance of thermal control coatings irradiated in vacuo with various combinations [AIAA PAPER 67-342] 12 p1959 A67-26056

UV stability of several white thermal control coatings spectrally characterized in vacuum for application to Lunar Orbiter project [AIAA PAPER 67-345] 12 p1959 A67-26059

Pressure effect on interband reflectivity spectra of germanium and related semiconductors 13 p2179 A67-27158

Polarization and directional variation effect on radiant heat transfer through long specular reflecting passages [ASME PAPER 66-WA/HT-32] 15 p2579 A67-29319

Absolute spectral reflectance measurement

in solar region in vacuo for applications to thermal control coatings 15 p2487 A67-29542

Energy band structure of crystals of groups IV, III-V and II-VI and magnesium silicide type crystals 18 p3095 A67-33448

Spectral brightness, reflectivity and polarization characteristics of clouds in IR band, measuring angular structure of underlying radiation field 18 p3073 A67-33563

IR reflection spectra of tellurium and zinc doped indium arsenide single crystals, discussing reflection minima and spectral curves given 19 p3306 A67-35705

Hemispherical reflectance of metal surfaces investigated for relation of wavelength and surface roughness 22 p3920 A67-40420

Dual beam bidirectional reflectance attachment permitting sample plane tilting in spectroscopic measurements 23 p4002 A67-41261

Thermal radiation properties measurement for materials in spacecraft design, discussing apparatus, instruments, techniques, devices and methods 23 p4083 A67-41368

Solar wind and UV exposure effects on spacecraft thermal control coatings, using in situ spectral reflectance measurements 24 p4174 A67-42040

Spectral reflectance of water and carbon dioxide cryodeposits in vacuum integrating sphere as function of incidence angle, substrate material and cryodeposit thickness 24 p4253 A67-42046

SPECTRAL RESOLUTION

Mass spectrometer resolution improved by variable focus at any arbitrary ion current through three-element unipotential lens 02 p0248 A67-12700

Lunar occultation of celestial radio sources noting brightness distribution and spectral resolution 05 p0891 A67-16402

Spectral resolution improvement by photoelectric Raman spectrometer with He-Ne laser excitation, noting results for carbon disulfide, carbon tetrachloride and azobenzene 09 p1492 A67-21561

Complex organic compounds analysis by fast-electrical-scanning high resolution mass spectrometry and gas chromatography 14 p2259 A67-28425

Optimum spacing arrangement for 1100101 array of four antennas in straight line with spectral sensitivity in switched and unswitched cases 14 p2284 A67-28435

Variable field Thomson mass spectrograph application to analysis of mass composition of plasmoids 15 p2526 A67-29258

Time-resolved spectra for hypervelocity spheres and cones in free-flight ballistic range obtained by large aperture spectrograph and image converter camera 17 p2862 A67-33290

Fabry-Perot interferometer improvements for high resolution rocket photography of solar Fraunhofer spectrum 20 p3440 A67-36359

Spectrometer SNR improvement without affecting resolution by using larger inlet and outlet slit openings 20 p3441 A67-36365

SPECTRAL THEORY

Temperature dependence of lifetime of electrons and holes in GaAs, noting trapping effect of recombination centers and capture levels 01 p0128 A67-10091

Statistical and spectral density analyses of stationariness and behavior law of atmospheric turbulence 01 p0054 A67-11087

Stationary methods in continuous spectra perturbation theory of nonrelativistic quantum-mechanical scattering in Hilbert space 02 p0268 A67-12726

Spherical harmonics integration of low order spectral form of primitive meteorological equations 06 p1025 A67-18051

Spectral theory of Wiener-Hopf type integral operators on generalized Sobolev spaces 10 p1674 A67-22968

Numerical techniques for process identification in automatic control systems, discussing methods such as autocorrelation, spectral density, differential approximation, etc 15 p2480 A67-30310

Spectral density of stationary random signals corrupted by multiplicative noise 17 p2812 A67-32303

German book on differential operators of mathematical physics covering Hilbert space h, Schroedinger spectral theory, etc 20 p3475 A67-36434

SPECTROGRAM

- High dispersion spectrograms of Mars examined for water vapor presence, results indicate amount depends on size of polar cap
[JPL-TR-32-1048] 09 p1566 A67-22235
- Photographically recorded spectra for absolute intensity processed by computer program, providing digitally recorded densities on magnetic tape 21 p3624 A67-37851
- SPECTROGRAPH**
SA SOLAR SPECTROGRAPH
SA ULTRAVIOLET SPECTROGRAPH
- Transmittance measurements and consequent cloud top determination by Gemini V hand-held spectrographic camera 01 p0061 A67-11396
- Optical systems crossing in Fabry-Perot interferometer to determine instrumental function of spectrographic device 02 p0246 A67-12479
- Jarrell-Ash model 75 spectrograph adapted for time resolved spectroscopy of transient plasma produced by exploding wire and shock waves 03 p0426 A67-14401
- Slit size effect on magnetograph observations of solar magnetic field in near polar regions 06 p1082 A67-18015
- Fluor molecule emission spectrum between 4500 and 8500 angstroms, discussing results of rotational vibration analysis [DVL-624] 11 p1750 A67-25003
- High luminosity spectrograph using inverse Wadsworth mounting constructed for recording auroral spectra in far UV 14 p2315 A67-28157
- Electro-optical spectrograph producing dynamic spectrograph continuous in both frequency and time 14 p2319 A67-28444
- Helium afterglow observation at high latitudes, determining He line intensity on IR spectrograph and giving time-dependent seasonal variations 17 p2849 A67-32959
- Time-resolved spectra for hypervelocity spheres and cones in free-flight ballistic range obtained by large aperture spectrograph and image converter camera 17 p2862 A67-33290
- Spectra broadening mechanism on reflector of Vilnius Observatory 18 p3044 A67-33659
- Interference and spectroscopic devices improving photographic detection of astronomical telescopes on ground and in space 18 p3048 A67-34189
- SIMAC spectrography, discussing brightness, speed, etc. of electronic camera and photographic plate recording 20 p3439 A67-36350
- SPECTROGRAPHY**
SA X-RAY SPECTROGRAPHY
- Nitrogen wavelengths obtained from precision measurements of various nitrogen lines, using vacuum UV spectrograph 05 p0846 A67-16781
- Resonance emission of H and K lines of ionized calcium during twilight spectrographically observed, suggesting meteoritic origin 06 p0998 A67-18704
- Interferometer producing focusing hologram diffraction grating, noting photograph of spectrum 10 p1658 A67-23788
- Developments in techniques of meteor spectral observations 13 p2197 A67-26503
- Meteor radiation and methods of meteor spectrography, discussing chemical composition, spectral characteristics, green oxygen line and photoelectrical color sensors 13 p2197 A67-26504
- Spectrographic observations of late stages of limb flare by achromatic coronagraph 14 p2381 A67-28835
- Photographic spectra of ablating plastics in thermodynamic environments related to species and temperatures in boundary layers [AIAA PAPER 66-132] 15 p2582 A67-30206
- February 11, 1958 aurora observation during IGY, determining specific aurora features by all-sky camera and spectrographic techniques 17 p2849 A67-32964
- Shock waves and spectrographic properties of emitted light during high energy linear discharge in ionized gaseous filament 19 p3176 A67-35133
- Instrumentation for observing limb darkening of solar continuum during annular eclipse of May 1966 20 p3529 A67-37502
- Nitrogen role in oxidation of titanium in air at elevated temperatures studied by spectrographic analysis 21 p3643 A67-37828

SPECTROHELIOGRAPH

- Solar chromospheric structure noting network pattern of absorption in He 10830 angstrom region 03 p0514 A67-14312
- Observations of sun at Stanford on May 20, 1966 at 9.1 cm after annular eclipse in Greece and Turkey 07 p1251 A67-19914
- Extreme UV emission, discussing chromospheric coarse mottling and network characteristics of He II 304 angstroms 10 p1707 A67-23224
- Inadequacy of formula for correction of foreshortening of Ca plages, attempting to determine directly new correction factor 10 p1712 A67-23806
- Solar studies in extreme UV using stabilized Skylark rockets, including data on chromospheric and coronal spectra and XUV spectroheliograms 12 p2008 A67-25826
- Photoelectric measurements of continuum intensity differences and concave grating spectra of faculae and undisturbed photosphere 14 p2378 A67-27846
- Photoelectric solar spectroscopy at Nice Observatory, discussing suitability of location and results 14 p2387 A67-28592
- Solar radio emission spectroheliograms at different millimeter wave frequencies 14 p2388 A67-28834
- Extreme UV solar spectrum, reviewing echelle spectrum, soft X-rays and coronal emission 20 p3528 A67-37467
- SPECTROMETER**
SA EBERT SPECTROMETER
SA FABRY-PEROT SPECTROMETER
SA INFRARED SPECTROMETER
SA MASS SPECTROMETER
SA SCINTILLATION SPECTROMETER
SA ULTRAVIOLET SPECTROMETER
- Three-body and wall recombination coefficients of atomic nitrogen, using electron spin resonance spectrometer for concentration measurements 01 p0117 A67-10883
- Sweep spectrometer study of effect of strong magnetic field on characteristics of plasma beam produced by titanium plasma source 02 p0278 A67-12622
- Simplified 180 degrees focusing beta-ray spectrometer, noting electron trajectory radius, shape of vacuum chamber walls, etc 05 p0806 A67-16500
- Mossbauer nuclear resonance fluorescence effect spectrometer using Doppler principle, with applications to aerospace 05 p0843 A67-16544
- Atmospheric temperature profile to 30 km determined by balloon-borne grating spectrometer of radiance of earth between 2100 and 2700 reciprocal cm [JPL-TR-32-1080] 07 p1171 A67-19394
- Astrospectrometer, instrument for recording high definition star spectra 07 p1186 A67-19425
- Vibrational and rotational temperature at altitudes between 50 to 250 km determined from analysis of airglow in OH bands, using Fastie-Ebert spectrometer 07 p1172 A67-19582
- Spectral resolution improvement by photoelectric Raman spectrometer with He-Ne laser excitation, noting results for carbon disulfide, carbon tetrachloride and azobenzene 09 p1492 A67-21561
- Laser for length measurement, checking absolute wavelength stability by Fabry-Perot spectrometer 09 p1499 A67-22148
- Near IR atmospheric absorption over 25-km horizontal path at sea level 10 p1629 A67-22744
- Frequency stabilization of power klystron used in spectrometer for relaxation time measurement 11 p1767 A67-24752
- Lithium drifted germanium detector with cylindrical annular shape permitting standardization of gamma spectroscopy techniques 12 p1945 A67-25861
- Transmittance and reflectance measurements on wirecloth and metallic meshes using vacuum grating spectrometer for design of transmission band pass filter in far IR 13 p2121 A67-27354
- Sweep spectrometer study of effect of strong magnetic field on characteristics of plasma beam produced by titanium plasma source 13 p2170 A67-27378
- Solar spectrum observations in oxygen regions, describing prism-grating spectrometer, photoelectric recording and scan-averaging by digital computer [AFCLR-67-0478] 16 p2749 A67-31417

- Spectrometers onboard satellite, studying cosmic ray particle energy spectra and chemical composition 17 p2935 A67-32248
- Short wave spectrometer for measuring total and scattered sky radiation, spectral brightness and fluxes of direct and reflected solar radiation 19 p3227 A67-34860
- Solar X-ray spectra below 25 angstroms from crystal spectrometer mounted on solar pointer flown on satellite 19 p3318 A67-35198
- Enhancement of faint photographic spectra using signal averaging digital computer 19 p3232 A67-35698
- Wave field behind transmission grating illuminated by plane wave examined by Fourier spectrometry based on grating resonances 20 p3437 A67-36338
- Very high resolution Fourier transform spectrometer, discussing path difference variation 20 p3438 A67-36346
- Switched Proton Electron Channeltron Spectrometer /SPECS/ developed for measurement of charged particles in space 20 p3443 A67-36517
- Superconducting magnet spectrometer using lithium drifted silicon detectors for measurement of electron spectra 20 p3444 A67-36523
- Grazing incidence spectrometer and low inductance spark source used for energy level identification in various elements 20 p3378 A67-37468
- Rapid scan spectrometer for carbon dioxide laser studies noting time dependent effects 21 p3641 A67-38460
- Rapid scan spectrometer used to measure Stark broadened H lines in plasma column, determining electron density 23 p4032 A67-40957
- SPECTROMETRIC TRACKING**
Temperature distribution in argon plasma jet with variable mass flow measured, using grating spectrometer [ASME PAPER 66-WA/HT-50] 04 p0669 A67-15434
- South Atlantic proton radiation anomaly measurements using rocket flown spectrometer, examining variation of counting rates with altitude 12 p1995 A67-25771
- SPECTROMETRY**
SA MASS SPECTROMETRY
SA NEUTRON SPECTROMETRY
SA X-RAY SPECTROMETRY
- Double crystal spectrometer measurement of X-ray Compton and thermal scattering accompanying Bragg reflection from Si and Ge single crystals 01 p0132 A67-10456
- Charged particle solid state detectors, considering neutron intensity and energy and spectral and/or dose measurements 02 p0244 A67-12210
- Longitudinal Kerr and Faraday effects in Ni and permalloy films using photoelectric polarization spectrometer, choosing various refractive indices and gyroelectric constants 05 p0865 A67-16972
- Spectrometric and colorimetric observations of luminescence on moon surface 08 p1390 A67-21020
- Langmuir probe and spectrometric electron temperature measurements in negative glow plasma compared, finding probe temperatures significantly higher 11 p1788 A67-23963
- Time course of blue-to-red light intensity ratio of visible solar spectrum during and after sunset 11 p1786 A67-24116
- Spectrometric investigation of Mars in five spectral regions applied to color analysis of Martian continents and oceans for probable coloring of Martian vegetation 11 p1867 A67-24845
- Spectrometry of primary and solar protons at Skogar-Iceland using apparatus consisting of scintillation and Cerenkov counters 12 p1991 A67-25114
- Gas laser properties, noting usefulness in physics, chemistry and optics 13 p2129 A67-27364
- Comet 1963 III spectrometric observations showing important continuous spectrum of comet, spectrum wavelengths identification, etc 17 p2946 A67-32731
- Statistical properties of strong light intensity fluctuations propagating in ground layer of atmosphere investigated to measure frequency spectra 19 p3254 A67-36017
- Selective modulation spectrometry, discussing problem of spectrometry without slit 20 p3438 A67-36348

Spectrometer SNR improvement without affecting resolution by using larger inlet and outlet slit openings 20 p3441 A67-36365
 ESRO V satellite-borne solar-proton spectrometry experiment to study proton and alpha particle energy spectra emitted during solar activity 21 p3629 A67-38663
 Atmospheric ion mobility spectrograms measured with aspiration 22 p3810 A67-40524
 Laser radiation in calibration of spectrometer scanning function by duplicating spatial coherence characteristics of radiation 23 p4014 A67-41023
 Hakenmethode theory and experimental technique, presenting basic arrangement for hook formation in crossed interferometer-spectrometer system 23 p4002 A67-41264
 Al 26 content of stony meteorites by coincidence spectrometry noting cosmic ray exposure ages for eight meteorites 24 p4234 A67-42630

SPECTROPHOTOMETER

SA INFRARED SPECTROPHOTOMETER

Black body spectral radiance calibration procedure incorporating Beckman IR-4 double-beam spectrophotometer with thermocouple, lead sulfide detector and two NBS-certified black bodies 01 p0069 A67-11023

Cameras used in auroral and airglow experiments including SP3 spectrophotometer, three-channel photometer and all-sky camera 03 p0419 A67-13376

Spectrum of meteorite luminescence emission after irradiation with protons and UV radiation, using spectrophotometer 08 p1390 A67-21021
 Atomic beam resonance spectrophotometer used with solar telescope to observe solar line oscillation 11 p1861 A67-24494

Thermal radiation properties of oxide films of variable thickness on metal substrates, using radio-recording spectrophotometer at various wavelengths [AIAA PAPER 67-286] 12 p1958 A67-26003
 Spectrophotometric observations used to construct empirical curve relating radiation intensity and magnetic field strength in sunspots 17 p2946 A67-32728

Second order absorption spectra of symmetric cyanine dyes in methanol solution using spectrophotometer 22 p3757 A67-39444

SPECTROPHOTOMETRY

SA STELLAR SPECTROPHOTOMETRY

SA ULTRAVIOLET

SPECTROPHOTOMETRY

High resolution spectrophotometric system for measuring atmospheric transmittance spectra 02 p0263 A67-12645
 Adenine and guanine amounts in DNA determined spectrophotometrically by dialysis of DNA 04 p0564 A67-14406

Spectrophotometry of Arend-Roland comet, estimating radiation from comet emission bands and continuous spectrum 05 p0891 A67-16338

Automatic dielectric film filter method in spectrophotometry 05 p0805 A67-16370

Spectrophotometric results for H-alpha and K line contours of August 21, 1959 chromospheric flare 05 p0892 A67-16496

Spectrophotometric study of H, K and He spectral line characteristics of chromospheric flare of June 25, 1960 07 p1247 A67-19166

Cosmos LXI spectrophotometric measurements of atmosphere-reflected UV radiation spectra 07 p1178 A67-19801

Middle and far IR spectra of silicate minerals for remote sensing of lunar or planetary surface composition 08 p1385 A67-20934

Rapid remote sensing of lunar surface by IR spectrum matching technique using simple matching device or scanning instrument 08 p1385 A67-20935

Spectrophotometric data correlations between color and red shifts of quasars 08 p1398 A67-21231

Spectrum of quasi-stellar source PHL 5200 with rapidly expanding envelope 08 p1400 A67-21253

Characteristic optical density and equilibrium of alkyl-sodium and aromatic hydrocarbons as function of temperature and wavelengths, correlating electron affinity with enthalpy values 09 p1458 A67-22214
 Photometry of coronal emission line 5303

angstrom on Mt. Lomnicky Stit 10 p1705 A67-22897

Photometric measurements of eclipses of artificial solar satellite 1960 Eta 2 at sunrise and sunset in Lyman alpha and violet spectral range 10 p1706 A67-23221

Brightness of night glow measured in several spectral ranges by Cosmos 92 satellite-installed colorimeter 10 p1647 A67-23276

Cosmos 65 spectrophotometric measurements of atmosphere-reflected UV radiation spectra 10 p1647 A67-23277

Center-to-limb variations for continuum, faint iron lines and core of strong Fraunhofer lines measured along polar and equatorial diameters of solar disk 11 p1861 A67-24492

Metallic element concentrations in metals studied using atomic absorption spectrophotometry, noting chemical and bulk effect interferences 12 p1947 A67-26127

Silicon oxide and nitride film thickness determined with interference technique, using spectrophotometer in UV and visible wavelength range 17 p2854 A67-32191

Space-time properties of hydroxyl emission observed by spectrophotoelectrometry, giving diagrams of periodic variations and measurement errors 17 p2848 A67-32954

High latitude night sky emissions observed by photographic spectrography, examining oxygen, nitrogen and hydrogen lines 18 p3037 A67-33610

Spectrophotometric study of multiple reaction zones of premixed trimethylaluminum-oxygen flames, emphasizing microstructure 18 p3109 A67-33840

Moon spectrophotometric measurements from space probe compared with solar spectrum structure, calculating lunar albedo curve 18 p3122 A67-34140

Ionized gas produced by exploded lithium wires, presenting physical measurements, finding self-consistent solution of temperature and electron concentration 19 p3261 A67-35162

Photometry and spectrophotometry of short-period variable stars 19 p3330 A67-36076

SPECTROSCOPE

Molecular beam electric resonance /MBER/ spectrometer for hyperfine structure of rubidium fluoride 11 p1821 A67-23961

SPECTROSCOPIC TELESCOPE

All-mirror Schmidt telescope system for space research providing easier switchover from photography to slitless spectroscopy 10 p1657 A67-23561

Detecting planetary life from earth 11 p1747 A67-24063

Atmospheric spectral analysis of planets and stars by using computer, telescope and interferometer system 24 p4232 A67-42572

SPECTROSCOPY

SA AURORAL SPECTROSCOPY

SA COLORIMETRY

SA ELECTRON MICROSCOPY

SA GAS SPECTROSCOPY

SA INFRARED SPECTROSCOPY

SA MAGNETIC SPECTROSCOPY

SA MASS SPECTROSCOPY

SA MOLECULAR SPECTROSCOPY

SA NUCLEAR SPECTROSCOPY

SA OPTICAL EMISSION SPECTROSCOPY

SA RADIO SPECTROSCOPY

SA RAMAN SPECTROSCOPY

SA ULTRAVIOLET SPECTROSCOPY

SA VACUUM SPECTROSCOPY

SA X-RAY SPECTROSCOPY

Partial coherence theory to describe Fourier /autocorrelation/ spectroscopy, showing resolving power dependence upon parameter of measuring instrument and radiation 01 p0018 A67-10504

Stroke and Restrick method used in Fourier transform application to spectroscopy and astronomy and in obtaining holograms 01 p0069 A67-11008

Tetrafluoroethylene dissociation in nitrogen behind shock waves and thermoequilibrium constants studied, using shock tube and optical absorption spectroscopy 05 p0759 A67-16840

Remote sensing cross-beam cross correlation methods of determining spatially resolved average thermodynamic properties [AIAA PAPER 67-149] 06 p1004 A67-18477

Local mode absorption bands for Al impurities in InSb and for P impurities in GaAs at various temperatures, using grating spectroscopy 06 p1059 A67-18910

Laser studies at RCA Victor Research Laboratories, Montreal, discussing spectroscopic, interferometric and plasma diagnostic research 07 p1194 A67-19082

Laser spectroscopy, discussing advantages, precision attainable, line shape and position measurements 07 p1194 A67-19087

Thermodynamic equilibrium composition of Venus atmosphere computed from atomic composition deduced spectroscopically 07 p1256 A67-20022

Spectroscopic studies of plasma pulse discharge on hard electrodes in vacuum, determining excitation temperatures for various portions of jet 09 p1544 A67-21852

Echelle spectrograph for middle UV solar spectroscopy from rockets 10 p1653 A67-22735

Book on spectroscopic gas temperature measurement covering principles, radiometric and spectroscopic methods, instruments, applications to pyrometry, etc 12 p1940 A67-25431

Holographic imaging methods for improving luminosity, detection and resolution of spectroscopic and astronomical instruments 12 p1948 A67-26238

Time resolution amplification of flash spectroscopy apparatus equipped with switched laser 13 p2126 A67-26599

Spectroscopic measurements of plasma parameters in thermionic converters 13 p2056 A67-27385

Spectroscopic observation of sunspot structure, detailing sunspot model on basis of magnetic field and large scale motions interpretation 13 p2203 A67-27425

Spectroscopic methods applied to plasma electron temperature and density measurements 14 p2322 A67-29045

Stark-broadened isolated ion line agreement between theory and experiment obtained by Griem theory or by impact approximation of GBKO theory 15 p2520 A67-29678

Spectroscopic study of gas discharge parameters in argon ion lasers to determine level inversion mechanism in continuous or pulsed regime of generation 15 p2501 A67-30003

Spectroscopic measurements of cold plasma charged particle concentrations, specifically spectral broadening due to Stark effect, forbidden-line intensities affected by internal electric fields and autoionization line intensities 17 p2896 A67-32161

High resolution spectroscopy, using incoherent light mixed with coherent laser light, for astronomical purposes 17 p2854 A67-32234

Laser applications utilizing power density for studying reflectance, Raman spectra, photography, holography, etc 17 p2868 A67-32691

Spin-exchange frequency pulling of ground state hyperfine transition in atomic hydrogen analyzed for self-excited oscillation in hydrogen maser 17 p2889 A67-33225

Spectroscopic study of gas discharge parameters in argon ion lasers to determine level inversion mechanism in continuous or pulsed regime of generation 18 p3059 A67-33760

Hypersensitization procedure for spectroscopic plates, minimizing nonuniformities of plate fog by use of stop bath 18 p3047 A67-33883

Time signal transmission and reception, noting development of UHF spectroscopy and atomic frequency scales 18 p3004 A67-34400

Ionizing and charge transfer processes following heavy particle collisions in ionized gas analyzed using spectroscopic technique 19 p3264 A67-35069

Bulgarian research in spectroscopy, solar system, ionosphere, gravitation equations, astrophysics, etc 19 p3320 A67-35283

Spectroscopic properties of ionic beam source, discussing particle densities, source purity, etc 19 p3231 A67-35682

Two-beam interferometric spectroscopy, discussing digital computers role and quality of spectral and angular measurements 19 p3232 A67-35872

New methods of instrumental spectroscopy - Conference, Paris University, April

1966 20 p3436 A67-36334
 Fourier spectroscopy problems including source noise effects on interferogram modulation and maximum SNR attainable in spectrum estimated from given interferogram 20 p3437 A67-36336
 Fundamental intensity error in Fourier spectroscopy noting requirement that interferograms be inverted by Fourier transformation 20 p3437 A67-36337
 Real time Fourier transform synthesizer for spectral distribution of interferogram 20 p3437 A67-36341
 Planetary spectra improvement by Fourier spectroscopy, discussing modulation method reduction of atmospheric turbulence effects and fast transmission 20 p3438 A67-36345
 White light reflection holography, discussing recording, reconstruction and color images 20 p3438 A67-36349
 Divalent Eu ion ground state splitting in C3h symmetry sites and associated color centers in EPR spectrum study of Eu ion doped lanthanum trichloride 22 p3863 A67-40003
 Stimulated emission and spectroscopic investigations of double lanthanum-sodium molybdate single crystals with neodymium impurities, considering applicability in lasers 23 p4039 A67-40901
 Fully ionized barium plasma column generating device, discussing spectroscopic measurements of ion motions, densities, temperatures and electron temperature 23 p4033 A67-41215
 Dual beam bidirectional reflectance attachment permitting sample plane tilting in spectroscopic measurements 23 p4002 A67-41261
 Microwave plasma observed using spectroscopic and mass spectrometric techniques, discussing standing wave operation mode, emission and resonance lines 23 p4034 A67-41435

SPECTRUM

SA ABSORPTION SPECTRUM
 SA ASTRONOMICAL SPECTRUM
 SA DIFFRACTION GRATING
 SA ELECTRON SPECTRUM
 SA EMISSION SPECTRUM
 SA ENERGY SPECTRUM
 SA INFRARED SPECTRUM
 SA LINE SPECTRUM
 SA LYMAN SPECTRUM
 SA MASS SPECTRUM
 SA MICROWAVE SPECTRUM
 SA MOLECULAR SPECTRUM
 SA NEUTRON SPECTRUM
 SA NOISE SPECTRUM
 SA OPTICAL SPECTRUM
 SA OXYGEN SPECTRUM
 SA PLASMA SPECTRUM
 SA POWER SPECTRUM
 SA RADIATION SPECTRUM
 SA RADIO SPECTRUM
 SA RAMAN SPECTRUM
 SA SCHUMANN-RUNGE BAND SYSTEM
 SA SHOCK SPECTRUM
 SA SOLAR SPECTRUM
 SA SPECULAR REFLECTION
 SA STELLAR SPECTRUM
 SA ULTRAVIOLET SPECTRUM
 SA VIBRATIONAL SPECTRUM
 SA VISIBLE SPECTRUM
 Orbit, luminescence and spectrum of July 5, 1962 bolide orbit, luminescence and spectrum of July 5, 1962 bolide orbit, luminescence and spectrum of July 5, 1962 13 p2197 A67-26502

SPECULAR REFLECTION

Thermal emittance and reflectance of diffuse-bottomed specular-walled groove in solar radiant-flux environment [AIAA PAPER 66-459] 02 p0342 A67-11939
 Outward flux and intensity of scattered radiation for top of Rayleigh atmosphere lying above smooth water surface that reflects radiation according to Fresnel law [AIAA PAPER 65-664] 03 p0411 A67-13044
 Spherical concentric geometry for designing absorber materials for application to curved surfaces determined by specular radar cross section 03 p0371 A67-13863
 Total specular reflectance of rough metal surfaces calculated, using Maxwell equations and approximation via Kirchhoff diffraction theory [AIAA PAPER 65-424] 04 p0723 A67-15232
 Radiative heat exchange between specularly reflecting surfaces with direction

dependent properties 04 p0738 A67-15869
 Critical fields of thin superconducting films determined by specular reflection of electrons from surfaces 10 p1694 A67-23596
 Radar measurements of Doppler spectra and power reflectivity of Mars interpreted as surface elevation differences between dark and bright areas 11 p1867 A67-24776
 Spectrometric investigation of Mars in five spectral regions applied to color analysis of Martian continents and oceans for probable coloring of Martian vegetation 11 p1867 A67-24845
 Thermal radiation characteristics of spacecraft temperature control louvers in solar space environment, discussing specular reflection [AIAA PAPER 67-307] 12 p2036 A67-26022
 Reflectance function for stainless steel with various surface roughnesses, comparing incident and reflected monochromatic fluxes of assigned directions [AIAA PAPER 67-321] 12 p1957 A67-26036
 Spatial distribution of deuterium and hydrogen molecules and helium scatterer from /111/ plane of epitaxially grown silver 13 p2099 A67-26948
 Noble gas molecular beam quasi-specular scattering from metal surfaces noting effects of beam incidence angle, molecular weight and gas temperature 13 p2099 A67-26949
 Lobular scattering of 1 eV energy chopped argon beams from silver, mica and brass surfaces, noting distributions and contamination effects 13 p2099 A67-26950
 Selective polarization filtering during hologram construction enhancing reconstructed image resolution and tonal range by eliminating specular reflection recording 15 p2488 A67-29818
 Infrared reflectance and optical constants of tektites for origin mode, noting constituent dependence on geographic location 16 p2753 A67-31697
 Spacecraft package temperature control by interior louver panel system, calculating net heat transfer [ASME PAPER 67-HT-64] 20 p3549 A67-36746
 Alfvén two-dimensional problem extended to charged-particle motion in dipole magnetic field with electric field determining forbidden band size, shape and specular reflection points position 21 p3621 A67-39015
 Energy transmitting characteristics and wall local energy absorption distribution of curved specular reflecting duct irradiated by collimated beam 23 p4028 A67-41271

SPEECH

Verbal communication intelligibility in man-rated altitude simulator with nitrogen or helium added to oxygen atmosphere 08 p1287 A67-20484
 Degradation factors in speech channels of multiple access communications satellites 11 p1754 A67-24719

SPEECH DISCRIMINATION

Model of speech perception against noise background, hypothesizing that acoustic stimuli are mapped in segments 05 p0763 A67-16706
 Hearing discrimination in hyperbaric air explained by fact that increased ambient pressure causes disturbances of sound conduction 09 p1453 A67-21729
 Phonemic analysis of consonants in helium speech 10 p1597 A67-23312
 Speech distortion caused by respiration in helium-oxygen atmosphere, discussing standard and advanced correcting techniques 10 p1597 A67-23313
 Pressure transducer for speech articulation to detect minute changes in articulator gesture for possible application as control element 22 p3754 A67-39163
 Speech audiometry for hearing loss examinations of middle aged pilots 22 p3753 A67-40545
 Aerospace and Harvard PB word lists for speech discrimination testing of aircrew members while screening against possibility of Meniere disease and vertigo 23 p3963 A67-41542

SPEED

S AIR SPEED
 S CRITICAL SPEED
 S HYPERSONIC SPEED
 S LANDING SPEED
 S LIGHT, SPEED OF
 S PERCEPTUAL SPEED
 S ROTOR SPEED

S SONIC SPEED
 S SUBSONIC SPEED
 S SUPERSONIC SPEED
 S TIME MEASUREMENT
 S TIP SPEED
 S TRANSONIC SPEED
 S ULTRASONIC SPEED
 S VELOCITY

SPEED BRAKE

Main landing gear door and aerodynamic speed brake combination in F-111 aircraft, considering weight minimization and control of landing gears 05 p0753 A67-16163

SPEED REGULATION

Critical speed control by squeeze-film oil damper between two nonrotating parts in parallel with flexible bearing support, using mathematical model [SAE PAPER 670347] 17 p2865 A67-32989
 Hydrodynamic equations for automatic control of speed and coordinates of craft with underwater foils moving on disturbed body of water 18 p3074 A67-33416

SPHERE

SA CELESTIAL SPHERE
 SA HEMISPHERICAL SHELL
 SA OGIVE
 SA ROTATING SPHERE
 Mie scattering and plane wave diffraction theory for small angle light dispersion from sphere 01 p0112 A67-10131
 Diffusely transmitting integrating sphere with solid state photodiode used in laser output measurement 01 p0089 A67-10445
 Excitation of metal sphere with large electric diameter by arbitrary electric and magnetic current distribution 02 p0191 A67-11577
 Radar cross section minimization on sphere using symmetrically attached wires 03 p0369 A67-13683
 Apparent mass increase of sphere accelerated from rest and before boundary layer separation in cylinders of oil or water [ASME PAPER 66-WA/UNT-6] 04 p0601 A67-14483
 Slow periodic motions of viscous incompressible fluid past sphere in infinitely long circular cylinder, using Navier-Stokes motion equations 04 p0602 A67-14618
 Mass and oscillation damping of rigid sphere in cylindrical tube containing viscous liquid [ASME PAPER 66-WA/UNT-5] 04 p0608 A67-15442

Chapman-Enskog method applied to kinetic equation describing evolution of singlet distribution function in dense gas of perfectly rough spheres 04 p0658 A67-15507
 Strain gauge measurements of resistance of sphere to MHD turbulent flow of mercury in rectangular tube 04 p0670 A67-15530
 Transverse elastic impact of isotropic sphere against thin rectangular anisotropic plate 05 p0922 A67-17174
 Fixed vertical plane surface effect on velocity of solid sphere in free fall in laminar region of incident viscous flow for various Reynolds numbers 06 p0983 A67-17928
 Energy losses in explosions in sphere to determine specific heat, heats of dissociation and formation, chemical bond energies and other thermochemical values 06 p1113 A67-17963

Resistance coefficient of circular cylinder and sphere in range of Reynolds and Stuart numbers 06 p1045 A67-18692
 Rotational motion of rigid sphere about z axis in elastic medium taking into account surface adhesion 07 p1223 A67-19219
 Equations of pulsations of spherically symmetrical configurations in general relativity theory, considering oscillation frequency and instability of singular sphere 07 p1248 A67-19483

Upper atmospheric density, pressure and temperature profile obtained from drag acceleration measurements on falling sphere 07 p1181 A67-19938
 BGK intermolecular collision model of sphere drag at high Knudsen numbers and low Mach numbers 08 p1322 A67-21140

Hydromagnetic wake around nonconducting sphere moving in current carrying fluid 08 p1324 A67-21410
 Electromagnetic wave scattering measurements using spheres moving randomly within slab region container, obtaining data for coherent phase, average intensity, etc 09 p1461 A67-21597
 Comparison of distribution functions from

reduced data records for scattering of electromagnetic waves by randomly moving spheres in container 09 p1461 A67-21598

Zero Reynolds limit of steady incompressible viscous fluid motion in sphere due to Landau source at center proved to be Stokes flow 09 p1487 A67-21665

Rarefied gas flow past sphere studied by multibeam interferometry of density profile and shock structures 09 p1438 A67-22216

Stokes flow for sphere in arbitrary external flow pattern solved using Green function, showing uniqueness solution 10 p1629 A67-23831

Heat transfer from isothermal sphere to low Prandtl number fluid in steady and nonsteady potential flow compared with Stokes flow 11 p1882 A67-24119

Viscous flow around spheres, considering mass efflux effect, using Navier-Stokes equations and finite difference methods 12 p1927 A67-25282

Stress concentration of hollow sphere under uniformly distributed impact loads along inner and outer surfaces 13 p2215 A67-26526

Attainable sets and generalized geodesic spheres, noting set properties and meaning of conjugate points 13 p2088 A67-27096

Fluid turbulence effect on rate of heat transfer from spheres in vertical wind tunnel indicate turbulent Reynolds number as important parameter 13 p2225 A67-27466

Aerodynamic characteristics of sphere and blunt cone in highly rarefied gas flow, noting molecular collision effect 13 p2052 A67-27620

Effect of Reynolds number on hypersonic flow of rarefied gas past sphere obtained from pressure distribution at surface 14 p2240 A67-27996

Current carrying incompressible viscous fluid past nonconducting sphere taking fluid inertia into account, noting eddy formation and flow separation 15 p2469 A67-29224

Heat transfer through rarefied gas between concentric circular cylinders and spheres, using Krook kinetic equation 15 p2579 A67-29570

Rarefied gas flow interaction with sphere analyzed using multiple wave interferometer, noting transition region from continuous medium to free molecular flow 16 p2656 A67-30453

Drag coefficient of sphere at supersonic velocities dependence on specific heat ratio of argon, air, carbon dioxide and freon 16 p2593 A67-31122

Lobb empirical relation applied to method for computing flow past blunt body when predicting sphere shock standoff distance 17 p2793 A67-33026

Incompressible fluid drag force on sphere rolling at constant speed in closed-end tube [ASME PAPER 67-APM-18] 17 p2840 A67-33149

Diffraction of stress pulse by spherical cavity embedded in infinite linear homogeneous isotropic elastic medium [ASME PAPER 67-APM-27] 17 p2965 A67-33154

Rarefied gas flow past sphere studied by multibeam interferometry of density profile and shock structures 18 p2982 A67-33755

Spherical shape changes of droplet of viscous substance of high surface tension under variable external force and small deformation 18 p3028 A67-34220

Vector wave functions for boundary value problems in compressible plasma for spherical geometry, noting Fourier series, acoustic wave, etc 18 p3090 A67-34382

Ionized gas flow past cylinder and sphere, determining ionization and dissociation effect on displaced shock wave form 19 p3170 A67-35449

Heat-transfer coefficient effect on final magnitude of stresses in elastoplastic spherical body subjected to cooling process 19 p3340 A67-35510

Radiative effects in pair of spherical particles in radiation field produced by omnidirectional gravitational quanta 19 p3325 A67-35556

Inviscid hypersonic axisymmetric flow over cylinder and sphere near stagnation point, including dissociation and detached shock wave 19 p3171 A67-35722

50 degree semivertex angle sphere-cone Voyager configuration wind tunnel tested in dry nitrogen for aerodynamic characteristics,

pressure and heat transfer distribution 20 p3356 A67-36562

Bow shock and combustion zone studies of spheres fired through H2-O2 mixtures show ignition zone separation 20 p3359 A67-37128

Radial adiabatic motion of spheres of uniform density and isotropic pressure in general relativity, giving bounce occurrence conditions 20 p3486 A67-37273

Transient temperature distribution for spherical region subjected to variable heat flux at boundary represented by terms of known functions and quadratures 20 p3555 A67-37610

Electromagnetic scattering from adsorbing spheres near resonances calculated from extinction efficiency factor and angular scattering function dependence on refractive index 21 p3656 A67-37856

Scattering amplitude of frequency spectrum components of isolated exponential acoustic pulse incident on hard sphere 21 p3657 A67-38057

Simplified formulas and curves for electromagnetic wave diffraction on small ideally conducting sphere, examining electric field components 21 p3580 A67-38121

Oscillation of liquid sodium drop in dielectric medium in presence of constant magnetic field 21 p3665 A67-38245

Polytrope structure from integrodifferential equation assuming metric, energy momentum tensor for static spherical symmetry and polytropic equation of state 21 p3658 A67-38615

Interpolation of Poisson equation by method adjusting equations to insure existence of discrete solution 23 p4023 A67-40865

Electromagnetic scattering from free-space impedance homogeneous spheres, discussing null production in backscattering cross section 23 p3973 A67-40882

Forces on spheres inside diffusers noting instability onset 23 p3932 A67-41734

Viscoelastic lubricant in squeeze film configuration for sphere impinging on lubricant covered plane, noting pressure peak sensitivity to viscoelastic constants [ASME PAPER 67-LUB-24] 24 p4164 A67-42682

Contact region of glass ball rolling on viscoelastic plate at various velocities analyzed by interference microscope photography [ASME PAPER 67-LUB-25] 24 p4176 A67-42683

SPHERICAL CAP

Dynamic snap-through buckling of shallow spherical caps of elastic material 12 p2030 A67-25923

Boundary imperfections in buckling of clamped spherical caps 13 p2220 A67-27452

Dynamic stability of spherical segments subjected to impact loading, discussing buckling in relation to rise in center and time dependence 22 p3910 A67-39456

Homogeneous and sandwich spherical caps axisymmetric vibration natural frequencies solved approximately, noting application to shallow and spherical shell problems 23 p4073 A67-40617

Homogeneous and sandwich spherical caps and circular plate torsional frequency calculations based on sandwich and spherical shell equations 23 p4073 A67-40618

Electromagnetic backscatter from edge scattering centers found on cylinders and flat-backed cones, discussing hemispheric scattering 23 p3973 A67-40839

SPHERICAL HARMONICS

Book of physics and mathematics as foundation for application of satellites to geodesy including spherical harmonics, matrices, orbital geometry, statistical implications and data analysis 04 p0611 A67-14466

Drag free motion of satellite of oblate planet determined by differential equation expressing planet gravitational potential as spherical harmonics 06 p1081 A67-17777

Spherical harmonics integration of low order spectral form of primitive meteorological equations 06 p1025 A67-18051

Crustal features of moon and Mars analyzed for mantle convections, noting correspondence to spherical harmonics of various orders 08 p1397 A67-21208

Cosmos XLIX measurements of magnetic field intensity compared with calculation from spherical harmonic

coefficients 10 p1632 A67-22812

Geomagnetic field values obtained fromOGO-2 satellite-mounted rubidium vapor magnetometer 10 p1641 A67-23244

Equivalent dipole moment of geomagnetic field in terms of earth radius deduced from spherical harmonic analyses 10 p1652 A67-23492

Theory of statistical analysis of data distributed over sphere 10 p1652 A67-23547

Nonradial oscillations of homogeneous sphere examined on basis of general fourth order problem 11 p1819 A67-24783

Sputnik III data application to plotting of total magnetic field intensity chart above U.S.S.R., using spherical harmonic analysis 12 p1933 A67-25652

Linear Fokker-Planck collision operator expanded in terms of surface spherical harmonics, showing distribution function governed by differential-integral equations and eigenvalue spectrum 12 p1962 A67-26177

Earth gravitational potential field determined by satellite measurements, showing field in spherical harmonics form 13 p2116 A67-27395

Spinor algebra application to Fourier series transformation of spherical harmonics expansion representing earth gravitational potential at space location 15 p2561 A67-30055

Spherical dipole for Italian satellite, calculating radiation impedance and pattern, input admittance, efficiency, radiated field and antenna Q factor 17 p2826 A67-32780

Curves in polar plot representing auroral arcs over polar region organized in geomagnetic coordinate system and corrected by spherical harmonic terms 17 p2850 A67-33189

Lunar gravitational field obtained from Lunar Orbiter tracking data, with gravity potential as spherical harmonics series and lunar gravitational constant determined 19 p3318 A67-35190

Continuous spectrum of eigenvalues related to Fokker-Planck collision integral 19 p3285 A67-35341

Artificial satellite motion determination of external earth gravity field compared with surface measurements, orbit theory, etc 20 p3432 A67-37205

Reception vectors for first and second spherical harmonics of cosmic ray distribution calculated for neutron monitor stations 21 p3699 A67-39018

Separation of geomagnetic field into anomalous and normal components, analyzing spectral relation 21 p3622 A67-39024

Schuster method calculation of constant geomagnetic field spherical harmonics coefficients 21 p3623 A67-39045

Fourth order multipole parameters derived from spherical harmonic function coefficients for geomagnetic field potential 24 p4146 A67-41784

Cosmos XLIX measurements of magnetic field intensity compared with calculations from spherical harmonic coefficients 24 p4150 A67-42149

SPHERICAL SHELL

Dynamic stresses in thick walled spherical shell of Voigt material subjected to internal pressure load 01 p0164 A67-11174

Nonlinear influence coefficient obtained by extension of Reissner nonlinear analysis to include uniform pressure loading over surface of spherical shell 01 p0164 A67-11178

Discrete element technique applied to natural vibrations of deep spherical shells satisfying geometric and force boundary conditions 01 p0164 A67-11184

Axially symmetric motion of elastic spherical sandwich shell, determining natural frequencies and effects of shear deformation, normal stress and rotatory inertia 03 p0522 A67-13212

Nonlinear boundary value problem solution as applied to effect of uniformly distributed pressure and concentrated load on spherical dome 03 p0524 A67-13623

Spherical concentric geometry for designing absorber materials for application to curved surfaces determined by specular radar cross section 03 p0371 A67-13863

Radiation diffusion in gas analyzed by solving transport equation for homogeneous absorbing isotropically scattering spherical shell with point source in center 04 p0695 A67-14656

Tensile-instability mechanism concept

determination of ultimate strength of most ductile materials under uniaxial or biaxial tension conditions
[ASME PAPER 66-WA/MET-15]

Nonstationary heat conductivity solution for hollow sphere with varying inner surface and various outer surface
conditions

Integration of nonhomogeneous equations for axisymmetric bending of spherical shells by variation of parameters

Infinite series and finite difference solutions of elastic response of thin walled spherical shell to axisymmetric transient blast loading

[ASME PAPER 66-APM-EE]

Dynamic surface loads, transient displacement and stresses in elastic cylindrical shell under radial and torsional vibration and elastic spherical shell under radial symmetric vibration, using finite Hankel transformation

Eigenfunction expansion solution for axisymmetric vibrations of shallow spherical shell with concentrated mass

Stressed state of spherical shell under action of axisymmetric temperature field arbitrarily varying along meridian

Stress concentration for steep spherical shell with arbitrary elliptic hole

Dynamic displacements of thin spherical shell buckling under uniform pressure

Hole-weakened spherical body represented by deformation of two spherical shells with reinforcing rings under uniform internal load beyond elastic limit

Quasi-steady state temperature distribution in thick walled spherical satellite under solar radiation

Finite difference method stability analysis of deformed eccentrically stiffened shells of revolution, accounting for finite prebuckling rotations

[AIAA PAPER 67-110]

Initial geometric and boundary condition imperfection effect on stability of shallow spherical shells under uniform pressure

[AIAA PAPER 67-111]

Statistical analysis discrepancy in physical experimental values of buckling pressures of spherical shells

Thermal stresses in thin walled open spherical shell of constant thickness

Spherical plastic shell theory and design methods

Second order equations of motion for free axisymmetric deformation of thin spherical shells, discussing membrane and composite mode of solution

Numerical solution methods of invariant imbedding equation for reflection function of spherical shell with absorption and isotropic multiple scattering

Pressure shell structures for space noting materials, machining, assembly, welding, testing, etc

Bifurcation phenomena in spherical shells under concentrated and ring loads taking into account finite prebuckling deformation

Initial postbuckling behavior of spherical shell under external pressure determined using Koiter theory, analyzing effects of imperfections on buckling strength of structures

Stability analysis of symmetrically loaded thin walled spherical shell, noting construction of asymptotic expansion, error estimation and application of elasticity theory

Dynamic problem of shell of revolution in axial rotation under action of plane compression wave

Lower critical load determination of elastic spherical shell with rigidly fastened edge

Infinite systems of equations for multiply connected finite regions in shells obtained by extending solutions for stressed state in infinite multiply connected regions

Asymptotic elastoplastic condition of spherical shell weakened by circular hole and sustaining residual deflections

Dynamic response of clamped shallow thin elastic spherical shells under time dependent loads

[AIAA PAPER 66-446]

Effect of axisymmetric impact against water on shallow clamped aluminum spherical shell-type caps

Holzer method extended to analysis of free vibration of spherical shells, solving boundary value problem as set of initial value problems until all boundary conditions can be satisfied

Adiabatic gravitational collapse of spherically symmetrical distribution of matter, investigating nonvanishing internal pressure gradient, using Einstein field equation

Creep effects in structures obtained by elastic solution applied to pressurized shells containing discontinuities

Stresses due to external forces and moments acting on elastic nonradial circular cylindrical nozzle attached to spherical shell

Imperfections effect on buckling of complete electroformed spherical shells under uniform external pressure examined in rigid and soft testing systems

Finite difference method stability analysis of deformed eccentrically stiffened shells of revolution, accounting for finite prebuckling rotations

[AIAA PAPER 67-110]

Rayleigh-Ritz method used to predict elastic buckling of prolate spheroidal shells under hydrostatic pressure

Laser energy output measured using formed calibrated hollow sphere of thin insulated copper wire as calorimeter

Free vibrations frequency of ideal fluid in elastic bottom cylinder in form of spherical shell

Steady state heat transfer by simultaneous conduction and radiation through spherical shell

[ASME PAPER 67-HT-20]

Stress concentration near hole in large radius sphere solved by approximation method for Helmholtz equations in coordinated system

Approximate method for calculating interaction between flow and soft spherical shell

Aluminum alloy creep rates with changing temperature and stresses in hollow sphere, using time dependent viscosity coefficient

Plane wave approximation for dilatational mode response of thin hollow spherical shell embedded in elastic medium and subjected to asymmetric pressure wave

Shell of revolution stability under axial compressive loading with changes in curvature due to initial imperfections effects

Elastic spherical shell stability under thermal stresses from abrupt temperature change at shell equator solved, using Fredholm integral equation

Natural frequencies and shape of axisymmetric oscillations of thin spherical shell under initial stress calculated via boundary value problem, using computer method

Incompressible hydromagnetic fluid oscillation in rotating spherical shell pervaded by strong toroidal and weak poloidal magnetic field for geomagnetic secular variation hypothesis

Displacement and stress distribution in shallow spherical shell under concentrated loads including normal force, tangential force and bending moment

Unloaded thin walled spherical shell rigidly hinged along edge noting existence of nontrivial form of equilibrium and negative lower critical load

Shallow spherical shell dynamic stability under variable moment

load

Mode acceleration method for axisymmetric dynamic response due to time dependent loading in spherical and cylindrical shells

Axisymmetric vibrations of homogeneous and sandwich spherical shells obtained from generalized variational motion equations including thickness-shear deformation effect

Stress-strain relationship effect on r-power steady creep of pressurized thin spherical shell with sealed opening for various edge load boundary conditions

Bifurcation phenomena in spherical shells under concentrated and ring loads taking into account finite prebuckling deformation

Elastic buckling loads of shallow spherical shells supported by edge rings including nonlinear prebuckling effects

Radio evidence for two supernova remnants in Southern Milky Way and observations of shell type radio sources, considering shell model fitting problem

Einstein field equations derived for thin spherical shell of charged dust falling on spherically symmetric field of massive charged body, considering bounce

SPHERICAL TANK

Heat leak and pressure decay for single phase cryogenic storage in nonequilibrium calculated for spherical tanks, using simplifying assumptions

Aerodynamic investigation of spherical chambers, determining swirling velocity, tangential velocity and regions of air suction

SPHERICAL WAVE

Asymptotic evaluation for k approaching infinity of antenna field emerging from currents induced on surface of reflector with incident spherical wave

Thermoelasticity theorems for harmonic vibrations of continuum, examining spherical wave propagation

Covariance of log amplitude fluctuations for propagation of spherical wave in turbulent medium over horizontal path to obtain phase structure function

Cosmic ray distribution, discussing method of diurnal variations, zonal harmonics and spherical analysis

Spherical wave propagation in infinite elastic body with transverse isotropy

Spherical wave Fourier holography modifications using different scheme for incidence of reference beam and illumination of object

Modes in unstable optical resonators and lens waveguides, noting spherical wave characteristics of geometrical eigenmodes

Energy accumulation of spherical and cylindrical shock waves in inhomogeneous gas

Equations describing one-, two-, and three-layer earth model spheroidal oscillations derived and solutions obtained, considering constant density and constants differing for each layer

Cosmic ray distribution, discussing method of diurnal variations, zonal harmonics and spherical analysis

SPHEROID

SA GEOID

SA PROLATE SPHEROID FUNCTION

Behavior of magnet and ball in gravitational field in five-dimensional continuum

Deviation from sphere shape of drop moving through viscous media and dependence on Weber number, size, etc

Spheroidal coordinate method for obtaining gravitational potential of oblate planet

Rayleigh-Ritz method used to predict elastic buckling of prolate spheroidal shells under hydrostatic pressure

Determination of magnetic field of spreading currents in continuous conducting media separated by spheroidal surface

22 p3911 A67-39683

23 p4075 A67-40667

23 p4079 A67-41343

23 p4080 A67-41728

23 p4080 A67-41729

24 p4230 A67-42332

24 p4189 A67-42599

02 p0223 A67-12796

07 p1264 A67-20222

10 p1678 A67-22712

10 p1698 A67-22778

13 p2217 A67-26633

15 p2486 A67-29237

15 p2497 A67-29391

15 p2472 A67-29694

23 p3994 A67-40714

24 p4209 A67-42114

Finite-amplitude oscillations of Maclaurin spheroids preserving ellipsoidal nature of surface and generating internal motions of uniform vorticity 19 p3263 A67-36078

Current-voltage characteristics of semiconductor diode with spheroidal contact 22 p3769 A67-39571

SPHYGMOGRAPHY

S PULSE RECORDER

SPICULE

H-alpha line profiles and motions of spicules in solar chromosphere studied by spectral photographs taken with noneclipse coronagraph 02 p0328 A67-12483

He I excitation as result of ionization and recombination at chromospheric spicule temperature 02 p0328 A67-12484

H-alpha line profiles and motions of spicules in solar chromosphere studied by spectral photographs taken with noneclipse coronagraph 10 p1708 A67-23351

He I excitation as result of ionization and recombination at chromospheric spicule temperature 10 p1708 A67-23352

Kinetic energy transport outwards in transition region between chromosphere and corona discussed qualitatively, postulating connection with spicules 17 p2952 A67-33393

Spicules and inhomogeneities in corona and interplanetary plasma compared assuming mutual relationship spicules and inhomogeneities in corona and interplanetary plasma compared assuming mutual 21 p3711 A67-39028

SPIDER

Saturn IB flight test loads, comparing measured and calculated bending moment, noting launch time wind profile 10 p1713 A67-23734

SPIKE NOZZLE

Fluidics applications to ramjet control systems incorporating sensing, logic and actuation functions to inlet duct, flow-air ratio and coolant control 17 p2927 A67-31981

SPIKING

S LASER OUTPUT

SPIN

SA ANGULAR MOMENTUM

SA ELECTRON SPIN

SA ELECTRON SPIN RESONANCE

SA ISOTOPIC SPIN

SA NUCLEAR SPIN

Shear-spinning technique for manufacturing molybdenum alloy missile nose tips 18 p3054 A67-34365

SPIN DECOUPLING

Coupled spin, electromagnetic and plasma waves in ferrites 04 p0686 A67-15973

SPIN DYNAMICS

Spin calculations corroborating vertical wind tunnel tests on delta wing aircraft, noting aerodynamic parameters [ONERA-TP-388] 05 p0751 A67-16477

Spin scale factor of Frick for scaling body fixed motion equations analyzed, deriving near optimum factor and near maximum time interval of integration for spinning missiles 05 p0906 A67-17362

Linear and nonlinear attitude control law synthesis for spinning aerospace vehicles, including analog simulation for control designs based on frequency symmetry 07 p1257 A67-19359

Ballistic propellant combustion alteration and thermal effects due to dynamic spinning observed on solid propellant sounding rockets 08 p1408 A67-20522

Balancing operations for rocket vehicles and payloads, defining terms, establishing relation between static and dynamic imbalance and flight vehicle motions, etc 08 p1408 A67-20535

Spinning rocket attitude control technique including theory, system mechanization and performance 08 p1409 A67-20539

Two-impulse torquing scheme for reorienting spin axis of asymmetric spinning vehicle 08 p1413 A67-21510

Steady state dynamic properties of large spinning net-like antenna suitable for radio signal reception from 10 p1727 A67-23753

Hamiltonian for free particle of arbitrary spin and mass formulated in terms of spin matrix polynomials, noting independence of expansion coefficients 11 p1824 A67-25074

Solar spin-down problem, noting oblateness effect on perihelion precession of Mercury 17 p2940 A67-32208

Alouette I and Explorer XX /S-48/ spin behavior explained by solar heating of

antennas and solar radiation pressure 21 p3712 A67-37784

Fast and slow oscillatory spinning of aircraft, examining equations of motion by approximate methods based on Brodetsky analysis 22 p3744 A67-39197

Quasi-cylindrical approximation theory on swirling nozzle flow in relation to spin effect on rocket nozzle performance 22 p3742 A67-40118

Close binary protostellar system formation using model with stellar wind mass loss and primeval magnetic field 22 p3896 A67-40520

Lunar orbit precession due to quadrupole moment of sun arising from solar oblateness 23 p4066 A67-41014

Spin characteristics of VJ 101 C VTOL airplane via numerical integration of motion equations including mass coupling effects and nonlinear aerodynamics 23 p3934 A67-41313

SPIN FORGING

Shear spun 300-grade maraging steel evaluated for pressure vessel applications, discussing fracture toughness [ASM PAPER C6-2.4] 23 p4020 A67-41412

SPIN-LATTICE RELAXATION

Spin-lattice relaxation time dependence on temperature and magnetic field in neutron-irradiated quartz with paramagnetic defects at helium temperature range 01 p0127 A67-10064

Zeeman field spatial orientation of paramagnetic spin-lattice relaxation for 2T2 states in rhombic symmetry, emphasizing application to Fe-doped potassium cobalticyanide and potassium ferricyanide 01 p0129 A67-10150

High resistivity silicon single crystals, discussing carrier lifetime, photoconductivity and recombination levels 02 p0297 A67-11832

Measurement method for spin relaxation and longitudinal decay of optically pumped vapors in weak magnetic fields 02 p0248 A67-12699

Spin-lattice relaxation time of dirty type II superconductor alloys in mixed state in almost upper critical field 03 p0493 A67-13472

Magnetic field gradient relaxation mechanism by random excitation of transitions in F equals 1 level of ground state of hydrogen atoms in maser 05 p0817 A67-16635

Chromium ion concentration and temperature effects on spin-lattice relaxation times in ruby at liquid He temperatures in zero magnetic field 05 p0817 A67-16637

Highly spin polarized carriers for studying neutral impurity scattering in P doped silicon 06 p1063 A67-18937

Spin lattice relaxation times of donor electrons in Si, noting electric field effect on relaxation rate 06 p1068 A67-18971

X-band ruby maser design with liquid hydrogen cooling for high gain at low pumping power 07 p1194 A67-19131

Interrelation between relaxation center in tungsten and molybdenum and high temperature internal friction background of spectrum 07 p1210 A67-20010

Temperature variation of spin-lattice relaxation time and spin-spin relaxation time in superconducting and normal states of vanadium compounds 07 p1236 A67-20139

Transient behavior of three-level paramagnetic maser, discussing rate equations, spin-lattice relaxation, time measurement, etc 11 p1801 A67-24667

Orbach spin lattice relaxation of shallow donors in silicon 13 p2180 A67-27162

Spin-lattice relaxation times in grown ruby in one phonon region, noting temperature dependence and undulation of lattice planes 16 p2728 A67-31054

Resonance absorption and zero-field nuclear spin relaxation in normal and superconducting aluminum, studying phase change 19 p3303 A67-35044

Population inversion and spin-lattice relaxation effect on maser operation 19 p3304 A67-35547

Tl isotopes nuclear magnetic resonance in hexagonal Tl metal showing d-like conduction-electron states at Fermi level by spin-lattice relaxation 24 p4203 A67-42109

SPIN-ORBIT INTERACTION

Complex band structure properties in diamond type crystals, discussing symmetry of various surface states with and without

spin-orbit coupling 01 p0134 A67-10786

Galvanomagnetic effect in ferromagnetic metals, developing theory of planar Hall effect in terms of spin-orbit interaction of electrons 03 p0501 A67-14368

Spin relaxation times of ground state of atomic cesium in aromatic gases measured using optical pumping, noting dependency on temperature 04 p0680 A67-14611

Energy spectrum of semiconductor compounds with chalcopyrite structure analyzed, using perturbation theory, noting changes resulting from crystalline and spin-orbital interactions 05 p0861 A67-16393

Relativistic trajectory and orbital precession of spinning satellite under nonspherically symmetric gravitational field 05 p0906 A67-16849

Thermal excitation and de-excitation of alkali atoms in inert gas heat bath 07 p1265 A67-19075

Room temperature electroluminescence spectra of several materials with Ge, zinc blende and wurtzite structures by electrolyte technique 10 p1691 A67-23401

Spin-projected unrestricted self-consistent field /SCF/ methods for spin density calculations used to determine hyperfine coupling constants 13 p2160 A67-26540

Orbach spin lattice relaxation of shallow donors in silicon 13 p2180 A67-27162

Far IR absorption spectra of chromium and titanium ions in aluminum oxide crystal, indicating Jahn-Teller effect reduction of trigonal field and spin-orbit coupling 14 p2370 A67-28714

Potentials occurring in excitation of highly ionized ions by electron impacts 15 p2520 A67-29527

Absolute reflectance of RbI and KI between 300 and 77 degrees K, noting spin orbit interaction effects and values of dielectric parameters 15 p2520 A67-29768

Valence band structure of wurtzite type crystals 16 p2725 A67-30802

Capture probability at Venus resonant rotation rate implying fluid core similar to earth 18 p3136 A67-34587

Close binary protostellar system formation using model with stellar wind mass loss and primeval magnetic field 22 p3896 A67-40520

SI and S ion oscillator strengths for resonance lines in solar spectrum, discussing spin-spin and spin-other orbit interactions 23 p4067 A67-41235

Exact calculation of indirect exchange interaction isotropic and nonisotropic terms in rare earth metals, with free electron model for conduction band 24 p4203 A67-42110

SPIN REDUCTION

SA DESPINNING

Ekman pumping in solar core noting slow meridional-current distribution in spinning core determined by energy balance 24 p4225 A67-41834

SPIN RESONANCE

SA ELECTRON SPIN RESONANCE

Temperature dependence of La-139 nuclear quadrupole resonance in lanthanum fluoride 01 p0129 A67-10149

Magnetic characteristics of ferromagnetic thin films obtained by ferromagnetic and spin wave resonance techniques 12 p1981 A67-25241

Combined resonance transition in indium antimonide induced by single photon absorption 13 p2178 A67-27083

Resonance rotation of Venus, discussing spin period determinations and retrograde nature of rotation from radar observations 19 p3317 A67-34952

Electromagnetic interactions in hyperfine structure of vibrational and rotational states in rubidium and potassium /isotopes/ fluorides, using electric resonance method 22 p3839 A67-39203

SPIN-SPIN COUPLING

Oscillations in burnt gas coupling to gas dynamical interactions occurring at detonation wave front 03 p0402 A67-13465

Temperature variation of spin-lattice relaxation time and spin-spin relaxation time in superconducting and normal states of vanadium compounds 07 p1236 A67-20139

Ammonia inversion transition hyperfine structure for nitrogen 14 and 15 nuclear masses measured with two-cavity maser spectrometer 20 p3462 A67-37565

Spin-spin coupling constants from perturbation-variation and first order

- perturbed trial function 21 p3658 A67-38003
 assumptions 21 p3658 A67-38003
 Microscopic theory of zero-bias magnetic tunneling anomalies covering weak and strong coupling limits in p-n semiconductors and tunnel junctions 21 p3682 A67-38385
 Quadratic Stark effect in argon II calculated assuming LS coupling 21 p3659 A67-38408
 Si and S ion oscillator strengths for resonance lines in solar spectrum, discussing spin-spin and spin-other orbit interactions 23 p4067 A67-41235
- SPIN STABILIZATION**
 Flexible antenna effect on stability of spin-stabilized satellite in viscous damped oscillator model 02 p0330 A67-11927
 Dynamics of spin-stabilized satellite with nonrigid extendible antennas, noting effects of terrestrial magnetic and gravitational field 02 p0333 A67-12309
 Mathematical technique of midcourse guidance for spin stabilized interplanetary spacecraft, specifically computer simulation for flight to Jupiter 02 p0264 A67-12369
 Rocket probe design for studying physical structure, chemical composition and interaction with sun of Tuttle-Giacobini-Kresak comet 03 p0518 A67-13497
 Synchronous orbit stationkeeping techniques, examining thrust control requirements of spin-stabilized spacecraft 06 p1094 A67-17679
 Simulation of deployment dynamics of spinning spacecraft, discussing test methods emphasizing gravity compensating techniques [AIAA PAPER 67-207] 06 p0980 A67-18325
 Solar radiation field interaction with flexible antenna as possible explanation of anomalous rapid spin decay of satellites [AIAA PAPER 67-39] 06 p1096 A67-18350
 Command laws for DC magnetic attitude control of spin-stabilized earth satellites by means of coil of axis parallel to spin, including effects of orbital eccentricity and magnetic dipole 07 p1257 A67-19361
 Time optimal position and velocity control of spinning vehicle with reaction jet [AAS PAPER 66-115] 07 p1259 A67-19974
 Spin rate effect on stability and transient response of vehicle treated by root locus technique 08 p1405 A67-20507
 Simplified approach to predicting onset of spin-yaw instability of rapidly ascending rolling ballistic missile in absence of asymmetric forces 08 p1406 A67-20509
 Nutation divergence during atmosphere exit of spin stabilized probe shown to be analogous to pendulous gyro with time dependent spring 08 p1406 A67-20511
 Dynamic flight characteristics of spin-stabilized sounding rockets during passage through atmosphere, emphasizing roll resonance and motions leading to roll lock-in and angle of attack 08 p1407 A67-20514
 Passive attitude control using gravity torques, solar torques and spin stabilization 08 p1410 A67-20622
 Aspect system on Pioneer VI and VII incorporates digital computer for accurate time sector division of spin stabilized vehicle 11 p1870 A67-24441
 Missile dynamic behavior analysis using linear aeroballistic theory in conjunction with numerical computations of motion equation 14 p2395 A67-29058
 Military surveillance satellite for high resolution photography noting design, application and projected performance 15 p2564 A67-29400
 Elastic components influence on attitude stability of motion of spinning satellite 16 p2761 A67-30742
 Configuration study for ELDO-PAS test satellite based on communications requirements 17 p2955 A67-32396
 Asteroid belt study with spin-stabilized flyby probes 19 p3322 A67-35317
 Motion equations of spin-stabilized rocket under thrust with jet damping, variable mass and momentum effects and all angular disturbances 19 p3334 A67-35938
 Manual control stationkeeping simulation, studying tether visual rendezvous techniques and fuel economy [AIAA PAPER 67-617] 19 p3337 A67-36006
 Simplified approach to predicting onset of spin-yaw instability of rapidly ascending rolling ballistic missile in absence of asymmetric forces 22 p3904 A67-40103
- Dynamic flight characteristics of spin-stabilized sounding rockets during passage through atmosphere, emphasizing roll resonance and motions leading to roll lock-in and angle of attack 24 p4242 A67-42917
- SPIN TEST**
 Spin effects on rocket nozzle performance show higher combustion pressures and burning rates due to blockage of nozzle throat 02 p0303 A67-11947
- SPIN WAVE**
 Magnon phonon scattering relaxation time as function of temperature and wave vector, calculating thermal conductivity of YIG 05 p0869 A67-17191
 Spectral analysis of interacting electromagnetic, plasma and spin waves in antiferromagnetic semiconductors and metals with easy-axis and plane type anisotropy 09 p1555 A67-22073
 Spin wave theory of thin ferromagnetic films, Curie temperature decreases monotonically with decreasing film thickness spin wave theory of thin ferromagnetic films analyzed, showing Curie temperature decreases 12 p1981 A67-25239
 Spin wave interaction in YIG with acoustic, magnetoplastic and relaxation oscillations excited by laser and microwave 12 p1953 A67-25749
 Simple metal spin-density-wave state analyzed using electron-electron exchange interaction 12 p1985 A67-25849
 Frequency selective parametric limiting by parallel pumping of subharmonic magnetoelastic waves in YIG 13 p2077 A67-26523
 Spin waves in two-band ferromagnetic metal assuming electron interaction via Coulomb potential 13 p2178 A67-27138
 Transient growth of magnetostatic modes in yttrium garnet subject to pulsed longitudinal pumping 16 p2732 A67-31704
 Associated nonuniform electron-nucleus oscillations in ferromagnetic substances studied to determine feasibility of maser, using magnetic-reversal nuclear magnetic resonance 16 p2686 A67-31731
 Optical exciton-magnon absorption in manganese fluoride, experimental results and theory of interactions 17 p2926 A67-33382
 Spinning detonation, deflagration instability and normal detonation characteristics 19 p3346 A67-35574
 Data and theories on stationary spin waves in ferromagnetic thin layers, considering modes, dispersion law and spectra interpretation 20 p3507 A67-36318
 Spin-density waves effect on electronic properties and Fermi surface of antiferromagnetic metals 21 p3676 A67-37817
- SPINAL CORD**
 Terminal connections of spinothalamic and distribution in human thalamus, noting pain relay question 06 p0953 A67-18775
 Aminosine injection and electrolysis effects on formative reticularis of animals after exposure to hypoxia 20 p3367 A67-36255
 Gamma irradiation effect on spinal cord timed differently, considering time factor in reactions of nervous system in guinea pigs 23 p3943 A67-40767
 Guinea pigs exposed to vibrations alternating with intermittent gamma radiation studied for effects on spinal cord activity, noting reflex response depression and paralytic stimulations 23 p3943 A67-40768
- SPINE**
 Identification and localization of center median nucleus of Luys, noting CM projects primarily upon putamen 08 p1288 A67-21356
- SPINEL**
 Relation between changes in ferrite lattice parameter at magnetic conversion temperature and changes in ferrite metal ion charges due to electron exchange 18 p3095 A67-33444
- SPINNING RECOVERY**
 Spin characteristic of fighter type aircraft investigated by using Kerr criteria, noting yawing velocity and recovery 09 p1439 A67-21836
 Fast and slow oscillatory spinning of aircraft, examining equations of motion by approximate methods based on Brodetsky analysis 22 p3744 A67-39197
- SPIRAL**
 Thermal distortion due to viscous heating in fluid film effects on load capacity of spiral-grooved gas-lubricated thrust-bearing [ASME PAPER 66-LUB-10] 03 p0432 A67-13765
 Conservative fields of force admitting spiral trajectories and dependence on constancy of energy level 16 p2748 A67-31137
- SPIRAL ANTENNA**
 Ultrashort antenna with conical spiral, noting effect of negative reactance component of impedance [ONERA-TP-373] 01 p0039 A67-10948
 Electromagnetic excitation by vertical magnetic dipole located above spiral anisotropic plane 04 p0586 A67-15672
 Boundary value solutions for current density and radiation patterns in spiral excited sheath antennas in terms of Hankel function 09 p1482 A67-22696
 Calculation of dimensions of effective radiation regions for conical spiral antennas 13 p2080 A67-27030
 Short conical spiral antennas for trajectory plotting of small nose cones 14 p2279 A67-27900
- SPIRAL BAND**
 Membrane stress state of spiral coiled tube surface, reducing stress components to second order differential equation 22 p3913 A67-40009
- SPIRAL GALAXY**
 Upper limit to neutral atomic hydrogen density in halo regions of spiral galaxies 04 p0694 A67-14480
 Principal mechanism of galactic structure based on stellar dynamics principles, discussing spiral pattern in presence of rotation and mathematical theory 08 p1379 A67-20353
 LF galactic emissions, noting spiral arms and spherical halo on galactic hub, signal strength variation and terrestrial atmosphere role 08 p1385 A67-20866
 Spiral and irregular galaxies total mass to neutral hydrogen mass ratio derived from mass-luminosity relations 11 p1858 A67-23995
 Stellar dynamics and galactic spiral structure analyzed using gas and plasma dynamics 11 p1863 A67-24534
 Polarization of extragalactic radiation sources and evidence of irregularities of magnetic field in our Galaxy 13 p2198 A67-26791
 Association of radio sources with peculiar galaxies in symmetrically distributed pairs 14 p2388 A67-28830
 Unified theory for galaxy spiral formation and radio galaxy and quasar evolutionary dynamics, discussing galactic dipole magnetic field generation 22 p3893 A67-40504
 Galactic rotation effects on gaseous spiral arm stability for magnetic critical wavelength less than Jeans critical wavelength case 22 p3893 A67-40506
 Spiral field rotation with motion integrals as distribution function arguments, discussing potential, density and spiral arm stability 22 p3893 A67-40507
 Jacobi high energy ellipsoid orbits in barred spirals valid at galactic time scales 23 p4063 A67-40898
 Microwave background in steady state universe explained by starlight absorption and microwave reemission by interstellar dust, discussing young spiral galaxies 24 p4226 A67-41875
- SPLEEN**
- S BLOOD**
- SPLINE FUNCTION**
 Interpolation between given data points by using spline functions 09 p1468 A67-22048
 Variation diminishing spline approximation method of linear interpolation 13 p2147 A67-27468
 Smoothing experimental values of function based on choice of regularity and repeatability criteria, noting infinite number values, derivatives, spline functions, etc [ONERA-TP-463] 18 p3072 A67-34460
 Spline friction effect on multiple disk brake and clutch packs, including torque and load variation and pressure distribution equations [ASME PAPER 67-LUB-26] 24 p4164 A67-42684
- SPOILER**
 S Q-SPOILING
 S WING SPOILER
SPOILER-SLOT AILERON
 Spoilers for aircraft steering, discussing wind tunnel tests, banking moment and spoiler-slot aileron 22 p3739 A67-39535

SPONTANEOUS EMISSION

Spontaneous emission spectra and ratio of number of photons in various oscillation modes of laser with nonlinear filter type lock 02 p0251 A67-11573
 Luminescent intensity and spectral energy distribution determined for exciton luminescence of anthracene crystals for spontaneous and stimulated emission 03 p0436 A67-13136

Spontaneous emission in inversely populated medium examined for uniform ruby rod laser with uniform pumping distribution 03 p0438 A67-14186
 Raman laser physics covering gain formula, stimulated and spontaneous scattering and cavities 12 p1953 A67-26124

SPONTANEOUS IGNITION TEMPERATURE

Free radicals in gas phase oxidation and spontaneous ignition 02 p0341 A67-11502

Effect of diffusion-pump fluid contamination and degradation on explosion hazard of operating diffusion pumped system 06 p0979 A67-17632

Fire resistance of aircraft fluids, analyzing likelihood of spontaneous ignition by flashpoint and isothermal enclosure methods 09 p1521 A67-22247

Ignition of flammable fluids by hot surfaces tested on static hot plate rig and on wind tunnel rig, noting data on kerosene, lubricating oil and hydraulic fluid 09 p1580 A67-22248

Spontaneous ignition temperature of flammable fluid in facsimile high speed aircraft hydraulic system 09 p1521 A67-22249

Self-ignition and fuel combustion at blade cascade taking place at velocities and temperatures comparable to those of gas turbines 13 p2187 A67-26746

Factors influencing rocket ignition pressures and conditions leading to large ignition overpressures, estimating residual propellant in rocket combustor [AIAA PAPER 67-515] 18 p3114 A67-33978

Spontaneous inflammability temperatures of Al, Mg and Al-Mg alloy powders measured noting moisture effect 22 p3919 A67-40325

SPORADIC E LAYER

Statistical properties of echoes from meteoric trails during forward scattering, determining diurnal variations for number, duration and fill factor of reflected signals 01 p0025 A67-10791

Diurnal variations of boundary frequencies of sporadic c-type E layer, deriving cosine law not dependent on sunspot cycle 01 p0061 A67-11289

Existence of anomalously close radio reflections from sporadic ionization zone linked with polar aurora 02 p0193 A67-11674

Relation of sporadic E layer to magnetic fluxes based on observations of diurnal variations 02 p0237 A67-11675

Properties of equatorial sporadic E layer irregularities studied by HF observation, including scattering spectrum and diffraction pattern formed by reflection from ground 03 p0406 A67-12823

Fading characteristics of radio waves reflected from sporadic E layer of ionosphere over magnetic equator 03 p0406 A67-12824

Electron number density profile measurements of moderate and heavy sporadic E over Arecibo by incoherent backscatter technique 03 p0409 A67-12946

Magnetometer predictions of geomagnetic disturbances and intense sporadic E layer occurrences at various sunspot cycle times in auroral zone and effects on VHF absorption 03 p0415 A67-14118

Diurnal variation of sporadic E at high latitude as function of geomagnetic activity 04 p0615 A67-14972

Sporadic E layer behavior noting seasonal variations and duration 04 p0616 A67-15223

Ionospheric sporadic E layer propagation characteristics and signal strength calculation, noting decrease in antenna gain when using highly directional antennas 04 p0576 A67-15503

Radio Aurora and formation mechanism of ionospheric D and F regions, examining HF and VLF propagation via computer ray tracing, ionospheric storms and equatorial sporadic E layers 05 p0795 A67-16010

Sporadic E layer stratification and morphology of M and N reflections produced

by transparent and semitransparent E layer 05 p0799 A67-17029

Diurnal and short period h sporadic E layer and critical frequency sporadic E layer variations analyzed from data obtained at Ashkhabad station 05 p0800 A67-17129

Ionospheric electron density profiles determined by impedance probe and Doppler effect probe aboard rockets 06 p0993 A67-17595

Fast regular scintillation of VHF signals received from earth satellites distinguished from scintillation associated with irregular ionospheric diffracting phase screen, showing correlation with sporadic E layer 07 p1141 A67-19416

Sporadic E ionization and anomalous increase in rate of radar meteor counts during 1963 in mid-latitude European stations 07 p1172 A67-19424

Effects of technical parameters of station on results of observations of sporadic E layer, noting that frequencies depend weakly on receiver and transmitter 07 p1173 A67-19689

Parametric analysis of stability of reflection from sporadic E layer during 11-year solar cycle 07 p1174 A67-19704

Diurnal and seasonal variations of sporadic layer in auroral zone 07 p1178 A67-19823

Formation mechanism of ionospheric narrow sporadic E layers by high energy electron fluxes captured by geomagnetic field 07 p1179 A67-19835

Geomagnetic field variations in temperate zone sporadic E layer according to wind-shear theory 07 p1179 A67-19849

Electron and ion temperature changes in sporadic E layer based on wind shear theory, using energy equation 08 p1327 A67-21366

Seasonal observations of nocturnal ionospheric absorption, noting connection with structural state of sporadic E layer 09 p1491 A67-21930

Sporadic E layer in middle latitude by method of forward ultrashort wave scattering 10 p1630 A67-22792

Tidal force effect on variations of critical frequencies of sporadic E layer 10 p1631 A67-22806

Ionization density as decisive factor in integral radio wave absorption increase accompanying increase in critical sporadic E layer frequency 10 p1631 A67-22807

Intense diurnal activity in sporadic E layer interpreted as effect of Omicron-Cetid meteoric stream 10 p1633 A67-22896

Ionospheric electron content calculated from beacon satellite data on Faraday rotation 10 p1641 A67-23235

Ionospheric drift velocities observed by spaced receiver method compared with neutral winds from luminous rocket trails 10 p1643 A67-23252

High incidence and erraticism of sporadic E occurrence in temperate zones where horizontal component of geomagnetic field is greatest attributed to horizontal wind shear 10 p1644 A67-23255

Neutral wind structure and time variation over height in lower thermosphere observed using gun-launched trails, noting relation to sporadic E layer 10 p1644 A67-23257

Wind shear theory of formation of temperate zone blanketing sporadic E layers, noting motion equation for ions in ionospheric E region 10 p1644 A67-23258

Neutral wind structure effects on ionospheric sporadic E layer variations, noting daytime evolution, nighttime characteristics and electron density profiles 11 p1783 A67-23924

Aerobee rocket sounding of ionospheric sporadic E layer, noting abundance of metallic ions in layer and NO above and below 11 p1784 A67-23926

Ionospheric radio wave absorption, noting inverse correlation between solar activity with stability of reflections from sporadic E layer 12 p1933 A67-25544

Solar activity dependence of sporadic E layer, noting cyclic variation in 1964 12 p1933 A67-25545

Sporadic E backscatter noting two peaks in activity, motion, temporal component parameters and cause 13 p2107 A67-26306

Relation between diurnal, seasonal and cyclic variations of stratifications in E layer and fine structure of sporadic E layer and

E-2 layer 13 p2110 A67-26550

Diurnal variations in sporadic E layer parameters during solar cycle based on Moscow observations 13 p2111 A67-26570

Sporadic E layer generated by meteoritic ionization noting critical frequency 13 p2111 A67-26601

Sporadic E layer formation and possible creation of more favorable conditions by high meteor activity 13 p2201 A67-27391

Limiting frequencies median values suggested as suitable characteristics of relation between solar activity and sporadic E layer behavior 14 p2307 A67-27913

Absorption intensity in ionospheric sporadic E layer 14 p2308 A67-27935

Sporadic E layer scintillation effects on amplitude of 137 MHz radio waves from Early Bird 14 p2270 A67-28577

Diurnal and seasonal variations in occurrence probability of screening and semitransparent types of sporadic E layer 15 p2474 A67-29387

Occurrence frequency of midlatitude blanketing sporadic E studied for seasonal, diurnal and latitudinal variations 15 p2476 A67-29622

Nightglow measurements noting intensity relation to spread-F and sporadic E [AGARDOGRAPH 95] 15 p2485 A67-30308

Existence of anomalously close radio reflections from sporadic ionization zone linked with polar aurora 16 p2624 A67-31089

Relation of sporadic E layer to magnetic fluxes based on observations of diurnal variations 16 p2665 A67-31090

Diurnal variations asymmetry in critical frequency ratio of E layer for morning and evening values 16 p2668 A67-31895

Relationship between variations of critical frequencies of sporadic E layer and solar activity cycle 16 p2669 A67-31903

Semitransparency range of sporadic E layer as solar radiation function, noting diurnal and seasonal variations 16 p2669 A67-31904

Sporadic E layer shows small negative relation to magnetic disturbances from 1958 to 1963 16 p2669 A67-31905

Coefficient characterizing stability of continuous radio signal reflections declining occurrence probability from sporadic ionospheric layer 16 p2669 A67-31907

Ionization in E region due to influx of micrometeorites 17 p2943 A67-32542

Geomagnetic activity effect correlation with sporadic E occurrence in African zone, showing longitude dependence 17 p2844 A67-32546

Anomalous magnetic field charts for heights in ionosphere useful for studying auroras spatial distribution and sporadic E layer distribution 17 p2847 A67-32948

Time constants of sporadic E layer formation influenced by wind field containing strong vertical gradients 20 p3428 A67-36375

Screening frequency dependence on reflection cut-off frequency in sporadic E layer 20 p3428 A67-36762

Irregular pulsations of diminishing periods /IPDP/, discussing cause and low energy electron flux variations 20 p3431 A67-37097

Diurnal and short period h sporadic E layer and critical frequency sporadic E layer variations analyzed from data obtained at Ashkhabad station 21 p3618 A67-38472

Seasonal and long term variations in duration of continuous radio signal reflections from sporadic E layer 21 p3623 A67-39038

Duration of continuous occurrence of sporadic E layer dependence on incidence of sporadic E layer critical frequency maximum value 21 p3623 A67-39039

Meteor activity radar observations and simultaneous ionosphere probe to establish relation between sporadic E layer ionization and sporadic meteors 21 p3623 A67-39040

Field-aligned irregularity instabilities in ionization vertical gradient, showing unstable E region for irregularities of scale size 20 m-6 km 22 p3789 A67-39475

Sporadic E blanketing frequencies during November 1965 as indicator of wind structure in lower ionosphere and meteor influx 23 p3995 A67-40806

Sporadic E layer in middle latitude by method of forward ultrashort wave scattering 24 p4149 A67-42128

Tidal force effect on variations of critical

frequencies of sporadic E layer 24 p4150 A67-42143

Ionization density as decisive factor in integral radio wave absorption increase accompanying increase in critical sporadic E layer frequency 24 p4150 A67-42144

SPORADIC METEOR

Goniometric measurements of two angles defining direction of incoming 30 MHz wave reflected by meteor streams, using radio link 14 p2390 A67-28900

Meteor activity radar observations and simultaneous ionosphere probe to establish relation between sporadic E layer ionization and sporadic meteors 21 p3623 A67-39040

SPORE

Sporulation mutations induced by heat in *Bacillus subtilis* 08 p1287 A67-20983

SPOROCIDAL COMPOUND

Antimicrobial properties for various spacecraft materials, discussing impregnation methods for bactericides and two-stage sterilization 19 p3179 A67-35229

SPOT WELDING

SA ARC WELDING

Nondestructive test development to meet inspection requirements of advanced aircraft design, discussing titanium fusion and resistance spot welds and adhesive bonding honeycomb components 05 p0808 A67-17087

Antonov An-24V Soviet high wing monoplane and use of electrical spot welding and metal bonding in construction 06 p0944 A67-17597

Resistance spot-welded adhesive bonds between aluminum alloy components, using thermosetting film 09 p1502 A67-21688

Weldability of titanium alloy sheets, noting quality through spot welding 09 p1520 A67-22621

Ultrasonic spot welding of dissimilar metals, discussing bond mechanisms and threshold curves relating clamping force, power level and weld strength 12 p1950 A67-25737

Aluminum welding techniques, evaluating various filler alloys and forms for welding ease and efficiency 14 p2323 A67-27819

Properties of adhesive bonding compared with spot welding and riveting in aircraft industry 19 p3236 A67-35821

Resistance spot welding process, using heating, cooling and stress development data to compute internal behavior 20 p3456 A67-37697

SPRAY

S DROP

S PROPELLANT SPRAY

SPRAYED PROTECTIVE COATING

Spray and brush repair of zinc oxide-potassium silicate spacecraft thermal control paint, describing tests, surface preparation and coating application 22 p3826 A67-40111

SPRAYING

S FLAME SPRAYING

S PLASMA ARC METAL SPRAYING

SPRAYING APPARATUS

Monodisperse sprays production technique using Rayleigh criterion for breakup of capillary jets by mechanically vibrating uniform size capillary needles arranged in parallel 12 p1946 A67-25983

Plasma spray gun as possible method of applying resin, ceramic and metallic bonded solid film lubricants [ASLE PREPRINT 67AM 7A-4] 14 p2326 A67-28792

Automatic apparatus for flooding or spraying test specimens with liquid corrosive media according to predetermined program 21 p3715 A67-37827

SPREAD-F

Spread-F occurrence dependency on F layer height variations with time, season and longitude and plasma wave generation near geomagnetic equator 03 p0415 A67-14115

Equatorial spread-F and tropical disturbances, supplying data on typhoon, geomagnetic activity and atmospheric pressure waves 04 p0612 A67-14653

Diffusion reflections during cycle of solar activity, showing frequency changes according to increase in solar activity 05 p0800 A67-17127

Spread-F effects on WWV transequatorial propagation of HF radio waves 06 p0964 A67-18575

Spread-F and effects upon radiowave propagation and communication - NATO/AGARD Conference, Copenhagen,

August 1964 [AGARDOGRAPH 95] 15 p2479 A67-30273

Observation methods, mechanisms, geomorphology, time variations and associated effects of equatorial type spread-F [AGARDOGRAPH 95] 15 p2480 A67-30274

Time and space study of onset and early development of single occurrence of spread-F in equatorial region [AGARDOGRAPH 95] 15 p2480 A67-30275

Satellite topside sounder investigation of spread echoes at mid and high latitudes in Northern Hemisphere [AGARDOGRAPH 95] 15 p2480 A67-30276

Field aligned structure of ionization associated with boundaries of spread-F at middle latitudes studied by combining topside and fast-sweeping ground-based ionograms [AGARDOGRAPH 95] 15 p2480 A67-30277

Angular spread of backscattered spread-F echoes compared with that associated with normal F region returns [AGARDOGRAPH 95] 15 p2480 A67-30278

Influence of spread-F upon apparent reflection coefficients of F region for HF radio waves [AGARDOGRAPH 95] 15 p2481 A67-30279

Data analysis from oblique incidence soundings during spread-F conditions [AGARDOGRAPH 95] 15 p2481 A67-30280

Diurnal, annual, latitudinal and sunspot cycle-influenced variations of spread-F intensity at very high latitudes [AGARDOGRAPH 95] 15 p2481 A67-30281

Diurnal, seasonal and geographic variations of frequency of spread-F occurrence over Antarctica [AGARDOGRAPH 95] 15 p2481 A67-30282

Partial correlation coefficients between ionospheric, solar and geomagnetic parameters and spread-F occurrence probability [AGARDOGRAPH 95] 15 p2481 A67-30283

Statistical analysis of spread-F and scintillation data in middle latitude noting diurnal and seasonal variations [AGARDOGRAPH 95] 15 p2481 A67-30284

Broadband radio star Cassiopeia A scintillations observed with swept frequency interferometer [AGARDOGRAPH 95] 15 p2563 A67-30288

Radio star Cassiopeia A scintillations and spread-F in auroral zone [AGARDOGRAPH 95] 15 p2482 A67-30289

F scatter, flutter fading and maximum usable frequency phenomenology from HF radio propagation studies near equator 15 p2438 A67-30297

Properties of irregularities responsible for spread-F, discussing hydromagnetic waves [AGARDOGRAPH 95] 15 p2484 A67-30303

Field-aligned irregularities caused by low energy charged particles penetrating to F layer heights [AGARDOGRAPH 95] 15 p2484 A67-30304

Spread-F occurrence studied using hourly soundings near magnetic equator [AGARDOGRAPH 95] 15 p2484 A67-30307

Nightglow measurements noting intensity relation to spread-F and sporadic E [AGARDOGRAPH 95] 15 p2485 A67-30308

Topside ionosphere irregularity studied by Alouette I ionograms and ground based ionosonde records, noting spread-f occurrence topside ionosphere irregularity studied by Alouette I ionograms and ground based ionosonde 16 p2667 A67-31515

Diffusion reflections during cycle of solar activity showing frequency changes according to increase in solar activity 21 p3618 A67-38470

Spread ionization in topside of ionosphere from satellite observations 24 p4148 A67-42060

SPREAD REFLECTION

Distribution of photons from point image in photographic emulsion calculated using diffusion equation, deriving limits on point spread functions and corresponding modulation transfer functions 09 p1496 A67-21708

Hologram reconstruction of objects in fog-like medium 20 p3450 A67-37027

SPRING

Amplitudes of two-mass single-spring system, using Rayleigh approach to determination of eigenfrequencies 01 p0159 A67-10282

Spring theory of ball bearing supporting

rotor and role in vibration analysis of system 02 p0248 A67-11468

Rational approximation of generalized Duffing equation, damped mass spring oscillator equation and generalized second order Riccati equation 04 p0647 A67-15660

Relaxation, creep and modulus of rigidity lowering in compression springs under high temperature 11 p1795 A67-24090

Liquid spring design characteristics noting fluid characteristics, precharge fluid pressure, friction, efficiency, gland configuration and application requirements 15 p2494 A67-30097

Cup spring designing method, with generatrix curvature included in approximation, gives better characteristic curve and stresses 18 p3144 A67-34262

SPUR

S SPACE POWER UNIT REACTOR /SPUR/

SPUTNIK III SATELLITE

Sputnik III data application to plotting of total magnetic field intensity chart above U.S.S.R., using spherical harmonic analysis 12 p1933 A67-25652

SPUTTERING

Silicon-tantalum oxide system prepared by reactive sputtering, noting characteristics of MOS diode of system 01 p0137 A67-11071

Deposition conditions effect upon growth and structure of evaporated and sputtered films and significance in relation to electrical, magnetic and mechanical behavior 02 p0285 A67-11703

High specific impulse thrust by sputter ejection of atoms from single crystals following ion bombardment, useful in space propulsion 02 p0308 A67-12716

Figure contact resistance between Al and Cr sputtered conductive and resistive films 03 p0491 A67-13248

Thin film deposition techniques, presenting vacuum evaporation and sputtering 04 p0631 A67-15992

RF sputtering of insulators noting deposition rate, film properties, etc 04 p0631 A67-15993

Sputtered film deposition processes, investigating low pressure sputtered germanium films 04 p0631 A67-15995

Basic diode and triode sputtering processes, describing channelled diode system and sheet beam 04 p0631 A67-15996

Thrust generation from neutral particle, sputtering from solid target, noting advantages such as storage, operating life, etc 05 p0873 A67-16515

Sputtering yields of aluminum, copper and titanium measured as function of cesium ion energies for use as electrodes on cesium ion engines [AIAA PAPER 66-203] 05 p0871 A67-17349

Radioactive tracer technique for measurement of yield and angular distribution of molybdenum sputtered by cesium ion beam 06 p1036 A67-18139

Device for controlling thickness of thin films prepared by sputtering in vacuum 06 p1003 A67-18195

Mass spectrometric investigation of composition of negative ion sputtering products of solid metal surfaces under cesium ion bombardment 06 p1036 A67-18425

Nature of forces causing adhesion of coatings produced by plasma jet sputtering techniques 07 p1190 A67-19304

Tungsten films with fcc structure obtained by ion beam sputtering in vacuum onto substrates of glass, rock salt and mica at various temperatures 07 p1232 A67-19557

Evaluation of requirements for ground testing of electric propulsion devices in vacuum, noting effects of sputtering phenomena 09 p1559 A67-22120

Cathode sputtering thin film preparation at low pressure, describing duoplasmatron and sputron ion sources 10 p1661 A67-23693

Mass spectrometry of background gases composition during sputtering of tantalum films in argon glow discharges 13 p2178 A67-27078

Molecular beam apparatus for measuring collision cross section and velocity distribution of sputtered particles 14 p2316 A67-28191

Thin films as passive and active electrical components in microminiaturization, noting characteristics obtained by vacuum evaporation, cathode sputtering, diffusion

and epitaxial growth 15 p2447 A67-29684
Yield and angular distribution of cesium ion-sputtered copper, noting dependence on angle of incidence, target temperature and energy 16 p2728 A67-31056
Thin-film and diffused passive component comparison, describing resistor and capacitor fabrication by using sputtered tantalum and indichrome through 16 p2640 A67-31528
Semiconductor-metal potential barriers for semiconductor devices obtained by silicon dioxide and silicon local sputtering in argon discharge 17 p2916 A67-32809
Single gallium arsenide crystals sputtered by normally incident low energy argon ions in mass spectrometer source 18 p3106 A67-34639
Sputtered films stable f₂ modification of several metals deposited at high temperatures, obtaining normal structures over 400 degrees C 21 p3677 A67-38091
Thin film integrated circuits, considering vacuum deposition and cathode sputtering 21 p3597 A67-38496
Evaporation of Saturn ice rings by UV and solar wind sputtering or by photospattering in IR and proton bombardment 21 p3705 A67-38599
Sputtering yields and energy-transfer efficiency measurements by ion beam sputtering of liquid metals indicate no justification for incorporation into low thruster [AIAA PAPER 67-683] 21 p3692 A67-38714

STABILITY
SA ACOUSTIC STABILITY
SA AERODYNAMIC STABILITY
SA AIRCRAFT STABILITY
SA BOUNDARY LAYER STABILITY
SA COMBUSTION STABILITY
SA CONTROL STABILITY
SA CONTROLLED STABILITY
SA DIMENSIONAL STABILITY
SA DIRECTIONAL STABILITY
SA DYNAMIC STABILITY
SA ELASTIC STABILITY
SA FLAME STABILITY
SA FLIGHT STABILITY TEST
SA FLOW STABILITY
SA FLYING PLATFORM STABILITY
SA FREQUENCY STABILITY
SA GUIDANCE STABILITY
SA GYROSCOPIC STABILITY
SA HOVERING STABILITY
SA HYDRODYNAMIC STABILITY
SA INSTABILITY
SA INTERFACE STABILITY
SA LATERAL STABILITY
SA LEONHARD STABILITY
SA LONGITUDINAL STABILITY
SA LOW SPEED STABILITY
SA MAGNETOHYDRODYNAMIC STABILITY
SA MOTION STABILITY
SA PLASMA STABILITY
SA ROTARY STABILITY
SA SHELL STABILITY
SA SPACECRAFT STABILITY
SA STABLE OSCILLATION
SA STATIC STABILITY
SA STORAGE STABILITY
SA STRUCTURAL STABILITY
SA SURFACE STABILITY
SA THERMOSTABILITY
Matrix analysis of resonant vibration stability conditions 01 p0113 A67-10675
Stability of solutions to general equations of steady state one-dimensional relaxed flow of perfect gas mixtures [ONERA-TP-360] 01 p0054 A67-11089
Necessary conditions for stability of trivial solutions of parabolic systems of partial differential equations 03 p0456 A67-12861
Stability analysis of spectrotron with external feedback based on time delay, inertia of nonlinear quadrupole and circuit phase shifts 03 p0377 A67-13092
Restriction and stability in solutions of difference equations 03 p0457 A67-13113
Quasi-rotational oscillatory solution to equation system with arbitrary degree of freedom with respect to parameter in given region 03 p0468 A67-13338
Conditions of existence of unbounded solution to unforced second order differential equation, considering global asymptotic stability 03 p0460 A67-13822
Tunnel diode circuit stability, equivalent circuit and conductivity hodograph 03 p0386 A67-13965

Finite difference method solution of diffusion equations, including analyses of stability and truncation errors 03 p0537 A67-14013
Periodic solutions for nonautonomous differential equations, discussing existence and stability criteria 04 p0644 A67-14853
Book on numerical realization of variational methods, discussing Hilbert space elements, Ritz and Bubnov-Galerkin stability processes, spectral and nonlinear problems, etc 04 p0645 A67-15009
Implicit difference methods for initial boundary value problems based on Wiener-Hopf factorization 04 p0645 A67-15085
Instability of amplification factor and stability of transmission coefficient of multistage transistorized amplifier without feedback 05 p0772 A67-16454
Stability of state of semiconductors with absolute negative conductivity 05 p0868 A67-17059
Inequalities for difference and pseudodifferential operators, providing sharp form of Garding inequality 06 p1025 A67-18642
Stability analysis of parametric phase-locked subharmonic tunnel diode oscillator circuits capable of bistable phase operation 07 p1153 A67-19610
Topological analysis of local stability and instability of nonlinear periodic RLC network based on Liapunov theorems 08 p1308 A67-20320
Stability of fourth order Runge-Kutta method for solving differential equation 08 p1349 A67-21259
Existence and uniqueness theorem for functional equation of optimal control problems, noting stability of solution 09 p1524 A67-21874
Stability of almost stationary periodic solution of Navier-Stokes equation, examining spectrum of relevant stationary problem 10 p1675 A67-23677
Periodic solutions for nonautonomous differential equations, discussing existence and stability criteria 11 p1813 A67-24730
Stability of points of equilibrium in restricted problem as influenced by perturbations of Coriolis force 11 p1866 A67-24773
Interpretation of results obtained by Liapunov method, using parallelepiped imbedded in region of asymptotic stability 12 p1919 A67-25912
Stability of discontinuous solutions of gas dynamic equations noting doubtful case with imaginary eigenvalues 13 p2093 A67-26379
Stability and asymptotic stability conditions for coefficients of system of linear first order differential equations 13 p2144 A67-26443
Stability of state of semiconductors with absolute negative conductivity 15 p2538 A67-29790
Stochastic Liapunov function existence demonstrated for continuous strong Markov process with certain stochastic stability properties 15 p2458 A67-29898
Stability of almost stationary periodic solution of Navier-Stokes equation, examining spectrum of relevant stationary problem 21 p3653 A67-38278

STABILITY AND CONTROL

SA LATERAL STABILITY AND CONTROL
SA LONGITUDINAL STABILITY AND CONTROL
SA STATIC STABILITY AND CONTROL
Stability theory application to control, circuit theory and aerospace systems 01 p0047 A67-11221
Real time digital simulation of stabilization and control systems /SCS/ for manned spacecraft noting transport delays, thruster duration, etc 02 p0228 A67-11788
Autopilot programmer design for automatic guidance in approach and stabilization along course of aerial photography aircraft 03 p0465 A67-14284
Time constant and control channel lag effects on size and configuration of platform stability region 04 p0552 A67-15883
Attitude stability of spinning rigid symmetric satellite in elliptic orbit examined for motion about equilibrium position with spin axis normal to orbit plane [AIAA PAPER 67-124] 06 p1095 A67-18312
Lift curve slope and aerodynamic center

for variable sweep wing configurations estimated using semiempirical technique [AIAA PAPER 67-135] 06 p0939 A67-18315
General lateral stability and control equations for steep gradient aircraft in terms of equivalent aircraft in level flight without inertial cross coupling 06 p0949 A67-18597
Book on flight characteristics, static stability, equations of motion, excitation and response 06 p0949 A67-18725
Advanced low thrust propulsion systems and propellants evaluation for stationkeeping and stability control of NASA Manned Orbital Research Laboratory [AIAA PAPER 66-226] 07 p1240 A67-19365
Azimuth stabilization of balloons, using frictionless bearing to decouple gondola 07 p1191 A67-19403
Feedback control system to position satellite in vicinity of unstable collinear libration point with application to lunar communication problem [AAS PAPER 66-132] 07 p1146 A67-19991
Aerodynamics of sounding rockets, discussing stabilization by fins, conical flares, etc [ONERA-TP-441] 08 p1275 A67-20498
Stabilized Skylark rocket using N-gas jet system, solar sensors and magnetometer to obtain three-axis control 08 p1408 A67-20537
Angular stabilization of flight vehicle by introduction of cubic terms of variable parameters into control law 10 p1678 A67-23319
Automatic flight control development for general aviation, discussing fluidics, electropneumatic servoactuator and microelectronics [SAE PAPER 670255] 12 p1895 A67-25505
Flutter characteristics of slab tail or stabilator installation, discussing prevention and design [SAE PAPER 670260] 12 p1895 A67-25509
Time optimal control of bounded phase coordinate process applied to unstable booster with actuator position and rate limits 12 p2012 A67-25911
Inertial navigation system with damping of oscillations for enhancement of stability of stationary platform 13 p2118 A67-26375
Feedback control system to position satellite in vicinity of unstable collinear libration point applied to lunar communication problem [AAS PAPER 66-132] 13 p2210 A67-27543
Three-step nonlinear analysis procedure for nonlinear stability for position-control servomechanical system applications 15 p2459 A67-30143
Gradient stabilization of cryogenic liquids in pendulum and sloshing motions, noting response to kinetic energy input, oscillation frequency period and stability criteria 17 p2836 A67-32053
Stability analysis of deformable space vehicle in torque free state noting gravitational effect, stability of spin motion, characteristic motion equations, etc 17 p2956 A67-32779
Attitude stability of spinning rigid symmetric satellite in elliptic orbit examined for motion about equilibrium position with spin axis normal to orbit plane 19 p3333 A67-35747
Criteria for determination of minimum usable approach speed for landing of carrier based aircraft [AIAA PAPER 67-578] 19 p3175 A67-35973
Aircraft performance, stability and control characteristics in nonsteady flight with high accuracy instrumentation system 20 p3442 A67-36466
Laser frequency control system using two optical discriminators for long and short term stability 20 p3459 A67-36519
Hydraulic support system for free flight simulation with Saturn V-Apollo vehicle, discussing stability requirements, upper bounds of system design, conversion from nonlinear to linear model, etc 21 p3807 A67-37796
Hydraulic servodrive with supply source, control valve, actuator and feedback components analyzed for stability, deriving motion equations 21 p3570 A67-38048
Triaxial attitude control stabilization for second-generation /TIROS/ meteorological satellite 22 p3897 A67-39156
Luna IX automatic station flight control complex, detailing communication,

- orientation and stabilization systems
operation after separation from acceleration
module 22 p3897 A67-39167
- Gyro power stabilizer in unsteady
equilibrium state becoming stable under dry
friction defined for controllability in phase
space 24 p4155 A67-42299
- Stabilization and control techniques for
future unmanned commercial space vehicles,
emphasizing application of projected
technological advances in instrumentation
[AIAA PAPER 67-878] 24 p4244 A67-42997
- STABILITY AUGMENTATION**
- Gust Alleviation and Structural Dynamic
Stability Augmentation System /GASDSAS/
design analysis 02 p0183 A67-12303
- [AIAA PAPER 66-999] 02 p0183 A67-12303
- Flywheel-augmented gravity gradient
stabilization /FLAGGS/ 02 p0333 A67-12312
- XC-142A flight control and stability
augmentation systems 17 p2794 A67-31996
- Degradation, training and instability in
superconducting coils, protection of windings
and related problems of superconducting
magnets for use in MHD
generators 18 p3099 A67-33711
- Digital program for stability-augmentation
system-gain values yielding desired pole-zero
locations for vehicle transfer functions of
flight conditions 21 p3568 A67-38539
- Lateral stability augmentation of
supersonic aircraft using linear multichannel
state-vector optimal feedback
control 22 p3746 A67-40155
- STABILITY DERIVATIVE**
- Dynamic stability tests of aircraft mockups
in transonic and supersonic flows, using
free-oscillation method
[ONERA-TP-390] 01 p0011 A67-11093
- Ljapunov method application to adaptive
loop redesign, using differential equations
for model system errors coupled with
squares of parameter
differences 01 p0045 A67-11202
- Slender body theory application in
obtaining aerodynamic stability derivatives
for reentry vehicles via electrical
analogy 03 p0354 A67-12918
- Influence on stability of masses which are
in relative motion with respect to projectile
determined, noting engine thrust effect on
attitude control system
performance 03 p0517 A67-13027
- Stability of solutions for differential-
difference equations with periodic
coefficients, establishing necessary and
sufficient criterion for boundedness of
parameter 03 p0459 A67-13642
- Least squares methods for calculating
stability derivatives of aircraft from
unsteady flight data 09 p1438 A67-22474
- Motion equations used in determining
lateral stability and control derivatives for
STOL aircraft 10 p1595 A67-23551
- Existence and stability of solutions for
equations of stationary thermal explosion in
bounded container 10 p1734 A67-23679
- Digital computer analysis of inviscid two-
dimensional parallel flow stability, using
finite difference method to solve resulting
initial value problem 11 p1778 A67-24220
- Stability of bilaterally symmetrical object
towed in air along straight line, obtaining
characteristic equation as test for lateral or
longitudinal stability 11 p1743 A67-24309
- Gyroviscosity of collisionless plasma in
strong magnetic field, duality theorem and
application to linear stability
analysis 11 p1839 A67-24547
- Propellant characteristics under impaired
combustion conditions, noting sufficiency of
Chulko-Margolin stability
criteria 12 p2039 A67-26112
- Internal stability of turbulent combustion,
developing analysis for one-dimensional
model and deriving sufficient instability
criterion 12 p2039 A67-26119
- Stable evaluation algorithm for
polynomials, discussing minimal Newton
forms, error estimation,
etc 14 p2342 A67-28003
- Integral equations in automatic control
theory, deriving theorem which leads to
Popov frequency domain stability
criterion 14 p2292 A67-28635
- Ljapunov function analysis applied to
derivation of general stability criterion for
control system 14 p2292 A67-28635
- Real autonomous smooth ODE system in
neighborhood of critical point, noting
stability dependence on sign of
eigenvalue 14 p2345 A67-28906
- Boltzmann kinetic equation solution for
completely ionized plasma in magnetic
field 14 p2363 A67-29071
- Parameter stability regions with frequency
response, noting interpretation for several
parameters 15 p2457 A67-29366
- Stability of feedback systems with
monotone and odd monotone
nonlinearities 15 p2457 A67-29374
- Numerical analysis of PDEs with singular
coefficients, noting equivalence of stability
and convergence 15 p2510 A67-29519
- Finite difference solution of third
boundary value problem for heat conduction
equation, obtaining conditions for
coefficients from stability
requirements 15 p2510 A67-29521
- Solution stability of parametric nonlinear
differential equation system, noting validity
of Popov criterion 15 p2518 A67-29660
- Suboptimal control function sequence
generation by combining approximation in
control policy space with stability criteria
from direct method of
Ljapunov 16 p2648 A67-31658
- Cross sectional variation effects on
velocity potential evaluated using slender
body theory 17 p2789 A67-32067
- Cauchy problem for homogeneous linear
difference scheme with constant complex
coefficients, giving stability
lemmas 17 p2877 A67-32677
- Single-step numerical integration stability
analysis applied to linear differential
equations with known root
locations 19 p3249 A67-34839
- Counter traveling wave regime stability in
ring gas laser, studying effects of atomic
collisions, isotopic state and wave
coupling 19 p3239 A67-34898
- Stability criterion for bandpass tunnel
diode amplifier, determining limitations on
diode series inductance as function of
negative resistance 19 p3196 A67-35662
- Existence and stability of solutions for
equations of stationary thermal explosion in
bounded container 21 p3731 A67-38280
- Stability criterion derivation involving
Markov determinants using second method
of Ljapunov 23 p4022 A67-40648
- Second order accurate approximation to
advection terms in hydrodynamics equations
noting aliasing effects, amplitude and phase
errors and stability 23 p4024 A67-40994
- Mathematical model, representing two-
dimensional panel fluttering in supersonic
flow, to study stability criterion via
Ljapunov second method 23 p4081 A67-41752
- Ionization fronts stability, finding no
instabilities for strong D type
fronts 24 p4224 A67-41816
- STABILITY TEST**
- SA FLIGHT STABILITY TEST**
- SA WIND TUNNEL STABILITY TEST**
- Stability theory based on functional
methods, examining feedback system with
linear time invariant and nonlinear
elements 01 p0046 A67-11208
- Frequency-time domain asymptotic
stability criterion for autonomous continuous
systems 01 p0046 A67-11209
- Oscillation formation by violation of
sufficient conditions of asymptotic stability
in linear system 01 p0047 A67-11215
- Sufficient condition for absolute bounded-
input-bounded-output stability for certain
class of nonlinear sampled data feedback
systems 02 p0224 A67-11586
- Second order autonomous differential
equation stability and boundedness obtained,
using computing algorithm based on tracking
function method 03 p0376 A67-13987
- Axisymmetric modes of loss of stability of
circular plates lying on elastic base in
inhomogeneous stress
field 03 p0529 A67-14163
- Gyro as force sensor in instrumentation
systems, discussing types, testing and
calibration procedures 04 p0626 A67-15732
- Matrix method formulation of vibration
and stability problems yielding upper bounds
for natural frequencies 05 p0917 A67-16301
- Instability modes of cantilevered bars
induced by fluid flow through attached
pipes, examining cases of torsional and
transverse flutter and torsional
buckling 05 p0921 A67-16882
- Circle criterion for stability of time
varying feedback systems 08 p1310 A67-20338
- Spectral stability criteria for numerical
integration procedure using Z transforms,
specifically finite difference
operators 08 p1296 A67-20600
- Stability of equilibrium of elastic systems
under nonconservative load, discussing
criteria of stability, modes of instability,
follower force problems,
etc 08 p1422 A67-21048
- Stability of stepwise solution methods of
initial value problems for second order
differential equations 09 p1524 A67-21935
- Stability of Fehrborg method when applied
to solution of initial value problems for
second order differential
equations 09 p1524 A67-21936
- Forced steady state response of linear
harmonic oscillator with impact absorber
attached, developing stability criterion
[ASME PAPER 67-VIBR-10] 11 p1795 A67-24170
- Bubble stabilization in pure viscous liquid
contained in sinusoidal vibrated tank
[ASME PAPER 67-FE-3] 14 p2304 A67-28356
- Captured Air Bubble /CAB/ vehicle
stability tests 14 p2246 A67-28731
- [AIAA PAPER 67-349] 14 p2246 A67-28731
- Effect of unconditional stability of loop in
phase lock demodulator on threshold
performance of loop, noting transfer
functions role 17 p2816 A67-32782
- Stability of periodic solution of nonlinear
systems with coefficients dependent on
amplitude and frequency 20 p3408 A67-37043
- Equations of motion of continuous single
loop adaptive control system with scan
modulated parameters, noting stability
analysis method 20 p3408 A67-37044
- Device for automatic recording of laser
emission and of energy of pumping
pulse 20 p3460 A67-37149
- Sufficient conditions for statistical
stability of motion in nonlinear
systems 20 p3409 A67-37225
- Hydrodynamic journal bearings in liquid
sodium, discussing stability characteristics of
different geometries and wear at high
temperatures 24 p4164 A67-42746
- STABILIZATION**
- SA GYRO-STABILIZED**
- SA MISSILE STABILIZATION**
- SA SIGNAL STABILIZATION**
- SA SPIN STABILIZATION**
- Quenching rate effect on athermal
stabilization of austenite
steel 06 p1014 A67-17801
- Ionospheric stabilization of interchange
mode calculation applied to electron debris
of Star Fish event, noting role of
ionospheric current 07 p1182 A67-19948
- Gyroscopic stabilization of relative
equilibrium-of satellite 11 p1869 A67-24067
- Optimum stabilization of axisymmetric
satellite by system of n reactive
jets 14 p2393 A67-27854
- RC network project for stabilization of
tunnel diode, noting stability conditions,
negative differential resistances,
etc 14 p2283 A67-28041
- Stabilization of current intensity in
superconducting coils noting two
characteristic intensities, measurements of
niobium compounds, effects of added
copper, etc 16 p2607 A67-30593
- Stabilization method for solution of
boundary value problems for second order
nonlinear ordinary differential
equation 16 p2696 A67-31482
- Stabilization method for solution of
boundary value problems for second order
nonlinear ordinary differential
equation 24 p4177 A67-42198
- STABILIZED PLATFORM**
- Gyrostabilized platform operating mode
and stabilization, for use in aircraft as
onboard position reference
system 04 p0624 A67-15537
- Time constant and control channel lag
effects on size and configuration of platform
stability region 04 p0552 A67-15883
- Triaxial gyrostabilized platform drift
determination, given oscillations of gyro
units relative to platform 06 p1003 A67-18176
- Optimum stability of body with fixed
point, using stabilizing
gyros 07 p1224 A67-20028
- Reading errors of oscillating plant
mounted gyrocompass assuming gyromoment
compensation and no friction, determining
motion through differential

equation 11 p1794 A67-25045
 Inertial navigation system with damping of oscillations for enhancement of stability of stationary platform 13 p2118 A67-26375
 Thermal gradients on surface of orbiting cylindrical stabilization boom determined, using computer simulation of earth orbital environment 16 p2764 A67-30957
 Gyromotor electromechanical moment effect on drift of triaxial gyro-stabilizer exposed to platform vibrations, formulating rotor motion equations 18 p3047 A67-33992
 Gyro-stabilized inertial navigation platform system upgraded by applying sampled model reference system, estimating gyro drift rates by stochastic approximation method 18 p3075 A67-34106
 Feedback control system using pneumatic computing components and vibration isolators for automatic platform tilt stabilization, performance characteristics, etc [AIAA PAPER 67-548] 19 p3208 A67-35946
 Stabilized platform for stratospheric balloons for IR, UV and X-ray astronomy 22 p3830 A67-39184
 Discrete methods for control network implementation using integrated circuitry to reduce inertial navigation systems complexity 22 p3800 A67-40184
 Strapdown system application studies related to surface to surface missile, considering angular vibration environment and constant rates about output and spin axes of gyro 22 p3833 A67-40186
 Expressions for determining directional gyroscope drift, considering random perturbations of base 22 p3809 A67-40481
 Book on inertial navigation covering laws of rational mechanics, gyroscopes, accelerometers, platform stabilization and control panels 23 p4025 A67-40633
 Inertial navigation system operation errors on moving power plant due to inaccurate initial data feeding into computer 24 p4182 A67-42300
STABILIZER
 SA CURRENT STABILIZER
 SA FIN
 Horizontal tail two-stage hydraulic servoactuator for F-111 horizontal stabilizer control 05 p0752 A67-16160
 Adhesive bonded honeycomb horizontal stabilizers, considering strength, aerodynamics, cost, endurance and serviceability 09 p1577 A67-22508
 Bird strike data on piston engine transport horizontal stabilizers summarized by bird weight, impact velocity, target-station distance and simulated and test load 22 p3746 A67-39845
 Bird strikes on high speed transport jet aircraft stabilizers 24 p4094 A67-42278
 Gyro power stabilizer in unsteady equilibrium state becoming stable under dry friction defined for controllability in phase space 24 p4155 A67-42299
STABLE OSCILLATION
 Discontinuous impact vibration absorber with small auxiliary mass sliding in slit of rigid body excited by sinusoidal oscillation 01 p0161 A67-10645
 Matrix analysis of resonant vibration stability conditions 01 p0113 A67-10675
 Stability of flute oscillations of rarefied plasma in constant electric field normal to magnetic field 02 p0278 A67-12619
 Higher harmonics computation of nonlinear steady oscillation in arbitrary system 05 p0846 A67-16438
 Optimal stabilization of small oscillations of body around center of mass in central field 05 p0901 A67-17117
 Automatic phase control (APC) loop for stabilization of phase shift in RF amplifier 05 p0778 A67-17395
 Triaxial gyro-stabilized platform drift determination, given oscillations of gyro units relative to platform 06 p1003 A67-18176
 Transverse oscillation stability in quasi-one-dimensional flow of conducting gas in magnetic field 07 p1227 A67-19119
 Stationary and transient processes in multiply stable pulsed element identified as autonomous system containing blocking generator, oscillatory circuit, detector and filter 09 p1473 A67-21959
 Existence, uniqueness and stability investigation of periodical solutions for nonlinear hyperbolic partial differential equations 10 p1674 A67-23387
 Fully stalled airfoil steady state pitching

oscillations in one degree of freedom, deriving torsional flutter equation [ASME PAPER 67-VIBR-12] 11 p1872 A67-24172
 Quasi-static analysis of nonsynchronous response effect of gas bearing pivoted pad design variables and application to operating machinery [ASME PAPER 67-VIBR-15] 11 p1796 A67-24175
 Stability analysis of long period Trojan librations treated as short period oscillations about long period reference solution 11 p1866 A67-24774
 Stability of flute oscillation of rarefied plasma in constant electric field normal to magnetic field 13 p2170 A67-27375
 Stability analysis of steady combination oscillations of single loop circuit, obtaining equations relating voltage harmonic of nonlinear capacitances 19 p3262 A67-35706
 IR emission in n-type gallium arsenide samples exhibiting current oscillations due to electron-phonon coupling 20 p3508 A67-36423
 Stability of three-dimensional oscillations of solid body coupled to periodically vibrating base by elastic springs 20 p3485 A67-36917
 Stationary and transient processes in multiply stable pulsed element identified as autonomous system containing blocking generator, oscillatory circuit, detector and filter 20 p3400 A67-37189
 Transverse oscillation stability in quasi-one-dimensional flow of conducting gas in magnetic field 21 p3664 A67-38164
 Oscillation stability of rotating cylindrical shell filled with ideal incompressible weightless fluid, determining instability region distribution 21 p3721 A67-38302
 CR self-oscillation circuits, discriminating CR oscillators from astable, monostable and bistable multivibrators 21 p3604 A67-38601
 Solitary pulse longitudinal waves existence in electron plasma related to trapped ions presence, studying ion pulse shape and oscillation stability 22 p3845 A67-39423
 Monograph on variable stars of RR Lyrae type covering spectrophotometric investigations of periodic brightness fluctuations and oscillations 22 p3880 A67-39463
 Simultaneous self-starting oscillations at unrelated frequencies in feedback loop containing one nonlinearity, calculating equivalent linear gain 23 p3984 A67-41157
 Stability boundary of periodic oscillation described by third order differential equations near Liapunov critical case 24 p4137 A67-43108
STACKING FAULT
 Stacking faults in steam-oxidized silicon wafers annealed in vacuum at 800, 1000 and 1200 degrees C observed by chemical etching and transmission electron microscopy 01 p0126 A67-10052
 Quantitative in situ X-ray diffractometer investigations of evaporated metal films and after annealing treatments ranging up to 370 degrees C 02 p0287 A67-11713
 Electron microscopic structure and lattice defects of martensite in commercially pure titanium 06 p1017 A67-17966
 Dislocations in Be, discussing twinning and deformation by climbing, stacking faults and condensation vacancies 07 p1210 A67-20163
 Chemical etching of dislocation and stacking fault structure of epitaxial GaAs, noting possible effect on electroluminescence 10 p1692 A67-23514
 Growth mechanisms and crystalline quality of diamond type compounds and crystals in III-V and II-VI groups 13 p2177 A67-27009
 Chemical etching examination of dislocations and stacking-fault structure of epitaxial gallium arsenic phosphide, considering doping level, growth rate and composition effects 14 p2366 A67-28421
 Fourier analysis of line profiles of X-ray-studied deformation faulting in titanium, zirconium and hafnium 14 p2340 A67-29033
 Stacking faults in tungsten specimen heated rigidly for short time by electric discharge 20 p3464 A67-36225
STACKING FAULT ENERGY
 Specific stacking fault energy of deformed fcc metals determined from electron microscope diffraction contrast of stacking fault dipoles 07 p1208 A67-19637
 Stacking fault tetrahedra in fatigued

stainless steel, describing mechanism for nucleation of triangular Frank dislocation loop during cyclic load 11 p1805 A67-24109
 Temperature dependence of bcc metals elastic limit at low temperature, assuming sessile-dissociated screw dislocations formation during microdeformation, stressing stacking fault energy effect 13 p2130 A67-26438
 X-ray diffraction analysis of polycrystalline brass deformed by tension, noting stacking fault probability, stress-strain curve, etc 18 p3064 A67-34084
 Dilute magnesium addition effect on growth and shrinkage of dislocation loops in aluminum studied by isothermal annealing of thin foils 21 p3644 A67-38088
 Stacking fault energy estimation in polycrystalline brass during tensile deformation by analyzing X-ray diffraction patterns 21 p3645 A67-38090
STADAN
S SATELLITE TRACKING AND DATA ACQUISITION NETWORK
STAGE
 S SECOND STAGE
 S SINGLE-STAGE ROCKET
 S THIRD STAGE
STAGE SEPARATION
 Solid booster thrust decay control for payload or upper stage separation, noting inert silvers with auxiliary retrorockets as separation control [AIAA PAPER 66-971] 02 p0304 A67-12293
 Second and third stage separation for ELDO A simulated in vacuum test 04 p0595 A67-14540
 Tip-off motion due to separation of stages or payload by multispring separation system with guided plungers 08 p1405 A67-20506
 Passive separation system for APL spacecraft providing despin, solar blade unfolding, yaw of injection rocket, battery elimination, etc 09 p1571 A67-22061
 Second and third stage separation for ELDO A simulated in vacuum test 20 p3413 A67-36413
 Optimization of staged ejector systems noting mathematical model development to represent performance characteristics 22 p3787 A67-40150
 Thrust staging for optimum thrust program without coasting phase for ascent from low orbit 23 p4071 A67-41314
STAGNATION FLOW
 Exact solutions to equations for compressible boundary layer in case of power-law dependence of initial profile of stagnation enthalpy on stream function 03 p0400 A67-12867
 Thermal choking in various devices having mixing processes between two flows with different stagnation enthalpies as possible limitation of mass flow rate [ONERA-TP-411] 05 p0792 A67-16934
 Cascade flow through compressor guide vanes and flow separation at top of vane profiles 05 p0750 A67-17323
 Base pressure fluctuations behind cone in supersonic flow due to presence of stagnant zone with subsonic reverse flow in shape of annular vortex 06 p0936 A67-17735
 High altitude supersonic isokinetic filter paper sampler for ALARR rocket, examining subsonic 3-D stagnation flow diffuser 08 p1276 A67-20500
 Fully stalled airfoil steady state pitching oscillations in one degree of freedom, deriving torsional flutter equation [ASME PAPER 67-VIBR-12] 11 p1872 A67-24172
 Unsteady perturbation effect of external velocity on laminar boundary layer 13 p2094 A67-26645
 Flow velocity determination by cylindrical magnifying probe, measuring stagnation and wake pressures difference, noting magnifying factor variation under Reynolds number and stem and blockage effects 15 p2471 A67-29529
 Three-dimensional rotational stagnation point flow solution noting surface curvature influence 17 p2789 A67-32039
 Stationary flow in viscous fluid film on rotating body of revolution, using differential equations 17 p2836 A67-32261
 Stationary laminar boundary layer equations of Ostwald-de Waele power law fluids, flow and temperature boundary layer differential equation solutions 17 p2836 A67-32262

Viscous fluid discharge from tubes of various cross sections under constant pressure gradient with longitudinal pulse along wall, noting short period stoppage 18 p3029 A67-34615

Parallel porous wall burner for studying premixed and diffusion flames in stagnation flows [CI PAPER 67-7] 19 p3345 A67-35002

Analysis of flow and points of stagnation of fluid circulating over cylinder 19 p3210 A67-35720

Heating rate and type effects on stationary flows stability, noting dependence on critical Rayleigh number 20 p3553 A67-36848

High altitude supersonic isokinetic filter paper sampler for ALARR rocket, examining subsonic 3-D stagnation flow diffuser 21 p3563 A67-37803

Laminar free convection of absorbing emitting gas analyzed in region of stagnation point of horizontal cylinder 22 p3920 A67-40418

High enthalpy supersonic wind tunnel performance, analyzing Teflon model stagnation ablation 23 p3931 A67-41477

STAGNATION POINT

Null point or transient copper calorimeter using single temperature response measurement to determine heat flux, correlating experimental with theoretical data 01 p0070 A67-11035

Boundary layer equations for pseudoplastic fluids solved for exact numerical solutions, specifically near stagnation point 04 p0609 A67-15599

Unsteady incompressible laminar forced convection around stagnation point due to arbitrary timewise-variant free stream velocity, considering skin friction and heat transfer 04 p0610 A67-15830

Thermal diffusion and diffusion thermoconduction coupling effects on transpiration cooling of porous bronze disk at axisymmetric stagnation point 04 p0733 A67-15839

Convective and radiative heat transfers at stagnation point of hemisphere cylinder model immersed in high enthalpy partially ionized supersonic flow in plasma wind tunnel 05 p0747 A67-16432

Atmospheric argon effect on hypersonic stagnation point convective heat transfer, using arc-heated shock tube simulating flight velocities up to 34,000 fps [AIAA PAPER 66-29] 05 p0928 A67-17337

Laminar boundary layer on ellipsoids of revolution situated at zero angle of attack in supersonic flow of perfect gas 06 p0936 A67-17740

Asymptotic method for solution of boundary layer equations for generalized three-dimensional flow of dissociated air at chemical equilibrium near stagnation point 06 p0984 A67-18113

Equilibrium air study extended to reentry speeds up to 70,000 fps, using transport and thermodynamic properties to examine stagnation point convective heat transfer including blowing rates 06 p0943 A67-18843

Simultaneous effects of heat and mass transfer on properties of stagnation point flows analyzed over full range of velocity gradients 08 p1276 A67-20568

Convective laminar heat transfer to hypersonic vehicle, deriving similarity relations between stagnation temperature profile and mass fractions of chemical species 09 p1579 A67-21699

Behavior of inviscid supersonic conical flow fields near crossflow stagnation points studied by constructing coordinate expansions of exact conical flow equations [AIAA PAPER 66-491] 10 p1591 A67-23112

Magnetoaerodynamic flow relations for axisymmetric blunt bodies with shock layers in shifting equilibrium 10 p1591 A67-23114

Approximate method for calculating stagnation point laminar boundary layer equations taking into account chemical reactions in gas phase and surface of body 12 p1928 A67-25673

Hypersonic flow near stagnation point of blunt body taking radiation into account, noting large enthalpy and density gradients 13 p2050 A67-26897

Existence of three-dimensional solution of boundary layer equations of viscous incompressible flow in neighborhood of stagnation point 13 p2050 A67-26912

Coupled nonlinear equations integration in boundary layer theory with specific reference to heat transfer near stagnation point in three-dimensional flow 13 p2224 A67-27463

Asymptotic and numerical solutions of Goulet integrodifferential equation describing hypersonic flow near stagnation point past blunt bodies, allowing for radiative transfer effects 14 p2296 A67-27981

Supersonic viscous flow near blunt body stagnation line, using Navier-Stokes equations 14 p2240 A67-27993

Heat transfer and skin friction increase for gas stream with liquid-droplet suspension flowing over blunt-nosed body near stagnation point 14 p2405 A67-28126

High Mach number low Reynolds number flow over two-dimensional circular cylinder, obtaining surface pressure and heat transfer distributions 14 p2242 A67-28174

Molecular speed ratio in low density flows determined via stagnation point heat transfer and flat plate heat transfer measurements 14 p2301 A67-28182

Axisymmetric blunt bodies shock standoff distances in hypersonic flow determined by numerical and analytic methods 14 p2244 A67-29056

Hypersonic stagnation point flow between strong shock wave and body involving radiation, conduction and dissociation 15 p2415 A67-29309

Hypersonic trim angle of attack of lifting entry vehicles, correlating stagnation point values obtained from heat shield ablation and pressure distribution measurements 15 p2417 A67-29447

Mach and Reynolds number, cone angle, base geometry, etc, effect on near wake flow of conical vehicle moving at high speed 15 p2418 A67-30215

Interaction of convection and radiation heat transfer in axisymmetric two-dimensional stagnation point low-speed flow of gray absorbing and emitting gas 16 p2591 A67-30939

Flow field and heat transfer in radiating stagnation-point shock layer of atmospheric-entry vehicles 16 p2591 A67-30940

Heat transfer in stagnation-point laminar boundary layer with mass injection and absorption of incident radiation 16 p2658 A67-30941

Vortex breakdown treated as failure of quasi-cylindrical approximation for viscous axisymmetric flow 16 p2658 A67-30948

Pressure measurement at stagnation point of cylindrical missile with spherical nose cone during free flight in ballistic testing 16 p2593 A67-31123

Two-dimensional inviscid flow pattern of gas behind shock front in neighborhood of stagnation point of cylindrical body acting as magnetic field source 16 p2723 A67-31581

Three-dimensional rotational stagnation point flow solution noting surface curvature influence 17 p2789 A67-32039

Transport property difference effect on flow prediction of blunt body stagnation region heat transfer, noting laminar flow and compressible boundary layer equations 17 p2793 A67-33025

Mach and Reynolds numbers effect on rarefied supersonic gas flow pattern near forward stagnation point of blunt body, noting decrease in density 18 p3028 A67-34209

Heat transfer in steady axisymmetric MHD flow near stagnation point, with series solutions for velocity, magnetic field and temperature 18 p3161 A67-34381

Temperature distribution within two-dimensional thermal boundary layer due to flow of second order fluid past flat plate 19 p3210 A67-35447

Analysis of flow and points of stagnation of fluid circulating over cylinder 19 p3210 A67-35720

Transient nature of heterogeneous boundary layer chemical reaction at stagnation point studied analytically, deriving stability conditions 19 p3211 A67-35740

Heat and mass transfer conditions in ablation of shear thinning and thickening fluids investigated at stagnation point [ASME PAPER 87-HT-78] 20 p3551 A67-38756

Rear stagnation point solution for viscous incompressible electrically conducting MHD flow 20 p3499 A67-36850

Stagnation-point flow of rarified gas, using linearized BGK model of Boltzmann equation with small Mach number 20 p3425 A67-37673

Charged particle /ion/ collection rates using supersonic atmospheric sounding rocket with electrode at stagnation point, noting electric field effect 22 p3791 A67-39818

Rarefied gas axisymmetric stagnation point flow, clarifying relationship between continuum and Knudsen layer flow 22 p3784 A67-39836

STAGNATION PRESSURE

Turbulence as producer of noise in proportional fluid amplifiers, considering signal and noise at receiver entrance in terms of stagnation pressure 04 p0557 A67-15919

Isentropic compression due to motion of heavy piston in gun tunnel noting nozzle throat effect on motion and stagnation pressure 11 p1773 A67-24577

Stagnation pressure lower than atmospheric pressure in supersonic subatmospheric flow in magnetoaerodynamic generation nozzle, discussing Hall effects for energy conversion process 18 p3020 A67-34122

Interaction of first and second shocks of blast-bow wave in double-driver shock tube, examining stagnation point pressure prediction methods 19 p3206 A67-34812

Critical fluid flow rate analysis of two-phase nitrogen at stagnation pressure of 25 psia 22 p3784 A67-39967

STAGNATION REGION

Periodic surface distortion of molten layer in axisymmetric flat stagnation regions of cylindrical iron and copper rods 01 p0102 A67-11190

Wall temperature effect on behavior of hypersonic stagnation region shock layer in incipient merged layer flow, obtaining enthalpy function profile 08 p1278 A67-20928

Thin shock layer stagnation region analysis in hypersonic flow, emphasizing lateral asymmetry for planar and perturbed axisymmetrical cases 10 p1624 A67-22936

Fluid flow processes for secondary sonic jet injection into Mach 6 free stream, noting upstream flow into separated flow regions 12 p1893 A67-25934

Wind tunnel investigation of wake structure behind cone in supersonic flow 14 p2240 A67-27994

Stagnation region foreign gas injection in low Reynolds number hypersonic shock layer flow 16 p2591 A67-30936

Nonequilibrium air dissociation and ionization in stagnation region of blunt body investigated in merged layer regime 16 p2592 A67-30955

Counterflow diffusion flame in forward stagnation region of porous cylinder, detailing flame stability and velocity gradient 18 p3155 A67-33842

Inviscid hypersonic flow in stagnation region of circular cylinder with detached shock wave, considering real-gas effects 19 p3171 A67-35713

Nonequilibrium quasi-one-dimensional nozzle flows in limit when relaxation time is large compared with characteristic flow time 19 p3172 A67-35800

Radiative heat loss effect on steady axisymmetric hypersonic flow past blunt body using gray gas approximation, with numerical solution for stagnation region 22 p3739 A67-39530

STAGNATION TEMPERATURE

Pressure and stagnation temperature distribution in test chamber of blowdown hypersonic wind tunnel 01 p0049 A67-10558

Internal temperature distributions of present and proposed calorimeter geometries operating at high pressure and extreme heating rates compared, using one- and two-dimensional heat conduction programs 01 p0070 A67-11033

Hypersonic low density wind tunnel for high Mach numbers and stagnation temperatures, analyzing measurements made, noting heater, nozzle, diffuser, etc 04 p0595 A67-14561

Oblique shock detection in conical nozzle with circular arc throat, noting measurement techniques 04 p0547 A67-14833

Flow properties in laminar and turbulent near wake of cones and wedges using hypersonic shock tunnels, obtaining wake centerline and stagnation temperature

- profile
[AIAA PAPER 67-30] 07 p1126 A67-19432
Stagnation temperatures from stagnation
point heat transfer rates measured in
hypersonic gun tunnel at Mach
9.8 09 p1486 A67-22414
Surface interaction of free molecular flows
or molecular beams, considering state
variables in highly rarefied gas in
Maxwellian equilibrium, stagnation
temperature, etc 13 p2159 A67-27299
Rocket launching pad exhaust deflector
investigated for uncooled efflux deflectors
design data, calculating heat transfer
coefficient and stagnation
temperature 19 p3207 A67-35520
- STAINLESS STEEL**
Cold rolled extra-thin stainless steel
application in construction of front and rear
interstage sections of second stage of
Europa I rocket 01 p0160 A67-10408
Mossbauer spectroscopy used to study
precipitation reactions in 17-7 PH stainless
steel and in 18Ni-8Co-5Mo maraging
steel 02 p0256 A67-12705
Residual stress effect on stress-strain
curve of uniaxial composite consisting of
stainless steel wire and aluminum alloy
matrix 03 p0444 A67-13432
Columbium additions to stainless steel for
steam turbine blading 03 p0446 A67-13543
Deformation and diffusion bonding of Al,
Ti and stainless steel alloys, discussing
surface condition, time, temperature, cold
work, heat treatment and intermediate
materials 03 p0430 A67-13692
Short-time tensile and long-time creep
rupture properties of HK-40 alloy and type
310 wrought stainless steel from room
temperature to 2000 degrees F
[ASME PAPER 66-WA/MET-2] 04 p0639 A67-15344
Rapid depressurization transients effect on
saturated pool boiling system from stainless
steel surface 04 p0734 A67-15848
Low endurance fatigue of aluminum alloy
and stainless steel in plane bending at
ambient and elevated
temperatures 05 p0920 A67-16810
Heating and cooling rates, hold time at
maximum temperature, phase temperature
between temperature and strain cycling
effects on thermal fatigue of stainless
steel 05 p0921 A67-17085
Diffusion welding of aluminum alloys and
austenitic stainless steel tubular
joints 07 p1190 A67-19214
Brazed graphite-stainless steel composites
for tube-to-armor joints of high temperature
graphite space radiators 07 p1223 A67-19462
Carbon and nitrogen mass transfer rates
by liquid potassium in 16 thermal convection
loops of type 316 stainless steel with
niobium/one-percent-zirconium and stainless
steel tabs at 1200 to 1600 degrees
F 07 p1223 A67-19465
Plastic strain distributions in
polycrystalline austenitic stainless steel and
titanium, using photoelastic
coating 08 p1343 A67-21333
Cryogenic low pressure seal to seal
aluminum or stainless steel
flanges 08 p1336 A67-21498
Material combination and hardness effect
in rolling contact fatigue life of high speed
tool steel, stainless steel and wear resistant
materials 09 p1505 A67-22191
Diffusion bonding of titanium and stainless
steel at high temperatures using pneumatic
hammer 09 p1520 A67-22436
Polybenzimidazole (PBI) structural
adhesives for bonding stainless steel,
beryllium and titanium
alloys 09 p1523 A67-22517
Stacking fault tetrahedra in fatigued
stainless steel, describing mechanism for
nucleation of triangular Frank dislocation
loop during cyclic load 11 p1805 A67-24109
Crack propagation for stainless steel and
Ti alloy at stresses below fatigue limit,
noting of alternating stress cycles crack
propagation for stainless steel and Ti alloy
at stresses below fatigue limit, noting
role 11 p1806 A67-24365
Martensitically hardened high strength
stainless steel, physical properties, heat
treatment effects, etc 11 p1810 A67-25103
Hot pressing technique for aluminum
sheet and stainless steel wire to produce
composite high tensile strength
plate 12 p1954 A67-25289
- Reflectance function for stainless steel
with various surface roughnesses, comparing
incident and reflected monochromatic fluxes
of assigned directions
[AIAA PAPER 67-321] 12 p1957 A67-26036
Ductile failure initiation by fractured
carbides in austenitic stainless
steel 13 p2133 A67-27008
Specifying temper for stainless steel
tubing, noting properties of various
techniques 13 p2124 A67-27175
Heat resistant stainless steel honeycomb
cores for cylindrical applications, measuring
energy absorption characteristics
[ASME PAPER 67-DE-14] 14 p2402 A67-28870
Phase composition of titanium containing
slag formed during alloying of stainless steel
with titanium, noting titanium
oxidation 16 p2687 A67-30842
Maraging stainless steel for high
temperature applications, discussing
properties, heat treatment and solution
temperature effect 17 p2875 A67-33049
Plasma arc process applied to stainless
steel and titanium plate welding, discussing
metallurgical and mechanical weld and
deformation tests 20 p3456 A67-37542
Cold forming properties and handling of
stainless steels and superalloys noting
contained extrusion and warm heading
techniques 21 p3634 A67-38177
Heat treatment practices for precipitation
hardening steels noting use in missile and
aerospace applications 21 p3634 A67-38178
Heat resistant stainless steels evaluated
experimentally for fatigue properties,
corrosion resistance, creep limit and tensile
strength 21 p3646 A67-39010
Additive elements studied for influence on
morphology, nature and hot plasticity of
sulfides in austenitic stainless
steels 21 p3646 A67-39077
Endurance fatigue characteristics of
weldable martensitic stainless steel, giving
data for butt and spot
welds 22 p3811 A67-39447
Co effect on precipitation hardening in high
strength stainless steels 23 p4018 A67-40871
Cratering produced by high velocity
impact of stainless steel threaded rod on
cold-rolled steel target 23 p4080 A67-41467
Rare earth metals effect on mechanical
properties of austenitic chromium steel at
high temperatures 24 p4169 A67-41920
Porous cermet tubular element fire
barriers of stainless steel powder for
increased safety in gas flame processes,
determining critical Peclet
values 24 p4159 A67-41957
Corrosion and hydrogen embrittlement
resistant nickel stainless maraging steel with
bcc martensite crystal structure for pressure
vessel applications 24 p4161 A67-42328
Lubricating action of electroplated gold on
stainless steel examined under load by
single rub block loaded against rotating disk
[ASLE PAPER 67-LC-16] 24 p4165 A67-42750
- STALL**
S ROTATING STALL
S WING STALL
STALLING
Deep-stall characteristics of T-tailed
aircraft configurations and recovery
procedures, noting parameters of pitch-up,
angle of attack, etc 03 p0350 A67-12912
[AIAA PAPER 66-13]
Stalling in swept wing jet aircraft with
reference to satisfying airworthiness
regulations and aerodynamic
problems 03 p0362 A67-14300
Rotor blade stall, comparing power,
flapping motion blade bending and vibratory
hub shears for illustration
[AHS PAPER 101] 16 p2595 A67-31818
- STAND**
S TEST STAND
STANDARD
SA FREQUENCY STANDARD
Product identification and traceability
standards for space system quality assurance
program for NASA space
systems 05 p0930 A67-17251
Microwave attenuation standard derived
using waveguide below critical frequency as
voltage divider to determine losses in
components 13 p2067 A67-26488
Global distribution of standard time by
VLF for synchronization with microsecond
accuracy 14 p2263 A67-28389
Impedance measurements in coaxial
waveguide systems propagating TEM wave,
- using precision coaxial line standards and
connectors 17 p2815 A67-32605
Laser energy and power measurement,
discussing radiation attenuation devices,
measurement standards, etc 17 p2867 A67-32612
Time signal transmission and reception,
noting development of UHF spectroscopy
and atomic frequency
scales 18 p3004 A67-34400
ISA Conference, Chicago, September 1967,
Volume 22, Part I, Measurement standards
instrumentation 23 p4003 A67-41334
- STANDARD ATMOSPHERE**
Effect of variation of vertical air density
profile on relative optical air mass for
ARDC standard model atmosphere 1959
compared with
measurements 10 p1652 A67-23622
- STANDARD DEVIATION**
Atmospheric turbulence compared with
associated radar echoes, noting correlation
coefficient for standard deviation of derived
gust velocity with maximum radar
reflectivity 04 p0649 A67-14687
- STANDARDIZATION**
SA CALIBRATION
Lithium drifted germanium detector with
cylindrical annular shape permitting
standardization of gamma spectroscopy
techniques 12 p1945 A67-25861
Standardization techniques for integrated
circuit production, particularly logic
circuits 12 p1918 A67-26215
Revision of military terminology for
weapon systems considering human factors,
safety and maintainability and reliability
relations 16 p2780 A67-30440
Maintainability program task requirements
covered by Military Standard
470 16 p2781 A67-30441
FAA certification standards for SST
engines and components, emphasizing
thermal environment testing and high
temperature materials
development 22 p3867 A67-39224
Test accelerometer comparison calibrations
via vibration standards, discussing
sensitivity, relative motion and error
analysis 23 p4003 A67-41336
Aircraft fasteners, airline operation and
maintenance requirements and improvement
of standardization 24 p4161 A67-42082
Emergency oxygen supply systems for
aircraft, discussing simplicity,
standardization, safety, reliability and
maintenance
[AIAA PAPER 67-965] 24 p4110 A67-43043
- STANDING WAVE**
Generating mode number in solid state
lasers using traveling wave and standing
wave 01 p0086 A67-10069
Alfven standing wave generation by
current injection and/or electromagnetic
induction in conducting
liquid 02 p0272 A67-11520
Plasma acceleration and retardation by
magnetic standing waves 04 p0688 A67-14564
Light waves traveling backward and
forward in very small filaments of optical
material result in standing waves producing
visible spatial beats, allowing detection of
changes in refractive
index 07 p1224 A67-19841
Resonant frequencies of standing wave
Bernstein modes propagating in magnetized
homogeneous plasma columns and effects of
anisotropy of unperturbed electron velocity
and ambipolar-diffusional electric
field 08 p1361 A67-21131
Generating mode number in solid state
lasers using traveling wave and standing
wave 08 p1339 A67-21452
Standing wave solution of homogeneous
waveguide field distribution for H-10 wave
after conformal mapping and effect of
capacitive and inductive
irises 10 p1607 A67-23571
Ruby laser output energy losses when
passing from normal to passive Q-switched
operation 11 p1800 A67-24241
Two-dimensional steady MHD flow with
resolution of neutral sheets into
intermediate and slow
waves 11 p1862 A67-24499
Benjamin theory of conjugate vortex flow
proved by alternate
method 13 p2095 A67-26909
Helical antenna radiation characteristics
under backfire operating conditions, noting
improvement over endfire

conditions 14 p2290 A67-29008
 Generalization of linearized equation of stationary waves in equilibrium gas dynamics applied to flow along two-dimensional sinusoidal wall 17 p2839 A67-32715
 Optical means for enhancing quantum efficiency of tri-alkali photocathode, discussing standing wave pattern in spaced-reflective and reflective photocathodes 17 p2861 A67-33287
 Soviet book on waveguide theory covering resonators, Maxwell equations role, eigenfunctions, etc 18 p3000 A67-33677
 Hydrogen-air reaction kinetics analyzed using standing wave normal shock, noting wall effects, ignition delay and recombination [AIAA PAPER 67-479] 18 p3157 A67-33948
 Magnetospheric boundary and standing shock wave for earth scaled down to apply to Mars 19 p3324 A67-35442
 Short-slit directional coupler functioning mode via boundary value problem indicating Chebyshev behavior of transfer coefficient and wideband subdivision 19 p3195 A67-35560
 Radar cross section measurement using standing wave method 19 p3184 A67-35826
 Spectral-line narrowing in ruby laser during standing wave field displacement with respect to active center of ruby crystal 19 p3241 A67-36023
 Electron beam deflection by standing light wave of laser shows momentum transfer resulting in Bragg relationship for reflection angle 20 p3461 A67-37185
 Resonance phenomena in bounded magnetoplasma shown on basis of dispersion relation as due to formation of standing waves of electromagnetic waves 20 p3503 A67-37671
 Plane deformation problem of instantaneous elasticity theory application to expansion of stationary elastic waves in infinite medium with cylindrical cavity 21 p3720 A67-38294
 Alfvén standing wave formation due to interaction of magnetosphere with geomagnetic pulsation 21 p3621 A67-39023
 Motion rate of pendulum with two antennas moving in electromagnetic field with standing wave measured by correlation meter 21 p3631 A67-39115
 Electron temperature spatial variation in late He afterglow due to standing wave microwave heating 22 p3844 A67-39353
 Standing waves in hot plasma traversed by quasi-neutral charged particle flux including numerical analysis of elongated wave occurrences 22 p3853 A67-40124
 Compensation method for longitudinal slot effects on propagation constant and characteristic impedance of rectangular waveguide used in standing wave meter 23 p4000 A67-41220
 Resonance in unbounded traveling and standing /harmonic oscillations/ waves, demonstrating equivalence of resonance states using wave equations 23 p4079 A67-41416
 Microwave plasma observed using spectroscopic and mass spectrometric techniques, discussing standing wave operation mode, emission and resonance lines 23 p4034 A67-41435
 Electric and magnetic field measurement by energy density antenna applicable to reducing signal fading encountered on mobile radio transmission path 24 p4131 A67-42340

STANDING WAVE RATIO
 Radiation pattern and standing wave ratio for antenna system consisting of paraboloidal cylindrical reflector and frequency-independent feed 02 p0213 A67-11644
 Communication relay to aircraft by satellite, discussing wave propagation characteristics, standing wave pattern, signal fading rates, etc 02 p0205 A67-12306
 Flexural wave velocity-amplitude relation indicates possibility of stationary waves for fixed ratio of wave amplitude and spinning membrane angular velocity 14 p2403 A67-29016
 Squinted, sum and difference radiation patterns interrelationships for amplitude monopulse antennas with impedance mismatch and mutual coupling between feeds 19 p3197 A67-35824
 Standing wave ratio and impedance measurement method for rectangular

waveguides at microwave frequencies 22 p3767 A67-39371
 Transistor parameters effect on microwave-circuit performance, tradeoffs and relation between tradeoffs, circuit performance and design 22 p3775 A67-40467

STANTON NUMBER
 Laminar flow on adiabatic surface measured, using Stanton tube and supersonic wind tunnel 04 p0547 A67-14849
 Mach number and temperature ratio effects on convective heat-transfer coefficient to flat plate through turbulent boundary layer in air and Stanton number calculation in terms of drag coefficient 04 p0731 A67-15820
 Heat transfer for wall adjacent to region of turbulent separated flow 06 p0985 A67-18131

STAR
 SA A STAR
 SA B STAR
 SA BINARY STAR
 SA CASSIOPEIA A
 SA CEPHEID
 SA GALAXY
 SA GIANT STAR
 SA MAIN SEQUENCE STAR
 SA NEUTRON STAR
 SA O STAR
 SA PROTOSTAR
 SA QUASI-STELLAR RADIO SOURCE /QSO/
 SA RADIO STAR SIGNAL
 SA STELLAR MASS
 SA T-AURI STAR
 SA TAU STAR
 SA VARIABLE STAR
 SA WHITE DWARF STAR
 Atmospheric turbulence effect on quality of star images based on telescopic observations of stars shows pronounced correlation 02 p0261 A67-11989
 Oscillations in turbulence angle in observations of quality of star images, considering role of synoptic front 02 p0261 A67-11990
 Ocular scattering in Gemini astronauts and imperceptibility of stars in daytime 06 p1089 A67-18647

STAR CLUSTER
 Clustering of radio sources analyzed using 4C catalog 05 p0902 A67-17289
 Artificial satellite UV photometry and polarimetry of galactic star clusters 06 p1077 A67-18065
 Chandrasekhar dynamical friction theory for star in cluster adapted to Fokker-Planck electron in two-component plasma theory and including multiple encounters 10 p1711 A67-23790
 Astronomical satellite for photoelectric spectrometry in UV region to measure stars of galactic clusters 12 p2002 A67-25460
 Stabilization of clusters of galaxies by ionized gas studied for recombination radiation 12 p2011 A67-26250
 Surface helium abundance in blue horizontal branch and halo B stars, considering depletion mechanism 17 p2947 A67-32764
 Stellar evolution and Brans-Dicke cosmological theory used to construct color-magnitude diagram of star cluster 19 p3330 A67-36077
 Statistical properties of optical variability of 3C 273 suggesting quasar nucleus as single body 20 p3521 A67-36297
 Search for IR stars at various temperature ranges reveals dense interstellar clouds, cool Mira Stars and circumstellar clouds 20 p3523 A67-36647
 Clustering process, examining self-gravitating system separation from expanding cosmic distribution 22 p3891 A67-40494
 Nonrandom optical red shift distribution of radio sources leading to uniform density over large volume possibility 22 p3892 A67-40500
 Globular star cluster, initial gravitational collapse and dynamical mixing, discussing numerical analyses for homogeneous spherical cluster with Maxwell velocity distribution 22 p3894 A67-40509
 IR nebula in Orion as protocluster with massive stars imbedded in opaque dust cloud, discussing collapse and lifetime 24 p4225 A67-41829

STAR FIELD
 Error correcting method for star pattern

and constellation identification process 04 p0619 A67-14552
 Large star fields outside earth atmosphere, using wide-angled photoelectric photometer for simultaneous UV and visible spectrum measurements of sky brightness 04 p0700 A67-15073
 Digital computer use to provide controllable display of star field for use with spacecraft simulator for optical sightings [AIAA PAPER 67-254] 07 p1149 A67-20051
 Error correcting method for star pattern and constellation identification process 13 p2153 A67-26579
 Palomar Schmidt telescope use as moon-star camera proved unpractical 18 p3049 A67-34315

STAR FISH PROJECT
 Star Fish debris from Cosmos V observation of gamma radiation burst 03 p0506 A67-12962
 Ionospheric stabilization of interchange mode calculation applied to electron debris of Star Fish event, noting role of ionospheric current 07 p1182 A67-19948

STAR TRACKER
 Spacecraft attitude sensor types, principles and future development 03 p0465 A67-14100
 Automatic star trackers for long range aircraft navigation, discussing instrumentation methods and use of pulse code modulation for sensor design 04 p0655 A67-15661
 Photomultiplier tubes for satellite instrumentation, discussing application as circuit components and star trackers 07 p1185 A67-19397
 Solid state celestial trackers development with special reference to photodiode, noting silicon photovoltaic sensor 09 p1526 A67-22394
 Star tracker using camera tube sensors and electronic scanning noting system errors reduction 13 p2154 A67-27491
 Canopus star sensor used for roll control of Mariner IV spacecraft 16 p2699 A67-30654
 Calibration of star tracker bias errors on OAO 17 p2955 A67-32479
 Unidentified landmark navigation from orbiting vehicle by computer simulation, noting instrumentation accuracies 17 p2882 A67-33018
 Automatic unique acquisition of Canopus for roll control of interplanetary spacecraft, discussing identification, discrimination and calibration [AIAA PAPER 67-585] 19 p3258 A67-35980
 Satellite attitude stabilization using gimbaled star trackers, analyzing satellite and star tracker motion in terms of angular velocity 22 p3830 A67-39170
 Star tracker error signal processor for onboard current satellite attitude control over wide range of gimbal angles 24 p4154 A67-42175

STAR TRACKING
 Automatic and semiautomatic devices for measuring scintillation of stellar images from traces of stars 02 p0242 A67-11994
 Astronomical Guidance System for Air Navigation which detects altitude and azimuth errors resulting from precomputed and preadjusted deviations 04 p0655 A67-15666
 Photogrammetric network for large-area phototriangulation using star-tracking airborne cameras, discussing theoretical and technical aspects 06 p0994 A67-17716
 Position determination for mobile luminous objects in sky by triangulation, using ballistic photographic chambers in positions pinpointed by star sightings 07 p1188 A67-19770
 BMK ballistic camera with equatorial and azimuthal mount for stellar geodetic satellite tracking and punch card controlled mono- and stereocomparators 07 p1188 A67-19773
 Oscillating plateholder for determining instantaneous focal length of large telescopes 11 p1791 A67-24459
 Gravitational satellite stabilization, star tracking, targets and sensors for orientation and inertial navigational instrumentation 14 p2347 A67-27878
 Strapdown star tracker for space vehicle attitude control, using scanning and error-signal determination method [AIAA PAPER 67-551] 19 p3233 A67-35948
 Surveyor spacecraft star sensor calibration

and spaceborne performance 19 p3233 A67-35982
Book on star trackers and systems design including technology, use for navigation and guidance, reference frames, error sources, atmospheric effects, etc 20 p3481 A67-36136
Stellar detectors components, describing optical receiving, image tracking and photometric devices 21 p3628 A67-38651
Photoelectric micrometer for automatic determination of meridian passage times, describing tracking servomechanism and collimation measurements 22 p3881 A67-39515

STARK EFFECT

Hydrogen line profile in Paschen series of solar spectrum, taking into account Stark effect and line broadening 04 p0702 A67-15567
Stark and Zeeman splitting in far IR spectra of erbium, dysprosium and samarium ethyl sulphate 04 p0686 A67-15778
Differential Stark effect in second excited state of alkali metal atoms described, using electric field level crossing spectroscopy 06 p1035 A67-17830
Electric field measuring methods, showing Stark effect in rotational spectra of gases as most promising 08 p1311 A67-20652
Expression for electron contribution to Stark broadening, using impact approximation with Lewis or Debye cut-offs 11 p1823 A67-24491
Stark broadening of hydrogen lines of large principal quantum number for RF transitions by electron and ion impact approximation 14 p2389 A67-28839
Stark-broadened isolated ion line agreement between theory and experiment obtained by Griem theory or by impact approximation of GBKO theory 15 p2520 A67-29678
Magnetic susceptibilities and anisotropies of manganous acetate tetrahydrate crystal measured at various temperatures 15 p2540 A67-30091
Spectroscopic measurements of cold plasma charged particle concentrations, specifically spectral broadening due to Stark effect, forbidden-line intensities affected by internal electric fields and autoionization line intensities 17 p2896 A67-32161
Stark effect in plasma, discussing theory, Lorentz symmetrical dispersion profile, atomic interaction, etc 17 p2901 A67-32404
Ionized gas produced by exploded lithium wires, presenting physical measurements, finding self-consistent solution of temperature and electron concentration 19 p3261 A67-35182
Significance of far field portion of plasma microfield 19 p3285 A67-35344
Electro-optical effect and Stark effect in exciton levels of cadmium sulfide 19 p3304 A67-35428
Absolute transition probabilities, Stark widths and shifts of S I and S II lines determined experimentally 19 p3266 A67-36089
Line profiles and Stark widths of singly ionized carbon and calcium atoms measured using plasma source 19 p3299 A67-36092
Transient Stark and Zeeman spectral line shifts in plasma emission measured with multiple beam Fizeau interferometer, discussing instrument errors 20 p3439 A67-36351
Quadratic Stark effect in argon II calculated assuming LS coupling 21 p3659 A67-38408
Stark effect spectral line broadening due to current or electron beam excitation of stochastic plasma 21 p3670 A67-38690
Energy difference between metastable levels of hydrogen-like atom determined by measuring lifetime in electrostatic field, yielding average Lamb shift in Li ion 22 p3839 A67-39202
He ions beam passing through electric field and inducing light intensity fluctuations when emitted from fine structure levels observed via Stark interference 23 p4029 A67-40956
Rapid scan spectrometer used to measure Stark broadened H lines in plasma column, determining electron density 23 p4032 A67-40957

STARLIFTER AIRCRAFT

S C-141 AIRCRAFT

STARTER

SA ENGINE STARTER
SA IGNITION SYSTEM
Starter cartridges for jet engines, discussing operational problems and mechanical design, igniter and propellant development, etc 15 p2423 A67-29982
Hydraulic power systems for V/STOL noting self-sufficiency on start-up and auxiliary power source 20 p3366 A67-37552

STATE

S ELECTRON STATE
S EXCITED STATE
S GROUND STATE
S SOLID STATE
S STEADY STATE
S TRIPLET STATE

STATE EQUATION

SA HUGONOT EQUATION OF STATE
Algorithm for reducing linear time-invariant differential systems to state form applied to systems described by transfer functions 01 p0047 A67-11219
State variable equation transformation to phase variable canonical form 01 p0047 A67-11222
State variables of shock induced states, analyzing calculations based on assumption of either constant volume or pressure from structural point of view 03 p0403 A67-13717
Book on propagation, reflection and superposition of shock waves in ideal gases based on theory of hyperbolic nonlinear PDEs 04 p0601 A67-14467
Solid-solid impact at hypervelocities using flow equations, noting variations of impact velocity, projectile shape and density and state equation 04 p0710 A67-15004
Regenerative thermomagnetic power devices, considering state equations for ferromagnetic material, power cycle and entropy change due to magnetization [ASME PAPER 66-WA/ENER-1] 04 p0555 A67-15414
Dynamic systems identification by digital computer modeling in state space formulation of ordinary differential equation [ASME PAPER 66-WA/AUT-10] 04 p0593 A67-15418
Network analysis with state variables describing system stored energy 05 p0781 A67-16022
Inverse operation for Jaumann derivative /integration/ applied to rheological equations of state for viscoelastic fluids 06 p0991 A67-18777
Dipole-dipole molecular interaction contribution to thermodynamics and state equation of excited molecular gas, noting dissociation possibility 06 p0991 A67-18802
Thermodynamic properties of hydrogen peroxide between 273 and 2000 K, deriving equations of state 07 p1265 A67-19123
Heat transfer in compressed gas evacuated from container, using numerical integration of state equation 07 p1287 A67-19324
Compressibility factors of gases determined by using sonic velocity measurements, providing reliable representations of equations of state 07 p1168 A67-19577
First two terms of high temperature equation of state for argon 08 p1355 A67-21255
Gas state equation determination from trajectory analysis of piston in hypersonic wind tunnel 11 p1782 A67-24759
Finite time stability of system trajectory under perturbing forces and within specified regions of state space 11 p1771 A67-24892
Equations in hodograph plane obtained for two-dimensional polytropic gas flow in presence of shock waves 12 p1892 A67-25443
State diagram structure of Ti-Cu system examined using metallographic, thermographic, X-ray and microhardness analyses 13 p2131 A67-26473
Equation of state for Debye continuum governing nonlinear propagation of perturbations terminating in shock wave at distance 14 p2374 A67-28982
Nonlinear differential equations of systems describable by state model solved by incremental linearization 15 p2458 A67-29908
Optimal control theory applied to extremum control in dynamic programming equation derivation for simplified extremum control problem 15 p2465 A67-30343
Hydrodynamic detonation theory, noting

equations of state, nonsteady detonation, further problem areas, etc 16 p2778 A67-30837

Scaling-law equation of state for gases in critical region 16 p2778 A67-31061
Process identification by decomposition method of multilevel systems analysis, noting computer estimation of state variables of discrete time systems 16 p2647 A67-31650
Optimal control of measurement subsystems within feedback control systems 16 p2650 A67-31676
Nonrotating, hydrostatic models of geochemically likely planets calculated using solar elemental abundances and equations of state for cold materials 16 p2754 A67-31748
State equation for interpolation and computations including parahydrogen thermodynamic properties using one set of 24 coefficients for all fluid states 16 p2780 A67-31763
Algorithm for constructing state equations corresponding to linear time varying system of differential equations 17 p2829 A67-32627
State variable difference equation method for HF solution of ordinary differential equations in digital simulation with nonlinearity 18 p3005 A67-33662
Unconfined nitromethane transient initiation, determining differential conservation, state and reaction rate equations, using two-dimensional computations 18 p3153 A67-33824
Regenerative thermomagnetic power devices, considering state equations for ferromagnetic material, power cycle and entropy change due to magnetization [ASME PAPER 66-WA/ENER-1] 18 p2989 A67-34128

Three-dimensional hypersonic flow past blunt cones calculated by modified method of characteristics, taking into account physicochemical equilibrium conversions 18 p2984 A67-34213
Dipole-dipole molecular interaction contribution to thermodynamics and state equation of excited molecular gas, noting dissociation possibility 18 p3029 A67-34421
High pressure equations of state including electron gas correlation energy, giving density vs pressure curves for various elements 18 p3104 A67-34594
Dynamic equations for adiabatic changes of state for mixtures of partially ionized gases with chemical reactions 19 p3286 A67-35348
LF acoustic/magnetoacoustic wave propagation in partially ionized plasmas studied within framework of macroscopic plasma dynamics, using dynamic adiabatic state equation 19 p3290 A67-35375
Classification of small amplitude waves, surfaces of weak discontinuity and shock waves in ideal MHD medium obeying adiabatic state equation 19 p3294 A67-35409
Strain rate history effects on strain hardening curve for aluminum described by state equation 19 p3245 A67-35448
Homomorphic decomposition set of state quantity of finite automation 19 p3202 A67-35605
Dynamic system with state at any instant represented by point in Euclidean space of n dimensions 19 p3203 A67-35902
Reentry trajectory optimization by repetitive computations of impulse response functions and state equations 19 p3190 A67-36072
State space equations formulated for general class of nonlinear networks, deriving block diagram of relationships 20 p3407 A67-36332
Dynamical consequences of thermostatic concept of stability within general framework of modern thermodynamics 20 p3543 A67-36428
Equations of state of matter at high pressures and temperatures, discussing temperature density regions, theoretical calculations, etc 20 p3485 A67-36929
Crystal deformation and uniaxial failure under complex loading due to stress and temperature variations, applying physical state equation 20 p3540 A67-37057
Exact equation of state for two-dimensional plasma of equal positive and negative charged particles interacting by Coulomb potential 20 p3501 A67-37293
Generalized Legendre-Clebsch condition applied to singular arc trajectory solutions

of state and adjoint equations for optimal control 21 p3602 A67-38023

Thermodynamic properties of hydrogen peroxide between 273 and 2000 K, deriving equations of state 21 p3731 A67-38167

Computational considerations for trajectory optimization in bounded state space, discussing necessary and sufficient condition 21 p3604 A67-38443

Polytrope structure from integrodifferential equation assuming metric, energy momentum tensor for static spherical symmetry and polytropic equation of state 21 p3658 A67-38615

Equations in hodograph plane obtained for two-dimensional polytropic gas flow in presence of shock waves 21 p3613 A67-38816

Liquid mercury equation of state and electrical resistivity at high temperatures and pressures 21 p3686 A67-39104

Eigenstate variables for representation of optimum orbital transfer problems, discussing numerical integrations 22 p3878 A67-39154

Optimal control problem with state variables subject to inequality conditions, deriving Pontryagin principle and differential equation 22 p3826 A67-39194

Classical scalar plasma with relativistic Hartree equilibrium approximation for energy, entropy and state equation noting effect of linear perturbation 22 p3842 A67-39209

Discontinuous integrands in calculus of variations formulations of trajectory optimization and maximum payload problems with discontinuous state variables 22 p3827 A67-39954

Real gas jet equations of motion, energy and continuity derived, transformed and solved for mixing region, discussing approximate state equation construction 23 p3989 A67-40729

Equilibrium state of two-dimensional lattice liquid-gas system using cluster variation method for nucleation and thin film growth studies 23 p4040 A67-40967

Temperature dependence of elastic constants of 1060 and 6061-T6 aluminum using ultrasonic pulse echo method, estimating high pressure state equation 23 p4021 A67-41469

Noninteraction and deadbeat response in linear sampled data multivariable systems synthesis by state difference equation 24 p4134 A67-42027

State variable approach to linear differential equations, coding for digital computation 24 p4179 A67-42933

STATE VECTOR

Phase-space collision domains corresponding to hard-sphere N-body problem in gas transport theory 01 p0112 A67-10144

Satellite rendezvous guidance laws applicable to circular, near-circular and elliptical orbits, using Lagrangian formulas for position and velocity in two-body orbit 02 p0264 A67-12315

State space method for navigation problems of nominal trajectories 06 p1028 A67-17927

Periodic oscillation mode of time invariant feedback system containing relay determined, using state space approach 06 p0978 A67-18719

Computation of optimal estimators synthesis reduced through partitioning of system state vector 11 p1764 A67-24443

State space methods approach to model referenced adaptive control systems design using differential equations 11 p1771 A67-24894

Derivation of moments of continuous stochastic system 15 p2459 A67-30131

Suboptimal control of large scale dynamic system consisting of two weakly coupled subsystems using aggregation 16 p2647 A67-31645

Synthesis technique applying Lapunov theory for state vector tracking of nonlinear multivariable control systems illustrated by reactor control design 16 p2649 A67-31662

Differential correction vectors for non-Keplerian reference orbits, reexamining rotating ellipses in Hansen type intermediaries 21 p3705 A67-38612

Lateral stability augmentation of supersonic aircraft using linear multichannel state-vector optimal feedback control 22 p3746 A67-40155

Serial/matrix technique extended to give multivariable linear system responses defined in state space 23 p3983 A67-40646

Errors in state vector from amplitude quantization in feedback control loop, noting finite word length in hybrid computer simulation 24 p4134 A67-42023

Design procedure for estimating state vector of discrete-time linear stochastic system with constrained memory estimator 24 p4135 A67-42185

STATIC AERODYNAMIC CHARACTERISTICS

Wind tunnel investigation of effect of ground level on static aerodynamic characteristics of sideslip for rectangular and delta wing with rudder assembly 07 p1126 A67-19886

Static characteristics of radial gas dynamic bearing, using differential equation for pressure distribution calculation 13 p2122 A67-26351

STATIC DEFORMATION

Functional analysis of plane problem of elastostatic theory for multiply-connected regions with given surface traction 01 p0160 A67-10516

Universal relations for static deformations in isotropic compressible elastic bodies determined by method that may be applied to isotropic incompressible elastic bodies 01 p0162 A67-10799

Plane oscillations of elastic pendulum with shaft undergoing bending deformation, determining principal zone of instability for action by longitudinal harmonic force 03 p0469 A67-14161

Heat treatment and microstructural observations in wrought Ni-base superalloy Udimet 700 in static creep, determining fracture and deformation properties 06 p1015 A67-17809

Static deflection of parallelogram plates with clamped edges subjected to uniformly distributed pressure studied by energy method 15 p2573 A67-29312

Apparatus for measuring metal/alloy hot hardness using indenter static impression and unilateral flattening 19 p3227 A67-34930

Stress functions for truncated conical shell buckling under uniform static pressure 23 p4081 A67-41760

STATIC ELECTRICITY

SA ATMOSPHERIC ELECTRICITY

SA ELECTROSTATICS

SA LIGHTNING

Agema Gemini electric charge monitor measures static charge difference between orbiting space vehicles 01 p0074 A67-11128

Aviation fuel static electricity elimination by Shell additive ASA-3 05 p0872 A67-16234

Explanation of anomalies of experimental static current-voltage characteristics of GaAs tunnel diode oscillators 12 p1917 A67-26098

Static electric fields produced in magnetosphere and effects such as motion of visual and radio aurora and currents in ionosphere 18 p3035 A67-33600

Static electricity as potential reliability problem in electronic equipment production, noting transistor failure 20 p3397 A67-36608

Null-field static dischargers location and maintenance on Convair 880/880M and 990 aircraft 22 p3745 A67-39733

Static characteristics of 2N1304 germanium junction transistor exhibited by two surfaces in three-dimensional space 24 p4128 A67-41925

Static electrification mechanism of particles in pseudofluidized bed in terms of causes of observed polarities of column wall and various particles 24 p4254 A67-42256

STATIC FIRING

Transducers role in problems associated with accurate and precise measurements during static firing tests of solid propellant motors 01 p0073 A67-11111

Role of large solid propellant rocket motor in U.S. space program noting design, technology, testing, cost, thrust-vector control systems, etc 01 p0142 A67-11447

Static firing ground testing of Saturn launch vehicle [AIAA PAPER 67-234] 07 p1165 A67-20057

Design criteria for NASA test facility for firings of 20 inch diameter solid rocket motors [AIAA PAPER 67-236] 07 p1241 A67-20059

STATIC FRICTION

Solid lubricants frictional behavior in

press-fit tests, measuring sliding speed, load and surface roughness as function of time [ASLE PREPRINT 67AM 5A-2] 14 p2325 A67-28786

STATIC LOADING

Structural loading, discussing stationary and nonstationary-random and severe loading processes 01 p0163 A67-11014

Discrete method strength calculation for round cylindrical shells applicable to computer solution of normal external loading problems 02 p0339 A67-12442

Micromechanical behavior of composite materials under static tension, bending, shear and fatigue loading investigated analytically and experimentally 03 p0455 A67-13440

Digital simulation of Gaussian random load forcing function and motion equations of nonlinear vibration of damped elastic beam 04 p0656 A67-14447

Molsture effect on slow crack propagation in thin sheets of SAE 4340 steel under static and cyclic loading [ASME PAPER 66-WA/MET-6] 04 p0639 A67-15340

Coupled system of thin elastic shells, giving response to static or harmonically oscillating loads or to unloaded natural frequencies and mode shapes, using Green matrix [AIAA PAPER 67-45] 06 p1103 A67-18351

Dynamic stress concentration due to elastic wave analyzed by high speed photoelasticity to clarify difference between dynamic and static stress distribution 07 p1262 A67-19414

Literature review on effect of static fatigue on filament wound fiberglass internal pressure vessels, noting program to test and expand data 08 p1415 A67-20432

Computer program for solving bending of plates of any shape and with any variation in boundary conditions for static loading and transverse vibration 10 p1731 A67-23843

Material hysteresis model for transient dynamic analysis 11 p1874 A67-24358

Elastic-plastic body and elastic work hardening materials under static loading, using maximum principle for computing procedures 11 p1876 A67-24622

Natural oscillations of elastic truncated conical shells of revolution under composite static load 12 p2026 A67-25613

Initial imperfection effects on free oscillation frequencies of cylindrical shell under static axial load 12 p2026 A67-25619

Equation for relation between critical stresses of cylindrical shell loading and minimum natural-oscillation frequency of unloaded shell 12 p2027 A67-25623

Beryllium joints and structures tested for static and repeated loading fatigue at room and high temperatures 13 p2123 A67-27132

Book on safety of structures 14 p2395 A67-28030

Static operating characteristics of diaphragm pneumatic logic device 14 p2275 A67-28347

Secure mechanically fastened assemblies in static and dynamic stress, showing effect of tightening preload [ASME PAPER 67-DE-3] 14 p2327 A67-28865

Cleaved surfaces of Mo cermet binary alloys structures annealed and fractured under static bending loads studied for surface properties 17 p2871 A67-32133

Fatigue strength calculated using fracture criterion for multiaxial alternating stress and combined alternating bending and torsional stresses 17 p2960 A67-32632

Brittle coatings for stress distribution analysis during static and dynamic loading, describing chemical composition and characteristics and giving formulas and diagrams 18 p3045 A67-33741

Tension and compression, dynamic and static flexural loading and vibration tests of bilaminate filament wound composite [SESA PAPER 1219] 18 p3141 A67-33889

General theory advanced for analysis of statically loaded elastic structures using concept of finite members interconnected in finite loaded joints 22 p3911 A67-39559

Silide wire strain gauge to measure static strains and stresses at high temperatures 22 p3809 A67-40476

Permanent deformation and interaction effects of rigid plastic clamped beam with constraints against axial displacements and subjected to transverse impulsive

loading 23 p4072 A67-40606

STATIC PRESSURE

SA HYDROSTATIC PRESSURE

Aerodynamic problems of turbomachinery, investigating effect of geometry and aerodynamic cascade parameters on flow deflection, static pressure difference and flow losses 04 p0547 A67-14985

Supersonic wind tunnel test providing static pressure measurements for use in cylinder flutter calculations 08 p1277 A67-20588

Wakes behind axisymmetric blunt based bodies, noting similarity among wakes through measurements of velocity, turbulence and static pressure 08 p1277 A67-20706

Gas flow velocity and static pressure profiles experimentally measured in combustion zone of gas turbine combustion chamber model under atmospheric conditions [SAE PAPER 670201] 09 p1561 A67-22545

Hemispheric pressure distributions, measuring effect of Mach number, hole size and angular position of hole on Pitot pressure 13 p2220 A67-27193

Axisymmetric free turbulent jet flow with swirling vortex motion over wide range of swirl degree 17 p2838 A67-32417

Supersonic combustion simulation for hypersonic flight in relation to scramjet operation, discussing auto-ignition limits [CI PAPER 67-6] 19 p3344 A67-35001

Static pressure probe nose derived from supersonic slender body theory and shaped for subsonic speeds 21 p3564 A67-38535

Second order weak interaction expansion for hypersonic flow past adiabatic flat plate, obtaining expressions for static pressure, displacement thickness and skin friction 21 p3566 A67-38892

Gas dynamic self-regulation of supersonic nozzle consisting of cylindrical channel with central body, measuring nozzle inlet and static pressures 22 p3868 A67-39544

STATIC STABILITY

Liapunov second method applied to elastostatic stability, discussing applicability of Dirichlet principle and Galerkin method 01 p0161 A67-10647

Boundary value analysis of static problems of transversely isotropic solid and hollow elastic cylinders 06 p1099 A67-17864

Book on flight characteristics, static stability, equations of motion, excitation and response 06 p0949 A67-18725

Inviscid equilibrium gas stability characteristics for pointed and spherically blunt bodies in unsteady supersonic flight in Mars atmosphere 07 p1258 A67-19380

Payload-apogee altitude performance, static stability and dynamic motions of Tomahawk vehicle analyzed for ability to meet 100 km sounding rocket requirement 08 p1404 A67-20494

Helmholtz velocity profile instability in atmosphere with unstable density gradient /negative Richardson number/ 08 p1323 A67-21388

Axisymmetrical deformation and static instability region of circular cylindrical shell under longitudinal compressive load 12 p2026 A67-25615

Aircraft handling qualities research with variable static stability aircraft used as in-flight simulator [SAE PAPER 670261] 13 p2054 A67-27296

Characteristic scales of thermal convection in unstable atmosphere, discussing time evolution of total kinetic energy and lifetime for dry air case 13 p2116 A67-27460

Low speed aerodynamic static stability of winged and wingless reentry configurations 14 p2239 A67-27796

Stability and asymptotic behavior of dynamical systems defined by autonomous functional or partial differential equation and conditions for applying Liapunov theorem 14 p2342 A67-28081

Theory of available potential energy and rate of change and variational approach to atmospheric energetics 18 p3074 A67-34096

Wing twist distortion effect on glider static longitudinal stability with stick fixed 18 p2986 A67-34373

Navy variable stability studies of longitudinal handling qualities in simulated carrier approach [AIAA PAPER 67-576] 19 p3174 A67-35971

DC potential solutions for low pressure Cs

diode with zero slope at emitter noting stability, oscillations and instability for ion/electron ratios 23 p4031 A67-40886

Stress-strain relation in viscoelastoplastic bodies noting static instability under conservative load 24 p4246 A67-41932

Tunnel diode low level detection characteristics under various bias conditions, discussing sensitivity performance and stability characteristics 24 p4131 A67-42444

Earth and planetary atmosphere entry problems for blunt nosed slender vehicles noting aerodynamics, stability, heating, ablation and interaction of effects [AIAA PAPER 67-803] 24 p4243 A67-42963

STATIC STABILITY AND CONTROL

Longitudinal static stability margin of glider for small lift coefficients showing effect of torsional deformation 16 p2596 A67-31001

Static and dynamic inventory control models for logistics planning and operational readiness with cost constraints 18 p3162 A67-34680

STATIC TESTING

Static and fracture tests with C-160 /Transall/ transport 01 p0048 A67-10212

Data acquisition techniques and system accuracies for static testing of solid propellant rocket engines 01 p0051 A67-11109

Titanium alloy forging tests covering notched tension, compression, shear, bearing, fracture toughness and smooth and axial fatigue 03 p0446 A67-13552

Mississippi Test Facility gas metal-arc welding of T-1 steel critical high pressure piping systems for Saturn V launch vehicle 03 p0430 A67-13691

Effect of locking dovetail joint geometry on static strength 03 p0528 A67-14077

Long term tensile stress-rupture strength of alloys calculated from static tensile strength tests at elevated temperatures [ASME PAPER 65-MET-12] 05 p0827 A67-16212

Transverse variation effects on accuracy of skin friction measurements determined via static hole pair 06 p1005 A67-18753

Model testing for design evaluation of major components and configurations of static test and launch facilities, noting hot jet model [AIAA PAPER 67-237] 07 p1165 A67-20060

Static and fatigue properties of repair welded aluminum and magnesium premium quality castings 08 p1333 A67-20360

Liquid hydrogen fuel tankage thermal protection in manned hypersonic vehicles, discussing results of tests in steady state conditions [AIAA PAPER 67-297] 12 p2035 A67-26012

Rocket nozzle design to reduce gas misalignment noting turning moment, nozzle geometry, cold gas tests, static and flight trials of motors, etc 15 p2547 A67-29995

Statistical probability distribution for determining systematic errors of potentiometer multiplier by Monte Carlo method /static testing/ 16 p2633 A67-30464

Kinetic approach to fatigue investigation in calculation of cyclic lifetime from static test data 23 p4074 A67-40663

STATION

S GROUND STATION

S METEOROLOGICAL STATION

S PLANETARY BASE

S SPACE STATION

S TRACKING STATION

STATIONARY ORBIT

Solid body motion equation about stationary point fixed at earth surface 02 p0267 A67-11961

Early Bird satellite measurement of ionospheric electron content obtained from Faraday rotation data [RASSA PAPER 1-10-131] 03 p0417 A67-14242

Broadcasting of TV by satellites, examining altitude effects, stationary satellite types, FM advantages, etc 06 p0956 A67-17560

Pacific equilibrium longitude for stationary satellite, discussing processing of Syncom III data, drift rate calculations, etc [AIAA PAPER 67-91] 06 p1086 A67-18338

Synchronous satellite communication systems including altitude and motion effects, time delay, control system, antenna, etc 12 p1907 A67-25991

Orbit determination of stationary satellites through data analysis, noting perturbation effect and estimation of Early Bird satellite

orbit 13 p2208 A67-27522

Time and frequency accuracies obtainable with geostationary satellites, noting measurement error 15 p2565 A67-29593

24-hr satellite positions studied for librations, using linear theory 15 p2560 A67-30043

Solid body motion about stationary point fixed at earth surface 17 p2886 A67-33278

Radiated power and frequency limitations of repeater in stationary satellite covering physical, legal and project viability limitations 18 p2999 A67-33657

Reliability, orbit achievement and control and increased power bandwidth as factors making communications satellites economically feasible 19 p3350 A67-35649

Pacific equilibrium longitude for stationary satellite, discussing processing of Syncom III data, drift rate calculations, etc [AIAA PAPER 67-91] 22 p3886 A67-40085

Stationary satellite to provide educational TV to underdeveloped lands noting design, transmission terminals and safeguards against control and propaganda [AIAA PAPER 67-963] 24 p4260 A67-43042

STATIONKEEPING

Gemini rendezvous results, discussing equipment, maneuvers, docking, stationkeeping, orbital calculation, etc 06 p1098 A67-18649

Orbital behavior and stationkeeping propulsion requirements for synchronous satellites, considering solar radiation and earth oblateness effects 09 p1571 A67-21697

Solar photon radiation reaction produced on body of satellite and utilized for satellite stationkeeping 13 p2213 A67-27489

Manual control stationkeeping simulation, studying tether visual rendezvous techniques and fuel economy [AIAA PAPER 67-617] 19 p3337 A67-36006

Solid propellant electric thruster /SPET/ using pulse plasma for spacecraft attitude control and stationkeeping [AIAA PAPER 67-661] 21 p3690 A67-38697

Satellite orbit adjustment, stationkeeping and attitude control of typical earth-and sun-synchronous satellites by electric propulsion systems [AIAA PAPER 67-719] 21 p3694 A67-38745

Thrust, power and performance requirements for synchronous satellite simulated for evaluating ion propulsion feasibility [AIAA PAPER 67-720] 21 p3694 A67-38746

Multijet electrothermal systems for attitude control and stationkeeping of synchronous communications satellite [AIAA PAPER 67-723] 21 p3694 A67-38748

Radiosotope heating for ionizer temperature of contact ionization thrusters for satellite attitude control and stationkeeping, studying power source mass saving [AIAA PAPER 67-735] 21 p3695 A67-38758

Electric propulsion applied to satellite stationkeeping and attitude control, noting ion engine resistojet combination providing complete redundancy [AIAA PAPER 67-722] 21 p3697 A67-38961

Colloid microthruster technology, discussing stationkeeping application, energy loss, diagnostic techniques, etc [AIAA PAPER 67-531] 22 p3867 A67-39200

STATISTICAL ANALYSIS

SA REGRESSION ANALYSIS

Binomial probability distribution applied to air battle analysis, discussing fire doctrines, attrition rates, weapon design classes and limitations of approach [AIAA PAPER 66-781] 01 p0169 A67-10527

Counting errors and amplitude spectra distortion in detectors for statistical characteristics of information contained in signals 01 p0066 A67-10653

Fluctuation noise effects on phase-locked automatic frequency control system obtained using Markov processes, determining phase difference probability density and statistical characteristics 01 p0037 A67-10713

Statistical-dynamical model for total chemical reaction cross sections using activated complex concept and integral equation 01 p0019 A67-10884

Statistical and spectral density analyses of stationariness and behavior law of atmospheric turbulence 01 p0054 A67-11087

Electron density fluctuations in turbulent wake, using stochastic analysis and statistical

- averaging [AIAA PAPER 65-818] 01 p0007 A67-11168
Methods, schedules and cost of applying computer technology to circuit design, including Apollo and LEM programs 01 p0031 A67-11335
Radiation stress effect on component reliability of electric circuits analyzed via mathematical statistics 02 p0210 A67-11527
Time-normalized Fourier transform of sampling function of stationary random process as bounded nonstationary random function of frequency 02 p0224 A67-11901
Stochastic process estimate of frequency and duration of weather events, using Monte Carlo simulation of probability distributions 02 p0261 A67-12079
Unreliability of mean-time-between-failures concept as standard quality measure for mechanical systems 02 p0249 A67-12426
Relation between Forbush decreases and chromospheric flares, obtaining longitudinal distributions before and after onset, using statistics 02 p0311 A67-12592
Statistical analysis of cosmic ray particle elastic scattering, noting isotropic nature of angular distribution 02 p0315 A67-12750
Statistical model of cost of elements of system undergoing gradual breakdown, giving optimal distribution of mean relative deviations of input and output parameters 03 p0389 A67-13090
Asymptotic behavior of distribution of maximum for class of processes with independent increments 03 p0458 A67-13340
Statistical theory for strength of laminar composites used to optimize biaxial and multidirectional tensile strength properties of laminated materials 03 p0522 A67-13442
Calculation of statistical sum of bounded states of electron in atom in Debye plasma 03 p0478 A67-13615
Test arrangement and statistical data analysis for remote sensing of local flow instabilities and turbulence 03 p0422 A67-13773
Statistical analysis for pulsed flow measurement evaluation using correlation and regression techniques 03 p0403 A67-13777
Meteor sighting probability and problem of actual number of meteors 03 p0511 A67-13815
Miscellaneous results connected with simple system alternating between two states, running or under repair 03 p0432 A67-13824
Statistical properties of newly identified radio galaxies, including monochromatic luminosity and linear extension distributions 03 p0512 A67-13878
Book on Monte Carlo method, method of statistical trials 03 p0462 A67-14256
Statistical investigation of characteristics of chains of type I solar radio bursts including distribution with midfrequency, position on solar disk, lifetime, etc 03 p0508 A67-14359
Nonlinear recognition procedures, discussing probability distribution approximation by orthogonal expansion and by-product of low order conditional probabilities 04 p0578 A67-14800
Statistical topological analysis of electric measurement precision and accuracy 04 p0657 A67-14887
Transfer functions and statistical properties of SST in atmospheric turbulence 04 p0620 A67-14893
Statistical analysis of high speed aircraft plotting, including wing and tail surface effects and pilot work load and performance 04 p0653 A67-14894
Statistical parameters of linear antenna arrays after removal of emitters 04 p0583 A67-15149
80-column punch card prototype for statistical generalization of cloud data from meteorological satellite 04 p0651 A67-15470
Aircraft piston engine components reliability characteristics determined from defect data survey, using statistics 04 p0691 A67-15902
Seismic refraction measurements, computing statistics for depth to Moho, crustal thickness and upper mantle velocity for geographical and geological provinces 05 p0796 A67-16152
Statistical characteristics of meteor radio echoes in Geminides stream noting duration, amplitudes, intervals and ranges 05 p0889 A67-16205
Objective statistical approach to tilt table data analysis using computer to define characteristics of cardiovascular deconditioning resulting from bed rest, water immersion and space flight 05 p0754 A67-16276
Synthesis and control strategy of optimal final value linear system under random environment statistically considered, using Bellman dynamic programming 05 p0783 A67-16442
Nonstationary response of closed loop control systems with random characteristics, noting statistical analysis of error response and conversion of random control system to constant parameter 05 p0783 A67-16443
Statistical method of calculation of atmospheric thermal, conservative and dynamic characteristics using measured ozone distribution 05 p0796 A67-16488
Statistical dislocation theory of crystal brittle fracture seen as stochastic process with microcrack formation and propagation under plastic deformation 05 p0919 A67-16504
Multiphoton absorption processes, coherence of radiation fields and statistical properties of laser light absorption 05 p0823 A67-16681
Multivariate statistical analysis of wind sounding data, applying high degree of correlation between two wind parameters and empirical density function [AIAA PAPER 66-353] 05 p0838 A67-17214
Statistical problems in use of EM data for remote sensing of geological attributes of lithosphere-atmosphere interface 05 p0803 A67-17387
Numerical handling of data in statistical study of servomechanism, noting circuitry and random function generator 06 p0966 A67-17586
Component, due to recombination-generation process, of overall noise from semiconductors under electric current, measuring probability densities by statistics 06 p0966 A67-17588
Probability estimation, discussing types, Bayesian method for binomial and multinomial distributions, sampling methods, etc 06 p1022 A67-17646
Analysis of differences in number of sunspot groups between Greenwich and Zurich observations 06 p1083 A67-18066
Histogram construction via algebraic Monte Carlo method, determining simultaneous effect of several input statistical variables on output variable [AIAA PAPER 67-210] 06 p1024 A67-18326
Atmospheric turbulence effects on statistical design and analysis of space vehicles [AIAA PAPER 67-134] 06 p1096 A67-18359
Analyzer of characteristic function of random phase of quasi-harmonic signal using statistics 06 p0972 A67-18392
Level quantization effect in statistical analysis of closed loop digital automatic systems 06 p0976 A67-18406
Oscillatory ground wind response of Atlas/Agema examined, using statistical theory of extreme values 06 p1104 A67-18492
Laser velocimeter measurement of point velocities in turbulent liquid flow in pipe, using statistical analysis to verify results [AIAA PAPER 67-179] 06 p0990 A67-18511
Long range weather forecasting, discussing necessity of nonadiabatic processes 06 p1027 A67-18605
Interdiurnal pressure variability as measure of kinetic energy of air masses 06 p1027 A67-18606
Comparison of VLF emissions of two conjugate stations, noting statistical results for diurnal variation, magnetic activity, hss, etc 06 p0997 A67-18698
Statistical analysis of aircraft accidents from 1938 to present 06 p0949 A67-18746
Statistical analysis discrepancy in physical experimental values of buckling pressures of spherical shells 06 p1111 A67-18876
Oscillations in stationary gas discharge, describing device for calculation of correlation function for electrical signals 07 p1227 A67-19120
Statistical analysis of distribution of cosmic ray ages of stone meteorites 07 p1249 A67-19540
Particle number fluctuation in single cell of Kastler photon set, discussing statistical properties of laser emission in multimode excitation regime 07 p1196 A67-19599
Curves of probability of detection vs signal to noise ratio for log-normal signals in Gaussian noise, considering correlated and uncorrelated signals 07 p1144 A67-19868
Definition and computation of daily solar flare activity index 07 p1251 A67-19945
Frequency response functions determined from correlation functions of force and response, using Bartlett triangular weighting function 08 p1353 A67-20592
Random deviation statistical analysis of acoustic and electromagnetic waves by comparatively large slope irregularities 08 p1294 A67-20820
Fracture of viscoelastic bodies, predicting statistical variability of rupture data for uniform and nonuniform excitation histories 08 p1421 A67-20913
Strength of laminar composites, discussing application of statistical theory to determine parameters 08 p1346 A67-20915
Lunar cratering statistics interpretation in terms of meteoroid impact hypothesis, noting equilibrium distribution function [AAS PAPER 66-183] 08 p1387 A67-20958
Book on electromagnetic wave propagation and turbulent media covering invariant imbedding method, turbulence generation, statistical methods of analysis, etc 08 p1295 A67-20964
Statistical analysis of errors in angular measurement of distant objects due to gravitational scattering along light path 08 p1398 A67-21232
Soviet book on random function theory application to statistical problems in radio physics 08 p1295 A67-21336
Geomagnetic storms due to solar flares statistically analyzed to obtain configuration of solar plasma flow generated by solar flares 08 p1377 A67-21360
Generalized Gaussian distribution functional for weak plasma turbulence neglecting three-point correlation function 08 p1366 A67-21415
Theory of superconductivity on basis of phonon model for finite temperatures, comparing four-fermion/electron interaction with Bardeen hamiltonian model theory of superconductivity on basis of phonon 08 p1372 A67-21491
Stochastic approximation method for determining real number from observation of random variables 09 p1524 A67-21933
Book on probabilistic theory of structural dynamics, analyzing responses of structures to random vibrations 09 p1575 A67-21983
Yield strength and reliability of structural cluster welds determined using statistical analysis 09 p1506 A67-22308
Statistical dynamics applications to evaluate system dynamic characteristics from operational data 09 p1469 A67-22460
Thermal equilibrium of quantum mechanical system composed of atom nuclei and electrons, using statistical method to eliminate divergence in sum of states of electron proton pair 09 p1550 A67-22664
Type II and IV solar radio bursts analyzed, determining nature and geoeffectiveness of causing agents 10 p1698 A67-22776
Monte Carlo and direct calculation methods analyzed in connection with microelectronic circuit designs 10 p1610 A67-22978
Statistical properties of dispersive waves in upper atmosphere analyzed, using correlation technique 10 p1639 A67-23206
Quantumstatistical thermodynamics with several temperatures for indivisible observation level 10 p1733 A67-23477
Theory of statistical analysis of data distributed over sphere 10 p1652 A67-23547
Statistical energy analysis for multimodal random vibration of complex system, discussing power flow, modal responses, kinetic energies, etc [ASME PAPER 67-VIBR-8] 11 p1872 A67-24168
Spatial variations in mean square response above lowest resonance frequency determined, using statistical analysis [ASME PAPER 67-VIBR-22] 11 p1872 A67-24181
Generalization of binary processes, discussing time domain and frequency domain analysis 11 p1813 A67-24312
Flight time estimation methods for iterative solutions of optimum trajectories

by numerical integration 11 p1859 A67-24436
Oscillating plateholder for determining instantaneous focal length of large telescopes 11 p1791 A67-24459
Inhomogeneous gas of weakly coupled relativistic electrons, deriving kinetic equation for particle electromagnetic field system 11 p1782 A67-24781
Statistical analysis of optimum control system design by parameter adjustment, finding systems transfer function through Wiener-Hopf integral 11 p1772 A67-25082
Statistical analysis of solar dm radio bursts in frequency range 536-2000 mc/s 12 p1993 A67-25132
Semirelativistic approximation of matter-radiation interaction 12 p1966 A67-25146
Long term variation in magnitude of diurnal anisotropy of solar cosmic rays analyzed quantitatively by applying statistical techniques to recorded data 12 p1993 A67-25205
Reliable decisions from unreliable measurements of electronic equipment via statistical method 12 p1949 A67-25524
Statistical performance confirmation of wideband random equalizer, emphasizing analysis technique, analyzer characteristics and power spectral density plot 12 p1942 A67-25692
Statistical method of calculation of atmospheric thermal, conservative and dynamic characteristics using measured ozone distribution 13 p2109 A67-26344
Flight Load Survey program, written in Fortran IV, for accurate and rapid sounding of wind-induced loads on aerospace launch vehicle [AIAA PAPER 66-470] 13 p2212 A67-26820
Statistical analysis of beryllium cross-rolled sheet, hot pressed block and ring rolled forgings 13 p2140 A67-27135
Statistical analysis of aluminum welds tested at cryogenic temperatures 13 p2124 A67-27674
Algorithm for minimal realization of linear finite-dimensional dynamical system displayed by Markov parameters 14 p2291 A67-28066
Stability, probability and reliability relationship presented together with statistical problems in structural stability 14 p2396 A67-28082
Eigenvalue distribution in random Hermitian matrices, considering self-adjoint operators in N dimensional unitary space 14 p2343 A67-28501
Total number and number of distinct particles in equilibrium system of recurrent Markov processes 14 p2345 A67-28907
Two-dimensional distribution of radio sources measured for random positioning using Poisson distribution function 14 p2393 A67-29026
Ionization probability of hydrogen atom by electron impact in terms of three-body problem of classical mechanics 14 p2351 A67-29072
Influence of higher order contributions to correlation function of intensity fluctuation in laser near threshold determined using Fokker-Planck equation 15 p2496 A67-29091
Statistical parameters of linear antenna arrays after removal of emitters 15 p2443 A67-29336
Sensitivity of cost functional in optimal control system with random variable parameters, noting system performance detection techniques 15 p2457 A67-29368
Diurnal and seasonal variations in occurrence probability of screening and semitransparent types of sporadic E layer 15 p2474 A67-29387
Statistical testing on digital computers for simulating current and voltage distribution in semiconductor rectifier circuits 15 p2439 A67-29416
Radiation hazard to man from solar proton events 15 p2429 A67-29450
Interpretation of tests for randomness of lunar craters, noting clustering and alignment 15 p2554 A67-29458
Correlation measurement in two-dimensional zero pressure gradient boundary layer, noting velocity fluctuation patterns 15 p2471 A67-29652
Confidence limits for percentile analysis of guidance system errors 15 p2515 A67-29740
Long term study for prediction of launch vehicle costs, emphasizing estimate accuracy and application of statistical

analysis 15 p2568 A67-29847
Electronic circuit tolerance analysis by digital computer, discussing data availability, analysis methods and interpretation of answers 15 p2440 A67-29938
Dynamical and statistical approach to range safety problems, noting impact-density function of space vehicle destruction at early launch stage [AAS PAPER 67-45] 15 p2572 A67-30113
Missile guidance accuracy, examining motion in central gravitational field along trajectory 15 p2572 A67-30177
Statistical analysis of spread-F and scintillation data in middle latitude noting diurnal and seasonal variations [AGARDOGRAPH 95] 15 p2481 A67-30284
Parameter estimation in automatic control systems using statistical techniques such as likelihood, Markov and least square estimates 15 p2460 A67-30311
Operator parameter identification on basis of digital treatment of experimental data, using algebraic means and static programming 15 p2460 A67-30313
Statistical dispersion methods for identification of nonlinear controlled plants 15 p2462 A67-30324
Interpolating/extrapolating computer programs noting application to analysis of industrial systems 15 p2462 A67-30327
Reliability statistics for repairable devices, proving Poisson distribution limitations and nonhomogeneous Poisson adequacy for analyzing stochastic processes 15 p2495 A67-30412
Reliability assessment on incomplete and inaccurate field removal data, using reliability scoreboard 15 p2496 A67-30419
Statistical methods and application to treatment of information in space domain, noting correlation functions 16 p2633 A67-30671
Book on analytical methods in vibrations covering general mathematical formulations of common features of various vibrating systems 16 p2765 A67-30999
Angle diversity performance of wire-grid lens antenna determined using statistical analysis 16 p2639 A67-31361
Solar flares causing Forbush effect, determining relevant parameters, variations with solar cycle and mutual relations 16 p2739 A67-31457
Sensitivity tests required to verify nonnormality in sample population, studied by computer simulation techniques 16 p2634 A67-31525
Adjoint simulation technique extended to signals consisting of continuous, sampled and multirate sampled systems with random inputs 16 p2652 A67-31684
Atmospheric modulation noise in optical heterodyne receiver, deriving signal power variance and mean-square frequency spread from propagation statistics for wave structure function 16 p2630 A67-31807
VLF worldwide comparison of atomic standards, noting statistical analysis of data and possible sources of error 16 p2632 A67-31860
Statistical processing of satellite data on spectral distribution of outgoing radiation 16 p2668 A67-31887
Statistical analysis of solar-diurnal and semidiurnal variations of cosmic ray neutron component with respect to geomagnetic field perturbations 17 p2932 A67-32081
Cosmic ray variation analysis using theory of random processes 17 p2935 A67-32107
Statistical behavior of two-way communication system with transmission delay 17 p2811 A67-32115
Book on statistical models in engineering covering probability theory, random variables, frequency distributions, etc 17 p2876 A67-32236
Statistical properties of wall pressure fluctuations in subsonic turbulent equilibrium boundary layer after transition from laminar flow 17 p2836 A67-32283
Wall-turbulence interaction for infinite flat plate inserted into homogeneous isotropic turbulence, measuring growth of inhomogeneity layer 17 p2837 A67-32286
Planetary influences on sunspot formation and disappearance showing periodicity in Zurich relative daily sunspot number 17 p2943 A67-32439
Linear/Monte Carlo method performance evaluation of intercept/rendezvous guidance

and navigation for advanced space missions 17 p2882 A67-32493
Statistically designed experiments in wind tunnel test programs dealing with exhaust nozzles, discussing data analysis techniques [AIAA PAPER 66-742] 17 p2834 A67-32571
Air safety statistics analysis based on set of intrinsic accident rates in takeoff, cruise and landing 17 p2797 A67-32580
Statistical particle acceleration mechanism in plasmas noting Cerenkov acceleration, particle state changes, wave generation, etc 17 p2905 A67-32921
Periodic variations in rotational temperatures of OH emission bands determined by spectroscopic measurements 17 p2849 A67-32956
Identification, coding and enumeration of distinguishable subnetwork configurations employing combinatorial analysis 18 p3016 A67-33496
Automatic control system for parameter evaluation, reducing stochastic errors by repeated measurements 18 p3017 A67-33991
Calculation of statistical sum of bounded states of electron in atom in Debye plasma 18 p3091 A67-34480
Statistical method for demonstrating reliability of clustered liquid propellant rocket engines 18 p3116 A67-34662
Relationship between acceptance test and operational reliability studied by multiple regression analysis 18 p3138 A67-34668
Statistical techniques for missile injection error analysis, discussing direct and adjoint methods 19 p3254 A67-34780
Strategy of holding higher performance rocket engines for critical missions analyzed statistically for increased payload 19 p3311 A67-34829
Book on electrodynamics of plasmas covering analysis of collective properties of plasma based on classical and quantum-statistical mechanics 19 p3267 A67-34866
Statistics of electron avalanche generating secondary effect at cathode through photon emission, obtaining excited molecule distribution 19 p3265 A67-35087
Systematic and random error effects on geodetic accuracy of results obtained by 3-station laser telemetry 19 p3182 A67-35240
Deformation characteristics of light concrete statistically compared to second concrete, determined through parameter similarity 19 p3341 A67-35630
Estimation and filtering in discrete linear systems with reference to Gaussian statistical hypothesis 19 p3250 A67-35910
Statistical properties of optical variability of 3C 273 suggesting quasar nucleus as single body 20 p3521 A67-36297
Probabilistic background of time series models which relate to spectral analysis and power spectrum and statistical inference for stationary stochastic processes 20 p3476 A67-36783
Foreshortening law for apparent area of flare derived using statistical method 20 p3518 A67-36841
COSMOS, Courtaulds system for matrix operations and statistics 20 p3391 A67-36932
Book on statistical theory of nonequilibrium processes in plasma, using microscopic equations to obtain two first moments of random functions 20 p3499 A67-36951
Statistical linearization of nonsingle valued nonlinearities considered as multidimensional inertialess functions of dependent variables 20 p3408 A67-37073
Bridge circuits with nonlinear resistances, calculating statistical characteristics by graphical method for functional transformer 20 p3451 A67-37151
Aircraft design by statistical methods, presenting samples for interceptor fighter, shorthaul jet and light twin-engine cargo aircraft 20 p3361 A67-37170
Sufficient conditions for statistical stability of motion in nonlinear systems 20 p3409 A67-37225
Minimum control system optimization, noting adaptation with respect to minimum mean square error, statistical criterion calculation, etc 20 p3410 A67-37227
Statistical dislocation theory of crystal brittle fracture seen as stochastic process with microcrack formation and propagation under plastic deformation 20 p3541 A67-37318
Particle number fluctuation in single cell of Kastler photon set, discussing statistical

properties of laser emission in multimode excitation regime 20 p3462 A67-37338
HF skywave propagation computer model for interference 20 p3387 A67-37646
prediction 20 p3387 A67-37646
Glued metal joints properties analyzed from test results by method using theory of probability and statistical sample 21 p3716 A67-37950
Oscillations in stationary gas discharge, describing device for calculation of correlation function for electrical signals 21 p3664 A67-38165
Limb darkening of earth deduced from statistical analysis of IR radiance data from measurements by Tros 21 p3655 A67-38579
satellites 21 p3655 A67-38579
Evaluation technique for correlation functions and power spectrum of randomly shaped pulse train using stationary point process 21 p3604 A67-38948
Statistical evidence of planetary and lunar modulation of geomagnetic activity 21 p3711 A67-39005
Statistical method for determining satellite orientation and rotation based on differential motion equation model 22 p3878 A67-39168
Electron mobility in He, using irreversible quantum statistics theory to obtain momentum dependent relaxation time 22 p3840 A67-39210
Statistical elasticity problems involving random stress and displacement tensor fields, proving uniqueness and minimum principle for boundary value 22 p3909 A67-39396
Approximation method for solution of Bellman equation in optimal control problems 22 p3777 A67-39828
Rocket engine cluster thrust and moment vectors analyzed statistically for thrust misalignment 22 p3869 A67-40170
Load and response design values determination by statistical method for structural systems such as launch vehicles, considering discrete forcing functions 22 p3907 A67-40178
Optimal filtering theory for horizon sensor data processing for orbital navigation, examining statistical characteristics 22 p3834 A67-40196
Statistical analysis of cosmic ray particle elastic scattering, noting isotropic nature of angular distribution 22 p3841 A67-40252
Impact crater size vs incidence analyzed statistically in study of validity of time dependence on saturation for moon and Mars 23 p4066 A67-41007
Solution of linear system of equations with singularity and stable with respect to small changes in matrix elements 23 p4023 A67-41048
Statistical radiative transfer in turbulent atmosphere underlying region 23 p4068 A67-41281
Electronic system reliability statistical estimates obtained from test results of components using series expansion 23 p3982 A67-41669
Statistical analog technique for complex logic control systems to obtain within single test series required reliability characteristics for various structural versions 23 p3985 A67-41670
Nonlinear sampled data automatic control system optimization by statistical method 23 p3985 A67-41673
Statistical significance of mathematical and logical foundations of information processing method applied to meteor stream 23 p4070 A67-41690
Type II and IV solar radio bursts analyzed, determining nature and geoeffectiveness of causing agents 24 p4209 A67-42112
High energy proton data from Telstar 1 satellite used to develop mathematical models of proton spatial distribution 24 p4210 A67-42334
Axis crossing intervals of sine wave plus noise 24 p4122 A67-42343

STATISTICAL COMMUNICATION THEORY

Book on statistical communications theory, digital communications, AM and FM CW communications, binary communications and noise 01 p0021 A67-10306
Statistical properties of input signals and effect on structure of optimal binary system of signal reception 01 p0024 A67-10722
Book on noise and effect on

communication covering random processes, fundamentals and spectra, nonlinear transformations /demodulation/, statistical theory of detection and information theory 01 p0024 A67-10725
Probabilistic structure of and establishment time for group synchronization in time-division-multiplex /binary code/ transmission systems 01 p0027 A67-11238
Statistical communication theory of antenna response to complex partially polarized nonisotropic random radio wave processes 02 p0191 A67-11588
Ground-Air-Ground /G/A/G/ communication channels analyzed in air traffic control 02 p0263 A67-12125
All phases of pseudorandom sequence obtained by N-stage shift register generator 02 p0203 A67-12133
Bit and message error rate dependence on variation of atmospheric noise statistical properties 02 p0203 A67-12165
Shannon expression of information entropy measure and average uncertainty 02 p0203 A67-12168
Statistical analysis of sidelobe region of offset-feed parabolic reflector antenna 03 p0382 A67-13673
Statistical theory for optimum direction-finding system for space-time signal processing against wideband fluctuation noise background 03 p0371 A67-13947
Equivalent linear antenna substitution for antenna with plane aperture in statistical analysis of antennas 03 p0386 A67-13958
Statistical distribution of AM laser signal envelope upon passage through turbulent atmosphere 03 p0438 A67-13988
Velocity azimuth display technique analysis of wind parameters, noting fundamental limitations 04 p0648 A67-14674
Book on phase coherent communication principles based on statistical communication theory, discussing coherent receivers and analog and digital modulation systems 04 p0578 A67-15616
Statistical properties of envelope of signal-noise mixture with random angular modulation 05 p0765 A67-16961
Subjective evaluation of telephone communications via Early Bird satellite and cable circuits 06 p0959 A67-17667
Converse of channel coding theorem, relating average probability of error to distortion measure of source sink pair 06 p0965 A67-17946
Iterative computation of a posteriori probability for M-ary nonsupervised adaptation 06 p0965 A67-17947
Information criteria for threshold setting in simple binary hypothesis tests 06 p0962 A67-17948
Bit synchronization during transmission of heavily biased information on PCM data systems 06 p0963 A67-18110
Equalization and cancellation model of binaural unmasking applied to data on interaural just-noticeable differences 08 p1290 A67-20482
Measurement interpreted as information process in terms of exactly defined basic concepts of information theory 10 p1654 A67-22756
Discrete signal optimal reception based on analysis of signal noise mixture 10 p1607 A67-23457
Lower bounds to minimum error probability using block coding on noisy discrete memoryless communication channels 11 p1752 A67-24270
Telemetry data processing problems noting error sources, probability distribution of counts in counting processes, sensor relay during motion in varying field, etc 12 p1905 A67-25779
Distinct state assignments for synchronous sequential machines, with modification of Dolotta-McCluskey algorithm 13 p2073 A67-27066
Optimal statistical adaptive model used in defining characteristics of control plants 15 p2461 A67-30321
Reliability through redundancy describing use of devices for averaging analog signals 16 p2649 A67-31667
Statistical analysis of observed relationship between independent air traffic and resultant communication channel loading parameters 17 p2810 A67-32110
Synthesis of radar ambiguity functions via burst-pulse time-frequency waveform coding,

employing Bayesian statistical analysis 18 p3000 A67-34109
Geometrical self-shadowing of random rough surface described by Gaussian statistics in wave backscattering phenomena 23 p3972 A67-40832

STATISTICAL CORRELATION
Statistical correlation theory of accuracy and error relationships of sensing element during parametric excitations caused by random vibrations 01 p0064 A67-10417
Analog device for measuring coefficient of space-time signal correlations and applications to statistical mechanics of turbulent fluids and random noise 01 p0054 A67-11090
Nonlinear Sturm-Liouville BVP with random forcing function 02 p0258 A67-11587
Ratio of Lagrange and Euler correlation scales determined from correlation of time fluctuation of transverse wind velocity and temperature variation 03 p0464 A67-14229
Optimal filtration of noise from useful signal based on statistical information and minimax principle 04 p0591 A67-14636
Analog circuits for statistical correlation in time measurements, with application to subsonic and supersonic flow turbulence 04 p0620 A67-14889
Autocorrelation function in statistical analysis of geomagnetic activity 04 p0613 A67-14897
Numerical solution of Wiener-Hopf equation in statistical identification of linear dynamic plant 04 p0644 A67-14903
Micropulsations of terrestrial electromagnetic field, noting statistical correlation between Pc-1 and Pc-2 type oscillations 04 p0616 A67-15219
Multiple correlation applications in design analysis of high reliability critical circuits 05 p0777 A67-17249
Invariants in inhomogeneous turbulent flow related to Loitsianskii integral 05 p0794 A67-17418
Statistical initial value problem for Burger model equation of turbulence, examining velocity correlation functions, energy spectra and other statistical properties 05 p0794 A67-17419
Correlation of meteoroid environments in solar system, analyzing meteor mass measurement results, hypervelocity impact and solar electromagnetic radiation effects [AIAA PAPER 67-151] 06 p1085 A67-18319
Approximation method of determining statistical characteristics of phase coordinates of linear automatic control systems 06 p0978 A67-18792
Statistical properties of radar signals with internal coherence reflected from rough surfaces 07 p1139 A67-19223
Quantization, sampling frequency and statistical scattering in correlation measurements 08 p1313 A67-21006
Statistical properties of coherent radiation noting correlation function, experiments on photon distribution, Bose-Einstein distribution, etc 11 p1799 A67-24106
Ratio of Lagrange and Euler correlation scales determined from correlation of time fluctuation of transverse wind velocity and temperature variation 12 p1964 A67-25485
Correlation of measurements of precipitated electrons with ionospheric effects of winter anomaly in midlatitude D layer 14 p2310 A67-28043
Geopotential and wind field calculations for Northern Hemisphere using statistical models 14 p2346 A67-28764
Seasonal variations in position and intensity of equatorial electrojet and correlation of latter with sunspot number 15 p2478 A67-30061
Correlation of rainfall rate with attenuation at various frequencies of microwaves 16 p2625 A67-31341
Statistical correlation of microwave range variation and dispersion differential measurements over 25 km tropospheric path 16 p2627 A67-31363
Statistical correlation of latitude with time of maximum darkening of Mars dark areas, noting consistency of 2 models 16 p2749 A67-31401
Correlation of monthly and nightly green line 5577 Angstroms /OI/ airglow intensity with sunspot number and 10.7 cm flux 16 p2749 A67-31404

Statistical correlation between phase and amplitude in first harmonic solar-diurnal variation of neutron component, noting longitude effect 17 p2931 A67-32078

Correlation of measurement data on electrical conductivity of nonequilibrium plasma with impurities 17 p2895 A67-32153

McIlwain coordinates correlated with vertical cut-off rigidities, estimating cosmic ray rigidities 17 p2936 A67-32537

Correlation of diameter of cirrus cloud shield and severity of thunderstorm complex 17 p2880 A67-32554

Auroral particle precipitation, establishing latitude vs time pattern from gross statistical data on optical-and radio-auroral phenomena 17 p2850 A67-33191

VLF emission associated with aurora and particle precipitation, describing receiving equipment, types of emission and occurrence patterns 18 p3039 A67-33621

Approximation method of determining statistical characteristics of phase coordinates of linear automatic control systems 18 p3018 A67-34457

Statistical correlation of type III solar radio burst activity with coronal green line over solar cycle 19 p3316 A67-36029

Correlation of north-south component of telluric currents and brightness fluctuations in quiet form auroras 20 p3431 A67-36994

EEG and rhythmical tremor in outstretched upper extremities in man analyzed by autocorrelation and cross correlation 20 p3373 A67-37525

Wind profile criterion for structural design of launch vehicles, representing wind statistically by bivariate-normal distribution function 21 p3712 A67-37813

Statistical dependence between frequency and amplitude deviations of FM wave perturbed by white noise, describing amplitude-phase correlation FM demodulator 22 p3758 A67-39271

Correlation of meteoroid environments in solar system, analyzing meteor mass measurement results, hypervelocity impact and solar electromagnetic radiation effects [AIAA PAPER 67-151] 23 p4070 A67-41719

Statistical entropy of nonequilibrium plasma assuming binary correlation functions, obtaining distribution function equation 24 p4196 A67-42158

STATISTICAL DECISION THEORY

Compound statistical decision theory for pattern recognition based on Bayes conditional probability theory 02 p0208 A67-12164

Self-organizing approach to structure adaptation in pattern recognition applied to handwritten numerals, spoken vowels and EEGs 04 p0578 A67-14797

Minimum average conditional entropy for minimum probability of error in statistical decision theory 04 p0644 A67-14885

Book on statistical decision theory and sensory processes in signal detection theory and psychophysics 07 p1136 A67-19726

Predicting structural reliability by recent developments in statistics, reliability, cost effectiveness analysis and decision theory [AIAA PAPER 66-503] 08 p1424 A67-21524

Loss structure models concerning age replacement policies, discussing mathematical aspects of maintenance with dynamic programming formulation 14 p2345 A67-28909

Formulation and analysis of class of optimization problems based on contraction mappings in theory underlying dynamic programming 15 p2511 A67-29891

Decision theory applied to angular resolution, deriving signal processing radar system beyond Rayleigh limits and target reliability 23 p3972 A67-40643

STATISTICAL FORECASTING PROJECT

Comparative evaluations of alternative weapon systems, discussing penetration cost effectiveness, attrition ratio, survivability, etc [AIAA PAPER 66-782] 01 p0169 A67-10528

Cost estimating techniques for military and NASA programs, comparing spacecraft resource forecasting with expenditure estimates [AIAA PAPER 67-809] 24 p4259 A67-42966

STATISTICAL MECHANICS

SA CONTINUUM MECHANICS

SA FLUCTUATION THEORY /STAT MECH/

SA FUNCTION SPACE

SA WEIGHTING /MATH/

Statistical mechanics applied to statistically occurring disturbance in flight mechanics 04 p0703 A67-14550

Statistical linearization of nonlinear aerodynamic coefficient of angle-of-attack moment of aircraft 04 p0549 A67-15884

Time constant determination for passive controlled plant with generalized nonlinear statistical characteristics, from response to sawtooth pulse probing 06 p0976 A67-18240

Statistical analysis of flare radiation intensity and brightness distribution of irregular and semiregular variables 07 p1248 A67-19486

Mathematical model for condensation point of first order phase transitions, examining free energy singularity and metastable phase 07 p1268 A67-20089

Electronic generation of stochastic step processes defined by stationary Markov chains 07 p1162 A67-20195

Steady state laser design, comparing balance method with method based on quasi-classical theory 07 p1197 A67-20245

Stochastic Markov model for transient amplitude variation in systems with damped free vibration compared with deterministic solution 10 p1724 A67-23709

Averaging method in nonlinear mechanics, discussing results of Bogoliubov studies 11 p1818 A67-24089

Formal expansion schemes in predicting statistical properties of turbulent flows at high Reynolds numbers 11 p1780 A67-24540

LF thermodynamic energy and pressure fluctuation-dissipation theorem for open systems with dynamic turbulence 11 p1821 A67-24974

Solution to Bogoliubov differential equation for distribution functions of particle system by functional integration technique 12 p1962 A67-26174

Partition functions applicability at high temperatures 14 p2405 A67-28131

Statistical band model used to compute spectral emissivity in carbon dioxide micronband as function of pressure, optical path and temperature 15 p2521 A67-30429

Kinetic equation for electron, ion and atom concentrations for Coulomb plasma taking into account inelastic processes 16 p2715 A67-31040

Non-Markovian evolution equation for velocities distribution in homogeneous gravitational system 16 p2748 A67-31139

Velocity distribution functions in statistical theory of turbulence, deriving moment equations and comparing properties with kinetic theory 16 p2660 A67-31220

Fracture theory statistical models, static and stochastic approach 16 p2771 A67-31294

Estimation of statistical sums of states of groups of oxides and fluorides at high temperatures 16 p2704 A67-31390

Temperature dependence of thermodynamic functions of polyatomic gases at high temperatures 16 p2704 A67-31391

Weakly interacting system statistical mechanics relation to macroscopic thermodynamic description, deriving entropy and absolute temperature 20 p3484 A67-36835

Monograph on equilibrium statistical thermodynamics using quantum mechanics 20 p3554 A67-37271

Time symmetry in oscillating cosmologies with locally irreversible processes, obtaining formalism for statistical processes and boundary conditions 21 p3706 A67-38844

Statistical properties of perturbations in rocket path determined to minimize statistical quantities 22 p3878 A67-39182

Mathematical model for vibrating characteristics of structures in statistical mechanics framework, noting closeness to Green function rather than to mode concept [ONERA-TP-467] 22 p3915 A67-40385

Statistical Newtonian mechanics and quantum physics, discussing classical, thermodynamical and biological time concepts 23 p4027 A67-41139

STATISTICAL PROBABILITY

Statistical description of signal filtration 01 p0043 A67-10237

Dynamic programming recursive estimation of modal trajectory for nonlinear non-Gaussian noise and comparison with Bayesian estimation and case of Gaussian white noise 01 p0047 A67-11214

Component performance and flight

operations of X-15 research airplane program, considering engine, auxiliary power and propellant system 01 p0011 A67-11341

Probability aspects of information transmission, deriving optimum coding and decoding algorithms 04 p0592 A67-14884

Numerical analysis of constraint effects on trial function selection in variational calculus problem of pure torsional vibration of cantilever beam of thin walled open cross section 05 p0917 A67-16418

Accuracy and limit analysis of statistical distribution of EM radiation field by photoelectron counting distributions from photodetector for single mode laser near threshold 05 p0815 A67-16624

Two-step procedure for high energy signal detection against noise background, based on statistical probability 05 p0765 A67-16954

Statistical probabilistic analysis of error propagation and tolerance limits in structural engineering design of assembled parts 05 p0813 A67-17258

Inertial guidance system accuracy and error sources, determining offset circular-or spherical-target error probabilities by approximate chi-square distribution 06 p1028 A67-17722

Structural reliability determined when stress and strength distributions are described by normal statistical distribution 09 p1575 A67-22298

Anomalies and irregularities in application of maximum probability method to stochastic processes 09 p1525 A67-22587

Model ten-member redundant structure under constant-amplitude loads analyzed, determining statistical distribution of consecutive failures for fail safe design applications 10 p1718 A67-23432

Structurally significant material properties effect on reliability of aircraft structures regarding unserviceability, ultimate load failure, etc, stressing stochastic concepts in strength analysis 10 p1718 A67-23433

Statistical properties of superposition of coherent and incoherent electromagnetic fields studied in terms of coherent state formalism 10 p1667 A67-23778

Statistical estimates for Gaussian random processes shown to be asymptotically normal and efficient 12 p1960 A67-25312

Lower bounds on error probability for communication in presence of white Gaussian noise with no bandwidth constraint 12 p1908 A67-26086

Statistical and instrumental fluctuations effect on distribution of first-harmonic amplitude and phase in harmonic analysis of cosmic radiation variation 13 p2191 A67-26565

Monte Carlo method applied to heat conduction problems, discussing steady state and transient situations with linear and nonlinear boundary conditions [ASME PAPER 65-WA/HT-1] 15 p2578 A67-29318

Recursive formula for updating determinant of covariance matrix of state estimation error after incorporation of measurement 15 p2512 A67-30213

Partial correlation coefficients between ionospheric, solar and geomagnetic parameters and spread-F occurrence probability [AGARDOGRAPH 95] 15 p2481 A67-30283

Worst distribution analysis for statistical circuit design 15 p2455 A67-30406

Statistical probability distribution for determining systematic errors of potentiometer multiplier by Monte Carlo method /static testing/ 16 p2633 A67-30464

Statistical probability for motion stability of nonlinear stochastic systems during time interval, discussing oscillation stability of pendulum with randomly oscillating bearing 16 p2703 A67-31145

Conservative series-parallel approximations to study systems models for reliability analysis and display 17 p2865 A67-32585

Structural design for gust loads on USAF aircraft based on continuous turbulence and failure probabilities 18 p2986 A67-34653

Multiple-photon ionization of atoms and molecules in strong varying electromagnetic field, measuring ionization probability dependence on field intensity 19 p3265 A67-35164

Variational procedure for sequential decoding scheme with mean error probability dependence on code limitation approximately same as for optimal

- decoding 19 p3185 A67-36096
 Statistical probability of fractures in polymethylmethacrylate by laser radiation 20 p3473 A67-36161
 Influence on hits and false alarms of response and signal events on preceding trial 20 p3372 A67-36962
 Approximating probability characteristics of mismatch for steady mode of operation of astatic servosystem with modulation 20 p3409 A67-37201
 Radar moving target indicating filters performance, describing method for including target Doppler frequency statistics in gain probability 20 p3386 A67-37498
 Discovery position plotting of various long period comets, showing tendency to cluster near sun in morning sky, orbit distribution and estimated probabilities 21 p3705 A67-38614
 Optimal choice of prototype set by mathematical-statistics estimation theory, using active part of set for identifying control image 21 p3605 A67-39113
 Final probabilities of ergodic Markov chain calculated by methods based on topological properties of stochastic graph 22 p3777 A67-39830
 Inhomogeneity formation probability in initially homogeneous Friedmann universe
 Inhomogeneity formation probability in initially homogeneous Friedman universe 22 p3891 A67-40493
 Random load fatigue life and reliability via fail-safe structural model, obtaining statistical distribution of 2024-T4 aluminum alloy bending strength 23 p4076 A67-40735
 Selection probability from multivariable normal populations in terms of noncentrality parameters 23 p4024 A67-41084
 Electromagnetic compatibility prediction using statistical descriptions of case emission and susceptibility 24 p4132 A67-42712

STATISTICS

- SA BAYESIAN STATISTICS
 SA BOSE-EINSTEIN STATISTICS
 SA CONFIDENCE LIMIT
 SA FACTOR ANALYSIS
 SA FERMIDIRAC STATISTICS
 SA FERMISTATISTICS
 SA MATHEMATICAL STATISTICS
 SA NULL HYPOTHESIS
 SA PROBABILITY THEORY
 SA STANDARD DEVIATION
 Test functions for testing location, scale and shape parameter hypotheses of Weibull distribution 01 p0107 A67-10931
 Perturbation theory for solving Vlasov equation for strong plasma turbulence, using statistical set of exact particle orbits 02 p0275 A67-12551
 Point and interval estimation, from one order statistic, of location parameter of extreme value distribution with known scale parameter and of scale parameter of Weibull distribution with known shape parameter 05 p0835 A67-16853
 Quantile system of data compression for space telemetry, discussing operation, efficiency and advantages [JPL-TR-32-772] 07 p1145 A67-19873
 Statistical quantities needed to fix scattering regime obtained from observations of radio scintillations, showing correlation length in electron density fluctuations 09 p1565 A67-22223
 Relationship between statistics of log amplitude and irradiance fluctuations due to atmospheric turbulence used to estimate effect of aperture in collecting scintillating light 10 p1603 A67-22711
 Asymptotic relative efficiency of mixed statistical threshold tests with Gaussian samples 20 p3412 A67-37495
 Two-mode laser beam electromagnetic field statistical properties tend to Bose-Einstein form 21 p3642 A67-39117
- STATOR**
 Stator whirl with rotors in bearing clearance noting jump and hysteresis phenomena [ASME PAPER 66-WA/MD-8] 04 p0629 A67-15346
 Sign-discriminating field mill design using one rotor and one stator 16 p2671 A67-30972
- STATOR BLADE**
 Axial compressor inlet stator tests determining pressure loss relationship to geometric parameters 20 p3516 A67-37082

STEADY FLOW

- Laminar Prandtl boundary layer arising during steady flow past blunt cone at angle of attack studied by finite difference method 03 p0349 A67-12868
 Steady flow possessing extremal kinetic energy compared to equivalent flow for stability analysis 03 p0402 A67-13618
 Flow pulsation effect on error of flow measurement by means of steady flow formula, noting manometer design requirements 03 p0403 A67-13767
 Idealized steady motion of aerosol particles and inertial deposition theory 03 p0404 A67-13836
 Stability and steadiness of gas flow of argon plasma jet analyzed, using dual grating spectrograph 04 p0664 A67-14848
 Piston motion effect on flow uniformity in hypersonic gun tunnel, using perforated plate technique to prevent piston fluctuation 05 p0791 A67-16430
 MHD steady laminar flow of viscous incompressible electrically conducting liquid in rectangular pipe between conducting plates 05 p0853 A67-16723
 Solution for parallel plates in steady state Hartmann flow extended to coaxial flow between concentric cylinders, noting role of magnetic field 05 p0856 A67-17356
 Steady two-dimensional MHD flow of ideal inviscid perfectly conducting compressible fluid with one nonzero component 06 p1040 A67-18115
 Characteristics solution breakdown near leading frozen characteristic for piston induced flow and relaxing gas flow 06 p0984 A67-18128
 Approximate solution of integral equations with aid of least squares for steady motions of viscous incompressible fluid in rotating cylinder 07 p1168 A67-19217
 Steady flow of anisotropic conducting medium in half-space under influence of magnetic field 07 p1230 A67-20033
 Shock wave tubes and wind tunnels for momentary generation of steady air flows for aerodynamic investigations at high supersonic velocities 07 p1127 A67-20121
 Oseen flow past semiinfinite plate and vertical force formulated by integral equations solved for drag and lifting singularities distribution, using Wiener-Hopf technique 08 p1319 A67-20350
 Compatibility relations and generalized finite difference approximation for three-dimensional steady supersonic flow 08 p1320 A67-20566
 Nonlinear viscoelastic fluids, discussing Couette flow, steady flow, periodic motion, wave propagation, thermomechanical coupling, etc 08 p1419 A67-20881
 Unsteady flow of rarefied gas under finite pressure gradient when starting from rest, varying gradient in time until steady flow is obtained 09 p1487 A67-21847
 Nozzle thrust increase through gas flow rotation noting dependence on nozzle length 10 p1590 A67-23027
 One-dimensional steady laminar premixed flame characterized by matched asymptotic expansions 10 p1733 A67-23145
 Two-dimensional steady MHD flow with resolution of neutral sheets into intermediate and slow waves 11 p1862 A67-24499
 Voltage-current characteristics measured by Fahleson alternate explanation, based on properties of Hartmann boundary layer in continuum type plasma 12 p1972 A67-25384
 Steady flow of conducting dissociating gas in channel of constant cross section in presence of magnetic field 12 p1929 A67-25756
 Linear stability of symmetrical parabolic flows of various types 13 p2092 A67-26276
 Analysis of steady flows of viscoelastic materials by introduction of two dimensionless groups 13 p2096 A67-26931
 Idealized steady motion of aerosol particles and inertial deposition theory 13 p2107 A67-27712
 Steady slow motion of time-independent non-Newtonian liquid through tapered tube, deriving motion equations 14 p2294 A67-27822
 Compression shocks in one-dimensional steady flow of Lighthill ideal dissociating gas studied, using semiempirical relation for relaxation equation 15 p2471 A67-29578
 Formula for thrust derived from thermodynamic steady flow energy

- equations 15 p2472 A67-29673
 Steady flow of anisotropically conducting fluid in plane or annular channel of MHD generator with nonequilibrium plasma at small Reynolds numbers 16 p2600 A67-30541
 Steady laminar flow of viscous, incompressible, electrically conducting fluid in insulated rectangular channel, with imposed oblique transverse magnetic field 16 p2713 A67-30860
 Inviscid steady partially cavitating flow through cascade of flat plate hydrofoils 16 p2662 A67-31550
 Reduction of steady viscous magnetohydrodynamic flows having orthogonal magnetic and velocity field distributions to associated flows having zero magnetic field 16 p2721 A67-31552
 Unsteady heat transfer in tube during heat-flux fluctuations 17 p2967 A67-32130
 Steady flow of ideal gas with conductivity past thin wedge in magnetic field studied for asymptotic properties of flow field 17 p2902 A67-32671
 Steady state magnetic field in transition region between magnetosphere and bow shock by MHD equations, noting solution by approximation method 17 p2951 A67-33186
 Steady flow adiabatic stirred reactor to study combustion mechanism of hydrogen-oxygen mixtures, determining reaction-kinetic constants 18 p3154 A67-33834
 Fuel consumption precision measurements for low thrust auxiliary rockets using impeller wheel and photometric devices [AIAA PAPER 67-507] 18 p2989 A67-33971
 Energy dissipation in turbulent steady isotropic homogeneous gas flow with suspended solid particles 18 p3028 A67-34385
 Heat transfer in steady flow of non-Newtonian fluid between two walls with periodic deformation considered, using perturbation method 18 p3161 A67-34616
 Instability of gas-cooled nuclear reactor passages in steady laminar flow studied by time-dependent analysis 19 p3260 A67-35743
 Plasma shock wave structure model, analyzing steady flow of electrically neutral fluid 20 p3493 A67-36144
 Steady flow of perfectly conducting inviscid liquid past thin symmetrical airfoil of finite conductivity in aligned magnetic field 20 p3494 A67-36146
 Compressible inviscid fluid MHD motion, stressing quasi-aligned field flows 20 p3496 A67-36272
 Steady flow equations with symmetry of revolution, obtaining first integrals for perfect fluid 20 p3420 A67-36395
 Color schlieren and high speed photography technique for transient flows in wind tunnels 20 p3445 A67-36537
 Rayleigh hypothesis applied to three-dimensional rotationally symmetric flows arising from rotating disk in rotating fluid compared with steady solutions 20 p3423 A67-37278
 Steady motion of electrically conducting viscous fluid due to slow rotation of thin dielectric disk inside housing immersed in magnetic field 21 p3665 A67-38247
 Steady motion of elasticoviscous liquid through annulus between two coaxial right circular porous cylinders with suction and injection 21 p3613 A67-38411
 Current sheet propagation transition to steady pattern in pulsed plasma accelerator, noting breakdown and current characteristics [AIAA PAPER 67-656] 21 p3689 A67-38692
 Concentration distribution time for heavy gas diffusing in light gas steady flow field 22 p3917 A67-39714
 Flow velocity profile analysis for pressure front steady motion with steady pressure on compressible fluid 22 p3784 A67-39826
 Theoretical collision efficiencies for cloud droplets in steady Stokes flow suggest near unity coalescence probability 23 p4024 A67-40636
 Friction and heat transfer effects on nonsteady flow behind Chapman-Joulet detonation to analyze transition to steady flow 23 p3993 A67-41744
 Inviscid steady axisymmetric flow inside closed annulus solution derived with extremal principle [ARL-66-0173] 24 p4140 A67-41807
 Heat and mass transfer processes in reacting laminar boundary layer flow with

- steady high speed gas flow 24 p4143 A67-42284
- Steady flow extremum principles for incompressible viscous fluid generalized to liquid flow containing suspended solid bodies and drops of another liquid 24 p4144 A67-42567
- One-dimensional steady MGD flow of polytropic gas with finite constant electric conductivity, noting flow patterns and oblique shock wave structure 24 p4198 A67-42707
- STEADY STATE**
- SA EQUILIBRIUM**
- Free energy of electron gas in compensating field at high temperatures determined from displacements in collective variables, using equation of statistical sum of steady state plasma 01 p0119 A67-10133
- Steady state two-coordinate problem of MGD solved for subsonic attached flow past simply connected profile 01 p0119 A67-10171
- Steady state oscillations and rotations, discussing time independency of parametric differential equations 01 p0113 A67-10285
- Vibroplate pickups for measuring mean values of nonsteady state forces, noting maximum permissible limits of frequency change of pickups 01 p0064 A67-10422
- Algorithm for reducing linear time-invariant differential systems to state form applied to systems described by transfer functions 01 p0047 A67-11219
- Ignition methods for strongly and weakly hypergolic hybrid propulsion systems, examining steady state combustion problems and combustion instability causes 01 p0139 A67-11416
- Steady state combustion analysis of solid propellant rocket motors extended by studying influence of grid sizes and number of steps used in numerical analysis 01 p0143 A67-11449
- Steady state charge distribution on surface of spaceship and in plasma beam emanating from ion engine under conditions of slight decomposition 02 p0302 A67-11549
- Steady state of earth external radiation belt, considering high energy electrons, kinetic instability, anisotropy, etc 02 p0306 A67-11655
- Stability analysis of steady state dynamic holonomic mechanical systems using Rouse, Kelvin, Poincare and Chetaev theorems 02 p0267 A67-11959
- Laminar diffusion flame stability analyzed, examining transient characteristics to infinitesimal disturbances of steady state solutions 02 p0342 A67-12028
- Steady state output ripple performance and sampling frequency choice for single and multirate direct digital control system with stochastic input 02 p0225 A67-12073
- Steady state heat balance on opaque inner wall of enclosure 02 p0343 A67-12413
- Book on conductive heat transfer covering lumped, integral and differential formulations, two-and three-dimensional periodic functions, unsteady problems, Laplace transforms, etc 03 p0535 A67-13075
- Steady state laser radiation during relaxation, discussing time-dependent spectral composition, oscillation modes and polarization characteristics 03 p0435 A67-13134
- Steady state response of viscoelastic cylindrical shells to moving loads, obtaining exact solution with correction for shear deformation and rotatory inertia effects via Fourier transforms 03 p0522 A67-13211
- Stabilization of steady state motion of controlled system described by nonlinear differential equations with time delays 03 p0392 A67-13588
- Flow meter for extremely low flow rates during steady state and pulse mode thruster operation 03 p0422 A67-13776
- Steady state oscillation regime of one-dimensional oscillator determined by replacing arbitrarily shaped hysteresis loop with ellipse of equivalent area, noting higher harmonics effect 03 p0530 A67-14176
- Response curves of steady state forced vibrations, cosinelike functions and periodic functions possessing amplitude 04 p0656 A67-14444
- Steady state regime and stability of two-photon laser, noting field dependence of intensity and duration of frequency pulse and resonance excitation curves 04 p0631 A67-14745
- Steady state axisymmetric thermoelastic problems in bispherical coordinate system [ASME PAPER 66-WA/APM-12] 04 p0713 A67-15403
- Dynamic response of cylindrical sandwich shell under axially symmetric moving ring load, considering steady state behavior 04 p0713 A67-15404
- Thermal properties of semiconductor diode under steady and pulsed operation 05 p0772 A67-16448
- Steady state analysis of switching circuit using combination of transistors and tunnel diodes, considering temperature effect and thermal stabilization of operating points 05 p0772 A67-16452
- Steady state kinetics and microstructures of simultaneous internal oxidation and external scale formation of Cb-Zr and Cb-Zr-Re alloys in pure oxygen at 1000 degrees C 05 p0828 A67-16471
- On-line digital computer used in optimizing control by prediction, including quadratic and steady state value 05 p0784 A67-16524
- Semiclassical and rate equations compared for determination of output power of steady state ruby laser 05 p0815 A67-16628
- Transient and steady state IR emission from low-lying vibrational levels of carbon dioxide in laser systems, using DC discharge 05 p0816 A67-16630
- Quenching of one pulsed ruby laser oscillation by another, noting coupled rate equations for steady state and transient behavior 05 p0823 A67-16682
- Steady state creep stress in shells under uniform internal pressure derived, using transition theory of Seth 05 p0920 A67-16722
- Shock wave structure in steady state monatomic relativistic gas 05 p0793 A67-17112
- Energy dissipation effect on vibrations of elastic element with one degree of freedom excited by steady state random Gaussian disturbance 05 p0923 A67-17182
- Two-component drag force anemometer design and performance, noting method for wind bearing and velocity measurements 05 p0808 A67-17308
- Digital computer programs for transient and steady state thermal analysis 05 p0929 A67-17452
- High temperature steady state creep rate analysis of pure Ag and internally ionized Ag-Mg alloys 06 p1014 A67-17805
- Steady state thermal conditions in semiconductor thermoelectric cooling device 06 p1113 A67-18180
- Solid propellant combustion research, discussing steady state combustion zone structure of propellants, composites, ignition, extinguishment and acoustic interaction [AIAA PAPER 67-67] 06 p1072 A67-18271
- Zero steady state error operation of feedback systems with time-varying nonlinear element 06 p0977 A67-18529
- Suction-preserved steady state vortex sheet on surface of infinite porous circular cylinder in viscous MHD liquid suddenly rotated about axis 06 p1046 A67-18891
- Solid propellant with heterogeneous surface reaction, noting agreement with steady state and acoustic response properties of JPN propellant 07 p1239 A67-19074
- Similarity relationships for study of transient and steady state thermal displacements, strains and stresses between model and prototype 07 p1262 A67-19413
- Electromagnetic induction in conducting sphere rotating in transverse field, extending results for steady state to unsteady rotation, determining magnetic moment 07 p1174 A67-19715
- Steady states in annealing of niobium and tantalum in oxygen atmosphere, noting relation of pressure to temperature 07 p1210 A67-20110
- Steady state laser design, comparing balance method with method based on quasi-classical theory 07 p1197 A67-20245
- Steady state temperature distribution in disk with radial flow of electric current derived with and without heat transfer conditions 08 p1427 A67-20929
- Steady state theory of discharge column, giving solutions to density and potential profiles for planar and cylindrical geometry 08 p1361 A67-21134
- Oxygen IV transition multiplet relative intensities for measuring decay rates, using triply ionized emitters 10 p1678 A67-22718
- Rate equation solution for density of excited atoms in He-Ne discharge for steady state 10 p1663 A67-22893
- Steady state dynamic properties of large spinning net-like antenna suitable for radio signal reception from space 10 p1727 A67-23753
- Steady state plasma belt in dipole magnetic field, measuring spatial variation of density and temperature, electron spin, gyration, etc 11 p1828 A67-23940
- Singular characteristics of dynamic systems with steady state motion, noting effect of constantly acting small perturbations 11 p1818 A67-24147
- Forced steady state response of linear harmonic oscillator with impact absorber attached, developing stability criterion [ASME PAPER 67-VIBR-10] 11 p1795 A67-24170
- Axisymmetric deformation of elastic slab with external crack interpreted as steady state problem of heat conduction 11 p1813 A67-24313
- Density attenuation within crossed particulate beams analyzed under steady state interaction, giving more exact solution than Beer law approximation 11 p1818 A67-24318
- Cesium plasma measurements to determine steady state parameters and LF oscillation characteristics 11 p1834 A67-24379
- Analytical expression for steady state rate of electric domain movement in semiconductors in terms of electric field distribution at domain center 11 p1846 A67-24482
- Cosmological distortion effect incorporating incident magnetic type gravitational field parameter upper limits measured from galactic cluster photographs 11 p1860 A67-24484
- Steady state properties of spheroidally symmetric static arcs with only conduction losses 12 p1970 A67-25290
- Steady state properties of collisionless cylindrical injected plasma of zero temperature in presence of longitudinal magnetic field steady state properties of collisionless cylindrical injected plasma of zero temperature in 12 p1974 A67-25455
- Steady state model of solar wind flow in equatorial plane solved for radial and azimuthal motions, taking into account pressure gradient, magnetic field and gravitational effects 12 p2010 A67-26241
- One-dimensional transport equations of p-n junction in steady state solved numerically 13 p2078 A67-26781
- Steady state forced sound propagation in semifinite gas induced by oscillating plane piston reflecting particles with Maxwellian distribution 13 p2100 A67-26957
- Equilibrium states of buckled elastic rings under stress 13 p2219 A67-27147
- Stability of solutions of Navier-Stokes equations for boundary value problem and convergence to steady state 13 p2106 A67-27455
- Comparison of steady state operator of Prigogine with T-matrix 13 p2159 A67-27730
- Travel-time effects on quasi-steady state operation characteristics occurring from electron optical characteristics of two-grid-controlled photomultiplier 14 p2277 A67-27769
- Steady state approach in competitive-consecutive gas reactions, establishing criterion for approach time estimation 14 p2407 A67-28548
- UBV values and red shifts of quasars interpreted within steady state and Friedman cosmological models 14 p2392 A67-28965
- Steady state one-dimensional carrier distribution in depth for electron beam excitation of semiconductors computed, including diffusion and surface recombination 15 p2442 A67-29180
- Recombination instability in plasma if temperature dependence is strong 15 p2522 A67-29208
- Steady state and transient analysis of digital phase-locked loops 15 p2458 A67-29939
- Burning rate vs pressure and other factors as function of composite solid propellant composition and oxidizer particle size distribution 15 p2580 A67-29985
- Relation between steady state behavior of regenerative traveling wave laser and linear

constant damping in medium 15 p2454 A67-30076

Observational evidence disproving cosmological steady state theory in favor of expanding universe 15 p2562 A67-30082

Solid propellant combustion research, discussing steady state combustion zone structure of propellants, composites, ignition, extinguishment and acoustic interaction [AIAA PAPER 67-67] 15 p2545 A67-30187

Steady state of earth external radiation belt, considering high energy electrons, kinetic instability, anisotropy, etc 16 p2738 A67-31070

Attachment and detachment processes effect on plasma quenching by electronegative gases, showing usefulness of steady state nitrogen afterglow flow system 16 p2720 A67-31238

Steady state charge distribution on surface of spaceship and in plasma beam emanating from ion engine under conditions of slight decomposition 16 p2736 A67-31615

Self-optimizing, type-one system design discussing steady state optimization problem 16 p2649 A67-31666

Control of output variables in discrete multivariable system at steady state noting design, application and performance 16 p2649 A67-31668

Numerical calculations of parameters of steady state HF high pressure vortical discharge of argon in air 16 p2723 A67-31769

Geometry of steady state annular electrodeless discharge in argon and xenon as function of discharge power, type of gas, gas pressure, etc 16 p2723 A67-31770

Mode-locked laser described in traveling light pulse terms, with saturable absorber, noting pulse width under steady state 16 p2686 A67-31808

Gyro-controlled rigid rotor system performance, noting steady state and transient response to various excitation [AHS PAPER 131] 16 p2599 A67-31845

Dispersion equations for long wavelength beam instability propagating through homogeneous plasma 17 p2895 A67-32160

Hall parameter instability and conductivity analysis applied to performance characteristics of subsonic flow generator 17 p2898 A67-32181

Microwave methods applied to plasma diagnostics restricted to steady state plasma 17 p2901 A67-32349

Thin airfoils in radiation gas dynamics, formulating linearized theory for plane steady motion via Fourier transform and obtaining solution for absorption coefficient 17 p2791 A67-32556

Stability analysis of steady state dynamic holonomic mechanical systems using Rouse, Kelvin, Poincare and Chetaev theorems 17 p2886 A67-33276

Steady state wave propagation in homogeneous anisotropic media governed by symmetric hyperbolic partial differential equations 18 p3077 A67-33429

Existence of affine solutions in natural convection along vertical flat heating plate, deriving expressions for thermal and dynamic boundary layers 18 p3025 A67-33685

Temperature gradient in steady state thermally operated solid state lasers, calculating end face curvatures and light paths for resonator mode correction 18 p3059 A67-33714

Physical and chemical conditions in rocket combustion chamber during starting transients and steady operation described by mathematical model intended for parametric studies [AIAA PAPER 67-517] 18 p3158 A67-33980

Steady state laminar and turbulent mixing in unsteady isothermal flow in wake behind body with incident shock wave 18 p2984 A67-34203

Steady state technique for measuring high temperature thermal conductivity of nonmetallic materials requiring heat flux and temperature gradient calculation 18 p3051 A67-34508

Plasma resonance in RF discharge excited with frequency higher than collision frequency, determining electron density 19 p3276 A67-35114

Steady state propagation of cosmic ray nuclei, discussing energy spectrum and path lengths 19 p3317 A67-36099

Steady state heat transfer by simultaneous

conduction and radiation through spherical shell [ASME PAPER 67-HT-20] 20 p3546 A67-36715

Steady state and transient temperature profiles for straight fins of trapezoidal profile with radiative heat transfer [ASME PAPER 67-HT-73] 20 p3550 A67-36753

Linear optimal stationary control system with state dependent white noise disturbances described by differential equation 20 p3408 A67-37077

Radial profiles of carrier density and energy in diffusion controlled plasma 20 p3501 A67-37239

Steady state model of system consisting of solar corona and interplanetary plasma, noting plasma efflux from sun 20 p3529 A67-37520

Convective heat flow nonlinear equations for fluid sphere having heat sources expressed in Boussinesq approximation as perturbation of steady state conduction solution 21 p3731 A67-37926

Steady state problem solution in linear formulation concerning movable load influence on thin elastic plate on ideal compressible fluid 21 p3720 A67-38300

Steady state plant performance optimization for unknown dynamic characteristics, determining periodic input signal 21 p3603 A67-38439

Steady state temperature field and stresses determined for infinite body with linear slit having definite heat resistance 21 p3729 A67-39007

Schuster method calculation of constant geomagnetic field spherical harmonics coefficients 21 p3623 A67-39045

Stationary state of collisionless plasma in magnetostatic and potential fields, deriving distribution functions and concentration formulas 22 p3842 A67-39243

Neodymium-glass laser amplifier gain saturation investigation using laser driving signal, discussing Schulz-DuBois steady state theory and inversion density 22 p3813 A67-39349

Steady state plasma in strong microwave electric field acting on electron component 22 p3845 A67-39431

Steady state nonlinear Landau damping of electron plasma wave obtained from random phase approximation by balancing nonlinear and collision effects 22 p3848 A67-39691

Nighttime variation of ionospheric winds over Barbados via luminous trails measurements, obtaining steady state components for seasonal variations 23 p3995 A67-40807

Nonlinear steady motions produced by stable stratification in rapidly rotating fluid, discussing Ekman layers 23 p3990 A67-41170

Microwave background in steady state universe explained by starlight absorption and microwave reemission by interstellar dust, discussing young spiral galaxies 24 p4226 A67-41875

Gyro power stabilizer in unsteady equilibrium state becoming stable under dry friction defined for controllability in phase space 24 p4155 A67-42299

Lithium-borling potassium test facility to investigate transient and steady state characteristics of Rankine cycle system for application to spacecraft nuclear-electric propulsion 24 p4183 A67-42492

Steady state and dynamic properties of cylindrical floating ring journal bearing with pressurized lubricant supply, considering turbulent flow and whirl instability [ASME PAPER 67-LUB-13] 24 p4162 A67-42674

STEADY STATE CREEP

Stokes creeping flow equations and steady flow of incompressible viscous fluid past liquid drop 01 p0051 A67-10458

Variation equation for steady state creep applied to semimomentless cylindrical shell 03 p0522 A67-13206

Steady state diffusional creep for materials with large grains and dislocations forming sinks for vacancies, obtaining strain rate 21 p3719 A67-38089

Steady state vertical displacements at surface of elastic half-space due to Rayleigh waves from sonic boom, obtaining shock amplification factors 23 p4074 A67-40632

Stress-strain relationship effect on r-power steady creep of pressurized thin spherical shell with sealed opening for various edge

load boundary conditions 23 p4079 A67-41343

Long cylindrical two-layer shell critical asymmetric buckling time for steady creep due to external pressure and axial compression, applying variational principle 24 p4250 A67-42306

STEADY STATE FLOW

Steady state flows without external forces becoming parallel in thermodynamic equilibrium at distance from body, noting relations between drag, shear, heat transfer, entropy, etc 01 p0005 A67-10281

Center of pressure stabilization for thin wing profile with downward deflected trailing edge, when placed in steady state flow of ideal incompressible fluid 02 p0179 A67-12438

Oscillation spectra of plasma in quasi-steady state characterized by self-consistent distribution of plasma particles and turbulent pulsation 02 p0274 A67-12455

Exact solutions to equations for compressible boundary layer in case of power-law dependence of initial profile of stagnation enthalpy on stream function 03 p0400 A67-12867

Steady state and dynamic characteristics of tilting pad journal bearing in laminar and turbulent flow regime [ASME PAPER 66-LUB-19] 03 p0431 A67-13756

One-dimensional steady state gas compression flow undergoing thermodynamic relaxation processes 03 p0405 A67-14258

Isothermal steady state process of fluid with constant density and kinematic viscosity coefficient flowing past thin plate 04 p0603 A67-14709

Nonisothermal steady state flow of fluid with constant density and kinematic viscosity coefficient past thin plate 04 p0603 A67-14710

Supersonic motion of plate in two-component medium in two dimensions 10 p1628 A67-23647

Behavior of solution of system of equations for unsteady boundary layer of two-dimensional liquid as time approaches infinity 11 p1782 A67-24669

Interaction of shock-induced flow in ideal gas and transverse magnetic field analyzed for steady state and transient one-dimensional effects 13 p2162 A67-26280

Onsager formalism of irreversible thermodynamics applied to steady state laminar hydromagnetic energy conversion, analyzing nature of coupling 13 p2055 A67-27001

Steady three-dimensional flow of electrically conducting gas in working section of linear MHD channel 13 p2169 A67-27310

Steady state fluid flow in thin passage analyzed using energy model and including compressibility effects 14 p2302 A67-28264

Steady state heat conduction approximation solution based on effective boundary conditions concept 14 p2408 A67-28805

Bifurcation of nonlinear operator equations to determine steady state axisymmetric homogeneous fluid flows between rotating cylinders 15 p2494 A67-29693

Time independent two-dimensional Navier-Stokes equations solutions from singular perturbation theory, determining properties 16 p2657 A67-30828

Integral equation derived for steady state temperature field in semifinite body with internal cylindrical heat source 16 p2779 A67-31204

Steady state heat flow and temperature fields in flat rectangular configurations with mixed boundary conditions 16 p2779 A67-31206

One-dimensional charged particle flow in bounded system, particularly overlapping steady state zero-temperature flow approximation solutions, noting instabilities 16 p2704 A67-31233

Unsteady heat transfer in tube in presence of variable gas flow rate 17 p2967 A67-32125

Unsteady convective heat transfer and hydrodynamic behavior of gas flows in channels 17 p2967 A67-32131

Steady flow in rectangular cavity with driving motion by uniform translation of one wall 17 p2836 A67-32277

Steady state relaxation hydrodynamic

theory with generalized Prandtl-Meyer flows in nonequilibrium hydrodynamics
[AFOSR-67-1992] 17 p2840 A67-31317

Slepián discharge /steady state DC crossed field discharge/, obtaining solutions for plasma velocity and potential to determine current-voltage characteristics 19 p3277 A67-35122

Hamiltonian description of irreversible steady state phenomena and elements of turbulence theory, noting entropy production 19 p3210 A67-35539

Finite conductivity effect on two-dimensional plasma flow in coaxial channel solved numerically, obtaining steady state flow regime by build-up method 21 p3665 A67-38240

STEAM GENERATOR
Steam generating technique for vacuum ejector system of high-altitude-simulating rocket test facility in West Germany [DVL-598] 03 p0394 A67-13030

STEAM TURBINE
Potassium metal Rankine cycle power system, testing turbines, bearings and seals, potassium boiler and steam topping cycle analysis obtaining high heat-transfer coefficients [AIAA PAPER 66-1009] 02 p0184 A67-12307

Potassium metal Rankine cycle power system, testing turbines, bearings and seals [AIAA PAPER 66-10009] 17 p2802 A67-32052

STEARATE
Langmuir-Blodgett multimonolayers of stearic acid investigated as thin film dielectric 16 p2728 A67-31020

STEEL
SA AUSTENITIC STEEL
SA CARBIDE
SA CHROMIUM STEEL
SA FERRITE
SA HIGH STRENGTH STEEL
SA IRON ALLOY
SA MARAGING STEEL
SA MARTENSITIC STEEL
SA NOTCHED STEEL
SA STAINLESS STEEL

Solderability of 15 CDV 6 25 mm thick steel using argon arc and electric arc, noting mechanical properties of resulting alloy 01 p0078 A67-10270

Titanium carbide coating depositions on steel and subsequent annealing redistribution of elements in interface 01 p0093 A67-10301

Mississippi Test Facility gas metal-arc welding of T-1 steel critical high pressure piping systems for Saturn V launch vehicle 03 p0430 A67-13691

Nickel effect on tensile strength, impact toughness and cold shortness threshold of low carbon steel 04 p0636 A67-14750

Mechanical properties of Kh21G7AN5 steel at liquid hydrogen 04 p0636 A67-14751

Fatigue cracks and fatigue cycles effect on brittle fracture behavior of annealed 4140 steel [ASME PAPER 66-WA/MET-17] 04 p0639 A67-15332

Heating and cooling rates, hold time at maximum temperature, phase temperature between temperature and strain cycling effects on thermal fatigue of stainless steel 05 p0921 A67-17085

Maraging, 15CDV6 and 40CDV20 steel for missile and aircraft construction 05 p0830 A67-17269

Relation between effective porosity and differential pressure of rigid steel and elastic nylon ribbon grids of various forms and porosities 06 p0944 A67-17630

New metals replacing steels noting titanium, beryllium and niobium in French industry 06 p1017 A67-17994

Soviet papers on structure and properties of aviation steels and alloys 07 p1198 A67-19238

Carbide forming elements effect on kinetics of isothermal transformation of austenite and mechanical properties of manganese-molybdenum steel 07 p1199 A67-19239

Hardness of heat resistant steels at elevated temperatures as function of alloying and heat treatment 07 p1199 A67-19240

Ce and Pr effect on structure, hardness and mechanical properties of cast steel at 800 degrees C 07 p1199 A67-19242

Fracture behavior of creep resistant alloy

steel and nickel-chromium alloy subjected to cyclic loading at elevated temperatures 09 p1517 A67-21556

Stress corrosion resistance of explosively deformed high strength steels and aluminum alloy [ASTME PAPER WES-7-63] 10 p1667 A67-23009

Laser beam effect on hardening of steel 12 p1955 A67-25372

Low endurance fatigue tests for reversed torsional strain cycling of two steels 12 p2015 A67-25421

Tensile and torsional fracture of low carbon steel at cryogenic temperatures, studying temperature and stress gradient effect 16 p2689 A67-31309

High pressure hydrogen environment effects on mechanical properties of steels at high temperatures 16 p2689 A67-31327

Thermal fatigue of 18-8 and 13 Cr steels under transient cross-sectional temperature gradients, noting crack mechanics, tensile stresses, plastic strain range, etc 18 p3140 A67-33651

Silicon and phosphorus role in crack formation in manually welded high temperature resistant steel plate 18 p3063 A67-33673

Nickel effect on tensile strength, impact toughness and cold shortness threshold of low carbon steel 18 p3066 A67-34408

Mechanical properties of Kh21G7AN5 steel at liquid hydrogen 18 p3066 A67-34409

Chromizing of steel by HF induction heating in vacuum using low-carbon ferrochrome and electrolytic chromium mixture 19 p3236 A67-34920

Cumulative damage observed for biaxial fatigue stress tests on tubular steel specimens 19 p3341 A67-35552

Sliding friction between spherical steel rider and gold-plated steel flat measured for varied loading, steel combinations and gold film thicknesses 19 p3237 A67-35837

Electron beam welded D6AC steel plates evaluated after heat treated condition /stress relief/ for mechanical properties 20 p3456 A67-37695

Rotating bending fatigue limit and true stress/true strain parameters correlation for steels extended to axial load fatigue tests 21 p3719 A67-38132

Tensile mean stress effect on dormancy of fatigue edge crack in mild steel 23 p4079 A67-41344

Cementite formation during sintering in cermet compositions with titanium carbide base and steel or iron binder noting CO role 24 p4171 A67-41960

Steel dislocation structure under adsorption fatigue investigated by electron microscope, discussing surface active medium effect 24 p4174 A67-42724

STEEL STRUCTURE
Metal and alloy heat treatment intensification with ultrasonic techniques improve steel recrystallization, etc 01 p0095 A67-10640

Treatment of steel with laser beam, obtaining precision holes without affecting microhardness of metal 06 p1008 A67-18234

Niobium addition effect on mechanical properties of steel, noting improvement of tensile strength and cold brittleness threshold decrease 06 p1018 A67-18235

Push-pull low endurance fatigue of En 25 and En 32B steels at 20 and 450 degrees C 12 p2015 A67-25422

Low endurance fatigue analysis for steel and Al alloy under cyclic torsion with controlled shear strain amplitude 12 p2016 A67-25425

Shock wave compression effect on low carbon steels, noting hardness-explosive correlation 12 p1957 A67-28117

Fracture concept for two-phase structures analyzed on basis of crack-tip displacement, discussing macro- and microstructural cases 14 p2400 A67-28424

Effect of defects distribution on behavior of steel structures analyzed for plastically relaxed model of slit 16 p2788 A67-31282

Inclusion type, forging ratio and heat treatment effect on properties of longitudinal and transverse steel specimens 16 p2689 A67-31310

Metal and alloy heat treatment intensification with ultrasonic techniques improve steel properties, recrystallization,

etc 18 p3066 A67-34404

Kaufman thruster with curved stainless steel accelerating-grid system, studying operation, efficiency, plasma instability, etc [AIAA PAPER 67-725] 21 p3694 A67-38750

Aging effect on structure and properties of complex alloyed heat resistant steel 24 p4173 A67-42190

STEEP GRADIENT AIRCRAFT
S HELICOPTER
S STOL AIRCRAFT
S VTOL AIRCRAFT

STEEPEST ASCENT METHOD
Optimization of Atlas-Agena trajectories via steepest ascent computer program 15 p2514 A67-29602

Steepest ascent method for trajectory optimization 16 p2744 A67-30734

Steepest-ascent optimization program developed for flight path of current vehicles, particularly supersonic transport vehicles 19 p3257 A67-35958

Mass optimal trajectory problems with variable endpoints solved using initial and terminal coasting arcs 22 p3884 A67-39955

STEEPEST DESCENT METHOD
Parameter optimization in systems subject to worst bounded disturbance that maximizes chosen performance index 01 p0046 A67-11204

Asymptotic behavior of distribution of maximum for class of processes with independent increments 03 p0458 A67-13340

Numerical procedure for optimizing stability of linear dynamic system by applying steepest descent method 05 p0845 A67-16437

Approximation of space wave plus complex wave using modified saddle point technique 05 p0766 A67-17297

Numerical method solution of nonlinear two-point boundary value problem associated with optimum transfer of spacecraft [AIAA PAPER 67-58] 06 p1023 A67-18267

Minimum energy problems in Hilbert function space for continuous and discrete linear systems, noting operator transformation into linear differential equations 07 p1216 A67-19908

MHD equations for spectral energy tensors of weak homogeneous magnetoturbulent field and derivation of asymptotic decay law by method of steepest descent 08 p1359 A67-21122

Soviet book on numerical solution of nonlinear boundary value problems for differential equation systems, determining eigenvalues and eigenfunctions 08 p1349 A67-21337

Boundary between applicability ranges of network and steepest descent methods in equation integration of Timoshenko theory in analysis of plate deformation 11 p1871 A67-24159

Two LMS algorithms related to steepest descent method, obtaining generalized theorems 13 p2147 A67-27173

Zeros of polynomials with real or complex coefficients determined, using steepest descent method in convergent procedure 13 p2148 A67-27496

Aerodynamic characteristics of helicopter main rotor during steep descent, using ring vortices method 20 p3356 A67-36443

STEERABLE ANTENNA
Large multiplate steerable-beam antenna built by using independent reflectors that redirect energy from desired direction to focus 02 p0210 A67-11592

Structural and mechanical concept, design and testing of fully steerable radome-enclosed parabolic Haystack antenna 03 p0396 A67-13750

Design, fabrication and erection of 210-ft parabolic fully steerable tracking antenna for deep space instrumentation facility /DSIF/ 03 p0383 A67-13751

Mechanical design of parabolic steerable antenna structure of 150-ft diam having superior accuracy and resonant frequency resulting from high stiffness-to-weight ratio 03 p0396 A67-13752

Ground-based steerable paraboloid spherical reflector and multiplate type antennas, noting cost per unit area for unit wind speed of 30 mph and frequency of 1400 mc, performance, restrictions, etc [AIAA PAPER 66-324] 06 p0967 A67-17685

Electronic self-steering techniques applied to satellite communications system with high gain antennas, noting transdirective array

and self-phasing array
[AIAA PAPER 66-326] 06 p0967 A67-17690

X-band circularly polarized nonreciprocal ferrite phase shifter for phased array antennas 08 p1305 A67-21226

Ground station antenna steering system for satellite communication, noting design 11 p1758 A67-24061

Independent control of angular location of independent zeros of directional pattern for linear array 11 p1762 A67-24290

Short wavelength large steerable radio telescope design, considering wind, heat, gravity effects and economics 11 p1768 A67-24777

Determinants of electronically steerable antenna arrays 12 p1917 A67-26158

Spacecraft high aperture efficiency small scan communication antenna, noting radar installation 14 p2289 A67-28911

Signal phase acquisition techniques for arrays of large aperture steerable antennas discussing SNR role 16 p2638 A67-31264

Antennas featuring steerable notch in omnidirectional pattern as alternative to narrow beam antenna for certain applications 16 p2638 A67-31335

Necessity of incremental phase shift during IF time delay steering of antenna array main beam 16 p2639 A67-31354

Large aperture, low noise, steerable antennas for ground station commercial satellite communication networks 16 p2641 A67-31532

Component selection of antenna steering system in satellite communication system, discussing tracking system characteristics and servo operation modes 17 p2833 A67-32190

Narrow beam microwave integrated circuit phased array system design for tactical communications satellite requirements 17 p2956 A67-32497

Coupled integral equations for transverse and axial currents for asymmetrically cylindrical antenna driven by EMF 17 p2826 A67-32618

Chilbolton 25 m steerable antenna for radio wave propagation research 20 p3400 A67-37203

Efficient thermal design of steerable antennas, considering space-environmental requirements 22 p3750 A67-40409

STEERING

SA ROCKET STEERING MOTOR

Steering laws synthesis for explicit guidance, noting generalization and solution of closed loop equations 15 p2514 A67-29603

Analog computer use in design of automatic steering control system of Apollo station ships for precision geographical track-keeping 16 p2701 A67-31659

STEFAN-BOLTZMANN LAW

Stefan-Boltzmann radiation law of fixed stars, calculating stellar temperature, diameter and luminosity 05 p0846 A67-16730

Nongray model atmospheres of Jovian planets constructed for different relative concentrations of helium and diatomic hydrogen and various likely effective temperatures as chief sources of thermal opacity 09 p1567 A67-22237

Book on radio astronomy covering history and fundamentals, wave propagation, radio sources, antennas and receivers, Boltzmann law, etc 17 p2943 A67-32432

STELLAR ATMOSPHERE

Synthetic line profiles generated for variety of model atmospheres containing linear and quadratic velocity fields, used to analyze solar chromosphere 02 p0323 A67-11690

Autoionization mechanism role in formation of astrophysical spectra 03 p0509 A67-13217

Brightness curves used to determine geometrical and physical parameters of eclipsing binary systems containing component with extended spherical atmosphere 04 p0701 A67-15553

Possible existence of circumstellar dust clouds emitting far IR radiation 04 p0702 A67-15588

Aerodynamic generation of noise in stellar convection zones, solving inhomogeneous wave equation when assuming isothermal disturbance 05 p0899 A67-17073

IR spectra of low temperature stars of type M, N/R/ and S, as well as NML objects in Cygnus and Taurus, noting atmospheric differences 09 p1566 A67-22224

Fe IR line excitation in solar corona, noting abundance of iron relative to H and linear polarization of IR lines in coronal streamer 12 p2010 A67-26242

Atmosphere model for pure helium star including only helium I and II transitions and electron scattering in calculating opacity 14 p2387 A67-28578

Methods in computational physics, Volume 7, Astrophysics 14 p2392 A67-28992

Model stellar atmosphere computations predict emergent radiation spectrum 14 p2392 A67-28993

Stellar pulsational instability phenomena calculated numerically for infinitesimal amplitude of central core motion 14 p2392 A67-28996

Stellar and solar atmosphere outermost layers structures, finding radiative equilibrium for massive stars 19 p3322 A67-35327

Stream instabilities in magnetotonic plasmas in presence of DC magnetic field, noting possibilities of growing waves 19 p3292 A67-35389

Recombination and bremsstrahlung continuum radiation measurements of atomic and ionic oxygen in plasma 19 p3299 A67-36093

Aerodynamic phenomena in stellar atmospheres - Conference, Nice, France, September 1965 23 p4067 A67-41275

Lithium content of T Tauri stars shown to exceed ionization of Li in solar atmosphere 24 p4227 A67-42161

Solar abundance determination, discussing composition parameters and Planck gradient method 24 p4237 A67-42654

STELLAR DOPPLER SHIFT

Red shifts and blue shifts relative frequency distribution for QSO 03 p0515 A67-14321

Radar observations of Venus at 23 cm noting flight time and Doppler shift measurements of reflected signals 05 p0889 A67-16297

Visual aspects of transstellar space flight 12 p2009 A67-26233

STELLAR EVOLUTION

SA GALACTIC EVOLUTION

SA HERTZSPRUNG-RUSSELL DIAGRAM

IR stars as supergiants of very late type and not objects in state of gravitational contraction as sustained by Penston theory 03 p0512 A67-13888

Luminosity and density evolution hypotheses concerning distribution of flux densities of quasars, testing validity with Einstein-de Sitter model 05 p0903 A67-17328

Evolution of sun and planets 06 p1091 A67-18995

Radio galaxy phenomena and quasars noting stellar evolution mechanism, energy generation and emission 07 p1246 A67-19055

Stellar evolution model compared with observation to determine interior structure of real stars 08 p1387 A67-20982

Plasma neutrino process as accelerating mechanism for evolution in UV dwarfs 08 p1396 A67-21180

Evolution of low mass stars, differences between solar system planets and black dwarfs and rotational angular momentum of G, K and M dwarfs 08 p1398 A67-21217

Evolution of low mass Population I stars from main sequence to red giant branch in Hertzsprung-Russell diagram, through energy generation phases of p-p chain reactions /dominating over C-N cycle reactions/ and hydrogen burning 09 p1566 A67-22225

Evolution of 2.25 M star from main sequence to helium burning phase noting lifetimes, nuclear burning of core, stellar mass fraction and stellar model algorithm 09 p1566 A67-22226

Contact binaries origin and evolution, discussing orbital angular momentum dissipation through mass ejection along magnetic lines of force 09 p1568 A67-22367

Lifetime of atomic state against decay induced by lepton coupling, estimating neutrino power radiation and astrophysical implications 11 p1821 A67-23959

Spiral and irregular galaxies total mass to neutral hydrogen mass ratio derived from mass-luminosity relations 11 p1858 A67-23995

Age and helium content correlations from recent mass determinations of two low mass binary star systems used in stellar evolution theory 11 p1858 A67-23996

Cold star relativistic collapse kinematics,

noting equilibrium and collapse of point masses system interacting by gravitation only 11 p1858 A67-24013

Solar corona and occurrence of solar wind and influence on evolution of red giant star 11 p1858 A67-24095

Evolution of radio spectral index of supernova remnants modeled to include synchrotron radiation energy distribution 11 p1859 A67-24114

One-dimensional model of stellar system evolution, using computer to calculate minimum energy configuration 11 p1862 A67-24500

Evolution in close binary star systems through mass exchange leading to white dwarf with relatively unevolved companion 11 p1864 A67-24581

Possible initial perturbations development into galaxies with dissipative effects associated with transport processes treated via Boltzmann equation 11 p1867 A67-24838

Element production in early stages of homogeneous expanding universe and within stars, noting nature of background microwave radiation 12 p2010 A67-26239

Primordial element formation, primordial magnetic fields and universe isotropy, showing correctness of big-bang relativistic theory, early anisotropy of universe, etc 12 p2010 A67-26240

Neutrinos in stellar evolution and cosmological processes, discussing production processes 14 p2383 A67-27969

Detectability of massive star from opaque dust cocoon through IR radiation 14 p2388 A67-28833

Methods in computational physics, Volume 7, Astrophysics 14 p2392 A67-28992

Nonlinear partial differential equations of stellar evolution theory solved under assumption of spherical symmetry of star 14 p2392 A67-28995

Hydrodynamics of gravitating stellar system numerically calculated for nonrotating spherically symmetric case 14 p2393 A67-28997

Density fluctuations and thermal conditions in expanding universe and creation of stars, quasars, galactic clusters and galaxies 15 p2551 A67-29138

Information on early history of solar system material obtained for neutron buildup processes of heavy element synthesis in stars 15 p2519 A67-29156

Supernova explosion and collapse theory using relativistic hydrodynamics 16 p2752 A67-31541

Origin and abundance distribution of heavy elements in stars, discussing theories 17 p2946 A67-32694

Energy transport, cosmic ray particle storage and triggering mechanism in solar flares, considering relation with stellar flares 17 p2939 A67-33398

Book on red giants and white dwarfs covering stellar evolution, planets and life, solar system origin, etc 18 p3117 A67-33430

Thermonuclear reactions occurring in supernova shock wave propagating through stellar envelope 18 p3136 A67-34726

Stellar evolution and Brans-Dicke cosmological theory used to construct color-magnitude diagram of star cluster 19 p3330 A67-36077

Planetary nebulae origin, examining posthorizontal branch stars structure and evolution 20 p3527 A67-37272

Core of two solar masses of gravitationally collapsing star, analyzing hydrodynamics, heating, helium 4 formation, neutron decay, nucleosynthesis, light output and mass ejection 22 p3882 A67-39622

Gravitational instability and star and galaxy formation and structure - Conference, Liege, Belgium, June 1966 22 p3890 A67-40491

Spiral arm magnetic field configuration model simplifies star formation theory, discussing theoretical and observational evidence 22 p3893 A67-40505

One-dimensional unstable cloud hydrodynamics analyzed numerically, noting collapse primarily in center and little density growth in outer region 22 p3895 A67-40515

Fragmentation and excess angular momentum problems in star formation theories, examining relevance to simplifying assumptions and physical situation 22 p3895 A67-40517

Rotation and magnetic field effects on

single and multiple stars
formation 22 p3895 A67-40519

Close binary protostellar system formation using model with stellar wind mass loss and primeval magnetic field 22 p3896 A67-40520

Small stellar systems evolution, double star formation and bound subgroup occurrence after condensation from collapsed cloud calculated numerically 22 p3896 A67-40521

Gravitational torque mechanism for radial outward angular momentum transport in solar nebula 24 p4223 A67-41790

Relativistic gravitational collapse, considering asymmetric nonrotating star collapse 24 p4226 A67-41885

Energetic nuclear bombardment effects on stellar surface element abundance calculated with statistical theory in A magnetic variable star abundance anomaly 24 p4228 A67-42263

Gravitational collapse considering space time diagrams and curvature of space, suggesting crushing body less than critical size 24 p4228 A67-42309

Density fluctuations and thermal conditions in expanding universe and creation of stars, quasars, galactic clusters and galaxies 24 p4239 A67-43061

STELLAR FIELD

Autonomous space navigation system using optical spatial filter techniques for recognition and tracking of planetary surfaces and star fields 02 p0264 A67-12316

Inertial frame of reference for measuring accelerations, considering external galaxies, stellar system in our galaxy and planetary system 07 p1250 A67-19678

Solar and stellar systems orbit theory - IAU Symposium, Salonika, Greece, August 1964 08 p1379 A67-20380

Pulsating model of closed universe, noting ordinary matter time-dependent scalar field interaction and equation for nonvanishing pressure 11 p1868 A67-24867

Finite value of escape velocity from stationary stellar system influence on residual velocities 16 p2746 A67-30836

STELLAR LUMINOSITY

Stellar interferometer at Narrabri, Australia, to determine angular diameters of approximately 50 bright stars 01 p0062 A67-10283

Correlation measurement of stellar interferometer at Narrabri, Australia 01 p0063 A67-10284

Intrinsic brightness of comet Alcock 1963 b obtained from visual observations in terms of stellar magnitudes 05 p0888 A67-16204

Various photometric standard systems assessed, noting use of photographic plates and filters in agreement with UVB system 05 p0805 A67-16335

Brightness and spatial luminosity distribution in comet heads analyzed for steady and variable emissive processes 05 p0891 A67-16339

Radio source diameter measurement through application of interplanetary scintillation, noting angular resolution 05 p0903 A67-17291

Stellar magnitude of 100 satellites 05 p0787 A67-17407

Stellar luminosity, discussing effect of nonuniform rotation on gravity darkening and limb darkening in rotating Roche model of star 06 p1089 A67-18709

Statistical analysis of flare radiation intensity and brightness distribution of irregular and semiregular variables 07 p1248 A67-19486

Central intensities and profiles of sodium D lines in solar spectrum, discussing atomic and photospheric data 10 p1704 A67-22885

Intermediate band pass photometric system properties and reduction and calibration procedures 11 p1792 A67-24778

Evolutionary scheme of radio galaxies based on radio luminosity vs volume emissivity diagram, noting similarity and parallelism between radio and X-ray intensities 12 p2007 A67-25787

Cosmic X-ray sources concentration toward galactic plane and variability 12 p1999 A67-26172

Statistical verification of hypothesis explaining observed scintillations of light curve of quasi-stellar radio sources by explosions of supernovas 13 p2198 A67-26766

Kinematic, spectroscopic and photometric

data for pygmy stars /blue ultradwarfs/ 17 p2945 A67-32645

Mean emissivity due to radio galaxies calculated, using assumption that total brightness temperature is uniform in universe 22 p3896 A67-40530

STELLAR MAGNETIC FIELD

Dynamic dissipation of magnetic field, examining mechanism by which magnetic energy is converted directly into fast particle energy 01 p0146 A67-11277

Data and theories on solar and stellar magnetic fields, including techniques for analyzing extraterrestrial magnetic phenomena 02 p0322 A67-11683

Steady state ionization fronts for H-2 regions with magnetic fields 03 p0514 A67-14316

Variable polarization of magnetic star HD 71866 studied by observational program between January and April 1966 04 p0697 A67-14759

Dynamo mechanism for formation of stellar magnetic field, considering effects of EM radiation emission and celestial body rotation 06 p1089 A67-18773

Solar corona and interplanetary gas corotation with sun and effects of solar wind, considering poloidal magnetic field of rotating star 08 p1399 A67-21239

Zeeman effect in measuring magnetic fields of sun and stars, noting apparatus 12 p2010 A67-26235

Magnetism and cosmos - Conference, University of Newcastle-upon-Tyne, England, April 1965 21 p3707 A67-38977

Oblique rotator model for magnetic stars supported by variability, line width, variable polarization and stellar rotation data 21 p3708 A67-38984

Stellar magnetic field origin theories, discussing fossil, dynamo and battery theories 21 p3708 A67-38985

Stellar and planetary magnetic field formation theory based on concept of existing ionized turbulent mass flow on these celestial bodies 24 p4230 A67-42352

STELLAR MASS

Dynamical model of steady state self-gravitating stellar system with finite total mass 05 p0897 A67-16804

Evolution of low mass stars, differences between solar system planets and black dwarfs and rotational angular momentum of G, K and M dwarfs 08 p1398 A67-21217

Spiral and irregular galaxies total mass to neutral hydrogen mass ratio derived from mass-luminosity relations 11 p1858 A67-23995

Age and helium content correlations from recent mass determinations of two low mass binary star systems used in stellar evolution theory 11 p1858 A67-23996

Evolution in close binary star system through mass exchange leading to white dwarf with relatively unevolved companion 11 p1864 A67-24581

Planetary system abundance for stellar system mass near solar mass determined from mass/angular momentum diagram 11 p1865 A67-24610

Detectability of massive star from opaque dust cocoon through IR radiation 14 p2388 A67-28833

Mass dependence of behavior of stellar core undergoing gravitational collapse examined, using improved equation of state and mean free path for energy transfer 15 p2553 A67-29183

Astronomical unit determination by dynamical method 15 p2555 A67-29577

Supernovae cosmical object model, discussing negative mass defect necessary for expansion to diffuse state 18 p3133 A67-34433

Stellar and solar atmosphere outermost layers structures, finding radiative equilibrium for massive stars 19 p3322 A67-35327

Mass accretion of compact star investigated for general properties and X-ray emission 19 p3316 A67-35801

Excited nuclei electromagnetic de-excitation rate by inelastic scattering in stellar particles calculated as function of temperature, density, transition energy and multipole functions 21 p3860 A67-38846

STELLAR MASS EJECTION

Contact binaries origin and evolution, discussing orbital angular momentum dissipation through mass ejection along magnetic lines of force 09 p1568 A67-22367

Aerobee rocket sounding of far UV spectra of six stars in Orion, extrapolating mass ejection from resonance absorption lines 11 p1861 A67-24488

STELLAR MOTION

Mean quadratic amplitude of star image deviation from average position dependence on zenith distance studied from stellar observation 02 p0261 A67-11988

Fluctuation of stellar images and analysis of systematic errors in guidance of telescope as result of atmospheric refraction and flexure of telescope 02 p0241 A67-11993

Automatic and semiautomatic devices for measuring scintillation of stellar images from traces of stars 02 p0242 A67-11994

Third integral of motion in series form derived by Contopoulos combined with known energy and field integrals describes orbits of axisymmetric star systems 04 p0699 A67-14981

Computational methods in stellar dynamics noting n-body problem approach, continuum technique and statistical method 06 p1081 A67-17780

Numerical analysis and third integral applications to n-body problem in stellar dynamics and relation to celestial mechanics 08 p1380 A67-20381

Radial velocities and spectral types for 13 stars, listing photoelectric magnitudes and colors for six 14 p2387 A67-28565

Stellar dynamics methods - Conference, Besancon, France, September 1966 16 p2748 A67-31136

Celestial mechanics and adaptation of perturbation methods and numerical integration techniques to stellar dynamics 16 p2748 A67-31141

Secular increase of stellar noncircular velocities in disk portions of galactic systems, noting gravitational disturbances [AROD-2160-19] 16 p2753 A67-31699

Equinox and equator corrections to FK3 system determined from meridian observations of Mars, Jupiter and minor planets 20 p3429 A67-36838

Declinations of major and minor planets /1951-1959/ determined from meridian observations and reduced to FK3 system 20 p3524 A67-36839

Head-on collision between stars at high initial relative velocity, considering one-dimensional driven shock motion in inhomogeneous medium 20 p3525 A67-36943

Angular momentum and vibrational energy transfer between nearly colliding stars 21 p3700 A67-37732

Spiral field rotation with motion integrals as distribution function arguments, discussing potential, density and spiral arm stability 22 p3893 A67-40507

Globular star cluster, initial gravitational collapse and dynamical mixing, discussing numerical analyses for homogeneous spherical cluster with Maxwell velocity distribution 22 p3894 A67-40509

Stability of stellar systems with different velocity distributions, considering nonlinear wave in stellar sheet leading to galactic stellar velocity distribution evolution 22 p3894 A67-40510

Protogalactic survival during metagalactic formation due to favorable orientation of equatorial planes to orbital planes 22 p3894 A67-40511

Normal modes of stellar internal motions, considering turbulent convection equations and weak-coupling approximation 23 p4068 A67-41277

STELLAR OCCULTATION

Irregularity of galactic magnetic field structure in vicinity of sun indicated by starlight polarization, interstellar cloud motion and Milky Way photography 01 p0151 A67-11275

Solar coronal reflection and occultation of 38 mc/sec galactic radio energy, using Taurus A and galactic equatorial continuum as occulted sources 05 p0891 A67-16403

Star occultation measurements accuracy for determining satellite orbit parameters, noting error sources 18 p3075 A67-34108

Quasar regarded as early stage in formation of system like galaxy nucleus, using model 19 p3317 A67-34950

STELLAR RADIATION

Solar and stellar X-ray astronomy, noting Crab Nebula occultation experiment 01 p0144 A67-10900

Night sky phenomena and atmospheric attenuation of light from Beta Canis Majoris photographed from Gemini
IX 01 p0151 A67-10965

X-ray emission from old novae noting possibility that hot coronas may arise from vibration
02 p0308 A67-12032

Ionization calorimeter measurement of contribution of ionizing particles of star radiation to electron induced ionization of cosmic ray shower
02 p0271 A67-12754

Radio emission from blue stellar objects and radio galaxies, comparing upper flux densities with quasi-stellar radio source emission densities
03 p0512 A67-14002

Nuclear physics of neutron emission in stellar interiors, reaction rates of neutron-producing processes evaluated with optical model of nucleus and uncertainties assessed
03 p0508 A67-14315

Observed interstellar polarization cannot be explained in terms of graphite-crystal color since polarization must increase monotonically from IR to UV
04 p0699 A67-14982

Anisotropy in stellar diurnal cosmic ray variations in Northern and Southern Hemispheres, noting distributions of stellar and antistellar vectors
05 p0881 A67-16120

Photoelectric observation results of short period variable DQ Cephei star
05 p0891 A67-16405

Luminosity of galactic disk in 12.8 micron radiation, obtaining from volume integral stellar photon flux density and thermal radio emission rate
05 p0892 A67-16412

Optical observation of brightest X-ray source in Scorpius, giving tabulated data as function of radius
05 p0892 A67-16414

Elliptical polarization of Crab Nebula radiation possibly explained without synchrotron hypothesis by analyzing photoelectric observations of Stokes parameters
05 p0882 A67-16593

Stefan-Boltzmann radiation law of fixed stars, calculating stellar temperature, diameter and luminosity
05 p0846 A67-16730

Dynamics of ionized stellar winds noting anisotropic effect of stress tensors and densities, velocities and electrostatic potentials distributions
[AIAA PAPER 87-146] 06 p1088 A67-18476

Closed form solution expressing transonic flow in idealized stellar wind and spherical accretion problems including viscosity and thermoconductivity effects
08 p1399 A67-21240

Calculation of gravitational radiation from pulsating and rotating objects according to weak field limit formula of general relativity and applied to neutron star data
09 p1562 A67-22227

Measuring atomic radiation and collision cross section coefficients of plasmas
11 p1839 A67-24551

Type I supernova exponential decrease in light output due to spontaneous nuclear gamma ray fission of Cf 254, including detection techniques using satellite or balloon-borne telescopes
12 p1995 A67-25765

Two-dimensional distribution of radio sources measured for random positioning using Poisson distribution function
14 p2393 A67-29026

Long-baseline-interferometer observations of radio sources to ascertain angular dimensions of radio sources at LF
15 p2437 A67-30031

Strong X-ray source in vicinity of constellation Crux compared to SCO xr-1, findings suggest similar physical nature
17 p2937 A67-32761

Electron temperature of H II region related to high temperature main sequence stars determined as function of electron density and radiation dilution
19 p3325 A67-35503

Ionization calorimeter measurement of contribution of ionizing particles of star radiation to electron induced ionization of cosmic ray shower
22 p3842 A67-40256

Solar neutrino astrophysics, universal neutrino sea, high energy neutrinos, neutrino detectors, stellar energy production, solar thermometry and gravitational constant time variation
23 p4056 A67-41111

Intervening galaxy effect on radiation from distant objects, studying Faraday rotation, 21-cm absorption, optical scattering and absorption lines
24 p4223 A67-41810

Relative radio source flux density at 8 GHz for various radio sources
24 p4224 A67-41824

IR line intensity of planetary nebula NGC 7027, noting presence of measurable continuum flux of stellar radiation
24 p4225 A67-41830

Anisotropy in stellar diurnal cosmic ray variations in Northern and Southern Hemispheres, noting distributions of stellar and antistellar vectors
24 p4214 A67-42796

STELLAR REFRACTION
Stellar differential chromatic refraction effects on guiding large-focal-length astronomical telescopes
02 p0325 A67-11983

STELLAR ROTATION
Discrepancies between various mass models of galactic systems, commenting on rotation curves
02 p0324 A67-11768

Stellar diurnal variation determined during reduced solar activity from crossed-telescope and neutron monitor data
02 p0311 A67-12594

Free oscillations of rotating star with equal angular velocity
04 p0698 A67-14915

Stability and dynamical response of small portions of differentially rotating stellar disks, noting decaying nonaxisymmetrical instabilities, epicyclic frequency, surface density, etc
05 p0892 A67-16410

Stellar luminosity, discussing effect of nonuniform rotation on gravity darkening and limb darkening in rotating Roche model of star
06 p1089 A67-18709

Calculation of gravitational radiation from pulsating and rotating objects according to weak field limit formula of general relativity and applied to neutron star data
09 p1562 A67-22227

Rotational velocity of Venus spots based on sidereal rotation measurements
13 p2198 A67-26588

Radial velocities and spectral types for 13 stars, listing photoelectric magnitudes and colors for six
14 p2387 A67-28565

Resonance rotation of Venus, discussing spin period determinations and retrograde nature of rotation from radar observations
19 p3317 A67-34952

Photometry and spectrophotometry of short-period variable stars
19 p3330 A67-36076

Oblique rotator model for magnetic stars supported by variability, line width, variable polarization and stellar rotation data
21 p3708 A67-38984

Rotation and magnetic field effects on single and multiple stars
22 p3895 A67-40519

STELLAR SPECTROPHOTOMETRY
Photoelectric observation results of short period variable DQ Cephei star
05 p0891 A67-16405

Far UV radiation flux measurement by satellite-borne telescopic stellar spectrophotometer
08 p1399 A67-21234

Metal deficiencies, UV excesses and other color anomalies in solar type disk population stars
08 p1400 A67-21249

Identification of forbidden nitrogen IR multiplet in Fraunhofer spectrum
14 p2382 A67-27848

Monograph on variable stars of RR Lyrae type covering spectrophotometric investigations of periodic brightness fluctuations and oscillations
22 p3880 A67-39463

STELLAR SPECTRUM
Nature and theories of quasi-stellar radio sources and observation of red shift in spectra, examining possible gravitational or cosmological origin of shifts
03 p0516 A67-14337

Astrospectrometer, instrument for recording high definition star spectra
07 p1186 A67-19425

IR spectra of low temperature stars of type M, N/R/ and S, as well as NML objects in Cygnus and Taurus, noting atmospheric differences
09 p1566 A67-22224

Red shift and absorption line of PKS 0237-23
09 p1567 A67-22242

Prism and grating spectra obtained during Gemini XI mission providing UV energy distribution data and Balmer discontinuity
10 p1706 A67-23060

Generalized integro-exponential weighting functions allow accurate computations of Fraunhofer lines in solar /intensity/ and stellar /flux/ spectra
11 p1859 A67-24113

Cosmic x-ray sources identified using Geiger counters aboard rockets, noting

clustering toward galactic disk
12 p1994 A67-25760

Precise position and spectra of Scorpio X-ray source and location of two weaker sources in galactic plane, describing instrumentation used
12 p1995 A67-25761

Classification of slit spectrograms of 185 bright stars in Morgan-Keenan system
14 p2387 A67-28560

Non-LTE line-transfer problem computational methods
14 p2351 A67-28994

Upper limit on concentration of molecular hydrogen in interstellar space by comparison of Lyman bands in absorption spectra of early type stars and laboratory source
17 p2945 A67-32651

Synchrotron radiation spectrum of self-absorbed radio sources for various electron distributions
17 p2947 A67-32755

Line broadening by collision damping, explaining solar and stellar curves of growth
21 p3700 A67-37731

X-ray spectrum and location measurements of several cosmic X-ray sources, using rocketborne proportional counters
21 p3698 A67-38564

Far UV spectra of brighter stars in vicinity of epsilon Orionis photographed with objective spectrograph carried by rocket
22 p3882 A67-39555

Strong radio sources at 1415 MHz, discussing flux density measurements and spectra of OQ208 source
24 p4225 A67-41831

Visual criteria for stellar spectral classification of Cordoba Observatory Atlas
24 p4227 A67-41967

Atmospheric spectral analysis of planets and stars by using computer, telescope and interferometer system
24 p4232 A67-42572

STELLAR STRUCTURE
Principal methods determining cosmic abundances of chemical elements, emphasizing quantitative spectral analysis of sun and fixed stars
03 p0510 A67-13538

Metaequilibrium state of one-dimensional star gas computed for interesting initial conditions corresponds to minimum energy configuration
07 p1256 A67-20017

Principal mechanism of galactic structure based on stellar dynamics principles, discussing spiral pattern in presence of rotation and mathematical theory
08 p1379 A67-20353

Franck-Condon factors and r centroids for C-X band system of astrophysically important zirconium oxide molecule found in S type stars
08 p1354 A67-20702

IR star in Orion nebula noting photometric result, comparing IR flux with energy distribution of black body as function of wavelength
09 p1567 A67-22239

Abnormal low helium abundance in atmospheres of old halo B star based on weak absorption lines in helium spectra
09 p1568 A67-22438

Scorpio X-1 physical characteristics noting ionization, possible stellar wind and pressure equilibrium effects
11 p1862 A67-24506

Neutron star structure and evolution from presupernovae stars including gravitational collapse and neutrino emission processes
12 p2007 A67-25766

Pulsation properties of star models with linear density distribution, considering radial, adiabatic contraction and dynamical stability
12 p2011 A67-26253

Surface stress effect on oblateness of sun and surface stress distribution, noting latitude dependence of angular velocity
17 p2940 A67-32207

Solar spin-down problem, noting oblateness effect on perihelion precession of Mercury
17 p2940 A67-32208

Synchrotron radiation spectrum of self-absorbed radio sources for various electron distributions
17 p2947 A67-32755

Surface helium abundance in blue horizontal branch and halo B stars, considering depletion mechanism
17 p2947 A67-32764

Radio emission flux from local solar sources relation to active solar regions structure, based on radio-astronomical observations
17 p2948 A67-32969

Origin of elements, discussing element formation and abundances, nucleosynthesis and cosmological theories
19 p3263 A67-35869

Planetary nebulae origin, examining posthorizontal branch stars structure and evolution
20 p3527 A67-37272

Static tufted magnetic field perturbing

effect on solar atmosphere small scale structure, noting pressure, density and temperature changes [SR-15] 24 p4222 A67-41767

Abundance anomalies in stellar surface layers by proton and alpha particle bombardment caused nucleus breakdown and buildup to lower and higher mass numbers respectively 24 p4228 A67-42264

Gravitational collapse considering space time diagrams and curvature of space, suggesting crushing body less than critical size 24 p4228 A67-42309

STELLAR WIND

SA SOLAR WIND

Dynamics of ionized stellar winds noting anisotropic effect of stress tensors and densities, velocities and electrostatic potentials distributions [AIAA PAPER 67-146] 06 p1088 A67-18476

STELLARATOR

Nuclear fusion, discussing magnetic confinement methods of hot plasma shell holding light nuclei 01 p0124 A67-10778
Radial transport of cesium plasma governed by resistive diffusion as shown by stellarator experiments in which surface recombination losses within plasma volume were negligibly small 01 p0125 A67-10914

Langmuir probe experiments on electric and magnetic field, density and temperature profiles, I-V characteristic, etc, for rotating plasma in B-3 stellarator 08 p1361 A67-21137
Velocity and current-driven universal instability of fluctuations in plasma of model C stellarator 08 p1365 A67-21406

Effect of low pressures on stability of plasma currents in closed hydromagnetic systems 11 p1826 A67-23877

Plasma wave drift in stellarator helical magnetic field, deriving equations for wave developing conditions 14 p2361 A67-28762

Ion cyclotron resonance heating limitation in shallow magnetic beach explained by wave reflection 15 p2523 A67-29212

Energetic plasma confined in magnetic mirrors shown to have little interaction with main plasma body 15 p2523 A67-29213

Soviet book on plasma physics covering magnetic traps, acceleration, radiation, etc 17 p2903 A67-32909

Toroidal stellarator magnetic trap with time-varying double coil magnetic field and external plasma injection 17 p2904 A67-32911

Particle motion and plasma equilibrium in helical magnetic field, discussing magnetic surface phenomena 17 p2904 A67-32914

Magnetic field line trajectories in toroidal stellarators, discussing rotational transforms on last closed surface and perturbation effects 21 p3662 A67-37753

STEP FUNCTION

Step procedure for synthesizing circular aperture patterns 02 p0212 A67-11609

Quantum dimensional effects in bismuth films by tunnel spectroscopy, showing energy dependence of state density having form of step function 02 p0281 A67-11632

Nonsimilar free convection boundary layer from vertical flat plate with step discontinuities in surface temperature [ASME PAPER 66-WA-HT-17] 04 p0739 A67-15930

Optimization of linear control systems when placing step limitations on control, using functional analysis 05 p0781 A67-16251

Magnetoelastic vibrations due to step function of mechanical radial force acting on perfectly conducting isotropic elastic cylinder placed in magnetic field 05 p0847 A67-17278

Transient response of Couette shear flow to step function change in blowing velocity across channel 05 p0751 A67-17420

Design procedure for meeting step-input specifications in piecewise single-valued nonlinear multivariate control system design 06 p0978 A67-18720

Electronic generation of stochastic step processes defined by stationary Markov chains 07 p1162 A67-20195

Temperature distribution, stress distribution and displacement components for circular disk when temperature distribution at disk rim is step function of time, considering inertial terms in thermoelasticity equations 08 p1418 A67-20723

Generalization of multistep methods for ordinary differential equations, noting associated operators and local discretization error 08 p1348 A67-21191

Accelerated fatigue testing using stepwise stress increase method 14 p2402 A67-28815

Static and dynamic parameter estimation of nonlinear transfer elements from step responses 15 p2463 A67-30331

Base pressure and geometry of separated region in boundary of supersonic accelerated flow analyzed and compared with Chapman-Korst model 16 p2592 A67-30951

Gas bearing stability determination by step-jump response using observation of growth or decay of motion amplitude [ASME PAPER 67-LUBS-5] 16 p2682 A67-31383

Asynchronous pulse modulation systems developed using step and linear segment approximations of message waveforms 17 p2812 A67-32318

Planar transistor collector current rise time determination with base driven by current step function and application procedures 20 p3395 A67-36299

Closed loop stepping motor as mechanical memory and time optimal control and digital servomechanism applications 21 p3570 A67-37787

Runge-Kutta integrations for all seasons by proceeding in blocks of N steps compared to predictor-corrector methods 21 p3652 A67-38173

Nonreflecting resistive loaded dipole antenna with step function internal impedance, measuring current amplitude, input admittance and radiation field pattern 23 p3978 A67-40826

Oscillating mass flow characteristics in modified Moore variometer configuration for step, triangular and infrasonic functions 23 p4000 A67-41221

Algebraic equations to predict time response to step input in free molecule, transition and continuum flow regimes 24 p4155 A67-42293

MHD lubrication flow in self-acting step type thrust bearing configuration, showing torque reduction 24 p4182 A67-42566

STEREOCHEMISTRY

Esterification rates of aliphatic carboxylic acids, acid terminated polybutadienes, etc, and steric environment in vicinity of acid groups 04 p0564 A67-14473

Reaction of lithium diphenyl phosphide with diphenylacetylene producing high yields of stereochemically pure vinyl phosphides in presence of primary or secondary amine 04 p0565 A67-14523

Esterification of secondary alcohols, using amino acids 06 p0956 A67-18576

Mass spectra of amino ketones and amino alcohols and related substances 09 p1458 A67-22057

Structures and stereochemistry of clivonine and clivimine analyzed through mass spectroscopy and nuclear magnetic resonance 09 p1458 A67-22059

Isomerization rate of iminocarbonates, discussing electronegative hetero-atom bonded to imino carbon 09 p1459 A67-22363

Stereoisomers of sulfur containing amino acids effect on local skin protection in X-irradiated mice 18 p2992 A67-34716

STEREOSCOPIC PHOTOGRAPHY

Conditional angular elements in external orientation of aerial photographs determined by orientating right photograph with baseline 01 p0068 A67-10855

Stereo interpretation of Nimbus II automatic picture transmission photography for cloud patterns [AFCLR-66-805] 02 p0241 A67-11970

Terrain relief appearance on aircraft radar determined from radar parallax and shadow parallax 02 p0239 A67-12539

Accuracy testing of Zeiss stereocomparator 03 p0419 A67-13263

Aerial photography processing problems using SD-3 and USD-1 05 p0809 A67-17549

Selenographic measurement including stereoscopic photography, crater wall heights and slopes, peak illumination limit methods, etc 08 p1396 A67-21166

Low spatial frequency white light hologram production on Diazo materials 09 p1493 A67-21572

Conditional angular elements in external orientation of aerial photographs determined by orientating right photograph with baseline 14 p2317 A67-28244

Time-microscopy methods using laser flashlight, roentgen flashlight and rapid

succession spark pulses in combination with stereo cameras 17 p2864 A67-33408

STEREOSCOPIC VISION

SA DEPTH PERCEPTION

Three-dimensional projections on cathode ray tube screens noting visual transformations linking retinal image to space scene 20 p3450 A67-36985

Multidimensional data stereoscopic graphic display principles, viewing and use in engineering design 24 p4157 A67-42434

STERILIZATION

SA CHEMICAL STERILIZATION

SA PURIFICATION

SA SPACECRAFT STERILIZATION

Lethal effect of high intensity sonic and ultrasonic waves on spores of Bacillus subtilis var. niger ATCC 9372 04 p0562 A67-14520

Heat sterilization of activated carbon at 135 degrees C for 24 hr or 165 degrees C for 3 hr for application to spacecraft 11 p1749 A67-24788

Microbial numbers relation to phosphate activity in soil, discussing seasonal variation, sterilization by irradiation and moisture content 18 p2991 A67-36860

Desiccated microbial populations of lyophilized Staphylococcus epidermidis cells and Bacillus subtilis spores studied for synergism in ethylene oxide-methyl bromide sterilization 19 p3180 A67-35279

Human microbial shedding using sterile stainless steel shedding chamber, discussing clean room clothing reducing shed rate 23 p3962 A67-40857

Sealed heat sterilizable high impact resistant battery for space missions, grafting acrylic acid and polyethylene by irradiation for separator 24 p4106 A67-42521

Reusable and disposable hydrosol filters tested with heavy bacterial suspension for ability to produce sterile filtrates 24 p4116 A67-42705

STEROID

S CHOLESTEROL

S CORTICOSTEROID

STIFF STRUCTURE

Test methods for determination of shear and flexural properties of sandwich panels 01 p0164 A67-11269

Beam-column analysis by finite element method, establishing end load-deformation relationship via stiffness matrices 03 p0523 A67-13457

Mechanical design of parabolic steerable antenna structure of 150-ft diam having superior accuracy and resonant frequency resulting from high stiffness-to-weight ratio 03 p0396 A67-13752

Matrix displacement approach to discrete element structural analysis for thin shell instability, emphasizing determination of membrane force distribution 05 p0925 A67-17352

Time dependent deflection behavior under compression loads of stiffened panel at high temperatures 06 p1100 A67-18011

Filamentary composite of boron and epoxy applied in design optimization of helicopter blade structure, considering filament orientation and stiffness [AIAA PAPER 67-176] 06 p1102 A67-18322

Invariants of triangular shell element stiffness matrices associated with polyhedral deflection distribution, discussing effect of geometry [AIAA PAPER 67-114] 06 p1103 A67-18356

Anisotropic sandwich constructions characteristics for orthotropic materials used for facings and cores, considering stiffness and buckling 06 p1108 A67-18655

Free vibration analysis for ring and stringer stiffened cylindrical shell, using Rayleigh-Ritz technique [AIAA PAPER 67-71] 07 p1262 A67-19434

Imperfection sensitivity of eccentrically axial and ring stiffened cylindrical shells under axial compression and hydrostatic pressure 08 p1417 A67-20552

Solar environment and aerodynamic drag effect on deflection of structural booms in space [AIAA PAPER 66-502] 08 p1413 A67-21512

Torsional stiffness of ribs effect on buckling strength of longitudinally stiffened plates compressed in direction of ribs 10 p1719 A67-23474

Book on matrices for structural analysis, including elementary algebra and detailed arithmetic of matrix methods applied to

structure theory 10 p1719 A67-23476
 Boron fiber reinforced epoxy matrix plastic composite for application to aircraft structures 10 p1723 A67-23697
 Structural design of stiffened cylindrical shells, discussing minimum weight, prevention of buckling modes, etc 10 p1726 A67-23719
 Skin-stiffened compression panel design with digital computer, obtaining optimal solutions for applied stress and local and general stability equation 10 p1726 A67-23720
 Prebuckling deformations, ring stiffeners and load eccentricity effect on buckling of stiffened cylinders 10 p1727 A67-23759
 Flexibility and mass distribution effect on vibration response of general continuous structures [ASME PAPER 67-VIBR-44] 11 p1873 A67-24196
 Stiffener eccentricity effect on critical load in cylindrical shells under axial compression 17 p2961 A67-32775
 Infinite edge-stiffener load diffusion into semilinear elastic sheet, noting interface sheet stress variation stiffener force distribution [ASME PAPER 67-APM-35] 17 p2965 A67-33160
 Biaxial buckling behavior of 45 degrees eccentric-stiffened waffle cylinders using prediction theory 19 p3341 A67-35525
 Compounded normal modes of free vibration of cantilever plates, determining component modes 20 p3541 A67-37491
 Stiffness matrix of unsymmetric nodal ring element for matrix displacement analysis of rib stiffened conical shells 22 p3914 A67-40191
 Stiffness matrix for shallow rectangular shell element and application of finite element displacement method 23 p4073 A67-40628
 Human spinal column stiffness under deflection rate /axial compression/ produced by impact 23 p3954 A67-41592
 Orthotropically stiffened cylinders elastic instability under torsional load 23 p4080 A67-41745

STIMULANT
SA CENTRAL NERVOUS SYSTEM
STIMULANT
 Reactivity of animals to caffeine and strychnine during transverse acceleration aftereffects 24 p4111 A67-41850

STIMULATED EMISSION
 Masers and lasers from Einstein discovery of stimulated emission to present 01 p0089 A67-10503
 Temperature dependence of threshold for stimulated emission of Nd trivalent ion in several host lattices estimated from intensity variation of laser active fluorescence component 01 p0091 A67-11085
 Self-excitation of nonsteady processes in two-photon laser 02 p0252 A67-12421
 Temperature induced and optical quenching of emission recombination in gallium arsenide Be-doped electroluminescent diode 02 p0254 A67-12741
 Powerful laser employing induced two-quanta luminescence 03 p0433 A67-12856
 Linear phase distortions of plane resonator with tilted mirrors and effects on generation of stimulated emission in ruby crystal laser 03 p0435 A67-13130
 Tunable dispersion resonator and broadening of laser emission spectral range to obtain operating frequency other than fundamental 03 p0435 A67-13131
 Luminescent intensity and spectral energy distribution determined for excitation luminescence of anthracene crystals for spontaneous and stimulated emission 03 p0436 A67-13136
 Effect of diffusion of excitation on conditions of multimode generation in laser radiation 03 p0437 A67-13207
 Population inversion of upper laser level of carbon dioxide molecules, noting electron-molecule collision and effect of neon addition 03 p0437 A67-13297
 Temporal-spatial variation of cross sectional flux distribution of stimulated emission from Nd glass pulsed laser 03 p0439 A67-14280
 Stimulated emission by electron beam bombardment of laser materials 03 p0439 A67-14394
 Population inversion of upper laser level of carbon dioxide molecules, noting electron-

molecule collision and effect of neon addition 04 p0631 A67-14722
 Degenerate stimulated four-photon interaction and four-wave parametric amplification observed in ruby laser and liquid cell arrangements 05 p0844 A67-16379
 Lamb self-consistent theory and rate equation approximation study of magnetic depolarization of vapor and polarization of monomode gas laser in magnetic field 05 p0818 A67-16644
 Double resonance effects extended to case of stimulated emission in excited states of neon, using gas laser in transverse DC magnetic field 05 p0818 A67-16645
 Loss measurement for ruby laser resonant cavity, comparing thresholds for R sub 1 and R sub 2 line operation 05 p0819 A67-16655
 Laser emission at 1.06 microns from ytterbium-neodymium glass, noting linearity of energy transfer with Yb concentration 05 p0820 A67-16664
 Semiconductor lasers with radiating mirrors developed by excitation, using electron beam and neodymium laser glass radiation 05 p0821 A67-16669
 Hypersonic excitations due to Brillouin scattering for case with Stokes feedback, deriving quantum equation of motion for creation of laser and Stokes modes and coupled acoustic mode 05 p0823 A67-16683
 Enhanced lasing of high pressure He-Ne laser, commenting on delay time of light pulse emitting through walls of discharge tube from start of exciting pulse 05 p0823 A67-16687
 Stimulated emission in triplet system of nitrogen molecule produced by pulsed laser discharge, identifying lines and interpreting intensity distribution in rotational band spectrum 05 p0824 A67-16785
 Stimulated emission of electromagnetic wave in decaying ionized plasma 05 p0855 A67-16998
 Light source devices for electronic functions, discussing p-n junction 07 p1231 A67-19081
 Traveling wave excitation of high power nitrogen and neon lasers with velocity matching that of stimulated emission 07 p1196 A67-20093
 Stimulated radiation from trivalent Nd ion doped barium crown glass fiber laser without resonator 08 p1337 A67-21203
 Stokes light generated in off-axis resonator for quantitative measurements of stimulated Raman effect in self-focusing materials 08 p1339 A67-21375
 Pinch discharge cumulation by using stimulated emission generated in high temperature plasma of strong current pinch discharge 08 p1366 A67-21501
 Complete vibrational population inversion in molecular product of chemical reactions, finding stimulated emission 09 p1511 A67-21746
 Stimulated emission in negative luminescence region of He-Ne glow discharge, noting effect of pressure and volt current 09 p1512 A67-21925
 Stimulated emission, absorption spectra and luminescence of neodymium-activated YAG crystals in pulsed laser 09 p1513 A67-22068
 Phonon lifetime variation effect on stimulated Brillouin and Raman scattering in gases by temperature, pressure and laser power variation and comparison with Stokes gain theories 10 p1662 A67-22758
 Energy propagation and partial self-focusing in laser beam 10 p1663 A67-22847
 Laser emission at band-band transitions in impurity semiconductor without conservation of quasi-momentum 10 p1666 A67-23653
 Stimulated emission in GaSb injection lasers with steep flat p-n junction, noting dependence of luminescence intensity on current density 10 p1667 A67-23665
 Stimulated Raman effects in anisotropic crystal potassium dihydrogen phosphate with Stokes generations 11 p1800 A67-24243
 Optical and laser properties of trivalent Nd and Eu ion doped yttrium orthovanadate 11 p1847 A67-24739
 Laser emission temperature dependence resulting from variation in radiationless transfer of excitation in trivalent erbium and thulium 11 p1803 A67-24836
 Room temperature laser threshold reduction and stimulated emission delay in GaAs diffused junction

diodes 11 p1803 A67-24911
 Stimulation of Jupiter radio emission by Io 12 p2000 A67-25204
 Fluorescein family organic dyes exhibiting laser action when excited by ruby and neodymium second harmonics 12 p1953 A67-25748
 Raman laser physics covering gain formula, stimulated and spontaneous scattering and cavities 12 p1953 A67-26124
 Gain narrowing and saturation broadening of Doppler broadened neon line in Zeeman scanned laser amplifier 13 p2129 A67-27485
 Laser gas-discharge tube /without resonator/ amplification relations, considering stimulating radiation, noting application as oscillator 14 p2328 A67-27771
 Coherent radiation frequency conversion and nonlinear optics methods, including stimulated Raman scattering and Mandelstam-Brillouin scattering 14 p2330 A67-28467
 Magnetoplasma radiation by microwave pulse excitation at gyrofrequency harmonics, considering single particle approach 14 p2360 A67-28557
 Stimulated emission from pulsed electrical discharge through helium with wavelength measured and transition identified with interferometer 15 p2497 A67-29395
 Probability distribution of number of photons and integrated intensity relation to normal and antinormal ordering of field operators in quantum optics 16 p2685 A67-30826
 Effective cross section of stimulated emission, noting fluorescence band profile during laser emission 17 p2866 A67-32293
 Laser emission at band-band transitions in impurity semiconductor without conservation of quasi-momentum 17 p2870 A67-33334
 Stimulated emission in GaSb injection lasers with steep flat p-n junction, noting dependence of luminescence intensity on current density 17 p2870 A67-33346
 Short stable gas laser construction and properties 18 p3058 A67-33658
 Stimulated coherent emission at upper hybrid resonance frequency from magnetoplasma excited by microwave pulse 18 p3090 A67-34468
 Models explaining long time delay between current-pulse application and generation of coherent oscillations in gallium arsenide junction lasers near room temperature 19 p3241 A67-36036
 Multiple stimulated Brillouin scattering from liquid within Q-switched ruby laser cavity, noting changes in pulse shape, output power and spectral characteristics 20 p3457 A67-36385
 Stimulated Raman scattering in IR active nontotally symmetric vibration of alpha quartz crystal, noting parametric oscillation 21 p3641 A67-38459
 Stimulated emission and spectroscopic investigations of double lanthanum-sodium molybdate single crystals with neodymium impurities, considering applicability in lasers 23 p4039 A67-40901
 Analysis of laser with selective resonator indicating stimulated emission basic characteristics determined by active medium band shape and Q-factor curve 23 p4013 A67-40907
 Stimulated Raman effects in calcite oscillator crystal, measuring gain index beta relative to Stokes wave 23 p4016 A67-41191
 Fluoride crystals for laser applications, discussing crystal absorption spectrum 24 p4166 A67-41983
 Threshold power dependence on temperature and photoelasticity for stimulated Brillouin scattering in crystalline and fused quartz 24 p4204 A67-42365

STIMULATION
SA PHOTIC STIMULATION
SA SENSORY STIMULATION
 Combustion chamber model for self-oscillating thermoacoustic system initiated by stimulation effect of acoustic shock 11 p1884 A67-24958

STIMULUS
SA AUDITORY STIMULUS
SA CALORIC STIMULUS
SA ELECTRIC STIMULUS
SA VISUAL STIMULUS
 Skilled response organization, discussing stimulus coherence, tracking task, spatial and temporal coherence, secondary task, sequence length and task

- coding 14 p2254 A67-28034
- TIRLING CYCLE**
- Gas turbines, regenerators, Wankel engine and Stirling engines, examining problem areas
- [AICE PREPRINT 45A] 04 p0691 A67-15944
- Unsteady state analysis of heat transfer and energy transformation processes in closed cycle regenerative heat energy converters, using differential equations [AIAA PAPER 67-216] 06 p0951 A67-18329
- Stirling cycle using dissociating gas 13 p2221 A67-26390
- Stirling type closed cycle cooling system for masers and other microwave electronic devices 14 p2278 A67-27784
- Unsteady state analysis of heat transfer and energy transformation processes in closed cycle regenerative heat energy converters, using differential equations 21 p3689 A67-37791
- Stirling, Brayton and Rankine dynamic cycles compatibility with isotope heat sources, emphasizing power system applications to long-duration earth orbital missions 24 p4185 A67-42542
- STOCHASTIC PROCESS**
- Final probabilities of ergodic Markov chain calculated by methods based on topological properties of stochastic graph 22 p3777 A67-39830
- STOICHIOMETRY**
- Mossbauer investigations of stoichiometric manganese-ferrite and two magnesium-manganese ferrites made at room and liquid nitrogen temperatures 04 p0676 A67-14925
- Crystalline structure of ZnTe thin films as function of stoichiometric and growth conditions 07 p1233 A67-19645
- Burning velocities, temperatures and burnt gas composition of flammable methane-rich perchloric acid mixtures 14 p2406 A67-28544
- Flame properties of flammable ethylene-rich perchloric acid mixtures 14 p2406 A67-28545
- Flame properties of flammable ethane-rich perchloric acid mixtures 14 p2406 A67-28546
- Nonstoichiometry of zirconium oxide and relation to tetragonal-cubic inversion in zirconium oxide 16 p2694 A67-31597
- Stoichiometric composition effect on semiconducting properties of gamma iron telluride at high temperature phase 17 p2911 A67-32220
- Solubility of impurities in semiconductors and mechanism for deviation from stoichiometry 18 p3096 A67-33449
- Ti-C-N system studied for stoichiometric range and thermodynamics using gas equilibration techniques, measuring nitrogen/carbon activities 19 p3248 A67-34865
- Superconductivity transition temperatures of metal carbides, showing stoichiometry as main feature for maximum temperature 19 p3303 A67-35040
- STOKES-BELTRAMI EQUATION**
- S VELOCITY POTENTIAL**
- STOKES LAW**
- Stokes creeping flow equations and steady flow of incompressible viscous fluid past liquid drop 01 p0051 A67-10458
- Stimulated Stokes emissions from Raman active media observed by using Q-switched ruby laser which emits multiple pulse in each shot 04 p0632 A67-14765
- Critical analysis of Stokes gravity formula derivations, noting truncation error effect 05 p0796 A67-16153
- Zero Reynolds limit of steady incompressible viscous fluid motion in sphere due to Landau source at center proved to be Stokes flow 09 p1487 A67-21665
- Distribution theory application to derive formula for deflections of vertical from Stokes formula 09 p1492 A67-22681
- Stokes flow for sphere in arbitrary external flow pattern solved using Green function, showing uniqueness solution 10 p1629 A67-23831
- Stokes problem solution for intensity of regularized gravity field around earth and at surface in form of rapidly converging series 11 p1812 A67-24162
- Stimulated Raman effects in anisotropic crystal potassium dihydrogen phosphate with Stokes generations 11 p1800 A67-24243
- Supersonic flow separation from corner of base compared to Stokes-type flow separation 14 p2240 A67-28111
- Copper and its solid solutions retarding force profiles studied for explanation of Cottrell-Stokes law 20 p3464 A67-36220
- Stimulated Raman effects in calcite oscillator crystal, measuring gain index beta relative to Stokes wave 23 p4016 A67-41191
- STOKES PARAMETER**
- Viscous shear flow past two-dimensional cavity of infinite depth by use of Stokes approximation, emphasizing flow pattern near dividing streamline 03 p0402 A67-13356
- Elliptical polarization of Crab Nebula radiation possibly explained without synchrotron hypothesis by analyzing photoelectric observations of Stokes parameters 05 p0882 A67-16593
- Hypersonic excitations due to Brillouin scattering for case with Stokes feedback, deriving quantum equation of motion for creation of laser and Stokes modes and coupled acoustic mode 05 p0823 A67-16663
- Isophotes of extended light sources in night sky, Stokes parameters, brightness and degree of polarization for Rayleigh-scattered light in earth atmosphere 08 p1326 A67-21243
- Electronic polarimeter applied to Stokes parameter measurement of lunar surface, determining reflected light ellipticity 15 p2552 A67-29147
- Automatic photopolarimeter as pilot model for scans of planetary disks on fly-by missions 15 p2492 A67-30435
- Counterpart of Stokes hydrodynamical paradox for linearized viscous fluid flow obtained from application of singular perturbation to Oseen equations 16 p2657 A67-30827
- Earth gravitational potential on geoid expressed by vertical and horizontal gradients for gravitational anomalies useful in earth figure determination 21 p3618 A67-38199
- Resonance electronic Raman effect and parametric induced anti-Stokes radiation in potassium vapor atoms 21 p3641 A67-38456
- Electronic polarimeter applied to Stokes parameter measurement of lunar surface, determining reflected light ellipticity 24 p4239 A67-43070
- STOL AIRCRAFT**
- SA SHIN MEIWA UF-XS AIRCRAFT**
- VTOL and STOL aircraft applications, Boston to Washington [AIAA PAPER 66-964] 02 p0182 A67-12638
- Boundary layer control systems on Buccaneer S. Mk 1 and S. Mk 2 carrier-based strike aircraft 03 p0353 A67-12846
- STOL aircraft characteristics compared with VTOL aircraft and helicopter, noting airport layout 03 p0357 A67-12969
- Lift-drag ratio, specific impulse, aspect ratio and weight of payload and power plant considered for STOL aircraft 03 p0358 A67-12980
- Future short haul air transportation in northeast corridor of U.S., considering conventional, STOL and VTOL air transport systems 03 p0538 A67-13783
- VTOL/STOL aircraft evaluation via performance characteristics 07 p1130 A67-20219
- STOL and VTOL aircraft performance and cost for intercity travel, discussing airport network 08 p1279 A67-20782
- OV-10A aircraft testing in landing and takeoff from fields, jungle clearings and primitive roadways 10 p1594 A67-23391
- Motion equations used in determining lateral stability and control derivatives for STOL aircraft 10 p1595 A67-23551
- Arava light twin-turboprop STOL transport aircraft operating from short rough airfield, noting wind tunnel results 11 p1743 A67-24213
- Military aircraft characteristics and performance evaluation procedure 11 p1885 A67-25102
- Three STOL commercial transports performance and cost compared with conventional transports 12 p1894 A67-25492
- High lift techniques for STOL aircraft compared based on maximum lift coefficient, noting airfoil stall characteristics and flow separation delay devices [SAE PAPER 670245] 12 p1894 A67-25500
- UF-XS Japanese STOL seaplane used to investigate slow speed flying quality and hydrodynamic characteristics of PX-S aircraft 14 p2245 A67-27743
- Yak 40, Soviet three-engine jet airliner, for operation off short natural-surface airfields 14 p2245 A67-27893
- Four engine STOL aircraft for short distance hauls, noting fuselage and wing design 16 p2595 A67-30601
- VTOL and STOL aircraft comparison, discussing advantages and disadvantages of hinged and folding rotors, hinged wings, jet thrust and fan-in-wing principle 17 p2798 A67-32833
- Circulation control rotor blades of circular or elliptical cross section for helicopters, VTOL and STOL and possible application to aircraft 18 p2987 A67-34707
- Hydraulic design of Japan YS-11 twin turboprop transport aircraft, noting component accessibility and ground service simplification 19 p3175 A67-34787
- Three STOL commercial transports performance and cost compared with conventional transports 20 p3362 A67-37530
- PT6 series of small shaft turboprop engines for STOL aircraft and high speed surface vehicles noting performance and environmental tolerance improvements [AIAA PAPER 67-744] 23 p4048 A67-40978
- Augmentor-Wing research program for developing high lift devices to reduce takeoff/landing speeds of jet aircraft [AIAA PAPER 67-741] 24 p4094 A67-42804
- STOL and VTOL takeoff and landing areas, discussing urban and suburban air transportation and operational weather requirements [AIAA PAPER 67-795] 24 p4258 A67-42956
- Reliability and safety for STOL aircraft and low airspeed operation, discussing automatic flight control system, air traffic control, etc [AIAA PAPER 67-797] 24 p4095 A67-42958
- STOMACH**
- S ABDOMEN**
- STONY METEORITE**
- SA ACHONDRITE**
- SA CHONDRITE**
- Cosmic ray variations studied by effects on Zaisan chondrite 02 p0310 A67-12581
- Emissivity, absorptivity and thermal inertia effects on calculation of iron meteoroid temperatures at earth distance from sun 04 p0699 A67-14965
- Chemical analysis of stony meteorites, noting analytical procedures and results 05 p0895 A67-16581
- Statistical analysis of distribution of cosmic ray ages of stony meteorites 07 p1249 A67-19540
- Meteoritic, solar and terrestrial rare earth distribution abundance in chondritic or ordinary stony meteorites 10 p1651 A67-23428
- Maskelynite-bearing stony meteorites, noting absence of crystalline structure 10 p1709 A67-23494
- Radioactive krypton content in stony meteorites determined via mass spectrometry, deriving spall ratios and radiation ages 11 p1866 A67-24692
- Iron and stony meteorite cooling rates determined by measuring kamacite bandwidth, bulk nickel content and composition 11 p1868 A67-24872
- Magnetic properties of meteorites, residual thermomagnetic capacity and determination of space magnetic fields 14 p2383 A67-27928
- Optical characteristics of cosmic and terrestrial surfaces, noting color distribution on moon, asteroids, stony meteorites, etc 15 p2516 A67-29152
- Farmington chondrite meteorite observations show two small granular cristobalite xenoliths surrounded by thin diopsidic clinopyroxene reaction rim 15 p2556 A67-29647
- Iron and iron-stony meteorites cooling rates in relation to Ni content and Widmanstätten structure suggest development in different thermal environments 16 p2750 A67-31453
- Chemical analyses of stony meteorite and iron meteorite with silicate inclusions 16 p2751 A67-31456
- Tektite formation and flight from large meteorite impact, discussing blast expansion flow 20 p3530 A67-37527
- Hypersthene chondrite postformational history, discussing native copper and ilmenite content of Newmann lamellae and flowage 24 p4232 A67-42613
- Al 26 content of stony meteorites by coincidence spectrometry noting cosmic ray exposure ages for eight meteorites 24 p4234 A67-42630
- Coexisting minerals and interstitial

- groundmass of chondrules of Mezo-Madaras chondrite 24 p4235 A67-42633
- Stony meteorite Fe, Ni, Co, Ca, Cr and Mn concentration determined by X-ray fluorescence 24 p4235 A67-42638
- Optical characteristics of cosmic and terrestrial surfaces, noting color distribution on moon, asteroids, stony meteorites, etc 24 p4190 A67-43075
- STORABLE PROPELLANT**
- Propellant combinations evaluation for minimum weight of high energy propellant reaction control systems [AIAA PAPER 66-947] 02 p0304 A67-12281
- STORAGE**
- SA AGING
- SA CRYOGENIC STORAGE
- SA DATA STORAGE
- SA ENERGY STORAGE
- SA HANDLING EQUIPMENT
- SA PROPELLANT STORAGE
- SA SPACE STORAGE
- Closed form expression for storage time of arbitrary base diode, noting diode transient behavior 03 p0380 A67-13489
- Failure rates and modes for nonoperating electronic packages, presenting solutions for reliability problem 05 p0780 A67-17469
- Prediction techniques developed under storage technology program, including nonoperating and operating time periods to determine operational readiness 15 p2495 A67-30416
- Growth of dendriform crystal contaminant in hydrocarbon fuel or hydraulic system during stagnant storage, discussing possible effects and corrections 17 p2801 A67-31991
- Solid chemical state O for spacecraft noting advantages over liquid and high pressure gas, discussing storage, handling, losses, shelf life, availability and containers 23 p3967 A67-41608
- STORAGE BATTERY**
- SA DRY CELL BATTERY
- Current stretch sensing for removing limitations to usable density of cryotron storage cells of random access memories 11 p1765 A67-24625
- Power conversion circuits of Surveyor spacecraft including distribution system, battery charging and central regulator units 17 p2803 A67-32510
- Book on high energy batteries covering electrochemistry of discharge plate materials, weight factors, polarization electrolytes, parasitic effects, etc 18 p2989 A67-34265
- Nonmechanical electric power sources - Conference, Brighton, England, September 1966 22 p3748 A67-40226
- Lithium in electrolyte and active metallic nickel formation effects on capacity and plate mechanical strength in alkaline storage batteries 22 p3748 A67-40229
- Sealed silver-cadmium batteries meeting space requirements, discussing high energy plates, cell design and packaging 22 p3749 A67-40230
- 30 cell 1 kw hydrogen fuel battery for room temperature operation, noting construction and performance 22 p3749 A67-40231
- Orbiting space vehicle secondary battery size and weight optimization based on cycle life and discharge depth 24 p4106 A67-42522
- STORAGE DEVICE**
- SA ENERGY STORAGE DEVICE
- Noise rejection properties of threshold devices with storage circuit calculated on basis of intersection probability of fixed level by storage circuit output voltage 02 p0205 A67-12533
- Direct view storage tubes for radar displays 09 p1528 A67-22628
- Noise rejection properties of threshold devices with storage circuit calculated on basis of intersection probability of fixed level by storage circuit output voltage 14 p2261 A67-28010
- Superconducting storage device with Josephson tunneling junction replacing cryotron 14 p2289 A67-28921
- Thermal annealing of silicon solar cells with direct solar heating or electric storage methods to avoid radiation damage 20 p3364 A67-37129
- High sensitivity information storage filter for spectrum analysis 21 p3601 A67-39067
- Q-switched laser single pulse visual recording by oscillograph with storage tube/photodiode
- combination 22 p3817 A67-40415
- STORAGE STABILITY**
- Storage reliability for electronic systems in missiles, noting factors affecting failure rates after dormant storage 11 p1768 A67-25010
- Decomposition and stability of diphenylamine compounds in nitrocellulose powder, determining activation energies 15 p2543 A67-29889
- Barium fluoride film electric hygrometer element aging and possible causes of calibration drift with time in storage 24 p4156 A67-42380
- Aerospace automatically activated electrochemical battery and DC-DC high voltage converter-regulator noting storage stability 24 p4108 A67-42541
- STORAGE TANK**
- SA CONTAINER
- SA FUEL TANK
- SA PROPELLANT TANK
- Transducer measuring water quantity in water storage tanks of LEM under zero g conditions 01 p0073 A67-11114
- Structural cryogenic vessels of chemical rocket stages 05 p0874 A67-17015
- Comparing shroud-mounted to tank-mounted high performance insulation systems 13 p2214 A67-27655
- Cooldown of shrouded spherical vessels in liquid nitrogen, determining smallest tank-shroud gap compatibility with rapid cooldown 13 p2229 A67-27666
- Variable thickness insulation system for transport of hydrogen propellant into earth orbit for docking transfer to lunar and interplanetary mission vehicles [ASME PAPER 67-HT-50] 20 p3548 A67-36732
- Hydrogen peroxide oxygen-water supply system as backup for long space flights noting storage tanks, catalytic reactor and heat exchanger 22 p3747 A67-39893
- STORAGE UNIT**
- Scan converter for Apollo TV performing time base conversion with destructive readout storage element and flicker correction with magnetic disk [SMPT PAPER 101-53] 12 p1904 A67-25468
- Universal array of complementary-symmetry MOS transistors applied to missile and surface radar beam steering phase array storage unit 18 p3015 A67-34563
- Batch fabrication method for storage elements using electrophoretic deposition of ferrite on platinum wire 22 p3812 A67-39915
- STORM**
- SA CYCLONE
- SA GEOMAGNETIC STORM
- SA GUST
- SA HURRICANE
- SA IONOSPHERIC STORM
- SA MAGNETIC STORM
- SA NOISE STORM
- SA RAINSTORM
- SA SOLAR STORM
- SA THUNDERSTORM
- SA TROPICAL STORM
- SA WIND
- Stress-related and other physiological variables on jet aircraft pilots participating in storm penetration and perimeter flights 17 p2805 A67-31955
- Soviet book on aeronautical meteorology covering wind and cloud effects on takeoff, landing and supersonic flying in storms and jet stream layers 18 p3074 A67-33676
- Summit areas of severe storms, measuring stratospheric-tropospheric interchange, air flow and hydrometeors 19 p3252 A67-35057
- STRAIN**
- SA BUCKLING
- SA CENTRIFUGAL STRAIN
- SA CRACK
- SA FAILURE
- SA FATIGUE
- SA INTERFACIAL STRAIN
- SA PRESSURE
- SA SHEAR STRAIN
- SA STRESS-STRAIN DIAGRAM
- SA STRESS-STRAIN DISTRIBUTION
- SA STRESS-STRAIN-TIME RELATION
- SA STRUCTURAL STRAIN
- SA UNIAXIAL STRAIN
- SA VOLUMETRIC STRAIN
- Degree of strain effect on kinetics of recrystallization of nickel and niobium monocrystals investigated by electron beam fusion in vacuum 01 p0101 A67-10940
- Taper in thickness of wing for special case of linear type analyzed, using triangular

- elements for matrix displacement method 04 p0707 A67-14441
- Moire patterns in determining partial derivatives of displacement components 05 p0909 A67-16142
- Distinct yield point appearance in vanadium alloys as function of composition strain temperature and strain rate 05 p0828 A67-16388
- Strain distribution measurement by optical grating 05 p0918 A67-16441
- Diffraction grating technique for measuring dynamic plastic strain exceeding 4 percent deformation at high strain rates in variable intensity light source 05 p0920 A67-16881
- Plastic strains in thick cylindrical segment under mechanical and thermal loads [AIAA PAPER 67-113] 06 p1102 A67-18301
- Photoelastic stress measurement techniques for birefringent high polymers extended to two- and three-dimensional linear viscoelasticity 08 p1420 A67-20887
- Degree of strain effect on kinetics of recrystallization of nickel and niobium monocrystals investigated by electron beam fusion in vacuum 22 p3820 A67-39793
- STRAIN AGING**
- Strain aging of ordered alloys at temperatures above and below critical points discussing yield point and hardening factor 01 p0101 A67-10933
- Constant load creep test determination of creep ductility and dimensional instability of nickel at 500 and 525 degrees C 02 p0256 A67-12701
- Fatigue mechanisms for fcc metals and alloys, reviewing research on crack initiation and propagation 03 p0447 A67-13804
- Yield point and strain aging in tantalum identifying interstitial atom in electron-beam melted tantalum after incremental plastic deformation 06 p1015 A67-17894
- Hot cracking and strain-age cracking in heat affected zone of Rene 41 alloy weldments 07 p1198 A67-19211
- Reversed speed effect and grain boundary diffusion as explanations of discrepancy of activation energy values for strain aging under fatigue or simple stress conditions 12 p2013 A67-25284
- Alloy steels response to dynamic strain aging in quenched, tempered and ausformed conditions, plotting strength and toughness against straining and tempering temperatures 16 p2688 A67-31300
- Strain age cracking characteristics in welded Rene 41 nickel base alloy, discussing test procedure used with circular patch test to evaluate contributing factors 20 p3471 A67-37698
- STRAIN-ENERGY**
- Modulated structure of aged Ni-Al alloys including electron micrograph and phase diagram studies of particle growth kinetics 01 p0092 A67-10051
- Equilibrium equations, boundary conditions and constitutive relations for nonlinear theory of elastic directed curves, examining double stress without moment 02 p0267 A67-12051
- Boundary layer phenomenon in nonlinear membrane theory, investigating problem of closing hole in membrane having John strain energy density 03 p0525 A67-13821
- Stiffness matrix evaluation on basis of strain energy 04 p0709 A67-14811
- Forming closed contour shells by straining with expandable punch 07 p1191 A67-19751
- Statistical basis for modified moment theory of elasticity that takes into account contribution of all deformation-tensor component gradients to deformation energy 09 p1574 A67-21911
- Friction stress acting upon moving dislocation derived from microstrain studies 09 p1518 A67-22021
- Cartesian formulation of membrane theory discussing equations of equilibrium, strain energy, variation formulation and boundary conditions 11 p1875 A67-24431
- Perturbation solutions for finite inflation under internal pressure, of elastic toroidal membrane of circular cross section 11 p1879 A67-25001
- Discrete analysis in plate and shell theories based on method of constructing difference equation, using strain energy of system 12 p2023 A67-25591
- High temperature strength of

- thermomechanical nickel dependent upon previous thermal and mechanical history, measuring elastic strain energy in matrix 14 p2337 A67-28418
- Heat resistant stainless steel honeycomb cores for cylindrical applications, measuring energy absorption characteristics [ASME PAPER 67-DE-14] 14 p2402 A67-28870
- Elastic interactions of cracks and dislocations of screw type in two-dimensional model 16 p2768 A67-31281
- Finite inflation of isotropic elastic toroidal membrane possessing strain-energy function by uniform internal pressure 17 p2956 A67-31932
- Axissymmetrical temperature fields for minimum functional of elastic deformation energy in infinite cylindrical shell 17 p2962 A67-32968
- Strain-energy function of hyperelastic material in terms of extension ratios, with natural rubber as example 18 p3145 A67-34642
- Group IV and V metal carbides ball-milled to determine mechanical strain effects 20 p3467 A67-37122
- Strain energy in thin isotropic elastic shells subject to arbitrary temperature distribution, considering large deflections and buckling 21 p3718 A67-38021
- Strain energy method for analyzing large deflections of trapezoidal plates with constant thickness and rigidly clamped edges under uniformly distributed load 21 p3725 A67-38794
- Nonlocal elasticity theory for materials with long range cohesive forces derived from lattice theory by writing strain energy in integral form 22 p3908 A67-39288
- Elastic strain energy change rate as related to notch depth considered for edge notches with finite radius 23 p4074 A67-40664
- Double cantilever beam /DCB/ specimen for fracture toughness testing, discussing elastic strain energy release rate and load and crack length extension relation 23 p4018 A67-40928
- Invariant form of strain-energy function of linearized elastic potential of isotropic thin shell using three-dimensional theory 24 p4249 A67-42156
- STRAIN FATIGUE**
- Strains in twisted blades with rectilinear axes, examining general relations and parameters in postulated new theory 03 p0528 A67-14080
- Strength criterion for complex loading, possible development based on strength criterion for symmetrical cyclic loading 03 p0529 A67-14168
- Cracking during welding of aluminum alloy noting effect of strain, maximum temperature and cooling rate [ASME PAPER 66-WA/MET-5] 04 p0639 A67-15341
- Mean strain cumulative damage and effect in low cycle fatigue of 2024-T351 aluminum alloy, covering strain cycling, fatigue life, residual ductility, etc [ASME PAPER 65-WA/MET-5] 05 p0827 A67-16214
- Second order strain accumulation in aluminum in reversed cyclic torsion at elevated temperatures 09 p1517 A67-21753
- Short life fatigue failures in multiaxial stress-strain system 10 p1719 A67-23486
- Cumulative strain behavior of nickel-chromium alloy and chromium martensitic type steel under action of cyclic loading 12 p2015 A67-25420
- Strain amplitude and flange width-to-thickness ratio effects on dynamic buckling in modified I-beams subjected to pure reverse bending 17 p2958 A67-32030
- Fatigue-damage evaluation system for transport aircraft, noting use of cumulative strain gauge that stores strain history 18 p3142 A67-33897
- Boron filament behavior in rotating-beam fatigue test 20 p3470 A67-37390
- Crack line loading methods for measuring fracture toughness noting advantages over remote loading test procedures 22 p3820 A67-39630
- Pressure effects on fatigue reported for Fe, Al and Ni wires subjected to oscillating strains, discussing several fatigue models 23 p4075 A67-40666
- Hysteresis loop measurement using Sonntag fatigue machine which produces sinusoidal force at 30 Hz fixed frequency 23 p4078 A67-41227
- Fatigue crack research effect on structural design of flight vehicle structures, discussing temperature effects, multiaxial strain effects and fatigue crack growth equations 24 p4247 A67-41942
- Fatigue fracture surface macroscopic and microscopic appearance as affected by prevailing stress intensity conditions at moving crack tip 24 p4170 A67-41946
- High temperature low cycle creep range strain fatigue behavior estimation from tensile and stress rupture properties 24 p4251 A67-42483
- STRAIN FIELD**
- Elastic strain distribution in structure of quasi-isotropic polycrystalline titanium 01 p0093 A67-10100
- Displacement potential for solutions of displacement equilibrium equations obtained by Mindlin for linear elastic medium where stresses are functions of strains and strain gradients 03 p0524 A67-13661
- Composite coatings provide temperature differences at surface of hot stamped blanks, thereby making it possible to control strain distribution over surface 04 p0630 A67-15901
- Quasi-static problem of generalized plane stressed state of thin plate, considering heat transfer on lateral surfaces and interaction between strain fields and temperature 05 p0913 A67-16186
- Generalized thermally stressed state of thin plate in presence of interaction between strain field and temperature, considering heat exchange with surrounding medium 05 p0913 A67-16187
- Plastic strain distributions in polycrystalline austenitic stainless steel and titanium, using photoelastic coating 08 p1343 A67-21333
- Instrument design for analyzing biaxial strain field in thin plate under creep, noting use of moire effect 08 p1332 A67-21461
- Plastic deformation and fracture of rotating turbine rotor model 09 p1502 A67-21554
- Invariant stress and deformation functions for doubly curved shells, noting reduction of equilibrium equations and surface strain-displacement relations into compatibility equation 10 p1730 A67-23834
- Stresses and displacements for any strain state of hollow cylinder 13 p2218 A67-26890
- Turbulent wake under homogeneous strain noting mechanism of transport and mixing 13 p2096 A67-26915
- Reciprocal theorem applied to linear and angular displacements due to creep or plastic strains in inelastic bodies 14 p2398 A67-28097
- Unsteady dynamic field excited by source moving along elastic half-plane boundary 21 p3716 A67-37967
- Relative and absolute error sign and magnitude shown to be functions of strain field, strain gauge mounting and angular error of mounting on test object 21 p3628 A67-38049
- Strain birefringence around tekite surface notches, discussing specimen quenched in air stream from 1000 degrees C 21 p3704 A67-38506
- Tungsten strain amplitude dependent dislocation damping measured as temperature function, discussing inconsistency with Friedel thermally activated breakaway theory 22 p3819 A67-39352
- Motor fields analysis in Cosserat continuum noting differential forms of stress and strain 22 p3837 A67-40006
- STRAIN GAUGE**
- Cryogenic strain gauge application to circumferential loads of Centaur hydrogen tank insulation while in launch configuration 01 p0069 A67-11016
- Si semiconductor strain sensors and miniature pressure transducers for cryogenic pressure measurements 01 p0069 A67-11017
- Electric-resistance strain gauge measuring techniques at high temperatures 01 p0071 A67-11096
- Digital computer compensation of strain gauge data to extend measuring bandwidth to transient or HF phenomena 01 p0030 A67-11098
- Signal conditioning variable resistance transducer excited by constant current power supply 01 p0071 A67-11099
- Strain gauge bridge outputs combined during flight to measure airloads directly and inexpensively in fatigue test program 01 p0030 A67-11103
- Strain gauges applied to epoxy laminates in liquid hydrogen insulation systems 01 p0072 A67-11107
- Contact resistance variation effect on strength tests, noting strain gauge reading error magnitudes 02 p0340 A67-12444
- Phosphorus-diffusion method in silicon with thin phosphorus containing layer used to produce working area of planar strain gauges 02 p0248 A67-12737
- Strain-gauge measurements of large-scale stationary mounted parts with gauges on foil substrate at high temperature 03 p0527 A67-14074
- Hole-drilling method of measuring residual stresses in elastic materials determined by empirically derived relation between magnitudes of principle stresses and strain relaxation about hole 03 p0531 A67-14360
- Strain gauge method for determining stress concentration in radial flow impellers 04 p0708 A67-14537
- DVL free piston shock tunnel and measuring systems of three-component balance based on use of strain gauges 04 p0546 A67-14575
- Compressor blade vibration, discussing prediction of amplitudes of vibration and interpretation of results of engine strain gauge tests in terms of component service life [ASME PAPER 66-WA/GT-14] 04 p0712 A67-15369
- Strain gauge measurements of resistance of sphere to MHD turbulent flow of mercury in rectangular tube 04 p0670 A67-15530
- Strain measurement at high temperature by vacuum deposition of thin films on specimens covered with insulating layer 04 p0626 A67-15745
- Separation of load eccentricity and initial deviation determined through column compressive tests, using aluminum alloy bars and strain gauges 05 p0919 A67-16588
- Reliable test method based on special strain gauge load transducer for embedment axial stress measurement in electronic modules 05 p0779 A67-17457
- Gross hydrostatic pressure effect as related to foil and wire strain gauges 07 p1185 A67-19412
- Experimental stress and strain analyses of solid propellant rocket engine grains under various loading conditions 08 p1419 A67-20886
- Stress-strain diagrams under dynamic conditions obtained by processing strain gauge data, using analog computer 09 p1492 A67-21560
- Hydrostatic pressure measurement by direct loading of semiconductor strain gauges 09 p1498 A67-22031
- Strain gauge measurement data on rotating impeller blades of aircraft turbines, discussing errors in determination of stress amplitude 09 p1576 A67-22458
- Compressor blade failure due to material fatigue, using destructive testing in stationary rig 12 p2014 A67-25413
- Semiconductor piezoresistive strain gauges and application to compressor blade vibratory stresses measurement 12 p2014 A67-25416
- Flat and stacked rosettes performance in linear and nonlinear stress fields 13 p2219 A67-27093
- Strain gauge bridge outputs combined during flight to measure airloads directly and inexpensively in fatigue test program 14 p2315 A67-28002
- High hydrostatic pressure effects on load cell using foil strain gauges and calibration for small uniaxial loads 17 p2855 A67-32393
- Tensometric properties of silicon whiskers and acicular single crystals studied under static and dynamic loads, estimating suitability as strain gauge sensors 18 p3097 A67-33473
- Tensile testing equipment using impact load facilitates rupture stress measurements by conventional strain gauges 18 p3141 A67-33719
- Strain and strain-rate sensor for measurements under dynamic conditions and without physical contact with deformation field being sensed 18 p3141 A67-33888
- High-elongation foil strain gauges

evaluation for measuring cyclic plastic strains, determining Poisson ratio 18 p3142 A67-33890
 Errors in high temperature electric-resistance strain gauge measurements 18 p3142 A67-33892
 Semiconductor strain gauge theory, application and installation 18 p3047 A67-33893
 Dynamometer using epoxy-bonded foil strain gauges for simultaneous two-force measurements for ultrahigh vacuum and high temperature applications, noting calibration [SESA PAPER 1209] 18 p3142 A67-33896

Fatigue-damage evaluation system for transport aircraft, noting use of cumulative strain gauge that stores strain history 18 p3142 A67-33897
 Steady thermal strains measurement in aero and industrial turbine and engine components, discussing fine wire behavior, bonding agent, performance, requirements, etc 18 p3143 A67-33900

Compressor blade vibration, discussing prediction of amplitudes of vibration and interpretation of results of engine strain gauge tests in terms of component service life [ASME PAPER 66-WA/GT-14] 18 p3115 A67-34132

Silicon semiconductor strain-gauge techniques applied to transducer design noting small light units, high sensitivity, silicon integrated circuits, reliability, etc 20 p3442 A67-36458

Relative and absolute error sign and magnitude shown to be functions of strain field, strain gauge mounting and angular error of mounting on test object 21 p3626 A67-38049

Comparative investigation of strain gauge testing methods 21 p3626 A67-38100

Silicon AC strain gauges performance investigated by employing oriented p-Si crystals operating in static and dynamic modes 22 p3798 A67-39569

Slide wire strain gauge to measure static strains and stresses at high temperatures 22 p3809 A67-40476

Book on two-dimensional and surface strain measurement for industrial application including strain gauges, photoelasticity and moiré methods 23 p4077 A67-40791

Testing procedure for determining strain gauge elongation limit, discussing gauge applications to strain measurements at LOX temperatures 23 p4007 A67-41389

Flight strain gauge system for Centaur /AC-6/ liquid hydrogen fuel tank skin 23 p4008 A67-41390

Si semiconductor strain gauge thermal coefficient of resistance /TCR/ reduction by high energy electron irradiation 23 p4008 A67-41391

Digital computer compensation of strain gauge data to extend measuring bandwidth to transient or HF phenomena 24 p4155 A67-42290

Metal-fatigue failure indicator-predictor gauge by correlating resistance changes with fatigue damage [AIAA PAPER 67-794] 24 p4251 A67-42955

STRAIN GAUGE ACCELEROMETER
 Piezoresistive strain gauge accelerometers with subcritical damping and high overload capabilities 01 p0075 A67-11138

Strain gauge accelerometer designed and constructed for vibration pickup use 06 p1004 A67-18580

Temperature effect on zero shift of piezoelectric crystal accelerometers under shock loading using Hopkinson bar technique 23 p4006 A67-41376

STRAIN GAUGE BALANCE

Strain gauged sting balance for use in small low speed wind tunnel for measuring lift, drag and pitching moment 01 p0051 A67-11270

V/STOL aircraft model wind tunnel tests on wing and propellers, describing strain gauge balances 22 p3745 A67-39728

Safety device to prevent overloading of models and sensitive wire strain gauge balance by aerodynamic forces during starting and switching off in wind tunnel 22 p3780 A67-39756

STRAIN HARDENING

Elastic-plastic solution for circular rigid inclusion in unidirectionally stressed flat plate of linearly strain-hardening

material 02 p0336 A67-11633
 Strain-hardening and temperature dependence of mechanical properties of ternary ordered alloys on nickel-iron base 02 p0255 A67-12875
 Bending moment change of curvature relation for large elastoplastic deflection of thin circular-arc cantilever beam, taking strain hardening materials into account 05 p0918 A67-16425

Ramberg-Osgood relation that adequately describes stress-strain curve of strain hardening material extended to formulate constitutive laws for creep 05 p0830 A67-16812

Hydrogen effect on high temperature plasticity failure and mechanical properties of titanium shown to be similar to that caused by strain hardening 07 p1200 A67-19248

Solution hardening in niobium by Ta, V, Zr and W, showing linearity with composition and relationship to sum of atomic size and elastic modulus differences 07 p1209 A67-19642

Strain hardening and softening of metals produced by cycles of plastic deformation explained in terms of Bauschinger effect 12 p2015 A67-25419

Low endurance fatigue analysis for steel and Al alloy under cyclic torsion with controlled shear strain amplitude 12 p2018 A67-25425

Strain hardening of high temperature titanium multiphase solid solution by deformation and subsequent rapid cooling 15 p2504 A67-29971

Cross slip and slip character related to fatigue, brittle fracture and strain hardening in crystal solids 16 p2772 A67-31299

Fatigue properties of explosively formed parts tested by repeated axial loading and results compared with statically formed specimens 17 p2871 A67-32433

Nonlinear flexural vibrations of rings studied without assuming zero midplane strain 17 p2963 A67-33032

Strain distribution in aluminum filament reinforced metal, investigating matrix plastic behavior and residual stresses, etc [ASTM PAPER 8] 18 p3067 A67-34573

Strain rate history effects on strain hardening curve for aluminum described by state equation 19 p3245 A67-35448

Multipoint equivalent cross section method for calculating finite deflections of beams of strain hardening material 20 p3541 A67-37285

Cyclic stress-strain in annealed and cold worked fcc polycrystalline metals and alloys studied for hardening and softening by transmission electron microscopy 22 p3821 A67-40033

STRAIN RATE

Loss in hydrodynamic thermostability of viscoplastic material with stress tensor deviator related to strain rate tensor deviator 01 p0052 A67-10682

Elastoplastic deformation under plane stress conditions determined, using method of photoelastic coatings 02 p0336 A67-11628

Mean tensile strength of aluminum alloys using torsion tests determined at high strain levels and compared with extrusion tests values 04 p0636 A67-14907

Plane strain equations for elastoviscoplastic compressible bodies without strain hardening 05 p0908 A67-16039

Stresses in solids moving during loading, using velocity vector and strain rate tensor as variables for instantaneous state of body motion 05 p0914 A67-16194

Diffraction grating technique for measuring dynamic plastic strain exceeding 4 percent deformation at high strain rates in variable intensity light source 05 p0920 A67-16824

Strain rate effects on low endurance fatigue noting constant frequency induced variations 07 p1261 A67-19059

Hydrogen brittleness in Ti alloys, noting conditions of development 07 p1206 A67-19283

Active slip volume /active crystal length/ concept in plasticity theory and relation to temperature and strain rate 07 p1232 A67-19636

Strain rate dependence of critical shear stress in cadmium single crystals used in activation energy determination 07 p1234 A67-20109

Rheologic and plastic phenomenological

analysis of viscoplasticity problems, discussing constitutive equations and stress propagation 08 p1414 A67-20312
 Viscoelasticity for micropolar solids, obtaining constitutive equations of strain and microrotation rate dependent materials 08 p1422 A67-20979
 Uniaxial tensile strain rate on stability of soft reinforced plastics with two-component fibrous base 10 p1671 A67-23605
 Irregularly spaced nozzle vanes effect upon blade vibration in radial flow gas turbine [ASME PAPER 67-VIBR-42] 11 p1797 A67-24195

Sollthane 113 urethane rubber composition analyzed via constant strain rate tests noting birefringent sensitivity and optical transmission properties 11 p1811 A67-24615
 Loss in hydrodynamic thermostability of viscoplastic material with stress tensor deviator related to strain rate tensor deviator 11 p1783 A67-25070

Molybdenum polycrystal plastic strain rate in pre-yield region studied by successive stress relaxation method for dislocation density and mobility characteristics 14 p2337 A67-28230

Cylindrical specimen behavior during high strain rate tensile test, using computer program 14 p2400 A67-28523

Griffith initiation criterion extended to fracture initiation and growth in viscoelastic materials using energy formulation 16 p2773 A67-31311

Low cycle fatigue behavior of metals at creep range temperature related to equivalent ductility and strain rate 16 p2774 A67-31321

Low strain rate and temperature effects on crack initiation and growth, recovery and boundary migration for Al and Al alloy 16 p2889 A67-31368

Oxygen concentration and strain rate effect on yield point phenomenon in electron beam refined niobium, showing relation to dislocation multiplication 18 p3063 A67-33486

Strain and strain-rate sensor for measurements under dynamic conditions and without physical contact with deformation field being sensed 18 p3141 A67-33888

Flow stress of aluminum related to strain, strain rate and temperature, discussing compression testing machine and results 18 p3064 A67-34078

Superplasticity resulting from high strain rate sensitivity observed in isothermal tension tests on several titanium and zirconium alloys 18 p3064 A67-34083

Strain rate history effects on strain hardening curve for aluminum described by state equation 19 p3245 A67-35448

Alloying effect on temperature and strain rate sensitivity of niobium-molybdenum bcc metal 19 p3248 A67-35730

Etch pitting and electron microscopy used for tungsten single crystals dislocation density measurements at different strain levels 19 p3248 A67-36028

Testing apparatus for rapid determination of tensile strength of fine filaments 20 p3537 A67-36522

Steady state diffusional creep for materials with large grains and dislocations forming sinks for vacancies, obtaining strain rate 21 p3719 A67-38089

Plastic deformation of single-crystal Ni-Al investigated for temperature, orientation and strain-rate dependence of tensile flow 21 p3645 A67-38774

Strain rate sensitivity and bending extension interaction in one degree of freedom deformation of clamped beam, considering vibration and load duration 23 p4072 A67-40607

Crack propagation through mild steel plates investigated by method using stress values at several places near crack and at crack tip 23 p4074 A67-40665

High speed information generation by projectile impact machine, explosive forming and capacitor-discharge energy with very high strain rates, presenting failure modes related to forming velocity 23 p4078 A67-40737

Testing machine operated by hydraulic pressure for mechanical properties of materials at medium rates of strain 23 p4079 A67-41332

Generalized dynamical thermoelasticity

theory formulated via heat transfer
equation, considering temperature/strain
rate coupling effect 24 p4252 A67-41955

RAIN SOFTENING
Nonlinear flexural vibrations of rings
studied without assuming zero midplane
strain 17 p2963 A67-33032

STRATIFICATION
SA ATMOSPHERIC STRATIFICATION
Stratification similitude laws for liquid
hydrogen determined and extrapolated to
full size tanks from small tank
data 13 p2186 A67-27643
Semiempirical description of stratification
in wall heated containers of cryogenic fluids,
noting decrease due to bottom
heating 13 p2227 A67-27644
Increase in mean electron energy shown
to be factor leading to plasma
stratification 14 p2353 A67-27756
Asymptotic stability of homogeneous
system of partial differential equations in
stratification wave theory, introducing
source function for local plasma disturbance
effect 17 p2907 A67-33101

STRATIFIED FLOW
Successive approximation method of
estimating effect of stratification and
dynamic nonuniformity of crosswind on
trajectory of circular turbulent
jet 01 p0053 A67-10824
Turbulent diffusion in nonuniform
stratification atmosphere, obtaining vertical
concentration profile by random walk
method
[AFCL-66-836] 02 p0262 A67-12081
Nonstationary models of cumuli and
thermals in stratified
atmosphere 02 p0262 A67-12641
Electron temperature, concentration and
potential distribution, measurement in
moving striations by Langmuir probe
method 19 p3273 A67-35095
Stratified shear flow instability examined
through two classical
models 19 p3210 A67-35611
Nonlinear steady motions produced by
stable stratification in rapidly rotating fluid,
discussing Ekman layers 23 p3990 A67-41170

STRATIFIED LAYER
Stratified and faceted forms on panoramas
obtained from Luna IX space station, noting
connection with mineral composition of
lunar surface 01 p0150 A67-10904
Structure of wind field in thermally
stratified atmosphere based on spectra of
horizontal wind speed 05 p0837 A67-16485
Parameters of small scale turbulence in
diabatic atmospheric surface layer,
examining structure characteristics of
temperature and vertical velocity field
components 05 p0837 A67-16487
Dynamic effective stiffness theory of
layered and unidirectionally fiber reinforced
composites, detailing field equations for
laminated composite 10 p1724 A67-23708
Thermal radiation properties of oxide
films of variable thickness on metal
substrates, using radio-recording
spectrophotometer at various wavelengths
[AIAA PAPER 67-286] 12 p1958 A67-26003
Structure of wind field in thermally
stratified atmosphere based on spectra of
horizontal wind speed 13 p2150 A67-26341
Parameters of small scale turbulence in
diabatic atmospheric surface layer,
examining structure characteristics of
temperature and vertical velocity field
components 13 p2150 A67-26343
Relation between diurnal, seasonal and
cyclic variations of stratifications in E layer
and fine structure of sporadic E layer and
E-2 layer 13 p2110 A67-26550
Fields generated by infinitesimal,
arbitrarily oriented, electric-dipole source
located in isotropic medium bounded by
parallel plane-stratified, anisotropic
media 16 p2632 A67-31858
Asymptotic solution for electromagnetic
field of electric dipole above stratified half-
space 22 p3763 A67-40311
Electromagnetic pulse distortion during
total internal reflection in stratified
troposphere, discussing reflecting medium
inhomogeneity effects on reflection
coefficients 23 p3973 A67-40837

STRATOFORTRESS AIRCRAFT
S B-52 AIRCRAFT

STRATOJET AIRCRAFT
S B-47 AIRCRAFT

STRATOSCOPE I TELESCOPE
Theoretical interpretation of fine
structure observations of sunspots by
stratoscope, discussing stability modes and
sunspot umbras 13 p2203 A67-27423
Relation between number of photospheric
granules and Wolf sunspot
number 14 p2387 A67-28582

STRATOSPHERE
Meteorological Rocket Network /MRN/
probing of stratosphere and lower
mesosphere and analysis of acquired
data 02 p0239 A67-12535
Carbon dioxide content in troposphere and
lower stratosphere measured at various
altitudes, showing seasonal
variations 03 p0414 A67-14086
Interdiurnal temperature variability
distribution in northern hemispheric
stratosphere in January and July, based on
synoptic weather maps 04 p0616 A67-15473
Rocket sounding of stratospheric
circulation, noting relationship between
minima in westerly zonal flow of 45-55 km
stratopause layer and tropospheric cut-off
lows 05 p0838 A67-17306
Zonal harmonics investigation of mean
temperature of stratospheric
layers 06 p0996 A67-18447
Book on structure of stratosphere and
mesosphere noting rocket exploration
results, synoptic observations, solar control
over temperature variations,
etc 07 p1172 A67-19603
Local peculiarities of vertical distribution
of ozone in equatorial and polar regions for
different turbulent dynamic models of
stratosphere 07 p1173 A67-19696
Stratospheric free air turbulence detection
from slant-range FPS-16 radar tracked
Jlimsphere balloons 10 p1676 A67-22815
Heat transfer equations for rocketborne
stratospheric temperature sensor in form of
spherical bead thermistor and experimental
analysis of physical, thermodynamic and
electrical characteristics of rocketsonde
[AIAA PAPER 66-385] 10 p1632 A67-22819
Meteorological rocket network
observations of complex circulation system
in middle and upper
atmosphere 10 p1643 A67-23247
Thermal oscillations of polar night
stratosphere and upward
propagation 10 p1643 A67-23248
Ionosphere-stratosphere coupling and
effect of atmospheric seasonal variations on
plasma behavior 10 p1645 A67-23266
Heat radiative flux divergences and
equilibrium temperature distribution with
altitude calculated for heat regime modeling
radiative transfer conditions in stratosphere
and mesosphere 10 p1647 A67-23275
Cosmic radiation intensity fluctuation in
stratosphere, noting absence of explanation
for anomaly 12 p1994 A67-25542
Modified RK-1 radiosonde circuit for
stratospheric cosmic ray
measurements 12 p1941 A67-25555
Seasonal variations in high latitude
stratosphere and
mesosphere 13 p2113 A67-26675
Temperature determination in stratosphere
via hydrodynamic equations taking into
account energy inputs and atmospheric
motion, suggesting existence of integral heat
sources 13 p2113 A67-26676
Mean meridional motions in biennial wind
oscillation in wind structure of low latitude
stratosphere 13 p2151 A67-26738
Vertical distribution of tropospheric and
stratospheric ozone based on observations of
U.S. ozonometric stations at various
latitudes 14 p2308 A67-27927
Radio probe to derive relations between
ozone content of lower stratosphere and
origin of air in layers 15 p2474 A67-29525
Stratospheric temperatures in north and
south polar regions shown to depend on
land mass temperatures 15 p2475 A67-29579
Evidence regarding possibility of
midwinter stratospheric
warmings in
Southern Hemisphere 17 p2880 A67-32553
Biennial oscillations effect on spring wind
reversal in stratosphere and mesosphere,
showing transition date dependence on
geographical location and
height 18 p3074 A67-34352
Stratospheric aerosol concentrations
observed by optical radar echoes compared

with expected return from molecular
atmosphere to obtain vertical
profile 18 p3042 A67-34493
Quasi-biennial zonal wind and temperature
oscillation in stratosphere and mesosphere,
discussing periodicity and oscillation
model 19 p3220 A67-35272
Vertical distribution of diffuse sky light in
stratosphere determined by rocket
measurements, noting intensity peak in
aerosol layer 19 p3221 A67-35273
Stratospheric mean adiabatic vertical
motion and temporal correlations with
temperature, isobaric height,
zonal/meridional wind and horizontal kinetic
energy computed based on seasonal
averages 19 p3224 A67-35529
On-the-ground optical determination
method of stratospheric aerosol particle
numbers and sizes from ruby laser radiation
measurement scattering 19 p3225 A67-35531
Stratosphere and mesosphere, discussing
energetics, energy transfer, ionospheric
currents, magnetic fields, atmospheric trace
components, solar UV radiation
measurements, etc 20 p3430 A67-36897
Semiannual wind variation in equatorial
stratosphere analyzed for origin from rocket
sounding data 22 p3828 A67-39466
Vertical distribution of thermal stability in
lower stratosphere compared with
atmospheric ozone from ozone and
temperature soundings 22 p3829 A67-40471
Stratospheric attenuation measurements in
near UV during rocket flight compared with
values computed for dust free
atmosphere 23 p3993 A67-40677
Cosmic ray intensity 19, 20 and 24 day
quasi-periodic global variations in
stratosphere related to solar activity
variations, comparing amplitudes with
Forbush effects 23 p4056 A67-41109

STRATOSPHERE RADIATION
Stratospheric cosmic ray intensity,
discussing Soviet measurements above
Antarctica 02 p0310 A67-12573
Stratospheric measurements of electrons
and gamma radiation in cosmic rays, using
plastic scintillator and lead sheet
supplemented Geiger
counters 02 p0310 A67-12584
Cosmic ray 27-day variations using
periodograms, with measured data processed
continuously from 1957 to
1964 02 p0311 A67-12591
Secular changes in stratospheric cosmic
ray intensity from 1962 to
1964 02 p0311 A67-12595
Direct solar radiation up to 30 km and
stratification of attenuation components in
stratosphere, noting aerosol extinction
properties in free
atmosphere 07 p1170 A67-19390
Angular intensity distribution of short
wave radiation measured by automatic
stratospheric balloons 07 p1220 A67-19453
Stabilized platform for stratospheric
balloons for IR, UV and X-ray
astronomy 22 p3830 A67-39184
Cosmic ray intensity increase in wake of
chromospheric flares from stratospheric
measurements 23 p4057 A67-41115

STRATUS CLOUD
Physical aspects of stratocumulus
including temperature, liquid water content,
drop size, wind effect, shape,
etc 03 p0462 A67-13499
Moisture transfer and thermal influx
equations solutions for atmospheric
boundary conditions of preinversion
intramass strata evolution
scheme 11 p1816 A67-24522

STREAK PHOTOGRAPHY
High speed cameras with image converter
tubes noting electrical
circuits 01 p0067 A67-10774
Lasers applied to photo-optical
instrumentation problems, detailing schlieren
systems, interferometry, high speed streak
photography and
transmissometer 02 p0245 A67-12243
Time resolution dependence on ambient
gas around rotating mirror in streak
camera 03 p0424 A67-13915
Streak and open shutter photography of
planar detonation wave in channel
transmitting through orifice, obtaining
induction distance for transition from
deflagration to detonation 06 p1119 A67-18596
Rotating mirror streak cameras, noting
development history and future

- needs 16 p2675 A67-31249
Displacement effects analyzed for one beam of laser streak interferometer relative to another on image intensity distribution 22 p3795 A67-39199
- STREAM**
S ACOUSTIC STREAMING
S FREE STREAM
S GAS STREAM
S JET STREAM
S SLIPSTREAM
S SOLAR STREAM
- STREAM FUNCTION**
MHD boundary layer development on accelerated body treated by reducing partial to ordinary differential equation, using stream function 01 p0121 A67-10190
Finite difference approximation of balance wind equation, discussing convergence of Liebmman relaxation process, Coriolis term and computer time 09 p1525 A67-21551
First approximation for MHD nozzle flows with end effects 09 p1550 A67-22589
Wind and pressure fields diagnostic relations substituted for classical equation of stream function and solved as boundary value problem 13 p2149 A67-26273
Benjamin theory of conjugate vortex flow proved by alternate method 13 p2095 A67-26909
Plane conducting fluid-into-fluid jet in presence of transverse magnetic field, examining series expansion of stream function 13 p2169 A67-27317
Current function of three eccentric dipoles representing main geomagnetic field 16 p2670 A67-31911
Hypersonic gas flow past slender body, obtaining pressure coefficient and shock wave curvature by linearizing differential equations involving stream function 17 p2791 A67-32868
Stream function of plane flow of incompressible viscous fluid around parabolic profile, using successive approximations method 20 p3420 A67-36394
Cascade flow in mixed flow pumps and turbines, solving boundary value problems for stream function by relaxation method 20 p3356 A67-36421
Perturbation method using stream function for investigating anisotropic wave propagation describable by hyperbolic differential equations 21 p3611 A67-37891
Stream functions correctness for pressurized metals plastic flow by analyzing streamlines of various materials 21 p3637 A67-38926
Cooling of cylinder moving through fluid assuming fluid properties permit boundary layer approximations 22 p3918 A67-39782
- STREAMLINE BODY**
Resistance coefficient of circular cylinder and sphere in range of Reynolds and Stuart numbers 06 p1045 A67-18692
Three-dimensional supersonic flow past pointed nonaxisymmetrical bodies characterized by great local surface curvature changes, using new approximation 13 p2051 A67-27617
Aircraft fuselage shapes analysis for drag reduction and maximum useful space based on streamlined bodies found in nature 20 p3375 A67-36887
- STREAMLINE FLOW**
Supersonic flow past blunt body with convex corner calculated to establish sonic point on body 03 p0349 A67-12862
Viscous shear flow past two-dimensional cavity of infinite depth by use of Stokes approximation, emphasizing flow pattern near dividing streamline 03 p0402 A67-13356
Streamline curvature computing procedures for turbomachinery and fluid flow problems, considering axisymmetric and nonaxisymmetric flow fields and compressible cascade flow [ASME PAPER 66-WA/GT-3] 04 p0607 A67-15358
Finite difference solution to nonsimilar laminar mixing of streams undergoing nonequilibrium chemical reactions 04 p0609 A67-15816
Skewed boundary layers over body of revolution rotating in axial stream 05 p0747 A67-18218
Flow field model for laminar hypersonic near-wake in inviscid expansion, viscous sublayer and recirculating flow [AIAA PAPER 67-63] 06 p0940 A67-18353
- Taylor series expansion of stream function, pressure and temperature about separation or reattachment points used to calculate incompressible closed streamline flows of unknown shape 06 p0989 A67-18468
Interaction of two cylindrical jets of uniform flow as far downstream as possible impinging at included angle of 60 degrees 06 p0944 A67-18888
Streamline matching technique for V/STOL wind tunnel wall corrections [AIAA PAPER 67-183] 07 p1163 A67-19439
Wall streamlines and detachment on circular cone at angle of incidence in supersonic flow 13 p2049 A67-26591
Reattachment of two-dimensional jet to adjacent plate assuming new hypothesis on path of dividing streamline 14 p2303 A67-28338
Mach number effect on location of head shock wave and flow stability at slightly supersonic velocities for various body shapes 16 p2593 A67-31129
Separation streamline for massive blowing in free stream for model injected into arc tunnel flow [AIAA PAPER 66-457] 17 p2839 A67-33007
Geometry of streamlines and field lines of MHD flow, using partial differential equations 17 p2910 A67-33351
Underexpanded jet boundary streamline calculations by exact and approximate methods 19 p3171 A67-35768
Two-dimensional potential flow through bend profile, obtaining streamlines and velocity distributions 20 p3356 A67-36533
Two-dimensional incompressible fluid jet penetration analyzed kinematically via free streamline theory and notched hodograph 20 p3422 A67-36845
Turbulent boundary layer theory for streamline flow over impermeable plate, noting viscous interface effect 20 p3424 A67-37461
Stream functions correctness for pressurized metals plastic flow by analyzing streamlines of various materials 21 p3637 A67-38926
Three-dimensional compressible laminar boundary layer with heat transfer in curvilinear coordinate system linked to streamlines of external flow, assuming transverse flow 21 p3615 A67-39127
Momentum equation examined by curvature of streamlines downstream from shock wave 22 p3783 A67-39727
Integral equation for discontinuous flows and free streamline solutions for axisymmetric bodies at zero and small angles of attack 22 p3743 A67-40166
Streamline curvature computing procedures for turbomachinery and fluid flow problems, considering axisymmetric and nonaxisymmetric flow fields and compressible cascade flow [ASME PAPER 66-WA/GT-3] 24 p4143 A67-42459
- STRENGTH**
S ELASTIC STRENGTH
S FIBER STRENGTH
S FIELD STRENGTH
S MUSCULAR STRENGTH
S NOTCH STRENGTH
S SHEAR STRENGTH
S WELD STRENGTH
S YIELD STRENGTH
- STRESS**
S ACCELERATION STRESS
S AXIAL STRESS
S BUCKLING
S COUPLED STRESS
S CRACK
S CRITICAL STRESS
S FAILURE
S FATIGUE
S FLIGHT STRESS
S INTERNAL STRESS
S MENTAL STRESS
S PHOTOSTRESS
S PRESTRESSING
S RESIDUAL STRESS
S SHEAR STRAIN
S SHEARING STRESS
S STRAIN
S STRESS-OPTIC LAW
S TENSILE STRESS
S THERMAL STRESS
S TORSIONAL STRESS
S VIBRATIONAL STRESS
S YIELD STRENGTH
- STRESS /BIOL/**
SA FATIGUE /BIOL/
SA FLIGHT STRESS
SA PATHOLOGICAL EFFECT
Oxygen balance of organism during prolonged accelerations, noting disturbed gas exchange between alveoles and capillaries 02 p0188 A67-12324
Fatigue failure induced by aging and disease of self-healing biological structure in mathematical model [ASME PAPER 66-WA/BHF-3] 04 p0564 A67-15399
Standard prolonged work test for evaluation of fatigue and stress man 10 p1600 A67-23811
Secondary determiners of anticipatory physical stress threat as components of perceived proximity of unpleasant event 10 p1601 A67-23824
Influence of different stresses on sugar content changes of blood and stabilization at another level as adaptation result of organism 14 p2255 A67-28221
Miniature multichannel pulse-duration modulated multiplex telemetry unit for medical monitoring of human subjects pulse temperature, airflow, etc., under stress 14 p2259 A67-28684
Plasma 17 hydrocorticotestosterone in healthy subjects after water immersion of 12 hr duration shows no stressful effect 15 p2427 A67-29274
Heat stress, skin and rectal temperatures, heat gain and water losses in Army pilots flying combat missions in Mohawk OV-10 aircraft in Vietnam 22 p3750 A67-39599
Physiological responses to cold in men during extended period of sleep loss 23 p3955 A67-41611
Water deficit effects on thermal sweating noting extraneous effects due to higher body temperature and wet skin 24 p4110 A67-41781
Autogenous and exogenous suggestion applied to changing of psychophysiological state of human organism after exposure to prolonged bed rest 24 p4112 A67-41855
- STRESS ANALYSIS**
Asymptotic method of refining classical theory of bending and stretching of plates by construction of two-dimensional equations for processes involved 01 p0163 A67-10996
Mechanical constitutive theory and methods of stress analysis for physically nonlinear solid propellants [AIAA PAPER 66-124] 01 p0139 A67-11151
Stiffness techniques based on numerical integration for explicit calculation of displacement functions and derivatives in subroutine 01 p0163 A67-11177
Accelerated stress testing and reliability estimation for electronic components 01 p0085 A67-11373
Homogeneous elastic stresses in evaporated gallium films, noting transition from compression to tensile stress 02 p0287 A67-11718
General problem in pure stress analysis obtaining direct characterization and specific properties of extremal fields 02 p0336 A67-11791
Equilibrium equations, boundary conditions and constitutive relations for nonlinear theory of elastic directed curves, examining double stress without moment 02 p0267 A67-12051
Temperature and stress dependence of electron lifetime in p-type Si-B and Ge-Zn between 1.5 and 4.2 degrees K 02 p0301 A67-12521
Acoustic fatigue tests of aircraft components, determining sound field and stresses using actual jet engine on simulation 03 p0521 A67-13021
Critical load equations for plate weakened by sharp stress raisers extended to account for effect of arbitrarily oriented external forces 03 p0522 A67-13121
Thermostability of ceramic coatings applied to W and Mo during cooling, in terms of temperature-dependent elastic modulus and linear expansion coefficients 03 p0446 A67-13631
Book on creep in structural engineering and uniaxial and multiaxial states of stress for stationary and nonstationary creep 03 p0525 A67-13811
Lagrange multiplier matrix in minimum weight and fully stressed optimum structural design techniques 03 p0525 A67-13961

- Computer program /MAST/ analyzing F-11 wing structure involving load and stress analyses 03 p0525 A67-13967
- Elasticity and shell theory solutions for long circular cylindrical shells compared by numerical analysis 04 p0709 A67-14811
- Optimal flexure solution for Saint Venant problem in circular cylinder, using Papkovitch-Neuber stress functions [ASME PAPER 66-WA/APM-19] 04 p0714 A67-15410
- Initial stress influence on frequency of three-dimensional vibrations of plates and rods 04 p0717 A67-15912
- Elastoplastic axisymmetric stressed state of circular cylindrical shell under unsteady temperature field, internal pressure and axial force, using differential equation 05 p0912 A67-16181
- Refrigeration process of freezing stresses at ambient temperature improves elastic and photoelastic properties and renders them comparable to those of nonplasticized epoxy resins [ONERA-TP-367] 05 p0919 A67-16480
- Slide grooving effect on measurements of plane strain fracture toughness 05 p0922 A67-17086
- TRIAX 6 element for axisymmetric analysis by matrix displacement method 05 p0922 A67-17105
- Finite element method for problems in structural mechanics extended to beam vibration including shear and rotary inertia effects 05 p0924 A67-17284
- Yielding and brittle cracking of orthotropic strip, using Wiener-Hopf technique and asymptotic method for isotropic case 06 p1102 A67-18317
- Rib elasticity effect on stressed state of circular cylindrical shell with rectangular cut in torsion 06 p1107 A67-18632
- Small oscillations and stability of hyperelastic incompressible rectangular strip under uniformly distributed biaxial load 06 p1111 A67-18892
- Similarity relationships for study of transient and steady state thermal displacements, strains and stresses between model and prototype 07 p1262 A67-19413
- Stress analysis of solid rocket engine propellant grains including linear viscoelasticity, thermal analysis and equilibrium, relaxation times, engine sizes, cooling, creep relaxation, etc 08 p1373 A67-20874
- Experimental stress and strain analyses of solid propellant rocket engine grains under various loading conditions 08 p1419 A67-20886
- Polarization-optical method for investigation of stresses - All-Union Conference, Leningrad, June 1964 08 p1423 A67-21329
- Design of three types of bonded metal-metal joints, discussing advantages of theoretical over empirical methods 09 p1576 A67-22501
- Stresses in ordinary lap joint compared to variable adhesive joint 09 p1577 A67-22504
- Stresses produced in elastoplastic sphere with spherical cavity by surface heating-cooling, reducing problem solution to first order ordinary differential equation and functional equation 10 p1716 A67-22940
- Correlation among room temperature creep stresses, fatigue and proportional limit in titanium alloys 10 p1669 A67-23325
- Incremental elastic-plastic analysis of two-dimensional stress system by finite element method 10 p1719 A67-23456
- Finite element approach for determining transverse deflections and stresses in randomly acoustically excited complex aerospace elastic structures 10 p1724 A67-23710
- Discrete element method for plastic analysis of complex built-up structures subjected to cyclic loading causing membrane stress and stress reversal 10 p1725 A67-23713
- Matched asymptotic expansions for solution of singular perturbation problem of stresses and deformations in pressurized toroidal membrane 11 p1871 A67-24086
- Soviet book on calculations of strength and vibrations of rocket engines 11 p1852 A67-24512
- Stress intensity analysis for flat plates loaded close to edge crackline, giving intensity dependence on crack length and specimen shape 11 p1875 A67-24588
- Theoretical calculations for minimum anticlastic cross section deformations of thin elastic strips with optimally tapered edges verified by moire method 11 p1875 A67-24613
- Static and kinematic formulation of plastic analysis of structures and duality in linear programming 11 p1876 A67-24623
- Plastic zone about circular hole in infinite plate under uniform hydrostatic tension 11 p1879 A67-24887
- Book on applied stress analysis covering fundamental concepts and applications 11 p1881 A67-25099
- Displacements, stresses and moments in orthotropic and bimetallic cylindrical shells under radial concentrated forces determined via computer method 12 p2025 A67-25608
- Universal endurance criterion for machine structural elements sustaining complex stresses, based on machine part lifetime assessment 12 p2032 A67-25964
- Handbook of engineering sciences, Volume 1, Basic sciences 13 p2155 A67-26266
- Constitutive equation for collapse load and limit analysis of elastoplastic structures 13 p2216 A67-26609
- Piezoresistive effect of homogeneous silicon diffused elements 13 p2175 A67-26656
- Creep rupture, fatigue strength and brittle-ductile transition of aluminum as affected by nuclear radiation 13 p2133 A67-27090
- Beryllium joints and structures tested for static and repeated loading fatigue at room and high temperatures 13 p2123 A67-27132
- Use of computer in aircraft design problems 13 p2074 A67-27191
- Stress analysis methods applied to hollow thin walled low-aspect-ratio wings, considering small deflection law 14 p2401 A67-28657
- Statistical service life prediction based on propellant grain structural integrity for Minuteman third stage motor, noting grain stress analysis 15 p2547 A67-29996
- Periodically fluctuating loading fracture propagation analysis with damage summation principle in stress and cracking time terms, deriving differential equation for fracture length 15 p2576 A67-30183
- Stresses in fiber-reinforced plate 16 p2776 A67-31544
- Stresses due to external forces and moments acting on elastic nonradial circular cylindrical nozzle attached to spherical shell 17 p2959 A67-32409
- Axisymmetric response of semilinear truncated cone striking smooth rigid obstacle, determining early stages of motion 17 p2960 A67-32422
- Moire stress analysis technique for transferring grid without master contact 17 p2855 A67-32456
- Stress analysis of semilinear plate containing reinforced notch on one side under uniform tension 17 p2961 A67-32777
- Third order moduli of GaAs by measurement of ultrasonic wave velocities as function of applied stress 17 p2922 A67-33057
- Immersion technique measurement of gravitational stresses using two- and three-dimensional photoelasticity [ASME PAPER 67-APM-11] 17 p2964 A67-33146
- Cracked rectangular beam stress analysis, considering longitudinal shear and Saint-Venant torsion and flexure [ASME PAPER 67-APM-21] 17 p2964 A67-33150
- Infinite edge-stiffener load diffusion into semilinear elastic sheet, noting interface sheet stress variation stiffener force distribution [ASME PAPER 67-APM-35] 17 p2965 A67-33160
- Thermostability of ceramic coatings applied to W and Mo during cooling, in terms of temperature-dependent elastic modulus and linear expansion coefficients 17 p2875 A67-33172
- Soviet book on dynamic effects of moving loads on beams supported by linear and nonlinear bearings and elastic bases 18 p3140 A67-33661
- Bond-layer compliances effect on flexural responses of sandwich beam, discussing homogeneous and composite beams, deformation equations, etc [SESA PAPER 1214] 18 p3142 A67-33895
- Temperature measurement for aircraft gas-turbine engine development 18 p3157 A67-33898
- Stress analysis of loaded boundaries in two-dimensional second boundary problems, studying mechanical and thermal strain, knife-edge device, etc [SESA PAPER 1194] 18 p3142 A67-33899
- Environmental stress use in conjunction with simulation testing 18 p3020 A67-34112
- Maximum entropy principle to derive reliability functions for creep failure modes of engineering materials at high temperatures, noting stress analysis, probability distribution, etc 18 p3145 A67-34675
- Stress analysis by polar coordinate system of turbine disks produced in various wound-fiber configuration 19 p3234 A67-34873
- Yield conditions for plastically incompressible isotropic and orthotropic materials with different yield stress in tension and compression, without using hydrostatic terms 19 p3339 A67-35053
- Plane elastic strip with stress-free edges concept studied, noting mechanical coherence for elasticity and bending, expressing results by meromorphic function 19 p3340 A67-35450
- Resolving equations of linear theory of isotropic viscoelastic shells subject to external load and steady temperature field 19 p3340 A67-35508
- Viscoelastic theories evaluated for ability to correlate linear dynamic data with nonlinear viscosity and normal stress data 19 p3210 A67-35614
- Fringe order estimation of principal stress difference in plastically deformed body shown useful for variable stress rate by calibration test in photoelastic stress analysis 20 p3536 A67-36419
- Circumferentially symmetrical stressed state of half-space determined using Polozhyl formulas in axisymmetric elasticity theory and p-analytic functions 20 p3538 A67-36918
- Differential equations for stressed thin orthotropic plates of variable thickness derived and solved in cylindrical coordinates 20 p3539 A67-36919
- Anisotropic composites viscoelastic analysis applied to orthotropic cylinder pressurization, glass fiber cooling and relaxation shear moduli problems 20 p3474 A67-37267
- Stress analysis in theory of circular cylindrical shell weakened by doubly periodic system of identical circular holes 20 p3542 A67-37664
- Stress analysis of ribbed shell of revolution, noting case of open shell of zero Gaussian curvature with cyclic symmetrical stresses 21 p3718 A67-37980
- Stress analysis of closed cylindrical shell under concentrated loading at free edge, solving differential equation by expanding functions into Fourier series 21 p3718 A67-37982
- Stress analysis of loaded boundaries in two-dimensional second boundary problems, studying mechanical and thermal strain, knife-edge device, etc 21 p3722 A67-38435
- Parachute stress analysis during inflation, evaluating magnitude and distribution of snap stress to prevent canopy failure 21 p3568 A67-38538
- Thermal stress analysis of epoxy encapsulants using mathematical model for predicting performance in thermal shock 21 p3723 A67-38630
- Reliability evaluation of passive electronic components of ceramic and mica condensers and carbon resistors, including defects and stress analysis 21 p3571 A67-38671
- Knoop hardness yield loci for two Ti alloys 21 p3646 A67-38777
- Soviet papers on strength and stability of elements of thin walled structures 21 p3723 A67-38778
- Conical shell of low aspect wing type, analyzing strength under distributed high/low pressures on surface, deriving equations and formulas for stresses 21 p3724 A67-38779
- Approximate solutions obtained in closed forms for low aspect wing stressed state under transverse load 21 p3724 A67-38780
- Compression strength analysis of plane and cylindrical multilayer skin panels reinforced by corrugated fillers, determining critical load and local stability loss 21 p3725 A67-38787
- Stress analysis for rib-reinforced

cylindrical shell subjected to rapidly varying pressure, calculating deflections and bending moments 21 p3725 A67-38790

Maximum stresses with changes in Poisson ratio for thin parallelogramic panels with nonlinear behavior 22 p3911 A67-39666

Circumferential crack in pressurized cylindrical shell analyzed for extensional and bending components of stresses 22 p3911 A67-39678

Metal stress relaxation effects under cyclic thermal loads, with endurance vs stress relaxation diagrams 22 p3912 A67-39686

Motor fields analysis in Cosserat continuum noting differential forms of stress and strain quantities 22 p3837 A67-40006

Membrane stress state of spiral coiled tube surface, reducing stress components to second order differential equation 22 p3913 A67-40009

Wing stress analysis, reviewing computer and variational methods for calculating structural strength 22 p3746 A67-40445

Book on linear mechanics of elastic structures covering work and energy, Saint Venant theory of torsion, stress analysis, etc 23 p4071 A67-40566

Stress interaction in cumulative fatigue damage studied to predict remaining life of machine structures 23 p4074 A67-40650

Soviet papers on dynamics and strength of machines, Issue 4 23 p4075 A67-40678

Discrete stress analysis method for shallow shells of double curvature and rectangular planform with various end conditions 23 p4075 A67-40679

Book on two-dimensional and surface strain measurement for industrial application including strain gauges, photoelasticity and moiré methods 23 p4077 A67-40791

Suitability of finite element method for stresses in composite materials, examining single broken fiber in matrix 23 p4077 A67-41156

Fracture-toughness tests described to obtain fracture data for transformation into allowable design stresses 23 p4079 A67-41413

Book on analysis and design of missile structure covering load and stress analysis 23 p4071 A67-41501

Fatigue crack propagation in aluminum alloy studied for influence of maximum stress, stress range and sequence of load application 24 p4171 A67-41954

Constrained torsion of thin walled rods with closed or open profiles, discussing stress-strain state of cross section sealed at one point 24 p4250 A67-42307

STRESS AND LOAD

Carrying capacity of cylindrical shells of arbitrary cross section calculated under transverse and longitudinal stresses 02 p0340 A67-12660

Beam-column analysis by finite element method, establishing end load-deformation relationship via stiffness matrices 03 p0523 A67-13457

Stress-strain concentration in plates of bilateral cut EI-437B heat resistant alloy and EI-481 austenitic steel under rapid tensile loading at high temperature 03 p0529 A67-14084

Plastic deformation of isotropic tubular samples of steel, brass, copper and duralumin under complex loading at constant stress rate 03 p0530 A67-14169

Destruction of heat resistant alloys by repeated heating and cooling, deriving formulas which are applied to thermocyclic loads under conditions of stressed state 03 p0447 A67-14192

Large deformations of circular membrane attached to ring subjected to action of uniform load 04 p0708 A67-14795

Elastoplastic deformation of cylinder under torque and tensile stress based on stress stabilization in yield zones 04 p0708 A67-14796

Three-dimensional stress distribution around elliptical crack under arbitrary shear loading, discussing Griffith-Irwin fracture theory [ASME PAPER 66-APM-N] 04 p0718 A67-15926

Bending of plates under moment induced and internal stresses 05 p0907 A67-16016

Elastoplastic deformation of nonuniformly heated rotating disk determined to verify validity of theory under nonisothermal load 05 p0907 A67-16019

Dynamic surface loads, transient displacement and stresses in elastic cylindrical shell under radial and torsional vibration and elastic spherical shell under radial symmetric vibration, using finite Hankel transformation 05 p0908 A67-16138

Concentrated tensile stresses induced by concentrated external loads applied to boundary of filament winding rectangular strip plate 05 p0914 A67-16216

Small plastic deformation theory determination of elastoplastic stressed state of thin walled isotropic incompressible shell of revolution under axisymmetric power loads and nonuniform heating 05 p0922 A67-17177

Plastic deformation under radial load determined, using plasticity equations that take into account Bauschinger effect 06 p1106 A67-18627

Apparatus for testing thin walled tubular samples under combined torsional and tensile load, using stressed state timer 06 p1107 A67-18639

Thermostability of refractory materials and effects of high brittleness on thermal stress resistance of structural elements under single and multiple heat treatment and loads 07 p1198 A67-19128

Book on aircraft materials strength calculations including load determination, heating problems, creep and fatigue strength, etc 07 p1128 A67-19578

Partial differential equations for displacement and stress functions of shallow shells expressed as Bessel functions 09 p1573 A67-21664

Durability of adhesive lap-shear joints with sustained stress, describing portable jig 09 p1578 A67-22522

Independent linearized solutions closely approximating Mises and Tresca M-T/limit loads in linear theory of plasticity for plane strain 10 p1718 A67-22933

Structurally significant material properties effect on reliability of aircraft structures regarding unserviceability, ultimate load failure, etc, stressing stochastic concepts in strength analysis 10 p1718 A67-23433

Hypersonic reentry heating problems for glider of composite structure with critical temperature condition, buckling, etc 11 p1869 A67-24092

Variational principle for elastic thin shells and panels of arbitrary shape and load conditions 11 p1876 A67-24624

Stress concentration calculated at holes in shallow shells subjected to finite deformation via iteration method 12 p2023 A67-25594

Stresses and displacements for any strain state of hollow cylinder 13 p2218 A67-26890

Displacement fields used in finite element representations to obtain upper bounds to limit loads of plane stress problems 14 p2403 A67-29014

Loading asymmetry effect introduced by short single edge crack specimen loaded in tension along center line 16 p2764 A67-30994

Cumulative fatigue at root of circular notch of coupon type aluminum alloy specimens subjected to low cycle compression-tension 17 p2957 A67-32028

Stress analysis of loaded boundaries in two-dimensional second boundary problems, studying mechanical and thermal strain, knife-edge device, etc [SESA PAPER 1194] 18 p3142 A67-33899

Hertzian fracture of brittle solid under spherical indenter, discussing path and stability crack in nonuniformly directed stress field 18 p3144 A67-34274

Accumulated plastic deformation during sequence of isothermal and nonisothermal loading 19 p3242 A67-34887

Ceramic materials fracture and deformation mechanisms, discussing stress role 20 p3473 A67-36645

Crystal deformation and uniaxial failure under complex loading due to stress and temperature variations, applying physical state equation 20 p3540 A67-37057

Pulse magnitude and distribution due to energy release in liquid, on walls of shells submerged in liquid, used to calculate loads 21 p3611 A67-38056

Stress analysis of loaded boundaries in two-dimensional second boundary problems, studying mechanical and thermal strain, knife-edge device, etc 21 p3722 A67-38435

Cracked cylindrical shell stress-strain state under symmetric load, discussing shell curvature effect and integral equation solution 22 p3911 A67-39684

Buckling loads in orthotropic circular cylindrical shells under simultaneous longitudinal and external peripheral pressure stresses 22 p3912 A67-39752

Stress-strain curves under variable stress sequences in high stress range 22 p3913 A67-40036

STRESS CALCULATION

SA ENERGY METHOD STRESS CALCULATION

SA MATRIX STRESS CALCULATION

Creep role in powder metallurgy sintering processes, considering plastic deformation stresses and material transport mechanism 01 p0096 A67-10692

Stresses in symmetrical three-layer circular disk rotating about own axis, with solutions in form of Fourier-Bessel integrals 01 p0080 A67-10777

Stresses calculated in centrifugal impeller with cover disk by two-dimensional stress analysis and digital computer program [ASME PAPER 65-WA/FE-17] 01 p0080 A67-10873

Computation by approximate methods of stress resultants for shell of revolution under distributed externally applied load 01 p0164 A67-11185

Closed form pseudostatic solutions for Kirchhoff bending stress fields associated with semilinear crack extending at uniform velocity in elastic plate 03 p0523 A67-13468

Displacement and stress fields in isotropic elastic solids determined by integrating displacements for point nuclei of strain 04 p0711 A67-15102

Stresses in solids moving during loading, using velocity vector and strain rate tensor as variables for instantaneous state of body motion 05 p0914 A67-16194

Stressed state in rotationally symmetric shell assuming ideally rigid plastic, determining yield condition in terms of stress resultants 05 p0917 A67-16244

Internal stress calculation in multilayer materials 05 p0919 A67-16590

Formulas for stress determination on surface of elastic right cylinder, sphere and circular cone taking into account geometrical nonlinearity 07 p1261 A67-19218

Stress field near surface of elastic solid during short time interval when heat flow occurs analyzed through strain theory for fracture location and probability 09 p1576 A67-22422

Sub-or supersonic wing leading edge in unsteady supersonic flow, presenting discontinuities in vibration modes and calculating wing stress forces 10 p1590 A67-22879

Second order gyroviscous stress in collisionless plasma for LF propagation quasi-perpendicular to magnetic field calculated by utilizing higher moments of Vlasov equation 10 p1685 A67-23331

Isolated force solution as Green function for formulation of plane problems for cracks along interface of two bonded half-spaces 10 p1731 A67-23848

Stability of elastically clamped annular plate for nonuniform stress field 13 p2218 A67-26889

Micro-yield stress determinations of cast and extruded beryllium as measure of dimensional stability 13 p2138 A67-27119

Influence coefficients for stresses at circular holes in shallow cylindrical shells with both flat and curved reinforcements [AIAA PAPER 67-365] 14 p2401 A67-28733

Stress states, structure deformation, failure criteria and constitutive relations in structural design noting tensile, strip and lap shear test and continuum model 15 p2575 A67-29977

Stresses computation at surface of contact between disk and circular ring under influence of concentrated loads 15 p2577 A67-30186

Activation energies of nucleation of crack and dislocation loops in crystals, noting crack propagation theories and temperature effect 16 p2772 A67-31303

Bending strength of spur gear teeth calculating methods to optimize design for high speed, lightweight aircraft gearing [AHS PAPER 118] 16 p2684 A67-31834

Strain due to even pressure in oval or

- circular tubes, calculating deformations 17 p2958 A67-32259
- Contact stresses and deformations between circular cylindrical shafts and sleeves obtained by numerical method, considering contact with and without friction 18 p3054 A67-34263
- Stresses acting in oblique cross sections of composite shells computed in reference to different orientations 19 p3342 A67-35719
- Thin walled structure bending in uniform temperature field, calculating stresses, deformations and creep 20 p3536 A67-36446
- Circumferential displacement and shearing stresses in out-of-plane elasticity problem for solid torus 20 p3538 A67-36672
- Triangular finite element under plane stress analyzed using stiffness matrix, including in-plane concentrated moments and nodal rotation 20 p3538 A67-36676
- Gravitational effect on thermal instabilities, discussing optimization techniques to calculate effects of surface stresses [ASME PAPER 67-HT-22] 20 p3546 A67-36717
- Stress field on epitaxial dislocation line in weakly alloyed titanium, calculating energy of phase boundary and contribution of latter to plastic deformation 20 p3467 A67-37117
- Unsteady dynamic field excited by source moving along elastic half-plane boundary 21 p3716 A67-37967
- Calculation method for mono-, two- and three-spar wings including membranes and plate, discussing stress formulas 21 p3722 A67-38525
- Stress determination in elastic plate with remanent elasticity and cylindrical anisotropy, using integral-operational method 21 p3723 A67-38555
- Elipatevskii method applied to axisymmetric deformation of two-layer cylindrical shell with helical glass fiber reinforcements, obtaining equations for stressed state 21 p3725 A67-38795
- Calculated stressed state of short thin walled shells under transverse loads and torsional moments 21 p3726 A67-38797
- Plate stability loss criterion for critical external load values without determining initial stresses applied to rectangular plate Sommerfeld problem 22 p3909 A67-39401
- Durability of conical rotating disks having asymmetric profiles and arbitrarily varying thickness 22 p3812 A67-39534
- Crack propagation through mild steel plates investigated by method using stress values at several places near crack and at crack tip 23 p4074 A67-40665
- Singular solutions for bending stresses in loaded infinite three-layer plate 23 p4079 A67-41415
- Optimal reinforcements of cuts in stressed plates, considering displacements and conditions in discrete points of contact contour 24 p4249 A67-42105
- STRESS COMPUTER PROGRAM**
- Displacement fields used in finite element representations to obtain upper bounds to limit loads of plane stress problems 14 p2403 A67-29014
- Computer program for solution of large deflection nonlinear problems of elastic flat plates using grid analogy 14 p2403 A67-29015
- Differential equations describing stressed state of revolving shell beyond elastic limit and solutions adaptable to computer programming 23 p4075 A67-40681
- STRESS CONCENTRATION**
- Stressed state in isotropic medium weakened by row of curvilinear holes, considering approximate effect of adjacent holes on concentration of stresses around each hole as loaded 01 p0158 A67-10217
- Concentration of stresses around curvilinear holes in thin shells solved with nonlinear law of elasticity, reducing problem by boundary shape perturbation 01 p0158 A67-10218
- Stress concentration in annular rotor with notch /or crack/ on inner surface, using integral equation 01 p0159 A67-10276
- Skin effect association with anisotropy of medium in solid mechanics, analyzing surface instability, internal buckling and surface wave propagation 01 p0113 A67-10406
- Stress concentration in plate weakened by infinite sequence of uniform holes and subject to elastoplastic strain 02 p0337 A67-11844
- Plane problems of moment theory of elasticity for plane weakened by finite number of circular apertures, obtaining uniqueness of solutions 02 p0338 A67-11954
- Stress concentration near elastic ring-reinforced hole in elongated nonlinear plate 02 p0341 A67-12665
- Strain gauge method for determining stress concentration in radial flow impellers 04 p0708 A67-14537
- Behavior and fatigue strength of graphite during testing, plotting curves in semilogarithmic coordinates 04 p0641 A67-14599
- Stress concentration effect on fatigue strength of mechanically heterogeneous welds 04 p0636 A67-14600
- Stress concentration in sheet with circular opening subjected to biaxial tension 04 p0711 A67-15198
- Diffraction of plane harmonic horizontally polarized shear waves by parabolic cylinder, obtaining dynamic shear-stress concentration for parabolic notch and rigid parabolic insert [ASME PAPER 66-WA/APM-13] 04 p0713 A67-15405
- Stress concentration in nonlinear creep of thin circular cylindrical shell loaded at one edge by symmetrical radial shear and bending moment 04 p0718 A67-15917
- Dynamic elastic response of ring loaded transiently on both edges 04 p0718 A67-15921
- Tensile stress concentration near rhombic hole taking into account physical nonlinearity of aluminum brass plate 05 p0907 A67-16020
- Classical elasticity theory determination of computational error of fibrous body treated as simply connected multiple hole disks 05 p0907 A67-16037
- Dynamic stresses at boundary of fluid filled cavity during passage of plane dilatational wave train 05 p0908 A67-16136
- Three-dimensional stress concentration around cylindrical hole in semilinear elastic body 05 p0909 A67-16140
- Temperature stresses in plane elements by unsteady heat fields examined via polarization optical method 05 p0914 A67-16195
- Stress concentration for steep spherical shell with arbitrary elliptic hole 05 p0916 A67-16223
- Dynamic thermoelastic problem solution for body of revolution with cuts satisfying boundary conditions 05 p0810 A67-16228
- Orthogonal function energy method calculation of stress concentration in ring under impact loads distributed along inner and outer edges 05 p0918 A67-16420
- Two-dimensional photoelasticity analysis of stress concentration in plate with large number of uniformly spaced circular holes under biaxial loading 05 p0918 A67-16423
- Design strength of plane notched elements under single mode vibration, obtaining equation for fatigue stress concentration factor 05 p0919 A67-16592
- Linearized elasticity theory of coupled stresses effect on stress concentration around finite crack 05 p0921 A67-16884
- Stress distribution at rigid ring-reinforced curvilinear hole in spherical shell 05 p0922 A67-17178
- Macroscopic brittle fracture theory for structural microheterogeneities effect on maximum macrostresses in plates with hyperbolic notches under tensile loads 06 p1100 A67-17950
- Stresses in elastic half-plane with rectilinear notch 06 p1101 A67-18181
- Stress concentration in infinite incompressible plate with circular hole under bilateral tension analyzed, using variational method 06 p1107 A67-18634
- Dynamic stress concentration for plate with square hole, using approximate method of boundary shape perturbation and conformal mapping 06 p1109 A67-18665
- Penny shaped crack embedded in isotropic material treated by linear elasticity, noting stress singularities 06 p1109 A67-18732
- Second order elastic effects in infinite isotropic compressible medium with elliptic hole subjected to uniform tangential force at boundary 07 p1283 A67-19729
- Surface defects effect on mechanical properties of sheet metal under tension and bending, tracking brittle fracture to stress concentrators 07 p1263 A67-19751
- Lower bound for limit pressure of cylindrical pressure vessel with unreinforced hole obtained by restricting stress directions of cylinder 08 p1421 A67-20921
- Fracture initiation at low stress concentration, noting effect of energetic conditions and independence of plastic zone length from applied stress and defect length 08 p1421 A67-20955
- Lower bounds for crack tip stress intensity factors of irregularly shaped planar cracks 08 p1422 A67-20956
- Stress concentration factors for two circular notches of variable radius and position superposed at edges of strip 09 p1574 A67-21839
- Plasticity correction for single edge cracked specimen in uniaxial tension, estimating axial rigidity 10 p1717 A67-23016
- Calculation method for concentrated forces arising at intersection line of two surfaces due to interaction of shock layers, based on Newton law 10 p1590 A67-23035
- Stresses and displacements in small circular stress-free crack at interface between thick elastic incompressible layer and rigid foundation 10 p1717 A67-23082
- Thin plate reinforcement around holes in plane sheets subjected to stresses at infinity 10 p1719 A67-23472
- Plane notch stresses in viscoelastic materials with equations obtained from three-dimensional elasticity theory 10 p1720 A67-23576
- Fiber aspect ratio, residual stress state and geometry of multifiber arrays studied in terms of influence on local stress concentration and matrix reinforcement 10 p1671 A67-23705
- Plane thermal stress at insulated hole under uniform heat flow in orthotropic medium 10 p1730 A67-23838
- Elastic wave diffraction around elliptical hole in thin plate, obtaining dynamic stress concentration coefficient through approximate solution 11 p1870 A67-23897
- Geometrically nonlinear effects of stress concentrations at holes in thin plate with large deformations 11 p1878 A67-24878
- Concentration of force and moments near circular holes in shells of revolution with large elastic displacements 11 p1878 A67-24879
- Stress concentration near holes in perturbed shallow shells of revolution 11 p1878 A67-24880
- Shear modulus magnitude effect on stress concentration at circular hole in cylindrical shell for various ratios of Youngs moduli 11 p1878 A67-24881
- Dynamic two-dimensional problem of moment theory of elasticity and viscoelasticity of medium with circular cylindrical cavity 11 p1879 A67-24883
- Stressed and strained state of orthotropic cylindrical shell weakened by circular hole 12 p2021 A67-25578
- Tensometry method to study stress concentration around circular hole in orthotropic glass-fiber reinforced cylindrical shell 12 p2021 A67-25579
- Stress concentration calculated at holes in shallow shells subjected to finite deformation via iteration method 12 p2023 A67-25594
- Stress concentration of hollow sphere under uniformly distributed impact loads along inner and outer surfaces 13 p2215 A67-26526
- Program attachment to fatigue testing machines intended for two-stage programs 13 p2217 A67-26796
- Ductile failure initiation by fractured carbides in austenitic stainless steel 13 p2133 A67-27008
- Stress dependence of dislocation configuration in deformed niobium 13 p2133 A67-27010
- Stress concentration factor role in evaluating notch toughness of aluminum alloy 13 p2220 A67-27185
- Stress effect on minority carrier mobility and concentration in germanium and silicon p-n junctions under uniaxial compression 14 p2364 A67-27825
- Hollow internally braced turbine blade design with uniform state of stress and temperature distribution 14 p2377 A67-28653
- Fatigue failure prevention noting load redistributing, stress concentration reduction, critical section size increases, mean stress reduction, etc 15 p2494 A67-30098

Stress concentrations around shaped holes in plates under uniform tension, deriving formulas by perturbation method 15 p2577 A67-30268

Photoelastic stress analysis on bonded interface of strip with different end configurations noting stress concentration, bonding problems, etc 16 p2764 A67-30933

Effect of defects distribution on behavior of steel structures analyzed for plastically relaxed model of slit 16 p2768 A67-31282

Electron fractography and analytical fracture mechanics application to fatigue crack propagation, noting stress-intensity-factor role 16 p2771 A67-31296

Cycles required to start crack, and cycles for crack propagation to failure estimated for notched specimen 16 p2771 A67-31297

Plastic accommodation in Mg O idealized as linear array of continuously distributed edge dislocations to study crack nucleation 16 p2775 A67-31326

Mechanical properties of titanium alloys at room and cryogenic temperatures 17 p2873 A67-32768

Zero-moment stressed state in shells of revolution under concentrated loading described by p-analytic functions 17 p2962 A67-32875

Plane problems of moment theory of elasticity for plane weakened by finite number of circular apertures, obtaining uniqueness of solutions 17 p2966 A67-33271

Stress concentration near curvilinear hole in infinite plate subjected to biaxial uniform stress field at infinity 18 p3144 A67-34172

Thermal stress concentration factors for rectangular flat plates penetrated by holes 19 p3337 A67-34823

Stress concentration in plates having average-depth cuts on both sides, determining applicability of infinitely shallow and deep cuts formulas 19 p3339 A67-34886

Heat-transfer coefficient effect on final magnitude of stresses in elastoplastic spherical body subjected to cooling process 19 p3340 A67-35510

Threshold equilibrium of brittle plate with polygonal hole in biaxial tension-compression 19 p3343 A67-35845

Stress concentration of plane curved beams with uniform cross section determined from photoelastic experiments 20 p3540 A67-37210

Stress distribution in imperfect filamentary composite material 20 p3474 A67-37270

Stress concentration near hole in large radius sphere solved by approximation method for Helmholtz equations in coordinated system 21 p3716 A67-37906

Stress concentration effects on stress rupture strength, noting applicability to short term creep 21 p3717 A67-37970

Random thermoelastic stress concentration near edge of circular cylindrical shell determined using axisymmetric formulation 21 p3718 A67-37979

Loading frequency influence on endurance characteristics of V95 aluminum alloy notched for stress concentration 21 p3644 A67-38051

Solution for elastic medium stressed state under axisymmetrical load, considering spherical cavity influence and moment stresses 21 p3720 A67-38301

Electrical simulation method of conformal mapping used in solving engineering problems in elasticity theory 21 p3727 A67-38839

Displacement and stress distribution in shallow spherical shell under concentrated loads including normal force, tangential force and bending moment 21 p3730 A67-39087

Anisotropic plate with two elliptical holes studied for stresses under edge load by solving linear algebraic equations infinite system 22 p3910 A67-39452

Fracture theory for amorphous high polymers below glass transition temperature, considering viscoelastic effects on structural defect stress concentration 22 p3824 A67-39740

Optimum tapers determined for circular and rectangular ties, comparing resultant flexural stiffness with untapered supports 22 p3914 A67-40066

Distribution function of durability in light structural alloys based on mass fatigue tests

analyzed for influence of scale factor and stress concentration 22 p3915 A67-40301

Stress intensity factors for infinite plate subjected to cylindrical bending with radial cracks from internal hole 23 p4073 A67-40615

Frozen stress photoelastic technique used to determine hoop and radial stresses at hole boundaries for different flat disk configurations 23 p4077 A67-41154

Surface waves in medium with coupled stresses, using Cosserat type medium for analysis of properties 23 p4079 A67-41417

STRESS CORROSION

Stress corrosion in titanium, examining preventive measures of surface treatment, reduction of design stress, environmental control and alloy modification 04 p0636 A67-14602

Stress-corrosion cracking, evaluating role of mechanical, electrochemical and surface energy theories of causation, including hydrogen and other factors 04 p0636 A67-14804

Metal single crystal use in structural design of stress resisting devices 06 p1013 A67-17795

Electron microscope analysis of stress corrosion crack failure 07 p1211 A67-20250

Stress corrosion resistance of explosively deformed high strength steels and aluminum alloy [ASTME PAPER WES-7-63] 10 p1667 A67-23009

Stress corrosion cracking of titanium alloys, noting tensile test data, crack propagation in salt solution and in pure solvents and metallurgical and electrochemical factors 10 p1670 A67-23701

Stress corrosion cracking of cold reduced austenitic stainless steels noting effects of marine atmosphere exposure, cold working, welding, etc 11 p1807 A67-24586

Microstructural variations of Ti-Mo-Al alloys due to stress corrosion cracking, noting increased resistance through heat treatment [ASME PAPER 67-GT-5] 11 p1808 A67-24793

Simple and stress corrosion problems in aircraft design emphasizing protection of joints 12 p1954 A67-25127

Book on stress corrosion of metals covering mechanisms, resistance techniques and tests 13 p2141 A67-27174

Stress corrosion resistance and control for aluminum alloys, noting types, causes and methods 14 p2335 A67-27806

Continuous total immersion stress corrosion testing of beryllium in synthetic sea water, discussing relationship between time-to-failure and tensile stress 14 p2336 A67-28147

Evaluating mechanical and corrosion suitability of materials [ASME PAPER 67-DE-7] 14 p2339 A67-28866

Slip step role in early stages of stress corrosion cracking in face centered iron-nickel-chromium alloy thin foils 16 p2690 A67-31384

Strength corrosion cracking of high strength steels and titanium alloys in flowing sea water using cantilever loaded test specimen 16 p2690 A67-31385

Alloys for failure-safe structures tested, determining fracture toughness, fatigue strength and stress-corrosion cracking resistance 17 p2875 A67-33048

Yielding effects in stress corrosion cracking in susceptible alloys 18 p3063 A67-33487

Aluminum alloy examined for dislocation arrangements and susceptibility to intergranular stress corrosion cracking, using electron microscopy 18 p3063 A67-34000

Electron fractographic techniques for failure analysis, examining fracture direction, differentiation between hydrogen embrittlement and stress corrosion in steels and cyclic stress 18 p3145 A67-34581

Stress corrosion test method determined from test program on precipitation hardening semiaustenitic steels 20 p3465 A67-36486

Stress corrosion characteristics of Ti alloy evaluated using cantilever beam testing procedure 20 p3470 A67-37465

Breakdown probability calculations to determine life span and reliability of structural components subjected to oscillations 22 p3908 A67-39284

Environmentally induced delayed failure

process incubation period of precracked steel from film formation 22 p3822 A67-40060

Ti stress corrosion in nitrogen tetroxide, detailing investigative techniques [ASM PAPER C6-2.2] 23 p4020 A67-41409

Basic guidelines for fastener system selection for use in exotic environment with unusual stress condition 24 p4160 A67-42077

Fracture toughness and stress corrosion cracking of titanium alloy weldments indicating resistance differences between base metal and weldment 24 p4161 A67-42329

STRESS CYCLE

Elastoplastic behavior of riveted joints subjected to pulsating and alternating stress and preliminary fatigue cycles 01 p0163 A67-11151

Fatigue crack propagation rates for aluminum cantilever beams in reversed bending under two-level constant amplitude and random excitation, noting stress cycle effect [ASME PAPER 66-WA/MET-3] 04 p0639 A67-15343

Fatigue strength of smooth and notched steel samples subject to bending in single plane, discussing effect of form of stress cycle on failure rate 05 p0923 A67-17181

Electron microscope study of plastic deformation mechanism of titanium alloy AT4 and fatigue strain mechanism in coarse grained specimens of alloy T-40 07 p1205 A67-19278

Friction stress acting upon moving dislocation derived from microstrain studies 09 p1518 A67-22020

Crack propagation for stainless steel and Ti alloy at stresses below fatigue limit, noting of alternating stress cycles crack propagation for stainless steel and Ti alloy at stresses below fatigue limit, noting role 11 p1806 A67-24365

Strain hardening and softening of metals produced by cycles of plastic deformation explained in terms of Bauschinger effect 12 p2015 A67-25419

Intermediate principal stress effect on fatigue of thick wall steel tubes under triaxial stresses 15 p2573 A67-29402

Engine materials investigated for optimum low cycle fatigue resistance by pull-pull and rotating-beam fatigue testing techniques [SAE PAPER 670336] 17 p2874 A67-32986

Low cycle thermal fatigue under uniaxial constraint, describing clamping device, time-temperature controller and programmer used 20 p3543 A67-37699

Mean stress level effect on corrosion fatigue strength of aluminum clad D16AT alloy sheet under asymmetrical loads 21 p3646 A67-39008

Variable loading effect on durability of D16T aluminum alloy exposed to continuous action of corrosive medium 21 p3642 A67-39009

Stress-strain curves under variable stress sequences in high stress range 22 p3913 A67-40036

High temperature low cycle creep range strain fatigue behavior estimation from tensile and stress rupture properties 24 p4251 A67-42483

STRESS DISTRIBUTION

Stress distribution in elastic anisotropic plate with row of elliptical holes reinforced by elastic rings 01 p0158 A67-10221

Plastic flow of axially symmetric notched bars pulled in tension, obtaining load factors 01 p0159 A67-10401

Ultrasonic machines used to determine fatigue strength of components subjected to repeated alternating stresses 02 p0338 A67-12043

Maximum limiting value of uniform deformation of metals and alloys by stretching, deriving hyperbola tangent to true-stress curve 02 p0341 A67-12676

Stress patterns in lubricated rolling contact elements calculated from surface pressures and temperature [ASME PAPER 66-LUB-16] 03 p0431 A67-13757

Strength of cylindrical shell deformed under radial temperature field 03 p0527 A67-14073

Stress distribution in fir-tree fastenings of turbine blades in alternate bending caused by blade oscillations under static tension 03 p0528 A67-14076

Stress distribution in vicinity of end of crack moving steadily along boundary joining

two elastic materials 03 p0529 A67-14167
Temperature and stress distributions in annulus partially filled with cold fluid 03 p0531 A67-14363
Stress field generation by screw dislocation pile-up at hard circular cylindrical inclusions obtained, using approximation of continuously distributed dislocations 04 p0707 A67-14403
Vibration modes, stress distribution, natural frequency and failure points in pin-fixed compressor blades [ASME PAPER 66-WA/GT-4]

04 p0711 A67-15359
Stress distribution due to pressurized exterior crack in infinite isotropic elastic medium with coaxial cylindrical cavity 04 p0717 A67-15799
Three-dimensional stress distribution around elliptical crack under arbitrary shear loading, discussing Griffith-Irwin fracture theory [ASME PAPER 66-APM-N]

04 p0718 A67-15926
Semiinfinite strip reinforced by flanges under concentrated load 04 p0719 A67-15933
Point load on thin shallow elliptic paraboloid with singular solutions expressed as power series 04 p0719 A67-15934
Classical elasticity theory determination of stress distribution on boundary plane of elastic half-space due to internal body force distribution 05 p0908 A67-16040
Tension of homogeneous anisotropic elastic semiinfinite plate with rigid stiffener attached on segment of straight boundary 05 p0910 A67-16150
Stressed state of viscoelastic cylinder with star shaped cavity caused by steady temperature field and distributed surface load in problem of elasticity 05 p0912 A67-16185

Quasi-static problem of generalized plane stressed state of thin plate, considering heat transfer on lateral surfaces and interaction between strain fields and temperature 05 p0913 A67-16186
Shape determination for uniform-strength clamped bar with constant dynamic stress distributions subjected to first order free vibrations 05 p0917 A67-16247
Inertial force effect on stress distribution around blade roots of turbine disk analyzed, using low Young modulus material and stroboscopy 05 p0811 A67-16602
Causal analysis of failure modes and failure rate, time and stress dependence, kinetic sensitivity and distribution 05 p0811 A67-16852

Stress distribution in thin walled shell during transfer of concentrated load to surface area of mechanical contact 06 p1106 A67-18623

Compression and tension of rod and plate with distribution of residual stresses such that deformation is partially plastic and elastic 06 p1107 A67-18633

Dynamic stress concentration due to elastic wave analyzed by high speed photoelasticity to clarify difference between dynamic and static stress distribution 07 p1262 A67-19414

Temperature distribution, stress distribution and displacement components for circular disk when temperature distribution at disk rim is step function of time, considering inertial terms in thermoelasticity equations 08 p1418 A67-20723
Energy factors of infinite straight dislocations and stresses of piecewise straight dislocation configurations expressed through Green functions of elasticity 08 p1418 A67-20798

Proof of Lothe theorem showing that knowledge of stresses around infinite straight dislocations leads to solution of dislocation problems 08 p1418 A67-20799
Fiber reinforced composite material behavior examined from shear loading tests, using finite difference analysis for representative PDEs 08 p1420 A67-20908

Stress distribution in unidirectional multifiber composite under external and residual shrinkage loads expressed via displacement potentials 08 p1420 A67-20912
Stress distribution at tip of crack expanded as power series, noting relation of various terms to crack propagation 08 p1421 A67-20954

Fourier integral and series approach to semiinfinite strip subject to general

symmetrical tractions along three edges 08 p1422 A67-20978

Stress distribution in elastic plate with circular hole, noting particular cases of general solution for simple boundary tractions 08 p1422 A67-21167

Stress distribution in dovetail compressor blade joint analyzed using frozen stresses method 08 p1424 A67-21335

Diffraction of plane longitudinal wave in interior of elastic solid, where wave is harmonic in time and impinging on surface of penny shaped crack 09 p1573 A67-21663

Mathematical model of microscopically heterogeneous medium undergoing elastoplastic deformation, deriving equations for stress-strain distribution under uniaxial loading 09 p1575 A67-21931

Incremental stress effects in transistors at emitter-base junction due to piezoresistive and piezoelectric effects 09 p1472 A67-21950
Interferometry analysis of stresses in plate due to pin 10 p1718 A67-23245

Stress distribution prediction in multilayered circular cylinder subjected to combined bending and axial loading exhibiting multilinear stress-strain relationships 10 p1724 A67-23706

Reducing stress levels on crack propagation growth rate investigated for aircraft design problems 11 p1804 A67-24037

Shear modulus effect on stress distribution of planar array of screw dislocations near bimetallic welded half-planes interface 11 p1804 A67-24107

Axisymmetric buckling of orthotropic circular plates with variable thickness in terms of lateral plate deflection and stress distribution 11 p1876 A67-24660

Existence of solution for equilibrium problem of circular symmetrically loaded membrane with stress free contour proven by Chaplygin method 11 p1876 A67-24680

Creep index determination by tests on stress relaxation with elastic members, noting importance of stress distribution at initial moment of loading 11 p1877 A67-24815
Plane stress state near circular hole in infinite anisotropic plate of rigid-plastic nonhardening material 11 p1879 A67-24882

Stress distribution in hole weakened shells of negative Gaussian curvature, noting linear nature of distribution and propagation direction of perturbation 11 p1879 A67-24888

Elastic-plastic deformation around circular hole in plate under cyclic loading, recording strain distributions, development of plastic zone, etc 12 p2016 A67-25423

Stress field in infinite plate with three circular holes under action of concentrated forces determined by solving associated boundary value problem 12 p2016 A67-25435

Equivalent reinforcement and contour of symmetrically shaped hole corresponding to plate subjected to bilateral tension 12 p2019 A67-25564

Semiinfinite thin plate with circular inclusion under uniform tension 13 p2215 A67-26525

Stressed state of conical shell with circular hole subject to tension and torsion 13 p2218 A67-26888

Stress and stability of stringer-reinforced circular cylindrical shell 13 p2218 A67-26892

Texture strengthening and fracture toughness of titanium alloy sheets biaxial stress fields at room and cryogenic temperatures 13 p2142 A67-27442

Three-dimensional elastostatic problems for infinite solid with geometric discontinuities solved using potential functions 13 p2221 A67-27735

Stress distribution in matrix of composite material for case of filler between one microfiber and two displaced semiinfinite microfibers 14 p2398 A67-28100

Inversely symmetrical edge effect in circular cylindrical shell with distributed stresses and moments 14 p2401 A67-28644

Moment stress effect on natural oscillation frequency, deriving motion equations of circular cylindrical shell 14 p2401 A67-28735

Nondestructive determination of stress distribution in three-layer tempered glass aircraft windshield by scattered-light photoelastic method 15 p2575 A67-30033

Screw dislocation and crack interaction when elastic field is independent of one of three Cartesian coordinates 16 p2764 A67-30993

Loading asymmetry effect introduced by

short single edge crack specimen loaded in tension along center line 16 p2764 A67-30994

Tensile stress of infinite plane weakened by hole or Zhukovskii profile with rounded edges 16 p2765 A67-31053

Stress distribution in thin plates containing curvilinear holes of various shapes 16 p2766 A67-31100

Plane and volume stressed states of discrete medium, analyzing deformation work of continuous elastic medium 16 p2766 A67-31144

Plastic yielding near crack tip, noting general solution for deformation and stress distributions for various loads 16 p2769 A67-31288

Wall jet compared to plane free jet examining equilibrium conditions of velocity profile of fluctuation and mean flow determining stress distributions 16 p2662 A67-31470

Surface stress effect on oblateness of sun and surface stress distribution, noting latitude dependence of angular velocity 17 p2940 A67-32207

Stress effect on electric properties of p-n junction of semiconductor diodes and means of control 17 p2912 A67-32252

Analyses of small-and large-deflection problems of clamped skewed plates under uniform pressure 17 p2958 A67-32407

Flexural rigidity of plates reinforced by parallel stiffeners for direction normal to stiffener orientation determined together with stresses induced by bending moment 17 p2959 A67-32408

Deformation and distribution of stresses in rotating disk with variable thickness and temperature gradient 17 p2960 A67-32687

Theoretical concepts about coercive forces in Permalloy films, considering variations as function of applied stress 17 p2920 A67-32889

External stress effect on coercive force in Permalloy film 17 p2920 A67-32890

Exact linear elastic analysis of end effect problems for isotropic cylinders 17 p2963 A67-33019

Gunther solution representation for stress fields noting tensor potential theorem, second order tensor fields, etc 17 p2964 A67-33136

Torsion of finite elastic cylindrical rod welded to elastic half-space [ASME PAPER 67-APM-30]

17 p2965 A67-33156
Cross sectional strain and stress distributions in cylindrical elastic bars subjected to pressure-step and velocity-impact loading [ASME PAPER 67-APM-33]

17 p2965 A67-33158
Analytic solution for finite radial expansion and consecutive unloading of circular hole in infinite elastic-plastic plate of initially varying thickness 17 p2966 A67-33347

Stress distribution in reinforced-material models consisting of isolated fiber embedded in brittle matrix analyzed by photoelastic technique 17 p2966 A67-33387

Monatomic step patterns on /100/ cleavage and tensile crack faces of NaCl crystals originate from dislocation processes of crack tip released by shear stress distribution 18 p3097 A67-33482

Shear stress distribution and dislocation processes at moving crack tips in ionic crystals 18 p3097 A67-33483

Elastic stress distribution in infinite plate having circular hole, applying coupled stresses theory 18 p3140 A67-33666

Brittle coatings for stress distribution analysis during static and dynamic loading, describing chemical composition and characteristics and giving formulas and diagrams 18 p3045 A67-33741

Hertzian fracture of brittle solid under spherical indenter, discussing path and stability crack in nonuniformly directed stress field 18 p3144 A67-34274

Shells of revolution produced by fiber-wound distributing internal and boundary stresses uniformly over fiber contours 19 p3337 A67-34871

Dissolution of single crystal silicon by aqueous solutions of hydrofluoric acid and chromium oxide studied as function of etchant composition 19 p3301 A67-34934

Cumulative damage observed for biaxial fatigue stress tests on tubular steel specimens 19 p3341 A67-35552

Plastic wave propagation in semiinfinite bar subjected to axially applied impact stress 20 p3536 A67-36416

Formulation of problem of elastoplastic torsion of rectangular or regular polygonal bar as variational problem 20 p3536 A67-36429

Stress distribution in imperfect filamentary composite material 20 p3474 A67-37270

Stress-strain relationships for single layer used to obtain stress distribution in orthotropic laminates subjected to axial and shear stresses [ASME PAPER 66-WA/RP-5] 20 p3542 A67-37611

Stress distribution in homogeneous isotropic body under finite elastic deformation rotating with constant angular velocity 20 p3542 A67-37680

Tangential and normal tearing stresses distribution in adhesive joint under various loads and bending moment 21 p3716 A67-37909

Deflection and stresses in corrugated diaphragm rigidly clamped on contour with distributed pressure and concentrated central force, using finite difference approximation 21 p3717 A67-37977

Characteristic method for determining stress field and plastic deformation mechanism during cutting, notching and punching processes 21 p3632 A67-38060

Orthotropic laminated layer with heat emission investigated for thermoconductivity and temperature stress distribution 21 p3731 A67-38299

Long cylindrical shell with externally loaded reinforcing ring, solving stress distributions and displacements 21 p3727 A67-38871

Stress distribution on boundaries of two unequal circular holes in infinite plate determined by mapping region conformally onto annulus 21 p3730 A67-39086

Surface active lubricant influence on internal stresses in sign variable slippage case, discussing chemisorption, wear resistance and stress distribution 22 p3810 A67-39219

Statistical elasticity problems involving random stress and displacement tensor fields, proving uniqueness and minimum principle for boundary value 22 p3909 A67-39396

Book on fiber reinforced materials covering theories, principles and experimental data noting stress distribution, fiber orientation effects, etc 22 p3820 A67-39590

Safety design for high strength low toughness materials assumed to have hidden flaws, formulating stress intensity factor for fracture mechanics 22 p3913 A67-39982

Triaxial state of residual stresses in long solid or hollow axisymmetric longitudinally uniform cylinder measured by boring out cut off specimen, analyzing process 22 p3913 A67-40034

Cylinder residual stress measurement, discussing stress distribution from Sachs equations 22 p3913 A67-40035

Low temperature transient creep behavior of polycrystalline aluminum investigated experimentally for recovery of surface layer stress 22 p3821 A67-40054

Transient displacement and strain distributions in fracturing notched magnesium plate, using moire-fringe technique and Q-spoiled laser 23 p4076 A67-40736

Elastic bending of thin shells and plates perforated with holes in various arrays, calculating stress distribution and concentration 23 p4077 A67-40749

Curved plates tested under axial compression to prove curved plate buckling and postbuckling behavior formula, discussing stress distribution measurement 23 p4080 A67-41476

Shallow spherical shell stress and displacement distribution calculated by integral equation 24 p4249 A67-42104

Stress distributions within materials sealed across planar interfaces compared with values measured in composite pairs of glass 24 p4175 A67-42374

Vibration modes, stress distribution, natural frequency and failure points in pin fixed compressor blades [ASME PAPER 66-WA/GT-4]

Fatigue crack initiation, comparing alpha brass and Al-Mg-Zn alloy, noting effect of increasing maximum pressure value in contact region 24 p4251 A67-42460

[ASLE PAPER 67-LC-5] 24 p4174 A67-42744

STRESS FUNCTION

SA AIRYS STRESS FUNCTION

General problem in pure stress analysis, obtaining direct characterization and specific properties of extremal fields 02 p0336 A67-11791

Displacement potential for solutions of displacement equilibrium equations obtained by Mindlin for linear elastic medium where stresses are functions of strains and strain gradients 03 p0524 A67-13661

Axiallysymmetric modes of loss of stability of circular plates lying on elastic base in inhomogeneous stress field 03 p0529 A67-14163

General solution of two-dimensional linear elasticity problem in polar coordinates in term of stress function satisfying biharmonic equation 06 p1111 A67-18873

Cosserat plane and shell theory development from considerations concerning equilibrium conditions with aid of introduced stress functions 07 p1263 A67-19885

Power series technique applied to single edge notches in semiinfinite region in plane elasticity problems, using mapping function and Muskhelishvili theory 08 p1414 A67-20347

Analytical solution, based on stress functions, for deflection of plastics sandwich beam under bending loads at center, agreeing with experimental results for short duration loading 09 p1579 A67-22612

Invariant stress and deformation functions for doubly curved shells, noting reduction of equilibrium equations and surface strain-displacement relations into compatibility equation 10 p1730 A67-23834

Stress and temperature dependence of motion of edge dislocations in nickel single crystals 11 p1809 A67-24920

Ribbed circular cylindrical shell under axial compression, reducing problem to determination of deflection and stress functions 12 p2020 A67-25571

Decomposition of stress functional with respect to small parameter 12 p2032 A67-26103

Sufficient condition providing nonlinear sampled system with set of initial conditions 15 p2458 A67-29473

Transversally isotropic cylindrical shell under periodically spaced axisymmetric band loads, comparing expressions derived for stresses and displacements by elasticity and shell theories 15 p2578 A67-30271

Beltrami stress functions, presenting completeness proof 17 p2884 A67-32717

Soviet papers on structure and properties of metal films 17 p2920 A67-32887

Plasticity and brittle fracture conditions combined for stability criteria derivation 18 p3144 A67-34174

Cup spring designing method, with generatrix curvature included in approximation, gives better characteristic curve and stresses 18 p3144 A67-34282

Hardening function form in flow theory, showing dependence on cosine of stress velocity vector angle with normal to yield surface 20 p3539 A67-36921

Nonlinear elastic anisotropic wedge deformation for short time loading moment applied to apex, approximating stress function 20 p3542 A67-37660

Elastodynamic problems using kinetic-stress functions 22 p3909 A67-39399

Equilibrium conditions of Cosserat continuum by complete stress function representation 22 p3837 A67-40007

Stress functions for truncated conical shell buckling under uniform static pressure 23 p4081 A67-41760

STRESS MEASUREMENT

SA PHOTOELASTIC STRESS MEASUREMENT

SA X-RAY STRESS MEASUREMENT

Temperature, stress and displacement in elastic bodies for random surface forces and randomly distributed environmental temperature 01 p0159 A67-10403

Tensile testing machine measuring mechanical properties under conditions of rapidly applied stresses 01 p0102 A67-11086

Hot wire measurement of tangential

velocity and Reynolds stresses in spiral laminar-turbulent flow 01 p0054 A67-11163

Internal stresses of thin metallic and dielectric films, discussing methods for stress measurement, stress models and formulas 02 p0287 A67-11717

Oscillatory magnetostriction in GaSb, noting stress effect on energy bands 02 p0296 A67-11819

Plane stressed state in plane contact problem of coupled plates under symmetrical load conditions 02 p0340 A67-12445

Hole-drilling method of measuring residual stresses in elastic materials determined by empirically derived relation between magnitudes of principle stresses and strain relaxation about hole 03 p0531 A67-14360

Stiffness matrix evaluation on basis of strain energy 04 p0709 A67-14813

Compressive stress effect on band gap widening and diffusion current in GaAs junctions 04 p0677 A67-15107

Fatigue life of thin walled shells with inside pressure and outside support during axial motion [ASME PAPER 66-WA/MET-13] 04 p0712 A67-15377

Approximation method for determining stress field of body from temperature field 05 p0914 A67-16196

Stressed state of spherical shell under action of axisymmetric temperature field arbitrarily varying along meridian 05 p0914 A67-16197

Stress in helical corrugated shell under axial tension examined as boundary value problem of ODE in cylindrical coordinate system 05 p0914 A67-16215

Soviet monograph on dynamics and durability of machines 05 p0915 A67-16219

Differential equation derivation for creep analysis using plastic interaction curve and associated flow rule 05 p0917 A67-16299

Reliable test method based on special strain gauge load transducer for embedment axial stress measurement in electronic modules 05 p0779 A67-17457

Plastic deformation of textured Ti alloy sheet examined, using tension testing along different directions and combined stress loading along principal axes of anisotropy 06 p1016 A67-17900

Stress distribution measurement by vibration method, applying hand-held extensometer place by place on surface of structure subjected to dynamic load of finite amplitude 06 p1100 A67-18001

General solution of two-dimensional nonlinear problems of elastoplasticity using finite element method, piecewise linear load deflection relationship and computational algorithm [AIAA PAPER 67-144] 06 p1104 A67-18457

Pressure distribution between lubricated rolling bearings, comparing static and dynamic stresses in cylindrical disks, noting film thickness 08 p1333 A67-20361

Stress induced velocity variations of longitudinal and shear ultrasonic waves in steel, Al and Cu, calculating third order elastic constant 08 p1415 A67-20481

Finite difference method for finding stress fields around parallel edge cracks 08 p1421 A67-20914

Environmentally induced stresses in encapsulated electronic modules measured using hydrostatically pressure-sensitive transducer, noting internal stress changes 08 p1306 A67-21418

Tensile residual stress measurement in area of failure origin in helicopter rotor blade, using laboratory tests and X-ray analysis [SAE PAPER 670154] 09 p1502 A67-21772

Generalization of Gaussian arbitrary constant sign curvature to shallow shells by introducing corrections in Lauricella-Sherman potentials 09 p1575 A67-21927

Stress measurement in metal components with photoelastic coatings and thin walled structures, using reflected light technique 09 p1575 A67-22169

X-ray diffraction residual stress measurements in aluminum alloy [SAE PAPER 670153] 09 p1509 A67-22543

Boundary value problems for thin elastic plates, discussing flexural stresses in neighborhood of crack, bending, etc 10 p1715 A67-22915

Bassall theory to calculate bending,

twisting moments and shearing forces for thin elastic plates under transverse flexure for structural design application 10 p1720 A67-23569

Short method measurement of Reynolds stresses in turbulent flow, using constant current hot-wire anemometer 10 p1629 A67-23845

Structural stress measurements in terms of induced temperature increments, using IR radiometer 11 p1877 A67-24827

Compressor blade failure due to material fatigue, using destructive testing in stationary rig 12 p2014 A67-25413

Semiconductor piezoresistive strain gauges and application to compressor blade vibratory stresses measurement 12 p2014 A67-25416

Stress field in infinite plate with three circular holes under action of concentrated forces determined by solving associated boundary value problem 12 p2016 A67-25435

Vlasov variational method application to stressed state of flexible plates and shells, linearizing partial differential equations by successive loadings 12 p2020 A67-25570

Continuum mechanics of Cosserat type, discussing kinematics generalization and existence of higher order displacement gradients in internal energy density equation 12 p1968 A67-26200

Flat and stacked rosettes performance in linear and nonlinear stress fields 13 p2219 A67-27093

Clinographic polariscope for surface measurement of stress-strain in building materials, noting operation and results 14 p2395 A67-27973

Accelerated fatigue testing using stepwise stress increase method 14 p2402 A67-28815

Refined plate bending theory taking into account edge effect 16 p2765 A67-31050

Stress space theory and application to fatigue fracture theory, noting geometrical formulations for deformation and stress of body 16 p2768 A67-31277

Energy necessary for fracture shown independent of lattice defects by low cycle fatigue tests at constant true mean stress amplitude 16 p2774 A67-31318

Model for hemispherical cratering of structural metals by hypervelocity impact, determining elastic-plastic threshold stress by true tensile strength measurement 17 p2958 A67-32217

Local stress measurement technique in metals using temperature changes due to elastic deformation 18 p3141 A67-33887

Errors in high temperature electric-resistance strain gauge measurements 18 p3142 A67-33892

Steady thermal strains measurement in aero and industrial turbine and engine components, discussing fine wire behavior, bonding agent, performance, requirements, etc 18 p3143 A67-33900

Holographic measurement of surface strains noting fringe pattern for displacements 21 p3625 A67-37944

Triaxial state of residual stresses in long solid or hollow axisymmetric longitudinally uniform cylinder measured by boring out cut off specimen, analyzing process 22 p3913 A67-40034

Cylinder residual stress measurement, discussing stress distribution from Sachs equations 22 p3913 A67-40035

Integral SI stress sensor with transverse and shear piezoresistance sensitivity, noting design and fabrication 23 p4005 A67-41371

Testing procedure for determining strain gauge elongation limit, discussing gauge applications to strain measurements at LOX temperatures 23 p4007 A67-41389

STRESS-OPTIC LAW

Total relative retardation in three-dimensional photoelastic model viewed under polarized light 07 p1264 A67-20259

Piezotransmission measurements of phonon-assisted transitions in semiconductors 13 p2179 A67-27157

Frame-camera interferogram data for Nd-doped glass rod during laser pumping analyzed through optical path length changes 18 p3062 A67-34623

STRESS PROPAGATION

Longitudinal oscillations of infinitely long linear viscoelastic rods to yield wave propagation in elastic rods 04 p0707 A67-14404

Book on strength under high transient

loads and nonlinear elastic and elastoplastic wave propagation 04 p0715 A67-15617

Rheologic and plastic phenomenological analysis of viscoplasticity problems, discussing constitutive equations and stress propagation 08 p1414 A67-20312

Stress waves propagating in half-space due to point load on surface studied initially in three-dimensional dynamic photoelasticity 17 p2959 A67-32415

Diffraction of stress pulse by spherical cavity embedded in infinite linear homogeneous isotropic elastic medium [ASME PAPER 67-APM-27] 17 p2965 A67-33154

STRESS RELAXATION

Stresses and stress relaxation in thin oxide films deposited by various methods on glass substrates from elastic or plastic deformation at elevated temperatures 02 p0288 A67-11719

Resolving kernel for analysis of creep and relaxation processes in materials possessing rheological properties 02 p0338 A67-12236

Anisotropy effect on strength of unwoven glass fiber reinforced plastic, ascertaining nature of stressed state arising at high temperature 05 p0912 A67-16183

Torsional creep measurements on natural rubber vulcanizates cross linked to various degrees complement studies on stress relaxation behavior and dynamic mechanical response 06 p1020 A67-17869

Stress-strain relations and relaxation in creep materials with elastic heredity and simple flow 06 p1107 A67-18637

Stress relaxation, creep and uniaxial elongation of polycrystals relationship as part of cumulative plastic deformation processes 06 p1109 A67-18809

Time dependent stress behavior of incompressible elastic fluid for various homogeneous deformation histories 07 p1169 A67-19728

Three-dimensional creep, stress relaxation and viscometric measurements of nonlinear viscoelastic materials in continuum 08 p1419 A67-20884

Creep, stress relaxation and vibrational measurements, sinusoidal torsional forced oscillations and stress wave propagation in polymeric linear viscoelastic solids 08 p1419 A67-20885

Portable X-ray equipment for measuring residual stresses in welded rocket motor case, machined aluminum parts and titanium welds [SAE PAPER 670152] 09 p1509 A67-22542

Relaxation, creep and modulus of rigidity lowering in compression springs under high temperature 11 p1795 A67-24090

Creep index determination by tests on stress relaxation with elastic members, noting importance of stress distribution at initial moment of loading 11 p1877 A67-24815

Stress relaxation dependence on heat deformation regime in Ti alloys VT14, VT3-1 and VTS-1 12 p1955 A67-25368

Strain hardening and softening of metals produced by cycles of plastic deformation explained in terms of Bauschinger effect 12 p2015 A67-25419

Approximate solution of creep and relaxation problem for plates and shells subject to bending moments and tensile forces 12 p2025 A67-25610

Crystal lattice defects as centers promoting dislocations during plastic deformation of ionic crystals 13 p2175 A67-26448

Analysis of steady flows of viscoelastic materials by introduction of two dimensionless groups 13 p2096 A67-26931

Molybdenum polycrystal plastic strain rate in pre-yield region studied by successive stress relaxation method for dislocation density and mobility characteristics 14 p2337 A67-28230

Constitutive equations describing small perturbations on viscometric flows, noting relations with stress-relaxation moduli flow 15 p2469 A67-29222

Hardness, toughness, stress relaxation, corrosion resistance, etc, of niobium-aluminum alloy with stable elastic modulus 15 p2504 A67-29973

Viscoelasticity and rubber-like elasticity continuum mechanical description under stress relaxation conditions [AIAA PAPER 67-489] 18 p3143 A67-33955

Mechanicochemical treatment for high

temperature strength increase in metals, noting effects on creep strength, stress relaxation, etc 19 p3247 A67-35852

Drawing technique for bundles of sheathed superalloy wires noting sheathing, stress relief, interfilament welding and oxide bonding 21 p3643 A67-37878

Metal stress relaxation effects under cyclic thermal loads, with endurance vs stress relaxation diagrams 22 p3912 A67-39686

STRESS RUPTURE

Stress-rupture data for refractory metals which yields linear relationship between Larson-Miller parameter and logarithm of applied stress 03 p0441 A67-13253

Analytical model developed for using creep data at constant stress to predict creep behavior under linearly increasing stress 03 p0447 A67-13797

Material strength parameter /coupling modulus/ dependence on crack propagation velocity when accounting for rupture kinetics 03 p0529 A67-14166

Long term tensile stress-rupture strength of alloys calculated from static tensile strength tests at elevated temperatures [ASME PAPER 65-MET-12] 05 p0827 A67-16212

Molybdenum and molybdenum alloy stress-rupture characteristics at 2200 degrees C for arc-cast and wrought sintered material 06 p1019 A67-18854

Monograph on creep and creep rupture as applied to aeronautics field noting problems in boundary and initial value, stability, stressed state, etc 07 p1264 A67-20301

Failure mechanism of solid propellant grain and stress criteria for solid motor design and evaluation 08 p1374 A67-20891

Filler effects on deformation and rupture of amorphous gum elastomers with various molecular structures, noting failure envelopes [JPL-TR-32-922] 08 p1420 A67-20892

Fracture of viscoelastic bodies, predicting statistical variability of rupture data for uniform and nonuniform excitation histories 08 p1421 A67-20913

Creep ductility, stress rupture and high temperature irradiation embrittlement of neutron-irradiated Hastelloy N 08 p1343 A67-21195

Plastic deformation and fracture of rotating turbine rotor model 09 p1502 A67-21554

Dynamic snap-through of shallow arches under stochastically varying transverse loads 10 p1725 A67-23711

Titanium carbide dispersion-strengthened nickel by internal carburization, with fair ductility and stress rupture properties at high temperatures 11 p1806 A67-24361

Titanium and aluminum additions to cobalt-base alloys improve tensile and stress rupture properties and heat resistance 11 p1807 A67-24703

Cobalt alloys precipitation hardening behavior, oxidation, thermal shock resistance and stress rupture strength 11 p1808 A67-24704

Gas turbine bucket alloy improvement via heat treatment, noting performance evaluation results from creep rupture tests [ASME PAPER 67-GT-55] 11 p1808 A67-24811

Stress rupture and creep behavior in binary and ternary vanadium alloys including tensile strength and activation energy, noting titanium role 12 p1954 A67-25140

High speed plastic deformation of bar studying relation of breaking strain vs tensile velocity and comparing values of former to static case 16 p2775 A67-31329

Aluminum content effect on stress-rupture properties of chromium-molybdenum-vanadium steel, noting notch sensitivity and ductility 16 p2693 A67-31869

Tensile testing equipment using impact load facilitates rupture stress measurements by conventional strain gauges 18 p3141 A67-33719

Blaxial prestressing in ceramic plates under nonuniform thermal stress for damage reduction study 20 p3538 A67-36778

Stability criteria in stress-rupture strength theory, deriving stress and moment influence functions and damage tensor 21 p3717 A67-37969

Stress concentration effects on stress rupture strength, noting applicability to short term creep 21 p3717 A67-37970

Heat treatment effect on microstructure

and notch-bar rupture life of INCONEL alloys 21 p3646 A67-38776
 Stress rupture strength and durability of elastic materials 22 p3824 A67-39221
 Coated columbium alloy potential as turbine vanes in gas turbine power plants, discussing stress rupture strength, oxidation erosion and thermal fatigue lives [ASM PAPER C6-1.4] 23 p4020 A67-41402
 Stress-rupture properties of composites containing refractory metal fibers and nickel alloys evaluated at high temperatures 24 p4174 A67-42475
 High temperature low cycle creep range strain fatigue behavior estimation from tensile and stress rupture properties 24 p4251 A67-42483

STRESS-STRAIN DIAGRAM

Plastic flow of axially symmetric notched bars pulled in tension, obtaining load factors 01 p0159 A67-10401
 Plastic deformation including instability of circular membrane subject to hydrostatic pressure, obtaining stress-strain curve 01 p0161 A67-10776
 Hardening during plastic deformation of steel samples under compression, deriving stress-strain state in cutting process 03 p0427 A67-13193
 Residual stress effect on stress-strain curve of uniaxial composite consisting of stainless steel wire and aluminum alloy matrix 03 p0444 A67-13432
 Interatomic force model calculation of shear and tensile strengths, predicting stress-strain curves for crystal structures 03 p0495 A67-13532
 Deformations and rupture criteria under cyclic loading using stress-strain diagram 03 p0531 A67-14361
 Elastic-plastic torsion of shafts with hyperbolic notches solved for Ramberg-Osgood and bilinear stress-strain curve 04 p0627 A67-14977
 Circular ring subjected to two diametrical, equal and opposite forces with results converted into stress-strain charts 04 p0715 A67-15603
 Combined elastic solutions-finite difference method for bending of compressible or incompressible rectangular metal plate beyond elastic limit 05 p0907 A67-16017
 Relations between mean stresses and strains of elastic body consisting of soldered isotropic layers, noting thermal effect 05 p0912 A67-16184
 Stressed and strained state of reinforced cylindrical shell under nonuniform heating and compression, noting three solutions to buckling problem 05 p0913 A67-16190
 Stress-strain relations of linear theory of shells extended to corresponding inversion with more complex results 06 p1100 A67-18111
 Transient stress-strain state of elastic system developing combination resonance analyzed, using approximate method 06 p1106 A67-18621
 Stress distribution in thin walled shell during transfer of concentrated load to surface area of mechanical contact 06 p1106 A67-18623
 Elastic equilibrium of circular plate with elliptical hole and tight washer, determining stress-strain state 06 p1106 A67-18631
 Material orthotropy effect on directions of principal stresses and strains in fiberglass and boron composites 06 p1108 A67-18654
 Stress-strain and Hooke law in orthotropic elasticity presented through matrix algebra and tensor coordinates 06 p1108 A67-18656
 Beading in thin walled pipes with localized heating, noting stress deformation state 07 p1192 A67-19752
 Single niobium crystal deformation, discussing stress-strain curves, slippage, orientation and asymmetry of slip 07 p1211 A67-20164
 Wave interaction between linear viscoelastic medium and thin cylindrical shell imbedded within it solved for uniform harmonic stress input applied to shell 08 p1415 A67-20486
 Compression strength and strain of solid propellants, noting internal loads developed during burning process 08 p1373 A67-20720
 Static and transient strain measurement in aerospace structural materials using extensometer and compressive test jig, determining Young modulus, creep rate,

etc 08 p1420 A67-20907
 Printed circuit board manufacturing process assuring crack-free plated-through hole 08 p1304 A67-21190
 Plane wave generation in metal plates by detonation of contact explosives, developing elastic-plastic deformation theory for finite stress-strain components 08 p1422 A67-21290
 Simulation of stress-strain state of metal under elastoplastic deformation, based on models used in polarization-optical techniques, analyzing stresses in high polymers 08 p1423 A67-21330
 Stress-strain diagrams under dynamic conditions obtained by processing strain gauge data, using analog computer 09 p1492 A67-21560
 Independent linearized solutions closely approximating Mises and Tresca /M-T/ limit loads in linear theory of plasticity for plane strain 10 p1716 A67-22933
 Nonlinearities in elastic energy release rate during load-deflection measurements of specimens with varying crack length 10 p1718 A67-23327
 Stress distribution prediction in multilayered circular cylinder subjected to combined bending and axial loading exhibiting multilinear stress-strain relationships 10 p1724 A67-23706
 Elastic-plastic analysis showing relationship between tangent modulus and initial strain methods 10 p1726 A67-23718
 Nonlinear membrane equations for extremely thin shell of revolution of very deformable material, assuming large displacements, rotations and strains 10 p1730 A67-23836
 Discontinuous yield phenomena for slip band dislocations, when frictional stress that hinders dislocation motion undergoes static or dynamic drop 11 p1807 A67-24568
 Low endurance fatigue tests for reversed torsional strain cycling of two steels 12 p2015 A67-25421
 Stress-strain state of thin cylindrical shell under effect of local forces 12 p2024 A67-25601
 Bending of thin plate of aluminum with nonlinear stress-strain relation analyzed, considering material compressibility effect 13 p2215 A67-26267
 Piezotransmission measurements of phonon-assisted transitions in semiconductors 13 p2179 A67-27157
 Stress vs strain curves and slip systems in compression and tension of niobium single crystals 14 p2339 A67-29030
 Effect of thermomechanical treatments on tensile properties of metastable austenitic steels 16 p2693 A67-31872
 Strength characteristics of single crystals of nickel aluminide /gamma phase/, discussing temperature and orientation dependence of work hardening 18 p3064 A67-34079
 Metal matrix composites compression-microstrain behavior at room temperature, discussing stress-strain curve, Youngs modulus, yielding, etc [ASTM PAPER 6] 18 p3067 A67-34571
 Dynamic microstrain of niobium, considering purity and temperature effects, obtaining activation energy band spectrum 20 p3469 A67-37385
 Structural modifications effect on PBI fiber critical properties, discussing strain-stress characteristics, target properties and crystallization 21 p3648 A67-37875
 Prestressing effects on stress-strain diagram of monodirectional transversely isotropic glass fiber reinforced plastic 21 p3650 A67-37911
 Creep buckling load for thin circular rings determined by tangent modulus theory together with isochronous stress-strain diagram 21 p3719 A67-38022
 Rotating bending fatigue limit and true stress/true strain parameters correlation for steels extended to axial load fatigue tests 21 p3719 A67-38132
 Pure plastic bending of sheet and strip at strains exceeding elastic limit analyzed by arbitrary stress-strain diagram 21 p3721 A67-38382
 Plasticity stress-strain approximation for initial elastic behavior and incompressible state approach 21 p3728 A67-38880
 Crack opening displacement and fracture toughness analyzed for uniaxial tension and edge-cracked plate 22 p3911 A67-39681

Stress-strain curves under variable stress sequences in high stress range 22 p3913 A67-40036
 Longitudinal oscillations with multiple degree of freedom obtained over sections of adopted stress-strain diagram, characterizing elastoplastic properties 23 p4076 A67-40683
 Metal creep behavior under step function stress application including elastic and plastic deformation 23 p4018 A67-40717
 Stress-strain relation in viscoelastoplastic bodies noting static instability under conservative load 24 p4246 A67-41932
 Silicon carbide and B filament reinforced Ti alloy composites analyzed metallurgically and micromechanically, noting stress-strain behavior [SAE PAPER 670862] 24 p4172 A67-42004
 Elastomer elastic deformation response in multiaxial stress field shown identical to uniaxial stress response 24 p4250 A67-42367

STRESS-STRAIN DISTRIBUTION
 Sanders equation for circular cylindrical elastic shell reduced to fourth order PDE 01 p0159 A67-10400
 Stress functional properties of plastic materials, discussing analyticity and continuity in terms of tensor analysis 02 p0336 A67-11630
 Stress concentration in plate weakened by infinite sequence of uniform holes and subject to elastoplastic strain 02 p0337 A67-11844
 Geometrical method for endurance theory using stress space, stress-strain relation and surface tensor 02 p0339 A67-12239
 Stress-strain state for elastic deformation of two-layer compressible nonlinearly elastic cylinder under internal and external loading 02 p0341 A67-12666
 Stress-strain calculations for thin walled axisymmetric shells with arbitrarily shaped midplane based on second order theory 03 p0521 A67-13018
 Exact field equations for motion of hyperelastic rod derived from general three-dimensional theory 03 p0522 A67-13391
 Griffith energy criterion and stress-strain environmental criterion for fractures in brittle cracked metallic plate 03 p0523 A67-13467
 Plastic strains in gas-turbine components under nonuniform cyclic heating, obtaining stress-strain relations 03 p0527 A67-14072
 Stress-strain concentration in plates of bilateral cut EI-437B heat resistant alloy and EI-481 austenitic steel under rapid tensile loading at high temperature 03 p0529 A67-14084
 Beryllium as substrate for mirrors of catadioptric lenses, noting strain-induced aberration 03 p0470 A67-14391
 Timoshenko beam theory equations and shear coefficient formula derived from three-dimensional elasticity theory [ASME PAPER 66-APM-C] 04 p0717 A67-15916
 Large elastoplastic deflection of simply supported plate subjected to uniform load, noting steel specimens 04 p0718 A67-15920
 Stressed state of anisotropic half-plane weakened by finite number of elliptical holes with centers on straight line perpendicular to boundary of half-plane 05 p0907 A67-16018
 Stress-strain relationships in materials under high rate of torsional loading and torsional plastic wave propagation in long Cu tube 05 p0909 A67-16144
 Ramberg-Osgood relation that adequately describes stress-strain curve of strain hardening material extended to formulate constitutive laws for creep 05 p0830 A67-16812
 Stress-strain relations and relaxation in creep materials with elastic heredity and simple flow 06 p1107 A67-18637
 Moire method of surface strain measurement 07 p1262 A67-19387
 Stress-strain state inside elastic quarter space activated by periodic or local normal loads at interfaces 07 p1264 A67-20221
 Constitutive equation describing stress-strain behavior of metallic and nonmetallic materials for strain rate 08 p1417 A67-20560
 Stress-strain analysis of effects of rapid loading rate of restraint harness webbing especially during air crash 08 p1289 A67-20613
 Elastic moduli of filled systems, discussing effects of filler size, shape, concentration

agglomeration, etc 08 p1421 A67-20916
 Analytical solution, based on stress functions, for deflection of plastics sandwich beam under bending loads at center, agreeing with experimental results for short duration loading 09 p1579 A67-22612
 Thermal stress distribution around crack in elastic solid of transversely isotropic material 10 p1718 A67-22934
 Fracture initiation in sheet specimens, noting correlation of crack-opening displacement and fracture toughness and dependence on applied stress 10 p1718 A67-23172
 Incremental elastic-plastic analysis of two-dimensional stress system by finite element method 10 p1719 A67-23456
 Stress-strain state of elements of thin walled shells of revolution with hinged meridional edges under effect of force and thermal distributed load satisfying end conditions 10 p1720 A67-23601
 Antisymmetric stress-strain state of thin walled isotropic and anisotropic sandwich shells of revolution with meridian of arbitrary shape for complex boundary conditions 10 p1720 A67-23603
 Nonlinear behavior of elastic structural systems, approximating displacement patterns, stress-strain ratios, post buckling behavior, etc 10 p1726 A67-23717
 Hydrostatic pressure effect on surface microstructure, dislocation substructure and stress-strain behavior of beryllium 11 p1805 A67-24110
 Stress-strain condition in thin walled shells having anisotropic moduli with one end clamped and torsion applied at other end 11 p1878 A67-24860
 Stress-strain state of circular cylindrical rod coupled to half-space when applying torsion to free end 11 p1879 A67-24884
 Approximate solution using finite difference method of bending of rectangular plate beyond elastic limit 11 p1879 A67-24886
 Stressed and strained state of infinite plate lying on elastic base weakened by finite number of arbitrarily located circular holes 11 p1879 A67-25053
 Aircraft flight and ground strain measurements for static strength clearance and fatigue life assessment, noting structural integrity evaluation problems 11 p1880 A67-25058
 Book on applied stress analysis covering fundamental concepts and applications 11 p1881 A67-25099
 Push-pull low endurance fatigue of En 25 and En 32B steels at 20 and 450 degrees C 12 p2015 A67-25422
 Stress-strain state of thin walled zero moment shell under uniformly distributed multiple load assuming various tensile and compression strengths 12 p2020 A67-25569
 Cylindrical shell stability under external radial load noting stress-strain states, critical load, etc 12 p2020 A67-25572
 Stressed and strained state of orthotropic cylindrical shell weakened by circular hole 12 p2021 A67-25578
 Stress-strain state of cylindrical shell analyzed based on elasticity theory, noting boundary value problem 12 p2022 A67-25583
 Approximate theory for stress-strain state of thin cylindrical shell reinforced with elastic ribs having bending rigidity 12 p2022 A67-25584
 Stress-strain state of thin sandwich plate consisting of arbitrary number of elastic isotropic layers rigidly coupled to each other 12 p2024 A67-25602
 Vlasov engineering theory of equilibrium of shells used to study stress-strain state of closed circular cylindrical shell loaded by internal pressure 12 p2028 A67-25632
 Reissner variational formulation of temperature distribution boundary value problem of axisymmetric thermal stresses in isotropic sandwich shells of revolution [AIAA PAPER 66-528] 12 p2030 A67-25917
 Stresses and strains in dual element and fibrous to steady state creep load calculated by considering individual properties of constituent elements 12 p2031 A67-25953
 Stress-strain state in elastoplastic range of notched Duralumin strip studied by photoelastic coatings 12 p2032 A67-26105
 Material deformation, showing functional dependence of thermodynamic potential on state parameters in theory of plasticity, creep and relaxation 12 p1938 A67-26197

Stress-strain state and corrosion and erosion produced by aggressive gas flows in surface layers of gas turbine nozzle blades of Zhs6-K alloy 13 p2187 A67-28451
 Friction stress acting upon moving dislocation derived by microstrain methods is meaningful under limited conditions 13 p2141 A67-27181
 Clinographic polariscope for surface measurement of stress-strain in building materials, noting operation and results 14 p2395 A67-27973
 Stress-strain problems in design load of commercial aircraft, noting role of frequency distribution curves 14 p2245 A67-28060
 Difference method for solution of plane problems in dynamic elasticity, noting equations of dynamic/elastic deformations under plain strain 14 p2400 A67-28256
 Stress-strain state of short cylindrical shell and square panel under axial compression hinged along edges 14 p2402 A67-28897
 Problem oriented language for mechanical problems programming applied to steady state vibrations, static problems and stress-strain relation 14 p2276 A67-29000
 Displacement equations of prestressed thin bending-resistant shells 15 p2574 A67-29699
 Bulk elastic deformation of continuous medium with coaxial stress-strain deviators, analyzing deformations in body with specified boundary conditions 15 p2576 A67-30181
 Extremal principle of possible simultaneous variations of stressed and strained states which follows from origin of virtual velocities 15 p2576 A67-30182
 Elastic deformation calculation using linear real tension-elongation law 16 p2764 A67-30855
 Inclusion problems involving tubular shells of isotropic incompressible materials yielding large deformations 16 p2766 A67-31099
 Stress-strain state determination of nonlinear plate with circular holes, deriving boundary conditions and basic equations 16 p2766 A67-31147
 Thermal stress concentration in physically nonlinear elastic plate with hole in presence of uniform heat flux 16 p2766 A67-31148
 Heating of flange joint solved with approximate method taking stresses at joint into account 16 p2766 A67-31205
 Bubble raft analog for analyzing short range repulsive forces at small strains that govern fractures 16 p2768 A67-31279
 Crack problems analyzed using Tresca yield conditions to obtain continuous distributions of dislocations 16 p2768 A67-31280
 Fracture stresses of cracked plates and flow stresses of polycrystalline aggregates as related to stresses and strains at ends of plano-discontinuities 16 p2769 A67-31285
 Crack extension and propagation experiments defining plane-stress regime and providing rationale for Dugdale-Mushkellshvili model, noting stress-strain relations 16 p2769 A67-31286
 Elasto-plastic stresses and strains in cracked plates analyzed by numerical method, noting stress singularities and stress-strain fields 16 p2769 A67-31287
 Ductile fracture depending on stress/strain history and material element rotation relative to stress/strain axes proposed for asymmetrically notched specimens 16 p2770 A67-31293
 Transient analysis of displacement, strain and stress fields around running crack tip in epoxy plate with central notch using Moire method 16 p2775 A67-31325
 Creep effects in structures obtained by elastic solution applied to pressurized shells containing discontinuities 16 p2776 A67-31558
 Etl pitting analysis of slips in Fe-Si bicrystals under plastic strains, noting effect of impingement of pure edge and pure screw slip bands 17 p2872 A67-32738
 Axially symmetric wave propagation in infinitely long two-layered cylinder, detailing displacement and stress distribution 17 p2961 A67-32778
 Photoelastoplastic method using creep and stress characteristics of epoxy resins under thermal cycle, discussing stress-strain behavior [SESA PAPER 1191] 18 p3141 A67-33886

X-ray diffraction analysis of polycrystalline brass deformed by tension, noting stacking fault probability, stress-strain curve, etc 18 p3064 A67-34084
 Evaluation of stored-energy function for elastomeric materials based on biaxial experiments [JPL-TR-32-1006] 18 p3145 A67-34486
 Aluminum-boron composites stress-strain behavior, considering synergism increasing over rule of mixtures [ASTM PAPER 7] 18 p3067 A67-34572
 Mechanical behavior of boron-aluminum composites subject to stress, strain and temperature, discussing melt infiltration, powder metallurgy and diffusion bonding production [ASTM PAPER 9] 18 p3067 A67-34574
 Mechanical behavior of fiber-reinforced aluminum and effect on engineering application [ASTM PAPER 10] 18 p3070 A67-34575
 Turbodynamo disk stress-strain state, with final deformations under unsteady operational conditions, noting plastic flow, continuity, tension, and disk equilibrium equations 19 p3234 A67-34880
 Axial residual stress determination in metal surface layers based on measuring strains 19 p3343 A67-35844
 Homogeneous beam consisting of two isotropic bars with different elastic properties but identical cross sections studied for perimeters stress-strain state under torsion 20 p3535 A67-36122
 Elastic and residual strains caused by friction load in polymer surface layers studied for dependence, slip rate and friction load duration 20 p3473 A67-36842
 Thermodynamic basis of plasticity, noting loading and unloading stress-strain relations 20 p3541 A67-37283
 Thermal stresses in orthotropic sandwich plate solved by boundary value and stress distribution 20 p3541 A67-37298
 Plane-strain problem of plasticity theory with two yield conditions applied to stress and velocity fields defined by differential equilibrium equations 20 p3541 A67-37299
 Stress-strain relationships for single layer used to obtain stress distribution in orthotropic laminates subjected to axial and shear stresses [ASME PAPER 66-WA/RP-5] 20 p3542 A67-37611
 Hardenable thin walled cylindrical metal sample stress-strain state under cyclic thermal load, determining plastic deformation 21 p3716 A67-37910
 Variationally derived finite difference equations for mixed boundary value problems of thermoelastic stress and strain 21 p3716 A67-37956
 Material point displacement velocity field of bending elements of sheet during profile shaping by roll forming, determining stress-strain condition 21 p3631 A67-38052
 Stress-strain distribution in clamped membrane during stamping, deriving formulas for plastic deformation of metals 21 p3632 A67-38061
 Stress-strain state in braces across elliptical hole in elastic plate, obtaining solution for eccentric load 21 p3721 A67-38305
 Square-law elasticity theory accounting for second order terms in load parameter of stress-strain relations 21 p3721 A67-38306
 Glass fiber reinforced plastics stress and strain, considering applications in structural design 21 p3650 A67-38519
 Shells and solid wall systems with/without symmetrical cross section, considering construction, stress-strain and calculation procedures 21 p3722 A67-38524
 Laterally flattened cylindrical shells under internal pressure representing aircraft sections strength analyzed, deriving formulas for stress-strain distribution 21 p3724 A67-38784
 Mathematical programming problem for automating design of optimum thin walled systems, noting stress-strain state factors 21 p3728 A67-38903
 Algorithm for selecting optimum parameters for mathematical programming problem in thin walled systems, noting stress-strain state characteristics 21 p3728 A67-38904
 Stress-strain state of tubular blanks expanding under uniform distributed

internal load 21 p3637 A67-38925
 Cracked cylindrical shell stress-strain state under symmetric load, discussing shell curvature effect and integral equation solution 22 p3911 A67-39684
 Stress distribution in shear-strained Cosserat prism containing deep notch 22 p3913 A67-40005
 Blade-spar thick walled cylindrical shell deformed under elastoplastic torsion, analyzing stress-strain ratio and torsional strain and displacement 22 p3916 A67-40458
 Yielding behavior of materials and structures examined via one-dimensional models noting stress-strain relations 23 p4072 A67-40605
 Stress-strain relationship effect on r-power steady creep of pressurized thin spherical shell with sealed opening for various edge load boundary conditions 23 p4079 A67-41343
 Composite, reinforced and porous elastic body isotropic deformation, deriving macroscopic moduli, mean stress and strain values and dispersion 24 p4249 A67-42102
 Thin toroidal elastoplastic shells of revolution loaded axisymmetrically, calculating force, moment, stress and strain interrelation for middle surface using complex representation 24 p4250 A67-42305
 Constrained torsion of thin walled rods with closed or open profiles, discussing stress-strain state of cross section sealed at one point 24 p4250 A67-42307

STRESS-STRAIN-TIME RELATION
 Loss in hydrodynamic thermostability of viscoplastic material with stress tensor deviator related to strain rate tensor deviator 01 p0052 A67-10682
 Dislocation model to explain creep curves, predicting linear relation between dislocation density and strain, for small strain 01 p0100 A67-10751
 Diffusion effect on thermal stresses in neighborhood of macrodefects in solid solution resulting in time dependent change of stress-strain state 03 p0521 A67-13121
 Stress-strain time relation in gallium doped p-type germanium, noting crystal dislocation and creep parameter temperature dependence 04 p0677 A67-15121
 Stressed and deformed state of plastic disk under cyclic loading in variable temperature field, using increments method 05 p0810 A67-16178
 Steady state creep stress in shells under uniform internal pressure derived, using transition theory of Seth 05 p0920 A67-16722
 One-dimensional acceleration waves and higher order waves propagating in general nonlinear Maxwellian materials with fading memory 06 p1099 A67-17834
 Viscoelasticity for micropolar solids, obtaining constitutive equations of strain and microrotation rate dependent materials 08 p1422 A67-20979
 Terrestrial behavior under action of time dependent periodic potential, treating earth as Maxwell body for shear processes 08 p1325 A67-21211
 Reformation processes effect on stress-time-to-fracture behavior of solids, considering governing differential equation 08 p1423 A67-21302
 Loss in hydrodynamic thermostability of viscoplastic material with stress tensor deviator related to strain rate tensor deviator 11 p1783 A67-25070
 Stresses and strains in nonlinear viscous elasticity, examining tensors in abstract form 12 p2016 A67-25444
 Stochastic thermoelectric time varying boundary effect in circular cylindrical shell 12 p2022 A67-25587
 Nickel and cobalt superalloys low cycle thermal fatigue test method under cyclical extension and temperature conditions, giving stress-strain-time relations [ASME PAPER 67-MET-19] 12 p1956 A67-25955
 Thermodynamic analysis of stress-strain relation for polymer type media 13 p2218 A67-26886
 Creep behavior at different stresses approximated through density of dislocation velocity, deriving strain time relation 14 p2400 A67-28420
 Physical state of material analyzed using non-Riemannian plasticity 16 p2768 A67-31278
 Fracture in viscoelastic bodies, considering stress-strain-time properties and analyzing

temperature and failure envelopes 16 p2694 A67-31313
 Plane plastic strain problem analyzed assuming absence of time effects and of intermediate principal stress 18 p3140 A67-33656
 Time dependent small-strain modulus of styrene-butadiene rubber, noting predictability from selected molecular parameters [AIAA PAPER 67-491] 18 p3143 A67-33956
 Stress-strain state of rod with end load and time variable load on other end, discussing forced and free oscillations 19 p3338 A67-34879
 Aluminum alloy creep rates with changing temperature and stresses in hollow sphere, using time dependent viscosity coefficient 21 p3643 A67-38019
 Stresses and strains in nonlinear viscous elasticity, examining tensors in abstract form 21 p3726 A67-38829
 Axisymmetric creep in cylindrical shells, noting creep buckling collapse after high temperature compression loading 21 p3727 A67-38872
 Dynamic stability of spherical segments subjected to impact loading, discussing buckling in relation to rise in center and time dependence 22 p3910 A67-39456
 Fatigue behavior of Cr steel and Ni-Cr alloy examined for influence of direction of first loading stroke of push-pull testing 23 p4019 A67-41155

STRESS TENSOR
SA MINKOWSKI THEORY
 Loss in hydrodynamic thermostability of viscoplastic material with stress tensor deviator related to strain rate tensor deviator 01 p0052 A67-10682
 Maxwell-Green tensor relating forces to displacements in structural elastic beam, showing role of Maxwell influence coefficient 02 p0336 A67-11482
 Stress functional properties of plastic materials, discussing analyticity and continuity in terms of tensor analysis 02 p0336 A67-11630
 Mohr circle geometric representation of transformation of two-dimensional symmetric stress tensors in using complex variable vectors /phasors/ 04 p0657 A67-14850
 Motion theory of discrete defects in linear elastic continuum 05 p0908 A67-16038
 Parity of components of stress functional in plasticity theory 05 p0925 A67-17477
 Material orthotropy effect on directions of principal stresses and strains in fiberglass and boron composites 06 p1108 A67-18654
 Two-fluid theory for plasma stability, obtaining equation on velocity field perturbation by considering Ohm law, stress tensor with Larmor radius and viscosity from collisions 10 p1865 A67-23465
 Polarizable dielectric viscous fluid model with nonsymmetrical stress tensor 10 p1828 A67-23674
 Bending strain in linear shell theory, noting surface differential geometry and rotation vector and tensor [ASCE PAPER 268] 11 p1874 A67-24430
 Loss in hydrodynamic thermostability of viscoplastic material with stress tensor deviator related to strain rate tensor deviator 11 p1783 A67-25070
 Gauss theorems for tensor with valence other than unity extended to include arbitrary orthogonal coordinates 14 p2349 A67-28738
 Inhomogeneous elastic medium with nonlocal interaction, considering case of point defects and obtaining Green tensor 20 p3540 A67-37056
 Polarizable dielectric viscous fluid model with nonsymmetrical stress tensor 21 p3612 A67-38275
 Solution for elastic medium stressed state under axisymmetrical load, considering spherical cavity influence and moment stresses 21 p3720 A67-38301

STRESS WAVE
 Steady state solutions of stress waves traveling in linear viscoelastic cylinder, considering torsional, longitudinal and flexural waves 04 p0716 A67-15794
 Shearing stress induced shock wave propagation in annealed aluminum under biaxial plastic prestresses [ASME PAPER 68-WA/APM-3] 05 p0909 A67-16143
 Stress-strain relationships in materials

under high rate of torsional loading and torsional plastic wave propagation in long Cu tube 05 p0909 A67-16144
 One-dimensional acceleration waves and higher order waves propagating in general nonlinear Maxwellian materials with fading memory 06 p1099 A67-17834
 Stress waves reflection and transmission in composite laminates and parameters affecting ability to resist fracture by hypervelocity impact [AIAA PAPER 67-140] 06 p1102 A67-18289
 Creep, stress relaxation and vibrational measurements, sinusoidal torsional forced oscillations and stress wave propagation in polymeric linear viscoelastic solids 08 p1419 A67-20885
 Matched pulses for two-layer laminates, discussing complete energy transfer to base and uniform momentum transfer 10 p1724 A67-23707
 Mathematical classification of differential equations governing elastic-plastic waves in plane strain 22 p3914 A67-40193
 Crack propagation related to stress wave emission number and amplitude for high strength steel, Al and Ti alloys 23 p4078 A67-41163

STRIP
 Theoretical calculations for minimum anticlastic cross section deformations of thin elastic strips with optimally tapered edges verified by moiré method 11 p1875 A67-24613
 Dynamic plastic buckling of thin strips, thin and moderately thick cylindrical shells and rods under longitudinal and radial impact and compression 14 p2397 A67-28088
 HF approximation to diffraction of plane wave by conducting strip, using cylindrical wave terms for higher order patterns 23 p3979 A67-40831
 Moebius strip self-irradiation coefficient calculated as function of relative width or area of strip 23 p4083 A67-41287

STROBOSCOPE
 Stroboscopic distortion during rotation of uniformly accelerated disk illuminated by light pulses 11 p1757 A67-23917
 Stroboscopic distortion during rotation of uniformly accelerated disk illuminated by light pulses 21 p3601 A67-38945

STROMGREN METHOD
 Stromgren family of periodic orbits in restricted problem 13 p2205 A67-27479

STRONTIUM
 Interpretation of profiles of middle strength Fraunhofer lines, especially strontium resonance line of microturbulence above hydrogen convection zone 05 p0899 A67-17072
 Sounding rocket-released artificial strontium and barium ion cloud motion in upper atmosphere, based on equations of ambipolar diffusion 10 p1644 A67-23254
 Electronic band structure calculations phase of Ca, Sr and Ba over wide range of atomic volumes under pressure electronic band structure calculations for fcc phase of Ca, Sr and Ba over wide range of 10 p1882 A67-23399
 Chondrites solidification age measured via rubidium-strontium pairs in component minerals, using phase separation method 21 p3702 A67-38125
 Strontium and rubidium 87 measurements on iron meteorite silicate inclusions, with age determination at 4.4 to 4.8 billion years 22 p3881 A67-39495

STRONTIUM COMPOUND
 Domain structure of strontium ferrite investigated by Bitter powder pattern method in basal planes, showing dependence on magnetic field intensity, temperature and thickness of crystals 04 p0673 A67-14482

STRONTIUM FLUORIDE
 Solid state CW optically pumped microwave masers using divalent Tm in calcium fluoride and strontium fluoride hosts 21 p3640 A67-38454

STRONTIUM TITANATE
 Superconductivity in strontium titanates and similar polar substances with transition temperature accounted for by electron-phonon interactions 03 p0491 A67-13259
 Temperature autostabilization in barium and strontium titanate solid solutions during dielectric heating 03 p0498 A67-13707
 Experimental evidence of conduction band of semiconducting strontium titanate 06 p1059 A67-18906
 Superconductivity in strontium titanate,

noting variability of critical temperature with carrier density and uniaxial stress 06 p1069 A67-18980

Uniaxial stress and static electric field effects on energy band structure of strontium titanate and derivation of optical selection rules in region of perturbed crystals 10 p1691 A67-23403

Electron mobility in semiconducting strontium titanate 13 p2180 A67-27160

Electric field enhanced Raman scattering and linear frequency shift of strontium titanate soft mode in random domain orientation and reorientation 18 p3098 A67-33520

Conduction band structure in n-type strontium titanate investigated by measuring oscillatory magnetoresistance in high magnetic fields 18 p3104 A67-34592

Superconducting transition temperatures and low field magnetization of ceramic mixed Ba, Sr and Ca-Sr titanates, showing particle nature of specimens 19 p3302 A67-35037

Conductivity and Hall coefficient measurements for electron mobilities in strontium titanate, discussing electron-phonon coupling and cryogenic experiments 22 p3863 A67-40002

Hydrostatic and uniaxial compressional stress effects on strontium titanate superconductive transition temperature 22 p3863 A67-40244

Evaporated metallic contacts to conducting strontium titanate single crystals measured for electric properties evaporated metallic contacts to conducting strontium titanate single crystals measured for 23 p4038 A67-40874

Second order Raman spectrum temperature dependence of strontium titanate and potassium tantalate 23 p4013 A67-40965

Low loss mechanically or magnetically tunable 1 to 12 GHz hybrid ferrimagnetic dielectric microwave bandpass filter with improved power handling 24 p4132 A67-42808

Semiconducting mixed titanate superconducting transition observed at 0.5 degrees K ascribed to change in valley numbers in conduction band 24 p4205 A67-43099

STRONTIUM 90

Radio nuclide generator using oxide of strontium 90 with thermionic converter, noting decaying characteristics 04 p0559 A67-15963

STRUCTURAL BEAM

SA CANTILEVER BEAM

SA I-BEAM

Titanium crossbeam design and fabrication [SAE PAPER 660647] 01 p0079 A67-10610

Maxwell-Green tensor relating forces to displacements in structural elastic beam, showing role of Maxwell influence coefficient 02 p0336 A67-11482

Flexural wave propagation along beam with arbitrary periodic concentrated load 02 p0340 A67-12501

Accuracy of central finite difference methods for solving boundary value problems in structural analysis governed by equations with variable coefficients 03 p0526 A67-13970

Fatigue crack propagation rates for aluminum cantilever beams in reversed bending under two-level constant amplitude and random excitation, noting stress cycle effect [ASME PAPER 66-WA/MET-3] 04 p0639 A67-15343

Free vibration of sandwich beams viscoelastic cores, examining equations of motion, natural boundary conditions and derivation of expressions for modal distribution of damping [ASME PAPER 66-WA/UNT-3] 04 p0713 A67-15382

Maximum thermoelastic stress and deflection in plate or beam as function of cross sectional shape, temperature and end conditions [ASME PAPER 66-WA/APM-1] 04 p0714 A67-15426

Distributed parameter transmission matrix analysis of bending vibrations of nonuniform elastic beam [SAE PAPER 660719] 04 p0716 A67-15782

Timoshenko beam theory equations and shear coefficient formula derived from three-dimensional elasticity theory

[ASME PAPER 66-APM-C] 04 p0717 A67-15916

Optimal plastic design of minimum cost structural beams with failure under given loads [ASME PAPER 66-WA/APM-22] 04 p0718 A67-15927

Finite element method for problems in structural mechanics extended to beam vibration including shear and rotary inertia effects 05 p0924 A67-17284

Potential damage to structural elements caused by sonic booms determined by considering effect of gap between beam and supports [AIAA PAPER 67-14] 06 p1101 A67-18253

Closed form solution for transverse-symmetric and asymmetric loadings on circular fixed beam 06 p1110 A67-18842

Transient response of beams using lumped parameter models calculated by Euler method to eliminate influence coefficient normally required 06 p1111 A67-18889

Beam equation for elastically supported clamped-clamped beam solved for conditions of initial, boundary and distributed load, using Hermitian operator 08 p1415 A67-20488

Bending oscillations of hinged and clamped three-layer beams 09 p1575 A67-22219

Analytical solution, based on stress functions, for deflection of plastics sandwich beam under bending loads at center, agreeing with experimental results for short duration loading 09 p1579 A67-22612

Book on torsion emphasizing beam stressed state calculation and civil engineering problems 10 p1720 A67-23578

Method of images series solution converging rapidly for simply supported Euler-Bernoulli beam with high velocity moving concentrated load 10 p1730 A67-23837

Large deflections of beam loaded and supported at two points 11 p1871 A67-24088

Composite loss factor and natural frequencies of vibrating beams composed of alternate layers of elastic and viscoelastic material [ASME PAPER 67-VIBR-6] 11 p1871 A67-24166

Natural and forced lateral vibration analysis of free-free beam by integration and finite difference methods, considering influence coefficients [ASME PAPER 67-VIBR-54] 11 p1873 A67-24202

Natural frequency and mode shape for nonuniform simply supported beam, using Fourier series to approximate deflection, mass and inertia moment 11 p1874 A67-24429

Bent and twisted bars analysis using finite element method 14 p2399 A67-28133

Creep deformation of composite beam subjected to combined axial and bending loads 14 p2403 A67-29002

Iterative procedures for elastic, plastic and creep deformation of beams 14 p2339 A67-29003

Bounds for natural frequency eigenvalues of simply supported uniform beam with constant end load and uniformly distributed axial load 14 p2403 A67-29005

Timoshenko beam equations modification necessary to account for normal pressure and Poisson ratio effects for application to thin walled circular tubes 14 p2403 A67-29013

Transform using eigenfunction as kernel generates universal solution for structural member vibration, noting application to Timoshenko beam 16 p2763 A67-30616

Thin walled unsymmetrical beam under bending and torsion studied for nonlinear elastic behavior 17 p2957 A67-32023

Torsion or coupled bending torsional wave theory for thin walled open section beams 17 p2959 A67-32413

Dynamic stability of homogeneous and inhomogeneous sandwich columns with pinned ends under pulsating periodic loads governed by Mathieu equation 17 p2963 A67-33036

Cracked rectangular beam stress analysis, considering longitudinal shear and Saint-Venant torsion and flexure [ASME PAPER 67-APM-21] 17 p2964 A67-33150

Transverse vibrations of tapered cantilever beam solved in terms of generalized hypergeometric function by Frobenius method [ASME PAPER 67-APM-25]

17 p2964 A67-33153

Soviet book on dynamic effects of moving loads on beams supported by linear and nonlinear bearings and elastic bases 18 p3140 A67-33661

Bending oscillations of hinged and clamped three-layer beams 18 p3141 A67-33770

Bond-layer compliances effect on flexural responses of sandwich beam, discussing homogeneous and composite beams, deformation equations, etc [SESA PAPER 1214] 18 p3142 A67-33895

Intrinsic frequencies and modes of periodic free vibrations of homogeneous beam with weakly nonlinear boundary conditions of Duffing type 19 p3340 A67-35509

Implications and ramifications of theory of cutouts in displacement method 19 p3343 A67-35771

Book on viscoelasticity covering linear theory as part of applied mechanics, differential equations, hereditary integrals, etc 20 p3535 A67-38138

Buckling analysis of sandwich beams with elastic orthotropic cores under axial compression 20 p3537 A67-38641

Rigidity estimation of parabolic reflector by comparison with beam resting on two bearings 20 p3542 A67-37512

Dynamic compliance of two degrees of freedom nonrotating beam undergoing flexural vibrations, taking into account internal friction 21 p3726 A67-38833

Curvature for variable cross section beam bending with arbitrary transverse and longitudinal loads calculated by computer 22 p3915 A67-40449

Permanent deformation and interaction effects of rigid plastic clamped beam with constraints against axial displacements and subjected to transverse impulsive loading 23 p4072 A67-40606

Dynamic response of large flexible space systems subjected to motion inputs and arbitrary force, analyzing joined Timoshenko beams 24 p4240 A67-42395

STRUCTURAL DESIGN

Cold rolled extra-thin stainless steel application in construction of front and rear interstage sections of second stage of Europa I rocket 01 p0160 A67-10408

Design, development and main assemblies of third stage of ELDO satellite launcher 01 p0078 A67-10409

Beryllium rudder and structures for F-4C aircraft, discussing weight factor, analysis, design, fabrication, ground tests and fail-safe flight test programs [SAE PAPER 660666] 01 p0094 A67-10574

Structural design and fatigue life of Chinook helicopter [SAE PAPER 660667] 01 p0010 A67-10575

C-141A cargo aircraft structural analysis, discussing design, load and gust criteria, flight and static test programs, vibration and noise control [SAE PAPER 660669] 01 p0010 A67-10576

Effects of subsonic, supersonic, hypersonic and orbital environments on structures [SAE PAPER 660671] 01 p0180 A67-10578

Manned and unmanned spacecraft structures, discussing environmental and functional requirements, influence of vibration and pressurized gas containment [SAE PAPER 660672] 01 p0153 A67-10579

Structural design of hypersonic vehicle flight tank for liquid hydrogen fuel, discussing loading, material, support system, stress analysis, testing and analytical problems [SAE PAPER 660679] 01 p0161 A67-10583

Titanium crossbeam design and fabrication [SAE PAPER 660647] 01 p0079 A67-10610

Structural loading, discussing stationary and nonstationary-random and severe loading processes 01 p0163 A67-11014

Aerodynamic, thermodynamic and structural design aspects of flight capsule entering low density Mars atmosphere from orbit 01 p0156 A67-11432

Structural design and temperature control influence on configuration of Mariner space probes 01 p0156 A67-11440

Structural design of large space chambers, examining outgassing rate and thermal stress in material selection 02 p0228 A67-11839

Saturn V Mobile Launcher configuration, design and testing 02 p0228 A67-11840

Winged lifting reentry hypersonic vehicles, discussing design, analysis, fabrication and testing of hot and cooled structures and materials [AIAA PAPER 65-367] 02 p0331 A67-11929

Second generation Saturn vehicles, discussing anomalies discovered during flight tests, development, etc [AIAA PAPER 66-839] 02 p0331 A67-12255

Ground testing, development of engines, stages and ground support equipment of Saturn V launch vehicle [AIAA PAPER 66-840] 02 p0331 A67-12256

Long wave spacecraft antenna design, deployment and stabilization, noting environmental effects such as thermal expansion, solar pressure, etc [AIAA PAPER 66-848] 02 p0221 A67-12258

Soviet book on aircraft building and air fleet equipment, Number 6 02 p0339 A67-12436

Air cushion vehicle design, calculating annular nozzle, air channel optimum parameters, power capacity, aerodynamic characteristics, etc 02 p0179 A67-12437

Computer algorithm for framework diagram in synthesizing thin walled shells strengthened by ribs 02 p0340 A67-12443

Structural design optimization by nonlinear programming noting Sequential Unconstrained Minimization Technique, use of variable metric, Powell direct search method, etc 02 p0209 A67-12711

San Marco satellite structural configuration for measurement of total force acting on satellite, electron content from satellite to earth and guided propagation 03 p0517 A67-12900

Aerodynamic qualities of flexible wings noting performance, lift drag ratio, application to powered aircraft and cargo gliders 03 p0359 A67-12993

Laminate optimization for filamentary composites, discussing applied spectrum of load requirement 03 p0453 A67-13413

Fiber reinforced rotor blades, discussing composite material selection for research, mass balance, dynamic response tuning and material design 03 p0453 A67-13416

Hollow-rib reinforced structure design from boron filament reinforced epoxy resin, describing fabrication equipment, techniques and test results 03 p0429 A67-13417

Fiber, matrix and interface contributions to composite material improvement 03 p0455 A67-13441

Attachment concepts and problems in fibrous composite aerospace structures 03 p0523 A67-13444

ESRO II satellite structural design, testing and material selection noting functions, vibration testing results, etc 03 p0518 A67-13600

Structural and mechanical concept, design and testing of fully steerable radome-enclosed parabolic Haystack antenna 03 p0396 A67-13750

Material selection and structural design problems for hypersonic vehicles 03 p0525 A67-13793

Lagrange multiplier matrix in minimum weight and fully stressed optimum structural design techniques 03 p0525 A67-13966

Computer program for automated design of hyperstatic truss structures under resonant frequency used in multisatellite Agena launcher 03 p0526 A67-13968

Mathematical formulation relating modal distribution of truncation errors to matrix conditioning and loading type on structure 03 p0526 A67-13969

Fan system of 14 by 9 ft open circuit wind tunnel structural principles and operation, discussing blade fabrication, hub design, spinner and motor fairing 03 p0397 A67-14104

Minimum weight structural designs for various types of behavior specifications including stiffness, elastic and plastic strength and stability 03 p0531 A67-14365

Structural design problems of hypersonic air vehicles with air breathing propulsion, discussing relation to future hypersonic commercial air transport 03 p0362 A67-14383

Material failure modes in engine components and improved structural design problems 03 p0505 A67-14387

Thermophysical properties of glass-fiber reinforced plastics for selecting optimum structural patterns when under

axisymmetrical load 04 p0708 A67-14787

Engineering methods for construction of electromagnetic wave absorbing walls for microwave darkroom applications at various frequency bands 04 p0576 A67-15504

Correlation between increased performance demands and cost of lightweight airframe structures [SAE PAPER 660674] 04 p0716 A67-15783

V/STOL transport aircraft structural problems related to propulsion, associated acoustical, thermal and debris conditions and weight/cost effectiveness requirements [SAE PAPER 660668] 04 p0552 A67-15784

Hypersonic thermal structural concepts to satisfy design requirements including insulated, insulated and cooled and hot load carrying approaches [SAE PAPER 660678] 04 p0716 A67-15789

Optimal plastic design of minimum cost structural beams with failure under given loads [ASME PAPER 66-WA/APM-22] 04 p0718 A67-15927

Soviet papers on thermal stresses in structural elements 05 p0910 A67-16174

Optimum design of bar profile, considering bending and torsion effect and variation of wall thickness 05 p0916 A67-16242

Reliability of finite automata determined from analysis of elements capable of misalignment, input errors and structural design 05 p0782 A67-16261

Thermal design of Isis A spacecraft, noting possibility of passive thermal control and computer programmed multinode heat balance analysis 05 p0904 A67-16294

Design strength of plane notched elements under single mode vibration, obtaining equation for fatigue stress concentration factor 05 p0919 A67-16592

ESRO II satellite project, describing systems and program 05 p0905 A67-16728

Fiber reinforced metal manufacture, discussing possible fiber-matrix combinations and high temperature applications 06 p1047 A67-17713

Metal single crystal use in structural design of stress resisting devices 06 p1013 A67-17795

Control law determination procedure for structural synthesis of combined automatic control systems for nonlinear plants 06 p0976 A67-18237

Economics and technology of efficient lightweight structural design 06 p1105 A67-18595

Performance-weight relations and shape parameters for Maxwell structures design, considering filament wound isotensoid container and tension shell decelerator 06 p1111 A67-18884

Unsteady temperature fields in structures calculated by moments method 07 p1266 A67-19145

Unsteady temperature field calculated by difference method, for application to structures with various geometric configurations 07 p1266 A67-19147

U.S. Passive Geodetic Satellite, describing fabrication, structural integrity, flight preparation, launch, etc 07 p1259 A67-19760

Flexible solar cell concept, discussing historical background, conceptual design and future plans 07 p1132 A67-19877

C-141A cargo aircraft structural analysis, discussing design, load and gust criteria, flight and static test programs, vibration and noise control [SAE PAPER 660669] 07 p1131 A67-20232

Spacecraft failures noting iron concentration, poor machining, nitriding and anisotropy as causes 07 p1193 A67-20253

Boron filament epoxy resin composites test program relative to mechanical design of reentry vehicle 06 p1345 A67-20424

Numerical procedure for proportioning members of complex structure with specified natural vibrational frequency based on finite element idealization 08 p1417 A67-20554

Static and dynamic combustion phenomena effects on grain structural design for solid propellant rocket engine 08 p1374 A67-20876

Structural design of solid propellant rocket engine and failure, deformation and fracture of reinforced propellant grains 08 p1420 A67-20888

Thermal design of attitude translational

control assembly /ACTA/ of lunar excursion module /LEM/ 08 p1303 A67-21062

Designing antisymmetrically loaded conical shells and elastic systems consisting of rings, plates and shells for machine elements 08 p1424 A67-21427

XV-4B vertical lift aircraft with lift engines noting stability, control, structural design, flight control system, etc 09 p1439 A67-22284

Design problems for hydraulic loading circuit with random variation of loading with time 09 p1451 A67-22472

Effect on stage characteristics of axial compressor of design procedure used for slightly elongated vanes 10 p1697 A67-23021

Bassali theory to calculate bending, twisting moments and shearing forces for thin elastic plates under transverse flexure for structural design application 10 p1720 A67-23569

Structural design of large orbiting radio telescope employing structural flexibility rather than rigidity for dimensional accuracy 10 p1723 A67-23698

Nonlinear behavior of elastic structural systems, approximating displacement patterns, stress-strain ratios, post buckling behavior, etc 10 p1726 A67-23717

Structural design of stiffened cylindrical shells, discussing minimum weight, prevention of buckling modes, etc 10 p1726 A67-23719

Skin-stiffened compression panel design with digital computer, obtaining optimal solutions for applied stress and local and general stability equation 10 p1726 A67-23720

Solid state diffusion bonding effect on structural design 10 p1662 A67-23733

Sterilization environment effects on structural systems design for interplanetary spacecraft 10 p1714 A67-23758

Spatial variations in mean square response above lowest resonance frequency determined, using statistical analysis [ASME PAPER 67-VIBR-22] 11 p1872 A67-24181

Equations for turbomachinery blades vibration control noting energy exchange, stress amplitude, mechanical damping, etc [ASME PAPER 67-VIBR-49] 11 p1797 A67-24199

Low speed wind tunnel design, structure, performance and cost 11 p1773 A67-24640

Relativity theory for solid media model design, deriving equations of state and closed system of differential equations based on variational principle 11 p1819 A67-24675

Short wavelength large steerable radio telescope design, considering wind, heat, gravity effects and economics 11 p1768 A67-24777

Material corrosion control techniques, considering initial structure design, coatings application and protective coatings specifications 11 p1773 A67-24940

Shrouds for space vehicles, discussing advantages of Al and Mg as materials and longitudinally split and over-nose type covers 11 p1870 A67-25006

Plastic foam pattern technique for producing vibration and shock fixtures 12 p1949 A67-25687

SR-N4 hovercraft, optimum size for coastal waters, structural features, performance, control, etc 12 p1895 A67-26168

ESRO I research satellite structural design test results for study of polar ionosphere, particularly auroras 13 p2211 A67-26583

Direct numerical method for finding optimal values of functionals and associated velocity fields in plastic limit analysis 13 p2219 A67-27153

Use of computer in aircraft design problems 13 p2074 A67-27191

Seismological equipment for space research applied to earthquake-resistant structural design 13 p2120 A67-27217

Dynamic stability problems in actual structures in vehicle design 14 p2397 A67-28084

Optimal structural design with failure probability constraints 14 p2399 A67-28122

One- and two-dimensional antenna synthesis for instruments of large resolving power and effective collecting area 14 p2284 A67-28433

Rocket cost dependence on weight and airframe resistance studied for design problem solutions 14 p2245 A67-28638

Structural, seal and sideboard design, propulsion and cavitation problems relevant

to operational requirements of captured air bubble vehicle
 [AIAA PAPER 67-346] 14 p2245 A67-28729
 Evaluating mechanical and corrosion suitability of materials
 [ASME PAPER 67-DE-7] 14 p2339 A67-28866
 Glass reinforced structural design fundamentals, discussing basic properties of filament materials, matrix material and composite materials
 [ASME PAPER 67-DE-16] 14 p2402 A67-28871
 Designing methods for meteoroid impact emphasizing minimum weight shield arrangement
 [ASME PAPER 67-DE-45] 14 p2402 A67-28878
 Operation, structure, performance and application of solid, molten and aqueous electrolyte fuel cells
 14 p2253 A67-29023
 Fluid sphere gyroscope designed for extreme shock, vibration, temperature and overrate, examining signal processing, design parameters, etc
 14 p2322 A67-29081
 Launcher for research and development on aerodynamic reentry
 15 p2564 A67-29094
 Influence of weapons on basic line, avionics, flight controls and handling qualities of future
 aircraft
 15 p2418 A67-29397
 Book on aircraft design covering turboprop, subsonic turbojet, supersonic and water-based aircraft, missiles, helicopters, etc
 15 p2419 A67-29417
 Design considerations in material selection for rocket motor cases, considering fracture toughness, ductile failure resistance and buckling under flight loading
 [AIAA PAPER 66-630] 15 p2573 A67-29418
 Spacecraft reliability requirements, discussing design parameters and performance standards
 15 p2493 A67-29606
 Book on computer programs for structural analysis covering flow charts, computer languages, matrix inversion, etc
 15 p2574 A67-29646
 Threaded fastener design and manufacture
 15 p2493 A67-29650
 Trends in technology for reusable launch vehicles
 15 p2569 A67-29854
 Structural technologies applicable to future large launch
 vehicles
 15 p2569 A67-29855
 Human factors information utilization by designers, noting test results on conceptual drawing of equipment configuration according to design
 specifications
 15 p2431 A67-29897
 Cost reduction of space vehicle structures and materials
 [AAS PAPER 67-81] 15 p2575 A67-29948
 Stress states, structure deformation, failure criteria and constitutive relations in structural design noting tensile, strip and lap shear test and continuum
 model
 15 p2575 A67-29977
 Electronic device modeling criteria expressing physical structure, representing significant properties and leading to useful equivalent circuits for circuit
 analysis
 15 p2452 A67-30013
 Stress concentrations around shaped holes in plates under uniform tension, deriving formulas by perturbation
 method
 15 p2577 A67-30268
 Concorde structural development noting effects of temperature on fatigue and creep strength of aluminum alloys
 [AIAA PAPER 67-402] 15 p2578 A67-30369
 Aircraft wheel and brake designs especially for 63 Series of DC-8 noting materials, properties, construction, etc
 [AIAA PAPER 67-404] 15 p2421 A67-30371
 Assurance and measurement of space vehicle alignment conforming to design requirements
 15 p2496 A67-30422
 Man-rated space-vehicle structural design considering space environment loads and material requirements, noting applicability of existing methods
 16 p2756 A67-30630
 Deflections and stresses of paraboloidal shells of revolutions under gravity loads for applications to paraboloidal reflector antenna construction
 16 p2783 A67-30678
 Book on matrix methods of structural analysis emphasizing force and displacement methods, noting civil and aircraft construction applications
 16 p2767 A67-31253
 Structures, charging into stage, thermal protection, ignition, and nozzles problems encountered in development of solid propellants
 16 p2736 A67-31617
 Structural design, analysis and tests

pertaining to hot cycle rotor system used on XV-9A aircraft
 [AHS PAPER 121] 16 p2598 A67-31836
 Soviet book on radio telescopes covering design and construction principles, structural considerations, astronomical data, antennas, parabolic reflectors, etc
 17 p2831 A67-31934
 Structural analysis and design of large area solar array, noting factors such as temperature distribution, dynamics, internal loads, permissible weight, etc
 17 p2954 A67-31980
 Metal-to-metal seal for separable joints /Bobbin seal/ utilizing elastic and plastic responses of seal structure and interface
 17 p2864 A67-31993
 Thermal gradients effect on separable tube connectors, discussing structural elements
 17 p2864 A67-32009
 Buckling of compressed thin walled structural sections, noting design concepts and flat plate theories
 17 p2957 A67-32025
 Program producing optimum structural design configurations when restrictions on variables and aims of design are given as input data
 [AIAA PAPER 66-531] 17 p2960 A67-32577
 Cup spring designing method, with generatrix curvature included in approximation, gives better characteristic curve and stresses
 18 p3144 A67-34262
 Book on high energy batteries covering electrochemistry of discharge plate materials, weight factors, polarization electrolytes, parasitic effects, etc
 18 p2989 A67-34265
 Design and construction of equipment for oxygen, nitrogen and hydrogen determination in aerospace materials
 [ONERA-TP-466] 18 p2998 A67-34461
 Measurement within rocket exhaust plumes
 18 p3051 A67-34507
 Structural design for gust loads on USAF aircraft based on continuous turbulence and failure probabilities
 18 p2986 A67-34653
 Soviet book on temperature fields and stresses in structural elements of flight vehicles, giving theoretical analysis and numerical calculation
 18 p3145 A67-34705
 Aerodynamic, thermodynamic, heat shield and structural design aspects of ballistic vehicle entering planetary atmosphere
 19 p3332 A67-35315
 Implications and ramifications of theory of cutouts in displacement
 method
 19 p3343 A67-35771
 Ride quality improvement on flexible aircraft by means of elastic structural bending mode suppression design technique
 [AIAA PAPER 67-571] 19 p3174 A67-35967
 Plane compressor and guide vane cascades design, deriving relations for angle of attack, angle of lag, etc
 20 p3358 A67-37081
 Structural rigidity of rotating parabolic reflector obtained by solving elastic strain problem
 20 p3542 A67-37511
 Aircraft structural form optimized through changes in geometry
 20 p3542 A67-37531
 Materials in airlift technology noting adaptation of titanium and beryllium
 20 p3471 A67-37533
 Man-made organic polymer properties and characteristics, considering crystallization, cross-linking and polymeric chain stiffening for structural applications
 20 p3474 A67-37713
 Wind profile criterion for structural design of launch vehicles, representing wind statistically by bivariate-normal distribution function
 21 p3712 A67-37813
 Soviet book on aerodynamics, flight dynamics, flight vehicle structural design and mechanical and control considerations for various aircraft
 21 p3566 A67-37833
 Design and applications of gas-lubricated journal and thrust bearings of self-acting and externally pressurized types
 21 p3632 A67-38137
 Despun antenna design, functioning and performance for communications satellites, discussing pattern, scanning and phase shifters
 21 p3591 A67-38205
 Satellite influence on microwave antenna design, discussing mount designs, multifunctional antenna feed systems, structural analysis and geometries for microwave antennas
 21 p3593 A67-38233
 Design, equipment and techniques of electronic packaging in Titan III program, stressing environmental levels and safety factors
 21 p3595 A67-38335

Glass fiber reinforced plastics stress and strain, considering applications in structural design
 21 p3650 A67-38519
 I-beam ratio of depth to flange width for minimum weight obtained via modulus of rupture
 21 p3722 A67-38546
 Interferometer standing on L-shaped base for velocity and distance measurements, noting tests on aircraft and rockets and solar reflections effect
 21 p3599 A67-38643
 Launch vehicles of post-Saturn class noting requirements for launch facilities at Kennedy Space Center
 21 p3608 A67-38808
 Minimum mass bar design for axial vibration of beam with load distribution at specified natural frequency
 21 p3728 A67-38890
 Supersonic transport structural materials design, considering fatigue behavior, crack propagation and residual static strength under temperature and cyclic load effects
 22 p3819 A67-39457
 Cryogenic rocket upper stage structural design, fabrication and testing
 22 p3899 A67-39533
 Aircraft engine turbine structure effect on blade tip clearance, analyzing clearance variations as function of rotor angular velocity
 22 p3868 A67-39546
 Systematic design of TEM equal stub admittance filters on basis of insertion loss
 22 p3773 A67-40061
 Handley Page Jetstream turboprop aircraft basic design requirements, emphasizing aerodynamic design
 22 p3746 A67-40129
 Handley Page Jetstream load carrying structural design, materials employed and structural test program
 22 p3746 A67-40130
 Efficient thermal design of steerable antennas, considering space-environmental requirements
 22 p3750 A67-40409
 VFW/Fiat joint project to develop single-seater fighter/reconnaissance aircraft noting structural design, power source and liftoff weight
 23 p3934 A67-41255
 Si and Cd solar cell arrays compared using rigid frame Si solar cell concept
 23 p3938 A67-41497
 Book on analysis and design of missile structure covering load and stress analysis
 23 p4071 A67-41501
 Fatigue crack research effect on structural design of flight vehicle structures, discussing temperature effects, multiaxial strain effects and fatigue crack growth equations
 24 p4247 A67-41942
 Fastener applications for gas turbine engines noting materials selection and design
 24 p4180 A67-42079
 Threaded fasteners for application to aerospace structures noting preload, torque and lubrication
 24 p4180 A67-42080
 Structural and mechanical design of Lunar Module Descent Engine, discussing component testing effect on development schedule
 24 p4207 A67-42394
 Structural problems in high power solar photovoltaic arrays technology, discussing configuration, materials selection, thermal control coatings and tests
 results
 24 p4251 A67-42897
 Materials and structural concepts for design of entry systems, discussing environmental factors, reuse potential and high reliability
 [AIAA PAPER 67-805] 24 p4251 A67-42964
STRUCTURAL DYNAMICS
 Effects of subsonic, supersonic, hypersonic and orbital environments on structures
 [SAE PAPER 660671] 01 p0160 A67-10578
 Estimated structural response to aeroacoustic pressure loading due to jet and rocket engines and boundary layer turbulence
 [SAE PAPER 660721] 01 p0010 A67-10625
 Dynamic response of simple beam and rectangular plate under traveling shock wave at supersonic speed, using Fourier transforms
 01 p0181 A67-10775
 Equations for one-dimensional model of macroscopically homogeneous linearly elastic medium of complex structure with spatial dispersion
 02 p0337 A67-11952
 Gust Alleviation and Structural Dynamic Stability Augmentation System /GASDSAS/ design analysis
 [AIAA PAPER 66-999] 02 p0183 A67-12303
 Exact field equations for motion of hyperelastic rod derived from general three-dimensional theory
 03 p0522 A67-13391

Soviet book on strength and dynamics of aircraft engines 03 p0526 A67-14068

Iteration method applied to integral equations arising in structural mechanics problems 03 p0461 A67-14079

Stiffness matrix evaluation on basis of strain energy 04 p0709 A67-14813

Vibration testing facilities for Apollo Saturn V launch vehicle, noting structural assemblies under dynamic testing 05 p0786 A67-16156

Vibrations of disk-drum rotor analyzed using matrix equation of discrete model 05 p0810 A67-16230

Matrix method formulation of vibration and stability problems yielding upper bounds for natural frequencies 05 p0917 A67-16301

Mathematical theory of dimensional analysis and similitude, application to spacecraft thermal design and experimental results 05 p0926 A67-16514

Structural dynamics of Gemini program, discussing environmental prediction, component testing, docking system, stability, etc 05 p0924 A67-17212

Book on aeroelastic static phenomena covering aerodynamic load characteristics, elastic deformation, drag effect on lift distribution, etc 05 p0924 A67-17227

Aerodynamic and structural data on supersonic decelerators, determining problem areas and voids [AIAA PAPER 67-201] 06 p0948 A67-18301

Analytical and empirical results on shell panel flutter boundaries compared, using nonlinear Donnell theory and linear piston theory approximation [AIAA PAPER 67-78] 06 p1104 A67-18452

General solution of two-dimensional nonlinear problems of elastoplasticity using finite element method, piecewise linear load deflection relationship and computational algorithm [AIAA PAPER 67-144] 06 p1104 A67-18457

Explosive loading and structural response measurement techniques for predicting large elastic-plastic dynamic and permanent deformations of shells under dynamic loading conditions 07 p1262 A67-19411

Free vibration analysis for ring and stringer stiffened cylindrical shell, using Rayleigh-Ritz technique [AIAA PAPER 67-71] 07 p1262 A67-19434

Mechanics and chemistry of solid propellants - Symposium on Naval Structural Mechanics, Purdue University, April 1965 08 p1418 A67-20872

Solid rocket engine propellant grain structural dynamics including elastic and viscoelastic deformations, stress and shear vibration modes, natural frequency calculations, etc, using Fourier Inversions and transforms 08 p1376 A67-20883

Dynamic properties of coupled systems derived from experimentally determined frequency response functions of component systems, noting cross correlation 09 p1573 A67-21752

Book on probabilistic theory of structural dynamics, analyzing responses of structures to random vibrations 09 p1575 A67-21983

Dynamic analysis of sandwich plate with clamped edges executing plane strain motions, using variational motion equation and Galerkin method 10 p1717 A67-23138

Field method application to linear differential equation for numerical solution of two-point boundary value problems in structural mechanics 10 p1679 A67-23147

Gurtin variational principles extended in application to dynamic problems of elasticity with finite deformation 10 p1720 A67-23598

Structures, structural dynamics and materials - AIAA/ASME Conference, Palm Springs, March 1967 10 p1721 A67-23696

Statistical energy analysis for multimodal random vibration of complex system, discussing power flow, modal responses, kinetic energies, etc [ASME PAPER 67-VIBR-8] 11 p1872 A67-24168

Energy techniques and matrix method for computer programming of dynamic response due to random and harmonic loading on structural systems [ASME PAPER 67-VIBR-56] 11 p1873 A67-24203

Material hysteresis model for transient dynamic analysis 11 p1874 A67-24358

Contact problem for elastic rectangle solved by reducing problem to solution of

quasi-fully regular infinite set of linear algebraic equations with bounded free terms 11 p1876 A67-24679

Structural influence coefficients of arbitrarily restrained system obtained from experimental results of free-free ground vibration test 12 p2030 A67-25918

Natural transverse vibrations of sandwich plates with rigid and lightweight fillers, deriving stability equations from eigenvalue equivalent problem 14 p2402 A67-28901

Matrix calculation of structures by parallel methods of forces and displacements [ONERA-TP-412] 15 p2576 A67-30125

Structural dynamic load and instability problems in launch vehicles and spacecraft in lunar exploration emphasizing reliability, crew safety and mission success 16 p2654 A67-30677

Equations for one-dimensional model of macroscopically homogeneous linearly elastic medium of complex structure with spatial dispersion 17 p2965 A67-33269

Yield conditions for plastically incompressible isotropic and orthotropic materials with different yield stress in tension and compression, without using hydrostatic terms 19 p3339 A67-35053

Parametric expansions in linear theory of cylindrical shells noting loading and boundary conditions, approximation formation, fiber elongation, etc 19 p3339 A67-35054

Sodium cloud between 85 and 110 km shows turbulent phenomena stratification exists and disappears with upward propagation of movements due to energy decreases 20 p3427 A67-36367

Ultrasonics as nondestructive means of measuring residual stresses 20 p3537 A67-36475

Circular plate on nonlinearly elastic base with uniform load force at center, tangential force and contour moments for plate deflection 20 p3539 A67-36923

Zero moment elliptical paraboloid translational shell under uniformly distributed load, reducing solution to Dirichlet problem 20 p3539 A67-36924

Analog simulation of differential equation system for Cardan-suspended gyro, considering dry friction, support and aircraft motion 20 p3454 A67-36954

Heat treating effects on molybdenum properties and structural characteristics 20 p3466 A67-36967

Temperature distributions and heat generation in viscoelastic isotropic solid resulting from mechanical deformations determined by energy equation 21 p3715 A67-37894

Cylindrical shell deflection by radial concentrated force, using digital computer for stability analysis 21 p3721 A67-38309

Thin plate idealization to Hrennikoff lattice model framework for linear stiffness method analysis 21 p3728 A67-38877

Shore hammer motion behavior, especially rebounding process frictional energy loss distribution 22 p3913 A67-40038

Strain rate sensitivity and bending extension interaction in one degree of freedom deformation of clamped beam, considering vibration and load duration 23 p4072 A67-40807

Permanent deformation of clamped plastic beam with central mass concentration subject to impulse loading 23 p4072 A67-40808

Soviet papers on dynamics and strength of machines, Issue 4 23 p4075 A67-40878

Fatigue crack propagation rate in sheet specimens under various loadings simulating rivet forces 24 p4247 A67-41944

Spacecraft structural criteria for lightweight photovoltaic solar arrays development, discussing Mariner type panel designs and power-to-weight ratios 24 p4108 A67-42557

Numerical procedure for structural systems analysis, discussing computer application to hydrodynamic, electric, magnetic, thermodynamic, elastostatic and elastodynamic problems [AIAA PAPER 67-955] 24 p4127 A67-43038

STRUCTURAL ENGINEERING

Mechanics Conference, Ukrainian Academy of Sciences, Institute of Mechanics, Kiev, April 1966 01 p0157 A67-10214

FR-1 satellite design difficulties such as material selection, insulation of structure,

making structure perfectly conducting, etc 03 p0518 A67-13601

Book on creep in structural engineering and uniaxial and multiaxial states of stress for stationary and nonstationary creep 03 p0525 A67-13818

Soviet monograph on dynamics and durability of machines 05 p0915 A67-16219

Statistical probabilistic analysis of error propagation and tolerance limits in structural engineering design of assembled parts 05 p0813 A67-17258

Ultrasonic immersion inspection apparatus for structural defects detection in turbine blades 06 p1007 A67-18103

Book on computer matrix analysis of structures 06 p1105 A67-18520

Book on matrices for structural analysis, including elementary algebra and detailed arithmetic of matrix methods applied to structure theory 10 p1719 A67-23476

Book on torsion emphasizing beam stressed state calculation and civil engineering problems 10 p1720 A67-23578

Composite materials potential in structural engineering 11 p1807 A67-24638

Thermoelastic piecewise homogeneous bodies 12 p2013 A67-25259

Book on engineering properties of ceramic materials covering high melting materials, physical, thermal and mechanical properties, thermal stress, oxidation, corrosion resistance, etc 12 p1960 A67-26201

Book on structural matrix analysis for engineers, giving examples of matrix algebra practical application and methods of linear equation investigation 16 p2764 A67-30966

Fiber shells of revolution under compression loads analyzed for use in pressurized balloons 19 p3338 A67-34872

Composite technology emphasizing fiber-reinforced metal matrix composites, discussing filaments, plastics, ceramics, fabrication methods, etc 21 p3643 A67-37953

STRUCTURAL ENGINEERING SYSTEMS

SOLVER /STRESS/

S STRESS COMPUTER PROGRAM

STRUCTURAL FAILURE

Anisotropy test examining failure behavior of aluminoborosilicate glass fibers under tensile and torsional loading [ACS PAPER 1-G-65F] 01 p0103 A67-10263

Vibration modes, stress distribution, natural frequency and failure points in pin-fixed compressor blades [ASME PAPER 66-WA/GT-4] 04 p0711 A67-15359

Tensile failure of whisker reinforced composites for loading in fiber direction 08 p1344 A67-20421

Micromechanical failure mechanism of fiber reinforced plastics under tension, compression and shear 08 p1344 A67-20422

Test method for aluminum and titanium alloys, estimating tendency toward brittle failure and recording kinetics of crack formation 08 p1342 A67-21176

Tensile residual stress measurement in area of failure origin in helicopter rotor blade, using laboratory tests and X-ray analysis [SAE PAPER 670154] 09 p1502 A67-21772

Materials failure laws based on combined analysis of cracks and fractures 09 p1575 A67-22166

Model ten-member redundant structure under constant-amplitude loads analyzed, determining statistical distribution of consecutive failures for fail safe design applications 10 p1718 A67-23432

Boron fiber reinforced epoxy matrix plastic composite for application to aircraft structures 10 p1723 A67-23697

Thermal mechanical treatments influence on strength, toughness and environmental failure resistance of low alloy high strength martensitic steel 11 p1806 A67-24363

Metallurgical investigations by electron microscopy of rolling contact fatigue, elucidating mechanisms of failure due to shearing stress 12 p1954 A67-25329

Crack propagation kinetics by thermal fluctuation induction, considering endurance and breakdown of metallic and semimetallic materials 12 p2029 A67-25666

Dent effect on buckling strength of aluminum alloy tubular columns subjected to axial compression [ASME PAPER 67-MET-12] 12 p2030 A67-25951

Constitutive equation for collapse load and

- limit analysis of elastoplastic structures 13 p2216 A67-26609
- Beryllium joints and structures tested for static and repeated loading fatigue at room and high temperatures 13 p2123 A67-27132
- Structural evaluation of sheet beryllium fabricated by three different methods 13 p2140 A67-27136
- Ultrasonic flaw detection of hidden cracks in turbine blades 14 p2395 A67-27872
- Book on safety of structures 14 p2395 A67-28030
- Single mode analysis of dynamic buckling of imperfection-sensitive elastic structure prone to catastrophic failure under time dependent load 14 p2396 A67-28083
- Optimal structural design with failure probability constraints 14 p2399 A67-28122
- Upper and lower bounds of survivorship function of redundant structure subjected to fatigue 16 p2774 A67-31319
- Failure safety design of rotary wing aircraft, emphasizing airline type operation [SAE PAPER 670349] 17 p2798 A67-32991
- Alloys for failure-safe structures tested, determining fracture toughness, fatigue strength and stress-corrosion cracking resistance 17 p2875 A67-33048
- Lifetime of structural sections subjected to creep deformation at high temperatures, showing relation to energy dissipation forces 20 p3540 A67-37058
- Failure mechanisms in semiconductor components under thermomechanical and electrical stresses for D2 satellite application 21 p3601 A67-39061
- Physicochemical interactions between components of refractory metals solid solutions, determining metal alloying effects on system structure and high temperature durability 22 p3818 A67-39319
- Kinetics of structural changes and failure formation and growth in high temperature alloys undergoing creep 22 p3818 A67-39320
- Molybdenum heat resistance improvement after structural polygonization by deformation and annealing, describing durability dependence on treatment conditions 22 p3819 A67-39324
- Safety design for high strength low toughness materials assumed to have hidden flaws, formulating stress intensity factor for fracture mechanics 22 p3913 A67-39982
- Air damping effect on structural fatigue failure evaluated mathematically as power function relating stress to number of cycles 22 p3915 A67-40405
- Stress interaction in cumulative fatigue damage studied to predict remaining life of machine structures 23 p4074 A67-40650
- Vibration modes, stress distribution, natural frequency and failure points in pin fixed compressor blades [ASME PAPER 66-WA/GT-4] 24 p4251 A67-42460
- Metal-fatigue failure indicator-predictor gauge by correlating resistance changes with fatigue damage [AIAA PAPER 67-794] 24 p4251 A67-42955
- STRUCTURAL FATIGUE**
- Environmental structural testing capabilities for orbital and space vehicles [SAE PAPER 680685] 01 p0154 A67-10589
- Ultrasonic fatigue damage indicator for inspection and design 01 p0165 A67-11362
- Long-haul transport aircraft structural considerations and effect on operating empty weight and on airframe maintenance [AIAA PAPER 66-882] 03 p0361 A67-14019
- Linear optimal control via root square locus to design simple effective structural bending control for four XB-70 coupled longitudinal bending modes [AIAA PAPER 66-970] 03 p0361 A67-14142
- Structural fatigue-failure under nonstationary random loading processes 04 p0716 A67-15749
- Book on aircraft materials strength calculations including load determination, heating problems, creep and fatigue strength, etc 07 p1128 A67-19578
- Structural fatigue in aircraft - ASTM Symposium, Seattle, October-November 1965 10 p1594 A67-23429
- Measurement of torsional fatigue loads on aircraft undercarriage under service conditions 11 p1880 A67-25057
- Aircraft flight and ground strain measurements for static strength clearance and fatigue life assessment, noting structural integrity evaluation 11 p1880 A67-25058
- Universal endurance criterion for machine structural elements sustaining complex stresses, based on machine part lifetime assessment 12 p2032 A67-25964
- Stochastic model to structural fatigue, obtaining probability distribution for number of load repetitions necessary for fatigue failure 15 p2578 A67-30270
- Alloys for failure-safe structures tested, determining fracture toughness, fatigue strength and stress-corrosion cracking resistance 17 p2875 A67-33048
- Flight control system for future large aircraft, obtaining structural fatigue reduction, better handling and smoother ride 21 p3570 A67-39133
- Initial tension and compression effects on fatigue strength of aluminum alloy structures during plastic cold working 22 p3911 A67-39549
- Transmission electron microscopy for microstructure observations at growing fatigue crack tips in aluminum alloys, discussing plastic dislocation morphology and density 24 p4170 A67-41947
- Deformation continuum mechanics near cracks, discussing fatigue load propagation applications and elastoplastic models 24 p4248 A67-41948
- Design methods to combat fatigue effects on economics of civil aircraft, discussing structural weight role, maintenance, inspection, etc 24 p4250 A67-42441
- Fail-safe design, nondestructive testing and inspection facilities at design stage for aircraft structures 24 p4250 A67-42442
- STRUCTURAL FOUNDATION**
- Computer program to aid analysis of tracking radar towers and foundations 03 p0396 A67-13753
- Dynamic measurements of heavy landings on experimental helicopter platform and of response to heavy vehicle loads on steel-and-concrete deck flyover 11 p1880 A67-25056
- STRUCTURAL HEATING**
- Stresses produced in elastoplastic sphere with spherical cavity by surface heating-cooling, reducing problem solution to first order ordinary differential equation and functional equation 10 p1716 A67-22940
- Heating of flange joint solved with approximate method taking stresses at joint into account 16 p2766 A67-31205
- Soviet book on temperature fields and stresses in structural elements of flight vehicles, giving theoretical analysis and numerical calculation 18 p3145 A67-34705
- Equations for transient temperature distribution and thermal stresses in heated idealized wing structure solved using heat flow analysis method 20 p3541 A67-37489
- Thermal protection methods for structures subject to aerodynamic heating, discussing heat dissipation methods and thermophysical materials 23 p4082 A67-41042
- STRUCTURAL MATERIAL**
- SA PANEL
- SA SKIN
- Materials for structural usage in high altitude/ high temperature supersonic transports, comparing aluminum, titanium, etc, alloys for mechanical and physical properties [SAE PAPER 680665] 01 p0094 A67-10573
- Space environmental effects on metallic and polymeric plastic structures including aluminum, magnesium, titanium, beryllium and stainless steel [SAE PAPER 680675] 01 p0094 A67-10581
- Mechanical property data on Lockalloy /62 Be, 38 Al/ and comparison with other lightweight structural metals [SAE PAPER 680652] 01 p0094 A67-10613
- Thermal field of cutting area of aircraft structural material analyzed, using differential equations of thermoconductivity 03 p0427 A67-13191
- Boron filaments for possible use as reinforcing phase in composite materials for aerospace structures 03 p0452 A67-13407
- Single crystal whisker composite methodology in plastics, metals and ceramics, emphasizing alignment and handling problems 03 p0453 A67-13410
- Potential payoffs of using high modulus filament reinforced composite materials in aerospace systems applications discussed in light of development programs 03 p0443 A67-13414
- Structures, materials and thermal protection systems for future manned reentry vehicles, emphasizing crew compartment compatible materials [AIAA PAPER 66-987] 03 p0520 A67-14143
- Thin shells and stability in aerospace structures [AIAA PAPER 66-1022] 03 p0529 A67-14154
- Beryllium properties and treatment for use in manned space flight noting thermal stress resistance, toxicity, honeycomb structures, etc 04 p0635 A67-14563
- Compression, shear and bending strengths of tubular synthetic products as materials for aircraft structural component 04 p0715 A67-15539
- Maraging, 15CDV6 and 40CDV20 steel for missile and aircraft construction 05 p0830 A67-17289
- Cermets as substitutes for common carbon and alloyed steels, iron and nonferrous metals, discussing powdered metal technology and applications to structural materials 06 p1015 A67-17842
- Newer titanium alloys compared with present production alloys from closed die forgings in typical airframe and engine configuration 06 p1017 A67-17999
- Automatic control system synthesis for fatigue testing of structural elements under random loads 06 p1101 A67-18239
- Filamentary composite of boron and epoxy applied in design optimization of helicopter blade structure, considering filament orientation and stiffness [AIAA PAPER 67-178] 06 p1102 A67-18322
- Orientation effects in mechanical behavior of anisotropic structural materials - Astm Symposium, Seattle, October-November 1965 06 p1107 A67-18653
- Anisotropic sandwich constructions characteristics for orthotropic materials used for facings and cores, considering stiffness and buckling 06 p1108 A67-18655
- Filament-metal matrix composite material research, considering reinforcement and binder 06 p1019 A67-18657
- Heat resistance of Ti alloy after thermomechanical treatment, noting properties as long lifetime structural material 07 p1206 A67-19284
- Book on aircraft materials strength calculations including load determination, heating problems, creep and fatigue strength, etc 07 p1128 A67-19578
- Shroud for Lunar Orbiter atop Atlas-Agena launch vehicle, noting structural alloys used 07 p1193 A67-20255
- Filamentary reinforced resin matrix composite materials for high specific strength and specific modulus necessary for aircraft structures 08 p1333 A67-20359
- Constitutive equation describing stress-strain behavior of metallic and nonmetallic materials for strain rate 08 p1417 A67-20560
- Static and transient strain measurement in aerospace structural materials using extensometer and compressive test jig, determining Young modulus, creep rate, etc 08 p1420 A67-20907
- Structures and materials for supersonic aircraft and space vehicles 09 p1576 A67-22429
- Thin shells and stability in aerospace structures [AIAA PAPER 66-1022] 10 p1715 A67-22767
- Structurally significant material properties effect on reliability of aircraft structures regarding unserviceability, ultimate load failure, etc, stressing stochastic concepts in strength analysis 10 p1718 A67-23433
- Structures, structural dynamics and materials - AIAA/ASME Conference, Palm Springs, March 1967 10 p1721 A67-23696
- Integrally formed compression panel efficiencies compared with other aerospace panel concepts 10 p1729 A67-23769
- Book on fracture of structural materials covering relation between design and fracture occurrence, fracture types, fracture resistance testing, etc 12 p2013 A67-25362
- Evaluating mechanical and corrosion suitability of materials [ASME PAPER 67-DE-7] 14 p2339 A67-28866
- Design considerations in material selection for rocket motor cases, considering fracture toughness, ductile-failure resistance and buckling under flight loading [AIAA PAPER 66-630] 15 p2573 A67-29418
- Design, mission and environment considered as criteria in material selection

- for use in spacecraft 15 p2502 A67-29539
- Epoxy casting resins as structural material in electronic industry, with tables of various hardener characteristics, viscosities, epoxy equivalents, etc 15 p2508 A67-29683
- Creep properties of glass fiber reinforced plastics for long-term bearing structures, noting elastic strain, creep rate, etc 16 p2694 A67-31486
- Sinusoidal vibration generator consisting of two rigid vibrodynes connected by synchronized shaft for testing structural material 16 p2776 A67-31556
- Mechanothermal treatment for high temperature strength increase in metals, noting effects on creep strength, stress relaxation, etc 19 p3247 A67-35852
- Electronic flat-pack processes covering sealing methods, material combinations, leakage determination, etc 21 p3634 A67-38621
- Book on inspection, construction, operation, maintenance and repair of aircraft and aerospace vehicles including metal, steel frames, wood structures and high temperature structural material 22 p3811 A67-39441
- Endurance fatigue characteristics of weldable martensitic stainless steel, giving data for butt and spot welds 22 p3811 A67-39447
- Fiber reinforced plastic components for structural materials noting high temperature polymers 22 p3825 A67-39854
- Performance reliability of reinforced plastics for structural load-bearing components using nondestructive testing, defining material-energy interactions 22 p3826 A67-39860
- Distribution function of durability in light structural alloys based on mass fatigue tests analyzed for influence of scale factor and stress concentration 22 p3915 A67-40301
- Strength and oxidation tests evaluated for coated fasteners in extreme temperature use 24 p4160 A67-42078
- Textile fabrication methods produce multidirectional materials, describing commercial use of 3-D materials 24 p4176 A67-42424
- Materials and structural concepts for design of entry systems, discussing environmental factors, reuse potential and high reliability [AIAA PAPER 67-805] 24 p4251 A67-42964
- ### STRUCTURAL RELIABILITY
- #### SA AIRCRAFT RELIABILITY
- Structural safety of Mercury and Gemini vehicles, noting fail-safe and fracture tolerant design [SAE PAPER 660681] 01 p0154 A67-10585
- Functional analysis method application to reliability testing of Polaris missile 01 p0155 A67-11346
- Integrated circuit reliability and nondestructive testing, noting component failure analysis, self-maintenance, network parameter determination, etc 02 p0224 A67-11526
- Triplex flight control system for VTOL aircraft noting new servomotor, simple mechanical construction and increased reliability 02 p0264 A67-12206
- History of selected reliability and maintainability committees and interested government agencies [AIAA PAPER 66-856] 02 p0343 A67-12259
- Aircraft structural design criteria and analysis methods, noting procedures which result in discrepancies between design loadings and actual flight test results [AIAA PAPER 66-881] 02 p0339 A67-12263
- Behavior and fatigue strength of graphite during testing, plotting curves in semilogarithmic coordinates 04 p0641 A67-14599
- Design strength calculation for materials as function of reliability level and number of components 04 p0627 A67-14705
- Mechanized data system for quality and reliability control, noting performance characteristics and computer program 05 p0814 A67-17264
- Construction of lunar landing module with high reliability and low weight 07 p1260 A67-20246
- Predicting structural reliability by recent developments in statistics, reliability, cost effectiveness analysis and decision theory [AIAA PAPER 66-503] 08 p1424 A67-21524
- Book on probabilistic theory of structural dynamics, analyzing responses of structures to random vibrations 09 p1575 A67-21983
- BAC 111 hydraulic system, discussing service experience, reliability, maintenance, performance characteristics, etc 09 p1444 A67-22128
- Hydraulic system of Boeing 737 jet transport, noting flight safety and system reliability throughout design 09 p1444 A67-22129
- Implementation of NASA NPC 250-1 /Reliability Program Provisions for Space Systems Contractors/ as applied to Saturn V Mechanical Ground Support Equipment Program 09 p1582 A67-22292
- Structural reliability determined when stress and strength distributions are described by normal statistical distribution 09 p1575 A67-22298
- Reliability methodology in design and development stage, discussing component stresses, performance variation, etc 09 p1572 A67-22310
- Structurally significant material properties effect on reliability of aircraft structures regarding unserviceability, ultimate load failure, etc, stressing stochastic concepts in strength analysis 10 p1718 A67-23433
- Principle of maximum entropy and application in reliability estimation of aircraft structures 10 p1726 A67-23730
- Constrained layer damping mechanism for optimum performance of plates, beams and tubular structures, using viscoelastic material [ASME PAPER 67-VIBR-26] 11 p1872 A67-24184
- Aircraft flight and ground strain measurements for static strength clearance and fatigue life assessment, noting structural integrity evaluation 11 p1880 A67-25058
- Executive aircraft structure safe-life fatigue analysis and tests [SAE PAPER 670257] 12 p2016 A67-25507
- Combined multishaker and gas flow tests as part of reliability test program for Saturn V, S-1C pneumatic systems 12 p1923 A67-25706
- Loss structure models concerning age replacement policies, discussing mathematical aspects of maintenance with dynamic programming formulation 14 p2345 A67-28909
- Computer partitioning for long term reliability in space, noting requirements for various phases of operation 15 p2439 A67-29306
- Strike aircraft design noting weapons compatibility, use of analytical and scale testing techniques, etc 15 p2418 A67-29396
- Apportioning system reliability requirements to various system components, using generalized failure mode and effects analysis for each equipment within system 15 p2492 A67-29605
- Hydraulic systems reliability and maintenance, designing corrective measures to eliminate fluid leakage [AIAA PAPER 67-403] 15 p2423 A67-30370
- System reliability study via detailed allocation method, selecting optimal solution in context of tradeoff analysis 15 p2512 A67-30409
- Static structural strengths, aeroelasticity and flutter problems for glider performance 16 p2776 A67-31466
- Helicopter structural elements safe life through variable-amplitude fatigue tests [AHS PAPER 122] 16 p2777 A67-31837
- Structural reliability of fatigue loaded rotorcraft estimated through S-N and spectrum testing [AHS PAPER 123] 16 p2777 A67-31838
- Hypersonic reentries with thermal and structural integrity problems studied by Saphir rocket firings 17 p2955 A67-32376
- Stress anomaly effect on structural integrity of Teflon laminates determined by photoelastic techniques 18 p3142 A67-33894
- Aircraft structural design criteria and analysis methods, noting procedures which result in discrepancies between design loadings and actual flight test results 21 p3568 A67-38537
- Space research experiments reliability requirements, considering structural components, project planning and measuring methods adaptation to ambient conditions 22 p3899 A67-39283
- Breakdown probability calculations to determine life span and reliability of structural components subjected to oscillations 22 p3908 A67-39284
- Nondestructive inspection of composite structures in helicopter rotor blades, discussing structure, loading and quality control capability 22 p3812 A67-39857
- ### STRUCTURAL RIGIDITY
- Stiffness techniques based on numerical integration for explicit calculation of displacement functions and derivatives in subroutine 01 p0163 A67-11173
- Ground resonance of helicopters with zero transverse flexibility analyzed 03 p0360 A67-13393
- Beam-column analysis by finite element method, establishing end load-deformation relationship via stiffness matrices 03 p0523 A67-13457
- Inelastic buckling of rib-cored orthotropic sandwich cylinders under external hydrostatic pressure, evaluating rigidity factor and Poisson ratio effect 04 p0719 A67-15936
- Resonance transition of hinged ponderable rod with nonlinear supports 06 p1109 A67-18666
- D1 satellite structure noting rigidity and shock absorbing properties 07 p1258 A67-19526
- Shell structures solved numerically, using network of partial panels 08 p1417 A67-20556
- Sandwich plate problem involving subjection to concentrated force of plate having filler flexural rigidity only, giving solution in form similar to that of thin isotropic plate 10 p1716 A67-22937
- Sandwich plate problem involving plate having filler flexibility only, giving solution via reciprocity theorem based on Rayleigh-Green equality in thin plate theory 10 p1716 A67-22938
- Torsional stiffness of ribs effect on buckling strength of longitudinally stiffened plates compressed in direction of ribs 10 p1719 A67-23474
- Straightforward method consistent with virtual work principle for accelerating convergence to exact solution in shell analysis by matrix displacement method 10 p1725 A67-23714
- Fiber spacing and array geometry effect on modulus of composites of laminate configurations used in aerospace structures 10 p1729 A67-23768
- Shells of revolution having arbitrary stiffness distribution of loads and temperatures 10 p1730 A67-23771
- Relaxation, creep and modulus of rigidity lowering in compression springs under high temperature 11 p1795 A67-24090
- Approximate theory for stress-strain state of thin cylindrical shell reinforced with elastic ribs having bending rigidity 12 p2022 A67-25584
- Selection of angular rigidity of shock absorbing system of gyroscopic device 15 p2490 A67-30173
- Double curvature influence on rigidity of shell of revolution analyzed for surface loading and cross sectional linear loading, using Fourier series 16 p2766 A67-31149
- Flexural rigidity of plates reinforced by parallel stiffeners for direction normal to stiffener orientation determined together with stresses induced by bending moment 17 p2959 A67-32408
- Large deflections of columns of variable flexural rigidity, assuming bending moment is proportional to curvature 17 p2963 A67-33020
- Stresses acting in oblique cross sections of composite shells computed in reference to different orientations 18 p3342 A67-35719
- Structural rigidity of rotating parabolic reflector obtained by solving elastic strain problem 20 p3542 A67-37511
- Rigidity estimation of parabolic reflector by comparison with beam resting on two bearings 20 p3542 A67-37512
- Unloaded thin walled spherical shell rigidly hinged along edge noting existence of nontrivial form of equilibrium and negative lower critical load 22 p3910 A67-39402
- Structural elastic deformations effect on aerodynamic steering loads of glider, examining lift changes caused by wing geometry variations 23 p3933 A67-40640
- Elastic wing twisting effect on longitudinal stability and controllability of glider,

considering wing rigidity 24 p4094 A67-42021
STRUCTURAL STABILITY
SA REINFORCED SHELL

Dispersion-strengthening by formation of carbides of Hf, Zr, Ta, Ti and Nb in wrought and recrystallized Cr, discussing structural stability 01 p0100 A67-10786

Flexural instability of foldable tube with elastic recovery for use as structural elements, pipes, antennas and masts 01 p0165 A67-11387

Stability of rectangular elastic orthotropic plates under distributed and concentrated loads, noting glass fiber reinforced plates 02 p0339 A67-12240

Stability problems of sandwich plates, considering buckling and wrinkling 02 p0341 A67-12713

Stability, wear and seizure characteristics of hydrodynamic journal bearings of various materials and designs in sodium at temperatures to 800 degrees F 03 p0428 A67-13227

Two stabilizing methods for externally pressurized thrust gas bearings using fluid restriction and fluid storage [ASME PAPER 66-LUB-5] 03 p0432 A67-13763

Strain-gauge measurements of large-scale stationary mounted parts with gauges on foil substrate at high temperature 03 p0527 A67-14074

Elastic-plastic continua with unstable elements obeying normality and convexity relations 04 p0708 A67-14622

Behavior of eigenvalues in stability of elastoplastic plates used in low rigidity structures 04 p0708 A67-14786

Parametric excitation of initially straight viscoelastic column represented by spring-dashpot model 04 p0709 A67-14814

Optimal control problem of variable structure system, deriving necessary and sufficient conditions for existence of trajectories 05 p0781 A67-16256

Phase recrystallization effect on structure and mechanical properties of cast monophase titanium alloys 05 p0830 A67-16760

Matrix displacement approach to discrete element structural analysis for thin shell instability, emphasizing determination of membrane force 05 p0925 A67-17352

Mechanical and structural properties of three-dimensionally reinforced plastic, noting composite cylinder 06 p1020 A67-18296

Finite rectangular plate under load solved by method involving Green function and Fourier sine transform 06 p1105 A67-18579

Second order elastic effects in infinite isotropic compressible medium with elliptic hole subjected to uniform tangential force at boundary 07 p1263 A67-19729

Skylark rocket attitude in free space determined from solar and magnetic sensor data used in least squares method 08 p1406 A67-20508

Mechanical impedance testing and analysis for spacecraft with single firing 08 p1422 A67-21285

Large size parabolic reflector with small deformation constructed with multibearing suspension 08 p1318 A67-21344

Radio telescope antenna phase errors due to structural rigidity and fabrication accuracy 08 p1306 A67-21346

Solar environment and aerodynamic drag effect on deflection of structural booms in space [AIAA PAPER 66-502] 08 p1413 A67-21512

Stability of nonprismatic and nonhomogeneous rods under compressive tangential force, calculating critical force and corresponding frequency 10 p1717 A67-22944

Linearization of hyperbolic equation for data analysis of stability of elastic column and plate structures, determining critical load 11 p1874 A67-24224

Tensile strength retaining characteristics of aluminum alloys determined after varied soaking periods at various elevated temperatures 11 p1805 A67-24271

Soviet book on calculations of strength and vibrations of rocket engines 11 p1852 A67-24512

Vibration response of Apollo shell structures to acoustic and aerodynamic noise 12 p2132 A67-25728

Compression load stability of nonuniformly rigid plates within and beyond elasticity limits solved by combined Galerkin and finite difference methods 12 p2031 A67-25961

Nickel-base superalloy technology, stressing structural stability and hot corrosion resistance 12 p1958 A67-26128

Two-mirror antenna with automatic phase error control, noting experimental model correlation 13 p2080 A67-27024

Relation between chromium cold-shortness temperature variations and structural changes under deformation, noting dependence on initial metallographic grain size 13 p2141 A67-27284

Dynamic stability of structures - Conference, Northwestern University, October 1965 14 p2396 A67-28078

Stability, probability and reliability relationship presented together with statistical problems in structural stability 14 p2396 A67-28082

Dynamic stability problems in actual structures in vehicle design 14 p2397 A67-28084

Axial vibration /pogo stick effect/ of Titan II, as Gemini launch vehicle, studied by analog computer simulation for instability influences 14 p2394 A67-28086

Energy method extended to stability analysis of linear system under action of nonconservative forces 14 p2398 A67-28094

Direct matrix method for analysis of critical loads and associated buckling modes for struts having various end constraints 14 p2403 A67-29017

Helicopter rotor and pylon stability investigated through motion equation 14 p2246 A67-29048

Sonic boom effect on structural behavior 15 p2573 A67-29401

Statistical service life prediction based on propellant grain structural integrity for Minuteman third stage motor, noting grain stress analysis 15 p2547 A67-29996

Rotating spacecraft attitude changes due to energy dissipation from angular deformation treated by modal method 15 p2572 A67-30201

Stability equation of multilayer sandwich plates with isotropic homogeneous facing layers and orthotropic homogeneous core layers 15 p2577 A67-30287

Stability of prismatic shaft rotating with constant angular velocity as function of mass and setting point of rotating mass 16 p2766 A67-31151

Vacuum chamber for plasma studies consisting of thin stainless steel shell strengthened by glass fiber reinforced plastic with epoxy compound as adhesive 16 p2676 A67-31397

Large size parabolic reflector with small deformation constructed with multibearing suspension 17 p2831 A67-31940

Radio telescope antenna phase errors due to structural rigidity and fabrication accuracy 17 p2822 A67-31942

Book on thin walled structures covering frame buckling, elastic buckling of rectangular flat plates, edge loading, anisotropic plate structures, etc 17 p2956 A67-32021

Elastic buckling of thin walled frames, discussing restraint effect on stability, symmetry effect on critical behavior and dead loads effect 17 p2957 A67-32022

Thin walled unsymmetrical beam under bending and torsion studied for nonlinear elastic behavior 17 p2957 A67-32023

Shear buckling of thin walled structural sections, noting reinforcement methods including use of swedges 17 p2957 A67-32026

Strain amplitude and flange width-to-thickness ratio effects on dynamic buckling in modified I-beams subjected to pure reverse bending 17 p2958 A67-32030

Thin elastic circular ring equilibrium stability in rigid cavity subjected to parallel loading, considering small ring separation region at buckling [ASME PAPER 67-APM-19] 17 p2958 A67-32406

Stability of cantilevered elastic bar with end under compressive follower force, noting shear deformation, rotary inertia and internal damping 17 p2959 A67-32420

Book on design and structural strength of aircraft gas turbine engines covering inlet and exhaust systems, compressors, combustion chambers, rotors, etc 17 p2928 A67-32564

Geometrical and equilibrium equations derived for circular plates, introducing Lagrange type coordinate as independent variable 17 p2961 A67-32807

Critical compressive forces causing instability of rigidly-fastened rectangular plate determined by method of summary representations 17 p2962 A67-32871

Structural section bending determined for fracturing tolerance 18 p3144 A67-34484

Blaxial buckling behavior of 45 degrees eccentric-stiffened waffle cylinders using prediction theory 19 p3341 A67-35525

High modulus high strength inorganic filament windings tested for tension and buckling-critical structures, considering weight decrease and operating temperature increase 19 p3245 A67-35553

Buckling of aging linearly viscoelastic beam columns with time variable mechanical properties, deriving integrodifferential equations and stability conditions 19 p3343 A67-35781

Adaptive control systems for stabilizing structural bending modes of Saturn V launch vehicle [AIAA PAPER 67-591] 19 p3336 A67-35987

Triangular elements under linearly varying strain used in matrix displacement method analysis of stability of membranes of arbitrary anisotropy 20 p3535 A67-36196

Asymmetric stability loss of nonuniformly heated circular plate rib, determining elastic properties and critical temperature jump value 20 p3536 A67-36447

Hardenable thin walled cylindrical metal sample stress-strain state under cyclic thermal load, determining plastic deformation 21 p3716 A67-37910

Soviet papers on strength and stability of elements of thin walled structures 21 p3723 A67-38778

Compression strength analysis of plane and cylindrical multilayer skin panels reinforced by corrugated fillers, determining critical load and local stability loss 21 p3725 A67-38787

Two-layer circular cylindrical shell stability under axial compression with transverse displacements, analyzing axisymmetric deformation of longitudinal strip 21 p3725 A67-38793

Discrete method extension for bending stability problem in sectorial plates, obtaining algorithm for solutions of boundary conditions and external loads 21 p3729 A67-38907

Three layer cylinders and cylindrical and plane panel optimum parameters using critical stress expressions from nonlinear elasticity theory 21 p3729 A67-38915

Elastic stability of cantilever column having fixed compressive and circulatory nonconservative loadings, determining critical loads 21 p3729 A67-39084

Plate stability loss criterion for critical external load values without determining initial stresses applied to rectangular plate Sommerfeld problem 22 p3909 A67-39401

Ring finite element analysis for shells of revolution improved by extending polynomials representing displacements 22 p3911 A67-39499

Environmental factors effect on stability of high performance polycarbonate 22 p3825 A67-39859

Heat treatment effect in various gaseous media on electrical properties of CdTe films with abnormally high photovoltage, noting structural stabilization 22 p3861 A67-39924

Optical properties of new and stable nonlinear optical ferroelectric potassium lithium niobate single crystal 22 p3863 A67-40236

Structural stability of welded joints of chromium steel used in power plant construction examined for structural stability 23 p4019 A67-41077

Stability of elastic structure in rest state based on break-point determinant, discussing bound, conjugated, affine and space and body-fixed load 23 p4078 A67-41196

Forces on spheres inside diffusers noting instability onset 23 p3932 A67-41734

Aerospace vehicle structure loading under structural integrity tests with simulated aerodynamic heating conditions, discussing computer relaxation solution for rod temperature distribution 24 p4172 A67-42036

Thermal vacancies in Ni-Al investigated by comparing separately determined dilatometric and lattice parameter of /100/ single crystal 24 p4173 A67-42165

Quenched structures and precipitation in Al-Cu alloys with and without traces of Cd studied electromicroscopically, showing possible CD stabilizing effect 24 p4173 A67-42166

Translucent material /Zyttrite/ obtained from cubic phase stabilization of Y and Zr alkoxides at low temperatures, noting high surface activity 24 p4175 A67-42373

STRUCTURAL STRAIN

SA INTERFACIAL STRAIN

Straining equipment for testing aircraft structures 04 p0708 A67-14584

Plane strain fracture toughness, strain instability, slow crack growth and different modes of cracking in metal alloys 06 p1014 A67-17806

Prediction and scaling of reflected impulse from strong blast wave, with experimental correlation 06 p0984 A67-18059

Structural change effects on plasticity and fracture characteristics on iron alloys with annealing 06 p1017 A67-18227

Carbon fibers of high strength and high breaking strain noting heat treatment, structure and mechanical properties 09 p1520 A67-21988

Dynamic analysis of sandwich plate with clamped edges executing plane strain motions, using variational motion equation and Galerkin method 10 p1717 A67-23138

Structural stress measurements in terms of induced temperature increments, using IR radiometer 11 p1877 A67-24827

Clinographic polariscope for surface measurement of stress-strain in building materials, noting operation and results 14 p2395 A67-27973

Effects of repeated loading of materials and structures - Conference, Mexico City, September 1966, Volume 3 17 p2957 A67-32027

Effects of repeated loading of materials and structures - Conference, Mexico City, September 1966, Volume 6 17 p2958 A67-32029

Strain due to even pressure in oval or circular tubes, calculating deformations 17 p2958 A67-32259

Stiffness matrix of thin flat triangular elements of nonzero Gaussian curvature derived by reducing geometrical idealization errors 19 p3342 A67-35750

Shell curvature variation parameter noting influence on equilibrium equations and error in equations of strain compatibility 21 p3718 A67-37981

X-ray structural analysis of ferromagnetic /ferrimagnetic/ bismuth ferrite single crystal 21 p3685 A67-38987

Bending of orthotropic strip to anticlastic surface by uniform moment, determining strain along neutral axis, bending moment and couple action 22 p3913 A67-40008

Mathematical classification of differential equations governing elastic-plastic waves in plane strain 22 p3914 A67-40193

Wing stress analysis, reviewing computer and variational methods for calculating structural strength 22 p3746 A67-40445

Book on linear mechanics of elastic structures covering work and energy, Saint Venant theory of torsion, stress analysis, etc 23 p4071 A67-40586

Reissner differential equation simplified for problems involving small strains in thin shells of revolution due to symmetrical deflections 23 p4073 A67-40612

Periodic pressure fluctuations relation to structure and propagation of combustion front in solid propellant rockets, giving perturbation frequencies 24 p4252 A67-41798

Book on nonlinear theory of thin shells covering deformation and stress state, surface kinetics, momentum conservation, etc 24 p4246 A67-41800

STRUCTURAL VIBRATION

Hybrid CDC 3200 digital computer acquisition of response data from acoustic and high force vibration tests 01 p0029 A67-11025

HF response of shell-type structures to buffeting aerodynamic environment [AIAA PAPER 68-81] 02 p0337 A67-11930

Elastic structural vibrations of vehicle effect on position of engine thrust vectors with respect to undisturbed nonvibrating

vehicle 02 p0335 A67-12732

Generalization of Weber theorem for problems of coupled thermoelasticity, considering vibrations varying with time 03 p0523 A67-13502

Characteristics of transverse vibrations of p-l-n jointed trusses obtained by use of rational method of lumping inertia forces 03 p0529 A67-14103

Coupled flatwise and edgewise vibrations of beam rotating about one end 04 p0707 A67-14492

High internal damping properties of magnesium alloy with zirconium addition 04 p0638 A67-15175

Vibrational problems of rotor blades in axial turbomachinery [ASME PAPER 66-WA/GT-12] 04 p0712 A67-15362

Free and forced vibrations of viscoelastic plate with consideration of rotatory inertia and shear deformation, noting rectangular plate 04 p0715 A67-15586

Ritz averaging method to determine free and forced vibratory response of beams and plates undergoing large amplitude steady state harmonic oscillations 04 p0715 A67-15659

Discrete model construction method for vibrating circular plates 05 p0810 A67-18231

Model analysis of radial oscillations of shaft with pounding of ball bearings 05 p0812 A67-17236

Vibratory energy dissipation of plates with riveted beams as induced by gas-pumping in structural joints 05 p0924 A67-17285

Intensity distribution in rotational structure of molecular spectra bands upon excitation by ion impacts 06 p1035 A67-17877

Stress distribution measurement by vibration method, applying hand-held extensometer place by place on surface of structure subjected to dynamic load of finite amplitude 06 p1100 A67-18001

Minimum structural response and acoustic radiation for panel excited by turbulent boundary layer [AIAA PAPER 67-12] 06 p0985 A67-18256

Tuned viscoelastic vibration dampers effect on responses of cantilever and clamped-clamped beams subject to Euler-Bernoulli beam equation, discussing loss factors based on transmissibility spectra 06 p1110 A67-18859

Dynamic analysis of lunar surface vehicle including power spectral density terrain definition, vehicle velocity limiting criteria and nonlinear analysis of vehicle freedom to pitch, bounce and roll 07 p1163 A67-19369

Transonic wind tunnel studies of ground-wind loads on aeroelastic models of Saturn launch vehicle, investigating structural damping, wind velocity and azimuth angle 07 p1257 A67-19371

Book on rotor stability self-excited vibration and nonlinear resonances 07 p1263 A67-19631

Level and duration of sine wave tests, discussing rocket design proof via random vibration testing 08 p1402 A67-20477

Shear deformation and rotatory inertia effects on modal data of nonuniform beam, with complex behavior defined by ordinary differential equations 08 p1416 A67-20533

Effective degrees of freedom of vibrating structure 10 p1718 A67-23153

Deflection of free three-layer strip under impact, determining displacement function and bending oscillations 10 p1721 A67-23610

Finite element approach for determining rms deflections and stresses in randomly acoustically excited complex aerospace elastic structures 10 p1724 A67-23710

Dynamic response of periodic liquid flow systems as function of structural support motions, noting resonance points and pressure amplitudes 10 p1628 A67-23737

Force-deflection relationship under arbitrary loading for structure exhibiting hysteresis behavior 10 p1727 A67-23751

Discrete mass technique for vibration analysis of thin shells [ASME PAPER 67-VIBR-23] 11 p1872 A67-24182

Flexibility and mass distribution effect on vibration response of general continuous structures [ASME PAPER 67-VIBR-44] 11 p1873 A67-24196

Equations for turbomachinery blades vibration control noting energy exchange,

stress amplitude, mechanical damping, etc [ASME PAPER 67-VIBR-49] 11 p1797 A67-24199

Determination of proper frequencies of vibration of thick-bladed turbine disk with interaction between disk, blades and shrouding [ASME PAPER 67-VIBR-52] 11 p1797 A67-24201

Laser for remote vibration measurement and detection without mechanical contact with structure under test 11 p1798 A67-24433

Soviet book on calculations of strength and vibrations of rocket engines 11 p1852 A67-24512

Stress-strain state of circular cylindrical rod coupled to half-space when applying torsion to free end 11 p1879 A67-24884

Cylindrical shell stability under external pressure, presenting critical load value and nature of undulation 11 p1880 A67-25054

Vibration environment of liquid propellant rocket engines 12 p1989 A67-25704

Stability and nonlinear vibrations of mechanical systems under harmonic excitation 14 p2397 A67-28087

Cabin noise reduction in DC-9 by tuned vibration absorbers attached to engine support structure [AIAA PAPER 67-401] 15 p2421 A67-30368

Transform using eigenfunction as kernel generates universal solution for structural member vibration, noting application to Timoshenko beam 16 p2783 A67-30616

Book on design and development of helicopters, Vol. 2 - Vibrations and dynamic stability 16 p2597 A67-31812

Effect of rotor control feedback loads of two-bladed rotor system on helicopter fuselage vibrations [AHS PAPER 133] 16 p2777 A67-31847

Vibro-acoustic test system for simulation of Saturn V dynamic launch environment on major space vehicle structures, discussing design and operation 17 p2832 A67-32005

Single frequency vibrations of beams and girders solved by applying asymptotic methods 17 p2962 A67-32881

Disk structural characteristics influence on rotors critical angular velocity 19 p3235 A67-34881

Axial compressor blades considered as thin walled elastic shells studied for vibration forms, frequencies, stress distribution and blade geometry change effects 19 p3235 A67-34882

Impedance and transmission matrices concepts applied to mechanical systems vibration, presenting formulations properties and interrelationships 19 p3261 A67-34960

Dynamic stability of beam columns undergoing weakly nonlinear vibrations studied using Ritz-Galerkin procedure 19 p3342 A67-35758

Generation threshold of substance with electronic-vibrational energy level studied for laser use 19 p3309 A67-36105

Axissymmetrical vibrations of cylindrical shell during HF internal pressure pulsations of gas flow containing uniformly distributed burning fuel droplets 20 p3536 A67-36445

Inertial effects of rotor on synchronous motion of simply supported and cantilever arrangements of rotor shaft systems 20 p3453 A67-36500

Surface vibration effect on nucleate pool boiling, measuring heat-transfer coefficient and proposing mechanism [ASME PAPER 67-HT-58] 20 p3549 A67-36740

Vibrating annular membrane problem, including load per unit area and asymmetry of load and vibration, using finite transform derivation 20 p3539 A67-37006

Radial adiabatic motion of spheres of uniform density and isotropic pressure in general relativity, giving bounce occurrence conditions 20 p3486 A67-37273

Deflection of free three-layer strip under impact, determining displacement function bending oscillations 20 p3542 A67-37540

Book on turbine blade vibration damping for increasing operational reliability 21 p3715 A67-37831

Dynamic model for magnetic field effect on vibrations of clock balance wheel having magnetized cross bar 21 p3625 A67-37988

Soviet papers on vibrations and strength of aircraft engine components 21 p3726 A67-38830

Shape of line of deflection in systems

subjected to flexural vibrations of rotating weightless shaft supporting eccentrically distributed mass points or disks 21 p3836 A67-38831

Vibrations of turbine disks of variable thickness calculated by Ritz method, applying functions approximating actual thickness of disk 21 p3836 A67-38836

Load carrying capacity of hydrostatic bearing having communicating chambers and operating with laminar flow of incompressible fluid, showing shaft vibration elimination 21 p3836 A67-38837

Mathematical model for vibrating characteristics of structures in statistical mechanics framework, noting closeness to Green function rather than to mode concept [ONERA-TP-467] 22 p3915 A67-40385

Aircraft flutter characteristics calculated from electromechanical analog using elastic mass vibration model and analog computer 22 p3746 A67-40451

Axially symmetric vibrations of homogeneous and sandwich spherical shells obtained from generalized variational motion equations including thickness-shear deformation effect 23 p4075 A67-40667

Aeroelastic phenomena in aircraft stability, control and airframe vibration characteristics, describing testing methods 23 p4077 A67-41046

STRUCTURAL WEIGHT

Resource allocation for maximum system reliability, noting weight allocation in spacecraft and Lagrange multiplier approach 01 p0084 A67-11354

Minimum weight member sizes determination for structural design, considering trussed and stiffened plate structures 03 p0525 A67-13895

Light aircraft design using fiberglass reinforced plastic primary structure for fibrous composite airframe 08 p1414 A67-20429

Elastic deformation due to structural weight sustained by 22-meter parabolic reflector of RT-22 radio telescope of U.S.S.R. Physics Institute 08 p1424 A67-21354

Elastic strains created in parabolic reflector /radio telescope antenna/ mounted on four supports by weight of structure in vertical position 08 p1424 A67-21355

Axially loaded cylindrical structures analyzed for optimum weight construction consistent with cost constraint, emphasizing beryllium-aluminum alloys 08 p1424 A67-21521

Weight savings derived from use of contrasting ring, stringer and wall materials in ST-stiffened axial compressed cylinders [AIAA PAPER 66-508] 08 p1424 A67-21522

Advanced structures and materials in future launch vehicles evaluated by design synthesis technique for component weight reduction, equivalent payload gained and cost ratio 10 p1723 A67-23699

Growth and operational capabilities of turboprop and reciprocating engines [SAE PAPER 670236] 12 p1989 A67-25494

Structures cost effectiveness in optimization weight-cost design in aerospace structures [AIAA PAPER 66-505] 13 p2220 A67-27590

Optimal structural design with failure probability constraints 14 p2399 A67-28122

Rocket cost dependence on weight and airframe resistance studied for design problem solutions 14 p2245 A67-28638

Designing methods for meteoroid impact emphasizing minimum weight shield arrangement [ASME PAPER 67-DE-45] 14 p2402 A67-28878

Structural technologies applicable to future large launch vehicles 15 p2569 A67-29855

Elastic deformation due to structural weight sustained by 22-meter parabolic reflector of RT-22 radio telescope of U.S.S.R. Physics Institute 17 p2956 A67-31950

Elastic strains created in parabolic reflector /radio telescope antenna/ mounted on four supports by weight of structure in vertical position 17 p2956 A67-31951

STRUCTURE

SA AIRCRAFT STRUCTURE

SA AIRFRAME

SA COMPOSITE STRUCTURE

SA CRYSTAL STRUCTURE

SA ELECTRONIC STRUCTURE

SA EXPANDABLE STRUCTURE

SA FINE STRUCTURE

SA FOLDING STRUCTURE

SA FRAME

SA HYPERFINE STRUCTURE

SA INFLATABLE STRUCTURE

SA INSULATED STRUCTURE

SA MEMBRANE STRUCTURE

SA MICROSTRUCTURE

SA MOLECULAR STRUCTURE

SA MULTILAYER STRUCTURE

SA NUCLEAR STRUCTURE

SA REDUNDANT STRUCTURE

SA RIGID STRUCTURE

SA RING STRUCTURE

SA SPACE ERECTABLE STRUCTURE

SA SPACECRAFT STRUCTURE

SA STEEL STRUCTURE

SA STELLAR STRUCTURE

SA STIFF STRUCTURE

SA SUBSTRUCTURE

SA VARIABLE GEOMETRY STRUCTURE

SA WELDED STRUCTURE

Structures, structural dynamics and materials - AIAA/ASME Conference, Palm Springs, March 1967 10 p1721 A67-23696

Structure dependent electric properties of anodized and unanodized tantalum-tantalum oxide thin film resistors, discussing aging, heat treatment, etc 13 p2082 A67-27366

STRUT

Direct matrix method for analysis of critical loads and associated buckling modes for struts having various end constraints 14 p2403 A67-29017

Theory and design methods of torsional-flexural buckling of thin walled elastic struts of open cross section, deriving basic differential equations 17 p2957 A67-32024

STRYCHNINE

Effects of radiation protective pharmacological agents /cystamine, serotonin AET, strychnine, etc/ on animals subjected to centrifugation, for application to astronauts 12 p1902 A67-25654

STURM-LIOUVILLE PROBLEM

Nonlinear Sturm-Liouville BVP with random forcing function 02 p0258 A67-11587

One-dimensional inverse problem of scattering theory, noting differential equation reduction, determining traveling wave coefficient 05 p0765 A67-17158

High altitude plasma-concentration diagnostics from magnetospheric oscillation spectra 17 p2846 A67-32940

Hybrid computer for co-current laminar-flow heat exchanger Sturm-Liouville problem 19 p3190 A67-36069

Recurrence formulas extending term computations in asymptotic expansions for eigenvalues of Sturm-Liouville systems and eigenfunction expansions using Horn method 24 p4178 A67-42692

STYRENE

S POLYSTYRENE

SUBCOOLING

Density wave type flow oscillations in boiling Freon 11 examined, noting effects of partial evaporation superheat and liquid inlet temperature on stability [ASME PAPER 66-WA/HT-49] 04 p0725 A67-15433

System induced instabilities of forced convection flows with subcooled boiling restricted to case of water flow in small circular channels, high L/D ratios, moderate temperature and pressure 04 p0736 A67-15858

Surface film boiling under free convection 13 p2222 A67-26532

SUBFLUID

S ANISOTROPIC FLUID

SUBGRAVITY

Upper torso exercises effect compared with torque maneuvers effect on oxygen metabolism under reduced gravity conditions 01 p0017 A67-10959

Subgravity traction simulation experiments to determine effects on metabolic rates during walking on treadmill 05 p0755 A67-16280

Liquid sloshing at simulated low gravity in rigid cylindrical tank, noting analytical model and experimental results [ASME PAPER 67-APM-14] 17 p2840 A67-33147

SUBHARMONIC OSCILLATOR

Signal suppression in ferrite frequency selective limiters evaluated using parametric subharmonic generator model 02 p0217 A67-12093

Parametric excitation of spectrotron with controllable p-n junction capacitance and intrinsic voltage feedback 03 p0378 A67-13241

Stability analysis of parametric phase-

locked subharmonic tunnel diode oscillator circuits capable of bistable phase operation 07 p1153 A67-19610

Forced nonlinear vibration of Duffing type experimentally simulated with models of isolating systems, obtaining response curves [ASME PAPER 67-VIBR-35] 11 p1873 A67-24192

Frequency selective parametric limiting by parallel pumping of subharmonic magnetoelastic waves in YIG 13 p2077 A67-26523

Current time variation for subharmonic parametric oscillator phase zero-transient switching 20 p3395 A67-36314

Steady random natural frequency variation and subharmonic resonance, discussing periodic right hand side Duffing type equation describing system 22 p3836 A67-39405

Subharmonic and summed and differential harmonic oscillations in multiple-degree-of-freedom system with asymmetric nonlinear spring characteristics, studying stability 22 p3910 A67-39408

SUBLIMATION

SA ABLATION

Low thrust reaction control system utilizing solid propellant which sublimates into low molecular weight vapor, noting heat sources 01 p0142 A67-11407

Sublimation and gaseous equilibria involving neodymium fluorides and barium fluorides 03 p0367 A67-13519

Ultrahigh vacuum produced by combination of turbomolecular and titanium sublimation pumping 06 p0950 A67-17752

Titanium for sublimation, using combination sublimation-getter ion pump 09 p1503 A67-22101

Comet head brightness diminution during perihelion passage due to sublimation calculated, using Clapeyron-Clausius equation and insulation effect 10 p1703 A67-22719

Solid film sublimation cooling effect in Couette gas flow simulating real rarefied gas flow heat transfer, for jet engine application 14 p2408 A67-28800

Temperature, valve and insulation criteria for designing low thrust subliming solid reaction systems 15 p2544 A67-29979

Neighbor model for computer simulation of field ion images in fcc point lattice 17 p2887 A67-32205

Thermionic properties, surface ionization, atomic and ionic sublimation of Re, Mo, Ta and W 19 p3264 A67-35082

Sublimation enthalpy of CdTe thin films in high vacuum determined from 350 to 400 degrees C 20 p3514 A67-37453

SUBLIMATION HEAT

Mass spectrometry of titanium subfluorides at high temperatures, determining sublimation pressures and heat and dissociation energy 20 p3377 A67-37135

Pulsed propulsive performance of low thrust subliming solid ammonium carbamate reaction jet, discussing transient response, apparatus, techniques, etc 21 p3697 A67-39152

SUBMARINE

Optimal control systems without complex controllers using variational calculus, for application to submarine diving control 08 p1309 A67-20331

Hardware and life-support systems on submarines and space vehicles, discussing oxygen supply, temperature-humidity control, etc [AIAA PAPER 67-364] 14 p2259 A67-28732

SUBMARINE CABLE

User reaction test results for comparison of telephone quality via Early Bird and via cable circuits based on callback interviews, service observations and circuit rejection counts 06 p0959 A67-17666

Subjective evaluation of telephone communications via Early Bird satellite and cable circuits 06 p0959 A67-17667

Seastations in conjunction with submarine cables for aviation communication, navigation and air traffic control 09 p1530 A67-22652

Communication satellite techniques future development 13 p2070 A67-27151

SUBMERGED BODY

Instability of ventilated cavities extending behind symmetric bodies, noting resonance frequency and pressure distribution fluctuation 04 p0600 A67-14457

Aerodynamic problems of low density high speed flow of rarefied gases past submerged

body 10 p1623 A67-22874
 Loads on bodies in wakes resulting from crossflow at submerged body or from wake translation over submerged body, noting dynamic instability 11 p1742 A67-24350
 Field spectrum developed from monochromatic temperature oscillations in bodies due to time variation of heat transfer coefficients caused by unsteady flow velocity 17 p2972 A67-33073
 Elliptic planform vertical submerged hydrofoils, determining circulation distribution over foil span at arbitrary Froude numbers 18 p3022 A67-33414
 Hydrodynamic equations for automatic control of speed and coordinates of craft with underwater foils moving on disturbed body of water 18 p3074 A67-33416
 Scuba diving relation to development of aviator decompression sickness, investigating decompression time before flying 21 p3574 A67-38078
 Inactivity and water immersion effects on fluid balance and tilt-table performance in dehydrated subjects, assessing vasopressin and positive pressure breathing effects 23 p3951 A67-41557
 Water immersion simulation, studying astronaut performance characteristics in Gemini and proposed Apollo missions [AIAA PAPER 67-773] 24 p4116 A67-42941
 Scaling laws and hydrodynamic model design techniques for high fidelity underwater simulation of zero and partial-g environments for manned space activities [AIAA PAPER 67-925] 24 p4140 A67-43021

SUBMERSION

S IMMERSION

SUBMILLIMETER WAVE

InSb submillimeter detector as mixer in superheterodyne receiver shows performance two orders less than ideal receiver 01 p0036 A67-10440
 Electromagnetic radiation absorption coefficient of atmospheric water vapor in long-wave portion of submillimeter range 02 p0190 A67-11568
 Submillimeter wave scattering by fog, comparing experiments in clear atmosphere and dense fog 02 p0199 A67-12078
 Power gain of submillimeter wave in traveling wave amplifier with periodic delay-line structure 03 p0380 A67-13557
 Submillimeter wavelength electronic devices, examining development of lasers and reflected wave tubes with overlapping effective wave range 05 p0825 A67-17168
 Cyclotron resonance in tellurium at submillimeter wavelengths, deducing relation time anisotropy 06 p1061 A67-18920
 Absorption coefficient of water vapor in relative windows of transparency for millimeter and submillimeter radio waves 08 p1294 A67-20817
 Central tuning dip in power output of continuous wave submillimeter molecular laser to measure radiative lifetime and collision line broadening 11 p1803 A67-24932
 Heterodyne detector of submillimeter radiation using CN maser as continuous wave source of coherent radiation 12 p1951 A67-25209
 Interferometry of resonator modes in submillimeter wave laser 13 p2129 A67-27347
 Sensitivity of radiometer operating in submillimeter range with multimode detector compared to crystal receiver equivalent noise temperature 16 p2877 A67-31501
 Absolute frequency measurements on continuous wave hydrogen cyanide submillimeter laser lines 24 p4166 A67-41861
 Submillimeter wave laser resonator mode calculation using laser-resonator interferometry 24 p4169 A67-43105

SUBROUTINE
S COMPUTER METHOD
SUBSONIC AIRCRAFT
 Isolated nacelle design for high by-pass ratio turbofan engines, particularly pylon mounted engine [SAE PAPER 660732] 01 p0140 A67-10632
 Nacelle design for high inlet pressure recovery and low external cowl drag, for high by-pass fan engine subsonic aircraft [SAE PAPER 660733] 01 p0140 A67-10633
 Boeing model 747 aircraft /large capacity subsonic transport/ engine aerodynamics and design objectives 02 p0181 A67-12248
 Long-haul intercontinental air

transportation, discussing passenger and cargo traffic increases and airport and airway crowding [AIAA PAPER 66-1017] 06 p0946 A67-17980
 Aircraft control system of subsonic airplanes operated over wide speed ranges, noting flight test results 11 p1744 A67-24578
 Aerodynamic factors effect on airframe design and power plant selection for medium Mach twin turboprop business aircraft [SAE PAPER 670244] 12 p1894 A67-25499
 ADAM II /air deflection and modulation/ propulsion system and application to long tube vertical propulsive wing aircraft configurations [SAE PAPER 670353] 17 p2929 A67-32993
 Boeing model 747 aircraft /large capacity subsonic transport/ engine aerodynamics and design objectives 21 p3568 A67-38542
 Sonic boom and subsonic aircraft noise test results 21 p3569 A67-39118

SUBSONIC FLOW

Steady state two-coordinate problem of MGD solved for subsonic attached flow past simply connected profile 01 p0119 A67-10171
 Optimal subsonic flow diffusers based on Walz laminar and turbulent boundary layer theory 01 p0006 A67-10648
 Flow field about subsonic jet exhausting into quiescent and low velocity air stream [AIAA PAPER 65-704] 01 p0055 A67-11254
 Graphs for momentum flux and mass flow calculations for use in subsonic compressible flow 01 p0007 A67-11268
 Tabulated data on specific losses in flow systems 02 p0233 A67-11995
 Turbulent boundary layer in subsonic or supersonic flow past pinched-waist bodies of revolution at various Mach numbers and pressure gradients 03 p0350 A67-12989
 Prediction of subsonic base drag of hypersonic reentry vehicles [AIAA PAPER 66-991] 03 p0353 A67-14144
 Simultaneous free and parametric oscillations of elastic cylindrical shell of infinite length and subsonic flow of ideal gas in shell 04 p0717 A67-15888
 Potential flow theory design of subsonic flow diffusers for centrifugal compressors, assuming compressible irrotational inviscid channel flow [ASME PAPER 66-WA/GT-9] 04 p0550 A67-15938
 Existence theorem for two-dimensional subsonic flow of compressible fluid, following Bers method 05 p0790 A67-16044
 Experiments on effect of subsonic inlet Mach number on performance of conical diffusers 05 p0748 A67-16811
 Subsonic compressible flow around profile obtained by conformal transformation, reducing to Dirichlet problem 05 p0749 A67-16845
 Oscillations of staggered plate cascade in plane subsonic gas flow, showing fluid compressibility effect on aerodynamic characteristics 06 p0935 A67-17729
 Correlation of local heat transfer and friction coefficients for subsonic turbulent flow of air through high temperature annulus 06 p1117 A67-18386
 Approximate analysis of subsonic compressible flow in annular nozzle of short duct fan engines and inner wall curvature effect on pressure 06 p0944 A67-18871
 Nonuniform two-dimensional subsonic and supersonic flow of compressible fluid past body, using small parameter method 07 p1125 A67-19322
 Subsonic jet flow past solids, examining two classes of exact solutions in ideal fluid for plane nonvortical steady state flow 08 p1321 A67-20836
 Functional extremals approximation method applied to compressible subsonic fluid flows 13 p2050 A67-27148
 Power jet and single control bubble region portion of fluid jet modulator modeled for studying static and dynamic properties 14 p2248 A67-28271
 Simple impact position model for predicting subsonic mass flow for opposing axisymmetric jet 14 p2303 A67-28331
 Elliptic nose shape bluntness effect on drag of bodies of revolution in axisymmetric subsonic flow 16 p2589 A67-30791
 Aeroelastic stability of two-dimensional flat panels in subsonic and transonic flow, noting flutter and

divergence 16 p2776 A67-31545
 Hall parameter instability and conductivity analysis applied to performance characteristics of subsonic flow generator 17 p2898 A67-32181
 Local turbulent properties of shear layer derived from covariance of two crossed perpendicular beams of radiation 17 p2855 A67-32282
 Statistical properties of wall pressure fluctuations in subsonic turbulent equilibrium boundary layer after transition from laminar flow 17 p2836 A67-32283
 Hall field intensity and asymptotic electron temperature of ionized argon-cesium mixture flow in transverse magnetic field with subsonic velocity 17 p2900 A67-32338
 Calculation of compressible subsonic potential flow through blade cascades, giving air outlet angle, velocity distribution around blade profile and critical Mach number 17 p2791 A67-32711
 Thin slightly curved profiles positioned at small angle of attack in subsonic gas flow and developing harmonic random vibrations studied for aerodynamic interference 17 p2792 A67-32903
 Pressure distribution in subsonic flow for vertical stabilizer calculated, using orthogonal function 18 p2982 A67-33655
 Approximate solution for subsonic gas flow, deriving approximation for Chaplygin function for use in boundary value problems 20 p3356 A67-36442
 Aerodynamic characteristics of plane compressor cascades with high subsonic flow analyzed, noting application in determining flow deflection angle and pressure loss coefficient 20 p3358 A67-37079
 Geometric parameters effect on aerodynamic characteristics of plane compressor cascade with high subsonic flow 20 p3358 A67-37080
 Book on thin wing and aerodynamic characteristics in subsonic gas flow 20 p3359 A67-37206
 Thrust and drag response to heat input directly behind and before body moving supersonically or subsonically 21 p3563 A67-37887
 Soviet book on aerodynamic flow calculations of axial flow turbines with subsonic and transonic blade cascade design method 21 p3565 A67-38766
 Gas-air mixing in coaxial flow engine based on one-dimensional ejector theory at subsonic flow velocities, discussing chamber design gas-air mixing in coaxial flow engine based on one-dimensional ejector theory at subsonic flow 23 p4048 A67-40638
 Oscillating infinitely thin wing profile in inviscid subsonic compressible flow, deriving perturbation pressure 23 p3929 A67-41250
 Momentum equation integration to determine two mixing parallel subsonic streams interface 23 p3991 A67-41667
 Numerical method together with stable difference scheme used to calculate sub-, trans- and supersonic flows in Laval nozzle inverse problem 24 p4091 A67-42160
 Lifting line theory for blade cascade in subsonic shear flow, noting compressibility effect dependence on harmonic mean upstream Mach number 24 p4091 A67-42204
 Three-dimensional flow across supersonic single rotor axial compressor subsonic at rotor entry and exit 24 p4092 A67-42661

SUBSONIC FLUTTER
 Static structural strengths, aeroelasticity and flutter problems for glider performance 16 p2776 A67-31466

SUBSONIC SPEED
 Turbulent subsonic gas jets, importance of Reynolds number and geometrical configuration of nozzle in determination of flow parameter 05 p0790 A67-16033
 Aerodynamic characteristics of wings of complex planform at subsonic velocities, calculating flows past wings at moderate angles of attack 06 p0935 A67-17730
 Sonic booms attributed to subsonic flight 12 p1895 A67-25936
 Retractable airfoil and hinged cowl modifications of supersonic inlet to reduce drag below choking point for subsonic operations 17 p2791 A67-32575
 Supersonic aircraft nozzle system aerodynamic performance at subsonic speeds [AIAA PAPER 67-452] 18 p2983 A67-33926

- Compressibility effects on airfoils during high subsonic and low speed stalls, considering Reynolds and Mach number effect 19 p3170 A67-35521
- Air temperature measurements at subsonic and supersonic flight speeds, discussing error sources and thermometer efficiency 22 p3797 A67-39542
- SUBSONIC WIND TUNNEL**
- Subsonic wind tunnel analysis of wake deformations produced by secondary velocities using models with flat base but various cross sections 02 p0233 A67-12228
- Interference of open and closed wind tunnels with ground board calculated and results applied to airfoils 16 p2590 A67-30854
- SUBSTRATE**
- Linearity of MOS transistor as variable resistor improved by keeping substrate floating and connecting substrate to drain 01 p0036 A67-10439
- Substrate doping, source bias and bulk contact effect upon DC characteristics of silicon MOS transistors 12 p1916 A67-26068
- Gold, silver, copper and tin condensed films, investigating dependence of structure and conductivity on substrate material 15 p2540 A67-30122
- Encapsulation material and process implementation for thick film substrates noting fabrication and quality problems 21 p3596 A67-38343
- Gallium arsenide substrate treatment methods effects on autoepitaxial layer perfection 21 p3685 A67-38972
- Epitaxial growth of gold on cadmium iodide surface studied with transmission electron microscopy, discussing diffraction patterns and substrates preparation 21 p3687 A67-39140
- Factors affecting tensile ductility minimum behavior of silicide coated niobium alloys investigated in air for intermediate temperature range 22 p3821 A67-40052
- Polished glass substrates for thin film microcircuits, analyzing surface resistivity and optical transmittance changes due to heat treatment 23 p4043 A67-41366
- Protective effect of substrates against ionizing radiation on enolase and lactic dehydrogenase [SAM-TR-66-264] 24 p4111 A67-41841
- Single crystal silicon films on insulating substrates, discussing preparation methods and chemical and structural perfection for use in field effect and bipolar devices 24 p4202 A67-42089
- Large lightweight rigid multi-kilowatt solar arrays, discussing substrate construction, design and testing 24 p4109 A67-42560
- SUBSTRUCTURE**
- Metallographic, X-ray and electron microscope studies of dislocation substructure and fatigue life extension in bending-fatigued Al and Ag crystals 06 p1013 A67-17798
- Substructural strengthening of carbide precipitation hardened molybdenum alloy by swaging and wire drawing 11 p1805 A67-24108
- SUBSURFACE**
- Combustion rate and subsurface activity of metallized burning polymers, stressing heat conduction role and applications to propellant combustion [CI PAPER 67-3] 19 p3344 A67-34998
- SUBSYSTEM**
- Sampling plans for identification of inadequate subsystems 01 p0084 A67-11370
- System reliability evaluation and identification of inadequate subsystems, with application to two missile-borne guidance systems 01 p0111 A67-11371
- Apollo lunar surface experiments package /ALSEP/ of scientific instruments and supporting subsystems [AIAA PAPER 66-919] 03 p0397 A67-14133
- Range instrumentation ships as major range subsystems, noting equipment used, accuracy and sources of errors 10 p1622 A67-22999
- Discretionary wiring method and polycell approach to large scale integration 15 p2444 A67-29456
- Reliability for redundant repairable systems using queuing theory, studying triplicate and similar/dissimilar subsystem systems 15 p2453 A67-30063
- Lapunov function for modeling and bounding solutions of distributed processes defined by interacting subsystems describable by stable differential equation 16 p2646 A67-31638
- Optimal control of measurement subsystems within feedback control systems 16 p2650 A67-31676
- SUCTION**
- Boundary layer flow having periodically distributed suction over permeable surface 01 p0052 A67-10794
- Sixth order polynomial calculation of axisymmetric laminar boundary layer of incompressible fluid removed by suction and arbitrary velocity distribution 05 p0749 A67-17184
- Boundary layer suction in two-component fluid flow around plate solved by method of partial averaging 06 p0985 A67-18204
- Suction requirements for elimination of turbulent boundary layer separation in adverse pressure gradient, based on mixing rate hypothesis and von Karman momentum integral [AIAA PAPER 67-197] 06 p0988 A67-18442
- Suction-preserved steady state vortex sheet on surface of infinite porous circular cylinder in viscous MHD liquid suddenly rotated about axis 06 p1046 A67-18891
- Navier-Stokes equation for viscous incompressible fluid flow between stationary and uniformly moving parallel plates with uniform suction along stationary plate 08 p1322 A67-21179
- Flight experiments to assess stalling behavior and handling problems arising in design, maintenance and operation of suction wing for high lift [AIAA PAPER 65-750] 09 p1441 A67-22483
- Lateral efflux from flow along wall into suction slot computed by conformal mapping contraction coefficient 10 p1627 A67-23559
- Difference method of solving boundary layer equation for laminar suction boundary layer using Crocco form 17 p2790 A67-32260
- Wall suction rate effect on turbulent flow in cylindrical circular porous duct, measuring distributions of velocity, pressure, friction coefficient and Reynolds stresses 17 p2837 A67-32380
- Laminar boundary layer for two-dimensional flow on bodies of revolution, noting suction velocity 19 p3210 A67-35721
- Air suction effect on moment characteristics of cranked slender profile, determining boundary layer control 21 p3564 A67-38043
- Compressible laminar boundary layer in pressure gradient, analyzing suction on basis of momentum and thermal integral equations 22 p3788 A67-40421
- Compressible laminar boundary layer on infinite swept cylinder analyzed for effects of suction on spanwise profile 23 p3993 A67-41746
- Effect of initial flow turbulence on optimum suction of fluid from boundary layer of porous plate 24 p4143 A67-42282
- SUD-AVIATION SA 330 HELICOPTER**
- SA 330 turbine-powered assault helicopter, noting flight tests, speed, altitude, transport capabilities, etc 04 p0550 A67-14468
- SUD VJ-101 AIRCRAFT**
- Control power usage for typical flight maneuvering in hover determined from flight test data of VJ-101 aircraft and of hover-rig with similar thrust-geometry and mass distribution [AIAA PAPER 66-816] 01 p0010 A67-10538
- German VJ101C VTOL fighter aircraft design and testing, with description of engines and telemetric testing 19 p3173 A67-35522
- Control power usage for typical flight maneuvering in hover determined from flight test data of VJ-101 aircraft and of hover-rig with similar thrust-geometry and mass distribution 21 p3568 A67-38541
- SUDDEN ENHANCEMENT OF ATMOSPHERIC /SEA/**
- Intensity observation of ELF electromagnetic field integral and SEA phenomena caused by solar flare-induced SID 01 p0060 A67-11240
- Magnetic storm enhancement of 5577 angstrom airglow emission intensity [AFCL-66-866] 03 p0505 A67-12836
- Geomagnetic pulsations accompanying storm sudden commencements and sudden impulses 05 p0795 A67-18026
- Crossing rates of atmospheric radio noise in high range of threshold field strength measured and compared with integrated field strength 14 p2306 A67-27881
- Magnetospheric ion density measurement possibility from association of pulsating radio auroral echoes with sudden geomagnetic field fluctuations 14 p2313 A67-28574
- Blast wave driven by solar flare ejecting plasma cloud proposed as origin of energy density increase causing sudden commencement of magnetic storm 15 p2476 A67-29625
- Solar flares, analyzing X-ray emission, radio emission and superposition of ionospheric effect 16 p2739 A67-31459
- Hydromagnetic mechanism explaining pulsating radio auroral echoes accompanying sudden commencements, considering Wentzel resonant interaction 17 p2845 A67-32766
- Morphological behavior of damped type geomagnetic pulsations associated with storm sudden commencements and sudden impulses 17 p2851 A67-33211
- SUDDEN IONOSPHERIC DISTURBANCE /SID/**
- Intensity observation of ELF electromagnetic field integral and SEA phenomena caused by solar flare-induced SID 01 p0060 A67-11240
- Sudden cosmic noise absorption and X-ray flares noting peak, nature of decay and theoretical and experimental values [RASSA PAPER 1-10-139] 03 p0373 A67-14247
- Spread in values of vertical magnetic field component during sudden commencements of magnetic storms attributed to local geoelectric conditions 07 p1174 A67-19712
- Geomagnetic disturbance and correlation with PCA in auroral zone on February 10, 1958 08 p1329 A67-21539
- Forecasting geomagnetic storms and disturbances from solar observations 12 p1931 A67-25110
- Detection of solar flare effect during severe geomagnetic disturbances from ionospheric flare effects 12 p1993 A67-25363
- Relation between solar flare, X-rays and sudden ionospheric disturbances (SID) using satellite measurements 12 p1905 A67-25801
- Magnetic and plasma observations of Explorer X and Mariner II confirmed that interplanetary shock waves give rise to sudden storm commencements magnetic and plasma observations of Explorer X 12 p2008 A67-25823
- Sudden cosmic noise absorption correlated with solar microwave flux to establish daily mean value 13 p2190 A67-26311
- Crossing rates of atmospheric radio noise in high range of threshold field strength measured and compared with integrated field strength 14 p2306 A67-27881
- Traveling ionospheric disturbance heat conduction waves excited in neutral gas of thermosphere by hydromagnetic waves from magnetopause 15 p2475 A67-29617
- Morphological behavior of damped type geomagnetic pulsations associated with storm sudden commencements and sudden impulses 17 p2851 A67-33211
- Polar auroral substorms, discussing mechanisms for dumping trapped particles 19 p3215 A67-35173
- Sudden commencement of November 13, 1960 caused by cosmic ray flare of November 12 20 p3517 A67-36284
- Sudden commencement and initial phase of magnetic storm explained in terms of currents induced in ionosphere 20 p3434 A67-37422
- VLF transmissions during SIDs for compatibility with general form of theory of waveguide mode propagation 24 p4149 A67-42067
- SUGAR**
- SUG GLUCOSE**
- SUIT**
- SA PRESSURIZED SUIT**
- SA SPACE SUIT**
- Antileakage assemblies evaluation in low temperature water, recording body heat loss and tolerance time for application to helicopter crews 17 p2807 A67-31959
- SULFATE**
- Spontaneous electro-optical effect in triglycin sulfate crystals spectrally studied, noting changes in double refraction along three crystallographic axes during ferroelectric phase transition 01 p0129 A67-10138
- Stark and Zeeman splitting in far IR spectra of erbium, dysprosium and samarium

ethyl sulphate 04 p0686 A67-15778

SULFATION

Ni-Cr superalloy oxidation and sulfidation, relating sulfidation resistance of uncoated Ni superalloys to matrix Cr content [ASM PAPER C6-18.5] 23 p4020 A67-41406

SULFIDE

SA BISMUTH SULFIDE

SA CADMIUM SULFIDE

SA CARBON DISULFIDE

SA COPPER SULFIDE

SA HYDROGEN SULFIDE

SA INDIUM SULFIDE

SA LEAD SULFIDE

SA MOLYBDENUM SULFIDE

SA ZINC SULFIDE

Temperature dependence of electroconductivity of As-Su-Ge system in vitreous state 06 p1052 A67-18610

Electric conductivity of AsSeGe-AsSbGe glasses 06 p1052 A67-18611

Electronic structure and electrophysical properties of d-transition metal sulphides 12 p1986 A67-26096

Additive elements studied for influence on morphology, nature and hot plasticity of sulfides in austenitic stainless steels 21 p3646 A67-39077

SULFUR

Technique for making thin sulfur targets mounted on solid backings for purpose of proton capture 02 p0247 A67-12698

Sulfur donor level associated with conduction bands of gallium antimonide in measurements of Hall coefficient vs temperature and resistivity vs pressure 04 p0673 A67-14476

Enthalpy of reaction of sulfur and nitrogen trifluoride 06 p0955 A67-17986

Impurity centers arising from sulfur in silicon identified, using IR absorption technique and uniaxial stress effect 06 p1061 A67-18924

SI and S ion oscillator strengths for resonance lines in solar spectrum, discussing spin-spin and spin-other orbit interactions 23 p4067 A67-41235

SULFUR COMPOUND

SA ACETAZOLAMIDE

Transition probabilities for S I multiplets measured from arc spectra running through sulphur chloride liquid vortex 06 p1038 A67-17656

Optical method observations of phase transition of ferroelectric monocystal SbSI 06 p1047 A67-17758

Electric conductivity of vitreous As-Se semiconductor 06 p1053 A67-18614

Electric conductivity of vitreous As-S-Te 06 p1053 A67-18615

Sulfur compound in carbonaceous chondrites explained by oxidation of troilite by oxygen and HOOH 07 p1249 A67-19539

Stereoisomers of sulfur containing amino acids effect on local skin protection in X-irradiated mice 18 p2992 A67-34716

Sulfur hexafluoride gas handling system for potential drop particle accelerator, considering design, fabrication and performance 20 p3413 A67-36181

Hydrogen peroxide and disulphane molecules force constant and vibrational spectra investigation indicates little change in elastic properties 22 p3757 A67-39583

SULFUR TETRAFLUORIDE

IR vibrational and Raman spectra of thiophosphoryl trichloride, thiophosphoryl dichlorodifluoride, thiophosphoryl chlorodifluoride and thiophosphoryl trifluoride 23 p4041 A67-41242

SULFURIC ACID

Mass spectrometric analysis of electrolyte degradation during electrolysis in sulfuric acid silica gel cell for oxygen recovery 23 p3970 A67-41705

SUM

Mean powers of r, sum rule and improved transition integrals computed for effective quantum number range up to 8.5, using Coulomb approximation wave functions 01 p0112 A67-10142

Calculation of statistical sum of bounded states of electron in atom in Debye plasma 03 p0478 A67-13615

Main properties of quasi-Cesaro method of summability 03 p0461 A67-13940

Ruby and neodymium glass lasers sum frequency generation using nonlinear electro-optical KDP crystal 06 p1009 A67-17754

Digital computer simulations of

pseudorandom noise generators, determining empirical sum distribution approximation of binomial variable 18 p3006 A67-34066

Calculation of statistical sum of bounded states of electron in atom in Debye plasma 18 p3091 A67-34480

Friedel sum rule applied to semiconductors, discussing Born approximation role 18 p3104 A67-34591

SUN

SA HELIOGRAPHY

SA INTERNATIONAL QUIET SUN

YEAR /QSY/

Deformation of Fraunhofer line linked to sound waves in solar disk 05 p0900 A67-17076

Photometric measurements of ash-moon, using large coronagraph 06 p1082 A67-18014

Absolute intensity of radiation from center of solar disk at wavelengths between 3288 and 12,480 angstroms 06 p1089 A67-18710

Solar oblateness effect on quadrupole moment and on perihelion of Mercury 10 p1709 A67-23487

Large scale structure of chromosphere examined using birefringent filter, comparing filtergrams with spectroheliograms of perturbed and active regions of solar disk 15 p2552 A67-29143

Astronomical unit determination by dynamical method 15 p2555 A67-29577

Computing transits of outer planets /Jupiter to Pluto/ over solar disk, as seen from another outer planet 17 p2948 A67-33095

Large scale structure of chromosphere examined using birefringent filter, comparing filtergrams with spectroheliograms of perturbed and active regions of solar disk 24 p4239 A67-43066

SUN TRACKER DEVICE

Balloon payload orientation system for viewing fixed position on celestial sphere 05 p0805 A67-16465

Balloon-borne telescope guidance by offset sun tracking 07 p1184 A67-19392

SUNRISE

Electron density profiles of Nike-Apache rocket observations of nitric oxide ionization by Lyman alpha radiation in E region at sunrise 03 p0415 A67-14114

Sunrise effect on atmospheric radio noise intensity, directional variations and formation of D region 04 p0618 A67-15575

VLF atmospheric noise level fluctuations, discussing daily variations as function of solar zenithal angles, sunrise and sunset and confusion of ionospheric propagation 07 p1171 A67-19422

Rocket measurement of quiet D-region electron number density profiles near sunrise 08 p1379 A67-21488

NO role in sunrise E region compared to Barth NO distribution, determining density profiles, relative ion ratios, etc 19 p3216 A67-35191

SUNSET

VLF atmospheric noise level fluctuations, discussing daily variations as function of solar zenithal angles, sunrise and sunset and confusion of ionospheric propagation 07 p1171 A67-19422

Time course of blue-to-red light intensity ratio of visible solar spectrum during and after sunset 11 p1786 A67-24116

Electron temperature and density profiles in lower ionosphere at sunset, describing temperature measurement technique 19 p3229 A67-35246

Balloon-borne diffusing system designed to measure absorption of minor atmospheric constituents, as sun set and passed below horizon 19 p3232 A67-35697

SUNSPOT

SA SOLAR FLARE

Longitudinal proper motion of sunspot groups shown to be function of size and relative extension in longitude [AFRL-66-801] 01 p0149 A67-10804

MHD wave generation in sunspots, examining depth of solar magnetic layer that affects magnetic convection 01 p0151 A67-11283

Sunspot magnetic field structure in model constructed from solution of boundary problem for semispace 02 p0329 A67-12489

Continuum brightness fluctuations and equivalent line widths in sunspot penumbral spectrum 02 p0330 A67-12715

Sunspot magnetic field and effect on solar cycles, noting wave propagation in inviscid conducting fluid 03 p0511 A67-13740

Computation of electric conductivity in sunspots and photosphere from empirically determined linear logarithmic relation 03 p0511 A67-13814

Identification of molecular bands of spectrum of large sunspot, detecting presence of magnesium oxide 03 p0512 A67-13887

Naked-eye observations of sunspots 03 p0514 A67-14184

Identification of diatomic H bands in large sunspot spectrum 04 p0698 A67-14918

East-west asymmetry of sunspots attributed to simultaneous action of rotation of sun, increase in sunspot area and sphericity of sun 04 p0699 A67-14980

Photospheric bridges over sunspots studied by meniscus photoheliograph at Tashkent Astronomical Observatory 04 p0701 A67-15552

Solar flare of August 28, 1968 associated with sunspot group which crossed sun face at 7 degrees N 05 p0882 A67-16577

Spoerer and Gleissberg laws for Babcock and Tuominen models of solar activity concerning migration in heliographic latitude of sunspot area and role of solar magnetic field 05 p0897 A67-16809

Solar atmosphere structure over sunspots studied from radio emission data 06 p1083 A67-18153

Oblong shape and Alfvén waves of looped expanding coronal prominence 06 p1078 A67-18157

Construction of model for chromospheric magnetic field over sunspot 09 p1563 A67-21628

Sunspot magnetic field structure in model constructed from solution of boundary problem for semispace 10 p1708 A67-23357

H-alpha and white light cinematograms of September 1963 flare/sunspot group and radio, ionospheric and magnetic field data 10 p1703 A67-23799

Inadequacy of formula for correction of foreshortening of Ca plages, attempting to determine directly new correction factor 10 p1712 A67-23806

Ionosphere rocket sounding for positive ion density, electron density and electron temperature, noting sunspot effect 11 p1787 A67-24843

Sunspot groups configuration preceding and following formation of type IV radio burst flares 12 p1892 A67-25130

Solar constant and sunspot relationship interpreted by solar radio flux effect on lower ionosphere density 12 p1832 A67-25342

Neutral /zero/ points and geometry of solar magnetic fields 12 p2002 A67-25534

Sunspots - Conference, Arcetri, Italy, September 1964 13 p2201 A67-27415

Sunspot phenomenon covering formation, penumbra, spot umbra, magnetic field, interpretation, radiative deficit in umbra and penumbra, energy flux through Evershed stream, etc 13 p2202 A67-27416

Statistics and evolution of sunspots, discussing frequency, shape, long solar cycle and secular variation 13 p2202 A67-27417

Magnetic field amplification within sunspot groups, considering convective zone and viscosity 13 p2202 A67-27419

Sunspot observation methods and techniques in white light, considering requirements, diffraction limitations on resolution, site selection and local seeing and telescope choice 13 p2202 A67-27421

Sunspot fine structure ground observations, considering umbras, penumbras, boundaries and photographs 13 p2203 A67-27422

Theoretical interpretation of fine structure observations of sunspots by stratoscope, discussing stability modes and sunspot umbras 13 p2203 A67-27423

Image and other techniques to measure and reduce stray and scattered light in sunspot photometry, emphasizing possibility of using partial solar eclipse 13 p2203 A67-27424

Spectroscopic observation of sunspot structure, detailing sunspot model on basis of magnetic field and large scale motions interpretation 13 p2203 A67-27425

Hot and cold component model of sunspot umbrae derived from observation of continuous and line spectra 13 p2203 A67-27427

Molecular spectra of sunspots and solar disk 13 p2203 A67-27428

Center-to-limb variation of Evershed effect for isolated symmetrical sunspot observations interpreted in terms of mass motions in penumbral fine structure 13 p2204 A67-27430

Line formation in sunspots taking into account magnetic field which greatly changes line profile, presenting transfer equations and solutions 13 p2204 A67-27431

Critical particle velocity and particles frozen in given point of magnetic field line, discussing effects of plasma compression and reflection levels 13 p2204 A67-27432

Sunspot groups and chromospheric features associated with magnetic fields of active region in light of supergranular structure of solar atmosphere 13 p2204 A67-27434

Static magnetic field effect on normal distribution of pressure, temperature and density in solar atmosphere, considering sunspots and velocity field effects [AFCL-66-679] 13 p2204 A67-27435

Sunspot magnetic field affecting convective energy transport so that resulting pressure gradient together with gravity force balances magnetic field 13 p2204 A67-27436

Experiment to represent sunspot model having mechanism of natural turbulent convection of liquid mercury inhibited in presence of magnetic field 13 p2171 A67-27437

Sunspot structure, discussing photospheric model, magnetic field influence, MHD structure and energy balance, and photospheric and chromospheric parts 13 p2205 A67-27438

Photographs of sunspots analyzed to obtain magnetic field strength data 14 p2384 A67-28076

Method for complete observation of magnetic field structure in sunspots 14 p2390 A67-28942

Heating of chromosphere above sunspot due to magnetoacoustic waves which develop into weak shock waves 15 p2551 A67-29142

Line contours for Fe-I-6302.5 angstrom across sunspot in west solar limb measured simultaneously with magnetic field strengths and direction and Evershed velocity 15 p2554 A67-29460

Solar atmosphere structure over sunspots studied from radio emission data 16 p2741 A67-30497

Oblong shape and Alfvén waves of looped expanding coronal prominence 16 p2737 A67-30501

Spectrophotometric observations used to construct empirical curve relating radiation intensity and magnetic field strength in sunspots 17 p2946 A67-32728

Sigma components of line split in young sunspots magnetic fields measured with spectrocomparator, showing broadening of iron line in intergranular space 17 p2952 A67-33394

Magnetic diffusion effects in sunspot region assuming Schroeter value for electric conductivity 17 p2952 A67-33395

Small scale magnetic fields observed in photosphere explained by sunspots made invisible by lateral heat 17 p2953 A67-33404

Influx 17 p2953 A67-33404

Upper ionospheric electron density profile variation with sunspot number controlled by temperature and ion composition as shown from rocket data 19 p3218 A67-35222

Model of nonradiative energy transport in sunspots, in which Alfvén waves generated in convectively unstable layer propagate upward into overlying stable layer 19 p3330 A67-36079

Radial motions in small and young sunspots indicating different cooling processes than regular sunspots 21 p3707 A67-38964

Solar magnetic field existence evidenced by transverse fields in sunspots, field vector spatial distribution around sunspots and granular pattern inside sunspots 21 p3708 A67-38966

Direction of sunspot magnetic force lines at any point of solar surface by fringe analysis of light polarization ellipse 21 p3709 A67-38987

Equations governing umbra structure of single spot integrated on spot axis, consistent model can be obtained only for narrow electron pressure range at surface 23 p4067 A67-41230

Velocity field around sunspots from H-alpha line spectra 23 p4067 A67-41239

K-line spectra from sunspots, discussing K-3 absorption line presence 23 p4067 A67-41241

Energy transfer in sunspot model with vertical magnetic field, noting magnetic pressure distribution and magnetohydrostatic equations 24 p4226 A67-41966

Magnetic field intensity effect of sunspot group on source radio noise flux 24 p4209 A67-42136

Heating of chromosphere above sunspot due to magnetoacoustic waves which develop into weak shock waves 24 p4239 A67-43065

SUNSPOT CYCLE

F-2 layer ion-atom interchange coefficients, ion-neutral diffusion coefficient and flux of solar ionizing radiation, comparing ionospheric data 01 p0056 A67-10108

Long term variation in relations of solar indices to E and F region character figures interpreted without assuming changes in solar radiation 01 p0056 A67-10110

Ionospheric D-region concentration of neutral NO estimated, based on dissimilarity of sunspot cycle variation 01 p0056 A67-10111

Forecasting length of solar cycle and maximum value of sunspot numbers, suggesting relation to joint tidal effect of Venus-Jupiter-earth 01 p0149 A67-10805

Solar prominences, proton flares and chromospheric flares in intensity of corona and solar radio emission and sunspots, noting maxima during eleven-year solar activity cycle 01 p0146 A67-11281

Diurnal variations of boundary frequencies of sporadic c-type E layer, deriving cosine law not dependent on sunspot cycle 01 p0061 A67-11289

Babcock theory of solar activity, quiet sun and 11-year magnetic cycle 02 p0330 A67-12639

Diurnal variations in F layer at Ibadan exhibit peak before noon during sunspot maximum and after noon during sunspot minimum 03 p0407 A67-12826

Solar flare mechanism, explaining absence of cosmic ray flares and occurrence of PCA events in years of sunspot minimum 03 p0506 A67-13651

Relative sunspot numbers and variations within each cycle and from cycle to cycle 03 p0511 A67-13809

Sunspot cycle coronal Fe XIV 5303 angstrom radiation emission and type IV bursts in solar flares 03 p0507 A67-13811

Sampling methods and data evaluation in climatological analyses of sunspot-weather relationship 03 p0463 A67-13935

VHF backscatter observations of radio auroral radar echo occurrence at sunspot maximum associated with spirals in geomagnetic latitude and time, magnetic disturbance levels and season 03 p0513 A67-14113

Solar proton streams apparently synodic in solar rotation interval during maximum epoch of recent solar cycle as indicated by polar cap absorption events 03 p0507 A67-14116

Magnetometer predictions of geomagnetic disturbances and intense sporadic E layer occurrences at various sunspot cycle times in auroral zone and effects on VHF absorption 03 p0415 A67-14118

Radar experiments of sun at 38 mc/s, presenting results on echo variation with sunspot number, coronal irregularities, etc 03 p0514 A67-14311

Solar cycle effect on geomagnetic activity and temperature of near-earth tropospheric layer 04 p0616 A67-15227

Proton flares and types of spot groups in 11-year cycle, discussing time-latitude occurrence combined with emissions of cosmic and subcosmic radiation 05 p0883 A67-16808

Diffusion reflections during cycle of solar activity, showing frequency changes according to increase in solar activity 05 p0800 A67-17127

Analysis of differences in number of sunspot groups between Greenwich and Zurich observations 06 p1063 A67-18066

Critical ionization frequencies in F-2 layer in near-polar region observed at Northern Hemisphere high latitude stations 07 p1179 A67-19832

Cyclic curves of F-2 layer critical frequencies based on seasonal phase variations in solar cycle 07 p1179 A67-19833

Longitude distribution of solar proton flares as function of recurrence period 08 p1377 A67-21248

Amplification of solar dipolar magnetic field by differential rotation investigated, noting implications of Sporer law 10 p1705 A67-22895

Solar K-line intensity and emission area at various phases of sunspot cycle 11 p1861 A67-24493

Secular variations of cosmic ray intensity governed by 11-year solar cycle 12 p1994 A67-25532

Sunspot decay and associated flare activity of coming minimum predicted, based on current cycle combined with sunspot lifetime and area distribution 13 p2202 A67-27418

Departures of maxima of solar activity from parabolic law 13 p2202 A67-27420

Long term solar cycle and seasonal variation of whistler dispersion 14 p2307 A67-27887

Relation between number of photospheric granules and Wolf sunspot number 14 p2387 A67-28582

Weighted mean latitudes of sunspots of new cycle during years of minimum solar activity, determining period 15 p2552 A67-29145

Seasonal variations in position and intensity of equatorial electrojet and correlation of latter with sunspot number 15 p2478 A67-30061

Diurnal, annual, latitudinal and sunspot cycle-influenced variations of spread-F intensity at very high latitudes [AGARDOGRAPH 95] 15 p2481 A67-30281

Correlation of monthly and nightly green line 5577 Angstroms /OI/ airglow intensity with sunspot number and 10.7 cm flux 16 p2749 A67-31404

Hysteresis phenomena in curves describing cosmic ray intensity dependence on number of sunspots 17 p2933 A67-32087

Planetary influences on sunspot formation and disappearance showing periodicity in Zurich relative daily sunspot number 17 p2943 A67-32439

Aurora Borealis and airglow history, discussing sunspot cycle influence, theories concerning origin, etc 18 p3032 A67-33579

S-current intensity variation and 10.7 cm radio noise flux show agreement with Schmidt sunspot numbers 19 p3221 A67-35432

Theory, similar to Babcock solar magnetic field theory, explaining magnetic stars variability 19 p3328 A67-35933

Night airglow research during IQSY noting correlation of low activity with sunspot minimum 20 p3430 A67-36905

Ionosphere thermal nonequilibrium during sunspot minimum noting electron density and temperature measurements and daily variations 21 p3616 A67-37999

Absorption of VHF waves in whistler mode at low latitudes calculated for various ionospheric conditions during sunspot activity 21 p3617 A67-38065

Diffusion reflections during cycle of solar activity showing frequency changes according to increase in solar activity 21 p3618 A67-38470

Sunspot cycles rise time and periodic variation probable values 21 p3704 A67-38511

Empirical model of sunspot activity within solar cycle limits indicating separate consideration of magnetic field generation and spot formation process 22 p3879 A67-39300

Annual and diurnal variations of geomagnetic anomaly in Australasian Zone during sunspot minimum, stressing role in transequatorial propagation of VHF radio signals 22 p3759 A67-39473

Ionospheric F-1 layer critical frequency at sunspot minimum and maximum, discussing critical frequency diurnal variation 22 p3789 A67-39476

Time dependency, anisotropy, propagation and spectral properties of cosmic radiation released by solar flares during sunspot activity 22 p3871 A67-39796

Solar flare occurrences probability, designating two-year period centered on sunspot minimum as safe time zone for vehicles on missions to Mars and Venus 22 p3873 A67-39929

Medium wave and global UV radiation, relative sunspot number and ozone density measurements and interrelationships 22 p3873 A67-40030

Cosmic ray yearly variation during solar activity cycle, discussing flare and acceleration mechanisms, stable coronal condensation and sunspot magnetic field 22 p3874 A67-40045

Double sunspot cycle or 22-yr variation in cosmic ray diurnal variation phase, discussing streaming mechanisms 22 p3874 A67-40046

Radar-derived results for midlatitude F-region densities and temperatures at sunspot minimum noting seasonal anomalies 22 p3793 A67-40080

Mean solar activity curves for 11-year and 80-year cycles from 1698 to 1964 reveal significant difference between two cycles 22 p3889 A67-40303

Periodicity of sunspot groups covering number and importance characteristics, formation frequency and long term spot period 22 p3890 A67-40428

Secularly smoothed data on sunspot frequency minima and maxima 23 p4067 A67-41240

Weighted mean latitudes of sunspots of new cycle during years of minimum solar activity, determining period 24 p4239 A67-43068

SUPERALLOY

Nickel-base superalloys hardened in part by precipitation of gamma phase examined by X-ray diffraction techniques 01 p0095 A67-10687

Sintered Ni-base heat resistant alloys, discussing composition-creep strength relation, grain size, prealloyed-powder production and thermal and structural shock properties 01 p0098 A67-10700

Light and electron microscopy used with X-ray diffraction and X-ray fluorescence analysis to study effects of temperatures and stress on As-cast nickel-base superalloy 02 p0256 A67-12706

Heat treatment and microstructural observations in wrought Ni-base superalloy Udimet 700 in static creep, determining fracture and deformation properties 06 p1015 A67-17809

Microstructural changes effect on mechanical properties of nickel base superalloys, with particular attention to wrought alloys 08 p1340 A67-20362

High strength alloys for gas turbines in Soviet Union, noting wrought and cast nickel-base alloys for turbine blades and vanes 10 p1688 A67-23012

Phase transformations in heat treated nickel-rich Ni-Co-Cr-Al-Ti-C cast alloys noting sigma formation 10 p1688 A67-23173

Nickel and cobalt superalloys low cycle thermal fatigue test method under cyclical extension and temperature conditions, giving stress-strain-time relations [ASME PAPER 87-MET-19] 12 p1956 A67-25955

Nickel-base superalloy technology, stressing structural stability and hot corrosion resistance 12 p1958 A67-26128

Structure, composition and morphology of carbide phases of nickel superalloy 13 p2131 A67-26573

High temperature corrosion and evaporation of Haynes 25 and Hastelloy X-280 in atmospheres of oxygen, carbon monoxide, carbon dioxide, water vapor and methane 14 p2338 A67-28148

High temperature superalloys for gas turbine applications noting alloys based on cobalt, iron, nickel and dispersion hardening 18 p2686 A67-30487

Temperature effect on low-cycle fatigue behavior of Udimet 700 superalloy, noting internal and surface cracking 16 p2693 A67-31870

Formation and degradation mechanisms of aluminide coatings on Ni-base superalloys, discussing experimental procedures 16 p2693 A67-31871

Elastic constants of directionally solidified Ni base superalloy considering consequences of anisotropy to design analysis 16 p2693 A67-31874

Heat treatment of nickel superalloys for high temperature applications, showing solution-temperature effect on mechanical properties 17 p2865 A67-33045

Alloy effects in low pressure diffusion

bonding of superalloys, presenting time, pressure, bond strength and temperature curves 17 p2866 A67-33200

Electrostream process for drilling very small diameter holes in superalloys for gas turbine and nozzle vane fabrication [ASTME PAPER MR67-141] 18 p3054 A67-34175

Superalloys for SST engine, discussing materials properties, structures, turbine disk production, welding, alloy design, coating-base metal interactions, etc 20 p3469 A67-37358

Unidirectional solidification of cast nickel-base superalloys, effect on creep behavior, stress-rupture properties and thermal shock resistance 20 p3469 A67-37383

Nickel-base single crystal superalloy tensile and creep properties, comparing single and multiple slip orientations 20 p3470 A67-37387

Drawing technique for bundles of sheathed superalloy wires noting sheathing, stress relief, interfilament welding and oxide bonding 21 p3643 A67-37878

Cold forming properties and handling of stainless steels and superalloys noting contained extrusion and warm heading techniques 21 p3634 A67-38177

Carbon content effect on properties and structures of nickel and nickel-iron base superalloys 22 p3818 A67-39223

Astroloy /Ni base superalloy/ disks for jet engine application, discussing chemical composition, basic ingot structure, forging and heat treatment 22 p3818 A67-39226

Closed die forging of nickel base superalloys for large turbine wheel components [ASM PAPER C6-18.4] 23 p4010 A67-41401

Protective coatings of Ni and Co base superalloys for gas turbine engines, discussing microstructure, chemistry and phase composition [ASM PAPER C6-4.2] 23 p4020 A67-41405

Ni-Cr superalloy oxidation and sulfidation, relating sulfidation resistance of uncoated Ni superalloys to matrix Cr content [ASM PAPER C6-18.5] 23 p4020 A67-41406

SUPERCAVITATING FLOW

Water tunnel investigation of unsteady partial, full and supercavitation in cascade flow, determining force coefficients [ASME PAPER 66-WA/FE-25] 04 p0607 A67-15355

Unsteady incompressible flow of two-dimensional supercavitating hydrofoils with finite cavity length, considering wake nature [ASME PAPER 87-FE-15] 14 p2304 A67-28363

Supercavitating engines noting design principles, performances of existing models and connection between parameters 18 p3023 A67-33417

Supercavitating engines, defining optimum curvature and thickness distribution, performance optimization, etc 18 p3023 A67-33418

Lift and drag coefficients of wing profile with elliptical pressure distribution calculated by approximate linearized theory 18 p3024 A67-33541

SUPERCHARGER

Pressurization of Mooney M22 aircraft by low cost exhaust-driven turbosupercharger based on diesel automotive unit [SAE PAPER 870287] 12 p1899 A67-25511

SUPERCONDUCTING MAGNET

Normal region distribution in superconducting solenoid measured after quenching by varying quenching current 01 p0137 A67-11065

Magnetic properties of second kind superconductivity of indium-lead alloys as function of temperature down to 0.38 degrees K 05 p0864 A67-16893

Inductance, flow current and external magnetic field effects caused by diamagnetism of superconducting solenoid winding 06 p1051 A67-18207

Traveling wave maser for radio astronomy interferometer noting superconducting magnet, dynamo and cryostat 07 p1197 A67-20115

Maser for traveling waves over large cm wave band used as low noise amplifier 09 p1482 A67-22481

Induced magnetic moment and surface fields of ideal superconducting torus in uniform magnetic field calculated using Legendre functions 11 p1850 A67-24918

Superconductive magnets at Lewis

Research Center of NASA 12 p1978 A67-25105

Magnet consisting of superconductive solenoid of niobium-zirconium wire with ferromagnetic insertions 15 p2422 A67-29127

Magnetic properties of superconducting vanadium calculated from cellular model 16 p2726 A67-30816

Inductance, flow current and external magnetic field effects caused by diamagnetism of superconducting solenoid winding 17 p2922 A67-33221

Degradation, training and instability in superconducting coils, protection of windings and related problems of superconducting magnets for use in MHD generators 18 p3099 A67-33711

Book on generation of high magnetic fields, discussing solenoids, cooling systems, superconducting and pulsed coils, etc 20 p3483 A67-36452

Superconducting magnet spectrometer using lithium drifted silicon detectors for measurement of electron spectra 20 p3444 A67-36523

Functional maser consisting of amplifier, low noise header and superconducting magnet for use in ATS satellite 20 p3459 A67-36595

Critical surface between superconducting and normal state determined for commercial niobium stannide ribbon and Nb-Zr wire 20 p3512 A67-37346

14-Tesla 15-cm bore superconductive magnet and test results 20 p3512 A67-37347

Liquid helium application in electromagnetic DC, LF and HF AC devices 22 p3838 A67-40397

Large model superconducting magnet for MHD central-station power generation, discussing performance and specifications 22 p3749 A67-40399

Gravity meter based on levitated superconducting ball over persistent current magnet 22 p3809 A67-40432

Intense continuous or long pulse magnetic fields in MHD generator, obtaining magnetic energy required for air gap, discussing superconducting magnets 24 p4098 A67-42414

SUPERCONDUCTIVITY

SA ELECTRIC CONDUCTIVITY Electron-based superconductivity mechanism involving two overlapping conduction bands in alloys 01 p0127 A67-10062

Superconductivity of nondegenerate semiconductor thin films, dependence on current carrier concentration, impurity level positions and film thickness 01 p0128 A67-10084

Mechanism leading to superconductivity even for particles with purely repulsive forces between them, examining general theory for weak short-ranged pair forces between particles 01 p0129 A67-10151

Superconducting transition temperature and critical field curve for pure Ga single crystals 01 p0130 A67-10153

Amplitude dependent attenuation in normal and superconducting lead for ultrasonic determination of superconducting energy gap 01 p0135 A67-10916

Clathrates exhibiting metallic conductivity and superconductivity at specific temperatures, noting transition temperature of nitrate salt 01 p0135 A67-10917

Vanadium-gallium wires with good superconducting properties fabricated by new stepwise diffusion process 01 p0137 A67-11064

Cryogenic computers based on superconductivity phenomena, discussing building and operating feasibility in outer space 01 p0031 A67-11443

Superconductivity of second kind in thin film, considering geometry dependent upper critical fields 02 p0291 A67-11738

Critical field for second order transition of superconductor to normal state, noting effect of vortex structure 02 p0291 A67-11739

Contact effect between superconductor and normal conductor and between two different superconductors, noting transition temperature 02 p0291 A67-11740

Shifts in normal state conductivity and superconducting transition temperature due to charge carrier changes in In, Tl and Sn films 02 p0291 A67-11741

Electron density effect on transition temperature of superconductivity, considering tantalum 02 p0291 A67-11742

Surface states and additional structure in McMillan-Anderson model for Tomasch effect in superconducting films 02 p0296 A67-11822

Gapless superconductivity by tunnel effect experiments on dirty superconducting alloys in high magnetic field 02 p0300 A67-12247

Boundary conditions at interface between superconductor-superconductor and superconductor metal 03 p0489 A67-12937

Superconducting critical temperatures of nonstoichiometric transition metal carbides and nitrides, correlating data with valence electron concentration 03 p0491 A67-13256

Superconductivity in strontium titanates and similar polar substances with transition temperature accounted for by electron-phonon interactions 03 p0491 A67-13259

Longitudinal microwave phonons inducing tunneling in Al-Pb, Al-Sn and Pb-Pb superconducting diodes 03 p0379 A67-13330

Cryogenic techniques for space power generators based on superconductivity, discussing MHD converters 04 p0560 A67-15967

Thermodynamic properties of superconducting thin films with interaction constant that varies with thickness 04 p0686 A67-15974

Degree of deformation effect on superconducting properties of niobium and vanadium 04 p0686 A67-15986

Superconductivity and transition temperature of technetium and technetium carbide 05 p0860 A67-16389

Superconductivity in aged Zr-Nb alloys, noting transition temperature increase of quenched alloy upon aging 05 p0828 A67-16469

X-ray structural analysis of superconducting Nb based alloys, noting two-phase region in annealed samples 05 p0863 A67-16690

Spin localization enhancement or hindrance by superconductivity 05 p0863 A67-16757

Isotope effects on superconducting transition temperature of molybdenum boride and tungsten boride 06 p1047 A67-17642

Limitation of Froehlich-Terreaux quasi-superconducting state, discussing experimental and observational difficulties 06 p1047 A67-17654

Increase in superconducting critical current density in diffusion layers of proton-irradiated niobium stannide and decrease at higher dosage 06 p1048 A67-17817

Solubility limit of Fe in close-packed hexagonal alpha-Ti noting temperature dependence and superconductivity 06 p1051 A67-18370

Metastable form of C12 type calcium disilicide when under high temperature and pressure, noting X-ray diffraction powder patterns and superconductivity 06 p1051 A67-18372

Superconductivity in degenerate semiconductors, applying Bardeen-Cooper-Schrieffer theory, calculating electron-electron interaction 06 p1069 A67-18979

Superconductivity in strontium titanate, noting variability of critical temperature with carrier density and uniaxial stress 06 p1069 A67-18980

Superconductivity in germanium telluride, noting critical magnetic field 06 p1069 A67-18981

Gap anisotropy increase in superconducting thallium transition temperature dependence on lattice defect density due to hydrostatic deformation 07 p1235 A67-20128

Pauli-paramagnetic superconductivity in Ti-16 at. percent Mo from specific heat measurements 07 p1235 A67-20130

Critical field for nucleation of superconductivity at tunneling barrier in magnetic field 07 p1235 A67-20131

Band structure effects and interacting electrons and phonons in superconductor, treating Dyson equations and various simplified models 07 p1235 A67-20133

Low temperature magnetic properties of superconducting Mo-Re alloys in fine wire form 07 p1236 A67-20135

Anisotropy of energy gap in superconducting Pb analyzed using superconductive tunneling 07 p1236 A67-20137

Dimensionality of superconductivity in alkali-metal-graphite lamellar

compounds 07 p1236 A67-20138

Superconductivity of metallic aluminum antimonide and comparison of results with measurements on InSb and GaSb 07 p1238 A67-20279

Superconducting properties of vanadium silicide noting high transition temperature, electron-phonon interaction, sound absorption, etc 08 p1369 A67-20990

Soviet book on electron properties of metals and alloys 08 p1371 A67-21490

Parallel critical field calculation of tunneling barrier extended to all temperatures in dirty limit 09 p1552 A67-21745

Phase diagram of Nb-Ti-Zr system and superconducting properties of alloys 09 p1518 A67-22029

Landau-Ginzburg theory extended to anisotropic superconducting energy gap, considering diffuse and specular boundary scattering 10 p1687 A67-22759

Millimeter microwave transmission and reflection through 50 angstrom superconducting tin and indium films near critical temperature 10 p1688 A67-22764

Electrical and thermal conductivity of tin films investigated in search for surface superconductivity induced by electric field 10 p1688 A67-22765

Cryogenic computers in space based on phenomenon of superconductivity 10 p1608 A67-22770

Stabilization of high temperature beryllium allotropes through transition element addition, noting appearance of superconductivity 10 p1688 A67-22890

Effect of liquation inhomogeneity on superconducting properties of ternary alloy, noting enhancement of critical current density in wire prepared from this alloy 10 p1689 A67-23089

Zirconium-niobium alloy analyzed by oxide replica technique, noting superconductivity and tunnel effect, determining relation between superconductivity current critical density and sample structural characteristics 10 p1689 A67-23090

Book on superconductivity of metals and alloys including fundamental properties, condensed state, analysis of Landau-Ginzburg equations, magnetic field effects, etc 10 p1690 A67-23160

Magnetically coupled superconducting films, showing fluxon size as function of film thickness 10 p1696 A67-23774

Transition temperatures of Be compounds, noting evidence for strong coupling to Mo localized mode from observed isotope effect 11 p1846 A67-24582

Type II superconductor voltage proportionality to time varying magnetic field under constant transport current and linear field sweep 11 p1846 A67-24583

Rare earth metal superconductive shielded magnetic lens for focusing high energy electrons 11 p1802 A67-24765

Porosity and particle size effects on magnetization curve of superconducting Nb sintered compacts with and without C added 12 p1978 A67-25139

Superconductivity of Nb3-Al-Mo3Al binary system 13 p2184 A67-27631

Degree of deformation effect on superconducting properties of niobium and vanadium 14 p2366 A67-28489

Transitional impurity effects on superconducting critical temperature of normal metals, stressing localized states with no magnetic moments 14 p2371 A67-28727

Superconducting solenoid producing oscillatory magnetic fields having peak to peak amplitudes, noting niobium-zirconium wire performance 14 p2288 A67-28747

Longitudinal acoustic wave attenuation in superconducting aluminum measured, verifying acoustic attenuation predictions 14 p2373 A67-28858

RCA papers on defense electronic products including search radar, superconductor devices, data and spacecraft communications, speech 14 p2274 A67-28910

X-ray structural analysis of superconducting Nb based alloys, noting two-phase region in annealed samples 15 p2539 A67-29860

Two-fluid hydrodynamic equations for London superconductors obtained in inviscid approximation 15 p2540 A67-30004

Superconducting mixed state of concentrated Mo-Nb alloy, evaluating free area of Fermi surface in k space 16 p2726 A67-30812

Superconducting niobium and tantalum compounds investigated for maximum transition temperatures 16 p2726 A67-30818

Microwave flux-flow resistivity transitions observed for strongly paramagnetically limited titanium-vanadium alloys 16 p2727 A67-30821

Superconducting materials for solenoids, noting simple form conductors and current carrying capacity as field function 17 p2912 A67-32264

Superconducting and superheated metastable state transition to normal state by beta irradiation 17 p2912 A67-32270

Superconducting transitions of three metastable states of Ga 17 p2915 A67-32707

Relationship between microhardness of niobium and other variables characterizing superconductivity 17 p2915 A67-32720

Zr-Nb alloy structure effect on critical superconductivity parameters determined, using electron microscopy of thin films 17 p2916 A67-32721

Electrical resistance of niobium single crystal at very low temperature from beginning of superconductivity transition 17 p2916 A67-32805

Critical parameters for vanadium-niobium alloys superconduction, giving curves for transition temperature and measuring critical electric fields 17 p2974 A67-32973

Self-consistency equation for nucleation of superconductivity in presence of magnetic field 17 p2924 A67-33372

Far IR measurements used to determine superconducting energy gap widths in niobium alloys 17 p2925 A67-33373

Magnetization in superconducting Mo measured in He 3 cryostat, noting transition temperatures and critical field 17 p2925 A67-33379

Coherent electromagnetic oscillation from voltage biasing of superconducting weak link producing coupled quantum oscillators 17 p2926 A67-33380

Correlation function method in superconductivity theory, formulating electric current density in terms of distribution function in phase space 18 p3100 A67-33712

Two-fluid hydrodynamic equations for London superconductors obtained in inviscid approximation 18 p3100 A67-33762

Zirconium-niobium alloys investigated for oxygen impurity effects on critical current density and superconducting properties 19 p3243 A67-34925

Superconducting transition temperatures and low field magnetization of ceramic mixed Ba, Sr and Ca-Sr titanates, showing particle nature of specimens 19 p3302 A67-35037

Superconductivity transition temperatures of metal carbides, showing stoichiometry as main feature for maximum temperature 19 p3303 A67-35040

Possibility of pressure destroying superconductivity in various metals, studying transition temperatures, critical pressures, etc 19 p3303 A67-35043

Microwave photon interaction with superconducting tunneling currents measured in aluminum-indium junctions, extended to tin-lead junctions, discussing phase shift 19 p3303 A67-35048

Existence and stability conditions of several-quanta flux lines in type II superconductors 20 p3505 A67-36206

Revised London theory of superconductivity destruction by current, using numerical methods for optimum phase-boundary configuration 20 p3505 A67-36208

Superconductor resistive behavior as hole motion in flux lattice under peak effect influence 20 p3505 A67-36209

Superconducting critical temperature of sandwich of two semiconducting films in contact 20 p3512 A67-37434

Superconducting critical temperature below Kondo temperature for metal solutions with magnetic impurities calculated, using Green function 21 p3680 A67-38350

Surface superconductivity of cylindrical niobium samples, discussing microscopic surface roughness and approximate character of theory 21 p3685 A67-38802

Superconductivity of Nb₃Al-Mo₃Al binary system superconductivity of Nb₃Al-Mo₃Al binary system 21 p3685 A67-38828

Superconducting property of kappa phase in Bi-Sn alloy at high pressure, with determination of transition to superconducting state and temperature interval to keep stable state 22 p3857 A67-39460

Nondestructive readout technique for superconductive memory cells, application and comparison with previous methods 22 p3765 A67-39699

Superconducting coils used for capacitors in pulsed operations to reduce size and weight of energy storage systems 22 p3747 A67-39900

Connections between superconductivity and electromagnetic potentials, presenting model for flow of superconducting electrons and quantization of fluxoid 22 p3863 A67-40198

Hydrostatic and uniaxial compressional stress effects on strontium titanate superconductive transition temperature 22 p3863 A67-40244

Surface superconductivity in dilute Ta-Nb alloy ascribed to decrease in mean free path due to lattice defects 23 p4036 A67-40657

Superconductivity enhancement in fine grained tungsten films, discussing structural changes and theoretical models 23 p4036 A67-40702

Thermal conductivity of clean and dirty type II superconductors, discussing finite temperature gradient effect on niobium 23 p4036 A67-40704

Positive isotope effect on superconducting transition temperature of alpha uranium 23 p4044 A67-41439

Destruction of superconductivity in niobium by current and external magnetic field intensity 23 p4047 A67-41691

Heat transfer from plate located on dielectric base to liquid helium in pulsed regime influencing kinetics of superconductivity in thin films 24 p4254 A67-42258

Strong coupling superconductivity in intermetallic compounds, possibly due to all electrons having same kinetic energy 24 p4205 A67-42738

Semiconducting mixed titanate superconducting transition observed at 0.5 degrees K ascribed to change in valley numbers in conduction band 24 p4205 A67-43099

SUPERCONDUCTOR

Dispersion relation of electron impurities in gapless superconductors and effect on period and damping of Tomasch oscillations 01 p0130 A67-10154

Motion of flux lines in type II superconductors at zero temperature, discussing friction, Magnus and other forces 01 p0133 A67-10750

London moment of rotating superconductors and relation to Lense-Thirring fields of general relativity 01 p0134 A67-10812

Peak effect in critical current of superconductors observed during deuteron irradiation at low temperature 01 p0135 A67-10880

Collective excitations influence on polarization operator of superconductor with P-pairing 02 p0301 A67-12734

AC measurements on hard superconductors exposed to magnetic field, obtaining critical surface current and density from voltage-time curves 03 p0487 A67-12809

Maximum current carrying capacity of type III hard superconducting wire in zero external field before superconductivity breaks down 03 p0488 A67-12814

Current carrying capacity of hard superconducting wire in zero external field determined from considerations of flux density distribution 03 p0488 A67-12815

Absorption dependence of ultrasonic waves in superconductors on amplitude of sound wave due to temperature 03 p0492 A67-13325

Energy gap of vanadium silicide measured by tunneling technique based on proximity effect 03 p0492 A67-13327

Spin-lattice relaxation time of dirty type II superconductor alloys in mixed state in almost upper critical field 03 p0493 A67-13472

Electron density effect on transition point

of superconductors 03 p0494 A67-13508

Parametric amplification and sideband oscillations in structured superconducting Sn thin films 03 p0496 A67-13568

Genness and Werthammer method generalization, developing theory of transition temperature of superconducting superposed films 03 p0499 A67-13874

Solutions for nonlinear Ginzburg-Landau equations in cylindrical symmetry for type I superconductor 03 p0499 A67-13876

Temperature and purity dependence of nuclear-spin relaxation time in type II superconductor gapless region and volume average of density states on Fermi surface 03 p0499 A67-13937

Magnetic properties of pure and impure double-band superconductors in vicinity of upper critical field treated by almost-free-electron approximation 03 p0500 A67-14196

V-I tunneling characteristics and energy gap anisotropy of Pb-Bi superconducting alloy, discussing mean free path 03 p0501 A67-14341

Superconducting-to-mixed state phase transformation in type II superconductors in applied magnetic field and accompanying onset of vortex filaments at surfaces 03 p0501 A67-14372

Order-disorder parameter determined from HF absorption in pure superconducting films 03 p0501 A67-14373

Acoustic wave energy absorption by superconductors in intermediate state 03 p0502 A67-14377

Energy gap anisotropy effects in pure single crystal superconductors investigated by factorable BCS-like model for effective electron-electron matrix element 04 p0673 A67-14518

Extreme variations of electronic effective mass with temperature cannot lead to satisfactory explanation of specific heat anomaly in superconducting lead 04 p0676 A67-14934

Flux jumps in hard superconductor AC and DC magnetic fields 04 p0682 A67-15328

Macroelectrodynamical equations for low temperature intermediate state of type I superconductors, noting magnetic field effect on structure 05 p0863 A67-16695

Josephson current in alternating field between two superconductors separated by dielectric barrier 05 p0853 A67-16697

Current dependence on voltage in Sn-Sn and Pb-Pb tunnel junctions attributed to electric gap anisotropy 05 p0863 A67-16754

Temperature and thickness dependence of critical field of superconducting Sn films measured and compared with nonlocal theoretical models 05 p0864 A67-16899

Quantum paramagnetic traveling wave amplifier using rutile with admixture of chromium and combined with magnet with superconducting coil 05 p0825 A67-17161

Microwave surface resistance of type II superconductors, from simultaneous measurements of real part of surface impedance and magnetization 05 p0871 A67-17375

Abnormal internal phenomena in superconducting coil during magnetic excitation and S-N transition 05 p0871 A67-17482

Tunnel current passing from type II superconductor into normal metal 05 p0871 A67-17490

Hysteresis losses in nonideal superconductors calculated, using phenomenological equations of flux motion 06 p1048 A67-17819

Resistive effects in type II superconductors near upper critical field examined, using Ginzburg-Landau equations 06 p1049 A67-17882

Superconducting tunnel diode for quantum generation and detection of incoherent phonons, discussing I-V characteristics 06 p1011 A67-18211

Superconducting switching and storage elements, examining physical properties, cryotron and continuous film memory cell 06 p0972 A67-18433

Tunneling measurements of energy gap anisotropy in thick and thin superconducting films of Al, Pb, In and Sn 06 p1052 A67-18571

Measuring equipment for critical current density of superconductors in strong magnetic field 06 p1005 A67-18722

Changes in ultrasonic attenuation of

superconducting niobium at low magnetic fields, considering effects of low critical field impurity phases 06 p1053 A67-18757

Weak superconductivity electrodynamic and EM wave propagation in Josephson tunnel junction in presence of vortices 06 p1054 A67-18806

Persistent current loops in hard superconducting wire formed when wire is magnetized by static transverse external field 07 p1232 A67-19554

Experimental tests of critical state model of hysteresis in type II superconductors, considering critical currents in field and transport currents in zero 07 p1233 A67-19842

Energy gap derived from I-V characteristics for pressure contacts between type II superconductors and normal metals 07 p1233 A67-19843

Effect of spin exchange scattering by magnetic impurities on electronic properties of superconductor 07 p1235 A67-20129

Superconducting energy-gap parameter anisotropy effect on critical field in presence of nonmagnetic impurities 07 p1235 A67-20132

Anisotropic energy gap in superconducting white tin obtained by expansion in tetragonal harmonics 07 p1235 A67-20134

Anisotropy and temperature dependence of upper critical field of type II superconductor single crystals with cubic structure 07 p1236 A67-20136

Constants of superconducting alloys for arbitrary temperatures and impurity concentrations, calculating free energy density by using Gorkov equation 07 p1236 A67-20140

Temperature dependence of critical field in superconducting vanadium 07 p1237 A67-20178

Sample standard resistor combination to shunt pulsed currents used to study superconducting-to-normal transition in short wire samples 08 p1367 A67-20378

Coulomb interaction in two-zone superconductor model, noting variation of critical electron-temperature and effect on superconductivity 08 p1369 A67-20838

Two energy gaps in superconducting compounds studied by NMR techniques 08 p1371 A67-21443

Growth of critical temperature of small superconductor samples explained within framework of BCS superconductivity theory without using electron pairing 08 p1372 A67-21502

Josephson and ordinary tunneling currents for two-band model superconductor, treating niobium-tin junction 09 p1551 A67-21667

Low temperature components for data processing, low noise amplifiers and microwave technology, noting superconductor elements like cryotron 09 p1463 A67-21760

Kinetic tunneling theory in superconductors clarifies conditions for onset of Josephson current 09 p1555 A67-22071

Pinning fluxoids by spatial inhomogeneities of Ti-Pb and Pb-In alloys, noting I-H characteristics and type II superconductor resistance 09 p1556 A67-22135

London superconductors in local approximation, obtaining solution to equation in form of gradient expansions 09 p1556 A67-22221

Occurrence, size and distribution of lattice defects in type III superconductor analyzed using electron microscopy, noting defect influence on critical current density 09 p1557 A67-22437

Continuous magnetic field satisfies conditions of stability, size, orientation, uniformity and controllability of maser type amplifier employing superconductor winding 09 p1516 A67-22482

Flow vortices in hollow cylinder made of type II superconductor 09 p1482 A67-22682

Cryogenic thermoconductivity of impure tin in superconducting and normal state, noting anisotropy and superconducting energy gap independence from impurity type 10 p1687 A67-22761

Correlation of anisotropic energy gap with thermal conductivity in pure and impure superconducting tin 10 p1687 A67-22762

Granular superconductor with thin insulating layer at boundary of each homogeneous superconductor grain, using isospin formulation of microscopic

theory 10 p1687 A67-22763
 Separation of effects of two factors
 controlling real contact area of
 superconducting contacts through number of
 individual contacts and 10 p1688 A67-22904
 size
 Critical fields of thin superconducting
 films determined by specular reflection of
 electrons from surfaces 10 p1694 A67-23596
 Nonlinearity in V-I characteristic of type
 II superconductor situated in external
 magnetic field 10 p1696 A67-23775
 Sensitive magnetic susceptibility
 measurements using superconducting circuits
 and magnetic shields 10 p1657 A67-23780
 Depression of superconducting transition
 temperature in narrow tin films, noting
 condition for maximum microwave
 enhancement of critical
 current 11 p1846 A67-24563
 Microwave surface absorption in static
 magnetic field affects surface resistance of
 superconducting alloys 11 p1846 A67-24584
 Superconducting energy gap of cubic and
 hexagonal LA obtained by point contact
 tunneling to bulk samples, noting V-I
 characteristics and temperature
 dependency 11 p1846 A67-24585
 Circuit Q of self-resonant coil of niobium
 stannide at RF low
 temperatures 11 p1767 A67-24726
 Probable upper limit of critical field for
 ternary and higher order ductile transition
 metal superconducting
 alloys 11 p1850 A67-24925
 Upper critical field limits for bulk type II
 superconductors 11 p1850 A67-24933
 Thermodynamics of vortex flow in
 superconductors, using combination of
 electrical currents and thermal
 gradient 12 p1983 A67-25477
 Microwaves parametric amplification
 experiments in superconducting Josephson
 tunnel junctions, showing signal
 amplification as function of temperature,
 absorption dip of rutile resonator,
 etc 12 p1915 A67-25745
 Low temperature deuteron irradiation
 effect on type II superconductors noting
 atomic displacement, resistivity increase and
 transition temperature
 decrease 12 p1985 A67-25845
 Response of superconducting sheath state
 of lead-indium in AC and DC magnetic fields
 studied, noting transition changes response
 of superconducting sheath state of lead-
 indium in AC and DC magnetic fields
 studied, 12 p1985 A67-25847
 Thin film superconducting bridge behavior
 in microwave field noting dependence of
 deviation from classical rectification on
 frequency, power, temperature and bridge
 width 12 p1985 A67-25848
 Structure effect on magnetization and
 critical current density in transverse
 magnetic field of superconducting V and Nb
 foils with different grain boundary
 orientations 12 p1986 A67-26067
 Electromagnetic wave propagation in type
 II superconductors, noting Hall angles
 influence 13 p2175 A67-26428
 Transition temperature change for thin tin
 and thallium superconducting films after
 deposition of dielectric
 substances 13 p2182 A67-27360
 Electrodynamic equations for pure and
 doped two-band superconductors, studying
 upper critical magnetic
 field 13 p2184 A67-27630
 Superconducting gyroscope for gimbaled
 platform application 13 p2122 A67-27683
 Frequency multiplication of microwaves by
 field electron emission in superconducting
 cavity 14 p2278 A67-27787
 Anisotropy in tunneling density of states
 in pure type II superconductors, examining
 ideal case of perfectly specular boundary
 scattering at tunneling
 junction 14 p2365 A67-28294
 Surface current change between critical
 paramagnetic and critical diamagnetic
 induced by temperature variation in type II
 superconductor immersed in static magnetic
 field 14 p2365 A67-28296
 Magnetic properties of pure and impure
 double-band superconductors in vicinity of
 upper critical field treated by almost-free-
 electron approximation 14 p2369 A67-28541
 Triangular flux line lattices observation by
 electron microscope in type II
 superconductors 14 p2369 A67-28599

Superconductor dynamic intermediate
 state DC voltage caused by flux motion
 shown by frequency spectrum measurements
 of noise voltage 14 p2369 A67-28600
 Two-zone superconductor with
 nonmagnetic impurity, noting
 correspondence of thermodynamic values to
 single-zone pure state except for
 density 14 p2369 A67-28672
 Autoelectric emission in superconductors
 near transition point noting variation with
 total field energy and normal
 component 14 p2370 A67-28673
 Decay of persistent currents in small ring-
 shaped superconductors due to detectable
 internal thermodynamic
 fluctuations 14 p2370 A67-28717
 Critical surface transport currents in type
 II superconductors interpreted by surface
 flux pinning model 14 p2370 A67-28718
 Two cases of critical surface current
 magnitude change in type II
 superconductors after transport current
 direction reversal 14 p2370 A67-28719
 HF localized and LF resonant impurity
 modes valence effect on energy gap and
 transition temperature in isotropic
 superconductors 14 p2370 A67-28720
 Theory of pure type II superconductors in
 high magnetic fields, calculating ultrasonic
 attenuation coefficient 14 p2370 A67-28721
 Bilinear current density induction of
 double-frequency laser beam from
 superconducting metal 14 p2371 A67-28722
 Superconducting indium-bismuth alloy
 films immersed in strong magnetic fields
 parallel and perpendicular to surface,
 studying film thickness effect by tunneling
 technique 14 p2371 A67-28723
 Electromagnetic properties of impure
 anisotropic strong-coupling superconductors,
 using Green function to obtain response,
 current density and Josephson tunneling
 current 14 p2371 A67-28724
 Effects of strong coupling and spin-flip
 scattering by magnetic impurities on
 superconductors, calculating conductivity and
 surface impedance at finite
 temperatures 14 p2371 A67-28725
 Magnetic field effect on microwave
 surface impedance of superconducting
 tantalum measured in various temperature
 ranges via dielectric-resonator
 techniques 14 p2371 A67-28726
 Thorium-gadolinium alloy magnetization
 curves confirming full Meissner effect,
 showing bulk properties of superconductors
 obey Abrikosov-Gorkov
 theory 14 p2373 A67-28859
 Perpendicular critical magnetic fields of
 superconducting aluminum, tin and gallium
 small grained films examined for
 superconducting transition temperature
 enhancement 14 p2373 A67-28860
 Superconducting microwave filters,
 discussing minimum insertion loss, loss
 dependence on various factors and effect of
 peak fields on maximum
 power 14 p2289 A67-28915
 High field type II superconductors,
 analyzing flux jumps 14 p2373 A67-28916
 Microwave frequency superconductor
 materials, applying bulk and thin film
 properties to filter, amplifier, oscillator,
 junction and Josephson effect
 devices 14 p2289 A67-28917
 Superconducting storage device with
 Josephson tunneling junction replacing
 cryotron 14 p2289 A67-28921
 Elastic vibrations in superconductors
 noting vortex effects, weaknesses of elastic
 moduli changes and decrease in ultrasonic
 attenuation 14 p2375 A67-28988
 Precipitate and dislocation structures
 associated with peak effect in niobium
 examined using electron
 microscopy 14 p2375 A67-28999
 Instrumentation using quantum effects in
 weakly coupled
 superconductors 14 p2375 A67-29043
 Ultrasonic measurement of temperature
 dependence of longitudinal sound absorption
 coefficient for main crystallographic
 directions in superconducting
 indium 14 p2375 A67-29070
 Possibility of Cerenkov effect in
 superconductors established from
 electromagnetic oscillation spectrum,
 calculating wave resistance and resonance
 maxima positions 14 p2375 A67-29079
 Density of states of pure type II

superconductors in high magnetic fields,
 deriving approximate expression for Green
 function 15 p2533 A67-29089
 Microwave harmonic generation from
 Josephson junction noting radiation
 waveguide coupling, bias point, input power
 level and Josephson
 equations 15 p2535 A67-29492
 Tunnel current modulation by acoustic
 wave in superconductors 15 p2537 A67-29708
 Macroelectrodynamics equations for low
 temperature intermediate state of type I
 superconductors, noting magnetic field
 effect on structure 15 p2539 A67-29866
 Josephson current in alternating field
 between two superconductors separated by
 dielectric barrier 15 p2530 A67-29868
 Oscillator with lumped parameter
 superconducting L-C tank circuit, noting
 frequency variations as function of
 temperature 15 p2451 A67-29916
 Stabilization of current intensity in
 superconducting coils noting two
 characteristic intensities, measurements of
 niobium compounds, effects of added
 copper, etc 16 p2607 A67-30593
 Phenomenological theory for
 thermomagnetic effects in type II
 superconductor flux flow
 state 16 p2724 A67-30609
 Nernst effect in type I superconductor,
 noting transverse voltages caused by
 longitudinal temperature
 gradients 16 p2727 A67-30819
 Broadening of lines emitted by tunnel
 superconductor, noting unfeasibility of
 simultaneous amplitude-frequency
 prescription of Josephson
 current 16 p2728 A67-31044
 Static and dynamic behavior of weakly
 connected superconducting rings, noting
 methods of measurement and
 results 16 p2728 A67-31058
 Acoustic wave attenuation coefficients for
 small gap superconductors, noting
 electromagnetic absorption and collisional
 drag as cause 16 p2729 A67-31059
 Flux observations in type II
 superconductors when changing magnetic
 field suddenly, with results used to deduce
 flux flow resistivity 16 p2730 A67-31169
 Type II superconductor flux flow
 resistivity theories, introducing Nozières-
 Vinen extension 16 p2731 A67-31170
 Electric field distribution inside local
 superconductor carrying steady case
 analyzed using Ginzburg-Landau equation,
 noting strong compressibility
 effect 16 p2731 A67-31171
 Electron-mirror microscopy for
 intermediate-state pattern of
 superconducting samples noting bulk, thin
 sheet and lead films 17 p2912 A67-32266
 Hysteretic superconductor, analyzing
 critical state and constrained reversibility
 relations in diamagnetic and temperature
 paths 17 p2912 A67-32269
 Superconductors and ferromagnetic
 domains proximity effects at critical
 temperature in resistive and tunneling
 effect measurements 17 p2912 A67-32271
 Thermal magnetic noise fluctuations
 reduction in superconductors below 4.2
 degrees K 17 p2913 A67-32272
 Quasi-particle recombination lifetimes in
 superconductors measured experimentally
 shown to differ from calculated
 lifetimes 17 p2913 A67-32370
 Thermal properties of anomalous
 superconductors, considering specific heat
 jump to normal state and thermal
 conductivity behavior 17 p2914 A67-32453
 Temperature dependence of upper critical
 fields for clean superconductors of second
 kind, noting role of electron-reflection
 properties of surface 17 p2915 A67-32693
 Electromagnetic properties associated with
 presence of overlapping bands in pure
 superconductors, discussing temperature
 dependence 17 p2915 A67-32718
 Temperature dependence of Josephson
 critical current in superconductor model
 having anisotropic energy
 gap 17 p2915 A67-32719
 Superconducting tunnel junction,
 discussing effect of exceeding critical
 current in one film 17 p2922 A67-33058
 Mean free path effects on critical field
 and density of states of small
 superconducting spheres 17 p2924 A67-33370
 Tunneling into thin superconducting films

in magnetic field, measuring field effect on density of states for finite mean free path 17 p2924 A67-33371

Magnetic field induced changes in Bardeen-Cooper-Schrieffer spectrum of electronic excitations in pure type I superconductor and effect on electromagnetic radiation absorption 17 p2925 A67-33374

Magnetization measurements in applied magnetic fields at cryogenic temperatures of dirty type II superconducting transition metal alloys 17 p2925 A67-33375

Electronic contribution to thermal conductivity of pure type II superconductor in high magnetic field, noting rapid conductivity drop and strong anisotropy 17 p2925 A67-33376

Transition temperature of phonon-coupling superconductor merged with that of type II superconductor critical field to obtain strong coupling corrections to critical field 17 p2925 A67-33378

Skin effect in type II superconductor, observing flux penetration into single crystal cylinder immersed in LF alternating magnetic field 17 p2926 A67-33381

Alpha particle irradiation effect at liquid-helium temperature on transition temperature of superconductive tin, indium and thallium foils 17 p2926 A67-33405

Relation between current, voltage and magnetic field of weakly connected double-contact junctions in superconductors 17 p2926 A67-33406

Hard superconductors electrical resistivity when subjected to increasing magnetic field, considering flux pinning and viscous motion of flux lines 18 p3098 A67-33518

Hall angle of various superconducting niobium-tantalum alloys in mixed state, noting dependence on current and temperature 18 p3098 A67-33519

Simultaneous AC and DC in ring-shaped hard superconductors, confirming critical AC and superimposed DC existence 18 p3098 A67-33521

London superconductors in local approximation, obtaining solution to equation in form of gradient expansions 18 p3100 A67-33765

Relation between current and voltage in type II superconductors situated in transverse magnetic field in flux-flow regime 18 p3101 A67-33987

Possible superconductive pairing of two electrons separated by barrier leading to higher transition temperature for superconductors and superconductivity in magnetic metals 18 p3101 A67-33988

Thin films deposited onto substrates cooled to low temperatures investigated for transition temperature in structures of superconductor-dielectric-superconductor 18 p3101 A67-33989

Magnetic field parallel component influence on depinning threshold of vortices in superconducting films 18 p3101 A67-33990

Weak superconductivity electrodynamics and EM wave propagation in Josephson tunnel junction in presence of vortices 18 p3102 A67-34425

Vortical structure of current and magnetic field distribution along superconducting film with magnetic field parallel to surface, discussing possible observation by optical diffraction 19 p3301 A67-34899

Automatic frequency-control system using superconducting resonator and reflex klystron 19 p3192 A67-34984

Hysteretic superconductor, showing trapped flux or remnant magnetic moment linear relationship with average internal field in low but not in high k superconductors 19 p3302 A67-35036

Time variations of order parameter, coupling to external perturbation and effect on various transport properties of dirty type II superconductors 19 p3302 A67-35038

Longitudinal and transverse collective fluctuation modes of order parameter in pure type II superconductor in high critical field region 19 p3302 A67-35039

Thin superconducting films behavior in perpendicular magnetic fields, studying sample geometry effect on reversible magnetization curve 19 p3303 A67-35041

Critical fields in strong coupling superconductors, using Ginzburg-Landau equations 19 p3303 A67-35042

Resonance absorption and zero-field

nuclear spin relaxation in normal and superconducting aluminum, studying phase change 19 p3303 A67-35044

Specific heat of superconductors containing paramagnetic impurities calculated, noting effect of ordering impurity spins 19 p3303 A67-35045

Peltier and Ettingshausen effects in flux-flow state of superconducting niobium, considering contribution to entropy flow 19 p3304 A67-35535

Temperature and frequency effects on amplitude-independent longitudinal ultrasonic attenuation in superconducting lead 19 p3304 A67-35536

High superconducting transition temperatures in molybdenum carbide compounds stressing crystal structures 19 p3245 A67-35729

Reports on progress in physics, volume 29, part II, covering type II superconductors, origin of elements, plasma oscillations, etc 19 p3263 A67-35867

Type II superconductors properties, studying Ginzburg-Landau equations, vortex lines, reversible magnetic behavior and irreversible phenomena in mixed state 19 p3307 A67-35868

Polarity reversal with DC bias in hot-carrier microwave diode 19 p3198 A67-36038

Type II superconductor suspended on elastic fiber in magnetic field investigated for oscillation dampings 20 p3505 A67-36203

Lossless small-area Josephson junction analyzed from viewpoint of quantum dynamics, considering system of two superconducting plates 20 p3505 A67-36207

Theory of superconductors in plane parallel thin films, discussing energy cut-off and termination of omega summation formulations of self-consistency conditions 20 p3507 A67-36328

Flux penetration and vortices formation in macroscopic type II superconductor shown to be favorable below thermodynamical critical field 20 p3508 A67-36426

Properties of steps appearing on volt-ampere characteristic of Josephson current in superconducting tunneling, noting nonlinear resonance effects 20 p3508 A67-36690

Superconducting niobium wire magnetic moment and heat development during external magnetic field variation, discussing irreversible behavior 20 p3511 A67-37240

Superconducting diode behavior in resonant electromagnetic radiation field, studying current-voltage-magnetic field relationship 20 p3511 A67-37241

Superconductors with overlapping bands, discussing copper pairing, heat capacity, critical field and ultrasonic attenuation 20 p3512 A67-37435

Longitudinal ultrasound attenuation in polycrystalline superconducting mercury at 9.3 GHz, studying temperature dependence 20 p3514 A67-37568

Alternating Josephson current and electromagnetic field interaction in generation of Pb-dielectric-Pb tunnel junction, noting steps in IV characteristics 21 p3677 A67-38096

Entropy and specific heat of superconductor in mixed state calculated using cellular model of vortex 21 p3680 A67-38349

Flux line lattice and laminar magnetic structure of mixed state in type II superconductors consisting primarily of lead 21 p3681 A67-38351

Nonideal type II superconductors, discussing flux motion and density, pinning force, magnetization, hysteresis, relaxation and energy loss 21 p3683 A67-38402

Nuclear relaxation time measurement in superconducting niobium near upper critical field 21 p3684 A67-38563

Superconducting bismuth investigated using tunnel effect method to measure electron energy spectrum gap and phonon spectrum distribution 21 p3685 A67-38801

Electrodynamical equations for pure and doped two-band superconductors, studying upper critical magnetic field 21 p3685 A67-38828

Time variation of magnetic flux distribution in type II superconductor under sinusoidal magnetic field, obtaining flux penetration rate, pinning forces and hysteresis loop 21 p3685 A67-39075

Mixed state existence in type I superconducting thin film, discussing microwave power absorption variation with perpendicular magnetic field 22 p3856 A67-39437

Limited instability and flux jumping variation with magnetic field for flux pinning and Lorentz forces equilibrium in mixed state of type II superconductor 22 p3856 A67-39438

LF permeabilities of superconductor due to surface currents calculated for magnetic field conditions 22 p3856 A67-39439

Generalized Ginzburg-Landau parameters and magnetic properties of type II superconductors near upper critical field 22 p3857 A67-39440

Flux penetration and dissipation measured on superconducting niobium slab samples with tangential applied field studied for effect of thickness 22 p3857 A67-39491

Pinning force in nonideal type II superconductors 22 p3858 A67-39519

Transition temperature, Knight shift and NMR line width variation in V-Au compounds as function of atomic ordering 22 p3858 A67-39520

Type II superconductor properties, discussing Ginzburg-Landau and London equations, surface superconductivity, vortex motion, etc 22 p3859 A67-39770

Direct solar to electric energy conversion using superconducting flux barrier, discussing superconductive phase change and magnetic properties 22 p3748 A67-40151

Superconducting devices utilizing transition, zero resistivity and diamagnetic properties of materials in that state 22 p3808 A67-40398

Physics of superconducting devices - Conference, University of Virginia, April 1967 22 p3864 A67-40430

Superconductors for high-Q microwave cavities construction, noting unloaded Q and resonant frequency measurements and surface properties 22 p3865 A67-40431

Current fluctuations in Josephson superconducting tunnel junctions 22 p3865 A67-40433

Zero magnetic field in superconducting lead shell using Meissner effect 22 p3865 A67-40438

Microwave mixing with weakly coupled Josephson superconducting diodes, discussing Fourier components 22 p3865 A67-40439

Superconducting parametric amplifier for measurements of small DC voltages in low impedance circuits 22 p3866 A67-40441

Book on low temperature physics covering Josephson effect, superfluid He flow, superconductivity, etc 22 p3866 A67-40548

Josephson effect and quantum coherence measurements in superconductors and superfluids, discussing perturbation theory and tunnel junctions interference effects 22 p3866 A67-40549

Ferromagnetic powder deposition on superconductor surface in vacuum used to obtain magnetic flux distribution in superconductors 23 p4035 A67-40652

Superconducting niobium energy gap determination by tunneling experiments 23 p4036 A67-40703

High oxygen Nb-Ti alloy solid solution critical superconducting current density and workability dependence on Th, Gd and Y solute content 23 p4036 A67-40705

Voltage-biased superconducting point contact Josephson radiation line width investigation for thermal noise contributions useful for low temperature thermometer 23 p4038 A67-40790

Niobium stannide, V-Ga and V-Si paramagnetic susceptibility, elastic constants and electric resistivity temperature dependence 23 p4038 A67-40794

Tunneling of electrons from normal metal to superconductor containing paramagnetic impurity atoms, discussing current voltage characteristics 23 p4043 A67-41300

Linear current-voltage characteristics in type II superconductors under flux flow conditions 23 p4044 A67-41440

Magnetization measurements for pure superconducting tin cylinders, discussing superheating effects 23 p4044 A67-41441

Magnetic field critical current density characteristics of Nb-Zr-Ti superconducting alloys, discussing peak effect and barrier height random

- distribution 23 p4044 A67-41451
- Magnetic field of flux jumping in synthetic high field superconductors measured as function of temperature and field sweep rate 23 p4044 A67-41452
- Rise rate dependence of transition current of superconducting solenoids on presence of electrical short circuit 23 p4045 A67-41457
- Tunnel current modulation by acoustic wave in superconductors 24 p4200 A67-41778
- Upper critical nucleation field at free surface of superconductor backed by normal metal 24 p4200 A67-41862
- Change of conductivity with temperature measurements for stabilized amorphous bismuth films 24 p4200 A67-41866
- Critical temperature near superconducting phase transition investigated for alloys and pure superconductors 24 p4200 A67-41867
- Edge effects in tunneling characteristics of thin film aluminum diodes in superconducting state, showing anomalies associated with quasi-particle tunneling through film edges 24 p4128 A67-41868
- Background noise measurement results using statistical model for vortex velocities, obtaining noise spectrum for type II superconductors 24 p4200 A67-41869
- Oscillating magnetic field influence on Hall effect and resistance of superconducting niobium 24 p4201 A67-41870
- Thermodynamic property of superconductors with nonmagnetic impurity analyzed using overlapping energy bands near Fermi energy 24 p4203 A67-42162
- Omega phase precipitation and superconducting critical transport currents in Ti-Nb wire samples 24 p4173 A67-42347
- Microwave absorption by magnetic field induced surface states in superconductors, showing anomalies consistent with quasi-particle decay 24 p4205 A67-42739
- Tin and indium superconducting films transverse voltages due to longitudinal temperature gradients calculated for entropy per flux quantum 24 p4205 A67-43098
- Electron tunneling into superconductors to investigate pressure induced energy shifts in Pb phonon spectrum 24 p4206 A67-43100
- SUPERCOOLING**
- Polarized light crystallization microanalysis for supercooled water droplets with additives applied to spherical single crystals of ice during droplet freezing 01 p0109 A67-11010
- Liquidified propane as fog dispersing agent 10 p1676 A67-22814
- Ice single crystal growth rate in supercooled water explained on basis of combined heat dissipation mechanism and molecular growth kinetics 23 p4024 A67-40973
- SUPERCritical PRESSURE**
- Elastoplastic deformation of circular cylindrical shells of ideally plastic incompressible material under uniform supercritical hydrostatic pressure 05 p0922 A67-17176
- Convective heat transfer through stabilized turbulent flow of chemically homogeneous liquid in circular pipe under supercritical pressure conditions 07 p1265 A67-19127
- Ferromagnetic film coercive force variation near supercritical state due to film thickness 12 p1981 A67-25243
- Lower critical load for deformation of cylindrical shell in torsion and hinged along edges 13 p2215 A67-26376
- Coolant passage axial curvature effect on heat transfer to endothermically dissociating supercritical nitrogen tetroxide [ASME PAPER 87-HT-59] 20 p3549 A67-36741
- Convective heat transfer through stabilized turbulent flow of chemically homogeneous liquid in circular pipe under supercritical pressure conditions 21 p3731 A67-38171
- SUPERFLUID FLOW**
- Hydrodynamic approximation of Green function for superfluid Bose system 18 p3029 A67-34386
- Book on low temperature physics covering Josephson effect, superfluid He flow, superconductivity, etc 22 p3866 A67-40548
- Josephson effect and quantum coherence measurements in superconductors and superfluids, discussing perturbation theory and tunnel junctions interference effects 22 p3866 A67-40549
- Energy dissipation and motion equations of superfluid helium flow through pores, describing technique to detect critical velocity in wide channels 22 p3839 A67-40550
- SUPERFLUIDITY**
- Helium 2 film free convection heat transfer, discussing mathematical analysis for vertical flat plate and horizontal circular cylinder [ASME PAPER 65-WA/HT-10] 03 p0536 A67-14007
- Book on experimental superfluidity covering He properties, low temperature production, temperature measurement, two-fluid model and macroscopic quantization, generalized hydrodynamic equations, etc 15 p2517 A67-29265
- SUPERHEATING**
- Rate dependent melting of polytetrafluoroethylene by differential thermal analysis, noting that amount of superheating is larger with higher molecular weight 04 p0641 A67-14528
- Condensation heat transfer in presence of noncondensables, interfacial resistance, superheating, variable properties and diffusion 04 p0720 A67-14644
- Probability of effervescence of superheated liquids as function of temperature and pressure, analyzing N-pentane and hexane under isobaric heating and reduced pressure 09 p1580 A67-21907
- Superheating in cylindrical pure niobium by suppressing end effects 14 p2369 A67-28597
- Superconducting and superheated metastable state transition to normal state by beta irradiation 17 p2912 A67-32270
- Magnetization measurements for pure superconducting tin cylinders, discussing superheating effects 23 p4044 A67-41441
- SUPERHETERODYNE RECEIVER**
- InSb submillimeter detector as mixer in superheterodyne receiver shows performance two orders less than ideal receiver 01 p0036 A67-10440
- Graphing spurious intermodulation responses in tunable superheterodyne receiver to determine susceptibility to RF environment 03 p0383 A67-13789
- Heterodyne and photon counting receivers compared for optical communications 07 p1185 A67-19398
- Superheterodyne receiver operating in K-band having solid state low noise characteristics 18 p3011 A67-34068
- Optical communication experiments to compare coherent and noncoherent optical detection fading characteristics in different weather conditions, using laser transmitter and optical superheterodyne receiver 19 p3184 A67-35685
- Radio signals from clouds to yield information on cloud physics, using superheterodyne microwave receivers 24 p4124 A67-42883
- SUPERNOVA**
- Radio sources and supernova theory of north polar Spur 05 p0903 A67-17292
- Evolution of radio spectral index of supernova remnants modeled to include synchrotron radiation energy distribution 11 p1859 A67-24114
- Cosmic X-ray sources attributed to thermal emission of hot condensations from supernova remnants in our galaxy or other galaxies 12 p1995 A67-25764
- Type I supernova exponential decrease in light output due to spontaneous nuclear gamma ray fission of Cf 254, including detection techniques using satellite or balloon-borne telescopes 12 p1995 A67-25765
- Neutron star structure and evolution from presupernovae stars including gravitational collapse and neutrino emission processes 12 p2007 A67-25768
- Statistical verification of hypothesis explaining observed scintillations of light curve of quasi-stellar radio sources by explosions of supernovas 13 p2198 A67-26766
- Supernova explosion and collapse theory using relativistic hydrodynamics 16 p2752 A67-31541
- Supernovae photometric properties, considering mean absolute photographic magnitude at maximum light, brightness decline rate, etc 18 p3119 A67-33857
- Thermonuclear reactions occurring in supernova shock wave propagating through stellar envelope 18 p3136 A67-34726
- Core of two solar masses of gravitationally collapsing star, analyzing hydrodynamics, heating, helium 4 formation, neutron decay, nucleosynthesis, light output and mass ejection 22 p3882 A67-39622
- Radio evidence for two supernova remnants in Southern Milky Way and observations of shell type radio sources, considering shell model fitting problem 24 p4230 A67-42332
- Novae and supernovae outbursts, suggesting mechanism which can account for both phenomena and for other problems concerned with quasi-stellar sources /quasars/ 24 p4231 A67-42451
- SUPEROXIDE**
- S PEROXIDE**
- SUPERSATURATION**
- Adiabatic flow of K vapor in supersaturated state noting supercompression, supercooling and equilibrium through condensation jump 11 p1881 A67-24029
- Condensation path of cooling gas of solar composition calculated considering barriers to homogeneous nucleation of condensed phase 16 p2751 A67-31454
- Critical supersaturations for homogeneous nucleation of ethanol, hexane, etc, investigated using thermal diffusion cloud chamber 20 p3555 A67-37562
- SUPERSONIC AIRCRAFT**
- SA BOEING 2707 AIRCRAFT
- SA F-111 AIRCRAFT
- SA HYPERSONIC AIRCRAFT
- Analytic processes for evaluation of supersonic aerodynamics of configuration treating drag, wing design, warp, interference and sidewash [AIAA PAPER 65-717] 03 p0354 A67-12914
- Parametric investigations of supersonic long-haul aircraft, discussing operational profile, optimal lift-drag ratio, takeoff weight, civilian and military aircraft 03 p0358 A67-12975
- Fuel requirements for high altitude high-Mach number aircraft noting thermal stability, autooxidation, self-ignition, specific heat, etc [DVL-599] 03 p0502 A67-13015
- Lubricant testing for supersonic aircraft, examining temperature requirements, viscosity, evaporation characteristics, etc [DVL-606] 03 p0426 A67-13016
- Aircraft noise characteristics and relationship to Lockheed SST design 03 p0360 A67-13920
- F-111 type hydraulic power supply system design for supersonic aircraft using ground support equipment and military materials 05 p0752 A67-16159
- Property damage caused by sonic booms, discussing recovery of damages under Federal Tort Claims Act 05 p0930 A67-16772
- Mesoscale temperature variability below 60,000 ft measured for calculation of supersonic aircraft fuel requirement 05 p0838 A67-17305
- Effects of 450 and 600 degrees F exposures on mechanical properties of glass-fiber polyimide resin sandwich panels to be used on large skin areas of SST aircraft [AIAA PAPER 67-174] 06 p1021 A67-18484
- Atmospheric effects on supersonic aircraft operations, particularly sporadic effects near ground and in free atmosphere, density variations, etc 07 p1219 A67-19066
- Handling and operation of XB-70A aircraft at Mach 3 speed noting folding wing tips, variable-geometry air inlet duct, etc 07 p1129 A67-19910
- Digital computer CPU control of kinetic heating processes in engine of supersonic aircraft under simulated flight conditions 08 p1315 A67-21007
- Aircraft noise characteristics and relationship to Lockheed SST design 09 p1439 A67-21703
- Methods to minimize sonic boom ground exposure, considering aircraft design and maneuverability as function of altitude 09 p1439 A67-21942
- Spontaneous ignition temperature of flammable fluid in facsimile high speed aircraft hydraulic system 09 p1521 A67-22249
- Adaptation scheme applied to pitch axis control system of supersonic aircraft, using stability analysis for system design 09 p1440 A67-22387
- Sonic boom measurements for supersonic aircraft, discussing techniques and results 09 p1440 A67-22457
- Boundary layer control for improvement of lift at lower angles of attack by carrier-

based supersonic aircraft
[AIAA PAPER 65-751] 09 p1441 A67-22484

Feasibility of effective aerodynamic round-
lip inlet for supersonic aircraft takeoff and
low speed flight 09 p1438 A67-22495

Three-dimensional flutter calculations
verification by wind tunnel results, using
flexible supersonic aircraft planform model
of determined characteristics to control
calculations 10 p1622 A67-22882

Bench and flight tests of twin spool axial
flow turbojet power plant for Concorde
aircraft
[ASME PAPER 67-GT-8] 11 p1854 A67-24796

Supersonic business jet designs, unswept
trapezoidal wing model and delta wing
model
[SAE PAPER 670246] 12 p1895 A67-25501

SST air inlet control system, considering
maintainability, impact on cockpit
procedures and component reliability effect
on dispatch reliability
[SAE PAPER 670325] 12 p1895 A67-25869

Supersonic aircraft effect on air traffic
control facility, radar and landing
aids 13 p2154 A67-26712

Future supersonic and hypersonic aircraft
horizontal liquid hydrogen fuel tank
requirements, discussing insulation
optimization using variable
thickness 13 p2054 A67-27657

Temperature stable lubrication of
supersonic aircraft
[ASLE PREPRINT 67AM 8A-1] 14 p2326 A67-28793

Flight test skin temperatures of
supersonic aircraft compared with
theoretical results, explaining measurement
discrepancies 14 p2243 A67-28977

Supersonic inlets for jet aircraft,
discussing positioning of terminal shock at
intake for most efficient engine
performance 15 p2415 A67-29303

Design requirements of commercial
supersonic aircraft engines
[AIAA PAPER 67-376] 15 p2549 A67-30423

Supersonic boom, discussing aerodynamic
field of aircraft, sonic ray characteristics
and noise suppression 16 p2589 A67-30832

Long distance air navigation aids, stressing
supersonic flight safety
requirements 16 p2701 A67-31248

Hydraulic power units for supersonic
aircraft noting trends in component power,
speed, flow, pressure, design,
etc 17 p2800 A67-31969

Engine nacelle location, size and shape
effects on drag due to wing thickness and
drag due to lift
[AIAA PAPER 66-665] 17 p2791 A67-32567

Direct numerical control by computer of
150 heating circuits for safe kinetic heating
test simulation of flying conditions for large
supersonic aircraft 17 p2820 A67-32748

Supersonic aircraft nozzle system
aerodynamic performance at subsonic speeds
[AIAA PAPER 67-452] 18 p2983 A67-33926

Supersonic aircraft evolution emphasizing
Dassault series, Northrop T-38 and F-5 and
Swedish Draken and Viggen 22 p3746 A67-39883

Lateral stability augmentation of
supersonic aircraft using linear multichannel
state-vector optimal feedback
control 22 p3746 A67-40155

Long range supersonic cruising aircraft
research and design techniques, methods
and approaches for optimizing efficiency,
drag and ATC
[AIAA PAPER 67-748] 23 p3987 A67-40982

Medical support for SR-71 aircraft crew
members, describing crew selection, flight
preparation and medical
examinations 23 p3966 A67-41600

Physiological Support Division facility for
training crew members of SR-71
aircraft 23 p3968 A67-41616

Supersonic civil aircraft, considering
journey time, safety and operating
economy 24 p4093 A67-41886

SUPERSONIC AIRFOIL

Linearized supersonic theory for favorable
thickness distributions and drag reduction
for wings in supersonic flow
[AIAA PAPER 65-716] 08 p1276 A67-20559

Nonlinear differential equation for shock
wave of several circular arc airfoils
integrated to give shock wave
location 14 p2239 A67-27797

SUPERSONIC COMBUSTION

Penetration of gaseous jets injected into

supersonic stream treated by solid body
drag model, noting application to hypersonic
ramjet combustion 02 p0232 A67-11935

Supersonic combustion ramjet
development 06 p1073 A67-17809

Chemical kinetics effects in supersonic
combustion noting three different zones in
chamber 06 p1113 A67-18027

Shock induced supersonic combustion of
fuel-air mixtures used to obtain induction
time, evaluating kinetic data and effect of
small contamination levels
[AIAA PAPER 67-105] 06 p1114 A67-18284

Fuel injection parameters effects on
mixing of gaseous hydrogen fuel with
supersonic air stream for hypersonic ramjet,
determining turbulent diffusion
coefficient 06 p1117 A67-18387

Supersonic combustion measurements by
thrust system method, optical probe and
gas-sample probe technique
[AIAA PAPER 67-223] 06 p1004 A67-18462

Specific impulse and thrust coefficient
performance as function of flight Mach
number and altitude for air augmented solid
propellant propulsion vehicle using
supersonic combustion
[AIAA PAPER 67-226] 06 p1097 A67-18517

Scramjet performance analysis stressing
construction problems and importance of
fuel choice 11 p1853 A67-24748

Supersonic combustion simulation facility
and duplicable static parameters for
hydrogen fuel
[AIAA PAPER 66-743] 15 p2465 A67-29437

Mechanism of electrode erosion by
supersonic flame jets during pulsed
discharge 16 p2724 A67-31775

Integration of propulsion system into
airframe of hypersonic cruise aircraft,
discussing configurations, cooling and
supersonic combustion 17 p2796 A67-32475

Aerodynamic effects of supersonic
combustion studied in wind
tunnels 18 p3154 A67-33829

Supersonic combustor length and contours
for optimum performance determined from
one-dimensional pressure-area
analysis 18 p3154 A67-33832

Supersonic combustion characteristics of
hypersonic ramjet predicted by analytical
method using constant-mass tube technique,
discussing flow field properties
[AIAA PAPER 67-494] 18 p2983 A67-33958

Fluid dynamics and chemical phenomena
near injector exit of idealized supersonic
combustion burner, noting parameters of
ignition delay length
[AIAA PAPER 67-496] 18 p3158 A67-33960

Flame stabilization with flame holders in
supersonic flow, discussing improved
combustion in ramjets at supersonic
velocities 18 p3116 A67-34609

Supersonic combustion simulation for
hypersonic flight in relation to scramjet
operation, discussing auto-ignition limits
[CI PAPER 67-6] 19 p3344 A67-35001

Shock induced supersonic combustion of
fuel-air mixtures used to obtain induction
time, evaluating kinetic data and effect of
small contamination levels
[AIAA PAPER 67-182] 21 p3732 A67-38858

SUPERSONIC COMBUSTION RAMJET

MISSILE /SCRAM/
Turboramjet developed from Griffon
aircraft capable of propelling hypersonic
vehicles 09 p1559 A67-22093

SUPERSONIC COMMERCIAL AIR

TRANSPORT /SCAT/
S BOEING 2707 AIRCRAFT

SUPERSONIC COMPRESSOR

Low altitude hypersonic flow simulation
by means of supersonic compressor,
considering capability of providing true
temperature sea-level flight duplication at
Mach 9 02 p0229 A67-11933

Parametric analysis of supersonic
compressors, determining relative
efficiencies of various leading and trailing
guide vane configurations 03 p0352 A67-13010

Pseudoshocks in pipe flow in supersonic
compressors represented as diffusion
process, noting application in cascade and
rotor configuration 03 p0352 A67-13011

Supersonic retardation cascades for
lossless reduction of supersonic flow to
subsonic in turbines and
compressors 03 p0503 A67-13012

Limitations on specific outputs and
compression ratio per stage in supersonic

compressors 05 p0874 A67-16746

SUPERSONIC DIFFUSER

Roy method in computing bladed
supersonic diffusers for centrifugal
compressors 02 p0235 A67-12792

Heat transfer in supersonic separated flow
over two-dimensional backward-facing step
found in entry enlargement region of
supersonic parallel
diffuser 04 p0546 A67-14640

Approximate single parameter solution for
compressible turbulent boundary layer in
supersonic diffuser 24 p4144 A67-42586

SUPERSONIC DRAG

Maximum lift/drag ratio wing for
supersonic environment 07 p1127 A67-20035

Drag coefficient of sphere at supersonic
velocities dependence on specific heat ratio
of argon, air, carbon dioxide and
freon 16 p2593 A67-31122

SUPERSONIC FLIGHT

Nonsteady state gas flows with small
entropy gradients corresponding to
supersonic flight 02 p0178 A67-11629

Biological effects of supersonic flight,
discussing radiation at high altitudes and
preventive measures 07 p1134 A67-19532

Aerodynamics survey emphasizing
supersonic speed 14 p2239 A67-27874

Endothermic hydrocarbon fuels for
supersonic aircraft, noting heat sink capacity
effect in overcoming thermal thicket and
usability as engine fuel 15 p2543 A67-29305

Sonic boom effect on structural
behavior 15 p2573 A67-29401

Soviet book on aeronautical meteorology
covering wind and cloud effects on takeoff,
landing and supersonic flying in storms and
jet stream layers 18 p3074 A67-33876

Aerodynamic effects of supersonic
combustion studied in wind
tunnels 18 p3154 A67-33829

Bluntness influence on nose cone heating
in laminar flow in supersonic flight
investigated to determine optimum design of
rocket or space vehicle nose 20 p3359 A67-37165

Soviet monograph on problem of
acceleration in aviation
medicine 20 p3375 A67-37466

High performance aerodynamic impulse
facility with shock tunnel, expansion tube
and accelerator for high velocity and high
Reynolds number environment 21 p3605 A67-37768

Oblique interaction between supersonic
vehicle in free flight and plane shock wave
simulated, noting large unbalanced
force 21 p3607 A67-37776

Air temperature measurements at subsonic
and supersonic flight speeds, discussing
error sources and thermometer
efficiency 22 p3797 A67-39542

Sonic boom and factors influencing shock
wave propagation during straight horizontal
supersonic flight 22 p3744 A67-39547

Supersonic aircraft evolution emphasizing
Dassault series, Northrop T-38 and F-5 and
Swedish Draken and Viggen 22 p3746 A67-39883

SUPERSONIC FLOW

Heat transfer and equilibrium temperature
of heat conducting sharp cones in supersonic
rarefied gas flow at zero angle of
attack 01 p0007 A67-10977

Linear formulation of electromagnetic
field effect on supersonic gas
flow 01 p0125 A67-10980

Three-dimensional supersonic gas flow
with shock waves around flat wing analyzed,
using integral relations method 01 p0007 A67-10981

Experimental study of turbulent transfer
phenomena in isobaric mixing layer of
supersonic flow containing preexisting
boundary layer [ONERA-TP-327] 01 p0054 A67-11003

Steady flow of jet from orifice at nose of
body and opposing supersonic free
stream 02 p0178 A67-11565

Tabulated data on specific losses in flow
systems 02 p0233 A67-11995

Hypersonic aerodynamic coefficients for
bodies of revolution in
yaw 02 p0179 A67-12314

Rutgers Axisymmetric Near-Wake Tunnel
for testing turbulent supersonic base flow,
temperatures and pressure distributions 02 p0230 A67-12361

- Diatomic gas flow past blunt bodies, noting effect of oscillation and dissociation relaxation on mean energy 02 p0180 A67-12465
- Fluctuations of potential isentropic supersonic gas flow in finite channel with oscillating walls 02 p0180 A67-12669
- Aerodynamic characteristics calculation for wing-fuselage assembly in supersonic flow 02 p0180 A67-12793
- Book on supersonic gas flow past blunt bodies under various conditions 03 p0349 A67-12851
- Supersonic flow past blunt body with convex corner calculated to establish sonic point on body 03 p0349 A67-12862
- Calculating shock wave separation and relaxation velocities for supersonic airflow past sphere 03 p0349 A67-12863
- Supersonic flow past sphere by hot gas mixture with detonation wave in cases when wave does not split and when splitting occurs 03 p0349 A67-12864
- Plane adiabatic flow of ideal gas behind separated shock wave for uniform supersonic symmetrical flow past smooth profile 03 p0349 A67-12873
- Approximate distribution of pressure friction and heat-transfer coefficients in laminar boundary layer separation during interaction with supersonic flow 03 p0401 A67-12877
- Turbulent boundary layer in subsonic or supersonic flow past pinched-waist bodies of revolution at various Mach numbers and pressure gradients 03 p0350 A67-12989
- Interference between plane surfaces in supersonic gas flow between two rectangular parallelepipeds 03 p0403 A67-13630
- Nozzle wall shape design based on Mach waves generation appearing when supersonic gas expands about corner 03 p0352 A67-13816
- Goursat problem of first order nonlinear hyperbolic equations, introducing characteristic parameters with reduction to standard form 03 p0462 A67-14109
- Heat transfer and equilibrium temperature of plate in supersonic flow of rarefied gas 04 p0546 A67-14783
- Oblique shock detection in conical nozzle with circular arc throat, noting measurement techniques 04 p0547 A67-14833
- Sudden expansion or compression effect on momentum thickness change in turbulent boundary layer calculated, using parameter of velocity layer profile 04 p0604 A67-14840
- Cryogenic pumping capability of liquid helium cooled plate in supersonic flow field at simulated high altitude 04 p0606 A67-14999
- 7-ft-diam shock tube for transonic and supersonic aerodynamic testing 04 p0598 A67-15254
- Supersonic conducting gas flow in coaxial channel in magnetic field formed by currents flowing over plasma 04 p0669 A67-15514
- Mass and heat transfer data from sweptback circular cylinders in Mach 2 wind tunnel with Reynolds number 100,000 04 p0549 A67-15824
- Approximate method for measuring distance between head wave and tip of body in supersonic flow past blunt tip body 04 p0550 A67-15884
- Deflection angle of supersonic gas flow with oblique shock wave and heat input in wake, choosing minimum entropy variation as measure of system optimality 04 p0550 A67-15898
- Numerical algorithm for supersonic gas flow past blunt bodies with shock wave separation, using Dorodnitsyn method of integral correlation 05 p0791 A67-16374
- Convective and radiative heat transfers at stagnation point of hemisphere cylinder model immersed in high enthalpy partially ionized supersonic flow in plasma wind tunnel 05 p0747 A67-16432
- Quasi-conical supersonic flow around lifting system with curved leading edge 05 p0749 A67-16843
- Supersonic flow around elliptic cone with symmetrical fins, determining perturbation velocity via Germain method 05 p0749 A67-16844
- Terminal shock-boundary layer interaction on slender cone-cylinder payloads at supersonic speeds and resulting flow separation [AIAA PAPER 66-471] 05 p0924 A67-17213
- Flow pressure structures of supersonic flow over rearward facing step, showing pressure changes and Reynolds number role 05 p0750 A67-17339
- Ion density profiles in boundary layers associated with supersonic flow of shock heated air over flat plate measured by cylindrical and flush-mounted electrostatic probes [AIAA PAPER 66-159] 05 p0856 A67-17345
- Supersonic flow past cone cylinder type body with circular groove 05 p0751 A67-17480
- Self-similar problems concerning supersonic flows of gaseous fuel mixtures with detonation waves and slow combustion fronts past wedges and cones 06 p0935 A67-17725
- Base pressure fluctuations behind cone in supersonic flow due to presence of stagnant zone with subsonic reverse flow in shape of annular vortex 06 p0936 A67-17735
- Plane vortex flow in vicinity of orthogonality point of sound line to velocity vector 06 p0936 A67-17738
- Linear supersonic conical flow past lower surface of triangular wing, obtaining homogeneous boundary value problem for analytical function of complex variable 06 p0936 A67-17739
- Laminar boundary layer on ellipsoids of revolution situated at zero angle of attack in supersonic flow of perfect gas 06 p0936 A67-17740
- Inviscid flow method predicting nonlinear supersonic and hypersonic lift component of highly swept wings with low aspect ratio 06 p0937 A67-18013
- Discontinuous solutions in supersonic reacting gas flows under nonequilibrium conditions 06 p0984 A67-18112
- Inviscid linearized perturbations of supersonic entropy layers analyzed, using approximating partial differential equations by simultaneous ordinary differential equations [AIAA PAPER 67-6] 06 p0938 A67-18249
- Base pressure behind supersonic vehicle, calculating existence conditions for wake solutions and location of stable and unstable singularities [AIAA PAPER 67-60] 06 p0986 A67-18269
- Source flow expansion of partially ionized gas into vacuum for predicting flow properties of low density free jet plasma expansions [AIAA PAPER 67-99] 06 p1041 A67-18281
- Flow field associated with tangential slot gas injection in supersonic flow, presenting turbulent mixing zone and stability and spark shadowgraphs [AIAA PAPER 67-198] 06 p0987 A67-18300
- Supersonic flow over axisymmetric bodies with continuous or discontinuous slope solved via parametric differentiation [AIAA PAPER 67-5] 06 p0939 A67-18303
- Skin friction under mass injection on porous flat plate in supersonic turbulent flow [AIAA PAPER 67-194] 06 p0987 A67-18341
- Hydrogen or nitrogen gas injection at various Mach numbers from nozzle in flat plate into Mach 2.72 free air stream [AIAA PAPER 67-225] 06 p0940 A67-18444
- Two-dimensional adiabatic laminar separated regions in supersonic flow, examining effects of blowing and suction at wall [AIAA PAPER 67-192] 06 p0988 A67-18459
- Time dependent computational method for three-dimensional blunt body flow fields traveling at supersonic speed including shock points, sphere cones and ellipsoid [AIAA PAPER 67-222] 06 p0941 A67-18461
- Stability of circular cylindrical shell in supersonic nonviscous conducting gas flow with unperturbed velocity and under magnetic field 06 p1106 A67-18622
- Quasi-MHD analysis of supersonic rarefied plasma flow near magnetic dipole 06 p1043 A67-18670
- Linearized long wave diffraction theory of supersonic inviscid flow past slender circular cylindrical bodies and thin wings 06 p0942 A67-18729
- Rational approximation method for calculating supersonic axisymmetric flow of perfect gas around given blunt body 06 p0943 A67-18846
- Radiation effect on hydrodynamic shock wave parameter distribution for bodies entering dense atmospheric layers at supersonic velocities 07 p1125 A67-19110
- Nonuniform two-dimensional subsonic and supersonic flow of compressible fluid past body, using small parameter method 07 p1125 A67-19322
- Numerical solution to time dependent Navier-Stokes equation for transient supersonic flow around right circular cylinder, using explicit-implicit finite difference method [AIAA PAPER 67-221] 07 p1169 A67-19625
- Simple method for determining deviation of supersonic or hypersonic plane parallel flow of inviscid gas caused by auxiliary jet in form of thin layer 07 p1127 A67-20208
- Aerodynamic characteristics /pressure distribution and wave drag/ or polygonal wings of symmetrical thickness in supersonic flow 07 p1127 A67-20209
- Unsteady supersonic flow about conical wing fuselage system with LF harmonic oscillatory motion 07 p1127 A67-20224
- Antisymmetrical thin delta wing with flow separation at subsonic leading edge 07 p1128 A67-20236
- Perfect fluid model for observed phenomena of plane transonic flow past given profile with attached shock wave, starting with lemma on possible hodograph configuration 07 p1128 A67-20282
- Surface pressure, heat transfer coefficient, wave structure and shock disturbances of inviscid supersonic flow field along corner of intersecting wedges [AIAA PAPER 66-128] 08 p1276 A67-20564
- Compatibility relations and generalized finite difference approximation for three-dimensional steady supersonic flow 08 p1320 A67-20566
- Flow field around porous wedge or cone immersed at zero angle of attack in uniform supersonic free stream when contact surface is straight 08 p1276 A67-20571
- Numerical wing analysis in steady or unsteady supersonic flow, calculating pressure coefficient, local loads and generalized forces from deformation law or wing slope 08 p1278 A67-20800
- Shock waves and periodic structures of supersonic plasma flows and effect on velocity of foremost luminous front 08 p1358 A67-20852
- Boundary value problem for Poisson-Vlasov equations resulting from interaction of conducting body and supersonic flow of rarefied plasma solved, using iterative method 08 p1363 A67-21368
- Test of probes designed to determine direction of supersonic flows in wind tunnels, using schlieren photography 09 p1496 A67-21693
- Supersonic flow velocity and density probe for direct measures of mass and momentum influx, noting solution of H-T diagram of argon and probe criteria 09 p1497 A67-21776
- Action of strong transverse magnetic field on supersonic current of ionized argon 09 p1540 A67-21787
- Sub-or supersonic wing leading edge in unsteady supersonic flow, presenting discontinuities in vibration modes and calculating wing stress forces 10 p1590 A67-22879
- Three-dimensional flow in supersonic stream in symmetry plane of region of shock boundary layer interaction in front of obstacle mounted on plate, noting penetration in separation region 10 p1590 A67-23026
- Supersonic flow of ideal thermodynamically perfect gas from nozzle into medium at rest 10 p1591 A67-23037
- Inviscid flow characterized by annular elliptical region between shock wave and ducted body calculated by integral relation method, noting contraction coefficient values 10 p1591 A67-23045
- Behavior of inviscid supersonic conical flow fields near crossflow stagnation points studied by constructing coordinate expansions of exact conical flow equations [AIAA PAPER 66-491] 10 p1591 A67-23112
- Approximate closed form solutions for supersonic separated and reattaching laminar flow problem with boundary layer/shock wave interaction 10 p1591 A67-23115
- Supersonic stream interaction with two-dimensional secondary jet from rectangular planform wedge 10 p1592 A67-23116
- Analytic solution to blunt body problem in supersonic flow of ideal gas approximated, using power series

[NOR REPORT 65-239] 10 p1593 A67-23454
 Supersonic motion of plate in two-component medium in two dimensions 10 p1628 A67-23647
 Supersonic delta wing problem, discussing new approach in determining flow parameters 10 p1593 A67-23687
 Approximate iterative calculation of non-Newtonian supersonic gas flow past highly blunt bodies 11 p1741 A67-24156
 Supersonic shear flow over cavity investigated, constructing velocity and shear stress coefficient profiles satisfying boundary conditions 11 p1778 A67-24218
 Laminar heat transfer rate to two-dimensional blunt base in supersonic flow evaluated for varying Reynolds, flow and shock Mach numbers 11 p1882 A67-24222
 Strong small perturbation solutions for steady supersonic flows of inert or reacting gas mixtures around plane corner 11 p1778 A67-24230
 Heat transfer between turbulent supersonic air stream and circular water-cooled tube at Mach 1 to 4, using two-dimensional flow model 12 p2035 A67-25753
 Spectroscopic measurement of combustion gas composition in supersonic flow [AIAA PAPER 65-580] 12 p1990 A67-25899
 Internal structure of highly underexpanded transverse jets in supersonic cross stream 12 p1892 A67-25900
 Hyperbolic region solutions of equation approximating Chaplygin equation near supersonic flow vacuum line in hodograph plane 12 p1962 A67-26181
 Wall streamlines and detachment on circular cone at angle of incidence in supersonic flow 13 p2049 A67-26591
 Three-dimensional supersonic flow for ideal fluids using Euler motion equation 13 p2050 A67-26648
 Parametric self-excited vibrations of plates of finite length in plane supersonic flow, applying linearized potential flow theory, deriving frequency equations 13 p2218 A67-26804
 Hemispheric pressure distributions, measuring effect of Mach number, hole size and angular position of hole on Pitot pressure 13 p2220 A67-27193
 Ionized gas flow past oscillating interface in presence of magnetic field, based on MHD boundary layer model with constant velocity profile 13 p2168 A67-27302
 Three-dimensional supersonic flow past pointed nonaxisymmetric bodies characterized by great local surface curvature changes, using new approximation 13 p2051 A67-27617
 Hartmann oscillator problem studied using hydraulic analogy between supersonic compressible gas dynamics and incompressible flows with free surface 14 p2295 A67-27903
 Gas dynamic functions for supersonic gas flow past axisymmetric bodies of various configurations 14 p2239 A67-27991
 Supersonic three-dimensional flows past smooth bodies, calculating flow parameters by characteristic method with analytical approximation of gas-dynamic functions 14 p2240 A67-27992
 Supersonic viscous flow near blunt body stagnation line, using Navier-Stokes equations 14 p2240 A67-27993
 Three-dimensional gas flow in region of incidence of shock wave on cylinder situated in high supersonic flow 14 p2297 A67-27995
 Shock wave structure in air at supersonic and hypersonic velocities studied by electron-beam density method 14 p2297 A67-27997
 Supersonic flow separation from corner of base compared to Stokes-type flow separation 14 p2240 A67-28111
 Thick laminar boundary layer effect on aerodynamic behavior of simple shapes in supersonic low density flow 14 p2241 A67-28170
 Low density shock layer structure on cylinders at Mach 4 noting magnitude, location of disturbances, existence of shock wave-like flows, recession of leading edge, etc 14 p2299 A67-28173
 Supersonic flow pressure and density perturbations caused by discrete or continuous mass and heat sources 14 p2302 A67-28316
 Two-dimensional supersonic fluid amplifier flow characteristics analyzed numerically by

digital computer 14 p2250 A67-28333
 Flow turning angle during two-dimensional turbulent supersonic reattachment to plane wall [ASME PAPER 67-FE-20] 14 p2305 A67-28367
 Parameter determination for flow field in space between shock wave of nonviscous supersonic gas flow and thin spherically blunt cone 14 p2243 A67-28659
 Propagation of small disturbances in general three-dimensional unsteady nonequilibrium MGD, noting influence of various parameters 14 p2361 A67-28904
 Supersonic gas-particle flow with chemical reactions 15 p2469 A67-29225
 Testing conditions for near-wake study of solids of revolution in supersonic and hypersonic flow, using streamlined supports in magnetic suspension [ONERA-TP-454] 15 p2416 A67-29379
 Weakly perturbed supersonic flows in presence of arbitrary number of nonequilibrium physicochemical processes 15 p2472 A67-29688
 Interaction of supersonic gas stream with inclined surface, calculating parameters and boundary of fluid spreading 15 p2472 A67-29776
 Laminar viscous wake interaction with supersonic external inviscid flow downstream treated by implicit finite difference method 15 p2417 A67-30188
 [AIAA PAPER 66-454] 15 p2417 A67-30188
 Supersonic internal axisymmetric conical flow obeying Taylor-Maccoll equation, discussing applications to wing surfaces and supersonic inlet leading edges 15 p2418 A67-30192
 Local turbulent properties of supersonic jet exhaust measured optically by crossed beam correlation technique 16 p2591 A67-30943
 Base pressure and geometry of separated region in boundary of supersonic accelerated flow analyzed and compared with Chapman-Korst model 16 p2592 A67-30951
 Collection of papers on aerophysical studies of supersonic flows covering shock tube experiments, gas density, interferometer and photographic measurements, etc 16 p2872 A67-31101
 Shock tube analysis of time dependent formation of supersonic flow near blunt bodies 16 p2592 A67-31102
 Argon and nitrogen flows past sphere at low supersonic velocities analyzing formation of bow shock wave 16 p2592 A67-31103
 Shadow method analysis of shock wave interaction with fixed bodies in shock tube at small and medium supersonic Mach numbers 16 p2673 A67-31105
 Variable heat capacity of gas effects on supersonic flow past blunt body analyzed using dimensionless system of equations 16 p2592 A67-31113
 Equations to investigate effect of simultaneous oscillation and dissociation relaxation on gas dynamic parameters of supersonic flow past blunt bodies 16 p2592 A67-31114
 Firing range for investigating Reynolds number effect on flow around bodies having complex design at transonic and supersonic velocities 16 p2655 A67-31116
 Photoelectric method measuring separation of head shock wave from supersonically-moving body, detailing equipment design and operation 16 p2674 A67-31128
 Mach number effect on location of head shock wave and flow stability at slightly supersonic velocities for various body shapes 16 p2593 A67-31129
 Shock-wave separation dependence on bluntness degree, Mach number and gas type during supersonic motion of ellipsoids of revolution 16 p2675 A67-31130
 Shape dependence of detached shock wave in supersonic gas flow of blunt-nosed models on Mach number, heat capacity and bluntness ratio 16 p2593 A67-31131
 Supersonic unsteady flow of cylindrical body past diaphragm model at interface between density-differing gases, studying flow patterns 16 p2593 A67-31133
 Heat conducting supersonic gas flow around corner considered calculating viscous corrections in expansion region 16 p2660 A67-31218
 Magnetically driven shock tube as tool for aerodynamic studies of high velocity high enthalpy flows 16 p2594 A67-31265

Soviet book on supersonic gas flows in perforated boundaries covering flow characteristics, dynamic property, supersonic nozzles, velocity regulation, etc 17 p2789 A67-32019
 Ionization of low temperature supersonic plasma jets, noting kinetics of elementary processes, gas dynamic parameters and effects of combustion and alkali metal admixtures 17 p2896 A67-32170
 Rarefied gas supersonic flows studied in wind tunnel for aerothermal/aerodynamic characteristics 17 p2790 A67-32231
 Book on aerodynamic and aerothermal experiments on circular cylinders at angle of attack in supersonic flow 17 p2790 A67-32379
 GaAs single crystals excited to stable longitudinal vibrations by supersonic absorption, determining resonance curve 17 p2914 A67-32401
 Velocity potential near disturbance boundary for steady supersonic flow past body-and-wing model 17 p2790 A67-32403
 Separated and reattaching flows emphasizing heat transfer considerations in calculations, especially in supersonic designs 17 p2790 A67-32448
 Integral relation method analysis of supersonic gas flow past blunt body of revolution 17 p2791 A67-32679
 Convection coefficient distribution in supersonic flow, noting wind tunnel measurement results at Mach 3.3 and at various angles of attack 17 p2791 A67-32702
 Gas ejection and boat-tailing effect on cylindrical afterbody in supersonic flow 17 p2793 A67-33041
 Boundary value problem for electrical potential and ion distribution function obeying Poisson-Vlasov equations when applied to rarefied plasma disturbance by supersonic body 17 p2909 A67-33205
 Finite length plate in plane supersonic flow analyzed for forced vibration by applying linearized potential flow theory 18 p3140 A67-33466
 Dynamic phenomena in two identical cylindrical shells placed side by side in inviscid supersonic flow of compressible fluid 18 p3024 A67-33540
 Turbulent base pressure in supersonic axisymmetric flow behind blunt body [AIAA PAPER 67-448] 18 p3026 A67-33922
 Stagnation pressure lower than atmospheric pressure in supersonic subatmospheric flow in magnetoaerodynamic generation nozzle, discussing Hall effects for energy conversion process 18 p3020 A67-34122
 Parameters of viscous supersonic compressible gas flow past corner, giving smooth coupling conditions for Navier-Stokes and boundary layer solutions 18 p3027 A67-34205
 High intensity heat flux formation during heat transfer on steel cylinder in region of incident shock wave in supersonic flow 18 p3027 A67-34206
 Three-dimensional detached flow patterns forming near secondary jet injected into supersonic flow 18 p3027 A67-34207
 Supersonic flow past windward side of delta wings with angles of attack from 0 to 80 degrees, verifying experimental and theoretical values 18 p2984 A67-34208
 Mach and Reynolds numbers effect on rarefied supersonic gas flow pattern near forward stagnation point of blunt body, noting decrease in density 18 p3028 A67-34209
 Supersonic fluid flow past elliptical and circular conical bodies at large angles of attack, using straight line method 18 p2984 A67-34211
 Supersonic flow past smooth body with internal duct incident at angle of attack 18 p2984 A67-34212
 Transition of supersonic flow of combustible gas mixture to Chapman-Jouguet regime 18 p3028 A67-34214
 Flow around thin delta wing under supersonic conditions, considering flow separation at leading edges 19 p3170 A67-35542
 Flat plate continuum Langmuir probe ion density measurements, analyzing boundary layer and sheath of supersonic flow behind shock wave 19 p3296 A67-35590
 Time dependent computational method for three-dimensional blunt body flow fields traveling at supersonic speed including

shock points, sphere cones and ellipsoid [AIAA PAPER 67-222] 19 p3171 A67-35736
Flutter of simply supported thin isotropic parallelogrammic flat panels in supersonic flow 19 p3342 A67-35751
Nonequilibrium-transition patterns of quasi-one-dimensional dissociating-gas flow through diverging supersonic nozzle 19 p3211 A67-35759
Dynamic stability analysis of bodies of revolution in supersonic flow, using characteristics method [AIAA PAPER 67-607] 19 p3172 A67-35998
Shape of minimum drag cruciform wing of symmetrical thickness in supersonic flow 20 p3355 A67-36192
Aerodynamic characteristics of polygonal wings with diamond-shaped profile in supersonic flow 20 p3355 A67-36194
Proton velocity distribution in solar wind flow around magnetosphere 20 p3518 A67-36653
Heat transfer coefficients from supersonic wind tunnel airflow through grid with rectangular bars [ASME PAPER 67-HT-74] 20 p3550 A67-36754
Supersonic viscous gas flow around body of revolution involving perturbation damping, analyzing Navier-Stokes and heat transfer equations for flow chart 20 p3357 A67-36810
Aerodynamic forces of harmonically oscillating cylindrical duct with supersonic internal flow within framework of potential flow theory 20 p3357 A67-37003
Theory of supersonic gas ejector with cylindrical mixing chamber, discussing low and high pressure gas flow 20 p3358 A67-37085
Incompressible cylindrical jet interaction with incompressible unbounded homogeneous stream, determining contact surface 20 p3360 A67-37661
Two-dimensional turbulent mixing of supersonic reacting and nonreacting gases studied with square shock tube 21 p3606 A67-37772
Hydrogen or nitrogen gas injection at various Mach numbers from nozzle in flat plate into Mach 2.72 free air stream 21 p3610 A67-37800
Thrust and drag response to heat input directly behind and before body moving supersonically or subsonically 21 p3563 A67-37887
Supersonic delta wing problem, discussing new approach in determining flow parameters 21 p3564 A67-38288
Characteristics method to determine radiative energy losses of supersonic gas flows past blunt cones 21 p3564 A67-38424
Insulator boundary layers in supersonic MGD channel noting heat transfer rate, current density, stagnation, pressure distribution and skin friction [AIAA PAPER 67-717] 21 p3673 A67-38743
Supersonic blunt body problem noting sonic point singularity for reformulated integral relations 21 p3614 A67-38879
Characteristic method computer program for calculating three-dimensional supersonic flow around blunt and pointed bodies of revolution in reasonable time 21 p3566 A67-38887
Roughness induced boundary layer transition in supersonic flow over blunt bodies 21 p3614 A67-38891
Base pressure measurements on elliptic cones in supersonic flow with turbulent boundary layer as function of geometry 21 p3566 A67-39083
Variable length foil fluttering in supersonic compressible gas flow, particularly case with end clamping of varying edges 22 p3910 A67-39454
Flutter of two cylindrical panels bonded by elastic filler in supersonic gas flow, showing flutter velocity increase with increasing filler elasticity 22 p3910 A67-39455
Self-similar solutions to motion equations are possible for internal heat generation in confined supersonic flow, assuming constant transport properties 22 p3784 A67-39781
Base pressure calculation of stepped axisymmetric body in supersonic flow based on turbulent mixing 22 p3740 A67-39944
Representation of characteristic surfaces of unsteady axisymmetric flow and steady three-dimensional supersonic flow by hyperbolic system of quasilinear differential

equations 22 p3785 A67-40010
Procedure for expanding parameter in asymptotic power series of any order to investigate viscous compressible supersonic gas flow past blunt body 22 p3740 A67-40014
Thin optimum wing contour constructing procedure having minimum wave drag in supersonic flow solved by linear approximation, obtaining numerical values for parameters 22 p3741 A67-40017
Navier-Stokes equations asymptotic solutions used for gas flow laminar boundary layer calculation near corner of body where supersonic gas flow passes through low pressure region 22 p3785 A67-40018
Supersonic three-dimensional flow fields of inviscid nonconducting gas around delta wing with blunt edges 22 p3741 A67-40025
Supersonic flow over flat and axisymmetric blunt bodies, discussing shock wave position, adiabatic index, surface pressure distribution and body geometric parameters 22 p3741 A67-40026
Two-dimensional adiabatic laminar separated regions in supersonic flow, examining effects of blowing and suction at wall [AIAA PAPER 67-192] 22 p3786 A67-40096
Velocity distribution determination method for supersonic flow around zero incidence cones in equilibrium air, discussing motion equation and flow field parameters 22 p3742 A67-40098
Shadow photography study of underexpanded nozzle ejected supersonic turbulent jet off-design behavior, discussing static pressure distribution, boundary layer and Mach number effect 23 p3928 A67-40732
Influence of sweepback wing leading edge geometry on boundary layer instability using supersonic flat plates 23 p3928 A67-41247
Nozzle form optimization from Mach distribution in supersonic region, defining perturbation functions 23 p3929 A67-41248
Reynolds number effect on base pressure behind wedge in supersonic and hypersonic flow based on Chapman wake flow recompression model 23 p3930 A67-41308
Skin friction under mass injection on porous flat plate in supersonic turbulent flow [AIAA PAPER 67-194] 23 p3991 A67-41713
Mathematical model, representing two-dimensional panel fluttering in supersonic flow, to study stability criterion via Liapunov second method 23 p4081 A67-41752
Total head tube in combination with electrostatic probe used in supersonic plasma diagnostics, measuring plasma and shock wave front parameters 24 p4197 A67-42355
Three-dimensional flow across supersonic single rotor axial compressor subsonic at rotor entry and exit 24 p4092 A67-42661
SUPERSONIC FLUTTER
Bending and torsion induced symmetric flutter of aircraft in supersonic flow 04 p0708 A67-14789
Supersonic flutter of thin walled circular cylindrical shells under compressive loading, comparing theory and experiment [AIAA PAPER 67-77] 06 p1103 A67-18354
Partial diaphragm when applying supersonic Mach box method for steady state condition and uniform downwash on wing compared with complete diaphragm 06 p0944 A67-18875
Supersonic flutter characteristics of thin cantilever plate surfaces with low aspect ratio 08 p1418 A67-20530
Supersonic wind tunnel test providing static pressure measurements for use in cylinder flutter calculations 08 p1277 A67-20588
Unsteady aerodynamic field with application to panel flutter in low supersonic flow 08 p1418 A67-20608
Nonlinear flutter of simply supported rectangular plate under thermal compression in supersonic gas flow 09 p1574 A67-21915
Three-dimensional flutter calculations verification by wind tunnel results, using flexible supersonic aircraft planform model of determined characteristics to control calculations 10 p1622 A67-22882
Free flight response of two panels subjected to turbulent pressure fluctuations at supersonic Mach numbers 10 p1719 A67-23558
Interaction between buckling and flutter of circular cylindrical shell subjected to

axial compression and placed in axial supersonic flow 14 p2398 A67-28092
Flutter of flat panels at low supersonic speeds, describing mounting which makes it possible to change tension of panel during testing at constant Mach number [ONERA-TP-487] 17 p2961 A67-32699
Supersonic flutter characteristics of thin cantilever plate surfaces with low aspect ratio 19 p3343 A67-35775
Panel flutter analysis of hinged closed circular cylindrical shell in supersonic gas flow, considering axial compression and structural damping 21 p3725 A67-38788
Supersonic flutter of thin walled circular cylindrical shells under compressive loading, comparing theory and experiment [AIAA PAPER 67-77] 21 p3727 A67-38869
SUPERSONIC HEAT TRANSFER
Ablative materials for thermal protection and minimum mass transfer of aircraft flying at hypersonic speeds [DVL-603] 03 p0532 A67-13026
Characteristic dimension selection for optimum supersonic heat transfer in axisymmetric body of prescribed shape 04 p0546 A67-14794
Ground simulation of Concorde aerodynamic heating effects by blowing air through ducts built over specimen surface 15 p2465 A67-29501
SUPERSONIC INLET
Starting phenomenon on reversed nozzle and multishock types of supersonic intakes 10 p1590 A67-22918
SST air inlet control system, considering maintainability, impact on cockpit procedures and component reliability effect on dispatch reliability [SAE PAPER 67-0325] 12 p1895 A67-25869
Retractable airfoil and hinged cowl modifications of supersonic inlet to reduce drag below choking point for subsonic operations 17 p2791 A67-32575
Semiempirical methods of spillage drag prediction for two-dimensional supersonic inlets operating in transonic flight [AIAA PAPER 67-449] 18 p2982 A67-33924
Equations for arc length derived for two-dimensional isentropic compression surface for ideal gas 22 p3742 A67-40102
Variable geometry in SST aircraft, discussing hardware, lift control system, compression inlet and full scale wing pivot [SAE PAPER 67-0878] 24 p4094 A67-42012
SUPERSONIC JET
Impingement of supersonic jet on flat plate studied for variety of jet Mach numbers, plate incidence angles and plate locations downstream of nozzle outlet 01 p0006 A67-10792
Turbulent reattachment of supersonic jet noting recompression region of flow, critical points and similarity law in evolution of wall pressures [ONERA-TP-326] 01 p0053 A67-11002
Combustion efficiency of supersonic ramjet, noting equations for chamber 01 p0141 A67-11149
Supersonic jet from finite length nozzle in supersonic stream at angle of attack, analyzing flow characteristics by using linearized theory 02 p0177 A67-11523
Supersonic underexpanded jet interacting with obstacle in numerical solution using integral relations and characteristics 03 p0350 A67-12879
Impact of supersonic jet against surface 05 p0795 A67-17479
Supersonic liquid jets produced by ballistic extrusion with velocities of 4.58 km/sec 06 p0982 A67-17603
Switching of supersonic gas jets in convergent-divergent duct by atmospheric venting, using phenomena of boundary layer separation 08 p1279 A67-20436
Collision of opposed supersonic jets in pulse discharges, noting formation of shock-constricted plasma regions between electrodes 09 p1544 A67-21855
Supersonic rarefied argon plasma jet, determining pressure distribution, electron concentration and temperature 11 p1842 A67-24963
Temperature and density measurements in supersonic free jets of nitrogen and shock waves 13 p2093 A67-26279
Axisymmetric supersonic jet injection from conical nozzle into supersonic wake flow or medium at rest 13 p2050 A67-26896
Apparent mass of supersonic jet stream

under off-design flow conditions 14 p2242 A67-28302

Supersonic jet expelled from plane nozzle solved by characteristic method to determine family of rarefaction waves and nozzles 16 p2656 A67-30455

Molecular nitrogen rotational relaxation time by probing of supersonic free jet 16 p2705 A67-31757

Supersonic free plasma jet with axial current, solving MGD equations for structure modifications due to self-magnetic forces 19 p3288 A67-35363

Houston intercontinental airport planning and development for supersonic jet, superjet and SST aircraft 22 p3779 A67-39374

Integral correlation technique used for first approximation solution in polar coordinate system to determine plane supersonic jet incidence on plane at arbitrary angle 22 p3786 A67-40020

Engine test facilities on Concorde examined for effect on supersonic Olympus engine development [AIAA PAPER 67-753] 23 p4049 A67-40987

Length of supersonic core of axisymmetric jet exhausting into quiescent atmosphere 23 p3992 A67-41739

Shock refraction effects due to velocity and temperature gradients in rocket nozzles investigated by studying leading shock in two-dimensional secondary fluid injection 23 p3992 A67-41740

Monograph on external burning in supersonic streams, discussing heat addition, fluid-mechanical model, use of characteristics method, Chapman-Jouget detonation, etc [TG-912] 24 p4254 A67-42386

SUPERSONIC NOZZLE

Supersonic nozzle producing lift force without downward deflection analyzed by characteristics method 04 p0545 A67-14440

Thrust and mass flow rate of supersonic nozzle with and without internal separation 04 p0602 A67-14568

Convective heat transfer in accelerated heated air flows through cooled conical supersonic nozzles of three different configurations 04 p0723 A67-14837

Low magnetic Reynolds number two-dimensional and axisymmetric MHD flow of conducting ideal gas through supersonic nozzle 06 p1043 A67-18669

SST nozzle geometry for high efficiency operation over large exhaust pressure variation 06 p0942 A67-18745

Thrust vector control by supersonic splitline gimbaled nozzle, considering linear aerodynamics to understand magnitude of spring rate torque component 07 p1126 A67-19378

Effect of fairing contraction into two-dimensional supersonic nozzle for wind tunnel, avoiding pressure gradients along walls unfavorable to boundary layer flow development 07 p1126 A67-19630

Optimum thrust nozzle contours for chemically reacting gas flows, obtaining set of partial differential equations for gas dynamic properties [AIAA PAPER 66-638] 10 p1592 A67-23118

Soviet book on supersonic gas flows in perforated boundaries covering flow characteristics, dynamic property, supersonic nozzles, velocity regulation, etc 17 p2789 A67-32019

Perfect frictionless supersonic MHD gas flow model for shock wave control, noting nozzle geometry 18 p3088 A67-34123

Turbulent boundary layer flow in conical supersonic nozzle, discussing convective heat transfer and adverse pressure gradient effect 19 p3169 A67-34814

High altitude variable Mach number test cell for testing intake system of Concorde aircraft Olympus 593 20 p3414 A67-36497

Laval nozzles performance under off-design conditions, noting shock wave formation in region of supersonic velocity 21 p3564 A67-38420

Axial electron density profile in weakly ionized seeded argon plasma expanding through supersonic nozzle determined experimentally using microwave interferometer [AIAA PAPER 67-704] 21 p3672 A67-38731

Pressure fluctuation onset conditions in jet engine combustion chambers with supersonic nozzles, discussing design factors effect on combustion process

stability 21 p3696 A67-38909

Swirling mass flow in supersonic nozzle indicates discharge coefficient falls nonlinearly with swirl 22 p3739 A67-39527

Gas dynamic self-regulation of supersonic nozzle consisting of cylindrical channel with central body, measuring nozzle inlet and static pressures 22 p3868 A67-39544

Helium argon mixture shock wave density profile measurements, discussing shock wave production in flow field at supersonic nozzle exit 22 p3783 A67-39709

Radiating hydrogen two-dimensional equilibrium flow with variable absorption coefficient in axisymmetric nozzle analyzed in presence of gray radiation, examining transfer equation in diffusive approximation 22 p3785 A67-40013

Optimum blowing angle of gas into supersonic nozzle determined by supersonic wind tunnel investigation of flow interaction 22 p3743 A67-40452

Numerical method together with stable difference scheme used to calculate sub-, trans- and supersonic flows in Laval nozzle inverse problem 24 p4091 A67-42160

SUPERSONIC PRESSURE DISTRIBUTION

Rectangular and inverted wedge recompression step effect on recovery factor, heat-transfer coefficient, velocity profile and pressure distribution in open cavity flow [ASME PAPER 65-WA/HT-37] 08 p1278 A67-21320

Vortex separated delta wing leading edge in supersonic flow, noting effect on pressure distribution and role of flow equation 09 p1438 A67-22496

Flow pattern in front of cylinder mounted on plate at Mach 3 in wind tunnel, noting supersonic region between cylinder surface and shock wave 10 p1590 A67-23025

Buffet limit for aircraft wings in transonic region based on boundary layer theory, determining transonic pressure distribution and separation points 23 p3931 A67-41311

SUPERSONIC SPEED

Effects of subsonic, supersonic, hypersonic and orbital environments on structures [SAE PAPER 660671] 01 p0160 A67-10578

Equivalency coefficient dependence on angle of attack, Mach number and angle of incidence for subsonic and supersonic gas flow past plate grid 03 p0353 A67-14082

Three-dimensional plane shock wave intersection in space, noting parameter range for which two solutions exist 07 p1169 A67-20036

Aerodynamic design of swept wing-fuselage combination for cruising at transonic and supersonic speeds, noting pressure distribution role 10 p1589 A67-22872

Identical flutter boundaries of multibay and one-bay panels with clamped edges in high and low supersonic regions 12 p2030 A67-25930

Skin friction drag coefficient at supersonic-hypersonic speeds as function of transition on delta wing 13 p2051 A67-27597

Rotary wing decelerator for sonic and supersonic operation, noting components and potential application 17 p2796 A67-32517

Unsteady aerodynamic forces due to gusts on supersonic bodies of revolution 19 p3172 A67-36001

Static pressure probe nose derived from supersonic slender body theory and shaped for subsonic speeds 21 p3564 A67-38535

Generator installation for supersonic gust simulation to measure wing forces, discussing calibration 21 p3609 A67-38889

Charged particle /ion/ collection rates using supersonic atmospheric sounding rocket with electrode at stagnation point, noting electric field effect 22 p3791 A67-39818

Perturbed region behind diffracting shock wave on plane-walled convex corners at supersonic speed 23 p3990 A67-41172

SUPERSONIC TRANSPORT

SA BOEING 2707 AIRCRAFT

Pump loop testing and operational evaluation of SST hydraulic fluids [SAE PAPER 660664] 01 p0103 A67-10572

Materials for structural usage in high altitude/ high temperature supersonic transports, comparing aluminum, titanium, etc, alloys for mechanical and physical properties

[SAE PAPER 660685] 01 p0094 A67-10573

Combination ground support and self-sufficiency concept in Boeing SST aircraft, discussing engine removal, accessory drive, wing pivot bearing, inlet control, inertial navigation and back-up support [SAE PAPER 660702] 01 p0049 A67-10596

Flight environment effect on lubrication requirements of Pratt-Whitney SST engine [SAE PAPER 660711] 01 p0013 A67-10601

Jet fuel lubricity noting poor performance due to polar compounds, improving lubricity by surface active additives 01 p0139 A67-10602

Titanium mill products intended to meet requirements of C5A and SST aircraft, describing specially designed mill processing equipment [SAE PAPER 660651] 01 p0079 A67-10612

High temperature stability of SST turbine fuel samples from refineries and airports [SAE PAPER 660710] 01 p0139 A67-10624

Jet-engine problem areas in relation to SST 01 p0141 A67-11200

Concorde SST aircraft, discussing airframe, engine, ancillary power plant, afterburner, etc 01 p0081 A67-11253

Design and construction of Franco-British Concorde SST, examining cabin, noise problem, production and tests 02 p0180 A67-12040

Supersonic transport design using double delta wing planform 03 p0360 A67-13918

SST servicing and maintenance characteristics and suitability of existing and planned airports 03 p0360 A67-13919

Near field and far field sonic boom signature of supersonic transport, noting structural response 03 p0360 A67-13921

Clear air turbulence effect on ride quality and flight profile of SST 03 p0463 A67-13922

Sonic boom decay and aural response in relation to SST configuration constraints and flight performance characteristics [AIAA PAPER 66-941] 03 p0361 A67-14139

Supersonic transport design using double delta wing planform 03 p0362 A67-14299

British-French cooperation in aeronautics, discussing Concorde SST, variable geometry aircraft, Olympus 593 turbojet, etc 03 p0362 A67-14379

SST sonic boom acceptance by public and problems of control 04 p0551 A67-14623

Transfer functions and statistical properties of SST in atmospheric turbulence 04 p0620 A67-14893

Meteorological problems connected with design and future operations of supersonic transport, noting particular hazards of mountain-like cumulonimbus clouds 04 p0652 A67-15542

Variable geometry SST project and expected support program 05 p0752 A67-16753

Composite aerospace transport for spacecraft launching, particularly French projects 06 p1094 A67-17993

Wind and temperature effects on transitory and cruise phases of supersonic flight 07 p1219 A67-19067

Supersonic transport navigation system accuracy, reliability, directional measurement, inertial speed, etc 07 p1221 A67-19068

Supersonic transport engine requirements in light of past jet transport operation [SAE PAPER 660296] 07 p1129 A67-19624

SST flight performance as affected by wind, temperature and radiation 07 p1129 A67-19679

Fundamentals of technology and operation of SST aircraft for commercial aviation 07 p1131 A67-20292

Fire hazard testing of hydraulic fluids, coolants and lubricants in aircraft with reference to SST hot wing compartment conditions 09 p1521 A67-22246

Near field and far field sonic boom signature of supersonic transport, noting structural response 11 p1743 A67-24038

Boeing SST inlet, control and power system development, discussing test program, design objectives and cost [SAE PAPER 670318] 12 p1990 A67-25886

Jet fuel lubricity noting poor performance due to polar compounds, improving lubricity by surface active additives [SAE PAPER 660712] 12 p1988 A67-26163

Book on air transport economics in supersonic era covering air cargo operational problems, mechanical loading, VTOL

transport operation, etc 13 p2052 A67-26256
 Clear air turbulence at high altitudes, showing occurrence where sharp kink in temperature profile exists near core of jet stream 13 p2150 A67-26331
 Mach 2 plus Olympus 593 turbojet power plant for Anglo-French SST, analyzing fuel system, lubrication and cooling on test run 13 p2187 A67-26701
 Hydraulic, pneumatic and electric circuits for twin loop engine control system of Olympus 593 in Concorde SST 13 p2187 A67-26702
 Navigation of SST with respect to optimum trajectory, flight system and traffic control 13 p2153 A67-26710
 SST and military aircraft simulation exercises under various terrain and traffic conditions 13 p2053 A67-26711
 Piloted flight simulator studies influence on design of SST instruments, discussing pitch indicator, landing and sonic boom limitation display systems 13 p2154 A67-27269
 Liquefied natural gas application to SST, noting improvement in engine performance with use of methane 13 p2185 A67-27439
 Liquid hydrogen for SST fuel compared with hydrocarbons, considering range, payload, weight, drag, engine design, storage and safety 13 p2186 A67-27635
 Cosmic radiation problems in space flights and in SST flights, examining biological effects, shielding methods, dosimetry and warning systems 14 p2255 A67-28217
 Possible decompression effects in supersonic transport cabin in terms of biomedical considerations for passenger safety 14 p2258 A67-28666
 Supersonic transport vehicle throttle schedule, comparing point performance, indirect and gradient optimization techniques 15 p2418 A67-29406
 Planning integration of Boeing 747 jet aircraft into commercial airline [AIAA PAPER 67-394] 15 p2421 A67-30361
 Concorde structural development noting effects of temperature on fatigue and creep strength of aluminum alloys [AIAA PAPER 67-402] 15 p2578 A67-30369
 Economic factors controlling development of high capacity supersonic transport aircraft 16 p2782 A67-30838
 Competition aspects of United States supersonic transport, discussing various aircraft designs 16 p2596 A67-31246
 Digital onboard checkout system for SST and other commercial/military aircrafts to discover in-flight malfunctions digital onboard checkout system for SST and other commercial/military aircraft to discover in-flight 16 p2596 A67-31493
 Satellite relay to provide communication paths for aircraft-ground communication over ocean, considering system design for ATC using reflex repeater 16 p2629 A67-31530
 Concorde SST third and fourth flying prototypes described, discussing structural design, power plant, control systems, landing gear, etc 16 p2597 A67-31785
 Concorde aircraft fuel, discussing fuel transfer, problem of boiling, in-flight environment simulation, payload/mass ratio, etc 16 p2734 A67-31809
 Flight control hydraulic systems for Boeing 2707 SST noting absence of radical changes in operating procedures 17 p2793 A67-31968
 SST Concorde hydraulic system noting design and hydraulic fluid selection resulting from high ambient temperatures, weight and space limitations, etc 17 p2800 A67-31971
 Controls Development /CODE/ program for proving design validity of B2707 SST flight control and hydraulic systems prior to flight 17 p2795 A67-32004
 Thermal stability aspects of commercial kerosene for supersonic transport [AIAA PAPER 66-670] 17 p2926 A67-32570
 Fuel control system of GE4 engine for supersonic transport noting main and augmentation fuel and control subsystems [SAE PAPER 670326] 17 p2929 A67-32982
 Diagnostic devices for sensing performance deterioration and mechanical malfunctions in supersonic aircraft engines [SAE PAPER 670363] 17 p2930 A67-33000
 Boeing SST maintenance requirements considered in terms of aircraft characteristics, economics, facilities, operations, etc

[SAE PAPER 670373] 17 p2798 A67-33003
 Supersonic transport size determination for competitive operation in air traffic market using traffic volume, aircraft type and flight frequency forecasts [SAE PAPER 670371] 18 p2985 A67-33569
 Subsonic diffuser with vortex generator as integral design feature for supersonic transport aircraft inlet [AIAA PAPER 67-464] 18 p2983 A67-33935
 Fuel requirements for Concorde SST stressing flame luminosity, radiant heat, spontaneous ignition, fuel viscosity and density 18 p3110 A67-34533
 Solutions for aviation crisis of congestion, delays and noise, including problems anticipated with jumbo and SST jets 19 p3207 A67-34968
 Atmospheric condition effects on SST aircraft, noting Concorde performance data analysis results 19 p3173 A67-35309
 Steepest-ascent optimization program developed for flight path of current vehicles, particularly supersonic transport vehicles 19 p3257 A67-35958
 SST flight control system electronic and hydraulic systems, discussing system design, components, reliability and test programs [AIAA PAPER 67-570] 19 p3174 A67-35966
 Ride quality improvement on flexible aircraft by means of elastic structural bending mode suppression design technique [AIAA PAPER 67-571] 19 p3174 A67-35967
 Supersonic transport variable sweep wing design, showing root glove and Mach number effects on aerodynamic center of strike aircraft 20 p3361 A67-36499
 Superalloys for SST engine, discussing materials properties, structures, turbine disk production, welding, alloy design, coating-base metal interactions, etc 20 p3469 A67-37358
 Modernizing air traffic control, governmental procedures, airports and support facilities to accommodate Boeing 747 and supersonic transports 20 p3418 A67-37442
 Planned introduction of Boeing 747 into airline service noting advances in technology for passenger comfort, cargo handling and rate reduction 20 p3361 A67-37443
 Provision of additional metropolitan airport facilities to accommodate supersonic transportation noting noise abatement, traffic growth and off-airport processing 20 p3556 A67-37444
 SST aircraft influence on fuel quality requirements, considering use of liquefied gaseous hydrocarbon fuels 21 p3688 A67-38192
 FAA certification standards for SST engines and components, emphasizing thermal environment testing and high temperature materials development 22 p3867 A67-39224
 Creep properties of sheet materials in SST environment for selection of optimal airframe materials 22 p3818 A67-39225
 Concorde SST economics noting short/medium haul characteristics, flight times, sonic boom problems, load factor, etc 22 p3744 A67-39339
 Airport terminal facilities - Conference, Houston, April 1967 22 p3778 A67-39373
 Houston Intercontinental airport planning and development for supersonic jet, superjet and SST aircraft 22 p3779 A67-39374
 Supersonic transport structural materials design, considering fatigue behavior, crack propagation and residual static strength under temperature and cyclic load effects 22 p3819 A67-39457
 Navigation satellites for information during movements of manned/unmanned terrestrial vehicles containing position determination, communications and weather relay service and scientific sensors 22 p3831 A67-39524
 Boeing SST competition, cost, operation, design, airport noise and sonic boom 22 p3746 A67-39882
 Technological and economic factors affecting airline progress, discussing fares, traffic, SST and terminal areas 22 p3922 A67-40062
 SST fleet size, flight time, station stop time, seat mile costs, fuel consumption, noise and sonic boom problems affecting airline economics 23 p3933 A67-40983
 [AIAA PAPER 67-749] 23 p3933 A67-40983
 US SST airframe prototype, surveying hardware developments, flight control,

pivoting system, landing performance and pilot cabin [AIAA PAPER 67-750] 23 p3933 A67-40984
 Factors for SST safety and airworthiness requirements, discussing environment, engineering level, learning and flying quality [AIAA PAPER 67-751] 23 p3933 A67-40985
 Engine air intake design and development for Concorde aircraft, discussing design constraints [AIAA PAPER 67-752] 23 p4048 A67-40986
 Steady state matching of inlets, engines and exhaust nozzle for SST [AIAA PAPER 67-754] 23 p3928 A67-40988
 Materials selection for external structures of transport aircraft flying at Mach 3 speeds, noting characteristics of maraging steels 23 p4019 A67-41045
 Radiobiological risk of SST flights from heavy ions of cosmic radiation, discussing methods of radiation detection 23 p3945 A67-41074
 Design characteristics of various SST, discussing Mach numbers and wing configuration 23 p3935 A67-41398
 Altitude chamber studies of passively pressurizing partial pressure suit for possible use by SST crew 23 p3969 A67-41647
 Supersonic civil aircraft, considering journey time, safety and operating economy 24 p4093 A67-41886
 Crack propagation rate and residual static strength of fatigue cracked Ti and steel cylinders for SST design data 24 p4247 A67-41943
 SST engines design, combustion and thrust augmentation systems, engine controls and complications facing users [SAE PAPER 670865] 24 p4207 A67-42005
 Variable geometry in SST aircraft, discussing hardware, lift control system, compression inlet and full scale wing pivot [SAE PAPER 670878] 24 p4094 A67-42012
 Wing pivot joint and actuation system configurations for SST variable geometry design [SAE PAPER 670883] 24 p4160 A67-42017
 SST variable sweep wing actuation system and pivot bearing reliability [SAE PAPER 670884] 24 p4098 A67-42018
 SST aircraft effect on overall situation of commercial airline traffic in Canada [SAE PAPER 670901] 24 p4257 A67-42019
 Automatic flight management of future high performance aircraft [AIAA PAPER 67-847] 24 p4183 A67-42983
SUPERSONIC TURBINE
 Engine design for civil operation from military supersonic engine [SAE PAPER 670316] 17 p2929 A67-32978
 Reliability methods used to insure reliability of supersonic transport engine [SAE PAPER 670317] 17 p2929 A67-32979
SUPERSONIC VEHICLE
 Asymmetric interaction of supersonic vehicle intercepted with oblique shock wave [AIAA PAPER 67-180] 06 p0989 A67-18486
 Structures and materials for supersonic aircraft and space vehicles 09 p1576 A67-22429
 Singularities causing numerical instabilities used in steady gas dynamic Cauchy problem solution, exemplifying with supersonic blunt body 12 p1893 A67-25932
SUPERSONIC WAKE
 Schlieren and hot-wire anemometric observation of supersonic wakes in wind tunnel turbulent flows [ONERA-TP-417] 05 p0748 A67-16482
 Laminar boundary layer separation and near wake flow for smooth blunt body at supersonic and hypersonic speeds [AIAA PAPER 67-62] 06 p0986 A67-18270
 Viscous interaction theory for laminar supersonic near wake applied to calculation of recirculation region for range of flow conditions [AIAA PAPER 67-61] 06 p0941 A67-18467
 Near wake uniqueness and criticality condition in Crocco-Lees mixing theory, obtaining critical point from boundary layer equations of motion [AIAA PAPER 67-65] 07 p1168 A67-19433
 Axisymmetric compressible turbulent wake fluctuating characteristics measured using supersonic wind tunnel, including radial velocity and temperature distribution, density, etc 12 p1893 A67-25928
 Wind tunnel investigation of wake structure behind cone in supersonic flow 14 p2240 A67-27994

Laminar boundary layer separation and near wake flow for smooth blunt body at supersonic and hypersonic speeds [AIAA PAPER 67-62] 14 p2240 A67-28112

SUPERSONIC WIND TUNNEL

Laminar flow on adiabatic surface measured, using Stanton tube and supersonic wind tunnel 04 p0547 A67-14849

Steady and unsteady aerodynamic coefficients determined by free flight analysis of trajectory and attitude variations in supersonic wind tunnel 05 p0748 A67-16765

Supersonic laminar two-dimensional boundary layer separation in compression corner with and without cooling [AIAA PAPER 67-191] 06 p0940 A67-18361

Shock wave tubes and wind tunnels for momentary generation of steady air flows for aerodynamic investigations at high supersonic velocities 07 p1127 A67-20121

Wind tunnel study of strong-deflection supersonic cascade decelerating flow past turbine blades 07 p1128 A67-20296

High altitude supersonic isokinetic filter paper sampler for ALARR rocket, examining subsonic 3-D stagnation flow diffuser 08 p1276 A67-20500

Supersonic wind tunnel test providing static pressure measurements for use in cylinder flutter calculations 08 p1277 A67-20588

Flow pattern in front of cylinder mounted on plate at Mach 3 in wind tunnel, noting supersonic region between cylinder surface and shock wave 10 p1590 A67-23025

Axisymmetric compressible turbulent wake fluctuating characteristics measured using supersonic wind tunnel, including radial velocity and temperature distribution, density, etc 12 p1893 A67-25928

Wind tunnel investigation of wake structure behind cone in supersonic flow 14 p2240 A67-27994

Aerothermodynamic testing of heat protective systems in arc tunnel 15 p2466 A67-29538

Radio telemetry system for aerodynamic data acquisition from free-flight models in supersonic wind tunnels 16 p2675 A67-31259

Color schlieren and high speed photography technique for transient flows in wind tunnels 20 p3445 A67-36537

Transpiration cooled porous surface in high temperature forced convection environment, applying transient energy balance with heat-transfer coefficient measurement [ASME PAPER 67-HT-27] 20 p3546 A67-36720

Heat transfer coefficients from supersonic wind tunnel airflow through grid with rectangular bars [ASME PAPER 67-HT-74] 20 p3550 A67-36754

High altitude supersonic isokinetic filter paper sampler for ALARR rocket, examining subsonic 3-D stagnation flow diffuser 21 p3563 A67-37803

Safety device to prevent overloading of models and sensitive wire strain gauge balance by aerodynamic forces during starting and switching off in wind tunnel 22 p3780 A67-39756

High enthalpy supersonic wind tunnel performance, analyzing Teflon model stagnation ablation 23 p3931 A67-41477

SUPPLY

S POWER SUPPLY

SUPPORT

SA CHASSIS

Stress effects of simple supports on radiation emission from turbulent flow near plane compliant surface, using acoustic equivalence to extended dipole system 05 p0748 A67-16813

Resonance transition of hinged ponderable rod with nonlinear supports 06 p1109 A67-18666

RCA papers on systems support and aerospace systems 08 p1303 A67-21056

Very low heat background calorimeter design for heat-short experiments and checking analytical predictions for propellant tank insulation 13 p2228 A67-27658

Lemmas and theorems for support functions of plurisubharmonic functions proved, discussing complex variables and linear maps 22 p3828 A67-40555

SUPPORT INTERFERENCE

Parametric oscillations of counterbalanced rotors 13 p2216 A67-26628

Vibration problems in high speed turbines including stability, critical speeds and

support structure effect on rotor response [ASME PAPER 67-DE-8] 14 p2402 A67-28867

SUPPORT SYSTEM

SA GROUND OPERATIONAL SUPPORT SYSTEM /GOSS/

SA GROUND SUPPORT SYSTEM

SA LIFE SUPPORT SYSTEM

Fluid power support equipment for space vehicles outside earth atmosphere, based on earth environment effect on various systems [SAE PAPER 660708] 01 p0013 A67-10600

Requirements of economical and effective orbital logistics support system [AIAA PAPER 66-863] 03 p0519 A67-14129

IEEE Automatic Support Systems Symposium for Advanced Maintainability, Clayton, Missouri, November 1966 03 p0397 A67-14201

Maintainability efforts in support of Acceptance Checkout Equipment/Apollo-Spacecraft /ACE-S/C/ program 03 p0398 A67-14205

Analysis of existing support systems and guide for planning of new systems presenting example of manual test system and automatic test system 03 p0424 A67-14214

Software configuration management by engineering methods, considering application to automatic support equipment /ASE/ for Saturn S-IVB stage 03 p0538 A67-14221

Launch vehicle parameter design for optimal support of communications satellites 06 p1093 A67-17678

Book on range instrumentation covering optical, radar, support systems, etc 10 p1604 A67-22992

Range instrumentation support systems, describing approaches to timing, firing and communications systems 10 p1605 A67-22998

Supporting equipment for space vehicles - Conference, Athens, September 1965

Supporting equipment for space vehicles - IAF Conference, Athens, September 1965, Volume 3 16 p2620 A67-30667

Requirements of economical and effective orbital logistics support system [AIAA PAPER 66-863] 19 p3331 A67-34809

Mission simulator for manned space flight support used for real time training 20 p3414 A67-36538

S-band telemetry data during spacecraft launch phases, discussing mission support problems 20 p3380 A67-36561

Missile and space support systems reliability, flight equipment and redundancy 22 p3781 A67-40342

Spacecraft equipment in-space maintainability design criteria 23 p4070 A67-40591

Earth orbital integrated logistics system extendable to space and lunar operations, considering technical and economic feasibility 23 p4061 A67-40592

Astronauts and astronaut support personnel training 23 p3960 A67-40594

SUPPRESSOR

SA DYNAMIC SUPPRESSOR

SA ECHO SUPPRESSOR

SA NOISE SUPPRESSOR

General equation for suppressor controlled transconductance of pentode useful for circuit analysis 16 p2635 A67-30794

SURFACE

SA CONTROL SURFACE

SA CRYSTAL SURFACE

SA CURVED SURFACE

SA EARTH SURFACE

SA FERMI SURFACE

SA FLAT SURFACE

SA INTERFACE

SA LAMBERT SURFACE

SA LIFTING SURFACE

SA LIQUID SURFACE

SA LUNAR SURFACE

SA MARS SURFACE

SA METAL SURFACE

SA PLANE

SA PLANETARY SURFACE

SA SOLID SURFACE

SA SUBSURFACE

Comparative evaluation of methods for determining microbial contamination on various types of surfaces 10 p1601 A67-23348

SURFACE CHEMISTRY

Electron processes at semiconductor surface in presence of chemisorption, noting conductivity and impurity distribution 03 p0492 A67-13315

Integral method to study surface

chemistry interaction due to combustion and attendant mass transfer on isothermal graphite cone in nonsimilar boundary layer flow 08 p1320 A67-20570

Oxygen chemisorption and oxidation on tungsten ribbon studied by flash desorption, using mass spectrometer 09 p1457 A67-22023

Vitreous silica and molten Al reaction, penetration rate of Al, reaction rate and effect of Bi and Sb on rates by lamellar compound formation 10 p1669 A67-23381

Surface cleaning of electrical and electronic equipment through water and oil removal by chemical compositions 14 p2327 A67-28822

Electron processes at semiconductor surface in presence of chemisorption, noting conductivity and impurity distribution 16 p2724 A67-30491

SURFACE COATING

Titanium susceptibility to corrosion, achieving protection by passive self-healing films forming on metal surface 20 p3466 A67-36638

Optimization for selection of optical coating patterns of external surfaces of spacecraft for temperature control [ASME PAPER 67-HT-55] 20 p3548 A67-36737

Radiation pattern lobing structure elimination for recessed annular slot in coated metal cylinder 22 p3767 A67-39274

Fastener and fastened joint technology noting influence of hole preparation, surface coating, thread lubricants and fit on fatigue life 24 p4161 A67-42081

SURFACE COOLING

Surface property effects on effectiveness of mass transfer cooling in laminar boundary layers with hydrogen injected into free stream of nitrogen or carbon dioxide 04 p0733 A67-15840

Supersonic laminar two-dimensional boundary layer separation in compression corner with and without cooling [AIAA PAPER 67-191] 06 p0940 A67-18361

Stresses produced in elastoplastic sphere with spherical cavity by surface heating-cooling, reducing problem solution to first order ordinary differential equation and functional equation 10 p1716 A67-22940

Cooling and heating effectiveness of plane surface in turbulent air flow by injection of air film, noting temperature effect 11 p1881 A67-23898

Spectral reflectance of water and carbon dioxide cryodeposits in vacuum integrating sphere as function of incidence angle, substrate material and cryodeposit thickness 24 p4253 A67-42046

SURFACE CRACK

Anomalous cooling of moon surface during lunar eclipse explained possibly by lunar surface roughness in form of cracks and declivities at centimeter scale 02 p0320 A67-11460

Three-dimensional stress distribution around elliptical crack under arbitrary shear loading, discussing Griffith-Irwin fracture theory [ASME PAPER 66-APM-N] 04 p0718 A67-15926

Gas saturation effect on titanium alloys undergoing heat treatment, discussing microhardness and surface crack formation 07 p1205 A67-19277

Nickel-base alloy static and dynamic creep test, examining fatigue zone fracture surface 11 p1806 A67-24364

Elastic interactions of cracks and dislocations of screw type in two-dimensional model 16 p2768 A67-31281

Cracked rectangular beam stress analysis, considering longitudinal shear and Saint-Venant torsion and flexure [ASME PAPER 67-APM-21] 17 p2964 A67-33150

Parallel contours of fracture surface at optical magnifications obtained by method based on microhardness indentations 22 p3823 A67-40300

SURFACE DIFFUSION EFFECT

Substrate temperature effect on structure of, evaporated alloy thin films 02 p0287 A67-11716

Equation of surface diffusion of indium in germanium solved by taking into account effect of external electric field 03 p0489 A67-13150

Laser action delay due to plasma-tube-surface decomposition resulting from bombardment by neon

ions 04 p0633 A67-15110
Dynamics of narrowing effect of surface and spatial dispersing agents on radiation line of ruby laser with nonresonance feedback 06 p1012 A67-18797
Equation of surface diffusion of indium in germanium solved by taking into account effect of external electric field 10 p1690 A67-23099
Surface and volume diffusion in thin films of system Ag-Se investigated by electron diffraction and microscopic studies 12 p1979 A67-25179
Electrical conductivity measurements of NaCl as function of particle size and temperature used to study subsurface diffusion 12 p1987 A67-26191
View function to images of surface in nonplanar specular reflector determined by general mathematical expressions [JPL-TR-32-939] 15 p2516 A67-29131
Pure molecular flow coupled with surface diffusion applied to cesium transport 15 p2520 A67-29494
Metallic adhesion between Mo-Mo and Ti-Ti couples, showing contact resistance useful in determining contamination at conducting interface 17 p2871 A67-32465
Dynamics of narrowing effect of surface and spatial dispersing agents on radiation line of ruby laser with nonresonance feedback 18 p3061 A67-34416
Surface, volume and grain-boundary diffusion role in metal sintering process, discussing theoretical equations 19 p3247 A67-35836
Scattering from hard surface solved numerically assuming constant potentials, relating potential present values to retarded values and to incident field 21 p3658 A67-39058
Alloying effect on diffusion thermopower in relation to Fermi surface variations in dilute silver-gold alloys [JPL-TR-32-1095] 24 p4200 A67-41840
Structure of image of diffused surface in coherent illumination investigated for mean intensity and noise-like obscuring component 24 p4155 A67-42336

SURFACE DISTORTION

Skin effect association with anisotropy of medium in solid mechanics, analyzing surface instability, internal buckling and surface wave propagation 01 p0113 A67-10406
Stokes creeping flow equations and steady flow of incompressible viscous fluid past liquid drop 01 p0051 A67-10458
Perturbations of gas-dynamic parameters behind shock wave front propagating from rarefied into dense gas with boundary between interfaces 01 p0053 A67-10984
Periodic surface distortion of molten layer in axisymmetric flat stagnation regions of cylindrical iron and copper rods 01 p1012 A67-11190
Free surface distortion and subsequent gas ingestion in emptying cylindrical tank, emphasizing maximum height of liquid surface when gas reaches outlet 02 p0233 A67-11945
Instrument designed for rapid measurement of surface deformations of 210-ft radio telescope at Parkes, Australia 02 p0229 A67-12069
Fermi surface of tin telluride approximated by four distorted surfaces located at L points of Brillouin zone as shown by Fourier analysis 06 p1065 A67-18950
Moire method of surface strain measurement 07 p1262 A67-19387
Infinitely small bending deformations of convex surfaces with boundary condition of generalized slip, formulating boundary value problem for bending of surface 18 p3144 A67-34482
Bending of orthotropic strip to anticlastic surface by uniform moment, determining strain along neutral axis, bending moment and couple action 22 p3913 A67-40008
Adsorbed ions and organic molecules effect on mobility of half-loops dislocation introduced by indenter into MgO surfaces 23 p4035 A67-40655
Laser irradiation effect on semiconductor crystals surfaces using pulsed ruby laser 23 p4045 A67-41470

SURFACE ENERGY

Surface charge after annealing of aluminum-silicon dioxide-silicon structures in inert atmospheres, analyzing effect of

applied electric field 01 p0032 A67-10004
Dynamic control for two-phase liquid-gas medium under weightlessness solved by surface energy, using computer for boundary value problem involved 02 p0231 A67-11540
Theory of influence of surface states on impedance of semiconductor-insulator interface, determining relaxation times which directly affect cut-off frequency of device 03 p0487 A67-12810
Surface photoelectromotive force in GaAs type semiconductors with short duration minority carriers 04 p0686 A67-15969
Phase shift as quantitative measure of relationship between surface convection and charge relaxation 11 p1825 A67-23862
Surface conditions effects on silicon planar transistor current gain 11 p1759 A67-24139
Electrical properties of degenerate intrinsic semiconductor noting spherical energy surfaces, parabolic density of states, acoustic phonon scattering, etc 15 p2535 A67-29487
Measurement methods for determining semiconductor surface properties stressing Garrett and Brattain calculations 15 p2449 A67-29810
Dynamic control for two-phase liquid-gas medium under weightlessness solved by surface energy, using computer for boundary value problem involved 16 p2683 A67-31606
Potential energy flux across isobaric surfaces in atmosphere indicates flux direction dependent on correlation sign between temperature and vertical velocity at surfaces 19 p3224 A67-35526
Electron energy spectrum, showing intensity maxima from surface plasma oscillations, noting thin films effect on surface losses 19 p3307 A67-35789
Computer program for determining net thermal energy incident on satellite by computing projected surface area [ASME PAPER 67-HT-56] 20 p3549 A67-36738
Oxidized silicon surface properties affected by diffused oxygen and gold, finding parasitic n-type layer formations and positive surface charge 21 p3678 A67-38149
Indium antimonide hole surfaces approximated within second order perturbation theory, discussing energy contours, Baguley cyclotron resonance data and maximum energy value 21 p3679 A67-38255
Ti additive effect on aluminum oxide particle growth in Ni matrix from 1000 to 1350 degrees C 24 p4171 A67-41959

SURFACE EROSION
Ground surface erosion due to rocket breaking, calculating flow-induced force parameters 01 p0156 A67-11434
Heating and scattering of plasma produced by giant laser pulse focused on solid target 03 p0486 A67-14194
Aircraft corrosion protection, discussing eloxation and electrophoretic deposition of multilayer synthetic resin 04 p0636 A67-14576
Erosion destruction mechanism in polycrystalline graphite, noting effect of gas flow over surfaces, flow pulsation frequency and generated aerodynamic loads 04 p0642 A67-15761
Debris ingestion into engine arising from ground erosion effects on jet lift V/STOL aircraft 06 p0945 A67-17906
Radiation cooled reentry heat shield of graphitic surface over graphite felt insulation with receding surface [AIAA PAPER 67-153] 06 p1115 A67-18320
Gas flow erosion effect on rough surfaces, noting pulsating pattern 06 p0991 A67-18815
Reversible and irreversible limitation of maximum power output from GaAs by thermal heating and surface damage 10 p1665 A67-23520
Microhill hypothesis for Martian wave of darkening noting developments 11 p1859 A67-24223
Lunar surface erosion by rockets simulated in laboratory to study hazards of retrorocket landing on airless planetary bodies 12 p1922 A67-25701
Heating and scattering of plasma produced by giant laser pulse focused on solid target 14 p2360 A67-28539
Small particle bombardment of stone and iron meteorites, obtaining comparative erosion rates 21 p3704 A67-38504

Real gases examined for application as working fluid in Brayton cycle power plant, considering radiator area reduction to Rankine cycle 24 p4102 A67-42488

SURFACE FINISH
Optical methods and equipment used in checking surface finish and volume and surface inhomogeneities of active media and interferometric mirrors of lasers 03 p0436 A67-13143
Emissive power of germanium and silicon with various surface finishes in temperature range from 700 to 1200 degrees K 04 p0674 A67-14719
Aluminum impact extrusion process design 14 p2323 A67-27814
Qualitative and quantitative methods of surface finish, discussing equipment 15 p2493 A67-29643
Strength increase of parts or system to prevent fatigue failure, noting bulk and material considerations and elimination of fretting, scoring, corrosion, sharp corners, etc 17 p2962 A67-32824
Holographic testing of large optical surfaces, using laser sources and interferometer guidance 17 p2863 A67-33301
Silicon surface depth damage determination technique, with confirmation by Sirtl etching, oxidation and epitaxial deposition 18 p3103 A67-34565
Integrodifferential equations for product surface area changes and grinding process development obtained by assuming proportionality between fracturing probability and particle size 19 p3236 A67-35725
Incipient boiling prediction extended from forced flow water to other fluids and natural flow conditions [ASME PAPER 67-HT-61] 20 p3549 A67-36743
Performance factors affecting size, shape and operation of piston and bore including hydraulic lock, viscous drag, oil contamination, etc 20 p3366 A67-37367
Honsel Plastic Mold /HPM/ process for high surface quality, discussing cost, materials and solidification time 21 p3637 A67-38976
Boiling heat transfer to liquid helium, discussing heat flux as temperature difference function and surface finish effect 22 p3920 A67-40390
Domain structures in YIG slices after polishing strains elimination, noting spike domains 23 p4041 A67-41185
Automatic plating system insuring quality finishes by selectively phosphating or chromating parts after zinc plating 23 p4010 A67-41351
Nickel on chromium carbide base cermet polishing by synthetic diamond wheels shown to have little effect on strength 24 p4159 A67-41963

SURFACE GEOMETRY
Reflecting surface geometry calculated by reflection and scattering of light source 02 p0268 A67-12446
Computer derivation of best-fit hyperbolic and parabolic surfaces using total parameter variation method 03 p0388 A67-14122
Two-dimensional incompressible potential flow theory for airfoil design with prescribed velocity distribution over surface 09 p1437 A67-21740
Curvature tensor in definition of affine branch point induced by Riemann branch point on isotropic hypersurface 09 p1534 A67-22566
Man-Computer Graphics /MCG/ allows operator control through oscilloscope via light sensitive pen 11 p1756 A67-24251
Bending strain in linear shell theory, noting surface differential geometry and rotation vector and tensor [ASCE PAPER 268] 11 p1874 A67-24430
Measures and reductions for 1868 points on Yerkes lunar photograph No. 1269, listing uncorrected and refraction-free photographic coordinates 11 p1860 A67-24463
Approximate solutions for boundary value problems of cylindrical shells of arbitrary geometry 12 p2021 A67-25576
Thermal coordinate analysis of lunar IR scan data for directional effects caused by surface geometry, illumination and sensor angle [AIAA PAPER 67-291] 12 p2009 A67-26008
VHF transistor, attempting design of 60 MHz passband amplifier 13 p2077 A67-26653
Rigidity of surface with flattened point

proved by Cauchy-Riemann equations, considering case where contact of surface with tangential plane approaches infinity 16 p2698 A67-31912

Computer graphics for surface generation, stressing Coons surfaces and parametric representation 17 p2820 A67-32783

Thermal conditions effect on moon figure, reviewing methods for determining lunar geometric form 17 p2949 A67-33122

Isostatical equilibrium form of moon model having homogeneous semimolten core and homogeneous solid crust 17 p2949 A67-33123

Interferometric comparison between two nearly identical shapes by superimposing hologram reconstruction of one onto real surface of second 17 p2864 A67-33388

Surface geometry demonstrated to be insignificant in production of lunar hot spots during eclipse 18 p3135 A67-34545

Friction data, elastoplastic deformation and surface geometry of rubbing surfaces 19 p3237 A67-35851

Local properties of limiting surfaces, giving hypothesis for surface separating two unconnected regions 19 p3204 A67-35903

Finite-amplitude oscillations of Maclaurin spheroids preserving ellipsoidal nature of surface and generating internal motions of uniform vorticity 19 p3263 A67-36078

Fin surface geometry optimization with respect to gross heat-transfer coefficient [AICHE PAPER 6] 20 p3552 A67-36827

Soviet monograph on geometry of earth ellipsoid describing analytic geometry methods for solving geodetic problems on spheroid surface 21 p3616 A67-37965

Analytic representation of absolute topography of isobaric surfaces by linear combination of arbitrary surfaces represented by Chebyshev polynomials 21 p3654 A67-38087

Surface geometrical variations in electrochemical shaping process for hydrodynamic removal of dissolved processed metal, deriving partial differential equations 21 p3636 A67-38897

Electrochemical shaping precision analysis, discussing efficiency, current losses, energy consumption, surface geometry and electrolyte properties 22 p3812 A67-39543

Representation of characteristic surfaces of unsteady axisymmetric flow and steady three-dimensional supersonic flow by hyperbolic system of quasilinear differential equations 22 p3785 A67-40010

Equations for arc length derived for two-dimensional isentropic compression surface for ideal gas 22 p3742 A67-40102

Aircraft fuselages, wings, fillets, ducts and other free form surfaces defined using man-machine graphical interaction with computer [AIAA PAPER 67-895] 24 p4126 A67-43004

SURFACE INTERACTION

Gaposchkin satellite gravity results compared with surface gravimetry data 01 p0056 A67-10041

Particle emission from surface interacting with laser beam 02 p0252 A67-12180

Potassium atom reactive scattering from oriented methyl iodine molecules, determining variation of chemical reactivity over molecular surface 03 p0367 A67-13524

Time harmonic Rayleigh wave attenuation in elastic half-space by surface impedance 03 p0371 A67-13945

Forces holding hydroxyl ions to surfaces of MgO particles 04 p0642 A67-15087

Wave diffraction on surface impedance discontinuity in coaxial waveguide 06 p0968 A67-17856

Fixed vertical plane surface effect on velocity of solid sphere in free fall in laminar region of incident viscous flow for various Reynolds numbers 06 p0983 A67-17928

Perpendicular magnetic field induced change in electron temperature of current carrying semiconducting plates 06 p1054 A67-18805

Interaction of two cylindrical jets of uniform flow as far downstream as possible impinging at included angle of 60 degrees 06 p0944 A67-18888

Surface recombination velocities and diffusion lengths in GaAs determined by variation of cathodoluminescence intensity with voltage of exciting electron beam 06 p1063 A67-18936

Integral method to study surface chemistry interaction due to combustion and

attendant mass transfer on isothermal graphite cone in nonsimilar boundary layer flow 08 p1320 A67-20570

CdTe properties evaluated through pulse height response of surface barrier devices to monoenergetic alpha particles normally incident to surface 08 p1356 A67-21308

Ultrahigh vacuum cold welding in dynamic load elevated temperature environment, noting surface oxide in vacuum 10 p1670 A67-23742

Asymptotic solution method for frozen dissociated laminar boundary layer flow over flat plate surface with arbitrarily distributed catalytic 11 p1781 A67-24573

Reduction or elimination of secondary asymmetry voltage in germanium Hall generators noting effect of surface recombination, temperature distribution stabilization, etc 12 p1939 A67-25278

Momentum and energy imparted by collisions of gas molecules with atoms of cold rigid wall for arbitrary interaction potential 13 p2050 A67-26883

Velocity distribution function of re-emitted molecules effect on slip flow boundary conditions 13 p2102 A67-26970

Surface interaction of free molecular flows or molecular beams, considering state variables in highly rarefied gas in Maxwellian equilibrium, stagnation temperature, etc 13 p2159 A67-27299

Superheating in cylindrical pure niobium by suppressing end effects 14 p2369 A67-28597

Semiconductor photoconductivity kinetics as affected by surface recombination, considering bi-and monopolar photoconductivity 14 p2372 A67-28756

Interaction of supersonic gas stream with inclined surface, calculating parameters and boundary of fluid spreading 15 p2472 A67-29776

Numerical calculations of interactions of monatomic gas particles with ideal and contaminated crystal surfaces at epithermal energies 15 p2434 A67-30197

Damping effect of conduction electrons on ultrasonic surface and body waves propagating in CdS crystals, plotting damping against conductivity 17 p2921 A67-32971

Interaction of finite amplitude pressure pulse with combustion region at surface of burning solid propellant 18 p3108 A67-33830

Perpendicular magnetic field inducer change in electron temperature of current carrying semiconducting plates 18 p3102 A67-34424

Interaction of three-dimensional model of gas with solid surface, discussing atomic velocity distribution from surface reflection, energy and momentum accommodation coefficients, etc 19 p3264 A67-34936

Interaction between environment, oxide layer and surface slip formation in aluminum during cyclic bending 19 p3247 A67-35788

Surface vibration effect on nucleate pool boiling, measuring heat-transfer coefficient and proposing mechanism [ASME PAPER 67-HT-58] 20 p3549 A67-36740

Incompressible cylindrical jet interaction with incompressible unbounded homogeneous stream, determining contact surface 20 p3360 A67-37661

Electric domains in high resistance GaAs single crystals, measuring electric field intensity with Pockels electro-optic effect noting surface state role 22 p3857 A67-39459

Mass spectrometric study of oxygen adsorption, determining condensation coefficient and tungsten surface work function for various concentrations 24 p4172 A67-42073

Benzene and related molecules adsorption on uniform graphite surfaces investigated for lateral interaction and localization of lattice sites 24 p4118 A67-42195

Very long nuclear spin relaxation times in gaseous He by suppressing He surface interactions measured in highly spin polarized samples 24 p4191 A67-42247

Soviet book on molecular flow in vessels covering mass balance, energy exchange, rarefied gas, etc 24 p4191 A67-42359

SURFACE IONIZATION

Semiconductor surface barrier Si n-type detector yielding fast resolution curve in alpha-gamma radiation coincidence experiment 01 p0066 A67-10657

Surface charge and impedance of plasma

excited by incident electromagnetic waves 02 p0190 A67-11507

Surface recombination velocity of thermally oxidized silicon structures exposed to X irradiation 03 p0496 A67-13677

Surface charge distribution effect on stability of conducting fluid in presence of magnetic field 03 p0481 A67-13731

Cesium ionization and transport phenomena for developing porous-surface ion sources 04 p0689 A67-15013

Electron and ion emission from iridium in lithium vapor, noting surface ionization, work functions and experimental setup 04 p0660 A67-15108

Fluctuation spectra of Cs and K plasmas produced by surface ionization in Q-3 device 05 p0859 A67-17443

Refractory metals and metal alloys analyzed regarding electron work function and threshold temperature for surface ionization in all-metal guard ring diode with directly heated wire 06 p1035 A67-18137

[AIAA PAPER 66-223] Surface ionization detector of hydrogen in presence of air at one atm 08 p1330 A67-20376

Saha-Langmuir formula applied to description of temperature dependence of positive ion current in surface ionization of silicon atoms, comparing work functions by methods using contact potential, thermionic emission and Richardson graphs 09 p1554 A67-22006

Cesium vapor thermionic diode operation in electron-rich surface ionization mode noting transport effects 11 p1849 A67-24902

Surface charge and impedance of plasma excited by incident electromagnetic waves 14 p2261 A67-28071

Cesium ion emission patterns from rear-fed porous refractory metals studied by thermal emission microscope 17 p2888 A67-33059

Thermionic properties, surface ionization, atomic and ionic sublimation of Re, Mo, Ta and W 19 p3264 A67-35082

Surface ionization of atoms and molecules on nonmetals, determining work functions and activation energies for dissociation 19 p3264 A67-35083

SURFACE LAYER

Fluctuations of refraction index of surface layers of atmosphere observed directly in daytime and parameters of fluctuation distribution 02 p0325 A67-11985

Anomalous gravitational field representation without using integral equation for density of auxiliary surface layer 03 p0411 A67-13345

Metal-semiconductor surface barrier and prediction using concepts of covalent and ionic crystals 03 p0494 A67-13475

Majority carrier current flow in metal-semiconductor barriers according to theory incorporating Schottky diffusion theory and Bethe thermionic emission theory 03 p0494 A67-13476

Diffusion coefficient for electroactive impurity in semiconductor based on current carrier concentration variations during successive removal of surface layers 03 p0498 A67-13841

Velocity, energy and concentration fields in laminar boundary layers with arbitrarily distributed mass transfer at surface 04 p0603 A67-14643

Environmental effects on mechanical behavior of metals in vacuum and gases normally found in atmosphere, considering surface oxide layer 04 p0638 A67-14996

Turbulent vertical diffusion in surface layer of atmosphere 04 p0652 A67-15568

Wind profile effect on turbulent diffusion for infinite linear source in surface layer of unstable stratified atmosphere 04 p0652 A67-15569

Orientation dependence of surface charge on anodized indium antimonide from MOS capacitance measurements 05 p0869 A67-17093

Corbino magnetoresistance experiments for n-type surface layers on p-type indium arsenide crystals as function of surface electric field 06 p1064 A67-18941

Geochemical differentiation in terrestrial environments, noting vertical planetary differentiation 06 p0999 A67-19015

Well logging methods for study of composition of planetary near surface layers, noting electric, nuclear and acoustic measurement methods 06 p1092 A67-19016

Conductivity changes in flash evaporated p-GaAs films caused by field effect and optical and thermal excitation at temperatures about 100 degrees K 07 p1232 A67-19564

Lunar photography application to creation of selenographic coordinates enveloping near and far sides of moon 08 p1388 A67-21000

Selective surface obtained experimentally by deposition of stack of thin layers 09 p1558 A67-22599

Anodic behavior of GaAs single crystals at increased current densities in alkaline and acidic solutions, discussing etch tunnels 11 p1848 A67-24743

C domain wall motion in barium titanate crystals is dependent on A domains and activation fields throughout whole crystal 11 p1849 A67-24900

P atoms distribution in doped surface layer of silicon photoconverter for various thermomdiffusion conditions exhibiting typical concentration curves slope 12 p1982 A67-25322

Stress-strain state and corrosion and erosion produced by aggressive gas flows in surface layers of gas turbine nozzle blades of ZhS6-K alloy 13 p2187 A67-26451

Charge motion on outer silicon oxide surface of MOS structure, estimating surface resistance and dependency on humidity and other factors 13 p2176 A67-26707

Origin of excessive reverse current in silicon p-n junction, discussing surface layer channel formation 14 p2283 A67-28040

Surface current change between critical paramagnetic and critical diamagnetic induced by temperature variation in type II superconductor immersed in static magnetic field 14 p2365 A67-28296

Expression for surface field components obtained for plane electromagnetic wave at nose-on incidence on seminfinit cone 14 p2261 A67-28376

Turbulent spectral density of radio refractive index in surface layer of atmosphere 14 p2262 A67-28379

Theoretical determination of polished metals emission factors, using model where emission depends on surface layer temperature and electric resistivity 14 p2407 A67-28558

Two cases of critical surface current magnitude change in type II superconductors after transport current direction reversal 14 p2370 A67-28719

Lateral heating and sublimation of arbitrary thick two-layer plate using thermal flux time-dependent on plate surface 14 p2408 A67-28802

Surface heat balance shown to be useful thermal boundary condition at sea-air-land interface for earth surface mean temperature and macroclimate models 15 p2513 A67-30060

Transmission coefficient associated with internal reflection from absorbing surface layer derived from reflection coefficient, noting relation to absorption 17 p2883 A67-32204

Lunar structure from lunar moments of inertia, noting thick layer denser than lead near surface 17 p2947 A67-32757

Barium adsorption on individual crystal planes of tungsten field emitter studied for thermally equilibrated and unequilibrated adsorbate layers 17 p2922 A67-33259

Thin semiconductor layers, studying surface conductivity variation with semiconductor thickness and surface band curvature 19 p3299 A67-34759

Au and P doped n-type Si, noting formation of p-type surface layer of increasing thickness when heat treated 19 p3299 A67-34761

180 degree domain formation in ferroelectric crystals unaffected by presence of shorted electrodes due to surface layer properties differing from bulk 19 p3304 A67-35047

Radiation surface effects in semiconductor devices, noting positive space charge buildup in passivated device dielectric surface layer 19 p3306 A67-35674

Axial residual stress determination in metal surface layers based on measuring strains 19 p3343 A67-35844

Elastic and residual strains caused by friction load in polymer surface layers studied for dependence, slip rate and friction load duration 20 p3473 A67-36842

Inverse layer effect on p-type silicon MOS structure surface, examining deviation from equilibrium space charge theory 20 p3511 A67-37141

Germanium and cadmium telluride edge absorption, noting lattice imperfections causing absorption coefficient increase in indirect transition region 20 p3511 A67-37143

Electric conductivity of surface space charge layers in semiconductors, solving Boltzmann equation and determining current density and carrier mobility 20 p3511 A67-37144

Critical surface between superconducting and normal state determined for commercial niobium stannide ribbon and Nb-Zr wire 20 p3512 A67-37346

Nitrogen role in oxidation of titanium in air at elevated temperatures studied by spectrographic analysis 21 p3643 A67-37828

Germanium conductivity dependence on surface and space charges in transverse magnetic field 21 p3676 A67-37862

Surface potential of semiconducting gallium arsenide through temperature dependence measurements of transverse conductivity of clamped contact 21 p3676 A67-37869

Donor surface states and bulk acceptor traps in silicon on sapphire films due to activation of absorbed impurities 21 p3677 A67-38012

High endurance thermionic cathodes for Kaufman thrusters, discussing emissive coatings and emissive layer starvation [AIAA PAPER 67-678] 21 p3696 A67-38929

Estimated thickness of fragmental surface layer of Oceanus Procellarum from laboratory impact cratering studies 22 p3885 A67-39977

Low temperature transient creep behavior of polycrystalline aluminum investigated experimentally for recovery of surface layer stress 22 p3821 A67-40054

Lunar surface layer soil density limits estimated in simulation study of adhesion, composition, grain size and grain shape effects 23 p4066 A67-41008

Defects in surface layer of silicon crystals during deep diffusion of phosphorus studied by X-ray diffraction 23 p4042 A67-41295

Deposited Al layer thickness on Si determined using X-ray spectrometric technique 24 p4200 A67-41803

Upper critical nucleation field at free surface of superconductor backed by normal metal 24 p4200 A67-41862

Second optical harmonic generation of pulsed ruby laser emission in GaSe crystal suggesting only surface layer contribution to generation 24 p4167 A67-42074

Cathode outer oxide surface heating for pulsed emission current measured in intervals between retarding current pulses and different repetition frequencies 24 p4129 A67-42231

Energetic nuclear bombardment effects on stellar surface element abundance calculated with statistical theory in A magnetic variable star abundance anomaly 24 p4228 A67-42263

Abundance anomalies in stellar surface layers by proton and alpha particle bombardment caused nucleus breakdown and buildup to lower and higher mass numbers respectively 24 p4228 A67-42264

Space charge layers on surfaces of lead sulfide photoconducting film noting Hall coefficients 24 p4204 A67-42363

Mezo-Madaras chondrite polymict structure differs from structure in light-dark meteorites 24 p4237 A67-42648

Steel dislocation structure under adsorption fatigue investigated by electron microscope, discussing surface active medium effect 24 p4174 A67-42724

SURFACE PRESSURE

Stress patterns in lubricated rolling contact elements calculated from surface pressures and temperature [ASME PAPER 66-LUB-16] 03 p0431 A67-13757

Reynolds number effect on surface pressure distributions and boundary layer velocity profiles on three-quarter power law bodies of revolution in hypersonic flow 05 p0747 A67-16431

Shock tunnel data on surface pressure resulting from hypersonic stream interaction with two transverse jets [AIAA PAPER 67-190] 06 p0939 A67-18299

Vertical interpolation of data from constant pressure to constant density surfaces for meteorological purposes 06 p0999 A67-18741

Film thickness effect on pressure generation of parallel surface thrust bearing investigated, using dynamic instrumentation mounted in moving surface 09 p1505 A67-22192

Elevation differences between Martian dark areas /maria/ and bright areas /deserts/, discussing surface pressure and temperature 10 p1706 A67-22957

Low aspect ratio wings at high incidence in wind tunnel study of surface pressure and vortex flow 10 p1593 A67-23549

Pressure measurements on surface and in wake of circular cylinder at rest and in vortex excited oscillation at subcritical Reynolds numbers [ASME PAPER 67-VIBR-31] 11 p1777 A67-24189

Rigid disk impact against ideal fluid surface in cylinder, deriving formula for impulse pressure at disk surface 12 p1928 A67-25669

Martian atmosphere models with different composition, pressure and temperature 12 p2003 A67-25685

Effect of Reynolds number on hypersonic flow of rarefied gas past sphere obtained from pressure distribution at surface 14 p2240 A67-27996

Low density hypersonic wind tunnel, noting surface pressure and flow field measurements 14 p2293 A67-28166

Thick laminar boundary layer effect on aerodynamic behavior of simple shapes in supersonic low density flow 14 p2241 A67-28170

High Mach number low Reynolds number flow over two-dimensional circular cylinder, obtaining surface pressure and heat transfer distributions 14 p2242 A67-28174

Two-dimensional flow through bends with turning vanes, using Green theorem to obtain surface pressure distributions [ASME PAPER 67-FE-13] 14 p2304 A67-28362

Inconsistency in Martian surface pressure as calculated by Gray explained, using Leighton and Murray observations 14 p2389 A67-28842

Formula for pressure vs flow deflection at hypersonic speeds, useful in studies involving pressure on inclined surfaces 15 p2472 A67-29675

Mars atmosphere surface pressure, radiative equilibrium temperatures, sunlight resonance scattering distribution, etc 18 p3123 A67-34152

Relation between surface pressure and atmospheric brightness in optically thin Rayleigh scattering atmosphere, considering application to Mars 18 p3134 A67-34536

Pressure fluctuations beneath incompressible turbulent boundary layer with mass addition 18 p3030 A67-34742

Surface pressure spatial correlation function for rigid infinitely long cylinder in three-dimensional diffuse sound field 20 p3537 A67-36646

Surface pressure distribution on tubelattice cluster with transverse gas flow to determine aerodynamic characteristics 20 p3359 A67-37306

Shock tunnel data on surface pressure resulting from hypersonic stream interaction with two transverse jets 21 p3610 A67-37799

Waveguide model for turbulent shear flow, calculating streamwise dependence of cross-power spectral density using Orr-Sommerfeld equation 22 p3782 A67-39529

Supersonic flow over flat and axisymmetric blunt bodies, discussing shock wave position, adiabatic index, surface pressure distribution and body geometric parameters 22 p3741 A67-40026

Planetary surface pressure and temperature of lower atmosphere determined from orbiting spacecraft with carbon dioxide laser 22 p3805 A67-40357

Reentry vehicle surface pressure measurement, obtaining accuracy and reliability in stable high level pressure transducer 23 p4006 A67-41378

Shock waves and boundary layer structure near tip of slender cone in rarefied hypersonic flow, discussing surface pressure peaks 23 p3932 A67-41762

SURFACE PROPERTY SA HARDNESS

Surface effect on temperature, I-V and watt-ampere characteristics of p-n junction semiconductor injection laser diode as coherent light source 01 p0087 A67-10077

Localized electron states of semiconductor surface due to lattice defects, determining excited state, ground state and bonding energies 01 p0128 A67-10078

IR spectral signatures of rocks and soils in identifying bulk composition by comparison to standard spectral curves 01 p0058 A67-10311

Terrain information from high altitude side-looking radar imagery of Arctic area 01 p0059 A67-10328

Spectral polarimetry signature of terrestrial and planetary materials through remote sensing 01 p0059 A67-10331

Interdependent microwave radar-and radiometer-sensor measurements of backscatter and albedo characteristics of earth surface 01 p0021 A67-10333

Electric conductivity on clean cleaved surface of degenerate germanium 01 p0131 A67-10340

Surface effects in quasi-classical energy quantization of conduction electron subject to arbitrary law of dispersion in metallic film 01 p0133 A67-10748

Basic problems of thin film physics - International Conference, Clausthal-Goettingen, West Germany, September 1965 02 p0281 A67-11701

Bremsstrahlung, transient and plasma radiation as affected by surface properties of silver bombarded by electrons 02 p0291 A67-11737

Hypervelocity crater size and target strength, relating force per unit area of crater surface to tensile strength of material 02 p0338 A67-12034

MOS capacitance measurements combined with neutron activation analysis, showing positive charge increase at oxidized silicon surfaces by sodium presence 02 p0300 A67-12518

Boundary conditions at interface between superconductor-superconductor and superconductor metal 03 p0489 A67-12937

Reflective properties of natural surfaces, noting dependence on surface properties of total reflected energy, spectral distribution, polarization degree of radiation, etc [AIAA PAPER 65-665] 03 p0411 A67-13045

Thermal conductance at interface of two materials in contact, investigating surface and lubrication effects [AIAA PAPER 65-662] 03 p0534 A67-13068

Room temperature measurements determining mean slope and peak-to-valley height influences on bidirectional spectral reflectance of V-grooved surfaces 03 p0426 A67-14398

Conducting surface boundary effect on current plasma instability in terms of potential fluctuations 04 p0687 A67-15208

Ultrasonic reflectivity of liquid-solid interface used as indicator of near surface properties of solid in cold work, grain orientation, etc 04 p0621 A67-15264

Gas flow, convective heat transfer, enthalpy rise and surface mass transfer for bodies in cross flow, with application to circular cylinder 04 p0733 A67-15841

Radiative heat exchange between specularly reflecting surfaces with direction dependent properties 04 p0738 A67-15869

Classical elasticity theory determination of stress distribution on boundary plane of elastic half-space due to internal body force distribution 05 p0908 A67-16040

Stability and dynamical response of small portions of differentially rotating stellar disks, noting decaying nonaxisymmetrical instabilities, epicyclic frequency, surface density, etc 05 p0892 A67-16410

Large signal AC field effect measurements on A and B real surfaces of InSb exposed to different ambients 05 p0862 A67-16604

Hardness of polyesters copolymerized with styrene, determining reticulation and temperature effects 05 p0759 A67-16767

Microwave surface resistance of type II superconductors, from simultaneous measurements of real part of surface impedance and magnetization 05 p0871 A67-17375

Semiconductor surface photovoltage under small signal conditions, when quasi-equilibrium approximation will be valid in space charge layer 06 p1047 A67-17600

Fracture mechanism for formation of dimpled fracture surface morphology 06 p1105 A67-18562

Surface generation-recombination and channel effects on p-n junctions and transistors exposed to ionizing radiation 06 p1054 A67-18822

Mundrabilla meteorite, describing iron meteorites found in Australia 07 p1247 A67-19058

Pencil-beam radio telescope adjustment via methods of control of surface of optical telescopes 07 p1189 A67-20244

Radar methods in lunar probing, discussing data obtained from surface soundings [AAS PAPER 66-186] 08 p1387 A67-20961

Bibliography on thin dielectric films, interfaces and surfaces 08 p1370 A67-21188

Surface effect on temperature, I-V and watt-ampere characteristics of p-n junction semiconductor injection laser diode as coherent light source 08 p1339 A67-21455

Localized electron states of semiconductor surface due to lattice defects, determining excited state, ground state and bonding energies 08 p1371 A67-21456

Electronic processes on semiconductor device surfaces analyzed using scanning light beam, for application to Si planar transistors 09 p1472 A67-21949

Large part inspection via ultrasonic and eddy current techniques, discussing surface and discontinuity dimension analysis 10 p1660 A67-23324

Surface parameter measurements of stannic oxide in powder, ceramic and gel forms by nitrogen adsorption techniques 10 p1603 A67-23398

Earth figure determination from relation between gravitational potential and vertical gradient anomalies and surface and sea level potential 11 p1783 A67-23899

Exponential point method measurement of heat fluxes and surface temperature in unsteady regime 11 p1882 A67-24030

Wavelength selectivity in solar collector design, noting role of scatter in determining radiative properties of surfaces 11 p1817 A67-24052

Barrier height between tungsten silicide films and n-type silicon base determined, using photoelectric response measurements 11 p1850 A67-24924

Bidirectional spectrophotometer for reflectance of solid and powder samples [AIAA PAPER 67-313] 12 p1946 A67-26028

Preparation and characterization of metal surfaces for study of emittance properties as function of surface roughness and oxidation [AIAA PAPER 67-318] 12 p1957 A67-26033

Proton radiation effects on mirror reflectance in high vacuum at various temperatures, degradation by blistering found to be highly temperature-dependent [AIAA PAPER 67-341] 12 p1957 A67-26055

Planar silicon transistors with improved performance and reliability due to metallic protection, noting low noise and surface potential stabilization 13 p2077 A67-26652

Surface effects in quasi-classical energy quantization of conduction electron subject to arbitrary law of dispersion in metallic film 13 p2176 A67-28777

Lambert diffuse reflection from general quadric surfaces 13 p2158 A67-26877

Magnetic field effect on microwave surface impedance of superconducting tantalum measured in various temperature ranges via dielectric-resonator techniques 14 p2371 A67-28726

Optical characteristics of cosmic and terrestrial surfaces, noting color distribution on moon, asteroids, stony meteorites, etc 15 p2516 A67-29152

Measurement methods for determining semiconductor surface properties stressing Garrett and Brattain calculations 15 p2449 A67-29810

Oscillator with lumped parameter superconducting L-C tank circuit, noting frequency variations as function of temperature 15 p2451 A67-29916

Charge curves for germanium and silicon surface obtained by field effect measurements, noting nature and mechanism of effect 15 p2542 A67-30249

Conducting surface boundary effect on current plasma instability in terms of potential fluctuations 15 p2532 A67-30256

Field effect behavior of thin InSb films noting semiconductor surface properties, mobility decrease with temperature and increase of impurity concentrations 16 p2732 A67-31527

Surface impedance of cylindrically stratified anisotropic ionosphere in presence of static magnetic field, calculating propagation parameters 16 p2631 A67-31853

Rigidity of surface with flattened point proved by Cauchy-Riemann equations, considering case where contact of surface with tangential plane approaches infinity 16 p2698 A67-31912

Cleaved surfaces of Mo cermet binary alloys structures annealed and fractured under static bending loads studied for surface properties 17 p2871 A67-32133

Surface potential contrast induced by electron beam of scanning microscope on unbiased planar transistors, investigating beam voltage effect on contrast formation 17 p2823 A67-32197

Surface leakage current and reverse current flow in silicon p-n junction diode affected by positive ion bombardment and oxygen adsorption 17 p2911 A67-32202

Temperature dependence of upper critical fields for clean superconductors of second kind, noting role of electron-reflection properties of surface 17 p2915 A67-32693

External features of South Vietnamese tektites noting structure, surface characteristics and possible formation mechanism 17 p2947 A67-32774

Subthreshold electron irradiation effects on surface recombination properties of n-and p-type germanium and silicon crystals 17 p2916 A67-32834

Mechanisms of atomic recombination at surfaces analyzed, considering behavior of insulators and semiconductor oxides 18 p2997 A67-33794

Slowly decaying broad maximum of parallel conductance explained by tunneling for surface states near Si-silicon oxide interface 18 p3101 A67-34018

Metal surface property improvement by thermal-spray coating noting flame plating 18 p3055 A67-34483

Surface recombination velocities relationship in depletion, inversion and accumulation surface layers of p-type silicon, using ambipolar carrier transport formulation 18 p3104 A67-34593

Ultrasonic energy, used for removing microorganisms from various surfaces for enumeration, noting texture, pretreatment and heat effects on recovery efficiency 19 p3179 A67-34911

Various boundary layer parameters and transducer shape effect on Measurement error of random pressure field by finite size transducer 19 p3228 A67-34964

Finite difference heat conduction method for surface subliming processes in space vehicles 19 p3346 A67-35755

Electron emission utilized in evaluating metal surface properties, particularly sintered material porosity 19 p3247 A67-35849

Local properties of limiting surfaces, giving hypothesis for surface separating two unconnected regions 19 p3204 A67-35903

MOS devices electrical characteristics controlled by physical parameters studied for approximate relations between loads, potentials and surface fields 20 p3507 A67-36319

Electron deflection instrument for measuring surface electric field strength 20 p3444 A67-36524

Rohsenow nucleate pool-boiling data correlation, stressing coefficients dependence on surface preparation and liquid-surface combination [ASME PAPER 67-HT-33] 20 p3547 A67-36723

Measuring methods for high energy molecules accommodation coefficients, determining dependence on energy, incidence angle, surface nature and outgassing 20 p3489 A67-36939

Solution for boundary value problems in elasticity theory for ellipsoid of revolution and cavity with surface loading, determining coefficients in closed form 21 p3718 A67-37984

Lubrication and wear problems of surfaces of solid materials noting influence of contact area, adhesion, speed, etc, on friction 21 p3633 A67-38139

Oxidized silicon surface properties

affected by diffused oxygen and gold, finding parasitic n-type layer formations and positive surface charge 21 p3678 A67-38149

MOS transistors surface properties and leakage current affected by gold, showing positive charge 21 p3678 A67-38150

Time average of autocorrelation function measured by CW radar illuminating moon calculated without lunar surface properties knowledge 21 p3703 A67-38189

Book on electrical properties of semiconductor surfaces covering space charge layer theory, solid state theory, etc 21 p3682 A67-38365

Mixed state existence in type I superconducting thin film, discussing microwave power absorption variation with perpendicular magnetic field 22 p3856 A67-39437

Surface states effect on frequency dependence of elements of equivalent circuit of n-type semiconductor/metal contact 22 p3859 A67-39578

Type II superconductor properties, discussing Ginzburg-Landau and London equations, surface superconductivity, vortex motion, etc 22 p3859 A67-39770

Superconductors for high-Q microwave cavities construction, noting unloaded Q and resonant frequency measurements and surface properties 22 p3865 A67-40431

Surface superconductivity in dilute Ta-Nb alloy ascribed to decrease in mean free path due to lattice defects 23 p4036 A67-40657

Resistance properties of thin continuous Au, Ag, Cu and Al films influenced by superimposed thin films, discussing resistance change and surface scattering 23 p4039 A67-40879

Lloyd mirror experiment applied to testing flatness of large surfaces, using moiré technique for visualizing and measuring fringe deviation 23 p4002 A67-41263

Static characteristics of 2N1304 germanium junction transistor exhibited by two surfaces in three-dimensional space 24 p4128 A67-41925

Phenomena between evaporated metal and semiconductor surface affecting potential barrier by metal electrons extraction potential and semiconductor fast state concentration 24 p4204 A67-42410

Optical characteristics of cosmic and terrestrial surfaces, noting color distribution on moon, asteroids, stony meteorites, etc 24 p4190 A67-43075

SURFACE REACTION

Functional analysis of plane problem of elastostatic theory for multiply-connected regions with given surface traction 01 p0160 A67-10516

Homogeneous transfer equation in line formation, noting correlation between thermalization length and line source function of two-level atom 02 p0266 A67-11898

Surface origin of LF noise power spectrum demonstrated via silicon MOS field effect structures 02 p0296 A67-11820

Surface states and additional structure in McMillan-Anderson model for Tomasch effect in superconducting films 02 p0296 A67-11822

Switching from transmission direction to barrier direction in junction diode at high injection levels 02 p0223 A67-12677

Boron filament preparation on fused silica substrates by decomposition of diborane 03 p0454 A67-13420

Screening effect on Coulomb interaction, electron-ion recombination and surface neutralization 03 p0473 A67-13512

Anomalous high photoconductivity of indium antimonide thin films due to negative charge transfer to oxide surface layer during illumination 04 p0683 A67-15650

Solid propellant regression rate in hybrid rocket motor examined via combustion process model, assuming homogeneous flow in central channel 05 p0874 A67-18786

Flow of thin layer of liquid on surface of rotating body of revolution in moving system of coordinates connected with body 06 p0991 A67-18817

Solid propellant with heterogeneous surface reaction, noting agreement with steady state and acoustic response properties of JPN

propellant 07 p1239 A67-19074

Diffusion bonding of Be, Mo and W by interdiffusion of mating surfaces through solid or liquid-state reactions 07 p1192 A67-20248

Oxide film surface effect on electrophysical characteristics of Ge surface, noting potential changes and recombination rate 08 p1367 A67-20412

Surface effects for solid propellant combustion, discussing flame profile and instability, surface burning mechanism, temperature distribution, etc 08 p1373 A67-20642

Effect of surface recombination and parasitic capacitance on linear buildup of photoconductivity in semiconductors, noting germanium photoresistor 09 p1551 A67-21668

Plasma characteristics of partially dissociated and ionized air due to alpha emissions from radioisotope surface material 09 p1543 A67-21819

Short aging test results on GaAs diodes, noting surface changes and dependence of nonradiative excess current component on device perimeter 09 p1472 A67-21952

Impurity free CsF effect on work function of tungsten surface, discussing amount of impurities, type and control 09 p1450 A67-22354

Perturbed zone stability of body immersed in equilibrium plasma during surface electron emission 10 p1683 A67-22782

Asymptotic calorimetry, developing general relationship between temperature and unperturbed heat transfer coefficient for steady state nonisothermal heating 10 p1656 A67-23139

Microwave surface absorption in static magnetic field affects surface resistance of superconducting alloys 11 p1848 A67-24584

Photovoltage measurement across lifetime junction produced by electron irradiation and by changing surface recombination velocity 11 p1850 A67-24917

Impurity effects on nucleation of Se vapor onto Pyrex glass noting degree of critical supersaturation, production of phase with nonequilibrium structure, etc 11 p1821 A67-24992

Microwave reflection analysis of plasma surface phenomena, noting dependence on electron density and collision frequency 11 p1844 A67-25097

Effective gap thickness and gap number relation determined from correlation of parameters of thermal contact conductance [AIAA PAPER 87-317] 12 p2037 A67-26032

Ablative behavior of low and high density phenolic nylon in diffusion controlled surface combustion regime [AIAA PAPER 87-328] 12 p2038 A67-26042

Thermal stress field effects on materials for idealized situation, discussing problem of half-space and elastic layer under nonuniform surface heating, crack, etc 12 p2032 A67-26198

IR surface photoconductivity of silicon as function of surface potential and current carrier parameters 13 p2174 A67-26397

Gas-surface interactions, energy exchange and scattering between particles and surface 13 p2097 A67-26935

Gas atom scattering from solid surface, analyses and comparisons 13 p2097 A67-26937

Molecular beam apparatus for determining momentum accommodation coefficients for neutral particle surface interactions 14 p2316 A67-28192

Aerodynamic flow deflection over convex curved surface noting occurrence of hysteresis 14 p2305 A67-28978

Unique determination for parameters of surface recombination centers in n-type germanium semiconductors 15 p2534 A67-29326

Surface reactions and structure determinations of oxides of niobium, tantalum and vanadium with /110/ surfaces from CO and oxygen 15 p2504 A67-29881

Surface coupled heat release effect on oscillatory amplitude of pressure coupled response in solid propellant 15 p2544 A67-29983

Combustion stability in solid propellant rockets, reviewing Soviet T-sub s and Q models 15 p2581 A67-29986

Rates of surface chemical reactions in well-defined flow systems theoretically investigated by data reduction techniques

and quantitative predictions 18 p2997 A67-33795

Deflagration of ammonium perchlorate studied using cleaved sections of large single crystals grown from water solution, discussing burning rate and combustion zone 18 p3108 A67-33814

Vapor volumetric fraction during forced convection, calculating true local vapor weight, volumetric fraction, location of bubble departure, etc 18 p3160 A67-34163

S-shaped boiling curves analyzed in terms of nucleation characteristics of heat transfer surface, correlating temperature driving force and density of centers 18 p3160 A67-34164

Chromizing of steel by HF induction heating in vacuum using low-carbon ferrochrome and electrolytic chromium mixture 19 p3236 A67-34920

Adsorption, surface reaction and mutual displacement of carbon monoxide, carbon dioxide and oxygen on titanium film, using mass spectrometer 19 p3244 A67-34941

Pressure dependent surface reaction effects on acoustic response of composite solid propellants studied for various coatings 19 p3309 A67-35010

Electron, X-ray and UV radiation effects on oxidized silicon surfaces and planar devices, noting space charge buildup 19 p3305 A67-35621

Transient nature of heterogeneous boundary layer chemical reaction at stagnation point studied analytically, deriving stability conditions 19 p3211 A67-35740

Surface-reaction effects on solid propellant acoustic-response functions characterizing transient combustion process 19 p3311 A67-35777

Gas chromatography and IR spectrophotometry used to examine monomethyl hydrazine air oxidation, showing evidence of surface catalyzed reaction 21 p3578 A67-38841

Surface states effect on current-voltage characteristics of metal-semiconductor contact from kinetic coefficients of electron exchange 22 p3858 A67-39570

Measuring method for minority carriers recombination rate at base surfaces of /n-m/ contact without passing DC through contact 22 p3858 A67-39575

Clean MOS structure bias and temperature /BT/ treatment at high electric fields causing electrochemical reaction affecting surface charge density 22 p3774 A67-40461

Perturbed zone stability of body immersed in equilibrium plasma during surface electron emission 24 p4195 A67-42118

SURFACE ROUGHNESS

Composite surface and composite correlation approaches to frequency dependence and surface roughness problems of lunar surface signal scattering 01 p0020 A67-10019

Optical surface roughness measurement using coherent radiation produced by helium-neon laser sigma-polarized at 6328 angstroms 01 p0020 A67-10020

Local geologic interpretation from intensity of radar return energy modified by illumination, surface roughness and object shape 01 p0058 A67-10310

Radar backscatter return interpretation in identifying terrain phenomena and composition 01 p0059 A67-10330

Centimeter-and millimeter scale roughness of lunar surface produced by micrometeorite impact 01 p0150 A67-10893

Self-preserving flow in turbulent boundary layer passing over surfaces with different roughness 02 p0232 A67-11561

Quantitative study of radar cross polarization factor D in order to obtain data on lunar surface roughness and dielectric properties 02 p0192 A67-11603

Turbulence structure in pipe flow with rough surfaces 04 p0604 A67-14845

Rough surface recrystallization of heated polyethylene extended-chain crystals 04 p0566 A67-15201

Temperature distribution effect on roughness of contacting surfaces of two juxtaposed solid materials 05 p0928 A67-16596

Analogy between radiation angular spectrum reflected from rough surface and frequency spectrum of carrier burst related to radio propagation 06 p0957 A67-17579

Magnification in profile drag of airfoil due

to effect of pressure gradients on boundary layer downstream of isolated roughness element 06 p0990 A67-18748

Gas flow erosion effect on rough surfaces, noting pulsating pattern 06 p0991 A67-18815

Statistical properties of radar signals with internal coherence reflected from rough surfaces 07 p1139 A67-19223

Resistance of magnetic structure of Ni-Fe thin films deposited on metal substrate with anisotropic surface roughness to effect of orthogonal pulsed fields 12 p1980 A67-25238

Preparation and characterization of metal surfaces for study of emittance properties as function of surface roughness and oxidation [AIAA PAPER 67-318] 12 p1957 A67-26033

Aluminum pretreating and finishing agents noting cleaning, etching, roughening and coatings 14 p2324 A67-27821

Asymptotic curve for single arbitrary reflection of atom from plane with weak surface roughness, calculating total momentum and energy 14 p2351 A67-28636

Solid lubricants frictional behavior in press-fit tests, measuring sliding speed, load and surface roughness as function of time [ASLE PREPRINT 67AM 5A-2] 14 p2325 A67-28786

Qualitative and quantitative methods of surface finish, discussing equipment 15 p2493 A67-29643

Electromagnetic wave diffraction by convex spherical surface considered in terms of mutual impedance between two radial electric dipoles, using integral equation 17 p2817 A67-32930

Lunar surface roughness and brightness temperature anomalies from IR image study 18 p3134 A67-34537

Skidding accident reduction investigated for runway and highway safety noting worn tires, smooth surface texture, locked wheels and pilot technique 19 p3173 A67-35930

Plane electromagnetic wave reflection from rough surface, calculating energy and polarization characteristics 21 p3580 A67-38115

Surface superconductivity of cylindrical niobium samples, discussing microscopic surface roughness and approximate character of theory 21 p3685 A67-38802

Hemispherical reflectance of metal surfaces investigated for relation of wavelength and surface roughness 22 p3920 A67-40420

Geometrical self-shadowing of random rough surface described by Gaussian statistics in wave backscattering phenomena 23 p3972 A67-40832

Vector field theory of time dependent backscatter from distant slightly rough sphere for pulsed and sinusoidally steady state sources 23 p3974 A67-41200

SURFACE ROUGHNESS EFFECT

Surface roughness effect on laminar MHD flow through rectangular duct, deriving relation between transition friction factor and Reynolds and Hartmann numbers 01 p0120 A67-10186

Anomalous cooling of moon surface during lunar eclipse explained possibly by lunar surface roughness in form of cracks and declivities at centimeter scale 02 p0320 A67-11480

Gaussian noise model of shadowing effect on wave backscatter from one-dimensional random rough surface 02 p0192 A67-11602

Thermal emissivity and absorptivity of trapezoidal grooves and paneled tubular radiators, obtaining parametric relations by numerical solutions via computer 02 p0342 A67-12331

Spectral emittance of metallic and nonmetallic materials, discussing surface roughness effects [AIAA PAPER 65-675] 03 p0467 A67-13042

Controlling radar cross section of long thin bodies by employing corrugated structures operating in nonpropagating mode 03 p0370 A67-13862

Controlled three-dimensional roughness effect on hypersonic laminar boundary layer transition [AIAA PAPER 66-26] 04 p0547 A67-14819

Total specular reflectance of rough metal surfaces calculated, using Maxwell equations and approximation via Kirchhoff diffraction theory [AIAA PAPER 65-424] 04 p0723 A67-15232

Airflow in small wind tunnel with roughened heat transfer surface, using flow visualization techniques 04 p0727 A67-15801

Heat-transfer coefficient measurements in separated flow regions in heated duct with circumferential grooves, ribs and enlargements, by visual flow techniques 04 p0729 A67-15810

Tip bluntness, surface roughness and angle of attack effects on laminar boundary layer for 10 degree cone, measuring heat transfer and detecting transition 04 p0549 A67-15823

Tests at Mach 8 on cone, analyzing effect of roughness elements and variable entropy on transition and heat transfer distribution [AIAA PAPER 67-132] 06 p0940 A67-18357

Aerodynamic characteristics of rough cylinders, noting effect on head drag coefficient and Reynolds number 07 p1126 A67-19323

Electromagnetic wave scattering by rough surface computed by approximate method 07 p1147 A67-20237

Perturbation technique used to study random response of airplanes to effect of runway roughness 08 p1279 A67-20480

High resolution radar correlometer measurement of spatial correlation radius of RF radiation scattered by disturbed ocean surface 08 p1294 A67-20819

Random deviation statistical analysis of acoustic and electromagnetic waves by comparatively large slope irregularities 08 p1294 A67-20820

Turbulent spots and wall roughness effects in shock tube boundary layer transition, noting stable region behind shock 08 p1322 A67-21382

Stability of various surfaces with respect to electron bombardment heating, noting influence of roughness on electron trapping 09 p1500 A67-22428

Surface treatment effect in field effect anomaly of cleaved and etched n-type indium antimonide at high magnetic fields 10 p1688 A67-22903

Acoustic waves omnidirectional scattering by rough imperfectly reflecting surfaces analyzed using physical optics method 10 p1680 A67-23314

Microhill hypothesis for Martian wave of darkening noting developments 11 p1859 A67-24223

Measurement of radiation reflectively scattered from optical surfaces in far UV, noting role of overcoating with metal films 11 p1819 A67-24666

Electromagnetic scattering from rough finitely conducting surface of uniform infinitely extended medium, considering intensity and polarization 12 p1906 A67-25945

Rough metal surface bidirectional reflectance, using Davies and Beckmann models [AIAA PAPER 67-319] 12 p2037 A67-26034

Surface roughness effect on spectral and total emittance of platinum, noting spatial distribution of polarized components [AIAA PAPER 67-320] 12 p1957 A67-26035

Reflectance function for stainless steel with various surface roughnesses, comparing incident and reflected monochromatic fluxes of assigned directions [AIAA PAPER 67-321] 12 p1957 A67-26036

Wire screen roughnesses effect on turbulent boundary layer along flat plate without pressure gradient 13 p2093 A67-26529

Displacement and momentum loss thickness in boundary layer of rough flat plate at low velocities as function of wall roughness, pressure gradient, etc 13 p2095 A67-26809

Signal spectral characteristics when reflected from rough surface exposed to monochromatic and frequency modulated oscillations from moving airborne emitter 13 p2154 A67-27038

Structure and properties of thin films in terms of deposition conditions, noting conditions for continuity, surface roughness, grain size, lattice defect density, crystalline orientation, purity, etc [AIAA PAPER 66-727] 13 p2054 A67-27591

Terrain irregularity influences on radio wave propagation and reflection 14 p2264 A67-28398

Electrodynamics applied to two-dimensional problem of determining resolution of images reproduced from ideally plane infinitely thin holograms 15 p2489 A67-30006

Laminar boundary layer transition in hypersonic shock tunnel of cone, noting effect of high Mach numbers and tip surface roughness, using surface heat transfer gauges [AIAA PAPER 66-494] 15 p2418 A67-30191

Influence of surface roughness and humidity on endurance of rubbed films of various lamellar solids on steel 16 p2681 A67-30853

Polarization characteristics of radio emission from rough lunar surface, analyzing averaging effects of antenna radiation pattern and surface roughness 16 p2628 A67-31495

Thermal radiation dependence of perfectly conducting materials on large and small surface roughnesses thermal radiation dependence of perfectly conducting materials on large and small surface 16 p2779 A67-31502

Steady motion of craft with aerial lifting surfaces over rough water, defining conditions for safe operation 18 p3022 A67-33415

Electrodynamics applied to two-dimensional problem of determining resolution of images reproduced from ideally plane infinitely thin holograms 18 p3046 A67-33767

Wave scattering phenomenon on uneven surfaces 18 p3004 A67-34380

Tungsten cermet emissivity study using electron heating 20 p3466 A67-36913

X-band propagation over rough earth when illuminated by radiation, studying scattering problems 20 p3388 A67-37647

Model for lunar surface roughness effect on emission of thermal IR radiation and casting of shadows in sunlight 21 p3702 A67-38188

Roughness induced boundary layer transition in supersonic flow over blunt bodies 21 p3614 A67-38891

Combined frequency and space correlation of wave fields scattered by rough surfaces where conditions of applicability of Kirchhoff approximation hold true 22 p3760 A67-39660

Polarized and depolarized scattering from perfectly conducting rough surface, theory based on Fourier transform and small perturbations polarized and depolarized scattering from perfectly conducting rough surface, using theory 22 p3762 A67-40076

Directional characteristics in optical heterodyne detection processes including finite sources, bandwidth, random phase sources and rough surfaces 23 p4012 A67-40877

SURFACE STABILITY

SNAP-10A high emittance white coating, noting stability at 600 degrees F, irradiation and vacuum and mechanical vibration [AIAA PAPER 65-652] 03 p0448 A67-13057

Dynamic response, sloshing frequencies and stability of free surface of liquid in circular cylindrical elastic tank with flexible bottom [AIAA PAPER 67-76] 06 p0986 A67-18274

Control surface instabilities of lifting body configurations at very high speeds and with separated flows analyzed by wind tunnel tests for unsteady control surface load problems [AIAA PAPER 67-15] 07 p1258 A67-19430

Dynamic response, sloshing frequencies and stability of free surface of liquid in circular cylindrical elastic tank with flexible bottom [AIAA PAPER 67-76] 21 p3614 A67-38868

Molecular sieves as casings filler for semiconductor devices, discussing stabilization of electrical parameters and absorptive capacity of synthetic zeolites 23 p4042 A67-41274

SURFACE TEMPERATURE

Pressure and density of heat flux at surface of pointed or blunt nosed obstacle in divergent truncated cone of hypersonic nozzle 01 p0005 A67-10255

Radiation techniques for surface temperature measurement, considering optical and radiation pyrometers, projection thermography and photographic techniques 01 p0062 A67-10274

Airborne surface temperature measurement relating surface appearances to radiation parameters 01 p0063 A67-10327

Epitaxial temperature for Si films vacuum deposited on silicon as function of substrate

crystallographic orientation observed by low energy electron diffraction patterns 01 p0132 A67-10372

Book on radiative heat transfer between surfaces and participating media 01 p0166 A67-10378

Thermoelectric probe in calibrating surface temperature transducers, noting results on various materials 01 p0075 A67-11134

Saturation effect dependence on electrode surface temperature and bulk gas temperature in MHD generator duct 01 p0126 A67-11186

Atmospheric and surface temperature profile measurement using balloon mounted IR spectrometer 01 p0061 A67-11391

Two-layer model of lunar surface analyzed, using criteria of transparency to microwave radiation 02 p0324 A67-11700

Thermal and pressure effects of rocket exhaust impinging on flat plate surface at high vacuum [AIAA PAPER 66-46] 02 p0341 A67-11934

Temperature control of orbital Titan III-C transtage space booster, noting thermal design, configuration and materials test program support 02 p0335 A67-12395

Mean surface temperature-time solution of heat absorbed by seminfinitesimal solids [ASME PAPER 66-WA/HT-58] 04 p0725 A67-15437

Nonsimilar free convection boundary layer from vertical flat plate with step discontinuities in surface temperature [ASME PAPER 66-WA/HT-17] 04 p0739 A67-15930

Surface temperature of Venus 05 p0886 A67-16029

Molecular fluxes in lunar atmosphere relationship to gas source distribution, surface temperature and gas emission laws 05 p0904 A67-17404

Axisymmetric modes and frequency vibration of thin conical shells subjected to rapid surface heating 06 p1100 A67-18000

Local radiation equilibrium temperatures in semigray enclosures, with reference to thermal design of spacecraft [AIAA PAPER 67-211] 06 p1115 A67-18327

Radiative heat exchange and equilibrium surface temperature in space environment [AIAA PAPER 67-212] 06 p1115 A67-18328

Surface temperature of deflagrating ammonium perchlorate crystals calculated from crystal phase transition thickness [AIAA PAPER 67-68] 06 p1073 A67-18469

Oceanographic measurements with instrumented satellites, examining surface temperature surface waves, tides, albedo, heat flux and coordination of airborne and seaborne sensing systems 06 p0999 A67-19000

Lunar radio brightness distribution measured at various wavelengths, determining surface temperature decrease and dielectric constant 08 p1390 A67-21023

Ignition of flammable fluids by hot surfaces tested on static hot plate rig and on wind tunnel rig, noting data on kerosene, lubricating oil and hydraulic fluid 09 p1580 A67-22248

Steady state Leveque problem generalized to include time dependence, obtaining eight solutions for surface temperature 10 p1732 A67-22727

Approximate solution of heat transfer problems with phase change for time dependent surface temperatures 10 p1733 A67-23119

Refractory and ablating polymeric reentry heat shield materials evaluated under high radiant fluxes, measuring surface temperature, recession rate, flux emittance, etc refractory and ablating polymeric reentry heat 11 p1811 A67-24054

Transient heat conduction problems involving time varying radiation boundary condition at surface solved by Goodman integral method 11 p1883 A67-24575

Nonstationary gunpowder combustion at various pressures analyzed for combustion rate and surface temperature dependency on pressure and initial temperature 11 p1884 A67-24957

Bending of three-layer plate freely supported along four edges in presence of variable surface heating 12 p2022 A67-25588

Martian atmosphere models with different composition, pressure and temperature 12 p2003 A67-25685

Heat transfer through various silicate

powders measured for lunar surface temperature studies, comparing theoretical results [AIAA PAPER 67-285] 12 p2035 A67-26002

Surface temperature of one-dimensional homogeneous thermally isotropic body impervious to radiation 13 p2222 A67-26610

Temperature measurements of grassland, desert and water surfaces using IR radiometer found to compare favorably with miniature thermistors 13 p2117 A67-27606

Theoretical determination of polished metals emission factors, using model where emission depends on surface layer temperature and electric resistivity 14 p2407 A67-28558

Thermal stresses in isotropic plate analyzed using Hankel transform, obtaining surface temperature for various cases 14 p2402 A67-28813

Aerodynamic heating through turbulent boundary layer of flat plate determined using Ferrari formula 15 p2415 A67-29328

Combustion stability in solid propellant rockets, reviewing Soviet T-sub s and Q models 15 p2581 A67-29986

Geographical distribution of surface temperature of ground and/or clouds and mean relative humidity of upper troposphere 15 p2513 A67-30059

Surface heat balance shown to be useful thermal boundary condition at sea-air-land interface for earth surface mean temperature and macroclimate models 15 p2513 A67-30060

Radiative power of toothed surface when ambient medium is black body at zero temperature 16 p2778 A67-30714

Oil Mist Deposits Test for differentiating deposit forming tendencies of jet engine lubricants, discussing mechanism and threshold temperature 16 p2683 A67-31755

Rotation and heating of planet Mercury, examining insolation and surface temperatures from coupling of orbital and rotational periods 17 p2940 A67-32210

Ammonium perchlorate solid propellant ignition characteristics recording preignition surface exotherms 17 p2927 A67-33027

Preignition phase of solid propellant burning, determining concentration of volatilized species as function of surface temperature 17 p2927 A67-33028

Heat-transfer coefficients for heat transfer from gas to blade surface in gas turbine under operating conditions 17 p2973 A67-33077

Volcanic and tectonic activity on Venus inferred from high surface temperature, considering possible effect on atmosphere obscuration 17 p2951 A67-33232

Error factors in cloud and underlying surface temperature determination from weather satellites in various spectral intervals 18 p3073 A67-33558

Composite ammonium perchlorate propellant temperature profile beneath burning surface, discussing main decomposition energy, heat sources, etc composite ammonium perchlorate propellant 18 p3107 A67-33811

Semiconductor surface thermocouples, determining heat-transfer rates associated with wind tunnel testing 18 p3048 A67-34103

Martian atmosphere circulation model from Mariner IV occultation experiment, studying lateral eddy viscosity, winds, surface temperature and stress 18 p3124 A67-34153

Gold resistance thermometers for measuring surface temperature of semitransparent materials 18 p3051 A67-34505

Local radiation equilibrium temperatures in semigray enclosures, with reference to thermal design of spacecraft [AIAA PAPER 67-211] 19 p3344 A67-34820

Current-voltage characteristics for double probe measured in seeded combustion products by low temperature surface emission 19 p3345 A67-35079

Surface-temperature conditions in disks and gears stressing heat transfer coefficient and lubricated contact 19 p3237 A67-35840

Open-cycle MHD generator thermal characteristics, direct thermal energy conversion into electricity and optimum front surface temperature 20 p3362 A67-36115

Sinusoidal surface vibration effect on nucleate pool boiling reveals lowered surface temperature for low heat flux, LF and high

acceleration [ASME PAPER 67-HT-49] 20 p3548 A67-36731

Thermocouple surface temperature measurement errors in space simulation chambers due to heat conduction and radiation of wires [ASME PAPER 67-HT-57] 20 p3447 A67-36739

Heating rate and type effects on stationary fluids stability, noting dependence on critical Rayleigh number 20 p3553 A67-36848

Combustion stability of powder in semiclosed volume, taking into account propellant surface temperature dependence on pressure and temperature gradient 21 p3732 A67-38526

Surface temperature of deflagrating ammonium perchlorate crystals calculated from crystal phase transition thickness [AIAA PAPER 67-68] 21 p3688 A67-38859

Photoelectric method for measuring temperatures in metal cutting 21 p3631 A67-38921

Surface temperatures of two rubbing bodies and heat partition between them determined numerically, using Fredholm integral equation solution 21 p3638 A67-39091

Prediction of lunar surface temperature through digital computer program noting heat transfer equations 22 p3884 A67-39930

Thermal diffusivities of thermal energy storage materials from solid surface temperature measurements, discussing advantages of transient method [ASME PAPER 66-WA/ENER-5] 22 p3919 A67-40349

Thermal boundary layer condensation enhancement of diffusion limited vaporization rates, discussing heat of vaporization, critical supersaturation and surface temperature 22 p3920 A67-40423

Temperature of metal surface irradiated by giant pulse laser beam by measuring energy of emitted thermal ions 23 p4015 A67-41035

Isohars of adsorption of Ce on faces of W crystal measured for adsorption heat dependence on atom surface density 23 p4042 A67-41298

Aircraft cockpit and surface temperatures after solar radiation exposure in desert, showing inadequacies of meteorological data for thermal stress predictions 23 p3935 A67-41593

Ground and water surface temperature measurements using IR radiometers onboard aircraft 24 p4181 A67-41789

Venus surface temperature measured using difference between optical and radar radii, cloud temperatures and adiabatic lapse rate 24 p4225 A67-41827

Cathode outer oxide surface heating for pulsed emission current measured in intervals between retarding current pulses and different repetition frequencies 24 p4129 A67-42231

Temperature field within multidimensional body in nonlinear heat conduction process in terms of known temperature distribution along coordinates 24 p4254 A67-42254

Surface temperature oscillations of externally cooled working blades of gas turbine with air-liquid mixtures 24 p4254 A67-42255

SURFACE TENSION

SA LIQUID-LIQUID INTERFACE

Inverse optimization for calculating refractive index and electrical resistivity of plasma in reentry and surface tension coefficient in epihydrodynamics 02 p0333 A67-12347

Fluid equilibrium shape under gravity force and surface tension analyzed via variational method 03 p0401 A67-12881

Surface charge distribution effect on stability of conducting fluid in presence of magnetic field 03 p0481 A67-13731

Surface tension and equilibrium surfaces in weightless liquids, with application to spacecraft systems design 03 p0404 A67-13890

Small oscillations of viscous incompressible fluid in container with free surface under action of potential force field 05 p0791 A67-16373

Differential equation of motion of meniscus of MHD fluid in capillary in TM field due to surface tension 06 p1044 A67-18681

Temperature induced surface tension variation effect on motion of bubbles and drops, noting surface active

- substances 08 p1321 A67-20711
Heat pipe, device with thermoconductivity greater than solid conductors, based on surface tension and latent heat of working fluid 08 p1427 A67-21051
Sessile drop technique to study effect of atmosphere and alloy additions of Ti and Cr on surface tension and contact angle of N on sapphire substrated at 1500 degrees C 08 p1343 A67-21543
Adhesive bonding of solid propellants in rocket motors, emphasizing propellant liner interface and bonding at 09 p1578 A67-22514
Significant-structure theory of liquids applied to rocket fuels, calculating vapor pressure, thermal expansion, dielectric constant, etc 16 p2734 A67-31537
Surface tension principles for propellant management devices, discussing static retention and dynamic control of spacecraft fuels 17 p2801 A67-31985
Thermal problems peculiar to cryogenics stored in reduced gravity environment 17 p2966 A67-32010
Surface stress effect on oblateness of sun and surface stress distribution, noting latitude dependence of angular velocity 17 p2940 A67-32207
Nusselt results concerning heat transfer extended to include surface tension effect on heat transfer coefficient 17 p2970 A67-32461
Spherical shape changes of droplet of viscous substance of high surface tension under variable external force and small deformation 18 p3028 A67-34220
Gravitational effect on thermal instabilities, discussing optimization techniques to calculate effects of surface stresses [ASME PAPER 67-HT-22] 20 p3546 A67-36717
Cesium propellant systems utilizing surface tension to position and transfer liquid propellant in zero-g environment studied with high voltage electrical isolation methods [AIAA PAPER 67-681] 21 p3692 A67-38712
Liquid sloshing cylindrical tank with elastic bottom for investigating surface tension effect at liquid gas interface of partly filled container 22 p3787 A67-40179
Liquid surface tension effect on maximum particle size in two-phase nozzle flow, discussing drag exerted by accelerating gas stream 22 p3787 A67-40225
Explosion of ovoid copper wire conductors observed with pulsed X-rays noting effect of magnetic pressure 23 p4028 A67-41461
Nonlinear analysis of cellular convection induced by surface tension in finite amplitude heated liquid layer, discussing prediction of hexagonal flow pattern 24 p4255 A67-42569
- SURFACE TO SURFACE MISSILE**
Strapdown system application studies related to surface to surface missile, considering angular vibration environment and constant rates about output and spin axes of gyro 22 p3833 A67-40186
- SURFACE TREATMENT**
Contact angle measurements for epoxy resin on boron filaments, demonstrating surface treatment effects 03 p0429 A67-13427
Surface treatment and interface stability of boron filaments reinforcing plastic composite materials 03 p0455 A67-13428
Aircraft corrosion protection, discussing eloxation and electrophoretic deposition of multilayer synthetic resin coatings 04 p0636 A67-14576
Stress corrosion in titanium, examining preventive measures of surface treatment, reduction of design stress, environmental control and alloy modification 04 p0636 A67-14602
V-I characteristics of p-n junctions on In-Sb base, noting effects of surface etching, temperature and impurity concentration 04 p0680 A67-15157
Effects of dry and wet preoxidation on characteristics of MOS transistor using silicon 09 p1552 A67-21768
Vapor-deposited tungsten formed by hydrogen reduction of tungsten hexachloride or hexafluoride, noting effect of crystal orientation and surface treatment on work function 09 p1451 A67-22357
Surface preparation for aluminum and bond strength dependence on cure temperature, humidity and
- impurities 09 p1507 A67-22519
Metal surface preparation by mechanical and chemical processing for adhesive bonding 09 p1507 A67-22520
Bond strength of magnesium alloys as affected by surface preparations, specific alloy and adhesive type 09 p1507 A67-22521
Surface treatment effect in field effect anomaly of cleaved and etched n-type indium antimonide at high magnetic fields 10 p1688 A67-22903
Semiconductor surface potential in ultrahigh vacuum and under controlled atmosphere 10 p1696 A67-23694
Adhesive bonding techniques for aluminum, advantages, drawbacks, joint design and surface treatment before bonding 14 p2323 A67-27820
Aluminum pretreating and finishing agents noting cleaning, etching, roughening and coatings 14 p2324 A67-27821
Nickel protective coating on large parts through chemical reduction of nickel salt by sodium hypophosphite, discussing technological and economic aspects 14 p2324 A67-28609
V-I characteristics of p-n junctions on InSb base, noting effects of surface etching, temperature and impurity concentration 15 p2534 A67-29344
Surface treatment of metal to ensure strength of bonded joints, discussing causes of aluminum-alloy corrosion during pickling 19 p3237 A67-35822
Gallium arsenide substrate treatment methods effects on autoepitaxial layer perfection 21 p3685 A67-38972
Spray and brush repair of zinc oxide-potassium silicate spacecraft thermal control paint, describing tests, surface preparation and coating application 22 p3826 A67-40111
Chemical milling of aluminum alloy parts by dimensional etching, discussing protective coatings 23 p4009 A67-40641
Beryllium part fabrication by metal removal, discussing machining and surface treatment methods [SAE PAPER 670803] 24 p4159 A67-41990
- SURFACE VEHICLE**
SA LUNAR SURFACE VEHICLE
Disturbance theory linearized initial value problems for free trajectories passively moving above smooth earth surface 02 p0320 A67-11465
Open and closed cabin lunar roving vehicles including unmanned Tumbling Explorer /TEX/ surface vehicle 03 p0396 A67-13889
Airline strategy for domination of Northeast Corridor despite improvements in high speed ground transportation [AIAA PAPER 66-942] 03 p0361 A67-14021
Surface mobility systems for lunar exploration and vehicle characteristics of chosen concepts 09 p1486 A67-22407
PT6 series of small shaft turboprop engines for STOL aircraft and high speed surface vehicles noting performance and environmental tolerance improvements [AIAA PAPER 67-744] 23 p4048 A67-40978
Vehicular traffic and rail transportation surveillance or coordination aids possibilities using earth orbiting satellite [AIAA PAPER 67-788] 24 p4242 A67-42951
Traffic prediction for high speed aircraft and surface vehicles and VTOL aircraft city-center to city-center transportation [AIAA PAPER 67-802] 24 p4259 A67-42962
- SURFACE WAVE**
Plane problem of surface electromagnetic wave scattering along rectangular dielectric wedge 02 p0191 A67-11579
Surface waves in current-carrying plasma filament of finite radius 02 p0277 A67-12614
Multimode surface waves for plane structures in generalized impedance boundary condition, noting electromagnetic field arising from magnetic dipole source located above plane structure 03 p0469 A67-13657
Multimode surface wave diffraction phenomenological theory extended to right-angled wedge configuration [NYU-EM-213] 03 p0369 A67-13660
Dispersion relations and wave power of isotropic compressible lossy plasma slab bounded by free space and ground plane and excited by line sources 03 p0487 A67-14354
Helicon wave propagation along multilayered structure, calculating Bloch
- waves, fields and dispersion 04 p0665 A67-15119
Millimeter wavelength transmission line deficiencies reduced by using channeling systems in form of elastic dielectric tape on thin metallic strips 04 p0575 A67-15167
Frequency range in which Vavlov-Cerenkov surface wave exists in plasma-vacuum boundary 04 p0688 A67-15273
Plane wave interaction with surface waves at plasma boundary 04 p0668 A67-15274
Field distribution at bends in circular zero-normal H and cylindrical surface waveguides 04 p0586 A67-15635
Nonlinear lateral sloshing in rigid tanks various geometries, noting frequency-amplitude response 05 p0790 A67-16135
Surface plasma wave dispersion in metals, noting method for solving Kulk equation 05 p0864 A67-16761
Stress effects of simple supports on radiation emission from turbulent flow near plane compliant surface, using acoustic equivalence to extended dipole system 05 p0748 A67-16813
Doppler effect on emission spectrum and energy of moving oscillator and intensity of surface wave excited by it 05 p0765 A67-17160
Shock wave incident on unknown free boundary surface calculated in spatial method of characteristics 07 p1125 A67-19141
Behavior of infinite arrays including radiation pattern approach yielding expressions for gain and periodic structure approach yielding input impedance variation with scan angle 07 p1154 A67-19783
Sensitivity of dielectric rod terminal impedance to surface wave coupling when no resonance regions exist within energy-carrying cross section 07 p1158 A67-20299
Monochromatic wave interaction with isotropic electron-plasma, determining field and surface wave generated on basis of Maxwell equations 09 p1464 A67-22012
Attenuation and coupling impedance of backward dipole surface wave on cylindrical plasma column with reference to oscillator design 09 p1546 A67-22281
Geomagnetic micropulsation excitation by solar wind flow around magnetosphere, noting surface wave propagation 10 p1699 A67-22797
Interaction of transverse distributed surface vibration with adjacent laminar flow, superimposing oscillatory pressure and velocity field developed in boundary layer fluid over idealized steady fluid flow 10 p1623 A67-22861
Rectangular terminal block in rectangular waveguide and dispersion equation for surface wave propagating along waveguide 10 p1613 A67-23445
Liquid film flowing instability down inclined plane with respect to Tollmien-Schlichting wave compared with surface wave formation 11 p1774 A67-23860
Elastic surface waves excitation method in quartz at high frequencies, noting absorption temperature dependence 11 p1848 A67-24835
Lower modes and frequencies of natural elastic oscillations of vessel formed by liquid-filled shell of revolution taking into account fluid surface wave and shell inertia 12 p2020 A67-25566
Cylindrical partially filled waveguides of rectangular cross section, formulating boundary value problem and characteristic equation 12 p1906 A67-25980
Fluid vibratory behavior in rigid containers, noting surface wave behavior governed by linearized boundary value solution 12 p1931 A67-26182
Theory of Rayleigh waves at surface of elastic half-space, determining ratio of horizontal to vertical component of motion 13 p2156 A67-26602
Surface waves in current-carrying plasma filament of finite radius 13 p2170 A67-27370
Radial variation of plasma electron density determined by surface wave resonances 14 p2355 A67-27822
Helical antenna radiation characteristics under backfire operating conditions, noting improvement over endfire conditions 14 p2290 A67-29006
Electromagnetic surface wave propagation in plasma, studying oscillation spectra dependence on surface wave field amplitude 15 p2529 A67-29711

Scattering of surface wave incident upon junction of two semi-infinite planes joined together by step analyzed using Wiener-Hopf equation 16 p2826 A67-31348

Radiation from dielectric antenna, noting erroneous radiation formula applications 17 p2824 A67-32308

Two-stream instability in semiconductor InSb plasmas, noting collision conditions, surface space charge, wave growth, etc 17 p2921 A67-33052

Shock wave incident on unknown free boundary surface calculated in spatial method of characteristics 17 p2840 A67-33213

Semiconductor surface electromagnetic oscillations excitation in presence of strong electric and magnetic fields, obtaining damping and dispersion law 20 p3504 A67-36163

Admittance function for burning surface by solving differential equation and satisfying boundary conditions, discussing frequency peaks qualities 20 p3554 A67-37255

Surface plasma oscillations at optical frequencies detected by radiation from optical grating metal surface, measuring dispersion relation 20 p3514 A67-37569

Attenuation function of surface wave propagating over spherical earth having surface layers with different electric impedances, studying interaction with space wave 21 p3580 A67-38122

Discontinuity problem between empty rectangular waveguide and one filled with transversely magnetized ferrite solved by introducing metal surface wave 22 p3758 A67-39272

Dispersion characteristics of surface waves excited in infinitely long axially magnetized cold plasma by electric dipole 22 p3847 A67-39621

Long period surface gravity waves in atmosphere 22 p3792 A67-39974

Launcher for trapped surface waves over ice-covered sea by ferrite loaded horn device 22 p3763 A67-40306

MF surface wave launching over earth, considering field strength at ground for given radiated power 22 p3763 A67-40315

Surface wave pole contribution to admittance of rectangular waveguide-fed slot into dielectric slab 23 p3979 A67-40829

Surface waves in medium with coupled stresses, using Cosserat type medium for analysis of properties 23 p4079 A67-41417

Plasma column and plasma-electron beam interaction properties by Langmuir and SHF probes noting resonance, coupling and microwave surface waves 24 p4194 A67-41911

Surface wave propagation around sharp corners in single wire transmission lines, calculating and measuring radiation loss and pattern 24 p4119 A67-41971

Electromagnetic wave fluctuations in semiminfinite plasmas, deriving correlation functions for electromagnetic parameters, considering surface waves 24 p4195 A67-42075

Geomagnetic micropulsation excitation by solar wind flow around magnetosphere, noting surface wave propagation 24 p4209 A67-42133

Dispersion of surface waves propagating in elliptical and rounded flat helices, discussing resonance effects 24 p4121 A67-42236

SURGE

Association rate between solar surges and flares 17 p2938 A67-32820

SURGERY

Surgical technique for implanting and maintaining arterial and venous catheters in monkeys 10 p1601 A67-23627

Aeromedical problems associated with surgical procedures for relief of otosclerosis 13 p2060 A67-26928

Lasers in ophthalmology, discussing surgery and hazards 23 p3962 A67-41051

SURVEILLANCE

SA RECONNAISSANCE

SA SPACE SURVEILLANCE SYSTEM

Vehicular traffic and rail transportation surveillance or coordination aids possibilities using earth orbiting satellite [AIAA PAPER 67-788] 24 p4242 A67-42951

SURVEILLANCE RADAR

Cost and effectiveness of surveillance device for anti-aircraft weapon system 03 p0538 A67-13695

SDS radar, surveillance radar designed to detect moving targets on ground extended to detection of low flying

aircraft 04 p0573 A67-15038

Automatic radar system for low level target detection, obtaining Doppler resolution and eliminating fixed atmospheric noise 04 p0573 A67-15043

ARSR Weather Surveillance System design, operation and performance 07 p1142 A67-19542

Digital data processing, transfer and display equipment applied to ATC terminal operations, using surveillance radars and radar beacons 08 p1351 A67-20677

Secondary surveillance radar system design, discussing interrogator interference, decoding and display systems 09 p1530 A67-22648

Secondary surveillance radar /SSR/ as principal sensor in future air traffic control service 09 p1466 A67-22657

Australian ATC radar network describing long range surveillance and control of neighboring airport 17 p2834 A67-32749

Aircraft position determination and surveillance requirements for ATC 19 p3256 A67-35860

SURVEYING

SA GEODETIC SURVEYING

SA MAGNETIC SURVEY

Surveying earth resources from high flying aircraft and earth orbiting satellites 10 p1735 A67-23688

SURVEYOR I SPACECRAFT

Component reliability screening techniques for Syncom, Early Bird, ATS Satellites and Surveyor spacecraft 01 p0155 A67-11343

Surveyor telecommunications system from standpoint of actual subsystem implementation and performance, detailing reliability, flexibility, redundancy and data transmission modes 02 p0196 A67-11998

Surveyor I photographs of lunar surface in support of theories that no mechanism exists on moon for sorting different sized particles into layers 03 p0512 A67-13892

Surveyor I spacecraft exploration results of lunar surface 08 p1386 A67-20939

Thermal properties of lunar surface as observed from Surveyor I spacecraft 08 p1386 A67-20940

Radar characteristics of lunar surface from Surveyor I spacecraft 08 p1386 A67-20941

Lunar surface mechanical properties at Surveyor landing site according to telemetry data and photographs 08 p1386 A67-20942

TV pictures of Surveyor I compartment radiators taken on June 11 and July 12, 1968, discussing cause of some changes in dust locations 08 p1386 A67-20944

Soil mechanics surface sampler experiment for Surveyor 08 p1410 A67-20945

Mosaic construction and image analysis for Surveyor TV pictures 08 p1333 A67-21504

Propellant composition variation for improving cooling characteristics of Surveyor vernier propulsion system [AIAA PAPER 66-627] 08 p1374 A67-21517

Reliability effect on design of lunar soft landing spacecraft /Surveyor/, Syncoms I, II and III, Applications Technology Satellites, Early Bird and four Intelsat IIs 09 p1582 A67-22302

Lunar surface according to Luna IX and Surveyor I 09 p1568 A67-22405

Far field radiation patterns of Advanced Antenna System presented by Surveyor I on lunar surface [JPL-TR-32-1079] 11 p1763 A67-24298

TV subsystem of Surveyor I, discussing operation-design constraints, camera configuration, video sequence, etc [SMPT PAPER 101-43] 12 p1904 A67-25461

Lunar environment effects on Surveyor I components, particularly white paint degradation as function of time 15 p2579 A67-29451

Lunar surface photographs taken by Luna IX and Surveyor I showing linear and circular ground features, rock blocks and dust 17 p2948 A67-33094

Size-frequency distribution of particles and craters and optical, thermal, radio and other properties of lunar surface obtained from Surveyor I landing 19 p3318 A67-35179

Surveyor I spacecraft location and identification on moon surface by photographs taken by Orbiter III 20 p3524 A67-38649

TV in lunar environment, discussing development and performance of instrument used during Surveyor I mission 21 p3629 A67-38658

Surveyor I landing site soil data covering mechanical, optical, thermal and electrical properties 23 p4064 A67-40950

Lunar surface layer soil density limits estimated in simulation study of adhesion, composition, grain size and grain shape effects 23 p4068 A67-41008

SURVEYOR III SPACECRAFT

Surveyor III lunar surface sampler for picking, digging, scraping and transporting material, noting design and operation 23 p4005 A67-41370

SURVEYOR PROJECT

Terminal descent design for unmanned vehicle soft lunar landing in Surveyor project [AIAA PAPER 64-644] 02 p0263 A67-11923

Surveyor throttleable liquid propellant rocket engine for operation on propellants saturated with dissolved liquid gas [AIAA PAPER 66-949] 02 p0304 A67-12283

Lunar surface chemical composition analysis by Surveyor-borne instrument based on alpha interaction with matter [JPL-TR-32-1090] 08 p1411 A67-20946

Vertical component seismograph for use in Surveyor lunar landing missions 08 p1411 A67-20947

Surveyor study of lunar ejecta fragments expelled from lunar surface during hypervelocity impact 08 p1411 A67-20948

Surveyor touchdown-dynamics experimental study of spacecraft motion and landing site surface 08 p1411 A67-20949

Surveyor vernier propulsion system, discussing design of thrust chamber, propellant tank assemblies, functions of VPS, etc [AIAA PAPER 66-593] 08 p1413 A67-21516

Launch-on-time capability performance measuring for Surveyor program 08 p1413 A67-21528

Surveyor system and camera design for photographic mission on Mars surface 09 p1570 A67-21680

Surveyor throttleable liquid propellant rocket engine for operation on propellants saturated with dissolved liquid gas [AIAA PAPER 66-949] 13 p2188 A67-26834

Surveyor guidance program for midcourse and terminal information, noting redundancy in design, decision making telecommunications, etc 15 p2514 A67-29599

Spaceborne programming language for Surveyor guidance, discussing impact on flight software development 15 p2439 A67-29600

Surveyor spacecraft reliability from test data, examining assessment outputs, basic definitions and mathematical models 15 p2493 A67-29608

Surveyor project composite telemetry processing system including signal processor, ground equipment, computer data program, etc 20 p3393 A67-37458

Surveyor variable and fixed focal length TV camera lenses, discussing zoom lens design criteria, focal plane shutter and color filter wheel 22 p3807 A67-40375

Surveyor TV system calibration, determining transfer functions for various parameters 22 p3807 A67-40376

Lunar geology using probe data to distinguish impact and volcanic surface shaping processes [AIAA PAPER 67-862] 24 p4238 A67-42986

SURVEYOR SPACECRAFT

Acceptance criteria of space materials, discussing materials for surveyor 15 p2508 A67-29559

Power conversion circuits of Surveyor spacecraft including distribution system, battery charging and central regulator units 17 p2803 A67-32510

Conventional guidance-problem parameters and basic parameters applicable to Surveyor in relation to accuracy of lunar landing 19 p3257 A67-35943

Surveyor spacecraft star sensor calibration and spaceborne performance 19 p3233 A67-35982

Real time performance, ground control and data processing of Surveyor spacecraft during maneuvers [AIAA PAPER 67-644] 20 p3419 A67-37625

Environmental, thermal and foreign particle effects on Surveyor vidicon performance and expected tube life [SMPT PAPER 102-32] 22 p3807 A67-40373

Surveyor TV system signal processing and transmission, analyzing performance and

computer simulation of some effects [SMPTE PAPER 102-41] 22 p3808 A67-40379
Methodology used to implement high reliability objectives for Surveyor pressure vessels, tabulating burst test results [ASM PAPER C6-2.1] 23 p4071 A67-41411
Surveyor V scientific experiment, comparing lunar surface sampling with that in Surveyor III, noting resemblance to granular terrestrial soil 24 p4228 A67-42308

SURVIVAL

SA LIFE SUPPORT SYSTEM

Fatigue process theory for general broadband random loading, calculating mean damage and survival probability 15 p2576 A67-30094

Antileakage assemblies evaluation in low temperature water, recording body heat loss and tolerance time for application to helicopter crews 17 p2807 A67-31959

In-flight escape of helicopter personnel using Navy fuselage capsule, describing devices for recovery, protection and survival 17 p2794 A67-31999

Tactical aircraft survivability in North and South Vietnam, discussing missile and interceptor ineffectiveness and limited-war considerations for aircraft 17 p2796 A67-32434

Air Force rescue radio equipment evolution, describing models 17 p2814 A67-32516

Terrestrial microorganisms survival in space, noting inactivation effect by solar radiation 19 p3178 A67-35221

Terrestrial microorganism survival in space aboard Gemini satellite, discussing lethal effects of solar radiation 19 p3178 A67-35223

Analytical model for microbial population survival times during heat sterilization studied for spacecraft applications, considering environment and exposure time 19 p3180 A67-35264

Ionospheric and stratospheric UV radiation effects on survival of microorganisms 19 p3178 A67-35271

Planetary quarantine problem for Martian survival of microorganisms investigated, using systems analysis 19 p3180 A67-35274

Anatomical locus of behavior reinforcement, discussing survival mechanism development in animals and humans 20 p3373 A67-37432

Bacillus brevis var. G-B survival ratio dependence on space flight factors, noting no induction of dissociation products nor appearance of auxotrophic mutants 21 p3577 A67-38597

Survival times of rats studied from positive and negative acceleration test exposure in special centrifuge 22 p3753 A67-40540

Qualitative safety and survival factors in emergency escape and relation to complete ejection event via functional diagramming 23 p3964 A67-41546

Death and survival during water immersion in plane crashes near Cape Cod and Hamilton Bay 23 p3970 A67-41707

Space flight emergency contingency planning for survival, evaluating physiological effects and remedial system effectiveness [AIAA PAPER 67-825] 24 p4116 A67-42972

Military flight clothing tested in actual survival conditions for ability of subject to withstand moderate sea water environment [AIAA PAPER 67-968] 24 p4118 A67-43046

SUSCEPTIBILITY

SA MAGNETIC SUSCEPTIBILITY

Propagation coefficients of leaky waveguide modes improved by corrections to radial line susceptance arising from uniform slot in wall of circular waveguide 17 p2812 A67-32317

Audioconducted and RF radiated susceptibility thresholds of active low pass filter circuits, determining limitations and meeting specification requirements 20 p3406 A67-37652

SUSPENSION

SA MAGNETIC SUSPENSION

SA SOLID SUSPENSION

Nonlinear macroscopic rheological behavior of dilute suspensions of deformable spheres 17 p2887 A67-32280

SUSPENSION SYSTEM

SA SPRING

Excitation of phosphor suspensions in solid dielectric by mechanical energy analyzed via impact

theory 01 p0113 A67-10354
Stability of motion of gyro suspension, noting gyrohorizon compass operation for constant suspension point and angular velocities 03 p0424 A67-14158

Mechanical suspensions for instrument components 06 p1007 A67-18061

Large size parabolic reflector with small deformation constructed with multibearing suspension 08 p1318 A67-21344

Excitation of phosphor suspensions in solid dielectric by mechanical energy analyzed via impact

theory 11 p1851 A67-25027
Optimal suspension systems synthesis, discussing dynamic programming theory 13 p2159 A67-27300

Mark 27 gyrocompass, discussing suspension by flotation 14 p2322 A67-29083

Hydrodynamic gas spin bearing gyroscope design for long duration space missions 14 p2322 A67-29084

Liquid spring design characteristics noting fluid characteristics, precharge fluid pressure, friction, efficiency, gland configuration and application requirements 15 p2494 A67-30097

Large size parabolic reflector with small deformation constructed with multibearing suspension 17 p2831 A67-31940

Miniature electrostatic accelerometer featuring suspension and force rebalance systems, discussing performance, applications and accuracy acceleration measurement 17 p2858 A67-32484

Error of three degrees of freedom astatic gyro motion owing to viscous friction moments in suspension in case of irregular rocking of base 22 p3810 A67-40484

SWAN BAND

Shock tube study of oscillator strength of diatomic molecular carbon Swan bands 11 p1750 A67-25066

Lunar crater Alphonsus emission flare noting C-2 Swan system proposal 20 p3528 A67-37470

SWEATING

Water deficit effects on thermal sweating, noting extraneous effects due to higher body temperature and wet skin 24 p4110 A67-41781

SWEDEN

Swedish space research organization, participating groups and experiments 19 p3321 A67-35302

SWEEP

SA VARIABLE SWEEP

Successive release evaluation by periodometer and memory oscillograph of viscous damping of one degree of freedom system 17 p2884 A67-32698

SWEEP FREQUENCY

Sweep random vibration test using narrow band random excitation with feedback control from variable gain stage 01 p0034 A67-10155

Extended theory of cumulative damage in fatigue when stress amplitude varies from cycle to cycle throughout life of structure [SAE PAPER 680720] 01 p0161 A67-10607

Microwave swept frequency measurements on RF transmission line systems and development of VSWR and insertion loss test set 01 p0039 A67-11038

Swept frequency modulation program, emphasizing lack of design information for optimizing performance and networks design with large time bandwidth products 02 p0202 A67-12124

Shock and vibration test specifications, contrasting approaches requiring exact duplication of environment with those simulating damaging characteristics 06 p0981 A67-18366

HF limits for radio transmission calculated from oblique and vertical sweep frequency records over 2000 km north-south subauroral path 07 p1142 A67-18446

Ultrasonic nondestructive inspection of adhesively bonded components, discussing pulse echo reflection, pulsed through transmission and sweep frequency coupling methods and scanning equipment 09 p1507 A67-22526

Ionospheric electron density measurement by gyroplasma probe, using sweep frequency impedance technique 10 p1648 A67-23291

Radio noise spectrum on VLF bands in ionosphere observed by sounding rocket K-9M-19 14 p2307 A67-27886

Broadband radio star Cassiopeia A

scintillations observed with swept frequency interferometer

[AGARDOGRAPH 95] 15 p2563 A67-30288
Ionospheric movement detection using frequency swept sounder and rhombic antenna

[AGARDOGRAPH 95] 15 p2484 A67-30301
Nonuniformity of mm wave detected by wideband frequency sweep control backward wave oscillator 16 p2643 A67-30896

Swept measurement techniques, discussing reflection coefficient and slotted line accuracy using signal flow graph 17 p2815 A67-32610

Electronically swept coherent frequency synthesizer for various bands 17 p2827 A67-32799

Electron density measurement in ionosphere-magnetosphere transition region using rocketborne gyroplasma swept frequency probe, discussing electron density profile and plasma medium 19 p3229 A67-35201

Magnetic field of flux jumping in synthetic high field superconductors measured as function of temperature and field sweep rate 23 p4044 A67-41452

SWEEPBACK ANGLE

Aerodynamic heating from turbulent boundary layer to swept surface symmetrical to surface line dividing flow obtained from momentum and energy integral equations 04 p0549 A67-15825

SWELLING

Swell generation by means of flat paddle board in translational motion 22 p3783 A67-39648

SWEPT FREQUENCY TOPSIDE SOUNDER

S ALOUETTE SATELLITE

S TOPSIDE PROGRAM

SWEPT WING

Pivot center position effect on aerodynamic characteristics of variable sweepback wings during rotation 03 p0351 A67-12994

Variable sweepback wing noting design problems, adaptability, controllability and comfort 03 p0351 A67-12995

Stalling in swept wing jet aircraft with reference to satisfying airworthiness regulations and aerodynamic problems 03 p0362 A67-14300

F-111 wing sweep actuator with irreversible Acme-thread jackscrew driven by hydraulic servomotor 05 p0752 A67-16157

Variable sweep wing F-111 aircraft cooling systems for temperature control of hydraulic fluid of type II system 05 p0752 A67-16161

Span loading of swept wing which produces minimum induced drag with constraints on lift and pitching moment 06 p0937 A67-18010

Inviscid flow method predicting nonlinear supersonic and hypersonic lift component of highly swept wings with low aspect ratio 06 p0937 A67-18013

Lift curve slope and aerodynamic center for variable sweep wing configurations estimated using semiempirical technique [AIAA PAPER 67-135] 06 p0939 A67-18315

Aerodynamic design of swept wing-fuselage combination for cruising at transonic and supersonic speeds, noting pressure distribution role 10 p1589 A67-22872

Three-dimensional turbulent boundary layers over swept wing calculated using entrainment equation 10 p1628 A67-23473

Four combat aircraft designs /tailless delta, swept wing, variable geometry and VTO aircraft/ using same bypass engines /Pratt Whitney-SNECMA

TF-306/ 15 p2419 A67-29670
Gulfstream II maintainability program, examining support department responsibility, insurance and material support [AIAA PAPER 67-383] 15 p2421 A67-30352

Three-dimensional turbulent boundary layer flow over infinite swept wing calculated using entrainment and momentum integral equations 16 p2657 A67-30617

Flow turbulence on leading edge of attachment line of swept wing studied in wind tunnel 16 p2589 A67-30618

Flight test program for F-111A variable sweep tactical weapon system, discussing afterburning turbofan engine, crew module, escape and survival 17 p2795 A67-32214

Supersonic transport variable sweep wing design, showing root glove and Mach number effects on aerodynamic center of strike aircraft 20 p3361 A67-36499

Variable sweep pivoted wing fighter aircraft structural and aerodynamic design considerations, noting journal bearing endurance and aircraft fatigue life [SAE PAPER 670881] 24 p4094 A67-42015

SWEEPBACK WING
Influence of sweptback wing leading edge geometry on boundary layer instability using supersonic flat plates 23 p3928 A67-41247

SWIRLING WAKE
Unsteady incompressible flow of two-dimensional supercavitating hydrofoils with finite cavity length, considering wake nature [ASME PAPER 67-FE-15] 14 p2304 A67-28363
Vortex breakdown treated as failure of quasi-cylindrical approximation for viscous axisymmetric flow 16 p2658 A67-30948
Aerodynamic investigation of spherical chambers, determining swirling velocity, tangential velocity and regions of air suction 16 p2594 A67-31209
Swirl effect on nozzle flow applied to solid propellant nozzles assuming irrotational flow so that tangential velocity field has free vortex characteristics 19 p3311 A67-34826
Friction and heat transfer characteristics of turbulent swirl flow under large transverse temperature gradients [ASME PAPER 67-HT-24] 20 p3546 A67-36718
Exact solutions of incompressible Navier-Stokes equation for irrotational Beltrami nonconvective two-dimensional swirl and axially symmetric cross flows 21 p3609 A67-37737
Quasi-cylindrical approximation theory on swirling nozzle flow in relation to spin effect on rocket nozzle performance 22 p3742 A67-40118

SWITCH
SA ECHO SUPPRESSION
SA ELECTRONIC SWITCH
Electro-optic intra-cavity color switching in krypton ion Fabry-Perot laser 06 p1010 A67-17888

SWITCHING
SA BEAM SWITCHING
SA MAGNETIC SWITCHING
SA MICROWAVE SWITCHING
Fast switching microwave phase shifters for high power array radars, describing drive control techniques 04 p0581 A67-15053
IF amplifier circuit diagrams, obtaining logarithmic amplitude characteristic by switching nonlinear elements to plate or cathode circuits 06 p0972 A67-18899
Soviet book on magnetic switching elements in radio electronics covering magnetic materials properties with rectangular hysteresis, shift registers, logic circuits, etc 11 p1785 A67-24515
Mean power gain for diversity reception system with lobe switching 11 p1768 A67-24988
Optimum spacing arrangement for 1100101 array of four antennas in straight line with spectral sensitivity in switched and unswitched cases 14 p2284 A67-28435
Solid state switching applied to aircraft electric systems noting design, performance and contactless switching concept 17 p2825 A67-32513
Book on shift register sequence theory, discussing applications in communications, computers and switching theory 19 p3187 A67-35832
Neodymium doped YAG Q-spooled laser system for switching high voltage spark gap at 50 pps with nanosecond jitter 22 p3813 A67-39258
Time optimal adaptive control system synthesized via adaptive switching hypersurface and function generator /off-line memorization and on-line interpolation/ 24 p4134 A67-42177

SWITCHING CIRCUIT
SA DUPLEXER
Trigger circuits for generating sharply defined rectangular waves phase locked to repetitive signal 01 p0036 A67-10451
Counting control methods for multistable elements containing nonlinear quadrupole with comb type amplitude characteristic, using short-term action on LF filter 01 p0044 A67-10497
Method based on static characteristics for limit of saturation used to find relationships between voltages and currents in transformer in saturation region 01 p0037 A67-10714
Nondissipatively regulated variable

frequency DC to DC converter with variable on time and variable off time 02 p0183 A67-12117
Graphical derivation of switching trajectories of transistor-tunnel diode logic circuits 03 p0389 A67-12803
Avalanche transistor pulser designed to drive GaAs radar-laser diode 03 p0376 A67-12964
Fluid logic elements based on binary arithmetic, and/or algebra and DeMorgan inversion, using gate 03 p0374 A67-13169
Multipactor in T-R switch for improved recovery time 03 p0383 A67-13827
Switching circuit malfunctions analysis, discussing modeling for failure, simulation of failure and timing problems and sequential networks 03 p0394 A67-14219
Nonlinear recognition procedures, discussing probability distribution approximation by orthogonal expansion and by-product of low order conditional probabilities 04 p0578 A67-14800
Book on digital transistor circuits in semiconductor devices based on Boolean algebra and logical and switching circuit principles 04 p0622 A67-15268
Steady state analysis of switching circuit using combination of transistors and tunnel diodes, considering temperature effect and thermal stabilization of operating points 05 p0772 A67-16452
Transient cut-off processes of transistorized switch with LC load 05 p0773 A67-16460
Laser digital devices, discussing use as switching circuit in digital computer 07 p1194 A67-19088
Coanda device as pressure maintainer and as switch or selector 08 p1281 A67-20453
PDM/FM high efficiency voltage regulator design, switching theory and regulation theory 08 p1286 A67-21030
Variable-duty-cycle spacecraft power switching circuit design giving high efficiency crewman illumination control of reticle within optical alignment sight 10 p1597 A67-23308
Counting control methods for multistable elements containing nonlinear quadrupole with comb type amplitude characteristic, using short term action on LF filter 10 p1621 A67-23619
Relay testing under operational voltages and currents, discussing timing circuits and sequencing and computer inputs outputs 12 p1922 A67-25698
P-I-n diode switches, discussing driving techniques for series and parallel biased switches, pulse leakage and RF turn-off delay minimization 12 p1917 A67-26194
MOS transistor digital switch integrating methods, presenting operating conditions and design factors for IC inverter 12 p1918 A67-26218
Static current amplification factor of transistor dependence on operating conditions in switching circuits 13 p2075 A67-26347
Large scale monolithic integration of subassemblies combined with upside-down assembly technique for more complex low cost high performance microcircuits 13 p2077 A67-26658
Satellite telecommunication with automatic routing noting switching concept and modulating methods 13 p2087 A67-26721
Satellite telecommunication with automatic routing noting switching 13 p2087 A67-26722
Charge equation of enhancement-type MOS transistors, determining waveforms and switching times of resistor-coupled switching circuit 13 p2078 A67-26786
Computer-implemented minimization techniques used to determine realizability of N-variable switching function with single threshold-element device 13 p2073 A67-27065
Distinct state assignments for synchronous sequential machines, with modification of Dolotta-McCluskey algorithm 13 p2073 A67-27066
High Noise Immunity Logic Family /HNIL/ digital switching microcircuits for long distance signal transmission operating at high voltage 14 p2282 A67-28028
Fluidic pulse switching network hazards at high operating speeds, suggesting digital computer simulation to anticipate and rectify hazards before hardware fabrication 14 p2251 A67-28348

Design of simple circuit for high speed transmission gating of analog signals with fast switching diode and small overshoot 14 p2287 A67-28686
Book on large signal transistor circuits covering device physics and equivalent circuits 15 p2454 A67-30233
High-intensity and high-voltage current switching devices, noting strong pulsed magnetic field production 17 p2803 A67-32350
Power conversion circuits of Surveyor spacecraft including distribution system, battery charging and central regulator units 17 p2803 A67-32510
Glass semiconductor threshold switches application in memory-addressing circuits, decoding matrices and current dividers 18 p3012 A67-34489
Slow response of cadmium selenide thin film transistors related to trapping levels in insulator 18 p3015 A67-34557
Relationship between switching time, transient suppression and filter complexity for filter-type diode switches 19 p3196 A67-35659
Current time variation for subharmonic parametric oscillator phase zero-transient switching 20 p3395 A67-36314
MOS transistors handling, mounting and utilization compared to FETs 20 p3396 A67-36322
Transistor circuit containing magnetic cores with rectangular hysteresis loop analyzed for switching processes using differential equations 20 p3399 A67-37114
Low noise transistor switch design capable of switching 1A and meeting military current probe EMI specifications 20 p3406 A67-37853
Design procedure for production of radiation resistant NOR gate logic circuit 21 p3603 A67-38185
Switching behavior equations derived for FET with solutions applied to MOS and junction gate FET circuits 21 p3602 A67-39069
Breakdown temperature of pulsed switching circuit using high power transistors depends on transistor property 22 p3771 A67-39827
Frequency doubler and divider using transistorized synchronized switching phase detectors with closed feedback circuit 22 p3762 A67-39872
Learning threshold element circuit employing electrochemical controllable resistors as weight factors 22 p3809 A67-40480
Design and operation of loudness level meter /8051A/ which uses analog switching circuits 22 p3810 A67-40561
Pyroelectric effect using single barium titanate crystals with liquid electrodes extending ferroelectric switching time measurements to low fields 24 p4203 A67-42090
Inductive energy storage and control system using Ignitron 24 p4197 A67-42249

SWITCHING ELEMENT
SA FLUID SWITCHING ELEMENT
Nuclear radiation intensity effect on switching time of fast diodes, examining produced stability changes 01 p0066 A67-10655
Switching and dynamic characteristics of germanium peak diodes used as AM devices 02 p0210 A67-11531
Mode switching in tunnel diode, noting change from relaxation to microwave oscillation mode 02 p0217 A67-12090
V-I characteristics of low voltage trlnistors 03 p0377 A67-13237
Transient response of junction transistors in case of inductive load, deriving switching-on time, switching-off voltage maximum value, etc 03 p0386 A67-13978
X sub L band waveguide switches using p-I-n diodes for switching elements in SPST, SP2T, SP4T and SP8T microwave switches 04 p0580 A67-14863
Equilibrium photocurrents in silicon switching diodes from nondestructively measured electrical parameters 04 p0588 A67-15698
Elastic and inelastic flux switching, explaining different types of domain wall displacement in terms of variations of energy gradient vs wall position 05 p0774 A67-16832
Superconducting switching and storage

elements, examining physical properties, cryotron and continuous film memory cell 06 p0972 A67-18433

Asynchronous control of information transmission in networks consisting of independent sequential circuits 07 p1161 A67-19884

Three-port 35-GHz ferrite circulator latching switch, discussing geometric configurations, effects on performance characteristics, ferromagnetic materials selection, etc 08 p1304 A67-21225

GaAs p-n-i-n diode as light activated switch, noting electrical and optical properties 08 p1306 A67-21295

Monograph on high power semiconductor-magnetic pulse generators, noting saturable inductors and silicon controlled rectifiers, circuit analysis, voltage regulator, etc 09 p1482 A67-22698

Transient switching process of semiconductor planar diode with retarding electric field in base operated by short forward current pulses 11 p1764 A67-24469

Charge ratios of recovery abruptness and figure of merit in switching diode with base field 11 p1765 A67-24470

Giant pulse operation of many-element laser with composite Q-switch consisting of spinning prism and saturable glass plate 13 p2126 A67-26729

Full-wave rectifier using field effect transistor switches 13 p2078 A67-26780

Diode and transistor transient switching characteristics determined from analog computer simulation of differential equations 15 p2449 A67-29803

Field effect transistor intrinsic and extrinsic transients, switching behavior and relation to time constant by charge concept 15 p2449 A67-29806

Time optimal adaptive control system synthesis using off-line memorization with simple on-line calculations to determine control signal 16 p2650 A67-31672

Germanium pulse switching triode with fused p-n-p junction 18 p3009 A67-33477

/n-m/ junction structures transient characteristics, forward and back bias cases show inductive and capacitive element behavior respectively 22 p3858 A67-39574

Solid state linear digital amplifier with external modulation using high operating efficiency of transistors as saturated switching elements 22 p3771 A67-39841

Josephson junction as switching device or logic element, discussing tunneling states and transition characteristics 22 p3865 A67-40437

SWITCHING FUNCTION

Fundamental theorem for diode switches proved, using scattering matrix formulation permitting generalization of theorem to nonreciprocal structures 01 p0032 A67-10010

Partitions of n-space by hyperplanes, examining applications in switching theory 01 p0106 A67-10733

Low order model to determine approximate time optimal switching function for given plant in stability analysis of predictive control system [AFOSR-67-1339] 01 p0046 A67-11207

Junction type field effect transistors and metal oxide semiconductor devices for switching functions in digital circuitry 02 p0215 A67-11971

All-solid state airborne low level PAM multileader that employs N-channel FETs for all analog switching functions of system 02 p0216 A67-12013

Necessary conditions for optimal fixed-time powered transfers with multiple coasts and thrusts between circular orbits 02 p0328 A67-12402

Nonuniform p-type base width effect on forward switching voltage of diffused alloyed thyristor devices, comparing empirical and theoretical values 03 p0380 A67-13483

Optimum switching function of relay servosystem subjected to stationary Gaussian random input found by perturbation method 05 p0783 A67-16445

Bang-bang control for feedback systems, applying computer to optimization of switching time from state to state of linear systems 05 p0784 A67-16854

Switching process for silicon p-n-p structures, deriving relations for delay and response times and transient period as function of parameters 05 p0865 A67-16911

Area of Safe Operation for transistors in switching mode defined, using thermal feedback model 07 p1157 A67-19902

Large signal transient response of junction transistor in switching and pulse operation treated by charge control analysis 10 p1603 A67-22772

Comparison of operator performance when using rotary selector, thumbwheel and digital pushbutton 15 p2430 A67-29135

Switching process for silicon p-n-p structures, deriving relations for delay and response times and transient period as function of parameters 16 p2727 A67-30888

Second order discontinuous attitude control system using fixed impulse, determining average number of switchings before escape from vertical switch line 16 p2762 A67-31640

Switching tunnel diodes, discussing amplitude discrimination and binary memory 19 p3193 A67-35065

Indirect measurement of differential switching parameters examined for admittance matrix of common emitter coupling for field effect and junction transistors 20 p3396 A67-36379

Suboptimal controller generating linear combination of state coordinates shown to give optimal performance when using linear controller preceding relay 20 p3410 A67-37251

Digital switching functions and pattern recognition realization through computer-programmable algorithm for designing feed-forward threshold logic 21 p3588 A67-38182

High reliability sequence programmers for DIAMANT satellite booster switching functions 21 p3655 A67-38207

P-n-p transistor overcomes bandwidth and switching time deficiencies to enhance minority carrier transport 21 p3598 A67-38570

Large angle flux reversal of Permalloy magnetic films investigated from experimental results of switching characteristics 22 p3860 A67-39903

MOSFET integrated circuits for use in analog computers noting simplicity and switching qualities for control of hybrid devices 22 p3775 A67-40465

HF and switching characteristics of junction transistors analyzed using power series expansions 24 p4201 A67-41900

Piecewise linear switching functions design for suboptimal regulation of linear plants with relay controller in regard to transient response performance criterion 24 p4135 A67-42179

SWITZERLAND

Swiss space research programs noting experiments, technology, etc 19 p3321 A67-35301

SYMBOL

Digital computer-aided circuit sensitivity analysis using symbols, with example of band pass filter analysis 04 p0578 A67-15088

SYMMETRICAL BODY

SA GEOID

Attitude stabilization and control system for rotationally symmetric gyroscopic body with two degrees of freedom 15 p2490 A67-30156

Radial adiabatic motion of spheres of uniform density and isotropic pressure in general relativity, giving bounce occurrence conditions 20 p3486 A67-37273

SYMMETRY

SA AXISYMMETRY

SA ISOTROPISM

Symmetry groups of motion equation determined, using generators of Lie spatial groups 02 p0268 A67-12424

Symmetry principles at high energy - Conference, University of Miami, January 1968 14 p2350 A67-27798

Gauss theorems for tensor with valence other than unity extended to include arbitrary orthogonal coordinates 14 p2349 A67-28738

Symmetry removal from linear relations between forces and fluxes, concluding that fading memory in viscoelastic materials results from irreversible entropy 18 p3159 A67-34005

Symmetry and self-duality in nonlinear programming investigated for class of nondifferentiable convex problems 20 p3475 A67-36482

Weak electromagnetic decays of hyperons in broken SU(3) model 20 p3489 A67-37093

Solution methods for Cauchy problem and ideal unstable gas motion in cylindrical and spherical symmetry, discussing shock wave occurrence 21 p3565 A67-38562

Symmetry principles at high energy - Conference, University of Miami, January 1967 22 p3840 A67-39582

SYNCHROCYCLOTRON

Adjustment and test of 300 Mev proton extraction system for NASA 600 Mev synchrocyclotron 20 p3413 A67-36182

SYNCHRONIZATION

SA BIT SYNCHRONIZATION

SA FREQUENCY SYNCHRONIZATION

Mean time analysis of PCM synchronization, noting pattern synchronization in presence of noise 02 p0197 A67-12020

Clock synchronization via communications satellite Relay II 09 p1494 A67-21617

Cardiovascular and renal 24 hr synchronized and desynchronized circadian rhythm 11 p1747 A67-24785

Global distribution of standard time by VLF for synchronization with microsecond accuracy 14 p2263 A67-28389

Clock synchronization with artificial satellites for precise time and frequency, comparing two-and one-way transmission and reception 14 p2263 A67-28391

Human circadian rhythms in activity, body temperature and other physiological functions, discussing oscillator multiplicity, internal desynchronization and entrainment 15 p2426 A67-29110

Diversity-reception systems used in discontinuous radio communication, considering error probability and channel utilization factors 18 p3001 A67-34181

Eastern Test Range time synchronization system, analyzing errors and limitations 20 p3414 A67-36535

Three geodetic measurement bases synchronized to within 100 microseconds by transporting atomic clock 23 p3997 A67-40573

SYNCHRONIZATION CODE

Non dissipatively regulated variable frequency DC to DC converter with variable on time and variable off time 02 p0183 A67-12117

Code-division-multiplex decentralized control system for communication satellites based on use of pseudorandom PM signals of wide bandwidth 06 p0959 A67-17672

Synchronous sequential multiphase pulse generator using unit distance cyclic code 07 p1162 A67-20199

PCM frame synchronization with self-varying threshold 11 p1764 A67-24434

Self-variable threshold method for synchronization code detection of PCM telemetry signal 21 p3583 A67-38641

SYNCHRONIZED OSCILLATOR

Phase locking, mode selection and noise problems in synchronous operation of microwave silicon avalanche diode oscillators to obtain large coherent output power 01 p0033 A67-10016

Standard frequency transfer to local oscillator, removing modulation and producing continuous stable carrier 02 p0210 A67-11530

Synchronous phase LC oscillator 03 p0378 A67-13290

Radiation transport in spectral lines as consecutive photon absorptions and emissions, discussing contemporary theories, approximation methods and applications spark shadow projections in air for giant pulse 06 p1010 A67-18090

UHF oscillator synchronization correlation with various parameters 06 p0969 A67-18119

Phase lock loop of synchronized time code translator, noting design and application 15 p2445 A67-29587

Pull-in range in feedback synchronization, discussing multistage filter and results obtained with graphical, computer and theoretical methods 15 p2446 A67-29588

Noise in injection-synchronized oscillators, deriving inequality 18 p3011 A67-34221

HF oscillators phase bridge based on phase synchronization of identical and adjacent frequencies 21 p3590 A67-37947

Synchronous motions in dynamic bearing system of nonlinear plants with one degree of freedom interacting through weak coupling 22 p3836 A67-39395

Carcinotron hyperfrequency power oscillator with tube of same noise

characteristics as control developed for space telecommunications 23 p3982 A67-41431

SYNCHRONOUS COMMUNICATIONS /SYNCOM/ SATELLITE

Ground signal station tasks and problems, examining Early Bird satellite and Ralsting station in Germany 01 p0023 A67-10453

Syncom III satellite measurement of time variation of total ionospheric electron content [RASSA PAPER 1-10-129] 03 p0417 A67-14240

Mission requirements and cost effectiveness comparison of Syncom satellites and associated network synthesis for defense communications systems 06 p0960 A67-17677

International Telecommunications Satellite /INTELSAT/ Consortium and COMSAT participation in program [AIAA PAPER 66-332] 06 p1120 A67-17707

Pacific equilibrium longitude for stationary satellite, discussing processing of Syncom III data, drift rate calculations, etc [AIAA PAPER 67-91] 06 p1086 A67-18338

Latitudinal variations of ionospheric irregularities studied via synchronous and 1000 km satellites, noting Early Bird data, scintillation index graphs, radio star signals, etc 10 p1640 A67-23234

Attitude determination and hydrogen peroxide control system for spacecraft orientation in Syncom, Early Bird and ATS [AIAA PAPER 67-532] 19 p3334 A67-35934

Pacific equilibrium longitude for stationary satellite, discussing processing of Syncom III data, drift rate calculations, etc [AIAA PAPER 67-91] 22 p3886 A67-40085

SYNCHRONOUS COMMUNICATIONS SATELLITE PROJECT P

Synchronous satellite communication systems including altitude and motion effects, time delay, control system, antenna, etc 12 p1907 A67-25991

Fundamental design features that have made synchronous communications satellites practical 16 p2759 A67-30690

Synchronous orbit communication satellite electric thruster, considering space charge neutralized ion accelerator 23 p4049 A67-41428

SYNCHRONOUS DETECTOR

Performance characteristics of transistorized synchronous demodulator 02 p0219 A67-12113

Book on asynchronous detection and reception of pulsed radio signals at HF and Shf against background of fluctuating noises 05 p0761 A67-16172

Synchronous detection for signal phase gap measurements and Diana type satellite tracking, discussing hypothetical carrier 21 p3583 A67-38644

SYNCHRONOUS GYROSCOPE

Inertial effects of rotor on synchronous motion of simply supported and cantilever arrangements of rotor shaft systems 20 p3453 A67-36500

SYNCHRONOUS METEOROLOGICAL SATELLITE /SMS/

Automated spacecraft flights and cost /1965 to September 1966/, discussing Voyager, Jupiter probe, technology satellite, synchronous meteorological satellite and voice/TV broadcast 05 p0904 A67-18384

SYNCHRONOUS MOTOR

Small size cylindrical gear reduction system design for servomotors of synchro systems in electronic equipment 11 p1745 A67-24553

SYNCHRONOUS SATELLITE SA DODGE SATELLITE

Satellite placing in synchronous orbit using ELDO PAS booster for telecommunications purposes 01 p0156 A67-11418

Automatic directional-antenna position control system for ATS synchronous orbit spin-stabilized satellite 01 p0156 A67-11426

Earth-based radio reference signal in obtaining attitude and pointing information for synchronous communications satellites 02 p0331 A67-12151

Equilibrium positions of synchronous equatorial satellite situated in directions of extremum positions of radius of equatorial section of synchronous geoid 02 p0327 A67-12370

Orbital resonance caused by tesseral harmonics, examining perturbations of synchronous satellite in eccentric

orbits 02 p0328 A67-12400

Exploration of role of Lagrangian points of earth-moon system within solar system exploration program, using libration point satellites 02 p0328 A67-12405

Technical properties of Early Bird communications satellite noting launching, positioning, worldwide system establishment, etc 03 p0367 A67-12898

Early Bird circuits and development of communications systems using synchronous satellites 03 p0370 A67-13830

Synchronous satellite orbits exploration, ground track plots show effects of varying orbit eccentricity and inclination 04 p0694 A67-14503

Ground track of earth-period synchronous /24-hr/ satellites, discussing equatorial, circular and elliptical orbits 04 p0704 A67-14826

Characteristics and performance of synchronous satellite military communication system 06 p0979 A67-17668

Synchronous orbit stationkeeping techniques, examining thrust control requirements of spin-stabilized spacecraft 06 p1094 A67-17679

Minimum cost ground receiving station for synchronous satellite system [AIAA PAPER 66-311] 06 p0979 A67-17691

Synchronous stationary satellite system for networking television and radio material to broadcast stations, noting frequency requirements and constraints 06 p0961 A67-17697

Lunar communication satellites, discussing satellite relay, librational, random and synchronous satellite design, lunar orbits, etc [AIAA PAPER 66-315] 06 p0961 A67-17705

Orbital behavior and stationkeeping propulsion requirements for synchronous satellites, considering solar radiation and earth oblateness effects 09 p1571 A67-21697

Tabulated altitudes, periods and velocities for Martian satellites in circular parking orbits 09 p1564 A67-21716

Configurations of hyperbolic position-fixing systems using synchronous satellites, showing Loran-like networks on earth resulting from these configurations 09 p1526 A67-22393

Navigation aids for ATC, discussing ground reference aids in terms of accuracy 09 p1530 A67-22649

Seasonal variations in ionospheric total electron content measured by observing Faraday rotation of linearly polarized wave from geostationary satellite Syncom III 10 p1651 A67-23346

Communications satellites for high power transmission of TV and VHF signals, considering synchronous satellites, antennas, stabilizing systems and weight 11 p1870 A67-24706

VHF antenna array, electronically despun, designed for spin-stabilized synchronous-altitude communications 14 p2288 A67-28693

Illumination impinging on geocentric satellite during eclipse by earth 16 p2761 A67-30958

Reaction control system for spinning synchronous satellite noting selection criteria, tradeoff methods, etc 17 p2953 A67-31972

Multiple laser communication design, considering links between ground stations and earth-synchronous satellite with single telescope and laser 17 p2813 A67-32495

Multipath effect measurement in propagation path at UHF frequencies from synchronous satellite to aircraft 17 p2816 A67-32626

Earth-based radio reference signal in obtaining attitude and pointing information for synchronous communications satellites 18 p3137 A67-34113

Effective geopotential at synchronous height determined using observations of Syncom satellites during free drift periods, noting longitude dependence 18 p3041 A67-34251

Reduction of dynamic data from geodetic satellites noting satellite tracking station position, gravitational potential, gravity coefficients, synchronous satellites, etc 20 p3429 A67-36891

Thrust, power and performance requirements for synchronous satellite

simulated for evaluating ion propulsion feasibility [AIAA PAPER 67-720] 21 p3694 A67-38746

Multijet electrothermal systems for attitude control and stationkeeping of synchronous communications satellite [AIAA PAPER 67-723] 21 p3694 A67-38748

Gravity gradient stabilization experiments using DODGE satellite at synchronous orbit 21 p3714 A67-39149

Minimum fuel flight plans for injecting synchronous satellite into circular equatorial orbit, developing four methods 22 p3886 A67-40116

SYNCHRONOUS SATELLITE SYSTEM

Cable suspension of daughter satellite from parent satellite, examining synchronous rotation at less than synchronous altitude 10 p1712 A67-23148

Rain effects at random antenna elevation 11 p1753 A67-24303

Reliability, orbit achievement and control and increased power bandwidth as factors making communications satellites economically feasible 19 p3350 A67-35649

DODGE TV system for evaluating attitude control system in gravity gradient stabilization at synchronous altitude 20 p3452 A67-37571

SYNCHROTRON S PARTICLE ACCELERATOR

SYNCHROTRON NOISE

Nuclear explosion effects on radio propagation, noting new ionization in ionosphere and radio signals generation 14 p2266 A67-28417

SYNCHROTRON RADIATION

Time varying energy distribution of high energy electrons producing solar microwave impulsive bursts and X-ray bursts by emission of gyrosynchrotron radiation 01 p0145 A67-11145

Intense radio emission from galaxies may be due to large scale explosions in galactic nuclei, examining characteristics of synchrotron emission 03 p0516 A67-14335

Negative absorption in cosmic radio sources of synchrotron radiation 04 p0700 A67-15200

Variations in RF spectra of 3C 84, 3C 273, 3C 279 and other radio sources 05 p0891 A67-16401

Diffuse omnidirectional inverse Compton and synchrotron X and gamma radiation from cosmic distributions of fast electrons and thermal photons 05 p0882 A67-16404

Synchrotron nature of Sagittarius A central component radio spectrum and injection of relativistic cosmic particles 06 p1078 A67-18166

Ionized medium effect on synchrotron emission spectra in solar corona proposed to account for LF cut-off in type IV radio bursts 08 p1402 A67-21464

Variation of radio brightness of synchrotron radiation from Van Allen belts as function of direction and frequency, using satellite receiver 11 p1855 A67-23944

Electron synchrotron as source of extreme UV radiation noting design 11 p1788 A67-23965

Electron component of primary cosmic radiation 11 p1856 A67-24104

Evolution of radio spectral index of supernova remnants modeled to include synchrotron radiation energy distribution 11 p1859 A67-24114

Synchrotron radiation of relativistic electrons in magnetic field of dipole 12 p1994 A67-25535

Net polarization of celestial X-rays could lead to specification of source mechanism producing radiation 14 p2381 A67-28617

Synchronous and cyclotron wave behavior of electron flux in resonator with transverse electric field varying sinusoidally along wave propagation direction 14 p2288 A67-28807

Nonthermal X-ray radiation accompanying solar flares, comparing spectral power of synchrotron radiation, Compton radiation and bremsstrahlung as possible generation mechanisms 15 p2549 A67-29141

Synchrotron nature of Sagittarius A central component radio spectrum and injection of relativistic cosmic particles 16 p2737 A67-30510

Interpretation of UVB measurements of quasi-stellar sources 17 p2944 A67-32637

Thermal and synchrotron cosmic X-ray sources 17 p2937 A67-32639

Synchrotron radiation spectrum of self-

- absorbed radio sources for various electron distributions 17 p2947 A67-32755
Microwave and type IV solar bursts, examining gyrosynchrotron emission and various electron acceleration mechanisms 17 p2939 A67-33391
Book on vacuum UV spectroscopy techniques noting Lyman continuum, synchrotron radiation, Bremsstrahlung radiation, UV radiation, resolution, etc 20 p3446 A67-36664
Solar flare microwave radio bursts, suggesting synchrotron radiation from relativistic positrons, calculating positron yield and synchrotron spectrum 20 p3519 A67-37101
Decimeter radiation from Jupiter originating in synchrotron radiation of ultrarelativistic energy electrons in 1 gauss field 21 p3710 A67-38996
Synchrotron radiation intensity of relativistic electron moving in anisotropic medium 22 p3851 A67-39735
Synchrotron X-ray radiation by high energy electrons in magnetic field with enhancement due to outward propagating hydromagnetic waves proposed as Crab Nebula emission mechanism 23 p4051 A67-40914
Nonthermal X-ray radiation accompanying solar flares, comparing spectral power of synchrotron radiation, Compton radiation and bremsstrahlung as possible generation mechanisms 24 p4222 A67-43064
- SYNCOM PROJECT**
S SYNCHRONOUS COMMUNICATIONS
SATELLITE PROJECT
SYNCOM SATELLITE
S SYNCHRONOUS COMMUNICATIONS /SYNCOM/ SATELLITE
SYNOPTIC METEOROLOGY
Oscillations in turbulence angle in observations of quality of star images, considering role of synoptic front 02 p0281 A67-11990
Aerologic and synoptic weather forecasting 06 p1026 A67-18599
Weather forecast deduction from field distribution of meteorological elements 06 p1027 A67-18600
Filtering problem in numerical weather forecasting, discussing use of truncated diagnostic and complete primitive field equations 06 p1027 A67-18601
Long range weather forecasting, discussing synoptic, statistical and physical approaches 06 p1027 A67-18604
Upper atmospheric condition noting solar activity effect, synoptic meteorology, etc 06 p1027 A67-18607
Book on structure of stratosphere and mesosphere noting rocket exploration results, synoptic observations, solar control over temperature variations, etc 07 p1172 A67-19603
Solid and hybrid propulsion relationship to sounding rocket vehicle design and mission analysis, particularly application to synoptic meteorology 08 p1374 A67-20492
Rocket vehicles for synoptic meteorology, evaluating vehicle concepts, performance characteristics and costs 08 p1404 A67-20497
General atmospheric circulation for mean state conditions, using synoptic charts 10 p1833 A67-22868
Atmospheric ozone data on basis of meteorological observations and synoptic maps on ship in Atlantic 11 p1785 A67-23958
Satellite radiation data application to synoptic weather analysis including cloud pattern mapping, tropospheric relative humidity and vertical cloud structure inference 13 p2149 A67-26274
Nondeepening synoptic scale tropical disturbance showing dependence on in situ development and decay in upper troposphere 13 p2152 A67-27805
Synoptic charting of high latitude geomagnetic field distribution during magnetic storm, discussing ring current behavior 14 p2309 A67-27942
Numerical methods for calculating pseudoadiabatic characteristics of saturated air parcels 17 p2879 A67-32549
- SYNOPTICAL MEASUREMENT**
Synoptical and monitoring projects for solar activity, interplanetary space, magnetosphere, ionosphere, aeronomy, etc 19 p3223 A67-35475
- SYNTHESIS**
SA FREQUENCY SYNTHESIS
SA NETWORK SYNTHESIS
SA NUCLEOSYNTHESIS
SA PHOTOSYNTHESIS
SA PLASMA JET SYNTHESIS
One-and two-dimensional antenna synthesis for instruments of large resolving power and effective collecting area 14 p2284 A67-28433
Earth rotation synthesis using arrays of small antennas for better low declination sensitivity 14 p2284 A67-28434
- SYNTHETIC ARRAY**
Fabrication of small geometry planar bipolar transistors by using electron beam 13 p2064 A67-27574
Method of radiation pattern synthesis for equally and unequally spaced arrays 14 p2285 A67-28451
Discretionary wiring method and polycell approach to large scale integration 15 p2444 A67-29456
- SYNTHETIC FIBER**
SA NYLON
SA POLYAMIDE
SA POLYBENZIMIDAZOLE
SA POLYESTER
Boron filament preparation on fused silica substrates by decomposition of diborane 03 p0454 A67-13420
Boron carbide filament production by vapor deposition from organoboranes 03 p0454 A67-13421
Viscoelastic properties of capron under torsion at infrasonic frequencies and polymer resin complex shear modulus temperature dependence 21 p3647 A67-37866
High temperature resistance fibers - ACS conference, Phoenix, January 1966 21 p3647 A67-37870
High temperature properties of aromatic polyimide fibers, noting thermal and dimensional stability 21 p3648 A67-37874
Aromatic poly-1, 3, 4-oxadiazole fiber preparation noting thermostability, property retention at high temperature and resistance to hydrolytic degradation 21 p3648 A67-37877
Laboratory equipment for R and D on fibrous refractory materials 21 p3649 A67-37883
Continuous filament ceramic fibers via viscose process involving lattice forming, spinning, weaving and firing 21 p3649 A67-37885
Polycrystalline boron nitride fibers structure, determining density, defects, resistance, thermostability, etc 21 p3649 A67-37886
- SYNTHETIC MICROSTRUCTURE**
Synthetic pink-ruby crystal demagnetization characteristics when employed as coolant in cryostat, noting temperature dependence 11 p1851 A67-25033
- SYNTHETIC RESIN**
SA PHENOL RESIN
SA PLASTIC
SA POLYCARBONATE
SA POLYESTER
SA POLYETHYLENE
SA POLYMETHYL METHACRYLATE
SA POLYPROPYLENE
SA POLYSTYRENE
SA POLYTETRAFLUOROETHYLENE
SA POLYURETHANE
SA POLYVINYL CHLORIDE
SA TEFLON
Compression, shear and bending strengths of tubular synthetic products as materials for aircraft structural component 04 p0715 A67-15539
Roving machine for impregnating glass fibers with synthetic resins 06 p1007 A67-18023
System, incorporating Teflon membrane, to selectively remove carrier gas from column effluent prior to entry into mass spectrometer 10 p1602 A67-22946
Vapor cured resins for aerospace applications 15 p2506 A67-29544
Thermoplastic-resin film with UV sensitive dispersed compound for carbon-dioxide laser-radiation photography 19 p3240 A67-35694
Synthetic lubricants noting chemical and physical properties of nonhydrocarbons, classes of synthetics, etc 20 p3455 A67-37264
Plastic based bearings, discussing polymer chemistry, use of fillers, incorporation into matrices of various resins, etc 20 p3455 A67-37266
Plastics in aircraft and rocket parts construction noting silicon oils and solid polysiloxanes, discussing temperature resistance and rubber-elastic properties 23 p4021 A67-41400
- SYNTHETIC RUBBER**
SA ELASTOMER
SA POLYBUTADIENE
SA POLYISOBUTYLENE
SA VULCANIZATE
Elastomer application in spacecraft launching, flight and reentry such as binder, sealant, base for adhesives, heat shielding, etc [ONERA-TP-407] 05 p0833 A67-16479
Time dependent small-strain modulus of styrene-butadiene rubber, noting predictability from selected molecular parameters [AIAA PAPER 67-491] 18 p3143 A67-33956
Viscoelastic behavior of pure gum rubbers and relationship between filler characteristics and mechanical properties of inert filled composite materials 19 p3249 A67-35888
Highly elastic materials temperature dependence of contact area and sliding friction forces affected by elastic modulus decrease with temperature under load 23 p4021 A67-40596
- SYSTEM**
S AEROSPACE SYSTEM
S AIR DEFENSE SYSTEM
S AIRCRAFT HYDRAULIC SYSTEM
S AUTOMATIC DATA PROCESSING SYSTEM
S CARDIOVASCULAR SYSTEM
S CARRIER SYSTEM
S CIRCULATORY SYSTEM
S CLOSED LOOP SYSTEM
S CODING SYSTEM
S COMMAND SYSTEM
S COMMUNICATION SYSTEM
S CONJUGATED SYSTEM
S CONTINUOUS FLOW SYSTEM
S CONTROL SYSTEM
S COOLING SYSTEM
S COORDINATE SYSTEM
S DATA HANDLING SYSTEM
S DATA READOUT SYSTEM
S DEICING SYSTEM
S DEWAR SYSTEM
S DIGESTIVE SYSTEM
S DIGITAL CAPACITANCE SYSTEM
S DISPLAY SYSTEM
S EARTH-MOON SYSTEM
S ECOLOGICAL SYSTEM
S ELASTIC SYSTEM
S EMERGENCY LIFE SUSTAINING SYSTEM
S ENDOCRINE SYSTEM
S ENGINE MONITORING SYSTEM
S EXHAUST SYSTEM
S FAIL-SAFE SYSTEM
S FEED SYSTEM
S FLOTATION SYSTEM
S FREQUENCY TRANSLATION SYSTEM
S FUEL SYSTEM
S FUEL TANK PRESSURIZATION SYSTEM
S GASTROINTESTINAL SYSTEM
S GODDARD RANGE AND RATE SYSTEM
S GROUND OPERATIONAL SUPPORT SYSTEM /GOSS/
S GUIDANCE SYSTEM
S HOT GAS SYSTEM
S HYDRAULIC SYSTEM
S HYPERBOLIC SYSTEM
S IGNITION SYSTEM
S INDUCTION SYSTEM
S INTERFEROMETER SYSTEM
S JETTISON SYSTEM
S LANDING SYSTEM
S LEARNING SYSTEM
S LINEAR SYSTEM
S LUBRICATION SYSTEM
S MAN-MACHINE SYSTEM
S MECHANICAL SYSTEM
S METAL-GAS SYSTEM
S MISSILE DEFENSE SYSTEM
S MISSILE SYSTEM
S MONOPOLE ANTENNA SYSTEM
S MOTOR SYSTEM
S MULTIPLE-DEGREE-OF-FREEDOM SYSTEM
S NAVIGATION SYSTEM
S NERVOUS SYSTEM
S NONLINEAR SYSTEM
S OXYGEN SYSTEM
S PIGGYBACK SYSTEM
S PROPULSION SYSTEM
S PULSE TRANSMISSION SYSTEM
S PULSED DOPPLER SYSTEM

S RADAR SYSTEM
 S RAIN REMOVAL SYSTEM
 S RECEIVING SYSTEM
 S REDUNDANT SYSTEM
 S REFLECTOR SATELLITE SYSTEM
 S REPRODUCTIVE SYSTEM
 S RESPIRATORY SYSTEM
 S RHO-THETA SYSTEM
 S ROTOR SYSTEM
 S SAMPLED DATA SYSTEM
 S SCHUMANN-RUNGE BAND SYSTEM
 S SELF-ADAPTIVE SYSTEM
 S SELF-REPAIRING SYSTEM
 S SOLAR POWER SYSTEM
 S SOLAR SYSTEM
 S SPACE SURVEILLANCE SYSTEM
 S SUBSYSTEM
 S SUPPORT SYSTEM
 S SUSPENSION SYSTEM
 S SYNCHRONOUS SATELLITE SYSTEM
 S TAKEOFF SYSTEM
 S TERNARY SYSTEM
 S THERMIONIC CONVERSION SYSTEM
 S THERMOELECTRIC CONVERSION SYSTEM
 S THERMOMAGNETIC CONVERSION SYSTEM
 S TRACKING SYSTEM
 S TRAJECTORY MEASURING SYSTEM
 S TWO-ELECTRON SYSTEM
 S TWO-PHASE SYSTEM
 S VACUUM SYSTEM
 S VARIABLE MASS SYSTEM
 S VASCULAR SYSTEM
 S VISUAL SYSTEM
 S VOICE DATA PROCESSING SYSTEM
 S VOR SYSTEM
 S WEAPON SYSTEM
 S WIRING SYSTEM
 SYSTEM FAILURE
 SA ENGINE FAILURE
 Monte Carlo techniques use of random numbers, noting Buffon needle problem, Laplace equation, number generation and radar target detection
 simulation 01 p0104 A67-10158
 Optimum tests for check of working order of system with minimal material losses of safe or fault system
 functioning 01 p0043 A67-10240
 Matching reliability methods to real situations in system-assessment
 context 01 p0078 A67-10514
 Reliability Symposium, San Francisco, January 1966 01 p0081 A67-11332
 System effectiveness critical activities covering reliability, maintainability, quality, design guides, etc, for aerospace industry 01 p0170 A67-11333
 Reliability estimation techniques adaptable to computer implementation for complex manned systems 01 p0031 A67-11338
 Reliability improvement effect on cost in tactical aircraft, examining obsolescence, risk factor determination, etc 01 p0170 A67-11350
 Full-life product warranty approach in reducing military avionics support costs by tying supplier profits to reliability attainment 01 p0171 A67-11351
 Reliability modeling utilizing conditional probability logic to simplify dependency and complex redundancy 01 p0083 A67-11353
 Electronic device degradation and failure analysis in terms of changes in atomic and molecular levels 01 p0041 A67-11356
 Physics of failure techniques applied in reliability failure analysis of intermittent operation of ceramic capacitors 01 p0041 A67-11358
 Failure rate and failure mechanism schools test philosophies combined to know and improve integrated circuits
 reliability 01 p0042 A67-11366
 Sampling plans for identification of inadequate subsystems 01 p0084 A67-11370
 Modified long-term system reliability models for redundant systems, considering imperfect failure detection, repair and sparing 01 p0043 A67-11378
 Prediction method for system reliability in early proposal and feasibility phases of program 01 p0085 A67-11379
 Markov chains used in construction of reliability mathematical models for systems with dependence between components, noting differential equations 01 p0085 A67-11383
 Reliability optimization relation to program time and costs and schedule for cost reduction keeping time

constant 01 p0085 A67-11384
 Unreliability of mean-time-between-failures concept as standard quality measure for mechanical systems 02 p0249 A67-12428
 Book on electronics reliability, calculation and design 03 p0377 A67-13232
 Miscellaneous results connected with simple system alternating between two states, running or under repair 03 p0432 A67-13824
 Failure mechanism of ceramic fibers in fiber-metal composites determined by high amplitude fatigue tests 03 p0525 A67-13871
 Deterministic and quasi-deterministic methods of failure prediction in electronic systems for prevention strategy in system test or checkout program 04 p0581 A67-14879
 Failure occurrence paradox capable of resolution by small change of attitude 04 p0584 A67-15480
 Approximation method determining follow-up failure conditions for nonlinear automatic systems in presence of control and noise signals 05 p0781 A67-16255
 Product identification and traceability standards for space system quality assurance program for NASA space systems 05 p0930 A67-17251
 Mathematical models properties analyzed for system reliability and maintainability, namely mission availability, discussing relationship to failure and action rate and time constraint 05 p0813 A67-17252
 Statistical procedures for analyzing test data to determine extent of dependence of failures in redundant components 05 p0813 A67-17256
 Relation between packaging design and cooling, vibration, RF interference and reliability of microelectronic systems used in space vehicles 05 p0779 A67-17467
 System reliability increased by introducing redundant elements or structural changes in elements 06 p1008 A67-18546
 Launch-on-time probability, showing dependence on initial countdown reliability and cumulative percentage of failures [AIAA PAPER 87-271] 07 p1260 A67-20080
 Leakages in hydraulic system of Hawker Siddeley Trident jet transport due to cavitation erosion 07 p1132 A67-20149
 Multithreading design of reliable aerospace computer, showing inverse proportionalities between speed capacity and reliability 08 p1298 A67-20667
 Systematic approach using weight factor for apportioning mean corrective times of equipment based upon maintainability, usage and reliability data 08 p1315 A67-20670
 Sealed Ni-Cd battery developments including oxygen recombination, temperature effect, separator reliability, electrochemical failure modes, etc 09 p1445 A67-22177
 Failure reporting, analysis and correction on satellite programs, discussing system reliability 09 p1480 A67-22289
 Implementation of NASA NPC 250-1 /Reliability Program Provisions for Space Systems Contractors/ as applied to Saturn V Mechanical Ground Support Equipment Program 09 p1582 A67-22292
 Nondestructive tests designed to increase reliability of coated specimens by elucidating failure mechanisms 09 p1519 A67-22303
 Logical redundancy technique based on failure-erasure circuitry for masking P-1 failures in P identical elements connected in parallel 09 p1470 A67-22868
 Material considerations in establishing failure mechanism of Nimbus solar array drive 10 p1713 A67-23741
 Interplanetary flight reliability problem treated by availability concept in terms of function, duty cycle and subsequent reliability 11 p1869 A67-24339
 Evaluation facility for rotor containment/control devices [SAE PAPER 870332] 12 p1925 A67-25873
 Boeing SST inlet, control and power system development, discussing test program, design objectives and cost [SAE PAPER 870318] 12 p1990 A67-25886
 Relay failure in spacecraft subsystem analyzed via vibration testing 13 p2085 A67-27697
 Reliability of electromechanical relays, discussing test equipment, data analysis, etc 13 p2085 A67-27698
 Gunn diodes using Sn-Ag and In-Au contacts studied for electrical properties and

failure mechanisms 14 p2290 A67-28927
 Efficiency criterion in form of probability of task completion estimated for dynamic systems with random parameters 15 p2455 A67-29121
 Systems approach to reliability, integrating cost and performance and demonstrating tradeoff decisions 15 p2448 A67-29800
 Transistor failure analyses by measuring electric parameters, repeating production phases on opened transistors, destructive testing and defect production by extreme artificial stress 15 p2449 A67-29811
 Stress states, structure deformation, failure criteria and constitutive relations in structural design noting tensile, strip and lap shear test and continuum model 15 p2575 A67-29977
 Mean time between failures for repairable system in terms of MTBF and availability of constituent units by reducing reliability block diagram 15 p2453 A67-30062
 Fatigue failure prevention noting load redistributing, stress concentration reduction, critical section size increases, mean stress reduction, etc 15 p2494 A67-30098
 Systems approach for product and test equipment failure information reporting, including cause and corrective and preventive measures 15 p2584 A67-30410
 Reliability statistics for repairable devices, proving Poisson distribution limitations and nonhomogeneous Poisson adequacy for analyzing stochastic processes 15 p2495 A67-30412
 System reliability for single-time demand interval, calculating distribution function for time to system failure 15 p2495 A67-30413
 Standard life-testing experiment in which n similar units are cycled to failure 15 p2495 A67-30414
 Engineering approach to nonelectric reliability in design, stressing mechanical aspects 15 p2495 A67-30415
 Environmental adjustment factors for operating and nonoperating failure rates 15 p2495 A67-30417
 Effectiveness for automatic control systems estimated by comparing performance with ideally functioning systems 16 p2643 A67-30919
 Reliability of multilayer printed wiring boards as interconnection device 16 p2642 A67-31726
 Structural reliability of fatigue loaded rotorcraft estimated through S-N and spectrum testing [AHS PAPER 123] 16 p2777 A67-31838
 Electronic systems for V/STOL fighter aircraft, considering operational capabilities, reliability, maintenance and protection 17 p2795 A67-32032
 Iterative on-line reliability calculation of automatically repaired space computer, noting reliability and performance 17 p2820 A67-32501
 Strength increase of parts or system to prevent fatigue failure, noting bulk and material considerations and elimination of fretting, scoring, corrosion, sharp corners, etc 17 p2962 A67-32824
 Twin spool zero-NPSP /net positive suction pressure/ turbopump selected for NERVA rocket after assessing turbopump, engine, vehicle and mission related systems [AIAA PAPER 87-476] 18 p3075 A67-33946
 Mathematical model for computer diagnosis of system failure, developing optimal policy for searching malfunctions with observable symptoms 18 p3008 A67-34065
 Markov processes applied to synchronization failure in phase-lock AFC loop subjected to external fluctuations 18 p3000 A67-34086
 Reliability and maintainability Conference, Cocoa Beach, Florida, July 1967, Volume 6 18 p3055 A67-34648
 Reliability demonstration during category II and III testing of missile and airborne radar fire control system, emphasizing coordination between factory and field 18 p3138 A67-34652
 Flight failures in complex unmanned spacecraft systematically studied for Voyager spacecraft design, discussing component failure, design deficiencies and space environment 18 p3138 A67-34656
 Detection of contaminating processes in integrated circuits, describing characteristics

associated with incipient failure in operational equipment 18 p3057 A67-34665

Development and maintenance of equipment containing integrated circuits, discussing processing, fault isolation and human error 18 p3016 A67-34670

Process control program including failure mode and effects analysis, critical characteristics determination, safety features and test equipment 18 p3058 A67-34673

Manned mission reliability and maintainability requirements in future systems 18 p2995 A67-34686

AH-56A /AAFSS/ safety engineering, failure effects method, Army role, etc 18 p2987 A67-34690

System safety management/engineering procedures and techniques for safety requirements application 18 p3163 A67-34691

Space systems reliability design problems, discussing estimation, weight-reliability tradeoffs, spare parts and redundancy 18 p3139 A67-34698

Reliability prediction with inadequate data in flight control systems, using nonelectric approach combining failure data with judgment 18 p3058 A67-34699

Integrated reliability program for Scout launch vehicle in terms of design specification, review functions, malfunction reporting, failed parts analysis, quality control, standardization and certification 18 p3139 A67-34702

Reliability analysis and mathematical models to evaluate crew safety applicable to system safety analysis, discussing component failure data, failure mode effect, etc 18 p3139 A67-34704

System reliability and effectiveness in manned and unmanned geological/geophysical space missions 19 p3332 A67-35323

Techniques and methods of automation in air-traffic control, discussing reliability, operation time reduction, etc 19 p3255 A67-35808

Reliability contribution of pilot using manual backup control for first stage of Saturn V tested using simulation [AIAA PAPER 67-554] 19 p3335 A67-35851

Reliability criteria of systems with recovery, noting mean time to failure of system and mean time of system operation between failures 20 p3454 A67-37037

Navigational system accuracy and breakdown detection, discussing efficiency criterion for logic device 20 p3399 A67-37069

System reliability prediction and confidence limits for several component failure probability distributions, using Monte Carlo simulation on digital computer 20 p3455 A67-37314

Optimum redundancy of multistage parallel systems using variational technique to maximize profit 20 p3558 A67-37316

Digital diagnostic program evaluation based on selective path simulation, tracing option and backtrace 20 p3392 A67-37456

Method 20 p3392 A67-37456

Ultrareliable six redundant sensor attitude reference system for Manned Orbital Laboratory /MOL/ with limited sparing capability 21 p3624 A67-37786

Launch-on-time probability, showing dependence on initial countdown reliability and cumulative percentage of failures [AIAA PAPER 67-271] 21 p3712 A67-37808

Parachute stress analysis during inflation, evaluating magnitude and distribution of snap stress to prevent canopy failure 21 p3568 A67-38538

Maintenance time reduction for multimode airborne weapons through built-in test equipment and integrated program 21 p3601 A67-38947

Solar electric propulsion for space missions, evaluating modularized ion propulsion systems to determine effect of electric isolation on system reliability, weight, etc 21 p3697 A67-38959

Graphic optimization technique for mass reduction in solar powered ion propulsion system with acceptable reliability constraint [AIAA PAPER 67-701] 21 p3697 A67-38960

Space research experiments reliability requirements, considering structural components, project planning and measuring methods adaptation to ambient

conditions 22 p3899 A67-39283

System reliability increased by introducing redundant elements or structural changes in elements 22 p3812 A67-39745

Complex technical systems servicing, considering operation cost as optimization criterion 22 p3812 A67-39746

LF solid state equipment improves mission reliability through use of integrated molecular circuit and modular redundancy 22 p3771 A67-39840

Protective devices in electrodynamic vibration exciters, examining design, operational principles and possible cause of failures 22 p3781 A67-40403

Scanning electron microscope signal processing and application to electronic devices failures, processes variations, integrated circuits and thin film circuit continuity 22 p3774 A67-40411

Procedures, facilities and equipment used in contamination control of Saturn S-IVB stage hydraulic system 23 p3935 A67-40848

Operational error analysis program /OEAP/ use with multiprocessing in air traffic control application 23 p3976 A67-41059

Electronic system reliability statistical estimates obtained from test results of components using series expansion 23 p3982 A67-41669

Statistical analog technique for complex logic control systems to obtain within single test series required reliability characteristics for various structural versions 23 p3985 A67-41670

Critical strain parameter concept for adhesive bond joints noting strength dependence on geometry and material elastic properties [SAE PAPER 670856] 24 p4160 A67-42003

Hydraulic failure detection system in Titan booster servo injector module featuring anticipation and correction of servomodule failure 24 p4099 A67-42426

Electronic equipment components unreliability in guided weapon systems, discussing packaging, environmental conditions and customer-manufacturer relations 24 p4161 A67-42479

Thermionic converter arrays output characteristics determined as function of interconnection resistance, failure modes and patterns, etc 24 p4103 A67-42500

Reliability assessment test program for determining capabilities and limitations of 2 kw hydrogen-oxygen fuel cell stacks 24 p4109 A67-42896

System-safety mathematical model for commercial jet airplanes using fault-tree modeling technique [AIAA PAPER 67-910] 24 p4086 A67-43017

Aircrew safety emphasizing prior to abort aspects in detection of catastrophic failure and initiation of abort sequence [AIAA PAPER 67-934] 24 p4245 A67-43024

Mathematical model for identification and control of systems safety in manned space programs using Monte Carlo techniques [AIAA PAPER 67-936] 24 p4245 A67-43026

SYSTEM FOR NUCLEAR AUXILIARY POWER /SNAP/ PROGRAM

S SNAP-8

S SNAP PROGRAM

S SNAP-10A

S SNAP-19

S SNAP-27

SYSTEM LIFE

Operational reliability components in four military systems, analyzing replacement data by digital and computer type circuitry employing semiconductors 01 p0041 A67-11344

System reliability improvements based on design and reliability experience producing increased success percentage of NASA systems from 62 to 87 percent 01 p0083 A67-11345

Reliability assessment methods for dormant weapons noting failure modes, redundancy, large parameter change, system design, derating, etc 15 p2495 A67-30418

SYSTEM STABILITY

Lateral motion of simply supported axially loaded viscoelastic column governed by system of linear ordinary differential equations with periodic coefficients 01 p0106 A67-10732

Liapunov second method in treating system stability properties 01 p0107 A67-10967

Variable-stability feedback control low range air speed system for X-22A

aircraft 01 p0073 A67-11121

Modified Bode criterion for feedback system stability 01 p0045 A67-11198

Stability of feedback single-loop systems with one differentiable nonlinear element, noting Popov criterion 01 p0046 A67-11210

Stability and sensitivity requirements considered simultaneously in control system design, minimizing time domain sensitivity index and incorporating transient response characteristics 01 p0047 A67-11217

Closed loop gain of two-loop linear feedback system calculated, using computer 01 p0047 A67-11211

Stability theory application to control circuit theory and aerospace systems 01 p0047 A67-11221

Stability of sampled data feedback systems with time-varying gain by restriction with memoryless element and nonanticipative linear time-invariant subsystem 01 p0048 A67-11226

Asymptotic stability of nonlinear systems, noting application to systems with control and Liapunov function role 01 p0048 A67-11318

Stability analysis of nonlinear stochastic systems in presence of random and Gaussian perturbations, determining validity of law of large numbers and amplified law of large numbers 02 p0267 A67-11958

Stability analysis of steady state dynamic holonomic mechanical systems using Rouse, Kelvin, Poincare and Chetaev theorems 02 p0267 A67-11959

Stabilizability of class of linear stochastic systems 02 p0259 A67-12064

Mechanical impact attenuation system for Apollo spacecraft provides stable land landing platform, noting deployed heat shields, extended legs, pneumatic bags, etc [AIAA PAPER 66-989] 02 p0333 A67-12300

Nonconservative oscillatory systems studied for stability and frequency characteristics, using analog computer and equation transformation 02 p0227 A67-12420

Stability in the sense of Liapunov, Poincare, Lagrange and others for dynamical systems 02 p0268 A67-12502

Analog computer solution to autonomous systems with one degree of freedom capable of self-excited oscillation or excited by external periodic force 02 p0209 A67-12712

Role of second order internal resonance in problem of stability of equilibrium of system neutral in linear approximation 03 p0467 A67-12860

Partially invariant relay systems 03 p0389 A67-13085

Stability of stochastic difference systems in case of continuous perturbations subject to Markov random effect 03 p0467 A67-13111

Absolute stability criterion for nonlinear sampled data automatic systems 03 p0392 A67-13596

Stability experiments on partially grooved gas journal bearing, comparing data with previous theoretical analysis [ASME PAPER 66-LUB-6] 03 p0432 A67-13764

Pulse amplitude range estimated for which PWM system is asymptotically stable, using method of Murphy and Wu 03 p0393 A67-13983

Stability criterion for PWM feedback systems containing one integrating element 03 p0393 A67-13984

Imbalance of elastically deformed rotor after starting only once with trial load, noting role of oscillation modes of rotor 03 p0528 A67-14078

Popov stability of distributed parameter dynamical systems with multiple nonlinearities 04 p0591 A67-14419

Stability analysis of multiloop multirate sampled systems using identities expressing Laplace transforms of sampled signals in terms of shifted transforms of same signals sampled with smaller periods 04 p0591 A67-14825

Adjoint field in elastic stability problems for nondissipative nonconservative systems 04 p0709 A67-14834

Book on lambda-matrices for treating linear vibrating systems 04 p0644 A67-14869

Stability and identification of parametric system with periodically varying rectangular wave excitation 04 p0592 A67-14912

Global stability of second order autonomous differential equations 04 p0647 A67-15743

Bounded-input bounded-output stability of time-varying differential system analyzed through extension of Yoshizawa definitions and methods 04 p0594 A67-15877

Stability of two-impacts-per-cycle motion of impact damper 04 p0631 A67-15911

Stability region of complex linear self-conjugate systems of differential equations containing skew-Hermitian matrix 04 p0647 A67-15980

Stability of finite connection of linear passive time-variable circuits demonstrated by Liapunov second method 05 p0785 A67-17300

Ripple instability in closed loop control systems with thyristor amplifiers whose sampling action is noted in presence of alternating component 05 p0777 A67-17302

Controllability limit of human pilot for unstable second order system with positive static stability analyzed by modified transfer function and servomechanism 05 p0757 A67-17354

Steady state rotations in perturbed autonomous systems 05 p0847 A67-17475

Stability and asymptotic stability of control systems with multiple nonlinearities and inputs, using frequency criterion in connection with transfer function 06 p0973 A67-17601

Stability of steady motions of holonomic mechanical systems in cyclic coordinates, using method based on theorems of Routh, Poincare, Kelvin and Chetaev 06 p1031 A67-17838

Liapunov theory of stochastic stability, discussing use to obtain information about random trajectories 06 p0974 A67-17931

Sufficient conditions for stabilization of motion of nonstationary controlled system 06 p0975 A67-18036

Asymptotic stability of periodic solutions of nonautonomous quasi-linear systems with two degrees of freedom 06 p0975 A67-18037

Improving estimates of solutions of linear perturbed-motion equations of mechanical systems with variable coefficients 06 p1023 A67-18038

Hypothetical control system with 30 db/decade attenuation characteristic and constant phase margin of 45 degrees, presenting phase angle stabilization technique that improves actual systems 06 p0977 A67-18416

Validity of equations for bending, natural oscillations and stability of three-layer solid circular plate with rigid filling and asymmetric structure 06 p1106 A67-18628

Stability of elastic systems in small and in large, determining bending deformation of rod, noting presence of upper and lower critical loads 06 p1108 A67-18663

Sufficient conditions of absolute stability of nonlinear discrete systems based on matrix majorant concept 06 p0978 A67-18793

Synthesis methods for structures equivalent to self-adjusting systems for plants with variable parameters 07 p1160 A67-19201

Stability requirements placed on subsystems of coherent impulse radars 07 p1140 A67-19232

Effects of unmodeled errors on minimum variance estimators, with application to tracking complex self-calibration estimation scheme [AAS PAPER 66-107] 07 p1216 A67-19967

Growth of solutions of forced oscillations of nonlinear oscillator driven by white noise 07 p1218 A67-20268

Iterative algorithm for increasing stability of adaptive control systems 08 p1308 A67-20319

Nonlinear DC circuits analyzed by digital computer for application to path integrals and stability problems 08 p1346 A67-20333

Circle criterion for stability of time varying feedback systems 08 p1310 A67-20338

Instability and periodic solutions in nonlinear feedback systems obtained using perturbation theory of Hale and Cesari 08 p1310 A67-20339

Stability and inverse receptance of multidegree systems under harmonic excitation 08 p1415 A67-20479

Simplified approach to predicting onset of spin-yaw instability of rapidly ascending rolling ballistic missile in absence of asymmetric forces 08 p1406 A67-20509

Elastic postbuckling involves coupled

modes when critical loads corresponding to buckling modes of two degrees of freedom system are equal 08 p1422 A67-21032

General dynamical system in metrical space, extending Liapunov method to analyze stability properties by using single Liapunov functional 09 p1532 A67-21661

Pressure feedback in electrohydraulic servomechanisms for high inertia loads to increase stability, using dynamic analysis and differential equations 09 p1442 A67-21687

Reliability-cost trade-off analysis of complex system using mathematical model involving constant percentage increase in MTE with cost 09 p1572 A67-22306

Stability of linear systems with time delay analyzed by introducing stability indicative function, noting applications to differential-difference equations 10 p1679 A67-22916

Liapunov stability theory applied to control system, noting stability of function and stochastic differential equations 10 p1620 A67-23422

Stability of optimal control problem in nonlinear process and linear regulator 10 p1620 A67-23423

Local potential variational method to study runaway stability of electrons in two-component plasma 11 p1826 A67-23872

Lock-on band determination for inertial system of phase automatic frequency control in presence of fluctuation noises 11 p1750 A67-23910

Mean square asymptotic stability of linear system described by nth order equation with random coefficients 11 p1818 A67-24161

Unbalance vibration of rotor analyzed for application to rotor bearing system with dynamic forces represented by spring and damping coefficients [ASME PAPER 67-VIBR-27] 11 p1796 A67-24185

Local and overall stability of nonlinear discrete system with variable modes consisting of linear filter preceded by impulse modulator 11 p1770 A67-24751

Finite time stability of system trajectory under perturbing forces and within specified regions of state space 11 p1771 A67-24892

Higher order resonance rotations of arbitrary order of nonlinear system 12 p1967 A67-26102

Conditional stability of class of controlled systems, noting aircraft controlled by autopilot 12 p1919 A67-26104

Zeta transformation applied to numerical integration operator to determine stability of solution to system of linear differential equations on digital differential analyzer 13 p2072 A67-26348

Compensation technique for improving stability of certain nonlinear autonomous systems by addition of zero networks 13 p2086 A67-26413

Alserman problem concerning absolute stability of zero solution to nonlinear third order system of differential equations 13 p2087 A67-26616

Iteration solution for system of equations for nonlinear deflection and stability of anisotropic plates 13 p2217 A67-26632

Stability analysis of minimum variance estimations used to self-calibrate missile tracking instrumentation complex 13 p2120 A67-26815

Elastic deformation effects on stability of rotating satellite composed of elastically connected rigid bodies 13 p2212 A67-26905

Stability analysis of computer controlled linear hydraulic antenna control system 13 p2088 A67-26996

Ordinary and time lag root locus diagram generating algorithm for adaptation to programming on digital computer 13 p2074 A67-27223

Stability analysis of adaptive aircraft control system with random disturbance 13 p2088 A67-27241

Effect of unmodeled errors on minimum variance estimators, with application to tracking complex self-calibration estimation scheme [AAS PAPER 66-107] 13 p2154 A67-27525

Single parameter family of two-layer difference schemes with decomposing operators for general linear second order parabolic equations with mixed derivatives and variable coefficients 13 p2149 A67-27814

Absolute stability criterion for nonlinear sampled data automatic systems 14 p2290 A67-27842

Stability of motion of continuous dynamical systems analyzed via computing machines 14 p2348 A67-28080

Stability problems in control system of Saturn launch vehicles 14 p2393 A67-28085

Stability and nonlinear vibrations of mechanical systems under harmonic excitation 14 p2397 A67-28087

Necessary and sufficient conditions for boundary of absolute stability domain of nonlinear automatic control systems 15 p2455 A67-29120

Mechanical impact attenuation system for Apollo spacecraft provides stable land landing platform, noting deployed heat shields, extended legs, pneumatic bags, etc [AIAA PAPER 66-989] 15 p2564 A67-29423

Stability of nonlinear controlled systems with infinite degrees of freedom 15 p2458 A67-29696

Three-step nonlinear analysis procedure for nonlinear stability for position-control servomechanical system applications 15 p2459 A67-30143

Stability of systems with controlled plant and correcting system, based on analysis of stabilizability conditions in certain natural frequency regions 15 p2518 A67-30176

Nonlinear nonconservative systems stability analysis by approximate method based on principle of energy conservation 15 p2519 A67-30194

Similarities between model-reference adaptive control systems and parameter identification by adjustable models 15 p2464 A67-30337

Parameter estimation representing differential equation coefficient of controlled system for quick-response adaptive identification 15 p2464 A67-30338

Dynamic imbalance of rotors determined and eliminated using angular oscillation and electrical erosion techniques 16 p2681 A67-30469

Powered flight rotor instabilities using analysis of second-order flap-lag coupling effects of torsionally rigid blades 16 p2595 A67-30927

Conditions for stability of solutions of second order linear differential equation with periodic coefficients 16 p2696 A67-31010

Realization of invariant multiloop control in case of near-critical and critical plant parameters 16 p2643 A67-31379

Gas bearing stability determination by step-jump response using observation of growth or decay of motion amplitude [ASME PAPER 67-LUBS-5] 16 p2682 A67-31383

Liapunov function for modeling and bounding solutions of distributed processes defined by interacting subsystems describable by stable differential equation 16 p2646 A67-31638

Asymptotic stability criterion for autonomous feedback system with single odd monotonic nonlinearity, using functional analysis 16 p2646 A67-31639

Adaptive controller synthesis for unstable mechanical system driven by bang-bang actuator adaptive controller synthesis for unstable mechanical system driven by bang-bang actuator 16 p2648 A67-31656

Triple input describing functions noting application to stability analysis of forced nonlinear control systems 16 p2650 A67-31673

Nonlinear discrete system equivalence of integral pulse frequency modulation /ipfm/ feedback systems, discussing Lagrange stability criterion 16 p2652 A67-31685

Exact stability criteria for kinetics equations of coupled-core nuclear reactors, using Pontryagin theorem and models for time-distribution of coupling neutrons [ASME PAPER 66-WA/AUT-16] 17 p2882 A67-32015

Nonuniform error quantization effects on stability of feedback control systems, investigating limit cycles existence and giving optimum quantizer design procedure 17 p2829 A67-32016

Motion of dynamically symmetric satellite under action of gravitational moments, discussing stability and nonlinear oscillations 17 p2955 A67-32243

Tolerance of nonlinearities in input transducer of time-varying optimal control systems, using Liapunov function 17 p2829 A67-32307

Stability of equilibrium of nonconservative continuous systems with slight

damping 17 p2959 A67-32414
 Asymptotic stability of homogeneous system of partial differential equations in stratification wave theory, introducing source function for local plasma disturbance effect 17 p2907 A67-33101
 Liapunov approach to obtain sufficient conditions for stability of parametrically excited random vibrational system [ASME PAPER 67-APM-9]

17 p2886 A67-33145
 Sufficient conditions guaranteeing asymptotic stability of class of linear dynamic systems with bounded narrow band parametric excitation [ASME PAPER 67-APM-24]

17 p2830 A67-33152
 Stability of steady motions of holonomic mechanical systems in cyclic coordinates, using method based on theorems of Routh, Poincare, Kelvin and

Chetaev 17 p2886 A67-33216
 Stability analysis of nonlinear stochastic systems in presence of random and Gaussian perturbations, determining validity of law of large numbers and amplified law of large numbers 17 p2886 A67-33275

Stability analysis of steady state dynamic holonomic mechanical systems using Rouse, Kelvin, Poincare and Chetaev theorems 17 p2886 A67-33276

Instability zones for vibration equations system having periodic acceleration matrices, damping and spring forces 18 p3140 A67-33464

Stability and instability of tridiagonal linear system, noting application to stability analysis of differential equation system 18 p3070 A67-33644

Soviet book on stability and oscillations of elastic systems covering theory, equilibrium breakdown, dynamic loading, aeroelastic oscillations, etc 18 p3140 A67-33674

Plasticity and brittle fracture conditions combined for stability criteria derivation 18 p3144 A67-34174

Existence of entropy as consequence of asymptotic stability 18 p3160 A67-34285

Relationship between stability and continuity for dynamical systems analyzed using functional analysis, discussing connection to boundedness 18 p3079 A67-34286

Sufficient conditions of absolute stability of nonlinear discrete systems based on matrix majorant concept 18 p3018 A67-34458

Voltage amplitude limiting for improving stability of correlation detector of electronic cross correlation systems, noting variation of SNR 18 p3012 A67-34524

Definition of asymptotic stability conditions and instability of zero solutions of differential equations system 18 p3080 A67-34605

Planar highly conducting liquid jet kink mode stability in electric field and feedback stability control of spatially growing wave 18 p3029 A67-34735

Parabola test for absolute stability, replacing Popov test for nonlinear sectors having nonzero lower bound 19 p3199 A67-34785

Algebraic method applied for control optimization of nonlinear systems, acquiring asymptotic stability by using Liapunov function 19 p3199 A67-34825

Flowgraph models of thermal and electrical parameters interaction in solid state devices, examining performance characteristics, system stability, etc 19 p3191 A67-34845

Coupled systems stability constraints and oscillatory behavior, discussing feedback path nonlinearities using differential equations 19 p3200 A67-34849

Stability range of feedback networks determined with respect to independent circuit parameter using root

hodographs 19 p3201 A67-34910

Stability of equilibrium of holonomic system in critical cases by means of search for Liapunov functions, using power series 19 p3261 A67-35050

Geometric prediction method extension to quaternary liquid-liquid equilibria in two-phase systems comprising two type I ternaries 19 p3346 A67-35612

Identification, optimization and stability of automatic systems - Conference, Sclay, France, May 1965 19 p3203 A67-35901

Macroscopic physical system with behavior

described in terms of differential equation system studied for stability in presence of small delay 19 p3205 A67-35912

Method for influence range determination of stationary points of nonlinear recurrence of order greater than one corresponding to rational functions 19 p3205 A67-35913

Jet attitude control system analysis when subjected to external disturbing torques [AIAA PAPER 67-537] 19 p3174 A67-35939

Analog computer solution of linear algebraic equations system modified to eliminate negative coefficients, guaranteeing computational system stability 19 p3187 A67-36032

Design and stability of wideband tunnel diode amplifiers for microwave radiolink receivers 20 p3395 A67-36248

Laser frequency control system using two optical discriminators for long and short term stability 20 p3459 A67-36519

Efficiency of using self-adjustment with respect to input signal in automatic control systems, estimating gain and stability 20 p3409 A67-37198

Soviet book on time-frequency remote control systems theory and design 20 p3412 A67-37632

Equilibrium stability conditions for mechanical system of solid bodies derived using Liapunov function 21 p3626 A67-37991

Two plates bounded by adhesive layer in plane stressed state, calculating system stability 21 p3719 A67-38050

Rotor bearing stability, describing incompressible and compressible fluid film bearings, calculating thresholds of instability 21 p3632 A67-38136

Stability and instability properties of differential system, discussing matrix and roots 21 p3653 A67-38558

Discontinuous systems proved for stability and instability, using almost-reducible linear approximations 21 p3654 A67-38850

Rapid parameter identification system for linear time-invariant plant with only input and output measurable 21 p3604 A67-38867

Lock-on band determination for inertial system of phase automatic frequency control in presence of fluctuation noises 21 p3585 A67-38938

Computer program based on tracking function method setup for investigating nonlinear second order autonomous system stability and boundedness 21 p3604 A67-39076

Satellite-gyroscope asymptotic equilibrium positions obtained by general motion equation, calculating gravitational and aerodynamic moment effects 22 p3898 A67-39187

Modified Poincare method for studying nonlinear oscillations taking into account circumstances causing fictitious degeneration of system 22 p3836 A67-39393

Synchronous motions in dynamic bearing system of nonlinear plants with one degree of freedom interacting through weak coupling 22 p3836 A67-39395

Thermodynamic stability conditions determined by potential functions of system potential at constant temperature and pressure 22 p3917 A67-39584

Stability and response time of quantified pulse-position modulation feedback control circuit consisting of nonlinear sampler and first order continuous part 22 p3776 A67-39647

Stability of nonlinear sampled data control systems, investigating pulse frequency modulation using Liapunov function 22 p3777 A67-39829

Simplified approach to predicting onset of spin-yaw instability of rapidly ascending rolling ballistic missile in absence of asymmetric forces 22 p3904 A67-40103

Stability margins for hybrid continuous discrete data control systems, developing open loop transfer function 22 p3778 A67-40157

Vehicle systems interaction effect on guidance system stability 22 p3907 A67-40194

Longitudinal oscillations with multiple degree of freedom obtained over sections of adopted stress-strain diagram, characterizing elastoplastic properties 23 p4076 A67-40683

Popov method extension for absolute stability of nonlinear feedback systems containing distributed elements 23 p3984 A67-40870

Multivariable Popov criterion application to stable and to state feedback law linear

finite-dimensional systems, noting toleration of nonlinearities 23 p3984 A67-41158

Stability analysis of two-dimensional nonlinear multivariable systems with nonlinearities, finding limit cycle of symmetric and antisymmetric cases from characteristic equations 23 p3984 A67-41160

Algebraic and transcendental equations solutions using analog computer model described by differential equations, noting Liapunov stability theorem and asymptotic equilibrium 23 p3976 A67-41392

Nonlinear sampled data system instability, discussing arbitrary single-valued nonlinearities and arbitrary modulation law /PAM, PWM or PFM/ 23 p3985 A67-41674

Matrix version of Kalman-Yacubovich lemma for deriving stability conditions for continuous time dynamical systems with m-feedback nonlinearities 23 p3985 A67-41726

Stability of ideal mechanical system with damping forces, obtaining motion equations 23 p4028 A67-41757

Integral pulse FM effect on feedback control, obtaining stability of equivalent nonlinear discrete system 24 p4135 A67-42182

Bounded-input bounded-output stability on nonlinear time varying discrete control system using Liapunov function extension 24 p4135 A67-42183

Stability of feedback systems containing single odd monotonic nonlinearity 24 p4136 A67-42187

Klystron amplifier stability during double interaction in output circuit determined assuming zero HF potential and electron flow not bunched 24 p4129 A67-42193

Relation between earth-moon orbital inclinations indicates incompatibility of dynamical figures with assumptions of hydrostatic equilibrium and homogeneous density distribution 24 p4229 A67-42320

Book on stability of nonlinear mechanical systems covering qualitative methods, one degree of freedom systems, etc 24 p4188 A67-42375

Sloshing stability of three-stage ELDO A launch vehicle during first stage flight 24 p4241 A67-42396

Gas bearing Brayton cycle turboalternator rotor system stability and dynamic response to electromagnetic forces 24 p4102 A67-42487

SYSTEMS ANALYSIS

Lubricant testing system optimizing with respect to machine ability and cost 01 p0077 A67-10121

Measurement systems control in rocket engine testing via real-time surveillance, computation, error correction and graphic display 01 p0076 A67-11144

Control system analysis and design using parameter space method 01 p0047 A67-11216

System reliability evaluation and identification of inadequate subsystems, with application to two missile-borne guidance systems 01 p0111 A67-11371

Reliability matrix analysis of AFSCM 375 management system 01 p0171 A67-11375

Stability of single-frequency solutions to quasi-linear autonomous systems with two degrees of freedom 03 p0468 A67-13625

Future onboard checkout systems including integrated onboard checkout, in-flight maintenance, onboard checkout modes and onboard/ground checkout 03 p0398 A67-14202

Analysis of existing support systems and guide for planning of new systems presenting example of manual test system and automatic test system 03 p0424 A67-14214

Optimization via information flow in system without memory, discussing ideal correction minimal and maximal error 04 p0592 A67-14904

Pulse type nonlinear automatic systems and systems with single nonlinear element 04 p0593 A67-15753

System and cost effectiveness analysis throughout program life cycle of weapon or support system to aid decision making [SAE PAPER 660724] 04 p0740 A67-15780

Network analysis with state variables describing system stored energy 05 p0781 A67-16022

Three and six degrees of freedom missile subsystem design analysis using flight simulation by hybrid computer 05 p0789 A67-17515

Real time approximation of continuous system performance on digital computer

- using difference equations obtained from digitized transfer function 05 p0768 A67-17518
- Systems analysis applied to identification of Saturn V launch vehicle support system requirements and establishment of baseline logic for vehicle prelaunch processing simulation and systems optimization [AIAA PAPER 67-248] 07 p1165 A67-20066
- Circuit and system theory - Allerton Conference, University of Illinois, October 1966 08 p1307 A67-20317
- Sensitivity models in terms of influence of time variation in given part on behavior of whole system 08 p1309 A67-20325
- Algorithms for dichotomous representation of macrocircuits, considering computer programs and establishment of flow graphs 08 p1299 A67-20326
- High resolution aerial photography, detailing photographic films, optical design, camera systems and methods of system analysis 08 p1330 A67-20645
- Experiment selection process for specific flights in Apollo applications program /AAP/, using algorithms [AAS PAPER 66-142] 08 p1411 A67-20967
- MORL system reliability analysis, discussing Monte Carlo simulation, major parameters, constraints, program contingencies, etc 08 p1411 A67-21073
- Titan III system capability for space support and logistics, discussing parameters of assessment 08 p1412 A67-21076
- Optimal control analysis of system behavior described by linear stochastic differential equations 08 p1313 A67-21325
- Self-adjusting control systems with models, reviewing basic theoretical problems of analysis and synthesis 08 p1313 A67-21328
- GSFC program in telemetry data archiving, discussing necessity of data accessing capability 09 p1467 A67-21685
- Optimal control of variable structure system in presence of perturbation, discussing quality control and preservation of sliding plane 09 p1483 A67-22081
- Doppler tracking systems as velocity measuring systems, including introduction methods for necessary position knowledge, one-and two-way systems analyses, etc 10 p1605 A67-22995
- Systems constraints imposed on spacecraft utilizing long flexible rods with attached tip masses, specifically deployment and retraction problems 10 p1714 A67-23757
- Computer application to aerospace missions, discussing operation and equipment parameters, reliability, man-machine interaction, etc 11 p1756 A67-24248
- On-line computation and man-computer interactive languages, discussing JOSS, MADCAP and Klerer-May systems 11 p1756 A67-24249
- Known and unknown principles of biological chronometry 11 p1747 A67-24937
- Total asymptotic stability by nonlinear compensation 13 p2086 A67-26415
- Sampled data control system analysis, determining gain margin in unsampled loops 13 p2086 A67-26416
- Aircraft noise monitoring system for Zurich airport 13 p2052 A67-26535
- Technical and economical possibilities of fast interplanetary space flight systems 13 p2211 A67-26577
- Theoretical design of equivalent mechanical system naturally matched to self-oscillating system 13 p2216 A67-26626
- Self-excited systems sensitivity function maximum value attained via time dependency on natural frequency and damping factor only 13 p2216 A67-26627
- Satellite Telecommunications with Automatic Routing /STAR/ system modulation techniques, channel capacity and Start-Stop /SS/ operation 13 p2067 A67-26718
- Satellite Telecommunications with Automatic Routing /STAR/ system transmission system operation and modulation techniques 13 p2068 A67-26719
- Satellite telecommunication with automatic routing noting switching 13 p2067 A67-26722
- Experiment selection process for specific flights in Apollo applications program /AAP/, using algorithms [AAS PAPER 66-142] 13 p2214 A67-27548
- Dynamical systems control problem in connection with differential equations with lagging arguments 14 p2291 A67-28384
- Approximate model for simplification of linear dynamic system, neglecting effect of higher order time constants 15 p2457 A67-29370
- Confidence limits for percentile analysis of guidance system errors 15 p2515 A67-29740
- Steady state and transient analysis of digital phase-locked loops 15 p2458 A67-29939
- Book on creation and use of computer simulation models and routines for study of systems 15 p2440 A67-30133
- Nonlinear nonconservative systems stability analysis by approximate method based on principle of energy conservation 15 p2519 A67-30194
- Interpolating/extrapolating computer programs noting application to analysis of industrial systems 15 p2462 A67-30327
- Systems with asymmetric nonlinearities analyzed and synthesized by setting up mathematical model applicable to control and adaptive systems 15 p2463 A67-30333
- Circuit analysis by computer, noting programs for reliability and quality control 15 p2441 A67-30408
- System reliability study via detailed allocation method, selecting optimal solution in context of tradeoff analysis 15 p2512 A67-30409
- Systems approach for product and test equipment failure information reporting, including cause and corrective and preventive measures 15 p2584 A67-30410
- Minimum realization of linear time-varying nonanticipative system characterized by its impulse response matrix 16 p2697 A67-31426
- Component parameter identification, discussing techniques and applications 16 p2647 A67-31649
- Process identification by decomposition method of multilevel systems analysis, noting computer estimation of state variables of discrete time systems 16 p2647 A67-31650
- Linear programming algorithm for optimizing channel assignments in satellite communication systems 17 p2810 A67-32111
- Systems recommended to meet area navigation requirements, considering pictorial display/ course line computer /PD/CLD/ application 17 p2881 A67-32391
- Heat transfer analysis for cavitation and boiling, noting vapor bubble formation 17 p2970 A67-32463
- Systems analysis with computer techniques to examine future weapons system, discussing logistic simulation, interpretation, maintenance, engineering, management, documentation and reliability 17 p2833 A67-32490
- Conservative series-parallel approximations to study systems models for reliability analysis and display 17 p2865 A67-32585
- System performance in electrooptical telemetry noting receiver, transmitter, silicon photodiode, shot, thermal and background noise, etc 17 p2817 A67-32931
- Algorithms for dichotomous representation of macrocircuits, considering computer programs and establishment of flow graphs 18 p3005 A67-33498
- Systems thinking and systems management in rocket motor manufacture 18 p3111 A67-33638
- Northrop program for v/STOL aircraft including systems studies, propulsion, aerodynamics, flight control technology, performance characteristics and operation and testing northrop program for V/STOL aircraft including 18 p2987 A67-34708
- Fault tree analysis concept development for predicting possible undetected safety hazards within complex missile systems 19 p3331 A67-34827
- Planetary quarantine problem for Martian survival of microorganisms investigated, using systems analysis 19 p3180 A67-35274
- Systems approach combining human experience and logic with computer technology to implement navigation management function 19 p3254 A67-35313
- Convolution technique applied to time domain to evaluate system capability 19 p3186 A67-35326
- Identification problem solution by gradient and Newtonian methods, using algorithm simplified by sensitivity function 19 p3205 A67-35914
- Variational problem in optimal interaction systems with control constraints solved by dynamic programming and Pontryagin principle applications 20 p3407 A67-36440
- Data reduction system noting magnetic tape data collection, data transfer, random data analyzer, system analysis with transfer function analysis, etc 20 p3442 A67-36460
- Computer simulation model for Saturn V launch vehicle system analysis 20 p3414 A67-36536
- Extremal systems having auto-oscillating optimizers and controlled plants, investigating performance improvement by complex modification of input signal 20 p3409 A67-37110
- Nonlinear automatic control systems characteristics analyzed for various possible error accumulations 20 p3412 A67-37382
- Equivalent quadrupoles for analyzing ultrasonic systems using piezotransducer disks operating at any frequency 20 p3401 A67-37454
- Systems analysis applied to identification of Saturn V launch vehicle support system requirements and establishment of baseline logic for vehicle prelaunch processing simulation and systems optimization [AIAA PAPER 67-248] 21 p3607 A67-37806
- Analytical methods for control systems applied to engine governor systems 21 p3602 A67-38129
- System effectiveness analysis with particular attention to availability, concepts and sample results 21 p3734 A67-38184
- Digital frequency synthesizers analysis and synthesis, considering clocked-pulse and sine-wave systems to obtain guidelines for DFS system designs 21 p3601 A67-38974
- Motion equation derivation permitting analysis of gyrosystems mounted on fixed or moving plants, determining instrumental errors 22 p3795 A67-39230
- Complex technical systems servicing, considering operation cost as optimization criterion 22 p3812 A67-39746
- Cost Analysis Model - Parametric /CAMP/ computer method of estimating hardware and logistics life cycle costs for air vehicles in design stage 23 p4085 A67-40589
- Spacecraft equipment in-space maintainability design criteria 23 p4070 A67-40591
- Distributive systems interaction between feedback and sensitivity noting parameter variations effects on external characteristics 23 p3983 A67-40644
- Coates flow graph gain formula modification by introducing loop-set and two-loop-set for linear systems analysis 23 p3984 A67-40649
- Analysis of system described by heat equation where disturbance propagates with infinite speed as function of time 23 p4024 A67-41086
- Chemical dynamic hydraulic power unit /HPU/ performance, weight and volume efficiencies, noting applications to solid and liquid propellants 24 p4107 A67-42531
- Synthesis of self-adaptive systems with variable structure, obtaining relationships between systems dynamics and characteristics of logical control law 24 p4137 A67-42699
- Mathematical model to aid in determination of need for technological advances in transportation [AIAA PAPER 67-799] 24 p4258 A67-42960
- Advanced systems planning with limited funds in terms of payoff from advancing technology through R and D [AIAA PAPER 67-811] 24 p4259 A67-42967
- Commuter airline planning using systems analysis to examine technical, managerial, legal and economic aspects [AIAA PAPER 67-843] 24 p4259 A67-42981
- Numerical procedure for structural systems analysis, discussing computer application to hydrodynamic, electric, magnetic, thermodynamic, elastostatic and elastodynamic problems [AIAA PAPER 67-955] 24 p4127 A67-43038

SYSTEMS DESIGN

- Changing environmental condition effects on spacecraft structure from launch through orbit to entry and recovery [SAE PAPER 660680] 01 p0154 A67-10584
- Fluid power support equipment for space vehicles outside earth atmosphere, based on earth environment effect on various systems [SAE PAPER 660708] 01 p0013 A67-10600
- Administrative considerations in systems effectiveness programs [SAE PAPER 660731] 01 p0170 A67-10631

Linear optimal control techniques used as synthesis tool in designing control system for Short Range Station Keeping /SRSK/ task of assault helicopter, noting closed loop dynamics 01 p0111 A67-11201

Functional analysis method application to reliability testing of Polaris missile 01 p0155 A67-11346

Reliable electronic design by suppression of adverse interactions among system levels 01 p0083 A67-11348

Inaccurate estimate effect on national budgets when evaluating systems efficiency 01 p0170 A67-11349

Language and system design of numerical analysis problem solving system /NAPSS/ 02 p0206 A67-11803

Data system requirements for large space vehicles and flexible telemetry system design for all stages of Saturn IB and V vehicles 02 p0196 A67-12000

Integrated circuit design of CLEM functional electronic block /FEB/ breadboards 02 p0219 A67-12109

Ground-Air-Ground /G/A/G/ communication channels analyzed in air traffic control 02 p0263 A67-12125

Triplex flight control system for VTOL aircraft noting new servomotor, simple mechanical construction and increased reliability 02 p0264 A67-12206

Requirements for radiation detection and measuring systems in aerospace environment, considering safety, design, circuit techniques, etc 02 p0220 A67-12208

Dielectrophoretic propellant orientation systems design, noting electrode requirements and avoidance of electrohydrodynamic instabilities [AIAA PAPER 66-922] 02 p0301 A67-12275

Voyager spacecraft guidance and control system analysis, examining systems design requirements, problems of redundancy implementation for critical functions and gyro system 02 p0265 A67-12381

Line scan TV for earth observation satellites noting camera design, coverage, systems effectiveness and performance results 02 p0335 A67-12398

Pattern recognition, property filtering and lunar feature data experiments coupled with Tiros cloud photographs demonstrate preprocessing for systems design [SMPT PREPRINT 100-13] 03 p0376 A67-13805

Telemetry design factors, discussing interference problems, antenna design, oscillator stability, preamplifiers, etc 03 p0372 A67-14120

Systems application in orbital launch operations [AIAA PAPER 66-908] 03 p0519 A67-14132

Linear optimal control via root square locus to design simple effective structural bending control for four XB-70 coupled longitudinal bending modes [AIAA PAPER 66-970] 03 p0381 A67-14142

Vibration shielding and shock absorbing systems design noting control function 03 p0530 A67-14180

Computer aided circuit design, synthesis, analysis, optimization and fabrication 03 p0376 A67-14276

Signal design and principle of vernier FM radar system to measure surface characteristics of small target at long distance and range 04 p0570 A67-14877

Numerical solution of Wiener-Hopf equation in statistical identification of linear dynamic plant 04 p0644 A67-14903

Group dynamics approach to resistance or counterpart of planning, conversion and management of automatic data processing systems design [ASME PAPER 66-WA/MBT-10] 04 p0740 A67-15334

Flexibility required to establish systems facility necessary to support Agena vehicle during development, testing and activation phases 04 p0600 A67-15781

Synthesis problem of optimum dynamic characteristics of multivariate linear control systems with random input signals 05 p0781 A67-16252

Construction of functional converter with several inputs 05 p0782 A67-16322

Book on applied microelectronics for system and subsystem designer 05 p0775 A67-17035

Integrated plan for reliability

demonstration through safety margin testing 05 p0813 A67-17253

Mechanical design and packaging of transceiver mounted in spacesuit helmet for intercommunication among astronauts and space vehicles 05 p0779 A67-17466

Packaging failures in reentry/recoverable aerospace equipment due to design deficiencies in parts, materials and/or processes associated with physical hardware 05 p0779 A67-17468

Data processing and control by spaceborne computer on instrumentation satellite used for analyzing space scientific properties, noting factors influencing system design 05 p0768 A67-17516

Applications of computer generated displays, technologies and systems design in man-machine interaction 05 p0769 A67-17520

System design analysis of laser methods of deep space communication, examining local heterodyne system /LHS/, direct detection system /DDS/ and transmitted reference system 06 p0957 A67-17635

Parametric analysis, penalty-effectiveness tradeoff and system selection for communications satellites, using block digital computer synthesis with subroutines for operational requirements [AIAA PAPER 66-330] 06 p0960 A67-17693

Hypothetical control system with 30 db/decade attenuation characteristic and constant phase margin of 45 degrees, presenting phase angle stabilization technique that improves actual systems 06 p0977 A67-18416

Megawatt ion-propulsion power conditioning system design for manned interplanetary missions, noting payload-mass ratio problems, advantages, etc [AIAA PAPER 67-52] 06 p1075 A67-18449

Digital simulation program for systems design of long-duration space station of MORL type [AIAA PAPER 67-208] 06 p0981 A67-18512

Optimal parameter problem of controlled dynamic systems, considering antagonism between designer and nature, applying results to space flight mechanics 06 p1088 A67-18616

Flexibility and rigidity requirements imposed on vibration damping systems of optimized precision devices 06 p1106 A67-18618

Design procedure for meeting step-input specifications in piecewise single-valued nonlinear multivariate control system design 06 p0978 A67-18720

Ion extractor system for electrostatic thrusters designed, using salient features of digital computer and electrolytic tank analog methods 06 p1075 A67-18877

Reliability in improving program quality and design decisions as in planetary exploration program 07 p1259 A67-19617

Optimized equipment systems design studies for handling and transportation of large solid fuel rocket motors [AIAA PAPER 67-266] 07 p1164 A67-20047

Test procedure for direct use of digital computer, noting utilization of software simulation technique and various applications [AIAA PAPER 67-235] 07 p1149 A67-20058

Model reference control systems design using Liapunov synthesis technique 07 p1162 A67-20203

Components and design improvement for FM and AM fluidic circuits 08 p1282 A67-20469

Adaptable large scale integrated military and space systems, discussing microelectronic circuit, logistics and dynamic redundancy 08 p1311 A67-20665

Millimeter wave satellite communications, considering propagation, orbital and system design parameters, antenna pointing and equipment 08 p1292 A67-20671

System design decisions through static and rotating magnetic memories reliability as applied to command and control systems 08 p1299 A67-20685

Information processing requirements for command systems, using particular form of simulation of system information 08 p1299 A67-20686

Dynamic programming for control system synthesis, noting invariant embedding and optimality principle use in optimum design problems 08 p1312 A67-20752

Management of engineering changes in manufacturing processes to prevent design or systems deficiencies resulting from poor control of changes 08 p1430 A67-21049

Fluidic system design including coded tape valves, vibrating reed frequency sensor, flow control, pneumatic switches, etc 08 p1286 A67-21053

Book on modern analytical design of instrument servomechanism noting computer programming, optimization, amplifier saturation, gear stiffness, etc 08 p1332 A67-21171

Program for satellite supported air traffic control 09 p1526 A67-21679

Design analysis for vacuum systems using diffusion pumps and getter ion pump, comparing parallel and series pumping 09 p1503 A67-22113

Hydraulic system of Boeing 737 jet transport, noting flight safety and system reliability throughout design 09 p1444 A67-22129

Five hundred kw traveling wave tube for X-band, considering design and matching of clover leaf structure and higher order mode spectrum 09 p1478 A67-22255

Survey and bibliography of works on optimum control system design and statistical signal descriptions 09 p1483 A67-22386

Adaptation scheme applied to pitch axis control system of supersonic aircraft, using stability analysis for system design 09 p1440 A67-22387

Frequency sharing and compatibility of satellite and terrestrial radio relay systems design, discussing interference effects 09 p1464 A67-22411

Air traffic control systems engineering and design - Conference, London, March 1967 09 p1527 A67-22626

Secondary surveillance radar system design, discussing interrogator interference, decoding and display systems 09 p1530 A67-22648

Flexible flight plan processing system with high continuity of service, using differing degrees of redundancy and having comprehensive system monitoring and control facilities 09 p1531 A67-22656

Integrated circuit technology for microwave equipment including guidelines and system design 10 p1610 A67-22973

Qualitative vibration data reduction techniques for application to design problems, noting examples involving power spectra and probability-density functions 10 p1680 A67-23315

Design equations and computer calculated curves to achieve varactor-tuned octave bandwidth transistor oscillators by using transmission line 10 p1613 A67-23412

Advanced structures and materials in future launch vehicles evaluated by design synthesis technique for component weight reduction, equivalent payload gained and cost ratio 10 p1723 A67-23699

System design of Voyager-class Mars Probe/Lander, considering selections of entry aeroshell, landed capsule and descent and postimpact instrumentation 10 p1714 A67-23756

Sterilization environment effects on structural systems design for interplanetary spacecraft 10 p1714 A67-23758

IBM System/360 Model 91 systems design using decomposition algorithm and three-cycle multiplication 11 p1755 A67-23948

IBM System/360 Model 91 machine organization alleviating disparity between storage time and circuit speed 11 p1755 A67-23949

Floating point execution unit of IBM System/360 Model 91, emphasizing design of instruction oriented units to reveal techniques employed to match burst instruction rate of one instruction per cycle 11 p1755 A67-23951

IBM System/360 Model 91 storage system design concepts 11 p1755 A67-23952

Terrain following pulsed radar system without continuous scanning noting computer simulation, antenna and pitch control 11 p1752 A67-24259

Axial lead package and stack design of batch fabricated matrices to speed integrated circuit assembly 11 p1760 A67-24260

Systematic design of matrix network, consisting of hybrids with phase delays in

interconnecting lines, used for antenna beam steering 11 p1763 A67-24300

Design, tests, operation and limitations of Apollo man-rated environmental control system simulation 11 p1748 A67-24340

Synthetic target scenes generation technique by general purpose digital computer for early analytical evaluation of sensor concepts 11 p1791 A67-24456

Soviet book on magnetic switching elements in radio electronics covering magnetic materials properties with rectangular hysteresis, shift registers, logic circuits, etc 11 p1765 A67-24515

Small size cylindrical gear reduction system design for servomotors of synchro systems in electronic equipment 11 p1745 A67-24553

Automatic technique of root location and determination of nth order polynomial equation using simple linear computing elements 11 p1756 A67-24639

Equation for solid state differential amplifier-circuit configuration effect on overall system accuracy and performance 11 p1768 A67-24823

Differential thermocouple device design for temperature measurements from 300 to 450 degrees K 11 p1793 A67-24886

Optimum distributed parameter system described by N-dimensional wave equation with unconstrained boundary control function 11 p1770 A67-24889

Optimum control integral criterion function for class of distributed parameter systems subject to control signal saturation 11 p1770 A67-24890

State space methods approach to model referenced adaptive control systems design using differential equations 11 p1771 A67-24894

Clean room techniques for Apollo/Saturn Instrument Unit, noting that environmental and guidance systems parts must be supercleaned to qualify for man-rated space vehicle 11 p1773 A67-24938

Statistical analysis of optimum control system design by parameter adjustment, finding systems transfer function through Wiener-Hopf integral 11 p1772 A67-25082

Interconnecting techniques for modules contained by printed circuit boards, noting usage of pin sockets and effect on maintainability and reliability 12 p1910 A67-25266

Modular xenon solar simulator for large area solar simulation, discussing source, transfer optical system and Cassegrain module, including fill-in optics 12 p1925 A67-25735

SST air inlet control system, considering maintainability, impact on cockpit procedures and component reliability effect on dispatch reliability [SAE PAPER 870325] 12 p1895 A67-25869

Evaluation facility for rotor containment/control devices [SAE PAPER 870332] 12 p1925 A67-25873

Shutter type thermal control system design for Nimbus spacecraft [AIAA PAPER 87-309] 12 p2012 A67-26024

Soviet book on pulsed self-adjusting and extremal automatic control systems covering theory and practice 13 p2086 A67-26459

Theoretical design of equivalent mechanical system naturally matched to self-oscillating system 13 p2216 A67-26626

Satellite Telecommunications with Automatic Routing /STAR/ system composition and operation, detailing signal relaying procedure 13 p2067 A67-26717

Lossless gyrator transistor realization using parallel connected positive and negative amplifiers in reverse direction 13 p2078 A67-26789

Thermal design of molten carbonate fuel cells using transpiration heating for reducing heat loss and control of temperature 13 p2055 A67-26842

Passive reactive circuit conversion into circuit that shapes radio pulse with rectangular envelope 13 p2069 A67-27042

Dynamical equations for optimal nonlinear filtering and representation of conditional expectation as solution to stochastic differential equation 13 p2146 A67-27094

Rectangular pulse thyatron-type generator design and operational principles 13 p2081 A67-27276

Optimal suspension systems synthesis,

discussing dynamic programming theory 13 p2159 A67-27300

Systems approach as systematic investigation of research, engineering and management activities for technological or sociological gain 13 p2231 A67-27513

Solid state technology limitation, discussing obsolescence within framework of digital application 13 p2183 A67-27561

Medical factors involving ATC information displays 13 p2064 A67-27564

Project NERO /near earth rescue and operations/ design study of MIT students as part of advanced space systems engineering course 13 p2214 A67-27700

Integrated circuit interconnection system design exemplified by 920 M digital computer 14 p2274 A67-28025

Highly adaptive phase lock coherent receiving system fulfilling requirements of data and Doppler tracking receivers 14 p2271 A67-28691

Block coded frequency multiplexed PM communication system design and performance, considering simplification, cost and weight 14 p2271 A67-28694

Cartridge-actuated thruster system design for jettisoning Apollo spacecraft heat shield for recovery system deployment [ASME PAPER 87-DE-34] 14 p2394 A67-28875

Design principles for air-cushion vehicles, noting possible application to aircraft landing gear [ASME PAPER 87-DE-61] 14 p2246 A67-28884

Wideband solar-burst spectrum analyzer noting antenna design and operation 14 p2382 A67-28966

Hover augmentation system reducing VTOL pilot task in maintaining position by providing damping signals for automatic flight modes with accurate path control 14 p2246 A67-29082

ONERA hot-shot wind tunnel flow stability and homogeneity and measurement of plasma electromagnetic field, skin friction, etc [ONERA-TP-447] 15 p2465 A67-29377

Concorde automatic flight control system noting autostabilization, autopilot, electric trim, autothrottle, etc 15 p2419 A67-29508

Flight recorder system designed to satisfy present and future mandatory requirements in accident recording and to provide economic solution to limited maintenance recording 15 p2487 A67-29510

Apportioning system reliability requirements to various system components, using generalized failure mode and effects analysis for each equipment within system 15 p2492 A67-29605

High resolution CRT for system designers to scan film or record photosensitive materials 15 p2447 A67-29734

CRT design factors for optimum tube design for display systems 15 p2447 A67-29735

Hot-water rocket design by dimensionless method, noting GRILLO rockets 15 p2567 A67-29840

Effect of payload weight, density and type on performance and design of reusable launch systems 15 p2568 A67-29841

French concept for aerospace transporter capable of horizontal takeoff from existing major airstrips 15 p2568 A67-29842

British reusable booster concept

MUSTARD /multiunit space transport and recovery device/ using rocket-propelled VTO lifting bodies, noting feasibility and development cost 15 p2568 A67-29843

Digital cardiometer design noting binary counter, clock, operation cycle, etc 15 p2432 A67-29921

System requirements effect on ballistic and hardware design of cast double-base solid propellant rocket motors 15 p2548 A67-30000

Liquid spring design characteristics noting fluid characteristics, precharge fluid pressure, friction, efficiency, gland configuration and application requirements 15 p2494 A67-30097

Onboard data systems selection and design and relation to ground networks [AAS PAPER 87-54] 15 p2440 A67-30118

Parameter estimation in automatic control systems using statistical techniques such as likelihood, Markov and least square estimates 15 p2460 A67-30311

Aircraft wheel and brake designs

especially for 63 Series of DC-8 noting materials, properties, construction, etc [AIAA PAPER 87-404] 15 p2421 A67-30371

Automatic all-weather landing system design having integration of autopilot and flight director [AIAA PAPER 87-406] 15 p2516 A67-30373

DC-9 environmental control design and first year service experiences [AIAA PAPER 87-407] 15 p2423 A67-30374

Magnetic device design optimization for satellite attitude control, noting equations and charts 15 p2572 A67-30385

Frequency shifting technique using auxiliary coil to produce magnetic field for masers in high power radar applications 15 p2439 A67-30392

System-effectiveness concept for turbine and piston engine development 15 p2584 A67-30402

Probability and prediction techniques related to maintainability discussed with application to early design, time constraints and maintenance goals 16 p2681 A67-30439

Design disclosure format /DDF/ linking program managers, review teams and contractors 16 p2781 A67-30443

System design of automated laboratory and associated entry vehicle for unmanned Martian exploration 16 p2653 A67-30628

Extravehicular space maneuvering units, manned and unmanned, in satellite laboratory systems, describing space flight requirements and systems configuration 16 p2615 A67-30631

Thermodynamic system design in Biosatellite program noting mission and spacecraft 16 p2757 A67-30632

System design for maximum reliability when gross weight of system is assigned or minimum weight when system reliability is designated 16 p2681 A67-30635

Satellite telemetry system transmitter optimization, noting error probability criterion, average power constraint, etc 16 p2622 A67-30693

Space systems design course for fourth- and fifth-year students at MIT noting departmental, industrial and governmental cooperation 16 p2781 A67-30784

Space systems engineering course, noting unmanned Mars exploration vehicle project and world weather system project 16 p2782 A67-30785

Trace /tape controlled recording automatic checkout equipment/ system design to accommodate aircraft ground support task 16 p2635 A67-30834

Design and operation of orbital space station, determining orbit altitude, payload weight, tracking and communication system support requirements, recovery operations, etc 16 p2761 A67-30961

Sign-discriminating field mill design using one rotor and one stator 16 p2671 A67-30972

Design and construction principles of radio telemetry recording systems for gasdynamic observations in ballistic testing 16 p2624 A67-31124

Design for light-gas gun with light piston by successive parameter computation of various parts 16 p2655 A67-31125

Book on communication principles emphasizing digital radio communication system design, frequency and binary phase shift keying, filtering, fading, etc 16 p2624 A67-31254

Method to extend operation range of FM altimeters, with block diagram of proposed system 16 p2676 A67-31274

Design guides for efficiency, bandwidth and resonant frequency derived from slot antenna analysis, using variational methods 16 p2638 A67-31334

Satellite relay to provide communication paths for aircraft-ground communication over ocean, considering system design for ATC using reflex repeater 16 p2629 A67-31530

Design schemes for magnetic systems of vortex MGD generators with external and internal winding 16 p2609 A67-31585

Quantization error effect for digital control system design 16 p2646 A67-31637

Optimal feedback control system design to account for differences between physical system and mathematical model in terms of parameters 16 p2647 A67-31641

Lapunov-derived fixed gain flight control system design to fulfil response requirements over wide range of parametric

variations 16 p2763 A67-31644
 Synthesis and design of on-line self-organizing control of multiple goal, multiple actuator systems 16 p2648 A67-31654
 Adaptation technique for on-line steady-state optimizing control using updated control algorithm 16 p2648 A67-31655
 Analog computer use in design of automatic steering control system of Apollo station ships for precision geographical track-keeping 16 p2701 A67-31659
 Self-optimizing, type-one system design discussing steady state optimization problem 16 p2649 A67-31666
 Algebraic characterization of optimal singular control for autonomous linear plants, using explicit closed form representation of singular strip 16 p2649 A67-31669
 Sensitivity analysis application to nonlinear system modeling and compensation noting minimization procedure parameter determination and performance 16 p2650 A67-31674
 Modern control theory applied to digitally controlled tracking telescope design, emphasizing accuracy and response 16 p2629 A67-31688
 Attitude control for orbiting astronomical observatories, noting system design and performance characteristics 16 p2763 A67-31689
 Optimum speed capability evaluation of aerial weapons system in relation to value and cost, noting aircraft performance characteristics 16 p2783 A67-31830
 Effective engine protection system for CH-54A Flying Crane helicopter, consisting of an engine-inlet air-particle separator, noting Vietnam performance [AHS PAPER 117] 16 p2737 A67-31833
 Pneumatic power for attitude control of long-life orbiting satellite, considering parameters, mission objectives, etc 17 p2801 A67-31983
 Permanent joints for Agena pressure systems, discussing retention of pressurized gases in connector tubing system 17 p2801 A67-31984
 C-5A landing gear, discussing design and evolution of requirements such as kneeling, steering, weight and flotation 17 p2794 A67-31988
 Evolution and future objectives of ejection-seat escape systems design, noting characteristics and deficiencies in conventional ejection seats 17 p2795 A67-32002
 Vibro-acoustic test system for simulation of Saturn V dynamic launch environment on major space vehicle structures, discussing design and operation characteristics 17 p2832 A67-32005
 Cryogenic fluid storage subsystems for Gemini program, noting more advanced designs for Apollo, Lunar Module, Biosatellite, Manned Orbiting Laboratory, etc 17 p2954 A67-32013
 Nonuniform error quantization effects on stability of feedback control systems, investigating limit cycles existence and giving optimum quantizer design procedure 17 p2829 A67-32016
 Soviet book on SHF radio receivers covering theoretical and engineering aspects of component design, control, signal detection, etc 17 p2822 A67-32020
 Interconnecting fluid elements and hardware components for construction of complex systems 17 p2802 A67-32229
 System for information transmission over optical path using microwave subcarrier, noting satisfactory SNR 17 p2812 A67-32237
 Operation and design principles of 200 MHz counter/shift register, noting integrated circuit fabrication techniques 17 p2824 A67-32306
 High-intensity and high-voltage current switching devices, noting strong pulsed magnetic field production 17 p2803 A67-32350
 ELDO-PAS program principles, objectives, ground stages, orbital injection, etc 17 p2955 A67-32399
 Digital simulation role in advanced avionics system development such as air to air/air to ground weapon delivery, noting advantages, performance, etc 17 p2833 A67-32492
 VLF transmitter design criteria and characteristics for global time and navigation signal network 17 p2824 A67-32494

IBM CP-2 militarized digital computer noting design, maintainability and performance 17 p2820 A67-32500
 Organizational techniques and trade-offs for low power operation in spaceborne data processing systems 17 p2820 A67-32503
 Solid state switching applied to aircraft electric systems noting design, performance and contactless switching concept 17 p2825 A67-32513
 High power frequency multiplication using beam lead varactors in arrays noting construction, technique and conversion loss 17 p2826 A67-32623
 Synthesis of mechanical system with variator having drive unit in steady or steadily increasing motion, deriving and solving dynamic equations 17 p2885 A67-32967
 Fuel control system of GE4 engine for supersonic transport noting main and augmentation fuel and control subsystems [SAE PAPER 870326] 17 p2929 A67-32982
 Data selection, collecting and processing for automatic performance recording and monitoring of aircraft gas turbine engine, considering hardware and software [SAE PAPER 870360] 17 p2835 A67-32999
 Materials engineering for electronic hardware, discussing design, development and construction, including tables on metallic finishes, coatings for printed wiring, etc 17 p2865 A67-33047
 East-west parabolic reflector array for design of high resolution multiple element interferometer for solar noise observations 17 p2864 A67-33402
 Large orbiting astronomical telescope design, discussing minimum waver, high resolution image recording, compactness and thermal warpage 18 p3043 A67-33493
 Crystals for UV and IR optics, discussing solubility, hardness, melting, expansion coefficients and design factors 18 p3078 A67-33565
 Design problems in IR optical systems including materials limitation, reflection losses, environmental requirements, etc 18 p3078 A67-33566
 Reliability studies for optimization of aerospace systems and military engineering design and manufacture 18 p3053 A67-33637
 Design considerations for reliable microwave power packs noting redundancy, independent module system and intrinsic reliability 18 p3010 A67-33665
 Book on analysis and design of pneumatic systems covering nozzle flow, transfer functions, root locus, plenum chambers, servomotor, etc 18 p2988 A67-33754
 Construction of functional converter with several inputs 18 p3017 A67-33874
 Subsonic diffuser with vortex generator as integral design feature for supersonic transport aircraft inlet [AIAA PAPER 87-464] 18 p2983 A67-33935
 Descent engine for lunar module specifications and operational requirements covering throttling, firing duration, crushable nozzle skirt, etc [AIAA PAPER 87-521] 18 p3115 A67-33984
 Parallel plate transmission system for reflection, diffraction and transmission measurements at microwaves, noting design criteria 18 p3002 A67-34224
 Image motion compensation tracking study for earth reconnaissance from space, investigating computer and manual tracking modes, control dynamics and gain and magnification 18 p2993 A67-34337
 Operational system for handling and processing aerospace-system human-factors task data in government/contractor environment 18 p2994 A67-34343
 RF design of satellite communications ground stations, giving hardware data on receivers, transmitters, tracking systems, power amplifiers and reliability 18 p3003 A67-34349
 Control and measurement of temperatures of Mariner IV 18 p3052 A67-34514
 Design of large scale integrated MOS-FET devices for general logic circuit applications 18 p3014 A67-34554
 Microelectronic systems design problems and solutions, discussing system adaptability concept and influence on design methods and technology 18 p3015 A67-34561
 Structural reinforced plastic composite materials for cryogenic temperature application evaluated noting tensile, compression, shear, flexural and bearing

properties 18 p3070 A67-34577
 [ASTM PAPER 16]
 Solid state pulsed carrier IF-AGC system design for microwave receivers noting input network, video circuit, AGC loop gain, etc 18 p3016 A67-34597
 Alkaline-metal-plasma machine design, studying operating modes with electric probes 18 p3091 A67-34631
 Quantification for effective human performance implementation into system designs during conceptual, design and acquisition phases 18 p2994 A67-34655
 Factors degrading reliability in use phase, developing analysis method for determining optimum corrective measures 18 p3057 A67-34667
 Human engineering research to aid system designers to optimize mans role as control element in space systems 18 p2995 A67-34687
 Ground system design approach integrating reliability and maintainability with performance requirements, using Saturn V simulation as example 18 p3139 A67-34694
 Oxygen concentration system for aviator breathing 18 p2995 A67-34717
 Low thrust cold-gas reaction jets in vacuum studied for pulsed propulsive performance for use in spacecraft attitude control 18 p3310 A67-34805
 Strip transmission lines used for microwave circuits noting applications, design data, discontinuity information, etc 19 p3191 A67-34945
 Design of optimal waveforms for optimal estimation or prediction of state of linear dynamical system in presence of Markov and white noise 19 p3201 A67-34965
 Empirical formulas for optimal operation of extremal controllers, design data generation and cost index determination 19 p3201 A67-34992
 Microelectronics fabrication in terms of specific systems, discussing input and waste piping systems design, electrical distribution, exhaust, contamination control, etc 19 p3193 A67-35030
 Time-shared computer system design and application, noting memory, remote terminals, program debugging, etc 19 p3186 A67-35078
 Formula manipulation by computer, noting simplification, pattern matching, complex number handling, etc 19 p3187 A67-35079
 Programming system design for incremental data assimilation in open ended man-computer information systems 19 p3187 A67-35080
 SST flight control system electronic and hydraulic systems, discussing system design, components, reliability and test programs [AIAA PAPER 87-570] 19 p3174 A67-35086
 Linear optimal control technique for flexible-booster control system design, showing drift minimum model with matrix transformations for closed-loop dynamics 19 p3336 A67-35088
 System/semiconductor interface with complex integrated circuits, examining different designs 19 p3199 A67-36055
 Graphical display technique for complex curve display, discussing system components, experimental results and relevant software 19 p3188 A67-36059
 Hybrid simulation for analysis and design of nuclear reactors feedback control systems 19 p3189 A67-36068
 Book on star trackers and systems design including technology, use for navigation and guidance, reference frames, error sources, atmospheric effects, etc 20 p3481 A67-36136
 Sulfur hexafluoride gas handling system for potential drop particle accelerator, considering design, fabrication and performance 20 p3413 A67-36181
 Analog and digital long range automatic radar tracking systems design characteristics and implementation by solid state components 20 p3379 A67-36244
 Aircraft AC electrical systems using changeover contactors and rapid fault clearance, discussing reliability and maintenance 20 p3362 A67-36316
 Design, construction and operation of multichannel photoelectric spectrometer, using Fabry-Perot etalon and axicon 20 p3439 A67-36353
 Apollo Manned Spacecraft Program systems design requirements, emphasizing instrumentation system and Phase I

- spacecraft 20 p3443 A67-36469
- Semipermanent optical memory design using laser light source, acoustic light deflector and hologram array as information storage elements for address selection 20 p3390 A67-36511
- Satellite retrieval system called Space Bola, employing passive/active grappling units depending on target vehicle dynamic characteristics 20 p3532 A67-36556
- Real time telemetry data system for Air Force Eastern Test Range 20 p3381 A67-36614
- Book on functional mechanisms for engineering design, presenting kinematic characteristics of output motion, planar linkage and spatial cycloidal crank and flexural mechanisms 20 p3454 A67-36766
- Power supply family synthesized from series of modules evaluated for packaging design, treating module interconnection methods and optimum thermal characteristics 20 p3399 A67-36926
- Reflectometer based on goniometer design employing beam reversal and beam splitter for measuring exit beam intensity 20 p3448 A67-36955
- Automatic test computer programming problems, discussing system planning, documentation, personnel, system compromises, etc 20 p3391 A67-36972
- Microminiaturized systems for fault analysis and indication design and application to built-in test equipment 20 p3449 A67-36983
- Onboard Checkout System /OCS/ design, considering system selection techniques, design development, equipment, etc, with orientation on OCS design by NASA/MSC 20 p3417 A67-36988
- Time optimal control problem solved by calculating boundary condition changes with system structure 20 p3409 A67-37222
- Concorde fire protection system based on Firewire Triple FD equipment, discussing extinguishant toxicity, low vapor pressure, etc 20 p3364 A67-37245
- Design and performance of frequency multiplexed phase-modulated communication systems 20 p3385 A67-37353
- Nonlinear fluid mechanical systems design using numerical least squares method in fitting second order differential equation to straight line approximation of state variable 20 p3366 A67-37368
- Fluid control system design by third order linear differential equation with transient response, showing relationship to frequency response 20 p3368 A67-37370
- Mach-Zehnder-Rozhdestvenskii interferometer design for training studies of supersonic and subsonic gas flows and anomalous dispersion 20 p3452 A67-37556
- Receiver performance related to signal and interference conditions for AM voice communication system analyzed for use in systems design 20 p3387 A67-37637
- Receiver mixer design characteristics effect on prediction of spurious response levels 20 p3405 A67-37648
- Synthesis procedure for linear automatic feedback control systems, examining time-domain response 20 p3413 A67-37679
- Soviet book on electronic and semiconductor devices of servosystems, examining theoretical principles, computational methods, design principles, analog and digital computers, etc 20 p3406 A67-37700
- Magnetic annular arc /MAARC/ driven shock tube design, construction and performance, stressing radiation loss prevention 21 p3806 A67-37774
- Lubrication and wear - Conference, London, September 1967, Session 6, Synthesis 21 p3633 A67-38144
- Sequential circuits design possessing distinguishing sequences and with very short fault detection experiments 21 p3588 A67-38183
- Approximate method for design of FM systems using variable capacitance varactor diodes, noting time varying differential equation 21 p3593 A67-38234
- Book on optimal adaptive control systems, detailing material on game theory for use in control system design 21 p3603 A67-38266
- Design and construction of power supply without hookup cables for manned lunar vehicle 21 p3571 A67-38337
- Packaging design of modular power supplies for airborne computers 21 p3596 A67-38341
- Thick film design considerations covering material and micropart selection, circuit cost, reliability, substrate size and delivery schedule 21 p3596 A67-38346
- Book on analysis and design of digital and linear integrated circuits covering transistor models, system parameters, etc 21 p3597 A67-38500
- Transient performance of delay equalized low pass filters studied for optimal response 21 p3582 A67-38529
- Pressure gauge using acoustic techniques designed for gas pressure measurements, discussing limitations, sensitivity and experimental results 21 p3630 A67-38767
- Mathematical programming problem for automating design of optimum thin walled systems, noting stress-strain state factors 21 p3728 A67-38903
- Digital frequency synthesizers analysis and synthesis, considering clocked-pulse and sine-wave systems to obtain guidelines for DFS system designs 21 p3601 A67-38974
- Lunar Orbiter flight programmer, electronic design, development, application and performance 21 p3601 A67-39062
- Perturbation scheme for linear system performance determination based on component performance 21 p3654 A67-39063
- Essential additional operator, essential transformed system and cross correlation function methods for self-adjusting circuit design, considering sign of gradient component 21 p3604 A67-39110
- Invariance principle proposed for controller analytical design for nonlinear invariant systems by reducing problem to quasi-linear problem 21 p3604 A67-39111
- Man-machine design for Apollo spacecraft navigation, guidance and control systems 22 p3830 A67-39180
- Aircraft skin friction balance components for hostile environments noting system design 22 p3795 A67-39188
- Magnus version of first harmonic approximation method for nonlinear systems engineering, using analog computer simulation for accuracy 22 p3776 A67-39327
- Microminiaturization problems associated with design and preparation of solid state Si microdiode matrices 22 p3769 A67-39580
- Low altitude atmospheric turbulence analysis methods 22 p3828 A67-39665
- Nonstationary second order linear differential equation for near time optimal space vehicle guidance system design solved by linear transform 22 p3832 A67-39966
- Gemini program engineering aspects compared to Gemini/Mercury, discussing basic design rules adopted and Apollo Applications Project objectives 22 p3904 A67-40064
- Radome antenna systems design utilizing dielectric structure applicable in aircraft, spacecraft and missile systems 22 p3775 A67-40468
- Logistics in 1970s - Conference, Washington, D.C., September 1967 23 p4084 A67-40579
- Maintainability problems analyzed noting Apollo/ Saturn program 23 p4070 A67-40581
- Systems planning for transportation of large launch vehicles and spacecraft noting land transporter and seagoing barge used for Apollo booster 23 p4070 A67-40584
- Logistics resource development and approaches to life cycle economics in 1970s 23 p4085 A67-40587
- Distribution theory in control system design, discussing sensitivity improvement by feedback for application to time invariant systems 23 p3984 A67-40755
- Basic displacement transducers, electromagnetic transducer theory and design 23 p4008 A67-41422
- Flight performance and power system design of Mariner IV Mars probe 23 p3939 A67-41509
- Noninteraction and deadbeat response in linear sampled data multivariable systems synthesis by state difference equation 24 p4134 A67-42027
- Digital controller design for tracking telescope, discussing tracking accuracy and response time 24 p4154 A67-42176
- Design parameters and performance characteristics for overdriven varactor upper sideband upconverter 24 p4131 A67-42446
- NASA test program to evaluate performance and design point characteristics of 3-kw closed recuperated Brayton cycle power conversion system 24 p4102 A67-42486
- Heat pipe dynamics analyzed for thermionic converter heat pipe radiator design criteria, discussing working fluid selection 24 p4104 A67-42503
- Large long-life power supply system designed for earth orbiting spacecraft, discussing radioisotope interchangeability, controlled intact reentry, etc 24 p4184 A67-42505
- Solar cell array design techniques for temperature extremes induced by space environment, discussing orbital flight requirements 24 p4104 A67-42510
- Large area solar array design for photovoltaic system for manned space systems based on orbital perturbations and mechanical and thermal environment considerations 24 p4105 A67-42516
- Analysis of satellite power systems for maximum utilization of power 24 p4108 A67-42540
- Integrated thermoelectric SNAP-8 Rankine power system for manned lunar base missions, studying man-system interactions effect on design criteria 24 p4185 A67-42544
- Repetitive circuit arrays combined with multilayer interconnections using discretionary wiring to improve array yield 24 p4132 A67-42688
- Charge time determined as circuit constants function in designing linear detectors 24 p4158 A67-42716
- Alkali metal Rankine cycle space power system component and systems design 24 p4186 A67-42887
- Advanced radioisotope thermoelectric generator /RTG/ system designs employing SiGe direct radiating power conversion subsystems 24 p4110 A67-42899
- Manned space flight safety, discussing system design, operations planning, staffing, training and simulation [AIAA PAPER 67-824] 24 p4243 A67-42971
- Commercial earth orbital manned space station power system requirements, estimating operational and logistical costs for isotope and reactor designs [AIAA PAPER 67-879] 24 p4187 A67-42998
- Implementation of safety provisions in manned systems [AIAA PAPER 67-937] 24 p4096 A67-43027
- Computer-aided design of space systems, discussing design morphology and process [AIAA PAPER 67-956] 24 p4127 A67-43039
- SYSTEMS ENGINEERING
- Problems in fuel systems associated with chemical impurities such as sulfur and chlorine compounds, examining effects of particulate matter and free water [SAE PAPER 680714] 01 p0140 A67-10603
- DOD/NASA management practice program ensuring identification, communication and achievement of mission success requirement [SAE PAPER 680729] 01 p0170 A67-10629
- Overall system performance optimization for specified cost [SAE PAPER 680730] 01 p0170 A67-10630
- Reliability and maintainability requirements and electronic systems division /AFSC/ application 01 p0042 A67-11368
- System engineering techniques applied to analysis of spacecraft sterilization objectives and available technology 02 p0186 A67-11928
- Analytical, test and coordinative methods in reliability problems in aerospace systems 04 p0627 A67-14579
- Laboratory payload concept of automated laboratories for planetary exploration, noting systems engineering advantages 04 p0706 A67-15237
- Progress in control engineering, Volume 3, covering dynamic programming, adaptive control systems, sampled data systems, etc 08 p1312 A67-20751
- Management systems planning for control and information systems for Voyager project, with attention to work breakdown and scheduling [AAS PAPER 66-141] 08 p1429 A67-20966
- Management of engineering changes in manufacturing processes to prevent design or systems deficiencies resulting from poor control of changes 08 p1430 A67-21049
- Shortcomings in complex reentry system design caused by human

factors 09 p1456 A67-22290
 Air traffic control systems engineering and design - Conference, London, March 1967 09 p1527 A67-22626
 Project NERO /near earth rescue and operations/ design study of MIT students as part of advanced space systems engineering course 13 p2214 A67-27700
 Communication system engineering handbook covering system design, programming, modeling, switching, multiplexing, etc 14 p2269 A67-28508
 Systems approach to reliability, integrating cost and performance and demonstrating tradeoff decisions 15 p2448 A67-29800
 System engineering approach to commercial aircraft crew requirements [AIAA PAPER 67-399] 15 p2433 A67-30366
 Graphic information acquisition, processing and analysis noting requirements, application of computer, etc 16 p2781 A67-30636
 Computerized mathematical procedures application in advanced large-scale automated systems 16 p2834 A67-31568
 F-111 MK 2 avionics system evaluation and parameter tradeoff considerations 17 p2819 A67-32499
 AFSCM 375-5 as methodology for system engineering, discussing management, documentation, applications, development, operation, design, etc 18 p3161 A67-33494
 Systems engineering in computer-driven CRT displays for man-machine communication, emphasizing hardware-software tradeoffs and communication-transmission factors systems engineering in computer-driven CRT 18 p3005 A67-33499
 Control engineering in systems management applied to missile control and guidance 18 p3162 A67-33636
 Human performance relation research relationship with aerospace mission oriented simulation studies, discussing methodological resolution and limitation 18 p2994 A67-34341
 AH-56A /AAFSS/ safety engineering, failure effects method, Army role, etc 18 p2987 A67-34690
 System safety management/engineering procedures and techniques for safety requirements application 18 p3163 A67-34691
 Rapid Availability of Information and Data for Safety /RAIDS/ system as tool of system safety engineering 18 p3007 A67-34703
 Built-in tests /BIT/ for AN/AWG-10 Missile Control System 20 p3417 A67-36990
 Theoretical and experimental research methods for engineering reliability operations 23 p4010 A67-41320
 Shock testing to aid design analysis and for qualification and certification 23 p3987 A67-41414
 Solar cell power supply design to satisfy whole satellite, discussing power supply size and solar cell panel fabrication 23 p3939 A67-41508

T

T TAIL SURFACE

Deep-stall characteristics of T-tailed aircraft configurations and recovery procedures, noting parameters of pitch-up, angle of attack, etc [AIAA PAPER 66-13] 03 p0350 A67-12912

T-TAURI STAR

Lithium content of T Tauri stars shown to exceed ionization of Li in solar atmosphere 24 p4227 A67-42161

TABLE

SA INTERFERENCE FACTOR TABLE

SA MATHEMATICAL TABLE

Black ball radiation tables and radiative equilibrium temperatures

computation 05 p0838 A67-17277

Catalog tabulating 1600 comet tail orientation observations 14 p2386 A67-28481

Epoxy casting resins as structural material in electronic industry, with tables of various hardener characteristics, viscosities, epoxy equivalents, etc 15 p2508 A67-29683

Chronological table of artificial satellites launched during 1966 including lifetimes, weights, dimensions and orbital details 20 p3531 A67-36307

U.S.S.R. astronomical almanac for 1970 21 p3703 A67-38200

TACAN

S TACTICAL AIR NAVIGATION

/TACAN/

TACHOMETER

Tachometer measuring angular velocity from time of definite number of rotations, noting diagram of basic circuit 01 p0062 A67-10164

TACTICAL AIR NAVIGATION /TACAN/

TACAN off-track airborne navigation computer and suitable indicator provide nonradial straight course as aid to ATC 09 p1531 A67-22658

GaAs laser reflectance measurements of tactical landing terrain samples 17 p2858 A67-32483

TACTILE DISCRIMINATION

SA CUTANEOUS PERCEPTION
 Properties of favorable coding schemes, applying results to text transmission through auditory and tactile senses 12 p1907 A67-26081

TACTILE SENSATION

Temporary irritation by anti-g and change in vestibular motor reflex action under laboratory conditions 14 p2257 A67-28224

TAIL

SA AIRFRAME

Geomagnetic field disturbance due to earth passage through tail of Halley comet, 1910 II 02 p0236 A67-11654

Geomagnetic field disturbance due to earth passage through tail of Halley comet, 1910, II 16 p2865 A67-31069

TAIL ASSEMBLY

Spin conditions for aircraft with nose-and tail-heavy longitudinal moment 07 p1130 A67-20148

TAIL PLANE

Wing twist distortion effect on glider static longitudinal stability with stick fixed 18 p2986 A67-34373

TAIL SURFACE

S HORIZONTAL TAIL SURFACE

S T TAIL SURFACE

TAKEOFF AND LANDING

SA AIRCRAFT LANDING

Vertical takeoff technology effect on aircraft design noting flexibility, reliability, decreased takeoff distance, etc 04 p0550 A67-14410

Control data acquisition during takeoff and landing of VTOL type vehicles 05 p0841 A67-16535

Statistical analysis of heart rates of Navy carrier pilots during bombing attacks compared with those for launch and landing 09 p1455 A67-21718

Dust content of air flow created by piston engine Mi-1 and Mi-4 helicopters in landing and takeoff 11 p1744 A67-24530

Soft gravel and aerated concrete material of various sizes tested to safely decelerate aircraft overshooting runway during takeoff and landing 14 p2246 A67-28817

Landing gear for operating off rough terrain and unprepared airstrips in OV-10A Bronco aircraft for counter insurgency 17 p2794 A67-31989

Soviet book on aeronautical meteorology covering wind and cloud effects on takeoff, landing and supersonic flying in storms and jet stream layers 18 p3074 A67-33676

Navigation system for long range transport aircraft providing accurate and reliable fixing, discussing takeoff and landing 19 p3254 A67-35312

Aircraft tracking problems in airport approach zone solved using cameras, descriptive geometry and vector computations 21 p3568 A67-38809

Noise reduction in residential areas near landing strips using Tu-124 aircraft studied with suggested takeoff and landing piloting techniques 21 p3569 A67-38928

Parametric investigation of propulsion system effect on takeoff weight of VTOL subsonic ground combat aircraft 23 p3934 A67-41315

STOL and VTOL takeoff and landing areas, discussing urban and suburban air transportation and operational weather requirements [AIAA PAPER 67-795] 24 p4258 A67-42956

TAKEOFF SYSTEM

SA CATAPULT

Glider takeoff using tow winch, emphasizing flight path and aerodynamic loads and forces 24 p4093 A67-41917

TALOS MISSILE

Tactical checkout missile test installations for Terrier, Tartar and Talos missiles 20 p3416 A67-36971

TANDEM

Changes in length measured by tandem laser device investigating mirror separation modulation by piezoelectric materials 16 p2871 A67-30823

TANDEM-ROTOR HELICOPTER

Flight tests of two X-22A dual tandem rotatable ducted propeller V/STOL research aircraft 06 p0948 A67-18201

Rotorcraft technology developments and possible improvements by mid-1970s 11 p1744 A67-24589

Rotor blade airload and dynamic response of large tandem rotor helicopter measured, using computer programs 20 p3536 A67-36466

TANK

SA CONTAINER

SA CYLINDRICAL TANK

SA FUEL TANK

SA PROPELLANT TANK

SA SPHERICAL TANK

SA STORAGE TANK

Axisymmetric vibration modes of cylindrical-hemispherical membrane tank partly filled with liquid [AIAA PAPER 67-75] 06 p0986 A67-18273

TANK GEOMETRY

Structural design of hypersonic vehicle flight tank for liquid hydrogen fuel, discussing loading, material, support system, stress analysis, testing and analytical problems [SAE PAPER 660679] 01 p0161 A67-10583

Eigenvalues and eigenfunctions of free oscillations of viscous incompressible fluid in arbitrarily shaped vessel under gravitational field, asymptotically expressed 02 p0233 A67-11950

Electrolytic tank analog for magnetic field configurations in design of plasma containment device 02 p0279 A67-12693

Continuous nucleonic oil quantity gauging system requiring no tank penetrations 05 p0842 A67-16538

Shape and stability of liquid-gas interface in annular tank in force field determined by numerical integration of boundary value problem and eigenvalue [AIAA PAPER 66-425] 05 p0793 A67-17218

Fuel container design for space vehicles, discussing impact protection, reusability and long term cryogenic storage 13 p2212 A67-27218

Eigenvalues and eigenfunctions of free oscillations of viscous incompressible fluid in arbitrarily shaped vessel under gravitational field asymptotically expressed 17 p2841 A67-33267

Propellant dependent inert weight for any propellant combination or venting condition for Mars mission 22 p3902 A67-39942

TANTALUM

Dislocation structure in tantalum single crystals deformed in tension to various strains at 373 degrees K studied by transmission electron microscopy 01 p0092 A67-10057

Deformation in niobium and tantalum by wire drawing at room temperature, producing changes in shape and position of X-ray diffraction peak 01 p0095 A67-10686

Hydrogen diffusion in tantalum at temperature interval of 0 to 100 degrees C 01 p0102 A67-10941

Oxidation and ablation characteristics of tantalum in hyperthermal arc tunnel filled with oxygen-nitrogen mixtures 01 p0102 A67-11153

Electron density effect on transition temperature of superconductivity, considering tantalum 02 p0291 A67-11742

Oxygen impurity effect on recrystallization temperature of annealed and rolled tantalum 02 p0255 A67-11868

Hybrid thin film microelectronics circuitry, using tantalum films as basis for passive components 02 p0218 A67-12197

Kinetics of degassing of tantalum-nitrogen solid solutions by annealing in high vacuum at various high temperatures 04 p0637 A67-14906

Various combinations of preanneal and diffusion anneal conditions used in experiments for determining environmental effects on diffusion of Ta 182 in bcc titanium 04 p0637 A67-14937

Electron diffraction scanner structural analysis of Ta and Mo very thin film growth 04 p0677 A67-15101

Tantalum thin film integrated circuits

noting fabrication techniques, applications, cost and advantages 05 p0770 A67-16239

Tantalum interaction with nitrogen and air show retardation of grain growth 05 p0832 A67-17507

Steady states in annealing of niobium and tantalum in oxygen atmosphere, noting relation of pressure to temperature 07 p1210 A67-20110

Niobium and tantalum purification from interstitial impurities by high vacuum annealing, noting effect on electric resistivity 07 p1210 A67-20112

Flashed getters for production of ultrahigh vacuum, tantalum most promising based on residual gas analysis 08 p1354 A67-21496

Temperature dependence of thermal diffusivity of tantalum and niobium 11 p1804 A67-24035

Sputtered beta-tantalum thin films produced in two-chamber vacuum system with applied negative anode bias voltage 13 p2177 A67-27077

Mass spectrometry of background gases composition during sputtering of tantalum films in argon glow 13 p2178 A67-27078

Porous cesium ionizer with improved lifetime obtained by adding secondary tantalum to tungsten powder [AIAA PAPER 66-219] 14 p2376 A67-28124

Magnetic field effect on microwave surface impedance of superconducting tantalum measured in various temperature ranges via dielectric-resonator techniques 14 p2371 A67-28726

Internal friction of annealed and cold-worked niobium and tantalum wires containing oxygen and nitrogen measured, noting cold-work peaks in addition to Snoek peaks 15 p2503 A67-29748

Balanced broadband microwave transistor amplifiers using tantalum integrated circuitry 15 p2452 A67-29927

Thin-film and diffused passive component comparison, describing resistor and capacitor fabrication by using sputtered tantalum and inductors through nichrome/gold 16 p2640 A67-31528

Electrical and thermal conductivity and integral degree of blackness of tantalum at temperatures above 1000 degrees C 16 p2692 A67-31771

Surface morphological changes of tantalum single crystals during plastic deformation, studying orientation dependence of yield stress in tension and compression 19 p3245 A67-35727

Tantalum interaction with nitrogen and air show retardation of grain growth 21 p3644 A67-38035

Hydrogen diffusion in tantalum at temperature interval of zero to 100 degrees C 22 p3820 A67-39794

Hafnium-tantalum coated refractory metals investigated for use in high temperature rocket motors 22 p3821 A67-39891

TANTALUM ALLOY

Work function of solid solutions of tungsten with molybdenum and tantalum explained by surface adsorption effects 01 p0093 A67-10092

Oxidation test and mechanical property data to determine suitability of columbium and tantalum alloys as thermal protective materials for use in multicycle earth reentry vehicles [SAE PAPER 660660] 01 p0094 A67-10618

Line broadening due to cold working Ta-10 percent Re and W-20 percent Re studied by Fourier analysis, integral breadth measurements and variance analysis 02 p0256 A67-12701

Structure and certain properties of niobium-tantalum alloys containing tungsten and molybdenum show these alloying elements form continuous series of hard solutions 05 p0831 A67-17503

Oxidation of tantalum coated with aluminum and aluminum-chromium alloys at high temperatures and various oxygen pressures, using X-ray diffraction, electron microscopy, etc 08 p1341 A67-20764

Carburization of niobium and tantalum-base alloys through exposure to gaseous mixture of benzene-hydrogen, noting results of creep rupture tests 08 p1341 A67-20765

Tantalum alloy slip line observations, stress-strain curves, yield stresses and anisotropic elastic constants in compression

deformation 11 p1810 A67-25091

Temperature dependence of Youngs modulus of tantalum alloy determined together with free-free vibrations and resonance frequency 12 p1954 A67-25141

Mo, V, Re, Zr and Ti additions effect on mechanical properties, forming stability and recrystallization temperature of Ta alloy with Nb 18 p3065 A67-34293

Brazing alloys and high remelt and conventional techniques developed and evaluated for use in tantalum honeycomb structures 20 p3456 A67-37696

Structure and certain properties of niobium-tantalum alloys containing tungsten and molybdenum show these alloying elements form continuous series of hard solutions 21 p3644 A67-38030

Surface superconductivity in dilute Ta-Nb alloy ascribed to decrease in mean free path due to lattice defects 23 p4036 A67-40657

Precipitation processes in Ta-Cr solid solutions investigated for temperature dependence and change in alloy properties resulting from precipitation 23 p4018 A67-40712

TANTALUM CARBIDE

Diffusion constant of carbon in carbide phases of tantalum determined from growth rate of carbide layers forming on tantalum surfaces 04 p0636 A67-14908

Diffusion coefficient of carbon in nonstoichiometric tantalum monocarbide at very high temperatures, noting increase with decreasing carbon content 06 p1016 A67-17901

Refractory carbides for high temperature applications, stressing use of metal-impregnated tantalum carbide [ONERA-TP-453] 15 p2502 A67-29378

TANTALUM COMPOUND

Minimum N and O content in degassing determined from equilibrium pressures in Nb-O and Ta-O systems 09 p1518 A67-22125

Tantalum thin film resistors for integrated circuits, noting manufacture and applications 14 p2280 A67-28015

Superconducting niobium and tantalum compounds investigated for maximum transition temperatures 16 p2726 A67-30818

TANTALUM NITRIDE

Niobium and tantalum nitrides physical properties including microhardness, electric and thermal conductivities, Hall coefficient and thermal EMF 22 p3861 A67-39917

TANTALUM OXIDE

Silicon-tantalum oxide system prepared by reactive sputtering, noting characteristics of MOS diode of system 01 p0137 A67-11071

Niobium and tantalum oxides from decomposition of zircon-pyrochlor concentrate by silicon 04 p0637 A67-14941

Electron transfer in thin film tantalum-tantalum oxide diodes, noting tunnel and Schottky emission 04 p0582 A67-15106

Electric conduction through tantalum oxide thin films, showing dependence of V-I characteristics on tunneling and Schottky effect 05 p0862 A67-16525

Anodic oxides of titanium, tantalum and niobium from thin dielectric film preparations compared, determining nature and characteristics 13 p2175 A67-26654

Anisotropy in thin dielectric films of tantalum and titanium anodic oxide from various measurements explained by transistor-like model 13 p2175 A67-26655

Structure dependent electric properties of anodized and unanodized tantalum-tantalum oxide thin film resistors, discussing aging, heat treatment, etc 13 p2082 A67-27366

Ionizing radiation effect on polymers used in electronics, producing temporary effects also found in mineral insulators like anodic tantalum oxide 17 p2917 A67-32841

TAPE

S MAGNETIC TAPE

S PLASTIC TAPE

TAPE RECORDER

SA MAGNETIC TAPE RECORDER

Reconstructing serial pulse train from parallel data recorded on magnetic tape, examining flutter performance 02 p0242 A67-12021

Predetection telemetry tape combiner 17 p2813 A67-32496

Sterilization of spacecraft tape recorder, noting component design for individual sterilization compatibility 19 p3230 A67-35583

Electromagnetic interference and tape recorder jitter control problems in data

management system for manned spacecraft 20 p3442 A67-36468

High data rate storage system for Nimbus B tested by simulation 20 p3445 A67-36547

TAPERED COLUMN

Large deflections of columns of variable flexural rigidity, assuming bending moment is proportional to curvature 17 p2963 A67-33020

TAPERED WING

Taper in thickness of wing for special case of linear type analyzed, using triangular elements for matrix displacement method 04 p0707 A67-14441

Incompressible potential flow about thick wing profiles and cascades for blade profiles with angular and round tapered trailing edges 23 p3929 A67-41254

TAPERING

Notch steepness of open circuit transfer function of loaded exponentially tapered RC notch filter 01 p0041 A67-11317

Reflection coefficient of tapered waveguide determined via coupled mode theory, noting error estimation and design of reflectionless tapers 03 p0376 A67-12802

Empiric design of taper for increasing efficiency of coupled cavity travelling wave tube 09 p1476 A67-22211

Theoretical calculations for minimum anticlastic cross section deformations of thin elastic strips with optimally tapered edges verified by moire method 11 p1875 A67-24613

TAR

S ASPHALT

TARGET

SA RADAR TARGET

Inertial guidance system accuracy and error sources, determining offset circular-or spherical-target error probabilities by approximate chi-square distribution 06 p1028 A67-17722

Class of problems of parametric linear programming of set of convex polyhedron having only target function coefficients dependent on parameter 07 p1219 A67-19167

Optimal value of target function in optimization theory 13 p2087 A67-26618

TARGET ACQUISITION

Permittivity and permeability of smooth convex body, using ray tracing technique for vector fields 01 p0020 A67-10014

Guidance equations for multistage boosters offer target change on launch pad and in flight 02 p0265 A67-12718

Target homing of tracking systems receiving signal packages only in absence of fading 04 p0591 A67-14659

Search and acquisition problem to relate spacecraft radar parameters and mission parameters, illustrating optimization and emphasizing radar power aperture product 04 p0572 A67-15030

Continuous wave radar application for obtaining velocity and range information on single targets at large distances 04 p0574 A67-15046

Real time evaluation of radar signals processed by digital detector used in automatic target tracking 04 p0574 A67-15058

Pulsed ruby laser rangefinder with high maximum repetition frequency and digital range readout for data acquisition for determining airborne target trajectories 09 p1465 A67-22622

Phased-array microwave antenna system for scanning simultaneous targets whose distance and direction are changing rapidly 13 p2083 A67-27566

Rapid acquisition of sun in solar energy conversion systems based on momentum exchange from rotating flywheels used to platform 15 p2423 A67-30130

Airborne optical satellite tracking, discussing accuracy limitations and comparing to ground stations 16 p2630 A67-31799

Target location systems functioning in daylight, darkness and under adverse weather conditions 17 p2814 A67-32507

Lunar Orbiter Attitude Control System design and space flight performance [AIAA PAPER 67-533] 19 p3334 A67-35935

Automatic unique acquisition of Canopus for roll control of interplanetary spacecraft, discussing identification, discrimination and calibration 19 p3258 A67-35980

Satellite retrieval system called Space Bola, employing passive/active grappling units depending on target vehicle dynamic

characteristics 20 p3532 A67-36556
Pulse radar on Air Force Eastern Test Range, discussing precision, sensitivity, acquisition, signature and multiple target capability 20 p3381 A67-36581
Optimal system determined from maximum probability criteria of target hitting 20 p3410 A67-37226
Radar station with antenna system for three target coordinates simultaneous measurements 21 p3582 A67-38498
Sensors for acquisition and aiming of solar direction aboard D-2 satellite, discussing operating principles 21 p3629 A67-38866
Camera for multispectral color aerial photography noting four-band interpretation on companion viewer and application to target acquisition 22 p3797 A67-39451
Resolution, contrast and time factors in visual target acquisition 22 p3755 A67-40410
Unresolvable targets producing single radar return estimation from slow amplitude fluctuation, discussing scattering cross section effects and computer simulation verification 23 p3974 A67-41198

TARGET AIRCRAFT
S JINDIVIK TARGET AIRCRAFT
TARGET PENETRATION
SA PROJECTILE PENETRATION
Impact of cylindrical or spherical projectiles of dural and polyethylene at high velocities in semiminfinite targets, analyzing crater shape and relation to kinetic energy 04 p0710 A67-15002
Hypervelocity impact of polythene projectiles on semiminfinite aluminum targets at various obliquity angles, using RARDE gas launcher 04 p0710 A67-15003
Momentum transfer during impact, penetration depth, crater form and mass loss at various velocities, using spherical aluminum projectiles and aluminum targets 04 p0710 A67-15005
Plasma formed by laser pulse on tungsten target, measuring radius, temperature and radiative properties, developing model 06 p1041 A67-18149
Thin plate targets response to hypervelocity impact to determine effectiveness of meteoroid bumpers composed of two layers of distinct materials 10 p1725 A67-23716
Avionics, ordnance and military aircraft as totally integrated system, noting need of accurate navigation, target accuracy and improved communications 15 p2444 A67-29398
Metal projectiles plastic deformation impacting on rigid targets defined, obtaining computer code through direct analysis 22 p3914 A67-40182
Ion energies in expanding plasma stream generated by intense giant pulse laser light in focus on solid LID and LIH targets 23 p4033 A67-41152
Cratering produced by high velocity impact of stainless steel threaded rod on cold-rolled steel target 23 p4080 A67-41487

TARGET RECOGNITION
Direction finder accuracy optimization, considering automatic tracking of target angular coordinates 01 p0024 A67-10721
Flying target detection and tracking with fixed antennas having radiation pattern scanning and multibeam characteristics 02 p0205 A67-12730
Two spatial distributions transformed simultaneously with single lens heterodyning Fourier transform of spatial spectra 03 p0423 A67-13904
Signal design and principle of vernier FM radar system to measure surface characteristics of small target at long distance and range 04 p0570 A67-14877
Radar target resolution and limits as function of environment, number of targets and size of delay Doppler space 04 p0572 A67-15034
Stationary antenna arrays for target detection and tracking noting radiation patterns, radar systems, etc 04 p0654 A67-15538
Radioisotopes for army aviation applications, stressing need for ballistic protection of crew members and critical components 05 p0841 A67-16534
Scheme for switching from automatic target search to range tracking, finding error distribution of backup system 05 p0767 A67-17473

Waveform and filter design for acceptable performance in clutter environment 07 p1145 A67-19880
Angular resolution of plane circular array with multiple targets 07 p1145 A67-19881
Optical range gated filter for detecting moving targets in clutter background, using laser beam for application to MTI radar 08 p1293 A67-20687
Matched filter detection of target shape in photographs using both coherent and incoherent illuminations 09 p1496 A67-21712
Effect of image smear and dimension on target recognition measured on differently oriented, moved and remote Landolt C 09 p1455 A67-21723
Helmet mounted sight as operational element in quick reaction boresighting system, using static and moving targets, obtaining field test data 09 p1456 A67-22371
Automatic tracking in aircraft identification and updating of flight prediction parameters for air traffic control 09 p1529 A67-22636
Mathematical treatment of sequential detection and application to detection of radar targets 10 p1607 A67-23570
Synthetic target scenes generation technique by general purpose digital computer for early analytical evaluation of sensor concepts 11 p1791 A67-24456
Radar resolution performance in moving target determined by cross section of desired target compared with combined cross section of all interfering targets 12 p1907 A67-26083
Probability density functions for power from Rayleigh target 13 p2067 A67-26520
Book on new concepts in radars covering ideal reception, moving targets, autocorrelation, SNR, amplitude distribution, clutter, etc 13 p2071 A67-27224
Method of implementing training problems for site simulator in simulated system training 13 p2090 A67-27233
Recognition thresholds for lunar crater sizes, noting elliptical image measurements and generation of appropriate computer program 15 p2431 A67-29894
Matched-filter systems waveform dependence investigated for signal detection in nonstationary clutter 15 p2438 A67-30135
Predictive identification and fast moving target recognition technique for adaptive control and tracking systems 15 p2463 A67-30330
Airborne low light level TV facility for reconnaissance, target recognition and acquisition, evaluating five sensor combinations 17 p2803 A67-32505
Target location systems functioning in daylight, darkness and under adverse weather conditions 17 p2814 A67-32507
Raster scan parameters influencing target identification in image recognition experiments using video display 17 p2859 A67-32508
Airborne imagery screening using automatic target recognition device 17 p2859 A67-32509
Aerodynamic deceleration system for target drone recovery with reduced impact damage, discussing design improvements 17 p2797 A67-32573
Bottle radar display effectiveness in target detection compared with conventional Plan Position Indicator /PPI/ [TR-750-7] 17 p2807 A67-32630
Radar target designation tracking performance in simulated high speed low altitude aircraft, using closed loop analyses 17 p2830 A67-33181
Pulse radar on Air Force Eastern Test Range, discussing precision, sensitivity, acquisition, signature and multiple target capability 20 p3381 A67-36581
Stability of automatic systems for tracking point targets, noting nonlinear dependence of signals on channel mismatch and its limiting values 20 p3410 A67-37234
Microwave and acoustic frequency holography and possible application to target shape recognition and inverse scattering in radar 21 p3628 A67-38063
Coherent acceleration and velocity observation in real time /CAVORT/ analog radar signal processor for matched filtering pulse trains from radial accelerated targets 21 p3586 A67-38953
Devices to help pilot detection of aircraft evaluated for systematic relationship

between detection functions under fixated conditions and in visual search 22 p3755 A67-39848
Decision theory applied to angular resolution, deriving signal processing radar system beyond Rayleigh limits and target reliability 23 p3972 A67-40643
Mobile laser transceiver for atmospheric targets detection, discussing real time technique for determining atmospheric function 23 p4014 A67-41022
Psychophysical study of irradiation phenomena effects on target size perception by investigating luminance, fixation position and corrections 23 p3969 A67-41643
Radar information automatic extraction by digital techniques, outlining information quantization, target detection and coordinate measurement principles 24 p4122 A67-42407

TARGET SIMULATION
Radar range and Doppler effect simulation by stationary target outlining passive electronic countermeasure technique 07 p1146 A67-19882
Collector target complex eliminating target life time and test equipment contamination by sputtered target material, applied in testing of electrical propulsion systems [AIAA PAPER 66-500] 11 p1852 A67-24341
Remote maneuvering unit control during satellite inspection in simulated conditions 14 p2258 A67-28669
Solid state and electron beam delay line features compared in optimal selection for radar system target simulation 23 p3982 A67-41503

TARGET THICKNESS
Yield variation of excited hydrogen atoms formed by charge exchange with gas target thickness described by analytical model 16 p2714 A67-30874
Thin self-supporting beryllium foils preparation for use as atomic and molecular ion beam targets 17 p2866 A67-33360
Secondary neutron spectral data measured by proton recoil spectrometer from targets bombarded by 180 Mev protons 23 p4028 A67-40739

TARTAR MISSILE
Tactical checkout missile test installations for Terrier, Tartar and Talos missiles 20 p3416 A67-36971

TARTARIC ACID
S DICARBOXYLIC ACID

TASK
SA AUDITORY TASK
SA VISUAL TASK
Secondary task interference in tracking 13 p2061 A67-26490
Maintainability program task requirements covered by Military Standard 470 16 p2781 A67-30441
Perceptual motor-skills forgetting in simple printing task, attributing decrements to retroactive interferences 21 p3576 A67-39099

TASK COMPLEXITY
Improvements in management control of complex projects, considering network analysis 11 p1885 A67-24656
Secondary verbal task effect on tracking performance 13 p2061 A67-26491
Computer techniques for data problems encountered by task analysts 13 p2063 A67-27260
Man-machine compatibility in very low altitude flight determined by two-phase controlled field experiments on obstruction avoidance task 14 p2256 A67-27742
Skilled response organization, discussing stimulus coherence, tracking task, spatial and temporal coherence, secondary task, sequence length and task coding 14 p2254 A67-28034
Intermittent visual stimulus influence on perceptual motor skills in aviation 14 p2258 A67-28668
Human factors and anthropotechnology in development of weapon systems 18 p2993 A67-33643
Interactionist models of human performance in complex system or formal work organization, discussing multidimensional models 18 p2994 A67-34654
Changing role of technical writers and editors during next decade 20 p3556 A67-36587
Visual display for aircraft, presenting simplest visual picture compatible with current pilot task 20 p3375 A67-36873

Anthropotechnical reliability establishing methods considering ability of man to assimilate amount of information in unit of time 22 p3754 A67-39280

Feasibility of short radius centrifuge incorporation in space station, testing radius effects on operator performance of tasks 23 p3965 A67-41567

Urinary catecholamine excretion in pilots relation to physical mental expenditure of energy and flight deck work loads 23 p3952 A67-41577

Vehicle volume and design criteria for manned lunar roving vehicles investigated by evaluating subjects performance under prolonged simulated lunar environment 23 p3970 A67-41658

TAU STAR

Flux intensity and energy spectra of galactic X-ray sources, Tau X-1 and other celestial bodies studies, using three sensitive Geiger counters 01 p0144 A67-10562

TAYLOR INSTABILITY

Taylor vortices intensity and viscous losses determined for viscous flow of liquid between concentric rotating cylinders, solving equation by numerical method 03 p0405 A67-14030

Electrohydrodynamic equilibrium showing continuum feedback control of Rayleigh-Taylor type instability 05 p0856 A67-17414

Negative critical Taylor number for stability of swirling fluid with variable density in circular magnetic field 05 p0859 A67-17442

Combined Rayleigh-Taylor and Kelvin-Helmholtz instability for incompressible plasmas carrying uniform magnetic field including Hall current 08 p1359 A67-20902

Electric analog simulation of periodic nonuniform heat transfer mechanism in film boiling from coated plate 08 p1427 A67-21321

Numerical technique for time dependent calculation of two incompressible fluids interaction to study viscous and inviscid Rayleigh-Taylor instability 11 p1774 A67-23859

LF loss cone instabilities of plasma in Taylor minimum-B configurations, discussing instability conditions and growth rate 12 p1969 A67-25199

Taylor instability in circular Couette flow reexamined as eigenvalue problem noting suppression of geometry effect 23 p3988 A67-40601

Taylor vortices and turbulence in flow between eccentric rotating cylinders [ASME PAPER 67-LUB-12] 24 p4145 A67-42673

TAYLOR THEOREM

Series integration of linear differential equations with deviating argument 01 p0104 A67-10289

Harmonic generation in Taylor vortices between rotating cylinders, measuring amplitude of each harmonic, noting agreement with Davey theory 04 p0601 A67-14462

Taylor theorem test as tool for determining completeness and convergence properties of finite element displacement functions, showing application to axisymmetric shell and conductive heat transfer [AIAA PAPER 67-143] 06 p1103 A67-18440

Taylor columns occurrence criterion in Jupiter atmosphere investigated experimentally, giving flow patterns 21 p3614 A67-38999

Experimental method for studying Taylor columns over hills and holes in Jupiter atmosphere 21 p3614 A67-39000

TECHNETIUM

Superconductivity and transition temperature of technetium and technetium carbide 05 p0860 A67-16389

TECHNICAL DRAWING

S MECHANICAL DRAWING

TECHNICAL WRITING

Changing role of technical writers and editors during next decade 20 p3556 A67-36587

Rapid Evaluation System To Repair Equipment /RESTORE/ approach to technical manual preparation on digital equipment 23 p4085 A67-40582

TECHNIQUE

S CULTURE TECHNIQUE

S DIGITAL TECHNIQUE

S FARADAY-DOPPLER TECHNIQUE

S HIGH RESOLUTION COVERAGE

ANTENNA TECHNIQUE

S IMAGING TECHNIQUE

S MODULATION TECHNIQUE

S MULTILAUNCH TECHNIQUE

S REACTION JET ATTITUDE CONTROL TECHNIQUE

S SCREENING TECHNIQUE

S VERNEUIL TECHNIQUE

TECHNOLOGY

SA AEROSPACE TECHNOLOGY

SA BIOTECHNOLOGY

SA MILITARY TECHNOLOGY

SA REACTOR TECHNOLOGY

New aerospace-related technology in nonaerospace applications, noting NASA and petroleum industry 07 p1269 A67-20263

Gallium arsenide International Symposium, Reading, Berks., England, September 1966 10 p1613 A67-23509

Planning and decision-making system in technological evolution and revolution 13 p2231 A67-27506

Book on ultrasonic machining of intractable materials covering basic principles, vibrator design, machine tools, technology, processes involved and applications 17 p2865 A67-32200

Fundamentals of silicon integrated device technology, Volume 1, Oxidation, diffusion and epitaxy 18 p3096 A67-33453

Soviet book on semiconductor technology and microelectronics covering photoelectric functional converters, junction characteristics, etc 18 p3008 A67-33467

Collection of papers on integrated circuit technology covering instrumentation and techniques for measurement, process and failure analysis 19 p3192 A67-35018

HF transistor design principles, considering current technology 20 p3396 A67-36493

TECTONIC MOVEMENT

Continental-oceanic boundaries of earth and relevance to tectonic speculations about moon and planets, noting role of radiogenic heat 06 p1091 A67-19003

Short period seismic radiation patterns from underground nuclear explosions and small magnitude earthquakes, noting propagation characteristics [SR-1] 20 p3434 A67-37430

Tectonic activity on Venus compared with earth, discussing convection currents and temperature gradients in crust and mantle 24 p4227 A67-42222

TEFLON

Quick change high vacuum window and heat transfer gauge installation for shock tubes 10 p1658 A67-23789

Potential hazards of Teflon gaskets in liquid fluorine systems 13 p2187 A67-27689

Heats of combustion in fluorine of Teflon and graphite and heats of formation of carbon tetrafluoride and carbon hexafluoride 15 p2433 A67-29765

Stress anomaly effect on structural integrity of Teflon laminates determined by photoelastic techniques 18 p3142 A67-33894

TEKTITE

Australites, Henbury impact glass and subgreywacke, comparison of abundances of 51 elements 03 p0512 A67-13900

Tektite structure and lunar ash flows, noting theoretical computations of pressure, temperature and voidage 03 p0512 A67-13936

Origin of Moung Nong type tektites detached by meteoritic impact, considering lunar origin based on diffusion rates in silicates 06 p1078 A67-17562

Composition of Marthas Vineyard and selected Georgia tektites mutually related to silica-rich bediasites 09 p1569 A67-22687

Normalization technique for analysis of heat transfer, considering thermal entrance length, ablation and tektite problems 10 p1732 A67-22931

Baddeleyite inclusion in Marthas Vineyard tektite identified by electron microscopy 11 p1858 A67-24065

Elastic properties of tektites measured using resonant sphere technique 11 p1864 A67-24558

Terrestrial origin hypothesis for tektites, moldavites and impact glass supported by krypton-argon and fission track measurements 11 p1866 A67-24693

German book on space chemistry covering age and origin of earth, meteorites, tektites and impactites 12 p1903 A67-25427

Tektites and impactites composition and origin 12 p1903 A67-25430

Tektite origin, composition, identification,

strewn fields and configurations 12 p2009 A67-26232

Identification with tektites of microscopic glassy objects deposited in Australasian area during and after last geomagnetic field polarity reversal 13 p2198 A67-26792

Cosmic origin of tektites indicated by factors other than chronology 14 p2385 A67-28145

Australasian tektite origin criticized regarding magnitude of atmosphere removal 14 p2390 A67-28889

Tektite field origin hypotheses including terrestrial and lunar 15 p2551 A67-29093

High temperature vapor fractionation of silicate glass related to variations of oxygen isotopes in tektites 15 p2564 A67-30394

Infrared reflectance and optical constants of tektites for origin mode, noting constituent dependence on geographic location 16 p2753 A67-31697

Tektites presence in Australian sea sediments, suggesting relation between geomagnetic reversals and fossil plankton changes to cosmic bodies terrestrial intrusions 16 p2754 A67-31864

External features of South Vietnamese tektites noting structure, surface characteristics and possible formation mechanism 17 p2947 A67-32774

Vapor pressure of natural tektite melts at high temperatures determined by boiling point technique, applied to aerodynamic analysis 18 p3134 A67-34495

Tektite glasses crystallizing tendency studied by subjecting them to heat treatments above strain point and CN slow cooling from melting 20 p3527 A67-37274

Tektite formation and flight from large meteorite impact, discussing blast expansion flow 20 p3530 A67-37527

Strain birefringence around tektite surface notches, discussing specimen quenched in air stream from 1000 degrees C 21 p3704 A67-38506

Lunar origin related to earth rotational instability due to earth core formation 24 p4230 A67-42324

Chemical analysis of glass bombs from Ries crater area investigated for textural differences due to shock melting and cooling rates 24 p4233 A67-42621

Tektite classification by type based on external form, attributing surface sculpturing of type B to aerodynamic and not chemical processes 24 p4235 A67-42639

Rare earth and barium abundances in Ivory Coast tektites and rocks determined by isotope dilution 24 p4236 A67-42645

Antimony abundance in meteorites, tektites and terrestrial rock by neutron activation analysis 24 p4236 A67-42647

Tektite composition considered from results of high temperature vapor fractionation of silicates 24 p4237 A67-42649

TELECOMMUNICATION

Direct backscatter recordings from polar cap F-layer reflections used to predict communications 01 p0020 A67-10007

Satellite placing in synchronous orbit using ELDO PAS booster for telecommunications purposes 01 p0156 A67-11418

Surveyor telecommunications system from standpoint of actual subsystem implementation and performance, detailing reliability, flexibility, redundancy and data transmission modes 02 p0196 A67-11998

Operative satellite applications including telecommunications, meteorology and radionavigation 06 p1093 A67-17555

International Consortium for Telecommunications by Satellites /Intelsat/, noting Comsat connections 06 p0956 A67-17556

European Conference on Telecommunications by Satellites /CETS/, recommendations and patterns of cooperation 06 p1119 A67-17558

Data processing centers integration through ground and satellite telecommunications networks for global information network [AIAA PAPER 66-331] 06 p0961 A67-17700

Transfer logic of double dialog high security data transmission system using long loop principle 07 p1146 A67-20159

Computer generation of DB Margin Summaries for telecommunications links 08 p1292 A67-20653

Space communications between points on

earth by space vehicles and between earth and space vehicles 08 p1294 A67-20783

Aeronautical telecommunications in air transport for transmission and reception of signals, written messages, sounds and images 08 p1294 A67-20784

Seastations in conjunction with submarine cables for aviation communication, navigation and air traffic control 09 p1530 A67-22652

Working principle of echo suppressor used in telephone link with high propagation time based on selective attenuation by frequency and time divisions 11 p1754 A67-24651

Legal problems of space research connected with telecommunication and meteorological activity 12 p2042 A67-26142

International legal principles and cooperation requirements for worldwide radio and TV broadcasting by satellite telecommunications networks 12 p2043 A67-26144

Satellite Telecommunications with Automatic Routing /STAR/ system composition and operation, detailing signal relaying procedure 13 p2067 A67-26717

Telefactor system in control of space operations, describing master-slave manipulator servomechanism with TV network and electronic communication link 13 p2063 A67-27213

Telemetry, tracking and command /TTC/ communications, emphasizing 1970 requirements for manned and unmanned earth-orbital, lunar and planetary missions 13 p2074 A67-27449

High power laser emitting monochromatic radiation at single frequency applicable in spectroscopy, telemetry and telecommunication 14 p2330 A67-28469

Satellite telecommunication networks commercial, political and military implications 14 p2270 A67-28567

World telecommunication satellite developments, service, requirements, technical and financial elements 14 p2270 A67-28583

U.S. international telecommunications requirements through 1975 14 p2272 A67-28704

Demand, applications and technology for future satellite communications covering transoceanic and military telecommunication, TV network, weather data, etc 14 p2274 A67-28912

Laser applications to telemetry, radar, navigation, telecommunications, medicine, boring and welding 14 p2333 A67-28974

Spacecraft and ground equipment of Lunar Orbiter telecommunications system 17 p2811 A67-32119

Future satellite regional and intercontinental telecommunication network, considering weight, classes, performance and orbital factors 17 p2813 A67-32397

European Satellite Telecommunication Conference /CETS/, discussing government participation, INTELSAT projects, European technical program and juridical and administrative operations 17 p2974 A67-32398

Satellite telecommunication techniques including demodulation, detection, microwave amplification, antennas, etc 17 p2813 A67-32400

Laser research and development in France and applications to holography, metrology and gyros 17 p2868 A67-32745

Telecommunication equipment reliability and maintenance costs reduction to increase availability, noting corrective method by transistorization 18 p3002 A67-34229

Worldwide satellite telecommunication system, economic and political implications and effects on CEPT 18 p3162 A67-34357

Telecommunication system for lunar, planetary and deep space flight mission control and data acquisition 19 p3207 A67-35224

International Telecommunications Satellite Consortium /INTELSAT/ organization 19 p3349 A67-35640

TELEGRAPHY

S COMMUNICATION

TELEMETRY

SA PHYSIOLOGICAL TELEMETRY

SA RADIO TELEMETRY

Time multiplex telemetry equipment for FR-1 satellite that encodes data in PAM/FM wave train for transmission to ground 01 p0020 A67-10107

Radiotelemetric recordings of EEGs

aviation pilots during long flight 01 p0017 A67-10962

Decoder signaling system of Eldo satellite employing PCM telemetry channel, examining counters, shift registers, flip-flop circuit, etc 02 p0192 A67-11651

Multiprogramming system for computer controlled telemetry data reduction system 02 p0206 A67-11807

Telemetry - ITC Conference, Los Angeles, October 1966, Volume 2 02 p0195 A67-11996

Apollo launch data telemetry system development from inception through planning and into final hardware implementation 02 p0195 A67-11997

Data system requirements for large space vehicles and flexible telemetry system design for all stages of Saturn IB and V vehicles 02 p0196 A67-12000

Digital computer controlled telemetry ground station, examining six subsystems 02 p0229 A67-12002

White Sands Missile Range instrumentation modernization program, discussing advanced range testing, reporting and control /ARTRAC/ system, telemetry and electronic and optical sensors 02 p0229 A67-12003

Optimum telemetry system characteristics for shock, vibration and acoustic measurements and data bandwidth sufficiency 02 p0196 A67-12009

Compatible double sideband/single sideband/constant bandwidth FM telemetry system for wideband data 02 p0197 A67-12010

Resolution of telemetering event occurrence times with 1 and 2 microsecond accuracy, considering real time systems, delayed time systems and hybrid time systems 02 p0197 A67-12012

Data abbreviation application to actual range telemetry data recorded on magnetic tape, noting redundancy removal, processing time reduction, etc 02 p0197 A67-12017

Telemetry receivers capture ratio effect on overall system accuracy, determining effect of IF filter characteristics 02 p0197 A67-12022

Data quality assurance program for telemetry ground station operations, noting frequency division and time division formats 02 p0198 A67-12023

Polarization-diversity telemetry receivers for combining FM/FM penetrometer data, noting signal fading 02 p0198 A67-12024

AGC and noise controlled dual-channel optimal ratio predetection combiners, examining design and performance by studying diversity combining techniques 02 p0198 A67-12025

Solid state high power LF and VLF telemetry transmitters, considering power amplifier design, RF output network, cooling systems, etc 02 p0218 A67-12106

Analog magnetic recording in ground telemetry stations 03 p0418 A67-12896

DATA CORE, integrated launch area telemetry data system using high speed digital computers and analog or digital display 03 p0375 A67-13382

Telemetry design factors, discussing interference problems, antenna design, oscillator stability, preamplifiers, etc 03 p0372 A67-14120

NASA FM telemetry system for data acquisition and processing from Ariel satellites including methods for storage, transmission, handling, etc 04 p0568 A67-14437

Data acquisition system for Blue Streak flight trials noting telemetry and radar and relation to trajectory, autopilot, structure, etc 04 p0568 A67-14438

Coding method for transmitting digital data over IRIG-FM/FM telemetry system applied to German-American high altitude/space flight program 04 p0569 A67-14572

Telemetry systems, discussing PAM/FM/FM system, airborne equipment parts, ground support system and electronic testing procedures 04 p0577 A67-15728

Sensors and signal conditioners, discussing operation and calibration of resistance thermometers, strain gauge pressure transducers and potentiometric transducers 04 p0626 A67-15731

USAF Eastern Test Range, discussing telemetry, tracking, geodetic and time measurements 05 p0787 A67-16609

Data display for Real Time Telemetry Data System /RTTDS/ 05 p0765 A67-17042

Automatic telemetry checkout station for Saturn V systems using real time signal digitizer and general purpose computer 05 p0789 A67-17044

PCM telemetry system for satellite test vehicle of ELDO program using transistorized printed circuit technology 06 p0957 A67-17613

DFL mobile telemetry ground station participation in solar eclipse expedition of ESRO in Greece 06 p0980 A67-18020

Automatic telemetry checkout station for Saturn V systems using real time signal digitizer and general purpose computer 06 p1089 A67-18861

Meteorological telemetry system for gun launched probes for high altitude research 08 p1292 A67-20664

GSFC program in telemetry data archiving, discussing necessity of data accessing capability 09 p1487 A67-21685

Airport traffic control tower instrument panel displaying continuously telemetered data on current weather conditions of runway complex 10 p1656 A67-23087

Recording telethermometer for use at airports, noting performance characteristics including unattended reliability, rapid response time, etc 10 p1656 A67-23088

Use of onboard data processing for eliminating irrelevant information telemetered from satellite experiment 12 p1909 A67-25780

Parallel data decoding with high transmission rates close to channel capacity for space telemetry systems 12 p1909 A67-25781

Implant telemetry techniques and associated problems and potential of microelectronics 12 p1903 A67-26171

Pulse amplitude measurement from scintillation cosmic-ray counter 13 p2119 A67-26560

Limitations in conventional radar compared to new multichannel radar with discontinuous pulse compression 13 p2070 A67-27203

Nomogram to predict SNR for certain laser setups 14 p2330 A67-28289

Telemetry - Conference, San Francisco, May 1967 14 p2270 A67-28679

RF hardware implementation techniques utilizing devices illustrated in block diagrams 14 p2287 A67-28680

NASA STADAN and Apollo network antenna systems, analyzing tracking antenna systems, command systems and operational problems 14 p2287 A67-28681

Modulation and demodulation methods for multiplex telemetry, discussing PCM, PSK and SSB 14 p2271 A67-28682

Nuclear radiation damage to circuit elements of missile FM/FM telemetry system, analyzing changes in electric characteristics 14 p2271 A67-28685

Miniature multichannel pulse-duration-modulated multiplex telemetry unit for medical monitoring of human subjects pulse, temperature, airflow, etc, under stress 14 p2259 A67-28688

Multiple format telemetry programmer design using control signals 14 p2275 A67-28689

Laser applications to telemetry, radar, navigation, telecommunications, medicine, boring and welding 14 p2333 A67-28974

Telemetry systems for gun launched upper atmosphere probes 15 p2436 A67-29412

Mobile telemetry ground station and maximum reliability procedures for rocket telemetry transmission system used in solar eclipse 15 p2467 A67-29575

Satellite telemetry system transmitter optimization, noting error probability criterion, average power constraint, etc 16 p2622 A67-30693

Handbook of telemetry and remote control considering position measuring, missile guidance, flight control, data processing, feedback information, communications, etc 16 p2633 A67-31916

Ballistic range blast-traversal testing technique using scale models containing fast response FM telemetry system modulated by capacitance type pressure transducer [AIAA PAPER 66-777] 17 p2832 A67-32063

Probability density function of ratio of two nonzero mean Gaussian random variables derived and applied to calibrated

signal using noisy calibration levels 17 p2816 A67-32624

Characteristics, operation, technology and reliability of telemetering systems for ESRO I, HEOS A, TD 1 and TD 2 including control factors and coding 17 p2816 A67-32747

System performance in electrooptical telemetry noting receiver, transmitter, silicon photodiode, shot, thermal and background noise, etc 17 p2817 A67-32931

Reduced noise rejection regions in receiver of PSK telemetry signals in narrow band concentrated noise, using phase and polarity comparison methods 18 p3000 A67-34085

Logarithmic compression of digitally telemetered data for constant maximum percentage error throughout encoded range 18 p3006 A67-34115

French laser telemetry network, noting Q-switched ruby laser, Doppler effect measurement and local spatial geodesy program 19 p3182 A67-35239

Systematic and random error effects on geodetic accuracy of results obtained by 3-station laser telemetry 19 p3182 A67-35240

Tracking station network organization, equipment and operations of National Center for Space Studies /CNES/ in France 19 p3207 A67-35242

Digital telemetry system for maximum transmission efficiency of measurements performed on space vehicle 20 p3394 A67-36245

Real time telemetry data system for Air Force Eastern Test Range 20 p3381 A67-36614

PCM telemetry system for ELDO program, discussing data acquisition and processing 20 p3392 A67-37162

Integrated MOS-FET analog gate for pointing and logic of space telemetry switch 21 p3592 A67-38227

Radiation effect on MOS transistors in D-2 satellite telemetry coder 21 p3593 A67-38230

Short range FM transmitter-receiver system for shock measurements required to optimize shock absorber design 21 p3581 A67-38395

High reliability PCM digital telemetry system for onboard data transmission of analog and digital signals 21 p3583 A67-38635

Satellite automatic telemetry data processing system, noting development of high speed computer for real time 21 p3588 A67-38638

Self-variable threshold method for synchronization code detection of PCM telemetry signal 21 p3583 A67-38641

Receiving system for telemetering with orientable antenna error-measuring signal receiver and servo loops 21 p3599 A67-38645

Power consumption reduction problems in coded telemetry measurements for ESRO I and HEOS A satellites 21 p3584 A67-38646

PCM coder, programmer and analog switch of D-2 satellite, including systems characteristics and diagrams 21 p3599 A67-38647

Analog treatment of digital telemetering signals using a priori information about transmission, noting Q-factor, storage and use of existing emissions 21 p3584 A67-38660

Lasers as light source in optical telemetry, discussing laser radiation, solid state and gas lasers and critical parameters 22 p3800 A67-39981

Developments in tracking, telemetry and command transmission, discussing move toward higher frequencies and rain losses 22 p3763 A67-40338

TELEPHONE

User reaction test results for comparison of telephone quality via Early Bird and via cable circuits based on callback interviews, service observations and circuit rejection counts 06 p0959 A67-17666

Subjective evaluation of telephone communications via Early Bird satellite and cable circuits 06 p0959 A67-17667

VHF and UHF radio/telephone communication channels for air traffic control 09 p1465 A67-22633

TELEPHONY

SA ECHO SUPPRESSION

Differential far-end-operated half-echo suppressor design for telephone circuits with long propagation time 03 p0371 A67-13990

Laser application to laser telephone circuits, noting experimental data and

effects of fog 08 p1337 A67-20769

Working principle of echo suppressor used in telephone link with high propagation time based on selective attenuation by frequency and time divisions 11 p1754 A67-24651

TELEPHOTOMETRY

Far UV radiation flux measurement by satellite-borne telescopic stellar spectrophotometer 08 p1399 A67-21234

TELESCOPE

SA ASTRONOMICAL TELESCOPE

SA PROTON TELESCOPE

SA RADIO TELESCOPE

SA REFLECTING TELESCOPE

SA REFRACTING TELESCOPE

SA SPECTROSCOPIC TELESCOPE

SA STRATOSCOPE I TELESCOPE

SA X-RAY TELESCOPE

Geometrical factor and radiation pattern for single crystalline detectors and coaxial telescope 02 p0240 A67-11542

Directional telescope for measuring intensity and spectral composition of gamma rays in primary cosmic radiation 09 p1497 A67-21899

OAO structure for measuring absolute stellar energy in UV region 10 p1712 A67-22991

Spacecraft orientation during interplanetary flights, using system employing two rigidly connected telescopes, one aimed at sun and other aimed at stars 11 p1751 A67-24084

Mean declinations correction for Talcott pairs of 191 stars from zenith telescope observations 11 p1888 A67-25088

Geometrical factor and radiation pattern for single crystalline detectors and coaxial telescope 16 p2877 A67-31608

Digital controller design for tracking telescope, discussing tracking accuracy and response time 24 p4154 A67-42176

TELETYPE

Half-tone Teletypewriter prints out picture from slow scan digital TV source 05 p0808 A67-16622

TELEVISION

SA CLOSED CIRCUIT TELEVISION

SA COLOR TELEVISION

SA EDUCATIONAL TELEVISION

SA SATELLITE TELEVISION

SA SPACECRAFT TELEVISION

Deflection-modulation display method analyzed for presenting video signals 01 p0081 A67-10018

Transistor failure in inductive load circuits such as TV horizontal deflection circuits and relation to secondary breakdown data 02 p0223 A67-12656

Electro-optical imaging systems used in military aerial TV display, emphasizing variables involved in viewing related to visual interpretation 05 p0757 A67-16309

Laser sources emphasizing TV display output power needs 09 p1515 A67-22362

Scan-converted bright displays for air traffic control systems 09 p1528 A67-22635

Book on fundamentals of display systems covering cathode ray tubes, color techniques, photographic and electromechanical systems, etc 20 p3435 A67-36135

TELEVISION CAMERA

Ultimate sensitivity of space camera imaging devices with particular reference to slow scan vidicon 02 p0245 A67-12245

TV camera to be used by Apollo astronauts noting integrated circuits, optical system, light intensifier, etc 09 p1499 A67-22175

Automatic electrostatic image orthicon camera with small weight, volume and input power, having full low-light level sensitivity capability 17 p2858 A67-32481

Hydrogen fire visualization detection techniques including application of photography, TV and image converter in IR and UV regions 20 p3445 A67-36540

Image dissector camera providing high resolving power, photometric fidelity and long life for use in meteorological satellite 20 p3445 A67-36541

DODGE TV system for evaluating attitude control system in gravity gradient stabilization at synchronous altitude 20 p3452 A67-37571

DODGE satellite vidicon cameras and information processing system electronics design and performance 20 p3452 A67-37572

DODGE satellite TV cameras for black and white, plus color picture transmission with

photometric analysis and camera optics 20 p3452 A67-37573

Surveyor variable and fixed focal length TV camera lenses, discussing zoom lens design criteria, focal plane shutter and color filter wheel 22 p3807 A67-40375

TV camera reseau for engineering information on planetary missions and reducing geometric distortion [SMPT PAPER 102-39] 22 p3808 A67-40377

Integrated circuit for TV camera including photosensitive array and self-scanned solid state image sensor 23 p3998 A67-40868

TELEVISION EQUIPMENT

Line scan TV for earth observation satellites noting camera design, coverage, systems effectiveness and performance results 02 p0335 A67-12398

Image orthicon TV system and application to auroral observations, noting data acquisition mechanism 06 p0993 A67-17563

Apollo TV scan conversion, discussing equipment and performance 06 p0964 A67-18413

Image analyzer tube for IR TV based on phenomenon of accumulation at semiconductor junctions 07 p1189 A67-20158

TV subsystem of Surveyor I, discussing operation-design constraints, camera configuration, video sequence, etc [SMPT PAPER 101-43] 12 p1904 A67-25461

TV system with automatic target tracking capability 12 p1904 A67-25462

Vidicon TV design modifications for spacecraft applications noting reduced power requirements, improvement of heaters, narrowing of bandwidth, etc [SMPT PAPER 101-51] 12 p1914 A67-25471

Ranger Block III television system for lunar surface photography 16 p2620 A67-30643

Performance of fiber-optics coupled cascade image intensifier systems from standpoint of overall system noise, resolution, gain, contrast degradation and information rate 17 p2859 A67-32504

Airborne low light level TV facility for reconnaissance, target recognition and acquisition, evaluating five sensor combinations 17 p2803 A67-32505

Low light level TV as aid to nighttime air rescue, describing ionoscope and image orthicon of camera system 17 p2859 A67-32506

Spaceborne fiber optics TV system emphasizing image enhanced flexible front end optical assembly 20 p3445 A67-36554

TV in lunar environment, discussing development and performance of instrument used during Surveyor I mission 21 p3629 A67-38658

Optical communication systems modulation, discussing TV link, modulator, optical waveguides and materials availability 22 p3759 A67-39330

Future improvements in aeronautical field covering noise control, centralization, TV communication, ultimate speed, sonic boom and nuclear cargo aircraft 22 p3746 A67-39846

Surveyor TV power conditioning circuit and product design, discussing weight saving features, reliability and magnetic housing 22 p3807 A67-40374

Surveyor TV system calibration, determining transfer functions for various parameters 22 p3807 A67-40376

TELEVISION RECEPTION

Mosaic construction and image analysis for Surveyor TV pictures 08 p1333 A67-21504

Direct TV reception from satellites, discussing cost of Yagi and parabolic antennas, noting output tube 13 p2066 A67-26336

Visual image description with aid of spectral power redistribution functions, discussing input arrangement in TV recognition system 21 p3605 A67-39114

TELEVISION TRANSMISSION

SA AUTOMATIC PICTURE TRANSMISSION /APT/

Satellites for TV distribution and broadcasting system for Western Europe, considering increased antenna gain of ground station for minimum satellite energy consumption 01 p0027 A67-11417

Voice communications system using GaAs room-temperature injection laser and TV communications system using GaAs crystals as modulators for laser beams 02 p0194 A67-11786

Half-tone Teletypewriter prints out

picture from slow scan digital TV source 05 p0806 A67-18622

Operative satellite applications including telecommunications, meteorology and radionavigation 06 p1093 A67-17555

Broadcasting of TV by satellites, examining altitude effects, stationary satellite types, FM advantages, etc 06 p0956 A67-17560

Direct-to-home TV broadcasting satellite system for upper UHF, describing stabilization, thermal control, antenna, power amplifier, etc [AIAA PAPER 66-309] 06 p1094 A67-17689

Synchronous stationary satellite system for networking television and radio material to broadcast stations, noting frequency requirements and constraints 06 p0961 A67-17697

Future pattern of communications satellite systems, reviewing world requirements for telephony, telex, TV and radio [AIAA PAPER 66-319] 06 p0961 A67-17709

Experimental and operational communication satellite, discussing attitude stabilization, automatic routing, etc 06 p1094 A67-18050

Direct-to-home TV broadcasting satellite system for upper UHF, describing stabilization, thermal control, antenna, power amplifier, etc [AIAA PAPER 66-309] 06 p0964 A67-18414

Digital and analog TV transmission from spacecraft compared, noting data compression and development of hybrid system 06 p0964 A67-18415

X-ray image transformation, transmission and amplification directly into video signals for inspection of missile case walls and weldments 10 p1622 A67-22929

Pseudocolor technique, noting applicability to TV data presentation from space vehicles 11 p1789 A67-24250

Communications satellites for high power transmission of TV and VHF signals, considering synchronous satellites, antennas, stabilizing systems and weight 11 p1870 A67-24706

Behavior in atmosphere of laser beam modulated for black and white TV signal transmission 13 p2068 A67-26725

Telefactor system in control of space operations, describing master-slave manipulator servomechanism with TV network and electronic communication link 13 p2063 A67-27213

Optimum efficiency of high power klystrons for operation in fourth and fifth TV band, noting space charge effect 14 p2277 A67-27773

TV signal transmission over gas laser light beam with ADP crystal at 7GHz modulating frequency 16 p2684 A67-30610

World-educational space-televasting technical and operational problems 16 p2622 A67-30696

Lens arrays use in holograms 17 p2860 A67-32619

Simplex information transmission system using communication satellites, discussing technological and economical parameters 18 p3001 A67-34176

Intelsat and communications satellites economic, political and social consequences, UN General Assembly Resolutions and use of satellite facilities for distribution of TV transmissions to broadcasting stations 18 p3182 A67-34354

Ground station for satellite communications in Italy covering TV transmission 19 p3207 A67-35568

Satellite TV broadcasting systems with multiple independently controllable channels visualized after 1975 19 p3183 A67-35657

Design and characteristics of solid state UHF transmitters and receivers applicable in color TV systems 20 p3395 A67-36249

DODGE satellite TV cameras for black and white, plus color picture transmission with photometric analysis and camera optics 20 p3452 A67-37573

TV system with spark chamber detector for analysis and transmission of cosmic ray pictures to earth from satellites 21 p3599 A67-38655

Test signal techniques for measurement and video monitoring used in ORTF network 22 p3796 A67-39233

Bandwidth reduction for holographic data transmission systems noting application to TV 22 p3796 A67-39260

Earth shine illuminated lunar surface TV picture taking by modifying Surveyor equipment to provide light integration [SMPTE PAPER 102-40] 22 p3808 A67-40378

Surveyor TV system signal processing and transmission, analyzing performance and computer simulation of some effects [SMPTE PAPER 102-41] 22 p3808 A67-40379

TV system resolution improvement without bandwidth increase, discussing accuracy of random alphabetic characters 23 p3975 A67-41282

Video digital data compression technique, time-buffered coarse-fine /TBCF/, for redundancy reduction 24 p4123 A67-42806

TELLURIC CURRENT

SA GEOELECTRICITY

Diurnal variation of telluric currents near magnetic equator during IGY and IQSY suggests equatorial electrojet as main source for current 10 p1651 A67-23343

Coastal effects in magnetic and telluric current variations near complex land, shelving seawater 13 p2108 A67-26317

Signal extraction and scattering of telluric currents studied for random sheets, semlinfinite medium and interface separating medium of different resistivities 24 p4152 A67-42885

TELLURIC-CURRENT MICROPULSATION

Correlation of north-south component of telluric currents and brightness fluctuations in quiet form auroras 20 p3431 A67-36994

TELLURIDE

SA BISMUTH TELLURIDE

SA CADMIUM TELLURIDE

SA INDIUM TELLURIDE

SA LANTHANUM TELLURIDE

SA LEAD TELLURIDE

SA MERCURY TELLURIDE

SA TIN TELLURIDE

SA ZINC TELLURIDE

Photovoltaic effect in thin telluride layers and in contacts between layers and various metal electrodes, noting dependence on angle of deposition 02 p0294 A67-11758

Growth of spherulitic structure in thin layers of tellurides, noting nucleations and multiplicity of phases 02 p0295 A67-11766

Copper telluride-cadmium telluride thin film heterojunction fabrication and characteristics for solar cell applications 08 p1285 A67-20730

TELLURIUM

Hall coefficient variation with substrate temperature of thin films of tellurium, lead telluride and antimony 01 p0138 A67-11231

Internal conversion coefficients for M4 transition in Te, noting gamma energy magnitude, nuclear size effects and eigenvalue results 03 p0472 A67-13335

Parametric amplification of far IR in Te crystal pumped by carbon dioxide laser 03 p0437 A67-13572

Emission from tellurium single crystal pumped by two waves from carbon dioxide laser 04 p0632 A67-14914

Absorption spectra of Te, Sn, Pb, PbTe and SnTe at various energy ranges, noting role of wave functions involved in absorption by d-electrons 04 p0681 A67-15295

Optical absorption and oscillatory magnetoabsorption in tellurium, noting interband transition and lack of inversion symmetry 06 p1060 A67-18919

Cyclotron resonance in tellurium at submillimeter wavelengths, deducing relation time anisotropy 06 p1061 A67-18920

Band-to-band radiative recombination in semiconductor groups IV, VI and III-V, presenting data on diamond, Si, Ge, Se and Te 09 p1558 A67-22601

Time analysis of Mossbauer spectrum variation and isometric shift of source Te-125m in PbTe absorber following neutron irradiation in reactor 09 p1559 A67-22661

Xenon 129 and tellurium 128 formation intervals in chondritic meteorites as measure of neutron induced isotope production by solar nucleosynthesis 09 p1570 A67-22694

Self-diffusion in high-purity tellurium between 300-400 degrees 13 p2179 A67-27156

C

Tellurium nonlinear optical properties including absorption and refraction indices, discussing second harmonic radiation generation 20 p3507 A67-36324

Angular distributions of elastic and

inelastic alpha scattering from tellurium isotopes using Lewis cyclotron 24 p4192 A67-42732

TELLURIUM ALLOY

Electrical conductivity and Hall coefficient temperature dependence in pure and alloyed Te 03 p0492 A67-13344

Lanthanum for germanium partial substitution effect on thermoelectric properties of single phase and homogeneous samples of GeTe 03 p0500 A67-14231

Temperature-composition relationship for Hall coefficient inversion point in Ti-doped Te single crystals 03 p0500 A67-14232

Electrical conductivity and Hall coefficient temperature dependence in pure and alloyed Te 13 p2184 A67-27718

Second harmonic generation in Se and Te-Se using carbon dioxide laser, measuring nonlinear coefficients and synchronism direction 23 p4016 A67-41192

TELLURIUM COMPOUND

Optical transmission and transition in semiconductor single crystals of various unit cells, considering bismuth tellurium sulfide 02 p0289 A67-11725

GeTe solid solutions reviewed considering thermal EMF, temperature dependence and current carrier mobility 16 p2730 A67-31184

Stoichiometric composition effect on semiconducting properties of gamma iron telluride at high temperature phase 17 p2911 A67-32220

Indium arsenide-tellurium ternary compounds chemical bond, microhardness and structure 20 p3506 A67-36226

TELSTAR SATELLITE

Experimental and operational communication satellite, discussing attitude stabilization, automatic routing, etc 06 p1094 A67-18050

TEMPERATURE

S ATMOSPHERIC TEMPERATURE

S AUROREAL TEMPERATURE

S BODY TEMPERATURE

S BODY TEMPERATURE /BIOL/

S COMBUSTION TEMPERATURE

S CRYOGENIC TEMPERATURE

S DEBYE TEMPERATURE

S ELECTRON TEMPERATURE

S ENVIRONMENTAL TEMPERATURE

S FLAME TEMPERATURE

S ION TEMPERATURE

S IONOSPHERIC TEMPERATURE

S LUNAR TEMPERATURE

S OPERATIVE TEMPERATURE

S PLANETARY TEMPERATURE

S PLASMA TEMPERATURE

S RECOVERY TEMPERATURE

S ROOM TEMPERATURE

S SKIN TEMPERATURE

S SPACE TEMPERATURE

S STAGNATION TEMPERATURE

S STEFAN-BOLTZMANN LAW

S WALL TEMPERATURE

TEMPERATURE COMPENSATION

Control-voltage transducer synthesis with variable capacitor compensation of quartz resonator frequency-temperature characteristics 08 p1306 A67-21280

Design and operation of reference temperature compensator in thermoelectric temperature gauge 09 p1496 A67-21690

Loss in temperature compensation with varying frequency for quartz generators 11 p1757 A67-23909

Temperature compensated electronically controlled ferrite attenuator design and performance 17 p2825 A67-32524

Ferroelectric phase shifter temperature compensation, showing reduction in sensitivity by connecting in series two different ferroelectric materials 21 p3879 A67-38219

Loss in temperature compensation with varying frequency for quartz generators 21 p3600 A67-38937

Digital temperature compensation and statistical filtering procedures for fast reaction alignment of inertial navigators 22 p3831 A67-39886

TEMPERATURE CONTROL

SA CRYOSTAT

SA HEAT REGULATION

SA INSULATION

SA SKIN TEMPERATURE /BIOL/

Structural design and temperature control influence on configuration of Mariner space probes 01 p0156 A67-11440

Temperature control and complex heat path designs inertial components, platforms

and strap-down guidance systems, considering floated gyros and accelerometers 02 p0241 A67-11789

Thermal control subsystem for Apollo lunar surface experiments package, noting construction and operation 02 p0184 A67-12357

Thermal testing of critical systems module of meteoroid detection satellite without attaching sensor arrays 02 p0334 A67-12378

Apollo thermal control systems and concepts, discussing 02 p0334 A67-12390

Thermal control of Nimbus spacecraft by utilizing semipassive and passive thermal control elements to maintain temperature of overall spacecraft, subsystems and components 02 p0335 A67-12391

Temperature control of orbital Titan III-C transtage space booster, noting thermal design, configuration and materials test program support 02 p0335 A67-12395

Book on thermophysics and temperature control of spacecraft and entry vehicles 03 p0532 A67-13032

Optical damage of spacecraft thermal control coatings in simulated space radiation environment of geomagnetically trapped particles [AIAA PAPER 65-646] 03 p0448 A67-13051

Spacecraft thermal control surface damage by solar wind bombardment in hydrogen and helium plasmas, with measurements of solar spectral reflectance and thermal emittance [AIAA PAPER 65-647] 03 p0448 A67-13052

Absorptivity standard instrument to investigate solar absorbance of four surfaces used for spacecraft temperature control for Mariner IV on Mars mission [AIAA PAPER 65-650] 03 p0448 A67-13055

Ames emissivity experiment on OSO-II to measure thermal radiation properties of temperature control coatings exposed to space environment [AIAA PAPER 65-651] 03 p0448 A67-13056

Ranger and Mariner spacecraft temperature control design, test and flight results 03 p0517 A67-13071

Spacecraft thermal design problems including computer programs, thermal control coatings, testing, etc 03 p0517 A67-13072

Spacecraft thermal control design problems including insulation, interface conductances, testing, weight penalties, etc 03 p0517 A67-13073

Controls and control experimental program for nuclear rocket engine employing hot bleed cycle [AIAA PAPER 66-1005] 03 p0466 A67-14150

Passive heat transfer system for metabolic heat removal in extravehicular activity suit 03 p0364 A67-14295

Optimal temperature control design using IBM 7094 digital computer program for thermal environment simulation of stabilized multisurfaced earth-orbiting spacecraft structure [ASME PAPER 66-WA/HT-44] 04 p0724 A67-15430

Spacecraft thermal control coatings based on optical properties, discussing stability, environmental simulation in development, thermophototropic concepts, data retrieval and optical measurement techniques in ultrahigh vacuum [SAE PAPER 660653] 04 p0630 A67-15785

Hypersonic thermal structural concepts to satisfy design requirements including insulated, insulated and cooled and hot load carrying approaches [SAE PAPER 660678] 04 p0716 A67-15789

Gimballed platform thermal control system and design constraints on inertial system housing 04 p0626 A67-15791

Centaur electronic packages for space flight thermal and radiative environmental control 05 p0778 A67-17453

Passive thermocontrol techniques for electronic equipment near descent engine skirts and plumes [AIAA PAPER 67-158] 06 p1117 A67-18479

Temperature fluctuation of thin walled satellite passing periodically from sun to shade simulated by hybrid computer 07 p1257 A67-19375

One-dimensional adiabatic equilibration of plate with starting temperature compared with nonadiabatic equilibration and exoatmospheric cooling of cylindrical metallic and plastic shells 08 p1429 A67-21527

Thermal design of navigational satellites, obtaining reduction in discrepancy between operational orbital temperatures and preflight calculations through thermal vacuum testing 09 p1572 A67-22062

Temperature control and thermal coupling of cesium adsorption porous tungsten, charcoal and graphite reservoirs 09 p1450 A67-22350

Operational economy of dip brazing method of joining aluminum and reliability of ultrasonic printout procedures for inspection of assemblies 10 p1660 A67-23007

Electronic computer usage to control temperature during creep and long term strength tests of heat resistant steels 11 p1877 A67-24818

MHD generator working fluid temperature reduction 12 p1973 A67-25395

Space environment simulation facility for thermal control coatings to study synergistic and healing effects 12 p1924 A67-25711

Light sources used for solar simulation testing in terms of operational characteristics and effect of different spectral irradiance characteristics on thermal control coatings 12 p1925 A67-25723

Low to moderately high temperature emissometer, based on calorimetric method, to measure total hemispherical emittance of metals and coatings in vacuum [AIAA PAPER 67-299] 12 p1946 A67-26014

Thermal radiation characteristics of spacecraft temperature control louvers in solar space environment, discussing specular reflection [AIAA PAPER 67-307] 12 p2036 A67-26022

Pegasus thermal control louver system characteristics determined by environmental chamber testing, noting testing configuration [AIAA PAPER 67-308] 12 p2036 A67-26023

Shutter type thermal control system design for Nimbus spacecraft [AIAA PAPER 67-309] 12 p2012 A67-26024

Heat pipes and vapor chambers for thermal control of spacecraft, noting design and application [AIAA PAPER 67-310] 12 p2036 A67-26025

Spacecraft thermal joint conduction study covering surface conditions, external pressure, use of various fillers and parent materials and vacuum environment [AIAA PAPER 67-316] 12 p2037 A67-26031

Spacecraft thermal control coating experiments, discussing unreliability of degradation results due to failure to measure radiation properties, UV wavelength dependence and micrometeoroid damage [AIAA PAPER 67-329] 12 p2038 A67-26043

Thermal control coating degradation data from aluminum case containing four sensors aboard Pegasus spacecraft [AIAA PAPER 67-331] 12 p2038 A67-26045

Preflight testing of ATS-1 Thermal Coatings Experiment /TCE/, discussing cup designs, sensor and cup calibrations, etc [AIAA PAPER 67-333] 12 p2038 A67-26047

High energy particle and electromagnetic space radiation effects on thermal control coating, noting spectral absorbance for various conditions [AIAA PAPER 67-339] 12 p1959 A67-26053

Thermal control coating spectral sensitivity to UV induced degradation, noting rapidly increasing damage as incident radiation wavelength decreases [AIAA PAPER 67-340] 12 p1959 A67-26054

In situ measurements of diffuse hemispherical spectral reflectance of thermal control coatings irradiated in vacuo with various combinations [AIAA PAPER 67-342] 12 p1959 A67-26056

Low solar absorption surface coatings of aluminum, silver and silica with controlled emittance for spacecraft thermal control [AIAA PAPER 67-343] 12 p1959 A67-26057

UV stability of several white thermal control coatings spectrally characterized in vacuum for application to Lunar Orbiter project [AIAA PAPER 67-345] 12 p1959 A67-26059

Temperature control in design of ESRO I European research satellite 13 p2222 A67-26582

Spacecraft thermal control coating damage in simulated space-bombardment conditions, using plasma bombardment techniques 14 p2293 A67-28138

Parametric amplifiers as reliable low noise broadband microwave amplifiers 14 p2286 A67-28465

Ruby laser with Fabry-Perot interferometer selector studied for wavelength and thermal stability control 14 p2332 A67-28759

Effects of spacecraft sterilization procedures and Mars dust environment on thermal control coatings 15 p2503 A67-29541

Absolute spectral reflectance measurement in solar region in vacuo for applications to thermal control coatings 15 p2487 A67-29542

Thermal control materials for spacecraft, considering UV spectral distribution, radiation energy and flux, oxygen bleaching, etc 15 p2579 A67-29552

Fast warmup crystal oscillator, noting advantages and applications in equipment requiring low power consumption and frequency stability 15 p2445 A67-29584

Spacecraft surface temperature-control coating requirements, selection and performance in prelaunch and space environments 16 p2757 A67-30634

Diapason satellite thermal control noting external energy exchange calculation, coating, in-space simulation tests, temperature measurements, etc 16 p2762 A67-31018

Fluidics applications to ramjet control systems incorporating sensing, logic and actuation functions to inlet duct, flow-air ratio and coolant control 17 p2927 A67-31981

Thermal control surface contamination due to rocket exhaust plumes and effects on solar absorbance and IR emittance of protective coatings 17 p2833 A67-32076

Compact black body source utilizing thermoelectric heat pumping for uniform and stable temperature control 17 p2862 A67-33288

Control and measurement of temperatures of Mariner IV 18 p3052 A67-34514

Specific features of French Diademe satellites noting payload stabilization, thermal control observation carried, instrumentation, etc 19 p3333 A67-35500

Air conditioning system of P-3 aircraft, noting redesign to include auxiliary power unit for functioning during ground operation 20 p3363 A67-36512

Optimization for selection of optical coating patterns of external surfaces of spacecraft for temperature control [ASME PAPER 67-HT-55] 20 p3548 A67-36737

Spacecraft package temperature control by interior louver panel system, calculating net heat transfer [ASME PAPER 67-HT-64] 20 p3549 A67-36746

Environmental control for high performance military aircraft covering air conditioning, temperature and pressure control and oxygen supply systems 21 p3572 A67-39130

Spray and brush repair of zinc oxide-potassium silicate spacecraft thermal control paint, describing tests, surface preparation and coating application 22 p3826 A67-40111

Unmanned 0.1 AU /icarvs/ solar probe preliminary design, discussing thermal control and power supply problems unmanned 0.1 AU /ICARVS/ solar probe preliminary design, discussing thermal control and power 22 p3906 A67-40152

Experiments on undercooling and overcooling with liquid cooling garments, noting correct cooling defined by narrow biothermal response band 23 p3970 A67-41655

Liquid coolant space radiator system for manned spacecraft thermal control, investigating design and transient performance [SAE PAPER 670838] 24 p4252 A67-41994

Solar wind and UV exposure effects on spacecraft thermal control coatings, using in situ spectral reflectance measurements 24 p4174 A67-42040

Nuclear subsystem controls and instrumentation for NERVA noting automatic startup, override, power and temperature controller testing 24 p4183 A67-42471

Blower compressors for high altitude pressure and climate regulation in commercial aircraft 24 p4109 A67-42709

Simulated solar absorbance of spacecraft thermal control coatings determined calorimetrically in vacuum at room and cryogenic temperatures 24 p4256 A67-42913

TEMPERATURE DIFFERENCE

Heat flux sensor using piezoresistive thermometer for sensing small temperature differentials, discussing design, analysis and

- test 01 p0069 A67-11020
Comparison of temperature differences for similar liquids boiling on various surfaces, with graph correlating heat flux/temperature difference data 04 p0721 A67-14645
Forced-convective heat transfer in asymmetrically heated rectangular ducts as function of prandtl number, Reynolds number, aspect ratio and temperature difference 04 p0728 A67-15804
Composite coatings provide temperature differences at surface of hot stamped blanks, thereby making it possible to control strain distribution over surface 04 p0630 A67-15901
Heat losses in conductive and convective transfer through rarefied fluids investigated for dependence on temperature differences, static pressures, test geometries and fluids 10 p1731 A67-22725
Electron and ion temperature difference necessary to develop instability connected with loss cone of plasma with hot electrons placed in magnetic mirror 12 p1971 A67-25334
Radiometric observations of total lunar eclipse of December 19, 1964 at wavelength of 3.3 mm indicate no significant temperature difference [JPL-TR-32-1097] 12 p2011 A67-26245
Method to describe finite amplitude convection time dependence 14 p2295 A67-27901
Rocketsonde and radiosonde temperature comparisons and evaluation of computed rocketsonde pressure and density 14 p2347 A67-28885
Thermal accommodation coefficients determination in temperature jump region 15 p2580 A67-29883
Efficiency and thermodynamic parameters of possible closed-cycle flow schemes for base-load MHD generators 16 p2603 A67-30563
Mean flow refraction and temperature differences between mixing layer and outside fluid effect on HF component of jet noise 19 p3173 A67-34962
Temperature difference between solid and gas of transpiration cooled wall due to radiant heating [ASME PAPER 67-HT-29] 20 p3546 A67-36722
Noise occurrence during heat transfer from solid to liquid He 2 flux at high temperature difference, discussing heat flux 22 p3838 A67-40389
Boiling heat transfer to liquid helium, discussing heat flux as temperature difference function and surface finish effect 22 p3920 A67-40390
- TEMPERATURE DISTRIBUTION**
SA WALL TEMPERATURE DISTRIBUTION
Thermal stresses in isotropic circular cylinder under temperature distribution effect, reducing problem to solution of boundary value in form of Airy stress function 01 p0159 A67-10278
Pressure and stagnation temperature distribution in test chamber of blowdown hypersonic wind tunnel 01 p0049 A67-10558
Nonuniform temperature distribution effects on creep bending characteristics of linear viscoelastic columns of polymethyl methacrylate 01 p0160 A67-10560
Internal temperature distributions of present and proposed calorimeter geometries operating at high pressure and extreme heating rates compared, using one-and two-dimensional heat conduction programs 01 p0070 A67-11033
Hypersonic flow separation over simple geometries and aerodynamic controls, noting pressure gradients and heating-rate distributions [AIAA PAPER 65-753] 03 p0350 A67-12911
Pulsed laser techniques for measuring thermal diffusivity of graphites and chars between 500 and 5000 degrees F [AIAA PAPER 65-644] 03 p0449 A67-13062
Transient temperature distributions in simple bodies with internal cycled heat sources [AIAA PAPER 65-660] 03 p0534 A67-13065
Temperature and stress distributions in annulus partially filled with cold fluid 03 p0531 A67-14363
Temperature fluctuation in AC heated filaments and magnitude and phase of harmonic components of temperature 04 p0723 A67-15117
Temperature distribution in argon plasma jet with variable mass flow measured, using grating spectrometer [ASME PAPER 66-WA/HT-50] 04 p0669 A67-15434
Interdiurnal temperature variability distribution in northern hemispheric stratosphere in January and July, based on synoptic weather maps 04 p0616 A67-15473
Heat transfer in plane conducting fluid jet spreading over flat wall in transverse magnetic field, noting solution for temperature distribution for small MHD interaction parameters 04 p0670 A67-15520
Temperature and heat flux distribution in linear liquid-metal MHD device with direct cooling of winding 04 p0556 A67-15528
Temperature distribution and fluid flow in horizontal layer of liquid heated from below, having rigid-rigid and rigid-free upper surfaces 04 p0726 A67-15679
Transient temperature distribution in semiinfinite solid, plate, cylinder and sphere subjected to heating or cooling thermal radiation 04 p0737 A67-15865
Radiative heat transfer through openings of variable cross section, discussing temperature distribution and numerical results of right circular cone 04 p0738 A67-15870
Turbulent heat transfer in circular tube with circumferentially varying wall temperature and wall heat flux [ASME PAPER 66-WA/HT-3] 04 p0738 A67-15929
Stressed state of spherical shell under action of axisymmetric temperature field arbitrarily varying along meridian 05 p0914 A67-16197
Pebble-bed heater for hypersonic wind tunnel, evaluating heat-transfer coefficients from transient temperature distribution of bed 05 p0926 A67-16429
Temperature distribution effect on roughness of contacting surfaces of two juxtaposed solid materials 05 p0926 A67-16596
Coronal temperature and temperature distribution in transition region between chromosphere and corona, assuming photospheric wave propagation as essentially one-dimensional 05 p0900 A67-17077
Velocity and temperature profiles of optically thick planar Couette flow, obtaining heat transfer rates for Rosseland mean absorption coefficient variation with temperature 05 p0793 A67-17343
Plane flow of radiating gas over semiinfinite flat plate, considering upstream effect when energy equation becomes elliptical 05 p0928 A67-17358
Quasi-steady state temperature distribution in thick walled spherical satellite under solar radiation 05 p0906 A67-17368
Temperature distribution in isotropic solid with variable specific heat and thermoconductivity treated by Kantorovich method 05 p0929 A67-17373
Temperature distribution in two-layer plate during welding by laser light flux 05 p0814 A67-17548
Heat transfer in short circuit generalized MHD Couette flow for velocity field and temperature distribution, when walls are at equal and unequal temperatures in transverse magnetic field 06 p1039 A67-18070
Radiative heat exchange and equilibrium surface temperature in space environment [AIAA PAPER 67-212] 06 p1115 A67-18328
Static temperature-velocity distribution for zero pressure flat plate compressible turbulent boundary layer with heat transfer [AIAA PAPER 67-195] 06 p1116 A67-18362
Mathematical model for potential heating from gamma radiation source, determining transient temperature distribution for materials used in nuclear rockets 06 p1116 A67-18363
Radial temperature profile of magnetospheric plasma near equatorial plane observed by IMP 06 p0996 A67-18432
Temperature variation in wall of square channel due to heat transfer to turbulent flow of water and Hg 07 p1265 A67-19128
Time dependent temperature profile for stationary nitroglycerin powder combustion process 07 p1267 A67-19312
Phase effect during rectangular pulsations of heat transfer coefficient 07 p1267 A67-19325
Ranque effect, based on model of two-dimensional vortex flow of viscous thermoconductive gas, explains radial temperature distribution 07 p1268 A67-19351
Vertical velocities in atmospheric front motions, noting pressure and temperature field distributions and application of computer to solve obtained equations 07 p1219 A67-19356
Winter radio absorption anomaly at middle latitudes theory in terms of temperature and nitric oxide distributions in D region 07 p1171 A67-19415
Argon, helium and nitrogen high temperature plasma compositions used to calculate radial temperature distribution 07 p1229 A67-19566
Polarization and brightness temperature distributions across lunar disk observed with Parkes radio telescope at various wavelengths 07 p1251 A67-19854
Black Brant III sounding rocket analyzed via mathematical model to predict temperature distribution in ablation material 08 p1425 A67-20531
Surface effects for solid propellant combustion, discussing flame profile and instability, surface burning mechanism, temperature distribution, etc 08 p1373 A67-206422
Temperature distribution, stress distribution and displacement components for circular disk when temperature distribution at disk rim is step function of time, considering inertial terms in thermoelasticity equations 08 p1418 A67-20723
Heat transfer in constant property turbulent boundary layer with arbitrary distributions of wall temperature and stream velocity 08 p1428 A67-20927
Steady state temperature distribution in disk with radial flow of electric current derived with and without heat transfer conditions 08 p1427 A67-20925
Analytical solution for determining inlet and outlet temperature for space radiator with heat rejection rate for steady state conditions and zero irradiation environment 08 p1429 A67-21511
Time and local temperature distribution in semiconductor under heating pulse 09 p1579 A67-21700
Spectroscopic studies of plasma pulse discharge on hard electrodes in vacuum, determining excitation temperatures for various portions of jet 09 p1544 A67-21852
Nonuniform molecular density, pumping power and gas temperature distribution in evacuated space simulator 09 p1503 A67-22118
Temperature distribution in tail pipe of M701 engine, based on differences between readings obtained from onboard thermocouples 09 p1560 A67-22463
Light-beam waveguide using lens-like media with periodic hyperbolic temperature distribution, discussing construction, optimum design and operating conditions 10 p1606 A67-23066
Correlation of nitrogen vibrational-translational relaxation times for various measuring methods, noting temperature distribution of rate 10 p1733 A67-23151
Shape and location of diurnal bulge in upper atmosphere, analyzing density and temperature distribution at high latitude from satellite drag data 10 p1639 A67-23204
Cloud formation theory based on aircraft observations of low cloud layers, considering turbulent vapor and heat redistribution in layer 10 p1677 A67-23406
Shells of revolution having arbitrary stiffness distribution of loads and temperatures 10 p1730 A67-23771
Equilibrium and stability of K plasma with internal E field normal to confining magnetic field, noting wave propagation at ion momentum velocity 11 p1833 A67-24365
Approximate formulae for transient temperature prediction due to kinetic heating in aircraft type structures 11 p1883 A67-24601
Quantitative schlieren interferometry, measuring thermal distributions near heated vertical plate and horizontal cylinder 11 p1791 A67-24666
Heat transfer of fully developed laminar flow of Bingham material between parallel plates and linearly varying wall temperature, noting equations of state, velocity and temperature distribution 11 p1883 A67-24944
Reduction or elimination of secondary asymmetry voltage in germanium Hall

generators noting effect of surface recombination, temperature distribution stabilization, etc 12 p1939 A67-25278

High speed radial turbine rotor temperature distribution measured for pattern prediction of temperature 12 p1988 A67-25354

Reissner variational formulation of temperature distribution boundary value problem of axisymmetric thermal stresses in isotropic sandwich shells of revolution [AIAA PAPER 66-528] 12 p2030 A67-25917

Axisymmetric compressible turbulent wake fluctuating characteristics measured using supersonic wind tunnel, including radial velocity and temperature distribution, density, etc 12 p1893 A67-25928

Thermal properties of moon by comparing IR and microwave measurements of spectrum with theoretical calculation of upper layer temperature distribution [AIAA PAPER 67-289] 12 p2009 A67-26006

General heat flow problem with convolution integrals eliminated and unsteady temperature distribution expressed as sum of quasi-steady and transient fields, noting region geometry 12 p2040 A67-26185

26 month oscillation in zonal wind and temperature in equatorial atmosphere 13 p2150 A67-26440

Ablation study scheme enabling determination, for given environment and material, of ablation starting time and temperature distribution within mass of material 13 p2222 A67-26596

Thermo- and viscothermoelasticity foundations and problems 13 p2216 A67-26608

Random thermal-stress analysis for linearly elastic body assuming zero-stress state, uniform temperature and freely deformable surface of body 13 p2217 A67-26634

Water-vapor rotational band transmission function calculations by atmospheric inhomogeneity approximate methods 13 p2151 A67-26682

Thermal design of molten carbonate fuel cells using transpiration heating for reducing heat loss and control of temperature 13 p2055 A67-26842

Heat transfer and temperature distribution turbulence measurements with inclined hot wires 13 p2222 A67-26913

Hot wire response equations including tangential velocity effects and nonlinearities caused by high intensity turbulence 13 p2095 A67-26914

Turbulent mixing in plane nonisothermal jets, deriving solutions for velocity, temperature and pressure distribution 13 p2105 A67-27052

Temperature field in plates and shallow shells with internal heat sources noting solutions for various boundary conditions 13 p2224 A67-27056

Temperature field of coaxial cylinders obtained as infinite series of Bessel and trigonometric functions 13 p2224 A67-27057

Influence of grain-size purity relation beryllium fabrication and resulting mechanical properties 13 p2139 A67-27127

Distribution of radio brightness temperature over disk of Venus 13 p2200 A67-27333

Static magnetic field effect on normal distribution of pressure, temperature and density in solar atmosphere, considering sunspots and velocity field effects [AFCLR-66-679] 13 p2204 A67-27435

Heat equation for free boundary problem with prescribed flux at fixed and melting interface of semilinear slab 14 p2405 A67-28255

Solar corona temperature from intensity gradients measured during total eclipse of May 30, 1965 14 p2387 A67-28564

Hollow internally braced turbine blade design with uniform state of stress and temperature distribution 14 p2377 A67-28653

Lateral heating and sublimation of arbitrary thick two-layer plate using thermal flux time-dependent on plate surface 14 p2408 A67-28802

Radiative energy transfer through nongray medium bounded by two flat surfaces, obtaining temperature distribution and heat flux values 15 p2578 A67-29130

Temperature distribution for asymmetric heat transfer in turbulent flow between parallel plates 15 p2469 A67-29133

Aerodynamic heating through turbulent boundary layer of flat plate determined

using Ferrari formula 15 p2415 A67-29328

Temperature distribution from local regions of microscopically thin film junctions of metal structures, noting effect on average temperature 15 p2444 A67-29415

Temperature field of hollow cylinder with spatially distributed heat source, examining transient temperature distribution and thermal stresses in cylinder 15 p2574 A67-29775

Sensible heat transfer influence on dynamic stability of harmonic perturbations superimposed on zonal current, using Lorentz two-level model 15 p2512 A67-30057

Thermal stresses in three-layer cylindrical sandwich shell of finite length with rigid filler having temperature as function of radius only 16 p2765 A67-31049

Temperature distribution field of flame studied by applying holographic techniques in obtaining interferogram of inhomogeneity created by flame 16 p2672 A67-31066

Thermal turbulent boundary layer on flat plate with thermally insulated section, determining temperature distribution in presence of heat transfer 16 p2594 A67-31201

Antenna resolution by data processing noting limitations due to noise 16 p2639 A67-31339

Barometric and temperature coefficients determined from solar-diurnal, antisideral variation, atmospheric showers etc 16 p2741 A67-31900

Structural analysis and design of large area solar array, noting factors such as temperature distribution, dynamics, internal loads, permissible weight, etc 17 p2954 A67-31980

Thermoelasticity of thin cylindrical shells for linear temperature distribution and temperature independent elastic constants, deriving differential equations of heat conduction 17 p2958 A67-32034

HF electrodeless plasmatron working at atmospheric pressure, noting plasma discharge and temperature distribution characteristics, obtaining constricted plasma jet 17 p2897 A67-32175

Affine solutions for temperature/flux distribution on heated horizontal plate 17 p2838 A67-32701

Spark produced in cell containing argon when concentrating laser beam in small volume, calculating temperature distribution 17 p2869 A67-32804

Hydrogen and helium lateral flow in collisionless exosphere calculated on model for various sinusoidal temperature and concentration variations over exobase surface 17 p2852 A67-33235

A priori bound on difference between free boundary positions in two Stefan problems derived in terms of initial conditions and heat influxes 18 p3071 A67-33664

Temperature range approximation determination in unsteady thermal boundary layer formed in plane parallel flow around body, solving equation with boundary conditions 18 p3025 A67-33680

Rayleigh number effect on importance of convective heat transfer in self-heating gaseous reactions checked against thermal ignition theory 18 p3158 A67-33852

Plasma time-dependent luminosity from pulsed discharge in vacuum, determining excitation temperature distribution and discharge spectral lines 18 p3087 A67-34049

Vapor volumetric fraction during forced convection, calculating true local vapor weight, volumetric fraction, location of bubble departure, etc 18 p3160 A67-34163

Influence of dissipation of acoustic waves on temperature rise in chromosphere 18 p3125 A67-34192

Confined electric arc developed for gas-transport properties determination, noting measurement of flow pressure drop, radiative heat transfer, spectral temperature distribution, etc 18 p3091 A67-34731

Temperature distribution in vortex cooled hydrogen arc obtained by emission and absorption coefficients in plasma source 19 p3279 A67-35142

Electric arcs in cross flow with variable magnetic field across electrode space 19 p3281 A67-35154

Temperature, electron density, and relative particle density radial distribution and mass separation effect in free burning DC arc 19 p3281 A67-35156

Spectral composition of earth IR radiation

measured from satellites, giving radiation intensity and temperature distributions 19 p3219 A67-35253

Spacecraft surveys of earth used for city growth observations, draw land-use maps, etc 19 p3221 A67-35324

Temperature distribution within two-dimensional thermal boundary layer due to flow of second order fluid past flat plate 19 p3210 A67-35447

Thermal-stress distributions in circular disk due to instantaneous heat source on radius midpoint, assuming no temperature variation over thickness 20 p3536 A67-36418

Computer program for heat transfer calculation by temperature distribution along wall surface, using Fourier-Bessel series to determine distribution coefficients 20 p3544 A67-36450

Local heat transfer coefficients, mean temperature and velocity distributions in turbulent natural convection boundary layer on vertical plane surface [ASME PAPER 67-HT-17] 20 p3545 A67-36713

Approximate solution to heat transfer coefficient on flat plate in linear shearing flow [ASME PAPER 67-HT-46] 20 p3547 A67-36728

Transient temperature distribution of cylinder subject to radiation cooling, giving dimensionless computer-derived graphs [ASME PAPER 67-HT-71] 20 p3550 A67-36751

Heat transfer in fuel cell battery held in isothermal bath, giving charts for maximum temperatures at different Peclet numbers 20 p3364 A67-37016

Motion equations of incompressible nonisothermal fluid jet studied by closed similarity solutions, obtaining temperature distributions 20 p3423 A67-37209

Equations for transient temperature distribution and thermal stresses in heated idealized wing structure solved using heat flow analysis method 20 p3541 A67-37489

Transient temperature distribution for spherical region subjected to variable heat flux at boundary represented by terms of known functions and quadratures 20 p3555 A67-37610

Mathematical model for potential heating from gamma radiation source, determining transient temperature distribution for materials used in nuclear rockets 21 p3730 A67-37793

Temperature distributions and heat generation in viscoelastic isotropic solid resulting from mechanical deformations determined by energy equation 21 p3715 A67-37894

Strain energy in thin isotropic elastic shells subject to arbitrary temperature distribution, considering large deflections and buckling 21 p3718 A67-38021

Temperature variation in wall of square channel due to heat transfer to turbulent flow of water and Hg 21 p3731 A67-38170

Spatial electron temperature distribution in electrodeless discharge, noting thermal conduction effect [AIAA PAPER 67-692] 21 p3672 A67-38721

Electromagnetically driven confined viscous vortex flow with high positive radial Reynolds numbers, solving energy equation for temperature distribution [AIAA PAPER 67-730] 21 p3674 A67-38754

Atmospheric humidity effect on lower atmospheric layer turbulence above oceans, discussing velocity, temperature and humidity profile calculation formulas 22 p3828 A67-39220

Computer program charts for investigation of effect of temperature dependent thermal conductivity on transient temperature distribution of heated materials 22 p3916 A67-39481

Cooling of cylinder moving through fluid assuming fluid properties permit boundary layer approximations 22 p3918 A67-39782

Radial temperature distribution in high power argon arcs measured at atmospheric pressure and 5 atm for currents ranging from 200 to 500 amp 22 p3853 A67-40049

Variational formulation and Rayleigh-Ritz method for nonequilibrium viscous incompressible flows, obtaining velocity and temperature distributions 22 p3788 A67-40422

Thin plate temperature distribution from solving conduction equation, considering boundary convection losses and moving discrete heat source 22 p3920 A67-40424

Radiative heat transfer in radiating and

conducting media, calculating heat flux and temperature distribution for semisotropic model 23 p4083 A67-41718

Perturbation solution to one-dimensional nonadiabatic temperature distribution behind detached shocks taking into account absorption effects 23 p3992 A67-41738

Temperature distribution measurements behind shock wave front in discharge tube with air and Ar indicate undisturbed thermodynamic equilibrium of plasmas 24 p4141 A67-41936

Aerospace vehicle structure loading under structural integrity tests with simulated aerodynamic heating conditions, discussing computer relaxation solution for rod temperature distribution 24 p4172 A67-42036

Temperature variations of satellite with radiatively coupled isothermal inner shell having heat source analyzed via perturbation method for differential equations 24 p4253 A67-42051

Heat absorber temperature distribution, considering medium temperature and heat transfer coefficient arbitrary functions of time 24 p4154 A67-42215

Spectral lines diagrammed for temperature distribution in Ar plasma arc channel transverse emission with axial flow of working fluid 24 p4196 A67-42219

Temperature distribution of fluid in laminar boundary layer of flat plate and heat flow from fluid to plate wall 24 p4143 A67-42281

Temperature distribution in homogeneous eccentric annular layer with constant internal heat generation 24 p4254 A67-42286

Finite difference integration method for predicting flow velocity and temperature distribution of gaseous diffusion flame in axisymmetrical combustion chamber 24 p4091 A67-42383

Temperature distribution in solid rotating cylinder exposed to solar radiation using Fourier series expansion 24 p4255 A67-42482

TEMPERATURE EFFECT

SA HEAT EFFECT

Channel model examination of output-dependent radius of spherical plasma discharge in thermal equilibrium 01 p0118 A67-10045

Spin-lattice relaxation time dependence on temperature and magnetic field in neutron-irradiated quartz with paramagnetic defects at helium temperature range 01 p0127 A67-10064

Temperature dependence of complex initial magnetic permeability of cobalt-zinc ferrites over 0.1-2000 mc frequency range 01 p0128 A67-10079

Preparation temperature and condensation rate effect on current carrier mobility in lead selenide and telluride films 01 p0128 A67-10089

Temperature dependence of lifetime of electrons and holes in GaAs, noting trapping effect of recombination centers and capture levels 01 p0128 A67-10091

Photo-Hall effect and photoconductivity on compensated p-InSb at low temperatures, examining temperature dependence of carrier mobility 01 p0128 A67-10093

Peculiarities of Hall curves of n-type alpha silicon carbide, noting concentration of conduction electrons related to temperature 01 p0129 A67-10102

Energy levels in forbidden band of gallium arsenide alloyed with silver or gold, determining impurity levels from temperature dependence of electric conductivity and Hall constant 01 p0129 A67-10104

Temperature dependence of La-139 nuclear quadrupole resonance in lanthanum fluoride 01 p0129 A67-10149

Dilatometer for measurement of thermal expansion coefficient of solids and variation with temperature 01 p0062 A67-10195

Solvent and temperature effects on fluorescent emission of europium beta diketones 01 p0131 A67-10297

Temperature dependence of heat-pulse propagation in sapphire at low temperature intervals, noting phonon mean free path 01 p0131 A67-10341

Temperature dependence of optical phonon mean free paths and mean energy loss per collision predict avalanche multiplication and voltage breakdown of Si and Ge p-n junctions 01 p0132 A67-10374

Temperature, stress and displacement in

elastic bodies for random surface forces and randomly distributed environmental temperature 01 p0159 A67-10403

Ne-He laser output dependence on pressure and nonexcited atom concentration 01 p0090 A67-10512

Nonuniform temperature distribution effects on creep bending characteristics of linear viscoelastic columns of polymethyl methacrylate 01 p0160 A67-10560

Physical and environmental effects on energy dissipation characteristics of balsa wood [SAE PAPER 660657] 01 p0103 A67-10616

Anisotropy of Hall effect dependence on field and temperature in dysprosium crystal 01 p0133 A67-10743

Luminescence and conductivity of CdS single crystals, noting temperature effect and release mechanism of trapped electrons and holes 01 p0134 A67-10820

Amplitude-dependent internal friction and defect structures in pure aluminum measured by bridge-circuit method for difference temperatures 01 p0100 A67-10843

Electronic and molecular radial distribution functions for liquid carbon tetrafluoride using X-ray diffraction, determining orientational effects of carbon tetrachloride and temperature dependency 01 p0117 A67-10885

Clathrates exhibiting metallic conductivity and superconductivity at specific temperatures, noting transition temperature of nitrate salt 01 p0135 A67-10917

Buckling tests on uniformly heated thin cylindrical shells, noting load and temperature effects 01 p0163 A67-11013

Maximum alloying temperature and cooling rate of p-n junctions effect on volt-ampere characteristics of silicon diode and minority carrier lifetime 01 p0039 A67-11053

Temperature dependence of diffusion coefficient of Li in InSb prepared in wafer form 01 p0137 A67-11067

Optical transmittance of fused silica at elevated temperatures, showing shift in UV to IR absorption with increasing temperature 01 p0138 A67-11074

Temperature dependence of threshold for stimulated emission of Nd trivalent ion in several host lattices estimated from intensity variation of laser active fluorescence component 01 p0091 A67-11085

Response of temperature sensor bonded to metal strip pulse-heated by capacitor discharge technique 01 p0071 A67-11100

Hall coefficient variation with substrate temperature of thin films of tellurium, lead telluride and antimony 01 p0138 A67-11231

Temperature dependence of grain size in nonstoichiometric NbC between 1600 and 3300 degrees K in vacuum and Ar 01 p0102 A67-11245

Apparatus for measuring temperature dependence of thermoconductivity coefficient, thermal emf and specific electroresistance of cermet cylindrical shells 01 p0076 A67-11248

Neutrino flux recording for temperature determination of sun interior, discussing thermonuclear reactions 01 p0152 A67-11301

Integrated circuit reliability survey showing relationship of failure rate and temperature 01 p0042 A67-11365

Rankine and Brayton cycles for spacecraft power generation, discussing operation principles, advantages and performance characteristics 01 p0112 A67-11428

Geomagnetic field intensity measurement, based on observation that ferromagnetic minerals cooled in weak magnetic field from above Curie temperature acquire thermoremanent magnetization 02 p0236 A67-11477

Oscillatory low temperature photoconductive spectral response of p-type indium antimonide as function of electric field strength and temperature 02 p0280 A67-11487

Temperature effect in neutron component of cosmic rays and seasonal changes in intensity affected by interplanetary magnetic field 02 p0307 A67-11666

Substrate temperature effect on structure of evaporated alloy thin films 02 p0287 A67-11716

Electric resistance of discontinuous thin gold films as function of time and temperature 02 p0292 A67-11747

Electron transport through thin insulating barriers in various diodes, analyzing current dependence on temperature and film thickness for perfect and imperfect dielectrics 02 p0294 A67-11760

Electron-hole conductivity effect on temperature variations of Hall coefficient and Nernst-Ettingshausen effect in semiconductor 02 p0296 A67-11829

Hypervelocity crater size and target strength, relating force per unit area of crater surface to tensile strength of material 02 p0338 A67-12034

Long wave spacecraft antenna design, deployment and stabilization, noting environmental effects such as thermal expansion, solar pressure, etc [AIAA PAPER 66-848] 02 p0221 A67-12258

Relation between skin temperature and environmental air supply temperatures in fixed air-ventilated clothing assembly 02 p0188 A67-12346

Thermal atmospheric sounding, discussing carbon dioxide transmission function parameters, water vapor and temperature effect 02 p0239 A67-12377

Temperature dependence of elastic wave losses for bismuth germanium oxide, noting possible application for information storage VHF and microwave frequencies 02 p0300 A67-12507

Temperature tuning of lithium niobate optical parametric oscillator in visible spectrum, noting generated frequency dependence on pump frequency and longitudinal mode 02 p0253 A67-12511

Temperature and stress dependence of electron lifetime in p-type Si-B and Ge-Zn between 1.5 and 4.2 degrees K 02 p0301 A67-12523

Radiant equilibrium temperature of opaque absorbing body relation to radiative temperature variations of air 02 p0343 A67-12646

Temperature dependence of phase shift in magnesium-copper ferrite-chromite phase shifter as affected by microwave permeability 02 p0301 A67-12672

Strain-hardening and temperature dependence of mechanical properties of ternary ordered alloys on nickel-iron base 02 p0255 A67-12675

Temperature induced and optical quenching of emission recombination in gallium arsenide Be-doped electroluminescent diode 02 p0254 A67-12741

Anisotropy of magnetoresistance and Hall effect in n-GaAs, discussing conduction band structure in vicinity of edge 03 p0487 A67-12806

Optical phonons role in thermal conductivity of GaSb doped with Zn and Te in temperature range 80 to 600 degrees K 03 p0488 A67-12811

Temperature dependence of spectral distribution of radiation, excitation and quantum output of green luminescence of cadmium sulfide films 03 p0433 A67-12889

Lubricant testing for supersonic aircraft, examining temperature requirements, viscosity, evaporation characteristics, etc [DVL-606] 03 p0426 A67-13016

Optical properties of semiconductors by measuring spectral emittance of transparent and opaque solids and measurements on materials used in IR optics [AIAA PAPER 65-654] 03 p0418 A67-13034

Thermal emittance of nickel as function of oxide thickness measured, using filament in vacuum technique and microphotography [AIAA PAPER 65-673] 03 p0440 A67-13041

Determining dependences of criteria for metal cutting processes from studies of thermal effects 03 p0428 A67-13195

Cutting temperature and heat distribution in cutting tool and blank in superhigh speed cutting process for deformable aluminum alloys 03 p0428 A67-13197

Optical and electrical properties of barrier layers in Cu doped GaP, discussing intensity region of superlinearity dependence on temperature and IR light 03 p0491 A67-13202

Absorption dependence of ultrasonic waves in superconductors on amplitude of sound wave due to temperature 03 p0492 A67-13325

Energy exchange localization to cathode emitting area during field electron emission, noting dependence on temperature, work function and applied field 03 p0472 A67-13329

Longitudinal microwave phonons inducing tunneling in Al-Pb, Al-Sn and Pb-Pb superconducting diodes 03 p0379 A67-13330

Electrical conductivity and Hall coefficient temperature dependence in pure and alloyed Te 03 p0492 A67-13344

Hall mobility, Seebeck and Nernst coefficients measured in temperature range from about 100 to 350 degrees K for scattering mechanisms of conduction electrons in n type CdS 03 p0493 A67-13351

Temperature dependence of electrical properties of alpha-indium selenide n-type semiconductor single crystals 03 p0493 A67-13362

Boron filament preparation on fused silica substrates by decomposition of diborane 03 p0454 A67-13420

Fracture surfaces, Wallner lines and crack propagation velocity in precracked W monocrystals at 20-300 degrees K 03 p0445 A67-13471

Temperature effect on electron emission and stability of p-n junction using silicon and silicon carbide 03 p0494 A67-13487

Thermal conductivity and degree of blackness of aluminum oxide coatings at high temperatures, using argon plasma jets 03 p0536 A67-13608

Stabilizing effect of wall and thermal flux temperature variations over channel length on heat transfer coefficient of liquid flow 03 p0538 A67-13610

Temperature and purity dependence of nuclear-spin relaxation time in type II superconductor gapless region and volume average of density states on Fermi surface 03 p0499 A67-13937

Shrinkage process in zirconium diboride during sintering, noting variation with length of isothermal processing 03 p0456 A67-14191

Thermodynamic approach to flow phenomena based on temperature dependence of specific heat 03 p0537 A67-14304

Disintegration of alkali halide single crystals, polymers and glasses under laser radiation, noting parameters of disintegration region magnitude 03 p0439 A67-14367

Two-dimensional convective motion in rectangular cavity with vertical slides maintained at different temperatures, analyzing heat transfer 04 p0719 A67-14460

Domain structure of strontium ferrite investigated by Bitter powder pattern method in basal planes, showing dependence on magnetic field intensity, temperature and thickness of crystals 04 p0673 A67-14482

Metabolic reaction of deer mice to temperature and altitude, analyzing various enzyme systems 04 p0561 A67-14593

Spin relaxation times of ground state of atomic cesium in aromatic gases measured using optical pumping, noting dependency on temperature 04 p0660 A67-14611

Emissive power of germanium and silicon with various surface finishes in temperature range from 700 to 1200 degrees K 04 p0674 A67-14719

Temperature dependent thermal property models of lunar surface and radiative energy transport deduced from RF and IR observations 04 p0697 A67-14740

Thin walled elastic shell response to thermal excitation [AIAA PAPER 66-84] 04 p0709 A67-14841

Temperature dependence of migration of double positioning boundaries during growth of gold films inside electron microscope 04 p0675 A67-14924

Trivalent neodymium doped glass laser with internal imperfections due to optical pumping examined via optical metallography, transmission electron microscopy and electron diffraction techniques 04 p0632 A67-14927

Hydrogen oxidation noting explosive property as function of temperature, pressure, composition, etc 04 p0565 A67-15091

Carbon disulphide oxidation noting self-ignition temperature, explosion limits, reaction products, cool flame propagation, etc 04 p0566 A67-15093

Hydrogen sulfide oxidation, role of temperature and pressure, determining explosion levels 04 p0566 A67-15094

Stress-strain time relation in gallium doped p-type germanium, noting crystal dislocation and creep parameter temperature

dependence 04 p0677 A67-15121

Velocity measurements at various temperatures made with zinc sulfide thin film longitudinal acoustic wave transducers, used on germanium 04 p0621 A67-15127

Temperature dependence of electroconductivity of pure barium titanate and Fe-and Co-doped barium titanate crystals 04 p0678 A67-15130

Temperature and impurity ion concentration effect on minority carrier mobility in degenerate gallium arsenide 04 p0679 A67-15143

Temperature dependence of current-carrier concentration and electrical conductivity of p-type germanium containing beryllium and phosphorus 04 p0679 A67-15144

V-I characteristics of p-n junctions on In-Sb base, noting effects of surface etching, temperature and impurity concentration 04 p0680 A67-15157

Nonstationary flow of gas in transverse magnetic field, noting electric conductivity dependence on compressibility and temperature 04 p0685 A67-15178

Thermal conductivity of lanthanum and monochalcogenides, noting role and temperature dependence of crystal-lattice conductivity 04 p0680 A67-15287

Temperature and doping level effect on conduction band edge of n-type semiconductors, noting doublet shifts resulting in narrower forbidden energy gaps 04 p0681 A67-15292

Transverse magnetoresistance of n-type InAs, noting temperature effect and correlation with quantum theory 04 p0681 A67-15293

Cracking during welding of aluminum alloy noting effect of strain, maximum temperature and cooling rate [ASME PAPER 66-WA/MET-5] 04 p0639 A67-15341

Variation of elastic constants of molten silica at high temperatures measured, using pulse method 04 p0683 A67-15499

Thermal power and electrical conductivity of SnTe-InTe crystals, discussing temperature effect 04 p0683 A67-15581

Transient annealing following pulsed neutron exposure in silicon transistors and solar cells as function of temperature and injection level 04 p0684 A67-15693

Interchannel generation transfer and multichannel generation in laser with four unsplit levels, noting radiation density, temperature effect and variations in coefficients of losses 04 p0634 A67-15780

Simultaneous conductive-convective heat-transfer coefficient and heat flux temperature relation at solid moving liquid interface 04 p0730 A67-15817

Mach number and temperature ratio effects on convective heat-transfer coefficient to flat plate through turbulent boundary layer in air and Stanton number calculation in terms of drag coefficient 04 p0731 A67-15820

Temperature effect on diurnal variation of meson intensity at high latitudes, finding wave maximum amplitude in spring 05 p0796 A67-16117

Temperature perturbation in Thomas-Fermi functions for atom radius as related by Gilvarry to simpler Feynman-Metropolis-Teller case 05 p0848 A67-16132

Lifting capacity of two-layer cylindrical shell made of different elastically hardening materials, considering temperature effect 05 p0912 A67-16180

Elastoplastic deformation of cylindrical shell under cyclic axisymmetric unsteady temperature field 05 p0912 A67-16182

Anisotropy effect on strength of unwoven glass fiber reinforced plastic, ascertaining nature of stressed state arising at high temperature 05 p0912 A67-16183

Stressed state of viscoelastic cylinder with star shaped cavity caused by steady temperature field and distributed surface load in problem of elasticity 05 p0912 A67-16185

Quasi-static problem of generalized plane stressed state of thin plate, considering heat transfer on lateral surfaces and interaction between strain fields and temperature 05 p0913 A67-16186

Dynamic stability of coaxial cylindrical shells in nonuniform temperature field under uniformly distributed axial compression load 05 p0913 A67-16189

Progressive buckling of rectangular cross section bar under cyclic variations in temperature 05 p0913 A67-16193

Temperature stresses in plane elements by unsteady heat fields examined via polarization optical method 05 p0914 A67-16195

Quantum oscillations of Hall effect and longitudinal and transverse reluctance in n-indium antimonide, noting spin splitting and temperature and electron concentration effect on oscillation maximum 05 p0861 A67-16394

Steady state analysis of switching circuit using combination of transistors and tunnel diodes, considering temperature effect and thermal stabilization of operating points 05 p0772 A67-16452

Temperature variation of electric conductivity and carrier mobility in diffused germanium resistors doped with antimony for thermometry 05 p0773 A67-16464

Dislocation mechanisms for prismatic and basal slip in Ti at low temperatures, measuring critical shearing stress and temperature dependence of activation volume 05 p0828 A67-16467

Superconductivity in aged Zr-Nb alloys, noting transition temperature increase of quenched alloy upon aging 05 p0828 A67-16469

Electron spin resonance in phosphorus-doped silicon at various temperature ranges 05 p0861 A67-16499

Chromium ion concentration and temperature effects on spin-lattice relaxation times in ruby at liquid He temperatures in zero magnetic field 05 p0817 A67-16637

Hardness of polyesters copolymerized with styrene, determining reticulation and temperature effects 05 p0759 A67-16767

Magnetic properties of second kind superconductivity of indium-lead alloys as function of temperature down to 0.38 degrees K 05 p0864 A67-16893

Thermoelectric powers and conductivities of vanadium dioxide whiskers measured from 273 to 335 degrees K 05 p0864 A67-16898

Temperature and thickness dependence of critical field of superconducting Sn films measured and compared with nonlocal theoretical models 05 p0864 A67-16899

Temperature effect on impact ionization coefficient in SiC semiconductor p-n junctions with reversed current in strong electric field 05 p0865 A67-16916

LF photocurrent oscillation in high resistivity n-type GaAs, noting relation between amplitude temperature and light intensity 05 p0866 A67-16987

Temperature dependence of dielectric constant and existence of microwave dispersion in barium titanate above Curie point 05 p0868 A67-17060

Temperature dependence of electrical and galvanomagnetic properties of single crystal InSb dendrites 05 p0869 A67-17092

Magnon phonon scattering relaxation time as function of temperature and wave vector, calculating thermal conductivity of YIG 05 p0869 A67-17191

Optical absorption due to direct intervalence band transitions in Ge, noting effect of lattice temperature 05 p0869 A67-17192

Temperature dependence of three-phonon processes in solids noting application to Si, Ge, GaAs and InSb 05 p0870 A67-17198

Temperature dependence of emittance and electric resistance of tantalum, vanadium and niobium up to 2500 degrees C 05 p0831 A67-17312

Spectral emissivity of Ti from 1100 degrees K to melting point 05 p0831 A7-17318

Bias and random radiometersonde temperature errors effects in estimation of atmospheric downward, upward, net and equivalent IR irradiance 05 p0803 A67-17385

Annealing temperatures effect on Young modulus, temperature coefficient and crystallographic texture of Fe-Ni-Ti alloys after deformation 05 p0831 A67-17485

Temperature, admixtures, structural state and deformation rate on mechanical properties of refractory metals in niobium-tantalum and molybdenum-tungsten groups 05 p0831 A67-17502

Cold plastic deformation, rolling direction

and annealing temperature effect on mechanical properties of sheet niobium at room and high temperature 05 p0831 A67-17504

Titanium, zirconium and hafnium effect on recrystallization temperature and strength of alloys of molybdenum with carbon 05 p0832 A67-17508

Plasticity of cast molybdenum improved by vacuum-annealing at temperatures from 900 to 1200 degrees C 05 p0832 A67-17511

Brightness temperature of shock waves dependence on wave amplitude in xenon and air at high temperature 05 p0795 A67-17544

Cyclic load and temperature effects on creep behavior of Ni-base alloy Mar-M 200 between 1800 and 1900 degrees F 06 p1014 A67-17802

Temperature dependence of thermoconductivity of dysprosium between 1 and 4 degrees K 06 p1048 A67-17821

Superconducting transition temperature of thin film, showing growth of temperature and decrease in film thickness due to phonon electron interaction 06 p1049 A67-17886

Ambient medium temperature effects on microplasma phenomena and on breakdown voltage of silicon p-n junction 06 p1050 A67-17895

Properties of pyrolytically produced boron fibers, noting strength decrease with temperature increase 06 p1016 A67-17903

Burning rate of N powder dependence on light flux density and initial temperature range 06 p1112 A67-17958

Time lag in thermal coefficient of resistivity of Ge whisker explained in terms of point defect diffusion 06 p1050 A67-18144

Steady state thermal conditions in semiconductor thermoelectric cooling device 06 p1113 A67-18180

Heat treatment effect on structure, hardness, microhardness and corrosion resistance of VT1 titanium and OT4 titanium manganese-aluminum alloy sheets 06 p1018 A67-18236

Solubility limit of Fe in close-packed hexagonal alpha-Ti noting temperature dependence and superconductivity 06 p1051 A67-18370

Metastable form of C12 type calcium disilicide when under high temperature and pressure, noting X-ray diffraction powder patterns and superconductivity 06 p1051 A67-18372

Conductive heat transfer coefficient measurement from sphere to rarified gas mixtures over range of Knudsen numbers 06 p1117 A67-18388

Crack growth rate and measurements of temperature effect on low pressure fatigue of Al 06 p1019 A67-18561

Temperature dependence of electroconductivity of As-Su-Ge system in vitreous state 06 p1052 A67-18610

Temperature effect on electroconductivity of complex vitreous systems of K-Ti-Pb 06 p1053 A67-18613

Logarithmic particular solutions of nonhomogeneous equation of cyclic deformation of shallow conical shell under nonuniform heating 06 p1109 A67-18664

Thermally activated deformation relating flow stress to square root of dislocation density 06 p1053 A67-18755

Temperature dependence of threshold current in injection lasers in continuous operation under liquid nitrogen cooling 06 p1012 A67-18788

Far IR lattice bands in n-type indium antimonide single crystal 06 p1059 A67-18908

Anomalous temperature dependence of IR absorption in p-type germanium attributed to phonon induced effects 06 p1060 A67-18913

Emission spectrum of GaP diodes analyzed as function of current and temperature 06 p1062 A67-18931

Shubnikov-de Haas effect and electron band structure of cadmium arsenide, investigating temperature and orientation dependences 06 p1064 A67-18947

Quantum oscillations in magnetoresistance of n-type pure HgTe used to estimate electron effective mass and g value close to band edge 06 p1065 A67-18948

Magnetoresistance of heavily doped n-type silicon at liquid He temperature noting dependence on field strength and temperature 06 p1067 A67-18967

Reverse tunneling currents in GaSb tunnel diodes as function of temperature and voltage explained through band structure 06 p0972 A67-18977

Wind and temperature effects on transitory and cruise phases of supersonic flight 07 p1219 A67-19067

Isothermal kinetics and self-heating in binary mixtures of Mg and sodium nitrate as function of temperature and reactant composition 07 p1238 A67-19072

Diathermy, derivation of equation relating monochromatic/integral radiation energy ratio of solid material of fluid heat emitter to temperature 07 p1211 A67-19130

Temperature dependence of thermal emf, electrical conductivity, current carrier mobility and thermal conductivity of GeTe-GeSe solid solution 07 p1231 A67-19164

Hot cracking and strain-age cracking in heat affected zone of Rene 41 alloy weldments 07 p1198 A67-19215

Cooling rate from homogenization temperature effect on structure and properties of forged alloy KhN77TiLuR 07 p1199 A67-19241

Hydrogen distribution between phases in /alpha and beta/ titanium alloys at various temperatures 07 p1200 A67-19246

Hydrogen brittleness in Ti alloys, noting conditions of development 07 p1206 A67-19283

Temperature coefficient of combustion rate for mixtures of ammonium perchlorate with various hydrocarbons 07 p1287 A67-19311

Active slip volume /active crystal length/ concept in plasticity theory and relation to temperature and strain rate 07 p1232 A67-19636

Dislocation theory of slip geometry and temperature dependence of flow stress in bcc metals 07 p1209 A67-19641

Temperature dependence of residual resistivity of diffusing ions for electromigration of silver in copper and gold and self-diffusion of copper in aluminum 07 p1209 A67-19647

Temperature dependence of paramagnetic resonance spectral shifts in chromium-doped titanium oxide crystal of cross relaxation rutile maser 07 p1196 A67-19676

Deformation speed effect on structural changes in Ti, noting test results at 600 degrees C 07 p1209 A67-19735

Maximum permissible angle in beveling, springiness of beveled part and heating effect on beveling process analyzed, considering loading 07 p1191 A67-19747

Current constriction in p-n junction under thermal breakdown, deriving expressions for terminal voltage and radius of constriction 07 p1157 A67-19901

Second breakdown in transistors analyzed in terms of lumped parameters noting V-I characteristics, temperature effect, avalanche multiplication, etc 07 p1157 A67-19903

Effect of thermal escape on neutral hydrogen density above 120 km 07 p1181 A67-19936

Film resistance effect on low impedance tunneling measurements 07 p1234 A67-20101

Anisotropy and temperature dependence of upper critical field of type II superconductor single crystals with cubic structure 07 p1236 A67-20136

Temperature variation of spin-lattice relaxation time and spin-spin relaxation time in superconducting and normal states of vanadium compounds 07 p1236 A67-20139

Temperature effect on equilibrium carrier concentrations and intrinsic lattice defects in semiconductor with self-activated conductivity, considering cuprous oxide 07 p1237 A67-20177

Temperature dependence of critical field in superconducting vanadium 07 p1237 A67-20178

Current-voltage-temperature dependence of symmetric tunnel junctions, noting role of insulator thickness 07 p1237 A67-20184

Hot source temperature effect upon thermoelectric energy conversion, noting efficiency of various compounds 07 p1132 A67-20286

Unalloyed titanium properties dependence on deformation and temperature 07 p1211 A67-20290

Friction welding fundamentals noting bonding, heat effect, pressure, speed,

etc 08 p1333 A67-20357

Electric field domain motion in Ge samples with Au and Sb impurities, noting temperature and illumination effect on V-I characteristics 08 p1367 A67-20411

Temperature dependence of relaxation-type ultrasound attenuation maxima in plastic deformation of molybdenum and niobium single crystals 08 p1367 A67-20419

Temperature induced surface tension variation effect on motion of bubbles and drops, noting surface active substances 08 p1321 A67-20711

Aluminum alloy with various metal additions analyzed for aging, using electron microscope 08 p1342 A67-20806

Aging effect on structure of cobalt alloys annealed at 1200 degrees C suggests formation of laminar regions 08 p1342 A67-20812

Wall temperature effect on behavior of hypersonic stagnation region shock layer in incipient merged layer flow, obtaining enthalpy function profile 08 p1278 A67-20928

Sporulation mutations induced by heat in *Bacillus subtilis* 08 p1287 A67-20983

Electroconductivity variations in CdS and CdSe single crystals with SHF electric field strength, intensity of bias lighting and temperature in minus 70 to plus 70 degrees C interval 08 p1370 A67-20996

Lunar ablateness due to thermal effects associated with decrease of mean surface temperature from equator toward poles 08 p1389 A67-21012

Treatments of drift wave velocities in Cs and K plasmas, noting radial electric field effect made negligible by reducing cathode temperature gradient 08 p1362 A67-21147

Electron scattering mechanism in SiC polytypes, noting mobility limiting mechanism from 300 to 800 degrees K 08 p1370 A67-21293

Electron mobility measurements in n-type SiC polytypes noting temperature dependence 08 p1370 A67-21294

Approximation method for calculating self-ignition delay for monodisperse air-fuel mixtures 08 p1428 A67-21425

Temperature dependent variations in Hall coefficient of indium and indium-rich alloys with Pb, Cd, Ti and Hg 08 p1371 A67-21438

Theory of superconductivity on basis of phonon model for finite temperatures, comparing four-fermion/electron interaction with Bardeen hamiltonian model theory of superconductivity on basis of phonon 08 p1372 A67-21491

Forward bias V-I characteristics for heterojunction in which tunneling dominates, noting temperature effect 09 p1551 A67-21666

Second order strain accumulation in aluminum in reversed cyclic torsion at elevated temperatures 09 p1517 A67-21753

MHD flow of viscous conducting fluid jets and MHD flows with nonlinear temperature dependent conductivity 09 p1541 A67-21807

Shear modulus determination from free flexural vibrations of sandwich beams with steel facing, using filled elastomer as core 09 p1574 A67-21838

Temperature dependence of saturated vapor pressure of sodium and potassium 09 p1579 A67-21857

Average diffusion coefficient and apparent effective charges of components of alloys of Ti-S system 09 p1553 A67-21906

Probability of effervescence of superheated liquids as function of temperature and pressure, analyzing N-pentane and hexane under isobaric heating and reduced pressure 09 p1580 A67-21907

Thermoconductivity values as function of temperature for semiconductors, noting effect of doping, alloying, etc 09 p1553 A67-21943

Twinning and temperature effect in plastic deformation of titanium 09 p1518 A67-21965

Paramagnetic Knight shift in metals and semiconductors as affected by temperature and magnetic and electric field intensity 09 p1554 A67-21972

Hydrostatic pressure and temperature effect on current-voltage characteristics of tunnel p-n junctions in gallium arsenide 09 p1554 A67-21977

Response of fungi to diurnal temperature extremes, describing soil, simulated Martian temperature regime and fungi growth 09 p1454 A67-21991

Saha-Langmuir formula applied to

description of temperature dependence of positive ion current in surface ionization of silicon atoms, comparing work functions by methods using contact potential, thermionic emission and Richardson graphs 09 p1554 A67-22006

Stability of palladium oxide resistive glaze films, describing process variables affecting resistivity and TCR 09 p1473 A67-22019

Vacuum ionization gauge reading dependence on localized gas densities caused by chamber temperature nonuniformity 09 p1498 A67-22108

Laser radiation effect on solids, noting laser properties, temperature rise, melting, vaporization and particle emission of materials 09 p1513 A67-22144

Dynamic plane shear of incompressible viscoelastic material with temperature dependent viscosity determined, using electric transmission line analog 09 p1533 A67-22152

Temperature dependence of threshold voltage, effective mobility in inversion layer and channel conductance of MOS transistor below saturation 09 p1475 A67-22204

Operating temperature effect on vacuum emission stability of vapor-deposited tungsten clad UC-ZrC and uranium dioxide 09 p1449 A67-22347

Effects of additions of carbon, nitrogen or oxygen on properties of vapor deposited tungsten 09 p1519 A67-22348

Structures and materials for supersonic aircraft and space vehicles 09 p1576 A67-22429

Phonon lifetime variation effect on stimulated Brillouin and Raman scattering in gases by temperature, pressure and laser power variation and comparison with Stokes gain theories 10 p1662 A67-22758

Far IR reflectivity of potassium tantalate analyzed as function of temperature, noting soft mode as temperature lowers towards Curie temperature far IR reflectivity of potassium tantalate 10 p1688 A67-22766

Elastoplastic properties of copper, aluminum alloys and brass under explosive load, noting increased temperature effect on elastoplastic wave parameters 10 p1668 A67-23092

CdS solar cell model noting spectral response, V-I characteristic and temperature variation 10 p1596 A67-23164

Correlation among room temperature creep stresses, fatigue and proportional limit in titanium alloys 10 p1669 A67-23325

Temperature effect on microwave gain characteristics of bulk GaAs amplifier, interpreting results in terms of changing carrier concentration 10 p1612 A67-23371

Exponential sintering temperature dependence of conduction electrons density and attendant decrease of mobility due to ionized impurity scattering in cadmium oxide 10 p1691 A67-23503

GaAs semiconductor quantum generator heating during injection pulse, analyzing temperature effect on external quantum output and generator efficiency 10 p1666 A67-23568

Frequency temperature dependence of longitudinal and transverse hypersonic wave absorption coefficients in quartz and artificial ruby crystal 10 p1693 A67-23582

Temperature dependence of Hall constant and photoconductivity kinetics of gallium antimonide with different tellurium content 10 p1694 A67-23651

Temperature dependence of electrical properties of compensated GaAs 10 p1694 A67-23655

Temperature dependence of Hall coefficient of tellurium doped GaAs ternary compound, noting activation energy parameter 10 p1694 A67-23656

Wall temperature and speed ratio effects on free molecule flow number density distribution about flat plate 11 p1881 A67-23880

Cooling and heating effectiveness of plane surface in turbulent air flow by injection of air film, noting temperature effect 11 p1881 A67-23898

Single conduction band approximation of nature of increase with temperature of thermal conductivity of ZrC and NbC in terms of scattering and Fermi energy 11 p1804 A67-23902

Temperature dependence of total intensity in difference band systems, difference

transitions between nondegenerate vibrations compared with carbon dioxide band 11 p1821 A67-23960

Temperature dependence of thermal diffusivity of tantalum and niobium 11 p1804 A67-24035

Relaxation, creep and modulus of rigidity lowering in compression springs under high temperature 11 p1795 A67-24090

Temperature effect, including liquid helium temperature, on yield stress of commercial purity alpha titanium 11 p1805 A67-24111

Efficiency of electroluminescent lamps, noting dependence on arsenic pressure and temperature during GaAs crystal growth 11 p1845 A67-24140

Bulk reverse current in diffused Si power rectifiers, interpreting reverse characteristics in terms of thermal pair production 11 p1760 A67-24144

Tensile strength retaining characteristics of aluminum alloys determined after varied soaking periods at various elevated temperatures 11 p1805 A67-24271

Heat and mass transfer during stationary adiabatic vaporization of water ethanol and carbon tetrachloride 11 p1882 A67-24319

Heat regeneration and high gas temperatures for fuel economy in helicopter gas turbine engines 11 p1852 A67-24525

Superconducting energy gap of cubic and hexagonal LA obtained by point contact tunneling to bulk samples, noting V-I characteristics and temperature dependency 11 p1846 A67-24585

Fiber reinforcement theory, considering strengthened metal behavior at elevated temperatures and under work hardening conditions 11 p1807 A67-24635

Composite materials potential in structural engineering 11 p1807 A67-24638

Temperature effects in wave propagation on drifting carriers in semiconductors 11 p1847 A67-24720

Co-Ni system heterodiffusion and interdiffusion coefficients variation with temperature and composition 11 p1808 A67-24772

Dependence of creep, corrosion and thermal fatigue of gas turbine vanes and blades upon inlet temperature and rate of change [ASME PAPER 67-GT-17] 11 p1808 A67-24801

Elastic surface waves excitation method in quartz at high frequencies, noting absorption temperature dependence 11 p1848 A67-24835

Laser emission temperature dependence resulting from variation in radiationless transfer of excitation in trivalent erbium and thulium 11 p1803 A67-24836

Temperature dependence of elastic constants of molybdenum single crystals measured, using thin rod resonance techniques 11 p1809 A67-24908

Stress and temperature dependence of motion of edge dislocations in nickel single crystals 11 p1809 A67-24920

Nonstationary gunpowder combustion at various pressures analyzed for combustion rate and surface temperature dependency on pressure and initial temperature 11 p1884 A67-24957

Electric field intensity distribution over length of plasmatron arc stabilized by longitudinal vortex air flow 11 p1843 A67-24972

Temperature dependence of thermal conductivity and phonon and electron components in solid and liquid n- and p-type semiconductors 11 p1851 A67-24975

Synthetic pink-ruby crystal demagnetization characteristics when employed as coolant in cryostat, noting temperature dependence 11 p1851 A67-25033

Transistor noise coefficient dependence on acoustic frequency, temperature, emitter current and collector voltage 11 p1769 A67-25037

Temperature dependence of Youngs modulus of tantalum alloy determined together with free-free vibrations and resonance frequency 12 p1954 A67-25141

Temperature dependence of electroconductivity of pure barium titanate and Fe- and Co-doped barium titanate crystals 12 p1978 A67-25154

Temperature and impurity ion concentration effect on minority carrier mobility in degenerate gallium arsenide 12 p1979 A67-25166

Temperature dependence of current-carrier concentration and electrical conductivity of p-type germanium containing beryllium and phosphorus 12 p1979 A67-25167

Spin wave theory of thin ferromagnetic films, Curie temperature decreases monotonically with decreasing film thickness spin wave theory of thin ferromagnetic films analyzed, showing Curie temperature decreases 12 p1981 A67-25239

Magnetic ordering effect on electrical properties of antiferromagnetic semiconductor MnTe indicate temperature anomaly above 440 degrees K 12 p1982 A67-25326

Time variability of bearing clearance due to temperature and pressure treated by iterative-numerical calculation 12 p1949 A67-25330

Structural changes effect on creep resistance of heat resistant alloys 12 p1955 A67-25371

Temperature dependence of volt-ampere characteristics of silicon space charge limited diode compared with ordinary diodes 12 p1914 A67-25459

Crystallographic anisotropy of electrical properties of thin film CdS photoresistors explained via potential barrier orientation theory 12 p1984 A67-25520

Absorption spectra and luminescence of p-type copper diffusion doped Ga-As crystals, noting appearance of temperature dependent narrow spectral lines 12 p1984 A67-25522

Bending of three-layer plate freely supported along four edges in presence of variable surface heating 12 p2022 A67-25588

Double cantilever beam specimen for determining plain strain fracture toughness of metals 12 p1956 A67-25946

Temperature-dependent thermoconductivity of metal film on insulation laminations in relation to bulk parent material in insulation systems of cryogenic propellants [AIAA PAPER 67-295] 12 p2035 A67-26010

Heat capacity evaluation between 150 and minus 180 degrees C, using evaporated gold-black coating as primary standard [AIAA PAPER 67-303] 12 p1958 A67-26018

Thermal modeling applicability to steady state and transient conditions, considering material property changes with temperature [AIAA PAPER 67-305] 12 p2036 A67-26020

Proton radiation effects on mirror reflectance in high vacuum at various temperatures, degradation by blistering found to be highly temperature-dependent [AIAA PAPER 67-341] 12 p1957 A67-26055

Ionization dependence of Na, K, Ca, Mg, Al, Fe and Si on arc temperature, noting correlations between temperature and electron concentration independent of plasma composition 12 p1977 A67-26108

Shock tube analysis of oscillation relaxation in iodine between 1000 and 3800 degrees K 12 p1930 A67-26115

Concentration limits of ignition of methanol and formaldehyde mixtures at atmospheric pressure and from 20 to 280 degrees C 12 p2039 A67-26118

Hypersonic sound velocity dispersion in liquids of low viscosity analyzed using Mandelstam-Brillouin components 12 p1967 A67-26133

Solid solubility of boron in graphite as function of temperature and nature of solution from density and lattice constants 12 p1960 A67-26189

Electrical conductivity measurements of NaCl as function of particle size and temperature used to study subsurface diffusion 12 p1987 A67-26191

Time-integrated and time-resolved spectra of GaAs laser diode, noting temperature effect on spectral emission 13 p2125 A67-26427

Anomalous photovoltages in CdSe and CdS thin layers 13 p2175 A67-26429

Temperature dependence of bcc metals elastic limit at low temperature, assuming sessile-dissociated screw dislocations formation during microdeformation, stressing stacking fault energy effect 13 p2130 A67-26438

Temperature dependence of yield point of crystals described in terms of thermally activated motion of dislocations in external forces field 13 p2131 A67-26449

Rare earth metals effect on Neel temperature and plasticity of recrystallized

chromium at 1200 degrees C in vacuum 13 p2131 A67-26450

Conductivity, temperature dependence, thermal EMF Hall constant, thermal conductivity and resistivity of aluminides of transition metals 13 p2131 A67-26471

Prediction of total emissivity of nitrogen-broadened and self-broadened hot water vapor 13 p2155 A67-26493

Piezoresistive effect of homogeneous silicon diffused elements 13 p2175 A67-26656

Seasonal variations in high latitude stratosphere and mesosphere 13 p2113 A67-26675

Temperature and environmental effects on mechanical behavior of metals 13 p2132 A67-26697

Temperature dependence of small signal AC field effect kinetics in silicon within 170-300 K, considering majority carriers and one energy level theory 13 p2176 A67-26708

Anisotropy of Hall effect dependence on field and temperature in dysprosium crystal 13 p2176 A67-26772

High temperature destruction of solid where one portion transforms into gas or liquid while remaining part forms porous frame 13 p2222 A67-26884

Entrance region tube flow combined with rounded entrance flow meters to obtain theoretical solution relating flow rate, downstream pressure, pressure drop and temperature 13 p2120 A67-26932

Noble gas molecular beam quasi-specular scattering from metal surfaces noting effects of beam incidence angle, molecular weight and gas temperature 13 p2099 A67-26949

Temperature dependence of energy levels of shallow donor impurities in silicon, noting electron-phonon interaction 13 p2176 A67-26987

Hafnium oxidation between 300 and 1200 C, noting occurrence of faster stages in process 13 p2132 A67-26999

Beryllium aging kinetics when having different purities 13 p2136 A67-27105

Beryllium oxidation in high temperature range 13 p2136 A67-27107

Curves of fusion and alpha-beta transformation of beryllium as function of pressure 13 p2137 A67-27110

Plastic deformation mechanisms of polycrystalline beryllium to analyze temperature dependence of critical shear in prismatic plane 13 p2138 A67-27121

High purity beryllium mechanical properties obtained by double electrolysis 13 p2139 A67-27126

Self-diffusion in high-purity tellurium between 300-400 degrees C 13 p2179 A67-27156

High pressure, uniaxial stress and temperature effects on GaAs electrical resistivity 13 p2180 A67-27159

Electron mobility in semiconducting strontium titanate 13 p2180 A67-27160

General model for semiconductor-to-metal transition 13 p2180 A67-27163

Relation between chromium cold-shortness temperature variations and structural changes under deformation, noting dependence on initial metallographic grain size 13 p2141 A67-27284

Electrically conductive self-similar gas flow in medium with given back pressure, assuming medium conductivity as function of temperature and density 13 p2169 A67-27307

Thermal phenomena arising upon projectile impact on metal surface 13 p2220 A67-27383

Texture strengthening and fracture toughness of titanium alloy sheets biaxial stress fields at room and cryogenic temperatures 13 p2142 A67-27442

Electrical and energy performance of high efficiency GaAs solar cells compared to silicon photocells, discussing temperature effect and p-n junction depth 13 p2056 A67-27623

Diffraction losses in resonator cavity decreased by thermal deformation of neodymium-glass crystal due to pumping with periodic pulses 13 p2130 A67-27629

Superconductivity of Nb₃Al-Mo₃Al binary system 13 p2184 A67-27631

Organic contaminant effects on relay reliability, discussing materials, degassing and contamination reduction 13 p2084 A67-27694

Electrical conductivity and Hall coefficient temperature dependence in pure and alloyed

Te 13 p2184 A67-27718

Trapped magnetic field effect on hydrogen plasma parameters in theta pinch, noting density and temperature dependence on initial pressure 14 p2353 A67-27751

Aluminum alloy forgings design 14 p2323 A67-27815

Temperature dependence of electrical conductivity and Hall effect of barium-titanate crystals reduced by hydrogen, observing electron spin resonance and optical absorptions 14 p2363 A67-27824

Temperature and carrier concentration effect on threshold electric field of current saturation and saturation drift velocity in gallium arsenide 14 p2364 A67-27826

Argon plasma thermal conductivity at atmospheric pressure and various temperatures determined in central zone of arc column 14 p2404 A67-28031

Galvanomagnetic properties of single crystal antimony as function of temperature, deriving carrier mobilities and densities, detailing nature of Fermi surface 14 p2364 A67-28105

High temperature corrosion and evaporation of Haynes 25 and Hastelloy X-280 in atmospheres of oxygen, carbon monoxide, carbon dioxide, water vapor and methane 14 p2336 A67-28148

Cadmium sulfide crystal photoconductivity peaks near band edge, noting heat treatment, temperature and defects 14 p2364 A67-28229

Carbon diffusion mobility in fused carbides of vanadium and titanium, giving carbon diffusion coefficient temperature dependence equations 14 p2337 A67-28285

Surface current change between critical paramagnetic and critical diamagnetic induced by temperature variation in type II superconductor immersed in static magnetic field 14 p2365 A67-28296

Activation energy of molecular relaxation processes in terms of areas under loss factor and reciprocal temperature curves 14 p2259 A67-28299

Nb-N system diagram for five stable nitride phases, giving two reactions governing high temperature phase fields 14 p2337 A67-28419

Temperature dependence of Hall mobility of photoelectrons and electrons produced by X radiation in cadmium sulfide single crystals 14 p2367 A67-28525

Depth of capture levels determined from temperature dependence of kinetics of gamma-conductivity or photoconductivity of cadmium sulfide 14 p2367 A67-28526

Generation mechanism of laser emission in cadmium sulfide-cadmium selenide crystals in presence of two-photon excitation at various temperatures 14 p2331 A67-28534

198 Au isotope diffusion in n-type indium arsenide at different temperatures 14 p2368 A67-28537

Experimental forging of titanium by techniques not requiring machining 14 p2324 A67-28629

Internal friction in nickel chromium alloys heated to annealing temperature, noting 530 and 800 degree peaks and origin of latter 14 p2338 A67-28675

Magnetic field effect on microwave surface impedance of superconducting tantalum measured in various temperature ranges via dielectric-resonator techniques 14 p2371 A67-28726

CdSb single crystals doped with Au at liquid helium temperature studied for temperature dependence and Hall effect 14 p2372 A67-28757

Effect of semiconductor glass shield temperature on absorption coefficient, output energy, pulse duration and energy and peak power of ruby laser 14 p2332 A67-28857

Fastener performance in commercial and aerospace application, considering component thermal expansion [ASME PAPER 67-DE-18] 14 p2327 A67-28872

Enthalpy changes in ammonium perchlorate during linear heating, noting crystal structure transformation and subsequent decomposition 14 p2376 A67-28903

MOS transistor channel conductance measured as function of gate voltage, noting variation with temperature 14 p2289 A67-28924

Electrical property change of pressure sensitive electronic components upon

embedding in casting resins, noting results of inductance changes in ferrite core transformer 14 p2341 A67-28954

Thermal stresses in thin shell in contact with smooth rigid container 14 p2403 A67-29011

Entropy applied to theory of fuel cells, noting effect of operating temperature 14 p2252 A67-29018

Biological and engineering problems in spacecraft sterilization, noting heat treatment 15 p2430 A67-29099

Exobiology and effect of physical factors on microorganisms 15 p2427 A67-29117

Recombination instability in plasma if temperature dependence is strong 15 p2522 A67-29208

Temperature dependence of current carrier mobility in nickel and iron oxide, noting scattering due to magnetic field 15 p2533 A67-29315

V-I characteristics of p-n junctions on InSb base, noting effects of surface etching, temperature and impurity concentration 15 p2534 A67-29344

Yttrium and gadolinium borides thermionic emission properties, noting inferiority to lanthanum hexaboride 15 p2534 A67-29358

Temperature dependence of electrical conductivity, Hall effect and resistance in transverse magnetic field for tin-doped InSb 15 p2534 A67-29385

Temperature distribution from local regions of microscopically thin film junctions of metal structures, noting effect on average temperature 15 p2444 A67-29415

Similarity criteria for plastic behavior of polymers under combined effect of nonuniform temperature field and hydrostatic pressure 15 p2573 A67-29466

Lanthanum chromite activation energy determination from electrical resistivity and Hall coefficient variation as function of temperature and IR absorption spectrum 15 p2535 A67-29478

Temperature dependence of lifetime and Hall coefficient in InSb, measuring lifetime by phase shift method, concluding that recombination centers are lattice defects 15 p2535 A67-29483

Vacuum thermionic work function and thermal stability measurements on crystal surfaces, discussing results on carbides, diborides and disilicides 15 p2535 A67-29486

Apparatus for direct weight loss recording of space materials 15 p2486 A67-29543

Solid rocket components exposure to elevated temperatures, hard vacuum and UV radiation during space flight and reentry 15 p2507 A67-29548

Nonmetallic materials for unmanned spacecraft 15 p2507 A67-29553

Silicones performance in high vacuum, temperature extremes and radiation environments of outer space, noting outgassing effect 15 p2508 A67-29557

Adhesives for nuclear powered spacecraft tested for pressure, temperature and radiation effects 15 p2508 A67-29560

Stratospheric temperatures in north and south polar regions shown to depend on land mass temperatures 15 p2475 A67-29579

Threshold temperature variation, output power and emission spectrum of short ruby crystals operated in quasi-continuous mode 15 p2498 A67-29665

Temperature dependence of complex permittivity and spontaneous polarization of SbSI single-crystal whiskers in phase transformation region 15 p2537 A67-29707

Parameters for model of two valence bands of SnTe according to Hall effect measurements at high temperatures 15 p2537 A67-29709

Temperature dependence of dielectric constant and existence of microwave dispersion in barium titanate above Curie point 15 p2538 A67-29791

Oscillator with lumped parameter superconducting LC tank circuit, noting frequency variations as function of temperature 15 p2451 A67-29916

Temperature homogenization effect on structure of industrial aluminum, determining mechanical properties dependency on Fe/Si ratio 15 p2504 A67-29975

Viscosity and thermoconductivity values of partially ionized argon plasmas derived by investigating temperature decay and stream

velocity distribution in argon plasma jet 15 p2531 A67-30203

Temperature dependent noise spectra of InSb single crystals, noting deep energy level and impurity energy 15 p2541 A67-30235

Fast neutron bombardment and temperature effects on conductivity, photoconductivity and resistivity of Si single crystals, determining energy levels of defects 15 p2541 A67-30236

Conductivity and Hall effect in analysis of temperature dependence of current carrier concentration and mobility in silicon, explaining ionization energy 15 p2541 A67-30240

Concorde structural development noting effects of temperature on fatigue and creep strength of aluminum alloys [AIAA PAPER 67-402] 15 p2578 A67-30369

Effective pair potential obtained for quantum electron gas to determine thermodynamic properties over large temperature and density range 15 p2533 A67-30383

High temperature vapor fractionation of silicate glass related to variations of oxygen isotopes in tektites 15 p2564 A67-30394

Statistical band model used to compute spectral emissivity in carbon dioxide micronband as function of pressure, optical path and temperature 15 p2521 A67-30429

Optimum Mach number for nonequilibrium helium-cesium plasma flow in MHD generator, explaining effect of deceleration temperature and internal efficiency level on optimum pressure 16 p2604 A67-30570

Surface charge density of MOS as affected by bias and temperature treatment 16 p2724 A67-30602

Electron recombination and capture processes at deep centers in n-type GaAs 16 p2724 A67-30604

Temperature dependence of properties of acceptor center in iron doped gallium arsenide, noting delocalization of cluster electron density 16 p2726 A67-30814

Microhardness and microstructure of annealed industrial nickel filings studied, noting results obtained at 300 degrees C 16 p2687 A67-30846

Temperature effect on impact ionization coefficient in SiC semiconductor p-n junctions with reversed current in strong electric field 16 p2727 A67-30893

Silicon negative-resistance junction diodes, studying n-p-n structure and diode characteristics dependence on light, temperature, voltage and frequency 16 p2636 A67-30898

Diurnal temperature change effect on F-2 layer, noting maximum electron density height dependence on neutral-gas temperature variations 16 p2663 A67-30967

Gain control of common emitter cascade by varying transistor regime, taking into account effect of operating frequency and temperature 16 p2637 A67-31027

Spin-lattice relaxation times in grown ruby in one phonon region, noting temperature dependence and undulation of lattice planes 16 p2728 A67-31054

Multiphonon relaxation in neodymium doped lanthanum chloride, determining transition rates between stark levels with lifetime and quantum efficiency measurements 16 p2728 A67-31057

Temperature effect in neutron component of cosmic rays and seasonal changes in intensity affected by interplanetary magnetic field 16 p2738 A67-31081

Electric and thermal conductivity and Hall effect in solid solution of complex semiconductors noting temperature dependence 16 p2729 A67-31155

Temperature dependence of transverse and longitudinal Nernst-Ettingshausen effect and composition effects on Hall electron concentration in InSb-InTe solid solution 16 p2730 A67-31157

Double-walled cryostat with copper holder for probe measurements of temperature dependence of semiconductor galvanomagnetic effects 16 p2730 A67-31158

Impurity concentration and temperature dependence of reverse current in indium antimonide diodes, determining components 16 p2637 A67-31162

N-type InSb electron thermoconductivity temperature dependence, lattice thermoconductivity and thermal

resistance 16 p2730 A67-31163

GeTe solid solutions reviewed considering thermal EMF, temperature dependence and current carrier mobility 16 p2730 A67-31164

Temperature dependence of thermal diffusion factors in ternary system He-Ne-Kr by two-bulb method 16 p2661 A67-31223

Temperature gradient effect on stability of inhomogeneous magnetically-confined plasma with frequent ion collisions 16 p2720 A67-31239

Fracture surface appearance and crack propagation velocity variation with stress and temperature in tungsten 16 p2688 A67-31302

Activation energies of nucleation of crack and dislocation loops in crystals, noting crack propagation theories and temperature effect 16 p2772 A67-31303

Titanium alloys crystal structures determined using single crystal X-ray and powder neutron diffraction method, noting mechanical properties temperature dependence and martensitic transition 16 p2688 A67-31307

Tensile and torsional fracture of low carbon steel at cryogenic temperatures, studying temperature and stress gradient effect 16 p2689 A67-31309

Low strain rate and temperature effects on crack initiation and growth, recovery and boundary migration for Al and Al alloy 16 p2689 A67-31368

High purity single crystal molybdenum electrical resistivity dependence on deformation 16 p2689 A67-31370

Microstructure stability of aluminum reinforced with Al-Ni whiskers, noting tensile strength and mechanical property dependence on temperature 16 p2690 A67-31372

Temperature dependence of thermodynamic functions of polyatomic gases at high temperatures 16 p2704 A67-31391

Effect of temperature dependence of plasma conductivity on magnetohydrodynamic channel flows 16 p2721 A67-31392

Cesium impurities analyzed for behavior in thermionic converters, investigating equilibrium state as function of pressure and temperature 16 p2609 A67-31399

Magnetoplasma diffusion equation of F-2 layer allowing electric currents and temperature variations, noting transverse drift of field 16 p2686 A67-31402

Crossed film cryotron as single stage high gain amplifier, noting design features and performance 16 p2640 A67-31431

Electrical conductivity and Hall effect of indium arsenide solid solutions, noting temperature dependence and hole mobility 16 p2732 A67-31480

Slow oxidation of n-octane vapor /oxygen/ nitrogen mixtures at reduced pressures and temperatures 16 p2779 A67-31518

Plane shock wave reflected from heat-conducting wall analyzed by method of matched asymptotic expansions 16 p2662 A67-31555

Energy dissipation and transport coefficients temperature dependence effect on short wave perturbation development in magnetohydrodynamics 16 p2723 A67-31578

Effect of temperature, density, and amount of stabilization on elastic modulus of zirconia 16 p2695 A67-31701

Dielectric constant measurement of solids at microwave frequencies, noting performance of solid dielectrics as temperature function 16 p2678 A67-31720

Proton-irradiation darkening of rock powders, noting contamination, temperature effects and applications to solar wind darkening of moon [JPL-TR-32-1130] 16 p2753 A67-31743

Density of lithium, sodium and potassium up to 1600 degrees C, using pycnometer method, showing dependence of density on temperature 16 p2692 A67-31773

Spatial correlation coefficients and transverse temperature perturbation scales during turbulent nonisothermal flow of mercury in circular pipe 16 p2724 A67-31776

Temperature effect on low-cycle fatigue behavior of Udmet 700 superalloy, noting internal and surface cracking 16 p2693 A67-31870

Soviet book on cosmic rays including solar-diurnal, 11-year and 27-day variations,

temperature effect, geomagnetic field effect, etc 17 p2930 A67-32077

Solar-diurnal variations of neutron and muon components of cosmic rays based on IGY data, analyzing temperature effect 17 p2931 A67-32079

Diurnal variation of hard component near minimum solar activity, emphasizing temperature effects 17 p2932 A67-32080

Temperature effect measurement of neutron cosmic ray component, noting results of Chicago and Hobart geophysical stations 17 p2933 A67-32088

Temperature effect on diurnal variation of hard cosmic ray component based on radio probe observations 17 p2933 A67-32089

Atmospheric temperature effect on latitudinal curve of cosmic ray intensity determined from radio probe observations 17 p2933 A67-32090

H, C, N, O, Cl, Ca and Al negative ion formation in plasma, noting role of continuous radiation, formation temperature and metastable and stable states 17 p2893 A67-32136

Black body radiation, pressure and temperature dependences of equilibrium composition, enthalpy, specific heat and electron density of air-carbon plasmas 17 p2894 A67-32147

Geometric dimensional, plasma temperature and pressure effects on capillary discharge with evaporating wall /CDEW/ 17 p2897 A67-32177

Preparation of doped and undoped epitaxial InAs with open tube vapor-phase transport system noting properties, temperature effects, electron mobilities, etc 17 p2911 A67-32194

MOS instabilities from ion drift, temperature dependent deep trapping and fast interface states from temperature stress, noting instabilities elimination techniques 17 p2823 A67-32195

Nitiluculent cloud formation by agglomeration of oxygen/ozone molecules in mesosphere layers 17 p2879 A67-32323

Temperature effect of cosmic ray neutron component 17 p2936 A67-32381

Seasonal variations in afternoon and evening maxima of F-2 layer and dependence of temperature and frequency on minimum zenith angle of sun 17 p2842 A67-32384

Thermal conductivity model for planetary igneous differentiation, discussing melting behavior as function of pressure and temperature 17 p2942 A67-32387

Thermal conductivity relation to density and temperature for normal hydrogen in dense gaseous and liquid states 17 p2969 A67-32446

Critical heat flux value nonlinearly dependent on liquid bulk underheating to saturation temperature, deriving empirical formula 17 p2970 A67-32460

Esaki diodes noting hump in V-I characteristics, temperature variation effects, etc 17 p2826 A67-32621

Temperature dependence of upper critical fields for clean superconductors of second kind, noting role of electron-reflection properties of surface 17 p2915 A67-32693

Temperature dependence and order of magnitude of barium titanate and strontium titanate determined from three-phonon diffusion process 17 p2915 A67-32706

Electromagnetic properties associated with presence of overlapping bands in pure superconductors, discussing temperature dependence 17 p2915 A67-32718

Temperature dependence of Josephson critical current in superconductor model having anisotropic energy gap 17 p2915 A67-32719

Evaluation of plasticity, durability and impact ductility of nonbrittle austenitic steel during high and low temperatures 17 p2873 A67-32767

Mechanical properties of titanium alloys at room and cryogenic temperatures 17 p2873 A67-32768

Mechanical properties of welded junctions of rolled sheets of aluminum alloys at room and cryogenic temperatures 17 p2873 A67-32769

Temperature dependency of specific heat of titanium base alloys 17 p2873 A67-32770

MOST behavior under irradiation studied for defect creation and ionization, charge displacements and preexistent trap

ionization 17 p2918 A67-32852
 Molybdenum/tungsten films obtained by thermal decomposition in vacuum analyzed, noting surface morphological changes with temperature changes 17 p2921 A67-32892
 X-ray absorption in chromium in chromium silicon after thermal processing at high temperatures 17 p2921 A67-32893
 Carbon silica reaction during erosion of silica-phenolic composites noting silica removal mechanisms 17 p2809 A67-33034
 Thermal nitridation of maraging steels, noting effects on mechanical properties 17 p2875 A67-33046
 Minority carrier trapping analyzed from transient decay of photoconductivity in n-type polycrystalline films of InAs 17 p2922 A67-33064
 Temperature dependence of grain size in nonstoichiometric NbC between 1600 and 3300 degrees K in vacuum and Ar 17 p2875 A67-33168
 Apparatus for measuring temperature dependence of thermoconductivity coefficient, thermal EMF and specific electroresistance of cermet cylindrical shells 17 p2861 A67-33171
 Multipass welded Hastelloy joint age embrittlement from exposure in inert atmosphere at high temperature, stressing ductility, tensile and hardness tests 17 p2866 A67-33199
 Temperature dependence of sound velocity in liquid helium at saturation vapor pressure and cryogenic temperatures 17 p2886 A67-33231
 Paramagnetic Knight shift in metals and semiconductors as affected by temperature and magnetic and electric field intensity 17 p2923 A67-33309
 Hydrostatic pressure and temperature effect on current-voltage characteristics of tunnel p-n junctions in gallium arsenide 17 p2923 A67-33314
 Channel model examination of output-dependent radius of spherical plasma discharge in thermal equilibrium 17 p2910 A67-33323
 Temperature dependence of Hall constant and photoconductivity kinetics of gallium antimonide with different tellurium content 17 p2923 A67-33332
 Temperature dependence of electrical properties of compensated GaAs 17 p2923 A67-33336
 Temperature dependence of Hall coefficient of tellurium doped GaAs ternary compound, noting activation energy parameter 17 p2923 A67-33337
 Magnetic field induced changes in Bardeen-Cooper-Schrieffer spectrum of electronic excitations in pure type I superconductor and effect on electromagnetic radiation absorption 17 p2925 A67-33374
 Magnetization in superconducting Mo measured in He 3 cryostat, noting transition temperatures and critical field 17 p2925 A67-33379
 Alpha particle irradiation effect at liquid-helium temperature on transition temperature of superconductive tin, indium and thallium foils 17 p2926 A67-33405
 Temperature and composition effect on ductility transitions, yield stress and dislocation pinning strength in iron base alloys due to change in slip 18 p3063 A67-33485
 Flow stress of fresh dislocations in titanium and vanadium doped MgO single crystals, measuring dependence on heat treatment and test temperature 18 p3097 A67-33492
 Hall angle of various superconducting niobium-tantalum alloys in mixed state, noting dependence on current and temperature 18 p3098 A67-33519
 Upper limit in flux density of intergalactic gas UV radiation measured from interplanetary satellite, showing temperature effect 18 p3116 A67-33524
 Conduction mechanism in GaSb tunnel p-n junctions from 77 to 380 degrees K, noting temperature dependence of basic parameters, V-I characteristics, etc 18 p3098 A67-33573
 Temperature dependence of threshold current in injection lasers in continuous operation under liquid nitrogen cooling 18 p3059 A67-33730
 Local stress measurement technique in

metals using temperature changes due to elastic deformation 18 p3141 A67-33887
 Gas temperature increase effect on thin walled container during prepressurization of high pressure blowdown systems [AIAA PAPER 87-443] 18 p3137 A67-33920
 Start characteristics of LM Ascent Engine determined by test series, noting effects of altitude variation, propellant lead time, temperature and valve slow-down [AIAA PAPER 87-522] 18 p3115 A67-33985
 Transient heat conduction in inhomogeneous solids with periodic temperature boundary conditions, using Keller perturbation method 18 p3159 A67-34007
 Temperature and magnetic field intensity dependence of microwave emission from n-type indium antimonide 18 p3101 A67-34016
 Cesium viscosity coefficient over range of temperatures and pressures, assessing accuracy of results and collision integral values 18 p3087 A67-34050
 Degree of blackness of normal black body radiation for various metals, studying temperature and kinetic relations and blackness of opaque oxide films 18 p3064 A67-34052
 Flow stress of aluminum related to strain, strain rate and temperature, discussing compression testing machine and results 18 p3064 A67-34078
 Strength characteristics of single crystals of nickel aluminide /gamma phase/, discussing temperature and orientation dependence of work hardening 18 p3064 A67-34079
 S-shaped boiling curves analyzed in terms of nucleation characteristics of heat transfer surface, correlating temperature driving force and density of centers 18 p3160 A67-34164
 Temperature and thickness effect on thermoelectric power by calibration curves of bismuth in thin layers, determining mean free path 18 p3102 A67-34188
 Temperature effect on gas saturation in alpha and beta titanium alloys 18 p3065 A67-34292
 Temperature and frequency response of argon arc continuum emission coefficient, explaining unexpected deviations 18 p3089 A67-34299
 Reversible contribution to flow stress in Ni-Al alloy analyzed by temperature change as function of tensile strain and precipitation hardening 18 p3065 A67-34363
 Crystallographic anisotropy of electrical properties of thin film CdS photoresistors explained via potential barrier orientation theory 18 p3103 A67-34451
 Absorption spectra and luminescence of p-type copper diffusion doped Ga-As crystals, noting appearance of temperature dependent narrow spectral lines 18 p3103 A67-34453
 Thermal conductivity and degree of blackness of aluminum oxide coatings at high temperatures, using argon plasma jets 18 p3161 A67-34473
 Stabilizing effect of wall and thermal flux temperature variations over channel length on heat transfer coefficient of liquid flow 18 p3161 A67-34475
 Mechanical behavior of boron-aluminum composites subject to stress, strain and temperature, discussing melt infiltration, powder metallurgy and diffusion bonding production [ASTM PAPER 9] 18 p3067 A67-34574
 Structural reinforced plastic composite materials for cryogenic temperature application evaluated noting tensile, compression, shear, flexural and bearing properties [ASTM PAPER 16] 18 p3070 A67-34577
 Frame-camera interferogram data for Nd-doped glass rod during laser pumping analyzed through optical path length changes 18 p3062 A67-34623
 Pump radiation induced optical distortion in Nd-doped glass laser rods measured and compared to theory 18 p3062 A67-34625
 Currents in copper phthalocyanine thin films measured as function of temperature and ambient noting effect on conductivity, trap density, etc 18 p3104 A67-34627
 Noise theory for self-sustaining discharge verified for low frequencies, noting temperature dependence, silicon, etc 18 p3106 A67-34638
 Time and temperature dependent diffusion

of vaporized Zn and Cd in n-type InAs 19 p3299 A67-34760
 Band structure and current carrier scattering in hole-type SnTe, studying temperature dependence of electric conductivity, thermal EMF, Hall effect, etc 19 p3300 A67-34766
 Temperature dependence of electric conductivity and Hall effect in epitaxial layers of undoped and Fe-doped n-type GaAs samples 19 p3300 A67-34770
 Photon generation threshold energy temperature dependence for gallium-arsenic epitaxial injection lasers 19 p3238 A67-34773
 Temperature effect on gold diffusion in crystalline and glassy cadmium germanium arsenide samples 19 p3301 A67-34776
 Diffusion welding of commercially pure titanium investigated for process parameters, noting temperature effect 19 p3234 A67-34792
 Flowgraph models of thermal and electrical parameters interaction in solid state devices, examining performance characteristics, system stability, etc 19 p3191 A67-34845
 Ionized gas produced by exploded lithium wires, presenting physical measurements, finding self-consistent solution of temperature and electron concentration 19 p3261 A67-35182
 Upper ionospheric electron density profile variation with sunspot number controlled by temperature and ion composition as shown from rocket data 19 p3218 A67-35222
 Shock wave interaction with plasma arc discharge, investigating wave refraction, arc response to pressure and temperature pulses and aftershock flow field 19 p3294 A67-35407
 Ion-density data modifications due to temperature variations, discussing normalization and electron density relationship 19 p3224 A67-35491
 Heat-transfer coefficient effect on final magnitude of stresses in elastoplastic spherical body subjected to cooling process 19 p3340 A67-35510
 Temperature and frequency effects on amplitude-independent longitudinal ultrasonic attenuation in superconducting lead 19 p3304 A67-35536
 Thin CdAs films thermal deposited in vacuum on various substrates investigated for electric properties 19 p3305 A67-35577
 Transient effects of changes in applied radio frequency power to which latching ferrite phase shifters could be subjected in array applications 19 p3196 A67-35663
 Alloying effect on temperature and strain rate sensitivity of niobium-molybdenum bcc metal 19 p3246 A67-35730
 Noise spectral density measured at low temperature in sensitized GaAs, studying relaxation time, temperature effect, etc 19 p3307 A67-35733
 Thermal fatigue hysteresis loop shape variations for Coffin-type test samples, stressing temperature-cycle effect 19 p3343 A67-35820
 Flowgraph models describing relationships between thermal and electrical parameters of devices and associated circuits 19 p3206 A67-36034
 Low temperature dependence of relative efficiency of forward biased InAs diode emitter 19 p3198 A67-36046
 Effect of semiconductor glass shield temperature on absorption coefficient, output energy, pulse duration and energy and peak power of ruby laser 19 p3242 A67-36108
 Temperature effect on mechanical properties of solids with high melting point, with quasi-static hardness as strength measure at high temperatures 20 p3463 A67-36111
 Temperature dependence of oxide hardness relative to other materials, comparing oxide hardness data to carbide data 20 p3472 A67-36113
 Thin cadmium telluride bombardment with indium ions, finding doping efficiency dependence on ion energy and temperature 20 p3504 A67-36160
 Temperature dependence of diffusion coefficient of zinc in gallium arsenide 20 p3504 A67-36162
 Current saturation in evaporated gallium arsenide films observed noting temperature effect, X-ray measurements, etc 20 p3505 A67-36177

Ultrasonic attenuation measurements at high magnetic fields in mixed state for clean and dirty limits 20 p3483 A67-36205

Heat treatment of indium antimonide crystals with various dislocation densities noting change in conductivity 20 p3506 A67-36227

Thermal diffusion in topside ionosphere, stressing effect on ion density profiles 20 p3427 A67-36304

Temperature dependence and anisotropy of high temperature ferrimagnetic microwave resonance linewidth of Si-doped YIG, showing valence exchange effect on losses 20 p3508 A67-36390

Temperature effect on seeding atom emission in argon plasma laminar jet 20 p3497 A67-36397

Temperature dependence of electrical conductivity in organic semiconductors, examining compounds during transition from solid to liquid state 20 p3508 A67-36404

Resonance frequency shift analysis of autostabilized light modulator at microwave frequencies noting heat transfer, transition temperature, etc 20 p3459 A67-36503

Nonequilibrium current carrier lifetime in p-type InSb samples alloyed with Cu and Ge, noting hole concentration and temperature effects 20 p3510 A67-36761

Temperature dependent viscosity effects on heat transfer and drag on wedge-shaped body, calculating boundary layers on surface 20 p3421 A67-36824

Influence of palladium additives and sintering temperature on tungsten molding noting shrinkage, density, microhardness, durability and microstructure 20 p3466 A67-36910

Low molecular weight polymer flow behavior variation with shear rate, shear stress and temperature 20 p3473 A67-36914

Rocket measurements above England, noting relation of temperature maximum at stratopause to mesospheric wind maximum 20 p3480 A67-36966

Tungsten-molybdenum alloy heat-resistant properties noting vacuum testing and subjection to plastic deformation, with results related to molybdenum content and temperature 20 p3467 A67-36968

Book on transistor electrical characteristics, discussing transistor model correspondence with real transistors, temperature variation effects, etc 20 p3399 A67-37010

Ambient temperature variation effect on gravitational acceleration variations as measured by gravimeter, discussing possible measurement errors 20 p3450 A67-37030

Energy band pinch effect in laser-heated GaAs, studying temperature effect on radiative recombination rate 20 p3460 A67-37106

Hardening during deformation in stoichiometric nickel manganite alloy noting temperature effect, surface characteristics and electric resistance 20 p3467 A67-37118

Tungsten sheets examined for recrystallization, grain growth and ductile-brittle transition temperature /DBTT/ as function of thermal treatment and grain size 20 p3467 A67-37119

Electric conductivity variation with temperature for solid ammonium perchlorate, determining energy barrier and enthalpy of lattice defect formation and migration 20 p3377 A67-37134

Survival and growth of *Bacillus cereus* and *B. subtilis* in simulated Martian environment of diurnal temperature cycling and low moisture and oxygen level 20 p3372 A67-37160

Titanium plasticity and durability under large temperature range as affected by Re, Ta, Pd and La alloying elements 20 p3468 A67-37175

Molybdenum-boron system structural diagram, noting carbon effect on phase equilibria and temperature effects 20 p3468 A67-37177

Ni-Fe-Mn alloy, Youngs modulus and magnetic saturation temperature dependence, noting order-disorder effects on Curie point 20 p3468 A67-37178

Anisotropic composites viscoelastic analysis applied to orthotropic cylinder pressurization, glass fiber cooling and relaxation shear moduli 20 p3474 A67-37267

Dynamic microstrain of niobium,

considering purity and temperature effects, obtaining activation energy band spectrum 20 p3469 A67-37385

Time dependent variations in parameters of junction semiconductors investigated for stability 20 p3401 A67-37450

Computer interconnection resistance causing propagation delay in circuits, suggesting low temperature use as possible remedy 20 p3393 A67-37457

Remote preamplifiers in multielement antenna arrays of radio telescopes operating at meter wavelengths, noting noise temperature effect 20 p3403 A67-37508

Low temperature and irradiation environment effects on mechanical properties of engineering materials 20 p3418 A67-37532

Dependence of electric resistance of thin Permalloy films on substrate temperature during evaporation and vacuum heat treatment 20 p3514 A67-37555

Temperature /K-state/ effect on dislocation blocking stresses in nickel alloy studied by mechanical hysteresis method 20 p3471 A67-37558

Temperature dependence of far IR collision-induced absorption as probe of rare gas mixtures interatomic potentials 20 p3490 A67-37567

Longitudinal ultrasound attenuation in polycrystalline superconducting mercury at 9.3 GHz, studying temperature dependence 20 p3514 A67-37568

Zn doped polycrystalline GaAs film electrical properties temperature variation 20 p3514 A67-37602

InBi single crystal electrophysical properties, giving temperature dependences 20 p3514 A67-37605

Attenuation cross section at Lyman alpha for Xe deviation from Beer law indicating diatomic Xe molecule formation 20 p3491 A67-37688

Electric conduction in solids, considering impurity, temperature and light effects on resistivity to electric currents 20 p3515 A67-37716

Lifetime decrease of metastable state of chromium ion in ruby and emerald due to temperature raise, showing radiative transition 21 p3678 A67-37816

Current carrier recombination processes in pure, preheated and Cu-doped GaAs, studying temperature and concentration dependence of intrinsic and impurity photoconductivity 21 p3676 A67-37863

Aluminum alloy creep rates with changing temperature and stresses in hollow sphere, using time dependent viscosity coefficient 21 p3643 A67-38019

Temperature, admixtures, structural state and deformation rate on mechanical properties of refractory metals in niobium-tantalum and molybdenum-tungsten groups 21 p3644 A67-38029

Cold plastic deformation, rolling direction and annealing temperature effect on mechanical properties of sheet niobium at room and high temperature 21 p3644 A67-38032

Titanium, zirconium and hafnium effect on recrystallization temperature and strength of alloys of molybdenum with carbon 21 p3644 A67-38036

Plasticity of cast molybdenum improved by vacuum-annealing at temperatures from 900 to 1200 degrees C 21 p3644 A67-38039

Contaminant control in space cabins by systematic screening of materials and supplies used, noting significance of test temperature 21 p3577 A67-38077

Sputtered films stable fcc modification of several metals deposited at high temperatures, obtaining normal structures over 400 degrees C 21 p3677 A67-38091

Low temperature effect on physical and mechanical properties of engineering materials and cryogenic fluids, discussing heat generation and removal at rubbing surfaces 21 p3633 A67-38141

UV radiation detection using silicon carbide p-n junctions, showing wavelength increment at peak response and decreasing photovoltage with increasing temperature 21 p3591 A67-38156

HF resonance probes, giving theoretical results of nonzero electron plasma temperature effect and experimental results with plasma between plates of plane capacitor 21 p3626 A67-38220

Junction temperature current dependence in CW operated gallium arsenide laser diodes 21 p3639 A67-38256

Temperature effect on Ni thermal diffusivity measured using ruby laser pulse 21 p3640 A67-38262

Elastic spherical shell stability under thermal stresses from abrupt temperature change at shell equator solved, using Fredholm integral equation 21 p3721 A67-38308

Temperature effect on diffusion coefficient of radioactive phosphorus in epitaxial Si layer 21 p3681 A67-38361

Electron-temperature dependence of electron collision frequency in afterglow plasma 21 p3687 A67-38414

Frequency of noctilucent clouds studied as function of meteorological conditions of mesopause 21 p3618 A67-38447

Ruby laser radiation frequency temperature dependence, observing narrow spectral width with Fabry-Perot interferometer 21 p3640 A67-38451

Mechanical thermal pulse techniques for precision bonding, emphasizing band and joint type connection and bonding to unstripped plastic insulated wires and cables 21 p3635 A67-38625

Oxidation mechanisms for nickel-aluminum alloys studied for effects of temperature and alloy composition 21 p3645 A67-38773

Diffraction losses in resonator cavity decreased by thermal deformation of neodymium-glass crystal due to pumping with periodic pulses 21 p3642 A67-38825

Superconductivity of Nb₃Al-Mo₃Al binary system superconductivity of Nb₃Al-Mo₃Al binary system 21 p3685 A67-38828

Excited nuclei electromagnetic de-excitation rate by inelastic scattering in stellar particles calculated as function of temperature, density, transition energy and multipole functions 21 p3680 A67-38846

Normal stresses induced by temperature effects in thin walled bars, assuming nondeformability of contour and no displacements in middle surface 21 p3728 A67-38905

Electron beams applied during pressworking of sheet materials to provide temperatures favorable to microstructure defect healing 21 p3678 A67-38927

Measuring device for frequency and resistance change measurements in quartz crystals due to temperature variations 21 p3601 A67-38975

Pseudopotential-structure factor relation for small wave vector applied to liquid alkali metal electric resistivities and temperatures 21 p3686 A67-39102

Electrical conductivity, Hall coefficient and thermo-EMF measurements in Zn and Te doped gallium antimonide crystals for minority carrier role in impurity conduction 21 p3687 A67-39141

Ferroelectricity of barium titanate thin films noting dielectric, temperature, polarization and electric field variations 21 p3687 A67-39142

Metal-silicon nitride-silicon /MNS/ capacitor charge storage variation with temperature and time 22 p3767 A67-39257

Physicochemical interactions between components of refractory metals solid solutions, determining metal alloying effects on system structure and high temperature durability 22 p3818 A67-39319

Qualitative and quantitative variation in alloy phase composition with temperature and age hardening length, studying structural diagram 22 p3818 A67-39321

Temperature dependence of ferromagnetic parallel resonance line width in Ni-Fe alloy films, stressing surface oxidation role 22 p3855 A67-39350

Tungsten strain amplitude dependent dislocation damping measured as temperature function, discussing inconsistency with Friedel thermally activated breakaway theory 22 p3819 A67-39352

Magnetostriction of trivalent Yb and Ce ions in YIG, measuring temperature dependence, noting exchange and interaction of crystal field splitting for Yb 22 p3855 A67-39363

Generalized Ginzburg-Landau parameters and magnetic properties of type II superconductors near upper critical field 22 p3857 A67-39440

Supersonic transport structural materials design, considering fatigue behavior, crack propagation and residual static strength under temperature and cyclic load effects 22 p3819 A67-39457

Superconducting property of kappa phase in Bi-Sn alloy at high pressure, with determination of transition to superconducting state and temperature interval to keep stable state 22 p3857 A67-39460

Direct Josephson current dependence on magnetic field in tunnel junctions noting temperature dependence of oscillation periods 22 p3857 A67-39504

TiC and ZrC powder properties after sintering investigated for linear growth rates vs temperature, obtaining sintering activation energy values 22 p3820 A67-39564

Sensory discrimination, psychological and preference factors toward water reclaimed from urine, discussing identification from tap and distilled water, temperature and smoking effects 22 p3751 A67-39597

Partial differential equations solution in heat transfer between incompressible fluid and porous medium 22 p3917 A67-39640

Recombination centers in silicon transistor emitter-base junctions causing anomalous base current component studied via temperature dependence of forward characteristics 22 p3770 A67-39732

Aging of iron-nickel-titanium alloys during heating in reverse martensitic alpha to gamma transformation process, investigating phase parameter changes 22 p3820 A67-39824

Iron titanium oxides and oxygen fugacity in volcanic rocks noting temperature effect 22 p3792 A67-39975

Low temperature electron irradiation effects on undoped GaSb resulting in impurity conduction 22 p3862 A67-40000

Hot rolling finishing temperature and cooling rate effects on aged 250 grade 18 Ni maraging steel fracture toughness 22 p3822 A67-40057

Spin-disorder resistivity measurements in Gd-Yt alloys noting temperature and concentration effects 22 p3863 A67-40203

Interband and free carrier Faraday rotation in n-type InAs at room and low temperature, determining conduction band parameters 22 p3863 A67-40204

Temperature dependence and electro-optic coefficients in lithium niobate single crystal measured, noting relationship in paraelectric perovskites 22 p3863 A67-40235

Kinetic collisionless plasma diode model stationary regimes, discussing sheath achievement density value dependence on temperature difference and trapped particle distribution 22 p3774 A67-40322

Curves for Hall effect logarithms, current carrier mobility and electric conductivity vs high pressure and temperature effects in InSb 22 p3864 A67-40323

Performance of electromechanical pressure transducers tested environmentally for static and dynamic temperature, steady acceleration and vibrational acceleration 22 p3809 A67-40464

Highly elastic materials temperature dependence of contact area and sliding friction forces affected by elastic modulus decrease with temperature under load 22 p4021 A67-40596

Spectroscopic analysis of iron meteoroid radiation by emission growth curve method covering temperature factors and atom and electron concentrations 23 p4062 A67-40674

Precipitation processes in Ta-Cr solid solutions investigated for temperature dependence and change in alloy properties resulting from precipitation 23 p4018 A67-40712

Na and K introduced into Si by diffusion from thin layer of alkali metal and during electrolysis of molten alkali halogenides 23 p4037 A67-40721

Epitaxial growth of aluminum nitride on silicon carbide studied for influence of substrate temperature on perfection of crystal deposit 23 p4037 A67-40722

Niobium stannide, V-Ga and V-Si paramagnetic susceptibility, elastic constants and electric resistivity temperature dependence 23 p4038 A67-40794

Raman scattering for overdamped soft optic vibrational mode in barium titanate, giving temperature dependence of Raman spectrum 23 p4038 A67-40796

Oxidation of ultrahigh purity Co at various oxygen pressures and at high temperatures 23 p4018 A67-40872

Threshold voltage for onset of image-spot blurring of field-ion microscope screen and function of tip 23 p3998 A67-40896

Temperature dependence of Hall mobility of photoelectrons and electrons produced by X radiation in cadmium sulfide single crystals 23 p4039 A67-40932

Depth of capture levels determined from temperature dependence of kinetics of gamma-conductivity or cadmium sulfide 23 p4039 A67-40933

Generation mechanism of laser emission in cadmium sulfide-cadmium selenide crystals in presence of two-photon excitation at various temperatures 23 p4040 A67-40941

198 Au isotope diffusion in n-type indium arsenide at different temperatures 23 p4040 A67-40944

Second order Raman spectrum temperature dependence of strontium titanate and potassium tantalate 23 p4013 A67-40965

Low dose reactor irradiation effect on temperature dependence of dynamic modulus and internal friction of as-deposited pyrolytic graphite 23 p4021 A67-41075

Sidereal cosmic ray diurnal variations, taking into account data correction for barometric pressure and temperature effects 23 p4059 A67-41130

Black body visible light at 2800 degrees K changed into energy distribution at 5500 degrees K via Fabry-Perot filter for white light standards for colorimetry 23 p3999 A67-41180

Deterioration in permanent magnets at high temperatures and procedures to minimize detrimental performance 23 p4041 A67-41182

Temperature effect on structure of W films prepared by triode pulverization at low pressure and low power 23 p4041 A67-41194

Operating principles of Y-shaped ferrite circulator, discussing temperature and power variations effects on sensitivity 23 p4041 A67-41213

Solar hydrogen convection zone mean stratification derived from mixing length theory, discussing zone structure dependence on temperature and density dependence of opacity 23 p4068 A67-41278

Temperature field and critical thermal loads for fuel elements with varying convective heat transfer coefficient and ambient temperature 23 p4082 A67-41286

Magnetic moments of sublattices and of yttrium garnet calculated including biquadratic temperature dependent exchange 23 p4043 A67-41302

Tensile properties and notch toughness of aluminum alloy sheet and welded joints evaluated at room and subzero temperatures 23 p4020 A67-41348

Secondary temperature resonances in magnetized plasma slab with nonsymmetric inhomogeneous density profile, noting spectrum degeneracy in symmetric nonuniform profile 23 p4034 A67-41359

Temperature effect on zero shift of piezoelectric crystal accelerometers under shock loading using Hopkinson bar technique 23 p4006 A67-41376

Reinforced plastics, evaluating epoxy resin with glass fiber reinforcements for laminates, measuring tensile, compressive and flexural strengths [ASM PAPER C6-21.1] 23 p4022 A67-41403

Magnetic field of flux jumping in synthetic high field superconductors measured as function of temperature and field sweep rate 23 p4044 A67-41452

Bi and Ag nucleation on evaporated substrates studied as function of substrate temperature and impinging flux using electron microscopy 23 p4044 A67-41455

Temperature dependence of elastic constants of 1060 and 8061-T6 aluminum using ultrasonic pulse echo method, estimating high pressure state equation 23 p4021 A67-41469

Decreasing thickness and temperature variation effects on solar cell performance 23 p3937 A67-41489

Computer program for predicting silicon solar cell current-voltage characteristics as function of incident solar intensity and cell temperature over heliocentric

distances 23 p3939 A67-41513

Solar cell array model constrained at four points, with computer simulating V-I characteristics for environmental temperature and illumination intensity effects 23 p3940 A67-41515

Temperature dependence of carrier drift type transistor characteristic frequency, discussing temperature and diffusion coefficients 23 p3983 A67-41676

Temperature dependence of complex permittivity and spontaneous polarization of SbSi single-crystal whiskers in phase transformation region 24 p4199 A67-41777

Parameters for model of two valence bands of SnTe according to Hall effect measurements at high temperatures 24 p4200 A67-41779

Change of conductivity with temperature measurements for stabilized amorphous bismuth films 24 p4200 A67-41866

Critical temperature near superconducting phase transition investigated for alloys and pure superconductors 24 p4200 A67-41867

IR detectors analyzed for dependences of detectivities on temperature, noting noise role 24 p4201 A67-41907

Rare earth metals effect on mechanical properties of austenitic chromium steel at high temperatures 24 p4169 A67-41920

Positive effect of Zr on nickel plasticity, showing elimination of hot brittleness within wide range of temperatures 24 p4169 A67-41922

Deformable aluminum alloys low temperature mechanical properties 24 p4170 A67-41923

Electrode configurations producing various intense charged particle beams, deriving algorithm applicable to three-dimensional problems 24 p4153 A67-41928

Fatigue crack research effect on structural design of flight vehicle structures, discussing temperature effects, multiaxial strain effects and fatigue crack growth equations 24 p4247 A67-41942

Niobium carbide enthalpy, heat content and heat capacity variation in homogeneity domain from 1300 to 2500 degrees K 24 p4171 A67-41958

Emissance and specific heat determination by transient thermal vacuum technique using coatings as function of temperature 24 p4153 A67-42039

Aging effect on structure and properties of complex alloyed heat resistant steel 24 p4173 A67-42190

Rarefied gas mixtures viscosity and heat conduction temperature dependence calculated, analyzing empirical relations 24 p4142 A67-42220

CdS single crystal film trap energy spectrum studied with thermo-stimulated currents -/TSC/ noting effect of SiO layer 24 p4203 A67-42246

Na-acenaphthene reaction temperature dependence, studying optical density, precipitation, ion pair formation, coupling constants and hyperfine structure [JPL-TR-32-1144] 24 p4118 A67-42326

Threshold power dependence on temperature and photoelasticity for stimulated Brillouin scattering in crystalline and fused quartz 24 p4204 A67-42365

Temperature, fiber compositions and matrix resin effects on flexural properties of unidirectionally reinforced short fiber composites 24 p4175 A67-42422

Interfiber distance and temperature effects on critical aspect ratio in fiber composites obtained from modified pull-out test 24 p4173 A67-42474

Solar cell array design techniques for temperature extremes induced by space environment, discussing orbital flight requirements 24 p4104 A67-42510

Characteristics of high energy electron radiation and temperature and effect on N/P silicon solar cells 24 p4105 A67-42513

Methanol-air fuel cell development, discussing electrode performance, temperature effects and catalytic agents 24 p4106 A67-42520

Shield-radiator weight tradeoffs to optimize K Rankine cycle space power plant heat source operating temperature, noting burnup 24 p4185 A67-42537

Lubricants, metal high temperature and atmospheric environments effects on gear load-carrying capacity [ASME PAPER 67-LUB-27]

Hydrodynamic journal bearings in liquid sodium, discussing stability characteristics of different geometries and wear at high temperatures 24 p4164 A67-42685
[ASLE PAPER 67-LC-7] 24 p4164 A67-42746
Temperature effect on diurnal variation of meson intensity at high latitudes, finding wave maximum amplitude in spring 24 p4152 A67-42793
Excitation time of electronic states on nitrogen molecule at high temperatures 24 p4194 A67-42890
Effects of low density, temperature, proton radiation and electromagnetic radiation on thermal control materials, using synergistic testing 24 p4177 A67-42916

TEMPERATURE FIELD
Thermal field of cutting area of aircraft structural material analyzed, using differential equations of thermoconductivity 03 p0427 A67-13191
Classification of experimental methods used in analysis of thermal phenomena during metal cutting 03 p0427 A67-13194
Turbulent heat transfer in tube in conditions of axial symmetry, discussing variation of mean temperature of flow as function of axisymmetrical variation of wall temperature 03 p0535 A67-13395
Temperature and heat transfer conditions determination on rotating turbine wheel in jet power plant, using electric analogy 04 p0688 A67-14571
Submerged nonisothermal turbulent jets analyzed over wide temperature range, noting expansion angle and profile configuration dependency on initial density ratio 04 p0602 A67-14638
Analytic approximation method for thermal convection at large Rayleigh numbers 04 p0721 A67-14649
Book on methods of determining temperature fields in thin walled elements characteristic of structure of flight vehicles and engines 04 p0723 A67-15010
Temperature induced in medium due to suddenly applied pressure inside spherical cavity investigated, using iteration method 05 p0910 A67-16148
Creep problems during small, periodic, slow or rapid changes in temperature field, noting role of thermal stresses 05 p0912 A67-16176
Stressed and deformed state of plastic disk under cyclic loading in variable temperature field, using increments method 05 p0810 A67-16178
Elastoplastic axisymmetric stressed state of circular cylindrical shell under unsteady temperature field, internal pressure and axial force, using differential equation 05 p0912 A67-16181
Thermoelastic wave propagation in elastic layer with convective heat transfer between layer surfaces and surrounding medium, considering relations between temperature field and dynamic displacement 05 p0913 A67-16188
Approximation method for determining stress field of body from temperature field 05 p0914 A67-16196
Stressed state of spherical shell under action of axisymmetric temperature field arbitrarily varying along meridian 05 p0914 A67-16197
Temperature field of active medium of pulsed laser using variational methods, considering two approximate solutions 05 p0825 A67-16935
Nonstationary combustion of powder under action of pressure pulse to determine temperature field variation and burning rate during transient process 06 p1112 A67-17957
Method for observing thermal field of semiconductor device using temperature dependence of zinc sulfide phosphor 06 p0970 A67-18193
Temperature field of elements of thin shelled surfaces of satellites for radiant heat transfer 07 p1265 A67-19104
Asymptotic properties of fluid temperature field and Nu numbers in nonstationary heat transfer during passage of laminar flow of viscous incompressible fluid through rectilinear channel 07 p1265 A67-19125
Soviet book on methods of calculating temperature fields and thermal insulation of flight vehicles 07 p1266 A67-19144
Unsteady temperature fields in structures

calculated by moments 07 p1266 A67-19145
Unsteady temperature field calculated by difference method, for application to structures with various geometric configurations 07 p1266 A67-19147
Approximate solution of temperature field of thin isotropic cylindrical shell heated by time dependent thermal fluxes from two ambient media 07 p1266 A67-19162
Alloying effect on elastic modulus, strength and plasticity of titanium in temperature range from - 196 to 800 degrees 07 p1206 A67-19280
Thermoelastic stressed state of sandwiched plate in temperature field 07 p1261 A67-19326
Equations for nonstationary temperature field of n-layer plate, noting convective heat transfer on free surface of plate 07 p1267 A67-19327
Statistical characteristics of atmospheric ozone distribution, determining autocorrelation and cross correlation functions, concentration and temperature profiles 07 p1170 A67-19357
Electroanalog analysis of convective and conductive heat transfer and transient temperature field in solid propellant rocket nozzle head 07 p1268 A67-19568
Thermal conductivity of laminated GaSe monocrystals studied in two crystallographic directions between 90 and 600 degrees K and effect of unilateral compression 07 p1233 A67-19649
Thermal variation of emitter base voltage of bipolar transistor 07 p1155 A67-19792
Growth of critical temperature of small superconductor samples explained within framework of BCS superconductivity theory without using electron pairing 08 p1372 A67-21502
Free cooling of thin rod in constant temperature medium, finding temperature field for thermodynamics application 09 p1579 A67-21862
Temperature field measurement behind combustion chamber of turbojet engine 09 p1560 A67-22464
Concentration field of components in turbulent gas jet determined from temperature field of mixture 10 p1624 A67-23038
Two-dimensional problem of thermoelasticity solved using analytic functions 11 p1879 A67-24885
Two-dimensional temperature field analyzed for laminar gas flow in interspace between parallel thermally thin plates 12 p2033 A67-25319
Axisymmetric thermal convection flow in rotating fluid annulus 12 p1963 A67-25340
Stochastic thermoelastic time varying boundary effect in circular cylindrical shell 12 p2022 A67-25587
Heat equation of thin closed cylindrical shell exact solution analyzed using least squares method 12 p2034 A67-25606
Temperature field distortion in region of thermocouple junction which arises when thermal conductivity of junction differs from object whose temperature is to be measured 12 p1943 A67-25754
Temperature and wind fields in stratosphere obtained with rocket probes, noting diurnal and annual temperature variation differences for heights beyond 35 km 13 p2113 A67-26679
Burn-pond concept of test facility for disposing of hydrogen at high flow rates 13 p2092 A67-27652
Infinite plate temperature field determined by approximate method when heat transfer coefficient is time dependent 14 p2407 A67-28647
Thermal field of solid rod of uniform cross section and arbitrary profile with time dependent heat transfer 14 p2408 A67-28658
Space-time region division method for reducing nonlinear heat conduction to subordinate linear multilayer system problems, assuming stationary time characteristics and coordinates 14 p2408 A67-28804
Spectral distribution of absorption coefficient in polycrystalline films of cadmium sulfide over wide temperature range 14 p2372 A67-28852
Forward conduction characteristics of contacts between gold n-type silicon measured at different

temperatures 14 p2373 A67-28925
Nonaxisymmetric temperature fields for orthotropic hollow cylinder and sphere solved using Bessel functions, noting heat transfer between external and internal surfaces 15 p2579 A67-29697
Approximate iteration procedure for determining temperature field in plate for simultaneously radiative and convective heat transfer 15 p2580 A67-29779
Integral equation derived for steady state temperature field in semiminfinite body with internal cylindrical heat source 16 p2779 A67-31204
Steady state heat flow and temperature fields in flat rectangular configurations with mixed boundary conditions 16 p2779 A67-31206
Free convection oscillatory flow from horizontal plate having periodic temperature variations analyzed for LF and HF ranges 17 p2969 A67-32445
Steady state temperature field of uniform body containing heat sources, examining nonlinear boundary value problems of unsteady thermal radiation 17 p2971 A67-32870
Axisymmetrical temperature fields for minimum functional of elastic deformation energy in infinite cylindrical shell 17 p2962 A67-32968
Limiting value calculation for temperature field criteria, analyzing heat-conduction equation solution and boundary value problems 17 p2972 A67-33068
Variational technique for temperature field determination in plane system with given heat distribution sources, based on Galerkin-Ritz method 17 p2972 A67-33069
Field spectrum developed from monochromatic temperature oscillations in bodies due to time variation of heat transfer coefficients caused by unsteady flow velocity 17 p2972 A67-33073
Temperature fields in cross section of gas turbine blade with internal coolant during variation of local heat-transfer coefficient 17 p2973 A67-33076
Three-component heat transfer system for regulating system of three heat conductors, analyzing temperature regime 17 p2973 A67-33078
Unsteady heat conduction and transfers by electrical simulation methods, determining temperature field in canonical metal bodies 17 p2973 A67-33082
Unsteady temperature field of thin cylindrical shell of finite length determined, using quadratic trinomial form 18 p3145 A67-33570
Inhomogeneous temperature field arising during laser welding of different materials with imperfect contact, deriving and solving heat conduction equations 18 p3053 A67-33630
Temperature field and electron concentration in electric arc moving along parallel electrodes in magnetic field, giving propagation rate, arc intensity, etc 18 p3087 A67-34046
Soviet book on temperature fields and stresses in structural elements of flight vehicles, giving theoretical analysis and numerical calculation 18 p3145 A67-34705
Energy balance of high current argon arc, showing main energy supply supported by cathodic plasma beam, measuring temperature decay and field 19 p3279 A67-35143
Resolving equations of linear theory of isotropic viscoelastic shells subject to external load and steady temperature field 19 p3340 A67-35508
Logarithmic, diffusion and high temperature creep in metals 19 p3248 A67-35854
Temperature field distribution and heat flux in thin narrow semiminfinite composite plate with moving point source 19 p3347 A67-36051
Transient mean wall temperature of flat plate with time dependent heat source and cooled by incompressible turbulent flow, discussing heat-transfer coefficient [ASME PAPER 67-HT-45] 20 p3547 A67-36727
Size and longitudinal conduction influence on wall temperature field and effectiveness of heat exchangers determined by differential equations [ASME PAPER 67-HT-80] 20 p3551 A67-36758
Solar wind velocity relationship to

tropospheric temperature field 20 p3428 A67-36814

Zirconium addition effect on dynamic strengthening temperature range of niobium alloys, discussing process mechanism 20 p3468 A67-37123

Sublimation enthalpy of CdTe thin films in high vacuum determined from 350 to 400 degrees C 20 p3514 A67-37453

Book on thermoelectric and thermomagnetic effects in metals, semimetals and semiconductors subjected to electric, magnetic and temperature fields, discussing transport theory 20 p3514 A67-37464

Asymptotic properties of fluid temperature field and Nu numbers in nonstationary heat transfer during passage of laminar flow of viscous incompressible fluid through rectilinear channel 21 p3731 A67-38169

Cordwood packaging concept for electronics thermal control in LEM, obtaining electronic package temperature field from finite difference equations 21 p3594 A67-38329

Displacements and temperature accompanying deformation in unbounded thermoelastic medium determined for concentrated force and heat source, using Green functions 21 p3723 A67-38559

Instability of plasma with anisotropic ion velocity distribution, deriving equations for temperature variations and magnetic field energy changes 21 p3669 A67-38680

Steady state temperature field and stresses determined for infinite body with linear slit having definite heat resistance 21 p3729 A67-39007

Kolter theorem generalized for examining unstable temperature field cyclic effects concerning progressive failure in elastoplastic bodies 22 p3910 A67-39453

Stresses, bending moments and displacements of variable rigidity toroidal shell in steady temperature field derived assuming independent thermal expansion coefficient and physical constants 23 p4075 A67-40680

Deriving stability and asymptotic stability properties of temperature fields governed by quasi-linear heat equations 23 p4081 A67-40745

Temperature field and critical thermal loads for fuel elements with varying convective heat transfer coefficient and ambient temperature 23 p4082 A67-41286

Different surface potential barrier models studied for T-F emission current density, energy distribution and Nottingham effect 24 p4201 A67-41893

Turbulent fluid flow velocity and temperature fields in annular and plane gaps calculated by integral approximation for turbulent viscosity and heat conduction coefficients 24 p4142 A67-42213

Temperature field within multidimensional body in nonlinear heat conduction process in terms of known temperature distribution along coordinates 24 p4254 A67-42254

Temperature field in solids with time-varying heat-transfer coefficient, giving numerical results for plate, cylinder and sphere 24 p4256 A67-42591

TEMPERATURE GRADIENT

Current instability of plasma injected into germanium, noting effect of strong electric field in presence of temperature gradient 02 p0297 A67-11833

Optimum averaging periods in measurements of wind velocity profile, temperature gradient, vertical thermal turbulent flow and atmospheric drag 02 p0263 A67-12644

Hydrodynamic drift-dissipation instability of plasma with nonuniform temperature 03 p0476 A67-13296

Arbitrary profile disk design, taking into account temperature gradient, based on simultaneous solution of integral equations 03 p0429 A67-13331

Temperature and magnetic field gradient effects on magnetothermomechanical interaction of viscous incompressible ferrofluid with cold wall 04 p0600 A67-14446

Hydrodynamic drift-dissipation instability of plasma with nonuniform temperature 04 p0663 A67-14721

Quasi-static stresses due to moving temperature discontinuity on plane boundary 05 p0908 A67-16137

Ohm law in multicomponent nonisothermal plasmas derived as function of electric and magnetic fields and temperature and pressure gradients, using transport equation 05 p0857 A67-17422

Decay of mean, variance and gradient variance of temperature and velocity measured in initially heated wake of sphere in water tunnel 06 p0987 A67-18347

[AIAA PAPER 67-20] 06 p0987 A67-18347

Heat transfer by steady laminar forced convection in noncircular ducts, analyzing effects of viscous dissipation due to constant axial temperature gradient 06 p1116 A67-18384

Gas lens focusing of light beams, using highly transparent gas with weakly varying refractive index to guide coherent transmission with small losses 07 p1188 A67-19789

Treatments of drift wave velocities in Cs and K plasmas, noting radial electric field effect made negligible by reducing cathode temperature gradient 08 p1362 A67-21147

Spectral characteristics of turbulence in presence of mean velocity and temperature gradients 11 p1815 A67-23955

Thermoconductivity of heat resistant materials during cooling at room temperature, using photopyrometer to record temperature gradients 11 p1789 A67-24021

Axisymmetric deformation of elastic slab with external crack interpreted as steady state problem of heat conduction 11 p1813 A67-24313

Highly ionized plasma with excitation and damping of density and temperature drift waves in stable regime 11 p1835 A67-24382

Microwave spectral brightness measurements of Venus compared with several model atmospheres 11 p1865 A67-24601

Thermodynamics of vortex flow in superconductors, using combination of electrical currents and thermal gradient 12 p1983 A67-25477

Sonic booms attributed to subsonic flight 12 p1895 A67-25936

One-dimensional heat flow to confined ideal gas solved on digital computer, discussing energy equations, thermal gradient induced fluid motion, etc [AIAA PAPER 67-337] 12 p2039 A67-26051

Ion temperature gradients causing plasma instabilities when magnetic shear is present, deriving governing integral equation 13 p2162 A67-26284

Tests analysis of buckling caused by thermal gradient and fatigue due to thermal cycling in restrained combustor-cooling tubes 15 p2572 A67-29164

Nernst effect in type I superconductor, noting transverse voltages caused by longitudinal temperature gradients 16 p2727 A67-30819

Thermal gradients on surface of orbiting cylindrical stabilization boom determined, using computer simulation of earth orbital environment 16 p2764 A67-30957

Drift instabilities in nonuniform collision-free plasma stabilized by magnetic shear noting longitudinal currents, electron and ion temperature gradients, etc 16 p2718 A67-31226

Temperature gradient effect on stability of inhomogeneous magnetically-confined plasma with frequent ion collisions 16 p2720 A67-31239

Thermal gradients effect on separable tube connectors, discussing structural elements 17 p2864 A67-32009

Estimation of lower bounds to minimum Rayleigh number inducing state of convective motion in quasi-incompressible fluid with temperature gradient in body force direction 17 p2968 A67-32410

Formulas for potential temperatures derived from thermodynamic principles, considering four stages of reversible adiabatic transformation of humid air 17 p2844 A67-32566

Deformation and distribution of stresses in rotating disk with variable thickness and temperature gradient 17 p2960 A67-32687

Thermal fatigue of 18-8 and 13 Cr steels under transient cross-sectional temperature gradients, noting crack mechanics, tensile stresses, plastic strain range, etc 18 p3140 A67-33651

Temperature gradient in steady state

thermally operated solid state lasers, calculating end face curvatures and light paths for resonator mode correction 18 p3059 A67-33714

Highly ionized two-fluid plasma confined magnetically analyzed for stability 18 p3086 A67-33986

Steady state technique for measuring high temperature thermal conductivity of nonmetallic materials requiring heat flux and temperature gradient calculation 18 p3051 A67-34508

Traveling-wave bulk electroconvection induced in slightly conducting liquid with temperature gradient, giving velocity profile equations for plane flow 18 p3029 A67-34736

Temperature gradient and thermal effects on ceramic transducer sensors used on spacecraft for cosmic dust experiments 19 p3229 A67-35170

Langevin similarity theorem applied to ballistic perturbation theory, deriving formulation containing temperature gradient, descent acceleration and kinetic height parameters 19 p3326 A67-35578

Thermal buckling of conical shells under circumferential temperature gradients analyzed using Rayleigh-Ritz method 19 p3343 A67-35772

Friction contact between semiconductor and rotating metal disk studied for sign shifts causing sharp temperature gradient producing thermal EMF 20 p3503 A67-36123

Forced convection of laminar flow in tubes of various cross sections, assuming constant temperature gradient and internal heat generation 20 p3420 A67-36317

Optical system using moire patterns to measure refractive index gradients in boundary layer, showing relation to temperature and density gradient [ASME PAPER 67-HT-3] 20 p3447 A67-36702

Friction and heat transfer characteristics of turbulent swirl flow under large transverse temperature gradients [ASME PAPER 67-HT-24] 20 p3546 A67-36718

Convective secondary flow in channel flow of quasi-incompressible fluid noting temperature gradient role [ASME PAPER 67-HT-26] 20 p3546 A67-36719

Motion of rotating plasma cylinder under gravity force assuming temperature type dependency 21 p3663 A67-37931

Printed circuit thermal design, discussing edge-to-center temperature gradient and circuit board models 21 p3594 A67-38330

Combustion stability of powder in semiclosed volume, taking into account propellant surface temperature dependence on pressure and temperature gradient 21 p3732 A67-38526

Thermal conductivity of clean and dirty type II superconductors, discussing finite temperature gradient effect on niobium 23 p4036 A67-40704

Optical measurement of atmospheric refractive index gradient showing approximate accuracy and simplicity for reasonably large gradients 24 p4188 A67-42093

Tectonic activity on Venus compared with earth, discussing convection currents and temperature gradients in crust and mantle 24 p4227 A67-42222

Heat transfer to end wall of shock tube after shock wave reflection through steep temperature gradient analyzed using variational method 24 p4257 A67-43092

Tin and Indium superconducting films transverse voltages due to longitudinal temperature gradients calculated for entropy per flux quantum 24 p4205 A67-43098

TEMPERATURE INDICATOR

Cholesteric liquid crystals and use in visualizing small thermal gradients for thermal nondestructive testing 02 p0250 A67-12538

Thermochromic materials application in display devices 05 p0860 A67-16307

Fluidic temperature sensor using frequency beating technique for generating analog pressure signal proportional to frequency differences 14 p2318 A67-28345

TEMPERATURE MEASUREMENT

SA CALORIMETRY

SA INTERNATIONAL PRACTICAL TEMPERATURE SCALE /ITS/

SA OPTICAL PYROMETER

SA THERMOCOUPLE

SA THERMOCOPY

Thermoluminescence of achondrite meteorites on lunar surface based on rate of

temperature rise of lunar
terminator 01 p0146 A67-10249

Radiation techniques for surface
temperature measurement, considering
optical and radiation pyrometers, projection
thermography and photographic
techniques 01 p0062 A67-10274

Tiros VII satellite IR measurement data
used to determine sea surface temperature
gradients, examining problem of cloud
cover 01 p0109 A67-10321

Plane temperature wave method for
measuring thermal diffusivity and
conductivity of solid and friable bodies
without using heat
detectors 01 p0166 A67-10364

Spectrographic method for measurement
of temperature in plasma jets at
atmospheric pressure, using amplification of
beta line of hydrogen 01 p0124 A67-10773

Heat flux measurement with narrow view
angle radiometers, discussing equipment
design, performance characteristics and
results 01 p0069 A67-11021

Rotational temperatures measured in static
low density air with electron beam
probe 01 p0071 A67-11105

Calorimeter for measuring heat flux to
ablating surface, noting theory of
device 01 p0071 A67-11106

Hybrid computer simulation of reentry
guidance for lifting vehicle, noting
compatibility of temperature rate flight
control system with other vehicle
controls 01 p0051 A67-11438

Thermal radio emission measurements at
wavelengths 7.93, 11.0, 14.2 and 20.8 cm,
discussing phase
dependence 02 p0322 A67-11581

Analysis of additional terms in Reynolds
flux equation when under unsteady
conditions, using wind and temperature
measurements, noting role in
micrometeorology 02 p0238 A67-12077

Rutgers Axisymmetric Near-Wake Tunnel
for testing turbulent supersonic base flow,
temperatures and pressure
distributions 02 p0230 A67-12361

Plasma electron temperature measured
from soft X-ray bremsstrahlung absorption
by beryllium foil 02 p0274 A67-12461

Neutron irradiation effect on twinning
behavior and transition temperature of
niobium-vanadium alloy 02 p0256 A67-12709

Nuclear cascade process in iron absorber
of ionization calorimeter, comparing
empirical and experimental
values 02 p0248 A67-12747

Ionization calorimeter measurement of
contribution of ionizing particles of star
radiation to electron induced ionization of
cosmic ray shower 02 p0271 A67-12754

Microwave radiometry application to
navigation, thermonuclear diagnostics,
astronomical temperature measurements,
etc 03 p0367 A67-12805

Problems of temperature data from
Explorer and Ariel II satellites including
magnetometer failure, poor conduction, paint
degradation, etc 03 p0518 A67-13074

Solar corona temperature measurements,
noting discrepancy between results from
observations of forbidden emission lines and
ionization balance
calculations 03 p0470 A67-13218

Temperature determination for collector
p-n junction of transistors in class B power
amplifier by thermal equivalent circuit
analysis 03 p0378 A67-13249

Stress patterns in lubricated rolling
contact elements calculated from surface
pressures and temperature
[ASME PAPER 66-LUB-16] 03 p0431 A67-13757

Gennes and Werthammer method
generalization, developing theory of
transition temperature of superconducting
superposed films 03 p0499 A67-13874

Ratio of Lagrange and Euler correlation
scales determined from correlation of time
fluctuation of transverse wind velocity and
temperature variation 03 p0464 A67-14229

Spin temperature of intergalactic atomic
hydrogen calculated as function of electron
density and kinetic
temperature 03 p0515 A67-14319

Mean values of methane wavelengths in
Uranus spectrum measured for
determination of atmospheric
temperature 03 p0515 A67-14327

Radiation losses effects on temperature
measurements with transparent sheathed
thermometers 03 p0426 A67-14344

Plasma electron density as function of
radius compared with ion cyclotron heating
theory and stability criteria
[AIAA PAPER 66-158] 04 p0664 A67-14823

Base spreading resistance and junction
temperature of uniform base junction
transistors 04 p0582 A67-15098

Temperature perturbations produced by
internal sensors embedded parallel to heated
surface of low conductivity material
[ASME PAPER 66-WA/HT-8] 04 p0724 A67-15427

Venus brightness temperature and
polarization of integral radio emission at 3.75
cm wavelength 04 p0702 A67-15566

Axial temperature and velocity
measurements made in water at various
aspect ratios, Grashof number and bottom-
to-side heat flux ratios for turbulent free
convection in closed
container 04 p0731 A67-15827

Shock wave from release of gas at 230 km
altitude indicated luminosity due to
scattered sunlight and temperature of 743
degrees K 05 p0795 A67-16027

Gas temperature decay characteristics for
interrupted high pressure arcs at various
current intensities 05 p0850 A67-16068

Radio emission from Jupiter, Saturn and
Mercury noting disk temperatures
[AD-653438] 05 p0892 A67-16409

Time resolved spectroscopic measurements
of intensity and Stark width during decay of
hydrogen plasma produced by ruby laser,
determining electron density and
temperature decay 05 p0852 A67-16653

Stefan-Boltzmann radiation law of fixed
stars, calculating stellar temperature,
diameter and luminosity 05 p0846 A67-16730

Rocket observations of temperatures and
winds in upper atmosphere, discussing
physical interpretation of
results 05 p0797 A67-16856

Atmospheric temperature and wind
velocity in mesosphere measured by rocket
grenade method 05 p0798 A67-16857

Continuous absorption cross section of
argon from measurements of continuous
emission of arc plasma in visible UV regions
of spectrum and from temperature
determination 05 p0854 A67-16988

Si and Ge heat capacities in terms of
equivalent Debye temperature, obtaining
coefficient of leading anharmonic
contribution to free
energy 05 p0870 A67-17199

Vacuum effect on sintering temperature,
describing measuring
apparatus and
results 06 p1006 A67-17559

Geometric model of radiative atmospheric
space used in research on mean radiation
temperature of space by
frigorimeter 06 p1025 A67-17637

Isotope effects on superconducting
transition temperature of molybdenum
boride and tungsten
boride 06 p1047 A67-17642

Spectroscopic measurement of
temperature, electron density and
conductivity in RF plasma
torch 06 p1039 A67-17825

Length-temperature measurements for
several polymers and mixtures for detection
of transitions and determination of location
and magnitude of expansion coefficient
changes 06 p1019 A67-17851

Difference equations for heat transfer
from liquid to solid and conductivity for
solid applied to calculation of local
temperatures within multilayer
walls 06 p1113 A67-17990

Zonal harmonics investigation of mean
temperature of stratospheric
layers 06 p0996 A67-18447

Continuous absorber effect on spectral
line reversal gas phase temperature
measurement
[AIAA PAPER 67-108] 06 p1004 A67-18503

Local temperature drops at central line of
annular solar eclipse of May 20,
1966 06 p1028 A67-19049

Vibrational and rotational temperature at
altitudes between 50 to 250 km determined
from analysis of airglow in OH bands, using
Fastie-Ebert spectrometer 07 p1172 A67-19562

V-I characteristics and turnover
phenomenon in Si devices in relation to
second breakdown in

transistors 07 p1156 A67-19898

Second breakdown in transistors examined
by thermal concept, noting transient
junction temperature rise 07 p1156 A67-19900

Constants of superconducting alloys for
arbitrary temperatures and impurity
concentrations, calculating free energy
density by using Gorkov
equation 07 p1236 A67-20140

Superconducting properties of vanadium
silicide noting high transition temperature,
electron-phonon interaction, sound
absorption, etc 08 p1369 A67-20990

Photometric, polarimetric and IR study of
lunar surface including polarization of
moonlight, thermal measurements, lunar
radar echo signals, etc 08 p1395 A67-21160

Equilibrium temperatures of Fe and Mg
ions in chondritic
meteorites 08 p1400 A67-21266

Upper atmospheric temperature
measurement by analysis of AIO
spectra 08 p1327 A67-21370

Rotational temperatures of CO molecule
oscillative-rotational bands in solar
atmosphere refute assumed temperature
nonuniformities 09 p1563 A67-21626

Design and operation of reference
temperature compensator in thermoelectric
temperature gauge 09 p1496 A67-21690

Melting temperatures of ZrC-HfC, TaC-ZrC
and TaC-HfC compacts obtained via Pirani
method 09 p1518 A67-21879

Dependence of thermal conductivity of
lunite on temperature, noting properties of
moon surface 09 p1565 A67-21987

Rise and decay times of spike burst
during type IV event of February 5, 1965,
noting electron stream velocities and coronal
temperature 09 p1562 A67-22233

LF temperature pulsations in turbulent
MHD flow of electrolyte 09 p1549 A67-22385

Temperature measurement in hypersonic
gun tunnel, using modified line reversal two-
beam optical pyrometer with measurements
in shock layer at front of
cylinder 09 p1486 A67-22413

Stagnation temperatures from stagnation
point heat transfer rates measured in
hypersonic gun tunnel at Mach
9.8 09 p1486 A67-22414

Measuring and calculating methods in
testing of aircraft - Conference, Prague,
April 1966 09 p1500 A67-22453

Aircraft instrumentation for oceanographic
measurement platform including radiation
thermometer, wave meter and expendable
bathythermograph
[AIAA PAPER 66-695] 09 p1441 A67-22498

Temperature and tolerance behavior of
transistor determined, based on equivalent
drift sources of transistor obtained from
intrinsic series coupling 09 p1482 A67-22611

Fluid and solid temperature determination
in regenerative heat exchangers at any time
and location 10 p1731 A67-22726

Fluctuations in measurements of hurricane
clouds, determining frequency domains for
dominant mode of activity via variance
spectrum analysis 10 p1676 A67-22817

Heat transfer equations for rocketborne
stratospheric temperature sensor in form of
spherical bead thermistor and experimental
analysis of physical, thermodynamic and
electrical characteristics of rocketsonde
[AIAA PAPER 66-385] 10 p1632 A67-22819

High resolution measurement of air
temperatures and temperature differences
applied in conjunction with data processing
equipment 10 p1654 A67-22821

Antenna temperature in wings of line
centered at 61.506 GHz, comparing
experimental and theoretical values on
atmospheric oxygen 10 p1632 A67-22857

Temperature measurement methods in
sulfur hexafluoride compared with reaction
separation 10 p1684 A67-22892

Mineral insulated thermocouple
applications in nuclear reactor, automobiles,
steel, concrete, plastics, textiles, ceramics
and heavy machinery 10 p1656 A67-23080

Recording telethermometer for use at
airports, noting performance characteristics
including unattended reliability, rapid
response time, etc 10 p1656 A67-23088

Asymptotic calorimetry, developing
general relationship between temperature
and unperturbed heat transfer coefficient
for steady state nonisothermal
heating 10 p1656 A67-23139

Mesosphere ice point temperature, atomic

oxygen concentration and total density measurement with heat recorder 10 p1656 A67-23207

Mass spectrometric measurements of upper atmosphere temperature 10 p1639 A67-23214

Evaluating accuracy of substitute term in Einstein equation, noting inconsistency with zero and second law of thermodynamics 10 p1680 A67-23496

Temperature of moving body in relativistic frame of reference 10 p1680 A67-23497

Potential sensitivity of energy radiation detectors, examining measurement error causes for radiation power of natural and artificial sources 10 p1607 A67-23589

Reduced thermodynamic potentials of large classes of refractory metal carbides and nitrides 11 p1804 A67-23901

Langmuir probe and spectrometric electron temperature measurements in negative glow plasma compared, finding probe temperatures significantly higher 11 p1788 A67-23963

Exponential point method measurement of heat fluxes and surface temperature in unsteady regime 11 p1882 A67-24030

Velocity and temperature measurements in turbulent swirling butane-propane air flames in high exit velocity range 11 p1882 A67-24217

Transient radiative heat exchange on moon surface observed in 8 to 12 micron band during lunar eclipse, using model for quantitative comparisons transient radiative heat exchange on moon surface observed in 8 to 12 micron band during lunar 11 p1865 A67-24604

Solar temperatures from observations of July 1963 eclipse with horn antenna in left and right circular polarization, noting magnetization 11 p1867 A67-24779

Larenz, two-line and calorimetric methods for plasma jet temperature measurements 11 p1793 A67-24825

Structural stress measurements in terms of induced temperature increments, using IR radiometer 11 p1877 A67-24827

Differential thermocouple device design for temperature measurements from 300 to 450 degrees K 11 p1793 A67-24866

Localized instantaneous plane heat sources position and strength determined using inert thermometers and time integrals of observed temperature transient 11 p1883 A67-24901

Automatic temperature programmed station for calibrating cryogenic sensors [ISA PAPER 12-11-2-66] 11 p1795 A67-25060

Microwave radiometric measurements of planetary disk temperature of Venus, Mars, Jupiter and Saturn 11 p1869 A67-25094

Cryostat, combination device for test and calibration of gauges for cryogenic temperature 12 p1938 A67-25187

Spectroscopic methods for measuring plasma temperatures from 1000 to 10,000 degrees K, distinguishing optically thick and thin media 12 p1938 A67-25188

Recovery factor associated with moving fluid temperature measurement is dependent on thermodynamic and transport properties of fluid, noting probe errors 12 p1928 A67-25353

Book on spectroscopic gas temperature measurement covering principles, radiometric and spectroscopic methods, instruments, applications to pyrometry, etc 12 p1940 A67-25431

Ratio of Lagrange and Euler correlation scales determined from correlation of time fluctuation of transverse wind velocity and temperature variation measurements 12 p1964 A67-25485

Japanese rocket observations of upper atmospheric wind and temperatures in relation to new Cira model atmosphere 12 p1937 A67-25841

Neel temperature in NiO and MnO with divalent Fe measured using Mossbauer effect 12 p1985 A67-25844

Verification of thermal mathematical model for artificial satellite using thermal vacuum chamber, noting error analysis [AIAA PAPER 67-304] 12 p2036 A67-26019

Thermoconductivity and diffusivity of amorphous solids determined simultaneously by refined line source technique [AIAA PAPER 67-314] 12 p2037 A67-26029

Optical interferometry in plasma diagnostics, discussing degree of ionization,

time dependent electron density distribution, etc 12 p1976 A67-26073

Temperature and density measurements in supersonic free jets of nitrogen and shock waves 13 p2093 A67-26279

Solar wind properties studied using Vela electrostatic analyzers, noting velocity ranges, proton temperature and ion density 13 p2190 A67-26319

Heat receiver with correcting device for instantaneous temperature measurements in unsteady gas flow, discussing matching of time constants and heat-transfer coefficients 13 p2118 A67-26352

Ultrasensitive miniature temperature sensor using pyroelectric material on gate of MOS transistor 13 p2119 A67-26517

Temperature determination in stratosphere via hydrodynamic equations taking into account energy inputs and atmospheric motion, suggesting existence of integral heat sources 13 p2113 A67-26676

Temperatures on hot days at Vandenberg AFB 13 p2152 A67-26845

Distribution function and temperatures in monatomic gas under steady expansion into vacuum determined by integrating Bhatnagar-Gross-Krook /BGK/ model equation and moment equations respectively 13 p2104 A67-26982

Hot-wire anemometry, discussing constant current and constant temperature measurement systems 13 p2120 A67-27020

Metal-to-semiconductor transition measurements of hydrostatic pressure shift and uniaxial stress of temperature 13 p2180 A67-27164

Remote sensing of surface and cloud temperatures using 899 cm spectral interval 13 p2152 A67-27355

Nozzle thermocouple for low flow rate measurement of high temperature gases, discussing calibration curves and taking into account Reynolds number effect 13 p2121 A67-27464

Temperature measurements of grassland, desert and water surfaces using IR radiometer found to compare favorably with miniature thermistors 13 p2117 A67-27606

Pressure and temperature in orifice set in body located in free molecular flow, checking first moment of distribution function 14 p2302 A67-28198

Fluoric pressure, temperature and angular rate sensors for military and commercial applications [ASME PAPER 67-DE-12] 14 p2252 A67-28869

Error possibility in temperature measurements of 30-60 km region, noting solar irradiation effects on thermistor bead 15 p2474 A67-29202

Temperature measurement of ruby laser rods during pulsed pumping from birefringence dependence on temperature and resulting thermoelastic stresses 15 p2499 A67-29721

Causes of ignition failure in solid-fuel rocket motors, obtaining simultaneously pressure and temperature data 15 p2543 A67-29773

Electronic, vibrational and rotational temperatures in laser-produced flames measured spectroscopically 15 p2433 A67-29879

Aerodynamic heat flux measurements in frozen boundary layer flows taken in hypothermal wind tunnel, considering surface catalytic effects 15 p2468 A67-30154

Energy exchange mechanism of cryogenic sensor dynamic behavior, noting error sources 15 p2490 A67-30155

Spectroscopic techniques for plasma parameter measurements in high temperature range, discussing methods employed and experimental setups 15 p2533 A67-30424

Magnetic properties of superconducting vanadium calculated from cellular model 16 p2726 A67-30816

Diapason satellite thermal control noting external energy exchange calculation, coating, in-space simulation tests, temperature measurements, etc 16 p2762 A67-31018

Interferometrically-measured ion temperatures compared to electron temperatures in pure barium and barium-cesium plasmas produced by contact ionization 16 p2720 A67-31243

Brightness temperature reduction of Venus at decimeter wavelengths determined

from 49.1 cm measurements 16 p2749 A67-31409

Ion temperature measurements in upper atmosphere to determine diurnal variation 16 p2666 A67-31416

Melting point and microhardness of carbon-saturated TIC-VC solid solutions, noting temperature of eutectic of TIC-VC with graphite 16 p2691 A67-31588

Enthalpy measurement of anhydrous crystalline aluminum trifluoride with ice calorimeter and drop method obtaining thermodynamic properties 16 p2620 A67-31761

Color temperature measurement in first stage of electrical explosion of copper, silver and constantan wires as function of magnitude of energy input for various heating times 16 p2703 A67-31779

Dynamic thermocouple for measuring plasma temperature up to 4000 degrees C, deriving relations for heating curve as function of time 17 p2854 A67-32162

Italian sensing devices for measuring temperature, pressure, acceleration, heat shield and vibration on ELDO satellite 17 p2854 A67-32227

Stationary laminar boundary layer equations of Ostwald-de Waele power law fluids, flow and temperature boundary layer differential equation 17 p2836 A67-32262

Excitation temperatures of electron levels of CH molecule in photosphere 17 p2941 A67-32326

Tropospheric water vapor analysis via Tiros IV satellite, determining spatial and temporal temperature, humidity and mass variations 17 p2880 A67-32550

Activities and relative partial molar free energies of CuPt alloys, noting formation mechanism, ordering temperatures, etc 17 p2872 A67-32739

Copper-constantan and chromel-copel microthermocouples installation in capillary tubes for measuring coolant temperature 17 p2860 A67-32831

Hydroxyl emission at high latitudes during winter months of 1960 through 1963 measured with spectroscope 17 p2848 A67-32955

Linear temperature measuring system and automatic regulating system accuracy, investigating heat transfer with random input for recipients of various forms 17 p2973 A67-33074

Error factors in cloud and underlying surface temperature determination from weather satellites in various spectral intervals 18 p3073 A67-33558

Spectrum and excitation mechanisms in aurora, discussing variations, excitation, ionization, hydrogen lines and temperature measurement 18 p3032 A67-33582

Kinetic temperature measurements of 5577 angstrom line night airglow with Fabry-Perot interferometer, discussing nightly mean temperatures 18 p3037 A67-33609

Probability distribution of square of temperature difference between two points of turbulent flow measured by pulsation thermometer 18 p3026 A67-33757

Combustion processes studied by shock tubes, discussing experimental techniques of combustion science, high temperature measurement by spectrum line reversal method, etc 18 p3019 A67-33779

Velocity and temperature measurements in turbulent swirling burning free jets of butane-propane-air mixture 18 p3151 A67-33815

Temperature measurement for aircraft gas-turbine engine development 18 p3157 A67-33898

Mars atmosphere surface pressure, radiative equilibrium temperatures, sunlight resonance scattering distribution, etc 18 p3123 A67-34152

Wall heat flux in turbulent air flow using inner law correlations for velocity and temperature 18 p3160 A67-34165

Sun effective disk temperature from measurement of solar radiation during May 1966 eclipse 18 p3125 A67-34195

Grid electrostatic probe for ionospheric measurement of electron density and temperature, examining measurement errors due to environmental disturbances 18 p3048 A67-34225

Calibration and recording method for transmission coefficients of thermal wall heat flows, using ONERA wind tunnel

[ONERA-TP-470] 18 p3020 A67-34463
 Temperature Measurements Society
 Conference, Hawthorne, California, March
 1967 18 p3050 A67-34501
 Inert thermometers, discussing heat
 capacity and contact resistance as sources
 and effect and 18 p3050 A67-34502
 applications 18 p3050 A67-34503
 Thermistor theory and special
 applications 18 p3050 A67-34503
 Gold resistance thermometers for
 measuring surface temperature of
 semitransparent materials 18 p3051 A67-34505
 Reentry vehicle heat shield materials
 thermal diffusivity measurements by flush
 method, using pulsed laser and xenon flash
 lamp 18 p3051 A67-34506
 Measurement within rocket exhaust
 plumes 18 p3051 A67-34507
 Ultrasonic thermometry in solids and
 gases at elevated 18 p3051 A67-34509
 temperatures 18 p3051 A67-34509
 Temperature sensing device development
 for temperature ranges from cryogenic to
 ambient 18 p3051 A67-34510
 Linear bridge for use with platinum
 resistance temperature
 sensors 18 p3052 A67-34511
 Heat flux measurements in fluid systems
 using joule heating accomplished with single
 calibration and without flow rate
 measurements 18 p3052 A67-34513
 Body temperature monitoring in external
 auditory meatus in pre-in-flight testing,
 showing correlation between sublingual and
 aural temperatures 18 p2995 A67-34709
 Mesospheric temperature possible
 relationship to occurrence of noctilucent
 clouds studied using rocket
 soundings 19 p3251 A67-34951
 Flame structure of hydrazine burning in
 oxidizing atmosphere determined by
 measuring temperature and specific
 contractions at 90 degrees from stagnation
 point 19 p3310 A67-35014
 Corona temperature and logarithmic
 intensity gradients determined by pointwise
 three-color photoelectric photometry during
 solar eclipse 19 p3318 A67-35017
 Possibility of pressure destroying
 superconductivity in various metals, studying
 transition temperatures, critical pressures,
 etc 19 p3303 A67-35043
 Temperature convection and vertical
 velocity fluctuations measured and compared
 with similarity theory of free convection and
 laboratory heated plates
 experiments 19 p3252 A67-35059
 High pressure, high power argon arc
 studied using cascade apparatus, showing
 spectral line absorption increases and
 temperature decreases with increasing
 pressure 19 p3278 A67-35136
 Rocket observations of upper atmospheric
 winds, electron density, electron
 temperature, and neutral temperature in
 auroral region with Langmuir
 probes 19 p3214 A67-35169
 Electron temperature and density profiles
 in lower ionosphere at sunset, describing
 temperature measurement
 technique 19 p3229 A67-35246
 Stratosphere and mesosphere wind and
 temperature measurements, noting additional
 cosmic radiation measurements during 1966
 solar eclipse in Argentina 19 p3320 A67-35287
 Electron density and temperature
 measurements using RF capacitance probe
 and double Langmuir probe in auroral
 zone 19 p3222 A67-35455
 High superconducting transition
 temperatures in molybdenum carbide
 compounds stressing crystal
 structures 19 p3245 A67-35729
 X-ray diffusion intensity by transverse
 polarization phonons in indium antimonide at
 various temperature
 ranges 19 p3307 A67-35793
 Plasma spectroscopy, discussing line
 profiles, local thermal equilibrium, methods
 of measuring number densities and
 temperatures 19 p3298 A67-35855
 Active impurities concentration in p-type
 semiconductors by measuring temperature at
 zero thermoelectric
 potential 19 p3308 A67-35875
 Temperature measurement problem in
 high temperature chemistry and
 International Practical Temperature
 Scale 20 p3435 A67-36117
 Installation for measuring wear rate,

friction force, etc, of plane surfaces in
 alternating motion 20 p3453 A67-36198
 E and F region electron density and
 temperature measurements, using
 electrostatic probe and MOS
 electrometer 20 p3441 A67-36383
 Tungsten-rhenium thermocouple systems
 evaluated for high temperature
 measurement 20 p3443 A67-36515
 Radiometric technique for absolute
 temperature measurement of microwave
 noise sources under field
 conditions 20 p3444 A67-36521
 Langmuir probe for electron density and
 temperature measurements in lower
 ionosphere 20 p3444 A67-36526
 Thermocouple surface temperature
 measurement errors in space simulation
 chambers due to heat conduction and
 radiation of wires 20 p3447 A67-36739
 [ASME PAPER 67-HT-57] 20 p3447 A67-36739
 Excitation temperature of low pressure
 magnetically confined argon plasma, using
 spectroscopic transition
 probability 20 p3499 A67-37028
 Convective heat transfer stability in fluid
 contained in cubic chamber shown from
 temperature
 measurements 20 p3422 A67-37064
 Physical properties of thin layers of
 cadmium telluride-metal systems analyzed
 for metal concentration and temperature of
 base at time of
 deposition 20 p3513 A67-37448
 Ultrasonic and line reversal methods for
 measuring gas temperatures behind reflected
 shock waves 21 p3624 A67-37740
 Electron temperature of shock-heated
 argon plasma determined by measuring
 microwave noise radiation and
 absorption 21 p3660 A67-37741
 Differential magnetic loop, density profile
 and gas laser interferometer measurements
 of beta, n and ion temperature in theta
 pinch operation 21 p3662 A67-37755
 Surface potential of semiconducting
 gallium arsenide through temperature
 dependence measurements of transverse
 conductivity of clamped
 contact 21 p3678 A67-37869
 Photoelectric device measuring cutting-
 tool temperature for automatic control of
 state of cutting edges 21 p3628 A67-38059
 Shock tube measurements of end-wall
 radiative heat transfer behind reflected
 shock waves in air, stressing radiative
 cooling and self-absorption effects
 [AIAA PAPER 67-695] 21 p3732 A67-38724
 Photoelectric method for measuring
 temperatures in metal
 cutting 21 p3631 A67-38921
 Air temperature measurements at subsonic
 and supersonic flight speeds, discussing
 error sources and thermometer
 efficiency 22 p3797 A67-39542
 Plasma electron and positive ion
 temperatures measurement using orbit
 magnetic analyzer probes 22 p3798 A67-39626
 Temperature determination of wire
 explosion plasma from expansion and
 resistivity measurements, showing existence
 of two phases of electric
 arcs 22 p3847 A67-39644
 Ground based atmospheric and ionospheric
 particle temperature measurements,
 examining methods and thermosphere heat
 sources 22 p3870 A67-39676
 Ionospheric and magnetospheric
 temperature measurements using rockets
 and satellites including neutral particle, ion
 and electrons 22 p3871 A67-39677
 Radial temperature distribution in high
 power argon arcs measured at atmospheric
 pressure and 5 atm for currents ranging
 from 200 to 500 amp 22 p3853 A67-40049
 Integrated transport cross sections
 obtained for nitrogen as function of
 temperature using gaskinetic
 formulas 22 p3841 A67-40050
 Soviet papers on thermoelectric
 measurements and
 monitoring 22 p3801 A67-40212
 Spectral and probe methods of plasma
 temperature measurement, discussing
 current-voltage
 characteristics 22 p3853 A67-40216
 Nuclear cascade process in iron absorber
 of ionization calorimeter, comparing
 empirical and experimental
 values 22 p3801 A67-40249
 Ionization calorimeter measurement of

contribution of ionizing particles of star
 radiation to electron induced ionization of
 cosmic ray shower 22 p3842 A67-40256
 Thermal diffusivities of thermal energy
 storage materials from solid surface
 temperature measurements, discussing
 advantages of transient method
 [ASME PAPER 66-WA/ENER-5] 22 p3919 A67-40349
 Planetary atmosphere radiation spectral
 distribution sounded with 4.3 micron carbon
 dioxide band to determine temperature
 profile 22 p3805 A67-40355
 Weighting function calculation for remote
 temperature sensing of terrestrial
 atmosphere using selective chopper
 radiometer 22 p3805 A67-40356
 Pressure, volume, temperature and
 internal energy data for He using constant
 volume calorimeter and gas thermometer,
 discussing He melting 22 p3920 A67-40392
 Vertical distribution of thermal stability in
 lower stratosphere compared with
 atmospheric ozone from ozone and
 temperature soundings 22 p3829 A67-40471
 Radiometric determination of absorption
 by earth atmosphere and solar brightness
 temperature at 5.65 mm
 frequency 22 p3897 A67-40560
 Deuterium-tritium plasma temperature
 measurement using neutron detector,
 assuming Kerr cell ruby laser produced
 thermonuclear reaction heating in
 gas 23 p4031 A67-40892
 Helium RF discharge radiation
 temperature as magnetic field function
 measured, discussing enhanced diffusion role
 in radiation temperature
 determination 23 p4032 A67-40897
 Equivalent temperature of cosmic
 microwave background radiation at 3.2 cm
 wavelength, discussing Dicke type
 radiometer and error
 sources 23 p4063 A67-40922
 Rocket instrumentation and sensing
 techniques for collecting stratospheric wind
 and temperature data 23 p4025 A67-41445
 Ground and water surface temperature
 measurements using IR radiometers onboard
 aircraft 24 p4181 A67-41789
 Effective temperature for late type stars
 with or without water vapor opacity
 calculated for several masses, determining
 convective energy transport
 efficiency 24 p4224 A67-41818
 Venus surface temperature measured
 using difference between optical and radar
 radii, cloud temperatures and adiabatic lapse
 rate 24 p4225 A67-41827
 Absolute measurement of Ar II transition
 probabilities using tungsten ribbon lamp as
 calibration standard 24 p4194 A67-41888
 Temperature distribution measurements
 behind shock wave front in discharge tube
 with air and Ar indicate undisturbed
 thermodynamic equilibrium of
 plasmas 24 p4141 A67-41936
 Emittance and specific heat determination
 by transient thermal vacuum technique
 using coatings as function of
 temperature 24 p4153 A67-42039
 Cathode outer oxide surface heating for
 pulsed emission current measured in
 intervals between retarding current pulses
 and different repetition
 frequencies 24 p4129 A67-42231
 Calorimeter for measuring heat flux to
 ablating surface, noting theory of
 device 24 p4155 A67-42289
TEMPERATURE PROBE
 Nonthermal radiation of Na in CO
 medium, analyzing temperature, pressure
 and composition variation effects of
 ambient 01 p0166 A67-10051
 Hot-wire probe measurement of friction
 temperature and convection coefficient of
 low pressure flows and wake of
 cylinder 01 p0006 A67-10757
 Theoretical analysis of heat transfer in
 solid propellant rocket exhaust plumes by
 use of temperature probe located in plume
 environment 01 p0071 A67-11101
 Semiautomatic potentiometer measurement
 of nitrogen specific heat at small intervals,
 noting applicability of logarithmic law for
 other temperature ranges 03 p0532 A67-12929
 Liquid hydrogen pressure, temperature,
 flow and liquid level measuring
 techniques 05 p0807 A67-17019
 Thermobimetallic sensing elements tested
 by compensation method 07 p1187 A67-19740

Recovery factor associated with moving fluid temperature measurement is dependent on thermodynamic and transport properties of fluid, noting probe errors 12 p1928 A67-25353

Electrical property change of pressure sensitive electronic components upon embedment in casting resins, noting results of inductance changes in ferrite core transformer 14 p2341 A67-28954

Periodic variations in rotational temperatures of OH emission bands determined by spectroscopic measurements 17 p2849 A67-32956

Current-voltage characteristics for double probe measured in seeded combustion products by low temperature surface emission 19 p3345 A67-35079

Radiation heat transfer by flames to wire temperature sensor corrected by technique combining radiative input and catalytic activity 21 p3733 A67-38883

Measurement of rapidly varying temperatures of gas flows with resistance thermometers taking into account heat transfer between heat probe and holders 21 p3630 A67-38914

Chromel-alumel thermocouple for high enthalpy gas flow temperature measurement, discussing design and measurement accuracy 23 p4081 A67-40569

TEMPERATURE PROFILE

Temperature field of thin plate with circular region containing pulsed heat source 01 p0168 A67-10365

Successive approximation method of estimating effect of stratification and dynamic nonuniformity of crosswind on trajectory of circular turbulent jet 01 p0053 A67-10824

Atmospheric and surface temperature profile measurement using balloon mounted IR spectrometer 01 p0061 A67-11391

Design technique predicting hot spot temperature and location in thin film circuit, determining power rating 02 p0215 A67-11972

Michelson type interferometer for Nimbus meteorological satellite to obtain vertical temperature, humidity and ozone profile 02 p0246 A67-12365

Boundaries and attenuating media effect on radiometric sounding of planetary atmospheres by remote sensing techniques 02 p0239 A67-12406

Maximum temperature profile in phenolic resin-siliceous fiber heat shields on ICBM and Mercury spacecraft [AIAA PAPER 65-638] 03 p0533 A67-13058

Temperature-vorticity analogy validity in laminar turbulent flows extended to compressible fluids, noting temperature relation to shear stress 04 p0727 A67-15680

Von Karman-Pohlhausen boundary layer analysis of temperature and velocity profiles in inlet region between two parallel planes with relative motion and pressure gradient 04 p0729 A67-15808

Atmospheric temperature profile to 30 km determined by balloon-borne grating spectrometer of radiance of earth between 2100 and 2700 reciprocal cm [JPL-TR-32-1080] 07 p1171 A67-19394

Convective laminar heat transfer to hypersonic vehicle, deriving similarity relations between stagnation temperature profile and mass fractions of chemical species 09 p1579 A67-21699

Greenhouse effect in semiminfinite scattering atmospheres, describing steady state distribution of thermal radiation 09 p1567 A67-22238

Falling sphere measurements of atmospheric density, noting temperature and density profiles, pressure distribution, etc 10 p1639 A67-23205

High altitude atmospheric models, discussing Harris-Priester and Nicolet theories 10 p1640 A67-23217

Thermal plasma measurements in magnetosphere for electron and ion density and thermal profiles, noting Maxwell energy distribution and charge neutrality 10 p1649 A67-23295

Radiative recombination processes in GaAs p-n junctions, noting correlation between temperature behavior and carrier transport mechanism 10 p1693 A67-23523

Absorption and brightness temperature variations of atmosphere on basis of statistical characteristics of vertical

temperature and humidity structures 11 p1785 A67-23956

Depression of superconducting transition temperature in narrow thin films, noting condition for maximum microwave enhancement of critical current 11 p1846 A67-24563

Temperature profile of single stage axial flow turbine disk and blades determined by approximation method using impingement cooling [ASME PAPER 67-GT-14] 11 p1854 A67-24799

Integral equations for radiative heat transfer inside solid whose solution leads to temperature-distance profile integral equations solution for radiative heat transfer inside solid leads to temperature- [AIAA PAPER 67-287] 12 p2035 A67-26004

Mathematical model for predicting temperature and life of silver-zinc battery system in spacecraft [AIAA PAPER 67-334] 12 p1901 A67-26048

Clear air turbulence at high altitudes, showing occurrence where sharp kink in temperature profile exists near core of jet stream 13 p2150 A67-26331

Temperature profile in stratosphere, noting contribution to heat budget by turbulent thermoconductivity and UV radiation absorption in ozone layer 13 p2113 A67-26677

Priestley constant H of free convection temperature profile approaching atmospheric value for increasing Rayleigh number 13 p2151 A67-26737

Heat transfer for gas with internal degrees of freedom between parallel plates, noting temperature profiles and jumps 13 p2100 A67-26959

Thermal boundary layer equation reduced to ordinary differential equation for flat plate with given heat conductivity 13 p2224 A67-27048

Energy equation for laminar flow of compressible Newtonian fluid, calculating temperature profiles of fluid 13 p2224 A67-27049

Semilempirical description of stratification in wall heated containers of cryogenic fluids, noting decrease due to bottom heating 13 p2227 A67-27644

Atmospheric wind effects on guided propagation of VLF infrasonic waves over long distances, including variable wind and temperature profiles 13 p2117 A67-27702

Local flow field measurements of static temperature, density and local impact pressure of hypersonic rarefied flow over 10 degree cone 14 p2241 A67-28169

Laminar Couette flow analyzed for gas injection effects on heat transfer to surface, temperature profile and convection interaction with radiation 15 p2578 A67-29129

Electrically conducting compressible viscous free jet in presence of transverse magnetic and electric fields solved analytically by perturbation technique 15 p2523 A67-29215

Arc operation under nonsteady electrical inputs noting initial conditions, energy equation solution, temperature profiles, application of Green function for moving boundary problem, etc [AIAA PAPER 66-480] 15 p2531 A67-30204

Estimation of statistical sums of states of groups of oxides and fluorides at high temperatures 16 p2704 A67-31390

Time-dependent mean-mass temperature of argon jet produced by arc plasmatron with powdered metal carbides injected into jet calculated using heat transfer equations 16 p2721 A67-31393

Quartz sand particles descending motion and heat transfer in gas vertical tube, determining temperature profile 17 p2967 A67-32132

Thermodynamic properties of plasmas in pressure and temperature equilibrium, showing evaluation accuracy to 4 percent 17 p2894 A67-32146

Response of bare wire thermocouple to temperature variation in jet engine intake, noting temperature pickup selection for desired response 17 p2859 A67-32589

Temperature dependency of specific heat of titanium base alloys 17 p2873 A67-32770

Composite ammonium perchlorate propellant temperature profile beneath burning surface, discussing main decomposition energy, heat sources, etc composite ammonium perchlorate

propellant 18 p3107 A67-33811

Chemical structure of premixed flames of methane and perchloric acid vapor diluted with argon obtained in terms of composition, temperature and velocity profiles 18 p3109 A67-33841

Criticality criteria and temperature profiles in thermal explosions, studying exothermic decomposition of gaseous methyl nitrate 18 p3156 A67-33851

Transfer function use in outgoing IF radiation temperature measurement of vertical profile over Caspian Sea by airborne modulation radiometer 18 p3040 A67-34001

Mars emission spectrum computed for two atmospheric models, presenting weighting functions for different wave numbers 18 p3125 A67-34159

Turbulent boundary layer in liquid hydrogen tank, determining attachment point, velocity and temperature profiles 19 p3310 A67-34810

Long-wave radiation cooling effect in troposphere/stratosphere calculated based on vertical temperature and moisture profiles from nighttime probe 19 p3213 A67-34852

Adsorption of oxygen upon clean nickel surface and beginning of oxidation 19 p3244 A67-34937

Perfectly stirred reactor /PSR/ theory application to flame analysis, obtaining temperature or concentration profiles as function of time or distance 19 p3345 A67-35011

Radial and axial temperature profiles of free-burning argon arc at various pressures, measuring continuum intensities [DVL-625] 19 p3278 A67-35135

Density, temperature and pressure profiles variations in upper atmosphere obtained from rocketborne experiments 19 p3218 A67-35219

Electron temperature and density profiles in lower ionosphere at sunset, describing temperature measurement technique 19 p3229 A67-35246

Temperature and wind profiles in stratosphere and mesosphere during winter and summer determined by grenade soundings, noting diurnal variations 19 p3226 A67-35924

Natural convection in finite nonzero length vertical channels, using integral technique to derive results for two wall conditions [ASME PAPER 67-HT-16] 20 p3545 A67-36712

Laminar boundary layer with heat transfer in liquids with variable fluid properties, including velocity and temperature profiles [ASME PAPER 67-HT-69] 20 p3550 A67-36749

Steady state and transient temperature profiles for straight fins of trapezoidal profile with radiative heat transfer [ASME PAPER 67-HT-73] 20 p3550 A67-36753

Theoretical prediction of temperature profiles within heated cylinder and on surface to determine thermal conductivities at high temperature [AIChE PAPER 16] 20 p3552 A67-36829

Volumetric absorption coefficient effect on Rosseland equilibrium radiative heat transfer and temperature profiles in optically thick fluid flowing past flat plate 20 p3553 A67-36936

Resistance spot welding process, using heating, cooling and stress development data to compute internal behavior 20 p3456 A67-37697

Tethered sonde for micrometeorological soundings of lower atmosphere noting pressure transducer, servoswitching system, thermistor, hygistor, data acquisition, etc 21 p3628 A67-38582

Electrical conductivity of nitrogen plasma seeded with potassium, noting nonuniform temperature profile in flow [AIAA PAPER 67-716] 21 p3673 A67-38742

Empirical orthogonal functions, determining vertical atmospheric temperature profiles from radiometric satellite measurements 22 p3828 A67-39325

Electron temperature spatial variation in late He afterglow due to standing wave microwave heating 22 p3844 A67-39353

Self-similar solutions to motion equations are possible for internal heat generation in confined supersonic flow, assuming constant transport properties 22 p3784 A67-39781

Planetary atmosphere radiation spectral distribution sounded with 4.3 micron carbon dioxide band to determine temperature

profile 22 p3805 A67-40355
 Atmospheric temperature profile to 75 km by remote sounding, using satellite measurement of molecular oxygen resonance line at 5 mm 22 p3806 A67-40360
 Model for straight fin nucleate boiling onset criterion, discussing boiling section length expression, heat flux and temperature profile 22 p3919 A67-40387
 Flame activation energy and combustion process order based on homogeneous reactor model for mean temperature coefficient determination 23 p4082 A67-41141
TEMPERATURE REGULATION
S HEAT REGULATION
TEMPERATURE TRANSDUCER
 Heat flux measurement with narrow view angle radiometers, discussing equipment design, performance characteristics and results 01 p0069 A67-11021
 Response of temperature sensor bonded to metal strip pulse-heated by capacitor discharge technique 01 p0071 A67-11100
 Thermoelectric probe in calibrating surface temperature transducers, noting results on various materials 01 p0075 A67-11134
 Pyroelectric effect in barium titanate ceramics used for weak thermal radiation recording 03 p0421 A67-13709
 Temperature sensor controller in form of linear monolithic integrated silicon device 04 p0619 A67-14595
 Control-voltage transducer synthesis with variable capacitor compensation of quartz resonator frequency-temperature characteristics 08 p1306 A67-21280
 Pyroelectric heat-transfer sensor performance compared with thin skin thermocouple heat sensors, noting discrepancy in measurement results in severe environment 11 p1790 A67-24453
 Heat flux measurements in fluid systems using joule heating accomplished with single calibration and without flow rate measurements 18 p3052 A67-34513
 Radiative and convective heat flux measuring instruments calibration for aerospace industry 23 p4006 A67-41375
TEMPERING
 Quenching from alpha region and subsequent tempering effect on mechanical properties of titanium alloy VT5-1 07 p1200 A67-19249
 Specifying temper for stainless steel tubing, noting properties of various techniques 13 p2124 A67-27175
TENSILE CREEP
 Centrifugal machines generating creep-design data by spinning specimens at identical temperature 03 p0395 A67-13542
 Stress-strain time relation in gallium doped p-type germanium, noting crystal dislocation and creep parameter temperature dependence 04 p0677 A67-15121
 Short-time tensile and long-time creep rupture properties of HK-40 alloy and type 310 wrought stainless steel from room temperature to 2000 degrees F [ASME PAPER 66-WA/MET-2] 04 p0639 A67-15344
 Atmospheric nitrogen contamination effect on tensile creep of chromium-tantalum alloys 06 p1018 A67-18369
 Tensile creep properties of chromium alloys affected by type of ceramic used as heating element core 08 p1341 A67-20766
 Relaxation, creep and modulus of rigidity lowering in compression springs under high temperature 11 p1795 A67-24090
 Heat resistance, bending and tensile creep of multicomponent Ti alloys 12 p1955 A67-25366
 Creep rupture, fatigue strength and brittle-ductile transition of aluminum as affected by nuclear radiation 13 p2133 A67-27090
 Testing techniques for electroformed thin shells noting tensile properties 13 p2219 A67-27184
 Tensile creep behavior of thick walled aluminum titanium alloy cylinders under internal pressure at high temperature 14 p2339 A67-29001
TENSILE DEFORMATION
 Room temperature microstrain behavior of zone-refined single crystal beryllium examined as function of prestrain 01 p0092 A67-10058
 Tensile deformation behavior of

commercial aluminum-5 percent magnesium alloy, correlating uneven yielding regions with occurrence of markings on specimen surface 01 p0093 A67-10060
 Linear solutions for large deflections of diamond-shaped frames under compressive loading 01 p0160 A67-10404
 Elastoplastic deformation under plane stress conditions determined, using method of photoelastic coatings 02 p0336 A67-11628
 Topographic X-ray analysis of deformation in tension of silicon crystal 03 p0493 A67-13452
 Stress-strain concentration in plates of bilateral cut EI-437B heat resistant alloy and EI-481 austenitic steel under rapid tensile loading at high temperature 03 p0529 A67-14084
 Tensile plastic instability in axisymmetric deformation of sheet metals 04 p0710 A67-14976
 Rate controlling mechanism in graphite creep, noting basal slip systems causing general deformation 05 p0833 A67-16892
 Thermally activated deformation relating flow stress to square root of dislocation density 06 p0153 A67-18755
 Changes in microhardness, elastic modulus and shear orientation at boundary between plastic and plastic deformation in steel under tensile stress 07 p1210 A67-20011
 Plastic flow and instability behavior of thin walled tubes of nickel-chrome steel subjected to constant ratio tensile stress 10 p1719 A67-23485
 Uniaxial tensile strain rate on stability of soft reinforced plastics with two-component fibrous base 10 p1671 A67-23605
 Carbon action effect on tensile deformation in single and polycrystalline beryllium in terms of solutionized and precipitated states 13 p2137 A67-27112
 Beryllium deformation under hydrostatic pressure 13 p2139 A67-27124
 Hydrogen influence on fracture propagation of titanium alloy during tension tests 14 p2337 A67-28286
 Stress states, structure deformation, failure criteria and constitutive relations in structural design noting tensile, strip and lap shear test and continuum model 15 p2575 A67-29977
 Si-Fe deformation in tension/compression noting orientation dependence of yield stress, slip band formation and direction of screw dislocations 17 p2872 A67-32741
 Matrix method for calculating behavior of rod of constant cross section stressed by bending and stretching or compression loading 19 p3343 A67-35815
 Stacking fault energy estimation in polycrystalline brass during tensile deformation by analyzing X-ray diffraction patterns 21 p3645 A67-38090
 Tensile properties and notch toughness of aluminum alloy sheet and welded joints evaluated at room and subzero temperatures 23 p4020 A67-41348
TENSILE STRENGTH
 Whisker strength measurement methods, noting role in reinforcement of ductile metal matrices 01 p0163 A67-11152
 Resistance of copper-tungsten fiber composites to repeated tension cycles 02 p0254 A67-11793
 Insert size, shape and core undercut diameter and depth effect on insert tensile strength of honeycomb sandwich fasteners 02 p0248 A67-11943
 Hypervelocity crater size and target strength, relating force per unit area of crater surface to tensile strength of material 02 p0338 A67-12034
 Variations in tensile and creep-rupture properties of niobium caused by nitrogen additions that produce single-phase and two-phase structures studied at room and high temperatures 02 p0256 A67-12703
 Metallurgical and geometrical factors affecting high temperature tensile properties of discontinuous tungsten fiber reinforced composites 03 p0441 A67-13272
 Fiberizing of oxides by hot deformation in metal matrices of unalloyed columbium or tantalum, preparing composites by powder metallurgy 03 p0441 A67-13273
 Strength characteristics of whisker crystals, microcrystals and macrocrystals influencing selection and use of composite reinforced materials 03 p0449 A67-13306

Mechanical characterization and structural perfection of alpha aluminum oxide wool whiskers in diameter range of 0.6 to 4.0 microns 03 p0449 A67-13307
 Tensile strength affecting factors in metals reinforced with strong fibers 03 p0442 A67-13311
 Boron filament manufacturing process using chemical vapor plating with boron trichloride and hydrogen onto tungsten filament substrate 03 p0453 A67-13419
 Boron filament preparation on fused silica substrates by decomposition of diborane 03 p0454 A67-13420
 Boron carbide filament production by vapor deposition from organoboranes 03 p0454 A67-13421
 Synthesis route to form continuous filaments of SiC, noting tensile strength, elastic modulus and density of product 03 p0454 A67-13422
 Boron-modified SiC continuous filament fabrication by vapor deposition on hot W wire substrate and tensile testing 03 p0454 A67-13423
 Boron fiber-reinforced aluminum composites fabrication by plasma spraying and tensile testing 03 p0444 A67-13431
 Statistical theory for strength of laminar composites used to optimize biaxial and multidirectional tensile strength properties of laminated materials 03 p0522 A67-13442
 Interatomic force model calculation of shear and tensile strengths, predicting stress-strain curves for crystal structures 03 p0495 A67-13532
 Load carrying capacity of thin plates of rigid perfectly plastic material with different tensile and compressive yield strength, using method of limit analysis 03 p0531 A67-14366
 Nickel effect on tensile strength, impact toughness and cold shortness threshold of low carbon steel 04 p0636 A67-14750
 Mechanical properties of Kh21G7AN5 steel at liquid hydrogen temperature 04 p0636 A67-14751
 Mean tensile strength of aluminum alloys using torsion tests determined at high strain levels and compared with extrusion tests values 04 p0636 A67-14907
 Maraging steel properties, discussing composition, strengthening mechanism, tensile and impact toughness, mechanical and fatigue properties, etc 04 p0640 A67-15458
 Long term tensile stress-rupture strength of alloys calculated from static tensile strength tests at elevated temperatures [ASME PAPER 65-MET-12] 05 p0827 A67-16212
 Fusion weld evaluation in 2014-T6 material by eddy current, electric conductivity and hardness plots, noting aging effects, mechanical property degradation, etc 06 p1007 A67-17640
 Tensile tests performed on alpha titanium between -321 and 75 degrees F, discussing ductile-to-brittle transition, microcrack formation and brittle fracture mechanics 06 p1014 A67-17807
 Factors affecting strength of whisker reinforced metals noting characteristics [ASME PAPER 66-MD-8] 06 p1015 A67-17835
 Plastic deformation of textured Ti alloy sheet examined, using tension testing along different directions and combined stress loading along principal axes of anisotropy 06 p1016 A67-17900
 Macroscopic brittle fracture theory for structural microheterogeneities effect on maximum macrostresses in plates with hyperbolic notches under tensile loads 06 p1100 A67-17950
 Niobium addition effect on mechanical properties of steel, noting improvement of tensile strength and cold brittleness threshold decrease 06 p1018 A67-18235
 Effects of 450 and 600 degrees F exposures on mechanical properties of glass-fiber polyimide resin sandwich panels to be used on large skin areas of SST aircraft [AIAA PAPER 67-174] 06 p1021 A67-18484
 Mechanical properties of continuous carbon filament/graphite binder composite including tensile, compressive, flexure, fatigue and shear properties [AIAA PAPER 67-173] 06 p1021 A67-18509
 Elastic behavior of bodies composed of materials with different characteristics of compression and tensile strengths, noting

applicability of various variational equations 06 p1106 A67-18624

Fusion welding of nickel maraging steel to lower strength steels to produce leaf spring subjected to tensile impact loading 07 p1198 A67-19213

Heat resistance of Ti alloy after thermomechanical treatment, noting properties as long lifetime structural material 07 p1206 A67-19284

Tensile and bending strengths as suitability criteria of pressworking of materials 07 p1192 A67-19755

Metal composite technology, emphasizing degree of success attained in fabricating reproducible tensile specimens by five techniques 08 p1340 A67-20358

Reinforced plastics - SPI Conference, Washington, D.C., January-February 1967 08 p1344 A67-20420

Tensile failure of whisker reinforced composites for loading in fiber direction 08 p1344 A67-20421

Polar properties of fiberglass fabric laminates effect on strength for aerospace applications 08 p1345 A67-20431

Nickel composite with tungsten filament and aluminum oxide whiskers, noting parameters of tensile strength after annealing 08 p1342 A67-20909

Fracture of viscoelastic bodies, predicting statistical variability of rupture data for uniform and nonuniform excitation histories 08 p1421 A67-20913

Finite difference method for finding stress fields around parallel edge cracks 08 p1421 A67-20914

Strength of laminar composites, discussing application of statistical theory to determine parameters 08 p1346 A67-20915

Tensile strength and cross sectional area measurement of aluminum oxide whiskers 10 p1669 A67-23326

Substructural strengthening of carbide precipitation hardened molybdenum alloy by swaging and wire drawing 11 p1805 A67-24108

Tensile strength retaining characteristics of aluminum alloys determined after varied soaking periods at various elevated temperatures 11 p1805 A67-24271

Test conditions effects on glass fiber strength data 11 p1811 A67-24587

Titanium and aluminum additions to cobalt-base alloys improve tensile and stress rupture properties and heat resistance 11 p1807 A67-24703

Filamentary materials for wound structures, particularly rocket motor cases, noting fabrication equipment, physical properties, etc 11 p1811 A67-25008

Failure mode at tip of crack predicted using cleavage strength and shear strength of perfect crystals, noting tungsten and iron 11 p1880 A67-25090

Stress rupture and creep behavior in binary and ternary vanadium alloys including tensile strength and activation energy, noting titanium role 12 p1954 A67-25140

Stress-strain state of thin walled zero moment shell under uniformly distributed multiple load assuming various tensile and compression strengths 12 p2020 A67-25569

Effect of V, Zr, and Y additions on mechanical properties of 1 mm sheet molybdenum 13 p2130 A67-26392

Aluminum oxide whiskers structure and properties 13 p2141 A67-27186

Aluminum and aluminum alloys properties for service at cryogenic temperatures 14 p2323 A67-27816

Tension equations for oval thin walled cylinders reinforced with lateral rigid ribs noting wall strength, complex bending moment computation, etc 15 p2577 A67-30185

Mechanical strength of medium formulated as microscopic behavior in continuum obtaining time-dependent macroscopic fracture strength 16 p2771 A67-31295

Inclusion type, forging ratio and heat treatment effect on properties of longitudinal and transverse steel specimens 16 p2689 A67-31310

Sapphire whisker strength coated with thin metal film determined at room and elevated temperatures 16 p2694 A67-31522

Effect of thermomechanical treatments on tensile properties of metastable austenitic steels 16 p2693 A67-31872

Model for hemispherical cratering of structural metals by hypervelocity impact, determining elastic-plastic threshold stress

by true tensile strength measurement 17 p2958 A67-32217

Nickel effect on tensile strength, impact toughness and cold shortness threshold of low carbon steel 18 p3066 A67-34408

Mechanical properties of Kh21G7AN5 steel at liquid hydrogen temperature 18 p3066 A67-34409

Fiber orientation and morphology effect on anisotropic tensile behavior of Al-Ni whisker reinforced aluminum, studying solidification rate, etc 18 p3067 A67-34569

[ASTM PAPER 3]

Short time tensile and long time creep-rupture properties of HF and HH iron-chromium-nickel alloys at high temperatures [ASTM PAPER 52] 18 p3068 A67-34582

Graphite material strength prediction by nondestructive test techniques consisting of bulk density and eddy current measurements 18 p3070 A67-34584

[ASTM PAPER 54]

Boron filaments mechanical properties and chemical compatibility compared with nickel and titanium matrices 19 p3245 A67-35728

Correlations between elastic limit, tensile strength and elongation in foundry aluminum alloys used in control reliability 20 p3465 A67-36479

Testing apparatus for rapid determination of tensile strength of fine filaments 20 p3537 A67-36522

Thermostable fibers from ordered heterocycle amide copolymers tested for tensile and high temperature properties 21 p3647 A67-37872

Loading rate effect on unidirectional fiberglass reinforced plastics under tension, examining mechanical characteristics and determining tensile strength and elastic modulus 21 p3649 A67-37908

Cold forming properties and handling of stainless steels and superalloys noting contained extrusion and warm heading techniques 21 p3634 A67-38177

Tensile strength of charred ablation material under rapid heating conditions tested using plasma arc flow and miniaturized specimen 21 p3650 A67-38874

Heat resistant stainless steels evaluated experimentally for fatigue properties, corrosion resistance, creep limit and tensile strength 21 p3646 A67-39010

Carbon content effect on properties and structures of nickel and nickel-iron base superalloys 22 p3818 A67-39223

Copolymers containing imidazopyrrolone and imide groups tested for thin film tensile properties, degradation by strong acids and bases and thermal stability 22 p3824 A67-39851

Factors affecting tensile ductility minimum behavior of silicide coated niobium alloys investigated in air for intermediate temperature range 22 p3821 A67-40052

High tensile strength of composite amorphous boron filament, discussing Weibull relationship and measurements 23 p4018 A67-40787

Aluminum alloy sheet welds with high silicon and magnesium content analyzed for tensile properties and fracture toughness 24 p4161 A67-42330

TENSILE STRESS

Stress required for brittle fracture of alumina at room temperature based on theory of dislocation movement of cracks 01 p0092 A67-10054

Stressed state in isotropic medium weakened by row of curvilinear holes, considering approximate effect of adjacent holes on concentration of stresses around each hole as loaded 01 p0158 A67-10217

Anisotropy test examining failure behavior of aluminoborosilicate glass fibers under tensile and torsional loading [ACS PAPER 1-G-65F] 01 p0103 A67-10263

Nickel-thoria powder produced by pressure hydrometallurgy techniques and dispersion-strengthened by compaction and rolling, noting tensile stress-rupture properties revealed by optical and electron microscopy 01 p0097 A67-10697

Stresses and stress relaxation in thin oxide films deposited by various methods on glass substrates from elastic or plastic deformation at elevated temperatures 02 p0288 A67-11719

Stress concentration near elastic ring-reinforced hole in elongated nonlinear plate 02 p0341 A67-12665

Shape of limiting-state curve for high strength steel predeformed to yield point by repeatedly applying internal load 02 p0255 A67-12667

Thermal emf in plastic deformation of copper, considering effects of crystal lattice defects and lattice elastic distortions 02 p0301 A67-12740

Aluminum alloy composite bulkhead fabrication under tensile stress with improved bonding 03 p0430 A67-13556

Data interpretation for sun grazing family of comets deriving formulas for compressive and tensile stress in spherical bodies for tidal, rotational and self-gravitating fields 03 p0512 A67-13923

Elastoplastic deformation of cylinder under torque and tensile stress based on stress stabilization in yield zones 04 p0708 A67-14796

Tensile stress concentration near rhombic hole taking into account physical nonlinearity of aluminum brass plate 05 p0907 A67-16020

Concentrated tensile stresses induced by concentrated external loads applied to boundary of filament winding rectangular strip plate 05 p0914 A67-16216

Tensile analog data reduction technique for determination of principal stress differences history at points of two nonhomogeneous photoviscoelastic models 05 p0921 A67-16826

Stability loss in thin walled plastic shell under tensile loading in plane stress conditions 07 p1261 A67-19190

Tensile residual stress measurement in area of failure origin in helicopter rotor blade, using laboratory tests and X-ray analysis [SAE PAPER 670154] 09 p1502 A67-21772

Fibrous model of shell shaped grid noting discrete network, properties of cross section surface and stress 10 p1715 A67-22920

Cyclic torsion interaction with axial load, showing torsion angle larger than fatigue limit and applied tensile stress larger than Bauschinger yield 10 p1669 A67-23438

Approximate solution of creep and relaxation problem for plates and shells subject to bending moments and tensile forces 12 p2025 A67-25610

Continuous total immersion stress corrosion testing of beryllium in synthetic sea water, discussing relationship between time-to-failure and tensile stress 14 p2336 A67-28147

Cylindrical specimen behavior during high strain rate tensile test, using computer program 14 p2400 A67-28523

Mechanical response of highly filled elastomer in complex triaxial tensile stress field, demonstrating dewetting effect, need for more testing, etc 15 p2575 A67-29978

Loading asymmetry effect introduced by short single edge crack specimen loaded in tension along center line 16 p2764 A67-30994

External dislocation effect on conditions for complete fracture from coplanar wedge shaped crack in presence of applied stress 16 p2765 A67-30996

Tensile stress of infinite plane weakened by hole or Zhukovskii profile with rounded edges 16 p2765 A67-31053

Tensile and torsional fracture of low carbon steel at cryogenic temperatures, studying temperature and stress gradient effect 16 p2689 A67-31309

High speed plastic deformation of bar studying relation of breaking strain vs tensile velocity and comparing values of former to static case 16 p2775 A67-31329

Stress analysis of semiminfinite plate containing reinforced notch on one side under uniform tension 17 p2961 A67-32777

Stress effects on structure of oriented crystallizing polymers, noting long periods changes due to displacement of crystallites in amorphous layers 18 p3068 A67-33489

Free radical formation correlated with breaking time and creep rate in solid polymers subject to crushing, breakdown and deformation 18 p3068 A67-33490

Flow stress of fresh dislocations in titanium and vanadium doped MgO single crystals, measuring dependence on heat treatment and test 18 p3097 A67-33492

Thermal fatigue of 18-8 and 13 Cr steels under transient cross-sectional temperature

gradients, noting crack mechanics, tensile stresses, plastic strain range, etc 18 p3140 A67-33651

Reversible contribution to flow stress in Ni-Al alloy analyzed by temperature change as function of tensile strain and precipitation hardening 18 p3065 A67-34363

Surface morphological changes of tantalum single crystals during plastic deformation, studying orientation dependence of yield stress in tension and compression 19 p3245 A67-35727

Alloying effect on temperature and strain rate sensitivity of niobium-molybdenum bcc metal 19 p3246 A67-35730

Threshold equilibrium of brittle plate with polygonal hole in biaxial tension-compression 19 p3343 A67-35845

Tensile properties of fiber-reinforced metals, discussing failure at notch root 20 p3464 A67-36417

Biaxial prestressing in ceramic plates under nonuniform thermal stress for damage reduction study 20 p3538 A67-36778

Truncated elastic shell of revolution stability under tensile stress 21 p3718 A67-37978

Netting analysis of reinforced sheets for load envelopes which combine tension and shear, determining optimum fiber arrangements 21 p3729 A67-39082

Change in brittle fracture work during combined impact and tensile load of polymer noting variation according to maximum law 23 p4072 A67-40595

Fatigue behavior of Cr steel and Ni-Cr alloy examined for influence of direction of first loading stroke of push-pull testing 23 p4019 A67-41155

Dislocation structure of tension deformed Si samples investigated by electron microscopy 23 p4042 A67-41296

Tensile mean stress effect on dormancy of fatigue edge crack in mild steel 23 p4079 A67-41344

Fabrication under tensile stress of large double contour composite structures, obtaining improved bonding [ASM PAPER C6-21.2] 23 p4010 A67-41410

Tensile to shear transition behavior of fatigue crack fronts during cycling of sheet materials, noting correlation of shear with crack stress intensities 24 p4170 A67-41950

Microstructure of SGBF graphite under tensile and compressive stresses noting crack generation in layer planes [ACS PAPER 6-N-66F] 24 p4175 A67-42372

TENSILE TESTING MACHINE

Extensometer for measuring small changes of specimen on tensile testing vacuum furnace at high temperatures, using CW gas laser as light source 01 p0070 A67-11036

Tensile testing machine measuring mechanical properties under conditions of rapidly applied stresses 01 p0102 A67-11086

Tensile test equipment and methods to determine modulus of elasticity and ultimate tensile strength of single boron filaments at room and elevated temperatures 03 p0455 A67-13445

Elevated-temperature tensile testing of thin Rene 41, Hastelloy X and TD Nickel sheet 03 p0446 A67-13553

Titanium alloys test results at 20 and 400 degrees C and at different grip speeds, using various tensile testing machines 03 p0448 A67-13566

Vacuum testing machine to determine tensile and creep properties of heavily drawn W wires at temperatures up to 2500 degrees F 06 p1013 A67-17799

Laser extensometer measuring small dimensional changes of specimen in tensile testing furnace at high temperatures 06 p1012 A67-18778

Impact bending and tension processes using drop hammer technique evaluated with improved method using oscillography for high quality load-time measurements 13 p2215 A67-26391

Tensile testing equipment using impact load facilitates rupture stress measurements by conventional strain gauges 18 p3141 A67-33719

TENSION

SA CARBON DIOXIDE TENSION

SA OXYGEN TENSION

SA SURFACE TENSION

Tension of homogeneous anisotropic elastic semiinfinite plate with rigid stiffener attached on segment of straight

boundary 05 p0910 A67-16150

Equilibrium configuration and tension of flexible cable in uniform flow field, considering tangential drag force and weight effects 13 p2051 A67-27587

TENSION TESTING MACHINE

Tensile strength and cross sectional area measurement of aluminum oxide whiskers 10 p1689 A67-23326

Cerium addition effects on magnesium workability evaluated by sample elongation in tension test and plate working limit in cold rolling 15 p2505 A67-30398

High speed plastic deformation of bar studying relation of breaking strain vs tensile velocity and comparing values of former to static case 16 p2775 A67-31329

Sapphire whiskers mechanical behavior obtained by static tension testing 16 p2694 A67-31523

High modulus high strength inorganic filament windings tested for tension and buckling-critical structures, considering weight decrease and operating temperature increase 19 p3245 A67-35553

Testing machine operated by hydraulic pressure for mechanical properties of materials at medium rates of strain 23 p4079 A67-41332

TENSOMETER

Tensometry method to study stress concentration around circular hole in orthotropic glass-fiber reinforced cylindrical shell 12 p2021 A67-25579

Tensometric properties of silicon whiskers and acicular single crystals studied under static and dynamic loads, estimating suitability as strain gauge 18 p3097 A67-33473

Adhesive and water resistance properties of epoxy resin for bonding tensometers and underwater sealing 21 p3650 A67-38919

TENSOR

SA STRESS TENSOR

SA TRANSFORMATION TENSOR

Curvature tensor in definition of affine branch point induced by Riemann branch point on isotropic hypersurface 09 p1534 A67-22566

TENSOR ANALYSIS

Stress functional properties of plastic materials, discussing analyticity and continuity in terms of tensor analysis 02 p0336 A67-11630

Matter tensor of generally relativistic perfect fluid derived from invariant integral by Marx variational principle 03 p0468 A67-13392

Second order spectral tensor equations governing turbulence occurring in presence of uniform magnetic field at low magnetic Reynolds numbers 03 p0483 A67-13883

Energy impulse vectors and kinetic moment tensor associated with body in gravitational field analyzed, using Brouwer theorem 04 p0658 A67-15494

Approximation method for determining stress field of body from temperature field 05 p0914 A67-18196

Stress-strain and Hooke law in orthotropic elasticity presented through matrix algebra and tensor coordinates 06 p1108 A67-18656

Einsteinian gravitation equations stated in terms of three-dimensional tensor analysis as applied in conformal space 08 p1354 A67-20843

Energy and momentum localization of gravitational field by direct field measurements 09 p1531 A67-21559

Antisymmetric tensor theory of gravitation in flat space-time with energy and momentum conserved 09 p1532 A67-21979

Complex vectorial formalism in general relativity, discussing Riemann connection related to representation of Lorentz group by three-dimensional linear space 09 p1525 A67-22625

Covariant decomposition of tensor and gravitational Cauchy problem in Riemann space 10 p1679 A67-22841

Equations for continuous media in finite case formulated in Eulerian and Lagrangian form 11 p1819 A67-24621

Properties of anisotropic continuous media with energy and stresses depending on deformation tensor gradients and other tensor magnitudes 11 p1876 A67-24876

Ordinary waves in viscoelastic mediums analyzed, using Green tensor relation to Kirchhoff tensor 11 p1877 A67-24750

Random motion transport relation to heat

propagation noting tensor characteristics, entropy effects and path dependence 11 p1819 A67-24757

Stresses and strains in nonlinear viscous elasticity, examining tensors in abstract form 12 p2016 A67-25444

Light diffraction by elastic waves in YIG noting values of photoelastic tensor components 12 p1984 A67-25746

Continuum mechanics of Cosserat type, discussing kinematics generalization and existence of higher order displacement gradients in internal energy density equation 12 p1968 A67-26200

Book on elasticity covering engineering, Cartesian tensor and vector-dyadic notation, etc 14 p2395 A67-27891

Computer programs for calculating curvature tensors and motion equations [JPL-TR-32-1122] 14 p2276 A67-28847

Boundary perturbation theory in electromagnetism noting application to conducting sphere with surface perturbation 15 p2435 A67-29186

Compatibility of some spectral functions with Heisenberg theory in axisymmetric turbulence and in equilibrium range [ONERA-TP-461] 15 p2470 A67-29381

Arbitrary electrode MHD generator electrical characteristics, considering end effects and determining internal conduction matrix 16 p2600 A67-30534

Schwarz transformation methods for electrical studies of MHD generators with tensor conductivity 16 p2600 A67-30535

Effective conductivity tensor of nonhomogeneous plasma in homogeneous external magnetic field 16 p2711 A67-30539

Stress space theory and application to fatigue fracture theory, noting geometrical formulations for deformation and stress of body 16 p2768 A67-31277

Second order incompressible fluid equation of motion, compatibility equation and dissipation function 16 p2663 A67-31703

Galactic and solar ray behavior equations, with cosmic ray drift velocity and diffusion tensor determined for interstellar space in anisotropic-diffusion approximation 17 p2935 A67-32109

Kinetic model of matter for energy momentum tensor of general relativity, noting freedom of divergence 17 p2883 A67-32360

Book on continuum mechanics including kinematics, principles and linear theories of continuum mechanics, elasticity and viscoelasticity 17 p2963 A67-33092

Gunther solution representation for stress fields noting tensor potential theorem, second order tensor fields, etc 17 p2964 A67-33136

Wave surfaces of Einstein-Schrodinger theory and nonlinear electrodynamics brought together using antisymmetric tensor 18 p3078 A67-33688

Necessary and sufficient conditions for space-time curvature tensor and isotropic vector field associated with double 2-form to satisfy higher order field equations 18 p3078 A67-33689

Structure of curved space-time in which electromagnetic wave propagation takes place without tail formation 18 p3079 A67-33761

Energy flux in steady inhomogeneous turbulent gas flow with arbitrary mean velocity field, deriving velocity spectra and pressure-velocity correlation tensors 18 p3030 A67-34741

Elastic potential used to study Green and Neumann tensors through series expansion for Dirichlet problem 19 p3341 A67-35541

Prestressed-shell buckling, using Budianski-Kolter tensor nonlinear equilibrium equations by numerical analysis 19 p3343 A67-35778

Stability criteria in stress-rupture strength theory, deriving stress and moment influence functions and damage tensor 21 p3717 A67-37969

Orthonormalized vector reference in coupling between symmetrical tensors in continuum mechanics, deriving expansion coefficients 21 p3717 A67-37971

Stresses and strains in nonlinear viscous elasticity, examining tensors in abstract form 21 p3726 A67-38829

Tensor calculation of origin of local concentration of matter in universe model, considering effect of gravitational

perturbations 22 p3880 A67-39314
Computer formulation of motion equations using tensor calculus to extend area of application of digital computers 22 p3827 A67-39418

TENSOR FIELD

Tensor components of thermal emf of CdSb measured by method without producing thermoelectrical eddy currents 01 p0129 A67-10137
Uniform velocity MHD channel flow of nonequilibrium plasma with tensor electroconductivity 02 p0275 A67-12552
Virial theorem for electron plasma obtained by defining potential tensor and superpotential of electric field 03 p0482 A67-13746
Electric potential and current density distribution in MHD channel allowing for anisotropy in conductivity 04 p0668 A67-15190
Variational derivations of field equations for relativistic mechanical, EM and gravitational fields in space-time continuum 06 p1033 A67-18582
Inverse operation for Jaumann derivative /integration/ applied to rheological equations of state for viscoelastic fluids 06 p0991 A67-18777
Asymptotic behavior of curvature tensor in certain asymptotically Euclidean Riemannian space-time manifold 11 p1819 A67-24763
Electromagnetic field tensor created by point charge provided with universal velocity and acceleration is equal to outer product of universal vectors 13 p2156 A67-26594
Second order conductivity tensor of isotropic electron gas theory, using thermodynamic Green functions 16 p2713 A67-30803
Gunther solution representation for stress fields noting tensor potential theorem, second order tensor fields, etc 17 p2964 A67-33136
Ideal fluid energy-momentum tensor derivation of Crocco-Vazsonyi equation for ideal fluid relativistic hydrodynamics, discussing continuity equation for specific entropy 19 p3210 A67-35707
Gravitational effects and cosmic phenomena reconciliation with Einstein relativity scalar-tensor theories 20 p3524 A67-36834
Einstein vacuum equation solution interpretation for gravitation, space and time concepts, using vector fields oriented in time and Riemann tensorial equations 20 p3487 A67-37684
Plasma conductivity tensor in steady magnetic field in terms of electric field correlation using Kubo transport theory 20 p3503 A67-37692
Tensor conductivity effect on continuum and collisionless MPD flows past slender bodies [AIAA PAPER 67-731] 21 p3674 A67-38755
Statistical elasticity problems involving random stress and displacement tensor fields, proving uniqueness and minimum principle for boundary value 22 p3909 A67-39396
Motor fields analysis in Cosserat continuum noting differential forms of stress and strain 22 p3837 A67-40006

TERBIUM

Energy transfer mechanisms involving trivalent terbium and europium, noting that at 295 degrees K thermal effects cause overlap permitting dipole-dipole transfer to occur 01 p0134 A67-10874
Luminescence spectra of terbium complex compounds with pyrazolone derivatives 03 p0433 A67-12888
Luminescence spectra of terbium complex compounds with pyrazolone derivatives 06 p1012 A67-18768
X-ray analysis of lattice structure of terbium crystals at 120 to 300 degrees K 09 p1555 A67-22066
Laser activity from terbium trifluoroacetate in p-dioxane and acetonitrile at room temperature 11 p1803 A67-24833

TERMINAL

SA ELECTRIC TERMINAL
Airport terminal facilities - Conference, Houston, April 1967 22 p3778 A67-39373
Gate arrival terminal design for Kansas City MCI airport noting loading positions,

maintenance hangars, service roads, post office, etc 22 p3779 A67-39375
Air terminal complex at Pittsburgh noting construction and expansion proposed under master plan 22 p3779 A67-39376
Development of major air terminal buildings at Canadian airports by maximum operational capacity, land availability, noise contours and capital investment 22 p3779 A67-39377
Aircraft terminal apron design, considering passenger convenience, variations in aircraft configuration and changes in aircraft mix and loading facilities 22 p3779 A67-39379

TERMINAL GUIDANCE

Singularity in motion equations of closed loop optimal guidance systems 01 p0111 A67-11224
Terminal descent design for unmanned vehicle soft lunar landing in Surveyor project [AIAA PAPER 64-644] 02 p0263 A67-11923
Time-optimal rendezvous in three dimensions with bounds on thrust and propellant, comparing various methods 02 p0330 A67-11924
Evasive guidance and maneuvering during terminal phase of co-orbital rendezvous 02 p0330 A67-11926
Minimum tracking data in guidance technique functioning comparable to proportional navigation homing system, noting tests in computer simulations and in laboratory model 02 p0263 A67-12158
Lunar and planetary terminal point guidance using optical correlator 02 p0264 A67-12317
Optimum terminal missile maneuver and evasion strategy with Gaussian process 03 p0465 A67-13267
Proportional navigation, emphasizing time-varying behavior of basic parameters, applied to exoatmospheric interception of satellite 04 p0654 A67-15550
Rendezvous problem of ascent and injection into transfer orbit and terminal phase 06 p1082 A67-17790
Minimum normed operator application to optimal terminal control system problems 06 p0974 A67-17925
Digital data processing, transfer and display equipment applied to ATC terminal operations, using surveillance radars and radar beacons 08 p1351 A67-20677
Flight instrumentation aiming at improving safety of approach and landing of commercial aircraft [SAE PAPER 67-0327] 17 p2860 A67-32983
Navigation system for long range transport aircraft providing accurate and reliable fixing, discussing takeoff and landing 19 p3254 A67-35312
Optimal terminal guidance law for linearized equations of air-to-surface missile 19 p3258 A67-35975
Optimum two-impulse orbital transfer for arbitrary terminal conditions, discussing analytic characteristics 19 p3329 A67-35979
Terminal guidance concept for soft and accurate lunar landing of unmanned spacecraft [AIAA PAPER 67-594] 19 p3259 A67-35990
Adaptive terminal guidance scheme for circular orbit rendezvous to provide near optimal trajectory 22 p3832 A67-39964
Terminal guidance problem involving optimal control for deviations in systems with transport lag 22 p3833 A67-40158
V/STOL all-weather guidance system developments and flight experimentation, discussing enroute navigation compatibility and terminal area operations [AIAA PAPER 67-796] 24 p4183 A67-42957
Performance and feasibility of staged propulsion during terminal phase of Mars soft landing [AIAA PAPER 67-987] 24 p4246 A67-43059

TERNARY ALLOY

Phase diagram of W-Zr-Ti ternary alloy 01 p0093 A67-10291
Room temperature recombination radiation induced by Lorentz field in InSb and ternary alloy of mercury, cadmium and tellurium under cross field conditions 03 p0496 A67-13675
Lattice thermal conductivity of disordered alloys of ternary compound semiconductors Cu₂/Sn, Ge/ /Se/S₃, /Ag, Pb, Sb/Te₂ and /Ag, Sn, Sb/Te₂ 04 p0675 A67-14760
Microscopic and X-ray analysis of cast and annealed W-Mo-Ti alloys, plotting

polythermal cross sections 04 p0638 A67-15203
Ternary alloys compounded with Ti, Zr, Hf, Fe, Ni, Co, Cu, Al, Ga, noting crystalline structures 05 p0830 A67-16919
Transmission electron microscopy analysis of microstructural phase properties of Ti-8Al-1V-1Mo alloy after duplex and mill annealing treatments 06 p1013 A67-17797
Temperature dependence of electroconductivity of As-Su-Ge system in vitreous state 06 p1052 A67-18610
Temperature effect on electroconductivity of complex vitreous systems of K-Ti-Pb 06 p1053 A67-18613
Physicochemical properties of Ti-Al-O solid solutions 07 p1203 A67-19260
Titanium carbide-molybdenum carbide interaction and structure of resulting Ti-Mo-C 07 p1203 A67-19261
Phase equilibrium and physicochemical properties of titanium aluminide-titanium stannide-zirconium quasi-ternary alloy 07 p1204 A67-19264
Aerospace castings from light ternary Mg-Li-Si alloy, discussing fabrication development 07 p1193 A67-20254
Effect of liquation inhomogeneity on superconducting properties of ternary alloy, noting enhancement of critical current density in wire prepared from this alloy 10 p1689 A67-23089
Probable upper limit of critical field for ternary and higher order ductile transition metal superconducting alloys 11 p1850 A67-24925
Coherent ordered precipitates formation in Ni-Cr-Al alloy, discussing spacing, shape and size of gamma prime particles as function of time 12 p1954 A67-25344
Ternary alloys compounded with Ti, Zr, Hf, Fe, Ni, Co, Cu, Al, Ga, noting crystalline structures 14 p2337 A67-28259
Slip step role in early stages of stress corrosion cracking in face centered iron-nickel-chromium alloy thin foils 16 p2690 A67-31384
Chemical reactions in Ni-Ti-Nb system, examining via X-ray diffraction formation of ternary intermetallic compounds 16 p2691 A67-31593
X-ray structural and diffraction analysis of Mo-Ni-Bo system at high temperatures noting isothermal sections of phase diagram 16 p2691 A67-31595
Structures from two-step aging of aluminum-magnesium-silicon alloy, discussing effect on needle precipitation 18 p3065 A67-34362
Ti-C-N system studied for stoichiometric range and thermodynamics using gas equilibration techniques, measuring nitrogen/carbon activities 19 p3248 A67-34865
Indium arsenide-tellurium ternary compounds chemical bond, microhardness and structure 20 p3506 A67-36226
Ni-Fe-Mn alloy, Youngs modulus and magnetic saturation temperature dependence, noting order-disorder effects on Curie point 20 p3468 A67-37178
W-Ta-Re system equilibrium diagrams examined, measuring diffusion layer element concentration by X-ray spectral analysis method 20 p3468 A67-37180
Aging of iron-nickel-titanium alloys during heating in reverse martensitic alpha to gamma transformation process, investigating phase parameter changes 22 p3820 A67-39824
Hf, Mo and W influence on maximum interstitial solid solubility of N in Nb rich ternary systems 24 p4172 A67-41977
Lifetimes of n-type Cd-Hg-Te alloy, showing Hall-Shockley-Read type recombination at low temperatures 24 p4205 A67-42664
Fatigue crack initiation, comparing alpha brass and Al-Mg-Zn alloy, noting effect of increasing maximum pressure value in contact region [ASLE PAPER 67-LC-5] 24 p4174 A67-42744

TERNARY SYSTEM

Crystallographic structure of hexagonal ferrites of BaO-MeO-ferric oxide system and applications in UHF and microwave regions 02 p0301 A67-12787
X-ray and thermal analyses and phase diagram of titanium chromide-tantalum chromide-niobium chromide solid solution at high temperatures 03 p0447 A67-13640
Visible and X-ray photoelectric emissions in layers of Se-As-Tl intrinsic semiconductor

films in vacuum 03 p0498 A67-13838
 Synthesis method for generating p-level pseudorandom signals derived from corresponding m-sequences, using standard binary logic elements 03 p0393 A67-13997
 X-ray analysis of Nb-Ni-Al solid solutions, noting solubility of Nb and construction of phase diagram 04 p0638 A67-15204
 Structure and mechanical properties of niobium alloys containing vanadium and titanium, showing relation between behavior in thermal etching and content of alloying element 05 p0831 A67-17505
 Electric conductivity of vitreous As-S-Th 06 p1053 A67-18615
 Mechanical properties of alloys of systems Al-Zn-Li and Al-Zn-Li-Mg 07 p1201 A67-19253
 Microstructure of alloys of Ti-Fe and Ti-Cr-Fe systems, determining phase composition and incipient melting temperature 07 p1204 A67-19269
 Phase diagram of Ti-V-C system based on phase equilibria, using X-ray diffraction, microhardness measurements, etc 07 p1204 A67-19270
 Ternary system Ti-Al-V alloys analyzed using thermal, microstructural, etc, methods, plotting solidus surface in crystallization region of beta-solid 07 p1205 A67-19273
 Phase diagram of Nb-Ti-Zr system and superconducting properties of alloys 09 p1518 A67-22029
 Titanium-chromium-vanadium system isohardness and isothermal diagrams and characteristic micrographs 11 p1806 A67-24362
 Ternary phase diagram of Mo-Ti-Zr system from eleven isothermal cross sections 11 p1808 A67-24856
 Elastic properties of Ti alloys of ternary system Ti-Zr-Cr, showing sensitivity to heat treatment 13 p2143 A67-27710
 Visible and X-ray photoelectric emissions in layers of Se-As-Tl intrinsic semiconductor films in vacuum 13 p2184 A67-27719
 Laminar flame speeds and composition flammability limits at low pressure for ternary mixtures of hydrogen and oxygen with ammonia and nitrous oxide 14 p2406 A67-28547
 Transforms for regularizing two-body collisions in plane two-and three-body systems with aid of conformal mapping and function theory 15 p2559 A67-30037
 Ti-Zr-C and Ti-Hf-C alloy X-ray and microstructural studies noting homogenizing, annealing, quenching and phase equilibria 15 p2505 A67-30388
 Ternary semiconductors, analyzing physical and physicochemical properties, noting synthesis and preparation of single crystals 16 p2725 A67-30801
 Temperature dependence of thermal diffusion factors in ternary system He-Ne-Kr by two-bulb method 16 p2661 A67-31223
 X-ray and thermal analyses and phase diagram of titanium chromide-tantalum chromide-niobium chromide solid solution at high temperatures 17 p2875 A67-33173
 Ternary semiconductor composition found through valence equation 20 p3512 A67-37243
 Structure and mechanical properties of niobium alloys containing vanadium and titanium, showing relation between behavior in thermal etching and content of alloying element 21 p3644 A67-38033
 Oxygen interstitial solid solubility in niobium, noting decrease with addition of tungsten and molybdenum 22 p3823 A67-40211

TERRAIN
SA TOPOGRAPHY
 Multispectral photography in gathering data on static physical and man-made elements of urban environment 01 p0058 A67-10309
 Tilt angles for photographs of physically and geographically diverse terrains taken with different types of gyrostabilized aerial cameras 13 p2118 A67-26463
 Survey satellite potential uses in vegetation resources and terrain analysis, emphasizing satellite photography 19 p3231 A67-35654

TERRAIN FOLLOWING AIRCRAFT
 Laws for aircraft control in terrain-following and formation-flight modes of operation, applying solution of Euler-Poisson equation 08 p1351 A67-20700
 Terrain following pulsed radar system without continuous scanning noting

computer simulation, antenna and pitch control 11 p1752 A67-24259
 Project 666a Automatic Terrain Following Program and Automatic Flight Control System /AFCS/, with digital and analog simulation and test 19 p3174 A67-35965
 Low altitude flight load spectra for light aircraft 24 p4094 A67-42755

TERRESTRIAL DUST BELT
 Tektite structure and lunar ash flows, noting theoretical computations of pressure, temperature and voidage 03 p0512 A67-13936
 Forces acting on small dust particles orbiting near earth and in interplanetary space and existence or nonexistence of terrestrial dust belt 04 p0615 A67-14967
 Near-earth cosmic dust cloud and data obtained from satellite, rocket and ground measurement 06 p1083 A67-18161
 Dust cloud moons of earth, discussing results of photographic measurements 07 p1256 A67-20165
 Radar evidence for atmospheric dust layers around 80 km altitude 13 p2109 A67-26333
 Near-earth cosmic dust cloud and data obtained from satellite, rocket and ground measurement 16 p2741 A67-30505
 Micrometeoritic cloud existence near earth refuted by satellite incidence-frequency measurements, describing satellite measuring devices 17 p2850 A67-32975
 Gravitational capture of cosmic dust by sun and planets and evolution of circumterrestrial cloud 18 p3119 A67-33863
 Noctilucent cloud fine structure wave form due to visibility through ice condensed on dust particles in wave-like pattern 24 p4146 A67-41791

TERRESTRIAL MAGNETISM
S GEOMAGNETISM
TERRESTRIAL RADIATION
 Errors of IR-horizon pickups due to satellite determination of vertical 02 p0240 A67-11541
 Direct measurements of thoron from ground surface to height of 50 cm in atmosphere, describing turbulent diffusion of radioactive emanations from soil surface 02 p0237 A67-11853
 Radioisotope and radiation techniques for terrestrial and planetary gas and solid measurements 02 p0245 A67-12223
 Magnetic particle motion, analyzing effect of earth electric dipole field 02 p0311 A67-12585
 Terrestrial radiance in middle UV noting Rayleigh scattering, vertical distribution of air, oxygen and ozone, attenuation factors, etc 04 p0613 A67-14695
 Cosmos LXI spectrophotometric measurements of atmosphere-reflected UV radiation spectra 07 p1178 A67-19801
 Biological satellite research, discussing radiation effects on living organism as measured by Cosmos 110 07 p1136 A67-19867
 Heat radiation spectra of earth as measured by Cosmos satellites, comparing experimental and calculated results 10 p1637 A67-23194
 IR transition zone between earth and space studied by gyro-stabilized satellite 10 p1637 A67-23196
 Cosmos 65 spectrophotometric measurements of atmosphere-reflected UV radiation spectra 10 p1647 A67-23277
 Heat flow values correlated with major geological features by analysis of 2000 terrestrial heat flow observations 15 p2477 A67-29763
 Spectral composition of earth IR radiation measured from satellites, giving radiation intensity and temperature distributions 19 p3219 A67-35253
 Wind and cloudiness effects on terrestrial scintillation based on visual estimates and measurements 22 p3828 A67-39240
 Earth upper atmosphere background radiance measured by UV radiometer carried on Air Force satellite 22 p3794 A67-40364
 Solar and terrestrial thermal radiometer absolute calibration noting standards and methods 23 p4006 A67-41373

TERRIER MISSILE
 Terrier two-stage sounding rocket design, fabrication, flight testing and performance characteristics 08 p1408 A67-20527
 Tactical checkout missile test installations for Terrier, Tartar and Talos missiles 20 p3416 A67-36971

TESSERAL HARMONICS
 Corrections to Smithsonian astrophysical observing station coordinates and nonzonal harmonics from combination of dynamical and geometrical method 01 p0056 A67-10039
 Orbital resonance caused by tesseral harmonics, examining perturbations of synchronous satellite in eccentric orbits 02 p0328 A67-12400
 Six solutions for tesseral harmonic coefficients of geopotential from satellite determinations compared with gravimetry 03 p0414 A67-13933
 Orbital elements determination from reduced Baker-Nunn observations of satellites, noting disturbance by resonance effects of earth gravitational potential sectorial and tesseral harmonics 05 p0763 A67-16562
 Earth gravitational field parameters from near-surface satellite observations influenced by zonal and tesseral harmonics 05 p0800 A67-17080
 Zonal and tesseral harmonic perturbations of artificial satellite 08 p1382 A67-20399
 Coefficient of major axis of symmetry of spherical harmonic in satellite oscillations 08 p1383 A67-20587
 Orbit perturbations due to tesseral harmonics contained in series expansion of gravitational potential determined using computer program 09 p1467 A67-21885
 Tesseral harmonics of coordinates using Baker-Nunn data and geopotential and dynamical procedures, noting iterative cycle for correction 10 p1636 A67-23178
 High order tesseral harmonic effects on satellite orbit calculation 12 p2008 A67-25831
 Orbit determination from Minitrack observations, discussing effects of ionospheric refraction, atmospheric drag and earth tesseral harmonics 18 p3126 A67-34244
 Von Zeipel method and Hamiltonian perturbation mechanics used for orbits at resonance with tesseral harmonics of geopotential 19 p3328 A67-35959
 Theory on earth shape, considering surface of geoid assumed as equipotential surface at sea level, obtaining relations between zonal and tesseral harmonics coefficients 22 p3792 A67-39933

TEST
S ALTITUDE TEST
S BODY SWAY TEST
S COLD FLOW TEST
S COLD WEATHER TESTING
S COMPRESSION TESTING
S CORROSION TEST
S DESTRUCTIVE TESTING
S DROP TEST
S ELECTRONIC EQUIPMENT TESTING
S ENGINE TESTING
S ENVIRONMENTAL TESTING
S FATIGUE TEST
S FLIGHT TEST
S FUEL TESTING
S FUNCTION TEST
S GROUND TEST
S HEAT TEST
S IMPACT TEST
S LOAD TEST
S MATERIAL TESTING
S MISSILE TEST
S NONDESTRUCTIVE TESTING
S PATCH TEST
S PRELAUNCH TESTING
S PROPELLANT TESTING
S PSYCHOLOGICAL TESTING
S RANK TEST
S RESONANCE TESTING
S SPIN TEST
S STATIC TESTING
S ULTRASONIC TESTING
S UNDERWATER TEST
S VESTIBULAR TEST
S VIBRATION TESTING
S WEBER TEST
S WHIRLING TEST
S WING FLOW METHOD TEST

TEST BED
 Lunar environment simulation test bed, noting lunar gravity effect on astronaut performance 17 p2832 A67-32003
 Transiently loaded foundation on soil designed using graphical phase-plane analysis, considering soil stiffness and damping effect [AIAA PAPER 67-550] 19 p3208 A67-35947
 Electromechanical servosystem in conjunction with inductive pickup circuit for

thrust measurements in jet engine bed tests 22 p3797 A67-39536

TEST CHAMBER

SA ANECHOIC CHAMBER

Design, construction and operation of vacuum chamber space simulator for testing Gemini space capsule 01 p0049 A67-10303

Pressure and stagnation temperature distribution in test chamber of blowdown hypersonic wind tunnel 01 p0049 A67-10558

Undulatory radiation in space and simulation in space test chambers 03 p0395 A67-13495

Solar simulation tests on UK-3 satellite, evaluating thermal environment and sorting out interface problems between spacecraft and test chamber 09 p1486 A67-22434

Design, tests, operation and limitations of Apollo man-rated environmental control system simulation 11 p1748 A67-24340

Reverberation chamber for high intensity acoustic testing of specimen subjected to directionally predetermined spectral distribution of acoustic energy field 12 p1924 A67-25712

Rescue teams for manned testing in environmental chamber for Gemini spacecraft noting personnel, chamber and personal equipment, test operations and rescue function and drill 17 p2807 A67-32598

High altitude variable Mach number test cell for testing intake system of Concorde aircraft Olympus 593 20 p3414 A67-36497

Arc jet power efficiencies tested in insulated tank, comparing deuterium with hydrogen [AIAA PAPER 67-677] 21 p3691 A67-38710

Steady flow ammonia MPD arc jet thruster propulsion performance, discussing test chamber pressure variation, thrust data and cooling systems [AIAA PAPER 67-690] 21 p3696 A67-38930

Manned chamber testing of lunar module environmental control subsystem, describing equipment and support systems 24 p4139 A67-42050

TEST EQUIPMENT

SA CHECKOUT EQUIPMENT

SA CREEP TESTING MACHINE

SA DAMPING TESTING MACHINE

SA ENDSCOPE

SA FATIGUE TESTING MACHINE

SA FLIGHT TEST INSTRUMENT

SA FOKKER BOND TESTER

SA FREE FLIGHT TEST APPARATUS

SA HYPERSONIC TEST APPARATUS

SA IMPACT TESTING MACHINE

SA LOAD TESTING MACHINE

SA LUBRICATION TESTING MACHINE

SA SHOCK TESTING MACHINE

SA TENSILE TESTING MACHINE

SA TENSION TESTING MACHINE

SA VIBRATION TESTING MACHINE

Automatic testing and fault-isolation capabilities in advanced avionics systems 01 p0034 A67-10272

Metering and pumping equipment for test channel for high altitude permeability tests of parachute cloth, noting permeability of MIL-C-7350 B, type I fabric 02 p0182 A67-12789

Onboard test and decision-making requirements for spacecraft checkout system including computer and software, data link detail and test set detail 03 p0400 A67-14215

Indirect techniques such as IR and temperature sensing to overcome limitations of hard-wired test points but still monitor complete ensemble of components in built-in test equipment 03 p0388 A67-14216

Straining equipment for testing aircraft structures 04 p0708 A67-14584

Postmortem flaw detection methods and equipment for IC failure analysis 06 p0968 A67-18054

Apparatus for testing thin walled tubular samples under combined torsional and tensile load, using stressed state timer 06 p1107 A67-18639

Fluidic test equipment for measuring rapidly varying fluid parameters and flow visualization 07 p1186 A67-19634

Test platform isolated from random long period ground tilts used in calibration of gyroscopes, accelerometers, etc 08 p1314 A67-20580

Digital computer control of automatic test equipment 08 p1299 A67-21058

LF test generator producing ramp output for phase shift detection in electronic

systems at different input

voltages 08 p1307 A67-21537

Facility for testing third stage of ELDO rocket, discussing high vacuum equipment in Ottobrunn laboratory 09 p1485 A67-22124

Thermionic planar electrode converter and generator tests, noting test equipment and performance tables 09 p1449 A67-22344

Optical instrumentation for missile and space vehicle testing 10 p1655 A67-22993

Test rig for fuel system in Concord aircraft noting construction, control system, equipment, installation and operation 10 p1623 A67-23548

Space evacuation of NRC-2 insulation for liquid hydrogen tankage, noting vacuum test apparatus and cold plate test 10 p1734 A67-23727

Forced nonlinear vibration of Duffing type experimentally simulated with models of isolating systems, obtaining response curves [ASME PAPER 67-VIBR-35] 11 p1873 A67-24192

Automatic height control test equipment for V/STOL aircraft, discussing experimental setup and performance 11 p1772 A67-24268

Testing instrument for determination of lead wire mechanical properties and bond strengths within semiconductor devices 12 p1911 A67-25270

Vibration characteristics of turbine and compressor blading under rotation 12 p2015 A67-25418

Reliability of electromechanical relays, discussing test equipment, data analysis, etc 13 p2085 A67-27698

Random vibration testing of relays noting test equipment 13 p2085 A67-27698

Harmonic and impulse techniques for flight vibration testing to reduce data processing time [ONERA-TP-477] 14 p2395 A67-27899

Tester to check altimeter of Apollo lunar module 14 p2318 A67-28291

Noncontacting device for compressor-blade vibration measurement supplying data on all blades of one stage 15 p2545 A67-29165

Space vehicle lubrication methods, noting design and construction of test apparatus 15 p2492 A67-29558

Systems approach for product and test equipment failure information reporting, including cause and corrective and preventive measures 15 p2584 A67-30410

Prediction techniques developed under storage technology program, including nonoperating and operating time periods to determine operational readiness 15 p2495 A67-30416

Assurance and measurement of space vehicle alignment conforming to design requirements 15 p2496 A67-30422

Computer simulation model for cost effectiveness of built-in test equipment /BITE/ in airborne radar systems 17 p2833 A67-32491

Signal generator tuning to center frequency of narrow band receivers, noting test setup and procedure 17 p2827 A67-32800

Semiconductor strain gauge theory, application and installation 18 p3047 A67-33893

Optimal layout of turbofan jet engines, discussing experimental rig for high thrust measurement [AIAA PAPER 67-416] 18 p3111 A67-33903

Design and construction of equipment for oxygen, nitrogen and hydrogen determination in aerospace materials [ONERA-TP-466] 18 p2998 A67-34461

Stability tests on birdcage high temperature platinum resistance thermometer, presenting potential ratio bridge design 18 p3051 A67-34504

Process control program including failure mode and effects analysis, critical characteristics determination, safety features and test equipment complexity 18 p3058 A67-34673

Diagnostic methods of rotating bearing defects, describing types of bearings, oils and equipment used in tests 19 p3235 A67-34888

Automatic high speed IC test equipment and procedure 19 p3192 A67-35027

Instrument for measuring group delay time of microwave four-poles, using backward-wave tube as wave generator 19 p3193 A67-35032

Traction test apparatus for vacuum and high temperature testing of refractory

metals, with modifications for rupture and brittleness tests 20 p3463 A67-36112

Temperature dependence of oxide hardness relative to other materials, comparing oxide hardness data to carbide data 20 p3472 A67-36113

TRKI-12 predetection receiver/recorder subsystem examined for performance characteristics 20 p3380 A67-36550

Remote control pneumatic pressure test system for Saturn S-IC booster checkout with manual or automatic control, using computer 20 p3415 A67-36569

Computer based CRT display technique for servo system testing, discussing Saturn V display computer and simulation studies results 20 p3415 A67-36609

Automation in electronic test equipment - Conference, New York, August-September 1966, Volume 3, Built-in test and continuous monitoring 20 p3416 A67-36969

Automatic electronic test and checkout techniques, automatic test equipment history and high points of 1957-1959 DOD symposia 20 p3416 A67-36970

Tactical checkout missile test installations for Terrier, Tartar and Talos missiles 20 p3416 A67-36971

Automation in electronic test equipment - Conference, New York, August-September 1966, Volume 4, Built-in test and continuous monitoring 20 p3448 A67-36978

Sensors and display systems covering fiber optics, sensing of parameters for built-in equipment and passive monitors, passive chemical vapor/gas detection, etc 20 p3449 A67-36980

Nondestructive testing of electronic circuits with fiber optic scintillators, vidicon data sampling and pattern recognition displays, discussing TV data handling 20 p3449 A67-36982

Microminiaturized systems for fault analysis and indication design and application to built-in test equipment 20 p3449 A67-36983

Built-in tests /BIT/ for AN/AWG-10 Missile Control System 20 p3417 A67-36990

Automatic test system employing optical and electrical input signals based on pattern recognition with CRT display 20 p3392 A67-36991

Low cycle thermal fatigue under uniaxial constraint, describing clamping device, time-temperature controller and programmer used 20 p3543 A67-37699

Fatigue indicating meter attachment to integrate fatigue damage over any load/time spectra 21 p3719 A67-38130

Interferometer standing on L-shaped base for velocity and distance measurements, noting tests on aircraft and rockets and solar reflections effect 21 p3599 A67-38643

Measurement of cesium and mercury ion-atom resonance charge exchange cross section [AIAA PAPER 67-682] 21 p3660 A67-38713

Maintenance time reduction for multimode airborne weapons through built-in test equipment and integrated program 21 p3601 A67-38947

Automatic test equipment /ATE/ to ensure aircraft availability noting operation, circuitry, computer methods, etc 21 p3609 A67-39132

Sensitivity of explosives to shock waves tested by device using water as intermediate layer 22 p3866 A67-39489

Cryogenic insulation thermoconductivity measuring apparatus operable at high vacuum and nonsteady state conditions 22 p3803 A67-40295

Inertial instrument testing with precision centrifuges 22 p3781 A67-40384

Centrifugal disk photosedimentometer used for size analysis of latex emulsions 23 p3972 A67-41066

Transonic and supersonic grid wind tunnel loaned to Germany by NASA for testing blades 23 p3987 A67-41328

Shock testing to aid design analysis and for qualification and certification 23 p3987 A67-41414

Flash blindness effects on pilot performance simulating inadvertent exposure to nuclear bursts of light by xenon gas discharge tube 23 p3965 A67-41569

Human respiratory system impedance simulator for dynamic testing of aircraft breathing equipment to detect possible instabilities 24 p4114 A67-41782

SUBJECT INDEX

TEST FACILITY

Automatic test equipment for checkout and fault finding on Saab 37
Viggen 24 p4137 A67-41898
Cold welding under flight conditions of
ATS silver-plated beryllium copper damper
boom, discussing ultrahigh vacuum
equipment and test 24 p4160 A67-42033

Manned testing of EVA equipment in
simulated space environment, emphasizing
crewman ingress and egress and mission
objectives 24 p4115 A67-42049

Microelectronic integrated checkout
equipment interfacing subsystems under test
with test subsystem 24 p4133 A67-43036
[AIAA PAPER 67-952]

TEST FACILITY

SA LABORATORY

SA ROCKET TEST STATION

SA SIMULATOR

SA WIND TUNNEL

Environmental simulation techniques to
supplement facility capabilities for
environmental test program of Lunar
Excursion Module /LEM/ 24 p4133 A67-43036
[SAE PAPER 660682] 01 p0049 A67-10587

Fatigue testing facility for tubings in
aviation hydraulic systems 02 p0231 A67-12447

Fluid dynamics, structures and operations
research and development at Netherlands
National Aerospace Laboratory 02 p0231 A67-12640

High altitude test stands of DVL rocket
test range at Lampoldshausen, planning
considerations and preliminary results from
altitude simulation 03 p0394 A67-13029

Instrumentation and control /I and C/
system for ground test of Nerva propulsion
system 03 p0395 A67-13384

Directory of RCA environmental test
facilities 03 p0396 A67-13635

Engine test facility for measuring thrust
and propellant flow in pulsating
rockets 03 p0396 A67-13774

Wind tunnel testing of hypersonic vehicles
with complete simulation of entire
hypersonic environment is not yet
possible 03 p0396 A67-13794

Rover testing facilities of Nuclear Rocket
Development Station in Nevada
[AIAA PAPER 66-1003] 03 p0397 A67-14148

Design and construction of mobile test
plant for jet engines to avoid engine
removal during control and checkout
procedure 04 p0594 A67-14413

Moving and stationary fluid type facilities
to simulate aerodynamics of charged
particles in ionosphere 04 p0595 A67-14991

Flexibility required to establish systems
facility necessary to support Agena vehicle
during development, testing and activation
phases 04 p0600 A67-15781

Vibration testing facilities for Apollo
Saturn V launch vehicle, noting structural
assemblies under dynamic testing 05 p0788 A67-16156

Space age facilities - ASCE Conference,
Cocoa Beach, Florida, November
1965 05 p0788 A67-16606

Arnold Center advanced ground test
facilities for rocket and space vehicle
environmental testing 05 p0788 A67-16617

Arnold Engineering Development Center,
discussing aircraft and space vehicle
environmental simulation and testing 05 p0788 A67-16619

Medical, design and operational aspects of
quality requirements for reliability of man-
rated space environment simulation
chambers 05 p0788 A67-16621

Scramjet testing with wave superheater
hypersonic tunnel 06 p0980 A67-18343
[AIAA PAPER 67-182]

Testing facility and methods for FR-1 and
D-1 satellite control 07 p1163 A67-19530

Space environment simulation noting
various testing facilities for space
equipment 07 p1163 A67-19534

Design criteria for NASA test facility for
firings of 20 inch diameter solid rocket
motors 07 p1241 A67-20059
[AIAA PAPER 67-236]

Electrical systems except data acquisition
and instrumentation for ground testing of
large booster 07 p1167 A67-20079
[AIAA PAPER 67-270]

Remote vibration testing facility for
components while using hazardous cryogenics
[AIAA PAPER 67-278] 07 p1167 A67-20083

Building block visual simulation facility
using new generation and display techniques
combined with TV model image
generation 08 p1314 A67-20659

FAA simulation systems for air traffic
control noting computer simulated radar
target generation, display equipment,
etc 08 p1315 A67-20678

Preflight and operational status test set
/PTS/ for radiation testing of electronic
equipment on military aircraft 08 p1303 A67-21059

Ground test facilities for aircraft air
breathing propulsion system development 08 p1315 A67-21063

Program checkout facility designed to
perform operational checkout of navigation
systems by analyzing system under
simulated conditions 09 p1484 A67-21833

Collector target complex eliminating
target life time and test equipment
contamination by sputtered target material,
applied in testing of electrical propulsion
systems 11 p1852 A67-24341

[AIAA PAPER 66-500] Man-rated space simulation facility,
emphasizing checkout and qualification of
systems 12 p1921 A67-25689

Space environment simulation facility for
thermal control coatings to study synergistic
and healing effects 12 p1924 A67-25711

High intensity acoustic test facility for
electronic packages and structures 12 p1924 A67-25718

Three-channel g limiter for protecting
specimen during vibrational testing 12 p1943 A67-25719

Mass properties determination on
aerospace balancing systems 12 p1925 A67-25724

Evaluation facility for rotor
containment/control devices [SAE PAPER 670332] 12 p1925 A67-25873

UV stability of several white thermal
control coatings spectrally characterized in
vacuum for application to Lunar Orbiter
project [AIAA PAPER 67-345] 12 p1959 A67-26059

Model tests on free jet scramjet facility
configurations at high Mach numbers,
obtaining data on bypass flow pressure
recovery and diffusion process 13 p2089 A67-26830

Shock-on-shock effects explored in
aerodynamic test facility combining
blowdown wind tunnel and shock wave
generator 13 p2091 A67-27490

Burn-pond concept of test facility for
disposing of hydrogen at high flow
rates 13 p2092 A67-27652

Computer controlled dynamic test facility
to provide data on flight characteristics of
Apollo-Saturn V launch vehicle by measuring
vibration amplitudes 14 p2293 A67-28593

MHD accelerators for hypervelocity test
facilities, showing Faraday accelerator is
best suited to operation at high flow
densities required 14 p2294 A67-29042

Graphite cloth and felt as resistance
heating elements for calibration and
simulation facilities, achieving fast changes
in heat flux level without sacrificing power
efficiency 15 p2490 A67-30153

Experiments and design of low
temperature seeded inert gas MHD power
generator operating in nonthermal ionization
mode 16 p2601 A67-30548

Role of ground and flight simulation test
facility on past, current and future
developments in aerospace propulsion 16 p2654 A67-30709

Hermetically sealed ballistic facility design
and operating principles, for testing at
various Mach and Reynolds numbers to
calculate aerodynamic coefficients and flow
geometry 16 p2655 A67-31115

Manrating of space environment
simulators, emphasizing integration of
physical facility requirements and operation
procedure to provide safety 17 p2807 A67-31960

Engine development and manufacture in
Sweden 17 p2928 A67-32123

Space pressure and temperature
environment simulation facility for liquid
rocket space-ignition reliability testing
[AIAA PAPER 67-428] 18 p3112 A67-33912

Parametric data on gas ingestion and
ground proximity jet effects experienced by
jet-powered VTOL configurations [AIAA PAPER 67-440] 18 p2985 A67-33917

Rocket engine turbopump assembly test
capability design, facilities, cryogenic
systems, control requirements, computer
simulation, activation and checkout
[AIAA PAPER 67-441] 18 p3112 A67-33918

M-1 Engine Thrust Chamber Assembly test
facilities and analog computer simulation
during checkout [AIAA PAPER 67-455] 18 p3019 A67-33929

Test facility for 5000 mw nuclear rocket
propulsion modules, discussing effect on
design and flight conditions duplication
[AIAA PAPER 67-465] 18 p3020 A67-33936

Environmental stress use in conjunction
with simulation testing 18 p3020 A67-34112

Scramjet testing with wave superheater
hypersonic tunnel [AIAA PAPER 67-182] 19 p3208 A67-35767

Inertial guidance and navigation systems
and components testing facility 1100 feet
underground [AIAA PAPER 67-538] 19 p3208 A67-35940

Space and high altitude simulation
requirements for testing various rocket
engine and propulsion systems 20 p3415 A67-36544

Safety program for nuclear rocket engine
testing, discussing role of
cryogenics 20 p3482 A67-36565

Hypersonic flight programs, considering
Air Force, Navy and NASA research
programs on scramjets 20 p3517 A67-37447

High performance aerodynamic impulse
facility with shock tunnel, expansion tube
and accelerator for high velocity and high
Reynolds number environment 21 p3605 A67-37768

Hot shot tunnel F operation as combustion
test facility using air, discussing oxygen
depletion, particle contamination and
reservoir decay 21 p3606 A67-37775

Wave superheater based on shock tube
principles, discussing application in scramjet
design 21 p3608 A67-38800

Hot shot nitrogen gas source for pulsed
MHD accelerator to provide lunar
reentry 21 p3608 A67-38863

Generator installation for supersonic gust
simulation to measure wing forces,
discussing calibration problem 21 p3609 A67-38889

Motion simulator with spherical self-
regulating gas bearing for testing attitude
control, analyzing turbine and tilting
momentum 22 p3778 A67-39165

Hatfield V/STOL tunnel design problems
and tunnel model test results 22 p3780 A67-40063

Large diameter helicopter rotors and
V/STOL propellers /axis tilting in vertical
plane/ testing system of wind tunnel and
aerodynamic torque measuring apparatus 23 p3986 A67-40575

Mississippi Test Facility /MTF/ of NASA
noting rocket testing facilities, scientific
laboratories and industrial complex 23 p3986 A67-40588

Engine test facilities on Concorde
examined for effect on supersonic Olympus
engine development [AIAA PAPER 67-753] 23 p4049 A67-40987

German Gyroscope Testing Laboratory
noting revolving platform for simulating
rotational velocities, signal testing and signal
simulation 23 p4003 A67-41327

Cryogenic valve testing facility for nuclear
rockets using liquid hydrogen at high
pressures and flow rates 23 p3936 A67-41425

Space magnetic environment simulation
coil facility for spacecraft testing by
mapping magnetic fields 24 p4138 A67-42030

White Sands Test Facility /WSTF/
constructed by NASA for hot firing tests of
lunar module at simulated altitude 24 p4138 A67-42031

Real gases examined for application as
working fluid in Brayton cycle power plant,
considering radiator area reduction to
Rankine cycle 24 p4102 A67-42488

Lithium-boiling potassium test facility to
investigate transient and steady state
characteristics of Rankine cycle system for
application to spacecraft nuclear-electric
propulsion 24 p4183 A67-42492

Impact of future aeronautical vehicles on
development test facility planning
[AIAA PAPER 67-780] 24 p4139 A67-42947

Space simulator growth problems,
discussing advantages of orbiting space
laboratories [AIAA PAPER 67-814] 24 p4243 A67-42968

Lunar gravity, reduced pressure and suit encumbrance effects examined in lunar surface environment simulation test bed, assessing astronaut performance [AIAA PAPER 67-866] 24 p4117 A67-42989

TEST FIRING

Third 260-inch diameter solid propellant rocket engine test firing 15 p2548 A67-30150

Liquid fluorine closed flow loop and rocket engine test position design, construction and operation 17 p2832 A67-32012

M-1 injector baffles, ablative chamber and start system design and development, using subscale testing [AIAA PAPER 67-461] 18 p2988 A67-33932

TEST METHOD

Graphical estimation of reliability of test results 01 p0104 A67-10157

Automatic and manual testing compared within framework of integrated testing system [SAE PAPER 660694] 01 p0050 A67-10622

Interferential method of testing high resolution photographic emulsions, using laser as light source 01 p0091 A67-10832

Test methods for determination of shear and flexural properties of sandwich panels 01 p0164 A67-11269

Reliability and maintainability demonstration at Rome Air Development Center, discussing test methods 01 p0084 A67-11360

Lunar landing type of Doppler radar system evaluated by space dynamic simulation testing, using helicopter and various types of terrain 02 p0205 A67-12412

Complex testing method for two-stage rocket probe recovery system with aid of two successively opening parachutes 03 p0518 A67-13397

Test arrangement and statistical data analysis for remote sensing of local flow instabilities and turbulence 03 p0422 A67-13773

Analysis of existing support systems and guide for planning of new systems presenting example of manual test system and automatic test system 03 p0424 A67-14214

Compiler for general purpose automatic test system /GPATS/ using program language for automatic checkout equipment 03 p0376 A67-14222

Test system for static tests on combinative unit for comparing two quantities given in binary code 05 p0768 A67-16265

Reliable test method based on special strain gauge load transducer for embedment axial stress measurement in electronic modules 05 p0779 A67-17457

Thermobimetallic sensing elements tested by compensation method 07 p1187 A67-19740

Test method for aluminum and titanium alloys, estimating tendency toward brittle failure and recording kinetics of crack formation 08 p1342 A67-21176

Graphical method for ascertaining acceptance number and size of sample in destructive and expensive testing 09 p1506 A67-22197

Measuring and calculating methods in testing of aircraft - Conference, Prague, April 1966 09 p1500 A67-22453

Test set for automatically compensating for error sources in calculating FET transconductance values 11 p1760 A67-24258

Serial comparison technique for coding systems where weight of ascending bit is equal or greater than previous bit 11 p1756 A67-24266

Absolute gain measurements of vertically polarized HF test antennas over imperfect ground 11 p1761 A67-24278

Buckling test data for internal integral ring-stiffened aluminum cylinders under combinations of axisymmetrical axial load and external lateral pressure 11 p1875 A67-24611

Glass filament wound interlaminar shear specimen design and instrumentation 11 p1875 A67-24614

Simulated high speed aerodynamic testing methods, factors complicating prediction of actual aerodynamics and various tunnels used 11 p1774 A67-25012

Nickel and cobalt superalloys low cycle thermal fatigue test method under cyclical extension and temperature conditions, giving stress-strain-time relations

[ASME PAPER 67-MET-19]

12 p1956 A67-25955

Verification of thermal mathematical model for artificial satellite using thermal vacuum chamber, noting error analysis [AIAA PAPER 67-304] 12 p2036 A67-26019

Piezoelectric accelerometer capacitance measurement and computation involved in conversion of accelerometer voltage sensitivity from one external circuit capacitance to another 12 p1947 A67-26186

Soviet papers on mechanism of metal breakdown 13 p2130 A67-26446

Wind tunnel tests of sonic boom phenomena, noting weak pressure field measurement, construction of extremely small models, boundary layer effects, etc [AIAA PAPER 66-765] 13 p2091 A67-27594

Test method used in analysis of statistical distribution functions for fatigue strength response data of aluminum sheet 13 p2221 A67-27738

Test methods to determine wear coefficients and design calculations for solid film lubricants, covering wide temperature range [ASLE PREPRINT 67AM 5A-5]

14 p2325 A67-28787

Test procedure and apparatus for evaluating oxidation-corrosion characteristics of aircraft gas turbine engine lubricants at high temperature 14 p2326 A67-28794

Testing conditions for near-wake study of solids of revolution in supersonic and hypersonic flow, using streamlined supports in magnetic suspension [ONERA-TP-454] 15 p2416 A67-29379

Semiconductor device measurements and test methods - Conference, Budapest, April 1967 15 p2448 A67-29799

Test methods and measurements of semiconductor devices - Conference, Budapest, April 1967, Part 2 15 p2449 A67-29809

Transistor failure analyses by measuring electric parameters, repeating production phases on opened transistors, destructive testing and defect production by extreme artificial stress 15 p2449 A67-29811

High speed automatic testing of semiconductor devices, discussing wafers and integrated circuits 15 p2449 A67-29812

Ultraviolet camera lenses for space flight use discussing techniques for testing and evaluating performance 16 p2680 A67-31805

Numerical Fourier transform calculations for pulse testing procedures for controlled time function input systems 17 p2883 A67-32018

Ballistic range blast-traversal testing technique using scale models containing fast response FM telemetry system modulated by capacitance type pressure transducer [AIAA PAPER 66-777] 17 p2832 A67-32063

Imperfections effect on buckling of complete electroformed spherical shells under uniform external pressure examined in rigid and soft testing systems 17 p2960 A67-32454

Parabola test for absolute stability, replacing Popov test for nonlinear sectors having nonzero lower bound 19 p3199 A67-34785

Servo loop electronics reliability using continuous redundancy, integral self-test circuits, etc 19 p3191 A67-34847

Reliability evaluation of MOS large scale integration devices, using simplified circuit to test individual small elements 20 p3398 A67-36800

Asymptotic relative efficiency of mixed statistical threshold tests with Gaussian samples 20 p3412 A67-37495

Strain age cracking characteristics in welded Rene 41 nickel base alloy, discussing test procedure used with circular patch test to evaluate contributing factors 20 p3471 A67-37698

Electronic equipment in space booster, considering test methods, environment simulation and electronic packaging 21 p3592 A67-38229

Tensile strength of charred ablation material under rapid heating conditions tested using plasma arc flow and miniaturized specimen 21 p3650 A67-38874

Test signal techniques for measurement and video monitoring used in ORTF network 22 p3796 A67-39233

Test and control planning concepts for space travel projects, considering third stage

of booster rocket Europa 22 p3921 A67-39281

I

Crack line loading methods for measuring fracture toughness noting advantages over remote loading test procedures 22 p3820 A67-39630

Measuring device for aerodynamic coefficients during wind tunnel tests by forced oscillation method 23 p3986 A67-40570

Test procedure for Si microcircuit production consisting of bulk and junctions electric measurement, oxide thickness and junction position 23 p3977 A67-40660

Aeroelastic phenomena in aircraft stability, control and airframe vibration characteristics, describing testing methods 23 p4077 A67-41046

Hovercraft research noting internal and external aerodynamics, test techniques and instrumentation requirements 23 p3934 A67-41167

Depth sampler for testing dirt content of jet fuels, discussing settling effects 24 p4206 A67-42279

Digital computer system for testing complex aerospace subsystems 24 p4126 A67-42932

Astronaut role in balanced in-flight testing for manned spacecraft [AIAA PAPER 67-949] 24 p4245 A67-43033

TEST PILOT

Test pilots report on aircraft and spacecraft - SETP Symposium, Beverly Hills, September 1966 06 p0947 A67-18196

FAA test pilot training in intent and administration of regulations 14 p2256 A67-27740

TEST PROGRAM

Pump loop testing and operational evaluation of SST hydraulic fluids [SAE PAPER 660664] 01 p0103 A67-10572

Long-term biomedical instrumentation in Air Force space program 01 p0017 A67-11029

Reliability tests on aerospace and missile systems research and development component assemblies 01 p0085 A67-11376

Computer design test program to automate checkout process of Saturn I and V space boosters gradually while retaining manual checkout 01 p0051 A67-11427

Test information systems improved by coupling data sources to users through remote terminals connected directly to large time sharing computing systems 02 p0207 A67-12001

Test program on air-to-air propagation between two jet aircraft at high altitude and path lengths up to maximum radio line-of-sight, considering antenna gain and multipath fading 02 p0202 A67-12122

Troposcatter test program for evaluating megabit digital transmission system, using wideband frequency shift keyed modem 02 p0202 A67-12126

Sunde channel model applied to Air Force tropo transmission test for calculating pulse error 02 p0202 A67-12129

Modeling of spacecraft performance during reentry /intact and disintegrated/ for evaluating spacecraft design through thermal and structural integrity tests 02 p0230 A67-12358

Man-machine interface and automatic test operations in Saturn S-IVB system 03 p0398 A67-14204

Hydrodynamic journal bearing tests in molten lithium at 600 to 800 degrees F to support compact canned rotor liquid metal pump [ASME PAPER 66-WA/LUB-6] 04 p0629 A67-15338

Acceptance vibration testing program costs, benefits and test control 05 p0813 A67-17248

Integrated plan for reliability demonstration through safety margin testing 05 p0813 A67-17253

Joint NASA-USAF lifting body flight test program and M2/F2, HL-10 and SV-5P research vehicles 06 p0947 A67-18197

Flight test program of North American OV-10A COIN /counter-insurgency/ aircraft 06 p0947 A67-18199

Handling quality evaluation of seven general aviation aircraft of type operated under instrument flight conditions 06 p0947 A67-18200

Category II Systems Evaluation Test of C-141A aircraft 07 p1129 A67-19616

Test program to evaluate characteristics of

existing Atlas engine boots in flight environment and provide parameters for design change
[AIAA PAPER 67-277] 07 p1241 A67-20054
Thermal design of navigational satellites, obtaining reduction in discrepancy between operational orbital temperatures and preflight calculations through thermal vacuum testing 09 p1572 A67-22062
Resistance of aviation hydraulic fluids, mineral, snuffer, phosphate ester, siloxane and chlorosilicone to wheel brake fires, evaluating lab test techniques and simulation testing 09 p1521 A67-22250
Helmet mounted sight as operational element in quick reaction boresighting system, using static and moving targets, obtaining field test data 09 p1456 A67-22371
Helicopter rotor blade service life substantiation through tests with rotor excitation panels inducing blade bending moments 10 p1622 A67-23431
Test conditions effects on glass fiber strength data 11 p1811 A67-24587
Testing of transpiration air cooled turbine, discussing blade fabrication [ASME PAPER 67-GT-29] 11 p1854 A67-24807
Executive aircraft structure safe-life fatigue analysis and tests [SAE PAPER 670257] 12 p2016 A67-25507
Combined multishaker and gas flow tests as part of reliability test program for Saturn V, S-1C pneumatic systems 12 p1923 A67-25706
Instrumentation and data acquisition system used in Saturn V dynamic test program for design of flight control system 12 p1923 A67-25709
Mechanical cascade toroidal servo flight control system tested using simulator [SAE PAPER 670269] 12 p1895 A67-25867
Boeing SST inlet, control and power system development, discussing test program, design objectives and cost [SAE PAPER 670318] 12 p1990 A67-25886
Preflight testing of ATS-1 Thermal Coatings Experiment /TCE/, discussing cup designs, sensor and cup calibrations, etc [AIAA PAPER 67-333] 12 p2038 A67-26047
Laboratory test program to study problems associated with flight instrument parameter measurement 12 p1947 A67-26187
XH-51A compound research flight test program, discussing adaptation of rigid rotor concept 13 p2052 A67-26421
Aircraft handling qualities research with variable static stability aircraft used as in-flight simulator [SAE PAPER 670261] 13 p2054 A67-27296
Hydrogen vent flare stack performance in adverse weather conditions 13 p2186 A67-27651
Test program of Al-Zn-Mg alloy /A25G/ to determine strength, fracture toughness, weldability and physical properties for cryogenic application 13 p2142 A67-27673
Computer applications to test scheduling problem against probabilistic demand in heuristic environment [AAS PAPER 67-46] 15 p2467 A67-30114
C-141A engineering development test program, discussing flight, accelerated service and all-weather testing [AIAA PAPER 67-409] 15 p2422 A67-30376
Lunar orbiter quality assurance program, emphasizing management, design, procurement, fabrication, quality control, etc 16 p2783 A67-31629
Coordinated laboratory and flight test program, determining stability of solar concentrator reflective surfaces in orbital environment 17 p2832 A67-32060
Statistically designed experiments in wind tunnel test programs dealing with exhaust nozzles, discussing data analysis techniques [AIAA PAPER 66-742] 17 p2834 A67-32571
NERVA program, reactor and nonnuclear component development, full-scale testing, engine program, facilities and materials research [AIAA PAPER 67-487] 18 p3076 A67-33953
Start characteristics of LM Ascent Engine determined by test series, noting effects of altitude variation, propellant lead time, temperature and valve slow-down [AIAA PAPER 67-522] 18 p3115 A67-33985
Optimum short term screen tests developed for integrated circuits 18 p3018 A67-34649
Reliability demonstration during category II and III testing of missile and airborne

radar fire control system, emphasizing coordination between factory and field 18 p3138 A67-34652
Maintainability demonstration results and experience, describing field and plant testing procedures and controls 18 p3007 A67-34669
Reliability and maintainability case histories 18 p3005 A67-34696
Oxygen concentration system for aviator breathing 18 p2995 A67-34717
Sterilization of spacecraft tape recorder, noting component design for individual sterilization compatibility 19 p3230 A67-35583
Structural and systems design characteristics of British launch vehicle noting control and guidance system, flight development and test programs 19 p3333 A67-35841
SST flight control system electronic and hydraulic systems, discussing system design, components, reliability and test programs [AIAA PAPER 67-570] 19 p3174 A67-35966
Pulsed injection laser radar for rendezvous and docking operations, giving results of test performance [AIAA PAPER 67-606] 19 p3259 A67-35997
Stress corrosion test method determined from test program on precipitation hardening semiaustenitic steels 20 p3465 A67-36486
IR scanning nondestructive testing program for microwelds to evaluate quality 20 p3454 A67-36666
Automatic test computer programming problems, discussing system planning, documentation, personnel, system compromises, etc 20 p3391 A67-36972
Transistorized time delay system based on measurement of condenser discharge time to predetermined voltage 21 p3590 A67-37952
Programmer for operational strength tests during aircraft construction 22 p3912 A67-39755
Handley Page Jetstream load carrying structural design, materials employed and structural test program 22 p3746 A67-40130
Test planning and decision making in environmental testing approached from program formulation involving resources and equipment, degree of simulation and optimum levels 22 p3781 A67-40402
Visually controlled placing response tests for kittens reared without sight of limbs 24 p4113 A67-42221
Reliability assessment test program for determining capabilities and limitations of 2 kw hydrogen-oxygen fuel cell stacks 24 p4109 A67-42896
U.S. launch operations techniques emphasizing launch site testing prior to launch [AIAA PAPER 67-889] 24 p4140 A67-43002
TEST RANGE
SA MISSILE TEST RANGE
USAF Eastern Test Range, discussing telemetry, tracking, geodetic and time measurements 05 p0787 A67-18609
Eastern Test Range time synchronization system, analyzing errors and limitations 20 p3414 A67-36535
Pulse radar on Air Force Eastern Test Range, discussing precision, sensitivity, acquisition, signature and multiple target capability 20 p3381 A67-36581
Acoustic problems from SST and multimillion pound thrust launch vehicles studied at Eastern Test Range, using Launch Acoustics Measuring System /LAMS/ 20 p3415 A67-36593
Real time telemetry data system for Air Force Eastern Test Range 20 p3381 A67-36614
TEST REACTOR
SA MATERIALS TESTING REACTOR
NERVA radiation effects tests at cryogenic temperatures [AIAA PAPER 67-477] 18 p3076 A67-33947
TEST STAND
Test stand simulating high intensity heating processes which occur in combustion chambers of rocket and jet engines 02 p0231 A67-12440
Design features of high velocity test stand with arc heater and MHD accelerator 04 p0595 A67-14543
Thrust measurement for microthrustor mounted on platform suspended from cable whose motion is sensed by autocollimator system [ASME PAPER 66-WA/AUT-8] 04 p0599 A67-15390

German papers on space research with satellites and space probes, Volume 2, Control, test stands and direction finding 07 p1260 A67-20266
Direct microthrust measurement on swinging gate test stand with equalization network 11 p1774 A67-25014
Optimum tapers determined for circular and rectangular ties, comparing resultant flexural stiffness with untapered supports 22 p3914 A67-40066
P4 double test stand for ground testing third stage of ELDO launch vehicle 23 p3987 A67-41325
TEST TIME
Reducing disturbances of certain form to zero by generating modified form of test signal to be applied to cross correlator 15 p2461 A67-30322
TEST TRACK
Wind tunnel data predicted vertical forces for rocket sleds compared with measurement on test track noting disagreement 22 p3780 A67-40095
TEST VEHICLE
SA DRONE
Instrumentation and data acquisition system used in Saturn V dynamic test program for design of flight control system 12 p1923 A67-25709
Nike rocket boosted 20-ft-diam ribbon parachute for deployment at dynamic pressures above 400 psf 13 p2054 A67-27598
Saphir test vehicle, two-stage guided and controlled rocket 15 p2571 A67-30090
TETHERLINE
Mathematical models for retrieval systems for future extravehicular operations, discussing rotational and translational motion and constraint equations 22 p3753 A67-39157
TETRACHLORIDE
S CARBON TETRACHLORIDE
S SILICON TETRACHLORIDE
TETRAETHYL
SA ETHANE
High intensity triboluminescence in europium tetrakis /dibenzoylmethide/-triethylammonium crystals under mechanical impact 01 p0019 A67-10897
TETRAFLUORIDE
SA CARBON TETRAFLUORIDE
SA SULFUR TETRAFLUORIDE
Oxygen atoms reaction with tetrafluoroethylene in presence of molecular oxygen 04 p0567 A67-15949
TETRAHEDRON
Image reconstruction of nonexistent three-dimensional equilateral tetrahedron using theoretically calculated automatically plotted photo-reduced hologram 07 p1186 A67-19558
Stacking fault tetrahedra in fatigued stainless steel, describing mechanism for nucleation of triangular Frank dislocation loop during cyclic load 11 p1805 A67-24109
TFX AIRCRAFT
S F-111 AIRCRAFT
THALLIUM
Plastic deformation of indium and indium-thallium alloys, noting change of pure indium lattice to fcc with increase of thallium content 02 p0255 A67-11869
Temperature-composition relationship for Hall coefficient inversion point in Ti-doped Te single crystals 03 p0500 A67-14232
Pressure composition diagrams of thallium rich portion of thallium-indium system at high pressure-temperature 04 p0635 A67-14511
Transmission spectra of GaS, GaSe, InSe and TlSe single crystals obtained at 300 degrees K by means of IR spectrometer 04 p0676 A67-14932
Electric conductivity of vitreous As-S-Th 06 p1053 A67-18615
Gap anisotropy increase in superconducting thallium transition temperature dependence on lattice defect density due to hydrostatic deformation 07 p1235 A67-20128
Optical quenching effect and spectral distribution of photoconductivity and optical transmission of KRS-5 single crystals 09 p1552 A67-21673
Average diffusion coefficient and apparent effective charges of components of alloys of Tl-S system 09 p1553 A67-21906
Transition temperature change for thin tin and thallium superconducting films after deposition of dielectric substances 13 p2182 A67-27360

THEODOLITE

SA CINETHEODOLITE

Method for piloting aircraft along prescribed paths, particularly for manually controlled complete instrument landings 04 p0550 A67-14548

Relationship of layer thickness and/or wind speed to wind shear [AIAA PAPER 66-352] 05 p0838 A67-17304

Theodolite Astro-2 observation of azimuth and position of moving satellite 10 p1655 A67-22985

Astro-2 observation theodolite and optical and electronic systems for tracking 10 p1655 A67-22990

Theodolitic device for measuring coordinates of center of gravity of photographed missile in flight 16 p2674 A67-31120

Development of kinetheodolites for satellite tracking 18 p3048 A67-34238

THEOREM

S BERNOULLI THEOREM

S BINOMIAL THEOREM

S EXISTENCE THEOREM

S GAUSS-MARKOV THEOREM

S GREEN THEOREM

S HELLMANN-FEYNMAN THEOREM

S HELMHOLTZ S THEOREM

S NERNST HEAT THEOREM

S POYNTING THEOREM

S RECIPROCAL THEOREM

S TAYLOR THEOREM

S UNIQUENESS THEOREM

S VON NEUMANN THEOREM

THEOREM PROVING

LF thermodynamic energy and pressure fluctuation-dissipation theorem for open systems with dynamic turbulence 11 p1821 A67-24974

Proof of Kupka and Smale approximation theorem concerning differential equations defined on compact manifold 13 p2146 A67-27095

Extremal problems of conformal mapping for doubly and triply connected regions, noting formulation and proof of pertinent theorems 16 p2698 A67-31913

Dyadic formalism to prove Herglotz-Noether theorem for flat manifolds [JPL-TR-32-1125] 17 p2879 A67-32929

Positive linear second order differential equation solutions, with proof of general theorems about qualitative asymptotic behavior 21 p3652 A67-38195

Invariant measure existence condition derived for Markov processes, with several ergodic theorems for homogeneous Markov processes proved, noting transfer functions 22 p3827 A67-39877

Perturbation theory definitions and overlap theorem proved and applied to small Reynolds number flows 24 p4142 A67-42168

THEORETICAL PHYSICS

Cosmological model for universe based on astronomical observations and validity of einstein theory and existing laws of physics 16 p2752 A67-31540

Soviet book on stability and oscillations of elastic systems covering theory, equilibrium breakdown, dynamic loading, aeroelastic oscillations, etc 18 p3140 A67-33674

One-dimensional models for constricted anomalous glow discharge investigated for various applications 19 p3274 A67-35100

Statistical Newtonian mechanics and quantum physics, discussing classical, thermodynamical and biological time concepts 23 p4027 A67-41139

THEORY

S BENDING THEORY

S BIOKINETIC THEORY

S BOGOLIUBOV THEORY

S BORN-INFELD THEORY

S COMMUNICATION THEORY

S CONVOLUTION THEORY

S CRITICAL INCLINATION THEORY

S CROCCO-LEE THEORY

S DECISION THEORY

S DIFFUSION THEORY

S DISTURBANCE THEORY

S DYNAMO THEORY

S FIELD MODE THEORY

S FIELD THEORY

S FLOW THEORY

S FLUCTUATION THEORY /STAT

MECH/

S GAME THEORY

S GRAVITATION THEORY

S GRIFFITH FRACTURE THEORY

S GROUP THEORY

S HANSEN LUNAR THEORY

S HEISENBERG THEORY

S HILL LUNAR THEORY

S HODOGRAPH THEORY

S HUECKEL THEORY

S INFORMATION THEORY

S JEANS THEORY

S JENSEN THEORY

S KINETIC THEORY

S KOLMOGOROFF THEORY

S MANY-PARTICLE THEORY

S MEASURE THEORY

S MEMBRANE THEORY

S MINKOWSKI THEORY

S MOLECULAR THEORY

S MOMENTUM THEORY

S NEWCOMB DERIVATIVE

S NEWTON THEORY

S NONADIABATIC THEORY

S NUMBER THEORY

S PARTICLE THEORY

S PERTURBATION THEORY

S PISTON THEORY

S PLASMA THEORY

S PLATE THEORY

S POTENTIAL THEORY

S PREDICTION THEORY

S PROBABILITY THEORY

S QUANTUM THEORY

S RELATIVISTIC THEORY

S RELATIVITY THEORY

S SET THEORY

S SHELL THEORY

S SPECTRAL THEORY

S THOMAS-FERMI THEORY

S TRANSPORT THEORY

S VINTI THEORY

S VOLCANIC THEORY

THERAPY

SA BED REST

SA SURGERY

Space environment utilization for biological and medical research, physiological studies and therapeutic purposes, discussing orbital hospital and ambulance launch vehicle 19 p3181 A67-35653

THERMAL ABSORPTION

Mean surface temperature-time solution of heat absorbed by sem infinite solids [ASME PAPER 66-WA/HT-58] 04 p0725 A67-15437

Absorption of thermal radiation from gaseous fuel by transparent wall of nuclear light bulb rocket engine [AIAA PAPER 66-619] 15 p2516 A67-29426

IR absorption in alkali-halide crystals containing molecular ion impurities caused by intralonic vibrations 20 p3511 A67-37140

Heat absorber temperature distribution, considering medium temperature and heat transfer coefficient arbitrary functions of time 24 p4154 A67-42215

Simulated solar absorptance of spacecraft thermal control coatings determined calorimetrically in vacuum at room and cryogenic temperatures 24 p4256 A67-42913

THERMAL ACCOMMODATION

COEFFICIENT

Absolute manometer of Knudsen for any temperature ratios and arbitrary accommodation coefficient on boundaries 08 p1331 A67-20867

Exact theory of enclosed molecular radiometer using flow field solution from Wu-revised thermal transpiration theory in two cases 10 p1681 A67-22864

Plane layer type apparatus for measuring thermal conductivities and accommodation coefficients of gases over wide pressure 10 p1658 A67-23783

Formula for thermal accommodation coefficient as basis for accommodation coefficient of monatomic gas-solid system calculation 12 p2040 A67-26229

Unified theory of gas-solid energy transfer in perturbation approximation, examining physical principles 13 p2223 A67-26940

Thermal accommodation of rare gases on clean metal surfaces, computing energy interaction with linear nearest-neighbor lattice 13 p2098 A67-26941

Thermal accommodation coefficient measurements with rare gases and metals and alkali metal sets 13 p2223 A67-26942

Thermal accommodation coefficient of rare gases on clean tungsten surfaces with gas temperature above room temperature 13 p2223 A67-26943

Thermal accommodation coefficient of nitrogen and helium on nitrogen covered tungsten above room

temperature 13 p2223 A67-26944

Thermal conductances in collisionless gas between coaxial cylinders and concentric spheres obtained for arbitrary thermal accommodation coefficients 15 p2579 A67-29566

Thermal accommodation coefficients determination in temperature jump region 15 p2580 A67-29883

Heat loss from wires in nitrogen, helium and mixtures measured at low Reynolds numbers, finding agreement with theory of Kassoy 16 p2779 A67-31217

Thirteen-moment equations solved obtaining theory of thermal force acting on spherical particle for entire range of Knudsen numbers 16 p2661 A67-31221

THERMAL AGITATION

Properties of Si-Si interface subjected to thermal oxidation in dry and wet oxidizing gases, thermal decomposition of ethyltriethoxysilane and vacuum evaporation of SiO and quartz 02 p0293 A67-11751

Temperature tuning of lithium niobate optical parametric oscillator in visible spectrum, noting generated frequency dependence on pump frequency and longitudinal mode distribution 02 p0253 A67-12511

Quasi-particle recombination lifetimes in superconductors measured experimentally shown to differ from calculated lifetimes 17 p2913 A67-32370

Rapid adiabatic cooling of gas systems for population inversion states 21 p3638 A67-37942

Tungsten strain amplitude dependent dislocation damping measured as temperature function, discussing inconsistency with Friedel thermally activated breakaway theory 22 p3819 A67-39352

X-ray diffusion from thermal agitation oscillations coupled with plasma waves in indium antimonide, discussing phonon-plasmon interactions and Hall effect measurements 22 p3859 A67-39652

THERMAL BATTERY

Heat transfer in fuel cell battery held in isothermal bath, giving charts for maximum temperatures at different Peclet numbers 20 p3364 A67-37016

THERMAL BOUNDARY LAYER

Smoothness of thermal potential and existence of solution for second and third boundary value problems with directional derivative for parabolic equation 04 p0721 A67-14669

Laminar heat transfer in thermal viscous MHD flow past sem infinite flat plate 05 p0857 A67-17418

Numerical solution of class of nonlinear high order differential equations with two-point asymptotic boundary conditions for thermal boundary layers in laminar and turbulent flow 10 p1627 A67-23560

Wind tunnel studies of heat shield over plane surface with film cooling during injection through two tangential slots 11 p1884 A67-25055

Thermal electrode boundary layer for shock wave ionized air ohmic heating in discharge chamber, noting Joule heat consumption effect 12 p1975 A67-25894

Boundary layer equations for two-temperature plasma, showing distinction between electron and ion thermal boundary layer thickness 16 p2712 A67-30544

Temperature range approximation determination in unsteady thermal boundary layer formed in plane parallel flow around body, solving equation with boundary conditions 18 p3025 A67-33680

Lower thermal boundary layer of solar convection zone within framework of mixing length theory 18 p3133 A67-34378

Heat transfer in steady flow of non-Newtonian fluid between two walls with periodic deformation considered, using perturbation method 18 p3161 A67-34618

Temperature distribution within two-dimensional thermal boundary layer due to flow of second order fluid past flat plate 19 p3210 A67-35447

Heat transfer for one- and two-dimensional pulsating incompressible laminar flow in circular tube with two thermal boundary conditions [ASME PAPER 67-HT-65] 20 p3550 A67-36747

Thermal boundary layer condensation enhancement of diffusion limited

vaporization rates, discussing heat of vaporization, critical supersaturation and surface temperature 22 p3920 A67-40423

Perturbation solution to one-dimensional nonadiabatic temperature distribution behind detached shocks taking into account absorption effects 23 p3992 A67-41738

Temperature distribution in homogeneous eccentric annular layer with constant internal heat generation 24 p4254 A67-42286

Free convection thermal transfer in narrow horizontal channels and infinitely wide channels 24 p4255 A67-42587

THERMAL BUCKLING

Buckling tests on uniformly heated thin cylindrical shells, noting load and temperature effects 01 p0163 A67-11013

Stressed and strained state of reinforced cylindrical shell under nonuniform heating and compression, noting three solutions to buckling problem 05 p0913 A67-16190

Progressive buckling of rectangular cross section bar under cyclic variations in temperature 05 p0913 A67-16193

Buckling of truncated conical shells due to directional thermal loadings [AIAA PAPER 67-112] 06 p1103 A67-18355

Snap-through buckling of open bimetallic shallow spherical shell under uniform temperature field 06 p1105 A67-18590

Thermal buckling of prestressed cylindrical shells and rings where expansion coefficient of external layer is smaller [ONERA-TP-422] 09 p1574 A67-21848

Hypersonic reentry heating problems for glider of composite structure with critical temperature condition, buckling, etc 11 p1869 A67-24092

Tests analysis of buckling caused by thermal gradient and fatigue due to thermal cycling in restrained combustor-cooling tubes 15 p2572 A67-29164

Thermal buckling of conical shells under circumferential temperature gradients analyzed using Rayleigh-Ritz method 19 p3343 A67-35772

Strain energy in thin isotropic elastic shells subject to arbitrary temperature distribution, considering large deflections and buckling 21 p3718 A67-38021

Buckling of truncated conical shells due to directional thermal loadings [AIAA PAPER 67-112] 21 p3728 A67-38873

THERMAL COMFORT

Water cooled vest with insulated icebox and electric pump to reduce thermal strain and increase comfort for aircrew members in hot humid climates 05 p0756 A67-18284

Temporal characteristics of body temperature during high thermal stress, determining correlation between effective and rectal temperature 10 p1600 A67-23822

Helium-oxygen environment relation to biological-thermal requirements of spacecrew 20 p3374 A67-36582

Thermal comfort zone test for helium-oxygen and nitrogen-oxygen atmospheric mixture for 18-day continuous manned run 22 p3754 A67-39599

THERMAL CONDUCTOR

Thermal conductor of arbitrary shape, analogy with rectangular array of electrical resistance, detailing conformal transformation 01 p0167 A67-11015

Thermal conductance at interface of two materials in contact, investigating surface and lubrication effects [AIAA PAPER 65-662] 03 p0534 A67-13068

Thermal conductivity of lanthanum and monochalcogenides, noting role and temperature dependence of crystal-lattice conductivity 04 p0680 A67-15287

Spacecraft thermal joint conduction study covering surface conditions, external pressure, use of various fillers and parent materials and vacuum environment [AIAA PAPER 67-316] 12 p2037 A67-26031

Effective gap thickness and gap number relation determined from correlation of parameters of thermal contact conductance [AIAA PAPER 67-317] 12 p2037 A67-26032

Thermal radiation dependence of perfectly conducting materials on large and small surface roughnesses thermal radiation dependence of perfectly conducting materials on large and small surface 16 p2779 A67-31502

Three-component heat transfer system for regulating system of three heat conductors, analyzing temperature regime 17 p2973 A67-33078

Similar or dissimilar materials thermal contact resistance in vacuum with negligible film effect, obtaining constriction resistance 20 p3555 A67-37609

THERMAL CONVECTION

Local convection coefficient along windward line of axisymmetric obstacle in hypersonic flow with laminar boundary layer 02 p0178 A67-12061

Periodic oscillations in model of thermal convection, noting flow direction and speed 04 p0719 A67-14464

Convective mechanism in clear air, examining isolated plume by new model which differs from similarity model 04 p0648 A67-14647

Analytic approximation method for thermal convection at large Rayleigh numbers 04 p0721 A67-14649

Subcritical convective instability, discussing effects of internal heat generation and spatial variation of gravity field on onset of thermal convection 05 p0928 A67-16817

Aerodynamic generation of noise in stellar convection zones, solving inhomogeneous wave equation when assuming isothermal disturbance 05 p0899 A67-17073

Mass transfer rates of Nb-based alloys in high temperature Li determined in thermal convection loops under dynamic flow conditions 07 p1223 A67-19463

Carbon and nitrogen mass transfer rates by liquid potassium in 16 thermal convection loops of type 316 stainless steel with niobium/one-percent-zirconium and stainless steel tabs at 1200 to 1600 degrees F 07 p1223 A67-19465

Turbulent viscosity forces in nonlinear three-dimensional nonstationary problem of thermal convection 07 p1221 A67-20005

Axisymmetric thermal convection in rotating fluid annulus for various Peclet numbers, obtaining mean thermal structure and heat transfer 08 p1323 A67-21387

Thermal oscillations of polar night stratosphere and upward propagation 10 p1643 A67-23248

Thermal convection in rotating fluid annulus analyzed using Navier-Stokes equations as initial value problem 12 p1963 A67-25339

Axisymmetric thermal convection flow in rotating fluid annulus 12 p1963 A67-25340

Characteristic scales of thermal convection in unstable atmosphere, discussing time evolution of total kinetic energy and lifetime for dry air case 13 p2116 A67-27460

Thermodynamic possibility of thermal convection in earth mantle 13 p2117 A67-27577

Air stream turbulence effect on local and macroscopic transport from cylinder, measuring thermal transfer and pressure coefficients at various Reynolds numbers 14 p2407 A67-28624

Variational principle for heat conduction and convection, noting applicability to nonhomogeneous fluids with temperature dependent properties in turbulent flow 15 p2582 A67-30019

Numerical calculations for two-dimensional Benard convection between rigid boundaries compared with other results 16 p2660 A67-31215

Turbulent thermal convection properties measured in air between constant temperature horizontal plates, discussing structure 17 p2968 A67-32281

Flame propagation along interface between gas and reacting medium, studying fuel heating ahead of flame, noting radiation and convection role 18 p3151 A67-33816

Temperature convection and vertical velocity fluctuations measured and compared with similarity theory of free convection and laboratory heated plates experiments 19 p3252 A67-35059

Adiabatic pulsations of inhomogeneous gaseous mass consisting of convective core and radiative envelope 19 p3261 A67-35502

Bistatic radar cross section of coherent-dot radar angel in convective thermal model 20 p3480 A67-36286

Thermal boundary layer theory for steady cellular convection in viscous rotating flow 20 p3553 A67-36937

Local coefficient of heat exchange by natural convection on isothermal vertical flat plate in turbulent regime 22 p3917 A67-39648

Gaseous ternary diffusion instabilities

observed by ammonium chloride smoke technique, studying pressure and composition effects 22 p3917 A67-39713

Normal modes of stellar internal motions, considering turbulent convection equations and weak-coupling approximation 23 p4068 A67-41277

Nonlinear analysis of cellular convection induced by surface tension in finite amplitude heated liquid layer, discussing prediction of hexagonal flow pattern 24 p4255 A67-42569

THERMAL CURRENT

Thermally stimulated current peak distribution changes with illumination time and intensity for semi-insulating gallium arsenide 07 p1234 A67-20102

Cumulus convective cloud formation above isolated source of heat and water vapor 09 p1491 A67-21552

THERMAL CYCLING

Thermal dilation of titanium alloys during repeated cycling through alpha-beta transformation 03 p0440 A67-13252

Destruction of heat resistant alloys by repeated heating and cooling, deriving formulas which are applied to thermocyclic loads under conditions of stressed state 03 p0447 A67-14192

Progressive buckling of rectangular cross section bar under cyclic variations in temperature 05 p0913 A67-16193

Dislocation mechanisms for prismatic and basal slip in Ti at low temperatures, measuring critical shearing stress and temperature dependence of activation volume 05 p0828 A67-16467

Unsteady state analysis of heat transfer and energy transformation processes in closed cycle regenerative heat energy converters, using differential equations [AIAA PAPER 67-216] 06 p0951 A67-18329

Manufacturing process and life testing of bismuth telluride alloy based flat plate thermoelectric solar cells for near earth orbits 08 p1283 A67-20648

Humidity and simulated space environment effect on various cadmium-sulfide thin film solar cells, noting degradation rates 10 p1596 A67-23163

Two-phase liquid metal cycle MHD conversion, discussing thermodynamic aspect, hot gas system and possibility for use in spacecraft and ground power plants 12 p1896 A67-25121

Tests analysis of buckling caused by thermal gradient and fatigue due to thermal cycling in restrained combustor-cooling tubes 15 p2572 A67-29164

Thermal fatigue cycling of nimonic 80A solid cylinder specimen restrained by clamps 16 p2775 A67-31323

Multicycling metallic bladders for positive expulsion of cryogenic fluids stored in tanks [AIAA PAPER 67-444] 18 p3054 A67-33921

Collection of papers of high purity metals and alloys, discussing properties fabrication and testing 19 p3243 A67-34923

Dimensional changes of metals under simultaneous effects of thermal cycling and external load due to surplus point defects directional displacement 19 p3244 A67-34929

Absorptance and emittance of metal surfaces determined via cyclic incident radiation, noting error computation and method accuracy 19 p3346 A67-35742

Unsteady state analysis of heat transfer and energy transformation processes in closed cycle regenerative heat energy converters, using differential equations 21 p3689 A67-37791

Microelectronic performance degradation resistance under thermal sterilization cycling conditions 21 p3596 A67-38344

Magnetic film memory written and read by focused light studied using thermal cycle time and read bandwidth calculations 22 p3765 A67-39910

Cryogenically cooled rocket nozzle thermal fatigue analysis by thermal-cycle testing of specimens 22 p3834 A67-40183

Environmental testing of thin film solar cells, studying long term thermal cycling effect on CdS solar cell 23 p3937 A67-41496

THERMAL DECOMPOSITION

Vapor flux of trichloromethylsilane affects morphology of pyrolytic deposits of silicon carbide 01 p0103 A67-10252

Gas phase pyrolysis kinetics of tetranitromethane, noting pressure effect

and rate equation of thermal decomposition 01 p0019 A67-10765

Boron filament preparation on fused silica substrates by decomposition of diborane 03 p0454 A67-13420

Chemical reaction effect on heat transfer in thermally decomposing ozone system 05 p0925 A67-16270

Catalyzed thermal decomposition of ammonium perchlorate 05 p0759 A67-17374

Initiation of explosion by impact of plate against charge surface 06 p1112 A67-17955

Kinetics of two-phase decomposition of solid solution of magnesium-aluminum alloy using X-ray analysis, noting grain orientation and size 08 p1342 A67-20810

Occurrence, decomposition kinetics and phase equilibria of cohenite, noting almost exclusive presence in meteorites containing 8 percent Ni 09 p1564 A67-21737

Mechanism of decomposition of ammonium perchlorate in accord with experimental fact 10 p1697 A67-23157

Steady state approach in competitive-consecutive gas reactions, establishing criterion for approach time estimation 14 p2407 A67-28548

Self-deflagration process of hydrazine diphosphate studied for three suggested pressure regimes 14 p2376 A67-28551

Molybdenum/tungsten films obtained by thermal decomposition in vacuum analyzed, noting surface morphological changes with temperature changes 17 p2921 A67-32892

Physical chemistry of potassium sulphate at high temperatures and use for MHD seeding 18 p3086 A67-33710

Nitrogen oxide and carbon dioxide high pressure unimolecular decomposition noting high pressure rate constants, transition probabilities, potential surface shape, etc 18 p3082 A67-33793

Effect of copper chromite, carbon and other potential catalysts on thermal decomposition and ignition of ammonium perchlorate 18 p3108 A67-33813

Condensed phase thermal decomposition of ammonium perchlorate, studying pressure and additives effect on kinetics 19 p3309 A67-35003

Factors involved in initiation of reaction in cobalt /III/ amine azides, discussing thermal decomposition, activation energy, etc [CI PAPER 67-15] 19 p3309 A67-35009

Amino acid formation by formamide thermal decomposition, noting support for hydrogen cyanide oligomerization hypothesis 20 p3376 A67-36700

Ammonium perchlorate deflagration studied by flash pyrolysis and kinetic spectroscopy noting radical concentrations 22 p3867 A67-39639

THERMAL DEGRADATION

Thermal distortion due to viscous heating in fluid film effects on load capacity of spiral-grooved gas-lubricated thrust bearing [ASME PAPER 66-LUB-10] 03 p0432 A67-13765

Electronic component reliability as affected by thermal doses and ethylene oxide gas used in spacecraft sterilization 04 p0563 A67-15239

Surface aspects of thermal degradation of GaAs p-n junction lasers and tunnel diodes 04 p0585 A67-15620

IR images of lunar crater Tycho during lunar night provide evidence that thermal anomaly is produced by solar rather than internal heat 09 p1565 A67-22013

High temperature polyimide unidirectionally reinforced with silica fiber, noting precuring process to avoid porosity and strength degradation 11 p1811 A67-24441

Light sources used for solar simulation testing in terms of operational characteristics and effect of different spectral irradiance characteristics on thermal control coatings 12 p1925 A67-25723

Thermal stability and degradation of n-hexadecane, mineral oils, and oligomers measured as function of time and temperature 16 p2695 A67-31754

Epoxy resins thermal degradation, discussing degradation in oxidizing atmospheres and vacuum differential thermal analysis and hot-wire pyrolysis 19 p3248 A67-34994

Fibers of ordered aromatic copolyamides, performance characteristics and resistance to degradation at high

temperature 21 p3647 A67-37873

THERMAL DIFFUSION

Pulsed laser techniques for measuring thermal diffusivity of graphites and chars between 500 and 5000 degrees F [AIAA PAPER 65-644] 03 p0449 A67-13062

Convection heat transfer for turbulent flow in subsonic diffusers [ASME PAPER 65-HT-64] 03 p0352 A67-14010

Condensation heat transfer in presence of noncondensables, interfacial resistance, superheating, variable properties and diffusion 04 p0720 A67-14644

Ruby laser as energy source for measuring thermophysical properties of materials via flash technique 04 p0623 A67-15305

Thermal diffusion and diffusion thermoeconduction coupling effects on transpiration cooling of porous bronze disk at axisymmetric stagnation point 04 p0733 A67-15839

Cylindrical flame propagation in analytical solution derived from artificial reaction rate 07 p1265 A67-19076

Thermal diffusion separation of damping fluids in floated gyroscopes 07 p1168 A67-19381

Atmospheric composition data from Explorer XVII satellite, obtaining expression for thermal diffusion factor of He 07 p1181 A67-19937

Thermal diffusivity and specific heat of molybdenum at high temperatures measured, using variable heating in induction furnace 09 p1517 A67-21866

Transfer phenomena in polygenous solutions, noting canonic form of component flow equation 09 p1553 A67-21905

Temperature dependence of thermal diffusivity of tantalum and niobium 11 p1804 A67-24035

Constitutive theory for fluid mixtures admitting diffusion and chemical interaction with heat conduction and plane wave propagation 11 p1783 A67-25001

P atoms distribution in doped surface layer of silicon photoconverter for various thermoeconduction conditions exhibiting typical concentration curves 12 p1982 A67-25322

Voltage breakdown in selectively diffused p-n junction, analyzing dependence on radius of junction curvature 12 p1982 A67-25453

Thermoconductivity and diffusivity of amorphous solids determined simultaneously by refined line source technique [AIAA PAPER 67-314] 12 p2037 A67-28029

Book on high temperature oxidation of metals and alloys, fundamental aspects and reaction mechanisms 13 p2141 A67-27176

Potential model for helium-hydrogen interaction in thermal diffusion 13 p2161 A67-27729

High temperature diffusion of potassium in single crystal and polycrystalline molybdenum 15 p2504 A67-29972

Electron thermal diffusivity in room temperature neon afterglow plasma measured using Tonks-Dattner resonance, noting independence of electron density 15 p2532 A67-30381

Temperature dependence of thermal diffusion factors in ternary system He-Ne-Kr by two-bulb method 16 p2661 A67-31223

Heat transfer, thermal conductivity and thermal diffusivity of loose fibrous materials under vacuum 16 p2780 A67-31772

Finite propagation velocity in heat conduction, diffusion and viscous shear motion, studying assumptions of differential equation derivation 18 p3159 A67-34070

Nonlinear and second order thermal diffusion of electrons in ionized gas, using kinetic theory 18 p3083 A67-34401

Reentry vehicle heat shield materials thermal diffusivity measurements by flush method, using pulsed laser and xenon flash lamp 18 p3051 A67-34506

Thermal exposure effect on recrystallization and ductility of TZM molybdenum alloy sheet and foil 19 p3234 A67-34793

Chromizing of steel by HF induction heating in vacuum using low-carbon ferrochrome and electrolytic chromium mixture 19 p3236 A67-34920

Thermoeconduction term in particle flux equation, showing large electron temperature variation across low voltage arc plasma 19 p3279 A67-35140

Copper-doping technique for obtaining p-n

junctions in sintered cadmium sulfide polycrystals, suitable for use in photoelectric converters 19 p3304 A67-35427

Basic operating-time contribution to pulse behavior of diffused transistor components, introducing system function for semiconductor barrier-layer component 19 p3195 A67-35580

Kinetic thermodynamics applied to real gas transport properties analysis by generalization of mean-free-path theory 20 p3543 A67-36185

Thermal diffusion in topside ionosphere, stressing effect on ion density profiles 20 p3427 A67-36304

Critical supersaturations for homogeneous nucleation of ethanol, hexane, etc, investigated using thermal diffusion cloud chamber 20 p3555 A67-37562

Temperature effect on Ni thermal diffusivity measured using ruby laser pulse 21 p3640 A67-38262

Current distribution and electron temperature profiles in nonequilibrium crossed field devices, considering nonuniformities, thermal diffusion, boundary layers and finite reaction rates effects [AIAA PAPER 67-715] 21 p3673 A67-38741

Momentum, heat and magnetic field diffusion in viscous, thermal and magnetic boundary layers of different thicknesses in MHD fluid 22 p3850 A67-39721

Thermal diffusivities of thermal energy storage materials from solid surface temperature measurements, discussing advantages of transient method [ASME PAPER 66-WA/ENER-5] 22 p3919 A67-40349

Kinetic prediction theory for viscosity, thermal conductivity and diffusivity of binary liquid mixtures composed of molecules interacting with square-well potential 23 p4083 A67-41531

Thermal diffusivity measuring device for conducting or insulating flat samples by short signal method 24 p4153 A67-41906

Galilean invariance principle used to analyze system of multicomponent MHD equations to select reference system describing motions and transfer processes across magnetic field 24 p4197 A67-42351

THERMAL DISSOCIATION

Thermodynamic properties of hydrogen peroxide between 273 and 2000 K, deriving equations of state 07 p1265 A67-19123

Monograph on hypersonic heat transfer calculation methods for boundary layers in presence of surface catalyzed reactions 09 p1489 A67-22198

Hypersonic stagnation point flow between strong shock wave and body involving radiation, conduction and dissociation 15 p2415 A67-29309

Estimation of statistical sums of states of groups of oxides and fluorides at high temperatures 16 p2704 A67-31390

Vaporization by dissociation of amine-type perchlorates revealed by infrared spectroscopy, proving role of proton transfer reaction in perchlorates thermal decomposition 16 p2619 A67-31536

Mass spectrometry of titanium subfluorides at high temperatures, determining sublimation pressures and heat and dissociation energy 20 p3377 A67-37135

Thermodynamic properties of hydrogen peroxide between 273 and 2000 K, deriving equations of state 21 p3731 A67-38167

THERMAL EFFECT

One-dimensional compressible gas-channel flow under thermal and mechanical effects analyzed within generalized energy coordinates 01 p0119 A67-10170

Thermal radiation effect on sound propagation in gases treated on basis of relaxation of molecular degrees of freedom 01 p0114 A67-10840

Thermal design method for Japanese scientific satellite IAS, based on skin temperature determination and correlation with inner compartments 02 p0335 A67-12392

Transition time dependence between avalanche and second breakdown on input power to p-n silicon junction, noting thermal effects in semiconductors 02 p0222 A67-12650

Epitaxial transistor array on common heat sink with and without emitter series resistance, examining second breakdown mechanism 02 p0222 A67-12652

Effect of thermal processing in various atmospheres and of additives of group I and

III elements in periodic table on luminescent properties of cadmium sulfide 03 p0433 A67-12890

Book on thermal effects and cutting machinability of aircraft materials 03 p0427 A67-13190

Thermal distortion due to viscous heating in fluid film effects on load capacity of spiral-grooved gas-lubricated thrust bearing [ASME PAPER 66-LUB-10] 03 p0432 A67-13765

Light absorption in transparent materials measured using thermal lens method 03 p0439 A67-14395

Binding in hydraulic servo control valves as affected by heat transfer from valve housing to spool and to surroundings [ASME PAPER 66-WA/AUT-15] 04 p0555 A67-15391

Relations between mean stresses and strains of elastic body consisting of soldered isotropic layers, noting thermal effect 05 p0912 A67-16184

Conical shell stability during axial compression and internal pressure under conditions of heating, noting reduction of critical load 05 p0913 A67-16192

Laser brightness gain and single transverse mode operation by compensation for thermal distortion with external mirror 05 p0819 A67-16656

Manometer for measuring gas pressure from current required to heat platinum wire to certain temperature 06 p1003 A67-18192

Numerical calculation of critical hot spot thermal explosion conditions for plane slab, cylindrical and spherical symmetry 07 p1264 A67-19071

Thermal excitation and de-excitation of alkali atoms in inert gas heat bath 07 p1265 A67-19075

Light beam deflection with low losses, using thermal gradient effects in gases 07 p1141 A67-19406

Hall mobility and thermal emf in indium antimonide with mixed electron scattering mechanism 07 p1237 A67-20182

Ballistic propellant combustion alteration and thermal effects due to dynamic spinning observed on solid propellant sounding rockets 08 p1408 A67-20522

Inviscid hypersonic flow of radiating gray gas over sphere analyzed, noting temperature role in process 08 p1276 A67-20567

Heated rectangular plate nonlinear free flexural vibration problem involving initial deflection, temperature change, etc 10 p1715 A67-22825

Self-focusing processes of laser pulses in dissipative medium, analyzing temporal nonlinear aberrations connected with thermal effects 10 p1664 A67-23332

Thermal mechanical treatments influence on strength, toughness and environmental failure resistance of low alloy high strength martensitic steel 11 p1806 A67-24363

Possible thermal histories of intergalactic gas 11 p1860 A67-24485

Heat resistance, bending and tensile creep of multicomponent Ti alloys 12 p1955 A67-25386

Cyclic loading of thick tube with creep, plasticity and thermal effects 12 p2016 A67-25424

Crack propagation kinetics by thermal fluctuation induction, considering endurance and breakdown of metallic and semimetallic materials 12 p2029 A67-25666

Thermal and ablative lag induced by periodic heat input to oscillating flat plate in high velocity flow, showing crossover from dynamically stabilizing to destabilizing condition as oscillation frequency increases [AIAA PAPER 67-336] 12 p2039 A67-26050

Generalized hypoelasticity theory includes theory of anisotropic elasticity as special case and thermal effects 12 p2032 A67-26169

Oxidation of Be thin films in oxygen and carbon dioxide, noting decomposition of Be carbide and effects of heating by electron beam 13 p2132 A67-26998

Dislocation velocity measurements and thermally activated motion in molybdenum 13 p2133 A67-27011

Time dependence of semiconductor enhanced reflectivity by pulsed argon ion laser based on thermally generated electron hole plasma 13 p2177 A67-27016

Optical fluorescence, thermally tunable over significant portion of visible and near

IR spectrum, from phase-matched parametric system 13 p2127 A67-27081

Thermal behavior of vehicle entering earth atmosphere at velocities approaching 15 km/sec 13 p2224 A67-27325

Heat flux requirements for cutting low-plasticity metal sheets on lathe, noting thermal effect 14 p2325 A67-28654

Ultrasonic measurement of temperature dependence of longitudinal sound absorption coefficient for main crystallographic directions in superconducting indium 14 p2375 A67-29070

Linear signal multiplier using thermally stable InSb, InAs or GaAs sensors with Hall effect voltage linearly dependent on control current 15 p2444 A67-29386

Ground simulation of Concorde aerodynamic heating effects by blowing air through ducts built over specimen surface 15 p2465 A67-29501

Condensation droplet growth in supersaturated vapor and inert carrier gas, noting thermal and diffusion effects 15 p2582 A67-30198

Thermal slip rate of gas near solid surface determined by measuring gas-flow distribution function according to Bhattacharya, Gross and Krook 15 p2582 A67-30390

Hydrodynamics of liquid-gaseous metal mixture flowing through nozzles, discussing heat exchange rate and condensation effects 16 p2656 A67-30574

Hypersonic reentries with thermal and structural integrity problems studied by Saphir rocket firings 17 p2955 A67-32376

Values of rigidity coefficient and space occupied by vacancy compared for deformed nickel samples 17 p2874 A67-32897

Thermal conditions effect on moon figure, reviewing methods for determining lunar geometric form 17 p2949 A67-33122

Ignition conditions of pore walls in burning of porous charge, assuming ideal pores and same charge composition throughout system 17 p2974 A67-33142

Pauling empirical equation relating thermal effect of reaction to negative ionization potential of solid substances 18 p3094 A67-33438

Temperature gradient in steady state thermally operated solid state lasers, calculating end face curvatures and light paths for resonator mode correction 18 p3059 A67-33714

Thermal processes role in thin semiconducting and dielectric films, discussing current-voltage characteristics, thermal inertia, etc 18 p3100 A67-33766

Thermal perturbations on fused silica primary mirror in orbiting space telescope, with numerical analysis of radiation transfer in telescope tube 18 p3046 A67-33880

Linear theory of initially straight elastic rods, discussing wave propagation, thermal effects for extension and flexure and torsion 18 p3144 A67-34287

Thermocouple drift on Chromel-P vs Constantan under vacuum, high temperatures and time factor 18 p3052 A67-34516

Temperature gradient and thermal effects on ceramic transducer sensors used on spacecraft for cosmic dust experiments 19 p3229 A67-35170

Thermal tidal motions in lower ionosphere and differential charge mobility pictured as producing earth atmosphere electrical structure 19 p3220 A67-35255

Layer removal techniques with Hall effect and sheet resistivity measurements indicate carrier concentrations exceeding thermal equilibrium solubility for antimony implants into silicon 20 p3510 A67-36856

Spectral variations resulting from thermal processes in crystals subjected to focused ruby laser beam 20 p3460 A67-37146

Thermophototropic model providing active thermal control in spacecraft surface functions as variable absorptance coating to compensate for solar irradiation changes 21 p3730 A67-37792

Thrust and drag response to heat input directly behind and before body moving supersonically or subsonically 21 p3563 A67-37887

Printed circuit thermal design, discussing edge-to-center temperature gradient and circuit board models 21 p3594 A67-38330

Laser thermal and radiation effect on metals, discussing mechanical

damage 21 p3646 A67-39011

Hot-cracking and microstructure characteristics in weld heat resistant Ni alloys evaluated by synthetic specimen technique 22 p3819 A67-39449

Environmental, thermal and foreign particle effects on Surveyor vidicon performance and expected tube life [SMPTE PAPER 102-32] 22 p3807 A67-40373

Operational requirements for modern space environment test laboratory covering thermal vacuum, shock, vibration and combined testing 22 p3781 A67-40401

Frictional processes of metal surfaces under boundary lubrication conditions emphasizing initiation of seizure 23 p4010 A67-41063

Thermal vacancies in Ni-Al investigated by comparing separately determined dilatometric and lattice parameter of /100/ single crystal 24 p4173 A67-42165

Temperature effect on thermostability of high temperature synthetic lubricants for turbojets 24 p4162 A67-42484

Thermal treatment at melting temperature inducing acceptors of electric conductivity in indium antimonide crystals 24 p4204 A67-42577

THERMAL EFFICIENCY

Improved expressions for efficiency of infinite stage thermoelectric heat pump and generator 15 p2422 A67-29639

Closed-loop MHD cycle efficiency through thermal efficiency as function of net MHD output density 16 p2603 A67-30561

Optimization of Brayton cycle consisting of heat source, MPD generator, recuperator, etc, in terms of thermal efficiency and specific power 16 p2603 A67-30562

Generator parameters and thermal efficiencies optimization for gas-cooled MGD reactor system, studying temperature and partial-pressure relation to power density 16 p2604 A67-30571

Thermodynamics of MHD converter cycles with previously mixed liquid metal used as working body, discussing thermal, electrical and energetic efficiency 16 p2610 A67-31780

Liquid hydrogen heat exchanger for servicing Saturn V S-II stage 17 p2954 A67-32011

Thermodynamic analysis of thermal cycles with MGD generator and steam or gas turbine, noting thermal efficiency 17 p2803 A67-32336

Maximum efficiency at constant applied thermal power of thermoelectric generator noting power gain and materials employed 22 p3747 A67-39429

Real gases examined for application as working fluid in Brayton cycle power plant, considering radiator area reduction to Rankine cycle 24 p4102 A67-42488

Rankine cycle power plants using organic working fluids considered for near-term application 24 p4103 A67-42495

THERMAL EMISSION

IR imagery application in locating anomalously hot earth in Yellowstone National Park 01 p0059 A67-10332

Errors of IR-horizon pickups due to satellite determination of vertical 02 p0240 A67-11541

Thermal emittance and reflectance of diffuse-bottomed specular-walled groove in solar radiant-flux environment [AIAA PAPER 66-459] 02 p0342 A67-11939

Thermal emissivity and absorptivity of trapezoidal grooves and paneled tubular radiators, obtaining parametric relations by numerical solutions via computer 02 p0342 A67-12331

Measurement of sticking coefficient for thermal electrons in oxygen and air, using microwave circuits 02 p0274 A67-12466

Plasma probe in thermal emission converter with high cesium vapor, noting parameters of diffusion, electron concentration, etc 02 p0184 A67-12468

Thermal emittance of nickel as function of oxide thickness measured, using filament in vacuum technique and microphotography [AIAA PAPER 65-673] 03 p0440 A67-13041

Ames emissivity experiment on OSO-II to measure thermal radiation properties of temperature control coatings exposed to space environment [AIAA PAPER 65-651] 03 p0448 A67-13056

Luminosity of galactic disk in 12.8 micron radiation, obtaining from volume integral stellar photon flux density and thermal

radio emission rate 05 p0892 A67-16412
 X-rays from Coma cluster of galaxies, investigating origin by applying virial theorem 05 p0882 A67-16413
 Temperature dependence of emittance and electric resistance of tantalum, vanadium and niobium up to 2500 degrees C 05 p0831 A67-17312
 Potential on hot body in plasma as function of surface temperature and plasma characteristics, considering case where photoemission is present 07 p1251 A67-19812
 Radiometric maps of brightness temperature contours on lunar disk from measurements of 3.3 mm wavelength thermal emission [JPL-TR-32-1058] 08 p1399 A67-21242
 Calorimetric measurements of thermionic converter/ heat pipe system, discussing electron cooling of emitter, thermal emissivity and thermal balance 09 p1448 A67-22342
 Heat radiation spectra of earth as measured by Cosmos satellites, comparing experimental and calculated results 10 p1637 A67-23194
 Thermoemission properties of ZrC powder in vacuum and in cesium vapor under thermoelectronic conversion conditions 11 p1822 A67-24033
 Cosmic X-ray sources attributed to thermal emission of hot condensations from supernova remnants in our galaxy or other galaxies 12 p1995 A67-25764
 Thermal coordinate analysis of lunar IR scan data for directional effects caused by surface geometry, illumination and sensor angle [AIAA PAPER 87-291] 12 p2009 A67-26008
 Earth albedo calculation using Pegasus I thermal data, discussing Rayleigh scattering, spacecraft position, atmospheric reflection effects, etc [AIAA PAPER 87-332] 12 p1938 A67-26046
 Thermal explosion equations for first order catalytic reaction, discussing nonstationary effects superposed on quasi-stationary combustion pattern 12 p2039 A67-26111
 X-ray and metallographic examination of tungsten alloys, noting decrease of work function during thermal emission upon addition of lanthanum hexaboride 13 p2131 A67-26468
 Thickness, material type, environmental and surface emittance of radiation shield effects on thermal performance of multilayer insulation system 13 p2228 A67-27660
 Planetary radio emission measurements, noting no radio emission from Pluto 14 p2385 A67-28405
 Theoretical determination of polished metals emission factors, using model where emission depends on surface layer temperature and electric resistivity 14 p2407 A67-28558
 IR radiation measurements by spectrometers flown on board stratospheric balloons, considering sky brightness, vertical distribution and thermal atmospheric emissions 14 p2313 A67-28768
 Lunar radio emission in 30 to 60 cm range, showing mean radio temperature of moon as 225 degrees K and independence of wavelength 15 p2552 A67-29148
 Coated refractory metals thermal emittance measured at high temperatures for design of reentry vehicle under time-temperature-pressure profile 5 p2503 A67-29546
 Heat flow values correlated with major geological features by analysis of 2000 terrestrial heat flow observations 15 p2477 A67-29763
 Radiative power of toothed surface when ambient medium is black body at zero temperature 16 p2778 A67-30714
 Heat emission and equilibrium temperature of homothermal organism calculated using factors of surrounding medium 16 p2617 A67-30772
 Mid-IR spectral emittance measuring apparatus, discussing range of performance, systems response, etc 16 p2677 A67-31429
 Errors of IR-horizon pickups due to satellite determination of vertical 16 p2677 A67-31607
 Sky brightness temperature measurements at various millimeter wavelengths for possible isotropic electromagnetic emission

in universe 17 p2935 A67-32230
 Cesium ion emission patterns from rear-fed porous refractory metals studied by thermal emission 17 p2888 A67-33059
 microscope 17 p2888 A67-33059
 Electrode heating of arc burning in moving plasma in vacuum, giving setup, heat emission diagrams, etc 17 p2907 A67-33091
 IR thermal emission from lunar nighttime surface, noting anomalies location and observational procedure 18 p3134 A67-34497
 Current-voltage characteristics for double probe measured in seeded combustion products by low temperature surface emission 19 p3345 A67-35079
 Absorbance and emittance of metal surfaces determined via cyclic incident radiation, noting error computation and method accuracy 19 p3346 A67-35742
 Temperature effect on seeding atom emission in argon plasma laminar jet 20 p3497 A67-36397
 Jupiter internal structure and energy emission 20 p3525 A67-36867
 Tungsten cermet emissivity study using electron heating 20 p3466 A67-36913
 Model for lunar surface roughness effect on emission of thermal IR radiation and casting of shadows in sunlight 21 p3702 A67-38188
 Orthotropic laminated layer with heat emission investigated for thermoconductivity and temperature stress distribution 21 p3731 A67-38299
 Thermally activated inert gas ion injection into tungsten and gold to correlate energies associated with peaks in desorption spectrum 23 p4030 A67-41357
 Incompatibility of microwave phase effects measurements in Mercury thermal emission with simple model for thermal behavior of planet surface 24 p4226 A67-41837
 Utilization of lunar geothermal emissions for rocket propellants and life support [AIAA PAPER 87-903] 24 p4165 A67-43011
 Lunar radio emission in 30 to 60 cm range, showing mean radio temperature of moon as 225 degrees K and independence of wavelength 24 p4239 A67-43071
THERMAL ENERGY
 Unsteady laminar flow of incompressible fluid in gap between parallel disks with gap width varying with time, obtaining solutions for Navier-Stokes and thermal energy equations 02 p0231 A67-11469
 Numerical solution for laminar flow heat transfer in circular tubes with axial conduction and developing thermal and velocity fields [ASME PAPER 66-WA/HT-7] 04 p0726 A67-15446
 Entropy and available energy in operation of gas turbine, considering thermodynamic efficiency, heat balance and available energy balance 05 p0873 A67-16742
 Error due to electron thermal energy fluctuations in mean electron temperature measurement by line intensity ratio 06 p1042 A67-18540
 Indigenous lunar power from geothermal deposits of hot water-rich gases and brines 08 p1317 A67-21095
 Thermal IR inspection technique for bond flaw inspection in simulated solid propellant rocket engines 09 p1508 A67-22528
 Reliability of laboratory thermal rate coefficients for positive ion/neutral reactions in ionosphere 11 p1785 A67-23945
 Thermal dissipation of energy in ionized cesium plasma, obtaining plasma oscillation excitation which destroys electron drift motion 11 p1837 A67-24394
 Ionosphere rocket sounding for positive ion density, electron density and electron temperature, noting sunspot effect 11 p1787 A67-24643
 Kinetic energy distribution of ions produced by dissociative attachment dependence on ion thermal energy and electron affinity of oxygen 14 p2350 A67-28151
 Numerical calculations of interactions of monatomic gas particles with ideal and contaminated crystal surfaces at epithermal energies 15 p2434 A67-30197
 MHD conversion of thermal energy contained in cesium-seeded noble gas examined for conditions governing disk-type ducts use 16 p2603 A67-30566
 Thirteen-moment equations solved

obtaining theory of thermal force acting on spherical particle for entire range of Knudsen numbers 16 p2661 A67-31221
 Thermodynamic aspects of energy studied in forms of localized and isotropic magnitude and motion in single direction 16 p2780 A67-31557
 Molecular nitrogen and oxygen ions colliding with atomic sodium examined in crossed-beam experiment for resonance charge transfers 16 p2705 A67-31758
 Thermal propagation in gases studied through heat transfer equation resulting from Fourier law 17 p2968 A67-32221
 Computer program for determining net thermal energy incident on satellite by computing projected surface area [ASME PAPER 87-HT-56] 20 p3549 A67-36738
 Friction in solid parts of earth and moon considered as sink for tidal energy and as geophysical thermal energy source 24 p4229 A67-42316
 Lunar geothermal deposits, discussing recovery applications and energy tapping [AIAA PAPER 87-901] 24 p4239 A67-43009
THERMAL ENERGY STORAGE
 Thermal diffusivities of thermal energy storage materials from solid surface temperature measurements, discussing advantages of transient method [ASME PAPER 66-WA/ENER-5] 22 p3919 A67-40349
 Optimization of electric energy storage for solar thermal space power systems 24 p4108 A67-42543
THERMAL ENVIRONMENT
SA HIGH TEMPERATURE ENVIRONMENT
 Potential distribution between graphite and metallic electrodes of MHD generator in nonstationary heat conditions under induced or applied electric field 01 p0011 A67-10176
 Computer-simulated mathematical model of thermal environmental effects on expulsion system design parameters for liquid-propellant gas-generator rocket engine [AIAA PAPER 86-686] 02 p0303 A67-11944
 Centaur electronic packages for space flight thermal and radiative environmental control 05 p0778 A67-17453
 Solar simulation tests on UK-3 satellite, evaluating thermal environment and sorting out interface problems between spacecraft and test chamber 09 p1486 A67-22434
 Iron and iron-stony meteorites cooling rates in relation to Ni content and Widmanstätten structure suggest development in different thermal environments 16 p2750 A67-31453
 Thermally induced boundary layer flows in isothermal rigid body rotation 20 p3421 A67-36843
 Prediction of lunar surface temperature through digital computer program noting heat transfer equations 22 p3884 A67-39930
 Integral relations method for nonequilibrium hypersonic planetary entry, emphasizing flow fields and thermal environment determinations for blunt body vehicle configuration 22 p3740 A67-39936
 Base flow characteristics and thermal environment of launch vehicles with strap-on solid rocket motors 22 p3902 A67-39939
 Superorbital reentry environments, discussing materials, test environments and heat factors 22 p3919 A67-40383
THERMAL EXPANSION
 Anisotropy of thermal expansion and microstructural changes due to thermal stresses 03 p0448 A67-13564
 Linear expansion coefficient divergence of commercial titanium rod 07 p1208 A67-19297
 Condensed explosive ignition by conductive heat inflow from low thermoconductivity media 07 p1287 A67-19314
 Integral relation technique for approximate solution of dynamic and thermal expansion of laminar radial slot gas jets along plane wall 11 p1779 A67-24322
 All-glass electroluminescence readout panel design with active areas integral part of connector pin 11 p1766 A67-24628
 Age hardenable low-expansion alloy for cryogenic service 13 p2142 A67-27675
 Fastener performance in commercial and aerospace application, considering component thermal expansion [ASME PAPER 87-DE-18] 14 p2327 A67-28872
 Current damping, thermal expansion, radial oscillation, kinetic pressure and other dissipative processes effects on magnetic

- properties of plasmoids 15 p2524 A67-29244
Refractory materials thermal expansion at elevated temperatures measured with apparatus consisting of optical comparator and controlled gradient vacuum furnace 16 p2677 A67-31542
Thermal gradients effect on separable tube connectors, discussing structural elements 17 p2864 A67-32009
Least squares method for heat problems and approximate similarity law covering orthogonal expansions and compatibility between contradictory requirements 18 p3071 A67-33752
Electronic flat-pack processes covering sealing methods, material combinations, leakage determination, etc 21 p3634 A67-38621
- THERMAL EXPANSION COEFFICIENT**
Dilatometer for measurement of thermal expansion coefficient of solids and variation with temperature 01 p0062 A67-10195
Length-temperature measurements for several polymers and mixtures for detection of transitions and determination of location and magnitude of expansion coefficient changes 06 p1019 A67-17851
Modulus of elasticity of metals and titanium alloys as function of electron structure and binding 07 p1206 A67-19279
High temperature thermal expansion of Ti, Zr, Hf, Nb and Ta 10 p1697 A67-23380
Thermal expansion coefficient of ferromagnetic thin films compared with bulky samples by electronographic technique 12 p1939 A67-25242
Significant-structure theory of liquids applied to rocket fuels, calculating vapor pressure, thermal expansion, dielectric constant, etc 16 p2734 A67-31537
Kinetic and thermodynamic conditions for detonation during chemical reaction in infinite medium involving reaction heat, thermal expansion coefficient and reactants specific volumes 17 p2809 A67-32977
Stresses, bending moments and displacements of variable rigidity toroidal shell in steady temperature field derived assuming independent thermal expansion coefficient and physical constants 23 p4075 A67-40680
- THERMAL FATIGUE**
Heating unit of device for testing small samples of sintered materials for thermal fatigue 03 p0420 A67-13545
Heating and cooling rates, hold time at maximum temperature, phase temperature between temperature and strain cycling effects on thermal fatigue of stainless steel 05 p0921 A67-17085
Thrust chamber life estimation from calculable local heat flux and tube temperatures, using assumptions of elastic strain invariance and isotropic material properties 05 p0874 A67-17226
Soviet book on high temperature strength of materials noting test stands, stresses, loads, applications to jet and rocket technologies, etc 07 p1208 A67-19299
Book on aircraft materials strength calculations including load determination, heating problems, creep and fatigue strength, etc 07 p1128 A67-19578
Damage accumulation during thermal fatigue noting need for statistical analysis of law governing process 09 p1575 A67-22167
Test method for metal resistance to thermal fatigue under active creep conditions 09 p1519 A67-22168
Phenomenological process in thermal fatigue research, equipment, tests and evaluation 09 p1578 A67-22475
Dependence of creep, corrosion and thermal fatigue of gas turbine vanes and blades upon inlet temperature and rate of change [ASME PAPER 67-GT-17] 11 p1808 A67-24801
Nickel and cobalt superalloys low cycle thermal fatigue test method under cyclical extension and temperature conditions, giving stress-strain-time relations [ASME PAPER 67-MET-19] 12 p1958 A67-25955
Tests analysis of buckling caused by thermal gradient and fatigue due to thermal cycling in restrained combustor-cooling tubes 15 p2572 A67-29164
Thermal fatigue cycling of nimonic 80A solid cylinder specimen restrained by clamps 16 p2775 A67-31323
Mechanical properties used to estimate low cycle fatigue behavior in creep range of components in high-temperature systems 16 p2777 A67-31813
Thermal fatigue of 18-8 and 13 Cr steels under transient cross-sectional temperature gradients, noting crack mechanics, tensile stresses, plastic strain range, etc 18 p3140 A67-33651
Thermal fatigue hysteresis loop shape variations for Coffin-type test samples, stressing temperature-cycle effect 19 p3343 A67-35820
Low cycle thermal fatigue under uniaxial constraint, describing clamping device, time-temperature controller and programmer used 20 p3543 A67-37699
Cryogenically cooled rocket nozzle thermal fatigue analysis by thermal-cycle testing of specimens 22 p3834 A67-40183
Coated columbium alloy potential as turbine vanes in gas turbine power plants, discussing stress rupture strength, oxidation erosion and thermal fatigue lives [ASM PAPER C6-1.4] 23 p4020 A67-41402
- THERMAL INSTABILITY**
Thermal instability affecting factors for current distribution in power transistor 02 p0222 A67-12651
Rayleigh thermal instability in horizontal circular cylinder, discussing two approximate methods for calculating upper bounds to critical Rayleigh number 05 p0929 A67-17415
Thermal stability of ammonium perchlorate-lithium perchlorate mixture, noting explosion above 280 degrees C for various compositions 07 p1239 A67-19078
Mineral additive effect on thermal stability of phenolic resins in inert and oxidative atmospheres at atmospheric pressure [ONERA-TP-324] 09 p1520 A67-22155
Long time mechanical and thermal stability of polymeric materials predicted from accelerated testing at increased temperature-time relations 10 p1672 A67-23743
Gravitational instability from reformulation of Lifshitz relativistic theory for galaxy formation in expanding universe and comparison with Bonnor approach 11 p1859 A67-24121
Electric field effect in Q machine with uniform end plate temperature, noting deviation from thermal equilibrium and increment in ion loss rate for certain range of particle densities 11 p1833 A67-24370
Effect of metals and alloys on thermal stability of Avtur 50 aviation kerosene from ASTM-CRC and high temperature coker tests 13 p2185 A67-26703
Average heat of atomization in correlating composition and temperature limits of stability of NaCl type structure among IV-VI compound semiconductors 13 p2184 A67-27570
Thermal stability aspects of commercial kerosene for supersonic transport [AIAA PAPER 66-670] 17 p2926 A67-32570
Quiescent solar prominences general appearance described by theoretical model 19 p3324 A67-35436
Gravitational effect on thermal instabilities, discussing optimization techniques to calculate effects of surface stresses [ASME PAPER 67-HT-22] 20 p3546 A67-36717
Infinite horizontal fluid layer heated from below /classical Rayleigh thermal stability problem/ extended to fluid in rigid sphere heated nonuniformly 22 p3918 A67-39715
Copolymers containing imidazopyrrolone and imide groups tested for thin film tensile properties, degradation by strong acids and bases and thermal stability 22 p3824 A67-39851
Thermal instabilities in homogeneous primeval medium theory shown to play no role in galactic evolution 22 p3892 A67-40497
Electric power generation with closed cycle MHD conversion fluid having gases with high equilibrium conductivity, discussing ionization and electrothermal instability 24 p4099 A67-42416
- THERMAL INSULATION**
SA ASBESTOS
SA HEAT SHIELD
Strain gauges applied to epoxy laminates in liquid hydrogen insulation systems 01 p0072 A67-11107
Multilayer insulation system materials and design data for use on spacecraft in temperature range from 300 to 800 degrees K [AIAA PAPER 65-663] 03 p0534 A67-13069
FR-1 satellite design difficulties such as material selection, insulation of structure, making structure perfectly conducting, etc 03 p0518 A67-13601
Ablative materials for thermal insulation of space vehicles, considering tungsten, tantalum, niobium, etc, as backing metals 04 p0726 A67-15536
Thermal design of Isis A spacecraft, noting possibility of passive thermal control and computer programmed multinode heat balance analysis 05 p0904 A67-16294
Elastomer application in spacecraft launching, flight and reentry such as binder, sealant, base for adhesives, heat shielding, etc [ONERA-TP-407] 05 p0833 A67-16479
Liquid hydrogen tank insulation, content gauging and design of transfer lines and valves 05 p0789 A67-17018
Direct-to-home TV broadcasting satellite system for upper UHF, describing stabilization, thermal control, antenna, power amplifier, etc [AIAA PAPER 66-309] 06 p1094 A67-17689
Direct-to-home TV broadcasting satellite system for upper UHF, describing stabilization, thermal control, antenna, power amplifier, etc [AIAA PAPER 66-309] 06 p0964 A67-18414
Soviet book on methods of calculating temperature fields and thermal insulation of flight vehicles 07 p1266 A67-19144
Thermal insulation for flight vehicles under various conditions of gas-kinetic heating 07 p1266 A67-19146
Power output variation of solar Brayton space power plant with heat storage due to solid layer thermal resistance effects 09 p1442 A67-21698
Material properties effect on design of reentry vehicle heat shield 10 p1734 A67-23726
Space evacuation of NRC-2 insulation for liquid hydrogen tankage, noting vacuum test apparatus and cold plate test 10 p1734 A67-23727
Vacuum multilayer insulation for cryogenic space propulsion vehicles noting self-evacuation system and calorimetric test 10 p1734 A67-23728
Temperature-dependent thermoconductivity of metal film on insulation laminations in relation to bulk parent material in insulation systems of cryogenic propellants [AIAA PAPER 67-295] 12 p2035 A67-26010
Space vehicle thermal testing in cold vacuum chambers with and without solar simulation [AIAA PAPER 67-306] 12 p1926 A67-26021
Carbon dioxide purge and thermal protection system for liquid hydrogen tanks of hypersonic aircraft, comparing with helium purge system 13 p2227 A67-27647
Minimum weight combinations of shields and spacers for lowest heat flux, noting mounting technique and leakage effect 13 p2228 A67-27653
Comparing shroud-mounted to tank-mounted high performance insulation systems 13 p2214 A67-27655
Effective thermal conductivity parameter for multilayered insulation 13 p2228 A67-27656
Klegecell G-300 mechanical and thermal properties tested for thermal insulation for cryogenic stage for liquid hydrogen on space vehicle 13 p2228 A67-27659
Measurement of thermal conductivity of irradiated foam-type insulation materials 13 p2228 A67-27662
Asbestos reinforced plastics evaluated for physical and optical properties, thermal-vacuum and UV resistance 15 p2507 A67-29550
Material limitations in MHD induction generator, discussing effect of conducting channel walls and thermal insulation on performance 16 p2605 A67-30582
Spacecraft surface temperature-control coating requirements, selection and performance in prelaunch and space environments 16 p2757 A67-30634
Development of liquid hydrogen-oxygen propulsion stage in France, discussing structure, thermal isolation, storage,

etc 18 p3111 A67-33653
 Value analysis technique to compare competing high performance insulation systems on basis of differences in performance and cost [AIAA PAPER 67-469] 18 p3162 A67-33939
 Active thermal insulator technique for long term cryogenic storage 19 p3207 A67-34836
 Insulating foams at liquid hydrogen temperature, describing methods for measuring thermoconductivity, specific heat and density 19 p3346 A67-35567
 High insulating effectiveness required of cryogenic insulations, evaluating insulation capacities of powders, fibers, foams, honeycomb, etc 20 p3553 A67-36885
 Thermal conductivity measurements of insulating materials at cryogenic temperatures - ASTM Conference, Philadelphia, February 1967, Committee C-16 22 p3802 A67-40289
 Guarded hot plate apparatus for measuring thermal conductance of multilayer cryogenic insulation under vacuum conditions 22 p3802 A67-40291
 Thermal conductivities of cryogenic insulation systems determined by two methods using calorimetry measurement of boll-off rate of liquid cryogen 22 p3802 A67-40292
 Heat flow meter apparatus for rapidly measuring thermal conductivity of flat insulation specimens under cryogenic temperatures 22 p3802 A67-40293
 Double-guarded cold plate apparatus for measuring thermal conductivity of multilayer insulations, powders, fibers and foams 22 p3803 A67-40294
 Cryogenic insulation thermoconductivity measuring apparatus operable at high vacuum and nonsteady state conditions 22 p3803 A67-40295
 Guarded cold flat plate calorimeter for measuring insulation thermoconductivity 22 p3803 A67-40296
 Calorimeter for evacuated multilayer insulation materials to evaluate performance and measure heat transfer rate and thermoconductivity 22 p3803 A67-40297
 Long term cryogenic propellant storage in space, considering rigid open cell polyurethane foam as spacer in multilayer insulation system 24 p4254 A67-42480
 High temperature thermal insulation consisting of thin refractory metal foils separated by thin refractory oxide layers 24 p4103 A67-42501
 Voyager thermal insulation requirements noting tests of vapor deposited Au on Mylar and Kapton [AIAA PAPER 67-777] 24 p4257 A67-42945

THERMAL NEUTRON
 Electrical conductivity measurement of He 3 plasma induced by neutron irradiation 09 p1542 A67-21813
 Expected change in output voltage when W/W-26Re thermocouple is exposed to thermal neutrons, causing Re atom transmutation to Os 15 p2535 A67-29489
 Uranium content of chondrites measured by thermal neutron activation and delayed neutron counting 21 p3704 A67-38505

THERMAL NOISE
 Thermal, excess and shot noise in transducers, examining CW signal generator method for measuring average noise factor 01 p0039 A67-11196
 Noises in quantum amplifier due to heat fluctuations and spontaneous emission of active microparticles, discussing negative temperature state 03 p0368 A67-13139
 Spectral intensity of short-circuited noise current of space-charge-limited solid state diodes 03 p0380 A67-13486
 Noise spectra of double base diode for case of uniform field in base and comparison with experimental noise measurements 04 p0585 A67-15619
 Electrical noises of plasma of steady state HF discharge in magnetic field discussed from standpoint of universal plasma instability 04 p0671 A67-15640
 Equivalent circuit for field effect transistor, considering amplifying characteristics of component, noting use of thermal and shot noise 06 p0966 A67-17589
 Thermal noise limitation in space-charge-limited solid state diodes and triodes 06 p0971 A67-18224
 Noise comparators and associated thermal

standards to provide noise source calibration facilities at S-and 09 p1495 A67-21621
 X-bands
 Thermal noise in space-charge-limited solid state diodes, showing equivalence of noise resistance with DC 09 p1472 A67-21951
 Reduction of peak factor in FM system design leading to reduction of thermal noise and increase in spectrum truncation distortion 11 p1752 A67-24123
 Hyperfrequency receiver noise temperature measurement, calculating gain stability influence 12 p1952 A67-25296
 Parametric amplifiers of high gain stability for radio astronomy noting very low SNR and optimum noise temperature 12 p1912 A67-25298
 Tracking circuit performance, discussing squaring loop, Costas loop variants and delayed decision feedback loop 15 p2436 A67-29591
 Sensitivity of radiometer operating in submillimeter range with multimode detector compared to crystal receiver equivalent noise temperature 16 p2677 A67-31501
 Cassegrain antenna gain and noise temperature with dual reflector system derived from feed pattern and system geometry 17 p2824 A67-32395
 Noise measurement covering principles, switching radiometer, sources, factors and temperature 17 p2814 A67-32604
 Electron temperature of shock-heated argon plasma determined by measuring microwave noise radiation and absorption 21 p3660 A67-37741
 Low noise temperature traveling wave maser preamplifier for microwave reception, discussing design, applications and specific electron gain 21 p3641 A67-38640
 Metal bolometer impedance and noise generation, discussing Johnson and temperature fluctuation noises 22 p3797 A67-39343
 Microwave and mm radiometric sensor for passive satellite reconnaissance of earth atmosphere and terrain thermal noise 22 p3805 A67-40353
 Noise occurrence during heat transfer from solid to liquid He 2 flux at high temperature difference, discussing heat flux 22 p3838 A67-40389
 Millidegree noise thermometry based on linewidth of Josephson radiation 22 p3865 A67-40436
 Voltage-biased superconducting point contact Josephson radiation line width investigation for thermal noise contributions useful for low temperature thermometer 23 p4038 A67-40790
 Equivalent noise temperature of antennas located on earth surface, discussing cosmic, tropospheric and man-made noise classification 23 p3980 A67-41043

THERMAL PLASMA
 Channel model examination of output-dependent radius of spherical plasma discharge in thermal equilibrium 01 p0118 A67-10045
 Temperature dependence of spectral line intensity emitted by thermal plasma 01 p0124 A67-10867
 Thermalization rate of highly ionized plasma with initially hot ions and cold electrons, using laser scattering to observe time variation of electron temperature 01 p0125 A67-10912
 Electron density enhancement in thermal plasma by metastable atoms, computing ionization by method of Lagrange multipliers 02 p0272 A67-11519
 Anisotropic distributions of suprathermal electrons as explanation of observed line splitting for type II solar radio outburst and indirect determination of coronal magnetic fields 02 p0307 A67-11691
 Temperature-dependent wave propagation in slightly inhomogeneous hot nonuniform plasma, examining positive column of mercury vapor discharge 02 p0193 A67-11782
 Dielectric constant of homogeneous fully ionized two-temperature plasma for determining conditions under which ion waves can be found 02 p0275 A67-12555
 Thermally ionized cesium plasma confinement investigated in magnetic mirror geometry, in terms of collisional diffusion and end plate ion recombination 02 p0276 A67-12560

Warm plasma excitation by electric dipole 03 p0475 A67-13173
 Possible models for X-ray source SCO-X-1, discussing conditions of gravitational confinement 04 p0694 A67-14484
 Two-particle ring term for kinetic equation with Darwin interaction relationship to relativistic Landau equation 04 p0672 A67-15772
 Properties of dense plasma with preheated electrons in ion cyclotron resonance region, using magnetic mirror trap 05 p0853 A67-16755
 Hot electron plasma instability in magnetic mirror, discussing stabilization by cold plasma component and magnetic field line typing in conducting end plates 05 p0858 A67-17431
 Dispersion nucleus of homogeneous nonmagnetic hot plasma and functional properties of plasma waves 06 p1039 A67-18048
 Plasma jet applications, emphasizing generation of high temperatures for refractory coatings in form of intermetallic compounds and cermets 09 p1545 A67-22172
 Energy production sources in inner magnetospheric plasma near equatorial plane 10 p1634 A67-23058
 Thermal plasma measurements in magnetosphere for electron and ion density and thermal profiles, noting Maxwell energy distribution and charge neutrality 10 p1649 A67-23295
 LF instabilities and anomalous plasma processes in cesium discharge and thermal plasmas 11 p1829 A67-24000
 Thermal plasma device /Q machine/ design objectives and proposed features, noting association with normal mode oscillations in gas laser 11 p1830 A67-24006
 Diffusion measurements in potassium magnetoplasmas based on volume plasma loss properties of variable length single-ended Q device 11 p1835 A67-24386
 Transition to turbulence in thermal plasma examined, using model based on coupled Van der Pol oscillators, noting noise spectrum rise 11 p1836 A67-24390
 Electrostatic probe techniques for low density thermally ionized plasmas 11 p1838 A67-24408
 Enhanced plasma fluctuations produced by suprathermal electron effect on emission and scattering of electromagnetic waves, noting analogy with corona plasma 11 p1839 A67-24546
 Nonlinear mechanics of plasma-like distributed system studied with Q machine, noting mode locking 11 p1839 A67-24550
 Calculation of thermal excitation function and optimum temperature and pressure of atom and ion spectral line shift in two-component plasma 11 p1840 A67-24580
 Electron and ion temperature difference necessary to develop instability connected with loss cone of plasma with hot electrons placed in magnetic mirror trap 12 p1971 A67-25334
 Mathematical theories applicable to excitation and ionization of atoms in plasmas at thermal equilibrium, determining electron density and temperature 12 p1988 A67-25432
 Stabilization of thermally ionized potassium plasma by applying shear to confining magnetic field 12 p1975 A67-25476
 RF electromagnetic fields to control state of flowing thermal plasma 12 p1975 A67-25921
 Modal wave solutions of isotropic plasma-filled parallel-plate waveguide examined, using cold and warm plasma models without collision 12 p1915 A67-25943
 Thermally ionized low density alkali-metal plasma for simulating controlled fusion processes, noting high particle losses and instability 14 p2362 A67-29038
 Current and potential distribution for thermally-stable plasma of Faraday-type segmented electrode MHD generator, taking into account nonequilibrium ionization 16 p2599 A67-30530
 Hot electron nonequilibrium plasma use in MHD generators, considering energy transfer, plasma stability, magnetogasdynamics, etc 16 p2601 A67-30545
 Cleavage method to study pulsed pressure /energy content/ in dense gas-discharge hot plasma 16 p2714 A67-31037
 Nonconvective instability for hot plasmas from poles colliding through negative wave numbers 17 p2899 A67-32276

- Thermal and synchrotron cosmic X-ray sources 17 p2937 A67-32639
- Dispersion relations for coupled electromagnetism and longitudinal waves propagating along isotropic inhomogeneous cylindrical hot plasma column 17 p2908 A67-33107
- Model for distribution of thermal plasma in magnetosphere of Jupiter under assumption of corotation with planet 17 p2951 A67-33196
- Fluid flow around magnetosphere boundary analyzed, noting geomagnetic field effect on hot plasma 17 p2853 A67-33252
- Channel model examination of output-dependent radius of spherical plasma discharge in thermal equilibrium 17 p2910 A67-33323
- Instrument for generation of thermal plasmas in direct current-arc discharges and expansion to walls of coaxial corotating cylinder 17 p2835 A67-33389
- Three-dimensional equation for wave propagation through inhomogeneous warm compressible plasma in inhomogeneous static magnetic field 18 p3088 A67-34071
- Thermally ionized cesium plasma produced containing negative Cl ions 19 p3272 A67-35084
- Experiments with thermally ionized cesium plasma in magnetic field with variable curvature 19 p3288 A67-35365
- Electric field due to double grid excitation in circular waveguide partially filled with warm homogeneous plasma in infinite magnetostatic fields 19 p3290 A67-35379
- Variational formula for antenna impedance in warm magnetoplasma, considering force and fluid-flux distribution 19 p3194 A67-35513
- Current distribution on cylindrical dipole antenna in homogeneous warm plasma 19 p3194 A67-35515
- Influence of Langmuir probe losses on ion-density measurements in thermal cesium plasma with homogeneous magnetic field 19 p3296 A67-35589
- Model thruster designed and operated with argon and hydrogen for investigation of hybrid flow fields of plasma acceleration by thermal and magnetic forces [DVL-630] 19 p3297 A67-35601
- Electron-plasma oscillation damping in hot collisional plasma with external uniform magnetic field investigated using Fokker-Planck equation 20 p3503 A67-37693
- Biorthogonality relation derived between eigenfunctions of operator representing linearized anisotropic multifluid warm plasma and eigenfunctions of adjoint operator 20 p3503 A67-37711
- Magnetic curvature effect on drift cyclotron instabilities, considering density gradients, Maxwell plasmas and resonance 21 p3661 A67-37749
- Streaming thermal plasma /STP/ devices, discussing plasma jet synthesis of HCN from cold methane and thermal nitrogen plasma 21 p3578 A67-38393
- Standing waves in hot plasma traversed by quasi-neutral charged particle flux including numerical analysis of elongated wave occurrences 22 p3853 A67-40124
- Hot electron plasma production, discussing microwave power feeding across magnetic flux lines producing closed plasma shell structure 22 p3854 A67-40243
- Plasma energy and heat transfer to surface with and without electric current, discussing various energy transfer models 24 p4197 A67-42331
- Resonance rectification effects for wire probe in magnetoplasma observed in terms of warm plasma perpendicular permittivity component 24 p4199 A67-43101
- THERMAL POWER**
- Thermal power and electrical conductivity of SnTe-InTe crystals, discussing temperature effect 04 p0683 A67-15581
- Thermal regeneration in power dissipating elements and effects on transistor circuit failures 06 p0971 A67-18245
- Alloying effect on diffusion thermopower in relation to Fermi surface variations in dilute silver-gold alloys [JPL-TR-32-1095] 24 p4200 A67-41840
- THERMAL PROPERTY**
- Plane temperature wave method for measuring thermal diffusivity and conductivity of solid and friable bodies without using heat detectors 01 p0166 A67-10364
- Sintered Ni-base heat resistant alloys, discussing composition-creep strength relation, grain size, prealloyed-powder production and thermal and structural shock properties 01 p0098 A67-10700
- One-dimensional freezing of semimfinite isotropic homogeneous liquid-solid system with temperature-varying thermal properties 01 p0166 A67-10758
- Temperature dependent thermal property models of lunar surface and radiative energy transport deduced from RF and IR observations 04 p0697 A67-14740
- Thermal properties of semiconductor diode under steady and pulsed operation 05 p0772 A67-16448
- Primary-secondary voltage imbalance effect on multiplication and thermal properties of Hall generator 05 p0774 A67-16704
- Digital computer programs for transient and steady state thermal analysis 05 p0929 A67-17452
- Spectral sensitivity and temperature characteristics of light generated pairs of photoelectric converters 07 p1131 A67-19105
- Book on basic principles of physics of semiconductors and semiconductor devices including quantum theory, thermal properties of solid bodies, etc 07 p1231 A67-19301
- Energy dependence of semiconductor devices with respect to secondary breakdown explained on basis of transient thermal resistance 07 p1156 A67-19895
- Stress analysis of solid rocket engine propellant grains including linear viscoelasticity, thermal analysis and equilibrium, relaxation times, engine sizes, cooling, creep relaxation, etc 08 p1373 A67-20874
- Thermal properties of lunar surface as observed from Surveyor I spacecraft 08 p1386 A67-20940
- Thermal design of attitude translational control assembly /ACTA/ of lunar excursion module /LEM/ 08 p1303 A67-21062
- General solutions of heat equation in stationary homogeneous isotropic finite region with constant thermal properties 08 p1429 A67-21436
- Latent heat of fusion of titanium 10 p1670 A67-23640
- Thermal properties and environmental stability of barrier layer anodized aluminum surfaces in space, noting emittance and absorption values 10 p1671 A67-23744
- Electric, thermal and physical properties of pyrolytic carbides and nitrides of group IV metals 11 p1804 A67-23903
- Natural remanent magnetization with normal polarity of lower lava flow in Olduvai Gorge, showing stability via thermal demagnetization 11 p1788 A67-24698
- Volt-ampere and thermal characteristic of plasmatron with insert in electron gap 11 p1843 A67-24973
- Thermal properties of moon by comparing IR and microwave measurements of spectrum with theoretical calculation of upper layer temperature distribution [AIAA PAPER 67-289] 12 p2009 A67-26006
- Thermal modeling applicability to steady state and transient conditions, considering material property changes with temperature [AIAA PAPER 67-305] 12 p2036 A67-26020
- Thermal and electrical properties and width of forbidden bands of PbTe and PbSe from 90 to 800 degrees K 12 p1986 A67-26094
- Handbook of materials and techniques for vacuum devices covering high temperature properties, materials selection, joining processes, etc 14 p2339 A67-28829
- Dynamic components thermal characteristics determination by IR optic techniques, studying metal fatigue, wear and friction phenomena [ASME PAPER 67-DE-24] 14 p2328 A67-28873
- Density fluctuations and thermal conditions in expanding universe and creation of stars, quasars, galactic clusters and galaxies 15 p2551 A67-29138
- Thermal control materials for spacecraft, considering UV spectral distribution, radiation energy and flux, oxygen bleaching, etc 15 p2579 A67-29552
- Collection of articles on complex semiconductors investigating conductivity, thermal, electrical and other properties, and preparation methods 16 p2729 A67-31154
- Deformation effects on thermal conductivity, microhardness, and thermal EMF of annealed bismuth telluride bars 16 p2730 A67-31160
- Thermal properties of anomalous superconductors, considering specific heat jump to normal state and thermal conductivity behavior 17 p2914 A67-32453
- Transistor overload in active region operated by large pulse trains, discussing thermal response and resistance and operational frequency intervals 17 p2827 A67-32784
- Thermal and elastic properties of ternary diamond-like semiconductor compounds, determining ultrasonic wave propagation rates 18 p3096 A67-33452
- Refractory properties and mechanical characteristics of graphites and carbons, discussing maximum compatibility temperature of graphite 20 p3472 A67-36110
- Heat conductivity in materials ascribed to phonons, noting phonon radiation effects 20 p3515 A67-37715
- Photoresistors thermal characteristics in automatic semiconductor control devices studied in steady and pulsed modes of operation, determining current-voltage characteristic and thermoresistance 22 p3801 A67-40214
- Posistors barium titanate, lead titanate and potassium compound semiconductor and ferroelectric properties analyses indicating closely interrelated properties 22 p3801 A67-40215
- New semiconductor compounds derived by cross substitution of group IV semiconductors, giving thermal properties and phase diagrams 23 p4036 A67-40720
- Surveyor I landing site soil data covering mechanical, optical, thermal and electrical properties 23 p4064 A67-40950
- Adhesives to bond metal linings to filament-wound cryogenic pressure vessels evaluated by test series simulating fabrication and service conditions 23 p4010 A67-41347
- Equivalent circuit to study AC posistor temperature characteristics and determine active and reactive components of net resistance 24 p4130 A67-42253
- Density fluctuations and thermal conditions in expanding universe and creation of stars, quasars, galactic clusters and galaxies 24 p4239 A67-43061
- THERMAL PROTECTION**
- Oxidation resistant thermal protection materials for 4000 degrees F high velocity air environment [SAE PAPER 660659] 01 p0094 A67-10617
- Oxidation test and mechanical property data to determine suitability of columbium and tantalum alloys as thermal protective materials for use in multicycle earth reentry vehicles [SAE PAPER 660660] 01 p0094 A67-10618
- Ablative materials for thermal protection and minimum mass transfer of aircraft flying at hypersonic speeds [DVL-603] 03 p0532 A67-13026
- Uncertainties in thermophysical properties of char-forming ablatives in intense convective and radiative heat transfer environments and effect on mathematical and physics models [AIAA PAPER 65-639] 03 p0534 A67-13059
- Structures, materials and thermal protection systems for future manned reentry vehicles, emphasizing crew compartment compatible materials [AIAA PAPER 66-987] 03 p0520 A67-14143
- Spacecraft thermal control coatings based on optical properties, discussing stability, environmental simulation in development, thermophototropic concepts, data retrieval and optical measurement techniques in ultrahigh vacuum [SAE PAPER 660653] 04 p0630 A67-15785
- Tubular support heat shield effects on insulated noncooled thermal protection, noting Dyna-Flex thermoconductivity discrepancy [AIAA PAPER 67-215] 06 p1117 A67-18443
- Graphite thermochemical response tested in simulated environment for use as thermal shield for hypersonic reentry vehicles [AIAA PAPER 65-643] 08 p1428 A67-20561
- Lifting entry vehicles requirements for near earth and planetary missions, noting four thermal protection systems 09 p1572 A67-22671

- Superlight ablative systems for Mars Lander thermal protection 10 p1672 A67-23724
- Optimization of base thermal protection system for advanced Saturn II boosters employing strap-on solid propellant motors 10 p1735 A67-23729
- Pressure and thermal protection of man during earth-moon flight and life on moon surface 12 p1901 A67-25175
- Liquid hydrogen fuel tankage thermal protection in manned hypersonic vehicles, discussing results of tests in steady state conditions 12 p2035 A67-26012
- [AIAA PAPER 67-297] 12 p2035 A67-26012
- Aerothermodynamic testing of heat protective systems in arc tunnel 15 p2466 A67-29538
- Aerothermodynamics for Apollo spacecraft design and results of flight tests 16 p2761 A67-30935
- Structures, charging into stage, thermal protection, ignition, and nozzles problems encountered in development of solid propellants 16 p2736 A67-31617
- Coordinated laboratory and flight test program, determining stability of solar concentrator reflective surfaces in orbital environment 17 p2832 A67-32060
- Value analysis technique to compare competing high performance insulation systems on basis of differences in performance and cost 18 p3162 A67-33939
- [AIAA PAPER 67-469] 18 p3162 A67-33939
- Interplanetary space environment effect on surface thermal radiative properties, noting results of exposure to simulated solar plasma, solar UV, solar wind, etc 19 p3249 A67-35748
- Thermal design of electronic packaging of Nimbus satellite control system 21 p3594 A67-38328
- Cordwood packaging concept for electronics thermal control in LEM, obtaining electronic package temperature field from finite difference equations 21 p3594 A67-38329
- Forced air distribution systems for electronic equipment cooling 21 p3594 A67-38331
- Thermal protection technique using resin fiber ablative materials for use on reentry bodies during ascent, emphasizing nozzle 21 p3731 A67-38377
- Superlight ablative systems for Mars Lander thermal protection 22 p3826 A67-40088
- Multiple reflective metal foil structure with separating matrix transient thermal response, determining number of radiation shields for given thermal protection 22 p3919 A67-40115
- Thermal protection methods for structures subject to aerodynamic heating, discussing heat dissipation methods and thermophysical materials 23 p4082 A67-41042
- Heat exchanger cooling system for controlling aircraft high temperature and thermal inorganic salt for protection against cold for flying personnel 23 p3967 A67-41612
- Ventilated wet suit /VWS/ for varying flight cockpit environment and emergency condition thermal protection, assessing physiological responses 23 p3967 A67-41614
- Optimization of base thermal protection system for advanced Saturn II boosters employing strap-on solid propellant motors 24 p4256 A67-42915
- Effects of low density, temperature, proton radiation and electromagnetic radiation on thermal control materials, using synergistic testing 24 p4177 A67-42916
- Earth and planetary atmosphere entry problems for blunt nosed slender vehicles noting aerodynamics, stability, heating, ablation and interaction of effects [AIAA PAPER 67-803] 24 p4243 A67-42963
- Thermo-protective systems for ejected aircraft personnel noting cream product producing heat when dissolved in water [AIAA PAPER 67-967] 24 p4117 A67-43045
- Military flight clothing tested in actual survival conditions for ability of subject to withstand moderate sea water environment [AIAA PAPER 67-968] 24 p4118 A67-43046
- THERMAL RADIATION**
- SA INFRARED RADIATION**
- Classical meteoric ablation theory generalized to include thermal radiation, conduction and meteoroid heat capacity in causing fragmentation 01 p0147 A67-10357
- Heat flux measurement with narrow view angle radiometers, discussing equipment design, performance characteristics and results 01 p0069 A67-11021
- Thermal atmospheric sounding, discussing carbon dioxide transmission function parameters, water vapor and temperature effect 02 p0239 A67-12377
- Differential approximation for forward and backward radiative flux components for three-dimensional flows 02 p0235 A67-12566
- Calorimetric apparatus for measurement of low temperature emittance of materials as function of temperature 03 p0418 A67-13037
- [AIAA PAPER 65-703] 03 p0418 A67-13037
- Reflectance and emittance properties of binary coatings in sintered or compacted powder form in terms of properties of pure components 03 p0448 A67-13038
- [AIAA PAPER 65-870] 03 p0448 A67-13038
- Directional absorptivity characteristics of conical cavities and use as thermal model for lunar meteor craters 03 p0508 A67-13049
- [AIAA PAPER 65-869] 03 p0508 A67-13049
- Nature of lunar surface, discussing interpretations of Luna IX photographs by Jaffe and Kulper 03 p0512 A67-13934
- Monte Carlo computer program for simulation of thermal radiation among opaque surfaces in vacuum [ASME PAPER 65-WA/HT-40] 03 p0537 A67-14009
- Thermally radiating and absorbing plane piston problem, obtaining zero order approximation in series expansion in density ratio across shock layer 03 p0405 A67-14029
- Room temperature measurements determining mean slope and peak-to-valley height influences on bidirectional spectral reflectance of V-grooved surfaces 03 p0426 A67-14398
- Thermal and nonthermal cosmic radio sources explained by short circuit breakdown of predischarged field initiated by breakdown to thermally ionized arc discharge 04 p0691 A67-14433
- Fluid dynamic sources of radiation during atmospheric entry, considering equilibrium and nonequilibrium radiation, thermal radiation and relaxation processes in hypersonic flow 04 p0703 A67-14703
- High resolution equilibrium radiation spectra for shock layer of blunt bodies at reentry velocities and radiative recombination of N and O ions [AIAA PAPER 66-104] 04 p0546 A67-14816
- Laminar free convection of radiation absorbing-emitting fluid along flat plate noting interaction effects, solving problem by singular perturbation 04 p0727 A67-15682
- Transient temperature distribution in semiminfinite solid, plate, cylinder and sphere subjected to heating or cooling thermal radiation 04 p0737 A67-15865
- Thermal radiative property behavior of materials under elementary charged particle bombardment, determining effect of combined UV plus electron exposure and low energy proton 04 p0686 A67-15873
- High cloud surface effect on satellite measurements of radiation temperature of stratosphere 05 p0802 A67-17376
- Thermal radiation intensity measurement from heating rate of Cu detector exposed to radiation 07 p1184 A67-19354
- Simulator solar incidence factors for thermal analysis of imperfectly collimated radiation [AIAA PAPER 66-458] 07 p1268 A67-19374
- Moon and planet surfaces analyzed based on thermal radiation for information on parameters of material of upper layer 08 p1390 A67-21024
- Nongray model atmospheres of Jovian planets constructed for different relative concentrations of helium and diatomic hydrogen and various likely effective temperatures as chief sources of thermal opacity 09 p1567 A67-22237
- Greenhouse effect in semiminfinite scattering atmospheres, describing steady state distribution of thermal radiation 09 p1567 A67-22238
- Solution of angular distribution of outgoing thermal radiation from planetary atmosphere, using Chandrasekhar diffuse scattering and transmission functions 09 p1567 A67-22240
- Inviscid axisymmetric radiating flow over blunt body, analyzing paraboloidal shock wave thermal radiation effects on temperature, density, velocity, etc 10 p1592 A67-23453
- Optimization of base thermal protection system for advanced Saturn II boosters employing strap-on solid propellant motors 10 p1735 A67-23729
- Thin film thermal radiation detector noting construction, calibration, performance, error sources and advantages of pyroelectric over thin film gauges 11 p1790 A67-24454
- Transient heat conduction problems involving time varying radiation boundary condition at surface solved by Goodman integral method 11 p1883 A67-24575
- New thermal radiative flux gauge utilizing thin film resistance thermometer and short duration test techniques 11 p1792 A67-24821
- Reduction of radiation effect on thermocouple in thermal vacuum testing by using fiberglass tape with aluminized mylar backing 12 p1943 A67-25695
- Radiation MGD, considering flow problems with thermal radiation and electromagnetic field effect 12 p1975 A67-25889
- Thermal radiation properties of oxide films of variable thickness on metal substrates, using radio-recording spectrophotometer at various wavelengths [AIAA PAPER 67-286] 12 p1958 A67-26003
- Low to moderately high temperature emissometer, based on calorimetric method, to measure total hemispherical emittance of metals and coatings in vacuum [AIAA PAPER 67-299] 12 p1946 A67-26014
- Thermal radiation characteristics of spacecraft temperature control louvers in solar space environment, discussing specular reflection [AIAA PAPER 67-307] 12 p2036 A67-26022
- Closed form solution for determining total emissivity of metals and radiation conductivity of radiation shield for nongray metallic surfaces at low temperature [AIAA PAPER 67-335] 12 p2038 A67-26049
- Thermal radiation emission detection from interplanetary dust, showing that zodiacal dust extends to within 4 solar radii of sun and confirming Poynting-Robertson effect 13 p2189 A67-26264
- Thermal radiation characteristics of metallic surfaces, comparing metal dispersion relationships with experimental emissivity 13 p2130 A67-26439
- Seasonal variations in high latitude stratosphere and mesosphere 13 p2113 A67-26675
- Approximate iteration procedure for determining temperature field in plate for simultaneously radiative and convective heat transfer 15 p2580 A67-29779
- Solar simulation, comparing techniques for reproducing space thermal radiation environment with sun characteristics 16 p2654 A67-30674
- Unsteady heat transfer due to radiation of two opaque bodies of finite dimensions, solving nonlinear Volterra integral equation with respect to net radiation density 16 p2779 A67-31208
- Thermal radiation dependence of perfectly conducting materials on large and small surface roughnesses thermal radiation dependence of perfectly conducting materials on large and small surface 16 p2779 A67-31502
- Steady state temperature field of uniform body containing heat sources, examining nonlinear boundary value problems of unsteady thermal radiation 17 p2971 A67-32870
- Probabilities for two-photon absorption processes induced by coherent and thermal light when acting on atomic system 17 p2870 A67-33317
- Far IR surveys of sky for thermal radiation from interstellar grains and other sources of far IR radiation, using balloon sounding 17 p2952 A67-33362
- Flame propagation along interface between gas and reacting medium, studying fuel heating ahead of flame, noting radiation and convection role 18 p3151 A67-33816
- Origin of X radiation from radio galaxies Cygnus A and Virgo A, hypothesizing thermal radiation and bremsstrahlung 18 p3116 A67-33855
- Spectral coefficients of blackness in materials with low thermoconductivity determined by measuring radiation intensity

and solving equations derived from Planck and Kirchhoff laws 18 p3048 A67-34056

Thermal radiation resonance of plasma cylinder in presence or absence of magnetic field 18 p3090 A67-34435

Spectral measurements of reflected solar and emitted thermal radiations from earth and clouds, using spectrometer with interference filter wedge 19 p3225 A67-35690

Wave transformation effect on inhomogeneous plasma radiation noise, applying results to stable plasma thermal radiation 20 p3498 A67-36691

Wave interference and radiation tunneling phenomena influences on thermal radiation energy transfer between two separated solid dielectrics, noting spacing effect [ASME PAPER 67-HT-21] 20 p3546 A67-36716

Gas local thermodynamic equilibrium effect on calculated thermal radiation emission [ASME PAPER 67-HT-51] 20 p3548 A67-36733

Blockage effects of centrally located sample on reflectance measurement by modified integrating sphere [ASME PAPER 67-HT-54] 20 p3447 A67-36736

Thermocouple surface temperature measurement errors in space simulation chambers due to heat conduction and radiation of wires [ASME PAPER 67-HT-57] 20 p3447 A67-36739

Theoretical prediction of temperature profiles within heated cylinder and on surface to determine thermal conductivities at high temperature [AICHE PAPER 16] 20 p3552 A67-36829

Convex plasma thermal radiation at UHF, determining spectral composition using Fourier integrals 21 p3663 A67-37937

Viscous dissipation effect on heat transfer rates for laminar boundary layer flow of gray gas across flat plate 21 p3732 A67-38878

Laminar free convection of absorbing emitting gas analyzed in region of stagnation point of horizontal cylinder 22 p3920 A67-40418

Nonself-similar energy diffusion of thermal radiation front for plane parallel geometry, giving series and parametric solutions 23 p4081 A67-40887

Thermal radiation properties measurement for materials in spacecraft design, discussing apparatus, instruments, techniques, devices and methods 23 p4083 A67-41368

Solar and terrestrial thermal radiometer absolute calibration noting standards and methods 23 p4006 A67-41373

High emittance coatings radiation characteristics investigated for space applications, considering thickness effect on high temperature emittance and space environment effect at moderate temperatures [ASM PAPER C6-4.3] 23 p4020 A67-41404

Laser radiation model of superimposed coherent and incoherent radiation, determining statistics of photons 24 p4166 A67-41903

Thermal development method used for observing and recording laser oscillations from output of nitrogen-carbon dioxide systems 24 p4166 A67-41908

Emittance and specific heat determination by transient thermal vacuum technique using coatings as function of temperature 24 p4153 A67-42039

Optimization of base thermal protection system for advanced Saturn II boosters employing strap-on solid propellant motors 24 p4256 A67-42915

THERMAL RADIO EMISSION

Irregularities in fine structure of solar atmosphere with respect to radio emissions, electron density, temperature and flux density 01 p0150 A67-10891

Thermal radio emission from Mercury, Venus, Mars, Saturn and Uranus at various wavelengths, using radio telescope in Australia, determining emission spectrum 02 p0319 A67-11452

Thermal radio emission measurements at wavelengths 7.93, 11.0, 14.2 and 20.8 cm, discussing phase dependence 02 p0322 A67-11581

Balloon observation of thermal radio emission of molecular oxygen in terrestrial atmosphere 02 p0237 A67-11852

Thermal radio emission from Mercury at 1.9 cm monitored by 140 ft radio telescope using tunnel diode radiometer 07 p1246 A67-19056

Chromosphere observation at different millimeter radio wavelengths with 4.88-m-diam telescope establishing correlation between mm solar radiation and solar activities 13 p2206 A67-27488

THERMAL SHOCK

Thermal shock testing of adhesive strength and crack resistance of turbine vane protective coating 06 p1006 A67-17810

Cobalt alloys precipitation hardening behavior, oxidation, thermal shock resistance and stress rupture strength 11 p1808 A67-24704

Hypereutectic carbides from carbide graphite alloys exhibiting high thermal shock resistance 11 p1809 A67-25004

Oscillations of cylindrical shell containing compressible gas perturbed by heat induced shock wave 12 p2023 A67-25595

Ballistic aspects, structure and destructive power of Tungusk meteorite do not support thermal explosion hypothesis 15 p2558 A67-30010

Hydrogen thermal ionization rate behind strong shock wave, considering nonadiabatic collisions and various relaxation mode interactions in shock speed range 19 p3292 A67-35394

Brittle-ductile materials thermal shock characteristics explained by strains and elastic energy, noting ductile materials withstand more strains before failure 20 p3538 A67-36673

Unidirectional solidification of cast nickel-base superalloys, effect on creep behavior, stress-rupture properties and thermal shock resistance 20 p3469 A67-37383

Ballistic aspects, structure and destructive power of Tungusk meteorite do not support thermal explosion hypothesis 20 p3530 A67-37534

THERMAL SIMULATION

Thermal testing of critical systems module of meteoroid detection satellite without attaching sensor arrays 02 p0334 A67-12378

Thermally scaled model space station subjected to steady state and cyclical transient solar environments [AIAA PAPER 65-658] 03 p0534 A67-13063

Steady state and transient full-scale, half-scale and quarter-scale thermal models in simulated space environment [AIAA PAPER 65-659] 03 p0534 A67-13064

Transient temperature distributions in simple bodies with internal cycled heat sources [AIAA PAPER 65-660] 03 p0534 A67-13065

Thermal similarity study of models in space environmental chambers for deducing characteristics of typical space vehicle element [AIAA PAPER 66-460] 04 p0724 A67-15247

Microwave and thermal vacuum testing to demonstrate design maturity of LEM rendezvous radar during simulated mission 04 p0578 A67-15397

Optimal temperature control design using IBM 7094 digital computer program for thermal environment simulation of stabilized multisurfaced earth-orbiting spacecraft structure [ASME PAPER 66-WA/HT-44] 04 p0724 A67-15430

Simultaneous simulation of space and thermal conditions of spacecraft [ASME PAPER 66-WA/HT-29] 04 p0599 A67-15443

Mathematical theory of dimensional analysis and similitude, application to spacecraft thermal design and experimental results 05 p0926 A67-18514

Transient heat transfer analysis of Apollo Service Module [AIAA PAPER 67-157] 06 p1118 A67-18506

Temperature fluctuation of thin walled satellite passing periodically from sun to shade simulated by hybrid computer 07 p1257 A67-19375

Thermal design of navigational satellites, obtaining reduction in discrepancy between operational orbital temperatures and preflight calculations through thermal vacuum testing 09 p1572 A67-22062

Thermal vacuum performance testing of scaled models as technique for reducing development costs of spacecraft 11 p1773 A67-24346

Thermal modeling applicability to steady state and transient conditions, considering material property changes with temperature [AIAA PAPER 67-305] 12 p2036 A67-28020

Simulation of nonlinear radiant heat transfer for constant emitting heat source by circuit, using semiconductor and pentode 15 p2579 A67-29323

Environmental simulation for aerospace vehicle, discussing vibration, shock and high temperature testing and space and nuclear radiation simulation 22 p3781 A67-40343

Aerospace vehicle structure loading under structural integrity tests with simulated aerodynamic heating conditions, discussing computer relaxation solution for rod temperature distribution 24 p4172 A67-42036

Thermal testing techniques for solar probe spacecraft using analytical and experimental models 24 p4139 A67-42043

THERMAL STRESS

Thermal stresses in isotropic circular cylinder under temperature distribution effect, reducing problem to solution of boundary value in form of Airy stress function 01 p0159 A67-10278

Structural design of large space chambers, examining outgassing rate and thermal stress in material selection 02 p0228 A67-11839

Light and electron microscopy used with X-ray diffraction and X-ray fluorescence analysis to study effects of temperatures and stress on As-cast nickel-base superalloy 02 p0256 A67-12706

Diffusion effect on thermal stresses in neighborhood of macrodefects in solid solution resulting in time dependent change of stress-strain state 03 p0521 A67-13121

Thermal stresses generation in nozzle blades of gas turbines tested in near operating conditions 03 p0429 A67-13332

Anisotropy of thermal expansion and microstructural changes due to thermal stresses 03 p0446 A67-13564

Strength of cylindrical shell deformed under radial temperature field 03 p0527 A67-14073

Temperature and stress distributions in annulus partially filled with cold fluid 03 p0531 A67-14363

Beryllium as substrate for mirrors of catadioptric lenses, noting strain-induced aberration 03 p0470 A67-14391

Transient thermal stress and associated natural frequency variations in circular disk elements [ASME PAPER 66-WA/MD-2] 04 p0629 A67-15347

Transient heat transfer and thermal stresses for nuclear rocket due to sudden hydrogen coolant flow increase [ASME PAPER 66-WA/NE-4] 04 p0656 A67-15373

Optimum control of flow rate through nuclear rocket with constraint on thermal stress in fuel elements [ASME PAPER 66-WA/AUT-6] 04 p0656 A67-15419

Maximum thermoelastic stress and deflection in plate or beam as function of cross sectional shape, temperature and end conditions [ASME PAPER 66-WA/APM-1] 04 p0714 A67-15426

Failure mechanisms in silicon transistors deduced from step stress tests 04 p0584 A67-15482

Quasi-static stresses due to moving temperature discontinuity on plane boundary 05 p0908 A67-16137

Soviet papers on thermal stresses in structural elements 05 p0910 A67-16174

Creep problems during small, periodic, slow or rapid changes in temperature field, noting role of thermal stresses 05 p0912 A67-16176

Quasi-static equilibrium of thin plate heated by stationary circular source, obtaining expression for elastoplastic region at heating center, using continuous function 05 p0912 A67-16179

Generalized thermally stressed state of thin plate in presence of interaction between strain field and temperature, considering heat exchange with surrounding medium 05 p0913 A67-16187

Critical stresses of three-layer wing panel compressed by load distributed along two sides, determining temperature stresses in bearing layers and equilibrium equations 05 p0913 A67-16191

Temperature stresses in plane elements by unsteady heat fields examined via polarization optical

method 05 p0914 A67-16195
Thermal stress determination in thin conical shells of revolution using real function expression for forces, moments and displacements occurring during cyclic deformation 05 p0914 A67-16198
Water cooled vest with insulated icebox and electric pump to reduce thermal strain and increase comfort for aircrew members in hot humid climates 05 p0756 A67-16284
Elastic plate bending mechanical analog to two-dimensional thermoelastic problem, solving thermal stresses of solid propellant grain 05 p0917 A67-16417
Refrigeration process of freezing stresses at ambient temperature improves elastic and photoelastic properties and renders them comparable to those of nonplasticized epoxy resins
[ONERA-TP-367] 05 p0919 A67-16480
Thermal contact resistance between smooth rigid isothermal planes separated by elastically deformed smooth spheres [AIAA PAPER 66-461] 05 p0928 A67-17223
Thermoelastic bending of solid circular plate of variable thickness 06 p1105 A67-18581
Thermostability of refractory materials and effects of high brittleness on thermal stress resistance of structural elements under single and multiple heat treatment and loads 07 p1198 A67-19128
Thermoelastic stressed state of sandwiched plate in temperature field 07 p1261 A67-19326
Thermal stresses in thin walled open spherical shell of constant thickness 07 p1262 A67-19348
Similarity relationships for study of transient and steady state thermal displacements, strains and stresses between model and prototype 07 p1262 A67-19413
Nonstationary thermoelastic stresses analyzed using photoelastic technique based on polarized light 08 p1423 A67-21334
Nonlinear flutter of simply supported rectangular plate under thermal compression in supersonic gas flow 09 p1574 A67-21915
Stress field near surface of elastic solid during short time interval when heat flow occurs analyzed through strain theory for fracture location and probability 09 p1576 A67-22422
Thermal stress distribution around crack in elastic solid of transversely isotropic material 10 p1716 A67-22934
Stresses produced in elastoplastic sphere with spherical cavity by surface heating-cooling, reducing problem solution to first order ordinary differential equation and functional equation 10 p1716 A67-22940
Complex solution of equations in two-dimensional thermal stress theory applied to solution of boundary value problems 10 p1716 A67-22942
IR techniques for reliability enhancement of microelectronics 10 p1610 A67-22977
Existence and stability of solutions for equations of stationary thermal explosion in bounded container 10 p1734 A67-23679
Plane thermal stress at insulated hole under uniform heat flow in orthotropic medium 10 p1730 A67-23838
Temperature effect, including liquid helium temperature, on yield stress of commercial purity alpha titanium 11 p1805 A67-24111
Contact problem of half-plane inelasticity theory using Jacobi polynomials and taking into account thermal stresses and presence of adhesion and friction in contact area 11 p1876 A67-24677
Two-dimensional problem of thermoelasticity solved using analytic functions 11 p1879 A67-24885
High speed radial turbine rotor temperature distribution measured for pattern prediction of temperature 12 p1988 A67-25354
Stress relaxation dependence on heat deformation regime in Ti alloys VT14, VT3-1 and VTS-1 12 p1955 A67-25368
Critical stresses of compressed three-layer cylindrical shell of asymmetrical structure in presence of variable temperature 12 p2026 A67-25614
Reissner variational formulation of temperature distribution boundary value problem of axisymmetric thermal stresses in isotropic sandwich shells of revolution [AIAA PAPER 66-528] 12 p2030 A67-25917

Thermal stress field effects on materials for idealized situation, discussing problem of half-space and elastic layer under nonuniform surface heating, crack, etc 12 p2032 A67-26198
Random thermal-stress analysis for linearly elastic body assuming zero-stress state, uniform temperature and freely deformable surface of body 13 p2217 A67-26634
Apparatus for programming thermal cycles in fatigue tests of materials 13 p2218 A67-26797
Thermal stresses and displacement in flat wedges using optical polarization method 13 p2219 A67-27058
Unsteady thermoelastic stress calculation in plane wall 13 p2219 A67-27059
Thermodynamic possibility of thermal convection in earth mantle 13 p2117 A67-27577
Thermal stresses in isotropic plate analyzed using Hankel transform, obtaining surface temperature for various cases 14 p2402 A67-28813
Lattice thermoconductivity noting local equilibrium hypothesis theory, thermal resistance mechanism, etc 14 p2374 A67-28981
Thermal stresses in thin shell in contact with smooth rigid container 14 p2403 A67-29011
Mean diameter/wall thickness optimum ratio and corresponding maximum shear stress for thin walled cylinder under uniform pressure and radial heat transfer 15 p2574 A67-29528
Temperature measurement of ruby laser rods during pulsed pumping from birefringence dependence on temperature and resulting thermoelastic stresses 15 p2499 A67-29721
Temperature field of hollow cylinder with spatially distributed heat source, examining transient temperature distribution and thermal stresses in cylinder 15 p2574 A67-29775
Transparent plastic materials for aircraft application, noting glass developments and thermal stress conditions 16 p2694 A67-30980
Thermal stresses in three-layer cylindrical sandwich shell of finite length with rigid filler having temperature as function of radius only 16 p2765 A67-31049
Thermal stress concentration in physically nonlinear elastic plate with hole in presence of uniform heat flux 16 p2766 A67-31148
MOS instabilities from ion drift, temperature dependent deep trapping and fast interface states from temperature stress, noting instabilities elimination techniques 17 p2823 A67-32195
Large orbiting astronomical telescope design, discussing minimum waver, high resolution image recording, compactness and thermal warpage 18 p3043 A67-33493
Stress analysis of loaded boundaries in two-dimensional second boundary problems, studying mechanical and thermal strain, knife-edge device, etc 18 p3142 A67-33899
Steady thermal strains measurement in aero and industrial turbine and engine components, discussing fine wire behavior, bonding agent, performance, requirements, etc 18 p3143 A67-33900
Frame-camera interferogram data for Nd-doped glass rod during laser pumping analyzed through optical path length changes 18 p3062 A67-34623
Thermal stress concentration factors for rectangular flat plates penetrated by holes 19 p3337 A67-34823
Periodic stress and heating during creep, studying deformation adaptability of material for conditions experienced by aircraft engine components 19 p3338 A67-34885
Accumulated plastic deformation during sequence of isothermal and nonisothermal loading 19 p3242 A67-34887
Thermal-stress distributions in circular disk due to instantaneous heat source on radius midpoint, assuming no temperature variation over thickness 20 p3536 A67-36418
Blaxial prestressing in ceramic plates under nonuniform thermal stress for damage reduction study 20 p3538 A67-36778
Thermal stresses in orthotropic sandwich plate solved by boundary value and stress distribution 20 p3541 A67-37298
Equations for transient temperature distribution and thermal stresses in heated

idealized wing structure solved using heat flow analysis method 20 p3541 A67-37489
Existence and stability of solutions for equations of stationary thermal explosion in bounded container 21 p3731 A67-38280
Thermal-stress deformed condition on heated elastic bodies boundary containing inclusions of spherical thin film with homogeneous infinite heat flow 21 p3720 A67-38295
Orthotropic laminated layer with heat emission investigated for thermoconductivity and temperature stress distribution 21 p3731 A67-38299
Elastic spherical shell stability under thermal stresses from abrupt temperature change at shell equator solved, using Fredholm integral equation 21 p3721 A67-38308
Stress analysis of loaded boundaries in two-dimensional second boundary problems, studying mechanical and thermal strain, knife-edge device, etc 21 p3722 A67-38435
Thermal stress analysis of epoxy encapsulants using mathematical model for predicting performance in thermal shock 21 p3723 A67-38630
Normal stresses induced by temperature effects in thin walled bars, assuming nondeformability of contour and no displacements in middle surface 21 p3728 A67-38905
Steady state temperature field and stresses determined for infinite body with linear slit having definite heat resistance 21 p3729 A67-39007
Failure mechanisms in semiconductor components under thermomechanical and electrical stresses for D2 satellite application 21 p3601 A67-39061
Mission profiles involving new materials for missile and space structures reviewed for progress in computer applications 22 p3915 A67-40330
Thermal stress fracture of brittle ceramics studied for effect of relaxation by creep at high temperature under conditions of quasi-static heat flow 22 p3915 A67-40386
Wing stress analysis, reviewing computer and variational methods for calculating structural strength 22 p3746 A67-40445
Cockpit environment thermal stress effect on psychological test performance and biomedical parameters 22 p3753 A67-40539
Numerical data for plane thermal stresses in isotropic elastic square plate bounded by edge stiffeners and under symmetric temperature distributions 23 p4073 A67-40611
Aircraft cockpit and surface temperatures after solar radiation exposure in desert, showing inadequacies of meteorological data for thermal stress predictions 23 p3935 A67-41593
Water deficit effects on thermal sweating, noting extraneous effects due to higher body temperature and wet skin 24 p4110 A67-41781
Glass fiber reinforced gas turbine engine compressor blade thermal stability for short cycle heat stress damage 24 p4249 A67-42103

THERMIONIC CATHODE
Cathode noise voltage in low current arc at atmospheric pressure as function of arc cathode surface state 14 p2354 A67-27764
Convective electric arc stability and slanting in thermionic rail accelerator [AIAA PAPER 67-674] 21 p3671 A67-38707
High endurance thermionic cathodes for Kaufman thrusters, discussing emissive coatings and emissive layer starvation [AIAA PAPER 67-678] 21 p3696 A67-38929
Neutralizer for large mercury thruster systems using hollow cathode forming plasma bridge neutralizer for large mercury thruster systems using hollow cathode forming plasma bridge [AIAA PAPER 67-671] 21 p3697 A67-38958

THERMIONIC CONVERSION SYSTEM
Thermionic energy conversion principles and conversion systems for satellite and space use 04 p0554 A67-15025
Alkaline vapor refueling of solar thermionic converters, concept, development and tests 07 p1132 A67-20287
Storage of solar electric energy by electrolysis of water, separate storage and subsequent recombination of gases by fuel cells 07 p1132 A67-20288
Thermionic Conversion Specialist Conference, IEEE, San Diego, October 1965 12 p1899 A67-25559

Thermionic space power systems, examining solar, radioisotope and nuclear reactors as heat sources, discussing power density and electrode affinity 17 p2802 A67-32050

Thermionic conversion for space auxiliary power systems noting high reliability and longevity potential 20 p3364 A67-37019

Book on electromechanical, direct and nuclear energy conversion covering transducer design, nuclear structure, photoelectric conversion, reactor theory, thermionic conversion, etc 22 p3749 A67-40329

Power systems for long duration missions including photovoltaic solar energy, thermoelectric, Brayton cycle and thermionic conversion systems, discussing solid state components 22 p3749 A67-40339

SET VIII Thermionic generator, evaluating operational and long term performance characteristics for space applications 24 p4103 A67-42499

Thermionic converter arrays output characteristics determined as function of interconnection resistance, failure modes and patterns, etc 24 p4103 A67-42500

Heat pipe dynamics analyzed for thermionic converter heat pipe radiator design criteria, discussing working fluid selection 24 p4104 A67-42503

Co 60-Re alloy in externally fueled thermionic system shown economically desirable for multi-kwt terrestrial or undersea applications 24 p4185 A67-42535

THERMIONIC CONVERTER

Thermionic energy conversion, discussing surface and volume phenomena, vacuum and gaseous converters 01 p0013 A67-10557

Plasma probe in thermal emission converter with high cesium vapor, noting parameters of diffusion, electron concentration, etc 02 p0184 A67-12468

Capillary emitter of electrons and Cs ions for use in thermionic converters 04 p0664 A67-15015

Thermionic energy converters in West Germany, discussing vacuum magnetic triodes, Cs diodes and rare gas triodes 04 p0554 A67-15026

Radio nuclide generator using oxide of strontium 90 with thermionic converter, noting decaying characteristics 04 p0559 A67-15963

Fast and thermal reactors with thermionic converters in reactor core and nuclear system with converters outside core analyzed for power supply for space vehicles 04 p0559 A67-15964

Liquid metal MHD converter with multistage thermodynamic drive for use as power source in space vehicles as alternative to thermionic converter 04 p0559 A67-15965

SNAP-10A and SNAP-8, discussing reactor thermoelectric space power program 08 p1352 A67-21052

Electron space-charge neutralization in design of thermionic /heat-to-electricity/ converters 08 p1286 A67-21177

Output characteristics of cesium thermionic converter as function of size of electrode gap, using device with movable air-cooled stainless steel anode 09 p1444 A67-22007

Inert gas effect on performance characteristics of cesium thermionic converter, noting saturation current increase 09 p1444 A67-22008

Thermionic conversion - IEEE Specialist Conference, Houston, November 1966 09 p1446 A67-22330

Niobium and nickel as thermionic converter collector materials, comparing characteristics 09 p1447 A67-22331

Output characteristics of electroetched rhenium surface, bare and cesiated work function and performance 09 p1447 A67-22332

Efficiency increase in vapor-filled thermionic converter anticipated by introducing intermediate electrodes between emitter and collector of vapor-filled diode 09 p1447 A67-22333

Thermionic converter life-test results and failure mechanisms noting braze failure, collector deposit, emitter warpage and separation and cesium reservoir leak 09 p1447 A67-22334

Dynamic characteristics of thermionic converter noting influence of emitter heat transfer 09 p1447 A67-22335

Thermionic converter performance in presence of inert gases under conditions which avoid previous difficulties 09 p1448 A67-22339

Flame heated thermionic converter noting electrical, material and combustion problems of design of 100 watt device 09 p1448 A67-22341

Calorimetric measurements of thermionic converter/ heat pipe system, discussing electron cooling of emitter, thermal emissivity and thermal balance 09 p1448 A67-22342

Performance of thermionic converters, discussing voltage output, interelectrode spacing, rhenium-rhenium and rhenium-molybdenum electrode systems 09 p1449 A67-22343

Thermionic planar electrode converter and generator tests, noting test equipment and performance tables 09 p1449 A67-22344

Emitter material, emitter treatment, collector lateral area and interelectrode and lateral spacing effects on solar converter performance 09 p1449 A67-22345

Thermionic low voltage converter-regulator systems, discussing relation between thermionic source, electron cooling and impedance-matching characteristics 09 p1449 A67-22346

High temperature adsorption reservoir for automatic control of cesium pressure for use in thermionic converter 09 p1449 A67-22349

Temperature control and thermal coupling of cesium adsorption porous tungsten, charcoal and graphite 09 p1450 A67-22350

Electron transport phenomena in thermionic converter plasmas, emphasizing electron-ion collisions to electron momentum transfer collision frequency 09 p1450 A67-22351

Oxygen as steady state electronegative additive in cesium thermionic converter shown to improve performance without surface corrosion 09 p1450 A67-22355

Vapor-deposited tungsten formed by hydrogen reduction of tungsten hexachloride or hexafluoride, noting effect of crystal orientation and surface treatment on work function 09 p1451 A67-22357

Nuclear heated thermionic converter construction, V-I characteristics and comparison with electrical heating 09 p1451 A67-22359

Semipermeable Ag membrane as electron collector in oxygen diffusion process for cesium thermionic energy converters 11 p1746 A67-24923

Transfer of electrons from emitter or space charge region to collector in thermionic energy converter by negative ions 13 p2056 A67-27002

Spectroscopic measurements of plasma parameters in thermionic converters 13 p2056 A67-27385

Thermionic converter acceleration plate and excessive current flow effects, noting collector and cathode surface secondary electron removal, determining cut-off characteristic form 14 p2246 A67-27766

Direct and indirect converters emphasizing preconcentration of solar radiation, noting thermophotovoltaic generators of p-i-n type 16 p2608 A67-30713

Thermionic conversion system using mixed vapors for electric propulsion 16 p2608 A67-30715

Cesium impurities analyzed for behavior in thermionic converters, investigating equilibrium state as function of pressure and temperature 16 p2609 A67-31399

Cesium-neon mixture effect on thermionic-emission converter operation measured in experimental tube with plane electrodes, discussing volt-ampere characteristics 16 p2610 A67-31783

Cesium-vapor vacuum diode for thermionic conversion stressing role of electrode homogeneity, space charge and transport phenomena 17 p2823 A67-32222

Cesium thermionic converter extinguished-mode operation theory, deriving expressions for forward and reverse saturation output current densities and open circuit voltages 17 p2803 A67-32365

Low voltage arc phenomena in cesium vapor investigated in connection with cesium-diode application as thermionic converter, calculating voltage-current

characteristics 19 p3176 A67-35130

Duo-emitter cesium thermionic converter, discussing electron and cesium ion emission to increase transport efficiency 21 p3571 A67-38610

Plasma physics of thermionic converters, discussing simple physical models, I-V curve and converter operation region processes 22 p3747 A67-39342

Thermionic energy converter operation showing anomalous electron and ion currents in plasma mode, discussing heating power and emitter temperature 24 p4103 A67-42502

THERMIONIC DIODE

Weak longitudinal and transverse magnetic fields increase emf and optimum output voltage characteristics of thermionic diode introduced into autonomous mercury discharge plasma 01 p0034 A67-10135

Refractory metals and metal alloys analyzed regarding electron work function and threshold temperature for surface ionization in all-metal guard ring diode with directly heated wire [AIAA PAPER 66-223] 06 p1035 A67-18137

Efficiency increase in vapor-filled thermionic converter anticipated by introducing intermediate electrodes between emitter and collector of vapor-filled diode 09 p1447 A67-22333

Optimization of thermionic diode, with electrical conduction and heat transport represented by differential equations 09 p1448 A67-22336

Volt-ampere characteristics of grooved collector thermionic diode indicate ions generated in cavities diffuse to cavity free region and neutralize electron space charge 09 p1448 A67-22340

Performance of thermionic converters, discussing voltage output, interelectrode spacing, rhenium-rhenium and rhenium-molybdenum electrode systems 09 p1449 A67-22343

Emitter material, emitter treatment, collector lateral area and interelectrode and lateral spacing effects on solar converter performance 09 p1449 A67-22345

Thermionic diode conversion of thermal energy into electrical energy, noting cesium plasma diodes 10 p1595 A67-22989

Cesium vapor thermionic diode operation in electron-rich surface ionization mode noting transport effects 11 p1849 A67-24902

Cesium thermionic diode parameters including added noble gas pressure effect for ignited mode performance prediction and optimization 12 p1896 A67-25262

Anode emission influence on thermionic diode energy converter maximum efficiency 14 p2247 A67-28033

Thermionic reactor with uranium diodes core array, describing in-pile reactor uses, arcjet, heat pipe and conceptual design components [AIAA PAPER 67-498] 18 p3076 A67-33962

Electron flow in low density argon gas diode analyzed by Monte Carlo method 18 p3091 A67-34641

THERMIONIC EMISSION

SA SCHOTTKY EFFECT

Space charge formation during flow of electric current in plasma moving under thermal emission of electrons 01 p0118 A67-10043

Schottky emission as rate limiting factor in thermal oxidation of metals 04 p0677 A67-14947

Thermionic energy conversion principles and conversion systems for satellite and space use 04 p0554 A67-15025

Conductivity of working fluid in MHD generator using thermionic emission from suspended lanthanum conductivity of working fluid in MHD generator using thermionic emission from suspended lanthanum hexaboride powder 09 p1543 A67-21820

Saha-Langmuir formula applied to description of temperature dependence of positive ion current in surface ionization of silicon atoms, comparing work functions by methods using contact potential, thermionic emission and Richardson graphs 09 p1554 A67-22006

Operating temperature effect on vacuum emission stability of vapor-deposited tungsten clad UC-ZrC and uranium dioxide 09 p1449 A67-22347

Plasma mode work function measurement for studying thermionic emission from Hf,

Th and Tl in Cs vapor at reservoir temperature of 414 degrees K 09 p1450 A67-22353

Anisotropy of electronic metal work functions for zero and high electric fields perpendicular to surface measured by field emission and thermionic techniques 09 p1450 A67-22356

Collisionless instabilities in thermally ionized potassium plasma and effect of magnetic shear on oscillations and diffusion 11 p1834 A67-24378

Yttrium and gadolinium borides thermionic emission properties, noting inferiority to lanthanum hexaboride 15 p2534 A67-29358

Vacuum thermionic work function and thermal stability measurements on crystal surfaces, discussing results on carbides, diborides and disilicides 15 p2535 A67-29486

Electron emission current density for semiconductors for all conditions between limits of thermionic and field emission 16 p2725 A67-30805

Localized uniaxial force effect on voltage-current relationship of gold-potassium tantalate Schottky barrier diodes, noting reversible changes 16 p2637 A67-31036

Cesium-neon mixture effect on thermionic-emission converter operation measured in experimental tube with plane electrodes, discussing volt-ampere characteristics 16 p2610 A67-31783

Thermionic and electrical sorption properties of tungsten in alkali iodide vapors at high pressure 17 p2887 A67-32201

Thermionic work functions and electron emission S curves for contaminated copper surface in oxygen and cesium vapors, separate and mixed 17 p2887 A67-32203

Space charge formation during flow of electric current in plasma moving under thermal emission of electrons 17 p2910 A67-33321

Gas-borne suspensions of thermionically emitting particles as MHD working fluids 18 p3086 A67-33707

Enhanced radiation energy for visible and near IR during electron emission calculated by energy balance 19 p3176 A67-35081

Thermionic properties, surface ionization, atomic and ionic sublimation of Re, Mo, Ta and W 19 p3264 A67-35082

High endurance thermionic cathodes for Kaufman thrusters, discussing emissive coatings and emissive layer starvation [AIAA PAPER 67-678] 21 p3696 A67-38929

Energy distribution deviation of electrons emitted from plasma or solid via Maxwell distribution, deriving kinetic reflection coefficient in thermionic emission current expression 23 p4047 A67-41688

THERMIONIC REACTOR

Space vehicle power supply systems using thermionic reactors, noting power distribution in fission zone, cooling, shielding, etc 04 p0553 A67-14551

Nuclear thermionic propulsion system with low specific weight as interplanetary propulsion system [AIAA PAPER 67-229] 06 p1029 A67-18519

Thermionic reactor with uranium diodes core array, describing in-pile reactor uses, arcjet, heat pipe and conceptual design components [AIAA PAPER 67-498] 18 p3076 A67-33962

THERMIONICS

Physical/chemical characteristics of thermionic plasma noting equipment and technology involved 16 p2722 A67-31564

THERMISTOR

SA RADIOSONDE THERMISTOR

Low pressure measurement with thermistors noting equipment and accuracy obtained 06 p1000 A67-17618

Conductive heat transfer coefficient measurement from sphere to rarified gas mixtures over range of Knudsen numbers 06 p1117 A67-18388

Low velocity flow measurements by inexpensive thermistor probe 14 p2318 A67-28342

Error possibility in temperature measurements of 30-60 km region, noting solar irradiation effects on thermistor bead 15 p2474 A67-29202

Thermistor theory and special applications 18 p3050 A67-34503

Posistors barium titanate, lead titanate and potassium compound semiconductor and ferroelectric properties analyses indicating

closely interrelated properties 22 p3801 A67-40215

Rocket instrumentation and sensing techniques for collecting stratospheric wind and temperature data 23 p4025 A67-41445

Rocketsonde thermistor mount noting thin film configuration and long lead mount for heat dissipation 23 p4025 A67-41446

Photoelectromagnetic detector spectral sensitivity, magnetoresistance and time constants with optically polished thin elements fabricated from Ge, InAs, GaSb and InSb single crystals 24 p4154 A67-42243

Equivalent circuit to study AC posistor temperature characteristics and determine active and reactive components of net resistance 24 p4130 A67-42253

THERMOCHEMISTRY

SA AEROTHERMOCHEMISTRY

Thermomolecular flow effect caused by transverse and longitudinal forces, calculating force on hangdown fiber in microbalance 04 p0620 A67-14732

Thermal explosion laws under cooling conditions, examining linear cooling as method for studying thermal explosion of strongly self-accelerating reactions 06 p1112 A67-17962

Energy losses in explosions in sphere to determine specific heat, heats of dissociation and formation, chemical bond energies and other thermochemical values 06 p1113 A67-17963

Book on chemical bond in semiconductors and solids, evaluating strength and determining effect on properties of substances 13 p2182 A67-27486

Temperature measurement problem in high temperature chemistry and International Practical Temperature Scale 20 p3435 A67-36117

Partial molal entropies of doubly ionized aqueous Zn, Cd and mercurous and mercuric ions calculated, using literature data 20 p3376 A67-36792

Progress in high temperature physics and chemistry, Volume 1, covering air opacity and state equation 20 p3485 A67-36928

Change patterns in melting point and forbidden bandwidth for anion and cation substituted compounds of AlIIBV group 21 p3676 A67-37932

THERMOCONDUCTIVITY

SA FOURIER LAW

Charged and neutral impurities effect on heat conductivity of bismuth telluride crystal lattice 01 p0127 A67-10073

Supersonic MHD generator crisis possibility assuming quasi-one-dimensional nonequilibrium approximation at small Reynolds numbers and plasma scalar conductivity 01 p0011 A67-10177

Molecular weight sensitivity of thermoconductivity of polydimethylsiloxane and polyethyleneglycol 01 p0103 A67-10295

Thermocouple errors resulting from heat conduction along thermocouple wire embedded in low conductivity ablative material indicate helicoil wire for optimum design 01 p0071 A67-11104

Apparatus for measuring temperature dependence of thermoconductivity coefficient, thermal emf and specific electroresistance of cermet cylindrical shells 01 p0076 A67-11248

Possible lunar surface vacuum layer structure from effective thermoconductivity coefficient based on radioastronomical data 02 p0322 A67-11567

Thermoconductivity and thermal emf of Zn- and Te-doped GaSb 02 p0297 A67-11847

Impulse measurements of temperature conduction in n-type semiconductors 02 p0297 A67-11848

Existence of divergence in density expansion of viscosity and thermal conductivity coefficient of two-dimensional gas of rigid disks 02 p0234 A67-12545

Optical phonons role in thermal conductivity of GaSb doped with Zn and Te in temperature range 80 to 600 degrees K 03 p0488 A67-12811

Char generation and determination of thermal conductivity function under simulated entry heating conditions [AIAA PAPER 65-640] 03 p0534 A67-13060

Transient temperature distributions in simple bodies with internal cycled heat sources [AIAA PAPER 65-660] 03 p0534 A67-13065

Heat transfer between metallic surfaces in

contact [AIAA PAPER 65-661] 03 p0534 A67-13067

Thermal conductance at interface of two materials in contact, investigating surface and lubrication effects [AIAA PAPER 65-662] 03 p0534 A67-13068

Steady state thermal conductance coefficient at interface formed by nominally-flat rough contacting surface placed in vacuum environment [AIAA PAPER 66-42] 03 p0534 A67-13070

Book on conductive heat transfer covering lumped, integral and differential formulations, two- and three-dimensional periodic functions, unsteady problems, Laplace transforms, etc 03 p0535 A67-13075

Thermal field of cutting area of aircraft structural material analyzed, using differential equations of thermoconductivity 03 p0427 A67-13191

Perturbation solutions in differential analysis of radiation interactions with conduction and convection 03 p0378 A67-13288

Analogous studies of simultaneous conductive and radiative heat transfer across transparent laminar gas space, showing position of radiation shield between bounding surfaces 03 p0535 A67-13464

Thermoconductivity-temperature-diffusion coefficient relations for pure and mixed polyatomic gases 03 p0535 A67-13518

Thermal conductivity and degree of blackness of aluminum oxide coatings at high temperatures, using argon plasma jets 03 p0536 A67-13608

Heat transfer and velocity characteristics of thermal and hydrodynamic laminar flow in ducts of arbitrary cross section, considering boundary conditions at wall [ASME PAPER 65-WA/HT-13] 03 p0537 A67-14008

Cross section estimates for symmetric resonant charge exchange between ions differing by one electronic charge, noting effect on heat conduction in plasmas 03 p0484 A67-14038

Electron thermal conductivity of fully ionized Lorentz gas, determining energy transfer from Landau damping of plasma waves and collision parameters 03 p0484 A67-14039

First boundary value problem for thermal conductivity equation involving region with two angular points on boundary 04 p0721 A67-14661

Temperature dependent thermal property models of lunar surface and radiative energy transport deduced from RF and IR observations 04 p0697 A67-14740

Lattice thermal conductivity of disordered alloys of ternary compound semiconductors Cu₂/Sn, Ge/₂Se₃/3, /Ag, Pb, Sb/Te₂ and /Ag, Sn, Sb/Te₂ 04 p0675 A67-14760

Nonstationary heat conductivity solution for hollow sphere with varying inner surface and various outer surface conditions 04 p0726 A67-15594

Longitudinal conduction effect on fluid temperatures in multistream counterflow heat exchanger, based on characteristic function 04 p0728 A67-15806

Simultaneous conductive-convective heat-transfer coefficient and heat flux temperature relation at solid moving liquid interface 04 p0730 A67-15817

Thermal diffusion and diffusion thermoconduction coupling effects on transpiration cooling of porous bronze disk at axisymmetric stagnation point 04 p0733 A67-15839

Transient method for simultaneously determining thermal conductivity and specific heat, utilizing finite difference and statistical procedure called nonlinear estimation 04 p0734 A67-15851

Thermal conductance determinations on L-605 cobalt-base alloy panels of variable geometry made to around 2000 degrees F in high vacuum and air 04 p0735 A67-15852

Thermal conductivity measurement of fibrous insulations up to 2500 degrees F, determining relative contributions from gaseous conduction, solid conduction and radiation 04 p0735 A67-15855

Interaction between radiation and conduction and resultant total heat flux increase in plane layer studied by differential method 04 p0738 A67-15868

Approximate solution of thermoconductivity equation for multilayer

cylinder in constant-temperature medium 04 p0738 A67-15891

Steady one-dimensional heat conduction in rarefied gas at rest analyzed from viewpoint of kinetic theory to determine existence or possible departure from Fourier law 05 p0925 A67-16272

MHD wave propagation emphasizing viscosity, heat and electrical conductivity, Hall current, nonequilibrium phenomena and effect of medium inhomogeneity 05 p0851 A67-16364

Viscosity and thermoconductivity of partially ionized argon plasma at atmospheric pressure measured, using equilibrium plasma jet 05 p0851 A67-16508

Estimates of Green function in first boundary value problem of thermoconductivity equation for cylinder 05 p0927 A67-17002

Two-dimensional self-similar hot conducting gas outflow into vacuum, for power law variation of gas-vacuum interface temperature 05 p0793 A67-17007

Composite valence band in p-PbTe obtained from measurement of Hall effect, thermoelectric and optical effects 05 p0868 A67-17062

Temperature distribution in isotropic solid with variable specific heat and thermoconductivity treated by Kantorovich method 05 p0929 A67-17373

Thermal conduction paths for magnesium joints in cordwood mounting of electronic parts in heat conducting plate 05 p0929 A67-17451

Temperature dependence of thermoconductivity of dysprosium between 1 and 4 degrees K 06 p1048 A67-17821

Difference equations for heat transfer from liquid to solid and conductivity for solid applied to calculation of local temperatures within multilayer walls 06 p1113 A67-17990

Asymptotic expansion applied to strong explosion in heat-conducting gas 06 p0984 A67-18030

General solutions to heat conduction equations for three-dimensional unsteady heating of finite solid circular cylinder 06 p1113 A67-18124

Conductive heat transfer coefficient measurement from sphere to rarified gas mixtures over range of Knudsen numbers 06 p1117 A67-18388

Radial temperature profile of magnetospheric plasma near equatorial plane observed by IMP 06 p0996 A67-18432

Taylor theorem test as tool for determining completeness and convergence properties of finite element displacement functions, showing application to axisymmetric shell and conductive heat transfer [AIAA PAPER 67-143] 06 p1103 A67-18440

Quasi-stationary heat transfer equations and maximum possible heat-transfer coefficient for solid surface moving in very fluid rotating boiling medium 06 p1118 A67-18549

Electron-neutral particle collision and electron thermal conductivity effect on upper atmospheric electron and ion temperatures 06 p0998 A67-18702

Resistivity, magnetoresistance, Hall effect and thermal conductivity in n-type In-Sb at liquid He temperatures 06 p1068 A67-18968

Electron components for electrical, thermal conductivity and viscosity coefficients of gas mixtures calculated via molecular kinetic theory 07 p1225 A67-19116

Thermal conductivity coefficients of refractory materials at high temperatures determined by measuring one-dimensional stationary thermal flux at single point 07 p1265 A67-19124

Interaction between two rectangular parallel jets analyzed using heat conduction theory 07 p1167 A67-19151

Conductivity changes in flash evaporated p-GaAs films caused by field effect and optical and thermal excitation at temperatures about 100 degrees K 07 p1232 A67-19564

Thermal conductivity of laminated GaSe monocrystals studied in two crystallographic directions between 90 and 600 degrees K and effect of unilateral compression 07 p1233 A67-19649

Temperature dependence for n-n-n

epitaxial GaAs sandwich structures mounted on infinite half-plane of copper 07 p1155 A67-19797

Book on physical processes of heat and mass transfer including thermal conductivity and potential and various integral procedures 07 p1268 A67-20039

Temperature variation of thermoconductivity of helium-hydrogen gas mixtures and correlation of thermoconductivity curves with gas chromatograms 08 p1426 A67-20805

Heat pipe, device with thermoconductivity greater than solid conductors, based on surface tension and latent heat of working fluid 08 p1427 A67-21051

Closed form solution expressing transonic flow in idealized stellar wind and spherical accretion problems including viscosity and thermoconductivity effects 08 p1399 A67-21240

Transverse plasma instabilities as mechanism coupling motions of solar wind and cometary plasma, using thermal diffusion and conductivity transport coefficients to describe flow 08 p1401 A67-21367

Time and local temperature distribution in semiconductor under heating pulse 09 p1579 A67-21700

Thermal conductivity coefficient and integral hemispherical degree of blackness of niobium at temperatures above 1000 degrees C 09 p1517 A67-21856

Current voltage characteristic of gas discharge for one-dimensional stationary case with fixed temperatures at conductor end, noting voltage saturation 09 p1544 A67-21863

Viscosity and thermoconductivity of vapors of sodium and potassium 09 p1579 A67-21865

Thermoconductivity values as function of temperature for semiconductors, noting effect of doping, alloying, etc 09 p1553 A67-21943

Dependence of thermal conductivity of lunite on temperature, noting properties of moon surface 09 p1565 A67-21987

Two-dimensional problem for layer with mixed boundary conditions, obtaining solutions for Fredholm integral equations and relations for temperature distribution 09 p1580 A67-21994

Alternation direction methods /particular class of iterative methods/ applied to heat conduction problems 09 p1468 A67-22051

Pressure dependence of thermoconductivity of gases measured using thermoelectric power of semiconductor 09 p1499 A67-22424

Cryogenic thermoconductivity of impure tin in superconducting and normal state, noting anisotropy and superconducting energy gap independence from impurity type 10 p1687 A67-22761

Correlation of anisotropic energy gap with thermal conductivity in pure and impure superconducting tin 10 p1687 A67-22762

Electrical and thermal conductivity of tin films investigated in search for surface superconductivity induced by electric field 10 p1688 A67-22765

Ionospheric thermal conductivity effect on gravitational wave propagation 10 p1631 A67-22803

Thermal conductivity coefficient of refractory materials at temperatures to 1600 degrees C 10 p1621 A67-22828

Energy production sources in inner magnetospheric plasma near equatorial plane 10 p1634 A67-23058

Metal-beryllium oxide bond for semiconductors noting mechanical and electrical strength, thermal conductivity and refractivity 10 p1696 A67-23691

Plane layer type apparatus for measuring thermal conductivities and accommodation coefficients of gases over wide pressure 10 p1658 A67-23783

Properties of partially ionized Ar computed via Chapman-Enskog-Burnett expressions noting ambipolar diffusion coefficient, electron-atom momentum, electrical and thermal conductivity, etc 11 p1775 A67-23865

Plasma thermoconductivity in general force fields, showing validity of Meador-Staton results in case of ambipolar diffusion and nonuniform total pressure 11 p1827 A67-23884

Heat flow through Langmuir sheath in presence of electron emission and

application to limitation of energy loss rate by thermal conduction 11 p1828 A67-23894

Single conduction band approximation of nature of increase with temperature of thermal conductivity of ZrC and NbC in terms of scattering and Fermi energy 11 p1804 A67-23902

Thermoconductivity of heat resistant materials during cooling at room temperature, using photopyrometer to record temperature gradients 11 p1789 A67-24021

Thermoconductivity of nitrosyl bromide at 290-900 degrees K and 200-600 torr measured by hot filament techniques 11 p1881 A67-24022

Inverse problem of unsteady heat conduction equation for unbounded hollow cylinder, determining specific heat 11 p1882 A67-24031

Axisymmetric deformation of elastic slab with external crack interpreted as steady state problem of heat conduction 11 p1813 A67-24313

Kantorovich method applied to approximate solution of nonlinear problems of heat conductivity theory of plate 11 p1883 A67-24323

Transient heat conduction problems involving time varying radiation boundary condition at surface solved by Goodman integral method 11 p1883 A67-24575

Heat resistance of GaAs laser diodes from 77 to 300 degrees K, showing relationship to thermal conductivity 11 p1802 A67-24744

Thermal conductivity of low temperature silicon and germanium irradiated by fast neutrons noting differences, additive thermal resistivity and possible scattering mechanisms 11 p1849 A67-24899

Temperature dependence of thermal conductivity and phonon and electron components in solid and liquid n-and p-type semiconductors 11 p1851 A67-24975

Constitutive theory for fluid mixtures admitting diffusion and chemical interaction with heat conduction and plane wave propagation 11 p1783 A67-25001

Thermal conductivity of binary gas mixtures, estimating conductivity at high temperatures 12 p2033 A67-25217

Temperature field distortion in region of thermocouple junction which arises when thermal conductivity of junction differs from object whose temperature is to be measured 12 p1943 A67-25754

Thermophysical properties of heat-resistant solid solution of rhenium in tungsten produced by arc melting in vacuum 12 p1956 A67-25758

Acoustic measurement method for following motion of solid-liquid interface, obtaining solution for transient heat conduction problem 12 p1946 A67-25985

Temperature-dependent thermoconductivity of metal film on insulation laminations in relation to bulk parent material in insulation systems of cryogenic propellants [AIAA PAPER 67-295] 12 p2035 A67-26010

Thermoconductivity and diffusivity of amorphous solids determined simultaneously by refined line source technique [AIAA PAPER 67-314] 12 p2037 A67-26029

One-dimensional conduction model for predicting pressure variation of nonvented cryogenic propellant tanks in low gravity field [AIAA PAPER 67-338] 12 p2039 A67-26052

Fundamental solution of thermoconductivity equations for thin walled shallow shells and infinite plates with various instantaneous interval heat sources 13 p2221 A67-26374

Thermal history of earth based on thermal conductivity equation 13 p2110 A67-26453

Conductivity, temperature dependence, thermal EMF Hall constant, thermal conductivity and resistivity of aluminides of transition metals 13 p2131 A67-26471

Temperature profile in stratosphere, noting contribution to heat budget by turbulent thermoconductivity and UV radiation absorption in ozone layer 13 p2113 A67-26677

Thermal conduction and viscosity and energy propagation upward in atmospheric oscillation theory 13 p2114 A67-26742

High temperature destruction of solid where one portion transforms into gas or

liquid while remaining part forms porous frame 13 p2222 A67-26884

Heat conduction equation for inhomogeneous body, obtaining integrable solutions applicable to boundary value problems 13 p2224 A67-27055

Effect of mutual entrainment of electrons and phonons on Wiedemann-Franz law for semiconductors, calculating thermoconductivity 13 p2181 A67-27280

Effective thermal conductivity parameter for multilayered insulation 13 p2228 A67-27656

Measurement of thermal conductivity of irradiated foam-type insulation materials 13 p2228 A67-27662

Alloying elements and impurities effects on aluminum-alloy systems properties including neutron absorption, temperature changes, electric conductivity, etc 14 p2335 A67-27805

Relativistic thermodynamics in case of equilibrium with stationary co-moving metric and constant pocket temperature, deriving relativistic Fourier law of heat conduction 14 p2404 A67-27951

Heat conductivity effect on various one-dimensional flows solved by numerical integration of Navier-Stokes equations 14 p2296 A67-27980

Argon plasma thermal conductivity at atmospheric pressure and various temperatures determined in central zone of arc column 14 p2404 A67-28031

Thermal conductivities of unidirectional composite materials parallel and normal to filaments, using analogy to shear loading response 14 p2404 A67-28099

Two-dimensional thermal conductivity problems for hollow cylinder heated at constant rate, estimating axial heat flux effect 14 p2406 A67-28306

Asymmetric R and RC networks as electrical analogs for solving nonlinear equation of nonstationary thermal conductivity 14 p2274 A67-28315

Sensitized ignitions of methane and oxygen mixtures, with nitrogen oxides and inert gases added, and suggested reaction mechanisms 14 p2407 A67-28549

Variational integration principles used to integrate wave and Fourier thermoconductivity equations, noting solution by Ritz method 14 p2408 A67-28803

Space-time region division method for reducing nonlinear heat conduction to subordinate linear multilayer system problems, assuming stationary time characteristics and coordinates 14 p2408 A67-28804

Steady state heat conduction approximation solution based on effective boundary conditions concept 14 p2408 A67-28805

Lattice thermoconductivity noting local equilibrium hypothesis theory, thermal resistance mechanism, etc 14 p2374 A67-28981

Thermal lattice conductivity at high temperatures in compound semiconductors, linking dilatation coefficient of molecular theory to ionic nature of interatomic bonds 14 p2374 A67-28984

Thermal and electrical conductivity equations for constricted water-cooled arc 15 p2523 A67-29229

Monte Carlo method applied to heat conduction problems, discussing steady state and transient situations with linear and nonlinear boundary conditions [ASME PAPER 65-WA/HT-1] 15 p2578 A67-29318

High accuracy alternating direction implicit difference schemes for biharmonic, heat conduction and Laplace equations 15 p2510 A67-29520

Acceptance criteria of space materials, discussing materials for surveyor 15 p2508 A67-29559

Thermal conductances in collisionless gas between coaxial cylinders and concentric spheres obtained for arbitrary thermal accommodation coefficients 15 p2579 A67-29566

Traveling ionospheric disturbance heat conduction waves excited in neutral gas of thermosphere by hydromagnetic waves from magnetopause 15 p2475 A67-29617

Composite valence band in p-PbTe obtained from measurement of Hall effect, thermoelectric and optical effects 15 p2538 A67-29793

Variational principle for heat conduction and convection, noting applicability to nonhomogeneous fluids with temperature dependent properties in turbulent flow 15 p2582 A67-30019

Thermal conductivity variation of double-base solid propellants under acoustic irradiation compared with polymethyl methacrylate 15 p2545 A67-30199

Viscosity and thermoconductivity values of partially ionized argon plasmas derived by investigating temperature decay and stream velocity distribution in argon plasma jet 15 p2531 A67-30203

Electric and thermal conductivity and Hall effect in solid solution of complex semiconductors noting temperature dependence 16 p2729 A67-31155

Deformation effects on thermal conductivity, microhardness, and thermal EMF of annealed bismuth telluride bars 16 p2730 A67-31160

N-type InSb electron thermoconductivity temperature dependence, lattice thermoconductivity and thermal resistance 16 p2730 A67-31163

SnTe samples under uniform load studied for relation between electrical and thermal conductivity, thermal EMF and microhardness 16 p2730 A67-31165

Solution of uniform heat conduction equation with movable boundaries applied to problem of electric contacts 16 p2779 A67-31207

Thermal conductivity of group of molten and solid chalcogenides at various temperatures, estimating heat transfer mechanism role 16 p2731 A67-31388

Plane shock wave reflected from heat-conducting wall analyzed by method of matched asymptotic expansions 16 p2662 A67-31555

Electrical and thermal conductivity and integral degree of blackness of tantalum at temperatures above 1000 degrees C 16 p2692 A67-31771

Heat transfer, thermal conductivity and thermal diffusivity of loose fibrous materials under vacuum 16 p2780 A67-31772

Heat conductivity coefficient of cesium vapor at temperatures from 1000 to 1600 degrees K and 1 to 5 torr measured by hot tungsten filament method 17 p2895 A67-32156

Thermal conductivity coefficient experimentally determined for argon plasma at atmospheric pressure and temperatures from 10,000 to 13,000 degrees K 17 p2895 A67-32157

Thermal conductivities below one degree K of various very pure metals, noting normal and superconducting states 17 p2912 A67-32265

MHD generators theory and operation including superheat conductivity, strong magnetic field generation and MGD flow structure in ducts 17 p2803 A67-32335

Thermal conductivity relation to density and temperature for normal hydrogen in dense gaseous and liquid states 17 p2969 A67-32446

Heat transfer bibliography covering boundary layer, phase change, two-phase flow, channel flow, conduction, liquid metal, MHD, etc 17 p2969 A67-32450

Thermal properties of anomalous superconductors, considering specific heat jump to normal state and thermal conductivity behavior 17 p2914 A67-32453

Upper atmosphere ion temperature profile transitional behavior analyzed by fractional separation in terms of energy budget, including multiple ion effects 17 p2843 A67-32531

Temperature dependence and order of magnitude of barium titanate and strontium titanate determined from three-phonon diffusion process 17 p2915 A67-32706

Low temperature thermal conductivity measurement of fast-neutron-irradiated silicon and germanium, showing difference between bombardment induced scattering in two materials 17 p2919 A67-32855

Unsteady heat transfer between solid body and surrounding fluid flow, using convective fluid heat transfer and body thermoconductivity equations 17 p2972 A67-33071

Static /time-discrete/ electrical model for mathematical analogy of heat transfer processes and application to solution of nonlinear heat conduction

equations 17 p2821 A67-33079

Combined electrical modeling technique for solution of two-and three-dimensional problems of unsteady heat conduction 17 p2973 A67-33081

Unsteady heat conduction and transfers by electrical simulation methods, determining temperature field in canonical metal bodies 17 p2973 A67-33082

Apparatus for measuring temperature dependence of thermoconductivity coefficient, thermal EMF and specific electroresistance of cermet cylindrical shells 17 p2861 A67-33171

Modified hot-wire thermal conductivity cell for measuring effects of finite length, pressure and temperature on heat transfer from wire in rare gases 17 p2863 A67-33357

Electronic contribution to thermal conductivity of pure type II superconductor in high magnetic field, noting rapid conductivity drop and strong anisotropy 17 p2925 A67-33376

Changes in InSb, GaSb and Te crystal lattice structure and chemical bonds investigated for effects on thermoconductivity, thermal EMF and microhardness 18 p3096 A67-33451

Unsteady temperature field of thin cylindrical shell of finite length determined, using quadratic trinomial form 18 p3145 A67-33570

Inhomogeneous temperature field arising during laser welding of different materials with imperfect contact, deriving and solving heat conduction equations 18 p3053 A67-33630

Critical reaction rate for ignition, temperature rise and induction period for various geometries calculated for conductive theory, including reactant consumption 18 p3156 A67-33850

Lunar thermal history computed for different radioactive elements distribution 18 p3119 A67-33862

Value analysis technique to compare competing high performance insulation systems on basis of differences in performance and cost [AIAA PAPER 67-469] 18 p3162 A67-33939

Transient heat conduction in inhomogeneous solids with periodic temperature boundary conditions, using Keller perturbation method 18 p3159 A67-34007

High pressure vortical discharge in air and argon, solving differential equations for heat conduction and electromagnetic field by digital computer 18 p3088 A67-34062

Finite propagation velocity in heat conduction, diffusion and viscous shear motion, studying assumptions of differential equation derivation 18 p3159 A67-34070

Classical hydrodynamics equations accounting for dissipative processes 18 p3027 A67-34089

Two-dimensional self-similar hot conducting gas outflow into vacuum, for power law variation of gas-vacuum interface temperature 18 p3028 A67-34269

Thermal conductivity and degree of blackness of aluminum oxide coatings at high temperatures, using argon plasma jets 18 p3161 A67-34473

Steady state technique for measuring high temperature thermal conductivity of nonmetallic materials requiring heat flux and temperature gradient calculation 18 p3051 A67-34508

Thermoelectric and galvanomagnetic measurements on p-type bismuth compound, explaining anomalous rise in Hall coefficient with temperature and effective mass ratios change 18 p3105 A67-34632

Active thermal insulator technique for long term cryogenic storage 19 p3207 A67-34836

Combustion rate and subsurface activity of metallized burning polymers, stressing heat conduction role and applications to propellant combustion [CI PAPER 67-3] 19 p3344 A67-34998

Thermal conductivity of nitrogen plasma in cascade arc, solving Elenbaas-Heller equation 19 p3287 A67-35358

Thermal conductivity ionization coefficient of cesium plasma at high temperature and low pressure 19 p3287 A67-35359

Semiconductor thermoconductivity increase due to illumination on one face by radiated energy 19 p3304 A67-35461

Insulating foams at liquid hydrogen

temperature, describing methods for measuring thermoconductivity, specific heat and density 19 p3346 A67-35567

Finite difference heat conduction method for surface subliming processes in space vehicles 19 p3346 A67-35755

Steady state heat transfer by simultaneous conduction and radiation through spherical shell

[ASME PAPER 67-HT-20] 20 p3546 A67-36715

Analytical method yielding solutions for transient steady heat conduction in bodies with arbitrary boundary and initial conditions

[ASME PAPER 67-HT-44] 20 p3547 A67-36726

Variational formulation of Laplace transformed heat diffusion problem

[ASME PAPER 67-HT-77] 20 p3551 A67-36755

Size and longitudinal conduction influence on wall temperature field and effectiveness of heat exchangers determined by differential equations

[ASME PAPER 67-HT-80] 20 p3551 A67-36758

Theoretical prediction of temperature profiles within heated cylinder and on surface to determine thermal conductivities at high temperature

[AIChE PAPER 16] 20 p3552 A67-36829

Heat transfer of gas between parallel plates including radiation and rarefaction effects treated, using kinetic theory 20 p3553 A67-36935

Viscosity, heat conduction and diffusion coefficients for two-temperature three-component plasma 20 p3500 A67-37049

Unsteady transverse diffusion of passive impurity and mass and heat transfer in granular layer described by cell type models 20 p3554 A67-37054

Optimal geometry of certain isolated heat-conducting circular fins cooled by radiation 20 p3554 A67-37067

Transient temperature distribution for spherical region subjected to variable heat flux at boundary represented by terms of known functions and quadratures 20 p3555 A67-37610

Heat conductivity in materials ascribed to phonons, noting phonon radiation effects 20 p3515 A67-37715

Turbulent gas flow viscosity, thermoconductivity and friction coefficients in tube 21 p3611 A67-37912

Electron components for electrical, thermal conductivity and viscosity coefficients of gas mixtures calculated via molecular kinetic theory 21 p3659 A67-38161

Thermal conductivity coefficients of refractory materials at high temperatures determined by measuring one-dimensional stationary thermal flux at single point 21 p3731 A67-38168

High temperature gas transport property estimation with chemically reacting gas mixture conduction 21 p3613 A67-38391

Spatial electron temperature distribution in electrodeless discharge, noting thermal conduction effect 21 p3672 A67-38721

[AIAA PAPER 67-692] 21 p3672 A67-38721

Energy transfer and electron conduction in nonequilibrium argon arc column at one atmosphere

[AIAA PAPER 67-693] 21 p3672 A67-38722

Compressible turbulent boundary layer equations, discussing third order correlation terms role and eddy thermal conductivity definition 21 p3614 A67-38894

Binary gas mixtures transport coefficients calculation, comparing experimental and theoretical values of viscosity and thermoconductivity dependent upon interaction between unlike molecules 21 p3733 A67-39064

MGD boundary layer flow for thermally conducting flat plate, deriving equations for any heat transfer condition 21 p3675 A67-39090

Computer program charts for investigation of effect of temperature dependent thermal conductivity on transient temperature distribution of heated materials 22 p3916 A67-39481

Thermal conductivity measurements of insulating materials at cryogenic temperatures ASTM Conference, Philadelphia, February 1967, Committee C-16 22 p3802 A67-40289

Guarded hot plate technique for measuring thermal conductivity of low conductivity materials at cryogenic temperatures 22 p3802 A67-40290

Guarded hot plate apparatus for measuring thermal conductance of multilayer cryogenic insulation under vacuum conditions 22 p3802 A67-40291

Thermal conductivities of cryogenic insulation systems determined by two methods using calorimetry measurement of boil-off rate of liquid cryogen 22 p3802 A67-40292

Heat flow meter apparatus for rapidly measuring thermal conductivity of flat insulation specimens under cryogenic temperatures 22 p3802 A67-40293

Double-guarded cold plate apparatus for measuring thermal conductivity of multilayer insulations, powders, fibers and foams 22 p3803 A67-40294

Cryogenic insulation thermoconductivity measuring apparatus operable at high vacuum and nonsteady state conditions 22 p3803 A67-40295

Guarded cold flat plate calorimeter for measuring insulation thermoconductivity 22 p3803 A67-40296

Calorimeter for evacuated multilayer insulation materials to evaluate performance and measure heat transfer rate and thermoconductivity 22 p3803 A67-40297

Cryogenic thermoconductivity heat flow meter apparatus for felt, powder and block materials at atmospheric pressure 22 p3803 A67-40298

Recovery time of carbon dioxide laser excited by electric pulse discharge noting heat conduction toward walls 23 p4011 A67-40692

Thermal conductivity of clean and dirty type II superconductors, discussing finite temperature gradient effect on niobium 23 p4036 A67-40704

Radiative and convective heat transfer between solid body and heat generating medium in motion, calculating thermal conductivity 23 p4083 A67-41289

Kinetic prediction theory for viscosity, thermal conductivity and diffusivity of binary liquid mixtures composed of molecules interacting with square-well potential 23 p4083 A67-41531

Solution for coupled system of parabolic partial differential equations describing reactants diffusion and heat conduction in gas phase 23 p4048 A67-41764

Book on thermoelasticity associating elasticity and heat conduction theories for thermodynamics of irreversible processes and differential equation problems 24 p4246 A67-41891

Frequency dependence of attenuation coefficient for longitudinal ultrasonic waves in InSb over range 50 to 210 MHz for temperatures between 200 and 600 degrees K 24 p4202 A67-41980

Ionospheric thermal conductivity effect on gravitational wave propagation 24 p4150 A67-42140

Rarefied gas mixtures viscosity and heat conduction temperature dependence calculated, analyzing empirical relations 24 p4142 A67-42220

Temperature field within multidimensional body in nonlinear heat conduction process in terms of known temperature distribution along coordinates 24 p4254 A67-42254

Surface temperature oscillations of externally cooled working blades of gas turbine with air-liquid mixtures 24 p4254 A67-42255

Book on mechanics of continua covering elasticity, fluid dynamics, heat conduction, thermoelasticity and viscoelastic materials equations 24 p4189 A67-42382

High temperature polyatomic gas and gas mixture transport properties, discussing thermoconductivity, multiple intermolecular potentials and plasmas 24 p4256 A67-42742

Neutron irradiation effect on thermal conductivity of silicon at low temperature noting annealing stage 24 p4206 A67-43110

THERMOCONDUCTIVITY GAUGE

New thermal radiative flux gauge utilizing thin film resistance thermometer and short duration test techniques 11 p1792 A67-24821

Temperature, pressure and density change effects free thermal conductivity gauge system for upper atmosphere pressure measurements 22 p3829 A67-40470

THERMOCOUPLE

SA COUPLING

SA TEMPERATURE MEASUREMENT

Liquid metal level measurements using

thermocouple type probes as tank sensors, noting usage of electrical resistance of probe sheath 01 p0070 A67-11027

Thermocouple errors resulting from heat conduction along thermocouple wire embedded in low conductivity ablative material indicate helicoil wire for optimum design 01 p0071 A67-11104

Ultrahigh temperature thermocouple using pure and boron-doped pyrolytic graphite or tungsten and rhenium for operation in vibration and oxidation environment 01 p0076 A67-11139

Time constants of thermocouples as function of parameters on which they depend, using schlieren phenomena 04 p0624 A67-15417

Temperature perturbations produced by internal sensors embedded parallel to heated surface of low conductivity material [ASME PAPER 66-WA/HT-8] 04 p0724 A67-15427

Design and operation of reference temperature compensator in thermoelectric temperature gauge 09 p1496 A67-21690

Mineral insulated thermocouple applications in nuclear reactor, automobiles, steel, concrete, plastics, textiles, ceramics and heavy machinery 10 p1656 A67-23080

Thermoelectric power of thin layers of bismuth in thermocouple with solid copper 12 p1978 A67-25151

Reduction of radiation effect on thermocouple in thermal vacuum testing by using fiberglass tape with aluminized mylar backing 12 p1943 A67-25695

Temperature field distortion in region of thermocouple junction which arises when thermal conductivity of junction differs from object whose temperature is to be measured 12 p1943 A67-25754

Nozzle thermocouple for low flow rate measurement of high temperature gases, discussing calibration curves and taking into account Reynolds number effect 13 p2121 A67-27464

Dynamic thermocouple for measuring plasma temperature up to 4000 degrees C, deriving relations for heating curve as function of time 17 p2854 A67-32162

Response of bare wire thermocouple to temperature variation in jet engine intake, noting temperature pickup selection for desired response 17 p2859 A67-32589

Copper-constantan and chromel-copel microthermocouples installation in capillary tubes for measuring coolant temperature 17 p2860 A67-32831

Temperature and thickness effect on thermoelectric power by calibration curves of bismuth in thin layers, determining mean free path 18 p3102 A67-34188

Thermocouple drift on Chromel-P vs Constantan under vacuum, high temperatures and time factor conditions 18 p3052 A67-34516

Soviet book on high temperature nonmetallic thermocouples and sheaths covering thermal control automation of metallurgical processes, thermoelectric and refractory properties, electrodes, electromotive force, etc 19 p3227 A67-34922

Tungsten-rhenium thermocouple systems evaluated for high temperature measurement 20 p3443 A67-36515

Thermocouple surface temperature measurement errors in space simulation chambers due to heat conduction and radiation of wires

[ASME PAPER 67-HT-57] 20 p3447 A67-36739

Series/parallel connection of redundant elements in thermopile shown to increase reliability of array over simple series of thermoelectric elements 20 p3363 A67-36958

RF power meter design having coaxial thin film thermocouple in-line detector to sample incident power 21 p3589 A67-37916

THERMOCOUPLE GAUGE

Thermal differential method of determining critical points in flow past projection in pipe 11 p1741 A67-24032

Pyroelectric heat-transfer sensor performance compared with thin skin thermocouple heat sensors, noting discrepancy in measurement results in severe environment 11 p1790 A67-24453

Differential thermocouple device design for temperature measurements from 300 to 450 degrees K 11 p1793 A67-24866

Cryostat, combination device for test and calibration of gauges for cryogenic

- temperature 12 p1938 A67-25187
- Semiconductor surface thermocouples, determining heat-transfer rates associated with wind tunnel testing 18 p3048 A67-34103
- THERMOCOUPLE PYROMETER**
- Expected change in output voltage when W/W-26Re thermocouple is exposed to thermal neutrons, causing Re atom transmutation to Os 15 p2535 A67-29489
- Chromel-alumel thermocouple for high enthalpy gas flow temperature measurement, discussing design and measurement accuracy 23 p4081 A67-40569
- THERMODYNAMIC COUPLING**
- Variable laminar boundary layer equations for air flows over flat plate with injection of foreign gases through solid surface 06 p1116 A67-18380
- THERMODYNAMIC EFFICIENCY**
- Regenerative thermomagnetic power devices, considering state equations for ferromagnetic material, power cycle and entropy change due to magnetization [ASME PAPER 66-WA/ENER-1] 04 p0555 A67-15414
- Fin efficiencies in n-core stack heat exchanger [ASME PAPER 66-WA/HT-47] 04 p0724 A67-15432
- Entropy and available energy in operation of gas turbine, considering thermodynamic efficiency, heat balance and available energy balance 05 p0873 A67-16742
- Thermodynamic flow analysis of feasibility of coolant gas addition to nozzle flow for improved particle formation efficiency in mixed flow colloid thruster [AIAA PAPER 67-85] 06 p0941 A67-18500
- Thermodynamic cycle for solar power systems using hexafluorobenzene as working fluid, discussing efficiency and radiator area 07 p1131 A67-19366
- Optimum conditions for MHD power generation with Joulean dissipation derived from first and second law of thermodynamics 09 p1442 A67-21799
- Thermomagnetic generator with resonating current in load circuit to improve thermodynamic performance 09 p1452 A67-22697
- Miniature cryogenic refrigeration systems design for masers and parametric amplifiers, investigating efficiency and contamination 14 p2277 A67-27775
- Regenerative thermomagnetic power devices, considering state equations for ferromagnetic material, power cycle and entropy change due to magnetization [ASME PAPER 66-WA/ENER-1] 18 p2989 A67-34128
- MHD generators using liquid metals examined for advantages/limitations, discussing loop design 19 p3268 A67-35063
- THERMODYNAMIC EQUILIBRIUM**
- Steady state flows without external forces becoming parallel in thermodynamic equilibrium at distance from body, noting relations between drag, shear, heat transfer, entropy, etc 01 p0005 A67-10281
- Thermodynamic equilibrium of binary channel with noise at fixed temperature 03 p0372 A67-14057
- Radiation transfer effect on equilibrium temperature for laminar boundary layer flow of absorbing-emitting gas over flat plate [ASME PAPER 66-WA/HT-48] 04 p0739 A67-15940
- Shanlavskii multiply ionized gas model for theoretical calculation of thermodynamic equilibrium parameters of shock tube 05 p0790 A67-16249
- Heat emission from compression shock layer about meteors in thermodynamic equilibrium 05 p0903 A67-17313
- Local radiation equilibrium temperatures in semigray enclosures, with reference to thermal design of spacecraft [AIAA PAPER 67-211] 06 p1115 A67-18327
- Photometric measurements on deviations from equilibrium state in burnt gases of laminar premixed shielded flames at atmospheric pressure 06 p1072 A67-18345
- Equilibrium air study extended to reentry speeds up to 70,000 fps, using transport and thermodynamic properties to examine stagnation point convective heat transfer including blowing rates 06 p0943 A67-18843
- Thermodynamic equilibrium composition of Venus atmosphere computed from atomic composition deduced spectroscopically 07 p1256 A67-20022
- One-dimensional adiabatic equilibration of plate with starting temperature compared with nonadiabatic equilibration and exoatmospheric cooling of cylindrical metallic and plastic shells 08 p1429 A67-21527
- Normal temperatures for optically thin plasma in state of local thermodynamic equilibrium 09 p1536 A67-21557
- [DVL-644] Excitation-recombination statistics in semiconductors with donor and center interacting with both bands for given thermal disequilibrium, treating silicon 09 p1551 A67-21669
- Thermodynamic equilibrium composition of all combinations of C, H, O and N at average pressure and temperature calculated for atmospheres of earth, Venus, Mars and Jupiter 09 p1566 A67-22236
- Thermal equilibrium method for calculating parameters of plasma arc in atmosphere of hydrogen, air and air containing 0.1 percent sodium vapor 09 p1546 A67-22315
- Heat radiative flux divergences and equilibrium temperature distribution with altitude calculated for heat regime modeling radiative transfer conditions in stratosphere and mesosphere 10 p1647 A67-23275
- Derivation and computer method solution of equations describing thermodynamic equilibrium of gaseous products from oxidative combustion of methane 11 p1881 A67-24023
- Homogeneous solar photosphere and lower chromosphere model in hydrostatic and local thermodynamic equilibrium, reproducing continuous and line spectrum 11 p1858 A67-24112
- CH molecule solar spectral observations interpreted using several upper photosphere models and assuming local thermodynamic equilibrium approximation 11 p1861 A67-24495
- Electron and ionic temperatures from incoherent diffusion spectra, noting dependence on height and permanent thermodynamic equilibrium below 130 km 12 p1931 A67-25108
- Plasma equilibrium from gas discharge, role of electron concentration and contributions of excited atom transitions and quenching collisions 12 p1977 A67-26132
- Negative-ion gas laser with thermal excitation 13 p2125 A67-26386
- Orthogonal polynomial method to determine distribution function for equilibrium of single species two-temperature gas mixture 13 p2102 A67-26972
- Heat leak and pressure decay for single phase cryogenic storage in nonequilibrium calculated for spherical tanks, using simplifying assumptions 13 p2227 A67-27641
- Thermodynamic investigation of singularity properties of critical point of vapor-liquid equilibrium 13 p2230 A67-27725
- Relativistic thermodynamics in case of equilibrium with stationary co-moving metric and constant pocket temperature, deriving relativistic Fourier law of heat conduction 14 p2404 A67-27951
- Partition functions applicability at high temperatures 14 p2405 A67-28131
- Constant total pressure evaporation with heat reuse by built-in engine 14 p2407 A67-28623
- Decay of persistent currents in small ring-shaped superconductors due to detectable internal thermodynamic fluctuations 14 p2370 A67-28717
- Model stellar atmosphere computations predict emergent radiation spectrum 14 p2392 A67-28993
- Non-LTE line-transfer problem computational methods 14 p2351 A67-28994
- Perturbation stability in thermodynamic parameters of isotropic expanding universe which contains matter and radiation in equilibrium 15 p2554 A67-29459
- Gas circulation effect on temperature field of cylindrical combustion chamber with axisymmetric heat-release and gas-velocity fields 16 p2779 A67-31395
- Equilibrium deviation occurring in plasma with variable kinetic temperature due to radiation transport within plasma volume and outflow beyond limits of volume 16 p2723 A67-31767
- Ionization outside equilibrium and relaxation of ionization in cesium seeded argon 17 p2894 A67-32152
- Droplets and bubbles in liquids studied using general thermodynamic equilibrium criteria 17 p2971 A67-33043
- Band and total emissivities estimation procedures for polyatomic molecules, discussing empirical emissivity charts and radiative exchange at local thermodynamic equilibrium 18 p3152 A67-33817
- Triatomic molecules formation and abundance in solar photosphere estimated for thermodynamic equilibrium 18 p3119 A67-33858
- Local radiation equilibrium temperatures in semigray enclosures, with reference to thermal design of spacecraft [AIAA PAPER 67-211] 19 p3344 A67-34820
- Thermally ionized cesium plasma produced containing negative Cl ions 19 p3272 A67-35084
- Quantum-mechanical treatment of free-bound approximation for eigenstates and canonical partition function for plasma system in thermodynamic equilibrium 19 p3285 A67-35345
- Plasma spectroscopy, discussing line profiles, local thermal equilibrium, methods of measuring number densities and temperatures 19 p3298 A67-35855
- Dynamical consequences of thermodynamic concept of stability within general framework of modern thermodynamics 20 p3543 A67-36428
- Gas local thermodynamic equilibrium effect on calculated thermal radiation emission [ASME PAPER 67-HT-51] 20 p3548 A67-36733
- Weakly interacting system statistical mechanics relation to macroscopic thermodynamic description, deriving entropy and absolute temperature 20 p3484 A67-36835
- Volumetric absorption coefficient effect on Rosseland equilibrium radiative heat transfer and temperature profiles in optically thick fluid flowing past flat plate 20 p3553 A67-36936
- Nitric oxide reaction with triphenylmethylperoxy radical investigated in connection with study on reversible reaction 20 p3377 A67-37138
- Ionosphere thermal nonequilibrium during sunspot minimum noting electron density and temperature measurements and daily variations 21 p3616 A67-37999
- Negative-ion gas laser with thermal excitation 21 p3642 A67-38823
- Boundary condition problem at interface between immiscible fluids investigated for nonequilibrium thermodynamics 21 p3733 A67-39065
- Classical scalar plasma with relativistic Hartree equilibrium approximation for energy, entropy and state equation noting effect of linear perturbation 22 p3842 A67-39209
- Thermodynamic stability conditions determined by potential functions of system potential at constant temperature and pressure 22 p3917 A67-39584
- Nonequilibrium thermodynamics canonical equations determination on basis of variational principle for transport equations governing irreversible processes 22 p3918 A67-39786
- Integral equation derived to relate source function for spectral line formed by noncoherent resonance scattering to thermodynamics of radiating medium 22 p3896 A67-40529
- Differential departure from thermodynamic equilibrium and electron temperature in gaseous nebulae determined by observing RF emission lines 24 p4225 A67-41825
- Temperature distribution measurements behind shock wave front in discharge tube with air and Ar indicate undisturbed thermodynamic equilibrium of plasmas 24 p4141 A67-41936
- IR C atom multiplet in solar spectrum at 10,700 angstroms, noting C abundance dependence on convective velocities and deviations from black body function and local thermodynamic equilibrium 24 p4237 A67-42655
- Correlation between entropy of envelope fluctuation of UHF radio signal and corresponding thermodynamic stability of tropospheric common volume 24 p4124 A67-42810
- Isothermal equilibrium of constant volume

gas mixture under external mass forces field deriving from time independent potential 24 p4257 A67-43113

THERMODYNAMIC PROPERTY

Nonlinear equations for equilibrium composition of combustion products from methane burned with ionizing admixtures over various temperature and pressure ranges 01 p0139 A67-10046

Thermodynamic compatibility of B, SiC, BN, boron carbide and tin nitride with various metal matrices in fiber-reinforced composites 03 p0443 A67-13429

Errors in thermodynamic functions of ideal gases determined from molecular data 03 p0536 A67-13607

Enthalpy measurement for self-binding silicon carbide at high temperatures 03 p0446 A67-13609

State variables of shock induced states, analyzing calculations based on assumption of either constant volume or pressure from structural point of view 03 p0403 A67-13717

Isobaric-isothermal potential and entropy and enthalpy formation of GaAs from emf measurements at 643-741 degrees K 03 p0498 A67-13840

Solutions for nonlinear Ginzburg-Landau equations in cylindrical symmetry for type I superconductor 03 p0499 A67-13876

Thermodynamic properties of real air, deriving expressions for expansion in isothermal-isentropic mode from subcritical temperatures to 1500 degrees K 04 p0738 A67-15914

Thermodynamic properties of superconducting thin films with interaction constant that varies with thickness 04 p0686 A67-15974

Thermodynamic properties of binary Cu-Pt alloys determined, using Knudsen effusion technique 05 p0829 A67-16473

Thermodynamic analysis of flow in gas turbines, for two-and three-dimensional boundary layers and wakes 05 p0748 A67-16745

Computer simulated calculation of simple fluid properties using Monte Carlo method 05 p0927 A67-16890

Transpiration, torsion and gravimetric effusion experiments to obtain thermal functions and approximate composition of vapors over solid beryllium chloride 06 p1071 A67-17984

Nonisothermal changes in properties and composition during chemical and physical reactions, noting application to Knudsen cell vaporization [AIAA PAPER 67-156] 06 p0956 A67-18321

Thermodynamic limits on specific work and specific impulse of adiabatic chemical engines and nuclear engines [AIAA PAPER 67-227] 06 p1029 A67-18445

Remote sensing cross-beam cross correlation methods of determining spatially resolved average thermodynamic properties [AIAA PAPER 67-149] 06 p1004 A67-18477

Density-temperature formulae for coexisting liquid and vapor and for freezing liquid para hydrogen 06 p1118 A67-18521

Existence of maximum conductivity of ionized gas mixture as function of thermodynamic parameters 07 p1225 A67-19117

Thermodynamic functions of diatomic gases with molecules in 3-sigma electron state 07 p1225 A67-19121

Thermodynamic properties of hydrogen peroxide between 273 and 2000 K, deriving equations of state 07 p1285 A67-19123

Quasi-particle ensemble theory applied to Fermi fluid, noting relation of thermodynamic properties to grand canonical ensemble 07 p1224 A67-19504

Thermodynamic processes influencing choice of rocket engine propellants 07 p1239 A67-20088

Transport of free molar energy in system in interdiffusion 09 p1581 A67-22597

Thermal equilibrium of quantum mechanical system composed of atom nuclei and electrons, using statistical method to eliminate divergence in sum of states of electron proton pair 09 p1550 A67-22664

Intrinsic viscosity of linear homogeneous polystyrenes in decalin and toluene over large temperature ranges and molecular weights 10 p1802 A67-23384

Critical point thermodynamics, refuting criticism concerning Planck-Gibbs equation 11 p1882 A67-24036

Gas turbine design, considering thermodynamic and physical properties of various Rankine-cycle working fluids [ASME PAPER 67-GT-6] 11 p1745 A67-24794

Binary van der Waals mixture near solution critical point, noting anomalous behavior of heat capacity, shear viscosity and bulk viscosity 11 p1884 A67-24990

Recovery factor associated with moving fluid temperature measurement is dependent on thermodynamic and transport properties of fluid, noting probe errors 12 p1928 A67-25353

Parameters of gas behind incident and reflected shock waves calculated, using gas dynamic and chemical equilibrium equations for one-dimensional problem 12 p1930 A67-26134

Material deformation, showing functional dependence of thermodynamic potential on state parameters in theory of plasticity, creep and relaxation 12 p1938 A67-26197

Formation of compression shocks in calorically ideal real gases with thermodynamic relaxation analyzed in closed form 13 p2094 A67-26636

Earth aerospace thermodynamic properties from 100 to 100,000 km alt predicted, considering diurnal and extreme solar activity variations for engineering applications 13 p2114 A67-26821

Short duration technique providing simulation of thermodynamic properties and composition of exhaust products of liquid and solid propellant rocket engines [AIAA PAPER 66-760] 13 p2090 A67-26843

Two-zone superconductor with nonmagnetic impurity, noting correspondence of thermodynamic values to single-zone pure state except for density 14 p2369 A67-28672

Relative enthalpy and thermodynamic properties of beryllium aluminate from room temperature to melting point 15 p2508 A67-29764

Trifluoramine oxide IR spectrum measured, determining structure, symmetry and rotational, vibrational and thermodynamic properties 15 p2433 A67-29880

Effective pair potential obtained for quantum electron gas to determine thermodynamic properties over large temperature and density range 15 p2533 A67-30383

Efficiency and thermodynamic parameters of possible closed-cycle flow schemes for base-load MHD generators 16 p2603 A67-30563

Magnetohydrodynamic liquid metal power conversion systems investigated using thermodynamic properties 16 p2606 A67-30590

Thermodynamics of injector of magnetohydrodynamic power unit using two-phase vapor-liquid metallic working fluid 16 p2607 A67-30591

Carrousel magnetoaerodynamic generator, defining equations governing development of electric and thermodynamic properties of plasma 16 p2608 A67-30599

Ionization levels and thermodynamic functions of theoretical gas mixtures composed of various highly ionized atom types 16 p2720 A67-31387

Thermodynamic characteristics and plasma parameters of lithium vapor in wide pressure and high temperature range 16 p2721 A67-31389

Temperature dependence of thermodynamic functions of polyatomic gases at high temperatures 16 p2704 A67-31391

Enthalpy measurement of anhydrous crystalline aluminum trifluoride with ice calorimeter and drop method obtaining thermodynamic properties 16 p2620 A67-31761

State equation for interpolation and computations including parahydrogen thermodynamic properties using one set of 24 coefficients for all fluid states 16 p2780 A67-31763

Nonlinear equations governing complex chemical and phase equilibria derived from thermodynamic principles and supplemented by solving algorithms and practical applications 16 p2620 A67-31815

Volatile liquid pressurization as expulsion method for storable propellants noting in-flight refueling system design parameters 17 p2953 A67-31973

Thermodynamic properties of plasmas in pressure and temperature equilibrium, showing evaluation accuracy to 4

percent 17 p2894 A67-32146

Black body radiation, pressure and temperature dependences of equilibrium composition, enthalpy, specific heat and electron density of air-carbon plasmas 17 p2894 A67-32147

Equilibrium thermodynamic and gas dynamic parameter calculation for low temperature plasma, using electromagnetic and diaphragm-type shock tubes 17 p2894 A67-32148

Local turbulent properties of shear layer derived from covariance of two crossed perpendicular beams of radiation 17 p2855 A67-32282

Formulas for potential temperatures derived from thermodynamic principles, considering four stages of reversible adiabatic transformation of humid air 17 p2844 A67-32566

Kinetic and thermodynamic conditions for detonation during chemical reaction in infinite medium involving reaction heat, thermal expansion coefficient and reactants specific volumes 17 p2809 A67-32977

Nonlinear equations for equilibrium composition of combustion products from methane burned with ionizing admixtures over various temperature and pressure ranges 17 p2927 A67-33324

Radial mass flow effect on electric arcs, obtaining higher axis temperature and enthalpy densities 17 p2910 A67-33366

Free energy, heat and entropy of formation of several semiconductors by measuring EMF 18 p3095 A67-33445

Phonon spectrum of Si calculated by Monte Carlo method, determining Si thermodynamic functions 18 p3098 A67-33629

General equation for explosion limits from unified thermal and chain theory, noting application to hydrogen and oxygen systems 18 p3156 A67-33849

Thermodynamic characteristics of equilibrium combustion products of methane-oxygen-nitrogen mixtures over wide range of parameters and compositions, using computer 18 p3159 A67-34051

MHD equation simplifications and MHD converter model for problem solving, discussing electrical and thermodynamic characteristics 18 p2989 A67-34125

Quantum statistics of high temperature plasma in thermodynamical balance, introducing effective potentials for partition function evaluation and calculating free energy 18 p3089 A67-34300

Errors in thermodynamic functions of ideal gases determined from molecular data 18 p3161 A67-34472

Enthalpy measurement for self-binding silicon carbide at high temperatures 18 p3066 A67-34474

Type II superconductors properties, studying Ginzburg-Landau equations, vortex lines, reversible magnetic behavior and irreversible phenomena in mixed state 19 p3307 A67-35868

Mean absorption coefficients for IR radiation of gases expressed as functions of gas spectroscopic and thermodynamic properties [ASME PAPER 67-HT-10] 20 p3545 A67-36708

Bubble frequency, departure diameter and rise velocity relationship in nucleate boiling 20 p3553 A67-36934

Density, morphology and melting data on extended chain linear polyethylene and high molecular weight polymethylene crystallized from melt under high pressure 20 p3474 A67-37398

Superconductors with overlapping bands, discussing copper pairing, heat capacity, critical field and ultrasonic attenuation 20 p3512 A67-37435

Magnetic properties of relativistic equilibrium plasma in magnetic field studied in Boltzmann and quantum cases, using thermodynamic functions 20 p3502 A67-37557

Existence of maximum conductivity of ionized gas mixture as function of thermodynamic parameters 21 p3659 A67-38162

Thermodynamic functions of diatomic gases with molecules in 3-sigma electron state 21 p3659 A67-38166

Thermodynamic properties of hydrogen peroxide between 273 and 2000 K, deriving equations of state 21 p3731 A67-38167

Sodium-potassium alloy thermodynamic properties and ordering, with pairing model

- for configurational entropy loss 21 p3733 A67-39106
- Motion and thermodynamic conditions of free piston ballistic compressor test gas taking into account gas leakage, viscous friction and heat losses 22 p3778 A67-39351
- Approximating method for predicting multilens exhaust geometry and thermodynamic properties with single reference engine 22 p3902 A67-39940
- Aerothermochemistry of high temperature multicomponent reactive systems, examining thermodynamic and transport characteristics and ionized and dissociated working fluid processes 22 p3921 A67-40447
- Thermodynamic properties of low temperature gaseous and liquid mixtures, discussing quantum effects in mixtures containing hydrogen isotopes and high density mixtures 22 p3921 A67-40553
- Lattice heat capacities, Debye temperatures, heat capacity, free formation energy and thermodynamic functions of groups II-IV semiconductors 23 p4047 A67-41533
- Carbon thermodynamic activity in molybdenum carbide alloyed with small additions of Fe, Ni and Ti 24 p4171 A67-41962
- Thermodynamic property of superconductors with nonmagnetic impurity analyzed using overlapping energy bands near Fermi energy 24 p4203 A67-42162
- Thermodynamic and electrical properties of MHD conversion fluid /K-seeded combustion products/ obtained by hydrocarbon fuel combustion, discussing electrical conductivity calculations 24 p4099 A67-42415
- Apollo fuel cell power system transient temperature and voltage response characteristics predicted by analytic model 24 p4106 A67-42523

THERMODYNAMICS

- SA AEROTHERMODYNAMICS
- SA CHEMICAL RELAXATION
- SA ENTHALPY
- SA ENTROPY
- SA FLUID MECHANICS
- SA HEAT TRANSFER
- SA NERNST HEAT THEOREM
- SA PLASMA PHYSICS
- SA POLYTROPIC PROCESS
- Thermodynamics of electronic carrier populations in pure or doped dissociable binary semiconductor 01 p0130 A67-10198
- Carnot cycle diagrams using heat and work as coordinates in addition to several thermodynamic variables 01 p0166 A67-10505
- Fuel cells from point of view of thermodynamics, electrochemical reaction kinetics and transport processes and state of development of representative types 01 p0013 A67-10554
- Surface effects in quasi-classical energy quantization of conduction electron subject to arbitrary law of dispersion in metallic film 01 p0133 A67-10748
- Clausius-Duhem inequality in general formulation of second law of thermodynamics 01 p0167 A67-10798
- Thermodynamics of epitaxial growth of GaAs-Ge heterojunctions in closed tube process 02 p0296 A67-11767
- Thermomolecular pressure differential in wide capillaries at low Knudsen numbers calculated, using irreversible thermodynamics 02 p0343 A67-12678
- Evaluation of Einstein conclusion that moving body appears to be cool 03 p0466 A67-12847
- Thermodynamics of metal cutting process, assuming plastic deformation accompanied by successive melting and solidification of metal area under deformation 03 p0427 A67-13192
- Thermodynamic parameters of combustible mixture and ignition system characteristics effect on energy of spark ignition of homogeneous gaseous mixture 03 p0535 A67-13396
- Wave propagation in elastic materials, noting extension to materials with memory 03 p0536 A67-13659
- Thermodynamic approach to flow phenomena based on temperature dependence of specific heat 03 p0537 A67-14304
- Entropy defect and source function in gray atmosphere thermodynamics 03 p0537 A67-14314

- Thermodynamics of shock compression of metals 04 p0637 A67-14975
- Lorentz invariance of special relativistic thermodynamics equations in inertial frame of observer 04 p0658 A67-15610
- Special relativity theory mechanical and thermodynamics laws for continuum 04 p0659 A67-15795
- Interaction between radiation and conduction and resultant total heat flux increase in plane layer studied by differential method 04 p0738 A67-15868
- Nonequilibrium thermodynamics of irreversible processes in approach based on fundamental inequality derived from second law of thermodynamics 04 p0718 A67-15925
- Stauchrohr experiments in thermodynamic acceleration process for liquid metal of MHD converter for space vehicle propulsion 04 p0560 A67-15966
- Exact expression for thermodynamic potential in reversible-transformation continuums, for isothermic case of finite deformations of homogeneous and isotropic elastic bodies without inner constraints 06 p1119 A67-18583
- Dipole-dipole molecular interaction contribution to thermodynamics and state equation of excited molecular gas, noting dissociation possibility 06 p0991 A67-18802
- Perfect thermodynamic vapor concepts and application to power conversion cycles 07 p1268 A67-19367
- Validity of Onsager-Casimir reciprocal relations with theoretical framework of macroscopic nonequilibrium thermodynamics 07 p1268 A67-19574
- Thermal turbomachines, Volume 1, Thermodynamics and fluid mechanics calculations, covering one-dimensional turbine stage theory, blade cascades, etc 07 p1127 A67-20040
- Classical macroscopic thermodynamics including entropy, equilibrium, accessibility, internal energy, absolute temperature, etc 07 p1268 A67-20277
- Free charged particles interaction with each other and neutral atoms in highly excited states effect on thermodynamic and gas dynamic parameters of shock wave propagating in cesium vapor, taking into account energy losses due to radiation 09 p1540 A67-21791
- Free cooling of thin rod in constant temperature medium, finding temperature field for thermodynamics application 09 p1579 A67-21862
- Fluid and solid temperature determination in regenerative heat exchangers at any time and location 10 p1731 A67-22726
- Heat transfer data obtained from film boiling for four liquid compositions, using flat plate geometry method 10 p1732 A67-22729
- Approximation equations of thermodynamic data of air-carbon plasma with arbitrary carbon content in atomic region 10 p1732 A67-22919
- Supersonic flow of ideal thermodynamically perfect gas from nozzle into medium at rest 10 p1591 A67-23037
- Evaluating accuracy of substitute term in Einstein equation, noting inconsistency with zero and second law of thermodynamics 10 p1680 A67-23496
- Reduced thermodynamic potentials of large classes of refractory metal carbides and nitrides 11 p1804 A67-23901
- Cosmochemical considerations, from thermodynamic viewpoint, of formation processes of earth, planets and meteorites 11 p1864 A67-24600
- LF thermodynamic energy and pressure fluctuation-dissipation theorem for open systems with dynamic turbulence 11 p1821 A67-24974
- Polytropic process of variations in state of system composed of gas and solid particles 12 p2033 A67-25317
- Thermodynamics and fluid mechanics - Conference, Liverpool, April 1966 12 p1927 A67-25345
- Thermodynamics of vortex flow in superconductors, using combination of electrical currents and thermal gradient 12 p1983 A67-25477
- Heat flow mechanisms and thermodynamics of supercritical cryogenic storage problems solved by digital computer simulation, using finite difference approximation 12 p1925 A67-25722

- Generalized hypoelasticity theory includes theory of anisotropic elasticity as special case and thermal effects 12 p2032 A67-26169
- Dispersion equations obtained for numerical forecasting of meteorological fields from basic hydrothermodynamic equations, using Reynolds stresses 13 p2149 A67-26272
- Biennial variations of zonal atmospheric circulation at equatorial latitudes analyzed using hydrothermodynamics 13 p2150 A67-26680
- Surface effects in quasi-classical energy quantization of conduction electron subject to arbitrary law of dispersion in metallic film 13 p2176 A67-26777
- Thermodynamics of elastic materials using corollary of Clausius-Duhem inequality 13 p2224 A67-27145
- Noether theorems describing continuum mechanics material applied to Hamiltonian principle for motion of piezotropic fluid or ideal gas undergoing polytropic process 13 p2105 A67-27397
- Thermodynamic possibility of thermal convection in earth mantle 13 p2117 A67-27577
- References on heat and mass transfer 15 p2580 A67-29780
- Photographic spectra of ablating plastics in thermodynamic environments related to species and temperatures in boundary layers [AIAA PAPER 66-132] 15 p2582 A67-30206
- Book on fluid mechanics and thermodynamics of turbomachinery covering application of dimensional analysis and performance laws 15 p2418 A67-30395
- Thermodynamic system design in Biosatellite program noting mission and spacecraft 16 p2757 A67-30632
- Thermodynamic evaluation of nuclear fuels, suggesting operation with deuterium-tritium and deuterium-helium mixture 16 p2702 A67-30718
- Thermodynamic aspects of energy studied in forms of localized and isotropic magnitude and motion in single direction 16 p2780 A67-31557
- Thermodynamics of MHD converter cycles with previously mixed liquid metal used as working body, discussing thermal, electrical and energetic efficiency 16 p2610 A67-31780
- Thermodynamic system for zero g venting, storage and transfer of cryogenic propellants, discussing heat exchanger 17 p2954 A67-32074
- Book on thermodynamics of irreversible phenomenon in liquid metals including Onsager symmetry relations, phenomenological theory, nuclear magnetic resonance, galvano-and thermomagnetic phenomenon, etc 17 p2968 A67-32233
- Thermodynamic analysis of thermal cycles with MGD generator and steam or gas turbine, noting thermal efficiency 17 p2803 A67-32336
- Soviet book on heat transfer and hydrodynamics in two-phase media 17 p2969 A67-32457
- Potential equations for hydrodynamic and thermoelastodynamic linear wave motions applied to linear wave motion of isotropic thermally conducting elastic solids and viscous fluids [ASME PAPER 67-APM-32] 17 p2886 A67-33159
- Soviet book on thermodynamic study of chemical bond in semiconductors 18 p3093 A67-33434
- Physical properties of semiconductors relation with energy and nature of interatomic bonds, discussing effect on elastic constant, thermodynamic functions, electric and dielectric properties 18 p3094 A67-33435
- Relativistic transformation formula for thermodynamics, with correspondence between energy change of reference system and energy change of moving body 18 p3159 A67-34119
- Soviet heat transfer bibliography covering heat conduction, convective and radiative heat transfer, mass transfer, drying processes, high temperature, etc 18 p3160 A67-34166
- Existence of entropy as consequence of asymptotic stability 18 p3160 A67-34285
- Dipole-dipole molecular interaction contribution to thermodynamics and state equation of excited molecular gas, noting dissociation possibility 18 p3029 A67-34421

Thermodynamics of ceramic systems - Conference University of London, April 1966 19 p3248 A67-34863

Knudsen cell used in mass spectrometry of thermodynamics of refractory substances vaporization 19 p3242 A67-34864

Ti-C-N system studied for stoichiometric range and thermodynamics using gas equilibration techniques, measuring nitrogen/carbon activities 19 p3248 A67-34865

Book on energy conversion covering heat engines, power sources, solar energy, SNAP generators, etc 19 p3177 A67-35892

Kinetic thermodynamics applied to real gas transport properties analysis by generalization of mean-free-path theory 20 p3543 A67-36185

Flux penetration and vortices formation in macroscopic type II superconductor shown to be favorable below thermodynamic critical field 20 p3508 A67-36426

AMICON 8000 kw plasma facility for simulating reentry environments for material and thermodynamic tests 20 p3415 A67-36551

Book on theory of energy transfers and conversions including thermodynamics and Legendre transform 20 p3484 A67-36650

Monograph on equilibrium statistical thermodynamics using quantum mechanics 20 p3554 A67-37271

Thermodynamic basis of plasticity, noting loading and unloading stress-strain relations 20 p3541 A67-37283

Thermodynamics of nonlinear materials with internal state variables, analyzing evolution equation, dynamic stability, dissipation, etc 20 p3555 A67-37563

Thermodynamic interpretation for Cauchy elasticity, showing formulation of constitutive equations in continua theories 21 p3733 A67-39085

Sign of energy gain and direction of energy flow shown invariant under Lorentz transformation for two relatively moving systems possessing equal proper temperature 21 p3733 A67-39124

Axiomatic foundation for continuum thermodynamics theory, discussing first law and second law inequality 22 p3918 A67-39741

Mathematical methods for incorporating thermodynamic data into least squares fit 24 p4177 A67-42083

Variational methods for nonequilibrium thermodynamic processes based on fluctuation theory, noting application to viscous heat conducting flows 24 p4255 A67-42554

Adiabatic constant formula which holds for ideal and real gas derived, noting application of thermodynamics and gas dynamics formulas to real gas 24 p4256 A67-42592

Validity of formula of relativistic heat transformation, discussing pressure concept definition 24 p4257 A67-43107

THERMOELASTICITY

Elastic stability theory formation by combining thermodynamic and mechanical stability 01 p0159 A67-10402

Generalization of Weber theorem for problems of coupled thermoelasticity, considering vibrations varying with time 03 p0523 A67-13502

Thin walled elastic shell response to thermal excitation [AIAA PAPER 66-84] 04 p0709 A67-14841

Steady state axisymmetric thermoelastic problems in bispherical coordinate system [ASME PAPER 66-WA/APM-12] 04 p0713 A67-15403

Boundary value problems for semilinear bars made of coupled thermoelastic material solved by new functions that are corrections to classic tabulated functions [ASME PAPER 66-WA/APM-24] 04 p0714 A67-15412

Maximum thermoelastic stress and deflection in plate or beam as function of cross sectional shape, temperature and end conditions [ASME PAPER 66-WA/APM-1] 04 p0714 A67-15426

Thermoelastic wave expansion in infinite medium discussed on basis of Duhamel-Neumann equation 04 p0715 A67-15577

Temperature induced in medium due to suddenly applied pressure inside spherical cavity investigated, using iteration method 05 p0910 A67-16148

Constitutive equations derived based on thermodynamics of irreversible processes

and coupled thermoelasticity, formulating variational and reciprocity theorems 05 p0910 A67-16165

Thermoelastic wave propagation in elastic layer with convective heat transfer between layer surfaces and surrounding medium, considering relations between temperature field and dynamic displacement 05 p0913 A67-16188

Approximation method for determining stress field of body from temperature field 05 p0914 A67-16196

Dynamic thermoelastic problem solution for body of revolution with cuts satisfying boundary conditions 05 p0810 A67-16228

Elastic plate bending mechanical analog to two-dimensional thermoelastic problem, solving thermal stresses of solid propellant grain 05 p0917 A67-16417

Thermoelastic stressed state of sandwiched plate in temperature field 07 p1261 A67-19326

Similarity relationships for study of transient and steady state thermal displacements, strains and stresses between model and prototype 07 p1262 A67-19413

Thermoelasticity theorems for harmonic vibrations of continuum, examining spherical wave propagation 07 p1264 A67-20222

Temperature distribution, stress distribution and displacement components for circular disk when temperature distribution at disk rim is step function of time, considering inertial terms in thermoelasticity equations 08 p1418 A67-20723

Magnetothermoelastic mechanism of exploding wire effect under high intensity current surge in pulsed generator for hydrodynamic and magnetoelastic pumping 08 p1354 A67-21046

Nonstationary thermoelastic stresses analyzed using photoelastic technique based on polarized light 08 p1423 A67-21334

Polynomial solutions for differential equations describing thermoelastic equilibrium of thin anisotropic plates 10 p1718 A67-23405

Moment stresses in thermoelasticity for medium described in terms of displacement and rotational vectors 10 p1720 A67-23599

Thermoelastic piecewise homogeneous bodies 12 p2013 A67-25259

Time variability of bearing clearance due to temperature and pressure treated by iterative-numerical calculation 12 p1949 A67-25330

Stochastic thermoelastic time varying boundary effect in circular cylindrical shell 12 p2022 A67-25587

Rectangular three-layer plate thermoelastic oscillations due to random pulses analyzed using series expansion 12 p2027 A67-25625

Thermo- and viscothermoelasticity foundations and problems 13 p2216 A67-26608

Unsteady thermoelastic stress calculation in plane wall 13 p2219 A67-27059

Temperature field of hollow cylinder with spatially distributed heat source, examining transient temperature distribution and thermal stresses in cylinder 15 p2574 A67-29775

Thermoelasticity of thin cylindrical shells for linear temperature distribution and temperature independent elastic constants, deriving differential equations of heat conduction 17 p2958 A67-32034

Local stress measurement technique in metals using temperature changes due to elastic deformation 18 p3141 A67-33887

Soviet book on temperature fields and stresses in structural elements of flight vehicles, giving theoretical analysis and numerical calculation 18 p3145 A67-34705

Thermal stress concentration factors for rectangular flat plates penetrated by holes 19 p3337 A67-34823

Virtual work principle shown equivalent to linear coupled thermoelasticity theory 19 p3342 A67-35763

Magnetoelasticity/magnetothermoelasticity theories concerned with externally applied magnetic field interacting effects on elastic/thermoelastic deformations of solid body 19 p3262 A67-35799

Longitudinal vibration formation by high density electric current pulses in rod, discussing thermoelastic excitation and electrodynamic radial compression 20 p3486 A67-37060

Thermoelastic coupling effect on

propagating discontinuities in stresses and particle velocities studied using characteristic method 21 p3715 A67-37893

Variationally derived finite difference equations for mixed boundary value problems of thermoelastic stress and strain 21 p3716 A67-37956

Random thermoelastic stress concentration near edge of circular cylindrical shell determined using axisymmetric formulation 21 p3718 A67-37979

Displacements and temperature accompanying deformation in unbounded thermoelastic medium determined for concentrated force and heat source, using Green functions 21 p3723 A67-38559

Three-dimensional heat conduction, heat and mass transfer and thermoelasticity problems solved by approximate method using functional parameters 23 p4083 A67-41290

Book on thermoelasticity associating elasticity and heat conduction theories for thermodynamics of irreversible processes and differential equation problems 24 p4246 A67-41891

Generalized dynamical thermoelasticity theory formulated via heat transfer equation, considering temperature/strain rate coupling effect 24 p4252 A67-41955

Coupled micropolar thermoelasticity equations using strict motion invariance conditions, presenting reciprocity and variational theorems 24 p4251 A67-42659

THERMOELECTRIC CONVERSION SYSTEM

Plasma probe measurement of distribution of electron concentration, temperature and space potential throughout entire interelectrode gap of thermoelectronic converters 01 p0012 A67-10353

Thermoelectric generator performance, materials, technology, electron transport theory and phenomenological basis of thermoelectric effects 01 p0013 A67-10555

Radionuclide generators with thermoelectric transformer for space application 04 p0559 A67-15960

Thermoelectric generator design and development for space application 04 p0559 A67-15961

SNAPPOODLE isotope thruster/electric power unit, discussing thermal analyses, thruster and electrical performance and mission applications 05 p0753 A67-16552

Thermoelectric powers and conductivities of vanadium dioxide whiskers measured from 273 to 335 degrees K 05 p0864 A67-16898

Thermoelectric generators, discussing design capabilities of SNAP series and thermoelectric materials 07 p1131 A67-19191

Hot source temperature effect upon thermoelectric energy conversion, noting efficiency of various compounds 07 p1132 A67-20286

Manufacturing process and life testing of bismuth telluride alloy based flat plate thermoelectric solar cells for near earth orbits 08 p1283 A67-20648

Voltage transformation and power/energy utilization of radiol isotopic thermoelectric generator source /RTG/ for space applications, analyzing components, inverter/convertor circuits, etc 08 p1284 A67-20694

Solar thermoelectric flat plate generator application to auxiliary power systems for incident solar fluxes from 130 to 1000 watts/square ft 08 p1286 A67-20737

SNAP-10A and SNAP-8, discussing reactor thermoelectric space power program 08 p1352 A67-21052

Thermoelectric generator modules with Si-Ge alloys, discussing material preparation and generator fabrication 09 p1445 A67-22180

Thermionic diode conversion of thermal energy into electrical energy, noting cesium plasma diodes 10 p1595 A67-22989

Characteristics of single circuit space power installation with thermoelectric converter noting capacity, temperature and heat transfer 10 p1596 A67-23019

SNAP-10A design, ground test and flight test 10 p1678 A67-23853

Thermoemission properties of ZrC powder in vacuum and in cesium vapor under thermoelectronic conversion conditions 11 p1822 A67-24033

Cesium vapor thermionic diode operation in electron-rich surface ionization mode noting transport effects 11 p1849 A67-24902

Plasma probe measurement of distribution of electron concentration, temperature and space potential throughout entire interelectrode gap of thermoelectronic converters 11 p1746 A67-25026

Improved expressions for efficiency of infinite stage thermoelectric heat pump and generator 15 p2422 A67-29639

Thermophotovoltaic conversion efficiency evaluation based on theory of photoelement operation 16 p2609 A67-31398

MHD conversion of heat into electricity noting nozzle behavior during long-lasting experiments, corrosion resistant conducting materials and electrical insulators 18 p2989 A67-34121

Input and output voltage and efficiency of thermal-to-electric energy conversion effect on fuel cells and insulation of thermoelectric generator 19 p3177 A67-35897

Open-cycle MHD generator thermal characteristics, direct thermal energy conversion into electricity and optimum front surface temperature 20 p3362 A67-36115

MHD transformation of heat energy into electricity, discussing plasmatron applications and plasma velocity and temperature measurements in MHD generators 21 p3664 A67-38236

Maximum efficiency at constant applied thermal power of thermoelectric generator noting power gain and materials employed 22 p3747 A67-39429

Book on electromechanical, direct and nuclear energy conversion covering transducer design, nuclear structure, photoelectric conversion, reactor theory, thermionic conversion, etc 22 p3749 A67-40329

Power systems for long duration missions including photovoltaic solar energy, thermoelectric, Brayton cycle and thermionic conversion systems, discussing solid state components 22 p3749 A67-40339

Planning and design of Voyager for future interplanetary flight, discussing RTG and spacecraft system redundancy 23 p4071 A67-40867

Systems optimization methodology to analyze radioisotope thermoelectric generators /RTG/ for spacecraft applications, discussing computer program 24 p4184 A67-42504

Large long-life power supply system designed for earth orbiting spacecraft, discussing radioisotope interchangeability, controlled intact reentry, etc 24 p4184 A67-42505

Cascaded and segmented thermoelectric module design, discussing SiGe and PbTe elements and performance 24 p4184 A67-42506

Thermoelectric converter designed for operation with SNAPOODLE /hybrid/ radioisotope thruster/ electric generator/, discussing test results 24 p4184 A67-42507

Integrated thermoelectric SNAP-8 Rankine power system for manned lunar base missions, studying man-system interactions effect on design criteria 24 p4185 A67-42544

SNAP-8 type reactors and shield subsystems for MORL and manned lunar base plants, discussing Rankine and thermoelectric power conversion 24 p4186 A67-42546

Thermoelectric nuclear energy conversion device operating inside reactor fuel element, discussing conversion efficiency 24 p4186 A67-42551

Advanced radioisotope thermoelectric generator /RTG/ system designs employing SiGe direct radiating power conversion subsystems 24 p4110 A67-42899

THERMOELECTRIC COOLING

Effective cooling of free electrons in plasma due to ambipolar diffusion and elastic collision with ions and neutrals 01 p0122 A67-10346

Thermoelectric /Peltier/ refrigeration technique for cooling complex electronic equipment in avionic weapon systems line replaceable units 05 p0754 A67-17454

Steady state thermal conditions in semiconductor thermoelectric cooling device 06 p1113 A67-18180

Thermoelectric cooling vs conventional cooling of electronic units 08 p1427 A67-21416

Effective cooling of free electrons in plasma due to ambipolar diffusion and elastic collision with ions and

neutrals 11 p1843 A67-25019

THERMOELECTRIC MATERIAL

Powder metallurgy techniques for thermoelectric materials particularly lead telluride, germanium bismuth telluride and zinc antimonide 01 p0099 A67-10709

Pure selenium conductivity, thermal emf and Hall effect 01 p0138 A67-11297

Thermoelectric power of series of gold films, noting thickness effect on electron diffusion and phonon drag 02 p0293 A67-11749

Thermal emf and electric conductivity in solid and liquid semiconducting copper-antimony-telluride 02 p0297 A67-11846

Thermoconductivity and thermal emf of Zn- and Te-doped GaSb 02 p0297 A67-11847

Lanthanum for germanium partial substitution effect on thermoelectric properties of single phase and homogeneous samples of GeTe 03 p0500 A67-14231

Seebeck and Hall coefficients, electrical and thermal conductivity and figure of merit measured as function of dopant concentration of n-type CuBr doped bismuth antimonide telluride 03 p0501 A67-14350

Impurity microsegregation substructure in n- and p-type bismuth telluride crystals grown according to Bridgman method, measuring electrical properties, thermal emf, Hall constant, etc 05 p0861 A67-16498

Temperature dependence of thermal emf, electrical conductivity, current carrier mobility and thermal conductivity of GeTe-GeSe solid solution 07 p1231 A67-19164

Thermoelectric generators, discussing design capabilities of SNAP series and thermoelectric materials 07 p1131 A67-19191

Resistivity, Hall effect and thermoelectric power of mercury selenide from 77 to 500 degrees K 09 p1557 A67-22556

Double valence band and thermoelectric properties of lead telluride-tin telluride solutions 10 p1688 A67-22848

Thermoelectronic properties of pure and barium-film coated face of tungsten single crystal thermoelectronic properties of pure and barium-film coated face of tungsten single crystal 10 p1694 A67-23646

Thermoelectric power of thin layers of bismuth in thermocouple with solid copper 12 p1978 A67-25151

Optimum multiscascade photocell constructing procedure from half-cells of arbitrary number, size and shape 13 p2174 A67-26370

CdSb polycrystals of different structural patterns investigated for dependence of electrical conductivity, Hall mobility and thermal EMF 14 p2372 A67-28758

Electric and thermoelectric effects in single crystals of zinc-cadmium-antimony solid solution, measuring electrical conductivity, Hall constant and thermoelectric power 15 p2540 A67-30029

Silver-gold and silver-germanium alloys tested for Fermi surface changes with alloying, using thermoelectric power measurements 16 p2731 A67-31448

Temperature and thickness effect on thermoelectric power by calibration curves of bismuth in thin layers, determining mean free path 18 p3102 A67-34188

Solar thermoelectric generator with cylindrical aluminum solar energy receiver using p and n type semiconductor materials and water cooled junctions 18 p2990 A67-34491

Thermoelectric and galvanomagnetic measurements on p-type bismuth compound, explaining anomalous rise in Hall coefficient with temperature and effective mass ratios change 18 p3105 A67-34632

Series/parallel connection of redundant elements in thermopile shown to increase reliability of array over simple series of thermoelectric elements 20 p3363 A67-36958

Anisotropy of piezothermal EMF in Si and Ge under uniaxial stress 20 p3511 A67-37147

Maximum efficiency at constant applied thermal power of thermoelectric generator noting power gain and materials employed 22 p3747 A67-39429

Carrier concentration dependence of thermoelectric power and Hall mobility of undoped and doped lead telluride explained by two-valence model 22 p3857 A67-39490

Pressure sintered GaSb-GaAs alloys investigated for densification and thermoelectric properties 24 p4204 A67-42346

THERMOELECTRICITY

SA THERMOCOUPLE

Thermoelectric current effect on stability of electric current and charge distribution in semiconductors 03 p0489 A67-13144

Electrical conductivity, Hall coefficient and absolute thermoelectric power of liquid antimonides and tellurides 03 p0495 A67-13533

Transverse magnetic field effect on thermoelectric properties of n-type polycrystals of bismuth-antimony alloys containing 0, 5, 12 and 19 percent antimony in bismuth [ASME PAPER 66-WA/ENER-4] 04 p0682 A67-15368

Mediterranean cooperation on solar energy use - General Spring Session, University of Marseille, May 1966 07 p1132 A67-20285

Thermoelectric current effect on stability of electric current and charge distribution in semiconductors 10 p1689 A67-23094

Nonequilibrium MHD plasmas investigated for electrothermal instabilities noting effect of plane wave fluctuations 12 p1972 A67-25391

Hall effect and thermoelectric power in doped, conductive titanium oxide ceramics, noting dependence on doping concentration 12 p1982 A67-25452

Thermoelectric power increase in low temperature metals not explained by residual resistivity in simple model calculation 15 p2540 A67-30096

Phonon drag part of thermoelectric power in metals formula, by assuming electron scattering description by relaxation time 16 p2731 A67-31445

Compact black body source utilizing thermoelectric heat pumping for uniform and stable temperature control 17 p2862 A67-33288

Active impurities concentration in p-type semiconductors by measuring temperature at zero thermoelectric potential 19 p3308 A67-35875

Book on thermoelectric and thermomagnetic effects in metals, semimetals and semiconductors subjected to electric, magnetic and temperature fields, discussing transport theory 20 p3514 A67-37464

Soviet papers on thermoelectric measurements and monitoring 22 p3801 A67-40212

Analogy between electric, thermal and magnetic phenomena considered in terms of molecular transfer theory, noting pure mathematical meaning with no physical content 22 p3837 A67-40213

THERMOGRAM

SA BATHYTHERMOGRAPH

Microwave thermography used to measure microwave optical field patterns, using Czerny IR thermosensitive transducer process 12 p1939 A67-25196

Thermographic method for investigation of kinetics of heat evolution 22 p3917 A67-39586

THERMOGRAVIMETRY

Radiation techniques for surface temperature measurement, considering optical and radiation pyrometers, projection thermography and photographic techniques 01 p0062 A67-10274

Thermogravimetric analysis and electron microscopy of agglomeration and chemical instability of submicron refractory dispersoids in tungsten 01 p0097 A67-10699

Molybdenum sulfide solid lubricant oxidation characteristics analyzed by thermogravimetry [ASLE PAPER 67-LC-14] 24 p4165 A67-42748

THERMOLUMINESCENCE

Lithium fluoride thermoluminescent responses to neutrons, studying first and second order kinetics of decay and phosphor experiment 04 p0685 A67-15716

Ruby laser efficiency increase, using gamma irradiation 09 p1515 A67-22430

THERMOMAGNETIC CONVERSION SYSTEM

Regenerative thermomagnetic power devices, considering state equations for ferromagnetic material, power cycle and entropy change due to magnetization [ASME PAPER 66-WA/ENER-1] 04 p0555 A67-15414

Thermomagnetic generator with resonating current in load circuit to improve thermodynamic performance 09 p1452 A67-22697

Regenerative thermomagnetic power

devices, considering state equations for ferromagnetic material, power cycle and entropy change due to magnetization [ASME PAPER 66-WA/ENER-1]

18 p2989 A67-34128

THERMOMAGNETISM

Nonlinear thermomagnetic wave theory and amplification in case of plasma instability

09 p1545 A67-22072

Galvano-and thermomagnetic phenomena in semiconductors analyzed using transient method, noting extraneous EMF influence on Hall effect

11 p1792 A67-24814

Impurities effect on electrical and thermomagnetic properties of cadmium tin arsenide

13 p2184 A67-27707

Magnetic properties of meteorites, residual thermomagnetic capacity and determination of space magnetic fields

14 p2383 A67-27926

Galvano and thermomagnetic effects in semiconductors determined by using Hall effect, resistance variations in magnetic field and Nernst-Ettingshausen transverse effect

14 p2365 A67-28314

Phenomenological theory for thermomagnetic effects in type II superconductor flux flow

16 p2724 A67-30609

Book on thermodynamics of irreversible phenomenon in liquid metals including Onsager symmetry relations,

phenomenological theory, nuclear magnetic resonance, galvano-and thermomagnetic phenomenon, etc

17 p2968 A67-32233

Thermomagnetic oscillation effect in arsenic, bismuth and antimony using cryostat, noting field strength variation

17 p2912 A67-32267

Thermal magnetic noise fluctuations reduction in superconductors below 4.2 degrees K

17 p2913 A67-32272

Transverse Nernst-Ettingshausen thermomagnetic effect in intrinsic conductivity region in InSb single crystals subjected to magnetic

19 p3300 A67-34763

Semiconductor galvano-thermomagnetic characteristics analyzed using all-metal device

19 p3228 A67-34989

Peltier and Ettingshausen effects in flux-flow state of superconducting niobium, considering contribution to entropy flow

19 p3304 A67-35535

Book on thermoelectric and thermomagnetic effects in metals, semimetals and semiconductors subjected to electric, magnetic and temperature fields, discussing transport

20 p3514 A67-37464

THERMOMECHANICS

Deformation processing of beryllium with respect to mechanical properties, economics and manufacturing considerations, examining production techniques

[SAE PAPER 660634]

01 p0078 A67-10608

Mechanical property and structural changes in titanium alloys subjected to high temperature thermomechanical treatment

01 p0095 A67-10641

Longitudinal waves in viscoelastic rod caused by sinusoidal stress applied at one end, noting temperature dependency of mechanical properties of rod

[ASME PAPER 66-WA/APM-29]

04 p0714 A67-15423

Thermomechanical energy converter for generating 500 watts, noting installation bearings testing device

04 p0559 A67-15962

High temperature thermomechanical treatment effects on VT10 titanium alloy fine structure

10 p1670 A67-23641

Fundamental field equations of continuum thermomechanics derived from balance of energy equation and entropy production inequality, using invariance

11 p1819 A67-24533

Thermomechanical theory of diffusing and chemically reacting mixture and application to elastic materials mixture subject to diffusion and heat

15 p2517 A67-29463

Mechanical property and structural changes in titanium alloys subjected to high temperature thermomechanical treatment

18 p3066 A67-34405

Thermal and thermomechanical treatments effect on structure and mechanical properties of Fe-Ni-base alloy with Al and Ti additions

19 p3247 A67-35834

THERMOMETER

SA BOLOMETER

SA RESISTANCE THERMOMETER

Environmental corrections for airborne IR radiation thermometer

01 p0063 A67-10313

Radiation losses effects on temperature measurements with transparent sheathed thermometers

03 p0426 A67-14344

Heat balance in rocketsonde semiconductor thermometers, noting dissipation constant dependence on altitude and solar radiation

13 p2117 A67-27608

Temperature Measurements Society Conference, Hawthorne, California, March 1967

18 p3050 A67-34501

Inert thermometers, discussing heat capacity and contact resistance as sources and effect and applications

18 p3050 A67-34502

THERMOMETRY

SA TEMPERATURE MEASUREMENT

GaAs semiconductor diodes for thermometric measurements in low and intermediate ranges, showing temperature dependence of injected current on emitter to collector voltage

11 p1766 A67-24650

Millidegree noise thermometry based on linewidth of Josephson radiation

22 p3865 A67-40436

THERMONUCLEAR ENERGY

Physics and efficiency of direct conversion of heat, light, nuclear, thermonuclear and chemical energy to electrical energy, avoiding mechanical

10 p1597 A67-23507

Energetic macroscopic particle production noting possible application in controlled thermonuclear power

12 p1966 A67-25252

THERMONUCLEAR EQUIPMENT

Minimum B magnetic field geometry for LF oscillations in Cs plasma of Topsy Q device

05 p0859 A67-17444

Gas discharge effects on materials employed in thermonuclear research

13 p2132 A67-26692

THERMONUCLEAR EXPLOSION

Mechanism of enhancement of Li resonance line in twilight airglow due to upper atmospheric thermonuclear explosions

06 p0998 A67-18705

Radioactivity of Cosmos III satellite after U.S. thermonuclear explosion over Johnston Island

07 p1242 A67-19112

THERMONUCLEAR PHENOMENON

Effect of low pressures on stability of plasma currents in closed hydromagnetic systems

11 p1826 A67-23877

Cooperative effect among electrons in presence of radial density gradient in cyclotron echo

11 p1836 A67-24391

Magnetic field line trajectories in toroidal stellarators, discussing rotational transforms on last closed surface and perturbation effects

21 p3662 A67-37753

THERMONUCLEAR PROPULSION

Thermoradioisotope propulsion and integrated power application to cislunar and planetary space missions

01 p0155 A67-11413

Thermodynamic evaluation of nuclear fuels, suggesting operation with deuterium-tritium and deuterium-helium mixture

16 p2702 A67-30718

THERMONUCLEAR REACTION

SA FUSION

Neutrino flux recording for temperature determination of sun interior, discussing thermonuclear reactions

01 p0152 A67-11301

Nuclear physics of neutron emission in stellar interiors, reaction rates of neutron-producing processes evaluated with optical model of nucleus and uncertainties assessed

03 p0508 A67-14315

Plasma instability as obstacle to controlled nuclear fusion noting causes, effects, forbiddenness phenomenon,

11 p1831 A67-24016

Plasma instabilities and controlled thermonuclear reactions

13 p2164 A67-26387

Relativistic velocity shock wave propagation in stellar high temperature high density plasmas with pair production, thermonuclear reactions and neutrino emissions

14 p2355 A67-27953

Experimental detection and evaluation of plasma instabilities, discussing research state in connection with thermonuclear and cosmic problems

14 p2360 A67-28556

Magnetic bottles leakage in fusion reactors, describing differences between microinstabilities and MHD

theories

16 p2724 A67-31865

Thermonuclear reactions occurring in supernova shock wave propagating through stellar envelope

18 p3136 A67-34726

Thermonuclear origin of neutron emission in theta pinch plasma, determining ion temperature from scattering of ruby laser beam

22 p3843 A67-39244

Stability of collisionless plasma with ions moving relative to electrons under electric field of ion cyclotron wave

22 p3852 A67-39989

Deuterium-tritium plasma temperature measurement using neutron detector, assuming Kerr cell ruby laser produced thermonuclear reaction heating in gas

23 p4031 A67-40892

THERMOPHYSICAL PROPERTY

Uncertainties in thermophysical properties of char-forming ablative in intense convective and radiative heat transfer environments and effect on mathematical and physics models

03 p0534 A67-13059

Thermophysical properties of glass-fiber reinforced plastics for selecting optimum structural patterns when under

04 p0708 A67-14787

axisymmetrical load

Ruby laser as energy source for measuring thermophysical properties of materials via flash technique

04 p0623 A67-15305

Thermophysical parameters of semiconductors measured with same instrument set through pulse method, for quality control application

09 p1495 A67-21655

High temperature behavior and testing techniques for refractory materials of different groups

12 p1939 A67-25321

Thermophysical properties of high temperature solid materials, Volume 3, Ferrous alloys

13 p2141 A67-27152

Book on heat transfer covering basic treatment of heat conduction, convection and radiation

14 p2404 A67-27792

Behavior study of titanium alloys of interest to aeronautics industry, stressing creep resistance

14 p2338 A67-28628

Thermal field of solid rod of uniform cross section and arbitrary profile with time dependent heat transfer

14 p2408 A67-28658

Copper phthalocyanine single crystal measurements for electric, thermoelectric and galvanomagnetic

14 p2376 A67-29086

Electrical and thermal conductivity and integral degree of blackness of tantalum at temperatures above 1000 degrees

16 p2692 A67-31771

Neutron irradiation effect on n-type and p-type semiconductors

19 p3307 A67-35874

Hall effect, resistivity, spin resonance and thermoelectric properties of poly(N-vinyl carbazole-iodine complex, demonstrating charge transfer state existence in system

24 p4205 A67-42602

THERMOPHYSICS

Book on thermophysics and temperature control of spacecraft and entry vehicles

03 p0532 A67-13032

Thermophysical properties of heat-resistant solid solution of rhenium in tungsten produced by arc melting in vacuum

12 p1956 A67-25758

Thermophysical research requirements for Venus Lander, Jupiter Entry Probe and Mercury Orbiter planetary exploration missions

24 p4227 A67-42041

THERMOPLASTIC

Fiberglass-reinforced thermoplastic production processes, discussing strength, rigidity, dimensional stability,

17 p2875 A67-31931

etc

High performance engineering thermoplastic/Polymer 360/ mechanical and electrical properties and environmental factors effects

22 p3825 A67-39858

Reinforced plastics pressed sheet materials series based on chrysotile asbestos fibers and thermoplastic resin combinations or thermoplastic and thermosetting resins

24 p4176 A67-42423

THERMOPLASTIC FILM

Theory and supporting experimental results on application of small heated film for skin friction measurements in laminar and turbulent boundary layers

16 p2659 A67-30950

Thermoplastic-resin film with UV sensitive dispersed compound for carbon-dioxide laser-radiation

16 p2659 A67-30950

photography 19 p3240 A67-35694
Recording and display programs
illustrating relative capabilities of
thermoplastic and direct electron beam on
photographic film
recording 20 p3449 A67-36984

THERMOPLASTICITY

Thermoplasticity theory of hardening
plastic material under nonuniform heating
applied to various
trajectories 05 p0911 A67-16175
Combustion and pyrolytic behavior of
thermoplastic polymer spheres burning in
quiescent atmospheres of air
[AIAA PAPER 67-103] 06 p1114 A67-18283
Thermoplasticity problem for circular
cylindrical shell subjected to arbitrary
axisymmetric heating and
loading 12 p2023 A67-25593
Mass, momentum and energy conservation
at wave fronts in coupled thermoplasticity,
noting propagation velocities for
isothermal/adiabatic
discontinuities 17 p2964 A67-33134

THERMOREGULATION**S BODY TEMPERATURE REGULATION****THERMOSETTING**

Resistance spot-welded adhesive bonds
between aluminum alloy components, using
thermosetting film
adhesive 09 p1502 A67-21688

THERMOSPHERE

Two-dimensional dynamic model of diurnal
variation of thermosphere 04 p0611 A67-14651
Midlatitude semidiurnal tide in lower
thermosphere determined from trails of
chemiluminescent vapor 04 p0615 A67-14969
Horizontal variability of properties of
model thermosphere with seasonal
changes 06 p0996 A67-18564
Large amplitude variations of intensity of
oxygen emission in night airglow and
structure of lower
thermosphere 10 p1634 A67-23051
Solar cycle variations in atmospheric
density deduced from meteor observations
and rocket measurements in mesopause and
thermosphere 10 p1638 A67-23204
Seasonal-latitudinal variations in lower
thermospheric density, temperature and
composition 10 p1639 A67-23210
High altitude atmospheric models,
discussing Harris-Priester and Nicolet
theories 10 p1640 A67-23217
Ionosphere as binary two-temperature gas
and transfer coefficients for elastic
collisions based on Boltzmann
equation 10 p1640 A67-23220
Lower thermospheric turbulence
investigated for scale size, turbulent velocity
spectra and energy dissipation
rate 10 p1643 A67-23250
Average rate of eddy mixing obtained
from some eddy transport problems in
thermosphere, noting molecular
diffusion 10 p1646 A67-23271
Eddy coefficients for diffusion and
turbulence parameters for dispersion of
vapor clouds in lower thermosphere from
vapor trail evidence 10 p1646 A67-23272
Model thermospheres, studying ducted
traveling acoustic gravity waves originating
in ionosphere 14 p2310 A67-28054
Traveling ionospheric disturbance heat
conduction waves excited in neutral gas of
thermosphere by hydromagnetic waves from
magnetopause 15 p2475 A67-29617
Lower thermosphere physical properties,
studying satellite drag for density profiles,
composition, data comparison,
etc 19 p3215 A67-35171
Lower thermosphere composition and
mean molecular weight analyzed for diurnal
and latitude effects, using mass
spectrometric
measurements 19 p3220 A67-35265

THERMOSTABILITY

Static accuracy of temperature
stabilization in thermostat increase by using
temperature dependences of heat regulators
and active resistance of output
transformer 01 p0064 A67-10424
High temperature stability of SST turbine
fuel samples from refineries and airports
[SAE PAPER 660710] 01 p0139 A67-10624
Loss in hydrodynamic thermostability of
viscoplastic material with stress tensor
deviator related to strain rate tensor
deviator 01 p0052 A67-10682
Magnetic properties of YGa and YGaGd
ferrites noting effect of increasing Gd

content 01 p0136 A67-11052
Fuel requirements for high altitude high-
Mach number aircraft noting thermal
stability, autooxidation, self-ignition, specific
heat, etc 03 p0502 A67-13015
Stabilizing effect of wall and thermal flux
temperature variations over channel length
on heat transfer coefficient of liquid
flow 03 p0536 A67-13610
Thermostability of ceramic coatings
applied to W and Mo during cooling, in
terms of temperature-dependent elastic
modulus and linear expansion
coefficients 03 p0446 A67-13638
Thermostability of WC-Co alloys,
discussing heat treatment, crack formation,
bending strength and thermal shock
resistance 03 p0447 A67-13641
Temperature autostabilization in barium
and strontium titanate solid solutions during
dielectric heating 03 p0498 A67-13707
Relaxation process leading to thermal
equilibrium behind ionizing shock waves in
argon analyzed, using optical
techniques 04 p0601 A67-14458
Steady state analysis of switching circuit
using combination of transistors and tunnel
diodes, considering temperature effect and
thermal stabilization of operating
points 05 p0772 A67-16452
Black ball radiation tables and radiative
equilibrium temperatures 05 p0838 A67-17277
Reliability and temperature stability of
metals used for contacts and
interconnections on semiconductor
devices 06 p0971 A67-18246
Thermostability of refractory materials
and effects of high brittleness on thermal
stress resistance of structural elements
under single and multiple heat treatment
and loads 07 p1198 A67-19128
Optimal conditions of thermostability of
anisotropic spherical ferrite microwave
resonator with various
orientations 07 p1153 A67-19597
Cryogenic stability, kinetics and energetics
of lower boron hydrides explored with
negative results, using mass
spectrometry 10 p1603 A67-23385
Enzymatic activity and inhibition, thermal
stability and electrophoretic properties of
induced and constitutive acid phosphatases
of *Engelmannia gracilis* 10 p1598 A67-23397
Polynomial solutions for differential
equations describing thermoelastic
equilibrium of thin anisotropic
plates 10 p1718 A67-23405
Loss in hydrodynamic thermostability of
viscoplastic material with stress tensor
deviator related to strain rate tensor
deviator 11 p1783 A67-25070
Shock front parameters in plasma
calculated from effective ratio of specific
heats and adiabatic
exponent 12 p1969 A67-25195
RC networks containing ferrite
microcomponents, noting thermal
stability 13 p2080 A67-27036
Jet fuels in U.S. and Great Britain,
chemical composition, technical
specifications, thermal stability and
corrosion effect 13 p2185 A67-27068
Discrete equilibrium temperatures of
hypothetical planet with atmosphere and
hydrosphere of one-component two-phase
system under constant solar
radiation 13 p2116 A67-27462
Porous cesium ionizer with improved
lifetime obtained by adding secondary
tantalum to tungsten powder
[AIAA PAPER 66-219] 14 p2376 A67-28124
Ruby laser with Fabry-Perot
interferometer selector studied for
wavelength and thermal stability
control 14 p2332 A67-28759
Temperature stable lubrication of
supersonic aircraft
[ASLE PREPRINT 67AM 8A-1]
14 p2328 A67-28793
Elastomeric materials thermostability in
simulated spacecraft environment tested to
obtain ignition point
values 15 p2466 A67-29545
Heat emission and equilibrium
temperature of homothermal organism
calculated using factors of surrounding
medium 16 p2617 A67-30772
Thermal plasma column instability concept
applied to determine Kaufmann Criterion,

calculating production coefficient, V-I
characteristics, etc 16 p2719 A67-31229
Wideband varactor upconverters for
satellites use, emphasizing transmission
characteristics and stability over wide
temperature range 16 p2640 A67-31531
Thermal stability and degradation of n-
hexadecane, mineral oils, and oligomers
measured as function of time and
temperature 16 p2695 A67-31754
Estimation of lower bounds to minimum
Rayleigh number inducing state of
convective motion in quasi-incompressible
fluid with temperature gradient in body
force direction 17 p2968 A67-32410
Steady state temperature field of uniform
body containing heat sources, examining
nonlinear boundary value problems of
unsteady thermal
radiation 17 p2971 A67-32870
Thermostability of ceramic coatings
applied to W and Mo during cooling, in
terms of temperature-dependent elastic
modulus and linear expansion
coefficients 17 p2875 A67-33172
Thermostability of WC-Co alloys,
discussing heat treatment, crack formation,
bending strength and thermal shock
resistance 17 p2875 A67-33174
Thermal stabilization of inverse current of
p-n junction by additional gate for minority
carriers extraction 18 p3009 A67-33478
Aircraft front windshields, discussing
thermal stability, clear vision maintenance,
bird impact, atmospheric pressure effect,
cabin pressure changes and tensile
strength 18 p2986 A67-34099
Electron conductivities calculated for
sodium-xenon and sodium-xenon-mercury
plasmas assuming local thermal equilibrium,
estimating plasma temperatures and electron
number densities 19 p3278 A67-35134
Heating rate and type effects on
stationary fluids stability, noting dependence
on critical Rayleigh
number 20 p3553 A67-36848
Convective heat transfer stability in fluid
contained in cubic chamber shown from
temperature
measurements 20 p3422 A67-37064
Optimal conditions of thermostability of
anisotropic spherical ferrite microwave
resonator with various
orientations 20 p3401 A67-37336
Electron temperature and density
distributions for helium plasma produced in
coaxial accelerator measured
spectroscopically, checking thermal
equilibrium assumption 21 p3661 A67-37752
Thermostable fibers from ordered
heterocycle amide copolymers tested for
tensile and high temperature
properties 21 p3647 A67-37872
High temperature properties of aromatic
polyimide fibers, noting thermal and
dimensional stability 21 p3648 A67-37874
Poly(phenylene/hydrazide) fibers
mechanical properties, thermal stability and
potential application 21 p3648 A67-37876
Aromatic poly-1, 3, 4-oxadiazole fiber
preparation noting thermostability, property
retention at high temperature and resistance
to hydrolytic degradation 21 p3648 A67-37877
Polycrystalline boron nitride fibers
structure, determining density, defects,
resistance, thermostability,
etc 21 p3649 A67-37886
Thermally stable polymers, discussing
synthesis and testing on pilot plant and
laboratory undeveloped
stages 22 p3825 A67-39856
150-180 watts at 1000 MHz tetrode,
examining mechanical durability and
temperature stability of metallic electrodes
and ceramic insulators 22 p3772 A67-39873
Temperature stable ferrite materials for
laminated memory arrays compatible with
integrated semiconductor drive
circuit 22 p3861 A67-39914
Vertical distribution of thermal stability in
lower stratosphere compared with
atmospheric ozone from ozone and
temperature soundings 22 p3829 A67-40471
Deriving stability and asymptotic stability
properties of temperature fields governed
by quasi-linear heat
equations 23 p4081 A67-40745
Polymeric materials for extreme
temperature emphasizing thermal
stability 23 p4021 A67-41228
Glass fiber reinforced gas turbine engine

compressor blade thermal stability for short cycle heat stress damage 24 p4249 A67-42103

Unstable radiant heat interaction between two plane parallel infinite plates of finite thickness analyzed to determine thermal stabilization processes 24 p4254 A67-42257

Temperature effect on thermostability of high temperature synthetic lubricants for turbojets 24 p4162 A67-42484

THERMOSTAT

SA CRYOSTAT

Static accuracy of temperature stabilization in thermostat increase by using temperature dependences of heat regulators and active resistance of output transformer 01 p0064 A67-10424

THERMOSYPHON

Heat transfer and circulation data for rotating mixed convection thermosyphon geometry for application to cooling certain rotating components 04 p0731 A67-15828

Cooling gas turbine blades by heat pipe effect for stationary blades and thermosyphon effect for moving blades 05 p0874 A67-16747

Heat transfer dependence in cavity of closed evaporative thermosyphon on device inclination angle and coolant filled fraction of cavity 21 p3625 A67-37913

THERMOVISCOELASTICITY

Anisotropy effect on strength of unwoven glass fiber reinforced plastic, ascertaining nature of stressed state arising at high temperature 05 p0912 A67-16183

THETA PINCH

Resonance conditions for maximum attainable induction acceleration of cylindrical plasma in space between two concentric glass tubes determined by solving MHD equations 01 p0119 A67-10168

Dense high temperature plasma produced by 30-kjoule theta pinch examined by IR maser-excited coupled resonator system [AIAA PAPER 66-151] 04 p0664 A67-14822

Plasma injected into magnetic trap with aid of conical theta pinch investigated to determine ion and electron energy, lifetime and charged particle concentration variation 04 p0668 A67-15279

Radial implosion of deuterium in theta pinch in which initial level of ionization was controlled, relating diamagnetism of plasma to mass of gas in motion 04 p0671 A67-15646

CW argon ion laser scattering in argon plasma, noting resonance and correlation between data and plasma properties 05 p0820 A67-16665

Plasma conductivity and temperature in theta pinch determined from magnetic field probe results 05 p0859 A67-17437

Faraday rotation measurement of trapped magnetic fields in theta pinch plasma, using gas laser beam 05 p0859 A67-17447

Plasma with axially varying equilibrium quantities, examining stability in theta pinch configuration via energy principle 08 p1361 A67-21132

End losses from linear theta pinch estimated from self-consistent calculation of structure of plasma and confining magnetic field 08 p1362 A67-21149

Energy coupling measurement through electrodeless discharges in coaxial tubes, discussing parameters, dynamic processes, etc 08 p1338 A67-21291

Stability of bumpy theta pinch plasma separated from vacuum by thin conducting surface 08 p1365 A67-21411

Electrodeless electromagnetic shock tube with large discharge chamber for high velocity shock waves, applying theta pinch effect 11 p1773 A67-24592

Magnetic field superposition technique for fast compression and long containment time of plasma in theta pinches 11 p1840 A67-24652

Local magnetic field, ion density flow and electric field in plasma measured downstream of theta-pinch accelerator in presence of uniform guide field [AIAA PAPER 66-155] 12 p1975 A67-25895

Relaxation effects in initially non-Maxwellian high temperature theta pinch using Fokker-planck equation for particle velocity distribution function relaxation effects in initially non-Maxwellian 13 p2163 A67-26288

Trapped magnetic field effect on hydrogen plasma parameters in theta pinch, noting density and temperature dependence on initial pressure 14 p2353 A67-27751

Drift of theta pinch plasma due to asymmetry of magnetic field analyzed, using high speed photography 14 p2357 A67-28233

Ruby laser light scattering by theta pinch plasma measured with Fabry-Perot spectrometer, noting cooperative density fluctuations superimposed on thermal density fluctuations 17 p2899 A67-32274

Radial hydromagnetic oscillation frequency of plasma cylinder, calculating g-factor and plasma mass 17 p2909 A67-33117

Holographic interferometry in fractional-fringe density plasmas, discussing sensitivity and advantages of combined method 19 p3232 A67-35691

Theta pinch plasma sheath and fields time development for relaxing radial electric field 21 p3662 A67-37754

Differential magnetic loop, density profile and gas laser interferometer measurements of beta, n and ion temperature in theta pinch operation 21 p3662 A67-37755

Probe for measuring three directional components of argon plasma magnetic field inside theta pinch conical coil, noting vortex structures [AIAA PAPER 67-659] 21 p3671 A67-38695

Optical interferometer for refractive plasma diagnosis, noting Q-switched ruby laser and pulsed arc lamp 21 p3630 A67-38768

Cooperative light scattering from density fluctuations in theta pinch plasmas, discussing peaks obtained 22 p3842 A67-39208

Theta pinch energy loss determined and electron temperatures measured, discussing Poynting flux and plasma diamagnetism decay 22 p3849 A67-39696

High beta plasmas in linear theta pinches and cusp compression devices, discussing various theta pinch and cusp experiments 22 p3851 A67-39983

Beta equals one theta pinch dynamic stabilization in all modes of m equal to or greater than one 23 p4031 A67-40793

Plasma dynamics with HF theta pinch discharges confined in magnetic field 24 p4198 A67-42575

THICK FILM

SA THIN FILM

Thick film hybrid microcircuit technology, fabrication and performance characteristics 08 p1301 A67-20790

Thick film integrated circuits drying and firing processes describing driers and furnaces for ambient air and synthesized atmospheres 16 p2641 A67-31619

Variables in screen printing and firing processes for thick film resistors affecting reproducibility 16 p2641 A67-31620

Assembly of thick film microcircuit production facility detailing equipment, materials, marketing, etc 16 p2641 A67-31621

Monolithic or thin film microcircuits design and performance limitations resolved by combining characteristics of thick and thin films 18 p3014 A67-34552

Encapsulation material and process implementation for thick film substrates noting fabrication and quality problems 21 p3596 A67-38343

THICK WALL

Dynamic stresses in thick walled spherical shell of Voigt material subjected to internal pressure load 01 p0164 A67-11174

Thick walled cylindrical shell mobility over wide frequency range, predicting vibration response based on normal mode series convergence 21 p3729 A67-39059

Hollow torus axisymmetric circumferential natural vibration eigenfrequencies and eigenmodes dependence on thickness and torus radius ratio 22 p3908 A67-39289

Blade-spar thick walled cylindrical shell deformed under elastoplastic torsion, analyzing stress-strain ratio and torsional strain and displacement 22 p3916 A67-40458

THICKNESS

S AIRFOIL THICKNESS

S FILM THICKNESS

S OPTICAL THICKNESS

S TARGET THICKNESS

THICKNESS RATIO

Optimum wedges and semicones in hypersonic viscous flow, examining effect of thickness ratio on lift-drag ratio 05 p0750 A67-17367

Supersonic flow over axisymmetric bodies with continuous or discontinuous slope solved via parametric differentiation [AIAA PAPER 67-5] 06 p0939 A67-18303

Strain amplitude and flange width-to-thickness ratio effects on dynamic buckling in modified I-beams subjected to pure reverse bending 17 p2958 A67-32030

Imperfections effect on buckling of complete electroformed spherical shells under uniform external pressure examined in rigid and soft testing 17 p2960 A67-32454

Aircraft wing drag noting relation between Mach number, thickness chord ratio, aspect ratio, airfoil shape and wing configuration 23 p3930 A67-41306

THIN AIRFOIL

Aerodynamic characteristics of thin airfoil of small camber in nonuniform flow 11 p1742 A67-24658

Effect of finite magnetic Prandtl number on hydromagnetic flow past thin airfoil 14 p2240 A67-28142

Thin airfoils in radiation gas dynamics, formulating linearized theory for plane steady motion via Fourier transform and obtaining solution for absorption coefficient 17 p2791 A67-32556

Uniformly valid approximation of two-dimensional subsonic flow along thin airfoil with blunt elliptical shape 18 p2982 A67-33663

Super-Alfvénic counterpart of transient sub-Alfvénic aligned-fields flow past airfoil 19 p3170 A67-35538

Steady flow of perfectly conducting inviscid liquid past thin symmetrical airfoil of finite conductivity in aligned magnetic field 20 p3494 A67-36146

Performance prediction of low solidity cascades from potential flow calculations 21 p3566 A67-39079

THIN BODY

MHD of thin body in oblique fields 12 p1976 A67-25939

Two-dimensional flow structure around thin body in dispersive medium, discussing flow equations and similarity law 19 p3208 A67-34901

Boundary value problems solution in steady two-dimensional compressible MHD flow past thin body 21 p3660 A67-37742

Perturbation theory for solving initial and boundary value problem in unsteady MHD flow past thin symmetrical bodies with inwardly diffusing magnetic field 22 p3850 A67-39707

Thin optimum wing contour constructing procedure having minimum wave drag in supersonic flow solved by linear approximation, obtaining numerical values for parameters 22 p3741 A67-40017

Compressible fluid with finite electrical conductivity in constant magnetic field hitting thin cylindrical obstacle, solving flow motion equations 24 p4199 A67-43080

THIN FILM

SA MAGNETIC FILM

SA PLATING

SA THICK FILM

Green function method applied to calculating resonance absorption of electromagnetic radiation for interlevel transitions in thin film 01 p0127 A67-10072

Superconductivity of nondegenerate semiconductor thin films, dependence on current carrier concentration, impurity level positions and film thickness 01 p0128 A67-10084

Variation of effective conductivity of thin metallic film with surface charge calculated by Boltzmann transport equation used with Fuchs-Sondheimer boundary conditions 01 p0130 A67-10204

Vacuum technology of thin film formation 01 p0131 A67-10298

Automatic control of evaporation and deposition of thin films under vacuum 01 p0078 A67-10299

Photon modulation of tunnel emission produced by IR irradiation of thin film semiconductor sandwich of aluminum-aluminum trioxide-tellurium-gold 01 p0131 A67-10369

Ferroelectric field effect device having drain current gate voltage characteristic reproducing hysteresis character of ferroelectric gate 01 p0036 A67-10463

Insulator 01 p0036 A67-10463

Time expansion device for photomultiplier circuit for high pulse frequency using recording system, readout, thin film memory and simulation unit 01 p0029 A67-10662

Indium arsenide thin films for field effect

transistors prepared by coevaporation, obtaining high Hall mobilities and good saturation 01 p0039 A67-10876

Attenuation characteristics of unsupported resistive thin film applied to one face of dielectric vane in microwave attenuator 01 p0039 A67-10899

Logarithmic dependence of energy losses on relativistic particle velocities in polystyrene films 01 p0125 A67-10926

Optical characteristics, including refractive indices, of thin layer amorphous titanium oxide films 01 p0115 A67-11048

Oscillation modes in film with free boundaries, determining phonon density 01 p0136 A67-11049

Ellipsometer study of anomalous absorption in very thin dielectric films on evaporated metals 01 p0138 A67-11075

Hall coefficient variation with substrate temperature of thin films of tellurium, lead telluride and antimony 01 p0138 A67-11231

Integrated ceramic printed and thin film circuitry in microelectronic technology 01 p0043 A67-11385

Vacuum evaporation of HgTe thin film, examining thermal treatment, electric properties as function of thickness, etc 02 p0280 A67-11463

Basic problems of thin film physics - International Conference, Clausthal-Goettingen, West Germany, September 1965 02 p0281 A67-11701

Nucleation theories, emphasizing relation with oriented growth of thin films condensing on solid foreign substrate 02 p0285 A67-11702

Deposition conditions effect upon growth and structure of evaporated and sputtered films and significance in relation to electrical, magnetic and mechanical behavior 02 p0285 A67-11703

Condensation mechanism and effect on physical properties of thin films 02 p0285 A67-11704

Peculiarities of substructure of thin metal films produced by condensation in vacuum studied by multibeam interferometric technique 02 p0285 A67-11706

Microstructure and microhardness of evaporated thin films as function of temperature of substrate during condensation 02 p0286 A67-11707

Interaction of crystalline film of one substance growing on surface of second substance, examining influence on film structure 02 p0286 A67-11708

Kinetics of formation of thin continuous films from isolated three-dimensional nuclei 02 p0286 A67-11709

Correlation of X-ray diffraction lines of thin films with theoretical forms of films made from large crystals in thin slabs of uniform thickness 02 p0287 A67-11714

Ti, Zr and La boride thin films by chemical conversion of thin films of these metals with gaseous boron hydrides 02 p0287 A67-11715

Substrate temperature effect on structure of evaporated alloy thin films 02 p0287 A67-11716

Internal stresses of thin metallic and dielectric films, discussing methods for stress measurement, stress models and formulas 02 p0287 A67-11717

Homogeneous elastic stresses in evaporated gallium films, noting transition from compression to tensile stress 02 p0287 A67-11718

Stresses and stress relaxation in thin oxide films deposited by various methods on glass substrates from elastic or plastic deformation at elevated temperatures 02 p0288 A67-11719

Interferometric technique for measuring thickness and optical constant of thin antimony trisulfide films 02 p0288 A67-11721

Optical properties of thin metallic films relative to electronic structure in microcrystals 02 p0288 A67-11722

Abnormal skin effect in thin films of noble metals near IR, taking into account wave penetration and magnitude of conducting electrons mean free path 02 p0288 A67-11723

Normal and abnormal optical absorption in thin zinc sulfide films with excited states in forbidden band surfaces 02 p0288 A67-11724

Optical transmission and transition in semiconductor single crystals of various unit

cells, considering bismuth tellurium sulfide 02 p0289 A67-11725

Index and thickness of absorbant thin film determined from reflection and transmission coefficients 02 p0289 A67-11727

Excitation and transport of electrons in metals studied by thin film methods 02 p0289 A67-11728

Secondary electron emission investigated by transmission and backscatter experiments with thin films, noting maximum exit depth dependence on energy 02 p0290 A67-11733

Physicochemical processes in thin evaporated films studied in terms of emf of galvanic cell with film acting as electrode 02 p0290 A67-11735

Superconductivity of second kind in thin film, considering geometry dependent upper critical fields 02 p0291 A67-11738

Critical field for second order transition of superconductor to normal state, noting effect of vortex structure 02 p0291 A67-11739

Semiconducting properties of lead telluride thin films, analyzing electron transport phenomena 02 p0294 A67-11756

Hall coefficient dependency on thickness of semiconducting thin metal films 02 p0294 A67-11757

Photovoltaic effect in thin telluride layers and in contacts between layers and various metal electrodes, noting dependence on angle of deposition 02 p0294 A67-11758

Thin layers of crystallized cadmium telluride of high electron mobility analyzed for electrical properties and photoconductivity 02 p0294 A67-11759

Electron transport through thin insulating barriers in various diodes, analyzing current dependence on temperature and film thickness for perfect and imperfect dielectrics 02 p0294 A67-11760

Surface states and additional structure in McMillan-Anderson model for Tomash effect in superconducting films 02 p0296 A67-11822

Electron angular distribution in copper and gold thin films attributed to individual close interaction scattering phenomena 02 p0297 A67-11834

Design technique predicting hot spot temperature and location in thin film circuit, determining power rating 02 p0215 A67-11972

Hybrid thin film microelectronics circuitry, using tantalum films as basis for passive components 02 p0218 A67-12107

Ceramic-based microcircuit manufacturing techniques 02 p0249 A67-12182

Continuously variable optical delay line using acoustic waves to diffract and frequency shift portion of argon ion laser beam 02 p0253 A67-12517

Low voltage photomeasurements in metal-insulator-metal films with opposing photocurrent separation 02 p0301 A67-12519

Composite metallic and dielectric insulators for high current arc electrodes 02 p0250 A67-12697

Solar absorbance and thermal emittance of aluminum coated with vacuum deposited films of aluminum oxide of various thicknesses [AIAA PAPER 65-656] 03 p0448 A67-13036

Ohm law deviation in island-structure thin metallic films and current dependence on field strength 03 p0490 A67-13159

Precision of thin film resistors and capacitors mounted on single base as affected by fabrication factors 03 p0491 A67-13242

Loss angle tangent of film capacitors with rectangular Al films and dielectric silicon monoxide interlayer 03 p0378 A67-13243

Epitaxial growth and control of low-resistivity n-type silicon layers on p-type boron-doped substrates 03 p0494 A67-13485

Cr-SiO cermet material used in precision thin film resistors for monolithic integrated circuits 03 p0381 A67-13663

Electric properties of thin ferroelectric films of barium titanate compound 03 p0498 A67-13708

Laser beam-induced recrystallization of amorphous Ge semiconductor thin films prepared by thermal deposition on glass 03 p0498 A67-13839

Texture and electric conductivity of cadmium sulfide thin films 03 p0498 A67-13868

Gennes and Werthammer method generalization, developing theory of

transition temperature of superconducting superposed films 03 p0499 A67-13874

Integrated circuits with evaporated thin film conductors, resistors and capacitors 03 p0387 A67-13999

Field effect transistor characteristics and operation 03 p0387 A67-14001

Order-disorder parameter determined from HF absorption in pure superconducting films 03 p0501 A67-14373

CdS thin film solar cells history, design, fabrication and performance 04 p0553 A67-14474

Thin film photoconverters using silicon cadmium sulfide and cadmium telluride 04 p0553 A67-14664

Quartz crystal oscillator measurements of effect of film deposition rate on resistance of chromium thin films 04 p0675 A67-14921

Topology of thin film RC circuits fabricated by depositing metallic and dielectric films on insulating substrate 04 p0582 A67-15079

Electron diffraction scanner structural analysis of Ta and Mo very thin film growth 04 p0677 A67-15101

Electron transfer in thin film tantalum-tantalum oxide diodes, noting tunnel and Schottky emission 04 p0582 A67-15106

Thin film piezoelectric transducers properties used in microwave acoustic delay lines and phonon generators for analysis of phonon-phonon interactions in dielectric materials 04 p0621 A67-15116

Vacuum deposition and mechanical properties of magnetic thin films of ferrite-borate mixtures 04 p0677 A67-15118

Velocity measurements at various temperatures made with zinc sulfide thin film longitudinal acoustic wave transducers, used on germanium 04 p0621 A67-15127

Vaporization of thin metallic films with focused laser beam, comparing theoretical and experimental results prepared by using pulsed high pressure helium-neon laser 04 p0630 A67-15478

Automatic electron beam balancing plant used for plane thin film resistor combinations provides automated electron beam machining by work conditional supplementary equipment 04 p0600 A67-15479

Electrical properties of thin and thick resistive films vacuum-deposited and nonvacuum-deposited by chemical and firing process 04 p0682 A67-15485

Three-resistor thin film network possessing minimum sensitivity to random variations in individual components compared with single thin film resistor with same terminal impedance 04 p0593 A67-15487

Wave flow of thinly layered fluid on vertical plane, noting fluid-gas interface stress 04 p0609 A67-15597

Anomalous high photoconductivity of indium antimonide thin films due to negative charge transfer to oxide surface layer during illumination 04 p0683 A67-15650

Optical self-absorption and dielectric constant of cadmium oxide thin film in case of high electron degeneration 04 p0683 A67-15655

Transient gamma ray effect on thin film insulated gate FETs compared with FETs fabricated on silicon substrate 04 p0589 A67-15717

Time-dependent response of polycrystalline cadmium selenide thin film transistor to transient high energy radiation 04 p0589 A67-15718

Strain measurement at high temperature by vacuum deposition of thin films on specimens covered with insulating layer 04 p0626 A67-15745

Anomalous photovoltaic effect in semiconductor Ge, Si, CdTe and GaAs thin films due to photodiffusion and microtransitions 04 p0685 A67-15758

Solar cell development and characteristics of Si, GaAs, CdS and CdTe types 04 p0558 A67-15955

Electron diffraction patterns for GaP semiconducting thin films deposited on indium oxide substrates, determining structure as function of film thickness 04 p0686 A67-15970

Thermodynamic properties of superconducting thin films with interaction constant that varies with thickness 04 p0686 A67-15974

Thin film deposition techniques, presenting vacuum evaporation and

- sputtering 04 p0631 A67-15992
- Vacuum deposition of thin films, noting importance of low pressure environment, with attention to diffusion and ion pumps 04 p0631 A67-15994
- Sputtered film deposition processes, investigating low pressure sputtered germanium films 04 p0631 A67-15995
- Aerodynamic detector measuring dynamic pressure distribution in laminar He jet heated by electric arc 05 p0850 A67-16035
- Tantalum thin film integrated circuits noting fabrication techniques, applications, cost and advantages 05 p0770 A67-16239
- Microwave integrated circuits combining tantalum thin film technology and beam lead devices, noting fabrication, advantages and performance 05 p0770 A67-16241
- Electric conduction through tantalum oxide thin films, showing dependence of V-I characteristics on tunneling and Schottky effect 05 p0862 A67-16525
- Optical properties of thin indium films of varying thicknesses 05 p0862 A67-16599
- Thin film refractive index and thickness calculated by ellipsometry 05 p0847 A67-16796
- Electron energy quantization phenomenon in thin film studied by using dielectric barrier sandwiched between semiconductor films of same conductivity type 05 p0865 A67-16966
- Equations for longitudinal Faraday and Kerr effects in gyroelectric thin films bounded by nonmagnetic medium, considering multiple inner reflections 05 p0865 A67-16971
- High voltage photo-emf in epitaxial zinc telluride films grown on halide substrates 05 p0868 A67-17061
- Piezoresistive elements of germanium thin films 05 p0871 A67-17481
- Thin film dielectric constant and loss tangent measured by HF capacitance meter 05 p0871 A67-17483
- Superconducting transition temperature of thin film, showing growth of temperature and decrease in film thickness due to phonon electron interaction 06 p1049 A67-17886
- Mercury telluride thin film properties and fabrication methods 06 p1050 A67-18185
- Device for controlling thickness of thin films prepared by sputtering in vacuum 06 p1003 A67-18195
- Resistivity, Hall coefficient and magnetoresistance of bismuth thin films at various temperatures, showing size dependence of effective mobilities of electrons and holes 06 p1070 A67-18985
- IR transmission measurements in single crystal thin film semiconductors, observing absorption band near plasma frequency 06 p1071 A67-18992
- Changes in giant molecule structure of polypropylene films under action of laser pulses analyzed by optical microscopy 07 p1211 A67-19169
- Effective triaxial anisotropy in exchange-coupled composite three-layered uniaxial ferromagnetic thin films 07 p1231 A67-19488
- Crystalline structure of ZnTe thin films as function of stoichiometric and growth conditions 07 p1233 A67-19645
- Film resistance effect on low impedance tunneling measurements 07 p1234 A67-20101
- Propagation coefficient of rectangular waveguide containing centrally placed semiconducting film 07 p1146 A67-20202
- Book on introduction to microelectronics including integrated circuits, thin film devices, etc 07 p1158 A67-20280
- Reciprocal time domain analysis of RC networks, thin film networks and minority carrier devices 08 p1310 A67-20340
- Nucleation during pulse remagnetization of thin films, showing domain structure of formation, growth of nuclei, etc 08 p1367 A67-20603
- SHF susceptibility of ferromagnetic thin films for constant magnetic fields far from electromagnetic resonance 08 p1367 A67-20605
- Semiconducting compounds for thin film photovoltaic devices using GaAs crystals, considering absorption coefficient 08 p1284 A67-20725
- Gallium arsenide epitaxial film on germanium obtained by vapor phase transport techniques 08 p1368 A67-20726
- Semiconductor thin film properties for photovoltaic cell applications 08 p1368 A67-20727
- Photovoltaic and photoresistant effects in cadmium sulfide thin films with recombination centers 08 p1368 A67-20728
- Copper telluride-cadmium telluride thin film heterojunction fabrication and characteristics for solar cell applications 08 p1285 A67-20730
- Solar photovoltaic cell properties and preparation using thin films of copper and cadmium telluride 08 p1285 A67-20731
- Electron and proton radiation effects on GaAs, CdS and CdTe thin film solar cells noting proton damage, estimates on cell life, etc 08 p1285 A67-20735
- Thin film circuit technology, discussing application to distributed parameter devices, cost, reliability, miniaturization, design flexibility, performance characteristics and manufacturing materials 08 p1301 A67-20789
- Thin film and semiconductor integrated circuits, discussing functional flexibility, fabrication by microengraving, isolation and computer fabrication 08 p1301 A67-20791
- Planar and sandwich resistor structures in Si thin film integrated circuits 08 p1302 A67-20793
- Surface oxide films and lifetime of vacancies in thin crystals analyzed for pure aluminum and dilute aluminum alloys 08 p1369 A67-20794
- Comparison of integrated microcircuits deposited on semiconductor and insulating substrates, noting vacuum deposition techniques 08 p1302 A67-20918
- Integrated semiconductor circuits and thin film hybrid circuits on insulating substrate developed in Europe for linear circuits 08 p1302 A67-20919
- Phase state of thin layers of vapor deposited InTe with 50-60 percent Te 08 p1369 A67-20994
- Dielectric properties including permittivity, losses, polarization, impurity conduction and forbidden bandwidths of thin films of praseodymium, cerium and neodymium fluorides 08 p1370 A67-20995
- Bibliography on thin dielectric films, interfaces and surfaces 08 p1370 A67-21188
- Surface blistering of metals due to low energy hydrogen ion bombardment, determining solar absorptance change in gold-plated specimens 08 p1343 A67-21520
- Thickness dependence of Hall constant, electrical conductivity and Hall mobility in polycrystalline thin layers of InSb 09 p1551 A67-21565
- Single crystal film structure of fcc metals evaporated in ultrahigh vacuum onto alkali halide surfaces cleaved in air and in situ 09 p1552 A67-21671
- Unusual electrode configuration for Hall effect measurements on thin films and field effect devices 09 p1472 A67-21955
- Stability of palladium oxide resistive glaze films, describing process variables affecting resistivity and TCR 09 p1473 A67-22019
- Parameter control during vacuum deposition of electronic film circuits for obtaining acceptable tolerances 09 p1503 A67-22099
- Thin film adhesion to substrate, considering effect of interposed thin film 09 p1503 A67-22100
- Evaporated thin film capacitor from silicon oxide, noting electron diffraction patterns and IR adsorption peaks 09 p1555 A67-22102
- Electrical characteristics of thin film nickel-chromium resistors dependency on variation in processing parameters including source and film composition, deposition rate, etc 09 p1555 A67-22103
- International Vacuum Congress, Stuttgart, June-July 1965, Volume 2, Part II 09 p1533 A67-22110
- Electronic carrier transport in semiconductor films, stressing active thin film devices and typical behavior 09 p1555 A67-22111
- Thin films of indium antimonide for active devices grown by various methods including atomic mixing, flash evaporation, etc 09 p1474 A67-22112
- IR absorption in high purity boron films, showing absence of absorption peaks at 2-15 microns 09 p1533 A67-22132
- Cut-off frequency, breakdown voltage and capacitance calculations for diffused junctions in thin epitaxial silicon layer for microwave diode design 09 p1556 A67-22206
- Single crystal thin semiconducting films prepared by short distance evaporation diffusion under isothermal conditions 09 p1557 A67-22573
- Millimeter microwave transmission and reflection through 50 angstrom superconducting tin and indium films near critical temperature 10 p1888 A67-22764
- Chemisorbed oxygen effect on Hall mobility and conduction electron concentration of spray deposited CdS thin films 10 p1689 A67-22910
- Thin shock layer stagnation region analysis in hypersonic flow, emphasizing lateral asymmetry for planar and perturbed axisymmetrical cases 10 p1624 A67-22936
- Electric field penetration of electrodes incorporated into theory of electron tunneling through dielectric layer 10 p1689 A67-22961
- Humidity and simulated space environment effect on various cadmium-sulfide thin film solar cells, noting degradation rates 10 p1596 A67-23163
- Vapor deposited GaAs thin film solar cells for application to solar power systems 10 p1596 A67-23165
- Analysis of current flow for different input conditions on double-gate thin film transistor 10 p1612 A67-23373
- Nonlinear dependence of current in electric field in thin semiconductor film in quantizing magnetic field 10 p1694 A67-23591
- Critical fields of thin superconducting films determined by specular reflection of electrons from surfaces 10 p1694 A67-23596
- Vapor deposition of thin films by decomposition of metallic alcoholates in luminescent discharge plasma 10 p1696 A67-23692
- Cathode sputtering thin film preparation at low pressure, describing duoplasmatron and sputron ion sources 10 p1661 A67-23693
- Magnetically coupled superconducting films, showing fluxon size as function of film thickness 10 p1696 A67-23774
- Wall creeping in thin magnetic Ni-Fe films analyzed as function of thickness, field pulse amplitude, etc, comparing results with existing theories 11 p1845 A67-23953
- Planar packaging concepts for avionics equipment systems and circuit boards developed from extensive use of microcircuits and thin film circuits [SAE PAPER 670251] 11 p1758 A67-23984
- Diagonalization procedure for Hamiltonian of ferromagnetic thin film, applying canonical transformation in direction of film thickness 11 p1845 A67-23992
- Optical transmission and electrical properties of complementary metallic meshes fabricated by formation of complement of agglomerated thin films 11 p1845 A67-24142
- Thin film thermal radiation detector noting construction, calibration, performance, error sources and advantages of pyroelectric over thin film gauges 11 p1790 A67-24454
- Depression of superconducting transition temperature in narrow tin films, noting condition for maximum microwave enhancement of critical current 11 p1846 A67-24563
- Sublimation technique applied to high mobility PbS and CdS thin film deposition under ultrahigh vacuum equilibrium conditions 11 p1847 A67-24738
- New thermal radiative flux gauge utilizing thin film resistance thermometer and short duration test techniques 11 p1792 A67-24821
- High resistivity cadmium selenide vacuum deposited films dielectric constant and electronic properties measured for different parameters 11 p1851 A67-25032
- Thermoelectric power of thin layers of bismuth in thermocouple with solid copper 12 p1978 A67-25151
- Surface and volume diffusion in thin films of system Ag-Se investigated by electron diffraction and microscopic studies 12 p1979 A67-25179
- Physics of thin ferromagnetic films - Conference, Kiev, June 1966 12 p1980 A67-25236
- Resistance of magnetic structure of Ni-Fe thin films deposited on metal substrate with anisotropic surface roughness to effect of orthogonal pulsed fields 12 p1980 A67-25238
- Spin wave theory of thin ferromagnetic films, Curie temperature decreases monotonically with decreasing film thickness

spin wave theory of thin ferromagnetic films analyzed, showing Curie temperature decreases 12 p1981 A67-25239

Magnetic characteristics of ferromagnetic thin films obtained by ferromagnetic and spin wave resonance techniques 12 p1981 A67-25241

Thermal expansion coefficient of ferromagnetic thin films compared with bulky samples by electronographic technique 12 p1939 A67-25242

Ferromagnetic film coercive force variation near supercritical state due to film thickness 12 p1981 A67-25243

Width of ferromagnetic resonance curve in nickel and permalloy thin films as function of preparation and thermal treatment techniques 12 p1981 A67-25244

Critical alternating-magnetization curves of permalloy films, clarifying theoretical experimental problems and effect of anisotropy field dispersion magnitude on curves 12 p1981 A67-25245

Electronic packaging technique in thin film technology using flip-chip bonding and MTFI techniques 12 p1910 A67-25264

Nucleation of titanium and titanium oxide thin films correlation to thickness obtained from fluorescent intensity measurement 12 p1981 A67-25276

Pore formation, lifetime and microstructure of thin electrolytic metal films under load and high temperature at grain boundaries 12 p1955 A67-25448

Trap density is lower in epitaxially grown GaAs crystals than in crystals grown by either horizontal Bridgman /HB/ or floating zone /FZ/ technique 12 p1983 A67-25457

Crystallographic anisotropy of electrical properties of thin film CdS photoresistors explained via potential barrier orientation theory 12 p1984 A67-25520

Thin film superconducting bridge behavior in microwave field noting dependence of deviation from classical rectification on frequency, power, temperature and bridge width 12 p1985 A67-25848

Microelectronics technique, particularly integrated circuits, basic theory and research 12 p1917 A67-26202

Thin film integrated circuit technology, discussing reliability, production, packaging, components, etc 12 p1917 A67-26204

Reliability and cost analysis of semiconductor integrated circuit and vapor deposited thin film IC, discussing failures and defects 12 p1918 A67-26207

High stability metal thin film resistors applied to thin film circuits, noting substrate properties and pattern design 12 p1918 A67-26209

Thin film capacitor dielectrics of silicon oxides and various metal oxides, noting influence on vacuum deposited compounds 12 p1918 A67-26210

Thin film technology and manufacturing 12 p1951 A67-26212

Thin film circular chromatography for determination of diphenylamine derivative products in propellant powders 13 p2185 A67-26425

Anomalous photovoltages in CdSe and CdS thin layers 13 p2175 A67-26429

Plane wave shielding effectiveness of thin films, using TEM mode 13 p2175 A67-26524

Anodic oxides of titanium, tantalum and niobium from thin dielectric film preparations compared, determining nature and characteristics 13 p2175 A67-26654

Anisotropy in thin dielectric films of tantalum and titanium anodic oxide from various measurements explained by transistor-like model 13 p2175 A67-26655

Lateral bipolar n-p-n transistors fabricated using heteroepitaxial films of silicon on sapphire 13 p2078 A67-28779

Nonequilibrium states in metal-to-semiconductor junction resulting from emission of high energy holes and hot free electrons in same direction 13 p2176 A67-26861

Stabilizing or destabilizing effect of electromagnetic force on liquid film flow 13 p2167 A67-26930

Oxidation of Be thin films in oxygen and carbon dioxide, noting decomposition of Be-carbide and effects of heating by electron beam 13 p2132 A67-26998

Recrystallization of Ge and Si thin films and structural changes due to electron bombardment and thermal

annealing 13 p2177 A67-27071

Sputtered beta-tantalum thin films produced in two-chamber vacuum system with applied negative anode bias voltage 13 p2177 A67-27077

Mass spectrometry of background gases composition during sputtering of tantalum films in argon glow discharges 13 p2178 A67-27078

Ferromagnetic resonance relaxation process in thin films 13 p2179 A67-27142

Uniaxial anisotropy and rotational hysteresis in thin gadolinium films 13 p2179 A67-27144

Maximeter in monitoring thin films differing in optical thickness 13 p2181 A67-27232

Transition temperature change for thin tin and thallium superconducting films after deposition of dielectric substances 13 p2182 A67-27360

Structure dependent electric properties of anodized and unanodized tantalum-tantalum oxide thin film resistors, discussing aging, heat treatment, etc 13 p2082 A67-27366

Photolithographic and metal aperture masks for integrated and thin film circuit manufacturing 13 p2124 A67-27390

Evaporated silicon thin-film transistors operating by field effect conductivity modulation of n-type inversion layer at p-type film surface 13 p2083 A67-27573

Structure and properties of thin films in terms of deposition conditions, noting conditions for continuity, surface roughness, grain size, lattice defect density, crystalline orientation, purity, etc [AIAA PAPER 66-727] 13 p2054 A67-27591

Laser beam-induced recrystallization of amorphous Ge semiconductor thin films prepared by thermal deposition on glass 13 p2185 A67-27720

Tantalum thin film resistors for integrated circuits, noting manufacture and applications 14 p2280 A67-28015

Thin film technique interconnecting integrated circuits by ultrasonic welding and multilayer thin film conductor networks 14 p2280 A67-28016

Steady state fluid flow in thin passage analyzed using energy model and including compressibility effects 14 p2302 A67-28264

Thin film passive elements for monolithic integrated circuits, using cermet and dielectrics 14 p2286 A67-28610

Thin film resistive and capacitive circuit design 14 p2287 A67-28611

Chemical deposition of dielectrics for thin film circuits and components 14 p2369 A67-28612

Evaluation method for deposited thin film interfacial interconnections 14 p2369 A67-28613

Test methods to determine wear coefficients and design calculations for solid film lubricants, covering wide temperature range [ASLE PREPRINT 67AM 5A-5] 14 p2325 A67-28787

Optical properties of thin aluminum and silver layers subjected to proton beam bombardment 14 p2373 A67-28855

Microwave frequency superconductor materials, applying bulk and thin film properties to filter, amplifier, oscillator, junction and Josephson effect devices 14 p2289 A67-28917

Measurement of resistance of thin metal films and kinetics of charge drain from surface 15 p2485 A67-29126

Tunnel diode logarithmic amplifier circuit design using thin film passive components and tiny inductors 15 p2442 A67-29166

Temperature distribution from local regions of microscopically thin film junctions of metal structures, noting effect on average temperature 15 p2444 A67-29415

Structure of thin tungsten films as function of nature and temperature of substrate, noting partial crystallization of fcc structure 15 p2535 A67-29477

Mathematical models for loss measurements in thin Permalloy films with ramp drives 15 p2536 A67-29649

Thin films as passive and active electrical components in microminaturization, noting characteristics obtained by vacuum evaporation, cathode sputtering, diffusion and epitaxial growth 15 p2447 A67-29684

Hole mobility produced by single pulses of electrons in films of polyvinyl acetate

semiconductors with sputtered gold electrodes, determining relation between film conductivity and mobility 15 p2537 A67-29703

High voltage photo-EMF in epitaxial zinc telluride films grown on halide substrates 15 p2538 A67-29792

Polymorphism in IV-VI compounds induced by high pressure and thin film epitaxial growth 15 p2539 A67-29822

Silicon nitride deposition on metal coated substrates for studying resistivity, breakdown strength and other electrical properties of thin dielectric films 15 p2540 A67-29932

Cathode sputtering, evaporation and anodic oxidation for thin film deposition in integrated circuit technology 15 p2453 A67-30066

Phenomenological theory for thermomagnetic effects in type II superconductor flux flow state 16 p2724 A67-30609

Influence of surface roughness and humidity on endurance of rubbed films of various lamellar solids on steel 16 p2681 A67-30853

Density, crystallinity and electric properties of thin metal films deposited on rotating cylindrical substrate 16 p2727 A67-30899

Langmuir-Blodgett multimonolayers of stearic acid investigated as thin film dielectric 16 p2728 A67-31020

Vacuum deposited amorphous and semicrystalline gallium phosphide film properties analyzed by electron diffraction 16 p2729 A67-31065

Book on microelectronics in U.S. covering semiconductor and thin film integrated circuits, hybrid circuits, fabrication, applications, etc 16 p2637 A67-31255

Sapphire whisker strength coated with thin metal film determined at room and elevated temperatures 16 p2694 A67-31522

Field effect behavior of thin InSb films noting semiconductor surface properties, mobility decrease with temperature and increase of impurity concentrations 16 p2732 A67-31527

Thin-film and diffused passive component comparison, describing resistor and capacitor fabrication by using sputtered tantalum and inductors through nichrome/gold 16 p2640 A67-31528

Compatible integrated circuits using thin films on silicon for application in space telemetry systems 16 p2641 A67-31559

Extreme pressure /EP/ films from lubricants containing borate esters, studying structure and mode of action 16 p2683 A67-31756

Strength and durability in friction tests of soft, vacuum deposited, thin-metal gold film lubricants, noting dependence on film-substrate interface 16 p2684 A67-31816

Refractive index of amorphous boron films determined from interference of transmission curves 16 p2734 A67-31884

Energy loss function of thin film deposited metals, using optical measurement method 17 p2913 A67-32294

Electrical design, mechanical fabrication and performance data of integrated broadband balanced transistor amplifier 17 p2825 A67-32599

Thin film single-sideband demodulator using time-varying RC networks and containing extremely selective filter 17 p2825 A67-32600

Zr-Nb alloy structure effect on critical superconductivity parameters determined, using electron microscopy of thin films 17 p2916 A67-32721

Structure and substructure effect on thin film properties, discussing vacuum deposition mechanism of metals, alloys, dielectrics and semiconductors 17 p2920 A67-32888

Theoretical concepts about coercive forces in Permalloy films, considering variations as function of applied stress 17 p2920 A67-32889

External stress effect on coercive force in Permalloy film 17 p2920 A67-32890

Structure of Ge-Sn thin films vacuum deposited on glass substrates analyzed by electron diffraction methods 17 p2920 A67-32891

Abnormally high photostresses in semiconductor films under monochromatic light studied, using angular dependence

observation technique 17 p2921 A67-32970
 Mean free path effects on critical field and density of states of small superconducting spheres 17 p2924 A67-33370
 Tunneling into thin superconducting films in magnetic field, measuring field effect on density of states for finite mean free path 17 p2924 A67-33371
 InSb-InAs solid solution thin films absorption spectra, noting band structure, temperature change and Hall EMF reduction 18 p3096 A67-33450
 Optical properties of magnesium fluoride in EUV from reflectivity measurements on crystal and thin films 18 p3099 A67-33692
 Thermal processes role in thin semiconducting and dielectric films, discussing current-voltage characteristics, thermal inertia, etc 18 p3100 A67-33766
 Evaporation of thin films of high melting point materials by focused laser beam and reflectance and relative transmittance in vacuum UV 18 p3059 A67-33885
 Thin films deposited onto substrates cooled to low temperatures investigated for transition temperature in structures of superconductor-dielectric-superconductor 18 p3101 A67-33989
 Magnetic field parallel component influence on depinning threshold of vortices in superconducting films 18 p3101 A67-33990
 Point charges interaction energy in semiconductor thin film 18 p3101 A67-34091
 Absorption, reflection and emission spectra of gold chloride at low temperatures 18 p3101 A67-34187
 Temperature and thickness effect on thermoelectric power by calibration curves of bismuth in thin layers, determining mean free path 18 p3102 A67-34188
 Nonvolatile block-oriented random access memory /BORAM/ combining thin magnetic films and scanning strain waves 18 p3012 A67-34347
 Crystallographic anisotropy of electrical properties of thin film CdS photoresistors explained via potential barrier orientation theory 18 p3103 A67-34451
 Glass semiconductor threshold switches application in memory-addressing circuits, decoding matrices and current dividers 18 p3012 A67-34489
 Thin film resistor used to improve performance of picosecond silicon integrated digital circuit with p-n junction isolation 18 p3014 A67-34551
 Monolithic or thin film microcircuits design and performance limitations resolved by combining characteristics of thick and thin films 18 p3014 A67-34552
 Slow response of cadmium selenide thin film transistors related to trapping levels in insulator 18 p3015 A67-34557
 Thin film hybrid subaudio active filter design and fabrication, discussing power consumption, circuit broadband performance, etc 18 p3015 A67-34559
 Computer method for determining time-frequency-domain response specifications of transversal linear wave filters, using thin film RC distributed networks 18 p3015 A67-34560
 Space charge limited currents in copper phthalocyanine thin films measured as function of voltage, temperature, thickness and illumination 18 p3104 A67-34626
 Currents in copper phthalocyanine thin films measured as function of temperature and ambient noting effect on conductivity, trap density, etc 18 p3104 A67-34627
 Thin films of cuprous sulfide, selenide and telluride prepared by flash evaporation, discussing resistivity and absorption coefficient 18 p3106 A67-34637
 Thin semiconductor layers, studying surface conductivity variation with semiconductor thickness and surface band curvature 19 p3299 A67-34759
 Lubrication mechanisms defined via electrodeposited solid film systems, noting porous structure formation 19 p3233 A67-34789
 Vortical structure of current and magnetic field distribution along superconducting film with magnetic field parallel to surface, discussing possible observation by optical diffraction 19 p3301 A67-34899
 Processes and instrumentation for forming contacts on microelectronics devices 19 p3236 A67-35022
 Thin superconducting films behavior in

perpendicular magnetic fields, studying sample geometry effect on reversible magnetization curve 19 p3303 A67-35041
 PbTe thin films vacuum-vaporized onto amorphous or oriented substrates studied for crystallographic properties as function of deposition temperature, film thickness, etc 19 p3304 A67-35422
 Thin CdAs films thermal deposited in vacuum on various substrates investigated for electric properties 19 p3305 A67-35577
 Indium-antimony alloy thin film preparation by vacuum evaporation, noting effect of heating and annealing on electrical resistivity 19 p3305 A67-35609
 Irradiation effect on minority carrier lifetime for p-n junction devices in epitaxial film and single crystal forms 19 p3306 A67-35670
 Electron energy spectrum, showing intensity maxima from surface plasma oscillations, noting thin films effect on surface losses 19 p3307 A67-35789
 Resistance and Hall effect measurements on PbTe thin films prepared by vacuum evaporation on amorphous or oriented substrates 19 p3307 A67-35795
 Fast thin film main memory system design noting 200 nsec cycle time and 160 nsec access time 19 p3189 A67-36063
 Thin cadmium telluride bombardment with indium ions, finding doping efficiency dependence on ion energy and temperature 20 p3504 A67-36160
 Adsorption effect of various metals on electrical conductivity and Hall effect of thin nickel films 20 p3504 A67-36166
 Miniature resonator consisting of piezoelectric cadmium sulphide transducer evaporated onto single-crystal quartz wafer 20 p3393 A67-36176
 Current saturation in evaporated gallium arsenide films observed noting temperature effect, X-ray measurements, etc 20 p3505 A67-36177
 Transport phenomena in semiconducting thin films studied using transport equation, obtaining relaxation time relationship to semiconductor 20 p3506 A67-36217
 Nonohmic electrical conduction of semiconducting thin films in strong electric fields analyzed using electron temperature approximation 20 p3506 A67-36219
 Data and theories on stationary spin waves in ferromagnetic thin layers, considering modes, dispersion law and spectra interpretation 20 p3507 A67-36318
 Theory of superconductors in plane parallel thin films, discussing energy cut-off and termination of omega summation formulations of self-consistency conditions 20 p3507 A67-36328
 Electron tunneling through thin dielectric films and damping relation to electron energy calculated, using band model and matrix methods 20 p3508 A67-36424
 Technological methods for depositing thin films in vacuum, considering evaporation, scattering, etc 20 p3453 A67-36472
 Germanium films crystallization when deposited by evaporation on silicon single crystals studied by optical microscopy and electron diffraction 20 p3509 A67-36473
 Heated thin film anemometer used to measure fluctuating velocity in airflow, noting relation of dynamic sensitivity to static calibration 20 p3447 A67-36846
 Superconducting critical temperature of sandwich of two semiconducting films in contact 20 p3512 A67-37434
 Physical properties of thin layers of cadmium telluride-metal systems analyzed for metal concentration and temperature of base at time of deposition 20 p3513 A67-37448
 Sublimation enthalpy of CdTe thin films in high vacuum determined from 350 to 400 degrees C 20 p3514 A67-37453
 Dependence of electric resistance of thin Permalloy films on substrate temperature during evaporation and vacuum heat treatment 20 p3514 A67-37555
 Thin films applications in electronic engineering - Conference, London, July 1966 21 p3589 A67-37915
 RF power meter design having coaxial thin film thermocouple in-line detector to sample incident power 21 p3589 A67-37916
 Thin film circuits for narrow band radar receivers, discussing manufacture of inductors, capacitors and LC resonant

circuits 21 p3589 A67-37917
 Quantum size effects in electric conductivity of thin films 21 p3678 A67-38099
 Charge instability problems in metal-nitride-semiconductors /MNS/ solved by using thin silicon dioxide layer between silicon nitride film and substrate 21 p3678 A67-38151
 Thin film cadmium telluride solar cells, discussing efficiencies and photoelectric properties of junction 21 p3679 A67-38224
 Thermal-stress deformed condition on heated elastic bodies boundary containing inclusions of spherical thin film with homogeneous infinite heat flow 21 p3720 A67-38295
 500 to 1000 MHz ultrahigh RF hybrid amplifier fabricated with microelectronic multilayer thin film technique, noting performance of components 21 p3596 A67-38342
 Thin film integrated circuits, considering vacuum deposition and cathode sputtering 21 p3597 A67-38496
 Quality control methods to ensure thin film circuitry integrity and reliability, showing need for better nondestructive testing techniques 21 p3635 A67-38623
 Pore formation, lifetime and microstructure of thin electrolytic metal films under load and high temperature at grain boundaries 21 p3646 A67-38827
 Electron energy loss calculations for nonnormal incidence in thin dielectric foil, with excitation probabilities and dispersion relations for bulk and surface plasmons 21 p3686 A67-39135
 Ferroelectricity of barium titanate thin films noting dielectric, temperature, polarization and electric field variations 21 p3687 A67-39142
 Temperature dependence of ferromagnetic parallel resonance line width in Ni-Fe alloy films, stressing surface oxidation role 22 p3855 A67-39350
 Hall coefficient and mobility measured for annealed polycrystalline and epitaxially grown gold, silver and copper films, discussing size effect 22 p3855 A67-39355
 Mixed state existence in type I superconducting thin film, discussing microwave power absorption variation with perpendicular magnetic field 22 p3856 A67-39437
 Dielectric thin film negative resistors for oscillator circuits compared to multilayer p-n-p-n structures for output frequency voltage temperature dependence 22 p3769 A67-39576
 Copolymers containing imidazopyrrolone and imide groups tested for thin film tensile properties, degradation by strong acids and bases and thermal stability 22 p3824 A67-39851
 Dynamic energy losses in thin Ni-Fe films during magnetization reversal studied by observation of M-H loop 22 p3860 A67-39902
 Scanning electron microscope signal processing and application to electronic devices failures, processes variations, integrated circuits and thin film circuit continuity 22 p3774 A67-40411
 Ti thin film microcircuit fabrication and electrical properties 23 p3977 A67-40661
 Design and performance of high gain amplifier consisting of cadmium sulfide single crystal and thin film transducers 23 p3977 A67-40690
 Resistance properties of thin continuous Au, Ag, Cu and Al films influenced by superimposed thin films, discussing resistance change and surface scattering 23 p4039 A67-40879
 Injection and emission of hot electron in thin film tunnel diodes 23 p4039 A67-40885
 Equilibrium state of two-dimensional lattice liquid-gas system using cluster variation method for nucleation and thin film growth studies 23 p4040 A67-40967
 Path-probability method applied to thin film nucleation and growth on substrate by vapor deposition, deriving kinetic equations 23 p4040 A67-40968
 Velocity distribution of evaporated Au and incident velocity on nucleation of Au on rocksalt studied by velocity selector 23 p4009 A67-41015
 Evaporated thin Au and Ni films electric conductivity measurements, obtaining electron mean free path and bulk resistivity 23 p4040 A67-41016

Device for metering variety of metals for high vacuum evaporation designed for thin film metal-insulator-metal diodes fabrication 23 p4001 A67-41223

Computer-operated following ellipsometer for monitoring buildup and removal of thin anodic oxide film 23 p4001 A67-41260

Automatic plating system insuring quality finishes by selectively phosphating or chromating parts after zinc plating 23 p4010 A67-41351

Mass spectrometry used for simultaneous measurements of adsorption and crystal nucleation processes 23 p4043 A67-41355

Polished glass substrates for thin film microcircuits, analyzing surface resistivity and optical transmittance changes due to heat treatment 23 p4043 A67-41366

Rocketsonde thermistor mount noting thin film configuration and long lead mount for heat dissipation 23 p4025 A67-41446

Photovoltaics - IEEE Conference, Cocoa Beach, Florida, March 1967, Volume 1, Thin film cells 23 p3936 A67-41482

Implantation process for thin silicon solar cell fabrication, discussing leakage losses and efficiency 23 p4046 A67-41488

Decreasing thickness and temperature variation effects on solar cell performance 23 p3937 A67-41489

Thin film GaAs solar cell fabrication and operating characteristics, describing two-cell types 23 p4046 A67-41493

Clevite thin film CdS solar cell fabricated with two different substrate structures noting design changes, improvements and performance characteristics 23 p3937 A67-41494

CdTe thin film solar cell, examining spectral response, sputtered Pt photovoltaic barrier-forming method and integrated array fabrication 23 p4046 A67-41495

Environmental testing of thin film solar cells, studying long term thermal cycling effect on CdS solar cell 23 p3937 A67-41496

Solar arrays constructed of CdTe thin film solar cells are feasible and competitive if space sunlight conversion efficiency can be maintained at level greater than 6 percent 23 p3938 A67-41498

Thin silicon, dendritic and cadmium sulfide solar cells technology and large-area lightweight arrays 23 p3939 A67-41512

Hole mobility produced by single pulses of electrons in films of polyvinyl acetate semiconductors with sputtered gold electrodes, determining relation between film conductivity and mobility 24 p4199 A67-41773

Edge effects in tunneling characteristics of thin film aluminum diodes in superconducting state, showing anomalies associated with quasi-particle tunneling through film edges 24 p4128 A67-41868

Radiation resistance and reactance of thin film inductor in microwave integrated circuit determined using Fourier transform 24 p4128 A67-41924

CdS single crystal film trap energy spectrum studied with thermo-stimulated currents /TSC/ noting effect of SiO layer 24 p4203 A67-42246

Heat transfer from plate located on dielectric base to liquid helium in pulsed regime influencing kinetics of superconductivity in thin films 24 p4254 A67-42258

Demagnetizing fields in thin magnetic films, considering saturation, film thickness and anisotropy 24 p4204 A67-42338

Barium fluoride film electric hygrometer element aging and possible causes of calibration drift with time in storage 24 p4156 A67-42380

Hall potential difference for thin film in magnetic leakage field of domain interface between ferro-and ferrimagnetic 24 p4204 A67-42457

Cryogenic flexibility of single and multiple ply thin polymeric film tested for porosity, cycle life and film thickness relation 24 p4176 A67-42468

Cryogenic mechanical properties of poly/ethylene terephthalate/ film studied for effects of stretch and heat set temperature and time 24 p4176 A67-42469

Solar cell/battery power systems for post-1975 satellites, discussing oriented thin film CdS solar cell array 24 p4105 A67-42515

Conversion of solar-thermal to electrical

energy by capacitance-change pumping of thermoelectric thin films, noting space environmental chamber tests 24 p4108 A67-42555

Viscoelastic lubricant in squeeze film configuration for sphere impinging on lubricant covered plane, noting pressure peak sensitivity to viscoelastic constants [ASME PAPER 67-LUB-24] 24 p4164 A67-42682

Monolithic integrated circuit design, considering thin film techniques and MOS devices 24 p4132 A67-42687

Tin and indium superconducting films transverse voltages due to longitudinal temperature gradients calculated for entropy per flux quantum 24 p4205 A67-43098

Structural studies of FeNi-FeNiMn type thin films with ferro-antiferromagnetic coupling by Lorentz electron microscopy 24 p4206 A67-43109

THIN FILM TRANSISTOR /TFT/

S FIELD EFFECT TRANSISTOR /FET/

THIN PLATE

Quadrature solution method for bending of arbitrarily loaded thin slab whose circular edge is supported by elastic rod 01 p0158 A67-10223

Temperature field of thin plate with circular region containing pulsed heat source 01 p0166 A67-10365

Capacitance pickups with nonelectrical quantity causing transverse bending of plates and change in transducer capacitance, used in recordings of mechanical quantities 01 p0063 A67-10416

Load carrying capacity of thin plates of rigid perfectly plastic material with different tensile and compressive yield strength, using method of limit analysis 03 p0531 A67-14366

Orthogonal double series solutions of nonlinear deflections of thin rectangular plate 04 p0707 A67-14445

Isothermal steady state process of fluid with constant density and kinematic viscosity coefficient flowing past thin plate 04 p0603 A67-14709

Nonisothermal steady state flow of fluid with constant density and kinematic viscosity coefficient past thin plate 04 p0603 A67-14710

Quasi-static equilibrium of thin plate heated by stationary circular source, obtaining expression for elastoplastic region at heating center, using continuous function 05 p0912 A67-16179

Quasi-static problem of generalized plane stressed state of thin plate, considering heat transfer on lateral surfaces and interaction between strain fields and temperature 05 p0913 A67-16186

Generalized thermally stressed state of thin plate in presence of interaction between strain field and temperature, considering heat exchange with surrounding medium 05 p0913 A67-16187

Bending equations for thin elastic anisotropic plates, using Goldenvelzer method 06 p1106 A67-18630

Nonlinear problems of thin plate bending, using successive approximations method 06 p1108 A67-18661

Simplified equations for equilibrium problem in large deflection theory for thin annular plates 08 p1414 A67-20348

Partial differential equations for plate motion, considering transverse shear and rotary inertia, solved for plates bounded by elliptical and hyperbolic cylinders 08 p1416 A67-20489

Hypersonic rarefied gas flow past plate with sharp leading edge, determining rarefaction effect on induced pressure distribution and value 08 p1278 A67-20924

Instrument design for analyzing biaxial strain field in thin plate under creep, noting use of moiré effect 08 p1332 A67-21461

Boundary value problems for thin elastic plates, discussing flexural stresses in neighborhood of crack, bending, etc 10 p1715 A67-22915

Sandwich plate problem involving subjection to concentrated force of plate having filler flexural rigidity only, giving solution in form similar to that of thin isotropic plate 10 p1718 A67-22937

Sandwich plate problem involving plate having filler flexibility only, giving solution via reciprocity theorem based on Rayleigh

Green equality in thin plate theory 10 p1716 A67-22938

Titanium alloy thin foil preparation using window method and electropolishing conditions, noting phase transformation 10 p1668 A67-23175

Interferometry analysis of stresses in plate due to pin 10 p1718 A67-23245

Polynomial solutions for differential equations describing thermoelastic equilibrium of thin anisotropic plates 10 p1718 A67-23405

Bassall theory to calculate bending, twisting moments and shearing forces for thin elastic plates under transverse flexure for structural design application 10 p1720 A67-23569

Thin plate targets response to hypervelocity impact to determine effectiveness of meteoroid bumpers composed of two layers of distinct materials 10 p1725 A67-23716

Elastic wave diffraction around elliptical hole in thin plate, obtaining dynamic stress concentration coefficient through approximate solution 11 p1870 A67-23897

Meteorite penetration through relatively thin shield 11 p1869 A67-24077

Boundary between applicability ranges of network and steepest descent methods in equation integration of Timoshenko theory in analysis of plate deformation 11 p1871 A67-24159

Flow induced vibrations of rigid plate in narrow channels, noting flow rate dependence on channel width [ASME PAPER 67-VIBR-32] 11 p1777 A67-24190

Micrographs of thin Ti layers through electron microscope showing dislocation distribution 11 p1806 A67-24428

Variational principle for elastic thin shells and panels of arbitrary shape and load conditions 11 p1876 A67-24624

Geometrically nonlinear effects of stress concentrations at holes in thin plate with large deformations 11 p1878 A67-24878

Two-dimensional temperature field analyzed for laminar gas flow in interspace between parallel thermally thin plates 12 p2033 A67-25319

Wiener-Hopf and Aleksandrov methods solve plane and axisymmetric problems of equilibrium longitudinal cracks in thin plates with edges free of stresses 12 p2019 A67-25565

Bending of thin plate of aluminum with nonlinear stress-strain relation analyzed, considering material compressibility effect 13 p2215 A67-26267

Seminfinite thin plate with circular inclusion under uniform tension 13 p2215 A67-26525

Thin elastic plate with uniformly distributed load over area and Navier condition on edge solved for deflection 13 p2217 A67-26631

Convective self-propulsion of continents 14 p2313 A67-28620

Existence conditions of periodic solution of equations describing nonlinear oscillations of thin plates with allowance for damping and application of Galerkin method 15 p2575 A67-29887

Elastic stability of simply supported uniformly-thin rectangular plate under unequal compressive stresses at two opposite edges due to constant body force 15 p2577 A67-30218

Stress distribution in thin plates containing curvilinear holes of various shapes 16 p2766 A67-31100

Fatigue crack propagation in thin plates under fluctuating plane extension and cylindrical bending 16 p2770 A67-31290

Boundary conditions influence on flutter critical boundary character considering nonlinearities of physical nature 16 p2776 A67-31471

Electron-mirror microscopy for intermediate-state pattern of superconducting samples noting bulk, thin sheet and lead films 17 p2912 A67-32286

Analyses of small-and large-deflection problems of clamped skewed plates under uniform pressure 17 p2958 A67-32407

Electron microscopy of titanium alloys noting preparation, heat treatment of samples, crystallographic structure, etc 17 p2872 A67-32722

Finite length plate in plane supersonic

- flow analyzed for forced vibration by applying linearized potential flow theory 18 p3140 A67-33466
- Determining resistivity and Hall coefficient using four point contacts placed on Hall plate isotropic uniformly thick two-dimensional sheet with perpendicular magnetic field 19 p3308 A67-36041
- Temperature field distribution and heat flux in thin narrow seminfinite composite plate with moving point source 19 p3347 A67-36051
- Nonlinear approximation of thin elastic plane plates noting influence of elastic medium and strain tensor deformations 20 p3535 A67-36279
- Differential equations for stressed thin orthotropic plates of variable thickness derived and solved in cylindrical coordinates 20 p3539 A67-36919
- Differential equation for bending of homogeneous plates of variable stiffness 20 p3541 A67-37284
- Steady state problem solution in linear formulation concerning movable load influence on thin elastic plate on ideal compressible fluid surface 21 p3720 A67-38300
- Thin plate idealization to Hrennikoff lattice model framework for linear stiffness method analysis 21 p3728 A67-38877
- Anisotropic plate with two elliptical holes studied for stresses under edge load by solving linear algebraic equations infinite system 22 p3910 A67-39452
- Homogeneous isotropic elastoplastic thin flat plate under uniform unidirectional stress, studying plastic flow, fracture, distortion and slip plane inclination 22 p3915 A67-40220
- Thin plate temperature distribution from solving conduction equation, considering boundary convection losses and moving discrete heat source 22 p3920 A67-40424
- Thin plate strong bending generalized and smooth solutions existence 23 p4076 A67-40716
- Plane problems with contained elastoplasticity, considering thin plates with small apertures as free boundary problem in continuum mechanics 23 p4077 A67-40754
- Thin boundary problems of bimaterial plates bonded along circular arcs behaving like crack imperfections under bending, using fracture mechanics to predict failure 23 p4078 A67-41164
- Flow past disk at angle to stream with marked periodic motions caused by vortex ring shedding increasing with angle of incidence 23 p3990 A67-41171
- First approximation analysis of rarefied hypersonic gas flow asymptotic properties near surface and front edge of thin plate, determining macroparameters 24 p4142 A67-42272
- Finite difference solution accuracy for potential gradient along conductor boundary near reentrant corner of thin plate 24 p4131 A67-42447
- THIN WALL**
- Stress analysis methods applied to hollow thin walled low-aspect-ratio wings, considering small deflection law 14 p2401 A67-28657
- Differential equations determining time-dependent torsional moment and stresses in thin walled rods in creep presence 17 p2821 A67-32830
- Soviet papers on aircraft construction and techniques used by Air Force covering theory, engines, design, manufacture and operation 21 p3568 A67-38901
- Mathematical programming problem for automating design of optimum thin walled systems, noting stress-strain state factors 21 p3728 A67-38903
- Algorithm for selecting optimum parameters for mathematical programming problem in thin walled systems, noting stress-strain state characteristics 21 p3728 A67-38904
- Normal stresses induced by temperature effects in thin walled bars, assuming nondeformability of contour and no displacements in middle surface 21 p3728 A67-38905
- Fast response thin skinned calorimeters for high heat flux profiles of arc jet flows 23 p4006 A67-41381
- THIN WALLED SHELL**
- Concentration of stresses around curvilinear holes in thin shells solved with nonlinear law of elasticity, reducing problem by boundary shape perturbation method 01 p0158 A67-10218
- Marguerre-Vlasov equations accuracy analysis based on equations for thin walled shallow shells derived, using series expansion 01 p0159 A67-10275
- Load carrying capability of thin walled pressurized tanks under compression and bending with postwrinkling included, improved by addition of jettisonable shell [SAE PAPER 660683] 01 p0161 A67-10586
- Arbitrary shallow shell under action of space-time homogeneous random load 01 p0163 A67-10995
- Numerical solution of nonlinear differential equations governing finite axisymmetric deformation of thin shells of revolution 01 p0164 A67-11176
- Stability equation of elastic bodies subjected to body and pressure forces derived using virtual work principle, noting specialization to thin shells 01 p0165 A67-11307
- Torsional oscillations of hollow cylinder of finite length encased in thin elastic shell 02 p0337 A67-11932
- Computer algorithm for framework diagram in synthesizing thin walled shells strengthened by ribs 02 p0340 A67-12443
- Elastoplastic equilibrium of thin arbitrary shells of revolution with finite deflection comparable to shell thickness 02 p0340 A67-12661
- Calculation of cylindrical minimum weight stringer shell in axial compression loading 02 p0340 A67-12662
- Stability of thin walled conical shells under axially symmetric loading determined from nonlinear shell theory [DVL-605] 03 p0521 A67-13020
- Ultimate bending moment capability of thin walled pressure stabilized cylinder with typical axial loads demonstrated to be 50 percent greater than bending moment at which compressive wrinkling occurs 03 p0522 A67-13230
- Comparative efficiencies of thin wall aerospace pressure vessels, emphasizing primary structural weight 04 p0709 A67-14810
- Thin walled elastic shell response to thermal excitation [AIAA PAPER 66-84] 04 p0709 A67-14841
- Book on methods of determining temperature fields in thin walled elements characteristic of structure of flight vehicles and engines 04 p0723 A67-15010
- Tensile-instability mechanism concept determination of ultimate strength of most ductile materials under uniaxial or biaxial tension conditions [ASME PAPER 66-WA/MET-15] 04 p0712 A67-15378
- Natural frequencies and mode shapes for axisymmetric vibration of thin elastic and ellipsoidal shells 04 p0714 A67-15424
- Nonlinear elastic thin shell theory in parallel approach based on Kirchhoff hypothesis 04 p0715 A67-15585
- Stress concentration in nonlinear creep of thin circular cylindrical shell loaded at one edge by symmetrical radial shear and bending moment 04 p0718 A67-15917
- Infinite series and finite difference solutions of elastic response of thin walled spherical shell to axisymmetric transient blast loading [ASME PAPER 66-APM-EE] 04 p0718 A67-15918
- Stress calculation comparison of computer data and photoelastic data for series of pressure vessels with hemispherical and torispherical heads [ASME PAPER 66-WA/PVP-5] 04 p0719 A67-15931
- Buckling phenomena involving formation of indentation in thin circular cylindrical shells under axial compression 05 p0907 A67-18021
- Zero moment boundary value problem of thin walled helicoidal shell in asymptotic lines 05 p0915 A67-18221
- Dynamic displacements of thin spherical shell buckling under uniform pressure 05 p0920 A67-18825
- Small plastic deformation theory determination of elastoplastic stressed state of thin walled isotropic incompressible shell of revolution under axisymmetric power loads and nonuniform heating 05 p0922 A67-17177
- Matrix displacement approach to discrete element structural analysis for thin shell instability, emphasizing determination of membrane force distribution 05 p0925 A67-17352
- Inertia effects of internal liquid column on vibration of thin walled pressurized elastic cylindrical bellows type container [AIAA PAPER 67-38] 06 p0986 A67-18262
- Coupled system of thin elastic shells, giving response to static or harmonically oscillating loads or to unloaded natural frequencies and mode shapes, using Green matrix [AIAA PAPER 67-45] 06 p1103 A67-18351
- Supersonic flutter of thin walled circular cylindrical shells under compressive loading, comparing theory and experiment [AIAA PAPER 67-77] 06 p1103 A67-18354
- Stability of truncated conical thin shells under torsional load 06 p1105 A67-18592
- Stress distribution in thin walled shell during transfer of concentrated load to surface area of mechanical contact 06 p1106 A67-18623
- Rotation of thin walled elastoplastic tube of circular cross section after bending 06 p1107 A67-18635
- Apparatus for testing thin walled tubular samples under combined torsional and tensile load, using stressed state timer 06 p1107 A67-18639
- Approximate solution of temperature field of thin isotropic cylindrical shell heated by time dependent thermal fluxes from two ambient media 07 p1266 A67-19162
- Stability loss in thin walled plastic shell under tensile loading in plane stress conditions 07 p1261 A67-19190
- Wall thickening of aircraft structural components by compression of blanks to produce counter force 07 p1191 A67-19749
- Beadling in thin walled pipes with localized heating, noting stress deformation state 07 p1192 A67-19752
- Displacement formulations of first order linear thin elastic shell equations in terms of stress resultant and middle surface, using modified Kirchhoff hypothesis 08 p1417 A67-20551
- Stiffness and consistent mass matrices for finite cylindrical shell element with admissible displacement state 10 p1717 A67-23128
- Stress-strain state of elements of thin walled shells of revolution with hinged meridional edges under effect of force and thermal distributed load satisfying end conditions 10 p1720 A67-23601
- Antisymmetric stress-strain state of thin walled isotropic and anisotropic sandwich shells of revolution with meridian of arbitrary shape for complex boundary conditions 10 p1720 A67-23603
- Dynamic stability of cylindrical shell reinforced by thin walled rigid longitudinal ribs 10 p1721 A67-23604
- Boundary value problem solution governed by system of partial differential equations applied to analysis of curved thin walled shells of revolution 10 p1729 A67-23765
- Linear motion equations including effects of transverse shear deformation and rotary inertia derived for thin elastic isotropic conical shells of revolution 10 p1729 A67-23767
- Stability analysis of symmetrically loaded thin walled spherical shell, noting construction of asymptotic expansion, error estimation and application of elasticity theory 11 p1871 A67-24152
- Discrete mass technique for vibration analysis of thin shells [ASME PAPER 67-VIBR-23] 11 p1872 A67-24182
- Nonlinear membrane theory for thin elastic inflatable shells during pressurization phase 11 p1875 A67-24432
- Stress-strain condition in thin walled shells having anisotropic moduli with one end clamped and torsion applied at other end 11 p1878 A67-24860
- Stress-strain state of thin walled zero moment shell under uniformly distributed multiple load assuming various tensile and compression strengths 12 p2020 A67-25569
- Approximate theory for stress-strain state of thin cylindrical shell reinforced with elastic ribs having bending rigidity 12 p2022 A67-25584

Matrix integral equations to calculate critical stresses and natural frequencies of oscillation of thin walled isotropic shells of revolution 12 p2022 A67-25585

Oscillation and stability of system of thin elastic shells in potential inviscid and incompressible fluid flow 12 p2023 A67-25589

Deflection function of glass fiber reinforced circular cylindrical shells under axial supercritical compressive loading 12 p2023 A67-25590

Elastic filler effect on thin cylindrical sandwich shell stability subjected to compression along generatrix 12 p2023 A67-25592

Dynamics of rigid plastic thin walled shells for short term constant high intensity load 12 p2025 A67-25607

Variational methods solutions for thin shell deformation mechanics 12 p2027 A67-25621

Equilibrium equations modified in nonlinear theory of thin walled elastic shells 12 p2028 A67-25634

Asymptotic integration technique for small axisymmetrical oscillations of thin walled elastic shell of revolution for case of double reversal point 12 p2029 A67-25675

Laminated thin shell theory applied to calculation of elastic coefficients of fiber reinforced shells [AIAA PAPER 66-526] 12 p2030 A67-25914

Dynamic response of clamped shallow thin elastic spherical shells under time dependent loads [AIAA PAPER 66-446] 12 p2030 A67-25915

Buckling of thin walled circular cylindrical shells under external pressure treated by Sanders theory 12 p2030 A67-25940

Axisymmetrical stability loss problem in thin walled cylindrical shell with continuous elastic filler 12 p2031 A67-25958

Fundamental solution of thermoconductivity equations for thin walled shallow shells and infinite plates with various instantaneous interval heat sources 13 p2221 A67-26374

Nonlinear dynamic response of thin walled shells of revolution 14 p2397 A67-28090

Thermal stresses in thin shell in contact with smooth rigid container 14 p2403 A67-29011

Timoshenko beam equations modification necessary to account for normal pressure and Poisson ratio effects for application to thin walled circular tubes 14 p2403 A67-29013

Thickness transition configurations for cylindrical pressure vessels with hemispherical heads, noting weight, load effects, etc 15 p2573 A67-29419

Mean diameter/wall thickness optimum ratio and corresponding maximum shear stress for thin walled cylinder under uniform pressure and radial heat transfer 15 p2574 A67-29528

Displacement equations of prestressed thin bending-resistant shells 15 p2574 A67-29699

Tension equations for oval thin walled cylinders reinforced with lateral rigid ribs noting wall strength, complex bending moment computation, etc 15 p2577 A67-30185

Boundary conditions for thin shells and physical meaning analyzed according to Kirchhoff-Love theory 16 p2764 A67-30862

Deformation energy of thin elastic shell expressed as function of deformations of reference surface other than mean surface 16 p2777 A67-31708

Book on thin walled structures covering frame buckling, elastic buckling of rectangular flat plates, edge loading, anisotropic plate structures, etc 17 p2956 A67-32021

Elastic buckling of thin walled frames, discussing restraint effect on stability, symmetry effect on critical behavior and dead loads effect 17 p2957 A67-32022

Thin walled unsymmetrical beam under bending and torsion studied for nonlinear elastic behavior 17 p2957 A67-32023

Buckling of compressed thin walled structural sections, noting design concepts and flat plate theories 17 p2957 A67-32025

Shear buckling of thin walled structural sections, noting reinforcement methods including use of swedges 17 p2957 A67-32026

Stress calculation comparison of computer data and photoelastic data for series of pressure vessels with hemispherical and torispherical heads [ASME PAPER 66-WA/PVP-5]

18 p3143 A67-34127

Resonances of thin shell model of earth-ionosphere cavity with dipolar magnetic field 18 p3042 A67-34427

Stability of reinforced thin structurally-orthotropic cylindrical shell problem, discussing rib eccentricity, axial compression load, torsional load, etc 19 p3338 A67-34874

Stiffness matrix of thin flat triangular elements of nonzero Gaussian curvature derived by reducing geometrical idealization errors 19 p3342 A67-35750

Thin walled structure bending in uniform temperature field, calculating stresses, deformations and creep 20 p3536 A67-36446

Hardenable thin walled cylindrical metal sample stress-strain state under cyclic thermal load, determining plastic deformation 21 p3716 A67-37910

Strain energy in thin isotropic elastic shells subject to arbitrary temperature distribution, considering large deflections and buckling 21 p3718 A67-38021

Creep buckling load for thin circular rings determined by tangent modulus theory together with isochronous stress-strain diagram 21 p3719 A67-38022

Oscillation and stability of two irregular thin elastic cylindrical shells in potential flow of compressible fluid 21 p3720 A67-38296

Soviet papers on strength and stability of elements of thin walled structures 21 p3723 A67-38778

Ten thin walled cylindrical shells under internal load investigated for bending stability, comparing experimental and analytical results 21 p3724 A67-38785

Calculated stressed state of short thin walled shells under transverse loads and torsional moments 21 p3726 A67-38797

Supersonic flutter of thin walled circular cylindrical shells under compressive loading, comparing theory and experiment [AIAA PAPER 67-77] 21 p3727 A67-38869

Unloaded thin walled spherical shell rigidly hinged along edge noting existence of nontrivial form of equilibrium and negative lower critical load 22 p3910 A67-39402

Cylindrical thin walled open section structures heated nonuniformly, calculating various elastic parameters, torsion properties and shearing stress 22 p3916 A67-40450

Reissner differential equation simplified for problems involving small strains in thin shells of revolution due to symmetrical deflections 23 p4073 A67-40612

Differential equations describing stressed state of revolving shell beyond elastic limit and solutions adaptable to computer programming 23 p4075 A67-40681

Elastic bending of thin shells and plates perforated with holes in various arrays, calculating stress distribution and concentration 23 p4077 A67-40749

Stress-strain relationship effect on r-power steady creep of pressurized thin spherical shell with sealed opening for various edge load boundary conditions 23 p4079 A67-41343

Simplified equations for thin circular cylindrical shells under loading investigated for possible elimination of inconsistencies 23 p4080 A67-41664

Book on nonlinear theory of thin shells covering deformation and stress state, surface kinetics, momentum conservation, etc 24 p4246 A67-41800

Invariant form of strain-energy function of linearized elastic potential of isotropic thin shell using three-dimensional theory 24 p4249 A67-42156

Revolving thin elastic shell free axisymmetric oscillation described by equation system derived by asymptotic integration technique with single reversal point 24 p4250 A67-42304

Thin toroidal elastoplastic shells of revolution loaded axisymmetrically, calculating force, moment, stress and strain interrelation for middle surface using complex representation 24 p4250 A67-42305

Constrained torsion of thin walled rods with closed or open profiles, discussing stress-strain state of cross section sealed at one point 24 p4250 A67-42307

Thin elastic shell nonlinear buckling theories, studying circular cylinder and truncated cone cases 24 p4252 A67-43096

THIN WING

Center of pressure stabilization for thin

wing profile with downward deflected trailing edge, when placed in steady state flow of ideal incompressible fluid 02 p0179 A67-12438

Asymptotic expansion of transient forces on finite thin wing in oscillatory upwash field treated by derived expression for change of generalized aerodynamic damping coefficients with respect to frequency parameter 03 p0352 A67-13896

Linearized long wave diffraction theory of supersonic inviscid flow past slender circular cylindrical bodies and thin wings 06 p0942 A67-18729

Unsteady aerodynamic forces on thin wing oscillating in transonic flow, discussing acoustic ray paths and signal transmission times [AIAA PAPER 67-16] 06 p0943 A67-18841

Antisymmetrical thin delta wing with flow separation at subsonic leading edge 07 p1128 A67-20236

Complex velocity and circulation around thin wing 09 p1439 A67-22564

Aerodynamic characteristics of wedge wings determined for hypersonic viscous flow 11 p1742 A67-24347

Solution of volterra type equation for oscillations of thin profiles of grid in incompressible inviscid flow 13 p2218 A67-26899

Flow pattern of thin jet-flapped wing with small deflection angle in proximity to ground 15 p2415 A67-29308

Thin rectangular vortex wing in uniform flow, solving nonlinear equations by successive approximations 20 p3356 A67-36439

Oscillating infinitely thin wing profile in inviscid subsonic compressible flow, deriving perturbation pressure 23 p3929 A67-41250

THIOCYANATE

IR spectra of gaseous, solid and matrix-isolated HNCS and DNCS, studying frequency shift, bending modes, fundamental vibrations, gas phase, etc 19 p3181 A67-35016

THIRD STAGE

SA MISSILE

SA PAYLOAD

SA SATELLITE

Checkout system for third stage of ELDO A program 04 p0595 A67-14534

German firm participation in designing and constructing third stage of ELDO launch vehicle EUROPA I 16 p2763 A67-31789

Development, reliability and acceptance tests for third stage of ELDO satellite launcher, discussing components, time schedules, personnel training, etc 18 p3136 A67-33639

Checkout system for third stage of ELDO A program 20 p3413 A67-36414

P4 double test stand for ground testing third stage of ELDO launch vehicle 23 p3987 A67-41325

THURONUM

S PSEUDOURA

THOMAS-FERMI THEORY

Electron energy spectrum for alloyed semiconductors, determining state densities via Thomas-Fermi statistical method 04 p0681 A67-15296

Temperature perturbation in Thomas-Fermi functions for atom radius as related by Gilvarly to simpler Feynman-Metropolis-Teller case 05 p0848 A67-16132

Effective diffusion cross section for meteor atoms in atmosphere, using Thomas-Fermi-Dirac and dumbbell molecule models 13 p2111 A67-26553

THOMSON EFFECT

SA PELTIER EFFECT

Lasers used to extend RF plasma diagnostic procedures to optical frequencies by interferometric and Thomson diffusion methods 03 p0477 A67-13474

Modified Thomson mass spectroscopy for visual observation of energy spectra of ion component of plasmoid 15 p2486 A67-29260

Protonosphere heating by photoelectrons escaping from F region, estimating protonosphere opacity and daytime escape flux 19 p3221 A67-35280

THOR LAUNCH VEHICLE

Thor SLV upper stage Burner 2 design, performance and cost 21 p3713 A67-38379

THORAX

Radiographic analysis of thoracic cardiovascular rupture during abrupt deceleration associated with crashes [ARL-TR-67-17] 08 p1287 A67-20614

Human cardiac output estimated using

- impedance plethysmography, discussing simultaneous indicator dilution curves /Dye/ and impedance records 23 p3951 A67-41563
- Thorax radiological changes associated with physiological and posture changes, discussing chest dynamics 23 p3956 A67-41625
- THORIUM**
- Strength of cobalt alloys at elevated temperatures improved by dispersion of submicron thorium particles 01 p0093 A67-10517
- Plasma mode work function measurement for studying thermionic emission from Hf, Th and Tl in Cs vapor at reservoir temperature of 414 degrees K 09 p1450 A67-22353
- THORIUM ALLOY**
- Thorium-gadolinium alloy magnetization curves confirming full Meissner effect, showing bulk properties of superconductors obey Abrikosov-Gorkov theory 14 p2373 A67-28859
- THORON**
- Direct measurements of thoron from ground surface to height of 50 cm in atmosphere, describing turbulent diffusion of radioactive emanations from soil surface 02 p0237 A67-11853
- THREE-BODY PROBLEM**
- Phase-space collision domains corresponding to hard-sphere N-body problem in gas transport theory 01 p0112 A67-10144
- Analytic continuation method proof of existence of class of periodic orbits of three-dimensional three-body problem, Part II 01 p0148 A67-10381
- Existence of class of quasi-periodic solutions of three-body problem for near-circular inclined planetary and lunar orbits, Part I 01 p0148 A67-10382
- Existence of two points near any planet where third body, given appropriate initial conditions, would remain in libration gravitational equilibrium 02 p0324 A67-11814
- Collision paths of free particle in Newtonian gravitational field examined, using analogy of circular restricted three-body problem 02 p0328 A67-12403
- Self-consistent three-body calculation of pion-nucleon scattering using off-energy shell theory 04 p0660 A67-14858
- Third integral of motion in series form derived by Contopoulos combined with known energy and field integrals describes orbits of axisymmetric star systems 04 p0699 A67-14981
- Three-body problem of orbital motion, examining periodic librations of planetoid around triangular equilibrium point 06 p1079 A67-17762
- Long period of nonperiodic librational motion about equilateral points of restricted three-body problem 06 p1080 A67-17765
- Nonperiodic librational motions in restricted three-body problem for relatively elliptic motion of two finite masses 06 p1080 A67-17766
- Regularization of three-body equations for case of binary collisions, using Sundman equation transformation in celestial mechanics problems 06 p1022 A67-17776
- Restricted problem of three bodies, two of which are assumed to be point masses, determining motion of third 06 p1081 A67-17779
- Electron-phonon interaction in semiconductors, considering three-phonon process and third order elastic constant 06 p1066 A67-18957
- Lagrangian dynamical system determined under parametric form of motions applied to two-and three-body problems 07 p1216 A67-19722
- Motion of vehicle in transition region of restricted three-body problem in which earth centered and moon centered conics were connected at mean sphere of action /MSA/ [AAS PAPER 66-97] 07 p1252 A67-19961
- Higher order perturbations of elements in three-body problem determined using methods of Krylov-Bogolubov and Poincare [AAS PAPER 66-99] 07 p1252 A67-19962
- Periodic solutions of elliptical and restricted four-body problems about libration points of restricted three-body problem [AAS PAPER 66-101] 07 p1252 A67-19963
- Feedback control system to position satellite in vicinity of unstable collinear libration point with application to lunar communication problem 07 p1146 A67-19991
- Numerical analysis of plane restricted three-body problem with two bodies of equal mass moving on circular orbit 08 p1380 A67-20386
- Canonical transformation in two-dimensional three-body problem giving power series Hamiltonian 08 p1380 A67-20387
- Elliptic restricted problem of periodic Trojan orbit and nonperiodic librational frequency and angular motion of Jupiter 08 p1381 A67-20388
- Long period effects in nearly commensurable cases of restricted three-body problem analyzed via Poincare, isolating secular and critical terms of disturbing function 08 p1381 A67-20389
- Three-body problem with all perturbations of first order represented by elliptic integrals 08 p1381 A67-20390
- Nearly commensurable periods in restricted problem of three bodies, calculating long period variations in interior 2/1 case, noting solutions to Poincare problem 08 p1381 A67-20391
- Harmonic series of coordinates of moon in three-body problem of sun-earth-moon treated by numerical method 08 p1382 A67-20395
- Periodic solutions for restricted three-body problem 08 p1384 A67-20619
- Numerical integration of restricted problem of three bodies for finding lunar trajectories, using motion equations and Taylor series 08 p1396 A67-21181
- Restricted problem of three bodies analyzed using Birkhoff variables and power series representing motion equations, obtaining coefficients for collision orbit 08 p1396 A67-21182
- Periodic solutions of three-dimensional restricted problem, noting existence of orbits for various combinations of eccentricity and inclination 08 p1396 A67-21183
- Elliptic restricted three-body problem solved for eigenvalues and orbital series solutions of Lagrangian triangular point 08 p1397 A67-21214
- Stability analysis of long period Trojan librations treated as short period oscillations about long period reference solution 11 p1866 A67-24774
- Equilateral position stability of equilibrium in planar restricted problem of three bodies for mass ratio values 13 p2205 A67-27477
- Stromgren family of periodic orbits in restricted problem 13 p2205 A67-27479
- Integrals of motion in three-dimensional restricted three-body problem as generalizations of angular momentum 13 p2205 A67-27480
- Computer program using Birkhoff normalization of Hamiltonian of restricted problem of three-bodies problem at L sub 4 13 p2208 A67-27521
- Feedback control system to position satellite in vicinity of unstable collinear libration point applied to lunar communication problem [AAS PAPER 66-132] 13 p2210 A67-27543
- Position and width of lowest elastic scattering resonances in three-body atomic system, showing resonance shape dependence upon observation angle and angular resolution 14 p2351 A67-28152
- Ionization probability of hydrogen atom by electron impact in terms of three-body problem of classical mechanics 14 p2351 A67-29072
- Selection of two regularizing functions reduced to one by evaluating relations between them in restricted three-body problem 15 p2557 A67-29875
- Family of periodic orbits around triangular libration points in restricted three-body problem 15 p2557 A67-29876
- New integral in restricted three-body problem expressed in terms of Delaunay variables 15 p2557 A67-29877
- Canonical elements for variables of Levi-Civita regularizing binary collisions in restricted three-body problem, noting existence of periodic orbits 15 p2557 A67-29878
- Motion analysis near triangular libration point within framework of elliptic restricted three-body problem 15 p2559 A67-30036
- Perturbation theory applied to periodic motions in three-body restricted problem 15 p2560 A67-30040
- 24-hr satellite positions studied for librations, using linear theory 15 p2560 A67-30043
- High altitude satellites orbital curves, considering moon effect 15 p2560 A67-30044
- Runge-Kutta-Fehlberg method for systems of ordinary first and second order differential equations applied to numerical solution of many-body problem 15 p2561 A67-30052
- Three-body problem reduced to two-body problem in general relativity theory 16 p2745 A67-30747
- Motion in ternary stellar system consisting of central body and close and distant companions 16 p2746 A67-30956
- Secular and periodic perturbations of orbits of artificial satellites of earth and moon by attraction of external bodies 16 p2746 A67-30981
- Birkhoff normalization of Hamiltonian function in neighborhood of stable equilibrium position in connection with Trojan orbits in three-body problem 16 p2747 A67-30985
- Particle trajectory analysis with perturbation series, noting position and velocity error estimation for restricted three-body problems 16 p2749 A67-31425
- Closed form regularized solutions in polar coordinates of two-body problem obtained and applied to restricted three-body problem 17 p2943 A67-32440
- Restricted three-body problem in post-Newtonian approximation, obtaining equations of motion 17 p2943 A67-32441
- Representation of rotating gaseous emission rings in eclipsing binary systems by periodic orbits around more massive component in restricted three-body problem 17 p2944 A67-32640
- Three-body problem of Jupiter satellites orbits under solar influence, computing initial elements, determining orbital stability and solving satellite motion equations 17 p2946 A67-32753
- One-dimensional three-body problem, noting shell model for two particles and coordinate transformation 17 p2888 A67-32926
- Regions forbidden to motion in three-body problem determined in barycentric coordinate system for nonzero modulus of momentum vector 18 p3117 A67-33627
- Book on theory of orbits covering restricted problem of three bodies, two bodies in rotating coordinate system and periodic orbits 18 p3120 A67-34032
- Bounded isoenergetic displacement of periodic orbits in restricted circular three-body problem 18 p3135 A67-34542
- Integrals of motion in plane elliptic restricted three-body problems for orbits with small eccentricity near primaries 18 p3136 A67-34588
- Regularization of restricted three-body problem extended to case where three primaries of any mass revolve in circular orbits around common center of mass and fourth body of infinitesimal mass moves in their field 18 p3136 A67-34589
- Restricted three-body problem with two masses under Newtonian gravitation and third obeying semi-Newtonian laws 19 p3327 A67-35864
- Ionization and recombination effects on MHD wave propagation through three-component magnetoplasma, deriving nonlinear motion equations 21 p3660 A67-37743
- Electron-ion three-body recombination rate in nonequilibrium dense nitrogen plasma measured spectroscopically [AIAA PAPER 67-703] 21 p3672 A67-38730
- Three-dimensional generalization of Birkhoff transformation for regularization of Keplerian motion in three-body problem noting differential equations system 22 p3881 A67-39513
- Analytic form of solutions of first order variational equations of restricted three-body problem 23 p4061 A67-40622
- General Pythagorean three-body problem solved completely using numerical method 23 p4062 A67-40624
- Lunar gravitational fields based on Cassini and Euler rotation laws compared with solar, Saturnian and Jovian effects on Saturn and Jupiter satellites 24 p4229 A67-42311

Stable libration points of degenerate three-body problem with negligible space vehicle mass 24 p4231 A67-42401

Three-body problem application to nuclear reactions involving neutron, proton and heavy nucleus, parametrizing two-body interactions in terms of s-wave separable potentials 24 p4191 A67-42593

Solution to Burrau three-body problem including historical and scientific background 24 p4232 A67-42605

THREE-DIMENSIONAL BOUNDARY LAYER

Three-dimensional boundary layer and inviscid hypersonic flow interaction on infinitely thin triangular wing 01 p0007 A67-10982

Algorithm for numerical calculation of three-dimensional boundary layer of incompressible fluid 03 p0401 A67-12876

Three-dimensional turbulent boundary layer characteristics predicted by method which assumes cross flow is small [ASME PAPER 66-WA/GT-10] 04 p0607 A67-15361

Hot-wire probe measurements of time average velocity, flow directions, turbulence intensities and growth of skewed three-dimensional turbulent boundary layers in low speed flow [ASME PAPER 66-WA/FE-2] 04 p0608 A67-15386

Thermodynamic analysis of flow in gas turbines, for two-and three-dimensional boundary layers and wakes 05 p0748 A67-16745

Three-dimensional laminar boundary layer equations solved by finite difference methods for application to boundary layer flow on blunted cone, noting effect on crossflow [AIAA PAPER 67-159] 06 p0989 A67-18480

Three-dimensional boundary layer flow over windward side of flat delta wing in hypersonic flow at moderate angle of attack, examining viscous-inviscid interaction [AIAA PAPER 66-492] 06 p0943 A67-18848

Three-dimensional turbulent boundary layers over swept wing calculated using entrainment equation 10 p1626 A67-23473

Integral energy equation for three-dimensional laminar boundary layer element on porous surface in presence of suction 11 p1783 A67-25052

Three-dimensional boundary layer for gas flow past generatrix of cylinder of arbitrary transverse cross section 20 p3360 A67-37658

Three-dimensional compressible laminar boundary layer with heat transfer in curvilinear coordinate system linked to streamlines of external flow, assuming transverse flow 21 p3615 A67-39127

Friction and heat flow resistances for three-dimensional compressible laminar gas boundary layer over ellipsoid of revolution at angle of attack 22 p3786 A67-40028

Dynamic impossibility of free stream velocity distributions admitting similarity solutions, calculating laminar boundary layers 23 p3992 A67-41741

THREE-DIMENSIONAL FLOW

Three-dimensional supersonic gas flow with shock waves around flat wing analyzed, using integral relations 01 p0007 A67-10981

Differential approximation for forward and backward radiative flux components for three-dimensional flows 02 p0235 A67-12566

Three-dimensional unsteady flow in uniformly expanding layer and dispersion of gas in vacuum 03 p0402 A67-13627

Approximate method of treating three-dimensional laminar incompressible boundary layer equations when cross flow is small [ASME PAPER 66-WA/FE-34] 04 p0607 A67-15365

Three-dimensional flow separation over structures with various geometric configurations, calculating limiting streamlines for subsonic laminar boundary layer conditions 05 p0747 A67-16293

Forms of function connecting deviation angle and axial velocity ratio of exit flow in three-dimensional cascade flow 05 p0791 A67-16428

Three-dimensional flow past blunt nosed cones 05 p0751 A67-17478

Three-dimensional flows with Mach interaction between shock waves, drawing conclusions on possible types of interference between wing and wall 06 p0936 A67-17736

Asymptotic method for solution of

boundary layer equations for generalized three-dimensional flow of dissociated air at chemical equilibrium near stagnation point 06 p0984 A67-18113

Time dependent computational method for three-dimensional blunt body flow fields traveling at supersonic speed including shock points, sphere cones and ellipsoid [AIAA PAPER 67-222] 06 p0941 A67-18461

Three-dimensional internal flows in intakes and exhaust nozzles computed by combined characteristics and finite difference method [AIAA PAPER 67-224] 06 p0942 A67-18516

Three-dimensional boundary layer flow of incompressible second order viscous fluid near spinning cone 06 p0992 A67-18868

Three-dimensional plane shock wave intersection in space, noting parameter range for which two solutions exist 07 p1169 A67-20036

Compatibility relations and generalized finite difference approximation for three-dimensional steady supersonic flow 08 p1320 A67-20566

Three-dimensional flutter calculations verification by wind tunnel results, using flexible supersonic aircraft planform model of determined characteristics to control calculations 10 p1622 A67-22882

Static and kinematic indeterminate states in three-dimensional plastic flow analyzed by replacing Haar-Karman yield conditions 10 p1716 A67-22932

Three-dimensional flow in supersonic stream in symmetry plane of region of shock boundary layer interaction in front of obstacle mounted on plate, noting penetration in separation region 10 p1590 A67-23026

Numerical finite difference solution of three-dimensional equations of motion for laminar natural convection, noting Navier-Stokes equation transformation 11 p1774 A67-23861

Three-dimensional flow in single stage axial flow fan rotor with prescribed and variable circulation along span 12 p1893 A67-25971

Three-dimensional supersonic flow for ideal fluids using Euler motion equation 13 p2050 A67-26648

Steady three-dimensional flow of electrically conducting gas in working section of linear MHD channel 13 p2169 A67-27310

Coupled nonlinear equations integration in boundary layer theory with specific reference to heat transfer near stagnation point in three-dimensional flow 13 p2224 A67-27463

Three-dimensional supersonic flow past pointed nonaxisymmetrical bodies characterized by great local surface curvature changes, using new approximation 13 p2051 A67-27617

Three-dimensional flow of ideal fluid past body enveloped by air cavern, deriving normal velocity components 14 p2239 A67-27985

Supersonic three-dimensional flows past smooth bodies, calculating flow parameters by characteristic method with analytical approximation of gas-dynamic functions 14 p2240 A67-27992

Three-dimensional gas flow in region of incidence of shock wave on cylinder situated in high supersonic flow 14 p2297 A67-27995

Three-dimensional turbulent boundary layer flow over infinite swept wing calculated using entrainment and momentum integral equations 16 p2657 A67-30617

Three-dimensional slender wings of maximum lift/drag ratio in hypersonic flow studied by variational calculus under several lift and volume conditions 16 p2592 A67-30964

Multidimensional unsteady flow field of inviscid fluid calculated with application of method of characteristics and digital computer 16 p2662 A67-31535

Three-dimensional laminar boundary layer flow, calculating skin friction and velocity profiles 17 p2790 A67-32284

Three-dimensional detached flow patterns forming near secondary jet injected into supersonic flow 18 p3027 A67-34207

Supersonic flow past smooth body with internal duct incident at angle of attack 18 p2984 A67-34212

Three-dimensional hypersonic flow past

blunt cones calculated by modified method of characteristics, taking into account physicochemical equilibrium conversions 18 p2984 A67-34213

Shadow photometer conversion to various interferometer types for studying inhomogeneous three-dimensional fluid flows in transparent media 19 p3228 A67-34985

Three-dimensional flow in axial fan, consisting of rotor only, having finite number of blades, by method of isolated airfoil of finite span 19 p3171 A67-35712

Three-dimensional flow through rotor of single stage axial fan with prescribed spanwise variable circulation 19 p3171 A67-35711

Three-dimensional vortex flow inverse problem through axial fan solved using isolated airfoil method 19 p3171 A67-35723

Time dependent computational method for three-dimensional blunt body flow fields traveling at supersonic speed including shock points, sphere cones and ellipsoid [AIAA PAPER 67-222] 19 p3171 A67-35736

Three-dimensional incompressible flow with colinear magnetic field, studying stability by numerical method 20 p3423 A67-37242

Rayleigh hypothesis applied to three-dimensional rotationally symmetric flows arising from rotating disk in rotating fluid compared with steady solutions 20 p3423 A67-37278

Characteristic method computer program for calculating three-dimensional supersonic flow around blunt and pointed bodies of revolution in reasonable time 21 p3566 A67-38887

Supersonic three-dimensional flow fields of inviscid nonconducting gas around delta wing with blunted edges 22 p3741 A67-40025

Conformal mapping method for overcoming difficulties caused by limiting line in computing flow field about blunt body supporting paraboloidal shock wave 23 p3932 A67-41730

Prandtl equation system for two-dimensional incompressible flows expanded to construct solutions for three-dimensional unsteady flows by straight lines method 24 p4177 A67-42200

Three-dimensional disturbance after perturbation of supercritical Poiseuille flow between parallel planes treated by initial value method 24 p4144 A67-42562

Three-dimensional flow across supersonic single rotor axial compressor subsonic at rotor entry and exit 24 p4092 A67-42661

Two-and three-dimensional laminar viscous boundary layer flow nonlinear partial differential equations solved analytically, studying difference equation substitution 24 p4145 A67-43087

THREE-DIMENSIONAL MOTION

Three-dimensional problem of optimizing motion of two-stage rocket in homogeneous parallel force field with limited thrusts in engine of both stages 01 p0154 A67-10993

Analytical and p-analytical functions of complex variable used to solve three-dimensional axisymmetric problems in elasticity theory 02 p0338 A67-11967

Low thrust engine spacecraft control during boost phase, independent of velocity vector determination, by stabilizing osculating orbit plane relative to planetocentric coordinate system 11 p1869 A67-24088

Electromagnetic component /Vectorsyn/ for improving mass element restraint and support for three-axes acceleration measurement system 12 p1947 A67-26123

Three-dimensional elastostatic problems for infinite solid with geometric discontinuities solved using potential functions 13 p2221 A67-27735

Integral multiplicity calculation procedure for meson component of cosmic rays based on three-dimensional elementary event model, noting meteorological effects 17 p2934 A67-32104

Stress waves propagating in half-space due to point load on surface studied initially in three-dimensional dynamic photoelasticity 17 p2959 A67-32415

Analytical and p-analytical functions of complex variable used to solve three-dimensional axisymmetric problems in elasticity theory 17 p2966 A67-33284

Nonlinear analysis of earth-moon system motion stability in three dimensions near L4

- libration point when perturbed by sun 19 p3328 A67-35962
- Stability of three-dimensional oscillations of solid body coupled to periodically vibrating base by elastic springs 20 p3485 A67-36917
- Three-dimensional generalization of Birkhoff transformation for regularization of Keplerian motion in three-body problem noting differential equations 22 p3881 A67-39513
- Peripheral jet GEM pitching characteristics analysis by longitudinal static stability and dynamic pitching motion 22 p3745 A67-39837
- Cosmic ray fluctuations without imposing limitations on particle scattering, deriving expressions using three-dimensional cascade shower theory 22 p3873 A67-39880
- Three-dimensional periodic motion about collinear Lagrangian equilibrium points, determining motion, variational and orbit equations and numerical integration 22 p3889 A67-40427
- THREE-FLUID MODEL**
- Wave equations for disturbances in partly ionized gas due to current sources determined, using three-fluid-model 17 p2906 A67-33056
- THRESHOLD**
- SA NOISE THRESHOLD**
- Threshold energy for electron radiation damage in Ag compared for liquid He and liquid Ni temperatures 04 p0638 A67-15115
- Absolute threshold of cat optic nerves determined by inspection of poststimulus time histograms, computed from responses of identical flashes of white light 10 p1598 A67-23581
- Stimulus thresholds for perception of angular acceleration in man 15 p2427 A67-29267
- Measurement of ensemble distribution of intensity fluctuations of laser radiation at threshold 18 p3098 A67-33522
- Threshold characteristics of systems for multistate orthogonal transmission of coded analog signals in communication systems 18 p3000 A67-34023
- Threshold power dependence on temperature and photoelasticity for stimulated Brillouin scattering in crystalline and fused quartz 24 p4204 A67-42365
- THRESHOLD CURRENT**
- Pulse length of collector current pulse, which causes secondary breakdown in transistors, measured at constant forward or reverse base current 02 p0223 A67-12657
- Threshold current density dependency on photon energy in gallium arsenide laser diodes 03 p0379 A67-13480
- High magnetic field effect on interband semiconductor laser, particularly electromagnetic modes and coupling and threshold current conditions 05 p0822 A67-16673
- Refractory metals and metal alloys analyzed regarding electron work function and threshold temperature for surface ionization in all-metal guard ring diode with directly heated wire [AIAA PAPER 66-223] 06 p1035 A67-18137
- Temperature dependence of threshold current in injection lasers in continuous operation under liquid nitrogen cooling 06 p1012 A67-18788
- Room temperature laser threshold reduction and stimulated emission delay in GaAs diffused junction diodes 11 p1803 A67-24911
- Ionized multiwatt argon lasers, discussing relation between output power and discharge current, gas pressure, magnetic field and tube bore size 12 p1953 A67-26159
- Temperature and carrier concentration effect on threshold electric field of current saturation and saturation drift velocity in gallium arsenide 14 p2364 A67-27826
- Ionization threshold energy of electrons and holes in silicon 14 p2368 A67-28535
- Transverse magnetic field effect on induced emission of GaAs diodes 15 p2543 A67-30251
- Temperature dependence of threshold current in injection lasers in continuous operation under liquid nitrogen cooling 18 p3059 A67-33730
- Glass semiconductor threshold switches application in memory-addressing circuits, decoding matrices and current dividers 18 p3012 A67-34489
- Destructive breakdown conduction in aluminum-silicon oxide-aluminum capacitors, discussing voltage threshold, etc 18 p3105 A67-34630
- Photon generation threshold energy temperature dependence for gallium-arsenic epitaxial injection lasers 19 p3238 A67-34773
- Conditions of stable burning of electric arc stabilized by gas stream in DC plasma arc torch, determining threshold current 19 p3281 A67-35150
- Multiquantum photoionization applied to laser-induced breakdown thresholds in cesium and rubidium vapors 19 p3241 A67-35810
- Generation threshold of substance with electronic-vibrational energy level studied for laser use 19 p3309 A67-36105
- Radiation effects on MOS devices, analyzing electrical characteristics degradation mode and conduction threshold voltage variation 20 p3396 A67-36321
- Near-threshold behavior of phase-locked devices, noting phase error processes 20 p3385 A67-37350
- Volt-ampere characteristics of n-type GaAs at high fields above Gunn threshold, showing saturation, space charge effect and current controlled negative resistance 21 p3679 A67-38260
- Solution grown GaAs laser diodes with Fabry-Perot cavity, measuring threshold current density variation with reciprocal laser diode length 21 p3641 A67-38457
- Threshold properties of CW laser oscillation at 7525.5 angstroms in DC-excited KrII discharge 22 p3818 A67-40490
- Threshold voltage for onset of image-spot blurring of field-ion microscope screen and function of tip temperature 23 p3998 A67-40896
- Ionization threshold energy of electrons and holes in silicon 23 p4040 A67-40942
- THRESHOLD DETECTOR**
- Automatic threshold control formulation and probability distribution of adaptive detection mode for matched and mismatched clutter model 02 p0203 A67-12139
- Noise rejection properties of threshold devices with storage circuit calculated on basis of intersection probability of fixed level by storage circuit output voltage 02 p0205 A67-12533
- Probability density and distribution function of random function threshold overshooting 04 p0657 A67-14888
- Multichannel sequential detection in case of reception through independent multiple channels with noise 05 p0765 A67-16953
- Threshold characteristics of photoresistors with noiseless contacts on CdS base 07 p1152 A67-19592
- Solid state microwave square law detectors, comparing threshold response for unit video bandwidth using Noise Equivalent Power /NEP/ concept 08 p1304 A67-21220
- PCM frame synchronization with self-varying threshold detector 11 p1764 A67-24434
- Noise rejection properties of threshold devices with storage circuit calculated on basis of intersection probability of fixed level by storage circuit output voltage 14 p2261 A67-28010
- Threshold characteristics of photoresistors with noiseless contacts on CdS base 20 p3401 A67-37331
- Self-variable threshold method for synchronization code detection of PCM telemetry signal 21 p3583 A67-38641
- THRESHOLD GATE**
- Anomalous shift in gate threshold voltage of high transconductance p-channel MOSFETs during exposure to space-like radiation 13 p2076 A67-26516
- MOS transistor channel conductance measured as function of gate voltage, noting variation with temperature 14 p2289 A67-28924
- Photomultiplier gate for stimulated spontaneous light scattering discrimination, showing high cut-off efficiency, linearity and absence of spurious effects 17 p2863 A67-33353
- Noise factor variations with source resistance for MOST in common-gate and common-source connections, showing advantage of low noise operation 22 p3773 A67-40309
- THRESHOLD LOGIC**
- Computer-implemented minimization techniques used to determine realizability of N-variable switching function with single threshold-element device 13 p2073 A67-27065
- Nonlinear decision surfaces determined by pattern-recognizing adaptive threshold device via generation of polynomial discriminant functions and computer programs 18 p3006 A67-34064
- Digital switching functions and pattern recognition realization through computer-programable algorithm for designing feed-forward threshold logic nets 21 p3588 A67-38182
- THRESHOLD SHIFT**
- Threshold reduction in phase locked loop by retarding phase of return signal from voltage controlled oscillator to phase detector 06 p0969 A67-18109
- Field emission from sharply pointed CdS single crystals photon-enhanced by illumination from pulsed argon-ion laser 11 p1845 A67-24133
- Anomalous shift in gate threshold voltage of high transconductance p-channel MOSFETs during exposure to space-like radiation 13 p2076 A67-26516
- THROAT**
- SA PHARYNX**
- SA THYROID**
- Turbulent heat transfer to noncircular throat bodies with and without water film cooling 04 p0728 A67-15803
- THROTTLING**
- Internal ballistic considerations in hybrid rocket design, noting throttling and regimes of operation involving effects of surface-or gas-phase reaction kinetics [AIAA PAPER 66-628] 07 p1240 A67-19377
- Supersonic transport vehicle throttle schedule, comparing point performance, indirect and gradient optimization techniques 15 p2418 A67-29406
- Design for throttling and pulsing operation of rocket engine, discussing test data [AIAA PAPER 67-506] 18 p3113 A67-33970
- THRUST**
- S DUAL THRUST**
- S JET THRUST**
- S MICROTHRUST**
- S NOZZLE THRUST COEFFICIENT**
- S ROCKET THRUST**
- S VARIABLE THRUST**
- THRUST AUGMENTATION**
- Jet engine thrust augmentation by controlled mixing of exhaust gases with ambient air 07 p1242 A67-20119
- Thrust augmentation ratio for hovercraft, lift ratio obtained by annular jets of same mass flow and total energy in ground effect and free flight conditions 15 p2419 A67-29674
- European heavy launching vehicle development potential and economy, discussing communication satellites, thrust augmentation, zero stages, synchronous orbit, etc 18 p3137 A67-34353
- Thrust augmented maneuvering /TAM/ for lifting reentry vehicle compared with other glide vehicles using lift/drag ratio 20 p3533 A67-36584
- Helicopter maximum speed increase by generating supplementary forward thrust or additional wings 22 p3744 A67-39540
- SST engines design, combustion and thrust augmentation systems, engine controls and complications facing users [SAE PAPER 670865] 24 p4207 A67-42005
- THRUST BEARING**
- Thermal distortion due to viscous heating in fluid film effects on load capacity of spiral-grooved gas-lubricated thrust bearing [ASME PAPER 66-LUB-10] 03 p0432 A67-13765
- MHD lubrication flow in externally pressurized thrust bearing analyzed, including fluid inertia effects 04 p0627 A67-14461
- Book on spiral groove thrust bearings calculation, use and transmitting force in direction of axis of rotation 06 p1007 A67-17893
- Film thickness effect on pressure generation of parallel surface thrust bearing investigated, using dynamic instrumentation mounted in moving surface 09 p1505 A67-22192
- High speed linear bearing to take launch uploads in aircraft-launching steam catapult 12 p1948 A67-25328
- Design and applications of gas-lubricated journal and thrust bearings of self-acting and externally pressurized

types 21 p3632 A67-38137
 Gas bearings with wide pockets
 investigated theoretically and experimentally
 for pressure distribution, flow quantity and
 load capacity 23 p4010 A67-41065
 MHD lubrication flow in self-acting step
 type thrust bearing configuration, showing
 torque reduction 24 p4162 A67-42566
 Boundary layer theory in gas bearing
 lubrication problems, obtaining pressure
 asymptotic expansions for infinitely long
 slender squeeze-film bearing
 [ASME PAPER 67-LUB-7] 24 p4162 A67-42671

THRUST CHAMBER**S COMBUSTION CHAMBER****S ROCKET CHAMBER****THRUST CONTROL**

Solid booster thrust decay control for
 payload or upper stage separation, noting
 inert slivers with auxiliary retrorockets as
 separation control 02 p0304 A67-12293
 [AIAA PAPER 66-971]

Synchronous orbit stationkeeping
 techniques, examining thrust control
 requirements of spin-stabilized
 spacecraft 06 p1094 A67-17679

Thrust magnitude and restart control of
 solid propellant motor by injection of
 fluorine and chlorine trifluoride 08 p1376 A67-21518

Optimum propulsion control law selection
 for limited motion capacity in mass
 accumulation regime determined, considering
 two-dimensional problem of vehicle
 motion 12 p1989 A67-25659

Electron bombardment ion thrusters with
 two accelerator-grid systems for producing
 ion beams in directions 180 or 90 degrees
 apart [AIAA PAPER 66-284] 12 p1990 A67-25891

Pontryagin maximum principle application
 to solution of one-dimensional minimum
 time rendezvous problem for thrust limited
 rocket with initial and final mass
 specified 12 p2012 A67-25922

Spacecraft guidance problem, examining
 general and one specific solution using
 boundary value problem and correction
 function 13 p2153 A67-26620

Nongeometric derivation of solution
 equations for cotangential orbital
 transfer 14 p2384 A67-28134

Analytic solution obtained for minimum
 impulse transfer between two neighboring
 low eccentricity orbits 15 p2554 A67-29405

Set of linearized motion equation for ferry
 vehicle to obtain optimal-thrust during
 rendezvous attempt with orbital
 satellite 15 p2571 A67-30049

Continuous nonlinear feedback law for
 controlling thrust direction to produce
 minimum time spacecraft rendezvous with
 nonmaneuvering target 16 p2758 A67-30651

Liquid-bipropellant pressure-fed propulsion
 systems in lower thrust range and use for
 spacecraft maneuvering 16 p2736 A67-30707

Design for throttling and pulsing operation
 of rocket engine, discussing test data
 [AIAA PAPER 67-506] 18 p3113 A67-33970

Conditions for optimal planar
 intermediate-thrust /singular/ trajectory in
 inverse-square-law field analyzed
 graphically 19 p3333 A67-35749

Manual control stationkeeping simulation,
 studying tether visual rendezvous techniques
 and fuel economy [AIAA PAPER 67-617] 19 p3337 A67-36006

Economical Hohmann type orbital transfer
 between coplanar circular orbits with fixed
 duration and limited thrust 20 p3527 A67-37258

Iterative guidance mode, deriving
 alternate expressions for thrust direction
 control angle for time savings on Saturn
 launches 22 p3831 A67-39957

Propulsion and time requirements for low
 gravity liquid settling obtained from known
 Bond number 22 p3869 A67-40171

THRUST EFFECT

Flight performance and low speed
 behavior of V/STOL aircraft, noting
 correlation between thrust angle and aircraft
 attitude 02 p0180 A67-11524

Optimal rocket trajectories, discussing role
 and significance of intermediate thrust arcs
 of rocket extremals in vacuum 02 p0335 A67-12397

Specific impulse and thrust coefficient
 performance as function of flight Mach
 number and altitude for air augmented solid

propellant propulsion vehicle using
 supersonic combustion 06 p1097 A67-18517
 [AIAA PAPER 67-226]
 Escape of rocket vehicle from vicinity of
 planet, using tangential thrust
 [AAS PAPER 66-120] 07 p1254 A67-19979
 Expressions showing possibilities to
 change independently all orbital elements of
 spacecraft by means of small continuous
 thrusts achieved through electric
 propulsion 08 p1413 A67-21365
 Optimal transfer of thrust limited vehicle
 between coplanar circular orbits 09 p1571 A67-21694

Asymptotic calculation of effect of small
 tangential thrust on satellite motion problem
 solved for satellite orbit in first and second
 approximation 11 p1870 A67-24684

Space vehicle flight control with minimum
 total characteristic velocity, determining
 optimum points for applying correcting
 acceleration 13 p2213 A67-27320

Escape of rocket vehicle from vicinity of
 planet, using tangential thrust
 [AAS PAPER 66-120] 13 p2209 A67-27534

Approximate analytical solution for
 satellite circular orbits subjected to small
 tangential thrust or drag 14 p2384 A67-28117

THRUST MEASUREMENT

Space inertial sensors for long-term
 orbiting satellites and interplanetary
 missions will require capability of measuring
 very low-level acceleration 01 p0074 A67-11125

Engine test facility for measuring thrust
 and propellant flow in pulsating
 rockets 03 p0396 A67-13774

Thrust and mass flow rate of supersonic
 nozzle with and without internal
 separation 04 p0602 A67-14568

Impulse measurements of small electric
 engines by vacuum microbalance technique,
 also suitable for average thrust
 measurements in millipound and micropound
 ranges 04 p0620 A67-14734

Thrust measurement for microthruster
 mounted on platform suspended from cable
 whose motion is sensed by autocollimator
 system [ASME PAPER 66-WA/AUT-8] 04 p0599 A67-15390

Supersonic combustion measurements by
 thrust system method, optical probe and
 gas-sample probe technique [AIAA PAPER 67-223] 06 p1004 A67-18462

Axial current distribution in exhaust of
 magnetic annular arc, examining effect of
 entrainment on thrust measurement 06 p1075 A67-18850

Rocket engine thrust measuring system
 for accuracy analysis 08 p1375 A67-20779

Electron bombardment thrusters using
 liquid mercury cathodes noting lifetime,
 propellant and power efficiency, feed
 system, temperature limits, etc 13 p2188 A67-26822

Local mass flux and local impact pressure
 measurement in arc jet exhaust flow
 fields 17 p2861 A67-33029

Optimal layout of turbofan jet engines,
 discussing experimental rig for high thrust
 measurement [AIAA PAPER 67-416] 18 p3111 A67-33903

M-1 Engine Thrust Chamber Assembly test
 facilities and analog computer simulation
 during checkout [AIAA PAPER 67-455] 18 p3019 A67-33929

Lithium and ammonia MPD arc thrusters
 tests in low environmental pressure
 [AIAA PAPER 67-685] 21 p3692 A67-38716

Instrumentation systems for measuring
 thrust and electric power input of
 electromagnetic induction plasma thruster
 [AIAA PAPER 67-739] 21 p3695 A67-38761

Colloid microthruster technology,
 discussing stationkeeping application, energy
 loss, diagnostic techniques, etc [AIAA PAPER 67-531] 22 p3867 A67-39200

Electromechanical servosystem in
 conjunction with inductive pickup circuit for
 thrust measurements in jet engine bed
 tests 22 p3797 A67-39536

THRUST POWER

Radioisotope application to spacecraft
 propulsion and integrated power noting
 potential sources, thruster design concepts
 and mission types 04 p0855 A67-14554

Propulsion systems for satellite attitude
 control, considering weight and thrust
 efficiency parameters 05 p0905 A67-16729

Finite thrust explicit guidance law for

nearly circular orbital
 rendezvous 05 p0906 A67-17208
 Radioisotope application to spacecraft
 propulsion and integrated power noting
 potential sources, thruster design concepts
 and mission types 13 p2155 A67-26578

Formula for thrust derived from
 thermodynamic steady flow energy
 equations 15 p2472 A67-29673

Vehicle mass requirements for optimal
 high and low thrust propulsion systems for
 manned and unmanned planetary
 missions 20 p3533 A67-37125

Thrust staging for optimum thrust
 program without coasting phase for ascent
 from low orbit 23 p4071 A67-41331

Performance and feasibility of staged
 propulsion during terminal phase of Mars
 soft landing [AIAA PAPER 67-987] 24 p4246 A67-43059

THRUST PROGRAMMING
 SA OPTIMUM THRUST PROGRAMMING
 Graphic solution of Lambert time of flight
 equation for spacecraft correctional
 maneuvers with respect to initial
 velocity 01 p0152 A67-11399

Thrust deflection in hypersonic air
 breathing vehicles, noting increased cruise
 range and effects of gross thrust/ram drag
 ratio 09 p1441 A67-22497

Rocket control using analog computers,
 determining thrust vectors for
 trajectory 21 p3655 A67-38208

THRUST REVERSER
 Thrust reversers for business jet aircraft
 noting limitations, performance gains,
 technical aspects of analysis and testing, etc
 [SAE PAPER 670235] 12 p1989 A67-25493

Turbofan jet propulsion system reversed-
 thrust, discussing momentum net change,
 external drags, clamshell and annular targets
 and cascade reversers [AIAA PAPER 67-418] 18 p2982 A67-33905

THRUST TERMINATION
 Dynamic ballistics of combustion
 termination by fluid injection in solid
 propellant motors, describing termination
 mechanisms 21 p3733 A67-38893

THRUST VECTOR CONTROL /TVC/
 Propellant and time-optimum trajectories
 with thrust vector rotational velocity at
 flight beginning and termination taken as
 additional boundary condition analyzed,
 using maximum principle 01 p0146 A67-10209

Thrust reverser efficiency on high by-pass
 ratio turbofan engines [SAE PAPER 660736] 01 p0140 A67-10635

Thrust deflection and vectoring in
 European V/STOL aircraft, noting single-
 sided deflector, tilting-pod engine
 configuration and vectoring nozzle
 [SAE PAPER 660738] 01 p0140 A67-10637

Jet direction variation via secondary fluid
 injection resulting in booster trajectory
 control, increased payload and
 reliability 01 p0142 A67-11409

Elastic structural vibrations of vehicle
 effect on position of engine thrust vectors
 with respect to undisturbed nonvibrating
 vehicle 02 p0335 A67-12732

TVC flight dynamics and trajectory
 optimization analysis of pulse, singular and
 sliding regimes 03 p0509 A67-13184

Microthrust ion engine system with thrust
 vector control, using ion beam deflection
 [AIAA PAPER 66-204] 04 p0706 A67-15241

Burning, staging and thrust direction
 programs for range maximization of particle
 in planar motion under downward
 gravitational acceleration and linear
 drag 05 p0905 A67-16780

Primer vector of fixed-time impulsive
 thrust trajectories [AIAA PAPER 67-54] 06 p1086 A67-18352

Structural compliance induced cross axis
 coupling effect on gimballing system
 stability of rocket engine two-axis attitude
 TVC system [AIAA PAPER 67-42] 06 p1097 A67-18423

Thrust vector control by supersonic
 splitline gimbal nozzle, considering linear
 aerodynamics to understand magnitude of
 spring rate torque component 07 p1126 A67-19376

Manual thrust vector control development
 for Apollo Command and Service Module
 Stabilization and Control System
 [AIAA PAPER 67-243] 07 p1260 A67-20043

Digital fluoric amplifier of gyroscopic
 signals for proportional thrust
 control 08 p1282 A67-20465

Low thrust engine spacecraft control during boost phase, independent of velocity vector determination, by stabilizing oscillating orbit plane relative to planetocentric coordinate system 11 p1869 A67-24068

Thrust vector controls for solid rockets, discussing liquid secondary injection, jet tabs, direct chamber bleed, omnialxial movable nozzle and lockseal 15 p2545 A67-29136

Hohmann-type orbital transfer between two coplanar concentric circular orbits by short duration powered flight with finite constant thrust 16 p2744 A67-30736

Lunar orbiter velocity control system design, discussing interface problems between actuator electronics and flight control system [AIAA PAPER 67-504] 18 p3137 A67-33968

Rocket control using analog computers, determining thrust vectors for trajectory 21 p3655 A67-38208

Rocket engine cluster thrust and moment vectors analyzed statistically for thrust misalignment 22 p3869 A67-40170

Structural compliance induced cross axis coupling effect on gimballing system stability of rocket engine two-axis attitude TVC system [AIAA PAPER 67-42] 24 p4242 A67-42909

THRUST-WEIGHT RATIO

Design aspects of power plants for V/STOL aircraft, examining lift jets, thrust vectoring and lift fans [ASME PAPER 67-GT-7] 11 p1744 A67-24795

Geomagnetic thruster, noting superiority over electric or chemical propulsion for thrust durations of more than few weeks 11 p1855 A67-25009

Jet VTOL aircraft problems, considering vertical thrust/aircraft weight, thrust application to aircraft gravity center, stability in hovering, thrust exertion, etc 17 p2796 A67-32392

Ascent of satellite of variable mass from elliptic orbit along spiral trajectories by low thrust 17 p2948 A67-33022

Optimal thrust-weight ratio for lifting engines of VTOL aircraft 18 p3110 A67-33544

Commercial aircraft noise system solution, considering engines, nacelles, operational procedures and airport options [AIAA PAPER 67-761] 23 p3933 A67-40992

Parametric investigation of propulsion system effect on takeoff weight of VTOL subsonic ground combat aircraft 23 p3934 A67-41315

THRUSTOR

SA PROPELLANT ACTUATED DEVICE

Resistojet and axisymmetric electromagnetic space propulsion thrusters 02 p0305 A67-12340

Colloid particle electrostatic thrusters for lunar ferry missions in specific impulse range 1000-3000 sec 03 p0503 A67-13492

Flow meter for extremely low flow rates during steady state and pulse mode thruster operation 03 p0422 A67-13776

Electric propulsion status of thruster performance, promises and potentialities [AIAA PAPER 66-1024] 03 p0504 A67-14155

Comparison of performance of atom-ion and colloidal thruster systems for orbital transfers, noting influence of various parameters on mission 04 p0688 A67-14560

Thrust measurement for microthruster mounted on platform suspended from cable whose motion is sensed by autocollimator system [ASME PAPER 66-WA/AUT-8] 04 p0599 A67-15390

SNAPOODLE isotope thruster/electric power unit, discussing thermal analyses, thruster and electrical performance and mission applications 05 p0753 A67-18552

Electric thrusters and electric propulsion, examining overall efficiency as function of specific impulse 05 p0874 A67-16933

Solar electric spacecraft performance in specific Mars orbiter-lander mission evaluated, using characteristic length concept 06 p1074 A67-18276

Electric propulsion unit using electron cyclotron resonance plasma thruster for spacecraft 06 p1074 A67-18418

Advanced low thrust propulsion systems and propellants evaluation for stationkeeping and stability control of NASA Manned Orbital Research Laboratory

[AIAA PAPER 66-226] 07 p1240 A67-19365

Solid propellant highly restartable electric trigger microthruster, noting triggering electrode and feed system 11 p1746 A67-25013

Cartridge-actuated thruster system design for jettisoning Apollo spacecraft heat shield for recovery system deployment [ASME PAPER 67-DE-34] 14 p2394 A67-28875

Primary electric propulsion application to satellite and other space missions, considering auxiliary systems and experimental thruster systems [AIAA PAPER 67-426] 18 p3112 A67-33910

Cathode phenomena in plasma thrusters with self-magnetic acceleration low mass-flow rates 19 p3297 A67-35600

Model thruster designed and operated with argon and hydrogen for investigation of hybrid flow fields of plasma acceleration by thermal and magnetic forces [DVL-630] 19 p3297 A67-35601

Comparison of performance of atom-ion and colloidal thruster systems for orbital transfers, noting influence of various parameters on mission 20 p3515 A67-36407

Solid propellant electric thruster /SPET/ using pulse plasma for spacecraft attitude control and stationkeeping [AIAA PAPER 67-661] 21 p3690 A67-38697

Single nozzle thermal storage resistojet thruster for low thrust satellite attitude and orbit control applications, noting design and performance [AIAA PAPER 67-662] 21 p3690 A67-38698

Liquid metal cathode electron bombardment thruster operable at high temperatures, noting stability in neutralizer current range [AIAA PAPER 67-667] 21 p3690 A67-38701

Optimum discharge chamber configuration of permanent magnet mercury-bombardment thruster for SERT II mission [AIAA PAPER 67-668] 21 p3691 A67-38702

Anode heat transfer in MPD arc, discussing configurations and thrusters [AIAA PAPER 67-673] 21 p3691 A67-38706

Arc jet power efficiencies tested in insulated tank, comparing deuterium with hydrogen [AIAA PAPER 67-677] 21 p3691 A67-38710

Conventional and composite grid designs tested with low voltage Kaufman thruster [AIAA PAPER 67-680] 21 p3692 A67-38711

MPD plasma accelerator for spacecraft propulsion system, performance data and proposed acceleration mechanisms [AIAA PAPER 67-688] 21 p3693 A67-38719

Space electric rocket test /SERT/ II thruster system, discussing flight worthiness and mercury bombardment discharges [AIAA PAPER 67-700] 21 p3693 A67-38728

Kaufman thruster with curved stainless steel accelerating-grid system, studying operation, efficiency, plasma instability, etc [AIAA PAPER 67-725] 21 p3694 A67-38750

Charged particles generation by liquid subjected to high electric field for efficient bipolar microthruster [AIAA PAPER 67-728] 21 p3694 A67-38752

Radioisotope heating for ionizer temperature of contact ionization thrusters for satellite attitude control and stationkeeping, studying power source mass saving [AIAA PAPER 67-735] 21 p3695 A67-38758

High endurance thermionic cathodes for Kaufman thrusters, discussing emissive coatings and emissive layer starvation [AIAA PAPER 67-678] 21 p3696 A67-38929

Steady flow ammonia MPD arc jet thruster propulsion performance, discussing test chamber pressure variation, thrust data and cooling systems [AIAA PAPER 67-690] 21 p3696 A67-38930

Mass flow rate, viscosity and conductivity changes effects on single needle colloid thruster [AIAA PAPER 67-530] 21 p3696 A67-38957

Neutralizer for large mercury thruster systems using hollow cathode forming plasma bridge neutralizer for large mercury thruster systems using hollow cathode forming plasma bridge [AIAA PAPER 67-671] 21 p3697 A67-38958

Colloid microthruster technology, discussing stationkeeping application, energy loss, diagnostic techniques, etc [AIAA PAPER 67-531] 22 p3867 A67-39200

Synchronous orbit communication satellite electric thruster, considering space charge neutralized ion accelerator 23 p4049 A67-41428

Primary electric propulsion application to satellite and other space missions, considering auxiliary systems and experimental thruster systems [AIAA PAPER 67-426] 24 p4208 A67-42901

Kaufman mercury-ion thruster grid design, discussing radial slot configuration 24 p4208 A67-42929

THUNDERSTORM

Weather satellite system determining worldwide occurrence and distributions of thunderstorms and associated atmospheric effects 02 p0262 A67-12399

Geometric and thermal height of shower and storm cells using radar observations 13 p2150 A67-26433

Atmospherics characteristics at source and propagation 14 p2265 A67-28412

Correlation of diameter of cirrus cloud shield and severity of thunderstorm complex 17 p2880 A67-32554

Thunderstorm electric circuit physics with atmospheric electric conductivity and variation with height, noting atmospheric electric fields and currents 18 p3074 A67-33996

Main processes pertinent to convective storm development, with emphasis on structure and mechanics of storms already formed 18 p3074 A67-34094

Thunderstorms endanger air traffic and travel, considering turbulence, ice formation, hail and lightning 23 p4025 A67-41303

THYRATRON

Multiunit thyatron generator for producing complex shaped pulses through rectifier control 03 p0388 A67-14267

Pulsed radar transmitter research in U.K., noting beam type microwave tubes, solid state switches, hydrogen thyratrons, etc 04 p0581 A67-15052

Generators of sonic and ultrasonic frequencies using thyristors 05 p0773 A67-16458

Memory device for matrix time meter, discussing use of logic thyatron to improve stability of memory matrix 16 p2674 A67-31119

Ring circuit using glow-discharge thyratrons to combine functions of pulse indicator and pulse counter with decimal readings 19 p3228 A67-34990

Thyatron circuit for generating high repetition rate high energy pulses, discussing design considerations and modifications 20 p3397 A67-36527

THYRISTOR

Thyristor assemblies /dimers/, for control of power supply, noting operation principles and examples cited 16 p2641 A67-31566

Power semiconductor devices, emphasizing thyristors and silicon rectifier diodes applications 20 p3397 A67-36643

Laser-diode impulse generator construction by four-layer diodes and thyristors supplying high current intensity short impulses to low resistance load 21 p3639 A67-37945

High power thyristor used with battery to operate pulse repeating sonar transducer 22 p3747 A67-39255

RF generation in VLF/LF thyristor transmitter for applications in long distance communications and navigation 22 p3771 A67-39842

THYROID

Rats exposed to simulated altitude studied for acute changes in iodine metabolism, noting dichotomy between thyroidal iodine uptake and secretion rates 15 p2428 A67-29279

Mammalian porcine thyrocalcitonin extract effect on concentrations of serum calcium and phosphate in catfish 20 p3372 A67-37277

THYROXINE

S HORMONE

TIDAL OSCILLATION

Forecasting length of solar cycle and maximum value of sunspot numbers, suggesting relation to joint tidal effect of Venus-Jupiter-earth 01 p0149 A67-10805

Objection to Martin ionospheric drift theory based on dynamo electric field, atmospheric tidal wind field and F-2 layer drift motion 05 p0796 A67-16063

Tidal friction and effect on evolution of earth-moon system with respect to moon capture 08 p1389 A67-21015

Lunar orbit evolution caused by tidal friction in earth and moon interiors 09 p1563 A67-21634

Tidal force effect on variations of critical frequencies of sporadic E layer 10 p1631 A67-22806

Eigenvalue and Hough functions for diurnal and semidiurnal components and both symmetric and antisymmetric modes of atmospheric tides 10 p1634 A67-23052

Atmospheric tides, shorter period gravity waves and shear waves 10 p1643 A67-23249

Partial coherence functions to investigate contribution of solar radiation and gravitational tide in causing geomagnetic variations /ionospheric tides/ 11 p1785 A67-23938

Eigenvalues of Laplace equation for diurnal and semidiurnal tidal oscillations solved using Galerkin method 13 p2112 A67-26668

Thermal conduction and viscosity and energy propagation upward in atmospheric oscillation theory 13 p2114 A67-26742

Lunar periodic variation of geomagnetic field on Khels Island in Franz Joseph Land 14 p2309 A67-27938

Ionospheric E region dynamical processes, discussing energy phenomena of planetary waves, tidal oscillations and gravity waves 14 p2311 A67-28408

Planetary influences on sunspot formation and disappearance showing periodicity in Zurich relative daily sunspot number 17 p2943 A67-32439

Tidal force effect on variations of critical frequencies of sporadic E layer 24 p4150 A67-42143

Friction in solid parts of earth and moon considered as sink for tidal energy and as geophysical thermal energy source 24 p4229 A67-42316

TIDE

SA ATMOSPHERIC TIDE

SA LUNAR TIDE

Tidal friction theory of lunar origin and dynamic evolution [AAS PAPER 66-192] 08 p1387 A67-20965

TIG

S TUNGSTEN INERT GAS /TIG/ WELDING

TILT-WING AIRCRAFT

XC-142A tilt-wing deflected slipstream aircraft designed to take off and land in virtually any terrain and achieve 430 plus mph 03 p0357 A67-12971

VTOL aircraft configurations features and characteristics including helicopter, compound, composite, tilt-wing, lift-fan, lift/cruise and lift engine [SAE PAPER 67-0686] 24 p4093 A67-41987

TILTED PROPELLER AXIS

Large diameter helicopter rotors and V/STOL propellers /axis tilting in vertical plane/ testing system of wind tunnel and aerodynamic torque measuring apparatus 23 p3986 A67-40575

TIME

S ELECTRON DECAY TIME

S EPHEMERIS TIME

S FIRING TIME

S FLIGHT TIME

S LAUNCH TIME

S LIFETIME

S PULSE DURATION

S PULSE TIME MODULATION /PTM/

S REACTION TIME

S REAL TIME

S RELAXATION TIME

S REVERSE TIME

S TEST TIME

S TRANSIT TIME

S UNIVERSAL TIME

TIME CONSTANT

Time constants of thermocouples as function of parameters on which they depend, using schlieren phenomena 04 p0624 A67-15417

Time constant and control channel lag effects on size and configuration of platform stability region 04 p0552 A67-15883

Onset of oscillation in He-Ne laser analyzed using Lamb theory, obtaining time constant value for population of lower laser level 05 p0824 A67-16821

Time constant determination for passive controlled plant with generalized nonlinear statistical characteristics, from response to sawtooth pulse probing 06 p0976 A67-18240

Vector equation for determining missile maximum roll rate for effective navigation

ratio and time constant for guidance systems 11 p1816 A67-24215

Plasma column deviation from static state analyzed for time constants, considering conductivity and temperature change rates 12 p1973 A67-25394

Heat receiver with correcting device for instantaneous temperature measurements in unsteady gas flow, discussing matching of time constants and heat-transfer coefficients 13 p2118 A67-26352

Ablation study scheme enabling determination, for given environment and material, of ablation starting time and temperature distribution within mass of material 13 p2222 A67-26596

Time resolution amplification of flash spectroscopy apparatus equipped with switched laser 13 p2126 A67-26599

Charge equation of enhancement-type MOS transistors, determining waveforms and switching times of resistor-coupled switching circuit 13 p2078 A67-26786

Automatic signal gain control system under constraints, determining time constants for signal filtering 13 p2088 A67-27041

Giant pulse time evolution influenced by pump-induced material inhomogeneities studied by analyzing laser rate equations 15 p2498 A67-29484

Field effect transistor intrinsic and extrinsic transients, switching behavior and relation to time constant by charge concept 15 p2449 A67-29806

Celestial mechanics and Dirac hypothesis 15 p2563 A67-30123

Static and dynamic parameter estimation of nonlinear transfer elements from step responses 15 p2463 A67-30331

Time constants of fast photodetectors measured, using mercury wetted relay and epitaxial indium arsenide diode laser 18 p3046 A67-33746

Slowly decaying broad maximum of parallel conductance explained by tunneling for surface states near Si-silicon oxide interface 18 p3101 A67-34018

Multichannel radar formula for discriminating power in distance corresponding to time resolution constant 18 p3002 A67-34228

Electric conductance exponential decay in column of wall stabilized nitrogen arc after current interruption 19 p3282 A67-35157

Steering equation derived from dynamic equation of velocity gain, as function of booster state for rocket vehicle ballistic trajectory [AIAA PAPER 67-595] 19 p3259 A67-35991

Quantum mechanical transition time shown to be electron tunneling characteristic time 20 p3505 A67-36178

Time constants of sporadic E layer formation influenced by wind field containing strong vertical gradients 20 p3428 A67-36375

Distillation process in spherical pyranometer studied for time constants and sensitivity in calibration until reaching balanced state 21 p3627 A67-38445

Gyrostabilizer feedback circuit transfer function with two-phase asynchronous motor equivalent to unit having time constant as function of transmission band of amplifier 22 p3810 A67-40483

Explicit nonlinear numerical integration method for solution of large systems of ordinary differential equations 23 p4024 A67-41394

Photoelectromagnetic detector spectral sensitivity, magnetoresistance and time constants with optically polished thin elements fabricated from Ge, InAs, GaSb and InSb single crystals 24 p4154 A67-42243

Steering equation derived from dynamic equation of velocity gain as function of booster state for rocket vehicle ballistic trajectory [AIAA PAPER 67-595] 24 p4182 A67-42910

TIME DELAY

SA CHRONOTRON

Current injection effect on time delay of GaAs laser radiation 01 p0087 A67-10083

Trigger circuits for generating sharply defined rectangular waves phase locked to repetitive signal 01 p0038 A67-10451

Frequency correlation of clutter by considering signal received by radar at time t after it has transmitted pulse 01 p0023 A67-10468

AC differential correlator for measuring small delays between two identical binary output waveforms 01 p0037 A67-10482

Pulsed chronotron vernier for precise time expansion, discussing circuit configuration operation and performance 01 p0087 A67-10658

Time expansion device for photomultiplier circuit for high pulse frequency using recording system, readout, thin film memory and simulation unit 01 p0029 A67-10662

All-pass RC filter network design for constant signal delay in LF systems, noting cascade phase characteristics 01 p0045 A67-11197

Perceived noise level calculator for immediate and continuous measurement in PNdB to overcome time delay 02 p0266 A67-11471

Resolution of telemetering event occurrence times with 1 and 2 microsecond accuracy, considering real time systems delayed time systems and hybrid time systems 02 p0197 A67-12012

Continuous linear programming problems with time delays in constraints, noting construction of solutions to dual problems from solution to primal problem 02 p0207 A67-12059

Kinetically based mathematical model of hypergolic ignition in space ambient engines for predicting delay time and conditions from which pressure spikes result [AIAA PAPER 66-950] 02 p0302 A67-12284

Stability analysis of spectrotron with external feedback based on time delay, inertia of nonlinear quadrupole and circuit phase shifts 03 p0377 A67-13092

Solution of optimum filtering problems when input signals of automatic control system are described by different differential equations at successive time intervals 03 p0390 A67-13099

Approximation of variable time delays and design of constant and variable delay circuits, noting simulation of delays in automatic control systems by computers 03 p0390 A67-13104

Linear optimal systems with time delays 03 p0392 A67-13270

Lumped-constant filters whose bandpass depends only on one parameter of transmission coefficient, having lower bandpass for given transient process delay time 03 p0380 A67-13582

Stabilization of steady state motion of controlled system described by nonlinear differential equations with time delays 03 p0392 A67-13588

Stability problem of steady motions, using differential equations with time delay 03 p0468 A67-13616

System Utilizing Signal-processing for Automatic Navigation, for moving vehicles, using time delays and frequency multiplication 04 p0653 A67-14870

Special modulation and detection processes enable radar target to be analyzed into dimensions of time delay and Doppler shift simultaneously 04 p0699 A67-15031

Computer simulation of hydraulic system using time delay elements independently of boundary conditions [ASME PAPER 66-WA/AUT-18] 04 p0555 A67-15413

Enhanced lasing of high pressure He-Ne laser, commenting on delay time of light pulse emitting through walls of discharge tube from start of exciting pulse 05 p0823 A67-16687

Hook whistler discovered in VLF radio noise data from Injun III satellite, noting time delay difference between components 05 p0799 A67-16888

Time delay measurements and radar echo determinations of planetary motions compared with IAU values 05 p0900 A67-17082

Simultaneous estimate of delay time and drift of carrier frequency during nonoptimum reception against correlated noise background 05 p0766 A67-17166

Errors by mutual interference in frequency-time coding in satellite communications systems, deriving expressions relating commissive and omissive error rates, simultaneous users per unit bandwidth, etc 06 p0961 A67-17696

Time optimal search algorithms in pulsed extremal control systems with inertial or transport delays for case with known time

constants and delay time 06 p0978 A67-18794
Formative time lag for pulsed RF breakdown in dry air as function of gas pressure and power of slot antenna 07 p1153 A67-19607
Time behavior of pulsed water vapor laser, noting spiking from far IR emission lines 07 p1197 A67-20095
Critical tracking task for man-machine research related to operator effective delay time 07 p1136 A67-20171
Delay time of avalanche discharge in silicon p-n junction as function of overvoltage 07 p1238 A67-20256
Maximal error estimation arising from delay in output functions of servomechanisms provided bandwidth, maximum oscillation and slope are known 08 p1286 A67-20780
Current injection effect on time delay of GaAs laser radiation 08 p1340 A67-21460
Stability of linear systems with time delay analyzed by introducing stability indicative function, noting applications to differential-difference equations 10 p1679 A67-22916
Time delay between geomagnetic storm and corresponding maximum in atmospheric density obtained from satellite drag data 10 p1639 A67-23209
Waveform independent condition for transmission coefficient in linear time-independent transmission system to provide upper limit to signal distortion 10 p1620 A67-23572
Satellite measurement of upper atmospheric density variations due to geomagnetic disturbances, correlating time delay with geographic latitude 11 p1783 A67-23922
IBM System/360 Model 91 machine organization alleviating disparity between storage time and circuit speed 11 p1755 A67-23949
Costs involved in delays occasioned by either ATC or airport acceptance rate for New York-Boston-Washington complex [SAE PAPER 670264] 11 p1884 A67-23987
Delay equalization in UHF range by allpass networks with symmetric three-conductor transmission lines 11 p1760 A67-24231
Transient emission characteristics of pulsed argon ion laser, noting capillary discharge due to radiation trapping effect 11 p1801 A67-24649
Forbush decreases associated with type IV burst flares, particularly in relation to PCA events, noting delay time and magnetic western boundary 12 p1992 A67-25129
Simulation of sampled data systems for pure servo delay by analog computer using potentiometer 12 p1919 A67-25203
Low cost time delay and multiple programmer for space research 12 p1909 A67-25230
Active filter design combining flat amplitude response with flat time delay 12 p1915 A67-25973
Determinants of electronically steerable antenna arrays 12 p1917 A67-26158
Contact-free controlled delay unit using shift register and clock-pulse generator for binary signals designed with wide range of time delay variation 13 p2088 A67-26798
System for rupturing diaphragms in single pulse shock tube, noting time decay role 13 p2090 A67-27060
Ordinary and time lag root locus diagram generating algorithm for adaptation to programming on digital computer 13 p2074 A67-27223
Frequency spread in ionospheric radio propagation 14 p2273 A67-28712
Planetary masses, radii and orbital element and astronomic unit determinations from radar time delay and Doppler shift measurements 15 p2556 A67-29871
Arc image ignition of solid propellants compared to conductive ignition, outlining corrective steps and deriving ignition time delay 15 p2581 A67-29987
Ionospheric movement detection using frequency swept sounder and rhombic antenna [AGARDOGRAPH 95] 15 p2484 A67-30301
Electronic equipment for generating delay times corresponding to missile velocity during optical recording by numerous sensors distributed along ballistic firing range 16 p2674 A67-31118
Necessity of incremental phase shift during IF time delay steering of antenna

array main beam 16 p2639 A67-31354
Plasma produced transit time delay of reflected pulses for collisionless inhomogeneous plasma 17 p2810 A67-32070
Hysteresis phenomena in curves describing cosmic ray intensity dependence on number of sunspots 17 p2933 A67-32087
Statistical behavior of two-way communication system with transmission delay 17 p2811 A67-32115
Delay time between current pulse and light emission of GaAs laser diodes, noting nonlinearity between current and delay time 17 p2824 A67-32316
Fluid dynamics and chemical phenomena near injector exit of idealized supersonic combustion burner, noting parameters of ignition delay length [AIAA PAPER 67-496] 18 p3158 A67-33960
Apollo ranging code with phase locked loop for bit synchronization, plotting SNR vs error probability and acquisition time 18 p3000 A67-34102
Geomagnetic activity effect derived from Explorer IX drag data, with atmospheric temperature as geomagnetic storm intensity function and atmospheric density increase 18 p3042 A67-34255
Synthesis of optimal and quasi-optimal sampled data control systems applied to various order plants 18 p3017 A67-34281
Human operator performance in continuous pursuit tracking with advanced and delayed visual display 18 p2994 A67-34339
Periodic solutions for quasi-harmonic time-lag system, proposing calculation for periodic regimes in form of integral series 18 p3079 A67-34371
Time optimal search algorithms in pulsed extremal control systems with inertial or transport delays for case with known time constants and delay time 18 p3018 A67-34459
Additives effect on ignition delay and pressure of hypergolic hydrazine-nitrogen tetroxide propellant systems 19 p3310 A67-35012
Instrument for measuring group delay time of microwave four-poles, using backward-wave tube as wave generator 19 p3193 A67-35032
Photon transmission delaying processes and secondary ionization growth time dependence on overvoltage in neon 19 p3264 A67-35086
Trigatron spark gap using low voltage plasma jet as switch analyzed for properties, time lag and mechanisms 19 p3298 A67-35602
Kinetically based mathematical model of hypergolic ignition in space ambient engines for predicting delay time and conditions from which pressure spikes result 19 p3311 A67-35744
Macroscopic physical system with behavior described in terms of differential equation system studied for stability in presence of small delay 19 p3205 A67-35912
Models explaining long time delay between current-pulse application and generation of coherent oscillations in gallium arsenide junction lasers near room temperature 19 p3241 A67-36036
Boundary value problem of oscillatory system with time lag quasi-linear partial differential equation 19 p3251 A67-36050
Retrofit accountability system requirements, environment, purpose and future applications 20 p3556 A67-36545
Bow shock and combustion zone studies of spheres fired through H2-O2 mixtures show ignition zone separation 20 p3359 A67-37128
Timing considerations in sequential fluid power circuits design in terms of stray delay concept and safety of asynchronous circuit 20 p3365 A67-37362
Time delay of remote-resonance trace of polarized electromagnetic pulse propagating through topside ionosphere 20 p3527 A67-37403
Laplace transformation of solution of linear differential equations with variable coefficients and time lags, analyzing motion stability 20 p3478 A67-37579
Maximum principle for hereditary processes optimal control with constant time lag and parameters 20 p3412 A67-37583
Transistorized time delay system based on measurement of condenser discharge time to predetermined voltage 21 p3590 A67-37952
Delay time of quenching response and recovery in gallium arsenide injection laser 21 p3640 A67-38261

Two base diode circuit having rectangular voltage pulse applied to one of base contacts investigated for front pulse delay phenomenon 22 p3769 A67-39572
Terminal guidance problem involving optimal control for deviations in systems with transport lag 22 p3833 A67-40158
Injector inlet conditions effects on combustion delay time in liquid bipropellant rocket engine, noting propellant atomization and droplet vaporization 22 p3868 A67-40161
Onset delaying of rotating stall in axial flow compressors 22 p3744 A67-40563
Very short pulse measurements by deriving delayed pulse from measured waveform, describing detector circuit 23 p3981 A67-41273
He-Ne laser pulse delay when excited in optical resonator noting dependence on gas pressures 24 p4167 A67-42207
Noise immunity in binary detection and temporal shift measurement of pseudorandom amplitude keyed echo signal in multichannel system 24 p4120 A67-42233
System parameters of linear time-variant space communication channels from input-output viewpoint, measuring correlation functions and Doppler spread 24 p4123 A67-42476
Stability boundaries of double-dead-time model describing chugging in liquid bipropellant rocket engine 24 p4207 A67-42689
Functional half-adder using optical coupling in injection laser noting design criteria and mode propagation delay 24 p4169 A67-42822

TIME DEPENDENCY

SA HELMHOLTZ EQUATION

Convergence theorems for sequence of expected values or random variables of stochastic learning process with time-dependent probabilities 01 p0104 A67-10280
Steady state oscillations and rotations, discussing time independency of parametric differential equations 01 p0113 A67-10285
Charged particle injection into magnetic traps through mirror, using annular electron gun 01 p0122 A67-10350
Heat dissipation rate in straight bar of constant cross section generating heat internally, using Laplace transforms 01 p0166 A67-10551
Stability theory application to control, circuit theory and aerospace systems 01 p0047 A67-11221
Drift velocities change in F layer as function of time explained by movement of reflection point over ionospheric surface 01 p0061 A67-11262
Unsteady laminar flow of incompressible fluid in gap between parallel disks with gap width varying with time, obtaining solutions for Navier-Stokes and thermal energy equations 02 p0231 A67-11469
Time limited receiver signals design for minimizing error probability under energy and frequency constraints 02 p0204 A67-12171
Computer simulation for turbulence/upset studies on jet transports, emphasizing time dependency and nonlinear aerodynamics [AIAA PAPER 66-1002] 02 p0181 A67-12304
Unreliability of mean-time-between-failures concept as standard quality measure for mechanical systems 02 p0249 A67-12426
Cauchy problem for Euler-Poisson-Darboux equation solved for all values of time and specified values of parameter 02 p0260 A67-12431
Time evolution of laser induced fractures in glass, noting crack propagation accompanied by sparking 02 p0253 A67-12508
Atomic and molecular time-dependent quantum-mechanical perturbation theory with differential equation formulation within Hartree-Fock approximation 02 p0268 A67-12725
Time dependence of current in In-CdS-In sandwich plate system at various voltages, using X-and Z-cut monocrystal CdS 03 p0490 A67-13157
Time-dependent photochemical model for space-time variations of oxygen allotropes in 20 to 100 km layer 03 p0414 A67-14087
Anomalous pulsed microwave emission at cyclotron frequency in partially ionized plasmas analysis extended to show that emission is not stationary with time 04 p0663 A67-14615
Steady blunt body problem solution via time-dependent technique, performing

computation in shock layer 04 p0546 A67-14818
 Photographic measurement of plasma jet velocity using time shift in brightness fluctuation 04 p0666 A67-15188
 Unsteady laminar flow of viscous incompressible fluid between two infinite parallel rotating disks with angular velocities varying with time 04 p0609 A67-15605
 MHD stability of plasma cylinder in time dependent magnetic field 04 p0671 A67-15643
 Time-dependent response of polycrystalline cadmium selenide thin film transistor to transient high energy radiation 04 p0589 A67-15718
 Differential equation derivation for creep analysis using plastic interaction curve and associated flow rule 05 p0917 A67-16299
 Satellite orbit major axis determination by using coincidence of time when satellite crosses plane of tracking station parallel with time of crossing topocentric celestial equator 05 p0894 A67-16560
 CW argon ion laser scattering in argon plasma, noting resonance and correlation between data and plasma properties 05 p0820 A67-16665
 Relation between terrestrial gravitational and magnetic field variations and time-dependent changes in shape, density and magnetization of disturbing bodies 05 p0799 A67-17027
 Self-consistent field approach to nonstationary time dependent turbulence 05 p0794 A67-17417
 Particle motion in vicinity of triangular libration point in earth-moon system solved in form of analytical expressions with time-dependent coordinates 06 p1079 A67-17763
 Geodetic error effect on time dependence of satellite tracking data received by ground station 06 p1080 A67-17769
 Time dependent geopotential variations analyzed, using straight line techniques 06 p0994 A67-17863
 Time dependent deflection behavior under compression loads of stiffened panel at high temperatures 06 p1100 A67-18011
 Time dependent computational method for three-dimensional blunt body flow fields traveling at supersonic speed including shock points, sphere cones and ellipsoid [AIAA PAPER 67-222] 06 p0941 A67-18461
 Mean number of random process ejections over arbitrary time period at output of receiver with time and frequency selectivity 06 p0965 A67-18897
 Numerical solution of hydrodynamic equations adaptable to finite difference methods 07 p1167 A67-19157
 Approximate solution of temperature field of thin isotropic cylindrical shell heated by time dependent thermal fluxes from two ambient media 07 p1266 A67-19162
 Electric signal transmission noting shape, properties, types, time dependency and use of Fourier transforms in calculations 07 p1141 A67-19338
 Numerical solution to time dependent Navier-Stokes equation for transient supersonic flow around right circular cylinder, using explicit-implicit finite difference method 07 p1169 A67-19625
 Time dependence of electron density in afterglow of electrodeless discharge in hydrogen plasma measured, using microwave interferometer 07 p1229 A67-19682
 Correlation of time variations of proton and electron intensity of outer radiation belt and dependence on geomagnetic environment 07 p1243 A67-19828
 Barometric coefficient for neutron monitor noting long term and altitude dependence 07 p1188 A67-19954
 Invariant imbedding and time dependent scattering processes including applications to particles moving in rod, radiative transfer in slab, photon diffusion and homogeneous diffusion processes 07 p1224 A67-20274
 Temperature distribution, stress distribution and displacement components for circular disk when temperature distribution at disk rim is step function of time, considering inertial terms in thermoelasticity equations 08 p1418 A67-20723
 Active component of voltage behavior in channel of helium pulse discharge measured, obtaining time dependence of channel resistance, input velocity and energy magnitude 08 p1357 A67-20848

Time variation of positional angle of polarization plane of radio sources due to Faraday rotation 08 p1388 A67-20987
 Terrestrial behavior under action of time dependent periodic potential, treating earth as Maxwell body for shear processes 08 p1325 A67-21211
 Time dependent Green function for electromagnetic radiation in moving simple media 08 p1296 A67-21430
 Time dependence of low energy proton belts noting spatial and differential energy distribution 08 p1378 A67-21470
 Recombination processes in decaying helium plasmas as indicated by time dependence of spectral line intensities and ion number density 09 p1548 A67-22361
 Power spectrum of irradiance for precessing cylinder computed as function of time for given value of phase angle 10 p1652 A67-22714
 Steady state Leveque problem generalized to include time dependence, obtaining eight solutions for surface temperature 10 p1732 A67-22727
 Asymptotic properties of solutions to kinetic coefficient equation system, noting mass velocity dependence on time 10 p1625 A67-23042
 Time dependence of current in In-CdS-In sandwich plate system at various voltages, using X-and Z-cut monocrystal CdS 10 p1690 A67-23105
 Properties of solar cosmic rays causing polar cap absorption measured with satellites 10 p1700 A67-23188
 Polar cap absorption with solar cosmic ray properties from balloons and relation to processes in terrestrial atmosphere 10 p1637 A67-23189
 Approximate method for diurnal variation of peak electron density in F-2 layer, estimating effect of time varying drifts 10 p1650 A67-23336
 Waveform independent condition for transmission coefficient in linear time-independent transmission system to provide upper limit to signal distortion 10 p1620 A67-23572
 Radio burst produced by solar flare on August 28, 1966, analyzing flux increases as function of time and frequency 10 p1703 A67-23803
 Numerical technique for time dependent calculation of two incompressible fluids interaction to study viscous and inviscid Rayleigh-Taylor instability 11 p1774 A67-23859
 Elastic medium dynamic response to time dependent pressure in spherical cavity with cavity wall under ablation process 11 p1871 A67-23964
 Cesium plasma confinement time measured in Q device by observing plasma density decay after atomic beam shut off 11 p1835 A67-24385
 Power output at 119 micron in water vapor laser, noting inhibition of laser action during discharge current pulse 11 p1801 A67-24728
 Pulsating model of closed universe, noting ordinary matter time-dependent scalar field interaction and equation for nonvanishing pressure 11 p1868 A67-24867
 Charged particle injection into magnetic traps through mirror, using annular electron gun 11 p1844 A67-25023
 Time variability of bearing clearance due to temperature and pressure treated by iterative-numerical calculation 12 p1949 A67-25330
 Premature generation breakdown in ruby laser, noting effect of additional media on pumping level/generation time 12 p1953 A67-25445
 Equations for elastic system free oscillations with parallelogram shaped hysteresis loop derived from kinetic energy changes, describing system time dependent dynamic behavior 12 p1967 A67-25660
 Time dependent large scale electric potential field effect on motion of geomagnetically trapped particles 12 p1997 A67-25809
 Time variations of intensity in outer belt and near boundary deduced from Elektron I and II data, noting comparison with magnetic field variations 12 p1997 A67-25815
 IR emission measurement of lunar-like materials during simulated eclipse, noting dependence on time 12 p2009 A67-26007
 [AIAA PAPER 67-290]

Sporadic E backscatter noting two peaks in activity, motion, temporal component parameters and cause 13 p2107 A67-26330
 Time dependence of coherent emission wavelength shift of GaAs-P laser diode during flat-topped current pulsation 13 p2125 A67-26511
 Self-excited systems sensitivity function maximum value attained via time dependency on natural frequency and damping factor only 13 p2216 A67-26622
 Condensation spectrum, evolution of cloud droplets 13 p2151 A67-26668
 Time dependent orientation of body fixed coordinate system relative to stars for spinning rigid torque-free body 13 p2154 A67-26661
 Kinetic model with velocity dependent collision frequency applied to forced wave propagation in half-space and other unsteady problems 13 p2100 A67-26995
 Time dependence of semiconductor enhanced reflectivity by pulsed argon ion laser based on thermally generated electron hole plasma 13 p2177 A67-27011
 Laser output pulse time dependence in acetone and nitrogen mixture, using indium antimonide detector 13 p2127 A67-27011
 Radar antenna synthesis for maximum SNR and minimum error dispersion in target bearing, reducing problem to filter synthesis 13 p2069 A67-27033
 Beryllium alloys age hardening noting increase in flow stress with time 13 p2136 A67-27101
 Dielectrophoretic methods for positioning cryogenic liquids in zero gravity environment, solving one-dimensional nonlinear problem for time history 13 p2106 A67-27644
 Method to describe finite amplitude convection time dependence 14 p2295 A67-27900
 Time dependent viscous flow between two rotating spheres analyzed by extension of numerical methods 14 p2296 A67-27900
 Electron production time variations in L layer during solar activity 14 p2378 A67-27900
 Coulomb interaction effect on time dependent variations of electron ion distributions in Van Allen belt, using kinetic equation 14 p2378 A67-27911
 Duration of initial stage of geomagnetic storm based on observations from 1954 through 1959 14 p2308 A67-27922
 Nonlinear theory of cyclotron instability of earth radiation belt covering time-dependent instability evolution, radiation belt stationary state, etc 14 p2379 A67-27933
 Electron number density profiles and polar cap absorption of radio waves time history during weak solar cosmic ray event 14 p2380 A67-28044
 Barium titanate polycrystal dielectric constant aging, discussing 90 degree splitting in domain structure 14 p2364 A67-28223
 Time varying magnetic field in shock tube analyzing electric current diffusion layer 14 p2358 A67-28223
 Time dependent pressure distribution and threshold acceleration for bubble formation in longitudinally vibrating flexible liquid filled cylinder 14 p2304 A67-28333
 [ASME PAPER 67-FE-1] Quiet sun current system effects of seasonal variations of critical frequency in region, noting dependence on local time and latitude 14 p2312 A67-28566
 Infinite plate temperature field determined by approximate method when heat transfer coefficient is time dependent 14 p2407 A67-28864
 Thermal field of solid rod of uniform cross section and arbitrary profile with time dependent heat transfer 14 p2408 A67-28864
 Chemiluminescent reactions of atomic oxygen with carbonyl sulfide and hydrogen sulfide in flow system as function of reaction time and reactant concentrations 14 p2260 A67-28870
 Solid lubricants frictional behavior in press-fit tests, measuring sliding speed, load and surface roughness as function of time [ASLE PREPRINT 67AM 5A-2] 14 p2325 A67-28870
 Lateral heating and sublimation arbitrary thick two-layer plate using thermal flux time-dependent on plate surface 14 p2408 A67-28864
 Time dependent problems of heat transfer in laminar flow of viscous incompressible

- fluid in cylinder and cylindrical annulus 14 p2408 A67-28892
- Time dependent heat conduction and diffusion equations for fuel-rich H-O flame solved by finite difference method 14 p2409 A67-29064
- Time-dependent Green function for moving isotropic nondispersive medium 15 p2509 A67-29199
- Approximate model for simplification of linear dynamic system, neglecting effect of higher order time constants 15 p2457 A67-29370
- Lunar environment effects on Surveyor I components, particularly white paint degradation as function of time 15 p2579 A67-29451
- P-n semiconductor junction widening due to impurity diffusion and drift, noting first order differential equations describing space-charge width variation with time 15 p2535 A67-29488
- Acquisition behavior of phase locked loops, determining time and pull in range of loop for input step in frequency 15 p2446 A67-29590
- Time and frequency accuracies obtainable with geostationary satellites, noting measurement error sources 15 p2565 A67-29593
- Initially isotropic turbulence, characterized by three dimensionless numbers, suppressed by applying uniform magnetic field 15 p2471 A67-29656
- Mean variations of total electron density with latitude and local time during winter obtained from dispersive Doppler investigations 15 p2477 A67-29666
- Advanced space vehicle planning analyzed from economic approach to decision making, noting cost decrease with time 15 p2566 A67-29833
- Recombination-regeneration formula for hole-electron pairs in randomly doped semiconductor materials 15 p2539 A67-29915
- Nuclear explosion effects on atmospheric pressure, electron density, and F-2 layer height, noting dependence on time, season, etc 15 p2478 A67-30067
- Carbon monoxide chemisorption on polycrystalline molybdenum studied by radiotracer, noting desorption at various temperatures as time function 15 p2434 A67-30099
- Backward and forward algorithms of dynamic programming for time dependent systems, noting advantages of forward algorithm for optimization of system 15 p2440 A67-30157
- Rayleigh problem solution and accuracy and utility of discrete ordinate method for time dependent problems as applied to Couette flow problems 15 p2473 A67-30214
- Satellite scintillation in auroral zone depends on time of observation and on magnetic activity 15 p2483 A67-30294
- Accuracy of mathematical models in control system identification estimated on basis of deterministic test signals for simulation in time and frequency domains 15 p2461 A67-30318
- Collision integral for Landau plasma in strong magnetic field to obtain time evolution of one-particle distribution function 15 p2532 A67-30382
- Mixed crystals with fluoride base, investigating spectrum and time behavior of laser emission for operation below room temperature 16 p2725 A67-30809
- Motion and continuity equations for atomic and molecular oxygen density solved numerically as time dependent problem 16 p2664 A67-30975
- Rapidly varying high pressure measurement requirements, treating pressure transducer as seismic system and analyzing feed channel distortion 16 p2671 A67-31004
- Ion-acoustic interaction in weakly turbulent plasma deriving time variation of plasmon number 16 p2715 A67-31046
- Shock tube analysis of time dependent formation of supersonic flow near blunt bodies 16 p2592 A67-31102
- Mechanical strength of medium formulated as microscopic behavior in continuum obtaining time-dependent macroscopic fracture strength 16 p2771 A67-31295
- Time dependent fracture of viscoelastic materials, considering defect initiation relation as approximation to crack growth history 16 p2773 A67-31312
- Internal fracture of solids analyzing initiation by converging tensile pulses in prolate spheroid and crack propagation in infinite solid 16 p2773 A67-31315
- Time-dependent mean-mass temperature of argon jet produced by arc plasmatron with powdered metal carbides injected into jet calculated using heat transfer equations 16 p2721 A67-31393
- Diffusion coefficient dependence on solar particle energy and distance from sun noting time variation 16 p2740 A67-31892
- Response of one degree of freedom system with power law time dependent damping and restoring forces using WKB approximation 17 p2958 A67-32128
- Unsteady heat transfer in tube in presence of variable gas flow rate 17 p2967 A67-32129
- Zonal and meridional distributions of 5-day averaged outgoing long wave radiation and relation to Northern Hemisphere circulation 17 p2879 A67-32548
- Algorithm for constructing state equations corresponding to linear time varying system of differential equations 17 p2829 A67-32627
- Differential equations determining time-dependent torsional moment and stresses in thin walled rods in creep presence 17 p2821 A67-32830
- Response of capacitors irradiated by pulses of transient nuclear radiation 17 p2828 A67-32863
- Toroidal stellarator magnetic trap with time-varying double coil magnetic field and external plasma injection 17 p2904 A67-32911
- Field spectrum developed from monochromatic temperature oscillations in bodies due to time variation of heat transfer coefficients caused by unsteady flow velocity 17 p2972 A67-33073
- Averaging method extended to physical systems described by differential equations simultaneously dependent on almost periodic fast time and periodic slow time 17 p2885 A67-33140
- Cosmic radiation anisotropy variation with time and direction described on intensity contour map, noting application for neutron monitors data reduction 17 p2938 A67-33209
- Contribution to friction coefficient from time correlations between hard and soft molecular interactions evaluated, using linear trajectory approximation 17 p2890 A67-33263
- Worldwide auroral morphology, discussing latitude and local time distribution and temporal variations 18 p3032 A67-33581
- Geomagnetic time and latitude distribution of magnetic disturbances at auroral and polar cap latitudes 18 p3032 A67-33583
- Initial loss in TWT with lossless slow wave circuit connection to drift tube, expressing field components by sums of normal modes 18 p3010 A67-33645
- Critical reaction rate for ignition, temperature rise and induction period for various geometries calculated for conductive theory, including reactant consumption 18 p3156 A67-33850
- Time dependent small-strain modulus of styrene-butadiene rubber, noting predictability from selected molecular parameters [AIAA PAPER 67-491] 18 p3143 A67-33956
- Plasma time-dependent luminosity from pulsed discharge in vacuum, determining excitation temperature distribution and discharge spectral lines 18 p3087 A67-34049
- Thermocouple drift on Chromel-P vs Constantan under vacuum, high temperatures and time factor conditions 18 p3052 A67-34516
- Time dependence of avalanche in silicon junctions including effects of different ionization rates and velocities of charge carriers 18 p3105 A67-34628
- Numerical solutions of hypersonic sharp leading edge flows, with full time-dependent Navier-Stokes equations solved 18 p2984 A67-34739
- Time and temperature dependent diffusion of vaporized Zn and Cd in n-type InAs 19 p3299 A67-34760
- Time dependent expression for droplet-size distribution function of clouds undergoing forcible modification or natural evolution 19 p3251 A67-34862
- Nonleptonic sigma decay modes described by four complex amplitudes with phases given by time-reversal invariance 19 p3263 A67-34892
- Zero-crossing times for signals, performing transformations of time sequence to determine distribution functions 19 p3201 A67-34905
- Perfectly stirred reactor /PSR/ theory application to flame analysis, obtaining temperature or concentration profiles as function of time or distance 19 p3345 A67-35011
- Time variations of order parameter, coupling to external perturbation and effect on various transport properties of dirty type II superconductors 19 p3302 A67-35038
- Analytical model for microbial population survival times during heat sterilization studied for spacecraft applications, considering environment and exposure time 19 p3180 A67-35264
- Time dependency, anisotropy degree and spectral composition of cosmic radiation generated during July 1966 solar flares as observed by Pioneer VI 19 p3314 A67-35270
- Basic operating-time contribution to pulse behavior of diffused transistor components, introducing system function for semiconductor barrier-layer component 19 p3195 A67-35580
- Image velocity sensing technique applying moving reticle scanners, with time-dependent correlation function analyzed by frequency discriminator 19 p3231 A67-35689
- Time dependent computational method for three-dimensional blunt body flow fields traveling at supersonic speed including shock points, sphere cones and ellipsoid [AIAA PAPER 67-222] 19 p3171 A67-35736
- Instability of gas-cooled nuclear reactor passages in steady laminar flow studied by time-dependent analysis 19 p3260 A67-35743
- Wave propagation in real gases, considering one-dimensional time-dependent disturbances semiinfinite in extent, emphasizing matched asymptotic expansion and coordinate stretching methods 19 p3212 A67-35798
- Existence problem in control theory noting time independence and control set 19 p3204 A67-35905
- Ethylene-oxygen reaction in shock waves, studying induction period and time dependency of mixture composition, ionization and chemiluminescence 20 p3376 A67-36232
- Relative intensity contribution and time dependency of primary cosmic rays, splash albedo and reentrant albedo measured by polar orbiting satellite 20 p3517 A67-36306
- Electron-ion radiative recombination influence on time-dependent luminous intensity of various spectrum lines in cesium vapor 20 p3488 A67-36436
- Time-dependent current flow equations solved for insulator with traps if injected space charge produces negligible perturbation on external electric field 20 p3509 A67-36506
- Color schlieren and high speed photography technique for transient flows in wind tunnels 20 p3445 A67-36537
- Field determination when produced by symmetrical plasmoid with time dependent current distribution traveling along cylindrical waveguide, using Wiener-Hopf method 20 p3497 A67-36680
- Transient mean wall temperature of flat plate with time dependent heat source and cooled by incompressible turbulent flow, discussing heat-transfer coefficient [ASME PAPER 67-HT-45] 20 p3547 A67-36727
- Thermodynamic basis of plasticity, noting loading and unloading stress-strain relations 20 p3541 A67-37283
- Parametric resonance in magnetosonic waves through analysis of perturbed particle trajectories in modulated plasma field, determining velocity time dependence 20 p3501 A67-37296
- Time dependent variations in parameters of junction semiconductors investigated for stability 20 p3401 A67-37450
- Electron density time and location dependence in Z-pinch calculated from emission measurements 20 p3502 A67-37528
- Theta pinch plasma sheath and fields time development for relaxing radial electric field 21 p3662 A67-37754
- Condensation spectrum evolution of cloud droplets 21 p3654 A67-38432
- Steady state plant performance

optimization for unknown dynamic characteristics, determining periodic input signal 21 p3603 A67-38439

Rapid scan spectrometer for carbon dioxide laser studies noting time dependent effects 21 p3641 A67-38460

Premature generation breakdown in ruby laser, noting effect of additional media on pumping level/generation time ratio 21 p3642 A67-38819

Magnetic field rotation, satellite Io and interplanetary propagation effects accounting for time variation of Jupiter magnetic flux and polarization 21 p3710 A67-38998

Time variation of magnetic flux distribution in type II superconductor under sinusoidal magnetic field, obtaining flux penetration rate, pinning forces and hysteresis loop 21 p3685 A67-39075

Euler motion generalization of solid body, discussing inertial and kinetic moments 22 p3836 A67-39403

Fatigue in fibers and plastics, use of cumulative extension testing and time dependent effects in fatigue tests 22 p3824 A67-39562

Vibrating neutron stars, discussing damping, heating, energy storage and X-ray emission possibilities at 1000 years range 22 p3882 A67-39619

Weakly turbulent spatially uniform ensemble of Vlasov plasmas, discussing time evolution of correlations due to collective interactions 22 p3849 A67-39701

Time dependency, anisotropy, propagation and spectral properties of cosmic radiation released by solar flares during sunspot activity 22 p3871 A67-39796

Numerical program integrating motion equation of charged particles from realistic geomagnetic field model, with trajectory calculations for solar cosmic rays 22 p3872 A67-39810

Temporal and spatial low energy solar proton intensity variations indicating interplanetary medium changes effects on magnetospheric configuration 22 p3873 A67-39813

Energetic outer radiation belt electron spectra spatial and time variations 22 p3873 A67-39822

Time dependent relation between coloring and spontaneous conductivity increase in barium titanate single crystals by strong electric field 22 p3861 A67-39918

Booster autopilot in bounded phase coordinates subject to disturbances, determining extremal control as function of time 22 p3833 A67-40149

Mode acceleration method for axisymmetric dynamic response due to time dependent loading in spherical and cylindrical shells 22 p3914 A67-40190

Geomagnetic crotchets of solar flares based on materials analysis recorded at Hurlanovo, discussing time factors and characteristics 23 p4049 A67-40670

Quasi-linear relaxation dynamics of unstable distribution function for potential drift waves, deriving law governing average wave number time variation 23 p4032 A67-40911

Impact crater size vs incidence analyzed statistically in study of validity of time dependence on saturation for moon and Mars 23 p4066 A67-41007

Interplanetary space cosmic ray intensity variation with time and distance from sun measured by Zond III and Venera II simultaneously 23 p4055 A67-41102

Solar neutrino astrophysics, universal neutrino sea, high energy neutrinos, neutrino detectors, stellar energy production, solar thermometry and gravitational constant time variation 23 p4056 A67-41111

Vector field theory of time dependent backscatter from distant slightly rough sphere for pulsed and sinusoidally steady state sources 23 p3974 A67-41200

Liquid drop impact on liquid, calculating velocity potential, initial pressure and time dependence of cavity depth and wall velocity 23 p3991 A67-41459

Space distribution function of Knudsen gas in closed volume investigated using gas model noting dependence of time 24 p4190 A67-41902

Interaction between broadening plasmoid and external magnetic field assuming time dependent conductivity and magnetic field

as function of time 24 p4195 A67-41929

Measurement of time varying spectra of argon plasma in coaxial gun for two different gun geometries 24 p4198 A67-42730

Pulsed ion flow energy and mass spectra analyzer suitable for 1 to 3 msec duration and time variation over 10 msec 24 p4158 A67-42741

Cosmogenic radioactivity in freshly fallen meteorites measured and compared to calculate terrestrial and exposure ages and spatial and time dependence 24 p4238 A67-42884

TIME DISCRIMINATION

Noise rejection properties of time discrimination method of pulsed signals improved by using exponential rather than selecting function 02 p0194 A67-11909

Passage of pulsed coherent useful and noise signals through two-channel time discriminator 07 p1140 A67-19237

Time resolution spectroscopy applied to electron recombination in H plasma due to azimuthal pinch 11 p1841 A67-24769

Known and unknown principles of biological chronometry 11 p1747 A67-24937

Time discretization method applied to determination of peak duration distribution of normal noise envelope 11 p1754 A67-24987

Fine structure profiles of solar radio bursts observed with high time resolution 14 p2381 A67-28579

TIME DIVISION MULTIPLEX

Time multiplex telemetry equipment for FR-1 satellite that encodes data in PAM/FM wave train for transmission to ground 01 p0020 A67-10107

Probabilistic structure of and establishment time for group synchronization in time-division-multiplex /binary code/ transmission systems 01 p0027 A67-11238

Data quality assurance program for telemetry ground station operations, noting frequency division and time division formats 02 p0198 A67-12023

Time division multiplexing system for LF bioelectric signals, noting operation parameters and modes 02 p0218 A67-12075

PCM/TDM and influence of channel on signal determined, using mathematical model 02 p0202 A67-12130

Time combined with frequency division multiplex multichannel communication system for transmission of digital information over tropospheric scatter communication channel 02 p0203 A67-12132

Multiple-access worldwide satellite communication system for aircraft terminals with limited antenna gain and transmitter power 06 p0960 A67-17874

Multiple access modulation techniques /frequency-division, time-division, spread-spectrum and pulse-address/ for use in communications satellites 06 p0960 A67-17894

Time division multiple access /TDMA/ modulation technique for satisfying anticipated demand by many small users for communication satellite facilities 06 p0961 A67-17695

Modulation devices for pulsed systems, discussing signal preparation and channel grouping for time multiplex systems 07 p1150 A67-19341

Asynchronous delta modulation system for cases with no time division multiplexing such as asynchronous multiplex communication 10 p1806 A67-23063

Working principle of echo suppressor used in telephone link with high propagation time based on selective attenuation by frequency and time divisions 11 p1754 A67-24651

Resonant-transfer sampling technique stressing bandpass filtering design and time division multiplex 20 p3379 A67-36243

TIME DOMAIN REFLECTOMETER

S REFLECTOMETER

TIME FACTOR

Thermalization rate of highly ionized plasma with initially hot ions and cold electrons, using laser scattering to observe time variation of electron temperature 01 p0125 A67-10912

Stability of sampled data feedback systems with time-varying gain by restriction with memoryless element and nonanticipative linear time-invariant subsystem 01 p0048 A67-11226

Reliability optimization relation to program time and costs and schedule for cost reduction keeping time constant 01 p0085 A67-11384

Reaction of human organism to time shifts experienced during flights of modern aircraft [DVL-611] 02 p0185 A67-12422

Closed form expression for storage time of arbitrary base diode, noting diode transient behavior 03 p0380 A67-13489

Adrenal corticosterone concentration changes in response to various doses of ACTH and time pattern of changes in hypophysectomized rats 04 p0560 A67-14523

Analysis technique for determining analog to-digital converter time aperture error taking into account nonlinear A-D conversion process 04 p0578 A67-14887

System of n first order differential equations relating coordinates and time using matrix methods for solution 06 p1022 A67-17773

Zero steady state error operation of feedback systems with time-varying nonlinear element 06 p0977 A67-18522

Time vs space in antenna theory and frequency variation 07 p1152 A67-19544

Electron precipitation from outer radiation belt as cause of ionospheric disturbances noting relation to time 07 p1245 A67-19928

Calculation of time behavior of forenoon anomaly in diurnal variations of critical frequency of normal E layer 07 p1183 A67-20118

Sensitivity models in terms of influence of time variation in given part on behavior of whole system 08 p1309 A67-20322

Systematic approach using weight factors for apportioning mean corrective times of equipment based upon maintainability, usage and reliability data 08 p1315 A67-20677

Optimum transient response for bang-bang control system with finite time control activation 09 p1483 A67-22607

Dead time instability effect on neutron monitor performance 10 p1699 A67-22799

Time variations in flux density of some quasi-stellar sources, discussing relationships with component age and thickness 10 p1705 A67-22958

Rise time in solid state detectors considering equivalent circuit, plasma, times etc 11 p1789 A67-24103

Aspect system on Pioneer VI and VII incorporates digital computer for accurate time sector division of spin stabilized vehicle 11 p1870 A67-24444

Motion stability during final time interval for case of two zero roots determined by analysis of nonlinear functions structure 11 p1813 A67-24511

Isentropic compression due to motion of heavy piston in gun tunnel noting nozzle throat effect on motion and stagnation pressure 11 p1773 A67-24577

Interdisciplinary perspectives of time Conference, New York, January 1966 11 p1820 A67-24933

Reversed speed effect and grain boundary diffusion as explanations of discrepancy of activation energy values for strain aging under fatigue or simple stress conditions 12 p2013 A67-25282

Modified quasi-linearization method for numerically solving trajectory optimization problems with undetermined terminal time 12 p2008 A67-25913

Piezoelectric accelerometer capacitance measurement and computation involved in conversion of accelerometer voltage sensitivity from one external circuit capacitance to another 12 p1947 A67-26186

Time-integrated and time-resolved spectra of GaAs laser diode, noting temperature effect on spectral emission 13 p2125 A67-26422

Travel-time effects on quasi-steady state operation characteristics occurring from electron optical characteristics of two-grid controlled photomultiplier 14 p2277 A67-27767

Fastener performance in commercial and aerospace application, considering component thermal expansion [ASME PAPER 87-DE-18] 14 p2327 A67-26877

Nonstationary disturbance effect on electron producing bound s-state during slow collision of atoms 14 p2352 A67-29077

Stability of feedback systems with monotone and odd monotone nonlinearities 15 p2457 A67-29377

Worldwide network of Doppler observation stations, discussing frequency and time monitoring for enhanced measurement accuracy 15 p2436 A67-29599

Mean time between failures for repairable system in terms of MTBF and availability of constituent units by reducing reliability block diagram 15 p2453 A67-30062

Ionospheric irregularity observation near F layer maximum, determining traveling velocities [AGARDOGRAPH 95] 15 p2484 A67-30302

Random noise and measurement errors limitation upon system identification in time domain 15 p2463 A67-30332

Standard life-testing experiment in which n similar units are cycled to failure 15 p2495 A67-30414

Random instability of nonlinear oscillations of dynamic system with time behavior described by equation 16 p2702 A67-30447

Noise and vibration effect on human mental work capacity with increasing time limitation indicating efficiency reduction 16 p2614 A67-30917

Unsteady motion stability over given time interval of mechanical systems described by nonlinear differential equations 16 p2702 A67-31052

Analysis of discrete nonlinear time-varying systems, noting computational simplicity, application to feedback system, etc 16 p2650 A67-31675

Active damping concept for gravity gradient satellite attitude control to reduce oscillation time constant, initial capture time and oscillation magnitude 17 p2954 A67-32073

Tolerance of nonlinearities in input transducer of time-varying optimal control systems, using Liapunov function 17 p2829 A67-32307

Sodium effect on dwell time and transport rates of various elements using DC arc, stressing spectral consequences 17 p2888 A67-32377

Rate constant of atomic oxygen ions reaction with vibrationally excited nitrogen molecules 17 p2889 A67-33201

Many-element lasers spiking emission for Fabry-Perot and confocal geometry, including time resolved spectroscopy and far and near field patterns 17 p2870 A67-33298

Long time behavior of weakly interacting nonlinear waves, emphasizing mathematical features common to physical situations 18 p3079 A67-34002

Conditions of time-symmetry for four classes of flows, discussing instabilities 18 p3079 A67-34004

Development of quantitative logistics performance parameters related to time, resources and cost in Concept Formulation Phase and Contractual Definition Phase 18 p3162 A67-34678

Maintainability demonstration methods and statistical techniques for test data reduction 18 p3163 A67-34700

Silicon transistors transient defect annealing from pulsed particle irradiation, stressing time factors 19 p3305 A67-35667

Fast thin film main memory system design noting 200 nsec cycle time and 160 nsec access time 19 p3189 A67-36063

Prognostic equation asymptotic solution for atmospheric pressure forecast 20 p3479 A67-36125

Quantum mechanical transition time shown to be electron tunneling characteristic time 20 p3505 A67-36178

Planar transistor collector current rise time determination with base driven by current step function and application procedures 20 p3395 A67-36299

Current time variation for subharmonic parametric oscillator phase zero-transient switching 20 p3395 A67-36314

Measurement of variation of formation time of Q-switched ruby laser as function of loop gain 20 p3458 A67-36432

Cross-spectral method application problems in feedback system analysis, identification and linear time invariant system 20 p3407 A67-36785

Economical Hohmann type orbital transfer between coplanar circular orbits with fixed duration and limited thrust 20 p3527 A67-37258

Minimizing time for deployment of infantry force by airlift analyzed by computer procedures based on loading, effectiveness and productivity 20 p3361 A67-37529

Soviet book on time-frequency remote control systems theory and design 20 p3412 A67-37632

Sunspot cycles rise time and periodic variation probable values 21 p3704 A67-38511

Time symmetry in oscillating cosmologies with locally irreversible processes, obtaining formalism for statistical processes and boundary conditions 21 p3706 A67-38844

Duration of dynamic system output for given input time calculated by computer programming 22 p3764 A67-39336

Aircraft autopilot system in longitudinal flight stabilization regime, using synthesis method based on time characteristics 22 p3831 A67-39609

Solar proton event /February 1965/, time history of low energy protons was more complex than that of higher energy particles 22 p3872 A67-39812

Propulsion and time requirements for low gravity liquid settling obtained from known Bond number 22 p3869 A67-40171

Resolution, contrast and time factors in visual target acquisition 22 p3755 A67-40410

Recovery time of carbon dioxide laser excited by electric pulse discharge noting heat conduction toward walls 23 p4011 A67-40692

Distribution theory in control system design, discussing sensitivity improvement by feedback for application to time invariant systems 23 p3984 A67-40755

Gamma irradiation effect on spinal cord timed differently, considering time factor in reactions of nervous system in guinea pigs 23 p3943 A67-40767

Statistical Newtonian mechanics and quantum physics, discussing classical, thermodynamical and biological time concepts 23 p4027 A67-41139

Relation of time between flights to accident potential of pilots 23 p3970 A67-41696

Interstellar gas and magnetic field periodic system stability noting free-fall time 24 p4224 A67-41814

Dead time instability effect on neutron monitor performance 24 p4209 A67-42135

Design procedure for estimating state vector of discrete-time linear stochastic system with constrained memory estimator 24 p4135 A67-42185

Charge time determined as circuit constants function in designing linear detectors 24 p4158 A67-42716

Stack of alternating lead layers, nuclear emulsions, X-ray films with graphite cosmic-ray receiving shield on top used for determining distribution in time of events 24 p4217 A67-42832

Time factor in onboard checkout and in-flight maintenance of manned spacecraft, discussing mission events and man-machine interaction [AIAA PAPER 67-950] 24 p4245 A67-43034

TIME FUNCTION

Stability theory based on functional methods, examining feedback system with linear time invariant and nonlinear elements 01 p0046 A67-11208

Real function interpolation method for synthesis of electric networks in time domain by sinusoidal exponential series 03 p0458 A67-13505

Mean surface temperature-time solution of heat absorbed by semiinfinite solids [ASME PAPER 66-WA/HT-58] 04 p0725 A67-15437

Rocket wind trajectory dispersion reduction by adjusting thrust-time curve without increasing total impulse 08 p1406 A67-20512

Maximal error estimation arising from delay in output functions of servomechanisms provided bandwidth, maximum oscillation and slope are known 08 p1286 A67-20780

Meteor burst radio propagation channel clock synchronization experiment to determine frequency offset between two remotely located frequency standards 09 p1494 A67-21618

Recombination processes determined from data of time dependence of spectral line intensities and number density in decay plasmas produced in neon and helium-neon mixtures 09 p1548 A67-22360

Synthesis of time functions with finite number of discontinuities by constructing functional scheme of system from Laplace transform of output 11 p1769 A67-24122

Generalization of binary processes, discussing time domain and frequency

domain analysis 11 p1813 A67-24312

Finite time stability of system trajectory under perturbing forces and within specified regions of state space 11 p1771 A67-24892

Dispersion of number of positive zeros as function of time for realization of quasi-harmonic random signal 11 p1754 A67-24985

Coherent ordered precipitates formation in Ni-Cr-Al alloy, discussing spacing, shape and size of gamma prime particles as function of time 12 p1954 A67-25344

Shock spectrum synthesis and analysis as environmental test technique compared with time function shock testing 12 p2030 A67-25681

Regularity properties in time variable of solutions of n-dimensional Navier-Stokes system 13 p2145 A67-26509

Regularity properties in temporal variable of solutions of n-dimensional Navier-Stokes system, using various interpolation methods 13 p2145 A67-26604

Interplanetary particle diffusion model analysis in terms of energy, position in space, direction and time 13 p2193 A67-27250

Stability and asymptotic behavior of dynamical systems defined by autonomous functional or partial differential equation and conditions for applying Liapunov theorem 14 p2342 A67-28081

Recursive algorithm for identification of time varying parameters of system, noting use for matrix inversion 15 p2509 A67-29371

Cross correlation bounds and positivity of nonlinear operators, examining criteria for positive composition 15 p2457 A67-29373

Dynamic characteristics of normal exploitation processes determined with controlled equivalent model 15 p2464 A67-30335

Probability that random function with known correlation function will not fall outside regions with given boundaries within given time 16 p2696 A67-30920

Energy loss spectrum in CsI at small atmospheric depths, discussing time variation of 0.5-mev gamma-ray flux 16 p2739 A67-31406

Exact stability criteria for kinetics equations of coupled-core nuclear reactors, using Pontryagin theorem and models for time-distribution of coupling neutrons [ASME PAPER 66-WA/AUT-16] 17 p2882 A67-32015

Numerical Fourier transform calculations for pulse testing procedures for controlled time function input systems 17 p2883 A67-32018

Dynamic thermocouple for measuring plasma temperature up to 4000 degrees C, deriving relations for heating curve as function of time 17 p2854 A67-32162

Time resolved measurements of phase fluctuations of coherent beam at emergence from turbulent layer 17 p2817 A67-33304

Time and space development equations for longitudinal and transverse modes in Vlasov plasma 18 p3092 A67-34745

Point-by-point measurements of magnitude and phase of repetitive pulsed time functions using commercial equipment 19 p3182 A67-35031

Convolution technique applied to time domain to evaluate system capability 19 p3186 A67-35326

Quantization error bounds for hybrid control systems by time varying function 19 p3202 A67-35625

Optimality and invariance conditions for linear free-time problem 20 p3412 A67-37582

Suboptimal radial guidance scheme based on cubic time function of optimal trajectories radius vector modulus from simultaneous data analysis 22 p3830 A67-39164

Metal-silicon nitride-silicon /MNS/ capacitor charge storage variation with temperature and time 22 p3767 A67-39257

WC-NbC-Co alloys oxidation resistance in air studied by sintering powdered WC and NbC with Co, finding oxidation rate linear function of time 22 p3820 A67-39565

Fokker-Planck equation describing distribution of geomagnetically trapped electrons as function of longitude, time, energy and mirror-point field intensity 22 p3791 A67-39808

Cosmic ray intensity from balloon sounding, discussing proton to He ratio behavior as time function within Parker solar modulation model 23 p4051 A67-40809

Haskell viscous flow equations describing very slow linearly viscous liquid with initially crater shaped surfaces solved and applied to lunar craters 23 p4065 A67-40998

Analysis of system described by heat equation where disturbance propagates with infinite speed as function of time 23 p4024 A67-41086

Interaction between broadening plasmoid and external magnetic field assuming time dependent conductivity and magnetic field as function of time 24 p4195 A67-41929

Sensitivity analysis of linear differential-difference equations with hereditary influences 24 p4134 A67-42026

Heat absorber temperature distribution, considering medium temperature and heat transfer coefficient arbitrary functions of time 24 p4154 A67-42215

Velocity and path of vertical motion of constant thrust rocket in homogeneous gravitational field, giving hyperbolic acceleration expression as time function 24 p4241 A67-42578

Rocket wind trajectory dispersion reduction by adjusting thrust-time curve without increasing total impulse 24 p4242 A67-42919

Data handling capabilities of periodic time function for given bandwidth using Fourier series in sinusoidal spectrum analysis 24 p4124 A67-42931

TIME MEASUREMENT

Time measurement with semiconductor device, noting parameter variation effect and experimental results 01 p0066 A67-10652

Neutron spectrometric measurements, discussing starting time determination and conversion of travel time into amplitude spectrum 01 p0066 A67-10656

Time resolving capabilities of RCA C-70045, 56 AVP and XP 1020 photomultipliers 01 p0067 A67-10659

Subnanosecond time interval measurements with recirculating transmission line memory 02 p0243 A67-12092

Mechanical gears to convert universal time to sidereal time, discussing range of validity of results with regard to one century 02 p0267 A67-12202

Multichannel tunnel diode chronotron circuit for measuring picosecond time intervals directly with sequence of timing circuits 02 p0246 A67-12684

Syncom III satellite measurement of time variation of total ionospheric electron content [RASSA PAPER 1-10-129] 03 p0417 A67-14240

Analog circuits for statistical correlation in time measurements, with application to subsonic and supersonic flow turbulence 04 p0620 A67-14889

Pulse measurement of nanosecond intervals using time expansion chronometer 06 p1002 A67-18055

Evaluation of minimum-time courses for aircraft and inherent error 07 p1222 A67-19680

Clock synchronization via communications satellite Relay II 09 p1494 A67-21617

Electrostatic separation probe to measure electronic velocity distribution function, showing evolution of distribution function relationship to plasma oscillation growth 11 p1789 A67-24409

Timekeeping unit calibration, on basis of signals emitted by HBG transmitter, permitting measurement of state and performance of quartz oscillators 11 p1792 A67-24782

Known and unknown principles of biological chronometry 11 p1747 A67-24937

Absolute gravitational acceleration determined by timing symmetrical free motion of body moving under attraction of gravity 12 p1965 A67-25126

Plasma concentration diagnostics in exosphere from delay time of forward frequency as function of parameter of whistler trajectory 13 p2111 A67-26563

High speed correlation technique to measure time development of width of ultrashort pulses generated by mode locked Nd trivalent ion glass laser 13 p2126 A67-27014

Relativistic effect of atomic clocks, noting error and magnitude increase with experiment duration 14 p2348 A67-27866

Global distribution of standard time by VLF for synchronization with microsecond accuracy 14 p2263 A67-28389

Clock synchronization with artificial satellites for precise time and frequency, comparing two-and one-way transmission and reception 14 p2263 A67-28391

Book on third international operation of longitudes as part of IGY covering history, characteristics, standard hour, etc 14 p2314 A67-28957

Atomic clock application for Universal Time determination, describing various corrective measures, atomic beam technique, etc 15 p2487 A67-29581

Phase lock loop of synchronized time code translator, noting design and application 15 p2445 A67-29587

Memory device for matrix time meter, discussing use of logic thyatron to improve stability of memory matrix 16 p2674 A67-31119

Nanosecond baseband pulse rise time measurement, discussing real time and sampling oscillography, pulse comparison, basic instrumentation, etc 17 p2814 A67-32603

Buildup time for nonequilibrium argon ionization at inlet of MHD generator channel 18 p2989 A67-34048

Cesium plasma confinement time measurement in Q machine by plasma density decay observation 18 p3093 A67-34757

Photoelectric micrometer for automatic determination of meridian passage times, describing tracking servomechanism and collimation measurements 22 p3881 A67-39515

Three geodetic measurement bases synchronized to within 100 microseconds by transporting atomic clock 23 p3997 A67-40573

Irregular earth rotation velocity variation analyzed by comparing universal time with atomic time 24 p4150 A67-42312

Excitation time of electronic states on nitrogen molecule at high temperatures 24 p4194 A67-42890

TIME OPTIMAL CONTROL

Propellant and time-optimum trajectories with thrust vector rotational velocity at flight beginning and termination taken as additional boundary condition analyzed, using maximum principle 01 p0146 A67-10209

Low order model to determine approximate time optimal switching function for given plant in stability analysis of predictive control system [AFOSR-67-1339] 01 p0046 A67-1207

Time-optimal rendezvous in three dimensions with bounds on thrust and propellant, comparing various methods 02 p0330 A67-11924

Minimax rendezvous time of two linear uniform control plants, constructing optimal pursuit 02 p0225 A67-11956

Computational method for optimization of infinite time control problem for linear systems and quadratic indexes of performance 02 p0226 A67-12148

Optimal tradeoff function where expense is increased for saving time in orbital transfer to rendezvous, considering impulse modes 02 p0328 A67-12407

In-flight bending moment and terminal drift minimization for flexible vehicle, applying two-point boundary value problem solution for optimum rigid body control system 04 p0706 A67-15422

Gain adjustment of nonlinear time variant control systems with random inputs 05 p0783 A67-16444

Time-optimum transition of VTOL aircraft takeoff to forward flight [DVL-627] 06 p0944 A67-17627

Uniqueness of extremal controls for minimum fuel problems pertaining to single input linear time-invariant systems 06 p1098 A67-18523

Minimum time and fuel problems for PFM systems, deriving optimal control by heuristic argument 06 p0977 A67-18524

Relationship between optimum gain and time constant settings for multiple time constant self-adjusting models 06 p0977 A67-18530

Time-weighted minimal energy control of nth order plant 06 p0977 A67-18531

Time optimal search algorithms in pulsed extremal control systems with inertial or transport delays for case with known time constants and delay time 06 p0978 A67-18794

Time optimum control of alignment process for gyrocompasses 07 p1186 A67-19629

Time optimal position and velocity control

of spinning vehicle with reaction jet [AAS PAPER 66-115] 07 p1259 A67-19974

Combined use of time-domain waveforms, detection probability and false alarm probability for selection of optimum sample period and quantization interval for detection of impulse waveforms 09 p1459 A67-21582

Synthesis of control device for one class of nonlinear sampled data systems, obtaining processes with minimum control time 09 p1483 A67-22082

Automatic control with prediction, discussing optimal least time systems for trajectories satisfying maximum principle 10 p1608 A67-23322

Discrete signal optimal reception based on analysis of signal noise mixture 10 p1607 A67-23457

Eigenvector scalar product solutions for closed loop time optimal control of linear systems 11 p1771 A67-24897

Time optimal control of bounded phase coordinate process applied to unstable booster with actuator position and rate limits 12 p2012 A67-25911

Minimax time elapsing until meeting of pursuing and pursued controlled motion 13 p2085 A67-26382

Transient response in closed transmission systems evaluated and compared to time optimum process 13 p2087 A67-26614

Time optimum control in n-dimensional linear dynamic system with constant coefficients determined by matrix method 13 p2087 A67-26615

Time optimal control problems of linear systems with state and control vectors 13 p2087 A67-26723

Solution algorithm for boundary problem generated by necessary conditions for optimality in variational problem 14 p2341 A67-27840

Second order optimal control system simulation by computer, describing method for generating time optimal controls 15 p2458 A67-29907

Optimal control problem for nonlinear systems with constrained sample times 16 p2646 A67-31633

Time optimal control of system with multiple control inputs and bounded phase coordinates for design of autopilot for booster 16 p2762 A67-31643

Time optimal adaptive control system synthesis using off-line memorization with simple on-line calculations to determine control signal 16 p2650 A67-31672

Continuous control process with random variable stopping time of known probability distribution, presenting optimal feedback control, trajectory and minimum cost 16 p2651 A67-31681

Time optimal control for parabolic equations, proving bang-bang principle, smoothness, existence of minimum, etc 17 p2877 A67-32559

Linear continuous time stochastic optimal control process, obtaining optimum performance achievable as function of total effort at initiation of optimization period 17 p2830 A67-33013

Minimax rendezvous time of two linear uniform control plants, constructing optimal pursuit 17 p2831 A67-33273

PERT /Program Evaluation and Review Technique/ planning method gives project management means for controlling project to accomplish task in shortest possible time 18 p3161 A67-33633

Synthesis of time optimal control for discrete plants described by difference equations, deriving algorithm defining surface in phase space of variables 18 p3017 A67-33873

Construction and uniqueness of time optimal control of multidimensional linear system with constraints on control signal amplitudes and rates 18 p3017 A67-34286

Time optimal search algorithms in pulsed extremal control systems with inertial or transport delays for case with known time constants and delay time 18 p3018 A67-34451

Formulation of problem of guiding low thrust spacecraft back to nominal trajectory [AIAA PAPER 67-618] 19 p3260 A67-36000

Time optimal feedback control using extension of Hermes approximation theorem 20 p3408 A67-37077

Time optimal control problem solved by calculating boundary condition changes with

- system structure 20 p3409 A67-37222
Closed loop stepping motor as mechanical memory and time optimal control and digital servomechanism
applications 21 p3570 A67-37787
Minimax time elapsing until meeting of pursuing and pursued controlled motion 21 p3604 A67-38818
Fuel optimal control conditions in attitude correction of satellite in circular orbit determined using maximum principle, solving resulting boundary value problem 21 p3715 A67-39153
Quasi-optimum three-axis attitude control law for minimum time of rigid body, noting gyroscopic cross axis coupling 22 p3899 A67-39190
Optimal control problem with state variables subject to inequality conditions, deriving Pontryagin principle and differential equation 22 p3826 A67-39194
Nonstationary second order linear differential equation for near time optimal space vehicle guidance system design solved by linear transform theory 22 p3832 A67-39966
Time optimal adaptive control system synthesized via adaptive switching hypersurface and function generator /off-line memorization and on-line interpolation/ 24 p4134 A67-42177
- TIME RESPONSE**
Time variation in intensity of light emitted from CW GaAs laser diodes 01 p0088 A67-10243
Digital feedback control system compensation of pulse input to improve time response of controlled variable 01 p0045 A67-10673
Frequency-time domain asymptotic stability criterion for autonomous continuous systems 01 p0046 A67-11209
Adaptive control by predictive identification and optimization in terms of time response 02 p0225 A67-12142
Choosing coefficients of prefiltering, series and feedback compensators for given time response specifications despite plant parameter variations 02 p0225 A67-12143
Time resolution dependence on ambient gas around rotating mirror in streak camera 03 p0424 A67-13915
Matrix method determination of time response of time invariant linear systems to range of deterministic functions 06 p0976 A67-18402
Ionospheric effect of sudden magnetic storm eruption, noting propagation of disturbance above terrestrial surface 07 p1174 A67-19705
Photon modulated tunneling in Te-Al oxide-Al structures, noting increased spectral response and detection range 10 p1689 A67-22907
Time varying electromagnetic field pattern of prolate spheroid antenna with rotationally symmetric current distribution motion pictures generated by computer 11 p1758 A67-24115
Conductance-and capacitance-voltage curves of MOS capacitors analyzed for temperature dependence of inversion layer frequency response in n-type silicon 11 p1846 A67-24234
Time behavior of radiation field of infinite cylindrical antenna upon DC voltage pulse at input 11 p1762 A67-24292
Reduction of order technique pertaining to plant and reference model in controller design for linear plants transfer functions with zeros and slowly varying parameters 11 p1771 A67-24895
Formation of Maxwell and non-Maxwell distribution in gases, noting reduction of time reversible to time irreversible equations 12 p1968 A67-26114
Book on modern control systems covering feedback control theory within framework of frequency and time domain analysis 16 p2643 A67-30621
Modern control theory applied to digitally controlled tracking telescope design, emphasizing accuracy and response time 16 p2629 A67-31688
Control display linkages tested with human subjects for response time 18 p2993 A67-34338
Computer method for determining time-frequency-domain response specifications of transversal linear wave filters, using thin film RC distributed networks 18 p3015 A67-34560
Evoked potential display procedures yielding photographic superposition of large number of average responses 19 p3179 A67-34955
Air density variations at heights near 150 km determined by analyzing satellite orbit changes, noting solar activity effect 19 p3215 A67-35181
Time variations of electron intensity in outer radiation belt observed by satellites, studying electron radial diffusion and drift velocity 19 p3313 A67-35257
Time variation of Doppler broadened resonance line profile determined by assuming complete frequency redistribution 19 p3329 A67-36030
Synthesis procedure for linear automatic feedback control systems, examining time-domain response 20 p3413 A67-37679
Flight mechanics of gust absorber for high speed aircraft, discussing transient effects and short response time 21 p3568 A67-38378
Aircraft circuit and installation requirements referring to short time characteristics of cables and effect on circuit protection, coordination and weight saving 21 p3572 A67-39072
Stability and response time of quantified pulse-position modulation feedback control circuit consisting of nonlinear sampler and first order continuous part 22 p3776 A67-39647
Serial/matrix technique extended to give multivariable linear system responses defined in state space terms 23 p3983 A67-40646
Digital controller design for tracking telescope, discussing tracking accuracy and response time 24 p4154 A67-42176
Photoelectromagnetic detector spectral sensitivity, magnetoresistance and time constants with optically polished thin elements fabricated from Ge, InAs, GaSb and InSb single crystals 24 p4154 A67-42243
Algebraic equations to predict time response to step input in free molecule, transition and continuum flow regimes 24 p4155 A67-42293
Semilimplicit numerical methods for time transient gas-lubrication Reynolds equation stressing numerical stability [ASME PAPER 67-LUB-18] 24 p4163 A67-42677
- TIME SCALE**
SA HELMHOLTZ-KELVIN TIME SCALE
Calculating past states of earth-moon system based on three time scales for dynamical change 04 p0698 A67-14854
Physical foundations of modern kinetic theory, showing interpretation of particular form of Liouville equation in terms of time scales appropriate to system 11 p1823 A67-24545
Characteristic scales of thermal convection in unstable atmosphere, discussing time evolution of total kinetic energy and lifetime for dry air case 13 p2116 A67-27460
Reynolds stress in turbulent flow dependence on mean velocity field determined by rational sequence of approximations 21 p3609 A67-37734
Solar X-ray emission below 20 angstroms made by Explorer XXX, discussing analog real time records and time resolution 23 p4050 A67-40805
Jacobi high energy ellipsoid orbits in barred spirals valid at galactic time scales 23 p4063 A67-40898
- TIME SERIES**
Adaptive technique determination of optimum operations for pure prediction of discrete time series with respect to mean square error cost function 02 p0207 A67-12138
Solar proton streams apparently synodic in solar rotation interval during maximum epoch of recent solar cycle as indicated by polar cap absorption events 03 p0507 A67-14116
Relation among sampling theorem, Z transformation and time series method for applications to network analysis 07 p1146 A67-20194
Generating time series for amount of solar radiation falling on horizontal surface of unit area at top of atmosphere per unit time 15 p2477 A67-29628
Extrapolation of time series with discrete Laguerre polynomials, deriving general recursion relation for expansion coefficients 16 p2697 A67-31418
Long term gyro drift rate evaluation involving time series detrending and autoregression, periodogram, autocorrelation, spectral density and mathematical model analysis 17 p2858 A67-32486
Spectral analysis of time series - Conference, University of Wisconsin, October 1966 20 p3476 A67-36782
Probabilistic background of time series models which relate to spectral analysis and power spectrum and statistical inference for stationary stochastic processes 20 p3476 A67-36783
Numerical spectrum analysis procedures, discussing fast Fourier transform techniques, classical spectrum windows and complex demodulation process for time series studies 20 p3476 A67-36784
Cross-spectrum analysis in meteorology, considering property fluxes and time series, discussing turbulent energy flux, solar activity, etc 20 p3480 A67-36786
Signal model with white noise fitted to time series, discussing signal proportion estimation methods 20 p3476 A67-36788
Prediction procedure for nonstationary stochastic processes with slow spectral density function variation with time 20 p3477 A67-36789
Stochastic models for forecasting seasonal and nonseasonal time series using iterative method 20 p3477 A67-36790
- TIME SHARING**
Computerized method for on-line data analysis, elucidating SLIP language, request, processing, interpretation, time sharing, background activity, etc 17 p2821 A67-32865
Program providing man-machine communication for electronic circuit analyses using time sharing computer 19 p3186 A67-35619
Time-sharing system with single central processing unit and several graphic display consoles for single high speed computer among human operators 19 p3188 A67-36060
Optimum word length for signal simultaneous digital transmission in real time through single channel 21 p3581 A67-38179
Real time systems and applications 23 p3976 A67-41056
Boeing Huntsville Simulation Center emphasizing ALPINE system and Interim Time Sharing System /ITSS/ [AIAA PAPER 67-896] 24 p4126 A67-43005
- TIME SIGNAL**
Receiver design for LF time signals on kilometer waves 02 p0190 A67-11481
Troposcatter transmission technique called frequency time shift keying, deriving optimum noncoherent receiver configuration and error performance 02 p0202 A67-12123
Time signal transmission and reception, noting development of UHF spectroscopy and atomic frequency scales 18 p3004 A67-34400
- TIMING**
Range instrumentation support systems, describing approaches to timing, firing and communications systems 10 p1605 A67-22998
Timing error and noisy phase reference joint effect on system performance of coded partially phase coherent reception 17 p2811 A67-32116
- TIMING APPARATUS**
SA ACCELEROMETER
SA ATOMIC CLOCK
SA CHRONOTRON
SA CLOCK
SA PENDULUM
SA TACHOMETER
Combination flash photolysis-flash pyrolysis system with timing circuit, using Tektronix pulse generators and ignitron circuit for firing spectroscopic lamp 02 p0247 A67-12689
Modular 100 MHz digital time analyzer using flexible plug-in logic 06 p1001 A67-17852
Atomic clock design using beam method or optical pumping method to make transitions observable 07 p1186 A67-19527
Electronic clocks, with frequency and phase variation negligible, as means of making air and space navigation exact 07 p1222 A67-19681
Rectangular terminal block in rectangular waveguide and dispersion equation for surface wave propagating along waveguide 10 p1613 A67-23445

Low cost time delay and multiple programmer for space research 12 p1909 A67-25230

Low cost accurate mechanical timers [ASME PAPER 67-DE-39] 14 p2321 A67-28877

Eastern Test Range time synchronization system, analyzing errors and limitations 20 p3414 A67-36535

TIN

Parametric amplification and sideband oscillations in structured superconducting Sn thin films 03 p0496 A67-13568

K-shell ionization cross sections of silver, tin and gold from electron bombardment 04 p0661 A67-15762

Temperature and thickness dependence of critical field of superconducting Sn films measured and compared with nonlocal theoretical models 05 p0864 A67-16899

Anisotropic energy gap in superconducting white tin obtained by expansion in tetragonal harmonics 07 p1235 A67-20134

Laser transition in B 2, Br 2 and Sn in pulsed discharges of boron chloride, hydrogen bromide and stannic chloride respectively 08 p1339 A67-21379

Josephson and ordinary tunneling currents for two-band model superconductor, treating niobium-tin junction 09 p1551 A67-21667

Cryogenic thermoconductivity of impure tin in superconducting and normal state, noting anisotropy and superconducting energy gap independence from impurity type 10 p1687 A67-22761

Correlation of anisotropic energy gap with thermal conductivity in pure and impure superconducting tin 10 p1687 A67-22762

Electrical and thermal conductivity of tin films investigated in search for surface superconductivity induced by electric field 10 p1688 A67-22765

Transition temperature change for thin tin and thallium superconducting films after deposition of dielectric substances 13 p2182 A67-27360

Perpendicular critical magnetic fields of superconducting aluminum, tin and gallium small grained films examined for superconducting transition temperature enhancement 14 p2373 A67-28860

Magnetization measurements for pure superconducting tin cylinders, discussing superheating effects 23 p4044 A67-41441

TIN ALLOY

Creep deformation of hot-rolled Zn-Ti alloys, noting secondary flow originating from strain induced grain growth 03 p0440 A67-13251

Continuous gas deposition of triniobium-tin alloy on moving refractory wire without reaction chamber contamination by by-products 03 p0500 A67-14065

Continuous gas deposition of triniobium-tin alloy on moving refractory wire without reaction chamber contamination by by-products 13 p2185 A67-27721

Superconducting property of kappa phase in Bi-Sn alloy at high pressure, with determination of transition to superconducting state and temperature interval to keep stable state 22 p3857 A67-39460

TIN COMPOUND

Amine-tin antioxidant systems for aliphatic hydrocarbons and related alkyl substituted fluids 20 p3474 A67-37594

TIN OXIDE

Surface parameter measurements of stannic oxide in powder, ceramic and gel forms by nitrogen adsorption techniques 10 p1603 A67-23398

Tin oxide films in microscopic quantities on glass and quartz substrates studied for transparency, reflectivity and roughness 12 p1982 A67-25324

TIN TELLURIDE

Thermal power and electrical conductivity of SnTe-InTe crystals, discussing temperature effect 04 p0683 A67-15581

Fermi surface of tin telluride approximated by four distorted surfaces located at L points of Brillouin zone as shown by Fourier analysis 06 p1065 A67-18950

Double valence band and thermoelectric properties of lead telluride-tin telluride solutions 10 p1688 A67-22848

Parameters for model of two valence bands of SnTe according to Hall effect measurements at high temperatures 15 p2537 A67-29709

SnTe samples under uniform load studied

for relation between electrical and thermal conductivity, thermal EMF and microhardness 16 p2730 A67-31165

Band structure and current carrier scattering in hole-type SnTe, studying temperature dependence of electric conductivity, thermal EMF, Hall effect, etc 19 p3300 A67-34766

Parameters for model of two valence bands of SnTe according to Hall effect measurements at high temperatures 24 p4200 A67-41779

TIP

S WING TIP

TIP CONTROL

Systems constraints imposed on spacecraft utilizing long flexible rods with attached tip masses, specifically deployment and retraction problems 10 p1714 A67-23757

Effect of rotor control feedback loads of two-bladed rotor system on helicopter fuselage vibrations 16 p2777 A67-31847

[AHS PAPER 133] 16 p2777 A67-31847

Aircraft engine turbine structure effect on blade tip clearance, analyzing clearance variations as function of rotor angular velocity 22 p3868 A67-39546

TIP SPEED

Propulsion-lift system interrelationship in compound helicopter and design parameters affects performance vs speed such as disk loading, solidity and tip speed schedule [ASME PAPER 67-GT-18] 11 p1854 A67-24802

JT9D engine design from viewpoint of incorporated noise reduction features [SAE PAPER 67-0331] 17 p2929 A67-32984

TIRE

SA AIRCRAFT TIRE

Skidding accident reduction investigated for runway and highway safety noting worn tires, smooth surface texture, locked wheels and pilot technique 19 p3173 A67-35930

TIROS III SATELLITE

Satellite radiation data application to synoptic weather analysis including cloud pattern mapping, tropospheric relative humidity and vertical cloud structure inference 13 p2149 A67-26274

TIROS IV SATELLITE

Radiation data measured by Tiros IV satellite for determination of global distribution of atmospheric water vapor 10 p1677 A67-23195

TIROS VII SATELLITE

Tiros VII satellite IR measurement data used to determine sea surface temperature gradients, examining problem of cloud cover 01 p0109 A67-10321

TIROS OPERATIONAL SATELLITE SYSTEM

Tiros satellite development and Tiros operational satellite /TOS/ system noting design, camera orientation, spin-rate control, etc 06 p1096 A67-18412

ESSA meteorological satellite system noting mission requirements, design and performance [SMPT PAPER 101-56] 12 p2011 A67-25472

TIROS satellite program accomplishments since 1960, describing operational system, TOS ground-station network and ESSA satellites 22 p3899 A67-39608

Photographic research of small scale meteorological disturbances /cloud formations/ observed by Tiros satellites 22 p3829 A67-39972

TIROS SATELLITE

SA ESSA SATELLITE

Tiros satellite photography used to forecast British Isles weather 12 to 24 hr in advance 01 p0108 A67-10225

Problems encountered in preparation of final meteorological radiation tapes, using Tiros IR radiation data 01 p0108 A67-10320

Evolution of Tiros meteorological satellite operational system noting orbital inclination, solar illumination, data storage ground stations, etc 02 p0334 A67-12371

Pattern recognition, property filtering and lunar feature data experiments coupled with Tiros cloud photographs demonstrate preprocessing for systems design [SMPT PREPRINT 100-13] 03 p0376 A67-13805

Automatic plotting of cloud information map on Setun digital computer from Tiros meteorological satellite data 04 p0652 A67-15471

Stabilite system, three-axis attitude control system utilizing single reaction wheel 06 p1094 A67-17681

Tiros satellite development and Tiros

operational satellite /TOS/ system noting design, camera orientation, spin-rate control, etc 06 p1096 A67-18412

Sensor beam, scan mode and perinadinal nadir angle determination for Tiros IR data using simplified graph 13 p2117 A67-27612

Evolution of Tiros meteorological satellite operational system noting orbital inclination, solar illumination, data storage ground stations, etc 15 p2565 A67-29761

Tiros satellites characteristics including ESSA I 15 p2565 A67-29762

Meteorological satellite program results discussing Tiros satellites cloud picture storm warning, etc 19 p3253 A67-35633

Limb darkening of earth deduced from statistical analysis of IR radiance data from measurements by Tiros satellites 21 p3655 A67-38577

Triaxial attitude control stabilization for second-generation /TIROS/ meteorological satellite 22 p3897 A67-39156

Clouds over equatorial and tropical Pacific investigated by comparing photographs from Tiros satellites and jet aircraft 24 p4181 A67-42661

TIROS WHEEL SATELLITE

Tiros IX wheel satellite design and performance and relation to earlier Tiros satellite 16 p2756 A67-30624

TISSUE

SA ADIPOSE TISSUE

Electric conduction models for biological tissues as anisotropic medium 08 p1288 A67-20600

Tissue protein synthesis in hypodynamic rats studied with aid of carbon 14 and sulfur 35 tagged amino acids 13 p2059 A67-26755

Ionizing radiation received by biological tissue during space flights measured by nuclear-emulsion technique 20 p3368 A67-36268

Inert gas effect on oxygen consumption in living tissue studied by polarographic and Warburg techniques 23 p3960 A67-41700

Tissue oxygenation during hemorrhage in dogs at 1 and 3 atm oxygen, noting oxygen at high pressure /OHP/ does not prevent stagnant hypoxia [SAM-TR-66-258] 24 p4111 A67-41800

TITAN I ICBM

Checkout equipment development over Titan I to III span and effect on GSI [AIAA PAPER 67-287] 07 p1166 A67-20077

TITAN II ICBM

Checkout equipment development over Titan I to III span and effect on GSI [AIAA PAPER 67-287] 07 p1166 A67-20077

Axial vibration /pogo stick effect/ of Titan II, as Gemini launch vehicle, studied by analog computer simulation for instability influences 14 p2394 A67-28008

TITAN III LAUNCH VEHICLE

Dynamic load analysis of Titan III booster structure using dynamically scaled model vibration survey [SAE PAPER 660684] 01 p0154 A67-10588

Facilities, ground handling and transport equipment for Titan III ITL system [SAE PAPER 660706] 01 p0050 A67-10599

Temperature control of orbital Titan III-transtage space booster, noting thermal design, configuration and materials test program support 02 p0335 A67-12399

Titan III launch vehicle for multiple payload delivery into precise space trajectory [AIAA PAPER 66-836] 03 p0519 A67-14122

Titan III launch vehicle assembly 05 p0787 A67-16611

Checkout equipment development over Titan I to III span and effect on GSI [AIAA PAPER 67-287] 07 p1166 A67-20077

Automatic checkout system /ACS/ and digital guidance programs for titan III and Apollo 08 p1297 A67-20633

Titan III program, considering DOD and USAF development of improved system acquisition policies and regulations [AAS PAPER 66-154] 08 p1430 A67-20977

Titan III system capability for space support and logistics, discussing parameter of assessment 08 p1412 A67-21077

Titan III program, considering DOD and USAF development of improved system acquisition policies and regulations [AAS PAPER 66-154] 13 p2232 A67-27551

Titan IIIB launch vehicle spent stage

recovery experiment, evaluating feasibility of refurbishment and reuse 15 p2569 A67-29853

Design, equipment and techniques of electronic packaging in Titan III program, stressing environmental levels and safety factors 21 p3595 A67-38335

Hydraulic failure detection system in Titan booster servo injector module featuring anticipation and correction of servomodule failure 24 p4099 A67-42426

TITAN LAUNCH VEHICLE

Storable propellant pressure vessel design for Titan launch vehicles and compatibility and stress-load-corrosion analysis [SAE PAPER 660677] 01 p0160 A67-10582

TITANATE

S BARIUM TITANATE

S LEAD TITANATE

S STRONTIUM TITANATE

TITANIUM

Change in resistance of titanium films deposited in high vacuum from argon ion bombardment, noting dependence on energy value 01 p0129 A67-10099

Elastic strain distribution in structure of quasi-isotropic polycrystalline titanium 01 p0093 A67-10100

Hall coefficient tensor in single crystals of titanium measured at room temperature as function of crystallographic orientation in magnetic field 01 p0132 A67-10375

Titanium fabrication techniques for XB-70 and space booster [SAE PAPER 660650] 01 p0079 A67-10611

Titanium mill products intended to meet requirements of C5A and SST aircraft, describing specially designed mill processing equipment [SAE PAPER 660651] 01 p0079 A67-10612

Electric resistance of titanium evaporated films in thickness range of path length effects 02 p0292 A67-11744

Effects of order-disorder state and film thickness on structure and electric conductivity of evaporated nickel, titanium and silver films 02 p0292 A67-11745

Sweep spectrometer study of effect of strong magnetic field on characteristics of plasma beam produced by titanium plasma source 02 p0278 A67-12622

Rate controlling mechanism during yielding and flow of alpha-titanium below 0.4 times melting point 03 p0441 A67-13258

Stress corrosion in titanium, examining preventive measures of surface treatment, reduction of design stress, environmental control and alloy modification 04 p0636 A67-14602

Effect of beryllium, boron, titanium, etc., additions on recovery and recrystallization processes in pure aluminum, using differential calorimetric techniques 04 p0637 A67-14910

Various combinations of preanneal and diffusion anneal conditions used in experiments for determining environmental effects on diffusion of Ta 182 in bcc titanium 04 p0637 A67-14937

High vacuum welding of cermet seals with titanium 04 p0630 A67-15632

Spectral emissivity of Ti from 1100 degrees K to melting point 05 p0831 A67-17318

Tensile tests performed on alpha titanium between -321 and 75 degrees F, discussing ductile-to-brittle transition, microcrack formation and brittle fracture mechanics 06 p1014 A67-17807

Electron microscopic structure and lattice defects of martensite in commercially pure titanium 06 p1017 A67-17966

Transformation twins in titanium, discussing relationship between twins and martensite crystal, using electron microscopy 06 p1017 A67-17967

New metals replacing steels noting titanium, beryllium and niobium in French industry 06 p1017 A67-17994

Hydrogen effect on high temperature plasticity failure and mechanical properties of titanium shown to be similar to that caused by strain 07 p1200 A67-19248

Optimal thickness of protective action of crucible lining in smelting of titanium 07 p1200 A67-19250

Mutual diffusion characteristics of titanium-tungsten mixtures at high temperatures, noting discontinuity on concentration curve due to two-phase region

presence 07 p1204 A67-19266

Obtaining high strength titanium welds without hardening by heat treatment 07 p1190 A67-19295

Linear expansion coefficient divergence of commercial titanium rod 07 p1208 A67-19297

Deformation speed effect on structural changes in Ti, noting test results at 600 degrees C 07 p1209 A67-19735

Unalloyed titanium properties dependence on deformation and temperature 07 p1211 A67-20290

Plastic strain distributions in polycrystalline austenitic stainless steel and titanium, using photoelastic coating 08 p1343 A67-21333

Deoxidative capacity and activity of titanium in nickel-chromium alloys 09 p1518 A67-21964

Twinning and temperature effect in plastic deformation of titanium 09 p1518 A67-21965

Titanium for sublimation, using combination sublimation-getter ion pump 09 p1503 A67-22101

Plasma mode work function measurement for studying thermionic emission from Hf, Th and Ti in Cs vapor at reservoir temperature of 414 degrees K 09 p1450 A67-22353

Diffusion bonding of titanium and stainless steel at high temperatures using pneumatic hammer 09 p1520 A67-22436

Emission and absorption bands in K spectral region of titanium, using single setup 10 p1668 A67-23093

Latent heat of fusion of titanium 10 p1670 A67-23640

Temperature effect, including liquid helium temperature, on yield stress of commercial purity alpha titanium 11 p1805 A67-24111

Micrographs of thin Ti layers through electron microscope showing dislocation distribution 11 p1806 A67-24428

Temperature, strain rate and purity effects on alpha-titanium deformation yield and flow stresses, ascertaining thermal activation rate controlling mechanism 11 p1807 A67-24567

Coating of titanium with aluminum and silicon by immersion of titanium samples in molten aluminum or in aluminum/silicon melts 12 p1955 A67-25360

Pulsed inert gas metal-arc welding technique for titanium 721, investigating arc characteristics in argon, argon/helium and helium 12 p1950 A67-25738

Strengthening of sapphire single crystals by precipitates containing titanium 12 p1987 A67-26190

Sweep spectrometer study of effect of strong magnetic field on characteristics of plasma beam produced by titanium plasma source 13 p2170 A67-27378

Formation of hydride zinc film on titanium activated for deposition of galvanic coating 14 p2336 A67-27868

Absolute oscillator strengths of three titanium resonance lines from absorption measurements in atomic beam 14 p2351 A67-28581

Experimental forging of titanium by techniques not requiring machining 14 p2324 A67-28629

Far IR absorption spectra of chromium and titanium ions in aluminum oxide crystal, indicating Jahn-Teller effect reduction of trigonal field and spin-orbit coupling 14 p2370 A67-28714

Fourier analysis of line profiles of X-ray-studied deformation faulting in titanium, zirconium and hafnium 14 p2340 A67-29033

Nonlinear effects during titanium plasma source operation, investigating plasma nature and magnetic field effects on injector operation and plasma parameters 15 p2529 A67-29719

Spectral linewidth and shift of Ti I lines produced by neutral argon atoms analyzed using high pressure arc as light source 16 p2703 A67-30665

Density, crystallinity and electric properties of thin metal films deposited on rotating cylindrical substrate 16 p2727 A67-30899

Marshall plasma gun with titanium electrodes saturated with deuterium for filling magnetic collector 16 p2676 A67-31400

X-ray K-absorption spectra of titanium, vanadium germanium in germanides 16 p2691 A67-31594

Metallic adhesion between Mo-Mo and Ti-Ti couples, showing contact resistance useful in determining contamination at conducting interface 17 p2871 A67-32465

Titanium plasma source design features, performance, ion mean free path, energy spectrum and energy distribution 17 p2904 A67-32912

Mass composition, contamination dynamics and jet structure of titanium plasma source 17 p2904 A67-32913

Knoop hardness anisotropy in unalloyed titanium and iodide titanium sheets, discussing orientation, hardness variations, rolling, cross section planes and indentation [ASTM PAPER 53] 18 p3068 A67-34583

Diffusion welding of commercially pure titanium investigated for process parameters, noting temperature effect 19 p3234 A67-34792

Adsorption, surface reaction and mutual displacement of carbon monoxide, carbon dioxide and oxygen on titanium film, using mass spectrometer 19 p3244 A67-34941

Titanium susceptibility to corrosion, achieving protection by passive self-healing films forming on metal surface 20 p3466 A67-36638

Materials in airlift technology noting adaptation of titanium and beryllium 20 p3471 A67-37533

Plasma arc process applied to stainless steel and titanium plate welding, discussing metallurgical and mechanical weld and deformation tests 20 p3456 A67-37542

Hyperfine interaction between unpaired trapped electron and adjacent titanium 47 and 49 nuclei in F center ESR line in barium titanate 21 p3684 A67-38417

Heterodiffusion of metallic impurities in body-centered phases of doped zirconium and titanium, determining diffusion coefficients via radioactive isotopes 22 p3820 A67-39823

Ti thin film microcircuit fabrication and electrical properties 23 p3977 A67-40661

Ti stress corrosion in nitrogen tetroxide, detailing investigative techniques [ASM PAPER C6-2.2] 23 p4020 A67-41409

Soviet metallurgical, chemical and electrochemical studies and industrial applications of titanium 24 p4169 A67-41918

Ti additive effect on aluminum oxide particle growth in Ni matrix from 1000 to 1350 degrees C 24 p4171 A67-41959

Ti thin films use as getter in electron microscopy of Mo particles at high temperature with minimum oxidation 24 p4172 A67-41978

Ti isotopes nuclear magnetic resonance in hexagonal Ti metal showing d-like conduction-electron states at Fermi level by spin-lattice relaxation time 24 p4203 A67-42109

TITANIUM ALLOY

Phase diagram of W-Zr-Ti ternary alloy 01 p0093 A67-10291

Mechanical properties and corrosion resistance of titanium alloy forgings used as compressor parts 01 p0093 A67-10546

Plasma arc welding produces butt type joints in thick titanium aerospace structures [SAE PAPER 660646] 01 p0078 A67-10609

Titanium crossbeam design and fabrication [SAE PAPER 660647] 01 p0079 A67-10610

Mechanical property and structural changes in titanium alloys subjected to high temperature thermomechanical treatment 01 p0095 A67-10641

Metastable phase formation in Ti alloys, noting nature and properties of different phases 01 p0095 A67-10642

Plasma arc welding for joining thick titanium, examining data for three common titanium alloys, three welding positions and process variables such as plasma gas composition and travel rates 01 p0081 A67-11039

Atom distribution in double matrix cell of ordered solid solution in alnico-titanium alloy 02 p0254 A67-11864

Structural changes during early stages of decomposition of oversaturated solid solution of titanium in cobalt, noting secondary diffusive reflection 02 p0255 A67-11865

Creep deformation of hot-rolled Zn-Ti alloys, noting secondary flow originating from strain induced grain growth 03 p0440 A67-13251

Thermal dilation of titanium alloys during

repeated cycling through alpha-beta transformation 03 p0440 A67-13252

Ti-Mg alloy production under high pressure, noting existence of solid solution of one weight-percent Mg 03 p0441 A67-13255

Titanium alloy forging tests covering notched tension, compression, shear, bearing, fracture toughness and smooth and axial fatigue 03 p0446 A67-13552

Titanium alloys test results at 20 and 400 degrees C and at different grip speeds, using various tensile testing machines 03 p0446 A67-13566

Deformation and diffusion bonding of Al, Ti and stainless steel alloys, discussing surface condition, time, temperature, cold work, heat treatment and intermediate materials 03 p0430 A67-13692

Soviet monograph on vacuum arc melting of titanium alloy ingots noting crystallization process, structural changes and properties of end-products 03 p0447 A67-13925

Plastic deformation in titanium at low temperatures, noting prevalence of twinning and suitability as construction material in cryogenic technology 04 p0636 A67-14752

Oxygen content effect on mechanical properties and phase transformations of VT 16 titanium alloy during thermal treatment 04 p0637 A67-14942

Annealing effect on texture of titanium alloys with electrodeposited chromium and nickel 04 p0637 A67-14944

Molten-Ti slag chlorination in automatic optimization based on mathematical model 04 p0637 A67-14945

Monograph on formation of Ti-based solid solutions and behavior at high temperature under tension 04 p0638 A67-15008

Microscopic and X-ray analysis of cast and annealed W-Mo-Ti alloys, plotting polythermal cross sections 04 p0638 A67-15203

Biaxial fracture strength of textured titanium alloy for design of liquid fuel tankage 04 p0711 A67-15242

Plastic deformation and aging effect on kinetics of beta phase decay, dispersion and alpha phase distribution of TC6 by optical and electron microscopy and measurements of hardness and mechanical properties in tension 04 p0640 A67-15976

Effect of structure of beta titanium alloy on crack propagation resistance 04 p0641 A67-15985

Titanium surface alloying in aluminum melts at temperatures from 700 to 1000 degrees C 05 p0828 A67-16328

Two oxidation mechanisms for Ti-Al alloys based on increased diffusion rate and decreased oxidation rate 05 p0829 A67-16492

Phase recrystallization effect on structure and mechanical properties of cast monophase titanium alloys 05 p0830 A67-16760

Plastic deformation of textured Ti alloy sheet examined, using tension testing along different directions and combined stress loading along principal axes of anisotropy 06 p1016 A67-17900

Newer titanium alloys compared with present production alloys from closed die forgings in typical airframe and engine configuration 06 p1017 A67-17999

Diffusion and nondiffusion transformations in titanium alloys, noting martensitic transformation 06 p1018 A67-18231

Heat treatment effect on structure, hardness, microhardness and corrosion resistance of VT1 titanium and OT4 titanium manganese-aluminum alloy sheets 06 p1018 A67-18236

High temperature condensed phase equilibria in Ti-W-O system examined, using sealed capsule technique 06 p1018 A67-18371

Isothermal transformation diagrams for titanium-molybdenum alloys 07 p1199 A67-19243

Isothermal transformations in hypo- and hypereutectoid titanium-chromium alloys 07 p1200 A67-19244

Kinetics of growth of beta grain in titanium alloy 07 p1200 A67-19245

Hydrogen distribution between phases in /alpha and beta/ titanium alloys at various temperatures 07 p1200 A67-19246

Hydrogen effect on processes occurring in alloy VT3-1 during aging shown to increase beta phase 07 p1200 A67-19247

Quenching from alpha region and subsequent tempering effect on mechanical

properties of titanium alloy VT5-1 07 p1200 A67-19249

Soviet papers on metallochemistry of titanium alloys [JPL-TR-32-807] 07 p1202 A67-19259

Physicochemical properties of Ti-Al-O solid solutions 07 p1203 A67-19260

Microstructural and X-ray analysis of intermediate phases of Ti-Ir and Ti-Rh intermetallic compounds, including microhardness and fusion point variations 07 p1204 A67-19263

Phase equilibrium and physicochemical properties of titanium aluminide-titanium stannide-zirconium quasi-ternary alloy 07 p1204 A67-19264

Chemical and crystal structural analysis of solid solution of titanium chromide and zirconium chromide metallides 07 p1204 A67-19265

Phase diagram of titanium-rich alloys of system Ti-Al, measuring resistivity and hardness through X-ray diffraction, thermal analysis, etc 07 p1204 A67-19267

Heats of solution and formation of Ti-Al alloys in region of alpha-solid solution determined, using calorimetry 07 p1204 A67-19268

Microstructure of alloys of Ti-Fe and Ti-Cr-Fe systems, determining phase composition and incipient melting temperature 07 p1204 A67-19269

Structural changes in titanium alloys during heat treatment 07 p1205 A67-19271

Ternary system Ti-Al-V alloys analyzed using thermal, microstructural, etc, methods, plotting solidus surface in crystallization region of beta-solid solution 07 p1205 A67-19273

Fine structure of two-phase alloys of titanium VT14 and structures effect on mechanical properties 07 p1205 A67-19274

Ni, Si and Nb effect on oxidation of binary alloys of titanium in air at high temperature, discussing heat resistance 07 p1205 A67-19275

Gas saturation effect on titanium alloys undergoing heat treatment, discussing microhardness and surface crack formation 07 p1205 A67-19277

Electron microscope study of plastic deformation mechanism of titanium alloy AT4 and fatigue strain mechanism in coarse grained specimens of alloy T-40 07 p1205 A67-19278

Modulus of elasticity of metals and titanium alloys as function of electron structure and binding energy 07 p1206 A67-19279

Alloying effect on elastic modulus, strength and plasticity of titanium in temperature range from - 196 to 800 degrees 07 p1206 A67-19280

Physical properties of quenched binary alloys of titanium 07 p1206 A67-19281

Heat treatment effect on mechanical properties and structure of Ti alloys, noting phase state variation as function of quenching temperature 07 p1206 A67-19282

Hydrogen brittleness in Ti alloys, noting conditions of development 07 p1206 A67-19283

Heat resistance of Ti alloy after thermomechanical treatment, noting properties as long lifetime structural material 07 p1206 A67-19284

Titanium alloy mechanical and physical characteristics, noting dependence on chemical and phase composition 07 p1206 A67-19285

Heat treatment effect on yield point, impact toughness and plasticity characteristics of Ti alloys 07 p1207 A67-19286

AT13 Ti alloy preparation noting physical and mechanical properties and heat treatment induced phase transformation 07 p1207 A67-19287

Heat resistance and fatigue strength of Ti alloys examined, using bending techniques 07 p1207 A67-19288

Mechanical properties and heat resistance of titanium alloyed with low and high proportions of Al and Sn 07 p1207 A67-19289

VT15 Ti alloy weld plasticity and strength as affected by additives, hardening and plastic deformation 07 p1207 A67-19290

Titanium alloy weld properties as affected by boron, beryllium and lanthanum additions 07 p1207 A67-19291

Phase transformations and welding

characteristics of alpha and /alpha plus beta/ titanium alloys 07 p1207 A67-19292

Delayed fracture and brittle properties of titanium alloys 07 p1207 A67-19293

VT15 titanium alloy weld properties as affected by machining and postwelding heat treatment 07 p1208 A67-19294

Diffusion zones formed during soldering of AT3 OT4 Ti alloys 07 p1190 A67-19296

Pauli-paramagnetic superconductivity in Ti-16 at percent Mo from specific heat measurements 07 p1235 A67-20130

Qualitative and quantitative methods for correlating preferred crystallographic orientation with biaxial strengths of titanium alloys 08 p1340 A67-20363

Fracture behavior of Ti alloys in aqueous environment, noting process to increase fracture toughness 08 p1340 A67-20364

Microstructure interpretation of 5Al-2.5Sn titanium alloy, examining high optical magnification and polarized light illumination 08 p1340 A67-20365

Scaling of binary titanium alloys in carbon dioxide at high temperatures using kinetic, metallographic and electron probe microanalysis [AAS PAPER 66-190] 08 p1341 A67-20763

Test method for aluminum and titanium alloys, estimating tendency toward brittle failure and recording kinetics of crack formation 08 p1342 A67-21176

Cold brittleness, impact toughness and crack resistance of titanium alloys at low temperatures 09 p1518 A67-21866

Thermal etching study of rod shaped formations caused by structural dislocations during heating and cooling of Ti-Mo-Fe-Al system 09 p1518 A67-21867

Alloying element selection for heat resistant titanium alloys, obtaining characteristic temperatures and mean quadratic displacement 09 p1518 A67-21968

Phase diagram of Nb-Ti-Zr system and superconducting properties of alloys 09 p1518 A67-22029

X-ray structural study of phase transformations during heat treatment of VT3-1 titanium alloy 09 p1518 A67-22030

Polybenzimidazole /PBI/ structural adhesives for bonding stainless steel, beryllium and titanium alloys 09 p1523 A67-22517

Weldability of titanium alloy sheets, noting quality through spot welding 09 p1520 A67-22621

Titanium alloy thin foil preparation using window method and electropolishing conditions, noting phase transformation 10 p1668 A67-23175

Correlation among room temperature creep stresses, fatigue and proportional limit in titanium alloys 10 p1669 A67-23325

Random-loading fatigue crack growth behavior of airframe aluminum and titanium alloys under sinusoidal, narrow band and broad band random loading 10 p1669 A67-23434

Bending fatigue tests of unmachined, mechanically machined and chemically machined panels of aluminum and titanium alloys 10 p1669 A67-23437

High temperature thermomechanical treatment effects on VT10 titanium alloy fine structure 10 p1670 A67-23641

Gas saturated layer effects on VT5 titanium alloy mechanical properties variation with temperature 10 p1670 A67-23642

Stress corrosion cracking of titanium alloys, noting tensile test data, crack propagation in salt solution and in pure solvents and metallurgical and electrochemical factors 10 p1670 A67-23701

Diffusion bonding of titanium sandwich structure for Saturn tank wall application 10 p1661 A67-23702

Titanium-chromium-vanadium system isohardness and isothermal diagrams and characteristic micrographs 11 p1806 A67-24362

Crack propagation for stainless steel and Ti alloy at stresses below fatigue limit, noting of alternating stress cycles crack propagation for stainless steel and Ti alloy at stresses below fatigue limit, noting role 11 p1806 A67-24365

Titanium and aluminum additions to cobalt-base alloys improve tensile and stress rupture properties and heat resistance 11 p1807 A67-24703

Microstructural variations of Ti-Mo-Al alloys due to stress corrosion cracking, noting increased resistance through heat treatment
[ASME PAPER 67-GT-5] 11 p1808 A67-24793
Direct observation on precipitation and aging behavior in Cu-Ti alloys by transmission electron microscopy 11 p1809 A67-24948
Heat resistance, bending and tensile creep of multicomponent Ti alloys 12 p1955 A67-25366
Stress relaxation dependence on heat deformation regime in Ti alloys VT14, VT3-1 and VTS-1 12 p1955 A67-25368
Intermediate phases in alloys of Ti with Ir, Rh and Qs indicate possibility of polymorphism 13 p2131 A67-26472
State diagram structure of Ti-Cu system examined using metallographic, thermographic, X-ray and microhardness analyses 13 p2131 A67-26473
Stability of titanium-aluminum alloys during oxidation in air 13 p2142 A67-27287
Texture strengthening and fracture toughness of titanium alloy sheets biaxial stress fields at room and cryogenic temperatures 13 p2142 A67-27442
Elastic properties of Ti alloys of ternary system Ti-Zr-Cr, showing sensitivity to heat treatment 13 p2143 A67-27710
Hydrogen influence on fracture propagation of titanium alloy during tension tests 14 p2337 A67-28286
Titanium-vanadium alloy microstructure investigated under quenching and aging through electron microscopy 14 p2338 A67-28423
Effect of structure of beta titanium alloy on crack propagation resistance 14 p2338 A67-28488
Titanium alloys research and development for aeronautics industry 14 p2338 A67-28627
Behavior study of titanium alloys of interest to aeronautics industry, stressing creep resistance 14 p2338 A67-28628
Experimental forging of titanium by techniques not requiring machining 14 p2324 A67-28629
Methods for transformation of titanium alloys by forging or die stamping to meet particular requirements 14 p2324 A67-28630
Alpha-beta Ti alloys weldability, considering underwater applications 14 p2327 A67-28821
Heat resistance of Ti alloys, emphasizing significance of chemical interactions, polymorphic transformations and phase diagrams for high temperature performance 15 p2504 A67-30007
Machinability of high strength steels, titanium alloys and refractory alloys, examining cutting and RF current induction for heat treatment 15 p2505 A67-30126
Ti-Zr-C and Ti-Hf-C alloy X-ray and microstructural studies noting homogenizing, annealing, quenching and phase equilibria 15 p2505 A67-30388
Heat treating effects on titanium alloy properties, discussing ductility and strength annealing, etc 16 p2681 A67-30486
Microwave flux-flow resistivity transitions observed for strongly paramagnetically limited titanium-vanadium alloys 16 p2727 A67-30821
Phase composition of titanium containing slag formed during alloying of stainless steel with titanium, noting titanium oxidation 16 p2687 A67-30842
Aluminum renewal from titanium electrolytes by reacting electrolyte melt at high temperature 16 p2687 A67-30843
Elastic properties of hardened Ti alloys discussed for behavior of elastic and shear moduli vs annealing temperature 16 p2687 A67-30848
Titanium alloys crystal structures determined using single crystal X-ray and powder neutron diffraction method, noting mechanical properties temperature dependence and martensitic transition 16 p2688 A67-31307
Strength corrosion cracking of high strength steels and titanium alloys in flowing sea water using cantilever loaded test specimen 16 p2690 A67-31385
Technological, physical, mechanical and heat resistance properties of new titanium alloy developed on titanium aluminide 16 p2691 A67-31590
Vanadium and molybdenum effect on

properties and phase transformations of titanium chromide 16 p2691 A67-31591
Electron microscopy of titanium alloys noting preparation, heat treatment of samples, crystallographic structure, etc 17 p2872 A67-32722
Mechanical properties of titanium alloys at room and cryogenic temperatures 17 p2873 A67-32768
Temperature dependency of specific heat of titanium base alloys 17 p2873 A67-32770
High strength Ti alloys in development of compressor blades, considering yield strength, impact energy absorption, ductility, fracture toughness and fatigue resistance [SAE PAPER 670335] 17 p2874 A67-32985
Two oxidation mechanisms for Ti-Al alloys based on increased diffusion rate and decreased oxidation rate 17 p2875 A67-33175
Superplasticity resulting from high strain rate sensitivity observed in isothermal tension tests on several titanium and zirconium alloys 18 p3064 A67-34083
Temperature effect on gas saturation in alpha and beta titanium alloys 18 p3065 A67-34292
Mechanical property and structural changes in titanium alloys subjected to high temperature thermomechanical treatment 18 p3066 A67-34405
Metastable phase formation in Ti alloys, noting nature and properties of different phases 18 p3066 A67-34406
Plastic deformation in titanium at low temperatures, noting prevalence of twinning and suitability as construction material in cryogenic technology 18 p3066 A67-34410
Atmospheric corrosion resistance of titanium alloys [ASTM PAPER 31] 18 p3068 A67-34579
Surface hardening of titanium alloys by carbon and nitrogen, using high-frequency induction heating 19 p3242 A67-34919
Structural transformations in alnico alloy with titanium studied by X-ray 19 p3245 A67-35467
Diffusion of nickel in solid solution and two-phase alloys of nickel-titanium system 19 p3245 A67-35468
Stress field on epitaxial dislocation line in weakly alloyed titanium, calculating energy of phase boundary and contribution of latter to plastic deformation 20 p3467 A67-37117
Titanium plasticity and durability under large temperature range as affected by Re, Ta, Pd and La alloying elements 20 p3468 A67-37175
Beta-Ti alloy mechanical properties variation with hydrogen content for various temperatures and hydrogen embrittlement mechanism 20 p3468 A67-37176
Ti-Al alloys ordering transformation studied by electron microscopy and electron and X-ray diffraction, showing existence of three phase fields 20 p3470 A67-37386
Stress corrosion characteristics of Ti alloy evaluated using cantilever beam testing procedure 20 p3470 A67-37465
Titanium alloy resistivity and aircraft structure role as current return and electromagnetic shield, discussing greater use of wire for susceptible circuits to achieve EMC 20 p3405 A67-37643
Knoop hardness yield loci for two Ti alloys 21 p3646 A67-38777
Trimming methods for Ti alloy materials including plasma arc cutting, band sawing, shearing, milling, nibbling and blanking 22 p3811 A67-39308
Low pressure diffusion welding and brazing process producing joints with mechanical properties close to titanium 6Al-4V 22 p3811 A67-39446
Phase transformations in commercial titanium alloys compared for mechanical properties, emphasizing decomposition of metastable beta phases on quenching, aging or deformation 22 p3822 A67-40055
Heavy section forgings of Ti and high tensile strength Ti alloys with thicknesses up to 10 inches 22 p3822 A67-40197
Omega phase morphology by transmission electron microscopy of Ti-Nb indicating ellipsoids with major axes parallel to /111/ directions in matrix 23 p4017 A67-40653
High oxygen Nb-Ti alloy solid solution critical superconducting current density and workability dependence on Th, Gd and Y solute content 23 p4036 A67-40705
Magnetic field critical current density characteristics of Nb-Zr-Ti superconducting

alloys, discussing peak effect and barrier height random distribution 23 p4044 A67-41451
Silicon carbide and B filament reinforced Ti alloy composites analyzed metallurgically and micromechanically, noting stress-strain behavior [SAE PAPER 670862] 24 p4172 A67-42004
Fracture toughness and stress corrosion cracking of titanium alloy weldments indicating resistance differences between base metal and weldment 24 p4161 A67-42329
Omega phase precipitation and superconducting critical transport currents in Ti-Nb wire samples 24 p4173 A67-42347
TITANIUM BORIDE
Titanium diboride densification at high pressure and high temperature, noting grain growth 01 p0098 A67-10704
TITANIUM CARBIDE
Titanium carbide coating depositions on steel and subsequent annealing redistribution of elements in interface 01 p0093 A67-10301
Neutron bombardment effect on titanium and chromium carbides before and after heat treatment, giving results of X-ray and micrographical analyses, electric resistance, brittleness and microhardness measurements 03 p0447 A67-13639
Titanium, zirconium and hafnium effect on recrystallization temperature and strength of alloys of molybdenum with carbon 05 p0832 A67-17508
Carbon content effects on properties of WC-TiC-Co alloys vacuum sintered 06 p1017 A67-17968
Titanium carbide-molybdenum carbide interaction and structure of resulting Ti-Mo-C 07 p1203 A67-19261
X-ray study of component atomic scattering and structural defects for titanium and carbide atoms in titanium carbide 07 p1208 A67-19306
Titanium carbide dispersion-strengthened nickel by internal carburization, with fair ductility and stress rupture properties at high temperatures 11 p1806 A67-24361
Carbon diffusion mobility in fused carbides of vanadium and titanium, giving carbon diffusion coefficient temperature dependence equations 14 p2337 A67-28285
Reaction kinetics of liquid titanium and hafnium with carbon using layer-growth method 16 p2690 A67-31373
Solid solutions of titanium, tungsten, chromium prepared by carburization of mixtures in hydrogen medium and obtained as fine-grained carbide powders 16 p2691 A67-31587
Melting point and microhardness of carbon-saturated TiC-VC solid solutions, noting temperature of eutectic of TiC-VC with graphite 16 p2691 A67-31588
Titanium, zirconium and hafnium effect on recrystallization temperature and strength of alloys of molybdenum with carbon 21 p3644 A67-38036
Field ion images from single crystals of titanium carbide, noting development of two crystallographic regions 21 p3645 A67-38093
TiC and ZrC powder properties after sintering investigated for linear growth rates vs temperature, obtaining sintering activation energy values 22 p3820 A67-39564
Cementite formation during sintering in cermet compositions with titanium carbide base and steel or iron binder noting CO role 24 p4171 A67-41960
TITANIUM COMPOUND
Titanium silicide preparation by simultaneous hydrogen reduction of silicon tetrachloride-titanium tetrachloride mixtures at 1200 degrees C 01 p0093 A67-10292
Titanium shavings application preventing iron oxidation during heating 01 p0095 A67-10643
Ferroelectric properties and morphotropic phase boundary in phase diagram of ternary system of compounds of lead, titanium and nickel 03 p0498 A67-13704
Dislocation mechanisms for prismatic and basal slip in Ti at low temperatures, measuring critical shearing stress and temperature dependence of activation volume 05 p0828 A67-16467
Titanium oxidation characteristics, determining activation energy of scale formation, oxygen absorption of base metal and total oxygen 05 p0829 A67-16759

X-ray emission and absorption spectra, electron structure and properties of metallic compounds of titanium 05 p0831 A67-17484

Phase diagrams of various titanium-phosphorus compounds and mixtures with up to 45 atomic percent P and microstructural characteristics of Ti-P alloys 07 p1203 A67-19262

Titanium shavings application preventing iron oxidation during heating 18 p3066 A67-34407

Ti-C-N system studied for stoichiometric range and thermodynamics using gas equilibration techniques, measuring nitrogen/carbon activities 19 p3248 A67-34865

Mass spectrometry of titanium subfluorides at high temperatures, determining sublimation pressures and heat and dissociation energy 20 p3377 A67-37135

TiNi-TiFe system equilibrium diagram, studying melting points and heat treatment effects on microstructure 20 p3468 A67-37179

TITANIUM DIBORIDE

High pressure hot-pressing fabrication of transition metal diborides without lower-melting metal additives 03 p0450 A67-13308

High temperature thermal expansion of Ti, Zr, Hf, Nb and Ta diborides 10 p1697 A67-23380

Densification and wear resistance of hot pressed pure and binary systems of diboride established with TaC and other refractory additives 17 p2875 A67-33407

TITANIUM OXIDE

Magnetic susceptibility studies show semiconductor to metal transition in titanium pentoxide and titanium trioxide, clarifying electronic nature of phase transition 01 p0132 A67-10376

Optical characteristics, including refractive indices, of thin layer amorphous titanium oxide films 01 p0115 A67-11048

Aluminum-titanium dioxide-silicon varactor equivalent circuit, noting measurement of parameters 03 p0377 A67-13240

Ferric-doped-rutile 8 mm traveling wave maser, noting operating range and performance characteristics 03 p0438 A67-13986

Temperature dependence of paramagnetic resonance spectral shifts in chromium-doped titanium oxide crystal of cross relaxation rutile maser 07 p1196 A67-19676

Nucleation of titanium and titanium oxide thin films correlation to thickness obtained from fluorescent intensity measurement 12 p1981 A67-25276

Hall effect and thermoelectric power in doped, conductive titanium oxide ceramics, noting dependence on doping concentration 12 p1982 A67-25452

Quenching examination of phase equilibrium in system lead oxide-titanium oxide-zirconium oxide, determining isotherms lines, melting points, etc 12 p1986 A67-26188

HF properties of laser cavities with anisotropic dielectric filling, calculating Q-factor and shunt resistance 13 p2075 A67-26399

Anodic oxides of titanium, tantalum and niobium from thin dielectric film preparations compared, determining nature and characteristics 13 p2175 A67-26654

Anisotropy in thin dielectric films of tantalum and titanium anodic oxide from various measurements explained by transistor-like model 13 p2175 A67-26655

Rutile in meteorites, noting presence of titanium oxide as result of electron microprobe studies 14 p2386 A67-28476

Phase composition of titanium containing slag formed during alloying of stainless steel with titanium, noting titanium oxidation 16 p2687 A67-30842

High temperature oxidation of titanium at reduced oxygen pressures governed by dissolution of oxygen in metal 17 p2873 A67-32812

Nitrogen role in oxidation of titanium in air at elevated temperatures studied by spectrographic analysis 21 p3643 A67-37828

Bainite beta to alpha transformation in titanium-oxygen system, using high temperature metallography techniques 22 p3821 A67-39825

Iron titanium oxides and oxygen fugacity in volcanic rocks noting temperature effect 22 p3792 A67-39975

TOCOPHEROL

Vitamins A and E deficiency effects on

rats exposed to pure oxygen noting less weight gain and growth 23 p3952 A67-41568

TOLERANCE

SA HEAT TOLERANCE

SA IMPACT TOLERANCE

SA NOISE TOLERANCE

SA ORTHOSTATIC TOLERANCE

Statistical probabilistic analysis of error propagation and tolerance limits in structural engineering design of assembled parts 05 p0813 A67-17258

Contamination control of hydraulic system achieved when contamination level of fluid is within contamination tolerance level of system components 20 p3365 A67-37363

TOLERANCE /BIOL/

S ACCELERATION TOLERANCE

S ALTITUDE TOLERANCE

S HUMAN TOLERANCE

S RADIATION TOLERANCE

TOLLMEIN-SCHLICHTING WAVE

Interaction of transverse distributed surface vibration with adjacent laminar flow, superimposing oscillatory pressure and velocity field developed in boundary layer fluid over idealized steady fluid flow 10 p1623 A67-22861

Liquid film flowing instability down inclined plane with respect to Tollmien-Schlichting wave compared with surface wave formation 11 p1774 A67-23860

TOMAHAWK ROCKET

S NIKE-TOMAHAWK ROCKET

TONOMETRY

SA BLOOD PRESSURE

SA PRESSURE MEASUREMENT

Tonometric and tonographic investigations of intraocular tension in hypoxia 06 p0953 A67-17995

TOOL

S MACHINE TOOL

TOOLING

SA MACHINING

Laser system for diamond piercing in wire-drawing dies and closed circuit TV viewing system for monitoring operation 04 p0628 A67-15309

TOOTH

S GEAR TOOTH

TOPOGRAPHY

SA GEODESY

SA LUNAR TOPOGRAPHY

SA MAPPING

SA SURFACE GEOMETRY

SA TERRAIN

Errors in estimates of lunar crater slope angles and surface roughness in Ranger VII and Ranger VIII pictures due to interpretation of dark areas as shadows [JPL-TR-32-994] 01 p0147 A67-10319

Terrain relief appearance on aircraft radar determined from radar parallax and shadow parallax 02 p0239 A67-12539

Formulas for extraterrestrial potential, anomalous gravity force gradient on earth topographic surface, deflections of vertical, etc 04 p0617 A67-15565

High resolution X-ray diffraction topography of dislocation structure of Si crystal 05 p0860 A67-16078

Astronomical theory of main features of earth crust based on fact that celestial bodies do not rotate en bloc 06 p0997 A67-18658

Automatic system for classifying and delineating terrain features in aerial photography, using general purpose computer 07 p1187 A67-19744

Earth topography in spherical harmonic analysis of land, ocean and ice 08 p1325 A67-20937

Planetary mapping mission system requirements for photography, IR and radar imagery, radar reflectivity and spectroscopy with data analysis techniques 11 p1859 A67-24438

Ries Kessel meteoritic crater /Germany/ analyzed by Fourier data smoothing technique, noting impact center, entry direction, etc 11 p1864 A67-24559

Systematic local errors in radio leveling of aircraft for different scales and tracks, using aerial camera 13 p2118 A67-26462

Errors, due to inaccurate tentative aerial observations, in determination of identification points for vertical aerial photography 13 p2118 A67-26464

Millimeter wave radiometry to study atmospheric properties, topographic relief, planets, medical and industrial research 14 p2265 A67-28402

Fracture surface markings and topography for transgranular and intergranular paths studied with electron microscope 16 p2772 A67-31300

Fracture surface topography related to micro-and macro-mechanics of fracture for plastic, cleavage and fatigue cases 16 p2772 A67-31301

Moire topography techniques for partial slope and macroscopic curvature measurements of cylindrical and conical shells due to loading 17 p2960 A67-32455

Martian clouds analysis and topographical relationships, discussing white and yellow classification and frequency of occurrences 18 p3124 A67-34156

Microelectronic failure mechanism, examining manufacture and processing methods and production of uniform and versatile material 19 p3193 A67-35029

Friction data, elastoplastic deformation and surface geometry of rubbing surfaces 19 p3237 A67-35851

Satellite geodesy results compared to other determinations, noting topography-gravity correlation confirmation, gravity field, etc 20 p3429 A67-36892

Analytic representation of absolute topography of isobaric surfaces by linear combination of arbitrary surfaces represented by Chebyshev polynomials 21 p3654 A67-38087

Lunar missions evaluated for scientific effectiveness via use of earth analogs assuming hypothetical terrestrial objectives parallel to lunar program 22 p3887 A67-40142

TOPOLOGY

SA OROGRAPHY

Network analysis shortcut by topological representation of impedance in node and loop equations 03 p0389 A67-12963

General variational problem and necessary conditions formulated in setting of locally convex linear topological space 03 p0458 A67-13268

Quality principle for automorphic forms on semisimple Lie groups extended to include arbitrary topological unimodular groups 03 p0458 A67-13387

Statistical topological analysis of electric measurement precision and accuracy 04 p0657 A67-14887

Lebesgue space in measure theory on Borel sets and Banach algebra over compact semigroups 07 p1214 A67-19211

Tame subsets of spheres in Euclidean-3 space, showing tameness of closed subset F of 2-sphere S 07 p1215 A67-19507

Topological properties of networks containing resistors, capacitors, self-inductors and controlled current generators 07 p1162 A67-20200

Topological analysis of local stability and instability of nonlinear periodic RLC network based on Liapunov theorems 08 p1308 A67-20320

Topology of three-dimensional integral surface projection of section of energy integral by third integral 08 p1380 A67-20382

Network analysis and synthesis using centrally located tree to generate connected linear graph trees 10 p1618 A67-22704

Singular point topological classification and analytical criteria relating singular points to generalized Liapunov-Krasovskii functions 14 p2342 A67-28381

Concept of extremal state in topological space, discussing existence conditions and criteria concerning extremal and stationary points 14 p2343 A67-28632

Extension of Vainberg method for studying nonlinear integral equations with aid of Hart theorem to cover Urysohn type equations 15 p2511 A67-29888

Motion of particles trapped in magnetic field, discussing conditions leading to spiral family of trajectory curves 15 p2551 A67-30387

Proof of continuity of Haar measurable almost periodic functions 17 p2876 A67-32385

Alternative approaches to particle solutions obeying Einstein gravitation theory 18 p3077 A67-33553

Magnetospheric open split tail topology noting stability of geometry in all solar wind and interplanetary medium conditions 22 p3792 A67-39820

Electronic network analysis using topological techniques of signal flow graphs, flow graphs and k-trees 22 p3778 A67-40556

General convergence theorems for Newton

method applied to convex operators for partially ordered topological linear spaces 23 p4023 A67-40863

TOPPING CYCLE
Maximum chamber pressure obtained with topping cycle at present, future and ultimate theoretical values 01 p0141 A67-11398
Potassium metal Rankine cycle power system, testing turbines, bearings and seals, potassium boiler and steam topping cycle analysis obtaining high heat-transfer coefficients 02 p0184 A67-12307
[AIAA PAPER 66-1009] 02 p0184 A67-12307
Potassium metal Rankine cycle power system, testing turbines, bearings and seals [AIAA PAPER 66-1009] 17 p2802 A67-32052

TOPSIDE PROGRAM
International Satellites for Ionospheric Studies /ISIS/ program using radio sounders 01 p0057 A67-10293
Calculation method for distortion of envelope of pulses during reflection from inhomogeneous ionospheric plasma during topside sounding 05 p0765 A67-17125
Ionic composition measurements of topside ionosphere from mass spectrometer flown on Explorer XXXI satellite 06 p0996 A67-18646
Ionospheric sounding data obtained principally by ground-based ionosondes, topside sounders and incoherent backscatter systems 10 p1630 A67-22775
Early results from topside sounder experiments in Alouette II satellite, presenting ionograms, plasma spike, electron number density and scale height 10 p1649 A67-23302
Nighttime topside ionosphere composition, measuring concentrations of H, He and O by mass spectrometry 13 p2108 A67-26310
Global response of topside ionosphere to magnetic disturbances at solar minimum studied from electron concentration measurements at 640 km 15 p2475 A67-29610
Satellite topside sounder investigation of spread echoes at mid and high latitudes in Northern Hemisphere 15 p2480 A67-30276
[AGARDOGRAPH 95] 15 p2480 A67-30276
Ionospheric movement detection using frequency swept sounder and rhombic antenna 15 p2484 A67-30301
Ionospheric irregularities following solar proton flare of July 1966 observed with Alouette topside sounders 19 p3312 A67-35176
Thermal diffusion in topside ionosphere, stressing effect on ion density profiles 20 p3427 A67-36304
Changes in topside ionosphere during large magnetic storm, studying electron density, slab thickness, scale height, etc 20 p3427 A67-36305
Ionosphere information via rocket and satellite measurements covering ion temperatures and concentration, electron content variation, etc 20 p3430 A67-36907
Rate of transequatorial plasma diffusion along geomagnetic field lines in topside ionosphere, considering electron distribution asymmetries in equatorial F-2 layer 20 p3431 A67-37098
Plasma scale height errors from Alouette I topside sounder ionogram analysis 20 p3433 A67-37409
Calculation method for distortion of envelope of pulses during reflection from inhomogeneous ionospheric plasma 21 p3582 A67-38468
Topside ionospheric swept-frequency pulsed sounder onboard Alouette 2 satellite, discussing transmitter power, large range receiver and antenna array 21 p3583 A67-38636
Particle and energy continuity equations derived and solved by computer method ion composition and plasma temperature measured by Explorer XXII particle and energy continuity equations derived and solved by computer method for ion composition 22 p3790 A67-39804
Electron scale heights from topside ionograms studied for radiation effects during quiet and disturbed conditions, noting relation to ionospheric plasma temperature 24 p4147 A67-42055
Electron concentration from topside ionograms for heights, below satellite 24 p4147 A67-42056
Storm behavior of topside ionosphere studied from electron concentration satellite data, discussing height and latitude

effects 24 p4148 A67-42058
Solar eclipse effects on topside ionosphere electron concentration, noting decrease for magnetic quiet conditions 24 p4148 A67-42059
Spread ionization in topside of ionosphere from satellite observations 24 p4148 A67-42060
Electron-resonance spikes on Alouette I ionograms observed for proton gyro-effects in topside ionosphere 24 p4148 A67-42062
Electron content of topside ionosphere studied for equatorial anomaly during diurnal variations 24 p4148 A67-42063
Diurnal variations of electron concentration in topside ionosphere studied at low and middle latitudes using satellite data, noting secondary nighttime maximum 24 p4148 A67-42064

TORCH
RF plasma torch coupling efficiency shown insensitive to input power and gas flow rate 12 p1976 A67-25925

TORNADO
Electrostatic motor action in rotational momentum of tornado funnels, noting that driving power removal by electric discharge may cause dissipation 12 p1963 A67-25383

TOROID
Generalized Zubov formulation from Liapunov function of limit cycle behavior in third order nonlinear systems 08 p1311 A67-20345
Specific resistance of semiconductor plates measured by change in effective loss component of toroidal coil 11 p1792 A67-24812
Induced magnetic moment and surface fields of ideal superconducting torus in uniform magnetic field calculated using Legendre functions 11 p1850 A67-24918
Antisymmetric toroidal containment systems with line closure 12 p1970 A67-25251
Natural frequencies of elastic toroids experimentally determined compared with theoretical results 13 p2219 A67-27091
Circumferential displacement and shearing stresses in out-of-plane elasticity problem for solid torus 20 p3538 A67-36672

TOROIDAL DISCHARGE
Plasma diffusional flow in toroidal axially symmetric discharge in presence of helical electric field and circular magnetic field 01 p0126 A67-11300
Plasma density variation in toroidal gas discharge stabilized by weak longitudinal magnetic field 02 p0277 A67-12617
Flute type instability of ideally conducting plasma in toroidal discharges with strong longitudinal magnetic field 03 p0476 A67-13343
Plasma diagnostics, comparing microwave toroidal resonator, cylindrical resonator and probe methods 03 p0477 A67-13466
Toroidal screw pinch equilibrium and stability in rapidly rising helical magnetic field, discussing experimental setup and results 11 p1827 A67-23888
High intensity runaway electron fluxes accelerated by external field in toroidal plasma discharge, noting pressure effect 13 p2162 A67-26270
Plasma density variation in toroidal gas discharge stabilized by weak longitudinal magnetic field 13 p2170 A67-27373
Flute type instability of ideally conducting plasma in toroidal discharges with strong longitudinal magnetic field 13 p2172 A67-27715
Electrical conductivity of plasma /produced in toroidal discharge chamber by injection method/ relation to electric field 16 p2721 A67-31483
Ionization rate at higher electron densities in DC fields measured in toroidal discharge tube 19 p3272 A67-35078

TOROIDAL PLASMA
Plasma trap configuration parameters inside solenoid wound about circular torus, noting magnetic surface distortion as function of screw axis period and curvature 01 p0121 A67-10342
Plasma equilibrium in toroidal magnetic traps, discussing readjustment of small denominators in nondisturbance equation 01 p0123 A67-10508
Nuclear fusion, discussing magnetic confinement methods of hot plasma shell holding light nuclei 01 p0124 A67-10778
Axisymmetric minimum average B configuration of triply connected system 05 p0809 A67-17446

Toroidal plasma containment, noting equilibrium theory consistency with first order orbit theory 08 p1364 A67-21395
Electron cloud equilibrium in toroidal magnetic and electric fields due to space and image charges 08 p1364 A67-21396
Latitude dependent plasmasphere oscillations, providing toroidal and standing wave solutions for MHD equations 08 p1365 A67-21407
Stability of plasma toroidal configurations under effect of component of magnetic field curvature which lies within magnetic surface 10 p1686 A67-23467
Toroidal machine velocity space instabilities, rapidly saturating, with long time scale remaining relaxation 11 p1826 A67-23876
Plasma ring acceleration produced by pulsed azimuthal electric field, noting magnetic field role in stabilization 11 p1828 A67-23893
Calculations of plasma distributions and field configurations with particle containment and stability within particular framework 11 p1843 A67-24997
Plasma trap configuration parameters inside solenoid wound about circular torus, noting magnetic surface distortion as function of screw axis period and curvature 11 p1843 A67-25015
Plasma equilibrium in toroidal magnetic traps, discussing readjustment of small denominators in nondisturbance equation 11 p1844 A67-25071
Static equilibrium for two-dimensional toroidal plasma configurations with inner fields and purely meridional electric currents 17 p2903 A67-32709
Toroidal stellarator magnetic trap with time-varying double coil magnetic field and external plasma injection 17 p2904 A67-32911
Formation of high energy plasma in toroidal system by neutral atom injection, discussing differential equations 17 p2908 A67-33110
Plasma finite orbits instability due to plasma particle shift, discussing collision frequency role 19 p3267 A67-34896
Intense runaway electron stream from wave-plasma interaction in magnetic field noting microwave radiation and disruption time 19 p3291 A67-35381
Extremely fast varying and low intensity plasma emissions analyzed with reflection multichannel Fabry-Perot interferometer 20 p3439 A67-36352
Toroidal plasma instabilities analyzed, justifying use of two-dimensional slab models with varying gravitational field simulating magnetic lines curvature effect 21 p3661 A67-37747
Flows superimposition on toroidal hydromagnetic equilibrium, stressing stationary motion of plasma layers between neighboring magnetic surfaces 21 p3661 A67-37751
Magnetic field line trajectories in toroidal stellarators, discussing rotational transforms on last closed surface and perturbation effects 21 p3662 A67-37753
Coordinate system with straight current and magnetic field lines used for hydromagnetic resistive interchange instabilities studies in toroidal configurations provides negative criterion generalization 22 p3846 A67-39486

TOROIDAL SHELL
Toroidal shell of circular cross section free of bending under uniform normal hydrostatic pressure 02 p0336 A67-11589
Initial postbuckling behavior of double curvature shell segments under several loading conditions determined, using Koiter theory 05 p0921 A67-16885
Frequency response of pressurized torus shell held free or rigidly [AIAA PAPER 67-73] 06 p1104 A67-18470
Stability of toroidal shell under uniform external pressure solved using series expansion, considering buckling modes 08 p1417 A67-20557
Closed toroidal shell stability under effect of uniformly distributed external pressure 10 p1720 A67-23602
Dirichlet problem of toroidal segment, noting integral transformation of spherical function 10 p1875 A67-23669
Matched asymptotic expansions for solution of singular perturbation problem of stresses and deformations in pressurized

toroidal membrane 11 p1871 A67-24086
 Perturbation solutions for finite inflation, under internal pressure, of elastic toroidal membrane of circular cross section 11 p1879 A67-25002
 Free vibrations of freely supported toroidal shell, noting elastic motion equations in terms of toroidal coordinates and boundary conditions applicable to polar motion 16 p2775 A67-31423
 Finite inflation of isotropic elastic toroidal membrane possessing strain-energy function by uniform internal pressure 17 p2956 A67-31932
 Dirichlet problem of toroidal segment, noting integral transformation of spherical function 21 p3652 A67-38270
 Hollow torus axisymmetric circumferential natural vibration eigenfrequencies and eigenmodes dependence on thickness and torus radius ratio 22 p3908 A67-39289
 Stresses, bending moments and displacements of variable rigidity toroidal shell in steady temperature field derived assuming independent thermal expansion coefficient and physical constants 23 p4075 A67-40680
 Thin toroidal elastoplastic shells of revolution loaded axisymmetrically, calculating force, moment, stress and strain interrelation for middle surface using complex representation 24 p4250 A67-42305

TORQUE
 Acceleration perturbations, gravity gradient torques and nutational motions effects on pendulums and gyrocompasses used as vertical indicating devices 01 p0064 A67-10644
 Gas squeeze film stiffness and damping torques on circular disk oscillating about diameter [ASME PAPER 66-LUB-4] 03 p0432 A67-13762
 Thrust vector control by supersonic splitline gimbaled nozzle, considering linear aerodynamics to understand magnitude of spring rate torque component 07 p1126 A67-19378
 Force /or torque/ electrohydraulic servocontrols, considering transfer function, compatibility conditions and hydraulic perturbation 07 p1132 A67-20113
 Two-impulse torquing scheme for reorienting spin axis of asymmetric spinning vehicle 08 p1413 A67-21510
 Periodic length of day /lod/ fluctuations, interplanetary torques and variations in earth rotation 24 p4229 A67-42313
 Parasitic torques of squeeze-film cylindrical journal bearings in output axis of high performance gyroscopes, discussing tolerance errors [ASME PAPER 67-LUB-5] 24 p4162 A67-42669

TORQUE MEASURING APPARATUS
 Thrust measurement for microthrustor mounted on platform suspended from cable whose motion is sensed by autocollimator system [ASME PAPER 66-WA/AUT-8] 04 p0599 A67-15390
 Torque effect on characteristics of burner flame based on principles of fluid mechanics 08 p1425 A67-20305
 MHD lubrication flow in self-acting step type thrust bearing configuration, showing torque reduction 24 p4162 A67-42566

TORQUE MOTOR
 Apollo Guidance and Navigation System positioning by electrically torquing gyros, discussing error sources 01 p0073 A67-11115
 Moving coil and variable air gap electromagnetic actuators, discussing characteristics and applications 14 p2247 A67-28266

TORQUE
 Rod configuration determined optimum for gyro torquer controlled spinning space station subject to impulse disturbance 17 p2955 A67-32477
 Strapdown and gimbaled inertial navigation systems history, engineering progress and current developments 19 p3256 A67-35859

TORSION
 Torsion of infinite hollow cylinder with axially symmetric load, discussing deformations in terms of integral equations 03 p0529 A67-14164
 Torsional problem of hemisphere in spherical coordinates based on Fredholm

integral equation of second kind 05 p0919 A67-16584
 Second order strain accumulation in aluminum in reversed cyclic torsion at elevated temperatures 09 p1517 A67-21753
 Cross section central line algorithm developed and applied to torsional problems of rods with polyconal cross section 14 p2401 A67-28739

TORSIONAL STRESS
 Anisotropy test examining failure behavior of aluminoborosilicate glass fibers under tensile and torsional loading [ACS PAPER 1-G-65F] 01 p0103 A67-10263
 Stresses in elliptical cross section rod subjected to elastoplastic torsion, using Legendre transforms 03 p0524 A67-13622
 Legendre series solution to contact problem of torsion of elongated ellipsoid of revolution under arbitrary torsional loading 03 p0530 A67-14199
 Mean tensile strength of aluminum alloys using torsion tests determined at high strain levels and compared with extrusion tests values 04 p0636 A67-14907
 Elastic-plastic torsion of shafts with hyperbolic notches solved for Ramberg-Osgood and bilinear stress-strain curve 04 p0627 A67-14977
 Stress-strain relationships in materials under high rate of torsional loading and torsional plastic wave propagation in long Cu tube 05 p0909 A67-16144
 Spherical elastic inclusion in transversely isotropic material under axisymmetric torsion field 05 p0910 A67-16149
 Optimum design of bar profile, considering bending and torsion effect and variation of wall thickness 05 p0916 A67-16242
 Torsional creep and creep recovery behavior of amorphous 1, 3, 5-tri-alpha-naphthyl benzene close to or below glass transition temperature 06 p1019 A67-17827
 Membrane solution of spirally corrugated shell under axial and torsional loading determined from thin shell bending equations 06 p1110 A67-18856
 Shape of interaction curve for axial compression vs torsional buckling of conical shells 06 p1110 A67-18858
 Dislocation density and magnetic hysteresis in superconducting state of 110-oriented Nb single crystals as function of angle of torsion 07 p1209 A67-19646
 Elastic-plastic torsion of square bar twisted by terminal couples formulated as variational minimum problem 07 p1264 A67-20293
 Torque effect on characteristics of burner flame based on principles of fluid mechanics 08 p1425 A67-20305
 Statistical basis for modified moment theory of elasticity that takes into account contribution of all deformation-tensor-component gradients to deformation energy 09 p1574 A67-21914
 Cyclic torsion interaction with axial load, showing torsion angle larger than fatigue limit and applied tensile stress larger than Bauschinger yield 10 p1669 A67-23438
 Torsional stiffness of ribs effect on buckling strength of longitudinally stiffened plates compressed in direction of ribs 10 p1719 A67-23474
 Book on torsion emphasizing beam stressed state calculation and civil engineering problems 10 p1720 A67-23578
 Elastic response of circular cylinder under torsion 11 p1871 A67-24118
 Torsional buckling stress of orthotropic cylindrical shells with high order terms due to internal pressure rise 11 p1876 A67-24701
 Stress-strain condition in thin walled shells having anisotropic moduli with one end clamped and torsion applied at other end 11 p1878 A67-24860
 Stress-strain state of circular cylindrical rod coupled to half-space when applying torsion to free end 11 p1879 A67-24884
 Measurement of torsional fatigue loads on aircraft undercarriage under service conditions 11 p1880 A67-25057
 Low endurance fatigue tests for reversed torsional strain cycling of two steels 12 p2015 A67-25421
 Low endurance fatigue analysis for steel and Al alloy under cyclic torsion with controlled shear strain amplitude 12 p2016 A67-25425
 Semilinear cylinder dynamic torsional problem, considering self-balanced and self-

unbalanced boundary perturbation expansion 12 p2029 A67-25664
 Numerical solution of elastoplastic torsion of rods by method of local variations 12 p2029 A67-25667
 Lower critical load for deformation of cylindrical shell in torsion and hinged along edges 13 p2215 A67-26376
 Stability of inhomogeneous anisotropic cylindrical shells containing elastic cores under pressure, axial load and torsion 14 p2399 A67-28119
 Treating bending-torsion problem of straight beam using Trefftz definition of shear center 15 p2572 A67-2931
 Maneuvering stability analysis of single rotor correctable gyrocompass with fluid torsional suspension of sensitive element 15 p2490 A67-30170
 Tensile and torsional fracture of low carbon steel at cryogenic temperatures, studying temperature and stress gradient effect 16 p2689 A67-31309
 Thin walled unsymmetrical beam under bending and torsion studied for nonlinear elastic behavior 17 p2957 A67-32023
 Theory and design methods of torsional-flexural buckling of thin walled elastic struts of open cross section, deriving basic differential equations 17 p2957 A67-32024
 Torsion or coupled bending torsional wave theory for thin walled open section beams 17 p2959 A67-32413
 Fatigue strength calculated using fracture criterion for multiaxial alternating stress and combined alternating bending and torsional stresses 17 p2960 A67-32632
 Differential equations determining time-dependent torsional moment and stresses in thin walled rods in creep presence 17 p2821 A67-32830
 Orthotropic circular cylindrical shell of elastic material instability under combined torsion and hydrostatic pressure investigated for simply supported and clamped ends 17 p2963 A67-33016
 Stability of cylindrical shells under torsion 18 p3144 A67-34171
 Axisymmetric mixed boundary value problem for solid elastic cylinder under torsion 18 p3144 A67-34173
 Fatigue characteristics of chromium-molybdenum steels subjected to various heat treatments, comparing tension-compression and torsion 18 p3065 A67-34258
 Linear theory of initially straight elastic rods, discussing wave propagation, thermal effects for extension and flexure and torsion 18 p3144 A67-34287
 Stability of reinforced thin structurally-orthotropic cylindrical shell problem, discussing rib eccentricity, axial compression load, torsional load, etc 19 p3338 A67-34874
 Homogeneous beam consisting of two isotropic bars with different elastic properties but identical cross sections studied for perimeters stress-strain state under torsion 20 p3535 A67-36122
 Formulation of problem of elastoplastic torsion of rectangular or regular polygonal bar as variational problem 20 p3536 A67-36429
 Viscoelastic properties of capron under torsion at infrasonic frequencies and polymer resin complex shear modulus temperature dependence 21 p3647 A67-37866
 Exact solutions for elastic displacements and stresses in composite circular cylinder under torsion in Fourier series form 21 p3723 A67-38560
 Calculated stressed state of short thin walled shells under transverse loads and torsional moments 21 p3726 A67-38797
 Constrained torsion computation for multispar box with elastic diaphragms assuming applied stresses at end ribs 21 p3728 A67-38906
 Cylindrical thin walled open section structures heated nonuniformly, calculating various elastic parameters, torsion properties and shearing stress 22 p3916 A67-40450
 Blade-spar thick walled cylindrical shell deformed under elastoplastic torsion, analyzing stress-strain ratio and torsional strain and displacement 22 p3916 A67-40458
 Orthotropically stiffened cylinders elastic instability under torsional load 23 p4080 A67-41745
 Constrained torsion of thin walled rods with closed or open profiles, discussing stress-strain state of cross section sealed at

one point 24 p4250 A67-42307
Torsion creep theory for circular and
noncircular tubes using Bredt equation,
measuring anisotropy in tubes, calculating
torsion stresses 24 p4250 A67-42381

TORSIONAL VIBRATION
Receptance and support receptance
methods in iterative solution of torsional
vibration problems 01 p0164 A67-11271
Torsional oscillations of hollow cylinder of
finite length encased in thin elastic
shell 02 p0337 A67-11932
Torsional constraints in calculation of
vibrational frequencies of compressor
blade 03 p0528 A67-14081
Bending and torsion induced symmetric
flutter of aircraft in supersonic
flow 04 p0708 A67-14789
Thin rod bending and twisting theory
applied to critical speed of rotating shaft
under axial loading and tangential torsion,
using Galerkin approximation
[ASME PAPER 66-WA/MD-1] 04 p0629 A67-15348
Instability modes of cantilevered bars
induced by fluid flow through attached
pipes, examining cases of torsional and
transverse flutter and torsional
buckling 05 p0921 A67-16882
Amplitude of limit cycle torsional motion
of helicopter blades as function of pitch
angle and reduced frequency 06 p0946 A67-17916
Bending torsional flutter of uniform swept
wing with velocity component aerodynamic
strip theory [AIAA PAPER 66-475] 06 p1110 A67-18860
Flexural-torsional vibration of rotating
shaft with distributed parameters 07 p1264 A67-20104
Forced torsional vibration of
inhomogeneous hollow cylinder solved for
radial variation of shear modulus and mass
density 07 p1264 A67-20234
Creep, stress relaxation and vibrational
measurements, sinusoidal torsional forced
oscillations and stress wave propagation in
polymeric linear viscoelastic
solids 08 p1419 A67-20885
Dynamic instability in undamped bellows
face seals operating in cryogenic
environment with torsional oscillation and
diametrical rocking as primary motion
[ASLE PAPER 66AM 2C2] 08 p1336 A67-21039
Torsional vibrations of reciprocating
engine with allowance for vibration of
second type treated by transfer-matrix
method 10 p1720 A67-23577
Fully stalled airfoil steady state pitching
oscillations in one degree of freedom,
deriving torsional flutter equation
[ASME PAPER 67-VIBR-12] 11 p1872 A67-24172
Electrodynamic vibration absorber
attached to single degree of freedom
vibrating system as passive or active device
with or without feedback
[ASME PAPER 67-VIBR-18] 11 p1796 A67-24177
Torsional vibration and steady state
response of geared system, noting computer
programming [ASME PAPER 67-VIBR-63] 11 p1797 A67-24205
Torsional wave propagation in anisotropic
nonuniform cylindrical rod for constant and
variable Youngs moduli 13 p2218 A67-26902
Elastic rod, string or torsional member
under effect of accelerating axial load,
solving differential equation of motion in
fixed end condition 14 p2399 A67-28140
Powered flight rotor instabilities using
analysis of second-order flap-lag coupling
effects of torsionally rigid
blades 16 p2595 A67-30927
Plasma concentration diagnostics by
hydromagnetic probing method, determining
concentration profile from latitude
dependence of torsional
vibrations 16 p2668 A67-31890
Torsion of finite elastic cylindrical rod
welded to elastic half-space
[ASME PAPER 67-APM-30] 17 p2965 A67-33156
Natural torsional vibration frequency
calculation method, with frequency as
algebraic equations with real roots,
discussing example 19 p3341 A67-35711
Uniform cantilevered bar subject to

eccentric compressive follower force,
considering warping rigidity, bending-
torsional flutter and stability 20 p3538 A67-36674
Torsional disturbance propagation in
Gutenberg-Bullen earth model through
spectral seismograms, discussing travel times
and S wave amplitude 20 p3435 A67-37675
Analog computer method application for
determining critical frequency and critical
flutter speed of wing having torsional
bending vibrations in airflow 21 p3718 A67-37992
Method for finding bending vibration
modes patterned on Holzer method for
determining torsional
vibration 21 p3728 A67-38881
Flexure-torsion cascade flutter of airfoils
with two degrees of translational and
torsional vibration 22 p3914 A67-40040
Homogeneous and sandwich spherical caps
and circular plate torsional frequency
calculations based on sandwich and spherical
shell equations 23 p4073 A67-40618

TOUGHNESS
S FRACTURE TOUGHNESS
TOWED BODY
Stability of bilaterally symmetrical object
towed in air along straight line, obtaining
characteristic equation as test for lateral or
longitudinal stability 11 p1743 A67-24309
Equilibrium configuration and tension of
flexible cable in uniform flow field,
considering tangential drag force and weight
effects 13 p2051 A67-27587
Glider towing cable configuration taking
into account aerodynamic drag forces, using
digital computer for numerical calculations
and integrations 22 p3745 A67-39551
Dynamic longitudinal stability of rigid
glider towed by rigid aircraft with elastic
cable subjected to aerodynamic loads,
deriving motion differential
equations 23 p3935 A67-41418
Glider takeoff using tow winch,
emphasizing flight path and aerodynamic
loads and forces 24 p4093 A67-41917

TOWER
S UMBILICAL TOWER
TOWNSEND AVALANCHE
Size distribution of electron avalanches in
methane gas under electric field no longer
satisfy Furry distribution due to first
Townsend ionization coefficient 03 p0473 A67-13463
Diffused base punchthrough avalanche
transistor /PAT/ at high recurrence
frequency having capacitance dependence of
pulse width 10 p1609 A67-22839
Penning cell discharge ignition in high
vacuum magnetic field in terms of
Townsend avalanche theory, with discharge-
ignition curves 19 p3272 A67-35089

TOWNSEND DISCHARGE
Penning cell discharge ignition in high
vacuum magnetic field in terms of
Townsend avalanche theory, with discharge-
ignition curves 19 p3272 A67-35089
Ion mobility and reactions in argon
measured using Townsend and Tyndall
techniques with mass analysis 20 p3492 A67-37690

TOXICITY
S OXYGEN TOXICITY
TOXICITY AND SAFETY HAZARD
Materials evaluation and selection for
compatibility with manned spacecraft
environment 15 p2507 A67-29551
Hazards of rocket launching noting
propellant toxicity, airborne fragmentation,
inadvertent ignition and nuclear
radiation 22 p3900 A67-39884
Toxicity of radioprotective amino ethyl
isothiolurium bromide from animal studies
noting hazardous effects in human
organism 22 p3753 A67-40546
Beryllium component machine tool
installations and operation, discussing
contamination protective systems for toxic
dust 23 p4009 A67-40687

TOXICOLOGY
S PHARMACOLOGY
TRACAC SATELLITE
Nonlinear resonant coupling between
damped and undamped vibrations for
damping roll in TRAAC and elastic dumbbell
satellites [AIAA PAPER 67-568] 19 p3329 A67-35964

TRACE CONTAMINANT
Gas-off products from space cabin
materials determined by continuous
recording instruments, gas chromatography
and IR analysis 02 p0189 A67-12388
RF spark source mass spectrometer to
detect and identify trace amounts of vapor
molecular carbide species for refractory
metal carbides 03 p0367 A67-13228
Methylene role in atmospheric tritiated
methane, specifically nitric oxide
interference 13 p2117 A67-27604
NASA and USAF experiment on mans
contribution to trace contaminants in space
cabin simulator at 760 mm of
Hg 15 p2430 A67-29278
Extraterrestrial life detection studied
from knowledge of major and trace
components of
atmospheres 23 p3944 A67-40999
Trace contaminant experiment for
studying effect of hyperoxic environment at
high total pressure on human blood
constituents 23 p3960 A67-41703

TRACE ELEMENT
Australites, Henbury impact glass and
subgreywacke, comparison of abundances of
51 elements 03 p0512 A67-13900
Rare earth trace element variations in
anorthosite and quartz mangerite
determined, using stable isotope dilution
technique of analysis 03 p0513 A67-14006
Trace formulas of difference between two
ordinary differential operators of higher
order 07 p1214 A67-19175
Ultramafic rock content of Na, Mn, Cr, Sc
and Co determined by neutron activation
technique 07 p1183 A67-20142
Trace element concentration in iron
meteorites determined using lithium drifted
Ge semiconductor detector 09 p1569 A67-22686
Neutron activation analysis to determine
trace elements in iron
meteorites 14 p2391 A67-28947
Testing for leak-proof encapsulation of
semiconductor devices by use of krypton 85
as radioactive tracer gas 17 p2823 A67-32297
Interphase exchange coefficient for gas
phase moving through fluidized bed analyzed
by tracer gas technique 18 p3160 A67-34290

TRACER
Emission, collection and analysis of
radioactive rare gas xenon 133 as
atmospheric tracer whose inert
characteristics allow diffusion processes to
be followed 02 p0237 A67-11854
Calculation method for energetic
photoelectric photometry system for tracing
behind radiative source or for distance
measurement 08 p1331 A67-21055
Radiotracer propellant gauge for zero
gravity space environmental conditions using
radioactive krypton 85 gas 10 p1656 A67-23078
Radioactive isotopes from cosmic ray
action in atmosphere and nonatmospheric
sources, discussing geophysical mixing and
dispersion 14 p2380 A67-27967
Radio carbon dioxide fixation, glutamate
labeling and Krebs cycle in ribose-grown
Hydrogenomonas facilis 20 p3370 A67-36796
Autotrophic and heterotrophic carbon
dioxide fixation regulation in
Hydrogenomonas, discussing two Calvin cycle
enzymes 20 p3370 A67-36797
Tracer experiments using tritiated ethanol
on surface of MOS capacitor to indicate
field-induced proton transport 20 p3510 A67-36857
Radioactively labeled coupling agents
adsorption on E-glass surfaces, noting
continuous film formation with covalent
bonding occurring at
interface 20 p3474 A67-37269
Calculation method for energetic
photoelectric photometry system for tracing
behind radiative source or for distance
measurement 22 p3797 A67-39417

TRACK
S GROUND TRACK
S PARTICLE TRACK
S TEST TRACK
TRACKING
SA COMPENSATORY TRACKING
SA LUNAR TRACKING
SA MISSILE TRACKING
SA OPTICAL TRACKING
SA PHOTOGRAPHIC TRACKING
SA PURSUIT TRACKING
SA RADAR TRACKING

SA RADIO TRACKING
 SA RANGE AND RANGE RATE TRACKING
 SA RAY TRACING
 SA SATELLITE TRACKING
 SA SPACECRAFT TRACKING
 SA SPECTROMETRIC TRACKING
 SA STAR TRACKING
 SA SUN TRACKER DEVICE
 SA VISUAL TRACKING
 Secondary task interference in tracking 13 p2061 A67-26490
 Laser technology noting applications to range finding, target illumination, tracking, welding, etc 14 p2332 A67-28818
 Autonomous landmark tracking by holography for space navigation 17 p2881 A67-32436
 Inertial tracker position error evolution, discussing equations and applicability to vehicle on ground or in circular orbit 17 p2882 A67-32725

TRACKING ANTENNA

Flying target detection and tracking with fixed antennas having radiation pattern scanning and multibeam characteristics 02 p0205 A67-12730
 Deep space and missile tracking antennas - ASME Conference, New York, November-December 1966 03 p0383 A67-13748
 Design, fabrication and erection of 210-ft parabolic fully steerable tracking antenna for deep space instrumentation facility /DSIF/ 03 p0383 A67-13751
 X-band Cassegrainian tracking antenna for space rendezvous position and rate information for navigation and guidance computations 04 p0569 A67-14502
 Stationary antenna arrays for target detection and tracking noting radiation patterns, radar systems, etc 04 p0654 A67-15538
 ELDO guidance station noting master antenna for automatic tracking of third stage 04 p0576 A67-15627
 Mechanical and electrical performance requirements of satellite communications antenna using Cassegrain configuration, noting relation to design 07 p1157 A67-20092
 High efficiency S-band monopulse focal point tracking feed, discussing aperture geometry design theory 08 p1300 A67-20654
 Ground station antenna steering system for satellite communication, noting design 11 p1758 A67-24061
 Phased-array microwave antenna system for scanning simultaneous targets whose distance and direction are changing rapidly 13 p2083 A67-27566
 NASA STADAN and Apollo network antenna systems, analyzing tracking antenna systems, command systems and operational problems 14 p2287 A67-28681
 Broadband monopulse three-element tracking feeds for spherical Luneberg lens scanning antenna, discussing radiator design, radiation pattern and cross coupling between error channels 15 p2451 A67-29924
 Modes of boresight shift in conical-scan and sequential-lobing types of amplitude sensitive angle-tracking antennas 17 p2814 A67-32523
 Systematic boresight and off-boresight tracking errors in planar monopulse phased rectangular arrays produced by analog phase shifters with nonlinear transfer characteristics 17 p2825 A67-32617
 S-band telemetry data during spacecraft launch phases, discussing mission support problems 20 p3380 A67-36561
 Target-tracking antenna design with primary feed system suitable for slewing of mobile radar equipment 22 p3760 A67-39592

TRACKING FILTER

Simulation results of adaptive tracking filter application to stabilization of structural bending modes of SI-B launch vehicle 13 p2212 A67-26818
 Image velocity sensing technique applying moving reticle scanners, with time-dependent correlation function analyzed by frequency discriminator 19 p3231 A67-35689
 Decoupled shifting memory filter method for radio tracking of space vehicles flight 21 p3587 A67-39146

TRACKING RADAR

SA SEARCH RADAR

All-weather carrier landing system using precision tracking radar and microelectronic data link aboard carrier 01 p0026 A67-10969
 Computer program to aid analysis of

tracking radar towers and foundations 03 p0396 A67-13753

Photographic techniques developed for photographing ballistic missiles and associated explosive reactions, including shadowgraph and schlieren techniques [SMPTE PREPRINT 100-59] 03 p0423 A67-13807

Radar target clutter, fluctuation, echo level, direction error and noise in tracking system 03 p0372 A67-14093

Simultaneous radiation of center-fed slotted rectangular waveguide array antenna for monopulse tracking radar 04 p0590 A67-15905

Continuous and discontinuous tracking of weapon system radar, discussing principles, characteristics, advantages and disadvantages 05 p0766 A67-17270

Radar search and tracking system developments 06 p0957 A67-17584

Range determination with CW tracking radar controlling rms error, noting SNR role in holding target echo 06 p0957 A67-17593
 Apollo lunar module /LM/ rendezvous radar system and tracking device 06 p0962 A67-18056

Noise and signal fluctuation effects on angle tracking radar with amplitude comparison system 07 p1147 A67-20239

Future radar developments noting range instrumentation deployment and employment, tracking, data acquisition radar sensors, changing cost patterns, etc [AIAA PAPER 67-55] 15 p2438 A67-30119

Millimeter wave passive radiometry noting design, capability, detectability and aerial reconnaissance 17 p2814 A67-32521

External noise levels effect on angular accuracy of tracking radar pencil-beam antennas, emphasizing radome noise and dielectric coating characteristics 17 p2826 A67-32685

Indonesian space center, describing radar and optical tracking systems, launch complex telemetry system, etc 19 p3207 A67-35234

Pulse radar on Air Force Eastern Test Range, discussing precision, sensitivity, acquisition, signature and multiple target capability 20 p3381 A67-36581

Tracking interruption probability determination in radars reduced to Kolmogoroff equation in dimensionless form taking dynamic error into account 21 p3585 A67-38815

S and X band ignitor design eliminating spike leakage variations in tracking radar tubes 24 p4131 A67-42350

TRACKING STATION

SA GROUND STATION

Standard earth geodetic coordinate system and Baker-Nunn camera station positions 01 p0056 A67-10038

Synthesis of multichannel transponder for radio guidance and tracking station and associated parameters 02 p0264 A67-12355

Satellite orbit major axis determination by using coincidence of time when satellite crosses plane of tracking station parallel with time of crossing topocentric celestial equator 05 p0894 A67-16560

Installation for measuring Doppler effect of satellites, investigating limits, optimization, SNR and orbital parameter accuracy 06 p0979 A67-18018

Smithsonian observatory tracking network and geodetic results 07 p1177 A67-19774

Simultaneity circles used in space geodesy to obtain synchronous observation of trials of satellites and determination of absolute directions in space of lines joining tracking stations 07 p1177 A67-19778

Optical and radio orbit tracking facilities, analyzing data accuracy levels, minitrack functions, etc 09 p1464 A67-22055

Satellite geodesy program at Smithsonian Astrophysical Observatory, with emphasis on twelve Baker-Nunn tracking stations 10 p1636 A67-23177

Ground based conversion of Lunar Orbiter II video signals into photographic images, describing reconstruction electronics, signal processor, etc 12 p1940 A67-25466

High accuracy radio guidance and tracking station, discussing relation between basic station parameters, error sources and associated error components 14 p2260 A67-27972

Guidance station for ELDO third stage, describing equipment and function 16 p2700 A67-30657

Interferometric system of Diane satellite tracking stations permits high altitude tracking and measurements with larger solid angle 16 p2621 A67-30680

Diamant satellite series, describing design and construction of Diapason and Diadem orbital satellites 17 p2956 A67-32746

Space center under construction in French Guiana for launching rocket probes and satellites with aid of Diamant booster, discussing optical sites, storage tanks, LOX factory, etc 18 p3019 A67-33652

Artificial satellites tracking by Smithsonian Astrophysical Observatory, discussing station locations, instrumentation, operation modes, interface and selection 18 p3003 A67-34236

Radio and radar tracking at Royal Radar Establishment at Malvern, discussing equipment, accuracy, alignment, performance, operation, drag and decay 18 p3048 A67-34239

Phase measuring equipment and instrumental performance of radio tracking station at Winkfield 18 p3048 A67-34240

Estimate of dynamical center from four lunar surface impact points determined by tracking Ranger probes from three earth-based stations 18 p3131 A67-34324

Tracking station network organization, equipment and operations of National Center for Space Studies /CNES/ in France 19 p3207 A67-35242

Mexican space research activities noting studies in meteorology, aeronomy, solar radiation, communications, tracking, astronomy and geomagnetism 19 p3321 A67-35298

South African space research, describing ground-based observations and tracking stations 19 p3321 A67-35304

VLF radio wave tracking stations for ionospheric propagation investigation using atomic clock 20 p3386 A67-37481

Electromagnetic compatibility operational problems aboard Apollo spacecraft tracking ship 20 p3387 A67-37641

Movable device for tracking rocket probes, discussing characteristics and requirements 21 p3608 A67-38673

Radio interferometry at Diane satellite tracking station, noting synchronous demodulation technique 21 p3587 A67-39052

Noise model for simulating tropospheric turbulence effects on radio guidance and tracking range and angular measurements for optimum filter synthesis 21 p3587 A67-39147

Determination of coordinates from satellite observations noting triangulation method and optical technique 23 p3994 A67-40700

TRACKING STUDY

Tracking interruption probability in second order astatic system, obtaining solution from Fokker-Planck equation and computer simulation 03 p0390 A67-13100

Extraterrestrial radiation source spectrum determined by comparing main beam and sidelobe signal power received on suitable bandwidth 03 p0371 A67-13946

Second order autonomous differential equation stability and boundedness obtained, using computing algorithm based on tracking function method 03 p0376 A67-13987

Human reactions and attention shifts during flight tracking tasks 04 p0562 A67-14544

Tracking geometry and dynamics of lunar satellite, estimating orbital elements and lunar gravitational field parameters through earth based range and range rate observations [AIAA PAPER 66-39] 05 p0902 A67-17207

Geodetic error effect on time dependence of satellite tracking data received by ground station 06 p1080 A67-17769

Critical tracking task for man-machine research related to operator effective delay time 07 p1136 A67-20171

Verbal-analytical model of human operator performance in compensatory tracking 10 p1618 A67-22733

Secondary verbal task effect on tracking performance 13 p2061 A67-26491

Sine wave tracking, studying operator manual control performance 17 p2808 A67-33179

Radar target designation tracking performance in simulated high speed low altitude aircraft, using closed loop

analyses 17 p2830 A67-33181
 Simultaneous recording of rocket trajectory and rapid auroral variations using high sensitivity image orthicon TV system 18 p3034 A67-33594
 Radio, radar and optical methods for close earth satellites tracking, advantages and limitations 18 p3003 A67-34235
 Image motion compensation tracking study for earth reconnaissance from space, investigating computer and manual tracking modes, control dynamics and gain and magnification 18 p2993 A67-34337
 Aircraft tracking problems in airport approach zone solved using cameras, descriptive geometry and vector computations 21 p3568 A67-38809
 Inverted pendulum and VTOL control experiments with and without motion cues, discussing various motion effects 22 p3755 A67-40087
 Factors in recovery from performance decrement, activation, inhibition and warm-up [NAVTRADEVCE-1H-72] 24 p4114 A67-41809

TRACKING SYSTEM

SA POLYSTATION DOPPLER /POLYDOP/ TRACKING SYSTEM
 SA SATELLITE TRACKING AND DATA ACQUISITION NETWORK
 Accuracy of real-time tracking of space vehicles using radar or L-shaped interferometer 01 p0110 A67-10266
 Amplitude and phase direction-finding characteristics of monopulse automatic tracking system operating on sum-difference principle 02 p0214 A67-11904
 Minimum tracking data in guidance technique functioning comparable to proportional navigation homing system, noting tests in computer simulations and in laboratory model 02 p0263 A67-12158
 Autonomous space navigation system using optical spatial filter techniques for recognition and tracking of planetary surfaces and star fields 02 p0264 A67-12316
 Digital range tracking system using integrated circuits at SPANDAR radar site 03 p0370 A67-13831
 Range instrumentation developments for trajectory measurements including cinetheodolites and tracking radars, noting error sources, weapons systems problems, etc 04 p0568 A67-14436
 Target homing of tracking systems receiving signal packages only in absence of fading 04 p0591 A67-14659
 Evaluation of tracking performance of various systems for airspace management using concept of real and apparent tracks, considering turn-following tracking 04 p0654 A67-15059
 Tracking in air traffic control environment, noting differences with military environment and cooperative tracking methods 04 p0654 A67-15060
 Adaptive flight control using parameter tracking mechanism functioning with any type of disturbance as input, for adjustment of control system parameters [ASME PAPER 66-WA/AUT-22] 04 p0552 A67-15393
 Book on electronic testing covering RF interference, tracking systems, receivers and transmitters, flight control equipment, digital computers, etc 04 p0577 A67-15726
 Range safety and tracking systems, discussing C-band beacon, CW transponder and command-destruct receiver operation and testing 04 p0577 A67-15729
 High accuracy tracking system for measurement of missile and rocket trajectories during lift-off phase 05 p0762 A67-16530
 Effects of unmodeled errors on minimum variance estimators, with application to tracking complex self-calibration estimation scheme [AAS PAPER 66-107] 07 p1216 A67-19967
 Digital communications on pseudonoise tracking link using sequence inversion modulation, noting bit error probability 09 p1459 A67-21581
 Effects of display magnification, proprioceptive cues, displacement aiding, etc, on decreasing tracking error assessed, using heavy inertia tracking simulator 09 p1458 A67-22372
 Automatic tracking in aircraft identification and updating of flight

prediction parameters for air traffic control 09 p1529 A67-22636
 Off-line autotracking evaluation system, discussing track initiation, following and termination 09 p1530 A67-22647
 Astro-2 observation theodolite and optical and electronic systems for tracking 10 p1655 A67-22990
 Doppler tracking systems as velocity measuring systems, including introduction methods for necessary position knowledge, one-and two-way systems analyses, etc 10 p1605 A67-22995
 Range instrumentation ships as major range subsystems, noting equipment used, accuracy and sources of errors 10 p1622 A67-22999
 Lasers for tracking and geometric geodesy as used in Explorer and Geos satellite missions 10 p1664 A67-23071
 Doppler frequency-measuring tracking system in which tracking filter or retuned heterodyne is used for definition of signal with unknown frequency 10 p1607 A67-23452
 TV system with automatic target tracking capability 12 p1904 A67-25462
 Automatic laser tracker system for close-up photographic coverage of rocket test [SMPTE PAPER 101-90] 12 p1905 A67-25474
 Apollo spacecraft-earth two-way communications provided by vehicle-mounted variable gain antenna array, automatically tracking ground-transmitted signals 13 p2068 A67-26802
 Stability analysis of minimum variance estimations used to self-calibrate missile tracking instrumentation 13 p2120 A67-26815
 Effect of unmodeled errors on minimum variance estimators, with application to tracking complex self-calibration estimation scheme [AAS PAPER 66-107] 13 p2154 A67-27525
 French space program /1966-1970/ techniques and installations for satellite launching and tracking 14 p2409 A67-28605
 MSQ-1 radar system for rocket tracking used to measure distance, elevation and azimuth during May 20, 1966 solar eclipse 15 p2467 A67-29574
 Worldwide network of Doppler observation stations, discussing frequency and time monitoring for enhanced measurement accuracy 15 p2436 A67-29592
 Simulation and error analysis of range-only location and tracking utilizing satellite system to obtain range measurements 15 p2514 A67-29597
 Satellite visibility calculation for individual ground stations of telemetry and tracking network as function of orbital injection parameters 15 p2561 A67-30047
 Range sum Doppler system for early launch tracking system to get warnings of possible impact in neighborhood of critical installations [AAS PAPER 67-42] 15 p2437 A67-30111
 Capabilities, goals and scientific and engineering problems associated with missile trajectory analysis, detailing tracking equipment [AAS PAPER 67-43] 15 p2438 A67-30112
 Range instrumentation ships electronic capabilities, operation, electronic systems function, accuracy and future role [AAS PAPER 67-52] 15 p2468 A67-30117
 Accuracy of satellite orbit prediction for rendezvous mission related to ground-based tracking network sensors by digital computer simulation 15 p2441 A67-30165
 Predictive identification and fast moving target recognition technique for adaptive control and tracking systems 15 p2463 A67-30330
 Evaluation and calibration of missile and space tracking systems including test-by-test analysis, lofted rockets, self-calibrating systems, etc 16 p2821 A67-30682
 Design and operation of orbital space station, determining orbit altitude, payload weight, tracking and communication system support requirements, recovery operations, etc 16 p2781 A67-30961
 Modern control theory applied to digitally controlled tracking telescope design, emphasizing accuracy and response time 16 p2629 A67-31688
 Satellite tracking and data acquisition network of receiving stations /TRANET/ that acquires and processes Doppler frequency shift data 16 p2630 A67-31740

Airborne photographic instrumentation system for photometric observation of total solar eclipse, noting automatic tracking system 16 p2678 A67-31794
 Component selection of antenna steering system in satellite communication system, discussing tracking system characteristics and servo operation modes 17 p2833 A67-32190
 Associative processors and application to automatic radar tracking and correlation, using digital computer 17 p2813 A67-32471
 Compensatory tracking experiments between single and two-axis tracking systems, determining training effects on model parameters of human operator 17 p2808 A67-33178
 U.S. Navy Doppler geodetic Tranet system configuration and operation, discussing tropospheric and ionospheric refraction, timing and frequency errors 18 p3003 A67-34241
 Data and orbit analysis supporting Navy satellite Doppler system Tranet, discussing editing and archiving of Doppler data and orbital ephemerides 18 p3003 A67-34245
 Analog and digital long range automatic radar tracking systems design characteristics and implementation by solid state components 20 p3379 A67-36244
 Parametric comparison between tracking with solar cell arrays and nontracking systems with respect to space power supplies 20 p3363 A67-36585
 Stability of automatic systems for tracking point targets, noting nonlinear dependence of signals on channel mismatch and its limiting values 20 p3410 A67-37234
 Space vehicle tracking noting significance of accuracy and rapidity in determination of position, velocity and acceleration 21 p3583 A67-38642
 Coherent responder used in distance Doppler tracking system, obtaining radial distance by using phase compression 21 p3656 A67-38650
 Developments in tracking, telemetry and command transmission, discussing move toward higher frequencies and rain losses 22 p3763 A67-40338
 Single channel self-adaptive servosystem synthesized for optimal tracking of diffusion type signal with drift 23 p3983 A67-40598
 Tracking ground station on Ascension Island to relay communication with Apollo spacecraft via INTELSAT II 23 p3986 A67-40706
 Digital controller design for tracking telescope, discussing tracking accuracy and response time 24 p4154 A67-42176
TRADESCANTIA
 Chromosome configuration and mitosis impairment in micropores Tradescantia paludosa due to space flight effects of Voskhod I 07 p1133 A67-19109
TRAFFIC CONTROL
SA AIR TRAFFIC CONTROL
 Adaptive utilization of communication satellite systems optimizing dynamic traffic handling of combined ground and satellite communications complex, noting network configurations 06 p0959 A67-17670
 Airport accessibility, discussing rail extensions to airports, bus lanes and bus-rail vehicles [SAE PAPER 670322] 12 p1925 A67-25868
 Proposed worldwide navigation, communication and traffic control system for all weather to guide aircraft and vessels, locate distressed vehicles and direct rescue operations at sea [AAS PAPER 67-102] 15 p2515 A67-29957
 Evolutionary concept for mass transportation system [AIAA PAPER 67-381] 15 p2420 A67-30351
 Computer application to planning and operating simultaneous access European ground station network 18 p3003 A67-34355
 Worldwide navigation satellite system in next decade, studying economical, organizational, technological, operational and safety aspects 19 p3255 A67-35658
 Technological and economic factors affecting airline progress, discussing fares, traffic, SST and terminal areas 22 p3922 A67-40062
 Vehicular traffic and rail transportation surveillance or coordination aids possibilities using earth orbiting satellite [AIAA PAPER 67-788] 24 p4242 A67-42951

Traffic prediction for high speed aircraft and surface vehicles and VTOL aircraft city-center to city-center transportation [AIAA PAPER 67-802] 24 p4259 A67-42962 Highway, ramp, terminal, runway and approach congestion problems for airports, suggesting separated general aviation airports and runways to alleviate big jet airports [AIAA PAPER 67-871] 24 p4139 A67-42992

TRAIL

-S METEOR TRAIL
S SMOKE TRAIL
S VORTEX TRAIL

TRAILING EDGE

Improved numerical procedure for harmonically deforming lifting surfaces from supersonic kernel function method [AIAA PAPER 66-78] 01 p0007 A67-11162 Ramjet external-combustion engine noting design of trailing edge, nomograms of pressure, temperature, thrust component, etc 04 p0688 A67-14578

Spence integrodifferential equation for flow around slender slightly curved profile with jet at trailing edge 05 p0749 A67-16842 Base bleed effects on flow behind two-dimensional model with blunt trailing edge, measuring base pressure, shedding frequency and vortex formation 21 p3566 A67-39078

Boundary layer control by suction at trailing edge to reduce profile drag of helicopter rotor blades 22 p3742 A67-40133

Two-dimensional incompressible flow near airfoil trailing edge treated by inviscid flow model, with constant vorticity inducing velocity field causing flow retardation 23 p3928 A67-41245

High lift characteristics of various aircraft configurations in wind tunnel model using different leading and trailing edge lift augmentation devices 23 p3934 A67-41309

TRAINER

State-of-the-art trainers for military applications, airborne trainers, aerospace ground equipment, aircraft weapons control system trainer and ground crew training devices 01 p0049 A67-10532

Future potential and requirements of digital simulation noting design, construction, cost, etc 13 p2090 A67-27265

TRAINING

SA ASTRONAUT TRAINING
SA FLIGHT SIMULATION
SA FLIGHT TRAINING
SA INSTRUCTION
SA LEARNING
SA MEMORY

SA PILOT TRAINING
SA SIMULATOR TRAINING
SA TRANSFER OF TRAINING

Airline operation, reliability, personnel and training techniques [SAE PAPER 670343] 12 p2041 A67-25879

Simulation and training - Conference, New York, April 1967 13 p2063 A67-27259

Impact of microelectronics on utilization and training of maintenance personnel 18 p2994 A67-34342

TRAINING AIRCRAFT

German SIAT 223 Flamingo sports, trainer and cross-country aircraft, noting design, components and tabulated technical data 18 p2985 A67-33641

TRAINING EQUIPMENT

SA FLIGHT SIMULATOR

Navy simulation techniques for pilot training [ASME PAPER 66-WA/AV-3] 04 p0599 A67-15396

Method of implementing training problems for site simulator in simulated system training 13 p2090 A67-27233

Aircraft technician training levels, methods and equipment analysis indicating need for specialty training equipment development 13 p2091 A67-27266

Airline pilot recruitment, role, capability and training 18 p2993 A67-34073

Mach-Zehnder-Rozhdestvenskii interferometer design for training studies of supersonic and subsonic gas flows and anomalous dispersion 20 p3452 A67-37556 Gas laser simulation technique to facilitate teaching of laser physics 22 p3816 A67-39923

TRAJECTORY

SA ABORT TRAJECTORY
SA ASCENT TRAJECTORY
SA BALLISTIC TRAJECTORY
SA CIRCUMLUNAR TRAJECTORY

SA DESCENT TRAJECTORY
SA EARTH-MOON TRAJECTORY
SA ELECTRON TRAJECTORY
SA FLIGHT PATH
SA HOHMANN TRAJECTORY
SA INTERPLANETARY TRAJECTORY
SA LUNAR TRAJECTORY
SA MISSILE TRAJECTORY
SA MOON-EARTH TRAJECTORY
SA PARTICLE TRAJECTORY
SA REENTRY TRAJECTORY
SA RENDEZVOUS TRAJECTORY
SA ROUND-TRIP TRAJECTORY
SA SPACE TRAJECTORY PROGRAM
SA SPACECRAFT TRAJECTORY

Conservative fields of force admitting spiral trajectories and dependence on constancy of energy level 16 p2748 A67-31137

TRAJECTORY ANALYSIS

Orbits, altitudes, viewing geometry, coverage and resolution pertinent to satellite observations of earth and atmosphere 01 p0147 A67-10325

Optimal one-and two-impulse orbital transfer maneuvers, considering shallowly intersecting coplanar orbits 01 p0148 A67-10426

Graphic solution of Lambert time of flight equation for spacecraft correctional maneuvers with respect to initial velocity 01 p0152 A67-11399

Trajectories of electromagnetic rays across terrestrial atmosphere and computer program 01 p0028 A67-11419

Disturbance theory linearized initial value problems for free trajectories passively moving above smooth earth surface 02 p0320 A67-11465

Accuracy problems for interplanetary trajectory correction system design and development, discussing orientation circuits and standards 02 p0321 A67-11537

Flight path control in software system for Lunar Orbiter, discussing optimization program for midcourse aim point and lunar injection point 02 p0265 A67-12382

Qualitative dynamic stability analysis of motion equations with two zeros and trajectories near singular line 03 p0467 A67-12887

Lunar gravitational field determined from orbital motion of Luna X satellite 03 p0510 A67-13341

Approximate method of computing attitude of sounding rockets from magnetometer data 03 p0519 A67-13782

Ascent or descent from initially Keplerian orbit by constant low thrust analyzed by two-variable expansion 04 p0704 A67-14828

Book on qualitative behavior of trajectories of system of differential equations characterizing rate of growth of solutions by Liapunov indices 04 p0645 A67-15011

Effects of reentry vehicle physical characteristics and trajectory constraints on variation of velocity-atmospheric density ambient value function 04 p0706 A67-15244

Optimal interorbital transfer between elliptical orbits in central Newtonian force field analyzed in terms of minimum characteristic velocity 05 p0886 A67-16047

Plane problem of optimum interorbital transfer in central Newtonian force field, classifying initial orbits and transfer trajectories 05 p0886 A67-16048

Variational problem of rocket dynamics in homogeneous gravitational field in empty space reduced to differential equation system 05 p0904 A67-16049

Tungusk comet trajectory and orbit with radiant in constellation Cetus 05 p0889 A67-16210

Reconnaissance missions to outer solar system using energy derived from midcourse planetary encounter 05 p0893 A67-16520

Trajectories of artificial celestial bodies - Symposium, Paris, April 1965 05 p0893 A67-16554

Steady and unsteady aerodynamic coefficients determined by free flight analysis of trajectory and attitude variations in supersonic wind tunnel 05 p0748 A67-16765

Mars/Venus flyby missions with manned Mars landers, showing trajectory profile for mission 05 p0902 A67-17221

Approximation for low thrust trajectory without singularity at escape and having correct behavior up to and beyond escape, using motion equation 05 p0903 A67-17363

Three and six degrees of freedom missile subsystem design analysis using flight simulation by hybrid computer 05 p0789 A67-17515

Rendezvous problem of ascent and injection into transfer orbit and terminal phase 06 p1082 A67-17790

State space method for navigation problems of nominal trajectories 06 p1028 A67-17927

Scaling equations for wind tunnel simulation of trajectory of jettisoned stores from aircraft 06 p0979 A67-18006

Construction and operational characteristics of device for photographic recording of gyroscopic pendulum trajectory 06 p1003 A67-18177

Optimum trajectory control for minimum heating paths during manned vehicle reentry at hyperbolic speeds 06 p1095 A67-18268

[AIAA PAPER 67-59] Science subsystems for Jupiter flyby missions, discussing equipment selection, mission planning, spacecraft design and trajectory and constraints on vehicle configuration 06 p1084 A67-18287

[AIAA PAPER 67-120] Mars stopover mission with Venus swingby technique, discussing velocity requirements, trip times and initial mass in earth orbit [AIAA PAPER 67-27] 06 p1085 A67-18332

Trajectory modes for manned and unmanned missions to Mercury, 1980-2000 [AIAA PAPER 67-28] 06 p1086 A67-18333

Sequential trajectory estimation improved by implementing simple running estimates of observation error variances [AIAA PAPER 67-89] 06 p1086 A67-18337

Radio-controlled reusable sounding rocket design characteristics, trajectory analysis, drag and lift, reentry stress control system, guidance, stabilization, etc 06 p1098 A67-18763

Optimal control system having nonunique solution of Pontryagin equation and having separatrix between two strategies 07 p1160 A67-19203

Trajectory characteristics of high thrust Mars missions and effect on other aspects of mission planning 07 p1248 A67-19358

Trajectory possibilities for Venus swingby mission and role in manned exploration of Mars [AIAA PAPER 66-37] 07 p1248 A67-19363

Lunar landing problem, determining position, velocity and acceleration as functions of time from ignition to shutdown [AAS PAPER 66-121] 07 p1254 A67-19980

Interplanetary trajectories for vehicles using high and low thrust propulsion systems, considering three two-body transfers and role of hyperbolic excess speeds [AAS PAPER 66-128] 07 p1241 A67-19987

Generalized Zubov formulation from Liapunov function of limit cycle behavior in third order nonlinear systems 08 p1311 A67-20345

Rocket wind trajectory dispersion reduction by adjusting thrust-time curve without increasing total impulse 08 p1406 A67-20511

Trajectory design and computer programs for planetary mission analysis 08 p1384 A67-20617

Hodograph theory of Newtonian mechanics for trajectory hodograph analysis, noting powered trajectories and multiple body problems 08 p1384 A67-20618

Qualitative relationship between trajectories of proportional navigation and initial parameters determining motion 08 p1351 A67-20830

Mariner IV trajectory analysis and importance of flight-path selection in construction of basic mission profile [AIAA PAPER 65-516] 08 p1413 A67-21507

Variation of functional determined on trajectories of differential equation systems with discontinuities, discussing application to optimal control problems 09 p1525 A67-22076

Closed form solution for gliding lateral turn at constant height over flat earth of unpowered vehicle, using linearized aerodynamic coefficients 09 p1441 A67-22488

Corrections to station coordinates and nonzonal coefficients of geogravitational potential from Baker-Nunn observations by combined dynamical and geometrical method 10 p1636 A67-23179

First and second adiabatic invariants of

- charged particle motion in calculating trajectory in combined electric-magnetic field 10 p1651 A67-23395
- Closed form solution to three-dimensional rocket trajectory problem, considering flight velocity and acceleration laws for guidance design applications 10 p1709 A67-23484
- Polynomial approximation method for determining satellite orbits from large-time-interval trajectory measurements 11 p1858 A67-24066
- Absence conditions for periodic trajectories in regions of possible existence 11 p1819 A67-24686
- Existence and uniqueness of periodic solution to ordinary differential equations, defining position in plane of closed integral curves 11 p1813 A67-24749
- Gas state equation determination from trajectory analysis of piston in hypersonic wind tunnel 11 p1782 A67-24759
- Vertical cut-off rigidities in South Atlantic analyzed via sixth degree simulation of geomagnetic field, obtaining results from trajectory analysis of cosmic rays [AFRL-67-0082] 12 p1996 A67-25774
- Meteor hyperbolic motion and geocentric trajectory determination 13 p2196 A67-26497
- Relationship between Pons-Winnecke comet and certain types of meteor showers 13 p2196 A67-26498
- Space trajectory analysis of nuclear-electric propelled vehicle 13 p2199 A67-27169
- Lunar landing problem, determining position, velocity and acceleration as functions of time from ignition to shutdown [AAS PAPER 66-121] 13 p2209 A67-27535
- Interplanetary trajectories for vehicles using high and low thrust propulsion systems, considering three two-body transfers and role of hyperbolic excess speeds [AAS PAPER 66-128] 13 p2214 A67-27539
- Lunar gravitational field determined from orbital motion of Luna X satellite 13 p2211 A67-27714
- Algorithm construction for processing of telemetry data in determination of space vehicle trajectories, applying dynamic filtering method 14 p2382 A67-27853
- Short conical spiral antennas for trajectory plotting of small nose cones 14 p2279 A67-27900
- Linearized manual space navigation incorporating redundant measurements to compensate for instrumentation inaccuracies 14 p2347 A67-28128
- Nongeometric derivation of solution equations for cotangential orbital transfer 14 p2384 A67-28134
- Constructing example of isolated stationary point 14 p2343 A67-28387
- Associated force field applied to phase trajectories of nonlinear systems, analyzing conditions of conservatism and normalization 14 p2349 A67-28744
- Ballistic reentry vehicle recovery via low speed water impact or air snatch after vehicle has flown unperturbed trajectory down to altitude of maximum dynamic pressure 15 p2564 A67-29424
- Mass point motion in central mass gravitational field determined from mass point position and velocity coordinates, obtaining Kepler orbits 15 p2559 A67-30035
- Finite terms interpretation of Groebner method for differential equations applied to trajectory calculations in celestial mechanics 15 p2561 A67-30051
- Missile guidance accuracy, examining motion in central gravitational field along trajectory 15 p2572 A67-30177
- Deviation of path of orbiting body calculated from nominal or reference trajectory 16 p2744 A67-30729
- Orbits and trajectories for plane motion of material point in conservative field of force 16 p2748 A67-31138
- Peak altitude of multistage sounding rocket vertical trajectory in vacuum determined by dimensionless graphs 16 p2762 A67-31247
- Particle trajectory analysis with perturbation series, noting position and velocity error estimation for restricted three-body problems 16 p2749 A67-31425
- Real trajectories of n-body problem calculated by convergent integral iterations on basis of differential equations for motion of centers of gravity 16 p2750 A67-31441
- Accuracy problems for interplanetary trajectory correction system design and development, discussing orientation circuits and standards 16 p2752 A67-31603
- Iterative guidance mode with application to three-dimensional upper stage vacuum flight 17 p2881 A67-32058
- Mars stopover mission with Venus swingby technique, discussing velocity requirements, trip times and initial mass in earth orbit [AIAA PAPER 67-27] 17 p2940 A67-32059
- Flight trajectories having apogees unaffected by geomagnetic field, giving numerical solution, discussing radial propagation laws 17 p2941 A67-32239
- Simultaneous recording of rocket trajectory and rapid auroral variations using high sensitivity image orthicon TV system 18 p3034 A67-33594
- Trajectories of auroral charged particles accelerated in geomagnetic tail computed, using fields of magnetosphere reconnection model 18 p3038 A67-33614
- Periodic trajectories in n stationary attracting centers field, using arbitrary gravitational law 18 p3127 A67-34271
- Rocket launchings of French ballistic program, discussing trajectory study techniques 18 p3020 A67-34379
- Optimum trajectory control for minimum heating paths during manned vehicle reentry at hyperbolic speeds [AIAA PAPER 67-59] 19 p3331 A67-34815
- Trajectory analysis of EOLE meteorological balloons flights in troposphere over Southern Hemisphere 19 p3332 A67-35276
- Matched asymptotic expansion method applied to hypervelocity flight trajectories, obtaining solutions to flight dynamic equations 19 p3336 A67-35994
- Digital computer simulation of orbital launch window problem for departure-trajectory analyses [AIAA PAPER 67-615] 19 p3329 A67-36004
- Trajectory prediction for moving stochastic systems 20 p3392 A67-37196
- Switching surface construction using one to one correspondence between points in controllability region and points on surface of nth order system 20 p3410 A67-37230
- Trajectory modes for manned and unmanned missions to Mercury, 1980-2000 21 p3700 A67-37782
- Optimal interorbital transfer between elliptical orbits in central Newtonian force field analyzed in terms of minimum characteristic velocity 21 p3701 A67-37834
- Plane problem of optimum interorbital transfer in central Newtonian force field, classifying initial orbits and transfer trajectories 21 p3701 A67-37835
- Variational problem of rocket dynamics in homogeneous gravitational field in empty space reduced to differential equation system 21 p3701 A67-37836
- Spacecraft trajectory parameter estimation, discussing various time-varying error components 21 p3705 A67-38587
- Radio wave propagation in three-dimensional inhomogeneous magnetoactive ionosphere studied by geometrical optics method 21 p3582 A67-38592
- Radio wave refraction and refraction-induced errors calculated in determination of artificial satellite trajectories 21 p3582 A67-38593
- Second order theory used to provide nearly exact solution for entry mechanics including solution of nonoscillating and oscillating trajectories [AIAA PAPER 66-488] 21 p3706 A67-38865
- Autonomous solution to orbital navigation problem yielding direct measure of orbital parameters 22 p3830 A67-39179
- Cosmic ray trajectories in geomagnetic field, discussing asymptotic directions, rigidities, crossed telescope measurements and focusing effect 23 p4050 A67-40693
- Ion optical system for extraction of dense ion beams from plasma discharges, studying beam forming characteristics via automatic trajectory tracer model 23 p4034 A67-41463
- Sequential trajectory estimation improved by implementing simple running estimates of observation error variances [AIAA PAPER 67-89] 23 p4070 A67-41717
- Pursuit trajectory plotting in central field of gravity for pursuer and fugitive assuming motion can be predicted successively at small time intervals 24 p4228 A67-42273
- Rocket wind trajectory dispersion reduction by adjusting thrust-time curve without increasing total impulse 24 p4242 A67-42919
- Manned space flight safety through mission trajectory design, considering hardware, software and operational constraints [AIAA PAPER 67-822] 24 p4243 A67-42970
- Graphics system for space vehicle design and flight plan via light pen, trajectory computation and performance curve display on scope [AIAA PAPER 67-897] 24 p4126 A67-43006
- TRAJECTORY CONTROL**
- SA DRIFT
- SA OPTIMAL CONTROL
- SA OPTIMIZATION
- Interplanetary trajectory correction via radial heliocentric velocity pulses, noting calculation by linear approximation 02 p0321 A67-11538
- Tabular adaptive predictive model for trajectory following control of nonlinear plant with switched two-level input 02 p0225 A67-12136
- Closedness of set of trajectories or of solutions of contingent equation used in existence problems of optimal control and variational calculus 06 p0975 A67-18100
- Kalman filter alternate form extended to include multiple simultaneous correlated measurements, testing with ballistic model and using square root formulation for trajectory determination [AIAA PAPER 67-90] 06 p1023 A67-18277
- Satellite communications system noting instrumentation, design criteria, frequency range, propagation aspects and suitable trajectories 07 p1141 A67-19344
- Trajectory control scheme effect on performance of lifting entry vehicles [AIAA PAPER 66-407] 07 p1257 A67-19362
- Interplanetary trajectory design, considering energy and duration of mission, arrival velocity at target and earth, use of Hohmann transfer orbit, trajectory maps, etc 08 p1401 A67-21282
- Numerical analysis and programming techniques for orbit determination 09 p1467 A67-21835
- Effects of display magnification, proprioceptive cues, displacement aiding, etc, on decreasing tracking error assessed, using heavy inertia tracking simulator 09 p1456 A67-22372
- Vector equation for determining missile maximum roll rate for effective navigation ratio and time constant for guidance systems 11 p1816 A67-24215
- Optimum trajectory of pulsed coplanar orbital transfer in central Newtonian force field with restrictions placed on distance to attracting center 14 p2382 A67-27851
- Optimum trajectories between material points moving along same orbit in gravitational field of spherically symmetric central body, obtaining numerical solutions for circular initial orbit 14 p2382 A67-27852
- Modulation of L/D and bank angle to achieved heading, range and trajectory stabilization, using closed form equations 14 p2347 A67-28114
- Kalman filter alternate form extended to include multiple simultaneous correlated measurements, testing with ballistic model and using square root formulation for trajectory determination 15 p2563 A67-30202
- Evaluation and calibration of missile and space tracking systems including test-by-test analysis, lofted rockets, self-calibrating systems, etc 16 p2621 A67-30682
- Geometric restraints on orbit about Mars noting trajectories of unmanned Mars exploration satellite, payload, orbit inclination, etc 16 p2745 A67-30748
- Interplanetary trajectory correction via radial heliocentric velocity pulses, noting calculation by linear approximation 16 p2752 A67-31604
- Bang-bang control using adaptive-predictive model applied to least-square error trajectory control of settling-time nonlinear systems 19 p3199 A67-34784
- Particle trajectories analysis for drift instability mechanism, considering resonant and nonresonant particles 19 p3267 A67-34890
- Simulation evaluation of closed form lifting reentry guidance [AIAA PAPER 67-597] 19 p3259 A67-35993
- Space probe rendezvous with Halley comet, considering use of planetary gravity

field to modify trajectory
[AIAA PAPER 67-614] 19 p3329 A67-38003
Formulation of problem of guiding low thrust spacecraft back to nominal trajectory
[AIAA PAPER 67-618] 19 p3260 A67-38007
Optimal correcting strategy for vehicle moving close to nominal trajectory 20 p3407 A67-38809
Manual steering problem and function of lunar module /LM/ manual hybrid guidance system, with automatic guidance system produced trajectory 22 p3898 A67-39176
Flight control system for automatic interplanetary stations /AIS/, comparing Venera series orientation and correction system to Mariner systems 22 p3898 A67-39185

TRAJECTORY MEASURING SYSTEM

Computational method for determination corridors of launch vehicle trajectory and impact dispersions
[AIAA PAPER 66-483] 02 p0325 A67-11941
Calculation method for trajectories in central force field with arbitrary potential 02 p0327 A67-12375
Range instrumentation developments for trajectory measurements including clinetheodolites and tracking radars, noting error sources, weapons systems problems, etc 04 p0568 A67-14436
Integrated Trajectory System, measuring spatial positions, velocities, accelerations and scalar and vector miss distances for targets 04 p0654 A67-15045
High accuracy tracking system for trajectories during lift-off phase 05 p0762 A67-16530
Satellite trajectory determination through high accuracy observations, using short arcs 05 p0894 A67-16561
USAF Eastern Test Range, discussing telemetry, tracking, geodetic and time measurements 05 p0787 A67-16609
Sound-ranging technique for locating supersonic missiles 05 p0766 A67-17282
Semidaptive ancillary numerical filters for use in best estimate of trajectory computation, noting development of optimal differentiator for scalar function semidaptive ancillary numerical filters for use 08 p1288 A67-20663
Pulsed ruby laser rangefinder with high maximum repetition frequency and digital range readout for data acquisition for determining airborne target trajectories 09 p1465 A67-22622
High stability clocks for trajectory measurement with oscillator, using atomic or molecular transitions
[ONERA-TP-459] 10 p1655 A67-22880
Laser rangefinder limit for rocket, balloon or satellite tractography, noting effects of various parameters related to source, receiver, etc 10 p1663 A67-22881
Principles, methods of operation, techniques and limitations of phase comparison position-determining CW and pulse type systems 10 p1605 A67-22996
Trajectory measurement errors for powered spacecraft using matrix analysis
[AIAA PAPER 64-650] 11 p1817 A67-24335
Trajectory systems, discussing atomic clock and laser based equipment design, operation and performance
[ONERA-TP-446] 15 p2554 A67-29376
French laser telemetry network, noting Q-switched ruby laser, Doppler effect measurement and local spatial geodesy program 19 p3182 A67-35239
Ionization gauge circuit for studies of solid explosives initiation by gaseous detonation waves and reflected wave trajectories in shock tunnels 21 p3630 A67-38770

TRAJECTORY OPTIMIZATION

Propellant and time-optimum trajectories with thrust vector rotational velocity at flight beginning and termination taken as additional boundary condition analyzed, using maximum principle 01 p0146 A67-10209
Numerical trajectory optimization method based on indirect and direct approaches for computer of limited memory 01 p0046 A67-11205
Quasi-optimum control law for minimum-time bounded acceleration rendezvous in plane 01 p0111 A67-11212
Fourth necessary condition in optimal rocket trajectory using maximum thrust in

static gravitational field 01 p0152 A67-11306
Jet direction variation via secondary fluid injection resulting in booster trajectory control, increased payload and reliability 01 p0142 A67-11409
Variational problem of optimal motion in gravitational field, for limited-power propulsion system in combination with energy accumulator and engine with limited jet velocity 02 p0327 A67-12332
Mayer technique in calculus of variation for constrained error coefficient criterion function for missile trajectory optimization in aerospace guidance and control 02 p0265 A67-12389
Optimal rocket trajectories, discussing role and significance of intermediate thrust arcs of rocket extremals in vacuum 02 p0335 A67-12397
Necessary conditions for optimal fixed-time powered transfers with multiple coasts and thrusts between circular orbits 02 p0328 A67-12402
TVC flight dynamics and trajectory optimization analysis of pulse, singular and sliding regimes 03 p0509 A67-13184
Principles of suboptimal perturbation guidance and methods for polynomial approximation of guidance matrices 04 p0655 A67-15629
Program selection for motion equations, parameters and control functions maximizing composite flight vehicle probability of delivering payload to given region 04 p0552 A67-15882
Optimum guidance law simulation by analog computer using logic controlled analog, spatial analog and trajectory riding techniques 06 p1028 A67-17614
Algorithm encountered while solving trajectory optimization problems, discussing variational concepts, indirect, gradient, second variation and generalized Newton-Raphson methods 06 p1082 A67-17932
Fixed time rendezvous by two-impulse transfer maneuver in statistical optimization
[AIAA PAPER 67-57] 06 p1029 A67-18266
Numerical method solution of nonlinear two-point boundary value problem associated with optimum transfer of spacecraft
[AIAA PAPER 67-58] 06 p1023 A67-18267
Range control system for lifting body reentry vehicles, using closed form prediction equations for longitudinal and lateral range control
[AIAA PAPER 67-136] 06 p1095 A67-18316
Primer vector of fixed-time impulsive thrust trajectories
[AIAA PAPER 67-54] 06 p1086 A67-18352
Simplified gravity force model effect in computing state transition matrices along two-body orbits
[AIAA PAPER 67-123] 06 p1087 A67-18455
Natural trajectory optimization for lateral turn at constant height 06 p1098 A67-18865
Optimal coplanar orbit transfer treated by Contensou-Busemann approach with metric tensor completed by smallest possible convex hull 06 p1090 A67-18886
Optimum planetary approach of vehicle when direction of correcting pulses applied to trajectory plane is determined from maximum efficiency condition of pulse 07 p1247 A67-19093
Parameter optimization procedure in three degree of freedom trajectory simulation computer program for multistage vehicles
[AAS PAPER 66-111] 07 p1253 A67-19970
Combination numerical-analytical approach to ascent trajectory optimization 07 p1253 A67-19971
Optimal stage sizes and trajectory for multistage launch vehicle determined by various techniques
[AAS PAPER 66-113] 07 p1259 A67-19972
Asymptotic matching in optimization of minimum fuel power-limited interplanetary trajectory
[AAS PAPER 66-114] 07 p1253 A67-19973
Digital simulation of boundary value problems of trajectory optimization, using variational and functional analysis and IBM-FORMAC language
[AAS PAPER 66-116] 07 p1149 A67-19976
Minimum fuel vehicle transfers between coaxial orbits of coplanar and noncoplanar types, using impulses
[AAS PAPER 66-119] 07 p1253 A67-19978
Optimum deorbit positioning on planetocentric elliptic orbit for single impulse reentry treated by two coupled

quartic polynomials
[AAS PAPER 66-123] 07 p1254 A67-19982
Optimal control for linear system with respect to performance functional which includes trajectory sensitivity 08 p1309 A67-20327
Conjugate gradient minimization method in function space 08 p1310 A67-20337
Minimum fuel transfer between circular or elliptic orbits in central gravitational field 08 p1384 A67-20620
Optimum weight ratio for space vehicle with solar energy operated engine, noting dependence on distance from sun, trajectory optimization, etc 09 p1571 A67-21886
Optimization in terms of energy expenditure of problem of interorbital one and two-pulse satellite transfer in central gravitational field 09 p1564 A67-21888
Propellant cost optimization using minimum characteristic velocity solutions for extra-atmospheric part of rocket ascent trajectory, emphasizing final elliptical orbit of arbitrary orientation 10 p1704 A67-22877
Quasi-linearization determination of optimum finite thrust and impulsive orbital transfers 10 p1706 A67-23130
Automatic control with prediction, discussing optimal least time systems for trajectories satisfying maximum principle 10 p1608 A67-23322
Minimum fuel impulses for space trajectories under influence of gravitational and propulsive forces 10 p1678 A67-23424
Flight time estimation methods for iterative solutions of optimum trajectories by numerical integration 11 p1859 A67-24436
Analog computer applied to solve two-point boundary value problem for fourth order optimal control problem with applied Pontryagin maximum principle 11 p1771 A67-24893
Optimum three-dimensional ascent trajectories in model gravitational field using maximum principle 12 p2000 A67-25211
Modified quasi-linearization method for numerically solving trajectory optimization problems with undetermined terminal time 12 p2008 A67-25913
Root trajectory theory use in automation schemes for analysis and synthesis of optimum control systems, outlining applications 13 p2085 A67-26394
Book on mechanics of low thrust space flight covering physical principles and generalized characteristics of engine systems, problems in optimization of space vehicles, etc 13 p2211 A67-26460
Navigation of SST with respect to optimum trajectory, flight system and traffic control 13 p2153 A67-26710
Parameter optimization procedure in three degree of freedom trajectory simulation computer program for multistage vehicles
[AAS PAPER 66-111] 13 p2214 A67-27527
Combination numerical-analytical approach to ascent trajectory optimization
[AAS PAPER 66-112] 13 p2208 A67-27528
Optimal stage sizes and trajectory for multistage launch vehicle determined by various techniques
[AAS PAPER 66-113] 13 p2214 A67-27529
Asymptotic matching in optimization of minimum fuel power-limited interplanetary trajectory
[AAS PAPER 66-114] 13 p2208 A67-27530
Digital simulation of boundary value problems of trajectory optimization, using variational and functional analysis and IBM-FORMAC language
[AAS PAPER 66-116] 13 p2074 A67-27531
Minimum fuel vehicle transfers between coaxial orbits of coplanar and noncoplanar types, using impulses
[AAS PAPER 66-119] 13 p2209 A67-27533
Optimum deorbit positioning on planetocentric elliptic orbit for single impulse reentry treated by two coupled quartic polynomials
[AAS PAPER 66-123] 13 p2209 A67-27536
Real time meteorological system for ballistic high altitude multistage rocket trajectory, computation and prediction 13 p2091 A67-27610
Two-person zero sum games with differential equation rules, noting location of optimal trajectories, separation properties, etc 15 p2509 A67-29404
Optimization of Atlas-Agena trajectories via steepest ascent computer program 15 p2514 A67-29602

Capabilities, goals and scientific and engineering problems associated with missile trajectory analysis, detailing tracking equipment [AAS PAPER 67-43] 15 p2438 A67-30112

Steepest ascent method for trajectory optimization 16 p2744 A67-30734

Optimal transfers between coplanar and coaxial orbits /any 16 p2745 A67-30739

Ablation of low melting models on ballistic facility, giving ballistic trajectory optimum conditions and ablation parameters calculation method 16 p2593 A67-31134

Optimal trajectories for linear discrete system with respect to minlmax criteria using standard programming code 16 p2650 A67-31670

Optimal feedback control calculation for launch vehicle synthesizing optimal controller with sensitivity constraints to reduce trajectory dispersion 16 p2763 A67-31679

Continuous control process with random variable stopping time of known probability distribution, presenting optimal feedback control, trajectory and minimum cost 16 p2651 A67-31681

Earth-Mars round-trip flight maximum payload delivery variational problem, determining optimum trajectories and minimum flight time dependence on engine parameters 17 p2941 A67-32240

Optimization of extra-atmospheric phase of orbital ascent by assumption of certain hypotheses concerning atmosphere transit cost and nonnegligible-aerodynamic atmosphere thickness 17 p2946 A67-32695

Iterative solution of boundary value problem for optimal trajectory, applying smoothing procedure 17 p2830 A67-32869

Algorithm for computing matrix Riccati equation solution in optimization problems 19 p3249 A67-34781

Conditions for optimal planar intermediate-thrust /singular/ trajectory in inverse-square-law field analyzed graphically 19 p3333 A67-35749

Lunar terrain uncertainties effect on trajectory optimization using Kalman filter during lunar landing powered descent [AIAA PAPER 67-543] 19 p3256 A67-35942

Optimal payload lifting and nonlifting trajectories of winged boost-launch vehicle [AIAA PAPER 67-558] 19 p3335 A67-35955

Steepest-ascent optimization program developed for flight path of current vehicles, particularly supersonic transport vehicles 19 p3257 A67-35958

Linear segment pitch rate program for near optimum trajectory for rocket boosters 19 p3335 A67-35976

Singular optimal control and attitude problem in rocket guidance [AIAA PAPER 67-582] 19 p3258 A67-35977

Solar-electric powered vehicle trajectory optimization using variational calculus, assuming general forms for efficiency and solar power variation [AIAA PAPER 67-583] 19 p3329 A67-35978

Optimum two-impulse orbital transfer for arbitrary terminal conditions, discussing analytic characteristics 19 p3329 A67-35979

Manual optimal guidance scheme using predictive display applied to launch vehicles during boost for continuous generation of predicted fuel-optimal trajectory 19 p3259 A67-35989

Iterative guidance mode /IGM/ applied to effective gravity vector prediction, acceleration measurement of noise sensitivity and energy limitations [AIAA PAPER 67-620] 19 p3260 A67-36009

Reentry trajectory optimization by repetitive computations of impulse response functions and state equations solution 19 p3190 A67-36072

Payload and trajectories determination for consumption optimization for missiles moving in constant gravitational field, using Pontryagin maximum principle 20 p3531 A67-36409

Aerocruise maneuver for optimizing orbital plane change with respect to cruise speed 20 p3532 A67-36552

Extremal space trajectories problems of one-impulse flights and two-impulse orbital transfers in central gravitational field 20 p3522 A67-36617

Optimal correcting strategy for vehicle moving close to nominal

trajectory 20 p3407 A67-36809

Second order nonlinear optimal control system for various performance criteria using Pontryagin principle 20 p3410 A67-37252

Data return advantages of earth-Mars-earth flyby trajectories over more conventional Mars trajectories 20 p3530 A67-37626

[AIAA PAPER 67-646] 20 p3530 A67-37626

Generalized Legendre-Clebsch condition applied to singular arc trajectory solutions of state and adjoint equations for optimal control 21 p3602 A67-38023

Generalized indirect method solving two-point boundary value problems for rapid optimal trajectory computation 21 p3702 A67-38024

Trajectory optimization initial value problem, considering various conditions, methods of solution and reentry heating minimization 21 p3703 A67-38440

Computational considerations for trajectory optimization in bounded state space, discussing necessary and sufficient condition 21 p3604 A67-38443

Trajectory optimization, performance and other factors in analysis of low thrust solar electric propulsion Jupiter flyby mission [AIAA PAPER 67-710] 21 p3706 A67-38737

Time optimal flight trajectories in planar and spatial pursuit problems with constraints on pursuer, using Pontryagin maximum principle 21 p3712 A67-39151

Suboptimal radial guidance scheme based on cubic time function of optimal trajectories radius vector modulus from simultaneous data analysis 22 p3830 A67-39164

Statistical properties of perturbations in rocket path determined to minimize statistical quantities 22 p3878 A67-39182

Optimal flexible strategies for pulsed correction of close-to-nominal space vehicle trajectory, using fuel reserve limitation criterion 22 p3878 A67-39186

Open loop adaptive optimal control, calculating plant dynamic sensitivity coefficients for unknown disturbances, using digital computer on feedback path 22 p3776 A67-39411

Unmanned probe and launch vehicle selection for solar system exploration, considering tradeoffs in terms of reliability, cost, weight, experimental accuracy, etc 22 p3900 A67-39617

Discontinuous integrands in calculus of variations formulations of trajectory optimization and maximum payload problems with discontinuous state variables 22 p3827 A67-39954

Mass optimal trajectory problems with variable endpoints solved using initial and terminal coasting arcs 22 p3884 A67-39955

Minimum total impulse for optimum two impulse transfer trajectory between coplanar circular close orbits 22 p3884 A67-39958

Lagrange multipliers in two-point boundary condition problems for trajectory optimization estimated by direct method 22 p3885 A67-39963

Thrust history to produce maximum altitude for two-stage launch vehicle determined using simplifying assumptions and atmospheric drag 22 p3904 A67-40089

Suboptimal feedback solution to guidance and control in minimum time and fuel for low thrust orbital transfer 22 p3832 A67-40146

Rapidly converging iterative solutions to Min-H strategy applicable to trajectory optimization and payload maximization 22 p3888 A67-40148

Mathematical model of linear guidance law to dynamical system, noting reduction of two-point boundary value class error 23 p4026 A67-41732

TRANSALL C-160 AIRCRAFT

Static and fracture tests with C-160 /Transall/ transport 01 p0048 A67-10212

Transall C 160 aircraft wings, fuselage, tail surfaces, landing gear and power units 20 p3381 A67-36633

TRANSCENDENTAL FUNCTION

Complex roots of dispersion relations involving transcendental analytic functions 03 p0486 A67-14056

Diffraction of plane harmonic horizontally polarized shear waves by parabolic cylinder, obtaining dynamic shear-stress concentration for parabolic notch and rigid parabolic insert [ASME PAPER 66-WA/APM-13]

Self-similar solution generalization for Euler-Poisson wave equations, noting application to transonic gas dynamics 06 p1023 A67-17862

Approximation of zero of transcendental equation by iterative methods 09 p1468 A67-22049

Increasing modulus maximum of integral function relation to moduli of coefficients of power series 11 p1813 A67-24520

Numerical solution of Cauchy problem class of nonlinear integrodifferential equations 14 p2344 A67-28896

Algebraic and transcendental equations solutions using analog computer model described by differential equations, noting Liapunov stability theorem and asymptotic equilibrium 23 p3976 A67-41392

TRANSDUCER

SA DIGITAL TRANSDUCER

SA ELECTRONIC TRANSDUCER

SA IMAGE TRANSDUCER

SA MAGNETIC TRANSDUCER

SA PHOTOELECTRIC CELL

SA PRESSURE TRANSDUCER

SA QUARTZ TRANSDUCER

SA TEMPERATURE TRANSDUCER

Capacitance pickups with nonelectrical quantity causing transverse bending of plates and change in transducer capacitance, used in recordings of mechanical quantities 01 p0063 A67-10416

Thermal analysis of thin wafer heat flux transducer backed by finite heat sink subjected to reentry and rocket-nozzle heat transfer environments 01 p0071 A67-11095

Signal conditioning variable resistance transducer excited by constant current power supply 01 p0071 A67-11099

Transducers role in problems associated with accurate and precise measurements during static firing tests of solid propellant motors 01 p0073 A67-11111

Thermal, excess and shot noise in transducers, examining CW signal generator method for measuring average noise factor 01 p0039 A67-11196

Static and dynamic properties of servomechanical transducers for nonelectrical signals with help of electrical signals 04 p0618 A67-14412

Thin film piezoelectric transducers properties used in microwave acoustic delay lines and phonon generators for analysis of phonon-phonon interactions in dielectric materials 04 p0621 A67-15116

Cadmium sulfide film transducers for shear mode with various insertion losses, noting effect of uniformity in oblique c axes orientations 04 p0621 A67-15126

Velocity measurements at various temperatures made with zinc sulfide thin film longitudinal acoustic wave transducers, used on germanium 04 p0621 A67-15127

Reliable test method based on special strain gauge load transducer for embedment axial stress measurement in electronic modules 05 p0779 A67-17457

Piecewise linear approximation procedure for linearization of readings of nondifferential vibrating and string transducers 06 p1003 A67-18174

Fluidic digital rectilinear displacement indicator emphasizing transducer, logic circuitry and readout 08 p1281 A67-20456

FM of RC generator by connecting parametric voltage transducer output to phase shift network and applying generated voltage to transducer input through matching network 09 p1496 A67-21692

Pressure calibration methods for testing response of microphones in difficult conditions of temperature, pressure and frequency 09 p1484 A67-21938

Transducers, transmission systems and display and implementation systems of radio telemetry and effect upon measurement 10 p1605 A67-22997

Push-pull electrostatic loudspeaker for aircraft cockpit, helmet and ear-insert communication 11 p1767 A67-24702

Rectangular to cylindrical waveguide transducer which couples dominant rectangular and cylindrical transverse electromagnetic modes 11 p1767 A67-24733

Microwave thermography used to measure microwave optical field patterns, using Czerny IR thermosensitive transducer process 12 p1939 A67-25196

Signal to noise ratios of transistorized

constant current and constant temperature hot-wire anemometers 12 p1947 A67-26121
 Piezoresistive effect of homogeneous silicon diffused elements 13 p2175 A67-26656
 Piezoelectric transducer electromechanical properties compared to electromagnetic actuator, noting fluid control applications 14 p2248 A67-28267
 Noise cancelling devices for converting noise into equivalent electric energy, noting pressure, differential and throat microphones 15 p2489 A67-30088
 Temperature autostabilizing nonlinear dielectric element /TANDEL/ for electric measurement circuits and measurement transducers 17 p2828 A67-32829
 Electrodynamical transducer for liquid-borne ultrasonic pulse intensity measurements, considering limits, inductance and measuring system dimensions 18 p3043 A67-33463
 Temperature gradient and thermal effects on ceramic transducer sensors used on spacecraft for cosmic dust experiments 19 p3229 A67-35170
 Silicon semiconductor strain-gauge techniques applied to transducer design noting small light units, high sensitivity, silicon integrated circuits, reliability, etc 20 p3442 A67-36458
 High power thyristor used with battery to operate pulse repeating sonar transducer 22 p3747 A67-39255
 Miniature transducers for shock tunnel instrumentation, noting compensating system to reduce spurious signals from pressure and skin friction acceleration 22 p3809 A67-40463
 Design and performance of high gain amplifier consisting of cadmium sulfide single crystal and thin film transducers 23 p3977 A67-40690

TRANSEQUATORIAL PROPAGATION
 Spread-F effects on WWV transequatorial propagation of HF radio waves 06 p0964 A67-18575
 Oblique sounding of transequatorial path [AGARDOGRAPH 95] 15 p2438 A67-30298
 Rate of transequatorial plasma diffusion along geomagnetic field lines in topside ionosphere, considering electron distribution asymmetries in equatorial F-2 layer 20 p3431 A67-37098
 Annual and diurnal variations of geomagnetic anomaly in Australasian Zone during sunspot minimum, stressing role in transequatorial propagation of VHF radio signals 22 p3759 A67-39473

TRANSFER

S CHARGE TRANSFER
 S ELECTRON TRANSFER
 S ENERGY TRANSFER
 S HEAT TRANSFER
 S INTERPLANETARY TRANSFER
 S MASS TRANSFER
 S MOMENTUM TRANSFER
 S ORBITAL TRANSFER
 S PROPELLANT TRANSFER
 S RADIATION TRANSFER

TRANSFER FUNCTION

Taylor line source distributions as reference set of antenna transfer functions 01 p0023 A67-10481
 Invariant and optimal linear systems with periodic parameters analyzed by transfer function calculation 01 p0044 A67-10492
 Oscillating limiter effect on message modulation for band pass filter with flat amplitude and linear phase characteristics in input signal frequency range 01 p0025 A67-10859
 Linearization of nonlinear transducer output transfer function by digital voltmeter 01 p0076 A67-11143
 Modified Bode criterion for feedback system stability 01 p0045 A67-11198
 Algorithm for reducing linear time-invariant differential systems to state form applied to systems described by transfer functions 01 p0047 A67-11219
 Notch steepness of open circuit transfer function of loaded exponentially tapered RC notch filter 01 p0041 A67-11317
 Electrical properties and electron emission of sandwich cathodes prepared in vacuum by vapor phase condensation, deriving transfer constant 02 p0294 A67-11761
 Regularization method to minimize error in solving Wiener-Hopf integral equation to determine pulse transfer function 03 p0374 A67-13083
 Restrictions placed on transfer function of

linear system with input and output coordinates in presence of given plant in control loop 03 p0390 A67-13098
 Transfer function of pulse amplitude modulated sampled data control systems with element generating arbitrarily shaped pulses and first order element series connected with constant parameter elements 03 p0390 A67-13103
 Externally pressurized bearings treated as hydraulic closed loop servomechanism analyzed, using transfer functions [ASME PAPER 66-LUB-7]

03 p0431 A67-13759
 Synthesis of phase synchronization system providing maximum level filtering of external fluctuation noise, using generalized integral criterion 03 p0393 A67-13949
 Synthesis technique for RC network using two distributed RC elements, one negative impedance converter and one lumped capacitor 03 p0393 A67-13975
 Discrete gyroscopic servocontrol in presence of multidimensional random noise, ensuring optimal reproduction of input signal 03 p0465 A67-14157
 Transfer functions and statistical properties of SST in atmospheric turbulence 04 p0620 A67-14893
 LF instability of liquid propellant rocket motors, noting combustion time effect on phase relations and oscillation excitation, obtaining transfer function 04 p0723 A67-15193
 Transfer function and input impedance of pressurized fluid piping system, using distributed parameters and block diagram feedback methods [ASME PAPER 66-WA/AUT-13]

04 p0555 A67-15416
 Generalized charge control theory derivation of transfer function of nonparametric transistor amplifier in system with common emitter 05 p0769 A67-16168
 Transfer function parameters of stationary controlled plants in identification problem estimated, using Laplace transform and least squares method 05 p0782 A67-16319
 Iterative method determination of output signal, impulse response and transfer function of variable parameter linear sampled data system 05 p0784 A67-16705
 Fluidic circuit design, testing and performance noting transfer functions and differentiating and integrating circuits 05 p0754 A67-17200

Controllability limit of human pilot for unstable second order system with positive static stability analyzed by modified transfer function and servomechanism theory 05 p0757 A67-17354
 Real time approximation of continuous system performance on digital computer using difference equations obtained from digitized transfer function 05 p0768 A67-17518
 Stability and asymptotic stability of control systems with multiple nonlinearities and inputs, using frequency criterion in connection with transfer function matrix 06 p0973 A67-17601
 Matrix method determination of time response of time invariant linear systems to range of deterministic functions 06 p0976 A67-18402
 Control system synthesis based on approximation principle using transfer function expansion in Maclaurin series 06 p0978 A67-18559
 Gyrostat transfer motion from initial stage to predicted orientation maneuver with minimum consumption, using Pontryagin method 07 p1184 A67-19149

In-flight measurement of human response transfer characteristics of pilot [AIAA PAPER 67-240] 07 p1136 A67-20061
 Poles and zeros of amplifier transfer functions using digital computer, noting role in network analysis 07 p1157 A67-20091
 Force /or torque/ electrohydraulic servocontrols, considering transfer function, compatibility conditions and hydraulic perturbation 07 p1132 A67-20113
 Quality of optical images and physical receivers including both curve of modulation transfer and noise 07 p1146 A67-20155
 Transfer logic of double dialog high security data transmission system using loop principle 07 p1146 A67-20159
 Identification of unknown transfer function in nonlinear sampled data systems,

using iterative method 08 p1310 A67-20336
 Transfer function of linear system obtained from discrete values of input-output data 08 p1311 A67-20344
 Angular acceleration sensor for control system stabilization using MHD principles, obtaining transfer function 08 p1331 A67-20697
 Distribution of photons from point image in photographic emulsion calculated using diffusion equation, deriving limits on point spread functions and corresponding modulation transfer functions 09 p1496 A67-21708
 Solid state physics - Conference, Kiev June 1965 09 p1580 A67-21901
 Transfer phenomena in polygenous solutions, noting canonic form of component flow equation 09 p1553 A67-21905
 Imaging properties of gas lens, discussing ray trajectory, ray matrix lens formula, optical transfer function, etc 09 p1498 A67-22083
 Insulated gate to obtain depletion in channel of MOS-FET transistor, noting inversion layer and frequency response 09 p1475 A67-22202
 Relation between human mechanical impedance and coupling of human center of mass to environment, noting transfer function 09 p1456 A67-22370
 Nonlinear vibration damping functions for fluid film bearings [SAE PAPER 670061] 09 p1508 A67-22535
 Functional properties of semiconductor devices and integrated circuits, considering network design 10 p1610 A67-22976
 Traveling wave tube amplifiers for communications systems noting amplitude transfer function, two-tone and FM intermodulation, etc 10 p1613 A67-23440
 Torsional vibrations of reciprocating engine with allowance for vibration of second type treated by transfer-matrix method 10 p1720 A67-23577
 Invariant and optimal linear systems with periodic parameters analyzed by transfer function calculation 10 p1621 A67-23614
 Nonlinear sampled system with parameters in functional dependence on sign of error at discrete instants of sampling 11 p1769 A67-24056
 Optimum linear receiver for noisy PAM system using criterion of mean square interference 11 p1752 A67-24134
 Restoration of digitized turbulence-degraded images by corrective processing of harmonic representation according to measured optical transfer function 11 p1789 A67-24414
 Diffusion effect on hole mobility in base of semiconductor device with p-n-p-n structure 11 p1765 A67-24480
 Transfer process effect on stability of plane flame front, deriving revised approximate solution for large finite Reynolds numbers 11 p1883 A67-24672
 Reduction of order technique pertaining to plant and reference model in controller design for linear plants transfer functions with zeros and slowly varying parameters 11 p1771 A67-24895
 Statistical analysis of optimum control system design by parameter adjustment, finding systems transfer function through Wiener-Hopf integral 11 p1772 A67-25082
 Nonlinear Bayes detector synthesized for Gaussian signal and noise fields using Wiener filters 12 p1919 A67-26087
 Human transfer function problem and compensatory tracking, analyzing variance and determining average rate of stick motion as underlying variable 13 p2063 A67-26923
 Rigid lifting body movement transfer function derived from translational and angular velocity components transfer functions 14 p2393 A67-28081
 Transmittance of thin film field effect transistor with equivalent circuit with lumped constants and generalized transfer function of nonparametric amplifier 14 p2286 A67-28586
 Variable data rate modem for digital signal transmission on HF radio circuits 14 p2272 A67-28705
 Magnetic shielding properties of earth mantle obtained from power spectrum, deducing transfer function of mantle 14 p2314 A67-28887
 Plotting inverse of transfer function,

deriving equations for hodograph and for gain values which yield greater or equal damping ratios 15 p2457 A67-29372

Local types presented in Chang paper for systems with particular open-loop transfer function are only types possible for third order systems with no open-loop zeros regardless of nature of open-loop poles 15 p2457 A67-29375

Static and dynamic parameter estimation of nonlinear transfer elements from step responses 15 p2463 A67-30331

Experimental identification of systems by adapting parallel model 15 p2464 A67-30336

Rate variation of aerodynamic parameters of pitching equation for aircraft, identifying them with linear plant model for simulation studies 15 p2420 A67-30340

Transient plane wave magnetic field attenuation through semiinfinite plate using simplified Laplace transfer function, noting infinite product form for LPTF 16 p2626 A67-31349

Control of output variables in discrete multivariable system at steady state noting design, application and performance 16 p2649 A67-31668

Necessary and sufficient conditions for decoupling time-invariant linear multivariable system by state variable feedback, discussing transfer matrix consequences 16 p2652 A67-31692

Monte Carlo evaluation of linear and eigenvector-method for estimation of pulse transfer function of linear, time-invariant dynamic feedback system 16 p2653 A67-31695

Computer program for optimizing performance of high resolution airborne photo-optical recording system using modulation transfer function analysis 16 p2678 A67-31792

Airborne photographic systems defining performance criteria for quantitative analysis and application of transfer functions for evaluation 16 p2680 A67-31804

Ventilatory mechanical system response to stepwise-increasing pressure stress studied with Laplace-Carson transform, giving characteristics of linear differential equation governing system 17 p2807 A67-32238

Effect of unconditional stability of loop in phase lock demodulator on threshold performance of loop, noting transfer functions role 17 p2816 A67-32782

Phase and amplitude characteristics of microwave amplifiers obtained from response to short input pulse 17 p2827 A67-32791

Transfer functions in electrohydraulic servo systems through feedback instability properties, discussing root locus theory and typical servomechanism properties 17 p2830 A67-32932

Book on analysis and design of pneumatic systems covering nozzle flow, transfer functions, root locus, plenum chambers, servomotor, etc 18 p2988 A67-33754

Transfer function parameters of stationary controlled plants in identification problem estimated, using Laplace transform and least squares method 18 p3017 A67-33870

Transfer function use in outgoing IF radiation temperature measurement of vertical profile over Caspian Sea by airborne modulation radiometer 18 p3040 A67-34001

Unlock behavior of second order phase locked loop with and without interfering carriers 18 p3018 A67-34346

Computer program for handling of transform between spatial coordinate representation and spatial frequency representation of image 18 p3007 A67-34599

Random vibration testing by multiple electrodynamic exciter technique, analyzing electromechanics and structural feedback 19 p3339 A67-34961

H-01 waveguide irregularities causing transfer function fluctuation, calculating rms and relative distortion power from PCM signal 19 p3183 A67-35561

Wind penetration effects on flight simulations evaluated in frequency domain by solution of theoretical transfer function, showing relationship to angle of attack [AIAA PAPER 67-609] 19 p3208 A67-36000

Evaluation of transfer functions using Lagrangian equations, giving dynamic equations from energy expressions 19 p3206 A67-36033

Data reduction system noting magnetic tape data collection, data transfer, random

data analyzer, system analysis with transfer function analysis, etc 20 p3442 A67-36460

Heat exchanger transfer functions obtained from linearization of partial differential equations [ASME PAPER 67-HT-5] 20 p3544 A67-36704

Capacitance reduction in active RC synthesis noting RLC, transfer functions, canonic sections, etc 20 p3409 A67-37109

Synthesis procedure for linear automatic feedback control systems, examining time-domain response 20 p3413 A67-37679

Digital program for stability-augmentation system-gain values yielding desired pole-zero locations for vehicle transfer functions of flight conditions 21 p3568 A67-38539

Rapid parameter identification system for linear time-invariant plant with only input and output measurable 21 p3604 A67-38867

Optimal parameters of transfer function of low thrust power limited engines by approximate solution of differential equation 22 p3898 A67-39181

Optimal transfer function of static systems calculated, using measured data and substitution for higher order transitions through jointly operating PI controller 22 p3776 A67-39335

Invariant measure existence condition derived for Markov processes, with several ergodic theorems for homogeneous Markov processes proved, noting transfer functions 22 p3827 A67-39877

Integral equation with transfer function density restrictions defining characteristic function of Markov process functional, deriving several limit theorems 22 p3827 A67-39878

Optical transfer function relation between image aberration and diffraction, describing measuring methods 22 p3837 A67-40072

Stability margins for hybrid continuous discrete data control systems, developing open loop transfer function 22 p3778 A67-40157

Surveyor TV system calibration, determining transfer functions for various parameters 22 p3807 A67-40376

Modulation transfer theory for frequency response of optical system in temporal or spatial domains, discussing Fourier series and transform [SMPT PAPER 102-47] 22 p3808 A67-40380

Gyro stabilizer feedback circuit transfer function with two-phase asynchronous motor equivalent to unit having time constant as function of transmission band of amplifier 22 p3810 A67-40483

Serial/matrix technique extended to give multivariable linear system responses defined in state space terms 23 p3983 A67-40646

Stability analysis of two-dimensional nonlinear multivariable systems with nonlinearities, finding limit cycle of symmetric and antisymmetric cases from characteristic equations 23 p3984 A67-41160

Modulation transfer functions of various solar recording films using interference device, giving detectability threshold of two-dimensional emulsion patterns 23 p4001 A67-41237

Generalized curves of closed loop loci of peak amplitude, phase and frequency of third order control system 24 p4134 A67-42025

Controllability and observability of parallel and tandem connections of two linear time invariant differential systems of Jordan canonical form 24 p4135 A67-42181

Two-dimensional optical image analysis program for image prediction and enhancement, discussing transfer function 24 p4157 A67-42433

Linear optimal control in systems with uncertain parameters, noting application to design of compensating network for flexible booster for uncertain value of first bending mode 24 p4137 A67-42903

TRANSFER OF TRAINING

Flight simulators for present and future aircraft 13 p2090 A67-27263

Off-line training technique achieving practical closed loop, suboptimal control laws and controllers 16 p2648 A67-31653

Habituation transference in Coriolis stimulation for change from passive lateral chair tilts to various active head tilts during rotation 23 p3953 A67-41585

TRANSFER ORBIT

SA EULER-LAMBERT EQUATION

Boundary value problem for differential equations of perturbed satellite motion assuming perturbing accelerations defined by Vinti potential 13 p2200 A67-27323

TRANSFER VEHICLE

Airport terminal planning for Tampa eliminating long walk, using circular multistory structure with handling equipment for passengers and baggage [SAE PAPER 670319] 17 p2835 A67-32980

TRANSFORM

S FOURIER TRANSFORM

S HILBERT TRANSFORM

S LAPLACE TRANSFORM

S LEGENDRE TRANSFORM

S Z TRANSFORM

TRANSFORM INTEGRAL

Linear heat transfer problems inside equilateral region solved by integral transform series [ASME PAPER 67-HT-67] 20 p3550 A67-36748

Vertical distribution of mechanical wave energy density in lower atmosphere and energy fraction escaping to high altitudes derived by integral transform methods 21 p3655 A67-39088

TRANSFORMATION

S CONFORMAL TRANSFORMATION

S COORDINATE TRANSFORMATION

S LINEAR TRANSFORMATION

S LORENTZ TRANSFORMATION

S MANGLER TRANSFORMATION

S PHASE TRANSFORMATION

S SCHWARZ-CHRISTOFFEL TRANSFORMATION

TRANSFORMATION TENSOR

Multiparameter data sorting technique for one-parameter information represented by simple distribution described by appropriate transformation coefficients 12 p1909 A67-25863

Independent variable changes in dynamical systems and applications to systems regularization, giving canonical and Lagrangian motion equations with tensor notation 23 p4027 A67-41006

Energy-mass equivalence and relativistic transformation formulas application to extended bodies 24 p4188 A67-41905

Validity of formula of relativistic heat transformation, discussing pressure concept definition 24 p4257 A67-43107

TRANSFORMER

SA MODE TRANSFORMER

Static accuracy of temperature stabilization in thermostat increase by using temperature dependences of heat regulators and active resistance of output transformer 01 p0064 A67-10424

Inside-out differential transformer with control element placed outside exciting and sensing coils 01 p0075 A67-11137

Variable ratio DC transformer regulator used in voltage boost configuration of power system in Radio Astronomy Explorer /RAE/ spacecraft, noting RF interference reduction 08 p1284 A67-20692

Structural and technological problems connected with miniature electromechanical filters 10 p1609 A67-22876

MOS element utilization as impedance transformer at output of ceramic ferroelectric subminiaturized pressure pickup 20 p3435 A67-36323

Bridge circuits with nonlinear resistances, calculating statistical characteristics by graphical method for functional transformer 20 p3451 A67-37151

Power supply system consisting of two-piece coaxial cable and pulse transformer found to possess all characteristics for gas laser operation 22 p3817 A67-40414

TRANSIENT HEATING

Null point or transient copper calorimeter using single temperature response measurement to determine heat flux, correlating experimental with theoretical data 01 p0070 A67-11035

Steady state and transient full-scale, half-scale and quarter-scale thermal models in simulated space environment [AIAA PAPER 65-659] 03 p0534 A67-13064

Exact transient temperature distribution in spherical region subjected to axisymmetric-reentry heat flux compared with one-dimensional theory [ASME PAPER 65-WA/HT-53] 03 p0537 A67-14014

Transient heat transfer and thermal

stresses for nuclear rocket due to sudden hydrogen coolant flow increase
[ASME PAPER 66-WA/NE-4]

Interference conductance between two plates during transient heat transfer 04 p0656 A67-15373

Transient temperature distribution in semiminfinite solid, plate, cylinder and sphere subjected to heating or cooling thermal radiation 04 p0735 A67-15853

Transient temperature in slab insulated on one face and subjected to nonlinear thermal transfer at other face studied by perturbation technique 04 p0737 A67-15865

Mathematical model for potential heating from gamma radiation source, determining transient temperature distribution for materials used in nuclear rockets 06 p1116 A67-18363

Transient heat transfer analysis of Apollo Service Module [AIAA PAPER 67-157] 06 p1118 A67-18506

Unsteady energy transfer in gray radiating gas during expansion at atmospheric pressure for arbitrary optical radius 08 p1323 A67-21391

Transient radiative heat exchange on moon surface observed in 8 to 2 micron band during lunar eclipse, using model for quantitative comparisons transient radiative heat exchange on moon surface observed in 8 to 12 micron band during lunar 11 p1865 A67-24604

Approximate formulae for transient temperature prediction due to kinetic heating in aircraft type structures 11 p1883 A67-24661

Instrumenting techniques for models under aerodynamic transient heating 11 p1793 A67-24826

Localized instantaneous plane heat sources position and strength determined using inert thermometers and time integrals of observed temperature transient 11 p1883 A67-24901

Transients in He-Ne plasma laser operating at 0.6328 micrometers 13 p2128 A67-27088

Microwave sound generation by transient heating of material surface with laser pulses 20 p3457 A67-36386

Spectral emittance of melting or decomposing polystyrene determined, describing apparatus and experimental technique 20 p3446 A67-36663

Equations for transient temperature distribution and thermal stresses in heated idealized wing structure solved using heat flow analysis method 20 p3541 A67-37489

Mathematical model for potential heating from gamma radiation source, determining transient temperature distribution for materials used in nuclear rockets 21 p3730 A67-37793

Computer program charts for investigation of effect of temperature dependent thermal conductivity on transient temperature distribution of heated materials 22 p3916 A67-39481

TRANSIENT LOAD

Book on strength under high transient loads and nonlinear elastic and elastoplastic wave propagation 04 p0715 A67-15617

Infinite series and finite difference solutions of elastic response of thin walled spherical shell to axisymmetric transient blast loading [ASME PAPER 66-APM-EE] 04 p0718 A67-15918

Similarity relationships for study of transient and steady state thermal displacements, strains and stresses between model and prototype 07 p1262 A67-19413

Method of images series solution converging rapidly for simply supported Euler-Bernoulli beam with high velocity moving concentrated load 10 p1730 A67-23837

Single mode analysis of dynamic buckling of imperfection-sensitive elastic structure prone to catastrophic failure under time dependent load 14 p2396 A67-28083

Dynamic buckling of ring constrained in rigid circular surface and subjected to transiently applied inertial loading 14 p2398 A67-28093

Transiently loaded foundation on soil designed using graphical phase-plane analysis, considering soil stiffness and damping effect [AIAA PAPER 67-550] 19 p3208 A67-35947

Protection of equipment and systems using semiconductor devices by suppression of voltage transients 22 p3786 A67-39250

TRANSIENT OSCILLATION

SA LASER

Natural oscillations in dissipative oscillatory circuits containing inductance coil with magnetized ferrite core in presence of strong HF field 01 p0037 A67-10544

Hydrodynamics of lower solar photosphere, examining connection between small-scale oscillatory Doppler shifts and exponentially decaying continuum 03 p0511 A67-13650

Isocline method used to analyze quasi-linear equation for single-loop self-excited oscillator with periodically varying bias voltage and resonant frequency radio signal 04 p0588 A67-15876

Transient vibration of viscoelastic body, showing dynamic displacement expression in terms of static boundary value problem 14 p2400 A67-28143

Laser oscillation cessation with strong pumping, interpreting effect as consequence of line broadening due to pumping strokes 18 p3059 A67-33672

Soviet book on unsteady oscillations of mechanical systems with any number of degrees of freedom 18 p3078 A67-33678

Harmonic linearization, estimating quality of oscillatory transients in nonsearching self-adjusting systems described by high order differential equations 20 p3408 A67-37045

Decay instability of steady state waves in plasma, considering Alfvén wave 21 p3674 A67-38803

Transient interference studied for emission from pulsed ruby laser 23 p4012 A67-40883

TRANSIENT PRESSURE

Pressures and temperatures occurring in jet engine exhaust nozzles during speed changes on basis of compression and detonation wave theory 01 p0141 A67-11150

Rapid depressurization transients effect on saturated pool boiling system from stainless steel surface 04 p0734 A67-15848

Ignition pressure transient in solid rocket motors, examining chamber filling interval, flame propagation, heat transfer correlation, burning area, etc 05 p0873 A67-16513

High velocity metalworking /HVM/ techniques, applying transient pressure to specific workplace area 20 p3454 A67-36886

Ducted silo launchers transient pressures caused by rocket engine ignition and shutdown, treating wave propagation by one-dimensional theory 22 p3780 A67-40091

TRANSIENT RESPONSE

Optimization of sampled data systems with finite transient response time on basis of combined stochastically deterministic Q factors 01 p0043 A67-10202

Exact solution, using Laplace transform, for problem of transient characteristic of semiconductor diode, challenging Nosov view 01 p0035 A67-10398

Dynamic response of simple beam and rectangular plate under traveling shock wave at supersonic speed, using Fourier transforms 01 p0161 A67-10775

Transient response of vapor volumetric concentration to perturbation propagation and wave form in boiling forced convection system under oscillatory conditions 01 p0167 A67-10974

Stability and sensitivity requirements considered simultaneously in control system design, minimizing time domain sensitivity index and incorporating transient response characteristics 01 p0047 A67-11217

Graphical method of analyzing nonlinear problems of fluidic circuits 02 p0182 A67-11775

Transient response of frequency synchronization circuit determined with or without application of radar stability circuit 02 p0203 A67-12146

Impulse and step responses of band stop equal element filters with varying degrees of dissipation calculated for transient responses of resonant circuits 02 p0220 A67-12177

Dynamic behavior of electric angle drive unit in linear automatic control system, noting nonlinearities 02 p0227 A67-12197

Tunnel diode traveling wave amplifier, determining amplification coefficient and stabilization time of transient characteristics 03 p0377 A67-13234

Effect of sudden change in magnetic field and/or pressure gradient on Hartmann flow, assuming stationary and nonconducting plates 03 p0482 A67-13745

Anisotropic magnetoplasma diagnostics using transient reflected polarized signals [AFCLR-67-0065] 03 p0371 A67-13865

Asymptotic expansion of transient forces on finite thin wing in oscillatory upwash field treated by derived expression for change of generalized aerodynamic damping coefficients with respect to frequency parameter 03 p0352 A67-13896

Linear approximation of frequency and transient characteristics for field triodes with insulated gate of constant capacitance 03 p0386 A67-13956

Transient response of junction transistors in case of inductive load, deriving switching-on time, switching-off voltage maximum value, etc 03 p0386 A67-13978

Diffusion theory of vibration-dissociation coupling used to analyze transient effects in dissociation reactions behind shock waves 03 p0474 A67-14025

Transient behavior of charring ablator under various thermal environments by finite difference method 04 p0723 A67-14847

Transient annealing following pulsed neutron exposure in silicon transistors and solar cells as function of temperature and injection level 04 p0684 A67-15693

Transient radiation effects induced in silicon irradiated by electron pulses measured, using resistivity transient response and Hall effect voltages 04 p0685 A67-15695

Transient response of transistor exposed to ionizing radiation environment determined, using lumped model technique 04 p0588 A67-15697

Transient radiation effects on microcircuits 04 p0588 A67-15701

Transient response of MOS transistors and integrated circuits to ionizing radiation 04 p0589 A67-15719

Quenching of one pulsed ruby laser oscillation by another, noting coupled rate equations for steady state and transient behavior 05 p0823 A67-16682

Switching process for silicon p-n-p structures, deriving relations for delay and response times and transient period as function of parameters 05 p0865 A67-16911

Transient behavior of He-Ne lasers under pulsed HF excitation, discussing rate equations representing atomic population density and photon density 05 p0825 A67-16980

Transient analysis of control system with nonlinear damping and frequency 05 p0785 A67-17301

Transient response of Couette shear flow to step function change in blowing velocity across channel 05 p0751 A67-17420

Digital computer programs for transient and steady state thermal analysis 05 p0929 A67-17452

Wideband multichannel transient monitoring system for detection and analysis of electrical transient 05 p0809 A67-17537

Transient stress-strain state of elastic system developing combination resonance analyzed, using approximate method 06 p1106 A67-18621

Transient self-excitation in autonomous electromechanical system consisting of pump and MHD generator 06 p0952 A67-18686

Exact expression for transient response for step modulated carrier signal obtained, using parallel plate waveguide 06 p0964 A67-18767

Transient response of beams using lumped parameter models calculated by Euler method to eliminate influence coefficient normally required 06 p1111 A67-18889

Transient response of autonomous nonlinear systems examined using Liapunov function, obtaining time constant 08 p1310 A67-20341

Stability and transient response of nonlinear control systems treated by parameter plane techniques and describing function theory 08 p1310 A67-20342

Spin rate effect on stability and transient response of vehicle treated by root locus technique 08 p1405 A67-20507

Aerodynamic forces on flexible plate embedded in right half-space undergoing arbitrary temporal and spatial motion 08 p1424 A67-21433

- Transient phenomena in reverse current and capacitance in gallium arsenide Schottky barrier diode in monochromatic light 09 p1471 A67-21762
- Optimum transient response for bang-bang control system with finite time control activation 09 p1483 A67-22609
- Large signal transient response of junction transistor in switching and pulse operation treated by charge control analysis 10 p1603 A67-22772
- Transient component in breakdown voltage of silicon p-n junction rectifiers in region of intermittent microplasma 10 p1612 A67-23375
- Diode type lossless network description with excellent transient response and less settling time than conventional branch-line coupler phase shifter 10 p1613 A67-23414
- Transient switching process of semiconductor planar diode with retarding electric field in base operated by short forward current pulses 11 p1764 A67-24469
- Charge ratios of recovery abruptness and figure of merit in switching diode with base field 11 p1765 A67-24470
- Transient behavior of three-level paramagnetic maser, discussing rate equations, spin-lattice relaxation, time measurement, etc 11 p1801 A67-24667
- Laser holography combined with schlieren techniques to measure ray deviations in optically inhomogeneous field of transient phenomenon 11 p1794 A67-24927
- Ferromagnetic film coercive force variation near supercritical state due to film thickness 12 p1981 A67-25243
- Transient acoustical response of uniform flow to turbulence and noise in MHD generators 12 p1899 A67-25390
- Polarized harmonic electromagnetic wave propagation in plane stratified isotropic plasma of cold lossless electron gas, resolving inconsistency near resonance region 12 p1976 A67-25944
- Interaction of shock-induced flow in ideal gas and transverse magnetic field analyzed for steady state and transient one-dimensional effects 13 p2162 A67-26280
- Transient characteristics of doped silicon diodes with negative resistance, determining electron lifetime vs current, noting space charge role 13 p2076 A67-26489
- Transient response in closed transmission systems evaluated and compared to time optimum process 13 p2087 A67-26614
- Optimal transients for third order system with stepwise external controls, determining switching surfaces 13 p2089 A67-27705
- Equivalent circuit model for solid state junction devices with single energy level defect centers including transient properties 15 p2456 A67-29170
- Diode and transistor transient switching characteristics determined from analog computer simulation of differential equations 15 p2449 A67-29803
- Field effect transistor intrinsic and extrinsic transients, switching behavior and relation to time constant by charge concept 15 p2449 A67-29806
- Metal oxide semiconductor field effect transistor /MOSFET/ inverter transient response determination, noting mobility dependency on gate voltage 15 p2452 A67-29940
- Combustion instability, transient burning during ignition and extinction by depressurization investigated in nonsteady burning of solid propellants 15 p2580 A67-29984
- Switching process for silicon p-n-p structures, deriving relations for delay and response times and transient period as function of parameters 16 p2727 A67-30888
- Transient processes in nonlinear automatic control systems 16 p2643 A67-30926
- Transient analysis of displacement, strain and stress fields around running crack tip in epoxy plate with central notch using Moire method 16 p2775 A67-31325
- Transient plane wave magnetic field attenuation through semiinfinite plate using simplified Laplace transfer function, noting infinite product form for LPTF 16 p2626 A67-31349
- Asymptotic behavior of transient signal propagation in lossless, isotropic plasmas for stepmodulated sine wave input signal 16 p2627 A67-31351
- Elimination of electrical transients in high performance sleeve induction motors for missile guidance control systems 16 p2609 A67-31664
- Transient growth of magnetostatic modes in yttrium garnet subject to pulsed longitudinal pumping 16 p2732 A67-31704
- Gyro-controlled rigid rotor system performance, noting steady state and transient response to various excitation [AHS PAPER 131] 16 p2599 A67-31845
- Phase and amplitude characteristics of microwave amplifiers obtained from response to short input pulse 17 p2827 A67-32791
- Semiconductor device and transient ionizing radiation effects on monolithic integrated circuits 17 p2828 A67-32836
- Deficiencies of pulse-parameter representation used for semiconductor diodes, discussing generalized parameter describing transient processes relaxation 18 p3009 A67-33474
- Unconfined nitromethane transient initiation, determining differential conservation, state and reaction rate equations, using two-dimensional computations 18 p3153 A67-33824
- Physical and chemical conditions in rocket combustion chamber during starting transients and steady operation described by mathematical model intended for parametric studies [AIAA PAPER 67-517] 18 p3158 A67-33980
- Moon Blink project for detecting red or blue temporary color phenomena 18 p3134 A67-34535
- Nonrecurring phenomena analysis and detection describing optimum criteria recording and data processing facility 19 p3230 A67-35329
- Transient effects of changes in applied radio frequency power to which latching ferrite phase shifters could be subjected in array applications 19 p3196 A67-35663
- Transient nature of heterogeneous boundary layer chemical reaction at stagnation point studied analytically, deriving stability conditions 19 p3211 A67-35740
- Initial conditions effect on transient states of linear systems 19 p3205 A67-35909
- Electron mobility and trapping time in semi-insulating cadmium telluride through observing transient response to alpha particles 19 p3308 A67-36101
- Theory of small signal current transients applied to study of electron trapping in amorphous selenium 20 p3509 A67-36507
- Pulsar circuit for studying large signal transient response in plasma lasers 20 p3445 A67-36530
- Analytical method yielding solutions for transient steady heat conduction in bodies with arbitrary boundary and initial conditions [ASME PAPER 67-HT-44] 20 p3547 A67-36726
- Transient heat transfer through monatomic collisionless ideal gas enclosed between parallel walls analyzed for step change in one wall temperature [ASME PAPER 67-HT-53] 20 p3548 A67-36735
- Linear heat transfer problems inside equilateral triangular region solved by integral transform series [ASME PAPER 67-HT-67] 20 p3550 A67-36748
- Transient temperature distribution of cylinder subject to radiation cooling, giving dimensionless computer-derived graphs [ASME PAPER 67-HT-71] 20 p3550 A67-36751
- Steady state and transient temperature profiles for straight fins of trapezoidal profile with radiative heat transfer [ASME PAPER 67-HT-73] 20 p3550 A67-36753
- Effect of deviation of inlet fluid temperature change from step change on maximum slopes of transient response curves [ASME PAPER 67-HT-79] 20 p3551 A67-36757
- Laser Fokker-Planck equation transient solution in threshold region investigated for laser distribution function, mean intensity and mean squared deviation 20 p3461 A67-37183
- Maximum principle application to optimal control procedure, minimizing transient response and decreasing effect of random changes in system 20 p3410 A67-37232
- Hydraulic line models for fluid control system analysis, discussing frequency and transient response calculation
- simplification 20 p3366 A67-37365
- Fluid control system design by third order linear differential equation with transient response, showing relationship to frequency response 20 p3366 A67-37370
- Transient heating and cooling of current carriers in semiconductors and highly ionized plasma analyzed, using effective temperature method 20 p3513 A67-37438
- Transient radiation of electric dipole in uniaxially anisotropic plasma examined for signal frequency greater and less than plasma frequency 20 p3388 A67-37704
- Transient response and current distribution of thin vertical antenna coupled to pulse generator by electric network, determining radiation field 21 p3590 A67-38117
- Transient performance of delay equalized low pass filters studied for optimal response 21 p3582 A67-38529
- Transient gas motions for various waves, analyzing motion equations and classifying integral curve fields 21 p3565 A67-38556
- Reverse transient in p-n-p-n triode when reverse pulse is applied to gate 21 p3598 A67-38573
- Pulsed propulsive performance of low thrust subliming solid ammonium carbamate reaction jet, discussing transient response, apparatus, techniques, etc 21 p3697 A67-39152
- Optimal transfer function of static systems calculated, using measured data and substitution for higher order transitions through jointly operating PI controller 22 p3776 A67-39335
- /n-m/ junction structures transient characteristics, forward and back bias cases show inductive and capacitive element behavior respectively 22 p3858 A67-39574
- Multiple reflective metal foil structure with separating matrix transient thermal response, determining number of radiation shields for given thermal protection 22 p3919 A67-40115
- Transient displacement and strain distributions in fracturing notched magnesium plate, using moire-fringe technique and Q-spoiled laser 23 p4076 A67-40736
- Controlled transient signal distortion by shock monitoring instrumentation circuits using piezoelectric accelerometers 23 p4007 A67-41382
- Piecewise linear switching functions design for suboptimal regulation of linear plants with relay controller in regard to transient response performance criterion 24 p4135 A67-42179
- Transient behavior of autonomous nonlinear control system phase space domains, finding relative stability domains for special time dependent Liapunov function 24 p4135 A67-42186
- Transient processes and initial conditions of excitation of lower harmonic oscillations in resistance-capacitance nonlinear inductance circuit, noting graphical integration 24 p4189 A67-42418
- Apollo fuel cell power system transient temperature and voltage response characteristics predicted by analytic model 24 p4106 A67-42523
- Induced interference in open and shielded wire lines due to AC and transient currents, discussing electromagnetic coupling effects 24 p4137 A67-42713
- TRANSISTOR**
- SA FIELD EFFECT TRANSISTOR /FET/
- SA JUNCTION TRANSISTOR
- SA PHOTOTRANSISTOR
- SA SILICON TRANSISTOR
- SA UNIPOLAR TRANSISTOR
- Steady state and unsteady thermal regimes of transistor operating under high current conditions 01 p0038 A67-10720
- Single crystal transistor with metallic base, noting frequency, V-I and power characteristics, radiation resistance, etc 02 p0221 A67-12530
- Second breakdown in transistor with power-handling capabilities 02 p0222 A67-12648
- Thermal instability affecting factors for current distribution in power transistor 02 p0222 A67-12651
- Pulse length of collector current pulse, which causes secondary breakdown in transistors, measured at constant forward or reverse base current 02 p0223 A67-12657
- Transistor noise coefficient measuring

device for 30 kHz to 1.5 MHz frequency range 02 p0223 A67-12798

Minimum noise coefficient of various types of common-base transistors at 1 kHz to 1.5 MHz frequencies 02 p0224 A67-12799

Avalanche transistor pulser designed to drive GaAs radar-laser diode 03 p0376 A67-12964

Radial distribution of excess current carriers in base of p-n junction transistor with high injection levels 03 p0378 A67-13244

McIver and coupled mode theory derivations of equations for traveling wave transistor 03 p0382 A67-13667

Planar transistor stability under X-ray irradiation, showing drifts of variable importance according to type of transistor /p-n-p or n-p-n/ 03 p0387 A67-13996

Field effect transistor characteristics and operation 03 p0387 A67-14001

Transistor life expectancy and failure predictions from LF noise measurements 03 p0389 A67-14277

Emitter barrier capacitance effect on frequency characteristic of current amplification factor in drift transistors with accelerating field for minority carriers 04 p0585 A67-15502

Static V-I relationships in transistors at high injection level 04 p0585 A67-15621

Transient response of transistor exposed to ionizing radiation environment determined, using lumped model technique 04 p0588 A67-15697

Anomalous permanent changes in transistor gain after low exposure dosage of electron and/or gamma radiation related to recombination current-component buildup 04 p0588 A67-15705

Time-dependent response of polycrystalline cadmium selenide thin film transistor to transient high energy radiation 04 p0589 A67-15718

Harmonic components of current of HF transistor under sinusoidal excitation, using piecewise parabolic approximation 05 p0772 A67-16456

Storage time of drift transistors calculated as function of minority carriers effective lifetime 05 p0776 A67-17094

Avalanche transistor properties in dynamical state derived from relation between current, collector voltage and concentrated load in base 06 p0970 A67-18186

Transistorized electron counter using tunnel diodes, noting trigger 06 p1004 A67-18391

Surface generation-recombination and channel effects on p-n junctions and transistors exposed to ionizing radiation 06 p1054 A67-18822

Thermal variation of emitter base voltage of bipolar transistor 07 p1155 A67-19792

Current mode second breakdown in epitaxial planar transistors, describing V-I behavior 07 p1156 A67-19897

Second breakdown in N-channel MOS transistor 07 p1157 A67-19906

Theory of lateral transistor current gain and frequency response 09 p1472 A67-21948

Noise measurements on pulsed four-cavity electrostatically focused S-band klystrons 09 p1477 A67-22253

Temperature and tolerance behavior of transistor determined, based on equivalent drift sources of transistor obtained from intrinsic series coupling 09 p1482 A67-22611

Diffused base punchthrough avalanche transistor /PAT/ at high recurrence frequency having capacitance dependence of pulse width 10 p1609 A67-22839

Analysis of current flow for different input conditions on double-gate thin film transistor 10 p1612 A67-23373

Iron doped gallium arsenide transistor with better frequency performance and higher operating temperatures 10 p1617 A67-23538

Channel transistor characteristics for impurity distribution taking into account space charge penetration into gate 11 p1765 A67-24481

Transistor noise coefficient dependence on acoustic frequency, temperature, emitter current and collector voltage 11 p1769 A67-25037

Plastic molded transistors for hybrid integrated circuits, production and reliability 13 p0277 A67-26651

VHF transistor, attempting design of 60 MHz passband amplifier 13 p0277 A67-26653

Characteristic cut-off frequencies of transistors determined from simple LF measurements 13 p0277 A67-26659

Analytical representations of admittance matrix of transistors, describing methods of obtaining quality coefficients, equivalent circuit synthesis, etc 13 p0281 A67-27199

Digital circuits in resistor-transistor, diode-transistor and transistor-transistor logic 13 p0282 A67-27388

Evaporated silicon thin-film transistors operating by field effect conductivity modulation of n-type inversion layer at p-type film surface 13 p0283 A67-27573

Single crystal transistor with metallic base, noting frequency, V-I and power characteristics, radiation resistance, etc 14 p2279 A67-28007

Device design for measurement of noise factor of RF transistor 14 p2286 A67-28587

Thermal, mechanical stress and moisture resistance reliability tests of plastic encapsulated transistors 15 p2444 A67-29457

Diffused base transistor impurity concentration measured nondestructively to determine structure 15 p2448 A67-29801

Collector conduction resistance in saturated planar transistors determined from current distribution measurement on electrolytic model 15 p2448 A67-29802

Diode and transistor transient switching characteristics determined from analog computer simulation of differential equations 15 p2449 A67-29803

Transistor failure analyses by measuring electric parameters, repeating production phases on opened transistors, destructive testing and defect production by extreme artificial stress 15 p2449 A67-29811

Electronic device modeling criteria expressing physical structure, representing significant properties and leading to useful equivalent circuits for circuit analysis 15 p2452 A67-30013

Intermodulation distortion due to nonlinear elements in transistors analyzed using Volterra series representation 15 p2455 A67-30386

Transistor current-voltage characteristics when controlled by space-charge and transit-time effects, obtaining large negative conductances at HF 17 p2824 A67-32302

First order prediction of equilibrium photocurrent in silicon switching diodes and radiation storage time in silicon low power planar and mesa transistors from electrical measurements 17 p2918 A67-32851

Slow response of cadmium selenide thin film transistors related to trapping levels in insulator 18 p3015 A67-34557

Linear operation of diffused planar transistor in common emitter connection studied by mathematical models 20 p3396 A67-36377

Base impurity distribution design consideration for figure of merit of HF transistors, considering accelerating, decelerating and neutral electric field 20 p3398 A67-36770

Crystal frequency stabilization in relaxation-oscillator circuit, showing similar use in astable multivibrator instead of LC circuit 20 p3384 A67-37215

Low noise transistor switch design capable of switching 1A and meeting military current probe EMI specifications 20 p3406 A67-37653

Second breakdown in semiconductor devices, discussing measurement methods and techniques, development, breakdown mode and safe operating conditions 22 p3766 A67-39248

TRANSISTOR AMPLIFIER

Optical modulator using electro-optic effect in lithium tantalate for PCM transmission systems operating at 224 megacycle bit rate 01 p0033 A67-10013

Selective transistorized logarithmic amplifier design and logarithmic amplitude characteristic computation from cascade output voltages 02 p0215 A67-11978

Small signal RF amplification of VHF MOS transistors, considering TA2840 triode and TA7010 dual-insulated-gate transistors used as VHF amplifiers 02 p0218 A67-12101

Temperature determination for collector p-n junction of transistors in class B power amplifier by thermal equivalent circuit analysis 03 p0378 A67-13249

MOS-FET amplifier RC network design 03 p0382 A67-13670

Transistor and integrated circuits applications including high input impedance amplifier using MOSFET transistor, pulse forming circuit, stable sawtooth generator, etc 04 p0579 A67-14402

Theoretical study of common-mode rejection factor of differential amplifier, with application to valve and transistor type amplifiers at LF 04 p0586 A67-15628

Wide temperature and parameter range transistor amplifier stage stabilization circuit design based on linear approximation of characteristics in terms of H parameters for CE circuit 04 p0586 A67-15669

Book on transistor IF amplifier design for radio, television and radar receivers 05 p0769 A67-16071

Generalized charge control theory derivation of transfer function of nonparametric transistor amplifier in system with common emitter 05 p0769 A67-16168

Instability of amplification factor and stability of transmission coefficient of multistage transistorized amplifier without feedback 05 p0772 A67-16454

Maximum negative feedback depth in transistorized AC amplifier as function of cut-off frequency of logarithmic amplitude-frequency characteristic for given phase reserve 05 p0772 A67-16455

Short and ultrashort wave power amplifiers using Soviet transistors 05 p0773 A67-16457

Amplitude characteristic in transistorized selective logarithmic amplifier with video output, discussing circuitry of proposed multistage amplifier 05 p0773 A67-16459

Statistical properties of amplitude and phase of output signal of electron beam quadrupole amplifier with superposition of regular signal plus Gaussian noise at input 05 p0765 A67-17162

Wideband solid state intermediate frequency repeater for communications satellites, using waveguide-cavity diode down converter transistor amplifier and varactor upconverter 06 p0980 A67-17882

Quadrupole calculation of zero-level drift in transistorized DC amplifiers 06 p0970 A67-18172

Transistorized wideband and pulse type amplifiers for nanosecond frequency range 06 p0970 A67-18191

Semiconductor devices in radio transmitters, examining operation of transistorized amplifiers and varactor multipliers in output stage 06 p0971 A67-18214

Optimization of design of input-output matching networks for transistor microwave frequency amplifiers, using computer program 08 p1305 A67-21228

Planar-technique for germanium, outlining manufacture of planar transistor based on amplifier 09 p1555 A67-22037

Twelve-channel parallel action noise spectrum analyzer for LF noise measurement, using transistorized negative feedback amplifier 11 p1769 A67-25038

Power gain sensitivity of transistors with conjugate matched two-port amplifier 12 p1910 A67-25268

Packaging method for integrated microwave transistor amplifier constructed on ceramic substrates 12 p1910 A67-25265

Lossless gyrator transistor realization using parallel connected positive and negative amplifiers in reverse direction 13 p2078 A67-26789

HF transistorized pulse amplifier with rise of 1 nsec and output voltages of more than 4 v designed for trigger pulses and traveling wave oscilloscope 13 p2082 A67-27400

Resistive transistor stage with feedback, deriving input-output impedances, amplification factors, conductance and resistance 14 p2283 A67-28276

Transistorized resonant cascade amplifier with added active resistance for amplification, stability improvement 14 p2283 A67-28277

Balanced broadband microwave transistor amplifiers using tantalum integrated circuitry 15 p2452 A67-29927

Semiconductor devices in radio transmitters, examining operation of transistorized amplifiers and varactor multipliers in output stage 16 p2635 A67-30480

Gain control of common emitter cascade by varying transistor regime, taking into account effect of operating frequency and

- temperature 16 p2637 A67-31027
- Hyperfrequency amplification using electric field effect for conduction modulation of single crystal germanium sheet 16 p2732 A67-31705
- Electrical design, mechanical fabrication and performance data of integrated broadband balanced transistor amplifier 17 p2825 A67-32599
- Low noise transistorized amplifier at 408 MHz for synthesis radiotelescope 17 p2827 A67-32785
- Monolithic operational amplifiers with simplified frequency-compensated network using minimum stages and integrated circuit components 17 p2828 A67-32899
- Amplitude modulation using varicaps and p-n junction in transistorized transmitter, analyzing HF oscillator 18 p2999 A67-33507
- Bipolar and field effect transistor combinations for high gain amplifiers, discussing various circuitries 19 p3191 A67-34943
- Transistor admittance parameters for mathematical model formulation representing small signal operations, for wideband transistor amplifier design 20 p3394 A67-36236
- UHF amplification and frequency conversion using single transistor as amplifier and base-collector junction capacitance as varactor 20 p3398 A67-36773
- Intermodulation due to nonlinearities in transistor amplifiers, discussing design guidelines for optimizing 20 p3404 A67-37634
- Ionospheric ion and electron densities by Langmuir probes, stressing solid state logarithmic amplifier for spatial electrometry 21 p3592 A67-38223
- Frequency limitations of field effect transistor as amplifier in connection with impurity profile, discussing figure of merit 22 p3767 A67-39275
- Functional analysis of transistor amplifier with multiloop feedback, deriving equation for transfer constant increment 22 p3769 A67-39577
- Solid state linear digital amplifier with external modulation using high operating efficiency of transistors as saturated switching elements 22 p3771 A67-39841
- High gain wideband amplifier with rapid pulse trains, discussing silicon transistor response time, impedance, Q-factor and correction circuit 23 p3977 A67-40691
- TRANSISTOR CIRCUIT**
- Maximum power gain and admittance matrix for neutralized amplifier stages with three-terminal amplifier devices /electron tubes and transistors/ 01 p0035 A67-10432
- Pulsed chronotron vernier for precise time expansion, discussing circuit configuration, operation and performance characteristics 01 p0067 A67-10658
- Method based on static characteristics for limit of saturation used to find relationships between voltages and currents in transformer in saturation region 01 p0037 A67-10714
- Integrated digital logic circuits including resistor transistor, diode transistor, emitter coupled and transistor-transistor logic 01 p0038 A67-10760
- Transistor behavior in phase inverter at LF as function of type /p-n-p or n-p-n/ and value of internal capacity 01 p0038 A67-10770
- Saturated transistor logic circuit using rectifier diodes to provide nonlinear current feedback from collector to base of transistor 01 p0038 A67-10817
- Binary compound transistors, calculating parameters using T-shaped equivalent circuits 01 p0038 A67-10828
- Spectral density measurement of relative fluctuations of current amplification factor common-base transistor circuit 02 p0213 A67-11646
- Wide range vibrating-reed Mariner II electrometer, describing components, performance characteristics and results 02 p0241 A67-11681
- Improved frequency stability and specific transistor characteristics of transistor oscillators with AGC 02 p0216 A67-11981
- Equations for small signal sinusoidal operation of intrinsic field effect transistor, considering physical principles of operation of device 02 p0216 A67-12071
- Performance characteristics of transistorized synchronous demodulator 02 p0219 A67-12113
- Nondissipatively regulated variable frequency DC to DC converter with variable on time and variable off time 02 p0183 A67-12117
- Epitaxial transistor array on common heat sink with and without emitter series resistance, examining second breakdown mechanism 02 p0222 A67-12652
- Transistor failure in inductive load circuits such as TV horizontal deflection circuits and relation to secondary breakdown data 02 p0223 A67-12656
- High input-low output transistor follower circuit with voltage gain approaching unity 02 p0223 A67-12795
- Graphical derivation of switching trajectories of transistor-tunnel diode logic circuits 03 p0389 A67-12803
- Equivalent circuit for four-layer dinistor with frequency independent elements, noting dependence of network elements on dinistor parameters 03 p0377 A67-13238
- Dinistor trigger circuits with counting input, discussing flip-flop circuits 03 p0377 A67-13239
- Aluminum-titanium dioxide-silicon varactor equivalent circuit, noting measurement of parameters 03 p0377 A67-13240
- Attenuation of background noise and exterior static through use of low impedance links and use of light loading in transistorized assemblies 03 p0379 A67-13389
- Amplifier design using multistage transistor current mode, feedback systems and minimized voltage swings 03 p0386 A67-13977
- Transistor hybrid equivalent circuit of large amplitude sinusoidal voltage used in design of LC oscillators, power amplifiers, etc 03 p0387 A67-13998
- Microwave varactor tuned transistor oscillator design, considering collector base multiplication, oscillation and load matching conditions and theoretical tuning curve 04 p0581 A67-14864
- Traveling wave field effect transistors, discussing method of increasing transconductance and cut-off frequency 04 p0582 A67-15096
- Book on digital transistor circuits in semiconductor devices based on Boolean algebra and logical and switching circuit principles 04 p0622 A67-15268
- Figure of merit as evaluation criterion for HF transistors, using unidirectional available power gain 04 p0585 A67-15501
- Anomalous photocurrent generation in transistors, noting carrier generation and transport processes 04 p0685 A67-15696
- Transient radiation response and permanent radiation damage in monolithic silicon-junction-transistorized integrated circuit 04 p0589 A67-15720
- Steady state analysis of switching circuit using combination of transistors and tunnel diodes, considering temperature effect and thermal stabilization of operating points 05 p0772 A67-16452
- Operational characteristics of transistorized smoothing filter working with parallel transistor 05 p0772 A67-16453
- Generators of sonic and ultrasonic frequencies using thyristors 05 p0773 A67-16458
- Amplitude characteristic in transistorized selective logarithmic amplifier with video output, discussing circuitry of proposed multistage amplifier 05 p0773 A67-16459
- Transient cut-off processes of transistorized switch with LC load 05 p0773 A67-16460
- Three equivalent circuits of transistor mixer 05 p0784 A67-16943
- HF measurements of thin film CdSe transistors, discussing equivalent circuit, stability factor and power gain 05 p0776 A67-17091
- Multiple correlation applications in design analysis of high reliability critical circuits 05 p0777 A67-17249
- Transistor circuit realization of inductance with three transistors and one power supply 05 p0785 A67-17536
- Equivalent circuit for field effect transistor, considering amplifying characteristics of component, noting use of thermal and shot noise 06 p0966 A67-17589
- PCM telemetry system for satellite test vehicle of ELDO program using transistorized printed circuit technology 06 p0957 A67-17613
- Electrodynamics of combined operation of transistors and tunnel diodes in pulsed circuit 06 p0970 A67-18170
- Smoothing filter with output controlled parallel transistors, discussing empirical and experimental formulas and approximate circuit calculation 06 p0971 A67-18215
- Thermal regeneration in power dissipating elements and effects on transistor circuit failures 06 p0971 A67-18245
- Oscillatory process stability in n-circuit transistorized LC oscillators with inductive feedback 06 p0972 A67-18894
- Transistorized circuit modeling high-Q capacitances depending on voltage and having high maximum-to-minimum ratios 06 p0972 A67-18896
- Dependence of first harmonic averaged parameters of transistor on oscillation amplitude in common-emitter circuit in absence of bias current in base circuit 07 p1149 A67-19187
- Amplitudes and phase angles of harmonic components of output current of operating circuits of transistorized magnetic amplifiers 07 p1150 A67-19209
- Gallium arsenide planar technology using starting material obtained by vapor growth, noting doped silicon dioxide technique 07 p1155 A67-19889
- Energy dependence of semiconductor devices with respect to secondary breakdown explained on basis of transient thermal resistance 07 p1156 A67-19895
- Transconductance limitation in FET devices obtained through changes in Shockley theory, noting behavior and design of solid state devices 08 p1300 A67-20335
- Avalanche transistors circuit generating high current fast risetime pulses suitable for driving injection lasers 09 p1510 A67-21642
- Arbitrarily doped four-terminal field effect transistors /large and small signal models/ 09 p1475 A67-22199
- Monte Carlo and direct calculation methods analyzed in connection with microelectronic circuit designs 10 p1610 A67-22978
- Design equations and computer calculated curves to achieve varactor-tuned octave bandwidth transistor oscillators by using transmission line 10 p1613 A67-23412
- Binary compound transistors, calculating parameters using T-shaped equivalent circuits 10 p1613 A67-23459
- Mass production lines for monolithic integrated circuits 12 p1916 A67-25995
- Semiconductor devices for microcircuits, discussing MOS FET, metal base transistor, etc 12 p1918 A67-26208
- Static current amplification factor of transistor dependence on operating conditions in switching circuits 13 p2075 A67-26347
- Upper cut-off frequency and amplitude frequency response curve shape for wideband aperiodic amplifiers, examining five common transistor circuits 13 p2077 A67-26660
- Microminiaturizable transistorized circuit for generating wide frequency range high Q inductances from semiconductor devices for integrated selective circuits 13 p2081 A67-27201
- Transmittance of thin film field effect transistor with equivalent circuit with lumped constants and generalized transfer function of nonparametric amplifier 14 p2286 A67-28586
- Book on theory and practice of transistor circuits covering oscillator theory, transistor noise, frequency modulation, band filter linkage, etc 14 p2290 A67-29007
- Current saturation phenomena in junction-gate field effect transistor 15 p2446 A67-29637
- MOS transistor HF behavior noting phase shift, frequency dependence, etc 15 p2449 A67-29805
- Book on large signal transistor circuits covering device physics and equivalent circuits 15 p2454 A67-30233
- Smoothing filter with output controlled parallel transistors, discussing empirical and experimental formulas and approximate circuit calculation 16 p2635 A67-30481
- Thick film hybrid modules discussed for speed, circuit, power density and versatility 16 p2641 A67-31618
- Resonant gate transistor used in integrated circuits as frequency selector

element for tuning 16 p2642 A67-31724
 problems 16 p2642 A67-31724
 Circuitry of transistorized azimuthal
 supertelescope designed for measurement of
 general ionization component of cosmic
 rays 17 p2854 A67-32097
 Transistor overload in active region
 operated by large pulse trains, discussing
 thermal response and resistance and
 operational frequency intervals 17 p2827 A67-32784
 Radiation-hardened semiconductor
 electronic circuit design, noting radiation
 environment existing in spacecraft nuclear
 generator vicinity 17 p2919 A67-32857
 Amplitude modulation using varicaps and
 p-n junction in transistorized transmitter,
 analyzing HF oscillator 18 p2999 A67-33507
 Universal array of complementary-
 symmetry MOS transistors applied to missile
 and surface radar beam steering phase array
 storage unit 18 p3015 A67-34563
 Electronic circuits containing vacuum
 tubes and transistors analyzed by computer
 method using Bellerts algebra of structural
 numbers 19 p3201 A67-34907
 Bipolar and field effect transistor
 combinations for high gain amplifiers,
 discussing various circuitries 19 p3191 A67-34943
 Basic operating-time contribution to pulse
 behavior of diffused transistor components,
 introducing system function for
 semiconductor barrier-layer component 19 p3195 A67-35580
 Flowgraph models describing relationships
 between thermal and electrical parameters
 of devices and associated circuits 19 p3206 A67-36034
 Design and characteristics of solid state
 UHF transmitters and receivers applicable in
 color TV systems 20 p3395 A67-36249
 Semiconductor negative resistance devices
 to achieve analog to digital conversion 20 p3390 A67-36252
 Planar transistor collector current rise
 time determination with base driven by
 current step function and application
 procedures 20 p3395 A67-36299
 MOS transistor advantages in integrated
 circuits 20 p3395 A67-36320
 Equivalent circuits derived by
 mathematical model from experimental data
 on diffused planar transistor 20 p3396 A67-36378
 Book on transistor electrical
 characteristics, discussing transistor model
 correspondence with real transistors,
 temperature variation effects, etc 20 p3399 A67-37010
 Transistor circuit containing magnetic
 cores with rectangular hysteresis loop
 analyzed for switching processes using
 differential equations 20 p3399 A67-37114
 Transistorized time delay system based on
 measurement of condenser discharge time to
 predetermined voltage 21 p3590 A67-37952
 P-n transistor overcomes bandwidth and
 switching time deficiencies to enhance
 minority carrier transport 21 p3598 A67-38570
 Transistor oscillator design stressing
 output, efficiency and frequency stability at
 maximum load 21 p3598 A67-38602
 Distributed Esaki diode pulse
 characteristics in solid state transmission
 circuit 21 p3599 A67-38609
 Solid state photosensitive devices
 combining p-n diodes and MOS circuitry
 noting application in electrical readout,
 image and pattern detection 22 p3796 A67-39332
 Breakdown temperature of pulsed
 switching circuit using high power
 transistors depends on transistor
 property 22 p3771 A67-39827
 Transistorized LF LC filter with positive
 and negative feedback, analyzing circuit to
 increase Q-factor and narrow passband 22 p3772 A67-39869
 Frequency doubler and divider using
 transistorized synchronized switching phase
 detectors with closed feedback circuit 22 p3762 A67-39872
 Noise factor variations with source
 resistance for MOST in common-gate and
 common-source connections, showing
 advantage of low noise operation 22 p3773 A67-40309
 Transistor parameters effect on
 microwave-circuit performance, tradeoffs and

relation between tradeoffs, circuit
 performance and design 22 p3775 A67-40467
 Temperature dependence of carrier drift
 type transistor characteristic frequency,
 discussing temperature and diffusion
 coefficients 23 p3983 A67-41676
 Unipolar-bipolar transistor hybrids for
 stable temperature independent current
 generators, detailing circuit design 24 p4128 A67-41895
 Power amplifiers using IC, calculating
 average and peak power dissipation by final
 transistors of push-pull circuit with resistive
 and reactive load 24 p4131 A67-42411
 Nuclear radiation damage to circuits
 noting Compton effect, ionization current
 effects, resistance drops, electron-hole pair
 formation, etc 24 p4132 A67-42702
TRANSISTOR LOGIC
 Design balances, tradeoffs and approaches
 to system design of various types of
 transistor-magnetic logic for aerospace
 timing 02 p0216 A67-12014
 Packaging integrated circuit airborne tape
 control unit 12 p1911 A67-25273
 Metal oxide silicon transistors as high
 performance analog switching elements,
 noting design and performance 14 p2281 A67-28018
 Variable-ratio frequency divider using
 integrated circuits of resistor-transistor-
 micrologic type 17 p2827 A67-32798
 Book on analysis and design of digital and
 linear integrated circuits covering transistor
 models, system parameters, etc 21 p3597 A67-38500
 High level transistor/transistor logic 16-bit
 memory element function, characteristics
 and applications 23 p3975 A67-40698
TRANSIT IVA SATELLITE
 Ionospheric electron content measured
 using passage of transit IVA radio beacon
 satellite across view field of observing
 station 12 p1935 A67-25797
TRANSIT SATELLITE
 Electron cloud-like distribution in
 ionosphere shown from phase measurements
 of 162 and 324 mc emissions of Transit and
 Anna satellites [RASSA PAPER 1-10-135] 03 p0417 A67-14246
 Solar cell power systems design and
 control technique for use in satellite
 programs, specifically transit 3B and 4A,
 ionosphere Beacon satellite, etc 23 p3938 A67-41507
TRANSIT TIME
 Transition time dependence between
 avalanche and second breakdown on input
 power to p-n silicon junction, noting thermal
 effects in semiconductors 02 p0222 A67-12650
 Avalanche transit time diode, noting
 dynamic resistance mechanism of formation
 and linear and nonlinear diode behavior 04 p0583 A67-15154
 Small signal negative resistance and
 avalanche region of impact ionization
 avalanche transit time /IMPATT/ diodes,
 particularly Read diodes 05 p0777 A67-17319
 Frequency modes of Gunn effect
 oscillator 05 p0872 A67-17531
 Carrier drift velocity measurements in
 silicon at high electric fields, using time-of-
 flight technique 10 p1690 A67-23167
 HF negative resistance in dielectric diodes
 with high density of shallow traps taking
 into account transit time 14 p2367 A67-28521
 Doping distribution optimum for
 minimizing minority carrier transit time
 through base to improve overall HF
 performance of diodes and transistors 14 p2287 A67-28676
 Avalanche transit time diode, noting
 dynamic resistance mechanism of formation
 and linear and nonlinear diode behavior 15 p2443 A67-29341
 Noise and HF input conductance
 measurement of double-injection germanium
 space-charge-limited diode, noting transit-
 time effect 16 p2637 A67-31034
 Plasma produced transit time delay of
 reflected pulses for collisionless
 inhomogeneous plasma 17 p2810 A67-32070
 Superconducting and superheated
 metastable state transition to normal state
 by beta irradiation 17 p2912 A67-32270
 Transistor current-voltage characteristics
 when controlled by space-charge and transit-
 time effects, obtaining large negative
 conductances at HF 17 p2824 A67-32302
 IMPATT diode operation based on
 combination of avalanche-current

multiplication and transit-time delay to
 produce negative resistance 17 p2824 A67-32332
 Airport terminal planning for Tampa
 eliminating long walk, using circular
 multistory structure with handling
 equipment for passengers and baggage
 [SAE PAPER 670319] 17 p2835 A67-32980
 Computing transits of outer planets
 /Jupiter to Pluto/ over solar disk, as seen
 from another outer planet 17 p2948 A67-33095
 Cooling and illumination effect on Gunn
 oscillators resulting in abrupt shift from
 transit-time frequency mode to higher
 frequency 19 p3305 A67-35628
 Josephson junction as switching device or
 logic element, discussing tunneling states
 and transition characteristics 22 p3865 A67-40437
TRANSITION
 S BOUNDARY LAYER TRANSITION
 S ELECTRON TRANSITION
 S FORBIDDEN TRANSITION
 S OPTICAL TRANSITION
 S TRANSIT TIME
TRANSITION ELEMENT
 SA CHROMIUM
 SA COBALT
 SA HAFNIUM
 SA IRIIDIUM
 SA MANGANESE
 SA MOLYBDENUM
 SA NICKEL
 SA PALLADIUM
 SA PLATINUM
 SA RHENIUM
 SA RUTHENIUM
 SA SCANDIUM
 SA TANTALUM
 SA TITANIUM
 Powder metallurgy techniques and solid
 state reactions in alloy constitution research,
 examining advantages of sintering method
 over modern melting methods 01 p0099 A67-10711
 Ti, Zr and La boride thin films by
 chemical conversion of thin films of these
 metals with gaseous boron hydrides 02 p0287 A67-11715
 Superconducting critical temperatures of
 nonstoichiometric transition metal carbides
 and nitrides, correlating data with valence
 electron concentration 03 p0491 A67-13256
 High pressure hot-pressing fabrication of
 transition metal diborides without lower-
 melting metal additives 03 p0450 A67-13308
 Diffusion and melting techniques used to
 determine effect of Ni, W, Ti and Ta
 impurities on lifetime of minority carriers in
 n-base of silicon p-n junctions 05 p0865 A67-16967
 Physical properties of transition elements,
 alloys and compounds in terms of stable
 electron configurations, using Samsonov
 theory 06 p1035 A67-17844
 Chemical bonds formation during
 interaction between individual elements
 explained by total valence band energy
 theory 06 p1035 A67-17845
 Partial sum rules for transition and noble
 metals having resonant d state 07 p1238 A67-20216
 S-D interaction in electronic band
 structure of transition metals represented
 by model Hamiltonian, treating copper band
 structure 07 p1238 A67-20217
 Equilibrium and elastic properties of
 triangular and parallelogram bending
 elements for plate and shell networks,
 discussing transition element and matrix
 force methods 08 p1417 A67-20553
 Correlation of physical properties of
 transition elements with atomic electron
 structure, noting energetic stability of
 configurations 09 p1517 A67-21878
 Stabilization of high temperature
 beryllium allotropes through transition
 element addition, noting appearance of
 superconductivity 10 p1688 A67-22890
 High temperature thermal expansion of Ti,
 Zr, Hf, Nb and Ta diborides 10 p1697 A67-23380
 Exchange model of zero bias tunneling
 anomalies, discussing Hamiltonian,
 interference magnetic scattering and metal
 junctions 10 p1691 A67-23400
 Single conduction band approximation of
 nature of increase with temperature of
 thermal conductivity of ZrC and NbC in
 terms of scattering and Fermi

energy 11 p1804 A67-23902
 Probable upper limit of critical field for ternary and higher order ductile transition metal superconducting alloys 11 p1850 A67-24925
 Low temperature deposition of amorphous films of transition metals and alloys, noting atomic arrangement, comparing with case of metals condensed in crystalline state 12 p1982 A67-25451
 Electronic structure and electrophysical properties of d-transition metal sulphides 12 p1986 A67-26096
 Effect of V, Zr, and Y additions on mechanical properties of 1 mm sheet molybdenum 13 p2130 A67-26392
 Conductivity, temperature dependence, thermal EMF Hall constant, thermal conductivity and resistivity of aluminides of transition metals 13 p2131 A67-26471
 Approximate quantum numbers for d-band states in transition metals 13 p2179 A67-27155
 Semiconductor-to-metal transitions in transition metal compounds 13 p2181 A67-27165
 Ion temperature, cell temperature, cell voltage and current in electrolytic technique for reproducible growth of molybdenum /IV/ oxide crystals 15 p2533 A67-29295
 Electron-phonon interaction calculation for solid state transition metals justifying matrix element presented and using augmented plane wave 16 p2731 A67-31447
 X-ray K-absorption spectra of titanium, vanadium germanium in germanides 16 p2691 A67-31594
 Physical properties of transition elements, alloys and compounds in terms of stable electron configurations, using Samsonov theory 20 p3490 A67-37586
 Chemical bonds formation during interaction between individual elements explained by total valence band energy theory 20 p3490 A67-37587
 Ti isotopes nuclear magnetic resonance in hexagonal Ti metal showing d-like conduction-electron states at Fermi level by spin-lattice relaxation time 24 p4203 A67-42109

TRANSITION LAYER
SA BOUNDARY LAYER TRANSITION
 SA EKMAN LAYER
 Laminar, transitional and turbulent boundary layer flows with adverse pressure gradient on axisymmetric blunted conical flared body at Mach 10
 [AIAA PAPER 66-493] 06 p0943 A67-18844
 Spatial variation of quasi-Fermi potentials in symmetrical step and linearly graded p-n junctions 09 p1556 A67-22201
 Outer ionosphere and transition into interplanetary space noting altitude and structure characteristics 11 p1786 A67-24261
 Plasma conductivity measurement based on Hall current and Hall voltage relation to electrical resistance 11 p1839 A67-24424
 Laminar turbulent transition of nonisothermal incompressible forced flows in pipes measured for several working fluids and temperatures, using Reynolds number as criterion 11 p1781 A67-24574
 General model for semiconductor-to-metal transition 13 p2180 A67-27163
 Metal-to-semiconductor transition measurements of hydrostatic pressure shift and uniaxial stress of temperature 13 p2180 A67-27164
 Rotating vortex flow and transition phenomena in conical diffuser
 [AIAA PAPER 66-426] 14 p2240 A67-28109
 Transverse secondary flow effects on laminar turbulent transition of free axisymmetric jet 14 p2303 A67-28328
 Steady state magnetic field in transition region between magnetosphere and bow shock by MHD equations, noting solution by approximation method 17 p2951 A67-33186
 Channel flow transition to jet flow, discussing turbulence determination in flow boundary layer as Reynolds number function 18 p3028 A67-34218
 Transition in oscillating boundary layer flows studied for various parameters effect 19 p3209 A67-35413
 Nonequilibrium-transition patterns of quasi-one-dimensional dissociating-gas flow through diverging supersonic nozzle 19 p3211 A67-35759
 Plane and axisymmetrical boundary layer characteristics computation, estimating transition region length 20 p3424 A67-37344

Flute instability of maximally inhomogeneous rarefied plasma cylinder with thick transition layer amounting to two Larmor radii 21 p3667 A67-38371
 One-component nonviscous nonheatconducting perfect gas in container with gaseous adsorption at boundary, noting acoustic oscillation instability for certain frequency disturbances 22 p3836 A67-39719
 Structural stability of welded joints of chromium steel used in power plant construction examined for structural stability 23 p4019 A67-41077

TRANSITION POINT
 Superconducting transition temperature and critical field curve for pure Ga single crystals 01 p0130 A67-10153
 Contact effect between superconductor and normal conductor and between two different superconductors, noting transition temperature 02 p0291 A67-11740
 Shifts in normal state conductivity and superconducting transition temperature due to charge carrier changes in In, Tl and Sn films 02 p0291 A67-11741
 Electron density effect on transition temperature of superconductivity, considering tantalum 02 p0291 A67-11742
 Superconductivity in strontium titanates and similar polar substances with transition temperature accounted for by electron-phonon interactions 03 p0491 A67-13259
 Electron density effect on transition point of superconductors 03 p0494 A67-13508
 Gennes and Werthammer method generalization, developing theory of transition temperature of superconducting superposed films 03 p0499 A67-13874
 Variation of transition Reynolds number with wall to recovery temperature ratio at hypersonic speeds, comparing transition measurements with and without Pitot tube 04 p0604 A67-14836
 IR optical properties of vanadium dioxide above and below transition temperature 05 p0860 A67-16380
 Superconductivity in aged Zr-Nb alloys, noting transition temperature increase of quenched alloy upon aging 05 p0828 A67-16469
 Steady state creep stress in shells under uniform internal pressure derived, using transition theory of Seth 05 p0920 A67-16722
 Microwave surface resistance of type II superconductors, from simultaneous measurements of real part of surface impedance and magnetization 05 p0871 A67-17375
 Electric conductivity of hexamethylbenzene explained by molecular interaction conductivity change at transition point 05 p0871 A67-17379
 Isotope effects on superconducting transition temperature of molybdenum boride and tungsten boride 06 p1047 A67-17642
 Limitation of Froehlich-Terreaux quasi-superconducting state, discussing experimental and observational difficulties 06 p1047 A67-17654
 Plane vortex flow in vicinity of orthogonality point of sound line to velocity vector 06 p0936 A67-17738
 Superconducting transition temperature of thin film, showing growth of temperature and decrease in film thickness due to phonon electron interaction 06 p1049 A67-17886
 Tests at Mach 8 on cone, analyzing effect of roughness elements and variable entropy on transition and heat transfer distribution [AIAA PAPER 67-132] 06 p0940 A67-18357
 Transition from laminar to turbulent boundary layer flow at hypersonic Mach numbers, noting measurement techniques [AIAA PAPER 67-130] 06 p0989 A67-18474
 Gap anisotropy increase in superconducting thallium transition temperature dependence on lattice defect density due to hydrostatic deformation 07 p1235 A67-20128
 Remedies for deficiencies in approximations near transition point in asymptotic methods used for estimates of solutions to differential equations governing axisymmetric vibrations of thin elastic shells 08 p1414 A67-20346
 Superconducting properties of vanadium silicide noting high transition temperature, electron-phonon interaction, sound absorption, etc 08 p1369 A67-20990

Field effect transistor transition from pentode to triode-like characteristics with increasing drain bias 11 p1759 A67-24138
 Transition temperatures of Be compounds, noting evidence for strong coupling to Mo localized mode from observed isotope effect 11 p1846 A67-24582
 Neel temperature in NiO and MnO with divalent Fe measured using Mossbauer effect 12 p1985 A67-25844
 Low temperature deuteron irradiation effect on type II superconductors noting atomic displacement, resistivity increase and transition temperature decrease 12 p1985 A67-25845
 Transition temperature change for thin tin and thallium superconducting films after deposition of dielectric substances 13 p2182 A67-27360
 Superconductivity of Nb₃Al-Mo₃Al binary system 13 p2184 A67-27631
 Autoelectric emission in superconductors near transition point noting variation with total field energy and normal component 14 p2370 A67-28673
 HF localized and LF resonant impurity modes valence effect on energy gap and transition temperature in isotropic superconductors 14 p2370 A67-28720
 Perpendicular critical magnetic fields of superconducting aluminum, tin and gallium small grained films examined for superconducting transition temperature enhancement 14 p2373 A67-28860
 Rarefied gas flow interaction with sphere analyzed using multiple wave interferometer, noting transition region from continuous medium to free molecular flow 16 p2656 A67-30453
 Superconducting niobium and tantalum compounds investigated for maximum transition temperatures 16 p2726 A67-30818
 Critical parameters for vanadium-niobium alloys superconduction, giving curves for transition temperature and measuring critical electric fields 17 p2874 A67-32973
 Transition temperature of phonon-coupling superconductor merged with that of type II superconductor critical field to obtain strong coupling corrections to critical field 17 p2925 A67-33378
 Alpha particle irradiation effect at liquid-helium temperature on transition temperature of superconductive tin, indium and thallium foils 17 p2926 A67-33405
 Negative glow diffusion model evaluated via generation function determined by discharge voltage and dependence of reduced length of cathode fall 18 p3085 A67-33668
 Thin films deposited onto substrates cooled to low temperatures investigated for transition temperature in structures of superconductor-dielectric-superconductor 18 p3101 A67-33989
 Superconducting transition temperatures and low field magnetization of ceramic mixed Ba, Sr and Ca-Sr titanates, showing particle nature of specimens 19 p3302 A67-35037
 Superconductivity transition temperatures of metal carbides, showing stoichiometry as main feature for maximum temperature 19 p3303 A67-35040
 Possibility of pressure destroying superconductivity in various metals, studying transition temperatures, critical pressures, etc 19 p3303 A67-35043
 High superconducting transition temperatures in molybdenum carbide compounds stressing crystal structures 19 p3245 A67-35729
 Superconductivity of Nb₃Al-Mo₃Al binary system superconductivity of Nb₃Al-Mo₃Al binary system 21 p3685 A67-38828
 Steady state solutions for system of partial differential equations with two independent variables describing small perturbations of transonic gas flow near transition point 22 p3844 A67-39391
 Transition temperature, Knight shift and NMR line width variation in V-Au compounds as function of atomic ordering 22 p3858 A67-39520
 Fracture theory for amorphous high polymers below glass transition temperature, considering viscoelastic effects on structural defect stress 22 p3824 A67-39740
 Reflectivity spectra of YIG and YGG crystals, observing YTG structure attributed

to charge transfer enhanced crystal field transitions reflectivity spectra of YIG and YGG crystals, observing YIG structure attributed to charge 22 p3863 A67-40238

Hydrostatic and uniaxial compressional stress effects on strontium titanate superconductive transition temperature 22 p3863 A67-40244

Superconducting devices utilizing transition, zero resistivity and diamagnetic properties of materials in that state 22 p3808 A67-40398

Positive isotope effect on superconducting transition temperature of alpha uranium 23 p4044 A67-41439

Asymptotic solutions of eigenvalue problem with two transition points applied to Graetz problem involving heat transfer in fluid 23 p4083 A67-41668

Tensile to shear transition behavior of fatigue crack fronts during cycling of sheet materials, noting correlation of shear with crack stress intensities 24 p4170 A67-41950

TRANSITION PROBABILITY

Mean powers of r , sum rule and improved transition integrals computed for effective quantum number range up to 8.5, using Coulomb approximation wave functions 01 p0112 A67-10142

Radiative transition probabilities between laser vibrational levels of carbon dioxide, noting relaxation time and dipole moment 02 p0252 A67-11891

Line profile in one-electron approximation compared with impact approximation 02 p0270 A67-12521

Franck-Condon factors and transition probabilities of electron oscillatory transfers in diatomic molecules 03 p0471 A67-13314

Fe spectrum energy levels for various subshell configurations, calculating oscillator strengths and transition probabilities 03 p0511 A67-13649

Saturable optical absorption of light flux from high intensity Q-switched ruby laser 05 p0822 A67-16677

Gaseous laser output expressed in single or two-line oscillations as function of pumping rates and transition probabilities, considering concept of equivalent network 05 p0825 A67-16979

Transition probabilities for S I multiplets measured from arc spectra running through sulphur chloride liquid vortex 06 p1038 A67-17656

Information criteria for threshold setting in simple binary hypothesis tests 06 p0962 A67-17948

Correction of calculations of Einstein A coefficient for transition of OH 09 p1532 A67-21989

Oxygen IV transition multiplet relative intensities for measuring decay rates, using triply ionized emitters 10 p1678 A67-22718

Continuous spectra of atomic gases and low temperature plasma, analyzing photolionization cross section and electron transitions in neutral atom field 10 p1682 A67-23067

Cosmic ray nucleon interaction with high energies, estimating transition probability and interaction cross section of baryon in passive state 10 p1703 A67-23586

Information theoretic derivation of limit theorem for Markov chain with countable number of states and constant transition probabilities 11 p1770 A67-24421

Measuring atomic radiation and collision cross section coefficients of plasmas 11 p1839 A67-24551

Resonance transition probabilities in intermediate coupling for some neutral nonmetals, noting radiative lifetime measurements by phase shift 12 p1968 A67-26246

Dipole transition integrals for nonmetal resonance transitions 13 p2160 A67-26442

Absolute oscillator strengths of three titanium resonance lines from absorption measurements in atomic beam 14 p2351 A67-28581

Laser transition absorption cross section at room temperature for neodymium ion in yttrium-aluminum garnet determined by two methods 14 p2331 A67-28713

Processes influencing radiative decay in compound semiconductors 15 p2536 A67-29634

Franck-Condon factors and transition probabilities of electron oscillatory transfers in diatomic molecules 16 p2703 A67-30490

Partial Franck-Condon factors and r

centroids for zirconium oxide molecule, noting transition probabilities 16 p2704 A67-31174

Coupling between free electron and molecular vibrational temperatures in plasma environments, noting energy distribution, application to MHD generation, etc 17 p2894 A67-32150

All Markov transition functions in denumerable state space satisfying prescribed initial condition with given matrix 17 p2878 A67-32734

Homogeneous continuous Markov process without discontinuities of second kind and form of infinitesimal operator 17 p2878 A67-32735

Probabilities for two-photon absorption processes induced by coherent and thermal light when acting on atomic system 17 p2870 A67-33317

Probability of tunneling across impurity level of p-n junction 18 p3099 A67-33695

Diatomic gas vibrational relaxation by master equation analysis, discussing quasi-steady state vibrational population distribution and transition probability increases 18 p3081 A67-33782

Transition probabilities for molecular collision excitation by differential equation matrix, approximations, perturbation theory, etc 18 p3081 A67-33785

Nitrogen oxide and carbon dioxide high pressure unimolecular decomposition noting high pressure rate constants, transition probabilities, potential surface shape, etc 18 p3082 A67-33793

Argon plasma radiation emission and absorption measurement, determining transition probabilities 18 p3091 A67-34732

Absolute transition probabilities, Stark widths and shifts of S I and S II lines determined experimentally 19 p3266 A67-36089

Electronic energy transfer between metastable argon and nitrogen molecule, noting rotational enhancement 20 p3487 A67-36228

Excitation temperature of low pressure magnetically confined argon plasma, using spectroscopic transition probability 20 p3499 A67-37028

S-matrix computations for quantum transitions, considering close coupling case of homonuclear diatomic molecular rotational excitation 21 p3659 A67-38005

Absolute measurement of Ar II transition probabilities using tungsten ribbon lamp as calibration standard 24 p4194 A67-41888

TRANSLATIONAL MOTION

Translational motion of two rotating spherical symmetrical bodies in general relativity theory 02 p0268 A67-12490

Calculating shock wave separation and relaxation velocities for supersonic airflow past sphere 03 p0349 A67-12863

Influence on stability of masses which are in relative motion with respect to projectile determined, noting engine thrust effect on attitude control system performance 03 p0517 A67-13027

Theoretical analysis of translational motion and angular motion of flow induced vibration of blade suspended in flow channel [ASME PAPER 66-WA/NE-1] 04 p0712 A67-15372

Translational motion of two rotating spherical symmetrical bodies in general relativity theory 10 p1680 A67-23358

Plane electromagnetic wave reflection and refraction by semilinear dielectric medium moving uniformly parallel to surface analyzed for arbitrary incidence plane orientation 11 p1820 A67-24909

Finite displacements of solid body under effect of internal rotating flywheels and translational motion of masses 15 p2518 A67-30169

Existence and stability of rectilinear translation motions of blunt body submerged in potential flow of incompressible fluid at rest at infinity 18 p3027 A67-34183

Zero moment elliptical paraboloid translational shell under uniformly distributed load, reducing solution to Dirichlet problem 20 p3539 A67-36924

Swell generation by means of flat paddle board in translational motion 22 p3783 A67-39646

TRANSLATOR

Avalanche transit time diode used as sideband translator and combination local

oscillator-mixer at X-band 03 p0381 A67-13666

TRANSLUCENT MATERIAL

Translucent material /Zytrite/ obtained from cubic phase stabilization of Y and Zr alkoxides at low temperatures, noting high surface activity 24 p4175 A67-42373

TRANSMISSION

SA AUTOMATIC PICTURE TRANSMISSION /APT/

SA COAXIAL TRANSMISSION

SA COHERENT TRANSMISSION

SA DATA TRANSMISSION

SA FACSIMILE TRANSMISSION

SA HEAT TRANSMISSION

SA LIGHT TRANSMISSION

SA MICROWAVE TRANSMISSION

SA MULTIPLEX TRANSMISSION

SA NEURON TRANSMISSION

SA POWER TRANSMISSION

SA PULSE TRANSMISSION SYSTEM

SA RADAR TRANSMISSION

SA RADIO TRANSMISSION

SA SATELLITE TRANSMISSION

SA SIGNAL TRANSMISSION

SA SOUND TRANSMISSION

SA TELEVISION TRANSMISSION

Direction finder accuracy optimization, considering automatic tracking of target angular coordinates 01 p0024 A67-10721

Instability of amplification factor and stability of transmission coefficient of multistage transistorized amplifier without feedback 05 p0772 A67-16454

Transmission probability describing free molecular flow through vacuum systems obtained via Monte Carlo program 09 p1488 A67-22104

Mechanical systems with automatic retardation /self-braking/ for application to brake mechanism and frictional transmission, analyzing Painleve paradoxes 10 p1680 A67-23607

Impedance and transmission matrices concepts applied to mechanical systems vibration, presenting formulations properties and interrelationships 19 p3261 A67-34960

TRANSMISSION EFFICIENCY

Harmonic linearization of logic law control systems, deriving complex equivalent transmission coefficient for nonlinear part of circuit with variable structural elements 01 p0044 A67-10241

Lumped-constant filters whose bandpass depends only on one parameter of transmission coefficient, having lower bandpass for given transient process delay time 03 p0380 A67-13582

Automatic system auto-oscillations when transmission coefficient of nonlinear part of system depends on amplitude and frequency of input signal 05 p0782 A67-16323

Number transmission coefficients for isotropically incident electrons determined for spacecraft shield design [AIAA PAPER 66-511] 05 p0906 A67-17219

Device measuring uniaxial pressure effect on transmission factor of semiconductors in low absorption region 09 p1551 A67-21657

Waveform independent condition for transmission coefficient in linear time-independent transmission system to provide upper limit to signal distortion 10 p1620 A67-23572

Fourier transform for exact solution of current distribution and input admittance of infinite cylindrical dielectric-coated antenna 11 p1757 A67-23972

Transmission and reception properties of equatorial slot antenna on plasma clad reentry sphere 11 p1757 A67-23973

Optical configuration for long distance laser beam transmission determined from truncated Gaussian aperture distribution radiation patterns 11 p1754 A67-24724

Transient response in closed transmission systems evaluated and compared to time optimum process 13 p2087 A67-26614

Single-band radio transmitters and receivers and other types of advanced channel diversification and multiplex reception 14 p2273 A67-28861

LF and HF single stage RC filters with steep frequency characteristic slope in transition region 14 p2289 A67-28863

Transmission noise control to achieve helicopter cabin noise levels comparable to fixed wing jet aircraft, discussing system phasing of planetary gears [ASME PAPER 67-DE-58] 14 p2328 A67-28883

Magnesium fluoride double Rochon prism used as polarizer or analyzer in vacuum UV

wavelengths 15 p2491 A67-30425

Transmission coefficient associated with internal reflection from absorbing surface layer derived from reflection coefficient, noting relation to 17 p2883 A67-32204

Absorption 17 p2883 A67-32204

Automatic system auto-oscillations when transmission coefficient of nonlinear part of system depends on amplitude and frequency of input signal 18 p3017 A67-33875

Threshold characteristics of systems for multistate orthogonal transmission of coded analog signals in communication systems 18 p3000 A67-34023

Laser mirror transmissivity optimization in high power optical cavities noting reflection coefficient selection 19 p3241 A67-35701

Digital telemetry system for maximum transmission efficiency of measurements performed on space vehicle 20 p3394 A67-36245

Frequency multiplier operating from 10-30 GHz with easily tunable construction, obtaining lossy element influence approximation 20 p3398 A67-36863

Flat-top pulse waveform with high transmission efficiency, confined spectra and good electromagnetic compatibility 20 p3388 A67-37654

Diamant launcher transmitter characteristics noting anomalies during first two firings 21 p3581 A67-38226

Transmission buffer overflow prevention in telemetry data compressors using adaptive queueing control system 21 p3586 A67-38956

Crossed field cascade tubes as frequency oscillators and microwave generators, discussing improved performance and interaction efficiency of devices 22 p3775 A67-40559

TRANSMISSION LINE

SA ANTENNA COUPLER

SA COAXIAL CABLE

SA DELAY LINE

SA FLUID TRANSMISSION LINE

SA WAVEGUIDE

HF conducted and radiated RF interference suppression by dielectric and magnetic absorption, pseudoresonant or interfacial loss and artificial skin effect 01 p0024 A67-10500

Microwave swept frequency measurements on RF transmission line systems and development of VSWR and insertion loss test set 01 p0039 A67-11038

Waveform coefficient variation F-matrix analysis of electromagnetic wave propagation in light waveguide with gas lens, considering field distribution and impedance analogy 01 p0026 A67-11237

Gunn effect domain traveling wave parametric amplifier pumped by periodic impedance variations in boundary conductor of microstrip transmission line 01 p0040 A67-11309

Constant phase local oscillator distributing signals for radio telescope, measuring phase length of transmission line 02 p0212 A67-11608

Shielded coupled strip transmission line with three center conductors, noting electrical behavior, cross section dimension evaluation from characteristic immittances, etc 02 p0193 A67-11777

Synthesis of TEM directional couplers and fixed phase shifters consisting of multiple parallel coupled quarter wave sections 02 p0214 A67-11778

Wideband elliptic-function band-stop transmission line filter design, computing characteristic impedances of filter element 02 p0214 A67-11779

Reflection measurements with broadband FM using long transmission lines 02 p0193 A67-11783

Characteristic impedance of TEM mode transmission lines, extracting upper and lower bounds on finite difference solution of Laplace equation 02 p0194 A67-11784

Matrices of scattering transmission wave and normed cascade parameters of linear passive 2/m plus m/ terminal networks 02 p0221 A67-12528

Epitaxially grown junction as nonlinear transmission line 03 p0379 A67-13294

Computer and curve tracer method to generate photo masters for printed circuit microwave antennas, transmission lines and filters 03 p0383 A67-13790

Transmission line antenna tunable over

greater than octave

bandwidth 03 p0384 A67-13847

Bar line theory for electromagnetic wave propagation in system of triperiodic parallel multiwire lines 03 p0387 A67-14094

Two types of slit-coupled strip transmission lines especially useful for realization of multisection components, using printed circuit techniques 04 p0592 A67-14862

Millimeter wavelength transmission line deficiencies reduced by using channeling systems in form of elastic dielectric tape on which are mounted thin metallic strips 04 p0575 A67-15167

Scattering matrix properties of symmetrical octupoles 04 p0586 A67-15673

Pneumatic transmission line model for use in fluidic control systems, noting nomographs determining gain-vs-frequency curves 05 p0753 A67-16237

Parametric transformation of spectrum of video pulses in transmission line 05 p0762 A67-16359

Small signal admittance parameters of field effect transistors treated as analog RC transmission lines 05 p0777 A67-17298

High speed digital computer packaging for minimum transmission line wire length, backplane, module connections and maximum computation speed 05 p0778 A67-17455

TEM mode coupling between transmission lines applied to wideband directional couplers 06 p0969 A67-18118

Equivalent circuit synthesis for microwave band pass filter design consisting of interdigital or comb structure EM line-coupled resonators 07 p1149 A67-19132

German book on transmission of communications including transmission methods and shapes, signals, radio relays, terminal devices, etc 07 p1140 A67-19337

Open air lines and cables, stressing electric wave propagation along homogeneous and inhomogeneous circuits 07 p1141 A67-19340

Formation and expansion of electromagnetic shock waves in communication lines, using ferroelectric crystals 08 p1295 A67-20824

Miniaturized C-band digital latching phase shifter for combined advantages of waveguide and stripline design 08 p1305 A67-21227

Spatial coherence measurement in 3.2 mm horizontal transmission, considering amplitude and phase fluctuations received in two spaced antennas 09 p1461 A67-21599

Measuring techniques and limitations as related to small reflections in precision coaxial transmission line 09 p1495 A67-21624

Illinois 400-ft radio telescope with compromised branching system and traveling wave system as transmission line 09 p1486 A67-22443

Monostable high speed pulse circuit using tunnel diode and transmission line, noting possibility of cascade connection without coupling elements between stages 10 p1609 A67-22773

Design equations and computer calculated curves to achieve varactor-tuned octave bandwidth transistor oscillators by using transmission line 10 p1613 A67-23412

Delay equalization in UHF range by allpass networks with symmetric three-conductor transmission lines 11 p1760 A67-24231

Transmission line approach for determining input admittance of slotted antenna array covered by dielectric sheet 11 p1782 A67-24293

Nonuniform distributed network problems solved by Lie algebras 12 p1919 A67-25979

Parametric coupling between two waves noting losses 13 p2086 A67-26511

Dynamic characteristics of pneumatic transmission lines in regulation loops noting parameters effects, calculation methods, etc 13 p2055 A67-26799

Microwave design techniques for calculating even and odd mode characteristic impedances of miniature microstrip transmission lines 13 p2071 A67-27445

Multiple internal communications system concept using single coaxial cable handling information transfer by integrated circuits 13 p2083 A67-27448

Flexwell waveguide as low loss flexible microwave transmission line 13 p2084 A67-27581

HF power from transmitters in drop

capsules of tube used for weightlessness experiments, utilizing Goubau transmission line to guide signals toward receiver 14 p2279 A67-27897

Two port power flow analysis using generalized scattering parameters 14 p2287 A67-28625

Frequency doubler using two-diode varactor array to obtain double output power 15 p2442 A67-29176

Impedance and effective dielectric constant analysis for transmission line, with approximate theoretical solutions and experimental verification 15 p2444 A67-29455

Magnetic devices for microwave integrated circuits, discussing ferrite substrate use as medium for microstrip transmission lines 15 p2452 A67-29928

Hybrid microwave integrated circuits, discussing use of planar and passivated chip devices 15 p2452 A67-29929

Perturbation method for solution of linear matrix differential equations subject to initial and two-point boundary conditions applied to transmission lines 15 p2511 A67-30018

Segmented two-stage waveguide-slot scanning antennas with intersegment phase shifters connected in series in transmission line 16 p2637 A67-31026

Statistical behavior of two-way communication system with transmission delay 17 p2811 A67-32115

Impedance measurements in coaxial waveguide systems propagating TEM wave, using precision coaxial line standards and connectors 17 p2815 A67-32605

Microwave direct-coupled cavity filter design using single insertion loss formula for case of Chebyshev equal-ripple characteristic 17 p2828 A67-33084

Coupling factor between microwave resonator and transmission line determined by oscillographic recording of microwave field 18 p3010 A67-33508

Equivalent transmission circuits for electromagnet propagation in birefringent media 18 p3002 A67-34226

Optimal design of RC lines distributed parameter systems using gradient technique and variational calculus 19 p3200 A67-34841

Scattering and transmission parameter methods for semiconductor device measurement, discussing linear integrated circuit test requirement 19 p3191 A67-34944

Strip transmission lines used for microwave circuits noting applications, design data, discontinuity information, etc 19 p3191 A67-34945

Coaxial and strip-line passive microwave components stressing design of hybrid junctions, microwave mixers, filters, etc 19 p3195 A67-35549

Nonlinear interaction between two waves of multiple frequencies in communication line, nonlinear line capacitance being periodic function of line length 19 p3185 A67-36021

Propagation behavior analyzed for fundamental mode of parallel plate waveguide 21 p3597 A67-38566

Precursor waves in electromagnetically driven shock tube explained by considering tube as electromagnetic transmission line [AIAA PAPER 67-694] 21 p3613 A67-38723

Aircraft circuit and installation requirements referring to short time characteristics of cables and effect on circuit protection, coordination and weight saving 21 p3572 A67-39072

Design, performance and development of aircraft wiring cables noting need for high temperature operation 21 p3572 A67-39073

Characteristic impedance of waveguides from equivalent voltage and current definitions 22 p3765 A67-39212

Capacitance between strands of braided cable composed of identical insulated conductors 22 p3747 A67-39340

Wave-like behavior of precursor electron density front in electromagnetic shock tubes explained via transmission line model 22 p3850 A67-39711

S-band rectangular digital phase shifter combining advantages of waveguide design with compactness of strip transmission line structure 22 p3773 A67-39909

Cylindrical antenna admittance taking into account antenna to coaxial line junction geometry, using magnetic current mathematical model 23 p3980 A67-41205

- Currents in load impedance of transmission lines near cylindrical scatterer noting antenna field equations 23 p3981 A67-41209
- Propagation of signals in transmission lines with distributed capacitance and conductance for nonlinear parameters 23 p3982 A67-41396
- Surface wave propagation around sharp corners in single wire transmission lines, calculating and measuring radiation loss and pattern 24 p4119 A67-41971
- Transmission behavior of double tuned band filters with frequency dependent feedback and stagger tuning 24 p4129 A67-42206
- Errorless code transmission in specific nonbinary cyclic channels, describing effective decoding process 24 p4136 A67-42409
- Finite difference solution accuracy for potential gradient along conductor boundary near reentrant corner of thin plate 24 p4131 A67-42447
- Radio noise data compared for transmission lines, automotive traffic and RF stabilized arc welders 24 p4123 A67-42718
- TRANSMISSION LOSS**
- Intrinsic damping and eddy current-limited domain wall mobility in Ni-Fe alloy ferromagnetic thin films 02 p0298 A67-11890
- Transmission loss for ionospheric propagation over 4000 km path measured at several frequencies in HF band 05 p0760 A67-16005
- Transmission methods in satellite communications and power level decrease by noise reduction 09 p1463 A67-21758
- VLF transmission loss calculated from spectral components of atmospherics arriving from within adjustable azimuthal direction 09 p1464 A67-22442
- Radio blackout extent from simplified calculation of average sheath power loss for typical Apollo reentry trajectory 15 p2434 A67-29168
- Transmission decrease of various aqueous solutions under ruby laser irradiation 19 p3240 A67-35420
- Approximate method for evaluation of processing loss in delay line MTI receiver 22 p3758 A67-39211
- Systematic design of TEM equal stub admittance filters on basis of insertion loss 22 p3773 A67-40061
- Dissipation loss equation solved by graphic form for ripple values of Chebyshev band pass filters 22 p3774 A67-40344
- Laser output power determination technique by rotating plane parallel wafer in resonant cavity to vary value of total losses 22 p3817 A67-40412
- Mutual admittance of infinite conducting slot antennas covered by dielectric layer and impedance sheet, noting losses effects on waveguide modes 24 p4133 A67-42818
- TRANSMITTANCE**
- SA SCATTERING**
- Optical transmittance of fused silica at elevated temperatures, showing shift in UV to IR absorption with increasing temperature 01 p0138 A67-11074
- Twofold phase modulation in meters of microwave reflection and transmission coefficients 08 p1295 A67-21276
- Ruby laser cavity losses measurement by Fabry-Perot resonance 10 p1662 A67-22740
- Statistical band model applied to NO fundamental vibration band, discussing transmittance measurements and validity of linear region criterion 19 p3266 A67-35681
- Spectral transmittance of mixture of carbon monoxide and nitrous oxide for overlapping absorption bands 19 p3266 A67-35696
- TRANSMITTER**
- SA MULTICHANNEL TRANSMITTER**
- SA RADIO TRANSMITTER**
- Solid state high power LF and VLF telemetry transmitters, considering power amplifier design, RF output network, cooling systems, etc 02 p0218 A67-12106
- Satellite-borne transmitter operating at 136 MHz 07 p1151 A67-19523
- Instrument landing system transmitter monitors for automatic blind landing, noting near field monitors and internal monitors 07 p1222 A67-19654
- Omega navigation system composed of eight transmitters will give worldwide coverage on frequencies 10.2 kc and 13.6
- kc 09 p1527 A67-22627
- Parallel operation of same frequency transmitters on common antenna examining several designs 16 p2837 A67-31003
- Frequency modulated transmitter and receiver for audio high speed data transmission including discriminator for analyzing and distinguishing waveforms 20 p3379 A67-36247
- Diamant launcher transmitter characteristics noting anomalies during first two firings 21 p3581 A67-38226
- RF generation in VLF/LF thyristor transmitter for applications in long distance communications and navigation 22 p3771 A67-39842
- Logic gate with coupled integrated circuit transmitters 23 p3977 A67-40662
- TRANSOCEANIC COMMUNICATION**
- User reaction test results for comparison of telephone quality via Early Bird and via cable circuits based on callback interviews, service observations and circuit rejection counts 06 p0959 A67-17666
- Subjective evaluation of telephone communications via Early Bird satellite and cable circuits 06 p0959 A67-17667
- VHF and UHF communications between transoceanic commercial aircraft and ground stations by means of aeronautical communication satellites 06 p0961 A67-17701
- Transoceanic aircraft control and communication via satellite 09 p1466 A67-22641
- TRANSONIC AIRCRAFT**
- Frequency response of longitudinal control transmission of transonic aircraft 19 p3176 A67-35570
- TRANSONIC COMPRESSOR**
- Transonic axial flow compressor blade profile design, with incidence and deviation rules incorporating thickness and Mach number effects [ASME PAPER 67-GT-47] 11 p1742 A67-24808
- TRANSONIC FLIGHT**
- Semilempirical methods of spillage drag prediction for two-dimensional supersonic inlets operating in transonic flight [AIAA PAPER 67-449] 18 p2982 A67-33924
- TRANSONIC FLOW**
- Transonic plane gas flow equations with algebraic self-similar solutions used for analysis of flow in various nozzles 02 p0178 A67-11951
- Plane transonic gas flow past symmetrical convex profile at zero angle of attack along axis of channel with parallel walls 03 p0352 A67-13620
- 7-ft-diam shock tube for transonic and supersonic aerodynamic testing 04 p0598 A67-15254
- Integral representation for transonic flow about thick airfoils obtained from equations for two-dimensional inviscid flow and locally surface-orthogonal shock waves [AIAA PAPER 67-3] 06 p0939 A67-18331
- Existence or nonexistence of continuous shockless transonic flow around symmetric wing profile, using Oswatitsch integral equation 06 p0942 A67-18586
- Near-field solution for nonequilibrium transonic flow around corner near transonic-frozen flow field 06 p0942 A67-18587
- Unsteady aerodynamic forces on thin wing oscillating in transonic flow, discussing acoustic ray paths and signal transmission times [AIAA PAPER 67-18] 06 p0943 A67-18841
- Cascade flow in axial transonic compressor, examining boundary layer separation condition 07 p1127 A67-20123
- Transonic airfoil problem solved via differentiation of airfoil thickness ratio by infinitesimal perturbation method [AIAA PAPER 66-90] 08 p1276 A67-20563
- Closed form solution expressing transonic flow in idealized stellar wind and spherical accretion problems including viscosity and thermoconductivity effects 08 p1399 A67-21240
- Closed form solution for tricoml boundary value problem, noting application to transonic dynamics 09 p1524 A67-21929
- Unsteady transonic flow of moving compressible gas filling half-space created by sudden rupture of membrane separating gas from vacuum 11 p1743 A67-24962
- Method of characteristics used in solving nonlinear boundary value problem of thickness of delta wing with transonic leading edge 13 p2049 A67-26646

- Existence of continuous transonic flow and model representing velocity distribution by Oswatitsch integral equation 13 p2050 A67-26808
- Transonic gas flow past ducted bodies of revolution indicates shock wave asymptotic attenuation at infinity 14 p2296 A67-27989
- Plane-parallel transonic flow with direct shock wave analyzed for case where Tricoml equation replaces Chaplygin equation 14 p2297 A67-27990
- Heat loss and recovery temperature of fine wires in transonic transitional flow regime, noting experimental and computational results 14 p2405 A67-2817
- Nonlinear inviscid transonic flow in throat of two-dimensional curved nozzle, using approximate method [ASME PAPER 67-FE-11] 14 p2242 A67-28360
- Supersonic inlets for jet aircraft, discussing positioning of terminal shock at intake for most efficient engine performance 15 p2415 A67-29303
- Nozzle type similarity solution to axisymmetric viscous transonic equation, describing shock wave development at nozzle throat 15 p2417 A67-29654
- Firing range for investigating Reynolds number effect on flow around bodies having complex design at transonic and supersonic velocities 16 p2655 A67-31116
- Aeroelastic stability of two-dimensional flat panels in subsonic and transonic flow, noting flutter and divergence 16 p2776 A67-31545
- Transonic blade cascades determined by mixed analog-numerical method starting from velocity distribution law and hodograph method 16 p2594 A67-31710
- Transonic plane gas flow equations with algebraic self-similar solutions used for analysis of flow in various nozzles 17 p2841 A67-33268
- Approximation solution of three-dimensional problems associated with slender wing motion in transonic gas flow with perturbations 18 p2981 A67-33535
- Soviet book on aerodynamic flow calculations of axial flow turbines with subsonic and transonic blade cascade design method 21 p3565 A67-38766
- Steady state solutions for system of partial differential equations with two independent variables describing small perturbations of transonic gas flow near transition point 22 p3844 A67-39391
- Numerical method together with stable difference scheme used to calculate sub-, trans- and supersonic flows in Laval nozzle inverse problem 24 p4091 A67-42160
- TRANSONIC FLUTTER**
- Mach number effect on flutter characteristics of thin cantilever wings analyzed in transonic blowdown wind tunnel, presenting results as flutter speed ratios 05 p0747 A67-16440
- TRANSONIC SPEED**
- Nozzle requirements for hypersonic vehicle at transonic conditions, noting results of tests in high velocity wind tunnel 04 p0545 A67-14536
- Sonic booms attributed to subsonic flight 12 p1895 A67-25936
- Solution of nonlinear flow problems through parametric differentiation 15 p2469 A67-29221
- Downstream flow of shock waves created by wing section moving at speed of sound 16 p2594 A67-31712
- Transonic jet flow study with electric analogy methods, solving Frankl and Tricoml problems for mixed type PDE 18 p2982 A67-33684
- Launch vehicle response in lateral vibration modes to nonstationary random transonic buffeting 22 p3907 A67-40147
- Buffet limit for aircraft wings in transonic region based on boundary layer theory, determining transonic pressure distribution and separation points 23 p3931 A67-41311
- TRANSONIC WIND TUNNEL**
- Mach number effect on flutter characteristics of thin cantilever wings analyzed in transonic blowdown wind tunnel, presenting results as flutter speed ratios 05 p0747 A67-16440
- Transonic wind tunnel studies of ground-wind loads on aeroelastic models of Saturn launch vehicle, investigating structural damping, wind velocity and azimuth

- angle 07 p1257 A67-19371
Continuously operating transonic wind tunnel at Aerodynamic Research Institute noting design, electronic data processing equipment and tunnel calibration 23 p3987 A67-41312
- TRANSPARENCY**
Mechanism regulating total amount of earth and Mars atmosphere transparent to visible and IR radiation 06 p0995 A67-18052
Magnetic recording process in dynamic magnetic storage method with bias magnetization, using Preisch magnetic particle model for case of static transparency in information carrier 07 p1147 A67-19633
Tin oxide films in microscopic quantities on glass and quartz substrates studied for transparency, reflectivity and roughness 12 p1982 A67-25324
Atmospheric aerosol internal changes, studying atmospheric transparency for direct solar radiation 18 p3073 A67-33562
Optical pumping of sodium vapor with deuterium light, discussing optical transparency in excited state mixing cross sections 21 p3639 A67-38018
- TRANSPARENT MATERIAL**
Statistical effects during generation of second harmonic in optically transparent crystals, noting coefficient of correlation between harmonic and fundamental radiation power of solid state laser 03 p0467 A67-12928
Light absorption in transparent materials measured using thermal lens method 03 p0439 A67-14395
Material properties and capabilities of different types of optical waveguides including iterative electromagnetic wave beams, reflecting pipes, fiber guides, etc 12 p1906 A67-25976
Total hemispherical emittance of transparent materials at low temperatures measured using calorimetry 13 p2159 A67-27356
Transparent plastic materials for aircraft application, noting glass developments and thermal stress conditions elimination 16 p2694 A67-30980
Gold resistance thermometers for measuring surface temperature of semitransparent materials 18 p3051 A67-34505
Simultaneous absorption of two photons by transparent material at radiation frequency corresponding to only one photon 20 p3457 A67-36325
Hologram-moire interferometry for transparent objects of moderate optical quality 21 p3624 A67-37853
- TRANSPARATION**
SA EVAPORATION
SA FLUID TRANSPARATION
Exact theory of enclosed molecular radiometer using flow field solution from Wu-revised thermal transpiration theory in two cases 10 p1681 A67-22864
Mixing-length velocity profile in boundary layers with transpiration, discussing Tennekes theory and turbulent kinetic energy change rate 19 p3211 A67-35752
Coles equation representing nonequilibrium turbulent boundary layer without transpiration 19 p3212 A67-35776
- TRANSPARATION COOLING**
Noncontour transpiration cooled heat shield for possible application to hypersonic atmospheric flight 04 p0725 A67-15435
Skin friction drag of constant property turbulent boundary layer with uniform injection, corrections of experimental law-of-wall and velocity-defect law concepts 10 p1625 A67-23111
Performance capability of transpiration cooled constricted arc heater, treating hydrogen 10 p1698 A67-23122
Testing of transpiration air cooled turbine, discussing blade fabrication [ASME PAPER 67-GT-29] 11 p1854 A67-24807
Thermal design of molten carbonate fuel cells using transpiration heating for reducing heat loss and control of temperature 13 p2055 A67-26842
Water cooled copper anode operation compared to porous graphite transpiration cooled annular anode to study energy transfer in wall stabilized cascaded arc 19 p3279 A67-35141
Radial instreaming mass flow effect on cylindrically-symmetric arc with transpiration cooling, noting heat flux reduction 19 p3280 A67-35148
- Transpiration cooled porous surface in high temperature forced convection environment, applying transient energy balance with heat-transfer coefficient measurement [ASME PAPER 67-HT-27] 20 p3546 A67-36720
Temperature difference between solid and gas of transpiration cooled wall due to radiant heating [ASME PAPER 67-HT-29] 20 p3546 A67-36722
Transpiration cooled vehicles correlation with compressible turbulent boundary layer with mass transfer, emphasizing high Mach number 20 p3423 A67-37256
Vaporizing solid or liquid underlayers for transpiration cooling of reentry vehicles; discussing advantages, handling, storage and self-regulating system 22 p3901 A67-39934
- TRANSPONDER**
Synthesis of multichannel transponder for radio guidance and tracking station and associated parameters 02 p0264 A67-12355
Geodetic electronic ranging system of satellites with Sequential Collation of Range /SECOR/ transponder 07 p1177 A67-19772
Mathematical tool for system design of pseudorandom coded ranging system used in space programs, noting failure probabilities 07 p1145 A67-19869
Three-dimensional multielement transponder array designed to give directional replies toward source of interrogating signals 13 p2071 A67-27404
Structure of quasi-linear and wideband satellite transponders, discussing possible improvements 18 p3003 A67-34356
- TRANSPORT**
S GAS TRANSPORT
S JET TRANSPORT
S SUPERSONIC TRANSPORT
- TRANSPORT AIRCRAFT**
SA AIR TRANSPORTATION
SA ANTONOV AN-24 AIRCRAFT
SA AVRO WHITWORTH HS-748 AIRCRAFT
SA BAC 111 AIRCRAFT
SA BOEING 2707 AIRCRAFT
SA BOEING 747 AIRCRAFT
SA CANADAIIR CL-84 AIRCRAFT
SA CONCORDE AIRCRAFT
SA HANDLEY PAGE H.P. 137 AIRCRAFT
SA ILYUSHIN IL-18 AIRCRAFT
SA LOCKHEED L-500 AIRCRAFT
SA MIL MI-10 HELICOPTER
Carrier Onboard Delivery aircraft, discussing cost effectiveness by reduced delivery time of critical spare parts [AIAA PAPER 66-790] 01 p0009 A67-10533
Production program and MAC operational experience of C-141A jet cargo transport [AIAA PAPER 66-791] 01 p0009 A67-10534
C-141A cargo aircraft structural analysis, discussing design, load and gust criteria, flight and static test programs, vibration and noise control [SAE PAPER 660669] 01 p0010 A67-10576
Fuselage optimization for short haul transport aircraft 02 p0181 A67-12199
Mi-10 Soviet flying crane, very high four-wheeled landing gear enables it to drive over load and clamp it by hydraulically operated grips 02 p0181 A67-12201
Transport jet engine inspection with radioactive isotopes, noting techniques and results 02 p0303 A67-12219
Boeing model 747 aircraft /large capacity subsonic transport/ engine aerodynamics and design objectives [AIAA PAPER 66-821] 02 p0181 A67-12248
VTOL and STOL aircraft applications, Boston to Washington [AIAA PAPER 66-964] 02 p0182 A67-12638
Aerodynamic design of Boeing 737 covering data of analytical studies, wind tunnel and flight tests, aerodynamic parameters and drag, flap system size, efficiency, wing geometry and handling qualities [AIAA PAPER 65-739] 03 p0354 A67-12906
All-weather landing system for C-141 jet cargo transport using vertical navigation computer for military operations 03 p0464 A67-12907
Short-haul aircraft design for low direct operating costs, noting wings 03 p0357 A67-12968
Onboard equipment designed for transport aircraft landings with visibilities less than 200 ft and runways less than 2800 ft, having all devices duplicated 03 p0464 A67-13001
- Long-haul transport aircraft structural considerations and effect on operating empty weight and on airframe maintenance [AIAA PAPER 66-882] 03 p0361 A67-14019
Air cargo transport from 1960 to 1970, discussing new methods of traffic promotion [AIAA PAPER 66-1018] 03 p0361 A67-14024
Economic and technological analysis of jet transport and cargo aircraft relation to future air traffic problems [AIAA PAPER 66-820] 03 p0538 A67-14134
Lockheed 500, derivative of USAF C-5A transport, discussing logistic capabilities, economics and representative approaches [AIAA PAPER 66-1019] 03 p0362 A67-14152
V/STOL military transports purchase decisions based on analyses of operational employment, engineering design and economic utility 04 p0551 A67-14803
Long-haul intercontinental air transportation, discussing passenger and cargo traffic increases and airport and airway crowding [AIAA PAPER 66-1017] 06 p0946 A67-17980
Dual-purpose passenger/cargo aircraft noting design, passenger interior system, cargo handling system, compatibility, comparisons, etc 06 p0946 A67-18005
Category II Systems Evaluation Test of C-141A aircraft 07 p1129 A67-19616
Lockheed C-5A cargo aircraft, discussing airframe construction, landing gear, weight and balance system, use of TI and honeycomb materials, etc 07 p1130 A67-20230
Lockheed C-5 cargo transport aircraft design optimization 07 p1130 A67-20231
C-141A cargo aircraft structural analysis, discussing design, load and gust criteria, flight and static test programs, vibration and noise control [SAE PAPER 660669] 07 p1131 A67-20232
Air freight transport development by Alitalia, noting Fluminio terminal 08 p1429 A67-20785
Aerodynamic design of Boeing 737 covering data of analytical studies, wind tunnel and flight tests, aerodynamic parameters and drag, flap system size, efficiency, wing geometry and handling qualities [AIAA PAPER 65-739] 08 p1279 A67-21043
Hypersonic transport design, considering payload vs range and weight and power plant, aerodynamic, structural and flight profile problems 11 p1744 A67-24579
Book on air transport economics in supersonic era covering air cargo operational problems, mechanical loading, VTOL transport operation, etc 13 p2052 A67-26256
Hawker Siddeley 748 design noting utilization rates, maintenance costs and indefinite fatigue life 15 p2419 A67-29509
Airport requirements for Boeing model 747, including description of necessary modification of terminal facilities and ground equipment [AIAA PAPER 67-384] 15 p2468 A67-30353
Boeing 727 QC aircraft development, manufacture, design objectives, cargo pallet system, seat pallet system, etc [AIAA PAPER 67-395] 15 p2421 A67-30362
Economic factors controlling development of high capacity supersonic transport aircraft 16 p2782 A67-30838
Helicopter cargo restraint system program meeting prescribed operational and safety requirements [AHS PAPER 124] 16 p2598 A67-31839
Carrier Onboard Delivery aircraft, discussing cost effectiveness by reduced deliver time of critical spare parts 17 p2797 A67-32572
Locating general drop zone and desired impact point, identifying receiving unit and dropping supplies for aerial delivery systems 17 p2797 A67-32587
Flight instrumentation aiming at improving safety of approach and landing of commercial aircraft [SAE PAPER 670327] 17 p2860 A67-32983
Space vehicle checkout procedure application to near-future transport aircraft, noting NASA sponsored advances [SAE PAPER 670337] 17 p2835 A67-32987
Fatigue-damage evaluation system for transport aircraft, noting use of cumulative strain gauge that stores strain history 18 p3142 A67-33897
Parametric analysis on hydrogen-fueled hypersonic aircraft for long range passenger transport missions and launch vehicle

missions, noting propulsion system-airframe interactions

[AIAA PAPER 67-493] 18 p2985 A67-33957
Hawker Siddeley 748 short-to-medium range civil transport aircraft design features including take off/landing field length, pressurized cabin, engines, payload, etc 18 p2986 A67-34074

A-300 Airbus, economic subsonic passenger transport for short and medium ranges 18 p2986 A67-34075

Hydraulic design of Japan YS-11 twin turboprop transport aircraft, noting component accessibility and ground service simplification 19 p3175 A67-34787

Navigation system for long range transport aircraft providing accurate and reliable fixing, discussing takeoff and landing 19 p3254 A67-35312

Transall C 160 aircraft wings, fuselage, tail surfaces, landing gear and power units 20 p3361 A67-36633

Cabin pressurization characteristics of USAF and commercial transport aircraft, stressing decompression sickness 21 p3577 A67-38081

Boeing model 747 aircraft /large capacity subsonic transport/ engine aerodynamics and design objectives 21 p3568 A67-38542

German lighter than air technical and economic travel problems of medium speed dirigibles using helium and nuclear power drives 22 p3745 A67-39751

High speed helicopters and large transport capacity aircraft, discussing combination of rotors with wings and propeller drive, retractable blades and folding rotors 22 p3745 A67-39753

Civil high speed intercity VTOL aircraft using fan lift engines, discussing noise, installation, aerodynamics and thrust deflection

[AIAA PAPER 67-745] 23 p4048 A67-40979
Circulation control by blowing for gust insensitivity in stopped rotor aircraft application

[AIAA PAPER 67-747] 23 p3933 A67-40981
Automatic landing system introduction for civil transport aircraft noting certification program and requirements and development of operable system

[AIAA PAPER 67-757] 23 p4025 A67-40990
Short haul military requirements /1970-1980/, considering assault and logistic airlifts supporting ground forces and V/STOL aircraft

[SAE PAPER 670827] 24 p4093 A67-41992
VTOL aircraft operational expense estimation using standard method, measuring maintenance costs in various planning stages and in operation

[AIAA PAPER 67-828] 24 p4096 A67-42974
Commercial V/STOL transportation system, analyzing intraurban and short haul factors for concerned parties by computer simulation

[AIAA PAPER 67-969] 24 p4260 A67-43047

TRANSPORT COEFFICIENT

Existence of divergence in density expansion of viscosity and thermal conductivity coefficient of two-dimensional gas of rigid disks 02 p0234 A67-12545

Hydrogen atom-molecule exchange reaction effect on transfer coefficients of dissociating mixture, noting anisotropy and collision integrals 03 p0473 A67-13606

Viscous friction and heat flux for partially ionized medium flowing in plane channel with anisotropic transport coefficients 04 p0666 A67-15189

Mass transfer measurements of paradichloro benzene cylinders at various turbulent intensities and angles of attack, showing free flow turbulence effect on local mass transfer coefficient 04 p0548 A67-15493

Quantum mechanical calculation of transport coefficients of gas of loaded spheres, obtaining scattering amplitudes and cross sections 06 p1038 A67-19045

Quadrupole effects on gas diffusion, viscosity and thermal diffusion factors, computing collision integrals 06 p1038 A67-19046

Transport coefficients for minority carrier scattering in InSb 07 p1209 A67-19652

Transverse plasma instabilities as mechanism coupling motions of solar wind and cometary plasma, using thermal diffusion and conductivity transport coefficients to describe flow 08 p1401 A67-21367

Quantum mechanical kinetic theory of gas loaded spheres to obtain limit of transport coefficients and relaxation time 10 p1682 A67-23383

Properties of partially ionized Ar computed via Chapman-Enskog-Burnett expressions noting ambipolar diffusion coefficient, electron-atom momentum, electrical and thermal conductivity, etc 11 p1775 A67-23865

Transport coefficients for dense gases via Bogolubov theory of two-particle nonequilibrium distribution function 11 p1823 A67-24538

Nonequilibrium process in one dimension in presence of constant and oscillating electric field, using distribution function 11 p1824 A67-25078

Electron transport coefficients and electron energy equation closed formulation for two-temperature plasma, considering elastic and nonelastic collisions 12 p1973 A67-25397

Transfer coefficients of charged particles trapped in magnetic field of earth, examining concept of sudden pulses as basic mechanism 12 p1994 A67-25541

Green function theory of nonlinear transport coefficients 12 p1967 A67-25846

Transport coefficient expressions for collisions between rigid diatomic molecules, using perturbation method 14 p2259 A67-28298

Lenard-Balescu kinetic equation solved by Chapman-Enskog method for transport coefficients of plasmas noting diminishing value 15 p2522 A67-29210

Collision integral for Landau plasma in strong magnetic field to obtain time evolution of one-particle distribution function 15 p2532 A67-30382

Transport coefficients calculated from adiabatic excitation transfer in atomic gases 16 p2661 A67-31222

Energy dissipation and transport coefficients temperature dependence effect on short wave perturbation development in magnetohydrodynamics 16 p2723 A67-31578

Sodium effect on dwell time and transport rates of various elements using DC arc, stressing spectral consequences 17 p2888 A67-32377

Hydrogen atom-molecule exchange reaction effect on transfer coefficients of dissociating mixture, noting anisotropy and collision integrals 18 p3083 A67-34471

One-dimensional electron plasma model, transport coefficient determination, Lorentz plasma conductivity measurement, decay rate, etc 18 p3092 A67-34748

Wind tunnel measurement of turbulent transport terms for unstable curved mixing layer of incompressible flow 18 p3030 A67-34751

Wall temperature distribution effect on transport coefficients determination from arc plasmas 19 p3280 A67-35144

Transport coefficients of fully ionized hydrogen plasma in magnetic field calculated from Fokker-Planck equation 19 p3286 A67-35350

Many-body system interaction with quasi-particle with assigned orbit, discussing applications to transport coefficient, plasma stability, etc 20 p3495 A67-36155

Attachment coefficient and transport velocity in nighttime F region from backscatter N-h profiles, determining loss term integration 20 p3426 A67-36287

Binary gas mixtures transport coefficients calculation, comparing experimental and theoretical values of viscosity and thermoconductivity dependent upon interaction between unlike molecules 21 p3733 A67-39064

Chapman-Enskog expansion applied to Fokker-Planck equation for plasma allows transport coefficients calculation without further approximation in presence/absence of magnetic field 22 p3843 A67-39266

Surface states effect on current-voltage characteristics of metal-semiconductor contact from kinetic coefficients of electron exchange 22 p3858 A67-39570

Resonant particle diffusion of nonuniform plasma across magnetic field, calculating transport coefficients 22 p3848 A67-39687

Chapman-Enskog transport collision integrals calculated for repulsive and attractive screened Coulomb potentials in ionized gases 22 p3850 A67-39717

Integrated transport cross sections obtained for nitrogen as function of temperature using gaskinetic formulas 22 p3841 A67-40050

TRANSPORT EQUATION

Relaxation effect in electrical conductivity of semiconductors and metals, taking into account scattering by ionized impurities and Debye cloud polarization 02 p0280 A67-11480

Current density resulting from integration over energy of transport equation applicable to dielectric film 02 p0295 A67-11783

Upper and lower bounds for solutions to transport equation obtained, using collocation method and maximum principle [DVL-479] 04 p0602 A67-14591

Radiation diffusion in gas analyzed by solving transport equation for homogeneous absorbing isotropically scattering spherical shell with point source in center 04 p0695 A67-14656

Partially ionized two-temperature plasma, deriving distribution function of first approximation associated with viscosity 04 p0686 A67-15186

Magnetic field effect on transport equation, presenting relationship between classical Boltzmann equation and corresponding quantum mechanical formalism 04 p0659 A67-15773

Ohm law in multicomponent nonisothermal plasmas derived as function of electric and magnetic fields and temperature and pressure gradients, using transport equation 05 p0857 A67-17422

Diffusion and transport equation for turbulent atmosphere with variously heated air masses 06 p0999 A67-18740

Gas transport cross sections, angular distribution of elastic scattering of colliding gas particles and transport equation degeneration 07 p1225 A67-19125

Analytical method for solving nonstationary one-dimensional equation of ozone transport 07 p1172 A67-19457

Rarefied gas flow analyzed through transport equation in gas kinetics using bimodal two-stream distribution functions, with application to Couette flow 10 p1624 A67-22914

Plasma instability and anomalous transport - Conference, University of Miami, Coral Gables, May 1966 11 p1828 A67-23997

Heat flux in rarefied gas calculated via transport equations, noting validity of boundary temperature discontinuities 11 p1881 A67-24028

Behavior of line source function of low density gas in presence of nonthermal velocity field, examining strong shock situation and differential velocity via ordered velocity structure 11 p1861 A67-24489

Transport coefficients for dense gases via Bogolubov theory of two-particle nonequilibrium distribution function 11 p1823 A67-24538

Cesium vapor thermionic diode operation in electron-rich surface ionization mode noting transport effects 11 p1849 A67-24902

Kinetic equation for electron gas in classical limit derived from quantum mechanical transport equation, using equilibrium analogy 11 p1844 A67-25076

One-dimensional transport equations of p-n junction in steady state solved numerically 13 p2078 A67-26781

Proton mobility in ice when limited by lattice scattering calculated, using Boltzmann transport equation 13 p2160 A67-26991

Comparison of steady state operator of Prigogine with T-matrix 13 p2159 A67-27736

Spherically symmetrical planetary atmosphere brightness derivation using transport equation 14 p2313 A67-28766

Equivalent circuit model for solid state junction devices with single energy level defect centers including transient properties 15 p2456 A67-29171

Pure molecular flow coupled with surface diffusion applied to cesium transport 15 p2520 A67-29494

Fundamental relations for normal shock wave behavior in compressible fluid for classical and hydromagnetic cases 15 p2473 A67-30222

Cesium thermionic converter extinguished mode operation theory, deriving expression for forward and reverse saturation output current densities and open circuit voltages 17 p2803 A67-32365

- Differential transport equation system in n-dimensional anisotropic space solved using matrices, discussing heat conduction equations 17 p2972 A67-33070
- Radiative transfer for electron scattering atmosphere, obtaining eigenfunctions of transport equations 17 p2950 A67-33164
- Surface recombination velocities relationship in depletion, inversion and accumulation surface layers of p-type silicon, using ambipolar carrier transport formulation 18 p3104 A67-34593
- Rarefied gas cylindrical Couette flow noting Knudsen number, Bhatnagar-Gross-Krook model for Boltzmann equation, transport integrodifferential equation, etc 18 p3029 A67-34738
- Thermal conductivity of nitrogen plasma in cascade arc, solving Elenbaas-Heller equation 19 p3287 A67-35358
- Radiative heat flux for free burning methanol and acetone flames of arbitrary size and geometry predicted, using transport equation [ASME PAPER 67-HT-47] 20 p3547 A67-36729
- Gas transport cross sections, angular distribution of elastic scattering of colliding gas particles and transport equation degeneration 21 p3659 A67-38172
- Quantum transport theories for calculating multiple scattering in doped semiconductors 21 p3682 A67-38386
- Parameter diagnostics of low temperature plasma in cesium diode, comparing probe measurements with transport equation solutions 22 p3845 A67-39425
- Nonequilibrium thermodynamics canonical equations determination on basis of variational principle for transport equations governing irreversible processes 22 p3918 A67-39786
- Electronic transport in graded band gap semiconductor heterojunctions without space charges, using method based on intraband transitions between complete Hamiltonian eigenstates 22 p3864 A67-40381
- Integrated intensities for thermal radiation heat transfer in nongray nonscattering gas approximated, deriving effective absorption coefficient 22 p3920 A67-40442
- Kinetic equation for steady state electron-ion system with electrons drifting under electric field, calculating HF resistivity drift velocity dependence 23 p4033 A67-40962
- Optimization of capillary pumping of microgrooved heat pipes, discussing transport equation 24 p4255 A67-42552
- TRANSPORT PROPERTY**
- SA DIFFUSION**
- SA HEAT TRANSFER**
- SA KINETIC THEORY**
- Flame ignition from hot gas pocket, minimum size of gas bubble for flame propagation, dependence on chemical kinetic parameters and transport properties 02 p0342 A67-12030
- Hall mobility, Seebeck and Nernst coefficients measured in temperature range from about 100 to 350 degrees K for scattering mechanisms of conduction electrons in n type CdS 03 p0493 A67-13351
- NGe-pGaAs heterojunctions, diffusion or emission theories of current transport do not explain electrical characteristics but validate Anderson model, considering tunneling as transport mechanism 03 p0494 A67-13478
- Vertical ozone distribution in atmosphere and transport processes, noting results of tracer experiments 03 p0414 A67-14090
- Noon electron density variation of F-2 layer at low latitudes and associated transport processes, using modified least squares method 03 p0415 A67-14111
- Transport and ionization properties of molecular gases in transverse magnetic field, using ionization chamber 03 p0474 A67-14358
- Transport properties of model fluid whose molecules interact according to square-well potential used to calculate transport coefficients of krypton, xenon and argon 04 p0720 A67-14507
- Hall effect and transport properties of single crystals of iodine measured by alternating current technique, using field effect transistors 04 p0675 A67-14757
- Chapman-Enskog method applied to kinetic equation describing evolution of singlet distribution function in dense gas of perfectly rough spheres 04 p0658 A67-15507
- Correction for characteristic number of E layer based on electron transport processes and seasonal variations 04 p0618 A67-15573
- Anomalous photocurrent generation in transistors, noting carrier generation and transport processes 04 p0685 A67-15696
- Arc diffusion measurements of electron temperature and density profile across magnetic field 05 p0858 A67-17433
- Loss coefficient and vertical transport velocity for nighttime F region during solar activity 06 p0995 A67-17971
- F region effects following two severe magnetic storms, noting changes in electron density profile 06 p0995 A67-17972
- Avalanche transistor properties in dynamical state derived from relation between current, collector voltage and concentrated load in base 06 p0970 A67-18186
- Radiation transport theory and spatial radiative heat transfer in absorbing and isotropically scattering medium 06 p1118 A67-18552
- Equilibrium air study extended to reentry speeds up to 70,000 fps, using transport and thermodynamic properties to examine stagnation point convective heat transfer including blowing rates 06 p0943 A67-18843
- Hydrostatic pressure effect on energy gap, carrier concentration and electron and hole mobilities of indium antimonide 07 p1231 A67-19061
- Semiconductor dislocation noting velocities and effect on transport properties 07 p1237 A67-20162
- Plasma transport properties, discussing application of ionization level as indicator for electric conductivity and viscosity 08 p1357 A67-20591
- Modified Chapman-Enskog method for obtaining transport properties of nonequilibrium partially ionized gas, giving hydrodynamic equations 11 p1775 A67-23866
- Binary van der Waals mixture near solution critical point, noting anomalous behavior of heat capacity, shear viscosity and bulk viscosity 11 p1884 A67-24990
- Collective effects in collisionless plasmas in laboratory in case of Vlasov-Maxwell equations with Landau damping 14 p2362 A67-29037
- Temperature and transport properties of helium and argon at high temperatures from ultrasonic determination of sound velocity and sound absorption 15 p2580 A67-29882
- Equilibrium radiative transport properties of high temperature air coupled with aerodynamic flow field generated by planetary reentry vehicles 16 p2589 A67-30721
- Heat conducting supersonic gas flow around corner considered calculating viscous corrections in expansion region 16 p2660 A67-31218
- Silver-gold and silver-germanium alloys tested for Fermi surface changes with alloying, using thermoelectric power measurements 16 p2731 A67-31448
- Transverse magnetic field effects on heat transfer in turbulent flow of mercury in circular iron tube 17 p2899 A67-32186
- Transport property difference effect on flow prediction of blunt body stagnation region heat transfer, noting laminar flow and compressible boundary layer equations 17 p2793 A67-33025
- Time variations of order parameter, coupling to external perturbation and effect on various transport properties of dirty type II superconductors 19 p3302 A67-35038
- Charge, current, and self-consistent field transport properties of collisionless plasma derived using initial value solutions to Vlasov equation 19 p3285 A67-35343
- Kinetic theory of transport processes in weakly turbulent plasma with and without magnetic field 19 p3286 A67-35351
- Kinetic thermodynamics applied to real gas transport properties analysis by generalization of mean-free-path theory 20 p3543 A67-36185
- Transport phenomena in semiconducting thin films studied using transport equation, obtaining relaxation time relationship to semiconductor 20 p3508 A67-38217
- High temperature gas transport property estimation with chemically reacting gas mixture conduction 21 p3613 A67-38391
- Duo-emitter cesium thermionic converter, discussing electron and cesium ion emission to increase transport efficiency 21 p3571 A67-38610
- Electrical conductivity and transport properties of pure liquid metals 21 p3686 A67-39108
- N-type Hall effect in high temperature Li doped ceramic sample of MnO, measuring electric transport properties 22 p3858 A67-39521
- Self-similar solutions to motion equations are possible for internal heat generation in confined supersonic flow, assuming constant transport properties 22 p3784 A67-39781
- Aerothermochemistry of high temperature multicomponent reactive systems, examining thermodynamic and transport characteristics and ionized and dissociated working fluid processes 22 p3921 A67-40447
- Kinetic prediction theory for viscosity, thermal conductivity and diffusivity of binary liquid mixtures composed of molecules interacting with square-well potential 23 p4083 A67-41531
- Parametric analysis of heat pipes, design, operation principles and performance capabilities 24 p4255 A67-42553
- Hall effect, resistivity, spin resonance and thermoelectric properties of poly(N-vinyl carbazole-iodine complex, demonstrating charge transfer state existence in system [JPL-TR-32-1074] 24 p4205 A67-42602
- High temperature polyatomic gas and gas mixture transport properties, discussing thermoconductivity, multiple intermolecular potentials and plasmas 24 p4256 A67-42742
- TRANSPORT THEORY**
- SA INTEGRAL EQUATION**
- Thermoelectric generator performance, materials, technology, electron transport theory and phenomenological basis of thermoelectric effects 01 p0013 A67-10555
- Vertical transport of latent and sensible heat of IR cooling and short wave heating 09 p1490 A67-21550
- Anomalous transport phenomena in ring discharge studied for instability and losses due to noise, using mc RF oscillator [AROD-6398-2] 11 p1831 A67-24010
- Possible initial perturbations development into galaxies with dissipative effects associated with transport processes treated via Boltzmann equation 11 p1867 A67-24838
- Kinetic equation derivation for one particle species fluid using closure hypothesis 17 p2883 A67-32290
- Kinetic equation for inhomogeneous plasma in uniform external magnetic field, for application in studies of transport and high frequency wave phenomena 19 p3285 A67-35342
- Transport process instability theory, discussing collisionless plasma transport phenomena and relation to Ohm law 20 p3495 A67-36156
- Book on thermoelectric and thermomagnetic effects in metals, semimetals and semiconductors subjected to electric, magnetic and temperature fields, discussing transport theory 20 p3514 A67-37464
- Plasma conductivity tensor in steady magnetic field in terms of electric field correlation using Kubo transport theory 20 p3503 A67-37692
- Quantum transport theories and multiple scattering in doped semiconductors evaluated for screened Coulomb potentials 21 p3682 A67-38387
- Electron transport theory for energy below 10 Mev, reviewing interactions, scattering, thick targets, complex geometry and penetration in space environment [UCC/DSSD-267] 24 p4190 A67-41805
- TRANSPORT VEHICLE**
- SA MILITARY WEAPON TRANSPORT VEHICLE**
- Design evolution studies defining technological, operational and cost characteristics for reusable aerospace passenger transport 03 p0519 A67-13791
- Helicopter capabilities in solving interurban mass transport problems, particularly cost and time considerations [SAE PAPER 660336] 04 p0552 A67-15611
- Transportation of Douglas Saturn S-IVB stages to test and launch sites 05 p0787 A67-16610
- Mobile launcher and crawler transporter facilities for Apollo/Saturn V launch exploration vehicle 05 p0787 A67-16611
- Optimized equipment systems design studies for handling and transportation of large solid fuel rocket motors [AIAA PAPER 67-266] 07 p1164 A67-20047

Rules for comparing designs of aerospace transporters and selecting optimum configuration, based on overall cost criterion 10 p1713 A67-23482

Indications and contraindications for transportation of wounded by helicopter and ambulance 12 p1902 A67-25174

French concept for aerospace transporter capable of horizontal takeoff from existing major airstrips 15 p2568 A67-29842

Onboard and ground radio-engineering system for stratospheric transport balloon noting telemetering, remote control and localization functions integrated in system 21 p3581 A67-38213

Apron underground fueling systems, using experience in aircraft fueling to justify reduction or elimination of hydrant service vehicles 22 p3779 A67-39380

Apollo Crawler System analyzed by computer simulation for dynamic interactions of transporter and umbilical tower 22 p3782 A67-40466

Systems planning for transportation of large launch vehicles and spacecraft noting land transporter and seagoing barge used for Apollo booster 23 p4070 A67-40584

Turboramjet engine design for aerodynamic flight vehicles up to Mach number 6 23 p4049 A67-41318

Aerodynamic power and moment coefficients of space-transport configurations for hypersonic reentry and trajectory calculations 23 p3931 A67-41399

Traffic prediction for high speed aircraft and surface vehicles and VTOL aircraft city-center to city-center transportation [AIAA PAPER 67-802] 24 p4259 A67-42962

Lunar transportation systems for exploration logistics support after first Apollo flight, feasibility, candidates, selection and evolution [AIAA PAPER 67-873] 24 p4244 A67-42994

TRANSPORTATION

SA AIR TRANSPORTATION

SA RAIL TRANSPORTATION

Facilities, ground handling and transport equipment for Titan III ITL system [SAE PAPER 660706] 01 p0050 A67-10599

Transportation and handling of large solid rocket motors, considering program management aspects [SAE PAPER 660707] 01 p0169 A67-10623

Coordination of marine and air transportation, complementary aspects and necessity for government subsidy of shipping 05 p0920 A67-16603

Airport accessibility, discussing rail extensions to airports, bus lanes and bus-rail vehicles [SAE PAPER 670322] 12 p1925 A67-25868

Earth orbital transportation, proposing airline type system and composite nuclear-airbreathing engines for reusability with minimum refurbishment [AAS PAPER 67-84] 15 p2546 A67-29950

Commercial space utilization considering space transportation cost as fundamental factor [AAS PAPER 67-134] 15 p2571 A67-29968

Close coordination of aviation with other transportation facilities, considering airport/heliport planning within city planning, high speed train competition, highways congestion, etc 19 p3347 A67-34969

Hovercraft principle application noting development, sea-keeping problems, predicted capability and costs 22 p3745 A67-39663

Mathematical model to aid in determination of need for technological advances in transportation [AIAA PAPER 67-799] 24 p4258 A67-42960

TRANSURANIUM ELEMENT

S CALIFORNIUM

S PLUTONIUM

TRANSVERSE OSCILLATION

Transverse oscillated electron beam welding procedures of D6AC steel and mechanical properties evaluation show comparable results to corresponding gas tungsten arc welds 01 p0080 A67-10946

Oscillations in burnt gas coupling to gas dynamical interactions occurring at detonation wave front 03 p0402 A67-13465

Stability of transverse oscillation of thin finned elastic beam of revolution in gas flow acted upon by tracking 03 p0520 A67-14172

Finite elastic deformation theory applied to transverse nonlinear oscillation of cables

in rubber-like materials 06 p1111 A67-18863

Transverse oscillation stability in quasi-one-dimensional flow of conducting gas in magnetic field 07 p1227 A67-19119

Transversal mode excitation in electrostrictively operated scanning interferometer and optical matching to laser cavity 09 p1482 A67-21563

Transverse oscillations of vortex free fluid in circular cylinder with horizontal generatrix, determining first natural frequency by Rayleigh method 09 p1574 A67-21891

Transverse fluid flow stability between permeable boundaries for case with exact solution of perturbation spectrum 10 p1628 A67-23675

Cylinders of rectangular section as aeroelastic nonlinear oscillators, theory of galloping oscillation and force measurements on stationary cylinder [ASME PAPER 67-VIBR-50] 11 p1777 A67-24200

Piezoelectric type accelerometer transverse sensitivity ratio /TSR/, discussing measurements of vibrations and rotations 12 p1943 A67-25703

Unbounded laminar plate oscillations in bilateral potential ideal gas flow with uniform physical and mechanical parameters 15 p2575 A67-30009

Behavior of high speed, coherent, turbulent liquid jet in planar, standing, transverse acoustic field 16 p2658 A67-30945

Periodic relaxation pulses caused by thermal resonance drift, studying diffraction loss and other effects on transverse modes in crystal lasers 17 p2867 A67-32362

Transverse oscillations of elastic inhomogeneous rod with Young's modulus varying along length, solved in Bessel functions infinite series 17 p2962 A67-32873

Longitudinal and transverse collective fluctuation modes of order parameter in pure type II superconductor in high critical field region 19 p3302 A67-35039

X-ray diffusion intensity by transverse polarization phonons in indium antimonide at various temperature ranges 19 p3307 A67-35793

Unbounded laminar plate oscillations in bilateral potential ideal gas flow with uniform physical and mechanical parameters 20 p3542 A67-37539

Transverse oscillation stability in quasi-one-dimensional flow of conducting gas in magnetic field 21 p3664 A67-38164

Transverse fluid flow stability between permeable boundaries for case with exact solution of perturbation spectrum 21 p3612 A67-38276

Mariner IV flight magnetometer data, determining interplanetary field and geomagnetic variability 22 p3790 A67-39800

Systematic design of TEM equal stub admittance filters on basis of insertion loss 22 p3773 A67-40061

TRANSVERSE VIBRATION

Characteristics of transverse pulse produced by secondary particles created in active nuclear particle collision 02 p0271 A67-12752

Ground resonance of helicopters with zero transverse flexibility analyzed 03 p0360 A67-13393

Characteristics of transverse vibrations of p-l-n jointed trusses obtained by use of rational method of lumping inertia forces 03 p0529 A67-14103

Transverse shear and edge condition effect on nonlinear vibration and dynamic buckling of homogeneous and sandwich plates 05 p0910 A67-16146

Upper and lower bounds of transverse vibrational frequencies of variable cross section cantilever bars, considering transverse shear and rotary inertia effects 05 p0910 A67-16151

Linear shell theory for nonlinear transverse coupled vibrations of partially filled circular cylindrical elastic tank [AIAA PAPER 67-74] 06 p1101 A67-18272

Periodic vibrations of systems governed by nonlinear PDEs, examining perturbation method, transverse vibrations of bar, string, beam and membrane and sound waves in enclosure 06 p1034 A67-18640

Computer program for solving bending of plates of any shape and with any variation

in boundary conditions for static loading and transverse vibration 10 p1731 A67-23843

Rectangular to cylindrical waveguide transducer which couples dominant rectangular and cylindrical transverse electromagnetic modes 11 p1767 A67-24733

Natural transverse vibrations of sandwich plates with rigid and lightweight fillers, deriving stability equations from eigenvalue equivalent problem 14 p2402 A67-28901

Forced transverse vibrations of sandwich plates of symmetrical structure 16 p2776 A67-31547

Spatial correlation coefficients and transverse temperature perturbation scales during turbulent nonisothermal flow of mercury in circular pipe 16 p2724 A67-31776

Nonlinear flexural vibrations of rings studied without assuming zero midplane strain 17 p2963 A67-33032

Transverse vibrations of tapered cantilever beam solved in terms of generalized hypergeometric function by Frobenius method [ASME PAPER 67-APM-25] 17 p2964 A67-33153

Linear shell theory for nonlinear transverse coupled vibrations of partially filled circular cylindrical elastic tank [AIAA PAPER 67-74] 21 p3727 A67-38866

Characteristics of transverse pulse produced by secondary particles created in active nuclear particle collision 22 p3841 A67-40254

TRANSVERSE WAVE

HF random phase transverse wave transmission through turbulent plasma generating scattered waves at combination frequencies 01 p0121 A67-10343

Wave solutions for plane waves propagating in isotropic elastic solid using isotropic approximation 01 p0182 A67-10847

Self-focusing of transverse electromagnetic plane waves in magnetoplasma 02 p0191 A67-11571

Mutual coupling between TEM and TE 01 parallel-plate waveguides calculated, using wedge diffraction techniques 02 p0211 A67-11596

Unstable transverse waves in anisotropic multicomponent plasma, establishing stability criteria, noting role of electron distribution 02 p0276 A67-12562

Instabilities and dispersion during electromagnetic wave excitation and propagation in weakly turbulent plasma 02 p0278 A67-12627

Transverse wave behavior in reactive flow, analyzing refraction or reflection of acoustic waves at shock front, obtaining comparison of behavior in corresponding real flows 03 p0405 A67-14026

Laboratory-controlled nonlinear, nonresonant excitation of electron plasma oscillations with one transverse electromagnetic wave 03 p0485 A67-14052

Faraday fading rate of satellite signal as calculated from Appleton-Hartree formula for refraction index /without collision/ near transverse propagation [RASSA PAPER 1-10-127] 03 p0372 A67-14238

Transverse wave induced surface, compression and transverse waves in plasma, deriving expressions for amplitudes, phases and energies 04 p0663 A67-14744

TE modes propagation in rectangular waveguides containing two dielectric slabs, computing cut-off frequencies and propagation constants 04 p0570 A67-14860

Longitudinal and transverse waves transformation in nonuniform plasma 04 p0668 A67-15276

Transverse wave instabilities in collisionless hydrogen plasmas under magnetic field 05 p0858 A67-17429

Short wave asymptotics of diffraction field at sphere for incident plane transverse waves 06 p1100 A67-18032

Standing transverse hydromagnetic waves effect on longitudinal invariant of particle motion trapped along geomagnetic field 06 p0997 A67-18700

Impact problem of passage of longitudinal and transverse waves arising in elastic infinite thread over sequence of absolutely smooth nonrotating pulleys 07 p1261 A67-19163

Linear transformation of normalized static capacitance matrix used to describe TEM propagation on array of parallel conductors 08 p1304 A67-21224

- Transverse electromagnetic waves with constant phase velocity in fully ionized Vlasov plasmas 08 p1364 A67-21401
- Kinetics of nonuniform generation of longitudinal plasma waves by transverse wave beam with narrow spectrum, noting effect of magnetic field 09 p1545 A67-21995
- Transmission and reflection coefficients in coupling of transverse and longitudinal waves below second electron cyclotron harmonic 09 p1548 A67-22383
- Excitation of electroacoustic lateral waves in compressible plasma by nonelectromagnetic source 10 p1683 A67-22865
- HF random phase transverse wave transmission through turbulent plasma generating scattered waves at combination frequencies 11 p1843 A67-25016
- Field solution of TE sub k zero mode wave incidence on inductive iris in rectangular waveguide 13 p2066 A67-26475
- Instabilities and dispersion during electromagnetic wave excitation and propagation in weakly turbulent plasma 13 p2171 A67-27384
- Function of symmetrical gas-laser resonator analyzed to determine angle of divergence of laser beams generated by various transverse electromagnetic wave modes 14 p2332 A67-28854
- Heating of magnetized hot diffuse plasma using difference-frequency signal generated from two HF transverse waves 15 p2521 A67-29188
- Coulomb collisions effect on transverse wave along external magnetic field in dense plasma, noting damping of whistler mode and use of Fokker-Planck equation 16 p2713 A67-30608
- Transverse and longitudinal waves in ultrasonic light modulators, noting superiority of transverse waves in polarization rotations 17 p2815 A67-32614
- Traveling wave amplification by interaction of drifting carriers in semiconductors with external slow wave circuit 17 p2826 A67-32656
- Propagation modes and instabilities of transverse disturbances in solid state plasmas 17 p2925 A67-33377
- Transverse wave structure in detonations investigated using smoked-foil technique in gas mixtures, showing dependence on tube geometry and heat capacity 18 p3153 A67-33828
- Computer method for determining time-frequency-domain response specifications of transversal linear wave filters, using thin film RC distributed networks 18 p3015 A67-34560
- Oblique, normal and transverse ionizing shock waves 18 p3092 A67-34733
- Time and space development equations for longitudinal and transverse modes in Vlasov plasma 18 p3092 A67-34745
- Dispersion equations for two types of transverse interaction tubes analyzed numerically in presence of strong space charge 19 p3198 A67-36022
- Function of symmetrical gas-laser resonator analyzed to determine angle of divergence of laser beams generated by various transverse electromagnetic wave modes 19 p3242 A67-36106
- Dispersion equations and solution for transverse magnetic waves in parallel-plate waveguide partially filled with plasma slab, discussing existing modes 20 p3492 A67-36127
- Coupling coefficients for nonlinear interaction between two transverse waves and electron plasma wave in magnetic field 20 p3501 A67-37181
- Attenuation reduction by using hybrid wave in coaxial cables and resonators having supporting surfaces of enhanced reactance 20 p3384 A67-37214
- Characteristic admittances of comb-type and undulating waveguide filters, considering diaphragm thickness and TE propagation mode 22 p3770 A67-39662
- Long period hydromagnetic propagation in theta model geomagnetic tail, deriving TM and TE modes equations 22 p3791 A67-39815
- TM and TE mode uncoupling in oblique wave scattering from radially inhomogeneous cylinders 22 p3763 A67-40308
- Elliptically polarized electromagnetic wave propagation in homogeneous infinite plasma, solving Vlasov equations of nonlinear theory by successive approximation 23 p4030 A67-40597
- Plasma waves generation by transverse waves as function of phase relation of interaction 23 p4034 A67-41878
- Strong traveling transverse acoustic modes generated by rotating gas jet in cylindrical cavity 23 p3993 A67-41763
- TRAPEZOIDAL WING**
- Lift and drag of trapezoidal wing models in blown flow near free surface studied for sweepback angle effect on aerodynamic characteristics 13 p2093 A67-26595
- Steady state and transient temperature profiles for straight fins of trapezoidal profile with radiative heat transfer [ASME PAPER 87-HT-73] 20 p3550 A67-36753
- TRAPPED MAGNETIC FIELD**
- Faraday rotation measurement of trapped magnetic fields in theta pinch plasma, using gas laser beam 05 p0859 A67-17447
- Calculations of plasma distributions and field configurations with particle containment and stability within particular framework 11 p1843 A67-24997
- Trapped magnetic field effect on hydrogen plasma parameters in theta pinch, noting density and temperature dependence on initial pressure 14 p2353 A67-27751
- TRAPPED PARTICLE**
- SA GEOMAGNETICALLY TRAPPED PARTICLE**
- SA MAGNETICALLY TRAPPED PARTICLE**
- Luminescence and conductivity of CdS single crystals, noting temperature effect and release mechanism of trapped electrons and holes 01 p0134 A67-10820
- Charged particle traps installed in Luna X providing evidence for moon passing through tail of earth magnetosphere, noting effect of solar wind 01 p0145 A67-10908
- Drift velocity dependence on electric field in GaAs measured by analysis of reverse biased Schottky barrier response to step input of light 02 p0253 A67-12504
- Change in cosmic ray cut-off rigidity caused by currents from trapped particle motion, according to Chapman-Akasofu radiation belt model 05 p0880 A67-16111
- Standing transverse hydromagnetic waves effect on longitudinal invariant of particle motion trapped along geomagnetic field 06 p0997 A67-18700
- Satellite observations of energetic trapped electrons, August 1964 08 p1379 A67-21484
- Stability of various surfaces with respect to electron bombardment heating, noting influence of roughness on electron trapping 09 p1500 A67-22428
- Number and total mass of meteor particles captured by earth atmosphere from cosmic space to closed geocentric orbits 10 p1708 A67-23242
- Higher fast ion density achieved by fast neutral particle injection into closed-line magnetic trap 10 p1686 A67-23466
- Calculations of plasma distributions and field configurations with particle containment and stability within particular framework 11 p1843 A67-24997
- Solar wind trapping in solids using ion bombardment of aluminum foils at various energies and temperatures 11 p1825 A67-25079
- Energetic molecular hydrogen ions injected into resonant nonadiabatic magnetic mirror trap, studying particle mean lifetime, noting cold plasma stabilizing effect 12 p1969 A67-25248
- Trap density is lower in epitaxially grown GaAs crystals than in crystals grown by either horizontal Bridgman /HB/ or floating zone /FZ/ technique 12 p1983 A67-25457
- Time dependent large scale electric potential field effect on motion of geomagnetically trapped particles 12 p1997 A67-25809
- Spatial distribution of electrons and protons trapped by geomagnetic field and charged particle fluxes in interplanetary space 15 p2550 A67-29536
- One-dimensional propagation of stable negative-resistance domains for carriers interacting with single type of impurity level 16 p2727 A67-30852
- Space-charge-limited dielectric diode with quadratic I-V characteristics, noting shallow trap effects on detection properties 17 p2823 A67-32199
- Meteoritic satellites of earth, estimating capture region dimensions 17 p2941 A67-32324
- Resonant interactions between energetic trapped particles and transverse electromagnetic wave, suggesting geophysical applications and examining resonances suppression conditions 17 p2939 A67-33210
- Trapping of hydrogen ions in molybdenum, titanium, tantalum and zirconium measured by mass spectrometric technique 17 p2810 A67-33384
- Hysteretic superconductor, showing trapped flux or remnant magnetic moment linear relationship with average internal field in low but not in high k superconductors 19 p3302 A67-35036
- Polar ionosphere by satellite-borne electron traps, measuring electron density, temperature, quasi-energetic electron flux, etc 19 p3215 A67-35174
- Electron mobility and trapping time in semi-insulating cadmium telluride through observing transient response to alpha particles 19 p3308 A67-36101
- Reversible betatron acceleration mechanism during geomagnetic storm 20 p3434 A67-37425
- Counterstreaming ion electrostatic instability at cyclotron frequency to enhance trapping of injected ion beam 21 p3661 A67-37748
- Low energy, positive ion flux from inner radiation zone, noting losses due to charge exchange, night sky emissions and lifetimes 21 p3697 A67-37996
- Isolated longitudinal wave pulse amplitude and phase velocity dependence on trapped particle density in ion-electron and electron-positron plasmas 21 p3669 A67-38683
- Solitary pulse longitudinal waves existence in electron plasma related to trapped ions presence, studying ion pulse shape and oscillation stability 22 p3845 A67-39423
- Kinetic collisionless plasma diode model stationary regimes, discussing sheath achievement density value dependence on temperature difference and trapped particle distribution 22 p3774 A67-40322
- Plasma potential oscillations in traps, discussing flute instabilities, cyclotron instabilities and resonance electron wave excitation 23 p4034 A67-41680
- Neutral and charged particle trapping using waves, discussing wave attenuation from particle interaction, plasma waveguide and laser beam trapping 23 p4017 A67-41681
- Change in cosmic ray cut-off rigidity caused by currents from trapped particle motion, according to Chapman-Akasofu radiation belt model 24 p4214 A67-42787
- TRAPPED RADIATION**
- Instability effect in n-channel silicon MOS transistors bombarded with ionizing radiation 04 p0589 A67-15716
- Properties of self-trapped light filaments noting stimulated Raman emission and creation, containment and termination mechanisms 05 p0818 A67-16648
- Cloud melting zone, noting increased antenna temperature for radiation trapping between cloud layer and ground [AIAA PAPER 87-188] 06 p1026 A67-18491
- Charged particle motion in static magnetic fields without axial symmetry derived, employing Lagrange equation in transformed coordinate system and Alfvén motion 11 p1855 A67-23929
- Magnetic field variations in magnetosphere at distances of 3 to 6 earth radii attributed to distribution of trapped radiation 12 p1997 A67-25814
- High power argon ion laser with wall stabilized arc discharge determining laser output 16 p2685 A67-30825
- Radio wave trapping and guiding along magnetic field lines by irregularities in electron density 16 p2667 A67-31513
- Nature of trapping regions, using spherical harmonic expansion for magnetic field created by currents on geomagnetic cavity surface 17 p2938 A67-33207
- Self-focusing of laser light pulses in ruby and leucosapphire crystals, noting different damage forms for fundamental and second harmonics 21 p3639 A67-38094
- Trapped radiation levels via AP1-5 and AE1-3 model environments noting long term effects 23 p4061 A67-41517
- Cloud melting zone, noting increased antenna temperature for radiation trapping between cloud layer and ground [AIAA PAPER 87-188] 23 p4025 A67-41747

TRAPPING

SA CRYOTRAPPING

Adiabatic harmonic unitary transformations and relation between electron trapping energy and normal lattice modes associated with F center ground state 03 p0495 A67-13515

GaAs diodes measured for capacitance at 77 degrees K, noting change due to traps photoexcited in space charge layer 17 p2914 A67-32655

Slow response of cadmium selenide thin film transistors related to trapping levels in insulator 18 p3015 A67-34557

Currents in copper phthalocyanine thin films measured as function of temperature and ambient noting effect on conductivity, trap density, etc 18 p3104 A67-34627

Time-dependent current flow equations solved for insulator with traps if injected space charge produces negligible perturbation on external electric field 20 p3509 A67-36506

Theory of small signal current transients applied to study of electron trapping in amorphous selenium 20 p3509 A67-36507

SbS recombination center concentration, hole capture cross sections and trap energy levels 22 p3846 A67-39503

TRAUMA

SA BAROTRAUMA

Traumatic sickness in dogs due to high gravity impact noting enzymatic activity changes and immunizing reaction 21 p3575 A67-38509

Trauma in lateral impact at high entrance velocity compared with rearward and forward facing body orientations of baboons when restrained by lap belt only 22 p3750 A67-39594

TRAVELING CHARGE

Electromagnetic waves produced by charge traveling at constant velocity in medium with convective 05 p0762 A67-16353

TRAVELING SALESMAN PROBLEM

Markovian division process application for solving multicomponent preventive maintenance, work sampling and search theory problems 01 p0106 A67-10930

TRAVELING WAVE

Generating mode number in solid state lasers using traveling wave and standing wave 01 p0086 A67-10069

Charged particle motion in field of traveling electromagnetic waves used in studies for microwave amplifiers, particle accelerators, etc 01 p0022 A67-10352

Oscillation frequency of maser oscillator calculated using perturbation theory, noting traveling wave effect 01 p0089 A67-10395

Microwave negative conductance due to traveling space charge waves in n-type GaAs 01 p0133 A67-10487

Dynamic response of simple beam and rectangular plate under traveling shock wave at supersonic speed, using Fourier transforms 01 p0161 A67-10775

Microwave swept frequency measurements on RF transmission line systems and development of VSWR and insertion loss test set 01 p0039 A67-11038

Emission of point oscillator located in medium having permittivity varying according to traveling wave law 02 p0192 A67-11643

Propagation characteristics of cylindrical waveguide partially filled with dielectric light modulation material 02 p0193 A67-11780

McIver and coupled mode theory derivations of equations for traveling wave transistor 03 p0382 A67-13667

Traveling waves interaction in gas laser, explaining forcing-of-oscillations and traveling wave suppression effect 03 p0439 A67-14371

Traveling wave field effect transistors, discussing method of increasing transconductance and cut-off frequency 04 p0582 A67-15096

Harmonic generation by traveling waves in nonlinear dispersive medium for quasi-monochromatic signals, obtaining correlation function and spectrum of second harmonic for Gaussian processes 04 p0657 A67-15146

Effect of finite length of conducting body on ponderomotive forces acting on traveling magnetic field 04 p0670 A67-15526

Time-invariant Stokes, anti-Stokes and double emission processes in distributed traveling wave systems, calculating spatial

EM field distribution and estimated conversion length 05 p0762 A67-16355

Traveling wave ruby laser as radar transmitter noting power gain, coherence, frequency shift and single mode of operation 05 p0819 A67-16657

Induced electron cyclotron radiation application to generation and amplification of high power electromagnetic traveling waves 05 p0824 A67-16915

Approximation of space wave plus complex wave using modified saddle point technique 05 p0766 A67-17297

Linear nonrelativistic motion of charged particle in field of traveling electromagnetic wave 06 p0975 A67-18087

Synthesis of traveling wave regime in complex optical resonator with additional external mirrors 07 p1196 A67-19600

Resonant cavity technique for measurement of k/beta diagrams /dispersion relations/ of leaky wave structures 07 p1153 A67-19612

Electron concentration inhomogeneities during traveling gravity wave propagation through F layer 07 p1178 A67-19809

Light waves traveling backward and forward in very small filaments of optical material result in standing waves producing visible spatial beats, allowing detection of changes in refractive index 07 p1224 A67-19841

Effects of gain saturation by strong traveling fields in dilute laser media, noting atomic motion and line broadening 07 p1197 A67-20126

Generating mode number in solid state lasers using traveling wave and standing wave 08 p1339 A67-21452

Flow of ideal compressible electrically conducting fluid in traveling wave accelerator, using multiple coordinate method to approximate small perturbation solution 09 p1544 A67-21849

Nonlinear thermomagnetic wave theory and amplification in case of plasma instability 09 p1545 A67-22072

Dispersion and interaction impedance of slow wave structures from cold tests measured, using resonance methods 09 p1476 A67-22212

Lorentz transform applied to solution of problem in interaction of waves within nonlinear medium 09 p1465 A67-22478

Traveling wave V antenna, discussing parameter variation effect on radiation patterns 11 p1761 A67-24283

Charged particle motion in field of traveling electromagnetic waves used in studies for microwave amplifiers, particle accelerators, etc 11 p1755 A67-25025

Containment of transparent plasma produced by field of traveling wave in circular waveguide, noting plasma ion-current distribution 12 p1976 A67-26066

Self-excitation regime associated with traveling magnetic field interaction with ionized gas flow 12 p1977 A67-26077

Traveling waves onset in gas turbine bladed disks, considering resonant vibrations 12 p2033 A67-26231

Interconnection of transmitters with no noninteracting elements reduces input traveling wave ratio of antenna arrays with power supply systems 13 p2080 A67-27033

Model thermospheres, studying ducted traveling acoustic gravity waves originating in ionosphere 14 p2310 A67-28054

Expression for surface field components obtained for plane electromagnetic wave at nose-on incidence on semilinear cone 14 p2261 A67-28376

F region and magnetosphere observation by incoherent backscatter radar technique 14 p2265 A67-28410

Current density variation determination in plasma accelerated by traveling waves [ONERA-TP-472] 14 p2359 A67-28509

Two port power flow analysis using generalized scattering parameters 14 p2287 A67-28625

Interaction between oppositely moving traveling waves in helium-neon laser with annular resonator 14 p2332 A67-28856

Harmonic generation by traveling waves in nonlinear dispersive medium for quasi-monochromatic signals, obtaining correlation function and spectrum of second harmonic for Gaussian processes 15 p2517 A67-29333

Dispersion relations of moving striations in rare gases, noting wave nature and

dependence on discharge

current 15 p2472 A67-29733

Intense fluctuations observed above Arecibo during geomagnetically disturbed conditions, using ionospheric backscatter technique 15 p2483 A67-30299

Induced electron cyclotron radiation application to generation and amplification of high power electromagnetic traveling waves 16 p2685 A67-30892

Equivalent resistance of traveling wave phototube for large modulation index 16 p2636 A67-30897

Rhombic traveling wave antenna with feedback loop to utilize larger proportion of total power 17 p2824 A67-32313

Intensity and specific heat ratio effects for laminar compressible boundary layers arising behind traveling shock waves 17 p2837 A67-32347

Traveling wave amplification by interaction of drifting carriers in semiconductors with external slow wave circuit 17 p2826 A67-32656

Plasma acceleration by SHF waves, worldwide research and results 17 p2904 A67-32915

Vacuum UV and X-ray lasers from electron ejection from inner shells of atoms through photoionization 18 p3060 A67-34015

Symmetrical traveling-wave antenna design with given sidelobe level and amplification factor, determining coupling coefficient and maximum utilization 18 p3011 A67-34178

Traveling ionospheric disturbances effect on and measurement of direction of movement of downcoming F-2 region perturbation 18 p3043 A67-34526

Traveling-wave bulk electroconvection induced in slightly conducting liquid with temperature gradient, giving velocity profile equations for plane flow 18 p3029 A67-34736

Counter traveling wave regime stability in ring gas laser, studying effects of atomic collisions, isotopic state and wave coupling 19 p3239 A67-34898

Time-growing instability existences in distributed parametric media using dispersion relation 19 p3195 A67-35620

Interaction between oppositely moving traveling waves in helium-neon laser with annular resonator 19 p3242 A67-36107

Synthesis of traveling wave regime in complex optical resonator with additional external mirrors 20 p3462 A67-37339

Fringing effects on electric efficiency variation with slp for cylindrical induction MHD device operable as accelerator, generator or Joule heater [AIAA PAPER 67-714] 21 p3673 A67-38740

Resonance in unbounded traveling and standing /harmonic oscillations/ waves, demonstrating equivalence of resonance states using wave equations 23 p4079 A67-41416

Strong traveling transverse acoustic modes generated by rotating gas jet in cylindrical cavity 23 p3993 A67-41763

TRAVELING WAVE AMPLIFIER

Traveling wave amplification by interaction of drifting carriers in semiconductors with external slow wave circuit 01 p0132 A67-10377

Gunn effect domain traveling wave parametric amplifier pumped by periodic impedance variations in boundary conductor of microstrip transmission line 01 p0040 A67-11309

Tunnel diode traveling wave amplifier, determining amplification coefficient and stabilization time of transient characteristics 03 p0377 A67-13234

Traveling wave parametric amplifier circuit with series connected varactor diode 03 p0380 A67-13504

Power gain of submillimeter wave in traveling wave amplifier with periodic delay-line structure 03 p0380 A67-13557

Amplifier using electro-optic junction modulator combined with photodetector, showing gain at microwave frequencies 05 p0774 A67-16822

Quantum paramagnetic traveling wave amplifier using rutile with admixture of chromium and combined with magnet with superconducting coil 05 p0825 A67-17161

Nonlinear propagation of pulse signal in laser type traveling wave amplifier 05 p0825 A67-17232

Traveling wave tube amplifiers for

communications systems noting amplitude transfer function, two-tone and FM intermodulation, etc 10 p1613 A67-23440

HF transistorized pulse amplifier with rise of 1 nsec and output voltages of more than 4 v designed for trigger pulses and traveling wave oscilloscope 13 p2082 A67-27400

Quantum paramagnetic amplifiers in USSR, discussing physical characteristics and operation of resonators in decimeter band, antenna systems for noise reduction, etc 16 p2623 A67-31024

Interaction between electrostatic and guided electromagnetic wave, considering plasma wave amplification by pumping at microwave frequency 18 p3091 A67-34643

Traveling wave tube as hyperfrequency amplifier onboard satellites for reliable space communications 21 p3592 A67-38212

Helix spurious mode effects on TW amplifier performance analyzed for methods of elimination 22 p3775 A67-40462

Nonlinear electrical problems requiring partial differential equations including magnetic saturation, parametric amplifier, electron tube, traveling wave amplifier and semiconductor diodes 24 p4133 A67-43089

TRAVELING WAVE MASER

Microwave mixing in paramagnetic crystal using traveling wave maser with ruby as mixer element, noting frequency conversion 01 p0086 A67-10003

Ultralow-noise tunable S-band amplifier using TWM as second stage 01 p0034 A67-10106

Competition of two types of oscillations in traveling wave laser 01 p0089 A67-10362

RCA defense electronic products applied research 02 p0251 A67-11785

Traveling wave maser consisting of paramagnetic crystal /chromium doped rutile/, slow wave circuit and ferrite isolator, discussing performance, stagger tuning, etc 02 p0251 A67-11787

Ferric-doped-rutile 8 mm traveling wave maser, noting operating range and performance characteristics 03 p0438 A67-13986

Amplitude and frequency characteristics of traveling wave ring laser 04 p0635 A67-15777

Competition of two types of oscillations in traveling wave laser 06 p1009 A67-17620

Iron doped rutile traveling wave maser operating in 34-36 GHz frequency range 07 p1196 A67-19605

Traveling wave excitation of high power nitrogen and neon lasers with velocity matching that of stimulated emission 07 p1196 A67-20093

Traveling wave maser for radio astronomy interferometer noting superconducting magnet, dynamo and cryostat 07 p1197 A67-20115

C-band traveling wave maser for monopulse radar, analyzing saturation, recovery, duplexing and gain phase stability 08 p1293 A67-20691

Ultralow-noise two-channel tunable cascade amplifier system using upconverter and traveling wave maser 08 p1304 A67-21222

L-band rutile traveling wave maser, discussing slowing factor and inverted susceptibility 09 p1514 A67-22270

Amplification and detection of high power TW laser pulses, noting superradiance limit 09 p1514 A67-22273

Maser for traveling waves over large cm wave band used as low noise amplifier 09 p1482 A67-22481

Saturation effect on phase shift of traveling wave masers and reflex type cavity masers 11 p1800 A67-24468

C-band traveling wave maser using printed circuit technology results in reduced structure size, perfect contact between structure and ruby, etc 11 p1801 A67-24727

Traveling wave maser in radiometry receiver 12 p1951 A67-25295

Ultralow noise receiver configurations for cryogenically cooled microwave traveling wave masers and parametric amplifiers 14 p2260 A67-27776

Liquid helium traveling wave maser amplifier for low noise ground station satellite communication 14 p2329 A67-27777

Cooling system for maser amplifier for ground station satellite communication 14 p2277 A67-27778

Low noise preamplifier traveling wave

maser operated in closed cycle refrigerator for receiving Mariner IV picture transmissions 14 p2329 A67-27779

Low noise amplifiers in radio astronomy 14 p2286 A67-28466

Relation between steady state behavior of regenerative traveling wave laser and linear constant damping in medium 15 p2454 A67-30076

Propagation in rectangular waveguide solved for traveling wave maser design by Rayleigh-Ritz method reduced to matrix eigenvalue problem 17 p2828 A67-33086

Population inversion and spin-lattice relaxation effect on maser operation 19 p3304 A67-35547

Centimetric broadband traveling wave maser functioning, discussing physical phenomena involved 20 p3458 A67-36492

Functional maser consisting of amplifier, low noise header and superconducting magnet for use in ATS 20 p3459 A67-36595

Satellite low noise temperature traveling wave maser preamplifier for microwave reception, discussing design, applications and specific electron gain 21 p3641 A67-38640

Traveling wave maser saturation and signal distortion, determining magnetic moment 21 p3642 A67-38813

Ruby as active material for traveling wave maser /TWM/ noting advantages 24 p4167 A67-42238

TRAVELING WAVE MODULATION

Traveling wave electro-optic modulator tested at 6328 angstroms with CW drive power 09 p1471 A67-21644

Traveling wave IR and sub-mm light modulator design using free carrier absorption in reverse biased p-n junction diodes 11 p1759 A67-24137

Variation of radiation pattern of array of two traveling-wave V-antennas and use as spacecraft antenna 16 p2639 A67-31360

Charge density modulation from plasma-beam interaction 20 p3504 A67-36157

Electron space-charge and nonzero beam-coupling impedance effects on TWT, considering weakly saturated state 20 p3395 A67-36313

TRAVELING WAVE TUBE

Power amplification/bandwidth product of active device as measure of rate at which power supply energy converts to signal energy, noting TWT role 01 p0032 A67-10011

Output autocorrelation function and spectral density of CW and FM signals passed through TWT 01 p0025 A67-10858

Noise coefficient minimization for traveling wave tube, with account of current interception at delay system 03 p0386 A67-13961

Harmonic response due to compressibility in traveling wave plasma devices, discussing magnetoacoustic resonances for case of cylindrical symmetry 03 p0485 A67-14051

Optimum cavity beam hole diameter for traveling wave tube determined from beam parameters and slow wave structure parameters 04 p0583 A67-15153

Noise figure of low noise to TWT obtained by calculating equivalent noise impedance stage by stage 05 p0773 A67-16510

Nonlinear equations of traveling wave tube solved approximately, taking account of relativistic effects 05 p0776 A67-17164

Electron beam rotation experiments on linear spiratron with M-type electron gun 05 p0776 A67-17169

Single wave approximation of fields of cylindrical delay system with basic E-type wave propagating at variable phase velocity 05 p0767 A67-17398

Increased oscillation stability and efficiency of traveling wave tubes for global satellite communications 06 p0967 A67-17683

TWT delivering CW power in L, S, C and X-band designed for space environment, considering size, weight and voltage and comparing klystrons, amplifiers, circuit design, etc 06 p0967 A67-17688

Small signal nonlinear amplitude distortion and phase shift measurement in TWT 07 p1151 A67-19427

High power broadband traveling wave tube YH 1041 as transmitting tube for satellite radio communication, discussing mechanical layout and operational characteristics 08 p1307 A67-21446

Periodic permanent magnet assemblies for traveling wave tube design, employing magnet stack design curves and demagnetization curves 09 p1476 A67-22210

Empiric design of taper for increasing efficiency of coupled cavity traveling wave tube 09 p1476 A67-22211

Small signals of wideband and high gain multicavity klystron amplifier showing similarity to traveling wave tube 09 p1478 A67-22254

Five hundred kw traveling wave tube for X-band, considering design and matching of clover leaf structure and higher order mode spectrum 09 p1478 A67-22255

Multicavity klystrons and traveling wave tubes and use in ground stations 09 p1478 A67-22257

Transmission characteristics of high power traveling wave tubes for satellite ground stations 09 p1478 A67-22258

Grid modulated transmitting tubes for space applications, discussing metal capillary cathodes 09 p1478 A67-22259

S-band traveling wave phototube operating with He-Ne laser noting performance, design and methods of operation 09 p1479 A67-22279

Microwave oscillation-amplifying L-band platinotron tube to amplify peak power of radar transmitter 10 p1605 A67-23061

Two-cascade frequency multiplier with traveling wave tube at various input frequency ranges and high conversion coefficient 10 p1613 A67-23406

Electronic efficiency of three types of TWT and dependences on dimensionless and dimension parameters 11 p1764 A67-24465

Harmonic power at TWT taking into account effect of space charge on electron beam bunching 11 p1765 A67-24478

Mode-locked laser traveling pulses proved experimentally to be 180 degree pulses 14 p2330 A67-28292

Optimum cavity beam hole diameter for traveling wave tube determined from beam parameters and slow wave structure parameters 15 p2443 A67-29340

Prevention of burnout in high power linear beam traveling wave tubes by placing small negative electrode at end of collector opposite beam entrance 15 p2447 A67-29754

Multiple carrier measurements using TWT for application to satellite communications 15 p2438 A67-30140

Tunable microwave-frequency light modulator consisting of rectangular cross section coaxial cavity with two electro-optical crystals 15 p2501 A67-30141

Amplification of traveling-wave tube calculated to determine effect of continuous current interception along delay system 16 p2640 A67-31506

Initial loss in TWT with lossless slow wave circuit connection to drift tube, expressing field components by sums of normal modes 18 p3010 A67-33645

Coupling between slow waves and convective instabilities in solids, showing interaction inhibition for electron drift velocities greater than phase velocity 18 p3101 A67-34017

Electron space-charge and nonzero beam-coupling impedance effects on TWT, considering weakly saturated state 20 p3395 A67-36313

Extension of nonlinear TWT equations to floating drift relativistic klystron, noting formulas for first harmonic of current in two- and three-cavity klystron 22 p3770 A67-39655

Crossed field cascade tubes as frequency oscillators and microwave generators, discussing improved performance and interaction efficiency of devices 22 p3775 A67-40559

Parametric amplification of traveling wave tube through coupled wave method noting role of phase velocities of space charge waves 24 p4130 A67-42241

TREATMENT

S HEAT TREATMENT

S OXYGEN TREATMENT

S SURFACE TREATMENT

S THERAPY

TREE

Aerial and space photography for forestry 14 p2321 A67-28827

TRI-SERVICE TRANSPORT

S XC-142 AIRCRAFT

TRIANGULAR WING

Three-dimensional boundary layer and

inviscid hypersonic flow interaction on infinitely thin triangular wing 01 p0007 A67-10982
 Linear supersonic conical flow past low surface of triangular wing, obtaining homogeneous boundary value problem for analytical function of complex variable 06 p0936 A67-17739

TRIANGULATION

Satellite triangulation based on simultaneous observations from two stations defining space orientation of plane 01 p0055 A67-10037
 Taper in thickness of wing for special case of linear type analyzed, using triangular elements for matrix displacement method 04 p0707 A67-14441
 Geometric satellite triangulation system and relation to dynamical coordinate system 05 p0797 A67-16569
 Photogrammetric network for large-area phototriangulation using star-tracking airborne cameras, discussing theoretical and technical aspects 06 p0994 A67-17716
 Satellite three-dimensional triangulation accuracy, discussing orientation of camera axes and plate coordinates of satellite images as error sources 06 p0994 A67-17717
 European satellite triangulation network, discussing scientific, technical and organizational aspects 07 p1176 A67-19761
 U.S. Coast and Geodetic Survey satellite triangulation program based on optical tracking of passive satellites simultaneously from two or more mobile camera stations 07 p1176 A67-19764
 Maryland-Minnesota-Mississippi Echo I satellite observation triangle, discussing principles of triangulation method, camera systems and office data reduction techniques 07 p1176 A67-19765
 Astrometric processing of synchronous photographic observations of Echo I satellite 07 p1144 A67-19769
 Position determination for mobile luminous objects in sky by triangulation, using ballistic photographic chambers in positions pinpointed by star sightings 07 p1188 A67-19770
 Ballistic camera calibration method and triangulation of satellite position from camera observations 07 p1188 A67-19776
 Triangulation by photogrammetric use of geodetic satellites and data reduction methods 07 p1177 A67-19777
 Direct method for determining space directions and adjustment of satellite triangulation net 10 p1637 A67-23181
 Systematic errors in earthward coordinates of selenodetic points, noting results of triangulation 11 p1860 A67-24461
 Errors, due to inaccurate tentative aerial observations, in determination of identification points for vertical aerial photography 13 p2118 A67-26464
 Geometric satellite triangulation for position of fourth satellite, with position equations solved by least squares method and applied to geodetic satellites 20 p3429 A67-36890
 Space triangulation equalization method based on modified closing plane method, discussing error equations 21 p3618 A67-38196
 Terrestrial and satellite geodesy, discussing construction methods of geodetic system by triangulation, astrogeodetic leveling or satellite observation on stellar background 21 p3620 A67-38521
 Determination of coordinates from satellite observations noting triangulation method and optical technique 23 p3994 A67-40700

TRIATOMIC MOLECULE
 Triatomic molecules formation and abundance in solar photosphere estimated for thermodynamic equilibrium 18 p3119 A67-33858

TRIDENT AIRCRAFT
 S DE HAVILLAND DH-121 AIRCRAFT

TRIFLUORIDE
 S CHLORINE TRIFLUORIDE

TRIFLUOROAMINE OXIDE
 Trifluoramine oxide IR spectrum measured, determining structure, symmetry and rotational, vibrational and thermodynamic properties 15 p2433 A67-29880

TRIGATRON
 Trigatron spark gap using low voltage plasma jet as switch analyzed for properties, time lag and mechanisms 19 p3298 A67-35602

TRIGONOMETRIC FUNCTION

Interaction between atoms of solid surface and gas phase, obtaining closed-form solution of motion equations 01 p0118 A67-11295
 Optimal approximations by trigonometric polynomials for classes of periodic functions belonging to Banach space 03 p0459 A67-13645
 Newtonian analogues of trigonometric and exponential functions studied by series 13 p2146 A67-26851
 Temperature field of coaxial cylinders obtained as infinite series of Bessel and trigonometric functions 13 p2224 A67-27057
 First order generalized planetary theory from Poisson form, deriving trigonometric expansion of disturbing functions, periodic inequalities, etc 18 p3120 A67-33865

TRIM

Trimming methods for Ti alloy materials including plasma arc cutting, band sawing, shearing, milling, nibbling and blanking 22 p3811 A67-39308

TRINITRAMINE

S CYCLOTETRAMETHYLENE

TRINITRAMINE /RDX/

TRIODE

Welmer triode with contact rectifier for use as component of microminiature radio circuits, noting effect of contact rectification on current-voltage characteristics and amplifying power of such triodes 01 p0035 A67-10397
 Small signal RF amplification of VHF MOS transistors, considering TA2840 triode and TA7010 dual-insulated-gate transistors used as VHF amplifiers 02 p0218 A67-12101
 Linear approximation of frequency and transient characteristics for field triodes with insulated gate of constant capacitance 03 p0386 A67-13956
 Shunting of input current into collector region of planar triode 03 p0386 A67-13963
 Thermionic energy converters in West Germany, discussing vacuum magnetic triodes, Cs diodes and rare gas triodes 04 p0554 A67-15026
 Basic diode and triode sputtering processes, describing channeled diode system and sheet beam 04 p0631 A67-15996
 Penetration factor along grid of plane triode calculated from nomograms 05 p0774 A67-16937
 Thermal noise limitation in space-charge-limited solid state diodes and triodes 06 p0971 A67-18224
 Grid modulated transmitting tubes for space applications, discussing metal capillary cathodes 09 p1478 A67-22259
 Triode version of active LF directional coupler compared to passive coupler 13 p2081 A67-27198
 Silicon space charge limited triode considered as analog transistor noting I-V characteristics, current proportionality, voltage amplification and noise performance 13 p2083 A67-27571
 Signal-source noise mismatch and alignment in linear triode amplifier networks 14 p2289 A67-28884
 Current distribution parallel connected semiconductor triodes based on approximate transfer characteristics of diodes 18 p2634 A67-30462
 Germanium pulse switching triode with fused p-n-p junction 18 p3009 A67-33477
 Triode system of reflex klystron, stressing creation of modulated SHF oscillations device 20 p3451 A67-37148
 P-n-p-n triode turn-off characteristics showing forward biased center junction, establishing general turn-off criterion 21 p3591 A67-38154
 Reverse transient in p-n-p-n triode when reverse pulse is applied to gate 21 p3598 A67-38573
 General three-terminal p-n-p-n triode turn-on criterion equation derived and simplified for practical external-circuit arrangements 22 p3770 A67-39731

TRIOXIDE
 Carbon dioxide solid matrix study of carbon trioxide production, IR spectrum and molecular structure 05 p0759 A67-16838

TRIPLET EXCITATION
 Dissociation cross section of hydrogen molecule exchange excited by electron impact from ground to triplet state, using one-center wave functions 15 p2521 A67-30379

Triplet-to-singlet conversion of difluoromethylene radical by self-annihilation, noting reactions with oxygen atoms 20 p3378 A67-37561

TRIPLET STATE
 Analytic power series solution of nonrelativistic Schrodinger equation for two-electron atom, assuming fixed nucleus and singlet and triplet S states 15 p2520 A67-30158
 Triplet-to-singlet conversion of difluoromethylene radical by self-annihilation, noting reactions with oxygen atoms 20 p3378 A67-37561

TRITIUM
 Tritium production in atmosphere by galactic cosmic rays, by solar flare accelerated particles and accretion from sun 04 p0613 A67-14855
 Cosmogenic tritium content in Sikhote Alin iron meteorite irradiated with reactor neutrons 09 p1569 A67-22688
 Helium 3 anomaly in octahedrites and low spallogenic tritium content in freshly fallen iron meteorites caused by tritium loss due to solar heating in space 11 p1866 A67-24694
 Methylene role in atmospheric tritiated methane, specifically nitric oxide interference 13 p2117 A67-27604
 Rapid assay for thymidylate synthetase as specific and sensitive measure of enzyme activity 14 p2280 A67-28479
 Tritium diffusion from iron meteorite shortly after fall established by artificial proton irradiation 17 p2942 A67-32357
 Tracer experiments using tritiated ethanol on surface of MOS capacitor to indicate field-induced proton transport 20 p3510 A67-36857

TROJAN ORBIT
 Long period features of motion of Trojan planets in vicinity of equilateral triangle configurations 06 p1079 A67-17784
 Long period of nonperiodic librational motion about equilateral points of restricted three-body problem 06 p1080 A67-17785
 Elliptic restricted problem of periodic Trojan orbit and nonperiodic librational frequency and angular motion of Jupiter 08 p1381 A67-20388
 Stability analysis of long period Trojan librations treated as short period oscillations about long period reference solution 11 p1866 A67-24774
 Oscillating libration orbits with period rigorously commensurable in rational fraction to basic long period 11 p1866 A67-24775
 Birkhoff normalization of Hamiltonian function in neighborhood of stable equilibrium position in connection with Trojan orbits in three-body problem 18 p2747 A67-30985

TROPICAL METEOROLOGY
 Atmospheric jet streams in tropical latitudes, discussing velocities, seasonal variations, etc 04 p0652 A67-15474
 Atmospheric ozone distribution, air flows and temperature at high altitudes in equatorial latitudes of Atlantic Ocean 05 p0799 A67-17026
 Numerical modeling role in studies of general circulation of atmosphere 10 p1877 A67-23368
 Atmospheric ozone data on basis of meteorological observations and synoptic maps on ship in Atlantic 11 p1785 A67-23958
 Circulation patterns in upper atmosphere, using sounding rockets from Indian equatorial station during monsoon and winter periods 12 p1935 A67-25791
 Nondeepening synoptic scale tropical disturbance showing dependence on in situ development and decay in upper troposphere 13 p2152 A67-27605
 Clouds over equatorial and tropical Pacific investigated by comparing photographs from Tiros satellites and jet aircraft 24 p4181 A67-42667

TROPICAL STORM
 Absolute angular momentum of outflow winds and radar targets in hurricanes and typhoons 10 p1676 A67-22813

TROPISM
 S GEOTROPISM
 S ISOTROPISM
 S PHOTOTROPISM

TROPOPAUSE
 Position of tropopause in middle latitude jet flow 02 p0240 A67-12642
 Radar detection of tropopause and clear

air turbulence 04 p0649 A67-14682

TROPOSCATTER

Discrepancies between Boithias and other theories on troposcatter antenna-to-medium coupling loss, showing graph of path gain loss 02 p0213 A67-11621

Troposcatter transmission technique called frequency time shift keying, deriving optimum noncoherent receiver configuration and error performance 02 p0202 A67-12123

Troposcatter test program for evaluating megabit digital transmission system, using wideband frequency shift keyed mode 02 p0202 A67-12126

Sunde channel model applied to Air Force tropo transmission test for calculating pulse error 02 p0202 A67-12129

PCM/TDM and influence of channel on signal determined, using mathematical model 02 p0202 A67-12130

PPM-frequency time hopping for multichannel communication system to transmit digital data over tropospheric scatter path 02 p0202 A67-12131

Time combined with frequency division multiplex multichannel communication system for transmission of digital information over tropospheric scatter communication channel 02 p0203 A67-12132

Angle-of-arrival measurements over troposcatter path by simultaneous reception in angle diversity, using antenna beams 05 p0760 A67-15998

Millimeter waves in atmospheric research, discussing radar meteorology, radiometry, etc 13 p0202 A67-27493

Troposcatter techniques reviewed proposing analog voice waveform conversion into digital form by delta modulation or PCM for upgrading present operational systems 16 p2628 A67-31492

Digital error performance of transportable troposcatter facility evaluated as function of path length 17 p2811 A67-32118

Wideband troposcatter radio channel simulator exhibiting frequency flat or frequency selective fading over band greater than 10 MHz and centered at 70 MHz 20 p3385 A67-37354

TROPOSPHERE

Quasi-stationary solar corpuscular fluxes, examining effect on atmospheric pressure in earth polar cap regions 01 p0061 A67-11279

Distribution of solar-tropospheric disturbances over earth surface, based on simultaneous observations of 103 U.S.S.R. stations 01 p0061 A67-11280

Millimeter and centimeter radio wave propagation in near sea level tropospheric waveguides 02 p0191 A67-11569

Atmospheric agitation effect on image of extended celestial light sources, showing importance in long-range tropospheric propagation of ultrashort radio wave 02 p0325 A67-11986

Prediction of apparent elevation angle expected for object situated in troposphere at specified values of geometrical elevation angle height 02 p0199 A67-12083

Tropospheric pressure-altitude data by satellite radiometric topography mapping, using oxygen absorption band centered at 5 mm 02 p0262 A67-12367

Carbon dioxide content in troposphere and lower stratosphere measured at various altitudes, showing seasonal variations 03 p0414 A67-14086

Radio data suggests dielectric constant variations in troposphere limited to discrete scale sizes [RASSA PAPER 1-10-141] 03 p0417 A67-14249

Random tropospheric angle error prediction in microwave observations of Early Bird satellite 04 p0574 A67-15074

Solar cycle effect on geomagnetic activity and temperature of near-earth tropospheric layer 04 p0616 A67-15227

Power spectrum of horizontal components of clear air turbulence in upper troposphere, examining influence of degenerating gravity waves on nature of turbulence spectra 05 p0837 A67-16486

Power spectrum of horizontal components of clear air turbulence in upper troposphere, examining influence of degenerating gravity waves on nature of turbulence spectra 13 p2150 A67-26342

Vertical distribution of tropospheric and stratospheric ozone based on observations of U.S. ozonometric stations at various latitudes 14 p2308 A67-27927

Tropospheric refractive index variation measurement technique 14 p2264 A67-28394

Tropospheric turbulence and structure derived from phenomenon of electromagnetic wave 14 p2264 A67-28397

Geostrophic wind angular momentum transport at 500 mb in Northern Hemisphere, using zonal harmonic analysis, noting quasi-biennial cycle 15 p2512 A67-29201

Estimation of parameters of transverse diffusion in lowest atmospheric layer using Lagrange and Euler turbulence characteristics 16 p2698 A67-31095

Statistical correlation of microwave range variation and dispersion differential measurements over 25 km tropospheric path 16 p2627 A67-31363

Troposcatter techniques reviewed proposing analog voice waveform conversion into digital form by delta modulation or PCM for upgrading present operational systems 16 p2628 A67-31492

Tropospheric circulation observation through FR-2 satellite project, discussing instrumentation, ground stations, trajectory analysis, etc 19 p3332 A67-35243

Position, shape and motion of large scale cirrus bands relationship to meteorological properties of upper troposphere 19 p3252 A67-35527

Searchlight brightness measurements for vertical turbidity layer of troposphere using computing scattering functions 19 p3225 A67-35532

Solar wind velocity relationship to tropospheric temperature field 20 p3428 A67-36814

Far tropospheric propagation of radio waves due to coherent scattering, explaining signal level dependence on distance and wavelength and signal fading 21 p3585 A67-38814

High velocity tropospheric winds at 40 to 60 km altitude, discussing supergradient and subgradient winds and energy transport to mesosphere possibilities 22 p3793 A67-40032

Electromagnetic pulse distortion during total internal reflection in stratified troposphere, discussing reflecting medium inhomogeneity effects on reflection coefficients 23 p3973 A67-40837

Ice nucleating properties of meteoritic material 24 p4231 A67-42371

TROPOSPHERIC RADIATION

Radio astronomical observation technique, eliminating tropospheric radiation noise fluctuation effects on telescope 02 p0198 A67-12033

Tropospheric probe using vertically polarized signals scattered by clear air turbulence 04 p0649 A67-14683

Variations in long wave radiation field of free atmosphere within 7 to 10 hr time periods 07 p1220 A67-19455

Normal distributions of various quantities related to radiation budgets of tropospheric column, earth surface and troposphere-earth system over Northern Hemisphere 13 p2116 A67-27458

Vertical distribution of heating rate by radiative processes over Northern Hemisphere presented in zonal cross sections 13 p2116 A67-27459

TROPOSPHERIC WAVE

Internal gravity-shear waves in troposphere for two-and three-layer model of air density and horizontal velocity, noting phase velocities 02 p0238 A67-12190

Amplitude of perturbations about each interface in internal gravity-shear waves in troposphere according to three-layer model 02 p0239 A67-12191

Perturbation of vertical smoke trails and smoke puffs in lower troposphere explained by internal gravity-shear waves 02 p0239 A67-12192

Correlation between entropy of envelope fluctuation of UHF radio signal and corresponding thermodynamic stability of tropospheric common volume 24 p4124 A67-42810

TRUNCATION

Truncated conical shell stability under axial compression loads applied parallel to axis rather than along generatrix 06 p1105 A67-18593

Properties of solutions of second order nonlinear nonautonomous ordinary differential equations from study of

truncated version of equation 17 p2879 A67-32884

TRUNCATION ERROR

Continuous automatic interval computation for numerical integration of initial value problem 01 p0105 A67-10515

Mathematical formulation relating modal distribution of truncation errors to matrix conditioning and loading type on structure 03 p0526 A67-13969

Finite difference method solution of diffusion equations, including analyses of stability and truncation errors 03 p0537 A67-14013

Truncation error bounds for sampling representations of band limited signals 04 p0570 A67-14871

Stability and error analysis of Runge-Kutta-Fehlberg numerical integration method 04 p0645 A67-14986

Critical analysis of Stokes gravity formula derivations, noting truncation error effect 05 p0796 A67-16153

Spectrum signature data applied to interference analysis, noting data truncation 05 p0781 A67-17538

Numerical solutions of Poisson and motion equations for electron gun design, examining truncation error via perturbation theory 14 p2287 A67-28677

Computational errors in generation of direction cosine matrix in strapdown system 15 p2515 A67-29741

Random errors in ultrasonic measurements, discussing Students distribution measurement repetition effect and rounding-off error evaluation 18 p3044 A67-33735

Limiting values for remainder forms in Taylor series and error estimation procedures for power series approximations, including truncation error 18 p3072 A67-34398

Crank-Nicolson technique for first order linear time-invariant differential equation solution, discussing truncation error 20 p3477 A67-36933

Strapped-down inertial navigation computational problems solved by Euler parameter algorithms require less computer time 21 p3656 A67-38951

Explicit nonlinear numerical integration method for solution of large systems of ordinary differential equations 23 p4024 A67-41394

TRUSS

Computer program for automated design of hyperstatic truss structures under resonant frequency used in multisatellite Agena launcher 03 p0526 A67-13968

Characteristics of transverse vibrations of p-i-n jointed trusses obtained by use of rational method of lumping inertia forces 03 p0529 A67-14103

TUBE

SA BRONCHIAL TUBE
SA CATHODE RAY TUBE
SA CIRCULAR TUBE
SA DISCHARGE TUBE
SA ELECTROMAGNETIC SHOCK TUBE
SA ELECTRON TUBE
SA FLASH TUBE
SA GAS TUBE
SA IMAGE CONVERTER
SA IMAGE DISSECTOR TUBE
SA IMAGE ORTHICON TUBE
SA IMAGE TUBE
SA MICROWAVE TUBE
SA PHOTOTUBE
SA PIPE
SA PITOT-STATIC TUBE
SA PITOT TUBE
SA PRESSURE TUBE
SA PRESTON TUBE
SA TRAVELING WAVE TUBE
SA VACUUM TUBE
SA VENTURI TUBE

Flexural instability of foldable tube with elastic recovery for use as structural elements, pipes, antennas and masts 01 p0165 A67-11387

Exhaust processes of gases at high initial pressure from tubes, when flow is initiated by acceleration of solid body 02 p0235 A67-12788

Brittle fracture of Be tube under differential thermal contraction-induced plastic strain 03 p0445 A67-13470

Compression, shear and bending strengths of tubular synthetic products as materials for aircraft structural component 04 p0715 A67-15539

Bending of flexible tubes using variational calculus of Rayleigh-Ritz type 09 p1579 A67-22606

Optical instrument for measurement and control of tube flares in connections in liquid propulsion systems 18 p3054 A67-34366

Work of deformation during expansion of tubular blanks with varying hardening characteristics under uniform loading 21 p3631 A67-38054

Torsion creep theory for circular and noncircular tubes using Bredt equation, measuring anisotropy in tubes, calculating torsion stresses 24 p4250 A67-42381

TUBE HEAT EXCHANGER

Thermal emissivity and absorptivity of trapezoidal grooves and paneled tubular radiators, obtaining parametric relations by numerical solutions via computer 02 p0342 A67-12331

Heat-transfer coefficient of tube in transverse flow calculated from tube surface temperature distribution 04 p0726 A67-15598

Flow induced vibration and noise in tube bank heat exchangers due to Karman vortex streets analyzed, noting shedding frequency, lift, etc [ASME PAPER 67-VIBR-48] 11 p1777 A67-24198

Karman vortices in heat exchanger, noting no vortex shedding in supercritical Reynolds number range and wake turbulence 11 p1782 A67-24657

Plated-tube heat exchanger design for minimizing axial heat conduction losses and controlling heat transfer surfaces and core weight 13 p2229 A67-27665

Surface pressure distribution on tube-lattice cluster with transverse gas flow to determine aerodynamic characteristics 20 p3359 A67-37306

TUBING

Component design advances with fatigue tests on hydraulic tubes and outline of seal development 05 p0753 A67-18749

Dent effect on buckling strength of aluminum alloy tubular columns subjected to axial compression [ASME PAPER 67-MET-12] 12 p2030 A67-25951

Permanent joints for Agena pressure systems, discussing retention of pressurized gases in connector tubing system 17 p2801 A67-31984

Computer program for design and routing of external plumbing of aircraft gas turbine engines 17 p2928 A67-32006

Hydraulic tubing permanent joints, made by induction-brazing method, for installation on A-7A Corsair II aircraft 17 p2801 A67-32007

Weldable tube fittings, welding equipment and inspection methods for connecting tubing in aircraft and aerospace hydraulic systems 17 p2864 A67-32008

Thermal gradients effect on separable tube connectors, discussing structural elements 17 p2864 A67-32009

Empirical method predicting flexible hose flow losses, with Fanning friction factor as Reynolds number and internal hose geometry function 22 p3785 A67-39971

TUMBLING

Drag coefficients for random and planar tumbling satellites 21 p3563 A67-37809

TUNGSTATE

S CALCIUM TUNGSTATE

S LEAD TUNGSTATE

TUNGSTEN

Low energy electron diffraction study of interaction of thin deposit of amorphous boron with tungsten single crystal surfaces 01 p0093 A67-10205

Silicon carbide generation by pyrolysis of gas mixtures on tungsten wires, using X-ray diffraction to analyze structure 01 p0103 A67-10688

Thermogravimetric analysis and electron microscopy of agglomeration and chemical instability of submicron refractory dispersoids in tungsten 01 p0097 A67-10699

Gravity sintering and low pressure pressing of tungsten powders for economic production of large diameter W matrices 01 p0098 A67-10701

Tungsten composites strengthened by fibered or reacted additive 01 p0098 A67-10702

Porous high efficiency predictable-pore-density tungsten ionizers for cesium ion engine 01 p0140 A67-10703

Field electron emission measurements for determination of work function of single crystal /110/ planes of tungsten 01 p0135 A67-10878

Ultrahigh temperature thermocouple using pure and boron-doped pyrolytic graphite or tungsten and rhenium for operation in vibration and oxidation environment 01 p0076 A67-11139

Solubility of carbon in Mo, Re and W determined by isothermal carburization method 03 p0439 A67-12845

Fracture surfaces, Wallner lines and crack propagation velocity in precracked W monocrystals at 20-300 degrees K 03 p0445 A67-13471

Thermostability of ceramic coatings applied to W and Mo during cooling, in terms of temperature-dependent elastic modulus and linear expansion coefficients 03 p0446 A67-13638

Oxygen adsorption on tungsten crystal face studied by back-reflection low energy electron diffraction 03 p0447 A67-13647

Positive ion emission from tungsten surfaces laser irradiated studied, using time-of-flight spectrometer 05 p0819 A67-18651

Vacuum testing machine to determine tensile and creep properties of heavily drawn W wires at temperatures up to 2500 degrees F 06 p1013 A67-17799

Electric resistivity and electroconductivity of copper composites reinforced with fibrous felts of tungsten 06 p1015 A67-17808

Zr-coated tungsten cathode in reducing divergence of electron beam emission 06 p0968 A67-18091

Alkali ion scattering coefficient from tungsten single crystals surface and dependence on incidence angle 06 p1036 A67-18424

Mutual diffusion characteristics of titanium-tungsten mixtures at high temperatures, noting discontinuity on concentration curve due to two-phase region presence 07 p1204 A67-19266

Corrosion tests of W-, Mo-, Rh-based materials for compatibility in lithium at 2500, 2800 and 3000 degrees F 07 p1208 A67-19466

Tungsten films with fcc structure obtained by ion beam sputtering in vacuum onto substrates of glass, rock salt and mica at various temperatures 07 p1232 A67-19557

Oxygen chemisorption and oxidation on tungsten ribbon studied by flash desorption, using mass spectrometer 09 p1457 A67-22023

Reaction rate of oxygen jet impinging on tungsten samples at high temperature and various pressures, noting activation energy and diffusion effect 09 p1457 A67-22026

Operating temperature effect on vacuum emission stability of vapor-deposited tungsten clad UC-ZrC and uranium dioxide 09 p1449 A67-22347

Effects of additions of carbon, nitrogen or oxygen on properties of vapor deposited tungsten 09 p1519 A67-22348

Temperature control and thermal coupling of cesium adsorption porous tungsten, charcoal and graphite reservoirs 09 p1450 A67-22350

Vapor-deposited tungsten formed by hydrogen reduction of tungsten hexachloride or hexafluoride, noting effect of crystal orientation and surface treatment on work function 09 p1451 A67-22357

Thermoelectronic properties of pure and barium-film coated face of tungsten single crystal thermoelectronic properties of pure and barium-film coated face of tungsten single crystal 10 p1694 A67-23846

Failure mode at tip of crack predicted using cleavage strength and shear strength of perfect crystals, noting tungsten and iron 11 p1880 A67-25090

Thermal accommodation coefficient of rare gases on clean tungsten surfaces with gas temperature above room temperature 13 p2223 A67-26943

Thermal accommodation coefficient of nitrogen and helium on nitrogen covered tungsten above room temperature 13 p2223 A67-26944

Youngs modulus and shear modulus of inorganic filaments of tungsten and boron measured by oscillation technique 13 p2144 A67-27187

Book on tungsten and its compounds, physical, chemical and metallurgical data 14 p2336 A67-27890

Porous cesium ionizer with improved lifetime obtained by adding secondary tantalum to tungsten powder [AIAA PAPER 66-219] 14 p2376 A67-28124

Tungsten powder compacts impregnation technique by metallic halides solutions, obtaining even distribution of metal 14 p2338 A67-28614

Li film structure on compact tungsten faces by diffraction method, using free electron beams 14 p2372 A67-28760

Structure of thin tungsten films as function of nature and temperature of substrate, noting partial crystallization of fcc structure 15 p2535 A67-29477

Adsorptive interaction of oxygen with tungsten surface 15 p2434 A67-30100

Fracture surface appearance and crack propagation velocity variation with stress and temperature in tungsten 16 p2688 A67-31302

Reduced blackness coefficients measured for coaxial system of tungsten-molybdenum surfaces by calorimetric method 16 p2780 A67-31778

Oxygen caused bright spots in field ion microscope patterns of tungsten, noting oxygen variation effects 16 p2693 A67-31873

Thermionic and electrical sorption properties of tungsten in alkali iodide vapors at high pressure 17 p2887 A67-32201

Thermostability of ceramic coatings applied to W and Mo during cooling, in terms of temperature-dependent elastic modulus and linear expansion coefficients 17 p2875 A67-33172

Epitaxial growth of iron on tungsten field-emission points studied by field-emission microscopy 19 p3302 A67-34938

Interaction of oxygen with tungsten surface at room temperature 19 p3244 A67-34940

Low energy electron diffraction /LEED/ observations of interaction of tungsten surface with adsorbates 19 p3246 A67-35785

Adsorption of oxygen on tungsten surface, discussing electron diffraction 19 p3246 A67-35786

Etch pitting and electron microscopy used for tungsten single crystals dislocation density measurements at different strain levels 19 p3248 A67-36028

Electron emission and adsorption of potassium on tungsten single crystal faces, noting work function values 20 p3504 A67-36165

Cesium vapor ionization on porous tungsten substrate creates gradients in surface atom concentrations diminishing ionization efficiency 20 p3487 A67-36170

Stacking faults in tungsten specimen heated rigidly for short time by electric discharge 20 p3464 A67-36225

Tungsten cermet emissivity study using electron heating 20 p3466 A67-36913

Tungsten sheets examined for recrystallization, grain growth and ductile-brittle transition temperature /DBTT/ as function of thermal treatment and grain size 20 p3467 A67-37119

Grain boundary diffusion coefficients in tungsten at high temperatures, obtaining activation energy equation 20 p3470 A67-37388

Tungsten strain amplitude dependent dislocation damping measured as temperature function, discussing inconsistency with Friedel thermally activated breakaway theory 22 p3819 A67-39352

Oxygen interstitial solid solubility in niobium, noting decrease with addition of tungsten and molybdenum 22 p3823 A67-40211

Superconductivity enhancement in fine grained tungsten films, discussing structural changes and theoretical models 23 p4036 A67-40702

Temperature effect on structure of W films prepared by triode pulverization at low pressure and low power 23 p4041 A67-41194

Isobars of adsorption of Ce on faces of W crystal measured for adsorption heat dependence on atom surface density 23 p4042 A67-41298

TUNGSTEN ALLOY

Work function of solid solutions of tungsten with molybdenum and tantalum explained by surface adsorption effects 01 p0093 A67-10092

Phase diagram of W-Zr-Ti ternary

alloy 01 p0093 A67-10291
Line broadening due to cold working Ta-10 percent Re and W-20 percent Re studied by Fourier analysis, integral breadth measurements and variance analysis 02 p0256 A67-12701
Porous structures for ion engine application, discussing ionizer materials preparation, based on powder metallurgy and two-phase tungsten base alloy [AIAA PAPER 66-221] 08 p1341 A67-20576
Depressing effect of hafnium and zirconium on work function of tungsten, tantalum, niobium and rhenium 10 p1668 A67-23091
Thermophysical properties of heat-resistant solid solution of rhenium in tungsten produced by arc melting in vacuum 12 p1956 A67-25758
X-ray and metallographic examination of tungsten alloys, noting decrease of work function during thermal emission upon addition of lanthanum hexaboride 13 p2131 A67-26468
Structures in Mo-Re and W-Re systems examined by X-ray powder techniques, discussing occurrence of chromium oxide type structure 17 p2873 A67-32813
Influence of palladium additives and sintering temperature on tungsten molding noting shrinkage, density, microhardness, durability and microstructure 20 p3466 A67-36910
Rate of diffusion and degree of density during activated sintering of tungsten-molybdenum powders, noting influence of nickel additive 20 p3466 A67-36911
Tungsten-molybdenum alloy heat-resistant properties noting vacuum testing and subjection to plastic deformation, with results related to molybdenum content and temperature 20 p3467 A67-36968
Equilibrium phases in annealed NiCrTiAlW alloy using optical and electron microscopy and X-ray analysis 23 p4019 A67-41078
Mass spectrometric study of oxygen adsorption, determining condensation coefficient and tungsten surface work function for various concentrations 24 p4172 A67-42073
Chemical interactions in formation of oxidation resistant solid lubricant composites of tungsten diselenide-gallium alloys for use in ball bearing systems [ASME PAPER 67-LC-6] 24 p4164 A67-42745

TUNGSTEN CARBIDE
Aluminum and tungsten carbides formed from metal powders mixed with acetylene black and exposed to explosive shock 03 p0440 A67-12927
Thermostability of WC-Co alloys, discussing heat treatment, crack formation, bending strength and thermal shock resistance 03 p0447 A67-13641
X-ray study of phase composition of refractory alloys carbide solid solutions noting hardness, electric resistance and elastic deformation energy of crystal lattice 04 p0638 A67-15205
Carbon content effects on properties of WC-TiC-Co alloys vacuum sintered 06 p1017 A67-17968
Structural, physical and mechanical properties of hard alloys formed by sintering powdered VK 15 tungsten cobalt alloy with nonuniformly distributed carbide phase 07 p1208 A67-19305
X-ray analysis of lattice strain and crystallite size changes in tungsten carbide compressed at high pressure, noting annealing effect 11 p1809 A67-24949
Solid solutions of titanium, tungsten, chromium prepared by carbidization of mixtures in hydrogen medium and obtained as fine-grained carbide powders 16 p2691 A67-31587
Tungsten-carbon phase relations from DTA, X-ray and electron diffraction measurements noting disordered, ordered hexagonal and orthorhombic modifications 16 p2692 A67-31599
Thermostability of WC-Co alloys, discussing heat treatment, crack formation, bending strength and thermal shock resistance 17 p2875 A67-33174
WC-NbC-Co alloys oxidation resistance in air studied by sintering powdered WC and NbC with Co, finding oxidation rate linear function of time 22 p3820 A67-39565

TUNGSTEN COMPOUND
Metallurgical and geometrical factors

affecting high temperature tensile properties of discontinuous tungsten fiber reinforced composites 03 p0441 A67-13272
Hexagonal indexing of tungsten boride phase in reaction of boron with tungsten core, obtaining X-ray powder diffraction pattern 06 p1016 A67-17904

TUNGSTEN INERT GAS /TIG/ WELDING
Welding technique for thick nickel-base alloy using gas tungsten arc, noting inspection techniques, tensile test results, etc 12 p1950 A67-25736
Plasma arc welding processes compared with TIG method for speed, cost quality, etc [ASME PAPER 67-DE-46] 14 p2328 A67-28879
Aluminum alloy sheet welds with high silicon and magnesium content analyzed for tensile properties and fracture toughness 24 p4161 A67-42330

TUNGSTEN OXIDE
Rate of formation of tungsten oxide in porous sample, noting increase in rate of oxidation due to porosity effect 11 p1809 A67-24915
Adsorptive interaction of oxygen with tungsten surface 15 p2434 A67-30100
Criticism of McCarroll statement on oxide formation on tungsten surface at room temperature 19 p3244 A67-34942

TUNGUSK METEORITE
Cometary origin of Tungusk meteorite of 1908 supported by analysis of space trajectory and observed nightglow at time of fall 01 p0151 A67-11274
Tunguska meteorite composition, evaluating validity of theory attributing nucleon-antinucleon annihilation to antimatter composition 04 p0701 A67-15546
Tungusk comet trajectory and orbit with radiant in constellation Cetus 05 p0889 A67-16210
Parameters and shock wave characteristics of Tunguska explosion, postulating reaction mechanism 10 p1710 A67-23611
Tunguska meteorite transfer from heliocentric to geocentric orbit proved impossible by computer calculation 11 p1868 A67-24847
Ballistic aspects, structure and destructive power of Tungusk meteorite do not support thermal explosion 15 p2558 A67-30010
Ballistic aspects, structure and destructive power of Tungusk meteorite do not support thermal explosion 20 p3530 A67-37534
Parameters and shock wave characteristics of Tunguska explosion, postulating reaction mechanism 20 p3530 A67-37535

TUNING
Two-frequency volume resonator with independent tuning within wide frequency band 02 p0214 A67-11911
Tunable dispersion resonator and broadening of laser emission spectral range to obtain operating frequency other than fundamental 03 p0435 A67-13131
Microwave varactor tuned transistor oscillator design, considering collector base multiplication, oscillation and load matching conditions and theoretical tuning curve 04 p0581 A67-14864
Analogous tube and transistor tuned feedback amplifier analysis and use of nonunidirectional active network as amplifying element 04 p0586 A67-15670
Tuning of gas laser resonator 07 p1195 A67-19505
Dynamic vibration absorber for reducing transient vibrations of one degree of freedom system with tuning criteria formulated as function of root line of characteristic equation 10 p1715 A67-22913
Design equations and computer calculated curves to achieve varactor-tuned octave bandwidth transistor oscillators by using transmission line 10 p1613 A67-23412
Electrodynamic vibration absorber attached to single degree of freedom vibrating system as passive or active device with or without feedback [ASME PAPER 67-VIBR-18] 11 p1796 A67-24177
Central tuning dip in power output of continuous wave submillimeter molecular laser to measure radiative lifetime and collision line broadening 11 p1803 A67-24932
Automatic cavity tuning of hydrogen masers to achieve frequency source of absolute accuracy over unlimited time periods 13 p2125 A67-26512

Optical fluorescence, thermally tunable over significant portion of visible and near IR spectrum, from phase-matched parametric system 13 p2127 A67-27081
Resonant gate transistor used in integrated circuits as frequency selector element for tuning problems 16 p2642 A67-31724
Signal generator tuning to center frequency of narrow band receivers, noting test setup and procedure 17 p2827 A67-32800
Frequency multiplier operating from 10-30 GHz with easily tunable construction, obtaining lossy element influence approximation 20 p3398 A67-36863
Electrically tunable low pass filter using Permalloy films near resonance 22 p3772 A67-39906
Magnetically tunable multisection bandpass filter in ferrite-loaded evanescent waveguide 22 p3772 A67-39907

TUNNEL
SA HOTSHOT TUNNEL
SA HYDRODYNAMIC TUNNEL
SA SHOCK TUNNEL
SA WATER TUNNEL
SA WIND TUNNEL
Steady tunnel operation effects on tracked hovercraft air cushion performance, discussing tunnel entrance problems 22 p3746 A67-40067

TUNNEL DIODE
Negative resistance of waveguide-mounted tunnel diode decrease with frequency suggested as source of oscillations at frequencies above cut-off 01 p0032 A67-10001
Trapezoidal I-V characteristics in gallium arsenide at liquid nitrogen and room temperature 01 p0033 A67-10027
Inductive and capacitive tunable tunnel diode harmonic generator in waveguide 01 p0035 A67-10437
Nonsinusoidal pumping of tunnel diode mixers, calculating noise figure for zero bias as function of pump voltage 01 p0037 A67-10477
Multistable memory consisting of series of cascaded bistable tunnel diodes with low resolution time 01 p0037 A67-10660
Bistable logic delay circuit using tunnel diodes in circuit branches, noting fast response time and numerical division capability 01 p0044 A67-10661
Electron-tunneling measurements of energy gap in lanthanum explaining differences between various measurements 01 p0135 A67-10918
Electronic equipment for measuring peak and valley currents of tunnel diodes 02 p0216 A67-12037
Mode switching in tunnel diode, noting change from relaxation to microwave oscillation mode 02 p0217 A67-12090
Subnanosecond time interval measurements with recirculating transmission line memory 02 p0243 A67-12092
High speed magnetic logic circuits for operation in nuclear radiation environment 02 p0219 A67-12161
Electric characteristics of nGe-pGaAs heterojunctions in multistep recombination-tunneling model 02 p0299 A67-12189
Multichannel tunnel diode chronotron circuit for measuring picosecond time intervals directly with sequence of timing circuits 02 p0246 A67-12684
Graphical derivation of switching trajectories of transistor-tunnel diode logic circuits 03 p0389 A67-12803
Tunnel diode traveling wave amplifier, determining amplification coefficient and stabilization time of transient characteristics 03 p0377 A67-13234
Nonlinear distortions in parallel and series tunnel diode voltage amplifiers 03 p0377 A67-13235
Static characteristics of series connected tunnel diodes used in determining pulse duration and recovery time of driven multivibrator 03 p0377 A67-13236
Dinistor trigger circuits with counting input, discussing flip-flop circuits 03 p0377 A67-13239
Two frequency SHF tunnel diode trigger for automatic systems using frequency recorded information 03 p0378 A67-13245
Longitudinal microwave phonons inducing tunneling in Al-Pb, Al-Sn and Pb-Pb superconducting diodes 03 p0379 A67-13330
Relationships involving power and efficiency of self-excited tunnel diode

oscillator, calculating effect of parasitic TD parameters and circuit 03 p0381 A67-13584

Tunnel diode combined with backward diode improves rate of response and pulse waveform in tunnel diode circuits 03 p0381 A67-13585

Tunnel-diode amplifier sensitivity gain due to negative resistance variation 03 p0382 A67-13668

Book on network theory of negative-resistance tunnel diode linear and nonlinear sinusoidal circuits and application to amplifiers 03 p0383 A67-13817

Tunnel diode circuit stability, equivalent circuit and conductivity hodograph 03 p0386 A67-13965

Binary tunnel diode scaler and factors essential for reliable operation 03 p0376 A67-14266

Logarithmic tunnel diode amplifier design techniques and characteristics 04 p0580 A67-14597

Electron transfer in thin film tantalum-tantalum oxide diodes, noting tunnel and Schottky emission 04 p0582 A67-15106

Surface aspects of thermal degradation of GaAs p-n junction lasers and tunnel diodes 04 p0585 A67-15620

Pulse front shaping with monostable tunnel-diode generator by successive triggering through storage inductance 04 p0586 A67-15674

Radiation hardened sampled data recording system design, fabrication and testing incorporating parallel write-in, variable rate sampling and tunnel diode memory 04 p0625 A67-15709

Josephson tunnel effect in semiconductors 05 p0860 A67-16360

I-V characteristics of p-gallium antimonide based tunnel junction at various temperatures analyzed, finding secondary peaks exhibited by inverted diodes 05 p0861 A67-16395

Book on semiconductor devices including thermal processes and microwave frequency conversion in semiconductor diodes 05 p0771 A67-16447

Tunnel diode superregenerative amplification and detection in linear regime and volt-ampere characteristics of diode 05 p0772 A67-16450

Logic and memory circuits and operational dynamics of system of pulsed elements operating on tunnel diodes 05 p0772 A67-16451

Steady state analysis of switching circuit using combination of transistors and tunnel diodes, considering temperature effect and thermal stabilization of operating points 05 p0772 A67-16452

Current dependence on voltage in Sn-Sn and Pb-Pb tunnel junctions attributed to electric gap anisotropy 05 p0863 A67-16754

Performance characteristics of tunnel diode autodyne frequency converters 05 p0774 A67-16917

Tunnel diode amplifier distortion by finite impedance at zero frequency and second harmonic frequency 05 p0775 A67-16945

Tunnel diode capacitance relation to displacement interpreted in terms of impurity drift in nonuniform field of p-n junction in highly doped germanium diodes 05 p0865 A67-16959

Effect of copper on excess and tunneling current of As-doped Ge tunnel junctions 05 p0866 A67-16986

Noise factor dependence on frequency in tunnel-diode frequency mixers 05 p0777 A67-17172

Possibility of realization of multicascade tunnel diode frequency doublers without interscatter amplification 05 p0777 A67-17173

Electrodynamics of combined operation of transistors and tunnel diodes in pulsed circuit 06 p0970 A67-18170

Tunnel diode circuits for fast digital circuits, noting shift generator and comparator generator 06 p0970 A67-18203

Superconducting tunnel diode for quantum generation and detection of incoherent phonons, discussing I-V characteristics 06 p1011 A67-18211

Inductive correction effect on single stage tunnel diode RC amplifier, noting increase of upper frequency limit and shortening of wave front buildup time 06 p0970 A67-18213

Transistorized electron counter using tunnel diodes, noting trigger 06 p1004 A67-18391

Contact effects in degenerate semiconductors at low temperature based on Hall study of tunnel junctions 06 p1069 A67-18976

Reverse tunneling currents in GaSb tunnel diodes as function of temperature and voltage explained through band structure 06 p0972 A67-18977

Thermal radio emission from Mercury at 1.9 cm monitored by 140 ft radio telescope using tunnel diode radiometer 07 p1246 A67-19056

Short pulse start/stop control of tunnel diode oscillator 07 p1153 A67-19608

Stability analysis of parametric phase-locked subharmonic tunnel diode oscillator circuits capable of bistable phase operation 07 p1153 A67-19610

VHF tunnel diode frequency multiplier noting power gains and circuit 07 p1155 A67-19793

Electron barrier heights of Al-Al₂O₃-SnTe and Al-Al₂O₃-GeTe tunnel junctions, noting values of Fermi level and energy gap 07 p1155 A67-19893

Current-voltage-temperature dependence of symmetric tunnel junctions, noting role of insulator thickness 07 p1237 A67-20184

Parallel critical field calculation of tunneling barrier extended to all temperatures in dirty limit 09 p1552 A67-21745

Built-in voltage decrease in bulk germanium and Ge tunnel diodes under irradiation, noting Fermi level 09 p1471 A67-21764

Performance and stability of germanium tunnel-diode autodyne frequency converter 09 p1472 A67-21957

Operation of coupled mutually loaded tunnel diodes, considering short circuit mode 09 p1473 A67-21963

Effect of tunnel diode amplifier V-I characteristics on cross modulation products in electromagnetic spectrum 09 p1557 A67-22266

System characteristics of tunnel diode amplifiers, discussing noise figure, intermodulation, AM-PM conversion, etc 09 p1481 A67-22479

Monostable high speed pulse circuit using tunnel diode and transmission line, noting possibility of cascade connection without coupling elements between stages 10 p1809 A67-22773

Photon modulated tunneling in Te-Al oxide-Al structures, noting increased spectral response and detection range 10 p1889 A67-22907

Excess tunnel current due to inelastic electron molecule interactions near metal insulator interface 10 p1889 A67-23074

Monolithic gallium arsenide tunnel diode construction with epitaxial layer grown on semi-insulating substrate 10 p1817 A67-23542

Energy conservation analysis of step in negative resistance region of voltage-current characteristic curve of oscillating tunnel diode 11 p1759 A67-24132

Reflection amplifier design for use in tunnel diode UHF radio repeater 11 p1766 A67-24689

Subharmonic oscillations in tunnel diode circuits analyzed, including solutions to forced pumping oscillations and frequency characteristic equations 11 p1768 A67-24858

Energy distribution of electron tunneling through metal-insulator-metal diode noting dependence on temperature, film thickness and voltage 12 p1982 A67-25449

Three-channel particle spectrometer with semiconductor detectors and tunnel diode discriminators noting noise immunity, high signal level output, etc 12 p1944 A67-25853

Ten-channel tunnel diode analog-to-digital converter 12 p1909 A67-25856

Explanation of anomalies of experimental static current-voltage characteristics of GaAs tunnel diode oscillators 12 p1917 A67-26098

Two 8-cascade tunnel diode oscillators with HF oscillations and low resonant resistance 13 p2078 A67-26750

Distributed tunnel diode amplifier design noting magnitude of attenuation by shunt for LF and HF [AFOSR-67-1406] 13 p2079 A67-26876

Automatic frequency control circuit for SHF tunnel diode converter 13 p2069 A67-27043

RC network project for stabilization of tunnel diode, noting stability conditions,

negative differential resistances, etc 14 p2283 A67-28041

Low noise amplifiers in radio astronomy 14 p2286 A67-28466

Superconducting storage device with Josephson tunneling junction replacing cryotron 14 p2289 A67-28921

Minimum value of noise constant of tunnel diode, noting occurrence beyond point of inflection on I-V characteristic curve 14 p2290 A67-28930

Tunnel diode logarithmic amplifier circuit design using thin film passive components and tiny inductors 15 p2442 A67-29166

Volt-ampere characteristics of gallium arsenide tunnel diode oscillators 15 p2443 A67-29285

GaSb properties and perspective applications, noting junction formation, production processes, etc 15 p2536 A67-29700

DC and AC parameters of germanium tunnel diodes in 3 to 5 millamp range measured by ammeter dC and AC parameters of germanium tunnel diodes in 3 to 5 millamp range measured by ammeter 15 p2449 A67-29807

Variation of series resistance and junction capacity in tunnel diodes used in microwave switching 15 p2449 A67-29808

Inductive correction effect on single stage tunnel diode RC amplifier, noting increase of upper frequency limit and shortening of wave front buildup time 16 p2635 A67-30479

Performance characteristics of tunnel diode autodyne frequency converters 16 p2636 A67-30894

Book on analysis and synthesis of tunnel diode circuits including equivalent circuits, amplifiers, etc 16 p2636 A67-30997

Tunnel diode oscillator design from averaged and normalized current-voltage characteristics 16 p2637 A67-31028

Waveguide mounted tunnel-diode oscillator noting equivalent circuit, power output, frequency, etc 17 p2822 A67-32037

Circuitry and operation of instrument measuring entire DC response of tunnel diodes, describing measurement method 17 p2823 A67-32298

Superconducting tunnel junction, discussing effect of exceeding critical current in one film 17 p2922 A67-33058

Conduction mechanism in GaSb tunnel p-n junctions from 77 to 380 degrees K, noting temperature dependence of basic parameters, V-I characteristics, etc 18 p3098 A67-33573

Tunnel diode amplifier with single circuit, stability analysis and calculation of circuit parameters 18 p3011 A67-34179

Operating spectrum of tunnel diode oscillator developed according to waveguide techniques, determining optimal requirements 18 p3011 A67-34232

Switching tunnel diodes, discussing amplitude discrimination and binary memory 19 p3193 A67-35065

Oscillation conditions of microwave tunnel diode theoretically and experimentally evaluated for mounting at feed point of semicircular loop antenna 19 p3196 A67-35660

Stability criterion for bandpass tunnel diode amplifier, determining limitations on diode series inductance as function of negative resistance 19 p3196 A67-35662

Design and stability of wideband tunnel diode amplifiers for microwave radiolink receivers 20 p3395 A67-36248

Tunnel diode technology stressing electrical results 20 p3396 A67-36490

Memory-cell circuit employing Esaki diodes negative resistance characteristic, developing small memory pulse amplitude useful in minimizing cycle time 20 p3397 A67-36769

Voltage comparator with high speed analog-to-digital converter and tunnel diode circuit 20 p3398 A67-36771

Volt-ampere characteristics of tunnel diode analyzed to derive dependence of differential resistance on voltage 20 p3400 A67-37150

Performance and stability of germanium tunnel-diode autodyne frequency converter 20 p3400 A67-37187

Operation of coupled mutually loaded tunnel diodes, considering short circuit mode 20 p3400 A67-37193

Tunnel and excess currents in Esaki diodes compatible with reversible introduction of active intermediate tunneling

- levels 21 p3590 A67-38152
 Impurity effect on solubility of another
 impurity in p-n silicon tunnel diodes studied
 by measuring current-voltage
 characteristics 21 p3682 A67-38364
 Forced oscillation in distributed constant
 system with tunnel diode described by
 linear wave equation with nonlinear
 boundary conditions 21 p3598 A67-38606
 Microwave characteristics of coaxial
 mounted tunnel diodes investigated by
 equivalent circuit 21 p3602 A67-39070
 Junction potential measurement in
 irradiated tunnel diode showing no
 oscillation in any bias
 voltage 22 p3767 A67-39369
 High speed wideband L-band tunnel diode
 frequency deviator tunable over octave
 bandwidth by 160 mv change in input
 voltage
 [IEEE PAPER 19-TP-67-1175]
 Injection and emission of hot electron in
 thin film tunnel diodes 23 p4039 A67-40885
 Tunnel diode low level detection
 characteristics under various bias conditions,
 discussing sensitivity performance and
 stability characteristics 24 p4131 A67-42444
 Moderate bandwidth tunnel diode
 amplifier using directional filter as bandpass
 structure 24 p4131 A67-42445
 Gigahertz tunnel diode logic, static and
 dynamic behavior of circuits under DC worst
 case tolerance analysis, timing analysis,
 etc 24 p4133 A67-42825
- TUNNEL RESISTOR**
 Film resistance effect on low impedance
 tunneling measurements 07 p1234 A67-20101
 Tunnel current modulation by acoustic
 wave in superconductors 15 p2537 A67-29708
 Tunnel current modulation by acoustic
 wave in superconductors 24 p4200 A67-41778
 Magnetic impurities in tunnel junction
 barriers investigated for effect on junction
 resistance 24 p4200 A67-41865
- TUNNELING**
 Photon modulation of tunnel emission
 produced by IR irradiation of thin film
 semiconductor sandwich of aluminum-
 aluminum trioxide-tellurium-gold
 01 p0131 A67-10369
 Electron-tunneling measurements of
 energy gap in lanthanum explaining
 differences between various
 measurements 01 p0135 A67-10918
 Electron tunneling through space charge
 region of uniformly doped metal-
 semiconductor barriers calculated in
 effective-mass
 approximation 02 p0280 A67-11483
 Electron conduction in discontinuous metal
 films by transport of activated charge
 carrier creation and by tunneling for island
 sizes 02 p0292 A67-11746
 Electric conductivity in microcrystalline
 metal films in theory based on Kubo type
 formula and Bardeen-Harrison-Stratton
 treatment of tunneling 02 p0292 A67-11748
 Tunnel-current measurements of sandwich
 configurations, determining metal/metal-
 oxide work function 02 p0295 A67-11764
 Gapless superconductivity by tunnel effect
 experiments on dirty superconducting alloys
 in high magnetic field 02 p0300 A67-12247
 NGe-pGaAs heterojunctions, diffusion or
 emission theories of current transport do
 not explain electrical characteristics but
 validate Anderson model, considering
 tunneling as transport
 mechanism 03 p0494 A67-13478
 V-I tunneling characteristics and energy
 gap anisotropy of Pb-Bi superconducting
 alloy, discussing mean free
 path 03 p0501 A67-14341
 Radiative interband recombination in
 strong electric field of p-n junction,
 calculating radiation intensity as function of
 quantum energy and applied
 voltage 05 p0863 A67-16689
 Tunneling through junctions with
 nonuniform electric field, calculating
 probabilities and currents by WKB
 method 05 p0866 A67-16973
 Tunnel current passing from type II
 superconductor into normal
 metal 05 p0871 A67-17490
 Backward diode fabrication and properties
 for SHF detection, noting germanium
 diode 06 p0969 A67-18120
 Weak superconductivity electrodynamics
 and EM wave propagation in Josephson
 tunnel junction in presence of
 vortices 06 p1054 A67-18806
 Band structures of group V semimetals
 and IV-VI semiconductors analyzed using
 tunneling, noting data on band edge
 energies 06 p1069 A67-18975
 Reverse tunneling currents in GaSb tunnel
 diodes as function of temperature and
 voltage explained through band
 structure 06 p0972 A67-18977
 Electron motion in crossed fields with
 arbitrary ratio of electric and magnetic
 fields, considering simultaneously valence
 and conduction bands 06 p1069 A67-18978
 Critical field for nucleation of
 superconductivity at tunneling barrier in
 magnetic field 07 p1235 A67-20131
 Anisotropy of energy gap in
 superconducting Pb analyzed using
 superconductive tunneling 07 p1236 A67-20137
 Forward bias V-I characteristics for
 heterojunction in which tunneling dominates,
 noting temperature effect 09 p1551 A67-21666
 Josephson and ordinary tunneling currents
 for two-band model superconductor, treating
 niobium-tin junction 09 p1551 A67-21667
 Kinetic tunneling theory in
 superconductors clarifies conditions for
 onset of Josephson
 current 09 p1555 A67-22071
 Granular superconductor with thin
 insulating layer at boundary of each
 homogeneous superconductor grain, using
 Isospin formulation of microscopic
 theory 10 p1687 A67-22763
 Electric field penetration of electrodes
 incorporated into theory of electron
 tunneling through dielectric
 layer 10 p1689 A67-22961
 Zirconium-niobium alloy analyzed by oxide
 replica technique, noting superconductivity
 and tunnel effect, determining relation
 between superconductivity current critical
 density and sample structural
 characteristics 10 p1689 A67-23090
 Exchange model of zero bias tunneling
 anomalies, discussing Hamiltonian,
 interference magnetic scattering and metal
 junctions 10 p1691 A67-23400
 Tunneling assisted photon absorption
 process /Franz-Keldysh effect/ in
 semiconductor junctions studied, using
 differential photocurrent
 response 10 p1691 A67-23402
 Low bias non-Esaki current in tunneling p-
 n junction diodes with large excess
 currents 11 p1768 A67-24926
 Electron-phonon interaction and phonon
 spectrum observed for electron tunneling
 measurements in fcc alloys of Pb alloys,
 noting electron concentration
 changes 13 p2175 A67-26426
 Anisotropy in tunneling density of states
 in pure type II superconductors, examining
 ideal case of perfectly specular boundary
 scattering at tunneling
 junction 14 p2365 A67-28294
 Two opposing tunnel currents
 determination through transition zone of
 metal-oxide-metal
 structure 14 p2367 A67-28515
 Superconducting indium-bismuth alloy
 films immersed in strong magnetic fields
 parallel and perpendicular to surface,
 studying film thickness effect by tunneling
 technique 14 p2371 A67-28723
 MOS oxide-film thickness estimation by
 extrapolating MOS capacitance-voltage curve
 into accumulation region at high negative
 bias 15 p2539 A67-29815
 Radiative interband recombination in
 strong electric field of p-n junction,
 calculating radiation intensity as function of
 quantum energy and applied
 voltage 15 p2539 A67-29859
 I-V curve related to state densities on
 both sides of n-p junction of tunneling
 system 16 p2725 A67-30808
 Superconductors and ferromagnetic
 domains proximity effects at critical
 temperature in resistive and tunneling
 effect measurements 17 p2912 A67-32271
 Tunneling into thin superconducting films
 in magnetic field, measuring field effect on
 density of states for finite mean free
 path 17 p2924 A67-33371
 Probability of tunneling across impurity
 level of p-n junction 18 p3099 A67-33695
 Slowly decaying broad maximum of
 parallel conductance explained by tunneling
 for surface states near Si-silicon oxide
 interface 18 p3101 A67-34018
 Weak superconductivity electrodynamics
 and EM wave propagation in Josephson
 tunnel junction in presence of
 vortices 18 p3102 A67-34425
 Growth rate of oxide and other dielectric
 contact films on metal crystals computed for
 ionic diffusion and electron
 tunneling 18 p3103 A67-34590
 Image-force effects in normal state
 tunneling through lead-oxide-lead junctions
 exhibiting Josephson effect
 [JPL-TR-32-1154] 18 p3106 A67-34647
 Microwave photon interaction with
 superconducting tunneling currents
 measured in aluminum-indium junctions,
 extended to tin-lead junctions, discussing
 phase shift 19 p3303 A67-35046
 Potential delta well model for barrier in
 solid state tunneling 19 p3308 A67-36039
 Tunneling characteristics of metal-oxide-
 silicon semiconductors, observing band
 structure and interface-state densities
 influences 19 p3308 A67-36045
 Quantum mechanical transition time shown
 to be electron tunneling characteristic
 time 20 p3505 A67-36178
 Electron tunneling through thin dielectric
 films and damping relation to electron
 energy calculated, using band model and
 matrix methods 20 p3508 A67-36424
 E/k-relation for complex insulator band
 structure, explaining polarity effect on
 tunneling through asymmetric
 barrier 20 p3508 A67-36425
 Properties of steps appearing on volt-
 ampere characteristic of Josephson current
 in superconducting tunneling, noting
 nonlinear resonance effects 20 p3509 A67-36690
 Wave interference and radiation tunneling
 phenomena influences on thermal radiation
 energy transfer between two separated solid
 dielectrics, noting spacing effect
 [ASME PAPER 67-HT-21] 20 p3546 A67-36716
 Alternating Josephson current and
 electromagnetism field interaction in
 generation of Pb-dielectric-Pb tunnel
 junction, noting steps in IV
 characteristics 21 p3677 A67-38096
 Tunnel and excess currents in Esaki
 diodes compatible with reversible
 introduction of active intermediate tunneling
 levels 21 p3590 A67-38152
 Microscopic theory of zero-bias magnetic
 tunneling anomalies covering weak and
 strong coupling limits in p-n semiconductors
 and tunnel junctions 21 p3682 A67-38385
 Schottky tunneling measurements in GaAs
 with Au noting fine
 structure 22 p3861 A67-39996
 Current fluctuations in Josephson
 superconducting tunnel
 junctions 22 p3865 A67-40433
 Josephson junction as switching device or
 logic element, discussing tunneling states
 and transition
 characteristics 22 p3865 A67-40437
 Anisotropic energy gap measurements in
 niobium single crystals by
 tunneling 22 p3865 A67-40440
 Superconducting niobium energy gap
 determination by tunneling
 experiments 23 p4036 A67-40703
 Tunneling of electrons from normal metal
 to superconductor containing paramagnetic
 impurity atoms, discussing current voltage
 characteristics 23 p4043 A67-41300
 Edge effects in tunneling characteristics
 of thin film aluminum diodes in
 superconducting state, showing anomalies
 associated with quasi-particle tunneling
 through film edges 24 p4128 A67-41868
- TURBINE**
 SA AXIAL FLOW TURBINE
 SA GAS TURBINE
 SA SHROUDED TURBINE
 SA STATOR
 SA STEAM TURBINE
 SA SUPERSONIC TURBINE
 SA TWO-STAGE TURBINE
 Stress analysis by polar coordinate system
 of turbine disks produced in various wound-
 fiber configuration 19 p3234 A67-34873
 Cascade flow in mixed flow pumps and
 turbines, solving boundary value problems
 for stream function by relaxation
 method 20 p3356 A67-36421
 Optimal functional parameters of
 elastically damping turbine rotor bearing to

determine critical velocities of shaft 21 p3695 A67-38832

Real gases examined for application as working fluid in Brayton cycle power plant, considering radiator area reduction to Rankine cycle 24 p4102 A67-42488

Free thermal convection in axisymmetric rotating cavities 24 p4255 A67-42588

TURBINE BLADE

Velocity distributions at blade profiles in two-dimensional model of axial stage treated by numerical solution of Fredholm integral equations 01 p0006 A67-10525

Stress amplitude of gas turbine blades vibrating in resonance 02 p0336 A67-11466

Kryptonate /radioactive source with Kr 85/ for temperature profiles of turbine blades, missile gas analysis, corrosion, oxidation, etc 02 p0265 A67-12214

Dynamic stability and critical flutter of axial-flow-turbine blades in cascade, for natural frequencies slightly mismatched 03 p0520 A67-12880

Thermal stresses generation in nozzle blades of gas turbines tested in near operating conditions 03 p0429 A67-13332

Directional solidification and single-crystal casting for jet engine turbine blades 03 p0429 A67-13541

Columbium additions to stainless steel for steam turbine blading 03 p0446 A67-13543

Stress distribution in fir-tree fastenings of turbine blades in alternate bending caused by blade oscillations under static tension 03 p0528 A67-14076

Boundary layer measurements of friction losses due to finite thickness of leading edges of turbine blades 03 p0353 A67-14306

Coupling of turbomachine blade vibrations through rotor or disk in causing variations of natural frequencies and amplitudes [ASME PAPER 66-WA/GT-5] 04 p0711 A67-15360

Inertial force effect on stress distribution around blade roots of turbine disk analyzed, using low Young modulus material and stroboscopy 05 p0811 A67-16602

Materials evolution with high resistance to creep, mechanical and thermal fatigue, corrosion and impact, for gas turbine blades 05 p0829 A67-16744

Cooling gas turbine blades by heat pipe effect for stationary blades and thermosyphon effect for moving blades 05 p0874 A67-16747

Securing packets of reaction blades in turbine rotors and casings 05 p0811 A67-16841

Thermal shock testing of adhesive strength and crack resistance of turbine vane protective coating 06 p1006 A67-17610

Inflow boundary layer effect on secondary flow at blade tips of circular cascade of reaction turbine, considering tip and gap losses 06 p0937 A67-17991

Oscillogram interpretation during ultrasonic inspection of turbine and compressor blades 06 p1007 A67-18098

Ultrasonic immersion inspection apparatus for structural defects detection in turbine blades 06 p1007 A67-18103

Heat resistant nickel-based alloys for gas turbine blades and disks 06 p1018 A67-18232

Wind tunnel study of strong-deflection supersonic cascade decelerating flow past turbine blades 07 p1128 A67-20296

Heat-resistant casting alloy KhH65VMTiU for gas turbine guide vanes, noting structural stability and oxide film 09 p1519 A67-22376

Temperature field measurement behind combustion chamber of turbojet engine 09 p1560 A67-22464

Aerodynamic flow field past cascade of plane thin turbine blades subjected to small random vibrations [ONERA-TP-412] 09 p1439 A67-22588

Computer calculation of induced circulations and influence coefficients for turbine blades with arbitrary profiles and oscillation shift 10 p1591 A67-23044

Evaluation of wire lacing designs for damping of vibratory stresses on gas turbine blades [ASME PAPER 67-VIBR-47] 11 p1797 A67-24197

Determination of proper frequencies of vibration of thick-bladed turbine disk with interaction between disk, blades and shrouding [ASME PAPER 67-VIBR-52]

Vibratory motions of turbine blades, considering frequency determination, tangential mode, stress, damping and excitation source [ASME PAPER 67-VIBR-66] 11 p1797 A67-24201

Corrosion test on turbine blades with nickel and cobalt base conducted in burner rigs, using metallographic examinations [ASME PAPER 67-GT-2] 11 p1808 A67-24790

Dependence of creep, corrosion and thermal fatigue of gas turbine vanes and blades upon inlet temperature and rate of change [ASME PAPER 67-GT-17] 11 p1808 A67-24801

Testing of transpiration air cooled turbine, discussing blade fabrication [ASME PAPER 67-GT-29] 11 p1854 A67-24807

Rotating blades cascade performance in mixed flow turbomachines, noting flow characteristics and slip factors 12 p1892 A67-25350

Aerodynamic theory of blade vibration, discussing compressibility effect, stalling and design 12 p2014 A67-25412

Vibration characteristics of cantilever type pretwisted turbine blading, considering effects of taper, calculating frequencies and mode shapes 12 p2014 A67-25414

Natural frequencies of bladed disks calculated from receptances 12 p2014 A67-25417

Vibration characteristics of turbine and compressor blading under rotation 12 p2015 A67-25418

Gas turbine blade erosion from dust, discussing momentum separators and erosion-resistant coating 12 p1990 A67-25947

Auxiliary singularity-carrier-curve theorems derived for blade profile design calculations 12 p1893 A67-25970

Traveling waves onset in gas turbine bladed disks, considering resonant vibrations 12 p2033 A67-26231

Frequencies of turbine blade vibrations calculated by iteration method, considering coupling between bending and torsion 13 p2217 A67-28744

Self-ignition and fuel combustion at blade cascade taking place at velocities and temperatures comparable to those of gas turbines 13 p2187 A67-28746

Aerodynamic damping and frequency drift of turbomachine blades, discussing wind tunnel testing results for various geometric configurations 13 p2051 A67-27205

Heat transfer calculation to turbine blading in cascade in presence of secondary flow, considering flow velocity estimation, blade boundary layer and related heat transfer properties 13 p2225 A67-27465

Ultrasonic flaw detection of hidden cracks in turbine blades 14 p2395 A67-27872

Hollow internally braced turbine blade design with uniform state of stress and temperature distribution 14 p2377 A67-28653

Flow through blade cascade studied by averaging flow parameters behind cascade for testing internal combustion turbine guide vanes 16 p2736 A67-31005

Matrix method calculation for frequency, deformation, forces and moments of variable cross section in rotating turbine blade during natural bending oscillation 16 p2766 A67-31150

Transonic blade cascades determined by mixed analog-numerical method starting from velocity distribution law and hodograph method 16 p2594 A67-31710

Calculation of compressible subsonic potential flow through blade cascades, giving air outlet angle, velocity distribution around blade profile and critical Mach number 17 p2791 A67-32711

Powder-metallurgical methods using mechanical filling, isostatic pressing and high vacuum-high temperature sintering for fabrication of airfoil turbine-blade blocks 17 p2865 A67-32821

Temperature fields in cross section of gas turbine blade with internal coolant during variation of local heat-transfer coefficient 17 p2973 A67-33076

Heat-transfer coefficients for heat transfer from gas to blade surface in gas turbine under operating conditions 17 p2973 A67-33077

Tip losses in two types of turbine straight-blade cascades at several Reynolds numbers, noting vibration effect on stage

performance 18 p2983 A67-33999

High temperature operation of air-cooled turbine blades and vanes 18 p3115 A67-34377

Gas turbine theory based on Coanda effect and turbine efficiency from fluid flow analysis of depressive blade-fitted turbines 20 p3515 A67-36274

Local heat-transfer coefficients of turbine blades, evaluating local Nusselt number distribution, Reynolds numbers, and turbulent flow effects 20 p3515 A67-36451

Gas turbine cooling, discussing high temperature problems, solutions and benefits of air cooled blades and vanes 20 p3517 A67-37168

Book on turbine blade vibration damping for increasing operational reliability 21 p3715 A67-37831

Optimum relative angular velocity selected for cooled high temperature gas turbine stages, discussing blade mean cooling depth and cooling heat 22 p3870 A67-40456

Aerodynamic damping of turbine buckets and compressor blades noting flutter and frequency shift 23 p3927 A67-40669

Natural frequency vibration mode of turbine blades calculated by approximate theory of integral evaluation yield discrete models 23 p4076 A67-40684

Solution for flow through circular array of blades contained between two surfaces of revolution separated by small variable distance obtained by Akeret method 23 p3927 A67-40726

Turbine blade profile calculation by hybrid method 23 p3928 A67-41244

Matrix displacement method for coupled bending-bending vibrations of pretwisted blading 23 p4078 A67-41329

Coated columbium alloy potential as turbine vanes in gas turbine power plants, discussing stress rupture strength, oxidation erosion and thermal fatigue lives [ASM PAPER C6-1.4] 23 p4020 A67-41402

Variable gas pressure acting on turbine engine blades measured by piezoelectric sensors, discussing sensor structure and noise possibility 24 p4153 A67-42095

Surface temperature oscillations of externally cooled working blades of gas turbine with air-liquid mixtures 24 p4254 A67-42255

Coupling of turbomachine blade vibrations through rotor or disk in causing variations of natural frequencies and amplitudes [ASME PAPER 66-WA/GT-5] 24 p4251 A67-42461

TURBINE ENGINE

Digital electronic programmable turbine engine control system for reducing time and cost in engine-control system matching 01 p0030 A67-11094

Sonic analysis for determining performance and mechanical integrity of turbine engines by using phase-locked filter and frequency ratio 01 p0076 A67-11141

Turbine engine propulsion system development noting inlet temperatures, turbine-blade cooling methods, etc 02 p0302 A67-11817

Effects of improved refractory blade materials and internal cooling on inlet temperatures, design and performance of air breathing engines at supersonic speeds [AIAA PAPER 65-743] 03 p0502 A67-12904

Radial gap effect on effectiveness of turbine stage determined from gas leakage measurements by outlet cross section traversing techniques 04 p0690 A67-15895

Cooling induced hydraulic and thermodynamic energy losses in high pressure turbine and turbojet engines 04 p0690 A67-15896

Hypothetical turbine driven power shaft bearing arrangement for logical analysis and practical approach to selection of optimum rolling bearings [SAE PAPER 670060] 09 p1508 A67-22534

Mechanical difficulties in designing shaft, bearing and seal systems for three high speed turbine engines [SAE PAPER 670064] 09 p1560 A67-22537

Hot corrosion of aircraft gas turbine alloys operating in marine environment reproduced in laboratory test, analyzing nature of attack 11 p1804 A67-23918

Book on helicopter gas turbine engines 11 p1852 A67-24524

Pneumatic starting systems for gas turbine engines including energy sources, system

components and arrangements
[ASME PAPER 67-GT-15] 11 p1854 A67-24800
High pressure hot gas solid propellant cartridge starter for aircraft turbine engine
[ASME PAPER 67-GT-21] 11 p1854 A67-24803
Testing of transpiration air cooled turbine, discussing blade fabrication
[ASME PAPER 67-GT-29] 11 p1854 A67-24807
Light weight small gas turbine starter system permitting self-starting of high power turbo engines noting cost, flexibility, military application, etc 12 p1988 A67-25186
High speed radial turbine rotor temperature distribution measured for pattern prediction of temperature 12 p1988 A67-25354
Dynamic vibration in aircraft power plant components, noting responsiveness of parts and fatigue life evaluation
[SAE PAPER 670237] 12 p1989 A67-25495
Allison T63 engine sand and dust tolerance development and field experience
[SAE PAPER 670334] 12 p1990 A67-25875
Emulsified fuel mixture /JP-4 and water/ tested in model Allison T63 turbine engine
[SAE PAPER 670368] 12 p1987 A67-25883
Averaged axisymmetric vortex flow of ideal incompressible fluid in turbine engine 14 p2296 A67-27986
Test procedure and apparatus for evaluating oxidation-corrosion characteristics of aircraft gas turbine engine lubricants at high temperature 14 p2326 A67-28794
System-effectiveness concept for turbine and piston engine 15 p2584 A67-30402
Requirements for operating characteristics of single and twin gas turbine engines for military helicopters noting system response, deceleration, fuel control, etc 16 p2736 A67-30929
Parametric comparative study of helicopters powered with current-technology engines and advanced non-regenerative and regenerative twin-engine installations
[AHS PAPER 119] 16 p2598 A67-31835
Ch-54 A Flying Crane helicopter, discussing use in Vietnam in terms of field supply, transportation to Vietnam, etc
[AHS PAPER 126] 16 p2598 A67-31841
Optimum use of contingency power rating for increasing permissible operating gross weight in twin-turbine helicopters performing long continuous flights
[AHS PAPER 128] 16 p2599 A67-31842
Engine design for civil operation from military supersonic engine
[SAE PAPER 670316] 17 p2929 A67-32978
Operating economics in short-haul air transports noting advantages of conversion to turbine powered equipment
[SAE PAPER 670357] 17 p2975 A67-32996
Soviet book on combustion chambers of gas turbine engines covering fuels, working processes, heating, etc 18 p3111 A67-33675
Temperature measurement for aircraft gas-turbine engine 18 p3157 A67-33898
Variable turbine geometry in gas turbine engines, discussing part power fuel consumption, acceleration characteristics, etc
[AIAA PAPER 67-417] 18 p3111 A67-33904
Aircraft engine turbine structure effect on blade tip clearance, analyzing clearance variations as function of rotor angular velocity 22 p3868 A67-39546
Fuel burnout processes in inlet flow of secondary air stream to turbine combustion chamber determined by working mechanism in inlet section of chamber 22 p3869 A67-40453
Protective coatings of Ni and Co base superalloys for gas turbine engines, discussing microstructure, chemistry and phase composition
[ASM PAPER C6-4.2] 23 p4020 A67-41405
Variable gas pressure acting on turbine engine blades measured by piezoelectric sensors, discussing sensor structure and noise possibility 24 p4153 A67-42095
Space power system pulsed turbine concept using bipropellants, reviewing multistage and multiple pass reentry performance and operational characteristics 24 p4107 A67-42530
Aircraft and missile electric/hydraulic power supplies, describing turboalternator performance, design and applications 24 p4107 A67-42532
TURBINE NOZZLE
Thermal stresses generation in nozzle

blades of gas turbines tested in near operating conditions 03 p0429 A67-13332
Theoretical aspects and technological development of parametric optimization of centripetal turbine stage, including study of turbine nozzle and wheel profiling 07 p1239 A67-19298
Irregularly spaced nozzle vanes effect upon blade vibration in radial flow gas turbine
[ASME PAPER 67-VIBR-42] 11 p1797 A67-24195
Stress-strain state and corrosion and erosion produced by aggressive gas flows in surface layers of gas turbine nozzle blades of ZrS6-K alloy 13 p2187 A67-26451
NERVA components including nozzle and associated hot gas bleed port, turbopump, control valve, pressure vessel and thermocouples 22 p3834 A67-40172
TURBINE PUMP
Vibration problems in high speed turbines including stability, critical speeds and support structure effect on rotor response
[ASME PAPER 67-DE-8] 14 p2402 A67-28867
Configuration selection of turbopump for hot-bleed cycle nuclear engine, discussing performance optimization factors 22 p3834 A67-40162
TURBINE WHEEL
SA COMPRESSOR ROTOR
SA IMPELLER
Temperature and heat transfer conditions determination on rotating turbine wheel in jet power plant, using electric analogy 04 p0688 A67-14571
Dynamic rubber wheel model to supplement digital computer analysis for prediction of frequencies, mode shapes and stress distributions of vibrating rotor stages
[ASME PAPER 66-WA/GT-8] 04 p0712 A67-15364
Elastoplastic calculation of turbine disks, considering cyclic plastic deformation 05 p0810 A67-16177
Plastic deformation and fracture of rotating turbine rotor model 09 p1502 A67-21554
Determination of proper frequencies of vibration of thick-bladed turbine disk with interaction between disk, blades and shrouding
[ASME PAPER 67-VIBR-52] 11 p1797 A67-24201
Vibrations of turbine disks of variable thickness calculated by Ritz method, applying functions approximating actual thickness of disk 21 p3636 A67-38836
Astroloy /Ni base superalloy/ disks for jet engine application, discussing chemical composition, basic ingot structure, forging and heat treatment 22 p3818 A67-39226
Laminar flow field between rotating turbine disks solved for low Reynolds number and partial admission 23 p3988 A67-40614
Closed die forging of nickel base superalloys for large turbine wheel components
[ASM PAPER C6-18.4] 23 p4010 A67-41401
TURBOALTERNATOR
Aircraft and missile electric/hydraulic power supplies, describing turboalternator performance, design and applications 24 p4107 A67-42532
Reentry vehicle solid propellant and liquid fuel compact turboalternator electric power system operating characteristics and performance 24 p4108 A67-42534
TURBOCHARGER
SA CENTRIFUGAL COMPRESSOR
Instrumentation and fuel systems for turbocharged and/or pressurized aircraft, discussing vapor lock problem, hydrocarbon fuels and vapor pressure equipment
[SAE PAPER 670262] 12 p1899 A67-25510
TURBOCONVERTER
NASA radial flow turbine research related to Brayton cycle power generator, investigating size, Reynolds number and speed effects on efficiency and flow 24 p4102 A67-42489
TURBOELECTRIC CONVERSION
Potassium Rankine cycle turboelectric space power system, emphasizing vapor fin type of condensing radiator 20 p3364 A67-37018
TURBOFAN AIRCRAFT
Aerodynamics of nacelle used in selection and integration of exhaust systems producing highest thrust-minus drag cruise

performance
[SAE PAPER 660734] 01 p0140 A67-10634
ADAM II /air deflection and modulation/ propulsion system and application to long tube vertical propulsive wing aircraft configurations
[SAE PAPER 670353] 17 p2929 A67-32993
Turbofan jet propulsion system reversed-thrust, discussing momentum net change, external drags, clamshell and annular targets and cascade reversers
[AIAA PAPER 67-418] 18 p2982 A67-33905
TURBOFAN ENGINE
Isolated nacelle design for high by-pass ratio turbofan engines, particularly pylon mounted engine
[SAE PAPER 660732] 01 p0140 A67-10632
Nacelle design for high inlet pressure recovery and low external cowl drag, for high by-pass fan engine subsonic aircraft
[SAE PAPER 660733] 01 p0140 A67-10633
Thrust reverser efficiency on high by-pass ratio turbofan engines
[SAE PAPER 660736] 01 p0140 A67-10635
JT9D turbofan engine for Boeing 747 commercial transport aircraft, analyzing design and performance potentials
[AIAA PAPER 67-374] 15 p2548 A67-30346
Rolls-Royce three-shaft turbofan engine vibration, number of parts and maintainability
[AIAA PAPER 67-375] 15 p2548 A67-30347
Program for perceived noise levels reduction on ground of turbofan-powered commercial transport by acoustically absorptive lining of ducts
[AIAA PAPER 66-389] 15 p2548 A67-30357
High bypass ratio turbofan engine installation noting induction system, exhaust system, thrust reverser configuration requirements, accessories, etc
[AIAA PAPER 67-390] 15 p2548 A67-30358
Four engine STOL aircraft for short distance hauls, noting fuselage and wing design 16 p2595 A67-30601
Turbotip lift fan concept for VTOL propulsion system, noting control capability, future potential, etc
[AHS PAPER 115] 16 p2737 A67-31831
Flight test program for F-111A variable sweep tactical weapon system, discussing afterburning turbofan engine, crew module, escape and survival 17 p2795 A67-32214
JT9D engine design from viewpoint of incorporated noise reduction features
[SAE PAPER 670331] 17 p2929 A67-32984
Shaft power from conventional two-spool turbofan engines for composite aircraft applications
[SAE PAPER 670352] 17 p2929 A67-32992
Optimal thrust-weight ratio for lifting engines of VTOL aircraft 18 p3110 A67-33544
Optimal layout of turbofan jet engines, discussing experimental rig for high thrust measurement
[AIAA PAPER 67-416] 18 p3111 A67-33903
TURBOGENERATOR
Turbodynamo disk stress-strain state, with final deformations under unsteady operational conditions, noting plastic flow, continuity, tension, and disk equilibrium equations 19 p3234 A67-34880
TURBOJET
Optimal layout of turbofan jet engines, discussing experimental rig for high thrust measurement
[AIAA PAPER 67-416] 18 p3111 A67-33903
TURBOJET AIRCRAFT
Initial VGH data on small turbojet operations in commercial transport service relating to accelerations, airspeed operating practices and unusual events
[AIAA PAPER 67-408] 15 p2421 A67-30375
Temperature effect on thermostability of high temperature synthetic lubricants for turbojets 24 p4162 A67-42484
TURBOJET ENGINE
SA BRISTOL-SIDDELEY OLYMPUS 593
TURBOJET ENGINE
Flight environment effect on lubrication requirements of Pratt-Whitney SST engine
[SAE PAPER 660711] 01 p0013 A67-10601
Supercharging turbojet engine for light aircraft compared to piston and turbojet engines 03 p0502 A67-13006
Energy method analysis of flutter instabilities in turbojet engine rotors caused by interaction between unsteady air loading and coupled vibration modes
[ASME PAPER 66-WA/GT-8] 04 p0713 A67-15384

- Air-cooled rotor and guide vanes of turbojet engine 06 p1073 A67-17607
 Temperature field measurement behind combustion chamber of turbojet engine 09 p1560 A67-22464
 Extended plug nozzles in suppression of jet noise in small turbojet engines [SAE PAPER 670157] 09 p1561 A67-22544
 Nondestructive testing techniques for turbojet engines noting advantage of planned inspection [SAE PAPER 670339] 12 p1950 A67-25876
 Materials requirements for aircraft turbojet and ramjet engines 13 p2187 A67-26694
 Mach 2 plus Olympus 593 turbojet power plant for Anglo-French SST, analyzing fuel system, lubrication and cooling on test run 13 p2187 A67-26701
 Hydraulic, pneumatic and electric circuits for twin loop engine control system of Olympus 593 in Concorde SST 13 p2187 A67-26702
 Liquefied natural gas application to SST, noting improvement in engine performance with use of methane 13 p2185 A67-27439
 Technical, economic and operation criteria for airlines when switching from conventional engines to turboprops or turbojets 14 p2409 A67-28499
 Reliability methods used to insure reliability of supersonic transport engine [SAE PAPER 670317] 17 p2929 A67-32979
 Fuel control system of GE4 engine for supersonic transport noting main and augmentation fuel and control subsystems [SAE PAPER 670326] 17 p2929 A67-32982
 Airborne analyzer and digital recording system to assess, diagnose and predict turbojet engine health on immediate and long term basis [SAE PAPER 670359] 17 p2861 A67-32998
 Energy method analysis of flutter instabilities in turbojet engine rotors caused by interaction between unsteady air loading and coupled vibration modes [ASME PAPER 66-WA/GT-6] 18 p3115 A67-34130
 Integrated data processing for turbojet and turboprop engines high altitude test facility 20 p3413 A67-36464
 Gas turbine cooling, discussing high temperature problems, solutions and benefits of air cooled blades and vanes 20 p3517 A67-37168
 Steady state matching of inlets, engines and exhaust nozzle for SST [AIAA PAPER 67-754] 23 p3928 A67-40988
 Design criteria for VTOL tactical aircraft power plant using turbojets for attack aircraft in support of land troops 23 p4049 A67-41044
 Mixing effect in dual flow turbojet engines analyzed to obtain better conversion of combustion into kinetic energy 23 p3931 A67-41317
 Turbojet engine gasdynamic parameters dependence on reduced rotational velocity for in-flight characteristics determination, assuming variable compression and critical pressure ratio 24 p4207 A67-41916
- TURBOJET ENGINE CONTROL**
 Turboramjet engine transition phase noting problems in passing from turbojet to ramjet operation 12 p1988 A67-25185
- TURBOMACHINE**
 Gas lubricated bearings used in Brayton cycle closed loop system turbomachinery in design of two-shaft power plant [ASME PAPER 66-GT/CLC-9] 01 p0080 A67-10871
 Aerodynamic problems of turbomachinery, investigating effect of geometry and aerodynamic cascade parameters on flow deflection, static pressure difference and flow losses 04 p0547 A67-14985
 Protecting turbomachinery from unstable and oscillatory flow, noting resonance effect [ASME PAPER 66-WA/GT-13] 04 p0690 A67-15370
 Thermal turbomachines, Volume 1, Thermodynamics and fluid mechanics calculations, covering one-dimensional turbine stage theory, blade cascades, etc 07 p1127 A67-20040
 Fluid film and rolling element bearings effect on turbomachinery rotor dynamics including critical speeds, imbalance response, instability, turbulence, etc [SAE PAPER 670059] 09 p1508 A67-22533
 Numerically controlled milling for producing three-dimensional curved surfaces for turbomachinery [SAE PAPER 670096] 09 p1509 A67-22539
 Lubrication system design and component arrangements for several oil and gas lubricated closed looped gas turbine machines [ASME PAPER 67-GT-3] 11 p1799 A67-24791
 Quantitative graphical method of screening working fluids for Rankine cycle power plants using single stage turbines at different levels of diameter and rpm [ASME PAPER 67-GT-12] 11 p1746 A67-24798
 Relative eddy flows mechanism in mixed flow turbomachines 12 p1891 A67-25348
 Turbomachine rotating shaft and rotor systems critical speeds taking into account bearing support stiffness and clearances, noting vibration mode 12 p1949 A67-25410
 Vibration problems in high speed turbines including stability, critical speeds and support structure effect on rotor response [ASME PAPER 67-DE-8] 14 p2402 A67-28867
 Dynamic-seal technology in applications employing liquid metals, gas and standard organic fluids for ground, aerospace and space turbomachinery [ASME PAPER 67-DE-50] 14 p2328 A67-28881
 Book on fluid mechanics and thermodynamics of turbomachinery covering application of dimensional analysis and performance laws 15 p2418 A67-30395
 Axisymmetric flow equations for performance prediction of axial-flow turbomachines and stage design 20 p3355 A67-36186
 Protecting turbomachinery from unstable and oscillatory flow, noting resonance effect [ASME PAPER 66-WA/GT-13] 24 p4207 A67-42462
 Parametric analysis and system optimization of nuclear reactor heated Brayton cycle space power plants, discussing turbomachinery performance and shielding weight factors 24 p4186 A67-42550
- TURBOMACHINE BLADE**
 Boron filaments for reinforcement of aluminum alloys used in turbomachinery 03 p0444 A67-13436
 Streamline curvature computing procedures for turbomachinery and fluid flow problems, considering axisymmetric and nonaxisymmetric flow fields and compressible cascade flow [ASME PAPER 66-WA/GT-3] 04 p0607 A67-15358
 Circumferential inlet velocity distortion effect on normal force response and stall characteristics of rotating blade in axial flow turbomachine 06 p0938 A67-18255
 Production inaccuracy effects on oscillation frequency characteristics of turbomachine blades 07 p1261 A67-19134
 Equations for turbomachinery blades vibration control noting energy exchange, stress amplitude, mechanical damping, etc [ASME PAPER 67-VIBR-49] 11 p1797 A67-24199
 Effect of blade row interference on cascade flutter investigated using semiautator disk method 15 p2415 A67-29314
 Radial pressure gradients in clearance between two blade rims of axial turbomachine determined by introducing empirical function dependent on local twist exponent 15 p2417 A67-30144
 Circumferential inlet velocity distortion effect on normal force response and stall characteristics of rotating blade in axial flow turbomachine 21 p3565 A67-38536
 Streamline curvature computing procedures for turbomachinery and fluid flow problems, considering axisymmetric and nonaxisymmetric flow fields and compressible cascade flow [ASME PAPER 66-WA/GT-3] 24 p4143 A67-42459
- TURBOPROP**
 GE T64 engine operation on emulsified fuel /JD1/, noting corrosion effects on fuel system components due to water additive [SAE PAPER 670369] 17 p2927 A67-33002
- TURBOPROP AIRCRAFT**
 Quality control around twin turboprop utility plane MU-2 at experimental stage 05 p0812 A67-17245
 Arava light twin-turboprop STOL transport aircraft operating from short rough airfield, noting wind tunnel results 11 p1743 A67-24213
- TURBOPROP ENGINE**
 Reverse flow annular combustion system for TPE331 turboprop engine, noting fabrication and combustor efficiency [ASME PAPER 67-GT-25] 11 p1854 A67-24805
 Growth and operational capabilities of turboprop and reciprocating engines [SAE PAPER 670236] 12 p1989 A67-25494
 High temperature long life turbine design, noting role of air cooling of critical parts [SAE PAPER 670345] 12 p1990 A67-25880
 Integrated data processing for turbojet and turboprop engines high altitude test facility 20 p3413 A67-36464
 Handley Page Jetstream power plant, propeller design, turboprop engine operation and control 22 p3868 A67-40131
 PT6 series of small shaft turboprop engines for STOL aircraft and high speed surface vehicles noting performance and environmental tolerance improvements [AIAA PAPER 67-744] 23 p4048 A67-40978
- TURBOPUMP**
 Optimization of high energy turbopump unit engine for ELDO-B carrier rocket, employing system specific impulse 03 p0503 A67-13013
 Single-phase and two-phase cavitating flow regime performance of liquid propellant rocket engine turbopump inducers [ASME PAPER 66-WA/FE-23] 04 p0554 A67-15353
 Ultrahigh vacuum produced by combination of turbomolecular and titanium sublimation pumping 06 p0950 A67-17752
 Rocket engine turbopump assembly test capability design, facilities, cryogenic systems, control requirements, computer simulation, activation and checkout [AIAA PAPER 67-441] 18 p3112 A67-33918
 Twin spool zero-NPSP /net positive suction pressure/ turbopump selected for NERVA rocket after assessing turbopump, engine, vehicle and mission related systems [AIAA PAPER 67-476] 18 p3075 A67-33946
 M-1 engine system technology items noting thrust chamber assembly, gas generator, fuel turbopump, etc [AIAA PAPER 67-520] 18 p3115 A67-33983
 Liquid hydrogen pumping for Phoebus reactor, discussing feed systems, nozzles, configurations, design, testing, etc [AIAA PAPER 67-478] 18 p3077 A67-34402
 Single-phase and two-phase cavitating flow regime performance of liquid propellant rocket engine turbopump inducers [ASME PAPER 66-WA/FE-23] 24 p4143 A67-42464
- TURBORAMJET ENGINE**
 Turboramjet developed from Griffon aircraft capable of propelling hypersonic vehicles 09 p1559 A67-22093
 Turboramjet engine transition phase noting problems in passing from turbojet to ramjet operation 12 p1988 A67-25185
 Air breathing reusable rocket launchers for European development, comparing ramrocket and turboramjet propulsion 15 p2568 A67-29844
 Turboramjet engine design for aerodynamic flight vehicles up to Mach number 6 23 p4049 A67-41318
- TURBULENCE**
 SA ATMOSPHERIC TURBULENCE
 SA BOUNDARY LAYER CONTROL
 SA BOUNDARY LAYER TRANSITION
 SA CLEAR AIR TURBULENCE
 SA GUST
 SA HOMOGENEOUS TURBULENCE
 SA ISOTROPIC TURBULENCE
 SA LOW LEVEL TURBULENCE
 SA MAGNETOHYDRODYNAMIC TURBULENCE
 SA PLASMA TURBULENCE
 Diurnal and seasonal variations of ionospheric turbidity 02 p0236 A67-11670
 Shear flow generation by flat plate grid with added turbulence generator and roughened floor in wind tunnel 09 p1483 A67-21566
 Diurnal and seasonal variation of ionospheric turbidity 16 p2665 A67-31085
- TURBULENCE EFFECT**
 Turbulent reattachment of supersonic jet noting recompression region of flow, critical points and similarity law in evolution of wall pressures [ONERA-TP-326] 01 p0053 A67-11002
 Resolving power of circular-aperture antenna affected by plane turbulent layer between antenna and point of

observation 02 p0210 A67-11570
 Mass transfer measurements of
 paradichloro benzene cylinders at various
 turbulent intensities and angles of attack,
 showing free flow turbulence effect on local
 mass transfer coefficient 04 p0548 A67-15493
 Interpretation of profiles of middle
 strength Fraunhofer lines, especially
 strontium resonance line of microturbulence
 above hydrogen convection
 zone 05 p0899 A67-17072
 Free stream turbulence effects on
 boundary layer transition, discussing
 acoustical disturbance as source of velocity
 fluctuations 05 p0794 A67-17364
 Turbulent diffusion evaluation and
 determination of dependence of Lagrange
 turbulence scale and intensity on various
 factors in closed volume with artificial
 turbulence 06 p1112 A67-17959
 Atmospheric density, winds and
 turbulence relative influence on Saturn V
 vehicle control system and structural
 bending moment response during Atlantic
 Missile Range ascent flight
 [AIAA PAPER 66-341] 07 p1257 A67-19372
 Turbulent viscosity forces in nonlinear
 three-dimensional nonstationary problem of
 thermal convection 07 p1221 A67-20005
 Book on electromagnetic wave propagation
 and turbulent media covering invariant
 imbedding method, turbulence generation,
 statistical methods of analysis,
 etc 08 p1295 A67-20984
 Turbulence effects on laminar skin
 friction and heat transfer from plates and
 circular cylinders in incompressible flow,
 using two low turbulence wind
 tunnels 08 p1427 A67-21118
 Thermal and momentum eddy diffusivities
 computed from wind profile and turbulence
 of rocket released chemical
 clouds 08 p1328 A67-21478
 Sealing coefficient of visco seal for
 laminar and turbulent flow, noting Reynolds
 number effect 10 p1859 A67-22706
 Eddy coefficients for diffusion and
 turbulence parameters for dispersion of
 vapor clouds in lower thermosphere from
 vapor trail evidence 10 p1846 A67-23272
 Initial turbulence effect on characteristics
 of axisymmetric submerged air jets, using
 thermo-anemometer to measure averaged
 velocity and mean quadratic longitudinal
 pulsation rate component 11 p1779 A67-24320
 Transition to turbulence in thermal plasma
 examined, using model based on coupled
 Van der Pol oscillators, noting noise
 spectrum rise 11 p1836 A67-24390
 CH molecule solar spectral observations
 interpreted using several upper photosphere
 models and assuming local thermodynamic
 equilibrium 11 p1861 A67-24495
 Turbulence tensor within framework of
 hydrodynamic relativity, noting
 generalization of Weber
 equation 11 p1782 A67-24760
 LF thermodynamic energy and pressure
 fluctuation-dissipation theorem for open
 systems with dynamic
 turbulence 11 p1821 A67-24974
 Internal stability of turbulent combustion,
 developing analysis for one-dimensional
 model and deriving sufficient instability
 criterion 12 p2039 A67-26119
 Medical/human factors affecting pilots
 during atmospheric
 turbulence 13 p2064 A67-27262
 Fluid turbulence effect on rate of heat
 transfer from spheres in vertical wind
 tunnel indicate turbulent Reynolds number
 as important parameter 13 p2225 A67-27466
 Atmospheric fine structure deduced from
 radio observation and from turbulence
 theory 14 p2311 A67-28396
 Local turbulent properties of supersonic
 jet exhaust measured optically by crossed
 beam correlation
 technique 16 p2591 A67-30943
 Mean velocities, turbulence intensities,
 Reynold stresses and wall friction
 measurement in turbulent radial wall jet
 [ASME PAPER 67-APM-10] 17 p2838 A67-32419
 Distinction between macro-and
 microturbulence in solar photosphere
 studied from line profiles 17 p2944 A67-32641
 Small perturbations effect on internal gas
 dynamic structure of flame zone for slow
 combustion stability

criterion 17 p2974 A67-33144
 Turbulent base pressure in supersonic
 axisymmetric flow behind blunt body
 [AIAA PAPER 67-446] 18 p3026 A67-33922
 Mesosphere winds and turbulence
 observed by forming aluminum oxide smoke
 trails 18 p3043 A67-34496
 Hamiltonian description of irreversible
 steady state phenomena and elements of
 turbulence theory, noting entropy
 production 19 p3210 A67-35539
 Mass-transfer coefficients through plane
 surface in liquid-liquid systems, examining
 interphase turbulence
 effect 19 p3345 A67-35566
 Gas-side heat transfer at high temperature
 combustor sonic points, discussing Reynolds
 number effect, boundary layer transitions,
 turbulence intensity, etc 20 p3552 A67-36831
 [AIChE PAPER 27]
 Turbulent convective eddies effect on
 solar concentrated magnetic fields, plotting
 force lines 21 p3709 A67-38991
 Noise model for simulating tropospheric
 turbulence effects on radio guidance and
 tracking range and angular measurements
 for optimum filter
 synthesis 21 p3587 A67-39147
 Turbulence effect on accuracy of
 microwave cut-off measurements of plasma
 density suggests electromagnetic wave
 scattering 22 p3845 A67-39430
 Harmonic generation and turbulencelike
 spectrum from pulsed HF beam-plasma
 interaction, tabulating harmonic wave
 properties 22 p3847 A67-39615
 Laser beam expansion in turbulent
 medium using Huygens-Kirchhoff principle
 and Fresnel diffraction
 approximation 22 p3761 A67-39739
 Mean flow and motion turbulence
 characteristics after separation from conical
 afterbody for various initial boundary layer
 thickness and convergence
 angles 23 p3927 A67-40631
 Wind profiles properties application to
 launch vehicle design and operation,
 emphasizing wind shears and turbulence
 effects on vehicle dynamic
 response 24 p4242 A67-42918
TURBULENCE MEASURING APPARATUS
SA HOT-WIRE TURBULENCE
MEASURING APPARATUS
 Gust reduction equations governing
 numerical procedure for transforming to
 inertial frame continuous records of air
 turbulence velocity via matrix methods
 [AIAA PAPER 66-967] 02 p0246 A67-12290
 Power spectral density /PSD/ methods
 applied to prediction of aircraft responses to
 continuous turbulence 03 p0362 A67-14147
 [AIAA PAPER 66-1000]
 Laser applicability to line-of-sight
 atmospheric turbulence
 parameters 05 p0839 A67-17383
 Clear air turbulence problems including
 forecasting inadequacy, detection device
 requirements, categories,
 etc 09 p1526 A67-22390
 Space-time correlations of turbulent field
 measured by grid using high speed
 computer 11 p1780 A67-24541
 Internal scale measurements of
 atmospheric turbulence in 80 to 100 km
 altitude using alkaline clouds produced by
 ejecting sodium metal and trimethyl
 aluminum from rocket 12 p1935 A67-25793
 Clear air turbulence power spectra in free
 atmosphere near jet stream level, discussing
 CAT generation 15 p2513 A67-30058
 Local turbulent properties of shear layer
 derived from covariance of two crossed
 perpendicular beams of
 radiation 17 p2855 A67-32282
 Power spectral density /PSD/ methods
 applied to prediction of aircraft responses to
 continuous turbulence 17 p2797 A67-32582
 [AIAA PAPER 66-1000]
 Aircraft mounted recording accelerometers
 for excessive turbulence compared with
 direct turbulence
 measurement 17 p2798 A67-32700
 Wind tunnel measurement of turbulent
 transport terms for unstable curved mixing
 layer of incompressible
 flow 18 p3030 A67-34751
TURBULENT AIR CURRENT
 Clear atmosphere angels origin, clear air
 turbulence detection, radio propagation and
 atmospheric radar
 probing 14 p2264 A67-28395

Air stream turbulence effect on local and
 macroscopic transport from cylinder,
 measuring thermal transfer and pressure
 coefficients at various Reynolds
 numbers 14 p2407 A67-28624
TURBULENT BOUNDARY LAYER
 Estimated structural response to
 aeroacoustic pressure loading due to jet and
 rocket engines and boundary layer
 turbulence
 [SAE PAPER 660721] 01 p0010 A67-10625
 Turbulent velocity fluctuation field in
 isothermal boundary layer with homogeneous
 injection and combustion
 [AIAA PAPER 65-820] 01 p0054 A67-11169
 Two-dimensional shock induced separated
 flows in turbulent boundary layer, applying
 Crocco-Lee theory and calculating pressure
 rise coefficient 02 p0231 A67-11522
 Reynolds number effects and initial
 conditions effects on development of free
 shear in mixing layer from constant area
 nozzle 02 p0231 A67-11559
 Self-preserving flow in turbulent boundary
 layer passing over surfaces with different
 roughness 02 p0232 A67-11561
 Shear layer and internal flow arising from
 turbulent boundary layer separation and
 heat transfer over cavity 02 p0179 A67-12344
 Analogy between turbulent MHD channel
 flow at high Reynolds numbers and
 moderate Hartmann numbers and turbulent
 boundary layer flow with
 suction 02 p0277 A67-12569
 Turbulent boundary layer in subsonic or
 supersonic flow past pinched-waist bodies of
 revolution at various Mach numbers and
 pressure gradients 03 p0350 A67-12989
 Coolant injection in turbulent boundary
 layer for protection of surfaces from effects
 of high temperature and high energy gas
 flows 03 p0536 A67-13526
 Boundary layer measurements of friction
 losses due to finite thickness of leading
 edges of turbine blades 03 p0353 A67-14306
 Correlation scheme for mean velocity
 distributions in turbulent boundary layers
 developing in arbitrary adverse pressure
 gradients 04 p0601 A67-14459
 Transitional immersed cylinder heat
 transfer measurements used in conjunction
 with theory of boundary layer transition to
 determine free-stream turbulence
 intensity 04 p0601 A67-14508
 Thrust and mass flow rate of supersonic
 nozzle with and without internal
 separation 04 p0602 A67-14568
 Convective heat transfer in accelerated
 heated air flows through cooled conical
 supersonic nozzles of three different
 configurations 04 p0723 A67-14837
 Sudden expansion or compression effect
 on momentum thickness change in turbulent
 boundary layer calculated, using parameter
 of velocity layer profile 04 p0604 A67-14840
 Linearized Couette flow problem in
 rarefied gas solved, using one-dimensional
 radiative heat transfer
 analogy 04 p0606 A67-15183
 Unstalled two-dimensional diffusers
 performance prediction by method based on
 turbulent boundary layer integral theory
 [ASME PAPER 66-WA/FE-15] 04 p0548 A67-15351
 Three-dimensional turbulent boundary
 layer characteristics predicted by method
 which assumes cross flow is small
 [ASME PAPER 66-WA/GT-10] 04 p0607 A67-15361
 Hot-wire probe measurements of time
 average velocity, flow directions, turbulence
 intensities and growth of skewed three-
 dimensional turbulent boundary layers in
 low speed flow
 [ASME PAPER 66-WA/FE-2] 04 p0608 A67-15386
 Hydrogen and helium injection effect on
 local heat transfer to porous surface from
 dissociated turbulent boundary layer
 [ASME PAPER 66-WA/HT-24] 04 p0725 A67-15444
 Free stream turbulence and pressure
 gradient effects on flat plate boundary layer
 velocity profiles and heat transfer
 [ASME PAPER 66-WA/HT-4] 04 p0608 A67-15448
 Turbulent boundary layer-flat surface
 interfacial Stefan-Nusselt flow effects on
 apparent kinetics of heterogeneous chemical
 reactions in forced convective
 systems 04 p0567 A67-15681

Prediction of turbulent boundary layer development in conical diffusers, using kinetic energy deficit equation 04 p0549 A67-15750

Heat-transfer coefficient measurements in separated flow regions in heated duct with circumferential grooves, ribs and enlargements, by visual flow techniques 04 p0729 A67-15810

Preston tube measurements of skin friction and velocity profiles in incompressible turbulent boundary layer, considering pressure gradient effects 04 p0609 A67-15818

Wall shearing stress and heat transfer measurements through turbulent boundary layer on heated flat plate in accelerating and decelerating airflow 04 p0731 A67-15819

Mach number and temperature ratio effects on convective heat-transfer coefficient to flat plate through turbulent boundary layer in air and Stanton number calculation in terms of drag coefficient 04 p0731 A67-15820

Uniform property turbulent boundary layer heat transfer calculation, using solution of integral momentum and kinetic energy equations 04 p0731 A67-15821

Aerodynamic heating from turbulent boundary layer to swept surface symmetrical to surface line dividing flow obtained from momentum and energy integral equations 04 p0549 A67-15825

Asymptotic flow theory laws of friction and heat transfer in turbulent boundary layer 04 p0610 A67-15838

Heat-transfer coefficients and shearing stress in turbulent boundary layer along porous flat plate with uniform fluid injection 04 p0733 A67-15842

Turbulent boundary layer calculation, considering compressible and incompressible flows with pressure gradients and heat transfer 04 p0610 A67-15908

Momentum transfer mechanism in separated flow region of rectangular cavity facing oncoming turbulent boundary layer [AFCLR-66-851] 04 p0610 A67-15924

Stress effects of simple supports on radiation emission from turbulent flow near plane compliant surface, using acoustic equivalence to extended dipole system 05 p0748 A67-16813

Attenuation law of turbulent pulsations in viscous sublayer of turbulent boundary layer of incompressible fluid 06 p0982 A67-17741

Step-induced separation of low speed turbulent boundary layer in incompressible flow 06 p0985 A67-18132

Minimum structural response and acoustic radiation for panel excited by turbulent boundary layer [AIAA PAPER 67-12] 06 p0985 A67-18256

Mach number effect on mixing lengths and kinematic eddy viscosities in turbulent flat plate boundary layer [AIAA PAPER 67-199] 06 p0987 A67-18324

Turbulent boundary layer characteristics of compliant surfaces, using hot-wire anemometer to measure velocity profiles, Reynolds stresses and skin friction [AIAA PAPER 67-128] 06 p0987 A67-18336

Skin friction under mass injection on porous flat plate in supersonic turbulent flow [AIAA PAPER 67-194] 06 p0987 A67-18341

Static temperature-velocity distribution for zero pressure flat plate compressible turbulent boundary layer with heat transfer [AIAA PAPER 67-195] 06 p1116 A67-18362

Suction requirements for elimination of turbulent boundary layer separation in adverse pressure gradient, based on mixing rate hypothesis and von Karman momentum integral [AIAA PAPER 67-197] 06 p0988 A67-18442

Turbulent MHD boundary layer flow of constant-electroconductivity incompressible fluid past dielectric plate in TM field, for small magnetic Reynolds numbers 06 p1043 A67-18672

Local skin friction coefficient for turbulent boundary layers on smooth flat plates measured, using Preston tube 06 p0990 A67-18751

Laminar, transitional and turbulent boundary layer flows with adverse pressure gradient on axisymmetric blunted conical flared body at Mach 10 [AIAA PAPER 66-493] 06 p0943 A67-18844

Erosive burning of ammonium perchlorate

solid propellants for combustion in turbulent boundary layer determined, using flat plate heat transfer correlation 07 p1238 A67-19069

Velocity distribution of turbulent incompressible boundary layer along flat plate with assumed polynomials of shearing stress and mixing length 08 p1319 A67-20405

Velocity distribution for low drag airfoil with little tendency toward separation of turbulent boundary layer 08 p1275 A67-20407

Aerodynamic characteristics of flared bodies noting geometry, Reynolds number and boundary layer state effects on stability 08 p1275 A67-20499

Similarity law for wall region of turbulent boundary layers in compressible flow, discussing Coles theory 08 p1320 A67-20565

Irrational fluctuations near turbulent boundary layer in Phillips theory and relation between one- and two-dimensional wave number spectra 08 p1320 A67-20705

Heat transfer in constant property turbulent boundary layer with arbitrary distributions of wall temperature and stream velocity 08 p1426 A67-20927

Pressure gradients effects on boundary layers grown on wall of wind tunnel, obtaining equilibrium boundary layers of Clauser type 09 p1489 A67-22415

Flight experiments to assess stalling behavior and handling problems arising in design, maintenance and operation of suction wing for high lift [AIAA PAPER 65-750] 09 p1441 A67-22483

Skin friction drag of constant property turbulent boundary layer with uniform injection, corrections of experimental law-of-wall and velocity-defect law concepts 10 p1625 A67-23111

Three-dimensional turbulent boundary layers over swept wing calculated using entrainment equation 10 p1626 A67-23473

Screen and honeycomb effect on variation of skin friction in low speed wind tunnel, noting turbulent boundary layer growth 10 p1627 A67-23556

Free flight response of two panels subjected to turbulent pressure fluctuations at supersonic Mach numbers 10 p1719 A67-23558

Wall law for thick turbulent boundary layer with sublayer thickness compared to radius of transverse curvature, analyzing motion equations 10 p1629 A67-23847

Turbulent boundary layer phenomena, discussing parameters of production processes, relation with instability, etc 11 p1776 A67-24043

Turbulent boundary layer development noting representation of velocity profiles, skin friction and eddy viscosity 11 p1776 A67-24044

Skewed turbulent boundary layers, noting absence of pressure gradient and shearing stress measurements in experiments and applicability of similarity defect equation 11 p1776 A67-24048

Turbulent boundary layer of gas mixture with dissociation flowing at inlet section of tube 11 p1782 A67-24961

Surface mass addition into turbulent boundary layer for attaining equilibrium velocity profiles, determining development from start of injection 12 p1930 A67-25929

Wire screen roughnesses effect on turbulent boundary layer along flat plate without pressure gradient 13 p2093 A67-26529

Law for turbulent boundary layer dissipation integral 13 p2094 A67-26637

Resistance and heat transfer of plate situated in turbulent MHD boundary layer in compressible fluid 13 p2169 A67-27312

Hypersonic turbulent boundary layers transformation to incompressible form 14 p2297 A67-28137

Free stream turbulence and pressure gradient effects on flat plate boundary layer velocity profiles and heat transfer [ASME PAPER 66-WA/HT-4] 15 p2470 A67-29321

Obstacle effect on turbulence intensity in boundary layer, discussing results of hot-wire anemometer measurements 15 p2471 A67-29651

Correlation measurement in two-dimensional zero pressure gradient boundary layer, noting velocity fluctuation patterns 15 p2471 A67-29652

Turbulent energy equation converted into differential equation for boundary layer development calculation 15 p2472 A67-29657

Acoustic radiation of panels excited by random pressure fluctuation of turbulent boundary layer investigated, showing agreement with experiment 15 p2574 A67-29770

Turbulent boundary layer flow properties predicting velocity profiles in region of velocity maximum decay downstream 16 p2657 A67-30614

Three-dimensional turbulent boundary layer flow over infinite swept wing calculated using entrainment and momentum integral equations 16 p2657 A67-30617

Theory and supporting experimental results on application of small heated film for skin friction measurements in laminar and turbulent boundary layers 16 p2659 A67-30950

Lateral convex curvature and helium surface injection effect on turbulent wall boundary layer characteristics and skin friction 16 p2659 A67-30952

Turbulent boundary layer with large acceleration parameter studied for flow and heat transfer coefficient [JPL-TR-32-1119] 16 p2659 A67-30953

Shock tunnel experiments with hypersonic turbulent boundary layer flow over flat plates with blunt and sharp leading edges and wall of expansion nozzle 16 p2659 A67-30954

Thermal turbulent boundary layer on flat plate with thermally insulated section, determining temperature distribution in presence of heat transfer 16 p2594 A67-31201

Statistical properties of wall pressure fluctuations in subsonic turbulent equilibrium boundary layer after transition from laminar flow 17 p2836 A67-32283

Wall-turbulence interaction for infinite flat plate inserted into homogeneous isotropic turbulence, measuring growth of inhomogeneity layer 17 p2837 A67-32286

Law for velocity distribution through wall boundary layers derived from eddy viscosity model, considering turbulent shear variation and Reynolds number effect 17 p2839 A67-33008

Heat-transfer coefficients for heat transfer from gas to blade surface in gas turbine under operating conditions 17 p2973 A67-33077

Electron concentration in turbulent boundary layer of weakly ionized plasma when injecting electrons through pores in wall 18 p3087 A67-34053

Turbulent boundary layer on plane catalytic plate in nonequilibrium dissociating gas calculated by successive approximation technique 18 p3027 A67-34204

Channel flow transition to jet flow, discussing turbulence determination in flow boundary layer as Reynolds number function 18 p3028 A67-34218

Pressure fluctuations beneath incompressible turbulent boundary layer with mass addition 18 p3030 A67-34742

Turbulent boundary layer in liquid hydrogen tank, determining attachment point, velocity and temperature profiles 19 p3310 A67-34810

Turbulent boundary layer flow in conical supersonic nozzle, discussing convective heat transfer and adverse pressure gradient effect 19 p3169 A67-34814

Turbulent velocity fluctuations dynamics in and outside viscous sublayer examined by linearizing motion equation around known mean velocity profile 19 p3209 A67-35414

Laminar-turbulent boundary layer transition over aircraft components measured by method using negative-temperature-coefficient resistors compared to hot wire measurements 19 p3230 A67-35573

Critical Reynolds number of laminar-turbulent transition for Newtonian flow in rectangular ducts to verify minimum in curve as function of duct aspect ratio 19 p3210 A67-35616

Incompressible turbulent boundary layers with arbitrary pressure gradients and divergent or convergent cross flows predicted by effective viscosity hypothesis 19 p3211 A67-35738

Coles equation representing nonequilibrium turbulent boundary layer without transpiration 19 p3212 A67-35776

Mean heat transfer coefficient at flat plate with turbulent boundary layer at zero incidence Mach numbers mean heat-transfer

coefficient at flat plate with turbulent boundary layer at zero incidence
Mach 20 p3543 A67-36275

Heat transfer in region of separated flow over two-dimensional rectangular cavity facing oncoming turbulent boundary layer [ASME PAPER 67-HT-14] 20 p3545 A67-36711

Local heat transfer coefficients, mean temperature and velocity distributions in turbulent natural convection boundary layer on vertical plane surface
[ASME PAPER 67-HT-17] 20 p3545 A67-36713

Turbulent boundary layer and heat-transfer coefficients for air in conical nozzles, noting uncooled inlet length and convergence angle effects
[ASME PAPER 67-HT-28] 20 p3357 A67-36721

Laminar and turbulent free shear layers analysis unifying treatment of mixing layers, assessing Mach number, Prandtl number and temperature ratio effects on constant pressure mixing
[ASME PAPER 67-HT-81] 20 p3551 A67-36759

Wall turbulent boundary layer pressure resolution by piezoelectric transducer, noting attenuation of frequency component with size and frequency dependence 20 p3422 A67-37002

Transpiration cooled vehicles correlation with compressible turbulent boundary layer with mass transfer, emphasizing high Mach number 20 p3423 A67-37256

Turbulent boundary layer theory for streamline flow over impermeable plate, noting viscous interface effect 20 p3424 A67-37461

Physical analysis of convective heat transfer in laminar and turbulent flow through ducts and boundary layers, deriving trailing functions by variational method 21 p3730 A67-37736

Incident and reflected shocks from laminar and turbulent boundary layers measured over various Mach numbers 21 p3610 A67-37771

Turbulent MHD boundary layer in liquid with linear pressure gradient, discussing numerical integration, flow velocity and magnetic field distribution 21 p3665 A67-38244

Stability technique for gas flow past body impeding laminar-turbulent boundary layer transition via crossed electric and magnetic fields 21 p3666 A67-38251

Steady flow field from turbulent boundary layer separation in front of forward facing step, discussing pressure field 21 p3613 A67-38853

Compressible turbulent boundary layer equations, discussing third order correlation terms role and eddy thermal conductivity definition 21 p3614 A67-38894

Transitional and turbulent boundary layers on cold flat plate in hypersonic flow noting bluntness, Reynolds and Mach numbers effects 21 p3615 A67-39080

Base pressure measurements on elliptic cones in supersonic flow with turbulent boundary layer as function of geometry 21 p3566 A67-39083

Turbulent cylindrical wall jet flow field, velocity profile and surface friction coefficient noting transverse curvature effects 22 p3783 A67-39531

Heat transfer experiments with flat plate heated under constant heat flux, discussing wall temperature distribution, Prandtl number and Spalding function 22 p3918 A67-40041

Internal flow turbulent boundary layer separation for variable angle two-dimensional diffuser, discussing analytical model and model limitations
[ASME PAPER 66-WA/FE-14] 23 p3989 A67-40929

Turbulence structure of equilibrium boundary layers, discussing shear stress, thickness, eddy motion and intensity spectra 23 p3990 A67-41168

Turbulent boundary layer energy and motion equations, heat transfer through layers, energy exchange and phenomenological relations 23 p3991 A67-41249

Skin friction under mass injection on porous flat plate in supersonic turbulent flow
[AIAA PAPER 67-194] 23 p3991 A67-41713

Two-phase flow equations for turbulent boundary layer flows, considering solid particle effects 23 p3993 A67-41748

Heat transfer between gas flows and solid /carbon/ surfaces, considering chemical reactions 24 p4252 A67-41935

Approximate single parameter solution for compressible turbulent boundary layer in supersonic diffuser 24 p4144 A67-42586

Flared afterbody aerodynamic characteristic predictions for aircraft stability at high Mach numbers, discussing turbulent separation 24 p4093 A67-42924

TURBULENT DIFFUSION

Observed differences between lateral transport rates of heat and chemical species and of momentum in turbulent free shear flows accounted for by model
[AIAA PAPER 65-810] 01 p0054 A67-11167

Direct measurements of thoron from ground surface to height of 50 cm in atmosphere, describing turbulent diffusion of radioactive emanations from soil surface 02 p0237 A67-11853

Turbulent diffusion in nonuniform stratification atmosphere, obtaining vertical concentration profile by random walk method
[AFCLR-66-836] 02 p0262 A67-12081

Anomalous diffusion arising from LF flute instability in Penning discharge, measurements of turbulent fields used to determine statistical transport rates 02 p0276 A67-12559

Nonlinear theory of plasma instability in oscillating discharge, estimating oscillation energy and coefficient of turbulent diffusion 03 p0478 A67-13537

Relative dispersion of particle pairs in homogeneous turbulence using Lagrangian-history direct interaction closure approximation for convected scalar field, obtaining Richardson diffusion equation 03 p0405 A67-14031

Generalized mixing length argument in turbulent diffusion, obtaining integral equation for continuous case 04 p0603 A67-14648

Turbulent vertical diffusion in surface layer of atmosphere 04 p0652 A67-15568

Wind profile effect on turbulent diffusion for infinite linear source in surface layer of unstable stratified atmosphere 04 p0652 A67-15569

Hydraulic resistance determination for plane and axisymmetric channels with attached and separated flow, noting terminology 04 p0549 A67-15602

Turbulent diffusion evaluation and determination of dependence of Lagrange turbulence scale and intensity on various factors in closed volume with artificial turbulence 06 p1112 A67-17959

Decay of mean, variance and gradient variance of temperature and velocity measured in initially heated wake of sphere in water tunnel
[AIAA PAPER 67-20] 06 p0987 A67-18347

Fuel injection parameters effects on mixing of gaseous hydrogen fuel with supersonic air stream for hypersonic ramjet, determining turbulent diffusion coefficient 06 p1117 A67-18387

Laser velocimeter measurement of point velocities in turbulent liquid flow in pipe, using statistical analysis to verify results
[AIAA PAPER 67-179] 06 p0990 A67-18511

Diffusion and transport equation for turbulent atmosphere with variously heated air masses 06 p0999 A67-18740

Mean velocity and mean static pressure distribution on stability and space requirements of turbulent diffusion flames 08 p1425 A67-20304

Nonlinear effects produced by instability of nonpotential plasma waves in oscillating discharge, deriving wave kinetic equation 10 p1684 A67-22902

Eddy coefficients for diffusion and turbulence parameters for dispersion of vapor clouds in lower thermosphere from vapor trail evidence 10 p1646 A67-23272

Physical stabilization mechanism of helical instability of positive column in longitudinal magnetic field due to quasi-linear effects 11 p1831 A67-24012

Numerical integrations of equation for turbulent diffusion in atmosphere 13 p2152 A67-26863

Estimation of parameters of transverse diffusion in lowest atmospheric layer using Lagrange and Euler turbulence characteristics 16 p2698 A67-31095

Simultaneous ejection of two vapor trails

of different atomic mass, examining turbopump phenomena of atmospheric turbulence 17 p2853 A67-33254

Diffusion of free isothermal turbulent jet of incompressible fluid flowing from nozzle into coaxial surrounding uniform stream 19 p3209 A67-35443

Diffussing plane turbulent free jet compared with correspondent wall jet velocity distribution and variation and length scales 20 p3360 A67-37492

Limit diffusion flux on rotating ring electrode surface in turbulent regime, determining mass transfer constant 24 p4146 A67-43112

TURBULENT FLOW

Hot wire measurement of tangential velocity and Reynolds stresses in spiral laminar-turbulent flow 01 p0054 A67-11163

Turbulence in free shear layer in mixing region of circular jet, comparing statistical characteristics of mathematical and physical models
[AIAA PAPER 65-805] 01 p0054 A67-11164

Observed differences between lateral transport rates of heat and chemical species and of momentum in turbulent free shear flows accounted for by model
[AIAA PAPER 65-810] 01 p0054 A67-11167

Turbulence measured by flow direction indicators used as pressure probes 01 p0076 A67-11192

Pressure distribution in vicinity of wedge for separated turbulent flow analyzed, using modified Vasilu step solution 02 p0232 A67-11634

Oscillation spectra of plasma in quasi-steady state characterized by self-consistent distribution of plasma particles and turbulent pulsation 02 p0274 A67-12455

Instabilities and dispersion during electromagnetic wave excitation and propagation in weakly turbulent plasma 02 p0278 A67-12627

Optimum averaging periods in measurements of wind velocity profile, temperature gradient, vertical thermal turbulent flow and atmospheric drag 02 p0263 A67-12644

Turbulent annular airflows in turbulent film lubrication of high speed bearings
[ASME PAPER 66-LUB-14] 03 p0403 A67-13755

Turbulent lubrication analysis in fluid film theory and turbulent shear flow, with application to bearings
[ASME PAPER 66-LUB-12] 03 p0431 A67-13761

Test arrangement and statistical data analysis for remote sensing of local flow instabilities and turbulence 03 p0422 A67-13773

Convection heat transfer for turbulent flow in subsonic diffusers
[ASME PAPER 65-HT-64] 03 p0352 A67-14010

Propagation of vertical turbulent hot gas stream in fog from point source of heat 03 p0463 A67-14225

Probability distribution of square of vertical wind velocity difference during unstable stratification 03 p0463 A67-14228

Turbulent skin friction measurement with Preston tube, using similarity hypothesis for mean velocity profiles in turbulent flows 04 p0600 A67-14442

Pressure variational law effect along boundary layer of flat plate on formation of turbulent spots measured via hot-wire technique 04 p0602 A67-14598

Quantity of separated liquid deposited on wall of rectangular channel from turbulent air-water dispersed annular flow, calculating liquid flow rate 04 p0602 A67-14641

Turbulence structure in pipe flow with rough surfaces 04 p0604 A67-14845

Analog circuits for statistical correlation in time measurements, with application to subsonic and supersonic flow turbulence 04 p0620 A67-14889

Kinetic theory of gases through certain correlation functions known as product densities used to explain transitions from gaseous to liquid state 04 p0608 A67-15466

Turbulent MHD flows in prismatic and cylindrical pipes, particularly pipes with slot shaped cross section 04 p0669 A67-15513

Strain gauge measurements of resistance of sphere to MHD turbulent flow of mercury in rectangular tube 04 p0670 A67-15530

Temperature-vorticity analogy validity in laminar turbulent flows extended to

compressible fluids, noting temperature relation to shear stress 04 p0727 A67-15680

Velocity profile and friction in plane-parallel channel with developed turbulent compressible gas flow 04 p0609 A67-15684

Mathematical flow-intermittance model for turbulent patterns, noting viscosity effects 04 p0609 A67-15755

Mixing length flow theory of turbulent incompressible flow integral diffusion model extended for boundary layer, channel and Couette flows 04 p0609 A67-15811

Schlieren and hot-wire anemometric observation of supersonic wakes in wind tunnel turbulent flows 05 p0748 A67-16482

[ONERA-TP-417] 05 p0748 A67-16482

Relative diffusion of liquid particles in turbulent flow with shear, deriving formulas 05 p0837 A67-16490

Intermittent phenomena related to entrainment process in free turbulent flows, noting indentation of surface growth and decay cycle 05 p0792 A67-16814

Amplitude spectrum of turbulent flow rate fluctuations at flame temperatures measured via photoelectric method 05 p0927 A67-16942

Self-consistent field approach to nonstationary time dependent turbulence 05 p0794 A67-17417

Invariants in inhomogeneous turbulent flow related to Loitsianskii integral 05 p0794 A67-17418

Hot-wire anemometer measurements of transition in incompressible wake of cone at low Reynolds number 05 p0751 A67-17439

Heat transfer for wall adjacent to region of turbulent separated flow 06 p0985 A67-18131

Correlation of local heat transfer and friction coefficients for subsonic turbulent flow of air through high temperature annulus 06 p1117 A67-18386

Self-preserving turbulent jet ejector, solving equations of motion to determine system geometry corresponding to flow conditions [AIAA PAPER 67-127] 06 p0988 A67-18456

Transition from laminar to turbulent boundary layer flow at hypersonic Mach numbers, noting measurement techniques [AIAA PAPER 67-130] 06 p0989 A67-18474

Turbulent boundary layer properties for strong adverse pressure gradients, obtaining layer and displacement thickness, skin friction, heat transfer, etc [AIAA PAPER 67-196] 06 p0989 A67-18489

Dimensional analysis of turbulent MHD flow in interspace between two coaxial cylinders in rotating circular magnetic field and similarity criteria for EM power losses 06 p1042 A67-18548

Turbulent flow of mercury in flat channels plane perpendicular to magnetic field, noting reduction of flow resistance coefficient 06 p1044 A67-18678

Longitudinal magnetic field effect on convective heat transfer during turbulent MHD pipeflow of liquid Ga 06 p1044 A67-18682

Turbulent flow of electrically conducting fluid in pipe located in longitudinal magnetic field 06 p1044 A67-18689

Size and shape of roughness projections effect on resistance coefficient during turbulent pipe flow in transverse magnetic field 06 p1044 A67-18690

Preston tube in concentric annuli, discussing skin friction measurement in fully developed turbulent flow 06 p0990 A67-18749

Turbulence effect on burning velocity and physical structure of flame surface in turbojet-afterburner-like combustion chamber 07 p1265 A67-19073

Convective heat transfer through stabilized turbulent flow of chemically homogeneous liquid in circular pipe under supercritical pressure conditions 07 p1285 A67-19127

Turbulent flow of conducting fluid with free surface in presence of crossed magnetic and electric fields 07 p1227 A67-19321

Perturbation of two-dimensional viscous flows in finite region, noting exact solution of Navier-Stokes equation 08 p1319 A67-20352

Turbulence amplifiers design, characteristics and production 08 p1280 A67-20437

Empirical expression for resistance of small bore tubes to turbulent flow of compressible fluid in terms of mass flow and total head 08 p1320 A67-20461

Book on quantitative relationships for non-Newtonian systems, considering classification and fluid behavior of materials with anomalous flow properties 08 p1322 A67-21268

Turbulent spots and wall roughness effects in shock tube boundary layer transition, noting stable region behind shock 08 p1322 A67-21382

Approximation of electrical conductivity change in ideally conducting gas in turbulent MGD flow 09 p1544 A67-21860

LF temperature pulsations in turbulent MHD flow of electrolyte 09 p1549 A67-22385

Device for measuring potential fluctuations in turbulent flow of distilled water 09 p1501 A67-22562

Effects of fast expansion and consequent lip shock at shoulder of supersonic base or downstream-facing step, suggesting alleviation by shoulder modification 10 p1592 A67-23156

Binary turbulent reattachment type fluid amplifier to control submerged jet of fluid 10 p1597 A67-23389

Pressure drop correlation in developed, isothermal, laminar and turbulent flow in rectangular ducts 10 p1627 A67-23555

Numerical solution of class of nonlinear high order differential equations with two-point asymptotic boundary conditions for thermal boundary layers in laminar and turbulent flow 10 p1627 A67-23560

Cooling and heating effectiveness of plane surface in turbulent air flow by injection of air film, noting temperature effect 11 p1881 A67-23898

Heat transfer of electrolyte solutions, noting effect of magnetic field on turbulent flow and empirical relation to calculate Nusselt number 11 p1831 A67-24024

Turbulent boundary layer on smooth flat wall, measuring skin friction, turbulence intensity, shearing stress, transverse integral scale, etc 11 p1776 A67-24045

Turbulence research applicability to solution of internal flow problems 11 p1776 A67-24046

Separation and nonseparation of skewed boundary layer, considering two-dimensional wing of finite aspect ratio at large angle of incidence 11 p1777 A67-24051

Velocity and temperature measurements in turbulent swirling butane-propane air flames in high exit velocity range 11 p1882 A67-24217

Kraichnan turbulence theory analyzed by computer calculated solutions with correlation and regression functions derived from experiment, shows good agreement with theory 11 p1780 A67-24539

Formal expansion schemes in predicting statistical properties of turbulent flows at high Reynolds numbers 11 p1780 A67-24540

Random walks computer experiments on ensembles of random binary homogeneous velocity fields, using Eulerian and Lagrangian statistics 11 p1756 A67-24542

Laminar turbulent transition of nonisothermal incompressible forced flows in pipes measured for several working fluids and temperatures, using Reynolds number as criterion 11 p1781 A67-24574

Aerodynamic characteristics of thin airfoil of small camber in nonuniform flow 11 p1742 A67-24658

Wind tunnel studies of heat shield over plane surface with film cooling during injection through two tangential slots 11 p1884 A67-25055

Earth rotational and orbital motions interrelated by Loitsianskii theorem for turbulent fluid motion 12 p1932 A67-25190

Heat transfer and friction coefficients measured for turbulent flow of non-Newtonian fluids in rectangular and circular channels 12 p2033 A67-25315

Velocity profiles for turbulent ducted flow systems analyzed, showing profile decay rate for flow pattern 12 p1927 A67-25351

Free turbulent shear flows and bound turbulent shear layer flows 12 p1928 A67-25355

Propagation of vertical turbulent hot gas stream in fog from point source of heat 12 p1963 A67-25481

Probability distribution of square of vertical wind velocity difference during unstable stratification 12 p1963 A67-25484

Bulk properties of three-dimensional turbulent incompressible jets regarding axis

velocity decays, half-width boundaries, etc 12 p1892 A67-25901

Friction factors and velocity profiles in turbulent flow of viscoelastic non-Newtonian fluid, noting correlation between frictional characteristics and Reynolds number 12 p1929 A67-25904

Transition sticking in wake of slender hypersonic cone as Reynolds number increases 12 p1893 A67-25927

Nonhomogeneous turbulent motion of conducting fluid stabilized by longitudinal magnetic field 12 p1976 A67-26069

Extension of Loitsianskii hypothesis concerning localism of turbulent transfer processes in viscous flows to MHD flows, noting results for friction coefficient 12 p1976 A67-26070

Nonlinear equations in gas dynamics for turbulent nonpotential flows, emphasizing geometry of characteristic surfaces and numerical calculation 12 p1931 A67-26199

Turbulent flow through concentric annuli, measuring velocity profiles, finding maximum velocity radius different from value for laminar flow and dependent on Reynolds number 13 p2092 A67-26268

Higher order time correlations, skewness, flatness and nonGaussian probability density distribution in turbulent field 13 p2092 A67-26278

Relative diffusion of liquid particles in turbulent flow with shear, deriving formulas 13 p2093 A67-26345

Unsteady perturbation effect of external velocity on laminar boundary layer 13 p2094 A67-26645

Displacement and momentum loss thickness in boundary layer of rough flat plate at low velocities as function of wall roughness, pressure gradient, etc 13 p2095 A67-26809

Boundary layer of principal region of turbulent nonisothermal plane-parallel jet of real gas 13 p2095 A67-26885

Instabilities and dispersion during electromagnetic wave excitation and propagation in weakly turbulent plasma 13 p2171 A67-27384

Shear flow, determined by velocity and density profiles, is stable for small disturbances of all wavelengths and Richardson numbers, enumerating eigenvalues 14 p2295 A67-27904

Enthalpy and position in heated tube where liquid boiling begins, finding heat content in turbulent liquid flow 14 p2406 A67-28311

Transverse secondary flow effects on laminar turbulent transition of free axisymmetric jet 14 p2303 A67-28328

Frictional pressure drop for isothermal incompressible flow in isosceles triangular duct, with correlations for laminar and turbulent flow [ASME PAPER 67-FE-18] 14 p2243 A67-28365

Flow turning angle during two-dimensional turbulent supersonic reattachment to plane wall [ASME PAPER 67-FE-20] 14 p2305 A67-28367

Effect of wide angle screened diffuser on turbulent velocity fluctuations [ASME PAPER 67-FE-23] 14 p2243 A67-28368

Amplitude spectrum of turbulent flow rate fluctuations at flame temperatures measured via photoelectric method 14 p2406 A67-28490

Characteristics of sound formation in turbulent flow and mechanism of flow energy conversion into sound energy 14 p2305 A67-28519

Viscoseal operation in superlaminar flow regime noting pressure patterns, end effect, gas ingestion and sealing capacity 14 p2327 A67-28797

Critical region determination in viscous fluid flow using dye stream fuzziness or pressure drop discontinuity as measure of flow turbulence 14 p2305 A67-28801

Velocity profile analysis in turbulent concentric annular flow, emphasizing correlation of results in inner wall region 15 p2468 A67-29132

Temperature distribution for asymmetric heat transfer in turbulent flow between parallel plates 15 p2469 A67-29133

Solution of nonlinear flow problems through parametric differentiation 15 p2469 A67-29221

Constitutive equations describing small perturbations on viscometric flows, noting relations with stress-relaxation modul

flow 15 p2469 A67-29222
Analytical method, based on polarography, for measuring concentration of class of polymers in dilute aqueous solutions 15 p2433 A67-29676
Variational principle for heat conduction and convection, noting applicability to nonhomogeneous fluids with temperature dependent properties in turbulent flow 15 p2582 A67-30019
Generalized streamline hypothesis for turbulent boundary layer flow with spatial variation of viscosity 15 p2473 A67-30210
Laminar and turbulent MHD flows of liquid sodium in rectangular duct with conducting walls, determining wall and magnetohydraulic losses 16 p2712 A67-30573
Flow turbulence on leading edge of attachment line of swept wing studied in wind tunnel 16 p2589 A67-30618
Prandtl shear stress theory applied to similarity models of free turbulence 16 p2657 A67-30857
Dust remover using paper filters and wind tunnel with turbulence in cylindrical duct used for pressure determination 16 p2657 A67-30867
Local turbulent properties of supersonic jet exhaust measured optically by crossed beam correlation technique 16 p2591 A67-30943
Curved mixing layer measured for probability density of turbulent velocities at several positions in curved mixing layer 16 p2660 A67-31219
Velocity distribution functions in statistical theory of turbulence, deriving moment equations and comparing properties with kinetic theory 16 p2660 A67-31220
Turbulent channel flow of mercury in presence of uniform transverse magnetic field deducing skin friction coefficient 16 p2661 A67-31224
Turbulent channel flow of electrically conducting fluid in presence of magnetic field obtaining skin friction coefficient and velocity profiles 16 p2661 A67-31225
Probe measurements of friction drag coefficient and velocity profile of turbulent flow of mercury in circular tube in presence of longitudinal magnetic field 16 p2721 A67-31394
Transverse magnetic field effect upon convective heat transfer in turbulent flow in electrically conducting fluid in channel bounded by two parallel plates 16 p2722 A67-31572
Turbulent flow in circular cylindrical duct at various Reynolds numbers, analyzing fluctuations and mean value of velocity 16 p2663 A67-31702
Spatial correlation coefficients and transverse temperature perturbation scales during turbulent nonisothermal flow of mercury in circular pipe 16 p2724 A67-31776
Heat transfer in turbulent carbon dioxide pipeline at supercritical region 16 p2780 A67-31777
Transverse magnetic field effects on heat transfer in turbulent flow of mercury in circular iron tube 17 p2899 A67-32186
Turbulent thermal convection properties measured in air between constant temperature horizontal plates, discussing structure 17 p2968 A67-32281
Spectral distribution of turbulent energy, noting space-time correlations, instantaneous motion of fluid, existence of nonlinear inertial forces, etc 17 p2837 A67-32289
Wall suction rate effect on turbulent flow in cylindrical circular porous duct, measuring distributions of velocity, pressure, friction coefficient and Reynolds stresses 17 p2837 A67-32380
Karman similarity hypothesis extended to cylindrical geometry to establish conditions for universal velocity similarity in fully turbulent rotating flows [ASME PAPER 67-APM-23] 17 p2838 A67-32416
Transverse magnetic field effect on turbulent MHD jet flow in bounded space, noting channel wall conductivity 17 p2901 A67-32565
Separation shock near base of conical bodies at hypersonic speeds noting inflections in bow shock 17 p2793 A67-33044
Motion of small solid particles suspended in steady isotropic and locally uniform turbulent gas flow 18 p3025 A67-33626

Probability distribution of square of temperature difference between two points of turbulent flow measured by pulsation thermometer 18 p3026 A67-33757
Wall heat flux in turbulent air flow using inner law correlations for velocity and temperature 18 p3160 A67-34165
Velocity measurement in turbulent flow near smooth wall by hot-wire anemometer 18 p3027 A67-34184
Longitudinal magnetic field effect on conducting fluid turbulent flow found limited to dissipation mechanism occurrence 18 p3028 A67-34215
Energy dissipation in turbulent steady isotropic homogeneous gas flow with suspended solid particles 18 p3028 A67-34385
Grid geometry effect on longitudinal and lateral turbulence intensities, determining decay rate dependence 18 p3030 A67-34740
Energy flux in steady inhomogeneous turbulent gas flow with arbitrary mean velocity field, deriving velocity spectra and pressure-velocity correlation tensors 18 p3030 A67-34741
Probability function for turbulent velocity in duct flow determined from Doppler shift of scattered laser radiation 18 p3030 A67-34752
Jet flow turbulence energy balance, measuring point-pressure/velocity correlations and spatial mean gradients, giving energy equation 19 p3170 A67-35412
Hot-wire anemometer response in turbulent flow studied requires correction leading to constant results when applied to flat plate bluff body wakes normal to stream 19 p3230 A67-35523
Turbulent flow in circular duct, obtaining velocity distribution 20 p3419 A67-36276
Local heat-transfer coefficients of turbine blades, evaluating local Nusselt number distribution, Reynolds numbers, and turbulent flow effects 20 p3515 A67-36451
Ultrasonic field effects on nucleating fluid in flash boiling system and heat transfer dependence on bubble density parameters [ASME PAPER 67-HT-11] 20 p3545 A67-36709
Friction and heat transfer characteristics of turbulent swirl flow under large transverse temperature gradients [ASME PAPER 67-HT-24] 20 p3546 A67-36718
Transient mean wall temperature of flat plate with time dependent heat source and cooled by incompressible turbulent flow, discussing heat-transfer coefficient [ASME PAPER 67-HT-45] 20 p3547 A67-36727
Cross-spectrum analysis in meteorology, considering property fluxes and time series, discussing turbulent energy flux, solar activity, etc 20 p3480 A67-36786
Correlation method for local and average friction coefficients of laminar and turbulent gas flow through smooth tubes 20 p3422 A67-36941
Internal rotational relaxation effect on attenuation of HF turbulent vortices during degeneration of turbulence in viscous weakly elastic fluid 20 p3422 A67-37053
Transpiration cooled vehicles correlation with compressible turbulent boundary layer with mass transfer, emphasizing high Mach number 20 p3423 A67-37256
Heat transfer in circular channel containing revolving cylinder, considering turbulent flow with microvortices 20 p3359 A67-37343
Drag measurements for turbulent flow about circular cylinders joined to plane parallel walls, noting dependence on velocity profile 20 p3359 A67-37486
Langmuir probe current in weakly ionized gas flow, studying correlation between hydrodynamical turbulence and pressure fluctuations 20 p3503 A67-37674
Reynolds stress in turbulent flow dependence on mean velocity field determined by rational sequence of approximations 21 p3609 A67-37734
Turbulent gas flow viscosity, therm conductivity and friction coefficients in tube 21 p3611 A67-37912
Rotor bearing stability, describing incompressible and compressible fluid film bearings, calculating thresholds of instability 21 p3632 A67-38136
Convective heat transfer through stabilized turbulent flow of chemically homogeneous liquid in circular pipe under supercritical pressure conditions 21 p3731 A67-38171

Digital computer for simulating and analyzing fluid turbulence by applying laws governing behavior and energy transfer of fluid elements 21 p3612 A67-38193
Electromagnetic forces and pressure and hydraulic losses of turbulent mercury flow in annular channel under travelling magnetic field effect 21 p3666 A67-38249
Liquid fuel polydisperse jet total combustion time curve determined based on droplet of fuel and medium parameters 21 p3732 A67-38528
Incompressible two-dimensional turbulent channel flow, calculating velocity profile and obtaining resistance formula 22 p3782 A67-39409
Turbulence theory from local equilibrium breakdown macroscopic approach by imposing suitable conditions on correlation functions, discussing stochastic Navier-Stokes equations 22 p3782 A67-39500
Waveguide model for turbulent shear flow, calculating streamwise dependence of cross-power spectral density using Orr-Sommerfeld equation 22 p3782 A67-39529
Local coefficient of heat exchange by natural convection on isothermal vertical flat plate in turbulent regime 22 p3917 A67-39648
Correlation measurement in turbulent flow with hot wire anemometer downstream from grid, considering velocity effects 22 p3783 A67-39704
Wake turbulence regimes for flows behind typical hypersonic bodies 22 p3743 A67-40222
Physicochemical combustion of turbulent air-fuel mixture in straight flow combustion chambers, noting effects of various factors and intensification methods 22 p3921 A67-40448
Turbulent skin friction in incompressible flow with heat transfer, determining Preston surface pitot tube applicability 23 p4004 A67-41341
Partial differential equation in lubricant pressure based on mixing-length theory, presenting full journal bearings in turbulent and laminar regimes 23 p4010 A67-41342
Asymptotic perturbation of hypersonic flow over blunt slender cones and wedges showing oscillatory nature 23 p3931 A67-41665
Integral turbulent transfer model using velocity distribution function to develop mixing length flow theory 24 p4141 A67-41933
Turbulent fluid flow velocity and temperature fields in annular and plane gaps calculated by integral approximation for turbulent viscosity and heat conduction coefficients 24 p4142 A67-42213
Incompressible viscous fluid rotary turbulent flow microstructure between rotating cylinders, analyzing centrifugal force effects on turbulent heat transfer processes 24 p4142 A67-42214
Effect of initial flow turbulence on optimum suction of fluid from boundary layer of porous plate 24 p4143 A67-42282
Friction-drag and heat-transfer coefficients of plate in turbulent gas flow, estimating effect of turbulent Prandtl number 24 p4143 A67-42283
Stellar and planetary magnetic field formation theory based on concept of existing ionized turbulent mass flow on these celestial bodies 24 p4230 A67-42352
Three-dimensional disturbance after perturbation of supercritical Poiseuille flow between parallel planes treated by initial value method 24 p4144 A67-42562
Nondisturbing turbulent flow measurements applied to viscous sublayer in smooth square pipe, showing linear velocity gradient in layer adjacent to wall 24 p4144 A67-42607
Taylor vortices and turbulence in flow between eccentric rotating cylinders [ASME PAPER 67-LUB-12] 24 p4145 A67-42673
Steady state and dynamic properties of cylindrical floating ring journal bearing with pressurized lubricant supply, considering turbulent flow and whirl instability [ASME PAPER 67-LUB-13] 24 p4162 A67-42674
TURBULENT HEAT TRANSFER
Turbulent heat transfer in tube in conditions of axial symmetry, discussing variation of mean temperature of flow as function of axisymmetrical variation of wall temperature 03 p0535 A67-13395
Approximate theory for development of steady two-dimensional turbulent free

mixing shear layers from initial velocity profile, including effects of compressibility and heat transfer
[ASME PAPER 66-WA/FE-17]

Airflow in small wind tunnel with roughened heat transfer surface, using flow visualization techniques
04 p0606 A67-15352

Turbulent heat transfer to noncircular throat bodies with and without water film cooling
04 p0728 A67-15803

Axial temperature and velocity measurements made in water at various aspect ratios, Grashof number and bottom-to-side heat flux ratios for turbulent free convection in closed container
04 p0731 A67-15827

Rayleigh-Ritz method for turbulent heat transfer in curvilinear channel and heat flux magnitudinal and directional effects on stability of isothermal flow in laminar boundary layer
04 p0610 A67-15900

Turbulent heat transfer in circular tube with circumferentially varying wall temperature and wall heat flux
[ASME PAPER 66-WA/HT-3]

Turbulent heat transfer at semipermeable surface during foreign gas injection, solving energy equation
05 p0927 A67-17000

Temperature variation in wall of square channel due to heat transfer to turbulent flow of water and Hg
07 p1265 A67-19126

Numerical solution for heat transfer to reversibly reacting gas in turbulent boundary on surface of rotating cylinder
07 p1268 A67-19575

Atmospheric turbulence statistical characteristics dependence on stratification and elevation from heat flux and wind friction stress characteristics
11 p1815 A67-23954

Heat transfer between turbulent supersonic air stream and circular water-cooled tube at Mach 1 to 4, using two-dimensional flow model
12 p2035 A67-25753

Resistance and heat transfer of plate situated in turbulent MHD boundary layer in compressible fluid
13 p2169 A67-27312

Fluid turbulence effect on rate of heat transfer from spheres in vertical wind tunnel indicate turbulent Reynolds number as important parameter
13 p2225 A67-27466

Turbulent heat-transfer coefficients and eddy diffusivity profiles for momentum and heat in Newtonian and non-Newtonian fluids, giving equation for data correlation
19 p3344 A67-34869

Temperature variation in wall of square channel due to heat transfer to turbulent flow of water and Hg
21 p3731 A67-38170

Semiempirical solution for heat transfer during turbulent natural convection near vertical impermeable flat surfaces
24 p4253 A67-42251

V-I characteristics correlated with energy release from arc column, noting turbulent nature of heat transfer in arc with transverse blowing
24 p4255 A67-42589

TURBULENT JET

Successive approximation method of estimating effect of stratification and dynamic nonuniformity of crosswind on trajectory of circular turbulent jet
01 p0053 A67-10824

Flat turbulent jet ejected from thin slit into cross wind in experimental and theoretical comparison
03 p0401 A67-12878

Submerged nonisothermal turbulent jets analyzed over wide temperature range, noting expansion angle and profile configuration dependency on initial density ratio
04 p0602 A67-14638

Convective mechanism in clear air, examining isolated plume by new model which differs from similarity model
04 p0648 A67-14647

Intersecting turbulent jet mixing studied for velocity fields, pressure and temperature
04 p0609 A67-15592

Turbulent subsonic gas jets, importance of Reynolds number and geometrical configuration of nozzle in determination of flow parameter
05 p0790 A67-18033

Radial momentum equation of flow outward from axisymmetric turbulent wall air jet impinging on solid surface
05 p0792 A67-16819

Pizeau fringes produced in laser illuminated Fabry-Perot interferometer to obtain concentration profiles in turbulent

and laminar jets
05 p0794 A67-17371

Wind tunnel results for expansion problem of two-dimensional and axisymmetric turbulent jets with zero excess impulse
06 p0982 A67-17742

Gas dynamics and geometry in mixing zone of Freon 12, air and helium jets in wake air flow, determining effect of jet velocity, gas density, etc
06 p0982 A67-17743

Expansion of free turbulent air jet controlled by given frequency from disk pulsator
06 p0982 A67-17744

Growth of turbulent mercury jet issuing into low speed secondary flow and located in coaxial magnetic field
06 p1040 A67-18130

Constant pressure turbulent jet mixing between two compressible nonisoenergetic streams of identical composition with finite initial boundary layer effects
06 p0992 A67-18880

Internal turbulence scale for convection jets determined, using measurements of light intensity fluctuations
07 p1220 A67-20003

Attachment time of thin turbulent jet to adjacent parallel flat plate calculated using quasi-steady analysis and correlated empirically
08 p1280 A67-20440

Switching time of turbulent reattachment fluid amplifier in large scale model and in theory
08 p1281 A67-20447

Wall pressure distribution in turbulent reattachment bubble calculated by spitting bubble into large number of small control volumes
08 p1320 A67-20451

Spread of turbulent plane jet issuing into parallel moving air stream, noting Reynolds number variation
08 p1321 A67-20713

Laser interferometric measurement of power spectral density of integrated particle density fluctuations in turbulent exhaust of sonic jet
08 p1337 A67-21142

Air mass measurement during turbulent axial flow towards surface of rotating disk, noting entrainment rates for high and low Reynolds numbers
09 p1437 A67-22159

Feasibility of effective aerodynamic round-lip inlet for supersonic aircraft takeoff and low speed flight
09 p1438 A67-22495

Turbulent fluctuations in rotationally symmetrical jet, obtaining velocity profiles from integration of motion equations
09 p1490 A67-22548

Concentration field of components in turbulent gas jet determined from temperature field of mixture
10 p1624 A67-23038

Similarity laws for jet noise and shear flow instability as suggested by experiments
10 p1628 A67-23830

Symmetrical jets and wakes in streaming flow with pressure gradient, noting time-mean profiles of particular pressure fields
11 p1741 A67-24047

Constant Reynolds number applied to data evaluation for turbulent jet flow in converging-diverging axisymmetric tube using free turbulent jet
11 p1742 A67-24272

Acoustic characteristics of jet determined, using Lighthill equation for free turbulent jet when components of flow fluctuation rate, turbulent vortex volume and turbulent fluctuation frequency are known
14 p2302 A67-28301

Bounded and confined turbulent jets compared to two-dimensional turbulent free jet
14 p2302 A67-28323

Aspect ratio effect on noise in proportional fluid amplifiers
14 p2250 A67-28330

Reattachment of two-dimensional jet to adjacent plate assuming new hypothesis on path of dividing streamline
14 p2303 A67-28338

Attachment distance for two-dimensional jet shown unaffected by presence or absence of second sidewall and nozzle aspect ratio
14 p2303 A67-28339

Turbulent jet spread issuing into parallel moving airstreams
16 p2657 A67-30615

Behavior of high speed, coherent, turbulent liquid jet in planar, standing, transverse acoustic field
16 p2658 A67-30945

Axisymmetric free turbulent jet flow with swirling vortex motion over wide range of swirl degree
17 p2838 A67-32417

Velocity and temperature measurements in turbulent swirling burning free jets of butane-propane-air mixture
18 p3151 A67-33815

High speed liquid jet in standing acoustic

field with velocity vector transverse to jet axis, testing injector orifice diameter, viscosity, etc
[AIAA PAPER 67-473]

Diffusion of free isothermal turbulent jet of incompressible fluid flowing from nozzle into coaxial surrounding uniform stream
19 p3209 A67-35443

Sound and white noise effects on turbulent jet aerodynamic characteristics studied at several Reynolds numbers
22 p3785 A67-40019

Soviet papers on turbulent jets of air, plasma and real gas
23 p3988 A67-40727

High temperature turbulent jet gasdynamic behavior, discussing high temperature plasma jet experiments
23 p3989 A67-40728

Isobaric mixing chamber configuration determination method for maintaining constant static pressure along flow during turbulent jet mixing
23 p3927 A67-40730

Approximate solution for turbulent jet expansion in opposite gas flow, discussing hydraulic drag coefficient formula derivation
23 p3989 A67-40731

Shadow photography study of underexpanded nozzle ejected supersonic turbulent jet off-design behavior, discussing static pressure distribution, boundary layer and Mach number effect
23 p3928 A67-40732

Plane and turbulent fluid jets dynamic and thermal behavior expanding in magnetic field described by differential equations system
24 p4195 A67-41930

Mixed flow of five plane turbulent air jets discharged into atmosphere through slotted nozzles
24 p4143 A67-42285

TURBULENT MIXING

Incompressible plane jet turbulent mixing into external parallel flow
01 p0052 A67-10646

Experimental study of turbulent transfer phenomena in isobaric mixing layer of supersonic flow containing preexisting boundary layer
[ONERA-TP-327]

Warren momentum integral method for predicting compressible free mixing of two dissimilar gases
01 p0054 A67-11003

[AIAA PAPER 65-822]

Turbulent mixing of axisymmetric jet of partially dissociated nitrogen with ambient air, establishing mixing and decay characteristics
01 p0055 A67-11170

[AIAA PAPER 65-823]

Decay of dynamically passive reactant in stationary isotropic turbulent velocity field investigated, using direct interaction and modified quasi-normal closures
02 p0234 A67-12549

Equivalency coefficient dependence on angle of attack, Mach number and angle of incidence for subsonic and supersonic gas flow past plate grid
03 p0353 A67-14082

Flow field associated with tangential slot gas injection in supersonic flow, presenting turbulent mixing zone and stability and spark shadowgraphs
[AIAA PAPER 67-198]

Concentration field of components in turbulent gas jet determined from temperature field of mixture
10 p1624 A67-23038

Turbulent wake under homogeneous strain noting mechanism of transport and mixing
13 p2096 A67-26915

Turbulent mixing in plane nonisothermal jets, deriving solutions for velocity, temperature and pressure distribution
13 p2105 A67-27052

Turbulent mixing at interface of two different density media under influence of pressure gradient, considering diffusion
13 p2105 A67-27411

Planar incompressible free turbulent mixing with arbitrary velocity ratio and axial pressure gradient
[ASME PAPER 67-FE-9]

Mixture ratio distribution effect on rocket thrust chamber performance
15 p2545 A67-29431

Mathematical model for thermal and chemi-ionization processes in turbulent nonequilibrium afterburning rocket exhausts plume, studying neutral and charged species distribution
18 p3152 A67-33820

Steady state laminar and turbulent mixing in unsteady isothermal flow in wake behind body with incident shock wave
18 p2984 A67-34203

Two-dimensional turbulent mixing of supersonic reacting and nonreacting gases studied with square shock tube 21 p3606 A67-37772
Monograph on turbulent mixing of rotating jets in circular confined duct 21 p3615 A67-39128

TURBULENT WAKE

Cyclic formation of turbulence in wake of profiled obstacle with laminar boundary layer 01 p0053 A67-10943
Statistical characteristics of high speed turbulent wake boundaries [AIAA PAPER 65-808] 01 p0007 A67-11165
Mach-Zehnder interferometer study of fluctuations in turbulent wakes of slender cones and spheres in ballistic flight [AIAA PAPER 65-809] 01 p0007 A67-11166
Electron density fluctuations in turbulent wake, using stochastic analysis and statistical averaging [AIAA PAPER 65-818] 01 p0007 A67-11168
Subsonic wind tunnel analysis of wake deformations produced by secondary velocities using models with flat base but various cross sections 02 p0233 A67-12228
Free streamline theory of two-dimensional separated potential flow past bluff body and formation of periodic vortex turbulent wake 02 p0178 A67-12233
Density gradient effect on development of turbulent wake of reentry object determined by studying wake of heated object at low speed 02 p0179 A67-12356
Rutgers Axisymmetric Near-Wake Tunnel for testing turbulent supersonic base flow, temperatures and pressure 02 p0230 A67-12361
Projectile wake turbulence measurements using hot-wire anemometer 05 p0750 A67-17346
Turbulence in reaction zone of detonating liquid explosives, noting pressure irregularities in and around shock wave front 06 p1113 A67-18143
Schlieren techniques used in free flight range study of far wake of hypersonic cones [AIAA PAPER 67-31] 06 p0938 A67-18261
Space-time correlation measurements in fluctuating turbulent wakes behind projectiles 06 p0940 A67-18434
Turbulent wake of slender body analyzed to include dominant mode of laminar diffusion, deriving solution for linear electron chemistry 06 p0943 A67-18870
Statistical mechanics predictions of turbulent fluctuations in hypersonic wake from ballistic range experiments and theoretical stochastic model of gas particle motion [AIAA PAPER 67-22] 07 p1168 A67-19431
Flow properties in laminar and turbulent near wake of cones and wedges using hypersonic shock tunnels, obtaining wake centerline and stagnation temperature profile [AIAA PAPER 67-30] 07 p1126 A67-19432
Flow field in turbulent far wake at high Mach and Reynolds numbers, obtaining solution of boundary layer equations 08 p1277 A67-20577
Elliptical wake formation behind sharp edged elliptical bodies, noting turbulent energy periodicity 08 p1277 A67-20710
Double Langmuir probe measurement of turbulent structure and ionization intensity of hypervelocity projectile and spectral characteristics of probe signal 11 p1790 A67-24449
Karman vortices in heat exchanger, noting no vortex shedding in supercritical Reynolds number range and wake turbulence 11 p1782 A67-24657
Axisymmetric compressible turbulent wake fluctuating characteristics measured using supersonic wind tunnel, including radial velocity and temperature distribution, density, etc 12 p1893 A67-25928
Turbulent wake under homogeneous strain noting mechanism of transport and mixing 13 p2096 A67-26915
Vortices in plane flow behind circular cylinder at different Mach numbers, noting staggered pattern 14 p2296 A67-27988
Calculation of diffusive gas flame in turbulent wake, reducing problem to differential equations of motion 14 p2407 A67-28649
Shock tube performance of Langmuir

probe suitable for ballistic range applications, noting low pressure turbulent wakes 15 p2490 A67-30212
Schlieren techniques used in free flight range study of far wake of hypersonic cones [AIAA PAPER 67-31] 17 p2793 A67-33006
Wake plasma turbulence of projectiles studied using electrostatic probe array 17 p2861 A67-33023
Aerodynamic characteristics of wakes behind hypervelocity bodies [AIAA PAPER 66-53] 19 p3171 A67-35741
Wing tip vortices behind DC-8 measured for maximum circumferential velocities by research aircraft 24 p4091 A67-42276
TURNSTILE ANTENNA
Machine design, capillary control selection, hydraulic circuitry and oil selection of two two-surface angular hydrostatic bearings used for azimuth turntable of radar antenna pedestals 03 p0431 A67-13749
TVC
S THRUST VECTOR CONTROL /TVC/
TWENTY-FOUR HOUR ORBIT
SA STATIONARY ORBIT
Inclination variation with time of 24-hr low inclination orbits perturbed by solar-lunar gravitation 08 p1402 A67-21508
TWENTY-FOUR HOUR SATELLITE
SA SYNCHRONOUS SATELLITE
Solar-lunar perturbation of 24-hour satellite, independence of librational motion and impossibility of equilibrium 02 p0321 A67-11498
Von Zepel transformation solution small divisor problem arising from natural frequencies of orbital resonance motion of 24-hr artificial satellite 03 p0457 A67-13162
Synchronous satellite orbits exploration, ground track plots show effects of varying orbit eccentricity and inclination 04 p0694 A67-14503
Ground track of earth-period synchronous /24-hr/ satellites, discussing equatorial, circular and elliptical orbits 04 p0704 A67-14826
24-hr satellite positions studied for librations, using linear theory 15 p2560 A67-30043
Lunar-solar gravitational perturbation of satellite with sidereal day period, discussing stability 20 p3523 A67-36626
TWENTY-SEVEN DAY VARIATION
Profile and fine structure of diurnal variation of cosmic ray intensity during high and low solar activity 01 p0144 A67-10810
27-day changes in solar diurnal variation from 1957 to 1958 based on neutron component data, noting modulation of cosmic ray anisotropy 02 p0312 A67-12800
Solar cycle effect on geomagnetic activity and temperature of near-earth tropospheric layer 04 p0616 A67-15227
Amplitude of 27-day cosmic ray modulation in relation to solar and geomagnetic activities 05 p0881 A67-16122
Quasi-spiral nature of change in 27-day cosmic ray variation with solar activity shown by harmonic analysis 05 p0884 A67-17137
27-day cycle variation in various noncosmic ray electromagnetic complex phenomena 17 p2932 A67-32084
Effective volume of asymmetric solar wind shown to be independent of primary cosmic radiation energy, noting role of 27-day variation 17 p2932 A67-32085
Geomagnetic variations discussing attempts to explain 27-day recurrence tendency and to relate solar wind and magnetic indices 20 p3430 A67-36902
Quasi-spiral nature of change in 27-day cosmic ray variation with solar activity shown by harmonic analysis 21 p3698 A67-38480
Nuclear cosmic ray component intensity variation related to 27-day solar activity variation in Elektron II and IV analysis of modulating effect 23 p4055 A67-41104
Cosmic ray intensity 27 day variations during low and high solar activity periods noting lower amplitude and softer spectrum 23 p4056 A67-41108
27-day cosmic ray intensity variations noting possible selective effects of active spots on solar hemispheres and plasma corpuscular fluxes 23 p4056 A67-41110
Amplitude of 27-day cosmic ray modulation in relation to solar and geomagnetic activities 24 p4214 A67-42798

TWILIGHT

Artificial sodium cloud in twilight produced by French rocket studied, using auroral spectrophotometer and cameras 03 p0412 A67-13370
Artificial cloud produced in twilight over Wallops Island by payload containing sodium azide and lithium azide 03 p0412 A67-13371
Photometric analysis of twilight halo photographs by Vostok VI spacecraft 03 p0415 A67-14227
Atmospheric sounding of twilight phenomena in upper layers, solar ray illumination techniques and solar ray color spectral variation 04 p0617 A67-15475
Zodiacal-light photometric measurements, analyzing effect of twilight radiation on observable brightness 04 p0617 A67-15558
Molecular nitrogen ion emission in twilight, discussing intensities, rotational distribution, charge transfer zenith measurement and ion-atom interchange reaction 05 p0803 A67-17409
Twilight effects of solar ionizing radiation absorption, discussing ion production rates and fluorescence 05 p0885 A67-17410
Multiple scattering effect on brightness of twilight sky, noting changes in spectral composition due to radiation absorbing effect of ozone and height variation of multiple layer 07 p1219 A67-19148
Multiple air scattering in mesosphere as function of zenith distance of sun and brightness of twilight sky 11 p1785 A67-23957
Spectroscopic twilight airglow measurements for upper atmosphere interpreted using rocket flight data 11 p1786 A67-24263
Correlation between diurnal meteor activity and twilight emission of ionized calcium H and K lines confirmed by Quadrantides swarm 11 p1857 A67-24756
Photometric analysis of twilight halo photographs by Vostok VI spacecraft 12 p1932 A67-25483
Upper atmosphere observation at twilight, considering broad spectral regions and emission lines 18 p3033 A67-33585
Higher order atmospheric light scattering at zenith of twilight sky, tabulating ratio between higher order scattering and primary twilight intensity 18 p3040 A67-33631
Pressure scanned Fabry-Perot interferometer for twilight sky and zodiacal light observations 20 p3440 A67-36361
Upper atmosphere optical properties determined by simultaneous twilight balloon and ground measurements, establishing twilight sky luminance ratios to solar luminance 20 p3427 A67-36369
Brightness and contrast study of noctilucent clouds in twilight layer indicating preferability of satellite observation 20 p3434 A67-37426
TWIN ENGINE
Cessna tandem twin aerodynamics noting propeller slipstream variation effects, comparing front and rear engine operation [SAE PAPER 670243] 12 p1894 A67-25498
Parametric comparative study of helicopters powered with current-technology engines and advanced non-regenerative and regenerative twin-engine installations [AHS PAPER 119] 16 p2598 A67-31835
Optimum use of contingency power rating for increasing permissible operating gross weight in twin-turbine helicopters performing long continuous flights [AHS PAPER 128] 16 p2599 A67-31842
TWIN JET
Twin jet business aircraft Mystere XX /fan jet Falcon/ structural material, propulsion data and circuits 05 p0752 A67-17268
Gulfstream II maintainability program, examining support department responsibility, insurance and material support [AIAA PAPER 67-383] 15 p2421 A67-30352
Strong forward flow of engine exhaust gas in blast deflection flow field of twin jet F-111B 17 p2797 A67-32568
TWINNING
SA MECHANICAL TWINNING
Neutron irradiation effect on twinning behavior and transition temperature of niobium-vanadium alloy 02 p0256 A67-12709
Plastic deformation in titanium at low temperatures, noting prevalence of twinning and suitability as construction material in cryogenic technology 04 p0636 A67-14752

Transformation twins in titanium, discussing relationship between twins and martensite crystal, using electron microscopy 06 p1017 A67-17967

Dislocations in Be, discussing twinning and deformation by climbing, stacking faults and condensation vacancies 07 p1210 A67-20163

Twinning and temperature effect in plastic deformation of titanium 09 p1518 A67-21965

Twinning of copper, silver, iron, and gold alloys of beryllium pressurized in solid medium noting structural changes 16 p2690 A67-31371

Plastic deformation in titanium at low temperatures, noting prevalence of twinning and suitability as construction material in cryogenic technology 18 p3066 A67-34410

Twin lamellae in magnesium examined by electron microscopy reconfirms double twinning sequence 24 p4173 A67-42345

TWIST

S TORQUE

TWISTED WING

Elastic wing twisting effect on longitudinal stability and controllability of glider, considering wing rigidity 24 p4094 A67-42021

TWO-BODY ORBIT

Satellite rendezvous guidance laws applicable to circular, near-circular and elliptical orbits, using Lagrangian formulas for position and velocity in two-body orbit 02 p0264 A67-12315

Orbit determination between two radii vectors with specified periastron radius distance 16 p2746 A67-30959

Two-body system connected on circular orbit by spherical hinge examined for plane oscillations, finding all equilibrium positions with respect to orbital coordinate 17 p2954 A67-32242

Book on theory of orbits covering restricted problem of three bodies, two bodies in rotating coordinate system and periodic orbits 18 p3120 A67-34032

First order perturbation solution for transition matrix relating errors at one point of two-body orbit to errors at later point 19 p3317 A67-34832

Pursuit trajectory plotting in central field of gravity for pursuer and fugitive assuming motion can be predicted successively at small time intervals 24 p4228 A67-42273

TWO-BODY PROBLEM

SA MANY-BODY PROBLEM

Behavior of magnet and ball in gravitational field in five-dimensional continuum 01 p0060 A67-10366

Nominal trajectory in modified Encke special perturbation method, using two-body functions 01 p0148 A67-10384

Mechanics of celestial bodies including problems on Newton gravitation law, motion equations, two-body problem, Kepler law, etc 06 p1030 A67-17772

Generalization of Whittaker formula for periodic orbits to fields with arbitrary attraction law 06 p1082 A67-18039

Astrodynamic perturbation theory in which perturbed space-vehicle motion is described in terms of osculating hodograph applied to lunar landing [AIAA PAPER 67-25] 06 p1085 A67-18304

Energy variation of two-body system due to gravitational radiation studied within framework of Minkowski theory 12 p1966 A67-25145

Mass point motion in central mass gravitational field determined from mass point position and velocity coordinates, obtaining Kepler orbits 15 p2559 A67-30035

Aerodynamic heating about vehicle entering atmosphere for corridor and guidance requirements analyzed on basis of Newton two-body problem 15 p2417 A67-30046

Three-body problem reduced to two-body problem in general relativity theory 16 p2745 A67-30747

Second partial derivatives of position and velocity vectors components developed with respect to same vectors components at arbitrary epoch 16 p2696 A67-30960

Closed form regularized solutions in polar coordinates of two-body problem obtained and applied to restricted three-body problem 17 p2943 A67-32440

Integration of regularizing canonical and corresponding Hamilton-Jacobi equation applied to two-body problem for construction of perturbation theory 19 p3249 A67-34795

Two-body problem in classical mechanics, proving existence and quantization of circular orbits 20 p3487 A67-37581

Pursuit trajectory plotting in central field of gravity for pursuer and fugitive assuming motion can be predicted successively at small time intervals 24 p4228 A67-42273

Three-body problem application to nuclear reactions involving neutron, proton and heavy nucleus, parametrizing two-body interactions in terms of s-wave separable potentials 24 p4191 A67-42593

TWO-DIMENSIONAL BODY

Existence of divergence in density expansion of viscosity and thermal conductivity coefficient of two-dimensional gas of rigid disks 02 p0234 A67-12545

Force distribution and stress displacement relations for two-dimensional elasticity with coupled stresses 06 p1107 A67-18651

Computer program for gravity and magnetic profiles across two-dimensional bodies of arbitrary shape 06 p0998 A67-18736

Dynamic properties of elastic one- and two-dimensional continua using matrix method on digital computer and Hermitian polynomials 13 p2216 A67-26621

Stress distribution in matrix of composite material for case of filler between one infinite and two displaced semilinear microfibers 14 p2398 A67-28100

Slender two-dimensional wing lift-drag ratio at hypersonic speed maximized, assuming modified pressure coefficient 15 p2416 A67-29409

Two-dimensional flow past bluff body, comparing vortex street wake measurements to von Karman predictions 17 p2790 A67-32278

Stress analysis of loaded boundaries in two-dimensional second boundary problems, studying mechanical and thermal strain, knife-edge device, etc 18 p3142 A67-33899

[SESA PAPER 1194]

Stress analysis of loaded boundaries in two-dimensional second boundary problems, studying mechanical and thermal strain, knife-edge device, etc 21 p3722 A67-38435

Saint Venant principle in linear and nonlinear plane elasticity in two-dimensional isotropic body 22 p3912 A67-39743

Mathematical reduction of three-dimensional continua to one and two dimensions expressed by equilibrium equations with identical form 23 p4078 A67-41195

TWO-DIMENSIONAL FLOW

Swirling axisymmetric radial jet flow of conducting fluid in presence of axial magnetic field, citing conditions for singularity in two-dimensional case 01 p0124 A67-10800

Theory for incompressible two-dimensional flow of inviscid liquid past array of similar hydrofoils, behind each of which extends cavity of finite length 01 p0053 A67-10851

Two-dimensional shock induced separated flows in turbulent boundary layer, applying Crocco-Lee theory and calculating pressure rise coefficient 02 p0231 A67-11522

Free streamline theory of two-dimensional separated potential flow past bluff body and formation of periodic vortex turbulent wake 02 p0178 A67-12233

Nonlinear two-dimensional unsteady potential flow around arbitrarily shaped airfoil in inviscid and incompressible fluid, considering method of calculating pressure, forces and moments [AIAA PAPER 66-968] 02 p0178 A67-12291

Five calculations of plasma accelerators using quasi-one-dimensional and two-dimensional model for different nozzle shapes 02 p0274 A67-12337

Hydrodynamic stability Cauchy problem for continuous spectrum of two-dimensional parallel flow of nonviscous incompressible fluid 03 p0402 A67-13172

Approximate theory for development of steady two-dimensional turbulent free mixing shear layers from initial velocity profile, including effects of compressibility and heat transfer [ASME PAPER 66-WA/FE-17] 04 p0606 A67-15352

Existence theorem for two-dimensional subsonic flow of compressible fluid, following Bers method 05 p0790 A67-16044

Thermodynamic analysis of flow in gas turbines, for two- and three-dimensional boundary layers and

wakes 05 p0748 A67-16745

Steady two-dimensional MHD flow of ideal inviscid perfectly conducting compressible fluid with one nonzero component 06 p1040 A67-18115

Supersonic laminar two-dimensional boundary layer separation in compression corner with and without cooling [AIAA PAPER 67-191] 06 p0940 A67-18361

Numerical analysis of free boundary problem inviscid incompressible flow field of impinging jet and two-dimensional Joukowski airfoil in sheared wind tunnel flow [AIAA PAPER 67-217] 06 p0988 A67-18460

Hysteresis effects in steady laminar two-dimensional MHD flow of gas between moving planes and coaxial cylinders in TM field 06 p1043 A67-18671

Fluid flow through parallel cylinders when flow incidence is lateral and Reynolds numbers are small, determining particles trajectories 06 p0991 A67-18819

Nonuniform two-dimensional subsonic and supersonic flow of compressible fluid past body, using small parameter method 07 p1125 A67-19322

Perturbation of two-dimensional viscous flows in finite region, noting exact solution of Navier-Stokes equation 08 p1319 A67-20352

Surface pressure, heat transfer coefficient, wave structure and shock disturbances of inviscid supersonic flow field along corner of intersecting wedges [AIAA PAPER 66-128] 08 p1276 A67-20564

Gas dynamics of nonisentropic two-dimensional MHD flow of ideal inviscid perfectly conducting compressible fluid 08 p1357 A67-20593

Two-dimensional incompressible potential flow theory for airfoil design with prescribed velocity distribution over surface 09 p1437 A67-21740

Two-dimensional isothermal liquid flow electrically conducting in channel under electromagnetic fields, finding self-modeling solutions using Jacobi functions 09 p1544 A67-21861

Two-dimensional problem for layer with mixed boundary conditions, obtaining solutions for Fredholm integral equations and relations for temperature distribution 09 p1580 A67-21994

Laminar boundary layer calculated by approximation of momentum and kinetic integral equation for boundary conditions 09 p1489 A67-22158

Two-dimensional laminar jet of incompressible fluid issuing into uniform stream in direction of main flow, considering two coordinate type expansions 09 p1489 A67-22412

Supersonic stream interaction with two-dimensional secondary jet from rectangular planform wedge 10 p1592 A67-23116

Inviscid two-dimensional flow using extension of Hele-Shaw analogy, noting axisymmetric, compressible and MHD cases 10 p1627 A67-23554

Supersonic motion of plate in two-component medium in two dimensions 10 p1628 A67-23647

Two-dimensional steady MHD flow with resolution of neutral sheets into intermediate and slow waves 11 p1862 A67-24499

Rotating Ekman boundary layer stability and transition for two-dimensional roll vortices superimposed upon basic boundary layer flow 11 p1781 A67-24543

Behavior of solution of system of equations for unsteady boundary layer of two-dimensional liquid as time approaches infinity 11 p1782 A67-24669

Current distribution in incompressible fluid flow in magnetic field at low Reynolds number, estimating Lorentz force effect 11 p1842 A67-24952

Equations in hodograph plane obtained for two-dimensional polytropic gas flow in presence of shock waves 12 p1892 A67-25443

Heat transfer between turbulent supersonic air stream and circular water-cooled tube at Mach 1 to 4, using two-dimensional flow model 12 p2035 A67-25753

Linear stability of symmetrical parabolic flows of various types 13 p2092 A67-26276

MHD generator two-dimensional incompressible flow, obtaining expressions for power output, velocity, electrical efficiency, etc 13 p2055 A67-26417

Two-dimensional unsteady plasma flows in

coaxial channel formed by two profile electrodes calculated in case of finite conductivity in presence of Hall effect 13 p2168 A67-27301

Rayleigh problem in hydrodynamic stability for two-dimensional parallel flow of nonviscous incompressible fluid 13 p2106 A67-27456

Two-dimensional steady flow analysis in channels with variable cross sections under strong magnetic field action, calculating velocity distribution by series expansion 14 p2355 A67-27902

Two-dimensional self-similar problem for uniform penetration of plate into half-plane of perfect gas flow, determining flow pattern 14 p2239 A67-27982

Two-dimensional unsteady Navier-Stokes equations for compressible viscous gas in closed region, examining convective flow and heat transfer 14 p2296 A67-27987

Model of inviscid, incompressible and variable density airflow in long channel over mountain treated mathematically 14 p2346 A67-28004

Similarity solutions for two-dimensional unsteady compressible boundary layer equations using group theoretic methods 14 p2297 A67-28135

Nonlinear inviscid transonic flow in throat of two-dimensional curved nozzle, using approximate method 14 p2242 A67-28360

Two-dimensional flow through bends with turning vanes, using Green theorem to obtain surface pressure distributions [ASME PAPER 67-FE-13] 14 p2304 A67-28362

Flow turning angle during two-dimensional turbulent supersonic reattachment to plane wall [ASME PAPER 67-FE-20] 14 p2305 A67-28367

Intake aerodynamics of upper wing surface studied with two-dimensional potential flow models and suction models, considering inlet problems 14 p2243 A67-28702

MHD generator with uniform rectangular duct, considering ion slip and Hall effect in case of two-dimensional flow 15 p2422 A67-29906

Effect of magnetic field gradients at inlet and outlet on linear two-dimensional induction MHD generator calculated by bilateral Laplace transform 16 p2605 A67-30579

Counterpart of Stokes hydrodynamical paradox for linearized viscous fluid flow obtained from application of singular perturbation to Oseen equations 16 p2657 A67-30827

Time independent two-dimensional Navier-Stokes equations solutions from singular perturbation theory, determining properties 16 p2657 A67-30828

Interaction of convection and radiation heat transfer in axisymmetric two-dimensional stagnation point low-speed flow of gray absorbing and emitting gas 16 p2591 A67-30939

Two-dimensional viscous fluid flow with formulation and solution of weak shock reflection problems by numerical method 16 p2662 A67-31534

Two-dimensional inviscid flow pattern of gas behind shock front in neighborhood of stagnation point of cylindrical body acting as magnetic field source 16 p2723 A67-31581

Static equilibrium for two-dimensional toroidal plasma configurations with inner fields and purely meridional electric currents 17 p2903 A67-32709

Uniformly valid approximation of two-dimensional subsonic flow along thin airfoil with blunt elliptical shape 18 p2982 A67-33663

Wave number and Rayleigh numbers effect on stability of two-dimensional convection in layer heated from below 18 p3159 A67-34003

Two-dimensional flow structure around thin body in dispersive medium, discussing flow equations and similarity law 19 p3208 A67-34901

Temperature distribution within two-dimensional thermal boundary layer due to flow of second order fluid past flat plate 19 p3210 A67-35447

Laminar boundary layer for two-dimensional flow on bodies of revolution, noting suction velocity 19 p3210 A67-35721

Momentum integral method applied to

two-dimensional flow problem between flat plates 20 p3420 A67-36420

Two-dimensional potential flow through bend profile, obtaining streamlines and velocity distributions 20 p3356 A67-36533

Heat transfer for one-and two-dimensional pulsating incompressible laminar flow in circular tube with two thermal boundary conditions [ASME PAPER 67-HT-65] 20 p3550 A67-36747

Laminar boundary layer with heat transfer in liquids with variable fluid properties, including velocity and temperature profiles [ASME PAPER 67-HT-69] 20 p3550 A67-36749

Properties of kinetic energy and squared vorticity in two-dimensional inviscid turbulent flow, using Navier-Stokes equation and conservation laws 21 p3609 A67-37735

Exact solutions of incompressible Navier-Stokes equation for irrotational Beltrami nonconvective two-dimensional swirl and axially symmetric cross flows 21 p3609 A67-37737

Boundary value problems solution in steady two-dimensional compressible MHD flow past thin body 21 p3660 A67-37742

Toroidal plasma instabilities analyzed, justifying use of two-dimensional slab models with varying gravitational field simulating magnetic lines curvature effect 21 p3661 A67-37747

Two-dimensional turbulent mixing of supersonic reacting and nonreacting gases studied with square shock tube 21 p3606 A67-37772

Finite conductivity effect on two-dimensional plasma flow in coaxial channel solved numerically, obtaining steady state flow regime by build-up method 21 p3665 A67-38240

Rigid cylinder two-dimensional motion in rotating incompressible fluid compared to motion in isotropic incompressible conducting medium under magnetic field 21 p3668 A67-38552

Equations in hodograph plane obtained for two-dimensional polytropic gas flow in presence of shock waves 21 p3613 A67-38816

Base bleed effects on flow behind two-dimensional model with blunt trailing edge, measuring base pressure, shedding frequency and vortex formation 21 p3566 A67-39078

Self-aligning hot-wire probe for direction, velocity and turbulence measurements in two-dimensional flow 22 p3800 A67-40069

Two-dimensional two-fluid nonlinear computer model applicable to low beta plasma interchange modes 23 p4033 A67-40995

Inviscid instability of cylindrical two-dimensional free boundary layer vortex flow, using approximation by axisymmetrical vortex model 23 p3990 A67-41169

Energy equation solution procedure for heat transfer across two-dimensional oscillating laminar boundary layer 23 p4082 A67-41243

Two-dimensional incompressible flow near airfoil trailing edge treated by inviscid flow model, with constant vorticity inducing velocity field causing flow retardation 23 p3928 A67-41245

Force defect coefficient method applied to calculation of compressible jet flow discharge for asymmetric two-dimensional orifice 23 p3936 A67-41330

Shock refraction effects due to velocity and temperature gradients in rocket nozzles investigated by studying leading shock in two-dimensional secondary fluid injection 23 p3992 A67-41740

Wakes in two-dimensional flows studied by comparing mesoscale eddies in earth atmosphere with Karman vortex street, calculating wake parameters 24 p4146 A67-41786

High speed computer graphic techniques for airfoil sections characteristics in two-dimensional compressible flow [SAE PAPER 670845] 24 p4091 A67-41998

Singular perturbation methods for two-dimensional lifting low Reynolds number flow 24 p4091 A67-42169

Prandtl equation system for two-dimensional incompressible flows expanded to construct solutions for three-dimensional unsteady flows by straight lines 24 p4177 A67-42200

Delta wing with leading edge vortices, calculating inviscid incompressible flow field near center of rolled up vortex sheet

assuming conical velocity field 24 p4092 A67-42570

TWO-DIMENSIONAL JET

Incompressible plane jet turbulent mixing into external parallel flow 01 p0052 A67-10646

Local heat-transfer coefficients between isothermal flat plate and two-dimensional wall jet 04 p0732 A67-15835

Wind tunnel results for expansion problem of two-dimensional and axisymmetric turbulent jets with zero excess impulse 06 p0982 A67-17742

Two-dimensional jet plane problem, considering rheological solution for applications to ground effect machines 11 p1781 A67-24571

Subsonic-transonic drag of supersonic, two-dimensional and axisymmetric plug inlets 13 p2051 A67-27592

Bounded and confined turbulent jets compared to two-dimensional turbulent free jet 14 p2302 A67-28323

Reattachment of two-dimensional jet to adjacent plate assuming new hypothesis on path of dividing streamline 14 p2303 A67-28338

Attachment distance for two-dimensional jet shown unaffected by presence or absence of second sidewall and nozzle aspect ratio 14 p2303 A67-28339

Two-dimensional wall jet effectiveness measurements and calculation procedures for injection conditions 15 p2468 A67-29128

Solution of MHD boundary layers with magnetic field as exponential function of x coordinate, extended to transverse magnetic fields 16 p2722 A67-31570

Force on plane wire screen at right angle to turbulent incompressible two-dimensional jet axis determined, developing approximate theories in terms of screen K factor 17 p2836 A67-32127

Two-dimensional incompressible fluid jet penetration analyzed kinematically via free streamline theory and notched hodograph 20 p3422 A67-36845

Reattachment of two-dimensional compressible air jets to planes, discussing pressure maximum and inlet Mach numbers 22 p3786 A67-40068

Transverse magnetic field effect on two-dimensional jet of incompressible fluid 24 p4198 A67-42565

TWO-ELECTRON SYSTEM

Nonrelativistic energies of several states of two-electron atoms by Rayleigh-Ritz expansions in independent variables chosen as natural coordinates 04 p0661 A67-15512

Analytic power series solution of nonrelativistic Schroedinger equation for two-electron atom, assuming fixed nucleus and singlet and triplet S states 15 p2520 A67-30158

Rapidly converging analytic solution by integral series of nonrelativistic Schroedinger equation for He atom 15 p2520 A67-30159

Irreducible tensorial components of two-electron operator and second-order density matrix for spin-projected single-determinantal wave function 16 p2705 A67-31759

TWO-FLUID MODEL

Stability of self-gravitating two-fluid infinite plasma cylinder model in axial magnetic field 13 p2163 A67-26285

Finite ion Larmor radius effect on superposed fluid stability investigated for general perturbation direction, noting magnetically stabilized configurations become overstable 13 p2167 A67-26993

Motion equation for nonideal relativistic electron gas, reviewing hydrodynamics obtained from Landau equation 15 p2527 A67-29517

Singularities of two-fluid plasma equations, investigating compatibility and relation to boundary conditions 21 p3661 A67-37744

Plasma hydromagnetic jump conditions derived from two-fluid plasma model, discussing relevance to collisionless plasma shock 21 p3662 A67-37764

Linear MPD channel theory with heavy component in uniform state evaluated for investigation of electrical conductivity phenomena 22 p3747 A67-39277

MHD stability in two-fluid model examined for condition where resistivity and electron inertia are neglected 22 p3851 A67-39984

Laminar nonrelativistic finite amplitude

hydromagnetic wave propagation in low temperature ionized plasma, using two-fluid model 22 p3852 A67-39990
Two-stream instability in plasma analyzed using magnetic field association with charged particle motion and boundary effects 23 p4034 A67-41450

TWO-PHASE FLOW

Two-phase flow and material attrition problems for Rankine cycle liquid metal power plants [ASME PAPER 66-GT/CLC-4]

01 p0014 A67-10872
Single-phase and two-phase cavitating flow regime performance of liquid propellant rocket engine turbopump inducers [ASME PAPER 66-WA/FE-23]

04 p0554 A67-15353
Heat transfer and skin friction rates increase in gas-liquid droplet suspension system flowing over circular cylinder formulated by laminar boundary layer theory 04 p0725 A67-15439

Differential equations for local interfacial and wall shear stresses for one-dimensional annular two-phase flow 04 p0735 A67-15857
Heat transfer - AICE International Conference, Chicago, August 1966, Volume 5, Flow boiling and radiation 04 p0736 A67-15859

Radiation effects on heat transfer and friction characteristics in natural and forced convection film boiling in boundary layer flows [ASME PAPER 66-WA/HT-6]

04 p0739 A67-15939
Nucleonic quality gauging system for two-phase hydrogen pipeflow 05 p0842 A67-16539
Bibliography and subject index to two-phase gas-liquid flow literature 07 p1269 A67-20300

Effect of underheating on development of boiling crisis in two-phase nonequilibrium flows 10 p1732 A67-23018

MHD power generation using bifluid liquid metal system /such as Li and Cs/ with two-phase generation 12 p1901 A67-25897

Mass limiting two-phase flow compared in straight tube and in nozzle 13 p2093 A67-26541

Pressure drop study of near saturation Freon 11, noting flowing liquid quality condition for estimates 13 p2106 A67-27668

Critical two-phase flow of nitrogen and oxygen through orifices characterized by mass-limited conditions 13 p2106 A67-27669

Heat transfer and skin friction increase for gas stream with liquid-droplet suspension flowing over blunt-nosed body near stagnation point 14 p2405 A67-28126

Incompressible two-phase mixed flow through sharp edge orifice including shear force between phases 14 p2305 A67-29012

Heat transfer and skin friction rates increase in gas-liquid droplet suspension system flowing over circular cylinder formulated by laminar boundary layer theory [ASME PAPER 66-WA/HT-33]

15 p2579 A67-29322
Hydrodynamics of liquid-gaseous metal mixture flowing through nozzles, discussing heat exchange rate and condensation effects 16 p2656 A67-30574

Electrical conductivity measurement of liquid-vapor potassium mixture flowing in circular steel tube simulating MHD oscillator conditions 16 p2712 A67-30575

Magnetohydrodynamic generators operating with two-phase liquid metal flows, describing design and performance 16 p2604 A67-30577

Two-phase gas-liquid flow photography equipment and techniques, with applications to droplet mass transfer, flow pattern determination, etc 16 p2671 A67-30840

Maximum heating temperature of smallest particles of polydisperse material in two-phase flow by approximation method 17 p2970 A67-32462

Eigenvalue method prediction of two-phase fluid critical flow rates via energy model, comparing empirical and theoretical results 17 p2838 A67-32689

Gravity and buoyancy effects on slip ratio, void fraction, flow model and boiling heat transfer [ASME PAPER 67-HT-63]

20 p3549 A67-36745
Flow patterns of two-phase mixtures in cylindrical tubes, using high speed photography 20 p3423 A67-37161

Critical fluid flow rate analysis of two-

phase nitrogen at stagnation pressure of 25 psia 22 p3784 A67-39967

Discharge line fluid conditions in cryogenic container with self-pressurized draining, using Bernoulli, continuity and general energy equations and fluid properties 22 p3784 A67-39968

Liquid surface tension effect on maximum particle size in two-phase nozzle flow, discussing drag exerted by accelerating gas stream 22 p3787 A67-40225

Two-phase flow equations for turbulent boundary layer flows, considering solid particle effects 23 p3993 A67-41748

Two-phase mixture passing through magnetic field in MHD generator studied for effective electric conductivity 23 p3942 A67-41758

Electrical conductivity of high void fraction two-phase flow with and without magnetic field in MHD generator 23 p3942 A67-41759

Critical air-water flow in converging-diverging annular venturi noting pressure profiles 24 p4143 A67-42280

Single-phase and two-phase cavitating flow regime performance of liquid propellant rocket engine turbopump inducers [ASME PAPER 66-WA/FE-23]

24 p4143 A67-42464

TWO-PHASE SYSTEM

Liquid solid film lubrication of hydrodynamic bearings, including effects of solid particles in liquid base lubricant 01 p0077 A67-10122

Transient response of vapor volumetric concentration to perturbation propagation and wave form in boiling forced convection system under oscillatory conditions 01 p0167 A67-10974

Stability of dry patches forming in thin liquid film flowing over heated surface, noting effects of vapor thrust and thermocapillarity 01 p0167 A67-10975

X-ray structural analysis of superconducting Nb based alloys, noting two-phase region in annealed samples 05 p0863 A67-16690

Fine structure of two-phase alloys of titanium VT14 and structures effect on mechanical properties 07 p1205 A67-19274

Two-phase liquid metal cycle MHD conversion, discussing thermodynamic aspect, hot gas system and possibility for use in spacecraft and ground power plants 12 p1896 A67-25121

Polytropic process of variations in state of system composed of gas and solid particles 12 p2033 A67-25317

Criterion expressions for Nusselt numbers of mass transfer in two-phase film system at high Prandtl numbers which describe physical properties of both phases 14 p2405 A67-28303

X-ray structural analysis of superconducting Nb based alloys, noting two-phase region in annealed samples 15 p2539 A67-29860

Soviet book on heat transfer and hydrodynamics in two-phase media 17 p2969 A67-32457

Diffusion of nickel in solid solution and two-phase alloys of nickel-titanium system 19 p3245 A67-35468

Geometric prediction method extension to quaternary liquid-liquid equilibria in two-phase systems comprising two type I ternaries 19 p3346 A67-35612

Youngs modulus variation as function of external magnetic field in mixed state in niobium 20 p3464 A67-36221

Cluster variation method based on W. shaped cluster in triangular lattice for lattice-gas liquid, phase-separating binary alloy and Ising model 23 p3971 A67-40969

Electric power generation using two-phase liquid-metal cycles in MHD converter, discussing liquid metal dynamics 24 p4099 A67-42417

TWO-STAGE ROCKET
Three-dimensional problem of optimizing motion of two-stage rocket in homogeneous parallel force field with limited thrusts in engine of both stages 01 p0154 A67-10993

Nose selection and vehicle motion dynamics for second stage of two-stage sounding rocket system, discussing nose shapes effect on altitude performance, overall vehicle stability, bending moments, etc 08 p1406 A67-20513

Saphir test vehicle, two-stage guided and

controlled rocket 15 p2571 A67-30090

Thrust history to produce maximum altitude for two-stage launch vehicle determined using simplifying assumptions and atmospheric drag 22 p3904 A67-40089

TWO-STAGE TURBINE

Metallurgical and fluid dynamic results of 2000-hr endurance test at high temperatures on two-stage 200 hp turbine in wet potassium vapor [ASME PAPER 67-GT-9]

11 p1745 A67-24797

U**U.S.S.R.**

Short and ultrashort wave power amplifiers using Soviet transistors 05 p0773 A67-16457

High strength alloys for gas turbines in Soviet Union, noting wrought and cast nickel-base alloys for turbine blades and vanes 10 p1668 A67-23012

Russian and American practices and policies regarding planetary contamination in connection with COSPAR requirements 10 p1601 A67-23580

Legal forms of international cooperation of U.S.S.R. in peaceful exploration of outer space, discussing bilateral and multilateral agreements between government and nongovernment organizations 12 p2044 A67-26155

Analysis of eucrite-type meteorite which fell on June 10, 1939 near Chervonyi Kut in Ukraine 13 p2197 A67-26508

IQSY program in U.S.S.R. /1964-1966/ including meteorology, aurora studies, solar activity, etc 19 p3223 A67-35482

Cosmic ray intensity measurement data from Soviet 1966 expedition in Arctic Ocean 23 p4060 A67-41138

Soviet metallurgical, chemical and electrochemical studies and industrial applications of titanium 24 p4169 A67-41918

Collected papers of Kapitza, Volume 3 covering low temperature production, stereoscopic films, liquid He, etc 24 p4188 A67-42294

U.S.S.R. SPACE PROGRAM

Soviet program of planetary exploration with aid of automatic interplanetary stations, examining problems due to trajectory errors and communications breakdown 02 p0326 A67-12041

Soviet book on space and problem of world peace 03 p0538 A67-13200

Soviet 10 million lb thrust booster in manned lunar flight 03 p0519 A67-14099

Cosmic space exploration in U.S.S.R., discussing results obtained from Cosmos and Elektron earth satellites 08 p1394 A67-21110

Visual observations of earth, sea and sky made by astronauts and cosmonauts during space flights 09 p1569 A67-22604

Flight activities of Russian cosmonauts in assessment of medical preparedness for orbital flight 12 p1902 A67-25653

Unmanned exploration of moon, summarizing results on surface structure, back side and material composition 16 p2748 A67-31199

Soviet space effort and Cosmos satellites, deducing orbital parameters, transmission frequencies, launching time/place, nature of experiments, etc 17 p2956 A67-32724

Soviet northern cosmodrome location determination from data obtained through radio/visual observation of Cosmos satellites 18 p3004 A67-34358

Soviet national report to COSPAR, summarizing findings in upper atmosphere, on lunar surface and outer space from 1964 to 1966 19 p3322 A67-35308

Vostok launch vehicle design characteristics evaluated including performance, propellant weights, booster phase burning period, etc 19 p3334 A67-35843

Bacillus brevis var. G-B survival ratio dependence on space flight factors, noting no induction of dissociation products nor appearance of auxotrophic mutants 21 p3577 A67-38597

Russian rocket hardware exhibited in Paris noting Vostok launcher 22 p3899 A67-39523

Soviet space activity /1933-1967/ noting Sputnik, Venera I, Luna and Zond programs 23 p4086 A67-40919

Soviet meteorological rocket observation

and research, basic techniques and program results 23 p4025 A67-41447

UF-XS AIRCRAFT

S SHIN MEIWA UF-XS AIRCRAFT

UK-C

S ARIEL II SATELLITE

UK-E

Electrical system design and integration in UK-3 scientific satellite, noting noise control for receiver 01 p0156 A67-11423

UK-2

S ARIEL II SATELLITE

ULM

S ULTRASONIC LIGHT MODULATOR

/ULM/

ULTRA-SHORT-WAVE RADIO EQUIPMENT

Short and ultrashort wave power amplifiers using Soviet transistors 05 p0773 A67-16457

Diurnal and seasonal variations in radio echo observations from meteoric trains during forward ultrashortwave scattering 14 p2383 A67-27924

ULTRAHIGH FREQUENCY

Equivalent series resistance of semiconductor region of varactor diodes at UHF determined, using series resonance method 01 p0038 A67-10815

Environmental, physical and practical limitations imposed on telemetry system performance when operating in UHF band 02 p0196 A67-12005

System design analysis of Edwards high range UHF telemetry receiving station network, considering reliability, availability, design adequacy, antennas, initial and operating costs, etc 02 p0229 A67-12007

Data quality assurance program for telemetry ground station operations, noting frequency division and time division formats 02 p0198 A67-12023

40 watt solid state UHF AM transmitter at 225-400 mc 02 p0219 A67-12111

Optical and UHF Doppler /UDOP/ tracking for lift-off phase of Saturn SA-5 launch vehicle 03 p0368 A67-13383

Short wave and very short wave direction finding from aircraft 03 p0465 A67-13394

UHF ultrasonics, discussing generation and wave detection, progressive wave amplification, biological effects, power measurement, etc 03 p0468 A67-13546

VHF and UHF communications between transoceanic commercial aircraft and ground stations by means of aeronautical communication satellites 06 p0961 A67-17701

UHF oscillator synchronization correlation with various parameters 06 p0969 A67-18119

Frequency spectrum during UHF plasma oscillation excitation by monoenergetic primary electrons introduced into low pressure Hg discharge 08 p1358 A67-20869

Optical signal modulation to measure noise figure at UHF of photoparametric amplifier, using silicon mesa diode as both photodetector and varactor 09 p1476 A67-22208

UHF distance measuring equipment /DME/ using new type of ground beacon and only thermionic devices in transmitter power stage 09 p1530 A67-22650

Delay equalization in UHF range by allpass networks with symmetric three-conductor transmission lines 11 p1760 A67-24231

UHF susceptibility of uniaxial magnetic films in weak fields far from ferromagnetic resonance 12 p1981 A67-25240

UHF oscillations in GaAs thin epitaxial layers deposited on isolating substrates of same material 12 p1981 A67-25279

Possibility of using p-n-n /p-n-n, n-p-p/ structure with heterojunctions for rectifier designed for ultrahigh current densities 13 p2174 A67-26366

Extension of stripline circulator operation calculation by Davies and Cohen to include wider range of stripline geometries 13 p2076 A67-26482

Triple-tuned broadband UHF junction circulator using lumped element technique 13 p2076 A67-26483

UHF intensity-modulated light emanating from plasma observed with aid of photomultiplier radiometer 13 p2167 A67-27082

Semiconductor conductivity measurement from propagation irregularities of SHF electromagnetic waves in medium containing semiconductor 14 p2364 A67-27836

Ionospheric discontinuity motion in E layer at 100 km, using long distance

ultrashort-wave propagation data obtained by diversity-reception method 15 p2479 A67-30148

Exciting molecular emission spectra in cold plasma free of electrode-induced impurities by superhigh frequency source 16 p2704 A67-31478

Scattering and absorption of ultrashort coherent radiation pulses passing through electron gas applied to ionosphere 17 p2812 A67-32312

Differential phase-shift measurements at UHF and microwave frequencies, discussing standards, techniques and uncertainties in characteristics 17 p2815 A67-32608

Multipath effect measurement in propagation path at UHF frequencies from synchronous satellite to aircraft 17 p2816 A67-32626

Time signal transmission and reception, noting development of UHF spectroscopy and atomic frequency scales 18 p3004 A67-34400

UHF amplification and frequency conversion using single transistor as amplifier and base-collector junction capacitance as varactor 20 p3398 A67-36773

Convex plasma thermal radiation at UHF, determining spectral composition using Fourier integrals 21 p3663 A67-37937

Possibility of using p-n /p-n-n, n-p-p/ structure with heterojunctions for rectifier designed for ultrahigh current densities 21 p3680 A67-38322

500 to 1000 MHz ultrahigh RF hybrid amplifier fabricated with microelectronic multilayer thin film technique, noting performance of components 21 p3596 A67-38342

UHF sferics detection system receiving and display components for remote sensing by satellite of convective cloud development 22 p3806 A67-40358

ULTRAHIGH VACUUM

Ultrahigh vacuum measurement and total and partial pressure gauges, discussing operational and calibration problems 01 p0064 A67-10501

Ultrahigh vacuum installation using ion-getter pumps for analysis of adhesion between plastics and metals in space environment 02 p0228 A67-11552

Ultrahigh vacuum envelopes design, fabrication and use, emphasizing choice of materials and outgassing load 02 p0250 A67-12452

Ultrahigh vacuum effects on flow and fracture behavior of molybdenum 06 p1016 A67-17897

Flashed getters for production of ultrahigh vacuum, tantalum most promising based on residual gas analysis 08 p1354 A67-21496

Bakeout procedure for small glass ultrahigh vacuum system to obtain stable pressures 08 p1354 A67-21497

Sliding electrical contact material for ultrahigh vacuum with 300 amp/sq inch current density, 425 in/min sliding velocity and 10 psi brush pressure 11 p1805 A67-24345

Sublimation technique applied to high mobility PbS and CdS thin film deposition under ultrahigh vacuum equilibrium conditions 11 p1847 A67-24738

Gas pressure effect on electrical breakdown and field emission, discussing ion bombardment and whisker formation 11 p1820 A67-24921

Lunar soil density problem investigated by sieving clean powders of different materials with different grain sizes and drop heights under ultrahigh vacuum 12 p2000 A67-25207

Metallic couples ultrahigh vacuum adhesion experiments show contaminant dispersal as major barrier 15 p2492 A67-29493

Solid rocket components exposure to elevated temperatures, hard vacuum and UV radiation during space flight and reentry 15 p2507 A67-29548

Space vehicle lubrication methods, noting design and construction of test apparatus 15 p2492 A67-29558

Ultrahigh vacuum and air fatigue testing of aluminum alloy observing corrosion process influence on mechanism by latter 16 p2689 A67-31369

Refractory metal alloys tested in ultrahigh vacuum, measuring creep extension 16 p2690 A67-31524

Vacuometer modification permitting direct pressure difference measurements in high

and ultrahigh vacuum range 17 p2855 A67-32352

Rotating device for transmitting motion through walls of ultrahigh vacuum chambers, using circular motion of bellows envelope and internal gearing 17 p2863 A67-33358

Dynamometer using epoxy-bonded foil strain gauges for simultaneous two-force measurements for ultrahigh vacuum and high temperature applications, noting calibration [SESA PAPER 1209] 18 p3142 A67-33896

Contact potential difference between crystal surfaces of indium antimonide cleaved in ultrahigh vacuum measured by Kelvin method 19 p3302 A67-34939

Cold welding tendencies and frictional studies of clean metal combinations under ultra high vacuum 19 p3237 A67-35839

Lunar surface layer soil density limits estimated in simulation study of adhesion, composition, grain size and grain shape effects 23 p4066 A67-41008

Cold cathode ion source /CCIS/ quadrupole mass spectrometer for ultrahigh residual gas analysis 23 p4000 A67-41217

Cold welding under flight conditions of ATS silver-plated beryllium copper damper boom, discussing ultrahigh vacuum equipment and test techniques 24 p4160 A67-42033

Adhesive qualities of lunar soil simulated by rock comminuted in ultrahigh vacuum 24 p4227 A67-42034

ULTRALOW FREQUENCY

ULF emission at two conjugate points signaling onset of negative ionospheric storms 03 p0411 A67-13347

Relations between VLF emissions of whistler and dawn choruses types and that of ULF emissions /pearl type oscillations and rapid irregular pulsations/ 04 p0617 A67-15500

ULF radio emission of upper atmosphere and other related geophysical phenomena, analyzing hisses, choruses and contribution to earth radiation belt 08 p1324 A67-20862

ULF electromagnetic radiations related to magnetic bays and ionospheric phenomena at high latitudes 13 p2110 A67-26455

Earth magnetic field effect on ultralong radio wave propagation, considering directional effects from planetary inhomogeneities and reciprocity principle impairment 15 p2479 A67-30168

ULF radio emission properties determination and relation to other geophysical phenomena, noting experimental equipment and correlation with auroral activity 17 p2846 A67-32938

ULF radio emission associated with magnetic field disturbances, geomagnetic pulsations, auroras and exospheric particle acceleration 17 p2846 A67-32939

ULTRAPURE METAL

Soviet papers on physical properties of ultrapure metals and semiconductors, stressing epitaxial silicon layers 21 p3681 A67-38357

ULTRASONIC AGITATION

Ultrasonic energy applied to several metallurgical processes, exploring possible application to metal reinforcement 14 p2337 A67-28321

Electrodynamic transducer for liquid-borne ultrasonic pulse intensity measurements, considering limits, inductance and measuring system dimensions 18 p3043 A67-33463

Ultrasonic energy, used for removing microorganisms from various surfaces for enumeration, noting texture, pretreatment and heat effects on recovery efficiency 19 p3179 A67-34911

Centrifugal disk photosedimentometer used for size analysis of latex emulsions 23 p3972 A67-41066

ULTRASONIC LIGHT MODULATOR /ULM/

Electro-optical spectrograph producing dynamic spectrograph continuous in both frequency and time 14 p2319 A67-28444

Ultrasonic devices for coherent optical systems, discussing CdS transducers, laser scanners and microwave signal processing 15 p2500 A67-29912

Transverse and longitudinal waves in ultrasonic light modulators, noting superiority of transverse waves in polarization rotations 17 p2815 A67-32614

ULTRASONIC MACHINING

Metal and alloy heat treatment intensification with ultrasonic techniques

improve steel recrystallization, etc 01 p0095 A67-10640
 Book on nontraditional machining processes covering process parameters, shape and materials applications, tooling, chemical removal, etc 14 p2328 A67-28893
 Book on ultrasonic machining of intractable materials covering basic principles, vibrator design, machine tools, technology, processes involved and applications 17 p2865 A67-32200
 Metal and alloy heat treatment intensification with ultrasonic techniques improve steel properties, recrystallization, etc 18 p3066 A67-34404

ULTRASONIC RADIATION

Lethal effect of high intensity sonic and ultrasonic waves on spores of *Bacillus subtilis* var. niger ATCC 9372 04 p0562 A67-14520
 X-ray analysis of size reduction of coherent scattering regions of metal deformed in ultrasonic field 13 p2124 A67-27627
 Piezoelectric microphone for measuring pulsed ultrasonic radiation intensity and energy distribution, discussing principles, operating conditions and construction of instrument 18 p3046 A67-33745
 Ultrasonic attenuation measurements at high magnetic fields in mixed state for clean and dirty limits 20 p3483 A67-36205

ULTRASONIC SPEED

Temperature dependence of sound velocity in liquid helium at saturation vapor pressure and cryogenic temperatures 17 p2886 A67-33231

ULTRASONIC TESTING

Ultrasonic fatigue damage indicator for inspection and design 01 p0165 A67-11362
 Ultrasonic machines used to determine fatigue strength of components subjected to repeated alternating stresses 02 p0338 A67-12043
 Sonic resonator for nondestructive testing of composite structure operating only from one accessible surface 02 p0250 A67-12630
 Nondestructive test methods for monitoring service hardware during boron composite material development and correlation with results of destructive tests 03 p0455 A67-13447
 Nondestructive ultrasonic detection of surface or internal flaws 03 p0430 A67-13549
 Ultrasonic fatigue testing using magnetostriuctive vibrators 03 p0524 A67-13550
 Ultrasonic apparatus using echo method to record automatically formation and propagation of fatigue cracks on smooth specimens 03 p0420 A67-13567
 Nondestructive testing /NDT/ developments noting radiography for quality control, ultrasonic, continuous wave, resonance and pulse echo methods and applications to Polaris program 04 p0706 A67-15263
 Ultrasonic reflectivity of liquid-solid interface used as indicator of near surface properties of solid in cold work, grain orientation, etc 04 p0621 A67-15264
 Ultrasonic phase sensitive test procedure for adhesive bonded structures 04 p0622 A67-15265
 Nondestructive test development to meet inspection requirements of advanced aircraft design, discussing titanium fusion and resistance spot welds and adhesive bonding honeycomb components 05 p0808 A67-17087
 Oscillogram interpretation during ultrasonic inspection of turbine and compressor blades 06 p1007 A67-18098
 Ultrasonic immersion inspection apparatus for structural defects detection in turbine blades 06 p1007 A67-18103
 Ultrasonic techniques for nondestructive testing for Saturn honeycomb heat shields 07 p1192 A67-20166
 Stress induced velocity variations of longitudinal and shear ultrasonic waves in steel, Al and Cu, calculating third order elastic constant 08 p1415 A67-20481
 UVFD-1 ultrasonic velocimetric flaw detector for inspection of nonmetallic laminated structures and products 09 p1502 A67-22096
 Ultrasonic nondestructive inspection of adhesively bonded components, discussing pulse echo reflection, pulsed through transmission and sweep frequency coupling methods and scanning 09 p1507 A67-22526

Quality control system for adhesive bonding using Fokker bond tester ultrasonic resonance instrument 09 p1508 A67-22527
 Ultrasonic inspecting technique for reinforced plastic components and adhesive bonds of solid propellant booster nozzles 10 p1659 A67-22930
 Operational economy of dip brazing method of joining aluminum and reliability of ultrasonic printout procedures for inspection of assemblies 10 p1660 A67-23007
 Ultrasonic flow meter for directly measuring average stream velocity using sing-around velocimeter with piezoelectric ceramics 10 p1658 A67-23079
 Large part inspection via ultrasonic and eddy current techniques, discussing surface and discontinuity dimension analysis 10 p1660 A67-23324
 Electronic and ultrasonic principles defining pulse-echo high resolution and application to electronic and electroacoustic circuitry for testing aerospace structures 12 p1948 A67-25218
 Ultrasonic flaw detection of hidden cracks in turbine blades 14 p2395 A67-27872
 Ultrasonic measurement of temperature dependence of longitudinal sound absorption coefficient for main crystallographic directions in superconducting indium 14 p2375 A67-29070
 Random errors in ultrasonic measurements, discussing Students distribution measurement repetition effect and rounding-off error evaluation 18 p3044 A67-33735
 Aluminum welded joints investigated by radiographic and metallographic methods for bubbles and cracks 18 p3053 A67-33743
 Ultrasonic probes calibration for evaluation of propagating ultrasonic wave during nondestructive testing of materials 18 p3046 A67-33744
 Propagation of elastic waves through composite media studied with ultrasonic pulse technique, noting Poisson ratio, bulk modulus, etc 18 p3069 A67-34488
 Temperature and frequency effects on amplitude-independent longitudinal ultrasonic attenuation in superconducting lead 19 p3304 A67-35536
 Correlation and analysis of ultrasonic test results in evaluating reinforced resin laminates 19 p3249 A67-35554
 Ultrasonics as nondestructive means of measuring residual stresses 20 p3537 A67-36475
 Ultrasonic and line reversal methods for measuring gas temperatures behind reflected shock waves 21 p3624 A67-37740
 Metal mechanical properties determination during deformation by uniform ultrasonic loading 21 p3722 A67-38450
 Assessment of microbial contamination on surfaces of space hardware by ultrasonics 23 p3962 A67-40852
 Ultrasonic monitoring technique for fatigue damage and crack formation and propagation in aircraft structures [AIAA PAPER 67-793] 24 p4251 A67-42954

ULTRASONIC WAVE
 Amplitude dependent attenuation in normal and superconducting lead for ultrasonic determination of superconducting energy gap 01 p0135 A67-10916
 Temperature dependence of elastic wave losses for bismuth germanium oxide, noting possible application for information storage VHF and microwave frequencies 02 p0300 A67-12507
 Absorption dependence of ultrasonic waves in superconductors on amplitude of sound wave due to temperature 03 p0492 A67-13325
 Monostatic scattered ultrasonic wave calculated as function of distance of reflector projection from source 03 p0369 A67-13551
 Holograms of objects immersed in water and illuminated by 7-mc sound waves and reconstruction of optical images from sound holograms using laser light 03 p0420 A67-13570
 Damped oscillations and velocity of sound waves in semiconductors and metals in presence of strong magnetic field 03 p0501 A67-14370
 Vannier-Mott excitons effect on ultrasound absorption in piezoelectric semiconductors 04 p0678 A67-15134
 Frequency modulation of GaAs semiconductor laser by ultrasonic wave modulation of dielectric constant 05 p0821 A67-16671
 Optimal regime conditions in engineering calculation of generating device with self-parametric frequency multiplication, using nonlinear inductance in ultrasonic frequency range 06 p0970 A67-18171
 Low accuracy of interferometric measurement of coefficient of ultrasound absorption in gas 06 p1004 A67-18395
 Ultrasonic wave absorption in GaAs and GaSb compounds at temperatures from 95 to 300 degrees K 06 p1051 A67-18399
 Third order elastic constant for NaCl and KCl single crystals by ultrasonic pulse techniques 07 p1238 A67-20218
 Frequency temperature dependence of longitudinal and transverse hypersonic wave absorption coefficients in quartz and artificial ruby crystal 10 p1693 A67-23582
 Vannier-Mott excitons effect on ultrasound absorption in piezoelectric semiconductors 12 p1978 A67-25158
 Book on ultrasonic wave absorption and dispersion in gases, liquids and solids, discussing physical mechanisms involved in sound absorption 12 p1967 A67-26157
 Two-phonon absorption in ultrasonic paramagnetic resonance of uranium-doped calcium fluoride, relating wave attenuation to ultrasonic intensity and magnetic field angular variation 14 p2365 A67-28295
 Elastic vibrations in superconductors noting vortex effects, weaknesses of elastic moduli changes and decrease in ultrasonic attenuation 14 p2375 A67-28988
 Optical image producing method of complex ultrasonic field using light diffraction of laser beam 15 p2487 A67-29498
 Direct experimental verification of frequency modulating semiconductor injection laser using ultrasonic waves 15 p2499 A67-29731
 Ultrasonic wave amplification by supersonic flux of drift electrons in sandwich structure of piezoelectric dielectric and semiconductor 15 p2542 A67-30245
 Damping effect of conduction electrons on ultrasonic surface and body waves propagating in CdS crystals, plotting damping against conductivity 17 p2921 A67-32971
 Third order moduli of GaAs by measurement of ultrasonic wave velocities as function of applied stress 17 p2922 A67-33057
 Thermal and elastic properties of ternary diamond-like semiconductor compounds, determining ultrasonic wave propagation rates 18 p3096 A67-33452
 Systematic errors limiting velocity measurement accuracy of longitudinal ultrasonic waves when using pulse-delay methods, for application to ultrasonic equipment 18 p3044 A67-33734
 Ultrasonic correlating device for fabrication of pulse compression radar signals 18 p3002 A67-34227
 Apparatus for uniform sized liquid drop production by ultrasonic wave action on fluid jet, with drop formation recorded by photography 18 p3052 A67-34610
 Book on electrodeposition of metals in ultrasonic field, discussing effects on electrode potentials, concentration polarization, deposition rate, etc 19 p3235 A67-34914
 Ultrasonic field effects on nucleating fluid in flash boiling system and heat transfer dependence on bubble density parameters [ASME PAPER 67-HT-11] 20 p3545 A67-36709
 Superconductors with overlapping bands, discussing copper pairing, heat capacity, critical field and ultrasonic attenuation 20 p3512 A67-37435
 Longitudinal ultrasound attenuation in polycrystalline superconducting mercury at 9.3 GHz, studying temperature dependence 20 p3514 A67-37568
 Velocity of sound in liquids measurement using ultrasonic interferometry and laser diffraction spectra 21 p3630 A67-38772
 Three- and four-phonon processes in piezoelectric cadmium sulfide observed using ultrasonic amplifier confirm nonlinear theory of multiple wave interactions 22 p3854 A67-39246
 Ultrasonic wave absorption in high purity gallium single crystals in magnetic field, observing large magnitude geometric oscillations at cryogenic

temperature 22 p3859 A67-39653
 Frequency dependence of attenuation coefficient for longitudinal ultrasonic waves in InSb over range 50 to 210 MHz for temperatures between 200 and 800 degrees K 24 p4202 A67-41980
 Active delay line with amplifiers converting electromagnetic oscillations into ultrasonic vibrations and back again 24 p4130 A67-42237
 Laser pulse compression of RF signals using Bragg scattering produced in transparent solid by ultrasonic waves 24 p4188 A67-42368
ULTRASONIC WAVE TRANSDUCER
 Materials for energy transducers used in detection, generation or measurement of ultrasonic waves and materials for electrical filters 03 p0495 A67-13547
 Ferrite materials for resonators of magnetostrictive transducers and filters used in transmission and reception of ultrasonic waves 03 p0420 A67-13548
 GaAs epitaxial layer ultrasonic wave transducers fabricated from seminsulator material, for generation of longitudinal waves 03 p0426 A67-14302
 Piezoelectric grating /PEG-/ dispersive device using ultrasonic propagation in prismatic quartz block 04 p0574 A67-15056
 Power output of pulse laser measured in terms of ultrasonic vibration intensity induced in piezocrystals by radiation 15 p2485 A67-29125
 Temperature dependence of elastic constants of 1060 and 6061-T8 aluminum using ultrasonic pulse echo method, estimating high pressure state equation 23 p4021 A67-41469
ULTRASONIC WELDING
 High density microelectronic circuitry, discussing interconnection through use of advanced materials and techniques 08 p1303 A67-21189
 Ultrasonic spot welding of dissimilar metals, discussing bond mechanisms and threshold curves relating clamping force, power level and weld strength 12 p1950 A67-25737
 Bonding and packaging techniques in production of semiconductor integrated circuits, discussing chip, lead and thermopressure bonding methods 12 p1951 A67-26214
 Thin film technique interconnecting integrated circuits by ultrasonic welding and multilayer thin film conductor networks 14 p2280 A67-28016
 Flip-component technology discussing bonding of flip chips and face bonding of semiconductor devices 16 p2642 A67-31727
 Flip-chip bonding and dimensional transformation, low cost microcircuit production technique 18 p3014 A67-34549
 Ultrasonic joining techniques for plastic welding, metal insertion, staking and reactivation of adhesives, emphasizing lock-seal process 19 p3233 A67-34791
ULTRASONICS
 UHF ultrasonics, discussing generation and wave detection, progressive wave amplification, biological effects, power measurement, etc 03 p0468 A67-13546
 Generators of sonic and ultrasonic frequencies using thyristors 05 p0773 A67-16458
 Visible three-dimensional ultrasonic imaging of interior and exterior of optically opaque objects, using synthetic holographic technique 11 p1793 A67-24831
 Jet flame stabilization and audible noise reduction using ultrasonic acoustic energy 11 p1883 A67-24842
 Temperature and transport properties of helium and argon at high temperatures from ultrasonic determination of sound velocity and sound absorption 15 p2580 A67-29882
 Ultrasonic thermometry in solids and gases at elevated temperatures 18 p3051 A67-34509
 Equivalent quadrupoles for analyzing ultrasonic systems using piezotransducer disks operating at any frequency 20 p3401 A67-37454
ULTRAVIOLET
S FAR ULTRAVIOLET
S VACUUM ULTRAVIOLET
ULTRAVIOLET FILTER
 Solid organic filters using polymethyl siloxane resin as host material for 2000-3000 angstrom range 03 p0470 A67-14393

ULTRAVIOLET LIGHT
 Balloon-UV polarimetry using two different telescope-gondola systems 07 p1184 A67-19395
 Vacuum UV resonance lamp design to eliminate difficulty of window seal caused by discharge 08 p1329 A67-20354
 Hydrogen and He UV glow in night sky as ion and electron source, estimating intensities and ionization rate 10 p1633 A67-22949
 Optical properties of magnesium fluoride in EUV from reflectivity measurements on crystal and thin films 18 p3099 A67-33692
 Martian atmosphere transparency and visibility of surface details in blue and UV light, showing dark and semitone areas intensity, etc 18 p3124 A67-34154
 Primitive-earth atmosphere models irradiated with UV light and ionizing radiation for primordial organic synthesis 20 p3369 A67-36656
 Simultaneous UV photographs and radar cross section measurements of Venus, discussing atmospheric motion and rotation 21 p3705 A67-38611
 UV light photolyzing ozone dispersed in solid carbon dioxide matrix causes formation of new substance showing IR absorption 23 p3971 A67-40970
ULTRAVIOLET MICROSCOPY
 Premelting of predetermined sites in sodium-potassium alloys studied by transmission UV microscopy 14 p2339 A67-29032
ULTRAVIOLET PHOTOMETRY
 Vertical distribution of ozone measured by rocket, using UV absorption 02 p0238 A67-12065
 Artificial satellite UV photometry and polarimetry of galactic star clusters 06 p1077 A67-18065
 Plasma neutrino process as accelerating mechanism for evolution in UV dwarfs 08 p1396 A67-21180
 Far UV transmitting windows, particularly lithium fluoride, and response measurements below 2000 angstroms, noting fabrication on solar blind materials 12 p1947 A67-28161
 Magnesium fluoride double Rochon prism used as polarizer or analyzer in vacuum UV wavelengths 15 p2491 A67-30425
 Daytime ozone density distribution of mesospheric layer measured by using UV photometers in rockets 19 p3217 A67-35203
 Energy distribution of photometric spectra in solar UV continuum in 1550 to 2100 angstrom range, discussing radiation temperature decrease 24 p4225 A67-41835
ULTRAVIOLET RADIATION
 Solar autoionization line profiles for Al I in rocket UV spectrum 02 p0323 A67-11699
 Bidirectional reflectance measurements to determine optical degradation induced by UV radiation [AIAA PAPER 65-672] 03 p0419 A67-13040
 Radiation equilibria in UV light on air, oxygen, carbon dioxide, etc, analyzed by bromine lamp in connection with studies of planetary atmospheres 03 p0513 A67-14088
 Near UV optical constants of lanthanum fluoride 03 p0470 A67-14400
 Meteorological satellites noting necessity of radiation measurements 04 p0648 A67-14409
 Book on middle UV science and technology 04 p0612 A67-14690
 Atomic and molecular absorption and emission in middle UV region of electromagnetic spectrum, noting energy levels, electronic transitions and oscillator strengths 04 p0660 A67-14692
 Charged particle collision as UV radiation source examined, using electron-excitation analytic cross section equations 04 p0660 A67-14698
 Astronomical UV radiation noting galactic composition and extragalactic systems, stellar emission and molecular and atomic H 04 p0696 A67-14700
 Radiation from flames and chemical perturbations of atmosphere, examining flame structure, irreversible processes, photoemissive events, etc 04 p0721 A67-14701
 Nozzle exhaust plumes of rockets or supersonic ramjets with diffusion flames as source of UV radiation 04 p0721 A67-14702
 UV technology, discussing radiation sources, photodetectors, filters, polarizers, reflective coatings, etc 04 p0619 A67-14704
 Thermal radiative property behavior of

materials under elementary charged particle bombardment, determining effect of combined UV plus electron exposure and low energy proton 04 p0686 A67-15873
 Solar UV and zodiacal light, emphasizing importance and merits of rocket and balloon observations 05 p0799 A67-16873
 Solar chromosphere and corona activities during flare, noting UV radiation, echelle spectrum, radio wave, X-ray and fast particle emission 05 p0885 A67-17266
 Radiative lifetimes of UV molecular transitions, analyzing emission spectrum in vacuum monochromator 06 p1035 A67-17828
 Optical properties of zinc oxide analyzed by exposing samples to mechanical and thermal treatments and UV radiation [AIAA PAPER 67-214] 06 p1052 A67-18514
 UV radiation generation from output of Nd glass laser by frequency doubling in ammonium dihydrogen phosphate crystals 06 p1011 A67-18712
 UV sensitivity increase in sodium salicylate photomultiplier combination 07 p1185 A67-19405
 Techniques for calculating vertical distribution of atmospheric ozone from intensity of solar UV radiation at various altitudes 07 p1172 A67-19456
 Spectrum of meteorite luminescence emission after irradiation with protons and UV radiation, using spectrophotometer 08 p1390 A67-21021
 Metal deficiencies, UV excesses and other color anomalies in solar type disk population stars 08 p1400 A67-21249
 Pyrrolic compound formation by UV irradiation of delta-aminolevulinic acid 08 p1290 A67-21254
 Calorimetric measurement of source and broadband spectral absorbances of spacecraft thermal control coatings during exposure to UV in vacuum environment 09 p1534 A67-22452
 Flash spectroscopy apparatus with Q-switched ruby laser, discussing molecular electronic excitation 10 p1663 A67-22854
 Ozone number densities in 30 to 75 km altitude determined at night by rocket measurements of lunar UV radiation absorption in various bands 10 p1638 A67-23203
 Upper atmosphere dynamics, noting role of horizontal and vertical winds in shifting density phase and amplitude and UV radiation as energy source 10 p1640 A67-23218
 Extreme UV emission, discussing chromospheric coarse mottling and network characteristics of He II 304 angstroms 10 p1707 A67-23224
 UV solar radiation absorption in upper atmosphere determined from measurement of photoelectron currents emitted by planar metallic orthogonal photocathodes onboard Cosmos II satellite 10 p1647 A67-23282
 Electron synchrotron as source of extreme UV radiation noting design 11 p1788 A67-23965
 Relative solar abundance for O, Si and Fe determined from intensities of far UV emission lines of solar corona 12 p2001 A67-25225
 Multiple sample space UV simulation facility for in situ hemispherical spectral reflectance measurements [AIAA PAPER 67-312] 12 p1926 A67-26027
 Thermal control coating spectral sensitivity to UV induced degradation, noting rapidly increasing damage as incident radiation wavelength decreases [AIAA PAPER 67-340] 12 p1959 A67-26054
 In situ measurements of diffuse hemispherical spectral reflectance of thermal control coatings irradiated in vacuo with various combinations [AIAA PAPER 67-342] 12 p1959 A67-26056
 Optical materials properties analyzed for UV induced degradation under vacuum conditions [AIAA PAPER 67-344] 12 p1959 A67-26058
 Oscillator strengths for extreme UV resonance lines of ions in neon isoelectronic sequence calculated, based on single configurations in intermediate coupling 12 p1968 A67-26247
 Neutral silicon photolization cross sections for continuous UV absorption measured near ionization limits by shock tube technique 12 p1968 A67-26248

Temperature profile in stratosphere, noting contribution to heat budget by turbulent thermoconductivity and UV radiation absorption in ozone layer 13 p2113 A67-26677

Receivers for measuring UV radiation in upper atmosphere and outer space 13 p2121 A67-27335

UV radiation effect on mechanical characteristics of polyethylene terephthalate film in vacuum and atmospheric pressure 13 p2184 A67-27624

Intensity and polarization of hydrogen Lyman alpha lines in day airglow as function of altitude for principal far UV emission 14 p2314 A67-28849

Satellite drag analysis of atmospheric temperatures noting effects of UV, solar radiation and geomagnetic fluctuations 14 p2314 A67-29027

Absolute spectral reflectance measurement in solar region in vacuo for applications to thermal control coatings 15 p2487 A67-29542

Solid rocket components exposure to elevated temperatures, hard vacuum and UV radiation during space flight and reentry 15 p2507 A67-29548

Chromospheric solar radiation measured during solar eclipse with UV monochromator, using electromagnetic radiation photomultipliers 15 p2565 A67-29573

Chromosphere and corona UV emission spectrum provided by sounding rocket using photographic recordings 16 p2752 A67-31625

Photographic high atmosphere observations of hydroxyl and helium emission bands, determining solar UV radiation and electron flux 17 p2849 A67-32960

Upper limit in flux density of intergalactic gas UV radiation measured from interplanetary satellite, showing temperature effect 18 p3116 A67-33524

UV radiation observed beyond atmosphere in winter Milky Way, noting nebula detection and photographic apparatus 18 p3125 A67-34190

Ion-molecule chemistry of Jupiter upper atmosphere, studying equilibrium and nonequilibrium abundances of hydrocarbon products due to UV radiation reaction 18 p3135 A67-34540

Lethal effect of solar UV radiations on dried Coliphage T-1 exposed to space at sounding rocket altitudes 19 p3177 A67-35184

Electron density and temperature, solar UV radiation and upper atmosphere neutral components measured using rockets 19 p3218 A67-35215

Ionospheric and stratospheric UV radiation effects on survival of microorganisms 19 p3178 A67-35271

Rocket observations of visible and UV dayglow including emission rates and electron density and temperature 19 p3221 A67-35277

Ground based solar electromagnetic radiation environment studies in visible and radio windows 19 p3323 A67-35332

Thermoplastic-resin film with UV sensitive dispersed compound for carbon-dioxide laser-radiation photography 19 p3240 A67-35694

Total atmospheric ozone from satellite measurements of solar UV reflected radiation determined, using atmospheric model with Rayleigh scattering 19 p3226 A67-35923

Hydrogen fire visualization detection techniques including application of photography, TV and image converter in IR and UV regions 20 p3445 A67-36540

Book on vacuum UV spectroscopy techniques noting Lyman continuum, synchrotron radiation, Bremsstrahlung radiation, UV radiation, resolution, etc 20 p3446 A67-36664

Simultaneous oscillation in UV and IR and interaction of 1st and 2nd plus ve system of bands in molecular nitrogen laser 20 p3461 A67-37292

Extreme UV solar spectrum, reviewing echelle spectrum, soft X-rays and coronal emission 20 p3528 A67-37467

UV radiation detection using silicon carbide p-n junctions, showing wavelength increment at peak response and decreasing photovoltage with increasing temperature 21 p3591 A67-38156

UV and X-ray background measurements by Venus 3 may lead to mean density

estimation of matter in universe through determination of intergalactic medium density and thermal history 21 p3705 A67-38591

Vidicon type image tube sensitive in near UV developed for space applications 21 p3599 A67-38654

UV absorption of ammonia at high temperatures behind shock waves, discussing NH radical formation from shock tube ammonia decomposition 22 p3756 A67-39442

Medium wave and global UV radiation, relative sunspot number and ozone density measurements and interrelationships 22 p3873 A67-40030

Earth upper atmosphere background radiance measured by UV radiometer carried on Air Force satellite 22 p3794 A67-40364

Ozone parameters determination from measurements of radiation backscattered by earth atmosphere 22 p3794 A67-40365

Solar wind and UV exposure effects on spacecraft thermal control coatings, using in situ spectral reflectance measurements 24 p4174 A67-42040

ULTRAVIOLET REFLECTION

Solar UV reflection and scattering from earth atmosphere, use in determining total concentration and vertical distribution of ozone 07 p1178 A67-19815

UV reflectance measurements of granitic, gabbroic and serpentine rocks used to identify lunar silicates 09 p1569 A67-22689

Multiple sample space UV simulation facility for in situ hemispherical spectral reflectance measurements 12 p1926 A67-26027

[AIAA PAPER 67-312]

Rocketborne spectrograph measurement of UV reflectivity of Venus and Jupiter, noting atmospheric Rayleigh scattering effects 18 p3123 A67-34147

LIF freshly cleaved crystal reflectance spectrum between UV and 28 ev, computing dielectric response function and measuring gamma exciton band 23 p4038 A67-40774

ULTRAVIOLET SPECTROGRAPH

Echelle spectrograph for middle UV solar spectroscopy from rockets 10 p1653 A67-22735

Monochromatic UV photographs of limb of sun analyzed for evidence of solar granulation in 2000 angstrom spectral range 12 p2001 A67-25220

High resolution UV spectrograph with echelle, noting optical line-up for photographing H-Lyman alpha line at 1216 angstroms 16 p2680 A67-31875

Vacuum type lensless spectrograph in intermediate and far UV for evaluating shock compressed metals resulting from hypervelocity impact 22 p3799 A67-39749

Rocketborne UV radiometers for solar spectral intensity distribution, calculating irradiance and earth reflectivity 22 p3794 A67-40363

ULTRAVIOLET SPECTROMETER

Photomultipliers in DC output mode for extreme UV 10 p1653 A67-22737

Javelin rocket soundings with far UV scanning spectrometer, noting atomic hydrogen and oxygen radiation 12 p1934 A67-25787

Measurement of solar extreme UV radiation atmospheric attenuation to establish daytime variations in upper atmosphere composition 17 p2843 A67-32535

ULTRAVIOLET SPECTROPHOTOMETRY

Trace fluorocarbon effect on vibrational relaxation in nitrogen shock waves studied by UV spectrophotometric technique 06 p0955 A67-18251

Absolute intensity of radiation from center of solar disk at wavelengths between 3288 and 12,480 angstroms 06 p1089 A67-18710

Far UV rocket spectrophotometry of atmospheric phenomena such as airglow and auroras [JHU-TR-11] 10 p1653 A67-22739

Astronomical satellite for photoelectric spectrometry in UV region to measure stars of galactic clusters 12 p2002 A67-25460

Solar continuous spectrum observations indicating limb darkening around 2500 angstroms, using optical system mounted on Veronique rocket 12 p2007 A67-25820

Trace fluorocarbon effect on vibrational relaxation in nitrogen shock waves studied by UV spectrophotometric technique [AIAA PAPER 67-11] 17 p2809 A67-33035

UV spectrophotometer for continuous measurement in vacuum systems of

polyphenyl diffusion pump fluid film thickness 23 p4004 A67-41358

ULTRAVIOLET SPECTROSCOPY

Radiative lifetimes of UV multiplets in Si, P, S, O, Ne 2 and Ar 2 measured via phase shift method, correcting for transition cascading 05 p0892 A67-18411

Vacuum UV flash photolysis kinetic spectroscopy apparatus 05 p0807 A67-18782

Atmospheric scattering of solar flux in UV noting radiation transfer for airborne detector, air component absorption coefficient and spectra from rocket flight 10 p1629 A67-22736

Prism and grating spectra obtained during Gemini XI mission providing UV energy distribution data and Balmer discontinuity 10 p1706 A67-23060

UV spectra of Mg III and Mg IV investigated by sliding spark in vacuum, noting various ionization charges in vacuum 14 p2351 A67-28944

Book on vacuum UV spectroscopy techniques noting Lyman continuum, synchrotron radiation, Bremsstrahlung radiation, UV radiation, resolution, etc 20 p3446 A67-36664

ULTRAVIOLET SPECTRUM

Optical transmittance of fused silica at elevated temperatures, showing shift in UV to IR absorption with increasing temperature 01 p0138 A67-11074

Calibration procedures for earth albedo experimental package of Orbiting Solar Observatory 02 p0246 A67-12401

Rotational intensity distribution of vacuum UV absorption spectrum bands of carbon monoxide arising through mixing of D state with neighboring states 02 p0269 A67-12450

Lunar disk color index derivation by applying method of photographic photometry in UV and IR spectral regions 02 p0329 A67-12493

Autoionization effects in UV absorption spectra of hot atomic gases 03 p0471 A67-13222

Electron spectra in UV region noting excitation techniques, energy level mean lives and population distribution 03 p0472 A67-13324

Quark confusion with electric-dipole transition in far UV solar spectrum 04 p0694 A67-14479

Middle UV region of solar radiation, discussing rocket and balloon mounted spectrograph measurement results 04 p0695 A67-14691

Atmospheric ozone in middle UV spectral region, noting vertical distribution, destruction by solar radiation, lifetime below layer in photochemical equilibrium, etc 04 p0612 A67-14694

Terrestrial radiance in middle UV noting Rayleigh scattering, vertical distribution of air, oxygen and ozone, attenuation factors, etc 04 p0613 A67-14695

Second order scattering effect on earth albedo calculations in middle UV, noting distribution functions and parameters used 04 p0613 A67-14696

Solar radiation effect on planetary atmosphere noting charged particle bombardment, dayglow phenomena, auroral emission, etc 04 p0696 A67-14699

Forbidden absorption bands of carbon monoxide in vacuum UV region, noting rotational and vibrational constants and perturbations 05 p0848 A67-18847

Upper atmospheric rocket sounding experiment during solar eclipse over Brazil, noting instrumentation and participating agencies 06 p0981 A67-18382

Photolization and absorption coefficients of nitric oxide gas measured, using vacuum UV monochromator 06 p1037 A67-18573

Sensors of electromagnetic radiation in UV, visible and IR ranges, noting improvement through automatic data processing 06 p1006 A67-19013

Cosmos LXI spectrophotometric measurements of atmosphere-reflected UV radiation spectra 07 p1178 A67-19801

UV imaging system for lunar missions to detect luminescing minerals on lunar surface 08 p1331 A67-21079

Solar wavelength measurements for approximately 14 bands of CO fourth positive group in solar rocket UV spectrum 08 p1399 A67-21235

Cosmos 65 spectrophotometric measurements of atmosphere-reflected UV

radiation spectra 10 p1647 A67-23277
 Lunar disk color index derivation by
 applying method of photographic photometry
 in UV and IR spectral
 regions 10 p1708 A67-23361
 Vacuum UV wavelength standards and
 energy levels in first silicon spectrum from
 low pressure source 11 p1822 A67-24417
 Solar studies in extreme UV using
 stabilized Skylark rockets, including data on
 chromospheric and coronal spectra and XUV
 spectroheliograms 12 p2008 A67-25826
 Absolute reflectance of RbI and KI
 between 300 and 77 degrees K, noting spin
 orbit interaction effects and values of
 dielectric parameters 15 p2520 A67-29768
 Ultraviolet camera lenses for space flight
 use discussing techniques for testing and
 evaluating performance 16 p2680 A67-31805
 Magnesium oxide and lithium fluoride in
 far UV, noting refractive and absorption
 indices 16 p2734 A67-31881
 Silicon oxide and nitride film thickness
 determined with interference technique,
 using spectrophotometer in UV and visible
 wavelength range 17 p2854 A67-32191
 Solar UV spectrum interpretation taking
 into account dielectronic recombination
 processes in ionization equilibrium
 computation, obtaining spectral lines
 intensities, abundances and atmospheric
 structure indications 17 p2941 A67-32235
 Rydberg series in extreme UV observed in
 absorption spectrum of helium-nitrogen
 discharges and active nitrogen
 [AFRCL-66-835] 17 p2888 A67-32629
 Darkening of solar limb in UV spectral
 band observed through rocket
 sounding 17 p2945 A67-32647
 Crystals for UV and IR optics, discussing
 solubility, hardness, melting, expansion
 coefficients and design 18 p3078 A67-33565
 UV spectra of lunar surface photographed
 from Zond III automatic space
 probe 18 p3122 A67-34141
 Rocketborne spectrograph measurement of
 UV reflectivity of Venus and Jupiter, noting
 atmospheric Rayleigh scattering
 effects 18 p3123 A67-34147
 Photosynthesis of nitrosoformaldehyde and
 identification of spectrum consisting of
 diffuse band 18 p2998 A67-34277
 Doppler widths from plasma UV lines
 using fast scan Michelson
 interferometer 20 p3438 A67-36343
 Charge compensation defects influence on
 UV excitation spectrum of rare earth doped
 crystals fluorescence 22 p3856 A67-39384
 Far UV spectra of brighter stars in
 vicinity of epsilon Orionis photographed
 with objective spectrograph carried by
 rocket 22 p3882 A67-39555
 Interstellar extinction wavelength
 dependence, assuming ice particle radii
 distribution function obeys decreasing power
 law and graphite particles have Gaussian
 distribution function 22 p3889 A67-40304
 Stratospheric attenuation measurements in
 near UV during rocket flight compared with
 values computed for dust free
 atmosphere 23 p3993 A67-40677
 Low inductance three-electrode spark
 source for vacuum UV generating high
 degree ionization spectra 23 p4000 A67-41214
UMBILICAL TOWER
 Fixed service tower for flight preparation,
 buildup and servicing of launch vehicles
 [SAE PAPER 660705] 01 p0050 A67-10598
 Saturn V ground support instrumentation
 systems, emphasizing launcher umbilical
 tower /LUT/ 01 p0051 A67-11117
 External damper effectiveness in
 attenuating vibration of launch vehicle near
 launch umbilical tower 04 p0598 A67-15248
 Missile handling, from primitive
 techniques to Titan III ICBM mobile service
 towers 05 p0787 A67-16613
 Umbilical carriers and quick-disconnect
 facilities of Saturn V ground support
 equipment noting location, ejecting methods,
 etc 09 p1484 A67-22038
 Vibration qualification of fly-away
 umbilical by induced acoustic excitation
 testing method in Apollo
 project 12 p1924 A67-25714
 Apollo Crawler System analyzed by
 computer simulation for dynamic
 interactions of transporter and umbilical
 tower 22 p3782 A67-40466

UMBRA
SA LUNAR SHADOW
 Continuum brightness fluctuations and
 equivalent line widths in sunspot penumbral
 spectrum 02 p0330 A67-12715
 Sunspot fine structure ground
 observations, considering umbras,
 penumbras, boundaries and
 photographs 13 p2203 A67-27422
 Theoretical interpretation of fine
 structure observations of sunspots by
 stratoscope, discussing stability modes and
 sunspot umbras 13 p2203 A67-27423
 Model with hydrostatic gas pressure
 distribution to interpret equivalent widths
 of atomic and ionic lines in spectra of
 umbrae 13 p2203 A67-27426
 Hot and cold component model of sunspot
 umbrae derived from observation of
 continuous and line
 spectra 13 p2203 A67-27427
 Center-to-limb variation of Evershed effect
 for isolated symmetrical sunspot
 observations interpreted in terms of mass
 motions in penumbral fine
 structure 13 p2204 A67-27430
 Equations governing umbra structure of
 single spot integrated on spot axis,
 consistent model can be obtained only for
 narrow electron pressure range at
 surface 23 p4067 A67-41230
UNCERTAINTY
 Shannon expression of information entropy
 measure and average uncertainty
 measure 02 p0203 A67-12168
UNDERGROUND NUCLEAR EXPLOSION
 Short period seismic radiation patterns
 from underground nuclear explosions and
 small magnitude earthquakes, noting
 propagation characteristics
 [SR-1] 20 p3434 A67-37430
UNDERWATER ENGINEERING
 Invariance theory for automatically
 controlled underwater wings ensuring ship
 motion stability in perturbed
 medium 03 p0359 A67-13189
UNDERWATER SOUND
 Sofar bomb signature identification by
 separation of desired signal from multipath
 signals with digital
 computer 20 p3484 A67-36558
UNDERWATER TEST
 Water-immersion weightlessness simulation
 to determine astronaut EVA capabilities and
 man-machine interfaces
 [AIAA PAPER 66-903] 02 p0187 A67-12270
 Adapted Mueller-Franz portable breath-
 powered respirometer utilizing scuba-gear
 for measuring underwater
 metabolism 09 p1455 A67-21722
 Task load and type of underwater
 exposure effects on response time to signal
 light in visual periphery of novice
 divers 14 p2256 A67-28662
 Water-immersion weightlessness simulation
 to determine astronaut EVA capabilities and
 man-machine interfaces
 [AIAA PAPER 66-903] 15 p2431 A67-29439
 Adhesive and water resistance properties
 of epoxy resin for bonding tensometers and
 underwater sealing 21 p3650 A67-38919
 Scaling laws and hydrodynamic model
 design techniques for high fidelity
 underwater simulation of zero and partial-g
 environments for manned space activities
 [AIAA PAPER 67-925] 24 p4140 A67-43021
UNDERWATER VEHICLE
S SUBMARINE
UNIAXIAL STRAIN
 Uniaxial compression effect on two jump
 conductivity processes occurring in p-type
 silicon 04 p0679 A67-15145
 Tensile-instability mechanism concept
 determination of ultimate strength of most
 ductile materials under uniaxial or biaxial
 tension conditions
 [ASME PAPER 66-WA/MET-15] 04 p0712 A67-15378
 Impurity centers arising from sulfur in
 silicon identified, using IR absorption
 technique and uniaxial stress
 effect 06 p1061 A67-18924
 Deformation potential of valence band of
 indium antimonide, using piezoemission
 technique of shifting intrinsic recombination
 under uniaxial stress 06 p1062 A67-18932
 Electron scattering by neutralized
 acceptors investigated in Ge and Si through
 cyclotron resonance 06 p1063 A67-18939
 Thermal conductivity of laminated GaSe
 monocrystals studied in two crystallographic

directions between 90 and 600 degrees K
 and effect of unilateral
 compression 07 p1233 A67-19649
 Mathematical model of microscopically
 heterogeneous medium undergoing
 elastoplastic deformation, deriving equations
 for stress-strain distribution under uniaxial
 loading 09 p1575 A67-21931
 Uniaxial stress and static electric field
 effects on energy band structure of
 strontium titanate and derivation of optical
 selection rules in region of perturbed
 crystals 10 p1691 A67-23403
 Uniaxial tensile strain rate on stability of
 soft reinforced plastics with two-component
 fibrous base 10 p1671 A67-23605
 Uniaxial compression effect on two jump
 conductivity processes occurring in p-type
 silicon 12 p1979 A67-25168
 Mechanical response of highly filled
 elastomer in complex triaxial tensile stress
 field, demonstrating dewetting effect, need
 for more testing, etc 15 p2575 A67-29978
 Plastic energy dissipation rate at onset of
 rapid crack growth for predicting biaxial
 fracture 16 p2775 A67-31324
 Cross sectional strain and stress
 distributions in cylindrical elastic bars
 subjected to pressure-step and velocity-
 impact loading
 [ASME PAPER 67-APM-33] 17 p2965 A67-33158
 Low cycle thermal fatigue under uniaxial
 constraint, describing clamping device, time-
 temperature controller and programmer
 used 20 p3543 A67-37699
 Piezoresistance effect measurement in
 PbTe single crystals, obtaining coefficients
 for principal valence band through
 hydrostatic and uniaxial stresses in several
 crystallographic directions 21 p3683 A67-38389
 Crack opening displacement and fracture
 toughness analyzed for uniaxial tension and
 edge-cracked plate 22 p3911 A67-39681
 Hydrostatic and uniaxial compressional
 stress effects on strontium titanate
 superconductive transition
 temperature 22 p3863 A67-40244
UNIFIED FIELD THEORY
 Principles developed for founding of
 unified field theory of gravitation and
 electromagnetism, with space-time geodesics
 as charged particle motion
 equation 23 p4026 A67-40659
UNIFORM FLOW
 Variable thermal capacity of gas mixture
 taken into account in calculation of heat
 regeneration in gas turbine cycles, using
 working bodies 07 p1266 A67-19181
 Stream structure and bow waves in
 electromagnetic shock tube, establishing
 flow uniformity limitations through
 temperature and pressure
 measurements 19 p3294 A67-35404
 Thin rectangular vortex wing in uniform
 flow, solving nonlinear equations by
 successive approximations 20 p3356 A67-36439
UNIPOLAR TRANSISTOR
 Functional device based on interaction of
 two unijunction transistors to perform flip-
 flop circuit function, noting V-I
 characteristics and binary counter
 operation 04 p0593 A67-15489
 Unipolar-bipolar transistor hybrids for
 stable temperature independent current
 generators, detailing circuit
 design 24 p4128 A67-41895
UNIQUENESS
 Oseen equations inadequacy in ensuring
 uniqueness for flow past infinite
 body 08 p1319 A67-20351
 Simultaneous approximation of function
 and derivatives, ensuring uniqueness by
 imposing linear conditions on coefficients of
 polynomials 08 p1347 A67-20368
 Stokes flow for sphere in arbitrary
 external flow pattern solved using Green
 function, showing uniqueness
 solution 10 p1629 A67-23831
 Upper and lower bounds on distance
 between zeros of components of solutions of
 second order ordinary nonlinear differential
 equations 12 p1961 A67-26062
UNIQUENESS THEOREM
 Uniqueness and stability theorems for BVP
 involving degenerated elliptic differential
 operator 01 p0105 A67-10678
 Existence, uniqueness and reversion
 theorems, necessary optimality criteria and
 nonfixed time case for optimal control
 problem of n-dimensional linear parabolic

- equations 01 p0105 A67-10679
Existence and uniqueness theorem of Riccati equation arising in solution of optimal linear regulator problems in Hilbert space 01 p0047 A67-11213
Identity of uniqueness and convergence constants of interpolation problems, discussing Abel-Goncharov function 02 p0258 A67-11624
Free boundary problem for parabolic equation proving existence and uniqueness theorems for certain initial conditions 02 p0258 A67-11626
Cauchy and boundary value problems for homogeneous differential equations with two independent variables analyzed, establishing generalized solution existing on uniqueness maximal domain 02 p0260 A67-12432
Existence and uniqueness theorem and upper and lower Chaplygin function approximations for solutions of Cauchy problem for quasi-linear first order PDE 03 p0456 A67-12884
Conditions of solvability of Chaplygin problem 03 p0458 A67-13339
Tensile plastic instability in axisymmetric deformation of sheet metals 04 p0710 A67-14976
Existence and uniqueness in first and second boundary value problems for nonlinear second order differential equations 04 p0647 A67-15742
Boundary value problem of hyperbolic equation with discontinuous boundary conditions 05 p0834 A67-16371
Uniqueness and existence theorems for mixed problem of second order degenerate hyperbolic equation with discontinuous coefficients 05 p0834 A67-16494
Uniqueness of Cauchy problem when initial surface contains characteristic points 05 p0835 A67-16739
Error bounds for asymptotic solutions of differential equations, using Volterra equations for actual and formal solution vectors 06 p1021 A67-17565
Boundary value problem for heat equation, discussing Laplace transform solution and uniqueness theorem 06 p1111 A67-17645
Inverse problems of potential theory analyzed for uniqueness of solution 06 p1023 A67-17861
Uniqueness of extremal controls for minimum fuel problems pertaining to single input linear time-invariant systems 06 p1098 A67-18523
Well posed problems for PDEs, discussing continuous dependence and error bounds 07 p1213 A67-19158
Existence and uniqueness of 2k-fold continuously differentiable solutions to Dirichlet problem for nonlinear integrodifferential equations 07 p1215 A67-19476
Existence and uniqueness theorem for functional equation of optimal control problems, noting stability of solution 09 p1524 A67-21874
Existence, uniqueness and stability investigation of periodical solutions for nonlinear hyperbolic partial differential equations 10 p1674 A67-23387
Existence and uniqueness of periodic solution to ordinary differential equations, defining position in plane of closed integral curves 11 p1813 A67-24749
Existence, uniqueness and reversion theorems, necessary optimality criteria and nonfixed time case for optimal control problem of n-dimensional linear parabolic equations 11 p1814 A67-25067
Representation and uniqueness theorems for second order linear parabolic partial differential equations 12 p1961 A67-26061
Uniqueness of quasi-regular solution to boundary value problem for Chaplygin equation 13 p2145 A67-26444
Existence, uniqueness, stability and approximation of solutions of Prandtl system for nonstationary boundary layer 13 p2093 A67-26603
Chebyshev approximations of differentiable functions, giving uniqueness criterion 13 p2145 A67-26611
Uniqueness of solutions for Cauchy problem and some boundary value problems of general parabolic systems in class of increasing Holder 14 p2344 A67-28894
Continuous solutions of Cauchy problem for linear first order PDEs with discontinuous coefficients, noting conditions imposed 14 p2344 A67-28905
Uniqueness theorems for Adler fourth and fifth boundary value problems for heat conduction differential equation 14 p2409 A67-28936
Necessary and sufficient conditions to ensure existence of unique solutions of equations for active networks 15 p2456 A67-29238
Sufficient condition providing nonlinear sampled system with set of initial conditions 15 p2458 A67-29473
Uniqueness and existence of Cauchy problem solution considering Dirichlet limits, studying convergence requirements 16 p2695 A67-30829
Radiation conditions for derivatives of radiating functions, omitting prescribed asymptotic behavior 17 p2877 A67-32562
Scattering problem for partial difference equations with finite perturbation and inverse problem determining perturbation 17 p2817 A67-32885
Uniqueness theorem for general linear anisotropic time-variable viscoelastic body under boundary conditions, using Laplace transformation 17 p2964 A67-33135
Uniqueness of response of nonlinear continuous servosystem subjected to any signal 18 p3017 A67-34185
Existence and uniqueness theorem for axisymmetric problem with initial data for Euler equation in case of incompressible fluid 18 p3027 A67-34201
Existence and uniqueness of solutions of point boundary value problem for denumerable system of differential equations 18 p3073 A67-34606
Automatic control systems general theory with distributed parameters and delay, proving existence and uniqueness of solutions of partial differential equations solutions 19 p3251 A67-36048
Existence and uniqueness of classical solutions of nonstationary boundary and initial value problem in MHD 20 p3497 A67-36430
Uniqueness theorem for Cauchy problem, elliptic equations with double characteristics derived by imposing smoothness condition 20 p3475 A67-36456
Evolution problem investigated for invariant Einstein vacuum equation, discussing existence and uniqueness theorems 20 p3487 A67-37685
Helly problem of moment theory and optimum approximation of finite defect by subspace elements of continuous functions, examining uniqueness and existence 21 p3653 A67-38400
Statistical elasticity problems involving random stress and displacement tensor fields, proving uniqueness and minimum principle for boundary value 22 p3909 A67-39396
Elastohereditary /viscoelastic/ media mechanics, analyzing linear and nonlinear equilibrium equations, uniqueness and existence theorems and solution methods 23 p4077 A67-40750
Cauchy problem solution for linear partial differential equation with coefficients which are functions of three-dimensional variable, deriving maximal class of uniqueness of solution 23 p4024 A67-41692
Local existence, uniqueness and regularity theorems for Cauchy problem solution for Navier-Stokes system in space 24 p4177 A67-42155
Duhamel principle for internal radiation field in inhomogeneous finite atmosphere based on existence and uniqueness theorem for Milne integral equation 24 p4189 A67-42598
- regions, manpower, etc 06 p1120 A67-19038
Criteria used by Government patent departments in screening and evaluating inventions for patent 07 p1269 A67-19467
East-West motion of auroras analyzed in Idaho using radar echoes, noting velocity, direction reversal, etc 10 p1651 A67-23344
Russian and American practices and policies regarding planetary contamination in connection with COSPAR requirements 10 p1601 A67-23580
Vertical distribution of ozone over Tallahassee, noting maximum and minimum density altitudes, seasonal variations, etc 11 p1787 A67-24555
Economic regulatory powers of Civil Aeronautics Board 12 p2040 A67-25489
U.S. overall economic outlook in light of space technology and systems to year 2001 13 p2231 A67-27511
FAA test pilot training in intent and administration of regulations 14 p2256 A67-27740
U.S. international telecommunications requirements through 1975 14 p2272 A67-28704
FAA navigation improvement program, discussing approach and landing, short and long distance navigation and performance assurance 15 p2514 A67-29738
European recoverable and reusable aerospace transporter 15 p2566 A67-29829
Competition aspects of United States supersonic transport, discussing various aircraft designs 16 p2596 A67-31246
Air safety statistics analysis based on set of intrinsic accident rates in takeoff, cruise and landing 17 p2797 A67-32580
U.S. research program for IQSY 1964-1965 covering solar synoptic observations, zodiacal light, comet tails, atmosphere, etc 19 p3224 A67-35501
Evolution of U.S. space program since inception and future manned and unmanned exploration 23 p4086 A67-40917
U.S. space flight affairs and decisions /1957-1967/ 23 p4086 A67-40918
U.S. exploration of solar system with unmanned spacecraft 23 p4086 A67-40920
- UNIVAC 418 COMPUTER
Univac 418 real time executive computer design having storage speeds of 2 and 4 microseconds 02 p0206 A67-11806
- UNIVERSAL TIME
SA EPHEMERIS TIME
Mechanical gears to convert universal time to sidereal time, discussing range of validity of results with regard to one century 02 p0267 A67-12202
Solar flare data computerized, reducing reported values of importance and area to standard scales, considering universal time and day 11 p1856 A67-24497
Difference between ephemeris and universal time based on observations of lunar occultations 17 p2950 A67-33129
Ephemeris time corrections /1900-1966/ with respect to UT after revision of Brown lunar theory 22 p3881 A67-39516
Biennial component of seasonal variation in earth rotation rate using time observation data, calculating stratospheric zonal wind effect 23 p3996 A67-41085
Measuring methods for pole displacements and latitude variations, determining Universal Time from instantaneous pole coordinates, plotting polhody diagram 23 p3997 A67-41349
Irregular earth rotation velocity variation analyzed by comparing universal time with atomic time 24 p4150 A67-42312
- UNIVERSE
Structure of universe and role of gravitation in determining dynamic behavior, indicating that universe will stop expanding at certain critical maximum size 03 p0516 A67-14339
Gravitational instability due to small irregularities and implications for early universe and galaxy formation 11 p1860 A67-24483
Quasi-stellar objects red shift and optical magnitude measurements, noting discrepancies with zero and nonzero cosmological constant 11 p1863 A67-24508
Pulsating model of closed universe, noting ordinary matter time-dependent scalar field interaction and equation for nonvanishing

pressure 11 p1868 A67-24867
 Energy of system of particles defined as related to active gravitational mass, or to inertial mass and passive gravitational mass respectively, in expanding universe 13 p2199 A67-27004
 Opacity of universe to high energy photons, estimating spectra and absorption probability 13 p2161 A67-27734
 Line element describing gravitational field of charged particle embedded in expanding universe 14 p2336 A67-27892
 Perturbation stability in thermodynamic parameters of isotropic expanding universe which contains matter and radiation in equilibrium 15 p2554 A67-29459
 Hot model of universe supported by radioastronomical observations, estimating quark number density 15 p2555 A67-29640
 Gravitational fields for observation of soft cosmic neutrino and neutrino background predicted by different cosmological theories 15 p2555 A67-29641
 Primeval fireball /cosmic radio radiation/ concept based on Hubble observation of universe expansion, discussing predictions on its nature 15 p2562 A67-30085
 Sky brightness temperature measurements at various millimeter wavelengths for possible isotropic electromagnetic emission in universe 17 p2935 A67-32230
 Upper limit on mean mass density of luminous matter in universe from brightness of night sky 17 p2944 A67-32638
 Quantum cosmology, discussing continuous fluid models as representations of early dense universe 18 p3117 A67-33515
 Nonlinear effect of gravitational instability in expanding universe, calculating second-order density perturbations by iteration method 19 p3317 A67-34891
 Local condensation in early stage of universe suggested from observation of spatial inhomogeneity of cosmic black-body radiation 19 p3312 A67-34893
 Luminous and intergalactic matter, background radiation, radio sources, quasars, cosmic rays and other observational data relevant to cosmological models 19 p3327 A67-35870
 Quasar sources studies set limits on possible density inhomogeneity magnitudes in universe by measuring cosmic microwave background isotropy and homogeneity 20 p3525 A67-36868
 Tensor calculation of origin of local concentration of matter in universe model, considering effect of gravitational perturbations 22 p3880 A67-39314
 Inhomogeneity formation probability in initially homogeneous Friedmann universe inhomogeneity formation probability in initially homogeneous Friedman universe 22 p3891 A67-40493
 Book on universe covering development of astronomy from optical observation to radio, satellite and space probing investigations 24 p4223 A67-41783
 Friedman cosmological models describing spatially homogeneous and isotropic universe 24 p4231 A67-42454
UNIVERSITY PROGRAM
 Astronautics education for RAF and USAF officers 16 p2782 A67-30786
UNLOADING WAVE
 Ceylon and artificial graphite behavior under very high pressure, examining problem of metallic phase of carbon 01 p0104 A67-10833
 Unloading wave expanding in elastoplastic rod determined by integration of differential equation in quadratures 10 p1721 A67-23685
 Nonuniform elastic unloading wave propagation into perfectly plastically deformed region, obtaining solution of displacement field 11 p1879 A67-24941
 Unloading wave expanding in elastoplastic rod determined by integration of differential equation in quadratures 21 p3720 A67-38286
UNMANNED SPACECRAFT
SA MANNED SPACECRAFT
 Unmanned spacecraft systems design for deep space probes, examining flyby and orbiter missions, attitude stabilization, etc [AIAA PAPER 66-887] 02 p0331 A67-12266
 System design of integrated automated laboratory payloads in scientific planetary research unmanned spacecraft 02 p0334 A67-12349
 LEM optical astronomy package /OAP/ containing astronomical telescope,

spectrophotometer, data processing subsystem and other devices, for unmanned landing and life support 02 p0246 A67-12414
 Automated spacecraft flights and cost /1965 to September 1966/, discussing Voyager, Jupiter probe, technology satellite, synchronous meteorological satellite and voice/TV broadcast 05 p0904 A67-16384
 Propellant requirements for unmanned lunar and interplanetary soft landing vehicles presented with equations that couple injection, midcourse and terminal phases [AAS PAPER 66-129] 07 p1241 A67-19988
 Propellant requirements for unmanned lunar and interplanetary soft landing vehicles presented with equations that couple injection, midcourse and terminal phases [AAS PAPER 66-129] 13 p2214 A67-27540
 Soviet book on pilotless aircraft and missiles covering jet engine design, automatic control, radio engineering and aircraft aerodynamics 15 p2564 A67-29242
 Nonmetallic materials for unmanned spacecraft 15 p2507 A67-29553
 Future interplanetary unmanned space missions, examining velocity requirements and launch vehicle and payload sizes necessary for scientific investigation of solar system [AIAA PAPER 67-29] 15 p2562 A67-30104
 System design of automated laboratory and associated entry vehicle for unmanned Martian exploration 16 p2653 A67-30628
 Unmanned exploration of moon, summarizing results on surface structure, back side and material composition 16 p2748 A67-31199
 Unmanned rough-landing survival capsules design considerations for potential planetary payloads 19 p3332 A67-35335
 Terminal guidance concept for soft and accurate lunar landing of unmanned spacecraft [AIAA PAPER 67-594] 19 p3259 A67-35990
 Guidance system requirements for unmanned Martian propulsive landing capsule [AIAA PAPER 67-619] 19 p3260 A67-36008
 Unmanned spacecraft reliability, discussing design requirements, testing, lifetimes, performance and ball bearing failures 20 p3532 A67-36573
 General utility spacecraft family, orbital bus and multiple orbit/payload launch missions for reducing unmanned space research and development costs [AIAA PAPER 67-637] 20 p3534 A67-37617
 Multipurpose orbital bus-vehicle for alternate missions [AIAA PAPER 67-638] 20 p3534 A67-37618
 Unmanned spacecraft systems design for deep space probes, examining flyby and orbiter missions, attitude stabilization, etc 21 p3712 A67-37781
 Radar type instrument for measuring reflection coefficients of planetary surfaces from unmanned spacecraft 22 p3785 A67-39159
 Unmanned probes designed to land on planetary surfaces to obtain temperature, atmospheric measurement and ground samples chemical analysis 22 p3900 A67-39613
 Electric propulsion ion engine systems using solar power source for Mars and Jupiter exploratory unmanned spacecraft is adaptable to existing launch vehicles [AIAA PAPER 67-713] 22 p3868 A67-39844
 Saturn V launch vehicle and Apollo spacecraft hardware systems applied to unmanned exploration of Jupiter 22 p3887 A67-40138
 Unmanned 0.1 AU /Icarus/ solar probe preliminary design, discussing thermal control and power supply problems unmanned 0.1 AU /ICARUS/ solar probe preliminary design, discussing thermal control and power 22 p3906 A67-40152
 U.S. exploration of solar system with unmanned spacecraft 23 p4086 A67-40920
 Stabilization and control techniques for future unmanned commercial space vehicles, emphasizing application of projected technological advances in instrumentation [AIAA PAPER 67-878] 24 p4244 A67-42997
 Manned orbiting space station operation in association with unmanned observatory, comparing gimbal mounted, free floating, tethered and firmly fixed modes

[AIAA PAPER 67-926] 24 p4245 A67-43022
UNSTEADY FLOW
SA OSCILLATING FLOW
SA PULSATING FLOW
 Parametric representation derived for one-dimensional nonsteady flows, considering two distinct solutions of Martin Monge-Ampere equation 01 p0052 A67-10520
 Unsteady adiabatic centrally symmetric radial flow of ideal fluid in general theory of relativity 01 p0114 A67-10987
 Unsteady laminar flow of incompressible fluid in gap between parallel disks with gap width varying with time, obtaining solutions for Navier-Stokes and thermal energy equations 02 p0231 A67-11469
 Solution to boundary layer equations for unsteady flow of viscous incompressible fluid under injection or suction 02 p0233 A67-11948
 Analysis of additional terms in Reynolds flux equation when under unsteady conditions, using wind and temperature measurements, noting role in micrometeorology 02 p0238 A67-12077
 Nonlinear two-dimensional unsteady potential flow around arbitrarily shaped airfoil in inviscid and incompressible fluid, considering method of calculating pressure, forces and moments [AIAA PAPER 66-968] 02 p0178 A67-12291
 Three-dimensional unsteady flow in uniformly expanding layer and dispersion of gas in vacuum 03 p0402 A67-13627
 Nonsteady flow problems, solving fluid motion equations by characteristic method and obtaining boundary conditions 03 p0403 A67-13769
 Differential pressure flow meter for unsteady or transient fluid flow 03 p0422 A67-13775
 Numerical analysis of unsteady viscous fluid flow past circular cylinder, noting effect of Reynolds number 04 p0602 A67-14617
 Unsteady viscous fluid flow in MHD channel under action of pressure gradient solved for arbitrary load coefficient 04 p0669 A67-15519
 Unsteady laminar flow of viscous incompressible fluid between two infinite parallel rotating disks with angular velocities varying with time 04 p0609 A67-15605
 Unsteady incompressible laminar forced convection around stagnation point due to arbitrary time-wise-variant free stream velocity, considering skin friction and heat transfer 04 p0610 A67-15830
 Exact solution /by Hankel and Laplace transforms/ of unsteady motion of viscous MHD fluid in cylindrical vessel in axisymmetric constant strength magnetic field 05 p0850 A67-16134
 Book on methods of determining boundary conditions for unsteady state heat transfer 06 p1111 A67-17661
 Characteristics solution breakdown near leading frozen characteristic for piston induced flow and relaxing gas flow 06 p0984 A67-18128
 Unsteady aerodynamic forces on thin wing oscillating in transonic flow, discussing acoustic ray paths and signal transmission times [AIAA PAPER 67-16] 06 p0943 A67-18841
 Potential double waves at interface between two-dimensional nonsteady barotropic gas flow and region of undisturbed gas 07 p1169 A67-20034
 Unsteady supersonic flow about conical wing fuselage system with LF harmonic oscillatory motion 07 p1127 A67-20224
 Transonic airfoil problem solved via differentiation of airfoil thickness ratio by infinitesimal perturbation method [AIAA PAPER 66-90] 08 p1276 A67-20563
 Approximate solution of some nonstationary boundary layer problems with allowance for magnetic field, discussing nonsteady flow of viscous incompressible electrically conducting fluid past flat plate 08 p1362 A67-21202
 Unsteady flow of rarefied gas under finite pressure gradient when starting from rest, varying gradient in time until steady flow is obtained 09 p1487 A67-21847
 Unstable motion of incompressible viscous fluid in interspace between concentric spheres 09 p1487 A67-21928
 Numerical calculations of blast waves by standard and Hartree techniques compared

with analytical results and application of Richardson extrapolation method 10 p1625 A67-23110

Inverse problem of unsteady heat conduction equation for unbounded hollow cylinder, determining specific heat 11 p1882 A67-24031

Rarefied gas motion instability, constructing general solution for effect of various force fields 11 p1782 A67-24688

Unsteady transonic flow of moving compressible gas filling half-space created by sudden rupture of membrane separating gas from vacuum 11 p1743 A67-24962

Two-dimensional nonsteady airflow in shaped duct prediction, using numerical method 12 p1928 A67-25357

Shock wave diffraction and reflection problems on faces of angle situated in nonstationary gas flow 12 p1928 A67-25672

Heat receiver with correcting device for instantaneous temperature measurements in unsteady gas flow, discussing matching of time constants and heat-transfer coefficients 13 p2118 A67-26352

Similarity solutions for two-dimensional unsteady compressible boundary layer equations using group theoretic methods 14 p2297 A67-28135

Unsteady incompressible flow of two-dimensional supercavitating hydrofoils with finite cavity length, considering wake nature [ASME PAPER 67-FE-15] 14 p2304 A67-28363

Unsteady flow of inviscid, electrically conducting but thermally nonconducting gas at small magnetic Reynolds numbers in MHD generator channel unsteady flow of inviscid electrically conducting but thermally nonconducting gas at small magnetic 16 p2706 A67-30451

Nonsteady combustion MHD open cycle generator improving power density by modulation of conductivity and particle velocity 16 p2607 A67-30595

Linearized theory for unsteady flow about bodies of revolution in sonic stream 16 p2589 A67-30790

Supersonic unsteady flow of cylindrical body past diaphragm model at interface between density-differing gases, studying flow patterns 16 p2593 A67-31133

Multidimensional unsteady flow field of inviscid fluid calculated with application of method of characteristics and digital computer 16 p2662 A67-31535

Field spectrum developed from monochromatic temperature oscillations in bodies due to time variation of heat transfer coefficients caused by unsteady flow velocity 17 p2972 A67-33073

Solution to boundary layer equations for unsteady flow of viscous incompressible fluid under injection or suction 17 p2840 A67-33265

Unsteady plane parallel flow stability of viscous electrically conducting incompressible fluid in oscillating magnetic field 17 p2910 A67-33350

Initial phase of expansion of two-component plasma into vacuum analyzed, using extension of Sedov homogeneous relative deformation method 18 p3084 A67-33423

Nonstationary drag coefficient for unsteady flow for large Reynolds numbers determined experimentally, using analog computer method 18 p3023 A67-33425

Variable mass body rectilinear unsteady motion equations for movement at various levels in viscous fluid 18 p3023 A67-33426

Steady state laminar and turbulent mixing in unsteady isothermal flow in wake behind body with incident shock wave 18 p2984 A67-34203

Unsteady flow past blade cascade problem solved by splicing technique instead of conformal mapping 18 p2984 A67-34217

Unsteady discharge of compressed viscous gas from duct analyzed by finite-difference method 19 p3172 A67-35780

Flow due to rotating disk with center sink solved numerically by considering flow unsteady [ASME PAPER 67-FE-8] 20 p3425 A67-37599

Unsteady conducting fluid flow in MHD ducts with small magnetic Reynolds number and constant pressure 21 p3663 A67-37935

Nonlinearity of unsteady gasdynamic processes in internal combustion engine

exhaust systems, using unsteady sources and sinks 21 p3689 A67-38044

Unsteady airfoil stall noting frequency effects on velocity distribution and angle of attack for oscillating pitch 21 p3565 A67-38547

Instantaneous heat transfer of thin tungsten wires in unsteady transverse airflow 21 p3733 A67-38913

Unsteady spherically symmetric gas flows with gas particle radial velocity proportional to distance from symmetry center 22 p3739 A67-39216

Precise and approximate formulations for unsteady flows of conducting fluid in MHD channels with external electric circuit 22 p3853 A67-40023

Heat transfer, skin friction and shearing stress from similar solutions to compressible laminar boundary layer equations for flow over flat plate 23 p4082 A67-41246

Prandtl equation system for two-dimensional incompressible flows expanded to construct solutions for three-dimensional unsteady flows by straight lines method 24 p4177 A67-42200

Correction to parametric representations of nonsteady one-dimensional flows 24 p4145 A67-42691

UPCONVERTER

Ultralow-noise tunable S-band amplifier using TWM as second stage 01 p0034 A67-10106

Input impedances calculated for parametric up-converters, examining overall signal behavior 02 p0220 A67-12205

DC parametric device in which capacitance variation of silicon p-n junctions due to input signal causes FM 03 p0377 A67-13106

Ultralow-noise two-channel tunable cascade amplifier system using upconverter and traveling wave maser 08 p1304 A67-21222

Wideband varactor upconverters for satellites use, emphasizing transmission characteristics and stability over wide temperature range 16 p2640 A67-31531

Design parameters and performance characteristics for overdriven varactor upper sideband upconverter /USBUC/ 24 p4131 A67-42446

UPPER AIR

Upper air turbulence gusts, describing vertical component test method using F type radiosonde 10 p1676 A67-23085

UPPER ATMOSPHERE

SA IONOSPHERE

SA MAGNETOSPHERE

SA MESOSPHERE

Worldwide meteorological data acquisition capability proposal for improving upper air observations, noting satellite system role 02 p0231 A67-12383

Two-dimensional dynamic model of diurnal variation of thermosphere 04 p0611 A67-14651

Hydrogen diffusion in earth upper atmosphere near critical level 04 p0612 A67-14654

Atmospheric sounding of twilight phenomena in upper layers, solar ray illumination techniques and solar ray color spectral variation 04 p0617 A67-15475

Book on mass spectrometry principles and application to ion and neutral atom composition of upper atmosphere 04 p0624 A67-15587

Rocket observations of temperatures and winds in upper atmosphere, discussing physical interpretation of results 05 p0797 A67-16856

Upper atmospheric wind measurement by artificial cloud method which releases sodium at twilight and trimethyl aluminum at night 05 p0798 A67-16858

Upper atmospheric plasma measurements with impedance probe, determining gyro and hybrid resonance frequencies 05 p0798 A67-16861

ELF and sub-ELF hydromagnetic waves in upper atmosphere observed using five rocketborne cesium magnetometers 05 p0798 A67-16869

Meteoritic dust accumulations at low latitudes in upper atmosphere evidenced by observation of noctilucent clouds, estimating scattering function 05 p0802 A67-17329

Upper atmospheric turbulence and wind measurement by radio reflection from meteor tail 05 p0802 A67-17382

Upper atmospheric rotation speed reevaluated from satellite orbital inclination changes 05 p0803 A67-17412

Rotational speed of upper atmosphere obtained by measuring changes in orbital inclinations of satellites or movements of vapor trails 06 p0993 A67-17564

Density and temperature of upper atmosphere, satellite tracking, geodetic applications and long distance measurements, using laser output 06 p1008 A67-17591

Upper atmospheric formation of electron cloud produced by chemionization reactions of chemical release agents [AIAA PAPER 67-148] 06 p0995 A67-18360

Atomic and molecular processes in upper atmospheres of Venus, Mars and Jupiter investigated by atmospheric models, presenting solar-planetary relationship 06 p1087 A67-18429

Seasonal variation in temperature in nighttime F region through analysis of emission intensity of oxygen red line and upper atmosphere structure 06 p0996 A67-18431

Upper atmospheric condition noting solar activity effect, synoptic meteorology, etc 06 p1027 A67-18607

Height dependence of albedo in earth upper atmosphere, calculating total quantity of neutral hydrogen in ionosphere 07 p1170 A67-19103

Vertical flux and energy spectra of secondary gamma rays and electrons in upper atmosphere 07 p1242 A67-19621

Upper atmospheric neutral gas density determination from simultaneous satellite position measurements 07 p1172 A67-19626

Radio wave propagation in artificial ionized cloud in upper atmosphere determined, using geometrical optics 07 p1143 A67-19691

Upper atmosphere temperature, pressure and density determined by photographic observations of meteors, based on calculating height of homogeneous atmosphere 07 p1174 A67-19708

Effect of thermal escape on neutral hydrogen density above 120 km 07 p1181 A67-19936

Upper atmospheric density, pressure and temperature profile obtained from drag acceleration measurements on falling sphere 07 p1181 A67-19938

Chemiluminescence of upper atmospheric Ni and rocket probe measurement of Ni atom concentration at night 07 p1182 A67-19951

Meteorological telemetry system for gun launched probes for high altitude research 08 p1292 A67-20664

Rocket measurements of small scale structure of ionization profile and wind speed fluctuations, propagation of gravity shock waves and stratification in upper atmosphere 08 p1325 A67-20986

Upper atmospheric temperature measurement by analysis of AIO spectra 08 p1327 A67-21370

Punch card deck for serially completed upper wind observations as substitute for map scaling 09 p1525 A67-22691

Semiannual variations of magnetic activity 10 p1630 A67-22796

Variation of inner scale of turbulence in upper atmosphere with height studied from density variations of alkaline clouds ejected by rockets 10 p1638 A67-23201

Statistical properties of dispersive waves in upper atmosphere analyzed, using correlation technique 10 p1639 A67-23206

Mass spectrometric measurements of upper atmosphere temperature 10 p1639 A67-23214

Rocket measurements of electron fluxes in upper atmosphere of middle latitude at altitudes of 200-500 km 10 p1701 A67-23219

Surveillance of solar activity based on optical observations of satellites 10 p1606 A67-23222

Sounding rocket-released artificial strontium and barium ion cloud motion in upper atmosphere, based on equations of ambipolar diffusion 10 p1644 A67-23254

Free sodium atom distribution in upper atmosphere related to diurnal and nocturnal variation 10 p1645 A67-23262

Rotational speed of upper atmosphere determined from satellite measurements 10 p1652 A67-23493

Book for amateurs on observing earth satellites including methods and discoveries about upper atmosphere and shape of

earth 10 p1608 A67-23620
Spectroscopic twilight airglow
measurements for upper atmosphere
interpreted using rocket flight
data 11 p1786 A67-24263
Atmospheric number density measured by
attenuation of solar X-rays monitored when
satellite passes from darkness to
sunlight 11 p1857 A67-24605
High energy particle precipitation into
upper atmosphere at medium latitude after
magnetic storms, dependence on season and
latitude and correlation with geomagnetic
pulsation enhancement 12 p1991 A67-25113
Yellow-green luminosity accompanying
injection of triethylborane into upper
atmosphere 12 p1932 A67-25208
RF mass spectrometer with small
dimensions and power requirements and
high sensitivity designed for analysis of
upper atmosphere ion and neutral
composition 12 p1941 A67-25651
Atmospheric density distribution at
altitudes from 200 to 300 km based on
Soviet satellite observations during minimum
solar activity 12 p1934 A67-25788
Japanese rocket observations of upper
atmospheric wind and temperatures in
relation to new Cirra model
atmosphere 12 p1937 A67-25841
Vertical component of gusts in upper
atmosphere estimated from rotation rate of
ascending radioprobe fan 12 p1964 A67-26165
Spectrum and scales of upper atmospheric
turbulence determined by photographic
tracking 13 p2108 A67-26314
Cross correlation /by superposed epoch
method/ between upper atmospheric sodium
and stratospheric warmings at high
latitude 13 p2110 A67-26441
Diurnal, annual and seasonal variations of
high altitude turbulent motions in upper
atmosphere through observation of meteor
trails by coherent pulse
method 13 p2110 A67-26506
Initial energy spectrum and flux of low
energy protons responsible for luminescence
of H in auroras 13 p2110 A67-26542
Soviet papers on physics of upper layers
of atmosphere 13 p2111 A67-26667
Diurnal variations in structural parameters
of upper atmosphere determined via
differential equations of
hydrodynamics 13 p2112 A67-26669
Upper atmosphere hydrodynamic equation
additional terms account for hydrodynamic
effects of dissociative recombination and ion
molecule reactions 13 p2112 A67-26670
Photochemical reaction and turbulent
diffusion effect studied using mesospheric
model, establishing relation between
composition and dynamic
state 13 p2113 A67-26681
Atmospheric boundary layer dynamics
models, similarity hypothesis and
theories 13 p2151 A67-26687
Approximate determination of satellite
lifetime by nomogram constructed on basis
of known upper atmosphere density
data 13 p2213 A67-27324
Receivers for measuring UV radiation in
upper atmosphere and outer
space 13 p2121 A67-27335
Upper atmosphere densities and
temperatures at 105-165 km from diffusion
and spectral intensity of aluminum oxide
trails 14 p2310 A67-28050
Upper atmospheric turbulence velocity
probability density investigated in 90 to 110
km region 14 p2346 A67-28058
Atmospheric warming over Central Europe
related to low solar and magnetic
activity 14 p2313 A67-28621
Electron density perturbations caused by
descending rocket in ionosphere studied by
radio pulse signals 14 p2313 A67-28622
Electrodynamic forces and torques on
charged bodies moving through rarefied and
partially ionized earth magnetosphere and
upper atmosphere 14 p2362 A67-29039
Telemetry systems for gun launched upper
atmosphere probes 15 p2436 A67-29412
Chemiluminescent rate constant increase
in reaction of nitric oxide and oxygen in
upper atmosphere explained by clustering of
former 15 p2434 A67-29884
Geographical distribution of surface
temperature of ground and/or clouds and
mean relative humidity of upper
troposphere 15 p2513 A67-30059
Project High Altitude Research Program

/HARP/ directed toward use of guns for
scientific probing of upper atmosphere
[AIAA PAPER 67-38] 15 p2467 A67-30110
Ionospheric irregularities in F region
during night hours /1958-1960/
[AGARDOGRAPH 95] 15 p2483 A67-30300
Probe for measuring energy transfer
between satellite surface and upper
atmosphere 16 p2670 A67-30646
Upper atmosphere photoelectric processes
contributing to low energy electron content
of magnetosphere 16 p2664 A67-30973
Effect of ozone on mean meridional
circulation in upper atmosphere and
mesosphere 16 p2666 A67-31098
Monograph on upper atmosphere kinetics
noting Boltzmann equations, MHD processes,
thermal diffusion, etc 16 p2666 A67-31166
Radar observation of meteor echoes in
upper atmosphere, particularly deionization
of processes in meteor
trails 16 p2749 A67-31251
Heating of upper atmosphere electron gas
by indirect Joule dissipation of reverse
current in ambient electrons demonstrated
for high fluxes 16 p2739 A67-31405
Ion temperature measurements in upper
atmosphere to determine diurnal
variation 16 p2666 A67-31416
Soviet book on meteors in earth
atmosphere studied by radar discussing
meteor trails, upper atmosphere winds,
etc 16 p2754 A67-31866
Current function of three eccentric
dipoles representing main geomagnetic
field 16 p2670 A67-31911
Dust content in upper atmosphere of
earth from satellite light absorption
measurements 17 p2842 A67-32257
Upper atmosphere ion temperature profile
transitional behavior analyzed by fractional
separation in terms of energy budget,
including multiple ion
effects 17 p2843 A67-32531
Measurement of solar extreme UV
radiation atmospheric attenuation to
establish daytime variations in upper
atmosphere composition 17 p2843 A67-32535
Turbulence in upper atmosphere possibly
due to density fluctuations accompanying
internal gravity waves 17 p2843 A67-32538
Helium afterglow observation at high
latitudes, determining He line intensity on
IR spectrograph and giving time-dependent
seasonal variations 17 p2849 A67-32959
Hydrogen distribution in upper
atmosphere and geocorona, relating H-alpha
emission increase to solar activity
decrease 17 p2849 A67-32961
Strontium and Ba vapor releases in upper
atmosphere, testing yield of evaporated
metal for different chemical
reactions 17 p2851 A67-33194
Production modes, physical deactivation
with related electronic energy transfer and
chemical reactions of D oxygen atoms,
noting significance for upper
atmosphere 17 p2809 A67-33203
Production mechanism of atomic nitrogen
ions in upper atmosphere, showing
predominance of nitrogen molecule
dissociative
photolionization 17 p2851 A67-33204
Injun III rocket orbital parameters
determined by optical and radar
observations to provide inclination values
for studying upper atmosphere rotational
speed 17 p2952 A67-33251
Upper atmosphere observation at twilight,
considering broad spectral regions and
emission lines 18 p3033 A67-33585
Upper-atmosphere density determination
methods, with comparison of orbital decay
and instrument 18 p3041 A67-34254
Upper atmosphere density, temperature
and variation determined from satellite drag
data, proposing thermosphere
model 19 p3214 A67-34931
Upper atmosphere diurnal and seasonal
latitudinal variations satellite data, showing
diurnal bulge migration with subsolar point,
2 PM bulge peak, etc 19 p3215 A67-35178
Upper atmosphere rotational speed
determined by analyzing changes in
satellites orbital
inclinations 19 p3216 A67-35182
Daytime ozone density distribution of
mesospheric layer measured by using UV
photometers in rockets 19 p3217 A67-35203
Density, temperature and pressure profiles
variations in upper atmosphere obtained

from rocketborne
experiments 19 p3218 A67-35219
Developments in upper atmosphere
research noting atmospheric density,
temperature, diurnal variations, solar and
geomagnetic activity effects,
etc 19 p3218 A67-35225
Diurnal atmospheric density bulge shifts
observed by Explorer, showing latitudinal-
seasonal variation in helium
concentration 19 p3218 A67-35228
Arctic upper atmosphere neutral gas
composition and altitude distribution
studied, using meteorological
rockets 19 p3219 A67-35251
Upper atmosphere densities and scale
heights from Soviet earth satellite drag data,
noting diurnal variation 19 p3219 A67-35252
Molecular and atomic ion concentration in
earth upper atmosphere observed from low
altitude satellite, discussing diurnal variation
and solar effect 19 p3220 A67-35262
East Germany space research in satellite
tracking, coupling processes, upper
atmosphere, high energy particles,
etc 19 p3321 A67-35294
Pakistan space research noting facilities,
sounding rocket experiments and satellite-
and ground-based
observations 19 p3321 A67-35297
Soviet national report to COSPAR,
summarizing findings in upper atmosphere,
on lunar surface and outer space from 1964
to 1966 19 p3322 A67-35308
Air density variation at 220 km altitude
shown due to increased solar activity, from
satellite orbit observation 19 p3222 A67-35458
Earth-ionosphere whispering-gallery nature
at VLF analyzed, using mode equation for
idealized earth ionosphere
model 19 p3184 A67-35827
Electromagnetic wave propagation in
absorbing gyrotropic medium in terms of
geometrical optics, considering applicability
to radiowave propagation in upper
atmosphere 19 p3185 A67-36015
Metastable helium atom altitude
distribution and 10830 angstrom radiation
emission rate, discussing possible
explanation of helium loss from
atmosphere 20 p3427 A67-36310
Fabry-Perot spectrometer applied to upper
atmospheric emission measurements of
airglow and aurora 20 p3440 A67-36362
Upper atmosphere optical properties
determined by simultaneous twilight balloon
and ground measurements, establishing
twilight sky luminance ratios to solar
luminance 20 p3427 A67-36369
Upper atmospheric dynamics, considering
day-night density and pressure variation,
wind structure, gravity waves,
etc 20 p3429 A67-36896
Structure and composition of upper
atmosphere above stratopause, discussing
temperature, density and wind
variations 20 p3430 A67-36904
Upper atmosphere density measurement
systematic errors in orbiting pressure
gauges by neglecting adsorption and
desorption 20 p3450 A67-37103
Altitude variation of air scattering
coefficient determined from brightness
profile measurements of haze at planet limb,
using spacecraft
photography 20 p3432 A67-37238
Micrometeorite flux rate for Leonid
shower measured with Luster sounding
rocket collecting surface 20 p3528 A67-37424
Photochemical reaction and turbulent
diffusion effect studied using mesospheric
model, establishing relation between
composition and dynamic
state 21 p3618 A67-38426
Atmospheric boundary layer dynamics
models, similarity hypothesis and
theories 21 p3654 A67-38429
Upper atmosphere angular velocity
determined from changes in satellite orbital
inclinations, noting increase with
height 21 p3619 A67-38512
Ionospheric positive ion density as
function of altitude measured by Langmuir
probe 21 p3629 A67-38662
Antiproton production by primary cosmic
ray collisions with atmospheric nuclei
compared with interstellar
gas 21 p3620 A67-38843
Indium activity measurements to
determine epithermal neutron flux in
atmospheric upper layers, giving results in

terms of dependence on atmospheric depth 21 p3622 A67-39031

Boron oxide identified as radiating species causing molecular fluorescence spectrum in upper atmosphere at

twilight 21 p3623 A67-39123
80 km atmospheric backscattering enhancement detected by optical radar 22 p3759 A67-39558

Temperature, pressure and density change effects free thermal conductivity gauge system for upper atmosphere pressure measurements 22 p3829 A67-40470

OH Meinel band, nitrogen dioxide continuum and O IS to ID transitions maxima altitudes in midlatitude night airglow emissions from rocket radiometer measurements 23 p3995 A67-40813

Optical instrumentation for auroral and afterglow studies with applications of grating spectroscopic systems, monochromators, interferometers and photometers 23 p3996 A67-41256

Semiannual variations of magnetic activity 24 p4149 A67-42132

Booster for Skylark upper atmosphere research vehicle to increase altitude and reduce launching dispersion of single stage vehicle 24 p4206 A67-42580

UPPER IONOSPHERE

Outer ionospheric structure and transition into interplanetary medium 05 p0886 A67-16012

Outer ionosphere and transition into interplanetary space noting altitude and structure characteristics 11 p1786 A67-24261

Inhomogeneous formations and disturbances of electron concentrations in outer ionosphere indicated by Doppler shift differences measured by Elektron I satellite 12 p1936 A67-25800

Photochemical analysis of diurnal variations of electron concentration and temperature of upper ionosphere 16 p2669 A67-31902

Ion-molecule chemistry of Jupiter upper atmosphere, studying equilibrium and nonequilibrium abundances of hydrocarbon products due to UV radiation reaction 18 p3135 A67-34540

Outer ionospheric structure and transition into interplanetary medium 20 p3530 A67-37589

URANIUM

Positive isotope effect on superconducting transition temperature of alpha uranium 23 p4044 A67-41439

URANIUM COMPOUND

Operating temperature effect on vacuum emission stability of vapor-deposited tungsten clad UC-ZrC and uranium dioxide 09 p1449 A67-22347

URANIUM OXIDE

Equilibrium carbon monoxide pressures measured by torsion effusion studies of reaction of graphite with hafnium and uranium dioxides at high temperatures 01 p0018 A67-10763

Electric conductivity of calcium fluorite single crystals doped with uranium dioxide 12 p1980 A67-25183

URANIUM 235

Absolute age of earth, heavy elements and meteorites determined by radioactive decay measurements, comparing present and initial ratios of uranium 235 and 238 02 p0329 A67-12496

Absolute age of earth, heavy elements and meteorites determined by radioactive decay measurements, comparing present and initial ratios of uranium 235 and 238 10 p1709 A67-23364

URANIUM 238

Absolute age of earth, heavy elements and meteorites determined by radioactive decay measurements, comparing present and initial ratios of uranium 235 and 238 02 p0329 A67-12496

Absolute age of earth, heavy elements and meteorites determined by radioactive decay measurements, comparing present and initial ratios of uranium 235 and 238 10 p1709 A67-23364

URANUS

IR brightness temperature of Uranus used to establish current lower limit at which brightness temperature of celestial object can be measured 02 p0324 A67-11773

Mean values of methane wavelengths in Uranus spectrum measured for determination of atmospheric

temperature 03 p0515 A67-14327

Molecular hydrogen features in spectra of Saturn and Uranus 04 p0696 A67-14738

Uranus and Neptune spectral absorptions compared with laboratory spectra obtained with very long optical paths indicate methane role in planetary absorption 08 p1397 A67-21213

URANYL

Properties of uranyl-doped glass for application as saturable optical filter for use with lasers 01 p0032 A67-10009

UREA

S PSEUDOURA

URETHANE

SA POLYURETHANE

SA POLYURETHANE FOAM

Sollthane 113 urethane rubber composition analyzed via constant strain rate tests, noting birefringent sensitivity and optical transmission properties 11 p1811 A67-24615

URINATION

Biological effects of time-zone changes on circadian rhythms of urinary elimination of potassium and 17-hydroxycorticosteroids 22 p3751 A67-39606

Urinary catecholamine excretion in pilots relation to physical mental expenditure of energy and flight deck work loads 23 p3952 A67-41577

URINE

Urinalysis assessment of physiological response of eight pilots to 18-hr flight in F-4C aircraft 03 p0364 A67-14287

Urinary loss of calcium, phosphorus, nitrogen, sodium and chloride in men under prolonged bed rest at ground level or at simulated altitudes [SAM-TR-66-296] 07 p1134 A67-19857

Acceleration effect on rate of urine flow and urinary excretion of sodium, potassium and total solute in rabbits 07 p1134 A67-19861

Urine composition in twelve dehydrated subjects in periods of activity, water immersion and reclining in deck chair [SAM-TR-66-305] 09 p1453 A67-21730

Changes produced in urinary sodium, potassium, and calcium excretion in mice exposed to homogeneous magnetic field 10 p1600 A67-23819

Adrenal gland reaction to different pressure breathing types by urine analysis 22 p3752 A67-40538

Hydrazine effects on free amino acid concentrations of plasma and urine in dogs 23 p3952 A67-41570

Open cycle air evaporation urine processing system recovering potable water in space cabin simulator, discussing wick evaporator 23 p3969 A67-41631

UTILITY AIRCRAFT

SA MITSUBISHI MU-2 AIRCRAFT

Quality control around twin turboprop utility plane MU-2 at experimental stage 05 p0812 A67-17245

Lubricants for utility aircraft piston engines, cost, availability, compatibility, etc [SAE PAPER 670248] 12 p1989 A67-25502

Utility aircraft costs lower than specialized aircraft in meeting mixed mission requirements in counterinsurgency environment, considering changes, uncertainty and logistics 22 p3745 A67-39618

V

V/STOL AIRCRAFT

SA STOL AIRCRAFT

SA VTOL AIRCRAFT

Thrust deflection and vectoring in European V/STOL aircraft, noting single-sided deflector, tilting-pod engine configuration and vectoring nozzle [SAE PAPER 660738] 01 p0140 A67-10637

Mobile model test rigs and model instrumentation for CL-84 V/STOL aircraft 01 p0073 A67-11120

Flight performance and low speed behavior of V/STOL aircraft, noting correlation between thrust angle and aircraft attitude 02 p0180 A67-11524

By-pass propulsion systems development for V/STOL transports including aerothermodynamic aspects [AIAA PAPER 64-606] 03 p0502 A67-12902

Airborne V/STOL simulators used for handling qualities research at National Aeronautical Establishment, Ottawa

[AIAA PAPER 65-705] 03 p0394 A67-12915

XC-142A tilt-wing deflected slipstream aircraft designed to take off and land in virtually any terrain and achieve 430 plus mph 03 p0357 A67-12971

V/STOL transport aircraft design and application, noting performance with varying number of propulsion units 03 p0357 A67-12972

Gimballed jet engine development, noting application to V/STOL aircraft and design of plenum chamber burning engine 03 p0503 A67-13008

V/STOL military transports purchase decisions based on analyses of operational employment, engineering design and economic utility 04 p0551 A67-14803

V/STOL transport aircraft structural problems related to propulsion, associated acoustical, thermal and debris conditions and weight/cost effectiveness requirements [SAE PAPER 660668] 04 p0552 A67-15784

Noise and loading actions on helicopters, V/STOL aircraft and ground effect machines - Symposium, University of Southampton, August-September 1965 06 p0945 A67-17905

Debris ingestion into engine arising from ground erosion effects on jet lift V/STOL aircraft 06 p0945 A67-17906

Lifting rotor-propeller noise prediction for military helicopters and V/STOL aircraft in forward flight 06 p0945 A67-17909

Flight tests of two X-22A dual tandem rotatable ducted propeller V/STOL research aircraft 06 p0948 A67-18201

Aircraft sizing methodology and hover control comparative analysis on V/STOL fighter-bomber using lift plus lift cruise propulsion [AIAA PAPER 67-133] 06 p0948 A67-18358

Copy machining of thin walled propulsion duct pivot support tube used in Bell V/STOL aircraft 06 p1008 A67-18724

Streamline matching technique for V/STOL wind tunnel wall corrections [AIAA PAPER 67-183] 07 p1163 A67-19439

Flight and operational suitability testing of XC-142 V/STOL assault transport [AIAA PAPER 67-261] 07 p1130 A67-20074

V/STOL theory for equilibrium level flight, evaluating optimum performance over complete velocity spectrum 09 p1441 A67-22487

Bell X-22A VTOL research vehicle, assessing mechanical and aerodynamic characteristics, variable stability and control system, etc 11 p1743 A67-24097

Automatic height control test equipment for V/STOL aircraft, discussing experimental setup and performance 11 p1772 A67-24268

Design aspects of power plants for V/STOL aircraft, examining lift jets, thrust vectoring and lift fans [ASME PAPER 67-GT-7] 11 p1744 A67-24795

V/STOL aircraft gas turbine systems, discussing propulsion system configurations applied to fighter, fighter attack and transport cargo aircraft [ASME PAPER 67-GT-48] 11 p1744 A67-24809

Handling criteria for basic stability and control characteristics of slender wing and V/STOL aircraft 13 p2053 A67-27192

Avionics system development for V/STOL tactical aircraft, emphasizing onboard electrical system 13 p2053 A67-27222

Minimum power requirements of V/STOL aircraft 13 p2054 A67-27586

Rotor downwash angle and tunnel geometry effect on maximum size rotor that can be tested in closed throat wind tunnel 13 p2091 A67-27595

V/STOL transport testing and operational requirement, discussing hover rig, pedestal and simulator 14 p2245 A67-27746

Book on aerodynamics of V/STOL aircraft emphasizing use of momentum and finite wing theories, considering deflection of trailing vortex system 14 p2243 A67-28678

Air traffic control operations forecasting, stressing proposed STOL and VTOL port [AIAA PAPER 67-398] 15 p2515 A67-30385

XC-142A flight control and stability augmentation systems 17 p2794 A67-31996

LW-3B escape system for low and medium performance V/STOL aircraft 17 p2794 A67-32000

Electronic systems for V/STOL fighter aircraft, considering operational capabilities, reliability, maintenance and protection 17 p2795 A67-32022

Vectoring and nonvectoring nozzles of

different geometries for lift and lift/cruise engines 17 p2928 A67-32569
V/STOL all-weather operation
developments noting navigation and communications, operations under icing and noise problems
[SAE PAPER 670348] 17 p2798 A67-32990
Failure safety design of rotary wing aircraft, emphasizing airline type operation [SAE PAPER 670349] 17 p2798 A67-32991
Shaft power from conventional two-spool turbofan engines for composite aircraft applications
[SAE PAPER 670352] 17 p2929 A67-32992
Integrated electronic display for V/STOL flight evaluated, considering vehicle dynamics, handling qualities, etc., and presenting performance data 17 p2861 A67-33182
Northrop program for v/STOL aircraft including systems studies, propulsion, aerodynamics, flight control technology, performance characteristics and operation and testing northrop program for V/STOL aircraft including 18 p2987 A67-34708
Navigational requirements of V/STOL aircraft in high density urban areas 19 p3256 A67-35863
Aerodynamic interference effect with jet lift V/STOL aircraft under static and forward-speed conditions, stressing adverse flow 20 p3357 A67-36952
Aircraft design by statistical methods, presenting samples for interceptor fighter, shorthaul jet and light twin-engine cargo aircraft 20 p3361 A67-37170
Floating airports proposed as solution to short haul air traffic problems in New York 20 p3418 A67-37445
Hydraulic power systems for V/STOL noting self-sufficiency on start-up and auxiliary power source function 20 p3366 A67-37552
Rotary wing role in short haul intercity transportation, comparing V/STOL and STOL advantages over fixed wing aircraft, noting need for compound helicopter 21 p3734 A67-38013
Airport terminal facilities - Conference, Houston, April 1967 22 p3778 A67-39373
Airport requirements for V/STOL and short haul air transportation, stressing need for solution of noise problem 22 p3779 A67-39381
V/STOL aircraft model wind tunnel tests on wing and propellers, describing strain gauge balances 22 p3745 A67-39728
Hatfield V/STOL tunnel design problems and tunnel model test results 22 p3780 A67-40063
Large diameter helicopter rotors and V/STOL propellers /axis tilting in vertical plane/ testing system of wind tunnel and aerodynamic torque measuring apparatus 23 p3986 A67-40575
VFW/Flat joint project to develop single-seater fighter/reconnaissance aircraft noting structural design, power source and liftoff weight 23 p3934 A67-41255
Short haul military requirements /1970-1980/, considering assault and logistic airlifts supporting ground forces and V/STOL aircraft [SAE PAPER 670827] 24 p4093 A67-41992
Commercial V/STOL operating characteristics in Northeast Corridor, discussing commuter design and cost analyses [AIAA PAPER 67-769] 24 p4095 A67-42937
Conceptual aircraft suitability for short haul transportation systems, discussing operation, design, noise factors, flight profiles and V/STOL certification rules [AIAA PAPER 67-771] 24 p4095 A67-42939
V/STOL all-weather guidance system developments and flight experimentation, discussing enroute navigation compatibility and terminal area operations [AIAA PAPER 67-796] 24 p4183 A67-42957
V/STOL aircraft scheduling for passenger demand and equipment mix, optimizing airline earnings with mathematical programming model [AIAA PAPER 67-801] 24 p4259 A67-42961
V/STOL airline economics simulated with computerized dynamic programming model [AIAA PAPER 67-841] 24 p4096 A67-42979
Elevated vertiport and stolport configurations and design, investigating flight operations, supporting services and legal aspects

[AIAA PAPER 67-891] 24 p4140 A67-43003
V/stol concepts for short haul commercial aircraft compared for gross weight, operating cost, gust sensitivity and noise levels
[AIAA PAPER 67-938] 24 p4096 A67-43028
V/STOL and STOL concepts as applied to short haul transportation
[AIAA PAPER 67-941] 24 p4097 A67-43031
Commercial V/STOL transportation system, analyzing intraurban and short haul factors for concerned parties by computer simulation [AIAA PAPER 67-969] 24 p4260 A67-43047
V/STOL airbus transportation system schedules, travel times and fares for Northeast Corridor generated by computer method [AIAA PAPER 67-972] 24 p4127 A67-43049
V-4 AIRCRAFT
S XV-4 AIRCRAFT
V-9 AIRCRAFT
S XV-9A AIRCRAFT
VACILLATION
S PERIODICITY
VACUUM
SA HIGH VACUUM
SA ULTRAHIGH VACUUM
Plasma expansion wave propagation in vacuum after current cut-off 02 p0278 A67-12628
Two-dimensional self-similar hot conducting gas outflow into vacuum, for power law variation of gas-vacuum interface temperature 05 p0793 A67-17007
Exploding wire phenomena in air at atmospheric and reduced pressures 05 p0847 A67-17317
International Vacuum Conference, Stuttgart, June-July 1965, Volume 2, Part I 09 p1488 A67-22098
International Vacuum Congress, Stuttgart, June-July 1965, Volume 2, Part III 09 p1484 A67-22116
Plasma expansion wave propagation in vacuum after current cut-off 13 p2171 A67-27386
Electronics and vacuum physics - Conference, Prague, September 1965 14 p2352 A67-27747
Bibliography on electrical discharges in vacuum and properties of vacuum as electrical insulator 15 p2516 A67-29200
Terminology associated with hermetically sealed devices in terms of specification inconsistencies, backfill gas requirements and leak rate 16 p2683 A67-31728
Two-dimensional self-similar hot conducting gas outflow into vacuum, for power law variation of gas-vacuum interface temperature 18 p3028 A67-34269
Einstein-Maxwell fields exact solutions constructed from Einstein vacuum fields, discussing vacuum metric and transformations 23 p4028 A67-41150
VACUUM CHAMBER
Space vacuum simulation chambers for testing of ionic, plasma and other rocket engines 01 p0048 A67-10302
Design, construction and operation of vacuum chamber space simulator for testing Gemini space capsule 01 p0049 A67-10303
Prolonged high temperature creep and endurance testing of refractory materials in vacuum or inert media 01 p0051 A67-11247
Steam generating technique for vacuum ejector system of high-altitude-simulating rocket test facility in West Germany [DVL-598] 03 p0394 A67-13030
Vacuum simulation facility near Munich for testing third stage of ELDO rocket 03 p0394 A67-13031
Vacuum chambers operating at larger dynamic gas loads at lower pressure by means of ions, titanium sublimation and liquid nitrogen cryogenic pumping 04 p0598 A67-15174
Cyclotron ion wave interaction with HF plasma oscillations measured, using vacuum chamber and electron gun 04 p0667 A67-15209
High speed drive for rotating shafts inside high vacuum chambers [ASME PAPER 66-WA/PID-7] 04 p0628 A67-15330
Diamagnetic probe measurements of kinetic pressure of plasma in magnetic field 07 p1228 A67-19513
Vacuum ionization gauge reading dependence on localized gas densities caused by chamber temperature

nonuniformity 09 p1498 A67-22108
Nonuniform molecular density, pumping power and gas temperature distribution in evacuated space simulator 09 p1503 A67-22118
German space simulation chamber, discussing influences of cryogenic panel and solar simulation on vacuum system 09 p1485 A67-22123
Facility for testing third stage of ELDO rocket, discussing high vacuum equipment in Ottobrunn laboratory 09 p1485 A67-22124
Prevention system of short circuit in vacuum chambers due to glow discharges 10 p1622 A67-23316
Vacuum or low pressure contamination removal from space simulation chamber, using bakeout with externally and internally supplied heat 11 p1773 A67-24976
Satellite sealed subsystems individual leak rates in thermal-vacuum environment measured with mass spectrometer 12 p1921 A67-25690
Large and intermediate ultraclean vacuum chambers converted to sputter-ion and titanium sublimation pumping 12 p1921 A67-25691
Verification of thermal mathematical model for artificial satellite using thermal vacuum chamber, noting error analysis [AIAA PAPER 67-304] 12 p2036 A67-26019
Space vehicle thermal testing in cold vacuum chambers with and without solar simulation [AIAA PAPER 67-306] 12 p1926 A67-26021
Gears evaluation testing under vacuum chamber space simulation [ASLE PAPER 66AM-7A4] 13 p2123 A67-27099
Vacuum equipment application in semiconductor production 13 p2124 A67-27365
Space simulation chamber for industry and research 14 p2292 A67-28063
Ni XIX, Cu XX and Zn XXI spectra observation using vacuum spark chamber 14 p2389 A67-28840
Apparatus for direct weight loss recording of space materials 15 p2466 A67-29543
Cyclotron ion wave interaction with HF plasma oscillations measured, using vacuum chamber and electron gun 15 p2532 A67-30257
Vacuum chamber for plasma studies consisting of thin stainless steel shell strengthened by glass fiber reinforced plastic with epoxy compound as adhesive 16 p2676 A67-31397
Mid-IR spectral emittance measuring apparatus, discussing range of performance, systems response, etc 16 p2677 A67-31429
Behavior of perfect sphere rotating around axis and under no external force 16 p2677 A67-31715
Prolonged high temperature creep and endurance testing of refractory materials in vacuum or inert media 17 p2835 A67-33170
Rotating device for transmitting motion through walls of ultrahigh vacuum chambers, using circular motion of bellows envelope and internal gearing 17 p2863 A67-33358
Nitrogen ion drift velocities in plasma jet flowing into vacuum chamber noting ion mobilities in parent and foreign gas 19 p3271 A67-35075
Laboratory investigation of laser emission line absorption by atmospheric gases in vacuum multiple-pass cell, obtaining data free of aerosol scattering 20 p3386 A67-37606
Plasma production by pulsed laser irradiation of aluminum in space chamber vacuum 21 p3666 A67-38259
Electron beam welding of high temperature metals in vacuum 22 p3812 A67-39541
RCA papers on environmental sciences 22 p3781 A67-40400
Operational requirements for modern space environment test laboratory covering thermal vacuum, shock, vibration and combined testing 22 p3781 A67-40401
Safety control requirements in thermal-vacuum testing involving protection against electric equipment operation in pressure range for glow discharge 22 p3782 A67-40404
High venous pressures during exposure of dogs to near-vacuum conditions 23 p3960 A67-41699
Vacuum chamber contaminants, discussing silicone pumping fluid from diffusion pumped systems 24 p4138 A67-42035
Optimum solar simulator and design of thermal vacuum chamber around it 24 p4138 A67-42042

VACUUM DEPOSITION

Vacuum technology of thin film formation 01 p0131 A67-10298

Automatic control of evaporation and deposition of thin films under vacuum 01 p0078 A67-10299

Epitaxial temperature for Si films vacuum deposited on silicon as function of substrate crystallographic orientation observed by low energy electron diffraction patterns 01 p0132 A67-10372

Surface color explained using backscattering angle and diffraction properties of germanium films vacuum deposited onto heated substrate 01 p0138 A67-11076

Vacuum evaporation of HgTe thin film, examining thermal treatment, electric properties as function of thickness, etc 02 p0280 A67-11463

Basic problems of thin film physics - International Conference, Clausthal-Goettingen, West Germany, September 1965 02 p0281 A67-11701

Vacuum deposited metal film structure analyzed over wide temperature range, using electron diffraction and electron microscopy techniques 02 p0285 A67-11705

Microstructure and microhardness of evaporated thin films as function of temperature of substrate during condensation 02 p0286 A67-11707

Electron microscopy study using replica technique of cross section of films of Al and Si vacuum deposited on glass substrates reveal columnar growth of polycrystalline film 02 p0287 A67-11712

Solar absorptance and thermal emittance of aluminum coated with vacuum deposited films of aluminum oxide of various thicknesses [AIAA PAPER 65-656] 03 p0448 A67-13036

Topology of thin film RC circuits fabricated by depositing metallic and dielectric films on insulating substrate 04 p0592 A67-15079

Vacuum deposition and mechanical properties of magnetic thin films of ferrite-borate mixtures 04 p0677 A67-15118

Epitaxial gallium arsenide films prepared by vacuum evaporation of elements 04 p0678 A67-15124

Synthesis and growth of dendritic InSb films by electron beam microzone melting of vacuum deposited composite indium and antimony films, noting electrical properties 04 p0682 A67-15319

Electrical properties of thin and thick resistive films vacuum-deposited and nonvacuum-deposited by chemical and firing process 04 p0682 A67-15485

Strain measurement at high temperature by vacuum deposition of thin films on specimens covered with insulating layer 04 p0626 A67-15745

Thin film deposition techniques, presenting vacuum evaporation and sputtering 04 p0631 A67-15992

Vacuum deposition of thin films, noting importance of low pressure environment, with attention to diffusion and ion pumps 04 p0631 A67-15994

Multilayer technique for evaporation of ohmic contacts onto CdS, noting V-I characteristics and noise spectrum of recrystallized layer 06 p1050 A67-18142

Device for controlling thickness of thin films prepared by sputtering in vacuum 06 p1003 A67-18195

Interaction between layers of ferromagnetic films of different composition and coercivity separated by insulating quartz layer, obtaining films by vacuum deposition 08 p1369 A67-20811

Comparison of integrated microcircuits deposited on semiconductor and insulating substrates, noting vacuum deposition techniques 08 p1302 A67-20918

Parameter control during vacuum deposition of electronic film circuits for obtaining acceptable tolerances 09 p1503 A67-22099

Thin film adhesion to substrate, considering effect of interposed thin film 09 p1503 A67-22100

Thin films of indium antimonide for active devices grown by various methods including atomic mixing, flash evaporation, etc 09 p1474 A67-22112

Optical transmission and electrical properties of complementary metallic

meshes fabricated by formation of complement of agglomerated thin films 11 p1845 A67-24142

Sublimation technique applied to high mobility PbS and CdS thin film deposition under ultrahigh vacuum equilibrium conditions 11 p1847 A67-24738

Oriented growth of thick films of CdTe deposited on quartz plates in vacuum, discussing photovoltaic effect 12 p1982 A67-25450

Vacuum deposition techniques for production of optical film materials for neutral density filters and sunglasses, discussing dielectric, metallic, reflecting and semitransparent films 13 p2158 A67-27076

Sputtered beta-tantalum thin films produced in two-chamber vacuum system with applied negative anode bias voltage 13 p2177 A67-27077

Photolithographic and metal aperture masks for integrated and thin film circuit manufacturing 13 p2124 A67-27390

Variable composition samples method for preparation of lead telluride semiconductor films by vacuum deposition 14 p2372 A67-28823

Thin films as passive and active electrical components in microminiaturization, noting characteristics obtained by vacuum evaporation, cathode sputtering, diffusion and epitaxial growth 15 p2447 A67-29684

Strength and durability in friction tests of soft, vacuum deposited, thin-metal gold film lubricants, noting dependence on film-substrate interface 16 p2684 A67-31816

Optical properties of Mg layers evaporated in ultrahigh vacuum, noting results of reflectivity measurements 17 p2913 A67-32292

Structure and substructure effect on thin film properties, discussing vacuum deposition mechanism of metals, alloys, dielectrics and semiconductors 17 p2920 A67-32888

Structure of Ge-Sn thin films vacuum deposited on glass substrates analyzed by electron diffraction methods 17 p2920 A67-32891

Molybdenum/tungsten films obtained by thermal decomposition in vacuum analyzed, noting surface morphological changes with temperature changes 17 p2921 A67-32892

Epitaxial deposition of silicon on silicon substrates, discussing vapor and vacuum deposition, impurity distributions, layer thickness, etc 18 p3097 A67-33456

Vacuum siliconization of refractory metals in Mo-Si system noting thermomdiffusion layers, vapor phase, chemical reaction, diffusion and temperature gradient 19 p3236 A67-34918

PbTe thin films vacuum-vaporized onto amorphous or oriented substrates studied for crystallographic properties as function of deposition temperature, film thickness, etc 19 p3304 A67-35422

Thin CdAs films thermal deposited in vacuum on various substrates investigated for electric properties 19 p3305 A67-35577

Indium-antimony alloy thin film preparation by vacuum evaporation, noting effect of heating and annealing on electrical resistivity 19 p3305 A67-35609

Technological methods for depositing thin films in vacuum, considering evaporation, scattering, etc 20 p3453 A67-36472

Thin film integrated circuits, considering vacuum deposition and cathode sputtering 21 p3597 A67-38496

Ferromagnetic powder deposition on superconductor surface in vacuum used to obtain magnetic flux distribution in superconductors 23 p4035 A67-40652

Device for metering variety of metals for high vacuum evaporation designed for thin film metal-insulator-metal diodes fabrication 23 p4001 A67-41223

VACUUM EFFECT

Logarithmic dependence of energy losses on relativistic particle velocities in polystyrene films 01 p0125 A67-10926

Liquid propulsion systems operating in space and resulting problems of phase transformation, noting plug formation and flow stoppage 01 p0055 A67-11386

Sliding friction characteristics in vacuum of single and polycrystalline aluminum oxide in contact and with various metals 03 p0428 A67-13231

Physical properties of metals influence on friction, adhesion, wear and welding

tendency in vacuum 03 p0428 A67-13271

Cardiovascular responses of anesthetized dogs to repeated rapid decompressions in near vacuum 03 p0365 A67-14296

Divergence of fragments of force-free gas-filled vessel exploded in vacuum 04 p0708 A67-14793

Spacecraft environmental effects covering outgassing in high vacuum, deterioration of materials by evaporation, lubrication and changes in mechanical and electrical properties of plastics 04 p0704 A67-14995

Electron beam welding noting effects of pressure and vacuum 04 p0628 A67-15313

Vacuum effect on sintering temperature, describing measuring apparatus and results 06 p1006 A67-17559

Ultrahigh vacuum effects on flow and fracture behavior of molybdenum 06 p1016 A67-17897

Ball bearing life operating in vacuum with molybdenum disulfide and oils as lubricant [ASLE PAPER 66AM 7A3] 08 p1335 A67-21036

Gas desorption following Q-switched laser beam bombardment of tungsten target in vacuum 08 p1338 A67-21310

Experimental verification of predictions of conventional quantum electrodynamic vacuum effects by Compton and other scattering techniques 09 p1534 A67-22021

Calorimetric measurement of source and broadband spectral absorptances of spacecraft thermal control coatings during exposure to UV in vacuum environment 09 p1534 A67-22452

Effect of varying magnetic field, vacuum and ion density at 27 MHz on properties of cylindrical argon plasma column, using capacitive and inductive coupling 10 p1686 A67-23504

Semiconductor surface potential in ultrahigh vacuum and under controlled atmosphere 10 p1696 A67-23694

Optical materials properties analyzed for UV induced degradation under vacuum conditions [AIAA PAPER 67-344] 12 p1959 A67-26058

Physical properties of metals influence on friction, adhesion, wear and welding tendency in vacuum 14 p2324 A67-28000

Australasian tektite origin criticized regarding magnitude of atmosphere removal 14 p2390 A67-28889

Exobiology and effect of physical factors on microorganisms 15 p2427 A67-29117

Absolute spectral reflectance measurement in solar region in vacuo for applications to thermal control coatings 15 p2487 A67-29542

Simulated space effects on microelectronic device materials 15 p2466 A67-29549

Asbestos reinforced plastics evaluated for physical and optical properties, thermal-vacuum and UV resistance 15 p2507 A67-29550

Vacuum effect on oven-dried balsa wood strength 15 p2507 A67-29554

Silicones performance in high vacuum, temperature extremes and radiation environments of outer space, noting outgassing effect 15 p2508 A67-29557

Adhesives for nuclear powered spacecraft tested for pressure, temperature and radiation effects 15 p2508 A67-29560

Vacuum effect on tensile, creep and fatigue properties of magnesium polycrystals and on tensile properties of oriented magnesium single crystals 15 p2503 A67-29561

Vacuum-ignition phenomena in Apollo rocket engine when oriented in upward-firing attitude 18 p3114 A67-33977

Chromizing of steel by HF induction heating in vacuum using low-carbon ferrochrome and electrolytic chromium mixture 19 p3236 A67-34920

Isochronal annealing of proton-irradiated silicon solar cells studied in vacuum over various temperature ranges 19 p3305 A67-35669

Sliding friction characteristics in vacuum of single and polycrystalline aluminum oxide in contact and with various metals 19 p3237 A67-35838

Tungsten-molybdenum alloy heat-resistant properties noting vacuum testing and subjection to plastic deformation, with results related to molybdenum content and temperature 20 p3467 A67-36968

Similar or dissimilar materials thermal contact resistance in vacuum with negligible

film effect, obtaining constriction resistance 20 p3555 A67-37609

Full wave solutions for coupled modes corresponding to ionospheric propagation in vacuum, stressing numerical swamping problem 20 p3389 A67-37710

Soviet book on high temperature materials for vacuum or inert gas industrial processes 21 p3645 A67-38600

Cosmology and elementary particles, noting relationship hypothesis between cosmological asymmetry and particles via vacuum 22 p3880 A67-39337

Book on vacuum engineering covering space vacuum simulation, pressure measurement, gas flow and load, vacuum systems and technology 23 p4028 A67-41353

Anesthetized dogs subjected to near vacuum condition before and after clinical death, comparing data of venous and arterial pressure 23 p3952 A67-41572

Animal study of body volume increase and pressure changes causing lungs and thorax expansion during decompression to near vacuum 23 p3954 A67-41594

Titanium-magnesium and titanium-beryllium oxides physical properties under electron bombardment in vacuum indicate usability for SHF oscillation energy absorbers 24 p4202 A67-42069

VACUUM EQUIPMENT

Numerical analysis showing dependence of vacuum plasma accelerator geometrical and electrical parameters on plasma acceleration kinematics 01 p0122 A67-10347

Ultrahigh vacuum envelopes design, fabrication and use, emphasizing choice of materials and outgassing 02 p0250 A67-12452

Vacuum microbalance techniques - Conference on Vacuum Microbalance Techniques, Princeton, September 1965, Volume 5 04 p0619 A67-14730

Longitudinal thermomolecular flow theories at intermediate pressures, comparing similarities and discrepancies in forces acting on hangdowns or samples in microbalance measurements 04 p0603 A67-14733

Vacuum testing machine to determine tensile and creep properties of heavily drawn W wires at temperatures up to 2500 degrees F 06 p1013 A67-17799

Modulated molecular beam apparatus with chopper used in conjunction with field emission microscope for studies of atomic interactions with surfaces 09 p1499 A67-22114

Electron beam welding in vacuum and in atmosphere, describing rapid positioning, workplace guidance, beam control and observation 09 p1503 A67-22119

Vacuum apparatus for testing flat and cylindrical specimens of high melting point materials for creep and long term strength 11 p1877 A67-24817

Multiposition grips for automatic mounting of metal or plastic specimens for low temperature mechanical tests 11 p1877 A67-24819

Numerical analysis showing dependence of vacuum plasma accelerator geometrical and electrical parameters on plasma acceleration kinematics 11 p1844 A67-25020

Cathode spot phenomena in pulsed vacuum arc utilized for electric microthrusters, testing cathode materials by mass and momentum transfer 12 p1989 A67-25403

In situ measurements of diffuse hemispherical spectral reflectance of thermal control coatings irradiated in vacuo with various combinations [AIAA PAPER 67-342] 12 p1959 A67-26056

Vacuum equipment application in semiconductor production 13 p2124 A67-27365

Handbook of materials and techniques for vacuum devices covering high temperature properties, materials selection, joining processes, etc 14 p2339 A67-28829

Vacuum systems for microelectronic device fabrication, detailing pumping methods and related equipment 19 p3236 A67-35020

Traction test apparatus for vacuum and high temperature testing of refractory metals, with modifications for rupture and brittleness tests 20 p3463 A67-36112

Guarded hot plate apparatus for measuring thermal conductance of multilayer cryogenic insulation under vacuum 22 p3802 A67-40291

Cryogenic insulation thermoconductivity measuring apparatus operable at high vacuum and nonsteady state conditions 22 p3803 A67-40295

VACUUM FURNACE

Extensometer for measuring small changes of specimen on tensile testing vacuum furnace at high temperatures, using CW gas laser as light source 01 p0070 A67-11036

Vacuum processing in controlling contamination during joining of superalloy and refractory type metals 03 p0430 A67-13555

Antimony diffusion into germanium using vacuum furnace, giving graphs with variation of antimony concentration and depth of diffused p-n junction 05 p0869 A67-17089

High temperature vacuum furnace using electric furnace parts 06 p0950 A67-17751

Diffusion bonding of titanium sandwich structure for Saturn tank wall application 10 p1661 A67-23702

Refractory materials thermal expansion at elevated temperatures measured with apparatus consisting of optical comparator and controlled gradient vacuum furnace 16 p2677 A67-31542

VACUUM GAUGE

SA PIRANI GAUGE

Ultrahigh vacuum measurement and total and partial pressure gauges, discussing operational and calibration problems 01 p0064 A67-10501

Reduced X-ray photoelectric current in modified Bayard-Alpert ion gauge for vacuum pressure measurements below 10 to minus tenth torr 05 p0805 A67-16462

Vacuum gauge calibration error with conductance-determined pressure divider 09 p1498 A67-22109

Quick change high vacuum window and heat transfer gauge installation for shock tubes 10 p1658 A67-23789

VACUUM MELTING

Soviet monograph on vacuum arc melting of titanium alloy ingots noting crystallization process, structural changes and properties of end-products 03 p0447 A67-13925

Electron beam zonal vacuum fusion growth of Mo-Nb alloy single crystals 05 p0827 A67-16080

Nickel-base alloys refractory-melt reactions in vacuum induction melting investigated by measuring contact angles from photographs, noting carbon contact angles from photographs noting carbon effect 19 p3242 A67-34786

Oxygen determination in molybdenum using vacuum extraction 20 p3467 A67-37121

Sublimation enthalpy of CdTe thin films in high vacuum determined from 350 to 400 degrees C 20 p3514 A67-37453

VACUUM PUMP

Superhigh vacuum created by cryopump, using liquid nitrogen and helium 06 p0950 A67-17940

Monte Carlo computer program for calculating molecular gas flow with axisymmetric vacuum structures, showing applications on pumping speed test domes and measuring apparatus for sticking coefficients 09 p1488 A67-22105

Design analysis for vacuum systems using diffusion pumps and getter ion pump, comparing parallel and series pumping 09 p1503 A67-22113

Small liquid propulsion systems testing in space environment simulator with high vacuum and low pumping capacity 13 p2089 A67-26840

Large space simulation chamber for studying low temperature, absolute vacuum and solar radiation effects 15 p2466 A67-29571

High vacuum pump selection requirements, discussing contamination problems 17 p2884 A67-32596

Superhigh vacuum created by cryopump, using liquid nitrogen and helium 18 p2988 A67-33776

Monte Carlo method for molecular vacuum pump calculation, noting applicability to molecule-boundary and molecule-molecule collision conditions 22 p3785 A67-40012

Collection efficiency of plane acting as pump in vacuum system, discussing parameter measurements, partial pressure analyzer and kinetic theory values 23 p4004 A67-41354

Helium sorption by nitrogen, oxygen and argon cryodeposits, discussing pumping

speeds and capture coefficients 24 p4115 A67-42047

VACUUM SPECTROSCOPY

Rotational intensity distribution of vacuum UV absorption spectrum bands of carbon monoxide arising through mixing of D state with neighboring states 02 p0269 A67-12450

Vacuum cup electrode in spectrographic analysis of solutions of refractory metal alloys 05 p0758 A67-16369

Vacuum UV wavelength standards and energy levels in first silicon spectrum from low pressure source 11 p1822 A67-24417

UV spectra of Mg III and Mg IV investigated by sliding spark in vacuum, noting various ionization charges in vacuum 14 p2351 A67-28944

Plasma time-dependent luminosity from pulsed discharge in vacuum, determining excitation temperature distribution and discharge spectral lines 18 p3087 A67-34049

Book on vacuum UV spectroscopy techniques noting Lyman continuum, synchrotron radiation, Bremsstrahlung radiation, UV radiation, resolution, etc 20 p3446 A67-36664

Vacuum type lensless spectrograph in intermediate and far UV for evaluating shock compressed metals resulting from hypervelocity impact 22 p3799 A67-39749

VACUUM SYSTEM

Reliability testing improvement through developments in vacuum systems, vibration systems and triaxial shock testing 01 p0084 A67-11369

Effect of diffusion-pump fluid contamination and degradation on explosion hazard of operating diffusion pumped system 06 p0979 A67-17632

Ultrahigh vacuum produced by combination of turbomolecular and titanium sublimation pumping 06 p0950 A67-17752

Cesium vapor flow from orifices and tubes into vacuum analyzed, noting dependence of angular distribution and center line intensity on Knudsen numbers 08 p1324 A67-21495

Bakeout procedure for small glass ultrahigh vacuum system to obtain stable pressures 08 p1354 A67-21497

Transmission probability describing free molecular flow through vacuum systems obtained via Monte Carlo program 09 p1488 A67-22104

International Vacuum Congress, Stuttgart, June-July 1965, Volume 2, Part II 09 p1533 A67-22110

Design analysis for vacuum systems using diffusion pumps and getter ion pump, comparing parallel and series pumping 09 p1503 A67-22113

Evaluation of requirements for ground testing of electric propulsion devices in vacuum, noting effects of sputtering phenomena 09 p1559 A67-22120

Space evacuation of NRC-2 insulation for liquid hydrogen tankage, noting vacuum test apparatus and cold plate test 10 p1734 A67-23727

Vacuum multilayer insulation for cryogenic space propulsion vehicles noting self-evacuation system and calorimetric test 10 p1734 A67-23728

Vacuum vaporization of saturated liquids on weightlessness, showing that separated bubbles remain in nucleation sites 12 p2034 A67-25726

Vacuum system pressure measuring and monitoring by remote control methods as used in Gemini spacecraft test program 17 p2859 A67-32593

Instrumentation for space vacuum simulation used in testing operations, discussing pressure measurement requirements 17 p2860 A67-32594

Space simulation using cryogenic adsorption pumping 17 p2884 A67-32595

Vacuum simulation developments and trends, noting solar simulator hardware advances with cryogenic systems 17 p2834 A67-32597

Lithium plasma source current-voltage characteristics in vacuum, obtaining parameters valid for arcs burning under atmospheric pressure and nonzero magnetic fields 17 p2906 A67-33089

Vacuum systems for microelectronic device fabrication, detailing pumping methods and related equipment 19 p3236 A67-35020

Book on vacuum sealing techniques covering permanent seals, demountable

seals, current transmission, design, materials, etc 19 p3238 A67-35925

Leak detection methods in vacuum devices including compressed air, discharge tube, halogen tracers, radioactive krypton, pressure rebuild, etc 20 p3443 A67-36474

Double-guarded cold plate apparatus for measuring thermal conductivity of multilayer insulations, powders, fibers and foams 22 p3803 A67-40294

Book on vacuum engineering covering space vacuum simulation, pressure measurement, gas flow and load, vacuum systems and technology 23 p4028 A67-41353

Collection efficiency of plane acting as pump in vacuum system, discussing parameter measurements, partial pressure analyzer and kinetic theory values 23 p4004 A67-41354

UV spectrophotometer for continuous measurement in vacuum systems of polyphenyl diffusion pump fluid film thickness 23 p4004 A67-41358

Radiometer using black plate with radiation toward night sky balanced by IR radiation transfer in vacuum system 24 p4152 A67-41787

Boeing 20-ft solar simulator alignment, calibration, cleanliness, optical system, xenon light sources and vacuum system 24 p4139 A67-42045

Spectral reflectance of water and carbon dioxide cryodeposits in vacuum integrating sphere as function of incidence angle, substrate material and cryodeposit thickness 24 p4253 A67-42046

VACUUM TUBE

Structural book properties on and operational modes of electron-optic current controlling high vacuum gas-filled and solid state discharge devices 06 p0968 A67-17894

Negative immittance converter circuits deducible from one basic NIC, noting similarity to Steimel vacuum tube circuits 11 p1769 A67-24129

General equation for suppressor controlled transconductance of pentode useful for circuit analysis 16 p2635 A67-30794

Electronic circuits containing vacuum tubes and transistors analyzed by computer method using Bellert's algebra of structural numbers 19 p3201 A67-34907

150-180 watts at 1000 MHz tetrode, examining mechanical durability and temperature stability of metallic electrodes and ceramic insulators 22 p3772 A67-39873

VACUUM TUBE OSCILLATOR

Oscillator with lumped parameter superconducting L-C tank circuit, noting frequency variations as function of temperature 15 p2451 A67-29916

VACUUM ULTRAVIOLET

Metal photocathodes as secondary standards for absolute intensity measurements in vacuum UV 03 p0499 A67-13910

Vacuum UV photolysis of solid ethane films, measuring product distributions, presenting evidence for quenching of excited ethane and ethylene 05 p0758 A67-16128

Nitrogen wavelengths obtained from precision measurements of various nitrogen lines, using vacuum UV spectrograph 05 p0846 A67-16781

Vacuum UV flash photolysis kinetic spectroscopy apparatus 05 p0807 A67-16782

Rocket measurement of altitude dependence of flux intensity of solar vacuum UV radiation, using ionization chambers 05 p0799 A67-16874

Photolysis of hydrazine vapor in vacuum UV, examining emission as function of pressure and photolysis time 07 p1138 A67-20190

Equilibrium air total radiation mechanism, vacuum UV radiation and relation to hypervelocity entry studied, using shock tube blunt model test flow [AIAA PAPER 66-103] 08 p1426 A67-20569

Maksutov-Cassegrain type telescope for rocket mounting, design and performance 10 p1654 A67-22751

UV stability of several white thermal control coatings spectrally characterized in vacuum for application to Lunar Orbiter project [AIAA PAPER 67-345] 12 p1959 A67-26059

CH concentration measurement in flash photolysis of methane by means of kinetic spectroscopy 12 p1904 A67-26228

Generation of series limit continua with aid of sliding sparks for absolute measurements in vacuum UV, observing bremsstrahlung 13 p2155 A67-26271

Vacuum UV radiation measurement from high temperature nitrogen, detecting radiation from shock layer of ballistic model 16 p2675 A67-31267

Reflectance and optical constants of evaporated iridium films measured in vacuum ultraviolet 16 p2733 A67-31878

Evaporation of thin films of high melting point materials by focused laser beam and reflectance and relative transmittance in vacuum UV 18 p3059 A67-33885

Vacuum UV and X-ray lasers from electron ejection from inner shells of atoms through photolization 18 p3060 A67-34015

Low inductance three-electrode spark source for vacuum UV generating high degree ionization spectra 23 p4000 A67-41214

VALENCE

Composite valence band in p-PbTe obtained from measurement of Hall effect, thermoelectric and optical effects 05 p0868 A67-17062

Chemical bonds formation during interaction between individual elements explained by total valence band energy theory 06 p1035 A67-17845

Double valence band and thermoelectric properties of lead telluride-tin telluride solutions 10 p1688 A67-22848

Band structure of spinel-type semiconductors calculation, applying model potential to nearly free electron model 13 p2181 A67-27166

Parameters for model of two valence bands of SnTe according to Hall effect measurements at high temperatures 15 p2537 A67-29709

Composite valence band in p-PbTe obtained from measurement of Hall effect, thermoelectric and optical effects 15 p2538 A67-29793

Energy dependence on wave vector in valence band of diamond, Si, Ge and SiC, obtaining Coulomb and resonance integrals 15 p2541 A67-30237

Valence band structure of wurtzite type crystals 16 p2725 A67-30802

GeTe solid solutions reviewed considering thermal EMF, temperature dependence and current carrier mobility 16 p2730 A67-31164

Short range intermolecular interaction of two ground state hydrogen molecules, using rigorous valence bond approach and population analysis 17 p2890 A67-33262

Ternary semiconductor composition found through valence equation 20 p3512 A67-37243

Chemical bonds formation during interaction between individual elements explained by total valence band energy theory 20 p3490 A67-37587

Parameters for model of two valence bands of SnTe according to Hall effect measurements at high temperatures 24 p4200 A67-41779

VALKYRIE AIRCRAFT

S XB-70 AIRCRAFT

VALVE

S BOUNDARY VALVE

S EXTREMUM VALVE

VALVE

SA CONTROL VALVE

SA FUEL VALVE

SA GAS VALVE

SA HYDRAULIC VALVE

Performance and characteristics of valve for pulsed gas injection into working volume of coaxial plasma accelerator 01 p0119 A67-10136

Mathematical model describing nonlinear behavior of vortex valve in fluid circuits, noting effect of swirl on vortex valve flow characteristics 14 p2251 A67-28341

Equation derived for accurate approximation of viscous friction coefficient in spool and nozzle-flapper preamplifier stages of electrohydraulic servovalve 16 p2810 A67-31915

Vacuum jacketed cryogenic globe valve design providing tight sealing, low heat leak, low cool-down mass and high flow 23 p3936 A67-41426

VAN ALLEN BELT

SA INNER RADIATION BELT

SA OUTER RADIATION BELT

Van Allen radiation belt simulation, obtaining accurate values for satellite and semiconductor lifetimes in orbit

[AIAA PAPER 67-177] 06 p0981 A67-18510

First order correction to magnetic moment invariant in Van Allen radiation belt 07 p1246 A67-19955

Protection of communications satellites data transmission against interplanetary interference sources and Van Allen belts 10 p1604 A67-22899

Variation of radio brightness of synchrotron radiation from Van Allen belts as function of direction and frequency, using satellite receiver 11 p1855 A67-23944

Van Allen belt proton measurements by pulse height analysis, using thin low-Z scintillator to minimize large angle electron scattering 11 p1856 A67-24011

Stimulation of Jupiter radio emission by Io 12 p2000 A67-25204

Coulomb interaction effect on time dependent variations of electron distributions in Van Allen belt, using kinetic equation 14 p2378 A67-27918

Van Allen radiation belt simulation, obtaining accurate values for satellite and semiconductor lifetimes in orbit [AIAA PAPER 67-177] 15 p2465 A67-29446

Magnetosphere and auroral phenomena including Van Allen radiation zones, satellite telemetry, solar wind fluctuations and cyclotron resonance 17 p2844 A67-32664

Nature of trapping regions, using spherical harmonic expansion for magnetic field created by currents on geomagnetic cavity surface 17 p2938 A67-33207

Inner Van Allen belt proton dose rate and spectral charged particle environment profiles correlated, noting agreement with theoretical values 19 p3313 A67-35189

High energy proton and electron damage on silicon junctions measured and compared with Van Allen belt radiation damage 20 p3507 A67-36237

Solar emissions and magnetic storms and auroras, discussing ring current, solar flux and Van Allen belt energetic particle density 21 p3620 A67-38978

CNES rocket probe mobile launching unit for auroras, eclipses and Van Allen belt layer experiments 21 p3609 A67-39051

Outer Van Allen radiation zone intensity maximum position dependence on electron energy and magnetic activity, noting relation to diffusion theory 22 p3870 A67-39620

Dynamic equilibrium of Van Allen belts studied for self-consistency through saturation of trapped plasma 22 p3871 A67-39799

VAN DE GRAAFF ACCELERATOR

Measurement and control of corona-generated noise in aircraft, noting charge rate during takeoff via potential gradient method 02 p0190 A67-11501

VAN DER WAALS FORCE

Impact approximation of spectral line broadening by resonance and Van der Waals forces in air molecule electronic-vibrational systems 05 p0759 A67-16790

Binary van der Waals mixture near solution critical point, noting anomalous behavior of heat capacity, shear viscosity and bulk viscosity 11 p1884 A67-24990

Nonlocal elasticity theory for materials with long range cohesive forces derived from lattice theory by writing strain energy in integral form 22 p3908 A67-39288

VANADATE

Spectral properties of Nd doped yttrium vanadate grown from melt, noting reduced Stark splitting leading to laser action 07 p1195 A67-19559

VANADIUM

Hall effect and fine structure of X-ray fluorescence and absorption K spectrum of vanadium in silicides 01 p0101 A67-10935

Vanadium-gallium wires with good superconducting properties fabricated by new stepwise diffusion process 01 p0137 A67-11064

Degree of deformation effect on superconducting properties of niobium and vanadium 04 p0686 A67-15986

Temperature dependence of critical field in superconducting vanadium 07 p1237 A67-20178

K beta 5 emission band and fundamental K-edge absorption of vanadium analyzed and results compared with vanadium spectra from other series 08 p1342 A67-20808

Degree of deformation effect on superconducting properties of niobium and

vanadium 14 p2366 A67-28489
Magnetic properties of superconducting vanadium calculated from cellular model 16 p2726 A67-30816
Vanadium and molybdenum effect on properties and phase transformations of titanium chromide 16 p2691 A67-31591
X-ray K-absorption spectra of titanium, vanadium germanium in 16 p2691 A67-31594
germanides 16 p2691 A67-31594
Plastic deformation of single crystals of vanadium by bending and compressing at 298 and 77 degrees K showed etching but no evidence of mechanical twinning 18 p3101 A67-34077
Anodic oxidation usable for efficient phase analysis technique for V-Ga alloys, identifying interference colors in absence of oxygen impurities 23 p4036 A67-40713
VANADIUM ALLOY
Cutting ability of high melting binder cemented carbides with Cr and V alloys 01 p0100 A67-10724
Phase diagram of vanadium-gallium system by differential thermal analysis of thirty-five 10-g V-Ga alloy samples prepared in arc oven 05 p0827 A67-16326
Distinct yield point appearance in vanadium alloys as function of composition, strain temperature and strain rate 05 p0828 A67-16388
New steels for aerospace tooling, properties and applications 10 p1668 A67-23011
Stress rupture and creep behavior in binary and ternary vanadium alloys including tensile strength and activation energy, noting titanium role 12 p1954 A67-25140
Titanium-vanadium alloy microstructure investigated under quenching and aging through electron microscopy 14 p2338 A67-28423
Microwave flux-flow resistivity transitions observed for strongly paramagnetically limited titanium-vanadium alloys 16 p2727 A67-30821
Critical parameters for vanadium-niobium alloys superconduction, giving curves for transition temperature and measuring critical electric fields 17 p2874 A67-32973
VANADIUM CARBIDE
Carbon diffusion mobility in fused carbides of vanadium and titanium, giving carbon diffusion coefficient temperature dependence equations 14 p2337 A67-28285
Melting point and microhardness of carbon-saturated TiC-VC solid solutions, noting temperature of eutectic of TiC-VC with graphite 16 p2691 A67-31588
Orthorhombic, low temperature alpha modification of niobium and vanadium carbide 16 p2691 A67-31598
VANADIUM COMPOUND
Energy gap of vanadium silicide measured by tunneling technique based on proximity effect 03 p0492 A67-13327
Book on structure of metallic alloy including phase diagram of vanadium-gallium system 05 p0827 A67-16325
Temperature variation of spin-lattice relaxation time and spin-spin relaxation time in superconducting and normal states of vanadium compounds 07 p1236 A67-20139
Superconducting properties of vanadium silicide noting high transition temperature, electron-phonon interaction, sound absorption, etc 08 p1369 A67-20990
Anomalies in intensity of Compton diffusion of X-rays by vanadium noting energy-diffusion angle relation 13 p2181 A67-27210
Iodine refining of vanadium, presenting internal friction and shear modulus curves for estimating interstitial impurity concentrations 19 p3243 A67-34924
Transition temperature, Knight shift and NMR line width variation in V-Au compounds as function of atomic ordering 22 p3858 A67-39520
VANADIUM OXIDE
IR optical properties of vanadium dioxide above and below transition temperature 05 p0860 A67-16380
Thermoelectric powers and conductivities of vanadium dioxide whiskers measured from 273 to 335 degrees K 05 p0864 A67-16898
VANE
SA GUIDE VANE
Effect on stage characteristics of axial compressor of design procedure used for

slightly elongated vanes 10 p1697 A67-23021
Two-dimensional flow through bends with turning vanes, using Green theorem to obtain surface pressure distributions [ASME PAPER 87-FE-13] 14 p2304 A67-28362
Electrostream process for drilling very small diameter holes in superalloys for gas turbine and nozzle vane fabrication [ASTME PAPER MR67-141] 18 p3054 A67-34175
High temperature operation of air-cooled turbine blades and vanes 18 p3115 A67-34377
VAPOR
SA CESIUM VAPOR
SA FILM BOILING
SA LIQUID-VAPOR EQUILIBRIUM
SA LIQUID-VAPOR INTERFACE
SA MERCURY VAPOR
SA METAL VAPOR
SA SODIUM VAPOR
SA WATER VAPOR
Perfect thermodynamic vapor concepts and application to power conversion cycles 07 p1268 A67-19367
Viscosity and thermoconductivity of vapors of sodium and potassium 09 p1579 A67-21865
Condensation droplet growth in supersaturated vapor and inert carrier gas, noting thermal and diffusion effects 15 p2582 A67-30198
VAPOR DEPOSITION
Semiconductor-metal-semiconductor structure with metal vapor deposited, analyzing voltage-current characteristics for amplifier technology 02 p0293 A67-11754
Boron filament manufacturing process using chemical vapor plating with boron trichloride and hydrogen onto tungsten filament substrate 03 p0453 A67-13419
Boron carbide filament production by vapor deposition from organoboranes 03 p0454 A67-13421
Boron-modified SiC continuous filament fabrication by vapor deposition on hot W wire substrate and tensile testing 03 p0454 A67-13423
Refractory composites consisting of high strength high modulus filaments imbedded in vapor deposited refractory metals 03 p0444 A67-13433
Idealized steady motion of aerosol particles and inertial deposition theory 03 p0404 A67-13836
Continuous gas deposition of triniobium-tin alloy on moving refractory wire without reaction chamber contamination by by-products 03 p0500 A67-14065
Vapor phase epitaxial deposition of n-type GaAs contact layers for Gunn effect X-band oscillators 07 p1153 A67-19609
Manufacturing methods for continuous filament refractory fibers including extrusion and chemical vapor deposition 08 p1345 A67-20427
Surface blistering of metals due to low energy hydrogen ion bombardment, determining solar absorptance change in gold-plated specimens 08 p1343 A67-21520
Operating temperature effect on vacuum emission stability of vapor-deposited tungsten clad UC-ZrC and uranium dioxide 09 p1449 A67-22347
Effects of additions of carbon, nitrogen or oxygen on properties of vapor deposited tungsten 09 p1519 A67-22348
Vapor-deposited tungsten formed by hydrogen reduction of tungsten hexachloride or hexafluoride, noting effect of crystal orientation and surface treatment on work function 09 p1451 A67-22357
Vapor deposited GaAs thin film solar cells for application to solar power systems 10 p1596 A67-23165
Gallium arsenide characteristics and preparation noting epitaxial deposition and liquid phase, mobility, impurity and Hall effect data 10 p1692 A67-23512
Vapor deposition of thin films by decomposition of metallic alcoholates in luminescent discharge 10 p1696 A67-23692
Electron beam process for vapor plating aluminum on beryllium for welding 11 p1798 A67-24264
Low temperature deposition of amorphous films of transition metals and alloys, noting atomic arrangement, comparing with case of metals condensed in crystalline state 12 p1982 A67-25451
Structure and properties of thin films in terms of deposition conditions, noting

conditions for continuity, surface roughness, grain size, lattice defect density, crystalline orientation, purity, etc [AIAA PAPER 66-727] 13 p2054 A67-27591
Idealized steady motion of aerosol particles and inertial deposition theory 13 p2107 A67-27712
Continuous gas deposition of triniobium-tin alloy on moving refractory wire without reaction chamber contamination by by-products 13 p2185 A67-27721
YIG epitaxial growth condition on YAG and GdIG on YAG identified by X-ray, electron diffraction, microprobe and magneto-optic studies 15 p2539 A67-29824
Silicon nitride deposition on metal coated substrates for studying resistivity, breakdown strength and other electrical properties of thin dielectric films 15 p2540 A67-29932
Oil Mist Deposits Test for differentiating deposit forming tendencies of jet engine lubricants, discussing mechanism and threshold temperature 16 p2683 A67-31755
Structures in Mo-Re and W-Re systems examined by X-ray powder techniques, discussing occurrence of chromium oxide type structure 17 p2873 A67-32813
Epitaxial deposition of silicon on silicon substrates, discussing vapor and vacuum deposition, impurity distributions, layer thickness, etc 18 p3097 A67-33456
Glow-discharge silicizing of refractory metals by unilow gas method in silicon tetrachloride vapor and hydrogen atmosphere 19 p3242 A67-34917
Refractory metals and oxidation protection noting coating materials, application methods, etc 20 p3463 A67-36133
Germanium films crystallization when deposited by evaporation on silicon single crystals studied by optical microscopy and electron diffraction 20 p3509 A67-36473
Vapor deposition-prepared continuous silicon carbide filaments for use as reinforcement in high strength oxidation-resistant structural plastic composite 21 p3648 A67-37881
Chemical vapor deposition method to grow epitaxial YIG on YAG using high temperature hydrolysis oxidation at seed surface 22 p3860 A67-39896
Path-probability method applied to thin film nucleation and growth on substrate by vapor deposition, deriving kinetic equations 23 p4040 A67-40968
Evaporated thin Au and Ni films electric conductivity measurements, obtaining electron mean free path and bulk resistivity 23 p4040 A67-41016
Mass spectrometry used for simultaneous measurements of adsorption and crystal nucleation processes 23 p4043 A67-41355
Vapor growth of single crystal heterojunctions of GaAs on Ge or InAs on GaAs using iodine process in closed tube system 23 p4043 A67-41432
VAPOR JET
Rotational speed of upper atmosphere obtained by measuring changes in orbital inclinations of satellites or movements of vapor trails 06 p0993 A67-17564
Simultaneous ejection of two vapor trails of different atomic mass, examining turbopause phenomena of atmospheric turbulence 17 p2853 A67-33254
VAPOR PHASE
Electrical properties and electron emission of sandwich cathodes prepared in vacuum by vapor phase condensation, deriving transfer constant 02 p0294 A67-11761
Laser induced breakdown of complex organic molecules in vapor state, noting emission accompanied by formation of partially dissociated hot gas 02 p0252 A67-12451
RF spark source mass spectrometer to detect and identify trace amounts of vapor molecular carbide species for refractory metal carbides 03 p0367 A67-13228
Gallium arsenide microwave diodes prepared by vapor phase growth method with highest combination of reverse breakdown voltages and cut-off frequencies 03 p0379 A67-13477
Vapor phase IR spectrum of planar structure of trimethylenecyclopropane 04 p0566 A67-15511
Gallium arsenide epitaxial film on germanium obtained by vapor phase transport techniques 08 p1368 A67-20726

Adiabatic flow of K vapor in supersaturated state noting supercompression, supercooling and equilibrium through condensation jump 11 p1881 A67-24029
Epitaxial vapor growth of GaAs noting reduction of electron concentration and increase in electron mobility 11 p1848 A67-24746
Ignition and combustion characteristics of single aluminum and beryllium particles burning in gaseous environment, discussing oxides role 18 p3149 A67-33796
Heterogeneous reaction in metal combustion for vapor-phase burning noting collision efficiency 18 p3149 A67-33797
Vacuum silicization of refractory metals in Mo-Si system noting thermodiffusion layers, vapor phase, chemical reaction, diffusion and temperature gradient 19 p3236 A67-34918
Vapor phase decontamination for removing residual hypergolic propellants in Apollo propulsion system 20 p3516 A67-36578

VAPOR PRESSURE

Centrifugal pump with vapor core principle combined with spill nozzle for application to aero engine fuel and reheat systems 01 p0014 A67-11267
Vapor composition, evaporation rate and vapor pressure above chromium carbides determined by effusion method combined with mass spectrometry 03 p0456 A67-14193
Recombination coefficient measurement for He plasma during decay at high pressure in presence of K vapor admixture 04 p0667 A67-15215
Nonisothermal changes in properties and composition during chemical and physical reactions, noting application to Knudsen cell vaporization [AIAA PAPER 67-156] 06 p0956 A67-18321
Molecular association in Na, K and Cs vapors, noting existence of dimer and tetramer molecules 08 p1355 A67-21033
Temperature dependence of saturated vapor pressure of sodium and potassium 09 p1579 A67-21857
Semiempirical description of stratification in wall heated containers of cryogenic fluids, noting decrease due to bottom heating 13 p2227 A67-27644
High temperature corrosion and evaporation of Haynes 25 and Hastelloy X-280 in atmospheres of oxygen, carbon monoxide, carbon dioxide, water vapor and methane 14 p2336 A67-28148
Recombination coefficient measurement for He plasma during decay at high pressure in presence of K vapor admixture 15 p2532 A67-30263
Numerical methods for calculating pseudoadiabatic characteristics of saturated air parcels 17 p2879 A67-32549
Vapor pressure of natural tektite melts at high temperatures determined by boiling point technique, applied to aerodynamic analysis 18 p3134 A67-34495
Ionization decay in cesium vapor explained in terms of dissociative recombination and diffusion, showing strong dependence on vapor pressure 19 p3271 A67-35072
Charge recombination coefficient of decaying He and Ar plasmas with Cs vapor additions at increased pressures 19 p3271 A67-35073
Pressure measurement with McLeod type gauge in presence of saturated vapors condensed during compression 21 p3627 A67-38384

VAPOR PRESSURE APPARATUS

HF acid vapor technique for room temperature etching of photolithographic stage of planar silicon dioxide device 04 p0682 A67-15488

VAPOR TRAP

Instrumentation and fuel systems for turbocharged and/or pressurized aircraft, discussing vapor lock problem, hydrocarbon fuels and vapor pressure equipment [SAE PAPER 670262] 12 p1899 A67-25510

VAPORIZATION**SA ABLATION****SA BOILING**

Vaporization rate and diffusion of Cu, Mg and Cr in arc discharge plasma determined from curves of spectral-line emission energies 02 p0279 A67-12743
Laser radiation effect on solids, noting laser properties, temperature rise, melting, vaporization and particle emission of

materials 09 p1513 A67-22144
Physical and hydrodynamic processes induced in vaporizable solids by pulsed light radiation from sources using explosives 11 p1782 A67-24955
Vacuum vaporization of saturated liquids on weightlessness, showing that separated bubbles remain in nucleation sites 12 p2034 A67-25726
Knudsen cell used in mass spectrometry of thermodynamics of refractory substances vaporization 19 p3242 A67-34864

VAPORIZATION HEAT

Theoretical dimensionless correlation for vaporization times of drops in film boiling on flat plate in Leidenfrost state 04 p0734 A67-15850
Cleavage and separation of dye-doped ice and paraffin instantaneously heated by laser pulse, measuring mechanical pulse at energy concentrations below vaporization heat 06 p1119 A67-18807
Vaporization under laser radiation in terms of gas-dynamics, formulating boundary conditions 14 p2334 A67-29074
Vaporization by dissociation of amine-type perchlorates revealed by infrared spectroscopy, proving role of proton transfer reaction in perchlorates thermal decomposition 16 p2619 A67-31536
Vaporizing solid or liquid underlayers for transpiration cooling of reentry vehicles, discussing advantages, handling, storage and self-regulating system 22 p3901 A67-39934
Thermal boundary layer condensation enhancement of diffusion limited vaporization rates, discussing heat of vaporization, critical supersaturation and surface temperature 22 p3920 A67-40423

VARACTOR

Analytic performance calculation for varactor frequency doubler with various degrees of nonlinearity 01 p0040 A67-11234
Time domain analysis of bridge doubler circuit for varactor multiplier 02 p0218 A67-12100
S-band direct phase modulator using varactor diodes with extremely linear phase characteristics 04 p0580 A67-14596
Microwave varactor tuned transistor oscillator design, considering collector base multiplication, oscillation and load matching conditions and theoretical tuning curve 04 p0581 A67-14864
Electrical parameters of Polish-developed silicon varactors 04 p0581 A67-14920
Design equations and computer calculated curves to achieve varactor-tuned octave bandwidth transistor oscillators by using transmission line 10 p1613 A67-23412
Two-stage fixed-tuned parametric amplifier for satellite communications earth stations, considering circulator development and varactor 14 p2278 A67-27781
Low temperature parametric amplifiers, discussing varactors, circulators and demands on cooling systems 14 p2278 A67-27783
Space charge varactor compared to p-n junction varactor, noting applications 15 p2449 A67-29804
High power frequency multiplication using beam lead varactors in arrays noting construction, technique and conversion loss 17 p2826 A67-32623
Large-signal analysis for varactor frequency upconverter under overdriven conditions, obtaining equations for varactor charge, current and voltage 20 p3396 A67-36510
UHF amplification and frequency conversion using single transistor as amplifier and base-collector junction capacitance as varactor 20 p3398 A67-36773
Design parameters and performance characteristics for overdriven varactor upper sideband upconverter /USBUC/ 24 p4131 A67-42446

VARACTOR DIODE**SA PARAMETRIC DIODE**

Impedance measurement of silver bonded Ge diode at X band and in mm wave region, improving performance by usage in breakdown region 01 p0033 A67-10028
Varactor diodes and frequency multiplier surveyed for application in harmonic generation at microwave frequencies 01 p0034 A67-10165
Reflection-type amplifier in downrange guidance system, examining noise figure optimization, pump power requirements,

bandwidth and input resistance 01 p0035 A67-10410
Equivalent series resistance of semiconductor region of varactor diodes at UHF determined, using series resonance method 01 p0038 A67-10815
Frequency doubling by varactor diode, expressing principal parameters as function of normalized amplitude of input voltage 01 p0039 A67-10856
Output power of frequency multiplier using varactor diode for given output voltage and terminal resistances at various harmonics 01 p0039 A67-10857
Microwave harmonic power generator using varactor diode, noting effect of reverse bias on harmonic output 01 p0041 A67-11319
Varactor diode series resistance loss responsible for bandwidth loss in parametric delay lines used for signal processing 01 p0027 A67-11323
Aluminum-titanium dioxide-silicon varactor equivalent circuit, noting measurement of parameters 03 p0377 A67-13240
Traveling wave parametric amplifier circuit with series connected varactor diode 03 p0380 A67-13504
Multiple contact Schottky barrier microwave diode, comparing operation with single diode in mixing and small and large signal detection 05 p0780 A67-17526
S-band parametric amplifier pumped at J-band using balanced idler circuit with two varactor diodes incorporated in one encapsulation 06 p0966 A67-17580
Varactor diode measurement by transmission methods under natural resonance conditions 06 p0969 A67-18122
Varactor diode impedance behavior in parametric amplifiers under low temperature conditions 07 p1152 A67-19551
Power reflection technique for high quality varactor diode characterization 08 p1304 A67-21221
Low temperature characteristics of Ga-As varactor diode junction properties, calculating spreading resistance 09 p1471 A67-21827
Optical signal modulation to measure noise figure at UHF of photoparametric amplifier, using silicon mesa diode as both photodetector and varactor diode 09 p1476 A67-22208
Varactor junction diode frequency multipliers emphasizing maximum conversion power and efficiency 10 p1609 A67-22836
Impedance and admittance measurements of periodically time-varying dipole and application to microwave varactor diode 10 p1610 A67-22925
Diffused GaAs varactor diodes, showing planar processes applied to production of diode based on metal-GaAs junction 10 p1615 A67-23529
Measured efficiency departure in power varactor converters from theoretical estimation, finding three-frequency current spectrum responsible 11 p1766 A67-24647
High resistance region effect in neighborhood of linear junction on series resistance analyzed for microwave varactor design 12 p1912 A67-25280
Parametric amplifiers incorporating two varactor diodes, noting in-phase pumping for unilateral operation and large potential bandwidth 13 p2078 A67-26785
Frequency doubler using two-diode varactor array to obtain double output power 15 p2442 A67-29176
Fabrication and properties of p-n junction diodes, noting cut-off frequencies, junction characteristics, etc 17 p2826 A67-32620
Superheterodyne receiver operating in K-band having solid state low noise characteristics 18 p3011 A67-34068
Design and characteristics/gain, noise factor and bandwidth of parametric amplifier 19 p3194 A67-35548
Two varactor diode bandpass filter for parametric amplifier, analyzing bandwidth vs gain 24 p4128 A67-41968
Unilateral parametric amplifier using two varactor diode low pass filter with pumping phase difference, noting bandwidth and gain 24 p4128 A67-41969
Read type and avalanche type oscillations in silicon varactor diodes, noting parasitic series resistance and electric field peak effects 24 p4133 A67-42820

VARIABLE DIODE CIRCUIT

Cut-off frequency of varactor diode defined for variable series resistance factor 01 p0036 A67-10466

Wideband solid state intermediate frequency repeater for communications satellites, using waveguide-cavity diode down converter transistor amplifier and varactor upconverter 06 p0960 A67-17682

Semiconductor devices in radio transmitters, examining operation of transistorized amplifiers and varactor multipliers in output stage 06 p0971 A67-18214

Parametric amplifier varactor characteristics, construction methods and qualities for hyperfrequency low noise parametric amplification 12 p1913 A67-25299

Varactor multiplier circuit design and equations for harmonic currents 13 p2089 A67-27724

All solid state wideband telemetry transmitters realization by compact high-powered frequency multipliers 14 p2288 A67-28692

Gain-bandwidth product of parametric reflection amplifiers with line-type resonators 15 p2454 A67-30145

Semiconductor devices in radio transmitters, examining operation of transistorized amplifiers and varactor multipliers in output stage 16 p2635 A67-30480

Wideband varactor upconverters for satellites use, emphasizing transmission characteristics and stability over wide temperature range 16 p2640 A67-31531

Step recovery varactors in constant-component and microstrip CW duplexers 18 p3011 A67-34067

Microwave amplifier using varactor diode with coaxial signal, lumped element idler and waveguide pump circuit for broadband radio link at 20 db 20 p3401 A67-37357

Approximate method for design of FM systems using variable capacitance varactor diodes, noting time varying differential equation 21 p3593 A67-38234

Varactor inductance effects on design varactor tuned circuits above 50 MHz 23 p3982 A67-41504

VARIABLE

S COMPLEX VARIABLE
S DEPENDENT VARIABLE
S INDEPENDENT VARIABLE
S RANDOM VARIABLE
S REAL VARIABLE

VARIABLE AREA WING

Lift augmentation through drag reduction and variable wing profile in light aircraft 01 p0005 A67-10265

Mirage III-G, variable-geometry military aircraft evaluation considering multiple-mission capability 16 p2597 A67-31539

Variable sweep wing aerodynamic problems in subsonic, supersonic and hypersonic aircraft design [SAE PAPER 670880] 24 p4094 A67-42014

Variable sweep pivoted wing fighter aircraft structural and aerodynamic design considerations, noting journal bearing endurance and aircraft fatigue life [SAE PAPER 670881] 24 p4094 A67-42015

Variable sweep wing aircraft mechanical design, control and actuation equipment and wing mounted system interconnects [SAE PAPER 670882] 24 p4094 A67-42016

SST variable sweep wing actuation system and pivot bearing reliability [SAE PAPER 670884] 24 p4098 A67-42018

VARIABLE GEOMETRY STRUCTURE

British-French cooperation in aeronautics, discussing Concorde SST, variable geometry aircraft, Olympus 593 turbojet, etc 03 p0362 A67-14379

Variable-sweep aircraft developments, design and problems [AIAA PAPER 66-983] 04 p0551 A67-14663

Variable geometry SST project and expected support program 05 p0752 A67-16753

Flow around variable profile in analog study of Laplacian field according to Dirichlet data 07 p1128 A67-20225

Optimal control of variable structure system in presence of perturbation, discussing quality control and preservation of sliding plane 09 p1483 A67-22081

Future French Air Force combat aircraft limited to Mirage F-III or Franco-British Jaguar project variable geometry

types 10 p1595 A67-23621

Extension of stripline circulator operation calculation by Davies and Cohen to include wider range of stripline geometries 13 p2076 A67-26482

Mirage III-G, variable-geometry military aircraft evaluation considering multiple-mission capability 16 p2597 A67-31539

ADAM II /air deflection and modulation/ propulsion system and application to long tube vertical propulsive wing aircraft configurations [SAE PAPER 670353] 17 p2929 A67-32993

Variable turbine geometry in gas turbine engines, discussing part power fuel consumption, acceleration characteristics, etc [AIAA PAPER 67-417] 18 p3111 A67-33904

Performance requirements and design aspects of variable sweep aircraft, examining swing pivot systems 20 p3361 A67-36498

Supersonic transport variable sweep wing design, showing root glove and Mach number effects on aerodynamic center of strike aircraft 20 p3361 A67-36499

Variable geometry entry spacecraft making secondary use of extendable wings in space as antenna and as radiators 20 p3532 A67-36560

Approximation method for finite element bending analysis of variable structural plates, giving linear equations defining nodal values 23 p4073 A67-40627

Variable geometry in SST aircraft, discussing hardware, lift control system, compression inlet and full scale wing pivot [SAE PAPER 670878] 24 p4094 A67-42012

Design and flying qualities of variable geometry aircraft, discussing wing pivot location and longitudinal stability characteristics [SAE PAPER 670879] 24 p4094 A67-42013

Variable sweep wing aerodynamic problems in subsonic, supersonic and hypersonic aircraft design [SAE PAPER 670880] 24 p4094 A67-42014

Wing pivot joint and actuation system configurations for SST variable geometry design [SAE PAPER 670883] 24 p4160 A67-42017

VARIABLE MASS SYSTEM

Motion laws for variable mass system, discussing versions of law and problem of angular momentum 01 p0113 A67-10507

Variational problem of optimal motion in gravitational field, for limited-power propulsion system in combination with energy accumulator and engine with limited jet velocity 02 p0327 A67-12332

Weight factor effects on optimal motion parameters of variable mass system with limited velocity jet propulsion in gravitational field 02 p0327 A67-12333

Aperiodic motion of two bodies of variable mass across canonical cross section, constructing osculating orbit and deriving equations for variation rate 04 p0700 A67-15202

Variability of conveyor belt velocity during loading and operation, unloading and stopping under load analyzed, using distribution theory 05 p0908 A67-16043

Dynamic characteristics of variable mass slender elastic body, solving vector differential equations [AIAA PAPER 67-41] 06 p1095 A67-18263

Plane optimum transfer of point of variable mass between two elliptical orbits in centrally directed Newtonian force field 07 p1247 A67-19095

Gyrostad transfer motion from initial stage to predicted orientation maneuver with minimum consumption, using Pontryagin method 07 p1184 A67-19149

Isotropic mass loss effect on binary star system orbital elements and period eccentricity relationship 08 p1380 A67-20385

Motion of point of variable mass in Newtonian central gravitational field 13 p2199 A67-26894

Inverse problem of relativistic motion of point of variable mass 13 p2159 A67-27362

Motion of variable-mass mechanical system with friction described by 3N equations 13 p2159 A67-27709

Motion of holonomic mechanical system of points with variable mass under action of active forces 15 p2517 A67-29464

Dynamic characteristics of variable mass slender elastic body, solving vector differential equations [AIAA PAPER 67-41] 17 p2956 A67-33013

Variable mass body rectilinear unsteady motion equations for movement at various levels in viscous fluid 18 p3023 A67-33426

Solid body of variable mass with cavities filled with ideal incompressible fluid, analyzing differential equations of motion 18 p3080 A67-34604

Thomson motion equation derivation for variable mass system extended for flight simulation equations for variable mass inertially guided system 22 p3832 A67-40099

Energy-mass equivalence and relativistic transformation formulas application to extended bodies 24 p4188 A67-41905

Spacecraft motion with limited power jet engine, applying simulation technique to determine operation modes for engine and control system 24 p4240 A67-42296

VARIABLE STAR

Milky Way galaxy mechanism and evolution, examining correlation between period of pulsation of intrinsic variable and galactic velocity 03 p0516 A67-14334

Upper limits to high energy gamma flux from quasars 3C 147, 3C 196 and 3C 273 from Crab Nebula and from 53 Cam magnetic variable star 05 p0900 A67-17079

Intermediate band pass photometric system properties and reduction and calibration procedures 11 p1792 A67-24778

Cosmic X-ray sources concentration toward galactic plane and variability 12 p1999 A67-26172

Pulsation properties of star models with linear density distribution, considering radial, adiabatic contraction and dynamical stability 12 p2011 A67-26253

Scalar gravitational fields in pulsating stars, calculating scalar wave radiation rate and star relaxation time 17 p2952 A67-33319

Theory, similar to Babcock solar magnetic field theory, explaining magnetic stars variability 19 p3328 A67-35933

Photometry and spectrophotometry of short-period variable stars 19 p3330 A67-36076

Intrinsic optical polarization of Taurus IR source 19 p3330 A67-36081

Photoelectric observations of 27 long period variable stars on UVB photometric system 22 p3880 A67-39415

Monograph on variable stars of RR Lyrae type covering spectrophotometric investigations of periodic brightness fluctuations and oscillations stability 22 p3880 A67-39463

Vibrating neutron stars, discussing damping, heating, energy storage and X-ray emission possibilities at 1000 years range 22 p3882 A67-39619

Total to selective interstellar absorption ratio, with improved values calculated for six-star group, considering spectral energy distribution and color excesses 22 p3883 A67-39767

Energetic nuclear bombardment effects on stellar surface element abundance calculated with statistical theory in A magnetic variable star abundance anomaly 24 p4228 A67-42263

VARIABLE SWEEP

Variable sweepback wing noting design problems, adaptability, controllability and comfort 03 p0351 A67-12995

Variable-sweep aircraft developments, design and problems [AIAA PAPER 66-983] 04 p0551 A67-14663

F-111 wing sweep actuator with irreversible Acme-thread jackscrew driven by hydraulic servomotor 05 p0752 A67-16157

Variable sweep wing F-111 aircraft cooling systems for temperature control of hydraulic fluid of type II system 05 p0752 A67-16161

Lift curve slope and aerodynamic center for variable sweep wing configurations estimated using semiempirical technique [AIAA PAPER 67-135] 06 p0939 A67-18315

Flight test program for F-111A variable sweep tactical weapon system, discussing afterburning turbofan engine, crew module, escape and survival 17 p2795 A67-32214

Supersonic transport variable sweep wing design, showing root glove and Mach number effects on aerodynamic center of strike aircraft 20 p3361 A67-36499

Design and flying qualities of variable geometry aircraft, discussing wing pivot location and longitudinal stability characteristics [SAE PAPER 670879] 24 p4094 A67-42013

Variable sweep wing aerodynamic

problems in subsonic, supersonic and hypersonic aircraft design
[SAE PAPER 670880] 24 p4094 A67-42014

Variable sweep wing aircraft mechanical design, control and actuation equipment and wing mounted system interconnects
[SAE PAPER 670882] 24 p4094 A67-42016

SST variable sweep wing actuation system and pivot bearing reliability
[SAE PAPER 670884] 24 p4098 A67-42018

VARIABLE THRUST

MIRA 150A variable thrust rocket engine applied to manned lunar exploration flying systems
[AIAA PAPER 67-505] 18 p3113 A67-33969

VARIANCE

SA COVARIANCE

SA REGRESSION ANALYSIS

Optimal multichannel nonlinear filtering problem of minimum variance estimation of state of n-dimensional nonlinear system subject to stochastic disturbance
04 p0592 A67-15084

Variance of log amplitude of laser beam evaluated for horizontal propagation path through atmosphere by following Schmelzter results
10 p1603 A67-22713

Linear minimum variance estimation for random signal with complex phase errors, considering signal processing and optical propagation
18 p3001 A67-34111

Error divergence elimination in recursive minimum variance estimation of space vehicle trajectories
21 p3587 A67-39148

Minimum variance simulation for satellite attitude determination reliability using magnetic and solar measurements
21 p3715 A67-39150

VARIATION

S ANNUAL VARIATION

S DIURNAL VARIATION

S MAGNETIC VARIATION

S SEASONAL VARIATION

S TWENTY-SEVEN DAY VARIATION

S VOLTAGE VARIATION INDICATOR

S WIND VARIATION

VARIATION METHOD

Bryson gradient method of constructing optimal control laws applied to algorithm for numerical solution of variational problems in optimal control theory
02 p0224 A67-11535

Fluid equilibrium shape under gravity force and surface tension analyzed via variational method
03 p0401 A67-12881

Variation equation for steady state creep applied to semimomentless cylindrical shell
03 p0522 A67-13206

Stability regions for compressible fluid squeeze-film journal bearing of infinite length, considering motion along axis
[ASME PAPER 66-LUB-15] 03 p0431 A67-13758

General method of variations for univalent functions with bounded boundary rotation permitting study of extremum problems
04 p0643 A67-14583

Dispersion and damping of oscillations in Maxwellian plasmas with zero order density gradients examined, using Vlasov and Maxwell equations
04 p0665 A67-15103

Algorithm encountered while solving trajectory optimization problems, discussing variational concepts, indirect, gradient, second variation and generalized Newton-Raphson methods
06 p1082 A67-17932

Governing equation for bending of multilayered sandwich elastic plates composed of n membranes developed by variational method
06 p1110 A67-18857

Variational bound method applied to calculation of lower bounds on S-wave phase shifts for scattering of electrons by hydrogen atoms
07 p1226 A67-19499

Accelerated gradient method for numerical solution of parameter optimization with nonlinear constraints
[AAS PAPER 66-118] 07 p1217 A67-19977

Single and double integration in method of variation of parameters for mean longitude or anomaly analyzed for influence on set not including such function
08 p1347 A67-20397

Sufficient conditions for stability of solutions of nonlinear nonautonomous equation, examining pendulum of variable length
09 p1533 A67-22154

Fluctuations in measurements of hurricane clouds, determining frequency domains for dominant mode of activity via variance spectrum analysis
10 p1676 A67-22817

Local potential variational method to

study runaway stability of electrons in two-component plasma
11 p1826 A67-23872

Cartesian formulation of membrane theory, discussing equations of equilibrium, strain energy, variation formulation and boundary conditions
11 p1875 A67-24431

Stability analysis of long period Trojan librations treated as short period oscillations about long period reference solution
11 p1866 A67-24774

Multistage rocket motion optimization in uniform gravitational field formulated as coupled variational problem
13 p2213 A67-27321

Nonlinear equation systems solved using parameters and varying them to original form while simultaneously tracing roots
14 p2342 A67-27975

Flute oscillations in bounded nonuniform plasmas and effect of incoherently precessing ions, noting variational methods and perturbation analysis
14 p2360 A67-28555

Optimal control applications of Fletcher-Reeves conjugate gradient minimization method and comparison with second variational technique
15 p2456 A67-29362

Existence theorems for systems of nonlinear integral equations of Hammerstein type with positive definite kernels
16 p2687 A67-30859

Second partial derivatives of position and velocity vectors components developed with respect to same vectors components at arbitrary epoch
16 p2696 A67-30960

Bryson gradient method of constructing optimal control laws applied to algorithm for numerical solution of variational problems in optimal control theory
16 p2644 A67-31601

Variational technique for temperature field determination in plane system with given heat distribution sources, based on Galerkin-Ritz method
17 p2972 A67-33069

Estimation method for lower bounds of natural frequencies of circular closed cylindrical shell
19 p3338 A67-34876

Variational equations solved by numerical integration along with nonlinear differential equations with less computing and storage and higher accuracy
20 p3478 A67-37212

Variational approximation for ground state of perturbed Schrodinger equation with single variable wave function
20 p3479 A67-37600

Physical analysis of convective heat transfer in laminar and turbulent flow through ducts and boundary layers, deriving trailing functions by variational method
21 p3730 A67-37736

Nonlinear variational trial function for atomic hydrogen dynamic polarizability, discussing first order perturbed wave function and perturbation-variation method
21 p3659 A67-38004

Variational method used to obtain extremal flight conditions, considering flights between circular orbits and planets close to each other
21 p3705 A67-38585

Cantilever plate calculation under load and deflection by variation method, reducing problems to solutions of differential equations with constant or variable coefficients
21 p3724 A67-38781

Variation method of microwave diagnostics of homogeneous plasma based on attenuation coefficient measurements, determining collision frequency and plasma density
21 p3675 A67-39032

Liquid He 4 ground state studied by variation method, deriving radial distribution function
22 p3835 A67-39301

Two-finite burns minimum fuel rendezvous problem using dual phase plane description, determining control law
22 p3888 A67-40147

Laser output power determination technique by rotating plane parallel wafer in resonant cavity to vary value of total losses
22 p3817 A67-40412

Bound functionals for limit analysis of plastic solids by variational method, discussing safety factor and sandwich structures
23 p4074 A67-40629

Cluster variation method based on W-shaped cluster in triangular lattice for lattice-gas liquid, phase-separating binary alloy and Ising model
23 p3971 A67-40969

Mixed problems of antenna synthesis, solving approximately specified amplitude and phase radiation patterns and given antenna current amplitude or phase
24 p4129 A67-42228

Thin elastic shell neutral equilibrium

under axial compression and hydrostatic pressure, obtaining parametric terms for expressions by using quadratic functional
24 p4249 A67-42303

Variational methods for nonequilibrium thermodynamic processes based on fluctuation theory, noting application to viscous heat conducting flows
24 p4255 A67-42554

Bounded variation method for optimum load capacity hydrodynamic one-dimensional gas slider bearing, discussing film thickness
[ASME PAPER 67-LUB-6] 24 p4162 A67-42670

VARIATIONAL CALCULUS

Accelerated gradient method for numerical solution of parameter optimization problems with nonlinear constraints
01 p0104 A67-10428

Selection and weighting of direct measurements, evaluating result of variational series by number x alone, using arithmetical mean and median
01 p0068 A67-10854

Variational expression for dominant mode coupling coefficients between elements of infinite array
02 p0212 A67-11604

Optimum nozzle contours for expansion of Lighthill idealized dissociating gas in one-dimensional flow determined by methods of variational calculus
02 p0305 A67-12353

Mayer technique in calculus of variation for constrained error coefficient criterion function for missile trajectory optimization in aerospace guidance and control
02 p0265 A67-12389

Variational analysis of BVP of natural oscillations of orthotropic plates
02 p0341 A67-12663

Perturbation theory and quantum mechanical applications - Seminar, University of Wisconsin, Madison, October 1965
02 p0270 A67-12721

Variational perturbation equations and time-independent Schrodinger equation for two-, three- and four-electron atoms
02 p0271 A67-12724

Atomic and molecular time-dependent quantum-mechanical perturbation theory with differential equation formulation within Hartree-Fock approximation
02 p0268 A67-12725

Structural design of optimal control for n-order nonlinear plant, using variational calculus
03 p0391 A67-13185

General variational problem and necessary conditions formulated in setting of locally convex linear topological space
03 p0458 A67-13268

Integrable function representation by double singular integral at generalized Lebesgue point
03 p0461 A67-14107

Ascent or descent from initially Keplerian orbit by constant low thrust analyzed by two-variable expansion procedure
04 p0704 A67-14828

Variational approximation of normal velocity on oscillating wings including linear approximation, numerical integration and comparison to least squares method
04 p0547 A67-14842

Book on numerical realization of variational methods, discussing Hilbert space elements, Ritz and Bubnov-Galerkin stability processes, spectral and nonlinear problems, etc
04 p0645 A67-15009

Similarity constant variation method of aircraft design
04 p0552 A67-15892

General theory of variational problems of optimum control incorporating calculus of variations and Pontryagin maximum principle
04 p0647 A67-15981

Motion theory of discrete defects in linear elastic continuum
05 p0908 A67-16038

Exact and variational solutions to elastic wave propagation eigenvalue problem in constant Poisson ratio linear viscoelastic material
05 p0909 A67-16141

Numerical analysis of constraint effects on trial function selection in variational calculus problem of pure torsional vibration of cantilever beam of thin walled open cross section
05 p0917 A67-16418

Temperature field of active medium of pulsed laser using variational methods, considering two approximate solutions
05 p0825 A67-16935

Brachistochrone problem analyzed using variational calculus and optimal control theory
06 p0973 A67-17770

Convergence rate of method of gradients relationship to singularity of second

variation operator in optimal programming problems 06 p0975 A67-17935

Closedness of set of trajectories or of solutions of contingent equation used in existence problems of optimal control and variational calculus 06 p0975 A67-18100

Nonlinear transformations for solution of variational problems 06 p0976 A67-18407

Elastic behavior of bodies composed of materials with different characteristics of compression and tensile strengths, noting applicability of various variational equations 06 p1106 A67-18624

Stress concentration in infinite incompressible plate with circular hole under bilateral tension analyzed, using variational method 06 p1107 A67-18634

Optimal power design of conduction type MGD generator 06 p0951 A67-18674

Complementary energy method for flexural buckling of initially straight elastic bars 06 p1110 A67-18840

Second order method for nonlinear optimal control problems resulting in Riccati differential equations 07 p1213 A67-19155

Eigenvalues of five lowest lying states for three electron atomic systems obtained using conventional Rayleigh-Ritz variational method 07 p1226 A67-19500

Digital simulation of boundary value problems of trajectory optimization, using variational and functional analysis and IBM-FORMAC language [AAS PAPER 66-116] 07 p1149 A67-19976

Simulation of pursuit-evasion differential game using variational method, comparing performance of human pilot to optimal pursuer 07 p1136 A67-20170

Pontryagin maximum principle, discussing singular and nonsingular extremals classification by numerical integration techniques 07 p1162 A67-20273

Caratheodory unified approach to Hamilton-Jacobi theory in variational calculus problems of optimal control 07 p1162 A67-20275

Optimal control systems without complex controllers using variational calculus, for application to submarine diving control 08 p1309 A67-20331

Variational bounds on eigenphase shifts in scattering theory obtained by SB and R approaches 08 p1355 A67-20865

Imparting motion to system of two masses coupled by linear elastic shaft in infinite set of piecewise continuous loads, by variational method of influence functions 08 p1354 A67-21047

Electron streaming instability of plasmas with zero order density gradients from variational analysis of Vlasov-and Maxwellian-plasma perturbation wave propagation 08 p1360 A67-21128

Caratheodory equivalent formulation relative to variational problem, showing role of min operator 09 p1483 A67-22596

Bending of flexible tubes using variational calculus of Rayleigh-Ritz type 09 p1579 A67-22606

Variational problem for flow of plasma with variable electrical conductivity in channel of MHD generator solved, using Lagrange method of multipliers 10 p1684 A67-23023

Nonlinear programming and control problems in terms of variations, maximum principle and dynamic programming 10 p1619 A67-23418

Dynamic programming relationship to calculus of variations, developing second order transversality condition 10 p1620 A67-23420

Mathematical methods for two classes of variational problems analogous to optical reflection and optical refraction in connection with rocket flight 10 p1678 A67-23425

Absolute extrema of certain integrals from method for finding corresponding functions with prescribed endpoints 11 p1812 A67-24087

Absolute extremum existence in Boltz-Mayer type variational problem established by optimality principle 11 p1870 A67-24685

Penalty function method used for bounded phase coordinate optimal control problem for linear discrete systems with quadratic cost functionals 11 p1771 A67-24891

Variational derivation of nonlinear equilibrium equations for three-layer conical shell with rigid incompressible filler under external pressure 12 p2025 A67-25609

Variational methods solutions for thin shell deformation 12 p2027 A67-25621

mechanics 12 p2027 A67-25621

Variational methods for calculating small axisymmetrical oscillations of conical shell of revolution partially filled with ideal incompressible fluid 12 p2028 A67-25633

Numerical solution of elastoplastic torsion of rods by method of local variations 12 p2029 A67-25667

Reissner variational formulation of temperature distribution boundary value problem of axisymmetric thermal stresses in isotropic sandwich shells of revolution [AIAA PAPER 66-528] 12 p2030 A67-25917

Variational, quasi-static and integral equation analytic waveguide solutions, extending singular integral equation to homogeneous and inhomogeneous loaded waveguide junction 12 p1906 A67-25978

Dipole transition integrals for nonmetal resonance transitions 13 p2160 A67-26442

Solvable convergent difference schemes for nonlinear elliptic equations using variational method applied to differential equation 13 p2145 A67-26445

Variational method for linearized problems of rarefied gas dynamics applied to cylindrical Poiseuille flow and heat transfer from sphere, using BGK 13 p2101 A67-26966

Digital simulation of boundary value problems of trajectory optimization, using variational and functional analysis and IBM-FORMAC language [AAS PAPER 66-116] 13 p2074 A67-27531

Alternate approach for spacecraft design sensitivities treating vehicle design variables as special control variables 13 p2054 A67-27600

Solution algorithm for boundary problem generated by necessary conditions for optimality in variational problem 14 p2341 A67-27840

Selection and weighting of direct measurements, evaluating result of variational series by number x alone, using arithmetical mean and median 14 p2317 A67-28243

Vlasov variational method applied to circular cylindrical shell design for local loading 14 p2400 A67-28643

Dual formulation of variational problems with differential inequality constraints, noting relation between mathematical programming and variational calculus 14 p2345 A67-28908

Newton-Raphson computational procedure for finding extremal control policies for nonlinear processes 15 p2456 A67-29363

Parametric input/output relation of approximate controller with optimized performance index, obtaining specific optimal control designed in regard to worst initial state 15 p2456 A67-29365

Parameter and domain dependence of eigenvalues of elliptic partial differential equations 15 p2509 A67-29461

Linear single input optimal cooperative rendezvous problem with quadratic performance index solved using variational calculus 15 p2458 A67-29909

Optimal final value control theory, applying variational calculus and functional analysis to control function selection for dynamic systems 15 p2459 A67-30020

Optimal maneuvers for space rendezvous between earth satellite and propelled vehicle on circular orbits, studying fuel consumption and rendezvous time 16 p2758 A67-30652

Space vehicle optimal control, studying maximum principle application, developing numerical algorithms of dynamic programming type and describing variational problems 16 p2742 A67-30664

Steepest ascent method for trajectory optimization 16 p2744 A67-30734

Three-dimensional slender wings of maximum lift/drag ratio in hypersonic flow studied by variational calculus under several lift and volume conditions 16 p2592 A67-30964

Book on variational calculus and integral equations, examining extremum conditions, Fredholm and Volterra integral equations, Pontryagin maximum principle, etc 16 p2696 A67-31200

Design guides for efficiency, bandwidth and resonant frequency derived from slot antenna analysis, using variational methods 16 p2638 A67-31334

Interior penalty method for inequality constrained optimal control problems concerning convergence 16 p2651 A67-31677

First variation theory in extremal problems, noting generalization of classical variational problems and optimal control problems for functions with single independent variable 17 p2876 A67-32043

Variationally computed antenna impedances and accuracy of resulting current distributions 17 p2824 A67-32301

Axisymmetrical temperature fields for minimum functional of elastic deformation energy in infinite cylindrical shell 17 p2962 A67-32968

Kantorovich indirect variational method applied to MHD flow inside rectangular duct 17 p2906 A67-33038

Stochastic differential game with missile and radar, using linear theory in finding optimal strategies 18 p3075 A67-33495

Optimum thrust direction for horizontal jet flight of maximum duration determined, using variational calculus 18 p3136 A67-33557

Soviet book on numerical methods for calculating natural oscillation frequencies of liquids in bounded volumes 18 p3026 A67-33772

Theory of available potential energy and rate of change and variational approach to atmospheric energetics 18 p3074 A67-34096

Combination variational-difference numerical method applied to nonlinear boundary value problems, noting numerical functional minimization 18 p3071 A67-34264

Pulse-width modulated control system optimization, with necessary conditions derived by variational calculus, and numerical solution to resulting boundary value problem 19 p3199 A67-34783

Optimal design of RC lines distributed parameter systems using gradient technique and variational calculus 19 p3200 A67-34841

Flexural center location and torsional rigidity of bar calculated using elasticity theory and variational calculus 19 p3340 A67-35512

Variational formula for antenna impedance in warm magnetoplasma, considering force and fluid-flux distribution 19 p3194 A67-35513

Determining sign of second variation in optimal control theory 19 p3202 A67-35756

Invariant integral from use of Noether theorem of calculus of variations applied to optimal control problem 19 p3204 A67-35906

Spacecraft performance, operation and design optimization solved by variational analysis [AIAA PAPER 67-557] 19 p3174 A67-35954

Solar-electric powered vehicle trajectory optimization using variational calculus, assuming general forms for efficiency and solar power variation [AIAA PAPER 67-583] 19 p3329 A67-35978

Formulation of problem of elastoplastic torsion of rectangular or regular polygonal bar as variational problem 20 p3536 A67-36429

Variational problem in optimal interaction systems with control constraints solved by dynamic programming and Pontryagin principle applications 20 p3407 A67-36440

Variational formulation of Laplace transformed heat diffusion problem [ASME PAPER 67-HT-77] 20 p3551 A67-36755

Functional analysis applied to optimum control by reduction of variational problem to finite dimensional analysis and calculation of algorithms for use with digital computer 20 p3477 A67-37034

Optimum control problems solved by numerical methods based on variation in state space 20 p3477 A67-37035

Aircraft flight dynamics optimized in angle of attack by variational calculus, analyzing control system 20 p3361 A67-37377

One-dimensional nonstationary compressible gas flow studied with variational calculus, obtaining approximate analytical periodical solutions 20 p3360 A67-37678

Poiseuille flow of rarefied gases through cylindrical tube, solving integral equation, noting variational calculation of hydrodynamic velocity 21 p3609 A67-37738

Generalized Legendre-Clebsch condition applied to singular arc trajectory solutions of state and adjoint equations for optimal control 21 p3602 A67-38023

Book on calculus of variations and optimal

control theory covering function maximum and minimum theory, fixed end-point problem, etc 21 p3653 A67-38799

Optimal shock absorbers synthesis, showing reduction to variational problem and equations for one degree of freedom mass 22 p3776 A67-39394

Point-to-point mapping technique in combination with variational calculus for solving optimum control problems for piecewise linear dynamic systems 22 p3776 A67-39776

Discontinuous integrands in calculus of variations formulations of trajectory optimization and maximum payload problems with discontinuous state variables 22 p3827 A67-39954

Variational calculus for optimal attitude acquisition/stabilization controller synthesis for spinning and nonspinning space vehicles 22 p3904 A67-40105

Rapidly converging iterative solutions to Min-H strategy applicable to trajectory optimization and payload maximization 22 p3888 A67-40148

Variational formulation and Rayleigh-Ritz method for nonequilibrium viscous incompressible flows, obtaining velocity and temperature distributions 22 p3788 A67-40422

Optimum process theory methods applied to calculus of variations, examining sufficient conditions for optimality principle 22 p3778 A67-40446

Analytic form of solutions of first order variational equations of restricted three-body problem 23 p4061 A67-40622

Approximation method for finite element bending analysis of variable structural plates, giving linear equations defining nodal values 23 p4073 A67-40627

Caratheodory method in variational calculus and partial differential equations, discussing coordinate-free invariance usage and extremal theory 24 p4178 A67-42203

Coupled micropolar thermoelasticity equations using strict motion invariance conditions, presenting reciprocity and variational theorems 24 p4251 A67-42659

Intermolecular forces theory, considering hydrogen atom interaction through Born-Oppenheimer approximation and variational calculations [WIS-TCI-249] 24 p4191 A67-42666

Heat transfer to end wall of shock tube after shock wave reflection through steep temperature gradient analyzed using variational method 24 p4257 A67-43092

VARIATIONAL PRINCIPLE

SA RAYLEIGH-RITZ METHOD

Direct and inverse problems of optimization of quadratic functional in linear autonomous and controlled systems 01 p0044 A67-10490

Electron resonances of hydrogen ion calculated and illustrated by waves, using variational principle incorporating outgoing-wave boundary conditions 01 p0117 A67-10781

Variational principles for plate bending problems not subjected to boundary conditions 01 p0162 A67-10850

Hamilton-Ostrogradskii integral variational principle for holonomic systems with linear constraints 01 p0114 A67-10991

Integral variational principles in mechanics when initial position and velocity are known 02 p0267 A67-11965

System of equations derived governing behavior of ideal relativistic charged fluid by means of variational principle, through introduction of generalized Clebsch transform 02 p0273 A67-12195

Perturbation theory in molecular quantum physics using variational principles 02 p0270 A67-12722

Zero order Hamiltonian in perturbation theory for eigenvalue problems of atom in magnetic field 02 p0271 A67-12723

Asymptotic form of correlation functions facilitated by use of Hamiltonian 03 p0458 A67-13342

Matter tensor of generally relativistic perfect fluid derived from invariant integral by Marx variational principle 03 p0468 A67-13392

Computer derivation of best-fit hyperbolic and parabolic surfaces using total parameter variation method 03 p0388 A67-14122

Auxiliary system considered simultaneously with given dissipative system in variational formulations, noting motion equations 03 p0530 A67-14175

Reissner variational method stability analysis of small eccentricity nonlinearly elastic thin circular ring 03 p0531 A67-14230

Theoretical derivation of modification of shape of given airfoil which reduces moment values and sustains original lift 04 p0545 A67-14411

Variational analysis of Graetz problem of forced-convective laminar heat transfer in duct, for various cross sections and given wall temperature and temperature gradient 04 p0728 A67-15802

Variational problem of rocket dynamics in homogeneous gravitational field in empty space reduced to differential equation system 05 p0904 A67-16049

Constitutive equations derived based on thermodynamics of irreversible processes and coupled thermoelasticity, formulating variational and reciprocity theorems 05 p0910 A67-16165

Rayleigh thermal instability in horizontal circular cylinder, discussing two approximate methods for calculating upper bounds to critical Rayleigh number 05 p0929 A67-17415

Taylor theorem test as tool for determining completeness and convergence properties of finite element displacement functions, showing application to axisymmetric shell and conductive heat transfer [AIAA PAPER 67-143] 06 p1103 A67-18440

Variational derivations of field equations for relativistic mechanical, EM and gravitational fields in space-time continuum 06 p1033 A67-18582

Variational principle for anisotropic and nonhomogeneous elasticity theory in terms of elastic polarization tensor 08 p1422 A67-20981

Mott-Smith type moment method and restricted variational principle determinations of shock structure 08 p1355 A67-21141

Rosen restricted variational principle used to obtain surface integral applicable to solution of kinetic theory boundary value problems 08 p1324 A67-21408

Statistical basis for modified moment theory of elasticity that takes into account contribution of all deformation-tensor-component gradients to deformation energy 09 p1574 A67-21914

Gurtin variational principles extended in application to dynamic problems of elasticity with finite deformation 10 p1720 A67-23598

Direct and inverse problems of optimization of quadratic functional in linear autonomous and controlled systems 10 p1621 A67-23612

Variational principle for elastic thin shells and panels of arbitrary shape and load conditions 11 p1876 A67-24624

Complementary variational principles in neutron diffusion theory 11 p1824 A67-24632

Relativity theory for solid media model design, deriving equations of state and closed system of differential equations based on variational principle 11 p1819 A67-24675

Variational principle as basis for dynamics of elastic shell theory, discussing motion described by Timoshenko type equation 11 p1877 A67-24853

Variational principle extended to relativistic scalar hydrodynamics, deriving Hamilton equations 11 p1844 A67-25034

Variational principles and reciprocity theorems for dynamic problems of elastic shell theory, particularly motion described by linear equations of Timoshenko type 12 p2019 A67-25563

Asymptotic form of correlation functions facilitated by use of Hamiltonian 13 p2149 A67-27713

Diffraction field parts of slit aperture formed by two nonplanar screens satisfy variational principle 14 p2261 A67-28106

Variational integration principles used to integrate wave and Fourier thermoconductivity equations, noting solution by Ritz method 14 p2408 A67-28803

Formulation of upper and lower bounds on Knudsen flow rate of gas through channel of arbitrary geometry by reciprocal variational principles 15 p2469 A67-29195

Variational technique involving Lagrange function representation of Grad magnetohydrostatic equation extended to symmetrical solenoid field 15 p2530 A67-29727

Variational principle of dynamics applied

to linear theory of elasticity and given in form of two integrals 15 p2575 A67-30002

Variational principle for heat conduction and convection, noting applicability to nonhomogeneous fluids with temperature dependent properties in turbulent flow 15 p2582 A67-30019

Variational problem of maximum payload in mechanics of flights with limited propulsion power and energy storage unit 16 p2760 A67-30719

Flute instability for inhomogeneous plasma equilibria in inhomogeneous magnetic fields of mirror machines, solving Vlasov and Poisson equations 16 p2714 A67-30875

Flute instability in mirror machines at very low plasma densities, using variational principle for stability criterion derivation 16 p2714 A67-30876

Prigogine-Glansdorf local potential calculated for usual transport effects case using variational principle 16 p2681 A67-31440

Variational principles and methods of approximation for nonself-adjoint and nonlinear systems 17 p2969 A67-32449

Variational principle for determining fluid flow stability in differentially rotating self-gravitating stars and galaxies and for studying eigenfunctions properties 17 p2947 A67-32756

Integral variational principles in mechanics when initial position and velocity are known 17 p2887 A67-33282

Variational principle of dynamics applied to linear theory of elasticity and given in form of two integrals 18 p3141 A67-33769

General variational theorem for rigid perfectly plastic materials developed using Hill and Markov maximum plastic work principles, noting possible unified derivation of principles 18 p3143 A67-34006

Book on variational principles of mechanics covering basic concepts, calculus of variation, equations of motion, etc 18 p3079 A67-34100

Hamiltonian description of irreversible steady state phenomena and elements of turbulence theory, noting entropy production 19 p3210 A67-35539

Optimum redundancy of multistage parallel systems using variational technique to maximize profit 20 p3556 A67-37316

Variational principle as basis for dynamics of elastic shell theory, discussing motion described by Timoshenko type equation 20 p3542 A67-37541

Variational problem of rocket dynamics in homogeneous gravitational field in empty space reduced to differential equation system 21 p3701 A67-37836

Variational approach to error analysis in dynamic system computer simulation, applying maximum principle and Liapunov second method 21 p3588 A67-38180

Continuous phase medium gas representation used to derive variational principles for Liouville, coupled Bogolubov and kinetic equations 22 p3835 A67-39218

Linear equations of motion of concentrated defect in elastic medium using variational principle 22 p3909 A67-39292

Nonequilibrium thermodynamics canonical equations determination on basis of variational principle for transport equations governing irreversible processes 22 p3918 A67-39786

Cylindrical thin walled open section structures heated nonuniformly, calculating various elastic parameters, torsion properties and shearing stress 22 p3916 A67-40450

Long cylindrical two-layer shell critical asymmetric buckling time for steady creep due to external pressure and axial compression, applying variational principle 24 p4250 A67-42306

VARNISH

S FILLER

VASCULAR SYSTEM

SA CARDIOVASCULAR SYSTEM

Surgical technique for implanting and maintaining arterial and venous catheters in monkeys 10 p1601 A67-23627

Carbon dioxide breathing effects on forearm blood vessels, discussing vascular resistance and carbon dioxide role in blood flow regulation 20 p3373 A67-37584

VASOCONSTRICTION

Fundus oculi observation of retinal vessel caliber alteration during changes in arterial gas tensions 17 p2805 A67-31961

VASODILATION

Fundus oculi observation of retinal vessel caliber alteration during changes in arterial gas tensions 17 p2805 A67-31961

VECTOR

SA STATE VECTOR

Permittivity and permeability of smooth convex body, using ray tracing technique for vector fields 01 p0020 A67-10014

Format method for generating Liapunov and scalar functions for autonomous and nonautonomous systems 04 p0593 A67-15415

Equivalent vector method for obtaining Lorentz transformations of special relativity shown to have apparent

variants 08 p1347 A67-20366

Strong reflection from underlying surface effect on range-only radar measurements, deriving phase angle between side and carrier-frequency oscillation

vectors 16 p2624 A67-31030

Real-valued function integration with respect to additive set function with real Banach space 17 p2879 A67-32810

VECTOR ANALYSIS

Deterministic optimal control, discussing Bellman dynamic programming method, Pontryagin maximum principle, orbital transfer, interplanetary guidance, etc 01 p0047 A67-11220

Triangular iteration method of vector-matrix equation, noting role of continuous function 03 p0462 A67-14328

Mohr circle geometric representation of transformation of two-dimensional symmetric stress tensors in using complex variable vectors /phasors/ 04 p0657 A67-14850

Optimum quadratic detection of sample vector from signal random process imbedded in Gaussian noise 05 p0765 A67-17041

Book on principles of ideal fluid aerodynamics covering vector algebra and calculus, Euler equations, steady and unsteady acyclic motion, complex variable, lift, etc 05 p0793 A67-17151

Matrix and vector computational procedures for solution of partial and ordinary differential equations 06 p1022 A67-17788

Decomposition, in orthogonal universal vectors, of electromagnetic universal force created by point charge animated by universal velocity and acceleration 09 p1534 A67-22590

Resonance oscillations and rotations in mechanical systems having n-dimensional quasi-static vector analyzed and applied to triaxial ellipsoid with unbalanced mass 10 p1680 A67-23409

Anisotropic vector functions of vector argument connected with crystal symmetry 11 p1812 A67-24148

Vector equation for determining missile maximum roll rate for effective navigation ratio and time constant for guidance systems 11 p1816 A67-24215

Solution algorithm for boundary problem generated by necessary conditions for optimality in variational problem 14 p2341 A67-27840

Characteristic vectors theory and application to study of asymptotic behavior of solutions to differential systems 14 p2342 A67-28385

Rotational analysis theorem concerning earth satellite motion about angular-momentum vector with respect to inertial reference frame 15 p2519 A67-30209

Book on engineering mathematics covering differential equation solutions by numerical method, partial differential equations, Fourier series, integrals, vector analysis, etc 17 p2876 A67-31930

Control theory of hyperbolic PDEs examined, noting application to distributed parameter systems 17 p2877 A67-32561

Dyadic formalism to prove Herglotz-Noether theorem for flat manifolds [JPL-TR-32-1125] 17 p2879 A67-32929

Relativistic generalization of Bernoulli equation from three-dimensional vector analysis of acoustic and entropy waves 18 p3084 A67-33422

Necessary and sufficient conditions for space-time curvature tensor and isotropic vector field associated with double 2-form to satisfy higher order field equations 18 p3078 A67-33689

Vector wave functions for boundary value problems in compressible plasma for spherical geometry, noting Fourier series,

acoustic wave, etc 18 p3090 A67-34382

Book on methods for applying principles of dynamics to engineering problems covering three-dimensional approach, free-body system and derivation of motion equations 18 p3080 A67-34566

Book on optimal control covering theory and application of linear algebra, vector analysis, Euclidean space, Pontryagin principle, etc 18 p3018 A67-34758

Differential geometry and vector analysis used to design axisymmetric lens of arbitrary shape for observing phenomena in arbitrary flow field of revolution 21 p3610 A67-37810

Method for determining physical interactions in system of bodies with arbitrary perturbations, using vector form equation 21 p3657 A67-37987

Necessary and sufficient conditions for linear system response to input vector with limited amplitude and slope, noting singular case existence 21 p3603 A67-38175

Aircraft tracking problems in airport approach zone solved using cameras, descriptive geometry and vector computations 21 p3568 A67-38809

Geomagnetic field configuration and time change using dipole vector, noting variation role 21 p3620 A67-38979

Two-tilt compensating interferometers, using vector form of reflection law 22 p3796 A67-39236

Graduate text in general fluid mechanics covering magnetofluid dynamics and vector analysis 22 p3788 A67-40324

Fixed point probability row vector of regular or ergodic transition matrices simplified using generalized matrix inversion theory 23 p4023 A67-41032

Vector field theory of time dependent backscatter from distant slightly rough sphere for pulsed and sinusoidally steady state sources 23 p3974 A67-41200

Book on fluid mechanics foundations for introductory and/or secondary fluid mechanics course, with appendices containing vector analysis, inviscid fluid flow equations, etc 23 p3991 A67-41529

Vector eigenfunctions solution of three-dimensional elastic theory problems, reviewing literature on bodies of revolution in various coordinates 24 p4248 A67-42101

Poynting vectors difference obtained by using convection and polarization current models of moving plasma in Minkowski theory 24 p4124 A67-42812

VECTOR CALCULUS

Energy impulse vectors and kinetic moment tensor associated with body in gravitational field analyzed, using Brouwer theorem 04 p0658 A67-15494

Elliptically polarized wave reception by antenna, itself elliptically polarized, for use in interferometry problems, noting relation to complex vector 04 p0658 A67-15628

Error bounds for asymptotic solutions of differential equations, using Volterra equations for actual and formal solution vectors 06 p1021 A67-17565

Electromagnetic field tensor created by point charge provided with universal velocity and acceleration is equal to outer product of universal

vectors 13 p2156 A67-26594

Book on elasticity covering engineering, Cartesian tensor and vector-dyadic notation, etc 14 p2395 A67-27891

Optimal control of random dynamical systems analyzed, using first order vector differential or difference equations 14 p2292 A67-29062

View function to images of surface in nonplanar specular reflector determined by general mathematical expressions [JPL-TR-32-939] 15 p2516 A67-29131

Topocentric velocity of artificial satellite determined by introducing two pairs of unitary vectors in orbital plane 15 p2556 A67-29745

Artificial satellite radius vector determination examined for degree of accuracy, discussing geodetic applications 15 p2477 A67-29746

Vector equation describing particle motion under Newtonian force used for velocity and equation of particle path through application of law of areas 21 p3658 A67-38553

Motor fields analysis in Cosserat continuum noting differential forms of stress and strain

quantities 22 p3837 A67-40006

Vector Liapunov function existence during conditionally or asymptotically stable motion 24 p4189 A67-42690

VECTOR CONTROL

Successive approximations to determine vector in theory of optimal control 01 p0043 A67-10236

Optimality of totally singular vector controls governing dynamical systems and extension of Green theory approach to higher dimensions to evaluate optimality of such controls 04 p0594 A67-15875

Synthesis of stochastic optimal control for case of discrete input of feedback vector, noting dependency on coordinates characterizing probability density of plant vector 05 p0782 A67-16316

Duality and a priori estimates in Markovian nonlinear stochastic optimal control problems 05 p0784 A67-16778

Caratheodory unified approach to Hamilton-Jacobi theory in variational calculus problems of optimal control 07 p1162 A67-20275

Approaching and soft landing on planet surface in absence of atmosphere, finding optimum acceleration vector control as function of generalized parameters 09 p1571 A67-21889

Electromagnetic component /Vectorsyn/ for improving mass element restraint and support for three-axes acceleration measurement system 12 p1947 A67-26123

Time optimal control problems of linear systems with state and control vectors 13 p2087 A67-26723

Synthesis of stochastic optimal control for case of discrete input of feedback vector, noting dependency on coordinates characterizing probability density of plant vector 18 p3016 A67-33867

Suboptimal radial guidance scheme based on cubic time function of optimal trajectories radius vector modulus from simultaneous data analysis 22 p3830 A67-39164

VECTOR CURRENT

Vector potential of magnetic field of any axisymmetric electric current distribution used to compute field of two model magnetospheric ring currents 04 p0617 A67-15535

Electric vector expression of amplitude-modulated electromagnetic wave propagating in nonlinear dispersive medium 20 p3499 A67-36992

VECTOR SPACE

SA BANACH SPACE

SA HERMITIAN POLYNOMIAL

SA HILBERT SPACE

Control system analysis and design using parameter space method 01 p0047 A67-11216

Exact difference replacement for hyperbolic equation system where n x n symmetric matrices become coefficients of vectors in two-dimensional space 03 p0460 A67-13880

Truncated elliptic systems of partial differential equations for reducing two-point boundary value problems in vector space to initial value problems by projection 08 p1348 A67-21192

Bound solutions for elliptical equation in n-dimensional vector space obtained, using linear transformation into Martin boundary 11 p1814 A67-24852

Two LMS algorithms related to steepest descent method, obtaining generalized theorems 13 p2147 A67-27173

Definition of solutions of problem that constitutes generalization of infrapolynomial problem and best approximation problem in normed space 13 p2148 A67-27471

Constrained minimization problem extended to necessary conditions for characterizing noninferior points to determine vector-valued criteria in finite dimensional spaces 20 p3478 A67-37576

Einstein vacuum equation solution interpretation for gravitation, space and time concepts, using vector fields oriented in time and Riemann tensorial equations 20 p3487 A67-37684

Linear differential games associated with vector differential equation in arbitrary dimensional space noting square matrix and convex sets 22 p3826 A67-39214

Vector space convexity and nonmonotonicity proof, discussing 34-dimensional linear space and l-simplicial

convexity 24 p4179 A67-42729
 Uniformization of asymptotic expansions, constructing counterterms by nesting increasing number of extensions for both secular and singular perturbation terms 24 p4190 A67-43094

VEGARD-KAPLAN BAND
 Lifetime and diffusion coefficient of lowest excited state of molecular nitrogen from intensity decay measurements of Vegard-Kaplan band 17 p2889 A67-33243

VEGETATION
 Spectrometric investigation of Mars in five spectral regions applied to color analysis of Martian continents and oceans for probable coloring of Martian vegetation 11 p1867 A67-24845
 Synthesized summary of reports on radio propagation in nonionized media, noting meteorological radar and precipitation effect 14 p2264 A67-28393
 Vegetation mapping from K-band radar imagery using image discrimination, enhancement, combination and sampling system 19 p3227 A67-34798
 Survey satellite potential uses in vegetation resources and terrain analysis, emphasizing satellite photography 19 p3231 A67-35654
 Nervous and humoral mechanisms of extralabyrinthine effects on vegetative disturbances during space flight factors 24 p4111 A67-41843
 Forestry applications for remote sensing from earth orbiting vehicles for inventory and evaluation of resources [AIAA PAPER 67-765] 24 p4258 A67-42934

VEHICLE
 S AERODYNAMIC VEHICLE
 S AEROSPACE VEHICLE
 S AIR CUSHION VEHICLE
 S AIRCRAFT
 S BALLISTIC VEHICLE
 S CAPTURED AIR BUBBLE VEHICLE
 S FLIGHT VEHICLE
 S HYPERSONIC VEHICLE
 S LAUNCH VEHICLE
 S LUNAR ROVING VEHICLE /LRV/
 S MISSILE
 S POWER-LIMITED VEHICLE
 S REENTRY VEHICLE
 S RESEARCH VEHICLE
 S ROCKET
 S ROCKET VEHICLE
 S ROTATING VEHICLE
 S SATELLITE
 S SELF-PROPELLED VEHICLE
 S SHIP
 S SPACE VEHICLE
 S SPACECRAFT
 S SURFACE VEHICLE
 S TEST VEHICLE
 S TRANSFER VEHICLE
 S TRANSPORT VEHICLE
 S WATER VEHICLE
 S WINGED VEHICLE
 S WINGLESS VEHICLE

VEIN
 9-alphafluorohydrocortisone and venous occlusive cuffs effects on plasma volume and orthostatic tolerance following 28 to 78 days of bed rest 01 p0016 A67-10960
 Cumulative effects of venesection and lower body negative pressure on circulation 10 p1599 A67-23813

VELA PROJECT
 Properties and velocity distribution functions observed by Vela III satellites 07 p1244 A67-19919
 Vela II measurements of earth magnetopause and bow shock positions, showing relationship to magnetic disturbance index and thus also to solar wind velocity 07 p1180 A67-19920
 Interplanetary solar wind measurements during April 1965 geomagnetic storm using electrostatic analyzers on Vela satellite 13 p2189 A67-26303
 Growth and decay of geomagnetic storms of April 17-18, 1965 studied using data from 88 ground stations, Explorer XXVI and Vela satellites 23 p3995 A67-40814

VELOCITY
 SA ACCELERATION
 SA ACOUSTIC VELOCITY
 SA AIR SPEED
 SA ANGULAR VELOCITY
 SA ESCAPE VELOCITY
 SA EXHAUST VELOCITY
 SA FLOW VELOCITY
 SA GROUP VELOCITY

SA HYPERVELOCITY
 SA ORBITAL VELOCITY
 SA PHASE VELOCITY
 SA PROPAGATION VELOCITY
 SA RELATIVISTIC VELOCITY
 SA SOLAR VELOCITY
 SA SOUND VELOCITY
 SA WIND VELOCITY
 Stable domain propagation in gallium arsenide for nonzero constant diffusion coefficient, based on analytic approximation to velocity field 03 p0493 A67-13461
 Trajectory modes for manned and unmanned missions to Mercury, 1980-2000 [AIAA PAPER 67-28] 06 p1086 A67-18333
 Theoretical derivation of self-extension velocities of storable tubular extendible member /STEM/ 06 p1008 A67-18594
 Energy method extended to stability analysis of linear system under action of nonconservative forces 14 p2398 A67-28094
 Trajectory modes for manned and unmanned missions to Mercury, 1980-2000 21 p3700 A67-37782

VELOCITY DISTRIBUTION
 Origin of polarization of radiation from GaAs diodes, noting intensity dependence on current density and effect of anisotropic electron velocity distribution 01 p0034 A67-10090
 MGD flows in channels analyzed, using transformation of hodograph for vortical velocity distribution 01 p0119 A67-10172
 Identical particles gas with velocities distributed regularly in plane, analyzing compression and relaxation waves present in six- and eight-velocity models 01 p0051 A67-10228
 Vortex strength in wake of circular cylinders and comparison of vortex velocity distribution with that of Hoffman and Joubert, using hot-wire anemometers at various Reynolds numbers 01 p0005 A67-10256
 Velocity distributions at blade profiles in two-dimensional model of axial stage treated by numerical solution of Fredholm integral equations 01 p0006 A67-10525
 Flow of compressible fluids past straight cascades of arbitrary airfoils using Karman-Tsien method, obtaining velocity distribution around airfoil through continuity equation 02 p0177 A67-11470
 Synthetic line profiles generated for variety of model atmospheres containing linear and quadratic velocity fields, used to analyze solar chromosphere 02 p0323 A67-11690
 Measurement of ion velocity distribution in plasma stream of pulsed coaxial accelerator agreeing with computation from momentum transfer and mass flow measurements 02 p0276 A67-12568
 Numerical integration of averaged cross section for electron induced resonance charge exchange and ionization of accelerated beam of hydrogen atoms 02 p0278 A67-12629
 Laminar boundary layer with longitudinal pressure gradient in high velocity flow of uniformly dissociated gas for arbitrary external velocity distribution 03 p0401 A67-12875
 Heat transfer and velocity characteristics of thermal and hydrodynamic laminar flow in ducts of arbitrary cross section, considering boundary conditions at wall [ASME PAPER 65-WA/HT-13] 03 p0537 A67-14008
 Stationary waves and nonstationary multibeam flows in plasma with arbitrary electron velocity distribution 03 p0486 A67-14198
 Correlation scheme for mean velocity distributions in turbulent boundary layers developing in arbitrary adverse pressure gradients 04 p0601 A67-14459
 Velocity, energy and concentration fields in laminar boundary layers with arbitrarily distributed mass transfer at surface 04 p0603 A67-14643
 Velocity distribution in shock wave, emphasizing heat transmission, longitudinal viscosity friction and relaxation 04 p0605 A67-14984
 Low speed cascade tunnel experiments for improvement of airflow and testing techniques, noting porous sidewall suction effect on axial velocity changes [ASME PAPER 66-WA/GT-7] 04 p0548 A67-15385

Numerical solution for laminar flow heat transfer in circular tubes with axial conduction and developing thermal and velocity fields [ASME PAPER 66-WA/HT-7] 04 p0726 A67-15446
 Velocity field in MHD jet flow discharging into immersed bounded space 04 p0669 A67-15518
 Energy transfer rate between electrons and ions in plasma, noting velocity dependence of Coulomb logarithm 04 p0672 A67-15775
 Alfven velocity distribution in magnetosphere to understand nature of geomagnetic micropulsation 05 p0795 A67-16062
 Rotating Langmuir probes for flow velocity distribution measurements in highly ionized supersonic low density MPD arc 05 p0851 A67-16466
 Magnetic and kinetic energy calculated for geomagnetic storm as function of velocity distributions 05 p0801 A67-17133
 Sixth order polynomial calculation of axisymmetric laminar boundary layer of incompressible fluid removed by suction and arbitrary velocity distribution 05 p0749 A67-17184
 Nozzle type molecular beam measuring distribution of speeds after scattering incident beam from solid surface 05 p0849 A67-17276
 Statistical initial value problem for Burger model equation of turbulence, examining velocity correlation functions, energy spectra and other statistical properties 05 p0794 A67-17419
 Heat transfer in short circuit generalized MHD Couette flow for velocity field and temperature distribution, when walls are at equal and unequal temperatures in transverse magnetic field 06 p1039 A67-18070
 Boundary layer thickness in air measured in presence of sound field, determining flow velocity distribution in layer 06 p0988 A67-18400
 Velocity distribution function relaxation and runaway of electrons in weakly ionized plasmas 07 p1228 A67-19510
 Drift velocity variation with electric field calculated in GaAs, using Boltzmann equation and incorporating additional scattering process 07 p1232 A67-19561
 Nonlinear singularities method for calculating velocity distribution over thick wing of finite aspect ratio situated at zero angle of attack in incompressible frictionless potential flow 07 p1127 A67-19887
 Properties and velocity distribution functions observed by Vela III satellites 07 p1244 A67-19919
 MGD lubrication, obtaining motion equation of gas in electric or magnetic fields, velocity distributions, pressure differential equations, etc 07 p1192 A67-20210
 Velocity distribution of turbulent incompressible boundary layer along flat plate with assumed polynomials of shearing stress and mixing length 08 p1319 A67-20405
 Velocity distribution for low drag airfoil with little tendency toward separation of turbulent boundary layer 08 p1275 A67-20407
 Simultaneous effects of heat and mass transfer on properties of stagnation point flows analyzed over full range of velocity gradients 08 p1276 A67-20568
 Integral method to study surface chemistry interaction due to combustion and attendant mass transfer on isothermal graphite cone in nonsimilar boundary layer flow 08 p1320 A67-20570
 Dispersion equation for whistler mode for velocity distribution with loss cone, discussing critical stability 08 p1324 A67-20894
 Heat transfer in constant property turbulent boundary layer with arbitrary distributions of wall temperature and stream velocity 08 p1426 A67-20927
 Kinetic theory-plasma dynamics theory calculations of magnetospheric solar wind proton velocity distribution as function of particle speed 08 p1377 A67-21315
 Energy balance equations including effects of heating by electron gas, cooling and energy coupling obtained for various ion species, assuming each ion gas has Maxwellian velocity distribution 08 p1326 A67-21363
 Landau damping and growth applied to

- electron plasma waves for Maxwellian velocity distribution in slab and cylindrical geometries 08 p1365 A67-21403
- Two-dimensional incompressible potential flow theory for airfoil design with prescribed velocity distribution over surface 09 p1437 A67-21740
- D'Alembert initial value problem for cylindrical waves, obtaining linearized potential equation for plane and symmetrically spherical case 09 p1488 A67-21932
- Device for analyzing propagation of nonrotating jet in rotating ambient flow, noting graphs for longitudinal and tangential velocity distributions 09 p1490 A67-22594
- Generation of oscillations in solar atmosphere by separate granules modeled by bottom zone of isothermal gravitating photospheric layer overlaid by hot corona 10 p1704 A67-22721
- Asymptotic behavior of laminar boundary layer, reducing system to heat equation, noting viscosity effects and uniqueness of homogeneous solution [ONERA-TP-458] 10 p1623 A67-22878
- Gas flow and shock wave velocity distribution in diaphragmed shock tube photographically analyzed at various opening rates 10 p1626 A67-23407
- Two-fluid theory for plasma stability, obtaining equation on velocity field perturbation by considering Ohm law, stress tensor with Larmor radius and viscosity from collisions 10 p1685 A67-23465
- Laminar flow between parallel plates for arbitrary initial velocity distribution and time varying pressure gradient 10 p1629 A67-23842
- Toroidal machine velocity space instabilities, rapidly saturating, with long time scale remaining 11 p1826 A67-23876
- Shock wave structure theory using Navier-Stokes character of shock wings and measured thickness, noting dependence on number density 11 p1775 A67-23879
- Electron beam experimental methods for current density distributions, electron velocities and determining parameters for microwave tube design 11 p1758 A67-24094
- Electric field effect in Q machine with uniform end plate temperature, noting deviation from thermal equilibrium and increment in ion loss rate for certain range of particle densities 11 p1833 A67-24370
- Relaxation in space of electron velocity distribution due to electron-ion collisions, obtaining time independent solution 11 p1833 A67-24372
- Diffusion of particles across magnetic lines in dense and quiescent plasma compared with Bohm and collisional values 11 p1835 A67-24383
- Random walks computer experiments on ensembles of random binary homogeneous velocity fields, using Eulerian and Lagrangian statistics 11 p1756 A67-24542
- Electrostatic oscillations in electron plasma, noting effect of external electric field on electron velocity distribution 11 p1848 A67-24868
- Differential reaction cross section and internal excitation function from K and Br molecule crossed beam velocity analysis 11 p1750 A67-24991
- Partial differential equation of MHD converters, noting effects of converter width, side conductor materials and velocity distribution 12 p1896 A67-25374
- MHD induction generator with variable fluid and magnetic field velocity noting high power of cascading generator 12 p1897 A67-25377
- Axially symmetric compressible turbulent wake fluctuating characteristics measured using supersonic wind tunnel, including radial velocity and temperature distribution, density, etc 12 p1893 A67-25928
- Relaxation of velocity distribution to equilibrium in electron plasma, showing linearized collision operator covers continuous spectrum of eigenvalues 12 p1977 A67-26176
- Electron velocities distribution in plasma, studying boltzmann equation inelastic and superelastic collision operator, considering eigenfunctions and eigenvalues for electronic excitations and deexcitations 13 p2165 A67-26437
- Similarity solutions derived for describing propagation of strong compression shock in transversely expanding gas 13 p2094 A67-26643
- Existence of continuous transonic flow and model representing velocity distribution by Oswatitsch integral equation 13 p2050 A67-26808
- Three-dimensional hard spheres theory of gas atom scattering from solid surface noting velocity distribution, energy and momentum accommodation coefficients, etc 13 p2097 A67-26936
- Gas atom scattering from solid surface, analyses and comparisons 13 p2097 A67-26937
- Sound propagation in dilute monatomic gas confined in box and in unconfined rarefied monatomic gas assuming unidirectional perturbation of velocity distribution 13 p2100 A67-26955
- Kinetic theory description of flow over right circular cylinder at low speed based on Lees moment method 13 p2102 A67-26969
- Velocity distribution function of re-emitted molecules effect on slip flow boundary conditions 13 p2102 A67-26970
- Turbulent mixing in plane nonisothermal jets, deriving solutions for velocity, temperature and pressure distribution 13 p2105 A67-27052
- Direct numerical method for finding optimal values of functionals and associated velocity fields in plastic limit analysis 13 p2219 A67-27153
- Numerical integration of averaged cross section for electron induced resonance charge exchange and ionization of accelerated beam of hydrogen atoms 13 p2171 A67-27387
- Three-dimensional axisymmetrical boundary layer on spinning body of revolution in two-component fluid flow, discussing velocity distribution, drag and separation 14 p2295 A67-27835
- Two-dimensional steady flow analysis in channels with variable cross sections under strong magnetic field action, calculating velocity distribution by series expansion 14 p2355 A67-27902
- Upper atmospheric turbulence velocity probability density investigated in 90 to 110 km region 14 p2346 A67-28058
- Anisotropic velocity distribution function measurements in jet flows using electron beam fluorescence technique 14 p2300 A67-28181
- Axial and radial velocity distributions in axisymmetric free jets of pure gases and binary gas mixtures, noting molecular beam production 14 p2301 A67-28183
- Time of flight distribution measurement of weak molecular beam, noting limitations due to signal to noise ratio 14 p2316 A67-28185
- Intensity and velocity distribution in molecular beams from nozzle sources, discussing physical processes responsible for formation 14 p2301 A67-28186
- Collimation of low density hypersonic jet from shock tube for atomic beam production, noting relation between beam intensity and velocity distribution 14 p2301 A67-28188
- Molecular beam apparatus for measuring collision cross section and velocity distribution of sputtered particles 14 p2316 A67-28191
- Velocity distributions in surface scattered molecular beams, proposing broadband lock-in beam detection for signal to noise enhancement 14 p2317 A67-28195
- Two-dimensional supersonic fluid amplifier flow characteristics analyzed numerically by digital computer 14 p2250 A67-28333
- Attachment distance for two-dimensional jet shown unaffected by presence or absence of second sidewall and nozzle aspect ratio 14 p2303 A67-28339
- Stationary waves and nonstationary multibeam flows in plasma with arbitrary electron velocity distribution 14 p2360 A67-28543
- Large microwave field and small parallel DC field applied across GaAs sample altering conductivity related to carrier velocity-field characteristic 14 p2369 A67-28601
- Displacement fields used in finite element representations to obtain upper bounds to limit loads of plane stress problems 14 p2403 A67-29014
- Electron mobility and temperature due to electric field in polar semiconductor investigated assuming displaced Maxwellian velocity distribution 14 p2375 A67-29065
- Particle velocity distribution calculation in current-carrying electron-proton plasma by Lenard-Balescu-Guernsey form of Fokker-Planck equation 15 p2522 A67-29204
- Steady state velocity distribution in fully ionized plasma in DC electric field obtained through Bhatnagar-Gross-Krook equation 15 p2522 A67-29206
- Viscosity and thermoconductivity values of partially ionized argon plasmas derived by investigating temperature decay and stream velocity distribution in argon plasma jet 15 p2531 A67-30203
- Small signal power conservation in space charge waves of multiveLOCITY electron beam with rectangular velocity distribution 16 p2703 A67-30796
- Finite value of escape velocity from stationary stellar system influence on residual velocities distribution 16 p2746 A67-30836
- Non-Markovian evolution equation for velocities distribution in homogeneous gravitational system 16 p2748 A67-31139
- Velocity distribution functions in statistical theory of turbulence, deriving moment equations and comparing properties with kinetic theory 16 p2660 A67-31220
- Bounce model pinch stability, noting plasma and field separation by thin surface, with anisotropies in velocity distribution and angular momentum considered 16 p2718 A67-31227
- Electron velocity distribution function obtained for partially ionized gas in weak, steady electric field by solving Boltzmann-Fokker-Planck equation 16 p2704 A67-31235
- Ion mobility in gases determined, based on kinetic equation for ion velocity distribution function with particular reference to Chapman-Enskog method 16 p2704 A67-31250
- Reduction of steady viscous magnetohydrodynamic flows having orthogonal magnetic and velocity field distributions to associated flows having zero magnetic field 16 p2721 A67-31552
- Particle theory analysis of electromagnetic and electrostatic instabilities due to anisotropic velocity distributions 16 p2722 A67-31560
- Transonic blade cascades determined by mixed analog-numerical method starting from velocity distribution law and hodograph method 16 p2594 A67-31710
- Electron velocity distribution function in nonequilibrium plasma having spatial distribution governed by electron-electron and inelastic collisions 16 p2723 A67-31768
- Charged particles with Alfvén velocities distribution in magnetosphere analyzed based on cold plasma density, emphasizing data of OGO A 17 p2899 A67-32256
- Wall suction rate effect on turbulent flow in cylindrical circular porous duct, measuring distributions of velocity, pressure, friction coefficient and Reynolds stresses 17 p2837 A67-32380
- Axially symmetric free turbulent jet flow with swirling vortex motion over wide range of swirl degree 17 p2838 A67-32417
- Calculation of compressible subsonic potential flow through blade cascades, giving air outlet angle, velocity distribution around blade profile and critical Mach number 17 p2791 A67-32711
- Pulsations in electron intensities in postbreakup aurora, noting possibility of distant processes affecting electrons 17 p2844 A67-32765
- Law for velocity distribution through wall boundary layers derived from eddy viscosity model, considering turbulent shear variation and Reynolds number effect 17 p2839 A67-33008
- Temperature dependence of sound velocity in liquid helium at saturation vapor pressure and cryogenic temperatures 17 p2886 A67-33231
- Low speed cascade tunnel experiments for improvement of airflow and testing techniques, noting porous sidewall suction effect on axial velocity changes [ASME PAPER 66-WA/GT-7] 18 p2983 A67-34131
- Longitudinal magnetic field effect on conducting fluid turbulent flow found limited to dissipation mechanism occurrence 18 p3028 A67-34215

Plasma behavior in shock tubes with parallel conductors, discussing shape of front and velocity dependence on pressure and gas composition 18 p3089 A67-34297

Energy flux in steady inhomogeneous turbulent gas flow with arbitrary mean velocity field, deriving velocity spectra and pressure-velocity correlation tensors 18 p3030 A67-34741

Interaction of three-dimensional model of gas with solid surface, discussing atomic velocity distribution from surface reflection, energy and momentum accommodation coefficients, etc 19 p3264 A67-34936

Velocity distribution function in positive column plasma and implications for electron energy transfer mechanism on microscopic scale 19 p3267 A67-34948

Profile velocity distribution and shape determinations for flow around thin profile with jet flap 19 p3172 A67-35819

Turbulent flow in circular duct, obtaining velocity distribution 20 p3419 A67-36276

Two-dimensional potential flow through bend profile, obtaining streamlines and velocity distributions 20 p3356 A67-36533

Proton velocity distribution in solar wind flow around magnetosphere 20 p3518 A67-36653

Generalized Mott-Smith functions for shock wave structure in binary mixtures, relative diffusion velocity obtained and compared with Diakov solution 20 p3421 A67-36678

Local heat transfer coefficients, mean temperature and velocity distributions in turbulent natural convection boundary layer on vertical plate surface [ASME PAPER 67-HT-17] 20 p3545 A67-36713

Probability distribution errors effect in linear and planar impulse orbital transfers, considering angular orientation and impulsive velocity 20 p3527 A67-37259

Plane-strain problem of plasticity theory with two yield conditions applied to stress and velocity fields defined by differential equilibrium equations 20 p3541 A67-37299

Diffusing plane turbulent free jet compared with correspondent wall jet velocity distribution and variation and length scales 20 p3360 A67-37492

Power series expansion of electron velocity distribution function, computing harmonic electric current densities in plasma 21 p3661 A67-37745

Alfven velocity distributions in magnetosphere used to understand nature of geomagnetic micropulsation 21 p3616 A67-37849

Material point displacement velocity field of bending elements of sheet during profile shaping by roll forming, determining stress-strain condition 21 p3631 A67-38052

Magnetic and kinetic energy calculated for geomagnetic storm as function of velocity distributions 21 p3619 A67-38476

Inviscid incompressible flow of normal and slightly oblique static round jet impinging on ground, noting velocity distribution 21 p3565 A67-38544

Unsteady airfoil stall noting frequency effects on velocity distribution and angle of attack for oscillating pitch 21 p3565 A67-38547

Velocity and pressure distributions and free shape of conducting liquid in rotating circular cylinder under magnetic and electric fields 21 p3668 A67-38561

Gruber method for radial flow impellers of greatly cambered forward curved blading, analyzing parameter variation effect on velocity distribution curves 21 p3614 A67-39053

Unsteady spherically symmetric gas flows with gas particle radial velocity proportional to distance from symmetry center 22 p3739 A67-39216

Rapid randomization phenomena in unstable plasma sac for Mach numbers close to unity attributed to electron interaction with trapped electroacoustic waves 22 p3844 A67-39357

Incompressible two-dimensional turbulent channel flow, calculating velocity profile and obtaining resistance formula 22 p3782 A67-39409

Drag forces on body with nonuniform velocity distribution, considering gradient flow effects on drag coefficients 22 p3740 A67-39941

Velocity distribution determination method

for supersonic flow around zero incidence cones in equilibrium air, discussing motion equation and flow field parameters 22 p3742 A67-40098

Variational formulation and Rayleigh-Ritz method for nonequilibrium viscous incompressible flows, obtaining velocity and temperature distributions 22 p3788 A67-40422

Oscillating relativistic universe model from Einstein field equations, discussing Friedmann model matter and velocity distribution, Hubble law and universe volume oscillating relativistic universe model from 22 p3892 A67-40496

Nonlinear hydrodynamic equation term effects on rotational fluid motion in galactic plane, discussing velocity perturbations and discontinuities 22 p3893 A67-40502

Stability of stellar systems with different velocity distributions, considering nonlinear wave in stellar sheet leading to galactic stellar velocity distribution evolution 22 p3894 A67-40510

Velocity and pressure distributions and flow field for laminar incompressible source flow between two coaxial parallel disks rotating at different speeds 23 p3988 A67-40602

Helicopter maximum speed increase using rotor with controlled blade oscillation motion, studying flow velocity, distribution and asymmetry elimination 23 p3933 A67-40639

Velocity distribution of evaporated Au and incident velocity on nucleation of Au on rocksalt studied by velocity selector 23 p4009 A67-41015

Nozzle form optimization from Mach distribution in supersonic region, defining perturbation functions 23 p3929 A67-41248

Velocity fields in solar photosphere and chromosphere, discussing granulation, supergranulation, magnetic fields and oscillatory motions 23 p4068 A67-41276

Penetrative motion of individual elements in earth atmosphere and prediction of velocity field from convective overshoot 23 p4024 A67-41279

Rapid temperature increase due to lower photosphere turbulence generation of mechanical waves, discussing gravity wave generation and acoustic noise 23 p4068 A67-41280

Quasi-neutral ion beam focusing by axisymmetric electromagnetic field with closed electron drift, noting ion velocity distribution effects for longitudinal and azimuthal components 23 p4035 A67-41682

Dynamic impossibility of free stream velocity distributions admitting similarity solutions, calculating laminar boundary layers 23 p3992 A67-41741

Light gas escape flux from atmosphere velocity and angular distributions near critical level using Monte Carlo analysis 24 p4224 A67-41823

Integral turbulent transfer model using velocity distribution function to develop mixing length flow theory 24 p4141 A67-41933

Turbulent fluid flow velocity and temperature fields in annular and plane gaps calculated by integral approximation for turbulent viscosity and heat conduction coefficients 24 p4142 A67-42213

Irregular earth rotation velocity variation analyzed by comparing universal time with atomic time 24 p4150 A67-42312

Nondisturbing turbulent flow measurements applied to viscous sublayer in smooth square pipe, showing linear velocity gradient in layer adjacent to wall 24 p4144 A67-42607

Anomalous electron heating rate in plasma region traversed by magnetic shock wave obtained by electron velocity distribution observation 24 p4198 A67-42736

VELOCITY ERROR

Velocity aberration and atmospheric refraction pertaining to laser satellite communication experiments, obtaining equations for estimation of effects 02 p0198 A67-12054

Mariner IV midcourse 50-lb thrust pressure-controlled monopropellant hydrazine propellant system, predicting impulse and velocity error as function of burn time [AIAA PAPER 66-948] 02 p0304 A67-12282

Error in R-meter measurement of velocity spread of meteorological targets resulting from radar frequency

Instabilities 04 p0648 A67-14673

Errors in R-meter measurement of velocity spread of meteorological targets resulting from radar frequency 10 p1676 A67-22816

Instabilities 10 p1676 A67-22816

Mariner IV midcourse 50-lb thrust pressure-controlled monopropellant hydrazine propellant system, predicting impulse and velocity error as function of burn time 21 p3712 A67-37797

VELOCITY MEASUREMENT

SA ACCELEROMETER

SA TACHOMETER

SA WIND VELOCITY MEASUREMENT

Motion sensing using Mossbauer nuclear resonance effect with radiation source located on body in motion and detector in controlled motion 01 p0062 A67-10156

Velocity propagation of stable detonations in gas mixtures determined, using Doppler effect obtained by electromagnetic wave reflection 01 p6166 A67-10229

Helicopter and VTOL vehicle low air speed measuring techniques and devices including pitot-static tube, hot-wire anemometer, sphere sensor and exotic techniques 01 p0073 A67-11122

Hot wire measurement of tangential velocity and Reynolds stresses in spiral laminar-turbulent flow 01 p0054 A67-11163

Interplanetary trajectory correction via radial heliocentric velocity pulses, noting calculation by linear approximation 02 p0321 A67-11538

Induction velometry measurement of average velocity of free jet of ionized gas influenced by transverse uniform magnetic field 02 p0272 A67-11881

Subsonic wind tunnel analysis of wake deformations produced by secondary velocities using models with flat base but various cross sections 02 p0233 A67-12228

Nonionized atmosphere effect on radial velocity measurement of satellite via Doppler-Flizeau method 03 p0369 A67-13530

Radar observation of insects in free flight, noting backscatter and velocity measurement results [AFCRL-67-0127] 03 p0371 A67-13916

Doppler system for missile and bullet velocity measurements noting design parameters, equipment used and range improvement obtained 04 p0653 A67-15044

Continuous wave radar application for obtaining velocity and range information on single targets at large distances 04 p0574 A67-15046

Kinetic energies of ions produced by giant laser pulses, noting dependence of mean square ion velocity on pulse peak intensity 04 p0633 A67-15099

Velocity measurements at various temperatures made with zinc sulfide thin film longitudinal acoustic wave transducers, used on germanium 04 p0621 A67-15127

Axial temperature and velocity measurements made in water at various aspect ratios, Grashof number and bottom-to-side heat flux ratios for turbulent free convection in closed container 04 p0731 A67-15827

Rotating shutter telescopic observation for optical measurement of faint meteor velocity 05 p0897 A67-16805

Diffusion influence on radio determination of meteor velocity by diffraction method 05 p0897 A67-16807

Supersonic flow around elliptic cone with symmetrical fins, determining perturbation velocity via Germain method 05 p0749 A67-16844

Smear camera used to measure detonation front velocity of explosive or propellant 06 p1001 A67-17793

Interpreting short voltage pulse measurements of electron drift velocity in n-GaAs 06 p1048 A67-17815

Absolute angular velocity measurement with aid of linear accelerometers on body of aircraft 06 p1028 A67-18178

Decay of mean, variance and gradient variance of temperature and velocity measured in initially heated wake of sphere in water tunnel [AIAA PAPER 67-20] 06 p0987 A67-18347

Laser velocimeter measurement of point velocities in turbulent liquid flow in pipe, using statistical analysis to verify results [AIAA PAPER 67-179] 06 p0990 A67-18511

Langmuir probe velocity and acceleration measurements for coaxial Hall accelerators

[AIAA PAPER 66-196] 08 p1375 A67-20575
Wakes behind axisymmetric blunt based bodies, noting similarity among wakes through measurements of velocity, turbulence and static pressure 08 p1277 A67-20706
Self-contained midcourse guidance system with space velocity meter /SVM/ used in returning probe to earth vicinity for data retrieval and orbit control 08 p1331 A67-21101
Velocity spread on modulated electron beam of finite diameter analyzed as function of drive, drift length and 08 p1362 A67-21298
Aerosol particle velocity measurement using optical compensation and photoelectric particle counter 08 p1428 A67-21422
Doppler tracking systems as velocity measuring systems, including introduction methods for necessary position knowledge, one-and two-way systems analyses, etc 10 p1605 A67-22995
Ultrasonic flow meter for directly measuring average stream velocity using ring-around velocimeter with piezoelectric ceramics 10 p1656 A67-23079
Carrier drift velocity measurements in silicon at high electric fields, using time-of-flight technique 10 p1690 A67-23167
Mobile charge carrier velocity measurements in silicon at high field strengths 10 p1690 A67-23168
Space charge conductance and electron drift velocity measurements for avalanche p-n diode 10 p1611 A67-23169
Newton inverse square force for planets from invariant velocity components of Keplerian planetary motion by graphical model 10 p1711 A67-23791
Velocity and temperature measurements in turbulent swirling butane-propane air flames in high exit velocity range 11 p1882 A67-24217
Electrostatic separation probe to measure electronic velocity distribution function, showing evolution of distribution function relationship to plasma oscillation growth 11 p1789 A67-24409
Absolute speed determination from measurement of induced EMF resulting from movement in geomagnetic field 11 p1791 A67-24455
Light velocity measurement using hollow cathode discharge in Ne-H laser 11 p1818 A67-24479
Monograph on problems of cloud physics covering evolution of preinversion stratiforms and vertical velocities determination in lower atmospheric layer 11 p1816 A67-24521
Vertical atmospheric flow mean velocity determination within fixed area from wind probe observations at fixed points 11 p1816 A67-24523
EMF induced in ionized gas across magnetic field measured for flow velocity determination 12 p1973 A67-25392
Doppler radar and Doppler navigation system capabilities, applications, cost and reliability for supersonic and subsonic aircraft 12 p1964 A67-25870
[SAE PAPER 670328] 12 p1964 A67-25870
T-burner technique for determining acoustic pressure- and velocity-coupled responses of solid propellants 12 p1988 A67-25910
Two-velocity spatial correlation coefficients and lengths measured for wall jets 13 p2049 A67-26590
Hydraulic properties of duct of constant rectangular cross section functioning in closed circuit used to measure MHD flow velocity 13 p2165 A67-26593
Arc jet exhaust velocity compared with propagation velocity of random light fluctuations 13 p2188 A67-26839
Dislocation velocity measurements and thermally activated motion in molybdenum 13 p2133 A67-27011
Velocity measurement in electrically conducting fluid flow in presence of uniform magnetic induction normal to flow direction 13 p2167 A67-27206
Solar wind ion concentration and velocity measurements from Venus III and Pioneer IV 13 p2195 A67-27343
Radial velocities and spectral types for 13 stars, listing photoelectric magnitudes and colors for six 14 p2387 A67-28565
Velocity limitations of accelerated plasma

by momentum loss due to electrode impact of accelerated ions, proposing modified snowplow model 15 p2531 A67-30030
Errors of real accelerometer and instability of rotation effect on accuracy of angular velocity measurements of aircraft motion 16 p2670 A67-30468
Shock wave velocity measurement using photoelectric, piezoelectric ionization and continuous scanning methods 16 p2673 A67-31106
Velocity measurement and image recording of freely moving objects during ballistic tests by electronic and photographic methods 16 p2674 A67-31126
Electric manometer using electrolytic fluid for low velocity measurements with Pitot tube 16 p2675 A67-31210
Analytical plasma flow model for acceleration process in Hall current device, noting final velocity derivation, temperature, critical velocity, etc 16 p2719 A67-31237
Interplanetary trajectory correction via radial heliocentric velocity pulses, noting calculation by linear approximation 16 p2752 A67-31604
Conrad-type probe used to determine, in boundary layer of flattened ellipsoid, mean velocity of flow 16 p2663 A67-31711
Rotational velocity of neutral hydrogen subsystem in outer regions of Galaxy outside galactic plane 17 p2950 A67-33163
Devices for flight speed measurement 18 p3019 A67-33461
Nature of gravity, discussing universal radiation of gravitation quanta, gravity velocity determination, effects on earth formation, etc 18 p3077 A67-33549
Speed of light in vacuum determined by helium-neon gas laser, using Edlen dispersion equation 18 p3059 A67-33671
Wave propagation velocity in relativistic fluids determined using new hydrodynamic equations 18 p3025 A67-33683
Systematic errors limiting velocity measurement accuracy of longitudinal ultrasonic waves when using pulse-delay methods, for application to ultrasonic equipment 18 p3044 A67-33734
Random errors in ultrasonic measurements, discussing Students distribution measurement repetition effect and rounding-off error evaluation 18 p3044 A67-33735
Velocity and temperature measurements in turbulent swirling burning free jets of butane-propane-air mixture 18 p3151 A67-33815
Microwave experimental technique for continuous velocity measurement of shock and contact discontinuities bounding air plasma generated in cylindrical hypersonic shock tube 18 p3020 A67-34105
Velocity measurement in turbulent flow near smooth wall by hot-wire anemometer 18 p3027 A67-34184
Plane shock wave velocity measurement after interaction with obstacles in form of channeled diaphragms of various diameters, discussing stabilization 18 p3028 A67-34210
Measurement within rocket exhaust plumes 18 p3051 A67-34507
Pressure fluctuations beneath incompressible turbulent boundary layer with mass addition 18 p3030 A67-34742
Perfluorocyclobutane-fluorine combustion studies and measurement of detonation velocities and limits 19 p3345 A67-35013
[CI PAPER 67-23] 19 p3345 A67-35013
Average dwell times and velocities of Ba, Sr, Li, Tl, Sn, Bi, Be, Zn, and Hg in arc plasma 19 p3281 A67-35155
Phase velocity and attenuation of ionic plasma waves in weakly ionized gases measured in absence and presence of external magnetic fields 19 p3290 A67-35378
Velocity fields in solar atmosphere observed with magnetograph, studying magnetic field effect on oscillations amplitude and frequency 19 p3324 A67-35434
Experimental duct for plane deformation of homogeneous turbulence, measuring mean velocities in axis and symmetry plane 20 p3420 A67-36393
Velocity and altitude at bottom of first plunge for reentry-vehicle pitch-plane maneuvers compared with digital simulation 20 p3532 A67-36577
Relative velocity effect on vaporization times and heat-transfer coefficients of water drops in Leidenfrost film boiling on heated

rotating wheel 20 p3552 A67-36833
[AICHE PAPER 32] 20 p3552 A67-36833
Heated thin film anemometer used to measure fluctuating velocity in airflow, noting relation of dynamic sensitivity to static calibration 20 p3447 A67-36846
Minimum velocity increment for bielliptic transfer between noncoplanar circular orbits 20 p3526 A67-37126
Airflow velocity measurement device in cylindrical or rectangular tubes at low gas pressures 20 p3451 A67-37300
Flow velocity calculation by analog computer, discussing Laplace equation role 20 p3424 A67-37302
Plasma component velocity distribution and multiple plasmoid production indicated in spectrograms from high speed photography of coaxial injector discharge 21 p3664 A67-37939
Interferometer standing on L-shaped base for velocity and distance measurements, noting tests on aircraft and rockets and solar reflections effect 21 p3599 A67-38643
MPD Hall accelerator construction and operation using argon or helium propellants, measuring azimuthal velocities in plume [AIAA PAPER 67-672] 21 p3691 A67-38705
Propellants and propellant mixtures effects on MPD arc jet performance in test for ions and neutrals mixture acceleration to high velocity 21 p3688 A67-38715
[AIAA PAPER 67-684] 21 p3688 A67-38715
Diagnostic probe for low density plasma beam ion velocity distribution measurement in steady state and pulsed plasma exhausts [AIAA PAPER 67-706] 21 p3672 A67-38733
Velocity of sound in liquids measurement using ultrasonic interferometry and laser diffraction spectra 21 p3630 A67-38772
Optimal functional parameters of elastically damping turbine rotor bearing to determine critical velocities of shaft 21 p3695 A67-38832
Ion wave velocities and damping measurements in quiescent plasma used for diagnosis of temperatures and drift velocities 22 p3846 A67-39488
Design and operation of various recording instruments /speedobarographs/ for simultaneous measurements of aircraft altitude and speed 22 p3798 A67-39550
Self-aligning hot-wire probe for direction, velocity and turbulence measurements in two-dimensional flow 22 p3800 A67-40069
Dynamic processes in tail of Morehouse comet, discussing velocity measurements, structures and acceleration variations 22 p3888 A67-40205
Laser interferometric velocity measurements of moving objects, discussing accuracy improvements by recorder resolution power increase and atmospheric and seismic disturbance elimination 23 p3997 A67-40571
Primary cosmic ray energy and jet CMS velocity estimations by three methods corrected by analyzing known energy interactions 23 p4051 A67-40913
Calibration of shock accelerometers, discussing velocity change and impact force methods with specific examples of systems in use 23 p4003 A67-41335
Spray coating particle flow rate dependence on plasma jet flow velocity, specific weight and particle size measured by high speed filming 24 p4159 A67-41961
Wing tip vortices behind DC-8 measured for maximum circumferential velocities by research aircraft 24 p4091 A67-42276
VELOCITY MODULATION
Variability of conveyor belt velocity during loading and operation, unloading and stopping under load analyzed, using distribution theory 05 p0908 A67-16043
Experimental transmissions for navigation system monitored over 8500 km path to determine phase variations of VLF signals, for use in design of radio navigation aid 15 p2515 A67-30134
Nonsteady combustion MHD open cycle generator improving power density by modulation of conductivity and particle velocity 16 p2607 A67-30595
Pulse rebalance system in conjunction with pulse accumulator and comparator for precision velocity cut-off signals, presenting data and system characteristics 17 p2858 A67-32485
Temperature and/or velocity modulation of plasmas for generating MHD

power 18 p3085 A67-33702
 Electron component observation in
 studying solar modulation of galactic cosmic
 rays, discussing Parker model and Gloeckler-
 Jokipii model 19 p3315 A67-35496
 Time-growing instability existences in
 distributed parametric media using
 dispersion relation 19 p3195 A67-35620
 C-band solid state YIG serrodyne theory
 and operation, outlining phase velocity
 modulation of magnetostatic
 modes 19 p3196 A67-35661

VELOCITY POTENTIAL

Electron velocity-field characteristics of
 insulating GaAs measured using electron
 beam injected electrons 09 p1551 A67-21573
 Stability of rotational motion of body with
 cavity containing ideal fluid, considering
 fluid motion as potential flow, determining
 velocity potential and inertia
 moments 10 p1679 A67-23031
 Velocity dependence of total scattering
 cross sections for atom-atom collisions
 measured in high energy 13 p2161 A67-27361
 Three-dimensional flow of ideal fluid past
 body enveloped by air cavern, deriving
 normal velocity components 14 p2239 A67-27985
 Velocity potential near disturbance
 boundary for steady supersonic flow past
 body-and-wing model 17 p2790 A67-32403
 Nonstationary plane and axisymmetric
 flows, discussing acoustic and Oswatitsch
 theories, velocity potentials, differential
 equations of motion, etc 17 p2839 A67-32713
 Analytical solution for sloshing of liquid in
 vessel of complex geometry using
 homogeneous boundary
 condition 17 p2839 A67-32886
 Nonlinear theory of lifting wing surface of
 arbitrary aspect ratio, deriving velocity
 potential, lift coefficient and induced
 drag 18 p2981 A67-33536
 Gas flow around wing in presence of
 moving shock wave with variable gas
 parameters noting wave equation, velocity
 potential, etc 20 p3355 A67-36191
 Plane motion of container formed by two
 concentric cylinders and radial partitions
 partly filled with small vibrating ideal
 fluid 22 p3786 A67-40029
 Liquid drop impact on liquid, calculating
 velocity potential, initial pressure and time
 dependence of cavity depth and wall
 velocity 23 p3991 A67-41459

VELOCITY PROBE

Electrostatic separation probe to measure
 electronic velocity distribution function,
 showing evolution of distribution function
 relationship to plasma oscillation
 growth 11 p1789 A67-24409
 Von Karman gas dynamics counterflow
 facility for simulating model high velocities
 and altitudes of reentry
 conditions 16 p2655 A67-31261
 Diagnostic probe for low density plasma
 beam ion velocity distribution measurement
 in steady state and pulsed plasma exhausts
 [AIAA PAPER 67-706] 21 p3672 A67-38733

VELOCITY PROFILE**SA ZERO VELOCITY CURVE**

Experimental study of turbulent transfer
 phenomena in isobaric mixing layer of
 supersonic flow containing preexisting
 boundary layer
 [ONERA-TP-327] 01 p0054 A67-11003
 Circumferential asymmetry in axial flow
 compressors 01 p0008 A67-11272
 Stability of plane parallel flows in finite
 length tube at large Reynolds numbers,
 noting velocity profile 02 p0233 A67-11949
 Hypersonic flow past lower surface of
 slender delta wing for wide-range of angle
 of attack, determining velocity component,
 pressure and density distribution 03 p0350 A67-12874
 Elbow flow meters, comparing average
 coefficients with theoretical
 values 03 p0422 A67-13779
 Turbulent skin friction measurement with
 Preston tube, using similarity hypothesis for
 mean velocity profiles in turbulent
 flows 04 p0600 A67-14442
 Shock wave structure in viscous heat
 conducting gas, deriving preservation law for
 irreversible energy flux, equation for
 velocity profile and expression for integral
 curve 04 p0604 A67-14747
 Sudden expansion or compression effect
 on momentum thickness change in turbulent

boundary layer calculated, using parameter
 of velocity layer profile 04 p0604 A67-14840
 Linearized Couette flow problem in
 rarefied gas solved, using one-dimensional
 radiative heat transfer
 analogy 04 p0606 A67-15183
 Electromagnetic measurement of motion of
 explosion products behind detonation
 wavefront, calculating isentrope from mass
 velocity distribution 04 p0606 A67-15184
 Approximate theory for development of
 steady two-dimensional turbulent free
 mixing shear layers from initial velocity
 profile, including effects of compressibility
 and heat transfer
 [ASME PAPER 66-WA/FE-17] 04 p0606 A67-15352

Static pressure and velocity profiles of
 rotating flow with recirculation core in
 straight pipes determined by five-hole
 pressure probe
 [ASME PAPER 66-WA/FE-36] 04 p0607 A67-15367

Hot-wire probe measurements of time
 average velocity, flow directions, turbulence
 intensities and growth of skewed three-
 dimensional turbulent boundary layers in
 low speed flow
 [ASME PAPER 66-WA/FE-2] 04 p0608 A67-15386

Velocity profiles for infinite cylindrical
 journal bearing, using small eccentricity
 perturbation calculation and modified
 Reynolds number as parameter
 [ASME PAPER 66-WA/APM-17] 04 p0630 A67-15408

Free stream turbulence and pressure
 gradient effects on flat plate boundary layer
 velocity profiles and heat transfer
 [ASME PAPER 66-WA/HT-4] 04 p0608 A67-15448

Velocity profile and friction in plane-
 parallel channel with developed turbulent
 compressible gas flow 04 p0609 A67-15684
 Von Karman-Pohlhausen boundary layer
 analysis of temperature and velocity profiles
 in inlet region between two parallel planes
 with relative motion and pressure
 gradient 04 p0729 A67-15808

Preston tube measurements of skin
 friction and velocity profiles in
 incompressible turbulent boundary layer,
 considering pressure gradient
 effects 04 p0609 A67-15818

Reynolds number effect on surface
 pressure distributions and boundary layer
 velocity profiles on three-quarter power law
 bodies of revolution in hypersonic
 flow 05 p0747 A67-18431

Velocity and temperature profiles of
 optically thick planar Couette flow,
 obtaining heat transfer rates for Rosseland
 mean absorption coefficient variation with
 temperature 05 p0793 A67-17343

Plane vortex flow in vicinity of
 orthogonality point of sound line to velocity
 vector 06 p0936 A67-17738

Plasmoid structure produced by coaxial
 plasma gun with interchangeable polarity
 electrodes, noting experimental setup,
 particle velocity, density, energy,
 etc 06 p1040 A67-18085

Charged particle excitation by random
 electromagnetic field, obtaining velocity
 distribution function via all-order
 perturbation method 06 p1040 A67-18102

Turbulent boundary layer characteristics
 of compliant surfaces, using hot-wire
 anemometer to measure velocity profiles,
 Reynolds stresses and skin friction
 [AIAA PAPER 67-128] 06 p0987 A67-18336

Static temperature-velocity distribution for
 zero pressure flat plate compressible
 turbulent boundary layer with heat transfer
 [AIAA PAPER 67-195] 06 p1116 A67-18362

Nonsimilar solution to complex boundary
 layer problems, using matrix concept to
 integral relations via Taylor series expansion
 of parameters [AIAA PAPER 67-218] 06 p0988 A67-18364

Rectangular and inverted wedge
 recompression step effect on recovery
 factor, heat-transfer coefficient, velocity
 profile and pressure distribution in open
 cavity flow
 [ASME PAPER 65-WA/HT-37] 08 p1278 A67-21320

Helmholtz velocity profile instability in
 atmosphere with unstable density gradient
 /negative Richardson
 number/ 08 p1323 A67-21388

Viscosity effect on stability of plane flame
 front, showing destabilization from linearized
 equations of velocity and pressure
 disturbances 08 p1428 A67-21423

Pressure gradients effects on boundary
 layers grown on wall of wind tunnel,
 obtaining equilibrium boundary layers of
 Clauser type 09 p1489 A67-22415

Gas flow velocity and static pressure
 profiles experimentally measured in
 combustion zone of gas turbine combustion
 chamber model under atmospheric
 conditions [SAE PAPER 670201] 09 p1561 A67-22545

Turbulent fluctuations in rotationally
 symmetrical jet, obtaining velocity profiles
 from integration of motion
 equations 09 p1490 A67-22548

Wall friction coefficient measurement,
 using scale incorporated into
 wall 09 p1501 A67-22577

Dynamics of continuous media, proposing
 new equation in which action modifying
 intrinsic mass has no effect on
 velocity 09 p1534 A67-22580

Field buildup during sudden
 commencement of magnetic storms in
 magnetosphere determined from MHD wave
 and solar wind pressure
 measurements 10 p1630 A67-22777

Deformation of velocity profile in
 inhomogeneous magnetic field, noting
 anisotropic conductivity of
 flow 10 p1686 A67-23670

Knudsen low voltage discharge with hot
 cathode, determining electron distribution,
 velocity profiles, V-I characteristics,
 etc 11 p1831 A67-24020

Turbulent boundary layer phenomena,
 discussing parameters of production
 processes, relation with instability,
 etc 11 p1776 A67-24043

Turbulent boundary layer development
 noting representation of velocity profiles,
 skin friction and eddy
 viscosity 11 p1776 A67-24044

Turbulent boundary layer on smooth flat
 wall, measuring skin friction, turbulence
 intensity, shearing stress, transverse integral
 scale, etc 11 p1776 A67-24045

Symmetrical jets and wakes in streaming
 flow with pressure gradient, noting time
 mean profiles of particular pressure
 fields 11 p1741 A67-24047

Initial turbulence effect on characteristics
 of axisymmetric submerged air jets, using
 thermo-anemometer to measure averaged
 velocity and mean quadratic longitudinal
 pulsation rate component 11 p1779 A67-24320

Behavior of line source function of low
 density gas in presence of nonthermal
 velocity field, examining strong shock
 situation and differential velocity via
 ordered velocity
 structure 11 p1861 A67-24489

Heat transfer of fully developed laminar
 flow of Bingham material between parallel
 plates and linearly varying wall temperature
 noting equations of state, velocity and
 temperature distribution 11 p1883 A67-24944

Free plane jet compared with wall jet,
 noting more rapid lateral expansion of free
 jet 12 p1891 A67-25142

Hydrodynamic boundary layer velocity
 profile on disks in transverse airflow
 analyzed theoretically and by wind tunnel
 tests 12 p1891 A67-25318

Velocity profiles for turbulent ducted flow
 systems analyzed, showing profile decay rate
 for flow pattern 12 p1927 A67-25351

Friction factors and velocity profiles in
 turbulent flow of viscoelastic non-Newtonian
 fluid, noting correlation between frictional
 characteristics and Reynolds
 number 12 p1929 A67-25904

Surface mass addition into turbulent
 boundary layer for attaining equilibrium
 velocity profiles, determining development
 from start of injection 12 p1930 A67-25929

Solutions to Falkner-Skan equation,
 making similarity solutions for pressure
 gradient parameter physically
 acceptable 12 p1893 A67-25935

Turbulent flow through concentric annuli,
 measuring velocity profiles, finding
 maximum velocity radius different from
 value for laminar flow and dependent on
 Reynolds number 13 p2092 A67-26268

Hot wire response equations including
 tangential velocity effects and nonlinearities
 caused by high intensity

turbulence 13 p2095 A67-26914
 Ionized gas flow past oscillating interface in presence of magnetic field, based on MHD boundary layer model with constant velocity profile 13 p2168 A67-27302
 Shear flow, determined by velocity and density profiles, is stable for small disturbances of all wavelengths and Richardson numbers, enumerating eigenvalues 14 p2295 A67-27904
 Upstream velocity profile effect on free mixing of jets with ambient fluid 14 p2240 A67-28107
 Numerical analysis of boundary layer separation effect on evolution of wake, noting sensitivity to initial velocity profile 14 p2297 A67-28129
 Boundary layer in nozzle of arc-heated wind tunnel, obtaining velocity, temperature and density profiles 14 p2299 A67-28171
 Velocity distribution function measurement in rarefied gas flow, using principle based on time of flight of metastable molecules 14 p2316 A67-28193
 Velocity distribution function of gas measured with laser, noting relation to frequency variation of absorption coefficient across spectral line 14 p2317 A67-28194
 Fully developed velocity profile for prediction of hydrodynamic entrance lengths for ducts of arbitrary cross section [ASME PAPER 67-FE-4] 14 p2304 A67-28357
 Planar incompressible free turbulent mixing with arbitrary velocity ratio and axial pressure gradient [ASME PAPER 67-FE-9] 14 p2304 A67-28359
 Flow of conducting incompressible viscous fluid near accelerated plate under parallel plate and magnetic field, noting velocity profiles and stress role 14 p2361 A67-28814
 Two-dimensional wall jet effectiveness measurements and calculation procedures for injection conditions 15 p2468 A67-29128
 Velocity profile analysis in turbulent concentric annular flow, emphasizing correlation of results in inner wall region 15 p2468 A67-29132
 Electrically conducting compressible viscous free jet in presence of transverse magnetic and electric fields solved analytically by perturbation technique 15 p2523 A67-29215
 Free stream turbulence and pressure gradient effects on flat plate boundary layer velocity profiles and heat transfer [ASME PAPER 66-WA/HT-4] 15 p2470 A67-29321
 Correlation measurement in two-dimensional zero pressure gradient boundary layer, noting velocity fluctuation patterns 15 p2471 A67-29652
 Laminar boundary layer equations solved in presence of nonuniform velocity and enthalpy profiles in initial cross section or on bodies extending to infinity upstream and downstream 15 p2472 A67-29689
 Turbulent boundary layer flow properties predicting velocity profiles in region of velocity maximum decay downstream 16 p2657 A67-30614
 Turbulent jet spread issuing into parallel moving airstreams 16 p2657 A67-30615
 Properties of uniformly propagating stable domains in gallium arsenide calculated on basis of velocity-field and diffusion-field characteristics 16 p2727 A67-30851
 Kelvin instability following velocity discontinuity in current-carrying cold collisionless plasmas under magnetic field, deriving dispersion relation and instability criteria from fluid equations 16 p2714 A67-30872
 Argon and nitrogen shock wave damping along tube in absence of effects of oscillation excitation, gas dissociation, ionization and emission 16 p2659 A67-31104
 Hydrodynamic stability of plane incompressible viscous wall jet subjected to small disturbances, determining critical Reynolds number, eigenvalues and eigenfunctions 16 p2660 A67-31213
 Probe measurements of friction drag coefficient and velocity profile of turbulent flow of mercury in circular tube in presence of longitudinal magnetic field 16 p2721 A67-31394
 Velocity profile of vortex region formed downstream of step-shaped wall calculated, assuming flow is turbulent, using similarity hypothesis 16 p2662 A67-31469
 Wall jet compared to plane free jet

examining equilibrium conditions of velocity profile of fluctuation and mean flow determining stress 16 p2662 A67-31470
 Decay and dispersion of disturbance pulse in fluid lines along pipe, considering velocity and pressure characteristics [ASME PAPER 66-WA/AUT-24] 17 p2835 A67-32017
 Three-dimensional laminar boundary layer flow, calculating skin friction and velocity profiles 17 p2790 A67-32284
 Hydrodynamic field of falling sphere in viscous liquid within cylindrical container noting streamlines, velocity variations, etc 17 p2837 A67-32288
 Gas ejection and boat-tailing effect on cylindrical afterbody in supersonic flow 17 p2793 A67-33041
 Correction for experimental velocity profile in compressible laminar boundary layer flow over flat plate 17 p2840 A67-33165
 Stability of plane parallel flows in finite length tube at large Reynolds numbers, noting velocity profile 17 p2841 A67-33266
 Counterflow diffusion flame in forward stagnation region of porous cylinder, detailing flame stability and velocity gradient 18 p3155 A67-33842
 Magnetosonic resonances location in exosphere, showing diagram of Alfvén velocity profile 18 p3042 A67-34389
 Traveling-wave bulk electroconvection induced in slightly conducting liquid with temperature gradient, giving velocity profile equations for plane flow 18 p3029 A67-34736
 Turbulent boundary layer in liquid hydrogen tank, determining attachment point, velocity and temperature profiles 19 p3310 A67-34810
 Aerodynamic forces pressure center on profile in plane rectangular blade cascade 19 p3169 A67-34884
 Rotational velocity and ion density profiles of plasma vortices by measuring radial electric field 19 p3288 A67-35361
 Turbulent velocity fluctuations dynamics in and outside viscous sublayer examined by linearizing motion equation around known mean velocity profile 19 p3209 A67-35414
 Longitudinal surface curvature effects on steady, two-dimensional incompressible laminar boundary layers, noting partial differential equations, computer solution, velocity profile, etc 19 p3209 A67-35415
 Mixing-length velocity profile in boundary layers with transpiration, discussing Tennekes theory and turbulent kinetic energy change rate 19 p3211 A67-35752
 Steady two-dimensional laminar flow of incompressible viscous fluid, noting asymptotic convergence of velocity profile in Prandtl boundary layer 19 p3212 A67-36031
 Natural convection in finite nonzero length vertical channels, using integral technique to derive results for two wall conditions [ASME PAPER 67-HT-16] 20 p3545 A67-36712
 Laminar boundary layer flow of water over flat plates, noting heat transfer effects on velocity profile stability [ASME PAPER 67-HT-41] 20 p3547 A67-36725
 Free convection effect on forced laminar flow of water in horizontal tube with uniform heat flux and velocity profile fully developed [ASME PAPER 67-HT-52] 20 p3548 A67-36734
 Laminar boundary layer with heat transfer in liquids with variable fluid properties, including velocity and temperature profiles [ASME PAPER 67-HT-69] 20 p3550 A67-36749
 Velocity and pressure fields in viscous incompressible fluid flow in inlet of flat channel 20 p3423 A67-37066
 Multistage rocket advantages compared to single stage rocket with respect to attainment of characteristic velocity 20 p3534 A67-37297
 Laminar MHD boundary layer over finite dielectric disk in presence of magnetic field, determining velocity profiles 20 p3501 A67-37305
 Drag measurements for turbulent flow about circular cylinders joined to plane parallel walls, noting dependence on velocity profile 20 p3359 A67-37486
 Velocity field in axisymmetric boundary layer described by nonlinear partial differential equations 20 p3425 A67-37677
 Terminal velocity theory of freely falling body with ballistic coefficient of 200 psf and

altitude region between zero and 60,000 ft 21 p3656 A67-37811
 Velocity profiles of boundary layer of conducting fluid rotating over stationary dielectric disk of infinite radius in magnetic field 21 p3665 A67-38246
 Deformation of velocity profile in inhomogeneous magnetic field, noting anisotropic conductivity of flow 21 p3666 A67-38271
 Mass injection effect on compressible three-dimensional laminar boundary layers analyzed for nonreacting gas, using conservation equations for flow velocity profiles 21 p3613 A67-38852
 Atmospheric humidity effect on lower atmospheric layer turbulence above oceans, discussing velocity, temperature and humidity profile calculation formulas 22 p3828 A67-39220
 Turbulent cylindrical wall jet flow field, velocity profile and surface friction coefficient noting transverse curvature effects 22 p3783 A67-39531
 Correlation measurement in turbulent flow with hot wire anemometer downstream from grid, considering velocity effects 22 p3783 A67-39704
 Flow velocity profile analysis for pressure front steady motion with steady pressure on compressible fluid surface 22 p3784 A67-39826
 Motion of small spherical particles entering upper atmosphere of earth with cosmic velocities studied for terminal velocities 22 p3890 A67-40472
 Dynamical interaction of interplanetary particles with upper atmosphere studied by simplification of motion equation 22 p3890 A67-40473
 High temperature turbulent jet gasdynamic behavior, discussing high temperature plasma jet experiments 23 p3989 A67-40728
 Velocity field around sunspots from H-alpha line spectra 23 p4067 A67-41239
 Transverse curvature parameter in hypersonic flow regime for modifying effects on velocity profile slope, skin friction and heat transfer rate 23 p3993 A67-41755
 Field buildup during sudden commencement of magnetic storms in magnetosphere determined from MHD wave and solar wind pressure measurements 24 p4149 A67-42113
 Velocity profiles of non-Newtonian fluid /polyisobutylene solution/ in helical flow by flow visualization technique, discussing Poiseville and viscometric flows 24 p4145 A67-42708
 Particle streams with greater than 1 TeV energy analyzed by Lobachevskii-Einstein velocity space images method to obtain kinematics 24 p4193 A67-42858
 Negative pion-and proton-nucleon reactions at 17 and 24 GeV/c, using Lobachevskii-Einstein velocity space images method to obtain kinematics 24 p4193 A67-42858
VENT
 Aircraft fuel tank pressurization and venting systems, evaluating refueling, defueling, inerting systems, recuperators and system integration 04 p0554 A67-14883
 Liquid venting concept for zero gravity environment by suppressing vapor generation with open loop refrigeration, using extracted liquid as working fluid 13 p2056 A67-27639
 Low gravity liquid hydrogen tank venting, considering systems with heat exchange for space missions 13 p2057 A67-27640
 Aircraft fuel tank pressurization, discussing pressure supply sources and control system, tank venting, system integration and equipment used 21 p3571 A67-38104
 Space cryogenic propellant storage utilizing vent gas recovery noting storability spectrum plot 22 p3906 A67-40164
 Analytical prediction of cryogenic propellant venting effects on orbital vehicle dynamic behavior, emphasizing vent thrusting and gas impingement 22 p3906 A67-40165
VENTILATION
SA HYPERVENTILATION
 Ventilated airfoil sections characteristics in free jet 05 p0793 A67-17321
 Ventilatory response to carbon dioxide

stimulus at spontaneous and consciously regulated rebreathing rates 07 p1133 A67-19479

VENTILATOR
SA FAN
Three-dimensional flow in axial fan, consisting of rotor only, having finite number of blades, by method of isolated airfoil of finite span 19 p3171 A67-35712
Three-dimensional flow through rotor of single stage axial fan with prescribed spanwise variable circulation 19 p3171 A67-35714

VENTURI TUBE
Transient air flow rates into gas turbine metered, using two critical flow circular arc venturi 03 p0421 A67-13770
Cavitation pitting and flow regime in cavitating venturi using water and mercury indicate microjet impingement is most important damaging mechanism [ASME PAPER 66-WA/FE-39] 04 p0608 A67-15447
Critical air-water flow in converging-diverging annular venturi noting pressure profiles 24 p4143 A67-42280

VENUS
Planetary proximity influence on motion of planetoid, with application to solar influence on Venus as studied by Mariner II 02 p0321 A67-11495
Radio observations of Mercury, Venus and Mars, discussing concepts concerning planets physical condition 03 p0509 A67-13317
Venus brightness temperature and polarization of integral radio emission at 3.75 cm wavelength 04 p0702 A67-15566
Masses of moon and Venus and astronomical unit determined from Mariner II Doppler data, noting sources of error 05 p0895 A67-16575
Venus swingby trajectory for manned Mars mission as possibility in 1978-1986 [AAS PAPER 66-125] 07 p1254 A67-19984
Flight trajectories to moon, Venus and Mars 08 p1394 A67-21115
Rotational velocity of Venus spots based on sidereal rotation measurements 13 p2198 A67-26588
Venus swingby trajectory for manned Mars mission as possibility in 1978-1986 [AAS PAPER 66-125] 13 p2209 A67-27538
Launching of space probes and data obtained on radiation particles and magnetic fields in space 14 p2392 A67-28960
Venus brightness temperature and atmosphere and Mars atmosphere sounded by Mariner II space probe, noting data on Mars magnetic field 14 p2322 A67-28964
Soviet book on radio physics /1965-1966/ reviewing radio-astronomical observations and radar probing of Venus 15 p2553 A67-29241
Cross section and angular scattering law for Venus and Mercury from delay and Doppler frequency shift radar echo measurements 15 p2556 A67-29870
Venus and Mercury intrinsic rotation rates and surface radar reflectivity of former from radar echo measurements 15 p2556 A67-29872
Radio observations of Mercury, Venus and Mars, discussing concepts concerning planets physical condition 16 p2741 A67-30493
Microwave spectrum and observation at 6 cm wavelength of Venus to determine total intensity and polarization of radiation 16 p2747 A67-30987
Brightness temperature reduction of Venus at decimeter wavelengths determined from 49.1 cm measurements 16 p2749 A67-31409
Radio and radar observations of Mercury, Venus and Mars 18 p3123 A67-34144
Radar studies of Venus noting values for rotation vector, latitudes and longitudes of several features and Earth influence on Venus rotation [JPL-TR-32-1081] 18 p3123 A67-34146
Capture probability at Venus resonant rotation rate implying fluid core similar to earth 18 p3136 A67-34587
21.2 cm spectra of Jupiter, Venus, Mars and Saturn noting mean effective brightness temperatures 21 p3709 A67-38993
Venus rotation, discussing radar and optical and UV photography observations 23 p4063 A67-40800
Venus surface temperature measured using difference between optical and radar radii, cloud temperatures and adiabatic lapse

rate 24 p4225 A67-41827
Tectonic activity on Venus compared with earth, discussing convection currents and temperature gradients in crust and mantle 24 p4227 A67-42222

VENUS ATMOSPHERE
Manned geophysical observations from satellites as training ground for planetary research, especially Venus atmosphere 01 p0155 A67-11395
Water vapor lines in spectrum of Venus obtained by photoelectric scanning of spectrum 02 p0324 A67-11769
Doppler-displaced lines of water vapor originating in atmosphere of Venus observed on three Coude spectrograms 02 p0324 A67-11774
Induced absorption coefficients in atmosphere model measured for calculation of Venus lower atmosphere properties from radio observations 03 p0394 A67-12949
Deep circulation in Venusian atmosphere model opaque to solar and planetary radiation but with differential heating 03 p0514 A67-14310
Interpretations of microwave emission from Venus through experiments in which anomalous signals have been observed in X-band from glow discharges 04 p0699 A67-14952
Surface temperature of Venus 05 p0886 A67-16029
Photometry of integrated light of Venus, inferring presence of ice in atmosphere from halo effect of brightness dispersion 05 p0892 A67-16407
Mariner Venus 1967 space probe, obtaining atmospheric pressure density and refractive index from radio signal frequency, intensity and phase changes [AIAA PAPER 67-118] 06 p1085 A67-18310
Thermodynamic equilibrium composition of Venus atmosphere computed from atomic composition deduced spectroscopically 07 p1256 A67-20022
Anisotropic nonconservative scattering in modified Schuster-Schwarzschild approximation and Venus cloud layer 08 p1385 A67-20931
Dielectric relaxation of gases and sharp rise in microwave absorption coefficient in Cytherean atmosphere 08 p1401 A67-21372
Venus atmosphere spectra obtained by Michelson interferometer, finding HCl lines consistent with 2-mm Amagat of gas [JPL-TR-32-1106] 11 p1863 A67-24510
Microwave spectral brightness measurements of Venus compared with several model atmospheres 11 p1865 A67-24601
Voyager project goals, orbital operations, capsule descent, navigational systems, etc 12 p2002 A67-25232
Distribution of radio brightness temperature over disk of Venus 13 p2200 A67-27333
Radiant energy transfer below cloud cover in Venus atmosphere, noting greenhouse effect caused by atmosphere containing components capable of IR absorption 14 p2383 A67-27859
Voyager project goals, orbital operations, capsule descent, navigational systems, etc 16 p2751 A67-31487
Two-layer model of Venusian atmosphere satisfying radioastronomic and radar self-radiation measurements 17 p2941 A67-32322
Upper limits on liquid water content in Venus atmosphere 17 p2945 A67-32652
Ashen light and magnetic field of Venus 17 p2948 A67-33096
Volcanic and tectonic activity on Venus inferred from high surface temperature, considering possible effect on atmosphere obscuration 17 p2951 A67-33232
Atomic and molecular processes in Cytherean, Martian and Jovian upper atmospheres 18 p3124 A67-34158
Venus surface temperature and microwave emission, discussing ionospheric model, greenhouse effect, microdischarge model, radio aurora, etc 18 p3135 A67-34543
Venus and Mars atmosphere and surface studied by radio astronomy 19 p3317 A67-34796
High resolution spectra of Venus and Jupiter using image intensifier and solar spectrograph, measuring abundances in planetary atmospheres 20 p3521 A67-36309
Nonthermal radio emission from electric discharges within Venus water

clouds 20 p3529 A67-37480
Simultaneous UV photographs and radar cross section measurements of Venus, discussing atmospheric motion and rotation 21 p3705 A67-38611
Soviet book on planetary physics covering Martian, Venusian and Mercurian atmospheres, Venusian surface temperature and Jovian radio emission 21 p3707 A67-38933
Indigenous biology in Venus clouds, proposing isopycnic float bladder macroorganism ingesting water and minerals blown up from surface by pinocytosis 22 p3750 A67-39556
Mariner Venus 1967 space probe, obtaining atmospheric pressure density and refractive index from radio signal frequency, intensity and phase changes [AIAA PAPER 67-118] 22 p3886 A67-40094
Venus radiation spectrum in mm range from Venus atmosphere models 22 p3886 A67-40120

VENUS FLY TRAP ROCKET S COLLECTOR
VENUS PROBE
Trajectory possibilities for Venus swingby mission and role in manned exploration of Mars [AIAA PAPER 66-37] 07 p1248 A67-19363
Mariner IV spacecraft modification for Venus mission, discussing extent of changes 09 p1571 A67-21682
Scattered Lyman alpha radiation in geocorona analyzed using satellite mounted equipment 10 p1706 A67-23223
Meteoritic matter investigation with Venus II and Zond III probes, discussing impact rate and distribution along flight path 10 p1708 A67-23241
Radar, radio astronomic and IR spectroscopic observations of Venus surface and atmosphere, examining general and surface data, chemical composition and atmospheric model construction 11 p1867 A67-24843
Energy spectra of solar wind ion fluxes outside magnetosphere measured using Venus 3 space vehicle 13 p2194 A67-27331
Solar wind ion concentration and velocity measurements from Venus III and Pioneer IV 13 p2195 A67-27343
Micrometric measurement of lengthening of horns of Venus crescent, phase and moment of dichotomy 17 p2942 A67-32329
Thermophysical research requirements for Venus Lander, Jupiter Entry Probe and Mercury Orbiter planetary exploration missions 24 p4227 A67-42041

VENUS RADAR REFLECTION
Frequencies of radar echoes from Mercury and Venus measured, for testing Doppler formula 01 p0026 A67-10920
Radar observations of Venus at 23 cm noting flight time and Doppler shift measurements of reflected signals 05 p0889 A67-16297
Radar observations of Venus at 3.8 cm noting low value of cross section, echo spectrum, polarization characteristics, absorption cross section and atmospheric attenuation 05 p0889 A67-16298
Interpretation of radar observations of Venus, Mercury and Mars with outline of direction of current radar astronomical research 07 p1246 A67-19053
Bistatic CW radar observations of Venus conducted by U.S.S.R. and Great Britain during 1966 14 p2265 A67-28403
Resonance rotation of Venus, discussing spin period determinations and retrograde nature of rotation from radar observations 19 p3317 A67-34952
Simultaneous UV photographs and radar cross section measurements of Venus, discussing atmospheric motion and rotation 21 p3705 A67-38611

VERNEUIL TECHNIQUE
Apparatus for refractory single crystal fusion growth at high temperature using arc melting 21 p3636 A67-38769

VERNIER ENGINE
Surveyor vernier propulsion system, discussing design of thrust chamber, propellant tank assemblies, functions of VPS, etc [AIAA PAPER 66-593] 08 p1413 A67-21516
Propellant composition variation for improving cooling characteristics of Surveyor vernier propulsion system [AIAA PAPER 66-627] 08 p1374 A67-21517

VERONIQUE ROCKET

Solar X-ray emission centers photographed by Veronique rocket 04 p0698 A67-14917

VERTEBRAL COLUMN

Vertebral fractures in pilots from helicopter accidents in dorso-lumbar junction of spinal column 12 p1902 A67-25170
Radiological findings from pilots afflicted with vertebral fractures from ejection injuries 21 p3575 A67-38510
Human spinal column stiffness under deflection rate/axial compression/ produced by impact 23 p3954 A67-41592

VERTICAL AIR CURRENT

Wind tunnel technique for measuring frequency response of flexible airplane to vertical sinusoidal gusts [AIAA PAPER 65-787] 03 p0354 A67-12908
Monograph on problems of cloud physics covering evolution of preinversion stratiforms and vertical velocities determination in lower atmospheric layer 11 p1816 A67-24521
Vertical atmospheric flow mean velocity determination within fixed area from wind probe observations at fixed points 11 p1816 A67-24523
Power spectra and dissipation rate for vertical velocity fluctuations measured with sonic anemometers 19 p3251 A67-35056
Temperature convection and vertical velocity fluctuations measured and compared with similarity theory of free convection and laboratory heated plates experiments 19 p3252 A67-35059

VERTICAL DISTRIBUTION

Vertical distribution of ozone measured by rocket, using UV absorption 02 p0238 A67-12065
Michelson type interferometer for Nimbus meteorological satellite to obtain vertical temperature, humidity and ozone profile 02 p0246 A67-12365
Vertical ozone distribution in atmosphere and transport processes, noting results of tracer experiments 03 p0414 A67-14090
Topside ionosphere over American continents, noting electron density and scale height distribution [RASSA PAPER 1-10-132] 03 p0417 A67-14243
Laser radar returns from lower troposphere compared with vertical ozone distributions indicate inverse relationship 04 p0612 A67-14676
Radar measurement of vertical density profiles of clouds and precipitation 04 p0650 A67-14689
Terrestrial radiance in middle UV noting Rayleigh scattering, vertical distribution of air, oxygen and ozone, attenuation factors, etc 04 p0613 A67-14695
High altitude vertical photoelectron distribution from electron concentration measurements by Cosmos V and IMP I and II 05 p0795 A67-16061
Height profile of Sq current in ionosphere, showing dependence on electric field direction 05 p0799 A67-16872
Emf as cause of vertical downward and upward ionization drift in F region of ionosphere during magnetic storm 05 p0801 A67-17141
Vertical drift velocity of small scale ionization inhomogeneities in ionosphere, noting seasonal variation 05 p0802 A67-17146
Stormer height measurements of aurora, analyzing height distribution at various geomagnetic latitudes, noting relation to solar activity 06 p0997 A67-18694
Vertical interpolation of data from constant pressure to constant density surfaces for meteorological purposes 06 p0999 A67-18741
Vertical distribution of neutral composition of atmosphere between 100 and 200 km, comparing mass spectrometer with optical measurement 07 p1169 A67-19097
Local peculiarities of vertical distribution of ozone in equatorial and polar regions for different turbulent dynamic models of stratosphere 07 p1173 A67-19696
Vertical measurement of ionospheric absorption at continuously varying frequency, showing diurnal variation of absorption 07 p1174 A67-19706
Vertical and horizontal variations of intensities of auroral OI and molecular nitrogen ion emissions 08 p1328 A67-21480
Vertical transport of latent and sensible heat of IR cooling and short wave heating 09 p1490 A67-21550

Vertical profile of concentration of atmospheric electron-ion gas flux under action of gravitational field 10 p1631 A67-22804
Upper air turbulence gusts, describing vertical component test method using F type radiosonde 10 p1678 A67-23085
Distribution curves of ion density and condensation particle concentration in layers of atmosphere near sea level, noting criteria for instruments 10 p1657 A67-23695
Height distribution of Sq current intensity in midlatitude ionosphere as function of electrostatic field 11 p1786 A67-24333
Vertical distribution of ozone over Tallahassee, noting maximum and minimum density altitudes, seasonal variations, etc 11 p1787 A67-24555
Model for vertical eddy heat flux in stable atmosphere 13 p2149 A67-26275
Meridional and vertical wind components analyzed for angular momentum, balance, heat influx and internal friction 13 p2113 A67-26678
Interaction between different layers of homosphere, discussing separating and null layers and vertical interaction 13 p2115 A67-26864
Approximate determination of satellite lifetime by nomogram constructed on basis of known upper atmosphere density data 13 p2213 A67-27324
Vertical distribution of heating rate by radiative processes over Northern Hemisphere presented in zonal cross sections 13 p2116 A67-27459
Vertical distribution of tropospheric and stratospheric ozone based on observations of U.S. ozonometric stations at various latitudes 14 p2308 A67-27927
Seasonal and diurnal variation of parameters of vertical electron density distribution 14 p2308 A67-27934
Unlikelihood of obtaining useful information on atmospheric composition from indirect sensing of scale heights by satellites 14 p2310 A67-27959
Temperature and humidity fields vertical structure determined under conditions of stratified cloudiness 14 p2346 A67-28765
IR radiation measurements by spectrometers flown on board stratospheric balloons, considering sky brightness, vertical distribution and thermal atmospheric emissions 14 p2313 A67-28768
Radio probe to derive relations between ozone content of lower stratosphere and origin of air in layers 15 p2474 A67-29525
Free atomic sodium distribution in daytime upper atmosphere, noting thin layer formation and radiative transfer 15 p2475 A67-29616
Atmospheric ozone vertical distribution, discussing optical measurement method 16 p2676 A67-31375
Atmospheric ozone concentration measurement using potassium iodide method 16 p2676 A67-31376
Atmospheric ozone vertical distribution, measurement, discussing equipment design and underlying principles of method 16 p2676 A67-31377
Volume emission profile vs height of positively ionized nitrogen molecule first negative band at 4278 angstroms 16 p2666 A67-31408
Propagation rate distribution as function of geomagnetic latitude provides evidence for geomagnetic effects on vertical ionization drifts in F region of ionosphere 16 p2668 A67-31894
Vertical electron temperature and concentration distribution up to 480 km at middle latitudes from rockets 17 p2842 A67-32253
Vertical electron density profile method for determining altitude of lower boundary of ionosphere 17 p2842 A67-32383
Satellite technique for sounding atmospheric optical properties and height distribution of ozone and aerosols 18 p3040 A67-33853
Ionospheric and magnetospheric neutral and charged particles temperature vertical distribution, noting effects producing variations 18 p3040 A67-34033
Stratospheric aerosol concentrations observed by optical radar echoes compared with expected return from molecular atmosphere to obtain vertical

profile 18 p3042 A67-34493
Long-wave radiation cooling effect in troposphere/stratosphere calculated based on vertical temperature and moisture profiles from nighttime probe 19 p3213 A67-34852
Absorption of total solar radiation using vertical profiles from balloon observations, estimating attenuation due to aerosols 19 p3214 A67-34854
Atmospheric ozone content compared for discrepancies between theoretical and experimental results for vertical, latitudinal and seasonal variations 19 p3214 A67-34856
Height profile of atomic oxygen 6300 angstrom emission in night airglow determined by rocket photography 19 p3215 A67-35177
Arctic upper atmosphere neutral gas composition and altitude distribution studied, using meteorological rockets 19 p3219 A67-35251
Vertical distribution of diffuse sky light in stratosphere determined by rocket measurements, noting intensity peak in aerosol layer 19 p3221 A67-35273
Iranian ionospheric observations, giving monthly median values of vertical-incidence data and critical frequency graphs 19 p3224 A67-35489
Searchlight brightness measurements for vertical turbidity layer of troposphere using computing scattering functions 19 p3225 A67-35532
Stability of continuous baroclinic flow in zonal magnetic field examined for zonal-flow profile of hyperbolic tangent form 19 p3253 A67-35918
Vertical distribution of meteor showers obtained by measuring distribution in decay times of underdense radio echoes 20 p3521 A67-36303
Metastable helium atom altitude distribution and 10830 angstrom radiation emission rate, discussing possible explanation of helium loss from atmosphere 20 p3427 A67-36310
High altitude vertical photoelectron distribution from electron concentration measurements by Cosmos V and IMP I and II 21 p3615 A67-37848
EMF as cause of vertical downward and upward ionization drift in F region of ionosphere during magnetic storm 21 p3619 A67-38483
Vertical drift velocity of small scale ionization inhomogeneities in ionosphere, noting seasonal variation 21 p3619 A67-38488
Smith gyrofrequency model for determination of vertical electron concentration distribution in magnetosphere, using whistling atmospherics data 21 p3621 A67-39022
Master matrix containing initial values of geomagnetic inclination and gyrofrequencies for storage in computer memory to calculate ionospheric vertical profiles 21 p3623 A67-39046
Vertical distribution of mechanical wave energy density in lower atmosphere and energy fraction escaping to high altitudes derived by integral transform methods 21 p3655 A67-39088
Empirical orthogonal functions, determining vertical atmospheric temperature profiles from radiometric satellite measurements 22 p3828 A67-39325
Field-aligned irregularity instabilities in ionization vertical gradient, showing unstable E region for irregularities of scale size 20 m-6 km 22 p3789 A67-39475
Ozone parameters determination from measurements of radiation backscattered by earth atmosphere 22 p3794 A67-40365
Atmospheric density, temperature and composition altitude variation measured by satellite observation of laser backscatter Raman component 22 p3806 A67-40366
Vertical distribution of thermal stability in lower stratosphere compared with atmospheric ozone from ozone and temperature soundings 22 p3829 A67-40471
Vertical profile of concentration of atmospheric electron-ion gas flux under action of gravitational field 24 p4150 A67-42141
Vertical distribution of cloud condensation nuclei in free atmosphere investigated by flow type onboard photoelectric apparatus to calculate washout coefficients 24 p4181 A67-42163

VERTICAL FLIGHT

Tip vortex method for helicopter rotor design during vertical descent 14 p2243 A67-28641

VERTICAL MOTION

Three-dimensional oscillatory motions generation and propagation in solar atmosphere 05 p0900 A67-17074

Velocity of vertical motion of lower ionosphere determined, using radio spectral analysis 05 p0801 A67-17144

Vertical velocities in atmospheric front motions, noting pressure and temperature field distributions and application of computer to solve obtained equations 07 p1219 A67-19356

Statistical characteristics of atmospheric ozone distribution, determining autocorrelation and cross correlation functions, concentration and temperature profiles 07 p1170 A67-19357

Motion induced by sources and sinks distributed along vertical boundary of rotating fluid, noting role of ekman layers 09 p1489 A67-22416

Vertical ionospheric perturbations observed from January 1963 through May 1965 10 p1630 A67-22789

Vertically moving perturbations in nighttime ionosphere studied from vertical ionospheric sounding data, discussing type A4 which develops in F layer near maximum ionization 10 p1631 A67-22805

Lower thermospheric turbulence investigated for scale size, turbulent velocity spectra and energy dissipation rate 10 p1643 A67-23250

Divergent vertical helicopter oscillations resulting from physical presence of pilot in collective control loop 11 p1744 A67-24591

Motions of chromospheric fine structure in weak plage analyzed, using time resolved H-alpha spectra for estimating line-of-sight velocities of objects 12 p2001 A67-25222

Vertical component of gusts in upper atmosphere estimated from rotation rate of ascending radioprobe fan 12 p1964 A67-26165

Upper atmospheric turbulence velocity probability density investigated in 90 to 110 km region 14 p2346 A67-28058

Quartz sand particles descending motion and heat transfer in gas vertical tube, determining temperature profile 17 p2967 A67-32132

Linear theory for steady motions in rotating stratified fluid 19 p3209 A67-35410

Ion layer formation in E region, assuming sinusoidal vertical motions and ion-electron recombination following attachment law 19 p3222 A67-35456

Stratospheric mean adiabatic vertical motion and temporal correlations with temperature, isobaric height, zonal/meridional wind and horizontal kinetic energy computed based on seasonal averages 19 p3224 A67-35529

Velocity of vertical motion of lower ionosphere determined, using radio spectral analysis 21 p3619 A67-38486

Vertical ionospheric perturbations observed from January 1963 through May 1965 24 p4149 A67-42125

Vertically moving perturbations in nighttime ionosphere studied from vertical ionospheric sounding data, discussing type A4 which develops in F layer near maximum ionization 24 p4150 A67-42142

Velocity and path of vertical motion of constant thrust rocket in homogeneous gravitational field, giving hyperbolic acceleration expression as time function 24 p4241 A67-42578

VERTICAL TAKEOFF AND LANDING

/VTOL/

S VTOL

S VTOL AIRCRAFT

VERY HIGH FREQUENCY

Performance and design characteristics of solid state microwave converters for converting VLF telemetry receivers to L-and S-bands 02 p0196 A67-12006

Small signal RF amplification of VHF MOS transistors, considering TA2840 triode and TA7010 dual-insulated-gate transistors used as VHF amplifiers 02 p0218 A67-12101

Internal modulation and heterodyning in construction of highly linear large-deviation VHF solid state FM oscillator /FMO/ 03 p0381 A67-13636

VHF backscatter observations of radio auroral radar echo occurrence at sunspot

maximum associated with spirals in geomagnetic latitude and time, magnetic disturbance levels and season 03 p0513 A67-14113

VHF transistor, attempting design of 60 MHz passband amplifier 13 p2077 A67-26653

Vhf antenna array, electronically despun, designed for spin-stabilized synchronous-altitude communications 14 p2288 A67-28693

Nature of nighttime F-layer irregularities responsible for scintillation of VHF signals received from radio stars and earth satellites [AGARDOGRAPH 95] 15 p2482 A67-30290

VHF radar reflections from artificial earth satellites used to analyze amplitude scintillations in ionosphere [AGARDOGRAPH 95] 15 p2482 A67-30292

Reflection and scattering from lunar surface of meter radio waves emitted by lunar orbiter 17 p2948 A67-32976

Penning ionization gauge discharge nonlinear response to VHF signals, discussing resonance behavior 19 p3275 A67-35110

VERY HIGH FREQUENCY RADIO

EQUIPMENT

Aircraft-to-ground communications using Applications Technology Satellite B as repeater in VHF COM band 01 p0024 A67-10665

VHF antenna proposed as working gain standard, determining antenna gain by two-identical antenna method 03 p0385 A67-13859

Magnetometer predictions of geomagnetic disturbances and intense sporadic E layer occurrences at various sunspot cycle times in auroral zone and effects on VHF absorption 03 p0415 A67-14118

VHF and UHF communications between transoceanic commercial aircraft and ground stations by means of aeronautical communication satellites 06 p0961 A67-17701

VHF ILS equipment achieves necessary instrumental accuracy for automatic landing operation 09 p1529 A67-22643

Communications satellites for high power transmission of TV and VHF signals, considering synchronous satellites, antennas, stabilizing systems and weight 11 p1870 A67-24706

VERY LOW FREQUENCY

Characteristics of normal atmospheric, discussing VLF characteristics due to return strokes 01 p0109 A67-11228

Frequency spectra of VLF hiss near auroral zone analyzed by Injun III satellite 04 p0614 A67-14958

Nighttime magnetospheric auroral VLF hiss generation by suprathermal particle associated with coherent electron plasma radio emission 04 p0618 A67-15686

Japanese sounding rocket measurements of intensity and frequency time variations in ionosphere to determine VLF radio noise 05 p0763 A67-16888

Comparison of VLF emissions of two conjugate stations, noting statistical results for diurnal variation, magnetic activity, hiss, etc 06 p0997 A67-18698

VLF atmospheric noise level fluctuations, discussing daily variations as function of solar zenithal angles, sunrise and sunset and confusion of ionospheric propagation 07 p1171 A67-19422

VLF radio signal phase and amplitude interference observed on GBR-16.0 kc/s transmissions in November and December 1965 08 p1295 A67-20988

Dual frequency VLF timing system for synchronization of remotely located clocks, noting WWVL radio carrier frequency, signal generator, etc 09 p1494 A67-21619

Computer method study of reflection and transmission coefficients in VLF range, noting effect of ionospheric D region electron density profiles 11 p1752 A67-24219

Phase measurements of VLF transmission over long distance transequatorial path 12 p1906 A67-25942

Global distribution of standard time by VLF for synchronization with microsecond accuracy 14 p2263 A67-28389

VLF noise emissions originating in ionosphere and magnetosphere with reference to ground-based, rocket and satellite observations 14 p2265 A67-28414

Atmospheric noise properties possible influence on communication, measuring intensities and short term amplitude

functions 14 p2266 A67-28416

Vlf transequatorial wave propagation, noting phase cycle slipping during sunrise transition 16 p2630 A67-31848

Periodic field strength variations during, sunrise on vlf signals in long path propagation noting amplitude minima and stepwise phase increase 16 p2630 A67-31849

Modal interference of VLF radio waves investigation from field strength data, noting isotropic case 16 p2631 A67-31850

Sunrise variations of phase and amplitude of vlf signals over single long path interpreted as interference between waveguide modes 16 p2631 A67-31851

Multimode propagation and mode conversion at sunrise and sunset lines explaining diurnal variations on vlf paths 16 p2631 A67-31852

Attenuation rates at vlf from aircraft measurements presented as curves of dominant waveguide mode vs. geomagnetic bearing of propagation path 16 p2631 A67-31854

Frequency shifts on whistler mode signals from stabilized VLF transmitter from ionosphere and magnetosphere effects, noting electron density 16 p2631 A67-31856

Reflection coefficients of sharply bounded ionosphere for plane waves incident from arbitrary direction at magnetic equator 16 p2632 A67-31863

VLF transmitter design criteria and characteristics for global time and navigation signal network 17 p2824 A67-32494

Ionosphere collision frequencies and densities studied by rocket measurements of magnetic field of VLF wave radiated from ground 18 p3041 A67-34233

High latitude disturbances influence on VLF propagation, showing high correlation with auroral absorption 18 p3004 A67-34428

Earth-ionosphere whispering-gallery nature at VLF analyzed, using mode equation for idealized earth ionosphere model 19 p3184 A67-35827

Resonance for VLF waves by ionospheric propagation using Haselgrove whistler ray tracing method, interpreting path shape as function of gradients 20 p3427 A67-36372

Excitation of earth-ionosphere waveguide by VLF source for case of azimuth dependent properties of source and ionosphere 20 p3428 A67-36373

VLF radio noise during auroral display studied by ground and rocketborne receivers, suggesting emissions triggered by high energy electron fluxes 20 p3428 A67-36374

VLF radio wave tracking stations for ionospheric propagation investigation using atomic clock 20 p3386 A67-37481

VLF radio reception anomalies explained by ephemeral natural satellite still in orbit, assuming reflections taking place near satellite perigee 21 p3582 A67-38514

Satellite and ground observations of VLF emissions, summarizing intensity, diurnal and seasonal variation, emphasizing chorus and hiss characteristics 22 p3794 A67-40083

Magnetospheric discrete VLF emissions, discussing gyroresonance extension, resonant electron and emission frequency 23 p3995 A67-40802

VLF transmissions during SIDs for compatibility with general form of theory of waveguide mode propagation 24 p4149 A67-42067

Distant atmospheric waveform at night analyzed using digital computer for VLF phase spectra 24 p4149 A67-42068

VERY LOW FREQUENCY EMISSION RECORDER

Ionospheric electron density profile determined by local measurements of VLF fields radiated by ground emitter 03 p0413 A67-13531

Relations between VLF emissions of whistler and dawn choruses types and that of ULF emissions /pearl type oscillations and rapid irregular pulsations/ 04 p0617 A67-15500

FR-1 satellite data on VLF propagation in lower magnetosphere 10 p1649 A67-23301

Ion composition and natural electromagnetic emissions of VLF phenomena observed by Alouette I and II 10 p1649 A67-23303

Magnetospheric regions of amplification of VLF emissions and micropulsations 13 p2115 A67-26858

Higher harmonic components of tweeks as evidence of adequacy of waveguide mode theory of VLF propagation between earth and ionosphere 14 p2307 A67-27888

Pc 1 micropulsation signals classified as hydromagnetic whistlers and periodic hydromagnetic emissions, suggesting cyclotron instability process as generation mechanism of latter 17 p2853 A67-33253

VLF emission associated with aurora and particle precipitation, describing receiving equipment, types of emission and occurrence patterns 18 p3039 A67-33621

Enhanced VLF emissions near and south of auroral zone, discussing properties, geomagnetic disturbances, riometer absorption, time interval, polarity, etc 18 p3039 A67-33622

VESSEL

SA CIRCULATORY SYSTEM

SA PRESSURE VESSEL

Free and forced oscillations of body with cavity partially filled with viscous fluid 10 p1679 A67-23029

Forced and free oscillation characteristics of ideal incompressible fluid contained in cavity shaped as rectangular parallelepiped with free surface under deformations 10 p1679 A67-23030

Soviet book on molecular flow in vessels covering mass balance, energy exchange, rarefied gas, etc 24 p4191 A67-42359

VESTIBULAR APPARATUS

Cupular function of man under acceleration, noting electroencephalographic results on caloric nystagmus under 1.2, 3 and 4 g and postrotational nystagmus 05 p0756 A67-16324

Flight simulator experiments test pilots ability to disregard senses and trust only flight control instruments 14 p2255 A67-28220

Extraterrestrial vestibular research in orientation of humans in space, noting possible disorders due to radiation and lack of protection 15 p2425 A67-29106

Prolonged recording from single vestibular units in frog during plane and space flight, significance and technique 15 p2430 A67-29281

Effects of irritation of vestibular apparatus on adaptability of human eye to darkness, studying rate of recovery of sharpness of vision 16 p2614 A67-30918

Bibliography dealing with vibration, acceleration and ionizing radiation on vestibular apparatus, noting lack of information 23 p3943 A67-40764

Precentrifugation effect on radiation reactions of vestibular analyzer in guinea pigs, establishing substantial spontaneous electric activity stimulation in hind legs extensor muscles 23 p3944 A67-40773

Semicircular canal physiological response in cats recorded for case of parallel swing rotation, noting mechanical excitation mode of canal 23 p3952 A67-41576

Vestibular organ acceleration while walking at lunar and earth gravity 23 p3953 A67-41584

Electric stimulus effect on vestibular apparatus responses to acceleration increasing or decreasing reactions depending on applied voltage 24 p4112 A67-41859

VESTIBULAR EFFECT

Vestibular section of labyrinth contribution to postrotational changes in level of adrenalin and noradrenalin content in some tissues of white rats 03 p0365 A67-14330

Vestibular stimulation effect on activity of neurons of optical cortex of curarized cats under vertical acceleration 13 p2058 A67-26758

Temporary irritation by anti-g and change in vestibular motor reflex action under laboratory conditions 14 p2257 A67-28224

Visual arousal interaction and specificity of nystagmic habituation 17 p2805 A67-31958

Vestibular inaptitude in atmospheric and space flight environment [AD-640908] 19 p3178 A67-35884

Effects of electric stimulation of human vestibular apparatus recorded by monosynaptic H-reflex technique 20 p3369 A67-36270

Modification of rat sensitivity to rotation through vestibular end organ damage or previous vestibular experience, studying activity changes 20 p3371 A67-36818

Biomedical results for various human

medical systems during weightlessness experiments of Gemini program, noting vestibular function and EVA 22 p3752 A67-40534

Habituation transference in Coriolis stimulation for change from passive lateral chair tilts to various active head tilts during rotation 23 p3953 A67-41585

Involuntary vestibularly driven head movements in man during rotational simulation 23 p3959 A67-41659

VESTIBULAR TEST

Vestibular tests of caloric irrigations and mild angular accelerations of semicircular canals of professional figure skaters 03 p0364 A67-14288

Gemini inflight experiments on space perception via measurements of ocular counterrolling as test of otolith function 13 p2062 A67-26920

Flight simulator motion enhancement and potential for flight crew training, examining human vestibular system 13 p2064 A67-27268

Vestibular, tactual and proprioceptive information in judging Coriolis rotation and attitudes during rotation and pitching on piloted flight simulator 22 p3751 A67-39605

Inverted pendulum and VTOL control experiments with and without motion cues, discussing various motion effects 22 p3755 A67-40087

Equipment integration for Apollo Application Program /AAP/ physiological experiments, discussing design and dimensions [AIAA PAPER 67-846] 24 p4117 A67-42982

VHF OMNIRANGE

S VOR SYSTEM

VIBRATION

SA ACOUSTIC VIBRATION

SA BENDING VIBRATION

SA BREATHING VIBRATION

SA FLUTTER

SA FORCED VIBRATION

SA FREE VIBRATION

SA LATTICE VIBRATION

SA LINEAR VIBRATION

SA MAGNETOELASTIC VIBRATION

SA MISSILE VIBRATION

SA OSCILLATION

SA RANDOM VIBRATION

SA RESONANT VIBRATION

SA SELF-INDUCED VIBRATION

SA STRUCTURAL VIBRATION

SA TORSIONAL VIBRATION

SA TRANSVERSE VIBRATION

Heat transfer - AICE International Conference, Chicago, August 1966, Volume 3, Single phase, mass transfer and vibrations 04 p0732 A67-15837

Advances in applied mechanics, Volume 9, covering hydrodynamic stability, free oscillations, nonlinear vibrations and viscoplasticity 08 p1352 A67-20308

Geometric analysis of vibration of nonlinear systems with one degree of freedom 08 p1353 A67-20311

Calibration of vibrational transition of CO at various pressures to determine vibration-rotation wave numbers 13 p2160 A67-26600

Book on analytical methods in vibrations covering general mathematical formulations of common features of various vibrating systems 16 p2765 A67-30999

Test accelerometer comparison calibrations via vibration standards, discussing sensitivity, relative motion and error analysis 23 p4003 A67-41336

VIBRATION ABSORBER

Discontinuous impact vibration absorber with small auxiliary mass sliding in slit of rigid body excited by sinusoidal oscillation 01 p0161 A67-10645

Stability of two-impacts-per-cycle motion of impact damper 04 p0631 A67-15911

Dynamic vibration absorber for reducing transient vibrations of one degree of freedom system with tuning criteria formulated as function of root line of characteristic equation 10 p1715 A67-22913

Forced steady state response of linear harmonic oscillator with impact absorber attached, developing stability criterion [ASME PAPER 67-VIBR-10] 11 p1795 A67-24170

Frequency response, equation of motion, elastic restraint and structural flexibility of gyroscopic vibration absorber, noting antiresonant frequency functions [ASME PAPER 67-VIBR-13] 11 p1795 A67-24173

Electrodynamic vibration absorber attached to single degree of freedom vibrating system as passive or active device with or without feedback [ASME PAPER 67-VIBR-18] 11 p1796 A67-24177

Vibration absorbers effectiveness determined using stiffness and mobility method, noting detuning [ASME PAPER 67-VIBR-65] 11 p1873 A67-24206

Cabin noise reduction in DC-9 by tuned vibration absorbers attached to engine support structure [AIAA PAPER 67-401] 15 p2421 A67-30368

Cadmium telluride electrical light absorption oscillations noting comparisons between experiment and theory, electric field, temperature range, etc 19 p3301 A67-34772

VIBRATION DAMPER

Motion stability of unbalanced gyroscope in Cardan suspension mounted on rotating platform 04 p0620 A67-14790

External damper effectiveness in attenuating vibration of launch vehicle near launch umbilical tower 04 p0598 A67-15248

Tuned viscoelastic vibration dampers effect on responses of cantilever and clamped-clamped beams subject to Euler-Bernoulli beam equation, discussing loss factors based on transmissibility spectra 06 p1110 A67-18859

Electric analog and mechanical model used to investigate single particle impact dampers 07 p1262 A67-19410

Electrodynamic vibration absorber attached to single degree of freedom vibrating system as passive or active device with or without feedback [ASME PAPER 67-VIBR-18] 11 p1796 A67-24177

Freely precessible gyroscope viscous fluid nutation damping response to translational and vibration accelerations near critical frequencies 12 p1942 A67-25679

Normal mode analysis of multispan skin-stringer structure with isolated tuned viscoelastic dampers at arbitrary surface points 17 p2960 A67-32579

Incompressible fluid drag force on sphere rolling at constant speed in closed-end tube [ASME PAPER 67-APM-18] 17 p2840 A67-33149

Amplitude of forced flexural vibrations of free rotating shaft under arbitrary load with dampers, taking into account viscous friction 21 p3728 A67-38834

Cold welding under flight conditions of ATS silver-plated beryllium copper damper boom, discussing ultrahigh vacuum equipment and test techniques 24 p4160 A67-42033

VIBRATION DAMPING

Asymptotic expansion of transient forces on finite thin wing in oscillatory upwash field treated by derived expression for change of generalized aerodynamic damping coefficients with respect to frequency parameter 03 p0352 A67-13896

Patching method applied to nonlinear differential equation of forced oscillation of second order relay system with damping 03 p0393 A67-13901

Oscillating field of vessel effect on accuracy of readings of gyrocompass with negative fluid/pendulum 03 p0425 A67-14283

Vibrational damping of externally pressurized orifice journal bearings undergoing free vibrations with and without shaft rotation 04 p0627 A67-14432

Digital simulation of Gaussian random load forcing function and motion equations of nonlinear vibration of damped elastic beam 04 p0656 A67-14447

Book on lambda-matrices for treating linear vibrating systems 04 p0644 A67-14869

Dispersion and damping of oscillations in Maxwellian plasmas with zero order density gradients examined, using Vlasov and Maxwell equations 04 p0665 A67-15103

Energy dissipation calculation of damping factor for free oscillations of viscous liquid in circular cylindrical vessel 04 p0711 A67-15196

Rational approximation of generalized Duffing equation, damped mass spring oscillator equation and generalized second order Riccati equation 04 p0647 A67-15660

Optimum control of two-dimensional oscillating system when placing limitations

on control, using Butkovskii L-problem of moments 05 p0781 A67-16253

Rotation and vibration of conducting circular cylinder in magnetic field, noting motion retardation due to induced electric current interaction with field 05 p0851 A67-16434

Magnetic delay line vibration isolation system as heart of airborne special purpose computer in USN E-2A early warning aircraft 05 p0779 A67-17458

Flexibility and rigidity requirements imposed on vibration damping systems of optimized precision devices 06 p1106 A67-18618

Transonic wind tunnel studies of ground-wind loads on aeroelastic models of Saturn launch vehicle, investigating structural damping, wind velocity and azimuth angle 07 p1257 A67-19371

Pressure amplitude at resonance decreasing with increasing Mach number observed as effect of mean flow on wall damping of finite amplitude gas pulsations 07 p1168 A67-19576

Extremal control problem of undamped oscillatory plant analyzed using bounded phase-coordinate control theory 08 p1309 A67-20330

General method of averaging applied to slightly damped librations problem in perturbed one degree of freedom system 08 p1424 A67-21435

Shear modulus determination from free flexural vibrations of sandwich beams with steel facing, using filled elastomer as core 09 p1574 A67-21838

Nonlinear vibration damping functions for fluid film bearings [SAE PAPER 670061] 09 p1508 A67-22535

Vibration characteristics of two-layered plates of arbitrary thickness and differing materials, noting coupling effect between flexure and extension 10 p1718 A67-23140

Dynamic theory of vibration damping by controlled impact in forced oscillations in two-mass nonlinear system 10 p1721 A67-23683

Stochastic Markov model for transient amplitude variation in systems with damped free vibration compared with deterministic solution 10 p1724 A67-23709

Individual section dampers relation to modal damping of series mass spring in lumped parameter systems 10 p1729 A67-23770

Dispersion and damping characteristics due to flexural vibrations in elastic plate with viscoelastic coating, obtaining energy loss resulting from dissipation [ASME PAPER 66-WA/APM-20] 10 p1731 A67-23840

Composite loss factor and natural frequencies of vibrating beams composed of alternate layers of elastic and viscoelastic material [ASME PAPER 67-VIBR-6] 11 p1871 A67-24166

Vibrational experiments with honeycomb type core sandwich beams on lowest natural frequency, node locations and damping, noting core shear flexibility [ASME PAPER 67-VIBR-11] 11 p1872 A67-24171

Supercritical speed helicopter power transmission shaft for rotor synchronizing, noting viscous damper for controlling shaft vibrations [ASME PAPER 67-VIBR-20] 11 p1796 A67-24179

Constrained layer damping mechanism for optimum performance of plates, beams and tubular structures, using viscoelastic material [ASME PAPER 67-VIBR-26] 11 p1872 A67-24184

Unbalance vibration of rotor analyzed for application to rotor bearing system with dynamic forces represented by spring and damping coefficients [ASME PAPER 67-VIBR-27] 11 p1796 A67-24185

Amplitude control of wind induced oscillation in antenna system through cross section shape [ASME PAPER 67-VIBR-39] 11 p1777 A67-24194

Evaluation of wire lacing designs for damping of vibratory stresses on gas turbine blades [ASME PAPER 67-VIBR-47]

Equations for turbomachinery blades vibration control noting energy exchange, stress amplitude, mechanical damping, etc [ASME PAPER 67-VIBR-49] 11 p1797 A67-24197

Vibratory motions of turbine blades, considering frequency determination, tangential mode, stress, damping and excitation source [ASME PAPER 67-VIBR-66] 11 p1798 A67-24207

Stability in whirl theory, considering internal damping role on motion of elastic shaft 11 p1798 A67-24316

Magnetic effect and collision in damping of electron Langmuir oscillations 11 p1842 A67-24965

Viscous friction in axes of gyroscope suspension further damping of nutational oscillations and increases precession oscillations of inertial vertical 11 p1794 A67-25051

Aerodynamic theory of blade vibration, discussing compressibility effect, stalling and design 12 p2014 A67-25412

Equations for elastic system free oscillations with parallelogram shaped hysteresis loop derived from kinetic energy changes, describing system time dependent dynamic behavior 12 p1987 A67-25660

Inertial navigation system with damping of oscillations for enhancement of stability of stationary platform 13 p2118 A67-26375

Motion equations and middle position equations for damping of stochastic oscillation in measuring apparatus pointer 13 p2119 A67-26622

Self-excited vibration of cylindrical shell in coaxial rigid cylindrical duct with gas flowing past 13 p2218 A67-26806

Aerodynamic damping and frequency drift of turbomachine blades, discussing wind tunnel testing results for various geometric configurations 13 p2051 A67-27205

Long period vibrometer with small spring constant and minimized solid friction by HF vibration of support 14 p2348 A67-28257

Gravity-gradient oriented satellite stabilization by means of solar pressure torques on adjustable slats 14 p2395 A67-29051

Existence conditions of periodic solution of equations describing nonlinear oscillations of thin plates with allowance for damping and application of Galerkin method 15 p2575 A67-29887

Plasma spectrum, discussing electromagnetic oscillation damping on boundary of two media with different electrical properties 15 p2531 A67-30073

Relation between steady state behavior of regenerative traveling wave laser and linear constant damping in medium 15 p2454 A67-30076

Attenuation characteristics of longitudinal wave propagating in weakly inhomogeneous plasma, deriving expression for oscillations damping constant 16 p2828 A67-31498

Transverse magnetic field effect on barrier wake oscillation in electrically conducting liquid 16 p2723 A67-31714

Suppression of oscillatory vertical force transmission from helicopter rotor to driving shaft using higher harmonic pitch angle inputs [AHS PAPER 129] 16 p2777 A67-31843

Equation derived for accurate approximation of viscous friction coefficient in spool and nozzle-flapper preamplifier stages of electrohydraulic servovalve 16 p2610 A67-31915

Active damping concept for gravity gradient satellite attitude control to reduce oscillation time constant, initial capture time and oscillation magnitude 17 p2954 A67-32073

Stability of equilibrium of nonconservative continuous systems with slight damping 17 p2959 A67-32414

Damping effect of conduction electrons on ultrasonic surface and body waves propagating in CdS crystals, plotting damping against conductivity 17 p2921 A67-32971

Instability zones for vibration equations system having periodic acceleration matrices, damping and spring forces 18 p3140 A67-33464

Resonant vibrations in rotating blades with hinged joints analyzed for small and large damping values, determining damping

coefficient 19 p3235 A67-34883

Damping effect of HF field on instabilities occurring in form of moving striations within plasma of gas laser 19 p3241 A67-35814

Transiently loaded foundation on soil designed using graphical phase-plane analysis, considering soil stiffness and damping effect [AIAA PAPER 67-550] 19 p3208 A67-35947

Nonlinear resonant coupling between damped and undamped vibrations for damping roll in TRAAC and elastic dumbbell satellites [AIAA PAPER 67-568] 19 p3329 A67-35966

Free-rotor gyros active damping evaluated through experimental studies 19 p3233 A67-35986

Semiconductor surface electromagnetic oscillations excitation in presence of strong electric and magnetic fields, obtaining damping and dispersion law 20 p3504 A67-36163

Type II superconductor suspended on elastic fiber in magnetic field investigated for oscillation dampings 20 p3505 A67-36203

Nonstationary automatic control systems design by reaction quenching method 20 p3410 A67-37235

Electron-plasma oscillation damping in hot collisional plasma with external uniform magnetic field investigated using Fokker-Planck equation 20 p3503 A67-37693

Book on turbine blade vibration damping for increasing operational reliability 21 p3715 A67-37831

Dynamic theory of vibration damping by controlled impact in forced oscillations in two-mass nonlinear system 21 p3720 A67-38284

Panel flutter analysis of hinged closed circular cylindrical shell in supersonic gas flow, considering axial compression and structural damping 21 p3725 A67-38788

Dynamic compliance of two degrees of freedom nonrotating beam undergoing flexural vibrations, taking into account internal friction 21 p3726 A67-38833

Collisionless damping of temperature or secondary resonance spectrum of plasma column 22 p3845 A67-39482

Vibrating neutron stars, discussing damping, heating, energy storage and X-ray emission possibilities at 1000 years range 22 p3882 A67-39619

Electromechanical simulator of wing flutter with aileron under flight conditions 22 p3912 A67-39779

Collisionless small and large amplitude electron plasma wave damping compared, showing small amplitude waves damp exponentially and large amplitude waves exhibit amplitude oscillations collisionless small and large amplitude electron 22 p3853 A67-40242

Air damping effect on structural fatigue failure evaluated mathematically as power function relating stress to number of cycles 22 p3915 A67-40405

Aerodynamic damping of turbine buckets and compressor blades noting flutter and frequency shift 23 p3927 A67-40669

Raman scattering for overdamped soft optic vibrational mode in barium titanate, giving temperature dependence of Raman spectrum 23 p4038 A67-40796

Optimum stabilization system for manned space station with asymptotic damping of initial angular momentum 24 p4240 A67-42088

VIBRATION EFFECT

Space flight acceleration, vibration and ionizing radiation effects on body functions, oxidizing metabolism of central nervous system and fission processes of hemopoietic tissues 01 p0015 A67-10336

Structural loading, discussing stationary and nonstationary-random and severe loading processes 01 p0163 A67-11014

Vibrating-piston electrostatic field sensor for Gemini program, examining design improvements including unity-feedback preamplifier, noise reduction devices, etc 01 p0074 A67-11127

Combined linear and vibratory accelerations effects on human body dynamics and pilot performance 02 p0189 A67-12409

Effect on human performance of whole-body vibration at various frequencies, determining minimum G level producing significant decrement 02 p0189 A67-12632

Elastic structural vibrations of vehicle effect on position of engine thrust vectors with respect to undisturbed nonvibrating vehicle 02 p0335 A67-12732

Combined effect of gravitational and vibrational forces on formation of convection studied by method of averaging with respect to small vibrations 03 p0401 A67-12870

Constant component of Cardan error of directional gyro subject to regular rocking 03 p0425 A67-14282

Oscillating field of vessel effect on accuracy of readings of gyrocompass with negative fluid/ pendulum 03 p0425 A67-14283

Theoretical analysis of translational motion and angular motion of flow induced vibration of blade suspended in flow channel [ASME PAPER 66-WA/NE-1] 04 p0712 A67-15372

Human body response to stationary and nonstationary vibration [ASME PAPER 66-WA/BHF-15] 04 p0564 A67-15937

Transient and steady state IR emission from low-lying vibrational levels of carbon dioxide in laser systems, using DC discharge 05 p0816 A67-16630

Unbalance vibration of rotor analyzed for application to rotor bearing system with dynamic forces represented by spring and damping coefficients [ASME PAPER 67-VIBR-27] 11 p1796 A67-24185

Chemical kinetic processes in gasdynamic shock wave interactions, especially vibration in four-center transition states 11 p1773 A67-24535

Monodisperse sprays production technique using Rayleigh criterion for breakup of capillary jets by mechanically vibrating uniform size capillary needles arranged in parallel 12 p1946 A67-25983

Sound and vibration effects on convective heat transfer rates 12 p2039 A67-26167

Axial vibration /pogo stick effect/ of Titan II, as Gemini launch vehicle, studied by analog computer simulation for instability influences 14 p2394 A67-28086

Nonlinear dynamic response of thin walled shells of revolution 14 p2397 A67-28090

Long duration random vibration effects on human response in simulated low altitude high speed flights 14 p2257 A67-28660

Vibration problems in high speed turbines including stability, critical speeds and support structure effect on rotor response [ASME PAPER 67-DE-8] 14 p2402 A67-28867

Cardiovascular changes at onset of whole body, X-axis sinusoidal vibration in anesthetized mongrel dogs and unsedated humans 15 p2428 A67-29272

Noise and vibration effect on human mental work capacity with increasing time limitation indicating efficiency reduction 16 p2614 A67-30917

Liquid discharge from cylindrical container exposed to longitudinal vibration, noting flow retardation 16 p2658 A67-30946

Design criteria and configuration for long-life aircraft gas turbines [SAE PAPER 670344] 17 p2929 A67-32988

Gyromotor vibration level variation causes and ball rotation regimes permitting stabilization 18 p3047 A67-33994

Tip losses in two types of turbine straight-blade cascades at several Reynolds numbers, noting vibration effect on stage performance 18 p2983 A67-33999

Continuous exposure to random vertical vibrations studied for effects on compensatory tracking performance, noting decrement by peak vibration acceleration power location 18 p2993 A67-34336

Book on electrodeposition of metals in ultrasonic field, discussing effects on electrode potentials, concentration polarization, deposition rate, etc 19 p3235 A67-34914

Impmittance and transmission matrices concepts applied to mechanical systems vibration, presenting formulations properties and interrelationships 19 p3261 A67-34960

Vibration effect on task performance evaluated from test series, using vibration simulator 19 p3181 A67-35557

Vibrational excitation effects on shock wave behavior calculated analytically by linearizing problem 19 p3212 A67-35773

Sinusoidal surface vibration effect on nucleate pool boiling reveals lowered surface temperature for low heat flux, LF and high

acceleration [ASME PAPER 67-HT-49] 20 p3548 A67-36731

Surface vibration effect on nucleate pool boiling, measuring heat-transfer coefficient and proposing mechanism [ASME PAPER 67-HT-58] 20 p3549 A67-36740

Stability of three-dimensional oscillations of solid body coupled to periodically vibrating base by elastic springs 20 p3485 A67-36917

Acoustic vibration effect on heterogeneous mass transfer at sphere surface in high Prandtl number liquids 20 p3554 A67-37068

Vibrational energy levels leading to laser oscillation in UV, noting process using Lyman discharge 21 p3638 A67-37855

Wheel acceleration influence on landing gear operation at touchdown, noting effect on shock absorption system and elastic deformation of supporting legs 21 p3566 A67-37949

Dynamic modeling of complex rotor system to determine critical velocities, noting influence of number of mass concentrations on accuracy 21 p3689 A67-37951

Plane motion of container formed by two concentric cylinders and radial partitions partly filled with small vibrating ideal fluid 22 p3786 A67-40029

Flexural vibration of stiffened circular plates with respect to rotatory inertia, obtaining differential equation 23 p4073 A67-40613

Bibliography dealing with vibration, acceleration and ionizing radiation on vestibular apparatus, noting lack of information 23 p3943 A67-40764

Guinea pigs exposed to vibrations alternating with intermittent gamma radiation studied for effects on spinal cord activity, noting reflex response depression and parabolic stimulations 23 p3943 A67-40768

Functional relation between oxidation, metabolism, blood flow volume rate and brain temperature in rats exposed to vibration, noting temperature decrease and blood supply and oxygen consumption stimulation 23 p3943 A67-40769

Pilot capability in low level high speed flying analyzed for influence of roughness fatigue, control improvements, vibration and visual problems 23 p3963 A67-41068

Reduction and analysis of nonstationary missile flight vibration data, obtaining power spectral density 23 p4007 A67-41385

Pharmacological alterations of vibration tolerance 23 p3955 A67-41613

Forces on spheres inside diffusers noting instability onset 23 p3932 A67-41734

IR lasers using vibrational rotational transitions of carbon dioxide 24 p4166 A67-41799

Fourier transformation theory for shock and vibration data analysis, discussing programming considerations and computational efficiency [SAE PAPER 670874] 24 p4248 A67-42011

VIBRATION MEASUREMENT

Vibroplate pickups for measuring mean values of nonsteady state forces, noting maximum permissible limits of frequency change of pickups 01 p0064 A67-10422

Spring theory of ball bearing supporting rotor and role in vibration analysis of system 02 p0248 A67-11468

Soviet monograph on dynamics and durability of machines 05 p0915 A67-16219

Vibrations of disk-drum rotor analyzed using matrix equation of discrete model 05 p0810 A67-16230

Discrete model construction method for vibrating circular plates 05 p0810 A67-16231

Matrix method formulation of vibration and stability problems yielding upper bounds for natural frequencies 05 p0917 A67-16301

Imperfect excitation effect on vibration test results such as admittance, phase curve, damping coefficient, etc 05 p0920 A67-16769

Finite element method for problems in structural mechanics extended to beam vibration including shear and rotary inertia effects 05 p0924 A67-17284

Cruise error analysis for strapdown inertial navigation system with pulse torqued instruments in presence of small amplitude oscillations 06 p0947 A67-18007

Vibrational characteristics of composite shells, noting effects of circular joint connecting two components

[AIAA PAPER 67-72] 06 p1104 A67-18496

Small oscillations and stability of hyperelastic incompressible rectangular strip under uniformly distributed biaxial load 06 p1111 A67-18892

Free vibration analysis for ring and stringer stiffened cylindrical shell, using Rayleigh-Ritz technique [AIAA PAPER 67-71] 07 p1262 A67-19434

Vibration tolerance of rats previously irradiated by X-rays and hypothetical mechanisms of stress involved 09 p1452 A67-21719

Nonlinear system response to pulse excitation, solving problem via Poincare perturbation method 09 p1533 A67-22153

Spacecraft instrumentation, discussing selection criteria for signal conditioning, transducer sensors, photographic equipment, etc 10 p1655 A67-23000

Flow induced vibrations of rigid plate in narrow channels, noting flow rate dependence on channel width [ASME PAPER 67-VIBR-32] 11 p1777 A67-24190

Vibration absorbers effectiveness determined using stiffness and mobility method, noting detuning [ASME PAPER 67-VIBR-65] 11 p1873 A67-24206

Laser for remote vibration measurement and detection without mechanical contact with structure under test 11 p1798 A67-24433

Vibrational characteristics of composite shells, noting effects of circular joint connecting two components [AIAA PAPER 67-72] 12 p2030 A67-25916

Nonlinear oscillation effect on motion equation of elastic object under free flight conditions 12 p2032 A67-25966

Power output of pulse laser measured in terms of ultrasonic vibration intensity induced in piezocrystals by radiation 15 p2485 A67-29125

Vortex wakes of vibrating cylinders at low Reynolds numbers noting change in geometry along span 15 p2471 A67-29653

Holzer method extended to analysis of free vibration of spherical shells, solving boundary value problem as set of initial value problems until all boundary conditions can be satisfied 15 p2577 A67-30193

Italian sensing devices for measuring temperature, pressure, acceleration, heat shield and vibration on ELDO satellite 17 p2854 A67-32227

Successive release evaluation by periodometer and memory oscillograph of viscous damping of one degree of freedom system 17 p2884 A67-32698

Circular disk error magnitude determination by measuring rear-wall echo with angular probe 18 p3044 A67-33736

Calculation of vibration level populations of polyatomic molecules in electronic ground state 20 p3457 A67-36216

Differential piezoelectric accelerometer charge system for monitoring in-flight jet engine vibrations 23 p4007 A67-41384

VIBRATION MEASURING APPARATUS

SA SEISMOGRAPH

SA SEISMOMETER

Stress distribution measurement by vibration method, applying hand-held extensometer place by place on surface of structure subjected to dynamic load of finite amplitude 06 p1100 A67-18001

Shock and vibration sensors, discussing types for measuring strain, displacement, acceleration, velocity, pressure, etc 10 p1656 A67-23081

Laser interferometer for accurate determination of vibration amplitude, noting basic characteristics 12 p1943 A67-25696

Piezoelectric type accelerometer transverse sensitivity ratio /TSR/, discussing measurements of vibrations and rotations 12 p1943 A67-25703

Youngs modulus and shear modulus of inorganic filaments of tungsten and boron measured by oscillation technique 13 p2144 A67-27187

Noncontacting device for compressor-blade vibration measurement supplying data on all blades of one stage 15 p2545 A67-29165

Accelerometer using interference fringes of Fabry-Perot system for measurement of small vibratory disturbances 20 p3444 A67-36520

Absolute and relative vibration measurement in aeronautical engineering,

describing sensing units for vibration amplitude, rate and acceleration determinations 22 p3798 A67-39545

VIBRATION MODE

Vibration modes and relative frequencies of shells stiffened by angularly equidistant stringers, using Vlasov theory of circular cylindrical shells 01 p0163 A67-11148

Statistical dependence effect of normal mode response of complex structures to random excitation 01 p0163 A67-11172

Discrete element technique applied to natural vibrations of deep spherical shells satisfying geometric and force boundary conditions 01 p0164 A67-11184

Vibrations of elastic shells containing liquids 01 p0165 A67-11441

Spheroidal disturbances propagation on surface of heterogeneous spherical earth studied by superposition of contributions from normal free spheroidal vibration modes 02 p0237 A67-11790

Mode switching in tunnel diode, noting change from relaxation to microwave oscillation mode 02 p0217 A67-12090

B-52 structural response to random turbulence with various stability augmentation systems, noting rigid body motions, normal vibration modes and control surface rotations [AIAA PAPER 66-998] 02 p0181 A67-12302

Power amplifier used in electrodynamic shakers for transforming electrical into mechanical vibrations, examining range, deformations, humming and impedance 03 p0363 A67-13398

Adiabatic harmonic unitary transformations and relation between electron trapping energy and normal lattice modes associated with F center ground state 03 p0495 A67-13515

Existence theorems for periodic solutions of coupled nonlinear systems of two or more degrees of freedom, including normal mode vibrations 03 p0524 A67-13654

Electric current oscillation mode beyond Gunn effect threshold in n-type GaAs 03 p0496 A67-13669

Imbalance of elastically deformed rotor after starting only once with trial load, noting role of oscillation modes of rotor 03 p0528 A67-14078

Existence, convergence and divergence of periodic solutions for normal mode vibrations of system subject to small perturbations 04 p0656 A67-14448

Stator whirl with rotors in bearing clearance noting jump and hysteresis phenomena [ASME PAPER 66-WA/MD-8] 04 p0629 A67-15346

Vibration modes, stress distribution, natural frequency and failure points in pin-fixed compressor blades [ASME PAPER 66-WA/GT-4] 04 p0711 A67-15359

Natural frequencies and mode shapes for axisymmetric vibration of thin elastic and ellipsoidal shells 04 p0714 A67-15424

Force constants and local mode frequencies for vibrations of interstitial lithium positive ion in Si crystal, using covalent orbital bond model 04 p0683 A67-15609

Normal modal vibrations for some damped n degree of freedom nonlinear systems 04 p0659 A67-15935

Correspondence principle in linearized classical theory of viscoelasticity for free vibrations, emphasizing case of irrotational or solenoidal motion 05 p0909 A67-16145

Design strength of plane notched elements under single mode vibration, obtaining equation for fatigue stress concentration factor 05 p0919 A67-16592

Energy dissipation effect on vibrations of elastic element with one degree of freedom excited by steady state random Gaussian disturbance 05 p0923 A67-17182

Axisymmetric modes and frequency vibration of thin conical shells subjected to rapid surface heating 06 p1100 A67-18000

Vibrational characteristics of inflatable wing model, determining resonant frequencies and mode shapes by using influence coefficients 06 p1100 A67-18002

Quasi-steady aerodynamic and von Karman large deflection plate theory equations of nonlinear oscillations of fluttering plate for single mode subsonic and sonic or coupled mode supersonic oscillations

[AIAA PAPER 67-13] 06 p1101 A67-18252

Axisymmetric vibration modes of cylindrical-hemispherical membrane tank partly filled with liquid [AIAA PAPER 67-75] 06 p0986 A67-18273

Vibration mode of conical shells measured, showing variation with conical angle and circumferential wave number 06 p1105 A67-18591

Remedies for deficiencies in approximations near transition point in asymptotic methods used for estimates of solutions to differential equations governing axisymmetric vibrations of thin elastic shells 08 p1414 A67-20346

Axisymmetric plane-strain vibrations of thick layered orthotropic shell under internal and external pressures analyzed, using Fourier series for eigenmodes determination 08 p1415 A67-20487

Partial differential equations for plate motion, considering transverse shear and rotary inertia, solved for plates bounded by elliptical and hyperbolic cylinders 08 p1416 A67-20489

Solid rocket engine propellant grain structural dynamics including elastic and viscoelastic deformations, stress and shear vibration modes, natural frequency calculations, etc, using Fourier inversions and transforms 08 p1376 A67-20883

Vibration modes of conical frustum shells with free ends [AIAA PAPER 66-450] 08 p1424 A67-21533

Gunn diode efficiency for mixed resonant transit time and suppressed modes, using dynamic drift velocity field strength characteristic 09 p1474 A67-22039

Sub-or supersonic wing leading edge in unsteady supersonic flow, presenting discontinuities in vibration modes and calculating wing stress forces 10 p1590 A67-22879

Resonant frequencies compared with associated mode shapes of truncated conical shells with both edges free 10 p1718 A67-23455

Free flight response of two panels subjected to turbulent pressure fluctuations at supersonic Mach numbers 10 p1719 A67-23558

Optimal control of maneuver induced vibration in flexible aerospace vehicles 10 p1714 A67-23754

Kinematic nonlinearities effect on existence, properties and stability of vibrations in unison of particle with two degrees of freedom 11 p1818 A67-24085

Approximate normal mode technique, providing solution to sinusoidal and white noise randomly excited damped linear multi-degree of freedom system, for application to mathematical model [ASME PAPER 67-VIBR-2] 11 p1871 A67-24164

Discrete mass technique for vibration analysis of thin shells [ASME PAPER 67-VIBR-23] 11 p1872 A67-24182

Mode coupling effect on response of rigid body to random excitation analyzed, using two degree of freedom model [ASME PAPER 67-VIBR-36] 11 p1873 A67-24193

Natural and forced lateral vibration analysis of free-free beam by integration and finite difference methods, considering influence coefficients [ASME PAPER 67-VIBR-54] 11 p1873 A67-24202

Low temperature alkali plasmas in magnetic fields in terms of collisional drift modes, determining steady state frequencies, amplitudes, etc 11 p1834 A67-24381

LF drift waves effect upon anomalous transverse diffusion in fully ionized magnetoplasma, noting wave amplitude 11 p1835 A67-24387

Rectangular to cylindrical waveguide transducer which couples dominant rectangular and cylindrical transverse electromagnetic modes 11 p1767 A67-24733

Combustion chamber model for self-oscillating thermoacoustic system initiated by stimulation effect of acoustic shock 11 p1884 A67-24958

Cylindrical shell stability under external pressure, presenting critical load value and nature of undulation 11 p1880 A67-25054

Turbomachine rotating shaft and rotor systems critical speeds taking into account

bearing support stiffness and clearances, noting vibration mode 12 p1949 A67-25410

Natural frequencies of bladed disks calculated from receptances 12 p2014 A67-25417

Lower modes and frequencies of natural elastic oscillations of vessel formed by liquid-filled shell of revolution taking into account fluid surface wave and shell inertia 12 p2020 A67-25566

Reverberation chamber for high intensity acoustic testing of specimen subjected to directionally predetermined spectral distribution of acoustic energy field 12 p1924 A67-25712

Structural influence coefficients of arbitrarily restrained system obtained from experimental results of free-free ground vibration test 12 p2030 A67-25918

Vibrational mode behavior of rotating gravitational mass sensors and sensor design to minimize nonideal effect of manufacturing and external disturbances 12 p1945 A67-25919

Directional coupler classification 12 p1915 A67-25977

Vibration of cylindrical shell containing flowing incompressible perfect fluid 13 p2215 A67-26528

Parametric oscillations of counterbalanced rotors 13 p2216 A67-26628

Problem oriented language for mechanical problems programming applied to steady state vibrations, static problems and stress-strain relation 14 p2276 A67-29000

Bounds for natural frequency eigenvalues of simply supported uniform beam with constant end load and uniformly distributed axial load 14 p2403 A67-29005

Current dependent modes in pulsed avalanche diodes 15 p2442 A67-29174

Effect of blade row interference on cascade flutter investigated using semiactuator disk method 15 p2415 A67-29314

Gunn effect as only solid state effect capable of producing high output power in microwave range in pulsed and continuous operation, noting physical nature 15 p2536 A67-29530

Plasma characteristics and instability when plasma waves lead to current oscillations in bulk semiconductor 15 p2450 A67-29814

Infrared lattice vibration spectra of II-VI compounds analyzed by Drude dispersion, obtaining transverse-optical-mode frequency 16 p2724 A67-30603

Free vibrations of unsupported elliptical plates of lenticular section with flat or uniformly curved middle surfaces 16 p2764 A67-30841

Nonaxial oscillation modes in He-Ne laser interaction with spherical mirror resonator confocal cavity 16 p2685 A67-31038

Ultrasort light pulse generation by forcing oscillation modes, noting role played by dispersion of medium within resonator cavity 16 p2702 A67-31042

Distributed parameter concepts of propagation, reflection and characteristic termination applied to dynamic analysis and control of bending vibration 16 p2776 A67-31686

Normal mode analysis of multispan skin-stringer structure with isolated tuned viscoelastic dampers at arbitrary surface points 17 p2960 A67-32579

IR absorption measurements of Li localized vibrational modes in Li and Te doped GaAs 17 p2922 A67-33066

Oscillation mode in open-ended circular cylindrical microwave cavity resonant frequency computed by Laplace transform and Wiener-Hopf techniques 17 p2828 A67-33083

Rate of vibration-vibration energy exchange in gas mixtures 18 p3081 A67-33783

Emission equations describing radiation field amplitude and energy level populations of solid state laser with broad oscillation spectrum 18 p3061 A67-34358

Alkaline-metal-plasma machine design, studying operating modes with electric probes 18 p3091 A67-34631

Localized vibrational modes of lithium in lithium diffused p-type Ga-As doped with Mn, Cd or Zn 18 p3106 A67-34644

Time variations of order parameter, coupling to external perturbation and effect on various transport properties of dirty type II superconductors 19 p3302 A67-35038

Longitudinal and transverse collective

fluctuation modes of order parameter in pure type II superconductor in high critical field region 19 p3302 A67-35039

Intrinsic frequencies and modes of periodic free vibrations of homogeneous beam with weakly nonlinear boundary conditions of Duffing type 19 p3340 A67-35509

Adaptive control systems for stabilizing structural bending modes of Saturn V launch vehicle

[AIAA PAPER 67-591] 19 p3336 A67-35987

Finite-amplitude oscillations of Maclaurin spheroids preserving ellipsoidal nature of surface and generating internal motions of uniform vorticity 19 p3263 A67-36078

Generalized formulas and stability criteria applied to higher order electrostatic oscillation modes in Vlasov plasmas, considering double-stream amplifier designs 20 p3495 A67-36169

Phase-locking effects between longitudinal modes in lasers, treating several-mode oscillations 20 p3456 A67-36171

Panels response to oscillating and to moving shock waves, discussing mode excitation, magnification factor, Bessel function, etc 20 p3539 A67-37001

Skin stringer panel rows natural frequencies and normal modes predicted by transfer matrix method 20 p3539 A67-37008

Longitudinal vibration formation by high density electric current pulses in rod, discussing thermoelastic excitation and electrodynamic radial compression 20 p3486 A67-37060

Compounded normal modes of free vibration of cantilever plates, determining component modes 20 p3541 A67-37491

Ideal incompressible fluid axisymmetrical oscillations in elastic cylindrical shell, determining normal modes and natural frequencies of shell and fluid 21 p3613 A67-38789

Quasi-steady aerodynamic and von Karman large deflection plate theory equations of nonlinear oscillations of fluttering plate for single mode subsonic and sonic or coupled mode supersonic oscillations

[AIAA PAPER 67-13] 21 p3727 A67-38870

Method for finding bending vibration modes patterned on Holzer method for determining torsional vibration 21 p3728 A67-38881

Minimum mass bar design for axial vibration of beam with load distribution at specified natural frequency 21 p3728 A67-38890

Thick walled cylindrical shell mobility over wide frequency range, predicting vibration response based on normal mode series convergence solution 21 p3729 A67-39059

Subharmonic and summed and differential harmonic oscillations in multiple-degree-of-freedom system with asymmetric nonlinear spring characteristics, studying stability 22 p3910 A67-39408

Launch vehicle response in lateral vibration modes to nonstationary random transonic buffeting excitation 22 p3907 A67-40167

Mathematical model for vibrating characteristics of structures in statistical mechanics framework, noting closeness to Green function rather than to mode concept [ONERA-TP-467] 22 p3915 A67-40385

Existence and form of orthogonality condition on natural vibrational modes of linear elastic shell under boundary conditions 23 p4073 A67-40616

Natural frequency vibration mode of turbine blades calculated by approximate theory of integral evaluation yield discrete models 23 p4076 A67-40684

Coaxial rotors natural vibrations analysis by computer showing occurrence at rpms above first critical speed 23 p4009 A67-40685

Differential equations maximum parameter values for single mass nonlinear system passage through resonance point determined with approximate methods based on small parameter method 23 p4026 A67-40686

Raman scattering for overdamped soft optic vibrational mode in barium titanate, giving temperature dependence of Raman spectrum 23 p4038 A67-40796

Rapid magnetic field variations observed in magnetosheath evaluated in terms of transverse modes of plasma wave propagation 23 p3995 A67-40804

Oscillator diode in limited space charge accumulation oscillation mode, obtaining maximum DC to RF conversion efficiency for sine wave excitation for n-GaAs 23 p3979 A67-40875

Simultaneous self-starting oscillations at unrelated frequencies in feedback loop containing one nonlinearity, calculating equivalent linear gain 23 p3984 A67-41157

Optimal control of maneuver induced vibration in flexible aerospace vehicles 23 p4071 A67-41725

Vibration modes, stress distribution, natural frequency and failure points in pin fixed compressor blades [ASME PAPER 66-WA/GT-4] 24 p4251 A67-42460

VIBRATION PICKUP

Transmission of random sound and vibration through double wall analyzed by general method applicable to acoustics and thermodynamics 03 p0468 A67-13214

Strain gauge accelerometer designed and constructed for vibration pickup use 06 p1004 A67-18580

VIBRATION PROTECTION

Vibration shielding and shock absorbing systems design noting control function 03 p0530 A67-14180

Soviet book on calculations of strength and vibrations of rocket engines 11 p1852 A67-24512

Aircraft engine reliability, considering local surface stresses, engine component distortion under load, vibration problems and material variability 13 p2188 A67-27000

Two coupled resonant mechanical circuits with parameter in coupling element allowed to vary periodically 15 p2494 A67-29772

Optimization for linear vibration isolators considering vibration clearance tradeoff for random base motion 16 p2703 A67-31642

Electronic systems for V/STOL fighter aircraft, considering operational capabilities, reliability, maintenance and protection 17 p2795 A67-32032

Laboratory equipment protection from vibration environment, noting instrumentation and results 17 p2833 A67-32066

Space electronic equipment design, considering incorporation of vibration, vacuum, micrometeoroid and radiation protection 21 p3591 A67-38209

Book on reusable protective packaging of military, electronic and aerospace instruments and systems 22 p3771 A67-39832

VIBRATION SIMULATOR

Vibro-acoustic test system for simulation of Saturn V dynamic launch environment on major space vehicle structures, discussing design and operation characteristics 17 p2832 A67-32005

VIBRATION TESTING

Manned and unmanned spacecraft structures, discussing environmental and functional requirements, influence of vibration and pressurized gas containment [SAE PAPER 660672] 01 p0153 A67-10579

Dynamic load analysis of Titan III booster structure using dynamically scaled model in vibration survey [SAE PAPER 660684] 01 p0154 A67-10588

Hybrid CDC 3200 digital computer acquisition of response data from acoustic and high force vibration tests 01 p0029 A67-11025

Reliability overstress testing of Gemini inertial measuring unit system electronics package, discussing vibration and temperature/altitude environment 01 p0111 A67-11363

Reliability testing improvement through developments in vacuum systems, vibration systems and triaxial shock testing 01 p0084 A67-11369

Optimum telemetry system characteristics for shock, vibration and acoustic measurements and data bandwidth sufficiency 02 p0196 A67-12009

Ultrasonic fatigue testing using magnetostrictive vibrators 03 p0524 A67-13550

ESRO II satellite structural design, testing and material selection noting functions, vibration testing results, etc 03 p0518 A67-13600

Compressor blade vibration, discussing prediction of amplitudes of vibration and interpretation of results of engine strain gauge tests in terms of component service life

[ASME PAPER 66-WA/GT-14] 04 p0712 A67-15369

Energy method analysis of flutter instabilities in turbojet engine rotors caused by interaction between unsteady air loading and coupled vibration modes [ASME PAPER 66-WA/GT-6] 04 p0713 A67-15384

Human dynamic force response to impact examined, using spring-mass-damper system with refined parameter values 04 p0564 A67-15401

Vibration tests of hemispherical shell with free edge and constant thickness, exploring dynamic behavior through analytical methods 04 p0714 A67-15425

Vibration testing facilities for Apollo Saturn V launch vehicle, noting structural assemblies under dynamic testing 05 p0786 A67-16156

Inertia constants of rigid bodies determined, using ground vibration tests [ONERA-TP-386] 05 p0786 A67-16476

Global method application to vibration problems, discussing present trends in experimental methods [ONERA-TP-405] 05 p0919 A67-16478

Acceptance vibration testing program costs, benefits and test control 05 p0813 A67-17248

Shock and vibration test specifications, contrasting approaches requiring exact duplication of environment with those simulating damaging characteristics 06 p0981 A67-18366

Frequency response of pressurized torus shell held free or rigidly [AIAA PAPER 67-73] 06 p1104 A67-18470

Remote vibration testing facility for components while using hazardous cryogenics [AIAA PAPER 67-278] 07 p1167 A67-20083

Level and duration of sine wave tests, discussing rocket design proof via random vibration testing 08 p1402 A67-20477

Rectangular plate under periodic in-plane edge load investigated for transition mechanisms attendant to parametric vibrations [ASME PAPER 67-VIBR-5] 11 p1871 A67-24165

Vibrational experiments with honeycomb type core sandwich beams on lowest natural frequency, node locations and damping, noting core shear flexibility [ASME PAPER 67-VIBR-11] 11 p1872 A67-24171

Unidirectional vibration isolation systems, discussing viscous damping, Coulomb damping transmissibility and resonance characteristics [ASME PAPER 67-VIBR-21] 11 p1796 A67-24180

Adhesive properties testing and damping behavior of thin viscoelastic material under different cyclic loadings [ASME PAPER 67-VIBR-25] 11 p1872 A67-24183

Trapped fluid effect on high speed rotor vibration, discussing asynchronous and synchronous whirl for fully and partially wetted cavities [ASME PAPER 67-VIBR-29] 11 p1797 A67-24187

Vibration absorbers effectiveness determined using stiffness and mobility method, noting detuning [ASME PAPER 67-VIBR-65] 11 p1873 A67-24206

Vibration in cylindrical shafts, noting high stresses due to low mechanical damping, existence of two natural frequencies, etc 12 p1949 A67-25411

Accelerometer mountings evaluated covering attachment, calibration, resonance frequencies, tension-compression, bending, shear interface and cantilever effect 12 p1942 A67-25680

Shock spectrum synthesis and analysis as environmental test technique compared with time function shock testing 12 p2030 A67-25681

Field testing of self-powered recorder for vibration data in environmental studies 12 p1942 A67-25682

Plastic foam pattern technique for producing vibration and shock fixtures 12 p1949 A67-25687

Portable self-powered magnetic tape recorder for gathering data on vibration, temperature and shock on ground and in-flight aircraft 12 p1942 A67-25688

Vibration qualification of fly-away umbilical by induced acoustic excitation testing method in Apollo project 12 p1924 A67-25714

Three-channel g limiter for protecting specimen during vibrational testing 12 p1943 A67-25719

Vibration response of Apollo shell structures to acoustic and aerodynamic noise 12 p2012 A67-25728

Structural influence coefficients of arbitrarily restrained system obtained from experimental results of free-free ground vibration test 12 p2030 A67-25918

Fluid vibratory behavior in rigid containers, noting surface wave behavior governed by linearized boundary value solution 12 p1931 A67-26182

Relay failure in spacecraft subsystem analyzed via vibration testing 13 p2085 A67-27697

Random vibration testing of relays noting test equipment 13 p2085 A67-27699

Harmonic and impulse techniques for flight vibration testing to reduce data processing time [ONERA-TP-477] 14 p2395 A67-27899

Computer controlled dynamic test facility to provide data on flight characteristics of Apollo-Saturn V launch vehicle by measuring vibration amplitudes 14 p2293 A67-28593

Vibrations of helicopter rotor in Cardan suspension, dividing problem into three boundary value setups with special conditions at hub 15 p2576 A67-30175

Galerkin method analysis of vibrations of clamped rectangular plates, using polynomial approximation 17 p2962 A67-32823

Laser excited vibrational fluorescence measurements in carbon dioxide noting energy transfer rates, system kinetics, radiative coupling, etc 18 p3060 A67-34027

Energy method analysis of flutter instabilities in turbojet engine rotors caused by interaction between unsteady air loading and coupled vibration modes [ASME PAPER 66-WA/GT-6] 18 p3115 A67-34130

Compressor blade vibration, discussing prediction of amplitudes of vibration and interpretation of results of engine strain gauge tests in terms of component service life [ASME PAPER 66-WA/GT-14] 18 p3115 A67-34132

Diagnostic methods of rotating bearing defects, describing types of bearings, oils and equipment used in tests 19 p3235 A67-34888

Aerospace technology and hardware transference to commercial and architectural testing, noting application to flow measurements, hydraulic acoustics and helium leak detection 20 p3416 A67-36698

Hydraulic support system for free flight simulation with Saturn V-Apollo vehicle, discussing stability requirements, upper bounds of system design, conversion from nonlinear to linear model, etc 21 p3607 A67-37796

Electrodynamic exciter of mechanical vibration noting design, operation and characteristics 22 p3780 A67-39553

Environmental simulation for aerospace vehicle, discussing vibration, shock and high temperature testing and space and nuclear radiation simulation 22 p3781 A67-40343

RCA papers on environmental sciences 22 p3781 A67-40400

Operational requirements for modern space environment test laboratory covering thermal vacuum, shock, vibration and combined testing 22 p3781 A67-40401

Comparison calibration techniques for vibration transducers using quartz accelerometer 23 p4003 A67-41337

Comparison calibration of rectilinear vibration and shock pickups 23 p4004 A67-41338

Electronic assembly loose parts detection system using nondestructive vibration testing 23 p4005 A67-41369

Foundation apparent weight during force controlled vibration test simulated electronically 23 p3987 A67-41383

VIBRATION TESTING MACHINE

Sweep random vibration test using narrow band random excitation with feedback control from variable gain stage 01 p0034 A67-10155

Silp table fixture design for cryogenic and

vibration testing of liquid oxygen prevalue and flow meter 04 p0598 A67-15176

Vibration characteristics of turbine and compressor blading under rotation 12 p2015 A67-25418

Statistical performance confirmation of wideband random equalizer, emphasizing analysis technique, analyzer characteristics and power spectral density plot 12 p1942 A67-25692

Combined multishaker and gas flow tests as part of reliability test program for Saturn V, S-1C pneumatic systems 12 p1923 A67-25706

Sinusoidal vibration generator consisting of two rigid vibrodynes connected by synchronized shaft for testing structural material 16 p2776 A67-31556

Random vibration testing by multiple electrodynamic exciter technique, analyzing electromechanics and structural feedback 19 p3339 A67-34961

Protective devices in electrodynamic vibration exciters, examining design, operational principles and possible cause of failures 22 p3781 A67-40403

VIBRATIONAL FREQUENCY

Vibrational force constants of nitrogen fluoride, using lone pair of electrons model 01 p0117 A67-10764

Vibrational-rotational motion effect on electric and magnetic properties of diatomic molecules, calculating magnetic susceptibility and rotational magnetic moment 01 p0117 A67-10784

Frequency equation for purely radial vibrations of infinite isotropic composite hollow cylinder with two concentric elastic layers 01 p0162 A67-10818

Eigenfrequencies of flexural vibrations of circular cylindrical shells calculated by various methods and compared with measured values 01 p0162 A67-10839

Vibration modes and relative frequencies of shells stiffened by angularly equidistant stringers, using Vlasov theory of circular cylindrical shells 01 p0163 A67-11148

Effect on human performance of whole-body vibration at various frequencies, determining minimum G level producing significant decrement 02 p0189 A67-12632

Torsional constraints in calculation of vibrational frequencies of compressor blade 03 p0528 A67-14081

Dynamic rubber wheel model to supplement digital computer analysis for prediction of frequencies, mode shapes and stress distributions of vibrating rotor stages [ASME PAPER 66-WA/GT-8] 04 p0712 A67-15364

Initial stress influence on frequency of three-dimensional vibrations of plates and rods 04 p0717 A67-15912

Upper and lower bounds of transverse vibrational frequencies of variable cross section cantilever bars, considering transverse shear and rotary inertia effects 05 p0910 A67-16151

Radiative lifetimes of UV molecular transitions, analyzing emission spectrum in vacuum monochromator 06 p1035 A67-17828

Periodic vibrations of systems governed by nonlinear PDEs, examining perturbation method, transverse vibrations of bar, string, beam and membrane and sound waves in enclosure 06 p1034 A67-18640

Production inaccuracy effects on oscillation frequency characteristics of turbomachine blades 07 p1261 A67-19134

Numerical procedure for proportioning members of complex structure with specified natural vibrational frequency based on finite element idealization 08 p1417 A67-20554

Heated rectangular plate nonlinear free flexural vibration problem involving initial deflection, temperature change, etc 10 p1715 A67-22825

Flow induced vibration and noise in tube bank heat exchangers due to Karman vortex streets analyzed, noting shedding frequency, lift, etc [ASME PAPER 67-VIBR-48] 11 p1777 A67-24198

Torsional vibration and steady state response of geared system, noting computer programming [ASME PAPER 67-VIBR-63] 11 p1797 A67-24205

Natural frequency and mode shape for nonuniform simply supported beam, using

Fourier series to approximate deflection, mass and inertia moment 11 p1874 A67-24429

Vibration characteristics of cantilever type pretwisted turbine blading, considering effects of taper, calculating frequencies and mode shapes 12 p2014 A67-25414

Structural influence coefficients of arbitrarily restrained system obtained from experimental results of free-free ground vibration test 12 p2030 A67-25918

Vibration characteristics and fundamental frequency of circular plate with arbitrary cross section reinforcing ring 13 p2216 A67-26534

Suspension axes defects effect on gyro motion under base angular vibration analyzed, noting large gyro drift 14 p2320 A67-28741

Natural frequencies of vibration of supported sandwich plate [SESA PAPER 1175] 18 p3143 A67-33901

Axial compressor blades considered as thin walled elastic shells studied for vibration forms, frequencies, stress distribution and blade geometry change effects 19 p3235 A67-34882

Intrinsic frequencies and modes of periodic free vibrations of homogeneous beam with weakly nonlinear boundary conditions of Duffing type 19 p3340 A67-35509

Natural torsional vibration frequency calculation method, with frequency as algebraic equations with real roots, discussing example problems 19 p3341 A67-35711

Free vibrations frequency of ideal fluid in elastic bottom cylinder in form of spherical shell 20 p3420 A67-36441

Accelerometer using interference fringes of Fabry-Perot system for measurement of small vibratory disturbances 20 p3444 A67-36520

Vibrational frequency and amplitude effects on heat transfer intensity from vibrating cylinder into circular channel at low Reynolds numbers 20 p3554 A67-37303

Elastic bending vibrations amplitude and frequency effects on current oscillations in CdS single crystals 20 p3514 A67-37463

Fresnel Integrals for quadratures of motion for undamped vibrator, deriving equation for envelope of maximum amplitude 20 p3541 A67-37485

Stimulated Raman scattering in IR active nontotally symmetric vibration of alpha quartz crystal, noting parametric oscillation 21 p3641 A67-38459

Self-oscillations of axial compressor blades, taking into account variation in natural frequency of flexural vibrations between blades 21 p3727 A67-38835

Natural vibration frequencies of cylindrically orthotropic circular plate with linearly variable thickness, solving differential equation of motion 21 p3728 A67-38898

Upper and lower bounds for frequencies of free vibration developed for uniform rectangular cantilever plates 21 p3730 A67-39094

Homogeneous and sandwich spherical caps axisymmetric vibration natural frequencies solved approximately, noting application to shallow and spherical shell problems 23 p4073 A67-40617

VIBRATIONAL RELAXATION

Vibrational excitation and dissociative attachment in bombardment of hydrogen molecules by electrons of energies up to about 12 ev 01 p0117 A67-10782

Excitation of vibrational degrees of freedom in molecular collision from vibrational relaxation data and molecular beam elastic scattering experiments 01 p0118 A67-11302

Steady state laser radiation during relaxation, discussing time-dependent spectral composition, oscillation modes and polarization characteristics 03 p0435 A67-13154

Diffusion theory of vibration-dissociation coupling used to analyze transient effects in dissociation reactions behind shock waves 03 p0474 A67-14025

Vibration temperature of relaxing hypersonic gas flow measured by electron beam technique 04 p0545 A67-14542

Molecular gas laser Q-switching techniques, determining rotational collision sections for carbon dioxide and cross

sections for vibrational relaxation 05 p0816 A67-16632

Characteristics solution breakdown near leading frozen characteristic for piston induced flow and relaxing gas 06 p0984 A67-18128

Trace fluorocarbon effect on vibrational relaxation in nitrogen shock waves studied by UV spectrophotometric technique 06 p0955 A67-18251

Complete vibrational population inversion in molecular product of chemical reactions, finding stimulated emission 09 p1511 A67-21746

Equation of relaxation hydrodynamics for diatomic perfect gas when rotational and translational degrees of freedom are in equilibrium and dissipation has not set in 10 p1590 A67-23024

Correlation of nitrogen vibrational-translational relaxation times for various measuring methods, noting temperature distribution of rate 10 p1733 A67-23151

Expression derived for vibrational relaxation in recombining expanding nozzle exhaust gas, assessing effect of chemical reactions on this mechanism 12 p1929 A67-25755

Shock tube analysis of oscillation relaxation in iodine between 1000 and 3800 degrees K 12 p1930 A67-26115

Hypersonic sound velocity dispersion in liquids of low viscosity analyzed using Mandelstam-Brillouin components 12 p1967 A67-26133

Method for analyzing single and double thermal relaxation processes 15 p2580 A67-29771

Nonequilibrium flow relation to flow in thermal balance, describing irreversible processes in terms of entropy source field and relaxation resistance 16 p2662 A67-31467

Trace fluorocarbon effect on vibrational relaxation in nitrogen shock waves studied by UV spectrophotometric technique [AIAA PAPER 67-11] 17 p2809 A67-33035

Rate constant of atomic oxygen ions reaction with vibrationally excited nitrogen molecules 17 p2889 A67-33201

Depopulation of vibrational energy levels in fast chemical dissociation reactions 18 p2996 A67-33780

Kinetics of coupled atomic recombination and vibrational de-excitation in continuously expanding gas flow 18 p3081 A67-33781

Diatomic gas vibrational relaxation by master equation analysis, discussing quasi-steady state vibrational population distribution and transition probability increases 18 p3081 A67-33782

Rate of vibration-vibration energy exchange in gas mixtures 18 p3081 A67-33783

Atomic oxygen effect on vibrational relaxation of oxygen in shock waves at high temperatures, using laser schlieren technique 18 p3081 A67-33784

Density induction times for shock wave induced exothermic reaction in lean mixtures of deuterium, hydrogen, ethylene and ethane with oxygen 18 p3081 A67-33792

Vibrational and/or chemical relaxation effects behind various shock waves in hypersonic air streams determined for equilibrium and nonequilibrium conditions 19 p3169 A67-34813

Low-energy electron collisions and interactions with atoms and molecules, discussing vibrational excitation, ion formation, ionization cross section, etc 19 p3264 A67-35068

Relaxation times of carbon dioxide vibrational levels and afterglow pulsed gain for nonflowing gas laser amplifiers 22 p3814 A67-39354

Shock wave reflection with vibrational relaxation times investigated by matching characteristics equation to shock wave equation 24 p4144 A67-42564

VIBRATIONAL SPECTRUM

SA SHOCK SPECTRUM

Digital computer program for power spectral density analysis of vibration data, noting bandwidth variation with frequency [SAE PAPER 680715] 01 p0028 A67-10604

Dispersion of refractive index of NO in fundamental vibration-rotation band 03 p0468 A67-13473

Exact vibrational matrix elements for molecular hydrogen and intensity of quadrupole rotation-vibration spectrum 03 p0515 A67-14324

Force constants and local mode frequencies for vibrations of interstitial lithium positive ion in Si crystal, using covalent orbital bond model 04 p0683 A67-15609

Optical maser oscillation lines in HF discharge in mixture of Ar and Br 06 p1011 A67-18545

Frequency spectrum during UHF plasma oscillation excitation by monoenergetic primary electrons introduced into low pressure Hg discharge 08 p1358 A67-20869

Continuous spectrum of nonperiodic curves, discussing measurement of frequency spectra of periodic voltage curves 09 p1501 A67-22468

Vibration environment of liquid propellant rocket engines 12 p1989 A67-25704

Detection of vibrational structure of gases adsorbed on tungsten by low energy electron scattering 13 p2160 A67-27075

Electronic, vibrational and rotational temperatures in laser-produced flames measured spectroscopically 15 p2433 A67-29879

Trifluoramine oxide IR spectrum measured, determining structure, symmetry and rotational, vibrational and thermodynamic properties 15 p2433 A67-29880

Infrared lattice vibration spectra of II-VI compounds analyzed by Drude dispersion, obtaining transverse-optical-mode frequency 16 p2724 A67-30603

Coupling between free electron and molecular vibrational temperatures in plasma environments, noting energy distribution, application to MHD generation, etc 17 p2894 A67-32150

Photoelectron energy measurement and Franck-Condon factors for vibrational transitions of molecular ions when ejected by He resonance line 17 p2888 A67-32356

IR chemiluminescence in hydrogen-diatomic bromine and hydrogen-hydrogen bromide IR chemiluminescence in hydrogen-diatomic bromine and hydrogen-hydrogen bromide 18 p2996 A67-33788

Statistical band model applied to NO fundamental vibration band, discussing transmittance measurements and validity of linear region criterion 19 p3266 A67-35681

Phonon spectrum of neodymium trichloride crystal lattice determined from polarized vibronic transition spectra and Zeeman effect of trivalent Pr and Nd impurity ions 22 p3840 A67-39434

Hydrogen peroxide and disulphane molecules force constant and vibrational spectra investigation indicates little change in elastic properties 22 p3757 A67-39583

Carbon disulfide P-branch transitions with J equals 28 to 46 for 001-100 vibrational transition identified as laser lines in N-carbon disulfide gas system 23 p4011 A67-40789

IR vibrational and Raman spectra of thiophosphoryl trichloride, thiophosphoryl dichlorofluoride, thiophosphoryl chlorodifluoride and thiophosphoryl trifluoride 23 p4041 A67-41242

FM oscillations spectrum component amplitude formula for multiple frequency modulation using Bessel function 24 p4122 A67-42379

VIBRATIONAL STRESS

Extended theory of cumulative damage in fatigue when stress amplitude varies from cycle to cycle throughout life of structure [SAE PAPER 680720] 01 p0161 A67-10607

Stress amplitude of gas turbine blades vibrating in resonance 02 p0336 A67-11466

Dynamic surface loads, transient displacement and stresses in elastic cylindrical shell under radial and torsional vibration and elastic spherical shell under radial symmetric vibration, using finite Hankel transformation 05 p0908 A67-16138

Vibration tolerance of rats previously irradiated by X-rays and hypothetical mechanisms of stress 09 p1452 A67-21719

Evaluation of wire lacing designs for damping of vibratory stresses on gas turbine blades [ASME PAPER 67-VIBR-47] 11 p1797 A67-24197

Vibratory motions of turbine blades, considering frequency determination, tangential mode, stress, damping and excitation source [ASME PAPER 67-VIBR-66] 23 p3998 A67-40740

Photoelastic coating technique for measuring stress distribution in blades vibrating in resonant modes 12 p2014 A67-25415

Semiconductor piezoresistive strain gauges and application to compressor blade vibratory stresses measurement 12 p2014 A67-25416

Piezotransmission measurements of phonon-assisted transitions in semiconductors 13 p2179 A67-27157

Vibrational stress of clamped free rectangular rods of constant cross section under effect of instantaneous impulse 13 p2220 A67-27279

Cavitation correlation with sound pressure and vibration acceleration in closed circuit hydrodynamic tunnel, showing cavitation noise spectrum 14 p2295 A67-27870

Breakdown probability calculations to determine life span and reliability of structural components subjected to oscillations 22 p3908 A67-39284

Stress interaction in cumulative fatigue damage studied to predict remaining life of machine structures 23 p4074 A67-40650

VIBRATOR

S CHOPPER

VIBRATORY LOADING

Simplified resonance-amplitude analysis of unbalance vibration superimposed upon steady state eccentricity in aerodynamic bearings 09 p1509 A67-22613

Reducing stress levels on crack propagation growth rate investigated for aircraft design problems 11 p1804 A67-24037

Effect of rotor control feedback loads of two-bladed rotor system on helicopter fuselage vibrations [AHS PAPER 133] 16 p2777 A67-31847

VIBROCARDIOGRAM

Vibrophonocardiographic techniques for monitoring cardiac dynamics in flight environment 17 p2806 A67-31954

Vibrocardiogram used as cardiovascular monitor, applying signal averaging methods for parameter evaluation during severe subject stress 23 p3959 A67-41660

Vibrophonocardiograph developed for use in shirt-sleeve flight environment, previous design miniaturized without sacrificing performance characteristics 23 p3970 A67-41661

VIDEO DATA

Parametric transformation of spectrum of video pulses in transmission line 05 p0762 A67-16359

Measuring harmonic AM frequency of bell-shaped videopulses train for modulation-to-repetition-frequency ratio greater than unity 07 p1139 A67-19227

Spectrum of AM sequences of video pulse packages 07 p1140 A67-19233

Transformation of spectrum of AM periodic sequence of video pulse by inertial detector 07 p1140 A67-19234

Wideband video data transmission from near earth orbiting vehicle and over leased telephone lines 09 p1460 A67-21583

Picture coding systems and selection of pre-and post-quantizing filters 11 p1791 A67-24711

Picture quality in PCM transmission of low resolution monochrome still pictures as affected by system parameter changes 11 p1791 A67-24712

Lunar Orbiter photographic system readout for image conversion to video signals [SMPTE PAPER 101-45] 12 p1940 A67-25463

Ground based conversion of Lunar Orbiter II video signals into photographic images, describing reconstruction electronics, signal processor, etc 12 p1940 A67-25466

Test signal techniques for measurement and video monitoring used in ORTF network 22 p3796 A67-39233

Series and parallel pulse forming feed networks for generating microwave signals, comparing output parameters and limitations 22 p3774 A67-40444

Analog and digital data processes for interplanetary photoscience with reference to Mariner Mars flyby mission, discussing telemetric transmission and SNR [IEEE PAPER 19-TP-66-1134] 23 p3998 A67-40740

VIDEO EQUIPMENT

Amplitude characteristic in transistorized selective logarithmic amplifier with video

output, discussing circuitry of proposed multistage amplifier 05 p0773 A67-16459
 Half-tone Teletypewriter prints out picture from slow scan digital TV source 05 p0806 A67-16622
 X-ray image transformation, transmission and amplification directly into video signals for inspection of missile case walls and weldments 10 p1622 A67-22929
 Film camera and video transmission system onboard Lunar Orbiter II 10 p1657 A67-23624
 Video mapping technique making possible radar moving target indication for permanent echoes only 12 p1909 A67-25128
 Raster scan parameters influencing target identification in image recognition experiments using video display 17 p2859 A67-32508
 Nanosecond baseband pulse rise time measurement, discussing real time and sampling oscillography, pulse comparison, basic instrumentation, etc 17 p2814 A67-32603
 Devices for information exchange between man and machine, emphasizing video display equipment 21 p3577 A67-38158
 Video digital data compression technique, time-buffered coarse-fine /TBCF/, for redundancy reduction 24 p4123 A67-42806

VIDICON

SA FIBER OPTICS

Ultimate sensitivity of space camera imaging devices with particular reference to slow scan vidicon 02 p0245 A67-12245
 Vidicon TV design modifications for spacecraft applications noting reduced power requirements, improvement of heaters, narrowing of bandwidth, etc [SMPT PAPER 101-51] 12 p1914 A67-25471
 Electronic zoom by varying vidicon raster size 14 p2321 A67-28920
 DODGE satellite vidicon cameras and information processing system electronics design and performance 20 p3452 A67-37572
 Vidicon type image tube sensitive in near UV developed for space applications 21 p3599 A67-38654
 SNR performance of SEC vidicon image storage tube at optimum and reduced readout rates 22 p3773 A67-39961
 Environmental, thermal and foreign particle effects on Surveyor vidicon performance and expected tube life [SMPT PAPER 102-32] 22 p3807 A67-40373
 Brightness distortions quantitative determinations in digitized Tiros/ESSA satellite vidicon data to normalize scene to uniformly illuminated image 24 p4156 A67-42431

VIEW FACTOR

Optimization of display configurations for group viewing 03 p0365 A67-13299
 View function to images of surface in nonplanar specular reflector determined by general mathematical expressions [JPL-TR-32-939] 15 p2516 A67-29131
 Lighting and viewing conditions posing visibility problems for lunar landing mission 20 p3521 A67-36598

VIGILANCE

Effects of inhaled air ions on speed of response and attention level, heart and respiration rate and transepithelial DC potential of men 09 p1452 A67-21720
 Auditory vigilance task, assessing effects on performance of signal detection value, miss or false detection cost and set size from which signals were drawn 14 p2258 A67-28664

Lowering of psychic tone, absentmindedness and vigilance decline during astronaut weightlessness on long space flights 15 p2425 A67-29103

VINI THEORY

Boundary value problem for differential equations of perturbed satellite motion assuming perturbing accelerations defined by Vinti potential 13 p2200 A67-27323

VINYL

Free radical addition of perfluoroacetonitrile to vinyl fluoride, noting formation of one isomeric compound 09 p1459 A67-22365

N-vinyl carbazole reactions with anionic initiators, discussing radical anion and polymer formation and ESR spectra [JPL-TR-32-1126] 24 p4118 A67-42601

VINYL POLYMER

SA POLYVINYL CHLORIDE

Paramagnetic and electrical properties of organic polyvinyl-acetate-based

semiconductor films irradiated with electrons before and after heating 18 p3099 A67-33694
 Poly-N-vinyl carbazole-iodine charge transfer photovoltaic effect spectral and intensity dependence, noting possible radiation detection and energy conversion applications [JPL-TR-32-1138] 24 p4201 A67-41899

VIRGO STAR CLUSTER

Spin temperature of intergalactic atomic hydrogen calculated as function of electron density and kinetic temperature 03 p0515 A67-14319
 Origin of X radiation from radio galaxies Cygnus A and Virgo A, hypothesizing thermal radiation and bremsstrahlung 18 p3116 A67-33855
 X-ray survey of Virgo region revealing signals from radio sources 3C 273 and M 87 23 p4061 A67-41473

VIRIAL THEOREM

Virial theorem for electron plasma obtained by defining potential tensor and superpotential of electric field 03 p0482 A67-13746
 X-rays from Coma cluster of galaxies, investigating origin by applying virial theorem 05 p0882 A67-16413
 Second and third virial coefficient of quantum gas expressed in terms of two-particle scattering amplitude, starting from cluster expansion of partition function 05 p0849 A67-17316
 Plasma expansion in magnetic field, showing dominating effect of initial outward momentum 05 p0858 A67-17428
 Molecular quadrupole moments and shape parameters derived from viscosities and second virial coefficients 06 p1038 A67-19047
 Second virial coefficient for atomic gas with divergent potential energy curves 07 p1225 A67-19122
 Virial theorem for continuous systems used to seek information about equilibrium of insulated self-gravitating system 07 p1183 A67-20175
 Intermolecular forces in methyl chloride and benzene calculated using spherical shell central potential theory 07 p1138 A67-20191
 Ordinary and dielectric second virial coefficients for dipolar gases calculated by off-center dipole model using series expansion 11 p1821 A67-23962
 Second virial coefficient contribution to high temperature plasma free energy calculated by means of derived pseudopotential 22 p3851 A67-39785

VIRTUAL WORK

Stability equation of elastic bodies subjected to body and pressure forces derived using virtual work principle, noting specialization to thin shells 01 p0165 A67-11307
 Equilibrium equations, boundary conditions and constitutive relations for nonlinear theory of elastic directed curves, examining double stress without moment 02 p0267 A67-12057
 Straightforward method consistent with virtual work principle for accelerating convergence to exact solution in shell analysis by matrix displacement method 10 p1725 A67-23714
 Virtual work principle shown equivalent to linear coupled thermoelasticity theory 19 p3342 A67-35763
 Variational formulation of Laplace transformed heat diffusion problem [ASME PAPER 67-HT-77] 20 p3551 A67-38755
 Book on electrodynamics of moving media, deriving force distribution using Hamiltonian and virtual power principles in relativistic formulations 20 p3500 A67-37087

VIRUS

SA BACTERIA

SA BACTERIOPHAGE

Space cabin environmental changes studied for susceptibility of mice to viral infection 21 p3574 A67-38080

VISCERA

Clineradiographic analysis of human visceral responses to short duration acceleration impact 23 p3951 A67-41553

VISCOELASTIC CYLINDER

Nonuniform temperature distribution effects on creep bending characteristics of linear viscoelastic columns of polymethyl methacrylate 01 p0160 A67-10560
 Plane large deformation of heated viscoelastic cylinder with internal and

external pressure in generalized Boltzmann superposition principle 02 p0338 A67-12238
 Steady state response of viscoelastic cylindrical shells to moving loads, obtaining exact solution with correction for shear deformation and rotatory inertia effects via Fourier transforms 03 p0522 A67-13211
 Parametric excitation of initially straight viscoelastic column represented by spring-dashpot model 04 p0709 A67-14814
 Longitudinal waves in viscoelastic rod caused by sinusoidal stress applied at one end, noting temperature dependency of mechanical properties of rod [ASME PAPER 66-WA/APM-29] 04 p0714 A67-15423

Steady state solutions of stress waves traveling in linear viscoelastic cylinder, considering torsional, longitudinal and flexural waves 04 p0716 A67-15794
 Stressed state of viscoelastic cylinder with star shaped cavity caused by steady temperature field and distributed surface load in problem of elasticity 05 p0912 A67-16185

Wave interaction between linear viscoelastic medium and thin cylindrical shell imbedded within it solved for uniform harmonic stress input applied to shell 08 p1415 A67-20486
 Stability of linear viscoelastic columns with variable cross sections, obtaining and verifying buckling load 08 p1418 A67-20594
 Fracture of viscoelastic bodies, predicting statistical variability of rupture data for uniform and nonuniform excitation histories 08 p1421 A67-20913

Bending of viscoelastic cylindrical shell resting on viscoelastic base with monodirectional characteristic 10 p1717 A67-22945

VISCOELASTIC DAMPING

Channel flow of suddenly pressurized viscoelastic and electrically conducting fluid under influence of constant transverse magnetic field 03 p0483 A67-14035
 Longitudinal oscillations of infinitely long linear viscoelastic rods to yield wave propagation in elastic rods 04 p0707 A67-14404
 Free vibration of sandwich beams viscoelastic cores, examining equations of motion, natural boundary conditions and derivation of expressions for modal distribution of damping [ASME PAPER 66-WA/UNT-3] 04 p0713 A67-15382

Tuned viscoelastic vibration dampers effect on responses of cantilever and clamped-clamped beams subject to Euler-Bernoulli beam equation, discussing loss factors based on transmissibility spectra 06 p1110 A67-18859

Dispersion and damping characteristics due to flexural vibrations in elastic plate with viscoelastic coating, obtaining energy loss resulting from dissipation [ASME PAPER 66-WA/APM-20] 10 p1731 A67-23840

Adhesive properties testing and damping behavior of thin viscoelastic material under different cyclic loadings [ASME PAPER 67-VIBR-25] 11 p1872 A67-24183

Constrained layer damping mechanism for optimum performance of plates, beams and tubular structures, using viscoelastic material [ASME PAPER 67-VIBR-26] 11 p1872 A67-24184

Viscous friction in axes of gyroscope suspension further damping of nutational oscillations and increases precession oscillations of inertial vertical 11 p1794 A67-25051

Elastic and dynamic response of viscoelastic plate with finite thickness to rigid body impact 20 p3539 A67-36920

Viscoelastic theory solving Lighthill paradox by accounting for acoustic energy damping in fine grained isotropic turbulence 21 p3610 A67-37759

Response in fundamental mode of simple single span beam with tuned viscoelastic dampers attached at discrete locations, assuming harmonic loading 21 p3719 A67-38147

Energy dissipation criteria for object falling on viscoelastic foundation or vehicle impacting without mass separation from support structure 23 p4072 A67-40609

- Field-polar forces interaction effect on viscoelastic properties of polypropylene oxide, measuring dilatometric, modulus and damping constants [JPL-TR-32-1026] 24 p4174 A67-41806
- VISCOELASTIC FLOW**
- Mechanical impedance of device moving in liquid at resonance, determining viscoelastic magnitudes of Newtonian and non-Newtonian liquids under different dynamic conditions 02 p0240 A67-11521
- Free and forced vibrations of viscoelastic plate with consideration of rotatory inertia and shear deformation, noting rectangular plate 04 p0715 A67-15586
- Laminar shearing flows breakdown for second order viscoelastic fluids in channels of critical width 05 p0792 A67-16724
- Inverse operation for Jaumann derivative /Integration/ applied to rheological equations of state for viscoelastic fluids 06 p0991 A67-18777
- Nonlinear viscoelastic fluids, discussing Couette flow, steady flow, periodic motion, wave propagation, thermomechanical coupling, etc 08 p1419 A67-20881
- Viscoelasticity for micropolar solids, obtaining constitutive equations of strain and microrotation rate dependent materials 08 p1422 A67-20979
- Dynamic two-dimensional problem of moment theory of elasticity and viscoelasticity of medium with circular cylindrical cavity 11 p1879 A67-24883
- Friction factors and velocity profiles in turbulent flow of viscoelastic non-Newtonian fluid, noting correlation between frictional characteristics and Reynolds number 12 p1929 A67-25904
- Analysis of steady flows of viscoelastic materials by introduction of two dimensionless groups 13 p2096 A67-26931
- Viscoelastic flow, examining boundary layer approximation for flat plate with zero angle of incidence 20 p3424 A67-37503
- Steady motion of elasticoviscous liquid through annulus between two coaxial right circular porous cylinders with suction and injection 21 p3613 A67-38411
- Viscoelastic fluid isotropic turbulence decay approximating non-Newtonian effects by perturbation method 22 p3787 A67-40221
- Film thickness, pressure distribution and load carrying capacity of loaded line contact in presence of viscoelastic lubricant noting high pressure spike [ASME PAPER 87-LUB-23] 24 p4163 A67-42681
- Viscoelastic lubricant in squeeze film configuration for sphere impinging on lubricant covered plane, noting pressure peak sensitivity to viscoelastic constants [ASME PAPER 87-LUB-24] 24 p4164 A67-42682
- Non-Newtonian elastoviscous channel flow between rigid boundaries solved by asymptotic expansion in lubrication approximation 24 p4145 A67-43086
- VISCOELASTICITY**
- Nonlinear viscoelasticity theory for zone of rigid behavior of polymer materials 02 p0338 A67-12237
- Internally bonded polariscope incorporated into transparent model for three-dimensional photoviscoelastic material studies 03 p0531 A67-14364
- Nondestructive testing by oscillatory methods of viscoelastic properties of high molecular weight polymers as functions of frequency and temperature 04 p0641 A67-14587
- Exact and variational solutions to elastic wave propagation eigenvalue problem in constant Poisson ratio linear viscoelastic material 05 p0909 A67-16141
- Correspondence principle in linearized classical theory of viscoelasticity for free vibrations, emphasizing case of irrotational or solenoidal motion 05 p0909 A67-16145
- One-dimensional acceleration waves and higher order waves propagating in general nonlinear Maxwellian materials with fading memory 06 p1099 A67-17834
- Mathematical analysis of certain problems concerning longitudinal oscillations of compound bars consisting of elastic and elastoviscous sections 07 p1214 A67-19176
- Stress analysis of solid rocket engine propellant grains including linear viscoelasticity, thermal analysis and equilibrium, relaxation times, engine sizes, cooling, creep relaxation, etc 08 p1373 A67-20874
- NBS polyisobutylene relaxation modulus and Rouse functions for torsional molecular vibrations and internal rotation in viscoelastic theory of amorphous polymers 08 p1346 A67-20878
- Nonlinear continuum mechanics of viscoelastic materials with application to solid propellants 08 p1419 A67-20879
- Restrictions on relaxation moduli of anisotropic linear viscoelastic solid 08 p1419 A67-20880
- Quasi-static and dynamic linear viscoelasticity boundary value problems and elastic wave propagation theory 08 p1419 A67-20882
- Solid rocket engine propellant grain structural dynamics including elastic and viscoelastic deformations, stress and shear vibration modes, natural frequency calculations, etc, using Fourier inversions and transforms 08 p1376 A67-20883
- Three-dimensional creep, stress relaxation and viscometric measurements of nonlinear viscoelastic materials in continuum 08 p1419 A67-20884
- Creep, stress relaxation and vibrational measurements, sinusoidal torsional forced oscillations and stress wave propagation in polymeric linear viscoelastic solids 08 p1419 A67-20885
- Propagation mode of one-dimensional HF finite acceleration pulses in nonlinear viscoelastic solids, stressing shock formation and propagation 09 p1573 A67-21547
- One-dimensional steady solutions for shock wave propagation in class of nonlinear viscoelastic materials deduced from stated balance laws and representation theorem for compressive and expansive motions 09 p1578 A67-22410
- Quasi-static problems of isotropic viscoelastic shells subjected to external loading and steady temperature field 10 p1717 A67-22943
- Second order gyroviscous stress in collisionless plasma for LF propagation quasi-perpendicular to magnetic field calculated by utilizing higher moments of Vlasov equation 10 p1685 A67-23331
- Plane notch stresses in viscoelastic materials with equations obtained from three-dimensional elasticity theory 10 p1720 A67-23576
- Propagation of acceleration waves in elastic and viscoelastic materials 11 p1875 A67-24572
- Ordinary waves in viscoelastic mediums analyzed, using Green tensor relation to Kirchhoff tensor 11 p1877 A67-24750
- Thermo-and viscothermoelasticity foundations and problems 13 p2216 A67-28608
- Dynamic stability of structures, discussing parametric resonance, impulsive loading, circulatory loads, aeroelastic and buckling problems 14 p2396 A67-28079
- Stabilizing effects of viscoelastic cores on response of long circular cylindrical shells subjected to time dependent axial loads 14 p2399 A67-28118
- Transient vibration of viscoelastic body, showing dynamic displacement expression in terms of static boundary value problem 14 p2400 A67-28143
- Griffith initiation criterion extended to fracture initiation and growth in viscoelastic materials using energy formulation 16 p2773 A67-31311
- Time dependent fracture of viscoelastic materials, considering defect initiation relation as approximation to crack growth history 16 p2773 A67-31312
- Fracture in viscoelastic bodies, considering stress-strain-time properties and analyzing temperature and failure envelopes 16 p2894 A67-31313
- Internal fracture of solids analyzing initiation by converging tensile pulses in prolate spheroid and crack propagation in infinite solid 16 p2773 A67-31315
- Book on continuum mechanics including kinematics, principles and linear theories of continuum mechanics, elasticity and viscoelasticity 17 p2963 A67-33092
- Uniqueness theorem for general linear anisotropic time-variable viscoelastic body under boundary conditions, using Laplace transformation 17 p2964 A67-33135
- Constructing solution of Cauchy initial value problem when Riemann function is unknown for one-dimensional linear viscoelasticity 18 p3139 A67-33428
- Molecular theories for polymer elastic and viscoelastic properties near glass transition region [AIAA PAPER 87-488] 18 p3143 A67-33954
- Viscoelasticity and rubber-like elasticity continuum mechanical description under stress relaxation conditions [AIAA PAPER 87-489] 18 p3143 A67-33955
- Viscoelastic theories evaluated for ability to correlate linear dynamic data with nonlinear viscosity and normal stress data 19 p3210 A67-35614
- Buckling of aging linearly viscoelastic beam columns with time variable mechanical properties, deriving integrodifferential equations and stability conditions 19 p3343 A67-35781
- Viscoelastic behavior of pure gum rubbers and relationship between filler characteristics and mechanical properties of inert filled composite materials 19 p3249 A67-35888
- Book on viscoelasticity covering linear theory as part of applied mechanics, differential equations, hereditary integrals, etc 20 p3535 A67-36138
- Uniformly moving crack in infinite body, in antiplane strain, driven by loads in simultaneous travel 20 p3536 A67-36415
- Mechanical characteristics of materials determined using circular bending 20 p3537 A67-36476
- Anisotropic composites viscoelastic analysis applied to orthotropic cylinder pressurization, glass fiber cooling and relaxation shear moduli problems 20 p3474 A67-37267
- Viscoelastic properties of capron under torsion at infrasonic frequencies and polymer resin complex shear modulus temperature dependence 21 p3647 A67-37866
- Stability criteria in stress-rupture strength theory, deriving stress and moment influence functions and damage tensor 21 p3717 A67-37969
- Birefringent properties of Voigt type viscoelastic medium and Noll hygrosteric material during stress relaxation 21 p3657 A67-38409
- Viscoelastic behavior of laminated orthotropic plates, discussing single layer or homogeneous orthotropic viscoelastic plate problem 22 p3914 A67-40108
- Soviet book on elasticity and plasticity covering perforated plates and shells and elastohereditary media mechanics 23 p4077 A67-40748
- Elastohereditary /viscoelastic/ media mechanics, analyzing linear and nonlinear equilibrium equations, uniqueness and existence theorems and solution methods 23 p4077 A67-40750
- Stress-strain relation in viscoelastoplastic bodies noting static instability under conservative load 24 p4246 A67-41932
- Book on mechanics of continua covering elasticity, fluid dynamics, heat conduction, thermoelasticity and viscoelastic materials equations 24 p4189 A67-42382
- Contact region of glass ball rolling on viscoelastic plate at various velocities analyzed by interference microscope photography [ASME PAPER 87-LUB-25] 24 p4176 A67-42683
- VISCOMETRY**
- Three-dimensional creep, stress relaxation and viscometric measurements of nonlinear viscoelastic materials in continuum 08 p1419 A67-20884
- VISCOPLASTIC FLOW**
- Loss in hydrodynamic thermostability of viscoplastic material with stress tensor deviator related to strain rate tensor deviator 01 p0052 A67-10682
- Internal forced convection in viscoplastic fluids between two parallel plates with applied normal magnetic field 01 p0126 A67-11188
- Zone of quasi-solid motion in MHD flows of viscoplastic fluids 04 p0670 A67-15532
- Plane strain equations for elastoviscoplastic compressible bodies without strain hardening 05 p0908 A67-16039
- Loss in hydrodynamic thermostability of viscoplastic material with stress tensor deviator related to strain rate tensor deviator 11 p1783 A67-25070

VISCOPLASTICITY

MHD rotation of conducting viscoplastic fluid between two coaxial cylinders in crossed fields 01 p0120 A67-10180
Plastic flow effects on MHD Couette flow in annular gap between two coaxial cylinders in radial magnetic field 06 p1044 A67-18680
Advances in applied mechanics, Volume 9, covering hydrodynamic stability, free oscillations, nonlinear vibrations and viscoplasticity 08 p1352 A67-20308
Rheologic and plastic phenomenological analysis of viscoplasticity problems, discussing constitutive equations and stress propagation 08 p1414 A67-20312
Boundary value wave problem in elastoviscoplastic medium solved by approximate method using Courant concept 19 p3340 A67-35444

VISCOSITY

SA EDDY VISCOSITY

SA GAS VISCOSITY

Thrust and mass flow rate of supersonic nozzle with and without internal separation 04 p0602 A67-14568
Diffusion coefficients determination from viscosity measurements based on higher Chapman-Enskog approximations 04 p0658 A67-15510
Viscosity and thermoconductivity of partially ionized argon plasma at atmospheric pressure measured, using equilibrium plasma jet 05 p0851 A67-16508
Torsional creep and creep recovery behavior of amorphous 1, 3, 5-tri-alpha-naphthyl benzene close to or below glass transition temperature 06 p1019 A67-17827
Mach number effect on mixing lengths and kinematic eddy viscosities in turbulent flat plate boundary layer [AIAA PAPER 67-199] 06 p0987 A67-18324
Small additions of Y, La, Hf, V, Ti and Zr on structure of cleaved surfaces and viscosity of Mo cermet 07 p1198 A67-19184
Turbulent viscosity forces in nonlinear three-dimensional nonstationary problem of thermal convection 07 p1221 A67-20005
Viscosity and thermoconductivity of vapors of sodium and potassium 09 p1579 A67-21865
Spatial dispersion of viscosity coefficients of liquids near critical point 09 p1487 A67-21904
One-dimensional compressible flow, considering buoyancy forces as closed-form solution of Navier-Stokes equations for unknown temperature-dependent coefficient of viscosity 10 p1625 A67-23135
Intrinsic viscosity of linear homogeneous polystyrenes in decalin and toluene over large temperature ranges and molecular weights 10 p1602 A67-23384
Stability of motion of plane boundary interface between two different density coupled fluid jets analyzed to determine role of viscosity in drop formation 11 p1782 A67-24959
Influence of Hall effect and viscosity on flow relations and power output of MHD generator 13 p2165 A67-26642
Effective viscosity of blood in circulation for large, intermediate and small vessels 18 p2990 A67-33511
Cesium viscosity coefficient over range of temperatures and pressures, assessing accuracy of results and collision integral values 18 p3087 A67-34050
Temperature dependent viscosity effects on heat transfer and drag on wedge-shaped body, calculating boundary layers on surface 20 p3421 A67-36824
Solar oblateness and Mercury perihelion advance, showing turbulent viscosity forces acting on photospheric meridional currents as possible distortion cause 21 p3701 A67-37963

VISCOUS DAMPING
Energy dissipation calculation of damping factor for free oscillations of viscous liquid in circular cylindrical vessel 04 p0711 A67-15196
Mass and oscillation damping of rigid sphere in cylindrical tube containing viscous liquid [ASME PAPER 66-WA/UNT-5] 04 p0608 A67-15442
Schlieren techniques used in free flight range study of far wake of hypersonic cones [AIAA PAPER 67-31] 06 p0938 A67-18261
Unidirectional vibration isolation systems,

discussing viscous damping, Coulomb damping transmissibility and resonance characteristics [ASME PAPER 67-VIBR-21] 11 p1796 A67-24180

Vertical vee gyro damping system for gravity gradient satellite, considering scaling, inertia, time and torque factors and viscosity change effects 12 p1920 A67-25122
Successive release evaluation by periodometer and memory oscillograph of viscous damping of one degree of freedom system 17 p2884 A67-32698
Schlieren techniques used in free flight range study of far wake of hypersonic cones [AIAA PAPER 67-31] 17 p2793 A67-33006
Amplitude of forced flexural vibrations of free rotating shaft under arbitrary load with dampers, taking into account viscous friction 21 p3726 A67-38834

VISCOUS DRAG

Precessional motion of corrected gyroscope as affected by viscous friction 01 p0064 A67-10421
Viscous friction and heat flux for partially ionized medium flowing in plane channel with anisotropic transport coefficients 04 p0666 A67-15189
Free vortex decay above stationary boundary for varying viscosity, determining plate boundary layer solution for small nondimensional radial distances 06 p0985 A67-18135
Lift-drag ratio, lift and drag coefficients and angle of attack effects on Gemini and Apollo reentry vehicles measured in shock tunnel under free flight conditions [AIAA PAPER 67-165] 06 p0941 A67-18507
Viscous and Coulomb-friction forces effect on precessional motion of gyroscope mounted on stationary base 09 p1498 A67-22034
Viscous friction in axes of gyroscope suspension further dampens of nutational oscillations and increases precession oscillations of inertial vertical 11 p1794 A67-25051
Lift-drag ratio, lift and drag coefficients and angle of attack effects on Gemini and Apollo reentry vehicles measured in shock tunnel under free flight conditions [AIAA PAPER 67-165] 19 p3169 A67-34818
Performance factors affecting size, shape and operation of piston and bore including hydraulic lock, viscous drag, oil contamination, etc 20 p3366 A67-37367
Viscous degradation of hypersonic lift-drag ratio in manned spacecraft, noting free stream Mach and Reynolds numbers 22 p3742 A67-40113

VISCOUS FLOW

SA INVISCID FLOW

SA POHLHAUSEN SOLUTION

Motion equation solution to viscous conducting flow at inlet of diverging channel using difference method, noting magnetic field effect 01 p0120 A67-10184
Stokes creeping flow equations and steady flow of incompressible viscous fluid past liquid drop 01 p0051 A67-10458
Injection from half-plane located in steady viscous flow in Oseen approximation, noting skin friction 01 p0052 A67-10793
Mass transfer and first order boundary layer effects on sharp cone drag [AIAA PAPER 66-33] 01 p0007 A67-11161
Equilibrium burning of spherical nongaseous fuel drop in slow convective hot-oxidant flow in thin flame 02 p0341 A67-11562
Viscous incompressible flow past finite flat plate obtained under Oseen approximation for large and moderate Reynolds numbers, using Wiener-Hopf technique 02 p0234 A67-12546
Pressure patterns, gas ingestion and sealing capacity of viscoseals investigated using oil, water and liquid sodium as sealed fluids 03 p0428 A67-13226
Viscous shear flow past two-dimensional cavity of infinite depth by use of Stokes approximation, emphasizing flow pattern near dividing streamline 03 p0402 A67-13356
MHD equations, discussing dimensional and nondimensional parameters, modifications of Maxwell equations, vorticity and rate of circulation change in viscous flow, etc 03 p0480 A67-13724
MHD flow past bodies in electroconductive viscous incompressible flow 03 p0482 A67-13743

Taylor vortices intensity and viscous losses determined for viscous flow of liquid between concentric rotating cylinders, solving equation by numerical method 03 p0405 A67-14030
Temperature and magnetic field gradient effects on magnetothermomechanical interaction of viscous incompressible ferrofluid with cold wall 04 p0600 A67-14446
Generalized Couette-type flow with variable viscosity in plane and annular channels, liquid being injected or sucked through porous surfaces 04 p0602 A67-14639
Stafical electointegrator for numerical solution of boundary layer theory problems for incompressible fluid and compressible gas 04 p0603 A67-14642
Isothermal steady state process of fluid with constant density and kinematic viscosity coefficient flowing past thin plate 04 p0603 A67-14709
Nonisothermal steady state flow of fluid with constant density and kinematic viscosity coefficient past thin plate 04 p0603 A67-14710
Composite heat transfer and viscous friction of moving gray medium with large optical density, using laminar boundary layer equation, noting hydrodynamic state role 04 p0722 A67-14713
Gas flow with accelerated contact surface and attenuated shock wave as example of gas flow not explainable by ideal one-dimensional theory 04 p0604 A67-14782
Variational analysis of Graetz problem of forced-convective laminar heat transfer in duct, for various cross sections and given wall temperature and temperature gradient 04 p0728 A67-15802
Successive approximations applied to optimal control equation for self-similar viscous Couette flow between one stationary and one moving wall 04 p0610 A67-15885
Reynolds number effect on surface pressure distributions and boundary layer velocity profiles on three-quarter power law bodies of revolution in hypersonic flow 05 p0747 A67-16431
Transport of vorticity and enthalpy in flow field in nose region of blunt body in viscous hypersonic flow 05 p0749 A67-16820
Parallel Couette and Poiseuille flows of multicomponent viscous plasma in presence of pressure gradient and electric field 05 p0854 A67-16894
Wall of large circular formation on moon shown on Orbiter photographs as convex body resembling flow of viscous lava 05 p0901 A67-17202
Continuum viscous nonequilibrium flow partial differential equations in thin shock layer 05 p0750 A67-17335
Diffusion-viscosity coupling in stationary flow of nitrous oxide-carbon dioxide mixture in case of Maxwellian intermolecular forces 05 p0794 A67-17380
Attenuation law of turbulent pulsations in viscous sublayer of turbulent boundary layer of incompressible fluid 06 p0982 A67-17741
Navier-Stokes equations for two-dimensional sonic flow of viscous heat-conducting gas assuming particle velocity close to sound speed, studying asymptotic pattern 06 p0937 A67-18031
Three-dimensional Cauchy-Poisson problem for waves in viscous fluid 06 p0984 A67-18046
Viscous effects in expanding solar corona under conduction heating 06 p1078 A67-18158
Flow field model for laminar hypersonic near-wake in inviscid expansion, viscous sublayer and recirculating flow [AIAA PAPER 67-63] 06 p0940 A67-18353
Reynolds number scaling theory for hypersonic ablation, deriving heat and mass transfer relationship [AIAA PAPER 67-155] 06 p1117 A67-18478
Free boundary flows of viscous liquid, analyzing Stokes flow at zero Reynolds number 06 p0990 A67-18641
Shock tunnel heat transfer measurement and hypersonic viscous flow over pointed cones, particularly viscous-layer regime at low Reynolds numbers 06 p0943 A67-18845
Three-dimensional boundary layer flow over windward side of flat delta wing in hypersonic flow at moderate angle of attack, examining viscous-inviscid interaction [AIAA PAPER 66-492] 06 p0943 A67-18848
Viscous incompressible slow flow over circular arc wall projections or depressions with shear flow far from

- projection 06 p0992 A67-18887
- Approximations to Navier-Stokes equations corresponding to steady two-dimensional incompressible viscous flow about circular cylinders 07 p1167 A67-19156
- Perturbation of two-dimensional viscous flows in finite region, noting exact solution of Navier-Stokes equation 08 p1319 A67-20352
- Instability of plane Couette-Poiseuille flow of two superposed layers of different viscosities between two horizontal plates 08 p1321 A67-20709
- Book on theory of flow machines covering pumps, turbines, windmills, fluid dynamics, viscous flow fields, cascade flow, etc 08 p1321 A67-20758
- Elastic moduli of filled systems, discussing effects of filler size, shape, concentration, agglomeration, etc 08 p1421 A67-20916
- Navier-Stokes equation for viscous incompressible fluid flow between stationary and uniformly moving parallel plates with uniform suction along stationary plate 08 p1322 A67-21179
- Closed form solution expressing transonic flow in idealized stellar wind and spherical accretion problems including viscosity and thermoconductivity effects 08 p1399 A67-21240
- Rayleigh problem of compressible viscous heat-conducting radiating gray gas flow near flat plate set impulsively in motion in own plane 08 p1324 A67-21392
- Viscosity effect on stability of plane flame front, showing destabilization from linearized equations of velocity and pressure disturbances 08 p1428 A67-21423
- Sealing coefficient of visco seal for laminar and turbulent flow, noting Reynolds number effect 10 p1659 A67-22706
- Asymptotic behavior of laminar boundary layer, reducing system to heat equation, noting viscosity effects and uniqueness of homogeneous solution [ONERA-TP-458] 10 p1623 A67-22878
- Asymptotic analysis of radiative Rayleigh problem in flow of compressible viscous heat-conducting radiating gray gas extended to high plate Mach numbers 11 p1774 A67-23855
- Solid body translational movement in viscous incompressible conductive flow in magnetic field solved for case of zero magnetic Reynolds number 11 p1832 A67-24055
- Aerodynamic characteristics of wedge wings determined for hypersonic viscous flow 11 p1742 A67-24347
- Plane viscous problem of gas motion through weak straight line discontinuity of acceleration, noting formation of boundary layer 11 p1742 A67-24687
- Viscous flow around flat plate at various angles of incidences at high Mach number to evaluate shock wave intensity variation and wall pressure distribution 11 p1742 A67-24761
- Viscous flow around spheres, considering mass efflux effect, using Navier-Stokes equations and finite difference methods 12 p1927 A67-25282
- Navier-Stokes equations solved by finite difference methods at low Reynolds numbers for viscous flow around sphere, noting no flow separation 12 p1927 A67-25283
- Extension of Loitsianskii hypothesis concerning localism of turbulent transfer processes in viscous flows to MHD flows, noting results for friction coefficient 12 p1976 A67-26070
- Linear stability of symmetrical parabolic flows of various types 13 p2092 A67-26276
- Hodograph transformation in two-dimensional problems of MHD of viscous flow 13 p2170 A67-27318
- Asymptotic short wave flow equations simplified for various viscous heat conducting gas flows 14 p2295 A67-27838
- Time dependent viscous flow between two rotating spheres analyzed by extension of numerical methods 14 p2296 A67-27905
- Steady state fluid flow in thin passage analyzed using energy model and including compressibility effects 14 p2302 A67-28264
- Viscous operation in superlaminar flow regime noting pressure patterns, end effect, gas ingestion and sealing 14 p2327 A67-28797
- Critical region determination in viscous fluid flow using dye stream fuzziness or pressure drop discontinuity as measure of flow turbulence 14 p2305 A67-28801
- Time dependent problems of heat transfer in laminar flow of viscous incompressible fluid in cylinder and cylindrical annulus 14 p2408 A67-28892
- Constitutive equations describing small perturbations on viscometric flows, noting relations with stress-relaxation moduli flow 15 p2469 A67-29222
- Current carrying incompressible viscous fluid past nonconducting sphere taking fluid inertia into account, noting eddy formation and flow separation 15 p2469 A67-29224
- Generalized streamline hypothesis for turbulent boundary layer flow with spatial variation of viscosity 15 p2473 A67-30210
- Hypersonic weak and strong interaction theory for case of uniform flow past flat plate, discussing boundary layer characteristics 15 p2473 A67-30220
- Viscous effects in expanding solar corona under conduction heating 16 p2741 A67-30502
- Stagnation region foreign gas injection in low Reynolds number hypersonic shock layer flow 16 p2591 A67-30936
- Vortex breakdown treated as failure of quasi-cylindrical approximation for viscous axisymmetric flow 16 p2658 A67-30948
- Reduction of steady viscous magnetohydrodynamic flows having orthogonal magnetic and velocity field distributions to associated flows having zero magnetic field 16 p2721 A67-31552
- Flow of viscous incompressible conducting fluid in channel with porous walls 17 p2910 A67-33352
- Hard superconductors electrical resistivity when subjected to increasing magnetic field, considering flux pinning and viscous motion of flux lines 18 p3098 A67-33518
- Heat transfer due to flow of electrically conducting incompressible viscous fluid from rotating insulated disk under influence of axially oriented magnetic field 18 p3084 A67-33667
- Flow past circular cylinder started impulsively from rest, reexamining Navier-Stokes equations 18 p3026 A67-34008
- Finite propagation velocity in heat conduction, diffusion and viscous shear motion, studying assumptions of differential equation derivation 18 p3159 A67-34070
- Parameters of viscous supersonic compressible gas flow past corner, giving smooth coupling conditions for Navier-Stokes and boundary layer solutions 18 p3027 A67-34205
- Regularity of generalized solutions of general nonlinear and nonstationary Navier-Stokes equations, improving differential properties by data smoothness 19 p3209 A67-35445
- Concentrated vortex model for Karman street in two-dimensional viscous incompressible laminar flow past bluff body 19 p3210 A67-35446
- Flow of incompressible viscous fluid past plane body, when flow boundary layer detaches from body producing aerodynamic wake 19 p3171 A67-35632
- Stream function of plane flow of incompressible viscous fluid around parabolic profile, using successive approximations method 20 p3420 A67-36394
- Hypersonic weak-interaction similarity solutions for viscous heat-conducting compressible flow past flat plate, using Navier-Stokes equations 20 p3357 A67-36849
- Rear stagnation point solution for viscous incompressible electrically conducting MHD flow 20 p3499 A67-36850
- Thermal boundary layer theory for steady cellular convection in viscous rotating flow 20 p3553 A67-36937
- Turbulent boundary layer theory for streamline flow over impermeable plate, noting viscous interface effect 20 p3424 A67-37461
- Hypersonic boundary layer of sharp cone, considering boundary layer interaction with outer viscous flow 22 p3741 A67-40027
- High altitude hypersonic viscous flow degradation of L/D effects on entry vehicle lateral range capability 22 p3742 A67-40114
- Variational formulation and Rayleigh-Ritz method for nonequilibrium viscous incompressible flows, obtaining velocity and temperature distributions 22 p3788 A67-40422
- Haskell viscous flow equations describing very slow linearly viscous liquid with initially crater shaped surfaces solved and applied to lunar craters 23 p4065 A67-40998
- Externally pressurized gas bearings examined for mechanism of series restrictors on pressure distribution, flow quantity and load 23 p4010 A67-41064
- Chemical reaction effect on viscous boundary layer of hypersonic flow of reacting gas mixture past blunt body 24 p4091 A67-42270
- Steady flow extremum principles for incompressible viscous fluid generalized to liquid flow containing suspended solid bodies and drops of another liquid 24 p4144 A67-42567
- Viscous flow stability between concentric rotating cylinders with Taylor vortices, deriving velocity and pressure perturbation nonlinear partial differential equations 24 p4145 A67-43083
- Two-and three-dimensional laminar viscous boundary layer flow nonlinear partial differential equations solved analytically, studying difference equation substitution 24 p4145 A67-43087
- VISCOUS FLUID**
- Approximate solution of stationary boundary layer problems involving flow of viscous incompressible conducting fluid around flat plate in presence of magnetic field 01 p0123 A67-10540
- Laminar flow of elastico-viscous fluid between parallel planes obeying Noll constitutive equation, considering heat transfer 01 p0053 A67-10802
- Flow of viscous fluid in closed cylindrical space under rotating surface solved by grid method appropriate for computers 03 p0401 A67-12871
- Heat transfer in viscous fluid flow in gap between permeable isothermal surface and rotating disk, solving energy equation 03 p0536 A67-13611
- Series coefficients of flow stream functions for plane laminar flows of viscous incompressible fluids in channels and near corners at small Reynolds numbers 03 p0405 A67-14259
- Numerical analysis of unsteady viscous fluid flow past circular cylinder, noting effect of Reynolds number 04 p0602 A67-14617
- Slow periodic motions of viscous incompressible fluid past sphere in infinitely long circular cylinder, using Navier-Stokes motion equations 04 p0602 A67-14618
- Convective heat transfer in motion of fluid in initial section of cylindrical tube 04 p0722 A67-14716
- Connective heat transfer and viscous fluid friction at air pressure with high Reynolds numbers in cooled channels, noting coolant pressure effect 04 p0603 A67-14717
- Reynolds number assessment in analytical relations for convective heat transfer and viscous fluid friction 04 p0722 A67-14718
- Partially ionized two-temperature plasma, deriving distribution function of first approximation associated with viscosity 04 p0666 A67-15186
- Unsteady viscous fluid flow in MHD channel under action of pressure gradient solved for arbitrary load coefficient 04 p0669 A67-15519
- Unsteady laminar flow of viscous incompressible fluid between two infinite parallel rotating disks with angular velocities varying with time 04 p0609 A67-15605
- Mathematical flow-intermittance model for turbulent patterns, noting viscosity effects 04 p0609 A67-15755
- Exact solution /by Hankel and Laplace transforms/ of unsteady motion of viscous MHD fluid in cylindrical vessel in axisymmetric constant strength magnetic field 05 p0850 A67-16134
- Integral motion equations of rigid body with cavity partly filled with viscous incompressible fluid with free surface 05 p0921 A67-17005
- Liquid and gas viscosity correlation at 1 atm with reduced density for parahydrogen 05 p0873 A67-17224
- Laminar heat transfer in thermal viscous MHD flow past semiinfinite flat plate 05 p0857 A67-17416
- Unsteady circular motion of viscous fluid with hollow vortex, showing motion vorticality in boundary layer region on free surface 06 p0982 A67-17728
- Fixed vertical plane surface effect on velocity of solid sphere in free fall in

laminar region of incident viscous flow for various Reynolds numbers 06 p0983 A67-17928

Viscous interaction theory for laminar supersonic near wake applied to calculation of recirculation region for range of flow conditions 06 p0941 A67-18467

[AIAA PAPER 67-61] Motion about fixed point of solid body with cavity filled with viscous incompressible fluid 06 p0991 A67-18810

Three-dimensional boundary layer flow of incompressible second order viscous fluid near spinning cone 06 p0992 A67-18868

Asymptotic properties of fluid temperature field and Nu numbers in nonstationary heat transfer during passage of laminar flow of viscous incompressible fluid through rectilinear channel 07 p1265 A67-19125

Approximate solution of integral equations with aid of least squares for steady motions of viscous incompressible fluid in rotating cylinder 07 p1188 A67-19217

Approximate solution of some nonstationary boundary layer problems with allowance for magnetic field, discussing nonsteady flow of viscous incompressible electrically conducting fluid past flat plate 08 p1362 A67-21202

Zero Reynolds limit of steady incompressible viscous fluid motion in sphere due to Landau source at center proved to be Stokes flow 09 p1487 A67-21665

MHD flow of viscous conducting fluid jets and MHD flows with nonlinear temperature dependent conductivity 09 p1541 A67-21807

Cauchy problem for nonstationary linearized Navier-Stokes equations for fixed container partially filled with liquid 09 p1532 A67-21873

Motion equations and boundary conditions for viscous liquid, noting operator characteristics of viscosity coefficients near critical point 09 p1487 A67-21909

Unstable motion of incompressible viscous fluid in interspace between concentric spheres 09 p1487 A67-21928

Unsteady incompressible flow of viscous electrically conducting fluid near stagnation point, determining skin friction and heat transfer at wall 09 p1544 A67-21934

Viscosity variation effect on heat transfer and friction coefficient at wall during Couette flow 09 p1490 A67-22547

Free and forced oscillations of body with cavity partially filled with viscous fluid 10 p1679 A67-23029

Finite difference scheme for solving set of Prandtl equations for nonstationary flow of viscous incompressible fluid 10 p1628 A67-23672

Polarizable dielectric viscous fluid model with nonsymmetrical stress tensor 10 p1628 A67-23674

Transverse fluid flow stability between permeable boundaries for case with exact solution of perturbation spectrum 10 p1628 A67-23675

Steady flow of viscous conducting fluid in pipe under magnetic field analyzed for relations among Hartmann number, Reynolds number, skin friction, wall conductivity, etc 10 p1687 A67-23833

Cold starting and service test evaluation of SAE 10W30 aircraft engine oil [SAE PAPER 670249] 11 p1811 A67-23982

Adhesive properties testing and damping behavior of thin viscoelastic material under different cyclic loadings [ASME PAPER 67-VIBR-25] 11 p1872 A67-24183

Green integrals extended to movement of incompressible viscous conductive fluid in which magnetic field is generated 11 p1840 A67-24620

Motion of hollow body filled with viscous fluid at large Reynolds numbers, determining Zhukovskii potentials and examining small oscillations 11 p1782 A67-24673

Asymptotic solutions for free and forced oscillations of solid having cavity filled with viscous fluid, considering several degrees of freedom and arbitrary cavity shapes 12 p2029 A67-25657

Flow and heat transfer in viscous fluid layer expanding over rotating disk, calculating energy and motion equations 13 p2224 A67-27050

Viscous fluid flow stability in boundary layer on plate, applying perturbation

method, calculating critical values of modified Reynolds numbers 13 p2105 A67-27051

Supersonic viscous flow near blunt body stagnation line, using Navier-Stokes equations 14 p2240 A67-27993

Deviation from sphere shape of drop moving through viscous media and dependence on Weber number, size, etc 14 p2302 A67-28235

One-dimensional small signal linear model of fluid transmission line using finite lumped parameter elements and Navier-Stokes equations 14 p2247 A67-28265

Bubble stabilization in pure viscous liquid contained in sinusoidal vibrated tank [ASME PAPER 67-FE-3] 14 p2304 A67-28356

Linear symmetric modes of propagation for viscous compressible liquid in rigid and elastic conduits analyzed using Navier-Stokes equations 14 p2304 A67-28361

Convective self-propulsion of continents 14 p2313 A67-28620

Flow of conducting incompressible viscous fluid near accelerated plate under parallel plate and magnetic field, noting velocity profiles and stress role 14 p2361 A67-28814

Small parameter method to study steady state flow of viscous incompressible fluid in journal bearing 15 p2493 A67-29692

Counterpart of Stokes hydrodynamical paradox for linearized viscous fluid flow obtained from application of singular perturbation to Oseen equations 16 p2657 A67-30827

Steady laminar flow of viscous, incompressible, electrically conducting fluid in insulated rectangular channel, with imposed oblique transverse magnetic field 16 p2713 A67-30860

Viscous, compressible fluid flow through narrow gap, noting compressibility effect on pressure distribution 16 p2681 A67-31420

Two-dimensional viscous fluid flow with formulation and solution of weak shock reflection problems by numerical method 16 p2682 A67-31534

Energy conservation law concerning electromagnetohydrodynamics of viscous electrically conducting fluid showing that total energy in fixed volume changes 16 p2721 A67-31549

Approximation method for steady laminar flows of incompressible viscous fluid in curved pipes, obtaining flow rate 17 p2836 A67-32038

Stationary flow in viscous fluid film on rotating body of revolution, using differential equations 17 p2836 A67-32261

Steady flow in rectangular cavity with driving motion by uniform translation of one wall 17 p2836 A67-32279

Hydrodynamic field of falling sphere in viscous liquid within cylindrical container noting streamlines, velocity variations, etc 17 p2837 A67-32288

Method of finite integral transforms as format for employment of incomplete eigenfunctions, discussing application of equitriangular transform 17 p2876 A67-32423

Periodic solution of boundary value problem involving motion equation of viscous fluid 17 p2838 A67-32681

Affine solutions for temperature/flux distribution on heated horizontal plate 17 p2838 A67-32701

Potential equations for hydrodynamic and thermoelastodynamic linear wave motions applied to linear wave motion of isotropic thermally conducting elastic solids and viscous fluids [ASME PAPER 67-APM-32] 17 p2886 A67-33159

Slip flow of incompressible viscous fluid past permeable infinite plate during fluid seepage into main homogeneous outer flow 18 p3023 A67-33419

Variable mass body rectilinear unsteady motion equations for movement at various levels in viscous fluid 18 p3023 A67-33426

Successive approximation method analysis of flow around single barrier extending downstream and in direction of velocity at infinity upstream 18 p3025 A67-33682

Classical hydrodynamics equations accounting for dissipative processes 18 p3027 A67-34089

Spherical shape changes of droplet of viscous substance of high surface tension under variable external force and small

deformation 18 p3028 A67-34220

Integral motion equations of rigid body with cavity partly filled with viscous incompressible fluid with free surface 18 p3028 A67-34267

Heat transfer in viscous fluid flow in gap between permeable isothermal surface and rotating disk, solving energy equation 18 p3161 A67-34476

Viscous fluid discharge from tubes of various cross sections under constant pressure gradient with longitudinal pulse along wall, noting short period stoppage 18 p3029 A67-34615

Unsteady discharge of compressed viscous gas from duct analyzed by finite-difference method 19 p3172 A67-35780

Perfect fluid theory analyzed from resistance viewpoint and compared with flow past material body when viscous, discussing potential flow 20 p3419 A67-36189

Supersonic viscous gas flow around body of revolution involving perturbation damping, analyzing Navier-Stokes and heat transfer equations for flow chart 20 p3357 A67-36810

Internal rotational relaxation effect on attenuation of HF turbulent vortices during degeneration of turbulence in viscous weakly elastic fluid 20 p3422 A67-37053

Asymptotic properties of fluid temperature field and Nu numbers in nonstationary heat transfer during passage of laminar flow of viscous incompressible fluid through rectilinear channel 21 p3731 A67-38169

Finite difference scheme for solving set of Prandtl equations for nonstationary flow of viscous incompressible fluid 21 p3612 A67-38273

Polarizable dielectric viscous fluid model with nonsymmetrical stress tensor 21 p3612 A67-38275

Transverse fluid flow stability between permeable boundaries for case with exact solution of perturbation spectrum 21 p3612 A67-38276

Viscous non-Newtonian fluid radial flow between circular disks solved, using model equation reduced to power law equation 21 p3612 A67-38381

Procedure for expanding parameter in asymptotic power series of any order to investigate viscous compressible supersonic gas flow past blunt body 22 p3740 A67-40014

Peristaltic viscous fluid motion through axisymmetric pipes and symmetrical channels produced by pressure gradients and cross section changes, using Stokes approximation 23 p3990 A67-41174

Kinetic prediction theory for viscosity, thermal conductivity and diffusivity of binary liquid mixtures composed of molecules interacting with square-well potential 23 p4083 A67-41531

Plane shock wave disturbance development analysis by solving Cauchy problem, discussing low viscosity effect 24 p4141 A67-41931

Nondisturbing turbulent flow measurements applied to viscous sublayer in smooth square pipe, showing linear velocity gradient in layer adjacent to wall 24 p4144 A67-42607

VISIBILITY

SA LIGHT TRANSMISSION

Computer programming to predict performance of complex orbit navigation systems using simulation of landmark visibility from orbit as model 09 p1467 A67-21832

Satellite visibility calculation for individual ground stations of telemetry and tracking network as function of orbital injection parameters 15 p2561 A67-30047

Mars polar cap size changes, color and visibility from observations in 1963 17 p2942 A67-32330

Aircraft front windshields, discussing thermal stability, clear vision maintenance, bird impact, atmospheric pressure effect, cabin pressure changes and tensile strength 18 p2986 A67-34099

Photographic techniques for atmospheric attenuation in air to ground visibility 20 p3441 A67-36399

Lighting and viewing conditions posing visibility problems for lunar landing mission 20 p3521 A67-36598

Visibility in warm fog produced in cloud chamber by seeding with sodium chloride

particles, with application for aircraft landing clearance 22 p3828 A67-39338

Soviet book on atmospheric visibility noting photometry, range, threshold, runway visual range, atmospheric transmittance and atmospheric boundary layer problems 23 p4024 A67-40600

VISIBLE RADIATION

Sum and difference frequency mixing of visible and IR gas laser light in GaP at near reststrahl frequencies and relationship to spontaneous Raman scattering 04 p0682 A67-15464

Mechanism regulating total amount of earth and Mars atmosphere transparent to visible and IR radiation 06 p0995 A67-18052

Absolutely calibrated radiometer for CW laser radiation in visible and near IR bands which relies on heat flow through standard thermal impedance 09 p1502 A67-22615

Fringe visibility dependence on path length difference in laser illuminated two-beam interferometer 11 p1790 A67-24420

X-ray source in Crab Nebula size and position, showing visible light distribution having common center within 15-inch precision of measurement and finite angular extent 13 p2189 A67-26263

Spontaneous visible light emission due to laser action in carbon dioxide laser plasma, examining plasma current change with phase-lock technique 14 p2331 A67-28494

Enhanced radiation energy for visible and near IR during electron emission calculated by energy balance 19 p3176 A67-35081

Rocket observations of visible and UV dayglow including emission rates and electron density and temperature 19 p3221 A67-35277

Ground based solar electromagnetic radiation environment studies in visible and radio windows 19 p3323 A67-35332

Extensive cosmic ray shower bremsstrahlung in RF and optical bands noting intensity and incoherency 22 p3870 A67-39517

VISIBLE SPECTRUM

Three new visible CW laser lines in discharge in singly-ionized Cl 01 p0089 A67-10373

Flashlight /incoherent/ pumping of visible and IR, InSb and CdS-CdSe lasers 01 p0089 A67-10447

Light absorption by uranium glass in excited state, showing relaxation time relation to luminescence 03 p0436 A67-13141

Panoramic facsimile camera for unmanned space operation providing 360 degrees IR and visible spectrum imagery [SMPTTE PREPRINT 100-40] 03 p0423 A67-13806

Visible and X-ray photoelectric emissions in layers of Se-As-Tl intrinsic semiconductor films in vacuum 03 p0498 A67-13838

Continuous absorption cross section of argon from measurements of continuous emission of arc plasma in visible UV regions of spectrum and from temperature determination 05 p0854 A67-16988

Luminescence amplifier as intensifying tubes for faint or rapidly changing images 07 p1189 A67-20156

P-n junction fabrication in vapor phase grown GaAs-P alloys resulting in room temperature injection laser, thereby extending operation into visible spectrum 11 p1802 A67-24741

Two digital computer filing programs for determining ordinates of propagation curves of ground waves in visible region 13 p2070 A67-27202

Observational study of lunar visible emission according to study of line depths 13 p2210 A67-27601

Visible and X-ray photoelectric emissions in layers of Se-As-Tl intrinsic semiconductor films in vacuum 13 p2184 A67-27719

Visible continuous spectrum of comets rules out hypothesis of iron particles major role in scattering solar light 15 p2554 A67-29515

Refractive index dispersion of CdSSe and CdTe crystals in visible and infrared spectral range at room temperature 16 p2732 A67-31481

Absorption, reflection and emission spectra of gold chloride at low temperatures 18 p3101 A67-34187

Luminescence profiles of earth sunlit limb through visible spectrum for navigation and research 19 p3213 A67-34804

Sodium D lines in Comet Ikeya-Seki /1965 f/ near perihelion passage noting possible formation by resonance scattering at comet densities and temperatures 22 p3880 A67-39414

VISION

SA BINOCULAR VISION

SA EYE

SA FLASH BLINDNESS

SA MONOCULAR VISION

SA NIGHT VISION

SA PERSPECTIVE

SA STEREOSCOPIC VISION

Advanced vision research for extended space flight 15 p2430 A67-29274

VISUAL ACCOMMODATION

Photochemical cells and site involved in visual adaptation, reporting electroretinogram data 06 p0953 A67-18643

Independent effect of receptor adaptation level and pupil size on production of flashblindness by high intensity short-duration flashes 13 p2080 A67-28925

Peripheral vision displays for dynamic tracking information during difficult flight control tasks improve operator performance 14 p2258 A67-28663

Color normals differences, discussing classification and correlation methods 20 p3372 A67-37026

VISUAL ACUITY

Existence of fovea in human retina explained by blood supply interference with steady and acute vision 02 p0184 A67-11473

Flight simulation techniques covering digital computers, visual simulation and displays [ASME PAPER 66-WA/AV-1] 04 p0599 A67-15394

Visual acuity decrement from laser lesion in fovea of stump tail macaque monkeys 05 p0756 A67-16287

Effect of image smear and dimension on target recognition measured on differently oriented, moved and remote Landolt C 09 p1455 A67-21723

Retinal discrimination and visual acuity at different degrees of hypoxia by reading symbol E individually and combined, using oxygen-poor mixtures 21 p3575 A67-38507

VISUAL AID

Visual flight simulation, detailing all-weather operation 13 p2091 A67-27267

Air derived separation assurance /ADSA/ covering visual capabilities, passive visual enhancement, visual avoidance aids and nonvisual avoidance systems 15 p2515 A67-29942

Hydrogen fire visualization detection techniques including application of photography, TV and image converter in IR and UV regions 20 p3445 A67-36540

VISUAL CONTROL

Sudden strong stimulus effects on pilot simple visual reaction time and fatigued muscle strength 22 p3756 A67-40537

Visually controlled placing response tests for kittens reared without sight of limbs 24 p4113 A67-42221

VISUAL CUE

Apollo external visual simulation display systems, discussing optical methods applied during navigation, guidance and control tests [AIAA PAPER 67-253] 07 p1189 A67-20085

VISUAL DISCRIMINATION RECOVERY

Effects of irritation of vestibular apparatus on adaptability of human eye to darkness, studying rate of recovery of sharpness of vision 16 p2614 A67-30918

Retinal discrimination and visual acuity at different degrees of hypoxia by reading symbol E individually and combined, using oxygen-poor mixtures 21 p3575 A67-38507

Flash blindness, recovery time and aircraft control loss studied in flight simulator 23 p3966 A67-41580

VISUAL DISPLAY

Optimization of display configurations for group viewing 03 p0365 A67-13299

Command and control display system requirements noting dependence on human visual mechanism 03 p0365 A67-13300

Performance requirements of dynamic flight simulators and visual display systems in man-machine flight control problems 03 p0395 A67-13385

High power visible CW gas laser beam generation, modulation and deflection for application to visual display technology [SMPTTE PREPRINT 100-6]

03 p0438 A67-13801

Holography, discussing color reproduction, character recognition and vision by sound or ultrasound 04 p0623 A67-15301

Holographic laboratory experiments, discussing Lippman method and imagery through diffusing media contour line implantation 04 p0623 A67-15302

Society for Information Display, Symposium, Boston, October 1966 05 p0804 A67-16305

Hybrid nonlinear optical filter exhibiting different transmission properties in opposite paths applied to CRT display 05 p0804 A67-16306

Electro-optical imaging systems used in military aerial TV display, emphasizing variables involved in viewing related to visual interpretation 05 p0757 A67-16309

White light display of holograms 05 p0808 A67-17320

Laser displays application, performance and status of existing devices 06 p1001 A67-17887

Digital computer driven display system of electronic data and semiautomatic film plotters for rapid evaluation of aircraft carrier landing parameters 07 p1164 A67-19623

Man-machine interaction in visual displays of computer output 07 p1148 A67-19658

Digital computer use to provide controllable display of star field for use with spacecraft simulator for optical sightings [AIAA PAPER 67-254] 07 p1149 A67-20051

Lunar Module evaluation and test using analog and hybrid computer simulation with LM guidance and control hardware [AIAA PAPER 67-232] 07 p1184 A67-20056

Apollo external visual simulation display systems, discussing optical methods applied during navigation, guidance and control tests [AIAA PAPER 67-253] 07 p1189 A67-20085

Image storage tubes /cathode ray tubes with memory device to store visual information/ 07 p1189 A67-20157

Queueing model of many-instrument visual sampling 07 p1136 A67-20172

Fluidic digital rectilinear displacement indicator emphasizing transducer, logic circuitry and readout 08 p1281 A67-20456

Building block visual simulation facility using new generation and display techniques combined with TV model image generation 08 p1314 A67-20659

Radar applications to ATC, pictorial display and role of paper flight strip, present and future 09 p1484 A67-21678

Visual display of output patterns of IR lasers using heat sensitive phosphors 09 p1500 A67-22433

Visual presentation of data required for ATC task, noting possible traffic display and attributes 09 p1529 A67-22646

All-glass electroluminescence readout panel design with active areas integral part of connector pin 11 p1786 A67-24628

Optical resolution, light intensity and true perspective effect on imaging characteristics and parallax and image brightness influence on display realism of visual simulation 11 p1749 A67-24629

Visual presentation of geomagnetic displays using normal ionospheric current system with line separation inversely proportional to field perturbation intensity 11 p1788 A67-24699

Microwave optical field distribution patterns visualized using IR thermosensitive transducer method 11 p1792 A67-24714

Panel layout for rectilinear instruments 14 p2257 A67-28661

Large screen displays for group interaction simulation noting cost factors, techniques and performance characteristics 15 p2486 A67-29302

Color TV laser display using Ne-He and argon-ion laser in modulation and scanning system 15 p2489 A67-29914

Graphic information acquisition, processing and analysis noting requirements, application of computer, etc 16 p2781 A67-30636

Coordinatograph and electro-optical data visualization unit for digital computers noting details 16 p2634 A67-31633

Human operator performance in continuous pursuit tracking with advanced and delayed visual display 18 p2994 A67-34339

Book on fundamentals of display systems covering cathode ray tubes, color

techniques, photographic and electromechanical systems, etc 20 p3435 A67-36135

Two-dimensional displays conversion to three-dimensional, using uniaxial crystals to vary optical path length and digital control with electro-optic polarization switches 20 p3447 A67-36806

Visual display for aircraft, presenting simplest visual picture compatible with current pilot task 20 p3375 A67-36873

Built-in test features in Minuteman II intercontinental ballistic missile weapons system electronics, discussing ground equipment including self-test features and status display techniques 20 p3417 A67-36973

Automatic test system employing optical and electrical input signals based on pattern recognition with CRT display 20 p3392 A67-36991

Millimeter wave reflectance for semiconductor panel, air space and metal reflector arranged planarly, discussing reflectance variation with conductivity and complete absorption 20 p3510 A67-37025

Moving map display as cockpit navigation device useful when flying erratic routes at low altitude 23 p4003 A67-41283

Johnson touch display for updating flight data combining visual display and keyboard functions 24 p4152 A67-41780

Installation problems of head-up displays in commercial aircraft 24 p4152 A67-41896

Internal light applied to opaque-faced edge-lighted plastic display panels [SAE PAPER 670196] 24 p4097 A67-41986

High speed computer graphic techniques for airfoil sections characteristics in two-dimensional compressible flow [SAE PAPER 670845] 24 p4091 A67-41998

Digital imaging techniques used in sinusoidal frequency response modification with or without computer control and display on operator console 24 p4125 A67-42429

Multidimensional data stereoscopic graphic display principles, viewing and use in engineering design 24 p4157 A67-42434

VISUAL FIELD

Correlation between heart rate, landing error and field of view for binocular and monocular sphere of vision of jet pilots 09 p1455 A67-21717

Peripheral vision displays for dynamic tracking information during difficult flight control tasks improve operator performance 14 p2258 A67-28663

Independent effects of error magnification and field of view on compensatory tracking performance, analyzing display and optical magnification 14 p2258 A67-28667

VISUAL OBSERVATION

Zodiacal light and solar activity, examining results of visual observations and photometric measurements for correlation between phenomena 03 p0413 A67-13455

Naked-eye observations of sunspots 03 p0514 A67-14184

Intrinsic brightness of comet Alcock 1963 b obtained from visual observations in terms of stellar magnitudes 05 p0888 A67-16204

Tungusk comet trajectory and orbit with radiant in constellation 05 p0889 A67-16210

Cetus 05 p0889 A67-16210

Visual and photographic comet photometry problems, noting brightness estimates obtained by individual observers 05 p0890 A67-16330

Visual techniques for measuring comet total brightness based on nonfocality 05 p0890 A67-16331

Visual, photographic and photoelectric methods for comet polarimetry 05 p0890 A67-16334

Preliminary analysis of INTEROBS program observations in Hungary, noting determination of changes in period of satellite 05 p0763 A67-16556

Simultaneous visual observation of satellite 1960 sigma 3, obtaining quasi-nodal period 05 p0763 A67-16557

Simultaneous visual tracking data reduction for satellite period 05 p0763 A67-16558

Satellite orbital parameters determined from visual observations 05 p0894 A67-16559

Visual observations of comets Everhart and Alcock /1964-1965/ 05 p0903 A67-17314

Stellar magnitude of 100 satellites 05 p0767 A67-17407

Wind tunnel study of boundary layer transition structure on ogive nose cylinders

aligned parallel to flow [AIAA PAPER 67-129] 06 p0939 A67-18314

Visual observation of internal circuitry and interconnections of multilayer boards through failure analysis technique 08 p1307 A67-21419

Apparent size and hue variations of single spot of 6328 angstrom laser light, analyzing physical correlates 09 p1515 A67-22373

Visual observations of earth, sea and sky made by astronauts and cosmonauts during space flights 09 p1569 A67-22604

New endoscope for internal viewing [SAE PAPER 670361] 12 p1945 A67-25881

Titan IIIB launch vehicle spent stage I recovery experiment, evaluating feasibility of refurbishment and reuse 15 p2569 A67-29853

Color indices of visible meteors observed by naked eye and through color filters noting brightness dependence and meteor train distribution 16 p2751 A67-31462

Satellite tracking, noting radio, radar and laser methods, and visual and photographic observations 16 p2630 A67-31765

Mars polar cap size changes, color and visibility from observations in 1963 17 p2942 A67-32330

Criticism of classical theory of Mercury rotation period equal to revolution around sun 18 p3125 A67-34191

Low perigee satellite orbit determination by visual observation, comparing directional accuracy and orbital elements with Minitrack and Baker-Nunn 18 p3126 A67-34247

Examination of ability of man to determine drift angle of spacecraft with optical sight [AIAA PAPER 67-624] 19 p3337 A67-36013

Holographic interferometry in electrochemical studies, examining advantages in less critical alignment and preparation and observation of changes 20 p3450 A67-37137

Visual characteristics of welded wire joints, discussing correlation with metallurgical and mechanical properties 21 p3636 A67-38631

Wind and cloudiness effects on terrestrial scintillation based on visual estimates and measurements 22 p3828 A67-39240

VISUAL PERCEPTION

SA COLOR PERCEPTION

Model of retinal receptor incorporating various feedback control processes consistent with physiological and psychological evidence 01 p0044 A67-10465

NASA research on visual problems of extended spaceflight 02 p0189 A67-12408

Light propagation through Schwarzschild singular sphere, solving problem of visual image of emitting surface of gravitating sphere as seen by observer 03 p0467 A67-12932

Mammalian neuron networks for visual pattern recognition, noting equivalence of processing by memory neurons with matrix multiplication 04 p0563 A67-14798

Mathematical model for adaptive signal preprocessor, noting eye adaptation to changes in signal intensity and bandwidth 04 p0563 A67-14799

Contrast transfer characteristics of n tuple models of retinal receptive fields as function of optical signal size or spatial frequency 05 p0757 A67-17303

Naming sequentially presented letters and words 06 p0954 A67-18533

Ocular scattering in Gemini astronauts and imperceptibility of stars in daytime 06 p1089 A67-18647

Visibility of point sources approaching or receding from high luminance source in apparent frontal plane 08 p1351 A67-21103

In-space visual environment simulation, discussing photometric and geometric requirements, solar illumination characteristics and effects on human performance 12 p1922 A67-25700

Visual flight simulation, detailing all-weather operation requirements 13 p2091 A67-27267

Panel layout for rectilinear instruments 14 p2257 A67-28661

Control-display association preferences for concentric controls 14 p2258 A67-28665

Independent effects of error magnification and field of view on compensatory tracking performance, analyzing display and optical magnification 14 p2258 A67-28667

Three-dimensional projections on cathode

ray tube screens noting visual transformations linking retinal image to space scene 20 p3450 A67-36985

Visual noise induction methods investigated at seven noise levels, discussing pattern comparisons by 46 subjects 20 p3372 A67-37000

Diffusion model of perceptual memory process when observer compares two consecutive stimuli, noting visual and auditory discrimination 21 p3576 A67-39097

Visual aspects of carrier landing, discussing research program to evaluate pilot ability to make critical visual judgments 22 p3755 A67-39847

Devices to help pilot detection of aircraft evaluated for systematic relationship between detection functions under fixated conditions and in visual search 22 p3755 A67-39848

Soviet book on atmospheric visibility noting photometry, range, threshold, runway visual range, atmospheric transmittance and atmospheric boundary layer problems 23 p4024 A67-40600

Pilot capability in low level high speed flying analyzed for influence of roughness fatigue, control improvements, vibration and visual problems 23 p3963 A67-41068

Psychophysical study of irradiation phenomena effects on target size perception by investigating luminance, fixation position and corrections 23 p3969 A67-41643

VISUAL PHOTOMETRY

Semiconducting alloys of gallium investigated by photometric method using gallium and xylene orange 22 p3804 A67-40299

Visual criteria for stellar spectral classification of Cordoba Observatory Atlas 24 p4227 A67-41967

VISUAL SIGNAL

SA OPTICAL SIGNAL

Autodyne design and operational principles for EPR in weak fields, using coaxial resonator 11 p1793 A67-24865

VISUAL STIMULUS

Responses of lateral geniculate nucleus of monkey to light increment and decrement and encoding of brightness 04 p0561 A67-14592

Sensory input overload effects on performance of civil aviation pilots during simulated instrument flights in Link AN 2550-1 trainer 09 p1455 A67-21726

Vestibular stimulation effect on activity of neurons of optical cortex of curarized cats under vertical acceleration 13 p2058 A67-26758

Intermittent visual stimulus influence on perceptual motor skills in aviation 14 p2258 A67-28668

Visual arousal interaction and specificity of nystagmic habituation 17 p2805 A67-31958

VISUAL SYSTEM

Adaptive visual signal preprocessor with quantized weights 02 p0207 A67-12140

Mathematical model simulation of horseshoe crab eye lateral inhibition for nervous system pattern transformation, discussing human visual pattern recognition process 20 p3375 A67-37543

Blackout experimentation results, discussing centrifugation and ophthalmodynamometry blackout production and visual system effects 22 p3752 A67-39607

VISUAL TASK

Alertness during visual surveillance at night, noting correlation between cortical activity and performance 04 p0561 A67-14627

Effect on human performance of variations from true values in simulation of extraterrestrial visual environment [AIAA PAPER 67-251] 07 p1186 A67-20069

Task load and type of underwater exposure effects on response time to signal light in visual periphery of novice divers 14 p2256 A67-28662

Peripheral vision displays for dynamic tracking information during difficult flight control tasks improve operator performance 14 p2258 A67-28663

Control-display association preferences for concentric controls 14 p2258 A67-28665

Resolution, contrast and time factors in visual target acquisition 22 p3755 A67-40410

VISUAL TRACKING

Skilled response organization, discussing stimulus coherence, tracking task, spatial and temporal coherence, secondary task, sequence length and task coding 14 p2254 A67-28034

- Radar, radio, photographic and visual satellite tracking methods 15 p2437 A67-30084
- Tracking activity of human operator under effect of certain space flight factors, establishing relationship between control habits and level of hypoxia and hypercapnia 20 p3368 A67-36265
- Movable device for tracking rocket probes, discussing characteristics and requirements 21 p3608 A67-38673
- VISUALIZATION**
- S FLOW VISUALIZATION**
- VITAMIN A**
- S RETINENE**
- VITAMIN B 02**
- S RIBOFLAVIN**
- VITAMIN E**
- S TOCOPHEROL**
- VITAMIN G**
- S RIBOFLAVIN**
- VITREOUS MATERIAL**
- SA GLASS**
- Temperature dependence of electroconductivity of As-Su-Ge system in vitreous state 06 p1052 A67-18610
- Impurity effects on electroconductivity of vitreous AsSe 06 p1053 A67-18612
- Temperature effect on electroconductivity of complex vitreous systems of K-Tl-Pb 06 p1053 A67-18613
- Electric conductivity of vitreous As-Se semiconductor 06 p1053 A67-18614
- Electric conductivity of vitreous As-S-Th 06 p1053 A67-18615
- Fluctuation levels and induced photoconductivity in vitreous semiconductor thallium selenide and arsenic telluride mixture 09 p1553 A67-21969
- Identification with tektites of microscopic glassy objects deposited in Australasian area during and after last geomagnetic field polarity reversal 13 p2198 A67-26792
- Chemical analysis of meteorite impact glass from separated areas across Henbury strewnfield 16 p2667 A67-31452
- Adhesives for aircrafts and spacecrafts considering high temperature resistivity, waterproofing and brittleness 16 p2683 A67-31788
- Light interaction with solids, discussing photoconductivity and phototropy 17 p2913 A67-32373
- Fluctuation levels and induced photoconductivity in vitreous semiconductor thallium selenide and arsenic telluride mixture 17 p2923 A67-33306
- Tektite glasses crystallizing tendency studied by subjecting them to heat treatments above strain point and CN slow cooling from melting 20 p3527 A67-37274
- Anisotropy due to molecular structure orientation in vitreous inorganic glass fibers, noting phase equilibrium relation 21 p3648 A67-37880
- Chemical composition analysis of Macedon and Darwin natural glass 24 p4233 A67-42615
- Chemical analysis of glass bombs from Ries crater area investigated for textural differences due to shock melting and cooling rates 24 p4233 A67-42621
- Preatmospheric hypervelocity impact black glass in Cachari eucrite studied by optical microscopy, electron microprobe and X-ray diffraction 24 p4233 A67-42623
- VJ-101 AIRCRAFT**
- S SUD VJ-101 AIRCRAFT**
- VLASOV EQUATION**
- Marguerre-Vlasov equations accuracy analysis based on equations for thin walled shallow shells derived, using series expansion 01 p0159 A67-10275
- Perturbation theory for solving Vlasov equation for strong plasma turbulence, using statistical set of exact particle orbits 02 p0275 A67-12551
- Three-dimensional eigenmodes for collisionless electronic Vlasov plasma imbedded in magnetic field in electrostatic approximation, noting plasma stability 02 p0275 A67-12553
- Random phase approximation for plasma, establishing perturbed electron distribution in oscillating electric field 02 p0276 A67-12557
- Plasma streaming across magnetic field by beam polarization studied by Vlasov equation 03 p0484 A67-14042
- Approximate Vlasov equation for local stability of zero-moment shells of positive Gaussian curvature under arbitrary multiparameter subcritical load 05 p0923 A67-17186
- Parametric excitation of modes of infinite plasma by incident radiation using Vlasov equation, noting unstable oscillations for incident frequencies 07 p1228 A67-19502
- Effect of longitudinal plasma oscillations excited by external electric field on plasma stability, deriving dispersion relations by using Vlasov equation 07 p1229 A67-19518
- Electron streaming instability of plasmas with zero order density gradients from variational analysis of Vlasov-and Maxwellian-plasma perturbation wave propagation 08 p1360 A67-21128
- End losses from linear theta pinch estimated from self-consistent calculation of structure of plasma and confining magnetic field 08 p1362 A67-21149
- Generalized formulation of electrostatic oscillations and streaming instabilities in bounded and unbounded inhomogeneous Vlasov plasmas with transverse density gradients in strong axial magnetic field 08 p1363 A67-21305
- Boundary value problem for Poisson-Vlasov equations resulting from interaction of conducting body and supersonic flow of rarefied plasma solved, using iterative method 08 p1363 A67-21368
- Transverse electromagnetic waves with constant phase velocity in fully ionized Vlasov plasmas 08 p1364 A67-21401
- Second order gyroviscous stress in collisionless plasma for LF propagation quasi-perpendicular to magnetic field calculated by utilizing higher moments of Vlasov equation 10 p1685 A67-23331
- Vlasov equation for stationary distribution function of charged particles in plasma and self-consistent solution of Maxwell equations 10 p1685 A67-23463
- Perturbation theory developed to estimate magnetic surface stability against field irregularities, noting role of field resonances 10 p1686 A67-23468
- Hamilton-Jacobi solutions for Vlasov equation leading to nonsecular perturbation theory for macroscopic quantities 10 p1686 A67-23469
- WKB /Wentzel-Kramers-Brillouin/ approximation to solve linearized Vlasov equation for oscillations of inhomogeneous one-dimensional plasma 11 p1838 A67-24404
- Vlasov variational method application to stressed state of flexible plates and shells, linearizing partial differential equations by successive loadings 12 p2020 A67-25570
- Equilibrium equations of Vlasov engineering moment theory of shells of variable curvature 12 p2021 A67-25577
- Vlasov engineering theory of equilibrium of shells used to study stress-strain state of closed circular cylindrical shell loaded by internal pressure 12 p2028 A67-25632
- Third order Vlasov equation solved for nonlinear plasma oscillations in classical nonrelativistic collisionless Maxwell distribution electron gas 13 p2162 A67-26283
- Electron-cyclotron wave instability in plasma noting dispersion relation, growth rate frequency, destabilizing effect of electrons, etc 13 p2163 A67-26286
- Plasma EM instability in magnetic mirror configuration, solving linearized Vlasov equation for dispersion relation of transverse EM waves 13 p2164 A67-26293
- Kinetic equation for completely ionized plasma generalized for several particle species case 13 p2165 A67-26585
- Boundary value problems involving shallow cylindrical shells of given arbitrary configuration solved, using Vlasov moment theory 14 p2395 A67-27837
- Moment method treatment of collisionless plasma equilibria in confining magnetostatic fields, using Vlasov equation to determine distribution function of particles 14 p2360 A67-28554
- Vlasov variational method applied to circular cylindrical shell design for local loading 14 p2400 A67-28643
- Collective effects in collisionless plasmas in laboratory in case of Vlasov-Maxwell equations with Landau damping 14 p2362 A67-29037
- Fourier-Hermite solutions of Vlasov equations for electron motion against positive neutralizing background examined in linearized limit, noting Landau damping recovery 15 p2509 A67-29205
- Displacement equations of prestressed thin bending-resistant shells 15 p2574 A67-29699
- Flute instability for inhomogeneous plasma equilibria in inhomogeneous magnetic fields of mirror machines, solving Vlasov and Poisson equations 16 p2714 A67-30875
- Asymmetric proton injection into magnetosphere using Vlasov equation, with solution in terms of electric potential 16 p2666 A67-31403
- Unsteady Vlasov equation for class of beam-like initial distributions associated with ion engines 17 p2928 A67-32158
- Vlasov equation for anisotropic electron plasma in external magnetic field solved by Laplace transform of density perturbation in initial value problem 17 p2907 A67-33104
- Longitudinal and transverse collective effects contribution to energy loss rate in relativistic isotropic plasma subject to external fields and particles 17 p2908 A67-33111
- Boundary value problem for electrical potential and ion distribution function obeying Poisson-Vlasov equations when applied to rarefied plasma disturbance by supersonic body 17 p2909 A67-33205
- Electromagnetic wave scattering from plasma wave analyzed using Vlasov equations for anisotropic plasma, applying formulas to boundary value problems 18 p3088 A67-34090
- Time and space development equations for longitudinal and transverse modes in Vlasov plasma 18 p3092 A67-34745
- Collisionless electron plasma dynamics in one dimension, investigating nonlinear Vlasov equation for Landau damping and instability 18 p3092 A67-34747
- Fokker-Planck damping introduced into Fourier-Hermite representation of Vlasov equation produces Landau and Van Kampen treatments 18 p3030 A67-34754
- Charge, current, and self-consistent field transport properties of collisionless plasma derived using initial value solutions to Vlasov equation 19 p3285 A67-35343
- Plasma oscillations, discussing kinetics, macroscopic and Vlasov equations, Landau damping and beam instabilities [AFOSR-66-2823] 19 p3299 A67-35871
- Quasi-linear plasma waves model, considering Vlasov approximation, deriving distribution functions and electric field equations solution 20 p3494 A67-36149
- Guiding center plasma theory /GCP/ stability, potential, Vlasov and motion equations, etc 20 p3494 A67-36152
- Generalized formulas and stability criteria applied to higher order electrostatic oscillation modes in Vlasov plasmas, considering double-stream amplifier designs 20 p3495 A67-36169
- Two-stream instability calculations from phase-space boundary motion, using Vlasov equation in distribution function 21 p3662 A67-37763
- Flat plate bending and two-dimensional, axisymmetric and boundary value problems in elasticity theory investigated using Vlasov initial function method 21 p3725 A67-38792
- Malmberg-Wharton configuration electron plasma wave dispersion and damping 22 p3844 A67-39367
- Plasma stability investigated using constants of motion for solution of Vlasov equation 22 p3849 A67-39700
- Weakly turbulent spatially uniform ensemble of Vlasov plasmas, discussing time evolution of correlations due to collective interactions 22 p3849 A67-39701
- Thermal particles parallel velocity and transverse spatial diffusion coefficients found by studying test particle motion in weakly turbulent Vlasov magnetoplasma 22 p3849 A67-39702
- Approximate integrodifferential equations determining ensemble mean and covariance of particle distribution function of Vlasov plasma, discussing incompressible Navier-Stokes turbulence 22 p3850 A67-39703
- Quasi-linear perturbation expansion used to study evolution of localized disturbance in plasma 22 p3851 A67-39985
- Vlasov equation solved by taking continuous spectrum of infinite matrix belonging to moment equations into account, obtaining Landau damping results 22 p3852 A67-39992
- Two-body relaxation term in N-body self-gravitating gases of one and three dimensions and validity of Vlasov equation 22 p3894 A67-40508

Elliptically polarized electromagnetic wave propagation in homogeneous infinite plasma, solving Vlasov equations of nonlinear theory by successive approximation 23 p4030 A67-40597

VOCODER

Alternative modulation techniques for Satellite Telecommunications with Automatic Routing, considering start-stop operation with PCM-FDM system 13 p2068 A67-26720
Redundancy reduction techniques and error correction coding of digital communication systems including waveform, pattern recognition, vocoding, etc 18 p3004 A67-34613

**VOICE COMMUNICATION
SA ECHO SUPPRESSION**

Voice communications system using GaAs room-temperature injection laser and TV communications system using GaAs crystals as modulators for laser beams 02 p0194 A67-11786

Voice communications and control facilities at mission control center in Houston for support of manned space program conducted by NASA 02 p0229 A67-12120

Voice-bandwidth communication link analyzer /CLA/ system for making measurements on communication link, using periodic pulse stream with suitable spectral filtering 02 p0203 A67-12134

Subjective evaluation of telephone communications via Early Bird satellite and cable circuits 06 p0959 A67-17667

Verbal communication intelligibility in man-rated altitude simulator with nitrogen or helium added to oxygen atmosphere 08 p1287 A67-20484

Speech distortion caused by respiration in helium-oxygen atmosphere, discussing standard and advanced correcting techniques 10 p1597 A67-23313

Alternative modulation techniques for Satellite Telecommunications with Automatic Routing, considering start-stop operation with PCM-FDM system 13 p2068 A67-26720

Satellite telecommunication with automatic routing noting switching concept and modulating methods 13 p2087 A67-26721

Satellite telecommunication with automatic routing noting switching 13 p2087 A67-26722

Voice modulation effect on phase-lock demodulator for single channel voice communication extending definition of threshold for optimum link design 16 p2629 A67-31529

Receiver performance related to signal and interference conditions for AM voice communication system analyzed for use in systems design 20 p3387 A67-37637

Most efficient use of voice band channel in digital data transmission by direct use of passband [IEEE PAPER 19-TP-67-1262]

Proactive inhibition, recency and limited channel capacity under acoustic stress 24 p4116 A67-42701

VOICE DATA PROCESSING SYSTEM

Speech commands in control systems, discussing operation of bandpass, formant, scanning, harmonic and correlation voice coders 01 p0016 A67-10823

Speech distortion caused by respiration in helium-oxygen atmosphere, discussing standard and advanced correcting techniques 10 p1597 A67-23313

Simultaneous primary and secondary voice message monitoring, discussing methods and experimental setup 15 p2431 A67-29895

VOID FRACTION

Void effect on strength of filament reinforced composite materials 08 p1415 A67-20434

Electrical conductivity of high void fraction two-phase flow with and without magnetic field in MHD generator 23 p3942 A67-41759

VOLCANIC THEORY

Volcanism triggered by meteoritic impact suggested from comparison of volcanic and impact data, noting terrestrial, lunar and Martian craters 02 p0319 A67-11455

Martian and lunar craters and volcanic activity 06 p1089 A67-18648

Indigenous lunar power from geothermal deposits of hot water-rich gases and brines 08 p1317 A67-21095

Terrestrial rotation fluctuations and volcanic activity analyzed, considering

existence of viscous and liquid masses at interior of earth 11 p1788 A67-24780

Lunar surface rocks viscosity, volcanic origin, etc, with reference to Flamsteed Ring putative magma 15 p2553 A67-29159

Formation of Flamsteed Ring slopes on moon investigated, noting wall consistency with fragmental debris from moon quakes 15 p2553 A67-29160

Thermal conductivity model for planetary igneous differentiation, discussing melting behavior as function of pressure and temperature 17 p2942 A67-32387

Volcanic and tectonic activity on Venus inferred from high surface temperature, considering possible effect on atmosphere obscuration 17 p2951 A67-33232

Lunar craters and fragments compared with terrestrial low velocity secondary volcanic impact craters and ejecta on basis of distribution relations 18 p3134 A67-34538

Geomagnetic field polarity inversion, discussing reverse magnetization of volcanic rocks 21 p3821 A67-38982

Lunar silicate rock appearance and genesis conditions with emphasis on vesiculation processes 23 p4064 A67-40947

Seleno-geological evidence for lunar surface properties from Surveyor I, discussing weathering products and volcanic genesis 23 p4064 A67-40952

Lunar geology using probe data to distinguish impact and volcanic surface shaping processes [AIAA PAPER 67-862] 24 p4238 A67-42986

VOLCANICS

SA LAVA
Flamsteed P volcanic rings from Orbiter I and Surveyor I lunar photographs 07 p1249 A67-19659

Lead 206/lead 204 vs lead 207/lead 204 plots for young mantle-derived volcanics support upheaval predicted by lunar capture hypothesis 22 p3881 A67-39554

Iron titanium oxides and oxygen fugacity in volcanic rocks noting temperature effect 22 p3792 A67-39975

VOLT-AMPERE CHARACTERISTICS

Trapezoidal I-V characteristics in gallium arsenide at liquid nitrogen and room temperature 01 p0033 A67-10027

Volt-ampere characteristics and other properties of GaAs lasers with tellurium and Zn-doped epitaxial p-n junction 01 p0087 A67-10080

Wielmer triode with contact rectifier for use as component of microminiature radio circuits, noting effect of contact rectification on current-voltage characteristics and amplifying power of such triodes 01 p0035 A67-10397

Method based on static characteristics for limit of saturation used to find relationships between voltages and currents in transformer in saturation region 01 p0037 A67-10714

Frequency doubling by varactor diode, expressing principal parameters as function of normalized amplitude of input voltage 01 p0039 A67-10856

Current transmission through semiconductor with impurities, calculating V-I characteristics at high temperatures during acceptor level creation 01 p0135 A67-10925

X-ray radiation effect on p-n junctions of germanium diodes, noting changes in V-I characteristics 01 p0138 A67-11047

Maximum alloying temperature and cooling rate of p-n junctions effect on volt-ampere characteristics of silicon diode and minority carrier lifetime 01 p0039 A67-11053

Space-charge layer effect on volt-ampere characteristics of multilayer diffusion structures in silicon 02 p0281 A67-11504

Potential difference variation in circuits consisting of diode, capacitance and active resistor 02 p0209 A67-11509

Quantum dimensional effects in bismuth films by tunnel spectroscopy, showing energy dependence of state density having form of step function 02 p0281 A67-11632

Semiconductor-metal-semiconductor structure with metal vapor deposited, analyzing voltage-current characteristics for amplifier technology 02 p0293 A67-11754

Strong injection in nondegenerated p-n junction producing electron-hole plasma in n region near junction 02 p0296 A67-11827

Current-voltage characteristics peculiarities of fine cadmium sulfide single

crystals with nonohmic

contacts 02 p0296 A67-11831

Negative photoconductivity in germanium, noting breakdown and negative conductivity in In region, volt-ampere characteristics, etc 02 p0297 A67-11835

Solution grown epitaxial red light emitting p-n junctions in GaP preparation, electrical and optical properties, examining I-V characteristics 02 p0297 A67-11878

Implantation of Cs and Na ions into p-type silicon, effect on hot electron emission from p-n junction 02 p0299 A67-11897

DC and RF I-V characteristics, device fabrication and structure of epitaxial depletion mode n-type

MOS-FET 02 p0218 A67-12103

Electric characteristics of nGe-pGaAs heterojunctions in multistep recombination-tunneling model 02 p0299 A67-12189

Potential distribution, I-V characteristics and pulse shape of n-type Ge with sealed-in Sn, In-Sb, Sn-Sb and Pb-Sb contacts in strong electrical field 02 p0300 A67-12480

Single crystal transistor with metallic base, noting frequency, V-I and power characteristics, radiation resistance, etc 02 p0221 A67-12530

Second breakdown protection of Si power transistors by applying emitter resistances 02 p0222 A67-12654

Secondary breakdown characterization technique in Ge p-n-p alloyed junction transistors with open base condition 02 p0223 A67-12655

Field intensity probe measurements of potential distribution and I-V characteristics in AC arc plasma 03 p0475 A67-13087

Cadmium selenide single crystals subjected to gas discharge saturation of current-voltage characteristic, noting section with negative differential

resistance 03 p0489 A67-13146

Static characteristics of series connected tunnel diodes used in determining pulse duration and recovery time of driven multivibrator 03 p0377 A67-13236

V-I characteristics of low voltage trinitors 03 p0377 A67-13237

Equivalent circuit for four-layer dinistor with frequency independent elements, noting dependence of network elements on dinistor parameters 03 p0377 A67-13238

Longitudinal microwave phonons inducing tunneling in Al-Pb, Al-Sn and Pb-Pb superconducting diodes 03 p0379 A67-13330

NGe-pGaAs heterojunctions, diffusion or emission theories of current transport do not explain electrical characteristics but validate Anderson model, considering tunneling as transport mechanism 03 p0494 A67-13478

Forward voltage characteristics of thyristors in fired state, depending on injection level for high current density 03 p0380 A67-13482

Nonuniform p-type base width effect on forward switching voltage of diffused alloyed thyristor devices, comparing empirical and theoretical values 03 p0380 A67-13483

Rectification and detection characteristics of space-charge-limited solid state diode at VHF 03 p0380 A67-13488

Feedback effect on current voltage characteristic of device with negative feedback and reactivity of device in negative resistance region 03 p0380 A67-13583

Tunnel diode combined with backward diode improves rate of response and pulse waveform in tunnel diode circuits 03 p0381 A67-13585

Plasma electric conductivity around 2000 degrees K measured, using double probe with interelectrode section of controllable length 03 p0478 A67-13603

Polarization and volt-ampere characteristics of ferroelectrics simultaneously under static and alternating fields 03 p0382 A67-13710

Secondary breakdown relaxation oscillations and I-V characteristics of point contact n-type Ge diode 03 p0386 A67-13964

V-I characteristics and bias field/carrier concentration-sample length diagram of Gunn effect phenomena 03 p0500 A67-13993

Diode detector with exponential volt-ampere characteristics 04 p0579 A67-14452

V-I characteristics of stagnation point electrodes in lightly ionized atmospheric pressure plasma, calculating electric

resistance from conductivity
measurements 04 p0664 A67-14821

Current voltage characteristics of Cd-GaSe-Bi diode structure, rectification coefficient, activation energy and photocurrent spectral distribution 04 p0676 A67-14930

Electroluminescence, photoconductivity and I-V characteristics of niobium-niobium oxide-gold diode and possible existence of p-i-n junction in oxide 04 p0582 A67-15104

Electron transfer in thin film tantalum-tantalum oxide diodes, noting tunnel and Schottky emission 04 p0582 A67-15106

Compressive stress effect on band gap widening and diffusion current in GaAs junctions 04 p0677 A67-15107

Wave propagation in n-type semiconductor with negative differential resistance 04 p0678 A67-15129

I-V characteristic of GaAs diode with Fabry-Perot resonator, noting variations during amplification to generation transition 04 p0678 A67-15132

Emission spectra and I-V characteristics of diffusion p-n junctions in InP and spontaneous radiative recombination in presence of small current 04 p0679 A67-15138

Photoconductivity and negative resistance caused by carrier lifetime change in response to change in injection level in SiC p-n junctions 04 p0680 A67-15156

V-I characteristics of p-n junctions on In-Sb base, noting effects of surface etching, temperature and impurity concentration 04 p0680 A67-15157

Electric arc stabilization mechanism for nonconducting gas flow in chamber of DC plasma generator 04 p0686 A67-15191

Coaxial plasma source transition from high energy particle production to production of slow plasmoids, noting V-I characteristics and magnetic field distribution 04 p0667 A67-15212

Radiative recombination in space charge layer of p-n junction in silicon carbide determined from I-V characteristics and capacitance 04 p0681 A67-15298

Functional device based on interaction of two unijunction transistors to perform flip-flop circuit function, noting V-I characteristics and binary counter operation 04 p0593 A67-15489

Static V-I relationships in transistors at high injection level 04 p0585 A67-15621

I-V characteristics shift and radiation hardening of Mos transistors for low ionizing dose level 04 p0589 A67-15714

Book on semiconductor devices with negative resistance having decreasing section in volt-ampere characteristics 05 p0770 A67-16171

Energy input requirements of electric shock tube determined from empirical I-V relations at electrodes 05 p0786 A67-16248

I-V characteristics of p-gallium antimonide based tunnel junction at various temperatures analyzed, finding secondary peaks exhibited by inverted diodes 05 p0861 A67-16395

Tunnel diode superregenerative amplification and detection in linear regime and volt-ampere characteristics of diode 05 p0772 A67-16450

Electric conduction through tantalum oxide thin films, showing dependence of V-I characteristics on tunneling and Schottky effect 05 p0862 A67-16525

Josephson current in alternating field between two superconductors separated by dielectric barrier 05 p0853 A67-16697

Current dependence on voltage in Sn-Sn and Pb-Pb tunnel junctions attributed to electric gap anisotropy 05 p0863 A67-16754

I-V characteristics of alloyed contacts of germanium with Sn, Pb and In in wide range of resistivities and ambient temperatures, establishing correlation with work function 05 p0864 A67-16909

Effect of copper on excess and tunneling current of As-doped Ge tunnel junctions 05 p0866 A67-16986

Volt-ampere characteristics of epitaxial GaP-GaAs heterojunctions 05 p0867 A67-17054

Instability of electron hole plasma of semiconductor caused by nonlinear current-voltage characteristic 05 p0867 A67-17058

Silicon p-n junction avalanche breakdown voltages obtained from formula for ionization coefficient 05 p0869 A67-17090

Current-controlled NDR, electron-hole generation and switching to higher current

lower voltage state in GaAs 05 p0870 A67-17275

Langmuir probe analysis when immersed in slightly ionized collision-dominated plasma, computing current-voltage characteristics and Poisson and diffusion equations 05 p0856 A67-17341

Negative resistance regions in Si Zener diodes explained in terms of impact ionization and junction breakdown combination 06 p0968 A67-17814

X and electron irradiation effect on current-voltage characteristics of p-n junctions in gallium arsenide 06 p1049 A67-17859

Current pause during circuit overloading accompanied by filament explosion 06 p1031 A67-17867

P-i-n diode structure and behavior under direct and reverse-bias conditions 06 p0969 A67-18121

Multilayer technique for evaporation of ohmic contacts onto CdS, noting V-I characteristics and noise spectrum of recrystallized layer 06 p1050 A67-18142

Avalanche drift diode and application in microwave technology, analyzing dynamic negative resistance formation, volt-ampere characteristics and output power 06 p0970 A67-18169

Superconducting tunnel diode for quantum generation and detection of incoherent phonons, discussing I-V characteristics 06 p1011 A67-18211

Excess noise and oscillations in gold-doped germanium photodiodes attributed to generation-recombination fluctuations of large bulk resistance 06 p0971 A67-18220

Interaction between two high resistivity layers in Mn doped GaAs separated by region of bulk material 06 p1051 A67-18222

Silicon-gallium phosphide heterojunction fabricated by epitaxial deposition, presenting V-I characteristics and energy band diagrams 06 p1051 A67-18223

Perpendicular magnetic field induced change in electron temperature of current carrying semiconducting plates 06 p1054 A67-18805

Recombination radiation of p-n junctions in GaAs with and without Fabry-Perot cavity, discussing nonequilibrium current carrier kinetics and I-V characteristics 06 p1063 A67-18934

Nonlinear galvanomagnetic effects due to hot electrons in n-type InSb in quantum limit 06 p1065 A67-18953

Time dependence of V-I curves in n-type In-Sb at low temperatures, determining electron-hole pair generation rate 06 p1066 A67-18955

Current saturation and phonon amplification induced instabilities in CdS crystals 06 p1066 A67-18958

Oscillations in conductivity of electron-hole plasma in semiconductors due to nonlinearity of volt-ampere characteristics 06 p1070 A67-18988

Shottky theory and electron affinity of semiconducting CdSe from DC I-V characteristics and work function of Au, Ag and Cu contacts with 07 p1231 A67-19491

Short pulse start/stop control of tunnel diode oscillator 07 p1153 A67-19608

Energy gap derived from I-V characteristics for pressure contacts between type II superconductors and normal metals 07 p1233 A67-19843

Electron barrier heights of Al-Al₂O₃-SnTe and Al-Al₂O₃-GeTe tunnel junctions, noting values of Fermi level and energy gap 07 p1155 A67-19893

Current mode second breakdown in epitaxial planar transistors, describing V-I behavior 07 p1156 A67-19897

V-I characteristics and turnover phenomenon in Si devices in relation to second breakdown in transistors 07 p1156 A67-19898

Area of Safe Operation for transistors in switching mode defined, using thermal feedback model 07 p1157 A67-19902

Second breakdown in transistors analyzed in terms of lumped parameters noting V-I characteristics, temperature effect, avalanche multiplication, etc 07 p1157 A67-19903

Self-healing electric breakdown in MOS structures noting magnitude duration, temperature and propagation

characteristics 07 p1157 A67-19904

Current-voltage-temperature dependence of symmetric tunnel junctions, noting role of insulator thickness 07 p1237 A67-20184

Electric field domain motion in Ge samples with Au and Sb impurities, noting temperature and illumination effect on V-I characteristics 08 p1367 A67-20411

Adaptive power conditioning for optimal power transfer from solar cell array to load regardless of environment, impedance or volt-ampere characteristics 08 p1284 A67-20651

Pulsed sinusoidal bridge for simultaneous measurement of volt-capacitance and volt-ampere characteristics of relaxing p-n junction barriers 08 p1303 A67-20998

Capacitance voltage and V-I characteristics of four-layer p-n-nu-n semiconductor diode structures 08 p1303 A67-21054

Electron space-charge neutralization in design of thermionic /heat-to-electricity/ converters 08 p1286 A67-21177

Intermodulation rejection in mixers, discussing performance characteristics of various combinations 08 p1304 A67-21223

Semiconductor-insulator-semiconductor structure as negative resistance, noting V-I characteristics under various conditions 08 p1370 A67-21292

V-I characteristics in flame by double probe method at atmospheric pressure 08 p1428 A67-21426

Volt-ampere characteristics and other properties of GaAs lasers with tellurium and Zn-doped epitaxial p-n junction 08 p1340 A67-21457

IR photovoltaic response, quantum efficiency and V-I characteristics of InSb MOS structures 09 p1551 A67-21577

Forward bias V-I characteristics for heterojunction in which tunneling dominates, noting temperature effect 09 p1551 A67-21666

Negative slope mobility in n-GaAs from measurements of current-voltage characteristic 09 p1552 A67-21744

Electrostatic probes for collision dominated weakly ionized plasma noting mathematical formulation, density and V-A characteristics 09 p1539 A67-21782

Current-voltage characteristics of moving argon plasma, noting variation of plasma conductance with flush and filament electrodes 09 p1540 A67-21786

Current voltage characteristic of gas discharge for one-dimensional stationary case with fixed temperatures at conductor end, noting voltage saturation 09 p1544 A67-21863

Stress-dependence of Si p-n junctions with dense generation-recombination centers, showing that shifts in bias I-V characteristics are due to bandgap changes 09 p1553 A67-21947

High injection theories of p-n junction, commenting on corrections made in connection with junction voltage 09 p1472 A67-21953

Hydrostatic pressure and temperature effect on current-voltage characteristics of tunnel p-n junctions in gallium arsenide 09 p1554 A67-21977

Output characteristics of cesium thermionic converter as function of size of electrode gap, using device with movable air-cooled stainless steel anode 09 p1444 A67-22007

Microcircuitry leakage path detection using scanning electron microscopy 09 p1473 A67-22017

Point contact electrically formed semiconductor junction diodes, discussing harmonic generation by various material combinations 09 p1474 A67-22086

Small size CW He-Ne laser pumped by resonant cavity, examining current-voltage characteristics and current dependence of output power 09 p1513 A67-22170

Signal and noise response of Ge avalanche photodiodes noting design, fabrication, LF photomultiplication and static V-I characteristics 09 p1475 A67-22200

Thin film silicon-on-sapphire deep depletion MOS transistors 09 p1475 A67-22203

Effect of tunnel diode amplifier V-I characteristics on cross modulation products in electromagnetic spectrum 09 p1557 A67-22266

Circuit load effects on microwave properties of Gunn diodes, discussing equivalent circuit and graphical analysis of quenched and inhibited modes of

operation 09 p1479 A67-22268
 Electric current flow in moving decaying plasma and plasma diagnostics, deriving nonlinear V-I characteristics 09 p1547 A67-22317
 Two-frequency correlation method for determining time dependent mean statistical voltage and current values for DC arc 09 p1547 A67-22323
 Output characteristics of electroetched rhodium surface, bare and cesiated work function and performance 09 p1447 A67-22332
 Volt-ampere characteristics of grooved collector thermionic diode indicate ions generated in cavities diffuse to cavity free region and neutralize electron space charge 09 p1448 A67-22340
 Thermionic low voltage converter-regulator systems, discussing relation between thermionic source, electron cooling and impedance-matching characteristics 09 p1449 A67-22346
 Nuclear heated thermionic converter construction, V-I characteristics and comparison with electrical heating 09 p1451 A67-22359
 Current-voltage characteristics of Esaki diode composite circuit 10 p1609 A67-22837
 Electron bombardment type ionization gauge with logarithmic differential circuit 10 p1610 A67-22950
 Electric field penetration of electrodes incorporated into theory of electron tunneling through dielectric layer 10 p1689 A67-22961
 Cadmium selenide single crystals subjected to gas discharge saturation of current-voltage characteristic, noting section with negative differential resistance 10 p1689 A67-23095
 CdS solar cell model noting spectral response, V-I characteristic and temperature variation 10 p1596 A67-23164
 Capacitance of abrupt p-n heterojunctions and effects of interface states, noting capacitance-voltage characteristics 10 p1612 A67-23372
 Analysis of current flow for different input conditions on double-gate thin film transistor 10 p1612 A67-23373
 Distribution of injected carrier densities in strongly forward biased laser junctions 10 p1686 A67-23522
 Quantum efficiency of optimized GaAs diodes with Zn diffused in skin layer, noting dependence on junction depth 10 p1614 A67-23524
 Systematic degradation of GaAs light emitter quantum efficiency, noting relation to current density 10 p1615 A67-23525
 Factors of degradation of GaAs electroluminescent diodes, discussing surface leakage and change in spectral characteristics as major causes 10 p1615 A67-23526
 Nonlinearity in V-I characteristic of type II superconductor situated in external magnetic field 10 p1696 A67-23775
 Helical instability of positive plasma column in longitudinal magnetic field, using magnetic pickup coil 11 p1829 A67-23999
 Knudsen low voltage discharge with hot cathode, determining electron distribution, velocity profiles, V-I characteristics, etc 11 p1831 A67-24020
 Energy conservation analysis of step in negative resistance region of voltage-current characteristic curve of oscillating tunnel diode 11 p1759 A67-24132
 Space-charge-limited currents in p-type silicon noting I-V characteristics, theoretical values agreement, Hall coefficient measurements correlation, etc 11 p1845 A67-24135
 Bulk reverse current in diffused Si power rectifiers, interpreting reverse characteristics in terms of thermal pair production 11 p1760 A67-24144
 V-I characteristics of In and Ge structures with negative resistance, noting effect of four-layer substructures 11 p1765 A67-24474
 Type II superconductor voltage proportionality to time varying magnetic field under constant transport current and linear field sweep 11 p1846 A67-24583
 Superconducting energy gap of cubic and hexagonal LA obtained by point contact tunneling to bulk samples, noting V-I characteristics and temperature dependency 11 p1846 A67-24585

Volt-ampere characteristics of diffused silicon n-n junctions with negative resistance analyzed, noting preparation technique 11 p1768 A67-24859
 Microwave amplification and negative conductance for GaAs, InP and CdTe 11 p1850 A67-24916
 Computer analysis of curve for total emission from group of separate localized emission points on surface of high vacuum metallic cathode 11 p1820 A67-24922
 Volt-ampere and thermal characteristic of plasmatron with insert in electron gap 11 p1843 A67-24973
 Wave propagation in n-type semiconductor with negative differential resistance 12 p1978 A67-25153
 I-V characteristic of GaAs diode with Fabry-Perot resonator, noting variations during amplification to generation transition 12 p1951 A67-25156
 Emission spectra and I-V characteristics of diffusion p-n junctions in InP and spontaneous radiative recombination in presence of small current 12 p1979 A67-25161
 Cesium thermionic diode parameters including added noble gas pressure effect for ignited mode performance prediction and optimization 12 p1896 A67-25262
 Piezotransistor static characteristics approximated by exponential function of two variables 12 p1939 A67-25281
 Voltage-current characteristics measured by Fahleson alternate explanation, based on properties of Hartmann boundary layer in continuum type plasma 12 p1972 A67-25384
 Electric current conduction between cold electrodes in shock-ionized air plasmas, noting current-voltage characteristics in flow behind shock wave 12 p1974 A67-25401
 Temperature dependence of volt-ampere characteristics of silicon space charge limited diode compared with ordinary diodes 12 p1914 A67-25459
 Volt-ampere characteristics effect on thickness of contact materials of some heterojunctions and band structures obtained by epitaxial deposition 12 p1983 A67-25515
 Volt-ampere characteristics of diffused p-n junctions in epitaxial GaAsP film obtained by gas transport 12 p1984 A67-25519
 Electric conductivity, Hall effect and photoconductivity of epitaxial single crystal GaAs films obtained by gas transport method 12 p1984 A67-25521
 Axially flowing gas through arc discharge, examining effect on I-V characteristic and radial temperature distribution in arc column 12 p1975 A67-25751
 Constant density theory leads to analytical forms for current-voltage characteristics and electrical resistance associated with shock tube sidewall electrostatic probe problem 12 p1925 A67-25902
 Hall EMF measurement in base of negative resistance silicon diode 12 p1917 A67-26097
 Explanation of anomalies of experimental static current-voltage characteristics of GaAs tunnel diode oscillators 12 p1917 A67-26098
 Current voltage characteristics of alloyed p-n junctions in n-type InAs, discussing contribution of tunnel current 12 p1986 A67-26099
 Nonlinear effects in steady state volt-ampere characteristics of zinc compensated n-type silicon single crystals 13 p2172 A67-26356
 High energy density Zn/O battery system, noting good low oxygen pressure and low temperature performance characteristics 13 p2055 A67-26836
 Active and reactive impedance components of total resistance of p-n-n structures at high injection levels 13 p2081 A67-27278
 Current-voltage characteristics of germanium-silicon isotype heterojunctions with regard to capacitance and photoelectric measurements 13 p2183 A67-27569
 Silicon space charge limited triode considered as analog transistor noting I-V characteristics, current proportionality, voltage amplification and noise performance 13 p2083 A67-27571
 Current-voltage characteristics of cadmium sulfide crystal diodes with indium and gold cathodes 13 p2085 A67-27731
 Volt-ampere characteristics, generation and decay of interrupted and AC arcs in

nitrogen, air, argon and carbon dioxide at zero gravity 14 p2354 A67-27760
 Current voltage characteristics of argon cesium plasma in inductive hydrodynamic shock tube 14 p2354 A67-27761
 Field ion microscope design and operation, noting construction and experimental results 14 p2314 A67-27770
 Transient phenomena in capacitance and reverse current for n-type GaAs Schottky barrier diodes at different carrier concentrations 14 p2364 A67-27827
 Single crystal transistor with metallic base, noting frequency, V-I and power characteristics, radiation resistance, etc 14 p2279 A67-28007
 Threshold voltage control for complementary pair MOS transistors, discussing techniques used 14 p2281 A67-28019
 Two-step saturation of pulsed current in CdS single crystals, noting electron bunching mechanism and volt-ampere characteristics 14 p2365 A67-28238
 Performance characteristics of nonstoichiometrically doped p-n junctions in Cd-Hg-Te alloy operated as IR photovoltaic detector 14 p2366 A67-28496
 Two opposing tunnel currents determination through transition zone of metal-oxide-metal structure 14 p2367 A67-28515
 Characteristics of electroluminescent p-n junctions prepared on base of beryllium-doped silicon carbide 14 p2367 A67-28524
 Nonlinear volt-ampere characteristic of photosensitive GaAs plus copper atoms in strong electric field 14 p2368 A67-28532
 Double injection and oscillations of current-voltage dependence of alloyed diodes prepared on basis of p-type gallium phosphide 14 p2286 A67-28594
 Minimum value of noise constant of tunnel diode, noting occurrence beyond point of inflection on I-V characteristic curve 14 p2290 A67-28930
 Volt-ampere characteristics of gallium arsenide tunnel diode oscillators 15 p2443 A67-29285
 Diode detector with exponential volt-ampere characteristics 15 p2443 A67-29289
 Epitaxial deposition of p-GaAs on n-GaAs noting dislocations, packing defect concentrations and V-I characteristics 15 p2533 A67-29317
 Photoconductivity and negative resistance caused by carrier lifetime change in response to change in injection level in SiC p-n junctions 15 p2534 A67-29343
 V-I characteristics of p-n junctions on InSb base, noting effects of surface etching, temperature and impurity concentration 15 p2534 A67-29344
 Current-voltage characteristic determination for n-InSb Corbino disk, noting capacitance and internal resistance current source at cryogenic temperature 15 p2534 A67-29359
 Linear signal multiplier using thermally stable InSb, InAs or GaAs sensors with Hall effect voltage linearly dependent on control current 15 p2444 A67-29386
 Current saturation phenomena in junction-gate field effect transistor 15 p2446 A67-29637
 Substrate resistivity effect on threshold of surface inversion in MOS system, deriving expression for threshold voltage vs impurity concentration 15 p2446 A67-29638
 Excitation of potential LF electromagnetic waves in electron-hole plasma of solid body for negative volt-ampere characteristics of carrier current 15 p2537 A67-29702
 Tunnel current modulation by acoustic wave in superconductors 15 p2537 A67-29708
 Volt-ampere characteristics of epitaxial GaP-GaAs heterojunctions 15 p2538 A67-29785
 Instability of electron hole plasma of semiconductor caused by nonlinear current-voltage characteristic 15 p2538 A67-29789
 MOS oxide-film thickness estimation by extrapolating MOS capacitance-voltage curve into accumulation region at high negative bias 15 p2539 A67-29815
 Josephson current in alternating field between two superconductors separated by dielectric barrier 15 p2530 A67-29868
 Emitter-base voltage vs collector-current characteristic used to study stability of parallel pairs of HF high power transistors 15 p2453 A67-30017

Coaxial plasma source transition from high energy particle production to production of slow plasmoids, noting V-I characteristics and magnetic field distribution 15 p2532 A67-30260

Effect of capture levels on current-voltage characteristic of semiconductor p-n diode with ohmic back contact 16 p2635 A67-30471

Potential distribution and volt-ampere characteristics of ionized gas flows in ducts 16 p2713 A67-30598

I-V curve related to state densities on both sides of n-p junction of tunneling system 16 p2725 A67-30808

Nernst effect in type I superconductor, noting transverse voltages caused by longitudinal temperature gradients 16 p2727 A67-30819

I-V characteristics of alloyed contacts of germanium with Sn, Pb and In in wide range of resistivities and ambient temperatures, establishing correlation with work function 16 p2727 A67-30886

Analog-to-code converter using negative resistance of unijunction transistor, noting construction and results 16 p2836 A67-30900

Tunnel diode oscillator design from averaged and normalized current-voltage characteristics 16 p2837 A67-31028

Localized uniaxial force effect on voltage-current relationship of gold-potassium tantalate Schottky barrier diodes, noting reversible changes 16 p2837 A67-31036

Broadening of lines emitted by tunnel superconductor, noting unfeasibility of simultaneous amplitude-frequency prescription of Josephson current 16 p2728 A67-31044

Static and dynamic behavior of weakly connected superconducting rings, noting methods of measurement and results 16 p2728 A67-31058

Plasma probe diagnostic technique in shock tube, noting electron concentration, gas temperature and plasma potential from V-T characteristics 16 p2873 A67-31110

Surface etching effects on positively sloped current-voltage characteristics of p-n junctions in fused indium antimonide 16 p2730 A67-31161

Thermal plasma column instability concept applied to determine Kaufmann Criterion, calculating production coefficient, V-I characteristics, etc 16 p2719 A67-31229

Atmospheric ozone vertical distribution, measurement, discussing equipment design and underlying principles of method 16 p2876 A67-31377

Crossed film cryotron as single stage high gain amplifier, noting design features and performance 16 p2840 A67-31431

Heat transfer in cryogenic range, noting heat flux measurements, use of semiconductors, etc 16 p2780 A67-31533

Cesium-neon mixture effect on thermionic-emission converter operation measured in experimental tube with plane electrodes, discussing volt-ampere characteristics 16 p2610 A67-31783

Arc burning mechanism of vortex-stabilized plasmatrons, noting effect of arc shunting on volt-ampere characteristics 17 p2897 A67-32171

Composition, heat conduction and radiative energy transfer characteristics of hydrogen and argon plasmas produced by arc in cylindrical channel with cooled walls 17 p2897 A67-32172

Small signal current gain of p-n-p-n section of four-layer Si structure as function of current, noting effect of base width, minority carrier lifetime and doping level 17 p2911 A67-32193

Interface alloy technique for heterojunctions between GaAs and InSb single-crystal heterojunctions shown by X-ray analysis 17 p2911 A67-32196

Space-charge-limited dielectric diode with quadratic I-V characteristics, noting shallow trap effects on detection properties 17 p2823 A67-32199

Transistor current-voltage characteristics when controlled by space-charge and transit-time effects, obtaining large negative conductances at HF 17 p2824 A67-32302

Electric conductivity of flowing plasma, discussing boundary layer problem when measuring with immersed electrodes 17 p2900 A67-32343

High-intensity and high-voltage current switching devices, noting strong pulsed

magnetic field production 17 p2803 A67-32350

Esaki diodes noting hump in V-I characteristics, temperature variation effects, etc 17 p2826 A67-32621

Josephson junction as ideal zero impedance voltage source with discrete voltage for simultaneous application of microwave and magnetic fields 17 p2915 A67-32657

Wing slope techniques for analysis of Langmuir probe characteristics in low density plasma, using I-V characteristics and spherical and cylindrical geometries 17 p2906 A67-33054

Superconducting tunnel junction, discussing effect of exceeding critical current in one film 17 p2922 A67-33058

Minority carrier trapping analyzed from transient decay of photoconductivity in n-type polycrystalline films of InAs 17 p2922 A67-33064

Lithium plasma source current-voltage characteristics in vacuum, obtaining parameters valid for arcs burning under atmospheric pressure and nonzero magnetic fields 17 p2906 A67-33069

Voltage drop near electrode during plasma and electric field interaction in electrical discharge tube, giving plasma current-voltage curves 17 p2907 A67-33090

Hydrostatic pressure and temperature effect on current-voltage characteristics of tunnel p-n junctions in gallium arsenide 17 p2923 A67-33314

Relation between current, voltage and magnetic field of weakly connected double-contact junctions in superconductors 17 p2926 A67-33406

Niobium alloy semiconductor structures with nonlinear negative resistance, giving volt-ampere characteristics 18 p3009 A67-33472

Current-voltage characteristics of clamped metal/p-silicon diodes 18 p3009 A67-33475

Current-voltage characteristic of metal semiconductor point contact, taking into account rectifying effect of junction gap and majority and minority current carrier 18 p3097 A67-33476

Automatic AM control noting proportionate variation of carrier level to signal volume 18 p2998 A67-33502

Single circuit parametron with pulsed balance-modulated pumping voltage, showing existence of two independent subharmonic components 18 p3005 A67-33503

Impact ionization in gallium arsenide through fast pulse experiment, noting conflict between theoretical and measured current-voltage characteristics 18 p3097 A67-33517

Conduction mechanism in GaSb tunnel p-n junctions from 77 to 380 degrees K, noting temperature dependence of basic parameters, V-I characteristics, etc 18 p3098 A67-33573

Thermal processes role in thin semiconducting and dielectric films, discussing current-voltage characteristics, thermal inertia, etc 18 p3100 A67-33766

Relation between current and voltage in type II superconductors situated in transverse magnetic field in flux-flow regime 18 p3101 A67-33987

Electrode in low temperature air plasma containing potassium, investigating cathode potential drop, current density dependence, current-voltage characteristics, temperature, etc 18 p3088 A67-34054

High current arc operation characteristics in vertical-scheme plasmatron, determining current voltage characteristics 18 p3088 A67-34057

Experimental data applicability for DC arcs in construction of AC plasmatrons 18 p3088 A67-34058

Open circuit voltage, short circuit current and maximum power for silicon solar cells at low temperatures 18 p2989 A67-34101

Perpendicular magnetic field inducer change in electron temperature of current carrying semiconducting plates 18 p3102 A67-34424

Volt-ampere characteristics effect on thickness of contact materials of some heterojunctions and band structures obtained by epitaxial deposition 18 p3103 A67-34446

Volt-ampere characteristics of diffused p-n junctions in epitaxial GaAsP film obtained by gas transport

technique 18 p3103 A67-34450

Electric conductivity, Hall effect and photoconductivity of epitaxial single crystal GaAs films obtained by gas transport method 18 p3103 A67-34452

Plasma electric conductivity around 2000 degrees K measured, using double probe with interelectrode section of controllable length 18 p3090 A67-34468

Digital filters with ICs boost Q without inductors 18 p3012 A67-34490

Space charge limited currents in copper phthalocyanine thin films measured as function of voltage, temperature, thickness and illumination 18 p3104 A67-34626

Electron flow in low density argon gas diode analyzed by Monte Carlo method 18 p3091 A67-34641

Image-force effects in normal state tunneling through lead-oxide-lead junctions exhibiting Josephson effect [JPL-TR-32-1154] 18 p3106 A67-34647

Nonuniform stationary states of current in semiconductors having S-shaped current-voltage characteristics 19 p3301 A67-34900

Microwave photon interaction with superconducting tunneling currents measured in aluminum-indium junctions, extended to tin-lead junctions, discussing phase shift 19 p3303 A67-35046

Current-voltage characteristics for double probe measured in seeded combustion products by low temperature surface emission 19 p3345 A67-35079

Current-voltage characteristics of low pressure discharge in magnetron, giving integral equations and current stability 19 p3277 A67-35120

Slepián discharge/steady state DC crossed field discharge, obtaining solutions for plasma velocity and potential to determine current-voltage characteristics 19 p3277 A67-35122

Sinusoidal frequency oscillations in DC magnetron plasmas discharge, determining magnetic field, anode current and voltage and gas pressure dependence 19 p3277 A67-35124

Low voltage arc phenomena in cesium vapor investigated in connection with cesium-diode application as thermionic converter, calculating voltage-current characteristics 19 p3176 A67-35130

Dynamics of channel formation in nonisothermal pulsed discharge and nonequilibrium ionization in inert gas-cesium mixtures 19 p3278 A67-35132

Volt-ampere characteristics of long free-burning convection-free DC and AC arcs in nitrogen, argon and carbon dioxide 19 p3280 A67-35149

Measurement of column resistance during recovery of rapidly interrupted low current wall stabilized DC arc 19 p3282 A67-35158

Gold-doped silicon diode space charge and oscillation effect, discussing deviation from Ohm law at lowest voltages 19 p3198 A67-36043

Tunneling characteristics of metal-oxide-silicon semiconductors, observing band structure and interface-state densities influences 19 p3308 A67-36045

Current creep in selenium rectifier and effect on local conductivity channels in p-n junction of rectifier 20 p3508 A67-36403

Large-signal analysis for varactor frequency upconverter under overdriven conditions, obtaining equations for varactor charge, current and voltage 20 p3396 A67-36510

Properties of steps appearing on volt-ampere characteristic of Josephson current in superconducting tunneling, noting nonlinear resonance effects 20 p3509 A67-36690

Controlled differential negative resistance silicon junction diodes with cadmium alloyed base 20 p3397 A67-36696

Volt-ampere characteristics of tunnel diode analyzed to derive dependence of differential resistance on voltage 20 p3400 A67-37150

Superconducting diode behavior in resonant electromagnet radiation field, studying current-voltage-magnetic field relationship 20 p3511 A67-37241

I-V characteristics of many-valley semiconductors in strong electric field deviating from Ohm law with scattering by phonons 20 p3513 A67-37439

Avalanche drift diode and application in microwave technology, analyzing dynamic negative resistance formation, volt-ampere characteristics and output 20 p3404 A67-37592

Circular planar satellite electrostatic probe theory based on reversible particle trajectories, showing relation between boundary curve in velocity space and current-voltage characteristics 21 p3625 A67-37899

Alternating Josephson current and electromagnetic field interaction in generation of Pb-dielectric-Pb tunnel junction, noting steps in IV characteristics 21 p3677 A67-38096

Negative differential conductivity in semiconductor in acoustic instability mode and connection with sound amplification and number of electron traps 21 p3678 A67-38097

Carrier spatial redistribution under magnetic field effect of current in semiconducting crystal with intrinsic conductivity noting I-V curve shape 21 p3678 A67-38098

Volt-ampere characteristics of n-type GaAs at high fields above Gunn threshold, showing saturation, space charge effect and current controlled negative resistance 21 p3679 A67-38260

P-n-p diode volt-ampere characteristic qualitative calculation, analyzing device negative resistance with avalanche multiplication 21 p3593 A67-38289

Diode volt-ampere characteristics, considering space charge in base barrier layer and rear contact oxide film, noting vertical section appearing on direct branch 21 p3593 A67-38291

Nonlinear effects in steady state volt-ampere characteristics of zinc compensated n-type silicon single crystals 21 p3679 A67-38313

Impurity effect on solubility of another impurity in p-n silicon tunnel diodes studied by measuring current-voltage characteristics 21 p3682 A67-38364

Gunn effect applied to GaAs crystals for use as diodes, discussing current-voltage characteristics 21 p3684 A67-38444

Density, electric field and volt-ampere characteristics for spherical electrostatic Langmuir probe in collision plasma with weak ionization and recombination, using asymptotic method [AIAA PAPER 67-705] 21 p3672 A67-38732

Basic equation derived for I-V characteristics of p-n-p-n device with graphical solution for related p-n junctions 22 p3766 A67-39251

Concentric ring junction to prevent surface breakdown in planar p-n junctions 22 p3766 A67-39252

Avalanche breakdown voltage in Si planar p-n junctions studied for relation to impurity gradient 22 p3766 A67-39256

Plasma physics of thermionic converters, discussing simple physical models, I-V curve and converter operation region processes 22 p3747 A67-39342

Cold Cu electrode interaction with H plasma, measuring electrode I-V characteristics, interelectrode charge concentration, electron temperature, etc 22 p3846 A67-39505

Surface states effect on current-voltage characteristics of metal-semiconductor contact from kinetic coefficients of electron exchange 22 p3858 A67-39570

Current-voltage characteristics of semiconductor diode with spheroidal contact 22 p3769 A67-39571

Photoresistors thermal characteristics in automatic semiconductor control devices studied in steady and pulsed modes of operation, determining current-voltage characteristic and thermoresistance 22 p3801 A67-40214

Spectral and probe methods of plasma temperature measurement, discussing current-voltage characteristics 22 p3853 A67-40216

Heteroepitaxial Si films grown on sapphire studied for current voltage relations, finding space charge limited current 23 p4038 A67-40785

Current oscillations in Co-doped Si p-i-n diode devices noting SCL I-V characteristics 23 p3978 A67-40788

Space charge limited /SCL/ hole current in Si noting mobility, capacitance, current

density, I-V characteristics and double injection 23 p4038 A67-40878

Characteristics of electroluminescent p-n junctions prepared on base of beryllium-doped silicon carbide 23 p4039 A67-40931

Nonlinear volt-ampere characteristic of photosensitive GaAs plus copper atoms in strong electric field 23 p4039 A67-40939

Tunneling of electrons from normal metal to superconductor containing paramagnetic impurity atoms, discussing current voltage characteristics 23 p4043 A67-41300

Linear current-voltage characteristics in type II superconductors under flux flow conditions 23 p4044 A67-41440

Distributed model for photovoltaic cell via nonlinear least square techniques, discussing p-n silicon cells 23 p4046 A67-41487

High voltage solar cell made by integrated circuit processes noting fabrication and electrical characteristics 23 p3937 A67-41492

Thin film GaAs solar cell fabrication and operating characteristics, describing two-cell types 23 p4046 A67-41493

Computer program for predicting silicon solar cell current-voltage characteristics as function of incident solar intensity and cell temperature over heliocentric distances 23 p3939 A67-41513

Computer calculation of 1 Mev electron flux and irradiation degradation of solar cell I-V curves for charged particle environment 23 p3940 A67-41514

Solar cell array model constrained at four points, with computer simulating V-I characteristics for environmental temperature and illumination intensity effects 23 p3940 A67-41515

Li doped Si solar cells noting fabrication, preradiation behavior, changes with temperature, recovery and I-V characteristics after irradiation 23 p3941 A67-41526

Excitation of potential LF electromagnetic waves in electron-hole plasma of solid body for negative volt-ampere characteristics of carrier current 24 p4199 A67-41772

Tunnel current modulation by acoustic wave in superconductors 24 p4200 A67-41778

Solid state electrochemical solar cell using various anode metals and charge transfer complexes as cathodes, noting I-V characteristics and discharge curves [JPL-TR-32-1116] 24 p4097 A67-41804

Constant voltage steps of AC Josephson effect observed in drop-form junctions exposed to radiation 24 p4200 A67-41864

Axial component of electric field intensity in vortex stabilized arc measured by sectional channel and electrode spacing 24 p4195 A67-41940

Oscillating circuits with nonlinear active elements amplitude and phase frequency characteristics graphically plotted, noting effects on frequency 24 p4136 A67-42191

Hot Langmuir probe in Cs plasma studied for method of controlling current voltage characteristics 24 p4154 A67-42210

Logarithmic nature of I-V characteristics of silicon junction diodes for design of analog multiplier with differential operational amplifier 24 p4131 A67-42478

V-I characteristics correlated with energy release from arc column, noting turbulent nature of heat transfer in arc with transverse blowing 24 p4255 A67-42589

VOLTAGE

SA OVERVOLTAGE

Microwave swept frequency measurements on RF transmission line systems and development of VSWR and insertion loss test set 01 p0039 A67-11038

Initial saturation voltage effects in alloy-type transistors at high injection levels 02 p0215 A67-11977

Hall effect, voltage generation across current-carrying conductor perpendicular to magnetic field and galvanomagnetic effects based on Lorentz force 04 p0657 A67-15081

Primary-secondary voltage imbalance effect on multiplication and thermal properties of Hall generator 05 p0774 A67-16704

Small signal MIS capacitance vs bias characteristics measured over wide range of biases and sweep speeds 06 p1002 A67-17979

Method for receiving radio signals against background of strong amplitude-modulated noise signal 06 p0965 A67-18898

Thermal variation of emitter base voltage

of bipolar transistor 07 p1155 A67-19792

Active component of voltage behavior in channel of helium pulse discharge measured, obtaining time dependence of channel resistance, input velocity and energy magnitude 08 p1357 A67-20848

Reduction or elimination of secondary asymmetry voltage in germanium Hall generators noting effect of surface recombination, temperature distribution stabilization, etc 12 p1939 A67-25278

Voltage induced by magnetic field using shock tube with high velocity ionized argon flow 17 p2898 A67-32184

Input and output voltage and efficiency of thermal-to-electric energy conversion effect on fuel cells and insulation of thermoelectric generator 19 p3177 A67-35897

Depletion layer capacitance of p-n step junction with inclusion of effect of spillover charge as function of voltage 20 p3504 A67-36167

VOLTAGE AMPLIFIER

Nonlinear distortions in parallel and series tunnel diode voltage amplifiers 03 p0377 A67-12325

Silicon space charge limited triode considered as analog transistor noting I-V characteristics, current proportionality, voltage amplification and noise performance 13 p2083 A67-27571

VOLTAGE BREAKDOWN

Insulated gate FET tetrode with high drain breakdown potential 01 p0033 A67-10025

Temperature dependence of optical phonon mean free paths and mean energy loss per collision predict avalanche multiplication and voltage breakdown of Si and Ge p-n junctions 01 p0132 A67-10374

Oscillation frequency and breakdown voltage in GaAs p-n junction reverse-biased into avalanche region due to negative resistance arising from transit time effect 01 p0137 A67-11070

Forced convection effects on VHF CW and X-band antenna voltage breakdowns in wind tunnel experiments, using cold nonconducting gas 02 p0213 A67-11647

Selective transistorized logarithmic amplifier design and logarithmic amplitude characteristic computation from cascade output voltages 02 p0215 A67-11978

Transition time dependence between avalanche and second breakdown on input power to p-n silicon junction, noting thermal effects in semiconductors 02 p0222 A67-12650

Epitaxial transistor array on common heat sink with and without emitter series resistance, examining second breakdown mechanism 02 p0222 A67-12652

Transistor failure in inductive load circuits such as TV horizontal deflection circuits and relation to secondary breakdown data 02 p0223 A67-12656

Pulse length of collector current pulse, which causes secondary breakdown in transistors, measured at constant forward or reverse base current 02 p0223 A67-12657

Time dependent light emission due to voltage breakdown in mesoplasma region in Si on Si diode surfaces 02 p0301 A67-12658

Intensity of light emitted by individual microplasmas of silicon p-n junctions increases with voltage to maximum and then decreases 03 p0491 A67-13176

Book on microwave breakdown in gases covering electron collisions, Boltzmann equation for ionized gas, breakdown in atmosphere, etc 03 p0369 A67-13559

Image converter observation of radial striated light filaments during gas breakdown and current sheath buildup in dense plasma focus coaxial discharge 03 p0486 A67-14055

High altitude high voltage breakdown in electric propulsion flight test system 04 p0704 A67-14997

Localized breakdown in Ge mesa diodes due to inclusions 04 p0584 A67-15486

Input admittance of slot antenna after RF voltage breakdown 05 p0775 A67-16947

Bias voltage dependence of capacitance in n-type silicon p-n junctions with voltage breakdown 05 p0869 A67-17171

Ambient medium temperature effects on microplasma phenomena and on breakdown voltage of silicon p-n junction 06 p1050 A67-17895

Avalanche multiplication in Ge and GaAs p-n junctions, comparing experimental and

theoretical ionization rates, predicting voltage breakdown 06 p1065 A67-18954

Models for second breakdown, considering localized high temperatures in crystals and voltage drop mechanisms 07 p1156 A67-18984

Energy dependence of semiconductor devices with respect to secondary breakdown explained on basis of transient thermal resistance 07 p1156 A67-18985

X-ray diffraction study of crystallographic transistor defects causing secondary breakdown 07 p1156 A67-18986

V-I characteristics and turnover phenomenon in Si devices in relation to second breakdown in transistors 07 p1156 A67-18988

Avalanche characteristics and failure mechanisms in junction diodes, showing negative resistance regions due to space charge effect of carriers 07 p1156 A67-18989

Second breakdown in transistors examined by thermal concept, noting transient junction temperature rise 07 p1156 A67-19900

Current constriction in p-n junction under thermal breakdown, deriving expressions for terminal voltage and radius of constriction 07 p1157 A67-19901

Second breakdown in transistors analyzed in terms of lumped parameters noting V-I characteristics, temperature effect, avalanche multiplication, etc 07 p1157 A67-19903

Second breakdown and degradation in Ge alloy junctions, noting failure mechanism and preventive surface treatment 07 p1157 A67-19905

Second breakdown in N-channel MOS transistor 07 p1157 A67-19906

Electroexplosive devices, considering safety improvement for exploding and thermal bridgewire initiators 08 p1372 A67-20526

Junction curvature effect on avalanche breakdown for abrupt junctions in silicon 09 p1471 A67-21945

Cut-off frequency, breakdown voltage and capacitance calculations for diffused junctions in thin epitaxial silicon layer for microwave diode design 09 p1556 A67-22206

Large area 200-v planar voltage-variable capacitance diodes 09 p1475 A67-22207

Optimum design method for variable capacitance diodes with m-th power characteristic for wide voltage range, emphasizing impurity distribution 09 p1476 A67-22213

Transient component in breakdown voltage of silicon p-n junction rectifiers in region of intermittent microplasma conduction 10 p1612 A67-23375

Double diffused n-p-n gallium arsenide transistor, discussing ways oxygen modifies p-n junctions to increase voltage breakdown 10 p1617 A67-23537

Pulsed RF slot antenna breakdown controlled by preionization and diffusion 11 p1758 A67-24126

Laser-produced dielectric breakdown at particle sites in liquids with resulting absorption of secondary light beam 11 p1801 A67-24560

Breakdown and switching in CdS single crystals, noting formation of negative resistance and thickness effect on performance 11 p1847 A67-24729

P-type Au compensated Si diode with negative resistance, determining reversed conductivity recovery 11 p1768 A67-24861

Premature generation breakdown in ruby laser, noting effect of additional media on pumping level/generation time ratio 12 p1953 A67-25445

Voltage breakdown in selectively diffused p-n junction, analyzing dependence on radius of junction curvature 12 p1982 A67-25453

Breakdown voltage characteristics of Ge bonded diode in relation to microwave oscillation, noting avalanche breakdown 12 p1914 A67-25458

Electric conductivity, Hall effect and photoconductivity of epitaxial single crystal GaAs films obtained by gas transport method 12 p1984 A67-25521

Surface fields effect on breakdown voltage of planar silicon p-n junctions 13 p2079 A67-26873

Handbook of materials and techniques for vacuum devices covering high temperature properties, materials selection, joining processes, etc 14 p2339 A67-28829

Absorption of laser radiation in semiconductors and mechanisms of breakdown in process 15 p2537 A67-29704

Avalanche photodiode model with guarding for active area geometry 15 p2452 A67-30014

Current gain and collector-base saturation current and breakdown voltage in aged silicon transistors 15 p2453 A67-30064

Voltage breakdown measurement in various gases at low pressures during simultaneous excitation by RF in superimposed DC field 17 p2902 A67-32672

Lattice and junction imperfection effect on behavior of reverse biased p-n junctions, noting voltage breakdown parameters, origin of microplasma behavior, etc 18 p3102 A67-34344

Electric conductivity, Hall effect and photoconductivity of epitaxial single crystal GaAs films obtained by gas transport method 18 p3103 A67-34452

Data representing monopole antenna voltage breakdown in simulated Mars and Venus atmospheres 19 p3197 A67-35829

Voltage breakdown in undoped and chromium doped semiconducting GaAs 19 p3308 A67-36040

Distributed RC parameters influence on Hall voltage magnitude in high resistivity semiconductors, explaining voltage decrease 20 p3513 A67-37452

MOSFET gate breakdown nondestructively determined by measurement of leakage component 21 p3598 A67-38574

Current sheet propagation transition to steady pattern in pulsed plasma accelerator, noting breakdown and current characteristics [AIAA PAPER 87-656] 21 p3689 A67-38692

Premature generation breakdown in ruby laser, noting effect of additional media on pumping level/generation time ratio 21 p3642 A67-38819

Second breakdown in semiconductor devices, discussing measurement methods and techniques, development, breakdown mode and safe operating conditions 22 p3766 A67-39248

Concentric ring junction to prevent surface breakdown in planar p-n junctions 22 p3766 A67-39252

Avalanche breakdown voltage in Si planar p-n junctions studied for relation to impurity gradient 22 p3766 A67-39256

Neodymium doped YAG Q-spoiled laser system for switching high voltage spark gap at 50 pps with nanosecond jitter 22 p3813 A67-39258

Transistor parameters effect on microwave-circuit performance, tradeoffs and relation between tradeoffs, circuit performance and design 22 p3775 A67-40467

Low inductance three-electrode spark source for vacuum UV generating high degree ionization spectra 23 p4000 A67-41214

Absorption of laser radiation in semiconductors and mechanisms of breakdown in process 24 p4199 A67-41774

VOLTAGE GENERATOR

Fuel cell as low voltage power source 02 p0183 A67-12102

Voltage generator consisting of quadrupole injectors where output voltage is complex function of previously chosen input voltages 03 p0392 A67-13450

Neon tube staircase generator performing functions of frequency and voltage division 05 p0769 A67-16023

Circuits consisting of HF oscillator, kenotron heater, rectifier, etc, for low power HF voltage generator 05 p0780 A67-17499

FM of RC generator by connecting parametric voltage transducer output to phase shift network and applying generated voltage to transducer input through matching network 09 p1496 A67-21692

Random process generation methods using noise-voltage generators and electronic computers 13 p2088 A67-27023

Rectangular pulse thyatron-type generator design and operational principles 13 p2081 A67-27276

Hydrogen integrator in pulsed mode of operation used to determine current pulse integrals 22 p3795 A67-39228

Power conversion derivation in nonlinear resistive element in series with linear resistors 23 p3981 A67-41395

VOLTAGE REGULATOR

Linearity of MOS transistor as variable resistor improved by keeping substrate floating and connecting substrate to drain 01 p0036 A67-10439

Nondissipatively regulated variable frequency DC to DC converter with variable on time and variable off time 02 p0183 A67-12117

Tunnel diode combined with backward diode improves rate of response and pulse waveform in tunnel diode circuits 03 p0381 A67-13585

Threshold reduction in phase locked loop by retarding phase of return signal from voltage controlled oscillator to phase detector 06 p0969 A67-18109

Selenium stabiltron tubes for voltages of 1 v or less 07 p1149 A67-19165

Energy dependence of semiconductor devices with respect to secondary breakdown explained on basis of transient thermal resistance 07 p1156 A67-19895

Motion reproduction, analyzing control systems, dynamic fidelity, voltage command, etc [AIAA PAPER 87-252] 07 p1166 A67-20070

Variable ratio DC transformer regulator used in voltage boost configuration of power system in Radio Astronomy Explorer /RAE/ spacecraft, noting RF interference reduction 08 p1284 A67-20692

Pulse width modulation voltage regulator design for power conversion applications, considering interrelation of loop gain, switching frequency, etc 08 p1284 A67-20693

Voltage transformation and power/energy utilization of radioisotopic thermoelectric generator source /RTG/ for space applications, analyzing components, inverter/converter circuits, etc 08 p1284 A67-20694

DC-to-DC prime converter for anchored interplanetary monitoring platform spacecraft /AIMP/ transforming power from solar array into suitable level for instrumentation electronics 08 p1284 A67-20695

PDM/FM high efficiency voltage regulator design, switching theory and regulation theory 08 p1286 A67-21030

Control-voltage transducer synthesis with variable capacitor compensation of quartz resonator frequency-temperature characteristics 08 p1306 A67-21280

Direct coupling resistance component of transistorized voltage stabilizer 09 p1473 A67-21958

Thermionic low voltage converter-regulator systems, discussing relation between thermionic source, electron cooling and impedance-matching characteristics 09 p1449 A67-22346

Monograph on high power semiconductor-magnetic pulse generators, noting saturable inductors and silicon controlled rectifiers, circuit analysis, voltage regulator, etc 09 p1482 A67-22698

LC smoothing filter in rectifier for pulse supply source stabilized by pulse width modulation 10 p1611 A67-22980

Sawtooth voltage oscillation of triangular shape for pulse width modulation pulse shapers 13 p2089 A67-27704

Approximate solution to nonlinear problem of pull-in range of phase locked loops, noting filter configurations and methods of analysis 15 p2446 A67-29589

Direct coupling resistance component of transistorized voltage stabilizer 20 p3400 A67-37188

Motion reproduction, analyzing control systems, dynamic fidelity, voltage command, etc 21 p3608 A67-38540

Protection of equipment and systems using semiconductor devices by suppression of voltage transients 22 p3766 A67-39250

Aerospace automatically activated electrochemical battery and DC-DC high voltage converter-regulator noting storage stability 24 p4108 A67-42541

VOLTAGE VARIATION INDICATOR

Vibrating capacitor type device for measuring semiconductor contact potential and changes due to illumination or ambient atmosphere 06 p1005 A67-18728

Direct coupling resistance component of transistorized voltage stabilizer 09 p1473 A67-21958

Continuous spectrum of nonperiodic curves, discussing measurement of frequency

spectra of periodic voltage
curves 09 p1501 A67-22468
Voltage fluctuations on Pt filament probes
attributed to pressure
variations 09 p1490 A67-22576
Amplitude modulation using varicaps and
p-n junction in transistorized transmitter,
analyzing HF oscillator 18 p2999 A67-33507
Voltage comparator with high speed
analog-to-digital converter and tunnel diode
circuit 20 p3398 A67-36771
Direct coupling resistance component of
transistorized voltage
stabilizer 20 p3400 A67-37188

VOLTERRA EQUATION SA RADIATION

Comparison of variances evaluated by
Kolmogorov and Volterra techniques for
phase locked loop subjected to white
Gaussian input 01 p0044 A67-10480
Differential equation solution by
separation of multiplicative derivative, by
perturbation method, by reduction to
Volterra equation and by integral
series 01 p0107 A67-11250
Solution of second order differential
equation containing continuous function
expandable in Maclaurin series, using
Volterra integral equation 02 p0260 A67-12668
Energy moments of inverse problem in
theory of nuclear cascade determined, using
first order Volterra integral
equation 02 p0317 A67-12769
Volterra method used for two-dimensional
problems of pressure penetration and
penetration of small wedge into layer of
incompressible liquid 04 p0604 A67-14778
Error bounds for asymptotic solutions of
differential equations, using Volterra
equations for actual and formal solution
vectors 06 p1021 A67-17565
Stabilization of gyrostabilizer using motion
equations as given by
Volterra 06 p1002 A67-18043
Monograph on integral equations covering
Fredholm and Volterra equations,
applications to theory of differential
equations, properties of Cauchy type
integrals, etc 08 p1348 A67-20761
Solution of volterra type equation for
oscillations of thin profiles of grid in
incompressible inviscid
flow 13 p2218 A67-26899

Existence theorem for initial value
problems in differential equation leading to
Volterra integral equation in several
variables 13 p2149 A67-27736
Numerical solution of linear differential
equation and Volterra linear integral
equation of second kind based on Lobatto
four-point quadrature
formula 14 p2342 A67-27977

Intermodulation distortion due to
nonlinear elements in transistors analyzed
using Volterra series
representation 15 p2455 A67-30386

Book on variational calculus and integral
equations, examining extremum conditions,
Fredholm and Volterra integral equations,
Pontryagin maximum principle,
etc 16 p2696 A67-31200

Unsteady heat transfer due to radiation of
two opaque bodies of finite dimensions,
solving nonlinear Volterra integral equation
with respect to net radiation
density 18 p2779 A67-31208

Algorithm for Fredholm type integral
equation solution incorporating successive
approximations, kernel replacement by
degenerate kernel, averaging functional
corrections and band
methods 18 p3071 A67-34167

Energy moments of inverse problem in
theory of nuclear cascade determined, using
first order Volterra integral
equation 22 p3842 A67-40271

Integral equations for nonlinear problems
in partial differential equations, including
Volterra, boundary value and initial value
problems 24 p4180 A67-43088

VOLTMETER

Error of measurement of mean square
value of fluctuation signals due to voltmeter
calibration 10 p1607 A67-23451

VOLUME

SA BODY VOLUME /BIOL/

Numerical method for estimating capacity
of arbitrary surface noting relation to
Dirichlet problem 03 p0462 A67-14342
Load prediction method necessitated by
minimum weight and volume requirements

for spacecraft recovery system, considering
nonuniform opening of parachutes in
cluster 17 p2797 A67-32578

Pressure, volume, temperature and
internal energy data for He using constant
volume calorimeter and gas thermometer,
discussing He melting 22 p3920 A67-40392

VOLUMETRIC STRAIN

Exact expressions derived for deflection,
swept volume and ratio of balancing force to
total thrust due to pressure for flat circular
plate 01 p0164 A67-11273

Plane and volume stressed states of
discrete medium, analyzing deformation
work of continuous elastic
medium 16 p2766 A67-31144

Hexagonal cobalt single crystals plastic
deformation, determining stress, free
enthalpy and volume activation, temperature
and strain rate 17 p2873 A67-32815

Surface, volume and grain-boundary
diffusion role in metal sintering process,
discussing theoretical
equations 19 p3247 A67-35636

Volume strains in metals during
pressworking and rolling 21 p3637 A67-38922

VON KARMAN EQUATION

Von Karman-Pohlhausen boundary layer
analysis of temperature and velocity profiles
in inlet region between two parallel planes
with relative motion and pressure
gradient 04 p0729 A67-15808

Quasi-steady aerodynamic and von Karman
large deflection plate theory equations of
nonlinear oscillations of fluttering plate for
single mode subsonic and sonic or coupled
mode supersonic oscillations
[AIAA PAPER 67-13] 06 p1101 A67-18252

Section requirements for elimination of
turbulent boundary layer separation in
adverse pressure gradient, based on mixing
rate hypothesis and von Karman momentum
integral
[AIAA PAPER 67-197] 06 p0988 A67-18442

Two-dimensional flow past bluff body,
comparing vortex street wake measurements
to von Karman
predictions 17 p2790 A67-32278

Karman similarity hypothesis extended to
cylindrical geometry to establish conditions
for universal velocity similarity in fully
turbulent rotating flows
[ASME PAPER 67-APM-23] 17 p2838 A67-32416

Numerical integration solution for finite
elastoplastic deflections of circularly
symmetrical plates 19 p3340 A67-35511

Quasi-steady aerodynamic and von Karman
large deflection plate theory equations of
nonlinear oscillations of fluttering plate for
single mode subsonic and sonic or coupled
mode supersonic oscillations
[AIAA PAPER 67-13] 21 p3727 A67-38870

Maximum stresses with changes in Poisson
ratio for thin parallelogramic panels with
nonlinear behavior 22 p3911 A67-39666

VON NEUMANN THEOREM

Hyperbolic difference equations, reviewing
Courant-Friedrichs-Lewy paper in light of
recent developments 14 p2342 A67-28154

VON ZEIPPEL METHOD

Von Zepel transformation solution small
divisor problem arising from natural
frequencies of orbital resonance motion of
24-hr artificial satellite 03 p0457 A67-13162

Satellite orbit perturbation analysis for
lunar gravitational field determination using
von Zepel transformation 18 p3131 A67-34325

Von Zepel method and Hamiltonian
perturbation mechanics used for orbits at
resonance with tesseral harmonics of
geopotential 19 p3328 A67-35959

Von Zepel method to eliminate short
period terms in first order general planetary
theory noting system transformation into
canonical equations 22 p3881 A67-39514

VOR SYSTEM

Flush cavity VOR antenna for DC-9
aircraft permitting omnidirectional radiation
pattern characteristics 04 p0590 A67-15906

Air traffic control, navigation techniques,
requirements and equipment for general
aviation to end of
century 19 p3256 A67-35861

VORTEX

Motion of flux lines in type II
superconductors at zero temperature,
discussing friction, Magnus and other
forces 01 p0133 A67-10750

Vortex structures of cloud systems from
meteorological satellite

data 04 p0651 A67-15468
Cloud vorticity effects on ocean
roughness, from Tiros autumnal
observations 04 p0651 A67-15469

Weak superconductivity electrodynamic
and EM wave propagation in Josephson
tunnel junction in presence of
vortices 06 p1054 A67-18806

Weak superconductivity electrodynamic
and EM wave propagation in Josephson
tunnel junction in presence of
vortices 18 p3102 A67-34425

VORTEX BREAKDOWN

Forced and periodic breakdown of
confined vortex rotating in opposite
direction, measuring flow rates and wall
pressures
[ASME PAPER 66-WA/FE-7] 04 p0611 A67-15928

Free vortex decay above stationary
boundary for varying viscosity, determining
plate boundary layer solution for small
nondimensional radial
distances 06 p0985 A67-18135

Vortex breakdown theory, considering
small energy losses and small flow force
reduction /wave resistance
effects/ 13 p2095 A67-26908

Vortex breakdown effects on lift, drag and
pitching moment coefficients of slender
sharp-edged delta wings with different
aspect ratios 13 p2050 A67-27194

Vortex breakdown treated as failure of
quasi-cylindrical approximation for viscous
axisymmetric flow 16 p2658 A67-30948

Vortical stabilization of plasma column
within radial electric
field 20 p3500 A67-37062

VORTEX COLUMN

Sound wave generation by columnar-
starting vortex passing through reflected
plane shock front analyzed, revealing
alternate compression-rarefaction
nature 10 p1625 A67-23117

VORTEX DISTURBANCE

Cylinders of rectangular section as
aeroelastic nonlinear oscillators, theory of
galloping oscillation and force measurements
on stationary cylinder
[ASME PAPER 67-VIBR-50] 11 p1777 A67-24200

Karman vortices in heat exchanger, noting
no vortex shedding in supercritical Reynolds
number range and wake
turbulence 11 p1782 A67-24657

Axisymmetric free turbulent jet flow with
swirling vortex motion over wide range of
swirl degree 17 p2838 A67-32417

VORTEX FLOW

Vortex strength in wake of circular
cylinders and comparison of vortex velocity
distribution with that of Hoffman and
Joubert, using hot-wire anemometers at
various Reynolds numbers 01 p0005 A67-10256

Rotating fluid dynamics with results
derived from classical rules of vorticity,
noting various types of
waves 02 p0232 A67-11566

Pressure losses and improved heat
transfer in incompressible fluid flow through
tubes containing twisted
tapes 02 p0233 A67-12200

Vortex amplifier performance
characteristics in liquid and gas flow control
and chemical processing 03 p0363 A67-13170

Steady flow possessing extremal kinetic
energy compared to equivortex flow for
stability analysis 03 p0402 A67-13618

Harmonic generation in Taylor vortices
between rotating cylinders, measuring
amplitude of each harmonic, noting
agreement with Davey
theory 04 p0601 A67-14462

Convective vortex over horizontal surface
caused by nonuniform
heating 04 p0612 A67-14652

Swirling flow-induced spin effect on
rocket nozzle
performance 04 p0548 A67-15255

Curved flow effect on lift characteristics
of blade using Scholz method, noting role of
correction coefficient of lift curve slope and
zero lift angle 05 p0791 A67-16427

Earnshaw conjecture refuted for particle
in three-dimensional lamellar
motion 05 p0792 A67-16728

Transport of vorticity and enthalpy in
flow field in nose region of blunt body in
viscous hypersonic flow 05 p0749 A67-16820

Hot-wire anemometer measurements of
transition in incompressible wake of cone at

low Reynolds number 05 p0751 A67-17439
 Negative critical Taylor number for stability of swirling fluid with variable density in circular magnetic field 05 p0859 A67-17442
 Performance and flow field characteristics of vortex-flow fluid logic devices, discussing efficiency, velocity profiles and momentum profiles for amplifier, rate sensor, test apparatus, etc 06 p0982 A67-17719
 Unsteady circular motion of viscous fluid with hollow vortex, showing motion vorticality in boundary layer region on free surface 06 p0982 A67-17728
 Hypersonic laminar boundary layer on blunt cones, considering external flow vorticity caused by curved shock wave, calculating gas-enthalpy profile 06 p0936 A67-17734
 Base pressure fluctuations behind cone in supersonic flow due to presence of stagnant zone with subsonic reverse flow in shape of annular vortex 06 p0936 A67-17735
 Plane vortex flow in vicinity of orthogonality point of sound line to velocity vector 06 p0936 A67-17738
 Induction coupled argon plasma at atmospheric pressure, noting vortex stabilization on discharge 06 p1039 A67-18067
 Vortex periodicity in wakes as function of Reynolds and Rossby numbers, solving nonlinear viscous Navier-Stokes equations [AIAA PAPER 67-34] 06 p0987 A67-18349
 Pressure pulse and wall-to-jet heat transfer in discrete vortex zone of restrained gas jet in circular channel 06 p1118 A67-18550
 Boundary layer theory of heat exchange in vortex region of separated flow past cylinder 06 p1119 A67-18821
 Oscillating variables of flow past cylinder, calculating magnitude and frequency of lift 07 p1168 A67-19258
 Application limit of inviscid small perturbation theory to secondary flow in cascade, comparing experimental and calculated vortex strength 08 p1275 A67-20406
 Vortex devices characteristics and applications studied with vortex sink model 08 p1280 A67-20442
 Performance of vortex diode, scroll diode and fluid flow rectifier 08 p1283 A67-20473
 Vortex gas stabilization of arc and effect of current strength, flow rate and geometrical dimensions 09 p1547 A67-22320
 Vortex separated delta wing leading edge in supersonic flow, noting effect on pressure distribution and role of flow equation 09 p1438 A67-22496
 Flow vortices in hollow cylinder made of type II superconductor 09 p1482 A67-22662
 Axisymmetric vortex flow in neighborhood of point having sonic line orthogonal to velocity vector 10 p1824 A67-23034
 End-wall pressure distributions in confined vortex [JPL-TR-32-1099] 10 p1626 A67-23150
 Low aspect ratio wings at high incidence in wind tunnel study of surface pressure and vortex flow 10 p1593 A67-23549
 Spectral characteristics of turbulence in presence of mean velocity and temperature gradients 11 p1815 A67-23955
 Pressure measurements on surface and in wake of circular cylinder at rest and in vortex excited oscillation at subcritical Reynolds numbers [ASME PAPER 67-VIBR-31] 11 p1777 A67-24189
 Flow induced vibration and noise in tube bank heat exchangers due to Karman vortex streets analyzed, noting shedding frequency, lift, etc [ASME PAPER 67-VIBR-48] 11 p1777 A67-24198
 Rotating Ekman boundary layer stability and transition for two-dimensional roll vortices superimposed upon basic boundary layer flow 11 p1781 A67-24543
 Approximate similarity criterion for arc with self-adjusting length, burning in plasmatron with gas vortex stabilization, determined by shunting 11 p1843 A67-24969
 Electric field intensity distribution over length of plasmatron arc stabilized by longitudinal vortex air flow 11 p1843 A67-24972
 Dynamics of baroclinic geostrophic circumpolar vortex beta-plane flow in zonal magnetic field, noting applications to solar

rotation, hydromagnetic dynamo theory, etc 12 p1963 A67-25338
 Thermodynamics of vortex flow in superconductors, using combination of electrical currents and thermal gradient 12 p1983 A67-25477
 Vortical interaction between free jet boundary layer and outer flow in separation area of hypersonic gas flow past body 12 p1892 A67-25671
 Channel profiles for producing vortex flows in weakly ionized gases in transverse magnetic fields 12 p1977 A67-28076
 Lagrange and Euler representations of particle shapes and vortex theorems in hydrodynamic flow 13 p2094 A67-28644
 Orographic factors effect on stratospheric pressure field, obtaining ascending vortical fluxes and heat input equations, discussing refractive index for atmospheric perturbations 13 p2112 A67-28672
 Benjamin theory of conjugate vortex flow proved by alternate method 13 p2095 A67-26909
 Stability of multiple rows of vortices created behind tripping cylinders at low Reynolds number 14 p2294 A67-27795
 Averaged axisymmetric vortex flow of ideal incompressible fluid in turbine engine 14 p2296 A67-27986
 Wind tunnel investigation of wake structure behind cone in supersonic flow 14 p2240 A67-27994
 Rotating vortex flow and transition phenomena in conical diffuser [AIAA PAPER 66-426] 14 p2240 A67-28109
 Static and dynamic performance of pancake vortex flow field and application to pressure amplification 14 p2248 A67-28272
 Mathematical model describing nonlinear behavior of vortex valve in fluid circuits, noting effect of swirl on vortex valve flow characteristics 14 p2251 A67-28341
 Vortex valve performance power index 14 p2251 A67-28343
 Tip vortex method for helicopter rotor design during vertical descent 14 p2243 A67-28641
 Vortex flow about wings, fins and fuselages of slender aircraft and missiles analyzed using small water tunnel 15 p2465 A67-29399
 Designing propeller blades with maximum aerodynamic efficiency by vortex theory, considering engine power, propeller diameter, forward velocity, etc 15 p2417 A67-30079
 Velocity profile of vortex region formed downstream of step-shaped wall calculated, assuming flow is turbulent, using similarity hypothesis 16 p2662 A67-31469
 Arc burning mechanism of vortex-stabilized plasmatrons, noting effect of arc shunting on volt-ampere characteristics 17 p2897 A67-32171
 Vortex wake and aerodynamic load distribution of slender rectangular wings 17 p2790 A67-32215
 Two-dimensional steady flows of viscous fluid in external infinite region on basis of fourth order nonlinear Helmholtz equation in vortex terms 18 p2981 A67-33420
 Motion equation of system of two banked wings near solid surface with optimum circulation distribution 18 p3024 A67-33542
 Economical feasibility of open and closed cycle vortex-stabilized gaseous nuclear rocket engines, investigating vortex flow characteristics [AIAA PAPER 67-500] 18 p3076 A67-33964
 High pressure vortical discharge in air and argon, solving differential equations for heat conduction and electromagnetic field by digital computer 18 p3088 A67-34062
 Rotational velocity and ion density profiles of plasma vortices by measuring radial electric field 19 p3288 A67-35361
 Three-dimensional vortex flow inverse problem through axial fan solved using isolated airfoil method 19 p3171 A67-35723
 Type II superconductors properties, studying Ginzburg-Landau equations, vortex lines, reversible magnetic behavior and irreversible phenomena in mixed state 19 p3307 A67-35868
 Flux penetration and vortices formation in macroscopic type II superconductor shown to be favorable below thermodynamical critical field 20 p3508 A67-36426
 Test data for heat transfer in vortex flows in tubes with band type swirl generator,

determining effect of mass inertial forces 20 p3544 A67-36449
 Internal rotational relaxation effect on attenuation of HF turbulent vortices during degeneration of turbulence in viscous weakly elastic fluid 20 p3422 A67-37053
 Heat transfer in circular channel containing revolving cylinder, considering turbulent flow with microvortices 20 p3359 A67-37343
 Properties of kinetic energy and squared vorticity in two-dimensional inviscid turbulent flow, using Navier-Stokes equation and conservation laws 21 p3609 A67-37735
 Single parameter Ball cylindroids representation of multiply connected surface vortical motion axes congruence 21 p3611 A67-37902
 Congruence of screw axes attached to body with multiply connected surface in vortical motion in ideal fluid 21 p3611 A67-37905
 Electromagnetically driven confined viscous vortex flow with high positive radial Reynolds numbers, solving energy equation for temperature distribution [AIAA PAPER 67-730] 21 p3674 A67-38754
 Pinch-discharge source of ionizing plasmoids for aerophysical investigations at high pressures, emphasizing stabilization and passage of AC current through vortex 21 p3675 A67-38912
 Gas separation effects in Ranque-Hilsch vortex tube explained by dynamic model of axial flow 22 p3917 A67-39512
 Swirling mass flow in supersonic nozzle indicates discharge coefficient falls nonlinearly with swirl 22 p3739 A67-39527
 Type II superconductor properties, discussing Ginzburg-Landau and London equations, surface superconductivity, vortex motion, etc 22 p3859 A67-39770
 Vorticity component change rate expressions for arbitrary configuration inviscid flow, discussing local instabilities 23 p3990 A67-41166
 Inviscid instability of cylindrical two-dimensional free boundary layer vortex flow, using approximation by axisymmetrical vortex model 23 p3990 A67-41169
 Axial component of electric field intensity in vortex stabilized arc measured by sectional channel and electrode spacing 24 p4195 A67-41940
 Taylor vortices and turbulence in flow between eccentric rotating cylinders [ASME PAPER 67-LUB-12] 24 p4145 A67-42673
VORTEX GENERATION
 Superconducting-to-mixed state phase transformation in type II superconductors in applied magnetic field and accompanying onset of vortex filaments at surfaces 03 p0501 A67-14372
 Vorticity generation by interaction of waves with plasma in magnetic field 15 p2524 A67-29231
 Formation mechanism of luminous gas sphere/ionized vortex configuration/ due to atmospheric electrical discharge 21 p3655 A67-38902
 Base bleed effects on flow behind two-dimensional model with blunt trailing edge, measuring base pressure, shedding frequency and vortex formation 21 p3566 A67-39078
 Spiral flow in cylindrical annular chamber behind guide vanes /stators/ noting flow instability in outer region due to vortex generation 23 p3929 A67-41253
VORTEX GENERATOR
 Plasma vortex filaments produced in pairs as shown by image converter photographs of interfaces between magnetic field and accelerated plasma 03 p0486 A67-14054
 Initial turbulence effect on characteristics of axisymmetric submerged air jets, using thermo-anemometer to measure averaged velocity and mean quadratic longitudinal pulsation rate component 11 p1779 A67-24320
 Design schemes for magnetic systems of vortex MGD generators with external and internal winding 16 p2609 A67-31585
 Wing flap aerodynamic performance as affected by wing flap surface cavities, noting usefulness in flow stabilization at high pressure gradient 17 p2792 A67-32904
 Subsonic diffuser with vortex generator as integral design feature for supersonic transport aircraft inlet [AIAA PAPER 67-464] 18 p2983 A67-33935

VORTEX RING

- MHD phenomena in vortex ring in conducting fluid, noting intensification of initial field at high Reynolds numbers and self-excitation 07 p1229 A67-19684
- Circular vortex ring motion and decay in incompressible flow field considered for Navier-Stokes equations solution by boundary layer technique 16 p2660 A67-31212
- Aerodynamic characteristics of helicopter main rotor during steep descent, using ring vortices method 20 p3356 A67-36443
- Flow past disk at angle to stream with marked periodic motions caused by vortex ring shedding increasing with angle of incidence 23 p3990 A67-41171

VORTEX SHEET

- Nonlinear two-dimensional unsteady potential flow around arbitrarily shaped airfoil in inviscid and incompressible fluid, considering method of calculating pressure, forces and moments [AIAA PAPER 66-968] 02 p0178 A67-12291
- Suction-preserved steady state vortex sheet on surface of infinite porous circular cylinder in viscous MHD liquid suddenly rotated about axis 06 p1046 A67-18891
- Linear aerodynamic theory of rotor blades for predicting lift distribution, considering wake vortex sheet 13 p2051 A67-27589
- Limit of circulatory lift on wings with finite span, deriving lift and drag for flat and rolled up vortex sheets 17 p2789 A67-32035
- Unsteady plane parallel flow stability of viscous electrically conducting incompressible fluid in oscillating magnetic field 17 p2910 A67-33350
- Thin rectangular vortex wing in uniform flow, solving nonlinear equations by successive approximations 20 p3356 A67-36439
- Delta wing with leading edge vortices, calculating inviscid incompressible flow field near center of rolled up vortex sheet assuming conical velocity field 24 p4092 A67-42570

VORTEX STREET

- SA KARMAN VORTEX STREET
- Aerodynamic forces of oscillating lifting surfaces of large aspect ratio in subsonic range investigated by approximation method 03 p0351 A67-12996
- Two-dimensional flow past bluff body, comparing vortex street wake measurements to von Karman predictions 17 p2790 A67-32278
- Wakes in two-dimensional flows studied by comparing mesoscale eddies in earth atmosphere with Karman vortex street, calculating wake parameters 24 p4146 A67-41786

VORTEX TRAIL

- Vortex-rotor disk interaction effect on helicopter rotor performance in forward flight 06 p0945 A67-17907
- Correct image system and conditions for vortex model of wing body interference 08 p1277 A67-20596
- Vortices in plane flow behind circular cylinder at different Mach numbers, noting staggered pattern formation 14 p2296 A67-27988
- Book on aerodynamics of V/STOL aircraft emphasizing use of momentum and finite wing theories, considering deflection of trailing vortex system 14 p2243 A67-28678
- Vortex wakes of vibrating cylinders at low Reynolds numbers noting change in geometry along span 15 p2471 A67-29653
- Downstream flow of shock waves created by wing section moving at speed of sound 16 p2594 A67-31712
- Three-dimensional flow in axial fan, consisting of rotor only, having finite number of blades, by method of isolated airfoil of finite span 19 p3171 A67-35712
- Three-dimensional flow through rotor of single stage axial fan with prescribed spanwise variable circulation 19 p3171 A67-35714
- Wing tip vortices behind DC-8 measured for maximum circumferential velocities by research aircraft 24 p4091 A67-42276

VORTICITY EQUATION

- SA BALANCE EQUATION
- Predicting wake-induced nonuniform flow field in plane of rotor disk [AIAA PAPER 66-17] 03 p0354 A67-12909
- Vorticity jump across discontinuity surface which is not contact surface obtained on

- kinematical basis, recovering Hayes formula for gas dynamic 04 p0600 A67-14456
- Two-dimensional transient laminar natural convection heat transfer in partially filled liquid propellant tanks, solving vorticity and energy equations 04 p0731 A67-15828
- Two-cell solution to vorticity equations in unstably stratified atmosphere 06 p1026 A67-18565
- Computer solution of barotropic vorticity equation for weather forecasting 11 p1816 A67-24330
- Finite-amplitude oscillations of Maclaurin spheroids preserving ellipsoidal nature of surface and generating internal motions of uniform vorticity 19 p3263 A67-36078
- Predictions from barotropic vorticity equation in spectral form analyzed for errors 21 p3654 A67-38575

VORTICITY TRANSPORT HYPOTHESIS

- Temperature-vorticity analogy validity in laminar turbulent flows extended to compressible fluids, noting temperature relation to shear stress 04 p0727 A67-15680
- Noether theorems describing continuum mechanics material applied to Hamiltonian principle for motion of pleiotropic fluid or ideal gas undergoing polytropic process 13 p2105 A67-27397

VOSKHOD I SPACECRAFT

- Pre- and postflight medical examinations of Voskhod I cosmonauts 07 p1133 A67-19108
- Chromosome configuration and mitosis impairment in micropores Tradescantia paludosa due to space flight effects of Voskhod I 07 p1133 A67-19109
- Radiation doses measured by onboard dosimeters and those fastened to space suits of crews of Voskhod I and Voskhod II compared, noting radiation composition analysis by means of nuclear emulsions 14 p2256 A67-27863
- Electrophysiological tests performed onboard Voskhod I noting apparatus recording electroencephalograph, electrooculogram, dynamogram and motion coordination in writing of astronauts 16 p2616 A67-30760

VOSKHOD II SPACECRAFT

- Dynamic characteristics of human operator in tracking system under spaceflight conditions onboard Voskhod II spacecraft
- dynamic characteristics of human operator in tracking system under space flight conditions 07 p1135 A67-19106
- Medical tests of spacemen Bellaev and Lenov during training and orbital flight 11 p1748 A67-24080
- Radiation doses measured by onboard dosimeters and those fastened to space suits of crews of Voskhod I and Voskhod II compared, noting radiation composition analysis by means of nuclear emulsions 14 p2256 A67-27863
- Bellaev description of 17-orbit flight of Voskhod II including spacecraft design and control, life support system and walk-in-space 16 p2616 A67-30758
- First walk in space from Voskhod II described by Leonov, noting importance of simulated training 16 p2616 A67-30759

VOSKHOD MANNED SPACECRAFT

- Cloud cover space photography by Voskhod I and Voskhod II to determine spatial structure of clouds of various types and fields of brightness 01 p0110 A67-11429
- Physiological functions of cosmonauts during flight of Voskhod, discussing measurement results of ECG, EEG, dynamography, etc 02 p0185 A67-11545
- Physiological measurements of Soviet cosmonauts in Voskhod spacecraft, noting human performance characteristics and detection techniques 02 p0185 A67-11546
- Radiation types encountered and shielding used by Voskhod I and II manned spacecraft 02 p0308 A67-12321
- Medical observations of astronauts on Voskhod and Voskhod II 08 p1288 A67-21111
- Bacteria survival and mutation in radiation environment on Voskhod I and II 14 p2254 A67-27864
- Operational efficiency of astronauts evaluated on basis of Voskhod I and II flights, discussing manual operation, EVA memory efficiency, etc 18 p2618 A67-30780
- Physiological functions of cosmonauts during flight of Voskhod, discussing measurement results of ECG, EEG, dynamography, etc 16 p2614 A67-31611

- Physiological measurements of Soviet cosmonauts in Voskhod spacecraft, noting human performance characteristics and detection techniques 16 p2614 A67-31612

VOSTOK VI SPACECRAFT

- Photometric analysis of twilight halo photographs by Vostok VI spacecraft 03 p0415 A67-14227
- Photometric analysis of twilight halo photographs by Vostok VI spacecraft 12 p1932 A67-25483

VOSTOK SPACECRAFT

- Control signal generator and output characteristics of angular position and velocity sensors used in single-axis sun-oriented system of Vostok spacecraft 12 p1964 A67-25642
- Vostok launch vehicle design characteristics evaluated including performance, propellant weights, booster phase burning period, etc 19 p3334 A67-35843
- Russian rocket hardware exhibited in Paris noting Vostok 22 p3899 A67-39523

VOYAGER PROJECT

- Voyager project for planetary biological exploration 02 p0185 A67-11816
- Propulsion system selection considerations for Voyager spacecraft including Minuteman solid with liquid restartable midcourse, orbit trim system, LEM descent stage and transtage [AIAA PAPER 66-974] 02 p0305 A67-12296
- Voyager spacecraft guidance and control system analysis, examining systems design requirements, problems of redundancy implementation for critical functions and gyro system 02 p0265 A67-12381
- Automated spacecraft flights and cost /1965 to September 1966/, discussing Voyager, Jupiter probe, technology satellite, synchronous meteorological satellite and voice/TV broadcast 05 p0904 A67-16384
- Comparison between Monte Carlo and PERT models, noting PERT errors and Monte Carlo simulation for Voyager spacecraft development [AIAA PAPER 67-209] 06 p1097 A67-18513
- Planetary entry vehicle development, discussing mission objectives, vehicle requirements, Voyager capsule, etc [AAS PAPER 66-57] 07 p1259 A67-19994
- Voyager type landers on Mars surface noting instrumentation, operation, reliability, etc [AAS PAPER 66-61] 07 p1259 A67-19997
- Management systems planning for control and information systems for Voyager project, with attention to work breakdown and scheduling [AAS PAPER 66-141] 08 p1429 A67-20966
- Voyager project, orbital operations, objectives for 1971, etc 08 p1412 A67-21097
- System design of Voyager-class Mars Probe/ Lander, considering selections of entry aeroshell, landed capsule and descent and postimpact instrumentation 10 p1714 A67-23756
- Voyager project goals, orbital operations, capsule descent, navigational systems, etc 12 p2002 A67-25232
- Voyager project goals, orbital operations, capsule descent, navigational systems, etc 16 p2751 A67-31487
- Automated biological laboratory /ABL/, comprehensive integrated system for detection of life on Mars 16 p2762 A67-31488
- Flight failures in complex unmanned spacecraft systematically studied for Voyager spacecraft design, discussing component failure, design deficiencies and space environment 18 p3138 A67-34656
- Planetary quarantine and biological search strategy, discussing Voyager-Mars mission configuration, sterilization, back-contamination and decisions 19 p3180 A67-35233
- Flight phase constraints effect on design of Voyager orbiter-capsule mission 20 p3532 A67-36564
- Scientist role in automated laboratory for remote biological exploration of planets [AIAA PAPER 67-632] 20 p3375 A67-37615
- Mars landing guidance requirements for unmanned lander after separation from interplanetary flyby space vehicle 21 p3655 A67-37783
- Unmanned probes designed to land on planetary surfaces to obtain temperature, atmospheric measurement and ground

samples chemical analysis 22 p3900 A67-39613
 Planning and design of Voyager for future interplanetary flight, discussing RTG and spacecraft system
 redundancy 23 p4071 A67-40867
 Voyager thermal insulation requirements noting tests of vapor deposited Au on Mylar and Kapton
 [AIAA PAPER 67-777] 24 p4257 A67-42945
VTOL FIGHTER AIRCRAFT
 Four combat aircraft designs /tailless delta, swept wing, variable geometry and VTO aircraft/ using same bypass engines /Pratt Whitney-SNECMA
 TF-306s/ 15 p2419 A67-29670
VTOL
 Aerodynamic suckdown results obtained in investigation of VTOL ground-proximity effects 17 p2791 A67-32588
VTOL AIRCRAFT
 Optimum design safety for VTOL aircraft, noting noise and vibration elimination [AIAA PAPER 66-813] 01 p0008 A67-10031
 Hoverbug VTOL twin-jet flying simulator operational experience and management and construction techniques [AIAA PAPER 66-799] 01 p0009 A67-10537
 Control power usage for typical flight maneuvering in hover determined from flight test data of VJ-101 aircraft and of hover-rig with similar thrust-geometry and mass distribution [AIAA PAPER 66-816] 01 p0010 A67-10538
 Small-perturbation hover dynamics motion equations, characteristic modes, stability derivatives and dimensional analysis [SAE PAPER 660576] 01 p0010 A67-10570
 Helicopter and VTOL vehicle low air speed measuring techniques and devices including pitot-static tube, hot-wire anemometer, sphere sensor and exotic techniques 01 p0073 A67-11122
 Triplex flight control system for VTOL aircraft noting new servomotor, simple mechanical construction and increased reliability 02 p0264 A67-12206
 Objection to marine propeller application to VTOL aircraft 02 p0182 A67-12427
 VTOL and STOL aircraft applications, Boston to Washington [AIAA PAPER 66-964] 02 p0182 A67-12638
 Suppressor applications of nozzles in reduction of sound power level generated in exhaust jet wake and ground surface deterioration from VTOL lift jets 03 p0350 A67-12916
 VTOL jet transport noise effect on surrounding habitants and guidelines for airport design 03 p0357 A67-12973
 Operation of VTOL aircraft in vicinity of airport including safety, noise and air traffic control factors 03 p0357 A67-12974
 Altitude control for VTOL aircraft facilitates control of hovering flight, noting construction, operation principles and performance 03 p0363 A67-12981
 Sensitivity analysis of VTOL aircraft control in vertical-horizontal transition 03 p0358 A67-12982
 VTOL aircraft static and dynamic performance measurement technology, analyzing application of data processing methods 03 p0418 A67-12983
 Heli gyro configuration in autogyro, helicopter and VTOL aircraft design 03 p0359 A67-12987
 Autopilot requirements, particularly for VTOL aircraft and automatic instrument landing, noting introduction of redundant channels 03 p0464 A67-13004
 Effect of bleeding air behind compressor for VTOL stabilization on dynamic behavior of jet engine 03 p0503 A67-13009
 Future short haul air transportation in northeast corridor of U.S., considering conventional, STOL and VTOL air transport systems 03 p0538 A67-13783
 High lift rotor design for jet propulsion VTOL aircraft 03 p0360 A67-13891
 Vertical takeoff technology effect on aircraft design noting flexibility, reliability, decreased takeoff distance, etc 04 p0550 A67-14410
 VTOL power plant design noting jet deflection, lift fans, RB-162 engine, etc 04 p0687 A67-14435
 Simulation system and hovering vehicle prototype design for use in development of VTOL aircraft 04 p0600 A67-15540
 Control data acquisition during takeoff and landing of VTOL type

vehicles 05 p0841 A67-16535
 Time-optimum transition of VTOL aircraft takeoff to forward flight [DVL-627] 06 p0944 A67-17627
 Periodic aerodynamic loading prediction for helicopters and VTOL aircraft 06 p0945 A67-17908
 External noise characteristics of lifting systems for VTOL aircraft 06 p0946 A67-17912
 Tilt rotor VTOL aircraft stability, discussing results of wind tunnel tests on rotor-pylon behavior at different velocities [AIAA PAPER 67-17] 06 p0948 A67-18254
 VTOL test bed for ground effects test, noting environmental characteristics, configuration dependence of lift and hot gas ingestion [AIAA PAPER 67-181] 06 p0980 A67-18297
 Hovercraft and rotorcraft, discussing design, construction, operation and future 06 p0949 A67-18744
 Six-component balances installed under each of two test sections of Lockheed-Georgia wind tunnel designed for development of VTOL aircraft 07 p1164 A67-19672
 VTOL capability in military and civil aircraft, discussing Italian and German efforts 07 p1130 A67-20122
 VTOL/STOL aircraft evaluation via performance characteristics 07 p1130 A67-20219
 VTOL technique and advanced aircraft design 07 p1130 A67-20220
 STOL and VTOL aircraft performance and cost for intercity travel, discussing airport network 08 p1279 A67-20782
 XV-4B vertical lift aircraft with lift engines noting stability, control, structural design, flight control system, etc 09 p1439 A67-22284
 Inlet/door performance characteristic of VTOL lift engines studied in full scale wind tunnel tests [AIAA PAPER 66-655] 09 p1438 A67-22490
 VTOL short-haul transportation design requirements and configuration characteristics 13 p2053 A67-27067
 Status and possibilities of VTOL propulsion, noting weight/payload ratio role 13 p2189 A67-27499
 Hover augmentation system reducing VTOL pilot task in maintaining position by providing damping signals for automatic flight modes with accurate path control 14 p2246 A67-29082
 Optimum design safety for VTOL aircraft, noting noise and vibration elimination [AIAA PAPER 66-813] 15 p2419 A67-29411
 Commercial rotor VTOL for economic intercity transportation, discussing time-frame and design requirements and analyzing improvement factors [AIAA PAPER 67-410] 15 p2422 A67-30377
 VTOL aircraft with rotor or propeller lift systems for commercial transportation, discussing helicopter role in system development [AIAA PAPER 67-411] 15 p2422 A67-30378
 Bell Model 266 composite VTOL aircraft, discussing tilting rotor principle for conversion from helicopter to aircraft 16 p2595 A67-30495
 Compound aircraft flying quality improvement methods, noting VTOL characteristic and high speed as compared to pure helicopters [AHS PAPER 111] 16 p2598 A67-31827
 Turbotip lift fan concept for VTOL propulsion system, noting control capability, future potential, etc [AHS PAPER 115] 16 p2737 A67-31831
 Jet VTOL aircraft problems, considering vertical thrust/aircraft weight, thrust application to aircraft gravity center, stability in hovering, thrust exertion, etc 17 p2796 A67-32392
 VTOL and STOL aircraft comparison, discussing advantages and disadvantages of hinged and folding rotors, hinged wings, jet thrust and fan-in-wing principle 17 p2798 A67-32833
 Computer simulated flights of manual control for VTOL IFR operations indicate display and control subsystem deficiencies 17 p2808 A67-33183
 Controllability methods on VTOL transporters, developing model of pilot dynamic reaction to aircraft machinery 18 p2893 A67-33457

Optimal thrust-weight ratio for lifting engines of VTOL aircraft 18 p3110 A67-33544
 Exhaust gas recirculation for VTOL aircraft [AIAA PAPER 67-439] 18 p2985 A67-33916
 Parametric data on gas ingestion and ground proximity jet effects experienced by jet-powered VTOL configurations [AIAA PAPER 67-440] 18 p2985 A67-33917
 Circulation control rotor blades of circular or elliptical cross section for helicopters, VTOL and STOL and possible application to aircraft 18 p2987 A67-34707
 German VJ101C VTOL fighter aircraft design and testing, with description of engines and telemetric testing 19 p3173 A67-35522
 Bad weather landing of VTOL aircraft noting landing profiles, meteorological parameters and control system 20 p3361 A67-36455
 Control power usage for typical flight maneuvering in hover determined from flight test data of VJ-101 aircraft and of hover-rig with similar thrust-geometry and mass distribution 21 p3568 A67-38541
 Cost effectiveness of VTOL short range jet airlines, discussing significance of block time [AIAA PAPER 67-797] 21 p3568 A67-38543
 Civil high speed intercity VTOL aircraft using fan lift engines, discussing noise, installation, aerodynamics and thrust deflection [AIAA PAPER 67-745] 23 p4048 A67-40979
 Circulation control by blowing for gust insensitivity in stopped rotor aircraft application [AIAA PAPER 67-747] 23 p3933 A67-40981
 Design criteria for VTOL tactical aircraft power plant using turbojets for attack aircraft in support of land troops 23 p4049 A67-41044
 Spln characteristics of VJ 101 C VTOL airplane via numerical integration of motion equations including mass coupling effects and nonlinear aerodynamics 23 p3934 A67-41313
 Parametric investigation of propulsion system effect on takeoff weight of VTOL subsonic ground combat aircraft 23 p3934 A67-41315
 Performance and design parameters for VTOL fighter aircraft engine and wings, stressing takeoff weight factor 23 p3935 A67-41316
 VTOL aircraft configurations features and characteristics including helicopter, compound, composite, tilt-wing, lift-fan, lift/cruise and lift engine [SAE PAPER 670686] 24 p4093 A67-41987
 Hot cycle rotor/wing aircraft for high speed city-center transportation, estimating cost and performance [AIAA PAPER 67-770] 24 p4095 A67-42938
 Commercial VTOL airline system development through advanced helicopter application noting need for government sponsorship [AIAA PAPER 67-772] 24 p4095 A67-42940
 STOL and VTOL takeoff and landing areas, discussing urban and suburban air transportation and operational weather requirements [AIAA PAPER 67-795] 24 p4258 A67-42956
 All-weather flight requirements of VTOL aircraft, suggesting artificial stabilization by automatic control system [AIAA PAPER 67-798] 24 p4096 A67-42959
 Traffic prediction for high speed aircraft and surface vehicles and VTOL aircraft city-center to city-center transportation [AIAA PAPER 67-802] 24 p4259 A67-42962
 Commercial VTOL aircraft operating costs and cost reduction evaluation [AIAA PAPER 67-826] 24 p4096 A67-42973
 VTOL aircraft operational expense estimation using standard method, measuring maintenance costs in various planning stages and in operation [AIAA PAPER 67-828] 24 p4096 A67-42974
 Public and private financing of vertiports /VTOL aircraft terminals/ for intercity service, investigating financial self-supporting possibilities [AIAA PAPER 67-829] 24 p4259 A67-42975
 Short haul VTOL air transportation airport-community noise problem, examining propulsion systems and site planning [AIAA PAPER 67-867] 24 p4096 A67-42990
 Comparative projections of helicopters,

compound helicopters and tilting propotor
low-disk-loading VTOL aircraft for civil
applications 24 p4097 A67-43029
Rotor VTOL aircraft for future transport
noting rotor systems for low downwash
velocity, minimum noise and low fuel
consumption 24 p4097 A67-43030
[AIAA PAPER 67-940]
Commercial VTOL transport compared
with conventional aircraft and ground
transportation, discussing design and
operating costs 24 p4097 A67-43048
[AIAA PAPER 67-970]
V/STOL airbus transportation system
schedules, travel times and fares for
Northeast Corridor generated by computer
method 24 p4127 A67-43049
[AIAA PAPER 67-972]

VULCANIZATE

SA SYNTHETIC RUBBER

Torsional creep measurements on natural
rubber vulcanizates cross linked to various
degrees complement studies on stress
relaxation behavior and dynamic mechanical
response 06 p1020 A67-17869

VULNERABILITY

ILS as guidance component of all-weather
automatic landing system, discussing
operational need and specific
vulnerabilities 13 p2154 A67-26985

VZ-10 AIRCRAFT

S XV-4 AIRCRAFT

W

WAFER

Impurity concentration profiles in silicon
epitaxial wafer determined, using MOS
capacitors 05 p0866 A67-16985
Structure of wafer type point-contact
diodes 18 p3011 A67-34021
Microcircuit nondestructive IR inspection
and equipment used for mask
alignments 19 p3192 A67-35025

WAKE

SA AIRCRAFT WAKE
SA DOWNWASH
SA DRAG
SA HELICOPTER WAKE
SA HYPERSONIC WAKE
SA LAMINAR WAKE
SA SUPERSONIC WAKE
SA SWIRLING WAKE
SA TURBULENT WAKE

Vortex strength in wake of circular
cylinders and comparison of vortex velocity
distribution with that of Hoffman and
Joubert, using hot-wire anemometers at
various Reynolds numbers 01 p0005 A67-10256

Hot-wire probe measurement of friction
temperature and convection coefficient of
low pressure flows and wake of
cylinder 01 p0006 A67-10757

Instability and transition of wake behind
axisymmetric slender body with sound-
induced velocity fluctuation
amplification 02 p0177 A67-11560

Corresponding compressible and
incompressible jets and wakes in boundary
layer equations of turbulent and laminar
cases 03 p0350 A67-12988

Charged particle distribution in wake of
fast moving body in rarefied
plasma 05 p0855 A67-17123

Gas dynamics and geometry in mixing
zone of Freon 12, air and helium jets in
wake air flow, determining effect of jet
velocity, gas density, etc 06 p0982 A67-17743

Free and forced oscillation of disks and
right circular cylinders rotating in free
stream, noting turbulent wake
flow 06 p1101 A67-18136

Frequency effects in radar return from
turbulent weakly ionized missile wakes,
obtaining relationship between radar cross
section and electron density distribution
[AIAA PAPER 67-23] 06 p0963 A67-18258

Vortex periodicity in wakes as function of
Reynolds and Rossby numbers, solving
nonlinear viscous Navier-Stokes equations
[AIAA PAPER 67-34] 06 p0987 A67-18349

Criticism of Ivanov assumption regarding
IMP-I observation of lunar wake in solar
wind by magnetic field and plasma
measurements 07 p1243 A67-19829

Wakes behind axisymmetric blunt based
bodies, noting similarity among wakes
through measurements of velocity,
turbulence and static
pressure 08 p1277 A67-20706

Flow visualization technique study of wake
existence behind large air bubble rising
through quiescent liquid 08 p1321 A67-20712

Hydromagnetic wake around
nonconducting sphere moving in current
carrying fluid 08 p1324 A67-21410

Pressure measurements on surface and in
wake of circular cylinder at rest and in
vortex excited oscillation at subcritical
Reynolds numbers
[ASME PAPER 67-VIBR-31] 11 p1777 A67-24189

Loads on bodies in wakes resulting from
crossflow at submerged body or from wake
translation over submerged body, noting
dynamic instability 11 p1742 A67-24350

Linear aerodynamic theory of rotor blades
for predicting lift distribution, considering
wake vortex sheet 13 p2051 A67-27589

Numerical analysis of boundary layer
separation effect on evolution of wake,
noting sensitivity to initial velocity
profile 14 p2297 A67-28129

Wakes behind circular cylinders in free
molecule flow, noting inaccuracy in off-axis
impact pressure 14 p2300 A67-28175

Hypersonic decelerator deployment
investigated for interactions between
decelerator, connecting cable and wake of
forebody it tails 14 p2244 A67-29055

Testing conditions for near-wake study of
solids of revolution in supersonic and
hypersonic flow, using streamlined supports
in magnetic suspension 15 p2416 A67-29379

Flow velocity determination by cylindrical
magnifying probe, measuring stagnation and
wake pressures difference, noting
magnifying factor variation under Reynolds
number and stem and blockage
effects 15 p2471 A67-29529

Transverse magnetic field effect on
barrier wake oscillation in electrically
conducting liquid 16 p2723 A67-31714

Two-dimensional flow past bluff body,
comparing vortex street wake measurements
to von Karman
predictions 17 p2790 A67-32278

Steady state laminar and turbulent mixing
in unsteady isothermal flow in wake behind
body with incident shock
wave 18 p2984 A67-34203

Periodic spatial variations of parameters
of positive column plasma in magnetic field
along obstacle shadow due to electron
wakes 19 p3273 A67-35093

Flow analysis of compressible fluid in
wake behind body positioned symmetrically
with respect to flow direction, using
momentum and energy conservation
equations 19 p3170 A67-35610

Flow of incompressible viscous fluid past
plane body, when flow boundary layer
detaches from body producing aerodynamic
wake 19 p3171 A67-35632

Modifying effect of base bleed
investigated photographically for
incompressible wake behind two-dimensional
bluff body, estimating base
pressure 20 p3421 A67-36844

Charged particle distribution in wake of
fast moving body in rarefied
plasma 21 p3668 A67-38466

Diffusion flame shape in wake of falling
droplet taken as point source of fuel,
limiting analysis to Lewis and Prandtl
numbers unity 23 p4083 A67-41720

Reynolds number effect on slender high
speed cones wake-neck geometry, obtaining
measurements of location, diameter and
closure angle 23 p3932 A67-41754

Wakes in two-dimensional flows studied by
comparing mesoscale eddies in earth
atmosphere with Karman vortex street,
calculating wake
parameters 24 p4146 A67-41786

WAKEFULNESS
SA SLEEP DEPRIVATION

Evoked brain response to clicks as
measure of vigilance tested in work-rest
schedule and pressure suit-sleep
experiments on man 09 p1452 A67-21721

EEG baselines covering wide range of
states of wakefulness and sleep in astronaut
candidates estimated by computation and
pattern recognition 13 p2062 A67-26921

WALL
SA NOZZLE WALL

SA POROUS WALL

SA THIN WALL

SA WIND TUNNEL WALL

Principle of operation and static
performance data of fluoric AND gate, using
wall attachment principle 14 p2251 A67-28337

Physical and chemical wall effects on
mechanism of combustion reaction in gases
studied by introducing solids and measuring
ignition pressure 18 p3155 A67-33847

Shells and solid wall systems with/without
symmetrical cross section, considering
construction, stress-strain and calculation
procedures 21 p3722 A67-38524

WALL FLOW

Compressibility effects on rarefied gas
flow in Rayleigh problem, using BGK model
of Boltzmann equation 01 p0051 A67-10457

Knudsen layer in steady shear flow with
temperature gradient along infinite flat
wall 01 p0052 A67-10460

Heat transfer and distribution of velocity,
temperature and concentration in laminar
supersonic boundary layers with blowing of
light gas with desired pressure and heat
distribution 03 p0532 A67-12990

Aeromagnetic flutter of walls of plane
infinite channel with ionized gas
flow 03 p0524 A67-13503

Temperature and magnetic field gradient
effects on magnetothermomechanical
interaction of viscous incompressible
ferrofluid with cold wall 04 p0600 A67-14446

Solvability of parallel-wall cavitation flow
problem of perfect incompressible fluid past
symmetric smooth arc 04 p0606 A67-15195

Local heat-transfer coefficients between
isothermal flat plate and two-dimensional
wall jet 04 p0732 A67-15835

Heat transfer by array of two-dimensional
jets directed normal to surfaces including
effects of superposed wall-parallel
flow 04 p0732 A67-15836

Frozen layer that forms when warm liquid
flows over flat plate cooled below freezing
temperature of liquid by coolant flowing
along other side of plate 04 p0735 A67-15856

Differential equations for local interfacial
and wall shear stresses for one-dimensional
annular two-phase flow 04 p0735 A67-15857

Heat transfer for wall adjacent to region
of turbulent separated
flow 06 p0985 A67-18131

Wall profile construction of working zone
of flat MHD channel with ideal conductors
for both sides 06 p1044 A67-18691

Viscous incompressible slow flow over
circular arc wall projections or depressions
with shear flow far from
projection 06 p0992 A67-18887

Temperature variation in wall of square
channel due to heat transfer to turbulent
flow of water and Hg 07 p1265 A67-19126

Streamline matching technique for
V/STOL wind tunnel wall corrections
[AIAA PAPER 67-183] 07 p1163 A67-19439

Pressure amplitude at resonance
decreasing with increasing Mach number
observed as effect of mean flow on wall
damping of finite amplitude gas
pulsations 07 p1168 A67-19576

Steady state and switching characteristics
of OR/NOR and bistable wall attachment
elements 08 p1280 A67-20438

Jet deviation by curved convex wall and
Reynolds number explained as effect of
boundary layer separation 08 p1320 A67-20450

Similarity law for wall region of turbulent
boundary layers in compressible flow,
discussing Coles theory 08 p1320 A67-20565

Wall conductance effect on MHD flow
through finite cross section rectangular and
circular channels 08 p1356 A67-20572

Core and boundary layer flows in large
scale MHD generator, noting viscous friction
and heat transfer at walls 09 p1442 A67-21793

Wall friction coefficient measurement,
using scale incorporated into
wall 09 p1501 A67-22577

Wall law for thick turbulent boundary
layer with sublayer thickness compared to
radius of transverse curvature, analyzing
motion equations 10 p1629 A67-23847

Local heat transfer in water flow in
horizontal annular tube, estimating local
longitudinal and circumferential variations in
Nusselt number at tube wall as function of
Reynolds and Rayleigh
numbers 11 p1881 A67-24025

Integral relation technique for
approximate solution of dynamic and

thermal expansion of laminar radial slot gas jets along plane wall 11 p1779 A67-24322

Wall streamlines and detachment on circular cone at angle of incidence in supersonic flow 13 p2049 A67-26591

Unsteady ideal gas flow along moving wall treated by method of characteristics 13 p2093 A67-26635

Gas mixture component concentration in fluid film flowing down wall, determining quantity of gas component transported by fluid per unit time 13 p2094 A67-26638

Aeromagneto flutter of plane duct of finite length 13 p2218 A67-26805

Unsteady thermoelastic stress calculation in plane wall 13 p2219 A67-27059

Flight test skin temperatures of supersonic aircraft compared with theoretical results, explaining measurement discrepancies 14 p2243 A67-28977

Aerodynamic flow deflection over convex curved surface noting occurrence of hysteresis 14 p2305 A67-28978

Obstacle effect on turbulence intensity in boundary layer, discussing results of hot-wire anemometer measurements 15 p2471 A67-29651

Correlation measurement in two-dimensional zero pressure gradient boundary layer, noting velocity fluctuation patterns 15 p2471 A67-29652

Lateral convex curvature and helium surface injection effect on turbulent wall boundary layer characteristics and skin friction 16 p2659 A67-30952

Open-cycle gas generator as power supply source for MHD generators, noting reduction of wall effects 17 p2802 A67-32179

Wall-turbulence interaction for infinite flat plate inserted into homogeneous isotropic turbulence, measuring growth of inhomogeneity layer 17 p2837 A67-32286

Mean velocities, turbulence intensities, Reynold stresses and wall friction measurement in turbulent radial wall jet [ASME PAPER 67-APM-10] 17 p2838 A67-32419

Generalization of linearized equation of stationary waves in equilibrium gas dynamics applied to flow along two-dimensional sinusoidal wall 17 p2839 A67-32715

Law for velocity distribution through wall boundary layers derived from eddy viscosity model, considering turbulent shear variation and Reynolds number effect 17 p2839 A67-33008

Slip flow of incompressible viscous fluid past permeable infinite plate during fluid seepage into main homogeneous outer flow 18 p3023 A67-33419

Differential and boundary layer equations for free convection flow along vertical hot wall, investigating existence question 18 p3027 A67-34009

Concentration profiles in fixed laminar boundary layer with catalyst distribution on wall, discussing Schmidt number effect and approximations 18 p3159 A67-34161

Wall heat flux in turbulent air flow using inner law correlations for velocity and temperature 18 p3160 A67-34165

Velocity measurement in turbulent flow near smooth wall by hot-wire anemometer 18 p3027 A67-34184

Calibration and recording method for transmission coefficients of thermal wall heat flows, using ONERA wind tunnel [ONERA-TP-470] 18 p3020 A67-34463

Turbulent flow in circular duct, obtaining velocity distribution 20 p3419 A67-36276

Plane incompressible wall jet ejected from slot into boundary layer in case of stationary and nonstationary external flow with and without pressure increase 20 p3420 A67-36277

Test data for heat transfer in vortex flows in tubes with band type swirl generator, determining effect of mass inertial forces 20 p3544 A67-36449

Boundary layer theory applied to laminar flow with chemical reaction, considering coolant blown through porous wall and wall reaction with laminar boundary layer 20 p3424 A67-37345

Drag measurements for turbulent flow about circular cylinders joined to plane parallel walls, noting dependence on velocity profile 20 p3359 A67-37486

Laminar compressible boundary layer induced by plane shock wave passing over flat wall using empirical viscosity-

temperature relation for Prandtl number 21 p3611 A67-37928

Temperature variation in wall of square channel due to heat transfer to turbulent flow of water and Hg 21 p3731 A67-38170

Boundary conditions at wall for low density flow problems treated by kinetic theory, synthesizing relation between distribution functions of incident and reflected particles 21 p3614 A67-38861

Longitudinal wall curvature effect on boundary layer flow stability and generalization of Rayleigh theorems for nonviscous instability 23 p3992 A67-41733

High speed internal flow past cone with large wall injection velocities, calculating pressure of outer flow using contact surface initial slope as parameter 24 p4092 A67-42398

Nondisturbing turbulent flow measurements applied to viscous sublayer in smooth square pipe, showing linear velocity gradient in layer adjacent to wall 24 p4144 A67-42607

WALL JET

Radial momentum equation of flow outward from axisymmetric turbulent wall air jet impinging on solid surface 05 p0792 A67-16819

Pressure pulse and wall-to-jet heat transfer in discrete vortex zone of restrained gas jet in circular channel 06 p1118 A67-18550

Two-dimensional jet plane problem, considering rheological solution for applications to ground effect 11 p1781 A67-24571

Free plane jet compared with wall jet, noting more rapid lateral expansion of free jet 12 p1891 A67-25142

Two-velocity spatial correlation coefficients and lengths measured for wall jets 13 p2049 A67-26590

Laminar motion equation for conducting gas jet expansion along plane wall in presence of transverse magnetic field solved in series form 13 p2168 A67-27304

Upstream velocity profile effect on free mixing of jets with ambient fluid 14 p2240 A67-28107

Two-dimensional wall jet effectiveness measurements and calculation procedures for injection conditions 15 p2468 A67-29128

Hydrodynamic stability of plane incompressible viscous wall jet subjected to small disturbances, determining critical Reynolds number, eigenvalues and eigenfunctions 16 p2660 A67-31213

Wall jet compared to plane free jet examining equilibrium conditions of velocity profile of fluctuation and mean flow determining stress distributions 16 p2662 A67-31470

Mean velocities, turbulence intensities, Reynold stresses and wall friction measurement in turbulent radial wall jet [ASME PAPER 67-APM-10] 17 p2838 A67-32419

Plane incompressible wall jet ejected from slot into boundary layer in case of stationary and nonstationary external flow with and without pressure increase 20 p3420 A67-36277

Coanda effect shown to be caused by periodic system of vortices arising from nozzle edges 20 p3421 A67-36811

Diffusing plane turbulent free jet compared with correspondent wall jet velocity distribution and variation and length scales 20 p3360 A67-37492

Turbulent cylindrical wall jet flow field, velocity profile and surface friction coefficient noting transverse curvature effects 22 p3783 A67-39531

WALL PRESSURE

Internal wall pressure of obstacles in hypersonic wind tunnels with reflected shock waves measured by piezoelectric gauge system 01 p0005 A67-10259

Turbulent reattachment of supersonic jet noting recompression region of flow, critical points and similarity law in evolution of wall pressures [ONERA-TP-326] 01 p0053 A67-11002

Forced and periodic breakdown of confined vortex rotating in opposite direction, measuring flow rates and wall pressures [ASME PAPER 66-WA/FE-7] 04 p0611 A67-15928

Wall pressure distribution in turbulent reattachment bubble calculated by splitting

bubble into large number of small control volumes 08 p1320 A67-20451

Viscous flow around flat plate at various angles of incidences at high Mach number to evaluate shock wave intensity variation and wall pressure distribution 11 p1742 A67-24761

Statistical properties of wall pressure fluctuations in subsonic turbulent equilibrium boundary layer after transition from laminar flow 17 p2836 A67-32283

Coanda effect shown to be caused by periodic system of vortices arising from nozzle edges 20 p3421 A67-36811

Wall turbulent boundary layer pressure resolution by piezoelectric transducer, noting attenuation of frequency component with size and frequency dependence 20 p3422 A67-37002

Flow coefficient of various nozzles discharging into unbounded atmosphere for wall pressure distribution of potential rotational flow, using rheoelectric tank 23 p3989 A67-41140

Incidence angle effects on wall heat flux in symmetry plane of cone of revolution in hypersonic regime, discussing wall pressure measurements 24 p4092 A67-42660

WALL TEMPERATURE

Conductivity of plasma accelerated by progressive waves, noting wall thermal absorption effect on electron temperature [ONERA-TP-424] 02 p0279 A67-12794

Thermal creep in rarefied gas investigated using Boltzmann-Krook equation 03 p0402 A67-13359

Turbulent heat transfer in tube in conditions of axial symmetry, discussing variation of mean temperature of flow as function of axisymmetrical variation of wall temperature 03 p0535 A67-13395

Numerical solutions of equations of motion and energy for heating of non-Newtonian fluids in rectilinear axisymmetric laminar flow in circular tubes extended to case of cooling at constant tube-wall temperature 04 p0720 A67-14510

Wall temperature prediction for internal laminar heat transfer based on Graetz number 04 p0721 A67-14646

Variation of transition Reynolds number with wall to recovery temperature ratio at hypersonic speeds, comparing transition measurements with and without Pitot tube 04 p0604 A67-14836

Finite difference solution of parabolic equation for laminar heat transfer in inlet of rectangular duct as function of wall temperature and Nusselt number for different aspect ratios 04 p0728 A67-15805

Equilibrium temperatures of mass transfer cooled walls in high speed flow of absorbing-emitting gas 04 p0737 A67-15864

Turbulent heat transfer in circular tube with circumferentially varying wall temperature and wall heat flux [ASME PAPER 66-WA/HT-3] 04 p0738 A67-15929

Difference equations for heat transfer from liquid to solid and conductivity for solid applied to calculation of local temperatures within multilayer walls 06 p1113 A67-17990

Wall temperature effect on behavior of hypersonic stagnation region shock layer in incipient merged layer flow, obtaining enthalpy function profile 08 p1278 A67-20928

Steady state Leveque problem generalized to include time dependence, obtaining eight solutions for surface temperature 10 p1732 A67-22727

Absorption of thermal radiation from gaseous fuel by transparent wall of nuclear light bulb rocket engine [AIAA PAPER 66-619] 15 p2516 A67-29426

Wall radiation, temperature, pressure and electric field strength effects on electric conductivity, electron density and ionization time of nonequilibrium He-Ce plasma 16 p2709 A67-30515

Shock tunnel experiments with hypersonic turbulent boundary layer flow over flat plates with blunt and sharp leading edges and wall of expansion nozzle 16 p2659 A67-30954

Plane shock wave reflected from heat-conducting wall analyzed by method of matched asymptotic expansions 16 p2662 A67-31555

Nucleate boiling heat transfer correlations graphically estimated for design purposes to compute heat flux and wall

superheat 17 p2966 A67-32033
 Unsteady heat transfer in tube in presence of variable gas flow rate 17 p2967 A67-32129
 Unsteady heat transfer in tube during heat-flux fluctuations 17 p2967 A67-32130
 High vacuum enclosure problems solved by use of magnetic seal for joints of large valves and degassing by direct heating of wall surfaces 17 p2802 A67-32300
 Laminar boundary layer theory applied to heat transfer in low thrust rocket nozzles, checking with experimental wall temperature data [AIAA PAPER 67-447] 18 p3112 A67-33923
 Temperature difference between solid and gas of transpiration cooled wall due to radiant heating [ASME PAPER 67-HT-29] 20 p3546 A67-36722
 Transient mean wall temperature of flat plate with time dependent heat source and cooled by incompressible turbulent flow, discussing heat-transfer coefficient [ASME PAPER 67-HT-45] 20 p3547 A67-36727
 Energy equation for laminar convective heat transfer in combined hydrodynamic and thermal entrance region bound by parallel flat plates [ASME PAPER 67-HT-48] 20 p3548 A67-36730
 Transient heat transfer through monatomic collisionless ideal gas enclosed between parallel walls analyzed for step change in one wall temperature [ASME PAPER 67-HT-53] 20 p3548 A67-36735
 Size and longitudinal conduction influence on wall temperature field and effectiveness of heat exchangers determined by differential equations [ASME PAPER 67-HT-80] 20 p3551 A67-36758
 Shock tube measurements of end-wall radiative heat transfer behind reflected shock waves in air, stressing radiative cooling and self-absorption effects [AIAA PAPER 67-695] 21 p3732 A67-38724
 Infinite horizontal fluid layer heated from below /classical Rayleigh thermal stability problem/ extended to fluid in rigid sphere heated nonuniformly 22 p3918 A67-39715
 Similarity solutions for compressible laminar boundary layer, showing pressure and heat and mass transfer effects on wall temperature and shear stress 22 p3918 A67-39716
 Zonal method of determining radiative heat transfer between gray particle cloud and surrounding gray walls of enclosing system 24 p4253 A67-42252

WALL TEMPERATURE DISTRIBUTION

Laminar boundary layer on flat plate at high Prandtl number, obtaining temperature profile, recovery factor and heat transfer 01 p0052 A67-10795
 Thermal emittance and reflectance of diffuse-bottomed specular-walled groove in solar radiant-flux environment [AIAA PAPER 66-459] 02 p0342 A67-11939
 Stabilizing effect of wall and thermal flux temperature variations over channel length on heat transfer coefficient of liquid flow 03 p0536 A67-13610
 Variable laminar boundary layer equations for air flows over flat plate with injection of foreign gases through solid surface 06 p1116 A67-18380
 Stabilizing effect of wall and thermal flux temperature variations over channel length on heat transfer coefficient of liquid flow 18 p3161 A67-34475
 Heat transfer in steady flow of non-Newtonian fluid between two walls with periodic deformation considered, using perturbation method 18 p3161 A67-34616
 Wall temperature distribution effect on transport coefficients determination from arc plasmas 19 p3280 A67-35144
 Heat transfer experiments with flat plate heated under constant heat flux, discussing wall temperature distribution, Prandtl number and Spalding function 22 p3918 A67-40041

WANKEL ENGINE

Gas turbines, regenerators, Wankel engine and Stirling engines, examining problem areas [AICE PREPRINT 45A] 04 p0691 A67-15944

WAR GAME

Binomial probability distribution applied to air battle analysis, discussing fire doctrines, attrition rates, weapon design classes and limitations of approach [AIAA PAPER 66-781] 01 p0169 A67-10527

WARFARE

Utility aircraft costs lower than specialized aircraft in meeting mixed mission requirements in counterinsurgency environment, considering changes, uncertainty and logistics 22 p3745 A67-39618

WARMING

Evidence regarding possibility of midwinter stratospheric warmings in Southern Hemisphere 17 p2880 A67-32553

WARNING DEVICE

SA COLLISION WARNING DEVICE
 Hypoxia warning systems, discussing spurious warning avoidance and mask mounted sensor 23 p3968 A67-41629

WARNING SYSTEM

S EARLY WARNING SYSTEM

WASHOUT

Vertical distribution of cloud condensation nuclei in free atmosphere investigated by flow type onboard photoelectric apparatus to calculate washout coefficients 24 p4181 A67-42163

WASTE

S HUMAN WASTE

S LEAKAGE

S METABOLIC WASTE

S RADIOACTIVE WASTE

WASTE DISPOSAL

Spacecraft life support systems should ensure radiation protection, food, power supply, waste removal, etc 13 p2061 A67-26753

Electrochemical generator concept noting compactness, adaptability, methods of adding active agents, evacuation of reaction products and decarbonation 14 p2253 A67-29020

Fecal waste management unit for life support simulator or aerospace flights [SAE PAPER 670852] 24 p4115 A67-42001

WASTE UTILIZATION

Mineralization of human solid and liquid wastes by methods of thermal and thermocatalytic oxidation for autotrophic and heterotrophic organism use 02 p0187 A67-12326

Food, water and oxygen regeneration and reclamation techniques for long duration space flights, considering carbon dioxide removal, water reclamation from urine and contamination control 22 p3755 A67-40340

Open cycle air evaporation urine processing system recovering potable water in space cabin simulator, discussing wick evaporator 23 p3969 A67-41631

WATER

SA BODY FLUID

SA ICE

SA OVER-WATER FLIGHT

SA POTABLE WATER

SA SEA WATER

Far IR absorption and dielectric constant of liquid water 01 p0115 A67-11082

Transducer measuring water quantity in water storage tanks of LEM under zero g conditions 01 p0073 A67-11114

Dissociation pressures of mixed gas hydrates predicted from data for hydrates of methane, propane and nitrogen with water 02 p0190 A67-12234

Incidence, growth and detachment of boiling bubbles in saturated distilled water from artificial nucleation sites of given geometry and size in heated metal surface 04 p0734 A67-15847

Equilibrium concentrations for air water plasma at various temperatures tabulated for three densities, noting effect on electron concentration 05 p0850 A67-16131

Role of solar photon and corpuscular radiation in dissociation and ionization of water molecules in cometary atmospheres 05 p0888 A67-16203

Engine-oil-operated water/methanol system provides boosted takeoff power and maintains takeoff power at elevated temperatures 05 p0873 A67-16233

Temperature variation in wall of square channel due to heat transfer to turbulent flow of water and Hg 07 p1265 A67-19126

Device for measuring potential fluctuations in turbulent flow of distilled water 09 p1501 A67-22562

Effect of axisymmetric impact against water on shallow clamped aluminum spherical shell-type caps 12 p2030 A67-25937

Acoustic measurement method for following motion of solid-liquid interface, obtaining solution for transient heat conduction problem 12 p1946 A67-25985

Extraterrestrial life detection based on

catalysis of oxygen exchange between labeled oxyanions and water, noting equipment 15 p2426 A67-29113

GE T64 engine operation on emulsified fuel /JD1/, noting corrosion effects on fuel system components due to water additive [SAE PAPER 670369] 17 p2927 A67-33002

Economics related to practical extraction of logistics and water from moon, nearby planets and asteroids 19 p3327 A67-35652

Reflection in water of plane shock waves from rigid wall 21 p3611 A67-38058

Temperature variation in wall of square channel due to heat transfer to turbulent flow of water and Hg 21 p3731 A67-38170

Spectral reflectance of water and carbon dioxide cryodeposits in vacuum integrating sphere as function of incidence angle, substrate material and cryodeposit thickness 24 p4253 A67-42046

WATER BALANCE

Centrifugal force field with rotation or static impingement separation for water handling in absence of gravity 01 p0017 A67-10958

Polydipsia elicited by synergistic action of saccharin and glucose solution 24 p4113 A67-42099

WATER CONTENT

Quantitative estimation of liquid water content on Mars from thickness of snow blanket on planet polar cap 06 p1084 A67-18167

Martian transient phenomena correlations among mass motion of water in atmosphere, polar cap growth and white cloud appearance frequency 11 p1862 A67-24501

Crystallization of boric anhydride obtained only through maintaining high water content in reactive agent during thermal treatment 13 p2143 A67-26812

Low barometric pressure, high carbon dioxide concentration and water availability on simulated Mars environment related to survival and growth of bacillus cereus 15 p2426 A67-29111

Quantitative estimation of liquid water content on Mars from thickness of snow blanket on planet polar cap 16 p2742 A67-30511

Upper limits on liquid water content in Venus atmosphere 17 p2945 A67-32652

Microbial numbers relation to phosphatase activity in soil, discussing seasonal variation, sterilization by irradiation and moisture content 18 p2991 A67-33660

Manned spacecraft water supply microbial contamination detection using firefly bioluminescent reaction 23 p3968 A67-41627

WATER DEPRIVATION

S DEHYDRATION

WATER FLOW

Reynolds number and incidence angle effects on inducer cavitation in water [ASME PAPER 66-WA/FE-31] 04 p0607 A67-15363

Local heat transfer in water flow in horizontal annular tube, estimating local longitudinal and circumferential variations in Nusselt number at tube wall as function of Reynolds and Rayleigh numbers 11 p1881 A67-24025

Convective heat transfer for water flow in curvilinear short channel, noting flow and convection types at various sections 12 p2033 A67-25316

Laminar boundary layer flow of water over flat plates, noting heat transfer effects on velocity profile stability [ASME PAPER 67-HT-41] 20 p3547 A67-36725

Free convection effect on forced laminar flow of water in horizontal tube with uniform heat flux and velocity profile fully developed [ASME PAPER 67-HT-52] 20 p3548 A67-36734

WATER INJECTION

Water injection for alleviating reentry plasma sheath-induced communication blackout, analyzing spherical drop evaporation in free molecular flow 19 p3211 A67-35762

WATER INTAKE

Indigenous biology in Venus clouds, proposing isopycnic float bladder macroorganism ingesting water and minerals blown up from surface by pinocytosis 22 p3750 A67-39556

WATER JET

Disruption of water jet into large drops studied by photography 04 p0609 A67-15591

WATER LANDING

Model tests for determination of structural response of Apollo Command Module to water impact 07 p1257 A67-19368
Fatal injuries resulting from extreme water impact studied from necropsy data on persons jumping from Golden Gate Bridge 21 p3573 A67-38069

WATER LOSS

Urine composition in twelve dehydrated subjects in periods of activity, water immersion and reclining in deck chair [SAM-TR-66-305] 09 p1453 A67-21730
Heat stress, skin and rectal temperatures, heat gain and water losses in Army pilots flying combat missions in Mohawk OV-1 aircraft in Vietnam 22 p3750 A67-39595
Water deficit effects on thermal sweating, noting extraneous effects due to higher body temperature and wet 24 p4110 A67-41781
Na and water excretion, renal plasma flow and glomerular filtration rate lowered by lower body negative pressure /LBNP/, noting application to space flight [SAM-TR-65-329] 24 p4110 A67-41801

WATER MODERATED REACTOR

Control of water moderated nuclear reactor using neutron absorbing helium 3 gas control elements 04 p0656 A67-15989

WATER PRESSURE

Wind tunnel ejector and hot water supply for ramjet power plant attitude test stand, noting synchronization of ejector with test section 17 p2834 A67-32817
Sensitivity of explosives to shock waves tested by device using water as intermediate layer 22 p3866 A67-39489

WATER PURIFICATION

Chemical, physical, microbiological and radiological standards of aerospace system water potability 23 p3968 A67-41620

WATER RECOVERY

Centrifugal force field with rotation or static impingement separation for water handling in absence of gravity 01 p0017 A67-10958
Aerojet Carbothermal Process for oxygen manufacture from lunar resources, discussing experimental results from research operations 08 p1316 A67-21092
Lunar water sources, considering hydrous minerals, cold trapped volatile products of volcanic origin and dispersed hydrates 08 p1317 A67-21093
Solar energy role in lunar water production, evaluating efficiency of collector-absorber systems 08 p1317 A67-21094
Biological problems in prolonged space voyages including oxygen replacement, water supply and food regeneration 19 p3179 A67-35209
Sensory discrimination, psychological and preference factors toward water reclaimed from urine, discussing identification from tap and distilled water, temperature and smoking effects 22 p3751 A67-39597
Food, water and oxygen regeneration and reclamation techniques for long duration space flights, considering carbon dioxide removal, water reclamation from urine and contamination control 22 p3755 A67-40340
Open cycle air evaporation urine processing system recovering potable water in space cabin simulator, discussing wick evaporator 23 p3969 A67-41631
Continuous culture system for Hydrogenomonas bacteria in waste management of life support system [SAE PAPER 670854] 24 p4115 A67-42002
Potential benefits of lunar resources, discussing water deposits location, mining and processing [AIAA PAPER 67-876] 24 p4238 A67-42996

WATER TUNNEL

Water tunnel investigation of unsteady partial, full and supercavitation in cascade flow, determining force coefficients [ASME PAPER 66-WA/FE-25] 04 p0607 A67-15355
Force measurements and visual observations made in water tunnel on fully wetted and ventilated flows past family of conical ring wing hydrofoils having flat plate section geometry [ASME PAPER 66-WA/UNT-4] 04 p0608 A67-15383
Decay of mean, variance and gradient variance of temperature and velocity

measured in initially heated wake of sphere in water tunnel [AIAA PAPER 67-20] 06 p0987 A67-18347
Vortex flow about wings, fins and fuselages of slender aircraft and missiles analyzed using small water tunnel 15 p2465 A67-29399
Adhesives for bonding overlay materials to substrates for high speed hydrofoils, describing water tunnel and rotating arm tests 21 p3632 A67-38131

WATER VAPOR

SA HUMIDITY

Airborne double bolometer technique for deriving atmospheric water vapor profiles by solving radiative transfer equations 01 p0108 A67-10315
Total emissivity and upper limit of hot water vapor determined from IR spectral emissivity 01 p0187 A67-10973
Electromagnetic radiation absorption coefficient of atmospheric water vapor in long-wave portion of submillimeter range 02 p0190 A67-11568
Water vapor lines in spectrum of Venus obtained by photoelectric scanning of spectrum 02 p0324 A67-11769
Spectral distribution of net radiance at boundary of nonisothermal gas applied to water vapor band 02 p0342 A67-12051
Atmospheric water vapor distribution estimated from satellite measurements, using Planck radiance and assuming temperature distribution to be given 02 p0239 A67-12364
Thermal atmospheric sounding, discussing carbon dioxide transmission function parameters, water vapor and temperature effect 02 p0239 A67-12377
Barometric pressure coefficient, correcting terrestrial neutron monitor intensities, dependency on magnitude variations related to changes of atmospheric water vapor content 03 p0505 A67-12958
Width of spectral absorption line of water vapor at lambda equals 0.92 mm measured with aid of monochromatic radiation source and radiometer with thermal indicator 05 p0761 A67-16342
Atmospheric radio wave absorption at wavelengths ranging from 1.36 to 3.0 mm, determining absorption coefficients of molecular oxygen and water vapor 05 p0761 A67-16343
Microradiowave absorption in air by water vapor dimers 06 p0963 A67-18206
Frost phenomena on Mars examined on basis of Martian wave of darkening, noting necessity of deliquescent salts to attract and retain water on surface 06 p1089 A67-18645
Extreme IR atmospheric absorption calculation shown in graphs and compared with available results in submillimeter and millimeter range 06 p0998 A67-18717
Water vapor mass below upper limit of earth cloud cover estimated through earth brightness measurements 07 p1183 A67-20006
Time behavior of pulsed water vapor laser, noting spiking from far IR emission lines 07 p1197 A67-20095
High dispersion spectrograms of Mars examined for water vapor presence, results indicate amount depends on size of polar cap [JPL-TR-32-1048] 09 p1566 A67-22235
Radiation data measured by Tiros IV satellite for determination of global distribution of atmospheric water vapor 10 p1677 A67-23195
Mesosphere ice point temperature, atomic oxygen concentration and total density measurement with heat recorder 10 p1656 A67-23207
Cloud formation theory based on aircraft observations of low cloud layers, considering turbulent vapor and heat redistribution in layer 10 p1677 A67-23408
Power output at 119 micron in water vapor laser, noting inhibition of laser action during discharge current pulse 11 p1801 A67-24728
Prediction of total emissivity of nitrogen-broadened and self-broadened hot water vapor 13 p2155 A67-26493
Water-vapor rotational band transmission function calculations by atmospheric inhomogeneity approximate methods 13 p2151 A67-26682
Submillimeter-wave measurements for water-vapor detection from jet aircraft flying in stratosphere 13 p2114 A67-26795

Competitive and cascade coupling between transitions in CW water vapor laser 14 p2331 A67-28498
Single frequency, far IR and high power gas laser design and manufacturing 14 p2333 A67-28970
Vapor cured resins for aerospace applications 15 p2506 A67-29544
Water vapor and atomic oxygen concentration in mesosphere measured by meteorological rocket 16 p2665 A67-31097
High intensity electric field used to freeze out large quantity of droplets from supercooled artificial fog 16 p2699 A67-31717
Tropospheric water vapor analysis via Tiros IV satellite, determining spatial and temporal temperature, humidity and mass variations 17 p2880 A67-32550
Microradiowave absorption in air by water vapor dimers 17 p2817 A67-33219
Permafrost layer existence beneath lunar surface, noting possible detection techniques 17 p2952 A67-33250
Ignition kinetics of carbon monoxide-oxygen reaction 18 p3155 A67-33846
Absorption coefficients of radiation by water vapor and aerosols determined from atmospheric counter radiation 19 p3251 A67-34858
Water adsorption on oxide covered surface of germanium, studying chemisorption dependence on p-type doping 19 p3301 A67-34935
Density, temperature, water vapor and atomic oxygen concentration in mesosphere measured by heat method 19 p3216 A67-35183
Prebiotic synthesis of monocarboxylic acids suggested from mixture of methane and water exposed to semicorona discharge 19 p3181 A67-35882
High resolution far IR lamellar grating interferometer with double beam differencing 20 p3438 A67-36347
Relative velocity effect on vaporization times and heat-transfer coefficients of water drops in Laiden frost film boiling on heated rotating wheel [AICHE PAPER 32] 20 p3552 A67-36833
Nonthermal radio emission from electric discharges within Venus water clouds 20 p3529 A67-37480
Radiative heat transfer in nonisothermal nongray gas model, measuring absorption and emission in carbon dioxide and water gases [ASME PAPER 66-WA/HT-25] 20 p3555 A67-37607
Amplitude distributions of refractive index differences showing spikes superimposed on variations continuum due to water vapor clustering 21 p3617 A67-38187
Far IR maser oscillators with water and deuterium oxide, presenting construction and operating characteristics 21 p3639 A67-38253
Atmospheric ground layer water vapor absorption of 183.31 GHz electromagnetic wave 22 p3759 A67-39506
Precursor IR resonance radiation from hypervelocity ablating vehicles observed and related to photon absorption and water vapor presence in air 22 p3917 A67-39712
Attenuation of continuous and pulsed laser emission studied for various thicknesses of artificial water fog 22 p3816 A67-39921
Carbon dioxide and water vapor band emissivities determination, discussing spectral absorption, radiative heat transfer and energy distribution 22 p3918 A67-40042
Attenuation of plane sinusoidal acoustic waves due to electromagnetic radiative properties of carbon dioxide and water vapor bands 22 p3829 A67-40232
Earth atmosphere humidity profiles and cloud densities interpreted from 1 cm microwave absorption measurement, water vapor resonance and radiosonde measurement 22 p3806 A67-40359
Pulsed water vapor laser single wavelength operation using three diffraction gratings to make resonator frequency-selective 23 p4011 A67-40783
Mass spectrometric analysis of electrolyte degradation during electrolysis in sulfuric acid silica gel cell for oxygen recovery 23 p3970 A67-41705
Effective temperature for late type stars with or without water vapor opacity calculated for several masses, determining convective energy transport efficiency 24 p4224 A67-41818

WATER VEHICLE

Hot-water rocket design by dimensionless method, noting GRILLO rockets 15 p2567 A67-29840

WATERPROOFING

Adhesives for aircrafts and spacecrafts considering high temperature resistivity, waterproofing and brittleness 16 p2683 A67-31788
Adhesive and water resistance properties of epoxy resin for bonding tensometers and underwater sealing 21 p3650 A67-38919

WATTMETER

Noise injection and coherent detection to extend RF attenuation measurement range of series IF substitution 09 p1495 A67-21623
RF power meter design having coaxial thin film thermocouple in-line detector to sample incident power 21 p3589 A67-37916

WAVE

S ALFVEN WAVE
S BACKWARD WAVE
S BAROCLINIC WAVE
S BOW WAVE
S CAPILLARY WAVE
S COMBUSTION WAVE
S COMPRESSION WAVE
S CONTINUOUS WAVE
S CYLINDRICAL WAVE
S DETONATION WAVE
S DIFFUSION WAVE
S DILATATIONAL WAVE
S ELASTIC WAVE
S ELECTROACOUSTIC WAVE
S ELECTROMAGNETIC WAVE
S ELECTROSTATIC WAVE
S EXPANSION WAVE
S GRAVITY WAVE
S GROUND WAVE
S H-WAVE
S IONIC WAVE
S LEE WAVE
S LOADING WAVE
S LONGITUDINAL WAVE
S MAGNETOACOUSTIC WAVE
S MAGNETOELASTIC WAVE
S MAGNETOHYDRODYNAMIC WAVE
S MICROWAVE
S MILLIMETER WAVE
S MODULATED CONTINUOUS WAVE
S PLANE WAVE
S PLASMA WAVE
S PRESSURE WAVE
S RADIO WAVE
S RAREFACTION WAVE
S RAYLEIGH WAVE
S REFLECTED WAVE
S S-WAVE
S SEISMIC WAVE
S SHOCK WAVE
S SINE WAVE
S SKY WAVE
S SOUND WAVE
S SPHERICAL WAVE
S SPIN WAVE
S STANDING WAVE
S STRESS WAVE
S SUBMILLIMETER WAVE
S SURFACE WAVE
S TOLLMEIN-SCHLICHTING WAVE
S TRANSVERSE WAVE
S TRAVELING WAVE
S TROPOSPHERIC WAVE
S ULTRASONIC WAVE
S UNLOADING WAVE

WAVE ATTENUATION

SA ACOUSTIC ATTENUATION
SA MICROWAVE ATTENUATION
SA RADIO ATTENUATION
SA SHOCK WAVE ATTENUATION
Cerenkov and cyclotron absorption of Alfvén and fast magnetoacoustic waves in plasma with gas-kinetic pressure in quasi-linear approximation 01 p0124 A67-10747
Cylindrical resonator for high precision measurements of sound absorption in oxygen 01 p0067 A67-10838
Quasi-linear approximation of Cerenkov and cyclotron damping of electromagnetic waves in magnetoactive plasma, considering collisions of wave-absorbing resonance particles with plasma 03 p0475 A67-12934
Time harmonic Rayleigh wave attenuation in elastic half-space by surface impedance 03 p0371 A67-13945
Damping and phase characteristics of gas-filled metallic waveguides near cut-off frequency, noting ammonium case 04 p0576 A67-15656
Shock wave attenuation in shock tube in

Mach 4 to 7 range, noting equipment used and results 05 p0791 A67-16433

Deformation of Fraunhofer line linked to sound waves in solar disk 05 p0900 A67-17078

Attenuation and coupling impedance of backward dipole surface wave on cylindrical plasma column with reference to oscillator design 09 p1546 A67-22281

Transmission and reflection coefficients in coupling of transverse and longitudinal waves below second electron cyclotron harmonic 09 p1548 A67-22383

Acoustic waves amplification in CdS crystal by electron-phonon interaction 09 p1558 A67-22591

Galactic radio noise intensity decrease correlated with decline in solar activity, calculating D and F region absorption 11 p1784 A67-23934

Received signal degradation for coherent pulse transmission through rain scattering volume, calculating length and energy for various paths 11 p1752 A67-24285

Highly ionized plasma with excitation and damping of density and temperature drift waves in stable regime 11 p1835 A67-24382

Cosmic radio wave absorption dependence on frequency and number of electron-ion collisions during atmospheric magnetic storms 12 p1933 A67-25548

Harmonic ion cyclotron wave propagation and attenuation investigated experimentally 13 p2183 A67-26287

Attenuating electron waves in crystals corresponding to energy values in forbidden band used in calculating current across n-p junction 13 p2172 A67-26354

Cerenkov and cyclotron absorption of Alfvén and fast magnetoacoustic waves in plasma with gas-kinetic pressure in quasi-linear approximation 13 p2166 A67-26776

Two-phonon absorption in ultrasonic paramagnetic resonance of uranium-doped calcium fluoride, relating wave attenuation to ultrasonic intensity and magnetic field angular variation 14 p2365 A67-28295

Millimeter wave attenuation measurement in rain using low height antennas 14 p2274 A67-28923

Acoustic wave attenuation coefficients for small gap superconductors, noting electromagnetic absorption and collisional drag as cause 16 p2729 A67-31059

Path diversity in millimeter waves propagation through rain for various frequency 16 p2825 A67-31343

Transient plane wave magnetic field attenuation through semiinfinite plate using simplified Laplace transfer function, noting infinite product form for LPTF 16 p2828 A67-31349

Attenuation characteristics of longitudinal wave propagating in weakly inhomogeneous plasma, deriving expression for oscillations damping constant 16 p2828 A67-31498

Numerical analysis of ionospheric radio wave propagation, examining, attenuation polarization and power flow as function of electron density profiles 16 p2831 A67-31857

Attenuation of natural hydromagnetic waves ω_{ce}/ω in ionosphere, noting amplitude reduction and particle distribution in magnetosphere 17 p2843 A67-32536

Torsional Alfvén waves attenuation in decaying hydrogenous plasma 19 p3290 A67-35377

Phase velocity and attenuation of ionic plasma waves in weakly ionized gases measured in absence and presence of external magnetic fields 19 p3290 A67-35378

Phase velocity and attenuation of audiofrequency electromagnetic waves to derive electron density profiles 20 p3426 A67-36288

Bouguer law applicability for describing narrow collimated light beams attenuation in scattering media in terms of optical thickness 20 p3462 A67-37866

Growth and attenuation of acceleration waves and higher order waves derived from nonlinear fluid theory with internal state variables 21 p3610 A67-37739

Approximate method for calculating electromagnetic field structure of vertical antenna 21 p3590 A67-38118

Earth finite conductivity effect on directivity patterns of vertical antennas taking into account attenuation factor 21 p3590 A67-38119

Attenuation function of surface wave propagating over spherical earth having

surface layers with different electric impedances, studying interaction with space wave 21 p3580 A67-38122

Attenuating electron waves in crystals corresponding to energy values in forbidden band used in calculating current across n-p junction 21 p3679 A67-38311

Neutral and charged particle trapping using waves, discussing wave attenuation from particle interaction, plasma waveguide and laser beam trapping 23 p4017 A67-41681

WAVE DETECTION

Gravitational radiation measurements by HF gravitational wave detector 10 p1652 A67-23545

Optical communication experiments to compare coherent and noncoherent optical detection fading characteristics in different weather conditions, using laser transmitter and optical superheterodyne receiver 19 p3184 A67-35685

Real-time electrooptical spectrum analyzers with coherent detection 19 p3197 A67-35687

Tunnel diode low level detection characteristics under various bias conditions, discussing sensitivity performance and stability characteristics 24 p4131 A67-42444

WAVE DIFFRACTION

Mie scattering and plane wave diffraction theory for small angle light dispersion from sphere 01 p0112 A67-10131

Diffraction of plane plasma wave in rectangular dielectric wedge, considering cases of E-wave and H-wave 01 p0020 A67-10139

Interferences between waves diffracted by circular screens or thin wires and coherent background provided by laser, producing rings or rectilinear fringes 01 p0087 A67-10231

Operational notation characterizing basic optical elements as block diagrams gives results identical to those of Fresnel-Kirchhoff diffraction formula 01 p0028 A67-10433

Slow decay of solution of initial boundary value problem for wave equation in exterior of three-dimensional smooth star-shaped body 01 p0052 A67-10519

Diffraction of elastic waves in formulation of Young, including form of tensor potential for longitudinal waves 01 p0114 A67-10868

Propagation constant derived for electromagnetic waves propagating along array of parallel thin wires located in plane dielectric layer 02 p0192 A67-11642

Spherical diffraction solution obtained by reducing it to solution of diffraction problem for circular cylinder via coordinate transformation 02 p0205 A67-12529

Mitra three-receiver method improvement for measuring winds and diffraction of radioelectric waves in ionosphere 03 p0406 A67-12819

Spaced antenna technique for determining drift and anisotropy of equatorial E and F region irregularities 03 p0407 A67-12833

Multimode surface wave diffraction phenomenological theory extended to right-angled wedge configuration [NYU-EM-213] 03 p0369 A67-13660

Diffraction of plane wave at sinusoidally stratified dielectric grating, using hologram analysis 03 p0423 A67-13905

Plane electromagnetic wave diffraction at two parallel circular cylinders for TM and TE polarization 03 p0371 A67-13959

Interferences between coherent light background and light diffracted by small aperture in case of strongly astigmatic beam 04 p0631 A67-14416

Diffraction of plane harmonic horizontally polarized shear waves by parabolic cylinder, obtaining dynamic shear-stress concentration for parabolic notch and rigid parabolic insert [ASME PAPER 66-WA/APM-13] 04 p0713 A67-15405

Diffraction of plane harmonic polarized shear waves by half-plane crack extending under antiplane strain [ASME PAPER 66-WA/APM-18] 04 p0714 A67-15409

Density effect on Sommerfeld diffraction problem 04 p0715 A67-15583

Wave diffraction in rectangular waveguides passing through double ribbon barriers 05 p0775 A67-16956

Reduction of problems of diffraction of scalar and vector waves at open curvilinear screen to integral equations of second

kind 05 p0765 A67-17157

Surface impedance of nonhomogeneous plasma with sharply varying parameters, noting skin effect and permittivity gradient 05 p0766 A67-17231

Diffraction based criteria use for image quality in automatic optical design, reviewing aberration tolerance 06 p1030 A67-17573

Wave diffraction on surface impedance discontinuity in coaxial waveguide 06 p0968 A67-17856

Diffraction of angular spectrum of radio waves by phase changing screen 06 p0962 A67-17969

Short wave asymptotics of diffraction field at sphere for incident plane transverse waves 06 p1100 A67-18032

Sound diffraction by semilfinite elastic plate in moving medium 06 p1032 A67-18398

Electromagnetic diffraction at aperture, comparing three theories for case of partial polarized incident field 06 p1033 A67-18541

Multiple beam interference in opaque photocathodes, determining intensity function via multiplication of amplitude by complex conjugate 07 p1185 A67-19407

Electromagnetic plane wave diffraction on anisotropically conducting plane and shielding and reflecting activity of dense radial grating 07 p1143 A67-19589

Electromagnetic wave diffraction problems solved by two-dimensional Laplace transforms 07 p1147 A67-20298

Diffraction of plane longitudinal wave in interior of elastic solid, where wave is harmonic in time and impinging on surface of penny shaped crack 09 p1573 A67-21663

Electromagnetic wave diffraction on perfectly black screen in Kottler theory 09 p1464 A67-22054

Hologram copies by recording interference pattern between undiffracted and diffracted waves 10 p1654 A67-22754

Bispectral analysis of electromagnetic wave diffraction by ionosphere, obtaining information on altitude and scale of irregularities 10 p1604 A67-22888

Statistical properties of dispersive waves in upper atmosphere analyzed, using correlation technique 10 p1639 A67-23206

Irregular refraction of plane shock wave by hot gas wedge, analyzing relation to Mach number values 11 p1775 A67-23878

Electron plasma frequency instability, correlating coherent deceleration of electron beam with compression of interference pattern 11 p1827 A67-23890

Elastic wave diffraction around elliptical hole in thin plate, obtaining dynamic stress concentration coefficient through approximate solution 11 p1870 A67-23897

Diffraction of plane electromagnetic wave from ideally conducting ellipsoid of revolution 11 p1751 A67-23915

Plane electromagnetic wave diffraction by conducting half-plane embedded in uniaxial anisotropic medium 11 p1753 A67-24315

Electromagnetic wave diffraction on plasma cylinders calculated using wave equation and geometrical optics approximation 12 p1969 A67-25246

Shock wave diffraction and reflection problems on faces of angle situated in nonstationary gas flow 12 p1928 A67-25672

Light diffraction by elastic waves in YIG noting values of photoelastic tensor components 12 p1984 A67-25746

Deformed laser resonator mode, studying diffraction losses, amplitude and phase distribution during pumping pulse 13 p2127 A67-27087

Intensity fluctuations of waves diffracted by deeply modulated random phase screen 13 p2071 A67-27403

Data processing of signal reception from Soviet satellites indicates radio signals scintillation caused by diffraction of waves from ionospheric nonuniformities 14 p2280 A67-27857

Spherical diffraction solution obtained by reducing it to solution of diffraction problem for circular cylinder via coordinate transformation 14 p2261 A67-28006

Diffraction field parts of slit aperture formed by two nonplanar screens satisfy variational principle 14 p2261 A67-28106

General formulation and solution methods of electromagnetic wave diffraction and scattering problems 14 p2268 A67-28448

Slit width effect on accuracy of equivalent

width measurements, noting results with 10 angstrom/mm plates 14 p2319 A67-28591

Book on problems of optics covering emission, absorption, diffraction, dispersion, etc 14 p2349 A67-29006

Transition functions occurring in diffraction theory of plane stratified medium with increasing refractive index 14 p2349 A67-29063

Electromagnetic wave diffraction by infinite set of parallel metallic plates, obtaining exact solution by Wiener-Hopf technique 15 p2435 A67-29191

Diffraction of HF radio waves by ionospheric layer containing field-aligned inhomogeneities [AGARDOGRAPH 95] 15 p2482 A67-30291

Temperature distribution field of flame studied by applying holographic techniques in obtaining interferogram of inhomogeneity created by flame 16 p2672 A67-31066

Mutual coupling between sectoral horns side-by-side formulated in terms of rays, modes and mode caustics excited in each horn 16 p2639 A67-31355

Diffraction coefficients in Keller theory extended to near-field and shadow-boundary regions of edge, introducing two correction factors 16 p2627 A67-31365

Diffraction of plane electromagnetic waves on compressible plasma cylinder analyzed, obtaining scattering cross sections 16 p2628 A67-31503

High frequency asymptotic behavior of wave field in two-dimensional diffraction problem on inhomogeneous cylinder of arbitrary cross section 16 p2628 A67-31505

Refractive index of amorphous boron films determined from interference of transmission curves 16 p2734 A67-31884

Interference from laser light beam superposition at single photon level, noting existence of fringes 17 p2866 A67-32277

Electromagnetic wave diffraction by convex spherical surface considered in terms of mutual impedance between two radial electric dipoles, using integral equation 17 p2817 A67-32930

Diffracting shock wave profile for various corner angles and wall shock Mach numbers, comparing experimental and theoretical results 20 p3422 A67-36847

Electromagnetic plane wave diffraction on anisotropically conducting plane and shielding and reflecting activity of dense radial grating 20 p3384 A67-37326

Diffraction by cylinder in locally uniaxial medium with azimuthal optic axis, using Maxwell equation solution for plasma frequency 20 p3389 A67-37705

Green function for SH-line source in wedge-shaped medium with apex removed by circular cylinder, determining reflected and refracted fields 21 p3579 A67-37925

Incomplete expansion wave diffraction by corner, noting pressure discontinuity across boundary 21 p3584 A67-37929

Soviet papers on wave propagation and diffraction problems 21 p3579 A67-38107

Electromagnetic and acoustic waves diffraction at smooth convex body of arbitrary shape, solving field equations 21 p3579 A67-38108

Inversion formulas for parabolic functions solution to vibration equation in diffraction at paraboloid of revolution 21 p3652 A67-38110

Simplified formulas and curves for electromagnetic wave diffraction on small ideally conducting sphere, examining electric field components 21 p3580 A67-38121

Asymptotic solution for planar electromagnetic wave diffraction on ideally conducting cylinder surrounded by inhomogeneous plasma layer 21 p3585 A67-38811

Diffraction of plane electromagnetic wave from ideally conducting ellipsoid of revolution 21 p3586 A67-38943

YIG magnetically induced elastic wave dispersion, acoustic Faraday rotation and group velocity dispersion measured using Bragg diffraction 22 p3855 A67-39358

Integral equation for asymptotic expansions of plane electromagnetic and acoustic fields diffracted by convex surfaces of variable curvature 22 p3836 A67-39389

HF plane waves diffraction on plane circular diaphragm solved by functional theoretic methods for integral equation for Fourier transform of screen

covering 22 p3912 A67-39783

HF approximation to diffraction of plane wave by conducting strip, using cylindrical wave terms for higher order patterns 23 p3979 A67-40831

Perturbed region behind diffracting shock wave on plane-walled convex corners at supersonic speed 23 p3990 A67-41172

RF pulse compression by chirped shear microwave sound in sapphire, inducing self-focusing of Bragg diffracted light 24 p4188 A67-42369

Electromagnetic wave diffraction in magnetoactive plasma by conducting wedge using Laplace integral in rotating reference frame 24 p4123 A67-42706

WAVE DRAG

Thin optimum wing contour constructing procedure having minimum wave drag in supersonic flow solved by linear approximation, obtaining numerical values for parameters 22 p3741 A67-40017

WAVE EQUATION

SA HELMHOLTZ EQUATION

SA LAME WAVE EQUATION

Competition of two types of oscillations in traveling wave laser 01 p0089 A67-10362

Slow decay of solution of initial boundary value problem for wave equation in exterior of three-dimensional smooth star-shaped body 01 p0052 A67-10519

Geometrical optics method modified for asymptotic solution to scalar wave equation for wave penetrating caustic surface 02 p0192 A67-11637

Self-focusing of laser beam in plasma, solving wave equation for slab and cylindrical beam configurations 02 p0252 A67-12089

Quantum mechanical perturbation theory calculation of upper and lower bounds of energy eigenvalues using partitioning methods 02 p0269 A67-12727

Exact and approximate solutions to Cauchy problem for nonlinear wave equation in affine connection field theory 03 p0457 A67-13171

Half-plane elliptic boundary value problems involving mixed boundary conditions solved by considering generalized Tricomi equation containing damped wave equation 03 p0461 A67-13942

Asymptotic characteristic of eigenfunctions of two-dimensional scalar wave equation with boundary conditions at equidistant curves 04 p0570 A67-14743

Exterior Dirichlet problem for reduced wave equation treated by numerical method 05 p0835 A67-16738

Aerodynamic generation of noise in stellar convection zones, solving inhomogeneous wave equation when assuming isothermal disturbance 05 p0899 A67-17073

Competition of two types of oscillations in traveling wave laser 06 p1009 A67-17620

Self-similar solution generalization for Euler-Poisson wave equations, noting application to transonic gas dynamics 06 p1023 A67-17862

Multiple scattering of light in turbulent atmosphere noting relation to refraction index and power spectra, using Born series solution to wave equation 06 p1033 A67-18536

Periodic vibrations of systems governed by nonlinear PDEs, examining perturbation method, transverse vibrations of bar, string, beam and membrane and sound waves in enclosure 06 p1034 A67-18640

First order coupled wave equations for propagation in planar stratified compressible electron plasmas 07 p1230 A67-19851

Periodic solutions of hyperbolic equations containing small parameter by extending Cesar method for differential equations 07 p1218 A67-20213

Scalar wave equation of annular membrane for origin symmetric motion and arbitrary initial and boundary conditions 08 p1415 A67-20476

Series solution for average wave field in medium with random inhomogeneities by using Green function for wave equation 08 p1294 A67-20814

Latitude dependent plasmasphere oscillations, providing toroidal and standing wave solutions for MHD equations 08 p1365 A67-21407

Wave propagation in random medium analyzed by solving stochastic wave equation with random function for refractive index coefficient and applied to laser

beam 08 p1296 A67-21434

Criterion for spatial amplification or nontransmittance using double Laplace transforms in light of complex values of wave vector 09 p1463 A67-21992

Resonance in plasma magnetized by radial magnetic field solved, obtaining MHD wave equation, noting relation to micropulsations 09 p1545 A67-22196

Linear hyperbolic equations describing one-dimensional wave propagation, with stability conditions by harmonic analysis and second Liapunov method 09 p1533 A67-22400

Wave equation solution yielding steady absorption coefficient for laser diode 09 p1516 A67-22663

Method of averages in solving resonance problems in wave mechanics 10 p1679 A67-22842

Nonlinear effects produced by instability of nonpotential plasma waves in oscillating discharge, deriving wave kinetic equation 10 p1684 A67-22902

Plasma instabilities due to RF motion obtained by expanding fluid and electromagnetic wave equations in asymptotic series 11 p1825 A67-23870

Ray solution for point source in medium with varying propagation constant determined, using Green function for scalar wave equation 11 p1751 A67-23969

Averaging method in nonlinear mechanics, discussing results of Bogoliubov studies 11 p1818 A67-24089

Radiating slot on dielectric clad cylinder, solving wave equations and finding field expressions via harmonic series representation 11 p1761 A67-24280

Ordinary waves in viscoelastic mediums analyzed, using Green tensor relation to Kirchhoff tensor 11 p1877 A67-24750

Optimum distributed parameter system described by N-dimensional wave equation with unconstrained boundary control function 11 p1770 A67-24889

Electromagnetic wave diffraction on plasma cylinders calculated using wave equation and geometrical optics approximation 12 p1969 A67-25246

E and H waves in planar dielectric waveguides mounted on dielectric bases, deriving equations for wave dispersion and damping 13 p2069 A67-27028

Hyperbolic difference equations, reviewing Courant-Friedrichs-Lewy paper in light of recent developments 14 p2342 A67-28154

Variational integration principles used to integrate wave and Fourier thermoconductivity equations, noting solution by Ritz method 14 p2408 A67-28803

Momentum and energy of gravitational waves in terms of relativity theory 15 p2518 A67-30005

Successive approximation method for asymptotic solution of waves in inhomogeneous gyrotropic plasma 16 p2627 A67-31366

Radiation conditions for derivatives of radiating functions, omitting prescribed asymptotic behavior 17 p2877 A67-32562

Nonlinear interacting plasma wave equations derived by semiquantum analysis of wave-particle and wave-wave interactions 17 p2905 A67-32923

Wave equations for disturbances in partly ionized gas due to current sources determined, using three-fluid model 17 p2906 A67-33056

Wave equation solution for potential of cylindrical Dirac pulse incident on reflecting half-plane 17 p2817 A67-33139

Potential equations for hydrodynamic and thermoelastodynamic linear wave motions applied to linear wave motion of isotropic thermally conducting elastic solids and viscous fluids [ASME PAPER 67-APM-32] 17 p2886 A67-33159

Momentum and energy of gravitational waves in terms of relativity theory momentum and energy of gravitational waves in terms of relativity theory 18 p3079 A67-33763

Three-dimensional equation for wave propagation through inhomogeneous warm compressible plasma in inhomogeneous static magnetic field 18 p3088 A67-34071

Oblique, normal and transverse ionizing shock waves 18 p3092 A67-34733

Gas flow around wing in presence of moving shock wave with variable gas

parameters noting wave equation, velocity potential, etc 20 p3355 A67-36191

Wave equation for electromagnetic wave propagation in randomly varying refractive index medium, noting focusing for radio waves in interplanetary plasma 20 p3386 A67-37521

Ionospheric radio wave theory using coupled vacuum modes with set of coupled wave equations 20 p3389 A67-37709

Full wave solutions for coupled modes corresponding to ionospheric propagation in vacuum, stressing numerical swamping problem 20 p3389 A67-37710

Forced oscillation in distributed constant system with tunnel diode described by linear wave equation with nonlinear boundary conditions 21 p3598 A67-38606

Resonance in unbounded traveling and standing /harmonic oscillations/ waves, demonstrating equivalence of resonance states using wave equations 23 p4079 A67-41416

Shock wave reflection with vibrational relaxation times investigated by matching characteristics equation to shock wave equation 24 p4144 A67-42564

WAVE EXCITATION

Warm plasma excitation by electric dipole 03 p0475 A67-13173

Ion wave excitation due to Hall current compared with current parallel to static magnetic field in weakly ionized plasma on basis of two-fluid model 03 p0476 A67-13354

Excitation of dipole wave in circular small delay dielectric waveguide by sources with amplitudes and phases variously distributed over apertures 03 p0385 A67-13953

Dispersion relations and wave power of isotropic compressible lossy plasma slab bounded by free space and ground plane and excited by line sources 03 p0487 A67-14354

Stability and identification of parametric system with periodically varying rectangular wave excitation 04 p0592 A67-14912

Electromagnetic excitation by vertical magnetic dipole located above spiral anisotropic plane 04 p0586 A67-15672

Doppler effect on emission spectrum and energy of moving oscillator and intensity of surface wave excited by it 05 p0765 A67-17160

Electromagnetic wave emission excited by electron stream over diffraction grating lying on boundary of semilinear anisotropic dielectric 05 p0766 A67-17163

Electrostatic ion cyclotron oscillations excitation by electrode immersed in plasma 05 p0859 A67-17435

Wave excitation in compressible partially ionized plasma by electromagnetic and acoustic /or mechanical/ sources, describing set of linearized hydrodynamic and Maxwell equations 05 p0859 A67-17436

Traveling wave excitation of high power nitrogen and neon lasers with velocity matching that of stimulated emission 07 p1196 A67-20093

LF wave frequency-and amplitude-dependent transverse anomalous diffusion coefficient in fully ionized magnetoplasma in Q-machine 08 p1360 A67-21125

Excitation of ion-acoustic waves in potassium-cesium plasma when passing current through it, finding natural frequencies of system when plasma is drifting along axis 09 p1544 A67-21853

Electron beam excitation of longitudinal transverse waves in ionic semiconductors, obtaining amplitude increments and frequencies 09 p1554 A67-21978

Beam-generated plasma oscillation frequency expansion due to temperature, field and density 09 p1546 A67-22282

Gap excitation of waveguide loaded with plasma represented as charge-free medium with tensor dielectric constant 09 p1480 A67-22283

Excitation and damping of drift waves in stable regime of ionized plasma radially confined by axial magnetic field 09 p1550 A67-22679

Electrostatic wave excitation growth in collisionless plasma interaction and simultaneous modification with electron beam studied for weakly unstable situations 11 p1826 A67-23875

Highly ionized plasma with excitation and damping of density and temperature drift

waves in stable regime 11 p1835 A67-24382

Elastic surface waves excitation method in quartz at high frequencies, noting absorption temperature dependence 11 p1848 A67-24835

Parametric resonance excitation of Alfvén waves by small LF modulation of DC magnetic field imposed on ideal MHD plasma 11 p1844 A67-25062

Excitation of collisionless shock waves in low density plasma noting lifetime, discharge process, adiabatic contraction, etc 12 p1976 A67-26074

Ionospheric fine structure, considering excitation of ion-acoustic waves by vertical gradients of density 13 p2109 A67-26329

Cyclotron instability range in earth radiation belt analyzed taking into account wave absorption in atmosphere, using measurements of perturbation effects 14 p2378 A67-27916

Expression for surface field components obtained for plane electromagnetic wave at nose-on incidence on semilinear cone 14 p2261 A67-28376

Electromagnetic wave propagation, excitation and dispersion in metals in magnetic field 14 p2366 A67-28426

Growth and damping rates of resistive instability in gaseous plasma in crossed fields determined from empirical observations 15 p2530 A67-29823

Excitation of high and low frequency electromagnetic waves in unbounded plasma by external currents, deriving wave excitation intensity 16 p2721 A67-31477

Excitation of magnetoelastic waves at 200 to 3000 mc at room temperature in yttrium garnet single crystals obtained by gradual crystallization from yttrium and ferric oxides 16 p2733 A67-31733

Electron beam excitation of longitudinal transverse waves in ionic semiconductors, obtaining amplitude increments and frequencies 17 p2923 A67-33315

LF waves induced by superimposed electric and magnetic fields in semiconductor plasma 18 p3102 A67-34442

Electric field due to double grid excitation in circular waveguide partially filled with warm homogeneous plasma in infinite magnetostatic fields 19 p3290 A67-35379

Launching efficiency of PE-20 and PM-11 modes in dielectric-loaded trough waveguide excited by dielectric-loaded rectangular waveguide 19 p3194 A67-35514

Magnetoacoustic wave excitation and detection in rotating plasma accelerator, noting resonance and wave transition 19 p3298 A67-35746

Vibrational excitation effects on shock wave behavior calculated analytically by linearizing problem 19 p3212 A67-35773

Semiconductor surface electromagnetic oscillations excitation in presence of strong electric and magnetic fields, obtaining damping and dispersion law 20 p3504 A67-36183

Quasi-CW oscillation at 4880 angstrom of wide-bore AR II ion laser by plasma inductive excitation 20 p3458 A67-36387

LF and HF wave excitation in homogeneous plasma with external magnetic field, obtaining differential and integral wave intensities 20 p3501 A67-37142

Unsteady dynamic field excited by source moving along elastic half-plane boundary 21 p3716 A67-37967

Decay instability of steady state waves in plasma, considering Alfvén wave 21 p3674 A67-38803

Acoustic ion waves phase velocity and attenuation constant measurements verify predicted dependence on ion mass, with attenuation due to ion-neutral collisions 21 p3675 A67-39054

Backward waves effect on excitation of delay line by modulated electron beam with zero transit angle 22 p3767 A67-39422

Dispersion characteristics of surface waves excited in infinitely long axially magnetized cold plasma by electric dipole 22 p3847 A67-39621

Analytic model for output voltage of fluxgate magnetometer, demonstrating excitation function and core squareness effects 22 p3800 A67-39911

Plasma potential oscillations in traps, discussing flute instabilities, cyclotron instabilities and resonance electron wave

excitation 23 p4034 A67-41680

WAVE FRONT

SA SHOCK FRONT

Mach interactions and propagation mode of spinning detonation wave front in stoichiometric oxyhydrogen 02 p0232 A67-11564

Shock wave front structure in plasma, noting use of SHF diagnostics, electron concentration growth, etc 06 p0984 A67-18077

Deformation of surface of removable wave front discontinuity in acoustically anisotropic medium with variable sound velocity 06 p1032 A67-18396

Signal to noise ratio of optical-heterodyne detection system as affected by atmospheric distortion of optical wave front 07 p1144 A67-19786

Formation of compression shocks in calorically ideal real gases with thermodynamic relaxation analyzed in closed form 13 p2094 A67-26636

Extension to three dimensions of Wentzel-Kramer-Brillouin approximation method for quasi-classical wave function, applicable to axisymmetrical problems 16 p2703 A67-31920

Wave surfaces of Einstein-Schrodinger theory and nonlinear electrodynamics brought together using antisymmetric tensor 18 p3078 A67-33688

Soviet book on nonlinear problems of motion of compressible fluid with small disturbances, investigating pressure fronts, neighborhoods of wave fronts, etc 18 p3025 A67-33715

Air ionization behind shock wave front, estimating free electron concentration, ionization time and collision frequency 19 p3293 A67-35401

Energy dissipation of strong magnetosonic waves in rarefied plasma, discussing electrons ionizing collisions at wave front 19 p3293 A67-35402

Propagation rate of electromagnetic and gravity wave front in synchronous reference system in Riemann space 20 p3486 A67-37554

WAVE FRONT DEFORMATION

Spatial coherence of laser light beam after extreme wavefront distortions on diffraction explained on basis of Fraunhofer and Fresnel diffraction 01 p0115 A67-11062

Elastic nonlinearity due to acoustic wave-charge carrier interaction in CdS, noting waveform distortion for zero acoustic dissipation 08 p1353 A67-20485

Phase and amplitude measurements of laser wavefront using laser phase-locked loop 13 p2129 A67-27494

Spatial coherence and shape of emission wave front of giant pulse from ruby laser with Pockels cell shutter 18 p3058 A67-33526

Antenna array simulator using acoustic waves in water to simulate electromagnetic propagation 20 p3397 A67-36580

WAVE FRONT RECONSTRUCTION

Holographic techniques for recording and reconstructing three-dimensional objects 01 p0062 A67-10192

Fourier transform holography for diffusion of coherent laser light beam, examining distortion term in reconstructed image 01 p0070 A67-11063

Holograms of objects immersed in water and illuminated by 7-mc sound waves and reconstruction of optical images from sound holograms using laser light 03 p0420 A67-13570

Wavefront reconstruction with light of finite coherence length 03 p0424 A67-13911

Hologram copying by laser techniques using original hologram as object for second hologram 03 p0426 A67-14397

Wavefront reconstruction imaging technique and amplitude and phase recording techniques in hologram preparation 05 p0807 A67-16800

Fresnel-Kirchhoff diffraction theory interpretation of plane and three-dimensional hologram 06 p1003 A67-18105

Laser holography, discussing various methods of wave front reconstruction 07 p1183 A67-19092

Wave front reconstruction imaging technique for hologram production of aerial image of lens 07 p1188 A67-19787

Holographic technique for restoration of third-dimension information in recording of conventionally focused photographs 07 p1188 A67-19788

Prisms for dispersion compensation and single plane diffraction grating as correcting

element for achromatizing white light reconstruction of two-beam surface hologram 09 p1492 A67-21567

Reconstructions of visible images from reduced scale replicas of polarized microwave holograms 09 p1496 A67-21709

Hologram fixation by Gabor single beam method, using gas laser as light source 09 p1511 A67-21919

Hologram temporal filtering properties applicability to Doppler mapping of moving objects and wavefront reconstruction process on noncoherent object images 13 p2121 A67-27352

Hologram fixation by Gabor single beam method, using gas laser as light source 14 p2329 A67-28248

Images reconstructed from multiple-exposure hologram separated by selecting appropriate-reconstructed pupil 15 p2487 A67-29500

Optical image reconstruction from sampled hologram using wavefront reconstruction technique 15 p2488 A67-29819

Rayleigh-Sommerfeld diffraction formula to obtain imaging behavior of Gabor type holograms of transparencies for reconstructed wave forms with large diffraction angles 22 p3835 A67-39241

Photographic film nonlinearities effect in holographic recording of coherent wavefront using two-beam interferometry, describing phenomenological model 23 p4002 A67-41269

Digital image formation and reconstruction from photographic and direct electronically detected holograms 24 p4157 A67-42437

WAVE FUNCTION

Mean powers of r , sum rule and improved transition integrals computed for effective quantum number range up to 8.5, using Coulomb approximation wave functions 01 p0112 A67-10142

Isospin impurity mixing in distorted deuteron reaction 02 p0270 A67-12526

Approximate solution of Gelfand-Levitan equation leading to localized bound-state wave function examined in S -matrix approach to first order energy shift 02 p0270 A67-12637

Perturbation theory in molecular quantum physics using variational principles 02 p0270 A67-12722

Energy and wave functions of singly charged donor impurity centers in silicon and germanium 03 p0488 A67-12857

Autolocalization calculation describing scattering aspect of phenomenon 03 p0471 A67-13220

Close-coupling calculation of resonant structure of scattering amplitude of excited-state atoms and molecules in continuum 03 p0471 A67-13221

Internal conversion coefficients for M_4 transition in Te, noting gamma energy magnitude, nuclear size effects and eigenvalue results 03 p0472 A67-13335

Perturbation treatment of diatomic hydrogen ion, improving polarized hydrogen-atom treatment by using zero-order wave function 03 p0474 A67-14333

Approximate molecular orbitals, Part I 03 p0474 A67-14351

Approximate molecular orbitals, Part II 03 p0474 A67-14352

Absorption spectra of Te, Sn, Pb, PbTe and SnTe at various energy ranges, noting role of wave functions involved in absorption by d -electrons 04 p0681 A67-15295

Hartree, Hartree and Swirls calculations for oxygen repeated with superposition of configurations in determining wave functions and energy 06 p1034 A67-17847

Perturbation treatment for molecular configuration using product of atomic or molecular orbitals as zero-order wave function 06 p1034 A67-17826

Nucleon radius from pion-nucleon phase shift, assuming nucleon is p -wave bound state of pion and nucleon, using Gelfand-Levitan formalism 06 p1036 A67-18368

[AIAA PAPER 67-213] Thermal excitation and de-excitation of alkali atoms in inert gas heat bath 07 p1265 A67-19075

Multichannel photoionization of atomic systems obtained with dipole approximation assuming LS coupling, using wave functions 07 p1226 A67-19498

Electron capture cross section by protons in hydrogen atom obtained, using perturbed wave functions due to electric

field 07 p1226 A67-19501

Hellmann-Feynman theorem in curvilinear coordinates for exact and for floating variational wave functions 07 p1138 A67-20189

Integral equation for propagation of second order correlation function assuming statistical independence of wave function and refractive index fluctuations 09 p1460 A67-21594

Conductivity of high density plasma of MHD generator, noting quantum phenomena associated with overlapping electron wave functions 09 p1543 A67-21818

Unrestricted projected Hartree-Fock solutions for two-electron systems, with application to special configuration superposition 09 p1535 A67-22380

Condon loci geometry of molecular spectrum determined by plotting intensities on Deslandres diagram 10 p1681 A67-22959

Operator calculus, based on momentum operator choice, designed to take account of finite domain of wave functions in quantum mechanics 10 p1682 A67-23349

Relation between Slater screening constants and interchangeability of atomic orbitals 10 p1682 A67-23378

Optimum illumination for maximum power transfer between two opposed rotationally symmetric antennas 11 p1762 A67-24291

Spatial correlation and molecular properties in extended Hartree-Fock calculations, deriving first and second order density matrices for ground state of H, Li and F 11 p1824 A67-24993

Irreducible tensorial components of two-electron operator and second-order density matrix for spin-projected single-determinantal wave function 16 p2705 A67-31759

Atmospheric modulation noise in optical heterodyne receiver, deriving signal power variance and mean-square frequency spread from propagation statistics for wave structure function 16 p2630 A67-31807

Zeeman effect of germanium I and II, discussing configuration-interaction, deriving intermediate-coupling wave functions 16 p2733 A67-31876

Source size effect on resolution in Fourier transform holography comparing theoretical and experimental results 16 p2681 A67-31883

Extension to three dimensions of Wentzel-Kramer-Brillouin approximation method for quasi-classical wave function, applicable to axisymmetrical problems 16 p2703 A67-31920

Kronig-Penney model for electron potential in crystal adapted to semiconductor, discussing cubic lattice 17 p2914 A67-32386

Renormalizing approximate wave functions so that amplitude is correct by means of matrix, with applications to Born approximation 17 p2887 A67-33318

Integration scheme for variational r sub ij wave functions containing unlinked four-electron correlated terms for atoms up to neon 18 p3082 A67-34026

Vector wave functions for boundary value problems in compressible plasma for spherical geometry, noting Fourier series, acoustic wave, etc 18 p3090 A67-34382

Light absorption of single-band semiconductor calculated from wave function of electron-hole pairs located near charged impurities, obtaining pair lifetime 19 p3300 A67-34767

Nonuniform RC lines with hypergeometric and spheroidal wave functions solutions, calculating driving point impedance 19 p3190 A67-34840

Compound state resonances in molecular collisions, stressing scattering cross sections behavior for deuterium-xenon 19 p3266 A67-35881

Spin restricted, unrestricted, projected unrestricted and extended SCF wave functions energies compared, discussing calculation method for spin extended SCF functions 20 p3483 A67-36230

Electron-interference experiment using laser light, discussing electron wave function phase change and electron interference pattern displacement 20 p3460 A67-36999

Total energy of beryllium hydride molecule analyzed, using difference between SCF energies and single determinant wave function 20 p3377 A67-37139

Variational approximation for ground state of perturbed Schrodinger equation with single variable wave

function 20 p3479 A67-37600

Nonlinear variational trial function for atomic hydrogen dynamic polarizability, discussing first order perturbed wave function and perturbation-variation method 21 p3659 A67-38004

Liquid He 4 ground state studied by variation method, deriving radial distribution function 22 p3835 A67-39301

Interaction of two H atoms in ground states using Hirschfelder-Linnet wave function and Gaussian type 22 p3756 A67-39385

Long range interaction of two H atoms calculated with electrostatic Hellmann-Feynman theorem, determining part of second order molecular wave function 22 p3840 A67-39387

Matrix method to calculate energy eigenvalues and orbital wave functions for various singlet states of helium isoelectronic sequence 22 p3841 A67-40202

Intermediate range intermolecular forces with overlapping wave functions and exchange effects calculated for ionized H molecule using perturbation theory 23 p4029 A67-40971

Hyperfine coupling constants of lithium energy levels, using Weiss 4s-configuration wave functions 24 p4190 A67-42097

WAVE GENERATION

SA SHOCK WAVE GENERATOR

Nozzle wall shape design based on Mach waves generation appearing when supersonic gas expands about corner 03 p0352 A67-13816

Simple waves for nonlinear system of partial differential equations applied to multidimensional compressible inviscid flows 05 p0790 A67-16045

Induced electron cyclotron radiation application to generation and amplification of high power electromagnetic traveling waves 05 p0824 A67-16915

Aerodynamic generation of noise in stellar convection zones, solving inhomogeneous wave equation when assuming isothermal disturbance 05 p0899 A67-17073

Kinetics of nonuniform generation of longitudinal plasma waves by transverse wave beam with narrow spectrum, noting effect of magnetic field 09 p1545 A67-21995

Sound wave generation by columnar-starting vortex passing through reflected plane shock front analyzed, revealing alternate compression-rarefaction nature 10 p1625 A67-23117

Nonlinear wave processes in plasma in strong magnetic field, obtaining dispersion for fundamental and harmonic 11 p1836 A67-24392

High power pulsed microwave generation in gallium arsenide diode when operated at X-band frequencies 11 p1767 A67-24721

Generation rate of secondary HF wave from resonant interaction of two longitudinal waves in cold beam-plasma under external magnetic field 12 p1970 A67-25250

Oblique incidence of electromagnetic wave on plasma half-space 13 p2065 A67-26290

Plasma wave drift in stellarator helical magnetic field, deriving equations for wave developing conditions 14 p2361 A67-28762

Pulsed laser beam induced elastic waves in metals, noting experimental techniques and role of radiation pressure in wave generation 14 p2374 A67-28987

Laser emission under external signal, analyzing competition between amplification mode and parasitic generation arising at resonant frequency, noting signal role 15 p2498 A67-29469

Induced electron cyclotron radiation application to generation and amplification of high power electromagnetic traveling waves 16 p2685 A67-30892

Shock wave generation of electromagnetic radiation at magnetospheric boundary, discussing plasma oscillation excitation, plasma wave scattering, etc 17 p2846 A67-32935

Alfven and magnetosonic wave generation and propagation in magnetosphere, detailing azimuth number approaching infinity 18 p3042 A67-34391

Planar highly conducting liquid jet kink mode stability in electric field and feedback stability control of spatially growing wave 18 p3029 A67-34735

Instrument for measuring group delay time of microwave four-poles, using

backward-wave tube as wave generator 19 p3183 A67-35032

Low power pulsed reflex klystron used to produce hyperfrequency-wave trains for short time periods 19 p3193 A67-35416

Ion cyclotron frequency wave generation in plasma confined in magnetic well for maximal density 19 p3295 A67-35419

Electromagnetic wave generation and amplification extended from LF microwaves up to optical band 20 p3380 A67-36488

Acoustic wave generation in weakly ionized plasma by fusion and damping of two ion-sound waves 20 p3501 A67-37291

Growth and attenuation of acceleration waves and higher order waves derived from nonlinear fluid theory with internal state variables 21 p3610 A67-37739

Laser emission under external signal, analyzing competition between amplification mode and parasitic generation arising at resonant frequency, noting signal role 21 p3641 A67-38550

ULF radiation in polar auroral zone explained via plasma beam instability, assessing perturbation of particle fluxes in magnetosphere 21 p3621 A67-39016

Swell generation by means of flat paddle board in translational motion 22 p3783 A67-39646

Ruby and neodymium-glass lasers light emission mixing, noting created wave frequency is sum of two initial wave frequencies 22 p3815 A67-39765

Coherent high power millimeter and submillimeter wave generation by various free electron beam devices, noting periodic beam has greatest development potential 22 p3774 A67-40443

Transverse electric field generated by interaction of various longitudinal plasma waves in ion electron plasmas 23 p4033 A67-41151

Rapid temperature increase due to stellar photosphere turbulence generation of mechanical waves, discussing gravity wave generation and acoustic noise 23 p4068 A67-41280

Strong traveling transverse acoustic modes generated by rotating gas jet in cylindrical cavity 23 p3993 A67-41763

Mountain wave and air turbulence program using high altitude research aircraft measurements and stressing CAT 24 p4181 A67-42275

WAVE INCIDENCE CONTROL

Wave synchronization in gas laser with ring resonator cavity 09 p1513 A67-22063

Fabry-Perot etalon resonator studied for incidence angles for use as filter, test instrument and control device for laser output 22 p3809 A67-40469

WAVE INTERACTION

SA SHOCK WAVE INTERACTION

Photon interaction in plasma, determining energy density and collision frequency 02 p0272 A67-11583

Waveguide interactometer measurement of plasma parameters 03 p0477 A67-13458

Traveling waves interaction in gas laser, explaining forcing-of-oscillations and traveling wave suppression effect 03 p0439 A67-14371

Wave interaction dynamics of far IR electromagnetic radiation generation by coherent molecular vibrations or phonons excited by stimulated Raman scattering and resonant phase matching condition 04 p0657 A67-15113

Plasma wave behavior in strong external magnetic field, discussing scattering at ions, wave transformations and nonlinear wave interactions 04 p0667 A67-15206

Wave interactions in spatially dispersive media 05 p0849 A67-18013

Drift waves in finite pressure plasma, noting oscillation caused instabilities induced by Alfven type and slow magnetoacoustic wave interaction 05 p0852 A67-18693

Polytrope index for gas detonation products determined by velocity ratio for incident and reflected wave during collision of two detonation waves 05 p0927 A67-16999

Nonlinear interaction between plasma oscillation normal modes in hydrodynamic approximation 05 p0858 A67-17434

Nonlinear and quasi-linear transformation of HF waves in LF part of spectrum in inhomogeneous plasma 06 p1038 A67-17759

Wave coupling in varying density regions in hot anisotropic electron plasma, noting

effect of angle width between propagation vector and static magnetic field 07 p1228 A67-19509

Interaction between helicon waves and drift currents in layered lead telluride structure 07 p1232 A67-19555

Wave interaction in saturable absorbers, noting hole burning in dye switched ruby laser 07 p1234 A67-20094

Wave interaction between linear viscoelastic medium and thin cylindrical shell imbedded within it solved for uniform harmonic stress input applied to shell 08 p1415 A67-20486

Monochromatic wave interaction with isotropic electron-plasma, determining field and surface wave generated on basis of Maxwell equations 09 p1464 A67-22012

Spectral analysis of interacting electromagnetic, plasma and spin waves in antiferromagnetic semiconductors and metals with easy-axis and plane type anisotropy 09 p1555 A67-22073

Dispersion and interaction impedance of slow wave structures from cold tests measured, using resonance methods 09 p1476 A67-22212

Two positive kinetic power waves coupled in interaction for DC pumped quadrupole amplifier having low noise and high efficiency 09 p1478 A67-22260

Transmission and reflection coefficients in coupling of transverse and longitudinal waves below second electron cyclotron harmonic 09 p1548 A67-22383

Lorentz transform applied to solution of problem in interaction of waves within nonlinear medium 09 p1465 A67-22478

Scattering of circularly polarized electromagnetic wave in Coulomb field, noting coalescence of two-wave quanta into one quantum of double frequency 10 p1666 A67-23594

Ionospheric electron density profile measurement via radio wave interaction technique, noting superiority of partial reflection method 11 p1785 A67-23946

Plasma stability, discussing flute and Kadomtsev instabilities and possibility of anomalous diffusion for confined steady state 11 p1831 A67-24011

Nonreciprocal characteristics of long distance HF ionospheric propagation path interpreted as interaction of waves with transmitting and receiving antennas 11 p1754 A67-24718

Laser beam acceleration of inhomogeneous plasma by imparting high energies to oncoming ions 12 p1969 A67-25198

Spin wave interaction in YIG with acoustic, magnetoplastic and relaxation oscillations excited by laser and microwave 12 p1953 A67-25749

Detonation wave interaction with hydrogen-oxygen flow fields in clarifying rocket combustion instability and supersonic combustion 12 p1929 A67-25898

Approximate technique using perturbation theory in analyzing microwave interaction with gyrotropic media 12 p1908 A67-26183

Interaction between oppositely moving traveling waves in helium-neon laser with annular resonator 14 p2332 A67-28856

Vorticity generation by interaction of waves with plasma in magnetic field 15 p2524 A67-29231

Drift waves in finite pressure plasma, noting oscillation caused instabilities induced by Alfven type and slow magnetoacoustic wave interaction 15 p2530 A67-29864

Plasma wave behavior in strong external magnetic field, discussing scattering at ions, wave transformations and nonlinear wave interactions 15 p2532 A67-30254

Rarefied gas flow interaction with sphere analyzed using multiple wave interferometer, noting transition region from continuous medium to free molecular flow 16 p2656 A67-30453

Ion-acoustic interaction in weakly turbulent plasma deriving time variation of plasmon number 16 p2715 A67-31046

Shadow method analysis of shock wave interaction with fixed bodies in shock tube at small and medium supersonic Mach numbers 16 p2673 A67-31105

Nonlinear interacting plasma wave equations derived by semiquantum analysis of wave-particle and wave-wave interactions 17 p2905 A67-32923

Laminar slow wave coupler applied to

waveguide to detect very low power slow waves in indium antimonide subjected to combined effects of applied electric and magnetic fields 17 p2922 A67-33087

Long time behavior of weakly interacting nonlinear waves, emphasizing mathematical features common to physical situations 18 p3079 A67-34002

Coupling between slow waves and convective instabilities in solids, showing interaction inhibition for electron drift velocities greater than phase velocity 18 p3101 A67-34017

Weak turbulence theory for collisionless plasmas formulated in terms of test waves 18 p3092 A67-34744

Macroscopic cross-field instability occurring in ionized plasma studied by computer, discussing wave interactions between Fourier modes 18 p3092 A67-34746

UHF wave interaction between plasma and electron stream in magnetic field noting convective instability 19 p3291 A67-35382

Validity range for weak turbulence theory in case of wave resonant interaction mechanism, treating Fokker-Planck and nonlinear optics approximations 19 p3298 A67-35792

Nonlinear interaction between two waves of multiple frequencies in communication line, nonlinear line capacitance being periodic function of line length 19 p3185 A67-36021

Dispersion equations for two types of transverse interaction tubes analyzed numerically in presence of strong space charge 19 p3198 A67-36022

Interaction between oppositely moving traveling waves in helium-neon laser with annular resonator 19 p3242 A67-36107

Coupling coefficients for nonlinear interaction between two transverse waves and electron plasma wave in magnetic field 20 p3501 A67-37181

Wave interactions in spatially dispersive media 20 p3502 A67-37590

Plane wave approximation for dilatational mode response of thin hollow spherical shell embedded in elastic medium and subjected to asymmetric pressure wave 21 p3718 A67-38020

Attenuation function of surface wave propagating over spherical earth having surface layers with different electric impedances, studying interaction with space wave 21 p3580 A67-38122

Drift and ion acoustic waves and coupled waves in highly ionized dense plasma of finite ion temperature 21 p3667 A67-38412

Three- and four-phonon processes in piezoelectric cadmium sulfide observed using ultrasonic amplifier confirm nonlinear theory of multiple wave interactions 22 p3854 A67-39246

Wave correlation evolution in uniformly turbulent weakly nonlinear systems 22 p3843 A67-39287

Kinetic equation for spatially uniform unstable plasma with collision term containing wave effect /plasmons/ in system and Lenard-Balescu equation 22 p3848 A67-39690

Transverse electric field generated by interaction of various longitudinal plasma waves in ion electron plasmas 23 p4033 A67-41151

Synergetic approach to problems of nonlinear dispersive wave propagation interaction 24 p4125 A67-43093

WAVE MOTION

Concentration waves excited by internal modulation of charged particle concentrations in cross section of plasma flow analyzed for various velocities of flow 09 p1544 A67-21851

Interplanetary magnetic field effect on hydrodynamic supersonic expansion of solar corona noting solar wind velocity, nonradial flow, wave motion, etc 10 p1709 A67-23546

Approximate expression derivation for calculating propagation rate of strong shock wave in inhomogeneous cosmic medium 15 p2552 A67-29146

Potential equations for hydrodynamic and thermoelastodynamic linear wave motions applied to linear wave motion of isotropic thermally conducting elastic solids and viscous fluids 17 p2886 A67-33159

[ASME PAPER 67-APM-32]

Disintegrating liquid jet penetrating high speed gas stream investigated for amplification of capillary and acceleration waves 18 p3026 A67-33959

[AIAA PAPER 67-495] Finite amplitude elastic wave motions with only constitutive nonlinearities 20 p3540 A67-37282

Mesoscale structure of atmospheric winds analyzed using data obtained from FPS-16 radar/Jimsphere precision wind measuring system 21 p3855 A67-38576

Problem solving method based on averaging over periodic functions for steady waves in nonlinear one-dimensional distributed systems, deriving approximate equations 22 p3815 A67-39761

Peristaltic viscous fluid motion through axisymmetric pipes and symmetrical channels produced by pressure gradients and cross section changes, using Stokes approximation 23 p3990 A67-41174

Approximate expression derivation for calculating propagation rate of strong shock wave in inhomogeneous cosmic medium 24 p4239 A67-43069

WAVE NUMBER

S WAVELENGTH

WAVE OSCILLATOR

Oscillation spectral density of SHF oscillators measured, using frequency phase self-tuning system to eliminate LF component of phase fluctuations 08 p1302 A67-20833

Resonances in wave mechanics and anomalous light dispersion, obtaining value of displacement 17 p2884 A67-32704

Stimulated Raman effects in calcite oscillator crystal, measuring gain index beta relative to Stokes wave 23 p4016 A67-41191

WAVE PROPAGATION

SA SHOCK WAVE PROPAGATION

Auroral region disturbances generating atmospheric waves in F layer that produce atmospheric mixing 01 p0056 A67-10112

Second-order effects in propagation of elastic waves through homogeneous isotropic media 01 p0113 A67-10405

Skin effect association with anisotropy of medium in solid mechanics, analyzing surface instability, internal buckling and surface wave propagation 01 p0113 A67-10406

Elastic wave propagation in heterogeneous plates, discussing various plate theories, frequency equations, transverse shear deformations, etc 01 p0160 A67-10407

Optimal control of one-dimensional distributed oscillatory system and wave processes using momentum theory and propagating method 01 p0044 A67-10493

Wave propagation in continents and adjacent shelf areas used for study of seismic crustal refraction and reflection measurements 01 p0060 A67-10502

Nonlinear dispersive wave propagation analyzed by linearization, obtaining solution as Fourier integral through differential equation 01 p0024 A67-10737

Equations for nonlinear wave propagation in incompressible heat-conducting elastic material, noting propagation of shocks in isotropic material 01 p0162 A67-10846

Wave solutions for plane waves propagating in isotropic elastic solid using isentropic approximation 01 p0162 A67-10847

Electromagnetic theory of wave propagation modes in dielectric cylinders applied to coherent light transmission in optical fibers 02 p0190 A67-11528

Excitation of metal sphere with large electric diameter by arbitrary electric and magnetic current distribution 02 p0191 A67-11577

Approximate general bistatic radar scattering relationships derived for finite length metal cylinder for transverse electric /TE/ and transverse magnetic /TM/ cases 02 p0192 A67-11623

Temperature-dependent wave propagation in slightly inhomogeneous hot nonuniform plasma, examining positive column of mercury vapor discharge 02 p0193 A67-11782

Finite-amplitude plane wave propagation in elastic solids 02 p0336 A67-11792

Electromagnetic wave propagation along plasma column subjected to longitudinal magnetic field, calculating dispersion curves for two dipolar modes as function of wavelength and frequency 02 p0273 A67-12062

Forward and backward wave striations in constricted positive column of high pressure argon discharge 02 p0273 A67-12188

Communication relay to aircraft by satellite, discussing wave propagation characteristics, standing wave pattern, signal fading rates, etc 02 p0205 A67-12306

Criteria for cold plasma density necessary to stabilize grade B drift waves in finite length energetic plasmas 02 p0275 A67-12554

Characteristics method in numerical solution of one-dimensional problems of propagation 03 p0458 A67-13348

Nonionized atmosphere effect on radial velocity measurement of satellite via Doppler-Feizeau method 03 p0369 A67-13530

Wave propagation in elastic materials, noting extension to materials with memory 03 p0536 A67-13659

Small amplitude wave propagation in incompressible conducting fluid 03 p0480 A67-13725

Wave propagation in rarefied two-component plasma situated in uniform constant magnetic field with finite Larmor radius 03 p0483 A67-13875

Differential far-end-operated half-echo suppressor design for telephone circuits with long propagation time 03 p0371 A67-13990

Propagation of coupled electromagnetic, electron-acoustic and ion-acoustic waves in horizontally stratified and magnetized electron-ion plasma 03 p0372 A67-13991

Growing space charge wave phenomenon due to collision coupling in warm compressible dissipative electron plasma in uniform motion 03 p0483 A67-13995

Propagation of nonaxisymmetric Alfvén waves in linear discharge tube filled with nonuniform plasma 03 p0485 A67-14045

Space charge wave velocity in semiconductors, noting recombination type instability 04 p0676 A67-14928

Courant-Hilbert ray theory and Thomas singular surfaces theory of wave propagation in anisotropic homogeneous linearly elastic medium, based on growth equation 04 p0657 A67-15083

Helicon wave propagation along multilayered structure, calculating Bloch waves, fields and dispersion 04 p0665 A67-15119

Wave propagation in n-type semiconductor with negative differential resistance 04 p0678 A67-15129

Dispersion equation for electromagnetic waves propagating in uniform plasma layer along boundary parallel to external magnetic field 04 p0667 A67-15207

Waves with complex propagation constants in diaphragmed circular waveguide, solving dispersion equation for various frequencies and structural parameters of waveguide 04 p0575 A67-15214

Field and charge density distributions in semiconductor with hot electrons, showing domain movement type oscillations due to stationary wave propagation 04 p0680 A67-15286

Density wave type flow oscillations in boiling Freon 11 examined, noting effects of partial evaporation superheat and liquid inlet temperature on stability [ASME PAPER 66-WA/HT-49] 04 p0725 A67-15433

Thermoelastic wave expansion in infinite medium discussed on basis of Duhamel-Neumann equation 04 p0715 A67-15577

Coupled spin, electromagnetic and plasma waves in ferrites 04 p0686 A67-15973

Exact and variational solutions to elastic wave propagation eigenvalue problem in constant Poisson ratio linear viscoelastic material 05 p0909 A67-16141

Stress-strain relationships in materials under high rate of torsional loading and torsional plastic wave propagation in long Cu tube 05 p0909 A67-16144

Thermoelastic wave propagation in elastic layer with convective heat transfer between layer surfaces and surrounding medium, considering relations between temperature field and dynamic displacement 05 p0913 A67-16188

MHD wave propagation emphasizing viscosity, heat and electrical conductivity, Hall current, nonequilibrium phenomena and effect of medium inhomogeneity 05 p0851 A67-16364

Three-dimensional oscillatory motions generation and propagation in solar atmosphere 05 p0900 A67-17074

Acoustic wave propagation characteristics

in solar chromosphere, discussing resonant frequencies 05 p0900 A67-17075

Coronal temperature and temperature distribution in transition region between chromosphere and corona, assuming photospheric wave propagation as essentially one-dimensional 05 p0900 A67-17077

Single wave approximation of fields of cylindrical delay system with basic E-type wave propagating at variable phase velocity 05 p0767 A67-17398

Plasma in Ar positive column DC discharge examined for wavelike perturbations about equilibrium, noting striation dispersion relation, density variations and electron temperature 05 p0857 A67-17427

One-dimensional acceleration waves and higher order waves propagating in general nonlinear Maxwellian materials with fading memory 06 p1099 A67-17834

Similarity in propagation of detonation waves in gaseous and liquid explosives with respect to homogeneity explained in terms of single detonation reaction 06 p1112 A67-17960

Three-dimensional Cauchy-Poisson problem for waves in viscous fluid 06 p0984 A67-18046

Wave propagation in random medium, examining stochastic PDEs, solutions and method of regularization 06 p1032 A67-18101

Log amplitude covariance for horizontal and nonhorizontal propagation path of plane wave through turbulent atmosphere, noting refractive index effect 06 p1033 A67-18537

Exact expression for transient response for step modulated carrier signal obtained, using parallel plate waveguide 06 p0964 A67-18767

Graphical and analytical solutions to wave propagation in inhomogeneous media in conditions of wave number variations oscillating along coordinate 06 p1034 A67-18814

Small oscillations and stability of hyperelastic incompressible rectangular strip under uniformly distributed biaxial load 06 p1111 A67-18892

Open air lines and cables, stressing electric wave propagation along homogeneous and inhomogeneous circuits 07 p1141 A67-19340

Propagation of magnetodynamic disturbance through loss ionosphere and entry into earth surface 07 p1174 A67-19718

Nonlinear nonsteady wave propagation in plane flow analyzed by introducing perturbations of potential into equation of gas dynamics and equation of characteristics 07 p1169 A67-19731

Ionospheric disturbances from high altitude nuclear detonations observed as changes in F-2 layer critical frequency 07 p1181 A67-19939

Ionosphere-exosphere system response to bomb-like hydromagnetic source and resultant ground level magnetic fluctuations 07 p1181 A67-19940

Propagation coefficient of rectangular waveguide containing centrally placed semiconducting film 07 p1146 A67-20202

Stress induced velocity variations of longitudinal and shear ultrasonic waves in steel, Al and Cu, calculating third order elastic constant 08 p1415 A67-20481

Electrodynamics properties of homogeneous magnetoactive plasmas including wave propagation, excitation, scattering, etc 08 p1358 A67-20863

Plane wave growth associated with Cerenkov and cyclotron instabilities in plasma stream 08 p1358 A67-20893

Nonlinear constant profile plane waves in cold Vlasov hydrogen plasma under influence of external magnetic field 08 p1359 A67-20896

Resonant particle instabilities in uniform magnetic field of plasma waves propagating at arbitrary angle 08 p1359 A67-20897

Book on electromagnetic wave propagation and turbulent media covering invariant imbedding method, turbulence generation, statistical methods of analysis, etc 08 p1295 A67-20984

Ion beam excitation of drift waves in alkali plasma, discussing sinusoidal signal propagation characteristics, variations with beam velocity and with modulation frequency 08 p1361 A67-21135

Wave propagation in random medium analyzed by solving stochastic wave equation

with random function for refractive index coefficient and applied to laser beam 08 p1296 A67-21434

Growth rate along whistler path for waves propagating at angle to geomagnetic field 08 p1328 A67-21463

Removal of incident wave spectrum by background wind shears during atmospheric gravity waves propagation to ionosphere from lower regions 08 p1328 A67-21477

Wave propagation through random and nonrandom medium, discussing relation of phenomena to coherence theory 09 p1460 A67-21586

Stochastic waveguides containing media with constitutive parameters having random variations not necessarily small or statistically homogeneous [SR-2] 09 p1460 A67-21593

Integral equation for propagation of second order correlation function assuming statistical independence of wave function and refractive index fluctuations 09 p1460 A67-21594

Effect of weak random inhomogeneities on long distance wave propagation, calculating first two statistical moments 09 p1461 A67-21595

Electromagnetic wavefront perturbations from plane wave propagation resolved into random tilt and residual phase perturbation 09 p1461 A67-21596

Average far field intensity patterns of antennas calculated for quasi-monochromatic space-time stationary signals 09 p1470 A67-21607

Variation of phase constant and damping constant of SHF wave propagating in waveguide incorporating coaxial plasma-filled dielectric tube 09 p1473 A67-21999

Decimeter wave propagation over large distance indicates signal propagation does not follow great circle 09 p1492 A67-22593

Covariance of log amplitude fluctuations for propagation of spherical wave in turbulent medium over horizontal path to obtain phase structure function 10 p1678 A67-22712

Variance of log amplitude of laser beam evaluated for horizontal propagation path through atmosphere by following Schmelzter results 10 p1603 A67-22713

Plasma magnetization under action of circularly polarized wave, noting inverse Faraday effect 10 p1683 A67-22853

Frequency equation for harmonic wave propagation in composite circular cylindrical shells established, based on linear three-dimensional theory of elasticity 10 p1717 A67-23127

Optimal control of one-dimensional distributed oscillatory system and wave processes using momentum theory and propagating method 10 p1621 A67-23615

Converging cylindrical and spherical detonation wave behavior in polytropic perturbed medium, noting self-similar solution 10 p1628 A67-23684

Dissipative wave propagation in linearized compressible MHD flow, constructing solution for arbitrary values of dimensionless parameters and field orientation 11 p1825 A67-23867

Dispersion relation for large amplitude circularly polarized plane wave propagation along magnetic field in hot collision-free plasma, considering distribution function 11 p1826 A67-23881

Effect of finite aperture dimension of antenna in vertical plane on conditions of ultrashort wave propagation within limits of direct visibility 11 p1757 A67-23916

Elastic medium dynamic response to time dependent pressure in spherical cavity with cavity wall under ablation process 11 p1871 A67-23964

Scattering matrix equations for waveguide structure of varying surface impedance boundaries 11 p1751 A67-23968

Ray solution for point source in medium with varying propagation constant determined, using Green function for scalar wave equation 11 p1751 A67-23969

Wave dispersion phenomena in blood vessels analyzed as measures of cardiovascular parameters 11 p1748 A67-23990

Ionospheric absorption determination by measuring amplitudes of wave components of satellite transmission 11 p1786 A67-24059

Laser beam modulation by atmospheric turbulence as function of receiving aperture

size, range and atmospheric conditions 11 p1799 A67-24236

Sheath helix antenna with conducting core, noting variation of operation characteristics with core size and pitch angle 11 p1760 A67-24277

Polarization characteristics of antenna measured, using stereographic projections of polarization sphere and various graphical methods 11 p1761 A67-24279

Feed system design for spherical reflector illumination specifying required field distribution and primary gain 11 p1761 A67-24281

Current distribution and input admittance of infinitely long cylindrical antenna driven by slice generator and immersed in anisotropic plasma 11 p1761 A67-24284

Inclined log spiral antenna, noting back radiation reduction and frequency independence 11 p1763 A67-24294

Equilibrium and stability of K plasma with internal E field normal to confining magnetic field, noting wave propagation at ion momentum velocity 11 p1833 A67-24369

Quiescent plasma physics - Conference, Frascati, Italy, January 1967, Part 2 11 p1836 A67-24389

Alkali metal plasma generator design and performance, noting characteristics of LF wave propagation parallel to magnetic field 11 p1837 A67-24396

Electron plasma wave propagation along cylindrical plasma column in magnetic field, calculating damping and dispersion curves 11 p1837 A67-24401

Propagation of acceleration waves in elastic and viscoelastic materials 11 p1875 A67-24572

Magnetic field effect on electromagnetic wave propagation through free carrier plasmas in semiconductors, considering Faraday configuration 11 p1840 A67-24663

Atmosphere effects on laser beam propagation noting diameter, intensity amplitude and power dependence on transmitter and receiver aperture dimensions 11 p1801 A67-24665

Slotted inhomogeneous waveguide propagation behavior investigated, using transverse equivalent network 11 p1766 A67-24691

Temperature effects in wave propagation on drifting carriers in semiconductors 11 p1847 A67-24720

Nonuniform elastic unloading wave propagation into perfectly plastically deformed region, obtaining solution of displacement field 11 p1879 A67-24941

Cylindrical wave propagation in rarefied plasma, examining effect of compression on internal plasma-magnetic field by external field 11 p1842 A67-24964

Constitutive theory for fluid mixtures admitting diffusion and chemical interaction with heat conduction and plane wave propagation 11 p1783 A67-25001

Hydromagnetic wave propagation and energy transfer in stratified isothermal plasma embedded in parallel uniform gravity and magnetic fields 11 p1868 A67-25083

Wave propagation in n-type semiconductor with negative differential resistance 12 p1978 A67-25153

Plasmas of gas state and of solid state compared, considering density, temperature, and anisotropic mass, noting wave propagation electric discharges and confinement phenomena plasmas of gas state and of solid state compared, 12 p1980 A67-25202

Wave propagation in earth-ionosphere waveguide, obtaining modal solutions 12 p1904 A67-25216

MHD wave propagation in magnetoplasma-filled waveguide, discussing pressure, current inertia, resistivity, etc 12 p1969 A67-25247

Plasma models and methods used to study wave propagation phenomena, considering particle orbit, single species moment equations, velocity distribution function, etc 12 p1975 A67-25527

Transformation of magnetoacoustic waves in terms of ideal MHD by phase integrals method 12 p1976 A67-26072

Harmonic ion cyclotron wave propagation and attenuation investigated experimentally 13 p2163 A67-26287

Plasma EM instability in magnetic mirror configuration, solving linearized Vlasov

- equation for dispersion relation of transverse EM waves 13 p2164 A67-26293
- Electromagnetic wave propagation in type II superconductors, noting Hall angles influence 13 p2175 A67-26428
- Parametric coupling between two waves noting losses 13 p2086 A67-26511
- Elastic wave propagation in Cosserat continuum with free surface 13 p2217 A67-26630
- Spherical wave propagation in infinite elastic body with transverse isotropy 13 p2217 A67-26633
- Gravitational wave propagation from upper to lower atmospheric layers analyzed taking into account reflection and refraction 13 p2112 A67-26673
- Torsional wave propagation in anisotropic nonuniform cylindrical rod for constant and variable Youngs moduli 13 p2218 A67-26902
- Kinetic model with velocity dependent collision frequency applied to forced wave propagation in half-space and other unsteady problems 13 p2100 A67-26956
- Steady state wave propagation in homogeneous anisotropic media studied from near field behavior of Green matrix 13 p2158 A67-27179
- Energy propagation and Poynting vector for electromagnetic wave propagation in tube of square cross section 13 p2070 A67-27207
- Image transmission through optical fiber, discussing reconstruction of refracted image via holography 13 p2120 A67-27209
- Alfven wave propagation in viscous incompressible infinitely conductive fluid under effect of gradually varying magnetic field 13 p2170 A67-27363
- Infrasonic and hydromagnetic wave propagation in atmosphere and ionosphere measured by array of underwater and acoustic sensors 13 p2122 A67-27701
- Atmospheric wind effects on guided propagation of VLF infrasonic waves over long distances, including variable wind and temperature profiles 13 p2117 A67-27702
- Semiconductor conductivity measurement from propagation irregularities of SHF electromagnetic waves in medium containing semiconductor 14 p2364 A67-27836
- HF conductivity of weakly ionized plasma, establishing expression for Lorentz plasma conductivity 14 p2355 A67-27954
- Dispersion relation for two-component model of collisionless nonrelativistic plasma with external magnetic field acting on system 14 p2356 A67-28201
- Infinitesimal pressure disturbance propagation in chemically reacting gas, deriving general equation for process, solution shows wavefront propagation at sound velocity [ASME PAPER 67-FE-2] 14 p2304 A67-28355
- Linear symmetric modes of propagation for viscous compressible liquid in rigid and elastic conduits analyzed using Navier-Stokes equations [ASME PAPER 67-FE-12] 14 p2304 A67-28361
- Tropospheric turbulence and structure derived from phenomenon of electromagnetic wave propagation 14 p2264 A67-28397
- Terrain irregularity influences on radio wave propagation and reflection 14 p2264 A67-28398
- Diversity distances and loss in path antenna gain, noting association with beam width 14 p2264 A67-28399
- Characteristic momentary pictures of two-dimensional electromagnetic wave fields with all boundaries conformally transformed into parallel planes, taken from motion picture 14 p2268 A67-28447
- Macroscopic linear fluid model of plasma radiation and scattering restricted to bounded media, emphasizing physical interpretation of wave constituents 14 p2359 A67-28463
- Directional dependency of slow tail ELF atmospheric waveforms, noting generation by cloud to ground type lightning discharges 14 p2312 A67-28571
- Energy conservation during propagation of unsteady waves, obtaining formula for complex intensity 14 p2349 A67-28633
- Soviet atmospheric turbulence studies considering microstructure, wave propagation in turbulent atmosphere, turbulent exchange in atmospheric ground layers, etc 14 p2346 A67-28763
- Synchronous and cyclotron wave behavior of electron flux in resonator with transverse electric field varying sinusoidally along wave propagation direction 14 p2288 A67-28807
- Propagation of small disturbances in general three-dimensional unsteady nonequilibrium MGD, noting influence of various parameters 14 p2361 A67-28904
- Flexural wave velocity-amplitude relation indicates possibility of stationary waves for fixed ratio of wave amplitude and spinning membrane angular velocity 14 p2403 A67-29016
- Propagation of coupled electromagnetic and electroacoustic waves in magnetized compressible stratified electron plasma 15 p2521 A67-29177
- Generation of quiescent variable-parameter arc plasma in strong magnetic field 15 p2523 A67-29228
- Solitary waves, discussing electron and ion acceleration and transfer mechanism of solar wind ion kinetic energy to electrons 15 p2475 A67-29613
- Polarization of complex wave form geomagnetic micropulsations of natural and artificial origin, using physical optics 15 p2476 A67-29620
- Introduction to method of characteristics covering propagation processes, relation to long water waves, gas flows, etc 15 p2472 A67-29677
- Interaction between SHF field and created plasma in electron-cyclotron resonance state 15 p2529 A67-29715
- Tables of Fresnel intensity reflectances from classical electrodynamics noting characteristics for amplitude minima, polarization maxima and 90 degrees phase difference [RE-TR-67-7] 15 p2518 A67-29769
- Troposphere and ionosphere effects on different frequency radio wave propagation for space communication [AAS PAPER 67-93] 15 p2437 A67-29953
- Range of undistorted propagation of traveling disturbances, noting shape of altitude-frequency characteristics of ionosphere with parabolic electron density distribution 15 p2479 A67-30074
- Ionospheric discontinuity motion in E layer at 100 km, using long distance ultrashort-wave propagation data obtained by diversity-reception method 15 p2479 A67-30148
- Nonlinear drift wave propagation arising from inhomogeneity transverse to magnetic field in plasma 15 p2531 A67-30187
- Dispersion equation for electromagnetic waves propagating in uniform plasma layer along boundary parallel to external magnetic field 15 p2532 A67-30255
- Waves with complex propagation constants in diaphragmed circular waveguide, solving dispersion equation for various frequencies and structural parameters of waveguide 15 p2438 A67-30262
- Finite-ion Larmor radius effect on wave propagation in rarefied rotating plasma, noting solar corona application 15 p2533 A67-30396
- Changes in structure of gas detonation wave with changes in initial pressure 16 p2656 A67-30452
- Electrostatic wave propagating into region of decreasing electron density calculated using one-dimensional plasma with uniform electron density 16 p2715 A67-31063
- Collection of papers on aerophysical studies of supersonic flows covering shock tube experiments, gas density, interferometer and photographic measurements, etc 16 p2672 A67-31101
- Field distribution in plasma waveguide at LF and large densities, noting dispersion properties of E and H waves 16 p2718 A67-31189
- Turbulent plasma state from unstable, current driven drift waves, noting ion damping effect on amplitude of spectrum, density gradient, etc 16 p2719 A67-31231
- Numerical analysis of structure of one-dimensional unsteady magnetic compression waves propagating into collisionless plasma, using motion equations 16 p2719 A67-31232
- Radio gain between simple dipole antennas for single propagation paths, noting effect of resistance from imperfect ground 16 p2625 A67-31342
- Polarization and angle of arrival fluctuations for plane wave propagated through turbulent medium 16 p2625 A67-31344
- Asymptotic behavior of transient signal propagation in lossless, isotropic plasmas for stepmodulated sine wave input signal 16 p2627 A67-31351
- Propagation of shear acoustic waves traveling parallel to magnetic field along symmetry direction in metal crystal 16 p2731 A67-31446
- Vlf transequatorial wave propagation, noting phase cycle slipping during sunrise transition 16 p2630 A67-31848
- Surface impedance of cylindrically stratified anisotropic ionosphere in presence of static magnetic field, calculating propagation parameters 16 p2631 A67-31853
- Attenuation rates at vlf from aircraft measurements presented as curves of dominant waveguide mode vs. geomagnetic bearing of propagation path 16 p2631 A67-31854
- Atmosphere effect on laser beam scintillation measurements after propagating over 8 km path near ground for various collector sizes and environmental conditions 16 p2686 A67-31879
- Decay and dispersion of disturbance pulse in fluid lines along pipe, considering velocity and pressure characteristics [ASME PAPER 66-WA/AUT-24] 17 p2835 A67-32017
- Dispersion equations for long wavelength beam instability propagating through homogeneous plasma 17 p2895 A67-32160
- Steady state plasma accelerators different from gas dynamic accelerators with Laval nozzles due to variety of waves, electric/magnetic fields, etc 17 p2898 A67-32185
- Infrasonic waves from auroral and magnetic activity, origin in supersonic movement of large scale auroral forms 17 p2841 A67-32209
- Thermal propagation in gases studied through heat transfer equation resulting from Fourier law 17 p2968 A67-32221
- Axisymmetric response of semiinfinite truncated cone striking smooth rigid obstacle, determining early stages of motion 17 p2960 A67-32422
- Book on radio astronomy covering history and fundamentals, wave propagation, radio sources, antennas and receivers, Boltzmann law, etc 17 p2943 A67-32432
- Impedance measurements in coaxial waveguide systems propagating TEM wave, using precision coaxial line standards and connectors 17 p2815 A67-32605
- Linear theory of collision-induced instability of partially ionized gases for waves propagating along external magnetic field 17 p2902 A67-32669
- Hydromagnetic wave propagation in collisionless plasma based on Vlasov equation, finding Alfven, magnetoacoustic and nonoscillating waves 17 p2902 A67-32673
- Nonstationary plane and axisymmetric flows, discussing acoustic and Oswatitsch theories, velocity potentials, differential equations of motion, etc 17 p2839 A67-32713
- Axially symmetric wave propagation in infinitely long two-layered cylinder, detailing displacement and stress distribution 17 p2961 A67-32778
- Plane wave propagation in kinetic theory, discussing Boltzmann equation use and asymptotic results beyond critical frequency 17 p2905 A67-32927
- Plane wave propagation in kinetic theory, noting Boltzmann equation and kinetic model 17 p2885 A67-32928
- Third order moduli of GaAs by measurement of ultrasonic wave velocities as function of applied stress 17 p2922 A67-33057
- Propagation in rectangular waveguide solved for traveling wave maser design by Rayleigh-Ritz method reduced to matrix eigenvalue problem 17 p2828 A67-33086
- Mass, momentum and energy conservation at wave fronts in coupled thermoplasticity, noting propagation velocities for isothermal/adiabatic discontinuities 17 p2964 A67-33134
- Axisymmetric two-dimensional elastic wave propagation equations for finite elastic bar, considering continuous and discontinuous loadings at impact end [ASME PAPER 67-APM-22] 17 p2964 A67-33151
- Steady state wave propagation in

homogeneous anisotropic media governed by symmetric hyperbolic partial differential equations 18 p3077 A67-33429

Thermal and elastic properties of ternary diamond-like semiconductor compounds, determining ultrasonic wave propagation rates 18 p3096 A67-33452

Soviet book on waveguide theory covering resonators, Maxwell equations role, eigenfunctions, etc 18 p3000 A67-33677

Wave propagation velocity in relativistic fluids determined using new hydrodynamic equations 18 p3025 A67-33683

Inhomogeneous hydrodynamic motion and thermal particle velocities effect on MHD wave propagation 18 p3086 A67-34034

Linear minimum variance estimation for random signal with complex phase errors, considering signal processing and optical propagation 18 p3001 A67-34111

Propagation and radiation of waves excited by electric dipole in dispersionless uniaxial moving medium 18 p3002 A67-34199

Resonance effects arising during sub-and supersonic waves expansion in aerodynamic cascade 18 p2984 A67-34216

Absorption by atmospheric oxygen and rain of mm waves, using device permitting continuous frequency variation 18 p3002 A67-34230

Linear theory of initially straight elastic rods, discussing wave propagation, thermal effects for extension and flexure and torsion 18 p3144 A67-34287

Alfven and magnetosonic wave generation and propagation in magnetosphere, detailing azimuth number approaching infinity 18 p3042 A67-34391

Directional fluctuations in light waves propagating from edge of solar disk caused by atmospheric turbulence 18 p3080 A67-34436

Light intensity fluctuations along inclined inhomogeneous path with variable turbulence characteristics in lower atmospheric layer 18 p3080 A67-34437

Propagation of narrow beam of light in turbid medium with strongly extended scattering 18 p3080 A67-34438

Propagation of elastic waves through composite media studied with ultrasonic pulse technique, noting Poisson ratio, bulk modulus, etc 18 p3069 A67-34488

Electromagnetic wave reflection and transmission by moving plasma medium as function of velocity 18 p3091 A67-34633

Glow discharge positive column response to external perturbations, obtaining moving striations profile, structure and backward wave nature 19 p3273 A67-35094

Wave propagation and electron beam-plasma interaction in plasma column inside magnetic field, measuring plasma characteristics and spatial distribution 19 p3275 A67-35107

Ionizing wave in plasma gun with crossed electric-magnetic fields, obtaining burning voltage of discharge and bias magnetic field ratios 19 p3277 A67-35123

Soviet book on wave propagation in turbulent atmosphere covering geometric optics of electromagnetic and acoustic wave scattering and propagation, etc 19 p3182 A67-35206

Cyclotron harmonic wave propagation in warm magnetoplasmas predicted theoretically for perpendicular and oblique damping 19 p3288 A67-35371

LF acoustic/magnetoacoustic wave propagation in partially ionized plasmas studied within framework of macroscopic plasma dynamics, using dynamic adiabatic state equation 19 p3290 A67-35375

Nonlinear effects of laser radiation interaction with turbulent dense plasma, discussing wave propagation, plasma diagnostics, etc 19 p3291 A67-35385

Wave propagation and geometrical optics in random media, considering applications to solar corona heating by energy transfer, stellar scintillation and cosmic ray acceleration 19 p3261 A67-35507

Guidance of audio-frequency electromagnetic waves along earth magnetic field investigated in absence of field-aligned irregularities of ionization density 19 p3225 A67-35608

Linearized system of water waves initial value problem, obtaining eigenvalue with parameter in boundary condition 19 p3210 A67-35703

Wave propagation in real gases, considering one-dimensional time-dependent disturbances semiinfinite in extent, emphasizing matched asymptotic expansion and coordinate stretching methods 19 p3212 A67-35798

Wave propagation in anisotropic plasma in presence of electron density irregularities, noting Faraday effect 19 p3184 A67-35825

Plastic wave propagation in semiinfinite bar subjected to axially applied impact stress 20 p3536 A67-36416

Light beam propagation in atomic vapor, with atoms undergoing magnetic resonance, describing electromagnetic wave polarization 20 p3458 A67-36435

Wave propagation in ferrite-filled rectangular waveguide with transverse magnetization 20 p3382 A67-36864

Electric vector expression of amplitude-modulated electromagnetic wave propagating in nonlinear dispersive medium 20 p3499 A67-36992

Doppler effect wave radiation experiment correction equations developed for source, observer and medium 20 p3486 A67-37005

Guided waves on infinite cylindrical cavity in magnetotonic medium noting wave solutions, phase velocity, plasma frequencies, etc 20 p3383 A67-37107

Guided wave characteristics in infinite free space cylindrical cavity in magnetotonic medium noting resonance, transition, cut-off frequencies, phase velocity, etc 20 p3383 A67-37108

LF and HF wave excitation in homogeneous plasma with external magnetic field, obtaining differential and integral wave intensities 20 p3501 A67-37142

Ultrashort optical pulse propagation in two-level medium, describing pulse shapes by solving partial differential equation 20 p3461 A67-37286

Highly asymmetric equation for MHD resonance of guided poloidal mode solved using dipole coordinates 20 p3502 A67-37427

Plasma wave propagation dispersion in sodium and potassium at cryogenic temperature using Landau-Fermi liquid theory 20 p3514 A67-37570

HF skywave propagation computer model for interference prediction 20 p3387 A67-37646

X-band propagation over rough earth when illuminated by radiation, studying scattering problems 20 p3388 A67-37647

Wave propagation and flow past obstacle in fluid magnetodynamics 20 p3503 A67-37676

Plane waves propagation in microelastic medium having only coupled stresses 20 p3542 A67-37681

Wave propagation in nonuniform slightly gyrotropic medium with parameter less than one solved by differential equations 20 p3389 A67-37708

Ionization and recombination effects on MHD wave propagation through three-component magnetoplasma, deriving nonlinear motion equations 21 p3660 A67-37743

Ion cyclotron wave propagation in plasma, considering Larmor radius effects, quasi-static dispersion relation, phase velocity and cyclotron resonance 21 p3661 A67-37750

Perturbation method using stream function for investigating anisotropic wave propagation describable by hyperbolic differential equations 21 p3611 A67-37891

Thermoelastic coupling effect on propagating discontinuities in stresses and particle velocities studied using characteristic method 21 p3715 A67-37893

Wave propagation rate in elastoplastic bodies under completely plastic conditions, noting discontinuity magnitude 21 p3716 A67-37968

Absorption of VHF waves in whistler mode at low latitudes calculated for various ionospheric conditions during sunspot activity 21 p3617 A67-38065

Soviet papers on wave propagation and diffraction problems 21 p3579 A67-38107

Asymptotic representations of Whittaker functions /with terms of standard equation coefficients equal/ applicable to wave propagation in inhomogeneous media 21 p3652 A67-38109

Wave propagation in inhomogeneous half-space with refractive index depending on two coordinates analyzed, using parabolic equation method 21 p3580 A67-38114

Optimal wave path parameters determined by experimentally recorded pulsed signals processing, using least squares method 21 p3580 A67-38120

Axial shear wave radial propagation in nonhomogeneous elastic medium under axisymmetric loading solved by Laplace transform and characteristics method 21 p3719 A67-38146

Converging cylindrical and spherical detonation wave behavior in polytropic perturbed medium, noting self-similar solution 21 p3612 A67-38285

Dispersion equation for frequency dependence on wave amplitude propagated in plasma placed in constant magnetic field causing longitudinal oscillations 21 p3669 A67-38681

Isolated longitudinal wave pulse amplitude and phase velocity dependence on trapped particle density in ion-electron and electron-positron plasmas 21 p3669 A67-38683

Fast and slow magnetosonic wave propagation in plasma analyzed by Huygens principle 21 p3670 A67-38687

Effect of finite aperture dimension of antenna in vertical plane on conditions of ultrashort wave propagation within limits of direct visibility 21 p3600 A67-38944

Dispersion relations for elastic wave propagation in filamentary composites obtained, establishing averaging rules for elastic constants 21 p3729 A67-39055

Ducted acoustic gravity wave propagation in isothermal atmosphere, obtaining dispersion relations ducted modes and surface wave in incompressible medium 21 p3623 A67-39057

Boundary value problems of wave propagation in plane, investigating coverage, source distribution and velocity perturbations 21 p3615 A67-39093

Alfven, fast and slow magnetoacoustic and entropy hydromagnetic wave propagation in anisotropic collisionless magnetoplasma 22 p3843 A67-39268

Dispersion equation for extraordinary and plasma waves propagating through magnetoplasma perpendicular to external magnetic field studied near lower hybrid frequency 22 p3844 A67-39419

Ion wave velocities and damping measurements in quiescent plasma used for diagnosis of temperatures and drift velocities 22 p3846 A67-39488

Helical electromagnetic wave scattering and transformation during propagation in magnetoplasma, considering fluctuations 22 p3846 A67-39501

Microwave pulse compression filter using dispersive characteristics of propagating magnetostatic spin waves in single crystal YIG rods 22 p3773 A67-39908

Laminar nonrelativistic finite amplitude hydromagnetic wave propagation in low temperature ionized plasma, using two-fluid model 22 p3852 A67-39990

Ducted silo launchers transient pressures caused by rocket engine ignition and shutdown, treating wave propagation by one-dimensional theory 22 p3780 A67-40091

Coherent Raman amplification dynamics, considering pump depletion and coupling saturation and stimulated Raman scattering by polarization waves 22 p3816 A67-40318

Rapid magnetic field variations observed in magnetosheath evaluated in terms of transverse modes of plasma wave propagation 23 p3995 A67-40804

Ion wave propagation in weakly ionized gases 23 p4032 A67-40960

Wave propagation in wave optics transition to geometrical optics in general relativity theory using series expansion 23 p4027 A67-41146

Wave propagation in random plasma medium with inhomogeneous parabolic electron density profile background for ionospheric propagation applications 23 p3974 A67-41199

Compensation method for longitudinal slot effects on propagation constant and characteristic impedance of rectangular waveguide used in standing wave meter 23 p4000 A67-41220

Photoelectric records of DE and LZE in solar photosphere velocity fields, analyzing oscillations onset and lifetimes 23 p4066 A67-41229

Transmission phenomenon of

inhomogeneous electromagnetic wave in negative permittivity medium 23 p3975 A67-41480

Surface wave propagation around sharp corners in single wire transmission lines, calculating and measuring radiation loss and pattern 24 p4119 A67-41971

VLF transmissions during SIDs for compatibility with general form of theory of waveguide mode 24 p4149 A67-42067

Maxwell equations solved for Gaussian beam form in anisotropic medium, discussing laser applications 24 p4187 A67-42092

Geomagnetic field aligned irregularities, explaining ionospheric E-region scattered wave propagation 24 p4120 A67-42150

Dispersion of surface waves propagating in elliptical and rounded flat helices, discussing resonance effects 24 p4121 A67-42236

Parametric amplification of traveling wave tube through coupled wave method noting role of phase velocities of space charge waves 24 p4130 A67-42241

Wave propagation in plasma with anisotropic pressure studied using modified Burgers equations, examining effect of collisions 24 p4197 A67-42260

Propagation in periodically deformed circular and rectangular waveguides 24 p4121 A67-42287

Circularly polarized nonlinear electromagnetic waves in conservative centrally symmetric dielectric, considering reflection, transmission and propagation 24 p4168 A67-42481

Complex wave propagation and coupling in inhomogeneous media, discussing WKB type amplitude coefficients and electromagnetic and space charge waves 24 p4123 A67-42657

Synergetic approach to problems of nonlinear dispersive wave propagation interaction 24 p4125 A67-43093

WAVE RADIATION

SA SHORT WAVE RADIATION

Axial nonuniform perturbations of electromagnetic propagating structures analyzed, using nonlinear phase progression from perturbation theory of quantum mechanics 16 p2626 A67-31345

Scalar gravitational fields in pulsating stars, calculating scalar wave radiation rate and star relaxation time 17 p2952 A67-33319

Ionosphere collision frequencies and densities studied by rocket measurements of magnetic field of VLF wave radiated from ground 18 p3041 A67-34233

Doppler effect wave radiation experiment correction equations developed for source, observer and medium motion 20 p3486 A67-37005

Vertical distribution of mechanical wave energy density in lower atmosphere and energy fraction escaping to high altitudes derived by integral transform methods 21 p3655 A67-39088

WAVE RECORDER

IR spectroscopy using Michelson interferometer coupled with computer and wave analyzer 07 p1190 A67-20272

WAVE REFLECTION

Velocity propagation of stable detonations in gas mixtures determined, using Doppler effect obtained by electromagnetic wave reflection 01 p0186 A67-10229

Wave front scattering and refraction by laser spark studied by holograms of air plasma formed by giant ruby laser pulse 01 p0087 A67-10234

Behavior of stationary electromagnetic field produced by reflection of given incoming stationary field for small frequencies 01 p0024 A67-10523

Permittivity determination based on change in polarization of wave at reflection 02 p0191 A67-11578

Rectilinear and smooth multiwave transition 02 p0215 A67-11914

Spaced receiver method for measuring ground diffraction pattern of vertically reflected radio waves 03 p0407 A67-12830

Successive approximations for determining direct and backward wave in inhomogeneous medium and consequently reflection coefficient and total field 03 p0467 A67-12893

Reflection and refraction of plane MHD waves at plane interface discontinuity of two semilinear homogeneous conducting fluids of different densities 03 p0480 A67-13727

Refraction of plane shock wave by interface between different gases, reducing motion equation to polynomial of degree 12 04 p0601 A67-14465

Ultrasonic reflectivity of liquid-solid interface used as indicator of near surface properties of solid in cold work, grain orientation, etc 04 p0621 A67-15264

Stationary and reflected shock wave produced in moving argon plasma interacting with stationary magnetic field 05 p0850 A67-18067

Backscattering of centimeter waves from ruffled sea surface at small angles of slip 05 p0761 A67-18345

Approximate computer method solution to impact problem of elastoplastic wave reflection from flexible plates in resisting medium 05 p0919 A67-16495

Analogy between radiation angular spectrum reflected from rough surface and frequency spectrum of carrier burst related to radio propagation 06 p0957 A67-17579

Prediction and scaling of reflected impulse from strong blast wave, with experimental correlation 06 p0984 A67-18059

Plasma parameter determined from measurements of wave reflection coefficient in waveguide 06 p1041 A67-18187

Stress waves reflection and transmission in composite laminates and parameters affecting ability to resist fracture by hypervelocity impact [AIAA PAPER 87-140] 06 p1102 A67-18289

Reflection and transmission of birefringent plates surrounded by semilinear birefringent media with incident waves having polarized electric fields 06 p1033 A67-18544

Successive approximations for determining direct and backward wave in inhomogeneous medium and consequently reflection coefficient and total field 06 p1034 A67-18771

Nonlinear second harmonic generation of current density in inhomogeneous magnetoplasma and reflected electromagnetic wave from free space interface 06 p1046 A67-18825

Geometrical approximation of amplitude and surface-curvature parameters of wave front reflected or refracted from curvilinear boundary interface 08 p1294 A67-20815

Bending effect of spectral lines in plasma created by rotating HF dipole in quasi-steady magnetic field 08 p1358 A67-20854

Power reflection technique for high quality varactor diode characterization 08 p1304 A67-21221

Impossibility of three confluent shocks in two-dimensional irrotational flow proved independently of state equation 08 p1322 A67-21383

Trajectory of rebounding detonation wave in approximate analytic solution of nonlinear equation of motion 10 p1626 A67-23152

Plane electromagnetic wave reflection and refraction by semilinear dielectric medium moving uniformly parallel to surface analyzed for arbitrary incidence plane orientation 11 p1820 A67-24909

Reflection and transmission of electromagnetic waves at interface between stationary isotropic medium and moving anisotropic medium 11 p1820 A67-24919

Geometrical optics approximation of plane electromagnetic wave reflection from ideally electrically conducting triaxial ellipsoid 11 p1754 A67-24986

Reflection coefficients for electromagnetic waves obliquely incident on sinusoidally stratified half-space 13 p2066 A67-26481

Gravitational wave propagation from upper to lower atmospheric layers analyzed taking into account reflection and refraction 13 p2112 A67-26673

Refraction and reflection of shock waves from interface between media having different densities 13 p2105 A67-27414

Ionospheric structural studies via absorption measurements 14 p2378 A67-27911

Plane shock wave propagation in inviscid perfect gas colliding with right angle obstacle, determining flow in perturbed region 14 p2296 A67-27979

Bilinear current density induction of double-frequency laser beam from superconducting metal 14 p2371 A67-28722

Goniometric measurements of two angles defining direction of incoming 30 MHz wave reflected by meteor streams, using radio link 14 p2390 A67-28900

Ion cyclotron resonance heating limitation in shallow magnetic beach explained by wave reflection 15 p2523 A67-29212

High frequency asymptotic behavior of wave field in two-dimensional diffraction problem on inhomogeneous cylinder of arbitrary cross section 16 p2628 A67-31505

Two-dimensional viscous fluid flow with formulation and solution of weak shock reflection problems by numerical method 16 p2662 A67-31534

Plane shock wave reflected from heat-conducting wall analyzed by method of matched asymptotic expansions 16 p2662 A67-31555

Density and pressure in real gas behind plane shock wave upon reflection from solid surface 17 p2836 A67-32072

Propagation velocity of stable detonation wave in gaseous mixtures measured using Doppler effect resulting from reflection of electromagnetic wave from front of detonation wave 17 p2970 A67-32806

Optical means for enhancing quantum efficiency of tri-alkali photocathode, discussing standing wave pattern in spaced-reflective and reflective photocathodes 17 p2861 A67-33287

Continuous wave signals from Lunar Orbiter I after reflection from lunar surface, noting mapping use 17 p2817 A67-33364

Electromagnetic wave reflection and transmission by moving plasma medium as function of velocity 18 p3091 A67-34633

Holographic devices and principles, discussing application to plasma studies 19 p3228 A67-34949

Electromagnetic wave reflection by stratified magnetoplasma, obtaining formulas providing perturbation effect on reflection coefficients 19 p3183 A67-35457

Plasma wave influences on metal surface reflectivity investigated using Maxwell equation, calculating dielectric constant and conductivity 19 p3262 A67-35581

Electromagnetic radiation reflectivity on metal surface investigated using microscopic model to derive fields and boundary conditions 19 p3262 A67-35582

Millimeter wave reflectance for semiconductor panel, air space and metal reflector arranged planarily, discussing reflectance variation with conductivity and complete absorption 20 p3510 A67-37025

Electron beam deflection by standing light wave of laser shows momentum transfer resulting in Bragg relationship for reflection angle 20 p3461 A67-37185

Reflection of incident right and left hand circularly polarized plane electromagnetic waves from anisotropic helium afterglow plasma 20 p3389 A67-37707

Incident and reflected shocks from laminar and turbulent boundary layers measured over various Mach numbers 21 p3610 A67-37771

Green function for SH-line source in wedge-shaped medium with apex removed by circular cylinder, determining reflected and refracted fields 21 p3579 A67-37925

Reflection in water of plane shock waves from rigid wall 21 p3611 A67-38058

Reflected wave amplitude dependence on degree of inhomogeneity of medium 21 p3580 A67-38112

Plane electromagnetic wave reflection from rough surface, calculating energy and polarization characteristics 21 p3580 A67-38115

Two-tilt compensating interferometers, using vector form of reflection law 22 p3796 A67-39236

Lower ionospheric drift studied from signal recordings from distant medium wave broadcasting stations 22 p3788 A67-39467

Re-reflected shock wave from convergent cylindrical channel, showing secondary shock wave overtaking primary wave 22 p3783 A67-39720

Kinetic model of Tonks-Dattner absorption resonances in plasma positive column providing plasma wave reflection mechanism 23 p4031 A67-40782

Circularly polarized nonlinear electromagnetic waves in conservative centrally symmetric dielectric, considering reflection, transmission and propagation 24 p4168 A67-42481

Shock wave reflection with vibrational relaxation times investigated by matching characteristics equation to shock wave

equation 24 p4144 A67-42564
Heat transfer to end wall of shock tube after shock wave reflection through steep temperature gradient analyzed using variational method 24 p4257 A67-43092

WAVE RESISTANCE
Vortex breakdown theory, considering small energy losses and small flow force reduction /wave resistance effects/ 13 p2095 A67-26908
Possibility of Cerenkov effect in superconductors established from electromagnetic oscillation spectrum, calculating wave resistance and resonance maxima positions 14 p2375 A67-29079

WAVE SCATTERING
SA ATMOSPHERIC SCATTERING
Wave front scattering and refraction by laser spark studied by holograms of air plasma formed by giant ruby laser pulse 01 p0087 A67-10234
HF random phase transverse wave transmission through turbulent plasma generating scattered waves at combination frequencies 01 p0121 A67-10343
Gaussian noise model of shadowing effect on wave backscatter from one-dimensional random rough surface 02 p0192 A67-11602
Transformation of transverse oscillations of electron flux by short magnetic lenses studied by eigenvector concept 02 p0214 A67-11900
Dispersion equations of ring delay circuit formed by bending diaphragmed rectangular waveguide in H plane 02 p0214 A67-11903
Submillimeter wave scattering by fog, comparing experiments in clear atmosphere and dense fog 02 p0199 A67-12078
Monostatic scattered ultrasonic wave calculated as function of distance of reflector projection from source 03 p0369 A67-13551
Scattering of plane wave by grating of identical cylinder specialized for case in which individual elements of grating scatter isotropically 03 p0374 A67-14353
Scattering of line-source radiation by circular cylinder, noting plane wave approximation 03 p0374 A67-14356
Idempotent method solution of transport equations for radiative heat transfer in nonisothermal anisotropic scattering medium between two parallel plates [ASME PAPER 66-WA/HT-28] 04 p0725 A67-15441
Transmission coefficient for passage of electromagnetic wave through circular aperture in plane diaphragm 04 p0577 A67-15657
Radiative heat transfer and intensity distribution in one-dimensional absorbing isotropic scattering medium 04 p0737 A67-15862
Temperature dependence of dielectric constant and existence of microwave dispersion in barium titanate above Curie point 05 p0888 A67-17060
One-dimensional inverse problem of scattering theory, noting differential equation reduction, determining traveling wave coefficient 05 p0765 A67-17158
Angular distribution of intensity and phase of electromagnetic wave scattered by cylindrical plasma column 06 p1041 A67-18138
Radiation and scattering of transient gravity waves by thin vertical plates in deep ocean 06 p0985 A67-18188
Oscillatory magnetoabsorption of direct transition in layer compound gallium selenide near absolute 06 p1060 A67-18918
Plane wave scattering by medium with strong fluctuations of refractive index, noting reentry condition 07 p1141 A67-19441
Finite scattering matrix for plane wave excited infinite array in relating array number and active element properties 07 p1151 A67-19442
Electromagnetic and electroacoustic waves and scattering in compressible plasma 07 p1141 A67-19443
Optical and acoustic waves and scattering in compressible plasma treated by ray optical method 07 p1141 A67-19444
Microwave third harmonic generation in homogeneous semiconductors at low temperatures, noting ionized impurity scattering effect 08 p1388 A67-20701
High resolution radar correlometer measurement of spatial correlation radius of RF radiation scattered by disturbed ocean surface 08 p1294 A67-20819

Random deviation statistical analysis of acoustic and electromagnetic waves by comparatively large slope irregularities 08 p1294 A67-20820
Noise energy spectra created by wave-wave scattering of quasi-longitudinal waves in magnetoactive plasmas with different electron and ion temperatures 08 p1365 A67-21413
Comparison of distribution functions from reduced data records for scattering of electromagnetic waves by randomly moving spheres in container 09 p1461 A67-21598
HF random phase transverse wave transmission through turbulent plasma generating scattered waves at combination frequencies 11 p1843 A67-25016
Lunar radar echoes depolarization studied via lunar surface backscattering characteristics at 23 cm wavelength 14 p2261 A67-28374
Multiple scattering of electromagnetic waves by arbitrary configurations extended to three-dimensional vector case 15 p2435 A67-29197
Doppler effect method for measuring effective scatter area in laboratory 15 p2443 A67-29286
Temperature dependence of dielectric constant and existence of microwave dispersion in barium titanate above Curie point 15 p2538 A67-29791
Scattering of surface wave incident upon junction of two semi-infinite planes joined together by step analyzed using Wiener-Hopf equation 16 p2626 A67-31348
Interaction of incident H-wave with infinite conducting cylinder coated with inhomogeneous and anisotropic plasma sheath, noting far field pattern of scattered field 16 p2626 A67-31350
Magnetohydrodynamic wave dispersion theory at open end of semiinfinite plasma waveguide closed by conducting diaphragm 16 p2722 A67-31574
Extension to three dimensions of Wentzel-Kramer-Brillouin approximation method for quasi-classical wave function, applicable to axisymmetrical problems 16 p2703 A67-31920
Plane wave scattering by finite circular cylinder treated by geometrical diffraction theory, obtaining formulas for radar cross section 17 p2816 A67-32789
Electromagnetic wave scattering from plasma wave analyzed using Vlasov equations for anisotropic plasma, applying formulas to boundary value problems 18 p3088 A67-34090
Influence of dissipation of acoustic waves on temperature rise in chromosphere 18 p3125 A67-34192
Wave scattering phenomenon on uneven surfaces 18 p3004 A67-34380
Principal polarization radar cross sections as function of azimuth aspect angle for rectangular cylinder 19 p3183 A67-35518
Dispersion equations for two types of transverse interaction tubes analyzed numerically in presence of strong space charge 19 p3198 A67-36022
Scattering amplitude of frequency spectrum components of isolated exponential acoustic pulse incident on hard sphere 21 p3657 A67-38057
Electromagnetic wave scattering by rectangular geometry dielectric wedge, using precise boundary conditions 21 p3585 A67-38688
Far tropospheric propagation of radio waves due to coherent scattering, explaining signal level dependence on distance and wavelength and signal fading 21 p3585 A67-38814
Structures of glow discharge and evaporated silicon oxide films determined by measuring intensity of electron wave scattering at large angles, describing measurement method 21 p3687 A67-39139
Scattering of plane electromagnetic wave obliquely incident on surface of two coaxial disks investigated via separation of variables 22 p3758 A67-39306
Plane circularly polarized magnetoelastic and elastic wave scattering at plane discontinuity surface between ferromagnetic insulating medium and elastic medium 22 p3856 A67-39364
Turbulence effect on accuracy of microwave cut-off measurements of plasma density suggests electromagnetic wave scattering 22 p3845 A67-39430
Combined frequency and space correlation

of wave fields scattered by rough surfaces where conditions of applicability of Kirchhoff approximation hold true 22 p3760 A67-39660
Electrostatic relaxation wave dispersion in isotropic Lorentz gas, considering Landau damping and balancing of elastic electron-atom collisions 22 p3848 A67-39692
Tenuous high temperature plasma electromagnetic wave scattering, with relativistic corrections for scattered radiation spatial and spectral distribution 22 p3849 A67-39699
TM and TE mode uncoupling in oblique wave scattering from radially inhomogeneous cylinders 22 p3763 A67-40308
Field scattering by convex cylinders solved by asymptotes expressing reduced wave equations 23 p3972 A67-40751
[NYU-EM-217]
Geometrical self-shadowing of random rough surface described by Gaussian statistics in wave backscattering phenomena 23 p3972 A67-40832
Currents in load impedance of transmission lines near cylindrical scatterer noting antenna field 23 p3981 A67-41209
Dispersion equations for rectangular helix in presence of plasma 24 p4121 A67-42235
Scattering from half-loop on conducting plane obtained through image theory, considering electric and magnetic dipole contributions 24 p4121 A67-42265

WAVE SUPERHEATER
SA ENERGY TRANSFER
SA SHOCK HEATING
Wave superheater based on shock tube principles, discussing application in scramjet design 21 p3608 A67-38800

WAVEFORM
AC differential correlator for measuring small delays between two identical binary output waveforms 01 p0037 A67-10482
Rectilinear and smooth multiwave transition 02 p0215 A67-11914
Pneumatic oscillator producing triangular waveforms of pressure vs time, using freely floating disk [ASME PAPER 66-WA/AUT-4] 04 p0555 A67-15388
Signal design problem of optimal waveforms for transmission through phase incoherent channel 06 p0962 A67-17945
Charge transport equations used to determine transient waveforms of FET as function of gate current and drain current 07 p1153 A67-19614
Integrated film reading and display system, discussing characteristics of waveform display/ analyzer subsystems and scanning/recording requirements 07 p1148 A67-19742
Waveform and filter design for acceptable performance in clutter environment 07 p1145 A67-19880
Performance of wideband interferometers using interferometer ambiguity function for radar application 08 p1300 A67-20680
Waveform independent condition for transmission coefficient in linear time-independent transmission system to provide upper limit to signal distortion 10 p1620 A67-23572
Optimization techniques for linear matched filters to obtain maximum signal to noise ratio for certain signal waveforms 10 p1621 A67-23573
Spectrum, correlation and probability analysis of arbitrary waveforms 12 p1905 A67-25732
Matched-filter systems waveform dependence investigated for signal detection in nonstationary clutter 15 p2438 A67-30135
Analog-to-code converter using negative resistance of unijunction transistor, noting construction and results 16 p2636 A67-30900
Asynchronous pulse modulation systems developed using step and linear segment approximations of message waveforms 17 p2812 A67-32318
Multidigit delta modulation system using individual optimized stages developed by successive approximation of message waveform 17 p2812 A67-32319
Design of optimal waveforms for optimal estimation or prediction of state of linear dynamical system in presence of Markov and white noise 19 p3201 A67-34965
Flat-top pulse waveform with high transmission efficiency, confined spectra and

- good electromagnetic compatibility 20 p3388 A67-37654
- ELF waveforms spectral estimation at discrete frequencies of each polarity used for statistical comparison of mean spectra show normal distribution 22 p3789 A67-39474
- Noctilucent cloud fine structure wave form due to visibility through ice condensed on dust particles in wave-like pattern 24 p4146 A67-41791
- Distant atmospheric wave form at night analyzed using digital computer for VLF phase spectra 24 p4149 A67-42068
- Book on radar signals covering FM pulse compression signals, waveform, Doppler shift, time factor, etc 24 p4122 A67-42425
- WAVEGUIDE**
- SA BEAM WAVEGUIDE
- SA MICROWAVE FILTER
- SA PLASMAGUIDE
- SA RECTANGULAR GUIDE
- Negative resistance of waveguide-mounted tunnel diode decrease with frequency suggested as source of oscillations at frequencies above cut-off 01 p0032 A67-10001
- Expansion of E type symmetrical oscillations in axisymmetrical delay systems used in calculation of cylindrical resonators 01 p0035 A67-10394
- Inductive and capacitive tunable tunnel diode harmonic generator in waveguide 01 p0035 A67-10437
- Transmission power of dielectric waveguide 01 p0038 A67-10716
- Electromagnetic wave propagation in two waveguides with different cross section connected by long continuous slot 01 p0038 A67-10717
- Mode transformation due to slightly tilted waveguide tube treated as boundary value problem 01 p0040 A67-11233
- Waveform coefficient variation F-matrix analysis of electromagnetic wave propagation in light waveguide with gas lens, considering field distribution and impedance analogy 01 p0026 A67-11237
- Radio wave guiding along electron density discontinuity in magnetospheric exosphere, noting low dispersion modes 01 p0027 A67-11259
- Simulation of curvature in straight model earth-ionosphere waveguide, using planar structure loaded by inhomogeneous dielectric 01 p0040 A67-11310
- Millimeter and centimeter radio wave propagation in near sea level tropospheric waveguides 02 p0191 A67-11569
- Mutual coupling between TEM and TE 01 parallel-plate waveguides calculated, using wedge diffraction techniques 02 p0211 A67-11596
- Lambda 1 distribution in circular aperture energizer for low noise parabolic antennas 02 p0214 A67-11796
- Radio wave propagation in multimode waveguides of arbitrary height, assuming ionosphere boundary to be perfectly reflecting 02 p0198 A67-12070
- Electric motor energized by microwaves in waveguides at S-band, investigating speed, torque and frequency characteristics 02 p0183 A67-12116
- Kinetic theory for passage of electromagnetic wave through plasma layer in waveguide with metallic walls, assuming negligible transverse particle motion due to strong magnetic field 02 p0205 A67-12474
- Ferrite resonant isolators on coaxial, strip and rectangular waveguides with dielectric 02 p0223 A67-12670
- Reflection coefficient of tapered waveguide determined via coupled mode theory, noting error estimation and design of reflectionless tapers 03 p0376 A67-12802
- Critical conditions of waveguide with dielectric bushing for case of nonsymmetrical waves 03 p0378 A67-13287
- Waveguide Interactometer measurement of plasma parameters 03 p0477 A67-13458
- Excitation of dipole wave in circular small delay dielectric waveguide by sources with amplitudes and phases variously distributed over apertures 03 p0385 A67-13953
- Slot filters for H waves in circular waveguide 03 p0386 A67-13960
- Dispersion formula for waveguide irises with rounded inner edges 04 p0579 A67-14415
- X sub L band waveguide switches using p-i-n diodes for switching elements in SP2T, SP4T and SP8T microwave switches 04 p0580 A67-14863
- Radio propagation in microwave terrestrial model waveguide of variable surface impedance, using reciprocity theorem 04 p0570 A67-14865
- Field distribution at bends in circular zero-normal H and cylindrical surface waveguides 04 p0586 A67-15635
- Damping and phase characteristics of gas-filled metallic waveguides near cut-off frequency, noting ammonium case 04 p0576 A67-15656
- Omnidirectional slot antenna with two slots resonant at frequencies nearly octave apart and fed by single common waveguide 04 p0590 A67-15904
- Propagation constant of electromagnetic waves over earth surface 05 p0780 A67-16001
- Gas discharge in argon maintained within waveguide by microwave signal at cyclotron resonance, observing second harmonic radiation 05 p0850 A67-16046
- Electromagnetic field emission of infinite package of impedance half-planes produced by cophasal linear sources 05 p0762 A67-16352
- Total energy loss in weakly irregular multiwave waveguide accounted for by energy losses in weakly damped waves 05 p0775 A67-16965
- Single wave approximation of fields of cylindrical delay system with basic E-type wave propagating at variable phase velocity 05 p0767 A67-17398
- Wave diffraction on surface impedance discontinuity in coaxial waveguide 06 p0968 A67-17856
- MNT-VZ-V device for simulating electromagnetic field in radio waveguides by induced current method 06 p1001 A67-17937
- ELF and VLF wave propagation in earth-ionosphere waveguide at wide frequency range, giving amplitude spectra and mean phase velocity for day and night 06 p0994 A67-17970
- Resonators use for higher sound attenuation in waveguide with sound absorbing cladding 06 p1032 A67-18397
- Automatic phase sensor for waveguide combiner in S-band ground tracking and space communication 07 p1149 A67-19051
- Coupling coefficients of waves in variable cross section waveguides with impedance wall 07 p1143 A67-19602
- Amplitude and phase velocity of electromagnetic waves in 1-30 kc range near earth surface for plane and spherical earth-ionosphere waveguide 07 p1144 A67-19695
- Propagation coefficient of rectangular waveguide containing centrally placed semiconducting film 07 p1146 A67-20202
- Semiconductor loaded E plane T waveguide junction spectrometer for microwave measurement of transport parameters in semiconductors 08 p1329 A67-20375
- Higher order waveguide mode radiation incorporated antenna feed systems for performance improvement, evaluating S-and C-band dual frequency Cassegrain feed 08 p1300 A67-20681
- Miniaturized C-band digital latching phase shifter for combined advantages of waveguide and stripline design 08 p1305 A67-21227
- Stochastic waveguides containing media with constitutive parameters having random variations not necessarily small or statistically homogeneous [SR-2] 09 p1460 A67-21593
- Gas ionization by fast electron beam directed along waveguide leading to longitudinal distribution of secondary electron concentration 09 p1545 A67-22002
- Bidirectional waveguide theorems derived directly from transverse and longitudinal components of Maxwell equation and generalization to include nonbidirectional waveguides 09 p1464 A67-22091
- EH solutions of Maxwell equations describing guided electromagnetic waves in homogeneous isotropic medium at velocity of light 09 p1465 A67-22550
- Plasma column and plasma beam of same radius situated in coaxial waveguide under magnetic field, obtaining dispersion equation 09 p1465 A67-22551
- Ultrarapid AM of hyperfrequency mm wave in waveguide 09 p1465 A67-22568
- Light beam waveguide using lens-like media with periodic hyperbolic temperature distribution, discussing construction, optimum design and operating conditions 10 p1606 A67-23066
- Standing wave solution of homogeneous waveguide field distribution for H-10 wave after conformal mapping and effect of capacitive and inductive irises 10 p1607 A67-23571
- Lecher system with finlines providing transition to waveguides for incorporation in microwave interferometers with high spatial resolution 10 p1658 A67-23785
- Optimal reception of signal transmitted through channel with randomly varying parameters, measuring amplitude and phase 11 p1751 A67-23914
- Scattering matrix equations for waveguide structure of varying surface impedance boundaries 11 p1751 A67-23968
- Waveguide discontinuity problems solved through matrix iterative analysis 11 p1760 A67-24237
- Waveguide dispersion effect on radiation pattern and directivity of series-fed linear arrays 11 p1762 A67-24289
- Peak and average output power of cyanide laser in far IR measured, indicating usefulness of available oversize waveguide instrumentation at HF 11 p1801 A67-24715
- Rectangular to cylindrical waveguide transducer which couples dominant rectangular and cylindrical transverse electromagnetic modes 11 p1767 A67-24733
- MHD wave propagation in magnetoplasma-filled waveguide, discussing pressure, current inertia, resistivity, etc 12 p1969 A67-25247
- Advances in microwaves, Volume 1, covering stanford accelerator design, directional couplers, waveguide singular integral equations, Lie algebras, microwave network application, etc advances in microwaves, Volume 1, covering 12 p1906 A67-25975
- Material properties and capabilities of different types of optical waveguides including iterative electromagnetic wave beams, reflecting pipes, fiber guides, etc 12 p1906 A67-25976
- Variational, quasi-static and integral equation analytic waveguide solutions, extending singular integral equation to homogeneous and inhomogeneous loaded waveguide junction 12 p1906 A67-25978
- Cylindrical partially filled waveguides of rectangular cross section, formulating boundary value problem and characteristic equation 12 p1906 A67-25980
- Microwave power coupling from waveguide to helicon mode in doped indium antimonide by placing aluminum oxide cones on semiconductor surface 12 p1986 A67-26160
- Propagation characteristics in waveguide loaded with cylindrical semiconductor rod, calculating electric field distribution 12 p1918 A67-26222
- Book on open resonators and open waveguides 13 p2075 A67-26461
- Field solution of TE sub k zero mode wave incidence on inductive iris in rectangular waveguide 13 p2066 A67-26475
- Probability of ray position in beam waveguides 13 p2066 A67-26476
- Microwave attenuation standard derived using waveguide below critical frequency as voltage divider to determine losses in components 13 p2067 A67-26488
- Microwave field distribution in waveguide partially filled with solid state plasma for application to isolator 13 p2076 A67-26521
- E and H waves in planar dielectric waveguides mounted on dielectric bases, deriving equations for wave dispersion and damping 13 p2069 A67-27028
- Frequency scanning array of emitters on convex curve 13 p2069 A67-27031
- Performance of two versions of continuously operating electromechanical SHF phase converter 13 p2081 A67-27047
- Ionospheric waveguide channels for long distance radio links below maximum of F-2 layer 13 p2071 A67-27328
- Characteristics of waveguide resonant-iris filters for microwave generators 13 p2083 A67-27444
- Flexwell waveguide as low loss flexible microwave transmission line 13 p2084 A67-27581
- HF power from transmitters in drop capsules of tube used for weightlessness experiments, utilizing Goubau transmission

line to guide signals toward receiver 14 p2279 A67-27897

Jet driven fluoric oscillator 14 p2251 A67-28344

Faraday effect in semiconductors in cylindrical waveguides analyzed using numerical calculation 14 p2270 A67-28522

Mode correspondence between circular and square multimode tapered waveguide, noting similar behavior of coupling mechanism of waveguides 15 p2444 A67-29454

Measured admittance of X-band waveguide radiating into dielectric and plasma layers compared with computed admittance figures 16 p2627 A67-31352

Waveguide mounted tunnel-diode oscillator noting equivalent circuit, power output, frequency, etc 17 p2822 A67-32037

Electron beam interaction with plasma analyzed using nonquasi-static plasma model 17 p2895 A67-32159

Propagation coefficients of leaky waveguide modes improved by corrections to radial line susceptance arising from uniform slot in wall of circular waveguide 17 p2812 A67-32317

Impedance measurements in coaxial waveguide systems propagating TEM wave, using precision coaxial line standards and connectors 17 p2815 A67-32605

External mutual coupling of rectangular waveguide-slot emitters, deriving coefficient of reflection 17 p2826 A67-32683

Waveguide discontinuity problems solution by digital computer 17 p2827 A67-32792

Radiation from array of parallel plate waveguide with thick walls excited by TEM modes 17 p2828 A67-33085

Laminar slow wave coupler applied to waveguide to detect very low power slow waves in indium antimonide subjected to combined effects of applied electric and magnetic fields 17 p2922 A67-33087

Soviet book on waveguide theory covering resonators, Maxwell equations, role, eigenfunctions, etc 18 p3000 A67-33677

MNT-VZ-V device for simulating electromagnetic field in radio waveguides by induced current method 18 p3046 A67-33774

Operating spectrum of tunnel diode oscillator developed according to waveguide techniques, determining optimal requirements 18 p3011 A67-34232

H-01 waveguide irregularities causing transfer function fluctuation, calculating rms and relative distortion power from PCM signal 19 p3183 A67-35561

Earth-ionosphere whispering-gallery nature at VLF analyzed, using mode equation for idealized earth ionosphere model 19 p3184 A67-35827

Dispersion equations and solution for transverse magnetic waves in parallel-plate waveguide partially filled with plasma slab, discussing existing modes 20 p3492 A67-36127

Excitation of earth-ionosphere waveguide by VLF source for case of azimuth dependent properties of source and ionosphere 20 p3428 A67-36373

Electromagnetic wave propagation in waveguides calculated together with electric and magnetic fields by perturbation method 20 p3382 A67-36862

Monograph on waveguide junctions theory and microwave network analysis, stressing model characteristic definition and impedance 20 p3399 A67-36950

Guided waves on infinite cylindrical cavity in magnetotonic medium noting wave solutions, phase velocity, plasma frequencies, etc 20 p3383 A67-37107

Attenuation reduction by using hybrid wave in coaxial cables and resonators having supporting surfaces of enhanced reactance 20 p3384 A67-37214

Waveguide-below-cutoff bandpass filter theoretical design using equivalent circuit of filter to derive attenuation and bandpass properties 20 p3400 A67-37217

Coupling coefficients of waves in variable cross section waveguides with impedance wall 20 p3401 A67-37341

Continuous DC EMF in semiconductor with symmetrical nonlinear conductivity analyzed in variable AC waveguide magnetic field 20 p3513 A67-37449

Mode-matching technique for bifurcated anisotropic waveguide, discussing Bressler biorthogonality relationships to derive anisotropic guide mode equations 20 p3407 A67-37712

Schumann Resonance frequencies, Q-factor and waveguide propagation constant derived at ELF for ionospheric profiles 21 p3579 A67-37993

Long radio wave propagation in earth ionosphere waveguide channel, determining eigenvalues of boundary value problem from complex transcendental equation containing Bessel function 21 p3580 A67-38116

Propagation behavior analyzed for fundamental mode of parallel plate waveguide 21 p3597 A67-38566

Optimal reception of signal transmitted through channel with randomly varying parameters, measuring amplitude and phase 21 p3585 A67-38942

Waveguide dispersive line use in FM pulse compression system outlined for high resolution in S-band radar 21 p3601 A67-39068

Characteristic impedance of waveguides from equivalent voltage and current definitions 22 p3765 A67-39212

Discontinuity problem between empty rectangular waveguide and one filled with transversely magnetized ferrite solved by introducing metal surface wave 22 p3758 A67-39272

Permeability and permittivity values of homogeneous samples obtained by making transmission or reflection measurements in waveguides or coaxial cables 22 p3796 A67-39276

Electromagnetic wave propagation in moving media filled waveguides noting nondispersive dielectric and cold plasma cases 22 p3759 A67-39361

Waveguide model for turbulent shear flow, calculating streamwise dependence of cross-power spectral density using Orr-Sommerfeld equation 22 p3782 A67-39529

Damping constant of electromagnetic wave in plane parallel waveguide with ferrite resonant isolator, using perturbation theory, considering dielectric and magnetic losses 22 p3770 A67-39659

Reflection coefficient for arbitrary lossy waveguide with large number of identical periodically positioned inhomogeneities determined by iteration process 22 p3770 A67-39661

Characteristic admittances of comb-type and undulating waveguide filters, considering diaphragm thickness and TE propagation mode 22 p3770 A67-39662

Nonreciprocal waveguide device consisting of ferrite loaded coaxial branch and crystal diode useful as isolator, modulator and filter 22 p3774 A67-40459

Electron density between shock front and discharge plasma in electromagnetic shock tube determined by interferometric technique, using guided waves 22 p3810 A67-40523

Interaction between plasma stream and inhomogeneous field of electromagnetic wave studied for relation of plasma behavior to potential forces acting on charged particles 23 p4032 A67-40910

Electromagnetic mode propagation in anisotropic dielectric p-n junction waveguide models noting Pockel effect of electric field on light 23 p3982 A67-41466

Approximate solution to irregular waveguides with impedance boundary conditions based on amplitude of normal wave propagation 24 p4120 A67-42159

Electromagnetic wave propagation through two-layer shielded dielectric waveguide using dispersion equation 24 p4129 A67-42192

Propagation in periodically deformed circular and rectangular waveguides 24 p4121 A67-42287

Planar dielectric waveguide excitation at p-n junctions by externally incident electromagnetic field 24 p4121 A67-42337

Asymptotic functional dependences and eigenvalues of guided wave modes in uniform and nonuniform structures deduced by ray-optical techniques 24 p4124 A67-42807

Optical detector using length of single mode optical waveguide with photodetector at output for null detection 24 p4133 A67-42817

WAVEGUIDE ANTENNA

Reception antenna of ONERA weightlessness laboratory in form of surface waveguide [ONERA-TP-374] 01 p0039 A67-11004

Computer program for optimizing network components and evaluation of improvement of planar array match by compensation

through contiguous element coupling 02 p0211 A67-11597

Propagation characteristics of cylindrical waveguide partially filled with dielectric light modulation material 02 p0193 A67-11780

Point matching method, solving boundary value problem in uniform cylindrical waveguide with inserted conductor within conducting tube 02 p0193 A67-11781

Infinite cylindrical antenna insulated from surrounding uniaxially anisotropic plasma by concentric cylindrical sheath of free space 03 p0384 A67-13849

Waveguide-slot antenna design, considering interaction of radiators on principal wave 03 p0385 A67-13951

Slot couplings of rectangular single-mode waveguides analyzed by equivalent circuit and concentrated parameter methods 03 p0385 A67-13952

Electrical properties of slotted waveguide bridge section based on symmetric terminal network theory and classical thermodynamical methods 04 p0582 A67-15147

Control of polarization of radiation field of waveguide-slot antenna emitter 07 p1153 A67-19598

Properties of real radiators and effects of mutual coupling between pairs noting impedance, pattern and polarization characteristics 07 p1154 A67-19782

Coefficient of reflection of H-11 mode shock wave emitted from aperture of circular waveguide with infinite flange 08 p1302 A67-20825

Attenuation constant of model helix waveguide determined using approximate method, considering electromagnetic leakage due to wall irregularity 10 p1606 A67-23064

Approximation method calculation of propagation constants of dielectric loaded TE wire-grid leaky wave antenna for near endfire radiation 11 p1763 A67-24296

Simulator measurements of active impedance of phased array antenna element at two different scan angles by single element in waveguide 11 p1763 A67-24299

Transverse resonance method applied to slotted inhomogeneous circular waveguide with leaky wave mode propagation 11 p1766 A67-24690

Slotted inhomogeneous waveguide propagation behavior investigated, using transverse equivalent network 11 p1766 A67-24691

Waveguide structures for double beam leaky wave antennas 13 p2082 A67-27408

Electrical properties of slotted waveguide bridge section based on symmetric terminal network theory and classical thermodynamical methods 15 p2443 A67-29334

Segmented two-stage waveguide-slot scanning antennas with intersegment phase shifters connected in series in transmission line 16 p2637 A67-31026

Concentric ring array application to space tapering of planar arrays, noting obtainable frequency ranges and scan angles 16 p2640 A67-31526

Characteristics of dielectric rod excited with dominant propagating mode 18 p3011 A67-34020

Control of polarization of radiation field of waveguide-slot antenna emitter 20 p3401 A67-37337

S-band rectangular digital phase shifter combining advantages of waveguide design with compactness of strip transmission line structure 22 p3773 A67-39909

Radome antenna systems design utilizing dielectric structure applicable in aircraft, spacecraft and missile systems 22 p3775 A67-40468

Radiation from infinite aperiodic array of parallel plate waveguides, using Wiener-Hopf technique for edge effect evaluation 23 p3978 A67-40825

WAVEGUIDE FILTER

Waves with complex propagation constants in diaphragmed circular waveguide, solving dispersion equation for various frequencies and structural parameters of waveguide 04 p0575 A67-15214

Wideband solid state intermediate frequency repeater for communications satellites, using waveguide-cavity diode down converter transistor amplifier and varactor upconverter 06 p0960 A67-17682

Waveguide resonant-iris bandpass filter with very wide passband and stopbands that provide transmission and attenuation

characteristics for use with microwave generators 07 p1151 A67-19426
 Exact calculation of electrical performance of rectangular waveguide T-junction having arbitrary cross section used to find equivalent circuit 11 p1767 A67-24732
 Waves with complex propagation constants in diaphragmed circular waveguide, solving dispersion equation for various frequencies and structural parameters of waveguide 15 p2438 A67-30262
 Microwave direct-coupled cavity filter design using single insertion loss formula for case of Chebyshev equal-ripple characteristic 17 p2828 A67-33084
 Magnetically tunable multisection bandpass filter in ferrite-loaded evanescent waveguide 22 p3772 A67-39907
WAVEGUIDE TUNER
 Two-frequency volume resonator with independent tuning within wide frequency band 02 p0214 A67-11911
 Tuning techniques for waveguide band pass filters operating below cut-off frequency 03 p0387 A67-13994
 Nonlinear ferrite diaphragms in waveguides, discussing magnetic field effect on cavity tuning 24 p4119 A67-41972
WAVEGUIDE WINDOW
 Semiconductor laser generating oscillations in external cavity, finding Brewster window effective in suppressing modes within crystal 15 p2498 A67-29511
 Communication with and by space vehicles at ghz frequencies, using atmospheric windows [AAS PAPER 67-94] 15 p2478 A67-29954
 Impedance and reflection coefficient measurement in uniconductor waveguide noting experimental techniques, coefficient standards, etc 17 p2815 A67-32606
 Optical communication systems modulation, discussing TV link, modulator, optical waveguides and materials availability 22 p3759 A67-39330
WAVELENGTH
 Optical reflection, transparency and Faraday effect for indium antimonide, calculating effective electron mass, relation between energy and wave number, etc 01 p0128 A67-10095
 Far UV extinction curve and wavelength dependence of interstellar polarization by graphite grains 01 p0150 A67-10890
 Donor electron IR absorption coefficients in semiconductors in 3-10 micron range used to study wavelength dependence 04 p0674 A67-14608
 Nitrogen wavelengths obtained from precision measurements of various nitrogen lines, using vacuum UV spectrograph 05 p0848 A67-16781
 Wavelength dependence of spectrum of laser beams traversing atmosphere 05 p0763 A67-16793
 Wavelength dependence of characteristic curve of photographic emulsion 06 p1002 A67-17977
 Vibration mode of conical shells measured, showing variation with conical angle and circumferential wave number 06 p1105 A67-18591
 Lunar observation in wavelength range one to three mm, noting brightness temperature drop during total eclipse, obtaining dielectric constant 08 p1390 A67-21022
 Laser for length measurement, checking absolute wavelength stability by Fabry-Perot spectrometer 09 p1499 A67-22148
 Multiple wavelength and source holography with constant depth contours superimposed used in cross section tracing or contour mapping 10 p1652 A67-22710
 Wavelength selectivity in solar collector design, noting role of scatter in determining radiative properties of surfaces 11 p1817 A67-24052
 Vacuum UV wavelength standards and energy levels in first silicon spectrum from low pressure source 11 p1822 A67-24417
 Statistical analysis of solar dm radio bursts in frequency range 536-2000 mc/s 12 p1993 A67-25132
 Calibration of vibrational transition of CO at various pressures to determine vibration-rotation wave numbers 13 p2160 A67-26600
 Shear flow, determined by velocity and density profiles, is stable for small disturbances of all wavelengths and Richardson numbers, enumerating

eigenvalues 14 p2295 A67-27904
 Ruby laser with Fabry-Perot interferometer selector studied for wavelength and thermal stability control 14 p2332 A67-28759
 Stimulated emission from pulsed electrical discharge through helium with wavelength measured and transition identified with interferometer 15 p2497 A67-29395
 Axially symmetric wave propagation in infinitely long two-layered cylinder, detailing displacement and stress distribution 17 p2961 A67-32778
 Radiation power of He-Ne laser at 0.63, 1.15 and 3.39 microns, effect on electron concentration 18 p3060 A67-34038
 Spectral line wavelengths of solar violet bands of carbon /isotope/ nitride and hydride molecules, determining solar abundance ratios 22 p3889 A67-40207
 Hemispherical reflectance of metal surfaces investigated for relation of wavelength and surface roughness 22 p3920 A67-40420
 O and B stars surveyed with 154 cm Catalina reflector show discrepancies from mean interstellar polarization-wavelength dependence near Orion 23 p4062 A67-40626
WEAPON
SA AIRCRAFT
SA ORDNANCE
 Constant acceleration flows applied to high speed fixed geometry guns using H propellant in constant projectile acceleration problem 23 p3992 A67-41716
WEAPON SYSTEM
 Avionic computer testing and fault-locator of weapons systems and system control 01 p0034 A67-10273
 Computer programmed simulation for supporting resources of aircraft weapon systems from concept through production [AIAA PAPER 66-785] 01 p0169 A67-10529
 Evaluation of automatic test equipment for airborne weapon systems from standpoint of effect on readiness of weapon system 03 p0399 A67-14206
 Range instrumentation developments for trajectory measurements including cinetheodolites and tracking radars, noting error sources, weapons systems problems, etc 04 p0568 A67-14436
 Continuous and discontinuous tracking of weapon system radar, discussing principles, characteristics, advantages and disadvantages 05 p0766 A67-17270
 Thermoelectric /Peltier/ refrigeration technique for cooling complex electronic equipment in avionic weapon systems line replaceable units 05 p0754 A67-17454
 Helicopter armaments, discussing efficiency and performance of high fire-power chin-mounted turrets 07 p1131 A67-19481
 Operational phase of Minuteman program [AAS PAPER 66-162] 08 p1430 A67-20977
 Orion P-3 electrical power system changes effect on weapons system, noting power distribution and generation 09 p1452 A67-22677
 Supersonic combat biplane airframe, power plant, fuel, control and escape system, instrumentation and weapons system 13 p2052 A67-26420
 Operational phase of Minuteman program [AAS PAPER 66-162] 13 p2233 A67-27557
 Strike aircraft design noting weapons compatibility, use of analytical and scale testing techniques, etc 15 p2418 A67-29397
 Influence of weapons on basic line, avionics, flight controls and handling qualities of future aircraft 15 p2418 A67-29397
 Revision of military terminology for weapon systems considering human factors, safety and maintainability and reliability relations 16 p2780 A67-30440
 Reliability prediction relationship to system support costs, computing factors for undersupport and oversupport of tactical missile system 16 p2782 A67-31256
 Hueycobra helicopter design and configuration noting maneuverability range, endurance, crew protection, weapons system, etc [AHS PAPER 113] 16 p2598 A67-31829
 Optimum speed capability evaluation of aerial weapons system in relation to value and cost, noting aircraft performance characteristics 16 p2783 A67-31830
 Flight test program for F-111A variable

sweep tactical weapon system, discussing afterburning turbofan engine, crew module, escape and survival 17 p2795 A67-32214
 Systems analysis with computer techniques to examine future weapons system, discussing logistic simulation, interpretation, maintenance, engineering, management, documentation and reliability 17 p2833 A67-32490
 Digital simulation role in advanced avionics system development such as air to air/air to ground weapon delivery, noting advantages, performance, etc 17 p2833 A67-32492
 Airborne low light level TV facility for reconnaissance, target recognition and acquisition, evaluating five sensor combinations 17 p2803 A67-32505
 Human factors and anthropotechnology in development of weapon systems 18 p2993 A67-33643
 Static and dynamic inventory control models for logistics planning and operational readiness with cost constraints 18 p3162 A67-34680
 A-7A aircraft maintenance guarantee and role of training 18 p2987 A67-34681
 AH-56A weapons system design approach, detailing avionics subsystem 19 p3196 A67-35666
 Multiple internal communications system dealing with diversified information forms, discussing flexibility, reliability and other advantages for weapon systems 20 p3381 A67-36567
 Computer program for reproducing operational conditions and simulating environment in which weapons system operates 20 p3416 A67-36765
 Built-in test features in Minuteman II intercontinental ballistic missile weapons system electronics, discussing ground equipment including self-test features and status display techniques 20 p3417 A67-36973
 Digital computers for built-in self-test in airborne weapon system, with examples of mechanized tests from F-106/MA-1 system 20 p3392 A67-36989
 Built-in tests /BIT/ for AN/AWG-10 Missile Control System 20 p3417 A67-36990
 TSIS fire control equipment family, considering maximum cost effectiveness, discussing use in Dassault Mirage M-5 and RCAF CF-5 aircraft 20 p3364 A67-37244
 AH-56A Cheyenne compound aircraft weapon system and major subsystems, discussing fire control, navigation system and performance characteristics 21 p3568 A67-38133
 Utility aircraft costs lower than specialized aircraft in meeting mixed mission requirements in counterinsurgency environment, considering changes, uncertainty and logistics 22 p3745 A67-39618
 Simplified fire control system for helicopters, noting helmet sight, error source corrections and sighting and tracking convenience 22 p3755 A67-39849
 Combat helicopters with reference to HueyCobra noting stub wings, armor protection, rotor and weapon systems 23 p3932 A67-40619
WEAPON SYSTEM MANAGEMENT
 Comparative evaluations of alternative weapon systems, discussing penetration cost effectiveness, attrition ratio, survivability, etc [AIAA PAPER 66-782] 01 p0169 A67-10528
 Cost effectiveness of optimum military aircraft system, evaluating design alternatives in hardware and support concepts via Monte Carlo simulation and high speed digital computers [AIAA PAPER 66-786] 01 p0009 A67-10530
 Total systems management technique applied to ground equipment management in development and production of weapons system [SAE PAPER 660687] 01 p0169 A67-10591
 System effectiveness in weapon system development and acquisition decisions [SAE PAPER 660722] 01 p0169 A67-10626
 Mission reliability and effectiveness analysis of Army Missile Command weapon systems [SAE PAPER 660725] 01 p0154 A67-10627
 Findings, conclusions and recommendations of Weapon System Effectiveness Industry Advisory Committee /WSEIAC/, noting concept of cost effectiveness 01 p0170 A67-11334

Radar data handling and display systems used with pulsed radars, detailing military type for use of weapons control officer 04 p0578 A67-15057

F-111 fixed price contract management, discussing weapon system management, acquisition, controls and techniques to circumvent inherent problems 08 p1430 A67-20971 [AAS PAPER 66-153]

Titan III program, considering DOD and USAF development of improved system acquisition policies and regulations 08 p1430 A67-20972 [AAS PAPER 66-154]

Titan III program, considering DOD and USAF development of improved system acquisition policies and regulations 13 p2232 A67-27552 [AAS PAPER 66-154]

F-111 fixed price contract management, discussing weapon system management, acquisition, controls and techniques to circumvent inherent problems f-111 fixed price contract management, discussing weapon system management, acquisition, controls 13 p2233 A67-27554 [AAS PAPER 66-153]

Data utilization in Air Defense Command /ADC/ weapon systems management 13 p2233 A67-27560

Reliability assessment methods for dormant weapons noting failure modes, redundancy, large parameter change, system design, derating, etc 15 p2495 A67-30418

WEAR

SA ABRASION

SA CORROSION

SA EROSION

SA FRETTING CORROSION

SA FRICTION

Stability, wear and seizure characteristics of hydrodynamic journal bearings of various materials and designs in sodium at temperatures to 800 degrees 03 p0428 A67-13227

F Physical properties of metals influence on friction, adhesion, wear and welding tendency in vacuum 03 p0428 A67-13271

Friction, lubrication and wear, survey of work done during last decade 05 p0809 A67-16065

Wear effects in polymer-metal joints under frictional loads 07 p1211 A67-19170

Quantitative analysis of wear of metal-metal/polymer composite friction pairs as function of time and operational conditions 08 p1334 A67-20597

Lubrication and wear - IME Convention, Scheveningen, Netherlands, May 1968 09 p1505 A67-22190

Load, vibration, temperature, surface oxides, etc, effect on wear resistance of materials for aircraft gas turbine engines 09 p1506 A67-22194

Substrate metal hardness effect on performance of molybdenum disulfide films, noting wear rates 10 p1659 A67-22867

Impact and abrasion wear of axial and centrifugal helicopter compressor stages due to dust intake, showing direct proportionality to impact velocity and particle size 11 p1853 A67-24531

Lubrication and wear - IME Conference, Plymouth, England, May 1967 12 p1948 A67-25327

Machinery wear, galling and scuffing reduction by using graphite and molybdenum disulfide as dry film lubricants 14 p2324 A67-27999

Physical properties of metals influence on friction, adhesion, wear and welding tendency in vacuum 14 p2324 A67-28000

Rolling contact failure modes classification including wear, plastic flow, fatigue and bulk failure [ASLE PREPRINT 67AM 1C-3]

14 p2325 A67-28784

Wear lifetimes for three greases thickened with submicron boron nitride powder [ASLE PREPRINT 67AM 2C-2]

14 p2325 A67-28785

Test methods to determine wear coefficients and design calculations for solid film lubricants, covering wide temperature range [ASLE PREPRINT 67AM 5A-5]

14 p2325 A67-28787

Polyimide bonded solid lubricants development [ASLE PREPRINT 67AM 7A-1]

14 p2326 A67-28789

Wear life improvement of ceramic bonded solid film lubricant by compression and

artificial filling of film voids [ASLE PREPRINT 67AM 7A-2]

14 p2326 A67-28790

Friction and wear properties of resins and polymers with carbon fiber examined and compared for various amounts of fiber 16 p2694 A67-31021

Variation of friction and wear of solid lubricant film with thickness theory based on junction and wear particle size 16 p2683 A67-31751

Solid self-lubricating materials mechanically strong and resisting oxidation for high temperature air applications, examining friction-wear characteristics 16 p2683 A67-31752

Gyromotor vibration level variation causes and ball rotation regimes permitting stabilization 18 p3047 A67-33994

Polyimide bonded solid lubricants development 19 p3233 A67-34790

Wear, scaling and chemical resistance of carbide and boride diffusion coatings on refractory metals 19 p3243 A67-34921

Installation for measuring wear rate, friction force, etc, of plane surfaces in alternating motion 20 p3453 A67-36198

Lubrication and wear - IME Conference, London, September 1967, Session 2, Fluid film lubrication 21 p3632 A67-38134

Lubrication and wear - Conference, London, September 1967, Session 4, Lubrication and materials 21 p3632 A67-38138

Lubrication and wear - IME Conference, London, September 1967, Session 5, Specific environments 21 p3633 A67-38140

Lubrication and wear in high vacuum, considering inability to maintain oxide films, evaporation of lubricants, heat transfer and sliding friction 21 p3633 A67-38142

Lubrication and wear - Conference, London, September 1967, Session 6, Synthesis 21 p3633 A67-38144

Oxygen diffusion through lubricant to metal surface examined for influence in corrosive wear [ASLE PAPER 67-LC-4]

24 p4164 A67-42743

WEAR TESTING MACHINE

Wear and compatibility of liquid metal bearing materials, including surface coatings and cemented refractory carbides, analyzed for Rankine cycle power plants [ASME PAPER 66-WA/LUB-3]

04 p0630 A67-15350

Filament wound sleeve seal impregnated with solid lubricants dissipates heat in rubbing contact zone and provides wear characteristics for use in air compressor [ASLE PREPRINT 67AM 7A-3]

14 p2326 A67-28791

Lubrication and wear with reference to boundary lubrication, fluid and solid films, discussing dry and lubricated sliding and rolling theory 20 p3455 A67-37282

Soviet papers on friction and wear in machinery covering elastorheology and equilibrium stability of rigid rotor 22 p3811 A67-39315

Slough characteristics measuring methods for clean packaging materials, considering Taber-Abraser, tumble-box and reciprocating-style 23 p3986 A67-40847

Wear characteristics of polytetrafluoroethylene studied under various loading and sliding speeds in air and vacuum 23 p4009 A67-41062

Worm gear lubrication with bonded solid film lubricants, discussing efficiency and wear life test apparatus [ASLE PAPER 67-LC-18]

24 p4165 A67-42751

WEATHER

SA ZERO-ZERO WEATHER

Temperatures on hot days at Vandenberg AFB 13 p2152 A67-26845

WEATHER CONDITION

Atmospheric attenuation at millimeter wavelength measured noting correlation with weather conditions and solar flux effect 11 p1751 A67-23971

Saturn S-IB stage fuel system, studying LOX density fluctuations, heat transfer and boiling under various weather conditions 13 p2186 A67-27637

Boeing 727 automatic flight control and landing system [AIAA PAPER 67-573]

19 p3258 A67-35969

Bad weather landing of VTOL aircraft noting landing profiles, meteorological parameters and control 20 p3361 A67-36455

Optical system performance and atmosphere attenuation, analyzing absorption and scattering phenomena in terms of weather conditions 22 p3828 A67-39612

Weather effects on exposed and enclosed earth based satellite communications antenna systems, discussing performance characteristics under various meteorological conditions 22 p3763 A67-40408

Field strength data correlation with meteorological cyclonic parameters, noting possible prediction of scatter signal losses during frontal disturbances 24 p4124 A67-42823

STOL and VTOL takeoff and landing areas, discussing urban and suburban air transportation and operational weather requirements [AIAA PAPER 67-795]

24 p4258 A67-42956

WEATHER CONTROL

ARSR Weather Surveillance System design, operation and performance 07 p1142 A67-19542

Electrostatic motor action in rotational momentum of tornado funnels, noting that driving power removal by electric discharge may cause dissipation 12 p1963 A67-25383

Defogging procedure for all-weather aircraft landing, with operational results 18 p3021 A67-34608

Large scale atmospheric motions control, discussing weather control, long term effect and instability 24 p4182 A67-42756

WEATHER DATA RECORDER

Weather satellite system determining worldwide occurrence and distributions of thunderstorms and associated atmospheric effects 02 p0262 A67-12399

Computer processed air traffic control, automatic weather data collection and forecasting 13 p2153 A67-26665

Worldwide meteorological satellite system, operation, structure and functions 16 p2759 A67-30686

WEATHER FORECASTING

SA ATMOSPHERIC CONDITION EFFECT

SA LONG RANGE WEATHER FORECASTING

Tiros satellite photography used to forecast British Isles weather 12 to 24 hr in advance 01 p0108 A67-10225

Stochastic process estimate of frequency and duration of weather events, using Monte Carlo simulation of probability distributions 02 p0261 A67-12079

Existence theorem for smooth solution of short term weather forecasting problem 03 p0462 A67-13834

Sampling methods and data evaluation in climatological analyses of sunspot-weather relationship 03 p0463 A67-13935

Data processing activities and ancillary equipment used in advanced techniques of computer generated graphics for weather observing and forecasting system [AIAA PAPER 66-854]

03 p0376 A67-14128

Global weather forecasting system of meteorological balloons 03 p0464 A67-14278

Velocity azimuth display technique analysis of wind parameters, noting fundamental limitations 04 p0648 A67-14674

Weather information interpretation and utilization for air traffic control 04 p0650 A67-14688

Short term weather forecasting by determination of aerodynamic maps of cold front motion in terms of normal wind velocity component 04 p0652 A67-15472

Information display for weather forecasters 05 p0836 A67-16311

Nomograms and tables for calculation of Richardson number in relation to forecasting of clear air turbulence 05 p0838 A67-16710

Physical model of turbulence used in developing forecasting scheme of clear air turbulence /CAT/ over mountains [AIAA PAPER 67-184]

06 p1026 A67-18298

Weather forecasting - Symposium, Vienna, September 1965 06 p1026 A67-18598

Aerologic and synoptic weather forecasting 06 p1026 A67-18599

Weather forecast deduction from field distribution of meteorological elements 06 p1027 A67-18600

Filtering problem in numerical weather forecasting, discussing use of truncated diagnostic and complete primitive field equations 06 p1027 A67-18601

Retrospection of nondiverging waves, noting phase velocity dependence on atmospheric stability 06 p1027 A67-18603

Interdiurnal pressure variability as measure of kinetic energy of air masses 06 p1027 A67-18606

Data requirements for medium period weather prediction, discussing mathematical models and meteorological satellites 06 p1028 A67-18998

Cloud photographs obtained on board ATS-I satellite with camera equipped with reflecting telescope show feasibility of short-lived weather systems from synchronous altitude 10 p1657 A67-23367

Space technology developments for World Weather Watch, discussing satellites role in weather forecasting, meteorological sensor and instrumentation 10 p1677 A67-23369

Slice method forecasting of convective cloud cover, rain showers and hail 11 p1815 A67-24327

Computer solution of barotropic vorticity equation for weather forecasting 11 p1816 A67-24330

Forecasting geomagnetic storms and disturbances from solar observations 12 p1931 A67-25110

ESSA meteorological satellite system noting mission requirements, design and performance [SMPTE PAPER 101-56] 12 p2011 A67-25472

Computer processed air traffic control, automatic weather data collection and forecasting 13 p2153 A67-26665

Sea-level pressure specification from 700-mb height by applying screening regression techniques to 17 years of synoptic data 13 p2114 A67-26740

Computerized weather forecasting based on informational and probability logic 13 p2152 A67-27275

Tiros satellites characteristics including ESSA I 15 p2565 A67-29762

Proposed worldwide navigation, communication and traffic control system for all weather to guide aircraft and vessels, locate distressed vehicles and direct rescue operations at sea [AAS PAPER 67-102] 15 p2515 A67-29957

Design requirements for commercial orbital space stations intended for weather forecasting, agricultural prediction and industrial research 15 p2557 A67-29961

Optical system for earth observation satellite with line-scan television for weather forecasting discussing photometry and fiber optics 16 p2679 A67-31797

Zonal and meridional distributions of 5-day averaged outgoing long wave radiation and relation to Northern Hemisphere circulation 17 p2879 A67-32548

Space-time wind variability for forecasting from near ground surface sampling for ungulded rocket impact prediction 17 p2880 A67-32551

Physical model of turbulence used in developing forecasting scheme of clear air turbulence /CAT/ over mountains 17 p2880 A67-32552

Space research effects on science and technology, noting fields of application 17 p2974 A67-32771

Economic benefits from space systems used to survey food producing areas and weather 19 p3350 A67-35650

Satellites role in World Weather Watch /WWW/ program for weather analyses and forecasts 19 p3253 A67-35656

Clear air turbulence /CAT/ evaluated to alleviate effects on air traffic, noting forecasting techniques and in-flight and ground-based remote detectors 19 p3254 A67-35931

ATS-1 spin scan camera experiment for photographic recording of weather motions 20 p3448 A67-36610

Tatellites and balloons for earth surface observation surveyed by types noting operations concerning geodesy, weather, oceanography, vegetation and wildlife 24 p4150 A67-42201

Advanced meteorological satellite objectives, discussing storm warnings, weather forecasting and atmospheric pollution 24 p4240 A67-42392

ATS-1 spin scan camera experiment for photographic recording of weather motions 24 p4156 A67-42405

WEATHER FRONT

Field strength data correlation with meteorological cyclonic parameters, noting possible prediction of scatter signal losses

during frontal disturbances 24 p4124 A67-42823

WEATHER MAP

Automatic plotting of cloud information map on Setun digital computer from Tiros meteorological satellite data 04 p0652 A67-15471

Short term weather forecasting by determination of aerodynamic maps of cold front motion in terms of normal wind velocity component 04 p0652 A67-15472

Interdiurnal temperature variability distribution in northern hemispheric stratosphere in January and July, based on synoptic weather maps 04 p0616 A67-15473

Punch card deck for serially completed upper wind observations as substitute for map scaling 09 p1525 A67-22691

WEATHER RADAR

Microwave radiometric meteorological observations using twin-horn antenna technique, noting antenna resolution 01 p0108 A67-10314

Radar scatterometer remote sensing measurement of variation of radar scattering coefficient with angle, wavelength and polarization 01 p0021 A67-10317

Maritime precipitation analyzed using radar data and satellite photographs of cloud cover 02 p0262 A67-12404

Radar meteorology - AMS Conference, Oklahoma, October 1966 04 p0648 A67-14672

Error in R-meter measurement of velocity spread of meteorological targets resulting from radar frequency instabilities 04 p0648 A67-14673

Dual beam wind measurement by incoherent radar 04 p0648 A67-14675

Tracks of dot angels, insects and birds obtained by ultrasensitive multiwavelength radars 04 p0569 A67-14680

Radar detection of tropopause and clear air turbulence 04 p0649 A67-14682

Measurements by means of vertical beaming cloud pulsed radar operating simultaneously on two wavelengths 04 p0573 A67-15036

Raindrop and melting halstone absorption, scattering and backscatter cross sections of millimeter waves in satellite communications and weather radars 04 p0577 A67-15685

Airborne weather radar for general aviation aircraft, considering transmitter power, wavelength, target area, reflectivity characteristics, installation limitations, etc [SAE PAPER 670252] 12 p1905 A67-25503

Synthesized summary of reports on radio propagation in nonionized media, noting meteorological radar and precipitation effect 14 p2264 A67-28393

Japanese weather radar facility featuring network relay equipment functioning in PPI/RHI mode, noting parabolic horn antenna 14 p2290 A67-28998

WEATHER STATION

S METEOROLOGICAL STATION

WEATHERING

Seleno-geological evidence for lunar surface properties from Surveyor I, discussing weathering products and volcanic genesis 23 p4064 A67-40952

WEBER-FECHNER LAW

Soviet book on atmospheric visibility noting photometry, range, threshold, runway visual range, atmospheric transmittance and atmospheric boundary layer problems 23 p4024 A67-40600

WEBER TEST

Generalization of Weber theorem for problems of coupled thermoelasticity, considering vibrations varying with time 03 p0523 A67-13502

WEDGE

Diffraction of plane plasma wave in rectangular dielectric wedge, considering cases of E-wave and H-wave 01 p0020 A67-10139

Plane problem of surface electromagnetic wave scattering along rectangular dielectric wedge 02 p0191 A67-11579

Multimode surface wave diffraction phenomenological theory extended to right-angled wedge configuration [NYU-EM-213] 03 p0369 A67-13660

Pressure, heat transfer and Pitot pressure profiles measured on wedges and cones at high Mach and Reynolds numbers in hypersonic tunnel 04 p0600 A67-15822

Thermal stresses and displacement in flat wedges using optical polarization method 13 p2219 A67-27058

Steady flow of ideal gas with conductivity past thin wedge in magnetic field studied for asymptotic properties of flow field 17 p2902 A67-32671

Nonlinear elastic anisotropic wedge deformation for short time loading moment applied to apex, approximating stress function 20 p3542 A67-37660

Green function for SH-line source in wedge-shaped medium with apex removed by circular cylinder, determining reflected and refracted fields 21 p3579 A67-37925

Nonlinear differential equations for elastic spherical wedge distortion assuming isotropy, homogeneity and incompressibility 21 p3721 A67-38380

Electromagnetic wave scattering by rectangular geometry dielectric wedge, using precise boundary conditions 21 p3585 A67-38686

Asymptotic perturbation of hypersonic flow over blunt slender cones and wedges showing oscillatory nature 23 p3931 A67-41665

WEDGE FLOW

Pressure distribution in vicinity of wedge for separated turbulent flow analyzed, using modified Vasilu step solution 02 p0232 A67-11634

Optimum wedges and semicones in hypersonic viscous flow, examining effect of thickness ratio on lift-drag ratio 05 p0750 A67-17367

Lip shock from separation edge of half-angle wedge and resultant static-pressure recovery distribution along wake [AIAA PAPER 67-29] 06 p0986 A67-18260

Surface pressure, heat transfer coefficient, wave structure and shock disturbances of inviscid supersonic flow field along corner of intersecting wedges [AIAA PAPER 66-128] 08 p1276 A67-20564

Flow field around porous wedge or cone immersed at zero angle of attack in uniform supersonic free stream when contact surface is straight 08 p1276 A67-20571

Supersonic stream interaction with two-dimensional secondary jet from rectangular planform wedge 10 p1592 A67-23116

Flutter of panels mounted on wedges in hypersonic flow of perfect gas, neglecting acoustic waves 10 p1593 A67-23735

Reynolds number effect on base pressure behind wedge in supersonic and hypersonic flow based on Chapman wake flow recompression model 23 p3930 A67-41308

WEIBULL DISTRIBUTION

Anisotropy test examining failure behavior of aluminoborosilicate glass fibers under tensile and torsional loading [ACS PAPER 1-G-65F] 01 p0103 A67-10263

Test functions for testing location, scale and shape parameter hypotheses of Weibull distribution 01 p0107 A67-10931

Replacement policies for aircraft and missile parts that fail according to normal log-normal or Weibull continuous probability distribution 01 p0083 A67-11339

Point and interval estimation, from one order statistic, of location parameter of extreme value distribution with known scale parameter and of scale parameter of Weibull distribution with known shape parameter 05 p0835 A67-16853

Monte Carlo simulation studies for fatigue data analysis of rolling-contact bearings, using Weibull equation [ASLE PAPER 66AM 1B2] 08 p1336 A67-21038

High tensile strength of composite amorphous boron filament, discussing Weibull relationship and measurements 23 p4018 A67-40787

Rolling element bearing fatigue life for cyclic race oscillation, analyzing variation with load, speed and oscillation amplitude via Weibull statistics [ASME PAPER 67-LUB-22] 24 p4163 A67-42680

WEIERSTRASS FUNCTION

S ELLIPTIC FUNCTION

WEIERSTRASS PROBLEM

Weierstrass canonical product analog for integral functions of many complex variables, discussing existence problems and canonical function 22 p3827 A67-39215

WEIGHT

SA LIGHTWEIGHT
SA MOLECULAR WEIGHT
SA ORGAN WEIGHT
SA STRUCTURAL WEIGHT

SA THRUST-WEIGHT RATIO
Sensory information necessary for size-weight illusion 03 p0363 A67-12850

WEIGHT ANALYSIS
Weight and cost comparative analysis of ablative and combined ablative/radiative heat shields for SV-5 and SV-32 lifting reentry vehicles
[AIAA PAPER 66-990] 02 p0333 A67-12301
Dead weight/service load ratio effect on propulsive efficiency and fuel consumption of large helicopters with mechanical, gearless or jet-propulsion drives 03 p0358 A67-12984
Lagrange multiplier matrix in minimum weight and fully stressed optimum structural design techniques 03 p0525 A67-13966
Weight savings derived from use of contrasting ring, stringer and wall materials in J-stiffened axially compressed cylinders [AIAA PAPER 66-508] 08 p1424 A67-21522
Weight and cost comparative analysis of ablative and combined ablative/radiative heat shields for SV-5 and SV-32 lifting reentry vehicles
[AIAA PAPER 66-990] 15 p2564 A67-29421
Apparatus for direct weight loss recording of space materials 15 p2466 A67-29543
Empty-weight control in helicopters, with cost estimation of excess weight on helicopters sold to government [AHS PAPER 112] 16 p2783 A67-31828
Optimum use of contingency power rating for increasing permissible operating gross weight in twin-turbine helicopters performing long continuous flights [AHS PAPER 128] 16 p2599 A67-31842
Load prediction method necessitated by minimum weight and volume requirements for spacecraft recovery system, considering nonuniform opening of parachutes in cluster 17 p2797 A67-32578
Aircraft empty weight equations as function of takeoff weight, using mathematical statistics 21 p3567 A67-38041
Propellant dependent inert weight for any propellant combination or venting condition for Mars mission 22 p3902 A67-39942
Commercial aircraft balance and weight measurement using on-board system, discussing wind load, runway tilt, hard landings and extreme temperature variation effects 23 p4007 A67-41386
Criterion for minimum weight Carnot limited space power systems 24 p4103 A67-42496

WEIGHT FACTOR
Weight of moon, considering approaches of tides and force of attraction exerted by moon on element of earth 01 p0148 A67-10506
Propellant combinations evaluation for minimum weight of high energy propellant reaction control systems [AIAA PAPER 66-947] 02 p0304 A67-12281
Weight factor effects on optimal motion parameters of variable mass system with limited velocity jet propulsion in gravitational field 02 p0327 A67-12333
Clutter suppression by complex weighting of coherent pulse train 04 p0570 A67-14878
Propulsion systems for satellite attitude control, considering weight and thrust efficiency parameters 05 p0905 A67-18729
Nuclear thermionic propulsion system with low specific weight as interplanetary propulsion system [AIAA PAPER 67-229] 06 p1029 A67-18519
Weight factor of optimizing functional determined by distribution of roots for analytical design of optimal controls 06 p0977 A67-18547
Economics and technology of efficient lightweight structural design 06 p1105 A67-18595
Performance-weight relations and shape parameters for Maxwell structures design, considering filament wound isotensoid container and tension shell decelerator 06 p1111 A67-18884
Systematic approach using weight factor for apportioning mean corrective times of equipment based upon maintainability, usage and reliability data 08 p1315 A67-20670
Optimal structural design with failure probability constraints 14 p2399 A67-28122
Dynamic characteristics of normal exploitation processes determined with controlled equivalent model 15 p2464 A67-30335
Adjustment uniqueness in defining

dynamic characteristics with help of self-adjusting model 15 p2464 A67-30339
Launch vehicle performance and engineering trade-off, considering mass fraction, weight reduction, specific impulse, losses and stage selection 16 p2782 A67-31489
Initial weight prediction of single and multistage launching vehicles by coordinating practical and theoretical aspects 16 p2762 A67-31490
Reaction control system for spinning synchronous satellite noting selection criteria, tradeoff methods, etc 17 p2953 A67-31972
Book on high energy batteries covering electrochemistry of discharge plate materials, weight factors, polarization electrolytes, parasitic effects, etc 18 p2989 A67-34265
Space systems reliability design problems, discussing estimation, weight-reliability tradeoffs, spare parts and redundancy 18 p3139 A67-34698
Horizontal, solid, cantilever-beam profile with constant density, width and elasticity modulus determined, using Pontryagin principle 19 p3340 A67-35524
Electro-and permanent magnet configurations using different materials analyzed, determining lowest mass magnet system for MPD arcs [AIAA PAPER 67-686] 21 p3692 A67-38717
Graphic optimization technique for mass reduction in solar powered ion propulsion system with acceptable reliability constraint [AIAA PAPER 67-701] 21 p3697 A67-38960
Aircraft circuit and installation requirements referring to short time characteristics of cables and effect on circuit protection, coordination and weight saving 21 p3572 A67-39072
Weight factor of optimizing functional determined by distribution of roots for analytical design of optimal controls 22 p3776 A67-39747
Learning threshold element circuit employing electrochemical controllable resistors as weight factors 22 p3809 A67-40480
Performance and design parameters for VTOL fighter aircraft engine and wings, stressing takeoff weight factor 23 p3935 A67-41316
Foundation apparent weight during force controlled vibration test simulated electronically 23 p3987 A67-41383
Design methods to combat fatigue effects on economics of civil aircraft, discussing structural weight role, maintenance, inspection, etc 24 p4250 A67-42441
Parametric analysis and system optimization of nuclear reactor heated Brayton cycle space power plants, discussing turbomachinery performance and shielding weight factors 24 p4186 A67-42550
Spacecraft structural criteria for lightweight photovoltaic solar arrays development, discussing Mariner type panel designs and power-to-weight ratios 24 p4108 A67-42557
Large lightweight rigid multi-kilowatt solar arrays, discussing substrate construction, design and testing 24 p4109 A67-42560
Pressurized propellant tank system for rocket engine, discussing weight factors, propellant combinations and expellant gas pressure relations 24 p4241 A67-42754

WEIGHTING /MATH/
Selection and weighting of direct measurements, evaluating result of variational series by number x alone, using arithmetical mean and median 01 p0068 A67-10854
Adaptive visual signal processor with quantized weights 02 p0207 A67-12140
Frequency response functions determined from correlation functions of force and response, using Bartlett triangular weighting function 08 p1353 A67-20592
Time varying weight functions effect on convergence of polynomial expansions of isotropic distribution 08 p1323 A67-21385
Chebyshev approximation for calculating coefficients of rational function 09 p1469 A67-22053
Generalized integro-exponential weighting functions allow accurate computations of Fraunhofer lines in solar /intensity/ and stellar /flux/ spectra 11 p1859 A67-24113
Selection and weighting of direct

measurements, evaluating result of variational series by number x alone, using arithmetical mean and median 14 p2317 A67-28243
Precomputed approximation to weighting matrix in extended Kalman filter for ballistic reentry vehicle trajectories estimation 16 p2851 A67-31682
Analytic design of optimal digital controller, resolving problem of choice of weighting coefficients of functional representing generalized rms estimate of transient 20 p3408 A67-37046
Weighting function calculation for remote temperature sensing of terrestrial atmosphere using selective chopper radiometer 22 p3805 A67-40356

WEIGHTLESS FLUID
Numerical determination of axisymmetric equilibrium shapes of interface between two nonmixing liquids uniformly rotating in vessel under weak centrifugal and capillary forces and zero gravity conditions 03 p0402 A67-12882
Surface tension and equilibrium surfaces in weightless liquids, with application to spacecraft systems design 03 p0404 A67-13890
Asymptotic exponential laws of contraction of plane and axisymmetric jets of weightless fluids, obtaining expressions for stream function and velocity component 10 p1624 A67-23039
Interaction between gliding contour and ideal fluid flow 18 p3022 A67-33413
Potential flow stability of weightless incompressible fluid for specific flow geometries 18 p3028 A67-34219

WEIGHTLESSNESS
SA FREE FALL
Centrifugal force field with rotation or static impingement separation for water handling in absence of gravity 01 p0017 A67-10958
Transducer measuring water quantity in water storage tanks of LEM under zero g conditions 01 p0073 A67-11114
Fractional g levels for reducing effects of conditioning to zero gravity on prolonged space flights 01 p0018 A67-11397
Dynamic control for two-phase liquid-gas medium under weightlessness solved by surface energy, using computer for boundary value problem involved 02 p0231 A67-11540
Fluid motion in weightlessness, examining effects of weak forces normally suppressed by terrestrial gravitational field 02 p0233 A67-12322
Moments of inertia calculated for human body as whole and of certain parts in unsupported positions of weightlessness 02 p0187 A67-12325
Weightlessness effect on level of vigilance of cats and rats launched in rockets, examining electrical activity of cerebral cortex 03 p0364 A67-13927
Telemetering and programming equipment used by CERMA in nose cones of rockets containing cats and rats in state of weightlessness 03 p0366 A67-13928
Liquid-vapor interface in weightless environment noting dynamic behavior, configuration parameters and dependence on model size 04 p0605 A67-14988
Free convective heat transfer between hot and cold rotating disks in laminar steady azimuthally symmetric flow in zero-gravity field 06 p1119 A67-18864
Vacuum vaporization of saturated liquids on weightlessness, showing that separated bubbles remain in nucleation sites 12 p2034 A67-25726
Weightlessness and manned space flight medical data to date 12 p1902 A67-25727
Minimal value of artificial gravity for normal electroactivity of skeletal muscles determined for otherwise weightless condition 13 p2057 A67-26457
Liquid venting concept for zero gravity environment by suppressing vapor generation with open loop refrigeration, using extracted liquid as working fluid 13 p2056 A67-27639
Low gravity liquid hydrogen tank venting, considering systems with heat exchange for space missions 13 p2057 A67-27640
Dielectrophoretic methods for positioning cryogenic liquids in zero gravity environment, solving one-dimensional nonlinear problem for time history 13 p2106 A67-27642

Cooling system for maintaining uniform low temperature environment under low gravity conditions 13 p2227 A67-27645
 Volt-ampere characteristics, generation and decay of interrupted and AC arcs in nitrogen, air, argon and carbon dioxide at zero gravity 14 p2354 A67-27760
 HF power from transmitters in drop capsules of tube used for weightlessness experiments, utilizing Goubau transmission line to guide signals toward receiver 14 p2279 A67-27897
 Lowering of psychic tone, absentmindedness and vigilance decline during astronaut weightlessness on long space flights 15 p2425 A67-29103
 Caloric nystagmus in man clarified by test in weightless phase of parabolic flight 15 p2428 A67-29277
 Prolonged recording from single vestibular units in frog during plane and space flight, significance and technique 15 p2430 A67-29281
 Neutral buoyancy /water immersion/ technique for simulated space crewman performance, noting psychophysiological, man-machine and anthropomorphic parameters affecting space station design 15 p2431 A67-29282
 Weightlessness effect on human cardiovascular system noting mechanical forces, amount of work done to overcome hydrostatic pressure, etc 16 p2612 A67-30773
 Dynamic control for two-phase liquid-gas medium under weightlessness solved by surface energy, using computer for boundary value problem involved 16 p2663 A67-31606
 Thermodynamic system for zero g venting, storage and transfer of cryogenic propellants, discussing heat exchanger 17 p2954 A67-32074
 Radiation and weightlessness effect on human organism in space flights, discussing galactic cosmic, solar and Van Allen belt radiation 18 p3116 A67-33700
 Monkey psychomotor reactions during ballistic flight investigated noting alertness reduction during weightlessness 19 p3178 A67-35241
 Monkey psychomotor reactions during ballistic flight, noting alertness reduction during weightlessness 19 p3181 A67-35466
 Quadrant mechanical hypothesis /QMH/ on gravitation, gravitational chemistry and zero gravity effects in various chemical processes 20 p3484 A67-36546
 Weightlessness effect on human body noting brain hemodynamics, cardiovascular system, calcium metabolism, task performance, etc 20 p3369 A67-36668
 Aerodynamic lift, studying production of cosmic energy level supporting mechanism, explaining electromagnetic Magnus effect for gravity-free device 20 p3484 A67-36821
 Human engineering performance data for equipment design for manned space systems, discussing zero gravity maintenance and repair [AIAA PAPER 67-653] 20 p3375 A67-37630
 Performance characteristics in zero potential energy manual task, discussing work output 21 p3577 A67-38074
 Propellant sloshing effect on vehicle dynamics under zero gravity conditions studied by programming motion equation into digital simulation of spacecraft, control and propellant 22 p3907 A67-40180
 Biomedical results for various human medical systems during weightlessness experiments of Gemini program, noting vestibular function and EVA 22 p3752 A67-40534
 Zero gravity perturbation mechanisms affecting electrochemical systems noting transport processes and Curie theorem 23 p3972 A67-41607
 Human blood circulation times during weightlessness produced by parabolic flight 23 p3959 A67-41698
 Na and water excretion, renal plasma flow and glomerular filtration rate lowered by lower body negative pressure /LBNP/, noting application to space flight weightlessness [SAM-TR-65-329] 24 p4110 A67-41801
 Motion coordination under conditions of intermittent acceleration and weightlessness during parabolic aircraft flight 24 p4112 A67-41858
 Heat pipe performance in zero gravity field, discussing isothermal operation of

water heat pipe in earth orbit 24 p4256 A67-42926
 Materials development and testing in orbiting laboratory noting zero gravity benefits [AIAA PAPER 67-815] 24 p4139 A67-42969
 Zero gravity orbital manufacturing noting free fall casting and blowing and zero gravity surface tension casting and foaming, discussing Serpentator System engineering [AIAA PAPER 67-842] 24 p4165 A67-42980
WEIGHTLESSNESS SIMULATION
 Reception antenna of ONERA weightlessness laboratory in form of surface waveguide [ONERA-TP-374] 01 p0039 A67-11004
 Water-immersion weightlessness simulation to determine astronaut EVA capabilities and man-machine interfaces [AIAA PAPER 66-903] 02 p0187 A67-12270
 Prolonged weightlessness exposure and expected effects on man 12 p1902 A67-25725
 Gastroenterology in space medicine and physiological basis of cosmonaut nutrition 13 p2058 A67-26752
 Weightlessness simulation by bed rest and water immersion, evaluating validity of protective measures, recovery time and tilt response 15 p2424 A67-29102
 Plants in low gravity environment simulated by 2 rpm clinostat with horizontal axis, studying growth direction and respiratory metabolism 15 p2426 A67-29114
 Water-immersion weightlessness simulation to determine astronaut EVA capabilities and man-machine interfaces [AIAA PAPER 66-903] 15 p2431 A67-29439
 Physiological testing under simulated reduced gravity conditions with subject suspended and performing exercises on inclined treadmill 16 p2616 A67-30756
 Effect upon cardiovascular system of weightlessness simulated by immersion in brine 17 p2805 A67-31952
 Extravehicular activity /EVA/ simulator for zero gravity environment using servodrive and computer 17 p2832 A67-31994
 Animal study for motor reflexes under simulated weightlessness and during gravitational pulses 20 p3367 A67-36258
 Human sensor-motor coordination testing in simulated weightlessness 20 p3368 A67-36263
 Weightlessness state in atmosphere and vacuum applied to satellites and space probes, noting effects on passengers and equipment 20 p3418 A67-37260
 Low gravity slosh simulation parameters and scaling law used to extrapolate data to full scale spacecraft systems 24 p4141 A67-42032
WELD STRENGTH
 Stress concentration effect on fatigue strength of mechanically heterogeneous welds 04 p0636 A67-14600
 Eddy current conductivity technique for monitor of heat effects in nondestructive testing of 2014 Al alloy 05 p0813 A67-17260
 VT15 Ti alloy weld plasticity and strength as affected by additives, hardening and plastic deformation 07 p1207 A67-19290
 Titanium alloy weld properties as affected by boron, beryllium and lanthanum additions 07 p1207 A67-19291
 Phase transformations and welding characteristics of alpha and /alpha plus beta/ titanium alloys 07 p1207 A67-19292
 VT15 titanium alloy weld properties as affected by machining and postwelding heat treatment 07 p1208 A67-19294
 Obtaining high strength titanium welds without hardening by heat treatment 07 p1190 A67-19295
 Welding technique for thick nickel-base alloy using gas tungsten arc, noting inspection techniques, tensile test results, etc 12 p1950 A67-25736
 Gas-shielded stud welding of magnesium 12 p1950 A67-25739
 Statistical analysis of aluminum welds tested at cryogenic temperatures 13 p2124 A67-27674
 Alpha-beta Ti alloys weldability, considering underwater applications 14 p2327 A67-28821
 Welding characteristics of aluminum alloys, noting influence of quenching temperature, quenching process delay and cooling velocity on weld tensile

strength 15 p2503 A67-29781
 Microstructural features of Ni maraging steel weldments related to fracture toughness properties 16 p2692 A67-31868
 IR scanning nondestructive testing program for microwelds to evaluate quality 20 p3454 A67-36666
 Plasma arc process applied to stainless steel and titanium plate welding, discussing metallurgical and mechanical weld and deformation tests 20 p3456 A67-37542
 Cross-wire resistance welded metal joints for aerospace electronic packing assemblies, investigating embedment, mechanical strength and materials evaluation 21 p3635 A67-38629
 Microcracking susceptibility studies of Inconel 718 weld heat affected zones, noting hot ductility, weld circle patch and fillerless fusion welding tests 22 p3818 A67-39222
 Long term strength limit and fracture propagation of AKN22 /Nimonic 80/ alloy welds and AKN22-16/13 CrNi steel composites welds 23 p4019 A67-41079
WELDABILITY
 Augmented strain concept and Vareststraint test for hot-cracking sensitivity and weldability of filler metals 03 p0430 A67-13694
 Refractory metal alloys rating on basis of weldability emphasizing metallurgical considerations, taking into account process control and welding as thermal process 05 p0830 A67-16829
 Silicon and phosphorus role in crack formation in manually welded high temperature resistant steel plate 18 p3063 A67-33673
 Weldability of Al when used in low temperature container construction noting shielding with rare gases 24 p4159 A67-41839
WELDED JOINT
 Fracture toughness and critical defect sizes with welds of 18 percent nickel maraging steels 03 p0448 A67-13554
 Design strength calculation for materials as function of reliability level and number of components 04 p0627 A67-14705
 Narrow welded joint, discussing advantages and limitations of narrow gap, electron beam and plasma arc techniques 04 p0627 A67-14805
 Spacecraft plumbing systems, discussing tubing materials and types of joints 07 p1192 A67-20247
 Aircraft reliability as function of fatigue life of welded joints noting static strength variation, S-N curve and multiple safety factor 09 p1506 A67-22471
 Laser and electron beam welding techniques, noting weld joint characteristics and tungsten inert gas arc welding 10 p1660 A67-23008
 Dissimilar metal transition joints employing roll-bonded and friction welded components 13 p2124 A67-27685
 Plasma arc welding of pipes, studying effects of various gas combinations on weld characteristics 14 p2327 A67-28819
 Multipass welded Hastelloy joint age embrittlement from exposure in inert atmosphere at high temperature, stressing ductility, tensile and hardness tests 17 p2866 A67-33199
 Alloy effects in low pressure diffusion bonding of superalloys, presenting time, pressure, bond strength and temperature curves 17 p2866 A67-33200
 Inhomogeneous temperature field arising during laser welding of different materials with imperfect contact, deriving and solving heat conduction equations 18 p3053 A67-33630
 Aluminum welded joints investigated by radiographic and metallographic methods for bubbles and cracks 18 p3053 A67-33743
 Effectiveness of butt-welded joints and optimum heat treatment conditions for thin sheets of maraging steel containing 18 percent nickel 18 p3054 A67-34259
 Visual characteristics of welded wire joints, discussing correlation with metallurgical and mechanical properties 21 p3636 A67-38631
 Low pressure diffusion welding and brazing process producing joints with mechanical properties close to titanium 6Al-4V 22 p3811 A67-39446
 Hot-cracking and microstructure characteristics in weld heat resistant Ni alloys evaluated by synthetic specimen

technique 22 p3819 A67-39449
 Structural analysis of welded joints in composite welded panels using beam column concepts 22 p3813 A67-40181
 Structural stability of welded joints of chromium steel used in power plant construction examined for structural stability 23 p4019 A67-41077
 Tensile properties and notch toughness of aluminum alloy sheet and welded joints evaluated at room and subzero temperatures 23 p4020 A67-41348

WELDED STRUCTURE

Arc radiation and selective solute vaporization from arc spot region of weld pool used to explain formation of overlap segregation in aluminum alloy weldments 01 p0080 A67-10947
 High vacuum welding of cermet seals with titanium 04 p0630 A67-15632
 Yield strength and reliability of structural cluster welds determined using statistical analysis 09 p1506 A67-22308
 Portable X-ray equipment for measuring residual stresses in welded rocket motor case, machined aluminum parts and titanium welds
 [SAE PAPER 670152] 09 p1509 A67-22542
 Material corrosion control techniques, considering initial structure design, coatings application and protective coatings specifications 11 p1773 A67-24940
 Welds qualification system based on radiographically determined macrostructure defectiveness, classifying defects according to size and distribution 18 p3053 A67-37342
 Microchemical and microhardness properties of parallel gap welds for microstructure interpretation of metal joint 21 p3636 A67-38633
 Microsegregation and grain boundary liquation in heat affected zone of 18-Ni maraging steel welds 22 p3812 A67-39448
 Structural analysis of welded joints in composite welded panels using beam column concepts 22 p3813 A67-40181
 Cold welding under flight conditions of ATS silver-plated beryllium copper damper boom, discussing ultrahigh vacuum equipment and test techniques 24 p4160 A67-42033

WELDING

SA ACETYLENE
 SA ARC WELDING
 SA BRAZING
 SA DIFFUSION WELDING
 SA ELECTRIC WELDING
 SA ELECTRON BEAM WELDING
 SA FLAME PLATING
 SA FUSION WELDING
 SA GAS WELDING
 SA PRESSURE WELDING
 SA SPOT WELDING
 SA ULTRASONIC WELDING
 Weldability of quenched and tempered martensitic alloy steels of low to medium carbon content, particularly carbon-nickel-cobalt alloys 01 p0081 A67-11041
 Vacuum processing in controlling contamination during joining of superalloy and refractory type metals 03 p0430 A67-13555
 Cracking during welding of aluminum alloy noting effect of strain, maximum temperature and cooling rate [ASME PAPER 66-WA/MET-5] 04 p0639 A67-15341

Human performance correlation with changes in incentive conditions and weld lengths, using simulated welding tasks 05 p0756 A67-16072

Temperature distribution in two-layer plate during welding by laser light flux 05 p0814 A67-17548

Hot cracking and strain-age cracking in heat affected zone of Rene 41 alloy weldments 07 p1198 A67-19215

Friction welding fundamentals noting bonding, heat effect, pressure, speed, etc 08 p1333 A67-20357

Static and fatigue properties of repair welded aluminum and magnesium premium quality castings 08 p1333 A67-20360

Laser welding and machining - Seminar, Pennsylvania State University, June-July 1965 09 p1504 A67-22137

Energy problems in laser welding, examining maximum instantaneous heat flux metals can withstand 09 p1504 A67-22138

Pulsed laser welding process, discussing wire-to-wire welds, sheet-to-sheet welds and

circuit board weldings 09 p1504 A67-22139
 Laser as drilling and welding tool, noting industrial guidelines, pulse control techniques, micromachining, etc 09 p1504 A67-22140
 Laser radiation effect on solids, noting laser properties, temperature rise, melting, vaporization and particle emission of materials 09 p1513 A67-22144
 Industrial laser application, giving background information on laser theory 09 p1505 A67-22145
 Welding of niobium and nickel alloys by high energy pulsed laser, noting weld joint 09 p1505 A67-22147
 Weldability of titanium alloy sheets, noting quality through spot welding 09 p1520 A67-22621
 Structural and technological problems connected with miniature electromechanical filters 10 p1609 A67-22876
 Friction welding of dissimilar metals by inertial process, considering effects of flywheel rotation and weld-interface velocity and pressure [ASTME PAPER WES-7-51] 10 p1660 A67-23006

Laser and electron beam welding techniques, noting weld joint characteristics and tungsten inert gas arc welding 10 p1660 A67-23008

Ultrahigh vacuum cold welding in dynamic load elevated temperature environment, noting surface oxide in vacuum 10 p1670 A67-23742

Aluminum, Volume 3, Fabrication and finishing 14 p2323 A67-27818

Aluminum welding techniques, evaluating various filler alloys and forms for welding ease and efficiency 14 p2323 A67-27819

Laser applications to telemetry, radar, navigation, telecommunications, medicine, boring and welding 14 p2333 A67-28974

Welding processes covering high purity metals, plasma arcs, resistive slags, high energy beams and solid state 15 p2493 A67-29681

Fusion and resistance-welding techniques used in aircraft industry, discussing tungsten-arc and electron-beam welding principles 18 p3053 A67-33431

Ultrasonic joining techniques for plastic welding, metal insertion, staking and reactivation of adhesives, emphasizing lock-seal process 19 p3233 A67-34791

IR monitoring technique to improve accuracy of welding inspection using voltage feedback to regulate output 21 p3634 A67-38620

Endurance fatigue characteristics of weldable martensitic stainless steel, giving data for butt and spot welds 22 p3811 A67-39447

WELDING MACHINE
 Computer welding skate for automatic gas tungsten-arc welding of contoured or double-contoured parts, providing control without touching work surface with transducers 01 p0081 A67-11040

Modular liquid-cooled cylindrical ruby laser microwelder design and construction 04 p0628 A67-15310

Nonvacuum electron beam welder noting welding head 04 p0628 A67-15312

Electron beam welding parameters correlation for understanding welding process [ASME PAPER 66-WA/MET-18] 04 p0629 A67-15333

Laser equipment for fusion welding of aerospace structural materials, examining ruby laser properties, flash tube and overall system 09 p1504 A67-22141

Percussive arc mode welding applicability to delicate components and butt type joints 12 p1948 A67-25269

Weldable tube fittings, welding equipment and inspection methods for connecting tubing in aircraft and aerospace hydraulic systems 17 p2864 A67-32008

In-space hand-held electron beam welding gun design, testing and performance 20 p3454 A67-38575

Laser welding and welding processes noting evolution as specialized tool to supplement present welding equipment 21 p3635 A67-38622

Laser applications in welding and machining thin film and semiconductor integrated circuits 23 p3983 A67-41765

WEST FORD PROJECT

Radar measurements confirm West Ford dipoles reentered lower atmosphere in accord with predictions 04 p0618 A67-15841

WEST GERMANY

Passenger volume handled and area accommodated by commercial airports in West Germany 03 p0538 A67-12978

West German wartime military air transport requirements regarding fleet size and composition 04 p0551 A67-14566

Thermionic energy converters in West Germany, discussing vacuum magnetic triodes, Cs diodes and rare gas triodes 04 p0554 A67-15026

Tiros VIII, Nimbus I and II and Essa II weather satellites and radio reception of observational results by German meteorological service APT receiver stations 05 p0904 A67-16028

Aeronautical research facility in West Germany 06 p0981 A67-18754

German contribution to space flight and aerospace technology in international community 07 p1269 A67-19567

Space research in West Germany noting ionospheric physics, magnetosphere and solar and cosmic radiation 19 p3321 A67-35293

Isolated solar events effects on neutral and charged earth atmosphere studied in West Germany during IQSY 1964-1965 19 p3223 A67-35479

German Institute for Air and Space Travel, 1966 Annual Report 20 p3418 A67-37313

WETTING
 S SOAP

WHEATSTONE BRIDGE
 Parallel operation of same frequency transmitters on common antenna examining several designs 16 p2637 A67-31003

WHEEL
 SA REACTION WHEEL
 SA TURBINE WHEEL

Wheel trimming quality effect on thread grinding temperature for aircraft materials 03 p0428 A67-13196

Molded aircraft wheels of epoxy resin reinforced with noncontinuous glass filaments 06 p1007 A67-18026

Theoretical aspects and technological development of parametric optimization of centrifipetal turbine stage, including study of turbine nozzle and wheel profiling 07 p1239 A67-19298

Wheel acceleration influence on landing gear operation at touchdown, noting effect on shock absorption system and elastic deformation of supporting legs 21 p3566 A67-37949

WHEEL BRAKE
 Aircraft wheel and brake designs especially for 63 Series of DC-8 noting materials, properties, construction, etc [AIAA PAPER 67-404] 15 p2421 A67-30371

WHIRL INSTABILITY
 Propeller-rotor whirl flutter and effect of hinged blades and flexible twisted blades 06 p1099 A67-17920

Externally pressurized gas journal bearings, evaluating various design parameters for operating at high temperatures and high speeds [ASLE PAPER 66AM 4B2] 08 p1336 A67-21040

Simplified resonance-amplitude analysis of unbalance vibration superimposed upon steady state eccentricity in aerodynamic bearings 09 p1509 A67-22613

Rotor supported in fluid film journal bearings, eliminating self-excited vibrations through motion equation [ASME PAPER 67-VIBR-28] 11 p1797 A67-24186

Stability in whirl theory, considering internal damping role on motion of elastic shaft 11 p1798 A67-24316

Bearing mounted shaft-rotor system noting harmonic and stable whirl characteristics 12 p1949 A67-25409

Steady state and dynamic properties of cylindrical floating ring journal bearing with pressurized lubricant supply, considering turbulent flow and whirl instability [ASME PAPER 67-LUB-13] 24 p4162 A67-42674

WHIRLING TEST
 Rotor bearing clearance effects on whirling of gimbal-mounted gyroscope 14 p2328 A67-29004

WHISKER

Amorphous whiskers from cobalt-gold alloy by quenching molten material through electron-beam heating and anvil-cooling device 01 p0135 A67-10895

Whisker strength measurement methods, noting role in reinforcement of ductile metal matrices 01 p0163 A67-11152

Strength characteristics of whisker crystals, microcrystals and macrocrystals influencing selection and use of composite reinforced materials 03 p0449 A67-13306

Mechanical characterization and structural perfection of alpha aluminum oxide wool whiskers in diameter range of 0.6 to 4.0 microns 03 p0449 A67-13307

Single crystal whisker composite methodology in plastics, metals and ceramics, emphasizing alignment and handling problems 03 p0453 A67-13410

Single crystal fiber reinforced composites, discussing use of silicon carbide whisker as interstitial reinforcement 03 p0453 A67-13411

Coatings of nickel, chromium and Cu on SiC and aluminum oxide whiskers by electroforming and metalizing, using electron microscope techniques 03 p0444 A67-13434

High temperature reaction between refractory whiskers of silicon nitride and Al and Ni, observing results by electron microscopy 03 p0445 A67-13528

Comparative efficiencies of thin wall aerospace pressure vessels, emphasizing primary structural weight 04 p0709 A67-14810

Composite materials using whisker and short fiber reinforcements, discussing specific strength and specific moduli [SAE PAPER 660640] 04 p0642 A67-15787

Organic composites reinforced with single crystal fibers manufactured, using fiberization of whiskers 05 p0832 A67-16167

Thermoelectric powers and conductivities of vanadium dioxide whiskers measured from 273 to 335 degrees 05 p0864 A67-16898

Factors affecting strength of whisker reinforced metals noting characteristics [ASME PAPER 66-MD-8] 06 p1015 A67-17835

Metallic fibers development, noting research for continuous filaments, whiskers, staple fibers, materials, strength, etc 06 p1019 A67-18558

Filament-metal matrix composite material research, considering reinforcement and binder 06 p1019 A67-18657

Tensile failure of whisker reinforced composites for loading in fiber direction 08 p1344 A67-20421

Tensile strength and cross sectional area measurement of aluminum oxide whiskers 10 p1669 A67-23326

Eutectics use in composite material by growing single crystal whiskers aligned inside matrix 10 p1669 A67-23637

Aluminum oxide whiskers structure and properties 13 p2141 A67-27186

High strength and high elastic modulus in resin-matrix composite structures of single-crystal whiskers [ASME PAPER 67-DE-9] 14 p2340 A67-28868

Metal matrices reinforcement by whiskers demonstrating high strength at high temperatures [ASME PAPER 67-DE-35] 14 p2328 A67-28876

Temperature dependence of complex permittivity and spontaneous polarization of SbSI single-crystal whiskers in phase transformation region 15 p2537 A67-29707

Microstructure stability of aluminum reinforced with Al-Ni whiskers, noting tensile strength and mechanical property dependence on temperature 16 p2690 A67-31372

Sapphire whisker strength coated with thin metal film determined at room and elevated temperatures 16 p2694 A67-31522

Sapphire whiskers mechanical behavior obtained by static tension 16 p2694 A67-31523

Tensometric properties of silicon whiskers and acicular single crystals studied under static and dynamic loads, estimating suitability as strain gauge sensors 18 p3097 A67-33473

Sapphire whisker reinforced aluminum composites fabrication and evaluation [ASTM PAPER 2] 18 p3070 A67-34568

Fiber orientation and morphology effect on anisotropic tensile behavior of Al-Ni

whisker reinforced aluminum, studying solidification rate, etc 18 p3067 A67-34569

[ASTM PAPER 3]

Chemical polishing effects on sapphire whisker strength, obtaining correlation between fracture strength and whisker diameter 20 p3473 A67-36480

Electrical breakdown association with field emission observed through electron microscopy of whiskerlike projections on cathode surface 21 p3589 A67-37824

Temperature dependence of complex permittivity and spontaneous polarization of SbSI single-crystal whiskers in phase transformation region 24 p4199 A67-41777

WHISTLER

Radio whistler occurrence in nighttime and daytime during maximum and minimum solar activity 01 p0057 A67-10261

Relations between VLF emissions of whistler and dawn choruses types and that of ULF emissions /pearl type oscillations and rapid irregular pulsations/ 04 p0617 A67-15500

Whistler recordings on thermal plasma motions and ionization density near magnetospheric knee, noting whistler attenuation VLF noise, ion effects, electron temperature, etc 05 p0795 A67-16011

Japanese sounding rocket measurements of intensity and frequency time variations in ionosphere to determine VLF radio noise 05 p0763 A67-16868

Hook whistler discovered in VLF radio noise data from Injun III satellite, noting time delay difference between components 05 p0799 A67-16888

Micropulsation dynamic spectra showing nosed tones instead of usual tones explained by helium ion content increase in outer magnetosphere 05 p0803 A67-17406

LF whistler mode of electromagnetic waves propagating at angle to magnetic field in model plasma 05 p0857 A67-17426

Dispersion equation for whistler mode for velocity distribution with loss cone, discussing critical stability 08 p1324 A67-20894

Quasi-trapped whistler mode propagation and generation by trapped electrons in magnetosphere, noting refraction index and wave reflection 08 p1327 A67-21462

Growth rate along whistler path for waves propagating at angle to geomagnetic field 08 p1328 A67-21463

Ion composition and natural electromagnetic emissions of VLF phenomena observed by Alouette I and II 10 p1649 A67-23303

Dispersion relation for large amplitude circularly polarized plane wave propagation along magnetic field in hot collision-free plasma, considering distribution function 11 p1826 A67-23881

Plasma concentration diagnostics in exosphere from delay time of forward frequency as function of parameter of whistler trajectory 13 p2111 A67-26563

Magnetospheric electron density distribution determined from analytical calculations, using whistler travel-time integral 13 p2111 A67-26576

Low latitude nose whistlers, estimating path latitude and electron density distribution in intermediate region of magnetosphere 14 p2306 A67-27882

Horizontal loop antenna for observation of whistler-like ELF radio waves between 3 and 60 c/s 14 p2306 A67-27885

Long term solar cycle and seasonal variation of whistler 14 p2307 A67-27887

Dispersion of proton whistlers in plasma in motion with respect to observer 14 p2379 A67-27933

Measurement errors of arrival direction of radio whistler caused by propagation in earth-ionosphere waveguide 15 p2436 A67-29480

Statistics relating plasmopause position to three magnetic indices to clarify relationship between equatorial geocentric distance to plasmopause and worldwide magnetic activity level 15 p2477 A67-29627

Diurnal and annual variations of occurrence frequency and dispersion of whistlers during IGY and 15 p2478 A67-30068

ISQY Coulomb collisions effect on transverse wave along external magnetic field in dense plasma, noting damping of whistler mode

and use of Fokker-Planck equation 16 p2713 A67-30608

Whistler investigation below ionospheric layers at high magnetic latitudes in Sweden 17 p2845 A67-32793

Pc 1 micropulsation signals classified as hydromagnetic whistlers and periodic hydromagnetic emissions, suggesting cyclotron instability process as generation mechanism of latter 17 p2853 A67-33253

OGO-A satellite observations of hydromagnetic whistlers /pearls/ nature, showing linkage to magnetosphere 18 p3042 A67-34390

Resonance for VLF waves by ionospheric propagation using Haselgrove whistler ray tracing method, interpreting path shape as function of gradients 20 p3427 A67-36372

Absorption of VHF waves in whistler mode at low latitudes calculated for various ionospheric conditions during sunspot activity 21 p3617 A67-38065

Selective circuit with FM system and constant gain designed to determine radio whistler arrival direction as function of frequency 21 p3587 A67-39125

WHISTLER RECORDER

ULF recording of geohydromagnetic micropulsations /whistlers/ 01 p0060 A67-10892

Cyclotron resonance amplification of VLF and ULF whistlers, evaluating power transfer for various whistler distributions 07 p1179 A67-19915

Whistler observations near Sofia and in Czechoslovakia 14 p2307 A67-27914

Frequency shifts on whistler mode signals from stabilized VLF transmitter from ionosphere and magnetosphere effects, noting electron density 16 p2631 A67-31856

Whistler method detection of magnetospheric electric field associated with polar substorm 17 p2851 A67-33197

WHITE BLOOD CELL S LEUKOCYTE

WHITE DWARF STAR

Plasma neutrino process as accelerating mechanism for evolution in UV dwarfs 08 p1396 A67-21180

Evolution in close binary star system through mass exchange leading to white dwarf with relatively unevolved companion 11 p1864 A67-24581

Kinematic, spectroscopic and photometric data for pygmy stars /blue ultradwarfs/ 17 p2945 A67-32645

Book on red giants and white dwarfs covering stellar evolution, planets and life, solar system origin, etc 18 p3117 A67-33430

WHITE NOISE

Comparison of variances evaluated by Kolmogorov and Volterra techniques for phase locked loop subjected to white Gaussian input 01 p0044 A67-10480

Optimum signal reception against non-Gaussian noise background in presence of white Gaussian noise 03 p0368 A67-13274

First passage problems for lightly damped linear oscillator excited by white noise for two types of initial conditions and three types of barrier configurations 04 p0659 A67-15932

Linear system providing maximum signal to noise ratio for given parameters of correlation function of incoming quasi-harmonic signal mixed with white noise 05 p0767 A67-17396

Digital computer simulation of nonstationary Gaussian processes using Gaussian white noise, with application to simulation of structural response, ground acceleration, velocity and displacement of earthquake 06 p1109 A67-18839

Growth of solutions of forced oscillations of nonlinear oscillator driven by white noise 07 p1218 A67-20268

Power flow formulas for white noise driven vibratory systems, estimating average oscillation amplitude and plastic strain accumulation rate 10 p1731 A67-23841

Approximate normal mode technique, providing solution to sinusoidal and white noise randomly excited damped linear multi-degree of freedom system, for application to mathematical model [ASME PAPER 67-VIBR-2] 11 p1871 A67-24164

Lower bounds on error probability for communication in presence of white Gaussian noise with no bandwidth constraint 12 p1908 A67-26086

- Energy detection of unknown deterministic signal in white Gaussian noise by energy measuring device 13 p2067 A67-26510
- Automatic frequency control for estimating random signal frequency when received against whitenoise 13 p2069 A67-27037
- background 13 p2069 A67-27037
- Impulse response of dynamic systems using cross correlation techniques 13 p2081 A67-27220
- Convolutional encoder for orthogonal tree codes in presence of white Gaussian noise [JPL-TR-32-1120] 14 p2273 A67-28710
- Cost function to evaluate quasi-optimal amplitude meter for signal with random initial phase on white noise background with random correlation function 16 p2623 A67-31015
- Optimization for linear vibration isolators considering vibration clearance tradeoff for random base motion 16 p2703 A67-31642
- Added narrow band noises and tones influence on subjective response to shaped white noise 17 p2795 A67-32125
- Averaging principle applied to stochastic differential equations describing oscillatory system subject to white noise effects 17 p2885 A67-32878
- JT9D engine design from viewpoint of Incorporated noise reduction features [SAE PAPER 670331] 17 p2929 A67-32984
- Stochastic differential game with missile and radar, using linear theory in finding optimal strategies 18 p3075 A67-33495
- Feedback-signal lag and channel discreteness effect on rate of information transmission over Gaussian channel with feedback during symbolized coding 18 p2999 A67-33531
- Receiving system for detecting binary random signals in white noise, determining correlation functions and error probability 18 p3001 A67-34180
- Unlock behavior of second order phase locked loop with and without interfering carriers 18 p3018 A67-34346
- Design of optimal waveforms for optimal estimation or prediction of state of linear dynamical system in presence of Markov and white noise 19 p3201 A67-34965
- Signal model with white noise fitted to time series, discussing signal proportion estimation methods 20 p3476 A67-36788
- Linear optimal stationary control system with state dependent white noise disturbances described by differential equation 20 p3408 A67-37077
- Binary symmetrical channel noise effect on PCM picture quality compared with white Gaussian noise effect in PAM system 20 p3386 A67-37496
- Statistical dependence between frequency and amplitude deviations of FM wave perturbed by white noise, describing amplitude-phase correlation FM demodulator 22 p3758 A67-39271
- Binary and tetravalent signals quantitative comparison for noise sensitivity by computing transmission matrix during transmission via linear channel 22 p3761 A67-39787
- Output SNR dependence on difference between input signal and natural frequencies for quasi-optimal linear filters, noting improvement for mismatched input 22 p3761 A67-39867
- Sound and white noise effects on turbulent jet aerodynamic characteristics studied at several Reynolds numbers 22 p3785 A67-40019
- WHITTAKER FUNCTION**
- Asymptotic representations of Whittaker functions /with terms of standard equation coefficients equal/ applicable to wave propagation in inhomogeneous media 21 p3652 A67-38109
- WIDE ANGLE LENS**
- Prismatic wideband directional couplers of Brewster angle type, discussing basic theories, frequency characteristics, insertion loss and directivity 10 p1606 A67-23065
- WIDEBAND COMMUNICATION**
- Analog and digital wideband radar transmission and application to air traffic control 01 p0021 A67-10213
- Compatible double sideband/single sideband/constant bandwidth FM telemetry system for wideband data 02 p0197 A67-12010
- Troposcatter test program for evaluating megabit digital transmission system, using wideband frequency shift keyed modem 02 p0202 A67-12126
- Solid state pulse modulated 10 MHz/channel passband frequency switch design and reduction to microelectronic form 05 p0789 A67-17043
- High data rate laser communication system, discussing integration of laser and wideband modulator and experimental results under field conditions 08 p1292 A67-20672
- Adaptive antenna for ground reception of wideband RF signals in space communications systems 08 p1301 A67-20776
- Wideband video data transmission from near earth orbiting vehicle and over leased telephone lines 09 p1460 A67-21583
- Radar information transmission using wideband microwave links and conventional display techniques 09 p1465 A67-22637
- Diode type lossless network description with excellent transient response and less settling time than conventional branch-line coupler phase shifter 10 p1613 A67-23414
- Wideband and optimum antennas, using Lepidopter antenna as example 10 p1613 A67-23506
- Wideband miniature bridge constructed on basis of quarter wave two-conductor shielded line for UHF and SHF 11 p1757 A67-23911
- Telemetry transmitters using solid state wideband microwave voltage-controlled oscillators 11 p1753 A67-24442
- Statistical performance confirmation of wideband random equalizer, emphasizing analysis technique, analyzer characteristics and power spectral density plot 12 p1942 A67-25692
- Special purpose analog computer for analyzing wideband signals in two parts of network, with automatically plotting and coupling factor as function of frequency 13 p2089 A67-26410
- Wideband tank circuit using ferromagnetic core with negative frequency characteristic in induction coil 13 p2071 A67-27277
- Communication problems connected with deep space transmissions of interplanetary distances range 14 p2258 A67-28454
- All solid state wideband telemetry transmitters realization by compact high-powered frequency multipliers 14 p2288 A67-28692
- Pulse measuring system for observing structure of pulsed signals in rectangular phase-time coordinates 15 p2444 A67-29414
- Wideband communication systems, detailing sequenced and parallel complex signals concept 16 p2624 A67-31025
- Correlation reception of wideband signals from ionospheric inhomogeneities, considering effectiveness for signal distortion discrimination 16 p2632 A67-31909
- Predetection telemetry tape combiner 17 p2813 A67-32496
- Woodward ambiguity function extended to broadband signals including Doppler distortions of modulation function 18 p3001 A67-34114
- Structure of quasi-linear and wideband satellite transponders, discussing possible improvements 18 p3003 A67-34356
- Reliability, orbit achievement and control and increased power bandwidth as factors making communications satellites economically feasible 19 p3350 A67-35649
- Lasers for wideband planetary communication, describing heterodyne receiver and transmitter designs 20 p3381 A67-36566
- Wideband troposcatter radio channel simulator exhibiting frequency flat or frequency selective fading over band greater than 10 MHz and centered at 70 MHz 20 p3385 A67-37354
- KHz to GHz wide predetector bandwidth receiving system applicable to EMI evaluations of high data rate digital equipment 20 p3406 A67-37656
- Wideband miniature bridge constructed on basis of quarter wave two-conductor shielded line for UHF and SHF 21 p3600 A67-38939
- Optical and IR wideband communication between earth and interplanetary spacecraft, discussing tracking, detectors, pointing and beam formation 22 p3762 A67-39960
- High gain wideband amplifier with rapid pulse trains, discussing silicon transistor response time, impedance, Q-factor and correction circuit 23 p3977 A67-40691
- High speed wideband L-band tunnel diode frequency deviator tunable over octave bandwidth by 160 mv change in input voltage [IEEE PAPER 19-TP-67-1175] 23 p3978 A67-40743
- WIDMANSTATTEN PATTERN**
- Iron and stony meteorite cooling rates determined by measuring kamacite bandwidth, bulk nickel content and composition 11 p1868 A67-24872
- Iron and iron-stony meteorites cooling rates in relation to Ni content and Widmanstatten structure suggest development in different thermal environments 16 p2750 A67-31453
- Germanium distribution in metallic phases of various iron meteorites by electron probe microanalysis 22 p3885 A67-39976
- Anoka, Minnesota, iron meteorite noting composition, chemistry, structure and cooling rate 23 p4069 A67-41449
- Cooling rates for Widmanstatten pattern formation in iron meteorites used to obtain data on parent meteorite bodies 24 p4234 A67-42627
- WIDTH**
- S BANDWIDTH
- S SPECTRAL LINE WIDTH
- WIENER FILTER**
- Kalman filtering technique applied to classical Wiener problem, deriving equations for discrete and continuous processes 01 p0048 A67-11257
- Optimization via information flow in system without memory, discussing ideal correction minimal and maximal error 04 p0592 A67-14904
- Information theory assessment of optimizing criteria and approximation for steady state gain of optimum filter, based on Wiener type 04 p0586 A67-15639
- Optimal Wiener values of filter parameters in phase-lock loop, noting possibility of improved performance despite deviations 06 p0973 A67-17615
- Radar antenna synthesis for optimum and suboptimum filtering of spatial signals according to mean square error minimization 07 p1158 A67-20238
- Filter theory method applied in solving analytical construction problems for optimal controllers, noting existence of Fourier transform and Pally-Wiener condition 09 p1482 A67-22078
- Nonlinear Bayes detector synthesized for Gaussian signal and noise fields using Wiener filters 12 p1919 A67-26087
- Self-optimizing dual input Wiener digital filter by live input data processing derived for zero mean input case, noting applications to hybrid navigation systems 17 p2882 A67-32527
- WIENER-HOPF EQUATION**
- Algorithm for approximate solution of Wiener-Hopf integral equation 02 p0209 A67-12175
- Viscous incompressible flow past finite flat plate obtained under Oseen approximation for large and moderate Reynolds numbers, using Wiener-Hopf technique 02 p0234 A67-12546
- Regularization method to minimize error in solving Wiener-Hopf integral equation to determine pulse transfer function 03 p0374 A67-13083
- Numerical solution of Wiener-Hopf equation in statistical identification of linear dynamic plant 04 p0644 A67-14903
- Stresses in infinitely long strip of finite width containing seminfinit crack calculated for displaced clamped boundaries, using Wiener-Hopf technique 04 p0718 A67-15923
- Yielding and brittle cracking of orthotropic strip, using Wiener-Hopf technique and asymptotic method for isotropic case 06 p1102 A67-18317
- Oseen flow past seminfinit plate and vertical force formulated by integral equations solved for drag and lifting singularities distribution, using Wiener-Hopf technique 08 p1319 A67-20350
- Spectral theory of Wiener-Hopf type integral operators on generalized Sobolev spaces 10 p1674 A67-22968
- Density of Gaussian distributions and Wiener-Hopf integral equation 11 p1812 A67-24100
- Plane electromagnetic wave diffraction by

- p conducting half-plane embedded in uniaxial anisotropic medium 11 p1753 A67-24315
-
- p Statistical analysis of optimum control system design by parameter adjustment, finding systems transfer function through Wiener-Hopf integral 11 p1772 A67-25082
-
- p Wiener-Hopf and Aleksandrov methods solve plane and axisymmetric problems of equilibrium longitudinal cracks in thin plates with edges free of stresses 12 p2019 A67-25565
-
- p Variational, quasi-static and integral equation analytic waveguide solutions, extending singular integral equation to homogeneous and inhomogeneous loaded waveguide junction 12 p1906 A67-25978
-
- p Characteristic for kernels of certain integral equations on
- \pm
- semiaxis for determining solvability and number of possible solutions 14 p2344 A67-28809
-
- p Electromagnetic wave diffraction by infinite set of parallel metallic plates, obtaining exact solution by Wiener-Hopf technique 15 p2435 A67-29191
-
- p Scattering of surface wave incident upon junction of two semi-infinite planes joined together by step analyzed using Wiener-Hopf equation 16 p2626 A67-31348
-
- p Wiener-Hopf technique for class of nonhomogeneous difference-differential integral equations 17 p2877 A67-32560
-
- p Radiation from array of parallel plate waveguide with thick walls excited by TEM modes 17 p2828 A67-33085
-
- p Boundary value problem and singular integral equation applied to automatic control theory 20 p3475 A67-36652
-
- p Field determination when produced by symmetrical plasmoid with time dependent current distribution traveling along cylindrical waveguide, using Wiener-Hopf method 20 p3497 A67-36680
-
- p Plant parameter uncertainties sensitivity constraint for optimal linear control synthesis, discussing Wiener-Hopf equation condition 21 p3602 A67-38026
-
- p Radiation from infinite aperiodic array of parallel plate waveguides, using Wiener-Hopf technique for edge effect evaluation 23 p3978 A67-40825
-
- WIND**
-
- p SA ATMOSPHERIC CIRCULATION
-
- p SA GEOSTROPHIC WIND
-
- p SA GUST
-
- p SA SOLAR WIND
-
- p SA STELLAR WIND
-
- p Noise wave amplitude reduction method by suitable initial wind field adaptation to pressure field studied for applications to divergent barotropic model 19 p3253 A67-35530
-
- WIND CIRCULATION**
-
- p Numerical method for calculation of finite amplitude orographic disturbances by using finite difference algorithm 05 p0837 A67-16484
-
- p Finite difference approximation of balance wind equation, discussing convergence of Liebmann relaxation process, Coriolis term and computer time economy 09 p1525 A67-21551
-
- p Neutral wind structure effects on ionospheric sporadic E layer variations, noting daytime evolution, nighttime characteristics and electron density profiles 11 p1783 A67-23924
-
- p Numerical method for calculation of finite amplitude orographic disturbances by using finite difference algorithm 13 p2150 A67-26340
-
- p Mean meridional motions in biennial wind oscillation in wind structure of low latitude stratosphere 13 p2151 A67-26738
-
- p Geopotential and wind field calculations for Northern Hemisphere using statistical models 14 p2346 A67-28764
-
- p Fluctuations in stratospheric and mesospheric winds studied by meteorological sounding rockets, noting relation to solar activity 19 p3217 A67-35207
-
- p Windborne dust collections on Barbados Islands investigated by mesh technique for origin of cosmic dust 20 p3432 A67-37174
-
- p High velocity tropospheric winds at 40 to 60 km altitude, discussing supergradient and subgradient winds and energy transport to mesosphere possibilities 22 p3793 A67-40032
-
- WIND DIRECTION**
-
- p Wind velocity, direction and diffusion coefficients determined with aid of artificial luminescent cloud 10 p1675 A67-22795
-
- p Nondeepening synoptic scale tropical disturbance showing dependence on in situ development and decay in upper troposphere 13 p2152 A67-27605
-
- p Wind velocity and direction measurements by radar tracking of chaff /dipoles/ clouds 19 p3219 A67-35247
-
- p Wind velocity, direction and diffusion coefficients determined with aid of artificial luminescent cloud 24 p4181 A67-42131
-
- WIND EFFECT**
-
- p Auroral region disturbances generating atmospheric waves in F layer that produce atmospheric mixing 01 p0056 A67-10112
-
- p Effect of meridional wind on satellite orbit inclination 01 p0146 A67-10255
-
- p Design of gust alleviation controls for boost phase flight of missiles incorporating random winds, time-varying missile dynamics, control problem, etc [AIAA PAPER 66-969] 02 p0332 A67-12292
-
- p Physical aspects of stratocumulus including temperature, liquid water content, drop size, wind effect, shape, etc 03 p0462 A67-13499
-
- p Environmental wind tunnel investigation of wind velocity and discharge current effects on average charge per Trichel pulse in corona discharges 03 p0486 A67-14119
-
- p Altitude of gravitational division level, discussing wind currents above it 05 p0800 A67-17124
-
- p Wind variability effect on impact point of launch vehicle with reference to range safety at Western Test Range [AIAA PAPER 67-187] 06 p0980 A67-18323
-
- p Atmospheric turbulence effects on statistical design and analysis of space vehicles [AIAA PAPER 67-134] 06 p1096 A67-18359
-
- p Motor driven cup anemometer and freely rotating cup anemometer in free and artificial flows 06 p1006 A67-18836
-
- p Wind and temperature effects on transitory and cruise phases of supersonic flight 07 p1219 A67-19067
-
- p Atmospheric density, winds and turbulence relative influence on Saturn V vehicle control system and structural bending moment response during Atlantic Missile Range ascent flight [AIAA PAPER 66-341] 07 p1257 A67-19372
-
- p Rocket wind trajectory dispersion reduction by adjusting thrust-time curve without increasing total impulse 08 p1406 A67-20512
-
- p Wind compensation system at Kagoshima Space Center, University of Tokyo, consists of radar system for obtaining wind data and method for finding launch angle compensation 08 p1314 A67-20542
-
- p Optical effects of thermal structure in lower atmosphere 10 p1879 A67-22745
-
- p Approximate method for diurnal variation of peak electron density in F-2 layer, estimating effect of time varying drifts 10 p1650 A67-23336
-
- p Motion equations for planar simulation of flexible Saturn IB launch vehicles under in-flight winds using Appell equation, noting sloshing mode 10 p1713 A67-23750
-
- p Atmospheric turbulence statistical characteristics dependence on stratification and elevation from heat flux and wind friction stress 11 p1815 A67-23954
-
- p Amplitude control of wind induced oscillation in antenna system through cross section shape [ASME PAPER 67-VIBR-39] 11 p1777 A67-24200
-
- p Cylinders of rectangular section as aeroelastic nonlinear oscillators, theory of galloping oscillation and force measurements on stationary cylinder [ASME PAPER 67-VIBR-50] 11 p1777 A67-24200
-
- p Helicopter exhaust-gas expansion and contamination of intake air under unfavorable wind conditions 11 p1853 A67-24529
-
- p Flight Load Survey program, written in Fortran IV, for accurate and rapid sounding of wind-induced loads on aerospace launch vehicle [AIAA PAPER 66-470] 13 p2212 A67-26820
-
- p Real time meteorological system for ballistic high altitude multistage rocket trajectory, computation and prediction 13 p2091 A67-27610
-
- p Atmospheric wind effects on guided propagation of VLF infrasonic waves over long distances, including variable wind and temperature profiles 13 p2117 A67-27702
-
- p Book on safety of structures 14 p2395 A67-28030
-
- p Mesospheric wind components via rocket measurements of Northern and Southern Hemispheres, noting semiannual wind fluctuation near equator 18 p3030 A67-33552
-
- p Soviet book on aeronautical meteorology covering wind and cloud effects on takeoff, landing and supersonic flying in storms and jet stream layers 18 p3074 A67-33676
-
- p Wind variability effect on impact point of launch vehicle with reference to range safety at Western Test Range 19 p3207 A67-34834
-
- p Solar radiation-balance measuring device using polyethylene film to give protection from wind effects 19 p3240 A67-34855
-
- p Lift penetration and growth effects on space vehicle response based on slender body theory 19 p3337 A67-35999
-
- p Wind penetration effects on flight simulations evaluated in frequency domain by solution of theoretical transfer function, showing relationship to angle of attack [AIAA PAPER 67-609] 19 p3208 A67-36000
-
- p Landing characteristics of SV-5P lifting body vehicle analyzed using six degree of freedom piloted simulation, noting gust effect [AIAA PAPER 67-574] 20 p3533 A67-37133
-
- p Wind perturbation effects on performance of radio telescope servosystems, giving method for determining optimal system parameters 20 p3403 A67-37519
-
- p Latitude, altitude and local time variation of forces controlling 100 to 700 km atmospheric winds, noting effects on ionospheric phenomena 21 p3654 A67-37994
-
- p Altitude of gravitational division level, discussing wind currents above it 21 p3618 A67-38467
-
- p Wind and cloudiness effects on terrestrial scintillation based on visual estimates and measurements 22 p3828 A67-39240
-
- p Ion and neutral particle interaction effects on F region winds, considering plasma forces 22 p3789 A67-39479
-
- p Biennial component of seasonal variation in earth rotation rate using time observation data, calculating stratospheric zonal wind effect 23 p3996 A67-41085
-
- p Commercial aircraft balance and weight measurement using on-board system, discussing wind load, runway tilt, hard landings and extreme temperature variation effects 23 p4007 A67-41386
-
- p Rocket wind trajectory dispersion reduction by adjusting thrust-time curve without increasing total impulse 24 p4242 A67-42919
-
- WIND MEASUREMENT**
-
- p SA ANEMOMETER
-
- p Pilot experiment, recording simultaneously optical image position, atmospheric temperature fluctuations and wind direction 01 p0108 A67-10250
-
- p Mitra three-receiver method improvement for measuring winds and diffraction of radioelectric waves in ionosphere 03 p0406 A67-12819
-
- p Dual beam wind measurement by incoherent radar 04 p0648 A67-14675
-
- p Rocket observations of temperatures and winds in upper atmosphere, discussing physical interpretation of results 05 p0797 A67-16856
-
- p Upper atmospheric wind measurement by artificial cloud method which releases sodium at twilight and trimethyl aluminum at night 05 p0798 A67-16858
-
- p Multivariate statistical analysis of wind sounding data, applying high degree of correlation between two wind parameters and empirical density function [AIAA PAPER 66-353] 05 p0838 A67-17214
-
- p Rocket sounding of stratospheric circulation, noting relationship between minima in westerly zonal flow of 45-55 km stratopause layer and tropospheric cut-off lows 05 p0838 A67-17306
-
- p Upper atmospheric turbulence and wind measurement by radio reflection from meteor trail 05 p0802 A67-17382
-
- p Upper atmospheric wind measurements derived from vapor trail soundings 06 p1025 A67-17594
-
- p Mean monthly winds at low level calculated for equatorial station in East

Africa, noting monsoon patterns and jet streams 06 p1025 A67-18024

Inertial navigation equipment applied to meteorological research, using aircraft for vertical gust measurement 06 p1002 A67-18025

Oscillatory ground wind response of Atlas/Agema examined, using statistical theory of extreme values 06 p1104 A67-18492

Cyclogenetic processes from baroclinic instability occurring in zonal and meridional flow 06 p1027 A67-18602

Soviet book on aeronautical meteorology noting atmospheric conditions, clouds, ice formation, flight data utilization, Soviet Civil Aviation services, etc 07 p1220 A67-19579

COTIR wind weighting technique to reduce impact dispersion of sounding rockets 08 p1313 A67-20541

Real time meteorological system providing prelaunch impact prediction for unguided high altitude rocket firings, noting computer program 08 p1314 A67-20543

Rocket measurements of small scale structure of ionization profile and wind speed fluctuations, propagation of gravity shock waves and stratification in upper atmosphere 08 p1325 A67-20986

Orthogonal functions of time, describing daily perturbations in 100 mb circulation over eastern U.S. 09 p1562 A67-22684

Punch card deck for serially completed upper wind observations as substitute for map scaling 09 p1525 A67-22691

Constant temperature difference hot thermocouple anemometer, discussing operation principle and performance 10 p1654 A67-22822

Ionospheric diffusion spectra, obtaining information on neutral atmospheric winds and ionosphere dynamics 10 p1632 A67-22858

Meteorological probes using GHOST balloons for wind measurements 10 p1594 A67-23197

S-N wind components analyzed for diurnal and semidiurnal variations, noting results on amplitude and phase of components 10 p1638 A67-23200

Upper atmosphere dynamics, noting role of horizontal and vertical winds in shifting density phase and amplitude and UV radiation as energy source 10 p1640 A67-23218

Ionospheric drift velocities observed by spaced receiver method compared with neutral winds from luminous rocket trails 10 p1643 A67-23252

East-West ionospheric wind component measured by CW meteor radar 10 p1644 A67-23253

Vertical atmospheric flow mean velocity determination within fixed area from wind probe observations at fixed points 11 p1816 A67-24523

Japanese rocket observations of upper atmospheric wind and temperatures in relation to new Cirra model atmosphere 12 p1937 A67-25841

Meridional and vertical wind components analyzed for angular momentum, balance, heat influx and internal friction 13 p2113 A67-26678

Meteorological rocket measurement of wind patterns noting velocities, turbulences, stratospheric diffusion coefficients, etc 13 p2117 A67-27611

Mesospheric wind components via rocket measurements of Northern and Southern Hemispheres, noting semiannual wind fluctuation near equator 18 p3030 A67-33552

Martian atmosphere circulation model from Mariner IV occultation experiment, studying lateral eddy viscosity, winds, surface temperature and stress 18 p3124 A67-34153

COTIR wind weighting technique to reduce impact dispersion of sounding rockets 19 p3207 A67-34837

Stratosphere and mesosphere wind and temperature measurements, noting additional cosmic radiation measurements during 1966 solar eclipse in Argentina 19 p3320 A67-35287

Rocket and balloon studies of solar radiation, wind characteristics, equatorial electrojet and lower ionosphere electron density 19 p3223 A67-35474

Real time meteorological system providing prelaunch impact prediction for unguided high altitude rocket firings, noting computer program 21 p3607 A67-37812

Mesoscale structure of atmospheric winds

analyzed using data obtained from FPS-16 radar/Jimsphere precision wind measuring system 21 p3655 A67-38576

Mechanically and electrically simple cup-type anemometer developed with starting speed of 6 cm/sec and linear response 21 p3628 A67-38581

Lunar semidiurnal air tide distribution and small lunar gravitational excitation noting lunar diurnal tide detectable only with wind data 22 p3882 A67-39557

Nighttime variation of ionospheric winds over Barbados via luminous trails measurements, obtaining steady state components for seasonal variations 23 p3995 A67-40807

WIND PROFILE

Midlatitude semidiurnal tide in lower thermosphere determined from trails of chemiluminescent vapor 04 p0615 A67-14969

Vertical profiles of horizontal wind in lower ionosphere treated by spectral energy density estimates [AFCRL-67-0054] 04 p0615 A67-14970

Wind profile effect on turbulent diffusion for infinite linear source in surface layer of unstable stratified atmosphere 04 p0652 A67-15569

Structure of wind field in thermally stratified atmosphere based on spectra of horizontal wind speed fluctuations 05 p0837 A67-16485

Wind profiles obtained from meteorological tower plotting wind velocity, normalized by value of friction velocity, as function of measurement heights 07 p1220 A67-20002

Small perturbation analysis of observed organized cloud convection for arbitrary unidirectional wind 08 p1350 A67-20950

Cloudstreet formation by wind induced vorticity forces equal to buoyancy forces, noting Rayleigh number variation 08 p1350 A67-20951

Thermal and momentum eddy diffusivities computed from wind profile and turbulence of rocket released chemical clouds 08 p1328 A67-21478

Optimal gain settings for atmospheric turbulence in 407 atmosphere wind profiles [AIAA PAPER 66-484] 08 p1413 A67-21509

Absolute angular momentum of outflow winds and radar targets in hurricanes and typhoons 10 p1676 A67-22813

Rocket observation of upper atmospheric winds noting wind shear, velocity, pressure, wind vector rotation, etc 10 p1638 A67-23198

Neutral wind structure and time variation over height in lower thermosphere observed using gun-launched trails, noting relation to sporadic E layer 10 p1644 A67-23257

Turbulent transfer in diabatic conditions, deriving formulas for wind and temperature profiles 10 p1677 A67-23574

Saturn IB flight test loads, comparing measured and calculated bending moment, noting launch time wind profile 10 p1713 A67-23734

Neutral upper atmosphere winds near equator, discussing sodium vapor rocket observation results 12 p1934 A67-25790

Wind and pressure fields diagnostic relations substituted for classical equation of stream function and solved as boundary value problem 13 p2149 A67-26273

Structure of wind field in thermally stratified atmosphere based on spectra of horizontal wind speed fluctuations 13 p2150 A67-26341

Temperature and wind fields in stratosphere obtained with rocket probes, noting diurnal and annual temperature variation differences for heights beyond 35 km 13 p2113 A67-26679

Wind profile analysis from balloon sounding data, using Fourier series to filter out unwanted part of spectrum 16 p2668 A67-31742

Temperature and wind profiles in stratosphere and mesosphere during winter and summer determined by grenade soundings, noting diurnal variations 19 p3226 A67-35924

Zonal winds studied by meridional sections from observations made during same months over several years 20 p3480 A67-36965

Wind profile criterion for structural design of launch vehicles, representing wind statistically by bivariate-normal distribution 21 p3712 A67-37813

Correction technique validity determined by comparing parachute determined winds with chaff-determined wind profiles 21 p3654 A67-38186

Mountain lee waves, comparing wavelengths observed on satellite pictures with calculations assuming wind speed increase with height 21 p3655 A67-38578

Sporadic E blanketing frequencies during November 1965 as indicator of wind structure in lower ionosphere and meteor influx 23 p3995 A67-40806

Anabatic winds caused by solar heating of slope, investigating flow patterns useful for soaring purposes 24 p4181 A67-42022

Wind profiles properties application to launch vehicle design and operation, emphasizing wind shears and turbulence effects on vehicle dynamic response 24 p4242 A67-42918

WIND SHEAR

Wind, temperature, vertical motions and degree of turbulence measurements of cumulonimbus clouds interacting with wind field 03 p0463 A67-14224

Radar measurement of vertical density profiles of clouds and precipitation 04 p0650 A67-14689

Relationship of layer thickness and/or wind speed to wind shear [AIAA PAPER 66-352] 05 p0838 A67-17304

Geomagnetic field variations in temperate zone sporadic E layer according to wind-shear theory 07 p1179 A67-19849

Positive ion layers in E region explained by wind shear theory, obtaining steady state solutions for simple model 08 p1326 A67-21359

Electron and ion temperature changes in sporadic E layer based on wind shear theory, using energy equation 08 p1327 A67-21366

Removal of incident wave spectrum by background wind shears during atmospheric gravity waves propagation to ionosphere from lower regions 08 p1328 A67-21477

High incidence and erraticism of sporadic E occurrence in temperate zones where horizontal component of geomagnetic field is greatest attributed to horizontal wind shear 10 p1644 A67-23255

Wind shears and ionospheric electron densities measured by vapor trail method and rocketborne Langmuir probe respectively during twilight and night 10 p1644 A67-23256

Wind shear theory of formation of temperate zone blanketing sporadic E layers, noting motion equation for ions in ionospheric E region 10 p1644 A67-23258

Aerobee rocket sounding of ionospheric sporadic E layer, noting abundance of metallic ions in layer and NO above and below 11 p1784 A67-23926

Wind, temperature, vertical motions and degree of turbulence measurements of cumulonimbus clouds interacting with wind field 12 p1963 A67-25480

Time constants of sporadic E layer formation influenced by wind field containing strong vertical gradients 20 p3428 A67-36375

Wind profiles properties application to launch vehicle design and operation, emphasizing wind shears and turbulence effects on vehicle dynamic response 24 p4242 A67-42918

WIND TUNNEL

SA BLOWDOWN WIND TUNNEL

SA COMBUSTION WIND TUNNEL

SA HYPERSONIC WIND TUNNEL

SA HYPERVELOCITY WIND TUNNEL

SA LOW DENSITY WIND TUNNEL

SA LOW SPEED WIND TUNNEL

SA SHOCK TUNNEL

SA SLOTTED WIND TUNNEL

SA SUBSONIC WIND TUNNEL

SA SUPERSONIC WIND TUNNEL

SA TRANSONIC WIND TUNNEL

Heat flux to SNAP reactor system models in hypersonic continuum flow measured in shock and hyperthermal wind tunnels, using thin film resistance thermometer 01 p0112 A67-11022

Heat flux measurement in very short flows in short arc wind tunnels and shock tubes 01 p0168 A67-11091

Wind tunnel testing of ground effect machine, examining geometric dependence of aerodynamic characteristics, lift due to interference and peripheral jet, pressure

Increases, etc 02 p0180 A67-11534
 Forced convection effects on VHF CW and X-band antenna voltage breakdowns in wind tunnel experiments, using cold nonconducting gas 02 p0213 A67-11647
 Pivot center position effect on aerodynamic characteristics of variable sweepback wings during rotation 03 p0351 A67-12994
 Free stream conditions approaching oscillating body in low speed wind tunnel, employing unsteady Bernoulli equation 03 p0352 A67-13899
 Nozzle requirements for hypersonic vehicle at transonic conditions, noting results of tests in high velocity wind tunnel 04 p0545 A67-14536
 Upper atmospheric oxygen atom concentration profiles obtained via wind tunnel simulation of NO releases [AFCR-67-0053] 04 p0615 A67-14971
 Convective and radiative heat transfers at stagnation point of hemisphere cylinder model immersed in high enthalpy partially ionized supersonic flow in plasma wind tunnel 05 p0747 A67-16432
 Schlieren and hot-wire anemometric observation of supersonic wakes in wind tunnel turbulent flows [ONERA-TP-417] 05 p0748 A67-16482
 Wind tunnel results for expansion problem of two-dimensional and axisymmetric turbulent jets with zero excess impulse 06 p0982 A67-17742
 Reentry trim angle of attack and lift-drag ratios from Gemini flights compared to wind tunnel data for aerodynamic studies [AIAA PAPER 67-166] 06 p0939 A67-18295
 Wind tunnel study of boundary layer transition structure on ogive nose cylinders aligned parallel to flow [AIAA PAPER 67-129] 06 p0939 A67-18314
 Oscillatory ground wind response of Atlas/Agena examined, using statistical theory of extreme values 06 p1104 A67-18492
 Aeronautical research facility in West Germany 06 p0981 A67-18754
 Shear flow generation by flat plate grid with added turbulence generator and roughened floor in wind tunnel 09 p1483 A67-21566
 Aspect ratio effect on cascade performances, noting complex variation of boundary layer thickness and changes in axial velocity ratio 09 p1437 A67-21742
 Measurements of conductivity, electron density and ionization rate of cesium in argon on alkali shock tube, describing MHD generator wind tunnel experiment 09 p1540 A67-21789
 Pressure gradients effects on boundary layers grown on wall of wind tunnel, obtaining equilibrium boundary layers of Clauser type 09 p1489 A67-22415
 Total aerodynamic forces and moments of free flying body in wind tunnel determined from accelerations measured and telemetered by onboard instruments [AIAA PAPER 66-775] 11 p1773 A67-24349
 Hydrodynamic boundary layer velocity profile on disks in transverse airflow analyzed theoretically and by wind tunnel tests 12 p1891 A67-25318
 Multiple arc performance in 8000 kw plasma facility consisting of hyperthermal blowdown tunnel for ballistic flight simulation 12 p1974 A67-25404
 Electrode feed system for segmented electrode MHD wind tunnel 12 p1920 A67-25406
 Aerodynamic damping and frequency drift of turbomachine blades, discussing wind tunnel testing results for various geometric configurations 13 p2051 A67-27205
 Wind tunnel tests of sonic boom phenomena, noting weak pressure field measurement, construction of extremely small models, boundary layer effects, etc [AIAA PAPER 66-765] 13 p2091 A67-27594
 Wakes behind circular cylinders in free molecule flow, noting inaccuracy in off-axis impact pressure measurements 14 p2300 A67-28175
 Wind tunnel heat transfer measurements from circular cylinders to transverse air flow, noting recovery factor as function of Knudsen number 14 p2405 A67-28178
 First collision effects in rarefied high speed flows in low density wind tunnel, noting measurement techniques and apparatus used 14 p2317 A67-28197

Para-Foil models tested in wind tunnel and free flight for flight capability, L/D ratios, deployment, control and maneuverability, etc 14 p2246 A67-29054
 ONERA hot-shot wind tunnel flow stability and homogeneity and measurement of plasma electromagnetic field, skin friction, etc [ONERA-TP-447] 15 p2465 A67-29377
 Aerodynamic heat flux measurements in frozen boundary layer flows taken in hyperthermal wind tunnel, considering surface catalytic effects 15 p2468 A67-30154
 Flow turbulence on leading edge of attachment line of swept wing studied in wind tunnel 16 p2589 A67-30618
 Dust remover using paper filters and wind tunnel with turbulence in cylindrical duct used for pressure determination 16 p2657 A67-30867
 Reentry trim angle of attack and lift-drag ratios from Gemini flights compared to wind tunnel data for aerodynamic studies [AIAA PAPER 67-166] 17 p2789 A67-32061
 Rarefied gas supersonic flows studied in wind tunnel for aerothermal/aerodynamic characteristics 17 p2790 A67-32231
 Statistically designed experiments in wind tunnel test programs dealing with exhaust nozzles, discussing data analysis techniques [AIAA PAPER 66-742] 17 p2834 A67-32571
 Span loading on wing of complete aircraft configuration determined, using segmented wing in wind tunnel test technique and least squares method [AIAA PAPER 66-768] 17 p2834 A67-32576
 Convection coefficient distribution in supersonic flow, noting wind tunnel measurement results at Mach 3.3 and at various angles of attack 17 p2791 A67-32702
 Barometric sensors insensitive to high winds 17 p2860 A67-32816
 Wind tunnel ejector and hot water supply for ramjet power plant attitude test stand, noting synchronization of ejector with test section 17 p2834 A67-32817
 Tangentially injected plane jet spreading in slipstream at various Reynolds numbers at jet inlet slot studied in wind tunnel for dynamic behavior 17 p2839 A67-32906
 Calibration and recording method for transmission coefficients of thermal wall heat flows, using ONERA wind tunnel [ONERA-TP-470] 18 p3020 A67-34463
 Plasma layer effect on antenna performance from wind tunnel studies, discussing antenna transmission and breakdown in plasma jet flow 18 p3004 A67-34645
 Wind tunnel measurement of turbulent transport terms for unstable curved mixing layer of incompressible flow 18 p3030 A67-34751
 Heat transfer intensifying process experimented in wind tunnel by applying longitudinal/transverse pressure gradients through controlled flow pressure field 19 p3346 A67-35633
 Ablation characteristics investigated using plasma jet wind tunnel, discussing effective heat of ablation and free stream stagnation enthalpy 20 p3544 A67-36640
 Wind tunnel tests for load and pressure distributions on flat-top cylinders with thick boundary layer 20 p3421 A67-36781
 Sonic boom and factors influencing shock wave propagation during straight horizontal supersonic flight 22 p3744 A67-39547
 Hatfield V/STOL tunnel design problems and tunnel model test results 22 p3780 A67-40063
 Wind tunnel data predicted vertical forces for rocket sleds compared with measurement on test track noting disagreement 22 p3780 A67-40095
 Large diameter helicopter rotors and V/STOL propellers/axis tilting in vertical plane/ testing system of wind tunnel and aerodynamic torque measuring apparatus 23 p3986 A67-40575
 Transonic and supersonic grid wind tunnel loaned to Germany by NASA for testing blades 23 p3987 A67-41328
 Drag problems of Belfast aircraft solved by modifications developed in wind tunnel program 24 p4092 A67-42443
WIND TUNNEL APPARATUS
 Probe holder used in wind tunnels for shifting of flow measuring probes 02 p0228 A67-11554
 Rutgers Axisymmetric Near-Wake Tunnel

for testing turbulent supersonic base flow, temperatures and pressure distributions 02 p0230 A67-12361
 Ion concentration in D region, describing wind tunnel experiments to determine electrode configuration for Gerdien condenser rocket probe 03 p0412 A67-13367
 Fan system of 14 by 9 ft open circuit wind tunnel structural principles and operation, discussing blade fabrication, hub design, spinner and motor fairing 03 p0397 A67-14104
 Three-component wind tunnel balance capable of magnetically suspending test model 05 p0786 A67-16461
 Hypersonic testing methods at ONERA, discussing wind tunnel apparatus [ONERA-TP-371] 05 p0748 A67-16475
 Hypersonic wind tunnel for small gas densities noting vacuum pumps, diffuser, cooler, etc 05 p0786 A67-16591
 Scaling equations for wind tunnel simulation of trajectory of jettisoned stores from aircraft 06 p0979 A67-18006
 Test of probes designed to determine direction of supersonic flows in wind tunnels, using schlieren photography 09 p1496 A67-21693
 Ignition of flammable fluids by hot surfaces tested on static hot plate rig and on wind tunnel rig, noting data on kerosene, lubricating oil and hydraulic fluid 09 p1580 A67-22248
 Screen and honeycomb effect on variation of skin friction in low speed wind tunnel, noting turbulent boundary layer growth 10 p1627 A67-23556
 Atomic oxygen density profiles obtained from radiation intensity resulting from nitric oxide reaction 14 p2293 A67-28199
 Semiconductor surface thermocouples, determining heat-transfer rates associated with wind tunnel testing 18 p3048 A67-34103
 Generator installation for supersonic test simulation to measure wing forces, discussing calibration problem 21 p3609 A67-38889
 Spoilers for aircraft steering, discussing wind tunnel tests, banking moment and spoiler-slot aileron 22 p3739 A67-39535
 Wind tunnel pressure measurement installation, describing calibration bench and industrial testing 23 p3997 A67-40572
 Hypersonic aerodynamics, discussing tunnel testing, inviscid flows, airfoil shapes, real gas effect, shock wave theory and boundary layers 23 p3930 A67-41307
 Laser macrophotography for size distribution of particulate debris dispersed from ablating zirconium alloy specimen in hyperthermal wind tunnel ablation testing 23 p4006 A67-41380
WIND TUNNEL BALANCE
 Strain gauged sting balance for use in small low speed wind tunnel for measuring lift, drag and pitching moment 01 p0051 A67-11270
 Turning-arm apparatus operating in rarefied gas chamber and low pressure wind tunnel for drag measurements 04 p0596 A67-14993
 Aerodynamic balance for wind tunnel measurement of forces and moments on jet flap 07 p1163 A67-19350
 Six-component balances installed under each of two test sections of Lockheed-Georgia wind tunnel designed for development of VTOL aircraft 07 p1164 A67-19672
 Yaw force /Magnus/ of spinning projectile at angle of attack measured, using balance device in wind tunnel [AIAA PAPER 66-753] 14 p2292 A67-28132
 Safety device to prevent overloading of models and sensitive wire strain gauge balance by aerodynamic forces during starting and switching off in wind tunnel 22 p3780 A67-39756
WIND TUNNEL CALIBRATION
 Local density and temperature measurement in wind tunnels determined by 50-kev electron scattering, using air as test gas 11 p1790 A67-24446
 Electric manometer using electrolytic fluid for low velocity measurements with Pitot tube 16 p2675 A67-31210
 Wind tunnel pressure measurement installation, describing calibration bench and industrial testing 23 p3997 A67-40572
 Continuously operating transonic wind tunnel at Aerodynamic Research Institute

noting design, electronic data processing equipment and tunnel calibration 23 p3987 A67-41312

WIND TUNNEL DRIVE

Low turbulence wind tunnel driven by airfoil centrifugal blower, noting design for best performance 09 p1485 A67-22162

Limiting driven conditions corresponding to optimum expansion and low density shock tube flow for overexpanded nozzle 21 p3609 A67-38886

WIND TUNNEL MODEL

Subsonic wind tunnel analysis of wake deformations produced by secondary velocities using models with flat base but various cross sections 02 p0233 A67-12228

Wind tunnel tests of lifting reentry body at Mach numbers up to 16.5 and at angles of attack up to 50 degrees 04 p0546 A67-14567

Wind tunnel experiments extending range of data published in 1964 on flow field associated with sonic injection of gas 04 p0604 A67-14831

Heat transfer tests of blunt nosed cone containing cylindrical protuberances tested in AEDC tunnel, including effects of local Mach number, Reynolds number and sweepback angle 04 p0549 A67-15832

Glass fiber reinforced plastics experience for preparing high precision models of complex shape, noting wind tunnel application 06 p1007 A67-18019

Transonic wind tunnel studies of ground-wind loads on aeroelastic models of Saturn launch vehicle, investigating structural damping, wind velocity and azimuth angle 07 p1257 A67-19371

Shock wave tubes and wind tunnels for momentary generation of steady air flows for aerodynamic investigations at high supersonic velocities 07 p1127 A67-20121

Wind tunnel model for analysis of autorotating rotors for reentry space vehicles tested at transonic and supersonic regimes 09 p1440 A67-22285

Free flight hypersonic wind tunnel testing technique noting pneumatic launcher, data acquisition and processing 10 p1622 A67-23390

Low speed aerodynamic static stability of winged and wingless reentry configurations 14 p2239 A67-27796

Supersonic aircraft nozzle system aerodynamic performance at subsonic speeds [AIAA PAPER 67-452] 18 p2983 A67-33926

High lift characteristics of various aircraft configurations in wind tunnel model using different leading and trailing edge lift augmentation devices 23 p3934 A67-41309

High enthalpy supersonic wind tunnel performance, analyzing Teflon model stagnation ablation 23 p3931 A67-41477

WIND TUNNEL NOZZLE

Hypersonic low density wind tunnel for high Mach numbers and stagnation temperatures, analyzing measurements made, noting heater, nozzle, diffuser, etc 04 p0595 A67-14561

Effect of fairing contraction into two-dimensional supersonic nozzle for wind tunnel, avoiding pressure gradients along walls unfavorable to boundary layer flow development 07 p1126 A67-19630

Air condensation in hypersonic wind tunnel strongly related to flow expansion rate 18 p2657 A67-30708

WIND TUNNEL STABILITY TEST

Open jet wind tunnel testing of Meteor sailplane, examining aerodynamic merging of wings, fuselage and cockpit 01 p0006 A67-10970

Wind tunnel technique for measuring frequency response of flexible airplane to vertical sinusoidal gusts [AIAA PAPER 65-787] 03 p0354 A67-12908

Environmental wind tunnel investigation of wind velocity and discharge current effects on average charge per Trichel pulse in corona discharges 03 p0486 A67-14119

Power spectral density/PSD/ methods applied to prediction of aircraft responses to continuous turbulence [AIAA PAPER 66-1000] 03 p0362 A67-14147

Total pressure losses in hypersonic wind tunnel with Eiffel chamber, calculating coefficient of pressure recovery 04 p0546 A67-14780

Airflow in small wind tunnel with roughened heat transfer surface, using flow visualization techniques 04 p0727 A67-15801

Spin calculations corroborating vertical wind tunnel tests on delta wing aircraft,

noting aerodynamic parameters

[ONERA-TP-388] 05 p0751 A67-16477

Damping in yaw on jet-flap blowing model measured by decaying oscillation technique 06 p0979 A67-17919

Measurement techniques used in wind tunnel and free atmosphere parachute tests 06 p0979 A67-18017

Tilt rotor VTOL aircraft stability, discussing results of wind tunnel tests on rotor-pylon behavior at different velocities [AIAA PAPER 67-17] 06 p0948 A67-18254

Wind tunnel investigation of effect of ground level on static aerodynamic characteristics of sideslip for rectangular and delta wing with rudder assembly 07 p1128 A67-19886

Supersonic flutter characteristics of thin cantilever plate surfaces with low aspect ratio 08 p1416 A67-20530

Supersonic wind tunnel test providing static pressure measurements for use in cylinder flutter calculations 08 p1277 A67-20588

Turbulence effects on laminar skin friction and heat transfer from plates and circular cylinders in incompressible flow, using two low turbulence wind tunnels 08 p1427 A67-21118

Automatic carpet plotting applicability to reduction of wind tunnel data 08 p1278 A67-21530

Wind tunnel investigation of dynamic instabilities in cruciform finned missiles due to rolling motion 08 p1413 A67-21531

Aerodynamic characteristics of forced lead-lag rotor system, noting parameters of horizontal force, rolling and/or pitching moments 09 p1437 A67-21741

Three-dimensional flutter calculations verification by wind tunnel results, using flexible supersonic aircraft planform model of determined characteristics to control calculations 10 p1622 A67-22882

Wind tunnel test program for simulation of gas-particle rocket exhaust plume, separated flow around nozzle and base recirculation [AIAA PAPER 66-767] 11 p1773 A67-24351

Rotor downwash angle and tunnel geometry effect on maximum size rotor that can be tested in closed throat wind tunnel 13 p2091 A67-27595

Bell Model 266 composite VTOL aircraft, discussing tilting rotor principle for conversion from helicopter to aircraft 16 p2595 A67-30495

Power spectral density/PSD/ methods applied to prediction of aircraft responses to continuous turbulence [AIAA PAPER 66-1000] 17 p2797 A67-32582

Flutter of flat panels at low supersonic speeds, describing mounting which makes it possible to change tension of panel during testing at constant Mach number [ONERA-TP-487] 17 p2961 A67-32699

Time lag effect on dynamic stability determined, using wind tunnel tests with 10 degree cone as test body simulating ablation process by gas injection into boundary layer [AIAA PAPER 66-757] 17 p2792 A67-33004

Supersonic flutter characteristics of thin cantilever plate surfaces with low aspect ratio 19 p3343 A67-35775

V/STOL aircraft model wind tunnel tests on wing and propellers, describing strain gauge balances 22 p3745 A67-39728

Longitudinal stability and control wind tunnel results, considering swept and variable geometry wing aircraft during deep stall conditions 23 p3932 A67-40567

Measuring device for aerodynamic coefficients during wind tunnel tests by forced oscillation method 23 p3986 A67-40570

WIND TUNNEL WALL

Streamline matching technique for V/STOL wind tunnel wall corrections [AIAA PAPER 67-183] 07 p1163 A67-19439

WIND VARIATION

Atmospheric tides deduced from drifts of ionized meteor trains observed by Doppler shift of echoes 05 p0803 A67-17405

26 month oscillation in zonal wind and temperature in equatorial atmosphere 13 p2150 A67-26440

Space-time wind variability for forecasting from near ground surface sampling for unguided rocket impact prediction 17 p2880 A67-32551

Biennial oscillations effect on spring wind reversal in stratosphere and mesosphere,

showing transition date dependence on geographical location and height 18 p3074 A67-34352

Fluctuations in stratospheric and mesospheric winds studied by meteorological sounding rockets, noting relation to solar activity 19 p3217 A67-35207

Quasi-biennial zonal wind and temperature oscillation in stratosphere and mesosphere, discussing periodicity and oscillation model 19 p3220 A67-35272

Structure and composition of upper atmosphere above stratopause, discussing temperature, density and wind variations 20 p3430 A67-36904

Semiannual wind variation in equatorial stratosphere analyzed for origin from rocket sounding data 22 p3828 A67-39466

WIND VELOCITY

Energy spectrums, mean and eddy kinetic energies of atmosphere between surface and 50 km 03 p0463 A67-13930

Solitary waves in compressible atmosphere with arbitrary wind and density profiles, obtaining solution for critical speed by perturbation scheme 03 p0463 A67-14032

Probability distribution of square of vertical wind velocity difference during unstable stratification 03 p0463 A67-14228

Doppler technique application to radar measurement of clear air target motion 04 p0569 A67-14684

Short term weather forecasting by determination of aerodynamic maps of cold front motion in terms of normal wind velocity component 04 p0652 A67-15472

Cartwright-Longuet-Higgins-Rice theory on instantaneous maxima of stationary random variable for deriving instantaneous maximum gust ratio to mean wind speed 05 p0837 A67-16426

Multivariate statistical analysis of wind sounding data, applying high degree of correlation between two wind parameters and empirical density function [AIAA PAPER 66-353] 05 p0838 A67-17214

Probability distribution of square of vertical wind velocity difference during unstable stratification 12 p1963 A67-25484

Vertical component of gusts in upper atmosphere estimated from rotation rate of ascending radioprobe fan 12 p1964 A67-26165

Numerical integrations of equation for turbulent diffusion in atmosphere 13 p2152 A67-26863

Hydrogen vent flare stack performance in adverse weather conditions 13 p2186 A67-27651

Catalog tabulating 1600 comet tail orientation observations 14 p2386 A67-28481

Relationship between absorption of hydrogen fluoride by lined filter papers and exposure dosages investigated under controlled conditions of various factors 16 p2675 A67-31211

Concepts of wind drift and lateral maneuver applied in flight mechanics 17 p2798 A67-32591

Barometric sensors insensitive to high winds 17 p2860 A67-32816

Strontium and Ba vapor releases in upper atmosphere, testing yield of evaporated metal for different chemical reactions 17 p2851 A67-33194

WIND VELOCITY MEASUREMENT

Successive approximation method of estimating effect of stratification and dynamic nonuniformity of crosswind on trajectory of circular turbulent jet 01 p0053 A67-10824

Analysis of additional terms in Reynolds flux equation when under unsteady conditions, using wind and temperature measurements, noting role in micrometeorology 02 p0238 A67-12077

Optimum averaging periods in measurements of wind velocity profile, temperature gradient, vertical thermal turbulent flow and atmospheric drag 02 p0263 A67-12644

Ratio of Lagrange and Euler correlation scales determined from correlation of time fluctuation of transverse wind velocity and temperature variation measurements 03 p0464 A67-14229

Velocity azimuth display technique analysis of wind parameters, noting fundamental limitations 04 p0648 A67-14674

Atmospheric temperature and wind velocity in mesosphere measured by rocket grenade method 05 p0798 A67-16857

Two-component drag force anemometer design and performance, noting method for wind bearing and velocity 05 p0808 A67-17308

Rotational speed of upper atmosphere obtained by measuring changes in orbital inclinations of satellites or movements of vapor trails 06 p0993 A67-17564

Hot-wire anemometer for instantaneous measurements of rapidly time-varying wind flows 06 p1000 A67-17633

Wind profiles obtained from meteorological tower plotting wind velocity, normalized by value of friction velocity, as function of measurement heights 07 p1220 A67-20002

Doppler radar measurements of wind velocity horizontal components variation in rain and snow, calculating time correlation and structural functions for neutral and unstable stratifications 07 p1221 A67-20004

Supersonic flow velocity and density probe for direct measures of mass and momentum influx, noting solution of H-T diagram of argon and probe criteria 09 p1497 A67-21776

Wind velocity, direction and diffusion coefficients determined with aid of artificial luminescent cloud 10 p1675 A67-22795

Macroscopic neutral and ionized gas motions in ionospheric D and E layer interpreted from wind and radio wave scattering measurements 11 p1787 A67-24595

Ratio of Lagrange and Euler correlation scales determined from correlation of time fluctuation of transverse wind velocity and temperature variation 12 p1964 A67-25485

Atmospheric temperature, pressure, density and wind measurements between 30 and 80 km by Skylark rocket at Woomera, Australia 12 p1937 A67-25840

Ferrite-diode system with automatic gating of signal reflection used in radar wind velocity observations to reduce pulse interferences produced by meteor trails 13 p2197 A67-26505

Radar measurements of wind regime of meteor zone made by means of pulse-coherent method 13 p2110 A67-26552

Mesosphere winds and turbulence observed by forming aluminum oxide smoke trails 18 p3043 A67-34496

Rocket observations of upper atmospheric winds, electron density, electron temperature, and neutral temperature in auroral region with Langmuir probes 19 p3214 A67-35169

Wind velocity and direction measurements by radar tracking of chaff /dipoles/ clouds 19 p3219 A67-35247

Rocket measurements above England, noting relation of temperature maximum at stratopause to mesospheric wind maximum 20 p3480 A67-36966

Biennial component of seasonal variation in earth rotation rate using time observation data, calculating stratospheric zonal wind effect 23 p3996 A67-41085

Rocket instrumentation and sensing techniques for collecting stratospheric wind and temperature data 23 p4025 A67-41445

Wind velocity, direction and diffusion coefficients determined with aid of artificial luminescent cloud 24 p4181 A67-42131

WINDING

S FILAMENT WINDING
S HELICAL WINDING
S WIRE WINDING

WINDOW

SA LAUNCH WINDOW
SA WAVEGUIDE WINDOW

Interferoscope used in testing large glass panels for aircraft camera windows 10 p1652 A67-22701

Quick change high vacuum window and heat transfer gauge installation for shock tubes 10 p1658 A67-23789

Gemini window contamination due to outgassing of silicones 15 p2507 A67-29555

Fiber optic window fitted to stainless steel field ion microscope permitting use of direct contact photography for image recording 17 p2863 A67-33354

WINDSHIELD

Semipermanent repellant for aircraft windshields to overcome effect of visual errors caused by rain on windshields 08 p1279 A67-21042

Nondestructive determination of stress distribution in three-layer tempered glass aircraft windshield by scattered-light

photoelastic method 15 p2575 A67-30033

Aircraft front windshields, discussing thermal stability, clear vision maintenance, bird impact, atmospheric pressure effect, cabin pressure changes and tensile strength 18 p2986 A67-34099

WING

SA AIRFOIL
SA CAMBERED WING
SA CANTILEVER WING
SA CRUCIFORM WING
SA DELTA WING
SA FLEXIBLE WING
SA GOTHIC WING
SA HELICOPTER WING
SA LOW ASPECT RATIO WING
SA MISSILE WING
SA OSCILLATING WING
SA PIVOTED WING
SA RECTANGULAR WING
SA RING WING
SA ROTARY WING
SA ROTOR
SA SLENDER WING
SA SWEPT WING
SA SWEPTBACK WING
SA TAPERED WING
SA THIN WING
SA TILT-WING AIRCRAFT
SA TRAPEZOIDAL WING
SA TWISTED WING

Possio integral equation kernel derived in analytical form for wing flow 06 p0935 A67-17623

Partial diaphragm when applying supersonic Mach box method for steady state condition and uniform downwash on wing compared with complete diaphragm 06 p0944 A67-18875

Numerical wing analysis in steady or unsteady supersonic flow, calculating pressure coefficient, local loads and generalized forces from deformation law or wing slope 08 p1278 A67-20800

Flight experiments to assess stalling behavior and handling problems arising in design, maintenance and operation of suction wing for high lift [AIAA PAPER 65-750] 09 p1441 A67-22483

Book on aerodynamics of V/STOL aircraft emphasizing use of momentum and finite wing theories, considering deflection of trailing vortex system 14 p2243 A67-28678

Reinforced plastic materials for light aircraft wing structures, calculating torque strength 22 p3912 A67-39729

WING BODY

Statistical analysis of high speed aircraft plotting, including wing and tail surface effects and pilot work load and performance 04 p0653 A67-14894

Gas flow around wing in presence of moving shock wave with variable gas parameters noting wave equation, velocity potential, etc 20 p3355 A67-36191

Quasi-conical motion past wing-body lifting system, determining pressure distribution, potential expression and axial disturbance velocity 20 p3356 A67-36278

Thin optimum wing contour constructing procedure having minimum wave drag in supersonic flow solved by linear approximation, obtaining numerical values for parameters 22 p3741 A67-40017

WING FLAP

SA JET AUGMENTED WING FLAP

Gap size effect on pressure and aerodynamic heating over flap of blunt delta wing in hypersonic flow [AIAA PAPER 66-408] 05 p0749 A67-17220

Lift gain of flapped wing through use of wing-slot suction of friction layer near knee of flap 10 p1590 A67-22917

Flapped finite-span wing lift, center-of-pressure and hinge moment moving near solid wall determined as functions of flap length, rotation angle, etc 17 p2792 A67-32902

Wing flap aerodynamic performance as affected by wing flap surface cavities, noting usefulness in flow stabilization at high pressure gradient 17 p2792 A67-32904

WING FLOW METHOD TEST

Aerodynamic coefficients of finite wing with built-in lifting fans, noting additional lift and drag due to supercirculation at trailing end 01 p0006 A67-10769

Induced drag for idealized ground effect wing for optimum lift distribution 01 p0006 A67-10809

Airflow past wing profile with leading edge slot blowing foreign gases, noting

schlieren photographs of flow patterns and concentration distribution measurement 10 p1589 A67-22724

Semilempirical method for predicting aerodynamic interference of circular jet exhausting at right angles from wing, showing effect on lift loss 11 p1742 A67-24659

Lift and drag of trapezoidal wing models in blown flow near free surface studied for sweepback angle effect on aerodynamic characteristics 13 p2093 A67-26595

Thick laminar boundary layer effect on aerodynamic behavior of simple shapes in supersonic low density flow 14 p2241 A67-28170

Interference of open and closed wind tunnels with ground board calculated and results applied to airfoils 16 p2590 A67-30854

Limit of circulatory lift on wings with finite span, deriving lift and drag for flat and rolled up vortex sheets 17 p2789 A67-32035

Iterative method for design of bullet-like fairing, giving subsonic subcritical flow with desired velocities at junction of two wings 17 p2791 A67-32586

Approximation solution of three-dimensional problems associated with slender wing motion in transonic gas flow with perturbations 18 p2981 A67-33535

Nonlinear theory of lifting wing surface of arbitrary aspect ratio, deriving velocity potential, lift coefficient and induced drag 18 p2981 A67-33536

Supersonic flow past windward side of delta wings with angles of attack from 0 to 80 degrees, verifying experimental and theoretical values 18 p2984 A67-34208

Aerodynamic characteristics of polygonal wings with diamond-shaped profile in supersonic flow 20 p3355 A67-36194

V/STOL aircraft model wind tunnel tests on wing and propellers, describing strain gauge balances 22 p3745 A67-39728

Electromechanical simulator of wing flutter with aileron under flight conditions 22 p3912 A67-39779

WING-FUSELAGE COMBINATION

Open jet wind tunnel testing of Meteor sailplane, examining aerodynamic merging of wings, fuselage and cockpit 01 p0006 A67-10970

Aerodynamic characteristics calculation for wing-fuselage assembly in supersonic flow 02 p0180 A67-12793

Fuselage interference effect on annular airfoils determined by measuring lift and drag of model aircraft equipped with annular wing for each semispan and empennage 03 p0352 A67-13313

Slender wing basic shape for adaptation to fuselage of circular cross section [ONERA-TP-425] 05 p0748 A67-16762

Linearized long wave diffraction theory of supersonic inviscid flow past slender circular cylindrical bodies and thin wings 06 p0942 A67-18729

Aerodynamic effect of volume addition to high lift to drag wing-body ratio at Mach 6 07 p1126 A67-19382

Unsteady supersonic flow about conical wing fuselage system with LF harmonic oscillatory motion 07 p1127 A67-20224

Correct image system and conditions for vortex model of wing body interference 08 p1277 A67-20596

Fiat G91Y and G222 aircraft at Second International Aeronautical Exhibition, Turin, noting performance, physical characteristics and component parts 09 p1439 A67-22092

Aerodynamic design of swept wing-fuselage combination for cruising at transonic and supersonic speeds, noting pressure distribution role 10 p1589 A67-22872

Wing-fuselage section panels of hypersonic aircraft built by brazing welded refractory honeycomb 10 p1660 A67-23171

WING LOADING

Electron microscopy study of fracture surface topography permitting identification of fine scale fracture surface features, relating them to fracture formation mechanisms [AIAA PAPER 66-814] 01 p0077 A67-10034

Computer program /MAST/ analyzing F-111 wing structure involving load and stress analyses 03 p0525 A67-13967

Isolated compressor blade within framework of lifting line theory, expressing drag produced by tip-gap in terms of flow

rate and wing loading 09 p1437 A67-21739
 Action of concentrated loads in plane problem of mechanics of deformable solids 10 p1715 A67-22921
 Electron microscopy study of fracture surface topography permitting identification of fine scale fracture surface features, relating them to fracture formation mechanisms [AIAA PAPER 66-809] 10 p1661 A67-23552
 Propulsion-lift system interrelationship in compound helicopter and design parameters affects performance vs speed such as disk loading, solidity and tip speed schedule [ASME PAPER 67-GT-18] 11 p1854 A67-24802
 Accelerometer use for operational load measurements in aircraft, emphasizing automatic counting technique 11 p1880 A67-25059
 Transient buffet loads on wings due to gust or maneuver 13 p2215 A67-26533
 Span loading on wing of complete aircraft configuration determined, using segmented wing in wind tunnel test technique and least squares method [AIAA PAPER 66-768] 17 p2834 A67-32576
 Annular wing motion in compressible fluid axisymmetric flow, determining forces acting on wing cross section 18 p3022 A67-33411
 Pressure distribution in subsonic flow for vertical stabilizer calculated, using orthogonal function theory 18 p2982 A67-33655
 Flare and landing performance of glide vehicles with low lift-drag ratio, noting aerodynamic characteristics effect [AIAA PAPER 67-575] 19 p3335 A67-35970
 Approximate solutions obtained in closed forms for low aspect wing stressed state under transverse load 21 p3724 A67-38780
 Generator installation for supersonic gust simulation to measure wing forces, discussing calibration problem 21 p3609 A67-38889
 Poly I glider wing noting bonded aluminum sheet/honeycomb sandwich shell 22 p3811 A67-39302
 Wing stress analysis, reviewing computer and variational methods for calculating structural strength 22 p3746 A67-40445
 Buffet limit for aircraft wings in transonic region based on boundary layer theory, determining transonic pressure distribution and separation points 23 p3931 A67-41311

WING PANEL
 Critical stresses of three-layer wing panel compressed by load distributed along two sides, determining temperature stresses in bearing layers and equilibrium equations 05 p0913 A67-16191
 Supersonic internal axisymmetric conical flow obeying Taylor-Maccoll equation, discussing applications to wing surfaces and supersonic inlet leading edges 15 p2418 A67-30192

WING PLANFORM
 Supersonic transport design using double delta wing planform 03 p0360 A67-13918
 Supersonic transport design using double delta wing planform 03 p0362 A67-14299
 Aerodynamic characteristics of wings of complex planform at subsonic velocities, calculating flows past wings at moderate angles of attack 06 p0935 A67-17730
 Vibrational characteristics of inflatable wing model, determining resonant frequencies and mode shapes by using influence coefficients 06 p1100 A67-18002
 Sub-or supersonic wing leading edge in unsteady supersonic flow, presenting discontinuities in vibration modes and calculating wing stress forces 10 p1590 A67-22879
 Intake aerodynamics of upper wing surface studied with two-dimensional potential flow models and suction models, considering inlet problems 14 p2243 A67-28702
 Variable length foil fluttering in supersonic compressible gas flow, particularly case with end clamping of varying edges 22 p3910 A67-39454
 Wing shape and size selection for hypersonic velocities formulated as extremum problem of drag, aerodynamic property, temperature and coolant consumption for given wing volume 22 p3741 A67-40015
 V-shaped wings with plane sides and sharp edges investigated for aerodynamic properties, deriving equations for flow

parameters at Mach 6 22 p3741 A67-40016

WING PROFILE
 Three-dimensional supersonic gas flow with shock waves around flat wing analyzed, using integral relations method 01 p0007 A67-10981
 Flexible wing analysis based on slender body theory, calculating wing profiles, pressure distribution as function of stress and lift force values 03 p0351 A67-12992
 Aerodynamic forces of oscillating lifting surfaces of large aspect ratio in subsonic range investigated by approximation method 03 p0351 A67-12996
 Hypersonic flow in compressed layer between tapered blunt leading edge of wing and internal shock wave forming in front when nonuniform flow moves past, considering expansion plane 06 p0936 A67-17733
 Existence or nonexistence of continuous shockless transonic flow around symmetric wing profile, using Oswatitsch integral equation 06 p0942 A67-18586
 Maximum lift/drag ratio wing for supersonic environment 07 p1127 A67-20035
 Aerodynamic characteristics /pressure distribution and wave drag/ or polygonal wings of symmetrical thickness in supersonic flow 07 p1127 A67-20209
 Airflow past wing profile with leading edge slot blowing foreign gases, noting schlieren photographs of flow patterns and concentration distribution measurement 10 p1589 A67-22724
 Rogallo wing aerodynamic characteristics compared for various wing configurations and Mach numbers for possible application to spacecraft recovery 11 p1889 A67-24093
 Supersonic business jet designs, unswept trapezoidal wing model and delta wing model [SAE PAPER 670246] 12 p1895 A67-25501
 Pressure distributions and shock wave shapes on conical wings calculated by numerical solution of integral equations 16 p2589 A67-30619
 Downstream flow of shock waves created by wing section moving at speed of sound 16 p2594 A67-31712
 Electric vortex-field integrator using aluminum foil sheet and external field to simulate circular flow about wing profile at various angles of attack 17 p2834 A67-32905
 Wing slope techniques for analysis of Langmuir probe characteristics in low density plasma, using I-V characteristics and spherical and cylindrical geometries 17 p2906 A67-33054
 Wing profile effect on thin wing aerodynamic characteristics approaching screen in incompressible fluid potential flow 18 p2981 A67-33412
 Lift and drag coefficients of wing profile with elliptical pressure distribution calculated by approximate linearized theory 18 p3024 A67-33541
 Motion equation of system of two banked wings near solid surface with optimum circulation distribution 18 p3024 A67-33542
 Aerodynamic characteristics of wing profile employing boundary layer control by blowing with controllable jet 18 p2984 A67-34202
 Aerodynamic forces and pressure on wing model for Carafoli type MHT-C-04-04-10 profile characteristics, discussing applications to blade rotors 20 p3355 A67-36193
 Aerodynamic characteristics of polygonal wings with diamond-shaped profile in supersonic flow 20 p3355 A67-36194
 Book on thin wing and aerodynamic characteristics in subsonic gas flow 20 p3359 A67-37206
 Equations for transient temperature distribution and thermal stresses in heated idealized wing structure solved using heat flow analysis method 20 p3541 A67-37489
 Air suction effect on moment characteristics of cranked slender profile, determining boundary layer control 21 p3564 A67-38043
 Calculation method for mono-, two- and three-spar wings including membranes and plate, discussing stress formulas 21 p3722 A67-38525
 Supersonic aircraft evolution emphasizing Dassault series, Northrop T-38 and F-5 and Swedish Draken and Viggen 22 p3746 A67-39883

Multiple reflection of molecules effect on nonconvex wing aerodynamic characteristics for finite Mach number lateral free molecular flow 22 p3741 A67-40022
 Oscillating infinitely thin wing profile in inviscid subsonic compressible flow, deriving perturbation pressure 23 p3929 A67-41250
 Incompressible potential flow about thick wing profiles and cascades for blade profiles with angular and round tapered trailing edges 23 p3929 A67-41254
 Airfoil and profiles theories emphasizing boundary layer theory, lift augmentation and wing aerodynamics 23 p3930 A67-41305
 Aircraft wing drag noting relation between Mach number, thickness chord ratio, aspect ratio, airfoil shape and wing configuration 23 p3930 A67-41306
 Design characteristics of various SST, discussing Mach numbers and wing configuration 23 p3935 A67-41398
 DC-9 wing and high lift system aerodynamic design and development, discussing STOL field length design goals and flight test results [SAE PAPER 670846] 24 p4093 A67-41999

WING SPAN
 Flapped finite-span wing lift, center-of-pressure and hinge moment moving near solid wall determined as functions of flap length, rotation angle, etc 17 p2792 A67-32902

WING SPOILER
 F-111 aircraft wing spoilers controlled by hydraulic servoactuators 05 p0753 A67-16162

WING STALL
 High lift techniques for STOL aircraft compared based on maximum lift coefficient, noting airfoil stall characteristics and flow separation delay devices [SAE PAPER 670245] 12 p1894 A67-25500
 Separation and stall of impulsively started elliptic cylinder including interactions between boundary layer and outer flow [ASME PAPER 67-APM-31] 17 p2840 A67-33157
 Compressibility effects on airfoils during high subsonic and low speed stalls, considering Reynolds and Mach number effect 19 p3170 A67-35521
 Unsteady airfoil stall noting frequency effects on velocity distribution and angle of attack for oscillating pitch 21 p3565 A67-38547
 Longitudinal stability and control wind tunnel results, considering swept and variable geometry wing aircraft during deep stall conditions 23 p3932 A67-40567

WING TIP
 Wing tip vortices behind DC-8 measured for maximum circumferential velocities by research aircraft 24 p4091 A67-42276

WINGED VEHICLE
 Winged lifting reentry hypersonic vehicles, discussing design, analysis, fabrication and testing of hot and cooled structures and materials [AIAA PAPER 65-367] 02 p0331 A67-11929
 Invariance theory for automatically controlled underwater wings ensuring ship motion stability in perturbed medium 03 p0359 A67-13189
 Propulsion system development for very high speed winged vehicles application 03 p0505 A67-14382
 Book on variational problems in flight dynamics of winged aircraft and space vehicles 04 p0705 A67-15007
 Winged helicopter performance, stability and control with or without auxiliary propulsion 06 p0946 A67-17913
 Critical heating conditions in hypersonic glider reentry 06 p1113 A67-17981
 Low speed aerodynamic static stability of winged and wingless reentry configurations 14 p2239 A67-27796
 Optimal payload lifting and nonlifting trajectories of winged boost-launch vehicle [AIAA PAPER 67-558] 19 p3335 A67-35955

WINGLESS VEHICLE
 Low speed aerodynamic static stability of winged and wingless reentry configurations 14 p2239 A67-27796
 Soviet book on aerodynamics, flight dynamics, flight vehicle structural design and mechanical and control considerations for various aircraft 21 p3566 A67-37833

WIRE
 SA HOT WIRE
 Thermocouple errors resulting from heat conduction along thermocouple wire embedded in low conductivity ablative

material indicate heliocoil wire for optimum design 01 p0071 A67-11104

Maximum current carrying capacity of type III hard superconducting wire in zero external field before superconductivity breaks down 03 p0488 A67-12814

Magnesium wire as in-contact masking material, with surfaces precoated with thin silver layer 03 p0494 A67-13490

Persistent current loops in hard superconducting wire formed when wire is magnetized by static transverse external field 07 p1232 A67-19554

Resistivity changes in thin metallic wires with lattice defects measured by various methods 08 p1368 A67-20717

Hot pressing technique for aluminum sheet and stainless steel wire to produce composite high tensile strength plate 12 p1954 A67-25289

Heat loss and recovery temperature of fine wires in transonic transitional flow regime, noting experimental and computational results 14 p2405 A67-28177

Beryllium wire manufacture and uses, noting properties, drawing techniques, annealing effects, reinforcing filament use, etc 16 p2687 A67-30488

Heat loss from wires in nitrogen, helium and mixtures measured at low Reynolds numbers, finding agreement with theory of Kassoy 16 p2779 A67-31217

Drawing technique for bundles of sheathed superalloy wires noting sheathing, stress relief, interfilament welding and oxide bonding 21 p3643 A67-37878

Optimum tapers determined for circular and rectangular ties, comparing resultant flexural stiffness with untapered supports 22 p3914 A67-40066

WIRE BRIDGE CIRCUIT

SA WHEATSTONE BRIDGE

Linear bridge for use with platinum resistance temperature sensors 18 p3052 A67-34511

Remote control of monochromator prism rotation using balanced-bridge system to regulate flow 20 p3451 A67-37308

WIRE GRID LENS

Angle diversity performance of wire-grid lens antenna determined using statistical analysis 16 p2639 A67-31361

WIRE MESH

Evaluation of wire lacing designs for damping of vibratory stresses on gas turbine blades [ASME PAPER 67-VIBR-47] 11 p1797 A67-24197

Wire screen roughnesses effect on turbulent boundary layer along flat plate without pressure gradient 13 p2093 A67-26529

Transmittance and reflectance measurements on wirecloth and metallic meshes using vacuum grating spectrometer for design of transmission band pass filter in far IR 13 p2121 A67-27354

Pressure loss measurements of compressible flow through gauzes with different porosity 14 p2305 A67-29009

Force on plane wire screen at right angle to turbulent incompressible two-dimensional jet axis determined, developing approximate theories in terms of screen K factor 17 p2836 A67-32127

Far IR Fabry-Perot interference filters consisting of parallel close-spaced metal meshes 19 p3262 A67-35686

Windborne dust collections on Barbados Islands investigated by mesh technique for origin of cosmic dust 20 p3432 A67-37174

Mathematical models of flow and filtration performance of wire cloth filter media in series and parallel configuration 20 p3365 A67-37364

WIRE WINDING

Differential inductive sensor with correcting windings for monitoring and measuring various nonelectric quantities and processes 06 p1003 A67-18173

WIRING SYSTEM

Modular system for packaging microelectronic flat packs and miniature discrete electronic components 05 p0779 A67-17465

Developments in fire detection equipment noting continuous wire, armored wire and surveillance detectors 09 p1439 A67-21704

Wire-connected electronic packaging module system providing change capability, design flexibility, arrangement freedom and volumetric efficiency 12 p1912 A67-25275

Discretionary wiring method and polycell approach to large scale integration 15 p2444 A67-29456

Transistorized time delay system based on measurement of condenser discharge time to predetermined voltage 21 p3590 A67-37952

WOOD

Physical and environmental effects on energy dissipation characteristics of balsa wood [SAE PAPER 660657] 01 p0103 A67-10616

Vacuum effect on oven-dried balsa wood strength 15 p2507 A67-29554

WOOD AIRCRAFT CONSTRUCTION

Book on inspection, construction, operation, maintenance and repair of aircraft and aerospace vehicles including metal, steel frames, wood structures and high temperature structural material 22 p3811 A67-39441

WORK

S PHYSICAL WORK

S VIRTUAL WORK

WORK CAPACITY

Metabolic work requirement of man wearing pressure suit and associated biomechanical characteristics while locomoting on lunar gravity simulator 02 p0189 A67-12393

Subgravity traction simulation experiments to determine effects on metabolic rates during walking on treadmill 05 p0755 A67-16280

Absolute bed rest and recumbent exercise during bed rest effects on pulse rate response to submaximal work, cardiovascular functional capacity /maximal oxygen intake/, physical work capacity and orthostatic tolerance 05 p0755 A67-16283

High altitude effect on work capacity, discussing bicycle ergometer test results on physiological response of human subjects 10 p1598 A67-23393

Heat and exercise induced hypohydration effects upon physical performance of women, showing some deterioration in cardiovascular system 20 p3372 A67-37033

Performance characteristics in zero potential energy manual task, discussing work output 21 p3577 A67-38074

Maximal muscular static force vs physical stress measurement for optimal work conditions 23 p3954 A67-41598

Physiological measurements in obtaining energy expenditure and workloads during simulated lunar surface mission 23 p3959 A67-41657

Physical capabilities and work potential of man in terms of physiological elements and methodology 23 p3959 A67-41682

WORK FUNCTION

Work function of solid solutions of tungsten with molybdenum and tantalum explained by surface adsorption effects 01 p0093 A67-10092

Field electron emission measurements for determination of work function of single crystal /110/ planes of tungsten 01 p0135 A67-10878

Tunnel-current measurements of sandwich configurations, determining metal/metal-oxide work function 02 p0295 A67-11764

Energy exchange localization to cathode emitting area during field electron emission, noting dependence on temperature, work function and applied field 03 p0472 A67-13329

Electron and ion emission from iridium in lithium vapor, noting surface ionization, work functions and experimental setup 04 p0660 A67-15108

I-V characteristics of alloyed contacts of germanium with Sn, Pb and In in wide range of resistivities and ambient temperatures, establishing correlation with work function 05 p0884 A67-16909

Refractory metals and metal alloys analyzed regarding electron work function and threshold temperature for surface ionization in all-metal guard ring diode with directly heated wire [AIAA PAPER 66-223] 06 p1035 A67-18137

Shottky theory and electron affinity of semiconducting CdSe from DC I-V characteristics and work function of Au, Ag and Cu contacts with 07 p1231 A67-19491

Saha-Langmuir formula applied to description of temperature dependence of positive ion current in surface ionization of silicon atoms, comparing work functions by methods using contact potential, thermionic

emission and Richardson 09 p1554 A67-22006

graphs Thermionic converter life-test results and failure mechanisms noting braze failure, collector deposit, emitter warpage and separation and cesium reservoir leak 09 p1447 A67-22334

Operating temperature effect on vacuum emission stability of vapor-deposited tungsten clad UC-ZrC and uranium dioxide 09 p1449 A67-22347

Plasma mode work function measurement for studying thermionic emission from Hf, Th and Ti in Cs vapor at reservoir temperature of 414 degrees K 09 p1450 A67-22353

Impurity free CsF effect on work function of tungsten surface, discussing amount of impurities, type and control 09 p1450 A67-22354

Anisotropy of electronic metal work functions for zero and high electric fields perpendicular to surface measured by field emission and thermionic techniques 09 p1450 A67-22356

Vapor-deposited tungsten formed by hydrogen reduction of tungsten hexachloride or hexafluoride, noting effect of crystal orientation and surface treatment on work function 09 p1451 A67-22357

Work functions of monocrytalline and polycrytalline rhenium with electron emission current measured by copper collector 09 p1451 A67-22358

Depressing effect of hafnium and zirconium on work function of tungsten, tantalum, niobium and rhenium 10 p1668 A67-23091

Semipermeable Ag membrane as electron collector in oxygen diffusion process for cesium thermionic energy converters 11 p1746 A67-24923

X-ray and metallographic examination of tungsten alloys, noting decrease of work function during thermal emission upon addition of lanthanum hexaboride 13 p2131 A67-26468

Quasi-invariance and ergodicity in binary sequence space with respect to discrete groups of Bernoulli schemes, noting finite entropy distance formulation of measure equivalence 14 p2343 A67-28502

Vacuum thermionic work function and thermal stability measurements on crystal surfaces, discussing results on carbides, diborides and disilicides 15 p2535 A67-29486

I-V characteristics of alloyed contacts of germanium with Sn, Pb and In in wide range of resistivities and ambient temperatures, establishing correlation with work function 16 p2727 A67-30886

Thermionic work functions and electron emission S curves for contaminated copper surface in oxygen and cesium vapors, separate and mixed 17 p2887 A67-32203

Cesium vapor treatment effect on work function of high melting Ta and Zr carbides, evaporation products and graphite 19 p3176 A67-35080

Surface ionization of atoms and molecules on nonmetals, determining work functions and activation energies for dissociation 19 p3264 A67-35083

Measurement of work function changes of nickel films for oxygen and hydrogen chemisorption 19 p3246 A67-35787

Electron emission and adsorption of potassium on tungsten single crystal faces, noting work function values 20 p3504 A67-36165

Work of deformation during expansion of tubular blanks with varying hardening characteristics under uniform loading 21 p3631 A67-38054

Duo-emitter cesium thermionic converter, discussing electron and cesium ion emission to increase transport efficiency 21 p3571 A67-38610

Urinary catecholamine excretion in pilots relation to physical mental expenditure of energy and flight deck work loads 23 p3952 A67-41577

Electron beam retarding potential method to measure work function changes resulting from Cs, oxygen and hydrogen adsorption on /110/ Ta single crystal 24 p4201 A67-41892

Space charge effect on potential barrier in field emission, obtaining expression for work function increase using electrical image method 24 p4201 A67-41894

Mass spectrometric study of oxygen

adsorption, determining condensation coefficient and tungsten surface work function for various concentrations 24 p4172 A67-42073
Hot Langmuir probe in Cs plasma studied for method of controlling current voltage characteristics 24 p4154 A67-42210

WORK HARDENING

Second phase interface influence on work-hardening behavior of aluminum-5 atomic percent silver alloy, examining substructure development and flow stress behavior 01 p0092 A67-10055

Metal and alloy heat treatment intensification with ultrasonic techniques improve steel recrystallization, etc 01 p0095 A67-10640

Fiber strengthening theory, taking into account stress transfer between matrix and fiber in both elastic and plastic regions 03 p0449 A67-13257

Phase work hardening of austenitic Fe-Ni alloys in phase transformation process 04 p0635 A67-14430

Test on nickel and aluminum of Bailey-Orowan equation in relation to work hardening and recovery in creep 04 p0640 A67-15623

Nb embrittlement by H at ambient temperatures under work hardening effect, noting correlation between elastic limit and deformability in H 11 p1806 A67-24427

Elastic-plastic body and elastic work hardening materials under static loading, using maximum principle for computing procedures 11 p1876 A67-24622

Fiber reinforcement theory, considering strengthened metal behavior at elevated temperatures and under work hardening conditions 11 p1807 A67-24635

Stress vs strain curves and slip systems in compression and tension of niobium single crystals 14 p2339 A67-29030

Strength characteristics of single crystals of nickel aluminide /gamma phase/, discussing temperature and orientation dependence of work hardening 18 p3064 A67-34079

Metal and alloy heat treatment intensification with ultrasonic techniques improve steel properties, recrystallization, etc 18 p3066 A67-34404

Crack propagation in solid undergoing cyclic loading using Griffith model, stressing work hardening effect 22 p3911 A67-39680

WORK-REST CYCLE

Evoked brain response to clicks as measure of vigilance tested in work-rest schedule and pressure suit-sleep experiments on man 09 p1452 A67-21721

Cardiac output during rest and work determined via carbon dioxide method at 3800 m altitude 10 p1598 A67-23392

Two 15-day experiments of three subjects performing work-rest cycles in isolation chamber studying psychological functions, cardiovascular system, etc 16 p2613 A67-30912

Data on crew workload in C-141 aircraft used for extended mission living and working schedules, showing major disruptions in regular patterns 21 p3576 A67-38073

Subjective effects of fatigue on aircrew expressed in work cycle terms from data of continuing daily activity log 23 p3959 A67-41663

WORKING FLUID

Fabrication of columbium alloy liquid metal loop to study boiling and condensing characteristics of Na and K up to 1000 degrees F with gas tungsten arc welding in helium atmosphere 01 p0080 A67-10945

Closed Brayton cycle power conversion system development, discussing rotating components and single phase operating fluid [AIAA PAPER 66-889] 02 p0183 A67-12268

MHD heat transfer in finite duct for fully developed flow conditions with arbitrary oriented applied magnetic field and variable heat flux boundary conditions 04 p0673 A67-15872

Wall profile construction of working zone of flat MHD channel with ideal conductors for both sides 06 p1044 A67-18691

Variable thermal capacity of gas mixture taken into account in calculation of heat regeneration in gas turbine cycles, using working bodies 07 p1266 A67-19181

Thermodynamic cycle for solar power systems using hexafluorobenzene as working fluid, discussing efficiency and radiator

area 07 p1131 A67-19366
Classification of working fluids including applications in hydraulic control technology 07 p1212 A67-19733
Coanda device as pressure maintainer and as switch or selector 08 p1281 A67-20453
Heat pipe, device with thermoconductivity greater than solid conductors, based on surface tension and latent heat of working fluid 08 p1427 A67-21051

Theory of electrostatic probes in high pressure plasma, discussing ionization and recombination phenomena, diffusion boundary layer, spherical probe, etc 09 p1539 A67-21784

MHD generator using nonseeded inert gas as working fluid 09 p1444 A67-21812

Conductivity of high density plasma of MHD generator, noting quantum phenomena associated with overlapping electron wave functions 09 p1543 A67-21818

Conductivity of working fluid in MHD generator using thermionic emission from suspended lanthanum conductivity of working fluid in MHD generator using thermionic emission from suspended lanthanum hexaboride 09 p1543 A67-21820

Gas turbine design, considering thermodynamic and physical properties of various Rankine-cycle working fluids [ASME PAPER 67-GT-6] 11 p1745 A67-24794

Quantitative graphical method of screening working fluids for Rankine cycle power plants using single stage turbines at different levels of diameter and rpm [ASME PAPER 67-GT-12] 11 p1746 A67-24798

Test program for induction coupled MHD generator using liquid sodium as working fluid, noting equivalent single phase circuit for electrical characteristics 12 p1897 A67-25376

Three diagonal conducting wall MHD generators, discussing time averaged behavior, instabilities and working fluid conductivity 12 p1898 A67-25381

MHD generator working fluid temperature reduction 12 p1973 A67-25395

MHD power generation using bifluid liquid metal system /such as Li and Cs/ with two-phase generation 12 p1901 A67-25897

Direct current MHD generator having channel of constant cross section and using NaK as working fluid 13 p2056 A67-27315

Liquid venting concept for zero gravity environment by suppressing vapor generation with open loop refrigeration, using extracted liquid as working fluid 13 p2056 A67-27639

Experiments with 100-kw MHD generator free from secondary effects by choosing MHD interaction parameter values greater than unity 16 p2602 A67-30559

Efficiency and thermodynamic parameters of possible closed-cycle flow schemes for base-load MHD generators 16 p2603 A67-30563

MHD Brayton cycle power generation techniques, considering noble gases seeded with alkali metal vapors as working fluid 16 p2603 A67-30567

Energy conversion with liquid metal working fluids in MHD converter, proposing stepwise injection and expansion to reduce impact losses 16 p2604 A67-30572

AC MHD power generator and turbine described noting working fluid flow 16 p2605 A67-30581

Liquid metal magnetohydrodynamic power generation for space vehicle use 16 p2605 A67-30583

Fluid metal magnetohydrodynamic power conversion program 16 p2606 A67-30584

Magnetohydrodynamic generator functioning by emulsion consisting of gas or vapor in liquid metal 16 p2606 A67-30588

Liquid metal magnetohydrodynamic power generation systems using condensing ejector or two-phase jet pump 16 p2606 A67-30589

Thermodynamics of injector of magnetohydrodynamic power unit using two-phase vapor-liquid metallic working fluid 16 p2607 A67-30591

Striated layer flow of working fluid in duct of synchronous induction MGD generator studying stability by approximation 16 p2607 A67-30594

Large combustion-driven, self-excited Faraday-type MHD generator having multi-or single-circuit net power output, discussing design 16 p2608 A67-30596

Local loss coefficients for multiplate hydraulic actuators with various working fluid temperatures 16 p2608 A67-31007

Thermodynamics of MHD converter cycles with previously mixed liquid metal used as working body, discussing thermal, electrical and energetic efficiency 16 p2610 A67-31780

SST Concorde hydraulic system noting design and hydraulic fluid selection resulting from high ambient temperatures, weight and space limitations, etc 17 p2800 A67-31971

Synchronous and asynchronous idealized induction alternating current MGD generators 17 p2803 A67-32340

Gas-borne suspensions of thermionically emitting particles as MHD working fluids 18 p3086 A67-33707

Optimum consumption of inert mass working fluid in limited discharge velocity engine in terms of final speed gain 21 p3689 A67-37986

Aerothermochemistry of high temperature multicomponent reactive systems, examining thermodynamic and transport characteristics and ionized and dissociated working fluid processes 22 p3921 A67-40447

Plasma nonequilibrium electric conductivity in induced electric field investigated by MHD generator with Ar-K working fluid 24 p4196 A67-42209

Spectral lines diagrammed for temperature distribution in Ar plasma arc channel transverse emission with axial flow of working fluid 24 p4196 A67-42219

Real gases examined for application as working fluid in Brayton cycle power plant, considering radiator area reduction to Rankine cycle 24 p4102 A67-42488

Small scale Rankine cycle power conversion system using potassium working fluid under environmental, RF interference and ground performance tests 24 p4102 A67-42491

Organic Rankine cycle power system using monoisopropylbiphenyl /MIPB/ as working fluid noting advantages 24 p4103 A67-42494

Rankine cycle power plants using organic working fluids considered for near-term application 24 p4103 A67-42495

SNAP-8, nuclear electric power-conversion system /PCS/ designed for operation in space, using liquid metals as working fluids 24 p4184 A67-42497

Rotating boiler for high performance Rankine cycle power generator using water as test fluid, obtaining heat-transfer coefficients 24 p4184 A67-42498

Electrofluiddynamic /EFD/ power generator channel performance dependence on charge spreading for various geometries, noting stage efficiency and electric pressure 24 p4107 A67-42529

MPD energy conversion duct using heated inert gas working fluid, discussing Hall parameter operation and efficiency factors 24 p4109 A67-42898

WORLD DATA CENTER

Space technology developments for World Weather Watch, discussing satellites role in weather forecasting, meteorological sensor and instrumentation 10 p1677 A67-23369

Satellites role in World Weather Watch /WWW/ program for weather analyses and forecasts 19 p3253 A67-35656

WRINKLE

Stability problems of sandwich plates, considering buckling and wrinkling 02 p0341 A67-12713

WROUGHT ALLOY

Microstructural changes effect on mechanical properties of nickel base superalloys, with particular attention to wrought alloys 08 p1340 A67-20362

Statistical analysis of beryllium cross-rolled sheet, hot pressed block and ring rolled forgings 13 p2140 A67-27135

Commercial aluminum wrought alloys properties, describing temper designation and heat and nonheat treatment classification 14 A67-27808

WURTZITE

OPW calculation of six symmetry points in wurtzite Brillouin zone of CdS, using pseudopotential techniques 06 p1058 A67-18903

Valence band structure of wurtzite type crystals 16 p2725 A67-30802

Transverse and longitudinal electron effective masses for wurtzite type crystals 17 p2913 A67-32273

Elastic moduli, bond parameters and

effective ion charges for wurtzite and sphalerite binary crystal lattices 18 p3094 A67-33437

X

X-15 AIRCRAFT

Component performance and flight operations of X-15 research airplane program, considering engine, auxiliary power and propellant system 01 p0011 A67-11341
Flight data of X-15 research aircraft noting development, operation and economic aspects of performance 15 p2420 A67-29848

X-22 AIRCRAFT

Variable-stability feedback control low range air speed system for X-22A aircraft 01 p0073 A67-11121
Flight tests of two X-22A dual tandem rotatable ducted propeller V/STOL research aircraft 06 p0948 A67-18201
Bell X-22A VTOL research vehicle, assessing mechanical and aerodynamic characteristics, variable stability and control system, etc 11 p1743 A67-24097

X-BAND

Microwave mixer point contact diode with X-band intermediate frequency for good value of conversion loss 01 p0036 A67-10438
X-band Cassegrainian tracking antenna for space rendezvous position and rate information for navigation and guidance computations 04 p0569 A67-14502
X sub L band waveguide switches using p-i-n diodes for switching elements in SPST, SP2T, SP4T and SP8T microwave switches 04 p0580 A67-14863
Interpretations of microwave emission from Venus through experiments in which anomalous signals have been observed in X-band from glow discharges 04 p0699 A67-14952
Bistatic radar cross section of underdense turbulent plasma measured at X-band and results compared with theoretical scattering model 05 p0760 A67-15999
X-band Gunn oscillator with dielectric tuning system 05 p0775 A67-16951
Terrain backscattering characteristics at low grazing angles for X-band 05 p0768 A67-17527
X-band ruby maser design with liquid hydrogen cooling for high gain at low pumping power 07 p1194 A67-19131
Franck-Condon factors and r centroids for C-X band system of astrophysically important zirconium oxide molecule found in S type stars 08 p1354 A67-20702
X-band circularly polarized nonreciprocal ferrite phase shifter for phased array antennas 08 p1305 A67-21226
Noise comparators and associated thermal standards to provide noise source calibration facilities at S-and 09 p1495 A67-21621
X-bands 09 p1495 A67-21621
Five hundred kw traveling wave tube for X-band, considering design and matching of clover leaf structure and higher order mode spectrum 09 p1478 A67-22255
Apparatus producing voltage pulses in X-band magnetrons operating on pulse lengths of tens of nanoseconds 09 p1479 A67-22262
Phase locking experimental data on injection locked X-band Gunn effect microwave oscillators 11 p1759 A67-24128
Measured admittance of X-band waveguide radiating into dielectric and plasma layers compared with computed admittance figures 16 p2627 A67-31352
X-band propagation over rough earth when illuminated by radiation, studying scattering problems 20 p3388 A67-37647
Omnidirectional double slot array of thin X-band rectangular waveguides, noting design for slot conductance and power handling capacity 23 p3977 A67-40699
S and X band ignitor design eliminating spike leakage variations in tracking radar tubes 24 p4131 A67-42350

X-RAY

SA BREMSSTRAHLUNG SA PHOTON

Visible and X-ray photoelectric emissions in layers of Se-As-Tl intrinsic semiconductor films in vacuum 03 p0498 A67-13838
X-ray and gamma ray navigation systems for helicopter formation flying, examining accuracy and scanning requirements 04 p0653 A67-14605

X-ray effect on conductivity, carrier concentration and mobility in Si crystals and Si p-n junction 06 p1048 A67-17855
X and electron irradiation effect on current-voltage characteristics of p-n junctions in gallium 06 p1049 A67-17859
Flux and energy spectra of primary cosmic X and gamma rays between 20 kev and 1 mev from balloon-rocket measurements 10 p1701 A67-23231
X-ray source in Crab Nebula size and position, showing visible light distribution having common center within 15-inch precision of measurement and finite angular extent 13 p2189 A67-26263
Possible polarization of X-ray bremsstrahlung of solar flares due to sharply anisotropic electron beams 13 p2191 A67-26383
Visible and X-ray photoelectric emissions in layers of Se-As-Tl intrinsic semiconductor films in vacuum 13 p2184 A67-27719
Coherency relation between quasi-periodic X-ray and optical pulsations in auroras 17 p2844 A67-32543
Time-microscopy methods using laser flashlight, roentgen flashlight and rapid succession spark pulses in combination with stereo cameras 17 p2864 A67-33408
Critical comments on Shklovsky model for newly identified X-ray source Sco XR-1 20 p3527 A67-37394
Possible polarization of X-ray bremsstrahlung of solar flares due to sharply anisotropic electron beams 21 p3698 A67-38817

X-RAY ABSORPTION

Plasma electron temperature measured from soft X-ray bremsstrahlung absorption by beryllium foil 02 p0274 A67-12461
Emission of bremsstrahlung X-rays caused by electrons precipitating isotropically into upper atmosphere 10 p1633 A67-23048
X-ray K-absorption spectra of titanium, vanadium germanium in 16 p2891 A67-31594
Photoadsorption of X-rays by interstellar gas using photoionization cross sections, showing neon K edge as distinctive feature of spectrum 17 p2937 A67-32752
X-ray absorption in chromium in chromium silicon after thermal processing at high temperatures 17 p2921 A67-32893
Energy spectrum of cosmic X-rays background component, proving experimentally rocketborne detector counting rate proportionality to field of view 19 p3314 A67-35278
Electrical conductivity variation of low and high resistance germanium due to X-ray radiation absorption 20 p3508 A67-36405

X-RAY ANALYSIS

X-ray analysis applications - Conference, Denver, August 1965 01 p0095 A67-10685
Radioisotope and radiation techniques for terrestrial and planetary gas and solid measurements 02 p0245 A67-12223
Neutron bombardment effect on titanium and chromium carbides before and after heat treatment, giving results of X-ray and micrographical analyses, electric resistance, brittleness and microhardness measurements 03 p0447 A67-13639
Microscopic and X-ray analysis of cast and annealed W-Mo-Ti alloys, plotting polythermal cross sections 04 p0638 A67-15203
X-ray analysis of Nb-Ni-Al solid solutions, noting solubility of Nb and construction of phase diagram 04 p0638 A67-15204
X-ray Debye temperature thermal variation measurements of pure nickel and chromium 06 p1015 A67-17850
Microstructural and X-ray analysis of intermediate phases of Ti-Ir and Ti-Rh intermetallic compounds, including microhardness and fusion point variations 07 p1204 A67-19263
X-ray study of component atomic scattering and structural defects for titanium and carbide atoms in titanium carbide 07 p1208 A67-19306
X-ray line broadening in deformed magnesium by Fourier analysis of line shapes and analysis of line widths, noting lattice distortion 07 p1210 A67-20108
Plastic deformation of diamonds due to differences in initial defect distribution examined by birefringence, X-ray topography and electron microscopy 08 p1346 A67-20795

Kinetics of two-phase decomposition of solid solution of magnesium-aluminum alloy using X-ray analysis, noting grain orientation and size 08 p1342 A67-20810
Aging effect on structure of cobalt alloys annealed at 1200 degrees C suggests formation of laminar regions 08 p1342 A67-20812
X-ray structural and spectral analysis of changes in lattice constant, linear expansion coefficient and K-absorption edge of iron and manganese in ferrite with spinel structure 08 p1372 A67-21492
X-ray structural study of phase transformations during heat treatment of VT-3-1 titanium alloy 09 p1518 A67-22030
X-ray analysis of lattice structure of terbium crystals at 120 to 300 degrees K 09 p1555 A67-22066
Value of routine abdominal X-ray during aeromedical evaluation, noting number and significance of abnormalities detected 10 p1601 A67-23828
X-ray study of lanthanum borides to verify existence of homogeneous compounds within large range of variations in composition 11 p1810 A67-23905
X-ray analysis of lattice strain and crystallite size changes in tungsten carbide compressed at high pressure, noting annealing effect 11 p1809 A67-24949
Geomagnetic micropulsations and electron bremsstrahlung in northern auroral zone 13 p2108 A67-26321
X-ray and metallographic examination of tungsten alloys, noting decrease of work function during thermal emission upon addition of lanthanum hexaboride 13 p2131 A67-26468
State diagram structure of Ti-Cu system examined using metallographic, thermographic, X-ray and microhardness analyses 13 p2131 A67-26473
Polarization of cosmic X-ray produced by bremsstrahlung mechanism 13 p2191 A67-26713
X-ray analysis of size reduction of coherent scattering regions of metal deformed in ultrasonic field 13 p2124 A67-27627
X-ray examination of arms of pilots killed in aircraft collisions, determining from bone injuries degree of control before collision 14 p2255 A67-28227
Ti-Zr-C and Ti-Hf-C alloy X-ray and microstructural studies noting homogenizing, annealing, quenching and phase equilibria 15 p2505 A67-30388
Optical and stereoscan microscope scanning combined with X-ray microanalysis used to investigate results on collection surfaces of space probes 19 p3339 A67-35197
Broadening of Debye-Scherrer line profiles and structure recovery studied in cold-worked Ti, Zr and Hf specimens by X-ray analysis 19 p3247 A67-35835
Binary molybdenum-carbon system investigated using X-ray, metallographic, thermoanalytical and melting-point techniques 20 p3470 A67-37389
Structural properties of Si anodic oxide layers studied by X-ray analysis, using Laue photograph method 21 p3681 A67-38360
Powder X-ray structural analysis of compounds of Nb-Ni and Ta-Ni systems, establishing homogeneity region for NbNi 21 p3646 A67-38973
X-ray analysis of hydrate of diethylamine three-dimensional crystal structure, determining bond distances and angles 22 p3757 A67-39634
Auroral zone balloon measurement of 5 and 25 msec duration energetic electron burst fluxes 22 p3873 A67-39821
Softening and incipient recrystallization temperature of deformed niobium during annealing measured by X-ray analysis and mechanical properties examination 22 p3823 A67-40326
Equilibrium phases in annealed NiCrTiAlW alloy using optical and electron microscopy and X-ray analysis 23 p4019 A67-41078
Explosion of ovoid copper wire conductors observed with pulsed X-rays noting effect of magnetic pressure 23 p4028 A67-41461
Seven year follow-up X-ray survey for bone changes in low pressure chamber operators to determine long term effects of altitude decompression sickness 23 p3957 A67-41641
Crystal structure of rare earth Co

compounds prepared by levitation melting process investigated by
X-ray 24 p4172 A67-41975

Pionlic and muonic K-series X-rays studied by liquid He scintillation counter, obtaining separation peaks 24 p4192 A67-42735

X-RAY ASTRONOMY

Flux intensity and energy spectra of galactic X-ray sources, Tau X-1 and other celestial bodies studies, using three sensitive Geiger counters 01 p0144 A67-10562

Lunar X-rays excited by electrons of magnetospheric tail provide information on chemical composition of moon 01 p0144 A67-10563

Solar and stellar X-ray astronomy, noting Crab Nebula occultation experiment 01 p0144 A67-10900

Visual component identification of Sco X-1 X-ray source 01 p0151 A67-10963

Location of X-ray source Sco X-1 determined by instrumented payload flown on stabilized Aerobee rocket 02 p0308 A67-11771

Optical identification of position of X-ray astronomical source Sco X-1, noting similarity of certain properties with old novae 02 p0324 A67-11772

Powerful X-ray flare on sun detected by high altitude rocket, noting high energy electrons in superchromospheric layer 02 p0308 A67-11974

Apollo X-ray astronomy experiment, noting instrumentation techniques employed and advantages [AIAA PAPER 66-888] 02 p0246 A67-12267

X-ray emission from radio galaxies as possible bremsstrahlung radiation of hot gas, noting Crab Nebula 02 p0308 A67-12482

Energy spectrum of X-ray source in Cygnus constellation with 2 to 80 kev 03 p0507 A67-13917

Instrumental and observational aspects of balloon X-ray astronomy involving position, angular size, intensity and spectral measurements of X-ray sources [AIAA PAPER 66-1015] 03 p0514 A67-14151

Possible models for X-ray source SCO-X-1, discussing conditions of gravitational confinement 04 p0694 A67-14484

Detection of X-ray point sources from rocket and satellite experiments applied to astronomy 04 p0698 A67-14886

Observational X-ray astronomical advances since 1962 including improved sensitivity and angular resolution, identification of SCO-X1, spectral analyzers, etc [AIAA PAPER 66-1016] 04 p0702 A67-15589

Diffuse omnidirectional inverse Compton and synchrotron X and gamma radiation from cosmic distributions of fast electrons and thermal photons 05 p0882 A67-16404

Optical observation of brightest X-ray source in Scorpius, giving tabulated data as function of radius 05 p0892 A67-16414

Cosmic X-ray research with discussion of possible mechanism of X-ray generation with reference to observed spectra 05 p0883 A67-16875

Energy spectra of galactic X-rays observed with three types of counters borne on sounding rockets 05 p0883 A67-16876

Extrasolar X-ray observation regarded as astronomy in contrast to cosmic ray observation which is considered as local geophysical phenomena 05 p0884 A67-16881

X-ray astronomy of discrete sources in or near galactic plane, noting likely X-ray production mechanism 06 p1092 A67-19009

Search for 21 cm radiation near cosmic X-ray sources 07 p1242 A67-19062

Cosmic X-ray source scanning for 21 cm wavelength radiation, using radiometer and parabolic reflector 07 p1247 A67-19063

Balloon observation of X-ray sources in Cygnus region in energy range 20-130 kev 08 p1377 A67-21252

Energy spectra of galactic X-rays from four rocket measurements, observing Cygnus and Tau X-1 10 p1700 A67-23054

Energy spectra of Tau X-1 and isotropic component of galactic X-rays, using rocketborne scintillation and GM counters 10 p1701 A67-23229

X-ray emission from radio galaxies as possible bremsstrahlung radiation of hot gas, noting Crab Nebula 10 p1702 A67-23350

Aerobee rocket instrumentation for solar spectroscopy in soft X-ray region 10 p1712 A67-23804

Sco X-1 physical characteristics noting ionization, possible stellar wind and pressure equilibrium effects 11 p1862 A67-24506

Tabulated localized cosmic X-ray sources and survey of rocket probe identifications 11 p1857 A67-24633

Cosmic X-ray sources identified using Geiger counters aboard rockets, noting clustering toward galactic disk 12 p1994 A67-25760

Precise position and spectra of Scorpio X-ray source and location of two weaker sources in galactic plane, describing instrumentation used 12 p1995 A67-25761

Evolutionary scheme of radio galaxies based on radio luminosity vs volume emissivity diagram, noting similarity and parallelism between radio and X-ray intensities 12 p2007 A67-25767

Cosmic X-ray sources concentration toward galactic plane and variability 12 p1999 A67-26172

Space astronomy utilizing gains made by space science and stressing X-ray astronomy 13 p2206 A67-27510

Radio galactic X-ray emission noting possible cosmic radiation mechanism, history of X-ray astronomy, etc 14 p2381 A67-28427

X-ray astronomy emphasizing interpretation of observational results and relationship to radio and optical astronomy and cosmic ray physics 15 p2551 A67-30224

Solar X-ray flux for wavelength less than five angstroms measured, noting extreme variations in spectral slope and intensity 16 p2739 A67-31411

Thermal and synchrotron cosmic X-ray sources 17 p2937 A67-32639

X-ray scanning of Cygnus region with large area proportional counters flown on attitude-controlled sounding rocket 17 p2937 A67-32648

Optical search of sky near X-ray positions of Cyg X-1 and Cyg X-2 for identification purposes 17 p2937 A67-32649

Solar X-ray spectrum observed by rocket carried Bragg crystal spectrometers and pinhole cameras array 17 p2937 A67-32650

Primary diffuse X-ray flux and spectrum found isotropic by balloon measurements made in three particular directions 19 p3313 A67-35244

Secular behavior of optical properties of X-ray emitting object near Cygnus X-2 19 p3331 A67-36084

Cosmic X-ray sources in 20-180 kev energy range detected in balloon flights, giving energy spectra 20 p3520 A67-37475

X-ray spectrum and location measurements of several cosmic X-ray sources, using rocketborne proportional counters 21 p3698 A67-38564

Flare X-ray emission period determined, noting maximum radio emission and optical intensity 21 p3699 A67-38965

Stabilized platform for stratospheric balloons for IR, UV and X-ray astronomy 22 p3830 A67-39184

Vibrating neutron stars, discussing damping, heating, energy storage and X-ray emission possibilities at 1000 years range 22 p3882 A67-39619

Ionizing radiation effects on dark current and noise pulse spectrum of photomultiplier tubes used in balloon and satellite X-ray observations 23 p4000 A67-41216

X-ray survey of Virgo region revealing signals from radio sources 3C 273 and M 87 23 p4061 A67-41473

Instrumental and observational aspects of balloon X-ray astronomy involving position, angular size, intensity and spectral measurements of X-ray sources [AIAA PAPER 66-1015] 23 p4070 A67-41711

X-ray emissions from coronal condensation regions studied with pinhole camera, obtaining intensity profiles along intense X-ray regions 24 p4224 A67-41821

X-RAY DENSITY MEASUREMENT
X-rays from Coma cluster of galaxies, investigating origin by applying virial theorem 05 p0882 A67-16413

X-ray microburst correlation with impulsive microburst 07 p1246 A67-19949

Balloon measurements of auroral X-rays, discussing flux and energy spectrum variations and bursts relation to magnetic storms 18 p3038 A67-33613

X-RAY DIFFRACTION
Deformation in niobium and tantalum by wire drawing at room temperature, producing changes in shape and position of X-ray diffraction peak 01 p0095 A67-10688

Nickel-base superalloys hardened in part by precipitation of gamma phase examined by X-ray diffraction techniques 01 p0095 A67-10687

Silicon carbide generation by pyrolysis of gas mixtures on tungsten wires, using X-ray diffraction to analyze structure 01 p0103 A67-10688

Combined focusing X-ray diffractometer and nondispersive X-ray spectrometer for lunar and planetary analysis 01 p0067 A67-10689

X-ray diffraction-Fourier series analysis and electron microscopy analysis of annealing effects on structural properties of cold worked dispersion-strengthened alloys 01 p0097 A67-10698

Electronic and molecular radial distribution functions for liquid carbon tetrafluoride using X-ray diffraction, determining orientational effects of carbon tetrachloride and temperature dependency 01 p0117 A67-10885

Crystal orientation of grains during fatigue and plastic deformation analyzed on copper using X-ray diffraction, noting crystal behavior 02 p0254 A67-11467

Correlation of X-ray diffraction lines of thin films with theoretical forms of films made from large crystals in thin slabs of uniform thickness 02 p0287 A67-11714

Aging of Ni containing maraging steel and related alloys analyzed by electrical resistivity, X-ray diffraction and hardness measurements, noting nature of Co-Mo interaction 03 p0440 A67-13250

Crystallinity index measurements of poly(ethylene terephthalate) by X-ray diffractometric and differential scanning calorimetry index methods 04 p0641 A67-14527

High resolution X-ray diffraction topography of dislocation structure of Si crystal 05 p0860 A67-16078

Equilibrium diagram of niobium-nickel system determined by thermal analysis, microscopical metallography and X-ray techniques 05 p0828 A67-16387

Growth condition effect on perfection of single crystals of niobium examined, using X-ray diffraction techniques 05 p0828 A67-16470

X-ray structural analysis of superconducting Nb based alloys, noting two-phase region in annealed samples 05 p0863 A67-16690

Basal plane contraction and annealing of degraphitized carbon examined via X-ray diffraction techniques 05 p0833 A67-16891

Dislocation loops by gold diffusion into silicon crystals analyzed, using X-ray diffraction topography and optical microscopy 05 p0866 A67-16974

Local variations in spacing and orientation of lattice plane in silicon single crystal, measuring angular positions of diffraction peak by double crystal spectrometer 05 p0866 A67-16977

X-ray crystal structural analysis of tetraethyl titanate and monomethyltriethyl titanate, determining reason for difference in color 06 p0955 A67-17849

Metastable form of C12 type calcium disilicide when under high temperature and pressure, noting X-ray diffraction powder patterns and superconductivity 06 p1051 A67-18372

Phase diagram of titanium-rich alloys of system Ti-Al, measuring resistivity and hardness through X-ray diffraction, thermal analysis, etc 07 p1204 A67-19267

Phase diagram of Ti-V-C system based on phase equilibria, using X-ray diffraction, microhardness measurements, etc 07 p1204 A67-19270

X-ray diffraction study of crystallographic transistor defects causing secondary breakdown 07 p1156 A67-19896

Chemical and mineralogical composition of roederite found in Indarch meteorite, presenting electron probe analysis and X-ray diffraction pattern optical data 07 p1255 A67-20012

Oxidation of tantalum coated with aluminum and aluminum-chromium alloys at high temperatures and various oxygen pressures, using X-ray diffraction, electron microscopy, etc 08 p1341 A67-20764

Plastic flow peculiarities analysis based on X-ray diffraction effects obtained by

deforming single crystal molybdenum of various orientations 08 p1342 A67-20809

X-ray diffraction residual stress measurements in aluminum alloy [SAE PAPER 670153] 09 p1509 A67-22543

X-ray diffraction and metallographic investigation show iron meteorites shock at pressures of at least 130 kbar 10 p1705 A67-22954

Amphibole richterite found in graphite nodules of iron meteorite, using electron microprobe and X-ray powder diffraction 11 p1868 A67-24873

Anomalies in intensity of Compton diffusion of X-rays by vanadium noting energy-diffusion angle relation 13 p2181 A67-27210

Cohenite grains from iron meteorites studied by X-ray diffraction for establishing pressure scale, using solid state recrystallization 13 p2200 A67-27235

Niobium-cobalt alloys constitution, determining equilibrium diagram by thermal analysis, microscopic metallography and X-ray diffraction techniques 14 p2338 A67-28615

Fourier analysis of line profiles of X-ray-studied deformation faulting in titanium, zirconium and hafnium 14 p2340 A67-29033

Vacuum thermionic work function and thermal stability measurements on crystal surfaces, discussing results on carbides, diborides and disilicides 15 p2535 A67-29486

X-ray structural analysis of superconducting Nb based alloys, noting two-phase region in annealed samples 15 p2539 A67-29860

Spin-lattice relaxation times in grown ruby in one phonon region, noting temperature dependence and undulation of lattice planes 16 p2728 A67-31054

Titanium alloys crystal structures determined using single crystal X-ray and powder neutron diffraction method, noting mechanical properties temperature dependence and martensitic transition 16 p2688 A67-31307

Metal fatigue studied with X-ray diffraction technique 16 p2774 A67-31322

Chemical reactions in Ni-Ti-Nb system, examining via X-ray diffraction formation of ternary intermetallic compounds 16 p2691 A67-31593

X-ray structural and diffraction analysis of Mo-Ni-Bo system at high temperatures under isothermal sections of phase diagram 16 p2691 A67-31595

Tungsten-carbon phase relations from DTA, X-ray and electron diffraction measurements noting disordered, ordered hexagonal and orthorhombic modifications 16 p2692 A67-31599

Structural characteristics of Ni-Mo alloys analyzed using electron microscopy and X-ray diffraction scattering 17 p2872 A67-32723

Activities and relative partial molar free energies of CuPt alloys, noting formation mechanism, ordering temperatures, etc 17 p2872 A67-32739

Relation between molecular structure of In and Sb semiconductor compounds and fine structure of X-ray absorption spectra 18 p3095 A67-33441

X-ray diffraction analysis of polycrystalline brass deformed by tension, noting stacking fault probability, stress-strain curve, etc 18 p3064 A67-34084

Surface hillock-like features in epitaxially grown gallium arsenide studied by X-ray diffraction topography 18 p3106 A67-34636

High strength high modulus carbon fiber microstructure, studying crystallite size, orientation effect, electron micrographs and X-ray diffraction 19 p3248 A67-35426

Abnormal X-ray interference pattern change during aging of nickel-beryllium alloys 19 p3245 A67-35471

Ti-Al alloys ordering transformation studied by electron microscopy and electron and X-ray diffraction, showing existence of three phase fields 20 p3470 A67-37386

Structural changes due to fatigue in cladding layer of alloy D16AT studied by X-ray diffraction 21 p3642 A67-37826

Stacking fault energy estimation in polycrystalline brass during tensile deformation by analyzing X-ray diffraction patterns 21 p3645 A67-38090

X-ray structural analysis of ferromagnetic/ferrimagnetic/ bismuth ferrite single crystal 21 p3685 A67-38967

Interstitial oxygen solubility in niobium

using X-ray diffraction, micrographic and thermal techniques, discussing lattice structure 22 p3823 A67-40209

Defects in surface layer of silicon crystals during deep diffusion of phosphorus studied by X-ray diffraction 23 p4042 A67-41295

Dynamical theory of X-ray diffraction for optical holography noting anomalous light transmission at Bragg angle 23 p4009 A67-41462

Preatmospheric hypervelocity impact black glass in Chachari eucrite studied by optical microscopy, electron microprobe and X-ray diffraction 24 p4233 A67-42623

Microscopic and X-ray diffraction study of octahedrite shock history 24 p4234 A67-42631

X-RAY EQUIPMENT

X-ray spectrometer with cold cathode, discussing equipment design, principles, operation and performance 17 p2853 A67-32046

X-RAY FLUORESCENCE

Stony meteorite Fe, Ni, Co, Ca, Cr and Mn concentration determined by X-ray fluorescence 24 p4235 A67-42638

X-RAY FLUORESCENCE SPECTROSCOPY

Hall effect and fine structure of X-ray fluorescence and absorption K spectrum of vanadium in silicides 01 p0101 A67-10935

X-RAY INSPECTION

SA FLAW DETECTION

All-weather pulsed X-ray instrument for altitude measurement and terrain identification 05 p0806 A67-16528

X-ray image transformation, transmission and amplification directly into video signals for inspection of missile case walls and weldments 10 p1622 A67-22929

X-radiographic nondestructive testing and inspection for quality control of electronic and electromechanical devices including printed circuits, encapsulated modules, thin films, etc 10 p1611 A67-23311

Nondestructive testing methods noting applicability to flaw detection and quality control 12 p1948 A67-25138

Radiographic screening of relays for detection of solder balls, broken leads, cracks, etc 13 p2084 A67-27695

Relay testing for Saturn program including vibration scan, radiographic inspection, etc 13 p2084 A67-27696

Current saturation in evaporated gallium arsenide films observed noting temperature effect, X-ray measurements, etc 20 p3505 A67-36177

Electronic assembly loose parts detection system using nondestructive vibration testing 23 p4005 A67-41369

X-RAY IRRADIATION

X-ray irradiation effect on electrophysical properties of n-and p-type germanium, determining absorption coefficient 01 p0136 A67-11044

X-ray radiation effect on p-n junctions of germanium diodes, noting changes in V-I characteristics 01 p0136 A67-11047

Gamma, bremsstrahlung and X-ray radiation limitations in aerospace application 02 p0266 A67-12217

Planar transistor stability under X-ray irradiation, showing drifts of variable importance according to type of transistor /p-n-p or n-p-n/ 03 p0387 A67-13996

Reduced X-ray photoelectric current in modified Bayard-Alpert ion gauge for vacuum pressure measurements below 10 to minus tenth torr 05 p0805 A67-16462

Roentgen radiation effect on glycogen metabolism of rat brain 07 p1133 A67-19468

Spatial and temporal characteristics of bremsstrahlung X-ray due to energetic electron precipitation in auroral zone, noting measurement techniques 07 p1180 A67-19929

Scintillation analysis of hard X radiation from high power pulse discharges 08 p1357 A67-20846

Vibration tolerance of rats previously irradiated by X-rays and hypothetical mechanisms of stress involved 09 p1452 A67-21719

Dog study on microwave radiation and effect on response to X-ray irradiation 10 p1599 A67-23815

Remote aftereffect on hemopoietic tissue of mice under simultaneous irradiation and acceleration, using both X-rays and protons 13 p2057 A67-26458

Temperature dependence of Hall mobility of photoelectrons and electrons produced by X radiation in cadmium sulfide single

crystals 14 p2367 A67-28525

Net polarization of celestial X-rays could lead to specification of source mechanism producing radiation 14 p2381 A67-28617

Isochronous and isothermal annealing of indium antimonide irradiated by X-rays and gamma rays, studying changes in current-carrier concentration 15 p2542 A67-30247

Physiological regeneration on cornea epithelium and intestines exposed to fractional irradiation with fission neutrons, studying mitotic index and chromosome aberrations content 16 p2613 A67-30909

Ionizing radiation effect on field effect MOST transistors, noting irradiation degradations 17 p2919 A67-32856

Origin of X radiation from radio galaxies Cygnus A and Virgo A, hypothesizing thermal radiation and bremsstrahlung 18 p3116 A67-33855

Stereoisomers of sulfur containing amino acids effect on local skin protection in X-irradiated mice 18 p2992 A67-34716

Mass accretion of compact star investigated for general properties and X-ray emission 19 p3316 A67-35801

Hard X-ray emission by hot electron plasma trapped in discharge tube due to magnetic field rise 21 p3687 A67-38413

Nature of defects in InSb induced by gamma and X-ray irradiation, discussing recovery process 21 p3687 A67-39143

Synchrotron X-ray radiation by high energy electrons in magnetic field with enhancement due to outward propagating hydromagnetic waves proposed as Crab Nebula emission 23 p4051 A67-40914

Temperature dependence of Hall mobility of photoelectrons and electrons produced by X radiation in cadmium sulfide single crystals 23 p4039 A67-40932

Sulphydrylamine drugs effect for protection in rats exposed to high, low, sublethal, lethal and supralethal dose of X and gamma radiation 23 p3958 A67-41648

Preirradiated organism reaction to space flight acceleration studied in determination of admissible ionizing radiation dose 24 p4113 A67-42393

X-RAY PHOTOGRAPHY

Compact flash X-ray systems for radiographic measurement of moving objects, radar ranging, atmospheric density, radiation effects, etc 02 p0245 A67-12215

Spinning-image coded X-ray star camera, based on image coding, permitting reconstruction of two-dimensional image [AIAA PAPER 66-850] 03 p0424 A67-14016

Rocket photography of sun and spectrum in EUV and soft X-ray regions 10 p1707 A67-23225

Fresnel microzone plates for X-ray images of sun 10 p1707 A67-23232

Maskelynite-bearing stony meteorites, noting absence of crystalline structure 10 p1709 A67-23494

Mass of shaped charge accelerator generated fragments determined via high speed flash X-ray photography of projectiles in flight 11 p1790 A67-24448

Pinhole X-ray photography of sun obtained during rocket flight, showing correlation of bright emitting regions on disk with calcium plages and radio emission sources 12 p2007 A67-25762

Rocket photography of sun and spectrum in EUV and soft X-ray regions 13 p2200 A67-27334

Spinning-image coded X-ray star camera, based on image coding, permitting reconstruction of two-dimensional image [AIAA PAPER 66-850] 15 p2486 A67-29440

Aircraft radiography for turbojet engine integrity and serviceability determination [AIAA PAPER 67-380] 15 p2494 A67-30350

Limitations arising during reconstruction of plane-grating hologram with characteristic X radiation to operate at optical wavelengths 18 p3047 A67-33884

Flash X-ray source penetrates thick objects and records shadowgraphs directly on film 18 p3052 A67-34531

Physical changes in exploding wires before gas ionization observed by X-ray technique, studying resistivity variation with density 19 p3261 A67-35161

Rentgenographic kymography in evaluating cardiovascular apparatus in middle aged pilots 22 p3753 A67-40543

Clineradiographic analysis of human

visceral responses to short duration acceleration impact 23 p3951 A67-41553

Linear defects imaging in single crystals by interpreting anomalous behavior of propagating X-rays ascribed to structural defects 24 p4202 A67-42072

X-RAY SCATTERING

Double crystal spectrometer measurement of X-ray Compton and thermal scattering accompanying Bragg reflection from Si and Ge single crystals 01 p0132 A67-10456

Observational distinction between ice and graphite models of interstellar grains 06 p1082 A67-17978

Microburst precipitation of energetic electrons into auroral zone 18 p3035 A67-33596

X-ray diffusion intensity by transverse polarization phonons in indium antimonide at various temperature ranges 19 p3307 A67-35793

UV and X-ray background measurements by Venus 3 may lead to mean density estimation of matter in universe through determination of intergalactic medium density and thermal history 21 p3705 A67-38591

X-ray diffusion from thermal agitation oscillations coupled with plasma waves in indium antimonide, discussing phonon-plasmon interactions and Hall effect measurements 22 p3859 A67-39652

X-RAY SPECTROGRAPHY

Strong X-ray source in vicinity of constellation Crux compared to SCO xr-1, findings suggest similar physical nature 17 p2937 A67-32761

X-RAY SPECTROMETRY

Combined focusing X-ray diffractometer and nondispersive X-ray spectrometer for lunar and planetary analysis 01 p0067 A67-10689

Intensities of L, M and N X-ray spectra for wavelengths in region from 2 to 85 angstroms 01 p0116 A67-10690

X-ray emission from old novae noting possibility that hot coronas may arise from vibration 02 p0308 A67-12032

X-ray anomalous transmission used in analysis of gallium arsenide crystal perfection with various dislocation densities, determining ratios of anomalous absorption coefficient 04 p0674 A67-14620

Isotropic component of cosmic X-rays at balloon altitude 04 p0693 A67-14963

Sample orientation and electron beam incidence angle variation effects on X-ray spectrometer performance 04 p0621 A67-15114

Intensity of characteristic spectral lines of Si, Al and Mg of lunar surface rock made fluorescent by solar X-rays determined from Luna X measurements 05 p0886 A67-16051

Aurora photometry and stratospheric cosmic ray intensity, noting electron intrusion and correlation between aurora intensity and X-ray emission 05 p0879 A67-16102

Etching and X-ray spectrometric techniques to investigate distribution and density of dislocations in deformed and annealed GaAs and InSb crystal 05 p0865 A67-16920

Solar X-ray spectrum of Tousey analyzed using criteria of abundance of elements of Pottasch 10 p1707 A67-23227

Auroral X radiation, measured by balloon-installed X-ray spectrometer incorporating scintillation counter with high speed analyzer, correlated with ionospheric radioelectric absorption and solar magnetic field variations 10 p1702 A67-23304

Monograph on electron microprobe X-ray analyzer and application in mineralogy 10 p1603 A67-23632

X-ray spectral distributions and fluxes in low kev range of five cosmic sources at low galactic latitude and longitude, noting effective temperature 11 p1856 A67-24505

Solar X-ray emission measurement below 25 angstroms using airborne Bragg spectrometers, with data reduced by computer 11 p1867 A67-24839

Cosmic X-ray sources attributed to thermal emission of hot condensations from supernova remnants in our galaxy or other galaxies 12 p1995 A67-25764

Etching and X-ray spectrometric techniques to investigate distribution and density of dislocations in deformed and annealed Ga-As and InSb

crystal 14 p2365 A67-28260

Solar X-ray flux for wavelength less than five angstroms measured, noting extreme variations in spectral slope and intensity 16 p2739 A67-31411

X-ray spectrometer with cold cathode, discussing equipment design, principles, operation and performance 17 p2853 A67-32046

Solar X-ray spectrum observed by rocket carried Bragg crystal spectrometers and pinhole cameras array 17 p2937 A67-32650

Solar X-ray flare of July 1966 observed from satellite, giving curves describing energy flux, radiation intensity, etc 19 p3312 A67-35187

Auroral absorption events, discussing bremsstrahlung X-rays spectrum, electron densities and temperatures measured with rockets 19 p3312 A67-35188

Spectral analysis of K alpha type X-ray transitions in solar atmosphere and laboratory plasma 19 p3331 A67-36086

Proportional counter spectrometer for solar soft X-ray spectrum study 20 p3448 A67-36960

Intensity of characteristic spectral lines of Si, Al and Mg of lunar surface rock made fluorescent by solar X-rays determined from Luna X measurements 21 p3701 A67-37838

Deposited Al layer thickness on Si determined using X-ray spectrometric technique 24 p4200 A67-41803

Aurora photometry and stratospheric cosmic ray intensity, noting electron intrusion and correlation between aurora intensity and X-ray emission 24 p4213 A67-42778

X-RAY SPECTROSCOPY

X-ray emission and absorption spectra, electron structure and properties of metallic compounds of titanium 05 p0831 A67-17484

Crab Nebula X-ray spectrum from balloon observations, noting importance of correction for escaped iodine K component 07 p1251 A67-19944

Low energy cosmic ray photons in atmosphere, noting X-ray generation by bremsstrahlung effect of electron component 08 p1377 A67-21466

Diurnal variation of primary auroral electrons, average energy spectrum of 20-150 kev X-rays and time dependence of intensity and morphology 10 p1702 A67-23305

Structure of X-ray K absorption edge of iron in Fe compounds, noting nature of chemical bond and structure of electron energy spectrum 12 p1957 A67-26109

X-ray spectral analysis of bent aluminum single crystals with crystallographic plane parallel to reflecting surface of crystal 17 p2874 A67-32895

Covalent bonds found more prevalent than ionic bonds in X-ray spectral study of Al and Sb in A-III B-V type semiconductor compounds 18 p3095 A67-33443

Relation between changes in ferrite lattice parameter at magnetic conversion temperature and changes in ferrite metal ion charges due to electron exchange 18 p3095 A67-33444

Chemical effects in X-ray spectra and inner shell photoelectron spectra of sulfur and chlorine-oxygen anions and molecular orbital method 18 p2998 A67-34520

Nickel aluminate structure, examining arrangement of Ti, Cr and W in lattice via X-ray spectroscopy 20 p3467 A67-37116

W-Ta-Re system equilibrium diagrams examined, measuring diffusion layer element concentration by X-ray spectral analysis method 20 p3468 A67-37180

X-ray spectrum and location measurements of several cosmic X-ray sources, using rocketborne proportional counters 21 p3698 A67-38564

X-RAY STRESS MEASUREMENT

Gamma and X-radiographic radioactive sources for nondestructive testing of hydrogenous materials such as rubber, adhesives and explosives in steel or other metal assemblies 02 p0249 A67-12220

Topographic X-ray analysis of deformation in tension of silicon crystal 03 p0493 A67-13452

Elastic and inelastic lattice strain at oxide window edges determined from imperfections of n and p type 08 p1370 A67-21297

X-ray diffraction techniques and apparatus for measuring residual stresses in metals

[SAE PAPER 670151] 09 p1502 A67-21771

Portable X-ray equipment for measuring residual stresses in welded rocket motor case, machined aluminum parts and titanium welds

[SAE PAPER 670152] 09 p1509 A67-22542

Deformation behavior of matrix and fibers in aluminum-boron and copper-tungsten composites studied by X-ray lattice strain techniques 18 p3067 A67-34570

X-RAY TELESCOPE

Upper limits to hard X-ray flux from quiet sun analyzed by balloon-borne scintillation detector measuring celestial sources 13 p2189 A67-26302

X-Y PLOTTER

Phaseplot, on-line graphical output parametric display technique, noting hardware realizations and software requirements 13 p2073 A67-27063

XB-70 AIRCRAFT

Titanium fabrication techniques for XB-70 and space booster

[SAE PAPER 660650] 01 p0079 A67-10611

Linear optimal control via root square locus to design simple effective structural bending control for four XB-70 coupled longitudinal bending modes

[AIAA PAPER 66-970] 03 p0361 A67-14142

Exothermically brazed tubing joints for XB-70 hydraulic system 07 p1190 A67-19212

Handling and operation of XB-70A aircraft at Mach 3 speed noting folding wing tips, variable-geometry air inlet duct, etc 07 p1129 A67-19910

Performance characteristics of XB-70 flight test data acquisition system 20 p3442 A67-36487

XC-142 AIRCRAFT

XC-142A tilt-wing deflected slipstream aircraft designed to take off and land in virtually any terrain and achieve 430 plus mph 03 p0357 A67-12971

Flight and operational suitability testing of XC-142 V/STOL assault transport

[AIAA PAPER 67-261] 07 p1130 A67-20074

XC-142A flight control and stability augmentation systems 17 p2794 A67-31996

XENON

Exciton and impurity states in Kr and Xe crystals and in rare-gas solids containing Xe impurity calculated by pseudopotential theory 02 p0281 A67-11490

Emission, collection and analysis of radioactive rare gas xenon 133 as atmospheric tracer whose inert characteristics allow diffusion processes to be followed 02 p0237 A67-11854

Microwave cavity measurement of recombination coefficient of decaying plasma obtained by gamma ray induced ionization of xenon 02 p0274 A67-12463

Magnetically tunable IR masers of helium-xenon, considering experimental problem in applying tunable IR maser to IR spectroscopy 04 p0632 A67-14764

Brightness temperature of shock waves dependence on wave amplitude in xenon and air at high temperature 05 p0795 A67-17544

Focused coaxial xenon gun to accelerate plasmas of high atomic weight with high power fluxes, measuring ablative and radiative flux at boundaries 08 p1356 A67-20371

Origin of fissionogenic Xe isotopes in Pasamonte achondrite 08 p1386 A67-20938

Laser effect on electron gas and excited state populations in xenon discharges 08 p1338 A67-21306

Relaxation process and magnitude of nonthermal ionization in MHD generator, describing experimental equipment and results in xenon and in argon 09 p1540 A67-21790

Charge exchange cross sections measurements for ion-molecule pairs of hydrogen, argon, krypton, helium and xenon 09 p1535 A67-22381

Xenon 129 and tellurium 128 formation intervals in chondritic meteorites as measure of neutron induced isotope production by solar nucleosynthesis 09 p1570 A67-22694

Cosmic ray spallation and special anomaly in achondrites 11 p1866 A67-24696

Ionization rate in helium, argon and xenon plasmas determined by microwave technique 12 p1970 A67-25291

Isotopic composition and abundance of xenon and krypton in graphite of iron meteorite from Canyon Diablo examined for

anomaly pattern 16 p2750 A67-31438
 Spallation and fission xenon and krypton content in Pasamonte achondrite as evidence for extinct radioactivity in meteorites 16 p2754 A67-31747
 Excitation and ionization mechanisms in positive DC discharge columns in krypton and xenon 19 p3265 A67-35131
 Attenuation cross section at Lyman alpha for Xe deviation from Beer law indicating diatomic Xe molecule formation 20 p3491 A67-37688
 Xenon data from Murray and Renazzo carbonaceous chondrites reinterpreted, discussing large presence of fissionogenic xenon 24 p4234 A67-42626
 Isotope ratios of fission and spallation xenon in meteorites from abundance data analysis by least squares method 24 p4238 A67-42886
XENON LIGHT
 Gas laser measurement of electron density in xenon pulse discharge 09 p1512 A67-21922
 Gas laser measurement of electron density in xenon pulse discharge 14 p2330 A67-28251
 Large space simulation chamber for studying low temperature, absolute vacuum and solar radiation effects 15 p2466 A67-29571
 Single-mesh circuits design for driving xenon flashlamps, solving normalized nonlinear differential equation 19 p3192 A67-35015
 Boeing 20-ft solar simulator alignment, calibration, cleanliness, optical system, xenon light sources and vacuum system 24 p4139 A67-42045
XENON 129
 Gas laser spectroscopic analysis of hyperfine structure, paramagnetic properties, radiative lifetimes and Doppler-broadened transition saturation behavior of excited states of Xe 129 04 p0661 A67-15462
 Xenon-iodine dating, sharp isochronism in chondrites 12 p2002 A67-25525
 Isotopic composition and abundance of xenon and krypton in graphite of iron meteorite from Canyon Diablo examined for anomaly pattern 16 p2750 A67-31438
XENON 133
 Hermetically sealed semiconductor device tested for leaks with xenon 133 gas, determining radiation safety measures for personnel 14 p2324 A67-28280
XH-51 HELICOPTER
 Flights tests of XH-51A compound helicopter, discussing rigid rotor concept and results of compound flight research program [AIAA PAPER 87-262] 07 p1130 A67-20075
 XH-51A compound research flight test program, discussing adaptation of rigid rotor concept 13 p2052 A67-26421
XV-4 AIRCRAFT
 XV-4B vertical lift aircraft with lift engines noting stability, control, structural design, flight control system, etc 09 p1439 A67-22284
XV-9A AIRCRAFT
 Structural design, analysis and tests pertaining to hot cycle rotor system used on XV-9A aircraft [AHS PAPER 121] 16 p2598 A67-31836
XYLENE
 Semiconducting alloys of gallium investigated by photometric method using gallium and xylene orange 22 p3804 A67-40299

Y

YAG
 S YTTRIUM-ALUMINUM GARNET /YAG/ CRYSTAL
YAGI ANTENNA
 Direct TV reception from satellites, discussing cost of Yagi and parabolic antennas, noting output tube 13 p2066 A67-26336
YAW
 Simplified approach to predicting onset of spin-yaw instability of rapidly ascending rolling ballistic missile in absence of asymmetric forces 08 p1406 A67-20509
 Captured Air Bubble /CAB/ vehicle stability tests [AIAA PAPER 87-349] 14 p2246 A67-28731
 Mathematical model used to determine influence of nonlinear induced roll moment and yawing moment on dynamic stability of

cruciform tailed bomb 15 p2416 A67-29428
YAW ATTITUDE
 Hypersonic aerodynamic coefficients for bodies of revolution in yaw 02 p0179 A67-12314
YEAH
 Enzyme activity of light and heavy crude ribosomal fractions in Saccharomyces cerevisiae indicating subcellular sites of lipid synthesis 21 p3573 A67-37919
YF-12 AIRCRAFT
 Next generation interceptor aircraft to follow F-106A, including YF-12A and evolving F-111B, would serve largely as missile launching platforms 04 p0550 A67-14422
YIELD
 Yield surfaces for nonhomogeneous shells of revolution 03 p0523 A67-13501
 Coherent precipitation hardening theory treats yielding in nickel base alloy containing coherent stress-free ordered particles as dynamic process 18 p3064 A67-34080
YIELD POINT
 Strain aging of ordered alloys at temperatures above and below critical point, discussing yield point and hardening factor 01 p0101 A67-10938
 Shape of limiting-state curve for high strength steel predeformed to yield point by repeatedly applying internal load 02 p0255 A67-12667
 Strain-hardening and temperature dependence of mechanical properties of ternary ordered alloys on nickel-iron base 02 p0255 A67-12675
 Titanium alloys test results at 20 and 400 degrees C and at different grip speeds, using various tensile testing machines 03 p0446 A67-13566
 Distinct yield point appearance in vanadium alloys as function of composition, strain temperature and strain rate 05 p0828 A67-16388
 Heat treatment effect on yield point, impact toughness and plasticity characteristics of Ti alloys 07 p1207 A67-18286
 Cyclic torsion interaction with axial load, showing torsion angle larger than fatigue limit and applied tensile stress larger than Bauschinger yield 10 p1669 A67-23438
 Discontinuous yield phenomena for slip band dislocations, when frictional stress that hinders dislocation motion undergoes static or dynamic drop 11 p1807 A67-24568
 Effect of V, Zr, and Y additions on mechanical properties of 1 mm sheet molybdenum 13 p2130 A67-26392
 Temperature dependence of yield point of crystals described in terms of thermally activated motion of dislocations in external forces field 13 p2131 A67-26449
 Dynamic and physical testing of metals, discussing yield point, plastic deformation and oscillation damping characteristics 13 p2215 A67-26452
 Micro-yield stress determinations of cast and extruded beryllium as measure of dimensional stability 13 p2138 A67-27119
 Hydrostatic pressure effects on brittleness in Cr and yielding in center annealed iron specimen studying brittle-ductile transition of former 16 p2689 A67-31328
 Physical basis of yield and fracture - Conference, Oxford, England, September 1986 18 p3062 A67-33481
 Pressurization produced free dislocations effect on yielding and fracture in bcc metals 18 p3063 A67-33484
 Oxygen concentration and strain rate effect on yield point phenomenon in electron beam refined niobium, showing relation to dislocation multiplication 18 p3063 A67-33486
 Yield conditions for plastically incompressible isotropic and orthotropic materials with different yield stress in tension and compression, without using hydrostatic terms 19 p3339 A67-35053
 Knoop hardness yield loci for two Ti alloys 21 p3646 A67-38777
YIELD STRENGTH
 Contact resistance variation effect on strength tests, noting strain gauge reading error magnitudes 02 p0340 A67-12444
 Maximum limiting value of uniform deformation of metals and alloys by stretching, deriving hyperbolic tangent to true-stress curve 02 p0341 A67-12676

Indium antimonide specimens plastically bent to introduce excess of dislocations, examining dependence of lower yield stress for bending on direction of bend 03 p0498 A67-13870
 Effect of locking dovetail joint geometry on static strength 03 p0528 A67-14077
 Load carrying capacity of thin plates of rigid perfectly plastic material with different tensile and compressive yield strength, using method of limit analysis 03 p0531 A67-14366
 Book on strength under high transient loads and nonlinear elastic and elastoplastic wave propagation 04 p0715 A67-15617
 Book on dynamic strength, brittleness, plasticity and ductility of metals 05 p0907 A67-16031
 Lunar surface composition, strength and failure modes, determining ability to support LEM 05 p0895 A67-16612
 Plastic deformation of textured Ti alloy sheet examined, using tension testing along different directions and combined stress loading along principal axes of anisotropy 06 p1016 A67-17900
 Yielding and brittle cracking of orthotropic strip, using Wiener-Hopf technique and asymptotic method for isotropic case 06 p1102 A67-18317
 Strength of threaded joints compared under static and dynamic conditions 07 p1190 A67-19353
 Book on aircraft materials strength calculations including load determination, heating problems, creep and fatigue strength, etc 07 p1128 A67-19578
 Qualitative and quantitative methods for correlating preferred crystallographic orientation with biaxial strengths of titanium alloys 08 p1340 A67-20363
 Yielding phenomena in beryllium wire plastic composites, discussing static strength and moduli, failure modes and impact resistance 08 p1341 A67-20428
 Yield strength and reliability of structural cluster welds determined using statistical analysis 09 p1506 A67-22308
 Independent linearized solutions closely approximating Mises and Tresca /M-T/ limit loads in linear theory of plasticity for plane strain 10 p1716 A67-22933
 Influence of explosive forming characteristics on springback based upon tests in forming of gore sections for Saturn V rocket 10 p1660 A67-23170
 Yield surfaces for nonhomogeneous anisotropic shells of revolution under rotationally symmetric conditions of loading and support 10 p1719 A67-23544
 Boron fiber reinforced epoxy matrix plastic composite for application to aircraft structures 10 p1723 A67-23697
 Temperature effect, including liquid helium temperature, on yield stress of commercial purity alpha titanium 11 p1805 A67-24111
 Soviet book on ideal plasticity theory covering basic assumptions, general theorems, Tresca yield condition, etc 11 p1875 A67-24511
 Rigid plastic cylindrical shell axisymmetrical deformations in terms of Tresca yield condition and gradient law when under load 12 p2026 A67-25618
 Universal endurance criterion for machine structural elements sustaining complex stresses, based on machine part lifetime assessment 12 p2032 A67-25964
 Molybdenum polycrystal plastic strain rate in pre-yield region studied by successive stress relaxation method for dislocation density and mobility characteristics 14 p2337 A67-28230
 Solid self-lubricating materials mechanically strong and resisting oxidation for high temperature air applications, examining friction-wear characteristics 16 p2683 A67-31752
 Effect of thermomechanical treatments on tensile properties of metastable austenitic steels 16 p2693 A67-31872
 Si-Fe deformation in tension/compression noting orientation dependence of yield stress, slip band formation and direction of screw dislocations 17 p2872 A67-32741
 Strength increase of parts or system to prevent fatigue failure, noting bulk and material considerations and elimination of fretting, scoring, corrosion, sharp corners, etc 17 p2962 A67-32824

- Yielding effects in stress corrosion cracking in susceptible alloys 18 p3063 A67-33487
- Strength of single crystals, amorphous materials and other brittle materials lacking grain boundaries, noting loading rate dependence 18 p3069 A67-33491
- Surface morphological changes of tantalum single crystals during plastic deformation, studying orientation dependence of yield stress in tension and compression 19 p3245 A67-35727
- Alloying effect on temperature and strain rate sensitivity of niobium-molybdenum bcc metal 19 p3246 A67-35730
- Stress concentration effects on stress rupture strength, noting applicability to short term creep 21 p3717 A67-37970
- Safety design for high strength low toughness materials assumed to have hidden flaws, formulating stress intensity factor for fracture mechanics 22 p3913 A67-39982
- Crack stability for fracture of nonworkhardening elastoplastic material in plane strain or plane stress, using energy criterion 23 p4078 A67-41162
- YIG**
- S YTTRIUM-IRON GARNET /YIG/ CRYSTAL**
- YOUNGS MODULUS**
- Diffraction of elastic waves in formulation of Young, including form of tensor potential for longitudinal waves 01 p0114 A67-10868
- Dislocation-induced relaxation in silicon single crystals by measuring internal friction and Youngs modulus at temperatures from 77 to 300 degrees K 04 p0681 A67-15294
- Annealing temperatures effect on Young modulus, temperature coefficient and crystallographic texture of Fe-Ni-Ti alloys after deformation 05 p0831 A67-17485
- Static and transient strain measurement in aerospace structural materials using extensometer and compressive test jig, determining Young modulus, creep rate, etc 08 p1420 A67-20907
- Carbon fibers of high strength and high breaking strain noting heat treatment, structure and mechanical properties 09 p1520 A67-21988
- Effect of vanadium, zirconium, tantalum and tungsten concentration on Youngs modulus of niobium, noting temperature dependence and changes in elastic properties 09 p1519 A67-22398
- Fibrous model of shell shaped grid noting discrete network, properties of cross section surface and stress 10 p1715 A67-22920
- Temperature dependence of Youngs modulus of tantalum alloy determined together with free-free vibrations and resonance frequency 12 p1954 A67-25141
- Youngs modulus and shear modulus of inorganic filaments of tungsten and boron measured by oscillation technique 13 p2144 A67-27187
- Cylindrical bending of plate composed of strengthening and binding agents with different Youngs moduli 14 p2401 A67-28734
- Column consisting of flexible and rigid section measured for buckling load, using Southwell method 14 p2404 A67-29057
- Transverse oscillations of elastic inhomogeneous rod with Youngs modulus varying along length, solved in Bessel functions infinite series form 17 p2962 A67-32873
- Deformation behavior of matrix and fibers in aluminum-boron and copper-tungsten composites studied by X-ray lattice strain techniques 18 p3067 A67-33470
- Metal matrix composites compression-microstrain behavior at room temperature, discussing stress-strain curve, Youngs modulus, yielding, etc [ASTM PAPER 6] 18 p3067 A67-33471
- Youngs modulus variation as function of external magnetic field in mixed state in niobium 20 p3464 A67-36221
- Ni-Fe-Mn alloy, Youngs modulus and magnetic saturation temperature dependence, noting order-disorder effects on Curie point 20 p3468 A67-37178
- Elastic properties of filled and porous epoxy composites tested in compression and tension noting Youngs modulus relation to filler content 22 p3824 A67-39498
- YTTERBIUM**
- Polarization of ytterbium isotopes in atomic state using optical pumping with resonance line, calculating magnetic moments 10 p1665 A67-23479
- Optical and paramagnetic resonance of ytterbium ions in calcium fluoride, obtaining correlation between site geometry and optical absorption 12 p1984 A67-25843
- Magnetostriction of trivalent Yb and Ce ions in YIG, measuring temperature dependence, noting exchange and interaction of crystal field splitting for Yb 22 p3855 A67-39363
- YTTRIUM**
- Hartree-Fock-Slater calculation of internal conversion coefficients for magnetic multipoles for yttrium-87 with 0.05 or 0.15 mc-square gamma energy values 01 p0116 A67-10203
- Corrosion resistance of yttrium is higher at higher pH because of slower anodic process 12 p1954 A67-25358
- YTTRIUM ALLOY**
- Structural changes during oxidation of chromium-yttrium alloys determined by measuring gain in weight per unit surface of samples heated in Silit or molybdenum oven in open aluminum tubes 05 p0827 A67-18327
- Nitrogen behavior in Cr-Y alloy of varying interstitial concentration and thermal history 06 p1016 A67-17898
- YTTRIUM-ALUMINUM GARNET /YAG/ CRYSTAL**
- Electron spin resonance absorption spectrum of Pt in YAG at low temperatures, noting ionic orientation 03 p0492 A67-13326
- Crystal absorption and lamp emission spectra for CW pumping of Nd-doped YAG by water-cooled Kr arcs 03 p0437 A67-13576
- Output spectra of Nd doped YAG and ruby lasers, determining mechanisms responsible for observed overall linewidths 05 p0820 A67-16660
- YAG solid state laser system, discussing output, theoretical limits, performance characteristics, etc 07 p1194 A67-19084
- Stimulated emission, absorption spectra and luminescence of neodymium-activated YAG crystals in pulsed laser 09 p1513 A67-22068
- Design characteristics and operation of continuous neodymium laser 09 p1516 A67-22665
- CW solid state lasers, considering principal laser crystals 14 p2330 A67-28470
- Laser transition absorption cross section at room temperature for neodymium ion in yttrium-aluminum garnet determined by two methods 14 p2331 A67-28713
- YIG epitaxial growth condition on YAG and GdIG on YAG identified by X-ray, electron diffraction, microprobe and magneto-optic studies 15 p2539 A67-29824
- Neodymium doped YAG Q-spoiled laser system for switching high voltage spark gap at 50 pps with nanosecond jitter 22 p3813 A67-39258
- Chemical vapor deposition method to grow epitaxial YIG on YAG using high temperature hydrolysis oxidation at seed surface 22 p3860 A67-39896
- YTTRIUM COMPOUND**
- Magnetic properties of YGa and YGaGd ferrites noting effect of increasing Gd content 01 p0136 A67-11052
- Laser excited electronic Raman spectrum of trivalent Eu ion doped YGa garnet 01 p0091 A67-11084
- Formation conditions for yttrium boride-lanthanum boride solid solution by reduction of Y and La oxides in vacuum 01 p0138 A67-11244
- Spectral properties of Nd doped yttrium vanadate grown from melt, noting reduced Stark splitting leading to laser action 07 p1195 A67-19559
- Specific heat and magnetic susceptibility of yttrium solid solutions with magnetic impurities of Gd 08 p1369 A67-20870
- Paramagnetic resonance absorption spectrum of cerium in yttrium-gallium-garnet host crystal 08 p1371 A67-21312
- Crystallization phase in Pbnm orthorhombic space group of yttrium manganite under pressure and high temperature 09 p1557 A67-22572
- Optical and laser properties of trivalent Nd and Eu ion doped yttrium orthovanadate 11 p1847 A67-24739
- Absorption, fluorescence and laser emission spectra of triply ionized neodymium yttrium in compound below room temperature 16 p2728 A67-30810
- Transient growth of magnetostatic modes in yttrium garnet subject to pulsed longitudinal pumping 16 p2732 A67-31704
- Translucent material /Zytrite/ obtained from cubic phase stabilization of Y and Zr alkoxides at low temperatures, noting high surface activity 24 p4175 A67-42373
- YTTRIUM-IRON GARNET /YIG/ CRYSTAL**
- YIG dispersive delay line in ultrawide bandwidth pulse compression radar system 01 p0132 A67-10435
- Approximate numerical solution used to calculate delay of z-directed magnetoelastic wave in yttrium iron garnet 01 p0138 A67-11321
- Microwave echoes in axially magnetized yttrium iron garnet cylinders following application of two pulses, with second twice frequency of first 02 p0297 A67-11874
- Ferroacoustic resonance in yttrium ferrite garnet crystals, noting effect of magnetic field on pulse amplitude 05 p0868 A67-17064
- Magnon phonon scattering relaxation time as function of temperature and wave vector, calculating thermal conductivity of YIG 05 p0869 A67-17191
- Echo pulses in YIG crystal noting influence of lateral elastic HF signals 08 p1366 A67-20313
- C-band traveling wave maser using printed circuit technology results in reduced structure size, perfect contact between structure and ruby, etc 11 p1801 A67-24727
- Light diffraction by elastic waves in YIG noting values of photoelastic tensor components 12 p1984 A67-25748
- Spin wave interaction in YIG with acoustic, magnetoplastic and relaxation oscillations excited by laser and microwave 12 p1953 A67-25749
- Single crystal YIG phase shifter performance noting improved output with proper microwave circuit design 13 p2076 A67-26479
- Frequency selective parametric limiting by parallel pumping of subharmonic magnetoelastic waves in YIG 13 p2077 A67-26523
- Ferroacoustic resonance in yttrium ferrite garnet crystals, noting effect of magnetic field on pulse amplitude 15 p2538 A67-29795
- YIG epitaxial growth condition on YAG and GdIG on YAG identified by X-ray, electron diffraction, microprobe and magneto-optic studies 15 p2539 A67-29824
- Excitation of magnetoelastic waves at 200 to 3000 mc at room temperature in yttrium garnet single crystals obtained by gradual crystallization from yttrium and ferric oxides 16 p2733 A67-31733
- Frozen vacancies effect on microhardness and electrical resistance of nickel ferrite and yttrium garnet 18 p3097 A67-33480
- Silicon doped YIG containing iron ions, studying loss mechanism, low temperature anisotropy, annealing and rotational hysteresis 18 p3105 A67-34629
- C-band solid state YIG serrodyne theory and operation, outlining phase velocity modulation of magnetostatic modes 19 p3196 A67-35661
- Microwave delay-line techniques using YIG crystal, examining solid state dispersion characteristics 20 p3507 A67-36241
- Temperature dependence and anisotropy of high temperature ferrimagnetic microwave resonance linewidth of Si-doped YIG, showing valence exchange effect on losses 20 p3508 A67-36390
- Two-port magnetoelastic delay performance obtained in YIG rod by injecting longitudinal elastic waves along axis 21 p3877 A67-38007
- High efficiency tunable ferrite frequency doubler consisting of yttrium-iron-garnet disk at waveguide junction 21 p3598 A67-38572
- YIG magnetically induced elastic wave dispersion, acoustic Faraday rotation and group velocity dispersion measured using Bragg diffraction 22 p3855 A67-39356
- Magnetostriction of trivalent Yb and Ce ions in YIG, measuring temperature dependence, noting exchange and interaction of crystal field splitting for Yb 22 p3855 A67-39363
- Magnetics - Conference, Washington, D.C., April 1967 22 p3859 A67-39895
- Chemical vapor deposition method to grow epitaxial YIG on YAG using high temperature hydrolysis oxidation at seed surface 22 p3860 A67-39896

Nonreciprocity in YIG filters employing stripline or miniature coaxial line construction 22 p3772 A67-39905
Microwave pulse compression filter using dispersive characteristics of propagating magnetostatic spin waves in single crystal YIG rods 22 p3773 A67-39908
Heating and quenching of aluminum and gallium substituted YIG changes magnetization of material due to cations redistribution process 22 p3860 A67-39913
Reflectivity spectra of YIG and YGG crystals, observing YTG structure attributed to charge transfer enhanced crystal field transitions reflectivity spectra of YIG and YGG crystals, observing YIG structure attributed to charge 22 p3863 A67-40238
Measurements on YIG crystals showing magnetic crystal symmetry lowering by strong electric field 23 p4035 A67-40654
Faraday rotation in YIG studied from measurements at He-Ne laser wavelengths for applications to materials design 23 p4041 A67-41184
Domain structures in YIG slices after polishing strains elimination, noting spike domains 23 p4041 A67-41185
Magnetic moments of sublattices and of yttrium garnet calculated including biquadratic temperature dependent exchange 23 p4043 A67-41302

YTTRIUM OXIDE
Two photon stepwise absorption of low power He-Ne laser light in erbium doped yttrium oxide and lanthanum fluoride crystals 13 p2177 A67-27013

Z

Z TRANSFORM

Partial error analysis of Fowler z transform root-locus method for digital simulation of complex system 07 p1148 A67-19892
Relation among sampling theorem, Z transformation and time series method for applications to network analysis 07 p1146 A67-20194
Spectral stability criteria for numerical integration procedure using Z transforms, specifically finite difference operators 08 p1296 A67-20600
Z-transform and W-transform theory applied to dynamic compensation of linear sampled data control systems for attitude control of large booster 21 p3713 A67-38027

ZEEMAN EFFECT

Zeeman field spatial orientation of paramagnetic spin-lattice relaxation for 2T2 states in rhombic symmetry, emphasizing application to Fe-doped potassium cobalticyanide and potassium ferricyanide 01 p0129 A67-10150
Laser characteristics of narrow band type I solar radio burst and magnetic dipole transitions in split Zeeman sublevels of hydrogen atoms of solar corona in ground level 02 p0322 A67-11652
Sodium dayglow emission measurement by Zeeman photometer, presenting calculation of radiant energy absorption by sodium vapor in magnetic field 03 p0409 A67-12945
Stark and Zeeman splitting in far IR spectra of erbium, dysprosium and samarium ethyl sulphate 04 p0686 A67-15778
High resolution spectroscopy using Zeeman-tuned IR maser oscillating at transitions between 3 and 9 microns 05 p0816 A67-16633
Lamb self-consistent theory and rate equation approximation study of magnetic depolarization of vapor and polarization of monomode gas laser in magnetic field 05 p0818 A67-16644
Magnetic field strength effects on excited acceptor states of semiconducting diamond determined, using Zeeman splittings of main excited lines 06 p1062 A67-18927
Center frequency shifts of 6328 angstrom neon transition in Zeeman discharge cell measured in terms of discharge current and gas pressure 07 p1197 A67-20100
Zeeman effect in Ne-He gas laser operating in longitudinal magnetic field, noting dependence of frequency difference on field strength 09 p1512 A67-21920
Absolute frequency measurement and spectroscopy of gas laser transitions in far IR, analyzing Zeeman

effect 11 p1802 A67-24830
Zeeman Centennial Conference, Amsterdam, September 1965 12 p1987 A67-26234
Zeeman effect in measuring magnetic fields of sun and stars, noting apparatus 12 p2010 A67-26235
Hyperfine structure and modified Zeeman effect in trivalent holmium in hexagonal lanthanum trichloride 12 p1987 A67-26237
Coulomb long range interaction effect on refractive index dependence on light frequency and on absorption lines shape of dipole active excitons 13 p2173 A67-26365
Optical double-quantum transition in which atom passes from one Zeeman sublevel to another by absorption and successive reemission of optical photons 13 p2127 A67-27079
Anomalous polarization of four cosmic OH lines predicted from states of polarization in OH maser amplifier 13 p2161 A67-27289
Gain narrowing and saturation broadening of Doppler broadened neon line in Zeeman scanned laser amplifier 13 p2129 A67-27485
Zeeman effect in Ne-He gas laser operating in longitudinal magnetic field, noting dependence of frequency difference on field strength 14 p2330 A67-28249
Gas laser mode interaction in Zeeman laser, investigating transition in axial magnetic field 14 p2331 A67-28715
Method for complete observation of magnetic field structure in sunspots 14 p2390 A67-28942
Optical pumping and double resonance used to study magnetic resonance and Zeeman effect 14 p2333 A67-28969
Laser characteristics of narrow band type I solar radio burst and magnetic dipole transitions in split Zeeman sublevels of hydrogen atoms of solar corona in ground level 16 p2747 A67-31067
Zeeman effect of germanium I and II, discussing configuration-interaction, deriving intermediate-coupling wave functions 16 p2733 A67-31876
Transient Stark and Zeeman spectral line shifts in plasma emission measured with multiple beam Fizeau interferometer, discussing instrument errors 20 p3439 A67-36351
Fine structure of nitrogen 14 resonance in hydrazine analyzed for Zeeman effect 21 p3688 A67-38418
Solar magnetic fields, discussing Zeeman effect, solar activity regularity and filamentary current in force-free magnetic fields 21 p3709 A67-38990
Ion bombardment excitation used to extend excited state range for level crossing spectroscopy studies, giving Zeeman energy level diagram 22 p3835 A67-39239
Photoelectric records of DE and LZE in solar photosphere velocity fields, analyzing oscillations onset and lifetimes 23 p4066 A67-41229
Cesium vapor pumping by intensive polarized light used for studying Cs buffer gas collision influence on pumping cycle and Zeeman transitions effect on polarization 23 p4016 A67-41291

ZENER DIODE

Avalanche transit time diode used as sideband translator and combination local oscillator-mixer at X-band 03 p0381 A67-13666
Negative resistance regions in Si Zener diodes explained in terms of impact ionization and junction breakdown combination 06 p0968 A67-17814
Energy dependence of semiconductor devices with respect to secondary breakdown explained on basis of transient thermal resistance 07 p1156 A67-19895
Zener diode function generator eliminates need for external reference voltage source 08 p1307 A67-21538
Avalanche injection and application to fast pulse generation and switching 13 p2079 A67-26872
Pulsed operation of large-area silicon p-n junction avalanche diode oscillators for microwave frequencies 19 p3196 A67-35627

ZERO ANGLE OF ATTACK

Nonlinear singularities method for calculating velocity distribution over thick wing of finite aspect ratio situated at zero angle of attack in incompressible frictionless potential flow 07 p1127 A67-19887
Flow field around porous wedge or cone immersed at zero angle of attack in uniform

supersonic free stream when contact surface is straight 08 p1276 A67-20571
Mach number effect on hypersonic flow past delta wing with blunt edges at zero angle of attack 10 p1590 A67-23036
Fluid dynamic fields from hypersonic flow around slender bodies, using extension of Vallander tangent cone method for zero angle of attack 11 p1741 A67-24091
Integral equation for discontinuous flows and free streamline solutions for axisymmetric bodies at zero and small angles of attack 22 p3743 A67-40166

ZERO CROSSING

Zero-crossing times for signals, performing transformations of time sequence to determine distribution functions 19 p3201 A67-34905
Laminar boundary layer subject to local three-dimensional disturbance, studying growth, flow field and transition to turbulence 23 p3991 A67-41175

ZERO FORCE CURVE

Neutral /zero/ points and geometry of solar magnetic fields 12 p2002 A67-25534

ZERO GRAVITY

S WEIGHTLESSNESS

ZERO LIFT

Curved flow effect on lift characteristics of blade using Scholz method, noting role of correction coefficient of lift curve slope and zero lift angle 05 p0791 A67-16427

ZERO VELOCITY CURVE

Book on theory of orbits covering restricted problem of three bodies, two bodies in rotating coordinate system and periodic orbits 18 p3120 A67-34032

ZERO-ZERO WEATHER

Instrumentation development making it possible to land safely under poor visibility conditions, goal being zero-zero landing 14 p2347 A67-28990

All-weather landing systems for automatic and manual control, considering Category II and III operations 22 p3831 A67-39611

ZETA MACHINE

Z-pinch in electron hole plasma observed by microwave probe method, noting no minimum current exists for semiconductors 21 p3666 A67-38356

ZINC

Diffusion and electrical transfer of zinc in indium arsenide as affected by temperature 01 p0127 A67-10068
Fermi-Dirac statistics, transverse magnetoresistance and galvanomagnetic properties of hexagonal-close-packed Mg and Zn 03 p0495 A67-13511
Capture cross section of photons by zinc and mercury atoms in germanium determined from integral voltaic photosensitivity, using black body as radiation source 05 p0868 A67-17066
Photoconductivity of silicon alloyed with gold and zinc at various temperatures 05 p0871 A67-17492
Diffusion and electrical transfer of zinc in indium arsenide as affected by temperature 08 p1371 A67-21451
Effect of multiple zinc diffusions on threshold and CW output power of semiconductor laser 13 p2125 A67-26522
Ni XIX, Cu XX and Zn XXI spectra observation using vacuum spark chamber 14 p2389 A67-28840
Capture cross section of photons by zinc and mercury atoms in germanium determined from integral voltaic photosensitivity, using black body as radiation source 15 p2538 A67-29797
Time and temperature dependent diffusion of vaporized Zn and Cd in n-type InAs 19 p3299 A67-34760
Temperature dependence of diffusion coefficient of zinc in gallium arsenide 20 p3504 A67-36162
Partial molal entropies of doubly ionized aqueous Zn, Cd and mercurous and mercuric ions calculated, using literature data 20 p3376 A67-36792
Zn doped polycrystalline GaAs film electrical properties temperature variation 20 p3514 A67-37602

ZINC ALLOY

SA BRASS

Aging kinetics and lattice defects in Al-Zn and Al-Zn-Mg alloys 11 p1809 A67-24947
Automatic plating system insuring quality finishes by selectively phosphating or chromating parts after zinc plating 23 p4010 A67-41351

ZINC ANTIMONIDE

- Powder metallurgy techniques for thermoelectric materials particularly lead telluride, germanium bismuth telluride and zinc antimonide 01 p0099 A67-10709
- Zn-Sb intermetallic compounds preparation for single crystals in semiconductor phase 14 p2372 A67-28826
- Electric and thermoelectric effects in single crystals of zinc-cadmium-antimony solid solution, measuring electrical conductivity, Hall constant and thermoelectric power 15 p2540 A67-30029

ZINC COMPOUND

- High energy density Zn/O battery system, noting good low oxygen pressure and low temperature performance characteristics 13 p2055 A67-26836
- Formation of hydride zinc film on titanium activated for deposition of galvanic coating 14 p2336 A67-27868

ZINC OXIDE

- Optical properties of zinc oxide analyzed by exposing samples to mechanical and thermal treatments and UV radiation [AIAA PAPER 67-214] 06 p1052 A67-18514
- Electron paramagnetic resonance of photosensitive donors in zinc oxide with oxygen vacancies 06 p1054 A67-18832
- Lattice IR reflection and transmission spectra and Raman spectrum of monocrySTALLINE and hot pressed pellets of ZnSe 06 p1059 A67-18909
- Sharp line emission spectra due to alkali metal doping in ZnO crystals at low temperatures 06 p1060 A67-18914
- Far field pattern of sheet-like laser beam from electron bombarded CdS and ZnO single crystals 07 p1196 A67-19798
- Chemical stability of silver graphite, molybdenum disulfide, zinc oxide, boron nitride, muscovite and phlogopite mica solid lubricants 10 p1659 A67-22829
- Zinc penetration through regenerated cellulose membrane separators shown to be growth mechanism in silver-zinc cell 22 p3758 A67-40227

ZINC SELENIDE

- Extremely high reflective dielectric mirror coatings with zinc selenide for laser resonator cavities and interference filters 04 p0634 A67-15654
- Laser action in zinc selenide crystals at 4600 angstroms prepared under high pressure in closed container by gas phase reaction and following crystallization 07 p1197 A67-20183

ZINC-SILVER BATTERY

S SILVER-ZINC BATTERY

ZINC-SILVER OXIDE BATTERY

- Aerospace automatically activated electrochemical battery and DC-DC high voltage converter-regulator noting storage stability 24 p4108 A67-42541

ZINC SULFIDE

- Molecular spectroscopy of illumination effects on cobalt activated ZnS exposed to ruby laser pulses 01 p0090 A67-10683
- Light modulation by large single crystal ZnS with negligible strain birefringence 01 p0138 A67-11330
- Normal and abnormal optical absorption in thin zinc sulfide films with excited states in forbidden band surfaces 02 p0288 A67-11724
- Anomalous polarity-dependent electro-optic effect with noncubic symmetry observed in cubic single crystals of ZnS and ZnTe 03 p0496 A67-13569
- Electric conductivity and luminescence increase in luminophorous zinc sulfide films as aftereffect of negative resistance 05 p0866 A67-17023
- Molecular spectroscopy of illumination effects on cobalt activated ZnS exposed to ruby laser pulses 11 p1804 A67-25072
- Electric and photoelectric properties of p-n junction obtained by thermal diffusion of copper into n-ZnS-Cl single crystals 13 p2172 A67-28355
- Electric conductivity and luminescence increase in luminophorous zinc sulfide films as aftereffect of negative resistance 14 p2366 A67-28487
- ZnS two-photon absorption spectrum to establish two-photon pumping capabilities of semiconducting crystals 15 p2500 A67-29816
- Electric and photoelectric properties of p-n junction obtained by thermal diffusion of copper into n-ZnS-Cl single crystals 21 p3679 A67-38312
- Erosion processes and outflow phenomena

- in ZnS rocket fuel, noting aluminum addition and gas leaks 24 p4206 A67-42579

ZINC TELLURIDE

- Shallow hydrogenic type acceptor levels produced by Li and P doping in zinc telluride and cadmium telluride, noting heat treatment effects 02 p0280 A67-11484
- Recombination processes in aluminum doped zinc telluride single crystals, determining distance of r-centers from C-band 02 p0300 A67-12478
- Anomalous polarity-dependent electro-optic effect with noncubic symmetry observed in cubic single crystals of ZnS and ZnTe 03 p0496 A67-13569
- High voltage photo-emf in epitaxial zinc telluride films grown on halide substrates 05 p0868 A67-17061
- Lattice IR reflection and transmission spectra and Raman spectrum of monocrySTALLINE and hot pressed pellets of ZnSe 06 p1059 A67-18909
- Optical transitions at isoelectronic traps in GaP and ZnTe, presenting fluorescent spectra 06 p1062 A67-18929
- Crystalline structure of ZnTe thin films as function of stoichiometric and growth conditions 07 p1233 A67-19645
- Volt-ampere characteristics effect on thickness of contact materials of some heterojunctions and band structures obtained by epitaxial deposition 12 p1983 A67-25515
- High voltage photo-EMF in epitaxial zinc telluride films grown on halide substrates 15 p2538 A67-29792
- Mean values of characteristic temperatures and dynamic displacements of ions for lattice of solid substitution solutions of zinc telluride-cadmium telluride system 18 p3095 A67-33446
- Volt-ampere characteristics effect on thickness of contact materials of some heterojunctions and band structures obtained by epitaxial deposition 18 p3103 A67-34446
- Zinc telluride laser generation by electron-beam excitation noting high threshold values 21 p3641 A67-38458

ZIRCONIUM

- Epitaxial deposition of Van Arkel zirconium on sodium chloride and calcium fluoride cleavages at various temperatures 02 p0286 A67-11711
- Zr-coated tungsten cathode in reducing divergence of electron beam emission 06 p0968 A67-18091
- Carbon and nitrogen mass transfer rates by liquid potassium in 18 thermal convection loops of type 316 stainless steel with niobium/one-percent-zirconium and stainless steel tabs at 1200 to 1800 degrees F 07 p1223 A67-19465
- Depressing effect of hafnium and zirconium on work function of tungsten, tantalum, niobium and rhenium 10 p1668 A67-23091
- Fourier analysis of line profiles of X-ray-studied deformation faulting in titanium, zirconium and hafnium 14 p2340 A67-29033
- Zirconium addition effect on dynamic strengthening temperature range of niobium alloys, discussing process mechanism 20 p3468 A67-37123
- Heterodiffusion of metallic impurities in body-centered phases of doped zirconium and titanium, determining diffusion coefficients via radioactive isotopes 22 p3820 A67-39823
- Positive effect of Zr on nickel plasticity, showing elimination of hot brittleness within wide range of temperatures 24 p4169 A67-41922

ZIRCONIUM ALLOY

- Phase diagram of W-Zr-Ti ternary alloy 01 p0093 A67-10291
- X-ray microstructural and chemical analysis of sintering of zirconium diboride-molybdenum disilicide alloys 01 p0102 A67-11242
- Chemical and crystal structural analysis of solid solution of titanium chromide and zirconium chromide 07 p1204 A67-19265
- Phase diagram of Nb-Ti-Zr system and superconducting properties of alloys 09 p1518 A67-22029
- Zirconium-niobium alloy analyzed by oxide replica technique, noting superconductivity and tunnel effect, determining relation

- between superconductivity current critical density and sample structural characteristics 10 p1889 A67-23090
- X-ray, microstructural and chemical analysis of sintering of zirconium diboride-molybdenum disilicide alloys 17 p2875 A67-33167
- Superplasticity resulting from high strain rate sensitivity observed in isothermal tension tests on several titanium and zirconium alloys 18 p3064 A67-34083
- Zirconium-niobium alloys investigated for oxygen impurity effects on critical current density and superconducting properties 19 p3243 A67-34925
- Laser macrophotography for size distribution of particulate debris dispersed from ablating zirconium alloy specimen in hyperthermal wind tunnel ablation testing 23 p4006 A67-41380

ZIRCONIUM CARBIDE

- Titanium, zirconium and hafnium effect on recrystallization temperature and strength of alloys of molybdenum with carbon 05 p0832 A67-17508
- Single conduction band approximation of nature of increase with temperature of thermal conductivity of ZrC and NbC in terms of scattering and Fermi energy 11 p1804 A67-23902
- Thermoemission properties of ZrC powder in vacuum and in cesium vapor under thermoelectronic conversion conditions 11 p1822 A67-24033
- Titanium, zirconium and hafnium effect on recrystallization temperature and strength of alloys of molybdenum with carbon 21 p3644 A67-38038
- TiC and ZrC powder properties after sintering investigated for linear growth rates vs temperature, obtaining sintering activation energy values 22 p3820 A67-39564

ZIRCONIUM COMPOUND

- High pressure hot-pressing fabrication of transition metal diborides without lower-melting metal additives 03 p0450 A67-13308
- Shrinkage process in zirconium diboride during sintering, noting variation with length of isothermal processing 03 p0456 A67-14191

ZIRCONIUM OXIDE

- Niobium and tantalum oxides from decomposition of zircon-pyrophor concentrate by silicon fluorides 04 p0637 A67-14941
- Frank-Condon factors and r centroids for C-X band system of astrophysically important zirconium oxide molecule found in S type stars 08 p1354 A67-20702
- Rolling friction studies of intermetallic and zirconium oxide for control surface bearings for space reentry vehicle [ASLE PAPER 66AM 5D4] 08 p1335 A67-21037
- Baddeleyite inclusion in Marthas Vineyard tektite identified by electron microscopy 11 p1858 A67-24065
- Composite structure of glass with crystalline aluminum oxide and zirconium oxide inclusions tested for strength and elastic properties 11 p1811 A67-24642
- Quenching examination of phase equilibrium in system lead oxide-titanium oxide-zirconium oxide, determining isotherms lines, melting points, etc 12 p1986 A67-26188
- Electronic states and transitions of zirconium oxide, noting Frank-Condon factors and r centroids, calculated from Morse model 16 p2704 A67-31173
- Partial Frank-Condon factors and r centroids for zirconium oxide molecule, noting transition probabilities 16 p2704 A67-31174
- Nonstoichiometry of zirconium oxide and relation to tetragonal-cubic inversion in zirconium oxide 16 p2694 A67-31597
- Effect of temperature, density, and amount of stabilization on elastic modulus of zirconia 16 p2695 A67-31701
- Combination of monoclinic zirconia, second ceramic and metal in electrodes of MHD generators 18 p3099 A67-33709

ZODIACAL DUST CLOUD

- Possible existence of circumstellar dust clouds emitting far IR radiation 04 p0702 A67-15588
- Interplanetary gas, solar corpuscular activity and magnetic storms and zodiacal dust cloud from satellite observations during IQSY and use of cometary tail as plasma

probe 07 p1248 A67-19333
Thermal radiation emission detection from interplanetary dust, showing that zodiacal dust extends to within 4 solar radii of sun and confirming Poynting-Robertson effect 13 p2189 A67-26264
Zodiacal dust explained by radioactive Al 26 deposited in marine sediments and brought by micrometeorites exposed to solar protons 15 p2553 A67-29157
Heliocentric dust cloud noting correlation of meteor and comet model with observations 17 p2842 A67-32325
Zodiacal dust particle flux measurements from OGO 3 and Mariner IV spacecraft in cisplanar and interplanetary space 19 p3318 A67-35185
Observational consequences of geocentric dust cloud whose particles are concentrated toward plane of ecliptic and which contribute to zodiacal light 19 p3222 A67-35460
Braking and heating effects of atmosphere on meteors in zodiacal dust to 1-meter size, discussing interaction at air cap, entry, etc 20 p3525 A67-36949
Zodiacal light and interplanetary dust, discussing brightness, polarization, color, spectrum and dust cloud about earth 22 p3794 A67-40426
IR nebula in Orion as protocluster with massive stars imbedded in opaque dust cloud, discussing collapse and lifetime 24 p4225 A67-41829
ZODIACAL LIGHT
Night sky phenomena and atmospheric attenuation of light from Beta Canis Majoris photographed from Gemini IX 01 p0151 A67-10965
Zodiacal light brightness variation during solar activity cycle 03 p0413 A67-13454
Zodiacal light and solar activity, examining results of visual observations and photometric measurements for correlation between phenomena 03 p0413 A67-13455
Lunar and cisplanar observation of interplanetary medium including lunar magnetic field, solar wind, existence of collisionless shock wave, gegenschein, zodiacal light and recovery of interplanetary particles 04 p0700 A67-15072
Zodiacal-light photometric measurements, analyzing effect of twilight radiation on observable brightness 04 p0617 A67-15558
Comet disintegration as basic source of interplanetary dust based on zodiacal isophots 04 p0701 A67-15559
Solar UV and zodiacal light, emphasizing importance and merits of rocket and balloon observations 05 p0799 A67-18873
Surface brightness and polarization state of zodiacal light measured from sounding rocket 08 p1326 A67-21244
Solar activity effect on brightness and polarization of zodiacal light 13 p2109 A67-26332
Rocket sounding of zodiacal light brightness at 4300, 5300 and 8000 angstroms 19 p3216 A67-35192
Observational consequences of geocentric dust cloud whose particles are concentrated toward plane of ecliptic and which contribute to zodiacal light 19 p3222 A67-35460
U.S. research program for IQSY 1964-1965 covering solar synoptic observations, zodiacal light, comet tails, atmosphere, etc 19 p3224 A67-35501
Pressure scanned Fabry-Perot interferometer for twilight sky and zodiacal light observations 20 p3440 A67-36361
Advances in astronomy and astrophysics, Volume 5, covering zodiacal light, periodic oscillations, sunspot groups, etc 22 p3889 A67-40425
Zodiacal light and interplanetary dust, discussing brightness, polarization, color, spectrum and dust cloud about earth 22 p3794 A67-40426
Photometry of zodiacal light during IQSY, discussing extension to poles 24 p4152 A67-43114
ZONAL HARMONICS
Odd zonal harmonics in terrestrial gravitational potential determined from 14 well distributed satellite orbits 02 p0235 A67-11475
Unstable modes of barotropic horizontally sheared zonal current in stratified atmosphere 04 p0611 A67-14650
Estimation problems in determining even

zonal harmonics of external geopotential from secular satellite motion, examining least squares method 05 p0797 A67-16573
Earth gravitational field parameters from near-surface satellite observations influenced by zonal and tesseral harmonics 05 p0800 A67-17080
Zonal harmonics investigation of mean temperature of stratospheric layers 06 p0996 A67-18447
Numerical integration of quasi-geostrophic atmospheric model with asymmetric zonal current 06 p0999 A67-18739
Zonal harmonics determination through satellite observations processed using computer program, noting necessity for increased number of satellites [AAS PAPER 66-91] 07 p1183 A67-19956
Zonal and tesseral harmonic perturbations of artificial satellite 08 p1382 A67-20399
Orbital disturbances of satellite produced by zonal harmonics of gravitational field 09 p1564 A67-21884
Cosmic ray distribution, discussing method of diurnal variations, zonal harmonics and spherical analysis 10 p1898 A67-22778
Atmospheric circulation in weak easterly region in troposphere over northwest Pacific in summer 10 p1677 A67-23499
Satellite orbit analysis and computer program for earth zonal harmonics determination, considering orbit elements and gravitational constants [AAS PAPER 66-91] 13 p2116 A67-27518
Geostrophic wind angular momentum transport at 500 mb in Northern Hemisphere, using zonal harmonic analysis, noting quasi-biennial cycle 15 p2512 A67-29201
Sensible heat transfer influence on dynamic stability of harmonic perturbations superimposed on zonal current, using Lorentz two-level model 15 p2512 A67-30057
Coefficients of odd zonal harmonics in terrestrial gravitation evaluated from orbital eccentricity analysis of artificial satellites 17 p2853 A67-33249
Zonal gravity harmonics of moon from tracking data 18 p3135 A67-34539
Quasi-biennial zonal wind and temperature oscillation in stratosphere and mesosphere, discussing periodicity and oscillation model 19 p3220 A67-35272
Cyclogenesis due to baroclinic instability in zonal and meridional basic current showing relationship by superimposing perturbation 19 p3252 A67-35528
Geostationary satellite stability in presence of geopotential field zonal harmonics, using Liapunov theory 19 p3333 A67-35569
MHD instability of sub-Alfven equations for zonal flow outside diurnally oscillating boundary layer of precessing spheroid 20 p3494 A67-36147
Theory on earth shape, considering surface of geoid assumed as equipotential surface at sea level, obtaining relations between zonal and tesseral harmonics coefficients 22 p3792 A67-39933
Cosmic ray distribution, discussing method of diurnal variations, zonal harmonics and spherical analysis 24 p4209 A67-42114

ZOND II SPACE PROBE

Electron and proton fluxes at geocentric distance of 7 earth radii measured by charged particle traps on interplanetary station Zond 2 12 p1998 A67-25818

ZOND III SPACE PROBE

Table of names of formations on moon far side identified by Zond III lunar orbiter photographs 02 p0329 A67-12498
Zond III interplanetary probe lunar surface photographs analyzed, considering asymmetry of moon, far side and relation of moon to solar system 05 p0887 A67-16059
Measurement of cosmic ray intensity by Zond III automatic space probe 10 p1701 A67-23230
Table of names of formations on moon far side identified by Zond III Lunar Orbiter photographs 10 p1709 A67-23366
Type II solar radio bursts observed by Zond III space probe 18 p3119 A67-33859
Zond III interplanetary probe lunar surface photographs analyzed, considering asymmetry of moon, far side and relation of moon to solar system 21 p3701 A67-37846
Interplanetary space cosmic ray intensity variation with time and distance from sun

measured by Zond III and Venera II simultaneously 23 p4055 A67-41102
1 to 5 Mev solar proton emissions observed by increased counting rates on Venera II and III and Zond III interplanetary probes 23 p4056 A67-41112
ZONE
S AURORAL ZONE
S BRILLLOUIN ZONE
S NULL ZONE
S RECOVERY ZONE
ZONE MELTING
Zone melting peculiarities for two-component system where semiconductor is ring-shaped or straight 01 p0127 A67-10074
Synthesis and growth of dendritic InSb films by electron beam microzone melting of vacuum deposited composite indium and antimony films, noting electrical properties 04 p0682 A67-15319
Electron beam float-zone melting process applied to dielectric compound aluminum trioxide to obtain sapphire crystals 04 p0628 A67-15320
Electron beam zonal fusion growth of Mo, W and Ta single crystals without using crucible 05 p0827 A67-16079
Electron beam zonal vacuum fusion growth of Mo-Nb alloy single crystals 05 p0827 A67-16080
Structure and mechanical properties of molybdenum-niobium system monocrystalline melts prepared by electron beam zonal melting 05 p0830 A67-17024
Structure and mechanical properties of molybdenum-niobium system monocrystalline melts prepared by electron beam zonal melting 14 p2338 A67-28491
Fusion crust of meteorites noting similar properties and relations in zonal arrangement of mineral associations in their formation 16 p2750 A67-31437
Liquid-zone melting process for preparing alloy bars with variable compositions 18 p3065 A67-34294
Intrinsic and impurity photoconductivity kinetics over wide temperature and illumination range of p-type indium sulfide single crystals obtained by zone melting 21 p3676 A67-37859
Closed form equation with variable segregation coefficient for single pass zone melting in binary alloy systems 22 p3856 A67-39368
ZONE REFINING
Continuous horizontal zone refining system for purification of organic compounds, inorganic salts, metals, etc 02 p0247 A67-12691
Hydrogen and nitrogen effect on ductility of beryllium purified by zone refining 13 p2136 A67-27103
Plastic behavior of zone refined and prestrained beryllium single crystals 13 p2137 A67-27111



U. of ILL. LIBRARY

JAN 3 1968

CHICAGO CIRCLE

AIAA TECHNICAL INFORMATION SERVICE

750 THIRD AVENUE

NEW YORK, N. Y. 10017